ENCYCLOPEDIA OF THE EYE

EDITED BY

DARLENE A. DARTT
JOSEPH C. BESHARSE
REZA DANA

EDITOR-IN-CHIEF

Darlene A. Dartt
Schepens Eye Research Institute
Harvard Medical School
Boston, MA, USA

EDITORS BIOGRAPHIES

Darlene A. Dartt

Senior Scientist, the Harold F. Johnson Research Scholar, and Senior Scientist, Schepens Eye Research Institute; Associate Professor, Department of Ophthalmology, Harvard Medical School, Boston, MA, USA. At the Schepens Eye Research Institute Dr. Dartt served as the Acting Director of Research and the Director of Scientific Affairs for 10 years. She received her AB degree from Barnard College (Columbia University) in New York City and her PhD from the Department of Physiology at the University of Pennsylvania in Philadelphia. After postdoctoral fellowships at the University of Copenhagen, Denmark, and Tufts University School of Medicine in Boston, Dr. Dartt joined the Schepens Eye Research Institute in 1985. Her primary research interest is the neural regulation of tear production. Her research focuses on the signaling pathways used by nerves and growth factors in the lacrimal gland and conjunctival goblet cells to induce secretion and proliferation and how dysregulation of these pathways can lead to dry-eye syndromes in mouse models and humans, particularly after refractive surgery. She has been continuously funded by NIH since 1980 for this work. Dr. Dartt directs the Institute's Department of Defense Research Program; she also chaired four Military Vision Research Symposia. She served on and chaired the ARVO Cornea Program Planning Committee and served on the Members in Training Committee. She was a founding member, a member of the organizing committee, and more recently treasurer for the Tear Film and Ocular Surface Society. She has been on the organizing committee for the three Biennial Cornea Conferences in Boston, MA. She served as Vice President for North America for the International Society for Eye Research and a Councilor for the International Society for Contact Lens Wear. She is on the editorial board for *Investigative Ophthalmology and Visual Science, Experimental Eye Research*, and *The Ocular Surface*. She served on the review panel for Fight For Sight and has been an *ad hoc* member of numerous NEI and NIAMS study sections. She received the Lew R. Wasserman merit award by Research to Prevent Blindness and is a Gold Fellow of ARVO.

Joseph C. Besharse

Dr. Besharse is currently the Marvin Wagner Professor and Chair of the Department of Cell Biology, Neurobiology, and Anatomy at the Medical College of Wisconsin. He received his BA degree from Hendrix College (Conway, Arkansas) and MA and PhD degrees from Southern Illinois University. After a brief period on the faculty at Old Dominion University in Virginia, he moved to Columbia University as a Postdoctoral Fellow in Retinal Research. He was appointed to the faculty of Department of Cell Biology and Anatomy at Emory University School of Medicine in 1977, becoming full Professor in 1984. He assumed the position of Professor and Chair of Anatomy and Cell Biology at the University Kansas School of Medicine (Kansas City) in 1989 and moved on to his present position at Medical College of Wisconsin in 1997. Dr. Besharse's research has focused on membrane turnover, circadian clocks, and microtubule-based transport in photoreceptors, with special attention to fundamental pathways that are disrupted in photoreceptor degenerative diseases. His research has been continuously funded by the National Institutes of Health since 1978. In addition to his roles as Department Chair and a Principal Investigator, he directs an NIH funded training program in vision science. Dr. Besharse is a past member of the editorial boards of *Investigative Ophthalmology and Vision Science* and *Vision Neuroscience* and served as the Section Editor for the 'Retina' section of *Experimental Eye Research*. He has served as a trustee of the Association for Research in Vision and Ophthalmology, and has served two full terms as a member of two different NIH study sections. Among his awards are the Alcon Research Award for outstanding research in Vision Science (1993), the Alumni Achievement Award from Southern Illinois University (1998) and the Distinguished Service Award from the Association for Research in Vision and Ophthalmology (2005). He is a Gold Fellow of ARVO.

Reza Dana

In addition to his role as Senior Scientist and Co-Director of Research at the Schepens Eye Research Institute, Dr. Reza Dana holds the Claes H. Dohlman Chair in Ophthalmology at Harvard Medical School. He is Director of the Cornea and Refractive Surgery Service at the Massachusetts Eye and Ear, and serves as the Vice Chairman of the Harvard Department of Ophthalmology and Associate Chief of Ophthalmology for Academic Programs at Massachusetts Eye and Ear. After graduating *Summa Cum Laude* from St. Paul's School in New Hampshire, he completed his bachelor's (Phi Beta Kappa), graduate, and medical education at Johns Hopkins University. He performed his residency in

Ophthalmology at the Illinois Eye and Ear Infirmary in Chicago, followed by a clinical fellowship in cornea and external diseases at the Wills Eye Hospital in Philadelphia. Dr. Dana then completed additional fellowship training in immunology and uveitis at the Massachusetts Eye and Ear Infirmary, and in ocular and transplantation immunology at the Schepens Eye Research Institute. Dr. Dana also holds an MS degree in management from Harvard University. Reza has been a member of the full-time Harvard faculty since 1995. As a clinician-scientist, he has a particular interest in the molecular and cellular mechanisms of inflammation as they pertain to the ocular surface and anterior segment pathologies, including dry eye, allergy, wound healing responses, and transplant rejection.

EDITORS AFFILIATIONS

EDITOR-IN-CHIEF
Darlene A. Dartt
Schepens Eye Research Institute
Harvard Medical School
Boston, MA
USA

SENIOR EDITORS
Joseph Besharse
Department of Cell Biology,
Neurobiology and Anatomy
Medical College of Wisconsin
Milwaukee, WI
USA

Reza Dena
Massachusetts Eye and Ear Infirmary
Schepens Eye Research Institute
Harvard Medical School
20 Staniford Street
Boston, MA
USA

SECTION EDITORS
Barbara Battelle (Comparative Eye)
University of Florida
Whitney Laboratory
St. Augustine, FL
USA

David Beebe (Lens)
Washington University School of Medicine
Saint Louis, MO
USA

Peter Bex (Visual Optics)
Schepens Eye Research Institute
Harvard Medical School
Boston, MA
USA

Paul Bishop (Vitreous)
University of Manchester
Manchester
UK

Dean Bok (Retina)
Jules Stein Eye Institute
David Geffen School of Medicine
University of California,
Los Angeles, CA
USA

Patricia D'Amore (Vascular Biology)
Schepens Eye Research Institute
Harvard Medical School
Boston, MA
USA

Henry Edelhauser (Ocular Surface)
Emory University Eye Center
Atlanta, GA
USA

Linda McLoon (Orbit)
Departments of Ophthalmology and Neuroscience
University of Minnesota
Minneapolis, MN
USA

Jerry Niederkorn (Immune Homeostasis of the Eye)
University of Texas Southwestern Medical Center
Dallas, TX
USA

Thomas Reh (Retinal Developemnt)
University of Washington
School of Medicine
Seattle, WA
USA

Ernst Tamm (Aqueous Humor Dynamics and Optic Nerve)
Institute of Human Anatomy and Embryology
University of Regensburg
Regensburg
Germany

PREFACE

Eye research has grown explosively over the years, and simultaneously with it individual scientists have become more specialized. Coupled with this dichotomy is the wide range of disciplines covered in eye research, from visual optics to butterfly vision and corneal structure to blood vessel growth. These variables necessitate a reference work that provides concise, easily understandable information on a wide range of subjects, and gives guidance on the most important articles to read from the literature. The *Encyclopedia of the Eye* was created to serve as such a reference work.

Each article in the encyclopedia contains text (easily understandable for scientists outside the field of the article), a number of multimedia and color figures that illustrate the most important points of the article, and a list of references to provide more in-depth information. Articles are primarily directed at scientists looking for an entry point into a field tangential to their specialty as well as at graduate students and postdoctoral fellows in eye research. The articles will be especially useful to scientists designing introductory or generalized courses that cover diverse fields of eye research. Scientists writing review articles or chapters will also find the encyclopedia articles especially useful as a starting point. The many introductory articles are written at a level that university undergraduates can understand, but include enough information to satisfy the more advanced needs of graduate students and postdoctoral fellows. The more in-depth articles on specialist research areas are ideal for postdoctoral fellows and experienced scientists. The plentiful multimedia figures will be especially helpful in understanding the more complicated points as well as illustrating basic processes and anatomy.

The format of the *Encyclopedia of the Eye* was selected by the editor-in-chief in collaboration with two senior editors, Drs. Reza Dana and Joseph C. Besharse. We covered the field of eye research with focus on specialties in ocular surface, immunology, clinical research, and retina. To choose the articles to be included in the encyclopedia, we selected 11 major areas of eye research that cover the entire field, with the exception of visual processing. The areas included the ocular surface, ocular immunology, vascular biology, orbit, aqueous humor, lens, vitreous, retina, visual optics, comparative eye research, and ocular development. Thus, the scope of the encyclopedia includes all fields of eye research, except visual processing. The latter area has been the focus of several recent major reference works. A prominent scientist in each area was chosen as a section editor. Each of the section editors in collaboration with the editor-in-chief and senior editors developed a list of articles to cover all important topics in the 11 major areas. The introductory articles and those with in-depth discussions of more focused specialized areas both are included in the encyclopedia. The section editors then selected an expert as the author for each article. Finished articles were reviewed by three individuals, the section editors, senior editors, and the editor-in-chief. Thus, the *Encyclopedia of the Eye* is a collaborative product of the most eminent scientists in eye research.

Eye research has become specialized and compartmentalized over the years and, to a large extent, has split among anatomical lines from the anterior to the posterior eye. For example, cornea research and retina research follow different paths and are based on different underlying concepts of cellular organization. The *Encyclopedia of the Eye* bridges this gap by including articles on all facets of eye research. In particular, we have included several topics usually not found in vision research reference works. These include orbit, vitreous, comparative eye research, and ocular development. These areas have unique specializations that are fascinating by themselves and highlight differences among well-known tissue or organism functions. Two articles in particular illustrate these points: one on the metabolism of intraocular muscles, which is unique to these nonfatiguing muscles; the other on color vision in butterflies, which allows butterflies to recognize each other.

Importantly, study of the eye and its various components involves pathways found in other tissues and provides insight into the function of the other tissues and organs. In addition, eye research has been a pacesetting discipline in many areas. Thus, the *Encyclopedia of the Eye* will provide knowledge and insight to scientists from wide-ranging disciplines, in addition to eye research itself. For example, eye research has provided seminal discoveries that impact other fields, such as gene therapy, genetics of human disease, angiogenesis, and retinal signaling pathways. Several unique areas of eye research

include the immune-privileged response of the eye, the prevention of blood vessel growth in the cornea and lens, and the role of a GTP-binding protein coupled cascade in retinal photoreceptor signaling. For all these reasons the *Encyclopedia of the Eye* will be valuable for nonvision biomedical scientists.

Articles are arranged in alphabetical order. The best way to find an article is to look at the subject index, as both introductory and more specialized articles are included in the encyclopedia. It could be advantageous to start with an introductory article to obtain knowledge about anatomy and the basic functions and then follow up with a more specialized, in-depth article. Furthermore, a subject could be included in an introductory, broader article and perhaps under a name that is not the reader's first guess.

An experienced, prompt, reliable, and thorough editorial staff is essential to the success of a major reference work. The outstanding contribution of the senior and section editors are appreciatively acknowledged by the editor-in-chief.

The editor-in-chief would like to gratefully acknowledge the scientific and editorial help of Ms. Robin Hodges. Ms. Hodges provided invaluable help in keeping track of all the articles in their various stages of the editorial process, contacting authors to keep them on schedule, and assisting the senior editors Drs. Reza Dana and Joseph C. Besharse. Without the expert help of Ms. Hodges, the *Encyclopedia of the Eye* would not be the outstanding new major reference work that it is. The editor-in-chief would also like to acknowledge the extremely helpful advice of Dr. Richard Masland, whose experienced suggestions were invaluable in setting up the editorial team as well as Dr. Joe G. Hollyfield for his helpful suggestions for section editors.

DARLENE A. DARTT
Editor-in-Chief

FOREWORD

This is a very long book – if indeed it should be denominated as a book – but it does not need a long Foreword. The editors, who are well chosen scholars of the eye, have assembled a remarkable series of over 200 articles, that cover a vast landscape on the biology of the eye, and do so with clarity and depth. They cover the eye from the front to the back – from the corneal tear film to the axons of the optic nerve.

The coverage is judicious. Each subject has an article that reviews its basic biology, these are accompanied by more specialized topics, commonly those relating to disease processes. Because disease processes are socially important, they deserve this emphasis – and it should be noted that they also have things to teach about the basic biology. The basic biology is presented in substantial depth, not only as a token gesture in the direction of the fundamentals. This kind of balance between basic biology and clinical subjects is rarely achieved, and the effect is that this is not only a Google-ready reference work but one that can be read serially, like a traditional expository volume.

The Introduction to another encyclopedia in this series makes reference to Wikipedia, the free form "Encyclopedia of Everything" created by a community of volunteer authors. The present encyclopedia has in common with Wikipedia great breadth, accessibility to rolling revision, and the fact that its authors are paid almost nothing. It is a credit to the editors, to the authors, and to our scientific community that so many talented people would devote their skill and effort primarily *pro bono* – for the common good.

And it is a very great "good." I hope and believe that this will become a standard, universal source for information about the eye. In this it also has a communality with Google and the Internet, but also a major difference: the information that appears in the Encyclopedia of the Eye is curated, by the editors and by the authentic experts whom they have chosen to write the articles. So I see this as an ongoing venture, a core resource that will roll forward with new authors and new editors as the science moves forward. It is an ambitious venture and I wish it all success.

Richard H. Masland
Charles A. Pappas Professor of Neuroscience
Harvard Medical School

PERMISSION ACKNOWLEDGMENTS

The following material is reproduced with kind permission of Nature Publishing Group

Fig 1 of "Dynamic Immunoregulatory Processes that Sustain Immune Privilege in the Eye"
Fig 1 of "Molecular Composition of the Vitreous and Aging Changes"
Fig 2 of "Molecular Composition of the Vitreous and Aging Changes"
Fig 3 of "Molecular Composition of the Vitreous and Aging Changes"
Fig 6 of "Molecular Composition of the Vitreous and Aging Changes"
Fig 5 of "Pathological Retinal Angiogenesis"
http://www.nature.com/nature

The following material is reproduced with kind permission of American Association for the Advancement of Science

Fig 2 of "Immunopathogenesis of Onchocerciasis (River Blindness)"
Fig 6 of "Information Processing: Horizontal Cells"
Fig 1 of "Rod and Cone Photoreceptor Cells: Outer-Segment Membrane Renewal"
http://www.sciencemag.org

The following material is reproduced with kind permission of Taylor & Francis Ltd

Table 2 of "Drug Delivery to Cornea and Conjunctiva: Esterase- and Protease-Directed Prodrug Design"
Fig 6 of "Drug Delivery to Cornea and Conjunctiva: Esterase- and Protease-Directed Prodrug Design"
http://www.tandf.co.uk/journals

A

Abnormal Eye Movements due to Disease of the Extraocular Muscles and Their Innervation

A Serra, University of Sassari, Sassari, Italy
R J Leigh, Case Western University, Cleveland, OH, USA

Glossary

Amblyopia – Lazy eye with poor vision because of misalignment of the eyes during development.
Chronic progressive ophthalmoplegia (CPEO) – This term describes a number of disorders affecting the extraocular muscles that lead to progressive limitation of eye motion.
Diplopia – Double vision.
Esotropia – Misalignment of the eyes, one of which turns in (toward the nose)–cross-eyed.
Exotropia – Misalignment of the eyes, one of which turns out (away from the nose)–wall-eyed.
Kearns–Sayre syndrome – One cause of CPEO (see above) that is inherited from the mother and affects other tissues, such as the heart.
Myasthenia gravis – A disorder causing muscle fatigue that is due to failure of the nerves to stimulate the muscles to contract.
Nystagmus – An oscillation of the eyes (shimmering or jumping eyes).
Optokinetic reflexes – Eye movements induced by moving a visual pattern in front of the eyes.
Ptosis – Droopy lids.
Saccades – Rapid eye movements that are used to move the point of visual fixation from one feature of interest to the next.
Smooth pursuit – Eye movements that smoothly follow a moving object, such as a bird in the sky.
Strabismus – Misalignment of the eyes; the eyes point in different directions.
Vestibulo-ocular reflexes – Eye movements induced by head movements, which stimulate the balance mechanism in the inner ear.

Introduction

In this article we apply current knowledge of the extraocular muscles (EOMs) and their brainstem innervation to develop working hypotheses to account for a range of abnormal eye movements. To be concise, we have mainly selected diseases with well-defined processes that affect specific sites, from muscle to premotor neurons in the brainstem (**Figures 1** and **2**). This bottom-up approach is somewhat reductionist and simplified, but we hope that it will provide insights for readers with a broad range of interests. For more comprehensive reviews, readers can turn to sources listed at the end of this article.

A prerequisite for understanding disordered ocular motility is that eye movements can be systemically examined (**Table 1**). Thus, restricting attention to the most evident disturbance (e.g., strabismus) will impoverish interpretation of the underlying disorder. Conversely, considering the properties of saccades, pursuit, vestibular, and vergence eye movements, as well as the presence of any visual deficits, will enrich the understanding of the pathogenesis of the disorder.

Effects of Disorders of the EOMs on Eye Movements

The EOMs (**Figure 1**, site 1) possess unique properties that make them resistant to some diseases and susceptible to others. Thus, on the one hand, the EOMs are spared in Duchenne muscular dystrophy, even when the disease is well advanced, a finding that has prompted much research. On the other hand, EOMs are rich in mitochondria, which is appropriate for the sustained contraction required for precise gaze control, but which makes them susceptible to mitochondrial disorders. Although such disorders

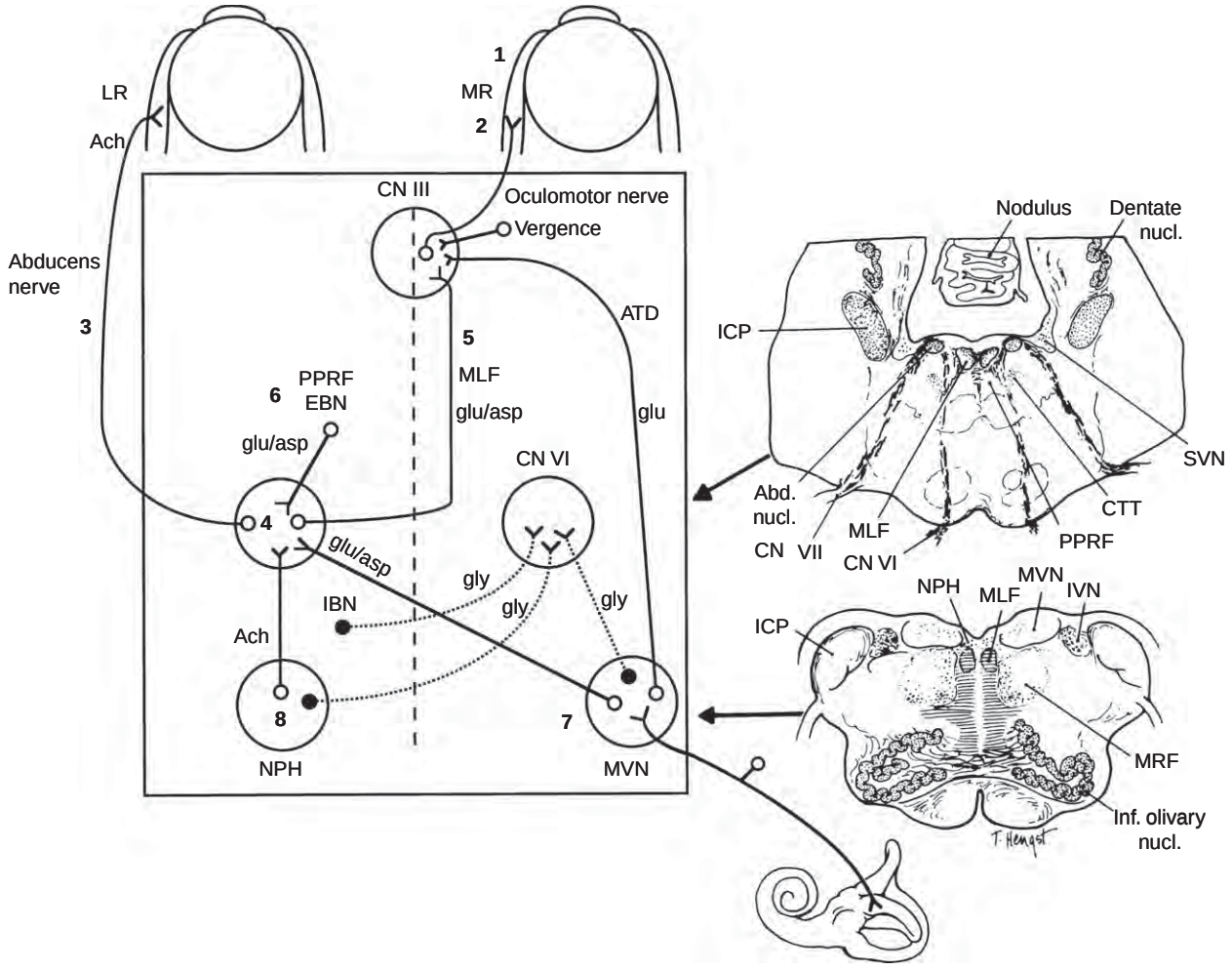

Figure 1 Anatomic scheme for the synthesis of signals for horizontal eye movements. The abducens nucleus (CN VI) contains abducens motoneurons that innervate the ipsilateral lateral rectus muscle (LR), and abducens internuclear neurons that send an ascending projection in the contralateral MLF to contact medial rectus (MR) motoneurons in the contralateral third nerve nucleus (CN III). From the horizontal semicircular canal, primary afferents on the vestibular nerve project mainly to the MVN, where they synapse and then send an excitatory connection to the contralateral abducens nucleus and an inhibitory projection to the ipsilateral abducens nucleus. Saccadic inputs reach the abducens nucleus from ipsilateral excitatory burst neurons (EBNs) and contralateral inhibitory burst neurons (IBNs). Eye position information (the output of the neural integrator) reaches the abducens nucleus from neurons within the nucleus prepositus hypoglossi (NPH) and adjacent MVN. The medial rectus motoneurons in CN III also receive a command for vergence eye movements. Putative neurotransmitters for each pathway are shown: Ach, acetylcholine; asp, aspartate; glu, glutamate; gly, glycine. The anatomic sections on the right correspond to the level of the arrowheads on the schematic on the left. Abd. nucl., abducens nucleus; CN III, oculomotor nerve; CN IV, trochlear nerve; CN VI, abducens nerve; CN VII, facial nerve; CTT, central tegmental tract; ICP, inferior cerebellar peduncle; IVN, inferior vestibular nucleus; Inf. olivary nucl., inferior olivary nucleus; MVN, medial vestibular nucleus; MRF, medullary reticular formation; SVN, superior vestibular nucleus. Numbers indicate lesion sites that are discussed in the text. Adapted from Leigh, R. J. and Zee, D. S. (2006). *The Neurology of Eye Movements*, 4th edn. New York: Oxford University Press.

may arise in childhood along with involvement of other tissues, such as heart muscle (Kearns–Sayre syndrome), these may present throughout adulthood with the syndrome of chronic progressive ophthalmoplegia (CPEO). Such individuals have ptosis and a limited range of eye movements. The complaint of diplopia is rare in CPEO, and although this had been ascribed to equal involvement of each of the eye muscles, another explanation seems more likely. Thus, slow progression of CPEO allows time for the visual system to adapt, and suppress images from one eye. Another interesting finding is that such patients may also make relatively quick eye movements (saccades or vestibular eye movements), despite a limited range of movement. This anomaly may be due to sparing of fast type myosin heavy chain (MyHC) EOM-specific global EOM fibers, which have fewer mitochondria.

Besides mitochondrial disorders, the EOM may be affected by other genetic diseases such as hereditary

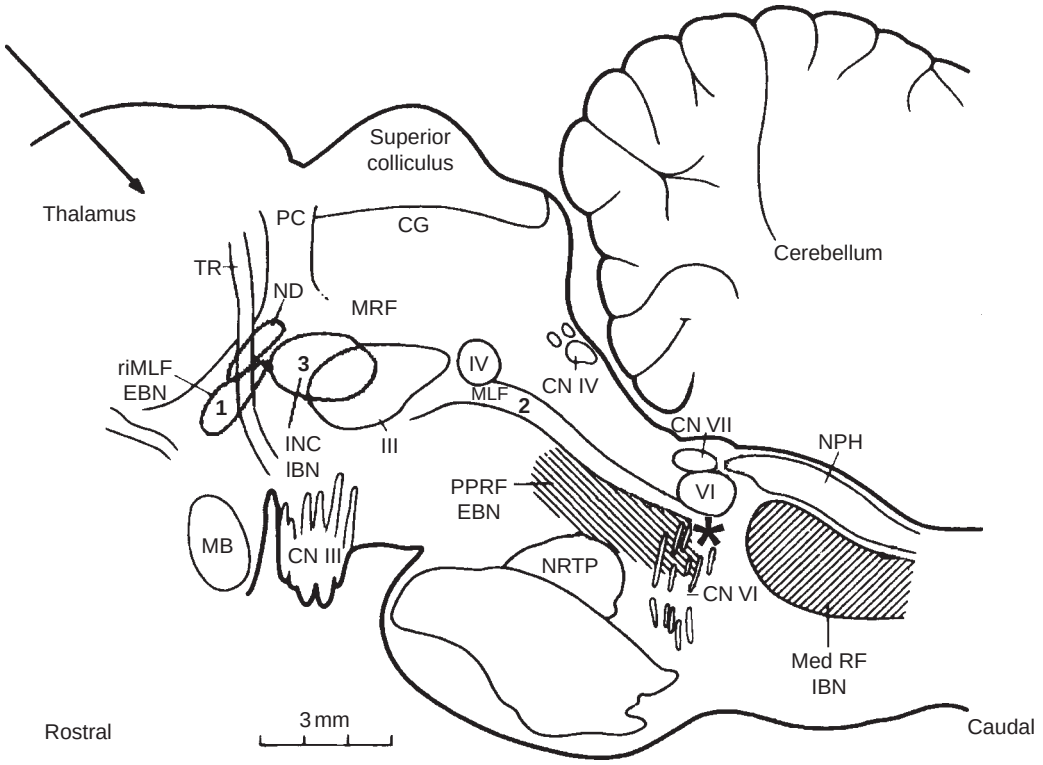

Figure 2 A sagittal section of the monkey brain stem showing the locations of premotor burst neurons: excitatory burst neurons for horizontal saccades lie in the paramedian pontine reticular formation (PPRF) and, for vertical and torsional saccades lie in the rostral interstitial nucleus of the medial longitudinal fasciculus (rostral iMLF). Burst neurons project to ocular motoneurons lying in the abducens nucleus (VI), the trochlear nucleus (IV) and the oculomotor nucleus (III). Omnipause neurons (indicated by an asterisk) lie in the midline raphe of the pons between the rootlets of the abducens nerve (CN VI) and gate the activity of burst neurons. CG, central gray; MB, mammillary body; MT, mammillothalamic tract; CN III, rootlets of the oculomotor nerve; CN IV, trochlear nerve; ND, nucleus of Darkschewitsch; NRTP, nucleus reticularis tegmenti pontis; PC, posterior commissure; NPH, nucleus prepositus hypoglossi; TR, tractus retroflexus. The arrow refers to the Horsley-Clarke plane of section. Numbers indicate lesion sites that are discussed in the text. Courtesy of Dr. Jean Büttner-Ennever).

disorders of myosin, or acquired disorders that present as a restrictive ophthalmopathy, such as thyroid disease. Thyroid ophthalmopathy, which has been attributed to accumulation of glycosaminoglycans in the orbit, often presents with vertical diplopia that is worse on wakening. Associated lid retraction and exophthalmia are common manifestations.

Effects of Disorders of the Neuromuscular Junction on Eye Movements

Eye movements are especially susceptible to a disease affecting the neuromuscular junction (**Figure 1**, site 2), classical myasthenia gravis, which is due to an abnormal immune attack on the postsynaptic acetylcholine receptor. In half of all patients with myasthenia gravis, diplopia or ptosis is the presenting complaint and, in about 80% of patients, movements of the eyes and lids are ultimately abnormal, with fluctuating weakness. Why are the EOMs so susceptible to diseases affecting the neuromuscular junction? One physiological reason arises from the demands made of eye movements to sustain the precise alignment of the eyes required for single binocular vision. It follows that fluctuating weakness due to myasthenia often causes ocular misalignment and diplopia. One morphological reason is that the postsynaptic junction of the EOM is poorly folded, thereby reducing the potential area for acetylcholine receptors. It follows that the EOM will be especially susceptible to loss of acetylcholine receptors. However, one subtype of EOM fibers, the MyHC EOM-positive myofibers (fast twitch/fatigable), which seems important for fast eye movements, does have substantial folding of its postjunctional membranes and, therefore, seems less susceptible to fatigue. Thus, it is interesting to note that patients with severe ocular myasthenia and little residual movement often retain the ability to make fast movements (quiver movements)-presumably due to preserved activity of their MyHC EOM-positive fast twitch myofibers.

Table 1 Functional classes of human eye movements

Class of eye movement	*Main function*
Vestibular	Holds images of the seen world steady on the retina during brief head rotations or translations
Visual fixation	Holds the image of a stationary object on the fovea by minimizing ocular drifts
Optokinetic	Holds images of the seen world steady on the retina during sustained head rotation
Smooth pursuit	Holds the image of a small moving target on the fovea; or holds the image of a small near target on the retina during linear self-motion; with optokinetic responses, aids gaze stabilization during sustained head rotation
Nystagmus quick phases	Reset the eyes during prolonged rotation and direct gaze toward the oncoming visual scene
Saccades	Bring images of objects of interest onto the fovea
Vergence	Moves the eyes in opposite directions so that images of a single object are placed or held simultaneously on the fovea of each eye

Adapted from Leigh, R. J. and Zee, D. S. (2006). *The Neurology of Eye Movements*, 4th edn. New York: Oxford University Press.

Why is diplopia a common complaint in ocular myasthenia but rare in CPEO? The view that the eyes move conjugately in CPEO but not in myasthenia is not supported by measurements of eye movements. A more cogent reason is that the weakness in ocular myasthenia is highly variable (hence the characteristic symptom of fatigue), whereas in CPEO it evolves slowly and steadily. Thus, in CPEO the visual system has time to adapt to the loss of binocular correspondence, whereas in ocular myasthenia visual inputs are continually varying. This is not to state that adaptation of eye movements does not occur in myasthenia: the converse is the case, and is often evident by the occurrence of abnormally large eye movements immediately following pharmacological reversal of the neuromuscular failure by intravenous injection of the acetylcholine esterase inhibitor, edrophonium.

Although ocular myasthenia is the most common disease to affect the EOM neuromuscular junction, other disorders that can impair eye movements include systemic botulism, neuromuscular blocking agents, and the Lambert-Eaton myasthenic syndrome (LEMS), which is due to the impaired release of acetylcholine secondary to autoimmune attack on presynaptic P/Q voltage-gated calcium channels. As opposed to myasthenia, in LEMS, repetitive saccades may change from hypometric (under-shooting) to hypermetric (over-shooting) as a consequence of the characteristic facilitation of muscle strength.

Effects of Disorders of the Oculomotor, Trochlear, and Abducens Nerves on Eye Movements

Palsies of the nerves innervating EOMs are common in clinical practice and cause diplopia and selective patterns of weakness of the muscles they supply. Such paralytic strabismus (misalignment of the visual axes) is greatest when the affected patient attempts to look in the direction of the weak muscle. Thus, in the case of left abducens palsy (**Figure 1**, site 3), the patient cannot abduct (turn out) the affected eye to the left. However, such weakness and the attendant diplopia is a stimulus to adapt the neural signals that move the eyes. Such adaptive changes are evident if the strong eye is covered and the weak eye forced to view the world. A similar situation occurs naturally if the weak eye is also the visually dominant eye. In either case, the level of innervation is increased in motoneurons supplying muscles that induce corresponding movements in each eye. Thus, in our example, the left lateral rectus, which turns the left eye out, and the right medial rectus, which turns the right eye in, would both receive increased innervation. One consequence of this adaptation is that movements of the weak eye may improve (unless paralysis is complete). A second consequence is that the strong eye, which also receives increased innervation, would, for example, make leftward saccades that overshoot the visual target. Such behavior is sustained for some time after adaptation even if the weak eye is covered and the strong eye views. This is a special example of plastic adaptation or motor learning, a property that depends heavily on the cerebellum, and which has been a subject of research interest for the past quarter-century. Because of the yoking mechanism by which eye movements are made conjugate in the brainstem circuitry (see the next section), there is a limitation to how much adaptive mechanisms can contribute to the recovery of the weakness due to nerve palsy. Nonetheless, such adaptive mechanisms undoubtedly contribute to the recovery from ocular motor nerve palsies. Paradoxically, in the case of trochlear nerve palsy, there is some recent evidence that such mechanisms may be maladaptive.

Effects of Disorders of the Brainstem Circuitry on Eye Movements

Horizontal Movements

The brainstem machinery whereby the eyes are coordinated to move together (conjugately) in the horizontal plane is summarized in **Figure 1**. The abducens nucleus, which lies in the pons, may be regarded as the horizontal gaze center (**Figure 1**, site 4). Thus, the abducens nucleus receives inputs for each functional class of eye

movements, including saccades, smooth pursuit, vestibular and optokinetic reflexes. It follows that each of these classes of conjugate eye movement (Table 1) may be independently affected by disease. The abducens nucleus contains two main groups of neurons: abducens motoneurons and abducens internuclear neurons. Axons of abducens motoneurons project in the sixth (abducens) cranial nerve to innervate the lateral rectus muscle. Axons of abducens internuclear neurons cross the midline and ascend in the contralateral medial longitudinal fasciculus (MLF, Figure 1, site 5) to contact medial rectus motoneurons in the oculomotor nucleus, which lies in the midbrain. Axons of medial rectus motoneurons project in the third (oculomotor) cranial nerve to innervate the medial rectus muscle.

It follows that lesions affecting the abducens nucleus (Figure 1, site 4) will impair movements of both eyes to the side of the lesion (horizontal gaze palsy). It also follows that lesions of the MLF (Figure 1, site 5) will impair the ability of the ipsilateral eye to adduct; this is called internuclear ophthalmoplegia (INO), because the coordination of the abducens motoneurons and oculomotor medial rectus motoneurons is disrupted. Multiple sclerosis (MS) is the most common etiology for an INO in young persons, especially when it is present bilaterally. Patients with INO due to demyelination of the MLF in MS show slowing or absent movements of the adducting eye because the MLF can no longer conduct high-frequency signals between the abducens and the oculomotor nuclei. However, vergence movements may be preserved either in abducens nucleus lesions or in INO, since vergence commands project directly to the oculomotor nucleus (Figure 1).

Horizontal saccades depend on premotor burst neurons, which lie in the paramedian pontine reticular formation (PPRF, Figure 1, site 6), and generate a high-frequency pulse of action potentials. Disorders affecting burst neurons of the PPRF selectively slow, or abolish, horizontal saccades. In contrast with abducens nucleus lesions, which cause complete horizontal gaze palsy, lesions of the PPRF usually spare ipsilateral smooth pursuit and vestibular eye movements.

The vestibulo-ocular reflex (VOR) for horizontal head rotations depends on vestibular afferents from the lateral semicircular canals, which relay their signal to the contralateral abducens nucleus via the medial vestibular nucleus (MVN, Figure 1, site 7). Wernicke's encephalopathy, a disorder due to thiamine deficiency that occurs in alcoholics, involves the vestibular nuclei and may impair the horizontal VOR.

The nucleus prepositus hypoglossi (NPH , Figure 1, site 8), the adjacent MVN, and the cerebellum play an important role in holding the eyes in an eccentric position (e.g., far right gaze) against the elastic pull of the orbital tissues. This function depends on mathematical integration of premotor (visual, vestibular, saccadic) signals by the NPH/MVN–cerebellar network. Impaired function of this network (leaky integration) due, for example, to intoxication with alcohol, causes the eyes to drift back to the center, leading to gaze-evoked nystagmus. It has also been postulated that the ocular motor neural integrator network may also become unstable causing either increasing velocity drifts away from center position or quasi-sinusoidal eye oscillations (acquired pendular nystagmus).

Vertical Movements

The coordination of eye movements in the vertical plane depends heavily upon neural circuits in the midbrain. However, there is no single vertical gaze center similar to the abducens nucleus for horizontal gaze. The oculomotor and trochlear nuclei (Figure 2) house motoneurons that innervate EOMs that rotate the eyes mainly vertically (superior and inferior rectus muscles) or mainly torsionally (around the line of sight-the superior and inferior oblique muscles). These motoneurons receive their saccadic input from the rostral interstitial nucleus of the medial longitudinal fasciculus (riMLF), which lies in the prerubral fields of the rostral midbrain. Bilateral lesions involving the riMLF (Figure 2, site 1) cause slow or absent vertical saccades, such as in progressive supranuclear palsy (PSP), a Parkinsonian disorder. Unilateral lesions of riMLF, such as in rostral brainstem strokes, cause loss of torsional rapid movements that rotate the top pole of the eye toward the side of the lesion.

The signals for vertical vestibular and pursuit eye movements ascend from the medulla and pons to the midbrain in the MLF and other pathways. Thus, bilateral MLF lesions (Figure 2, site 2), which occur in MS, cause impaired vertical pursuit and vestibular responses (as well as bilateral adduction failure during horizontal saccades, as described in the previous section). The interstitial nucleus of Cajal plays an important role in holding vertical eccentric gaze steady (e.g., far upward gaze); lesions here (Figure 2, site 3) cause gaze-evoked nystagmus on upward or downward gaze, postulated to be due to a leaky ocular motor integrator. The superior colliculus is a midbrain tectal structure that receives inputs from the cortical eye fields, and is important for triggering both horizontal and vertical saccades. Functional imaging studies in humans have demonstrated activation of the superior colliculus during generation of short-latency (express) saccades.

Neural circuits important for the generation of vergence eye movements are also located in the pretectum and midbrain, but pontine nuclei and their projections to the cerebellum also contribute. Thus, disturbances of vergence eye movements are encountered with lesions, such as strokes, throughout the brainstem. However, abducens nucleus lesions and INO (Figure 1, sites 4 and 5) usually spare vergence movements.

Congenital Misalignment of the Eyes (Infantile Strabismus) and Attendant Nystagmus

Ocular misalignment from infancy may be due to disorders of the orbital tissues, the innervation of EOM, or as a consequence of failure to develop binocular vision. The failure to develop binocular vision usually presents as the fusional maldevelopment nystagmus syndrome (FMNS), which includes amblyopia of one eye, strabismus (commonly esotropia and dissociated vertical deviation, with upward deviation of the covered eye) and latent nystagmus. Latent nystagmus is a jerk nystagmus comprising slow drifts of the eyes off target and a rapid resetting component that is absent when both eyes are viewing but appears when one eye is covered. The quick components of latent nystagmus beat away from the covered eye, and the nystagmus reverses direction upon covering of either eye. In most patients, the nystagmus is present (but low amplitude) when both eyes are uncovered, and is termed manifest latent nystagmus. Thus, although binocular viewing is possible, affected individuals almost invariably choose to fix with one eye and suppress the image from the other. Latent nystagmus can be induced experimentally in monkeys, either by depriving them of binocular vision early in life, or by surgically creating strabismus. In monkeys with latent nystagmus, the brainstem nucleus of the optic tract (NOT) shows abnormal electrophysiological properties. In normal monkeys, NOT neurons respond to visual stimuli presented to either eye. However, in monkeys with latent nystagmus, NOT neurons are driven mainly by the contralateral eye. Furthermore, inactivation of NOT with muscimol abolishes latent nystagmus in monkeys who have been deprived of binocular vision. Since the NOT projects to vestibular circuits concerned with gaze control during head rotations, one current view of the pathogenesis of latent nystagmus is that it represents the consequences of imbalance of visual inputs to the vestibular system, as if the subject was being rotated toward the side of the viewing eye.

Effect of Visual System Disorders on Eye Movements

Patients with a broad range of retinal disorders causing blindness is often a familial disorder. Both show continuous jerk nystagmus, with components in all three planes, which changes in direction over the course of seconds or minutes. The drifting null point, the eye position at which nystagmus changes direction, probably reflects an inability to calibrate the ocular motor system. Animals raised in a strobe illuminated environment, which deprives them of retinal image motion while still providing position cues, also develop spontaneous ocular oscillations. Gene therapy used to restore vision to dogs blind due to an inherited retinal disease resulted in a decrease in their associated nystagmus. Nystagmus is also a feature of albinism, which is associated with abnormal development of visual pathways and optic nerve hypoplasia.

Infantile Forms of Nystagmus in Individual with Normal Visual Systems

Infantile nystagmus syndrome (INS), or congenital nystagmus, may be present at birth but usually develops during infancy. The nystagmus is almost always conjugate and horizontal, even on up or down gaze, with a small torsional component. It is usually accentuated by the attempt to fix upon an object and by attention or anxiety. Up to 30% of patients with INS have strabismus but, even in individuals lacking strabismus, stereovision is usually degraded, partly due to retinal image motion. Head turns are common in INS and are used to bring the eye in the orbit close to the null point or zone, at which nystagmus is minimized. Some patients with INS also show head oscillations; such head movements could not act as an adaptive strategy to improve vision unless the VOR was negated. It seems possible that the head tremor and ocular oscillations in INS represent the output of a common neural mechanism. Measurements of nystagmus in INS demonstrate typical waveforms with increasing slow-phase velocity and the superimposed presence, during each cycle of oscillations (usually after a quick phase), of a brief period when the eye is still and is pointed at the object of regard. Such foveation periods are probably one reason why many individuals with INS have near-normal vision and why most do not complain of oscillopsia (illusory motion of the seen world), in spite of otherwise nearly continuous movement of their eyes.

INS, either with or without associated visual system abnormalities, is often a familial disorder. Both autosomal dominant and sex-linked recessive forms of inheritance have been reported. Although several hypotheses for the pathogenesis of INS have been offered, no animal models exist. At present, it seems possible that genetic studies will identify the underlying molecular mechanisms and point researchers to the neural disturbance causing INS.

Conclusions

Recent progress in understanding disorders of the EOMs and their innervation from the viewpoint of molecular biology and genetics is approaching the point where it can be combined with behavioral and electrophysiological studies. For example, recent evidence indicates that each functional class of eye movements (Table 1) is served by a separate population of ocular motoneurons

that receive specific premotor inputs. It follows that each functional class of eye movements may depend on distinct molecular mechanisms or morphological characteristics, from premotor neurons to EOM. Human diseases provide many opportunities to study behavioral effects of a disease when the disease process affects a specific site-such as the acetylcholine receptor in myasthenia gravis. In this way, insights from basic science have a growing impact on clinical ophthalmology and neurology, and vice versa.

See also: The Active Pulley Hypothesis; Congenital Cranial Dysinnervation Disorders; Cranial Nerves and Autonomic Innervation in the Orbit; Extraocular Muscles: Extraocular Muscle Anatomy; Extraocular Muscles: Extraocular Muscle Metabolism; Extraocular Muscles: Functional Assessment in the Clinic; Thyroid Eye Disease.

Further Reading

Kennard, C. and Leigh, R. J. (2008). Using eye movements as an experimental probe of brain function. A symposium in honor of Jean Büttner-Ennever. *Progress in Brain Research* 171: 1–603.

Leigh, R. J. and Zee, D. S. (2006). *The Neurology of Eye Movements,* 4th edn. New York: Oxford University Press.

Leigh, R. J. and Devereaux, M. W. (2008). *Advances in Understanding Mechanisms and Treatment of Infantile Forms of Nystagmus.* New York: Oxford University Press.

Accommodation

A Glasser, University of Houston, Houston, TX, USA

Glossary

Accommodation – The dioptric increase in optical power of the eye to focus at near. In the young phakic eye, this occurs through an increase in the lens surface curvatures.
Depth of field – The range of movement of an object in object space over which there is no perceptible change in focus of the image.
Depth of focus – The range of movement of the image in image space over which there is no perceptible change in focus of the image.

Optics of the Eye

The cornea and lens constitute the primary optical refracting surfaces of the eye. These are optical interfaces at which light is refracted because they are curved surfaces at which there exists a refractive index interface or boundary between the medium preceding the optical surface and the optical surface itself. The anterior corneal surface is the primary refracting surface of the eye which constitutes approximately 75% of the total optical refracting power of the eye. The cornea constitutes such an important and powerful optical surface because there is a greater refractive index boundary between air and the cornea than exists elsewhere in the eye. The posterior corneal surface and the anterior and posterior lens surfaces constitute the other primary optical interfaces of the eye. In addition, the lens has a gradient refractive index with a greater refractive index at the center than at the surface. This gradient also imparts additional optical power to the lens, resulting in a lens with greater overall optical power than if the lens had a uniform refractive index equal to the highest refractive index value at the center of the gradient. Light entering the eye is refracted at these optical interfaces and the gradient refractive index of the lens and drawn to a focus toward the retina.

Optics of Accommodation

Accommodation is defined as a dioptric increase in optical power of the eye with an effort to focus at near. A dioptric change means a change in optical power expressed in units of diopters where diopters are inverse or reciprocal meters. An unaccommodated emmetropic eye will form an in-focus image on the retina for objects at optical infinity (**Figure 1**). For the purposes of subjectively determining the refractive state or refractive error of an eye clinically, an object at a distance of 6 m from the eye is sufficient to constitute optical infinity for the eye. The vergence of light rays entering an eye from an object 6 m in front of the eye is calculated as $1/-6\,\text{m} = -0.16$ D. The minus sign is used to denote an object distance in front of the eye or rays that are diverging from the object toward the eye. The vergence of light rays entering the eye from an object at infinity would be $1/\infty\,\text{m} = 0$ D. The difference in vergence between 0 D and –0.16 D is undetectable for the eye and can be considered as negligible. Therefore, an emmetropic eye focused on an object at 6 m can be considered to be unaccommodated or relaxed. If a near object is placed in front of the eye, say at a point 0.5 m in front of the eye, the near object will have a vergence of $1/-0.5\,\text{m} = -2.0$ D. In an unaccommodated, emmetropic eye, the more divergent light rays from this near object would not be refracted sufficiently by the cornea and the unaccommodated lens to form a focused image on the retina. The rays reaching the retina would form a blur circle on the retina rather than a point image as the rays would not have converged to a point focus by the time they reach the retina. If the unaccommodated eye is to achieve an in-focus image of the near object on the retina, the eye must accommodate to increase its optical power. An increase in optical power of the eye will increase the vergence of the rays after refraction by the lens so that the rays leaving the posterior lens surface will converge to a focus on the retina. In the accommodated eye, the near object will form an in-focus image on the retina.

The Accommodative Anatomy

The ciliary muscle is elongated, triangular in shape, and located beneath the anterior sclera just posterior to the limbus. The shortest side of the triangular region faces anterior-inward and it is to this region of the ciliary body that the base of the iris inserts. The elongated, superficial, external surface of the ciliary muscle extends from the scleral spur posteriorly, curved along the inner surface of the anterior sclera. The apex of the ciliary muscle is oriented inward in the eye toward the lens equator and is covered by the pars plicata region of the ciliary processes. The inner surface of the ciliary muscle extends from the

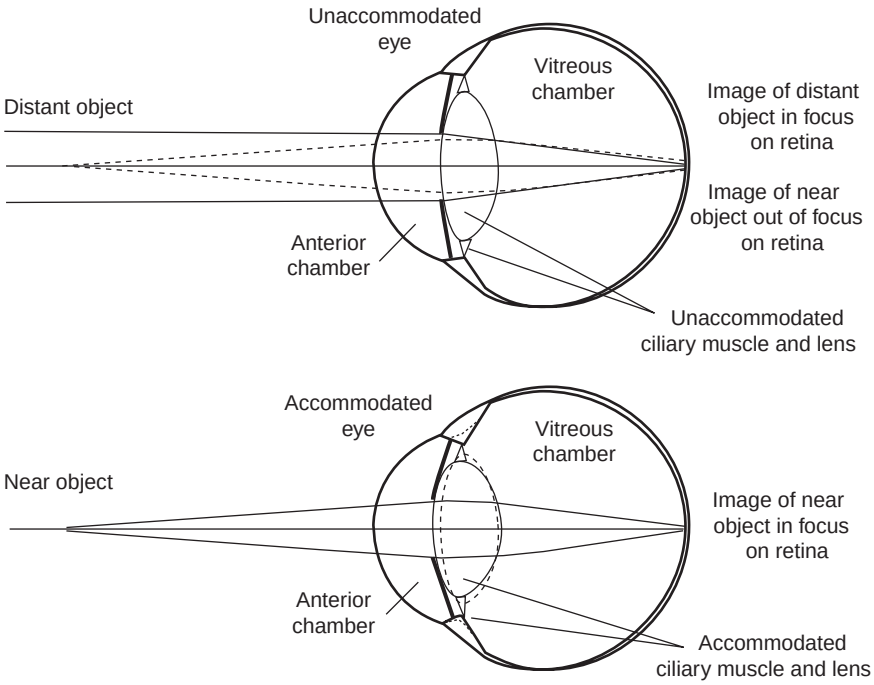

Figure 1 In an unaccommodated emmetropic eye, parallel rays from a distant object are refracted by the cornea and lens to form an in-focus image on the retina (upper diagram, solid rays). In the unaccommodated eyes, divergent rays from a near object would not be focused on the retina, resulting in an out-of-focus image on the retina (dashed rays). When the eye accommodated, the lens curvatures increase to increase the refraction of light such that the divergent rays from a near object are focused on the retina (lower diagram). Reproduced from Glasser, A. and Kaufman, P. L. (2002). Accommodation and presbyopia. In: Kaufman, P. L. and Alm, A. (eds.) *Adler's Physiology of the Eye: Clinical Applications,* 10th edn., pp. 197–233. St. Louis, MO: Mosby, with permission from Elsevier.

apex posteriorly toward the posterior insertion of the ciliary muscle and is covered by the pars plana region of the ciliary body. The ciliary muscle is composed of muscle fibers of three differing orientations. Most superficially, just beneath the sclera, are longitudinally oriented muscle fibers. These muscle fibers have their fixed origin at the scleral spur and their movable posterior insertion attached posteriorly to the choroid at the ora serrata of the retina. Deeper within the ciliary muscle and located more anteriorly toward the apex of the triangular-shaped region are the more radially oriented muscle fibers. Deeper still toward the apex of the triangular-shaped ciliary muscle are the circular muscle fibers. The muscle fibers are dually and reciprocally innervated by sympathetic and parasympathetic subdivisions of the autonomic nervous system. Although the muscle fiber orientations differ, the entire ciliary muscle contracts as a whole during accommodation. Contraction of the longitudinally oriented fibers acts principally to pull the posterior insertion of the ciliary muscle anteriorly; contraction of the radially oriented muscle fibers acts principally to consolidate and bulk up the apex of the triangularly shaped region; and contraction of the circularly oriented fibers acts principally to pull the apex of the triangle inward toward the lens equator. The pars plicate region of the ciliary body surrounding the anterior, inward-facing apical region of the ciliary muscle contains the dense vascular supply that provides oxygen and nutrients to the ciliary muscle. The ciliary muscle fibers have a greater abundance of mitochondria than any other muscle in the body, indicating the extraordinary high energy demands and requirements of this muscle. The lens is composed of transparent elongated lens fiber cells arranged in an onion-like shell structure. The central region of the lens, which is laid down earliest during embryological and postnatal development, is called the nucleus and, in the adult, is composed of anucleate lens fiber cells. Surrounding the nucleus is the developmentally younger lens cortex which is composed of the more recently differentiated lens fiber cells, some of which still contain nuclei. In the adult lens, the boundary between the nucleus and cortex is somewhat arbitrarily defined based on the appearance of optical zones of discontinuity due to refractive index boundaries visible from slit-lamp or Scheimpflug imaging. The lens is surrounded by a thin elastic membrane called the capsule. This is not of uniform thickness, but has an anterior midperipheral thickening ($\sim$10–15 μm) and thins toward the lens equator and around the lens posterior surface. The lens anterior surface is flatter than the posterior surface with radii of curvatures of approximately 10 mm and −6 mm, respectively. The lens axial thickness is approximately 4 mm and the lens equatorial diameter is approximately 10 mm. Dimensions of the lens change with age as the lens

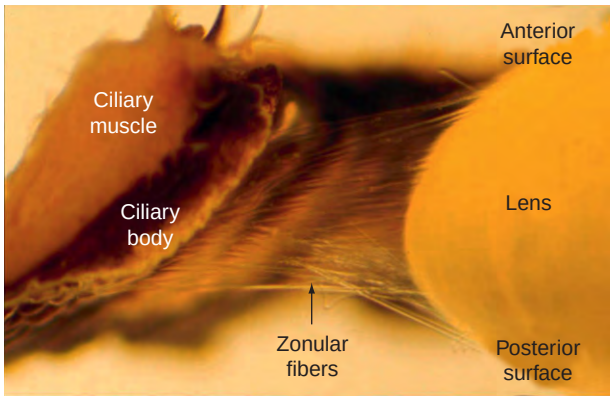

Figure 2 Photograph of a partially dissected human eye to show the accommodative structures. The cornea and sclera of the eye have been removed and the ciliary muscle and ciliary body have been cut through. The zonular fibers extend from all along the ciliary body across the circumlental space to insert into the capsule all around the lens equatorial region. Reproduced from Glasser, A. and Campbell, M. C. W. (1998). Presbyopia and the optical changes in the human crystalline lens with age. *Vision Research* 38: 209–229, with permission from Elsevier.

grows and also during accommodation, so these are approximate dimensions for an unaccommodated adult human lens. The lens is suspended by a fine meshwork of zonular fibers (**Figure 2**). These are fine elastic fibers and are inserted all around the lens equatorial region into the lens capsule, with no clear delineation into separate regional groups and with anterior–posterior crossing of zonular fibers visible. The zonular fibers extend from the lens equatorial region, through the valleys between the ciliary processes where they are anchored to the walls of the ciliary processes by a fine meshwork of anchoring fibers. The zonular fibers then continue their course posteriorly through the pars plicata region of the ciliary body forming a dense meshwork of fibers along the pars plana region of the ciliary body and finally insert into the ciliary epithelial tissue near the posterior insertion of the ciliary muscle.

The Accommodative Mechanism

The accommodative mechanism of the human eye has long been the subject of debate, but in recent years this debate has largely been quelled by numerous recent studies aimed at understanding why the eye gradually loses the ability to accommodate with increasing age in the condition called presbyopia. Early investigators studied the avian eye because of its relatively large size and ready availability in an effort to understand how the human eye accommodates. However, ultimately it has become clear that the accommodative mechanism in the avian eye differs between bird species and does not share much in common with the accommodative mechanism of the human eye. The varied accommodative mechanisms in birds led astray many early investigations into the accommodative mechanism. The relative inaccessibility of the structures involved in accommodation in the human eye also slowed progress in this area. Because of the similarity in anatomy and function between the eye of Old World monkeys and humans, much of our current understanding of the accommodative mechanism comes from studies on rhesus and cynomolgus monkeys, which share essentially the same accommodative mechanism as humans. Thanks to these studies, a consensus is developing regarding how the human eye accommodates.

The accommodative increase in optical power of the eye occurs through an increase in curvature of the anterior and posterior lens surfaces. In a young eye, the lens is relatively soft and pliable and is readily able to undergo a change in shape. When an object is moved toward the eye, the image on the retina becomes blurred. As the brain perceives that the near object is not in focus, it initiates a change in focus of the eyes. This begins with an increase in the frequency of the firing of the action potentials from the neurons in the midbrain Edinger–Westphal nucleus. Action potentials propagate down the preganglionic, parasympathetic long ciliary nerves to neurons in the ciliary ganglion. Postganglionic axons from the ciliary ganglion enter the globe via the short ciliary nerves, which enter the globe around the optic nerve, to innervate the ciliary muscle. The ciliary muscle contracts and the inner apex of the ciliary muscle moves toward the lens equator (**Figure 3**). The inward movement of the ciliary muscle and pars plicata of the ciliary body results in a release in the resting tension of the zonular fibers at the lens equator. When this zonular tension is released, the elastic capsule surrounding the lens molds the lens into a more spherical form. This causes a decrease in equatorial diameter of the lens (**Figure 4**), an increase in axial lens thickness, an increase in curvature of the anterior and posterior lens surfaces (**Figure 5**), a forward movement of the anterior lens surface, and a posterior movement of its posterior surface (**Figure 6**). These accommodative changes are qualitatively and quantitatively similar in humans and rhesus monkeys. The accommodative change in thickness of the lens is due to an increase in thickness of the lens nucleus without change in thickness of the anterior or posterior cortex. The anterior lens surface moves toward the cornea by about 75% of the increase in lens thickness and the posterior lens surface moves posteriorly toward the retina by about 25% of the increase in lens thickness. It is primarily the increase in the curvature of the anterior and posterior lens surfaces that results in the increase in optical power of the eye. These changes in the shape of the lens are linearly correlated with the increase in optical power of the eye during accommodation (**Figure 6**).

When an accommodative effort ceases, the ciliary muscle relaxes. In the young eye, the elastic posterior ciliary muscle, the elastic posterior tendons of the ciliary muscle and, possibly, the posterior zonular fibers pull the ciliary muscle back toward its unaccommodated state. As the

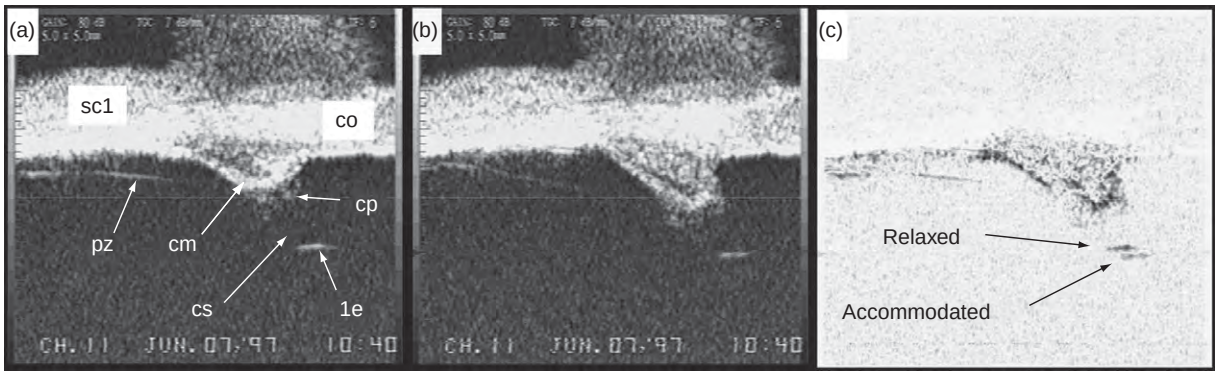

Figure 3 Ultrasound biomicroscopic (UBM) images of the temporal ciliary region of an iridectomized monkey eye (a) unaccommodated state and (b) accommodated to ~10 D, and the difference image (image (a) – image (b)) to show the movements of the accommodative structures. Only the extreme equatorial edge of the lens is seen in the UBM image. scl, sclera; co, cornea; pz, posterior zonular fiber bundle; cm, ciliary muscle; cs, circumlental space; cp, ciliary process; le, lens edge. Reproduced from Glasser, A. and Kaufman, P. L. (1999). The mechanism of accommodation in primates. *Ophthalmology* 106: 863–872, with permission from Elsevier.

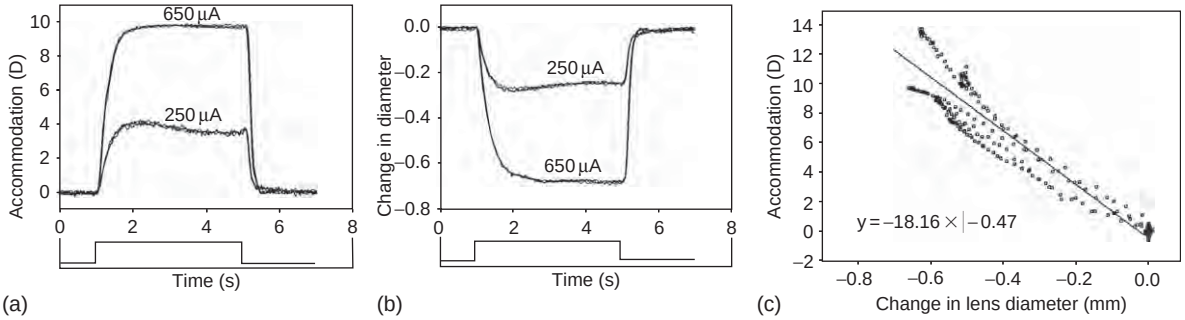

Figure 4 Graphs showing the decrease in lens diameter during centrally stimulated accommodation in iridectomized rhesus monkey eyes. (a) Accommodative refractive changes recorded dynamically with infrared photorefraction in response two different stimulus amplitudes (250 µA and 650 µA) delivered to the Edinger–Westphal nucleus of the brain. The lower graph represents the time course of the stimulus. Accommodative responses of about 4 D and 10 D, respectively, are produced. (b) Accommodative decreases in lens diameter recorded videographically, subsequent to the accommodative refractive changes, but using the same two different stimulus amplitudes. Decreases in lens diameter of about 250 and 650 µm, respectively, are produced. (c) Graph showing the correlation between accommodative refractive change and the accommodative decreases in lens diameter in the four eyes of two rhesus monkeys (with one experiment repeated in one eye). The data are from the accommodative phases only as seen in (a) and (b). Lens diameter decreases systematically with accommodation. Reproduced from Glasser, A., Wendt, M., and Ostrin, L. (2006). Accommodative changes in lens diameter in rhesus monkeys. *Investigative Ophthalmology and Visual Science* 47: 278–286, with permission from the Association for Research in Vision and Ophthalmology.

ciliary muscle is stretched posteriorly in the eye, the inner apex of the ciliary muscle and the ciliary body move outward at the lens equator. This causes an increase in tension on the zonular fibers at the lens equator, which pull the lens into its flattened, unaccommodated form via the elastic lens capsule. This results in a flattening of the anterior and posterior lens surface curvatures, a decrease in axial thickness of the lens and an increase in the equatorial diameter of the lens. The flattening of the lens results in a decrease in the optical power of the eye (**Figure 7**).

The most comprehensive, accurate, and widely known description of the mechanism of accommodation of the human eye was published by Helmholtz in 1855 (**Figure 8**). In actual fact, Antonie Cramer observed and published an earlier description of the changes in the curvature of the lens surface, quite possibly unbeknownst to Helmholtz. The accommodative mechanism, as is understood today, is often referred to as the Helmholtz accommodative mechanism. However, the mechanism originally described by Helmholtz was incomplete, due to limitations in early experimental methods. Subsequent investigators have added to the understanding of the accommodative mechanism. For example, although Helmholtz recognized that the lens undergoes an increase in thickness and a decrease in equatorial diameter during accommodation, he did not recognize how the lens changes its shape. Investigators prior to Helmholtz had suggested that the lens contained muscle fibers. In 1937, Fincham provided the first comprehensive description of the role of the capsule in accommodating the lens and, in 1979, Rohen offered a comprehensive description of the role of the zonular fibers. Only recently have studies identified limitations in

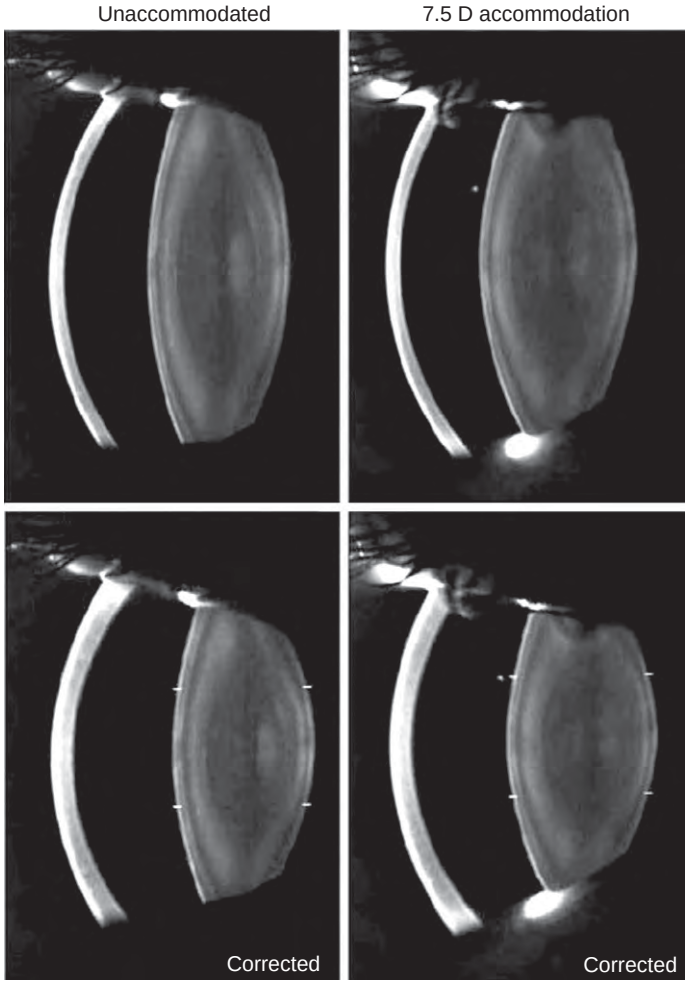

Figure 5 Scheimpflug images showing the accommodative change in the anterior chamber and lens from a 29-year-old human subject unaccommodated (left images) and accommodated to a 7.5-D accommodative stimulus (right images). The upper pair of images is uncorrected and the lower images have been corrected for the optical distortions through the preceding ocular media. As accommodation occurs, the lens surface curvatures become steeper, lens thickness increases, and anterior chamber decreases. Reproduced with permission from Dubbelman, M., van der Heijde, G. L., and Weeber, H. A. (2005). Change in shape of the aging human crystalline lens with accommodation. *Vision Research* 45: 117–132, with permission from Elsevier.

the mechanism described by Helmholtz. For example, Helmholtz and subsequent investigators believed that the posterior lens surface remains stationary during accommodation and undergoes little change in curvature. Recent studies however have documented a posterior movement of the posterior lens surface (see **Figure 6**) and an increase in curvature of the posterior lens surface during accommodation. Despite these modifications of the mechanism described by Helmholtz, the major tenets of the mechanism he described remain accurate and it is largely to his description that we owe our current understanding.

The Accommodative Triad

In a young individual, the effort to focus on a near object results in: (1) accommodation in both eyes, (2) constriction of the pupils, and (3) convergence of the eyes. These three events are together referred to as the accommodative triad. Accommodation, which is coupled in both eyes, increases the optical power of the eyes to allow focus on a near object. Convergence is required to achieve a single, fused image of the near object as viewed with both eyes. The pupil constriction increases the depth of field of the eye. As the pupil constricts, the cone of light converging toward the retina to form the image becomes narrower. A narrower cone of light means that there is a less perceptible change in focus of the image on the retina as the object is moved in object space. This represents an increased depth of focus of the eye and is closely related to the depth of field. The pupil constriction, therefore, further aids the actual accommodative optical change in power of the eye to allow near objects to be brought still closer to the eye without a perceptible change in focus. Convergence, pupil constriction, and

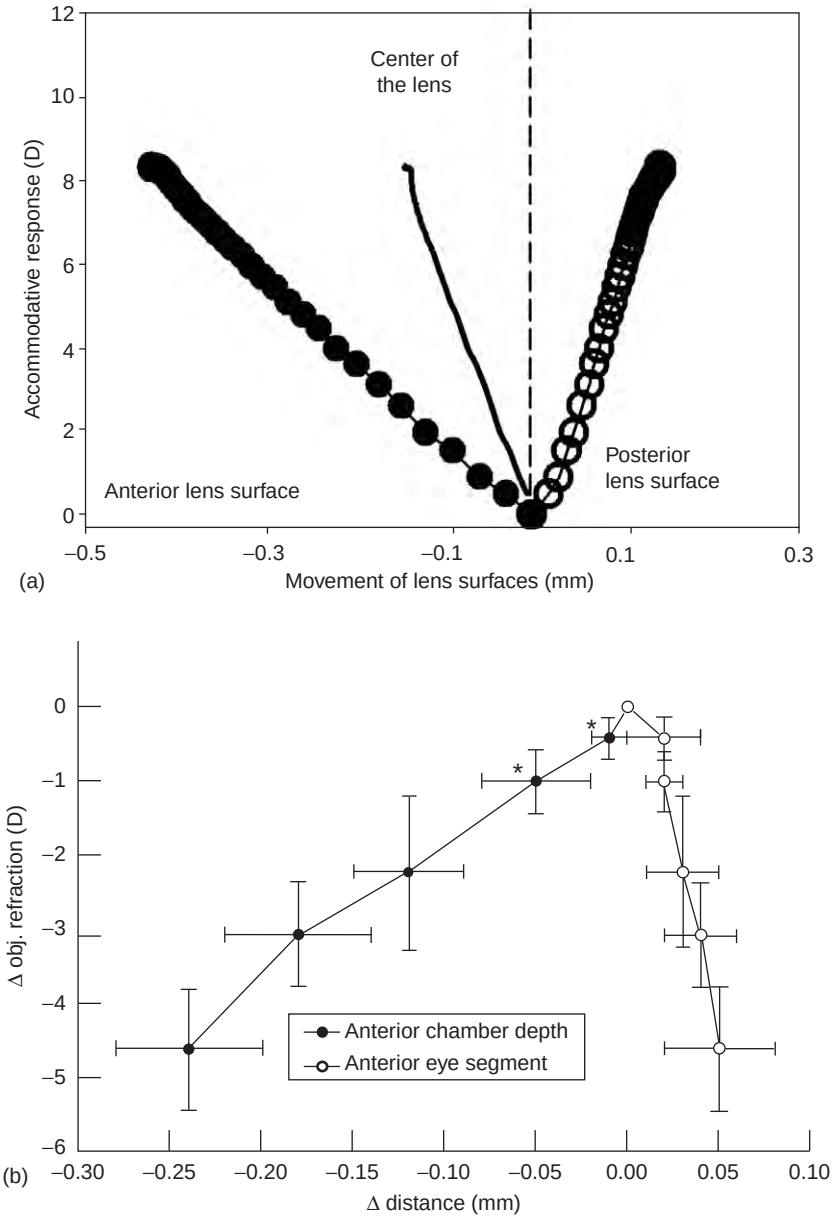

Figure 6 Axial accommodative biometric changes in the lens plotted as a function of the accommodative refractive changes in the eye in (a) an anesthetized rhesus monkey during Edinger–Westphal stimulated accommodation and (b) in 10 conscious human emmetropic subjects with a mean age of 23 years. Accommodation is represented as a positive number in (a) and as a negative number in (b). In both cases, the anterior lens surface moves toward the cornea (to the left in both graphs) and the posterior lens surface moves toward the retina (to the right in both graphs) relatively linearly with the accommodative refractive changes. The data from the monkey eye are both qualitatively and quantitatively similar to that from the human eyes. Reproduced from Vilupuru, A. S. and Glasser, A. (2005). The relationship between refractive and biometric changes during Edinger–Westphal stimulated accommodation in rhesus monkeys. *Experimental Eye Research* 80: 349–360, with permission from Elsevier and Bolz, M., Prinz, A., Drexler, W., and Findl, O. (2007). Linear relationship of refractive and biometric lenticular changes during accommodation in emmetropic and myopic eyes. *British Journal of Ophthalmology* 91: 360–365, with permission from BMJ Publishing Group Ltd.

accommodation are coupled in the brain. The act of initiating a convergence response to attain single binocular vision of a near object will also result in constriction of the pupils and accommodation. In the same way, accommodating to focus on a near object results in pupil constriction and a convergence response.

Changes in Optical Aberrations with Accommodation

The lens surfaces are aspheric and in conjunction with an aspheric cornea and the lens gradient refractive index; the eye is an imperfect optical system exhibiting optical

aberrations. Further, age-related changes in the lens and cornea result in age-related changes to the optical aberrations of the eye. The predominant aberration of the eye is spherical aberration. This is characterized by the light rays entering near the optical axis (paraxial rays) having a systematically different point of focus from the rays entering the eye at increasing distances from the optical axis. If the paraxial rays are focused to a point closer to the lens than the peripheral rays, this is called negative spherical aberration. The reverse situation, when the paraxial rays are focused further from the lens than the peripheral rays, is called positive spherical aberration. The young human lens has negative spherical aberration and with increasing age the spherical aberration becomes progressively more positive. After about 40 years of age, the human lens has predominantly positive spherical aberration. As the young eye accommodates, due to a combination of the changes in lens surface curvatures as well as a change in the form of the gradient refractive index of the lens, the lens and the eye undergo an increase in negative spherical aberration. This is due to a greater increase in optical power near the optical axis than toward the periphery of the lens. The pupil constriction that accompanies accommodation, in conjunction with the increase in negative spherical aberration of the eye, accentuates the overall increase in optical power of the eye by cutting off the more peripheral light rays that are focused further from the lens (**Figure 9**). Therefore, the pupil constriction is beneficial for increasing both the depth of field of the eye and in the overall optical power of the eye during accommodation.

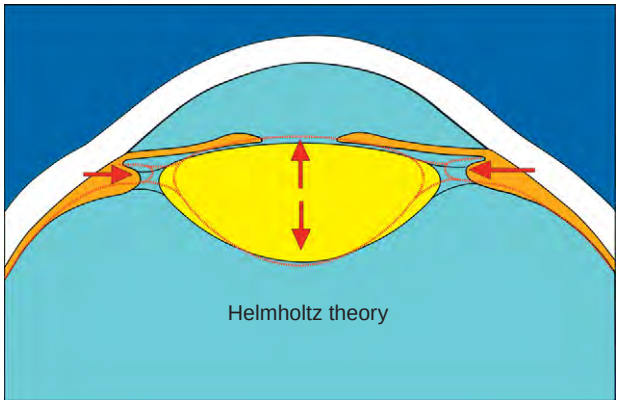

Figure 7 The accommodative changes in the ciliary body and the lens (red). The arrows depict the inward movement of the apex of the ciliary body (toward the axis of the eye) and the increase in lens thickness. Lens diameter decreases, the anterior lens surface moves anteriorly, the posterior lens surface moves posteriorly, and the anterior and posterior lens surface curvatures become steeper.

Other optical aberrations, such as astigmatism or coma, also aid in increasing the depth of field of the eye through degradation of the ocular image quality. In an eye with astigmatism or another optical aberration, the image formed on the retina is not ideal. For an eye with astigmatism, the image of a point object will appear as two orthogonal line foci separated by some distance (the interval of Sturm). The interval of Sturm is dependent on the magnitude of the astigmatism. As the object is moved in object space around the point of clearest vision in an unaccommodated eye with astigmatism, the image on the retina will transition gradually between one line foci and the orthogonal line foci. Therefore, although the appearance of the image on the retina will vary as the object is moved, there is no point of sharp image focus and hence no clear perception of a distinct change in image focus. As a consequence of the degraded image that is formed in an eye with astigmatism (or other optical

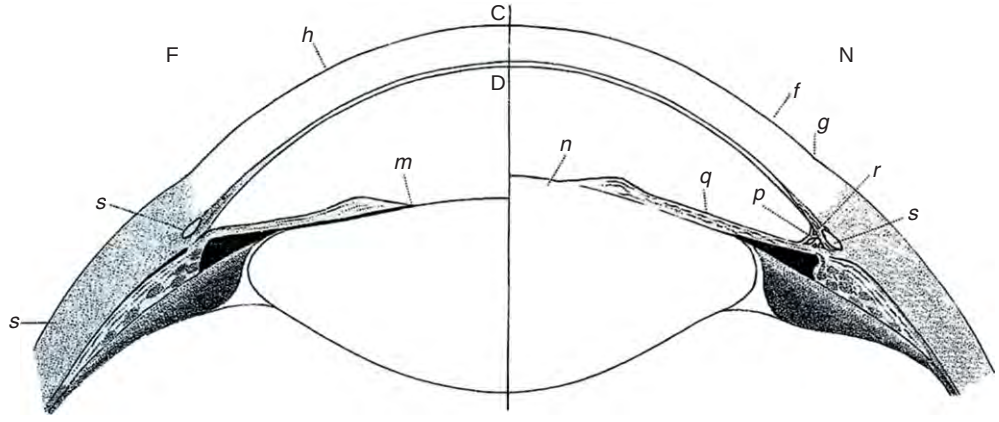

Figure 8 Helmholtz's diagram of the accommodative changes in the eye as he described it comparing the left unaccommodated side with the right accommodated side. Notice that there is no posterior movement of the posterior lens shown as is now known to occur. Reproduced from Helmholtz von, H. H. (1924). Mechanism of accommodation. In: Southall, J. P. C. (ed.) *Helmholtz's Treatise on Physiological Optics*, pp. 143–173. Baltimore, MD: The Optical Society of America. (Translated from the 3rd German edition, 1909.)

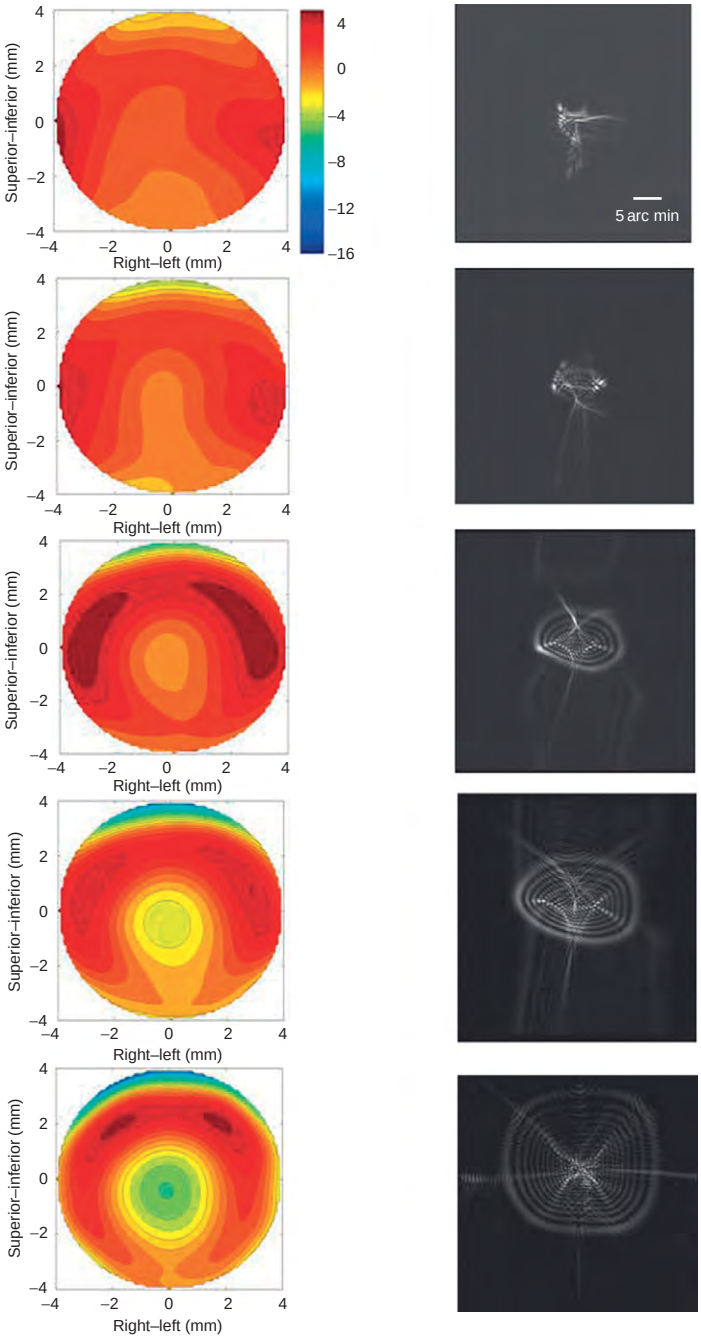

Figure 9 Measured wavefront maps with spherical defocus removed (left column) and calculated point spread function (PSF's) (right column) for 0 D, 1.41 D, 3.88 D, 5.93 D, and 10.91 D (top to bottom) of accommodation in the iridectomized of a rhesus monkey. There is a progressive increase in wavefront aberrations, especially near the center of the eye and a reduced image quality with accommodation. The false color scale is in microns and is the same for all wavefront maps. The predominant change in aberrations occurs in the central region with little change in the periphery which is normally obscured by the iris. The greatest change in optical power of the eye occurs at the center. Reproduced from Vilupuru, A. S., Roorda, A., and Glasser, A. (2004). Spatially variant changes in lens power during ocular accommodation in a rhesus monkey eye. *Journal of Vision* 4: 299–309, with permission from the Association for Research in Vision and Ophthalmology.

aberrations), the eye has an increased depth of field. Therefore, although the image quality is compromised by the optical aberrations, the object can be moved closer to the astigmatic eye without the subject reporting a perceptible change in image focus.

Measurement of Accommodation

Because of the many factors that affect the depth of field of the eye, such as ocular aberrations and small pupils, subjective measurement of near reading distance in a

distance-corrected eye, as is routinely performed clinically, is inappropriate for determining the true accommodative amplitude (the change in optical power of the eye during accommodation). Subjective push-up (or push-down) tests or subjective defocus tests, which rely on subjective blur cutoff criteria, inherently overestimate the true accommodative optical change in power of the eye, because they include the depth of field effects. The true accommodative optical change in power of the eye can only be measured with an objective optical instrument, such as autorefractors and wavefront aberrometers, which measures the refractive change in the eye with the effort to focus at near (**Figure 9**). To perform an objective measurement of accommodation, the refraction of the eye is first measured as the distance-corrected subject views a distant letter chart at 6 m. The subject is then presented with a near target at the closest near distance at which they can still maintain clear focus on the letters of a near letter chart and the refraction of the eye is again measured. The change in refraction between these two measurements represents the accommodative response amplitude. Subjective measurements of distance-corrected near reading distance overestimate the objectively measured accommodative amplitude by as much as 2–3 D in pre-presbyopic subjects (**Figure 10**). Subjective push-up tests suggest that accommodative amplitude is about 12–16 D at 10 years of age, which declines linearly to about 1 D by about age 55 years and remains at about 1 D thereafter. However, objective measurements in response to minus-lens-induced defocus show that there is an average of about 8 D of accommodative amplitude from age 5 to 25 years, which declines thereafter to essentially zero by age 55.

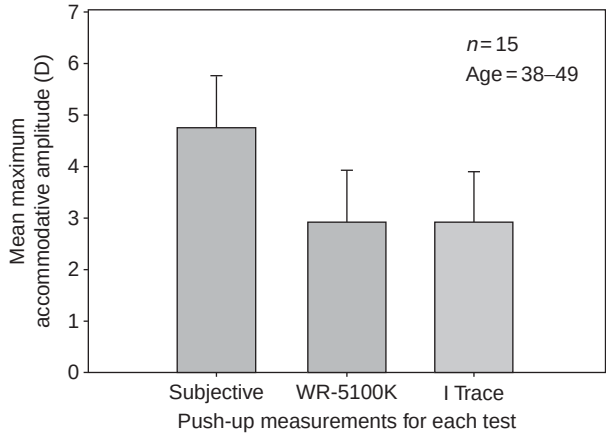

Figure 10 Comparison of the subjectively (subjective) and objectively (with a Grand-Seiko WR-5100K autorefractor or iTrace aberrometer) measured accommodative response amplitudes in pre-presbyopic subjects. Accommodation was stimulated with a real near-target progressively pushed-up toward the eyes. The subjective measurement of accommodation overestimates the objectively measured response amplitudes by between 1 and 3 D. Reproduced from Win-Hall, D. M. and Glasser, A. (2008). Objective accommodation measurements in prepresbyopic eyes using an autorefractor and an aberrometer. *Journal of Cataract and Refractive Surgery* 34: 774–784, with permission from Elsevier.

Stimulating Accommodation

Even when focused on a distant object, the young eye maintains a slight resting tonus of accommodation (sometimes referred to as the dark focus). This represents approximately 0.5–1 D of accommodation. Therefore, the normal resting refraction is slightly more myopic than the cycloplegic refraction, in which accommodation is completely paralyzed. The slight tonus of accommodation when focused for a distant object is called a lead of accommodation. To elicit an accommodative response, the eyes must be presented with an effective accommodative stimulus. This is best accomplished with a high-contrast stimulus that contains low-, mid-, and high-spatial-frequency visual cues. Letter charts or a Maltese cross represents visual targets often used to stimulate accommodation. There are several cues that can be effective for stimulating accommodation. Optical blur, proximity, and the requirement to converge to maintain single, binocular vision all offer cues that are important to facilitate an accommodative response. As a visual stimulus is moved progressively closer to the eyes, the target becomes blurred and this represents a cue to the eyes to start to elicit an accommodative response to attempt to maintain the target in clear focus. As the target is moved closer, the accommodative response falls behind the stimulus. This is called the lag of accommodation. As the target is moved toward the near point of the eyes, the eyes continue to accommodate within the amplitude of accommodation available. This is called the linear region of the accommodative stimulus/response curve. As the stimulus reaches the near point, the accommodative response reaches the maximum and asymptotes and the lag of accommodation becomes increasingly large as the stimulus is brought closer still. Since the eyes are no longer able to maintain clear focus on the stimulus, the accommodative response may begin to relax a little. To measure the maximum accommodative amplitude, the stimulus must be presented at the near point of the eyes and the refractive state of the eyes should then be measured objectively with an instrument such as an autorefractor or a wavefront aberrometer. The difference between this refraction measured when the eyes are focused on an object at the near point and the resting refraction when the eyes are focused on a distant target represents the objectively measured accommodative response amplitude.

Accommodative amplitude gradually declines with increasing age. This is the condition called presbyopia and ultimately results in a complete loss of accommodation.

See also: Astigmatism; Binocular Vergence Eye Movements and the Near Response; Lens Structure; Presbyopia; Pupil.

Further Reading

Cramer, A. (1853). Het accommodatievermogen der oogen, physiologisch toegelicht. Hollandsche Maatschappij der Wetenschappen te Haarlem 1:139-Haarlem: De Erven Loosjes.

Dubbelman, M., van der Heijde, G. L., and Weeber, H. A. (2005). Change in shape of the aging human crystalline lens with accommodation. *Vision Research* 45(1): 117–132.

Glasser, A. and Campbell, M. C. W. (1998). Presbyopia and the optical changes in the human crystalline lens with age. *Vision Research* 38 (2): 209–229.

Glasser, A. and Kaufman, P. L. (1999). The mechanism of accommodation in primates. *Ophthalmology* 106(5): 863–872.

Glasser, A. and Kaufman, P. L. (2002). Accommodation and presbyopia. In: Kaufman, P. L. and Alm, A. (eds.) *Adler's Physiology of the Eye: Clinical Applications,* 10th edn., pp. 197–233. St. Louis, MO: Mosby.

Glasser, A., Wendt, M., and Ostrin, L. (2006). Accommodative changes in lens diameter in rhesus monkeys. *Investigative Ophthalmology and Visual Science* 47(1): 278–286.

Helmholtz von, H. H. (1924). Mechanism of accommodation. In: Southall, J. P. C. (ed.) *Helmholtz's Treatise on Physiological Optics*, pp. 143–173. Baltimore, MD: The Optical Society of America. (Translated from the 3rd German edition, 1909.).

Rohen, J. W. (1979). Scanning electron microscopic studies of the zonular apparatus in human and monkey eyes. *Investigative Ophthalmology and Visual Science* 18(2): 133–144.

Rosales, P., Dubbelman, M., Marcos, S., and van der Heijde, R. (2006). Crystalline lens radii of curvature from Purkinje and Scheimpflug imaging. *Journal of Vision* 6(10): 1057–1067.

Rosales, P., Wendt, M., Marcos, S., and Glasser, A. (2008). Changes in crystalline lens radii of curvature and lens tilt and decentration during dynamic accommodation in rhesus monkeys. *Journal of Vision* 8(1): 18–12.

Vilupuru, A. S. and Glasser, A. (2005). The relationship between refractive and biometric changes during Edinger–Westphal stimulated accommodation in rhesus monkeys. *Experimental Eye Research* 80(3): 349–360.

Vilupuru, A. S., Roorda, A., and Glasser, A. (2004). Spatially variant changes in lens power during ocular accommodation in a rhesus monkey eye. *Journal of Vision* 4(4): 299–309.

von Helmholtz, H. H. (1855). Ueber die Accommodation des Auges. *Archiv für Ophthalmologie* 1(2): 1–74.

von Helmholtz, H. H. (1962). Mechanism of accommodation. In: Southall, J. P. C. (ed.) *Helmholtz's Treatise on Physiological Optics*, pp. 143–173. (transl. in 1924 and original German 1909). New York: Dover.

Wendt, M., Croft, M. A., McDonald, J., Kaufman, P. L., and Glasser, A. (2008). Lens diameter and thickness as a function of age and pharmacologically stimulated accommodation in rhesus monkeys. *Experimental Eye Research* 86(5): 746–752.

Acuity

M D Crossland, UCL Institute of Ophthalmology/Moorfields Eye Hospital, London, UK

Glossary

Cycles per degree – The number of complete phases of a grating (e.g., the distance between the center of a white bar and the center of the next bright bar in a square-wave grating; or the distance between two adjacent areas of maximum brightness on a sine-wave grating) contained in 1° of visual angle.
Minimum angle of resolution – The size of the angle subtended at the eye of the smallest feature which can be reliably identified on an optotype.
Minute of arc – One-sixtieth of a degree.
Optotype – A letter, symbol, or other figure presented at a controlled size to measure vision.
Visual angle – The angle, which a viewed object subtends at the eye.

Detection and Resolution Acuity

Visual acuity can be defined in two broad ways. Detection acuity is measured by determining the size of the smallest object which can be reliably seen (is there a circle on the first or second screen?). Detection can be elicited reliably with targets, which subtend an angle at the eye as small as 1 s of arc (1/3600°). Even a small point of light will stimulate several photoreceptors due to the point-spread function of the eye: that is, the way in which light is diffracted through the eye's optics (**Figure 1(a)**).

Tests that require the identification of a target are a measurement of resolution acuity. These tests frequently involve identifying a letter or reporting an object's orientation (what direction is this letter C facing?). Acuity for these tests depends on the separation of the target features: if they are too close, the point-spread function from each element will overlap and they will not be identified (**Figure 1(b)**). The smallest separation of the elements required for identification of the target (**Figure 1(c)**) is known as the minimum angle of resolution (MAR). For an adult observer with good vision, a typical MAR for a centrally presented, high-contrast target can be as good as 30 s of arc (1/120°). **Figure 2** shows the feature critical for the MAR for some commonly used tests of visual acuity.

Measurement of Visual Acuity

Visual acuity tests have been used for millennia: the ancient Egyptians are reported to have used discrimination of the twin stars of Mizar and Alcor as a measurement of vision. The most familiar clinical test of visual acuity, the Snellen chart, was introduced in 1862, and is still widely used today.

Detection acuity is often measured psychophysically by means of a temporal two-alternative forced-choice experiment (did the light appear in the first or the second interval?). Detection acuity is rarely measured clinically.

In psychophysical experiments of the visual system, resolution acuity is commonly measured by asking observers to report the orientation of a grating with variable separation between each dark and light bar (**Figure 2(b)**). In clinical practice, gratings are rarely used, with the exception of forced-choice preferential looking tests in preverbal children. These tests consist of a uniform gray field with an isoluminant grating toward one side of the chart (**Figure 3(a)**). In a featureless room, the test is presented to the child and the clinician observes whether the child looks toward the grating. The finest grating toward which the child repeatedly looks is recorded as the visual acuity.

For cooperative patients, optotypes are more often used to measure clinical resolution acuity. The Landolt C (**Figure 2(c)**) is the standard to which letter visual acuity tests are compared. This target consists of a ring of fixed width with a gap, of height equal to the stroke width, at the top, left, right, or bottom of the circle. The observer is asked to report the position of this gap. The smallest gap whose position can be reliably reported is equivalent to the MAR.

The National Academy of Sciences standard for visual acuity measurement advocates the presentation of 10 optotypes, of equivalent difficulty to the Landolt C, at each acuity size. The horizontal spacing between each optotype should be at least one character width, and vertical spacing between lines should be 1–2 times the height of the larger optotypes. It suggests that the number of characters on each line should be equal, and that the size difference between consecutive lines is 0.1 log units: in other words, for each target size, the next line should be approximately 1.26 times smaller.

The Snellen chart (**Figure 3(b)**) does not meet these recommendations: the number of letters per line and step

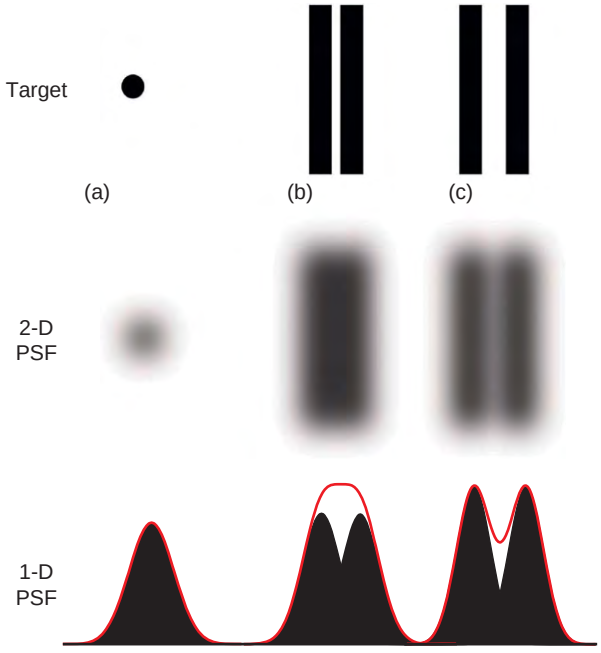

Figure 1 Schematic illustration of the point-spread function of three visual targets: (a) a point target; (b) two adjacent lines, too close to be resolved; and (c) two adjacent lines, with sufficient separation to be resolved. Middle row: two-dimensional representation of the target point-spread function; bottom row: one-dimensional representation of the point-spread function; and red line indicates the sum of energy incident on the retina. PSF, point-spread function.

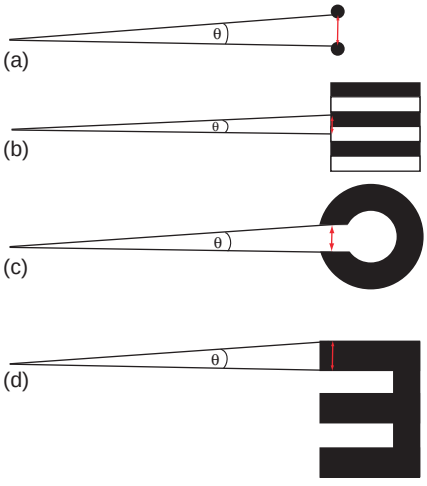

Figure 2 Examples of the limiting feature for four commonly used resolution tasks: (a) two-point discrimination task; (b) grating; (c) Landolt C; and (d) Sloan letter E (note that white gap size is equal in width to black bar elements).

size between the lines are variable, as is the horizontal and vertical spacing on the chart. There is also a marked difference in the legibility of different letters on the Snellen chart: a W, for example, has far less separation

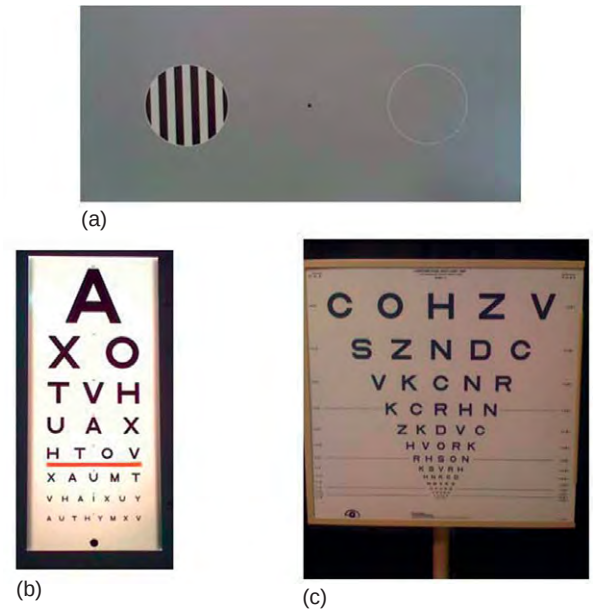

Figure 3 (a) A forced-choice preferential looking test consisting of a grating against an isoluminant background. Note the peephole in the center for the clinician to observe the child's visual behavior; (b) the Snellen chart; and (c) The ETDRS chart. ETDRS, Early treatment of diabetic retinopathy study.

between the elements of the letter and is more difficult to identify than a letter L. In the 1950s, Sloan suggested the use of 10 letters with a selection of vertical, horizontal, oblique, and round strokes which are each about as legible as a Landolt C. These Sloan letters are C, D, H, K, N, O, R, S, V, and Z. Each of the Sloan letters has a stroke width of the MAR and has a total height and width of five times the MAR.

The Bailey–Lovie chart, introduced before the recommendations of the National Academy of Sciences, conforms to most of these requirements, although it only has five letters per line. Further, the letters on the Bailey–Lovie chart are taller than they are wide: their height-to-width ratio is 5:4 and they are selected from the British Standards set of letters (D, E, F, H, N, P, U, V, R, and Z). The ETDRS chart (**Figure 3(c)**), developed for the early treatment of diabetic retinopathy study (ETDRS), is similar in design but does use the recommended 5×5 Sloan letters.

A criterion of 7/10 letters being read correctly for a line to be marked as seen was suggested by the National Academy of Sciences. This threshold reduces the chance of the line being scored correctly by chance (by a blind observer) to around 1 in 9 000 000. On a chart with five letters per line, recording a visual acuity where four of the five letters are read correctly equates to a chance success rate of 1 in 46 000. There is a theoretical advantage if the observer knows there are only 10 letters which can be presented on the chart: if an observer guesses from all 26 letters rather than the ten Sloan letters, the probability of the observer getting four out of five letters correct reduces to about 1 in 100 000.

Test–retest variability of the Snellen chart is around ±0.3 logMAR, while the ETDRS chart has far better repeatability (test–retest variability ~0.1–0.2 logMAR). Despite the many limitations of the Snellen chart, it is still widely used in clinical practice. While this is likely to be largely due to clinicians' familiarity with the Snellen chart, there is also a perception that Snellen acuity measurement is quicker than that on the Bailey–Lovie or ETDRS charts.

Various modified versions of the ETDRS chart exist: for example, a version with an altered letter set (A, B, E, H, N, O, P, T, X, and Y) has been developed for use by readers of most European languages, including those based on Cyrillic or Hellenic alphabets.

For observers unable to report letters on a sight chart, other frequently used optotypes include the tumbling E chart (formerly and less politically correctly known as the illiterate E chart), where a letter E is shown in each of four rotations; the HOTV chart, where only these four letters are used; symbols such as the Lea or Kay pictures; and simple shapes, such as the Cardiff card.

Reporting Visual Acuity

Clinicians have traditionally used Snellen fractions to record visual acuity, where the numerator is the test distance and the denominator the target size. The target size is expressed, counterintuitively, as the distance from which the target has an MAR of 1 min of arc. Therefore, a visual acuity of 6/6 indicates that from 6 m, letters with MAR 1-min arc are correctly identified, while a visual acuity of 3/36 indicates that from 3 m, the targets identified have a MAR of 1 min of arc when viewed from 36 m. The reciprocal of the Snellen fraction gives the visual acuity in MAR: so a visual acuity of 3/36 indicates a MAR of 12 min of arc.

In much of Europe, the Snellen fraction is reduced into a decimal fraction.

A further confusion with the Snellen system is that in countries not using the metric system, distances are expressed in feet rather than meters, with 20/20 being exactly equivalent to 6/6 but with a test distance of 20 ft rather than 6 m. Although Snellen recommended adoption of the metric system in 1875 and, in 1980, the US National Academy of Sciences favored adoption of a standard defined in meters, given the imminent adoption of the metric system, the feet system is still widely used in the USA, and among lay people in the UK.

The accepted standard for expressing visual acuity in clinical research, and increasingly in clinical practice, is to use the base 10 logarithm of the MAR (logMAR), such that 0.0 logMAR is equivalent to 6/6 or 20/20, and 1.0 logMAR is the same as 6/60 or 20/200. Table 1 gives approximately equivalent values in MAR, cycles per degree, Snellen fractions in meters and feet, decimal acuity, and logMAR for a range of visual acuities.

Optical and Neural Limits on Visual Acuity

Visual acuity is limited by many factors: the optics and refraction of the eye; the clarity of the optical media; the spacing and function of the retinal photoreceptors; the ratio of retinal ganglion cells to photoreceptors; and the resolution of the primary visual cortex and higher areas of visual processing.

Each diopter of myopia reduces visual acuity: a −1.00DS myope will typically have uncorrected visual acuity of around 0.5 logMAR (6/18; 20/60) and a two-diopter myope will have vision of around 0.8 logMAR on a distance test. Hypermetropia can often be relieved by accommodation in young people, but each diopter of hypermetropia

Table 1 Visual acuity conversion table[a]

MAR (min)	*Cycles/ degree*	*Snellen (metric)*	*Snellen (feet)*	*Decimal*	*Log MAR*
60	0.5	1/60	20/1200	0.017	1.8
20	1.5	3/60	20/400	0.05	1.3
10	3	6/60	20/200	0.1	1
6.3	4.7	6/36	20/120	0.17	0.8
4	7.5	6/24	20/80	0.25	0.6
3.2	9.4	6/18	20/60	0.33	0.5
2	15	6/12	20/40	0.5	0.3
1.6	18.8	6/9	20/30	0.67	0.2
1.3	23	6/7.5	20/25	0.8	0.1
1	30	6/6	20/20	1	0
0.83	36	6/5	20/17[b]	1.2	−0.1
0.67	44	6/4	20/13[b]	1.5	−0.2
0.5	60	6/3	20/10	2	−0.3
0.33	91	6/2	20/7	3	−0.4

[a]Each row contains approximately equivalent values of visual acuity. Log MAR values have been rounded to 1 decimal place.
[b]On US Snellen charts, these lines are 20/16 and 20/12 respectively.

beyond the accommodative ability of the eye will reduce visual acuity by a similar amount to an equivalent degree of myopia. Astigmatism, particularly where the meridia of astigmatism are oblique, will also reduce uncorrected vision significantly.

Other aberrations of the eye beyond defocus and astigmatism further limit visual acuity. Retinal image quality can be improved by viewing monochromatic stimuli (to reduce chromatic aberration) and by using a deformable mirror to correct coma, trefoil, and other higher-order aberrations of the eye. Under these ideal conditions, Williams and colleagues have shown that subjects are able to resolve gratings of up to 55 cycles per degree, equivalent to a visual acuity of approximately –0.30 logMAR (6/3; 20/10).

Assuming that an image is perfectly focused on the retina, the next limit on visual resolution is the spacing of the retinal photoreceptors. In order to detect a grating, alternate black and white bars must fall on adjacent photoreceptors. This theoretical limit of vision, known as the Nyquist limit, is equivalent to a grating with light to dark separation of $1/\sqrt{D}$, where D is the center-to-center separation of two photoreceptors. In the fovea, D is approximately 3 µm, equivalent to a visual angle of approximately 55 cycles per degree – almost identical to the value found by Williams. This confirms that in people with good vision, all of the limits on visual acuity are precortical. Amblyopia, where vision is reduced despite the absence of any eye disease, is dealt with elsewhere in the encyclopedia.

Visual Acuity across the Retina

Nonfoveal vision is limited by many elements. First, the eye's optics are not optimized for viewing off the visual axis, and peripheral vision is subject to greater aberration than central vision. Second, the size of photoreceptors increases and their density falls with increasing eccentricity. The number of photoreceptors per retinal ganglion cell also increases, from less than one photoreceptor per ganglion cell in the fovea to more than 20 photoreceptors per ganglion cell in the far periphery. The volume of visual cortex devoted to noncentral retina is also proportionally lower. It is unsurprising, therefore, that visual acuity falls quickly with increasing distance from the fovea (**Figure 4**). This is one reason for the severely reduced visual acuity of people with central vision loss from diseases such as age-related macular disease.

Visual Acuity over Life

Over the first year of life, visual acuity assessed by a preferential looking test appears to be reasonably stable

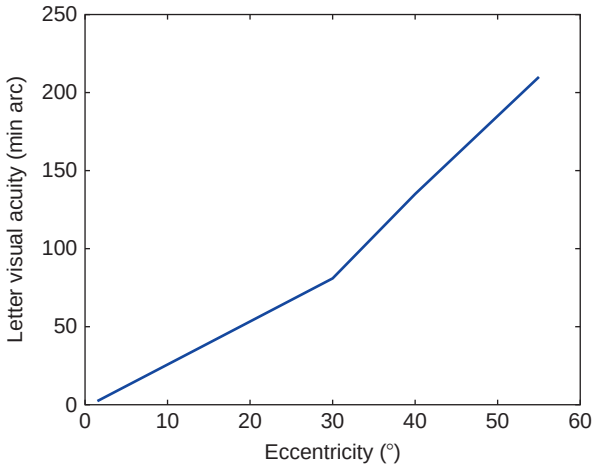

Figure 4 Letter visual acuity measured in peripheral vision as a function of degrees of eccentricity. Data from Anstis, S. M. (1974). Letter: A chart demonstrating variations in acuity with retinal position. *Vision Research* 14(7): 589–592.

at around 6 min of arc. Between a child's first and third birthday, visual acuity improves exponentially to reach 1 min of arc. A further small improvement in resolution ability to approximately 0.75 min of arc is achieved by age 5 years. In the absence of eye disease, this value remains relatively constant until the sixth decade. In a population-based study of nearly 5000 older adults, Klein found a decrease in visual acuity to a mean value of approximately 2 min of arc in those aged over 75 years. Of course, this reflects the age-related nature of many diseases which affect visual acuity, such as cataract, glaucoma, diabetic retinopathy, and age-related macular degeneration. **Figure 5** plots data from the studies of Mayer and Klein.

Visual Standards

In most countries, there is a visual-acuity requirement for car drivers. While the level and measurement technique varies between countries, the acuity limit is usually approximately 0.3 logMAR. Commercial airline pilots are required to have a binocular visual acuity of 0.0 logMAR.

Best corrected binocular visual acuity of 1.0 logMAR or poorer is used as a definition of low vision or partial sight in many countries, with acuity of worse than 1.3 logMAR being described as severe sight impairment.

Hyperacuity

Some visual tasks can be performed with a far greater degree of precision than would be suggested by the MAR. Alignment tasks such as Vernier discrimination (where the offset of one line with respect to another is detected, **Figure 6(a)**) can be performed with misalignment of less

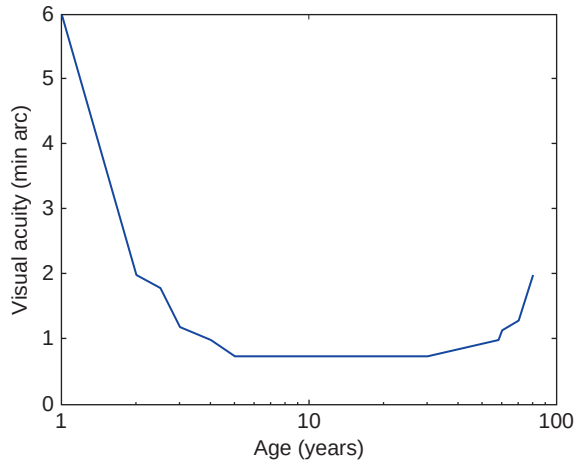

Figure 5 Variation in visual acuity over life. From Mayer, D. L. and Dobson, V. (1982). Visual acuity development in infants and young children, as assessed by operant preferential looking. Data from *Vision Research* 22(9): 1141–1151 and Klein, R., Klein, B. E., Linton, K. L., and De Mets, D. L. (1991). The beaver dam eye study: Visual acuity. *Ophthalmology* 98(8): 1310–1315.

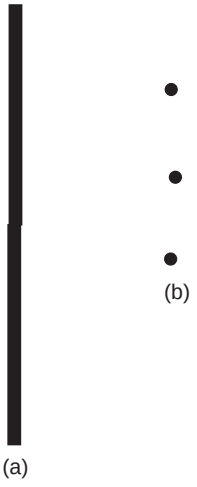

Figure 6 Examples of hyperacuity tasks. Misalignment of the lower element is easily visible. (a) Vernier alignment; (b) dot alignment: the offset of the middle dot with respect to the upper and lower dot is easily discerned.

than 5 s of arc – considerably less than the center-to-center spacing of a foveal photoreceptor. This is thought to be due to interpolation of the inputs of two or more adjacent neural elements.

Dynamic Visual Acuity

Throughout this article, visual acuity has been discussed for static targets. If the target is moved, central visual acuity decreases: the faster the target moves, the larger it must be for it to be seen. If a target moves with velocity of $40^\circ\ s^{-1}$, the MAR is increased to about 2 min of arc, while at $80^\circ\ s^{-1}$, acuity is about 3 min of arc.

In peripheral vision, slow image motion (less than $10^\circ\ s^{-1}$) slightly improves visual acuity for peripherally presented targets, perhaps because it breaks the phenomenon of Troxler fading.

Target motion at the retina can be induced by target movement, by eye motion, or by head motion. Many eye diseases, particularly those of the macula, are associated with poor fixation stability of the eye. This poor eye stability increases retinal image motion, and is significantly associated with poorer visual function. Small degrees of head motion do not significantly decrease visual acuity under normal conditions, but have a marked deleterious effect for subjects viewing through telescopic spectacles. Therefore, subjects with macular disease who have poor fixation stability and who view through telescopic low-vision aids have a marked impairment in their dynamic visual acuity.

See also: Acuity; Chromatic Function of the Cone; Contrast Sensitivity; Amblyopia; Photopic, Mesopic and Scotopic Vision and Changes in Visual Performance; Pupil.

Further Reading

Anstis, S. M. (1974). Letter: A chart demonstrating variations in acuity with retinal position. *Vision Research* 14(7): 589–592.

Bailey, I. L. and Lovie, J. E. (1976). New design principles for visual acuity letter charts. *American Journal of Optometry and Physiological Optics* 53: 740–745.

Bennett, A. G. and Rabbetts, R. B. (eds.) (1989). Visual acuity and contrast sensitivity. In: *Clinical Visual Optics*, pp. 23–72. Oxford: Butterworth-Heinemann.

Brown, B. (1972). Resolution thresholds for moving targets at the fovea and in the peripheral retina. *Vision Research* 12(2): 293–304.

Committee on vision. (1980). Recommended standard procedures for the clinical measurement and specification of visual acuity. Report of working group 39. *Advances in Ophthalmology = Fortschritte der Augenheilkunde = Progres en Ophtalmologie* 41: 103–148. Assembly of Behavioral and Social Sciences, National Research Council, National Academy of Sciences, Washington, DC

Crossland, M. D., Culham, L. E., and Rubin, G. S. (2004). Fixation stability and reading speed in patients with newly developed macular disease. *Ophthalmic and Physiological Optics* 24: 327–333.

Demer, J. L. and Amjadi, F. (1993). Dynamic visual acuity of normal subjects during vertical optotype and head motion. *Investigative Ophthalmology and Visual Science* 34(6): 1894–1906.

Klein, R., Klein, B. E., Linton, K. L., and De Mets, D. L. (1991). The beaver dam eye study: Visual acuity. *Ophthalmology* 98(8): 1310–1315.

Liang, J., Williams, D. R., and Miller, D. T. (1997). Supernormal vision and high-resolution retinal imaging through adaptive optics. *Journal of the Optical Society of America. A, Optics, Image Science, and Vision* 14: 2884–2892.

Mayer, D. L. and Dobson, V. (1982). Visual acuity development in infants and young children, as assessed by operant preferential looking. *Vision Research* 22(9): 1141–1151.

Plainis, S., Tzatzala, P., Orphanos, Y., and Tsilimbaris, M. K. (2007). A modified ETDRS visual acuity chart for European-wide use. *Optometry and Vision Science* 84(7): 647–653.

Rosser, D. A., Cousens, S. N., Murdoch, I. E., Fitzke, F. W., and Laidlaw, D. A. (2003). How sensitive to clinical change are ETDRS logMAR visual acuity measurements? *Investigative Ophthalmology and Visual Science* 44: 3278–3281.

Thibos, L. N., Cheney, F. E., and Walsh, D. J. (1987). Retinal limits to the detection and resolution of gratings. *Journal of the Optical Society of America. A, Optics, Image Science, and Vision* 4: 1524–1529.

Westheimer, G. (1987). Visual acuity. In: Moses, R. A. and Hart, W. M. (eds.) *Adler's Physiology of the Eye: Clinical Application*, pp. 415–428. St Louis, MO: Mosby.

Adaptive Immune System and the Eye: Mucosal Immunity

A K Mircheff, University of Southern California, Los Angeles, CA, USA

Glossary

CD80 and CD86 – B7 costimulatory ligands expressed by antigen presenting cells. They interact with coreceptors CD28 and CTLA4 on T cells and are necessary, but not sufficient for T-cell activation.

MHC class II (major histocompatibility complex class II molecules) – These molecules typically acquire autoantigen epitopes in endosomes and antigen processing compartments of antigen presenting cells and present them to antigen receptors of $CD4^+$ T cells.

TGF-β – Pleiotropic cytokine. One critical function in the mucosal immune system is to favor IgM-to-IgA isotype class switching; another is to promote differentiation of immature dendritic cells as regulatory antigen presenting cells. It may be mitogenic, antiproliferative, or pro-apoptotic, depending on target cell or synergistic interactions with other cytokines and growth factors.

The visual system interfaces with the external world at the epithelium of the corneal surface. The corneal epithelium is part of the convoluted yet topologically continuous surface that separates the body's *milieu intérieur* from the external world. Beyond the limbal and conjunctival epithelia, it ranges in one direction through the lacrimal excretory ducts and network of ducts to the acini of the lacrimal gland. In the other direction it ranges through the lacrimal drainage system to the oral and pharyngeal mucosae; through ducts to the acini of the salivary glands, through the airways to the alveoli of the lungs; through the mucosae of the esophagus, stomach, intestine, and colon; through ducts to the acini of the pancreas; and through ducts to the canaliculi of the liver. These moist tissues are linked topologically, via the epidermis, with the mucosal and glandular epithelia of the urinary tract, the reproductive tracts, and the mammary glands. They also are linked functionally, via the traffic of immune cells through the lymph vessels, secondary lymphoid organs, and vasculature, to comprise a physiological system, the mucosal immune system.

The metabolically active epithelial cells that comprise these surfaces perform diverse functions related to their roles in the visual, respiratory, gastrointestinal, liver, renal, and reproductive systems. However, they express several common functions. They either produce immense volumes of fluid, for example, saliva, gastric juice, bile, pancreatic juice, and occasionally diarrhea, or produce thin, largely aqueous, but physically and chemically complex, films as homeostatic *milieus extérieurs* for themselves. They also execute innate immune functions, and, at specialized inductive and effector sites, adaptive immune functions, which protect them, their underlying stromas, and the rest of the body from particulate irritants, noxious chemicals, and infectious microbes. The central principle of the adaptive immune strategy is to use noncomplement-fixing immunoglobulins (i.e., dimeric IgA and IgG1) to prevent infection while avoiding inflammatory processes that would damage host tissues and compromise their functions. As improved sanitary systems, antibiotics, and vaccines decrease morbidity and mortality due to infection, dysfunctions of mucosal immune system tissues that result in chronic inflammatory processes join other chronic inflammatory diseases among the main categories of afflictions that burden aging populations. The chronic inflammatory mucosal immune disorders of the visual system are subsumed under the prosaic rubric, dry eye disease. Other names have been suggested, including dysfunctional tear syndrome and lacrimal keratoconjunctivitis, or, as this author would prefer, dacryokeratoconjunctivitis.

Much of the current understanding of normal mucosal immune system physiology has come from studies of the gastrointestinal and respiratory systems. The gastrointestinal system must not only prevent infection by pathogens but it must also tolerate, and to a large extent, actively host, a rich flora of commensal microbes, which benefit the organism by processing or producing nutrients that would otherwise remain inaccessible or unavailable. When the mucosal immune barrier against infection fails, conventional innate and adaptive inflammatory mechanisms mount robust responses to rescue the host organism, but these responses typically induce diarrheal fluid loss, ulcerative damage to the mucosal and stromal tissues, and malabsorption of nutrients and electrolytes. The complex relationship the mucosal immune system maintains with its microbiota is paralleled by a nuanced relationship with the foods that the gastrointestinal system processes. Nutrient carbohydrates and proteins typically are digested to monosaccharides and amino acids before being absorbed across the intestinal epithelia. Nevertheless, antigen presenting cells continuously surveille the luminal contents, and both micropinocytosis and receptor-mediated transcytosis may transfer intact nutrient macromolecules across the epithelium. Clearly, it is in the organism's interest to avoid inflammatory responses against them.

While a smaller mass and less rich diversity of commensal and infectious microbial flora challenge the ocular surface tissues, the imperative to avoid inflammatory responses while preventing infection is no less urgent than it is in the gastrointestinal system. The executive decisions largely are made by antigen presenting cells, but these decisions are based on information conveyed by paracrine mediators that are produced by parenchymal cells and mesenchymal cells, as well as by neurotransmitters and neuropeptides.

Organized Inductive Sites

New generations of mucosal antigen presenting cells, T cells, and B cells are introduced to microbes and soluble molecules in organized signaling milieus that amplify B cells with high-affinity IgM and induce them to undergo somatic hypermutation and immunoglobulin isotype class switching while continuing to retain expression of the J chain. Some authors refer to the organized inductive sites generically as mucosa-associated lymphoid tissues (MALTs) and specifically as conjunctiva-associated lymphoid tissue (CALT), eye-associated lymphoid tissue (EALT), tonsils, adenoids, bronchus-associated lymphoid tissue (BALT), and Peyer's patches and gut-associated lymphoid tissue (GALT). Other authors include both the organized inductive sites and the less organized effector sites together as MALT.

Figure 1 illustrates stereotypical features of mucosal inductive site organization. The epithelial sheet that overlays an inductive site contains specialized cells with distinctive basal convolutions enfolding superficial dendritic cells. These so-called M cells phagocytose microbes and engulf soluble molecules at their apical surfaces, transcytose them to their basal surfaces, and release them to the underlying space. Dendritic cells in the immediate subepithelial areas again engulf the transcytosed microbes and soluble molecules, which then traffic to acidic endosomal compartments containing major histocompatibility complex class II (MHC class II) molecules and hydrolytic enzymes. Peptides that are exposed in superficial domains of the proteins being degraded have the greatest likelihood of entering the binding grooves of MHC class II molecules. Peptides that remain outside the binding grooves are exposed to further degradation. Peptide sequences that are protected from proteolysis become the dominant epitopes that the MHC class II molecules will present to $CD4^+$ T cells upon trafficking to the dendritic cells' surface membranes.

Whether or not a dendritic cell redistributes MHC class II molecules to its surface, upregulates expression of B7 costimulatory molecules, and migrates the short distance to the $CD4^+$ T-cell-rich zone may depend on signals received early in the encounter with the material it has internalized. The best understood of these signals are conveyed by lipopolysaccharides and double-stranded DNAs, which activate toll-like receptors (TLRs). The TLR activation induces a dendritic cell to downregulate chemokine receptors and homing receptors that favor retention in the subepithelial zone and to upregulate receptors that favor migration to the T-cell-rich zone. Typically, TLR activation also induces dendritic cells to upregulate surface expression of the costimulatory B7 ligands, CD80 and CD86, as they redistribute MHC class II molecule–epitope complexes to their surface membranes.

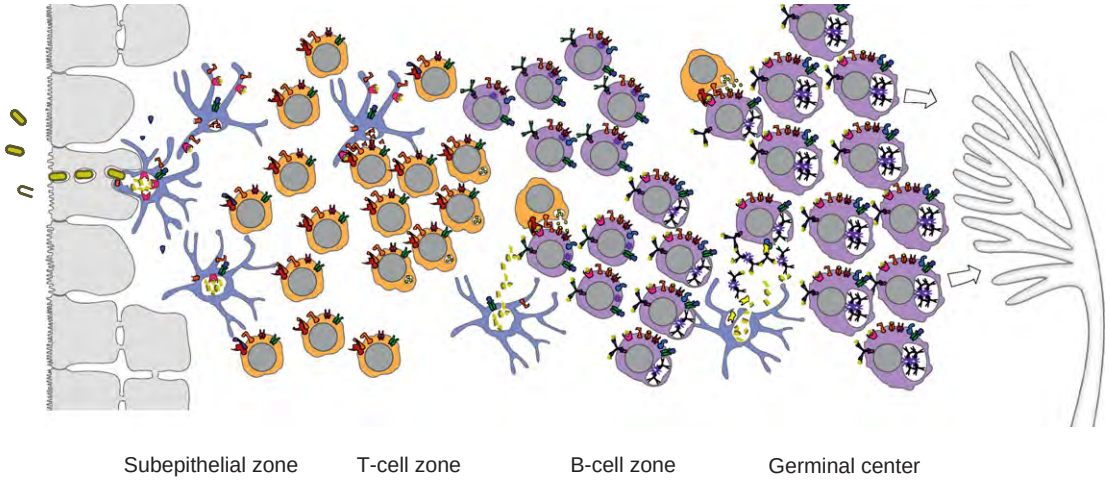

Figure 1 Stereotypical organization of mucosal immune inductive sites. After having taken up microbes or antigens transcytosed by M cells, dendritic cells may traffic directly to the B-cell zone, or they may migrate to the T-cell zone, where they activate antigen-specific $CD4^+$ cells to express T_H2 cytokines. B cells with antigen receptors of sufficient avidity internalize antigen, then use MHC class II molecules to present epitopes to activated T_H2 cells. Ongoing T_H2 activation promotes B-cell division and Ig hypermutation. In this signaling milieu, TGF-β induces IgM-to-IgA isotype class switching. In combination with B-cell growth factors, TGF-β in germinal centers promotes plasmablast proliferation and emigration via afferent lymph vessels.

While signals from engulfed microbes are decisive in determining whether the dendritic cell will undergo complete functional maturation and activation, the activated phenotype that the dendritic cell will assume is determined largely by paracrine mediators that are released by the overlaying epithelium and surrounding mesenchymal cells. The signaling mediators that are known to be predominant are transforming growth factor-beta (TGF-β) and interleukin (IL)-10, and they induce maturing dendritic cells to also express TGF-β and IL-10. An additional population of dendritic cells are distinguished by the absence of MHC class II molecule expression and expression of chemokine and homing signal receptors that lead them to bypass the T-cell-rich regions and enter B-cell-rich zones, where there they will release the material they had internalized.

Engagement of a naive $CD4^+$ T cell's antigen receptors by MHC class II molecule–epitope complexes generates the primary signal necessary, but not sufficient, for activation. Simultaneous engagement of CTLA-4 or CD28 at the T-cell surface by CD80 or CD86 at the dendritic cell surface provides the second signal essential for promoting T-cell activation and differentiation. However, the functional phenotype the activated $CD4^+$ T-cell expresses is determined by paracrine mediators in the immediate signaling milieu. These are secreted by dendritic cells, epithelial cells, and mesenchymal cells. They induce $CD4^+$ T cells to differentiate as T_H2 cells and to change their panel of chemokine receptors and homing receptors to favor migration from the T-cell-rich zones and into the B-cell-rich zone.

When molecules that dendritic cells have released encounter B cells with surface IgM antigen receptors that bind them with high enough affinity, they deliver a primary activation signal, which induces the B cell to endocytose the IgM–antigen complex to antigen-processing compartments and to begin expressing MHC class II molecules. Thus, $CD4^+$ T cells arriving from the interfollicular zone will be presented with dominant epitopes that maintain them in their activated state. They continue secreting the T_H2 cytokines needed to induce somatic hypermutation of B-cell immunoglobulin genes and promote selection of B-cell clones with increasing affinity for the determinant. The signaling milieus within some of the organized inductive sites, notably Peyer's patches, selectively induce IgM-to-IgA class switch recombination. The milieus in the inductive sites in the tonsils, adenoids, and airways may induce either IgM-to-IgA or IgM-to-IgG1 class switch recombination. In cases of IgA deficiency, the numbers of $IgG1^+$ cells and IgM cells may increase in compensation. Whether induced to express IgA or IgM, the activated B cells continue to express J chain. The IgA^+ B cells will express dimeric IgA (dIgA), while IgG1 B cells will express apparently irrelevant J chain.

The activated B-cell blasts amplify in germinal centers, and they alter their panel of chemokine receptors and homing receptors, so that they are induced to leave the inductive sites via lymph vessels, enter the circulation via the thoracic duct, and enter the mucosal immune effector sites. The IgA^+ B cells expressing CCR10, the receptor for CCL28, traffic to the lamina propria of the oral cavity, lower airways, and colon. The IgA^+ B cells expressing CCR9, the receptor for CCL25, traffic to the trachea, stomach, intestine, salivary glands, and mammary gland. The $IgG1^+$ B cells expressing CXCR4, the receptor for CXCL12, traffic to the bone marrow. In each setting, the plasmablasts will take residence and mature to become long-lived memory cells or plasmacytes.

Effector Sites

Specialized Niches

Stereotypical features of the mucosal immune effector site are illustrated in the upper panel of **Figure 2**. Like IgG^+ plasmablasts entering the bone marrow, the $dIgA^+$ plasmablasts that arrive in the mucosal effector sites receive signals that induce them to mature into plasmacytes. One of the critical mediators of maturation signaling at the mucosal effector sites is TGF-β. A mature plasmacyte's ongoing survival depends on the constant presence of additional signals to suppress the intrinsic apoptotic program. The candidate mediators of the survival signals include IL-6, B-cell activating factor (BAFF), a proliferation-inducing ligand (APRIL), and, perhaps, prolactin. In the rabbit lacrimal gland, which has been studied in some detail, epithelial expression of paracrine mediators is compartmentalized according to the epithelial histoarchitectural plan and vascular organization. Venules, the vascular elements that plasmablasts cross to enter the stromal space, tend to follow courses that parallel interlobular ducts. Epithelial cells of the interlobular ducts express TGF-β and prolactin at much higher levels than epithelial cells in the acini, and it appears they secrete these mediators both apically (i.e., into the fluid forming within the duct lumen) by way of their regulated exocrine secretory apparatus for proteins, and also basally, through either a constitutive paracrine secretory apparatus or a parallel paracrine apparatus that can be induced under certain circumstances. While TGF-β, as noted, induces $dIgA^+$ plasmablast-to-plasmacyte differentiation, it may not be conducive to the plasmacytes' ongoing survival. It appears that TGF-β signaling may be concentrated in the stromal spaces surrounding the venules and interlobular ducts. Preliminary findings in the author's laboratory suggest that transcripts for the extracellular matrix proteoglycan, decorin, are two orders of magnitude more abundant than TGF-β transcripts in lacrimal gland epithelial cells. Because decorin binds to the extracellular matrix and also binds the latent TGF-β, it may create a diffusion barrier that keeps latent TGF-β

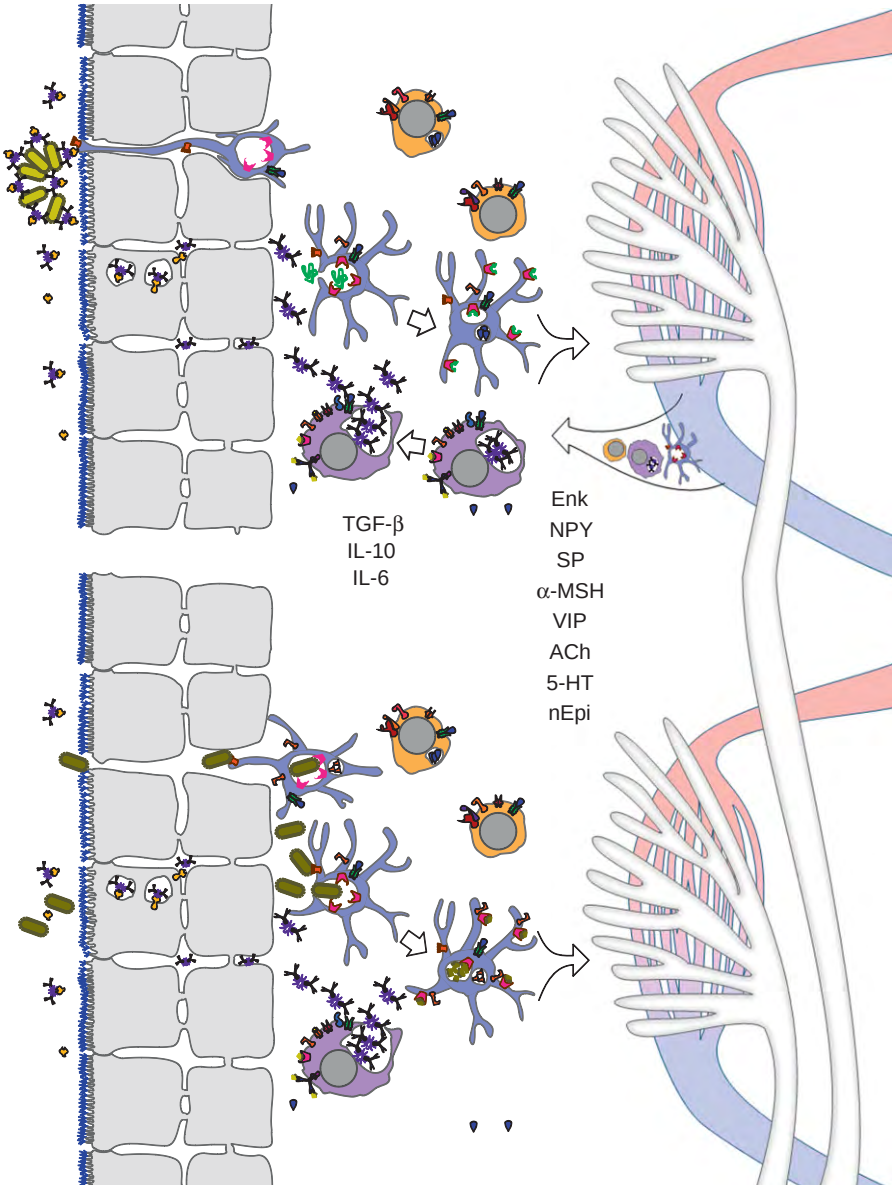

Figure 2 Normal (upper panel) and infected (lower panel) mucosal immune effector sites. IgA^+ J $chain^+$ plasmablasts, immature dendritic cells, and T cells enter the lamina propria of the conjunctiva and drainage system, stromal space of the lacrimal gland, and other effector sites from venules. Paracrine mediators induce plasmablasts to undergo terminal differentiation, then support their survival as plasmacytes. Of these mediators, TGF-β, IL-10, and IL-6 are provided, at least in part, by epithelial and stromal cells. Sensory, parasympathetic, and sympathetic nerve endings provide neurotransmitters and neuropeptides that may also influence plasmablasts, plasmacytes, dendritic cells, and lymphocytes. The normal signaling milieu induces dendritic cells that have taken up soluble proteins and cellular debris to mature as regulatory antigen presenting cells, which exit via afferent lymph vessels and induce regulatory T cells in the lymph nodes. The TLR activation by microbes that have evaded the immunospecific sIgA barrier induces dendritic cells to mature as immunoactivating antigen presenting cells that will elicit IgG responses in the lymph nodes.

concentrated in the periductal stroma. In contrast, prolactin may be free to equilibrate through the interstitial fluid, diffusing to plasmablasts throughout the gland's stromal spaces. Preliminary studies suggest that acinar epithelial cells may be able to express IL-6. In contrast, mRNAs for APRIL and BAFF appear substantially more abundant in whole gland extracts than in *ex vivo* acinar cells. If substantiated, this finding would imply that APRIL and BAFF are expressed by infiltrating lymphocytes, but it cannot exclude significant expression by ductal epithelial cells.

The information so far available about the cytophysiological mechanisms that secrete paracrine mediators to the stroma has come from immunohistochemical studies

of TGF-β, epidermal growth factor (EGF), fibroblast growth factor (FGF), and prolactin localizations in rabbit lacrimal gland and studies of the intracellular traffic of prolactin in *ex vivo* acinar cells from rabbit lacrimal gland. Under normal circumstances, the paracrine mediators are localized primarily in the apical cytoplasm, consistent with secretion into the duct lumen via the regulated exocrine secretory apparatus. Consistent with this inference, pilocarpine-induced lacrimal gland fluid contains high concentrations of TGF-β and prolactin. Two-color confocal immunofluorescence microscopy of the *ex vivo* model indicates that prolactin colocalizes with rab4, rab5, and rab11, which are effectors of traffic to and from endosomes, and electron microscopic-immunogold studies indicate that prolactin also is localized within mature secretory vesicles. These findings suggest that lacrimal epithelial cells may maintain two pools of the paracrine mediators they secrete: a large, often static, pool in the regulated exocrine secretory apparatus, and a small, but high throughput, pool in the paracrine apparatus.

Transfer of Immunoglobulins to the *Milieu Extérieur*

pIgR and dIgA

Several prominent aspects of lacrimal cytophysiology appear to reflect adaptations to the roles the epithelium plays in the mucosal immune system: maintaining the underlying stromal space as a niche for dIgA-secreting plasmacytes and then transferring dIgA from the stromal space to the fluid within the lumen of the acinus–duct system. The fundamental principles of the transcytotic mechanism for dIgA secretion were elucidated in studies of Madin-Darby canine kidney (MDCK) cells, derived from a canine kidney, which form continuous epithelial monolayers when cultured on microporous substrata. Renal tubular epithelial cells do not normally secrete IgA, but when MDCK cells are stably transduced to express the polymeric immunoglobulin receptor (pIgR), they gain the ability to internalize dIgA from their basal medium, which corresponds to the interstitial fluid, and secrete sIgA into their apical medium, which corresponds to the lumenal fluid of an exocrine gland or the surface fluid of a mucosal sheet. **Figure 3** illustrates the transcytotic apparatus as it is thought to function in conjunctival epithelial cells. The pIgR makes its way from the biosynthetic apparatus, that is, the endoplasmic reticulum and Golgi complex, through the trans-Golgi network (TGN) and endosomes, to the basal–lateral plasma membranes, hitchhiking in transport vesicles at each step. The pIgR may or may not bind the J chain and associated immunoglobulin while its ligand-binding domain is exposed at the basal–lateral membrane. In either case, it is internalized in an endocytotic transport vesicle that will traffic to the early endosome. Another transport vesicle will traffic pIgR and pIgR–dIgA complex to the recycling endosome, and yet another will traffic pIgR and pIgR–dIgA complex to the apical plasma membrane. Either during its transit through the recycling endosome, or upon arriving at the apical plasma membrane, the pIgR will encounter a protease that cleaves the extracytoplasmic, dIgA-binding domain, referred to as secretory component (SC), from the membrane-spanning domain. Thus, the cell releases both free SC and SC–dIgA complexes, that is, secretory IgA (sIgA), into the *milieu extérieur*. Consistent with the topological constraints that preclude traffic of transport vesicles between adjoining cells, expression of pIgR is concentrated in the apical-most layer of epithelial cells in the conjunctiva.

Acute Regulation of pIgR Traffic

The traffic of pIgR through lacrimal gland epithelial cells appears to be somewhat more complex than described in the MDCK cell paradigm. First, it appears that pIgR might cycle repeatedly to the basal–lateral plasma membrane from any compartment of the transcytotic apparatus, while free SC is preferentially trafficked from the recycling endosome to the apical plasma membrane. Second, some of the pIgR traffic from the TGN to the immature secretory vesicle, rather than to the transcytotic apparatus; SC derived from these pIgR remains in mature secretory vesicles until released into the lumen along with the classical secretory proteins. Interestingly, many of the classic lacrimal secretory proteins, such as β-hexosaminidase, lysozyme, and lactoperoxidase, are innate immune effector molecules. Free SC appears to perform important functions in the ocular surface fluid film, and the ability to sequester a portion of pIgR away from the transcytotic apparatus ensures that some free SCs always will be secreted, despite the large mass of dIgA that normally is present in the stromal space.

A considerable volume of membrane traffic flows through the lacrimal acinar cell's transcytotic apparatus. The micropinocytosis associated with endocytotic internalization of transport vesicles from the basal–lateral and apical surface membranes carries fluid phase markers into the cells, and such markers rapidly equilibrate throughout the aqueous phase within the lumena of the early endosome, recycling endosome, and TGN, as well as the late endosome, prelysosome, and lysosome. If *ex vivo* acinar cell models are acutely stimulated with the muscarinic acetylcholine receptor agonist, carbamylcholine (carbachol, CCh), they increase the rates at which they endocytose and exocytose fluid phase markers. If the CCh concentration is increased from 10 μM, which maximally accelerates fluid phase endocytosis but half-maximally accelerates protein secretion, to 100 μM, a concentration that maximally accelerates protein secretion, fluid phase endocytosis continues at the increased rate, but

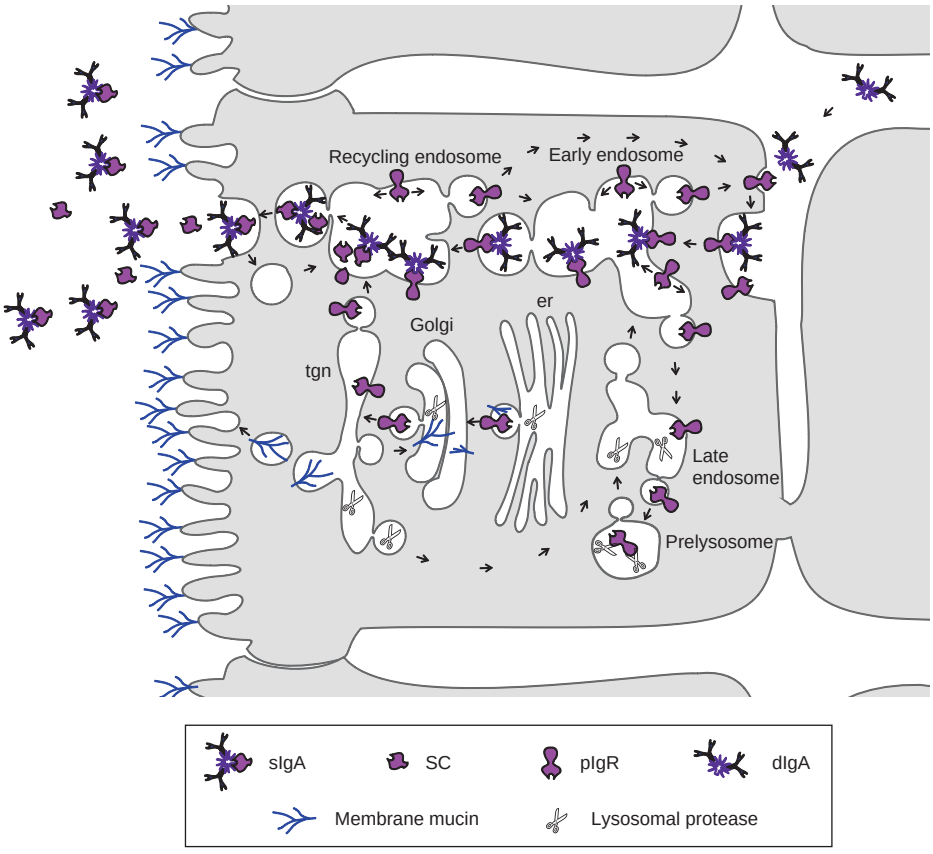

Figure 3 Transcytotic traffic of sIgA to the *milieu extérieur*. The apical-most layer of epithelial cells in stratified tissues, like the epithelial cells of lacrimal acini and ducts, express pIgR. At the basal–lateral surface membrane pIgR mediates endocytosis of dIgA, which it then chaperones through the early endosome and apical recycling endosome. Either within the apical recycling endosome or at the apical plasma membrane, the pIgR is cleaved by protease to release either free SC or dIgA–SC complex, that is, sIgA. In lacrimal gland epithelial cells, pIgR may cycle repeatedly through the TGN and transcytotic apparatus; it may enter immature secretory vesicles (not shown), where free SC is released and stored for subsequent secretion in response to secretagogue stimulation, or it may traffic through the late endosome, which is a gateway to the prelysosome and autophagic–lysosomal apparatus. The author proposes that the traffic of transport vesicles returning from the prelysosome and late endosome to the early endosome accounts for the constitutive release of an unusually heavy burden of autoantigens to the stromal space.

the volume of space that the fluid can reach decreases. If a marker is allowed to equilibrate through the fluid phases of the network of endomembrane compartments under resting conditions, subsequent acute stimulation with 100 μM CCh accelerates its release, but release then stops with a substantial portion of the marker remaining entrapped within the cell. These findings suggest that when the cell is maximally stimulated with CCh, it imposes a blockade of bidirectional traffic between proximal and distal compartments of the endocytotic pathway. Other studies indicate that the blockade affects traffic to the late endosome from both the early endosome and the TGN. A possible cytophysiological rationale for this phenomenon is suggested by preliminary studies of the kinetics of CCh-induced SC secretion. The CCh acutely induces a burst of secretory vesicle exocytosis, which releases SC along with the other secretory proteins. Secretory vesicle exocytosis is complete within 10 min. However, the cells continue to release SC at an increased rate for at least 60 min, while their total content of pIgR plus SC appears to remain unaltered. These phenomena suggest that the cell blockades traffic to the late endosome in order to divert an increased proportion of its newly synthesized pIgR from the degradative apparatus to the transcytotic apparatus.

A Mechanism That Constitutively Secretes Autoantigens to the Stroma

A consequence of the strategy of directing a large volume of transport vesicle traffic from the early endosome to the late endosome and prelysosome under nonstimulated conditions is that the reciprocal traffic of transport vesicles constitutively secretes lysosomal hydrolases and potential autoantigens that, in other cells, would remain in the autophagic–lysosomal apparatus and be degraded. Moreover, when traffic to the late endosome is blocked, the lysosomal hydrolases reflux into the compartments which remain accessible (i.e., the TGN), immature

secretory vesicle, early endosome, and recycling endosome. Of particular interest, at least some of the lysosomal proteases are catalytically active and may process other proteins that have accumulated with them in the same compartments. This phenomenon might lead to the degradation of dominant autoantigen epitopes and lead to the eventual presentation of epitopes that under normal circumstances are degraded.

FcγRn and IgG1

While the plasmacytes that produce dIgA reside in the stromal spaces of exocrine glands and the lamina propria of mucosal sheets, the plasmacytes that produce IgG1 typically reside in the bone marrow, and IgG1 must travel through the circulation to reach the epithelia that will secrete it. The same subcellular apparatus that transports SC and pIgR–dIgA complexes through epithelial cells likely also mediates the secretion of IgG1. However, IgG1 does not associate with J chain, and its traffic is mediated not by pIgR but by the neonatal Fcγ receptor, FcγRn. The association between IgG1 and FcγRn is regulated by pH, such that binding affinity is highest in relatively acidic endosomal compartments and lower at the pH of the interstitial fluid. In the tissues where it has been studied, the IgG1–FcγRn complex tends to bypass the late endosome in favor of the early endosome and recycling endosome. Because dissociation of IgG1 from FcγRn does not require proteolytic processing, FcγRn can mediate multiple cycles of IgG1 absorption as well as secretion. The FcγRn can also mediate absorption and secretion of IgG1-immune complexes, in some cases secreting opsonized microbes and immune complexes and in others absorbing them in a physical state that minimizes the risk of infection but perpetuates T-cell and B-cell responses. The extent to which FcγRn might be expressed in the lacrimal glands and drainage system has not been investigated; recently, however, it has been found to be present in epithelial cells of rat conjunctiva.

Mucosal Tolerance and Response to Infection

Commensal microbes in the gut are coated with sIgA, which normally prevents them from entering the epithelial lining. Notably, dendritic cells as well as dIgA-secreting plasmacytes populate the mucosal effector sites. They are present within the lamina propria and the epithelia and may extend processes that interdigitate between adjoining cells to surveille the *milieu extérieur*. As in the organized inductive sites, immature dendritic cells are endocytotically active, and under normal circumstances the material they internalize consists of soluble molecules and cellular debris. The robustness of the phenomenon of oral tolerance suggests that the TGF-β- and IL-10-rich milieu directs them to mature as regulatory antigen presenting cells, which, when they arrive in lymph nodes, induce food antigen- and, presumably, autoantigen-specific $CD4^+$ T cells to mature as T_H3 and T_R1 regulatory cells. The regulatory cells might function in both the effector sites and the lymph nodes to prevent inflammatory mediators or activated effect T cells from redirecting dendritic cells toward expression of immunoactivating phenotypes.

As illustrated in the lower panel of **Figure 2**, TLR on immature dendritic cells in the epithelium or lamina propria recognizes microbes that have evaded the immunospecific sIgA barrier, and TLR activation induces phagocytosis, redistribution of MHC class II molecules to the dendritic cell surface, and upregulation of surface CD80 and CD86. Certain microbes induce maturing dendritic cells to remain in the lamina propria and release antigen directly to B1 cells, stimulating activation independently of T-cell help. Typically, however, dendritic cells are activated to switch chemokine receptor and homing receptor expression to favor emigration via afferent lymph vessels. In the lymph nodes, they will induce activation of naive, antigen-specific $CD4^+$ T cells as T_H2 cells and generation of IgG-producing B cells.

Implications for Ocular Surface Pathophysiology

Contemporary paradigms hold that dry eye disease results from insufficiency of the ocular surface fluid film. Such might be the consequence of impaired lacrimal gland fluid production, excessive evaporation of water from the ocular surface fluid due to deficient production of lipids in the Meibomian glands, and excessive breakup of the fluid film due to deficiencies of the normally hydrophilic substratum provided by the apical surfaces of corneal and conjunctival epithelial cells. There is a general consensus that, whatever the etiology, the principal feature of pathophysiological state is inflammation of the ocular surface tissues. Inflammatory processes plausibly account for much of the cytopathology that occurs within the lacrimal gland and leads to quiescence of impairment of its exocrine functions. This seems to be the case, not only in Sjögren's syndrome, but also in graft-versus-host disease, sarcoidosis, Wegener's granulomatosis, and diffuse infiltrative lymphocytosis syndrome associated with HIV infection. A histopathological syndrome distinct from the familiar diagnoses and described primarily through postmortem studies is characterized by lymphocytic infiltration, acinar atrophy, ductal dilatation, and periductal fibrosis. Its underlying pathophysiological mechanisms have not been studied, although they appear not to involve production of autoantibodies.

The author suggests that these inflammatory processes normally are prevented by the same strategy that prevents immune responses to food antigens, soluble autoantigens, and cellular debris. There may be particular challenges to maintaining immunoregulation in the lacrimal glands, where vigorous traffic through the transcytotic apparatus releases an exceptionally heavy burden of potential autoantigens into the stromal space, and in the ocular surface tissues, where environmental stresses may induce release of inflammatory mediators that abrogate the local signaling milieu's ability to generate regulatory antigen presenting cells. Additional challenges may result from the epithelia's dependence on systemic hormones to maintain expression of the local signaling milieu.

See also: Adaptive Immune System and the Eye: T Cell-Mediated Immunity; Conjunctiva Immune Surveillance; Defense Mechanisms of Tears and Ocular Surface; Lacrimal Gland Overview; Tear Film; Tear Film Overview.

Further Reading

Brandtzaeg, P. and Johansen, F.-E. (2005). Mucosal B cells: Phenotypic characteristics, transcriptional regulation, and homing properties. *Immunological Reviews* 206: 32–63.

Cain, C. and Phillips, T. E. (2008). Developmental changes in conjunctiva-associated lymphoid tissue of the rabbit. *Investigative Ophthalmology and Visual Science* 49: 644–649.

Evans, E., Zhang, W., Jerdeva, G., et al. (2008). Direct interaction between Rab3D and the polymeric immunoglobulin receptor and trafficking through regulated secretory vesicles in lacrimal gland acinar cells. *American Journal of Physiology. Cell Physiology* 294: C662–C674.

Franklin, R. M, Kenyon, K. R., and Tomasi, T. B. (1973). Immunohistologic studies of human lacrimal gland: Localization of immunoglobulins, secretory component and lactoferrin. *Journal of Immunology* 110: 984–992.

Kaetzel, C. S. (2005). The polymeric immunoglobulin receptor: Bridging innate and adaptive immune responses at mucosal surfaces. *Immunological Reviews* 206: 83–99.

Kim, H., Fariss, R. N., Zhang, C., et al. (2008). Mapping of the neonatal Fc receptor in the rodent eye. *Investigative Ophthalmology and Visual Science* 49: 2025–2029.

Knop, E., Knop, N., and Claus, P. (2008). Local production of secretory IgA in the eye-associated lymphoid tissue (EALT) of the normal human ocular surface. *Investigative Ophthalmology and Visual Science* 49: 2322–2329.

Macpherson, A. J., McCoy, K. D., Johansen, F.-E., and Brandtzaeg, P. (2008). The immune geography of IgA induction and function. *Mucosal Immunology* 1: 11–22.

Meagher, C. K., Liu, H., Moore, C. P., and Phillips, T. E. (2005). Conjunctival M cells selectively bind and translocate Maackia amurensis leukoagglutinin. *Experimental Eye Research* 80: 545–553.

Mircheff, A. K., Wang, Y., de Saint Jean, M., Ding, C., and Schechter, J. E. (2007). Lacrimal epithelium mediates hormonal influences on APC and lymphocyte cycles in the ocular surface system. In: Zierhut, M., Rammensee, H. G., and Streilein, J. W. (eds.) *Antigen Presenting Cells and the Eye*, pp. 93–119. New York: Informa.

Rose, C. M., Qian, L., Hakim, L., et al. (2005). Accumulation of catalytically active proteases in lacrimal gland acinar cell endosomes during chronic *ex vivo* muscarinic receptor stimulation. *Scandinavian Journal of Immunology* 61: 36–50.

Seder, R. A., Marth, T., Sieve, M. C., et al. (1998). Factors involved in the differentiation of TGF-beta-producing cells from naive CD4+ T cells: IL-4 and IFN-γ have opposing effects, while TGF-β positively regulates its own production. *Journal of Immunology* 160: 5719–5728.

Spiekermann, G. M., Finn, P. W., Ward, E. S., et al. (2002). Receptor-mediated immunoglobulin G transport across mucosal barriers in adult life: Functional expression of FcRn in the mammalian lung. *Journal of Experimental Medicine* 196: 303–310.

Wang, Y., Chiu, C. T., Nakamura, T., et al. (2007). Traffic of endogenous, over-expressed, and endocytosed prolactin in rabbit lacrimal acinar cells. *Experimental Eye Research* 85: 749–761.

Weiner, H. L. (2001). Induction and mechanism of action of transforming growth factor-β-secreting Th3 regulatory cells. *Immunological Reviews* 182: 207–214.

Adaptive Immune System and the Eye: T Cell-Mediated Immunity

K C McKenna and R D Vicetti Miguel, University of Pittsburgh, Pittsburgh, PA, USA

Glossary

Antigen – A molecule recognized by receptors expressed by T cells (TCR) and B cells (immunoglobulin).
Complement – A system of serum proteins and cell surface proteins that combine to form the membrane attack complex that perforates cell membranes. Component proteins of the complement cascade have enzymatic activity and generate inflammatory mediators.
Cytokines – Soluble molecules that modulate immune responses.
Inflammation – The hallmark of an immune response characterized by edema, redness, and pain. Inflammatory mediators induce vasodilation of local vessels which are leaky and promote edema and facilitate immune cell infiltration. While inflammation controls infection, it can also cause tissue damage, as the effector function of the innate immune response is nonspecific.
Major histocompatibility complex (MHC) – Highly polymorphic molecule expressed on the cell surface that presents self and foreign peptides for T-cell recognition through the TCR.
Opsonization – The coating of cell surfaces with molecules that facilitate phagocytosis.
Phagocytosis – The process of pathogen engulfment through recognition of surface receptors.
Polymorphonuclear leukocytes (PMN) – Cells of the innate immune response characterized by a multilobed nucleus including neutrophils and eosinophils.
Signal transduction – The process by which signals received by the cell are converted into gene expression within the nucleus.

The human body and the microbes (bacteria, viruses, and parasites) that reside within it share the same simple mandate: to survive and to reproduce. The ground rules of the host are clear. The host–microbe relationship cannot cause damage that compromises the health of the host. When health is compromised, the host immune system eliminates or controls the growth of these unruly microbes, now termed pathogens. Immune responses in the eye are critical for protection from pathogens. For example, immune-suppressed HIV+ patients are more susceptible to ocular infection. However, ocular immune responses also pose a threat as inflammation can damage the delicate microanatomy of the eye and compromise vision. Examples of blinding inflammation include viral, bacterial, and parasitic keratitis, retinitis, bacterial endophthalmitis, and autoimmune uveitis, which are reviewed elsewhere in this encyclopedia. As an evolutionary adaptation to preserve vision, immune responses in the eye are normally tightly regulated to control pathogens while minimizing inflammation.

Innate and Adaptive Immunity

The two major arms of the immune system, innate and adaptive immunity, can be distinguished by the unique molecular structures they employ to recognize molecules expressed by pathogens or expressed by a host cell in response to a pathogen. The innate immune response utilizes a limited set of pathogen recognition receptors (PRRs) to detect pathogen-associated molecular patterns (PAMPs), which are conserved pathogen products. There are PRRs that recognize PAMPs expressed by all major classes of microbes for example: toll-like receptor (TLR) 4 recognizes lippopolysaccharide (LPS) of Gram-negative bacteria; TLR3 recognizes double-stranded RNA expressed by viruses; and TLR11 recognizes proteins expressed by parasites. PRRs can also recognize molecules associated with pathogen-induced cell death. For example, RAGE (receptor of advance glycation end products), TLR 2, 4, and 9 recognize nonoxidized high mobility group box 1 (HMGB1), which is released by normal cells upon necrotic but not apoptotic cell death. PRRs are expressed on epithelial cells at sites of microbial entry and on cells of the innate immune response which include: macrophages, dendritic cells (DC), and polymorphonuclear leukocytes (PMN).

Pathogen recognition by the adaptive immune response is not predetermined by a limited set of receptors. Rather, a random process of gene segment rearrangement by recombinase activation genes (Rag-1 and Rag-2) generates over a billion different receptors tailored to recognize essentially any molecule. Cells of the adaptive immune response include B cells, which express immunoglobulin (Ig) molecules and T cells that express T-cell receptors (TCRs). Individual B or T cells express receptors with a single specificity creating a repertoire of many B and T cells each with different specificities. B cells mediate humoral immunity through production of secreted Ig molecules (antibodies) which directly recognize

unique shapes, and conformations of pathogen-associated molecules including proteins, carbohydrates, lipids, nucleic acids, and simple chemical groups. Cellular immunity is mediated by T cells through TCR recognition of pathogen-associated proteins processed into peptides and presented on the cell surface by the major histocompatibility complex (MHC). These differences in antigen recognition specialize humoral immunity for defense against extracellular pathogens and cell-mediated immunity for defense against intracellular pathogens. The focus of this article is a general overview of T-cell-mediated immunity introducing how T-cell responses are regulated in the eye and conditions where ocular T-cell responses cause immunopathology.

Antigen Trafficking, Processing, and Presentation to T cells

The lymphatic system drains extracellular fluids through a network of collection channels and vessels that ultimately empty into the bloodstream through the thoracic duct. Interspersed between lymphatic vessels are lymph nodes that are filled with immune cells. This strategic placement of an immune organ within a drainage pathway allows the immune system to survey for foreign antigens contained within extracellular fluids from different regions of the body. For example, the eye is drained to cervical lymph nodes within the neck whereas the arms drain to axillary and brachial lymph nodes. Internal organs also have lymphatic drainage: lungs drain to mediastinal lymph nodes and intestine drains to mesenteric lymph nodes.

T cells, which have not encountered their antigen, are found in the lymph nodes, spleen, and blood but not in nonlymphoid tissues, such as the eye. Therefore, these naive T cells are not the first responders to an ocular pathogen. Rather, innate immunity is the first line of defense. Recognition of PAMPs through PRRs induces rapid expression of inflammatory cytokines (IL (interleukin)-1, IL-6, and tumor necrosis factor (TNF)) that increase the production of chemokines, such as IL-8 and acute phase proteins (e.g., C-reactive protein). Chemokines promote the migration of immune cells to the eye while acute phase proteins opsonize microbial surfaces where they activate complement and promote phagocytosis by macrophages and PMN. To control the pathogen, infiltrating PMN and macrophages produce reactive oxygen species, including superoxide which can be transformed into H_2O_2 by superoxide dismutase. H_2O_2 and chloride are substrates for myeloperoxidase which generates antimicrobial hypochlorous acid, the active ingredient of bleach. PMN and macrophages also release granules containing antimicrobial molecules and generate nitric oxide (NO) that reacts with superoxide to form the potent oxidant peroxynitrite. In addition to controlling the pathogen, DCs and macrophages which have internalized pathogens and/or pathogen products migrate to the lymph nodes through lymphatic vessels to activate pathogen-specific T cells.

Adaptive immune responses depend on innate immune responses, as T cells only recognize cell-associated antigens. Hence, antigens that flow freely into the lymph node or that are carried by DCs and macrophages from the pathogen site have to be processed and presented by antigen-presenting cells (APCs) for recognition by T cells. As a general rule, pathogen-expressed proteins from the extracellular milieu are digested by phagocytic APC and presented through MHC class II molecules for recognition by $CD4^+$ T cells, whereas intracellular pathogen-expressed proteins are processed and presented through MHC class I molecules for recognition by $CD8^+$ T cells (**Figure 1**). However, certain types of APC, for example CD8α+ CD11c+ DCs from mice, cross present extracellular proteins through MHC class I molecules.

T-cell activation

Very few T cells within the entire T-cell repertoire are specific for any one particular antigen. Therefore, to most effectively respond to a pathogen, these antigen-specific T cells undergo cell division to expand their numbers. This process of clonal expansion takes time, which explains why adaptive immune responses lag behind innate immune responses.

The activation of T cells to undergo proliferation results from several signals delivered from the APC. These signals initiate and sustain signal transduction cascades culminating in the transcription of genes necessary for T-cell proliferation, most importantly IL-2 (**Figure 2**). Transducing signals from the APC to T cells occurs by phosphorylation and dephosphorylation of intracellular substrates by kinases and phosphatases, respectively. Signal one is delivered by TCR engagement of MHC + peptide complexes, which results in a conformational change in the TCR that makes immunoreceptor tyrosine-based activation motifs (ITAMs) accessible on chains of the CD3 complex which is comprised of five distinct molecules (γ, δ, ε, ζ, and η). The CD3 complex is associated with the TCR and is necessary for signal transduction upon TCR engagement, as the TCR has a short cytoplasmic domain incapable of signaling. Upon TCR antigen recognition, CD3 ITAMS are phosphoylated by $p56^{lck}$, and $p59^{fyn}$ kinases, then bound by ZAP-70 ((CD3) zeta chain-associated protein of 70 kDa) kinase, which activates phospholipase Cγ1 (PLCγ1). PLCγ1 is an enzyme which catabolizes membrane-bound phosphatidlyinositol-1, 4-bisphosphate (PIP_2) into inositol-1,4,5-triphosphate (IP_3) and diacylglcerol (DAG). IP_3 induces an intracellular calcium increase which then activates the serine phosphatase calcineurin to dephosphorylate nuclear factor of activated T cells (NFAT). Dephosphorlated NFAT leaves the cytosol to enter the nucleus. DAG activates protein kinase C (PKC) initiating another cascade leading to degradation

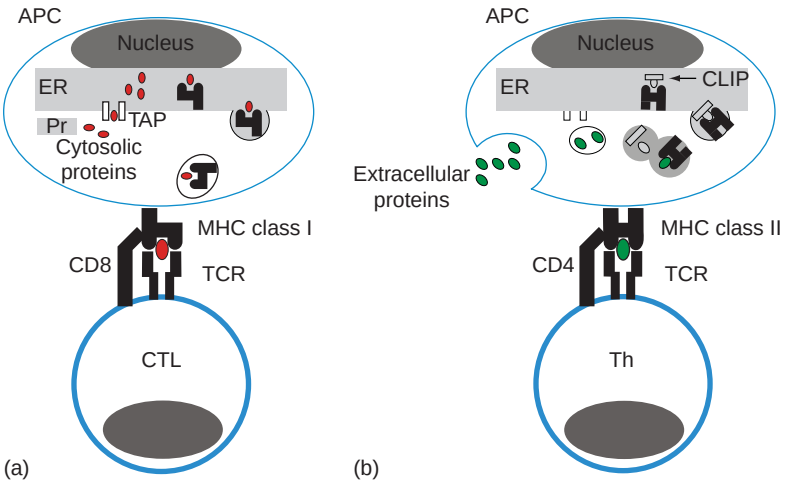

Figure 1 Antigen processing and presentation to T cells. (a) Proteins expressed within the cytosol are degraded into peptides by the proteasome (Pr), transported into the endoplasmic reticulum (ER) by the transporter associated with antigen processing (TAP) and then associate with newly formed MHC class I molecules which are transported to the cell surface for recognition by $CD8^+$ cytolytic T lymphocytes (CTL). (b) Extracellular proteins are degraded into peptides in endosomal vesicles that fuse with exocytic vesicles containing MHC class II molecules associated with the class II invariant chain peptide (CLIP). CLIP is then removed by the protein DM and replaced by peptides derived from extracellular proteins. MHC class II + peptide complexes are then transported to the cell surface for recognition by $CD4^+$ T helper (Th) cells.

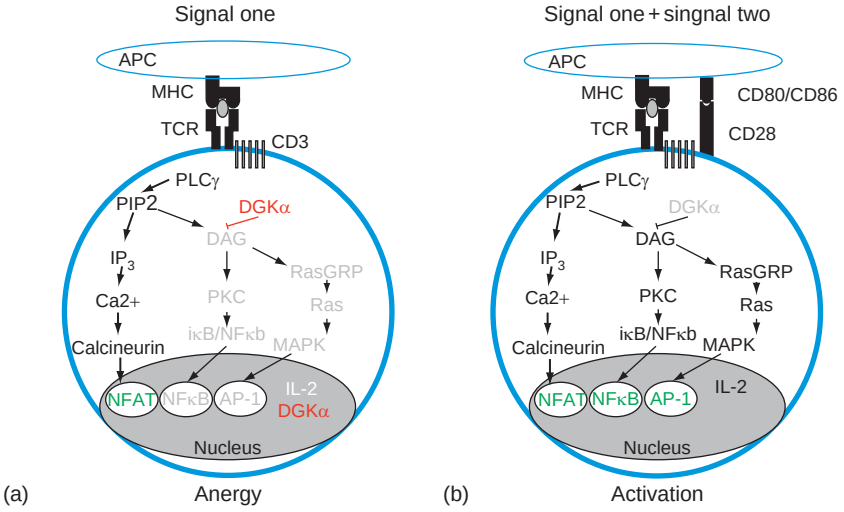

Figure 2 Signal transduction pathways of T-cell activation and anergy. (a) Engagement of TCR alone favors NFAT activation leading to inhibited IL-2 production and the induction of anergy-inducing genes. (b) Engagement of TCR along with co-stimulation provides balanced NFAT and NFκB activation and AP-1 formation leading to IL-2 production and repression of anergy-inducing genes. APC, antigen-presenting cell; MHC, major histocompatability complex; TCR, T-cell receptor; PLCγ, phospholipase Cγ; PIP_2, phosphatidylinositol-1,4 bisphosphate; IP_3, inositol 1,4,5-triphosphate; DGKα, diacylglycerol kinase alpha; DAG, diacylglycerol; PKC, protein kinase C; RasGRP, Ras guanyl releasing protein; MAPK, mitogen activated protein kinase; iκB, inhibitor of NFκB; NFκB, nuclear factor κB; NFAT, nuclear factor of activated T cells; AP-1, activator protein-1; IL-2, interleukin 2.

of the inhibitor of NFκB (i_kB) and subsequent translocation of NFκB from the cytosol to the nucleus. DAG also activates the Ras pathway, which through mitogen-activated protein kinase (MAPK) leads to formation and activation of the activator protein-1 (AP-1) molecule. NFAT, NFκB, and AP-1 are all transcription factors that cooperate to induce transcription of IL-2 and other T-cell activation genes. Signal one alone, however, is not sufficient to induce complete T-cell activation.

Signal two is delivered by invariant molecules expressed on the cell surface of APC that are upregulated after PRR engagement of PAMPs. The best characterized of these co-stimulatory molecules are CD80 (B7-1) and CD86 (B7-2), which bind to CD28 on T cells. CD28

engagement further activates the Ras/MAPK pathway to promote IL-2 production by making the IL-2 promoter accessible to transcription factors by chromatin remodeling, and by stabilizing IL-2 mRNA. Immediately, T-cell proliferation ensues.

The benefit of generating T cells with TCR capable of recognizing a tremendously diverse array of antigens carries the consequence that the same process generates TCR that recognize self molecules. While the most dangerous self-reactive T cells are deleted during T-cell development in the thymus by a process referred to as negative selection, many T cells with cross reactivity to both foreign and self-antigens escape negative selection. The requirement for two signals to induce T-cell activation may have developed to ensure that these cross-reactive T cells are activated only under appropriate circumstances; for example, when foreign antigen is encountered. During normal physiological conditions, APC that present self-antigens will not be activated by PAMPs to upregulate co-stimulatory molecules. Hence, signal one but not signal two will be delivered. Signaling through the TCR alone leads to long-lived T-cell unresponsiveness referred to as anergy, which is characterized by inhibited expression of IL-2. Therefore, anergy induction protects the body from the generation of autoimmunity while preserving the most extensive repertoire of TCR.

The current paradigm for anergy induction suggests that signal one induces NFAT activation with only partial AP-1 activation causing a signaling imbalance that leads to the expression of anergy-inducing genes, such as diacylglycerol kinase alpha (DGKα) (**Figure 2(a)**). DGKα phosphorylates DAG promoting its degradation and further decreasing activation of the Ras/MAPK and PKC pathways. Ultimately, the IL-2 promoter becomes inaccessible to transcription factors due to chromatin remodeling, and as a result, the cell becomes anergic. Anergy induction also involves T-cell expression of inhibitory co-stimulatory molecules, such as cytotoxic T-lymphocyte antigen 4 (CTLA-4), which antagonize activating co-stimulatory molecules.

T cell differentiation and effector function

Upon activation, T cells receive further instructions in the form of cytokines that promote differentiation that is best suited to respond to the offending pathogen. For example, $CD4^+$ T helper (Th) responses are directed toward at least four effector lineages: Th1, Th2, Th17, and adaptive T regulatory cells (Treg) by exposure to particular cytokines IL-12/ interferonγ (IFNγ), IL-4, transforming growth factor-β (TGF-β)/IL-6, or TGF-β, respectively (**Figure 3**). $CD8^+$ T cells differentiate into cytolytic T lymphocytes (CTLs) by exposure to IL-12 and express granzymes and perforin. $CD8^+$ T cells also produce cytokines and similar to Th cells are directed toward four effector lineages: Tc1, Tc2, Tc17, and Treg by exposure to IL-12/IFNγ, IL-4, TGF-β/IL-6, or TGF-β. PAMPs directly or indirectly induce the expression of these polarizing cytokines. For example, bacterial LPS and viral RNA induce DC expression of IL-12. The cellular source of IL-4 and TGF-β have not been defined. IL-6 is commonly expressed in inflammatory environments. These critical cytokines induce or repress the expression of key transcription factors. Th1 cells and CTL express T-bet while suppressing Gata-3 which is critical for Th2 development. Th17 cells do not express T-bet or Gata-3, but express retinoic acid-related orphan receptorγt (RORγt) which is fundamental for their development. Forkhead box P3 (FoxP3) is a signature transcription factor for Tregs. Each transcription factor promotes specific expression of subset-specific genes: Th1/Tc1 cells express IFNγ, Th2/Tc2 cells produce IL-4, 5, and 13, Th17/Tc17 cells produce IL-17, and Treg cells produce TGF-β.

The primary effector function of Th cells is to provide T cell help through co-stimulatory molecule expression and cytokine production, which orchestrates the immune response by inducing: T and B cell proliferation, Ig heavy chain class switching in B cells, and activation of innate cells. T follicular helper cells (Tfh) are another recently defined Th effector lineage characterized by expression of the chemokine receptor (CXCR5) and localization to B cell follicles within lymphoid tissues. Tfh cells promote B cell proliferation by production of IL-21. Activated B cells initially express IgM heavy chain molecules but upon engagement of Th cells through TCR and CD40L interactions, B cells change their Ig heavy chain isotype in response to Th expressed cytokines. For example, Th1-expressed IFNγ or Th2 expressed IL-4 promotes switching to IgG or IgE isotypes, respectively. Antibodies opsonize pathogen surfaces to: neutralize toxins, inhibit pathogen invasion by blocking cell surface receptors critical for binding host cells, and activate complement. In addition, antibody heavy chain isotypes are bound by Fc receptors expressed by innate cells to mediate antibody-dependent cellular cytotoxicity (ADCC). Antibody engagement of Fc receptors expressed by neutrophils (FcγRI), macrophages (FcγRI), NK cells (FcγRIII), and eosinophils (FcεR1), induces the release of lytic granules leading to targeted cell lysis. IgG molecules mediate ADCC through macrophages, neutrophils, and NK cells, whereas IgE molecules mediate ADCC through eosinophils.

Each Th lineage displays very different effector functions with clear protective and pathological consequences. Th1 cells mediate type IV delayed-type hypersensitivity responses (DTH) through production of IFNγ, which activates macrophages to increase their phagocytic activity and induce expression of TNF, NO, and reactive oxygen species. Hence, Th1 infiltration of the pathogen site amplifies inflammation initiated by PAMPs by further activation of macrophages. Th2 cells produce IL-4 and

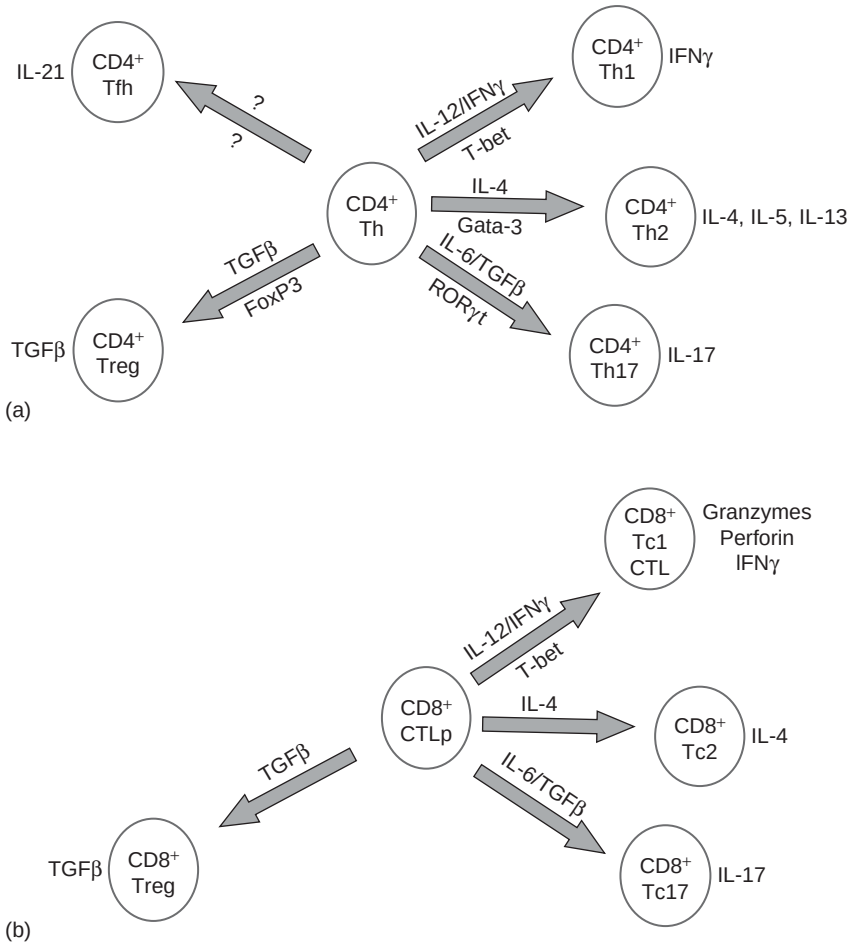

Figure 3 T-cell effector differentiation. $CD4^+$ Th cells (a) and $CD8^+$ T cells (b) differentiate into distinct subsets based on exposure to particular cytokines which induce unique transcription factor expression and cytokine expression. Th, T helper cell; Tfh, T follicular helper cells; Treg, regulatory T cells; TGFβ, transforming growth factor β; FoxP3, forkhead box P3; IL, interleukin; IFNγ, interferon gamma; RORγt, retinoic acid-related orphan receptor γt; CTLp, cytolytic T lymphocyte precursors.

IL-5, which control extracellular helminthic infections by activating eosinophils. The recently described Th17 subset produces IL-17 and has been implicated in the response against a wide variety of pathogens requiring a strong inflammatory response predominated by neutrophils. The nonspecific effector mechanisms elicited by macrophages, neutrophils, and eosinophils are associated with significant tissue damage. In contrast, Treg cells inhibit immune responses by expression of CTLA-4 and/or by the production of immunosuppressive cytokines such as TGF-β and IL-10, which inhibits T-cell proliferation and decreases co-stimulatory molecule and cytokine expression of APC. Tregs also suppress cytokine production and lytic activity of T cells, at sites of inflammation.

$CD4^+$ T helper cells are also critical for the generation of long-lived memory $CD8^+$ T cells that respond quickly and efficiently upon secondary exposure to antigen. $CD8^+$ T cells that expand in numbers to a pathogen in the absence of $CD4^+$ T cells rapidly undergo activation-induced cell death (apoptosis) through TRAIL/TRAIL receptor interactions upon secondary exposure to antigen. In addition, memory $CD8^+$ T cells generated in the presence of $CD4^+$ Th cells are not maintained if transferred to mice deficient in $CD4^+$ T cells, indicating that Th cells are somehow necessary to maintain long-lived memory $CD8^+$ T cells *in vivo*.

The primary effector function of $CD8^+$ T cells is control of intracellular pathogens. $CD8^+$ T cells differentiate into lytic effectors (CTL) which are characterized by expression of perforin and granzymes. CTL target infected cells by their expression of pathogen peptides presented on the cell surface by MHC class I molecules. Perforin molecules form pores in cell membranes which facilitate transfer of granzymes into the cytoplasm that activate caspases to induce apoptosis. Interestingly, granzyme B can also inhibit herpes simplex virus-1 (HSV-1) replication within latently infected neurons without

inducing apoptosis by caspase-mediated cleavage of viral proteins. Whether the neuron or the HSV-1 infection prevents apoptosis under this circumstance remains to be determined. $CD8^+$ CTL also produce IFNγ, which inactivates viral proteins and activates innate cells as previously mentioned.

Differentiation of T-cell effectors is coincident with the differentiation of long-lived memory T cells. Memory T cells are divided into central (Tc) and effector (Te) memory subpopulations based on their location and unique expression of cell surface molecules. Tc memory cells localize to lymph nodes and spleen through expression of the chemokine receptor7 (CCR7) and CD62L, whereas Te memory cells are present in nonlymphoid tissues and do not express these molecules. Several cell surface molecules have been useful in distinguishing naïve T cells from memory and effector T-cell populations. For example, naïve T cells express low levels of CD44 and killer cell lectin-like receptor G1 (KLRG1) and high levels of the IL-7 receptor (CD127). In contrast, both effector and memory T-cell populations express high levels of CD44. The retention or reexpression of CD127 along with low expression of KLRG1 distinguishes memory T cells from CD127 low KLRG1 hi T cell effectors.

The differentiation of effector and memory T cells from a single naïve T-cell precursor is an area of active research and several models are being tested. Lineage determination could involve dedifferentiation of effector cells. Another model suggests that the strength of signal delivered by APC to T cells may favor a particular lineage. For example, T effector generation may be favored when inflammation is high, whereas T memory generation may be favored when inflammation is low. Inverse regulation of T-bet and eomesodermin transcription factors by IL-12 expressed during inflammation may be critical for lineage determination. Alternatively, lineage commitment may be determined upon the first cell division by asymmetric distribution of critical lineage determining molecules to daughter cells.

T-cell immune responses in the eye

The eye was characterized as a site of immune privilege by the Nobel laureate Peter Medawar in 1948 based on the observation that foreign tissue transplanted in the anterior chamber persisted indefinitely whereas the same tissue transplanted in the skin was rapidly rejected by the host immune response. Based on the absence of demonstrable lymphatic drainage of the interior of the eye, Medawar concluded that ocular antigens were sequestered and the immune system was ignorant of their presence. However, subsequent investigations found that Medawar was incorrect. A reevaluation of ocular immune privilege almost 30 years later by Kaplan and Streilein indicated that soluble and cell-associated antigens injected into the anterior chamber escaped from the eye and induced systemic T-cell nonresponsiveness. Upon secondary exposure to the same antigen under immunogenic conditions, such as antigen administration with adjuvant, the magnitude of Th1 or Th2 type cell-mediated immune responses was markedly reduced in comparison to mice in which the first exposure to antigen was through a nonprivileged route (skin or conjunctiva of the eye). This phenomenon, termed anterior chamber-associated immune deviation (ACAID), is mediated by $CD4^+$ Tregs, which inhibit the induction of T-cell effector responses and $CD8^+$ Tregs, which inhibit the expression of T-cell effector responses specific for ocular antigens. ACAID may contribute to the tremendous success of corneal transplantation that does not routinely require donor/recipient MHC matching or systemic immunosuppression because mice that accept corneal allografts demonstrate reduced DTH responses to donor antigens.

Ocular immune privilege is also maintained by soluble molecules contained within the aqueous humor and by cell-associated molecules expressed on tissues lining the anterior chamber, which are immunosuppressive (**Table 1**). These molecules directly inhibit T-cell effector function, convert T effectors into Treg, or inhibit the activation of

Table 1 Immune suppressive factors that maintain ocular immune privilege

Factor	*Effect*
TGF-β (Transforming growth factor-beta)	Decreases expression of CD40 and production of IL-12 and increases production of TGF-β by antigen-presenting cells (APC) leading to generation of T-cell hyporesponsiveness and/or T regulatory cells (Treg) generation. Inhibits T-cell proliferation and T-cell effector function
αMSH (alpha-melanocyte stimulating hormone)	Conditions APC to generate $CD4^+$ Treg Converts $CD4^+$ Teffector into Treg Inhibits neutrophil function
VIP (vasoactive intestinal protein)	Inhibits T-cell proliferation
CGRP (calcitonin gene-related peptide)	Inhibits production of nitric oxide by macrophages
CD95 (FasL), TRAIL, and PD-L1	Induces apoptosis of effectors infiltrating the eye
Soluble FasL	Inhibits neutrophil function
CD86 (B7-2)	Expressed on pigmented cells of the eye Induces functional nonresponsiveness of T cells upon engagement of cytotoxic T-lymphocyte antigen 4 (CTLA-4)
MIF (macrophage migration inhibitory factor)	Inhibits natural killer (NK) cell activity

innate cells. These barriers to T-cell responses are thought to represent a necessary compromise to limit tissue damage during pathogen control. The inhibition of the adaptive immune response would suggest that the eye would be more susceptible to infection. However, this is not the case. Rather, the eye is more prone to immunopathology when T-cell responses break immune privilege to control an ocular pathogen.

Several ocular infections induce T-cell responses that promote immunopathology. Viral (HSV-1) and bacterial (*Pseudomonas aeruginosa*) infections of the cornea induce $CD4^+$ Th1 cells that infiltrate the cornea and orchestrate neutrophil infiltration leading to keratitis. Parasitic *Onchocerca volvulus* infections induce Th2 responses that contribute but are not alone sufficient to induce keratitis. Interestingly, endosymbiotic *Wolbachia* bacteria activate TLRs to induce infiltration of the cornea by neutrophils, which are the primary mediators of inflammation. Th17 and Th1 cells have been shown to contribute to immunopathology in experimental rodent models of uveitis. $CD4^+$ Th cells are also critical in the rejection of corneal allografts through induction of a classic DTH response in the cornea and mediate lacrimal keratoconjunctivitis in mice exposed to dessicating stress.

The factors that break immune privilege are not completely understood. However, changes in immunoregulatory elements due to inflammation must be involved. Interestingly, in animal studies, the type but not intensity of ocular inflammation has been shown to be critical in breaking immune privilege. For example, the induction of ACAID is preserved in mice with LPS-induced uveitis but not in mice with inflammatory pigmentary glaucoma, although neutrophil inflammation is more pronounced in uveitic mice. Differences in the duration of inflammation may distinguish whether privilege is broken, as LPS-induced uveitis resolves within days whereas glaucoma persists for months. Identification of the regulatory factors affected by pathogens that break immune privilege will be critical for our understanding of how T-cell responses to ocular antigens are modulated to promote the elimination of ocular pathogens while producing minimal tissue damage.

See also: Immunobiology of *Acanthamoeba* Keratitis; Immunobiology of Age-Related Macular Degeneration; Immunopathogenesis of Experimental Uveitic Diseases; Immunopathogenesis of Onchocerciasis (River Blindness); Immunopathogenesis of Pseudomonas Keratitis; Pathogenesis and Immunology of Bacterial Endophthalmitis; Pathogenesis of Fungal Keratitis; Pathogenesis of Uveitis in Humans.

Further Reading

Abbas, A. K. and Lichtman, A. H. (2009). *Basic Immunology: Functions and Disorders of the Immune System*, 3rd edn. Philadelphia, PA: Saunders/Elsevier.

Forrester, J. V., Dick, A. D., McMenamin, P. G., and Lee, W. R. (2008). *The Eye: Basic Sciences in Practice*, 3rd edn. Philadelphia, PA: Saunders/Elsevier.

Niederkorn, J. Y. and Kaplan, H. J. (2007). *Immune Response and the Eye, Chemical Immunology and Allergy*, vol. 92, 2nd, rev. edn. Basel: Karger.

Paul, W. E. (2008). *Fundamental Immunology*, 6th edn. Philadelphia, PA: Wolters Kulwer/Lippincot Williams and Wilkins.

Adaptive Optics

L Yin and D R Williams, University of Rochester, Rochester, NY, USA

Glossary

Deformable mirror – A mirror equipped with an array of actuators on the back surface that can warp the mirror surface by small amounts into arbitrary shapes, allowing the correction of the eye's aberrations.

Diffraction-limited resolution – The resolution of an optical system that has no aberrations, the image quality of which is reduced only by the diffraction of the light in the pupil of the system.

Lipofuscin autofluorescence – Lipofuscin is composed of many molecules that are by-products of the visual or retinoid cycle. These accumulate in the retinal pigment epithelium with aging and can be visualized in the living eye because they fluoresce when exposed to short wavelength light.

Point-spread function (PSF) – The light distribution in the image plane of an optical system such as the eye, formed from light from a point source outside the eye, such as a very distant star.

Retinal densitometry – A method to measure the density of photopigment in the living eye.

Shack–Hartmann wavefront sensor – A device capable of measuring the optical defects of an optical system such as the human eye. The output of a wavefront sensor can be used to control the shape of a deformable mirror in an adaptive optics system.

Stiles and Crawford effect – The fact that the eye is far more sensitive to light entering through a point near the center of the pupil than the pupil margin even though the irradiance at the retina is very little dependent on entry point in the pupil. This effect is caused by the waveguide properties of cone photoreceptors, which are more sensitive to light falling on their optical axes (which point near the center of pupil) than obliquely incident light.

The Benefit of Adaptive Optics in Vision Science

The history of ophthalmoscopy after its invention by Helmholtz until today is marked by efforts to extract the most information possible from the light reflected from the retina. Over the last two decades, there has been a concerted effort to improve the resolution of the imaging process in all three spatial dimensions. The development of optical coherence tomography (OCT) improved the resolution in the axial dimension, and has allowed the routine imaging of individual layers of cells in the retina. More recently, the introduction of adaptive optics (AO) has improved the resolution of fundus cameras in both transverse dimensions. The transverse resolution of the conventional fundus camera is limited not by the camera itself but by the optics of the human eye. The sources of image blur in the eye's optics include diffraction, aberrations, and scatter. Diffraction is the image blur that results from the wave nature of light as it passes through the eye's pupil. Blurring by diffraction is not inevitable; there are exciting techniques on the horizon that may eventually overcome the fundamental resolution limit set by diffraction, but no one has yet demonstrated this in the eye. A hypothetical eye that suffered only from diffraction would allow a resolution no smaller than about 1.4 μm when imaging wavelengths of light in the middle of the visible spectrum (550 nm). This is smaller than the smallest cells in the retina, so that if one could make the natural human eye limited only by diffraction, cellular and even subcellular features that are invisible in conventional fundus imaging could be seen. As shown in **Figure 1** (upper panels), in a diffraction-limited eye, the larger the pupil, the smaller the image of a single point of light and therefore the better the resolution.

The monochromatic and chromatic aberrations of all eyes further blur the retinal image. The monochromatic aberrations of the human eye alone are greater than those of even a mediocre man-made optical system. As shown in **Figure 1** (lower panels), increasing the pupil reduces the effect of diffraction, but exacerbates the effect of aberrations, with the best trade-off between the two occurring for pupil sizes around 3 mm. Light scatter, the third cause of loss in retinal image quality, is relatively unimportant in young eyes but it can greatly reduce retinal image contrast in older eyes, especially those with cataract. Not only is the retinal image blurred by the optical factors mentioned above, it is also exceedingly dim. The amount of light that can be delivered to the retina is limited for safety reasons and the retinal reflectance is low: 10^{-3}–10^{-5} across the spectrum. This would be less of a problem if it were easy to integrate light over long exposures, but the eye is always moving; even an eye with excellent fixation moves about ~20 μm root mean square (rms) velocity. Eye motion artifacts are all the more troublesome in instruments with high magnification that are designed to look at cellular

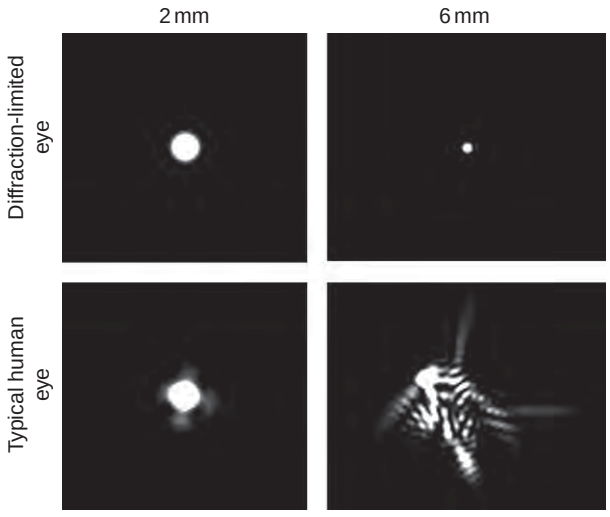

Figure 1 The point-spread function (PSF) for a diffraction-limited eye and a normal eye at two different pupil diameters. The PSF corresponds to the light distribution on the retina produced by a point source of light infinitely distant from the eye. For the hypothetical diffraction-limited eye, the PSF diameter decreases in inverse proportion to the pupil diameter such that large pupils produce the best image quality. However, in the typical human eye, aberrations increase with increasing pupil size, eliminating the benefit of escaping diffraction at the largest pupils. The goal of AO is to correct the aberrations to produce the PSF of a diffraction-limited eye with a large pupil. Adapted from Roorda, A. Garcia, C. A., Martin, J. A., et al. (2006). What can adaptive optics do for a scanning laser ophthalmoscope? *Bulletin de la Société Belge d'Ophthalmologie* 302: 231–244, Figure 1, with permission from Bulletin of the Belgian Societies of Ophthalmology (Copyright 2006).

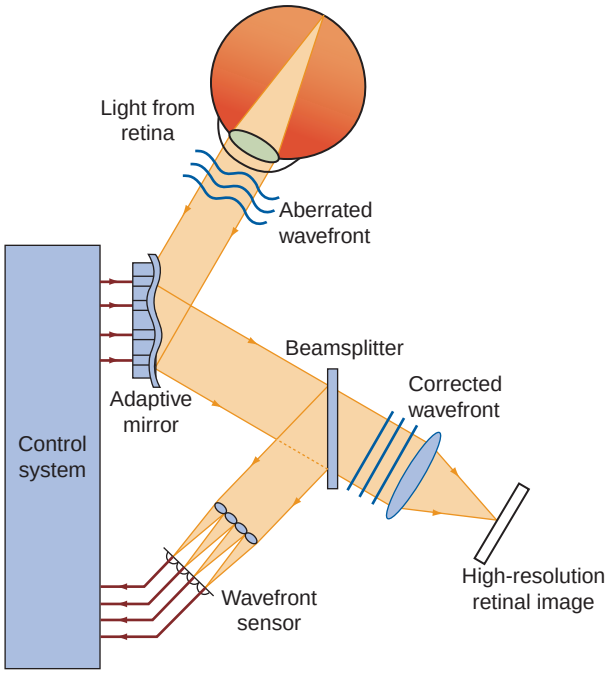

Figure 2 Principle of adaptive optics. The system contains two key parts: the wavefront sensor and wavefront corrector. The wavefront sensor, usually of the Shack–Hartmann type, measures the monochromatic aberration of the eye. It uses a 2-D array of lenslets conjugate with the eye's pupil to break the light from an infrared point source imaged on the retina into several hundred individual beams. Each beam is imaged on a CCD array. Its displacement on the CCD from where it would have landed had the eye been aberration-free indicates the slope of the wave aberration at that lenslet's location in the pupil. Information from all the lenslets is combined to compute the overall wave aberrations of the eye. These data are used to control a wavefront compensation device that corrects the wave aberration. The most commonly used device is a continuous surface deformable mirror. This mirror has a flexible surface overlying an array of actuators that can push or pull on the mirror surface locally. If the mirror surface is shaped so as to mimic the shape of the wave aberration but with half the amplitude of the wave aberration, the wavefront reflecting from the surface will be perfectly flat, and the monochromatic aberrations of the eye will have been corrected. Adapted from Carroll, J. Gray, D. C., Roorda, A., Williams, D. R. (2005). Recent advances in retinal imaging with adaptive optics. *Optics and Photonics News* 16: 36–42, Figure 1, with permission from Optical Society of America (Copyright 2005).

structures that are often far smaller than 20 μm. Despite all these formidable limitations, it is possible to design fundus cameras that address all of them with varying degrees of success, making microscopic resolution of the living retina possible as described below.

Correcting the Eye's Monochromatic Aberration

It is possible to overcome the eye's monochromatic aberrations with AO, a two-step process in which the eye's wave aberration is measured and corrected, usually in real time. **Figure 2** describes the principle of AO for imaging the eye. The monochromatic aberration of the eye is measured with a wavefront sensor. The measured aberration data are used to control a wavefront compensation device, usually a deformable mirror that corrects the wave aberration. Ideally, it would completely remove all the monochromatic aberrations, leaving diffraction and scatter as the only remaining sources of image blur. It usually takes several iterations of the measurement and correction loop to achieve the best correction, at which point it is possible to obtain a retinal image that is almost completely aberration free in eyes with normal amounts of aberrations. The rate of measurement and correction required to keep up with the temporal variations in the eye's wave aberration is relatively slow, at least compared with applications of AO in astronomy. Heidi Hofer has shown that measuring and correcting the wave aberration at 30 Hz or so is adequate to track the most important changes in the wave aberration, which are caused by microfluctuations in accommodation that have a temporal bandwidth of only a few Hertz. With complete wavefront correction, the point-spread function (PSF) is very

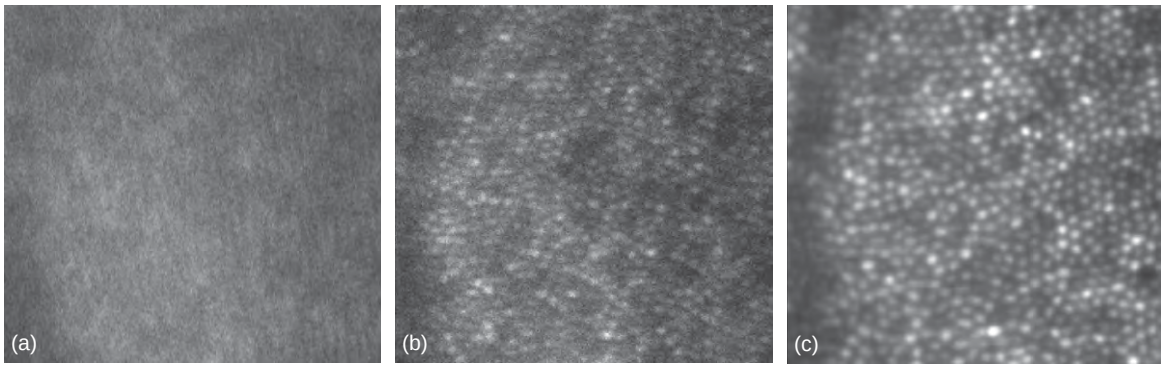

Figure 3 Adaptive optics and motion correction greatly improve the resolution of images of human cone mosaic. (a) Single frame of the reflectance image of the cone mosaic of a typical human eye at 1 degree of eccentricity imaged with all the aberrations of the eye, or (b) After the monochromatic aberrations of the eye were corrected with AO. (c) The summed frames of many images of the same cone mosaic with aberration and eye motion corrected with AO. The frames were registered before summing to correct for eye motion between frames, which increases the SNR over that obtained with single frames. The individual cones at this eccentricity are approximately 5 μm in diameter.

compact, approaching the light distribution produced by diffraction alone. Typically, one can achieve as much as an order of magnitude reduction in the rms wavefront error of a normal eye with this method. This provides a substantial improvement in image quality as shown in **Figure 3**.

Vision Correction with AO

One of the convenient features of AO correction is that the correction required to focus light onto the retina is the same as the correction required to image the retina at high resolution outside the eye. Many investigators have capitalized on the advantages of AO for vision correction as well as for retinal imaging. Correcting the higher order monochromatic aberrations (i.e., those other than defocus and astigmatism corrected by spectacles) produces a modest improvement in visual acuity and contrast sensitivity in the normal eye. The improvements can be dramatic in eyes with large amounts of higher-order aberrations such as those that suffer from keratoconus. The demonstration of these improvements in spatial vision with a deformable mirror has stimulated improvements in the control of laser ablation in refractive surgery as well as the fabrication of customized contact lenses that can correct higher-order aberrations. AO continues to be a valuable tool not only for correcting aberrations but also for generating specific patterns of aberrations so that their effects on vision can be studied conveniently. For example, it is possible to explore the design of contact lenses for presbyopes that increase the depth of field of the eye without the need to fabricate optical elements for each pattern one wishes to evaluate.

Retinal Imaging with AO

In retinal imaging, AO can be combined with almost any other imaging technology. David Williams' laboratory at the University of Rochester first demonstrated the value of a closed-loop AO system for retinal imaging, incorporating AO into a flood-illuminated system that acquired single snapshots of the retina with a resolution adequate to resolve cone photoreceptors near the fovea. Austin Roorda, then at the University of Houston, demonstrated that AO could also improve the resolution of the scanning laser ophthalmoscope (SLO). SLOs are potentially confocal devices and AO offers improvements in both axial and transverse resolutions. Moreover, AO improves the focus of the light on the confocal pinhole in front of detector, which increases the available signal. The AOSLO has a high lateral resolution of less than about 2 μm. The axial resolution of better than ~60 μm, though poor by OCT standards, is nonetheless adequate for some optical sectioning of the retina. AO has also improved the transverse resolution of OCT, allowing a resolution of less than 3 μm in all three spatial dimensions in the retina. AO systems can also be combined with other imaging modalities such as phase contrast microscopy, polarization imaging, or fluorescence microscopy.

Compensating for Eye Motion

In many cases, the signals acquired in a single video frame of an AOSLO are weak enough to warrant frame averaging to increase the signal-to-noise ratio (SNR) of the image (**Figure 4(a)**). Eye motion between frames, which is substantial in the high-magnification images of AO systems, must be corrected before frame averaging can be achieved. One correction method is to register successive frames with normalized cross-correlation, the benefit of which is shown in **Figure 3(c)**. However, it is not uncommon for single frames, such as the one shown in **Figure 4(a)**, to have inadequate SNR for this method. In the case, illustrated here of autofluorescence imaging by Jessica Morgan at the University of Rochester, there was typically less than

one photon for every 5 pixels in each frame. As shown in Figure 4(b), this problem can be solved by simultaneously recording infrared reflectance images of the cone mosaic at the same retinal location. Eye motion between frames can be reliably recovered from reflectance images of cone mosaic with an accuracy of one-fifth of the diameter of a foveal cone, and this information can be used to register the low SNR images as shown in Figure 4(b).

Eye movements can also produce warping artifacts within each frame. Austin Roorda and Scott Stevenson have developed methods in which the relative locations of local retinal features are compared across frames to compute and correct the eye movement warping within each frame as well as translation between frames. Figure 5 shows an AOSLO image motion before and after removing distortions from eye movements. Image motion after correction is reduced to a standard deviation of only 7 arcsec. David Arathorn at Montana State University, working in collaboration with Austin Roorda, has a fast software algorithm that can stabilize the retinal image in real time. This has very exciting applications for delivering light stimuli to single photoreceptors in both psychophysical and electrophysiological studies. Software registration approaches alone cannot address all the problems created by eye movements, particularly in AO instruments designed for routine clinical use where eye movements are much larger than the size of a single frame. In that case, successive frames do not share common features and cross-correlation cannot be

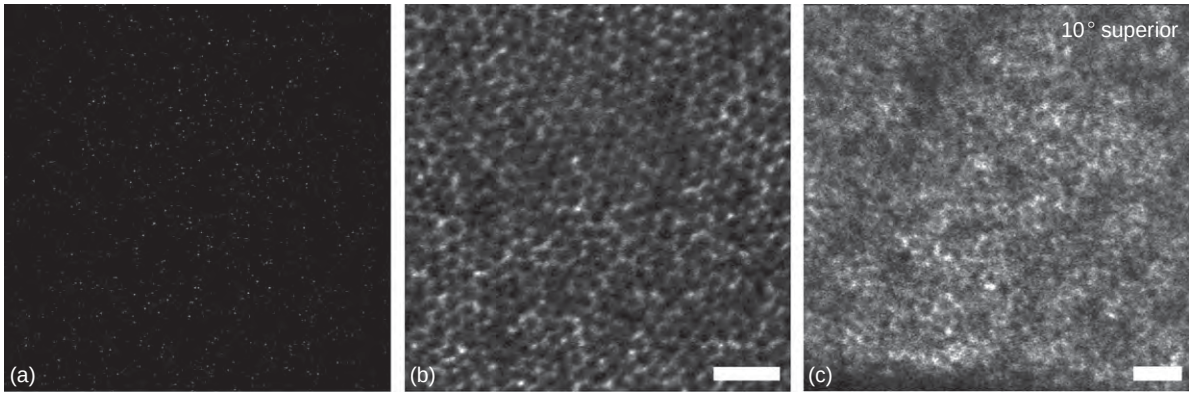

Figure 4 Dual registration improves the transverse resolution of autofluorescence images of the RPE mosaic. (a) Single frame of autofluorescence image of primate RPE mosaic. Because of the low SNR and photon density, the image does not have any apparent spatial structure. (b) 1000 frames of autofluorescence images of the same RPE mosaic shown in (a) summed with eye motion corrected using the dual-registration technique. The eye motion was calculated from reflectance images of the cone mosaic obtained simultaneously with the dim autofluorescence images, providing the translations necessary to register the autofluorescence images. The summed image reveals single cells in the RPE mosaic. (c) Autofluorescence image of human RPE mosaic at retinal eccentricity of 10 degrees. Bright regions in the images correspond to the accumulation of lipofuscin within the RPE cells. Dark regions correspond to the nuclei of RPE cells. Scale = 50 μm. Adapted from Morgan, J. I. Dubra, A., Wolfe, R., et al. (2009). In vivo autofluorescence imaging of the human and macaque retinal pigment epithelial cell mosaic. *Investigative Ophthalmology and Visual Science* 50: 1350–1359, Figure 5, with permission from Association for Research in Vision and Ophthalmology (Copyright 2009).

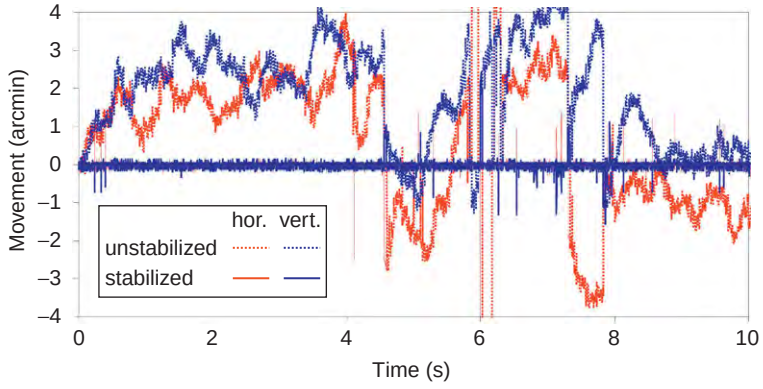

Figure 5 Eye motion in the AOSLO system before and after eye motion correction. Eye motion of a human subject within 10 s duration is captured at 480 Hz through AOSLO imaging (dotted red and blue lines: horizontal and vertical eye movements). After offline correction, the eye motion in the AOSLO images is reduced to flat lines (in red and blue: horizontal and vertical eye movement), with a standard deviation of 7 arcsec. This compares favorably with the most accurate methods to track the eye, having an accuracy that is roughly one-fourth of the diameter of the smallest foveal cones. Courtesy of A Roorda.

used. Dan Ferguson and Dan Hammer at Physical Sciences Incorporated have developed a hardware eye tracking system specifically for AO retinal imaging that complements the software approaches described above.

Imaging Cones

The ability to image cones at high resolution with AO opened a crucial window to examine both normal and abnormal processes in the retina. AO has made possible the first measurements of the antenna properties of single cones in the living human eye. Cone photoreceptors concentrate the image-forming light that passes through the pupil in the photopigment of the outer segment while simultaneously excluding stray light from sources that do not contribute to a sharp retinal image. This beneficial effect of the waveguide nature of cones gives rise to the psychophysical effect known as the Stiles and Crawford effect, in which the sensitivity of the eye declines dramatically for light beams that enter the margin instead of the center of the pupil. Austin Roorda and David Williams at the University of Rochester showed that nearby cones are remarkably well aligned with each other optically so that the angular tuning of a large group of cones is similar to the tuning function for a single cone.

Single cones imaged with AO in the living human eye show a striking variability in reflectance on a time scale of hours or days. The cause of this variability is unknown but could be related to the process of disc shedding in the cone outer segments. Don Miller at Indiana University has shown that, especially when the incoming light is highly coherent, there can be dramatic changes on very short time scales of 5–10 ms. These changes depend on the history of the cone's light exposure and provide an optical method to monitor to the response of cones to light. Kate Grieve and Austin Roorda have also reported increases in infrared reflectance following exposure to light that may provide an alternative method to monitor functional activity in single cones in the retina.

The Cone Mosaic and Color Vision

The first major scientific application of AO in the eye, undertaken at the University of Rochester, was to determine the organization of the human trichromatic cone mosaic. By combining AO retinal imaging with retinal densitometry, individual cones can be characterized by their sensitivity to long (L), middle (M), or short (S) wavelength light, according to the cone opsin it contains, as the example shown in **Figure 6**. Experiments using this method have shown that mosaic of L and M cones in the human are essentially randomly organized. It has been known for some time from indirect methods that the relative numbers of L and M cones varies greatly from eye to eye. AO revealed just how large this variation can be even across normal subjects where a variation in the order of 40-fold in L to M cone ratio has been observed. The human S cones are arranged randomly near the fovea but with slight tendency toward regular distribution, a tendency that is more pronounced in the macaque monkey.

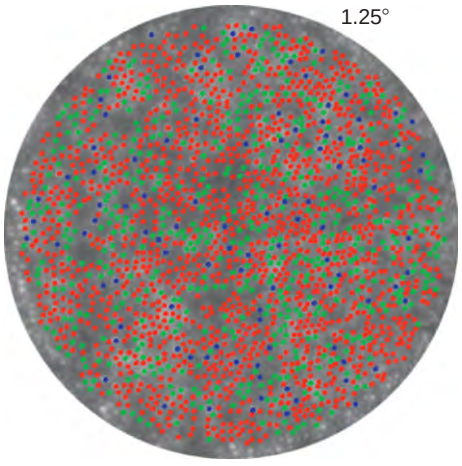

Figure 6 Cone mosaic of a human subject at a retinal eccentricity of 1.25 degree with normal color vision. Individual cones in each mosaic were categorized as L, M, or S cone types, using retinal densitometry, and false colored, respectively in red, green, and blue. Courtesy of O. Masuda.

The development of AO for the eye has also made it possible to study color vision in living human eyes in novel ways because it is now possible to deliver tiny flashes of light that are smaller than single cones. Heidi Hofer showed that near-threshold AO-delivered flashes of monochromatic light at a single wavelength produce a rich variety of color percepts. Indeed, for every subject she studied, the range of color experiences was too large to be explained by a simple model in which all cones of the same class produced the same color experience upon stimulation. David Brainard at the University of Pennsylvania has successfully described the range of color experiences in Heidi Hofer's data with a Bayesian model in which each cone feeds a specific circuit that provides the best estimate of the external stimulus given the local distribution of photon catches in the stimulated cone and its surrounding neighbors.

One of the most powerful applications of AO to date involves its use to characterize the topography of the cone mosaic in eyes in which the genotype is known. Until recently, it has been difficult to perform these studies with standard histological methods because of the difficulty in obtaining post-mortem tissue from eyes with specific and often rare genetic anomalies. Joe Carroll has shown that the cone mosaics of single gene dichromats appear completely normal despite the fact that they have two instead of the usual three cone photopigments (**Figure 7(b)**). On the contrary, dichromats with a specific polymorphism in one of the genes coding for a particular cone photopigment have a cone mosaic with numerous gaps corresponding to a spatially random loss of one class of cones (**Figure 7(c)**; also see **Figure 8** for another example).

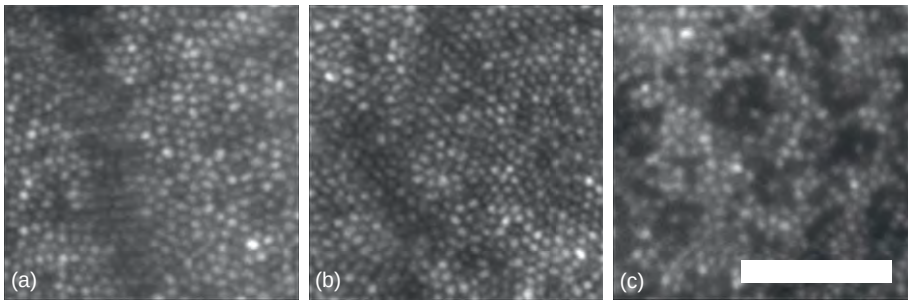

Figure 7 Pathological change of human cone mosaic in red or green dichromat. (a) Cone mosaic from a normal subject at approximately 1 degree of retinal eccentricity. (b) and (c) Cone mosaics at a similar eccentricity of two human subjects having red–green color-vision deficiency. In contrast to the normal cone mosaic in (a), the cone mosaic in (b) did not contain L cones, but appeared to have normal cone density. The cone mosaic in (c), did not contain M cones, and had reduced cone density with patches of functional loss of M cones. Scale = 50 μm for all panels. Reproduced from Carroll, J. Gray, D. C., Roorda, A., Williams, D. R. (2005). Recent advances in retinal imaging with adaptive optics. *Optics and Photonics News* 16: 36–42, Figure 3, with permission from Optical Society of America (Copyright 2005).

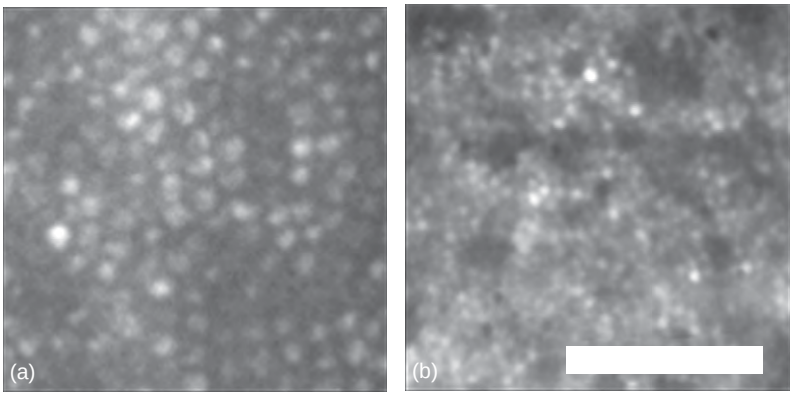

Figure 8 Pathological change of human cone mosaic in rod monochromat. (a) Cone mosaic from a normal subject at approximately 4 degrees of retinal eccentricity. (b) Possible rod mosaic of one subject who was a congenital achromat. The reason why the photoreceptors in (b) were believed to be rods is that their density and size match with the anatomical characteristic of the rod mosaic at this eccentricity, and differ greatly from the normal cones in (a). Scale = 50 μm for all panels. Reproduced from Carroll, J., Gray, D. C., Roorda, A., Williams, D. R. (2005). Recent advances in retinal imaging with adaptive optics. *Optics and Photonics News* 16: 36–42, Figure 3, with permission from Optical Society of America (Copyright 2005).

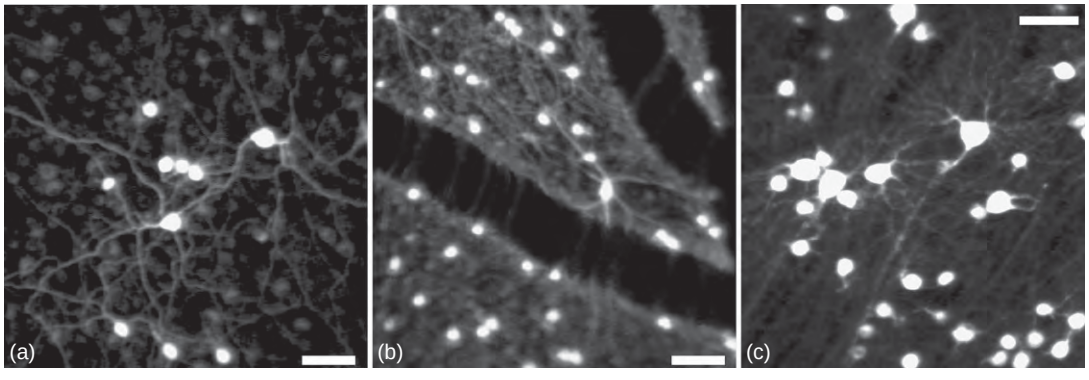

Figure 9 Fluorescence AOSLO images of primate retinal ganglion cells *in vivo.* (a–c) Fluorescence AOSLO imaging revealed the morphology of retinal ganglion cells labeled with fluorophore (rhodamine dextran) in living monkey eye. The transverse resolution of the images is fine enough to resolve the individual dendrites. The fluorophore was introduced into the ganglion cells through retrograde labeling through injections in the lateral geniculate nucleus (LGN). Scale = 50 μm for all panels. (a,c) Reproduced from Gray, D. C., Wolfe, R., Gee, B. P., et al. (2008). In vivo imaging of the fine structure of rhodamine-labeled macaque retinal ganglion cells. *Investigative Ophthalmology and Visual Science* 49: 467–473, Figures 1 and 5, with permission from Association for Research in Vision and Ophthalmology (Copyright 2008).

Imaging Retinal Pigment Epithelium

The retinal pigment epithelium (RPE) lies immediately behind the photoreceptors and plays several critical roles in maintaining their function. RPE cell damage is implicated in many retinal degenerative diseases such as age-related macular degeneration, retinitis pigmentosa, and Stargardt's disease. The ability to image these cells in the living retina and to track changes in them over time may prove valuable for understanding both normal RPE function and retinal disease. In AOSLO reflectance imaging, the more reflective photoreceptor mosaic normally obscures RPE cells. Occasionally, RPE cells can be seen in patients with retinal degenerative diseases, such as cone–rod dystrophy, where the overlying photoreceptors are absent. However, it has recently become possible to image the RPE mosaic in living human eyes in which the photoreceptor layer is intact, by taking advantage of the autofluorescence properties of lipofuscin in the RPE as shown in **Figure 4(c)**. Statistical characterization of the RPE mosaic, for example, packaging arrangement and cell density across eccentricity, in both normal subject and patients may eventually prove to be valuable for the clinical diagnosis of earlier stages of retinal degenerative disease. It may ultimately prove possible to use AO to image subcellular structures in RPE cells

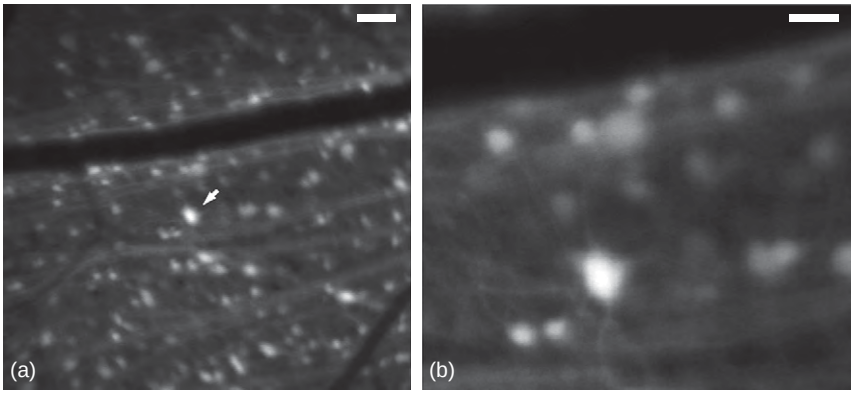

Figure 10 Fluorescence AOSLO images of rat retinal ganglion cells *in vivo.* (a) Fluorescence AOSLO image of rat retina with ganglion cell expressing EGFP. Scale = 50 μm. Image was taken at a large field of view (FOV). Gene encoding EGFP was delivered to ganglion cells through an AAV2 viral vector administrated intravitreally. The ganglion cell indicated by the white arrow was shown in (a) at higher magnification. Image at this view reveals the dendritic morphology of the cell. Such images could provide basis for morphological classification *in vivo*. Scale = 20 μm.

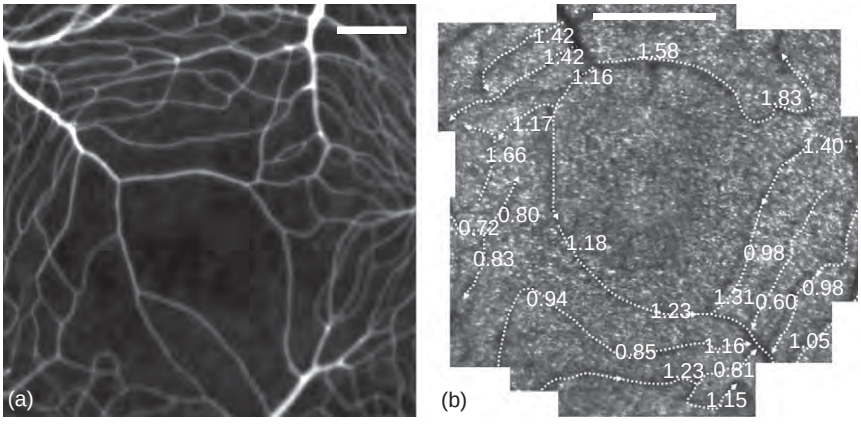

Figure 11 AOSLO images of retinal vasculature. (a) Retinal vasculature in the macular region in primate eye imaged by fluorescence AOSLO in combination with fluorescence angiography. Scale = 150 μm. (b) Direction of blood flow and leukocyte velocity within the capillaries of the macular region in human eye calculated from reflectance AOSLO images. Movement of discrete leukocytes was detected through an image-processing algorithm. The velocities of the leukocytes labeled on the images were in mm s^{-1}. Scale = 1 degree. (a) Reproduced from Gray, D. C., Merigan, W., Wolfing, J. I. et al. (2006). In vivo fluorescence imaging of primate retinal ganglion cells and retinal pigment epithelial cells. *Optics Express* 14(16): 7144–7158, Figure 6, with permission from Optical Society of America (Copyright 2006). (b) Adapted from Roorda, A., Garcia, C. A., Martin, J. A., et al. (2006). What can adaptive optics do for a scanning laser ophthalmoscope? *Bulletin de la Societé Belge d'Ophthalmologie* 302: 231–244, Figure 6, with permission from Bulletin of the Belgian Societies of Ophthalmology (Copyright 2006).

and/or to monitor changes in RPE cells over time. Jessica Morgan has already shown that it is possible to use AO to track the time course of lipofuscin autofluoresence bleaching and RPE damage following exposure to bright light.

Imaging Retinal Ganglion Cells

The retinal image is conveyed to the brain through an array of 17 or more parallel ganglion cell pathways in the primate. We know remarkably little about the functional significance of many of these morphologically distinct ganglion cell classes. One of the major impediments to learning more about them is that the less numerous cells are difficult to target with a microelectrode that is capable of recording from only one single cell at a time. The development of optical methods to record from many ganglion cells simultaneously in the intact living eye could greatly accelerate our understanding of ganglion cell function. There are numerous technical hurdles to overcome before this is feasible, but AO retinal imaging has now solved an important one: it is now possible to image ganglion cells along with some of their subcellular structure *in vivo* in nonhuman primate retina. This capability may also eventually prove useful in the study of diseases such as glaucoma, in which blindness results from the death of ganglion cells. New ways to image ganglion cells at a microscopic spatial scale may lead to earlier diagnosis and delivery of therapy.

Dan Gray, working in the AO group at the University of Rochester, imaged the dendritic morphology of macaque ganglion cells retrogradely labeled with fluorescent dye (rhodamine dextran) *in vivo*, with a transverse resolution of 1.6 μm (characterized as full width at half maximum;

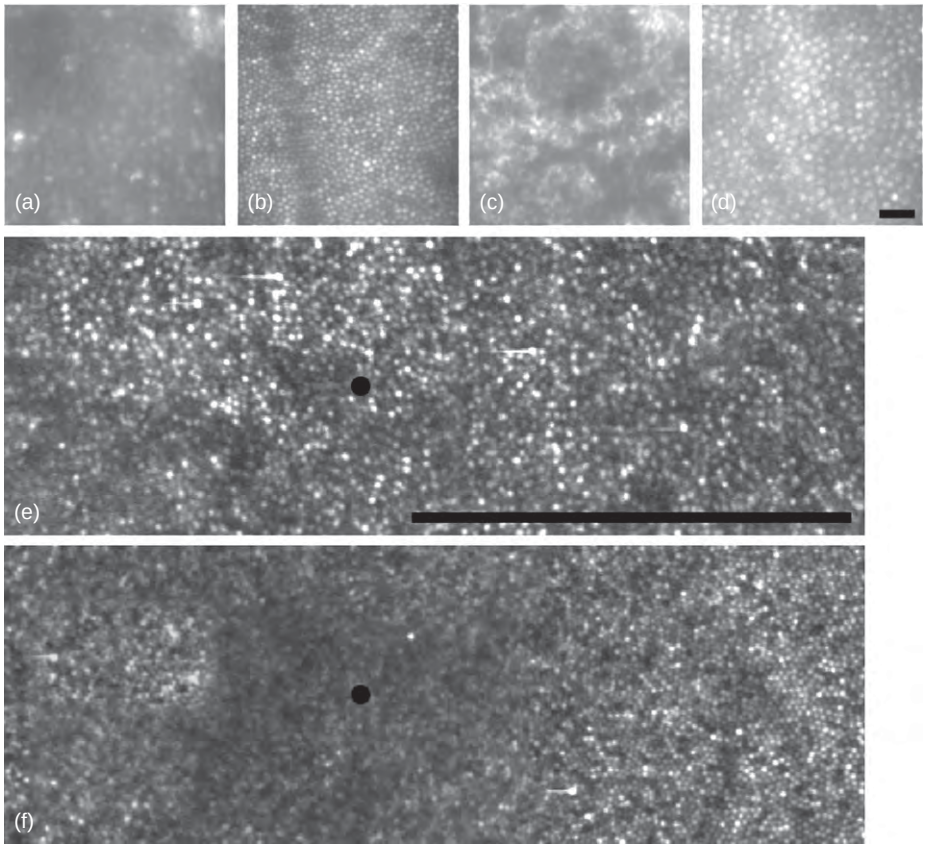

Figure 12 Structural change of cone mosaic of patients having retinal degenerative diseases. (a) and (c) Cone mosaics of a patient having cone–rod dystrophy compared, respectively with (b) and (d) cone mosaics of normal subjects at matched retinal eccentricity. For the patient, severe cone loss was apparent in (c), while in (a), cones still form a continuous mosaic, but the cone density is much decreased and cone size is much larger. Scale = 25 μm for panels (a–d). (e) and (f) Foveal cone mosaics of patients having disease caused by mitochondrial DNA (mtDNA) mutation. The two patients were affected by the disease at different severity. Cone mosaic of the less-affected patient in (f) showed normal cone spacing, while the cone mosaic of the more-affected patient in (e) showed increased cone size and cone spacing. The preferred fixation point of each subject is visualized as dark dots in (e) and (f). Scale = 1 degree for both panels. (a–d), Reproduced from Wolfing J.I., Chung, M., Carroll, J., et al. (2006). High-resolution retinal imaging of cone-rod dystrophy. *Ophthalmology* 113: 1014–1019, Figure 4, with permission from the American Academy of Ophthalmology, Elsevier Ltd (2006). (e,f) Adapted from Yoon, M.K., Roorda, A., Zhang Y., et al. (2009). Adaptive optics scanning laser ophthalmoscopy images in a family with the mitochondrial DNA T8993C mutation. *Investigative Ophthalmology and Visual Science* 50: 1838–1847, Figure 4, with permission from Association for Research in Vision and Ophthalmology (Copyright 2009).

Figure 9). Although in some cases, they were able to distinguish ganglion cell bodies at different depths in the retina, which is a valuable way to distinguish different classes, the depth resolution is modest, about 115 μm. Viral vector (e.g., AAV2)-mediated-gene delivery is another promising approach for delivering fluorophores (e.g., EGFP) to single cells. It requires a simpler intravitreal rather than an intracranial injection and can produce fluorescence that is essentially permanent in each cell that is transduced by the virus. Melissa Geng and Jason Porter at University of Rochester in collaboration with John Flannery at UC Berkeley combined this method with fluorescence AOSLO in the living rat eye (Figure 10). Another possibility is to use transgenics to create an animal whose cells express a fluorophore. Charles Lin and colleagues used this method to image microglia cells in living mouse eye. Work is underway to extend the viral vector method to nonhuman primate and to achieve expression of activity-dependent fluorophores such as G-CaMP (a green flurescent protein calcium probe) in single ganglion cells. These methods may ultimately allow AO retinal imaging to monitor the functional responses of ganglion cells.

Imaging Retinal Vasculature

Many retinal diseases, such as diabetic retinopathy or wet macular degeneration, have important effects on the retinal vascular structure and blood flow. AO combined with fluorescein angiography allows imaging of even the fine structure of the retinal capillary bed (Figure 11(a)). Austin Roorda, then at the University of Houston, showed that AO retinal imaging could image leukocyte motion in the smallest retinal capillaries without the need for fluorescein (Figure 11(b)). Steve Burns at University of Indiana has even succeeded in imaging the flow of erythrocytes by tracking movement of single erythrocytes in successive images of a single scan line superimposed on an oriented parallel to a small vessel.

Imaging Retinal Disease

The use of an AO to image retinal disease is one of the most exciting and also one of the most challenging applications. AO is at its best when the pupil is completely dilated and the ocular media are clear and scatter free. The challenge of imaging retinal disease lies in the fact that patients often have small pupils, poor fixation, and/or large amounts of light scatter. Despite these limitations, progress has been made in the deployment of AO in the clinical arena.

For many retinal degenerative diseases, the structural changes of the cone mosaic and the RPE mosaic of patients have been impressively documented *in vivo*. The diseases affecting cones include not only those relevant

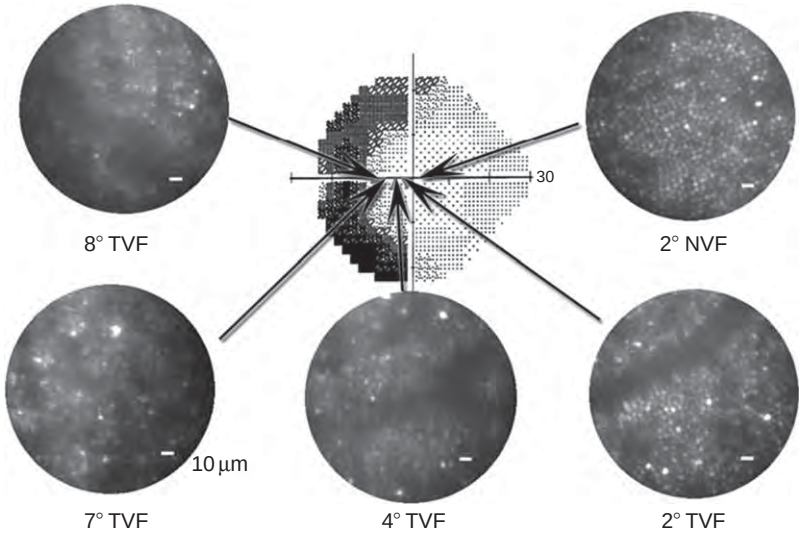

Figure 13 Correspondence between structural changes in the cone mosaic and functional measurement of visual sensitivity. Measured visual field sensitivity of a patient having rod–cone dystrophy is shown in the upper middle panel. The rest of the panels show the cone mosaics from retinal regions corresponding to locations in the visual field map. In those cone mosaic images, the darker regions indicate areas where cones are not reflecting light as in normal retina. From these images, it is not possible to determine if these dark regions represent loss of cones or structurally altered cones, hence became less effective in waveguiding and reflecting light. The extent of these dark regions strongly correlated with the level of visual sensitivity. The more extensive the dark regions (i.e., reduced cone density) were the lower the visual function (e.g., the comparison between the left and right panels). A strong positive relationship was found between the cone density and the level of visual sensitivity in patients with various types of retinal dystrophy. Adapted from Choi, S.S., Doble, N., Hardy, J.L., et al. (2006). In vivo imaging of the photoreceptor mosaic in retinal dystrophies and correlations with visual function. *Investigative Ophthalmology and Visual Science* 47: 2080–2092, Figure 5, with permission from Association for Research in Vision and Ophthalmology (Copyright 2006).

to color blindness mentioned previously, but also more common ones such as retinitis pigmentosa and photoreceptor dystrophy. As per the examples shown in **Figure 12**, cone loss can occur as a patchy, random dropout of cones that otherwise appear normal. In other cases, presumably when the mosaic has had the opportunity to remodel, the mosaic completely tiles the retina but the cones are larger and their density is reduced. Because the structure of the cone mosaic can be documented in living eyes, the specific structure in individual eyes can be correlated with the genotype of the patient, and also with functional measurements such as Humphrey visual field sensitivity, multifocal ERG, and contrast sensitivity (**Figure 13**).

Retinal degenerative diseases affect many other retinal structures, besides photoreceptors and RPE. As described in this article, AO imaging has enabled the accumulation of normative data of many retinal structures in both human and nonhuman primates, as well as data from animal disease models. These data will advance the clinical investigation of retinal degenerative disease. For example, the structure of lamina cribrosa was imaged in both normal primate eye and eye with experimentally induced glaucoma. Ultimately, AO imaging may play a role in the diagnosis of glaucoma and other retinal diseases in clinical practice.

See also: Color Blindness: Acquired; Color Blindness: Inherited; Optical Coherence Tomography.

Further Reading

Arathorn, D. W., Yang, Q., Vogel, C. R., et al. (2007). Retinally stabilized cone-targeted stimulus delivery. *Optics Express* 15: 13731–13744.

Artal, P., Chen, L., Fernandez, E. J., et al. (2004). Neural compensation for the eye's optical aberrations. *Journal of Vision* 4: 281–287.

Biss, D. P., Sumorok, D., Burns, S. A., et al. (2007). *In vivo* fluorescent imaging of the mouse retina using adaptive optics. *Optics Letters* 32: 659–661.

Carroll, J., Neitz, M., Hofer, H., Neitz, J., and Williams, D. R. (2004). Functional photoreceptor loss revealed with adaptive optics: An alternate cause of color blindness. *Proceedings of the National Academy of Sciences of the United States of America* 101: 8461–8466.

Carroll, J., Gray, D. C., Roorda, A., and Williams, D. R. (2005). Recent advances in retinal imaging with adaptive optics. *Optics and Photonics News* 16: 36–42.

Chen, L., Artal, P., Gutierrez, D., and Williams, D. R. (2007). Neural compensation for the best aberration correction. *Journal of Vision* 7(9): 1–9.

Geng Y., Greenberg K. P., Wolfe R., Gray D. C., et al. (2009). In vivo imaging of microscopic structures in the rat retina. *Investigative Ophthalmology and Visual Science* 50: 5872–5879.

Gray, D. C., Wolfe, R., Gee, B. P., et al. (2008). *In vivo* imaging of the fine structure of rhodamine-labeled macaque retinal ganglion cells. *Investigative Ophthalmology and Visual Science* 49: 467–473.

Hofer, H., Artal, P., Singer, B., Aragon, J. L., and Williams, D. R. (2001). Dynamics of the eye's wave aberration. *Journal of Optical Society of America A, Optics, Image Science, and Vision* 18: 497–506.

Hofer, H., Carroll, J., Neitz, J., Neitz, M., and Williams, D. R. (2005). Organization of the human trichromatic cone mosaic. *Journal of Neuroscience* 25: 9669–9679.

Hofer, H., Singer, B., and Williams, D. R. (2005). Different sensations from cones with the same photopigment. *Journal of Vision* 5: 444–454.

Liang, J., Williams, D. R., and Miller, D. T. (1997). Supernormal vision and high-resolution retinal imaging through adaptive optics. *Journal of Optical Society of America A, Optics, Image Science, and Vision* 14: 2884–2892.

Martin, J. A. and Roorda, A. (2005). Direct and noninvasive assessment of parafoveal capillary leukocyte velocity. *Ophthalmology* 112: 2219–2224.

Morgan, J. I., Dubra, A., Wolfe, R., Merigan, W. H., and Williams, D. R. (2009). *In vivo* autofluorescence imaging of the human and macaque retinal pigment epithelial cell mosaic. *Investigative Ophthalmology and Visual Science* 50: 1350–1359.

Morgan, J. I., Hunter, J. J., Masella, B., et al. (2008). Light-induced retinal changes observed with high-resolution autofluorescence imaging of the retinal pigment epithelium. *Investigative Ophthalmology and Visual Science* 49: 3715–3729.

Porter, J., Guirao, A., Cox, I. G., and Williams, D. R. (2001). Monochromatic aberrations of the human eye in a large population. *Journal of Optical Society of America A, Optics, Image Science, and Vision* 18: 1793–1803.

Porter, J., Queener, H., Lin, J., Thorn, K., and Awwal, A. A. S. (2006). Adaptive Optics for Vision Science: *Principles, Practices, Design and Applications*. Hoboken, NJ: Wiley-Interscience.

Roorda, A. and Williams, D. R. (1999). The arrangement of the three cone classes in the living human eye. *Nature* 397: 520–522.

Thibos, L. N., Hong, X., Bradley, A., and Cheng, X. (2002). Statistical variation of aberration structure and image quality in a normal population of healthy eyes. *Journal of Optical Society of America A, Optics, Image Science, and Vision* 19: 2329–2348.

Yoon, G. Y. and Williams, D. R. (2002). Visual performance after correcting the monochromatic and chromatic aberrations of the eye. *Journal of Optical Society of America A, Optics, Image Science, and Vision* 19: 266–275.

Zhong, Z., Petrig, B. L., Qi, X., and Burns, S. A. (2008). *In vivo* measurement of erythrocyte velocity and retinal blood flow using adaptive optics scanning laser ophthalmoscopy. *Optics Express* 16: 12746–12756.

Alternative Visual Cycles in Müller Cells

G H Travis, UCLA School of Medicine, Los Angeles, CA, USA

Glossary

Müller cell – A glial cell in the vertebrate retina that spans from the vitreal surface to the external limiting membrane, with apical processes that extend into the interphotoreceptor matrix. These cells perform multiple functions in the retina including the processing of visual retinoids.

Opsin visual pigment – A member of the G-protein-coupled receptor superfamily that functions as the light receptor in rods and cones. These pigments represent a complex between an opsin protein and a visual chromophore (see below).

Outer segment – An elongated light-sensitive structure attached to the connecting cilium of rod and cone photoreceptors. The rod outer segment in humans comprises a stack of approximately 1000 membranous disks. These disks are loaded with rhodopsin or cone opsin visual pigments.

Rpe65 – An abundant, membrane-associated protein in retinal pigment epithelium cells that functions as a retinoid isomerase. In particular, Rpe65 catalyzes the conversion of an all-*trans*-retinyl ester to 11-*cis*-retinol and a free fatty acid.

Visual chromophore – The light-absorbing molecular species in an opsin protein. The most common visual chromophore in vertebrates is 11-*cis*-retinaldehyde, which isomerizes to all-*trans*-retinaldehyde upon absorption of a photon.

Vision in vertebrates is provided by two types of photoreceptor cells, rods and cones. Rods mediate vision in dim light while cones mediate high-resolution color vision in bright light. Approximately 95% of photoreceptors in the human retina are rods. Nonetheless, cones are far more important for vision in humans. With the advent of artificial lighting, humans spend much of the time under conditions where the rod photoresponse is saturated and vision is mediated by cones. Both rods and cones contain a light-sensitive structure called the outer segment (OS) comprising a stack of densely packed membranous disks. These disks are packed with rhodopsin or cone-opsin visual pigment. The light-absorbing chromophore in most opsin pigments is 11-*cis*-retinaldehyde (11-*cis*-RAL). Absorption of a photon induces its isomerization to all-*trans*-retinaldehyde (all-*trans*-RAL), which activates the opsin pigment and stimulates the visual transduction cascade. After a brief period of activation, the pigment dissociates to yield free all-*trans*-RAL and apo-opsin, which is no longer light sensitive. The pigment is regenerated by recombination of apo-opsin with another 11-*cis*-RAL. To sustain light sensitivity, all-*trans*-RAL released by bleached opsin pigments is converted back to 11-*cis*-RAL by a multi-step enzyme pathway called the visual cycle (**Figure 1**).

Visual Cycle in Retinal Pigment Epithelium Cells

All but the first step of the visual cycle takes place within cells of the retinal pigment epithelium (RPE), an epithelial monolayer adjacent to photoreceptor OS. In brief, all-*trans*-RAL is reduced by all-*trans*-retinol dehydrogenase (all-*trans*-RDH) in rod and cone OS to all-*trans*-retinol (all-*trans*-ROL) or vitamin A. The all-*trans*-ROL is released by the OS into the extracellular space or interphotoreceptor matrix (IPM), where it is bound to interphotoreceptor retinoid-binding protein (IRBP). The all-*trans*-ROL is taken up by apical processes of RPE cells, where it binds to cellular retinol binding protein type-1 (CRBP1). Holo-CRBP1 is the substrate for lecithin:retinol acyl transferase (LRAT), which transfers a fatty acid from phosphatidylcholine in internal membranes to the all-*trans*-ROL. The resulting fatty-acyl ester of all-*trans*-ROL (all-*trans*-RE) is the substrate for Rpe65-isomerase. Rpe65 catalyzes hydrolysis of the carboxylate ester and utilizes the energy released for isomerization of all-*trans*-ROL to 11-*cis*-retinol (11-*cis*-ROL). The final catalytic step in the visual cycle is oxidation of 11-*cis*-ROL, by one of several 11-*cis*-ROL dehydrogenases (11-*cis*-RDH) to 11-*cis*-RAL. Both 11-*cis*-ROL and 11-*cis*-RAL are bound to cellular retinaldehyde binding protein (CRALBP) in the RPE. The 11-*cis*-RAL is released by the apical RPE to the IPM, where it binds IRBP. IRBP carries the 11-*cis*-RAL to the photoreceptor OS, where it is taken up and recombines with apo-opsin to reform a rhodopsin or cone-opsin pigment.

A Role for Müller Cells in Visual Pigment Regeneration

Evidence suggests that Müller glial cells in the retina also participate in the processing of visual retinoids. Müller cells span nearly the full thickness of the retina. The apical microvilli of Müller cells extend into the IPM and hence are well situated to exchange visual retinoids

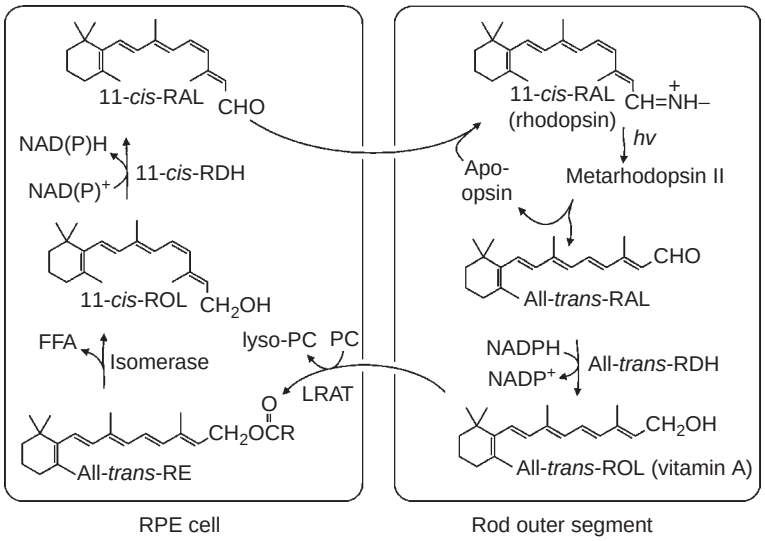

Figure 1 Visual cycle for rhodopsin regeneration. Absorption of a photon (*hv*) by a rhodopsin pigment molecule induces isomerization of 11-*cis*-RAL to all-*trans*-RAL, which converts the pigment to its active metarhodopsin II state. After deactivation, the pigment dissociates to yield apo-opsin and free all-*trans*-RAL. The all-*trans*-RAL is reduced to all-*trans*-ROL by one or more all-*trans*-RDHs that use NADPH as a co-factor. The all-*trans*-ROL is released by the OS to the IPM and is taken up by the apical RPE where it is esterified by LRAT to yield an all-*trans*-RE. The all-*trans*-RE is isomerized and hydrolyzed by Rpe65 to yield 11-*cis*-ROL. The 11-*cis*-ROL is oxidized by one or more 11-*cis*-RDHs to yield 11-*cis*-RAL chromophore. The 11-*cis*-RAL is released by the RPE into the IPM where it binds to IRBP. Finally, the 11-*cis*-RAL is delivered to the OS where it re-combines with apo-opsin to form a new visual pigment.

with rod and cone OS, similar to the apical microvilli of RPE cells. Importantly, Müller cells contain several proteins involved in the processing of visual retinoids. These include (1) CRALBP, (2) RPE-retinal guanine-nucleotide-binding protein (G-protein) coupled receptor (RGR-opsin), a non-photoreceptor opsin that effects light-dependent regulation of the visual cycle in RPE cells, (3) CRBP1, and (4) retinol dehydrogenases types 10 and 11. Müller cells neither express Rpe65 nor LRAT, which are both present in RPE cells. Therefore, Müller cells do not simply duplicate the function of RPE cells in the regeneration of visual chromophore.

A Second Source of Chromophore for Cones

Several lines of evidence suggest that an alternate source of chromophore precursor is available to cones but not rods. When frog retinas were separated from the RPE, cone opsins, but not rhodopsin, regenerated spontaneously after a photobleach. After photobleaching, isolated salamander cones recovered sensitivity with the addition of either 11-*cis*-ROL or 11-*cis*-RAL, while isolated rods only recovered sensitivity with the addition of 11-*cis*-RAL. Müller cells in primary culture were shown to take up all-*trans*-ROL and synthesize 11-*cis*-ROL, which they secreted into the medium. Salamander cones were shown to dark-adapt and regenerate visual chromophore in isolated retinas separate from the RPE. The intrinsic capacity of cones to recover sensitivity and regenerate visual chromophore in salamander retinas was lost after exposure to a selective Müller-cell toxin (α-aminoadipic acid), suggesting that Müller cells play a role in these processes.

Functional Differences between Rods and Cones

Although morphologically similar, rods and cones differ greatly in sensitivity, dynamic range, and speed of the photoresponse. Rods are single-photon detectors and show saturation of the photoresponse under relatively dim background illumination, producing 500 or more photoisomerizations per second. At saturation, all cyclic guanosine monophosphate (cGMP)-gated cation channels are closed and the rod no longer responds to light. Cones, on the other hand, are 100-fold less sensitive than rods but still exhibit a photoresponse to a light flash under bright background illuminations producing up to 10^6 photoisomerizations per second. The response kinetics of cones is also several-fold faster than rods. These disparities reflect differences in the properties of rhodopsin and the cone-opsin pigments. Rhodopsin is exceedingly quiet, with a spontaneous activation rate in the dark of one thermal isomerization every 2000 years. Cone opsins are much noisier than rhodopsin for two reasons. First, the spontaneous isomerization rate of cone opsin is 10 000-fold higher than of rhodopsin. Second, 11-*cis*-RAL spontaneously dissociates from cone-opsins. A dark-adapted

red cone contains approximately 10% apo-cone-opsin due to spontaneous dissociation of chromophore. In contrast, 11-*cis*-RAL combines almost irreversibly with apo-rhodopsin in rods. Apo-opsin, which results from dissociation of 11-*cis*-RAL, activates the transduction cascade, producing the phenomenon of dark light. These effects contribute to the noisy background of cones and explain their much lower sensitivity than rods.

Although the rod response is saturated in bright light, photon capture by rhodopsin continues unabated. Thus, in a rod-dominant retina under daylight conditions, the vast majority of photoisomerization events contributes nothing to useful vision. Under these circumstances, cones must compete with rods for the limited supply of 11-*cis*-RAL. The reversible binding of 11-*cis*-RAL to apo-cone-opsins and its irreversible binding to apo-rhodopsin confers a tendency of rods to steal chromophore from cones. This tendency aggravates the competition between rods and cones for limited chromophore.

An Alternate Retinoid Isomerase Activity in Cone-Dominant Retinas

Studies on the biochemistry of visual pigment regeneration in cone-dominant retinas suggest a mechanism whereby cones may escape competition from rods for visual chromophore. Experiments were performed on separated retinas and RPE from mice and cattle, as model rod-dominant species, and from chickens and ground squirrels, as model cone-dominant species. Measurement of endogenous retinoids showed that the rod-dominant species contain high levels of all-*trans*-retinyl esters (REs) in the RPE but no detectable REs in the retina. Cone-dominant species contain REs in both the RPE and retina, with predominantly 11-*cis*-REs in the retina. The activities of retinoid-processing enzymes were measured by incubating total homogenates or microsomes prepared from RPE or retinas with all-*trans*-ROL, then assaying for synthesis of new retinoids by high-performance liquid chromatography (HPLC). Incubation of RPE homogenates with all-*trans*-ROL resulted in rapid synthesis of all-*trans*-REs, due to the activity of LRAT. Only after accumulation of all-*trans*-REs was 11-*cis*-ROL synthesis detected, due to the activity of Rpe65. This profile of retinoid synthesis was observed with RPE homogenates from both rod- and cone-dominant species.

A strikingly different profile was observed when retina homogenates from cone-dominant chicken or ground squirrels were incubated with all-*trans*-ROL under similar conditions. Addition of all-*trans*-ROL resulted in rapid synthesis of 11-*cis*-REs and 11-*cis*-ROL, with negligible initial synthesis of all-*trans*-REs. Addition of palmitoyl coenzyme A (palm CoA) to the assay mixture increased synthesis of 11-*cis*-REs, again with minimal initial synthesis of all-*trans*-REs. Synthesis of 11-*cis*-ROL and 11-*cis*-REs from all-*trans*-ROL without prior formation of all-*trans*-REs suggests that the mechanism of retinoid isomerization is different in retina versus RPE. Instead of converting an all-*trans*-RE to 11-*cis*-ROL and a free fatty acid, as catalyzed by Rpe65 in RPE cells, cone-dominant retinas appear to catalyze the direct conversion of all-*trans*-ROL to 11-*cis*-ROL. This energetically unfavorable reaction appears to be driven by mass action through secondary esterification of the 11-*cis*-ROL product. Here, the energy of isomerization is indirectly supplied by hydrolysis of the thio-ester in palm CoA versus hydrolysis of the carboxyl ester in phosphatidylcholine, as catalyzed by Rpe65. The isomerase machinery in retinas may therefore involve two catalytic activities, as depicted in Figure 2. One is an isomerase that catalyzes the passive interconversion of all-*trans*-ROL and 11-*cis*-ROL. This enzyme has not yet been identified. The second is a palm-CoA-dependent RE synthase. Several proteins with acyl CoA:retinol acyltransferase (ARAT) activity have been described. At least one of these, diacylglycerol acyltransferase type-1 (DGAT1), is expressed in the retina.

11-*cis*-ROL Dehydrogenase Activity in Cones but Not in Rods

As discussed above, cones can regenerate visual pigments and restore light sensitivity with the addition of either 11-*cis*-RAL or 11-*cis*-ROL, while rods can only regenerate rhodopsin pigment and recover sensitivity with addition of 11-*cis*-RAL. Since 11-*cis*-RAL is the visual chromophore for both cone and rod pigments, these observations suggest that cones, but not rods, express an 11-*cis*-RDH activity that oxidizes 11-*cis*-ROL to 11-*cis*-RAL. Robust nicotinamide adenine dinucleotide phosphate (NADPH)-dependent 11-*cis*-RDH activity has been detected in cone

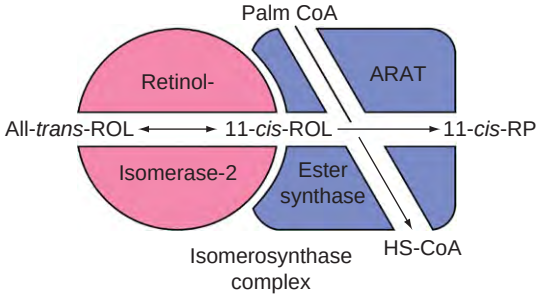

Figure 2 Proposed isomerase-2 complex in Müller cells. The isomerase in Müller cells appears to catalyze direct conversion of all-*trans*-ROL to 11-*cis*-ROL. This energetically unfavorable reaction appears to be driven by mass action through secondary esterification of 11-*cis*-ROL to an 11-*cis*-RE. This synthase uses palm CoA as an acyl donor, and hence is a type of ARAT. The isomerase-2/ARAT complex has been named isomerosynthase to denote its activities. Neither isomerase-2 nor its ARAT partner has been identified to date.

but not rod in photoreceptors. Reduction of all-*trans*-RAL to all-*trans*-ROL in bleached photoreceptors requires NADPH, and hence is an energy-consuming process. Oxidation of an 11-*cis*-ROL to 11-*cis*-RAL generates an NADPH reducing-equivalent. Since reduction of all-*trans*-RAL and oxidation of 11-*cis*-ROL occurs with 1:1 stoichiometry in a cone that is utilizing 11-*cis*-ROL as a chromophore precursor, the presence of reciprocal $NADP^+$/NADPH-specific dehydrogenases in cones affords a self-renewing supply of dinucleotide substrate at no energy cost to the cell. Eliminating the need for energy-dependent synthesis of NADPH may remove the metabolic bottleneck of all-*trans*-RAL-reduction in cones at high rates of photoisomerization.

An Alternate Visual Cycle that Mediates Pigment Regeneration in Cones

The observations outlined above can be explained by the hypothesized alternate visual cycle shown in Figure 3. According to this model, all-*trans*-ROL-isomerase (isomerase-2) and the 11-*cis*-ROL-specific ARAT are in Müller cells, which also express the 11-*cis*-ROL and 11-*cis*-RAL binding-protein, CRALBP. The major source of substrate for isomerase-2 is all-*trans*-ROL released by rods and cones during light exposure. Isomerization of all-*trans*-ROL to 11-*cis*-ROL and subsequent esterification of 11-*cis*-ROL to 11-*cis*-REs are probably limited by substrate availability. It has been shown that apo-CRALBP stimulates 11-*cis*-RE-hydrolase (11-*cis*-REH) in RPE cells. These observations suggest a regulatory mechanism for the proposed visual cycle: in the dark-adapted state, cones contain fully regenerated opsin pigment and hence do not use 11-*cis*-ROL. CRALBP is saturated with 11-*cis*-ROL and the level of 11-*cis*-REs are high in Müller cells. Both isomerase-2 and 11-*cis*-RE-synthase are inactive due to the absence of available substrate. With the onset of light and the bleaching of photopigments, cones begin to take up 11-*cis*-ROL. This results in desaturation of CRALBP, activation of 11-*cis*-REH, and mobilization of 11-*cis*-RE-stores in Müller cells. Rods and cones begin to release all-*trans*-ROL, which permits replenishment of 11-*cis*-REs through activation of isomerase-2 and 11-*cis*-RE-synthase. This pathway becomes progressively more active with increasing light intensity, availability of all-*trans*-ROL substrate, and consumption of the 11-*cis*-ROL product by cones.

A New Role for IRBP

IRBP is the major extracellular retinoid-binding protein in retinas. It has been suggested that the primary function of IRBP is to bind all-*trans*-ROL and 11-*cis*-RAL during translocation of these retinoids between OS and the RPE. However, loss of IRBP in $irbp^{-/-}$ mice has only a mild effect on rhodopsin regeneration. Might IRBP play another role? The endogenous ligands of IRBP have been studied.

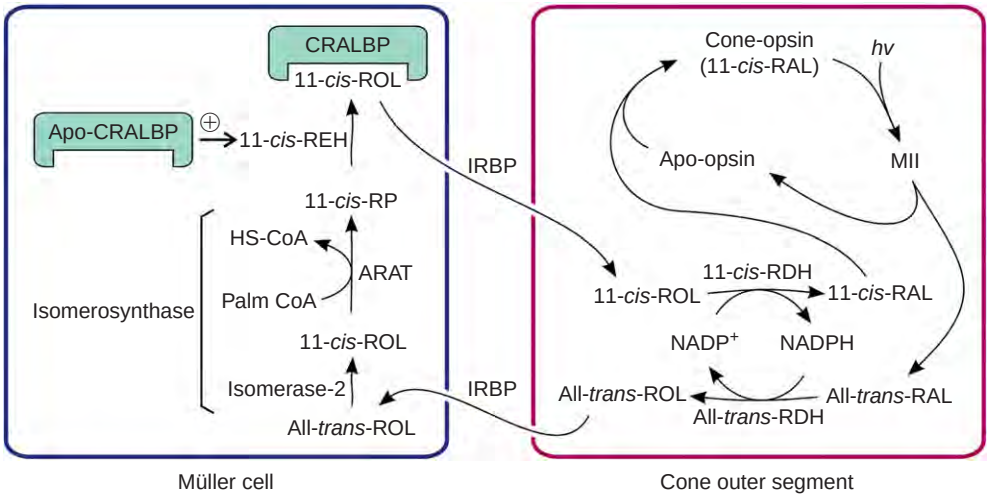

Figure 3 Proposed alternate visual cycle in Müller cells. Absorption of a photon (*hv*) induces 11-*cis* to all-*trans* isomerization of the retinaldehyde chromophore, resulting in activated opsin (MII) inside a cone outer segment. Decay of MII releases all-*trans*-RAL, which is reduced to all-*trans*-ROL by one or more NADPH-dependent all-*trans*-RDHs. The all-*trans*-ROL is released to the IPM where it binds IRBP and is carried to a Müller cell apical process. After uptake into the Müller cells, the all-*trans*-ROL is isomerized by isomerase-2 and esterified by ARAT to yield an 11-*cis*-RE (11-*cis*-RP). Müller cells also contain CRALBP, which binds 11-*cis*-ROL but not all-*trans*-retinol. 11-*cis*-REH is activated by apo-CRALBP to hydrolyze the 11-*cis*-RE, yielding 11-*cis*-ROL. Binding of 11-*cis*-ROL by CRALBP prevents its back-isomerization to all-*trans*-ROL. The 11-*cis*-ROL is released by CRALBP to IRBP in the IPM, where it is carried back to the cone OS. Within the cone, an $NADP^+$-dependent 11-*cis*-RDH oxidizes the 11-*cis*-ROL to 11-*cis*-RAL, which re-combines with apo-opsin to regenerate a new, light-sensitive cone pigment. The reciprocal reduction of all-*trans*-RAL and oxidation of 11-*cis*-ROL results in a self-renewing supply of NADP-co-factor at all rates of photoisomerization and no energy cost to the cell.

In light-adapted frog and bovine retinas, IRBP contains higher levels of 11-*cis*-ROL than 11-*cis*-RAL, in addition to all-*trans*-ROL. Moreover, IRBP immunoreactivity was found in association with cone but not rod OS. These observations suggest that the critical function of IRBP may not be exchange of all-*trans*-ROL and 11-*cis*-RAL between rods and RPE cells, as previously assumed, but rather exchange of all-*trans*-ROL and 11-*cis*-ROL between cones and Müller cells.

Alternate Visual Cycle in Rod-Dominant Species

Although clearly present in cone-dominant retinas, the evidence for an alternate visual cycle in Müller cells of rod-dominant species is less compelling. Endogenous 11-*cis*-REs and isomerase-2 catalytic activity were undetectable in homogenates from rod-dominant bovine and mouse retinas. The absence of 11-*cis*-retinoids in *rpe65*$^{-/-}$ mice has also been put forth as further evidence against the Müller-cell pathway in this species. However, this observation is difficult to interpret since *rpe65*$^{-/-}$ photoreceptors contain no visual chromophore, hence all-*trans*-ROL, the substrate for the alternative visual cycle, is not released following light exposure. The effective Michaelis constant (K_m) of all-*trans*-ROL for 11-*cis*-RE-synthesis by chicken retina homogenates is 13.5 μM. Thus, even in chickens, the alternate visual cycle is only active under conditions that yield high concentrations of all-*trans*-ROL. Recently, isolated mouse retinas were photobleached and analyzed physiologically for recovery of rod and cone light sensitivity. Cone sensitivity and the cone photoresponse recovered in these retinas despite the absence of RPE cells, while rod sensitivity and the rod response were dramatically attenuated. These physiological observations argue for existence of the alternate visual cycle in mouse retinas. The role of this pathway in rod-dominant retinas should be resolved upon identification of the proteins responsible for isomerase-2 activity, and measurement of their expression levels in rod- and cone-dominant retinas.

See also: Phototransduction: Phototransduction in Cones; Phototransduction: Phototransduction in Rods; Phototransduction: Rhodopsin; Phototransduction: The Visual Cycle.

Further Reading

Chen, Y. and Noy, N. (1994). Retinoid specificity of interphotoreceptor retinoid-binding protein. *Biochemistry* 33: 10658–10665.

Das, S. R., Bhardwaj, N., Kjeldbye, H., and Gouras, P. (1992). Muller cells of chicken retina synthesize 11-*cis*-retinol. *Biochemical Journal* 285: 907–913.

Fain, G. L., Matthews, H. R., Cornwall, M. C., and Koutalos, Y. (2001). Adaptation in vertebrate photoreceptors. *Physiological Reviews* 81: 117–151.

Jin, M., Li, S., Nusinowitz, S., et al. (2009). The role of interphotoreceptor retinoid-binding protein on the translocation of visual retinoids and function of cone photoreceptors. *Journal of Neuroscience* 29: 1486–1495.

Jones, G. J., Crouch, R. K., Wiggert, B., Cornwall, M. C., and Chader, G. J. (1989). Retinoid requirements for recovery of sensitivity after visual-pigment bleaching in isolated photoreceptors. *Proceedings of the National Academy of Sciences of the United States of America* 86: 9606–9610.

Kefalov, V. J., Estevez, M. E., Kono, M., et al. (2005). Breaking the covalent bond – a pigment property that contributes to desensitization in cones. *Neuron* 46: 879–890.

Mata, N. L., Radu, R. A., Clemmons, R., and Travis, G. H. (2002). Isomerization and oxidation of vitamin A in cone-dominant retinas. A novel pathway for visual-pigment regeneration in daylight. *Neuron* 36: 69–80.

Mata, N. L., Ruiz, A., Radu, R. A., Bui, T. V., and Travis, G. H. (2005). Chicken retinas contain a retinoid isomerase activity that catalyzes the direct conversion of all-*trans*-retinol to 11-*cis*-retinol. *Biochemistry* 44: 11715–11721.

Miyazono, S., Shimauchi-Matsukawa, Y., Tachibanaki, S., and Kawamura, S. (2008). Highly efficient retinal metabolism in cones. *Proceedings of the National Academy of Sciences of the United States of America* 105: 16051–16056.

Pugh, E. N. and Lamb, T. D. (2000). Phototransduction in vertebrate rods and cones: Molecular mechanisms of amplification, recovery and light adaptation. In: Stavenga, D. G., DeGrip, W. J., and Pugh, E. N., Jr (eds.) *Handbook of Biological Physics*, pp. 184–255. Amsterdam: Elsevier Science B.V.

Radu, R. A., Hu, J., Peng, J., et al. (2008). Retinal pigment epithelium-retinal G protein receptor-opsin mediates light-dependent translocation of all-*trans*-retinyl esters for synthesis of visual chromophore in retinal pigment epithelial cells. *Journal of Biological Chemistry* 283: 19730–19738.

Saari, J. C. and Bredberg, D. L. (1987). Photochemistry and stereoselectivity of cellular retinaldehyde-binding protein from bovine retina. *Journal of Biological Chemistry* 262: 7618–7622.

Stecher, H., Gelb, M. H., Saari, J. C., and Palczewski, K. (1999). Preferential release of 11-*cis*-retinol from retinal pigment epithelial cells in the presence of cellular retinaldehyde-binding protein. *Journal of Biological Chemistry* 274: 8577–8585.

Wang, J. S., Estevez, M. E., Cornwall, M. C., and Kefalov, V. J. (2009). Intra-retinal visual cycle required for rapid and complete cone dark adaptation. *Nature Neuroscience* 12: 295–302.

Yen, C. L., Monetti, M., Burri, B. J., and Farese, R. V., Jr. (2005). The triacylglycerol synthesis enzyme DGAT1 also catalyzes the synthesis of diacylglycerols, waxes, and retinyl esters. *Journal of Lipid Research* 46: 1502–1511.

Amblyopia

D M Levi, University of California, Berkeley, Berkeley, CA, USA

Glossary

Anisometropia – A condition in which the two eyes have unequal refractive power so that the two eyes are in different states of myopia.
Astigmatism – An optical defect causing blurred images due to failure to focus a point object into a sharp image on the retina.
Sensitive period – An early developmental period that is particularly sensitive to development of amblyopia.
Snellen acuity – Clarity of vision as measured by eye care professionals using a chart called the Snellen chart.
Strabismus – Misregistration or misalignment of the images from the two eyes preventing the development of binocular vision.

What Is Amblyopia?

Amblyopia (from the Greek, *amblyos* – blunt; *opia* – vision) is a developmental abnormality that results from physiological alterations in the visual cortex and impairs form vision. Amblyopia is clinically important because, aside from refractive error, it is the most frequent cause of vision loss in infants and young children, occurring naturally in about 2–4% of the population; and it is of basic interest because it reflects the neural impairment which can occur when normal visual development is disrupted. The damage produced by amblyopia is generally expressed in the clinical setting as a loss of visual acuity in an apparently healthy eye, despite appropriate optical correction; however, there is a great deal of evidence showing that amblyopia results in a broad range of neural, perceptual, and clinical abnormalities. Currently, there is no positive diagnostic test for amblyopia. Instead, amblyopia is diagnosed by exclusion: in patients with conditions such as strabismus and anisometropia, a diagnosis of amblyopia is made through the exclusion of uncorrected refractive error and underlying ocular pathology. Amblyopic patients (especially those with strabismic amblyopia) often exhibit crowding problems, meaning they have better visual acuity when letters are presented in isolation than when they are presented in a line or a full chart. Clinically, crowding may be a useful sign to aid in the diagnosis of amblyopia.

Amblyopia Is a Significant Public Health Problem

Amblyopia can easily be reversed or eliminated when diagnosed and treated early in life. Thus, there is a premium on early detection of amblyopia and its risk factors. It has been estimated that perhaps as many as three-quarters of a million preschoolers are at risk for amblyopia in the United States, and roughly half of those may not be detected before school age. Moreover, detection is likely to be more delayed in low socioeconomic areas. Improved vision screening and access to treatment could, in principle, eliminate amblyopia as a public health issue.

Types of Amblyopia

Amblyopia comes in different sizes (degree of loss) and flavors (types). The presence of amblyopia is almost always associated with an early history of abnormal visual experience: binocular misregistration (i.e., strabismus – a turned eye), image degradation (high refractive error and astigmatism, anisometropia), or, less commonly, form deprivation (congenital cataract, ptosis). The severity of the amblyopia appears to be associated with the degree of imbalance between the two eyes (e.g., dense unilateral cataract results in severe loss), and to the age at which the amblyogenic factor occurred. Precisely how these factors interact is as yet unknown, but it is evident that different early visual experiences result in different functional losses in amblyopia, and a significant factor that distinguishes performance among amblyopes is the presence or absence of binocular function. Binocular function is much more likely to be damaged when amblyopia results from binocular misregistration (strabismus) than from image blur (anisometropia).

The Site(s) of Amblyopia

A longstanding question is the site of damage in amblyopia. Current opinion places the earliest functional physiological abnormalities in cortical area V1. Exhaustive anatomical and physiological experiments failed to find retinal alterations in monkeys reared with experimentally induced amblyopia. These same animals had marked

abnormalities in V1. Moreover, although human electroretinogram (ERG) studies are equivocal, after optimizing optical focus, fixation alignment, and fixation stability, Robert Hess and colleagues found no pattern ERG deficit in deep amblyopes, in a spatial frequency range where there were obvious psychophysical deficits for the same stimuli. Although it is possible that retrograde degeneration may affect the lateral geniculate nucleus (where there is some shrinkage of the cells in the parvocellular layers) and retina, it seems unlikely that these effects contribute significantly to the behavioral losses. In contrast, amblyopia results in profound alterations in V1 both in cats and monkeys. In monkeys, visual deprivation (via lid suture) leads to a massive loss of neurons in V1 that can be driven by the deprived eye. Experimentally induced blur during development leads to a selective loss of V1 neurons tuned to high spatial frequencies and the spatial tuning of neurons may be markedly different when tested through the two eyes. Experimentally induced strabismus disrupts the binocular connections of cortical neurons. It is difficult to draw distinctions based on the type of rearing from the physiology, because the effects of abnormal visual experience are complicated by the onset, duration, and depth of deprivation; however, there is evidence that the physiological deficits in amblyopia do not fully explain the behavioral losses (in the same monkeys), suggesting that there may be deficits downstream from V1.

The most dramatic changes in V1 involve alterations in binocularity. Specifically, neurons that appeared to be monocular often demonstrate clear binocular interactions during dichoptic stimulation. In strabismic (prism-reared) monkeys, there is marked binocular suppression during dichoptic stimulation suggesting that inhibitory connections are less susceptible to the effects of strabismus than excitatory connections. Interestingly, even very brief periods (just 3 days) of prism-induced strabismus at the height of the critical period (4 weeks in monkeys, which translates to about 4 months in humans) increased the prevalence of V1 neurons that exhibited binocular suppression without altering their sensitivity to interocular spatial phase disparity. This result suggests that the earliest change in V1 is increased binocular suppression and, importantly, that the suppression originates at a site downstream from where information from the two eyes is first combined.

Very much less is known about the physiological effects of amblyopia on visual areas downstream from V1. Brain-imaging studies using positron emission tomography and functional magnetic resonance imaging show a clear deficit in V1, and several studies have also found deficits in other areas (e.g., V2). However, it is difficult to discern whether these downstream losses are simply a pass-through effect from V1 or whether the V1 losses are amplified downstream. However, several imaging and psychophysical studies are consistent with the idea that the abnormalities in V1 are amplified in V2 and possibly beyond. These studies show losses in second-order detection global form and motion integration, symmetry detection, and counting.

Sensitive Periods for the Development of Amblyopia

Clinicians are well aware that amblyopia does not develop after 6–8 years of age, suggesting that there is a sensitive period for the development of amblyopia; however, in humans with naturally occurring amblyopia, the age of onset of the amblyogenic condition(s) is difficult to ascertain, and the effects of intervention combine to make it difficult to obtain a clear picture of the natural history of amblyopia development. Thus, much of our current understanding of the development of amblyopia accrues from animal studies, and from retrospective studies of clinical records. Technological improvements in infant testing have also provided more direct data on the development of naturally occurring amblyopia in humans and monkeys. All of these studies provide strong evidence for amblyopia induced by early deprivation.

While the upper limit for susceptibility of binocular interactions (binocular summation and stereopsis) is not yet certain, it appears to be later than that for acuity or contrast sensitivity in monkeys, and may extend to at least 7 or 8 years (and possibly more) in humans. Psychophysical studies of interocular transfer in humans with a history of strabismus provide an indirect estimate of the period of susceptibility of binocular connections. The results of both studies suggest that binocular connections are highly vulnerable during the first 18 months of life, and remain susceptible to the effects of strabismus until at least age 7 years.

Traditional Treatment of Amblyopia

For centuries, the primary treatment for amblyopia has consisted of patching or penalizing the fellow preferred eye, thus forcing the brain to use the weaker amblyopic eye. Typically, patients with mild to moderate amblyopia are prescribed complete occlusion for 2–6 waking hours per day, over several months to more than a year. Patients with moderate to severe amblyopia are often prescribed 6–10 h or more a day, and some clinicians recommend more aggressive full-time occlusion for severe amblyopia. As reported in a recent large-scale clinical study of children (3–8 years of age), the dose–response rate for occlusion is approximately 0.1 log unit (1 chart line) per 120 h of occlusion, and the treatment efficacy is 3–4 logMAR lines. The dose–response curve appears to plateau only after 100–400 h. The treatment outcome is dependent on

occlusion dose, the depth of amblyopia, binocular status, fixation pattern, the age at presentation, and patient compliance. Recent clinical studies suggest that atropine penalization may be just as effective as patching.

The notion that there is a sensitive period (or periods) for the development of amblyopia has often been taken to indicate that there is also a critical period for the treatment of amblyopia. This concept grew out of the work of Claude Worth in 1903. Worth suggested that the presence of a sensory obstacle (e.g., unilateral strabismus) arrested the development of visual acuity (amblyopia of arrest), so that the patient's acuity remained at the level achieved at the time of onset of strabismus. In this view, the depth of amblyopia is a direct function of the age of onset of the sensory obstacle. Worth further suggested that, if amblyopia of arrest were allowed to persist, amblyopia of extinction could occur as a result of binocular inhibition. In Worth's view, only this extra loss of sensory function (i.e., the amblyopia of extinction) could be recovered by treatment. Although this latter notion is open to question in the light of present knowledge, the ideas of Worth have had a powerful influence upon both clinicians and basic scientists. Many of our currently held concepts of amblyopia, such as plasticity, sensitive periods, and abnormal binocular interaction, were already described more than a century ago, and gained currency with the work of Hubel and Wiesel in 1970 and the many anatomical and physiological studies that followed. Consequently, while amblyopia can often be reversed when treated early, treatment is generally not undertaken in older children and adults. Below we consider both experimental and clinical evidence for plasticity in the adult visual system that calls into question the notion of a sensitive period for treatment.

Clinical Studies

It is often stated that humans with amblyopia cannot be treated beyond a certain age; however, a review of the literature suggests otherwise. Recent clinical trials suggest that in children, 2 h of patching per day may be just as effective as 6 h per day. Moreover, treatment may be just as effective in older (13–17 years) patients who have not been previously treated as in younger (7–12 years) children.

Plasticity in adults with amblyopia is also dramatically evident in the report of amblyopic patients whose visual acuity spontaneously improved in the wake of visual loss due to macular degeneration in the fellow eye. There are also reports suggesting that some adult amblyopes recover vision in their amblyopic eye following loss of vision in their fellow (nonamblyopic) eye. These studies are consistent with the notion that the connections from the amblyopic eye may be suppressed rather than destroyed. Loss of the fellow eye would allow these existing connections to be unmasked, as occurs in adult cats with retinal lesions (**Figure 1**).

Experimental Treatment of Amblyopia Beyond the Sensitive Period

Adults are capable of improving performance on sensory tasks through repeated practice or perceptual learning ('yes, you can teach old dogs new tricks!'), and this learning is considered to be a form of neural plasticity that also has consequences in the cortex. Specifically, in adults with normal vision, practice can improve performance on a variety of visual tasks, and this learning can be quite specific (to the trained task, orientation, eye, etc.). Interestingly, similar neural plasticity exists in the visual system of adults with naturally occurring amblyopia due to anisometropia and/or strabismus, suggesting that perceptual learning may be a useful approach for amblyopia treatment. Perceptual learning can improve visual functions in amblyopia on a wide range of tasks, including: Vernier acuity, positional acuity, contrast sensitivity, and letter identification. Practicing each of these tasks results in improved performance on the practiced task.

The specificity of perceptual learning noted above poses some interesting difficulties. If the improvement following practice was solely limited to the trained stimulus, condition and task, then the type of plasticity documented here would have very limited (if any) therapeutic value for amblyopia, since amblyopia is defined primarily on the basis of reduced Snellen acuity. Importantly, perceptual learning of many tasks (e.g., Vernier acuity, position discrimination, contrast sensitivity) appears to transfer, at least in part, to improvements in Snellen acuity, as does practicing contrast detection. In addition to visual acuity improvement, other degraded visual functions such as stereoacuity and visual counting improve as well.

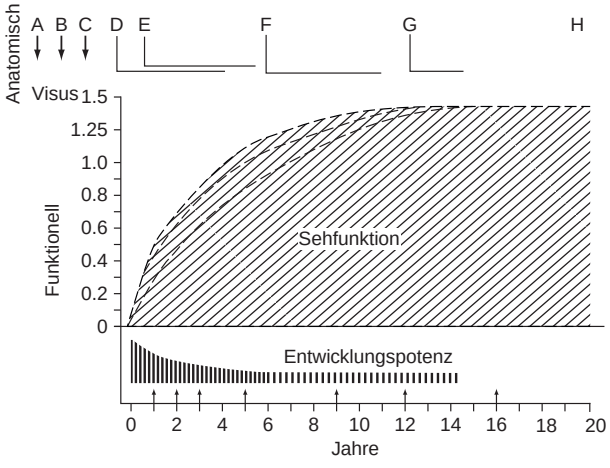

Figure 1 The postnatal development of visual function. Cartoon illustrating visual functions (*sehfunktion*) developing at somewhat different rates, while the developmental potential (*entwicklungspotenz*, in the lower panel) dissipates over the years (*Jahre*). Reproduced from Teller, D. Y. and Movshon, J. A. (1986) Visual Development. *Vision Research* 26: 1483–1506.

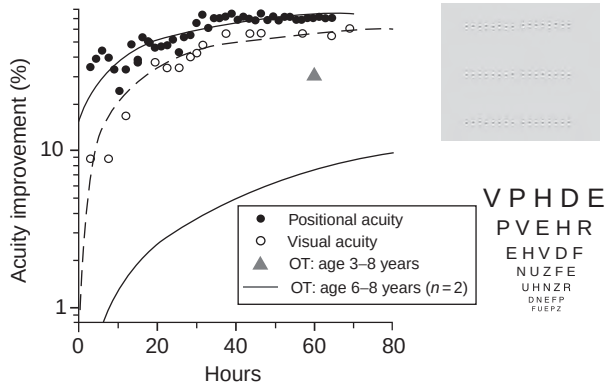

Figure 2 Improvement in positional acuity (solid circles) and Snellen acuity (open circles) of a severe juvenile amblyope (observer AL, 8.8 years old, with unilateral strabismus). The triangle shows the improvement based on occlusion alone. The gray line shows the improvement based on occlusion alone (OT: occlusion therapy) in 2 amblyopes (aged 6–8) with acuities similar to that of AL. Replotted from Li et al., 2007; Stewart et al., 2004, 2005, 2007.

Perceptual Learning as a Clinical Tool for Treating Amblyopia

Occlusion therapy is the gold standard method for treating amblyopia. In all previous perceptual learning studies, the subjects are occluded while performing the visual task, so it is reasonable to ask whether active perceptual learning actually provides an added benefit over occlusion alone. Recent work suggests that occlusion plus perceptual learning may be more effective than occlusion alone (**Figure 2**). Combining occlusion with perceptual learning may be a useful method for obtaining the optimal treatment outcome in the shortest possible time. Eliminating or reducing the need to wear an eye patch in public would eliminate, or at the very least reduce, the emotional stress that often accompanies occlusion therapy.

Over the centuries, there have been numerous attempts to increase the effectiveness of treatment. These attempts have a long and chequered history, ranging from the sublime to the ridiculous, and include: subcutaneous injection of strychnine, electrical stimulation of the retina and optic nerve, flashing lights, red filters and rotating gratings, administration of Levodopa/Carbidopa and shocks to the brain via transcranial magnetic stimulation. Few were subjected to rigorous scrutiny, and those that were often failed to stand up to it. Thus, any promising new method should be examined critically and there is a clear need for careful controlled studies.

Acknowledgment

This work was supported by National Eye Institute grant R01EY01728 from the National Eye Institute.

See also: Astigmatism; Binocular Vergence Eye Movements and the Near Response; Fundamentals of Stereopsis.

Further Reading

Ciuffreda, K. J., Levi, D. M., and Selenow, A. (1991). *Amblyopia: Basic and Clinical Aspects*. Stoneham, MA: Butterworth-Heinemann.

Fahle, M. (2004). Perceptual learning: A case for early selection. *Journal of Vision* 4: 879–890.

Harwerth, R. S., Smith, E. L., III, Duncan, G. C., Crawford, M. L. J., and von Noorden, G. K. (1987). Multiple sensitive periods in the development of the primate visual system. *Science* 232: 235–238.

Hubel, D. H. and Wiesel, T. N. (1970). The period of susceptibility to the physiological effects of unilateral eye closure in kittens. *Journal of Physiology (London)* 206: 419–436.

Kiorpes, L. (2006). Visual processing in amblyopia: Animal Studies. *Strabismus* 14: 3–10.

Levi, D. M. (2006). Visual processing in amblyopia: Human studies. *Strabismus* 14: 11–19.

Levi, D. M. and Carkeet, A. (1993). Amblyopia: A consequence of abnormal visual development. In: Simons, K. (ed.) *Early Visual Development, Normal and Abnormal*, pp. 391–408. Oxford: Oxford University Press.

Levi, D. M. and Polat, U. (1996). Neural plasticity in adults with amblyopia. *Proceedings of the National Academy of Sciences of the United States of America* 93: 6830–6834.

Li, R. W., Provost, A., and Levi, D. M. (2007). Extended perceptual learning results in substantial recovery of positional acuity and visual acuity in juvenile amblyopia. *Investigative Ophthalmology and Vision Science* 48: 5046–5051.

Mckee, S. P., Levi, D. M., and Movshon, J. A. (2003). The pattern of visual deficits in amblyopia. *Journal of Vision* 3: 380–405.

Polat, U., Ma-Naim, T., Belkin, M., and Sagi, D. (2004). Improving vision in adult amblyopia by perceptual learning. *Proceedings of the National Academy of Sciences of the United States of America* 101: 6692–6697.

Revell, M. J. (1971). *Strabismus: A History Orthoptic Techniques*. London: Barrie and Jenkins.

Stewart, C. E., Fielder, A. R., Stephens, D. A., and Moseley, M. J. (2005). Treatment of unilateral amblyopia: factors influencing visual outcome. *Investigative Ophthalmology and Vision Science* 46: 3152–3160.

Stewart, C. E., Moseley, M. J., Stephens, D. A., and Fielder, A. R. (2004). Treatment dose-response in amblyopia therapy: The Monitored Occlusion Treatment of Amblyopia Study (MOTAS). *Investigative Ophthalmology and Vision Science* 45: 3048–3054.

Stewart, C. E., Stephens, D. A., Fielder, A. R., and Moseley, M. J. (2007). Modeling dose-response in amblyopia: toward a child-specific treatment plan. *Investigative Ophthalmology and Vision Science* 48: 2589–2594.

Teller, D. Y. and Movshon, J. A. (1986). Visual Development. *Vision Research* 26: 1483–1506.

Vereecken, E. P. and Brabant, P. (1984). Prognosis for vision in amblyopia after the loss of the good eye. *Archives of Ophthalmology* 102: 220–224.

Wiesel, T. N. (1982). Postnatal development of the visual cortex and the influence of environment. *Nature* 299: 583–591.

Worth, C. A. (1903). *Squint: Its Causes, Pathology and Treatment*. Philadelphia: The Blakiston.

Wu, C. and Hunter, D. G. (2006). Amblyopia: Diagnostic and therapeutic options. *American Journal of Ophthalmology* 141: 175–184.

Anatomically Separate Rod and Cone Signaling Pathways

S Nusinowitz, UCLA School of Medicine, Los Angeles, CA, USA

Glossary

Neurotransmitter – A chemical substance that is released at synaptic connections that are used to relay, amplify, and modulate signals between cells and neurons.
Photopic vision – The scientific term for color vision mediated by multiple cone photoreceptor types in bright light. In the human retina, photopic vision is tri-chromatic.
Phototransduction – A process by which light is converted into electrical signals in rod and cone photoreceptor cells in the retina of the eye.
Retinal circuitry – It refers to the neuronal pathways in the retina that carry information from photoreceptor cells to ganglion cells.
Scotopic vision – Vision mediated by rod photoreceptors in dim light. Scotopic vision is color blind.
Spatio-temporal vision – A term commonly used to describe the spatial and temporal properties of human visual processing, and the neural mechanisms which underpin them.
Visual adaptation – A process by which vision adjusts to or gets used to a change in overall brightness, color, and other spatio-temporal properties, in order to maximize visual sensitivity.

Rod and Cone Photoreceptors

The process of vision is initiated by the absorption of light by a photoreceptor pigment molecule. The mammalian retina contains two classes of photoreceptors, referred to as rods and cones, each distinct in their structural morphology and in their behavior in response to light. Rod photoreceptors are highly sensitive to light and are capable of responding to a single photon. In contrast, cone photoreceptors are less sensitive to light, but are exquisitely tuned to mediate color and spatio-temporal vision. There are three types of cone photoreceptors in the human retina, each with different, but overlapping, spectral sensitivities, and the interaction of the output from these photoreceptor types mediates the ability to discriminate small color differences.

Based on studies of the evolution of visual pigments, it is hypothesized that rods evolved from cones. A single amino acid substitution has been shown to exchange the molecular properties of rod and cone visual pigments. This suggests that a single spontaneous amino acid substitution could have been one of the key steps in the divergence of rod- and cone-mediated vision. The first step in the formation of rods themselves may have been the spontaneous formation of disk membranes that were separated from the plasma membrane of the outer segment. This step is thought to have increased the light sensitivity of the photoresponse, a physiological property that is typical of rod photoreceptors. The post-receptoral retinal circuitry for rods is superimposed on pre-existing retinal circuitry mediating cone function. This feature of retinal circuitry predates the evolution of the rod photoreceptor itself and likely represents the pathway of a redundant cone photoreceptor that evolved into a rod. As described below, there are multiple sites in the retinal circuitry where rods have the opportunity to penetrate the cone system circuitry.

The absorption of a photon of light by a photoreceptor pigment molecule initiates a sequence of events referred to as the phototransduction cascade. Much of what we know about the specifics of the phototransduction cascade comes from the study of the rod photoresponse. In mammalian rods, the absorption of a photon of light by rhodopsin, the visual chromophore in rods, initiates a sequence of biochemical events that ultimately leads to a decrease in the intracellular level of cyclic guanosine 3,5′-monophosphate (cGMP) and the closure of the cGMP-gated ion channels in the outer segment. The resultant closure of the cGMP-gated channels in the outer-segment membrane decreases the circulating current by blocking inward current flow. This results in an hyperpolarization of the photoreceptor cell membrane and a decrease in the release of neurotransmitter at the photoreceptor synapse with second-order neurons. The biochemical steps in cone outer-segment phototransduction are thought to be similar to that which occurs in rods. In fact, there are corresponding components in rod and cone phototransduction at each step in the cascade, including rod and cone versions of visual pigment, tranducin, phosphodiesterase, arrestin, kinase, cGMP-gated channels, and Na^+/K^+, Ca^{2+} exchangers.

Cone Postreceptoral Circuitry

Consider first the retinal circuitry mediating cone function. Cone photoreceptor cells synapse with bipolar and horizontal cells in the outer plexiform layer of the retina

(see Figure 1). Cones release glutamate at a steady rate in darkness but this rate is slowed in a graded response that is correlated to the change in the outer-segment membrane potential after stimulation by light. The modulation of synaptic transmitter release drives signaling to second-order bipolar cells.

There are at least nine different types of cone bipolar cells in the mammalian retina that are distinguished on the basis of a number of features, including the number of cone photoreceptors contacting the bipolar cell, the spread of the dendritic terminals, and the stratification of their axon terminals in the inner plexiform layer. The precise function of each of these types of bipolar cells is not well understood but they are presumed to be tuned to process different aspects of the visual stimulus. Morphologically, bipolar cells can be subdivided into classes commonly referred to as diffuse and midget bipolar cells. Diffuse bipolar cells (of which there are at least six types) have broad dendritic spreads and make contact with 5–20 long (L-) and middle (M-) wavelength cones; the number of connections depends on where they are located in the retina. These cells are likely involved in tasks requiring broad spatial averaging and color processing but have poor spatial resolution. In contrast, midget bipolar cells have a narrow dendritic tree and can make contact with a single cone and with a single ganglion cell. This cone-mediated circuitry provides a mechanism for high spatial resolution of a scene and is thought to mediate an acuity channel. The midget bipolar cell also transmits color information by virtue of its one-on-one connections with L- and M-sensitive cones. In addition, bipolar cells that make specialized contacts with short (S-) wavelength sensitive cones have been described in the primate, rat, and mouse retina.

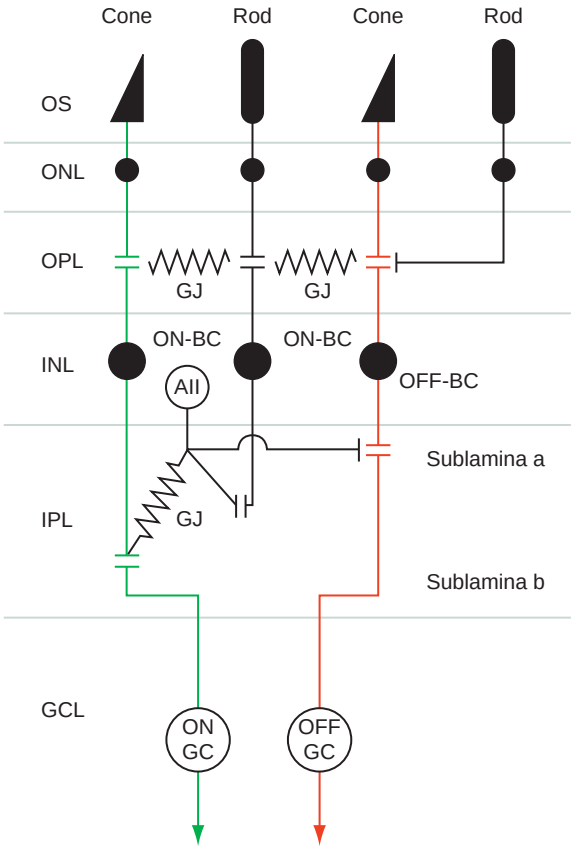

Figure 1 Cone signaling pathway in the mammalian retina. Cone photoreceptors respond to light with a graded hperpolarization and synapse with bipolar and horizontal (not shown) cells in the outer plexiform layer (OPL) of the retina. The release of glutamate at the synaptic terminal is modulated by the change in the outer-segment membrane potential. Cone signals are delivered to ON and OFF bipolar cells (BC) which carry signals to ON and OFF ganglion cells (GC) in the inner plexiform layer (green and red channels, respectively), thereby maintaining segregated cone pathways through the retina. ON and OFF bipolar cells provide excitatory and inhibitory inputs to amacrine cells and ganglion cells and respond with a graded depolarization (sign-inverting) or hyperpolarizing (sign-conserving) response, respectively. Cones communicate laterally with other cones (and rods) via electrical couplings called gap junctions (GJ). Lateral communication is also afforded by horizontal cells in the OPL and by amacrine cells in the IPL. Abbreviations: OS – outer segment, ONL – outer nuclear layer, OPL – outer plexiform layer, INL – inner nuclear layer, IPL – inner plexiform layer, GCL – ganglion cell layer, GJ – gap junction.

Functionally, there are two broad classes of bipolar cells in the mammalian retina mediating the cone signaling pathway. They are commonly referred to as ON and OFF bipolar cells, because of their expression of either excitatory glutamate receptors (mGluRs) or inhibitory glutamate receptors (iGluRs). ON cone bipolar cells make contact with photoreceptors through invaginations in the cone pedicle and are flanked by a pair of horizontal cell dendrites, an arrangement commonly referred to as a triad. The triads are apposed to a presynaptic ribbon, which is the release site for neurotransmitter mediating signal transfer to second-order neurons. There are typically about 25 invaginations in a cone pedicle, but as many as 50 invaginations have been reported. A recent study has identified the protein pikachurin, a previously unknown dystroglycan-binding protein, as critical for the apposition of photoreceptor and bipolar cells dendrites at the ribbon synapse. OFF bipolar cells make contact directly at the cone pedicle base where up to 500 contacts are made with postsynaptic cells.

ON bipolar cells that express mGluRs are depolarized (sign-inverting) by the light response in cone photoreceptor cells. Their dendritic processes terminate in sublamina B of the inner plexiform layer (see Figure 1). In contrast, OFF bipolar cells express iGluRs. In these cells glutamate expression is linked to Na^+ influx. OFF cone bipolar cells are hyperpolarized (sign-conserving) by the light response in cones and have processes that end in sublamina A of the inner plexiform layer. The two types of bipolar cells provide excitatory and inhibitory inputs to downstream cells

and tertiary neurons in response to light stimulation. In general, ON cone bipolar cells are excited by light that is brighter than its surround, whereas OFF cone bipolar cells are excited by light that is dimmer. This segregation of visual input is maintained in parallel signaling pathways to ON and OFF ganglion cells (see **Figure 1**).

Lateral Communication Networks

Signal transfer through the retinal layers, particularly for the rod system, depends on lateral communication between retinal cells. There are several cell types and neural connections within retinal layers that mediate lateral transfer of signal. The major cell types include amacrine and horizontal cells but lateral transfer is also accomplished by a class of low-resistance electrical gap junctions.

Gap Junctions

Low-resistance electrical gap junctions are ubiquitous in the mammalian retina. They enable the intercellular, bidirectional transport of ions, metabolites, and second-order messengers. These gap junctions are mediated by connexins of which several different types have been reported in the mammalian retina. The most abundant of these is neuronal Connexin36. Connexin36 is associated with processes in the outer and inner plexiform layers, consistent with expression in multiple cell types. In the outer plexiform layer, cone photoreceptors communicate laterally via Connexin36-mediated gap junctions between cone pedicles (see **Figure 1**). The gap junctions also permit signal transfer between cone pedicles and rod spherules. In the inner plexiform layer, the expression of Connexin36 co-localizes with the dendritic processes of AII-type amacrine cells. The latter gap junction mediates transfer of signal from AII amacrine cells to ON cone bipolar cells, a signaling pathway that is crucial for rod signals to infiltrate the cone postreceptoral signaling pathway. In addition, the gap junctions in the outer plexiform layer (between cone pedicles and rod spherules) allow rod signals to infiltrate the cone signaling pathway very early in visual processing. These pathways are described later in more detail.

Horizontal Cells

Horizontal cells are second-order, mainly inhibitory, neurons located in the outer plexiform layer. While these cells make synaptic connections with photoreceptors, they are also extensively coupled by either Connexin50 or Connexin57 gap junctions. Morphologically, three types of horizontal cells have been identified in the primate and human retina, referred to as HI, HII, and HIII. The HI-type horizontal cells have small dendritic fields (75–150 μm), but with long axons (300 μm) ending in a broad dendritic tree. HIII horizontal cells are similar to the HI horizontal cell but have larger dendritic trees at all retinal locations. In addition, HIII cells contact many more cones than HI. HII horizontal cells are more spidery and intricate in dendritic field characteristics than either of the other types. The three types of horizontal cells in the human retina demonstrate evidence of color-specific coding. HI horizontal cells contact primarily with green- and red-sensitive cones, with a smaller number of contacts with blue-sensitive cones. HII horizontal cells contact blue-sensitive cones primarily, and HIII horizontal cells contact only green- and red-sensitive cones.

Most, if not all, of the input to horizontal cells is derived from the response of cone photoreceptors to light and, depending on the type of horizontal cell, can make contact with many cones over broad retinal areas. In addition, because horizontal cells are extensively coupled via electrical gap junctions, their receptive fields can be much larger than their dendritic spreads. The connection to rod photoreceptors has traditionally been thought to occur at the axon terminal process, implying that signal transfer from cones to rods is unidirectional. However, rod inputs have been recorded in horizontal cell somata in the cat retina, presumed to be delivered via cone-rod gap junctions or direct dendritic connections. Like cone OFF bipolar cells, horizontal cells express iGluRs at their dendrites and are hyperpolarized in response to light.

In the primate retina, the transmitter release from cones that drives horizontal cells and bipolar cells is also regulated by feedback from horizontal cells. This feedback loop provides a mechanism for the inhibition of signals from adjacent cone photoreceptors. The precise mechanism by which horizontal cells produce this lateral inhibition is not well understood but may occur as a result of the modulated release of the inhibitory transmitter γ-aminobutyric acid (GABA) at the synaptic terminal of cones or via the modulation of the Ca^{2+} channels that regulate the release of glutamate. Regardless of the precise mechanism of lateral inhibition, the lateral interconnections provided by horizontal cells contribute to the formation of the antagonistic surrounds of bipolar cell receptive fields. The antagonistic center-surround interaction is thought to enhance the detection of edges but have also been implicated in the processing of color information where the center-surround configuration modulates antagonistic (or opponent) color information, and in illusory surface filling effects. In addition, the observation of rod and cone inputs at horizontal cell somata provides a mechanism for integrating light signals over broad retinal areas to ensure optimal retinal sensitivity over the entire intensity range.

Amacrine Cells

There are up to 30 types of amacrine cells located in the inner retina of the mammalian retina that have been

distinguished on the basis of morphological characteristics, physiological properties, and pharmacological criteria. While cells upstream from amacrine cells generate graded potentials in response to stimulation by light, the amacrine cell is the first site in the retina where action potentials are generated. Amacrine cells receive their input from bipolar cells, mediated by iGluRs at the synaptic terminals, and from ganglion cells and other types of amacrine cells. The main job of the amacrine cells is to provide a mechanism for transfer of signals from bipolar cells within and between sublamina of the inner plexiform layer, and with ganglion cells. However, amacrine cells, like horizontal cells, provide a mechanism for lateral signal communication between retinal cells, including providing a feedback loop to bipolar cells. They are assumed to play an important role in modulating activity in the antagonistic surrounds of ganglion cell receptive fields that shape higher visual functions, such as object segregation and spatio-temporal adaptation. The feedback from amacrine cells has also been implicated in switching the site of light adaptation between receptor and postreceptoral sites.

The extent of lateral transfer depends on the morphology of the amacrine cell. Wide-field amacrine cells transmit lateral information across a broad expanse of the inner plexiform layer and are present in many species, including the mouse, rat, cat, rabbit, salamander, and monkey. Small-field amacrine cells mediate local interactions between different sublaminae of the IPL. The best characterized of these is the AII amacrine cell which plays an important role in mediating signal transfer through the rod-mediated neural circuitry. Unlike cone bipolar cells, rod ON polar cells do not make direct contact with ON ganglion cells. Rather rod signals are transmitted to ON ganglion cells by AII electrical coupling (gap junctions) with ON cone bipolar cells and by synaptic connections with OFF-cone bipolar cells (see below). Another amacrine cell type, the A17 amacrine cell, has also been implicated in the rod-signaling pathway of the mammalian retina. Up to 11 other small-field amacrine cells have been identified in the cat, rabbit, and mouse, but their precise function is not well understood.

Ganglion Cells

Signals carried through the retinal layers converge on ganglion cells, the latter responsible for carrying information to higher-order visual centers. Up to 25 different types of ganglion cells have been identified in the mammalian retina, dependent on species. These retinal ganglion cells are broadly grouped into classes based on morphological characteristics and physiological properties. In the primate retina, for example, there are at least 18 different types of retinal ganglion cells that are classified morphologically into Pα (parasol), Pβ (midget), and Pγ types, and physiologically into two major types: parasol or magnocellular (M), and midget or parvocellular (P) cells. The parvocellular cells project exclusively to the parvocellular layers of the lateral geniculate nucleus (LGN) and play a key role in central acuity. Parasol ganglion cells are motion-sensitive cells and primarily project to the magnocellular layers of the LGN. Intrinsically photosensitive retinal ganglion cells (ipRGCs) containing melanopsin as the photosenstitive pigment have also been described recently. These neurons, which receive input from both rod and cone photoreceptors, have been implicated in nonimage-forming responses to environmental light such as the pupillary light reflex and circadian entrainment.

Multiple Rod Signaling Pathways

Cone photoreceptors synapse directly with both ON and OFF bipolar cells, which then transmit signals in parallel pathways to ON and OFF ganglion cells, respectively (**Figure 1**). In contrast, rod photoreceptors, which synapse with rod ON bipolar cells, do not make direct contact with ganglion cells, but rather transmit their signals to these cells through several alternate pathways. Consider first the evidence for multiple rod pathways. The alternative signaling pathways are described later and shown in **Figure 2**.

It is generally accepted that rod-mediated vision, like cone vision, involves multiple signaling pathways. The evidence in support of this hypothesis derives from early psychophysical experiments in humans in which critical fusion frequency (CFF; the intensity at which flicker can just be detected) was measured under conditions mediated by rods. These experiments revealed two distinct branches in the function that relates CFF and stimulus intensity. In the lower branch, over dim flash intensities, the CFF was no better than 15 Hz, and remained at this level over a broad range of stimulus intensities. However, at higher intensities, covering mesopic light levels, CFFs increased rapidly and could be as high as 28 Hz. The double-branched CFF versus intensity response function implied the existence of at least two signaling pathways mediating rod function in the mammalian retina. This hypothesis was supported by the observation that patients with achromatopsia, a retinal abnormality in which cone function is absent, also display the same response properties.

Additional support for at least dual rod signaling pathways comes from psychophysical measurements of rod flicker perception in humans. These experiments demonstrated that for 15 Hz flickering stimuli (the optimal stimulus presentation frequency for demonstrating the interaction), there is an intensity region, well above flicker detection threshold, where the perception of flicker is minimized or nulled. The perceptual nulling of flicker has been assumed to result from the mutual cancellation of signals originating from at least two signaling pathways

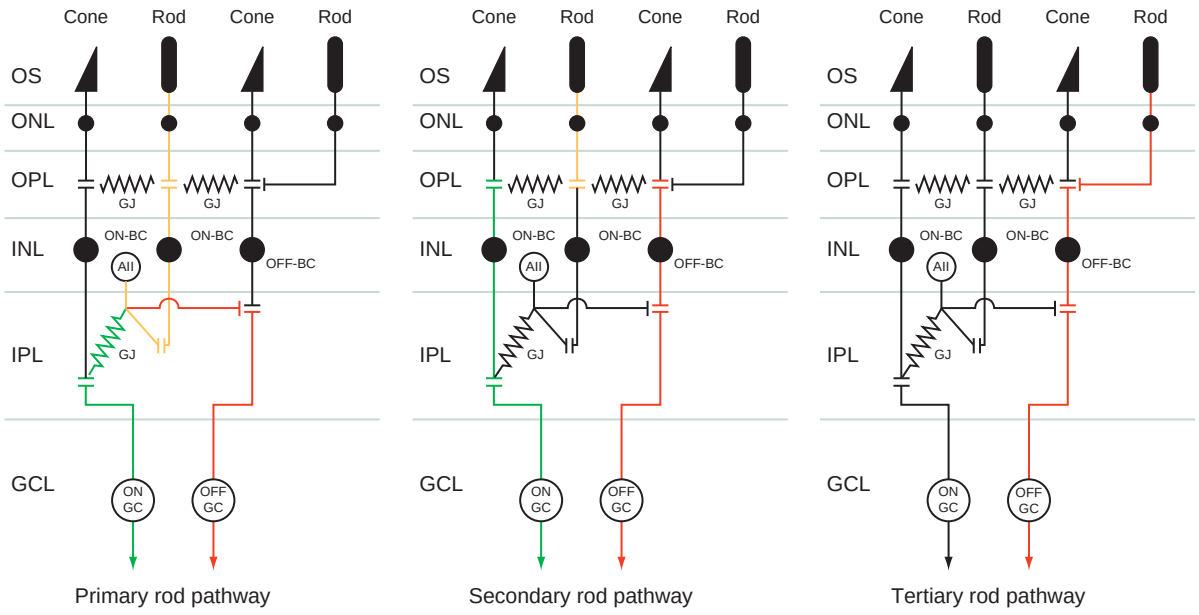

Figure 2 Rod signaling pathway in the mammalian retina. In the primary rod pathway (left panel), rod photoreceptors synapse with rod ON bipolar cells, which in turn make connections with amacrine AII cells in the inner plexiform layer (yellow pathway). Signals from the AII amacrine cells infiltrate the cone pathway by exciting ON cone bipolar cells via electrical gap junctions (green pathway) and via glycinergic (sign-inverting) synapses with OFF cone bipolar cells (red pathway). Rod signaling through the secondary rod pathway (middle panel) is mediated through rod-cone gap junctions between rod spherules and cone pedicles located in the outer plexiform layer. Through the rod-cone gap junction, rod signals have access to both ON and OFF cone bipolar cells and to ON and OFF ganglion cells (green and red pathways, respectively). A third pathway for rod signal transmission (right panel), in which rod photoreceptors bypass the rod ON bipolar cell and directly excite cone OFF bipolar cells, has also been hypothesized (red pathway). Abbreviations: OS – outer segment, ONL – outer nuclear layer, OPL – outer plexiform layer, INL – inner nuclear layer, IPL – inner plexiform layer, GCL – ganglion cell layer, GJ – gap junction.

having different speeds of signal transmission. The hypothesis argues that when signals are in phase, despite different speeds of transmission, they are mutually additive but, when out of phase, produce destructive interference, which contributes to the inhibition of signal strength and the flicker nulling perception. This mutual cancellation has also been demonstrated with the electroretinogram (ERG), which is a noninvasive measure of the massed response of the retina to light. It is assumed only to reflect activity of outer and middle retinal cells. As in the perceptual experiments described above, supportive evidence derives from a unique feature of the function that relates ERG signal amplitude and stimulus. A local response minimum is observed at an intensity that is well above ERG flicker detection threshold but still within the scotopic range of intensities and occurs at the same intensity where the perception of flicker in humans is also minimized.

Much of the electrophysiological evidence in support of the existence of multiple signaling pathways comes from experiments in which single unit extracellular recordings are made from ganglion cells in the mouse and rabbit retina. Using pharmacological agents to disrupt different cellular connections in the retinal circuitry, combined with animal models with known genetic defects affecting these connections, electrophysiological support for multiple rod pathways has come from what signals remain detectable at the ganglion cell level. On the basis of these types of experiments, rod photoreceptor signals are presumed to be transmitted to ganglion cells via three alternate pathways.

The anatomical substrates mediating rod postreceptoral signaling in the retina seem to be well established and are assumed to be conserved across mammalian species. They are illustrated in **Figure 2**. In the primary rod pathway (left panel), rod photoreceptors synapse with rod ON bipolar cells, via sign-inverting glutamatergic synapses. The output from the rod ON bipolar cell is then transmitted to AII amacrine cells in the inner plexiform layer via sign-conserving glutamatergic synapses. Signals from the AII amacrine cells then converge onto the cone pathway by exciting ON cone bipolar cells via electrical gap junctions and inhibit cone OFF bipolar cells via sign-inverting glycinergic synapses (see **Figure 2** for color coding).

Rod signaling through the secondary rod pathway (middle panel) converges onto the cone circuitry at an even earlier stage. The secondary rod pathway is mediated through rod-cone gap junctions that exist between rod spherules and cone pedicles located in the outer plexiform layer. Through the rod-cone gap junction, rod

photoreceptors can transmit signals directly to both ON and OFF cone bipolar cells and to ON and OFF ganglion cells. The circuitry for the primary and secondary rod pathways has been shown to exist in the cat, rabbit, primate, and more recently in the mouse.

A third pathway for rod signal transmission (right panel), in which rod photoreceptors bypass the rod ON bipolar cell and directly excite cone OFF bipolar cells, has also been hypothesized and supported by anatomical and physiological data. This alternative pathway has been demonstrated to exist using electrophysiological methods. In these experiments, a ganglion cell signal continues to be observed in animals without cones (thereby eliminating the rod–cone gap junction of the secondary pathway) and in which all signal transmission through the primary rod pathway is blocked with pharmacological agents.

Thus, the retinal circuitry comprising the rod system offers multiple signaling routes for carrying information from rod photoreceptors to inner retinal ganglion cells. While these signaling pathways provide the rod system with multiple opportunities for system redundancy, they also subserve specialized functions related to scotopic vision. It has been suggested that signal transfer from the primary to secondary rod signaling pathway affords the rod system the capability of enhanced temporal resolution at the expense of light sensitivity. However, further work is needed to better understand the precise role of each of the rod signaling pathways in the processing of visual information.

Concluding Statements

A major step in forming our perceptions of the visual world is accomplished in the retina, where information from rod and cone photoreceptors is filtered, processed, and channeled through multiple parallel signaling pathways. In addition to the different spectral sensitivities of rod and cone photoreceptors and the intensity range over which they operate, the different types of bipolar cells, amacrine cells, and horizontal cells are presumed to be tuned to capture or enhance specific attributes of a visual scene – color processing, brightness contrast, temporal processing, signal enhancement and integration, and adaptation mechanisms. Ultimately, these processed and filtered signals from the retina are transmitted to higher-order visual centers, such as the lateral geniculate nucleus and the primary visual cortex of the brain, where the information is optimized to form our perceptions of the visual environment.

Acknowledgments

The authors are grateful to Dr. William H. Ridder for reading the text and providing helpful comments and Bryan Chen for assistance with drawings.

See also: The Circadian Clock in the Retina Regulates Rod and Cone Pathways; Information Processing: Amacrine Cells; Information Processing: Bipolar Cells; Information Processing: Ganglion Cells; Information Processing in the Retina; Morphology of Interneurons: Amacrine Cells; Morphology of Interneurons: Bipolar Cells; Morphology of Interneurons: Horizontal Cells; Morphology of Interneurons: Interplexiform Cells; Phototransduction: Phototransduction in Cones; Phototransduction: Phototransduction in Rods.

Further Reading

Bloomfield, S. A. and Dacheux, R. F. (2001). Rod vision: Pathways and processing in the mammalian retina. *Progress in Retinal and Eye Research* 20: 351–384.

Dowling, J. E. (1999). Retinal processing of visual information. *Brain Research Bulletin* 50: 317.

Falk, G. and Shiells, G. (2006). Synaptic transmission: Sensitivity control mechanisms. In: Heckenlively, J. H., Arden, G. B., Nusinowitz, S., Holder, G., and Bach, M. (eds.) *Principles and Practice of Clinical Electrophysiology of Vision*, pp. 79–91. Cambridge, MA: MIT Press.

Fu, Y. and Yau, K. W. (2007). Phototransduction in mouse rods and cones. *Pflugers Archiv. European Journal of Physiology* 454: 805–819.

Kolb, H. (2006). Functional organization of the retina. In: Heckenlively, J. H., Arden, G. B., Nusinowitz, S., Holder, G., and Bach, M. (eds.) *Principles and Practice of Clinical Electrophysiology of Vision*, pp. 47–64. Cambridge, MA: MIT Press.

Kolb, H. and Famiglietti, E. V. (1974). Rod and cone pathways in the inner plexiform layer of cat retina. *Science* 186: 47–49.

Masland, R. H. (2001). The fundamental plan of the retina. *Nature Neuroscience* 4: 877–886.

Nickle, B. and Robinson, P. R. (2007). The opsins of the vertebrate retina: Insights from structural, biochemical, and evolutionary studies. *Cellular and Molecular Life Sciences* 64: 2917–2932.

Pugh, E. N., Jr. and Lamb, T. D. (1993). Amplification and kinetics of the activation steps in phototransduction. *Biochimica et Biophysica Acta* 1141: 111–149.

Schmidt, T. M., Taniguchi, K., and Kofuji, P. (2008). Intrinsic and extrinsic light responses in melanopsin-expressing ganglion cells during mouse development. *Journal of Neurophysiology* 100: 371–384.

Volgyi, B., Deans, M. R., Paul, D. L., and Bloomfield, S. A. (2004). Convergence and segregation of the multiple rod pathways in mammalian retina. *Journal of Neuroscience* 24: 11182–11192.

Wassle, H. (2004). Parallel processing in the mammalian retina. *Nature Reviews Neuroscience* 5: 747–757.

Anatomy and Regulation of the Optical Nerve Blood Flow

R Ehrlich, A Harris, and A M Moss, Indiana University, Indianapolis, IN, USA

Glossary

Anastamosis – A network of streams that both branch out and reconnect forming a communication between two blood vessels or other tubular structures.
Autoregulation – The intrinsic ability of a system to maintain constant blood flow despite changes in perfusion pressure and local vascular parameters to maintain homeostasis.
Choriocapillaris – A layer of capillaries in the choroid immediately adjacent to Bruch's membrane.
Central retinal artery – A branch of the ophthalmic artery which pierces the optic nerve close to the globe, sending branches to the internal surface of the retina.
Extraocular muscles – A group of six muscles that control the movements of the eye, including the superior, inferior, lateral, and medial recti, and the superior and inferior obliques.
Fenestration – From the Latin word for window (fenestra), a fenestration is an opening in a wall or membrane.
Hemodynamics – The study of the forces generated by the heart and the flow of blood through the cardiovascular system.
Ophthalmic artery – A branch of the internal carotid artery which enters the orbit through the optic canal, along with the optic nerve, to supply structures in the orbit.
Poiseuille's law – A physical law that describes slow, viscous, incompressible flow through a circular cross section. It states that for a laminar, nonpulsatile fluid flow through a uniform straight tube, the vascular resistance is inversely proportional to the fourth power of the radius of a vessel, and is directly proportional to the blood viscosity and length of the vessel.
Retrobulbar vessels – Blood vessels behind the eye.

Introduction

A thorough understanding of vascular anatomy is critical to appreciate the physiology of the optic nerve head (ONH). The study of blood flow and the metabolism of the eye are also important in understanding the role of the circulatory system in various eye diseases. The arterial supply to the optic nerve has been widely investigated; however, the precise anatomy of the anterior optic nerve microvasculature remains difficult to ascertain. Detailed assessment of this anatomy is limited by its small vessel caliber, its complex three-dimensional structure, and the relative inaccessibility of the microvascular bed. Although the evaluation of ocular hemodynamics continues to improve with the development of new imaging technologies, current techniques for measuring optic nerve blood flow do not directly evaluate the optic nerve. We summarize the vascular anatomy of the ONH, retina, and choroid, the regulation of blood flow in the ONH, and several imaging techniques used to measure blood flow in the eye.

Anatomy of the Vascular Supply

The ophthalmic artery (OA), which is the first branch of the internal carotid artery, provides the vast majority of the ocular blood supply (**Figure 1**). The OA enters the orbit through the optic canal and, in most individuals, runs inferolaterally to the optic nerve. After coursing nasally and anteriorly, the OA runs superior to the optic nerve, where it gives off most of its major branches. These branches include vessels to each of the extraocular muscles, the central retinal artery (CRA), and the posterior ciliary arteries (PCAs) (**Figure 2**). There are usually two to three PCA trunks, each dividing into approximately 10–20 short PCAs before, or, occasionally after, penetrating the sclera. The short PCAs supply the posterior choriocapillaris, peripapillary choroid, and the majority of the anterior optic nerve. The medial and temporal long PCAs pierce the sclera about 3–4 mm nasally and temporally from the optic nerve (**Figure 2**). They then travel anteriorly within the suprachoroidal space, along the horizontal meridians of the globe. Typically, the long PCAs divide in the vicinity of the ora serrata to supply the iris, ciliary body, and the anterior region of the choroid.

The CRA branches directly from the OA to pierce the medial aspect of the optic nerve sheath approximately 10–15 mm behind the globe. The CRA courses adjacent to the central retinal vein (CRV) through the center of the optic nerve. It emerges from the optic nerve within the globe, where it branches into four major vessels: the arteriola nasalis retinae superior, arteriola nasalis retinae inferior, arteriola temporalis retinae superior, and arteriola temporalis retinae inferior.

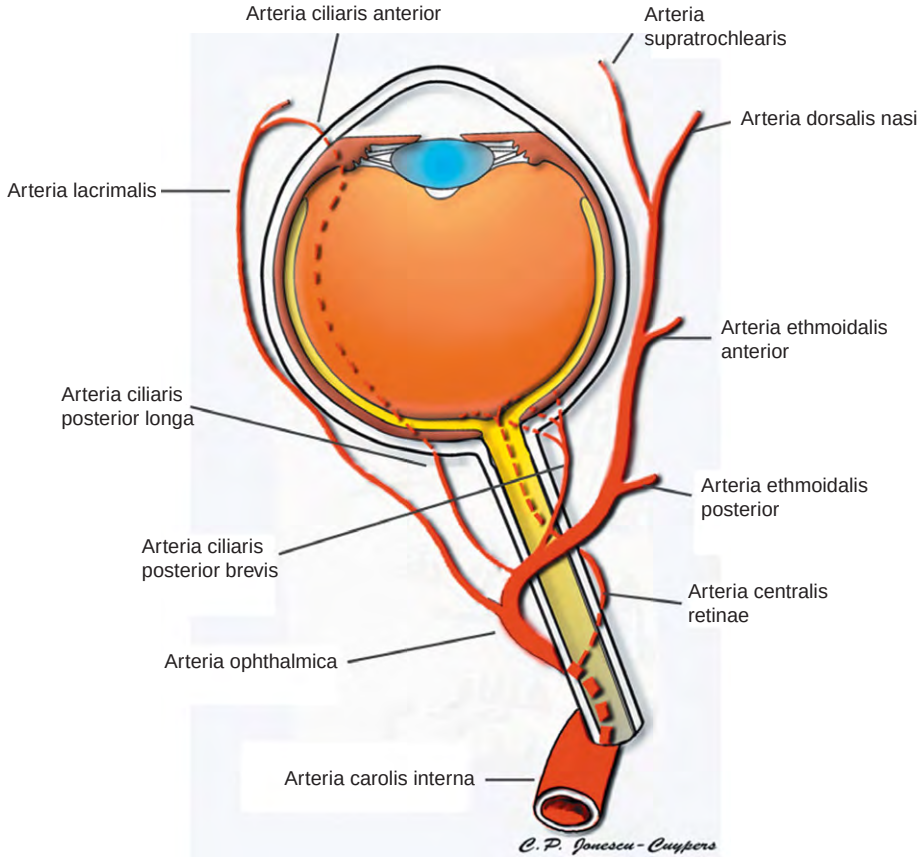

Figure 1 Schematic depicting the general vascular organization and the arterial feeds of the major and microciliary processes. The anterior and posterior arterioles that branch off the major arterial circle of the iris (MAC) supply the capillaries of the major and minor processes, respectively. Several smaller branches off the anterior arteriole feed into the marginal capillaries of the major process. Branches of the posterior arteriole feed the internal capillaries (ICs) of the major process. Blood supply to the capillaries of the minor processes is derived from more than one posterior arteriole. Anastomoses (green arrowheads) occur between the lateral branches, some marginal or central capillaries of the major processes and the basally located capillaries that extend posteriorly (white star). From Morrison, J. C. and van Buskirk, E. M. (1984). *American Journal of Ophthalmology* 97: 372–383 in Figure 11.25f in Bron, A. J., Tripathi, R. C., and Tripathi, B. J. (1997). The choroid and uveal vessels. In: *Wolff's Anatomy of the Eye and Orbit*, 8th edn., ch. 11. London: Chapman and Hall Medical.

The vasculature of the eye can be divided into two distinct systems: the retinal system and the uveal system. The retinal system provides blood flow to the inner two-thirds of the retina. The choroid and ciliary body are nourished by the uveal system. The retinal pigment epithelial layer, which is located between the retina and choroid, actively exchanges nutrients and metabolic waste products between the retina and the choroid. Thus, the outer layers of the retina receive their blood flow via the uveal system.

Retina

The retina receives its arterial blood supply from two distinct sources. The CRA provides blood flow to the inner two-thirds of the retina. The CRA branches on the surface of the optic disk, typically producing four main trunks which lie within the nerve fiber layer. Each trunk supplies its respective quadrant of the retina. The outer one-third of the retina, including the photoreceptors and bipolar cells, receives nourishment from the underlying choroid, specifically the choriocapillaris. Nutrients are actively transported between the choroid and retina via the retinal pigment epithelium. In approximately 30% of the people, a cilioretinal artery is present. Typically a branch of a ciliary artery, this vessel supplies a variably sized region of the retina temporal to the optic nerve. When present, the cilioretinal artery is an end artery, and therefore its territory receives no additional blood supply from any other vessels.

Retinal capillaries run parallel to the retinal nerve fiber layer, eventually coalescing into retinal veins, which empty into the CRV. The CRV exits the eye through the optic nerve, running parallel to the CRA. Once in the optic nerve, the CRV receives additional intraneural tributaries, and eventually empties into the superior ophthalmic vein. Although the CRV is normally the only outflow channel

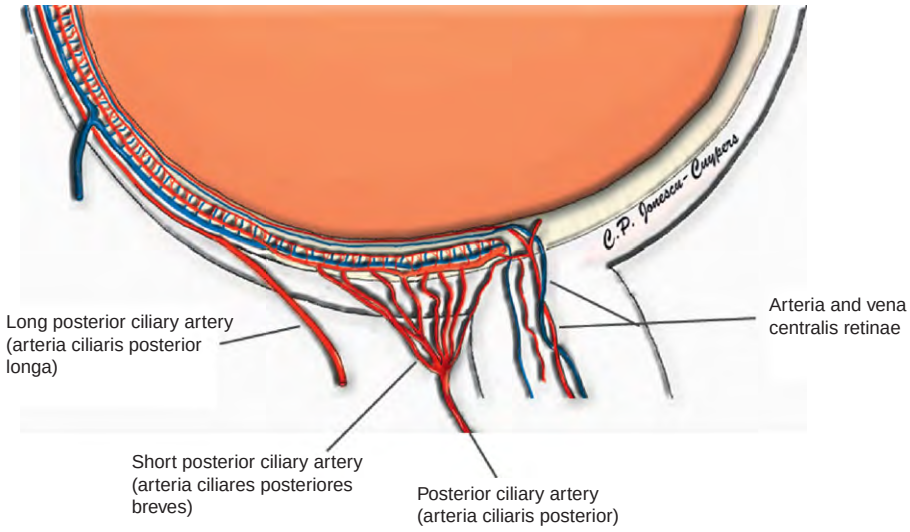

Figure 2 Drawing depicting the vascular territories of the ciliary processes. The first terroritory (outlined in the green box) includes the anterior arterioles, the lateral branches, and that feed the lateral branches, and the branches that drain into the basally located venules (white star). The second territory (indicated by the green arrows), includes the marginal capillaries and the capillary network (shown as short connections) that connect to these and the internal capillaries (IC) of the major process. The third territory (outlined in the purple box) includes the capillaries that branch off the posterior arterioles, and the vasculature of the minor processes. According to some authors the vessels in the posterior third of the major processes also fall within the third vascular territory. From Morrison, J. C. and van Buskirk, E. M. (1986). *Transactions of Ophthalmology Society* 105: 13 in Figure 10.28b in Bron, A. J., Tripathi, R. C., and Tripathi, B. J. (1997). The posterior chamber and ciliary body. In: *Wolff's Anatomy of the Eye and Orbit*, 8th edn., ch. 10. London: Chapman and Hall Medical.

for retinal circulation, potential anastamoses exist between the retinal and choroidal circulation. These alternate pathways are significant in the case of a CRV occlusion.

Choroid

The choroid supplies the outer retina with nutrients and maintains the temperature and volume of the eye. The choroidal circulation, which accounts for 85% of the total blood flow in the eye, is a high-flow system with relatively low oxygen content. The choroidal circulation is controlled mainly by sympathetic innervation and is considered not to be autoregulated. This lack of autoregulation makes the choroid more dependent on the ocular perfusion pressure.

The short PCAs supply the posterior choroid and the peripapillary region, while the anterior parts of the choroid are supplied by the long PCAs and the anterior ciliary artery. The anterior ciliary artery is a branch from the OA which accompanies the rectus muscle anteriorly to supply the iris and the anterior choriocapillaries.

The outer choroid, known as Haller's layer, is composed of large caliber, nonfenestrated, vessels. The inner choroid is referred to as Satler's layer, and is composed of significantly smaller vessels. The choriocapillaries of the innermost choroid are composed of richly anastomotic, fenestrated capillaries. The capillaries of the choriocapillaries are separate and distinct from the capillary bed of the anterior optic nerve.

Venous drainage from the choriocapillaries is primarily through the four vortex veins. Minor drainage also occurs through the ciliary body and the anterior ciliary vein. Venous anastomoses are frequent in the choroid. The vortex veins drain into the inferior and superior ophthalmic veins, which then exit the orbit through the superior and inferior orbital fissures, respectively.

Optic Nerve

The anterior optic nerve is divided into four anatomical regions: the superficial nerve fiber layer, the prelaminar layer, the laminar region, and the postlaminar region (**Figure 3**). The arterial supply to the ONH is derived from branches of the OA. The short PCAs penetrate the perineural sclera at the posterior aspect of the globe to supply the peripapillary choroid and anterior ONH. The circle of Zinn-Haller is a noncontinuous arterial circle surrounding the ONH within the perineural sclera. Formed by a network of small branches of the short PCAs, the circle of Zinn-Haller provides multiple perforating branches to various regions of the anterior optic nerve, peripapillary choroid, and pial arterial system. The capillaries of the anterior ONH are nonfenestrated, contain tight junctions, and form a rich anastomotic plexus. Some investigators surmise that the division of the short PCAs into branches

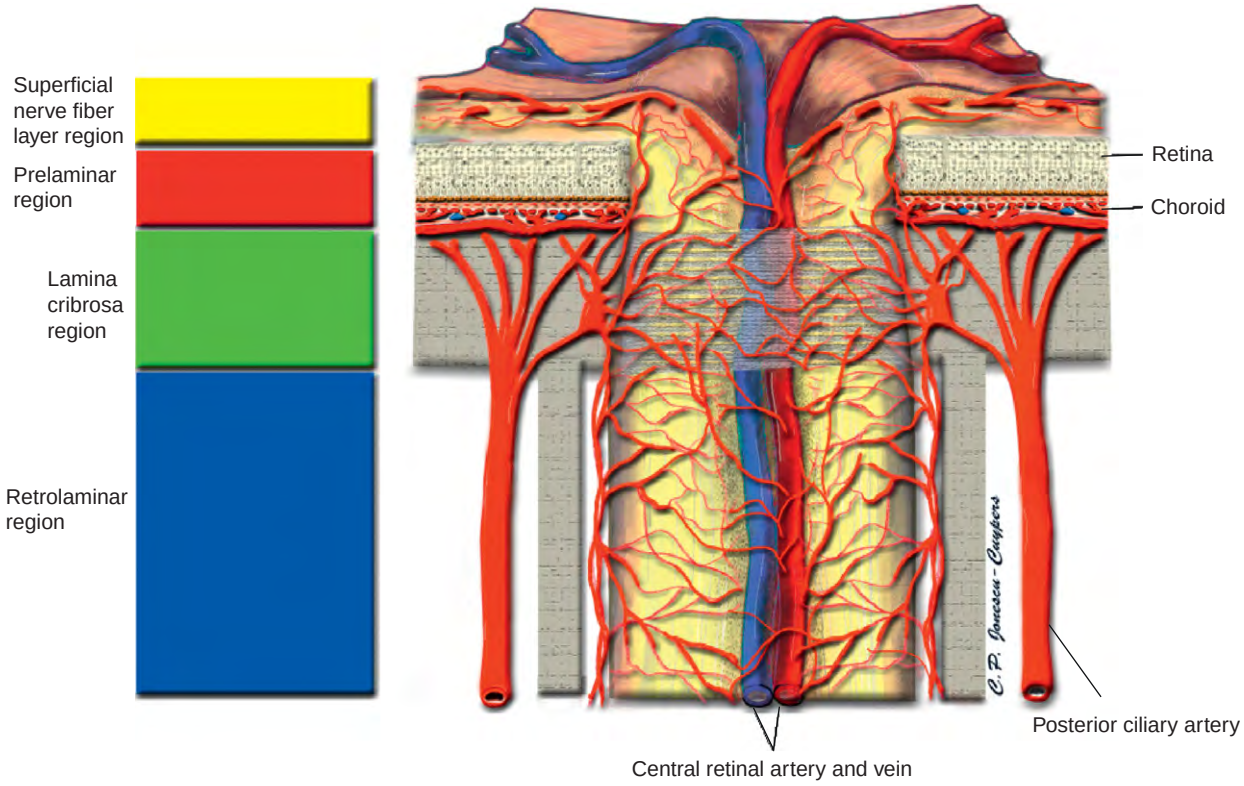

Figure 3 Left: anatomical regions of the optic nerve. Right: blood vessels of the anatomical regions of the optic nerve.

that supply the choroid and those supplying the ONH form the watershed zone near the ONH.

The superficial nerve fiber layer, which is continuous with the nerve fiber layer of the retina, receives its blood supply from recurrent arterioles arising from branches of the retinal arteries (**Figure 4**). These vessels, referred to as epipapillary vessels, originate in the peripapillary nerve fiber layer and run toward the center of the ONH. The temporal nerve fiber layer may receive additional arterial contribution from the cilioretinal artery when present.

Immediately posterior to the nerve fiber layer is the prelaminar region, which lies adjacent to the peripapillary choroid. In this region, ganglionic axons are grouped into bundles, surrounded by glial tissue septa, as they prepare for passage posteriorly through the lamina cribrosa. The prelaminar region is supplied primarily by branches of the short PCAs and, when present, by branches of the circle of Zinn-Haller (**Figure 5**). The amount of choroidal contribution may be difficult to determine, as there are branches from both the circle of Zinn-Haller and the short PCAs which course through the choroid and ultimately supply the optic nerve in this region. These vessels do not originate in the choroid, but merely pass through it. The choroid contributes little, if any, blood supply to this area of the ONH.

The laminar region is continuous with the sclera and is composed of fenestrated connective tissue lamellae which allow the passage of neural fibers through the sclera. This region, called the lamina cribrosa, receives its blood supply either from centripetal branches of the short PCAs or from branches of the circle of Zinn-Haller (**Figure 6**). These branches pierce the outer aspect of the lamina cribrosa before branching centrally to form an intraseptal capillary network throughout connective tissue. The larger peripapillary choroidal vessels occasionally contribute small arterioles to the lamina cribrosa region.

The retrolaminar region lies posterior to the lamina cribrosa, and is discernible by the beginning of the axonal myelination. Surrounded by the meninges of the central nervous system (CNS), the retrolaminar region is supplied primarily by branches of the pial arteries and the short PCAs (**Figure 7**). The pial system is an abundant anastomotic network fed by the OA, the circle of Zinn-Haller, and recurrent branches of the short PCAs. The pial branches are located within the pia matter and extend centripetally to perfuse the axons of the optic nerve. In addition, the CRA occasionally contributes small branches within the retrolaminar optic nerve.

Like that of the retina, the venous drainage from the ONH is through the CRV. In the superficial nerve fiber

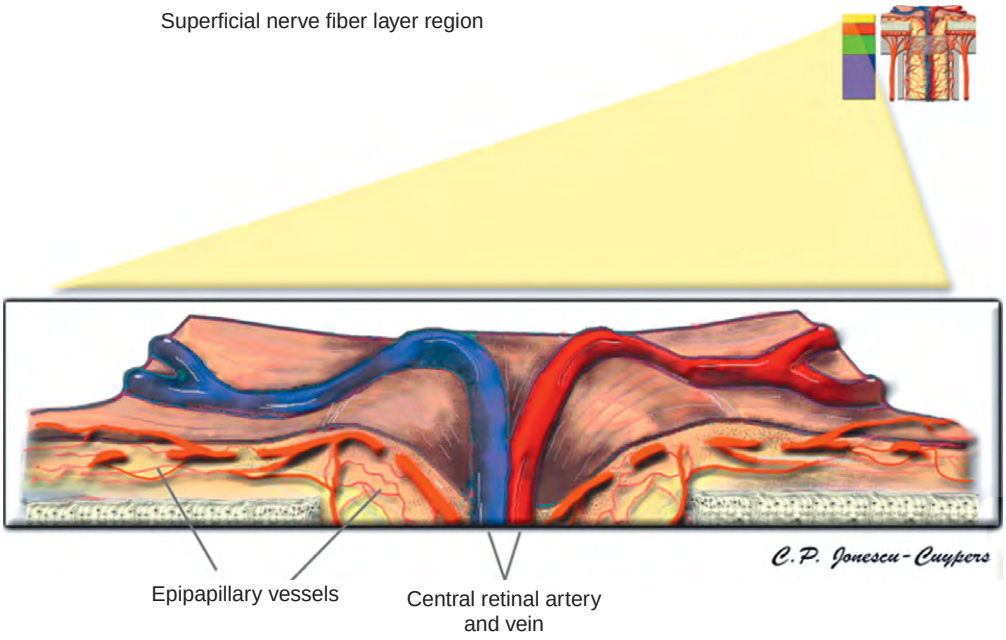

Figure 4 Schematic of the blood supply to the superficial nerve fiber layers.

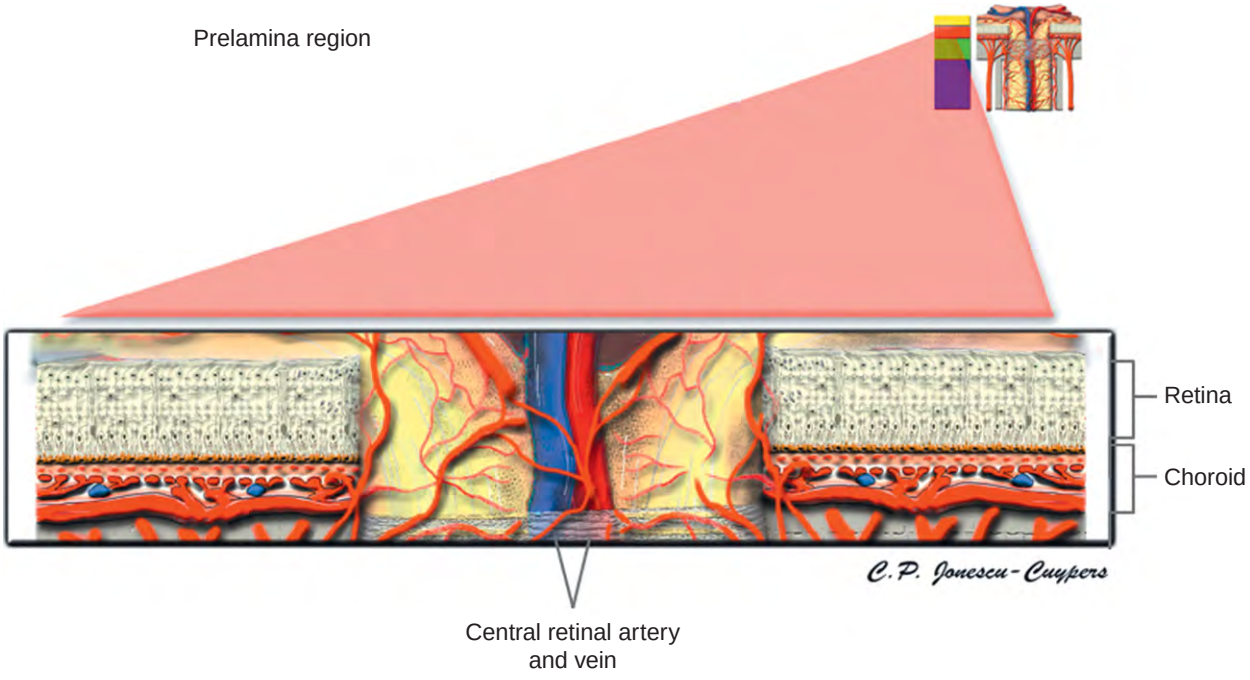

Figure 5 Schematic of the blood supply to the prelaminar region of the optic nerve.

layer, blood is drained by small, converging veins that empty into the CRV. In the other layers of the ONH, centripetal veins serve as tributaries, eventually emptying into the CRV. In the prelaminar region, there is also a noteworthy contribution from the peripapillary choroidal veins. Small portions of the peripheral region of the ONH may partially drain into the pial venous network, which ultimately joins together with the CRV as well.

Histology of Blood Vessels in the Optic Nerve

The anterior optic nerve is composed of nerve axons, neuroglia, blood vessels, and connective tissue. Large-caliber arteries of the optic nerve contain a muscularis layer, composed of multiple layers of smooth muscle, surrounded by the adventitia. The latter consists of

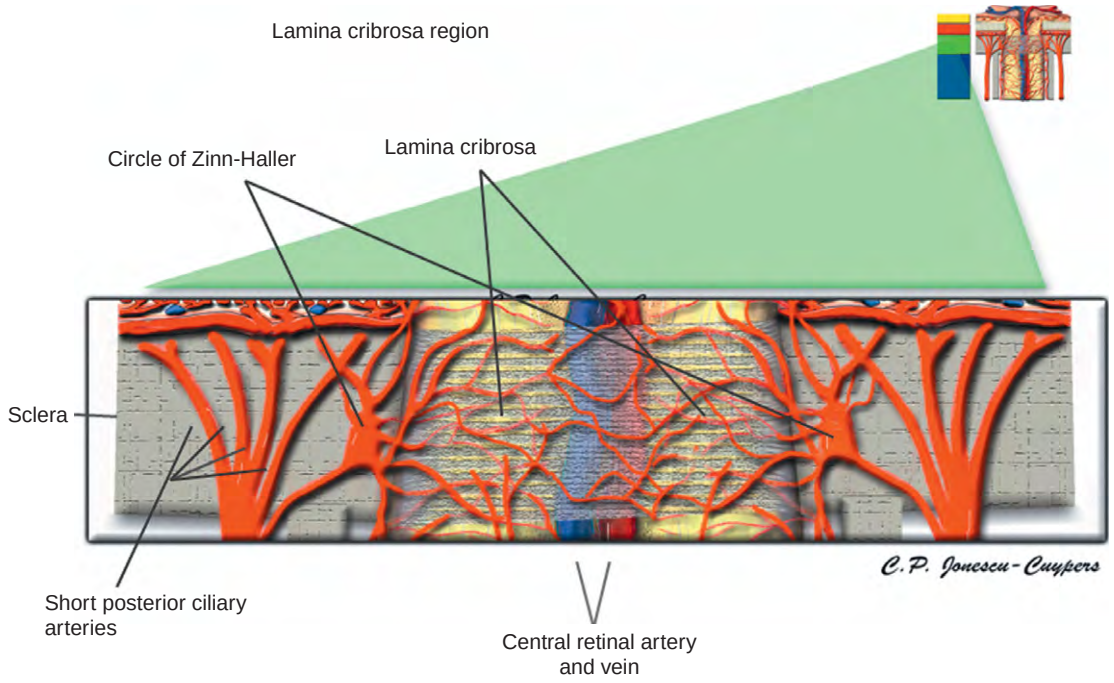

Figure 6 Schematic of the blood supply to the lamina cribrosa region.

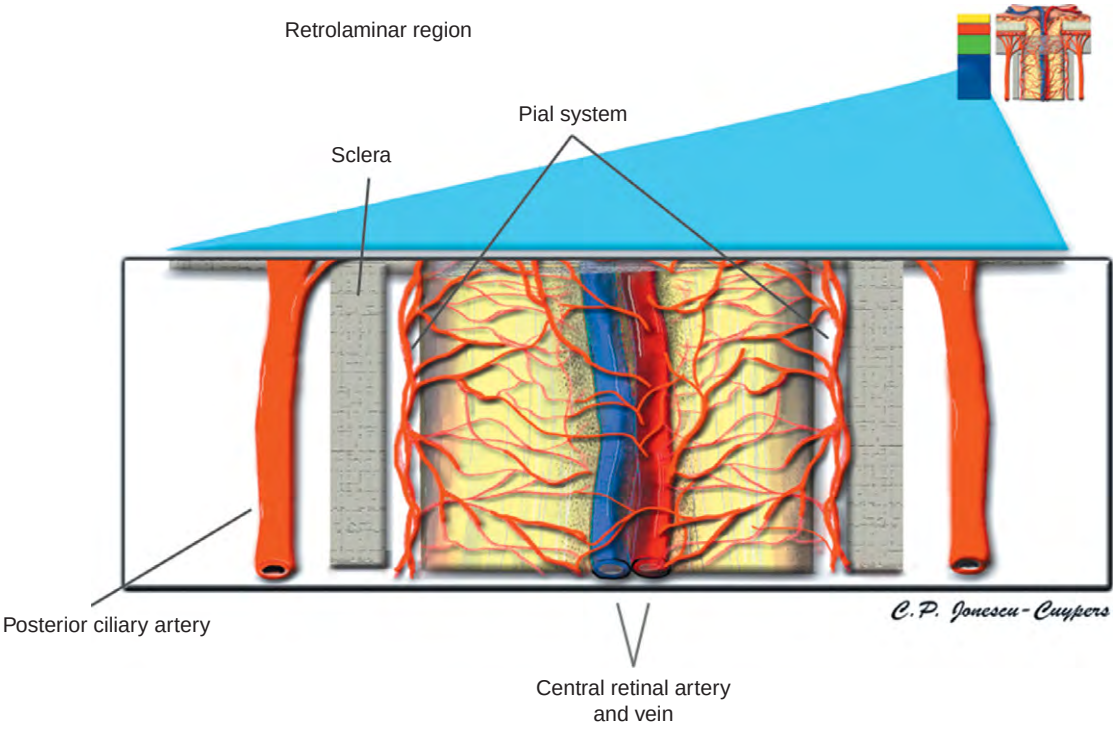

Figure 7 Schematic of the blood supply to the retrolaminar region of the optic nerve.

circumferential collagen fibers which blend with fibers from the perivascular space. On its luminal surface, the muscularis layer is separated from the endothelium by an inner elastic layer. The basement membrane lies between the endothelial cells and blends with the internal elastic lamina.

Arterioles of the optic nerve are much smaller in diameter, and have a single layer of smooth muscle.

They also possess minimal to no elastic lamina, but have a relatively dense reticular lining. The adventitia is continuous with collagen fibers of the intravascular space, and the endothelium is covered by a basement membrane.

Precapillaries and capillaries have a very thin wall and their basement membranes stain positively with the periodic acid-Schiff reaction. The endothelium, basement membrane, and mural cells of the venous structures are similar to that of the capillaries. The veins of the optic nerve are composed of an inner lining of endothelial cells, elastic fibers, thin adventitia, and intermittently, irregularly spaced, smooth muscle cells. When the venules enlarge, the basement membrane thickens accordingly.

Within the anterior ONH, the histology of the vasculature resembles that of the CNS, as the vessels contain a nonfenestrated endothelium with tight junctions. Capillaries predominate within the anterior ONH, and larger vessels are seldom visualized. Posteriorly, larger arterioles may be seen entering the lamina cribrosa. These capillaries and arterioles lack the internal elastic lamina and elastic tissue in the media that is characteristic of the larger vessels of the laminar and retrolaminar regions.

Regulation of Ocular Blood Flow

Autoregulation is the intrinsic ability of a system to maintain constant blood flow despite changes in perfusion pressure and local vascular parameters. The intrinsic control of blood flow involves chemical secretion by the cells in the immediate vicinity of the blood vessels. Within the eye, autoregulation is defined as local vascular constriction or dilation to alter vascular resistance, thereby maintaining a constant nutrient supply in response to perfusion pressure changes. Perfusion pressure is equal to the difference between the mean arterial pressure (MAP) and the venous pressure. The MAP is defined as the diastolic blood pressure plus one-third of the difference between systolic and diastolic blood pressure. Since the pressure in the central vein is normally slightly higher than the intraocular pressure (IOP), the IOP is used as an estimate of ocular venous pressure:

$$\text{Mean ocular perfusion pressure} = \frac{2}{3}\text{MAP} - \text{IOP}$$

$$\text{MAP} = \text{Diastolic BP} + \frac{1}{3}(\text{Systolic BP} - \text{Diastolic BP})$$

The maintenance of appropriate ocular blood flow is challenged by physiological changes in IOP, blood pressure, ocular perfusion pressure, and local tissue metabolic demands. As per Poiseuille's law, vascular resistance is inversely proportional to the fourth power of the radius of a vessel, and is directly proportional to the blood viscosity and length of the vessel. In the eye, vascular resistance is therefore dependent on the regulation of vessel diameter. In normal subjects, autoregulation is usually maintained until the IOP reaches approximately 40–45 mmHg. Failure of stable blood flow regulation may lead to ischemic damage of the optic nerve or retinal ganglion cells, which likely contributes to further impairment in vascular regulation. Several mechanisms, including neurogenic-, metabolic-, myogenic-, humoral-, and endothelial-mediated factors, have been demonstrated to play a role in the vascular regulation of ocular blood flow.

Fed primarily by the CRA, the retinal system is generally a low-flow, constant rate system that supplies a highly metabolically active tissue. Although it may only account for as little as 15% of the total ocular circulation, the retinal circulation is capable of providing relatively constant blood flow over a substantial range of IOPs. The retinal and anterior optic nerve head do not possess direct autonomic innervations. Although the retinal and optic nerve head have adrenergic and cholinergic receptors their role remains unclear. Consequently, retinal blood flow is locally autoregulated.

Several vasoactive molecules mediate retinal vascular autoregulation. Endothelial tone is determined by the balance between the vasoconstricting and vasodilating effects of secreted factors. Nitric oxide (NO) is produced by the oxidation of L-arginine by endothelial-derived nitric oxide synthase, which is present in both a constitutively active, membrane-bound form, and an inducible, cytosolic form. NO diffuses to nearby pericytes and smooth muscle, where it activates guanylyl cyclase, leading to the increase of cGMP and subsequent vasodilation. There are numerous stimuli for the production of NO, including increased shear force, bradykinins, insulin-like growth factor 1, acetycholine, and thrombin. Additionally, NO also inhibits platelet aggregation, platelet granule secretion, and leukocyte adhesion.

Vasoconstriction of the retinal microvasculature is stimulated by several vasoactive molecules. Endothelins, the most potent vasoconstricting agents known, are molecules that bind to receptors on pericytes and smooth muscle cells. A second vasoconstrictive substance is angiotensin II. Angiotensinogen is an inactive molecule that is constitutively produced by the liver. In response to physiologic stimuli, the kidneys release renin, which converts angiotensinogen into angiotensin I. Angiotensin converting enzyme (ACE), which is present on the surface of luminal endothelial cells, converts angiotensin I to angiotensin II, and also inactivates bradykinin. Once in its active form, angiotensin II moderates retinal vasoconstriction through the activation of smooth muscle cells and pericytes.

The choroidal vasculature is controlled extrinsically through hormonal influence and stimulation from the autonomic nervous system. It is characterized as a high-flow, variable-rate system which is tightly regulated by

the autonomic nervous system. The outer, larger vessels are composed of nonfenestrated endothelium, while the inner, smaller vessels form a richly anastomotic network of fenestrated capillaries. The vascular tone of the choroid is dominated by the sympathetic nervous system. Neurons course from the cranial cervical ganglion to the vascular bed, where vasoconstriction is mediated by the release of neuropeptide Y. The parasympathetic nervous system plays only a moderate and poorly defined role in the regulation of vascular tone. The presence of choroidal autoregulation is controversial and classically considered absent, though some autoregulatory response was reported during perfusion pressure changes.

Technology for Measuring Ocular Blood Flow

Color Doppler Imaging

Although originally developed for monitoring blood flow in the heart, carotid arteries, and peripheral vasculature, color doppler imaging (CDI) has proven to be useful in the study of retrobulbar vessels as well. By combining B-scan ultrasound images with velocity of measurements calculated from the Doppler shift of moving erythrocytes, CDI can be used to assess the velocity of blood flow through the retrobulbar vessels. The peak systolic velocity (PSV) and end diastolic velocity (EDV) can be measured and used to calculate the mean flow velocity (MFV). An index of resistance (RI) can be calculated as RI = (PSV – EDV)/PSV (Figure 8). Further research is necessary to determine the usefulness and application of the RI as it applies to the retrobulbar vasculature. Until recently, one critical limitation of this imaging technique had been that no quantitative information on vessel diameter was obtained, and therefore the calculation of total blood flow or flux was not possible. A recently developed analysis technique has made it possible to determine the diameter of the OA, allowing volumetric blood flow to be assessed. Further research is necessary to apply this technique to the assessment of blood flow through the other major vessels.

Angiography

Using sodium fluoroscein, angiography allows direct visualization of retinal blood flow. Most techniques measure the amount of time that it takes for the fluoroscein to pass through the retinal circulation. Using this technique, data can then be used to assess blood velocity through the retinal and optic disc circulation. Choroidal vessels are visualized in a similar fashion using indocyanine green, which is selected due to its increased binding to plasma proteins, preventing leakage from vessels to the surrounding tissue. Using videoangiography and scanning laser ophthalmoscopy, the arterio-venous passage time and retinal circulation time can be determined. This technology

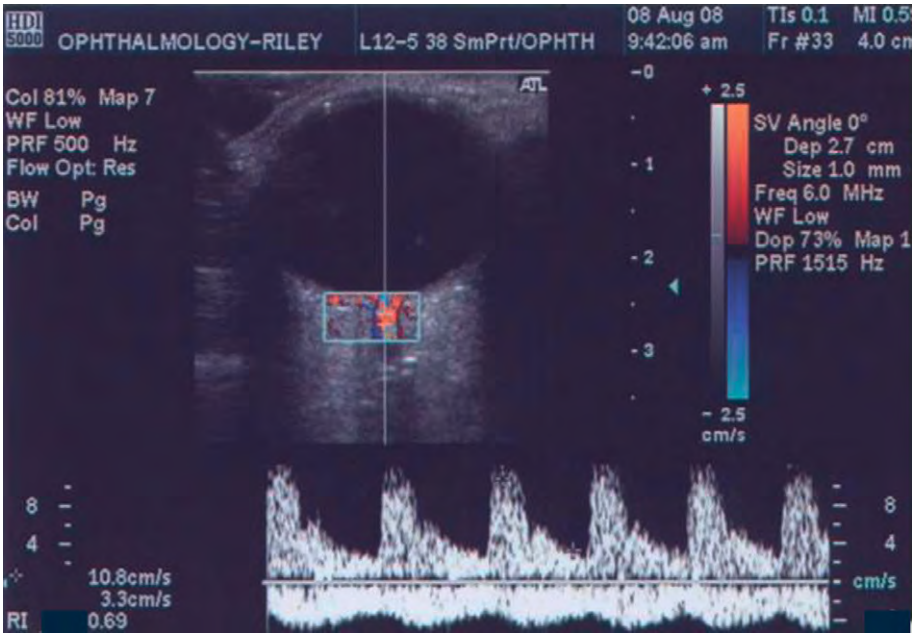

Figure 8 Color Doppler image of the central retinal artery and vein taken with a 7.5-MHz linear probe. The patient is placed comfortably in a half-supine position. An ultrasound probe is placed on closed eyelid and the optic nerve shadow of the optic nerve is identified. The vessels sampled include the ophthalmic artery, central retinal artery, and the nasal and temporal short posterior ciliary arteries. The Doppler-shifted spectrum (time–velocity curve) is displayed at the bottom of the image. Red and blue pixels represent blood movement toward and away from the transducer, respectively. The peak of the wave represents the peak systolic velocity (PSV) and the lower part of the wave the end diastolic velocity (EDV). The resistive index is calculated (PSV – EDV/PSV).

also has limitations, as it is based on the assumption that all of the blood of an area supplied by a specific artery is drained by a single corresponding vein.

Blue Field Entotpic Technique

The blue field entoptic phenomenon is produced by the different absorption of red and white blood cells when the retina is illuminated with blue light. Red blood cells absorb the short wavelength light, while passing white blood cells do not, thereby allowing the flux of the perimacular white blood cells to be estimated. This technique is limited by the assumption that leukocyte flux is proportional to retinal blood flow.

Laser Doppler Velocimetry

Laser Doppler velocimetry (LDV) is a technique that uses the optical Doppler shift of light to measure the blood flow velocities in retinal arterioles and venules. The Doppler shift of light is directly proportional to the blood velocity when the vessel is illuminated with a laser beam. The flow velocity in the vessel can be extrapolated from the range of frequency shifts of the power spectrum of the reflected laser light. The maximum frequency shift corresponds with the maximum velocity in the center of the vessel, assuming laminar flow.

Retinal Vessel Diameters

The aforementioned techniques can be utilized to provide information about ocular blood velocity, but lack the ability to calculate flux or flow rate. To determine blood flow, it is necessary to accurately measure the diameter of the vessel through which the blood is flowing. There are now commercially available systems that permit real-time assessment of retinal vessel diameter. The retinal vessel analyzer (RVA) is composed of a fundus camera and a sophisticated computer system which record vessel size in real time. One such system is the Canon Laser Doppler blood flowmeter, which combines the techniques of LDV and RVA. This approach is still limited to the study of larger vessels, and can only be performed on patients with clear ocular media.

Laser Speckle Technique

When the rough surface of the fundus is illuminated by coherent light, the backscatter of light produces a rapidly varying pattern. The rate of variation of this pattern produced by this laser speckle phenomenon can be measured to compute an estimate of the velocity of blood flowing through the retinal vessels. This laser speckle technique is limited by the fact that it provides only velocity information, as it cannot determine vessel diameter and therefore cannot be used to measure volumetric flow.

Laser Doppler Flowmetry

The scattering theory for light in tissue, formulated by Bonner and Nossal, assumes a randomization of light directions impinging on the erythrocytes. By directing a laser light on vascularized tissue that contains no large vessels, relative mean velocity of erythrocytes and blood volume can be calculated. Through two-dimensional mapping of the optical Doppler shift, blood flow to the juxtapapillary retina and ONH can be accurately evaluated. There is, however, significant variation in scattering of light between test subjects, likely a result of varying vascular densities and orientations. Thus, this technique can be used to compare changes in a given subject, but has less use in comparison of values between subjects.

Laser Doppler flowmetry can be combined with scanning laser tomography to provide a two-dimensional map of blood flow to the optic nerve and surrounding retina. The Heidelberg retina flowmeter (HRF) is one such commercially available system (**Figure 9**). This technique, however, is most sensitive to blood flow changes in the superficial layers of the ONH, and therefore provides only limited information about the deeper regions. This limits the ability to account for the retinal blood flow that is supplied by the choriocapillaris from the uveal system.

Pulsatile Ocular Blood Flow

Based on the changes in ocular volume and pressure during the cardiac cycle, it is possible to estimate pulsatile ocular blood flow. The pulse amplitude, which is the maximum IOP change during a cardiac cycle, is measured using a modified pneumotonometer. Alternatively, the

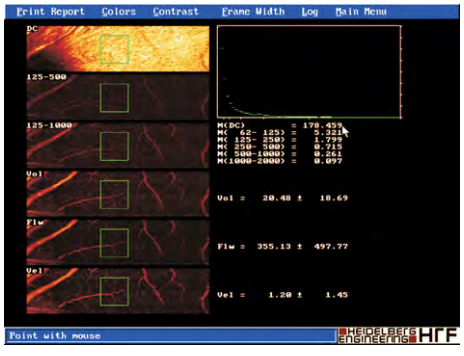

Figure 9 Confocal scanning laser Doppler flowmetry (Heidelberg retinal flowmeter) of optic nerve head and peripapillary retina. The patient is seated with the chin and forehead against the bar. The picture acquisition is performed without the need to dilate the patient's eye. The conventional 40 × 40 pixel measurement window collects flow values in arbitrary units from the entire retina except for large vessels.

ocular fundus pulsation amplitude can be determined by calculating the maximum change in distance between the retina and the cornea during a cardiac cycle. These two values have been shown to be useful in the calculation of pulsatile ocular blood flow, but lack information of the nonpulsatile component of ocular blood flow.

Optical Doppler Tomography

This technique combines the high-resolution cross-sectional imaging of optical coherence tomography with laser Doppler to measure velocity of blood flow in retinal arteries in real time.

Future Studies

Each of the previously discussed technologies quantifies some aspect of ocular blood flow. It is impossible, however, to interpret the impact of any single blood flow parameter measured within a single vascular bed on total retinal metabolism. The measurement of ocular blood flow is only a surrogate assessment of the metabolic status of the retina. Direct measurement of retinal tissue oxygenation would reveal the true impact of ischemia on retinal ganglion cell health and function.

New and emerging tools that assess metabolic parameters may help to reveal the relationship between reductions in ocular blood flow and tissue hypoxia. For example, Michelson and colleagues conducted a study in which they used imaging spectrometry to measure the oxygen saturation in retinal arterioles and venules in patients with glaucomatous optic neuropathy. In all examined eyes, the arteriolar oxygen saturation and the retinal arterio-venous differences in oxygenation were found to significantly correlate with the area of the patient's optic rim. Eyes with normal tension glaucoma, but not those with primary open angle glaucoma, showed significantly decreased arteriolar oxygen saturation. Although further advancements are still needed, these metabolic assessment tools may be very valuable in the evaluation of retinal hypoxia and in elucidating the effects of ocular ischemia. Obtaining accurate measurements of ocular tissue metabolism will greatly improve our understanding of disease pathophysiology, and will therefore lead to advancements in both diagnosis and treatment.

See also: Biomechanics of the Optic Nerve Head; Inherited Optic Neuropathies; Intraocular Pressure and Damage of Optic Nerve Axons; Ischemic Optic Neuropathy; Optic Nerve: Optic Neuritis; Orbital Vascular Anatomy; Retinal Ganglion Cell Apoptosis and Neuroprotection.

Further Reading

Bron, A. J., Tripathi, R. C., and Tripathi, B. J. (1997). The choroid and uveal vessels. *Wolff's Anatomy of the Eye and Orbit,* 8th edn. London: Chapman and Hall Medical.

Drexler, W. and Fujimoto, J. G. (2008). State-of-the-art retinal optical coherence tomography. *Progress in Retinal and Eye Research* 27: 45–88.

Hardarson, S. H., Harris, A., Karlsson, R. A., et al. (2006). Automatic retinal oximetry. *Investigative Ophthalmology and Visual Science* 47: 5011–5016.

Harris, A., Jonescu-Cuypers, C. P., Kagemann, L., Ciulla, T. A., and Krieglstein, G. K. (2003). *Atlas of Ocular Blood Flow*. Philadelphia, PA: Elsevier.

Harris, A. and Rechtman, E. (2008). Optic nerve blood flow measurement. In: Yanoff, M. and Duker, J. (eds.) *Ophthalmology,* 3rd edn., ch. 10.8, section 2, pp. 52–55. Edinburgh: Elsevier.

Hayreh, S. S. (2001). Blood flow in the optic nerve head and factors that may influence it. *Progress in Retinal and Eye Research* 20: 595–624.

Hayreh, S. S. (2008). Pathophysiology of glaucomatous optic neuropathy: Role of optic nerve head vascular insufficiency. *Journal of Current Glaucoma Practice* 2: 6–17.

Mackenzie, P. J. and Cioffi, G. A. (2008). Vascular anatomy of the optic nerve head. *Canadian Journal Ophthalmology* 43: 308–312.

Michelson, G. and Scibor, M. (2006). Intravascular oxygen saturation in retinal vessels in normal subjects and open-angle glaucoma subjects. *Acta Ophthalmologica Scandinavica* 84: 289–295.

Morrison, J. C. and van Buskirk, E. M. (1984). *American Journal of Ophthalmology* 97: 372–383.

Orgül, S. and Cioffi, G. A. (1996). Embryology, anatomy, and histology of the optic nerve vasculature. *Journal of Glaucoma* 5: 285–294.

Orgül, S., Gugleta, K., and Flamer, J. (1999). Physiology of perfusion as it relates to the optic nerve head. *Survey of Ophthalmology* 43: S17–S26.

Schmetterer, L. and Garhofer, G. (2007). How can blood flow be measured? *Survey of Ophthalmology* 52: 134–138.

Simon, B., Moroz, I., Goldenfeld, M., and Melamed, S. (2004). Scanning laser Doppler flowmetry of nonperfused regions of the optic nerve head in patients with glaucoma. *Ophthalmic Lasers, Surgery, and Imaging* 34: 245–250.

Angiogenesis in Inflammation

Z Szekanecz and L Módis, University of Debrecen Medical and Health Sciences Center, Debrecen, Hungary
A E Koch, University of Michigan Health System, Ann Arbor, MI, USA

Glossary

Angiogenesis – Physiological process involving the growth of new blood vessels from preexisting vessels.
Hypoxia inducible factors (HIFs) – Transcription factors that respond to decreases in oxygen.
Inflammation – A localized protective reaction of tissue to irritation, injury, or infection, characterized by pain, redness, swelling, and sometimes loss of function.
Neovascularization – Formation of functional microvascular networks with red blood cell perfusion.
Psoriatic arthritis – A form of rheumatoid arthritis usually affecting fingers and toes and associated with psoriasis.
Rheumatoid arthritis – A chronic autoimmune disease with inflammation of the joints and marked deformities.
Synovium – A thin layer of connective tissue with a free smooth surface that lines the capsule of a joint. Synovial fluid lubricates and facilitates movement of the joint.
Vascular endothelial growth factor – A signaling protein that regulates vasculogenesis.

Introduction

New capillary formation from preexisting blood vessels termed angiogenesis has been associated with inflammation and inflammatory diseases, as well as with malignancies. In inflammatory states, such as arthritis or psoriasis, the perpetuation of neovascularization increases the total endothelial surface and thus indirectly enhances leukocyte migration and accumulation into the involved tissue. There are numerous soluble and cell surface-bound mediators of angiogenesis, while angiostatic agents counterbalance neovascularization. The molecular mechanisms of angiogenesis and angiostasis, as well as angiogenesis in the eye are described in more detail elsewhere in this encyclopedia. Here we summarize the most relevant features of inflammation-related angiogenesis, as well as current therapeutic approaches to control angiogenesis in inflammatory states. Many of these therapeutic strategies have also been introduced to treat neovascular eye diseases. We have chosen rheumatoid arthritis (RA) as a prototype for inflammatory diseases, as the process of neovascularization, the most relevant angiogenic and angiostatic mediators and relevant anti-angiogenic therapies have been widely studied in context with inflammatory synovitis.

The Process and Models of Angiogenesis

In arthritis, there is excessive lymphocyte accumulation termed lymphoid neogenesis in the arthritic synovium. Inflammatory leukocytes migrate from the bloodstream through endothelia into the synovial tissue. Leukocyte adhesion to endothelium involves cell adhesion receptors, primarily integrins, selectins, and their respective ligands. Endothelial adhesion molecules, as well as several soluble mediators including growth factors, cytokines, chemokines, and others produced by synovial tissue macrophages and other cells may trigger synovial angiogenesis. First, these angiogenic mediators activate endothelial cells. Endothelium-derived proteolytic enzymes then digest the endothelial basement membrane and the perivascular extracellular matrix, thus enabling the proliferation and migration of endothelial cells into the interstitial tissue. The organization of these loose endothelial cells leads to the formation of primary and then further generation sprouts. Lumen formation within these endothelial sprouts leads to the genesis of capillary loops. Finally, new basement membrane is synthesized leading to new capillary formation.

There are several *in vitro* and *in vivo* models suitable to investigate the process of angiogenesis, the formation of new vessels on extracellular matrix substrata and to test anti-angiogenic compounds in preclinical studies. The corneal micropocket assay is the most relevant *in vivo* model of ocular angiogenesis. In this model, a micropocket is first prepared by cutting the cornea. The tested angiogenic compound is inserted into the pocket, and after 7–10 days vessel proliferation is induced toward the angiogenic compound (**Figure 1**).

Mediators of Angiogenesis

Numerous soluble and cell surface-bound mediators abundantly produced or expressed in inflammation exert angiogenic capacity (**Table 1**). There are endogenously

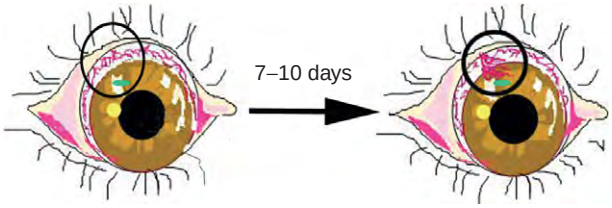

Figure 1 The rat corneal neovascularization model. The compound we wish to test for its angiogenic activity is inserted into the micropocket cut into the rat cornea. The degree of corneal neovascularization indicates the angiogenic activity of the compound.

Table 1 Some important mediators of inflammatory angiogenesis[a]

	Mediators
1. Growth factors	VEGF, aFGF, bFGF, HGF, HIF-1, HIF-2, PDGF, EGF, KGF, IGF-I, TGF-β
2. Cytokines	TNF-α, IL-1, IL-6, IL-8, IL-15, IL-17, IL-18, G-CSF, GM-CSF, oncostatin M, MIF
3. Chemokines/ receptors	IL-8/CXCL8, ENA-78/CXCL5, groα/CXCL1, CTAP-III/CXCL6, SDF-1/CXCL12, MCP-1/CCL2, fractalkine/CX3CL1 CXCR2, CXCR4, CCR2
4. Matrix molecules	Type 1 collagen, fibronectin, laminin, vitronectin, tenascin, proteoglycan
5. Cell adhesion molecules	β1 and β3 integrins, E-selectin, VCAM-1, ICAM-2, CD34, Lewis^y/H, MUC18, PECAM-1, endoglin, JAM-A, JAM-C
6. Proteolytic enzymes	MMPs, plasminogen activators
7. Others	Angiopoietin 1/Tie-2, angiotropin, pleiotrophin, angiogenin, survivin, COX/prostaglandin E2, PAF, nitric oxide (NO), endothelin-1, Serum amyloid A, histamine, substance P, adenosine, erythropoietin, prolactin, thrombin

[a]See text for abbreviations.

produced, natural inhibitors of neovascularization that try to counterbalance the effects of angiogenic agents; however, their amount and activity is usually insufficient to fully inhibit inflammatory angiogenesis so there is excess angiogenic over angiostatic capacity in inflammation, as well as in malignancies and other angiogenic diseases. Thus, anti-angiogenic therapies should be introduced by applying externally administered angiogenesis inhibitors in order to control pathological neovascularization in these disease states.

There are several angiogenic factors, including growth factors, cytokines, chemokines, extracellular matrix molecules, proteolytic enzymes, cellular adhesion molecules, and others implicated in inflammatory angiogenesis. In arthritis, these mediators are primarily released by macrophages and endothelial cells into the arthritic synovium. The most relevant molecules are listed in Table 1. Only angiogenic pathways also relevant for ocular neovascularization and anti-angiogenic treatment will be discussed in more detail.

There are numerous growth factors that are bound to heparin and heparan sulfate proteoglycans within the synovial matrix. Heparanase and plasmin produced during inflammation release these growth factors from the extracellular matrix. These growth factors include vascular endothelial growth factor (VEGF), basic (bFGF) and acidic fibroblast growth factors (aFGF), hypoxia-inducible factors 1 and 2 (HIF-1, HIF-2), as well as hepatocyte growth factor (HGF). In addition, some growth factors that do not bind to heparin, including platelet-derived growth factor (PDGF), epidermal growth factor (EGF), insulin-like growth factor-I (IGF-I), keratinocyte growth factor (KGF) and transforming growth factor-β (TGF-β) also promote neovascularization.

The hypoxia-HIF–VEGF-angiopoetin system is essentially involved in both inflammatory and ocular angiogenesis. In addition, as described later, VEGF is a primary target during angiogenesis. Hypoxia is a major feature of inflammation. In RA, there is intraarticular hypoxia, which induces branching of blood vessels. Hypoxia primarily acts by the stimulation of HIFs during angiogenesis and HIFs then stimulate the release of VEGF. (Hypoxia-induced neovascularization is discussed in more detail elsewhere in this encyclopedia.) As described recently, hypoxia may also act independently of HIFs by the peroxisome-proliferator-activated receptor-γ (PPARγ)/PPARγ coactivator 1α (PGC-1α) pathway. Upon ischemic injury, PGC-1α induces VEGF production and blood vessel reconstitution. Apart from PPARγ, activation of PPARβ/δ by specific ligands has also been recently implicated in VEGF production, inflammatory, and ocular angiogenesis.

Not only hypoxia and HIFs, but other proinflammatory mediators including tumor necrosis factor-α (TNF-α), interleukin-1 (IL-1), IL-6, IL-18, HGF, prostaglandins, and nitric oxide (NO) also promote VEGF release and capillary formation. VEGF stimulates angiogenesis, at least in part via cyclooxygenase-2 (COX-2) induction. VEGF also interacts with angiopoietin-1 (Ang1)/Tie-2, which promotes the stabilization of newly formed blood vessels. By contrast, Ang2, an antagonist of Ang1, inhibits vessel maturation. Survivin, an apoptosis inhibitor, has also been implicated in VEGF-induced angiogenesis. Thus, hypoxia, VEGF, HIF-1, HIF-2, Ang1, Tie2, and survivin are key players of inflammatory angiogenesis. Indeed, all these factors are abundantly expressed in the arthritic synovium. (More information on the molecular mechanisms of angiogenesis is available elsewhere in this encyclopedia.)

Pro-inflammatory cytokines may either directly induce neovascularization or may, as described above, act via VEGF-dependent pathways. The most relevant cytokines that have been implicated in arthritis-related

angiogenesis include TNF-α, IL-1, IL-6, IL-8, IL-15, IL-17, IL-18, oncostatin M, macrophage migration inhibitory factor (MIF), as well as granulocyte (G-CSF) and granulocyte-macrophage colony-stimulating factors (GM-CSF) (Table 1). As described above, TNF-α and IL-6 act via the induction of VEGF production. IL-17 exerts synergistic effects with TNF-α and thus stimulates the production of VEGF and other growth factors in synovitis. IL-18 also induces the production of VEGF, as well as that of angiogenic chemokines. Oncostatin M enhances adhesion molecule expression on RA synovial fibroblasts and vessels; it also stimulates endothelial cell migration and tubule formation. MIF is primarily produced by synovial macrophages and it acts via the release of VEGF and some angiogenic chemokines.

Some chemokines and chemokine receptors have also been implicated in inflammatory angiogenesis (Table 1). Chemokines are classified with respect to their chemical structure and the position of cysteine residues as CXC, CC, C, and CX_3C chemokines. In most angiogenic CXC chemokines the angiogenic capacity has been associated with the existence of glutamyl–leucyl–arginyl (ELR) amino acid motifs in their structure. The most relevant ELR^+ angiogenic CXC chemokines also abundantly produced in the inflamed synovium include IL-8/CXCL8, epithelial neutrophil activating protein-78 (ENA-78)/CXCL5, growth-related oncogene α (groα)/CXCL1, and connective tissue activating protein-III (CTAP-III)/CXCL6. Stromal cell-derived factor-1 (SDF-1)/CXCL12 is a key regulator of lymphoid neogenesis and the formation of lymphoid aggregates in the synovium. This chemokine lacks the ELR sequence; yet, it promotes neovascularization. Furthermore, hypoxia stimulates the release of SDF-1/CXCL12 in inflammatory synovitis. Among CC and CX_3C chemokines, MCP-1/CCL2 and fractalkine/CX3CL1 have been implicated in RA-associated angiogenesis. Among chemokine receptors, CXCR2 (the most important endothelial receptor for ELR^+ angiogenic CXC chemokines described above), CXCR4 (the receptor for SDF-1/CXCL12), and CCR2 (the receptor for MCP-1/CCL2) are all involved in chemokine-induced angiogenesis.

Inflammatory angiogenesis is associated with chemokine-driven recruitment of leukocytes through blood vessels into the synovium. This process involves cellular adhesion molecules, matrix macromolecules, as well as matrix-degrading proteolytic enzymes. Regarding adhesion molecules, most β_1 and β_3 integrins, E-selectin, selectin-related glycoconjugates including $Lewis^y$/H and MUC18, vascular cell adhesion molecule-1 (VCAM-1), intercellular adhesion molecule-2 (ICAM-2), platelet-endothelial cell adhesion molecule-1 (PECAM-1; CD31), endoglin (CD105), and junctional cell adhesion molecules A (JAM-A) and C (JAM-C) are expressed by endothelial cells and promote angiogenesis underlying inflammation. Among these adhesion receptors, the $\alpha_V\beta_3$ is of outstanding importance. This integrin mediates neovascularization, as well as osteoclast-mediated bone resorption and thus joint destruction in RA. During the process of angiogenesis, emigrating endothelial cells and soluble angiogenic mediators bind to extracellular matrix components. Thus, type I collagen, fibronectin, laminin, vitronectin, tenascin, and proteoglycans are also involved in neovascularization. Finally, matrix-degrading protease enzymes that digest the endothelial basement membrane and the interstitial matrix include various matrix metalloproteinases (MMPs) and plasminogen activators.

Other angiogenic mediators not mentioned above include endothelin 1 (ET-1), serum amyloid A (SAA), angiogenin, angiotropin, pleiotrophin, platelet-activating factor (PAF), substance P, histamine, erythropoietin, adenosine, prolactin, and thrombin. Among these mediators, ET-1 is released by endothelial as well as other cells. ET-1 stimulates VEGF production, endothelial proliferation, and angiogenesis. Abundant ET-1 production has been associated with RA, as well as scleroderma. SAA, an important acute-phase reactant in arthritis, stimulates endothelial proliferation, migration, and neovascularization.

Macrophages play a central role in angiogenesis related to arthritis and other types of inflammation. These cells express CXCR2 and CXCR4, which recognizes many angiogenic CXC chemokines described above. Macrophages also release numerous soluble angiogenic mediators, such as angiogenic CXC chemokines, TNF-α, IL-15, IL-18, VEGF, other growth factors, and MMPs. Finally, macrophages also secrete angiostatic factors such as CXCR3.

Angiogenesis Inhibition: Therapeutic Targeting of Angiogenesis in Inflammation

As a number of mediators are anti-inflammatory and also angiostatic, inflammation, and angiogenesis may be targeted simultaneously. Angiogenesis inhibitors relevant for inflammatory diseases, such as arthritis, are included in Table 2.

Naturally occurring endogenous angiogenesis inhibitors include interferons, IL-4, IL-13, CXC chemokines lacking the ELR motif including platelet factor 4 (PF4)/CXCL4, interferon-γ-inducible protein 10 (IP-10)/CXCL10 and monokine induced by interferon-γ (Mig)/CXCL9, thrombospondins, tissue inhibitors of MMPs, plasminogen activator inhibitors, and others. Theoretically all these inhibitors could be administered in high amounts in order to suppress neovascularization. Yet, only few compounds have been tested and found to be effective in animal models or humans (e.g., angiostatin, a fragment of plasminogen and endostatin, a fragment of

Table 2 Angiogenesis targeting strategies[a]

Endogenous inhibitors	• Angiostatin, endostatin
	• Thrombospondin 1 and 2
	• IL-4, IL-13
	• PF4/CXCL4
	• 2-Methoxyestradiol
Exogenous inhibitors	• VEGF inhibitors
	• HIF inhibitors
	• Ang1/Tie2 inhibitors
	• PPARγ, PPARβ/δ activators
	• Corticosteroids (triamcinolone)
	• Classical DMARDs
	• Biologics (infliximab, tocilizumab)
	• Thalidomide
	• Fumagillin analogues
	• Chemokine and chemokine receptor blockade (e.g., bicyclam)
	• $\alpha_v\beta_3$ integrin inhibitors (e.g., vitaxin)
	• Protease inhibitors
	• Endothelin-1 antagonists
	• Microtubule destabilizers (e.g., paclitaxel)

[a]See text for abbreviations.

type XIII collagen block $\alpha_V\beta_3$ integrin-mediated angiogenesis). Endostatin also inhibits VEGF receptor 2 signaling. Both compounds successfully abrogated arthritis, as well as arthritis-associated neovascularization in various rodent models. Recently, new molecules related to angiostatin or endostatin have been developed and are being tested in angiogenesis and arthritis models. These compounds include protease-activated kringles 1–5 (K1–5), kallistatin, arresten, canstatin, and tumstatin. Regarding human studies, both angiostatin and endostatin have been introduced to clinical trials in cancer. Thrombospondin-1 (TSP1) and TSP2 that are angiostatic extracellular matrix components naturally produced by RA synovial macrophages and fibroblasts. Both TSP1- and TSP2-derived peptides suppress synovial inflammation and angiogenesis in rodent models. IL-4 and IL-13 gene transfer inhibited synovial inflammation and angiogenesis in rats. The angiostatic PF4/CXCL4 chemokine has also been tried in rodent models of arthritis. 2-Methoxyestradiol (2-ME), a natural metabolite of estrogen with low affinity for estrogen receptors, inhibited angiogenesis by disrupting microtubules and by suppressing HIF-1 activity. In recent preclinical studies, 2-ME suppressed VEGF and bFGF gene expression, as well as arthritis in the rats.

Exogenously administered agents are not naturally found in human tissues. These compounds include currently used anti-inflammatory drugs, biological monoclonal antibodies, receptor antagonists, and other small molecule inhibitors that interfere with the activity of VEGF, chemokines, adhesion receptors, and other angiogenic mediators. Some of these agents, primarily VEGF and VEGF receptor antagonists, have been introduced to the therapy of ocular vascular diseases, as well as arthritis.

Among currently used antirheumatic, anti-inflammatory drugs, corticosteroids, chloroquine, sulfasalazine, methotrexate, azathioprine, cyclophosphamide, leflunomide, thalidomide, minocycline, and some anti-TNF agents primarily infliximab also inhibit endothelial cell migration and synovial angiogenesis. Triamcinolone is not only effective in the treatment of inflammatory diseases, but it suppresses VEGF and endostatin production and it has been used to treat ocular neovascularization, such as AMD. Recently, the anti-IL-6 receptor antibody tocilizumab decreased serum levels of VEGF.

Certainly today targeting of VEGF and VEGF-induced angiogenesis, as well as the hypoxia-HIF-VEGF-Ang1-Tie2 system is in the focus of cancer, inflammation, as well as ocular angiogenesis research. There have been several attempts to target VEGF by using synthetic VEGF and VEGF receptor inhibitors, anti-VEGF antibodies, and inhibitors of VEGF and VEGF receptor signaling. The VEGF-Trap construct is a composite decoy receptor based on the fusion of type 1 and type 2 VEGF receptors with IgG1-Fc. These VEGF and VEGF receptor inhibitors have primarily been tried in colorectal, lung, renal, and liver cancers. Some of these agents have recently been introduced to suppress angiogenesis related to arthritis, as well as neovascular eye diseases. Bevacizumab is a full-length human monoclonal antibody to VEGF that has been approved for the treatment of various types of cancer. Later it has become the first biological agent to suppress AMD. The use of bevacizumab has been suggested in other vascular eye diseases including diabetic macular edema, pathological myopia, retinal angiomatous proliferation, branch retinal vein occlusion, neovascular glaucoma, and several other forms of ocular neovascularization including corneal neovascularization. Preclinical and clinical trials on bevacizumab in arthritis are underway. Ranibizumab (an antigen-binding anti-VEGF antibody fragment) and pegaptanib (an anti-VEGF pegylated aptamer) have been successfully used to treat AMD. A soluble VEGF receptor 1 chimeric protein dose-dependently inhibited the proliferation of synovial endothelial cells. Vatalanib, sunitinib malate, sorafenib, vandetanib, and AG013736 are small molecule inhibitors of VEGF receptor tyrosine kinases, which have been introduced to cancer studies. Among these compounds, vatalanib also inhibited knee arthritis in rabbits.

HIF-mediated neovascularization may also be targeted in various ways. For example, YC-1, a soluble guanylyl cyclase stimulator originally developed to treat hypertension and thrombosis, is also a HIF-1 inhibitor. Microtubule destabilizers, such as 2-ME mentioned above, as well as paclitaxel, an anti-cancer agent, also suppress HIF-1α activity. 2-ME elicited anti-inflammatory and angiostatic properties in animal models of arthritis, while paclitaxel was effective and safe in a phase I human RA trial. Regarding the Ang-Tie system, Tie2 inhibition by adenoviral gene therapy attenuated the incidence and severity of arthritis

in mice. The role of PPARγ and PPARβ/δ in conjunction with hypoxia HIF VEGF-mediated angiogenesis is described above. The PPARγ ligands, rosiglitazone and pioglitazone, inhibit VEGF- and bFGF-mediated angiogenesis. Pioglitazone suppressed psoriatic arthritis in a small clinical trial. Furthermore, the use of both PPARγ agonists has been suggested in the treatment of AMD, diabetic retinopathy, and other neovascular ocular disorders. GW501516, a PPARβ/δ ligand currently under development for the treatment of dyslipidemia, also blocked VEGF-dependent endothelial cell proliferation and angiogenesis.

The suppression of chemokine- and chemokine receptor-mediated neovascularization may also be feasible. For example, blockade of CXCR2 inhibits tumor-induced angiogenesis, while Mig/CXCL9 chemokine gene therapy enhances the angiostatic effects of cytotoxic agents in cancer trials. Bicyclam (previously AMD3100), a highly selective antagonist of SDF-1/CXCL4, also inhibits neovascularization in various models.

Vitaxin, a humanized antibody to the $\alpha_V\beta_3$ integrin, inhibited synovial angiogenesis and inflammation in animal models of arthritis; however, it showed very little efficacy in a phase II human RA trial. Some MMP inhibitors have been tried in angiogenesis models. ET-1 antagonists currently used in the treatment of primary and scleroderma-associated pulmonary hypertension may also exert anti-angiogenic effects.

Thalidomide, currently in use to treat multiple myeloma but also tried in lupus and RA, is a potent TNF-α antagonist and angiogenesis inhibitor. Thalidomide suppressed both synovitis and angiogenesis in human models; however, it showed little efficacy in human RA trials.

Fumagillin is a naturally occurring product of *Aspergillus fumigatus*. TNP-470 and PPI2458 are synthetic derivatives of fumagillin that inhibit the methionine aminopeptidase-2 enzyme involved in angiogenesis. These compounds also attenuate VEGF production and VEGF-induced capillary formation. In rodent models, TNP-470 prevented arthritis when administered before the onset of the disease, while PPI2458 also suppressed the development of arthritis and joint erosions.

Theoretically most angiogenic mediators described above could be targeted to treat inflammatory angiogenesis. Indeed, many of these agents have already been introduced to either preclinical or clinical therapeutic trials, first in cancer and later in inflammatory diseases. Numerous VEGF and VEGF receptor antagonists gave promising results in cancer, arthritis, as well as neovascular ocular disease trials. However, it remains to be seen whether angiostatic strategies using targets with multiple actions may be more effective on the long-term than specific targeting of one single angiogenic mediator.

Acknowledgments

This work was supported by NIH grants AR-048267 and AI-40987 (A.E.K.), the William D. Robinson, M.D. and Frederick G.L. Huetwell Endowed Professorship (A.E.K.), funds from the Veterans' Administration (A.E.K.); and grant No T048541 from the National Scientific Research Fund (OTKA) (Z.S.).

See also: Angiogenesis in Response to Hypoxia; Angiogenesis in the Eye; Molecular Mechanisms of Angiostasis.

Further Reading

Agarwal, S. K. and Brenner, M. B. (2006). Role of adhesion molecules in synovial inflammation. *Current Opinion in Rheumatology* 18: 268–276.

Andreoli, C. M. and Miller, J. W. (2007). Anti-vascular endothelial growth factor therapy for ocular neovascular disease. *Current Opinion in Ophthalmology* 18: 502–508.

Brooks, P. C., Clark, R. A., and Cheresh, D. A. (1994). Requirement of vascular integrin alpha v beta 3 for angiogenesis. *Science* 264: 569–571.

Koch, A. E. (1998). Angiogenesis: Implications for rheumatoid arthritis. *Arthritis and Rheumatism* 41: 951–962.

Koch, A. E., Harlow, L. A., Haines, G. K., et al. (1994). Vascular endothelial growth factor. A cytokine modulating endothelial function in rheumatoid arthritis. *Journal of Immunology* 152: 4149–4156.

Lainer-Carr, D. and Brahn, E. (2007). Angiogenesis inhibition as a therapeutic approach for inflammatory synovitis. *Nature Clinical Practice Rheumatology* 3: 434–442.

Manley, P. W., Martiny-Baron, G., Schlaeppi, J. M., and Wood, J. M. (2002). Therapies directed at vascular endothelial growth factor. *Expert Opinion on Investigational Drugs* 11: 1715–1736.

Pablos, J. L., Santiago, B., Galindo, M., et al. (2003). Synoviocyte-derived CXCL12 is displayed on endothelium and induces angiogenesis in rheumatoid arthritis. *Journal of Immunology* 170: 2147–2152.

Petit, I., Jin, D., and Rafii, S. (2007). The SDF-1-CXCR4 signaling pathway: A molecular hub modulating neo-angiogenesis. *Trends in Immunology* 28: 299–307.

Piqueras, L., Reynolds, A. R., Hodivala-Dilke, K. M., et al. (2007). Activation of PPARβ/δ induces endothelial cell proliferation and angiogenesis. *Arteriosclerosis, Thrombosis, and Vascular Biology* 27: 63–69.

Strieter, R. M., Polverini, P. J., Kunkel, S. L., et al. (1995). The functional role of the ELR motif in CXC chemokine-mediated angiogenesis. *Journal of Biological Chemistry* 270: 27348–27357.

Szekanecz, Z. and Koch, A. E. (2007). Mechanism of disease: Angiogenesis in inflammatory diseases. *Nature Clinical Practice Rheumatology* 3: 635–643.

Szekanecz, Z. and Koch, A. E. (2008). Vascular involvement in rheumatic diseases: 'Vascular rheumatology'. *Arthritis Research Therapy* 10: 224.

Taylor, P. C. and Sivakumar, B. (2005). Hypoxia and angiogenesis in rheumatoid arthritis. *Current Opinion in Rheumatology* 17: 293–298.

Veale, D. J. and Fearon, U. (2006). Inhibition of angiogenic pathways in rheumatoid arthritis: Potential for therapeutic targeting. *Best Practice and Research Clinical Rheumatology* 20: 941–947.

Angiogenesis in Response to Hypoxia

Y Ozawa, K Tsubota, and H Okano, Keio University, Tokyo, Japan

Glossary

Erythropoietin (Epo) – Glycoprotein that controls angiogenesis as well as erythropoiesis.
Factor inhibiting HIF-1α (FIH-1) – Enzyme that hydroxylates and represses the transcription activity of HIF-1α.
Hypoxia-inducible factor-1α (HIF-1α) – A bHLH transcription factor regulated by hypoxia.
Oxygen partial pressure (pO_2) – Pressure of oxygen gas when it alone occupied the volume.
Proliferative diabetic retinopathy (PDR) – Most severe diabetes-induced retinopathy with pathological neovascularization.
Protein von Hippel-Lindau (pVHL) – E3-ubiquitin ligase that degrades ubiquitin-conjugated HIF-1α and a protein that determines the characteristic of von Hippel–Lindau syndrome.
Retinopathy of prematurity (ROP) – Disease that affects the newborn eye with disorganized growth of retinal vessels that may result in retinal detachment.
Vascular endothelial growth factor (VEGF) – Growth factor that controls angiogenesis and vascular permeability.

Introduction

Angiogenesis, the sprouting and branching of new blood vessels from the preexisting primitive network, involves several processes: endothelial cell proliferation and migration, degradation of the surrounding extracellular matrix (ECM) to allow migration, and vessel maturation by attracting pericytes and producing the basal lamina that surrounds the newly formed blood vessels. These processes are tightly regulated by the action of both stimulatory (angiogenic factors) and inhibitory (anti-angiogenic factors) molecules.

In the normal state, the action of angiogenic inhibitors dominates, and vessels are quiescent. However, under certain conditions that activate angiogenic factors, such as hypoxia or inflammation, the balance may shift in favor of angiogenesis. This mechanism contributes to the generation of new vessels not only during organogenesis, but also during the neovascularization associated with wound repair or pathological conditions in adults.

Pathological neovascularization is an important finding of vision-threatening diseases such as proliferative diabetic retinopathy (PDR) (Figure 1) and age-related macular disease (AMD). In PDR, vascular obliteration in the retina due to microangiopathy leads to extensive tissue hypoxia, which induces pathological angiogenesis; this angiogenesis leads to fibrovascular membrane formation, which causes severe vitreous hemorrhage, retinal detachment, and other detrimental conditions in the eye that result in vision loss. Worldwide, 194 million individuals have diabetes. Diabetic retinopathy is observed in 40% of individuals with diabetes, and over 8% of diabetic patients have vision loss from microvascular complications. In contrast, choroidal neovascularization in AMD is mainly caused by inflammatory reactions. More than 1.75 million people (1.5% of adults over 40) in the United States are estimated to have advanced AMD, which can induce registered legal blindness. The angiogenesis of both PDR and AMD is induced by the excessive expression of angiogenic factors and results in pathogenic conditions of the retina.

In this article, we focus on hypoxia-induced angiogenesis. We describe how angiogenic factors are regulated by hypoxia, and how they lead to pathological and physiological angiogenesis. The expression of two potent angiogenic factors, vascular endothelial growth factor (VEGF) and erythropoietin (Epo), is regulated by transcription factors called hypoxia-inducible factors (HIFs), and this regulation underlies most mechanisms that contribute to hypoxia-induced angiogenesis. Several pathways that regulate the HIFs under hypoxic conditions (and that, in turn, affect the levels of angiogenic factors regulated by the HIFs) are involved. Hence, hypoxia-induced angiogenesis is not mediated by a single pathway. The retina is a useful model system for studying angiogenesis in general, because it contains several thin vascular layers in which new vessels can be directly observed and quantified. This system has been used to elucidate the development of the vascular system and pathological neovascularization in the hypoxic retina. Here, we review the mechanisms of pathologic angiogenesis in the retina and describe supporting experimental data obtained from model animals in addition to human clinical data. We also discuss how hypoxia regulates vascular development in the retina.

Hypoxia and HIFs

One of the conditions regulating angiogenic factors is the local oxygen partial pressure (pO_2). While ambient air at sea level has a pO_2 of 149 mmHg (21% of the atmospheric

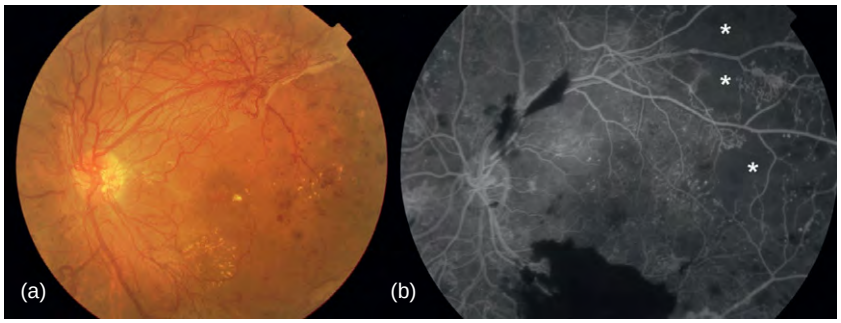

Figure 1 Fundus photograph of proliferative diabetic retinopathy. (a) Retinal neovascularization. (b) Fluorescent angiography shows areas of capillary nonperfusion in the retina (∗ in (b)).

pressure), the arterial oxygen content is as low as 75–100 mmHg (10–14%), and tissue pO_2 is lower still. For example, the pO_2 of resting skeletal muscle and ventricular myocardium is 30 mmHg (4%), which decreases to about 10 mmHg (1.4%) during contraction. Furthermore, the pO_2 in the inner segments of photoreceptor cells, where oxygen is supplied by diffusion from the choroidal vessels, decreases greatly during dark adaptation, to 5 mmHg (0.7%). In the dark, water and sodium flow passively into the photoreceptor cells from the surface membrane of their outer segment and are extruded by pumps in the inner segment. This dark current decreases during exposure to light, which promptly halts the pump action, thereby reducing the metabolism and oxygen uptake. Thus, oxygen consumption by photoreceptor cells is greater in darkness.

The condition of low pO_2 in normal tissue is called, physiological hypoxia. In a number of physiological and pathological processes, the tissue oxygen level may be further reduced due to poor circulation and/or rapid oxygen consumption. For example, in the diabetic retina, areas of capillary nonperfusion due to microangiopathy receive insufficient oxygen. During embryonic development, the rate of tissue expansion outpaces angiogenesis, creating an insufficient blood supply. Both of these situations lead to a very hypoxic environment in which various kinds of angiogenic factors can be simultaneously induced, to overcome the effects of insufficient blood flow.

Key molecules for promoting the expression of angiogenic factors are the HIFs. HIFs are heterodimers composed of an α subunit, HIF-1α (**Figure 2(a)**), HIF-2α (also known as HIF-1α-like factor; HLF), or HIF-3α, and a HIF-1β subunit. The subunits share a conserved domain structure, and, with the exception of HIF-1β, are upregulated by hypoxic conditions. The HIFα/HIF-1β heterodimeric complex forms a transcription factor that can bind to the HIF response element (HRE) (**Figure 2(b)**). In the HIF subunits, basic helix–loop–helix (bHLH) and PER-ARNT-SIM (PAS) motifs are required for dimerization, whereas a downstream basic region affords specific binding to the HRE sequence, 5′-RCGTG-3′. HIF-1α and HIF-2α activate the transcription of about 70 genes, including VEGF, Epo, and a VEGF receptor, VEGFR-1.

In the retina, HIF-1α is abundantly and broadly expressed during embryogenesis, when oxygen is supplied only by umbilical blood. Its expression is limited in the adult retina, but it can be induced again by hypoxic conditions. In contrast, HIF-2α is expressed generally in vascular endothelial cells.

HIF-1α is positively regulated by hypoxia through several pathways. A major pathway involves the stabilization of the protein by low levels of oxygen. In the presence of dioxygen, three oxygenases, prolyl hydroxylase domain proteins (PHD) 1-3, hydroxylate prolyl residues (proline residue 402 and/or 564) in human HIF-1α (**Figure 2(b)**). These residues are located in the N-terminal activation domain (TAD-N), within the oxygen-dependent degradation domain (ODDD) of HIF-1α. Hydroxylated HIF-1α is degraded by an E3-ubiquitin ligase, protein von Hippel–Lindau (pVHL), in a ubiquitin-proteasome-dependent pathway. However, under hypoxic conditions, PHD is inactivated and does not hydroxylate HIF-1α, and the degradation of HIF-1α by pVHL is, therefore, suppressed. HIF-2α also has an identical motif in the TAD-N, and HIF-3α has a partially identical one. The hydroxylation reaction by PHD requires Fe^{2+} and is inhibited by divalent cation chelators or cobalt chloride ($CoCL_2$). $CoCL_2$, which induces experimental neovascularization, promotes the induction of the angiogenic factor VEGF, and angiogenesis, by stabilizing HIFs. In addition, pVHL can degrade the RNA polymerase subunit, Rpb1, which may regulate the expression of HIFs both directly and indirectly.

Alternatively, factor inhibiting HIF-1α (FIH-1) represses the transcription activity of HIF-1α (**Figure 2(b)**). HIF-1α is hydroxylated by FIH-1 on asparagine residue 803, located in the C-terminal activation domain (TAD-C); this hydroxylation suppresses the binding of HIF-1α to its co-activators, p300/CBP. Thus, FIH-1 inhibits HIF-1α activity. This reaction is also dependent on Fe^{2+}, not only on oxygen. Moreover, PHD can bind to FIH-1, which together recruit histone deacetylase (HDAC) to repress the transcription of target genes.

Both of these HIF-1α regulatory pathways, that is, the PHD-pVHL-mediated protein degradation and the FIH-1-mediated inhibition of HIF-1α's function as a

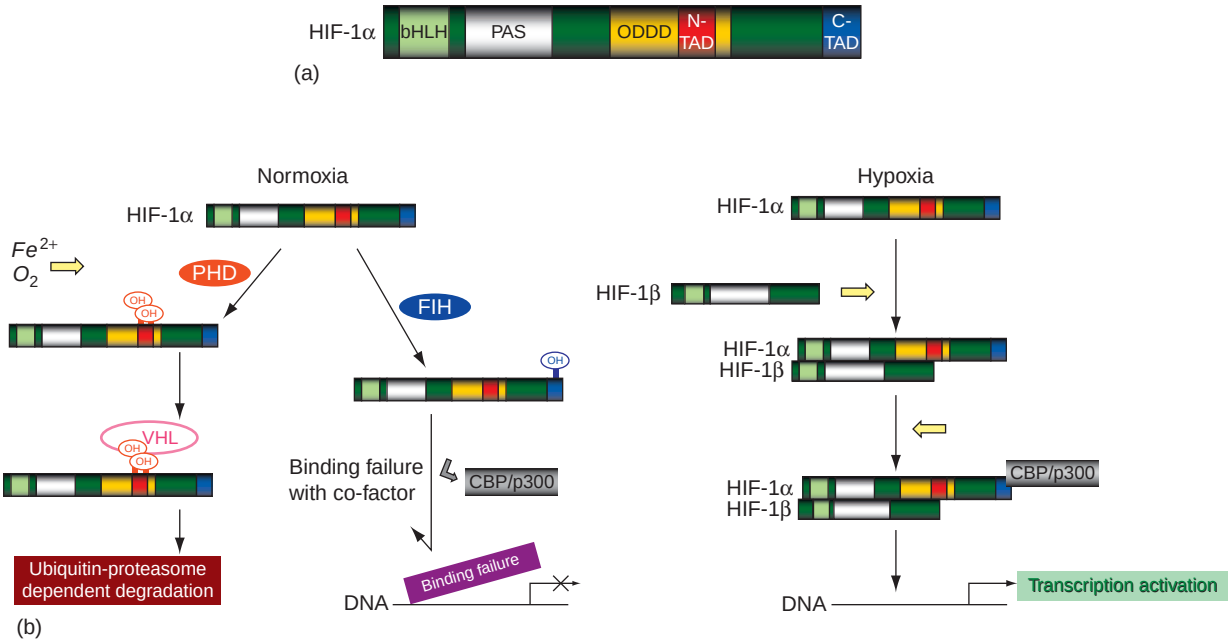

Figure 2 Regulatory systems of HIF-1α. (a) Structure of HIF-1α. (b) Molecular mechanism of HIF-1α regulation. PHD hydroxylates HIF-1α at N-TAD in the ODDD, leading to HIF-1α's ubiquitin-proteasome-dependent degradation by VHL protein. FIH-1 hydroxylates C-TAD, which inhibits HIF-1α transcriptional activity. The bHLH domain and PAS domain are required for HIF-1α dimerization to transactivate its target genes, binding with co-factors, CBP/p300. bHLH, basic helix loop helix; PAS, PER-ARNT-SIM; PHD, prolyl hydroxylase domain protein; N-TAD, N-activation domain; ODDD, oxygen-dependent degradation domain; VHL, von Hippel–Lindau; FIH-1, factor inhibiting HIF-1; C-TAD, C-activation domain.

transcriptional factor, are strictly pO_2 dependent. The K_m for O_2 in the PHD-pVHL-mediated reaction is 230–250 μM, and that in the FIH-1-mediated reaction is 90 μM. Therefore, a slight reduction in pO_2 is sufficient to inhibit the PHD-pVHL-mediated reaction, and if the hypoxia becomes more severe, the FIH-1-mediated reaction is inhibited, stabilizing HIF-1α function.

There are other pathways that regulate HIF-1α but are not dependent on pO_2. For example, the p42/p44 mitogen-activated protein kinase (MAPK) pathway suppresses the translocation of HIF-1α from the nucleus to the cytosol by phosphorylating HIF-1α serine residues 641 and 643. This mechanism prolongs HIF-1α's functioning as a transcription factor. A MAPK also phosphorylates a co-activator – p300 – to promote its interaction with HIF-1α. In addition, pVHL directly associates with and positively regulates the tumor suppressor p53 by inhibiting Mdm2-mediated ubiquitination, and p53 inhibits HIFs by directly binding to the ODDD of the HIF-1α subunit. p53 is induced to initiate apoptosis in response to DNA damage; thus, events following DNA damage may also regulate HIF activity.

Otherwise, HIF-1α regulation can also occur at the transcriptional level. The phosphatidylinositol 3 kinase (PI3K)/AKT signal-transduction pathway, which can be activated by insulin and by cytokines such as insulin-like growth factor (IGF)-1, promotes the transcription of HIF-1α gene.

HIFs and Angiogenic Factors

In this section, two major, potent angiogenic factors induced by hypoxia are discussed.

One of the most well-known angiogenic factors downstream of the HIFs is VEGF. VEGF (or VEGF-A) is a member of the platelet-derived growth factor (PDGF) family, molecules that function as dimeric glycoproteins. It also includes VEGF-B, VEGF-C, VEGF-D, and placental growth factor (PlGF). VEGF is a potent inducer of endothelial cell proliferation. In addition, it promotes the transcription of the *integrin V* gene. Since the selective display of integrin aVb3 and aVb5 on blood vessels guides endothelial cell migration, the induction of *integrin V* by VEGF promotes sprouting in angiogenesis.

Increased VEGF mRNA expression is reported in the human hypoxic retina in PDR. An increase in VEGF expression is strongly related to the transcriptional function of HIFs, and in addition, VEGF mRNA is stabilized by hypoxia posttranscriptionally. The hypoxia-induced RNA-stability factor, HuR protein, binds to an AU-rich element in the 3′-untranslated region (UTR) of VEGF mRNA, which extends the half-life of the VEGF mRNA 3–8 times. Moreover, HuR binds to and stabilizes HIF-1α mRNA, which also upregulates VEGF expression. Therefore, hypoxia induces VEGF through multiple pathways.

There are two homologous receptors for VEGF, VEGF receptor-1 (VEGFR-1/Flt-1) and VEGF receptor-2

(VEGFR-2/Flk-1/KDR), which are also targets of HIFs. VEGFR-1 is a target of both HIF-1α and HIF-2α, and VEGFR-2 is a target of HIF-2α. Although VEGFR-1 has a greater affinity for VEGF, VEGFR-2 induces tyrosine phosphorylation much more efficiently upon ligand binding, which, in endothelial cells, leads to mitogenesis, chemotaxis, and changes in cell morphology. The deletion of HIF-1α in endothelial cells disrupts an autocrine loop necessary for the hypoxic induction of VEGFR-2 by VEGF signaling through VEGFR-1. Disruption of the VEGF/VEGFR-1/VEGFR-2 autocrine signaling loop results in decreased endothelial cell proliferation and tube formation *in vitro*, and severely impairs tumor angiogenesis and tumor growth *in vivo*. Thus, the induction of VEGFR-2, not only of VEGFR-1, is also regulated by both HIF-1α, indirectly, and HIF-2α, directly. This positive feedback system promotes rapid and extensive angiogenesis under hypoxic conditions.

In the retina, VEGF is observed under normoxic conditions and is upregulated under hypoxic conditions in the inner nuclear layer cells, identified morphologically as Müller glial cells. VEGFR-1 is present in the retinal ganglion cells and retinal neural cells in the inner nuclear layer, and VEGFR-2 is mainly in the putative Müller glial cells and blood capillaries.

To date, six isoforms of human VEGF, which range in length from 121- to 206-amino acid residues (VEGF121–206), have been identified. Most VEGF-producing cells preferentially express VEGF121, VEGF165, and/or VEGF189. The splice variants differ in their ability to bind heparin and heparin sulfate, according to their size. The larger isoforms – VEGF189 and VEGF206 – have a high affinity for heparin and thus bind tightly to the cell surface and extracellular matrix (ECM). In contrast, the intermediate isoform, VEGF165, is moderately diffusible (up to half of it remains unbound), and the smallest isoform, VEGF121, is highly diffusible, due to a reduction in or lack of heparin-binding domains. The various isoforms of VEGF may play distinct roles during angiogenesis in the retina as well as during tumor proliferation. Diffusible VEGF165, secreted as a ~46-kDa homodimer, is the isoform responsible for inducing pathological angiogenesis. This function may partly be owing to the persistent potent downstream signaling that VEGF165 induces by binding to both VEGFR-2 and a co-receptor, one of the neuropilins (NRP1 or NRP2). The neuropilins enhance the binding of VEGF165 to VEGFR-2, and thus VEGF165's bioactivity.

Another angiogenic factor induced by hypoxia is Epo, a target of both HIF-1α and HIF-2α. Epo is a small, 30-kDa molecule that was originally reported as a regulator of erythropoiesis, but it also induces the proliferation and migration of endothelial cells. Epo mRNA is increased in the human retina with PDR where neovascularization is promoted. It is most abundant in the retinal ganglion cell and inner layers, and is expressed in vascular endothelial cells. In contrast, the Epo receptor mainly localizes to inner segments of photoreceptor cells and the region of synaptic complexes in the outer plexiform layer and, weakly, to the inner nuclear layer, as well as to the blood vessels.

HIFs and Ocular Angiogenesis

Hypoxia-induced angiogenesis is involved in diabetic retinopathy, and retinopathy of prematurity. In this section, human clinical data and experimental data that have helped to elucidate ocular angiogenesis are presented. Aiello and colleagues were the first to show, in 1994, that the VEGF is a mediating protein in retinal ischemia-induced intraocular neovascularization. The VEGF concentration was measured in ocular fluid obtained from 164 patients undergoing intraocular surgery. The 70 ocular fluid samples from patients with active PDR showed a higher VEGF concentration than the samples from patients with nonproliferative diabetic retinopathy (25 samples), quiescent PDR (41 samples), or nondiabetic patients (31 samples). The concentration of VEGF in the vitreous fluid was higher than in the aqueous fluid in 10 sample pairs obtained simultaneously from a single patient with active intraocular neovascularization. The persistently high level of VEGF in PDR has been confirmed by other research groups. In one study, the data were obtained from patients who had undergone vitrectomy for PDR. High levels of VEGF were found in the vitreous fluid collected at the time of fluid-air exchange during surgery, and several days after the primary operation.

The mechanism behind this hypoxia-induced VEGF expression in the diabetic retina has been little studied in animal models, because it is difficult to induce retinal vessel obliteration by artificial hyperglycemia. For example, in diabetic rats, acute intensive insulin therapy produces a transient worsening of the diabetic blood–retinal barrier breakdown via an HIF-1α-mediated increase in retinal VEGF expression; however, in this animal model, VEGF is induced by rapid insulin administration and not by hypoxia. Insulin-induced VEGF expression requires p38 MAPK and PI3K in this model, which may enhance HIF-1α stability and transcription. Another group showed that both a streptozotocin-induced mouse model of type 1 diabetes and the ob/ob mouse, a model of type 2 diabetes, show a high level of HIF-1α that leads to an increase in VEGF in the retina, but this effect is caused by insulin receptor substrate (IRS)-1 or 2 by binding to the insulin receptor.

There is an animal model of hypoxia-induced neovascularization associated with retinopathy of prematurity (ROP). This model is made by exposing young mice to a high pO_2 for several days to induce vessel obliteration, followed by normoxic conditions. The intra-retinal pO_2

declines just after the return to normoxic conditions – a relatively hypoxic state – but before the vessel occlusion is released, inducing HIF-1α expression in the inner nuclear layer. The HIF-1α expression profile coincides with VEGF expression, suggesting that VEGF may be a key molecule in ROP pathogenesis. However, Epo is also increased during ROP. Interestingly, Epo is not increased in HIF-2α-deficient mice following exposure to hyperoxia followed by normoxia, preventing ROP. In these mice, VEGF expression is unchanged. The article, therefore, showed that HIF-2α-induced Epo is required to induce ROP, which is compatible with the fact that HIF-2α has a higher affinity for the Epo than the VEGF promoter. It is also consistent with the finding that the HIF-1α expression in ROP models is only mildly and transiently increased, while the elevation of HIF-2α is large and rapid.

In contrast, ROP models in knockout mice of RTP801, a target of HIF-1α, show decreased levels of neovascularization. Moreover, a blockade of adenosine, which is synthesized by the HIF-1α-induced enzyme 5-nucelotidase (5 N), reduces neovascularization in ROP models, as shown by angiography. These data suggest the involvement of HIF-1α in ROP pathogenesis.

To complicate matters further, Epo is increased in the vitreous fluid of PDR patients independent of VEGF expression, suggesting that Epo is also a potent ischemia-induced angiogenic factor in the diabetic retina. These two separately proposed mechanisms of PDR and ROP generation – either by HIF-1α-induced VEGF or by HIF-2α-induced Epo – include the idea that several pathways are activated simultaneously in response to hypoxia. Further studies are required to elucidate how these multiple pathways are orchestrated to direct angiogenesis under various conditions.

The angiogenesis that occurs during development, following vasculogenesis, in which circulating or tissue-resident endothelial stem cells (angioblasts) proliferate and form the capillary plexus, may also be regulated by hypoxia. In the retina, vitreous vessels perfuse the retina during the embryonic stage; after birth they regress, and networks of vessels begin to form from the central to the peripheral retina. The pO_2 is low in the embryo, because the oxygen supply comes only from the umbilical flow, in which pO_2 is lower (up to 30 mmHg) than in the maternal venous blood flow. However, once that newborn is breathing on its own, the HIFs levels downregulate. Nonetheless, retinal vessel formation progresses in response to local gradient of pO_2 in the retina. Network of retinal astrocytes which guides vascular formation as templates during development is hypoxia sensitive. Retinal astrocytes proliferate under hypoxic condition and express HIF-1α and VEGF until they maturate to cease vascular induction in response to oxygen supply from newly formed vessels. Although oxygen may not be the only key molecule of vascular development, temporal and spatial regulation of HIFs and VEGF expression may be deeply involved in the retinal vascular development.

Recent studies have shown that anti-VEGF therapy reduces neovascularization in PDR, both in animal models and in human patients. However, as described above, VEGF is not the only regulator of angiogenesis; several other factors are also induced under hypoxic and pathologic conditions. It is not easy to completely regulate all of these factors therapeutically. Importantly, the HIF transcription factors can be regarded as master switches that regulate all oxygen-dependent retinal diseases. To date, several small-molecule inhibitors of HIF have been developed, and they are now being tested in clinical trials for the treatment of cancer-related disease. These HIF inhibitors may also be applicable to anti-angiogenic therapies for hypoxia-induced ocular diseases. Further studies are required to overcome the pathological angiogenesis.

See also: Angiogenesis in the Eye; Angiogenesis in Wound Healing; Developmental Anatomy of the Retinal and Choroidal Vasculature; Development of the Retinal Vasculature; Injury and Repair: Neovascularization; Molecular Mechanisms of Angiostasis; Pathological Retinal Angiogenesis; Retinal Vasculopathies: Diabetic Retinopathy; Retinopathy of Prematurity; Stability and Functional Integrity of New Blood Vessels; The Vascular Stem Cell.

Further Reading

Arden, G. B., Sidman, R. L., Arap, W., and Schlingemann, R. O. (2005). Spare the rod and spoil the eye. *British Journal of Ophthalmology* 89: 764–769.

Arjamaa, O. and Nikinmaa, M. (2006). Oxygen-dependent diseases in the retina: Role of hypoxia-inducible factors. *Experimental Eye Research* 83: 473–483.

Brahimi-Horn, C., Mazure, N., and Pouyssegur, J. (2005). Signalling via the hypoxia-inducible factor-1alpha requires multiple posttranslational modifications. *Cellular Signalling* 17: 1–9.

Carmeliet, P. (2005). Angiogenesis in health and disease. *Nature Medicine* 9: 653–660.

Fong, G. H. (2008). Mechanisms of adaptive angiogenesis to tissue hypoxia. *Angiogenesis* 11: 121–140.

Fruttiger, M. (2007). Development of the retinal vasculature. *Angiogenesis* 10: 77–88.

Gariano, R. F. and Gardner, T. W. (2005). Retinal angiogenesis in development and disease. *Nature* 438: 960–966.

Kvanta, A. (2006). Ocular angiogenesis: The role of growth factors. *Acta Ophthalmologica Scandinavica* 84: 282–288.

Liao, D. and Johnson, R. S. (2007). Hypoxia: A key regulator of angiogenesis in cancer. *Cancer Metastasis Reviews* 26: 281–290.

Masson, N. and Ratcliffe, P. J. (2003). HIF prolyl and asparaginyl hydroxylases in the biological response to intracellular O(2) levels. *Journal of Cell Science* 116: 3041–3049.

Robinson, C. J. and Stringer, S. E. (2001). The splice variants of vascular endothelial growth factor (VEGF) and their receptors. *Journal of Cell Science* 114: 853–865.

Walshe, T. E. and D'Amore, P. A. (2008). The role of hypoxia in vascular injury and repair. *Annual Review of Pathology* 3: 615–643.

Angiogenesis in the Eye

B Regenfuss and C Cursiefen, Friedrich-Alexander University Erlangen-Nuernberg, Erlangen, Germany

Glossary

Choroidal neovascularization – Formation of new blood vessels that are from the choroidal layer in the eye.
Hemangioblastoma – A benign tumor due to an abnormal growth of blood vessels.
Von Hippel–Lindau (VHL) disease – An inherited disorder involving the formation of tumors with abnormal growth of blood vessels.

Introduction: Angiogenesis in the Eye

The formation of new blood vessels can be achieved by two different mechanisms – angiogenesis and vasculogenesis. Both processes normally occur during embryonic development, whereas after birth most blood vessels remain in a quiescent state. Exceptions include physiological blood vessel growth in the adults during the hair cycle, during wound healing, and in the female reproductive system. Pathological blood vessel growth due to unregulated angiogenesis is associated with several disorders, including cancer, arthritis, and disorders such as corneal neovascularization, age-related macular degeneration (AMD), and diabetic retinopathy.

During embryonic development, the primary vascular plexus is established through a process called vasculogenesis. Vasculogenesis implies *de novo* blood vessel formation by differentiation of endothelial progenitor cells. From there on new blood vessels can be generated through angiogenesis, which means vessel growth is by sprouting from preexisting vasculature or by intussusception. During early development of the human fetal retina, both processes – vasculogenesis and angiogenesis – complement one another and contribute to meet the metabolic requirements of the developing retina. It has been suggested that vasculogenesis pioneers the establishment of a rudimentary vascular plexus, whereas angiogenesis provides further expansion of the vascular network and cares for increasing vessel density.

Steps of Angiogenesis

The formation of new blood vessels requires several steps comprising a degradation of the vascular basement membrane and remodeling of the extracellular matrix (ECM). Further on, endothelial cells need to proliferate and migrate in a defined manner, thereby invading the surrounding tissue and forming capillary-like tubes. Recent data suggest sprouting angiogenesis as a guided process with endothelial cells fulfilling specialized tasks.

Vessel vasodilatation and degradation of the ECM

One of the earliest steps in new blood vessel formation is vasodilatation, mainly effected by nitric oxide (NO), which itself can induce transcription of VEGF by endothelial cells. Vascular permeability factor (VPF) can increase vessel permeability and induce vascular leakage; thereby plasma proteins (such as fibrin/fibrinogen, and plasma-clotting proteins) can extravasate and form a fibrin gel, which serves as a temporary matrix for endothelial cell migration. To prevent excessive loss of plasma proteins, the organism has to provide mechanisms to regulate vascular permeability. Angiopoietin-1 (Ang1), a ligand for the endothelial receptor Tie-2 protects adult vessels from leakage. Ang1 and VEGF function together during vascular development and it is suggested that the coordinated action of Ang1 and VEGF contributes to vessel integrity in the adult.

For degrading the ECM, a prerequisite for endothelial cells to migrate, many proteolytic enzymes are necessary. Matrix metalloproteinases (MMPs) are thought to be primarily responsible for degrading ECM components and structures of the basement membrane. Their expression can be induced by growth factors, cytokines, interactions with the ECM, and is also regulated at the transcriptional and post-transcriptional levels. Both, MMP2 and MMP9 (gelatinase A and gelatinase B, respectively) can degrade collagen in the vascular basement membrane. The proteolytic activity of MMPs is controlled precisely and can be inhibited by endogenous factors such as tissue inhibitors of metalloproteinases (TIMPs). Besides their important role in degrading ECM components, MMPs are also involved in different pro- and antiangiogenic processes.

Endothelial cell proliferation, migration, and formation of tubular structures

After overcoming the ECM and loosening the endothelial cell–cell and cell–matrix adhesions, the endothelial cells proliferate and migrate to the chemotactic stimulus. Several factors, such as VEGF, basic fibroblast growth factor (bFGF), angiopoietins, and chemokines including monocyte chemotactic protein-1 (MCP-1) are involved in this process.

Endothelial cells that migrate to the ECM subsequently assemble as tubular structures whose diameter is regulated by several factors: for example, by different

isoforms of VEGF or through an interplay between VEGF and Ang1. Furthermore, endothelial cells can fuse with other existing vessels to form new ones and develop numerous cell–cell junctions. During further maturation of the vascular network, the endothelial cells differentiate to meet the local requirements due to specific tissues. To complete the maturation, a vascular basement membrane is deposited and periendothelial cells are recruited to stabilize the vessels by inhibiting endothelial cell proliferation and migration. The crucial role of pericytes and their interactions with endothelial cells becomes obvious, as intact pericyte–endothelial associations prevent vessels from regressing and aberrant remodeling. Additionally, activated transforming growth factor-β (TGF-β) produced in co-cultures of endothelial cells and pericytes inhibits further proliferation of endothelial cells and stabilizes the nascent vessels.

Corneal Angiogenesis

The cornea, the transparent window of the eye, normally is completely devoid of blood and lymph vessels, which is an indispensable prerequisite for good vision. Actively maintaining this avascularity, even under inflammatory or other pro-angiogenic conditions, is known as corneal angiogenic privilege. Deprivation of this privilege can lead to corneal neovascularization and to severe vision-threatening events. Therefore, angiogenic privilege is evolutionarily highly conserved and redundantly regulated by different molecular mechanisms, which are not completely elucidated to date. Corneal avascularity is already present during intrauterine development, at least from the gestational age of 17 weeks, suggesting that the cornea primarily is avascular and not as a result of regression of already existing vessels. An important mechanism for maintaining avascularity is the expression of vascular endothelial growth factor receptor-3 (VEGFR-3) on normal human corneal epithelial cells, where it can act as a decoy receptor to bind VEGF-C. VEGFR-3 is able to bind and neutralize pro-angiogenic molecules, thus inhibiting neovascularization in the limbus. Similarly, the soluble form of VEGFR-1 expressed in the cornea is believed to function as an endogenous VEGF-A trap, thereby inhibiting new vessel growth. As the angiogenic privilege is redundantly organized, a deficiency of a single antiangiogenic factor such as thrombospondin-1 (TSP-1) or TSP-2 does not result in a breakdown of the angiogenic privilege, at least during embryonic development. Nevertheless, the angiogenic privilege can be overcome and corneal neovascularization can occur (e.g., during severe inflammation). Neovascularization is induced by an imbalance of pro- and antiangiogenic molecules caused by upregulation of the pro-angiogenic factors and a downregulation of the antiangiogenic ones, thereby tilting the balance toward pro-angiogenic factors. Corneal neovascularization as a consequence of a temporary inflammatory stimulus (e.g., by placing sutures in the cornea of mice) seems to proceed in a defined manner. Initially, a parallel outgrowth of blood and lymphatic vessels occurs, both outgoing from the limbal vascular arcades. The outgrowth peaks around day 14 and is followed by vessel regression after removing the inflammatory stimulus, whereas lymphatic vessels regress earlier than blood vessels.

Angiogenic and Antiangiogenic Molecules

Several angiogenic and antiangiogenic molecules have been identified in the cornea over the years and are involved in corneal neovascularization. These include VEGFs, fibroblast growth factors (FGFs), MMPs, angiostatin, endostatin, TSPs, and pigment epithelium-derived factor (PEDF).

The VEGF growth factor family currently consists of five members: VEGF/VEGF-A, placental growth factor (PlGF), VEGF-B, VEGF-C, and VEGF-D, VEGF-A exists in five different isoforms, namely $VEGF_{115}$, $VEGF_{121}$, $VEGF_{165}$, $VEGF_{189}$, and $VEGF_{206}$ and are alternative splicing variants. VEGF-A can be released during hypoxia or inflammation and is upregulated in inflamed and vascularized human corneas. VEGF acts by binding to its cognate receptors VEGFR-1 and VEGFR-2 and stimulates endothelial cell proliferation and migration and also microvascular leakage, thereby promoting angiogenesis. Genetic polymorphism in the VEGF gene is implicated in eye diseases such as neovascular AMD and diabetic retinopathy. Furthermore, VEGF was suggested to induce not only hem-but also lymph-angiogenesis in an indirect manner through macrophage recruitment, which itself can release lymphangiogenic growth factors such as VEGF-C and VEGF-D.

VEGF-C and VEGF-D are the major lymphangiogenic growth factors with corresponding receptors VEGFR-2 and VEGFR-3, present on endothelial cells. VEGF-C plays a decisive role during lymphangiogenic development: homozygote as well as heterozygote VEGF-C-lacking mice were demonstrated to have severe defects in the formation of lymphatic vessels. Furthermore, VEGF-C is critically involved in corneal neovascularization and was also shown to promote angiogenesis *in vivo*. In its fully processed form, VEGF-C increases vascular permeability, migration, and proliferation of endothelial cells. *In vitro*, it stimulates migration of cultured endothelial cells.

bFGF/FGF-2 and acidic FGF (aFGF) belong to the FGF family. Their expression has been demonstrated immunohistochemically in the outer retina of rat and mouse. bFGF and aFGF seem to be involved in the development of choroidal neovascularization (CNV): both molecules are found to be expressed in retinal pigment epithelial cells from choroidal neovascular membranes from patients with AMD, but only little immunoreactivity for the growth factors was found in retinal pigment epithelial

cells from healthy eyes. As mice with a disruption of the bFGF-coding gene still can develop CNV, it is suggested that bFGF plays more of an indirect role in initiation of neovascularization and interacts with the signal transduction pathways of VEGF. Consistent with this fact, bFGF was found to be co-localized with VEGF in cells of epiretinal and choroidal neovascular membranes. To date, bFGF was analyzed in several corneal neovascularization models and was recently demonstrated to induce angiogenesis as well as lymphangiogenesis *in vivo* in a mouse corneal micropocket assay. Lymphangiogenesis was mediated by bFGF in an indirect way via VEGFR-3 and was suppressed after inhibition of VEGFR-3 signaling with antiVEGFR-3 antibodies.

Thrombospondins (TSPs) currently comprise a group of five multidomain extracellular glycoproteins that are involved in cell–cell or cell–matrix interactions. In this family, TSP-1, TSP-2, and TSP-5 are studied in detail, whereas only little is known about TSP-3 and TSP-4. TSP-1 was one of the first molecules shown to have an antiangiogenic activity. Its antiangiogenic activity was first observed in 1990. It was shown that a purified factor from baby hamster kidney (BHK) cells, similar to a fragment of the platelet and matrix protein thrombospondin, inhibited bFGF-induced corneal neovascularization. Since then, the impact of TSP-1 on angiogenesis has clearly been demonstrated in several *in vitro* and *in vivo* models. *In vitro* TSP-1 inhibits adhesion, proliferation, and tube formation of cultured endothelial cells and is implicated in inducing apoptosis in endothelial cells. *In vivo*, TSP-1 suppresses neovascularization in the chick chorioallantoic membrane (CAM) assay. TSP-2 is closely related to TSP-1 in its structure and amino acid identity and shows some similar properties, for example, an inhibitory effect on migration and proliferation on endothelial cells. Although TSP-1 and TSP-2 are the most similar in the TSP family and share such inhibitory functions, they differ significantly in promoter regulation and their expression patterns. In the eye, TSP-1 plays an important role in induction of immune deviation in the anterior chamber and thus contributes to the immune privilege of the eye. Furthermore, both TSP-1 and TSP-2 were shown to suppress corneal neovascularization in response to an inflammatory insult with a greater effect for TSP-1. In the case of developmental iris angiogenesis, a lack of TSP-1, TSP-2, or both leads to a significantly increased iris vessel density, with a more prominent role for TSP-2.

Diabetic Retinopathy and Retinal Angiogenesis

Diabetic retinopathy is one of the leading causes of blindness in Europe and North America. It is predominantly denoted to progressive vascular occlusion and increased vascular permeability and often leads to pathological neovascularization in the retina and the vitreous. Early stages of diabetic retinopathy are histologically characterized by the loss of pericytes from retinal capillaries and the formation of microaneurysm.

The mechanism of pericyte loss is still unclear but it might be caused by the accumulation of toxic products such as the sugar alcohol sorbitol and advanced glycation end products (the so-called AGEs) within the pericytes. An alternative hypothesis refers to an active elimination mechanism of the pericytes by upregulation of Ang-2 due to hyperglycemia. Recent data suggest that pericyte loss is due to pericyte migration, regulated by interactions of the Ang/Tie-2 system. The pericytes seem to control endothelial cell proliferation by releasing TGF-β. The pericyte drop-out leads to a disappearance of endothelial cells and subsequently to nonperfused acellular capillaries. Acellular capillaries characteristically can be found in histological sections of the ischemic retina.

Microaneurysms, one of the first clinical findings indicating a loss of pericytes, are mainly detected in hypoxic areas of occluded and unperfused capillaries (**Figure 1**). Hypoxia in diabetic retinopathy can occur due to several reasons including a thickening of the basement membrane, which impedes the diffusion of oxygen. Furthermore, the nonenzymatic glycosylation of membrane proteins of erythrocytes reduces cell plasticity and leads subsequently to an increased viscosity of the blood. Due to increased viscosity of the blood, the risk for thrombosis formation increases and can cause a lower perfusion and occlusion of the capillaries. Enduring retinal hypoxia can induce

Figure 1 Fluorescein angiography of diabetic retinopathy. Loss of pericytes leads to weak capillary walls and can result in microaneurysms, which are one of the first detectable signs in diabetic retinopathy (arrows).

neovascularization of the retina and the vitreous, whereas the extent of nonperfusion in the retina seems to be associated with the extent of neovascularization. Thus, VEGF plays a pivotal role in mediating the formation of the new blood vessels due to ischemia. *In vitro* studies have shown that VEGF mRNA is upregulated in cell cultures exposed to hypoxic conditions. Furthermore, VPF might be responsible for the fragility and increased permeability of the newly formed vessels. Due to the malformation of the proliferating vessels, their ingrowths can result in hemorrhage in the vitreous and thus leads to a compromised vision.

Central Retinal Vein Occlusion and Retinal Angiogenesis

Central retinal vein occlusion (CRVO), a common retinal vascular disorder, can be classified by means of the extent of retinal ischemia. According to the Central Vein Occlusion Study Group (CVOSG), it can be differentiated into the nonischemic and the ischemic CRVO, which are the milder and the more severe forms, respectively. Complications of the ischemic form are macular edema and neovascular glaucoma caused by iris neovascularization (Rubeosis iridis), which often results in vision loss. Due to an occlusion of the central retinal vein by a thrombus, the venous blood flow decreases and leads subsequently to an ischemic damage of circumjacent regions. It seems that VEGF is implicated in the pathophysiology of CRVOs. Several factors do support this hypothesis:

1. it was shown that cultured human retinal pigment epithelial cells synthesize and release VEGF;
2. hypoxia was shown to increase the level of VEGF mRNA in retinal cells;
3. furthermore, after induction of retinal ischemia in an animal model of retinal vein occlusion, upregulation of VEGF mRNA could only be found in the ischemic region; and
4. an upregulation of VEGF mRNA was also detected in the retinas of patients with CRVO.

Several studies have shown that excess VEGF application to tissues leads to the formation of leaky and hemorrhagic vessels, which can result in inflammatory responses with tissue swelling and edema. Capillary leakage induced by VEGF might be a pathogenic mechanism that contributes to the formation of macular edema in CRVO.

AMD and choroidal neovascularization

AMD is one of the main causes for vision disability among persons over 60 years of age. A metabolic disorder of the photoreceptors and the retinal pigment epithelial layer leads to the formation of yellow–white deposits (=drusen) that accumulate in the subretinal pigment epithelium of the eye (Figure 2). During late stages of the dry (nonexudative) form of AMD, a geographic atrophy can occur. In the case of the second form of AMD – wet (exudative) AMD – a detachment of the retinal pigment epithelium and CNV are significant. Clinically, visible signs during CNV are hemorrhage, retinal exudates, and serous or hemorrhagic pigment epithelial detachment. It is believed that the occurrence of pathological choroidal angiogenesis is due to the growth of new blood vessels from preexisting choroidal capillaries (angiogenesis) consequent to changes in Bruch's membrane. After rupturing the Bruch's membrane, choroidal vessels consequently grow in the subretinal or subpigmental epithelial space. Risk factors for the development of AMD include age, genetic dispositions, smoking, and other environmental factors.

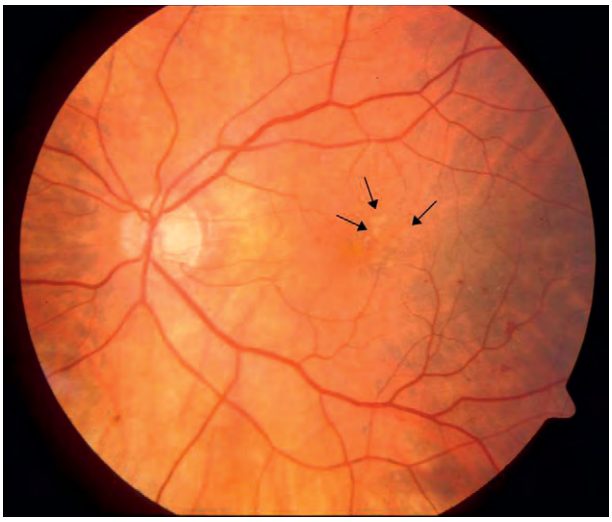

Figure 2 Central fundus photograph of AMD. Central fundus photograph with yellow–white deposits (=drusen, arrows) accumulating in the subretinal pigment epithelium due to a metabolic disorder of the photoreceptors and the retinal pigment epithelial layer.

Choroidal Neovascularization

Different factors seem to contribute to the pathogenesis of CNV, including hypoxia, inflammation, thickening of the Bruch's membrane, and angiogenic molecules, especially VEGF. As mentioned before, cultured human retinal pigment epithelial cells produce and secrete VEGF. Moreover, VEGF mRNA upregulation can be due to hypoxia.

Hypoxia can be induced in several ways. The eyes of pigeons show reduced thickness of the choroidea and decreased choroidal blood flow with increasing age.

Morphometric studies have revealed a thinning of the choroid in human eyes with increasing age. Another study showed a decrease in pulsatile ocular blood flow (a reliable parameter for evaluating chorioretinal circulation) occurring in aged human eyes. Furthermore, there is evidence that the choroidal blood flow in patients with AMD is modified. Due to the insufficient blood supply, a lower perfusion could result in hypoxia. Subsequently hypoxic conditions are known to upregulate VEGF mRNA, which can lead to a VEGF-induced choroidal angiogenesis. Lipid deposits within and around the Bruch's membrane and a thickening of the latter might also contribute to a disordered metabolism and reduced oxygen supply, which, in turn, can directly upregulate VEGF.

Chronic inflammatory processes, due to deposits in the Bruch's membrane, might also contribute to the development of AMD, which are associated with disorders of the complement regulatory system.

Besides VEGF, other molecules seem to be implicated in the pathogenesis of CNV during AMD. These include MMPs, especially MMP-2 and MMP-9, endostatin, PEDF, the angiopoietins, and NO. Nevertheless, the precise pathogenic mechanisms for the induction and the development of CNV are not completely elucidated to date.

Tumor Angiogenesis in the Eye

Since Judah Folkman first published his hypothesis in the early 1970s that tumor growth is depended on angiogenesis and the recruitment of capillary blood vessels, an extensive research has addressed this topic. A prerequisite for the development of new blood vessels is a shift of the balance between pro- and antiangiogenic molecules toward the pro-angiogenic ones (angiogenic switch). Thereafter, activated endothelial cells migrate to the tumor, proliferate, and form a new vessel network. Tumor neovascularization is a critical factor not only for tumor growth by supplying it with nutrients and oxygen, but also for tumor malignancy and metastasis, by providing an exit route for the tumor cells (**Figure 3**). Several pro-angiogenic molecules, including bFGF, PDGF, and VEGF, are produced by tumor cells. VEGF, a very potent inducer of neovascularization, is upregulated in many tumors and plays a pivotal role in tumor angiogenesis. Indeed, vascularization of microtumors in mice can be completely inhibited after treatment with a neutralizing antiVEGF antibody.

High levels of VEGF and VEGFR can be detected in the eyes of patients with retinoblastoma and choroidal melanoma. VEGF-targeted RNA-interference can suppress retinoblastoma growth and tumor angiogenesis.

The production of pro-angiogenic factors, like VEGF, by intraocular tumors is suggested to be a cause for breaking down the blood–retina barrier and subsequently for the formation of new vessels. VEGF also seems to be critically involved in the progression of tumors due to von Hippel–Lindau (VHL) disease, a hereditary cancer syndrome. Affected patients develop highly vascularized neoplasms called hemangioblastomas due to a germline mutation in the VHL tumor suppressor gene. An antiangiogenic therapy with VEGF-neutralizing antibodies or VEGFR inhibitors is an interesting tool for therapeutic treatments of ocular tumors.

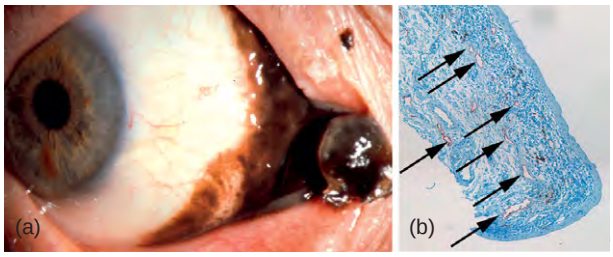

Figure 3 Malignant melanoma: (a) malignant melanoma of the conjunctiva; (b) immunohistochemistry shows various lymphatic tumor-associated lymphatic vessels (lymphatic vessels stained in red with LYVE-1 antibody, specific for lymphatic endothelium: arrows). Through these lymphatic vessels lymphatic metastasis in the regional lymph nodes can occur. Reproduced from Bock, F., König, Y., Dietrich, T., et al. (2007). Inhibition of angiogenesis in the anterior chamber of the eye/Antiangiogene Therapie am vorderen Augenabschnitt. *Ophthalmologe* 104(4):336–344, with permission from Springer Science + Business Media.

See also: Concept of Angiogenic Privilege; The Immunological Aspects of Aqueous Humor Turnover.

Further Reading

Ambati, J., Ambati, B. K., Yoo, S. H., Ianchulev, S., and Adamis, A. P. (2003). Age-related macular degeneration: Etiology, pathogenesis, and therapeutic strategies. *Survey of Ophthalmology* 48: 257–293.

Armstrong, L. C. and Bornstein, P. (2003). Thrombospondins 1 and 2 function as inhibitors of angiogenesis. *Matrix Biology* 22: 63–71.

Cai, J. and Boulton, M. (2002). The pathogenesis of diabetic retinopathy: Old concepts and new questions. *Eye* 16: 242–260.

Cai, J., Kehoe, O., Smith, G. M., Hykin, P., and Boulton, M. E. (2008). The angiopoietin/Tie-2 system regulates pericyte survival and recruitment in diabetic retinopathy. *Investigative Ophthalmology and Visual Science* 49: 2163–2171.

Campochiaro, P. A. (2000). Retinal and choroidal neovascularization. *Journal of Cellular Physiology* 184: 301–310.

Churchill, A. J., Carter, J. G., Lovell, H. C., et al. (2006). VEGF polymorphisms are associated with neovascular age-related macular degeneration. *Human Molecular Genetics* 15: 2955–2961.

Churchill, A. J., Carter, J. G., Ramsden, C., et al. (2008). VEGF polymorphisms are associated with severity of diabetic retinopathy. *Investigative Ophthalmology and Visual Science* 49: 3611–3616.

Conway, E. M., Collen, D., and Carmeliet, P. (2001). Molecular mechanisms of blood vessel growth. *Cardiovascular Research* 49: 507–521.

Cursiefen, C. and Kruse, F. E. (2005). New aspects of corneal angiogenesis. In: Krieglstein, G. K., Weinreb, R. N., Reinhard, T., and Larkin, F. (eds.) *Essentials in Ophthalmology, Cornea and External Eye*, pp. 83–100. New York: Springer.

Grisanti, S. and Tatar, O. (2008). The role of vascular endothelial growth factor and other endogenous interplayers in age-related macular degeneration. *Progress in Retinal and Eye Research* 27: 372–390.

Hammes, H. P. (2005). Pericytes and the pathogenesis of diabetic retinopathy. *Hormone and Metabolic Research* 37(supplement 1): 39–43.

Hughes, S., Yang, H., and Chan-Ling, T. (2000). Vascularization of the human fetal retina: Roles of vasculogenesis and angiogenesis. *Investigative Ophthalmology and Visual Science* 41: 1217–1228.

Pfister, F., Feng, Y., vom Hagen, F., et al. (2008). Pericyte migration: A novel mechanism of pericyte loss in experimental diabetic retinopathy. *Diabetes* 57: 2495–2502.

Shweiki, D., Itin, A., Soffer, D., and Keshet, E. (1992). Vascular endothelial growth factor induced by hypoxia may mediate hypoxia-initiated angiogenesis. *Nature* 359: 843–845.

Yancopoulos, G. D., Davis, S., Gale, N. W., et al. (2000). Vascular-specific growth factors and blood vessel formation. *Nature* 407: 242–248.

Zhang, S. X. and Ma, J. X. (2007). Ocular neovascularization: Implication of endogenous angiogenic inhibitors and potential therapy. *Progress in Retinal and Eye Research* 26: 1–37.

Angiogenesis in Wound Healing

Z-J Liu and O C Velazquez, University of Miami, Miami, FL, USA

Glossary

Angiogenesis – A physiological process involving the growth of new blood vessels from preexisting vessels.
Endothelial cells – The type of cells forming the interior surface of blood vessels; they create an interface between circulating blood in the lumen and the rest of the vessel wall.
Endothelial progenitor cells – They are bone marrow stem cell-derived cells that have the ability to differentiate into endothelial cells. EPCs exist in bone marrow, peripheral blood, umbilical blood, and fetal liver.
Neovascularization – The formation of new blood vessels by either angiogenesis and/or vasculogenesis.
Vasculogenesis – Formation of vascular structures from angioblasts or circulating endothelial progenitor cells, which proliferate into *de novo* blood vessels.
Wound healing – Cutaneous wound healing is the body's natural process of regenerating dermal and epidermal tissue.

Introduction

Angiogenesis, a process of formation of new blood vessels, is essential for wound repair. Healing of any skin wound other than the most superficial cannot occur without angiogenesis. The new blood vessels provide nutrients and oxygen to support cell growth and tissue repair, promote granulation matrix formation, and facilitate the clearance of debris in injured tissue. Neovascularization is a complex multistep process including the creation of pro-angiogenic factors in the injured tissue which stimulate the local existing blood vessels, the release of proteases, such as matrix metalloproteinases (MMPs), from activated endothelial cells with subsequent degradation of the basement membrane surrounding the blood vessel, formation of tip cells and sprouting, migration of endothelial cells into the interstitial space, proliferation of endothelial cells, and remodeling into new blood vessels. Recently, it has been proven that endothelial progenitor cells (EPCs) are also involved and, in fact, play a critical role in neovascularization. EPCs, derived from bone marrow stem cells, can be released into circulation, recruited into wound lesion, and undergo *in situ* differentiation to become matured endothelial cells and contribute to neovascularization. The processes mentioned above are dynamic and tightly regulated in a spatial and temporal manner by cell–cell, cell–extracellular matrix (ECM), and cell–soluble factor interactions, leading finally to a functional vascular network formation. A better understanding of the underlying mechanisms in neovascularization will bring new insights into wound-related diseases and offer novel therapeutic options in the treatment of wounds, in particular, chronic and nonhealing wounds, and would thus have tremendous benefit to both individual patients and society.

Cellular and Molecular Basis of Wound Healing

The healing of a wound requires a well-orchestrated integration of the complex biological and molecular events of cell migration, proliferation, differentiation, and ECM deposition. Normal wound healing requires proper circulation, nutrition, immune status, and avoidance of negative mechanical forces. The process usually takes 3–14 days to complete and has three phases: inflammation, proliferation, and remodeling with wound contraction (**Figure 1**). During the inflammatory phase, neutrophils and macrophages appear in the wounded area to phagocytize bacteria and debris. A functioning immune system and adequate supply of growth factors are necessary in this phase of wound healing. In the proliferative phase, fibroblasts produce a collagen matrix, new blood vessels invade the forming granulation tissue, and epidermal cells migrate across the wound surface to close the breach. During the remodeling phase, fibroblasts reorganize the collagen matrix and ultimately assume a myofibroblast phenotype to effect connective tissue compaction and wound contraction. Wounds gain about 80% of their final strength in the first 3 weeks of normal wound healing through collagen deposition, remodeling, and wound contraction. Each phase has unique cellular and substance constituents without which it cannot progress normally. A large variety of factors may influence any part of wound healing, including local factors (growth factors, edema and ischemia, low oxygen tension, and infection), regional factors (arterial insufficiency, venous insufficiency, and neuropathy), systemic factors (inadequate perfusion and metabolic disease), and other miscellaneous factors, such as nutritional state, preexisting

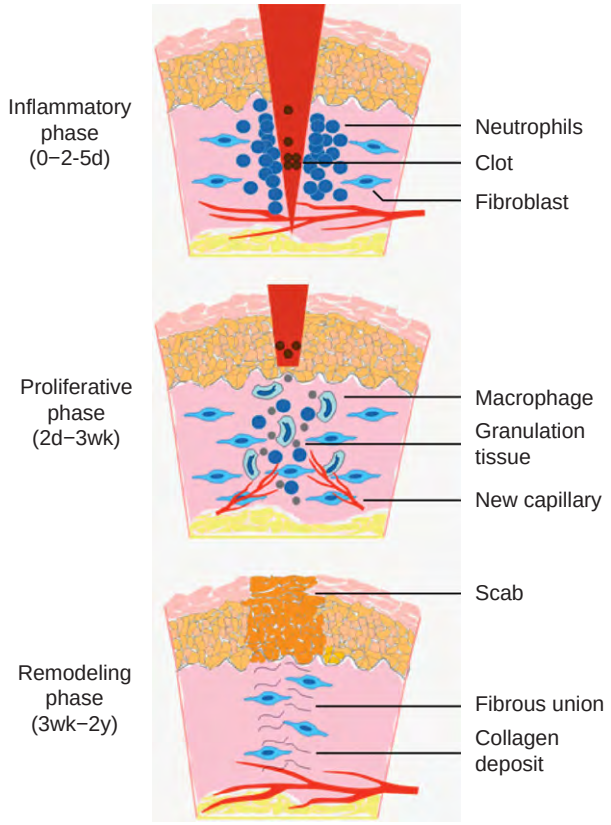

Figure 1 Schematic illustration of the three phases of acute wound healing. (1) Inflammatory phase: immediate to a few days. Immediately after the process of hemostasis, including vasoconstriction, platelet aggregation and thromboplastin production, injured tissue undergoes vasodilation and immune cells infiltrate and perform phagocytosis. (2) Proliferative phase: a few days to a few weeks. Fibroblasts lay a bed of collagen and fill the defect while new capillaries grow (granulation). Injured tissue undergoes contraction. Wound edges pull together to reduce the defect. Afterwards, epithelial cells migrate from the point of origin in all directions and cross the moist surface (epithelialization). (3) Remodeling phase: a few weeks to 2 years. During this phase, new collagen is formed and deposited, which increases tensile strength.

illnesses, exposure to radiation therapy, and smoking. When any of the components of the wound healing process is compromised, healing may be delayed. Chronic wounds are those that have failed to follow this sequence and do not achieve a sustained anatomic and functional result. Usually, a chronic wound requires a prolonged time (>8 weeks) to heal, or recurs, or even does not heal. The most prevalent forms of chronic wounds are leg ulcers caused by vascular insufficiency, and foot ulcerations associated with diabetic complications. It has been estimated that up to 2 million Americans have nonhealing lower extremity wounds. The economic costs associated with chronic wound are enormous and include hospital costs, disability, decreased productivity, and loss of independence.

Table 1 Pro-angiogenic and anti-angiogenic factors of angiogenesis

Pro-angiogenic factors	*Anti-angiogenic factors*
VEGF	Angiostatin
Angiopoietin	Anti-angiogenic anti-thrombin III
FGF	Endostatin (collagen XII fragment)
IL-8	Fibronectin fragment
PDGF-BB	Plasminogen activator inhibitor
Angiogenin	TSP-1
TGF-β	Retinoids

Abbreviations: VEGF, vascular endothelial growth factor; FGF, fibroblast growth factor; IL-8, interleukin-8; FGF, fibroblast growth factor; PDGF-BB, platelet-derived growth factor-BB; TGF, transforming growth factor; TSP-1, thrombospondin-1.

Molecular and Cellular Regulators of Wound Angiogenesis

Angiogenic Factors

Angiogenesis is tightly controlled by a variety of soluble factors and is determined by balance between pro-angiogenic and anti-angiogenic factors. In the physiological condition, the activity of inducers and inhibitors of angiogenesis maintains it in balance. When angiogenic factors are produced in excess of angiogenesis inhibitors, the balance is tipped in favor of blood vessel growth. When inhibitors are present in excess of stimulators, angiogenesis is stopped. Table 1 lists some most potent pro-angiogenic and anti-angiogenic factors.

Injury is the initiating factor with bleeding and microvascular damage. The clotting cascade is activated and injured vessels contract keeping blood loss to a minimum. Inflammatory cells are recruited rapidly, releasing vasoactive compounds that contribute to the leak of plasma and proteins into the wound allowing further effector cells to enter. Leukocytes secrete interleukin (IL)-8 and macrophage chemoattractant protein (MCP)-1. Platelets and monocytes can both release vascular endothelial growth factor (VEGF) when activated. Platelets also release platelet-derived growth factor (PDGF)-BB and transforming growth factor (TGF)-β (promoting angiogenesis and attracting macrophages), while monocytes release TGF-β and basic fibroblast growth factor (FGF). All these factors contribute to angiogenesis in healing wounds.

The angiogenic factors bind to specific receptors located on the endothelial cells of nearby preexisting blood vessels. Once angiogenic factors bind to their receptors, the endothelial cells become activated. Signals are sent from the cell's surface to the nucleus. The endothelial cell's machinery begins to produce new molecules including enzymes.

One of the most specific and critical regulators of angiogenesis is VEGF, which regulates endothelial

proliferation, permeability, and survival. VEGF family includes six members: VEGF-A (VEGF), -B, -C, -D, -E, and placenta growth factor (PLGF). VEGF stimulates vascular endothelial cells through VEGF receptors (VEGFRs). VEGFRs include VEGFR-1 (Flt-1), VEGFR-2 (KDR/Flk-1), and VEGFR-3 (Flt-4). VEGF associates VEGFR-1 and VEGFR-2, whereas VEGF-C and -D bind to VEGFR-2 and VEGFR-3, and primarily affect lymphangiogenesis. VEGF is a unique potent angiogenic factor that stimulates capillary formation *in vivo* and has direct mitogenic actions to endothelial cells. Human VEGF has at least four structurally related isoforms, $VEGF_{121}$, $VEGF_{165}$, $VEGF_{189}$, and $VEGF_{206}$. Of these, $VEGF_{165}$ has the most potent biological activity and is the most abundant subtype *in vivo*. VEGF is secreted by many cell types, and its expression is regulated by a number of growth factors and cytokines. For example, interleukin 1-β, PDGF-BB, and TGF-β stimulate VEGF production by smooth muscle cells.

It is known that VEGF acts on its receptor VEGFR-2, which stimulates increased intracellular calcium through phospholipase C activation and production of diacylglycerol and inositoltrisphosphate. This increase in intracellular calcium can then activate nitric oxygen synthase (NOS) through a calcium/calmodulin-dependent process, and the NO diffuses across the endothelial cell wall into the smooth muscle cells of the arterioles to result in muscle relaxation and vasodilatation. This results in increase in blood flow in injured tissues. This increase in blood flow is likely to have a significant effect on oxygen and glucose delivery and of course removal of CO_2, H^+, and lactate.

When sufficient neovascularization has occurred, angiogenic factors are downregulated or the local concentration of inhibitors increases. As a result, the endothelial cells become quiescent, and the vessels remain or regress if no longer needed.

Extracellular Matrix

The angiogenic response in the microvasculature is associated with changes in cellular adhesive interactions between adjacent endothelial cells, stromal cells, and surrounding ECM. In the process of active neovascularization, activated endothelial cells reorganize their cytoskeleton, express cell surface adhesion molecules such as integrins and selectins, secrete proteolytic enzymes, and remodel their adjacent ECM. The ECM is a complex mixture of matrix molecules, including the glycoproteins, fibronectin (FN), collagens, laminins, and proteoglycans. The ECM not only provides scaffolds for cellular support, but also participates in regulating wound angiogenesis by direct transduction of signals pivotal for cellular processes primarily via integrin interactions in concert with growth factor activation.

The interactions of endothelial cells with ECM involve diverse ECM molecules, which differ to some degree among vessels and certainly differ depending on the state of the vessel (quiescent, injured, or angiogenic). In resting vessels, endothelial cells are in contact with a basement membrane, which they share with pericytes in the case of small vessels. Vascular basement membranes contain laminins (predominantly laminin-8/laminin411 and laminin-10/laminin511), type IV collagens, perlecan, nidogens, collagen XVIII, and von Willebrand factor (vWF). The endothelial cells and pericytes in mature, quiescent vessels are nonproliferative and stably attached to the basement membrane. During vascular remodeling and angiogenesis, the quiescent endothelial layer becomes activated and endothelial cells breach the basement membrane and migrate into surrounding tissue containing different complements of ECM proteins, which can include collagens and FNs in interstitial ECM or fibrinogen and FNs in provisional matrices generated after vascular injury and during wound healing. Other ECM proteins encountered by endothelial cells and pericytes include vitronectin, thrombospondins, and tenascins. The effects of ECM on vascular cells therefore differ greatly, depending on the state of the vessel and, very probably, to a lesser degree among different vessels. It is evident that the switch from quiescence (adherent to laminins and probably other basement membrane proteins, stably assembled into tubes) to the angiogenic state (migratory, invasive, tube remodeling, and formation) involves marked changes in the cell–ECM interactions. It is also evident that different sorts of angiogenesis probably involve different forms of ECM and therefore different cell–ECM interactions.

Each of the many ECM proteins of vascular basement membranes or in the ECM during angiogenic sprouting has cell surface receptors, predominantly of the integrin family, although other ECM receptors (e.g., dystroglycan, GPIb, GPVI, and DDR collagen receptors) are also known. Integrins are a family of heterodimeric transmembrane proteins comprising at least 16 α and 8 β subunits in mammals. Different combinations of single α and β subunits dimerize to form approximately 24 different receptors with distinct and often overlapping specificity for ECM proteins. Integrins are widely recognized as important molecules for the transduction of positional cues from the ECM to the intracellular signaling machinery. For example, integrin ligation induces a wide range of intracellular signaling events, including the activation of Ras, mitogen-actived protein (MAP) kinase, focal adhesion kinase (FAK), Src, Rac/Rho/cdc42 GTPases, protein kinase C (PKC), and PI3K (phosphatidylinositol 3-kinase). In addition, integrin ligation increases intracellular pH and calcium levels, inositol lipid synthesis, cyclin synthesis, and the expression of immediate early genes and promotes cell survival.

On the other hand, MMPs play important roles in degradation and remodeling of ECM, permitting

endothelial cell migration during angiogenesis. For example, MMP2 is constitutively secreted as an inactive zymogen that is activated upon need by a complex of proteins on the surface of invading cells. The activation complex consists of tissue inhibitor of matrix metalloproteinase-2 (TIMP-2), membrane type I MMP (MT1-MMP), and integrin $\alpha V\beta 3$. Cells that express integrin $\alpha V\beta 3$ on their surface are able to bind active MMP2 (aMMP2) via the c-terminal hemopexin domain, and form an invasive front that enables migration. Eventually, the binding of aMMP2 to integrin $\alpha V\beta 3$ causes autocatalytic maturation that results in degradation of aMMP2 and the generation of PEX2, the 29–32 kDa hemopexin-like fragment. PEX2 is able to bind integrin $\alpha V\beta 3$ independently and compete with MMP2, preventing cell surface activation and thereby disrupting angiogenesis.

Pericytes and Stromal Cells in Angiogenesis

In addition to soluble factors and ECM, pericytes and surrounding stromal cells are critical in regulating neovascularization as well. Generally speaking, endothelial cells make up the blood vessel framework, but their assembly and stabilization are dictated by external signals from surrounding cells.

Pericytes are vascular mural cells which are embedded in the basement membrane of microvessels and play multiple roles in angiogenesis and maintenance of blood vessel morphology and stability. The relationship between endothelium and pericyte is for each to provide the other with growth factors and cell contacts that promote mutual proliferation and survival. At growing capillary tips, sprouting endothelium degrades the basement membrane, and releases PDGF-BB. PDGF-BB ligand is tethered to cell surfaces and matrix proteins, creating a polarized concentration gradient attracting $PDGFR\beta^+$ cells to vascular endothelium. Pericytes, in turn, release VEGF, which acts as a chemotactic agent and survival factor for proliferating endothelium. Pericytes are derived by differentiation of local mesenchymal cells and myofibroblasts, as well as by proliferation of existing pericytes. A proportion of pericytes is also derived by migration from the bone marrow.

Vasculature in skin granulation tissue is physically supported by connective tissue elements elaborated by resident fibroblasts. These fibroblasts provide a unique microenvironment that facilitates and sustains the microvasculature. Fibroblasts and their activated counterpart, the myofibroblast, play a pivotal role in regulating neovascularization in the process of wound healing by secreting various soluble factors, synthesis of ECM and direct cell–cell interaction. Fibroblasts, once activated, undergo a change in phenotype from their normal relatively quiescent state in which they are involved in slow turnover of the ECM, to a proliferative and contractile phenotype termed myofibroblasts. Myofibroblasts actively produce growth factors and ECM, and display an elongated spindle shape, and express contractile α-smooth muscle actin (α-SMA) and vimentin. Myofibroblasts can either arise from the local, resident fibroblasts or from circulating mesenchymal precursors/stem cells. It has been reported that fibroblasts located at chronic wound sites have been shown to be physiologically different from adjacent fibroblasts in nonaffected sites. Therefore, modulating the function of fibroblasts in wound tissue (in particular in chronic wound tissue) can be an alternative approach for the treatment of chronic, nonhealing wound.

Neovascularization and EPC

Until recently, neovascularization was thought to arise solely from preexisting vessels (angiogenesis). However, recent studies have proven that EPC can contribute to neovascularization (vasculogenesis) as well. In 1997, Asahara and colleagues first identified circulating EPCs contributing to neovascularization. Since then, increased evidence has suggested that bone marrow-derived EPCs can functionally contribute to neovascularization during wound healing, limb ischemia, postmyocardial infarction, endothelialization of vascular grafts, atherosclerosis, retinal and lymphoid organ neovascularization, vascularization during neonatal growth, and tumor growth. It has been estimated that EPCs contribute up to 25% of endothelial cells in newly formed vessels in animal models.

Although there have been conflicting reports regarding the importance of EPCs in neovascularization, a substantial amount of study in both animals and humans has provided strong evidence for the role of EPCs in neovascularization. Particularly, a very recent study showed that notwithstanding low numbers of EPC, recruitment of these EPCs is pivotal for the progression of avascular micrometastatic tumors to lethal macrometastatic ones. The lack of consensus may be due in part to heterogeneous phenotypic definitions of EPCs. In this aspect, two recent reports have shown that the subpopulations of EPCs with distinct phenotypes give rise to different outcomes, indicating an importance in defining the correct EPCs for such studies. Overall, however, these researchers clearly demonstrated a significant contribution of EPCs to neovascularization. Other factors, such as types of ischemic models or tumors (in which the profiles of chemoattractant factors may vary), time frame of the experiment, and method of *in situ* endothelial cell identification, may also contribute to some of the reported discrepancy. In general, it is now well accepted that at the site of tissue vascularization, endothelial cells originate from both adjacent preexisting blood vessels and recruitment of EPCs.

EPCs exist in peripheral blood, umbilical blood, bone marrow, and fetal liver. Multiple markers have been used

for characterization of EPCs and matured endothelial cells. Platelet endothelial cell adhesion molecule-1 (PECAM-1/CD31), VEGFR-2, von Willebrand factor (vWF), and vascular endothelial cadherin (VE-cadherin) are commonly used for the identification of endothelial cells. The ability to take up Dil-labeled acetylated low-density lipoprotein (Dil-Ac-LDL) has been used as a marker for the identification of endothelial precursors. CD34 is a marker for both endothelial and hematopoietic progenitor cells. In humans, EPCs (but not mature endothelial cells) express AC133 (CD133), a stem cell marker with as-yet unrecognized functions. Purified populations of $CD133^{+}VEGFR\text{-}2^{+}$ EPCs proliferate *in vitro* in an anchorage-independent manner and can be induced to differentiate into mature adherent $CD133^{-}VEGFR\text{-}2^{+}$ endothelial cells. Expression of various markers is a dynamic process. It is likely that different markers are present on EPCs and matured endothelial cells at various points along their differentiation cascade from immature progenitors to mature endothelial cells. Expression of CD133 will be turned off with the maturation of endothelial cells. Until now, the corresponding marker for CD133 in murine EPCs has not yet been substantiated. Murine EPCs are characterized as $Sca\text{-}1^{+}/c\text{-}Kit^{+}/Lin^{-}/VEGFR\text{-}2^{+}/CXCR4^{+}/Tie2^{+}$. With maturation, expression of stem cell marker Sca-1 and hematopoietic marker c-Kit will be turned off.

Interestingly, EPCs are not a single type of cell population and display tremendous heterogeneity in terms of phenotype and angiogenic potential. EPCs can be classified into two subpopulations: early EPCs and late EPCs. Early EPCs display spindle shape and show peak growth at 2–3 weeks and die at 4 weeks, whereas late EPCs have cobblestone shape and appear late at 2–3 weeks, show exponential growth at 4–8 weeks, and can live up to 12 weeks. Late EPCs are different from early EPCs in the expression of VE-cadherin, VEGFR-1, VEGFR-2, and CD45. Late EPCs produce more NO, incorporate more readily into human umbilical vein endothelial cells monolayer, and form capillary tubes better than early EPCs. Early EPCs secrete angiogenic cytokines (VEGF, IL-8) more so than late EPCs during culture *in vitro*. Both types of EPCs show comparable *in vivo* vasculogenic capacity. In addition, it has been reported that early EPCs can cause the disorganization of preexisting vessels, whereas late EPCs likely constitute and orchestrate vascular tube formation.

EPCs are embedded in a microenvironment (niche) of bone marrow and can be mobilized to the circulation (**Figure 2**). Under normal conditions, the number of circulating EPCs is relatively small but is increased in response to trauma or ischemia, which mobilizes these cells from the bone marrow and allows them to proliferate. The recruitment of EPCs from the bone marrow and circulation to homing sites of neovascularization is subject to regulation by many factors, including chemokines and growth factors. The precise mechanism of EPC mobilization is not entirely elucidated and is still under investigation. Many chemokines and cytokines trigger stem/progenitor cell release by induction of MMP-9 in bone marrow and NO-mediated signaling pathways have been previously proposed to be essential for EPC mobilization. Using VEGF as a proximal stimulus, Aicher and colleagues demonstrated that endothelial NOS (eNOS) becomes activated in bone marrow stroma, NO then S-nitrosylates by paracrine mechanisms and activates MMP-9, which releases the stem cell active cytokine, soluble Kit ligand. This agent shifts endothelial progenitor and hematopoietic stem cells from a quiescent to the proliferative niche and stimulates rapid stem cell mobilization to the peripheral blood. We have recently demonstrated that hyperoxia, induced by a clinically relevant hypoerbaric oxygen therapy (HBO) therapy protocol, can significantly enhance the mobilization of EPC from the bone marrow into peripheral blood. It has been shown that in the setting of trauma and ischemia, systemic VEGF levels rise following a time course that mirrors the rise in circulating bone marrow-derived EPC. In addition to the direct integration into vessel lumen and the contribution to neovascularization, recent studies have suggested that EPCs may promote local neovascularization by secreting angiogenic growth factors in a paracrine manner. In addition to VEGF, granulocyte colony-stimulating factor (G-CSF) and stromal cell-derived factor (SDF)-1α have been demonstrated to be able to enhance EPC mobilization. SDF-1α can promote EPC homing as well. Transplantation of EPCs into ischemic tissues may emerge as a promising approach in the therapy of diseases associated with blood vessel disorders.

Therapeutic Angiogenesis in Chronic Wound Healing

Chronic wounds continue to be a major clinical problem and novel therapeutic approaches are needed. Recent advances in the field of angiogenesis have led to very promising breakthroughs in the treatment of diabetic and other types of chronic wounds. The understanding of the crucial role of growth factors in wound healing has already led to the development and regulatory approval of topically applied growth factors, particularly PDGF-BB. Greater efficiency of delivery of growth factors by gene therapy or by cell therapy is now possible and being tested.

In addition to the use of growth factors, there has also been considerable interest in the application of ECM proteins to accelerate healing of diabetic foot ulcers, including collagen and hyaluronic acid.

Cell-based therapy is a promising therapeutic option for treating patients with diabetic, nonhealing wounds.

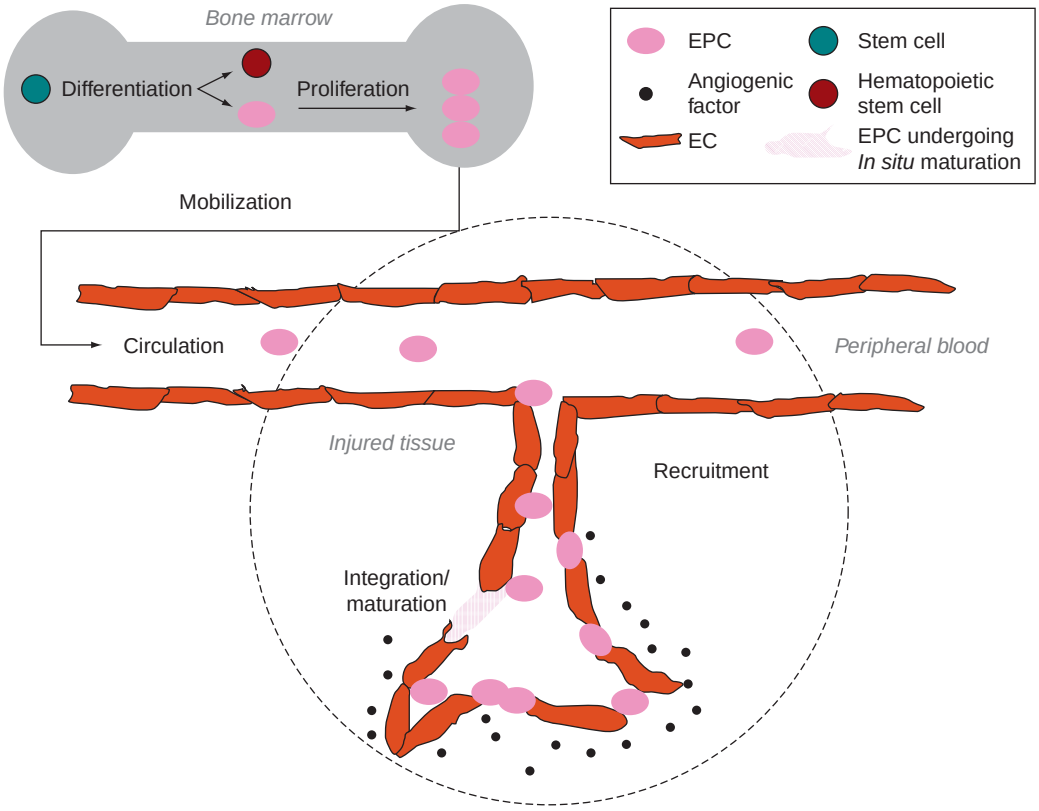

Figure 2 Overview of differentiation, mobilization, recruitment, and *in situ* maturation of endothelial progenitor cells (EPCs). Contribution of bone marrow-derived EPCs to wound healing involves multiple critical events. Bone marrow-derived EPCs are released from their niche into the circulation (mobilization). The circulating EPCs are recruited (homing) to injured tissue and contribute to neovascularization and wound healing (integration/*in situ* maturation). In addition, EPCs may contribute to neovascularization by secretion of soluble factors.

There is great interest in delivery of stem or progenitor cells, either applied topically or recruited from the circulation. Bone marrow is an enriched pool of stem and progenitor cells. Some preliminary work suggests that topically applied autologous bone marrow cells can heal human chronic wounds that are recalcitrant to other treatments, including growth factors and bioengineered skin. Of various different types of stem or progenitor cells, EPC is one type of cells which has been moved from experimental models to the clinic trials. EPC has thus far been tested in patients with acute and chronic ischemic disease and outcomes are very encouraging. A few properties, such as its endogenous, BM-derived character, ability to home to sites of pathological entities, and relative stability in terms of lineage specification in culture which allows genetic and epigenetic manipulation, make EPC a unique cell source and ideal candidate to be widely tested to formulate cell-based therapy for ischemic disorders, including chronic wound. The efficiency of cell therapy to augment recovery after ischemia depends on not only the sufficient amount of circulating EPCs, but also efficient recruitment of the cells to the target tissue. This is not surprising as the contribution of EPC to neovascularization is a coordinated sequence of multistep process, including mobilization, homing, *in situ* differentiation, and maturation, and each step is controlled by a specific mechanism(s). More important, some of these mechanisms are impaired with diabetes. Thus, a combination of therapeutic approaches which target individual steps, correct diabetes-inherited EPC deficits, and can synergize with each other's action, is likely to lead to a more successful treatment outcome for diabetic wounds.

Based on the importance of stromal cells in modulating neovascularization, targeting fibroblasts is a promising therapeutic option. Delivery of fibroblasts in an absorbable mesh, or in type 1 collagen, has been tested and the outcome is encouraging.

Advances in the treatment of chronic wounds, particularly diabetic wounds, are promising. In the future, we will probably see combination therapies of growth factors, ECM and EPC and/or stromal cells. It is believed that a better understanding the molecular and cellular etiologies of chronic, nonhealing wounds will eventually result in the development of clinically efficient and feasible therapies to prevent wound progression, eliminate amputations and promote rapid healing in patients with chronic, nonhealing wound.

See also: Angiogenesis in Response to Hypoxia; Concept of Angiogenic Privilege; Hemangiogenesis versus Lymphangiogenesis; Molecular Mechanisms of Angiostasis; Stability and Functional Integrity of New Blood Vessels; Vessel Regression.

Further Reading

Armulik, A., Abramsson, A., and Betsholtz, C. (2005). Endothelial/pericyte interactions. *Circulation Research* 97: 512–523.

Asahara, T. and Isner, J. M. (2002). Endothelial progenitor cells for vascular regeneration. *Journal of Hematotherapy and Stem Cell Research* 2: 171–178.

Bennett, S. P., Griffiths, G. D., Schor, A. M., Leese, G. P., and Schor, S. L. (2003). Growth factors in the treatment of diabetic foot ulcers. *British Journal of Surgery* 90: 133–146.

Clark, R. A. F. (1996). Overview of wound repair. In: Clark, R. A. F. (ed.) *The Molecular and Cellular Biology of Wound Repair,* 2nd edn., pp. 3–50. New York: Plenum Press.

Davis, G. E. and Senger, D. R. (2005). Endothelial extracellular matrix: Biosynthesis, remodeling, and functions during vascular morphogenesis and neovessel stabilization. *Circulation Research* 97: 1093–1107.

Eming, S. A., Krieg, T., and Davidson, J. M. (2004). Gene transfer in tissue repair: Status, challenges and future directions. *Expert Opinion on Biological Therapy* 4: 1373–1386.

Folkman, J. (1995). Angiogenesis in cancer, vascular, rheumatoid and other disease. *Nature Medicine* 1: 27–31.

Goldman, R. (2004). Growth factors and chronic wound healing: Past, present, and future. *Advances in Skin and Wound Care* 17: 24–35.

Hinz, B. (2007). Formation and function of the myofibroblast during tissue repair. *Journal of Investigative Dermatology* 127: 526–537.

Kopp, H. G., Ramos, C. A., and Rafii, S. (2006). Contribution of endothelial progenitors and proangiogenic hematopoietic cells to vascularization of tumor and ischemic tissue. *Current Opinion in Hematology* 13: 175–181.

Liu, Z. J. and Velazquez, O. C. (2008). Hyperoxia, endothelial progenitor cell mobilization, and diabetic wound healing. *Antioxidants and Redox Signaling* 11: 1869–1882.

Medina, A., Scott, P. G., Ghahary, A., and Tredget, E. E. (2005). Pathophysiology of chronic nonhealing wounds. *Journal of Burn Care and Rehabilitation* 26: 306–319.

Rafii, S. and Lyden, D. (2003). Therapeutic stem and progenitor cell transplantation for organ vascularization and regeneration. *Nature Medicine* 9: 702–712.

Singer, A. J. and Clark, R. A. F. (1999). Cutaneous wound healing. *New England Journal of Medicine* 341: 738–746.

Animal Models of Glaucoma

S I Tomarev, National Institutes of Health, Bethesda, MD, USA

Published by Elsevier Ltd.

Glossary

BAC – Bacterial artificial chromosome. It is a DNA construct based on a functional fertility plasmid, used for cloning in bacteria. The bacterial artificial chromosome's usual insert size is 150–350 kbp.
BAX – Proapoptotic BCL2-associated X protein. BCL2 is an integral outer mitochondrial membrane protein that blocks the apoptotic death of some cells.
Retrobulbar space – The area located behind the globe of the eye.
Synechia – An eye condition where the iris adheres to either the cornea (anterior *synechia*) or the lens (posterior *synechia*).
Tonometry – The procedure to determine the intraocular pressure.
TUNEL – Terminal deoxynucleotidyl transferase-mediated deoxyuridine triphosphate nick end labeling for detection of DNA fragmentation resulting from apoptotic programmed cell death.

Glaucoma is a complex disease, the initiation and progression of which involves interactions between different parts of the eye and brain. It is difficult to perform experiments directed toward elucidating pathogenic molecular mechanisms and potential treatments for glaucoma in human subjects and, as a rule, only postmortem material can be used for biochemical analysis. Experiments in cell culture or organ culture systems may only partially reproduce the complexity of the natural ocular environment. It is now well recognized that animal models may provide a very useful tool for understanding the underlying molecular mechanisms involved in glaucoma and for identifying new genetic components of the disease, including both causative and modifier genes. In addition, appropriate animal models are used to develop and test new regiments of glaucoma treatment as a prerequisite for clinical trials in humans. A number of animal models of glaucoma have been developed over the years. Since elevated intraocular pressure (IOP) is the most important risk factor in glaucoma, most of the animal models of glaucoma are based on elevation of IOP by surgical procedures or by genetic manipulations. Several models used to study death of the retinal ganglion cells (RGCs) include optic nerve crush or transaction, intravitreal injection of excitory amino acids (glutamate and *N*-methyl-D-aspartic acid (NMDA)), or retinal ischemia. Although these are not true glaucoma models, they allow the comparison of processes leading to RGC death induced by different initial insults. Such comparative analysis may lead to the identification of changes that are specific to glaucoma versus changes that are involved in more general RGC dysfunction. While none of the existing animal models is perfect, some of the existing models have been successfully used to uncover important features of glaucoma pathology in humans. Several factors should be considered in selecting a particular animal model of glaucoma for experimentation: (1) the similarity of the model visual system to the human eye; (2) the similarity in the time course of pathological changes in the model and human eyes; (3) ability to apply genetic manipulations; (4) training necessary to produce affected animals; (5) the size of the eye; (6) availability and difficulties of methods of analysis; (7) availability of animals; and (8) cost. This article briefly describes available animal models of glaucoma with emphasis on the strengths and weaknesses of each model.

Mammalian Models

Primate Models of Glaucoma

Monkey and human eyes are very similar both anatomically and functionally, making monkey models very attractive to study different eye pathologies including glaucoma. IOP in monkeys is measured using the same equipment that is used to measure IOP in humans. Moreover, tonometry and visual-field analysis can be performed in conscious, trained monkeys. This is an important factor since it is well documented that general anesthesia that is necessary to measure IOP in most other animal models results in rapid ocular hypotension. The main disadvantage of monkey models is that experiments with monkeys are expensive and require a highly skilled team of investigators. Moreover, large numbers of animals are required to assess effects of elevated IOP on the optic nerve head (ONH) and retina because of genetic variations between animals.

Several approaches have been used to develop pressure-induced glaucoma models in nonhuman primates. The most common method of IOP elevation in the monkey was originally developed more than 30 years ago and involves circumferential laser photocoagulation treatment of the trabecular meshwork. Several laser sessions are normally required to produce a sustained elevation of IOP. In the treated eyes, IOP rises several days after the laser treatment, normally to between 25 and 60 mmHg, and may last for more than a year. Other methods that have

been used to produce elevated IOP elevation in monkeys are less consistent than laser coagulation. They include injection of ghost red cells, latex microspheres, cross-linked polyacrylamide gels, or enzymes into the anterior chamber or application of topical steroids. A non-IOP-related monkey model of glaucoma involves the delivery of endothelin-1 to the retrobulbar space through osmotic pump for 6–12 months; this induces ischemia and leads to the preferential loss of large RGC axons. Ischemia-induced focal axonal loss is similar to human glaucoma and this model may reproduce some aspects of normal tension glaucoma.

A number of important observations have been made using the monkey photocoagulation model. Apoptosis as the primary mechanism of glaucomatous RGC death was first demonstrated in this model before later being confirmed in other models and in human glaucoma. Multifocal electroretinogram (ERG) techniques were used in monkeys to demonstrate that not only RGCs but also cells in the inner and outer nuclear layers are damaged in advanced glaucoma. The monkey glaucoma model has been successfully used to study changes in retinal gene expression patterns after the induction of ocular hypertension. It is also being used to efficiently test new drugs and techniques to reduce IOP. For instance, recombinant adenoviral delivery of the human $p21^{WAF\text{-}1/cip\text{-}1}$ gene to cause cell cycle arrest before filtration surgery in ocular hypertensive monkey eyes has shown a beneficial effect in long-term control of IOP.

Rodent Models of Glaucoma

Several rodent models of glaucoma have been developed over the last 20 years and new models are at different stages of development in several laboratories. These models have proven useful because the drainage structures of the rodent eye are similar to those in humans. Their utility was enhanced further by the development of new methods to measure IOP and analyze glaucomatous changes in these small eyes. Rodent models, and especially mouse models, are relatively cheap and allow extensive genetic manipulations. Rodent models are preferred when a significant number of animals are required to conduct genetic screens or to test different drugs and agents for neuroprotective or IOP-lowering effects. One of the main disadvantages of rodent models is that there are anatomical differences between rodent and human eyes, including the arterial blood supply to the ONH and the absence of a well-developed, collagenous lamina cribrosa. These variations, as well as differences in general physiology, may explain why expression of certain genes in mouse and human eyes (e.g., mutated myocilin) have differential effects.

Rat Models

Rats are easy to handle. The relatively large size of their eyes allows multiple noninvasive IOP measurements in awake trained animals with commercially available equipment. The TonoPen was the instrument of choice for IOP measurements for many years but has recently been superseded by an induction/impact tonometer, marketed as the TonoLab rebound tonometer. This instrument is easy to operate and can be used in both rats and mice.

Several rat models of pressure-induced glaucoma have been developed over the last 15 years. IOP elevation in the rat eye may be achieved by injection of hypertonic saline solution into the episcleral vein that leads to sclerosis of the aqueous humor outflow pathway. Sustained IOP elevation occurs 7–10 days after injection in most but not all rats. The saline injection generally produces a range of IOP elevation in different animals from a very minimal rise to twofold increase over IOP in control eyes, which can remain elevated for up to several months. Cauterization of two or more of the four large episcleral veins is another method of IOP elevation. In this model, IOP elevation occurs very quickly and there are some indications that this procedure impedes blood outflow from the globe and leads to ischemia. Reports indicate that IOP elevation may last from several weeks to several months without requiring retreatment. IOP increase can be also achieved by laser photocoagulation of the trabecular meshwork with or without injection of Indian ink into anterior chamber. Intracameral injection of hyaluronic acid or latex microspheres is another method of IOP elevation in rats. However, the repeated weekly injections required by this method may produce undesirable effects and are labor consuming. Topical application of dexamethasone for 4 weeks may also be used to induce ocular hypertension. These methods of chronic IOP elevation in rats are accompanied by death of the RGCs by apoptosis, optic nerve degeneration, and ONH remodeling similar to those observed in glaucoma in humans. Acute ocular hypertension, on the other hand, may be produced in rats by cannulation of the anterior chamber with a needle attached to a saline reservoir. Although such treatment leads to retinal ischemic injury, it has been suggested that this model mimics acute angle-closure glaucoma in humans.

A mutant rat strain with a unilateral or bilateral globe enlargement and IOPs that range from 25 to 45 mmHg have been described. In this strain, cupping of the ONH as well as reduction in the number of RGCs progress with age. Unfortunately, this strain was obtained from the Royal College of Surgeons colony that has a mutation in the receptor tyrosine kinase gene, leading to degeneration of the photoreceptors. This drastically limits the utility of this strain to study phenomena that are specific to glaucoma and not confounded by other neurodegenerative processes.

Rat models of glaucoma have been used to study effects of elevated IOP on the ERG, changes in the gene expression patterns in the retina, RGCs and optic nerve, and

changes in the protein spectrum of the retina. Rat models also are often used to study neuroprotection. For instance, the hypertonic saline model was used to demonstrate for the first time that agents targeting multiple phases of the amyloid-β pathway provide a therapeutic avenue in glaucoma management.

Mouse Models

Mouse models of glaucoma recently have become very popular. Although most mouse models of glaucoma are based on the elevation of IOP, information about IOP is essential even for the models that do not include experimental IOP manipulation. The mouse eye is much smaller than the human eye, and devices designed for tonometry in humans do not produce reliable data in the mouse. Thus, new methods to measure IOP in mice have been developed and, as a result, the development and acceptance of mouse models of glaucoma have been accelerated. Currently, several invasive and noninvasive methods of IOP measurements in mice exist. The oldest method remains as one of the most reliable and accurate methods and does not depend upon the mechanical properties of the cornea. It involves the insertion of a glass microneedle connected to a pressure transducer into anterior chamber of the eye. However, this procedure cannot be performed too frequently in the same eye, as adequate time is required for corneal wound healing. In addition, cannulation tonometry is technically difficult and training is required to develop sufficient expertise to obtain reliable IOP readings. Cannulation tonometry was used to demonstrate that common mouse strains exhibit different average IOPs in the range between 10 and 20 mmHg. Other methods of IOP measurements in mice were later developed including noninvasive techniques (TonoLab tonometer). Noninvasive techniques allow multiple IOP measurements within short periods of time without extensive training.

Pressure-induced mouse models

Surgical approaches similar to those that were used to produce elevated IOP in rats have also been developed in mice. Significant elevation of IOP in the C57BL/6J mouse eye is accomplished by combined injection of indocyanine green dye into the anterior chamber and diode laser treatment of the trabecular meshwork and episcleral vein region. IOP in operated eyes is significantly elevated 10 days after the surgery but returns back to normal 60 days after the procedure. Histological analysis of the treated eyes 65 days after the surgery revealed development of anterior synechia, loss of RGCs, thinning of all retinal layers, and damage to the optic nerve structures without evidence of prominent cupping. A reduction in the function of all retinal layers, as assessed by ERG studies, indicates that this model produces more dramatic changes in the retina compared to glaucoma in humans. Elevation of IOP may also be induced by argon laser photocoagulation of the episcleral and limbal veins in C57BL/6J mouse eyes or by cauterization of three episcleral veins in CD1 mouse eyes. In one study, mean IOP in the eyes that underwent laser treatment was about 1.5 times higher than in control eyes for 4 weeks. RGC loss was $22.4 \pm 7.5\%$ at 4 weeks after treatment with the majority of terminal deoxynucleotidyl transferase mediated deoxyuridine triphosphate (dUTP) nick end labeling (TUNEL)-positive apoptotic cells detected in the peripheral areas of the retina. Episcleral vein cauterization produced a maximum IOP elevation within 2–9 days after the procedure, which decreased progressively after that to baseline values in the following 24–33 days. This was associated with a 20% decline in the number of RGCs 2 weeks after the surgery.

The DBA/2J strain has become a popular mouse model of secondary-angle-closure glaucoma and is one of the best-characterized mouse models of glaucoma in general. DBA/2J mice have mutations in two genes, *Tyrp1* and *Gpnmb*, which lead to pigment dispersion, iris transillumination, iris atrophy, and anterior synechia. IOP is elevated in most mice by the age of 9 months. IOP elevation was accompanied by the death of the RGCs, optic nerve atrophy, and optic nerve cupping. Although no group of the RGCs appears especially vulnerable or resistant to degeneration, fan-shaped sectors of cell death and survival radiating from the ONH have been detected. It has been suggested that axon damage at the ONH might be a primary lesion in this model. Several important observations have been made using DBA/2J model. It was shown that proapoptotic protein BAX is required for RGC death but not for RGC axon degeneration in this model of glaucoma, suggesting that BAX may be a candidate human glaucoma susceptibility gene. Unexpectedly, high dose of γ-irradiation accompanied with syngenic bone marrow transfer protected RGCs in DBA/2J. Similar to the results obtained with rat and monkey models, genes involved in the glial activation and immune response are activated in DBA/2J retina as shown by array hybridization. Complement component C1q is upregulated in the retina in several animal models of glaucoma and human glaucoma with timing, suggesting that complement activation plays a significant role in glaucoma pathogenesis. Recent data suggest that complement proteins opsonize central nervous system synapses during a distinct window of postnatal development and that the complement proteins C1q and C3 are required for synapse elimination in the developing retinogeniculate pathway. In DBA/2J mice, C1q relocalizes to adult retinal synapses at an early stage of glaucoma prior to obvious neurodegeneration. These data indicate that C1q in adult glaucomatous retina marks synapses for elimination at early stages of disease, suggesting that the complement cascade mediates synapse loss in glaucoma.

Another DBA/2 substrain, DBA/2NNia, also develops elevated IOP and demonstrates RGC loss and optic nerve degeneration when aged. However, depletion of cells in the inner and outer nuclear layers and significant damage of the photoreceptor cells in 15-month-old mice have also been observed.

Transgenic and knock-out approaches have been used to prospectively develop several mouse models of glaucoma. The main advantage of these approaches is that animals within a particular line produce more uniform responses in terms of IOP elevation and damage to the retina and optic nerve as compared to surgically induced models. A large number of animals may be obtained and no training is needed to produce affected mice. Several lines of transgenic mice have been developed that contain BAC DNAs with a Tyr423His point mutation in the mouse or Tyr437His point mutation in the human *MYOCILIN* (*MYOC*) genes. Tyr437His mutation in the *MYOC* gene leads to severe glaucoma cases in humans, and mouse Tyr423His mutation corresponds to this human mutation. However, expression of mutated mouse or human myocilin in the eye-drainage structures of mice leads to moderate (about 2 mmHg at daytime and 4 mmHg at nighttime) elevation of IOP which is much less dramatic than IOP elevation in humans carrying the same mutation in the *MYOC* gene. Since these mice demonstrate progressive degenerative changes in the peripheral RGC layer and optic nerve with normal organization of the drainage structures, it has been suggested that these mice represent a mouse model of primary open-angle glaucoma. Another model of primary open-angle glaucoma was developed by the expression of a mutated gene for the α1 subunit of collagen type I. This mutation blocks the cleavage of collagen by matrix metalloproteinase-1. Transgenic mice expressing mutated collagen demonstrate elevated IOP which increases to a maximum of 4.8 mmHg greater than controls at 36 weeks.

A transgenic model of acute angle-closure glaucoma was developed by expression of calcitonin-receptor-like receptor under the control of a smooth muscle α-actin promoter. Overexpression of this receptor in the papillary sphincter muscle results in enhanced adrenomedullin-induced sphincter muscle relaxation that leads to abrupt transient rises in IOP in some mice up to a mean level of about 50 mmHg between 30 and 70 days of age. Although the aberrant ocular functions of adrenomedullin and calcitonin-gene-related peptide have not been associated with the pathogenesis of human acute glaucoma, it has been suggested that adrenomedullin and its receptor in the iris sphincter may present novel targets for the treatment of angle-closure glaucoma.

Normal-tension mouse models

Mice deficient in the glutamate transporters GLAST or EAAC1 show RGC death and typical glaucomatous damage of the optic nerve without elevation of IOP. It has been shown that the glutathione levels are decreased in Müller cells of GLAST-deficient mice, while administration of glutamate receptor blocker prevents loss of RGCs. RGCs are more sensitive to oxidative stress in EAAC1-deficient mice. These mice represent a model of normal tension glaucoma and are currently being used to develop therapies directed at IOP-independent mechanisms of RGC loss.

Developmental mouse models

Defects in genes involved in the development of the anterior eye segment may lead to relatively rare developmental glaucomas, which account for less than 1% of all human glaucoma cases. Several genes have been implicated in congenital glaucoma and anterior segment dysgenesis. They include *CYP1B1, FOXC1, FOXC2, PITX2, LMX1b*, and *PAX6*. Although *Cyp1b1* knock-out mice do not develop elevated IOP, they have ocular abnormalities similar to defects in humans with primary congenital glaucoma: small or absent Schlemm's canal, defects in the trabecular meshwork, and attachment of the iris to the trabecular meshwork and peripheral cornea. $Foxc1^{-/-}$ mice die at birth, while $Foxc1^{+/-}$ animals are viable but have defects in the eye-drainage structures in the absence of IOP changes. Similar eye defects are observed in $Foxc2^{+/-}$ mice. It has been suggested that $Foxc1^{+/-}$ and $Foxc2^{+/-}$ mice are useful models for studying anterior segment development and its anomalies, and they may allow identification of genes that interact with *Foxc1* and *Foxc2* to produce a phenotype with elevated IOP and glaucoma.

Transgenic mice overexpressing the ocular development-associated gene (ODAG) in photoreceptors under the control of mouse Crx promoter exhibit gradual protrusion of the eyeballs with dramatically increased IOP that is not attributable to mechanical block of the aqueous humor outflow. These transgenic mice demonstrate optic nerve atrophy and impaired retinal development. All retinal layers of these transgenic mice are affected, thereby differentiating this model from a typical glaucomatous retina where morphological changes are detected only in the RGC layer.

Other Mammalian Models

Several other mammalian models of glaucoma have been developed. Pig eyes are relatively large and, although the drainage outflow system of the pig eye is slightly different from that of the human eye, the porcine retina is more similar to the human retina than that of other large mammals (i.e., dog, goat, and cow). Cauterization of three porcine episcleral veins leads to a 1.3-fold elevation of IOP that is apparent 3 weeks after the surgery and persists for at least 21 weeks. It has been shown that endothelium leukocyte adhesion molecule 1 (ELAM-1), a molecular marker

for human glaucoma, is also elevated in the trabecular meshwork of pigs with elevated IOP.

Rabbits are a standard ophthalmic animal model for glaucoma filtration surgery and are often used for the development of new devices (e.g., drainage implants and degradable biopolymers) and medical therapies including gene therapy. At the same time, due to the unique anatomy of the rabbit eye, laser-induced elevation of IOP, like that in the monkey eye, is difficult to achieve. Alternatively, application of glucocorticoids has been successfully used to induce ocular hypertension in rabbit model. In addition, a line of rabbits with congenital glaucoma has been developed. Thick subcanalicular tissues and the deposition of extracellular matrix in the trabecular meshwork appear to contribute to the ocular hypertension exhibited by this model.

Several purebred dogs develop glaucoma with high frequency. Among North American breeds, the highest prevalence of primary glaucoma is observed in the American cocker spaniel (5.52%), basset hound (5.44%), and chow chow (4.70%), exceeding that in humans. Lens displacement resulting in secondary glaucoma is common in terrier breeds. The high prevalence of the glaucomas in these canine breeds suggests a genetic basis of pathophysiology.

It has been reported that topical application of corticosteroid induces reproducible elevation of IOP in the cow. The large amount of tissues available from the cow eye makes this model useful for biochemical studies.

Nonmammalian Models

Zebrafish

The zebrafish is an excellent model system to study complex diseases as it allows one to combine forward and reverse genetic approaches. The general organization of the zebrafish eye is similar to the human eye, although the fine details of individual ocular structures are rather different. In particular, there are significant differences in the organization of the iridocorneal angle between zebrafish and mammals. They include the trabecular meshwork and lack of iris muscles as well as ciliary folds in zebrafish as compared to mammals. Even with these limitations in mind, zebrafish have been used as a model organism for glaucoma studies. An accurate method exists to measure IOP in zebrafish which is based on servo-null electrophysiology. Using this method, baseline IOP differences have been demonstrated in genetically distinct zebrafish strains. Among tested strains, the long fin strain (LF) had the highest IOP (20.5 ± 1.2 mm Hg) while the Oregon AB strain (AB) has the lowest IOP (10.8 ± 0.3 mm Hg). At the same time, these differences in IOP do not lead to detectable defects of the retina or in visual function. Zebrafish have also been used to determine the function of several genes (*foxc1*, *lmx1b*, *wdr36*, *olfactomedin 1*, and *olfactomedin 2*) implicated in glaucoma. It has been shown that wdr36 functions in ribosomal RNA processing and interacts with the p53 stress-response pathway, while olfactomedin 1 is essential for optic nerve growth and targeting of the optic tectum. Thus, zebrafish system may be very useful to complement studies with other model organisms, but by itself should be used with caution to study glaucoma.

Other Nonmammalian Models

Open-angle glaucoma characterized by elevated IOP can be induced in domestic chickens or in Japanese quails when they are reared under continuous light. Besides, an unknown autosomal dominant mutation in a Slate line of domestic turkeys has been identified that leads to secondary angle-closure glaucoma. Although these models might be useful to study certain aspects of glaucoma in humans, one should remember that structural and physiological differences between human and bird eyes complicate direct comparison.

Drosophila eyes have been suggested as a useful system for the discovery of genes that are associated with glaucoma. However, the general organization of human and *Drosophila* eyes are very different and data obtained with *Drosophila* may not always be relevant to glaucoma in humans.

Conclusion

Animal models have already provided interesting new information about potential mechanisms of glaucoma in humans. However, even in monkey models which most closely mimic the human form of the disease, the time course of changes in the glaucomatous eyes may be significantly accelerated as compared with human glaucomatous eyes. Indeed, all of the previously discussed systems are, after all, just models of human glaucoma. Reactions to the same insult (IOP, expression of the same mutated protein, etc.) may be somewhat different between various animal models and humans. Results obtained with these models should not automatically be applied to human condition and should be confirmed by testing in human subjects when possible. Nevertheless, information on molecular mechanisms of glaucoma obtained using animal models might be extremely valuable to develop new therapeutic approaches for glaucoma treatment and prevention in humans.

See also: The Development of the Aqueous Humor Outflow Pathway; Functional Morphology of the Trabecular Meshwork; The Genetics of Primary Open-Angle Glaucoma: A Review; Molecular Genetics of Congenital and Juvenile Glaucoma; Myocilin; Primary Open-Angle Glaucoma; Steroid-Induced Ocular Hypertension and Effects of Glucocorticoids on the Trabecular Meshwork.

Further Reading

Anderson, M. G., Libby, R. T., Gould, D. B., et al. (2005). High-dose radiation with bone marrow transfer prevents neurodegeneration in an inherited glaucoma. *Proceedings of the National Academy of Sciences of the United States of America* 102: 4566–4571.

Baulmann, D. C., Ohlmann, A., Flügel-Koch, C., et al. (2002). Pax6 heterozygous eyes show defects in chamber angle differentiation that are associated with a wide spectrum of other anterior eye segment abnormalities. *Mechanisms of Development* 118: 3–17.

Harada, T., Harada, C., Nakamura, K., et al. (2007). The potential role of glutamate transporters in the pathogenesis of normal tension glaucoma. *European Journal of Clinical Investigation* 117: 1763–1770.

Iwata, T. and Tomarev, S. (2008). Animal models for eye diseases and therapeutics. In: Conn, P. M. (ed.) *Sourcebook of Models for Biomedical Research*, pp. 279–287. Totowa, NJ: Humana Press.

Levkovitch-Verbin, H., Quigley, H. A., Martin, K. R., et al. (2002). Translimbal laser photocoagulation to the trabecular meshwork as a model of glaucoma in rats. *Investigative Ophthalmology and Visual Science* 43: 402–410.

Libby, R. T., Anderson, M. G., Pang, I., et al. (2005). Inherited glaucoma in DBA/2J mice: Pertinent disease features for studying the neurodegeneration. *Visual Neuroscience* 22: 637–648.

McMahon, C., Semina, E. V., and Link, B. A. (2004). Using zebrafish to study the complex genetics of glaucoma. *Comparative Biochemistry and Physiology – Part C: Toxicology and Pharmacology* 138: 343–350.

Morrison, J. C., Johnson, E. C., Cepurna, W., and Jia, L. (2005). Understanding mechanisms of pressure-induced optic nerve damage. *Retinal Eye Research* 24: 217–240.

Pang, I.-H. and Clark, A. F. (2007). Rodent models for glaucoma retinopathy and optic neuropathy. *Glaucoma* 16: 483–505.

Rasmussen, C. A. and Kaufman, P. L. (2005). Primate glaucoma models. *Journal of Glaucoma* 14: 311–314.

Senatorov, V., Malyukova, I., Fariss, R., et al. (2006). Expression of mutated mouse myocilin induces open-angle glaucoma in transgenic mice. *Journal of Neuroscience* 26: 11903–11914.

Smith, R. S., John, S. W. M., Nishina, P. M., and Sundberg, J. P. (eds.) (2002). *Systematic Evaluation of the Mouse Eye*. Boca Raton, FL: CRC Press.

Weinreb, R. N. and Lindsey, J. D. (2005). The importance of models in glaucoma research Volume. *Journal of Glaucoma* 14: 302–304.

Anti-Angiogenic Properties of Vitreous

G A Lutty, Johns Hopkins Hospital, Baltimore, MD, USA

Glossary

Angiogenic factor – A factor that stimulates the growth of new blood vessels.
Anti-angiogenic factor – A factor that inhibits the growth of new blood vessels.
Hyalocytes – The monocytic cells that reside in vitreous through life and have been called the dendritic cell of vitreous. These cells are capable of producing many of the angiogenic and anti-angiogenic factors found in vitreous.
Hyaloid vasculature – This occupies the vitreous during fetal life and then regresses to become a vestige called Cloquet's canal. This vasculature has its origins in the central retinal artery and is composed of the hyaloid artery, the vasa hyaloidea propria, which nourishes retina before it is vascularized, and the tunica vasculosa lentis, which nourishes the lens during development.
Hyaluronic acid – A nonsulfated glycosaminoglycan that is a major component of vitreous and other extracellular matrices throughout the body.
Pigment-epithelium-derived factor (PEDF) – A monomeric peptide that is a member of the serpin serine protease inhibitor family that is neurotrophic as well as anti-angiogenic.
Sea fan neovascular formations – The extraretinal neovascularization formations found in patients with sickle cell disease.
Thrombospondin-1 (TSP-1) – A 450-kDa multifunctional extracellular matrix glycoprotein produced by many cells including smooth muscle, endothelial, and retinal pigment epithelial cells in the eye. The major source of this anti-angiogenic protein is platelet granules.
Transforming growth factor beta (TGF-β) – A ubiquitous dimeric polypeptide growth factor found in vitreous. It is produced by most cells in a large latent form and affects the differentiation, proliferation, and migration of many cell types, including inhibition of endothelial cell proliferation and migration.
Vascular endothelial growth factor (VEGF) – The major hypoxia-inducible, secreted angiogenic factor in the body. It also increases vascular permeability, is an endothelial cell survival factor, and is thought to be a major contributing factor in ischemic retinopathies and age-related macular degeneration.
Vitreous humor – The transparent gel of extracellular matrix material that fills the chamber of the eye between lens and retina. It is vascularized during development but avascular in normal adult mammals.

Vitreous

Vitreous humor is the transparent gel between the crystalline lens and the retina. It serves as a stabilizer and shock absorber for any movement or mechanical impact reaching retina and lens. The adult vitreous body is 80% of the volume of the human eye. Ninety-eight percent of vitreous is water and the major extracellular matrix (ECM) macromolecules are collagen type II and hyaluronic acid. Though seeming to be a simple transparent viscoelastic matrix, it is physically and biochemically partitioned and a complex mixture of macromolecules. It contains at least 121 distinct proteins, 38 of the proteins were known in 2003, and the protein concentration ranges from 0.45 to 1.1 mg ml^{-1}. In youth, vitreous is normally a gel but liquification or syneresis occurs with age, 50% being liquid by age 80 in humans. The concept that vitreous had anti-angiogenic properties arose from the fact that, in normal adult life, this gel is avascular even though it is surrounded by vasculatures of the retina and ciliary processes.

Development of Vitreous

The first evidence of vitreous in human development is during the third-to-fourth week gestation (WG) when neural ectoderm becomes separated from the surface ectoderm. The PAS-positive and Alcian-blue-positive material that bridges this space is the initial vitreous. Between 4 and 5 WG, mesodermal cells enter the vitreous space within the concave optic vesicle with the optic fissure fusing at 5 WG. The mesodermal cells will become the hyaloid vascular system, which includes the vasa hyaloidea propria (VHP), posterior tunica vasculosa lentis (TVL), and the hyaloid artery (**Figure 1**). The mesodermal cells may also become hyalocytes, which are of monocytic origin. We have recently demonstrated that the vascular development in vitreous occurs by hemo-vasculogenesis, development of blood vessels and blood cells from a common precursor,

Figure 1 Scanning electron microscope image of a 3-day-old mouse eye from which a temporal cap was removed. In the vitreous cavity, the artifactually broken hyaloid artery is present (arrow) supplying blood to the tunica vasculosa lentis on the posterior surface of the lens (L). The hyaloid artery also supplies the vasa hyaloidea propria (arrowhead), which has pulled away from retina (R) in processing. The round cells on the abluminal surface of the fetal vasculature are hyalocytes and macrophages. From Steve Wajer.

the hemangioblasts. This suggests that some of the mesodermal cells that enter vitreous are hemangioblasts, which will differentiate into the fetal vasculature and perhaps into the hyalocytes. Balazs and associates hypothesized that the monocytic cell that resides in vitreous through life, the hyalocyte, differentiated from the mesodermal cells as well. This cellular vitreous is termed the primary vitreous. The secondary vitreous forms by 12 WG between the VHP and the surface of the retina. It is virtually acellular and the major ECM molecules are collagen type II and hyaluronic acid.

The VHP will nourish inner retina until a retinal vasculature forms, while the posterior TVL will nourish the developing lens. The hyaloid vasculature reaches prominence at 9 WG and will regress thereafter. The VHP in human regresses first and then the posterior TVL. By 23 WG, flow ceases in the hyaloid artery. Adult vitreous is avascular and all that remains of the fetal vasculature of vitreous will be Cloquet's canal, a vestige of the hyaloid artery. Richard Lang and associates have demonstrated that macrophages mediate the regression of these transient vasculatures in vitreous and the anterior pupillary membrane through macrophage wingless-type MMTV integration site family, member 7B (WNT7B). The macrophage-induced apoptosis of select endothelial cells in turn causes obstruction of flow and widespread endothelial cell apoptosis. In human vitreous, apoptosis begins around 13–15 WG followed by necrosis. Other work suggests that hyalocytes (positive for major histocompatibility complex class I (MHC-1), MHC-II, cluster of differentiation 45 (CD45), and calcitonin-gene-related peptide-positive cells) are of two forms: dendritic, which associate with the regressing vasculature, and round in the secondary vitreous.

Switch from Pro-Angiogenic to Anti-Angiogenic in Development

The hyaloid vascular system regresses during the third trimester in human and postnatally in rodents with the vitreous remaining avascular for life in normal subjects. Judah Folkman and Arnall Patz noted a striking correlation between cartilage and vitreous: both tissues were vascularized during development and avascular during adult life. Folkman's lab had demonstrated that adult cartilage inhibited the growth of blood vessels induced by tumors and surmised that an anti-angiogenic agent was produced in adult cartilage. When tumor was implanted in vitreous, it only grew and became vascularized if it touched retina. An extract of vitreous in a slow-release polymer was then placed in corneal micropockets with tumor, and corneal neovascularization in response to the tumor was inhibited. Using the chick chorioallantoic membrane (CAM) assay, our lab demonstrated that bovine vitreous extract could inhibit retinal-derived growth-factor-induced angiogenesis. Furthermore, the major glycosaminoglycans (GAGs) in vitreous were not responsible for this inhibition of angiogenesis on the CAM assay. Our lab and others then demonstrated that the anti-angiogenic activity was heat stable and specifically inhibited endothelial cells *in vitro*. When the inhibitory effect of fetal bovine vitreous compared to adult was assessed during the author's dissertation studies, it was found that fetal vitreous stimulated endothelial cell proliferation, while adult vitreous inhibited; fetal vitreous that was heat treated inhibited endothelial cell proliferation (**Figure 2**). This suggested that while the hyaloid vasculature was present, the vitreous was pro-angiogenic but anti-angiogenic in adult life. Heat treatment also enhanced the inhibitory activity of adult bovine vitreous. This experiment also suggested that either the angiogenic factor(s) was heat labile or the inhibitor was heat activated. It was subsequently demonstrated in the author's dissertation that adult human, dog, rabbit, sheep, and chicken vitreous inhibited endothelial cell proliferation, and heat treatment enhanced the activity. The purification process demonstrated that the anti-angiogenic activity had many characteristics in common with transforming growth factor beta (TGF-β): binds to glass and most filters, heat stable and activated, acid stable and activated, activity lost under reducing conditions, inhibits mink lung epithelial cell proliferation, elutes from C-18 columns in 40% acetonitrile, and active form elutes in 8 M urea from molecular sieve columns with an apparent molecular weight of 25 kDa. The inhibitory activity from vitreous was then neutralized with antibodies against TGF-β. It was then demonstrated that the predominant species in vitreous was TGF-β2 but TGF-β1 was also present.

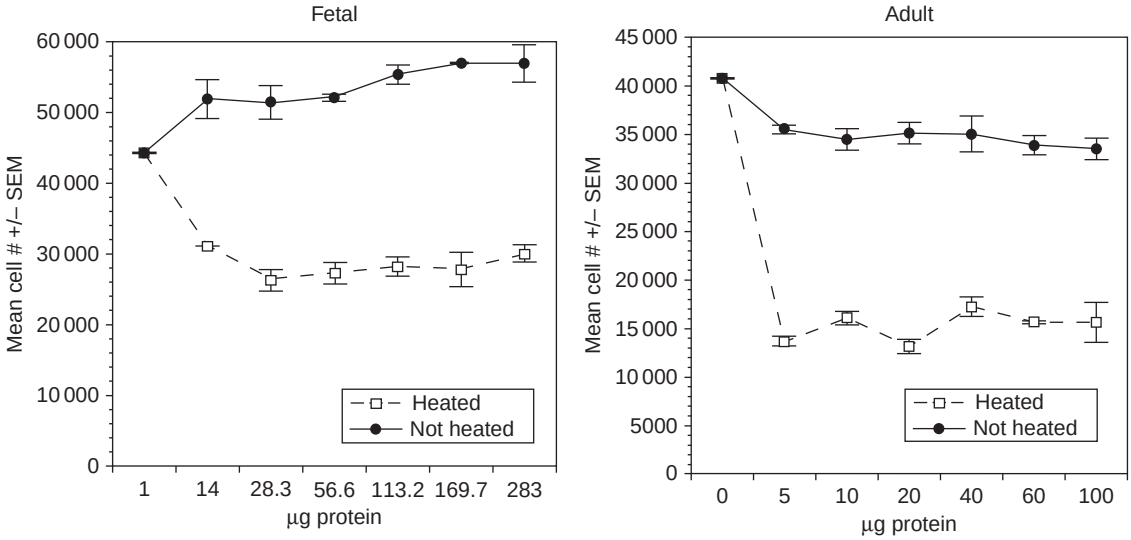

Figure 2 Effect of fetal (a) and adult (b) bovine vitreous on the proliferation of fetal bovine aortic endothelial cells. (a) Fetal vitreous stimulated proliferation (closed circles), but after heat treatment (95 °C for 10 min) inhibited proliferation (open squares). (b) Adult vitreous inhibited proliferation whether heated (open squares) or nonheated (closed circles).

Transforming Growth Factor Beta

TGF-β is a family member of dimeric polypeptide growth factors that includes bone morphogenic proteins (BMPs) and activins. Virtually every cell in the body, including epithelial, endothelial, hematopoietic, neuronal, and connective tissues, produces TGF-β and makes receptors for TGF-β. There are three isoforms in mammals: TGF-β 1, 2, and 3. They are synthesized as large precursor molecules, cleaved before the precursor is secreted, and most TGF-β is stored in ECM. The active form is a disulfide-linked dimer and the three isoforms share receptors. TGF-βs inhibit the proliferation of most epithelial, endothelial, and hematopoietic cells *in vitro*. TGF-β inhibits microvascular and macrovascular endothelial cell proliferation and migration. Ironically, early studies demonstrated that it was angiogenic *in vivo*, which was subsequently demonstrated to be due to an indirect effect of stimulating macrophage migration and then production of angiogenic cytokines by recruited macrophages. When TGF-β2 is knocked out in mice, the hyaloid vasculature does not regress and ocular pathology resembling persistent fetal vasculature results. The source of TGF-βs in vitreous may be hyalocytes or the pericytes of the fetal vasculature because pericytes are known to produce TGF-βs. Hyalocytes appear to produce and process TGF-β1 because both antiprepro-β1 and antisecreted-β1 localization were associated with them (**Figure 3**). Hyalocytes *in vitro* produce TGF-β2. They have a battery of acid hydrolases, which could be responsible for activating latent TGF-β. As the sole cellular occupant of normal adult vitreous, they then may control the rate of TGF-β activation in vitreous. It is noteworthy that hyalocytes also had immunoreactivity for TGF-β 2 and β3 (**Figure 3**); this was the only cell type in the posterior human eye that had immunoreactivity for all four forms of TGF-β evaluated: secreted TGF-β1, prepro-TGF-β1, TGF-β2, and TGF-β3. Ciliary epithelial cells as well as ciliary body stromal cells may also be a source of TGF-β1 and TGF-β2 in vitreous. When panretinal photocoagulation was performed in rats, the levels of both TGF-β1 and TGF-β2 were significantly elevated in vitreous. Therefore, the successful treatment of diabetic retinopathy with panretinal photocoagulation may be due to increased TGF-β production in the eye and its accumulation in the vitreous.

Pigment Epithelium-Derived Factor

In addition to TGF-β, there are many other substances in vitreous that have anti-angiogenic activity. PEDF is a 49.5-kDa monomeric protein, which is a member of the serine protease inhibitor (serpin) family. This was first purified from the conditioned medium of human retinal pigment epithelial (RPE) cells. It binds to many matrix components in vitreous, including collagen and hyaluronic acid. It is a neurotrophic factor that induces neurite outgrowth and promotes neurite survival. PEDF is a potent anti-angiogenic factor, inhibiting endothelial cell migration and proliferation and neovascularization in oxygen-induced retinopathy (OIR). There are high levels of PEDF in human vitreous. Some investigators found that PEDF levels were higher in patients with proliferative diabetic retinopathy (PDR) than in control subjects, while others claim that there is lower PEDF in PDR vitreous than in control subjects. Using immunohistochemistry,

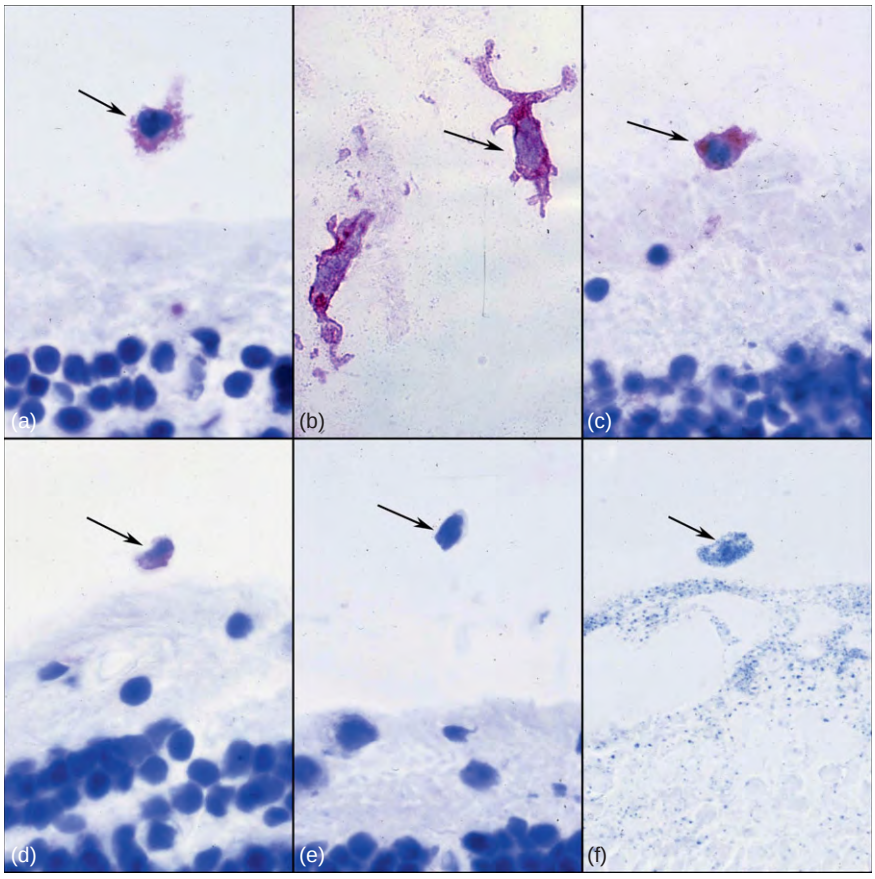

Figure 3 TGF-β isoforms expression in hyalocytes in human vitreous of a 71-year-old male subject who died of respiratory failure. (a) Antibody against prepro-TGF-β1 binds to a hyalocyte in cortical vitreous near the vitreoretinal interface. (b) Anti-secreted TGF-β1 immunoreactivity is prominent in amoeboid-shaped hyalocytes. (c) Anti-TGF-β2 labels a hyalocyte resting on the internal limiting membrane of retina. (d) Antibody to TGF-β3 labels a hyalocyte near the vitreoretinal interface. (e) There is no background labeling when a nonimmune IgG was used instead of anti-TGF-β antibodies. (f) Nonspecific esterase enzyme histochemistry labels a hyalocyte because they are of monocyte origin (arrow indicates hyalocytes in all; AEC immunoreaction product with hematoxylin counterstain).

we found high levels of PEDF in the vitreous of normal as well as sickle retinopathy subjects. During mouse development, levels of PEDF in vitreous change: at midgestation it was expressed in ciliary body and choroid; near term it was expressed in ganglion cell layer where levels remained high through 2 weeks postnatal; and then the levels decreased but persisted at low levels into adulthood. It is interesting that penetrating ocular wounds, such intravitreal injection, increases PEDF messenger RNA (mRNA) in retina and PEDF protein levels in vitreous. The injury and subsequent upregulation of PEDF in vitreous in those studies resulted in less intravitreal neovascularization in the rodent OIR model. Therefore, it would not be surprising if an injury like photocoagulation results in elevated levels of PEDF in human vitreous.

Endostatin

Endostatin, another endogenous inhibitor of angiogenesis, along with fragments of it were recently isolated from vitreous. Mouse endostatin consists of 184 amino acids at the noncollagenous carboxyl terminus of collagen XVIII (coll XVIII), and is released from coll XVIII through proteolytic cleavage. The production and liberation of endostatin is still poorly understood, but it has been found to be expressed in some differentiated tissues (e.g., kidney and liver) and freely circulating in serum. Endostatin blocks mitogen-activated protein kinase (MAPK) activation in endothelial cells. It specifically inhibits endothelial cell proliferation and migration *in vitro* and potently inhibits angiogenesis *in vivo*. Endostatin is currently being aggressively pursued as a candidate for cancer therapy in humans.

Coll XVIII, the source of endostatin, is widely expressed in mice and humans. In mouse, coll XVIII has been demonstrated prominently in all ocular basement membranes except Descemet's membrane. It is associated with collagen fibrils in vitreous that are connected to the internal limiting membrane. Intracellular endostatin was found in lens epithelium and nonpigmented epithelium of the ciliary body. It has been suggested that there is a ring

of extracellular endostatin around vitreous and the anterior chamber that might physiologically prevent neovascularization. Coll XVIII knock-out mice have delayed regression of the hyaloid vasculature and VHP. Novel mutations in coll XVIII have been associated with Knobloch syndrome and patients with this syndrome, who had no measurable endostatin in their serum, had persistent fetal blood vessels in the vitreous similar to the endostatin knock-out mouse.

Thrombospondin-1

TSP-1 was found in vitreous of normal rat and man. TSP-1 is a 450-kDa multifunctional ECM glycoprotein produced by endothelial cells, monocytes/macrophages, smooth muscle cells, platelets, and RPE cells. Since the major source of TSP-1 is platelet granules, one might assume that increased vascular permeability, as in diabetes, might result in greater levels in vitreous. However, TSP-1 was absent in vitreous of diabetic rats and endothelial cell production of TSP-1 was reduced in the presence of high glucose. As an anti-angiogenic factor, TSP-1 inhibits endothelial cell proliferation and migration, induces endothelial cell apoptosis, and it activates transforming growth factor. In the rat eye, TSP-1 inhibits corneal angiogenesis induced by pro-angiogenic factors: basic fibroblast growth factor and vascular endothelial growth factor (VEGF). Moreover, TSP-1 knock-out mice show more intense neovascularization than wild-type mouse in the cornea and have delayed regression of preretinal neovascularization in retinal angiogenesis models.

Other Anti-Angiogenic Factors in Vitreous

There have been reports on several other anti-angiogenic factors in vitreous that are less well known. Opticin was actually purified initially from bovine vitreous. This 90-kDa dimeric leucine-rich repeat ECM protein is O-linked glycosylated and binds hetereotypic collagen fibrils of vitreous. This protein binds growth hormone in vitreous and retina. Opticin-null mice showed increased neovascularization compared to wild-type mice after exposure to hyperoxia in the murine OIR model, whereas when recombinant opticin was injected into the vitreous there was decreased neovascularization compared to controls. The soluble form of VEGF receptor-1 (sflt-1) has been identified in vitreous. This form of VEGF receptor is thought to be one of the molecules responsible for the avascularity of normal cornea. Chondromodulin has also been found in vitreous. This 25 kDa endogenous anti-angiogenic factor was isolated from cartilage originally and, like TGF-βs, is made initially as a precursor form. mRNA for chondromodulin was found in ciliary body, ganglion, and RPE cells.

Two multifunctional cytokines with anti-angiogenic properties, interleukins (IL) 12 and 13, have been identified in vitreous by multiplex bead analysis. IL12 inhibits the proliferation of endothelial cells and corneal neovascularization induced by basic fibroblast growth factor or tumor. This was accomplished by inducing interferon gamma. IL12 inhibits tumor-induced neovascularization, which was the rationale for its evaluation as a cancer therapy. IL12 also inhibits choroidal neovascularization. IL13 inhibits endothelial cell migration and tube formation *in vitro* as well as the aortic ring assay. IL13 inhibits neovascularization in arthritic joints by upregulating endostatin. Its anti-angiogenic effect is through activation of janus kinase 2 (JAK2) and subsequent activation of signal transducer and activator of transcription 6 (STAT6).

Angiogenic Factors in Vitreous

Although normal adult vitreous is anti-angiogenic, vitreous can be angiogenic in disease states. Most angiogenic factors present in vitreous have been found in diseased states, especially in ischemic retinopathies. We found in our early studies that diabetic vitreous was angiogenic and that an 18-kDa, heat-labile molecule that eluted from heparin-Sepharose at 1.2 M NaCl could be isolated from diabetic vitreous. It was similar to the mitogen in brain extracts, which was subsequently identified as fibroblast growth factor (FGF). The angiogenic factor(s) could either be produced by cells in retina, usually in response to hypoxia, or they may leak from retinal blood vessels in diseases such as diabetes. More recently, the exact identity of these angiogenic factors has been determined.

VEGF was found in vitreous and it was significantly elevated in the vitreous of diabetic subjects and patients with iris neovascularization and central vein occlusion. It was assumed that ischemic retina had produced this heparin-binding growth factor and that it had diffused into vitreous. Soon thereafter, this was demonstrated experimentally when all branch retinal veins in monkey retina were occluded and increased levels of VEGF in aqueous humor and iris neovascularization were observed.

Another hypoxia-inducible, secreted angiogenic factor found in vitreous is erythropoietin (EPO). This increases with age in human vitreous between 12 and 24 WG, a period when the retinal vasculature is forming and the hyaloid system is regressing. This increase in EPO in vitreous was not paralleled by an increase in serum levels so it was assumed that it was produced locally. It is curious that the levels were still elevated at 24 WG when a significant retinal vasculature is present and retina should be less hypoxic. Increased levels of both VEGF and EPO were found in the vitreous of patients with diabetic retinopathy compared to no diabetic subjects. EPO levels in

vitreous are also higher than normal in subjects with diabetic macular edema.

Hepatocyte growth factor (HGF) or scatter factor has also been identified in human vitreous. HGF levels were higher in subjects with PDR and iris neovascularization than in normal subjects. Increased levels were also found in vitreous from subjects with proliferative vitreoretinopathy (PVR) and the level increased with severity of the disease. This is logical because HGF stimulates the proliferation of both endothelial and epithelial cells, cells present in PVR membranes. Insulin-like growth factor-1 (IGF-1), but not-2, is elevated in the vitreous of diabetic subjects compared to normal subjects and the level correlates with serum levels in the subjects, suggesting that serum was the source of vitreal IGF-1. Interestingly, IGF-binding proteins are also present in vitreous but there is no correlation of levels between vitreous and serum. Stromal-derived factor-1 (SDF-1), another hypoxia-inducible molecule, is elevated in vitreous of PDR and non-PDR and in subjects with diabetic macular edema. SDF-1 stimulates migration of endothelial cells and endothelial cell progenitors, but not their proliferation. Osteopontin has diverse functions, including angiogenesis, and increased levels of this factor were found in vitreous of diabetic subjects. Finally, fractalkine was found to be elevated in diabetic subjects compared to normal subjects.

Balance between Anti-Angiogenic and Angiogenic Factors

Although many angiogenic and anti-angiogenic proteins are found in human vitreous, we found that the net effect of normal human vitreous was anti-angiogenic (inhibits the proliferation of endothelial cells), while pathological diabetic vitreous is angiogenic most of the time, even after heat activation. From the previous section, it is apparent that there are many angiogenic factors normally in vitreous at very low levels or not present normally, but they are elevated in disease states such as diabetes. Conversely, there are many anti-angiogenic factors normally in vitreous and they may decline in disease states. Therefore, it is probable that the balance between pro- and anti-angiogenic factors determines if neovascularization forms in vitreous or whether the fetal vasculature in vitreous is viable or not.

Such a balance has been demonstrated between VEGF and PEDF levels in vitreous: levels of PEDF were significantly lower in PDR subjects compared to macular hole (MH) patients used as control; conversely, VEGF levels were significantly higher in PDR subjects compared to MH subjects. Vitreous PEDF levels were lower in PVR subjects than MH patients and higher in retinal detachment subjects, while VEGF vitreous levels were significantly higher with PVR than MH or retinal detachment subjects. When the vitreous of subjects with diabetic macular edema was analyzed, lower PEDF levels were observed with VEGF levels elevated compared to non-diabetic subjects and diabetic subjects without retinopathy. VEGF, of course, is not only angiogenic but increases vascular permeability as well. When we investigated PEDF and VEGF immunohistochemically in sickle cell retinopathy patients, we found that PEDF was not lower but VEGF levels were higher in sea fan neovascular formations and vitreous surrounding them, tipping the balance toward angiogenesis (**Figure 4**). Interestingly, infarcted sea fan formations had high PEDF and no VEGF immunoreactivity.

A balance has also been investigated between VEGF and endostatin. Endostatin levels in vitreous have been correlated with severity of DR: in PDR, VEGF was high and endostatin low, while VEGF was low and endostatin high in diabetics with quiescent DR. Levels of VEGF and endostatin in vitreous were predictive of outcome of DR: VEGF was higher and endostatin lower in a group of diabetics whose retinopathy progressed over the next 6 months, while endostatin was high and VEGF low in group whose retinopathy regressed.

Conclusions

Avascularity of vitreous is imperative for a transparent visual path. After macrophage-induced death of the fetal vasculature in vitreous, it will remain avascular and contain high levels of anti-angiogenic factors through normal adult life. The most prominent anti-angiogenic molecules in vitreous are either bound to matrix (PEDF, TGF-β) or are matrix proteins (endostatin, TSP-1), so their presence and accumulation in vitreous is logical since vitreous is a gelatinous matrix. Metabolic exchange from vitreous and equilibration may be so slow that clearance from vitreous is slowed and matrix-bound substances may accumulate with age. It is interesting that hyalocytes, the only resident cell of vitreous, produce some of the anti-angiogenic substances as well as the matrix components of vitreous. Basic FGF, which is found in vitreous and binds to heparan sulfate, makes hyalocytes morphologically round and stimulates their proliferation while TGF-β, which also binds GAGs, makes hyalocytes more amoeboid, inhibits their proliferation, and stimulates their production of GAGs. Therefore, the level and type of angiogenic and anti-angiogenic factor affects not only the anti-angiogenic properties of vitreous, but also the endogenous vitreous cells. The two types of hyalocytes that have been documented may actually be the same monocytic cell type exposed to different angiogenic and anti-angiogenic factors. It is apparent now that there are both angiogenic and anti-angiogenic factors in vitreous normally. The actual balance between them must be quite complex because there are many angiogenic and anti-angiogenic molecules found in vitreous that will determine the net effect of vitreous on

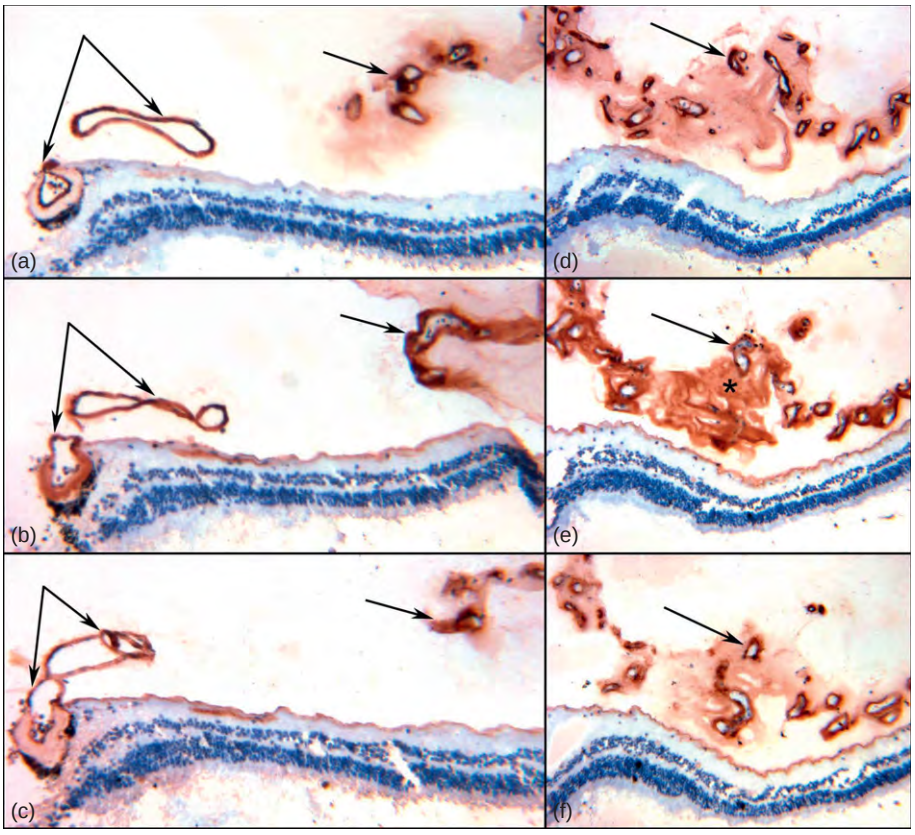

Figure 4 Localization of PEDF and VEGF in proliferative sickle cell retinopathy. A feeder vessel (a–c) and adjacent sea fan neovascularization formation (d–f) in a 58-year-old female SC subject. Heparan sulfate proteoglycan (HSPG) is prominent in vascular basement membranes in retina and the feeder vessel for the sea fan ((a); double arrow) and the sea fan blood vessels (arrow) and condensed vitreous around the vessels (d). PEDF is present in the wall of retinal blood vessels and the feeder vessel as well as condensed vitreous (b) and the sea fan, its matrix (*), and condensed vitreous associated with the membrane (e). VEGF localization is almost identical to HSPG in retinal blood vessels (c) and preretinal sea fan formation (f). (AEC immunoreaction product and hematoxylin counterstain in all.) Reproduced from Lutty, G. A. et al. (2003). *Experimental Eye Research* 77: 433–445.

angiogenesis and may even be predictive of disease progression. Undoubtedly, there is a dynamic balance between these two groups of factors that determines whether vitreous is avascular or not, which is apparent in animals with anti-angiogenic genes knocked out that have a persistent fetal vasculature and have more intravitreal neovascularization in the OIR model.

Acknowledgments

The studies mentioned in this article from the Lutty lab were funded by the Juvenile Diabetes Foundation International, Research to Prevent Blindness, the Helena Rubinstein Foundation, the Altsheler-Durell Foundation, and NIH grants EY09357 (GL), HL45922 (GL), and EY01765 (Wilmer). The author greatly appreciates Scott McLeod's creation of the figures and Steve Wajer for Figure 1, and Arnall Patz, M.D., for his guidance and support during these studies.

See also: Formation and Regression of the Primary Vitreous and Hyaloid Vascular System.

Further Reading

Adamis, A. P., Miller, J. W., Bernal, M.-T., et al. (1994). Increased vascular endothelial growth factor levels in the vitreous of eyes with proliferative diabetic retinopathy. *American Journal of Ophthalmology* 118: 445–450.

Balazs, E. A. (1960). Physiology of the vitreous body. In: Schepens, C. L. (ed.) *Importance of the Vitreous Body in Retina Surgery with Special Emphasis on Reoperation*, pp. 29–48. St. Louis, MO: C.V. Mosby.

Balazs, E. A. and Denlinger, J. L. (1984). The vitreous. In: Davis, H. (ed.) *The Eye*, pp. 533–600. New York: Academic Press.

Balazs, E. A., Toth, L. Z., and Ozanics, V. (1980). Cytological studies on the development of vitreous as related to the hyaloid vessel system. *Albrecht Von Graefes Archive for Clinical and Experimental Ophthalmology* 213: 71–85.

Becerra, S. P. (2006). Focus on molecules: Pigment epithelium-derived factor (PEDF). *Experimental Eye Research* 82: 739–740.

Blobe, G. C., Schiemann, W. P., and Lodish, H. F. (2000). Role of transforming growth factor beta in human disease. *New England Journal of Medicine* 342: 1350–1358.

Lazarus, H. S., Schoenfeld, C. L., Fekrat, S., et al. (1996). Hyalocytes synthesize and secrete inhibitors of retinal pigment epithelial cell proliferation *in vitro*. *Archives of Ophthalmology* 114: 731–736.

Lutty, G. A., Mello, R. J., Chandler, C., et al. (1985). Regulation of cell growth by vitreous humor. *Journal of Cell Science* 76: 53–65.

Lutty, G. A., Merges, C., Threlkeld, A. B., et al. (1993). Heterogeneity in localization of isoforms of TGF-β in human retina, vitreous, and choroid. *Investigative Ophthalmology and Visual Science* 34: 477–487.

Lutty, G. A., Thompson, D. C., Gallup, J. Y., et al. (1983). Vitreous: An inhibitor of retinal extract-induced neovascularization. *Investigative Ophthalmology and Visual Science* 24: 52–56.

Ogata, N., Nishikawa, M., Nishimura, T., et al. (2002). Unbalanced vitreous levels of pigment epithelium-derived factor and vascular endothelial growth factor in diabetic retinopathy. *American Journal of Ophthalmology* 134: 348–353.

Ogata, N., Tombran-Tink, J., Jo, N., et al. (2001). Upregulation of pigment epithelium-derived factor after laser photocoagulation. *American Journal of Ophthalmology* 132: 427–429.

Sebag, J. (1989). *The Vitreous: Structure, Function, and Pathology*. New York: Springer.

Sommer, F., Pollinger, K., Brandl, F., et al. (2008). Hyalocyte proliferation and ECM accumulation modulated by bFGF and TGF-β1. *Graefes Archive for Clinical and Experimental Ophthalmology* 246: 1275–1284.

Stitt, A. W., Graham, D., and Gardiner, T. A. (2004). Ocular wounding prevents pre-retinal neovascularization and upregulates PEDF expression in the inner retina. *Molecular Vision* 10: 432–438.

Antigen-Presenting Cells in the Eye and Ocular Surface

P Hamrah and R Dana, Harvard Medical School, Boston, MA, USA

Glossary

ACAID (anterior chamber-associated immune deviation) – Systemic inhibition of delayed-type hypersensitivity reactions to antigens which have previously been placed into the anterior chamber of the eye.
APC (antigen-presenting cell) – A cell that displays foreign antigen complex with major histocompatibility complex on its surface.
CX3CR1 – CX3CR1 (Fractalkine receptor) is important for homing of Langerhans-like dendritic cells to the corneal epithelium.
DC (dendritic cell) – Professional antigen-presenting cells.
DC-LAMP/CD208 – A member of the lysosome-associated membrane glycoprotein (LAMP) family, specifically expressed by mature dendritic cells.
DC-SIGN/CD209 – A type 2 transmembrane protein that also contains a mannose-binding (C-type lectin) domain, expressed on dendritic cells.
EAU (experimental autoimmune uveitis) – A disease of the neural retina induced by immunization with retinal antigens.
F4/80 – Antibody that recognizes both dendritic cells and macrophages.
GFP (green fluorescent protein) – Originally isolated from the jellyfish *Aequorea victoria* that fluoresces green when exposed to blue light. The GFP gene is frequently used as a reporter of expression. Animals have been created that express GFP as a proof-of-concept that a gene can be expressed throughout a given organism.
LCs (Langerhans cells) – Dendritic cells that typically reside in the epithelium or epidermis.
MHC class II (major histocompatibility complex class II) – These are necessary to present antigen to T cells.

Introduction

Antigen-presenting cells (APCs) serve as the immune sentinels to the foreign world and can be subdivided into professional and nonprofessional APCs. In the eye, professional APCs, such as dendritic cells (DCs), epithelial Langerhans cells (LCs), macrophages, and B cells, are derived from hematopoietic stem and progenitor cells in the bone marrow (BM), forming an integral part of the immune system. Nonprofessional APCs are found among nonlymphoid cells (e.g., vascular endothelial cells, corneal endothelial cells, and keratocytes) and have a low T-cell stimulatory capacity. However, they can gain requisite signals for T-cell priming under certain circumstances (e.g., inflammation).

DCs are specialized APCs that play a dual role in inducing adaptive immune responses to foreign antigens and in maintaining T-cell tolerance to self. DCs can also play an important role in innate immunity due to their capacity to respond acutely to inflammatory insults or danger signals in peripheral tissues. DCs consist of several distinct populations that can be differentiated by surface and intracellular phenotypic markers, immunological function, and anatomic location. In mice, DCs variously express the CD11c integrin and MHC class-II (MHC-II) molecules, and are further phenotypically distinguished by their differential expression of CD8α, CD4, and CD11b, as well as a growing list of other new markers. Irrespective of their phenotype and immunological role, DCs exert their activity in the eye remote from their place of origin, where they utilize their advanced migratory skills for navigation.

DC progenitors are not restricted to the BM and can be found in multiple locations. These progenitors can differentiate into DCs upon challenge in peripheral tissues. Fully differentiated DCs are found in healthy tissues as immunologically immature cells, being able to sample foreign antigens, but not able to prime naive T cells. Immature DCs express negligible amounts of MHC-II on their surface, and lack the requisite accessory (costimulatory) signals for T-cell activation, such as CD40, CD80 (B7-1), and CD86 (B7-2). In their immature state, they remain alert until signals in the extracellular milieu through inflammatory mediators (derived from microbes or distressed bystander cells) induce a rapid change in function, also known as activation or maturation. Maturation induces redistribution of MHC molecules from the intracellular endocytic compartments of DCs to the cell surface, allowing for T-cell stimulation.

Macrophages reside in virtually every tissue, are an integral part of the innate immune response, and synthesize and secrete a variety of powerful biological molecules. They develop from myeloid progenitor cells, enter the bloodstream as monocytes, and migrate into tissues as macrophages. Monocytes are circulating precursors for

tissue DCs and macrophages, being able to maintain or replenish populations in the peripheral tissues during homeostasis. Macrophages express low levels of MHC-II and costimulatory molecules that enable them to act as APCs, even though much less efficient than DCs. Macrophages are generally poorly responsive to activation signals, and also play a role in other processes, including immune regulation and suppression, tissue reorganization, angiogenesis, and lymphangiogenesis. APCs, including macrophages and DCs, are found in a variety of ocular tissues, including the cornea, conjunctiva, iris, ciliary body, sclera, retina, and choroid.

Antigen-Presenting Cells of the Ocular Surface

The immune-mediated responses of the ocular surface are influenced by its unique anatomy and physiology. The ocular surface consists of three distinct anatomical regions: the cornea, the limbus, and the conjunctiva that function both independently and in concert as specific barriers against microbial, immunogenic, and traumatic insults. Although the conjunctiva and cornea are anatomically proximate and are bathed in the same tear film, their immune responses are distinctly different from each other. Two populations of BM-derived cells, (1) macrophages or monocytes and (2) DCs/ LCs, form the main APC arm of the ocular surface immune response (Figure 1).

Corneal APCs

Epithelial Langerhans cells

During homeostasis, peripheral resident LCs, a subset of DCs, are the only cells that constitutively express MHC-II in the corneal epithelium (Table 1). While a large number of LCs are MHC-II^{+} in the periphery, a large population of MHC-II-negative immature LCs are present both in the periphery and the center of the epithelium, with the center being exclusively negative for MHC-II and costimulatory markers. These immature LCs are capable of expressing MHC-II and costimulatory markers during inflammation and migrate to draining lymph nodes (LNs) to present antigen. Phenotypically, both the peripheral and central murine LCs are CD11c^{+}CD11b^{-}, with the density of these cells decreasing from the limbus toward the center. These LCs have a classic dendritic morphology with long processes interdigitating among the corneal epithelial cells. In mice lacking the chemokine receptor CX3CR1, homing of immature LCs to the epithelium is markedly impaired.

APCs can be observed in living healthy corneas by modern *in vivo* confocal microscopy. Similar to rodents, the density of APCs declines from the limbus to the

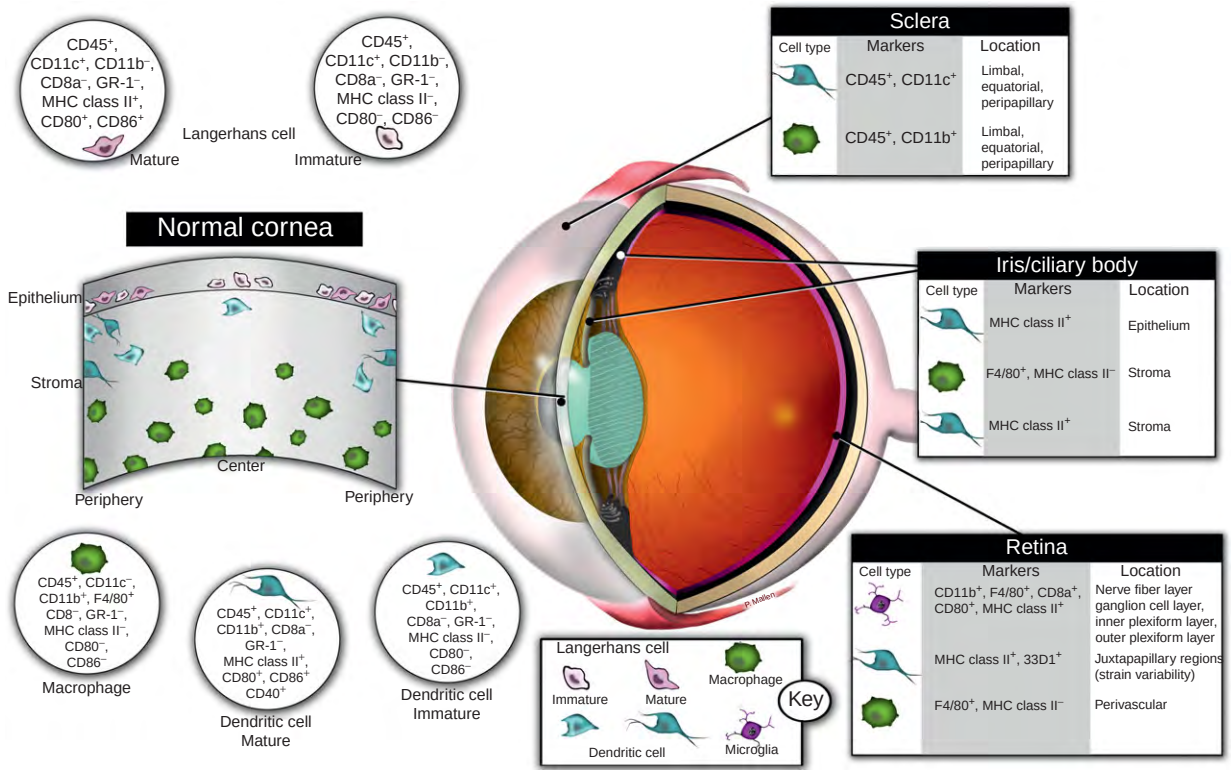

Figure 1 Schematic of antigen-presenting cells of various tissues in the eye.

Table 1 Antigen-presenting cell markers in *normal* corneal tissue

Tissue/cell type	*Markers*	*Location*
Corneal epithelium (Mouse)		
Langerhans cells (mature/immature)	$CD45^+$, $CD11c^+$, $CD11b^-$, $CD8a^-$ GR-1^-, MHC class $II^{+/-}$, $CD80^{+/-}$ $CD86^{+/-}$	Periphery
Langerhans cells (immature)	$CD45^+$, $CD11c^+$, $CD11b^-$, $CD8a^-$ GR-1^-, MHC class II^-, $CD80^-$, $CD86^-$	Center/periphery
Corneal epithelium (Human)		
Langerhans cells	$CD45^+$, $CD11c^+$, $CD207^+$, $CD1a^+$, HLA-DR^+, $CD11b^-$, DC-$SIGN^-$, DC-$LAMP^-$	Periphery
Langerhans cells	$CD45^+$, $CD11c^+$, $CD207^-$, $CD1a^-$, HLA-DR^-, $CD11b^-$, DC-$SIGN^-$, DC-$LAMP^-$	Center/periphery
Corneal stroma (Mouse)		
Dendritic cells (mature/immature)	$CD45^+$, $CD11c^+$, $CD11b^+$, $CD8a^-$ GR-1^-, MHC class $II^{+/-}$, $CD80^{+/-}$, $CD86^{+/-}$, $CD40^{+/-}$	Periphery
Dendritic cells (Immature)	$CD45^+$, $CD11c^+$, $CD11b^+$, $CD8a^-$ GR-1^-, MHC class II^-, $CD80^-$, $CD86^-$	Center/periphery
Macrophages	$CD45^+$, $CD11c^-$, $CD11b^+$, F4/80^+ $CD8^-$, GR-1^-, MHC class II^-, $CD80^-$, $CD86^-$	Center/periphery
Corneal stroma (Human)		
Dendritic cells	$CD45^+$, mostly $CD11c^+$, $CD11b^+$, HLA-DR^+, $CD207^-$, $CD1a^-$, DC-$SIGN^-$, few DC-$LAMP^+$	Periphery/few central
Dendritic cells	$CD45^+$, DC-$SIGN^-$, DC-$LAMP^-$ mostly $CD11c^+$, $CD11b^+$, HLA-DR^-, $CD207^-$, $CD1a^-$	Central/periphery
Macrophages	$CD45^+$, $CD11b^+$, $CD11c^-$, HLA-DR^-, $CD207^-$, $CD1a^-$, DC-$SIGN^-$, DC-$LAMP^-$	Periphery/few central

center in the healthy human cornea. In the corneal limbal epithelium, DCs are present in almost every healthy subject, while in the central cornea only some 20–30% of healthy controls show APCs. LCs are located at a depth of 35–60 μm, mostly at the level of basal epithelial cells and the subbasal nerve plexus. Phenotypically, peripheral LCs in freshly cultured human corneas are Langerin $(CD207)^+$/$CD1a^+$/$CD11c^+$/HLA-DR^+, with no Langerin expression on central LCs. The expression of high levels of CD1a and Langerin on peripheral LCs suggests a unique role of these cells in initiating immune responses to microbial pathogens.

Stromal APCs

Resident DCs reside in the periphery and center of the anterior corneal stroma. Phenotypically, these DCs are $CD11c^+CD11b^+CD8a^-$ demonstrating their monocytic lineage, although a small number of plasmocytoid DCs have been described. Peripheral stromal DCs are MHC-II^+ and positive for the costimulatory markers CD80, CD86, and CD40. The stromal center, however, contains exclusively MHC-$II^-CD80^-CD86^-$ DCs, similar to those of the highly immature LCs in the epithelium. The density of murine stromal DCs decreases from the limbus toward the center of the cornea. A population of undifferentiated monocytic precursor cells distinct from DC and macrophage populations also resides in the corneal stroma. Thus, in contrast to other organs, where terminally differentiated populations of resident DCs and/or macrophages outnumber colonizing precursors, large numbers of DCs within the cornea remain in a relatively undifferentiated state. The absence of MHC-II molecules in the normal cornea might actively maintain tolerance to foreign antigens, as antigen presentation to T cells by immature DCs can lead to anergy of T cells and subsequent tolerance, protecting the cornea from immune-mediated damage, when the insults are minor.

Resident $CD11c^-CD11b^+$ corneal macrophages are present in the posterior stroma of the normal mouse and human cornea, and are distinct from the DCs described in the anterior stroma. They are located in the peripheral, paracentral, and central regions. These resident stromal macrophages likely provide a critical first line of defense against pathogens that breach the epithelial barrier of the cornea by producing antimicrobial substances, as well as other inflammatory cytokines and chemokines to attract and activate additional macrophages, neutrophils, and DCs.

In freshly cultured human corneas, DCs express DC-SIGN and are detected mainly peripherally and in the anterior stroma, having only variable CD11c expression. Most of these cells are HLA-DR^-, with few mature DCs expressing DC-LAMP/HLA-DR or costimulatory markers. These DCs can be found in the cornea even after long-term culture. DC-$LAMP^+$ mature DCs are only partially DC-$SIGN^+$, implying that the peripheral stroma harbors two sets of rare mature DCs, those that coexpress DC-SIGN (mostly $CD11c^-$) and those that do not coexpress DC-SIGN ($CD11c^+$).

Studies in BM chimera mice have demonstrated a turnover rate for BM-derived cells in the stroma at around 24% at 2 weeks. Replenishment occurs initially in the peripheral cornea and the anterior stroma. By 8 weeks, turnover reaches 75%, reaching a plateau between 2 and 6 months. Close to one-third of migrating cells into the central and peripheral cornea are DCs.

Corneal APCs in Inflammation

Microbial products stimulate the immune system by interacting with toll-like receptors (TLRs) on APCs and other cells. The interaction between TLRs and their ligands activates APCs toward maturity. In addition, the release of proinflammatory cytokines, including interleukin (IL)-1β, GM-CSF, tumor necrosis factor (TNF)-α, and lipopolysaccharides (LPS), or heat-shock proteins from dying cells, creates a microenvironment that activates immature DCs. DCs themselves are also important producers of these proinflammatory cytokines, which act in an autocrine fashion to promote DC activation and maturation. Resident immature epithelial LCs and stromal DCs in the central cornea can significantly upregulate maturation markers, including MHC-II and costimulatory markers, within 24 h after induction of inflammation (Table 2).

In addition to the resident APC population, APCs are also recruited into the cornea from the limbal areas through upregulation of IL-1 and TNF-α during inflammation (Figure 2). In general, the migration of APCs to peripheral tissues requires the concerted activity of cell adhesion molecules and chemotactic factors. Cell adhesion molecules regulate both cell–cell and cell–matrix interactions, while chemokines provide directionality to local and infiltrating APCs. Suppression of these cytokines leads to downmodulation of APC migration into the cornea. IL-1 and TNF-α can act in concert to recruit APCs from the limbus into the cornea by mediating the expression of cell adhesion molecules and chemokines. Recruitment of macrophages into the cornea plays a crucial role in inducing inflammatory neovascularization by supplying or amplifying signals essential for pathological hemangiogenesis. Macrophages, but not DCs, physically

Table 2 Antigen-presenting cell markers in *inflamed* corneal tissue

Tissue/cell type	*Markers*	*Location*
Corneal epithelium (mouse)		
Langerhans cells (mature/immature)	$CD45^+$, $CD11c^+$, $CD11b^-$, $CD8a^-$ GR-1^-, MHC class $II^{+/-}$, $CD80^{+/-}$, $CD86^{+/-}$	Periphery/center
Corneal stroma (mouse)		
Dendritic cells (Mature/immature)	$CD45^+$, $CD11c^+$, $CD11b^+$, $CD8a^-$ GR-1^-, MHC class $II^{+/-}$, $CD80^{+/-}$, $CD86^{+/-}$, $CD40^{+/-}$	Periphery/center
Macrophages	$CD45^+$, $CD11c^-$, $CD11b^+$, F4/80^+ $CD8^-$, GR-1^-, MHC class II^-, $CD80^-$, $CD86^-$	Periphery/center

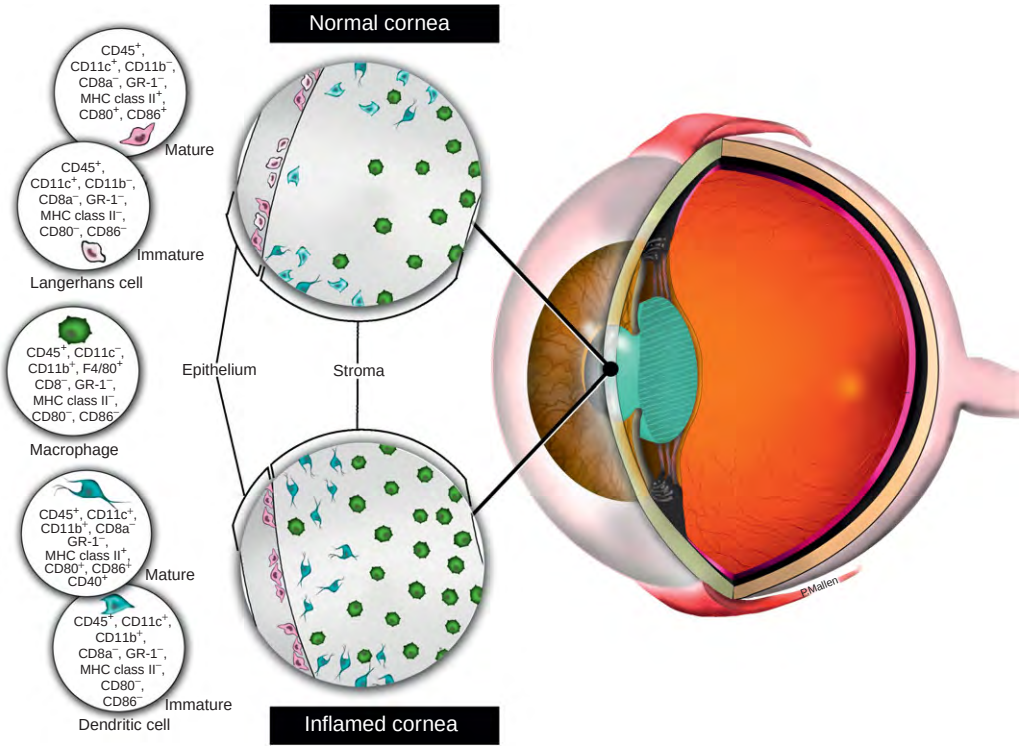

Figure 2 Schematic of the effect of inflammation on corneal antigen-presenting cells.

contribute to lymphangiogenesis under pathological conditions and express lymphatic endothelial markers such as LYVE-1 and Prox-1 under inflamed conditions. Macrophages are capable of forming tube-like structures that express LYVE-1 and podoplanin, and are actively involved in lymphangiogenesis.

The Function of APCs in Corneal Transplantation

The process of corneal transplant rejection includes an induction phase, called the afferent arm, and an expression phase, called the efferent arm. In the afferent arm the host becomes sensitized to the donor antigens by means of APCs , presenting antigens to T cells. This process can take place through two different pathways. The direct pathway, involving donor APCs that sensitize the host directly and the indirect pathway, involving host APCs that move toward the graft, take up donor antigens, and then present these antigens to T cells in draining LNs. While both direct and indirect alloreactive T cells can mediate graft rejection, host sensitization to donor antigens of corneal grafts occurs through both pathways of sensitization, especially in high-risk corneal grafting, where transplantation occurs in an inflamed bed. CD40 is a critical costimulatory molecule expressed by many APCs (including corneal DCs and LCs), whose ligation by CD154 leads to overexpression of other costimulatory molecules, and IL-12 – critical factors in priming a T-cell response. Blocking the interaction of CD40 with CD40 ligand/CD154 can block both the direct and indirect pathways of allosensitization, by preventing T-cell priming, but without promoting active tolerance.

Disruption of the eye–LN axis in the setting of corneal transplantation has been shown to lead to both complete prevention of host allosensitization and the indefinite survival of corneal grafts, demonstrating the functional relevance of corneal APC trafficking to draining LNs. Both donor and host-derived corneal APCs are capable of migrating efficiently to host LNs within 24 h after corneal transplantation. Since the cornea is alymphatic, this is achieved through sprouting of new lymphatic vessels into the cornea upon inflammation, and through migration of APCs toward the lymphatic-rich limbus and conjunctiva. Signaling through vascular endothelial growth factor receptor-3 (VEGFR-3) is critical for DC access to lymphatics, and selective blockade of this pathway can impair DC flow to LNs and the induction of alloimmunity, leading to reduction in the rate of graft rejection. On the one hand, migration of DC to LNs is facilitated by the interaction of the chemokine receptor CCR7 on their surface, with CCL21 secreted by the lymphatic vessels. On the other, CCR1 and CCR5 have been shown to be responsible for the recruitment of immature DCs in inflamed tissues, through their ligands CCL4, CCL5, and CCL7, with only stromal DCs expressing CCR1. Blockade of CCR1 leads to significant reduction in the rate of graft rejection, indicating the important role of stromal DCs in the alloimmune response. Interestingly, depletion of donor APCs before transplantation, however, does not have a significant effect on promoting graft survival, even in the high-risk setting, suggesting that these cells, other than promoting immunization, may also be relevant in the induction of maintenance of tolerance.

The Function of APCs in Microbial Keratitis

Herpetic stromal keratitis (HSK) is an inflammatory disorder induced by herpes simplex virus (HSV)-1 infection and is characterized by T-cell-dependent destruction of corneal tissues. The number of MHC-II$^+$ LCs present in the central areas of the cornea has been shown to correlate with the degree of corneal damage. Virally induced migration or maturation of LCs in the cornea precedes the development of HSK. Induction of LC migration into the central cornea before HSV-1 infection results in an accelerated and enhanced delayed-type hypersensitivity (DTH) response to HSV-1 antigens, and in an increased severity of HSK. Contrary, depletion of DCs reduces the incidence and severity of HSK, suggesting a role for DCs in the induction of a T-cell response. These findings have led to the conclusion that HSV-1 infection results in *de novo* migration of LCs from the limbus, which in turn might play a role in the immunopathology of HSK though presentation of antigens to T cells in the infected cornea.

Pseudomonas aeruginosa is an opportunistic pathogen associated with sight-threatening keratitis, whose outcome is largely determined by the host inflammatory response. Specific susceptible mouse strains challenged with *P. aeruginosa* undergo corneal perforation, while other strains are resistant. While induction of LCs into the central cornea of already susceptible strains before infection does not alter the outcome of disease, induction of LCs into the central cornea of resistant strains converts these to a susceptible phenotype. LCs in these mice express the costimulatory molecule B7-1, enhancing their capacity to present antigen to T cells. Further, macrophages control resistance to *P. aeruginosa* corneal infection through regulation of neutrophil number and apoptosis, bacterial killing and balancing pro- and anti-inflammatory cytokine levels.

Conjunctival APCs

In the naive conjunctiva, predominantly MHC-II$^+$ DCs are consistently detected from birth in the subepithelial layer and substantia propria. There are species and strain-specific differences in the numbers of these cells, with 200–400 LCs mm^{-2} in humans as compared to 100–150 LCs mm^{-2} in mice, with rat and guinea pig numbers intermediate between these two. Further, the

number of LCs is not static and increases with age. Moreover, a significant variability in LC density is also found in different regions of the conjunctiva. The largest number of epithelial LCs is found in the palpebral and inferior fornical region, followed by the medial and inferior epibulbar conjunctiva. DCs of the substantia propria are distributed most densely in the superior and medial epibulbar conjunctiva. This variability within the conjunctiva is interesting, and may be related to exogenous antigenic challenge secondary to the direction of normal tear drainage or to microenvironmental differences within the conjunctiva. Finally, macrophages have a density of 6.5 cells/mm^2 in the tarsal epithelium and 32.2 cells/mm^2 in the tarsal substantia propria, with similar numbers in the bulbar conjunctiva.

Role of APCs in Allergic Eye Disease

Allergic eye disease is a spectrum of diseases that share a common initiating mechanism and pattern of inflammation. While B cells and T cells are the mediators of the allergic immune response, DCs are the actual initiators and modulators of this response. Mast cells mediate the effector phase of the allergic response, whereas DCs are critical in determining the nature of the allergic response. During the sensitization phase, allergens encounter DCs on the ocular surface. Following allergen challenge, there is a marked influx of conventional DCs and plasmocytoid DCs into the subepithelial layer and throughout the substantia propria. DCs then process and present the allergen to T cells in association with the MHC-II. These T cells are then polarized in favor of the development of allergen sensitivity.

APCs of the Uvea

The uveal tract, the vascularized middle layer of the eye, consists of the iris, ciliary body, and choroid. It contains rich networks of F4/80$^+$ APCs that reside and traffic through the eye (**Figure 1** and **Table 3**). These populations include large numbers of macrophages and to a lesser extent, immature DCs, maintaining local immunological homeostasis, and play a role in inflammatory processes and immune-mediated diseases. Dendritiform and pleiomorphic macrophages are distributed in a regular array within the rat iris and ciliary body stroma (600–700 cells/mm^2). The iris contains a network of MHC-II$^+$ DC (400–600 cells/mm^2) within the iris stroma and ciliary epithelium, with few DCs in the uveal tract expressing costimulatory molecules. BM chimera studies demonstrate replenishment of BM-derived cells starting at 2 weeks, with almost complete turnover by 8 weeks in the iris stroma and posterior iris surface. Replenishment rates in the uveal tract are similar in the choroid, iris, and ciliary body stroma, although DCs in the ciliary epithelium replenish at a slightly slower rate starting at 4 weeks.

Table 3 Antigen-presenting cells of the *normal* uvea

Tissue/cell type	*Markers*
Iris/ciliary body stroma	
Macrophages	F4/80$^+$, MHC class II$^-$
Dendritic cells	MHC class II$^+$
Ciliary body epithelium	
Dendritic cells	MHC class II$^+$

Intraocular DCs, after contact with aqueous humor of the anterior chamber, migrate through the trabecular meshwork to the spleen. Additionally, they begin to secret IL-10 and transforming growth factor (TGF)-β in an autocrine fashion, thereby creating a microenvironment that is rich in tolerance-inducing mediators. These DCs promote the effective suppression of T-cell-dependent inflammatory reactions in the lymphoid organs, inducing sufficient levels of tolerance. DCs in the tissues lining the anterior chamber represent a rich network of APCs and are the most likely candidates for transmitting antigen-specific signals from the anterior chamber *in vivo* and in experimental models such as anterior chamber-associated immune deviation (ACAID).

Anterior Chamber-Associated Immune Deviation

The eye receives immune protection against pathogens, while avoiding inflammatory and immunological damage. The selective inability to develop delayed-hypersensitivity responses following antigen invasion into the anterior segment of the eye is highly dependent on DCs, which form the basis of an extraordinary phenomenon called ACAID. The immune response begins with intraocular capture of antigen by specialized ocular F4/80$^+$ APCs in the iris/ciliary body. ACAID-inducing APCs create a microenvironment rich in TGF-β and IL-10, but deficient in IL-12, thus failing to upregulate CD40. These APCs then migrate through the trabecular meshwork and the venous circulation, preferentially to the marginal zone of the spleen, where they become part of an intricate and highly specific cluster of immune cells. The end result is the emergence of a population of antigen-specific T-regulatory lymphocytes that return to the eye and suppress DTH response. A similar process has been described in the vitreous and other posterior compartments of the eye.

Role of APCs in Age-Related Macular Degeneration

AMD is the most common cause of legal blindness in elderly individuals of industrialized countries. The presence of complement factor proteins in drusen in AMD eyes and single nucleotide polymorphisms (SNPs) for complement factor regulatory genes in individuals with AMD implicate inflammation as an important component

in this disease. Choroidal macrophages are proposed as key players in the removal of age-related accumulation of extracellular debris at the choroidal–retinal interface. Observation of aging mice deficient in CCR2 or CCL-2 indicates that defective clearance or scavenging mechanism by resident choroidal macrophages may, in part, be responsible for the presence of drusen deposits at the choroidal–retinal interface. In addition to the potential role of choroidal macrophages, the discovery of age-dependent accumulation of subretinal microglia has recently implicated this population of cells as potential initiators of neovascularization and photoreceptor damage.

Role of APCs in EAU

Resident APCs of the normal human uvea are endowed with the complete LPS receptor complex and are strategically positioned in perivascular and subepithelial locations for surveying blood-borne or intraocular LPS. LPS may act as an adjuvant by activating APC maturation in the presence of the putative uveitogenic self-antigens and thus mediate the breakdown of peripheral tolerance resulting in the induction of an autoimmune response. APCs that capture self-antigens, present them to autoreactive T cells and induce T-cell tolerance by deletion or anergy, as these APCs are relatively immature. TLRs, however, can convert tolerogenic signals to activating signals by promoting APC maturation.

DCs and macrophages act as local APCs in the induction of uveoretinitis. Specifically, MHC-II$^+$ DCs appear at the time of disease onset and continue to be recruited during the inflammatory process, indicating their role in initiation if EAU. MHC-II$^-$ macrophages expressing antigens, however, are prominent during the peak phase of tissue damage in the retina and choroid. Depletion of these cells causes a delay in the onset and a reduction in the severity of EAU.

APCs of the Retina

The presence of the blood–retinal barrier and a predominantly immunosuppressive intraocular environment contribute to the suppression of local immune responses to retinal antigens. Nevertheless, retinal inflammation is not uncommon. Retinal antigen-specific T cells must encounter cognate antigen on APCs within the retina to initiate retinal inflammation. Several distinct populations of myeloid-derived cells reside in the retina, namely, the more prevalent retinal microglia (CD11b$^+$F4/80$^+$CD8a$^+$ CD80$^+$MHC-II$^+$), as well as perivascular macrophages (**Figure 1** and **Table 4**). Perivascular macrophages have poor antigen-presenting capability and are not thought to be absolutely essential for disease induction. Further, a population of BM-derived MHC-II$^+$ 33D1$^+$ DCs has been identified in mice, of which small numbers reside in the peripheral margin and juxtapapillary regions. Of note, the distribution and phenotype of these DCs within the retinas differs between mouse strains exhibiting different disease susceptibility. In EAU-resistant mice, DCs are MHC-II (low/–). Conversely, DCs are MHC-II$^+$ in EAU-susceptible mice.

Table 4 Antigen-presenting cells of the *normal* retina

Cell type	*Markers*	*Location*
Retinal microglia	CD11b$^+$, F4/80$^+$, CD8a$^+$, CD80$^+$, MHC class II$^+$	Nerve fiber layer ganglion cell layer, inner plexiform layer, outer plexiform layer
Dendritic cells	MHC class II$^+$, 33D1$^+$	Peripheral margin and juxtapapillary regions (strain variability)
Macrophages	F4/80$^+$, MHC class II$^-$	Perivascular

Microglia reside in the nerve fiber/ganglion cell layer, inner plexiform layer, and outer plexiform layer of the retina. Resting microglia play various roles in host defense, immunoregulation, and tissue repair and rapidly increase in numbers in response to various insults in the retina. Retinal microglia respond to photoreceptor light-induced injury or degeneration by migration from the inner retinal layers toward the photoreceptor layer and subretinal space, where they phagocytose photoreceptor debris and remain for prolonged periods. Resident host microglia residing in the inner retina are the principal source of the phagocytic microglia that accumulate in the photoreceptor layer and subretinal space during aging or retinal degeneration.

BM chimera studies demonstrate reconstitution of myeloid cells in the retina beginning at 4 weeks. Migrating cells are evident at the juxtapapillary margin and migrating deeper into the retinal layers, and almost completely replenish between 2 and 6 months, depending on the strain. Turnover of microglia within the retinal microenvironment occurs at a much slower rate than other peripheral tissue macrophages. When photoreceptor degeneration is induced, large numbers of microglia/macrophages are observed in the injured retina, starting at 12 h after injury, and peaking at 24 h. In addition, the number of MHC-II$^+$ cells in the retina increases greatly after retinal injury. In response to retinal damage, numerous BM-derived cells migrate to the retina from the ciliary body, optic nerve, and retinal vessels and differentiate into microglia. The higher rate of immunologic activation and the increased specificity to the damaged site appear to be the characteristic features of BM-derived microglia.

APCs of the Sclera

BM-derived cells have been described in the sclera. In BM chimeras, BM-derived cells replenish the sclera

Table 5 Antigen-presenting cells of the *normal* sclera

Cell type	*Markers*	*Location*
Dendritic cells	$CD45^+$, $CD11c^+$	Limbal, equatorial, peripapillary
Macrophages	$CD45^+$, $CD11b^+$	Limbal, equatorial, peripapillary

through limbal vessels and optic nerve vessels, migrating into the equatorial zone. These cells are $CD11c^+$ or $CD11b^+$ DCs and macrophages are found among the scleral fibroblasts (**Figure 1** and **Table 5**). During EAU, significant infiltration of these BM-derived cells takes place into the sclera, contributing to the ocular immune response.

Conclusions

The integrity of the visual system in the face of ever-changing immune challenges is vital. The unique immune homeostasis and immunological status of the eye and ocular surface is fascinating and continuously evolving. It is compelling that most of the APCs described herein were only discovered less than 10 years ago, emphasizing how much still has to be learned about APCs and their function in the eye. The constitutive presence of APCs in the ocular tissues has significant implications for a variety of infectious, autoimmune, and inflammatory responses in the eye. Since the presence of resident ocular APCs was largely unknown until very recently, many paradigms have already been shifted and many more will need to be rethought in the future. Understanding the mechanisms that lead to APC maturation, activation, and trafficking may well lead to novel approaches in the induction of tolerance, autoimmunity, and vaccine therapy.

See also: Adaptive Immune System and the Eye: Mucosal Immunity; Adaptive Immune System and the Eye: T Cell-Mediated Immunity; Dry Eye: An Immune-Based Inflammation; Dynamic Immunoregulatory Processes that Sustain Immune Privilege in the Eye; Immunosuppressive and Anti-Inflammatory Molecules that Maintain Immune Privilege of the Eye; Innate Immune System and the Eye; Penetrating Keratoplasty.

Further Reading

Dana, R. (2004). Corneal antigen-presenting cells: Diversity, plasticity, and disguise: The Cogan lecture. *Investigative Ophthalmology and Visual Science* 45: 722–727.

Hamrah, P. and Dana, R. (2007). Corneal antigen-presenting cells. *Chemical Immunology and Allergy* 92: 58–70.

Hamrah, P., Huq, S. O., Liu, Y., Zhang, Q., and Dana, M. R. (2003). Corneal immunity is mediated by heterogeneous population of antigen-presenting cells. *Journal of Leukocyte Biology* 74: 172–178.

Kezic, J. and McMenamin, P. G. (2008). Differential turnover rates of monocyte-derived cells in varied ocular tissue microenvironments. *Journal of Leukocyte Biology* 84: 721–729.

McMenamin, P. G. (1999). Dendritic cells and macrophages in the uveal tract of the normal mouse eye. *British Journal of Ophthalmology* 83: 598–604.

Novak, N., Siepmann, K., Zierhut, M., and Bieber, T. (2003). The good, the bad and the ugly – APCs of the eye. *Trends in Immunology* 24: 570–574.

Streilein, J. W. (2003). Ocular immune privilege: Therapeutic opportunities from an experiment of nature. *Nature Reviews Immunology* 3: 879–889.

Xu, H., Dawson, R., Forrester, J. V., and Liversidge, J. (2007). Identification of novel dendritic cell populations in normal mouse retina. *Investigative Ophthalmology and Visual Science* 48: 1701–1710.

Artificial Cornea

M A Rafat, University of Ottawa Eye Institute, Ottawa, ON, Canada
J M Hackett, University of Ottawa, Ottawa, ON, Canada
P Fagerholm, Linköping University Hospital, Linköping, Sweden
M Griffith, University of Ottawa Eye Institute, Ottawa, ON, Canada

Glossary

Bioengineered corneas – Are natural-based substitutes for human donor tissue that are designed to replace part or the full thickness of damaged or diseased corneas.
Collagen – The most common naturally occurring structural protein found in all multi-cellular animals and accounts for approximately 30% of all body proteins.
Interpenetrating polymeric networks (IPNs) – Polymeric structures comprising two or more networks that are interconnected on a molecular scale through chemical (covalent) and physical bonds.
Keratoprosthesis – A type of artificial cornea that is designed to be implanted in a patient who has severe bilateral corneal disease for which a corneal transplant is not an option.
Lenticles – A tiny disk slipped into the pocket of the patient's own cornea between corneal epithelium and Bowman's membrane for vision correction.
Penetrating keratoplasty – A surgical procedure where a damaged or diseased cornea is replaced by donated corneal tissue which has been removed from a recently deceased individual having no known diseases which might affect the viability of the donated tissue.
Photorefractive keratectomy (PRK), laser-assisted sub-epithelial keratectomy (LASEK), or laser-assisted *in situ* keratomileusis (LASIK) – Laser eye-surgery procedures for correcting a person's vision can reduce the need for glasses or contact lenses.

The Need for Artificial Corneas

The terms artificial corneas (ACs) or bioengineered corneas are widely used to describe corneal scaffolds that are designed to restore vision. These scaffolds are used as substitutes to human donor corneas, and can replace part or the full thickness of damaged or diseased corneas. Corneal scaffolds can range from solely synthetic ocular prostheses through to tissue-engineered hydrogels that allow some regeneration of the host tissues. In addition, bioengineered lenticles may be implanted into the cornea to improve vision. This is achieved by altering the refractive properties of the eye, which is an alternative procedure to laser-assisted *in-situ* keratomileusis (LASIK), laser-assisted sub-epithelial keratectomy (LASEK), and photorefractive keratectomy (PRK).

Compromising the transparency of the cornea interferes with its function. Once optical clarity is compromised, due to disease or damage, vision loss occurs and can result in corneal blindness (**Figure 1**). According to the World Health Organization (WHO), there are approximately 37 million people worldwide who possess bilateral blindness, as well as at least 124 million people who have impaired vision in both eyes. Corneal ulceration and ocular trauma are reported to be the major causes of corneal blindness, accounting for 1.5–2 million new cases annually. At present, transplantation of matched human donor tissue is the only widely acceptable treatment.

Corneas are the most successful organ transplants – with an 86% graft-survival rate at the 1-year postoperative follow-up, 73% after a 5-year period, 62% after 10 years, and 55% at 15 years. The success of the transplantation is dependent upon the availability of good-quality donor tissue, as well as the patient's condition. Inactive central scars or keratoconus are amenable to transplantation; however, alkali burns or neurotrophic scars that are secondary to Herpes zoster ophthalmicus have a poor prognosis. The cornea donor pool is in limited supply due to a longer life expectancy, combined with the aging population within North America. Demand for corneas is expected to increase, but a shortage in supply will most likely be experienced. The shortage is expected to be compounded by the increasing incidence of infectious diseases (HIV, hepatitis, Creutzfeldt–Jakob disease, etc.), as well as the growing popularity of refractive surgery. Surgically treated corneas are thinned, rendering them unacceptable as donor tissue. As alternatives to donor tissues, bioengineered corneas are designed to replace some or all of a damaged or diseased cornea. They range from prosthetic devices that solely address replacement of the cornea's function, to tissue-engineered hydrogels that permit regeneration of host tissues. This article focuses on the efforts employed to build an *in vitro* model of the visual system.

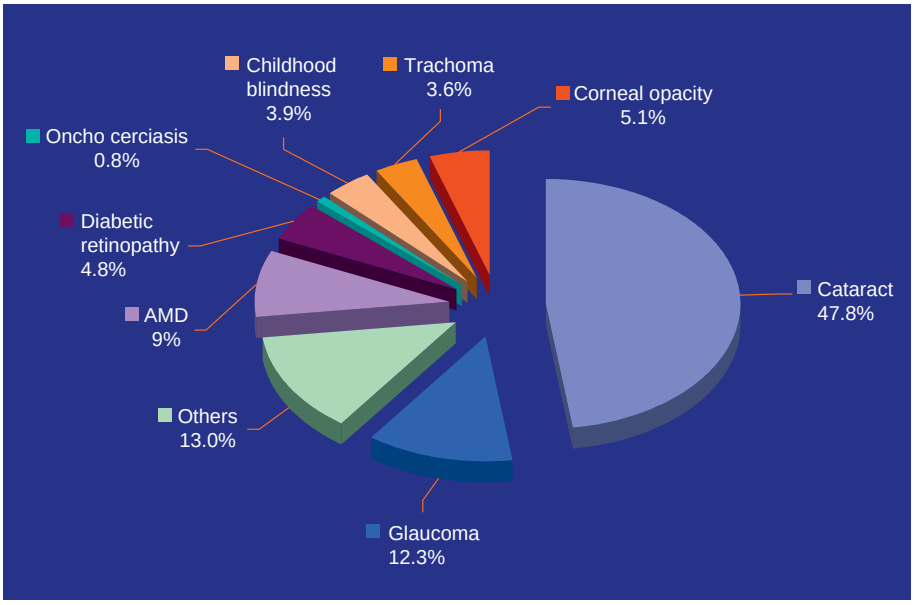

Figure 1 Global causes of blindness as a percentage of total blindness in the year 2002. Trachoma and corneal opacity are cornea-related diseases comprising about 10% of the total causes of blindness. Adapted with permission from **Fig. 1** in Resnikoff, S., Pascolini, D., Etya'ale, D., et al. (2004) Global data on visual impairment in the year 2002. *Bulletin of the World Health Organization* 82: 844–851, with permission from WHO Press.

In particular, we examine the development of novel biomaterials that serve as the building blocks for the fabrication of scaffolds in engineered tissues.

Desired Characteristics for an Implantable AC

In order to be clinically applicable, fabricated corneal substitutes need to replicate the functions of the human cornea. The human cornea forms a transparent window through which light is transmitted to the retina, enabling one to see. A unique property of the cornea is its optical clarity, which accounts for over 70% of the light that is transmitted to the retina for vision. Corneal clarity is now believed to result from a combination of refractive-index matching, and the presence of structural components that are well below the wavelength of visible light.

As alternatives to donor tissues, ACs are designed to replace some or all of a damaged or diseased cornea. They range from prosthetic devices that solely address replacement of the cornea's function, to tissue-engineered hydrogels that permit regeneration of host tissues. In instances where corneal stem cells have been depleted by injury or disease, tissue-engineered lamellar implants reconstructed with stem cells have been transplanted. *In situ* methods using ultraviolet A (UVA) cross-linking have also been developed to strengthen weakened corneas. In addition to the clinical need, bioengineered corneas are also rapidly gaining importance in the area of *in vitro* toxicology. In Europe, there is currently a ban on consumer product testing in animals (European Union Directive 76/768/EEC) that is expected to expand worldwide. Complex, fully innervated, physiologically active, three-dimensional (3D) organotypic corneal models are currently being developed and tested.

ACs must meet certain requirements, without exception, to be successful. To properly integrate into host tissue, AC must be biocompatible and noncytotoxic. A watertight junction with the host tissue is essential for preventing infection and epithelial down-growth. Epithelial cell growth must be supported over the anterior surface, allowing a wettable, self-renewing layer that promotes a healthy tear-film formation. Nerve innervations must be supported for high touch sensitivity. Penetration and proliferation of host fibroblast cells must be promoted for tissue regeneration. Optical transparency >80% and light scatter of <5% should be exhibited, as well as a suitable morphology and curvature to obtain the appropriate refractive index. In addition, flexibility and sufficient tensile strength is required to allow surgical manipulation and fixation, as well as to protect the eye. The AC should exhibit sufficient swelling in aqueous solutions similar to that of native cornea, but at the same time be permeable to oxygen, nutrients such as glucose, and serum albumin – which is a major water-soluble protein in the human cornea. Lastly, the AC must be inexpensive and easy to fabricate.

Artificial or bioengineered corneas developed to date range from prostheses – known as keratoprosthesis (KPro) – to naturally fabricated cell-based tissue equivalents, to bioengineered scaffolds that serve as templates for regeneration of host tissues.

Synthetic Artificial Corneas or Keratoprosthesis

Research into the development of an AC has existed for more than 200 years, with the original glass and quartz optics being put forward, in 1789, by Guillaume Pellier de Quengsy. Since then, there have been numerous attempts at developing ACs. Currently, four generations of KPros have been defined, according to the KPro Study group. KPros are synthetic implants designed to replace the central portion of an opaque cornea. First-generation KPros are comprised of monoblocks, or one-piece prostheses that are made from plastics such as poly methyl methacrylate (PMMA). An example of a second-generation KPros is the osteo-odonto keratoprosthesis (OOKP). This prosthesis, developed by Strampelli in 1964, consists of autologous tissue derived from tooth and bone, which surrounds a central PMMA optic. An osteodental skirt is preimplanted into the buccal mucosa, allowing colonization of fibroblasts to support its integration as an ocular implant. Third-generation KPros include a range of devices with plastic optics and metal parts that aid in anchoring the device to host tissues. Donor-tissue attachment can also be achieved through skirts, allowing for host integration. Fourth-generation KPros utilize the optic-skirt model, in which a solid optical core is surrounded by a porous skirt. This encourages biointegration with the adjacent host tissues to circumvent implant extrusion. Rigid synthetic polymers, such as PMMA, were used in the early attempts to develop artificial corneal transplants. While PMMA still remains a popular material, poly(2-hydroxyethyl methacrylate) (PHEMA) has been used more frequently in various types of KPros. In this article, we provide a synopsis of several examples of KPros that have either been tested clinically, or are currently in clinical use.

KPros currently in clinical use include the following: the OCULAID® KPro, Dohlman KPro, AlphaCor™ Kpro, OOKP KPro, BioKPro III, Seoul-type KPro, and Pintucci KPro. **Figure 2(a)** and **2(b)** represents the OCULAID® KPro, composed of an anti-conical shaped shaft that can be fixed into the host cornea or sclera. It creates a valve on the cornea to ensure a watertight environment. The pressure in the eye pushes the corneal rim around the 3-mm top of the KPro, while the steel-suture fixation on the sclera is designed to prevent extrusion. The Dohlman AC is a collar-button-design KPro, composed of PMMA. It consists of a central optical stem that penetrates the full thickness of the cornea. This stem is sandwiched between two plates and sutured into place similar to a penetrating keratoplasty (PKP) graft (**Figure 2(c)**).

The AlphaCor™ Kpro is one of the best-known keratoprosthetic devices fabricated as a one-piece device that comprises a transparent core and an opaque porous skirt. The implant is a 7-mm-diameter, one-piece, nonrigid synthetic cornea (**Figure 2(d)**). Composed of a transparent central optic core of PHEMA gel, the KPro is designed to allow the passage of light into the posterior of the eye. The outer porous skirt – an opaque, high-water PHEMA – is designed to allow cell infiltration from the host, which anchors the prosthesis into place. This device gained the Food and Drug Administration (FDA)-approval in 2002 for use in patients with scarred, vascularized, or diseased corneal tissues who are either ineligible for conventional donor-tissue transplants or have had multiple previous graft failures. Early results suggest that the AlphaCor™ Kpro, previously known as the Chirila KPro, is clinically safe. Associated complications include the formation of retroprosthetic membranes, corneal melt, retained lenticular material, optic depositions, and rare cases of device extrusion. Contraindications include abnormal tear film, as well as uncontrollable high intraocular pressure. Topical administration of medroxyprogesterone has been shown to limit corneal melting of the device. However, this KPro has been effectively used to restore a degree of vision in patients considered untreatable by conventional corneal transplantation.

The OOKP, described above, consists of autologous tissue derived from tooth, which surrounds a central PMMA optic. This KPro is one of the most successful, as it has a low extrusion rate due to the excellent integration of the skirt material with the host tissue. Associated complications with the OOKP include retroprosthetic membrane formation, glaucoma and decentration of the central optic, due to absorption of the osteodental skirt.

The BioKPro III, designed by the Legeais group, was recently clinically evaluated at the Moorfields Eye Hospital, London, UK. The BioKpro III consists of a central 5-mm-diameter, 500-mm-thick silicone optic, and a surrounding opaque skirt made of porous fluorocarbon. The device was implanted into seven patients with severe corneal scarring, and monitoring occurred between 18 and 48 months. The results showed that the KPro failed in six patients, due to extrusion occurring between 2 and 28 months postoperatively. One patient, who had a thermal burn, retained the KPro and reported an improvement in vision. However, this patient also reported mucous accumulation on the optic.

The Seoul-type KPro (S-KPro) consists of three sections: a long cylindrical optic surrounded by a mushroom-shaped anterior flange, a skirt for corneal fixation, and haptics for scleral fixation. The 4-mm diameter optic is made of PMMA; the anterior flange is composed of fluorinated silicone approximately 0.2-mm thick and 6 mm in diameter; while the skirt is fabricated from expanded polytetrafluoroethylene (e-PTFE). Preliminary results from the first human trial indicate that complications including retinal detachment, formation of a retroprosthetic membrane, and extrusion have been identified.

The Pintucci KPro consists of a 3-mm thick and 5-mm long optical cylinder made of PMMA. A woven, 0.7-mm

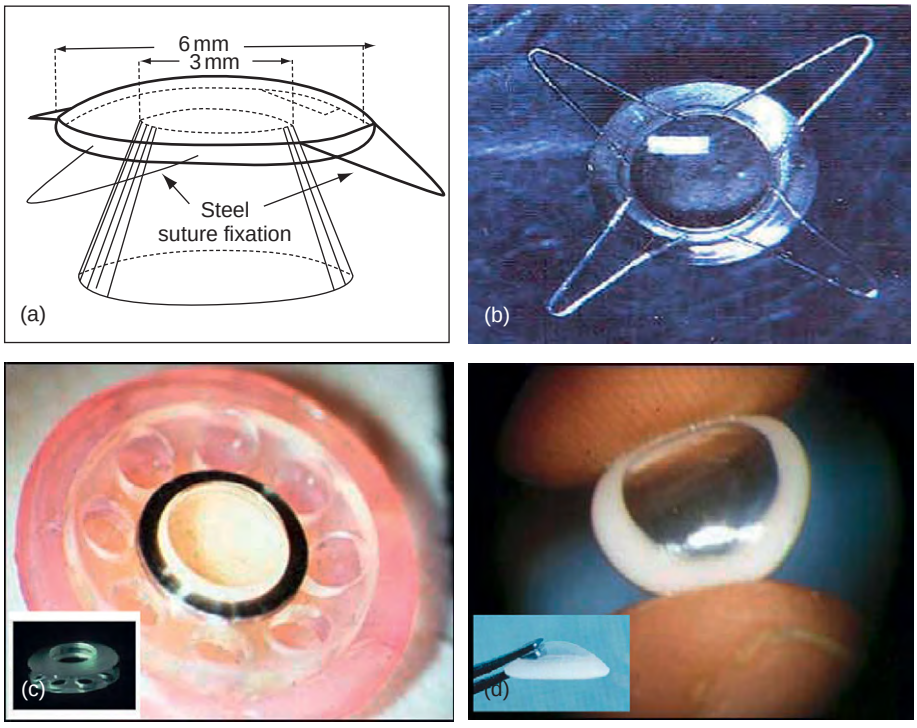

Figure 2 A glance at some of the keratoprostheses used in human clinical trials: (a) and (b) OCULAID® KPro, (c) Dohlman or Boston KPro, and (d) AlphaCor™ Kpro. (a) and (b) Adapted with permission from Dr. Jan Worst Research Group, the Netherlands. (c) Adapted with permission from Dr. Esen Akpek of the Wilmer Eye Institute at Johns Hopkins.

thick and 10-mm circular Dacron membrane is added to the KPro for tissue integration. Like the OOKP, this device is preimplanted into the patient for colonization of the skirt. Thirty-one patients have received implants from 1997 to 2004, by means of clinical trials. Results indicated that no infections or retroprosthetic membranes were reported. Seventy-seven percent of implanted eyes improved enough to enable the patients to function independently. However, approximately 40% of implanted eyes had complications, although only a few cases were vision threatening.

Recent developments in the design of KPros include a KPro developed by Storsberg and colleagues in Germany; the Stanford KPro; and recent work by Sheardown and colleagues on the coverage of KPros by extracellular matrix (ECM) proteins for enhanced epithelialization. The German KPro adheres to the eye without sutures, reducing inflammation and infection. Sheardown and colleagues have covalently attached cell-adhesion peptides to poly(dimethyl siloxane) (PDMS) surfaces. This surface modification has been effective, leading to a synergistic effect on corneal epithelial cell attachment when compared to single peptides only. The Stanford KPro has also been designed using a polymer network hydrogel, comprised of poly(ethylene glycol) and poly(acrylic acid) (PEG/PAA). When implanted in rabbit corneas, this hydrogel was retained and tolerated well in nine out of 10 cases for a 2-week period.

To date, however, no KPro meets the previously defined standards for a successful corneal implant. As such, no particular KPro is in widespread use to date, although recent versions appear to be promising.

Self-Assembled Corneal Equivalents

There have been various attempts at developing a natural-based self-assembled corneal equivalent. These range from the use of purely biological materials synthesized by cells in culture, to the use of noncorneal tissues as substitutes. Most bioengineering approaches to the restoration and repair of damaged tissue require scaffold materials upon which cells can attach, proliferate, and differentiate. Such scaffolds can be made using a self-assembly approach in which chemicals are used to stimulate the secretion of collagen, and other ECM molecules by fibroblast cells. Resulting sheets of scaffolds are stacked together to form a stroma, allowed to further integrate *in vitro*, and then epithelial cells are seeded on top of the stack. These constructs mimic corneal morphology, and the cells express appropriate tissue-specific markers. The main drawback is the time needed to produce enough self-assembled scaffolding for transplantation.

A cornea equivalent, composed of a 3D, bovine, dermal collagen matrix has been developed by Minami and

colleagues for *in vitro* studies. Zieske and colleagues also developed an *in vitro* cornea – fabricated using primary rabbit stromal cells. Funderburgh and colleagues have used keratocytes of the corneal stroma to produce a transparent ECM that may be useful in cell-based corneal therapy or for the development of bioengineered corneas. Funderburgh and colleagues also determined there is a population of cells present in adult mammalian corneal stroma having the ability to divide extensively, generating differentiated keratocytes. Previously, the authors reconstructed a human cornea using immortalized human corneal cell lines. Each cell line was subjected to electrophysiological, biochemical, and morphological tests. This was carried out to determine the phenotype, which was compared to postmortem human corneal cells, before being used in the 3D reconstruction. Collagen–chondroitin sulfate was the base scaffold in which keratocytes were integrated, before epithelial and endothelial cells were layered above or below. Two weeks following construction, the resulting corneal equivalent was found to behave similarly to a normal cornea, with respect to morphology, transparency, ion and fluid transport, and gene expression following injury. Although this human corneal equivalent shared functional properties with the natural cornea, it was not designed to meet the mechanical characteristics needed for transplantation. However, these studies represent an important future directive toward the development of bioengineered corneal implants. Reconstructed corneal equivalents presently have use in the biomedical world, as they are used as replacements for animals in toxicology testing and pharmacological studies.

Bioengineered ACs that Address Regeneration

To overcome the challenges of biocompatibility, inflammatory responses, and rejection, there have been attempts to promote varying degrees of corneal tissue regeneration through implants of bioengineered corneal ECM substitutes. In general, these matrix-mimetic materials range from simple cross-linked ECM macromolecules, such as collagen, to hybrids of ECM macromolecules and synthetic polymeric components. Prior to the assembly of these ECM mimetics for implantation, a bioactive scaffold material with accurate chemical/physical properties must be designed. It must be able to form robust scaffolds, promote cell differentiation/integration, and promote tissue formation in a uniform manner that is repeatable and reliable.

Polymeric blends of collagen have been previously used to emulate the collagen–glycosaminoglycans scaffolding of the ECM. Various tissue-engineering applications have utilized this technology, for example, as a scaffold for artificial liver, skin scaffolds with nerves and dermal models, membranes for controlled drug release, and as an *in vitro* model to test antineoplastic agents. Many efforts have been made to stabilize collagen, and its blends, by chemical cross-linking methods. These methods can be divided into two categories: bifunctional and amide-type. Several bi-functional reagents such as glutaraldehyde (GTA), polyethylene glycol diacrylate (PEGDA), and hexamethylene diisocyanate (HDC) have been used to bridge amine groups of lysine or hydroxylysine residues of collagen polypeptide chains. A major handicap of these cross-linking agents is the potential toxic effect of residual molecules and/or compounds released when the biomaterial is exposed to biological environments (i.e., during *in vivo* degradation).

Amide-type cross-linkers such as carbodiimide, especially 1-ethyl-3-(3-dimethylaminopropyl) carbodiimide (EDC), and *N*-hydroxysuccinimide (NHS) offer the main advantage of lower toxicity and better compatibility over GTA and HDC. However, collagen scaffolds stabilized by carbodiimide are not strong, yet are elastic enough for PKP transplantation. This is due to limited zero-length cross-links; in addition, there are reaction sites on collagen molecules that are not linkable by carbodiimide. It is reported that EDC and NHS (EDC/NHS) can link carboxylic acid and amino groups located within 1 nm from each other. Therefore, functional groups that are located on adjacent collagen microfibrils are too far apart to be bridged by carbodiimide. With systems such as EDC/NHS, the increase in tensile strength, especially when induced by the increasing of a cross-linking agent, is associated with the decrease in elasticity and toughness. This compromise in integrity may be due to restraints placed on the mobility of the polymer network, a decrease in scaffold porosity, and/or a diffusion of reactive residues and byproducts out of the scaffolds.

Despite the drawbacks, cross-linking agents have been used effectively to fabricate collagen based matrices. The application of these matrices has been mainly diagnostic; where the tissue is made and used *in vitro* for testing drug metabolism, uptake, and toxicity.

The authors have previously reported collagen-based materials, ranging from corneal scaffolds based on the copolymer poly(*N*-isopropylacrylamide-co-acrylicacid-co-acryloxylsuccinimide), to a simple EDC/NHS cross-linked collagen scaffold. These scaffolds allow regeneration of corneal cells and nerves, when implanted as lamellar grafts. However, these materials still lack the optimal toughness and elasticity required to withstand PKP surgical procedures, as well as normal day-to-day mechanical stresses.

In our most recent ongoing clinical study, we reported corneal regeneration following the implantation of a bioengineered corneal substitute, based on recombinant collagen. Visual acuity, ocular surface quality, and corneal sensitivity are continuously improving in the first recipients of the implants. **Figure 3** shows slit-lamp and optical coherence tomography (OCT) photographs of the operated cornea immediately following lamellar keratoplasty and at 9 months post operation. Such substitutes

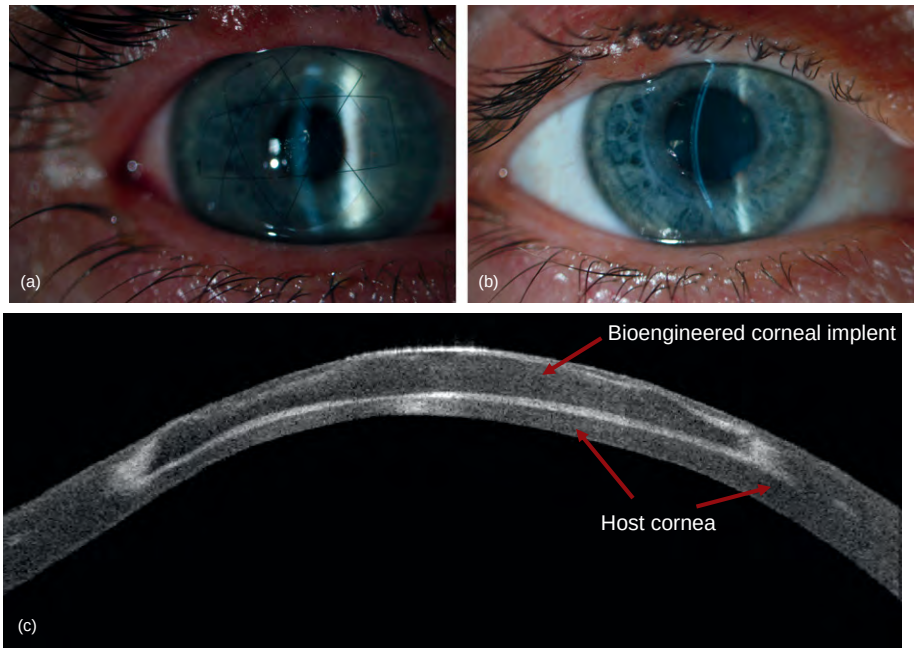

Figure 3 Operated cornea of a 37-year-old man following implantation of a bioengineered artificial cornea, which is transparent with a smooth corneal surface and is well accepted by the patient's eye: (a) slit-lamp photograph of the implanted cornea right after lamellar keratoplasty (LKP) anchored with three overlying 10-0 nylon sutures. (b) slit-lamp photograph of the cornea 9 months following the LKP, (c) OCT (optical coherence tomography) image (ASOCT, Visante, Carl Zeiss Meditec, Jena, Germany) 9 months following the LKP.

may find use as temporary or emergency corneal replacements, where human tissue is unavailable.

In several attempts to enhance mechanical properties of corneal substitutes, hybrid interpenetrating polymeric networks (IPNs) have been developed as ACs. Synthetic-based IPNs have been widely explored and used; however, bioengineered IPNs have not been investigated and examined for corneal applications until recently. Efforts were made by the authors to develop a bioengineered IPN as an AC. The goal was to develop an IPN scaffold that combines the bioactive features of biopolymers with the physical characteristics of synthetic polymers. Composite IPN structures – comprised of two or more interconnected networks on a molecular scale through chemical (covalent) and physical bonds – were developed.

The scaffold material used bio-functional polymers that naturally occur in the native tissue (e.g., collagen) as the core material. As an alternative, tissue-mimetic polymers such as chitosan, 2-methacryloyloxy ethyl phosphorylocholine (MPC) or chondroitin sulfate were used as bio-interactive components; with poly (ethylene glycol) dibutyraldehyde (PEG-DBA) or poly(ethylene glycol) diacrylate (PEG-DA) being used as a synthetic long-range cross-linker. Bio-inert short-range cross-linkers, including EDC and NHS, were also used in conjunction with long-range cross-linkers. This composition allowed the formation of hybrid IPNs that are mimetic of the natural cornea. The IPN scaffolds demonstrated significantly enhanced mechanical strength and elasticity compared to their non-IPN counterpart. In addition, they demonstrated excellent optical properties, optimum mechanical properties and suturability, and good diffusivity to glucose and albumin. The IPNs had excellent biocompatibility, and were further tested by being implanted into pig corneas. Over the 12-month monitoring period, it was demonstrated that there was seamless host–graft integration with successful regeneration of host corneal epithelium, stroma, and nerves. Figure 4 depicts an IPN-bioengineered AC compared to an eye-bank human donor cornea.

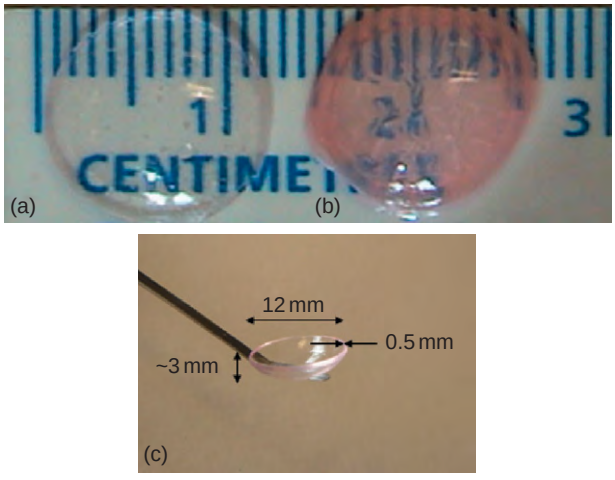

Figure 4 Corneal implants: (a) bioengineered artificial cornea (IPN), (b) eye-bank human donor cornea, and (c) dimensions of a typical bioengineered artificial cornea.

Future Directions

In the cornea, regeneration of the host cornea could overcome the rejection problems and other postoperative complications from donor-tissue transplantation and KPros. In addition, corneal implants that allow nerve- and host-tissue regeneration could also circumvent problems after surgery, found both in human donor tissue and in synthetic KPros. At the current pace of product development and testing, viable alternatives to donor corneas for transplantation are not far off. Processing procedures can affect both the native material properties and the subsequent clinical utility of scaffolds intended for certain tissue-engineering applications. Irrespective of the method, the AC must be engineered to mimic morphological, physiological, and biochemical properties of the natural tissue as closely as possible.

See also: Corneal Epithelium: Cell Biology and Basic Science; The Corneal Stroma; Cornea Overview; Penetrating Keratoplasty; Refractive Surgery and Inlays.

Further Reading

Chirila, T. V., Hicks, C. R., Dalton, P. D., et al. (1998). Artificial cornea. *Progress in Polymer Science* 23: 447–473.

Crawford, G. J., Hicks, C. R., Lou, X., et al. (2002). The Chirila keratoprosthesis: Phase I human clinical trial. *Ophthalmology* 109: 883–889.

Dohlman, C. H., Harissi-Dagher, M., Khan, B. F., et al. (2006). Introduction to the use of the Boston keratoprosthesis. *Expert Review of Ophthalmology* 1(1): 41–48.

Duan, D., Klenkler, B. J., and Sheardown, H. (2006). Progress in the development of a corneal replacement: Keratoprostheses and tissue-engineered corneas. *Expert Review of Medical Devices* 3: 59–72.

Funderburgh, M. L., Du, Y., Mann, M. M., Raj, N. S., and Funderburgh, J. L. (2005). PAX6 expression identifies progenitor cells for corneal keratocytes. *FASEB Journal* 19(10): 1371–1373.

Germain, L., Carrier, P., Auger, F. A., Salesse, C., and Guérin, S. L. (2000). Can we produce a human corneal equivalent by tissue engineering? *Progress in Retinal and Eye Research* 19: 497–527.

Griffith, M., Hakim, M., Shimmura, S., et al. (2002). Artificial human corneas: Scaffolds for transplantation and host regeneration. *Cornea* 21(7): S54–S61.

Griffith, M., Osborne, R., Munger, R., et al. (1999). Functional human corneal equivalents constructed from cell lines. *Science* 286: 2169–2172.

Hicks, C., Crawford, G., Chirila, T., et al. (2000). Development and clinical assessment of an artificial cornea. *Progress in Retinal and Eye Research* 19: 149–170.

Kalayoglu, M. V. (2006). In search of the artificial cornea: Recent developments in keratoprostheses. *Ophthalmology Technology Spotlight Medcompare*.

Leibowitz, H. M., Trinkhaus-Randall, V., Tsuk, A. G., and Franzbau, C. (1994). Progress in the development of a synthetic cornea. *Progress in Retinal and Eye Research* 13: 605–621.

Minami, Y., Sugihara, H., and Oono, S. (1993). Reconstruction of cornea in three-dimensional collagen gel matrix. *Investigative Ophthalmology and Visual Science* 34: 2316–2324.

Rafat, M., Li, F., Fagerholm, P., et al. (2008). PEG-stabilized carbodiimide crosslinked collagen–chitosan hydrogels for corneal tissue engineering. *Biomaterials* 29: 3960–3972.

Resnikoff, S., Pascolini, D., Etya'ale, D., et al. (2004). Global data on visual impairment in the year 2002. *Bulletin of the World Health Organization* 82: 844–851.

The National Coalition for Vision Health (2005). There's still a critical shortage of corneas for transplantation 2005. http://www.visionhealth.ca/news/insert/shortage.htm (accessed July 2009).

WHO (1997). Global initiative for the elimination of avoidable blindness. Geneva: World Health Organization. (unpublished document WHO/PBL/97.61/Rev 1). http://whqlibdoc.who.int/hq/1997/WHO_PBL_97.61_Rev.1.pdf.

WHO (2003). Human organ and tissue transplantation. World Health Organization, May 2003 (EB112/5 112th Session). http://www.who.int/ethics/topics/human_transplant/en (accessed July 2009).

Worst, J. (2007). The ''Champagne Cork'' keratoprosthesis (KP). http://www.janworst.com/projects/kp/frames/framekp1.htm.

Yaghouti, F., Nouri, M., Abad, J. C., and Power, W. J. (2001). Keratoprosthesis: Preoperative prognostic categories. *Cornea* 20: 19–23.

Relevant Website

http://www.asmr.org.au – The Australian Society for Medical Research, Following in the footsteps of Fred Hollow, Key Statistics 2006.

Astigmatism

M J Cox, University of Bradford, Bradford, UK

Glossary

Against-the-rule – Ocular astigmatism in which the meridian with greater optical power in the eye is horizontal.
Astigmat – An individual with ocular astigmatism.
Axis meridian – The meridian of a cylindrical surface that is flat and consequently has no optical power.
Emmetropization – The active process of reduction in refractive error toward an ideally focused system that occurs in the human eye during the first 2 years of development.
High-order wave front aberrations – Wave front aberrations that are expressed using cubic, or higher, powers of the light ray's distance from the pupil center to predict the amount of aberration.
Meridional amblyopia – A lack of contrast sensitivity to high and medium spatial frequency contours oriented along a particular meridian without any refractive error or ocular pathological process affecting the visual function.
Paraxial optics – Image forming through an optical system where only rays traveling close to the optical axis of the system and/or at small angles to this axis are considered.
Penetrating keratoplasty – A surgical procedure to remove corneal material and replace it with material from a donor cornea.
Stokes lens – A lens constructed from two symmetrically counter-rotating cylindrical lenses of equal absolute power but opposite sign. These combine to make a continuously variable power crossed-cylinder lens.
Wave front aberrations – Deviations of a wave front of light propagating through an optical system from a perfect spherical wave front.
With-the-rule – Ocular astigmatism in which the meridian with greater optical power in the eye is vertical.

The Definition and Etymology of Astigmatism

The earliest forms of correction for visual loss caused by refractive errors in the eye used spherical spectacle lenses. These are rotationally symmetrical about the optical axis and, considering paraxial optics, produce a point image from a point object on the axis of the lens. This type of image forming is known as stigmatic, from the Greek stigma, meaning a branding mark. Astigmatism describes an optical system where any nonpoint image is formed from a point object. In practice, astigmatism commonly refers to the simplest extension of stigmatic image formation, namely where the optical system forms two perpendicular line images from an axial point object, each at a different distance along the optical axis.

In an astigmatic optical system the power varies as a function of the meridian, with a maximum and minimum power in meridians that are perpendicular. This variation in power approximates very well to a sinusoidal function, as seen in the formula

$$F_\theta = F_{\text{Sph}} + \frac{F_{\text{Cyl}}}{2} + \frac{F_{\text{Cyl}}}{2}\cos[2(\theta - \alpha)] \qquad [1]$$

where F_θ is the power in the meridian at $\theta°$, measuring angles anticlockwise from the horizontal, F_{Sph} is the power in the meridian of minimum power, F_{Cyl} is the difference in power between the meridians of maximum and minimum power, and α is the angle of the meridian of maximum power.

The double angle $[2(\theta - \alpha)]$ in eqn [1] demonstrates that the power varies through a complete cycle as we rotate the meridian 180° around the optical axis.

Newton is said to be the first to describe the variation in optical power with meridian and the consequent formation of line foci, but did so in the rather specialized form of oblique astigmatism. It was left to Thomas Young to first describe and measure ocular astigmatism, a finding which was a by-product of his attempts to measure his own refractive error as a starting point for investigating accommodative mechanisms in the human eye. He found his own astigmatism to be around 1.75 D and even had additional evidence to suggest that its source was a tilt in his crystalline lens. Airy was the first individual to measure and correct his ocular astigmatism. Wollaston, Ostwalt, and Tscherning discovered means by which spectacle lenses could be manufactured to minimize lens-induced oblique astigmatism.

The above discussion concerns regular astigmatism, where two perpendicular axes of symmetry exist within the optical system and the relationship between power and the angle of the meridian is known. In irregular astigmatism this symmetry does not exist over the aperture through which light travels to form an image. Locally, over much smaller apertures, such symmetry may be present, but for

the purposes of image formation by the optical system or eye it is absent. This results in objects that do not form line images but rather two elongated spreads of light, even at best focus. Furthermore, these two elongated images are not oriented perpendicularly. All eyes contain some degree of irregular astigmatism but this is rarely visually limiting except in pathological processes where the irregular astigmatism is large. Examples of such pathology include keratoconus; lenticonus; corneal scarring, inflammation, dystrophy, and degeneration; pterygium; mechanical effects on the cornea from neighboring structures such as the lids or sclera or following the use of rigid contact lenses; lens dislocation; localized lens index changes; and polycoria and ectopic pupils. In ocularly healthy individuals with unusually large pupils and statistically higher levels of irregular astigmatism, visual function can be affected in low and medium light levels.

Ocular Astigmatism: Prevalence and Age-Related Changes

Ocular astigmatism is important for two main reasons. First, it prevents optimal retinal image formation and leads to a loss of contrast in the retinal image. It can be argued that it is more debilitating than either myopia or hypermetropia as, unlike myopia, there is no object distance at which a clear retinal image can be formed and unlike hypermetropia, it is not possible to overcome the refractive defect by using one's accommodation. Second, if the high levels of astigmatism that are naturally present during early infancy do not reduce during the process of emmetropization, then permanent meridional amblyopia can occur leading to lack of visual sensitivity to small oriented details in later years, even when the astigmatism has been refractively corrected. In addition, some suggest that visual blur during early life may help to drive the development of myopia in later years. Uncorrected ocular astigmatism may be one such cause of visual blur, and an association between ocular astigmatism and myopia development has been found.

Almost all neonates have significant amounts of astigmatism caused by an unusually steep cornea in one meridian, although the angle of this meridian with higher power is not consistent across the population. Early development reduces this cornea-generated astigmatism such that by 4–6 years of age only around one-twentieth of the population has ocular astigmatism in excess of 1 D and in the great majority of young astigmats, the meridian with the greatest power is vertical (or within 15° of vertical, the so called with-the-rule astigmatism). In later childhood (5–17 years of age) the proportion of individuals with at least 1 D of astigmatism increases up to around a quarter, with a higher risk for Asians and Hispanics (around a third), and a lower risk for African-Americans (around a fifth).

In adults, about two-thirds of the population have measureable astigmatism (> 0.25 D), but the majority of this is at low levels (<1 D). Estimates suggest that the prevalence of higher amounts of ocular astigmatism (>1 D) in adults ranges from about 10–20%, dropping to only 0.5% for astigmatism in excess of 4 D. A general trend can also be found in the adult population concerning the angle of the meridian of greatest power. In younger adults (<40 years of age) this is predominantly with-the-rule. In older adults it is predominantly against-the-rule. This change is believed to be due to the changes in the effects of the upper and lower lids on the cornea as the lids age and the tension generated by the lids on the cornea reduces. The lids squeeze on the upper and lower cornea in youth, flattening the cornea directly underneath them but steepening the corneal cap in the vertical meridian. The mechanical effects of the collagen structure within the cornea cause a consequent flattening of the cornea in the horizontal meridian. With aging, the cornea steepens overall, but the steepening in the vertical meridian is offset by the reduction in lid tension, leaving a steeper corneal curvature in the horizontal meridian and a consequent change from with-the-rule to against-the-rule ocular astigmatism.

The Origin of Ocular Astigmatism

The cornea is the major refracting surface in the eye and the ocular astigmatism is best correlated with the astigmatism generated by the cornea. Both the anterior and posterior surfaces of the cornea generate astigmatism and show similar changes in curvature as a function of meridian. Due to the aqueous humor immediately behind the cornea, the refractive power of the posterior surface is only about one-tenth of the anterior surface power and of opposite sign. Keratometers, when used to predict the refractive power of the cornea from anterior corneal curvature measurements in a meridian, account for this by adjusting the value used for the refractive index of the cornea. The physiological value of the corneal refractive index is believed to be close to 1.38, but the majority of keratometers (and their keratographic successors) utilize a value of 1.3375.

With the exception of corneal astigmatism associated with syndromic conditions, there is a complex pattern of heredity associated with corneal astigmatism in the general population, with some evidence of autosomal dominant inheritance patterns, but it seems likely that polygenic inheritance with variable penetrance exists. Unidentified environmental factors are also believed to influence the corneal astigmatism.

There is good evidence to suggest that the corneal shape, and hence the corneally generated ocular astigmatism, is influenced by lid position, tension, and shape.

Performing a task that alters the usual lid position, for instance prolonged reading, produces measureable but temporary changes in the corneal shape and astigmatism. Extra-ocular muscles may also influence the corneal shape, certainly showing effects following changes as dramatic as those induced by strabismus surgery where the extra-ocular muscles are recessed or resected.

Corneal astigmatism is also associated with some well-described syndromes, such as Down's syndrome and Treacher Collins syndrome (also known as Treacher Collins–Franceschetti syndrome or mandibulofacial dysostosis). Changes in the orientation of the palpebral aperture correlate with the axis of the astigmatism, the most powerful corneal meridian lying perpendicular to the axis connecting the inner and outer canthus.

In addition to ocular astigmatism being generated by the cornea, it is also influenced by the shape and position of the anterior and posterior surfaces of the crystalline lens, as well as the refractive index distribution of the crystalline lens. Accurate *in vivo* measurements of the shape of the anterior and posterior surfaces of the crystalline lens are difficult to make. Consequently, it is not known how great a contribution crystalline lens surface shape makes to ocular astigmatism, as opposed to the effect of surface position and refractive index changes. What is known is that the internal astigmatism, that is, that generated by the crystalline lens, partially compensates for the corneal astigmatism and it is believed that some active feedback process is responsible for this compensation. Decentration and tilt of the optical axis of the crystalline lens with respect to that of the cornea will also induce astigmatism. The average internal astigmatism is 0.5 D against-the-rule and this does not appear to alter significantly with age. This is too great to be explained by crystalline lens tilt alone, as the required tilt is 4–5 times the average tilt found for the crystalline lens.

Refractive index changes in the cortex of the crystalline lens, commonly associated with age-related cortical cataract, are also able to induce internal astigmatism, with the axis of the astigmatism believed to be associated with the long axis of the cortical opacity. Other pathological conditions that lead to abnormally large displacement of the crystalline lens also induce astigmatism, including sectoral weakness in the zonular supports of the crystalline lens in conditions such as Marfan's syndrome and homocystinuria, following blunt trauma, and associated with hypermature cataract. Lenticonus is a condition that results in conically shaped lens surfaces inducing large amounts of both regular and irregular astigmatism.

Image Formation and Refractive Specification in Astigmatism

The basic image-forming process that occurs in astigmatic imaging can be seen in Figure 1.

Standard Notation for Specifying Astigmatic Refraction

Here, the front surface of the lens is a cylindrical surface. Note the straight line section of the lens front surface in the XX′ meridian compared to the curved section in the YY′ meridian. This cylindrical surface is created by rotating a line about an axis. The orientation of this axis defines the axis meridian of the cylindrical surface. The distance of the line from the axis defines the radius of curvature, and hence power of the surface. The back surface of the lens is a spherical surface, and the lens is described as a sphero-cylindrical lens. Although used at one time in the production of spectacle lenses, such lens designs are now very uncommon and nearly all spectacle lenses used to correct

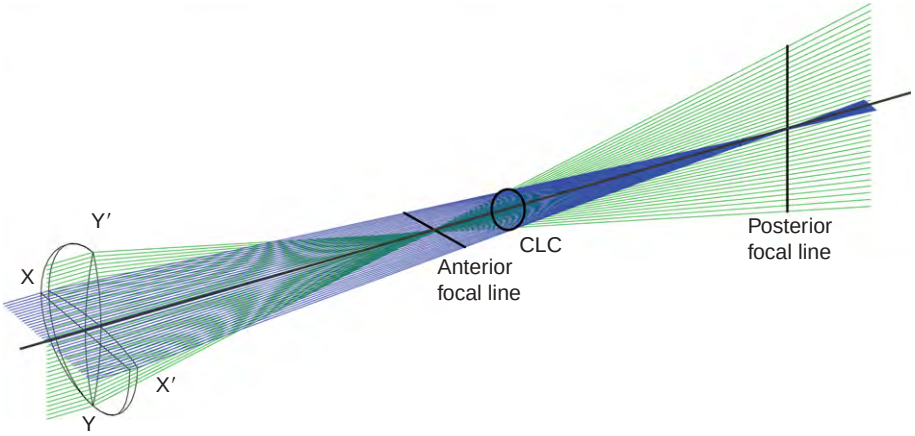

Figure 1 Image formation from a distant axial point object through a sphero-cylindrical lens. Blue rays are traveling in the horizontal meridian. Green rays are traveling in the vertical meridian. The front surface of the lens is cylindrical with a horizontal axis meridian, XX′. The bold lines show, from front to back, the anterior focal line, the circle of least confusion (CLC), and the posterior focal line.

astigmatism use a toric back surface, which is defined using two perpendicular radii of curvature.

The front surface power in the axis meridian is 0, while in the perpendicular meridian (the power meridian) it is F_{Cyl}. The angle of the axis meridian is measured from the perspective of looking at a person with astigmatism. An angle of 0° is represented by 180° but the degree sign is omitted. If the power of the spherical back surface in this lens was F_{Sph}, then we would denote the lens power as

$$F_{Sph}\text{DS}/F_{Cyl}\text{DC} \times 180$$

where DS is dioptres of spherical power. DC is dioptres of cylindrical power. F_{Cyl} is the difference in power between the meridians of maximum (F_{max}) and minimum (F_{min}) absolute power and is a signed value. Conversion between positive cylinder and negative cylinder notation is a straightforward process of

$$F_{Sph'} = F_{Sph} + F_{Cyl} \quad [2]$$

$$F_{Cyl'} = -F_{Cyl} \quad [3]$$

$$\text{Axis}' = (\text{Axis} + 90) \bmod 180 \quad [4]$$

A third much less commonly used notation is crossed-cylinder notation where the F_{max} and F_{min} meridians are considered as two separate cylindrical lenses. If F_{max} is +2.00 DC × 180 and F_{min} is +1.00 DC × 90 then the crossed-cylinder specification for the lens is

$$+1.00\ \text{DC} \times 90/+2.00\ \text{DC} \times 180$$

Ocular Image Formation in Astigmatism

The eye that suffers from astigmatism can usually be successfully studied by considering it to have a single toric corneal refracting surface with perpendicular meridians of maximum and minimum power. The image forming is very similar to that shown in **Figure 1**, where the more powerful meridian is vertical, denoting an eye having with-the-rule astigmatism. This astigmatic image pencil is known as the conoid of Stürm. Rays from a distant axial point that fan out in the vertical meridian (shown in green) are brought to a focus closer to the lens than the rays that fan out in the horizontal meridian (shown in blue). Hence, in the focal plane of the vertical meridian there is horizontal defocus and a horizontal line image is formed. In the focal plane of the horizontal meridian there is a vertical line image. Dioptrically (but not geometrically) equidistant between these two line images, the defocus in the horizontal and vertical (and all other) meridians is equal and the defocused image has its smallest spread, the circle of least confusion (CLC). At other image planes in the light pencil, the image is a horizontal ellipse if measured anterior to the CLC and a vertical ellipse if measured posterior to the CLC.

Paraxial optics can be used to determine the size and position of these astigmatic focal images. For a distant object (vergence of 0 D) and a pupil diameter d, the length of the anterior focal line is

$$\frac{dF_{Cyl}}{F_{max}} \quad [5]$$

The length of the posterior focal line is

$$\frac{dF_{Cyl}}{F_{min}} \quad [6]$$

The diameter of the CLC is

$$\frac{dF_{Cyl}}{F_{max} + F_{min}} \quad [7]$$

Given that F_{Cyl} found in human eyes is <1 D in around 80% of the cases, and the average value for F_{max} is around 60 D it is evident that eqns [5] and [6] will produce very similar results that are about twice the value of the result from eqn [7]. Thus, the focal lines give around twice as large an extent of blur as the CLC. This is helpful in explaining some of the effects of ocular astigmatism on human visual performance.

Classification of Ocular Astigmatism

Ocular astigmatism is divided into five categories depending upon where the retina lies with respect to the conoid of Stürm:

- The anterior focal line lies behind the retina – compound hypermetropic astigmatism;
- The anterior focal line lies on the retina – simple hypermetropic astigmatism;
- The anterior and posterior focal lines lie on either side of the retina – mixed astigmatism;
- The posterior focal line lies on the retina – simple myopic astigmatism;
- The posterior focal line lies in front of the retina – compound myopic astigmatism.

Most individuals with astigmatism have one or other form of compound astigmatism.

Astigmatic Blurring and Visual Perception

Unless the CLC is coincident with the retina, as is only possible in mixed astigmatism or hypermetropic astigmatism when accommodation is used, the retinal blur patches in an uncorrected astigmat will be oriented. In myopic astigmatism the long axis of the blur patch will typically be oriented along the more powerful corneal meridian, and in hypermetropic astigmatism along the

less powerful corneal meridian. Contours and edges in a scene that are parallel to the long axis of the blur patch will appear relatively clear, while those perpendicular to this axis will appear to be most blurred. As most scenes contain more contrast energy for horizontal and vertical orientations than for oblique orientations, there is often useful nonblurred information available to the viewer who has with-the-rule or against-the-rule astigmatism compared to a viewer with obliquely oriented astigmatism. This can be measured with visual acuity results, where with-the-rule and against-the-rule astigmatism produce a smaller loss of visual acuity than astigmatism along an oblique axis. In addition, as the line spacing in printed text is larger than the letter spacing, horizontal blurring is worse for reading than vertical blurring. An astigmat will benefit when reading printed text if he/she accommodates to a position where the vertical focal line is on the retina. For a with-the-rule astigmat, this would typically mean more accommodation is required to bring the vertical focal line (which is more posterior) onto the retina, compared with the accommodation required by an against-the-rule astigmat, for whom the vertical focal line is more anterior. If moderate to large amounts on myopia are present in addition, then the text would be best held at a distance that places the vertical focal line on the retina.

Figures 2 and **3** demonstrate the effects of astigmatic blur, compared to spherical blur, for Snellen letters and oriented contours (**Figure 2**) and an interior scene (**Figure 3**) when there is simple myopic astigmatism (or equivalent spherical error) present in with-the-rule (axis 180°), against-the-rule (axis 90°) and oblique (axis 135°) meridians. The images are taken from the viewer's perspective and the level of blur chosen is that of a narrow failure to pass the European vision standard for driving.

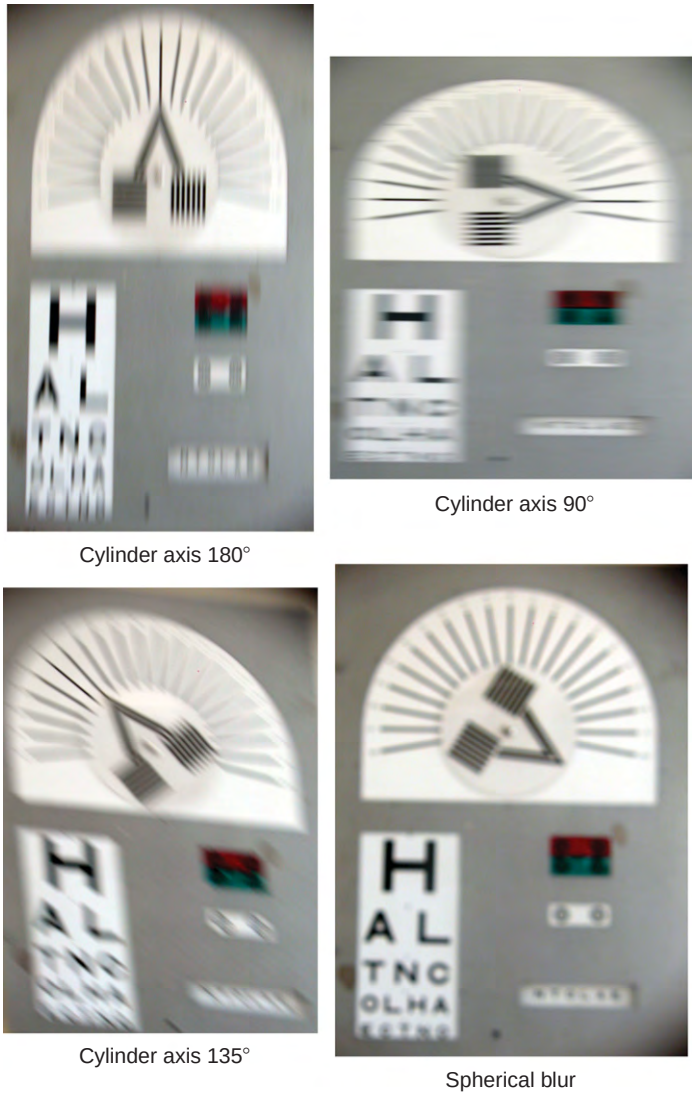

Figure 2 The effects of astigmatic blur, compared to spherical blur, for Snellen letters and oriented contours. Simple myopic astigmatism (or equivalent spherical error) is present in the following meridians: with-the-rule (axis 180°), upper left panel; against-the-rule (axis 90°), upper right panel; and oblique (axis 135°), lower left panel. The level of blur is that of a narrow failure to pass the European vision standard for driving.

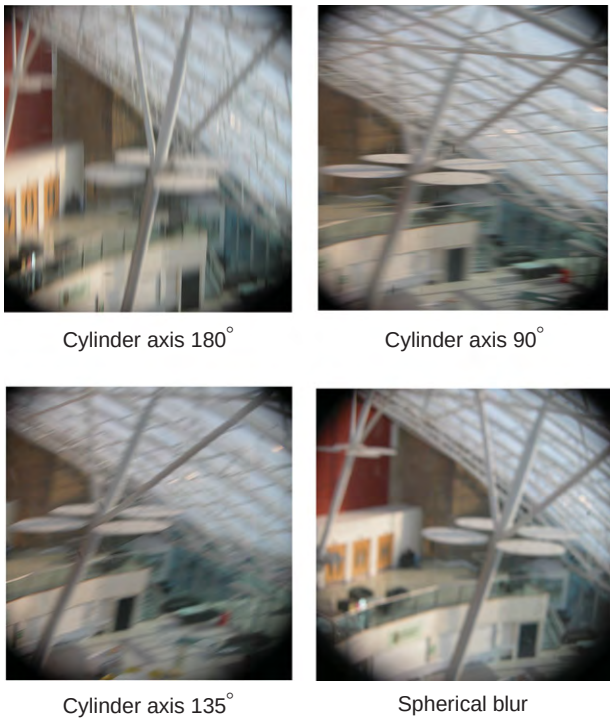

Figure 3 The effects of astigmatic blur, compared to spherical blur, for an interior scene. Simple myopic astigmatism (or equivalent spherical error) is present in the following meridians: with-the-rule (axis 180°), upper left panel; against-the-rule (axis 90°), upper right panel; and oblique (axis 135°), lower left panel. The level of blur is that of a narrow failure to pass the European vision standard for driving.

The induced spherical error is half that of the induced cylindrical error such that the diameters of the blur circle for the spherical lens and the CLC for the cylindrical lens would be matched.

Oblique Astigmatism

Even in an optical system that is rotationally symmetrical, the formation of images from off-axis object points will result in astigmatism, known as oblique astigmatism. This should not be confused with conventional astigmatism along an oblique axis meridian, which is due to different radii of curvature of the refracting surface in different meridians. In the eye, oblique astigmatism is important because the fovea is offset from the best approximation to an optical axis that the eye has, so that the objects that form an image on the fovea are nearly always slightly offset from this optical axis. It is also the dominant form of aberration in image formation for the peripheral retina.

Figure 4 shows the image-forming properties in oblique astigmatism. Rays in the tangential plane, the one containing the optical axis and the chief ray, form a line image oriented in the sagittal plane. Rays in the sagittal plane (the plane containing the chief ray that is perpendicular to the tangential plane) form a line image oriented in the tangential plane. In this biconvex lens, the tangential images form nearer the lens than the sagittal images, but for any given lens power the relative locations of the tangential and sagittal images depend upon the relative powers of the two surfaces of the lens, assuming that there is an aperture stop behind the refracting surface as is the case in the eye or when a spectacle lens is used in front of an eye. The distance from the tangential image to the image position found in a system free from oblique astigmatism is always three times the equivalent distance for the sagittal image. Circumferential image contours are formed clearly in the tangential image plane. In the sagittal image plane, radial image contours are formed clearly.

Any ocular astigmatism caused by oblique astigmatism at the fovea can be corrected with the usual refractive techniques and the oblique astigmatism that is present in the periphery of the visual field is unimportant in normal visual function as the retinal ganglion cell mosaic limits the visual resolving power of the eye to a greater extent than the optics. It is argued that ocular oblique astigmatism acts as a useful high spatial frequency filter to prevent aliasing and the consequent perception of reverse motion in the peripheral visual field.

Oblique astigmatism in refractive correction using spectacles is important. As the eye rotates to view different objects in the field of interest it will make different angles with the optical axis of any spectacle lens, and this will then cause different amounts of oblique astigmatism to be generated by the lens.

Ocular Astigmatism During Near Work

In addition to the nature of the visual task typically being different for near work compared to distance viewing, occasionally the ocular astigmatism itself, or its correction, can change. The power and/or axis of the ocular astigmatism at near compared to distance viewing may be affected by the following factors:

- when the eyes converge and depress for near work they tend to excyclotort;
- the suspensory ligaments of the crystalline lens may not be uniform, causing induced astigmatic changes in the lens during accommodation;
- the ciliary muscle fibers themselves may not exert uniform force on the crystalline lens;
- the crystalline lens may not be homogenously plastic, inducing irregular shape changes during accommodation;
- the pupil or lens may displace with respect to the corneal axis during accommodation inducing some change in the oblique astigmatism.

The power of the astigmatic correction using spectacles can change due to near vision effectivity when the astigmatic or spherical refractive error is large.

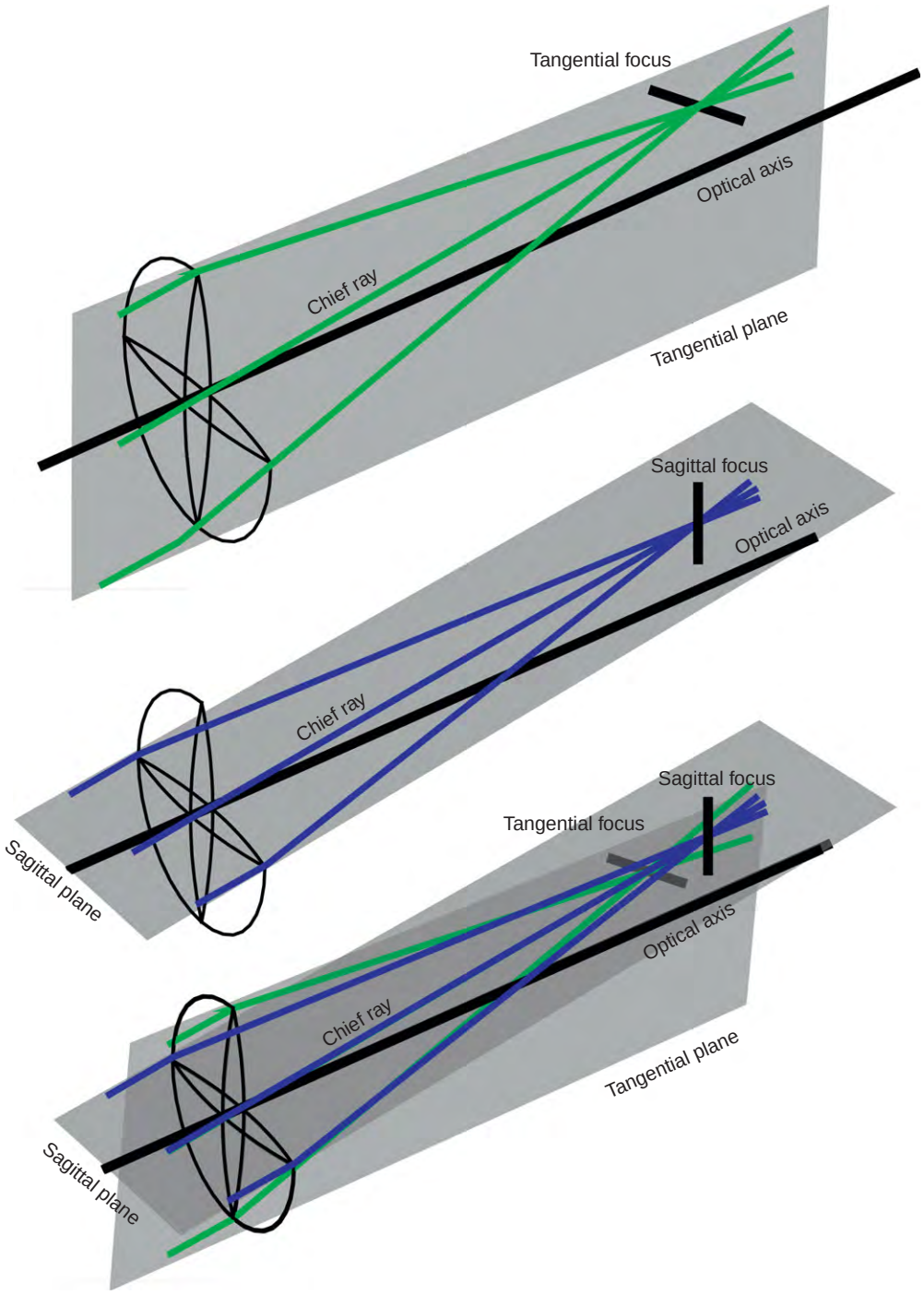

Figure 4 The image-forming properties for a biconvex spherical lens demonstrating oblique astigmatism for imaging a distant off-axis object point. Rays (green) in the tangential plane, upper panel, the one containing the optical axis and the chief ray, form a tangential focus, which is a line image oriented in the sagittal plane. Rays (blue) in the sagittal plane, middle panel, a plane perpendicular to the tangential plane that also contains the chief ray, form a sagittal focus, which is a line image oriented in the tangential plane. The lower panel demonstrates the relative position of these light rays and the induced astigmatism.

Specialized Notations for Specifying Astigmatic Refraction

In addition to the standard sphero-cylindrical notation used to specify astigmatic refractive errors, more specialized notations have been developed. The chief limitation of the standard notation happens when more than one refractive error needs to be considered, for instance when trying to determine population descriptive

statistics for refractive errors, assessing change in refractive error, or when trying to determine the effects of a refractive error when used in conjunction with other optical equipment or other induced refractive errors. Two main alternative forms of notation have been suggested: power vector notation and matrix notation.

Power vector notation resolves the optical power of any sphero-cylindrical lens into three components, a spherical component M, and two crossed-cylinder components, $\mathcal{J}_0$ and $\mathcal{J}_{45}$, with their axes at either 90°/180° or 45°/135°, respectively. Equal values of the components in this notation will lead to equal retinal blur circle sizes. Equations for computing the M, $\mathcal{J}_0$, $\mathcal{J}_{45}$ values from the conventional $F_{\text{Sph}}/F_{\text{Cyl}} \times \theta$ are given below:

$$M = F_{\text{Sph}} + \frac{F_{\text{Cyl}}}{2} \quad [8]$$

$$\mathcal{J}_\theta = -\frac{F_{\text{Cyl}}}{2}\cos(2\theta) \quad [9]$$

$$\mathcal{J}_{45} = -\frac{F_{\text{Cyl}}}{2}\sin(2\theta) \quad [10]$$

While this notation is useful for adding, subtracting, and multiplying by a scalar when dealing with thin sphero-cylindrical lenses, it is much less convenient to use when multiplying lens powers (as required when computing the powers of multiple lens systems or dealing with thick lens systems) or computing the prismatic effects of lens systems.

The alternative matrix representation of lens power is more general and can be used in the above-mentioned instances. A 2 × 2 matrix,

$$F = \begin{pmatrix} f_{11} & f_{12} \\ f_{21} & f_{22} \end{pmatrix}$$

is defined in thin lenses such that

$$f_{11} = F_{\text{Sph}} + F_{\text{Cyl}}\sin^2(\theta) = M + \mathcal{J}_\theta \quad [11]$$

$$f_{12} = f_{21} = -\frac{F_{\text{Cyl}}}{2}\sin(2\theta) = \mathcal{J}_{45}\sqrt{2} \quad [12]$$

$$f_{22} = F_{\text{Sph}} + F_{\text{Cyl}}\cos^2(\theta) = M - \mathcal{J}_\theta \quad [13]$$

It is interesting to note the simple transformations between these two systems in thin lenses and their relationship to the Zernike basis function representation of wave front aberrations now commonly used when considering irregular astigmatic refractive error. The Zernike astigmatism coefficients C_2^{-2} and C_2^{+2} are exactly $\frac{-r^2}{2\sqrt{6}}$ times the value of $\mathcal{J}_{45}$ and $\mathcal{J}_\theta$, respectively, given a pupil radius r, and using normalized variance terms. This has implications when measuring and correcting ocular astigmatism.

The Measurement of Ocular Astigmatism

Various techniques are employed to measure the extent of ocular astigmatism. The majority are based upon locating the meridians of maximum and minimum power and then minimizing the size of the retinal blur ellipses along those meridians. This may be done objectively or subjectively. Alternatively, different components of the astigmatic power may be measured and the final astigmatic refraction inferred from them.

Subjective methods include the Stenopaeic slit, Jackson's crossed-cylinder, fan and block, and Stokes lens techniques. Objective methods include retinoscopy, automated refraction, keratometry, and wave front analysis. It is the latter two that have benefited from the greatest development effort in the last few years.

Keratometry

In this method, the image magnification produced by using the anterior corneal surface as a convex mirror is measured along the meridians of maximum and minimum curvature. The sagittal radius of curvature is inferred from this magnification and the corneal astigmatism is inferred from the sagittal curvature the corneal refractive index and the presumed corneal back surface curvature. The ocular astigmatism is then inferred by assuming a fixed value for the internal astigmatism.

An extension to the principle of the keratometer is the corneal topographer that uses either reflected light from the cornea to measure the local curvature, or light (or even sound) scattered from the cornea – tear-film or cornea – aqueous interfaces to measure the local surface heights. It is possible to computer the local curvature from the local surface heights and vice versa. Unlike keratometers, such instruments clearly demonstrate the conicoidal nature of the cornea over most of its surface excluding the limbal region. Estimates of ocular astigmatism can be made by finding the best fitting overall match to the power map provided by the instrument. They also detect and measure irregular astigmatism much more accurately than keratometers. **Figure 5** shows a corneal keratometric power map and surface height map from the right eye of an individual with approximately 4.50 D of regular with-the-rule ocular astigmatism. The symmetric bow tie pattern in the curvature map is a typical finding in these types of representations of corneal power in astigmatism and the corneal axis of astigmatism can be clearly identified from both maps.

Wave Front Analysis

Most of the methods of refractive measurement estimate the refractive power of the eye along one meridian at a

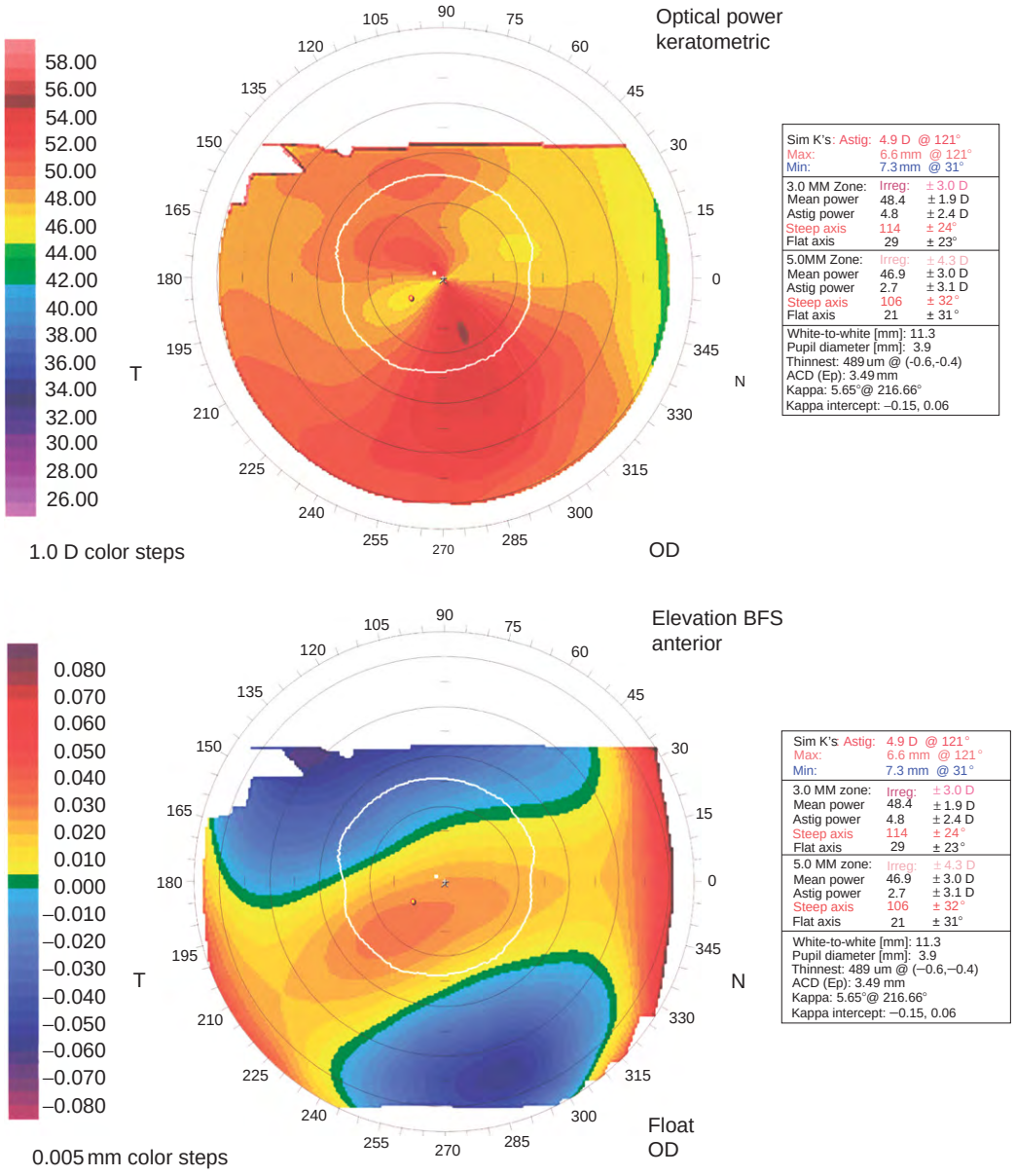

Figure 5 A corneal keratometric power map (upper image) and surface height map (lower image) from the right eye of an individual with approximately 4.50 D of regular with-the-rule ocular astigmatism. Color coding is for D in the upper map and millimeters in the lower one.

time. In these cases the refractive power in that meridian is a best fit to the combination of low-order refractive errors, high-order wave front aberration, and light scatter in the eye to produce the best perceived retinal image by viewing or varying light rays in only that meridian. If scatter or high-order aberrations are large (as in irregular astigmatism) then maximum and minimum power meridians may not be perpendicular giving a problem (albeit soluble) when attempting to arrive at a sphero-cylindrical refractive error. In addition, because change is restricted to one meridian at a time, and the imaging effects from the two meridians tested may interact, it is far from guaranteed that an optimum solution will be found. Furthermore, intermediate meridians will also influence image quality and these are not assessed.

The Stokes lens subjective method circumvents these problems to some extent by estimating along two perpendicular meridians at the same time. Corneal topography assessments can theoretically reduce the problem significantly by estimating ocular astigmatism from combining many individual samples of corneal power across the whole pupil area. Wave front analysis, where the refractive power of the eye is also sampled across multiple small apertures across the pupil, also estimates ocular astigmatism from this array of samples and is typically represented using Zernike polynomials. The Zernike terms are

orthogonal to each other and therefore theoretically do not influence one another over a circular pupil. By considering the measurement or expression of ocular astigmatism using this basis, as opposed to along meridians of maximum and minimum power, it is possible to arrive at an astigmatic correction that is optimized for reducing the wave front aberration given a limitation of being able to use only sphero-cylindrical refractive correction such as can be worked onto spectacle lenses, contact lenses, and intraocular lenses. The spherical element of the correction is not well predicted using an equivalent method, however, due to the extra importance of central versus peripheral pupil rays in the wave front. Techniques that can use asymmetrical surfaces, such as laser refractive corneal ablation, directly make use of the additional higher-order terms of the Zernike expression of the optical defect to provide further optimization of the refractive correction. However, neither corneal topography nor wave front analysis can account for the effects of ocular scatter.

The Correction of Ocular Astigmatism

Spectacles

Spectacles are the most common form of correction for ocular astigmatism. Except in unusual circumstances these lenses are successful in providing optimal visual function. In a limited number of individuals with unusually high irregular astigmatism and/or under conditions where the eye's pupil is very large, the other nonrotationally symmetric optical aberrations such as coma, trefoil, tetrafoil, and secondary astigmatism can reduce the visual performance significantly despite the correction of regular astigmatism.

Spectacle correction of high levels of regular astigmatism also produces spatial distortions due to the different levels of relative spectacle magnification in the different meridians. These make it difficult to binocularly fuse objects that are viewed through the more peripheral parts of the lenses. Patients corrected in this way will often learn to limit this effect by substituting head movement for eye movements when viewing outside a limited area from the optical center of the lens. Misperceived orientations of features and contours in the field of view also occur in high levels of regular astigmatism. Perceptual adaptation takes place over about a 2-week period to ameliorate this effect. Changing the power of the lenses significantly can, however, lead to a return of the perceptual problems.

Tscherning offered a solution to the problem of spectacle lens-induced oblique astigmatism by deriving the necessary lens forms (distribution of lens power between the front and back surfaces) to eliminate oblique astigmatism from spectacle lenses with a given refractive index and for use viewing objects at a given distance. These lens forms are known as punctal (or point focal) lenses. It is more common today to use minimum tangential error, where the tangential image plane is designed to be of a specified power that is independent of the angle of viewing. While this leaves a small residual astigmatic error, it reduces the spherical power error found in punctal lens designs where power changes as a function of viewing angle.

Spectacle lenses with an aspheric surface can also be used to reduce or eliminate oblique astigmatism with the additional benefit of a flatter front surface that makes the lens look less bulbous and also allows the lens to be thinner and hence lighter. The disadvantage is that aspheric lenses must be centered on the visual axis correctly or they induce, rather than reduce oblique astigmatism and other nonrotationally symmetric aberrations. Progressive addition lenses (PALs, also known as varifocals), with their aspheric surface induce astigmatism in a similar way as they can be centered for only two zones in the lens.

Contact Lenses

Contact lens correction of astigmatism can be with rigid or soft lenses. Spherical rigid contact lenses can eliminate the majority of regular or irregular corneal astigmatism. Ensuring the correct fitting of the rigid contact lens limits the amount of correction that can be provided with this method and bitoric lenses, with front and back toric surfaces, are needed for high degrees of astigmatism. Toric front surface rigid contact lenses can be used in cases of internal astigmatism that require correction. Most soft contact lenses flex sufficiently to align to the shape of the anterior corneal surface and so do not correct corneal astigmatism through a tear lens in the same way that rigid lenses do. Front surface toric soft contact lenses are required for the proper correction of ocular astigmatism.

In either rigid or soft contact lens correction of ocular astigmatism, many of the optical problems associated with spectacle correction are relieved. Meridional image magnification, near vision effectivity, and differential prismatic effects are all greatly reduced in contact lens correction. One of the principal difficulties in using contact lenses to correct astigmatism is in maintaining a stable rotational alignment between the contact lens and the cornea.

Surgery

Surgical control or correction of ocular astigmatism usually relies upon altering the shape of the cornea. This is most commonly done by making circumferential incisions in the corneal periphery. This reduces the tensile forces across the corneal stroma in that location, steepening the cornea locally, but flattening it across the pupil in the meridian which intersects with the incision. It is common because cataract surgery is common and most cataract surgery uses a corneal incision, the incision usually being

made in the steepest corneal meridian to reduce postoperative astigmatism. Penetrating keratoplasty is sometimes needed in severe cases of irregular corneal astigmatism. In this case, the resulting corneal shape can be altered by increasing or decreasing the tensile forces created by sutures. It is even possible to remove corneal material in one meridian, a wedge resection, to stretch the cornea, and change its shape. For healthy eyes, laser refractive surgery and conductive keratoplasty are the two techniques commonly used to treat ocular astigmatism. Toric intraocular lens implants also exist that can be used to correct ocular astigmatism and these may be used following cataract surgery or clear lens extraction.

Not Correcting Ocular Astigmatism

It is not always desirable or necessary to correct ocular astigmatism in adults. The most useful property of astigmatism is that, if one is accepting limited amounts of blur, it creates depth of focus in the eye. As mentioned earlier, for near tasks blur along a vertical meridian can usually be tolerated more readily than horizontal blur. An individual with against-the-rule simple myopic astigmatism will have vertical blur conjugate with a near distance equivalent to the amount of astigmatism and horizontal blur conjugate with distance vision. As long as this patient can tolerate the distance blur, they will have functional vision at both distance and near without accommodative effort. Such a situation would be useful for later presbyopes and pseudophakes and free the individual from needing any form of optical correction.

In addition, in some instances where individuals have very different ocular astigmatism in each eye the fusion difficulties that occur with spectacle correction make binocular vision impossible. If contact lenses cannot be tolerated and surgery is not an option, then there may be no alternative than to significantly undercorrect the astigmatism in the nondominant eye and allow visual suppression of the resulting blurred image to occur.

Finally, it is sometimes the case that an individual with high levels of ocular astigmatism has a measureable change in that astigmatism but is not complaining of any significant visual difficulties. One would be very cautious about changing any refractive correction in this individual as the perceptual adaptation to the meridional magnification differences would be affected by doing so and the person may end up feeling that he/she see worse rather than better. The same is true when large changes to the ocular astigmatism are found that do cause symptoms. Adapting to large changes in the correction can be intolerable for some people.

Summary

Although ocular astigmatism is very common, affecting two out of every three adults, visually disabling ocular astigmatism is much less common, affecting only one in five. Correcting this astigmatism is straightforward in the great majority of cases, although the measurement and correction of both irregular astigmatism and high degrees of regular astigmatism remain challenging. Astigmatism induced when looking obliquely through spectacles is well controlled by using the appropriate lens design and contact lens and surgical correction of astigmatism is successful in many instances, even though the uptake of these latter forms of refractive correction is still low. Measuring and correcting irregular astigmatism has improved with the use of more accurate assessment of the corneal surface and with wave front aberrometry to sample the local refractive powers across a fine array of pupil locations. Optimally correcting irregular astigmatism with custom contact lenses and surgical refractive correction is proving to be challenging but successful trials have been performed.

See also: Hyperopia; Myopia; Ocular Media Clarity and Straylight; Refractive Surgery.

Further Reading

Freeman, M. H. and Hull, C. C. (2003). *Optics*, 11th edn. London: Butterworth-Heinemann.

Harris, W. F., Raasch, T. W., and Thibos, L. N. (1997). *Optometry and Vision Science: Feature Issue on Visual Optics* 6: 339–463.

Rabbetts, R. B. (2007). *Bennett and Rabbetts' Clinical Visual Optics*, 4th edn. London: Butterworth-Heinemann.

Read, S. A., Collins, M. J., and Carney, L. G. (2007). A review of astigmatism and its possible genesis. *Clinical and Experimental Optometry* 90: 5–19.

Avascularity of the Cornea

R J C Albuquerque and J Ambati, University of Kentucky, Lexington, KY, USA

Glossary

Alloimmunity – A condition in which the body gains immunity, from another individual of the same species, against its own cells.
Aniridia – Congenital disorder characterized by the abnormal deficient development of the iris and associated with corneal angiogenesis and poor vision.
Atopic keratoconjunctivitis (AKC) – Allergic conjunctivitis where the conjunctiva is red and swollen. Untreated, AKC can progress to ulceration, scarring, cataracts, keratoconus, and corneal vascularization.
Hemangiogenesis – It pertains to the specific growth of blood vessels.
Limbus – The edge of the cornea where it joins the conjunctiva and the sclera.
Lymphangiogenesis – It pertains to the specific growth of lymphatic vessels.
Neovascularization – Formation of new blood and lymphatic vessels.
Perforating keratoplasty – Corneal transplant with replacement of all layers of the cornea, but retaining the peripheral cornea.

Light, the substrate of vision, is required to transverse the full diameter of the eye globe and reach retinal photoreceptors giving rise to the intricate biophysical phenomenon of sight. The cornea, interfacing the outer world and the intra-ocular tissues, serves as an entry window through which light comes into the eye. Avascularity and optical transparency are directly related and a requirement for optimal vision. The absence of vessels in the cornea is also one of the pillars of corneal immune privilege, an important physiological phenomenon that is associated with the maintenance of corneal clarity and responsible for the high success rate of corneal transplants. The growth of blood and lymphatic vessels into the normally avascular cornea (neovascularization) is considered pathological as it impairs the passage of light resulting in severely deteriorated vision or complete corneal blindness, which together afflict over 200 million people worldwide.

The absence of vascular structures in the cornea has been known for over 1000 years. But only recently, advances in molecular biology have led to improved understanding of the homeostatic mechanisms underlying such phenomenon. The absence of vasculature (blood and lymphatic vessels) in the cornea is remarkably intriguing given the highly vascularized nature of the neighboring tissues such as the ocular conjunctiva. The abrupt and precise delineation of the limbal vasculature (**Figure 1**) suggests that corneal avascularity is an active process in which endogenous pro- and anti-angiogenic mechanisms are in harmony and that these molecular modulators of angiogenesis are differently expressed in these interfaces between the cornea and its neighboring tissues preventing the blood and lymphatic vessels from invading the avascular cornea.

Corneal Histology

Histologically, the cornea is comprised of five layers (**Figure 2**). The epithelial layer coats its outermost surface and is composed of a thin nonkeratinized squamous stratified epithelium (only a few cells thick). Unlike the stratified squamous epithelium of the epidermis, that contains indented dermal papillae, the corneal epithelium lays flat on a thick basement membrane called Bowman's membrane. The subjacent layer of the cornea, its stroma or substantia propria, is formed by tightly packed collagen fibers that are uniquely organized in a parallel fashion affording the cornea its crystal clear disposition. The corneal stroma is devoid of blood and lymphatic vessels and is populated by fibroblasts. In addition to fibroblasts, the substantia propria is also endowed with a heterogeneous population of cells including bone-marrow-derived cells, and antigen presenting dendritic cells, most of which, under normal physiological conditions, are still immature and remain quiescent. Descement's membrane, a thick lamina propria, separates the corneal stroma from its innermost cellular layer: the corneal endothelium, which consists of a single layer of low cuboidal cells. The corneal endothelium is critical for water homeostasis as it actively transports excess fluid from the corneal stroma into the anterior chamber. This peculiar histological organization of the cornea with a thin epithelium layer and an active endothelium allows oxygen from the room-air and nutrients from the aqueous humor to diffuse through its full thickness. Because the loss of avascularity in the cornea results in impaired light transmission and poor vision, these unique histological features evolved over time and bestowed the cornea with the ability to remain viable and clear in the absence of a direct blood supply.

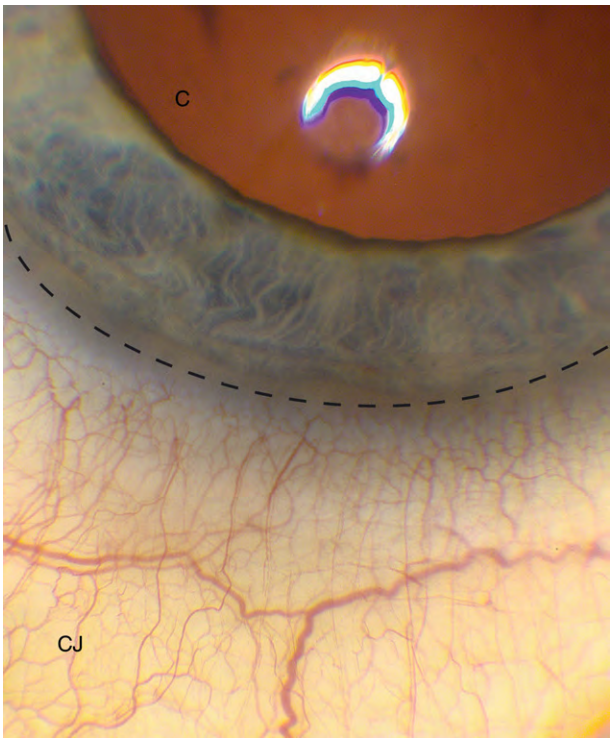

Figure 1 Photograph of the human limbus showing the abrupt termination of the conjunctival vasculature in the interface between the cornea (C) and the conjunctiva (CJ). Dotted line delineates the limbus.

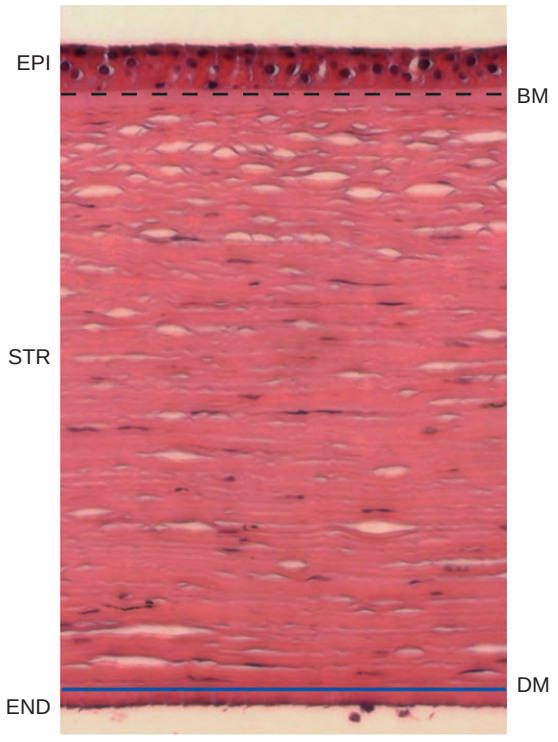

Figure 2 Photomicrograph of the human cornea stained with H&E showing its histological layers. The epithelial layer (EPI) overlaying Bowman's membrane (dotted line). The corneal stroma (STR) displaying its tightly packed parallel collagen fibers. Descement's membrane (DM) interfacing the substantia propria and the corneal endothelium (END).

Corneal Avascularity and Optical Clarity

The visual impairment associated with the loss of corneal avascularity is not only related to the physical obliteration caused by the opaque vessels within the visual field. Corneal neovascularization also reduces visual acuity because the infiltrating vasculature disrupts the tightly packed collagen bundles eliciting opacities, especially in areas surrounding the newly formed vessels. Vascular leakage and edema, usually associated with inflammatory neovascularization, overwhelms the endothelium drainage capacity, creates fluid accumulation, disrupts corneal clarity, and perturbs light transmission. Additionally, the neovascular corneas may also have diminished transparency due to lipid deposits. This is observed in vascularized corneas following corneal herpetic infections. Altogether, these observations speak of the tight correlation that exists between corneal avascularity, corneal transparency, and optimal optical performance.

Endogenous Anti-Angiogenic Mechanisms

The molecular homeostatic mechanisms supporting the lack of vessels in the cornea were unknown until recently. Long ago, it was postulated that corneal avascularity was a passive process. It was thought that the cornea was avascular simply because pro-angiogenic forces were not present. It is quite intriguing, however, that the avascular cornea is surrounded by extremely vascularized tissues, such as the ocular conjunctiva and iris. Because pro-angiogenic factors are a requirement for endothelial cell survival one may postulate that the cornea must be armed with angiostatic capabilities in order to counteract the constant angiogenic stimuli that derives from the adjacent vascular beds. This alternate hypothesis has challenged the previous beliefs, became accepted as a working hypothesis, and still stands as a paradigm of modern vascular biology. Currently, it is well known that corneal avascularity is an extremely active phenomenon, requiring an exact balance between pro- and anti-angiogenic forces, and not the mere absence of pro-angiogenic stimulation.

Extrinsic and intrinsic mechanisms have been proposed to underlie the absence of blood and lymphatic vessels in the cornea. The aqueous humor, fluid that circulates through the anterior chamber of the eye, has been regarded as a major extrinsic inhibitor of corneal angiogenesis. It contains several soluble angiostatic molecules including heparan sulfate proteoglycans. Because vascular endothelial growth factor (VEGF) and basic fibroblast growth factor (bFGF), the foremost studied angiogenic factors, bind to

these glycoproteins with relative high affinity, it has been proposed that the aqueous humor sequesters VEGF and bFGF from the cornea into the anterior chamber. However, it is important to bear in mind that not all isoforms of VEGF, like VEGF121, shown to be expressed in the cornea, bind heparan sulphate. This suggests that additional mechanisms are in place to secure corneal avascularity. In reality, it has long been suggested that corneal avascularity is a phenomenon supported by a redundant system. Additional factors contributing to corneal avascularity include the intrinsic synthesis of angiostatic molecules. It has been shown that the cornea expresses several of these anti-angiogenic factors, like angiostatin, endostatin, thrombospondins (TSPs), interleukin-1 receptor antagonist, pigmented epithelium-derived factor (PEDF), non vascular VEGF receptor-3 and soluble VEGF receptor-1.

The current paradigm of intrinsic angiostatic mechanisms in the cornea derived from the clinical observation that corneal epithelial dysfunction was often associated with neovascularization. This suggested that the anti-angiogenic powers of the cornea resided primarily in its epithelial layer. In fact, most of the anti-antiangiogenic factors identified in the cornea have been localized primarily to the corneal epithelium.

Angiostatin, a by-product of plasminogen, was first isolated in 1994. Its angiostatic effect was initially demonstrated in a cancerous tumor growth and metastasis model. Mechanistically, angiostatin is thought to inhibit ATP synthase activity, block endothelial cell migration and proliferation and also cause vascular endothelial cell apoptosis. Angiostatin has been detected in healthy human corneal extracts and it has been shown that human corneal epithelium in culture is capable of converting exogenous plasminogen into its angiostatic by-product. Angiostatin has also been implicated in the maintenance of angiogenic privilege in the normal cornea and after wound healing.

Endostatin was first described in 1997. It is a proteolytic fragment of the caroboxyterminus of collagen XVIII. It has been portrayed as a potent inhibitor of angiogenesis and tumor growth. Collagen XVIII is a component of the basement membrane ubiquitously expressed and it also has been shown to exist in ocular tissues. Immunohistochemical studies have localized collagen XVIII and endostatin to the corneal epithelium, principally in the basal epithelium. Endostatin has been shown to block VEGF-induced phosphorylation of VEGFR-2 and inhibit endothelial cell proliferation and migration. The synthesis of endostatin in the cornea is upregulated during injury and has been shown to inhibit injury-induced corneal neovascularization. Although endostatin has been shown in the uninflammed cornea, mice deficient in collagen XVIII have normal avascular corneas, suggesting that endostatin is only one of many factors contributing to the maintenance of corneal avascularity.

TSP-1 and -2 are potent anti-angiogenesis protein. TSP-1 directly inhibits the migration and survival of endothelial cells by activation transforming growth factor-beta (TGF-β). TSP-2 inhibits vascular endothelial cell proliferation independently of TGF-β activation. Both molecules have been detected in the mouse and human corneas under normal physiological conditions. Exogenous administration of TSP-1 and/or -2 have been associated with diminished suture-induced corneal angiogenesis. However, the systemic ablation of TSP-1 and -2 was not associated with spontaneous angiogenesis in the cornea, suggesting that alternate redundant angiostatic mechanisms are operative in the cornea.

Interleukin (IL)-1 receptor antagonist, a key modulator of IL-1 activity, was shown to be expressed in the normal human cornea. It was localized to the corneal epithelium and some stromal fibroblasts. In a mouse model of suture-induced corneal neovascularization IL-1 receptor antagonist was shown to have anti-angiogenic properties and its exogenous administration was also associated with diminished infiltration of inflammatory cells into the cornea. IL-1 receptor antagonist deficiency in mice had no bearing in corneal avascularity, once again implying that corneal avascularity is secured by a multifactorial and redundant system.

VEGFR-3, normally expressed in lymphatic endothelial cells (LECs), corneal dendritic cells, and macrophages, was shown to be ectopically expressed in corneal epithelial cells of human and mice. These ectopic receptors have been shown to work as an inhibitor of injury-induced corneal angiogenesis in mice.

Since its discovery in 1993, soluble VEGFR-1 (sVEGFR-1) has been extensively studied as a powerful inhibitor of VEGF-induced angiogenesis. It has been implicated in several pathological states, including pre-eclampsia, sepsis, arthritis, and cancer. Interestingly, VEGF, a powerful driver of angiogenesis, is expressed in the normal avascular cornea. Recently, it has been shown that sVEGFR-1 is co-expressed by the corneal epithelium serving as a VEGF manacle. Because the systemic ablation of VEGFR-1 gene is not compatible with survival, corneal specific deletion of VEGFR-1 was employed in mice and led to spontaneous corneal neovascularization. sVEGFR-1 is considered to be singularly essential for maintaining corneal avascularity of the uninjured cornea. The expression of sVEGFR-1 in the cornea was also shown to be conserved among mammals, including humans. One exception is the Manatee, whose cornea is spontaneously vascularized and lacks sVEGFR-1 expression. A similar splice variant of VEGFR-2, sVEGFR-2, was recently identified and described as the first specific endogenous inhibitor of lymphangiogenesis. In the cornea, sVEGFR-2 was shown to be singularly essential to maintaining the cornea devoid of lymphatic vessels, as its genetic deletion cause spontaneous invasion of lymphatic, but not blood vessels into the cornea.

Loss of Corneal Avascularity

Corneal neovascularization occurs when the precise equilibrium between pro- and anti-angiogenic forces is disrupted. The loss of corneal avascularity is pathological. Several ocular disorders are hallmarked by corneal neovascularization. These neovascular disorders of the cornea range from benign contact lens-associated neovascularization to congenital and hard to manage ocular anomalies such as aniridia.

Extended contact lens wear may induce neovascularization because the associated hypoxia triggers a steep rise in VEGF expression, overwhelming the natural anti-angiogenic barriers. Other corneal disorders are coupled with pathological angiogenesis because of direct damage to the corneal epithelium. Corneal trauma, such as corneal abrasions or chemical (alkali) burn of the ocular surface, infections (herpetic keratitis), immune diseases such as atopic keratoconjuctivitis or rheumatoid arthritis, limbal cell deficiency, or congenital anomalies such as aniridia are all associated with the loss of avascularity. These clinical entities commonly require surgical management, like refractive surgery or perforating keratoplasty, both of which are negatively impacted by the preexistence of vessels in the cornea. This represents a significant clinical predicament and speaks of the critical nature of unveiling molecular targets that may be manipulated to treat the aberrant and disordered growth of vessels into the cornea.

Immune Privilege of the Avascular Cornea

The absence of blood and lymphatic vessels in the cornea is known to play a critical role in maintaining its immune privilege, but other immune-protective mechanisms have been described. One such mechanism is referred to as anterior chamber-associated immune deviation (ACAID). ACAID is regarded as the ability of antigen-presenting cells (APCs) and antigens from anterior chamber-associated tissues (i.e., cornea) to directly enter the blood circulation through the trabecular meshwork homing to the spleen where immune tolerance is induced. Additionally, tissues from the anterior segment of the eye have been reported to express Fas-ligand which induces apoptosis in activated immune cells (Fas-receptor positive), thus protecting the cornea from damage by stimulated lymphocytes. These mechanisms are thought to collectively downregulate inflammation in the cornea, thereby preserving corneal clarity which is essential for optimal vision. Corneal avascularity is therefore one factor of several redundant active mechanisms aimed at preserving corneal transparency and optical light transmission.

Corneal Transplant and Avascularity

In 1905, ophthalmologist Edward Zim performed the first corneal transplant in a human subject. Since then, corneal transplants have become the most common type of solid tissue transplantation in the world. Nearly 46 000 corneal transplants are preformed yearly in the US. In addition to being the most prevalent, corneal allograft transplantation, it is also the most successful intervention among other commonly transplanted organs. However, the long-term outcome of this intervention is greatly influenced by pre-operative risk factors, with corneal neovascularization (high-risk group) being an important negative predictor of corneal allograft survival. While graft survival is approximately 90% in the low-risk group (no pre-operative inflammation or neovascularization), these numbers are drastically reduced to roughly 35% in the high-risk group. Recent studies targeting corneal angiogenesis with VEGF-A binding molecules (VEGF-trap®) demonstrated that allograft survival is inversely related to the amount of neovascularization in the murine corneal transplantation model corroborating the aforementioned epidemiological observations. The loss of corneal avascularity is therefore a significant clinical quandary.

The surgical procedures used in corneal allograft transplantation require delicate techniques to prevent adverse inflammatory reactions which may compromise outcome. The corneal graft is attached to the recipient's ocular surface with the placement of small sutures. Paradoxically, in a vastly employed injury model of corneal angiogenesis, similar intrastromal sutures are used as a method of eliciting blood and lymphatic vessel growth. Because suture placement is a requirement for corneal transplantation as well as a pro-angiogenic stimulus, it is critical to understand the molecular underpinnings related to the growth of blood and lymphatic vessels into the cornea, so potential molecular targets could be identified and manipulated to promote corneal avascularity, optimal optical performance, and prevent corneal blindness.

Corneal Alymphaticity and Allograft Rejection

Because the growth of blood and lymphatic vessels into the cornea are intimately intertwined, the individual contribution of each of these vasculatures to the fate of corneal allografts is not clearly understood. However, recent evidence suggests that the growth of lymphatic vessels into the cornea may be more tightly associated with loss of corneal immune privilege and critical for corneal allograft rejection than corneal hemangiogenesis.

Substantial progress in the study of corneal lymphangiogenesis has taken place since the discovery of VEGFR-3

and its ligands VEGF-C and –D. The identification of specific cellular makers preferentially expressed by LECs, such as LYVE-1, Prox1, and Podoplanin, has also propelled great advances to the field of lymphangiogenesis.

Corneal lymphangiogenesis generally occurs after corneal injury and inflammation, which in turn is associated with increased levels of VEGF-C. The newly formed corneal lymphatic vessels give rise to an afferent route through which corneal transudate and APCs are carried from the interstitial space into the lymphatic system and later back into the blood circulation. This drainage pathway becomes extremely deleterious in the context of corneal transplantation. Under these circumstances, the alternative route bypassing the standard outflow pathway (i.e., trabecular meshwork in the anterior chamber) allows for antigens from the donor cornea to escape through the lymphatic system and into the draining lymph node where a graft rejection reaction is initiated. The significance of this alternate drainage pathway to corneal alloimmunity and graft rejection has been portrayed in studies demonstrating that removal of cervical lymph nodes significantly increases the transplant survival rates in the low-(noninflamed, nonvascularized) and high-risk (neovascularized) groups. Together, these observations suggest that improved molecular understanding of corneal lymphangiogenesis, as well as the identification of endogenous compounds with the ability to uncouple lymphangiogenesis from hemangiogenesis would shed light into our current understanding of allograft rejection and potentially unveil therapeutic targets to enhance the survival of corneal allograft.

The Avascular Cornea as an Angiogenesis Study Platform

The avascular disposition and its ready accessibility have made the cornea an important platform for the study of angiogenesis allowing scientists to test the pro-and/or anti-angiogenic effects of several compounds *in vivo*. Numerous assays have been developed to study angiogenesis modulation utilizing the cornea. Direct intra-stromal injection of angiogenesis compounds have been performed in the mouse, rat and rabbit cornea. Models in which a transient chemical (alkali), physical (scraping), or thermal (cautherization) injury are incurred to the cornea to provoke an angiogenic response have been widely used. Prolonged injury of the cornea has been achieved with intra-stromal suture placement. The insertion of a small pellet containing pro-angiogenic molecules has also been described and termed corneal micropocket assay. The cornea stroma has even been utilized for the implantation of tumor cells. The reliability of these models and the easy visualization of corneal vessels have placed the cornea in the forefront of discovery and *in vivo* testing of drugs for the treatment of disorders hallmarked by aberrant angiogenesis, particularly cancer. The ability of analyzing these molecules *in vivo* provides valuable insight regarding the angio-modulatory effects of such compounds.

Conclusions

Avascularity of the cornea is intimately related to optical transparency and optimal vision. Hence, the loss of corneal avascularity is pathological and often results in impaired vision or corneal blindness. A precise balance between pro- and anti-angiogenic factors is essential to maintain the avascular disposition of the cornea. Even though it is well known that corneal immune privilege is a function of a constellation of factors, the absence of blood and lymphatic vessels in the cornea has proven to be one of its most important underlying mechanisms. A more precise understanding regarding the individual contribution of blood and lymphatic vessel growth to corneal alloimmunity is needed. The cornea, given its avascular nature and accessibility, is an ideal the platform for the *in vivo* testing of angiogenesis modulators.

See also: Angiogenesis in the Eye; Corneal Angiogenesis; Hemangiogenesis versus Lymphangiogenesis; Tear Drainage; Vessel Regression.

Further Reading

Albuquerque, R. J. C., Hayashi, T., Cho, W. G., et al. (2009). Alternatively spliced vascular endothelial growth factor receptor-2 is an essential endogenous inhibitor of lymphatic vessel growth. *Nature Medicine* 15: 1023–1030.

Ambati, B. K., Nozaki, M., Signh, N., et al. (2006). Corneal avascularity is due to soluble VEGF receptor-1. *Nature* 443: 993–997.

Azar, D. T. (2006). Corneal angiogenic privilege: Angiogenic and antiangiogenic factors in corneal avascularity, vasculogenesis, and wound healing (an American Ophthalmological Society thesis). *American Ophthalmological Society* 104: 264–302.

Cursiefen, C. (2007). Immune privilege and angiogenic privilege of the cornea. *Chemical Immunology and Allergy* 92: 50–57.

Cursiefen, C., Chen, L., Saint-Geniez, M., et al. (2006). Nonvascular VEGF receptor 3 expression by corneal epithelium maintains avascularity and vision. *Proceedings of the National Academy of Sciences of the United States of America* 103: 11405–11410.

Folkman, J. (2007). Angiogenesis: An organizing principle for drug discovery? *Nature Reviews Drug Discovery* 6: 273–286.

Hirsch, E., Irikura, V. M., Paul, S. M., et al. (1996). Functions of interleukin 1 receptor antagonist in gene knockout and overproducing mice. *Proceedings of the National Academy of Sciences of the United States of America* 93: 11008–11013.

Krachmer, J., Mannis, M., and Holland, E. (2004). *Cornea.* Amsterdam: Mosby.

Lawler, J. (2000). The functions of thrombospondin-1 and -2. *Current Opinion in Chemical Biology* 12: 634–640.

O'Reilly, M. S., Boehm, T., Shing, Y., et al. (1997). Endostatin: An endogenous inhibitor of angiogenesis and tumor growth. *Cell* 88: 277–285.

O'Reilly, M. S., Holmgren, L., Shing, Y., et al. (1994). Angiostatin: A novel angiogenesis inhibitor that mediates the suppression of metastases by a Lewis lung carcinoma. *Cell* 79: 315–328.

Spencer, W. H. (1996). *Ophthalmic Pathology: An Atlas and Textbook.* Philadelphia, PA: W.B. Saunders.

Whitcher, J. P., Srinivasan, M., and Upadhyay, M. P. (2001). Corneal blindness: A global perspective. *Bulletin of the World Health Organization* 79: 214–221.

Yamagami, S., Dana, M. R., and Tsuru, T. (2002). Draining lymph nodes play an essential role in alloimmunity generated in response to high-risk corneal transplantation. *Cornea* 21: 405–409.

B

Binocular Vergence Eye Movements and the Near Response

C M Schor, University of California at Berkeley, Berkeley, CA, USA

Glossary

Cyclo-vergence – The torsional rotations of the two eyes in opposite directions.
Horopter – The locus of points in space imaged on corresponding regions of the two retinae that results in identical visual directions (singleness).
Retinal disparity – The perspective differences between the two retinal images.
Torsion – The ocular rotation of the eye about the visual axis.
Vergence – The rotations of the eyes in opposite directions (horizontal, vertical, and torsional).

Vertebrates are equipped with two eyes that are either widely separated in the head to provide panoramic vision, or they are narrowly separated to provide stereoscopic depth perception but with a reduced extent of the binocular visual field. Panoramic vision provides a useful field of view for herbivores that graze throughout the day, and stereopsis provides a useful range finder for predators and hunter-gatherers. Stereopsis is stimulated by perspective differences between the two eye's retinal images that result from the small 6-cm separation between viewpoints of the two eyes.

Stereopsis is stimulated by horizontal disparities that result from the horizontal misalignment of the two retinal images from corresponding or homologous regions of the two eyes retinae. When objects in space are imaged on these corresponding points, they appear in identical visual directions, that is, single vision, and the surface in space where points are imaged on corresponding retinal points is referred to as the horopter. For the purpose of single vision, correspondence is between small areas (Panum's fusional area) that result in a singleness horopter surface in space that is approximately 0.5° thick and it passes through the point of binocular convergence. Figure 1 also describes the backward pitch of the horopter surface that results from a 2° shear between the corresponding vertical meridians of the two retinae. Only this small region of space described by the horopter surface appears single and all objects in front and behind the horopter appear double when one image is not suppressed.

Stereopsis is supported by two classes of eye movements that obtain and maintain registration or alignment of the two retinal images on corresponding retinal regions of the two eyes to produce single binocular vision. The two eyes rotate in a yoked fashion (versions) to maintain binocular image registration while the eyes change direction of gaze, and they rotate in opposite directions (vergence) to establish binocular registration. Misalignment of the two eyes with the viewing geometry of a given target produces a misalignment with corresponding points, referred to as binocular parallax or absolute disparity, and these absolute disparities stimulate vergence eye movements.

For the purpose of binocular eye alignment, absolute disparity can be described with three degrees of freedom, including horizontal, vertical, and cyclo-components. 'Cyclo' describes the twist of the eye about its visual axis. Binocular alignment minimizes all three components of disparity at the fovea with vergence control, and any residual disparities in the periphery are used to interpret relative depth and surface orientation. All three components of disparity are necessary to interpret space, because, by themselves, horizontal, vertical, and cyclo disparities are ambiguous. The same horizontal disparity can correspond to many different depth intervals that depend on distance and direction (azimuth) of targets relative to the observer. Similarly, many different slant angles correspond to the same cyclo and shear disparities. These disparities are disambiguated with information about distance and direction (azimuth) of objects relative to the head. This information can be obtained from extra-retinal information from the sense of eye position or from retinal information from vertical disparity.

Horizontal disparity is the primary stimulus for horizontal vergence (convergence). Disparities are defined with reference to the horopter, which passes through the

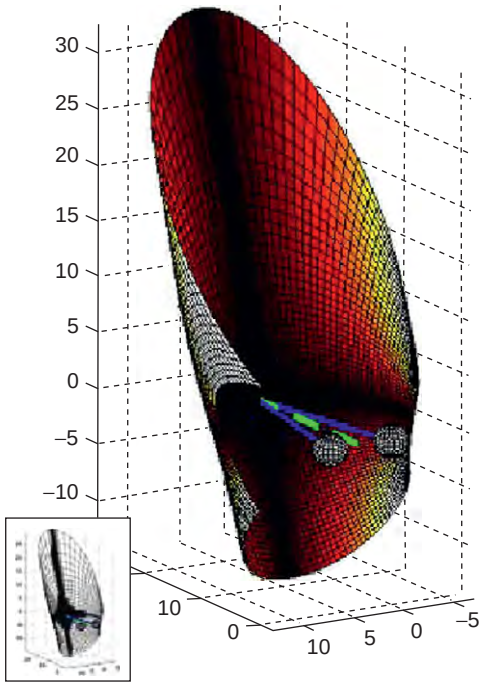

Figure 1 The horopter with a vertical shear deviation from a pattern of identical corresponding points. Gaze is straight ahead at a vergence of 10°.
The horopter with gaze straight ahead at a vergence angle of 20°.

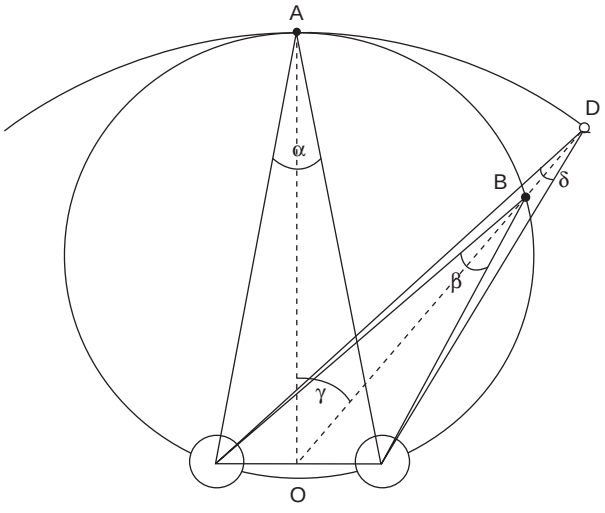

Figure 2 Plan view of iso-vergence circle (large complete circle), iso-accommodation circle (shown as an arc) and various azimuth angles. The two small circles represent the right and the left eye. The point A represents the spatial location that corresponds to matched stimuli for accommodation and convergence. ‡ = convergence angle at point A (angle made by the intersection of two lines of sight), β = convergence angle at point B, and $* = \beta$ along the iso-vergence circle, γ = lateral gaze angle. Note that at point D on the iso-accommodation circle, the convergence stimulus (δ) is lower than β at point B.

point of binocular convergence. Note that the distance corresponding to a fixed angle of convergence varies with gaze azimuth along an isovergence circle that passes through the two eyes centers of rotation. (**Figure 2**). The

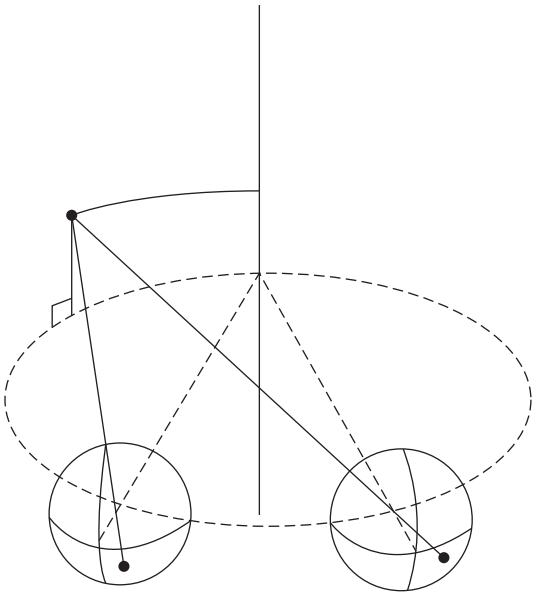

Figure 3 Optical geometry producing vertical disparity of points presented in tertiary directions at finite viewing distances.

iso-accommodation circle is also shown, which has a center at the point midway between the two eyes. Differences between these two circles are discussed below. If we assume that the nodal point of the eye is very close to the centers of rotation, then the horopter surface contains the isovergence circle. Targets lying in the horopter surface all subtend zero disparity, and targets lying at distances closer or farther than the horopter subtend crossed and uncrossed disparities respectively, which in turn stimulate convergence and divergence of the eyes.

Vertical disparity is subtended by all near targets lying in tertiary directions above and below the visual plane. These disparities arise from the difference in distance of the target from the entrance pupils of the two eyes (**Figure 3**). Normally binocular fixation of targets at near distances in a tertiary position requires that the abducting eye move up more than the adducting eye (Fick coordinates). This vertical vergence occurs automatically with gaze shifts, even when one eye is occluded.

Uniform cyclo-disparities along both horizontal and vertical meridians result from vergence errors. The uniform cyclo-disparities produced by ocular cyclo-torsion can be distinguished from nonuniform cyclo-disparities produced by slanted surfaces, which do not produce cyclo-disparity between horizontal lines imaged on the two foveas.

A Coarse-to-Fine Strategy for Vergence

Voluntary binocular gaze shifts respond to both perceived spatial location and retinal disparity. When the gaze shifts are between targets separated widely in depth, retinal disparity is too large to provide useful visual feedback and the primary cue for gaze is perceived spatial location.

As the voluntary response to perceived location proceeds, retinal-image disparity and blur are reduced into the effective stimulus-operating range of a fine adjustment or foveal-maintenance mechanism that utilizes visual feedback from retinal cues, including binocular disparity and blur. These perceptual and retinal classes of stimuli are used to control the vergence response in a coarse-to-fine strategy and their goal is to optimize stereopsis by minimizing horizontal, vertical, and cyclo-components of retinal-image disparity at the fovea.

Cross-Coupling of Voluntary and Involuntary Motor Responses and the Near Response

While all three vergence components respond to retinal cues of horizontal, vertical, and cyclo-disparity, only horizontal vergence responds voluntarily to perceptual cues. Vertical vergence and cyclo-vergence are only under involuntary control, and they do not respond directly to perceived target location. The two involuntary components of the vergence are cross-coupled with voluntary version and horizontal vergence eye movements. Involuntary components of vergence are guided by the attentionally driven voluntary components of version and convergence that change direction and distance of gaze in response to perceived space. The cross-coupled vergence responses reduce all three components of retinal-image disparity into the effective stimulus-operating range of all three components of vergence. Couplings that link involuntary components of vergence with convergence are collectively referred to as the near response.

Ideal Cross-Links for Three-Dimensional Viewing Geometry

Cross-links between voluntary and involuntary components of the near response are based upon predictable relationships between version and vergence components of eye position that reduce retinal-image disparity to zero. Horizontal, vertical, and cyclo-disparities are determined by target location and the coordinate systems that control horizontal and vertical eye position. These predictable relationships allow the cross-coupled involuntary responses to be scaled with version and horizontal vergence components of the voluntary response. Scale factors are used to describe the couplings quantitatively.

Horizontal Vergence Coupling

Coupling interactions have been described for all three components of vergence. The horizontal component of vergence, which is under voluntary control, can be guided by voluntary accommodation under conditions where an occluder, such as the nose, blocks one eye's view of a target. The linkage between accommodation and convergence is possible because both respond to optical–geometric properties of a common viewing distance. The linkage between horizontal convergence (C) with the accommodation response (A) to blur is described by the accommodative vergence ratio (K_c).

$$C = K_c \times A \quad [1]$$

Ideally, the K_c would be 1.0 for symmetrical convergence expressed in meter angles and accommodation in diopters. Empirical measures demonstrate a normal $K_c = 0.66$ MA/D. Accommodation (A) can also follow convergence responses (C) to disparity with a different empirical scalar value (K_a) of 1.0.

$$A = K_a \times C \quad [2]$$

The ideal K_c and K_a change with gaze azimuth. Ideal K_c is lower and ideal K_a is higher for targets viewed in eccentric horizontal gaze than in symmetrical convergence because constant stimuli for accommodation and convergence lie on different circles. **Figure 2** illustrates the iso-vergence circle and iso-accommodation circles that intersect one another in the midsagittal plane, but differ elsewhere. Empirical measures of K_c follow these changes in the ideal K_c with azimuth. The empirical K_c becomes reduced and a bias of K_a increases with increasing horizontal eccentric gaze in asymmetric convergence. The low empirical value of K_c is also a compromise of several different gaze azimuths.

Vertical Vergence Coupling

Binocular vertical alignment of foveal images is controlled by vertical vergence. In a Fick coordinate system that is often used to describe vertical disparity, the amplitude of vertical vergence is scaled proportionally with the vertical image size ratios of the two ocular images of a target viewed in a tertiary direction. In this application, vertical vergence is quantified as the ratio of vertical positions of the left and right eyes (V_l/V_r) that is necessary for bifoveal fixation of elevated targets in tertiary directions of gaze. In symmetrical convergence, the ratio equals 1.0 and in asymmetric convergence it depends upon both, convergence (C) and horizontal gaze eccentricity (H). Convergence is positive following a sign convention where left and down are positive values, and where convergence equals R–L eye position. In left-gaze, the ratio of left over right eye position is described by (in Fick coordinates)

$$V_l/V_r = K_v \tan^{-1}[\cos(H_l - C/2)]/\tan^{-1}[\cos(H_r + C/2)] \quad [3]$$

where H_l and H_r represent the azimuth of the left and right eye relative to primary position and V_l and V_r represent the elevation of the left and right eye in Fick coordinates. Empirical measures demonstrate a normal scalar value of

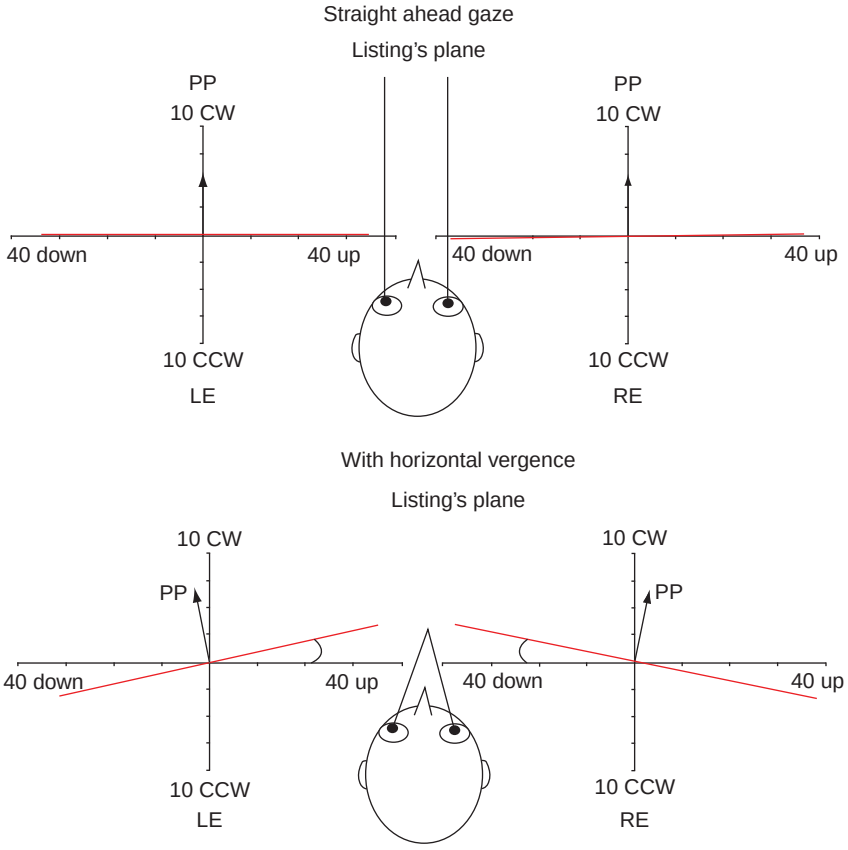

Figure 4 Changes in the divergence between Listing's planes with gaze at infinity (upper panel) and during convergence (lower panel). Primary position (PP) is orthogonal to Listing's plane. During distance viewing, the primary positions are nearly parallel, and during near viewing they diverge by approximately the angle of convergence.

$K_v = 1.0$. Note that when vertical vergence is described in a Helmholtz coordinate system,

$$V_l / V_r = K_v \qquad [4]$$

and K_v is independent of convergence or gaze angle. $K_v = 1.0$ for both the Fick or Helmholtz coordinate systems.

Cyclo-Vergence Coupling

Nearly 150 years ago, Donders recognized that the torsional orientation of the eye in any given direction of gaze was independent of the path the eye took to reach that position. This was noteworthy because spherical rotations of physical objects such as satellites are normally noncommutative, that is, the twist about the primary depth axis does depend on the path taken to reach a tertiary direction. The amount of ocular torsion was described by Listing as though the eye had rotated from a primary position about an axis that was in a common plane with other axes describing ocular torsion in other directions of gaze (**Figure 4** showing Listing's plane from old **figure 5**). Helmholtz referred to this as Listing's plane. Listing's law describes a coupling between cyclo-torsion and versional eye position that makes spherical rotations of the eye commutative.

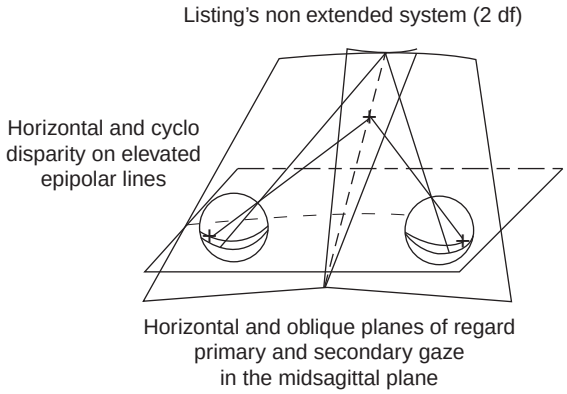

Figure 5 Torsional orientation of epipolar planes passing through the foveas with gaze horizontal and elevated gaze when Listing's law is not extended. The projections of the corresponding epipolar meridians (planes of regard) are extorted such that the horopter collapses to a single point where the visual axes intersect. Pure horizontal disparities (no vertical or cyclo-disparity) only exist along the line at the intersection of the planes of regard.

The orientation of Listing's planes changes with convergence. Hering first observed a binocular coupling between horizontal vergence, eye elevation, and cyclovergence. He observed that in upward gaze, the eyes

were intorted and in downward gaze, they were extorted relative to the orientations predicted by the orientation of Listing's planes located in the facial plane. In a Fick coordinate system, incyclo-vergence forms an A pattern between the vertical meridians of the retinae and excyclo-vergence forms a V pattern. This coupling between cyclo-vergence and eye elevation during convergence is part of the near response.

During convergence, ocular torsion is still described as commutative, as though the eyes had rotated about axes in two fixed planes, one for each eye, from their respective primary positions. However, the orientation of the planes is different from the orientation of the classical Listing's plane that lies in the facial plane when the eyes view distant targets. During near fixation, ocular torsion has a different pattern in which the eyes incyclo-verge in upward gaze and excyclo-verge in downward gaze. These changes follow Listing's law for Listing's planes that are diverged for the right and left eye by approximately the amount that the eyes have converged (**Figure 4**). The benefit of this change in cyclo-vergence with vertical gaze and convergence is described below.

Coupling between cyclo-vergence with vertical gaze and convergence is optimized to match viewing geometry. During symmetrical convergence, the torsional alignment of the horizontal meridians of the retinae is controlled by cyclo-vergence (T) that is scaled proportionally by K_t with combinations of convergence (C) and vertical eye position (V). Following a right-hand-rule sign convention, left, down, and clockwise ocular rotations are positive and convergence equals R–L eye position. Eye position is described in Helmholtz coordinates so that foveal alignment is achieved by equal elevation of the two eyes. The cyclo-vergence necessary for coplanar alignment of the planes of regard is described by

$$T = K_t \times 2\left(\tan^{-1}[\tan\ C/2 \times \tan\ V/2]\right) \quad [5]$$

When expressed in radians,

$$T = K_t \times V \times C/2 \quad [6]$$

The coupling between the diverged orientation of Listing's planes and convergence can be described by the scalar K_t as a ratio of the change in divergence difference between the two eyes' Listing's planes (ΔY) over the change in convergence (ΔC).

$$K_t = \Delta Y/\Delta C \quad [7]$$

Effects of Listing's Law and Coupling with Convergence on Stereoscopic Depth Perception

The change in orientation of Listing's planes with convergence makes it possible to have good stereoscopic depth for targets lying in the visual plane by twisting the horizontal meridians of the retinae of the two eyes so that they are coplanar and all targets along the visual plane can be imaged on corresponding points without any vertical disparity. The change in orientation of Listing's planes also makes it possible to have good stereopsis with gaze elevated, even in tertiary directions of gaze.

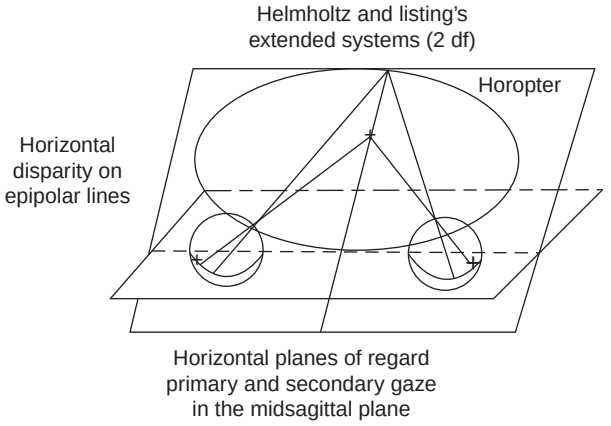

Figure 6 Coplanar orientation of epipolar lines and planes of regard passing through the foveas with horizontal and elevated gaze when Listing's law is extended. The longitudinal horopter exists in elevated gaze and any point in the elevated visual plane subtends pure horizontal disparity on epipolar meridians.

Figures 5 and **6** illustrate the torsional orientation of the two horizontal retinal meridians during two near-fixation conditions in symmetrical convergence. They illustrate variations of cyclo-torsion for the classical Listing's coordinate system and the extended Listing's coordinate system. Both fixation conditions are illustrated for symmetrical convergence. Either the eyes have zero elevation or gaze is elevated in the midsagittal plane. The arcs across the two retinae represent sections of great circles that pass through the horizontal meridians of the retinae and the foveas. The arcs describe epipolar meridians of the eye with gaze elevated. The planes in the figures describe projections of the horizontal meridians of the retinae through the entrance pupils (planes of regard) when gaze is elevated. The locus of points where the two planes of regard intersect represent points in space that subtend pure horizontal disparity without any vertical or cyclo-components.

During convergence, the only targets that can be viewed without retinal image cyclo-disparity must lie in the horizontal plane that passes through the nodal points of the two eyes and intersects the two foveas (i.e., the visual plane). When the eyes are converged in the zero-elevation position, all points lying in the visual plane will subtend pure horizontal disparities because the visual plane contains both planes of regard (i.e., it intersects both horizontal retinal meridians). If the orientation of the Listing's planes did not change during convergence (**Figure 5**), then when gaze was elevated, the planes of regard would become extorted. Images of most objects lying in the inclined

visual plane would be off the horopter and they would subtend complex combinations of horizontal, vertical, and incyclo-disparities. The torted planes of regard would not be coplanar, and they would only intersect along a line in the midsagittal plane. Only points on the line of intersection would be imaged with pure horizontal disparities and the fixation point would be the only point on the line of intersection that could be imaged on the horopter.

Figure 6 demonstrates how the oculomotor system remedies this situation and still obeys Listing's law during symmetrical convergence. In a binocular extension of Listing's law, cyclo-vergence intorts the eyes with gaze elevation and extorts the eyes with gaze depression to keep the horizontal meridians coplanar in symmetrical convergence. When gaze is elevated, an incyclo-rotation of the planes of regard makes them coplanar so that it is possible to image real targets on the longitudinal horopter. All targets in the inclined visual plane, whether they are nearer or farther from the fixation point, will be imaged on corresponding epipolar meridians of the eye with pure horizontal disparities. These gaze-dependent changes in cyclo-vergence are consistent with an outward or divergence of Listing's planes. Stereoscopic depth perception would be compromised if this torsional compensation did not occur. Interestingly, these same yaw rotations of Listing's planes preserve stereopsis in tertiary directions of gaze by keeping the horizontal meridians of the two retinae coplanar in gaze directions composed of combined elevation and azimuth.

Figure 1 describes the backward pitch of the horopter surface that results from a 2° shear disparity between the vertical meridians of the two retinae. When the eyes rotate downward to fixate in the ground plane, the horopter pitches back into the ground plane so that objects at all distances along the ground plane appear single. When the eyes fixate different viewing distances along the ground, changes in eye elevation cause changes in cyclo-vergence, predicted by Listing's law, that keep the horopter in the ground plane. The benefit of this is to have single vision over a large range of distances within the ground plane while converged in that plane at a single distance.

See also: Abnormal Eye Movements due to Disease of the Extraocular Muscles and Their Innervation; The Active Pulley Hypothesis; Cranial Nerves and Autonomic Innervation in the Orbit; Extraocular Muscles: Extraocular Muscle Anatomy; Extraocular Muscles: Functional Assessment in the Clinic.

Further Reading

Allen, M. J. and Carter, J. H. (1967). The torsion component of the near reflex. *American Journal of Optometry* 44: 343–349.

Alpern, M. and Ellen, P. (1956). A quantitative analysis of the horizontal movements of the eyes in the experiments of Johannes Muller. I. Methods and results. *American Journal of Ophthalmology* 42: 289–303.

Bradshaw, M. F. and Rogers, B. J. (1994). Is cyclovergence state affected by the inclination of stereoscopic surfaces? *Investigative Ophthalmology and Visual Science* 35: (ARVO Abstracts) 1316.

Bruno, P. and Van den Berg, A. V. (1997). Relative orientation of primary positions of the two eyes. *Vision Research* 37: 935–947.

Collewijn, H. (1994). Vertical conjugacy: What coordinate system is appropriate? In: Fuchs, A. F., Brandt, T., Buttner, U., and Zee, D. S. (eds.) *Contemporary Ocular Motor and Vestibular Research: A Tribute to David A. Robinson*, pp. 296–303. Stuttgart: Thieme.

Donders, F. C. (1848). Beitrag zur Lehre von den Bewegungen des menschlichen Auges. *Hollandische Beitrage zu den anatomischen und physiologischen Wissenchaften* 1: 105–145.

Fincham, E. F. and Walton, J. (1957). The reciprocal actions of accommodation and convertgence. *Journal of Physiology (Lond)* 137: 488–508.

Garding, J., Porrill, J., Mayhew, J. E. W., and Frisby, J. P. (1995). Stereopsis, vertical disparity and relief transformations. *Vision Research* 35(5): 703–722.

Haselwanter, T. (1995). Mathematics of three-dimensional eye rotations. *Vision Research* 35: 1727–1739.

Helmholtz, H. (1910). *Treatise on Physiological Optics*. In: Southal, J. P. C. (ed.). New York: Dover.

Hering, E. (1868). *The Theory of Binocular Vision* (ed. and trans. Bridgeman, B. and Stark, L. (1977)) New York: Plenum

Howard, I. P. and Kaneko, H. (1994). Relative shear disparities and the perception of surface inclination. *Vision Research* 34: 2505–2517.

Howard, I. P. and Rogers, B. J. (1995). *Binocular Vision and Stereopsis*. Oxford: Oxford University Press.

Mok, D., Cadera, A., Ro, W., Crawford, J. D., and Vilis, T. (1992). Rotation of Listing's plane during vergence. *Vision Research* 32: 2055–2064.

Nakayama, K. (1983). Kinematics of normal and strabismic eyes. In: Schor, C. M. and Ciuffreda, K. (eds.) *Vergence Eye Movements: Basic and Clinical Aspects*, ch. 16, pp. 543–564. Boston, MA: Butterworths.

Nguyen, D., Vedamurthy, I., and Schor, C. (2008). Cross-coupling between accommodation and convergence is optimized for a broad range of directions and distances of gaze. *Vision Research* 48: 893–903.

Panum, P. L. (1858). *Physiologische Untersuchungen uber das Sehen mit zwei Augen*. Keil: Schwers.

Schor, C. M., Alexander, J., Cormack, L., and Stevenson, S. (1992). A negative feedback control model of proximal convergence and accommodation. *Ophthalmic and Physiological Optics* 12: 307–318.

Schor, C. M., Maxwell, J., and Stevenson, S. B. (1994). Isovergence surfaces: The conjugacy of vertical eye movements in tertiary positions of gaze. *Ophthalmic and Physiological Optics* 14: 279–286.

Schor, C. M. and McCandless, J. W. (1995). Distance cues for vertical vergence adaptation. *Optometry and Visual Science* 72: 478–486.

Schreiber, K., Crawford, J. D., Fetter, M., and Tweed, D. (2001). The motor side of depth vision. *Nature* 410(6830): 819–822.

Schreiber, K. M., Hillis, J. M., Filippini, H. R., Schor, C. M., and Banks, M. S. (2008). The surface of the empirical horopter. *Journal of Vision* 8(3): 7.1–7.20.

Schreiber, K. M., Tweed, D. B., and Schor, C. M. (2006). The extended horopter: Quantifying retinal correspondence across changes of 3D eye position. *Journal of Vision* 6(1): 6, 64–74.

Somani, R. A. B., Desouza, J. F. X., Tweed, D., and Vilis, T. (1998). Visual test of listing's law during vergence. *Vision Research* 38: 911–923.

Tweed, D. (1997). Visual–motor optimization in binocular control. *Vision Research* 37: 1939–1951.

Van Rijn, L. J. and Van den Berg, A. V. (1993). Binocular eye orientation during fixations: Listing's law extended to include eye vergence. *Vision Research* 33: 691–708.

Walls, G. L. (1967). *The Vertebrate Eye and Its Adaptive Radiation*. New York: Hafner.

Ygge, J. and Zee, D. S. (1995). Control of vertical eye alignment in three-dimensional space. *Vision Research* 35: 3169–3181.

Biological Properties of the Trabecular Meshwork Cells

J Z Gasiorowski, University of Chicago, Chicago, IL, USA
P Russell, University of California at Davis, Davis, CA, USA

Glossary

Anisotropic substrates – Surfaces that have a regular pattern. Although cells typically grow on native basement membranes with isotropic surfaces, investigation of cellular responses to repeating biophysical cues are often useful as initial studies.
Biophysical cues – The signals that a cell obtains as a result of external characteristics upon which it is located. Biophysical cues involve both topographic features as well as the rigidity of the substratum.
Cell culture – The maintaining of cells generally from vertebrate species *in vitro*. Cells directly from donor tissue (primary) or from immortalized or transformed lines are supplied with a culture medium that provides nutrients necessary for survival and proliferation.
Oxidative stress – The damage to a cell as a result of exposure to an oxidative environment. In general, an oxidative environment contains reactive oxygen species, such as hydrogen peroxide or oxygen radicals.
Phagocytosis – A process in which the cell actively takes up material from the extracellular environment. Phagocytosis results in the expenditure of energy by the cell to engulf extracellular components. The process is usually performed by the cell to reconstruct the external environment or structures, or to remove noxious components.
Topography – The three-dimensional features of a surface. In the discussed biological context, this refers to the physical shapes and features of a native or fabricated extracellular matrix.

Introduction

In order to understand the relationship between the trabecular meshwork and glaucoma, one must appreciate the level of anatomical and physiological complexity in the eye, beginning with the aqueous humor. Aqueous humor is produced by the ciliary body of the eye and flows from the posterior chamber around the lens into the anterior chamber through the pupil. The fluid exits the eye by going through either the trabecular meshwork (TM), known as the conventional outflow pathway, or through the uveal–sclera pathway, the unconventional pathway. In humans, the majority of aqueous humor leaves the eye through the TM. The TM consists of cells and matrix and is believed to be the tissue that regulates intraocular pressure (IOP). To date, the exact mechanism by which IOP is regulated has not been elucidated. While a TM has been found in all animals studied from fish to humans, there is a wide variety of anatomical features in this tissue from one species to another. In the humans, the cell-covered trabeculae (beams) are present in the uveal and corneoscleral parts of the meshwork. In the outer part of the meshwork is the juxtacanalicular tissue (JCT) or cribiform region consisting of TM cells on an extracellular matrix (ECM) connecting with the inner-wall cells of Schlemm's canal. Curiously, the human TM has anatomical differences with other primates but has similarities to the mouse and the rat.

Even with humans, there are documented differences in the TM from one eye to the other in the same individual. Notable differences have been found in the cellularity (nuclei of TM cells per solid tissue area) as well as in the variation in cell number with deviations as high as 39%. In primary open-angle glaucoma (POAG), the cellularity difference between paired eyes was reported to be even higher. Even with these variations, the study of the human trabecular meshwork (HTM) and HTM cells is essential in understanding glaucoma.

Glaucoma is found in a number of species, but the anatomical differences between species make the study of the disease very complicated. Because of these differences, the study of glaucoma, particularly as it is influenced by changes in the regulation of outflow in humans, lacks adequate animal models. Currently, the progression of glaucoma in humans is studied by either *ex vivo* organ culture of human, primate, and other species TM or the tissue culture of HTM cells. Since organ culture of TM is complex and somewhat difficult, hypotheses are generally tested with cultured HTM cells first and then validated with organ culture.

Cell Culture

TM can be dissected from whole donor eyes or from unused corneal buttons. Cells from TM are generally separated from the tissue by enzyme digestion and placed

in tissue culture. HTM cells in culture will send out long processes to other cells; and after proliferation, a somewhat cobblestone appearance of cells can be observed. The cells can be passaged but will undergo senescence after an estimated seven passages. If cells are obtained from very young donors, the passage number can be increased before the cells become unusable. In general, work with HTM cells is often limited to five or six passages with the maximum passage level studied annotated in the report. The best way to test hypotheses about the glaucoma is to study normal and glaucomatous HTM cells in the same experiment. Unfortunately, the culture of glaucomatous HTM cells has proven very challenging. Although there have been some laboratories that are successful in their culture, most investigators have found that cells from glaucomatous donors are difficult to passage, and therefore, the number of cells obtained is insufficient for most experiments. The reason for the obstacles in culturing glaucomatous HTM cells is not yet understood. To circumvent this problem, different techniques are used to stimulate normal HTM cells to express glaucoma-like phenotypes.

HTM Cell Characteristics

Of all the proteins that have been identified in HTM cells, myocilin is perhaps the most characteristic. Myocilin was initially known as trabecular-meshwork-inducible glucocorticoid response protein (TIGR). After HTM cells are treated with dexamethasone for a period of time, myocilin is upregulated. This induction appears to be specific for HTM cells even though myocilin has been located in other cells in the eye, and can be used to determine if dissected, cultured cells are indeed HTM cells. Myocilin is one of the families of olfactomedin proteins and has the characteristics of a matricellular protein. Another protein that has been reported in cells in the JCT region of the TM is αB-crystallin. This protein, initially described in the lens of the eye, is actually found throughout the body. It is one of the small heat-shock proteins that can be induced with transforming growth factor-β (TGF-β), heat shock, and oxidative stress. This protein has been reported to be upregulated in glaucoma. The protein αB-crystallin has been shown to be present in normal TM only in the JCT region, suggesting that there may be more than one cell type present in the TM. Other proteins identified in the TM include: the alpha-2 adrenergic receptor, aquaporin-1, as well as acetylated and acetoacetylated low-density lipoproteins; however, these proteins are not specific to the TM and thus are not good markers for HTM cells. Therefore, it can be helpful to also use behaviors, such as phagocytosis, to help define cell types.

HTM Cell Phagocytosis

One characteristic of HTM cells is their pronounced capacity for phagocytosis. Pigment granules are phagocytized with aging, resulting in the TM looking pigmented when viewed in the dissected eye. Excessive amounts of pigment can overwhelm phagocytosis of the TM and this causes pigment dispersion glaucoma. An obvious reason that HTM cells engage in phagocytosis would be to maintain the pores and openings in the outflow pathway so that aqueous humor can readily flow through to Schlemm's canal. Maintaining homeostatic phagocytosis rates is important because a decline in phagocytosis can cause complications as well. The glaucoma that can follow glucocorticoid treatment results in part from the steroid-mediated decrease in phagocytosis by HTM cells. This decrease leads to the increased deposition of ECM material in the TM, which causes an increase in IOP. With phagocytosis, there is a loss of extracellular fibronectin and laminin, again indicative of a role for phagocytosis in ECM remodeling. Thus, besides removal of miscellaneous material that might be washed into the TM by aqueous humor, maintenance of the TM matrix would be another function for the phagocytosis observed. A number of studies have attempted to analyze TM phagocytosis using a variety of particles, such as latex beads, zymosan particles, and *Staphylococcus aureus* bioparticles. These studies have been conducted *in vivo*, in organ-cultured TM, as well as with HTM cells *in vitro*. In one study using cats, one eye was challenged with particles *in vivo*, while the fellow eye in organ culture was similarly challenged. More cells *in vivo* were engaged in phagocytosis, suggesting activation was occurring that was not present in organ culture. There is an indication that an inflammatory pathway might be responsible for this activation, since gamma-interferon has been shown to inhibit phagocytosis. This effect is thought to be related to the alteration of actin filaments in the cell that form the radial spoke-like arrangements during the process of phagocytosis. Conversely, platelet-derived growth factor was shown to enhance phagocytosis by limiting stress-fiber formation in TM cells.

Glaucoma Models

As stated previously, the use of cultured HTM cells allows investigators to test hypotheses about the initiation and progression of glaucoma. HTM cells *in vitro* do not always have the same characteristics that these cells have *in vivo*. It has been reported that gene expression and protein synthesis are often altered when cells are placed in tissue culture. Different culturing methods, described later in this article, discuss some specific steps that can be

taken to coerce the HTM cells into producing a protein expression profile that more closely mimics the whole TM. While cultured cells offer challenges, not the least of which is the short, productive life span, at least four different models that use external stimuli have been used to study glaucoma progression *in vitro*. It is important to note that all of these models possess limitations.

Glucocorticoid Treatment

One of the earliest *in vitro* models for glaucoma and the one that remains widely used today is the addition of glucocorticoids to the culture medium. This class of compounds produces a variety of effects depending on the presence of receptors and the transduction cascades they induce. Clinically, glucocorticoids can increase IOP in certain individuals; a discovery that stimulated the modeling of glaucoma in HTM cells with the glucocorticoid most typically used, dexamethasone. After several days of drug delivery, myocilin will increase in cultured HTM cells, which mimics the myocilin increase seen in the aqueous humor of glaucomatous individuals. Other hallmarks of glaucoma are also present in HTM cells treated with dexamethasone. Notably, a specific type of cross-linked actin network is formed with drug treatment. The HTM cells create dense actin networks, become less pliable, and are more likely to inhibit outflow. Furthermore, when HTM cells are subjected to 50-mmHg pressure, there is an upregulation of matrix metalloproteinase (MMP)-3. The increase in MMP-3 appears to be a response by the cells to elevated pressure and may help in degrading or remodeling the ECM to allow increased outflow. This upregulation of MMP-3, however, is blocked by dexamethasone, which can also downregulate MMP-2 and MMP-14. With dexamethasone treatment, there is also a decrease in the amount of endothelin-1 receptor B. Under normal conditions, the B receptor binds endothelin-1 and causes a release of nitric oxide, resulting in vasodilation. By decreasing the expression of the B receptor, nitric oxide levels will drop. The ligand will then bind the endothelin-1 receptor A, which starts a vasoconstrictive signaling cascade, leading to less outflow and increased IOP.

Transforming Growth Factor-β

Another model system for studying glaucoma is dependent on treatment of cultured cells with TGF-β, which is a superfamily of signaling proteins that includes the bone morphogenetic proteins (BMP). TGF-β2, which can exist in either an active or latent form, has been found in the aqueous humor of glaucoma patients at high levels. Thrombospondin-1, a TGF-β activator, is upregulated in glaucomatous HTM and may influence the signaling cascade. Thus, there is reason to hypothesize that the increased expression of TGF-β may lead to the progression of glaucoma. In cultured cells, TGF-β2, at levels reported in aqueous humor, will increase the expression of tissue transglutaminase, an enzyme that can cross-link ECM proteins; it will also upregulate fibronectin production. Both of these increases have the potential to modify ECM and reduce the facility of outflow. There is a balance between the TGF-β's and the BMPs, with the BMPs appearing to counter the effects of TGF-β in the TM and HTM cells under normal conditions. BMP2 is present in the TM, but appears to be downregulated when HTM cells are cultured. The effects of TGF-β on fibronectin expression can be blocked by co-treatment with BMP4, and BMP7 can similarly negate the effect of TGF-β on the expression of collagens IV and VI. In addition, several reports on specific proteins or results from gene array studies indicate increased TGF-β2 can initiate changes in expression of ECM components that could impede outflow. With glaucoma, there is increased expression of not only TGF-β2, but also gremlin, a protein that inhibits the action of the BMPs. Altogether, these data suggest that the important and delicate balance between these members of the TGF-β superfamily is disrupted with disease and needs to be studied further.

Oxidative Stress

There is evidence for increased oxidative modification of both DNA and lipids with glaucoma. With exposure to 40% oxygen for 10 days, HTM cells lose proteasome activity and have increased cell death. The inhibition of proteasome activity could contribute to decreased facility of outflow by preventing the degradation of both intra- and intercellular debris. Continuous exposure of HTM cells to oxidative stress results in the generation of reactive oxygen species, which stimulate nuclear factor kappa-light-chain-enhancer of activated B cells (NF-κB) and subsequent production of interleukins (ILs), particularly IL-1. A positive-feedback loop is generated between the activated NF-κB and IL-1, which may be a cellular response to lower IOP. Higher levels of NF-κB and IL-1 have been reported after phacoemulsification of the lens during cataract surgery. A lower IOP is typically observed after this surgery. This would support the hypothesis that this signaling pathway is an attempt by the TM to increase outflow in response to oxidative challenge. Curiously, when IL-1 is administered to rat eyes, aqueous humor flow is decreased. The relationship of the effects of oxidative stress both on the HTM cells and on the inflammatory signaling pathway is not clear at this point, but there is evidence that oxidative stress may play a key role in the progression of glaucoma.

Mechanical Stretch

The TM is subjected to mechanical stretch as a result of accommodation, contraction of the ciliary muscle, and elevated IOP in many cases of POAG. Mechanical stretching of HTM cells has revealed major changes in messenger RNA (mRNA) and protein expression patterns. A gene array study found that mechanical stretch resulted in a downregulation of 29 genes and an upregulation of over 100 genes. Tenacin C, fibronectin, TGF-β, and some collagens were among the many genes upregulated between 1.5- and 3.7-fold. Mechanical stretch also increases the expression of MMP-2 and MMP-14 through the intracellular signaling molecule mammalian target of rapamycin (mTOR). The upregulation of these two MMPs can modulate the remodeling of the ECM. In addition to regulating transcription of genes, mechanical stretch influences the alternative splicing of several mRNAs, including tenacin C, collagen XII, and CD44. The relative amounts of these variants change the composition and functionality of the meshwork ECM. Stretching also controls fibronectin splicing, and variants of this protein could influence outflow as a result of providing different binding domains within the ECM. Overall, mechanical stretch alters the ECM of the TM in many ways, all of which have downstream implications on outflow dynamics.

Biophysical Cues

While biochemical cues have been used to study HTM cells, the mechanical stretch model listed above illustrates the importance of also studying biophysical cues that the cells receive. *In vivo*, cells do not sense the hard, flat surfaces that are typically used to culture cells *in vitro*. Rather, the cells are provided with thousands of biophysical cues through cell-to-cell contact or cell-to-ECM attachment. All basement membranes that have been studied have a rich three-dimensional topography consisting of pores, bumps, and ridges. One can easily see that HTM cells are influenced by substrates that have the biomimetic topographic features in the nano- to micron-scale range. In **Figure 1**, HTM cells were plated onto anisotropic substrates consisting of repeating 600-nm grooves and 600-nm ridges (lower right-hand side) as well as a flat surface that was chemically identical (top and left side). The HTM cells orient parallel to the grooves and ridges and are dramatically elongated on these biomimetic substrates compared to the cells on the flat surfaces. In addition to the orientation and alignment differences, the actin cytoskeleton has been shown to align with the patterned substrate (**Figure 2**). Not surprisingly, gene expression is also dramatically altered with biophysical cues in the nano to micron size. Myocilin expression is upregulated on topography, independent of any dexamethasone

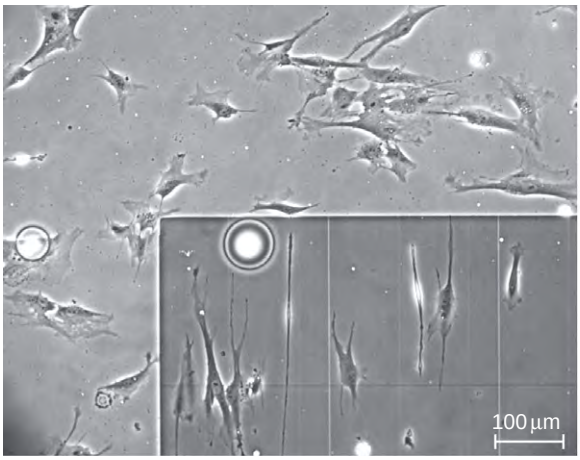

Figure 1 Human trabecular meshwork cells sensing biophysical cues from nanopatterned substrate. Human trabecular meshwork cells growing on a flat surface (top and left) and on a chemically identical nanopatterned substrate (bottom and right). The nanopatterned surface has parallel sets of grooves and ridges each of which are 600 nm in width. The direction of the grooves and ridges is marked. The cells orient parallel to the direction of the biomimetic pattern and become elongated. Cells will also migrate in the direction of these patterned surfaces.

stimulation. A 12-h time lapse of the HTM cells plated on the anisotropic surface and contiguous flat surface shows the random movement of the HTM cells on the flat surface. Cells on the 600-nm grooves and ridges can be seen to migrate along an axis parallel to the patterned substrate. Thus, biophysical cues present in basement membranes can influence basic cellular functions and gene expression. By culturing cells on flat plastic or glass, cells do not experience these cues and this may be the reason why cell-specific proteins or properties often appear to be downregulated when cells are first placed in tissue culture.

In addition to the topography, cells also sense a less rigid, more compliant substrate *in vivo*. Compliance also modulates HTM cell behavior. HTM cells plated onto polyacrylamide surfaces spread less and at a slower rate than cells plated onto stiff tissue culture plastic. The actin cytoskeleton has fewer stress fibers and focal adhesion kinase is minimally phosphorylated on the soft gels. Similar to the topographically patterned surfaces, myocilin expression is upregulated on the more compliant gels. These data, combined with the data reported on the biomimetically patterned surfaces, show the importance of biophysical cues on cells and the necessity to incorporate these features when growing cells *in vitro*.

Summary

The biological properties of HTM cells are varied and complex. While certain characteristics are known, the

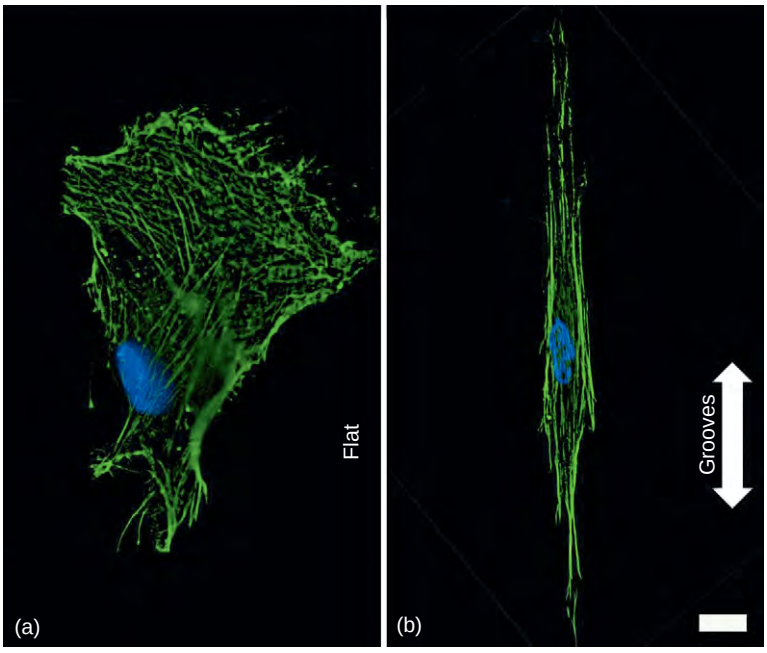

Figure 2 HTM cells orient and elongate with topographic cues. HTM cells were plated onto (a) a flat surface or (b) an anisotropically patterned surface with a repeating pattern of grooves and ridges. Both surfaces were chemically identical. The actin cytoskeleton (green) and nuclei (blue) of the HTM cells were stained 24 h after plating. HTM cells on the flat surface were spread out with actin stress fibers oriented in all directions, while the HTM cells plated on the topographic surface strongly aligned and elongated with the groove and ridge pattern. Scale = 10 μm.

complicated interaction of biochemical and biophysical cues that the HTM cells sense, particularly during the progression of glaucoma, requires additional research. The currently used models have limitations, but with the incorporation of biochemical and biophysical cues, a more accurate representation of HTM cell behavior can be realized. Eventually, a better comprehension of HTM cell properties will aid the development of new treatments for glaucoma.

Acknowledgments

The authors acknowledge support from the National Eye Institute (grant 1R01EY016134-01A1), the National Heart, Lung and Blood Institute (grant 5R01HL07912-02), and the National Science Foundation (grant DMR9632527).

See also: Animal Models of Glaucoma; The Biology of Schlemm's Canal; Biomechanics of Aqueous Humor Outflow Resistance; The Fibrillar Extracellular Matrix of the Trabecular Meshwork; Functional Morphology of the Trabecular Meshwork; The Genetics of Primary Open-Angle Glaucoma: A Review; Myocilin; Primary Open-Angle Glaucoma; Regulation of Extracellular Matrix Turnover in the Aqueous Humor Outflow Pathways; The Role of Oxidative Stress in the Trabecular Meshwork; Role of Proteoglycans in the Trabecular Meshwork; The Role of the Ciliary Body in Aqueous Humor Dynamics. Structural Aspects; Steroid-Induced Ocular Hypertension and Effects of Glucocorticoids on the Trabecular Meshwork.

Further Reading

Bradley, J. M., Kelley, M. J., Zhu, X., et al. (2001). Effects of mechanical stretching on trabecular matrix metalloproteinases. *Investigative Ophthalmology and Visual Science* 42: 1505–1513.

Caballero, M., Liton, P. B., Epstein, D. L., and Gonzalez, P. (2003). Proteasome inhibition by chronic oxidative stress in human trabecular meshwork cells. *Biochemical and Biophysical Research Communications* 308: 346–352.

Flugel-Koch, C., Ohlmann, A., Fuchshofer, R., Welge-Lussen, U., and Tamm, E. R. (2004). Thrombospondin-1 in the trabecular meshwork: Localization in normal and glaucomatous eyes, and induction by TGF-beta1 and dexamethasone *in vitro*. *Experimental Eye Research* 79: 649–663.

Fuchshofer, R., Yu, A. H., Welge-Lussen, U., and Tamm, E. R. (2007). Bone morphogenetic protein-7 is an antagonist of transforming growth factor-beta2 in human trabecular meshwork cells. *Investigative Ophthalmology and Visual Science* 48: 715–726.

Keller, K. E., Kelley, M. J., and Acott, T. S. (2007). Extracellular matrix gene alternative splicing by trabecular meshwork cells in response to mechanical stretching. *Investigative Ophthalmology and Visual Science* 48: 1164–1172.

Li, G., Luna, C., Liton, P. B., et al. (2007). Sustained stress response after oxidative stress in trabecular meshwork cells. *Molecular Vision* 13: 2282–2288.

Polansky, J. R., Wood, I. S., Maglio, M. T., and Alvarado, J. A. (1984). Trabecular meshwork cell culture in glaucoma research: Evaluation of biological activity and structural properties of human trabecular cells *in vitro*. *Ophthalmology* 91: 580–595.

Russell, P., Gasiorowski, J. Z., Nealy, P. F., and Murphy, C. J. (2008). Response of human trabecular meshwork cells to topographic cues on the nanoscale level. *Investigative Ophthalmology and Visual Science* 49: 629–635.

Schlunck, G., Han, H., Wecker, T., et al. (2008). Substrate rigidity modulates cell matrix interactions and protein expression in human trabecular meshwork cells. *Investigative Ophthalmology and Visual Science* 49: 262–269.

Tripathi, R. C. and Tripathi, B. J. (1982). Human trabecular endothelium, corneal endothelium, keratocytes, and scleral fibroblasts in primary cell culture. A comparative study of growth characteristics, morphology, and phagocytic activity by light and scanning electron microscopy. *Experimental Eye Research* 35: 611–624.

Wang, N., Chintala, S. K., Fini, M. E., and Schuman, J. S. (2001). Activation of a tissue-specific stress response in the aqueous outflow pathway of the eye defines the glaucoma disease phenotype. *Nature Medicine* 7: 304–309.

Wordinger, R. J. and Clark, A. F. (1999). Effects of glucocorticoids on the trabecular meshwork: Towards a better understanding of glaucoma. *Progress in Retinal and Eye Research* 18: 629–667.

Biomechanics of Aqueous Humor Outflow Resistance*

M Johnson, Northwestern University, Evanston, IL, USA
E R Tamm, University of Regensburg, Regensburg, Germany

Glossary

Conventional aqueous outflow pathway – Comprised of the trabecular meshwork, the juxtacanalicular connective tissue, the endothelial lining of Schlemm's canal, Schlemm's canal itself, the collecting channels, and aqueous veins.
Flow resistance – The flow resistance ($R=\Delta P/Q$) of a tissue is the ratio between the pressure drop across that tissue (ΔP) and the flow rate generated by that pressure drop (Q).
Giant vacuoles – The outpouchings of the inner-wall endothelium of Schlemm's canal into its lumen. They are caused by the pressure drop across inner-wall endothelial cells.
Hydraulic conductivity (L_p) – A measure of the ease with which a fluid passes through a tissue: $L_p=Q/A/\Delta P$ where A is the cross-sectional area of the tissue facing flow.
Inner-wall region – Comprised of the inner-wall endothelium of Schlemm's canal, its basement membrane, and the adjacent juxtacanalicular tissue.
Laser trabeculoplasty – The surgical treatment of glaucoma, in which a laser beam is focused on the trabecular meshwork making tiny, evenly spaced burns.

More than 135 years ago, in 1873, Leber recognized that the elevated pressure characteristic of primary open-angle glaucoma arises due to an increased resistance to the outflow of aqueous humor out of the eye. However, a conclusive determination of where in the outflow pathways this elevated outflow resistance is generated has been elusive. Surprisingly, the locus of aqueous humor outflow resistance in the normal eye has also not been unequivocally determined.

In 1921, Seidel, using light microscopy, stated "that the inner wall of Schlemm's canal stand in open communication with the anterior chamber, and that the aqueous humor directly washes around the inner wall endothelium of Schlemm's canal and is only separated from the lumen of Schlemm's canal by a thin, outer membrane." Our view is little different today. The locus of outflow resistance, both in the normal eye and the glaucomatous eye, is thought to arise either in the endothelial lining of Schlemm's canal, or very near to this location. In this article, current viewpoints on where that flow resistance might be generated are reviewed.

There are a number of excellent review articles (see the section titled 'Further reading') that describe the detailed morphology and physiology of the aqueous outflow pathway. Here, we first review the evidence leading to the conclusion that the region surrounding the inner-wall endothelium of Schlemm's canal generates the bulk of aqueous outflow resistance. We then turn our attention to the aspect of the outflow nearest to the endothelial lining of Schlemm's canal, and examine the transport characteristics of those structures.

The bulk of the aqueous humor flows out of the anterior chamber of the eye through the conventional aqueous outflow pathway comprised of the trabecular meshwork (TM), the juxtacanalicular connective tissue, the endothelial lining of Schlemm's canal, Schlemm's canal itself, the collecting channels, and aqueous veins, and, then finally, drains into the episcleral venous system, rejoining the venous system. A second unconventional outflow pathway exists, but carries less than 10% of the total flow in the adult human eye, and thus does not significantly contribute to the dynamics of aqueous humor outflow in the normal eye. This pathway is important, however, for the understanding of the mechanism of action of prostaglandins in the treatment of glaucoma.

Regions of Low Outflow Resistance

In this section, those aspects of the conventional aqueous humor outflow pathway that are generally agreed to have small or negligible outflow resistance are examined. These include the TM, Schlemm's canal, and the collector channels and aqueous veins.

The TM is made up of the uveal meshwork, corneoscleral meshwork, and the juxtacanalicular connective tissue (JCT). The former two regions are highly porous structures with numerous openings that range in size from 25 to 75 μm in the proximal regions of the uveal meshwork to 2–15 μm in the deeper aspects of the corneoscleral meshwork. In 1958, McEwen used Poiseuille's law to show that a single pore that is 100 μm long (the thickness of the TM) and 20 μm in diameter could carry the entire aqueous humor flow with a pressure drop of 5 mmHg, and thus concluded that there was negligible flow resistance in

*Adapted from Johnson, M. (2006). What controls aqueous humour outflow resistance? *Experimental Eye Research* 82: 545–557.

this region. In 1963, Grant provided experimental support for this conclusion by cutting through the proximal aspects of the meshwork of enucleated human eyes and found no effect on outflow resistance. The JCT is discussed in the next section.

Schlemm's canal and its endothelium, shown in Figure 1, exist between the JCT and the sclera.

While the canal is open at low intraocular pressures (IOPs), Johnstone and Grant, in 1973, showed that the TM expands and Schlemm's canal collapses as the IOP is increased. While the size of the canal at low IOP is much too large to generate a significant outflow resistance, the collapse of Schlemm's canal at higher IOP has led some to speculate that this might be a cause of primary open-angle glaucoma. However, in 1983, Johnson and Kamm pointed out that outflow resistance, when measured at high IOP in nonglaucomatous human eyes, is not nearly as high as that of a glaucomatous eye. Collapse of the canal would make a glaucomatous condition worse, but it could not cause the glaucoma.

After traveling circumferentially in Schlemm's canal, the aqueous humor enters one of approximately 30 collecting channels that connect Schlemm's canal with the aqueous veins. The collector channels and aqueous veins have diameters that are tens of microns across. The use of Poiseuille's law leads to the conclusion that these vessels should have negligible flow resistance.

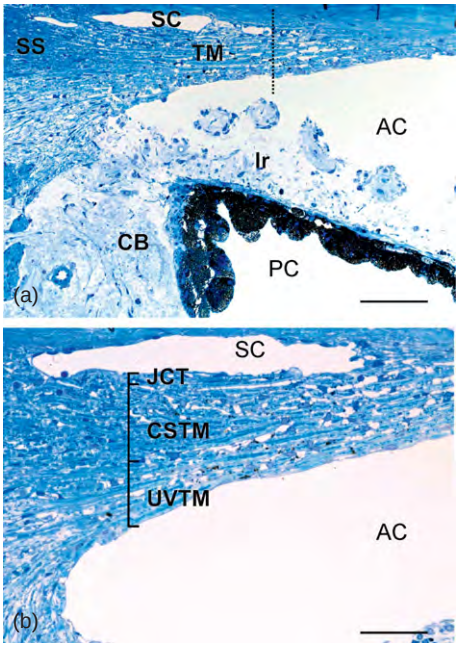

Figure 1 Light micrographs of meridional sections of the anterior chamber angle (a) and the trabecular meshwork (b). The dotted line in (a) marks the boundary between filtering and nonfiltering trabecular meshwork. SC, Schlemm's canal; TM, trabecular meshwork; SS, scleral spur; Ir, iris; CB, ciliary body; PC, posterior chamber; AC, anterior chamber; JCT, juxtacanalicular tissue; CSTM, corneoscleral trabecular meshwork; UVTM, uveal trabecular meshwork. Magnification: 100 μm (a), 50 μm (b). Adapted from Tamm, E. R. (2009). The trabecular meshwork outflow pathways. Functional morphology and surgical aspects. In: Shaarawy, T. M., Sherwood, M. B., Hitchings, R. A., and Crowston, J. G. (eds.) *Glaucoma*, vol. II, pp. 31–44. Philadelphia, PA: Saunders/Elsevier, with permission from Elsevier.

The experimental support for this conclusion is mixed. In 1992, Mäpea and Bill measured pressures in Schlemm's canal of primate eyes and found that the pressure there was little different from episcleral venous pressure. This is in agreement with the theoretical calculations. However, a 360° trabeculotomy, which would be expected to eliminate all flow resistance proximal to the collector channels and aqueous veins, leaves substantial flow resistance remaining. These disparate experimental results regarding the flow resistance of the collector channels and aqueous veins have not been reconciled, perhaps due to the fact that while a significant fraction of normal aqueous humor outflow resistance may be generated by the collector channels and/or aqueous veins, these vessels do not appear to be responsible for the elevated outflow resistance characteristic of the glaucomatous eye. Several observations lead to this conclusion. First, trabeculotomy was shown to eliminate nearly all elevated glaucomatous flow resistance in eight glaucomatous eyes. This result indicates that in primary open-angle glaucoma, the outflow obstruction is proximal to the collector channels and aqueous veins. Further support for this conclusion can be found in the success of laser trabeculoplasty (LTP) in reducing outflow resistance in glaucomatous eyes. While it is not known precisely where in the outflow pathway LTP acts, recent evidence suggests that the site of action is in the TM, and it seems very unlikely that LTP has a significant effect on the outflow resistance of the collector channels and/or aqueous veins.

The conventional wisdom now is that little, if any, significant flow resistance in the normal eye is found in the uveal meshwork, corneoscleral meshwork, Schlemm's canal, or the collector channels and aqueous veins. Furthermore, while some increased resistance might be found in these structures in the glaucomatous eye, they are not responsible for the bulk of the elevated outflow resistance characteristic of the glaucomatous eye. All evidences indicate that the bulk of normal aqueous humor outflow resistance resides in the region surrounding the inner wall of Schlemm's canal, and this is also the region where the elevated flow resistance characteristic of primary open-angle glaucoma likely arises.

The Inner-Wall Region of Schlemm's Canal

We use the term inner-wall region to refer to the inner-wall endothelium of Schlemm's canal, its basement membrane, and the adjacent JCT. Figure 2 shows a

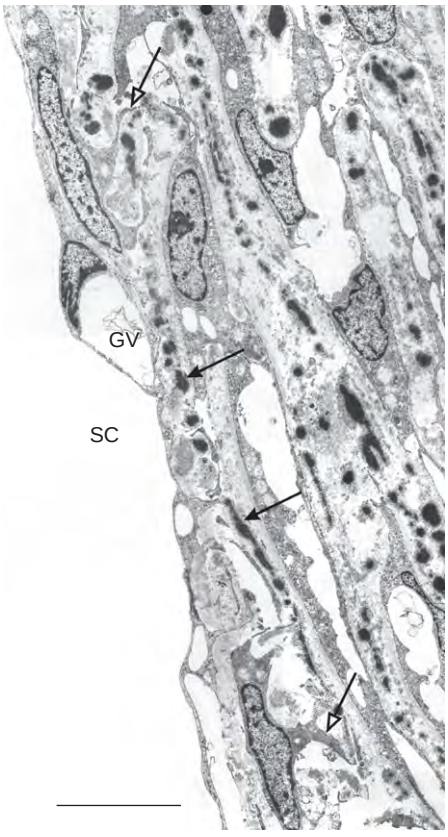

Figure 2 Electron micrograph of the inner-wall region including juxtacanalicular tissue and Schlemm's canal (SC) endothelium. The cells in the juxtacanalicular tissue form elongate processes (open arrows). Solid arrows mark the elastic fibers of the cribriform plexus. GV, giant vacuole. Magnification: 5 μm (a). Adapted from Tamm, E. R. (2009). The trabecular meshwork outflow pathways. Functional morphology and surgical aspects. In: Shaarawy, T. M., Sherwood, M. B., Hitchings, R. A., and Crowston, J. G. (eds.) *Glaucoma*, vol. II, pp. 31–44. Philadelphia, PA: Saunders/Elsevier, with permission from Elsevier.

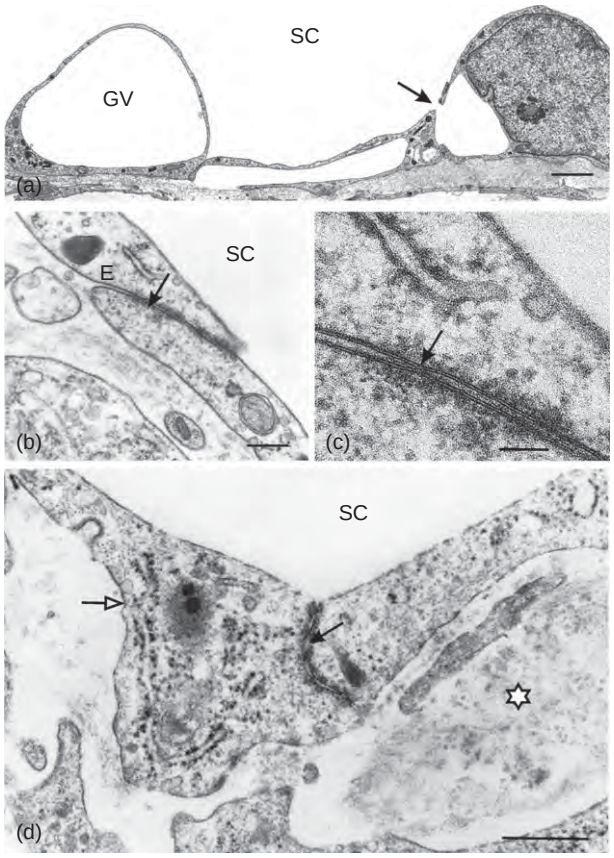

Figure 3 Electron micrographs of the endothelium of Schlemm's canal (SC) inner wall. (a) The inner-wall endothelium forms giant vacuoles (GV) in response to flow of aqueous humor. Pores (arrow) are often associated with the luminal side of the vacuoles. (b, c) Junctional complex (arrow) between two neighboring inner-wall endothelial cells; (c) is higher magnification of (b). The arrow in (c) denotes a tight junction. (d) The basal side of Schlemm's canal endothelial cells is in contact with fine fibrillar material (asterisk) and is often not covered by a basal lamina (open arrow). The solid arrow marks a junctional complex between two adjacent endothelial cells. Magnification: 2 μm (a), 250 nm (b), 125 nm (c), 500 nm (d). Adapted from Tamm, E. R. (2009). The trabecular meshwork outflow pathways. Functional morphology and surgical aspects. In: Shaarawy, T. M., Sherwood, M. B., Hitchings, R. A., and Crowston, J. G. (eds.) *Glaucoma*, vol. II, pp. 31–44. Philadelphia, PA: Saunders/Elsevier, with permission from Elsevier.

transmission electron micrograph (TEM) of the tissues that neighbors Schlemm's canal on its upstream side.

The endothelial lining of the inner wall of Schlemm's canal is typical in some ways of other vascular linings. The cells have their long axis parallel to the canal (in the direction of flow through the canal) with a length of 40–100 μm and a width of 5–15 μm. They are attached to one another with tight junctions.

This endothelium has several unique characteristics. First, structures known as giant vacuoles are seen in this layer (**Figure 3**). While they appear to be intracellular structures, giant vacuoles are really outpouchings of the endothelium into Schlemm's canal, caused by the pressure drop across inner-wall endothelial cells. In 1978, Grierson and Lee showed that these structures were invaginations into the canal with most having a large opening on the meshwork side of the vacuole and a smaller percentage (20–30%) also having a distal opening, a pore (**Figure 3**). Thus, some of the vacuoles are transcellular channels.

The distal openings, or pores, in these vacuoles are a second feature of the inner-wall endothelium that is relatively unique (**Figure 3**). Majority of these pores are transcellular, although a fraction of these pores are located at the border of two cells (border pores), and thus not transcellular but paracellular. These transcellular pores do not connect the extracellular fluid with the cytoplasm of the cell. Instead, they pass from the basal side of the cell to the apical side at a location on the cell surface where the cell membranes from the inner and outer surfaces of

the cell have come together and fused. The pore is thus membrane-lined on its surface. These pores usually form on giant vacuoles, since it is this region in which the cell is greatly attenuated and the cytoplasm becomes thin.

Fusion of the inner and outer cell membranes and the formation of transcellular pores are not entirely unique to these cells. Pores associated with giant vacuoles are also found on the arachnoid villi in the drainage pathway for the cerebrospinal fluid. When cell thickness is reduced below a critical measure, vascular endothelium can form transcellular pores involved in transport processes.

The inner-wall endothelium of Schlemm's canal is supported by a discontinuous basement membrane. This makes Schlemm's canal a somewhat unique vessel having a continuous endothelium with tight junctions between neighboring cells, supported by a discontinuous basement membrane. Blood vessel endothelia have a continuous endothelium with a continuous basement membrane, while lymphatics have a discontinuous endothelium with a discontinuous basement membrane.

The region immediately underlying the inner wall and basement membrane and extending to the last trabecular beam is the JCT. It has many large, apparently empty spaces and is typically 2–15 μm thick.

The Generation of Flow Resistance in the Inner-Wall Region of Schlemm's Canal

While there is agreement among most investigators that the bulk of aqueous humor outflow resistance is generated in the immediate vicinity of the inner-wall endothelium of Schlemm's canal, the precise location and the mechanism by which this dissipation occurs is still a topic of active debate and research.

The JCT

With its tortuous submicron-sized flow pathways, the JCT is a natural location to investigate as to its role in generating outflow resistance. Surprisingly, morphometric analyses combined with theoretical calculations have indicated that, unless these apparently open spaces are actually filled with an extracellular matrix gel, they would generate an insignificant fraction of the total outflow resistance.

This conclusion follows from porous media theory an approach that has been used to characterize flow resistance of other connective tissues. Several different parameters can be used to characterize the fluid transport capacity of a tissue. The flow resistance ($R = \Delta P/Q$) of a tissue is the ratio between the pressure drop across that tissue (ΔP) and the flow rate generated by that pressure drop (Q); the inverse of this quantity is known as the total hydraulic conductance of this tissue. The conductance per unit surface area is known as the hydraulic conductivity (L_p), while the conductance of the tissue normalized for surface area, tissue length in the flow wise direction (L), and fluid viscosity (μ) is known as the specific hydraulic conductivity (K).

Darcy's law relates the flow resistance (R) of a tissue to the specific hydraulic conductivity (K) of that tissue,

$$R = \frac{\Delta P}{Q} = \frac{\mu L}{KA} \quad [1]$$

and the specific hydraulic conductivity is related to the hydraulic conductivity as:

$$K = L_p \mu L \quad [2]$$

Typical values of K and L_p for a variety of tissues are found in **Tables 1** and **2**.

The K value that characterizes the flow resistance of a tissue can be measured experimentally by determining the other parameters in eqn [1], all of which are easy to determine or estimate for aqueous humor outflow with the exception of the length (L) over which the pressure drop occurs. However, since the bulk of the pressure drop occurs somewhere in or near the inner wall of Schlemm's canal, it can be concluded that this length is less than roughly 10 μm, or so, an estimate supported by experimental studies. Using

Table 1 Specific hydraulic conductivity (k) of connective tissues

Tissue	$K \times 10^{14}$ (cm^2)
Lens capsule[a]	0.1
Descemet's membrane[b]	0.1–0.2
Bruch's membrane[c]	0.5–1.5
Glomerulus basement membrane[d]	2
Aortic wall[e]	0.5–2.5
Corneal stroma[e]	0.5–2.5
Sclera[e]	1.4
Cartilage[f]	1–10
Synovium[g]	1.5–7
Vitreous humor[h]	1500–1800

[a]Fels, I. G. (1970). Permeability of the anterior bovine lens capsule. *Experimental Eye Research* 10: 8–14.
[b]Fatt, I. (1969). Permeability of Descemet's membrane to water. *Experimental Eye Research* 8: 34–354.
[c]Starita, C., Hussain, A. A., et al. (1997). Localization of the major site of resistance to fluid transport in Bruch's membrane. *Investigative Ophthalmology and Visual Science* 38: 762–767.
[d]Robertson, G. B. and Walton, H. A. (1989). Glomerular basement membrane as a compressible ultrafilter. *Microvascular Research* 38: 36–48.
[e]Levick, J. R. (1987). Flow through interstitium and other fibrous matrices. *Quarterly Journal of Experimental Physiology* 72: 409–437.
[f]Mow, V. C., Holmes, M. H., et al. (1984). Fluid transport and mechanical properties of articular cartilage: a review. *Journal of Biomechanics* 17: 377.
[g]Levick, J. R., Price, F. M., et al. (1996). Synovial matrix–synovial fluid system of joints. In: Comper, W. D. (ed.) *Extracellular Matrix*, vol I, pp. 328–377. Amsterdam: Harwood Academic.
[h]Fatt, I. (1977). Hydraulic flow conductivity of the vitreous gel. *Investigative Ophthalmology and Visual Science* 16: 565–568.

Table 2 Hydraulic conductivity (L_p: cm^{2*} s g^{-1}) for a variety of physiological membranes

Membrane	*Type*	$L_p \times 10^{11}$
Kidney epithelial cells (MDCK cells)	a	0.075
Xenopus oocytes[15]	a	0.2
Xenopus oocytes + CHIP28[15]	a	1.6
Proximal tubule epithelial cells[1,2]	a	1.2
Red blood cells[12,14]	a	1–1.6
Gall bladder epithelial cells[13]	a	4–9
Corneal epithelium[2,9]	b	0.04–0.7
Gall bladder epithelium[12,13]	b	1.3–3.6
Proximal tubule epithelium[1,12]	b	7.5–5.5
Retinal pigment epithelium[3]	b	16
Brain capillary[4]	c	0.03
Corneal endothelium[2,5]	c	0.14–5
Lung capillary[4]	c	3.4
Skeletal muscle capillary[4,7]	c	2.5–7
Cardiac muscle capillary[4,7]	c	8.6
Aorta[6]	c	9
Mesentery, omentum[4]	c	50
Intestinal mucosa[4,7]	d	32–130
Synovium (knee)[7]	d	120
Renal peritubulal capillaries[7]	d	225–700
Renal glomerulus[4,7]	d	400–3100
Descemet's membrane[9]	e	15–37
Lens capsule[10]	e	17–50
Bruch's membrane[11]	e	2000–12,500
Kidney tubule basement membrane[8]	e	6300–13,700

a: cell membranes, b: unfenestrated epithelium, c: unfenestrated endothelium, d: fenestrated epithelia, and e: basement membranes.

[1]Timbs, M. M. and Spring, K. R. (1996). Hydraulic properties of MDCK cell epithelium. *Journal of Membrane Biology* 153: 1–11.
[2]Klyce, S. D. and Russell, S. R. (1979). Numerical solution of coupled transport equations applied to corneal hydration dynamics. *Journal of Physiology* 292: 107–134.
[3]Tsuboi, S. (1987). Measurement of the volume flow and hydraulic conductivity across the isolated dog retinal pigment epithelium. *Investigative Ophthalmology and Visual Science* 28: 1776–1782.
[4]Renkin, E. M. (1977). Multiple pathways of capillary permeability. *Circulation Research* 41: 735–743.
[5]Hedbys, B. O. and Mishima, S. (1962). Flow of water in corneal stroma. *Experimental Eye Research* 1: 262–275.
[6]Vargas, C. B., Vargas, F. F., et al. (1979). Hydraulic conductivity of the endothelial and outer layers of rabbit aorta. *American Journal of Physiology* 236: H53–H60.
[7]Levick, J. R. (1987). Flow through interstitium and other fibrous matrices. *Quarterly Journal of Experimental Physiology* 72: 409–437.
[8]Welling, L. and Welling, D. (1978). Physical properties of isolated perfused basement membranes from rabbit loop of Henle. American *Journal of Physiology* 234: F54–F58.
[9]Fatt, I. (1969). Permeability of Descemet's membrane to water. *Experimental Eye Research* 8: 34–354.
[10]Fisher, R. F. (1982). The water permeability of basement membrane under increasing pressure: evidence for a new theory of permeability. *Proceedings of the Royal Society of London Series* B 216: 475–496.
[11]Starita, C., Hussain, A., et al. (1996). Hydrodynamics of ageing Bruch's membrane: implications for macular disease. *Experimental Eye Research* 62: 565–572; Bentzel, C. and Reczek, P. (1978). Permeability changes in Necturus proximal tubule during volume expansion. *American Journal of Physiology* 234: F225–F234.
[12]Gonzalez, E., Carpi-Medina, P., et al. (1982). Cell osmotic water permeability of isolated rabbit proximal straight tubules. *American Journal of Ophthalmology* 242: F321–F330.
[13]Persson, B. E. and Spring, K. R. (1982). Gallbladder epithelial cell hydraulic water permeability and volume regulation. *Journal of General Physiology* 79: 481–505.
[14]Solomon, A. K., Chasan, B., et al. (1983). The aqueous pore in the red cell membrane: band 3 as a channel for anions, cations, nonelectrolytes, and water. *Annals of the New York Academy of Sciences* 414: 97–124.
[15]Preston, G. M., Carroll, T. P., et al. (1992). Appearance of water channels in Xenopus oocytes expressing red cell CHIP28 protein. *Science* 256: 385–387.

a flow rate through the aqueous outflow pathway of 2 µl min^{-1} passing through a cross-sectional area of between 0.054 and 0.13 cm^2 (canal width of 150–350 µm; canal length around the eye of 3.6 cm), and a pressure drop of 5 mmHg, it can then determined that K of the resistance-causing region in the aqueous outflow pathway must be less than 65×10^{-14} cm^2. Unless the length over with the pressure drop occurs (L) is much lesser than 10 µm, the specific hydraulic conductivity of the connective tissue elements in the outflow pathway is greater than that of any other connective tissue with the exception of the vitreous humor (**Table 1**).

K can also be estimated from photomicrographs showing the ultrastructure of a tissue. This can potentially allow an evaluation of which structures in the aqueous outflow pathway are generating the measured outflow resistance. Carmen–Kozeny theory relates the structure of a porous medium to K as:

$$K = \frac{\varepsilon\, D_h^2}{80} \qquad [3]$$

where D_h is the hydraulic diameter of the open spaces available for flow and ε is the porosity, or fraction of open space of the medium (note that at porosities higher than roughly 0.8, this equation becomes inaccurate). Using Carmen–Kozeny theory combined with conventional TEM, it was found (in immersion-fixed eyes) that the porosity of the JCT was approximately 0.15–0.25, D_h was approximately 1–1.5 µm, and, most importantly, K of the JCT was calculated to be approximately 2000–10 000 10^{-14} cm^2 based on the photomicrographs. This is, at least, 30 times greater than K based upon measured properties of the outflow system.

In 1986, Ethier and coworkers concluded that the JCT, as visualized using conventional TEM, could not generate a significant fraction of outflow resistance. Other investigators have confirmed this conclusion, including studies in which the eyes were fixed by perfusion. It thus followed that either this region was filled with an extracellular matrix gel that was poorly visualized using

conventional TEM techniques, or, that this region was not the primary site of outflow resistance. The age-related accumulation of plaque-like material in this region that is reported to be enhanced in glaucomatous eyes would have no influence on this conclusion.

More recently, in 2002, Gong and coworkers used quick-freeze/deep-etch (QFDE) methodology to examine the apparent open spaces seen in the JCT region in greater detail. QFDE is a morphological technique that preserves the cellular and extracellular ultrastructure in exquisite detail and allows visualization of structures poorly preserved or not seen at all using conventional TEM tissue preparation techniques. A more elaborate and extensive extracellular matrix was seen in the JCT using QFDE as compared to conventional methods of preparation for TEM (**Figure 4**); however, micron-sized open spaces were still seen in this region, casting doubt on whether a significant fraction of outflow resistance could be generated in this region. An important caveat pointed out by the Gong group regarding their studies was that it was not clear whether or not QFDE can visualize the glycosaminoglycans (GAGs) in their uncollapsed state, and this leaves uncertain the question of generation of appreciable flow resistance in the JCT region.

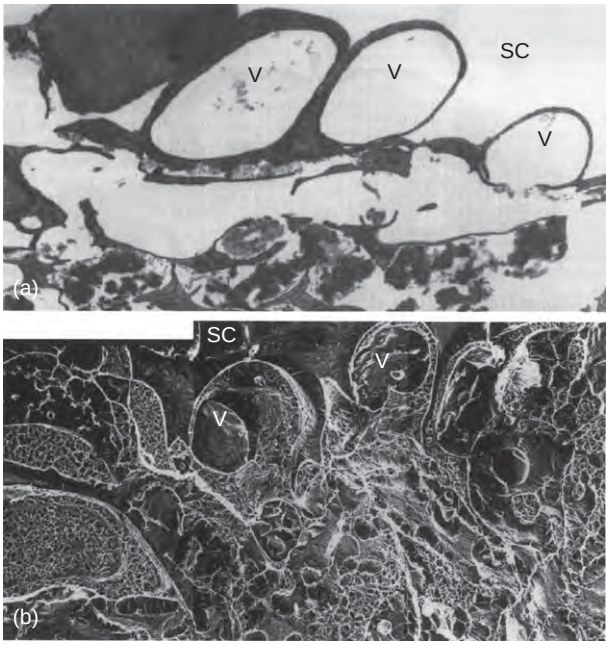

Figure 4 Enucleated human eye fixed by perfusion at 15 mmHg: (5A) vacuoles (V) in the inner wall of Schlemm's canal (SC) in tissue prepared for TEM using conventional methods; notice the large open space in the region of the JCT immediately under these vacuoles; (4B) the same region as seen in tissue prepared using QFDE; notice that while open spaces still exist under the vacuoles, a more complex and extensive extracellular matrix is seen. Magnification ×4860. Adapted from Gong, H., Ruberti, J., Overby, D., Johnson, M., and Freddo, T. F. (2002). A new view of the human trabecular meshwork using quick-freeze, deep-etch electron microscopy. *Experimental Eye Research* 75: 347–358, with permission from Elsevier.

The role that GAGs and other extracellular matrix elements found in the JCT might play in generating outflow resistance is unclear. While it has been shown that enzymes that degrade macromolecules (GAGases) increase outflow facility in a number of species (e.g., cow, guinea pig, dog, and rabbit), the evidence regarding primates is conflicting, and there has been no confirmed data yet showing that GAGases decrease outflow resistance in human eyes. Matrix metalloproteinases (MMPs) have been shown to reversibly increase outflow facility in perfused human anterior segment organ culture, and this is a strong indicator that the extracellular matrix may generate significant aqueous outflow resistance.

Perhaps the strongest experimental evidence implicating the JCT as a major site of outflow resistance is the 1992 study by Maepea and Bill in which they used micropipettes and localized the pressure drop to occurring somewhere between 7 and 14 μm from the inner wall of Schlemm's canal (i.e., in the JCT). While this result is frequently cited in the literature, it is not widely appreciated that this measurement was made with micropipettes whose tip sizes were as large as the measurement zone. When this reservation is combined with the fact that the inner wall of Schlemm's canal distends several to many microns during the process of penetration by the micropressure probe (unpublished work by Dr. Milko Iliev in collaboration with Dr. Johnson's laboratory), it leads to the conclusion that the bulk of the aqueous humor pressure drop occurs near the inner wall of Schlemm's canal (within 5–10 μm), but that no further quantitative conclusions are possible.

The basement membrane

The basement membrane of the inner wall of Schlemm's canal is another possible location for generation of outflow resistance. **Table 1** shows that the specific hydraulic conductivities of basement membranes (top four tissues in table) are among the lowest of connective tissues.

However, basement membranes tend to be quite thin and this limits the flow resistance they can generate (see eqn [1]). **Table 2** shows the hydraulic conductivity of a variety of physiological membranes, including cells membranes, epithelia, and basement membranes. The large variation in L_p of basement membranes is due not only to variation in the specific hydraulic conductivity of these tissues, but also to significant differences in their thicknesses (ranging from 0.15 μm for Bruch's membrane to 7 μm for Descemet's membrane).

It is interesting to compare the values seen in this table with the estimated value of the hydraulic conductivity of the outflow pathway. From the definition of hydraulic conductivity (or by combining eqns [1] and [2]), $L_p = Q/A/\Delta P$. Using the values characterizing the aqueous

outflow pathway presented above, we can estimate that L_p for the aqueous humor outflow pathway is between 4000 $\times 10^{-11}$ and 9000 $\times 10^{-11}$ cm^2 s g^{-1}. Note that this is not a theoretical calculation but an estimate based on measured quantities.

Table 2 shows that several basement membranes, in particular those of the renal system, have hydraulic conductivities similar to that of the aqueous outflow pathway. This suggests that the basement membrane of the inner-wall endothelium of Schlemm's canal might be an important contributor to aqueous humor outflow resistance.

However, as noted above, this basement membrane is discontinuous (Figure 3), as recently confirmed in 2002 by Gong and coworkers. If there are breaks in the basement membrane, it is difficult to see how a significant flow resistance could be generated by this tissue.

The inner-wall endothelium of Schlemm's canal

The inner-wall endothelium of Schlemm's canal has been an attractive candidate for the generation of outflow resistance since the time that light microscopes and later electron microscopes were focused on the inner-wall endothelium. Comparison of the hydraulic conductivity of this tissue (4000–9000 $\times 10^{-11}$ cm^2 s g^{-1}) with that of other endothelia and epithelia as seen in Table 2, leads one to conclude that this vessel lining must have one of the highest hydraulic conductivities in the body. Compared to other tissues in Table 2, it is clear that only fenestrated endothelia (and some basement membranes) have such high hydraulic conductivities.

While the inner-wall endothelium is not fenestrated, this endothelium is unique in that it contains micron-sized pores. It is interesting that even early investigators (e.g., Seidel) had concluded that such pores existed, long before they were first seen by electron microscopy. This conclusion was based on early filtration studies that examined the sizes of microparticulates that would pass through the outflow pathway. It was found in these studies that a filtration barrier existed for particles larger than roughly 0.5 µm or so, and thus it was concluded that pores nearly 1 µm in size must exist. More recent studies have confirmed this conclusion using microparticles and latex microspheres.

While there is some debate concerning the existence of these pores (which is discussed below), no group has offered an alternate explanation for the extraordinarily high hydraulic conductivity of the aqueous outflow pathway. Nor has any alternate explanation been offered for the relatively easy passage of microparticles 200–500 nm in diameter through the outflow pathway, except through these large pores. Since there are tight junctions (Figure 3) between the inner-wall cells (presumably to prevent blood reflux into the eye that can occur during periods of transient increases in ocular venous pressure), there are no other structures apparent in this endothelium that could explain the high hydraulic conductivity of this tissue or its filtration characteristics.

The flow resistance generated by these pores was first considered by Bill and Svedbergh in 1972. In an exhaustive study using scanning electron microscopy, they characterized the size distribution of these pores, and then used hydrodynamic theory to calculate for hydraulic conductivity of these pores. Using Sampson's law, that gives the hydraulic conductivity for a single pore of diameter d,

$$L_p = \frac{d}{6\pi\mu} \qquad [4]$$

they found that the inner-wall endothelium could present, at most, 10% of the outflow resistance. That is, the hydraulic conductivity of the pores in the inner-wall endothelium is, at least, 10-fold higher than the measured hydraulic conductivity of the outflow pathway. This conclusion has been confirmed in a number of studies.

These results would appear to rule out the inner-wall endothelium as a major site of outflow resistance. However, a number of experimental findings are at variance with this conclusion. In particular, when chelating agents (ethylenediaminetetraacetic acid (EDTA) and ethylene glycol tetraacetic acid (EGTA)) or a proteolytic enzyme (α-chymotrypsin) were perfused through the outflow pathway of live primates, it was found that ruptures of the inner-wall endothelium were produced by these agents that decreased outflow resistance more than could be explained by the calculated flow resistance of the inner-wall pores. A hydrodynamic interaction (the funneling effect) between the inner-wall pores and the JCT, which lies immediately below these pores, has been proposed as an explanation of the findings (see Figure 5).

In this scenario, the pores and vacuoles themselves contribute negligible flow resistance, but since they force aqueous humor to funnel through those regions of the JCT nearest the pores and vacuoles, the vacuole size

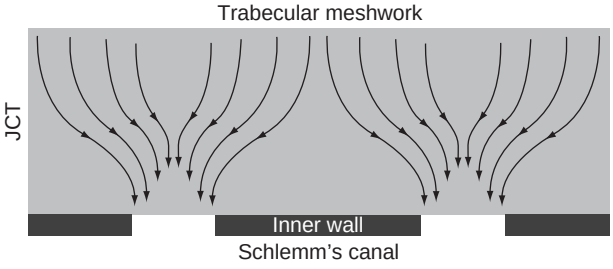

Figure 5 Schematic of the funneling of aqueous humor through the JCT, toward a vacuole and pore that allows this fluid to pass through the inner-wall endothelium. Adapted from Overby, D., Gong, H., Qiu, G., Freddo, T. F., and Johnson, M. (2002). The mechanism of increasing outflow facility during washout in the bovine eye. *Investigative Ophthalmology and Visual Science* 43: 3455–3464. ©The Association for Research in Vision and Ophthalmology.

and pore density can have a significant effect on the effective hydraulic conductivity (L_p) of the JCT:

$$L_p = \frac{2KnD}{\mu} \quad [5]$$

Here, K is the specific hydraulic conductivity of the JCT region, n is the number of pores per unit area in the inner wall, D is the diameter of the vacuoles in the inner wall, and μ is the viscosity of the aqueous humor.

The funneling model suggests that while the bulk of outflow resistance is actually generated in the JCT or basement membrane, its magnitude is modulated by the pores and vacuoles of the inner-wall endothelium of Schlemm's canal. This model explains many of the characteristics of the outflow pathways discussed above. However, two recent studies failed to find a correlation between outflow facility and inner-wall pore density as would be expected if eqn [5] describes the hydraulic conductivity of the outflow pathway. Furthermore, these studies found that at least some inner-wall pores may be artifacts of the fixation process.

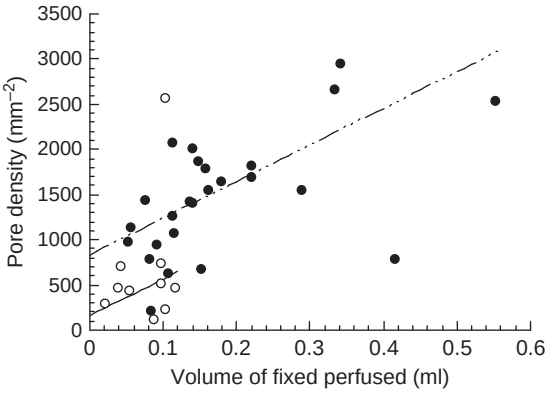

Figure 6 Pore density as a function of volume of fixative perfused through the outflow pathway of normal eyes (filled symbols) and eyes with POAG (open). Lines are best fit with outliers excluded. Adapted from Johnson, M., Chan, D., Read, A. T., et al. (2002). Glaucomatous eyes have a reduced pore density in the inner wall endothelium of Schlemm's canal. *Investigative Ophthalmology and Visual Science* 43: 2950–2955. ©The Association for Research in Vision and Ophthalmology.

Pores as possible fixation artifacts and the possible importance of flow through inner-wall cell junctions or through water channels

The micron-sized pores that pass through the endothelial cells of the inner-wall endothelium of Schlemm's canal are relatively unique to these cells and to the cells of the arachnoid villi, a tissue of the cerebrospinal fluid pathway. This unique character has led some investigators to doubt that these are physiologic structures, but instead consider them to be artifacts of the tissue-preparation process. The possibility that pores form during tissue preparation for electron microscopy was supported in recent studies that showed that during tissue fixation under flow conditions, the inner-wall endothelium pore density increased as a function of the volume of fixative perfused through the outflow pathway (see **Figure 6**).

It has been postulated by several investigators that instead of passing through the pores in the inner-wall endothelium, a significant fraction of the aqueous humor passes through gaps between the tight-junction strands of these cells. In 2001, Ethier and Chan found that cationized ferritin perfused into enucleated human eyes acted to decreased outflow facility and was seen accumulating in junctions between inner-wall endothelial cells. While Ethier and Chan argue that the decreased outflow facility caused by cationized ferritin was due to pore blocking that was also seen to occur in this study, others have interpreted their results as consistent with a significant flow through the junctional complexes.

There are a several reasons why this hypothesis is untenable. Two strong arguments against this possibility were suggested above, namely that the uniquely high hydraulic conductivity of the aqueous outflow pathway is inconsistent with flow through junctions, and that the relatively free passage of microspheres 200–500 nm in diameter through the outflow pathway would be precluded if transport was primarily through cell junctions. It is well known in the vascular system that macromolecules larger than roughly 10–20 nm are largely excluded from passing through cell junctions, for either fenestrated or nonfenestrated vessels.

In 1981, Raviola and Raviola examined the tight junctions of the inner-wall endothelium and calculated the flow that would be expected through these junctions. The gaps they found available for transport around the tight-junctional strands were nanometers in size, and they concluded that any flow that might occur through these spaces would be negligible. In 1997, Ye and coworkers used freeze-fracture techniques to examine these junctions in eyes fixed under flow conditions and did not report significant differences from the dimensions reported by Raviola and Raviola. The notion that microparticles that are roughly 0.5 μm in size could relatively easily pass through such openings seems improbable, at best.

The study of Ye and coworkers did find that the tight junctions of the inner-wall cells simplified with increasing IOP. They speculated that the junctional simplification that occurred with increasing perfusion pressure might lead to formation of pores at locations of focal separation in the tight junctions. While they did not find a statistically significant relationship between junctional complexity and outflow facility in this small series of eyes, they did find a trend in that direction, consistent with their hypothesis.

Thus, while there are a number of strong arguments against the possibility of transport of a significant quantity of aqueous humor across the inner wall of Schlemm's canal passing directly through cell junctions, simplification of these junctions might be involved in the process of pores formation. In particular, paracellular flow through border pores could be consistent with the 1991 findings of Epstein and Rohen of dilations of this paracellular space.

It has also been suggested that a fraction of outflow might pass through water channels (aquaporins) in the cell membrane of the inner-wall cells. Red blood cells and renal proximal tubules are cell types expressing high levels of aquaporin 1. The hydraulic conductivities of the water channels in these cell membranes have been measured, as have those of cells in which aquaporins are overexpressed (see **Table 2**). All of these values are more than 1000 times smaller than the hydraulic conductivity of aqueous outflow pathway. It goes without saying that water channels also cannot explain the relatively free passage of 0.5-μm-sized particles through the outflow pathway.

The only pathway that appears consistent with the available physiologic evidence is through the inner-wall pores whose existence was already postulated more than 80 years ago by Seidel in 1921, and that now are easily seen using scanning electron microscopy of this tissue. Importantly, the size of these pores is consistent with the predictions of Seidel. Whether this transport is primarily through border pores or is also through the transcellular pores remains to be determined.

The question remains as to why the number of these pores increases during the fixation process, as shown in **Figure 6**. A further finding of the studies was that the number density of pores in the inner-wall endothelium decreases as a function of postmortem time, something not expected of an artifact. Instead, it may be that fixation under flow conditions generates stresses in the inner wall due both to pressure-induced stretching of the inner wall of Schlemm's canal and also to shrinkage of the tissue following fixation. Pressure-induced stress is likely what causes the formation of these pores under physiologic conditions. Then, fixative-induced pore formation might be an artifact associated with a physiological process, namely stress on the inner-wall endothelium.

In this scenario, the y-intercepts of the lines seen on **Figure 6** would then represent the true physiological pore density of normal and glaucomatous eyes, respectively. Importantly, **Figure 6** shows this density to be greatly reduced in glaucomatous eyes. Through their importance to funneling (eqn [5]), a decrease of inner-wall pores would be expected to decrease the hydraulic conductivity of the outflow pathway and thereby increase IOP.

This decrease pore density in the inner-wall endothelium of Schlemm's canal may then represent the cause of the elevated pressure characteristic of glaucoma. Future work may then indicate why this pore density is decreased.

See also: Biological Properties of the Trabecular Meshwork Cells; The Biology of Schlemm's Canal; The Cytoskeletal Network of the Trabecular Meshwork; The Fibrillar Extracellular Matrix of the Trabecular Meshwork; Functional Morphology of the Trabecular Meshwork; Primary Open-Angle Glaucoma; Role of Proteoglycans in the Trabecular Meshwork; Structural Changes in the Trabecular Meshwork with Primary Open Angle Glaucoma; Uveoscleral Outflow.

Further Reading

Bill, A. (1975). Blood circulation and fluid dynamics in the eye. *Physiological Reviews* 55: 383–416.

Bill, A. and Mäepea, O. (1994). Mechanisms and routes of aqueous humor drainage. In: Albert, D. M. and Jakobiac, F. A. (eds.) *Principles and Practice of Ophthalmology. Vol I: Basic Sciences*, ch. 12, pp. 2577–2595. Philadelphia, PA: Saunders.

Bill, A. and Svedbergh, B. (1972). Scanning electron microscopic studies of the trabecular meshwork and the canal of Schlemm – an attempt to localize the main resistance to outflow of aqueous humor in man. *Acta Ophthamologica* 50: 295–320.

Epstein, D. L. and Rohen, J. W. (1991). Morphology of the trabecular meshwork and inner-wall endothelium after cationized ferritin perfusion in the monkey eye. *Investigative Ophthalmology and Visual Science* 32(1): 160–171.

Ethier, C. R. (2002). The inner wall of Schlemm's canal (review). *Experimental Eye Research* 74: 161–172.

Ethier, C. R., Coloma, F. M., Sit, A. J., and Johnson, M. (1998). Two pore types in the inner wall endothelium of Schlemm's canal. *Investigative Ophthalmology and Visual Science* 39: 2041–2048.

Ethier, C. R., Kamm, R. D., Palaszewski, B. A., Johnson, M. C., and Richardson, T. M. (1986). Calculations of flow resistance in the juxtacanalicular meshwork. *Investigative Ophthalmology and Visual Science* 27(12): 1741–1750.

Gong, H., Ruberti, J., Overby, D., Johnson, M., and Freddo, T. F. (2002). A new view of the human trabecular meshwork using quick-freeze, deep-etch electron microscopy. *Experimental Eye Research* 75: 347–358.

Gong, H., Tripathi, R. C., and Tripathi, B. J. (1996). Morphology of the aqueous outflow pathway. *Microscopy Research and Technique* 33: 336–367.

Grant, W. M. (1963). Experimental aqueous perfusion in enucleated human eyes. *Archives of Ophthalmology* 69: 783–801.

Johnson, M. (2006). What controls aqueous humour outflow resistance? *Experimental Eye Research* 82: 545–557.

Johnson, M. and Erickson, K. (2000). Mechanisms and routes of aqueous humor drainage. In: Albert, D. M. and Jakobiec, F. A. (eds.) *Principles and Practice of Ophthalmology. Vol. 4: Glaucoma*, ch. 193B, pp. 2577–2595. Philadelphia, PA: WB Saunders.

Johnstone, M. A. and Grant, W. M. (1973). Pressure dependent changes in the structures of the aqueous outflow system of human and monkey eyes. *American Journal of Ophthalmology* 75: 365.

Leber, T. (1873). Studien über den Flüssigkeitswechsel im Auge. *(Albrecht von Graefes) Archiv für Ophthalmologie* 19: 87–106.

Maepea, O. and Bill, A. (1992). Pressures in the juxtacanalicular tissue and Schlemm's canal in monkeys. *Experimental Eye Research* 54(6): 879–883.

Raviola, G. and Raviola, E. (1981). Paracellular route of aqueous outflow in the trabecular meshwork and canal of Schlemm. *Investigative Ophthalmology and Visual Science* 21: 52–72.

Seidel, E. (1921). Weitere experimentelle Untersuchungen über die Quelle und den Verlauf der intraokularen Saftströmung. IX Mitteilung. Über den Abfluss des Kammerwassers aus der vorderen AugenKammer. *Graefe's Archive for Clinical and Experimental Ophthalmology* 104: 357–402.

Tamm, E. R. (2009). *The trabecular meshwork outflow pathways. Functional morphology and surgical aspects*. In: Shaarawy, T. M., Sherwood, M. B., Hitchings, R. A., and Crowston, J. G. (eds.) *Glaucoma,* vol. II, pp. 31–44. Philadelphia, PA: Saunders/Elsevier.

Tripathi, R. C. (1974). Comparative physiology and anatomy of the aqueous outflow pathway. In: Davson, H. and Graham, L. T. (eds.) *The Eye. Comparative Physiology,* vol. 5, ch. 3, pp. 163–356. London: Academic Press.

Ye, W., Gong, H., Sit, A., Johnson, M., and Freddo, T. F. (1997). Interendothelial junctions in normal human Schlemm's canal respond to changes in pressure. *Investigative Ophthalmology and Visual Science* 38(12): 2460–2468.

Biomechanics of the Optic Nerve Head*

J C Downs, M D Roberts, and C F Burgoyne, Devers Eye Institute, Portland, OR, USA

Glossary

Anisotropic materials – These materials exhibit higher or lower stiffness properties along different directions. For instance, concrete may be isotropic by itself, but the introduction of rebar during fabrication would produce an anisotropic material with higher resistance to tension along the direction of the rebar.

Elastic materials – These materials exhibit no time-dependent stress–strain behavior.

Isotropic materials – These materials exhibit identical resistance to load in all directions.

Linear materials – These materials exhibit a stress–strain relationship in which stress is directly proportional to strain by a constant factor known as the Young's modulus.

Material properties – These describe the ability of a tissue to resist deformation under applied load and therefore relate stress to strain (i.e., load to deformation). Material properties can be thought of as the stiffness or compliance of a particular tissue or material that is intrinsic to the material itself. These properties are often described in terms of their material symmetry (isotropic or anisotropic), the nature of the relationship between load and deformation (linear or nonlinear), and the time dependence of their response to loading (elastic or viscoelastic).

Mechanical failure – It occurs at even higher strain, typically follows yield, and generally manifests in soft tissues as catastrophic rupture or pulling apart.

Mechanical yield – It occurs when a material is strained beyond its elastic limit, and is therefore unable to return to its undeformed shape. A material or tissue that has yielded in response to high strains is permanently damaged and deformed and is usually less resistant to further loading (hypercompliance).

Nonlinear materials – These materials have a varying proportionality between stress and strain that is generally dependent on the level of strain, and hence do not have a unique or constant Young's modulus. Connective tissues such as the sclera and lamina cribrosa generally get stiffer as they are stretched.

Strain – It is a measure of the local deformation in a material or tissue induced by an applied stress, and is usually expressed as the percentage change in length of the original geometry (e.g., a wire that was originally 10 mm long that has been stretched an additional 1 mm, exhibits 10% strain). It is important to recognize that strain, unlike stress, may be observed and measured and it is strain, not stress, which causes damage to tissues.

Stress – It is a measure of the load applied to, transmitted through, or carried by a material or tissue, and can be defined as the amount of force applied to a tissue divided by the cross-sectional area over which it acts (e.g., pressure is a stress and can be expressed in pounds per square inch (psi)).

Structural stiffness – It is a composite measure of the entire structure's resistance to deformation that incorporates both the material properties and geometry of a complex load bearing system. In the posterior pole, both the geometry and material properties of the sclera and lamina cribrosa contribute to their structural stiffness, and hence determine the ability of the optic nerve head (ONH) and peripapillary sclera to withstand strain when exposed to intraocular pressure (IOP). As such, individual ONH biomechanics is governed by the geometry (size and shape of the scleral canal, scleral thickness, regional laminar density, and beam orientation) and the material properties (stiffness) of the lamina cribrosa and sclera. Hence, two eyes exposed to identical IOPs may exhibit very different strain fields due to differences in their structural stiffness.

Viscoelastic materials – These materials exhibit a stress–strain response that is time dependent, that is, they have higher resistance when loaded quickly than when loaded slowly (similar to the behavior of a hydraulic shock absorber).

*Adapted from Downs, C., Roberts, M. D., and Burgoyne, C. F. (2009). Mechanical strain and restructuring of the optic nerve head. In: Shaarawy, T. M., Sherwood, M. B., Hitchings, R. A., Crowston, J. G. (eds.) *Glaucoma Medical Diagnosis and Therapy*, vol. 1, pp 67–90. Philadelphia, PA: Saunders Elsevier.

The Optic Nerve Head as a Biomechanical Structure

The optic nerve head (ONH) is of particular interest from a biomechanical perspective because it is a weak spot within an otherwise strong corneo-scleral envelope. While there are likely to be important pathophysiologies within the lateral geniculate and visual cortex as well as evidence both for and against direct, intraocular pressure (IOP)-induced damage to the retinal photoreceptors, most evidence suggests that the lamina cribrosa is the principal site of retinal ganglion cell (RGC) axonal insult in glaucoma.

The lamina cribrosa provides structural and functional support to the RGC axons as they pass from the relatively high-pressure environment in the eye to a low-pressure region in the retrobulbar cerebrospinal space. To protect the RGCs in this unique anatomic region, the lamina cribrosa in higher primates has developed into a complex structure composed of a three-dimensional (3D) network of flexible beams of connective tissue (**Figure 1**). The ONH is nourished by the short posterior ciliary arteries, which penetrate the immediate peripapillary sclera to feed capillaries contained within the laminar beams. This intra-scleral and intra-laminar vasculature is unique in that it is encased in load-bearing connective tissue, either within the scleral wall adjacent to the lamina cribrosa, or within the laminar beams themselves (**Figure 1**). Glaucoma is a multifactorial disease, and we believe that biomechanics not only determines the mechanical environment in the ONH, but also mediates IOP-related reductions in blood flow and cellular responses through various pathways (**Figure 2**).

Consideration of the anatomy of the lamina cribrosa and peripapillary sclera suggests that the classic mechanical and vascular mechanisms of glaucomatous injury are inseparably intertwined (**Figures 1 and 2**). For example, prior to structural damage, purely IOP-related stress could detrimentally affect the blood supply to the laminar segments of the axons through deformation of the capillary-containing connective tissue structures. Also, IOP-related remodeling of the extracellular matrix (ECM) of the laminar beams could limit the diffusion of nutrients to RGC axons in the ONH. Reciprocally, primary insufficiency in the blood supply to the laminar region could

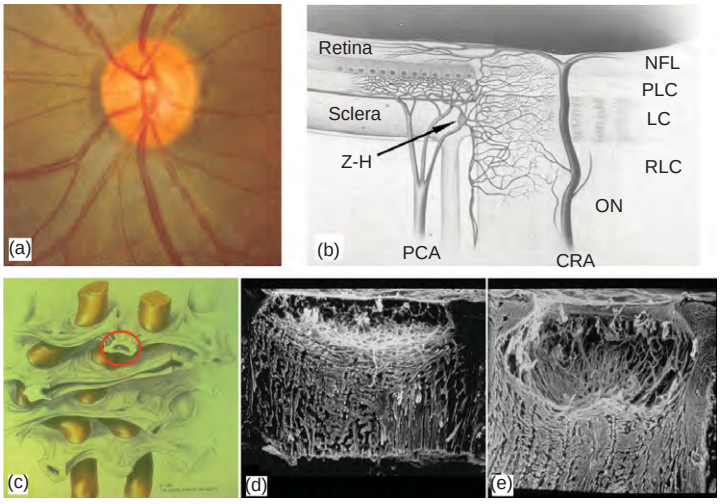

Figure 1 The optic nerve head (ONH) is a three-dimensional (3D) structure comprised of multiple interactive tissue systems that exist on different scales. This complexity has been a formidable deterrent to characterizing its mechanical environment. (a) While clinicians are familiar with the clinically visible surface of the optic nerve head (referred to as the optic disc), in fact the ONH is a dynamic, 3D structure in which the retinal ganglion cell (RGC) axons in bundles surrounded by glial columns, pass through the connective tissue beams of the lamina cribrosa. The blood supply for the connective tissues of the lamina cribrosa (b) derives from the posterior ciliary arteries and the circle of Zinn-Haller (Z-H), and capillaries inside the laminar beams supply the axons in the laminar region. The relationship of the axon bundles to the laminar beams and their contained capillaries is shown in schematic form in (c). Individual beams of the lamina cribrosa are lined by astrocytes. Together this system provides structural and metabolic support for the adjacent axon bundles. Within the lamina, the RGC axons have no direct blood supply, and axonal nutrition requires diffusion of nutrients from the laminar capillaries, across the endothelial and pericyte basement membranes, through the extracellular matrix (ECM) of the laminar beam, across the basement membranes of the astrocytes and through their processes to the adjacent axons. Chronic age-related changes in the endothelial cell and astrocyte basement membranes, as well as intraocular pressure (IOP)-induced changes in the laminar ECM and astrocyte basement membranes may diminish nutrient diffusion to the axons in the presence of a stable level of laminar capillary volume flow. In advanced glaucoma, the connective tissues of the normal lamina cribrosa (shown in (d) in a sagittal view of a trypsin-digested ONH; vitreous above, orbital optic nerve below), remodel and restructure into a cupped and excavated configuration (e). (b) reprinted with permission from Cioffi GA; (c) reprinted with permission from Quigley HA; (d, e) Courtesy of Harry A. Quigley, MD.

induce cell-mediated connective tissue changes that would serve to weaken the laminar beams, making them more prone to failure under previously safe levels of IOP-related mechanical stress.

To incorporate these concepts into a global conceptual framework, we have previously proposed that the ONH is a biomechanical structure. This paradigm assumes that IOP-related stress (force/cross-sectional area) and strain (local deformation of the tissues) are central determinants of both the physiology and pathophysiology of the ONH tissues and their blood supply (**Figure 2**) at all levels of IOP. These stresses and strains are complex and can be separated into three components that act simultaneously: tension, compression, and shear (**Figure 3**). The distributions of stress, strain, and deformation are determined by the complex material properties and geometries of the sclera and lamina cribrosa (**Figures 4** and **5**). IOP-related stress and strain induce changes in the tissues that include not only alterations to the load-bearing connective tissues of the lamina cribrosa and the peripapillary sclera, but also the cellular components of these tissues, including astrocytes, glial cells, endothelial cells, and pericytes, along with their basement membranes and the RGC axons in the ONH. Experienced over a lifetime at physiologic levels, they underlie normal ONH aging. However, acute or chronic exposure to pathophysiologic levels results in glaucomatous damage.

Although clinical IOP-lowering remains the only proven method for preventing the onset and progression of glaucoma, the role of IOP in the development and progression of the disease remains controversial. This largely arises from the clinical observation that significant numbers of patients with normal IOPs develop glaucoma (e.g., normotensive glaucoma), while other individuals with elevated IOP show no signs of the disease. While there is a wide spectrum of individual susceptibility to IOP-related glaucomatous vision loss, the biomechanical effects of IOP on the tissues of the ONH likely play a

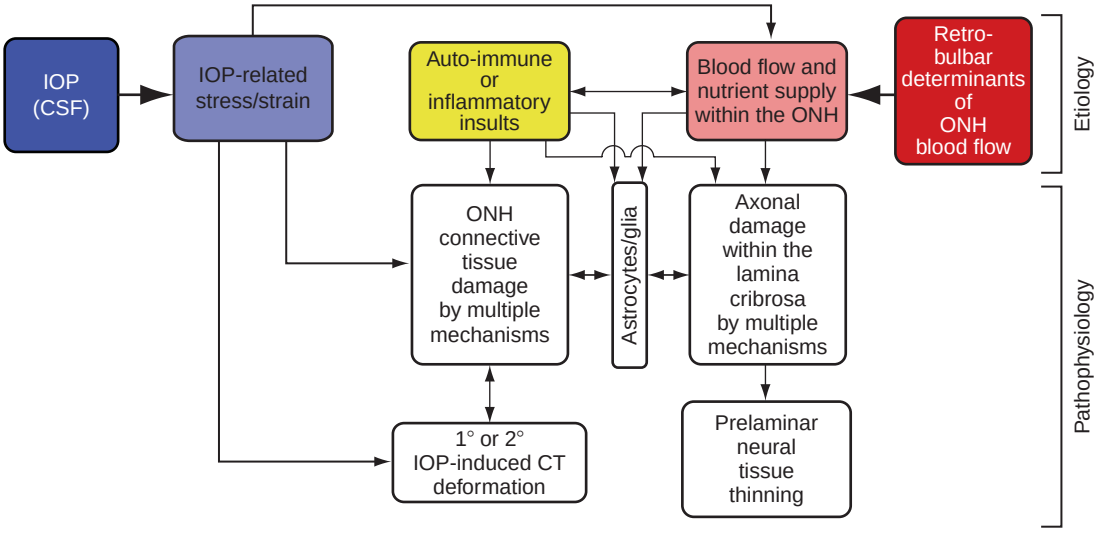

Figure 2 IOP-related stress and strain are a constant presence within the ONH at all levels of IOP. In a biomechanical paradigm, IOP-related strain influences the ONH connective tissues and the volume flow of blood (primarily), and the delivery of nutrients (secondarily) through chronic alterations in connective tissue stiffness and diffusion properties (explained in **Figure 1**). Non-IOP-related effects such as autoimmune or inflammatory insults (yellow) and retrobulbar determinants of ocular blood flow (red) can primarily damage the ONH connective tissues and/or axons, leaving them vulnerable to secondary damage by IOP-related mechanisms at normal or elevated levels of IOP. Based in part on Fig. 5, Burgoyne, C. F. and Downs, J. C. (2008). Premise and prediction – how optic nerve head biomechanics underlies the susceptibility and clinical behavior of the aged optic nerve head. *Journal of Glaucoma* 17(8): 318–328.

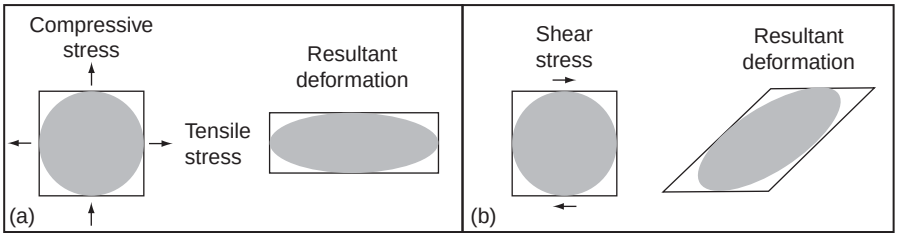

Figure 3 Normal and shear components of stress and strain. (a) The normal tensile and compressive stresses acting on a small square in the manner shown will act to elongate the region in one direction and compress it in the other. (b) The shear stresses acting on a similar region will act to distort the shape of the region.

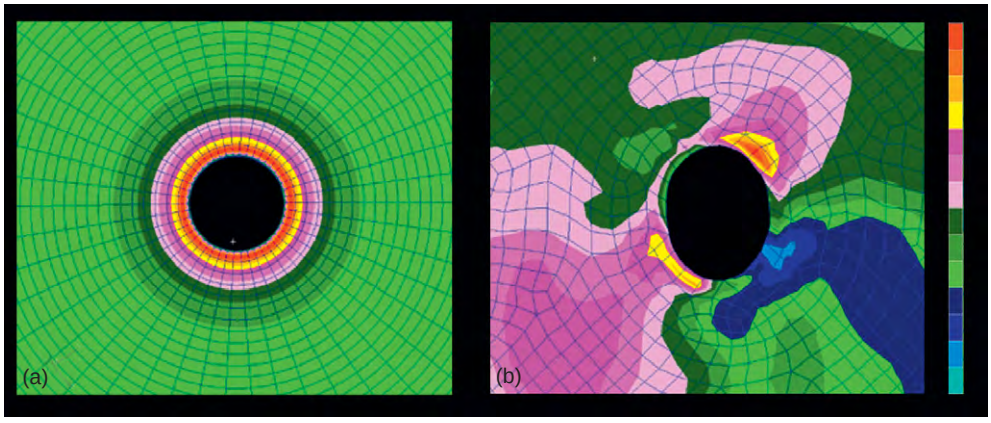

Figure 4 The material properties of the peripapillary sclera are influenced by nonlinearity and collagen fiber orientation (anisotropy). Separate from its thickness, the behavior of the sclera is governed by its material properties, which in turn are influenced by nonlinearity and fiber orientation. (a) Nonlinearity is an engineering term for tissues or structures whose material properties are altered by loading. Panel (a) demonstrates that the sclera becomes stiffer as it is loaded uniaxially (in one direction). In the case of the sclera, this is likely due to the fact collagen fibers embedded within the surrounding ground matrix start out crimped and progressively straighten as the load is increased. This conformational change in the fibrils accounts for the transition from an initially compliant, nonlinear response to a stiffened linear response as IOP increases. (b) Apart from nonlinearity, collagen fiber orientation (anisotropy) within the sclera strongly influences its mechanical behavior. Fiber orientation can be totally random (isotropic – not shown) or have a principal direction (anisotropic – three idealized cases shown). Finite element (FE) models of an idealized posterior pole with principal collagen fiber orientation in the circumferential, helicoidal, and longitudinal directions are shown. As the displacement plots show, the underlying fiber orientation can have profound effects on the deformation that occurs for a given IOP. Note that the displacement scale is exaggerated for illustrative purposes. Courtesy of Michael Girard.

central role in the development and progression of the disease at all IOPs. The individual susceptibility of a particular patient's ONH to IOP insult is likely a function of the biomechanical response of the constituent tissues and the resulting mechanical, ischemic, and cellular events driven by that response. Hence eyes with a particular combination of tissue geometry and stiffness may be susceptible to damage at normal IOP, while others may have a combination of ONH tissue geometry and stiffness that can withstand even high levels of IOP.

In this article, we focus on ocular biomechanics along two main themes: What is known about how mechanical forces and the resulting deformations are distributed in the posterior pole and ONH (biomechanics) and what is known about how the living system responds to those deformations (mechanobiology).

Mechanical Environment of the ONH and Peripapillary Sclera

Overview of the Mechanical Environment of the ONH and Peripapillary Sclera

From an engineering perspective, the eye is a vessel with inflow and outflow facilities that regulate its internal pressure. IOP imposes a pressure load normal to the inner surface of the eye wall, generating an in-wall circumferential stress known as the hoop stress (**Figure 6**). This IOP-generated stress is primarily borne by the stiff, collagenous sclera, while the more compliant retina and nerve fiber tissues bear little of the in-wall stress load and are therefore exposed primarily to the compressive stress of IOP. IOP is borne in the ONH by the fenestrated connective tissues of the lamina cribrosa, which span the scleral canal opening and tether into the stiff outer ring of circumferential collagen and elastin fibers in the peripapillary sclera (like a trampoline). While Laplace's law is useful to describe the pressure–deformation relationship in a spherical vessel of uniform thickness, it is inadequate for describing the eye's response to variations in IOP (**Figure 7**). There are several characteristics of the ocular load-bearing tissues that complicate the study of the mechanical environment to which the ONH and its resident cell populations are exposed.

First, the 3D connective tissue geometry of the eye is complex and difficult to measure. For instance, the thickness of monkey sclera can vary as much as fourfold from the equator to the peripapillary region and the 3D morphology of lamina cribrosa is more regionally complex and individualized than is generally appreciated. Second, the cornea, sclera and lamina cribrosa have extremely complex ECM microstructures with highly anisotropic collagen and elastin fibril orientations. As a result, the experimental characterization and theoretical/mathematical description of their constituent material properties are complex and difficult to obtain. Third, the cells that maintain the ocular connective tissues are biologically active. As such, the geometry and material properties of the sclera and lamina cribrosa change in response to both physiologic (age) and pathologic (IOP-related damage)

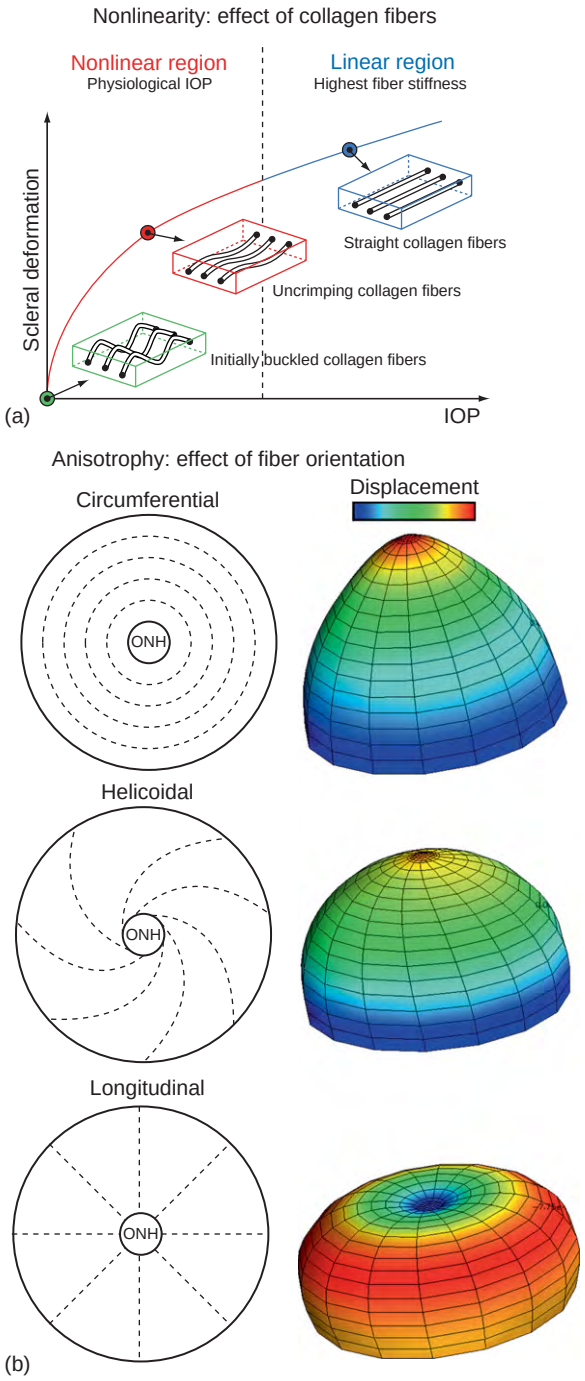

Figure 5 The thickness of the peripapillary sclera, and the size and shape of the scleral canal influence the magnitude and distribution of IOP-related stress within the peripapillary sclera. Stress plots within 3D biomechanical models of the posterior sclera and ONH demonstrate that stress concentrates around a defect (scleral canal) in a pressure vessel (eye) and varies according to the geometry of the peripapillary sclera and scleral canal. The idealized model in (a) shows the stress concentration around a circular canal in a perfectly spherical pressure vessel with uniform wall thickness (the ONH has been removed from these images for visualization purposes). The model in (b) shows the IOP-related stress concentration around an anatomically shaped scleral canal with realistic variation in peripapillary scleral thickness. In this case, the highest stresses (red) occur where the sclera is thinnest and the lowest stresses (blue) occur where the sclera is thickest, and also tend to concentrate around areas of the scleral canal with the smallest radius of curvature. The response of the sclera to this load is determined by its structural stiffness, which is the combination of geometry (how much tissue is bearing the load) and material properties (how rigid or compliant is the tissue).

factors. Fourth, the eye is exposed to ever changing loading conditions because IOP undergoes acute, short-term and long-term fluctuations ranging from blinks and eye rubs to circadian rhythms.

Finally, IOP-related stress generates strain patterns in the ONH and peripapillary sclera that are not only dependent on differing connective tissue geometries and material properties but are also influenced by complex loading conditions. The important factors contributing to this biomechanical component include the alignment and density of collagen fibrils in each tissue (stiffness and anisotropy), the rate of change in IOP (via tissue viscoelasticity), and the level of IOP-related strain at the time of altered loading (via tissue nonlinearity). In broad terms, the ONH connective tissues should be stiffer when there is already considerable strain present and/or if the IOP load is applied quickly. Conversely, the ONH should be more compliant in response to slow changes in IOP and/or at low levels of strain.

Mechanical Response of the ONH to Acutely Elevated IOP

It is important to note that the ONH responds to IOP elevations as a structural system, so the acute mechanical response of the lamina cribrosa is confounded with the responses of the peripapillary sclera, prelaminar neural tissues, and retrolaminar optic nerve. Also, because the lamina lies buried underneath the prelaminar neural tissues and the structural responses of these two tissue types to acute IOP elevations are quite different, acute laminar deformation cannot be directly measured or inferred by imaging the surface topography of the ONH. A final confounding effect is the cerebrospinal fluid pressure, which, along with IOP, determines the translaminar pressure gradient that must be borne by the lamina cribrosa.

Intuitively, it may seem that for a given acute increase in IOP, the lamina cribrosa should deform posteriorly and there have been several experimental studies designed to measure acute IOP-related laminar deformation. Yan and co-workers found that increasing IOP from 5 to 50 mmHg for 24 h produced an average posterior deformation of the central lamina of 79 μm in human donor eyes. Levy and Crapps reported a 12 μm average posterior movement of the central lamina with acute IOP elevations from 10 to 25 mmHg for shorter time periods in human eyes.

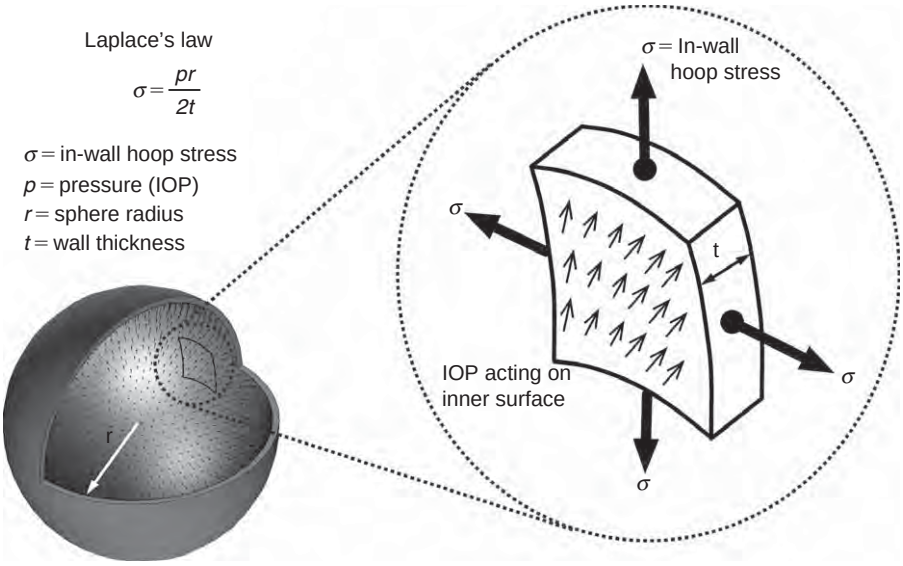

Figure 6 In-wall stress engendered by IOP loading. In an idealized spherical shell, the majority of the stress generated by IOP is transferred into a hoop stress borne within the thickness of the wall. Laplace's law, which relates the in-wall hoop stress to the internal pressure, is only applicable to spherical pressure vessels with isotropic material properties and uniform wall thickness, and can only be used to calculate very rough estimates of hoop stress in actual eyes. In pressure vessel geometries like the eye, with variable wall thickness, aspherical shape, and anisotropic material properties, the hoop stress may vary substantially by location.

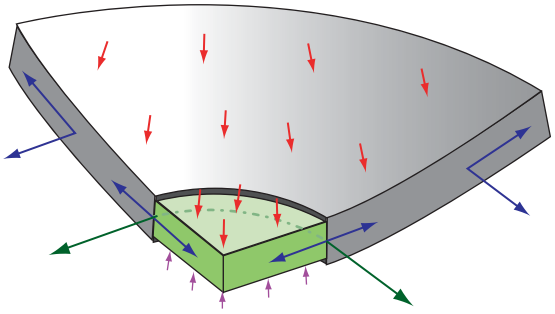

Figure 7 Stress, relative to IOP (red arrows) in the lamina cribrosa (light green) and peripapillary sclera (grey) engendered by IOP loading. Cut-away diagram of IOP-induced stress in an idealized spherical scleral shell with a circular scleral canal spanned by a more compliant lamina cribrosa. In this case, the majority of the stress generated by IOP (red arrows) is transferred into a hoop stress borne within the thickness of the sclera and lamina (blue arrows) that is concentrated circumferentially around the scleral canal (green arrows). Note that the difference between IOP (red arrows) and the retrolaminar cerebrospinal fluid pressure (pink arrows) is the translaminar pressure gradient that generates both a net posterior force on the surface of the lamina and a hydrostatic pressure gradient within the neural and connective tissues of the pre-laminar and laminar regions. Most importantly, note that the in-plane hoop stress transferred to the lamina from the sclera is much larger than stress induced by the translaminar pressure gradient.

More recently, Bellezza and colleagues reported a small but significant posterior laminar deformation of 10–23 μm (95% confidence interval (CI)) in a histologic evaluation of monkey eyes perfusion fixed with one eye at 10 mmHg and the contralateral eye at 30 or 45 mmHg for 15 min prior to death. However, these deformations, while statistically significant, did not substantially exceed the 95% CI for intra-animal physiologic differences (1–17 μm) between normal eyes bilaterally immersion fixed at an IOP of 0 mmHg.

The previous studies were performed using 2D measurements of laminar compliance within actual histologic sections. Angled sectioning, section warping, and the lack of a stable measurement reference plane can influence the accuracy of this technique. To overcome these problems, Downs, Yang and co-workers developed a technique for 3D delineation and measurement of ONH structures within high-resolution, digital 3D reconstructions (**Figure 8**). While our initial reports have concentrated on monkeys with early experimental glaucoma in one eye, preliminary data from a larger group of bilaterally normal monkeys perfusion fixed with both eyes at an IOP of 10 mmHg ($n = 5$), one eye at 10 mmHg, the other at 30 mmHg ($n = 3$), and one eye at 10 mmHg, the other at an IOP of 45 mmHg ($n = 3$) suggest that while acute IOP elevation causes expansion of the scleral canal, in most monkey eyes there is no net posterior laminar deformation from the plane of the sclera. Thus, our current understanding of the aggregate response of the young adult monkey ONH to acute IOP elevation is that expansion of the scleral canal tightens the lamina within the plane of the sclera, making it more resistant to posterior deformation out of that plane (**Figure 9**). These data are preliminary and our interpretation may change with further study.

It is important to note that the lack of laminar deformation in these eyes does not mean that the lamina is not

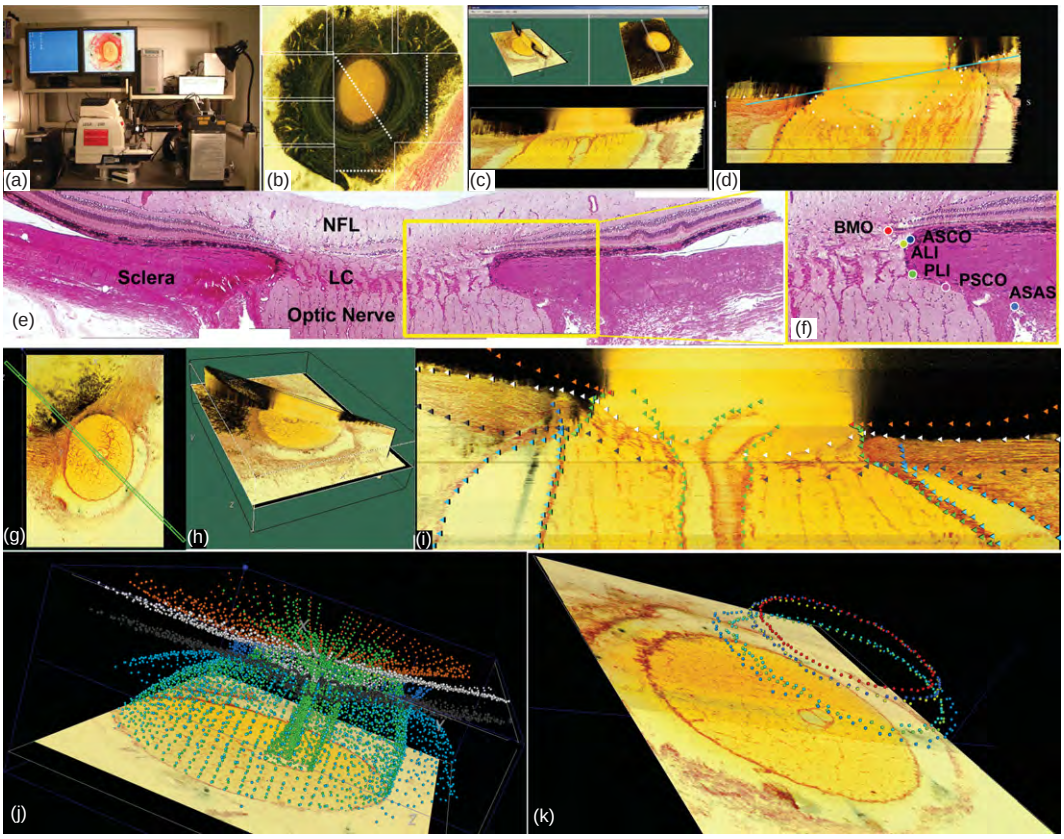

Figure 8 3D delineation of ONH and peripapillary scleral landmark points within digital 3D ONH reconstructions. (a) Photograph of our microtome-based 3D reconstruction device allows for serial sectioning and high-resolution image capture of the stained block face of embedded ONH specimens. (b) Images are acquired in a mosaic, then stitched into a composite of the entire 6-mm-diameter specimen, and stacked into a digital 3D reconstruction of the connective tissues of the ONH with 1.5 x 1.5 x 1.5 μm voxel resolution (c). Once loaded into custom software, the reconstruction can be digitally sectioned and landmarks delineated. In this view (d) our measurement reference plane, Bruch's membrane opening (BMO), is marked and shown with a light blue line. (e) Central horizontal histologic section through a representative normal monkey eye showing the ONH anatomy. (f) Magnified view of the nasal side of the neural canal showing the following landmark points: BMO (red), the anterior scleral canal opening (ASCO, dark blue), the anterior laminar insertion point (ALI, yellow), the posterior laminar insertion point (PLI, green), the posterior scleral canal opening (PSCO, pink), the anterior-most aspect of the subarachnoid space (ASAS, light blue). (g, h) With the 3D digital ONH reconstruction, a total of 40 radial, sagittal slices (each 7 voxels thick) are served to the delineator at 4.5° intervals. (i) A representative digital sagittal slice, showing the marks for seven landmark surfaces and six landmark point pairs. These features are interactively delineated within the 3D volume by viewing the position of a marking cursor displayed simultaneously within the sagittal (g) and transverse section images (h). (j) Representative 3D point cloud showing all delineated points for a normal monkey ONH in relation to the last section image of the reconstruction. (k) A subset of the 3D point cloud showing the neural canal landmarks depicted in (f).

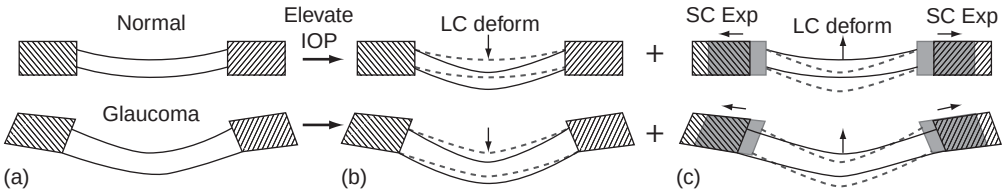

Figure 9 There are two components of acute IOP-induced ONH deformation in normal and early glaucoma eyes. (a) Sagittal section diagram of the ONH, showing the peripapillary sclera (hatched) and the lamina cribrosa for normal (upper) and early glaucoma (lower) eyes. Note that the early glaucoma eye has undergone permanent changes in ONH geometry including thickening of the lamina, posterior deformation of the lamina and peripapillary sclera, and posterior scleral canal expansion. Upon acute IOP elevation we believe two phenomena occur simultaneously and with interaction: the lamina displaces posteriorly due to the direct action of IOP (b), but much of this posterior laminar displacement is counteracted as the lamina is pulled taut by simultaneous scleral canal expansion (c). It is important to note that even though the net result of these IOP-related deformations is a small amount of posterior displacement of the lamina, substantial levels of IOP-related strain are induced in both the peripapillary sclera and lamina in this scenario.

strained. In this scenario, the expansion of the canal stretches the lamina cribrosa within the plane of the sclera generating substantial strain within the laminar beams. Estimation of laminar beam strain within these same 3D reconstructions is one of the outputs of finite element (FE) modeling, an engineering technique that is discussed in the section entitled 'Other acute, IOP-related changes in the ONH'.

The Contribution of the Sclera to ONH Biomechanics

The data described above, as well as the closed form analyses and computational models described in the next section suggest that the sclera plays an important role in ONH biomechanics. The peripapillary sclera provides the boundary conditions for the ONH. By this we mean that the peripapillary sclera is the tissue through which load and deformation are transmitted to the ONH, and that the structural stiffness of the peripapillary sclera, therefore, influences how the lamina deforms (**Figure 9**). This can be understood from the discussion above in which a compliant sclera allows the scleral canal to expand following an acute IOP elevation, tightening the laminar beams within the canal and thereby increasing laminar resistance to posterior deformation. In contrast, a rigid sclera allows less expansion of the canal or none at all, forcing the structural stiffness of the lamina alone to bear the IOP-related stress. Hence, characterization of both components of scleral structural stiffness (geometry and material properties) is essential to understanding the effects of IOP on the ONH.

Characterization of scleral geometry

Maps of the thickness variation for the posterior pole of human and monkey eyes show extreme spatial variation in scleral thickness, with very thin regions near the equator (as low as 300 μm in the human and 111 μm in the monkey). In both species the peripapillary sclera is notably thicker (1000 μm in the human and 415 μm in the monkey). Interestingly, this thick ring of peripapillary sclera is absent in the nasal quadrant of monkey eyes due to the oblique nasal insertion of the optic nerve through the scleral canal. Such variation in peripapillary scleral thickness as occurring naturally or in pathologic conditions such as myopia, may be important in assessing individual susceptibility to glaucomatous damage.

Characterization of scleral material properties

Several researchers have characterized scleral material properties in various species. Most recently, Downs and co-workers used a strain-rate controlled, servo-hydraulic materials testing system to determine the viscoelastic material properties of normal rabbit and monkey peripapillary sclera. They found that the material properties of peripapillary sclera are highly time dependent (viscoelastic), but reported no significant differences in material properties by quadrant.

However, uniaxial testing of scleral strips is limited in its ability to describe the nonlinear and anisotropic responses of the sclera (**Figure 5**), leading Girard and colleagues to develop a new 3D approach. Using a customized scleral shell pressurization apparatus, precise IOP control, and laser-based electronic speckle pattern interferometry, they measure the 3D deformation of the entire posterior scleral shell in response to small, stepped increases in IOP (from 5 to 45 mmHg). Results suggest that the monkey posterior sclera is highly nonlinear (it gets stiffer as IOP increases) and anisotropic (the underlying collagen fibril distribution is nonuniform and changes throughout the scleral shell, which affects directional stiffness) (**Figure 10**). By using an FE model backfitting method (see the following section), they have calculated the nonlinear, hyperelastic, anisotropic material properties for the entire posterior scleral shell of normal monkeys, and characterized changes in these properties due to age and stage of glaucomatous damage.

Engineering Models of Stress and Strain in the ONH and Peripapillary Sclera

Closed form solutions

Attempts to mathematically model the mechanical environment of the ONH generally fall into two broad categories – closed form solutions and numerical solutions. In closed form solutions, engineering principles are used to derive equations that can be analyzed to understand the effects of selected biological parameters. Examples of closed form approaches include work by Donqui, Edwards, and Good, and a hybrid cellular solid approach by Sander. The appeal of closed form solutions is that general conclusions may be drawn from a model cast in terms of a limited number of geometric and material parameters that are felt to be of interest or might be clinically measurable. However, closed form solutions may be of limited utility because of the complexity of the ONH and peripapillary scleral tissues (e.g., the nonuniform and asymmetric geometry and material properties). The most sophisticated of these studies suggest that the structural stiffness of the sclera is the most important determinant of macro-level ONH biomechanics.

Numerical solutions – FE analysis

To overcome the inherent limitations of closed form solutions, researchers often utilize numerical methods to study more complex biological systems. One of the most powerful of these is FE analysis. In FE analysis, complex load-bearing structures are broken into small, regularly shaped elements (**Figure 4**). Stress and strain within each element is calculated and then superposed to predict the mechanical response of the entire structure.

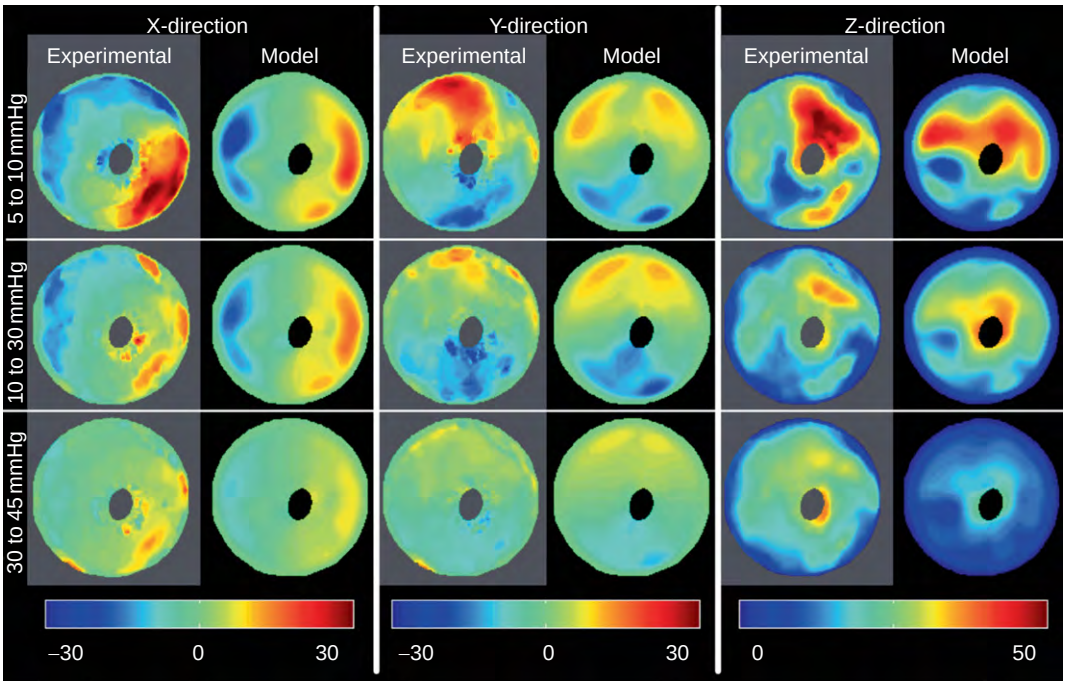

Figure 10 Experimental results and finite element (FE) model predictions of the nonlinear, anisotropic displacement behavior of an individual monkey posterior scleral shell as IOP increases from 5 to 10 mmHg (top row), 10 to 30 mmHg (middle row), and 30 to 45 mmHg (bottom row). Experimental (gray background) and predicted (model, black background) displacements for the X-direction (left-to-right), Y-direction (top-to-bottom), and Z-direction (in-and-out) are mapped onto the outer surface of the scleral shell of a right eye (for each map superior top, inferior bottom, temporal left and nasal right). The inhomogeneity of the experimental displacement patterns are indicative of underlying tissue anisotropy, and the much greater displacements seen in the 5–10 mmHg IOP elevation as compared to the 30–45 mmHg IOP elevation reflect the highly nonlinear behavior (i.e., the sclera is stiffer and therefore more resistant to deformation at higher levels of strain). Figure, including experimental and modeling results, courtesy of Michael Girard.

The power of FE analysis lies in its ability to model structures with highly complex geometries using material properties with varying levels of complexity as warranted (e.g., inhomogeneous, anisotropic, nonlinear, or viscoelastic material descriptions). The three components necessary as input for FE models are: the 3D geometry of the tissue structure to be modeled, the material properties of the different tissues in the model, and appropriate loading and boundary conditions. These requirements have spurred the development of methodologies to isolate and describe the 3D geometry of the ONH and peripapillary sclera (**Figure 8**) and experimentally characterize their constituent material properties (**Figure 10**).

There are two basic approaches to FE modeling of the ONH: parametric and individual specific. Parametric modeling involves computing stress and strain in average, idealized geometries that do not conform to any individual's particular anatomy. Within these models, parameters such as peripapillary scleral thickness and laminar stiffness can be varied independently to gauge the parameter's effects on ONH biomechanics as a whole. This is a similar approach to analytical modeling, but the analyzed geometries are much more fidelic and the results more relevant and intuitive. Although parametric FE models are by nature simplified in their geometries and there are limited cases that can be modeled, these investigations yield interesting insight into the contributions of individual anatomical elements and tissue material properties to overall ONH biomechanics.

Bellezza and colleagues used parametric FE modeling to study the mechanical environment of an idealized 3D model of the posterior pole. In this study, the effects of the size and shape (aspect ratio) of an elliptical scleral canal within a spherical scleral shell of uniform thickness were studied. Idealized beamlike structures spanning the ONH were also incorporated into the model to simulate the lamina cribrosa. This study illustrated that IOP-related stress concentrations within the load-bearing connective tissues of the ONH is substantial, even at low levels of IOP. Specifically, models with larger scleral canal diameters, more elliptical canals, and thinner sclera all showed increased stresses in the ONH and peripapillary sclera for a given level of IOP. In the peripapillary sclera and ONH, stresses were as much as one and two orders of magnitude greater than IOP, respectively. While the model used in this study was idealized in terms of its material properties and geometry, it served to reinforce the concept of the peripapillary sclera and ONH as a high stress environment even at normal levels of IOP.

Sigal and co-workers used idealized axisymmetric FE models to pursue a more complex parametric analysis of the factors that influence the biomechanical environment within the ONH (**Figure 11**). In these studies, various geometric and material details of a generic model were parametrized and independently varied to assess their impact on a host of outcome measures such as strain in the lamina cribrosa and prelaminar neural tissue (**Figure 11**). This work identified the five most important determinants of ONH biomechanics (in rank order) as: the stiffness of the sclera, the size of the eye, IOP, the stiffness of the lamina cribrosa, and the thickness of the sclera. The finding that scleral stiffness plays a key role in ONH biomechanics is especially interesting, and was also found to be important in the analytical models of Sander and co-workers. Parametric studies such as these are important because they can be used to identify important biomechanical factors that warrant more in-depth study, thus narrowing and focusing future experimental and modeling efforts.

To address the limitations of idealized geometric and material property descriptions inherent in parametric FE models, individual-specific FE models can be created from the reconstructed geometries of particular eyes. At present, individual-specific modeling is based on high-resolution 3D reconstructions of monkey and human cadaver eyes (**Figure 8**), with a long-term goal to build models based on clinical imaging of living eyes so as to use them in the assignment of target IOP. This is especially important given that the 3D geometry of the scleral canal and peripapillary sclera largely determines the stress and strain transmitted to the contained ONH (**Figure 7** notes specifically how the 3D geometry of the scleral canal and peripapillary sclera alter the stress environment). Anatomically accurate 3D models are necessary to capture the biomechanics of anisotropic scleral material properties (varying collagen fibril orientation), and scleral canals that are noncircular and have varying optic nerve insertion angles (i.e., the optic nerve inserts from the nasal side resulting in a thinner peripapillary sclera in that quadrant). When modeling an ONH with anatomic fidelity, the tissue geometries can be constructed either by serial histologic methods or by 3D imaging, and material properties are generally determined through direct mechanical testing (**Figure 10**). Unfortunately, imaging of the lamina *in vivo* is not yet possible at the resolutions required for modeling, and no technology exists for experimental biomechanical testing of laminar beams. As a result, ONH FE models are typically constructed from eyes that are perfusion or immersion fixed at a selected IOP, and then undergo *ex vivo* 3D reconstruction of their connective tissues.

Bellezza and co-workers developed a histologic technique to 3D reconstruct the trabeculated structure of the lamina cribrosa from individual monkey eyes that have been perfusion fixed at varying levels of IOP (**Figure 8**). The resulting 3D data sets form the geometries of individual-specific FE models of the ONH at the macro- and micro-scale. Roberts, Downs, and co-workers have developed macro-scale continuum FE models of the posterior pole and ONH connective tissues from individual monkey eyes (**Figure 12**). In these models, the laminar microarchitecture is modeled using a continuum approach, with anisotropic material properties assigned to each FE in the ONH based on the connective tissue volume fraction and the predominant beam orientation of the contained laminar microarchitecture (**Figure 13**). Regional variations in connective tissue volume fraction and predominant

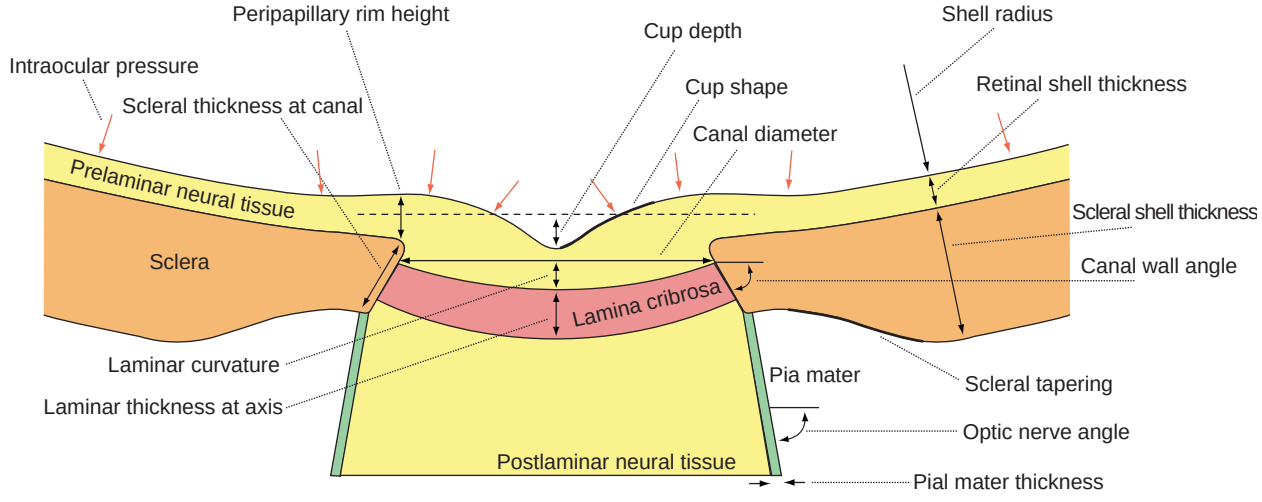

Figure 11 Parametric models can be used to study the influence of geometric and material property factors. To model the ONH, Sigal and colleagues created an idealized, axisymmetric (symmetric about the anterior-to-posterior axis) reference geometry and varied geometric and material property factors to assess their influence on various outcome measures of stress and strain within the model. This type of parametric sensitivity analysis is useful for identifying the tissues and anatomic structures that may be most important in the mechanical response of the ONH. Such information can serve to focus future biomechanics research and clinical device development efforts on the tissues and structures determined to be most important in ONH biomechanics. Figure courtesy of Ian Sigal.

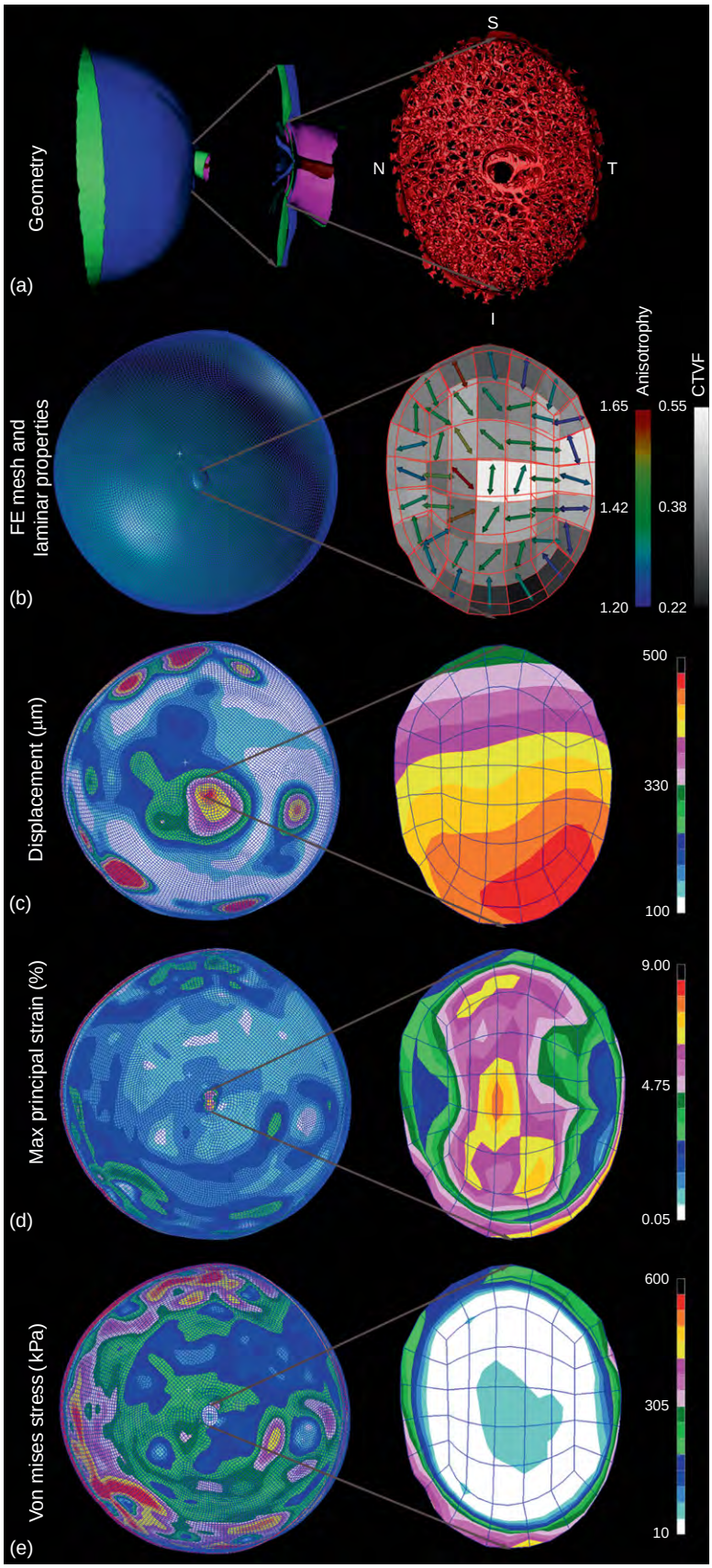

Figure 12 Construction and results from a macro-scale continuum FE model of the posterior scleral shell and ONH of a normal monkey eye. (a) To construct the model geometry, the 3D-delineated lamina cribrosa and surrounding peripapillary sclera (see **Figure 8**) of an individual eye are incorporated into a generic anatomic scleral shell with regional thickness variations mapped from previous

orientation are translated into variations in local oriented stiffness so that regions of higher and lower porosity reflect greater and lesser compliance, respectively. The inclusion of regional laminar material properties (connective tissue volume fraction and beam orientation) into FE models has a pronounced effect on the ONH's response to IOP (Figure 14). This indicates that the regional variations in laminar geometry and structural stiffness must be represented in models to fully capture the biomechanical behavior of the ONH and suggests that the lamina is biologically optimized to withstand IOP-induced deformation.

Downs and colleagues have also used the 3D reconstruction and continuum modeling approaches to characterize and explore laminar beam biomechanics. This micro-scale modeling approach utilizes a substructuring technique based on parent macro-scale FE models to calculate the IOP-related stress and strain fields in laminar beams (Figure 15). This technique reveals a complexity of IOP-related strains and stresses within the lamina cribrosa microarchitecture that is not available through macro-scale FE modeling. There have been several interesting preliminary results from this work. First, stress and strain in the laminar microarchitecture are likely higher than predicted by macro-scale models of the ONH. Second, even at normal levels of IOP, the micro-FE models predict that while the majority of laminar beams are within physiologic strain ranges, there are individual laminar beams with levels of IOP-related strain that are likely pathologic. Third, mean strain within the laminar beams of different

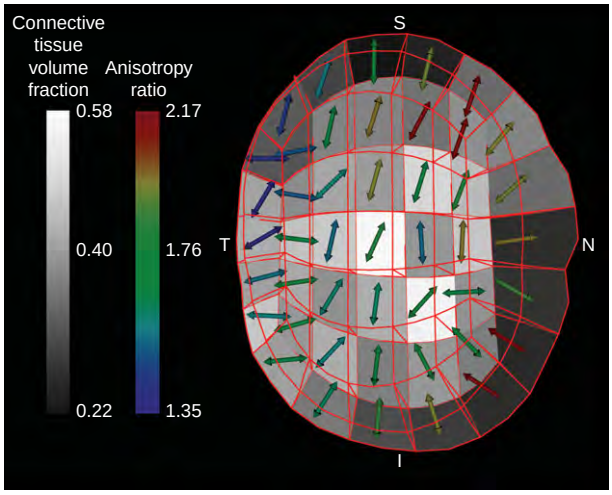

Figure 13 Regional differences in laminar microarchitecture in a normal monkey eye. Characterization of the laminar microarchitecture utilizes the element boundaries of a continuum finite mesh to partition the lamina cribrosa connective tissue into 45 subregions. The connective tissue volume fraction (CTVF) for each region is expressed as a percentage and mapped to a grayscale value in the background. The arrows indicate the predominant orientation of the laminar beams in each region, with higher values (color-coded) indicating regions in which the beams are more highly oriented. Note that in the peripheral regions of the lamina, the beams are tethered radially into the scleral canal wall.

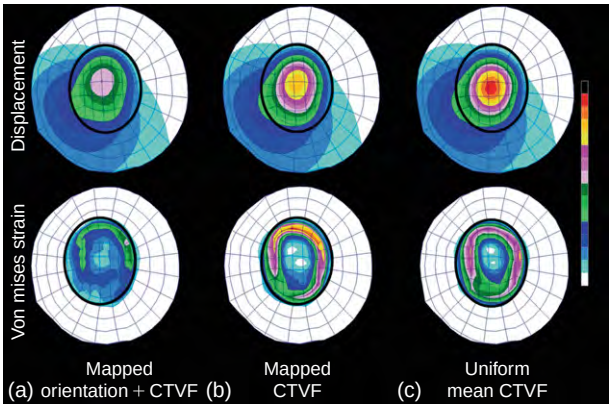

Figure 14 Incorporation of laminar beam orientation and connective tissue volume fraction into the material description of the lamina cribrosa affects the predictions of finite element (FE) models. Internal (vitreous) surface views of the displacement and strain in the ONH (within the heavy black outline) and peripapillary sclera in continuum models of the same eye following acute IOP elevation. In column (a), the stiffness of each laminar element is determined from both the predominant laminar beam orientation and connective tissue volume fraction (CTVF) of the contained lamina. In column (b) the orientation information (i.e., using an isotropic material stiffness), but retaining mapped CTVF produces a substantial increase in the displacement of the lamina with markedly higher strains. In column (c) all elements in the lamina are assigned the same isotropic material stiffness based on an average CTVF (with no beam orientation information). This model has slightly more central laminar displacement than case (b), but actually has lower strain in the superior lamina cribrosa owing to the fact that the superior elements in case (b) had lower CTVFs in that region (i.e., below the mean CTVF). These results suggest that representing regional laminar microarchitecture in FE models is essential to accurately predict ONH biomechanical behavior.

histologic measurements. The segmented 3D reconstruction of the laminar connective tissue (shown) is represented in each model. (b) A continuum FE mesh of the posterior pole is generated from the geometry. The sclera in this model is assigned uniform isotropic material properties based on previous experimental testing. The continuum elements representing the porous load-bearing laminar architecture are assigned anisotropic material properties that reflect the microstructure of the lamina enclosed by each laminar FE. This material property description is defined using a combination of the connective tissue volume fraction (CTVF) and the predominant laminar beam orientation. A visualization of the CTVF and predominant beam orientation are presented. Note that in this visualization, an anisotropy value of 1 would represent an isotropic material with no predominant orientation while larger values imply oriented laminar beams that impart higher stiffness in the direction of the plotted arrow. (c, d, e) FE results showing predicted displacement, strain, and stress distributions due to an increase in IOP from 10 to 45 mmHg. Note that in this eye, the model predicts that the ONH tilts inferiorly, the strains are highest along the superior–inferior axis of the ONH, and that the sclera bears most of the IOP-related stress.

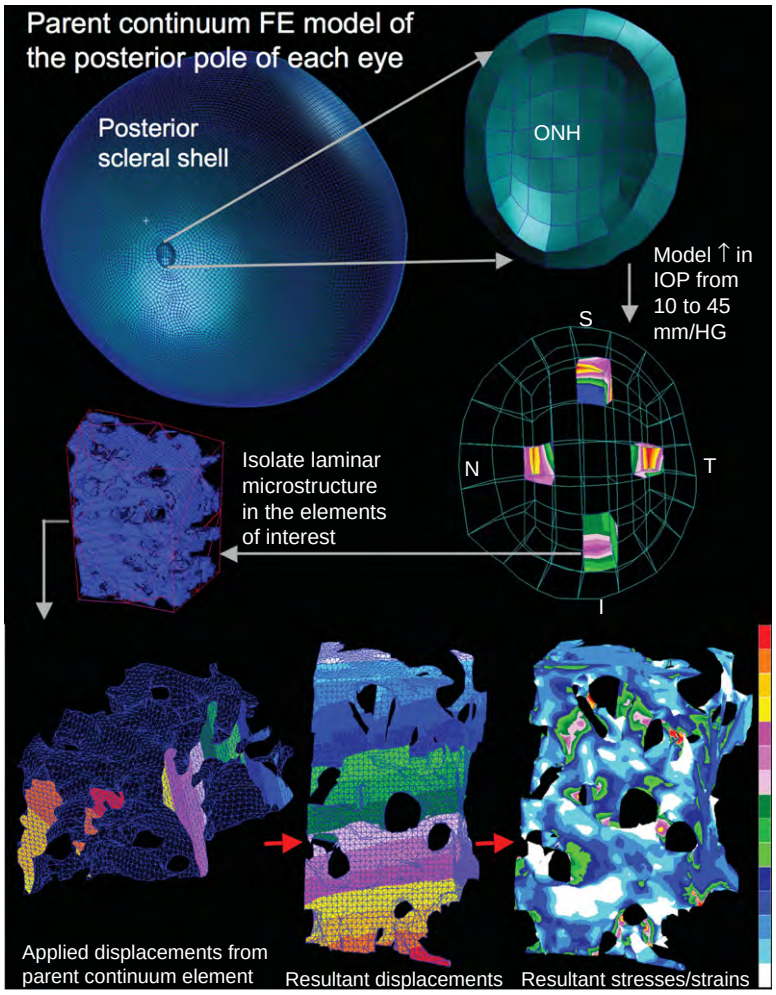

Figure 15 Construction and analysis of micro-FE models of the laminar microarchitecture of a monkey eye. The complexity of the stresses and strains at the laminar beam level is not captured in the macro-scale continuum FE models because the details of the microstructure are homogenized into a bulk material description. To address this limitation, a substructuring technique has been developed to characterize the beam-level strain environment within ONH models. The displacement field calculated from a continuum model is used along with individual element boundaries to define input loading conditions for micro-scale FE models of subregions of the 3D reconstructed lamina cribrosa. These micro-FE models illustrate that the stress and strain borne by the individual laminar beams are highly variable and complex. Modeling of individual beam mechanics will be necessary to predict the yield and failure of individual beams, model changes in blood flow in the laminar capillaries, and determine the strains to which laminar astrocyte basement membrane are subjected.

monkeys varies greatly, and is generally dependent on the 3D geometry of each eye's ONH connective tissues. Finally, strain is not equally distributed though the ONH, and are concentrated in regions with less dense laminar beams. This work, while still in its early stages, holds the possibility of testing hypotheses about failure mechanisms and cellular responses at the level of the laminar beams.

Other Acute, IOP-Related Changes in the ONH

ONH, retinal, and choroidal blood flow are all affected in different ways by acute IOP elevations. Previous studies using microspheres have suggested that volume flow within the prelaminar and anterior laminar capillary beds is preferentially diminished once ocular perfusion pressure (defined as the systolic arterial blood pressure plus one-third of the difference between systolic and diastolic pressures minus IOP) is less than 30 mmHg.

While a direct link to mechanical strain has not been established, axonal transport is compromised in the lamina cribrosa at physiologic levels of IOP and is further impaired following acute IOP elevations. Several hypotheses regarding this behavior emerge when considering ONH biomechanics. First, as the pores in the lamina cribrosa change conformation due to IOP-related mechanical strain, the path of the axons through those pores may be disrupted, thereby directly impeding axoplasmic

transport. Second, it may be that the IOP-related reduction in blood flow in the laminar region impairs the mitochondrial metabolism that drives axoplasmic transport. Finally, axoplasmic transport could be sensitive to the magnitude of the translaminar pressure gradient, and as that hydrostatic pressure gradient gets larger with increasing IOP (or lower cerebrospinal fluid pressure), the mechanisms driving that transport are unable to overcome the resistance of the pressure gradient (**Figure 7**).

In summary, while connective tissue dynamics should, by themselves, directly and indirectly influence astrocyte and glial metabolism and axonal transport, glaucomatous damage within the ONH may not necessarily occur at locations with the highest levels of IOP-related connective tissue strain, but rather at those locations where the translaminar tissue pressure gradient is greatest and/or where the axons, blood supply, and astrocytes and glia have been made most vulnerable. Further studies are necessary to elucidate the link(s) between IOP, mechanical strain, blood flow, astrocyte and glial cell homeostasis, and axoplasmic transport in the ONH, in both the physiologic and diseased states.

Restructuring and Remodeling of the ONH

Normal Aging

The ONH connective tissues are exposed to substantial levels of IOP-related stress and strain at normal levels of IOP (**Figure7**). We believe that physiologic levels of stress and strain experienced over a lifetime induce a broad spectrum of changes in both the connective tissues and vasculature that are central to normal aging. Thus, the restructuring and remodeling of glaucomatous damage (described in the following sections) should be understood to occur in the setting of the physiologic restructuring and remodeling inherent in normal aging.

Age-related alterations of the laminar ECM have been reported to include increased collagen deposition, thickening of astrocyte basement membranes, and increased rigidity of the lamina and sclera. Girard and colleagues have recently shown that the sclera in old monkeys is approximately twice as stiff than sclera from young monkeys at all IOPs. The aged ONH is thus more likely to have stiff connective tissues. Age-related hardening of the laminar ECM not only stiffens the connective tissues, it should also diminish nutrient diffusion from the laminar capillaries through the laminar ECM, across the astrocyte basement membranes, and into the adjacent axons (**Figure 1**). Thus, in addition to the effects of age-related decreases in the volume flow within the laminar capillaries, axonal nutrition in the aged eye may be further impaired as a result of diminished nutrient diffusion from the laminar capillaries to the center of the axon bundles.

Alterations in Connective Tissue Architecture, Cellular Activity, Axoplasmic Transport, and Blood Flow in Early Glaucoma

Pathophysiologic stress and strain induce pathologic changes in cell synthesis and tissue microarchitecture that exceed the effects of aging and underlie the two governing pathophysiologies in glaucoma: (1) mechanical yield and/or failure of the load-bearing connective tissues of the ONH (**Figures 2** and **16**) and (2) progressive damage to the adjacent axons by a variety of mechanisms (**Figure 2**).

Early glaucomatous damage has not been rigorously studied in humans because human cadaver eyes with well-characterized early damage are rare. In monkeys, following moderate experimental IOP elevations, we have described the following changes in ONH and peripapillary scleral connective tissue architecture and material properties at the onset of confocal scanning laser tomography-detected ONH surface change (clinical cupping): (1) enlargement and elongation of the neural canal (**Figure 17**); (2) posterior deformation and thickening of the lamina cribrosa accompanied by mild posterior deformation of the scleral flange and peripapillary sclera (**Figure 18**); (3) hypercompliance of the lamina in some cases; and (4) alteration in the viscoelastic material properties of the peripapillary sclera. These findings are accompanied by prelaminar neural tissue thickening and are summarized in **Figure 19**.

Roberts and coworkers have shown that in the monkey model of early experimental glaucoma, the volume of the laminar connective tissues is approximately 80% larger in the glaucoma eyes compared to their contralateral controls. The most surprising result of that work is the nature of that addition of laminar volume. Their results suggest that the connective tissues in glaucomatous eyes remodel in a way that the immediate retrolaminar septa add connective tissue and are recruited into the 3D load-bearing structure of the lamina.

The increase in laminar thickness in these early glaucoma monkey eyes is likely a combination of axonal swelling, tissue edema, gliosis, connective tissue remodeling, and new connective tissue synthesis. Preliminary quantification of the amount of connective tissue within our 3D reconstructions of the lamina suggests an increase in connective tissue volume of 50–100% in early glaucoma (**Figure 20**). These data strongly support the notion that connective tissue remodeling, and new connective tissue synthesis, are present at this early stage of the neuropathy.

Alterations in cellular activity, axoplasmic transport and blood flow in early glaucoma have not been rigorously studied. However, in a recent study in rat eyes (which has a very minimal lamina cribrosa), Johnson and colleagues used genomic techniques to characterize the alterations in the genome of ONH tissues following 5 weeks exposure to experimental elevated IOP. Within

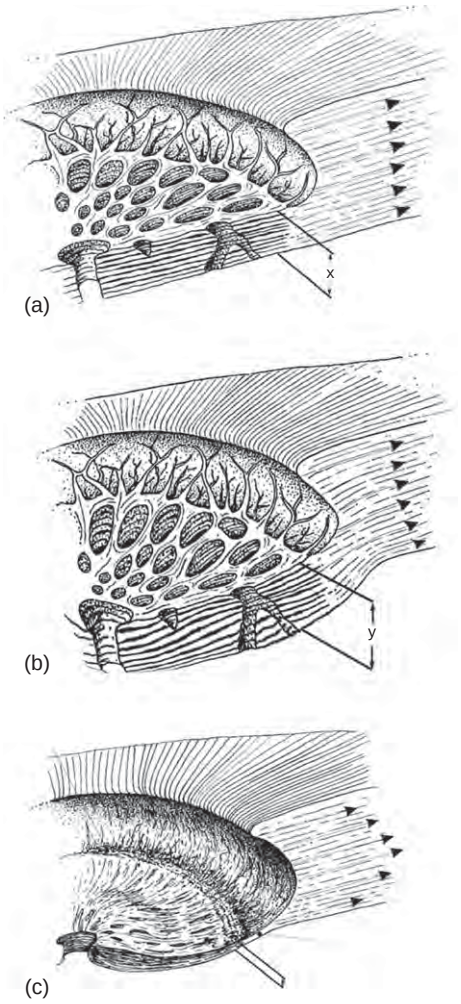

Figure 16 Progression of connective tissue morphology from normal health to early glaucoma to end-stage glaucoma. (a) Diagram of normal ONH connective tissue showing the thickness of the lamina cribrosa (x) and the in-wall hoop stress generated by IOP in the peripapillary sclera. (b) In early experimental glaucoma, our data to date suggests that rather than catastrophic failure of the laminar beams, there is permanent posterior deformation and thickening (y) of the lamina which occurs in the setting of permanent expansion of the posterior scleral canal. These changes indicate that a combination of mechanical yield and subsequent remodeling of the connective tissues occur very early in glaucoma that is not yet accompanied by physical disruption of the beams or frank excavation. (c) As the disease progresses to end-stage damage, we believe that the anterior laminar beams eventually fail, the lamina compresses (z) and scars, the laminar insertion into the sclera displaces posteriorly, and the scleral canal enlarges to the typical cupped and excavated morphology. Very little is known about the biomechanics, cellular processes, and remodeling that drives the morphological progression from the earliest detectable stage of glaucoma to end-stage damage, but it is likely that these processes continue to be driven by the distribution of IOP-related stress and strain within the connective tissues either primarily or through their effects on the capillaries contained within the laminar beams and the adjacent astrocytes. Modified from Burgoyne, C. F. and Downs, J. C. (2008). Premise and prediction – how optic nerve head biomechanics underlies the susceptibility and clinical behavior of the aged optic nerve head. *Journal of Glaucoma* 17(8): 318–328.

the large group of animals studied, a subset of eyes had an early focal stage of orbital optic nerve axon loss. Within these animals, expression of genes governing initiation of cell division was maximally elevated (compared to later stages of damage) as well as the genes for several ECM components including fibulin 2, tenascin C, and the matrix metalloproteinase inhibitor TIMP-1. While gene expression for transforming growth factor (TGFβ1) increased linearly with severity of damage in all studied eyes, gene expression for TGFβ2 was lowest in the focally damaged eyes suggesting differential expression of TGFβ isoforms at this early stage of the neuropathy. Similar to TGFβ2, gene expression for the principal water channel protein in astrocytes, aquaporin-4, demonstrated the largest degree of downregulation in focal damage. Most importantly, Johnson and co-workers characterized gene expression patterns in a group of 2-week optic nerve transection eyes and found a pattern of expression similar to the most severely damaged high IOP eyes, suggesting that the changes in gene expression in the focal group were likely IOP-related, not simply a reflection of early axonal loss.

Alterations in Connective Tissue Architecture, Cellular Activity, Axoplasmic Transport, and Blood Flow in Later Stages of Glaucomatous Damage

The classic descriptions of profound laminar deformation, excavation of the scleral canal beneath the optic disk margin, compression, and increased rigidity of the lamina are largely based upon human and monkey eyes with moderate, severe, and end-stage glaucomatous damage. Because these studies describe a broad range of damage that has occurred in response to an IOP insult that is uncharacterized in magnitude and duration, a common description of events has yet to emerge. However, astrocyte basement membrane disruption and thickening as well as damage to elastin, physical disruption of the laminar beams, and remodeling of the ECM are consistent phenomenon within these reports. It is assumed that IOP-induced alterations in the synthetic activities of the cells associated with these tissues underlie these changes.

Within the more severely damaged eyes in Johnson's study (above), expression of genes governing initiation of cell division was also elevated (compared to normals) but to a lesser degree than in eyes with focal damage. Genes associated with activation of microglia, immune response, ribosomes, and lysosomes were all linearly elevated in the more severely damaged eyes. Genes for the ECM components including fibulin 2, tenascin C, and the matrix metalloproteinase inhibitor TIMP-1 were elevated nonlinearly (most elevated in early damage, elevated less in more severe), whereas genes for periostin, collagen IV,

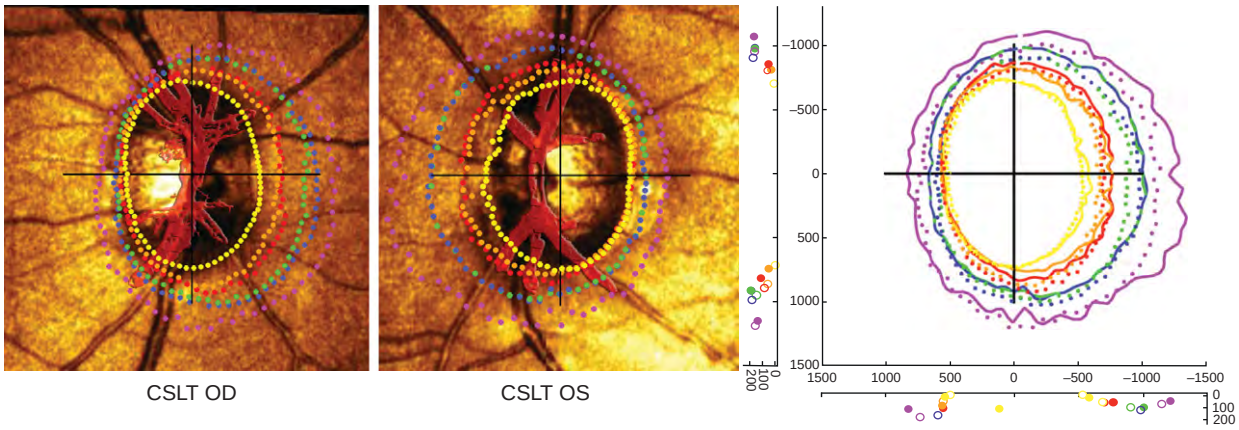

Figure 17 (left and middle) Our method of 3D reconstruction and delineation (**Figure 8**) includes the central retinal vessels, which allows clinical alignment of the delineated point clouds to clinical images and demonstrates the anatomic expansion of the neural canal under the clinically visible disc margin. Here just the Neural Canal landmark points are three-dimensionally overlaid onto Heidelberg Retinal Tomograph images of the normal (OD, left) and early experimental glaucoma (OS, middle) eye of a monkey. Note that the clinically visible disk margin in these eyes has been histomorphometrically determined to be BMO (yellow dots) in both eyes. Note also that the neural canal is not the size of the clinical visible disk margin, but rather it enlarges dramatically as it passes through the sclera. Because the data are digital, the left eye data can be converted to right eye orientation and overlaid onto the right eye data as shown in (right). Here the early glaucoma (solid line) and normal (dotted line) eye data can be directly compared. Note that expansion of the neural canal is present at the onset of early glaucomatous damage in the monkey eye and is greatest in the posterior aspects of the canal.

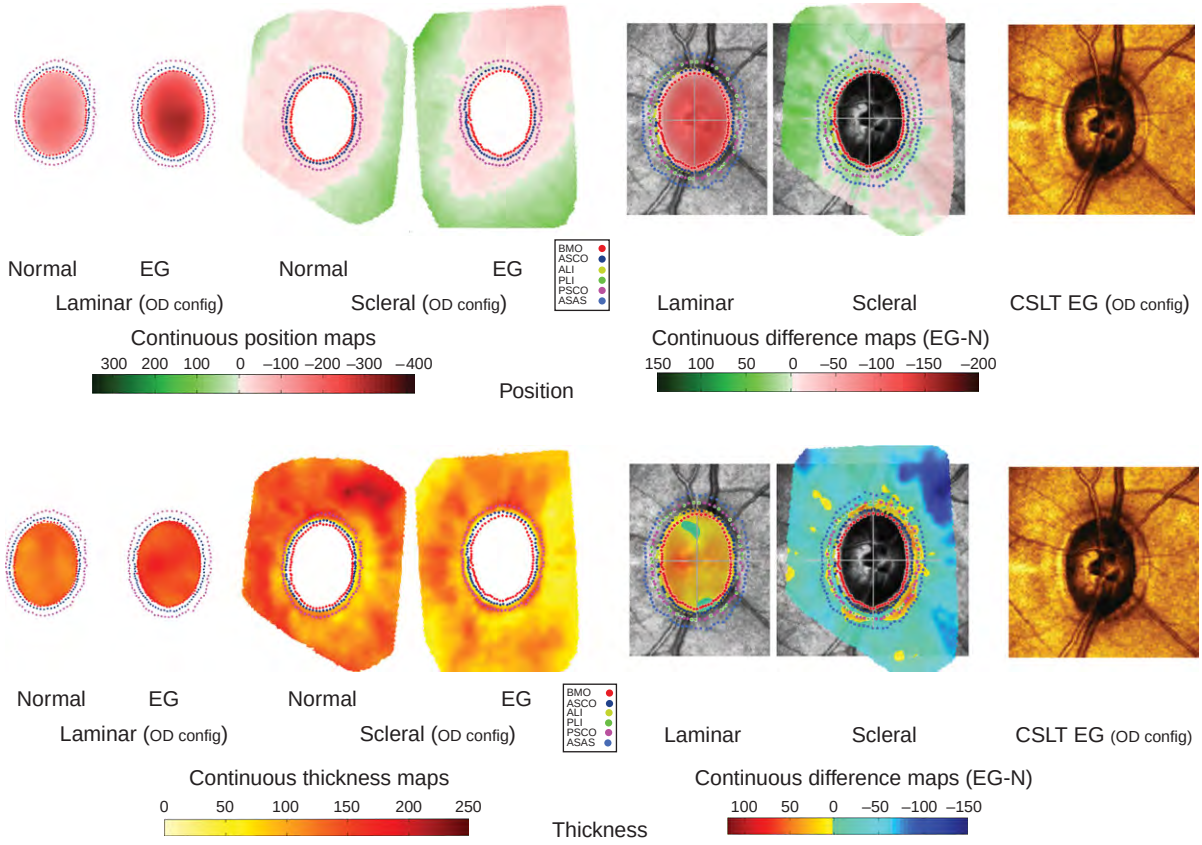

Figure 18 3D histomorphometric maps of laminar and peripapillary scleral position and thickness demonstrate profound permanent posterior deformation of the lamina cribrosa and peripapillary sclera and thickening of the lamina cribrosa in the early glaucoma eye of one monkey. Laminar and peripapillary scleral position (above) and thickness (below) are co-localized with the neural canal landmark points for both the normal and early glaucoma eyes of one monkey (left four columns). Early glaucoma eye difference maps for each parameter are shown in the first two columns to the right, followed by a Confocal Scanning Laser Tomograph image of the early glaucoma eye prior to sacrifice for orientation. These maps are typical for early glaucomatous changes in the monkey eye and demonstrate the permanent posterior deformation of the lamina and immediate peripapillary sclera, as well as the marked thickening of the lamina in the glaucoma eye compared to its contralateral control.

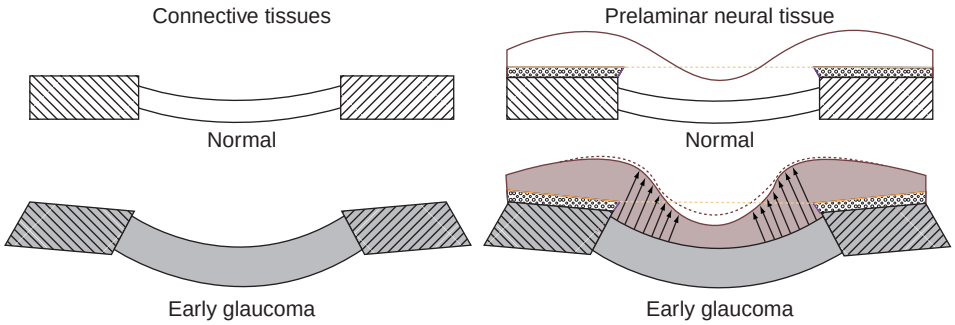

Figure 19 Remodeling and restructuring of the ONH in early experimental glaucoma. Sagittal section diagrams of the ONH, showing the peripapillary sclera (hatched) and the lamina cribrosa for normal and early glaucoma eyes. (left) The early glaucoma eye has undergone permanent changes in ONH geometry, including thickening of the lamina, posterior deformation of the lamina and peripapillary sclera, and posterior scleral canal expansion. (Right) Recent work has also shown that although the cup deepens relative to Bruch's membrane opening (dotted orange line) as can be detected by longitudinal confocal scanning laser tomography imaging (orange line) in early glaucoma, the prelaminar neural tissues (gray) are actually thickened rather than thinned. Reprinted with permission from Hongli Yang.

and collagen VI were elevated linearly. Differential gene expression for TGFβ1 and TGFβ2, as well as nonlinear expression of aquaporin are described above.

Axoplasmic transport alterations at the lamina cribrosa and a complicated array of ONH, retinal and choroidal blood flow alterations have been described following chronic IOP elevation in monkey and human eyes. However, direct observation of ONH blood flow at the level of the peripapillary sclera and lamina cribrosa capillaries is not yet possible either experimentally or clinically. We thus lack the ability to study primary interactions between IOP and non-IOP-induced alterations in ONH blood flow, ONH connective tissue integrity, ONH glial cell activity, and RGC axonal transport within individual human and animal eyes.

Integrins are mechanotransduction proteins that span the laminar astrocyte and capillary endothelial cell basement membranes to bind to ligands in the ECM and interact with the cell cytoskeleton. Morrison has described the location and alteration of integrin subunits in normal and glaucomatous human and monkey eyes and proposed them as an important link between laminar deformation and damage, laminar connective tissue remodeling, and laminar astrocyte mediated axonal insult in glaucoma.

Biomechanical Manipulation of ONH and Peripapillary Scleral Cells in Culture

Laminar astrocytes have been shown to respond to changes in hydrostatic or barometric pressure. However, the uncertain role of hypoxia and lack of astrocyte basement membrane deformation in the barometric pressure model has led to genomic and biochemical characterization of ONH astrocytes exposed to controlled levels of strain. At present, these strain-based techniques are in their infancy and a consistent stimulation cycle and pattern of gene and protein expression has yet to emerge. Eventually, strain predictions from FE models and data on IOP fluctuation from telemetric IOP monitoring studies will allow these experiments to more closely model physiologic/pathophysiologic conditions in the normal and glaucomatous human and animal eye.

Future Directions

Clinical Implications

There are currently no science-based tools to predict at what level of IOP an individual ONH will be damaged. As described herein, FE modeling is a computational tool for predicting how a biological tissue of complicated geometry and material properties will behave under varying levels of load. The goal of basic research FE modeling in monkey and human cadaver eyes is to learn what aspects of ONH neural, vascular, and connective tissue architecture are most important to the ability of a given ONH to maintain structural integrity, nutritional and oxygen supply, and axoplasmic transport at physiologic and nonphysiologic levels of IOP. In the future, clinical imaging of the ONH will seek to capture the architecture of these structures so as to allow clinically derived biomechanical models of individual patient ONHs to make predictions regarding physiologic and pathophysiologic levels of IOP. Eventually knowing the relationship between IOP, mechanical strain, systemic blood pressure, and the resultant astrocyte and axonal mitochondrial oxygen levels will drive the clinical assessment of safe target IOP. Clinical characterization of the actual IOP insult through telemetric IOP monitoring will eventually allow better-controlled studies of ONH directed neuroprotection. Finally, these FE modeling-driven targets for deep (subsurface) ONH imaging will likely allow early detection of lamina cribrosa deformation and thickening. Once clinically

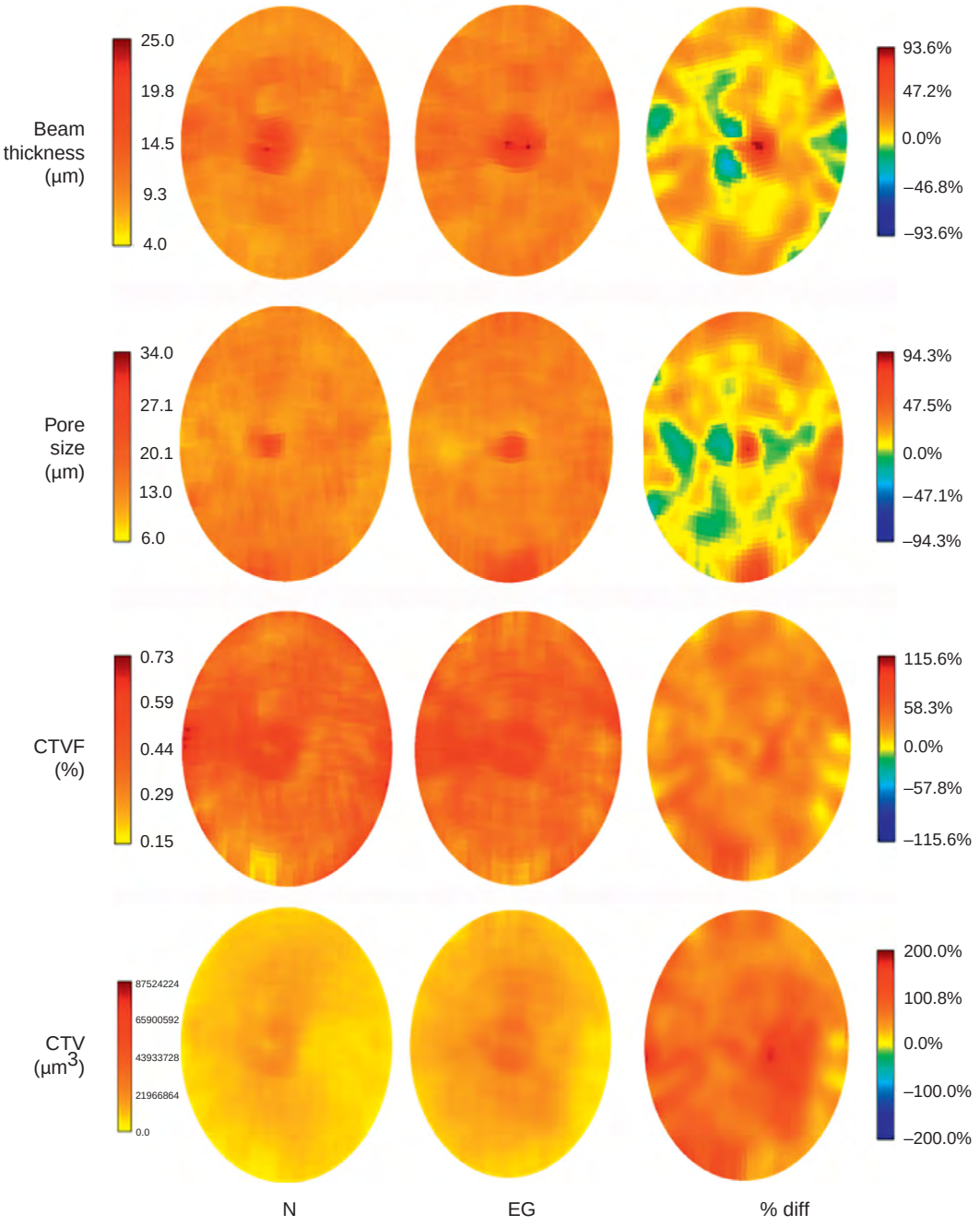

Figure 20 3D histomorphometric maps of laminar microarchitecture in paired and normal and early glaucoma eyes for three monkeys (left and center). Maps of laminar beam thickness, pore size, connective tissue volume fraction (CTVF), and connective tissue volume (CTV) for contralateral normal and early glaucoma eyes of a monkey derived from the same 3D reconstruction technique described in Figure 8. (Right) The differences between the normal and early glaucoma eyes for each parameter are mapped as a percentage. Note that CTVF is ratio of laminar connective tissue volume to total tissue volume in each regional sample. In early glaucoma, the CTVF and total laminar connective tissue volume increase significantly in all regions, and laminar beam thickness and pore size increase in most regions but decrease in others. These results together indicate that the increase in laminar thickness described in Figure 18 in early experimental glaucoma, is due not just to axonal swelling or tissue edema, but also contains a very substantial component of laminar connective tissue synthesis.

detectable, early stabilization, and perhaps reversal, of these laminar changes will become a new end point for target IOP lowering in most ocular hypertensive and all progressing eyes.

Basic Research Directions

From an engineering standpoint, large challenges remain to achieve basic and clinical knowledge regarding: (1) the mechanisms and distributions of IOP-related yield and

failure in the laminar beams and peripapillary sclera; (2) the mechanobiology of the astrocytes, scleral fibroblasts, and lamina cribrosa, and glial cells; (3) the mechanobiology of axoplasmic flow and within the lamina cribrosa; (4) the fluid dynamics governing the volume flow of blood within the laminar capillaries and scleral and laminar branches of the posterior ciliary arteries; and (5) nutrient diffusion to the astrocytes in young and aged eyes. We predict that knowledge gained from these studies will importantly contribute to new therapeutic interventions aimed at the ONH and peripapillary sclera of glaucomatous eyes.

See also: Animal Models of Glaucoma; Intraocular Pressure and Damage of Optic Nerve Axons; Primary Open-Angle Glaucoma; Retinal Ganglion Cell Apoptosis and Neuroprotection.

Further Reading

Albon, J., Purslow, P. P., Karwatowski, W. S., and Easty, D. L. (2000). Age-related compliance of the lamina cribrosa in human eyes. *British Journal of Ophthalmology* 84: 318–323.

Burgoyne, C. F. and Downs, J. C. (2008). Premise and prediction – how optic nerve head biomechanics underlies the susceptibility and clinical behavior of the aged optic nerve head. *Journal of Glaucoma* 17(8): 318–328.

Burgoyne, C. F., Downs, J. C., Bellezza, A. J., Suh, J. K.-F., and Hart, R. T. (2005). The optic nerve head as a biomechanical structure: A new paradigm for understanding the role of IOP-related stress and strain in the pathophysiology of glaucomatous optic nerve head damage. *Progress in Retinal and Eye Research* 24: 39–73.

Clark, A. F., Browder, S. L., Steely, H. T., et al. (1995). Cell biology of the human lamina cribrosa. In: Drance, S. M. and Anderson, D. R. (eds.) *Optic Nerve in Glaucoma*, pp. 79–105. Amsterdam: Kugler Publications.

Downs, J. C., Roberts, M. D., and Burgoyne, C. F. (2008). The mechanical environment of the optic nerve head in glaucoma. *Optometry and Vision Science* 85(6): 425–435.

Geijer, C. and Bill, A. (1979). Effects of raised intraocular pressure on retinal, prelaminar, laminar, and retrolaminar optic nerve blood flow in monkeys. *Investigative Ophthalmology and Visual Science* 18: 1030–1042.

Girard, M. J. A., Suh, J.-K. F., Bottlang, M., Burgoyne, C. F., and Downs, J. C. (2009). Scleral biomechanics in the aging monkey eye. *Investigative Ophthalmology and Visual Science* 50: 5226–5237.

Hernandez, M. R., Andrzejewska, W. M., and Neufeld, A. H. (1990). Changes in the extracellular matrix of the human optic nerve head in primary open-angle glaucoma. *American Journal of Ophthalmology* 109: 180–188.

Kirwan, R. P., Fenerty, C. H., Crean, J., et al. (2005). Influence of cyclical mechanical strain on extracellular matrix gene expression in human lamina cribrosa cells *in vitro*. *Molecular Vision* 11: 798–810.

Morrison, J. C. (2006). Integrins in the optic nerve head: potential roles in glaucomatous optic neuropathy (an American Ophthalmological Society thesis). *Transactions of the American Ophthalmological Society* 104: 453–477.

Quigley, H. and Anderson, D. R. (1976). The dynamics and location of axonal transport blockade by acute intraocular pressure elevation in primate optic nerve. *Investigative Ophthalmology and Visual Science* 15: 606–616.

Roberts, M. D., Grau, V., Grimm, J., et al. (2009). Remodeling of the connective tissue microarchitecture of the lamina cribrosa in early experimental glaucoma. *Investigative Ophthalmology and Visual Science* 50(2): 681–690.

Sigal, I. A., Flanagan, J. G., and Ethier, C. R. (2005). Factors influencing optic nerve head biomechanics. *Investigative Ophthalmology and Visual Science* 46: 4189–4199.

Sigal, I. A., Roberts, M. D., Girard, M., Burgoyne, C. F., and Downs, J. C. (2009). Biomechanical changes of the optic disk. In: Levin, L. A. and Albert, D. M. (eds.) *Ocular Disease: Mechanisms and Management,* 1st edn., ch. 20. London: Elsevier.

Yang, H., Downs, J. C., Girkin, C. A., et al. (2007). 3-D histomorphometry of the normal and early glaucomatous monkey optic nerve head: Lamina cribrosa and peripapillary scleral position and thickness. *Investigative Ophthalmology and Visual Science* 48: 4597–4607.

Blinking Mechanisms

C W McMonnies, University of New South Wales, Kensington, NSW, Australia

Glossary

Blepharospasm – The eye closure due to an uncontrolled contraction of the orbicularis muscle.
Goblet cell – A mucus-secreting epithelial cell found in the conjunctiva.
Levator palpebrae superioris – An eye opening muscle of the upper lid.
Meibomian glands – The specialist sebaceous glands opening onto the lid margin, and producing an oily sebum that reduces tear evaporation.
Orbicularis muscle – An eye-closing sphincter-like sheet of muscle of the lids that encircles the palpebral fissure.
Punctate keratopathy – The fine gray-white microdot opacities of the corneal epithelium that may require disclosure with sodium fluorescein stain and ultraviolet light examination.
Tear meniscus: lacrimal rivus – The concave strip of tears at the junction of the lid margin and ocular surface.

A blink is a brief eye closure, normally involving contraction of the palpebral portion of the orbicularis muscle in the closing phase, and the levator palpebral superioris in the opening phase. Most blinks are regular and spontaneous, occurring without any apparent external stimulation. However, spontaneous blinks may be spontaneous only in the sense that the stimulus is not readily apparent. For example, any sensation of tear evaporation from the corneal surface, or the associated loss of temperature, may be a stimulus for apparently spontaneous blinks. Strong, reflex, and most voluntary blinks involve the additional contraction of the orbital portion of the orbicularis muscle. The average time for a blink is about 0.25 s, with the closure phase about twice as fast as the opening phase. Blink velocity varies between individuals and for the same individual, depending on the type of blink. Reflex blinks take less time with, again, closure being much faster than opening. Reflex blinks may occur defensively when the eyes are exposed to real or perceived risk of injury. Strong lights, the sudden approach of an object toward the eyes, and loud noises are common stimuli for reflex blinks. For example, reflex blinks are a response to the irritation caused by a foreign body and, together with reflex lacrimation, will help to displace the irritant particles toward the nasal canthus. Blepharospasm involves strong eye closure, with the action of the orbicularis muscle being supplemented by the muscles of the eyebrow. Blepharospasm can accompany anterior segment diseases, especially those involving the cornea and pain sensations. Repetitive nonrhythmic involuntary blinks can occur as a tic or as a compulsive behavior in an obsessive compulsive disorder. A similar involuntary series of blinks can become an affectation that, for example, accompanies an attentive listening pose, or as part of an assumed pose of concern. High-speed recordings of the blink mechanism were developed by Marshal Doane, PhD, Schepens Eye Research Institute, Boston, MA. They show how the upper lid action is like a windshield wiper. However, the lower lid can be seen to make a horizontal movement of 2–5 mm toward the nose. In the case of a complete blink, and full contact of the lid margins, the lower lid tends to carry the top lid nasally. Doane's recordings show that there is no Bell's phenomenon (upward eye rotation) with normal blinks, only with forced blinks.

Inter- and Intrasubject Variations in Blink Rate

A review of studies that examined blink rates in human subjects indicated a range of mean blink rates between 10 and 22 blinks per minute. Apart from differences in the criteria used to select subjects for inclusion in these studies, the disparities between them demonstrate how blink rate is also dependent on varying experimental conditions for measurement. The nature of the visual task involved is a major factor. For example, blink rate during computer use was found to be four blinks per minute, only 20% of the rate recorded for the same subjects during a period of general conversation. Another group was found to record an average of eight blinks per minute while reading and 21 blinks per minute while engaged in general conversation. Blink rate has been found to reduce significantly as task difficulty increased from watching a film, to reading, and to counting the number of times the letter a appeared in a sample of reading material. These results are consistent with the finding that there is a tendency for nonblink periods to be sustained, until difficult target recognition tasks are completed. The results support the presence of a mechanism for inhibiting spontaneous blinks. The precentral gyrus appears to be responsible for both voluntary and inhibited blinking, but the parietal area appears to be exclusively related to blink inhibition. However, apart

from intrasubject blink rate variation, according to visual task demands, for example, there is also a large range of intersubject blink rate variation. For the same experimental conditions of watching an educational film, the blink rate for 20 subjects varied between 6 and 30 blinks per minute. Ambient humidity, air quality, presence of draughts, visual fatigue, general fatigue, interest in the film's subject matter, and many other factors, may contribute to variations in blink rate.

Benefits of Complete Blinks

The blinking mechanism makes a crucial contribution to the health of the ocular surface and to many eye and vision functions. Mechanical protection is provided for the delicate eye tissues, for example, when the lids close rapidly and repeatedly in response to a gust of wind and dust foreign bodies. Blinking is also a protective mechanism for the cornea and conjunctiva, by serving to maintain a tear layer over the ocular surface. The tear layer is necessary for epithelial health and optical performance. Complete blinks help to maintain a clean and wet anterior surface. These blinks cause debris to be swept into the inferior marginal tear strip, allowing a cleaner tear layer to be distributed as the upper lid ascends. Complete blinks maximize the extent of distribution of tarsal goblet cell mucin. The normal apposition of the lids during a complete blink is a means of promoting lipid secretion from meibomian glands. Forceful blinking can significantly increase lipid-layer thickness, provided the meibomian glands have adequate reservoirs of secretion, and the gland orifices are not blocked with clusters of keratotic cells. The lipid layer is spread across the cornea by the upper lid and incomplete blinking, or a reduced blink rate, may be associated with poor maintenance of lipid-layer integrity. For example, during prolonged reading, when blink rate is significantly reduced, the lipid layer can disappear and then reappear with conscious blinking. Apart from a critical multifaceted role in maintaining tear function and ocular surface health, efficient complete blinks also contribute to the comfort and vision performance of contact lenses.

Consequences of Incomplete Blinking

For a sample of normal subjects, under experimental conditions of watching an educational film, incomplete blinks were found, on average, to represent 10% of the total number. In another group of normal subjects, the rate of incomplete blinking for an unspecified vision task was 20% of the total. Apart from variations in experimental methods and sampling, the frequency of incomplete blinks will depend on the criteria for distinguishing between normal and incomplete blinks. For example, high-speed records of blinking performance indicate that most blinks are not fully complete, in the sense of full apposition of top and bottom lid margins at the point of maximum closure. However, the distinction between incomplete, partial, and twitch blinks does not appear to have been specified. Incomplete blinks appear to have occurred immediately prior to the photographs shown in **Figures 1(a)–1(c)** and **2(b)**. However, as is the case for overall blink rate, incomplete blink rates may vary widely between individuals. Incomplete blink rates may also vary for the same individual according to the ambient conditions and the state of fatigue and/or mental alertness, for instance, as well as the difficulty of the vision task involved. An incomplete blink may be the result of partial or unsuccessful inhibition of a spontaneous blink. Thus, visually and/or intellectually demanding tasks may be associated with higher-than-normal rates of incomplete blinking as well as reduced rates of all types of blinking. Fluorophotometry assessment shows that, following complete closure with a normal blink, tear layer thickness reduces over the inferior cornea. This phenomenon appears to be due to the spreading of tears as the top lid rises.

Evaporation can also substantially reduce tear film thickness, especially over the exposed (inferior) cornea. (**Figures 1(a)–1(b)** and **2(b)**). Evaporation is associated with long interblink intervals as well as incomplete blinking. Significant tear evaporation and breakup problems appear to be more likely to occur in regions of a deficient lipid layer. Close apposition of the lid margins during a complete blink may involve the combination of the tear meniscus of the upper and lower lids, providing a larger volume of tears for distribution over the cornea by the ascending upper lid. In contrast, an incomplete blink is only able to redistribute the tears of the upper lid tear meniscus and the superior cornea during the upper lid ascending phase. The bands of thinned tear layer, evident in **Figures 1(a)–1(b)** and **2(b)**, appear to have been created as the upper lid tear meniscus reforms during an incomplete blink. Assuming that the concave tear meniscus at the margin of the upper lid is deformed by any tears collected and pushed downward during the blink descending phase, reformation of the concave meniscus appears to draw fluid upward as the blink ascending phase commences. Thus, tear thinning inferiorly may sometimes be a consequence of an incomplete blink sequence. Loss of tear layer thickness inferiorly, possibly to critical levels, also appears to be at least partly due to longer evaporative interblink periods for the inferior cornea which are associated with an incomplete blink. In the case of a blink rate of $12\,\text{min}^{-1}$, (average interblink interval of 5 s) an incomplete blink creates an interblink interval of approximately 10 s for the corneal, conjunctival, and/or contact lens surface areas, which are exposed by the lack of

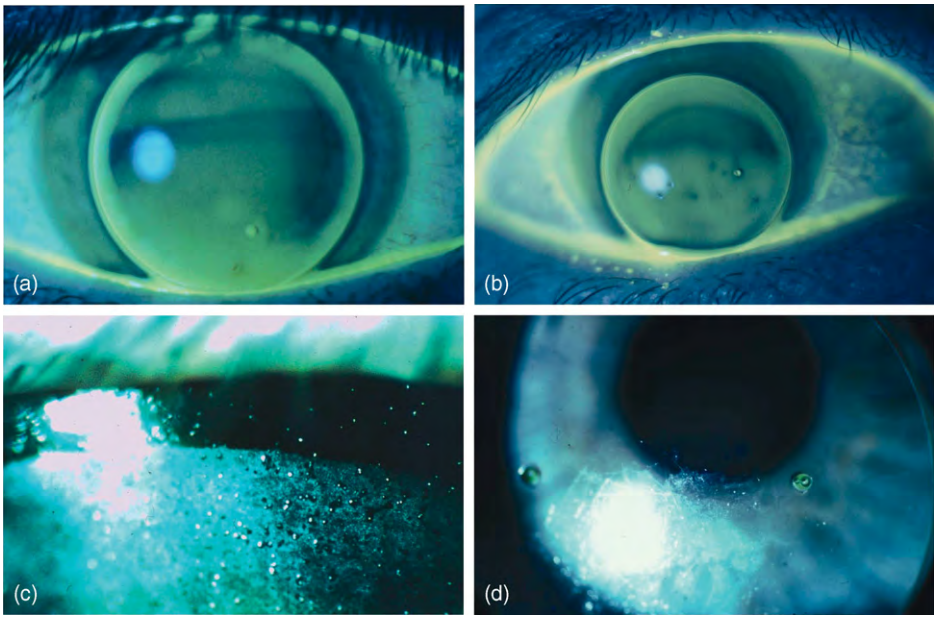

Figure 1 Reading clockwise from top left: (a) Top left: The band of thinned tear layer provides evidence of an incomplete blink prior to this photograph. (b) Top right: Downward lens displacement and tear breakup on the inferior lens surface following an incomplete blink. (c) Bottom right: An incomplete twitch blink appears to have occurred prior to this photograph of a rapidly drying lens surface.(d) Bottom left: Deposits that are restricted to the inferior contact lens surface on nonrotating (e.g., prism ballast) lenses appear to be due to incomplete blink habits. Reproduced from McMonnies, C. W. (2007). Incomplete blinking: Exposure keratopathy, lid wiper epitheliopathy, dry eye, refractive surgery, and dry contact lenses. *Contact Lens and Anterior Eye* 30: 37–51, with permission from the British Contact Lens Association.

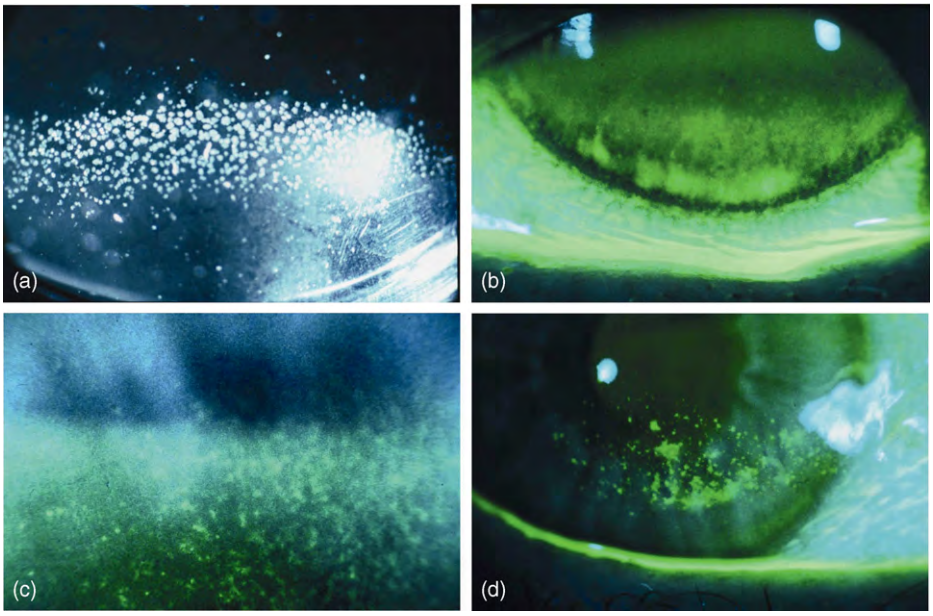

Figure 2 Reading clockwise from top left: (a) Top left: For a nonrotating (e.g., prism ballast) lens designs, a horizontal band of mid-peripheral deposits suggests that incomplete blinking, and associated tear thinning and evaporation, can play a crucial role in deposit precipitation. (b) Top right: The band of thinner tears immediately above the stained exposure keratopathy appears to define the limit of downward excursion of the top lid for the blink immediately prior to this photograph. The keratopathy below the thinned tear layer suggests that this type of incomplete blink is common. (c) Bottom right: Punctate inferior corneal epithelial keratopathy that developed with soft lens wear without symptoms and appears to indicate a high rate of incomplete blinking in association with intensive (proof) reading. (d) Bottom left: A causal role for incomplete blinking is suggested by exposure keratopathy that occurs following a laser-assisted keratomileusis procedure, especially when the keratopathy involves the normally innervated region outside the flap. Reproduced from McMonnies, C. W. (2007). Incomplete blinking: Exposure keratopathy, lid wiper epitheliopathy, dry eye, refractive surgery, and dry contact lenses. *Contact Lens and Anterior Eye* 30: 37–51, with permission from the British Contact Lens Association.

completeness. When the blink rate is reduced to 8 min^{-1} while reading, for example, the average interblink interval is 7.5 s and an incomplete blink increases the interblink interval for the exposed cornea, conjunctiva, or contact lens surface to approximately 15 s. However, when the blink rate is only 4 min^{-1} (e.g., during computer use), and the average interblink interval is 15 s, an incomplete blink creates an interblink interval of approximately 30 s for the exposed cornea, conjunctiva, or contact lens surface.

It is a well-known clinical phenomenon that desiccation occurs in the exposed cornea (**Figures 2(b)–2(d)**) in consistent partial blinkers. For example, incomplete blinking for subjects with superficial inferior punctate keratopathy was found to represent 90% of the total number of blinks. This finding raises the question as to what extent do incomplete blinking habits contribute to the development of inferior punctate keratopathy, and to what extent are they also partly a consequence of the epitheliopathy, and any associated symptoms. If symptoms of inferior punctate keratopathy irritation occur with blinking, blinking may be inhibited and/or the rate of incomplete blinks may increase. However, when the superior cornea is normal, and inferior punctate keratopathy is symptomless (**Figures 2(c)** and **2(d)**), the incomplete blinking rate, which appears to have contributed to the development of the keratopathy, does not appear to have been provoked by irritation. For example, **Figure 2(c)** shows inferior punctate keratopathy that developed without symptoms under a soft contact lens in association with a period of intensive proofreading.

To the extent that lipid secretion depends on lid margin contact, incomplete blinking appears likely to contribute to lipid-layer deficiencies. Incomplete blinking will not express the meibomian glands or reform those portions of the lipid layer that are not wiped by the blinks; the tear layer over the unwiped areas of cornea will continue to thin until re-wiped by a subsequent complete blink.

The classical view of tear film structure is that of an aqueous layer sandwiched between a very thin layer of mucus bound to the corneal epithelium, and a lipid layer. A review of the mucous contribution to tear film structure indicated that the classical aqueous layer is really an aqueous/mucous gel. The concentration of the mucous component reduces toward the lipid layer, from a maximum at the epithelial surface. Apart from the possibility of deficient meibomian gland secretion, and inadequate lipid spreading, incomplete blinking results in reduced opportunities for the tarsal goblet cells to contribute to the integrity of the mucin layer of the exposed cornea. In **Figure 2(b)**, the bottom of the zone of thinner tears, immediately above the stained exposure keratopathy, appears to have been the limit of downward excursion of the top lid for the blink immediately prior to this photograph. The relative normality of the epithelium (freedom from staining), in the zone above the exposure keratopathy, raises the possibility that tear thinning alone may not be a sufficient basis for keratopathy to develop. For example, reduced delivery of tarsal goblet cell mucin to the exposed area may be a more important factor for the development of keratopathy than a thinned tear layer.

Conjunctival stain is increased in symptomatic patients with both sodium fluorescein and lissamine green stains being discriminating factors for symptomatic noncontact lens wearers. However, only lissamine green staining could discriminate symptomatic from asymptomatic soft lens wearers. These findings suggest that the exposed conjunctiva may also be disadvantaged by incomplete blinking. It is assumed that deposits are more easily precipitated on a contact lens anterior surface when the pre-lens tear layer thins or evaporates, and leads to a concentration of tear constituents. In the case of nonrotating lens designs (e.g., prism ballast toric lenses), a horizontal band of deposits (**Figure 2(a)**) suggests that incomplete blinking can play a crucial role in deposition. It appears that incomplete blinks may thin the tear layer in the region of the deposit as well as allow the tear film over that area to evaporate, per medium of longer interblink intervals. It is presumed that regular surface re-wetting inhibits deposition over the superior portion of the lens in **Figure 2(a)**. The lower lid margin tear meniscus appears to have kept the lower region free of significant deposits by preventing tear layer thinning and evaporation (**Figure 2(a)**). Similar deposits appear unlikely to be as evident for the same patient wearing a lens design that is free to rotate and assume different meridional positions on the eye from day to day. In this case the deposits could be precipitated, but because they are distributed over 360° of the lens mid-periphery, the band of deposit would not develop, and the patient's incomplete blinking habits may not be as apparent. Incomplete blinking is frequently observed during a biomicroscopy examination (**Figures 1(a)–1(c)**) with patients having to be instructed to blink completely, in order that a clearer view of the cornea through a contact lens can be achieved.

Lid Wiper Epitheliopathy Mechanisms and Symptoms

A comparison of sodium fluorescein and rose Bengal staining of the marginal conjunctiva of the upper lid, that wipes the ocular and/or contact lens surface during a blink (lid wiper), was made between symptomatic dry eye patients and asymptomatic controls. Patients with dry eye symptoms (without corneal stain) were found to have lid wiper stain in 76% of cases, compared with 12% for the asymptomatic controls. Inadequate lubrication at the lid wiper–ocular surface interface with a concomitant increase in the frictional coefficient, and an increase in the potential damage to either, or both of these ocular surfaces, appears to be applicable in the case of lid

wiper epitheliopathy. Exposure keratopathy may result in increased friction between an abnormal epithelium of the lid wiper and the desiccated inferior cornea (**Figures 2(b)** and **2(d)**). This frictional increase may be greatest for the complete blink that follows an incomplete blink, because the tear layer over the desiccated exposed cornea may be thinnest, and its lubricant properties most deficient, at the end of the prolonged interblink interval that is associated with an incomplete blink. Consequently, the risk of mechanical trauma to the lid wiper epithelium appears to be significantly higher following an incomplete blink.

Lid wiper epitheliopathy may be difficult to treat and improved blink efficiency, which is achieved through a reduction in the rate of incomplete blinking, may be an important component of management. Lid wiper epitheliopathy was evident for 74% of ocular irritation symptomatic contact lens wearers, and 16% of an asymptomatic contact-lens-wearing control group. The prime sensory mechanism for lens awareness, or discomfort associated with an undamaged and well-fitted soft lens, appears to be the blink-related action of the lid wiper over the contact lens surface. The contrast in lubrication for the rewet and dry contact lens surface areas shown in **Figure 1(c)**), and the deposits in **Figure 2(a)**, indicates how lid wiper sensation and trauma may be associated with dry and/or harsh surfaces. Lack of wetness of the soft lens front surface (**Figure 1(c)**), and associated symptoms of dryness, may be an important factor in increasing or decreasing the overall blink rate, as well as the incomplete blink rate. For example, contact lens discomfort has been reported to have the effect of reducing the completeness and rate of blinking, so that awareness of lens dryness (and associated discomfort), that is detected by the lid wiper during a blink, may be a stimulus to reduced blink rate and/or incomplete blinks. Alternatively, awareness of lens dryness may be a stimulus to reflex tearing and blinking. However, the high frequency of dryness symptoms in soft contact lens wear suggests that awareness of a dry lens that is detected by the lid wiper, and any associated increased reflex aqueous production and blinking, is not usually an adequate stimulus for the significant relief of dryness symptoms.

Reflex tear production may be poorly sustained over long periods of dryness symptoms. In addition, any reflex tears may be diluted with respect to lipids and dissolved protein, for example, and their lubricant performance may be reduced accordingly. An association between lid wiper epitheliopathy, and symptoms, suggests the possibility of a lowered threshold for lid wiper sensation in dry eye and dry contact lens conditions. Loss of superficial epithelium from a traumatized lid wiper may expose nerve endings and increase sensitivity. Conversely, the occasional observation that some patients are able to wear contact lenses that are very soiled and/or unwet, without apparent discomfort, suggests that such patients have high thresholds for lid wiper sensation. It is possible that the lid wiper in these cases has become toughened, and desensitized, through the development of an increased epithelial thickness, including an increased density of keratinized cells.

Indications for Blink Efficiency Exercises

Exposure keratopathy may be successfully managed if efficient (complete) blinking habits can be developed, or restored, to help reestablish healthy corneal, conjunctival, and lid wiper epithelia. Improved regularity of complete blinks may contribute to reduced tear thinning and evaporation rates by improving mucin, lipid, and aqueous distribution. Accordingly, there may be the possibility of avoiding tissue changes and symptoms that result from tear evaporation and hyperosmolarity, as well as drying that increases friction between lid wiper and the ocular surface. Similarly, improved blink efficiency may help to maintain a wet and clean contact lens surface, with a concomitant reduction in friction-related trauma to the lid wiper, and any associated symptoms. Blink efficiency exercises should not be introduced into patient care without consideration of other aspects of dry eye and dry contact lens management. For example, patients with exposure keratopathy in association with incomplete blinking can benefit from tear substitutes in addition to improved blink efficiency. However, signs of exposure keratopathy may not be accompanied by symptoms. For example, post-laser-assisted *in situ* keratomileusis (LASIK) exposure keratopathy may be symptomless (**Figure 2(d)**). In addition, the keratopathy shown in **Figure 2(c)**, developed during soft lens wear and periods of intensive proofreading, in the absence of any symptoms. Nevertheless, these types of findings are an indication for blink efficiency exercises and tear substitutes, as well as representing a contraindication to extended contact lens wear, in particular, if they cannot be managed successfully.

The findings that chronic dry eye conditions increased the risk for refractive regression after LASIK, and that ocular surface management minimized the impact of LASIK on goblet cell density reduction and dry eye symptoms, suggest the possibility that blink efficiency exercises may also have a beneficial role for refractive surgery outcomes (even when symptoms are absent). Wound healing and refractive outcomes may be enhanced. Given prophylactically, ocular surface management that includes blink efficiency exercises may also serve to allow some patients to present for surgery with an improved prognosis for optimum refractive outcomes. Indications for blink efficiency exercises based on signs without symptoms may be more difficult to manage if patient

motivation to follow remedial recommendations is lacking. Conversely, the presence of symptoms may provide the basis for increased patient compliance with remedial blink efficiency instructions.

Post-LASIK symptoms are often reported in the absence of exposure keratopathy. Similarly, contact lens wear is often associated with symptoms without signs of exposure keratopathy. In some post-LASIK cases, and for some contact lens wearers, exposure keratopathy and/or lid wiper epitheliopathy may repair overnight and then return during the day following exposure to provocative conditions. For example, these provocative conditions may involve incomplete blinking that is associated with central heating, air-conditioning, computer use, reading, and other visually demanding tasks. An assessment in the early part of the day may not detect exposure keratopathy and/or lid wiper epitheliopathy, or may underestimate the significance of these findings. Similarly, contact lens soiling and unwetting that increases during the day may not be apparent at an assessment during the early part of the day.

Lubricant Therapy: Incomplete Blink Habit Reversal; Optimizing Lid Wiper and Corneal Therapy

Lubricant drops can be rapidly diluted and eliminated from the ocular surface by reflex blinking and lacrimation that follow drop instillation. Exposure keratopathy may respond more favorably from increased blink rate and completeness during the short period of presumed maximum therapeutic potential, immediately after drop instillation. The same principles apply to the use of contact lens rewetting drops. At this critical opportunity, full complete blink exercises ensure the therapeutic drop components are distributed over the exposed ocular or contact lens surface. The emphasis during blink efficiency exercises is for voluntary blinking that is complete, relaxed, and rapid as well as natural in appearance. According to the principles of behavior modification and habit reversal, patient education is a key element of these forms of therapy. Motivation to improve blink efficiency depends on an awareness of the significance of the problems associated with incomplete blinking. Explaining the links between incomplete blinks, the drying of the inferior corneal and/or contact lens surfaces, and symptoms, is greatly facilitated by the use of clinical photographs (**Figures 1(a)–1(d)** and **2(c)**). These are included in the consulting room (take-home) Blink Instruction Guide (BIG). The provision of take-home written instructions, which include these clinical photographs, is intended to assist the development and maintenance of patient motivation required to achieve optimum results. Often drop instillation is inconvenient, but blink efficiency exercises can nevertheless be beneficial at these times. As indicated in the BIG instructions, in order that conscious (practice-session-related) efficient blinks to become spontaneous, practice sessions need to be frequent. The goal for patients should be to perform the exercises frequently enough in order that improved blink completeness habits are generalized across all conditions of spontaneous blinking. A patient who can understand how complete blinks are critical to the maintenance of a wet corneal or contact lens surface is in a position to appreciate negative reinforcement that derives from symptoms of dryness, as well as positive reinforcement from a symptom-free period following blink completeness practice. Symptoms of dryness may serve as a prompt for performing blink efficiency exercises. However, symptom prevention, by performing the exercises routinely, and prior to the onset of symptoms is preferred.

Conclusions

An efficient blink mechanism is critical to ocular surface health and satisfactory contact lens performance. Inefficient blinking may be associated with, for example, low blink rates and/or incomplete blinking. Corneal surgery outcomes may also depend, in part, on blink efficiency. The consequences of inefficient blinking may be complicated by, for example, exposure to air conditioning, central heating, and demanding visual tasks. Any form of dry eye disease may be exacerbated by inefficient blinking. Consequently, improved blink efficiency may contribute to the amelioration of any dry eye condition.

See also: Corneal Angiogenesis; Defense Mechanisms of Tears and Ocular Surface; Dry Eye: An Immune-Based Inflammation; Tear Film; Tear Film Overview.

Further Reading

Albietz, J. M., Lenton, L. M., and McLennan, S. G. (2004). Chronic dry eye and regression after laser *in situ* keratomileusis for myopia. *Journal of Cataract and Refractive Surgery* 30: 675–684.

Doane, M. G. and Gleason, W. J. (1991). Tear layer mechanics. In: Bennett, E. S. and Weissman, B. A. (eds.) *Clinical CL Practice, p. 9.* Philadelphia, PA: Lippincott.

Doughty, M. J. (2001). Consideration of three types of spontaneous eyeblink activity in normal humans: During reading and video display terminal use, in primary gaze, and while in conversation. *Optometry and Vision Science* 78: 712–725.

Guillon, M. and Maissa, C. (2005). Bulbar conjunctival staining in CL wearers and non-lens wearers and its association with symptomatology. *Contact Lens and Anterior Eye* 28: 67–73.

Korb, D. R., Craig, J. P., Doughty, M. J., et al. (2002). *The Tear Film: Structure, Function and Clinical Examination.* Oxford: Butterworth-Heinemann.

Korb, D. R., Herman, J. P., Greiner, J. V., et al. (2005). Lid wiper epitheliopathy and dry eye symptoms. *Eye and Contact Lens* 31: 2–8.

McMonnies, C. W. (2009). Behaviour modification in the management of chronic habits of abnormal eye rubbing. *Contact Lens and Anterior Eye* 32(2): 55–63.

Patel, S., Henderson, R., Bradley, B., et al. (1991). Effect of visual display unit use on blink rate and tear stability. *Optometry and Vision Science* 68: 888–892.

Sugar, A., Rapuano, C. J., Culbertson, W. W., et al. (2002). Laser *in situ* keratomileusis for myopia and astigmatism: Safety and efficacy. A report by the American Academy of Ophthalmology. *Ophthalmology* 109: 175–187.

Wilson, S. E. (2001). Laser *in situ* keratomileusis-induced (presumed) neurotrophic epitheliopathy. *Ophthalmology* 108: 1082–1087.

York, M., Ong, J., and Robbins, J. C. (1971). Variation in blink rate associated with CL wear and task difficulty. *Journal of Optometry and Archives of American Academy of Optometry* 48: 461–466.

Young, G. and Efron, N. (1991). Characteristics of the pre-lens tear film during hydrogel lens CL wear. *Ophthalmic and Physiological Optics* 11: 53–58.

Blood–Retinal Barrier

J Cunha-Vaz, AIBILI, Coimbra, Portugal

Glossary

iBRB – The inner blood–retinal barrier is a situation of restricted permeability established at the level of the retinal vessels, between the blood and retinal tissue, by the tight junctions (zonula occludents) between neighboring retinal endothelial vessels and the retinal endothelial cells themselves.
oBRB – The outer blood–retinal barrier is a situation of restricted permeability established at the level of the retinal pigment epithelium, the blood, and the retinal tissue, by the tight junctions (zonula occludents) between neighboring retinal pigment epithelial cells and the retinal pigment epithelial cells themselves.
Retinal leakage analyzer – A method developed to perform localized measurements of blood–retinal barrier fluorescein leakage using a confocal scanning laser ophthalmoscope modified to obtain fluorescence measurements in the vitreous.
Tight junctions – Tight junctions are specialized junctions uniting neighboring cells by fusion of the outer leaflets of their cell membranes (zonulae occludentes) thus obliterating the intercellular space fusion and restricting paracellular diffusion.
Uveitis – Uveitis is inflammation of the uvea, which is the vascular layer of the eye sandwiched between the retina and the sclera. The uvea extends toward the front of the eye and consists of the iris, choroid layer, and ciliary body.
Vitreous fluorometry – A method developed to measure the fluorescence resulting from the presence of fluorescein in the vitreous after intravenous administration. It is a direct indicator of the permeability of the blood–retinal barrier to fluorescein.

The entire eye must function as the organ for vision and is organized with two major goals: normal function of the visual cell and the need to maintain ideal optical conditions for the light to access the visual cells, located in the back of the eye.

The blood–ocular barriers play a fundamental role in the preservation and maintenance of the appropriate environment for optimal visual cell function (Figure 1).

The blood–ocular barriers include two main barrier systems: the blood–aqueous barrier and the blood–retinal barrier (BRB) (Figure 2), which are fundamental to keep the eye as a privileged site in the body by regulating the contents of its inner fluids and preserving the internal ocular tissues from variations which occur constantly in the whole circulation. The blood–ocular barriers must not only provide a suitable, highly regulated, chemical environment for the avascular transparent tissues of the eye, but also serve as a drainage route for the waste products of the metabolic activity of the ocular tissues.

One of these barriers, the BRB, similar to the blood–brain barrier (BBB), is particularly tight and restrictive and is a physiologic barrier that regulates ion, protein, and water flux into and out of the retina.

It is also important to realize that once inside these barriers there are no major diffusional barriers between the extracellular fluid of the retina and adjacent vitreous; nor does the vitreous body itself significantly hinder the diffusional exchanges between the posterior chamber and the retinal extracellular fluid. This means that the functions of both barriers, blood–aqueous barrier and BRB, influence each other and must work in equilibrium.

Blood–Retinal Barrier

The presence of an intact BRB is essential for the structural and functional integrity of the retina and in clinical conditions where BRB breakdown occurs vision may be seriously affected.

The BRB consists of inner and outer components (inner BRB (iBRB) and outer BRB (oBRB)) and plays by itself a fundamental role in of the microenvironment of the retina and retinal neurons.

The BRB regulates fluids and molecular movement between the ocular vascular beds and retinal tissues and prevents leakage into the retina of macromolecules and other potentially harmful agents (Figure 3).

The iBRB is established by the tight junctions (TJs) (zonulae occludentes) between neighboring retinal endothelial cells. These specialized TJs restrict the diffusional permeability of the retinal endothelial layer to values in the order of $0.14 \times 10^{-5}\,\mathrm{cm\,s^{-1}}$ for sodium fluorescein. The retinal endothelial layer functions as an epithelium and in this way is directly associated with its differentiation and with the polarization of the BRB function. This continuous endothelial cell layer, which forms the main structure of the iBRB rests on a basal lamina that is covered by the processes of astrocytes and Müller cells. Pericytes are also present, encased in the basal lamina, in

close contact with the endothelial cells but do not form a continuous layer and, therefore, do not contribute to the diffusional barrier. Astrocytes, Müller cells, and pericytes are considered to influence the activity of the retinal endothelial cells and of the iBRB by transmitting to endothelial cells regulatory signals indicating the changes in the microenvironment of the retinal neuronal circuitry.

The oBRB is established by the TJs (zonulae occludentes) between neighboring retinal pigment epithelial (RPE) cells. The RPE is composed of a single layer of RPE cells that are joined laterally toward their apices by TJs between adjacent lateral cell walls. The RPE resting upon the underlying Bruch's membrane separates the neural retina from the fenestrated choriocapillaries and plays a fundamental role in regulating access of nutrients from the blood to the photoreceptors as well as eliminating waste products and maintaining retinal adhesion. The metabolic relationship of the RPE apical villi and the photoreceptors is considered to be critical for the maintenance of visual function.

In both, iBRB and oBRB, the cell TJs restrict paracellular movement of fluids and molecules between blood and retina, and the endothelial cells and RPE cells actively regulate inward and outward movements. As a result, the levels in the blood plasma of aminoacids or fatty acids fluctuate over a wide range while their concentrations in the retina remain relatively stable.

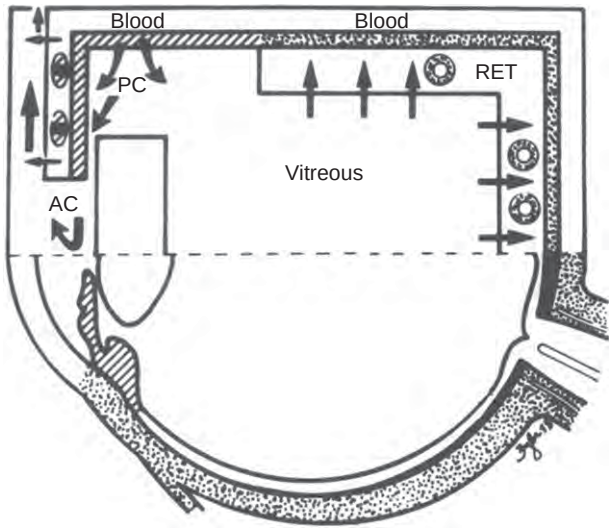

Figure 1 Schematic drawing of the blood–ocular barriers and main fluid movements. RET, retina; PC, posterior chamber; AC, anterior chamber.

Inner Blood–Retinal Barrier

Retinal endothelial cells

The endothelial cells of retinal capillaries are not fenestrated and have a paucity of vesicles. The function of these endothelial vesicles has been described as endocytosis or transcytosis that are receptor mediated. Pinocytotic residues are selectively decreased in the BRB endothelial cells. Receptor-facilitated transport mechanisms are used to move materials across the BRB (**Figure 4**). Channel-facilitated transport using transmembrane proteins is another mechanism for diffusion of specific substrates across the BRB. The glucose transporter Glut 1 is a good example, supplying the neuronal tissue with necessary glucose. Disruption of the iBRB in pathological conditions

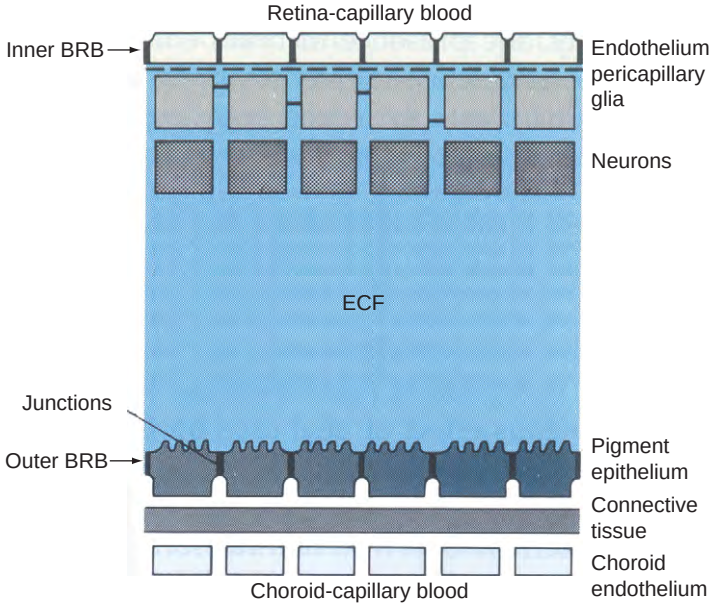

Figure 2 Schematic presentation of the inner and outer blood–retinal barriers (BRBs) and their relative location. ECF, extracellular fluid.

is associated with increased vesicle formation and disrupted endothelial membranes. These alterations may develop before opening of the TJs is detected on ultrastructural examination.

Retinal endothelial TJs

TJs or zonula accludentes of the retinal vascular endothelium are formed by fusion of the outer leaflets of adjacent endothelial cell membranes and were described for the first time in the retinal vessels in 1966.

The TJ obliterates the interendothelial space and confers highly selective barrier properties to the capillaries. Diffusion of molecules from the lumen to the tissue is significantly restricted by TJ.

These endothelial junctions have, like in the brain capillaries, extremely high electrical resistance, 1000–3000 ohm cm^2.

The TJ complex contains at least 40 proteins composing transmembrane and internal adapter proteins that regulated paracellular flux. Transmembrane proteins that make up the TJ are occludins, claudins, and junctional adhesion molecules (JAMs). Occludin is a 65-kDa protein and its changes correlate with permeability changes making it a likely candidate in regulating the opening and closing of the TJ. Claudins regulate small charged molecules and ion permeability. JAM is part of a family of proteins and is associated with adhesion molecules.

Numerous adapter proteins localize just below the membrane and act as TJ organizers and cytoskeleton anchors.

It is important to realize that TJs are dynamic structures that can be regulated by signal transduction through cyclic AMP levels, tyrosine kinases, etc.

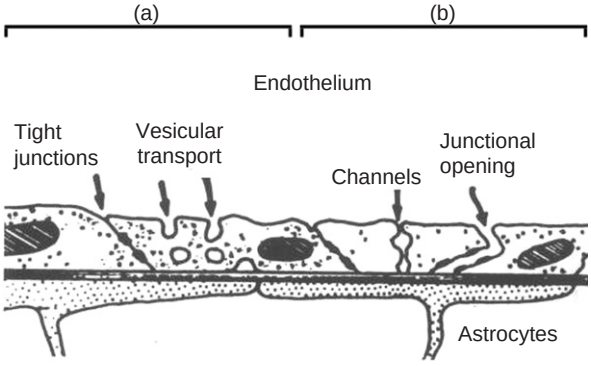

Figure 3 Pathways for solute movements across the inner blood–retinal barrier (retinal endothelial cells): (a) normal; (b) mechanisms of breakdown of iBRB.

Müller cells, astrocytes, and pericytes

A close spatial relationship exists between Müller cells and blood vessels in the retina suggesting a critical role for these cells in the formation and maintenance of the BRB, regulating the functions of barrier cells in the uptake of nutrients and in the disposal of metabolites under normal conditions. Barrier function is also impaired by matrix metaloproteinases (MMPs) from Müller cells as these MMPs lead to proteolytic degradation of the TJ protein occludin.

Astrocytes originate from the optic nerve and migrate to the retinal nerve fiber layer during retinal vascular development. They are associated closely with the retinal vessels and help to maintain their integrity. Astrocytes are known to increase the barrier properties of the retinal endothelium by enhancing the expression of TJ protein Z0.1 and may moderate TJ integrity. Astrocytes are considered to play an important regulatory role in the function of the BRB.

Finally, the pericytes have been shown to play a role in regulating vascular tone, secrete extracellular material, and being phagocytic. Pericytes are considered to play an accessory role in maintaining the integrity of the iBRB by inducing mRNA and protein expression of occludin and other protein junctions. There is evidence that pericytes interact with the endothelial cells contributing to their modulation.

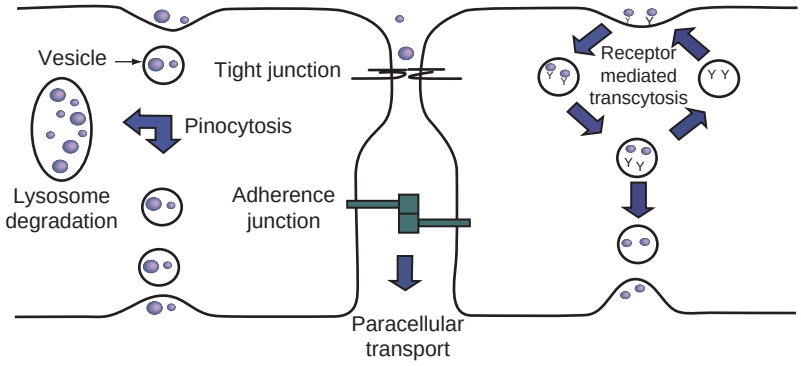

Figure 4 Transport mechanisms across retinal vascular endothelial cells. Modified from Philips, B. E. and Antonetti, D. A. (2007). Blood–retinal barrier. In: Joussen, A. M., Gardner, T. W., Kirchoff, B., and Ryan, S. J. (eds.) *Retinal Vascular Disease*, pp. 139–153. Berlin: Springer.

Outer Blood–Retinal Barrier

RPE cells

The RPE cells transport water from the subretinal space or apical side to the blood or basolateral side. Therefore, the RPE has the structural properties of an ion-transporting epithelium.

RPE cells regulate water content and lactic acid removal generated by the characteristic high metabolic rates in the retina. RPE cells transport water out of the retina and into the choroidal capillary plexus. The force generated by this water flux produces an adhesion force and helps to maintain retinal attachment. Water transport is linked with ion transport, organic anion transport, and other drainage mechanisms.

This outward molecular movement is largely dependent on active ionic transport associated with a relevant high oncotic pressure in the choroid.

RPE cells also have a fundamental role by transporting glucose and retinol, in the appropriate direction, from blood to the photoreceptors.

RPE tight junctions

Paracellular movement of larger molecules is restricted by the TJ between neighboring RPE cells. The paracellular resistance is 10 times higher than the transcellular resistance, classifying the RPE as a tight epithelium. Occludin, claudins, and adapter proteins have been detected at the RPE TJ as in TJ elsewhere. The TJs of the RPE are anchored to the actin cytoskeleton of RPE cells, interact with signaling molecules, and are important for the establishment of cell polarity.

In addition to TJ between RPE cells, the polarized distribution of RPE membrane proteins contributes to the function of the oBRB.

The outer retinal layers are nourished from the blood circulation through the fenestrated capillaries of the choriocapillaris and to subserve this function there is a necessity of a large baso-apical molecular movement from choroid to retina. Waste products of retinal metabolism are transported to the choroid through the oBRB.

Polarity of the outer and inner barriers: TJ modulation

Establishment of cell polarity is a characteristic of a tissue barrier. The endothelial cells of the retinal vessels and RPE develop distinct apical versus basal membrane surfaces. This cell polarity is associated with organization of the cytoskeleton, apical/basal cell membrane proteins, and organization of the junctional complexes between neighboring cells.

It is these TJ protein complexes that allow the establishment of the polarities of the BRB, restricting paracellular diffusion of blood–barrier compounds into the neuronal tissues.

Understanding the normal function of these TJs and the pathological changes that are induced by their alteration resulting in increased permeability is necessary to understand disease progression in retinal diseases such as diabetic retinopathy (iBRB primarily affected) and wet age-related macular degeneration (oBRB primarily affected).

Understanding the role of relevant proteins such as occludins, claudins, and JAMs in BRB physiology and in retinal pathology will certainly contribute to improved management of retinal disease.

Other factors regulating the molecular movement in the eye

Molecular movement from the retinal and choroidal vascular systems into, out, and across them is complex and limited by a variety of other ocular structures. There is a continuous molecular movement of small molecules (mainly water) from the vitreous cavity into the inner retina and through RPE to the choroid.

The major proportion of aqueous humor secreted by the ciliary body from its rich vascular supply provides a bulk flow of fluid through the anterior chamber of the eye but a smaller proportion enters the vitreous cavity where it is largely cleared across the retina and RPE to the choroidal circulation.

Molecular movement from vitreous to choroid is slowed by the cortical vitreous with its high concentration of hyaluronic acid stabilized in a relatively dense type II collagen matrix and the internal limiting membrane (ILM) of the retina. The ILM offers resistance to the diffusion of macromolecules of 148 kDa but allows the passage of smaller molecules. Movement through the retina of molecules that have crossed the iBRB into the retina is largely through the extracellular tissue spaces. Similary, Bruch's membrane that separates the basal RPE from the fenestrated capillaries appears, in health, to offer little resistance to molecular movement.

The presence of fenestrations in the choriocapillaris allows the passage of even large molecules such as albumin into the extravascular spaces of the choroid. The choriocapillaris, therefore, contributes little to the oBRB.

Molecular movement across the oBRB is, however, probably influenced by the very high rate of blood flow in the choroid. A possible explanation for the high blood flow in the choroid is that there is a need not only to supply oxygen and metabolites to the energy demanding retina and RPE, but also for the rapid removal of waste products of the retinal metabolism into the blood circulation.

Finally, the ciliary body may have a relevant regulatory role in the overall maintenance of the retinal

microenvironment. The large surface covered by the ciliary processes, their location where the aqueous and vitreous meet, and the multiple transport functions of the ciliary epithelium are all factors suggesting an important role for the ciliary body in the regulation of the inner ocular fluids.

The microenvironment of the retina, which closely resembles brain extracellular fluid and is in equilibrium with the vitreous is, therefore, maintained by a variety of facilitated and active transport processes which are located mainly in the iBRB and oBRB with the retinal endothelial cells and RPE playing fundamental roles.

The Blood–Retinal Barrier and Ocular Immune Privilege

The immune response has developed and evolved to protect the organism from invasion and damage by a wide range of pathogens. With time, the immune system has developed destructive responses that are specific for pathogens as well as tissues. Such tissue injury might, however, have a devastating effect on the function of an organ such as the eye that needs to maintain optical stability.

The existence of ocular immune privilege is dependent upon multiple factors such as immunomodulatory factors and ligands, regulation of the complement system within the eye, tolerance promoting antigen-presenting cells (APCs), unconventional drainage pathways, and, with particular relevance, the existence of the blood–ocular barriers.

The blood–ocular barriers provide a relative sequestration of the anterior chamber, vitreous, and neurosensory retina from the immune system and create the necessary environment for the existence of ocular immune privilege. The evolution of immune privilege as a protective mechanism for preserving the function of vital and delicate organs such as the eye has resulted in a complex system with multiple regulatory safeguards for the control of both innate and adaptative immurity. The consequences of inadvertent bystander tissue destruction by antigen-monspecific inflammation can be so catastrophic to the organ or host that a finely tuned regulatory system is needed to ensure the integrity of the ocular tissues and maintain optical relationships.

There are also several lines of evidence that points to immunosuppressive functions in the BRB cells, RPE, and retinal endothelial cells. These immunosuppressive effects are apparently due to the secretion of a variety of soluble factors, such as cytokines and growth factors.

Clinical evaluation of the blood–retinal barrier

Fluorescein angiography, an examination procedure performed routinely in the ophthalmologist's office, permits a dynamic evaluation of local circulatory disturbances and identifies the sites of BRB breakdown (**Figure 5**). It is, however, only semi-quantitative and its reproducibility depends on the variable quality of the angiograms.

Vitreous fluorometry was developed as a method capable of quantification of both inward and outward

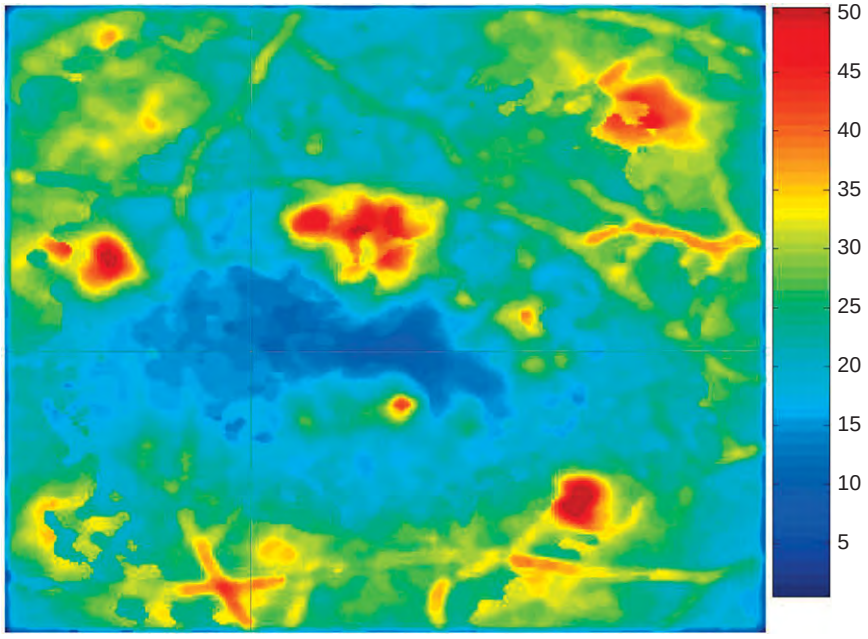

Figure 5 Sites of fluorescein leakage into the vitreous identified by the retinal leakage analyzer in an eye with nonproliferative retinopathy of a patient with diabetes type 2. Blue indicates minimal leakage; red indicates maximum leakage.

movements of fluorescein across the BRB system in the clinical setting. Protocols were devised, tested, and dedicated instrumentation developed.

With the development of vitreous fluorometry methodologies, a large number of clinical and experimental studies demonstrated convincingly the major role played by alterations of BRB in posterior segment disease.

In clinical situations, alterations of the BRB have been measured in pathologies of the RPE, aged-related macular degeneration, and macular edema, as well as in hypertension and diabetes. The clinical use of vitreous fluorometry, however, has declined because it offers only an overall measurement over the posterior role and because at the time of its development there were no drugs available for stabilizing the BRB. Nowadays, vitreous fluorometry is mostly used in experimental research and in drug development.

More recently, retinal leakage mapping has been introduced to identify the sites of BRB breakdown. Further developments of this methodology based on confocal scanning laser ophthalmology (SLO-Retinal Leakage Analyzer) associated with improved optical coherence tomography imaging are expected to contribute to earlier diagnosis of BRB alterations in retinal disease as well as improved testing of the effect of new drugs that are now becoming available for treatment of retinal disease.

Blood–retinal barrier and macular edema

Macular edema is the result of an accumulation of fluid in the retinal layers around the fovea, contributing to vision loss by altering the functional cell relationship in the retina and promoting an inflammatory reparative response.

Macular edema is only a nonspecific sign of ocular disease and not a specific entity. It should be viewed as a special and clinically relevant type of macular response to an altered retinal environment, in most cases associated with an alteration of the BRB. It occurs in a wide variety of ocular situations such as uveitis, trauma, intraocular surgery, vascular retinopathies, hereditary dystrophies, diabetes, age-related macular degeneration, etc.

The increase in water content of the retinal tissue that characterizes macular edema may be initially intracellular or extracelullar. In the first case, also called cytotoxic edema, there is an alteration of the cellular ionic distribution.

In the second case, more frequent and clinically more relevant, the extracellular accumulation of fluid is directly associated with an alteration of the BRB. In this later situation, the protective effect of the BRB is lost and the Starling law applies. When there is breakdown of the BRB, any changes in the equilibrium between hydrostatic and oncotic pressure gradients across the BRB contribute to further water movements and progression of the macular edema.

It is also of great relevance to keep in mind that the BRB cells, retinal endothelial cells, and retinal pigment epithelial cells, are both the target and producer of ecosanoids, growth factors, and cytokines. Breakdown of the BRB leading to situations of macular edema may be mediated by locally released cytokines and induction of an inflammatory reparative response creating the conditions for further release of cytokines, growth factors, etc.

Macular edema is also one of the most serious consequences of inflammation in the retinal tissue. Inflammatory cells can alter the permeability of the TJs that maintain the iBRB and oBRB. Cell migration may occur primarily through splitting the junctional complex or through the formation of channels or pores across the junctional complex.

Macular edema has particular relevance for its frequency in diabetic retinopathy. Leukocyte adhesion to retinal vessels and breakdown of the BRB appear to be mediated by nitric oxide (NO). NO upregulates intercellular adhesion molecule-1 (ICAM-1) and promotes the downregulation of TJ protein expression.

Relevance of BRB to Treatment of Retinal Diseases

When administered systemically, drugs must pass the BRB to reach therapeutic levels in the retina. Drug entrance into the retina depends on a number of factors, including the plasma concentration profile of the drug, the volume of its distribution, plasma protein binding, and the relative permeability of the BRB. To obtain therapeutic concentrations within the retina, new strategies must be considered such as delivery of nanoparticles, chemical modification of drugs to enhance BRB transport, coupling of drugs to vectors, etc.

The BRB must be considered as a dynamic interface that has the physiological function of specific and selective membrane transport from blood to retina and active efflux from retina to blood for many compounds, as well as degradative enzymatic activities.

From the viewpoint of drug delivery, designing drugs (including peptides) with greater lipophilicity to enhance BRB permeability seems to be an easy approach. However, such a strategy would not only increase the permeation into tissues other than the retina, but also decrease the bioavailability due to the hepatic first pass metabolism in the case of oral administration. Accordingly, for the development of retina-specific drug delivery systems for neuroactive drugs the most effective approach is to utilize the specific transport mechanisms active at the BRB. That would mean designing drugs that mimic the substrates to be taken by particular transporters or receptors existing in the BRB.

Eye drops are generally considered to be of limited benefit in the treatment of posterior segment diseases. Newer pro-drug formulations that achieve high concentrations of the drug in the posterior segment may have a

role in the future. Meanwhile, periocular injection is one modality that has offered mixed results.

Finally, the last years have seen a generalized and surprising safe utilization of intravitreal injections, a form of administration that circumvents the BRB. Steroids and a variety of anti-VEGF drugs have been administered through intravitreal injections to a large number of patients without significant side effects and demonstrating good acceptance by the patients. Intravitreal injections can achieve high drug concentrations in the vitreous and retina preserving the BRB function and its crucial protective function. At present the major challenge appears to be the need to decrease the number of intravitreal injections which in the case of anti-VEGF treatments are given every 6 weeks to maintain efficacy. The search for safe slow-delivery devices or implantable biomaterials is ongoing but the invasive approach to treat retinal diseases appears to be the only effective way of reaching rapidly therapeutic levels in the retina in the presence of a functioning BRB.

See also: Anatomy and Regulation of the Optical Nerve Blood Flow; Breakdown of the Blood–Retinal Barrier; Breakdown of the Retinal Pigmented Epithelium Blood–Retinal Barrier; Developmental Anatomy of the Retinal and Choroidal Vasculature; Dynamic Immunoregulatory Processes that Sustain Immune Privilege in the Eye; Immunosuppressive and Anti-Inflammatory Molecules that Maintain Immune Privilege of the Eye; Innate Immune System and the Eye; Macular Edema; Molecular Composition of the Vitreous and Aging Changes; Pathogenesis and Immunology of Bacterial Endophthalmitis; Physiological Anatomy of the Retinal Vasculature; Properties and Functions of the Vessels of the Ciliary Body; Retinal Pigment Epithelial–Choroid Interactions; Retinal Pigmented Epithelium Barrier; Stability and Functional Integrity of New Blood Vessels; Vitreous Anatomy, Aging, and Anomalous Posterior Vitreous Detachment.

Further Reading

Cocaprados, M. and Escribano, J. (2007). New perspectives in aqueous humor and secretion and in glaucoma: The ciliary body as multifunctional neuroendocrine gland. *Progress in Retinal Eye Research* 26: 239–262.

Cunha-Vaz, J. G. (1979). The blood–ocular barriers. *Survey of Ophthalmology* 23: 279–296.

Cunha-Vaz, J. G., Faria de Abreu, J. R., Campos, A. J., and Figo, G. (1975). Early breakdown of the blood–retinal barrier in diabetes. *British Journal of Ophthalmology* 59: 649–656.

Cunha-Vaz, J. G. and Maurice, D. M. (1967). The active transport of fluorescein by retinal vessels and the retina. *Journal of Physiology* 191: 467–486.

Cunha-Vaz, J. G. and Maurice, D. M. (1969). Fluorescein dynamics in the eye. *Documenta Ophthalmologica* 26: 61–72.

Cunha-Vaz, J. G. and Travassos, A. (1984). Breakdown of the blood–retinal barriers and cystoid macular edema. *Survey of Ophthalmology* 28: 485–492.

Cunha-Vaz, J. G., Shakib, M., and Ashton, N. (1966). Studies on the permeability of the blood–ocular barrier. I. On the existence, development and site of a blood–retinal barrier. *British Journal of Ophthalmology* 50: 411–453.

Kaplan, H. J. and Niederkorn, J. Y. (2007). Regional immunity and immune privilege. In: Niederkorn, J. Y. and Kaplan, H. G. (eds.) *Immune Response and the Eye. Chemical Immubology Allergy* vol. 92, pp. 11–26. Basel: Karger.

Lobo, C., Bernardes, R., and Cunha-Vaz, J. G. (1999). Mapping retinal fluorescein leakage with confocal scanning laser fluorometry of the human vitreous. *Archives of Ophthalmology* 117: 631–637.

Partridge, W. M. (1998). Introduction to the blood–brain barrier: Methodology and pathology. In: Partridge, W. M. (ed.) *Introduction to the Blood–Brain Barrier: Methodology, Biology and Pathology*, pp. 1–10. New York: Cambridge University Press.

Peyman, G. A. and Bok, D. (1972). Peroxidase diffusion in the normal and laser-coagulated primate retina. *Investigative Ophthalmology* 11: 35–45.

Philips, B. E. and Antonetti, D. A. (2007). Blood–retinal barrier. In: Joussen, A. M., Gardner, T. W., Kirchhof, B., and Ryan, S. J. (eds.) *Retinal Vascular Disease*, pp. 139–153. Berlin: Springer.

Rapoport, S. I. (1976). *Blood–Brain Barrier in Physiology and Medicine*. New York: Raven Press.

Reese, T. S. and Karnovski, M. J. (1967). Fine structural localization of a blood–brain barrier to exogenous peroxidase. *Journal of Cellular Biology* 34: 207–217.

Shakib, M. and Cunha-Vaz, J. G. (1966). Studies on the permeability of the blood–retinal barrier. IV. Junctional complexes of the retinal vessels and their role on their permeability. *Experimental Eye Research* 5: 229–234.

Strauss, O. (2005). The retinal pigment epithelium in visual function. *Physiological Review* 85: 845–881.

Breakdown of the Blood–Retinal Barrier

S A Vinores, Johns Hopkins University School of Medicine, Baltimore, MD, USA

Glossary

Fenestrations – Spaces between vascular endothelial cells that allow free fluid exchange between vessel and tissue. Fenestrations are characteristic of vessels found in tissues that do not have a blood–tissue barrier.

Leukostasis – The adhesion of leukocytes to the vascular endothelium as part of an inflammatory reaction.

Macular edema – Fluid accumulation, due to blood–retinal barrier (BRB) breakdown, in the area of the human or primate retina of highest visual acuity.

Tight junctions – Also referred to as zonula occludens, tight junctions are complex arrangements of microfilaments and other proteins that connect retinal vascular endothelial (RVE) or retinal pigment epithelial (RPE) cells and restrict the flow between them. Tight junctions are an integral component of the blood–retinal, blood–brain, or blood–nerve barrier.

Vesicular transport – The nonspecific transcellular transport of fluid and high-molecular-weight molecules from the luminal to the abluminal surface of the vascular endothelium by means of pinocytotic vesicles.

Uveitis – An inflammation of the uvea, or the middle layer of the eye. The uvea consists of three structures: the iris, the ciliary body, and the choroid.

Introduction

The blood–retinal barrier (BRB), which is analogous to the blood–brain barrier, maintains homeostasis in the retina by restricting the entry of blood-borne proteins from the retina and by maintaining strict ionic and metabolic gradients. When this barrier breaks down, excess fluid accumulates in the retina and this can result in macular edema, which is associated with ischemic retinopathies, including diabetic retinopathy (DR) and retinopathy of prematurity (ROP), ocular inflammatory diseases, retinal degenerative diseases, and a variety of other ocular disorders, or following ocular surgery. BRB breakdown can occur at the inner BRB, which is established at the retinal vasculature, at the outer BRB, which consists of the retinal pigment epithelial (RPE) cells, or at both sites. The BRB is established by the formation of tight junctions between the retinal vascular endothelial (RVE) cells and the RPE cells and a paucity of endocytic vesicles within these cells. The establishment and maintenance of the BRB is regulated by the perivascular astrocytes and pericytes, but the mechanism for this regulation is not entirely clear. Some studies have shown that cell to cell contact is necessary to establish and maintain the BRB, while others provide evidence that a soluble mediator is sufficient. BRB breakdown can result from a disruption of the tight junctions, which are composed of a complex network of junctional proteins, an upregulation of vesicular transport across the RVE or RPE, or by degenerative changes to the barrier-forming cells or to the regulatory cells, the pericytes and glia. In some cases, BRB breakdown is related to identifiable structural defects, such as loss of pericytes, astrocytes, or RPE cells or changes to the vascular endothelial cells, as would be caused by microaneurysm formation. In other cases, where retinal vascular leakage is diffuse, such as in uveitis, or when the leakage is remote from a lesion, such as a surgical wound or tumor, it is clear that diffusible factors are involved. Blood–tissue barriers exist only in the retina, brain, and nerve. Vascular endothelial cells in the choroid and in other tissues are fenestrated (**Figure 1(a)**), allowing large molecular weight molecules to freely pass from the blood to the tissue, and thus do not have a barrier function.

Tight Junctions

Tight junctions or zonula occludens consist of complex arrangements of over 40 proteins in the peripheral cytoplasm and apical plasma membrane that connect RVE or RPE cells and restrict flow between them (**Figure 1(b)**). Occludin and the claudins (over 24 isoforms), which form the junctional strands and are believed to constitute the backbone of the tight junction, span the plasma membrane and bind junctional proteins in adjacent cells. Zonula occludens proteins 1, 2, and 3 (ZO-1, -2, and -3) are intracellular proteins that associate with the cytoplasmic surface of the tight junctions and organize the complex. The binding of ZO-1 to occludin establishes the tight junction. Other integral components of the junctional complex are the junctional adhesion molecules, tricellulin, cingulin, 7H6, and symplekin. A breach of the tight junctions (**Figure 1(c)**) can result from an alteration in the content of the junctional proteins, their redistribution, or their

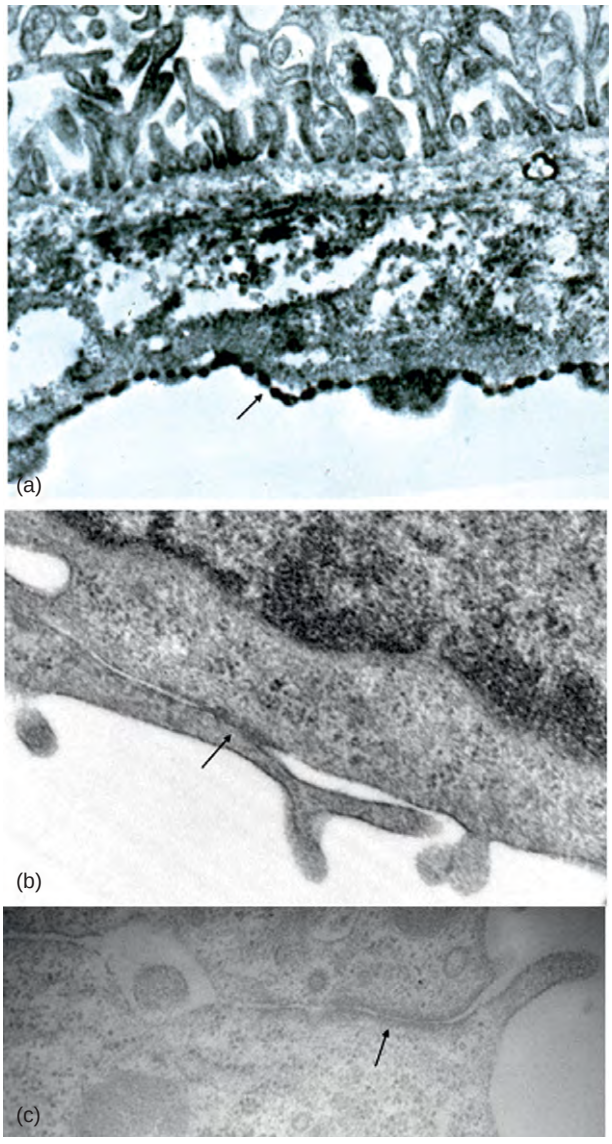

Figure 1 (a) Choroidal vessels are fenestrated (arrow) and, therefore, do not form a blood–tissue barrier. (b) A morphologically closed tight junction (arrow) in a normal retinal vessel. Note close apposition of vascular endothelial cells and an intact junctional complex. (c) A morphologically open tight junction (arrow) in a retinal vessel. The space between the vascular endothelial cells allows vascular leakage through the junction.

phosphorylation. Occludin content at the tight junction is higher in cells that have a tighter barrier and decreased occludin correlates with increased BRB permeability, but occludin knockout mice appear to form functional tight junctions, so the association is complex and not simply regulated by occludin. Increased occludin phosphorylation is also associated with increased BRB permeability. Altered expression of claudins can lead to changes in selectivity of the junctions and claudin-5 appears to be particularly important for maintenance of a functional tight junction.

Adenosine, prostaglandin E1 (PGE1), interleukin-1β (IL-1β), tumor necrosis factor-α (TNFα), and vascular endothelial growth factor (VEGF) appear to be capable of causing a morphological and functional opening of the RVE tight junctions. A significant number of interendothelial cell tight junctions appeared open along their entire length within 6 h of intravitreal injection of each agent into rabbits with TNFα showing the greatest effect (35.6% of the interendothelial cell junctions appeared open, morphologically). The effect of PGE1 on tight junctions appeared to be transient, that of VEGF and IL-1β were partially reversible by 24 h, and the effect of the adenosine agonist, *N*-ethylcarboxamidoadenosine was not reversible by 48 h. The demonstration of immunoreactive albumin, which would normally be confined to the lumens of vessels with a blood–tissue barrier, along the entire length of these junctions, from the luminal to the abluminal surface, suggests that they are also functionally open (**Figure 2(c)**).

Vesicular Transport

Since the tight junctions restrict the flow of molecules across the BRB, a series of pumps, channels, and transporter molecules are necessary to transport specific essential molecules from the blood to the retina. The nonspecific transport of high molecular weight molecules and fluids across the RVE by way of pinocytotic vesicles (**Figure 2(a)**) or caveolae is referred to as vesicular transport (**Figure 2(b)**) and serves as a transcellular means of BRB breakdown. This mechanism appears to be the predominant means for BRB compromise associated with VEGF-A-induced hyperpermeability in monkeys and in DR in humans, rats, and rabbits.

In addition to causing the opening of interendothelial cell tight junctions in the retina, adenosine, PGE1, IL-1β, TNFα, and VEGF also promote the formation of pinocytotic vesicles in RVE cells and the distribution of albumin-containing intraendothelial vesicles across the entire RVE cell and at both the luminal and abluminal surfaces suggests that active vesicular transport is occurring. Although infrequently seen, the vesiculo-vacuolar organelle, which is associated with VEGF in the vascular endothelium of tumors, was also evident in the RVE of VEGF-treated rabbits, but not monkeys, and is likely to play a role in VEGF-mediated vascular permeability. The effect of these mediators on the outer BRB is less clear.

Role of Inflammation

Inflammation has been associated with BRB breakdown in DR, choroidal neovascularization (CNV) associated with age-related macular degeneration, aging, ocular

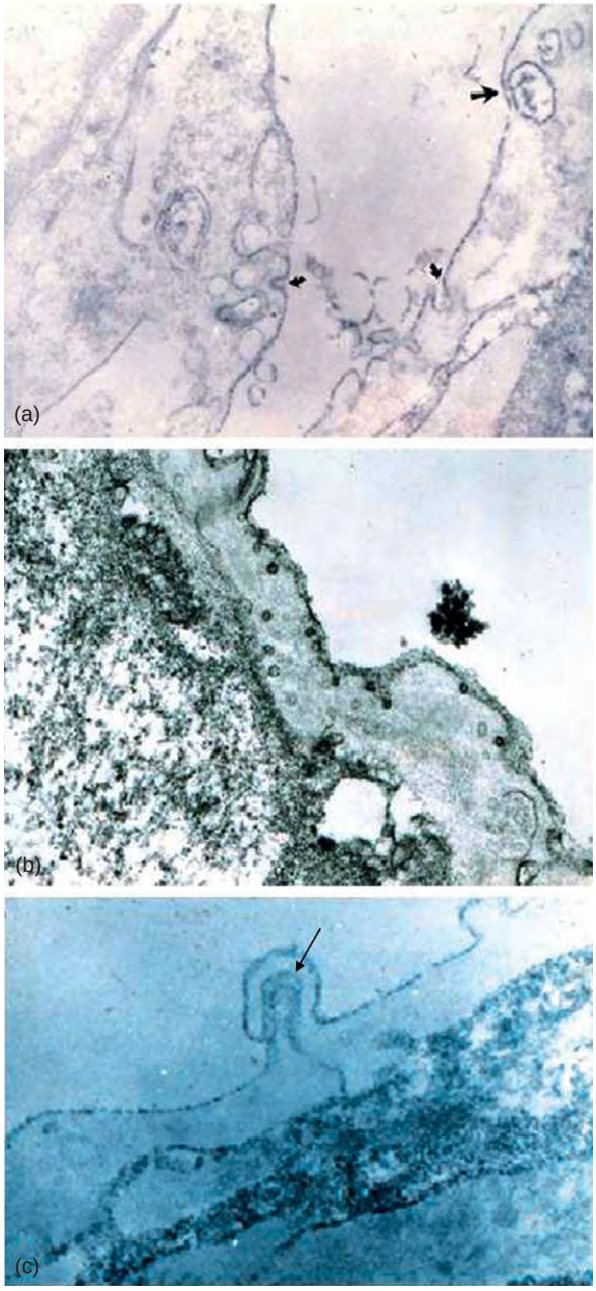

Figure 2 (a) Immunocytochemical staining for endogenous albumin shows the formation of pinocytotic vesicles (arrows) on the luminal surface of vascular endothelial cells in a 7 month galactosemic rat. Immunoreactive albumin is contained within the formed vesicles (top right). (b) Immunocytochemical staining for albumin demonstrates albumin filled vesicles throughout the cytoplasm of the vascular endothelial cells of a rabbit. The presence of these vesicles and the positive staining for albumin in the extracellular matrix (left) suggests that vesicles are actively transporting serum proteins across the endothelium and extruding their contents at the abluminal surface as a means of transcellular BRB breakdown. (c) Immunocytochemical staining for albumin along the entire length of the interendothelial cell junction (arrow) and in the basal lamina indicates that there is vascular leakage through the junction.

inflammatory disease, and the administration of pro-inflammatory molecules. The increased adhesion of leukocytes to endothelial cells in the retina is associated with increased expression of intercellular adhesion molecule-1 (ICAM-1), vascular cell adhesion molecule-1 (VCAM-1), CD18, and other adhesion molecules, which are upregulated by VEGF and other pro-inflammatory molecules in DR and other ocular disorders, and appear to be regulated, at least in part, by protein kinase C (PKC). Diabetic CD18 and ICAM-1 knockout mice have significantly fewer adherent leukocytes than diabetic mice with normal CD18 and ICAM-1 and the decreased leukostasis is associated with fewer damaged endothelial cells and reduced BRB breakdown, supporting the role of adhesion molecules in increased inflammation and the correlation of an inflammatory response with endothelial cell damage and permeability. It is not clear whether the same molecules that facilitate leukostasis also mediate BRB breakdown or if this is attributable to molecules secreted by the recruited leukocytes, or both, but there appears to be a direct correlation between increased leukostasis and vascular permeability in the retina and pro-inflammatory molecules, such as TNFα and IL-1β, are among the most potent inducers of BRB breakdown. Leukocyte adhesion to the diabetic vascular endothelium can promote endothelial apoptosis and inhibition of leukocyte adhesion to the retinal vessels can not only prevent endothelial degeneration, but also reduce the diabetes-associated loss of pericytes, which support the vascular endothelium and help to confer BRB integrity. Inflammation can also alter the distribution of astrocytes and their ensheathment of retinal vessels, leading to alterations in BRB integrity. Leukocytes have also been shown to cause a downregulation and redistribution of tight junctional proteins, which leads to a disruption of tight junctions and a transient breakdown of the BRB during retinal inflammation.

Molecular Mechanisms

The induction of BRB breakdown is a complex process that is mediated, not by a single factor, but by the interaction of multiple factors operating through different receptors and signaling pathways. The list of molecules that have been identified as playing a role in BRB breakdown, which is by no means all-inclusive, includes VEGF, hypoxia-indicible factors-1 and -2 (HIF-1 and -2), placental growth factor (PlGF), TNFα, IL-1β, platelet-activating factor, adenosine, histamine, prostaglandins (PGE1, PGE2, and PGF2α), platelet-derived growth factors A and B (PDGF-A and -B), insulin-like growth factor-1 (IGF-1), ICAM-1, VCAM-1, P-selectin, and E-selectin. The key will be to determine what the initiating event is and which events are parts of the

resulting cascade. By targeting the appropriate molecules, subsequent events leading to BRB failure may be blocked.

The various isoforms of VEGF and PlGF are members of the VEGF family. VEGF-A, a potent inducer of vascular permeability, binds to both VEGF type-1 (fms-like tyrosine kinase-1 or Flt-1) and type-2 (kinase insert domain-containing receptor, referred to as KDR in humans or Flk-1 in other species) receptors (VEGFR1 and VEGFR2), whereas PlGF binds only to VEGFR1, so comparing their activities may be a means of dissecting the respective roles of the VEGF receptor isoforms, since both receptors have been implicated in BRB breakdown. VEGFR1-mediated signaling appears to operate primarily through p38 MAPK (mitogen-activated protein kinase), while VEGFR2 signaling may be mediated through RAS, phosphoinositide 3-kinases (PI3K)/Akt, or phospholipase C (PLC)γ, but the interaction of VEGFR1 and VEGFR2 is complex and much remains to be learned about this interaction. Both receptors are associated with vascular permeability and angiogenesis, but in some circumstances, VEGFR1 can act as a negative regulator for VEGFR2.

VEGF is a key molecule in promoting increased retinal vascular permeability. This activity may be mediated, at least in part, by an upregulation of ICAM-1, E-selectin, and P-selectin as a means of facilitating its pro-inflammatory activity. VEGF-induced permeability showed a biphasic pattern with a rapid and transient phase followed by a delayed and sustained phase, the latter of which was blocked by antibodies to urokinase plasminogen activator or its receptor. VEGF receptor kinase inhibitors can suppress VEGF-mediated BRB breakdown, but this strategy shows that TNFα, IL-1β, and IGF-1 do not induce BRB leakage through an induction of VEGF, indicating that these mediators operate through distinct pathways that may also be targeted. Endothelial nitric oxide synthase activation and NO formation also appear to be implicated in VEGF-mediated vascular permeability, probably through activation of the serine/threonine protein kinase AKT/PKB, which can lead to an increase in nitric oxide production and ICAM-1 upregulation. Deletion of the hypoxia response element of the *Vegf* promoter also suppresses BRB breakdown in oxygen-induced ischemic retinopathy, demonstrating that HIF-induced VEGF is critical in this process.

TNFα and IL-1β are upregulated in DR and other ischemic retinopathies, as well as ocular inflammatory disease, and both molecules are associated with increased leukostasis and BRB breakdown. IL-1β has been shown to accelerate apoptosis of retinal capillary endothelial cells through activation of nuclear factor kappa light-chain enhancer of activated B cells and this is exacerbated in high glucose. IL-1β can also stimulate the production of reactive oxygen species, which in turn can induce the release of additional cytokines. Aspirin and etanercept are inhibitors of TNFα and each can reduce ICAM-1 levels, diabetes-related leukostasis, and BRB breakdown in diabetic rats without altering VEGF levels, showing that TNFα is involved in this process and that it operates through a distinct pathway from VEGF.

These data show that there are a number of potential target molecules for inhibitors to suppress BRB breakdown. The challenge will be to identify the best target or targets and develop the most effective therapeutic strategy.

Assessing BRB Breakdown

A variety of methods exist for the quantitative and qualitative assessment of the BRB, but each method has its particular limitations and sensitivity, so the choice of methods will largely depend on whether quantitative or qualitative data are desired and on the nature of the tissue being evaluated, whether it be fixed tissue, patients in a clinical setting, or experimental animal models. Since no single method can provide a quantitative assessment with precise localization of the site of BRB breakdown, multiple approaches may be necessary to provide an overall perspective. In addition, some methods can produce precise data in experimental models or on tissue specimens, but are not appropriate for use in the clinic.

To identify and compare factors that cause BRB breakdown and to evaluate the efficacy of new treatments designed to prevent or reduce macular edema, a reliable quantitative assay for assessing BRB function is essential. The most widely used protocols for the quantitative assessment of BRB breakdown utilize Evans blue or 3H-mannitol as tracers. With the Evans blue assay, the extracted dye is quantified in the retina following intravenous injection of the dye and subsequent perfusion with saline. A spectrophotometer, set at 620 nm, is used to quantify the leakage of dye into the retina. With the 3H-mannitol assay, a scintillation counter is used to determine the CPM/mg tissue, 1 h after an intraperitoneal injection of the tracer, and the data are expressed as a ratio of retina/lung or retina/kidney. Since the lung and kidney do not have a blood–tissue barrier, the ratio corrects for any variation in the amount of isotope injected or absorbed. These methods have been used to assess the BRB in several models of ocular disease and to determine the effect of various factors, agents, and genetic manipulations on the integrity of the BRB. Thus, these methods have been useful in identifying factors that initiate BRB compromise and for determining the relative efficacy of various agents at preventing or reducing BRB failure. Both methods produce highly reproducible results in an experimental setting, with the 3H-mannitol assay possibly being somewhat more sensitive due to the lower molecular weight of mannitol than Evans blue dye, but neither is applicable to the clinic. Vitreous fluorophotometry (VFP) is a more appropriate means of assessing BRB failure in

a clinical setting. Although these methods can provide a quantitative assessment of the BRB, they cannot localize the site of leakage or provide any insight into the mechanism, so alternative techniques are required to provide this information.

Fluorescein angiography has been used extensively in the clinic to visualize BRB breakdown, but it does not allow resolution at the cellular level. Magnetic resonance imaging (MRI) enhanced by the paramagnetic contrast agent gandoliniumdiethylene-triaminetetraacetic acid has been used to localize and quantify BRB breakdown in living animals. MRI is not subject to the optical limitations of VFP and allows the investigator to distinguish between inner and outer BRB failure in the rabbit. Its resolution is not as great as that resulting from microscopic evaluation of fixed tissue, but MRI allows *in vivo* analysis, thus enabling the investigator to monitor progressive changes in BRB integrity within the same animal. The use of exogenous tracer substances can provide a higher resolution, but several limitations are associated with their use. The use of tracers is impractical for clinical studies, the introduction of exogenous material may alter BRB integrity, and retrospective studies cannot be done on archival tissues. The immunolocalization of endogenous albumin (**Figure 3**) or IgG can circumvent most of these limitations and offers the following advantages for BRB assessment. The technique can be used with fixed surgical, autopsy, or archival specimens, no exogenous substance is introduced, and it can be used at the light and electron microscopic (EM) levels. Although, by nature, this is not a quantitative method, it can show the location and extent of BRB breakdown and, if used at the EM level, it can demonstrate the means by which serum proteins are extravasated from the retinal vessels or may transverse the RPE layer. This technique has been used to assess the BRB in a variety of human and experimental ocular disorders, including DR, retinitis pigmentosa, vascular occlusive disease, neoplastic disease, ocular inflammation or infection, and other diseases that develop macular edema, but for which pathological defects do not reveal a cause for BRB breakdown. EM immunocytochemical staining for albumin reveals that BRB breakdown can occur by the opening of tight junctions between RVE or RPE cells (**Figure 2(c)**), by an upregulation of trans-endothelial vesicular transport (**Figures 2(a)** and **2(b)**), or by increased surface membrane permeability of RVE or RPE cells resulting from degenerative changes associated with the disease process. It has also provided insights into how various factors, such as VEGF, TNFα, IL-1β, prostaglandins, adenosine, and others promote BRB breakdown. VEGF transiently opens some tight junctions and some leakage through the interendothelial cell tight junctions is induced by VEGF, but electron microscopy has revealed that the predominant mechanism for VEGF-A-induced hyperpermeability of the RVE in monkeys and diabetes-related BRB breakdown in humans, rabbits, and rats is an upregulation of pinocytotic vesicular transport.

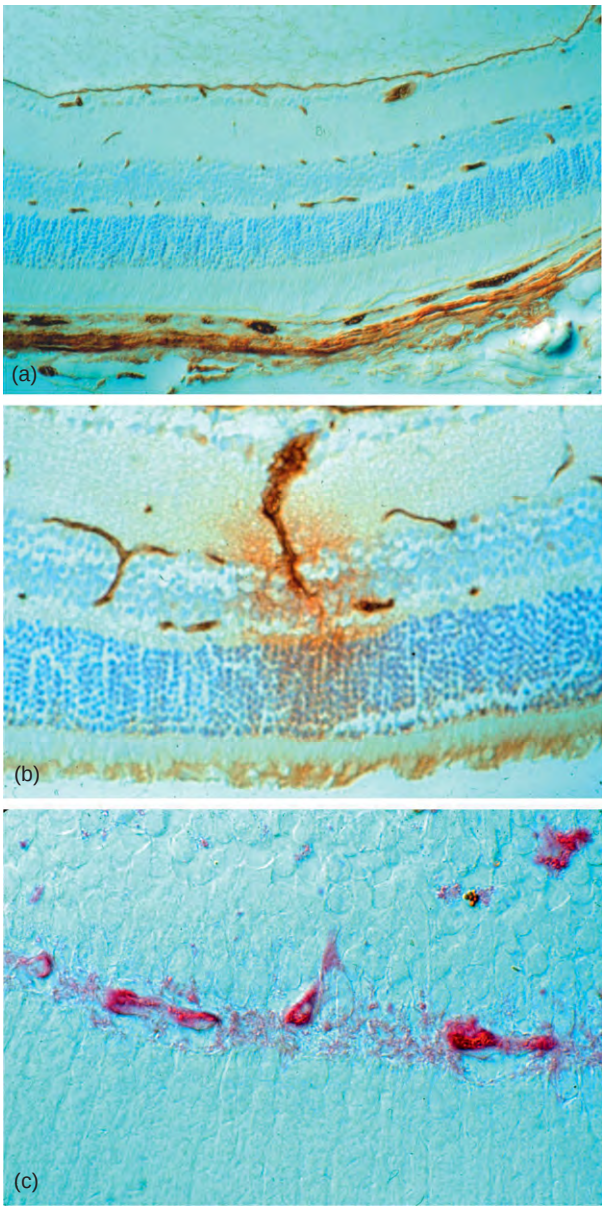

Figure 3 (a) In a normal mouse, immunohistochemical staining for albumin shows that, within the retina, albumin is confined to the vessels, indicating an intact BRB, but diffuse staining is demonstrated in the choroid (bottom) due to the fenestrated vessels and the absence of a blood–tissue barrier. (b) In a mouse infected with coronavirus, vascular leakage is demonstrated from a retinal vessel by immunohistochemical staining for albumin. (c) Immunohistochemical staining (red) shows that albumin has leaked from retinal vessels in a VEGF transgenic mouse. Vinores, S. A., et al. (2001). Blood–retinal barrier breakdown in experimental coronavirus retinopathy: Association with viral antigen, inflammation, and VEGF in sensitive and resistant strains. *Journal of Neuroimmunology* 119: 175–182, with permission from Elsevier.

Inhibiting BRB Breakdown

A variety of therapeutic approaches have shown success at inhibiting BRB breakdown, but generally not preventing it. Most of the agents currently in clinical trials target inflammatory processes or VEGF. Antibodies to key molecules, such as VEGF, PlGF, or TNFα, have been effective at suppressing BRB breakdown, as have inhibitors of these molecules. Drugs that block histamine receptors also reduce retinal vascular leakage in diabetic rats and humans. Bevacizumab (avastin), an anti-VEGF IgG1 antibody, Ranibizumab (lucentis), the Fab fragment of a humanized anti-VEGF antibody, Pegaptanib sodium (macugen), a VEGF aptamer, and VEGF trap, in which the binding domains of VEGFR1 and VEGFR2 are combined with the Fc portion of IgG to neutralize all VEGF family members, have all shown varying degrees of success in clinical trials for reducing macular edema by targeting VEGF. Corticosteroids inhibit BRB breakdown, but it is not clear whether this activity is mediated by their anti-inflammatory effect, which occurs, at least in part, through a downregulation of ICAM-1, their inhibition of VEGF expression, their induction of occludin and ZO-1 expression, their reversal of occludin phosphorylation, or a combination of these activities. Even though steroids may improve visual acuity, they carry a high risk of cataracts and glaucoma. The involvement of PKC in vascular permeability has been established and a PKC activator can promote BRB breakdown. PKC inhibitors can reduce retinal vascular permeability, particularly that mediated by VEGF or prostaglandins, but generalized inhibition of PKC is likely to have serious systemic consequences. A PKCβ inhibitor (LY333531) was also effective at suppressing retinal vascular permeability and may have fewer complications.

Prospects for the Future

As more studies are conducted, the complexity of BRB breakdown leading to macular edema becomes increasingly apparent. This process is not attributable to a single factor or event, but the interaction of an undetermined number of initiating events that generates a cascade of subsequent events, ultimately leading to BRB failure. Since this is a multifactorial process, a multifaceted or pleiotropic approach that restores the homeostatic balance is more likely to suppress BRB breakdown than targeting a single pathway with an inhibitor. That would explain why the currently used monotherapies may lead to a reduction of macular edema and improved visual acuity, but generally not a total resolution of the disorder. To develop more effective therapeutic strategies, a better understanding of the basic mechanisms in the pathogenesis of BRB breakdown is imperative. In addition, the frequent injections, high cost, and the occasional side effects associated with current therapeutic approaches emphasize the need for more effective treatment that is less invasive, less costly, and has little or no side effects.

Conclusions

BRB breakdown, leading to macular edema, occurs in a number of ocular disorders and can be due to structural changes or soluble mediators. Alteration in the content, distribution, or phosphorylation of junctional proteins can result in vascular leakage through the tight junctions. BRB breakdown can also result from an upregulation of transendothelial vesicular transport, which has been shown to be a major contributor to BRB failure caused by several mediators and in ocular disease models. Many of the same mediators can simultaneously promote opening of the tight junctions and upregulation of vesicular transport. Degenerative or structural changes to the RPE or RVE cells or to the pericytes and perivascular astrocytes that regulate the inner BRB can also lead to BRB breakdown. Inflammation promotes BRB breakdown, so the use of anti-inflammatory agents may be beneficial. BRB breakdown is not due to a single factor, but is a complex process involving multiple factors, receptors, and signaling pathways. Information on the molecular mechanisms is being revealed, but much remains to be learned. The complexity of the pathogenesis of BRB breakdown makes it likely that the greatest chance for success in preventing macular edema would be in targeting multiple molecules or pathways and a sensitive method for assessing the integrity of the BRB is necessary to monitor the efficacy of different therapeutic strategies.

Acknowledgment

Dr. Vinores is supported by grant R01EY017164 from the National Eye Institute, National Institutes of Health.

See also: Blood–Retinal Barrier; Breakdown of the Retinal Pigmented Epithelium Blood–Retinal Barrier; Macular Edema; Retinal Pigmented Epithelium Barrier; Retinal Vasculopathies: Diabetic Retinopathy; Retinopathy of Prematurity; Secondary Photoreceptor Degenerations: Age-Related Macular Degeneration.

Further Reading

Antonetti, D. A., Lieth, E., Barber, A. J., and Gardner, T. W. (1999). Molecular mechanisms of vascular permeability in diabetic retinopathy. *Seminars in Ophthalmology* 14: 240–248.

Erickson, K. K., Sundstrom, J. M., and Antonetti, D. A. (2007). Vascular permeability in ocular disease and the role of tight junctions. *Angiogenesis* 10: 103–117.

Gardner, T. W. and Antonetti, D. A. (2008). Novel potential mechanisms for diabetic macular edema: leveraging new investigational approaches. *Current Diabetes Reports* 8: 263–269.

Gardner, T. W., Antonetti, D. A., Barber, A. J., et al. (2002). Diabetic retinopathy: More than meets the eye. *Survey of Ophthalmology* 47(supplement 2): S253–S262.

Hofman, P., Blaauwgeers, H. G. T., Tolentino, M. J., et al. (2000). VEGF-A induced hyperpermeability of blood–retinal barrier endothelium *in vivo* is predominantly associated with pinocytic vesicular transport and not with formation of fenestrations. *Current Eye Research* 21: 637–645.

Joussen, A. M., Poulaki, V., Le, M. L., Koizumi, K., et al. (2004). A central role for inflammation in the pathogenesis of diabetic retinopathy. *FASEB Journal* 18: 1450–1452.

Leal, E. C., Santiago, A. R., and Ambrosio, A. F. (2005). Old and new drug targets in diabetic retinopathy: From biochemical changes to inflammation and neurodegeneration. *Current Drug Targets – CNS and Neurological Disorders* 4: 421–434.

Luna, J. D., Chan, C.-C., Derevjanik, N. L., et al. (1997). Blood–retinal barrier (BRB) breakdown in experimental autoimmune uveoretinitis: Comparison with vascular endothelial growth factor, tumor necrosis factor α, and interleukin-1β-mediated breakdown. *Journal of Neuroscience Research* 49: 268–280.

Rizzolo, L. J. (2003). Development and role of tight junctions in the retinal pigment epithelium. *International Review of Cytology* 258: 195–234.

Saishin, Y., Saishin, Y., Takahashi, K., et al. (2003). Inhibition of protein kinase C decreases prostaglandin-induced breakdown of the blood–retinal barrier. *Journal of Cellular Physiology* 195: 210–219.

Vinores, S. A. (1995). Assessment of blood–retinal barrier integrity. *Histology and Histopathology* 10: 141–154.

Vinores, S. A. (2007). Anti-VEGF therapy for ocular vascular diseases. In: Maragoudakis, M. E. and Papadimitriou, E. (eds.) *Angiogenesis: Basic Science and Clinical Applications*, pp. 467–482. Kerala, India: Transworld Research Network.

Vinores, S. A., Derevjanik, N. L., Mahlow, J., Berkowitz, B. A., and Wilson, C. A. (1998). Electron microscopic evidence for the mechanism of blood–retinal barrier breakdown in diabetic rabbits: Comparison with magnetic resonance imaging. *Pathology Research and Practice* 194: 497–505.

Vinores, S. A., Derevjanik, N. L., Ozaki, H., Okamoto, N., and Campochiaro, P. A. (1999). Cellular mechanisms of blood–retinal barrier dysfunction in macular edema. *Documenta Ophthalmologica* 97: 217–228.

Xu, Q., Quam, T., and Adamis, A. P. (2001). Sensitive blood–retinal barrier breakdown quantitation using Evans blue. *Investigative Ophthalmology and Visual Science* 42: 789–794.

Breakdown of the Retinal Pigmented Epithelium Blood–Retinal Barrier

M E Hartnett, Department of Ophthalmology, University of North Carolina, Chapel Hill, NC, USA

Glossary

Adherens junction – Cell–cell junction having transmembrane proteins called cadherins that connect to cadherins of epithelial cells through extracellular domains and to anchor proteins, known as catenins, through intracellular tails. Anchor proteins also bind to a continuous belt of actin filaments along cytoplasmic side of the cell plasma membrane, ultimately holding neighboring cells together.
Focal adhesions – Cell–matrix junctions having transmembrane proteins called integrins that connect cells to extracellular matrix and also to the actin cytoskeleton. Transmembrane proteins can trigger signaling within and between adjacent cells.
Inner blood-retinal barrier – It regulates the transport of fluid, ions, and metabolites between the neurosensory retina and the retinal vasculature.
Na,K,ATPase – Enzyme providing active transport mechanism in the retinal pigment epithelial and other cells. By catalyzing an ATP-dependent transport of three Na^+ ions out and two K^+ ions into the cell, a transmembrane sodium gradient is created (necessary for other Na^+ coupled transport systems) and an osmotic gradient (drives water toward the choroidal or basal side of the RPE and away from the subretinal space).
Outer blood-retinal barrier – It regulates the transport of fluid, ions, and metabolites between the neurosensory retina and the choroidal vasculature.
Tight junction – A cell–cell adhesion usually at the apical lateral aspects of polarized endothelia but can be present in other cells consisting of a number of proteins, including ZO-1, -2, -3, transmembrane protein, occludin, and claudins. The tight junction regulates paracellular permeability between adjacent cells and protein and lipid movement between apical and basal compartments of the cell.

Introduction

The retinal pigment epithelium (RPE) forms the outer blood-retinal barrier (BRB), which regulates the transport of fluid, ions, and metabolites between the neurosensory retina and the choroidal vasculature. The inner BRB is formed by retinal endothelial cells (RECs), which regulate the transport of fluid, ions, and metabolites between the neurosensory retina and the retinal vasculature. Together, the RPE and RECs collectively form the BRB that serves to exclude blood-borne substances from the neurosensory retina and regulates the ionic and metabolic gradients required for normal retinal function. The RPE barrier structures and functions will be broadly described below and for further detail, the reader is directed to other articles in this encyclopedia.

RPE Barrier Structure

The RPE is a polarized monolayer located deep to the neurosensory retina with its apical processes adjacent to the photoreceptors and its basal aspect on Bruch's membrane, a semipermeable collagen and elastin sandwich that separates the choroid from the RPE and neurosensory retina (**Figure 1**). The RPE helps to maintain the outer BRB through tight junctions that are located at the apical–lateral junctions of adjacent cells. Much of what is known about tight junctions was learned from studies of epithelial cells other than the RPE.

Tight junction-associated proteins include ZO-1, -2, -3, and several transmembrane proteins, including junction adhesion molecules and occludin, which bind ZO-1 and -2 that then bind the cytoskeleton. Occludin also has extracellular domains, which bind to those of adjacent cells to form the tight junctions. Claudin proteins are also important in this structure and have tissue and regional specificity. There are a number of other proteins that are important in the development and function of the tight junction.

Besides tight junctions, there are other points of contact between cells or cells and extracellular matrix. Adherens junctions have transmembrane proteins called cadherins that connect to cadherins of adjacent RPE cells through their extracellular domains and to anchor proteins, known as catenins, through intracellular tails. The anchor proteins also bind to a continuous belt of actin filaments along the cytoplasmic side of the cell plasma membrane. The resulting structure holds neighboring cells together. Focal adhesions have transmembrane proteins called integrins that connect cells to extracellular matrix and also to the actin cytoskeleton. Besides providing structure and connections, transmembrane proteins can trigger signaling pathways within and between adjacent cells.

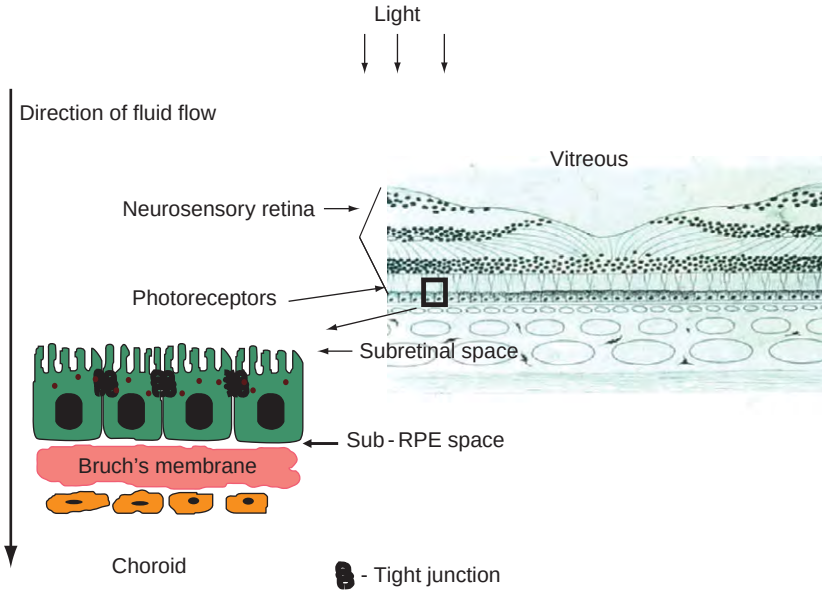

Figure 1 Artist diagram of RPE monolayer with tight junctions at the apical lateral junctions (see inset of RPE/Bruch's membrane/choroid in lower left corner) and in relation to the layers within the macula (shown as a diagram of cross-section of macula on right) and eye. Light is shown coming from above. Overall direction of fluid through the eye is represented by arrow on left.

In addition, a number of active processes regulate the flow of ions, glucose, and amino acids across the RPE. For example, ion fluxes and signaling processes are synchronized between cells through gap junctions, such as connexin 43.

RPE Barrier Functions

The RPE tight junctions regulate the passage of molecules across the paracellular pathway and this regulation depends on the selectivity and permeability of the tight junctions. The transcellular pathway requires pumps, such as Na,K-ATPase, channels, transporters, and metabolic modification to regulate transport across the cells of the monolayer. Breakdown of the RPE barrier may include disruption of the tight junction structure with reduced barrier properties of the RPE. To measure RPE barrier function in a living human, RPE barrier dysfunction is determined clinically by leakage of sodium fluorescein across the RPE seen on stereoscopic images of fluorescein angiograms following an intravenous injection of sodium fluorescein into the bloodstream. However, the distinction between dysfunction of the inner from the outer BRB is difficult in human diseases. This may be because broad BRB breakdown occurs from similar pathophysiologic mechanisms or because of limited resolution in optical imaging. Therefore, techniques are used *in vitro* to study the RPE barrier properties or *in vivo* to selectively poison the RPE and measure fluorescein leakage into the vitreous or eye in animal models (see below). When considering diseases associated with RPE barrier breakdown, it is useful first to understand the fluid flow and forces within the eye.

Transport and Fluid Flow within the RPE and Eye

The vitreous gel is within the eye adjacent to the inner retina, the ciliary body, zonule, and posterior lens capsule. The neurosensory retina includes retinal layers extending from the inner limiting membrane adjacent to the vitreous to the photoreceptors above the RPE. The subretinal space is the potential space between the photoreceptor outer segments and the apical processes of the RPE. The sub-RPE space is a potential space beneath the RPE basal infoldings and Bruch's membrane. The choroid is deep to Bruch's membrane (**Figure 1**). Historically, fluid tends to accumulate more easily in the subretinal than the sub-RPE spaces.

Passive and active transport mechanisms within the RPE and ocular forces within the eye are important when considering the pathophysiology of disease (**Figure 1**). These mechanisms serve to maintain a directional flow from inside the eye, that is, vitreous, to the choroid. Passive transport mechanisms include intraocular pressure and the osmotic pressure from the choroid. However, studies have shown that the RPE reduces directional fluid movement from the subretinal space to the choroid. When the RPE barrier is damaged in animal models (such as through chemicals like sodium iodate), fluid egress from the subretinal space to the choroid is faster than in conditions in

which the RPE has not been damaged. Therefore, in conditions in which there is increased fluid in the subretinal space and presumed RPE BRB breakdown, there is believed to be another pathophysiologic abnormality, such as increased perfusion pressure from the choroid from a vascular tumor, choroidal neovascular membrane, or hyperpermeable choroidal vessels, or reduced ability to accommodate extra fluid, such as with choroidal ischemia or inflammation.

RPE Na,K-ATPase pump

Since the RPE restricts fluid movement from within the eye toward the choroid, it is believed that one or more active transport mechanism is necessary to prevent fluid from accumulating in the subretinal space. The Na, K-ATPase pump is an important active transport mechanism in the RPE. This enzyme is located at the apical surface of the RPE and it is believed that the asymmetric positioning of this enzyme with other transporters, such as chloride channels, is important in creating directional fluid flow. The enzyme catalyzes an adenosine triphosphate (ATP)-dependent transport of three Na+ ions out and two K+ ions into the cell. This transmembrane sodium gradient is necessary for functions of other Na^+ coupled transport systems and creates an osmotic gradient, which helps drive water toward the choroidal or basal side of the RPE and away from the subretinal space. It has been shown *in vitro* using human RPE grown in polarized monolayers that Na,K-ATPase function is necessary for the structural integrity of tight junctions and their function. Inhibition of Na,K-ATPase using a K^+ free media or with ouabain led to increased ionic and nonionic permeability in association with a reduction in the number of contact points in the tight junctions as seen by transmission electron microscopy. Thus, Na,K-ATPase function is necessary to reduce paracellular permeability.

Methods to Assess RPE Barrier Structure and Function

Tight Junction Structure

ZO-1 staining is useful to define the hexagonal architecture of the RPE monolayer *in vitro*, but does not indicate that paracellular permeability is reduced and the barrier is tight. RPE is cultured in specific media to attain tight properties, and the tightness of the monolayer often correlates with the duration in culture and the immunolocalization of occludin to the cell junctions (Figure 2). However, lack of occludin can be associated with a functional tight junction and from this it has been shown that other proteins, including the claudins, are important. Therefore, ZO-1, occludin, and claudins, as well as other proteins, are important in the RPE tight junction function, and the reader is directed to other articles of this encyclopedia.

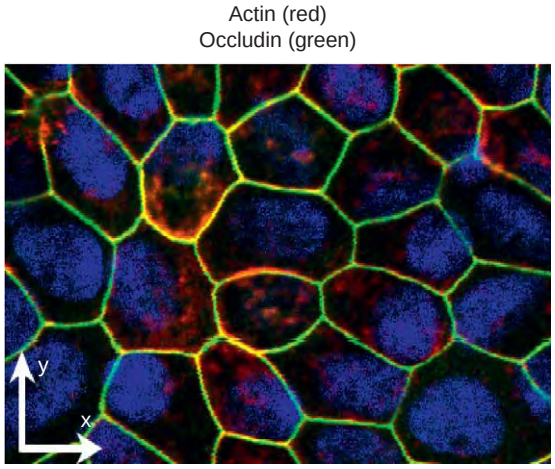

Figure 2 Immunolocalization of occludin (green), actin (red), and Hoechst nuclear stain (blue) in human fetal RPE cultured for >1 month.

When viewed with electron microscopy, it is noted that functional tight junctions have multiple contact points between cells, and that when functional assays show reduced tightness of the barrier, the number of contact points was reduced. The protein components of the tight junction and phosphorylation or activation of certain component, such as occludin, can be determined by immunoprecipitation and/or Western blot analysis.

Barrier Function

Electrophysiologic methods are used to measure barrier function. Transepithial electrical potential (TEP) measures the ion gradient across the monolayer generated by energy-driven ion pumps that regulate passage across the cells. Transepithelial electrical resistance (TER) measures resistance of substances through the paracellular space mainly through the fine structure of the tight junction structure. Permeability to nonionic compounds such as inulin or mannitol can be measured.

Assays That Measure Barrier Properties of RPE

In vitro. Measures of barrier function can vary depending on the RPE cell type, the components making up the media, and the duration of time in culture. Although a TER of 100 Ω cm^2 is sufficient to exclude movement from the apical and basal compartments of a monolayer of RPE, many investigators strive to obtain culture conditions in which the RPE monolayer develops a TER of 500 Ω cm^2. However, in RPE-choroid explants, a TER of 200 Ω cm^2 has been reported. Therefore, it remains unclear whether a higher TER than that *in vivo* indicates a physiologic condition or one in which the structure of the tight junction is

altered by an abnormal microenvironment. It is important in studies that compare the effects of agents on a barrier properties that the cell culture conditions be standardized and replicable.

Ex vivo. Explants of the RPE and choroid have been used in modified Ussing chambers to study the movement of compounds and to determine the barrier properties.

In vivo. Assessing the BRB function is performed with several assays that measure the amount of a substance leaked into the retina. In animal studies, quantitative assays include comparing blood concentration of Evans' blue dye to that measured within the retina after administration of a known concentration, or measuring the extravasation of albumin or inulin into the retina. In addition, qualitative and semi-quantitative assessment (i.e., measuring the area of fluorescein leakage) of fluorescein angiograms can be performed. However, it is difficult to distinguish leakage from the inner versus the outer BRB using these methods.

Clinical assays. Since direct measure of specific functions of the outer BRB is not possible in humans *in vivo*, *in vitro* testing and fluorescein angiography or vitreous fluorophotometry are performed. Vitreous fluorophotometry measures fluorescein leakage into the vitreous by measuring fluorescence.

Fluorescein angiography. When sodium fluorescein (376 Da) dye is activated with blue light (490 nm), it emits fluorescence in the green wavelength (520–530 nm). In a fluorescein angiogram, the dye is injected as a bolus (usually 500 mg/5 mL over 7 s) into the antecubital vein, and images of the fundus are obtained digitally or on film over time. At ~10 s following injection, a choroidal flush from filling of the choroid that is partly blocked by the RPE melanin occurs. Nearly simultaneously, filling of the retinal arterioles occurs. Subsequently, the veins fill (**Figure 3(a)**). Areas of abnormal hyperfluorescence can occur from loss of the RPE melanin or cell (known as window defects because of permitted fluorescence from the underlying choroidal vasculature) or from filling of abnormal vessels or pooling or leakage into spaces where fluid is not naturally present. Hypofluorescence can occur from blockage by pigment or blood, or from nonperfusion within any of the vascular structures in the eye (choroid, retinal vasculature, vessels of the optic nerve). Stereoangiography is helpful to determine the relative position within the retina where abnormal fluorescence was seen. Currently, clinicians gain additional data from optical coherence tomography (OCT).

OCT. Light is directed through a dilated pupil and reflects off different optical interfaces corresponding to layers within the retina (**Figure 3(b)**). Disorganization of the retinal architecture, invasion of tissue, and fluid-like cysts can occur within layers and be used in conjunction with the fluorescein angiogram to diagnose and manage several diseases (see below). Spectral domain OCT has provided better image quality than time domain OCT.

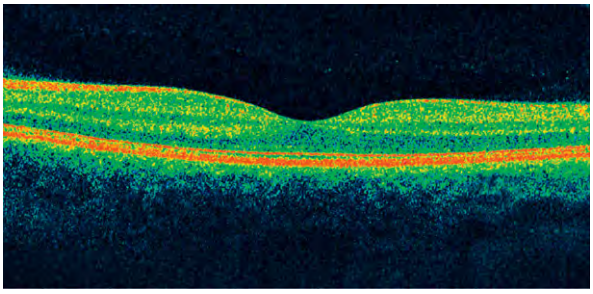

(b)

Figure 3 (a) Normal mid-phase fluorescein angiogram showing optic nerve at left (slightly out of focus) and filling of retinal arterioles and veins. (b) Spectral domain optical coherence tomogram (OCT) of adult macula showing reflective layers of retina (red – highly reflective) and natural foveal depression.

Clinical Conditions Associated with Breakdown of the RPE Barrier

Dysfunction of the BRB is believed to disrupt the normal health and function of the neurosensory retina in several diseases and lead to reduced visual function. RPE barrier dysfunction is diagnosed usually by the presence of hyperfluorescence in the deeper retina, unlike in normal, as determined by fluorescein angiography (cf. **Figures 3(a)** and **4(a)**). Occasionally, vitreous fluorophotometery is used, but this method does not distinguish leakage from the inner or outer BRB. Leakage of fluorescein from the RPE can appear as mild hyperfluorescence and staining, but may lead to intraretinal edema, seen as cystoid macular edema, shown by hyperfluorescence in early frames at the level of the RPE with petalloid hyperfluorescent within the retina in late frames (**Figure 4(b)**). However, most causes of CME are believed to involve several factors including leakage from the inner BRB and Müeller cell dysfunction.

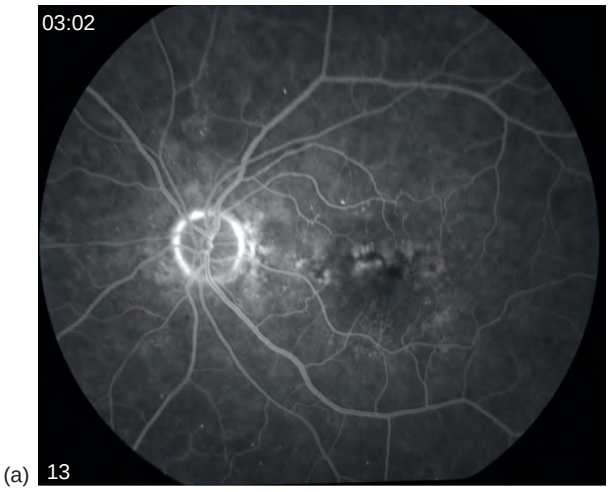

(a)

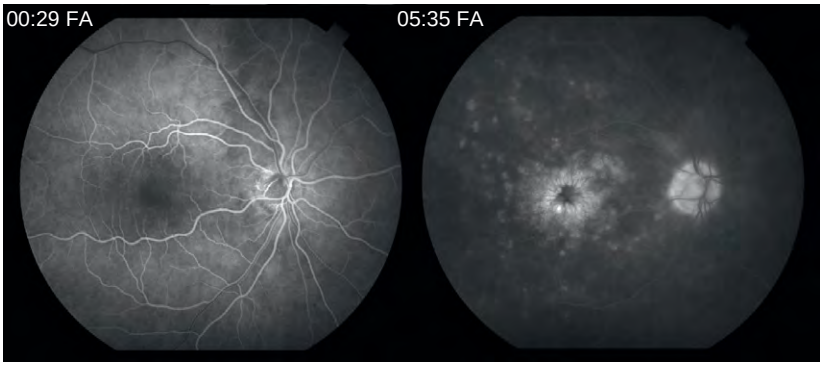

(b) Early frame FA Late frame FA

Figure 4 (a) Deep hyperfluorescence in macula of left eye seen on recirculation phase of fluorescein angiogram demonstrating subtle leakage at the level of the RPE barrier. (b) Early angiogram shows minimal hyperfluorescence surrounding the avascular zone of the macula, but in the recirculation frame of the angiogram, hyperfluorescence takes on a petalloid appearance in a patient with cystoid macular edema.

Inflammation/Infection

Inflammation reduces the BRB function and affects both the inner BRB of the RECs and the outer BRB of the RPE. Clinically, any disease that has an infectious or inflammatory component can compromise the BRB. Viral infections (such as human immunodeficiency virus (HIV), cytomegalovirus (CMV), Herpes) and bacteria (such as *Bacillus cereus*) have been shown to disrupt the tight junctions of the RPE *in vitro*. Factors such as tumor necrosis factor (TNF)-α, interleukins (IL)-6, -8, -1 disrupt tight junction barrier functions *in vitro* or *in vivo*. The RPE has been shown to have chemokine receptors, such as CXCR4, which can be activated by its ligand, stromal-derived factor (SDF-1), to release chemokines such as monocyte chemotactic protein-1 (MCP-1) and IL-8. Chemokines, like MCP-1, can attract leukocytes. Contact of RPE with monocytes results in additional secretion of IL-8 and MCP-1 through several pathways involving mitogen-activated protein kinases. Such pathways may amplify the effects of inflammation on BRB breakdown. As a model of human uveitis, experimental autoimmune uveoretinitis (EAU) is induced in animals by immunization with different proteins. For example, EAU can be induced in Lewis rats by immunization with S-antigen or in mice using peptides to interphotoreceptor retinoid-binding protein. A number of events occur in the EAU model and one is the movement of leukocytes into the retina. It has been shown that transient loss of ZO-1 occurs in RPE from IL-1 and MCP-1. (Transient loss of occludin-1 in RECs within venules was believed to play a role in permitting leukocyte diapedesis in the EAU model.) Inflammation in conditions such as Vogt Kayanagi Harada's disease, or choroidal inflammatory conditions can reduce RPE barrier function in humans.

Age-Related Macular Degeneration

Age-related macular degeneration (AMD) is a leading cause of nonreversible blindness worldwide. Clinical

evidence of RPE BRB dysruption is seen in fluorescein angiograms showing hyperfluorescence from the choroidal vascular normally blocked by healthy RPE, but where loss of melanin or RPE cells has occurred, as in atrophic AMD (**Figure 5**). Hyperfluorescence can also occur from leaky blood vessels that appear to disrupt the RPE barrier and lead to fluid accumulation in neovascular AMD (**Figure 6**). OCT provides additional evidence in neovascular AMD as to the location of the fluid: beneath the RPE (sub-RPE), above it (subretinal), or within the retina itself (intraretinal) (**Figure 7**). Neovascular AMD occurs in about 10% of AMD cases but accounts for 90% of severe vision loss.

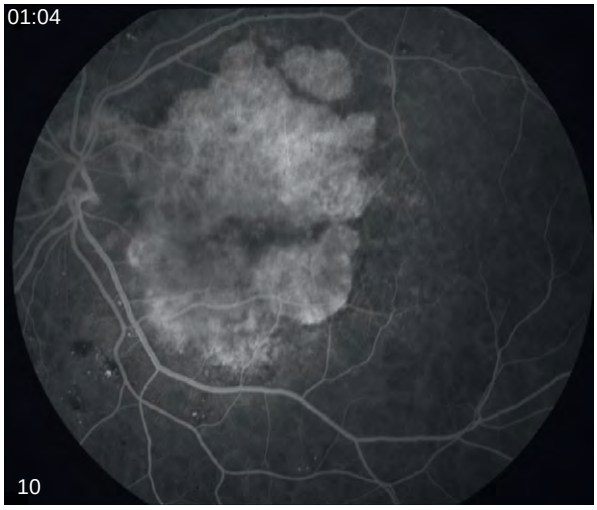

Figure 5 Presence of hyperfluorescence in late frame of fluorescein angiogram because of loss of RPE melanin, which naturally blocks fluorescence of underlying choroid.

Most of the neovascular AMD begins as ill-defined hyperfluorescence and late leakage noted on fluorescein angiography and had been initially called occult choroidal neovascularization (CNV). Later, occult CNV was characterized histopathologically as type 1 CNV, indicating that CNV remained beneath the RPE (**Figure 6**). This is in contrast to classic or well-defined CNV, characterized histopathologically as type II CNV in which the CNV has entered the neurosensory retinal space (compare **Figures 6 and 8**). (This distinction is useful as a model but in reality is not so clear-cut, since clinically there are often mixed types.) However, studies have provided support that when vision declines from neovascular AMD, more than half of the time it is from the transition from occult to classic CNV. This prompts the hypothesis that contact of the ECs with the RPE or its matrix can trigger signaling pathways leading to the release of angiogenic or chemotactic growth factors and the migration of choroidal ECs and movement of fluid into the neurosensory retina. These events would appear to involve a breakdown in the RPE BRB properties. Many stimuli that are believed to be involved in the pathophysiology of AMD also reduce BRB properties as determined in *in vitro* assays described earlier. These include, for example, oxidative stress (can disorganize tight junction proteins including occludin), inflammation (can reduce TER and disrupt tight junctions), activation of complement factors (RPE possess complement 5a receptors and can be stimulated by complement 5a to release several cytokines which can then regulate leukocyte function during inflammation), and contact of RPE or its extracellular matrix with endothelial cells (reduce TER and increase permeability of RPE through release of soluble forms of vascular

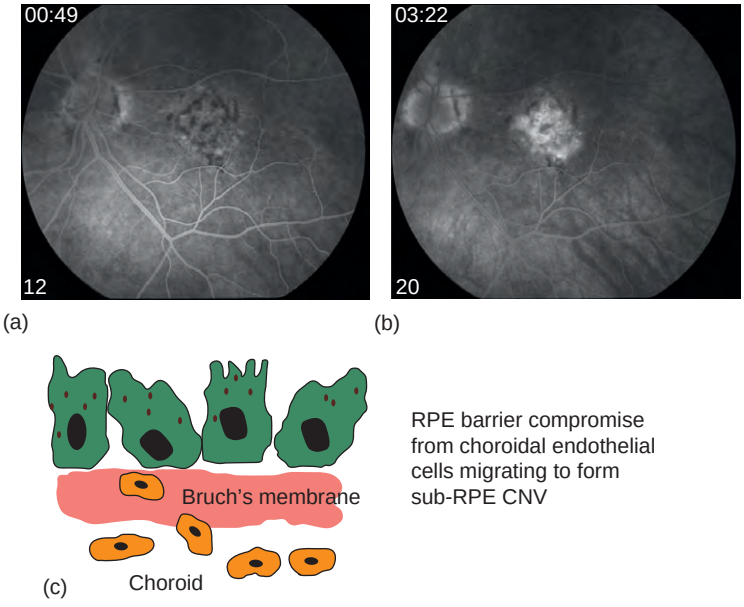

Figure 6 (a) Ill-defined hyperfluorescence in early frame with (b) leakage in late frame of fluorescein angiogram secondary to RPE barrier disruption from occult or type 1 choroidal neovascularization beneath the RPE depicted in (c).

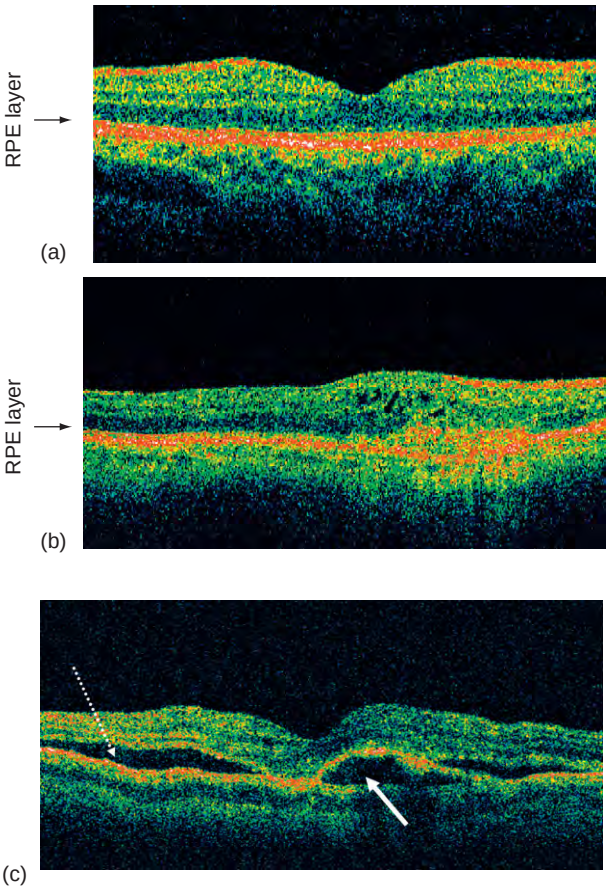

Figure 7 (a) Time domain optical coherence tomogram from patient with normal macula showing good definition of macular layers and normal foveal contour. (b) Optical coherence tomogram from patient with neurosensory retinal choroidal neovascularization, showing disruption of ordered architecture of the retinal layers, increased hyperreflectance (red) in layer near RPE/Bruch's membrane and intraretinal cysts, indicating intraretinal fluid (arrowhead). (c) Optical coherence tomogram showing subretinal fluid (dotted arrow – beneath the photoreceptors and above the RPE) and sub-RPE fluid (solid arrow – beneath the RPE and above Bruch's membrane).

endothelial growth factor (VEGF)). All these stimuli can lead to increased secretion of VEGF, which also increases permeability of blood vessels and RPE and choroidal endothelial migration, proliferation, and chemotaxis, all processes believed important in the development of neurosensory retinal choroidal neovascularization. Furthermore, RPE can release other cytokines that recruit leukocytes, including macrophages that can then release VEGF, or that interact with other processes important in the pathogenesis of AMD.

Diabetes Mellitus

In diabetic retinopathy, the inner BRB is impaired and is most easily appreciated clinically on fluorescein angiography, as leakage from microaneurysms, dilated capillaries, intraretinal microvascular abnormalities, and neovascularization that grows above the inner limiting membrane into the vitreous (**Figure 9**). However, fluorescein staining at the level of the RPE is seen on fluorescein angiograms of patients with diabetes. Also, hyperglycemia has been shown to impair the function of tight junctions of the RPE *in vitro*. Diabetic retinopathy also impairs vision through the development of macular edema, which occurs when there is fluid and solutes that leak from the vasculature into the neurosensory retina (**Figure 10**). It can occur through a breakdown of the inner and potentially outer BRBs. Besides the finding that hyperglycemia can reduce TER in cultured RPE, animal models of diabetic retinopathy have found that there is reduced Na,K-ATPase activity in the RPE. So, once retinal blood vessels leak fluid, lipids, and protein into the neurosensory retina, mechanisms to transport fluid and compounds out of the retina also appear to be impaired in the diabetic state.

Inflammation has been shown to play a role in the pathophysiology of diabetic retinopathy. In animal models, leukostasis or adherence of white blood cells to retinal capillaries has been found and postulated to be a mechanism of later capillary nonperfusion and endothelial damage, which precede the development of proliferative diabetic retinopathy and macular edema. Furthermore, diabetes can also cause a choroidal vasculopathy associated with leukostasis, which may cause choroidal ischemia and later angiogenesis both of which can interfere with intrinsic ocular flow from the vitreous toward the choroid.

Proliferative Vitreoretinopathy

Proliferative vitreoretinopathy (PVR) occurs when cellular contractile membranes develop on the surface of the retina and contract it and pull open breaks in the retina, which can lead to complex retinal detachments. It is the most common cause of failed retinal detachment repair. Vitreous fluorophotometry readings in animal models of PVR show a breakdown in the BRB associated with released cells into the vitreous cavity. It is believed that RPE cells, serum, and other factors have access to the vitreous cavity and are responsible for further breakdown of the BRB and growth of preretinal membranes.

The treatment for PVR, currently, is surgical, requiring vitrectomy and stripping of the membranes from the retina, and then methods to reattach the retina and create a permanent chorioretinal adhesion. However, ongoing research may provide medical means to prevent the formation of preretinal membranes.

Drug Toxicity

Several drugs, including thioridazine (Mellaril), thorazine, hydroxychloroquine, and chloroquine, have been shown to cause vision loss and toxicity with pigmentary changes. The exact effects on the RPE and BRB are unclear.

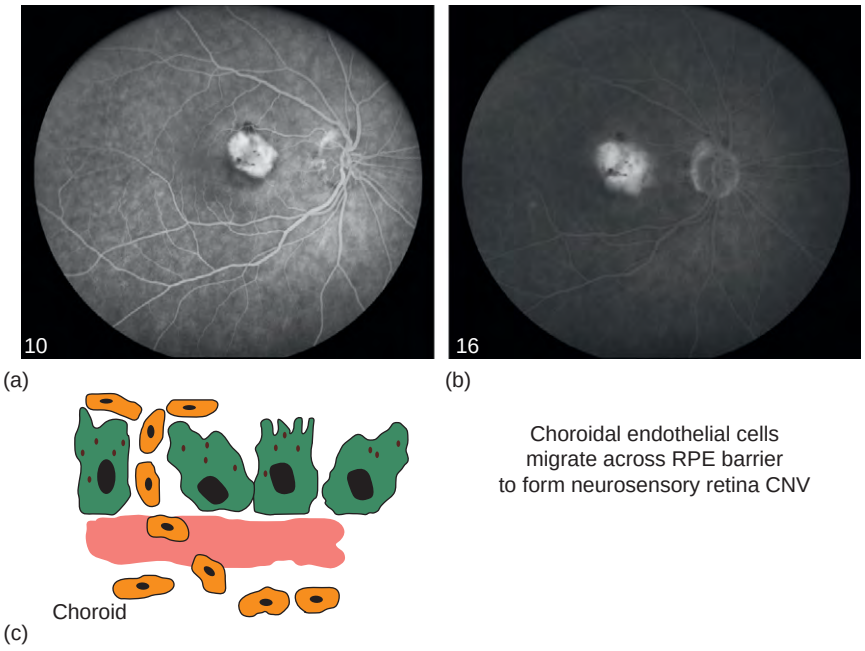

Figure 8 (a) Well-defined hyperfluorescence in early frame with (b) leakage in late frame of fluorescein angiogram from type II choroidal neovascularization (CNV) that has entered the neurosensory retina (depicted in (c)).

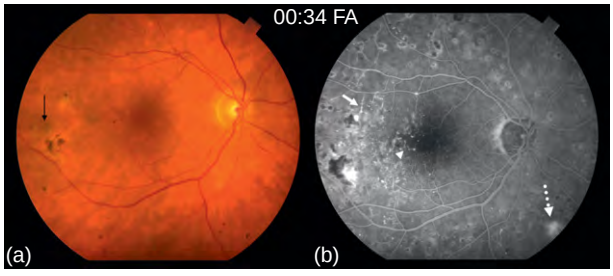

Figure 9 (a) Color images of right eye of patient with diabetic retinopathy previously treated with laser (examples of pigmented laser spots shown by arrows). (b) Fluorescein angiogram of same eye showing intraretinal microvascular abnormalities (arrow) and areas of avascular retina with dilated capillaries, an irregular foveal avascular zone, and microaneurysms (arrowhead). Dotted arrow shows area of hyperfluorescence from leaking neovascularization likely growing above the inner limiting membrane.

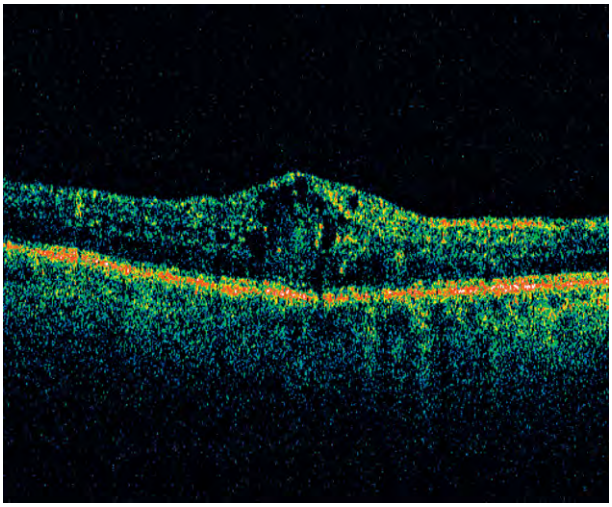

Figure 10 Example of intraretinal edema in a time domain optical coherence tomogram from a patient with diabetic macular edema. Note that the RPE reflective layer is intact in contrast to **Figure 7(b)** in which invasion of cells into the neurosensory retina has occurred in neovascular AMD.

Central Serous Retinopathy

Central serous retinopathy (CSR) is a clinical disease often occurring in young to middle-aged individuals, although it can also manifest or recur and become chronic in later life. Symptoms include reduced vision or inability to focus, and clinical examination shows the presence of a neurosensory retinal detachment within the macula. Fluorescein angiography shows focal areas of RPE leaks (**Figure 11**) or diffuse RPE disturbances. In chronic CSR, RPE decompensation occurs (**Figure 12**) and can lead to chronic subretinal leakage and accumulation of subretinal and intraretinal fluid. Although cases of CSR usually resolve without permanent vision loss, recurrent or chronic CSR can lead to permanent loss of visual acuity. Even when a sole leak appears to be present, CSR is believed to be associated with broad RPE dysfunction, because if only one area of dysfunction were present, the Na,K-ATPases of surrounding healthy RPE would pump out fluid from the subretinal space.

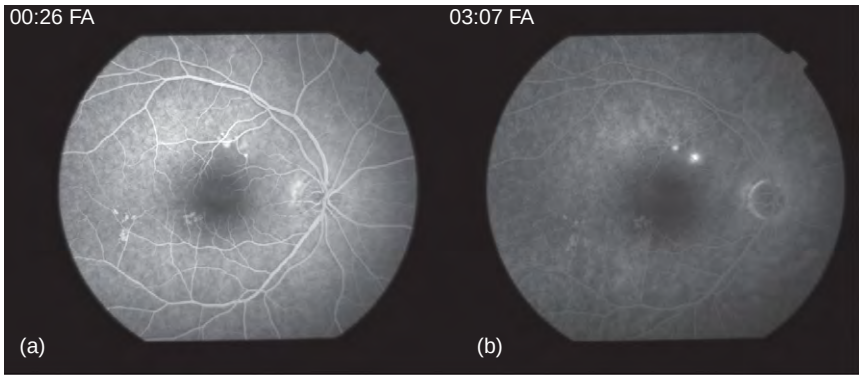

Figure 11 (a) Early hyperfluorescence at level of RPE in fluorescein angiogram from central serous retinopathy in 40-year-old male. (b) Late pooling of dye into the neurosensory retina from a leak in the RPE.

Figure 12 RPE decompensation showing broad area of hyperfluorescence in fluorescein angiogram from chronic long-standing central serous retinopathy in 60 year old male.

Angiograms using indocyanine green dye, which permits visualization of the choroidal vasculature, show that areas of choroidal hypoperfusion and later choroidal hyperpermeability are present in CSR. Although one might suspect inflammation to be a cause of the hyperpermeability, treatment with steroids can severely worsen CSR and should be avoided. Corticosteroids can affect the expression of adrenergic receptor genes and it is thought that this contributes to the overall effect of catecholamines on CSR. Some have postulated that the pathology may involve the adrenocorticotrophic hormone. Another unusual aspect of CSR is that treatment of a sole RPE leak on fluorescein angiography can hasten resolution of the serous detachment, even though it is believed that broad RPE dysfunction is present. Besides corticosteroids, hypertension also increases the risk.

CSR has long been believed to be associated with breakdown in the BRB particularly of the RPE. The cause remains unknown but it is associated with increased stress and a type A personality and is believed to be related to elevated cortisol and epinephrine, which affect the autoregulation of the choroidal circulation. In early studies, adult Japanese monkeys that received multiple daily (>30) injections of intravenous adrenalin developed serous retinal detachments and leaking RPE spots by fluorescein angiography similar in appearance to that seen in CSR. An intramuscular injection of prednisolone led to the same findings on fluorescein angiography but required fewer doses of adrenalin.

Retinitis Pigmentosa

Evidence of abnormalities in the localization of ZO-1, beta-catenin, and other associated adherens proteins in the $rho^{-/-}$ mouse, a model of autosomal dominant retinitis pigmentosa, provides support for tight junction and adherens junction-associated protein modifications in retinitis pigmentosa. Furthermore, in retinitis pigmentosa, there is cystoid macular edema often associated with hyperfluorescence of the RPE cells on fluorescein angiography, suggesting a breakdown of the RPE barrier. Toxins such as sodium iodate selectively poison the RPE and have been used to test the role of the RPE BRB in animal models in which fluid had been injected into the subretinal space or for studies in PVR. Although the toxin is selective for RPE, it poisons the RPE and therefore affects all functions of the RPE, not just the tight junctions.

Urethrane was used to test the BRB in earlier studies and was reported to lead to inhibition of intervesicular transport across endothelia and loss of RPE.

Growth Factors

Besides the role of VEGF in reducing RPE barrier properties, other growth factors play a role. Insulin-like growth factor-1 (IGF-1) can induce VEGF-related RPE barrier breakdown. Also, hepatocyte growth factor (HGF) can lead to disassembly of tight and adherens junctions in

association with reduced barrier properties. HGF has also been shown to be increased in human PVR.

Studies to Increase the Function of the BRB

Carbonic anhydrase inhibitors lead to acidification of the subretinal space, which, in turn, leads to an increase in chloride ion transport into the choroid, thus eliminating water from the subretinal space and retina and increasing the adhesiveness of the RPE. Carbonic anhydrase inhibitors have been associated with improved BRB function, based on reduced fluorescein leakage into the retina, in small clinical studies. However, larger clinical trials have shown a smaller benefit.

See also: Avascularity of the Cornea; Breakdown of the Blood–Retinal Barrier; Breakdown of the Retinal Pigmented Epithelium Blood–Retinal Barrier; Innate Immunity and Angiogenesis; Molecular and Cellular Mechanisms in Allergic Conjunctivitis; Pathogenesis of Uveitis in Humans; Photopic, Mesopic and Scotopic Vision and Changes in Visual Performance; Phototransduction in *Limulus* Photoreceptors.

Further Reading

Alberts, B., Johnson, A., Lewis, J., et al. (2002). Cell junctions, cell adhesion, and the extracellular matrix. In: Alberts, B., Johnson, A., Lewis, J., et al. (eds.) *Molecular Biology of the Cell*, pp. 949–1009. New York: Garland Science.

Bian, Z. M., Elner, S. G., Yoshida, A., and Elner, V. M. (2003). Human RPE-monocyte co-culture induces chemokine gene expression through activation of MAPK and NIK cascade. *Experimental Eye Research* 76: 573–583.

Campbell, M., Humphries, M., Kennan, A., et al. (2006). Aberrant retinal tight junction and adherens junction protein expression in an animal model of autosomal dominant retinitis pigmentosa: The Rho(–/–) mouse. *Experimental Eye Research* 83: 484–492.

Crane, I. J., Wallace, C. A., McKillop-Smith, S., and Forrester, J. V. (2000). CXCR4 receptor expression on human retinal pigment epithelial cells from the blood–retina barrier leads to chemokine secretion and migration in response to stromal cell-derived factor 1 alpha. *Journal of Immunology* 165: 4372–4378.

Dibas, A. and Yorio, T. (2008). Regulation of transport in the RPE. In: Tombran-Tink, J. and Barnstable, C. (eds.) *Ocular Transporters in Ophthalmic Diseases and Drug Delivery,* 1st edn., pp. 157–184. Berlin: Springer/Humana Press.

Fubuoka, Y., Strainic, M., and Medof, M. E. (2003). Differential cytokine expression of human retinal pigment epithelial cells in response to stimulation by C5a. *Clinical and Experimental Immunology* 131: 248–253.

Hartnett, M. E., Lappas, A., Darland, D., et al. (2003). Retinal pigment epithelium and endothelial cell interaction causes retinal pigment epithelial barrier dysfunction via a soluble VEGF-dependent mechanism. *Experimental Eye Research* 77: 593–599.

Hu, J. and Bok, D. (2001). A cell culture medium that supports the differentiation of human retinal pigment epipthelium into functionally polarized monolayers. *Molecular Vision* 7: 14–19.

Jin, M., Barron, E., He, S., Ryan, S. J., and Hinton, D. R. (2002). Regulation of RPE intercellular junction integrity and function by hepatocyte growth factor. *Investigative Ophthalmology and Visual Science* 43: 2782–2790.

Lodish, H., Berk, A., Zipursky, S. L., et al. (2000). Transport across cell membranes. In: *Molecular Cell Biology.* Basingstokes: WH Freeman.

Marmor, M. F. and Wolfensberger, T. J. (eds.) (1998). *The Retinal Pigment Epithelium.* New York: Oxford University Press.

Penn, J. S., Madan, A., Caldwell, R. B., et al. (2008). Vascular endothelial growth factor in eye disease. *Progress in Retina and Eye Research* 27(4): 331–371.

Rajasekaran, S. A., Hu, J., Gopal, J., et al. (2003). Na,K-ATPase inhibition alters tight junction structure and permeability in human retinal pigment epithelial cells. *American Journal of Physiology – Cell Physiology* 284: C1497–C1507.

Rizzolo, L. J. (2007). Development and role of tight junctions in the retinal pigment epithelium. In: Jeon, K. W. (ed.) *International Review of Cytology, a Survey of Cell Biology* vol. 258, pp. 195–234. San Diego, CA: Elsevier.

Sen, H. A., Robertson, T. J., Conway, B. P., and Campochiaro, P. A. (1988). The role of breakdown of the blood–retinal barrier in cell-injection models of proliferative vitreoretinopathy. *Archives of Ophthalmology* 106: 1291–1294.

Xu, H., Dawson, R., Crane, I. J., and Liversidge, J. (2005). Leukocyte diapedesis *in vivo* induces transient loss of tight junction protein at the blood–retina barrier. *Investigative Ophthalmology and Visual Science* 46: 2487–2494.

Yoshioka, H., Katsume, Y., and Akune, H. (1982). Experimental central serous chorioretinopathy in monkey eyes: Fluorescein angiographic findings. *Ophthalmologica* 185(3): 168–178.

C

Cellular Origin, Formation and Turnover of the Vitreous

W Halfter, M Balasubramani, C Ring, and B Schurer, University of Pittsburgh, Pittsburgh, PA, USA

Glossary

Basement membrane – Basement membranes are sheets of extracellular matrix that provide support and anchorage for epithelial and endothelial cells. Typical extracellular matrix components that are found in basement membranes include collagen IV, collagen XVIII, agrin, perlecan, laminin, and nidogen.
Heparin sepharose – This is a media used in chromatography that consists of beads coated with heparin. It is used to isolate heparin-binding molecules.
***In situ* hybridization** – A technique used to detect RNA or DNA. In this case, it is used to localize messenger RNA (mRNA) in tissue sections using labeled complementary RNA as a probe.
Nonpigmented ciliary epithelium – This is a monolayer of cells that is an anterior extension of neuroretina and lines the inner surface of the ciliary body. Underlying this layer is another monolayer of cells called the pigmented ciliary epithelium that is an anterior extension of the retinal pigment epithelium.
Sodium dodecyl sulfate-polyacrylamide gel electrophoresis (SDS-PAGE)/mass spectrometry – This is a technique, sometimes referred to as proteomics, for identifying multiple proteins in a sample. The proteins are separated by electrophoresis (in this case using sodium dodecyl sulfate-polyacrylamide gel electrophoresis). The individual proteins are then identified by tryptic digestion, measuring the mass of the resultant peptides by mass spectrometry and then interrogating databases to match to the distinctive peptide fingerprint of the protein.

The Composition of the Vitreous Body Extracellular Matrix

The vitreous body (VB) is a fibrillar meshwork of extracellular matrix (ECM) that fills the vitreous cavity of the eye (Figure 1(a)). Immunocytochemistry and western blot analysis revealed that major protein constituents of the VB include collagens II, V/XI, IX, and XVIII, and the noncollagenous components fibrillin, fibronectin, opticin, and tenascin (Figure 1(b)). Among the protein components, collagens and fibrillin establish the loose ECM meshwork that is responsible for the gelatinous nature of the VB, while the glycosaminoglycans of the chick vitreal chondroitin sulfate proteoglycans bind the large quantities of water, the most prominent component of the vitreous. The high concentration of water in VB is essential for providing the large volume of the VB and the intraocular pressure that is necessary for eye expansion during development and the close apposition of the retina to the pigment epithelium.

A sodium dodecyl sulfate-polyacrylamide gel electrophoresis (SDS-PAGE)/mass spectrometry analysis of embryonic chick VB extended the list of ECM proteins to about 40. The analysis not only confirmed the presence of the proteins already detected by western blotting, but also added vitronectin, FREM2, chondromodulin, fibulin, lumican, reelin, mimecan, and several basement membrane proteins that are found in the inner limiting membrane of the retina and lens capsule as an additional set of VB components (Table 1). Hyaluronic acid, a linear, high-molecular-weight carbohydrate polymer, is also found as a major VB constituent of mammalian eyes. Hyaluronic acid is not a major constituent of the vitreous in all species, since little is found in the avian eye. The constituents of the vitreous also include a variety of secretory proteins that are typically found in serum or other tissues fluids, such as albumin, transferrin, crystallins, apolipoproteins, immune globulins, $\alpha 2$ macroglobulin, and vitellogenins; they are not considered ECM proteins that do not contribute to the fibrillar matrix of the vitreous.

Collagen II establishes together with collagens V/XI and IX the dominant fibrillar network of the VB ECM that is responsible for the gel-like nature of vitreous. Many of the other ECM proteins, such as fibronectin, tenascin, and opticin are noncovalently associated with these collagen fibrils. Linear polymers of fibrillin establish

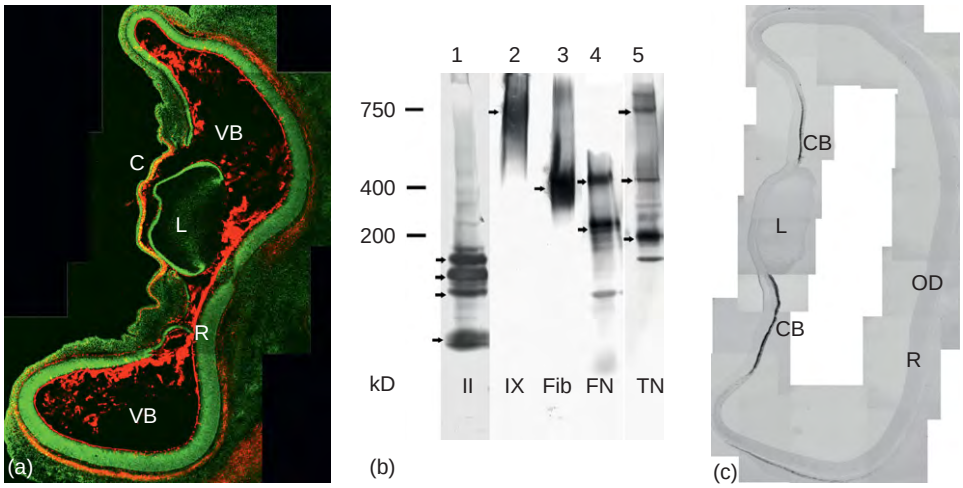

Figure 1 Localization, western blot analysis, and *in situ* hybridization of major VB proteins in the embryonic chick eye. Immunocytochemistry using an antibody to collagen II (a) shows the VB as a loose meshwork of ECM fibrils (red) that fills the entire lumen of the posterior eye. Particular high concentrations of collagen II are found in the cortical vitreous along the surface of the retina (R). Sytox-Green was used as a nuclear counter-stain (green). Collagen II is also found in the stroma of the cornea (C). Western blot analysis (B) of embryonic chick vitreous showed the multiple protein bands of collagen II (II), fibronectin (FN), and tenascin (TN). Fibrillin (Fib) and collagen IX (IX) appeared as long smears due to their extensive glycosylation. Specific bands are indicated by arrows. *In situ* hybridization (C) shows the high concentration of collagen IX mRNA in the ciliary body (CB), the main site of protein synthesis for the interior of the eye. The retina (R) and optic disk (OD) were not labeled, and thus, do not contribute in the synthesis of this protein.

a second ECM network that is ultrastructurally different from the collagen II fibrils. The water-binding and space-filling components of the VB are the highly charged glycosaminoglycans that exist either by themselves (i.e., hyaluronic acid) or are covalently connected to the core proteins of collagen IX and versican, the two chondroitin sulfate proteoglycans that have been detected in VB. The gelatinous nature and the very high water content of the vitreous are responsible for the transparency of the VB and allow passage of light to the retina. The high water concentration of the VB gel also buffers the interior of the eye, presses the retina against the pigment epithelium, and creates the intraocular pressure that promotes the expansion of the eye during ocular development.

Synthesis of VB Proteins in the Eye and Assembly of the VB Gel

Based on its localization next to the retina, most textbooks state that the VB proteins are synthesized by the retinal glial cells and (or) by the hyalocytes, the few macrophage-like cells that are found in the VB. However, the ECM of the VB is assembled from secreted proteins, and the sites of synthesis of these proteins cannot be predicted by location based on immunocytochemistry. A straightforward technique for the detection of the site of synthesis of VB proteins is the localization of their messenger RNA (mRNA) expression sites in the eye by means of *in situ* hybridization, reverse transcription polymerase chain reaction (RT-PCR), or Northern blotting. *In situ* hybridization is currently the method of choice to localize mRNA expression and to pinpoint the sites of synthesis of VB ECM proteins in the eye; particularly since Northern blotting and RT-PCR require microdissection of defined parts of the eye that is inherently prone to contamination from adjacent tissues. Several *in situ* hybridization studies have shown that the dominant site of mRNA expression for VB ECM proteins is the nonpigmented epithelium of the ciliary body, the nonneuronal epithelium that is an anterior extension of the retina located adjacent to the lens (**Figure 1(c)**). The retina contributes to VB protein synthesis to a minor degree: collagen II, for example, has been shown to originate in early embryonic development from the retina, and collagen IX apha1 mRNA has been detected in the retina as well. But even for these proteins, the dominant production site is the ciliary body, and the retina is only a secondary site of synthesis. Other minor sites of VB protein synthesis during eye development are the optic disk and the hyaloids blood vessels.

Independent support for the ciliary body as the dominant site of VB protein synthesis comes from mutant mice with targeted deletions of nectin 1 and 3. Both proteins are cell adhesion proteins that are essential for the morphogenesis of the ciliary body. Deletion of either of the proteins, or the expression of dominant negative constructs, results in an aborted development of the ciliary body and the absence of the VB.

Several of the serum-typical proteins, such as transferrin and α2-macroglobulin that have been detected in the

Table 1 List of ECM proteins from embryonic chick VB

AGRN	Agrin	x	IPI00597536.2	Retina
APP	Beta-amyloid protein		IPI00599595.1	?
CNTN2	Contactin-2 precursor		IPI00580259.1	?
COL11A1	Collagen alpha-1 (XI)	x	IPI00811594.1	?
COL18A1	Collagen alpha-1 (XVIII)	x	IPI00822542.1	CB, OD
COL1A1	Collagen alpha-1 (I)		IPI00572548.2	?
COL1A2	Collagen alpha-2 (I)		IPI00813745.2	?
COL2A1	Collagen alpha-1 (IIA)	x	IPI00589974.1	CB, retina
COL4A5	Collagen alpha-5 (IV)		IPI00818877.1	?
COL5A1	Collagen alpha-1 (V)	x	IPI00602965.1	?
COL5A2	Collagen alpha-2 (V)		IPI00594467.2	?
COL9A1	Collagen alpha-1 (IX)	x	IPI00819026.1	CB, retina
COL9A2	Collagen alpha-2 (IX)	x	IPI00571405.1	CB
COL9A3	Collagen alpha-3 (IX)	x	IPI00592081.1	CB
FBN1	Fibrillin1	x	IPI00591865.2	CB
FN1	Fibronectin	x	IPI00590535.2	?
FREM2	Frem2		IPI00593384.2	?
HSPG	Perlecan	x	IPI00597846.1	Lens
LAMA1	Laminin alpha-1	x	IPI00587004.2	CB, lens; BV
LAMB1	Laminin beta-1	x	IPI00586930.2	CB, lens; BV
LAMC1	Laminin gamma-1	x	IPI00822825.1	CB, lens; BV
LECT1	Chondromodulin-1		IPI00577635.1	?
LOC428086	Stromelysin-1		IPI00599690.2	?
LOC428148	Laminin alpha-5		IPI00578246.2	?
LUM	Lumican		IPI00592361.1	?
NID1	Nidogen-1	x	IPI00572382.2	CB, lens; BV
NLGN4X	Neurologin X isoform 2		IPI00819268.1	?
OGN	Mimecan		IPI00584733.3	?
OPTC	Opticin	x	IPI00592549.1	CB
RELN	Reelin		IPI00580862.2	Retina
SPARCL-1	SPARC-like protein 1		IPI00571290.2	?
SPON1	Spondin-1		IPI00600589.1	?
TNC	Tenascin, cytotactin	x	IPI00587380.1	CB, retina
VTN	Vitronectin		IPI00818472.1	?

The list of proteins was established from samples of E9 chick VB resolved by SDS-PAGE and analyzed by mass spectrometry. The proteins are listed in alphabetical order. The most abundant ECM protein in vitreous is collagen II. Proteins indicated by x were also detected by western blotting and (or) by immunocytochemistry. The proteins indicated in gray were detected after subfractionation of the vitreous by affinity chromatography using heparin sepharose. The sites of synthesis in the eye for each of the proteins, as determined by *in situ* hybridization, are listed in the last column. CB: ciliary body; BV: blood vessels; OD: optic disk; ?: unknown. Minor sites of synthesis are listed in a smaller font size. Note, that with few exceptions, most vitreous ECM proteins are synthesized by the ciliary epithelium, the dominant production site for ECM proteins of the interior of the eye. The IPI numbers refer to the International Protein Index.

vitreous, are also synthesized by the ciliary body. Thus, the current data indicate that the ciliary body is the dominant site of protein synthesis for the interior of the eye.

In vitro experiments, trying to recreate ECM fibril assembly of hyaline cartilage, have shown that mixtures of collagen II, IX, and V/XI, when incubated at physiological temperatures and at defined molar ratios, form long and uniform fibrils with a diameter of 20 nm. Since the VB shares many of its ECM proteins with cartilage, it is conceivable that a similar self-assembly of a fibrillar collagen network occurs in the vitreous chamber of the eye. What has not been established, though, is whether the self-assembled collagen II/IX and V/XI fibrils formed *in vitro* establish a transparent ECM gel with the same biomechanical stability as the vitreous gel. Further, *in vivo* experiments showed that a one-time liquefaction of the vitreous gel is irreversible, as the VB does not reconstitute to a gel even after collagen II and many of the remaining VB ECM proteins have reached normal concentrations again. It appears that a high concentration of collagen II alone may not be sufficient for the VB gel to assemble. Targeted gene deletion in mice has shown that collagen V/XI initiates collagen I fibrillogenesis; therefore, it is possible that collagen V/XI is required for the initiation of the collagen fibrillar network of the VB. It is worth noting that the mouse is not an optimum model system for studying VB assembly, since the vitreous cavity is very small and VB samples difficult to obtain.

The Turnover of VB Proteins

Western blotting showed that the monomeric ECM proteins in the VB are very abundant in the embryonic but almost undetectable in the adult eye. A time-course study in

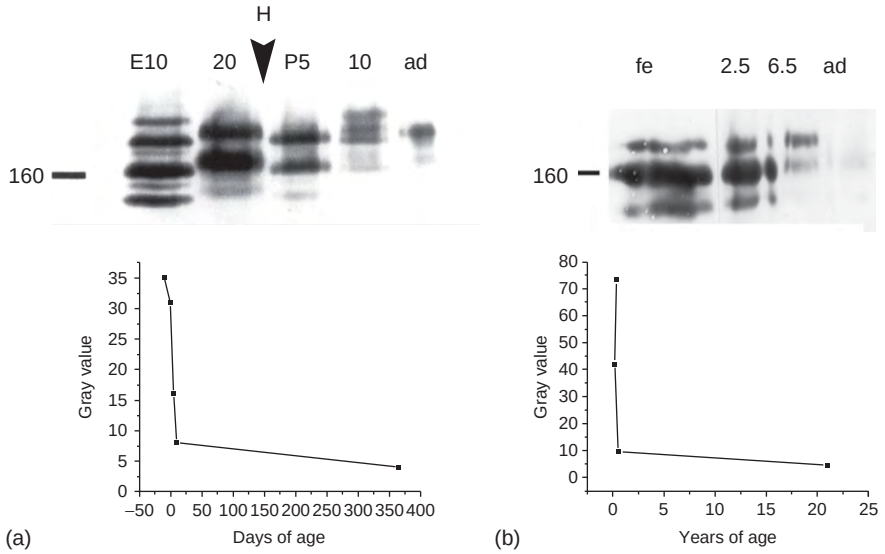

Figure 2 Time course of monomeric collagen II concentration in chick (a) and human (b) VB. The chick VB samples (a) were taken from E10, E20, posthatched (P) 5, P10, and adult chicken. The gray values of the bands was measured by densitometry and plotted against age showing the high concentration of collagen II in embryonic stages of development, and its rapid decline after hatching. The human VB samples (b) were from 20-week fetuses, from 2.5, 6.5 month, and adult humans. The gray values of the collagen II bands blotted against age shows the high concentration of collagen in fetal VB, its rapid decline postnatally and the very low abundance in the adult VB.

chick and human demonstrated a dramatic age-dependent decline in the abundance of the major ECM proteins from VB. In chick, the decline occurred in late embryonic stages, and the concentration of the VB ECM proteins reached very low levels already 10 days after hatching (**Figure 2(a)**). In human, the decline occurs in the first few months after birth, and plotting the data shows that monomeric collagen II is almost undetectable by the second year of life (**Figure 2(b)**).

The presence of monomeric VB ECM proteins during embryogenesis is indicative for active VB *de novo* assembly: for example, chick eyes grow between E2 and E20 by a factor of 20, and the high abundance of VB protein monomers at that stage of development allows for an instant assembly of new VB ECM during the rapid eye growth. The low abundance of monomeric VB proteins in the adult eye indicates a major reduction in the rate of *de novo* synthesis and reflects a slow turnover of the VB.

Quantification of mRNA expression for VB proteins in mouse eyes by Northern blotting at different stages of development confirmed the western blotting data: the mRNA concentrations for collagen II and IX peaked at mid-embryogenesis and then steeply declined postnatally approaching the detection limit. Thus, both western blotting and mRNA expression levels are consistent with the notion that the *de novo* synthesis of VB proteins is dramatically tuned down at early postnatal stages of development and remains at a low level throughout adult life. The data are consistent with the fact that the VB gel undergoes an age-dependent liquefaction and does not regenerate after vitrectomy. Further, immunostaining has shown that the density of collagen IX on the surface of the collagen II fibrils decreases with age, most likely due to protein degradation and insufficient *de novo* synthesis. Not all proteins in VB decrease in concentration over time: transferrin, a non-ECM protein that is synthesized by the ciliary body, remains steady from embryogenesis to old age. A similar steady expression was detected for fibronectin and α2-macroglobulin, the latter even increasing in concentration from embryonic to adult stages. It appears that the downregulation of VB protein expression is prominently targeted to ECM proteins with long half-lives.

It is tempting to speculate that the very long half-life of many of the ECM proteins in the body requires a major downregulation of protein synthesis. Several studies have shown that collagens in articular cartilage have half-lives of up to 100 years, and the half-life of collagen IX in human VB has been estimated to be 11 years. A continued high rate of synthesis of the very slowly metabolized ECM proteins in the eye would probably lead to an over-concentration of the proteins in the vitreous chamber resulting in an opaque vitreous that would interfere with vision.

It if of note that *de novo* synthesis of collagen II has been demonstrated in human eyes after vitrectomy; yet, the concentration was below the detection level of immunocytochemistry and western blotting. Other authors have also suggested that the vitreous is undergoing a constant renewal in the adult.

Acknowledgments

We would like to thank Robert Johnson from the Brain and Tissue Bank for Developmental Disorders (University of Maryland, Baltimore, MD) and Janice Anderson from the Center for Organ Recovery and Education (CORE) of Pittsburgh for providing the fetal and adult human eye samples and the National Science Foundation for support of the project (IBN# 0240774).

See also: Formation and Regression of the Primary Vitreous and Hyaloid Vascular System; Molecular Composition of the Vitreous and Aging Changes; Vitreous Anatomy, Aging, and Anomalous Posterior Vitreous Detachment.

Further Reading

Bishop, P. N. (2000). Structural macromolecules and supramolecular organization of the vitreous gel. *Progress in Retinal and Eye Research* 19: 323–344.

Bishop, P. N., Holmes, D. F., Kadler, K. E., McLeod, D., and Bos, K. J. (2003). Age-related changes on the surface of vitreous collagen fibrils. *Investigative Ophthalmology and Visual Science* 45: 1041–1046.

Bishop, P. N., Takanosu, M., le Goff, M., and Mayne, R. (2002). The role of the posterior ciliary body in the biosynthesis of vitreous humor. *Eye* 16: 454–460.

Blaschke, U. K., Eikenberry, E. F., Hulmes, D. J. S., Galla, H-J., and Bruckner, P. (2000). Collagen XI nucleates self-assembly and limits lateral growth of collagen fibrils. *Journal of Biological Chemistry* 275: 10370–10378.

Halfter, W., Dong, S., Schurer, B., et al. (2005). Embryonic synthesis of the inner limiting membrane and vitreous body. *Investigative Ophthalmology and Visual Science* 46: 2202–2220.

Ihanamaeki, T., Pelliniemi, L., and Vuorio, E. (2004). Collagens and collagen-related matrix components in the human and mouse eye. *Progress in Retinal and Eye Research* 23: 403–434.

Inagaki, M., Irie, K., Ishizaki, H., et al. (2005). Roles of cell-adhesion molecules nectin-1 and nectin-3 in ciliary body development. *Development* 132: 1525–1537.

Itakura, H. I., Kishi, S., Kotajima, N., and Murakami, M. (2005). Vitreous collagen metabolism before and after vitrectomy. *Graefe's Archive for Clinical and Experimental Ophthalmology* 243: 994–998.

Linsenmayer, T. F., Gibney, E., Gordon, M., et al. (1990). Extracellular matrices of the developing chick retina and cornea. Localization of mRNAs for collagen II and IX by in situ hybridization. *Investigative Ophthalmology and Visual Science* 31: 1271–1276.

Los, L. I., van der Worp, R. J., van Luyn, M. J. A., and Hooymans, J. M. M. (2003). Age-related liquefaction of the human vitreous body: LM and TEM evaluation of the role of proteoglycans and collagen. *Investigative Ophthalmology and Visual Science* 44: 2828–2833.

Wright, D. W. and Mayne, R. (1988). Vitreous humor of chicken contains two fibrillar systems: An analysis of their structure. *Journal of Ultrastructure Research* 100: 224–234.

Central Retinal Vein Occlusion

S S Hayreh, University of Iowa, Iowa City, IA, USA

Glossary

Demographic – The statistical study of a population, including geographical distribution, sex and age composition, and birth and death rates.
Electroretinography – The recording of the changes in electric potential in the retina by stimulating it by light.
Fluorescein fundus angiography – The visualization of blood vessels in the interior of the eye following intravenous injection of fluorescein.
Glaucoma – An eye disease caused by an increase in eye pressure, which causes changes in the optic nerve and loss of vision.
Hematological – Dealing with the blood and blood-forming tissues.
Histopathological – Dealing with the minute structure of diseased tissues.
Lamina cribrosa – The perforated portion of the back part of the white of the eye (sclera) through which nerve fibers from the retina exit.
Multifactorial – Related to, or arising through the action of many factors.
Neovascularization – The formation of abnormal new blood vessels.
Ophthalmoscopy – The examination of the interior of the eye with the instrument called ophthalmoscope.
Panretinal photocoagulation – The application of an intense beam of laser light to the entire retina.
Pathogenesis – The mechanisms of development of a disease.
Perimeter – An apparatus used to test the visual field.

Retinal vein occlusion is the most common retinal vascular occlusive disorder. In general, there is a tendency to regards this as one disease; that is not only incorrect but also causes much confusion. From the point of view of pathogenesis, clinical picture, prognosis, and management, retinal vein occlusion in fact consists of six distinct clinical entities that are categorized as follows:

1. Central retinal vein occlusion (CRVO), which comprises
   a. nonischemic CRVO, and
   b. ischemic CRVO.
2. Hemi-central retinal vein occlusion (HCRVO), which comprises
   a. nonischemic HCRVO, and
   b. ischemic HCRVO.
3. Branch retinal vein occlusion, which includes
   a. major BRVO, and
   b. macular BRVO.

It is beyond the scope of this article to discuss all the six types of retinal vein occlusion; hence, we restrict our discussion only to CRVO. Over the last 150 years, a large volume of literature has accumulated on the subject of CRVO. The objective of this article is to provide a brief review of the current state of our knowledge on the subject.

Pathogenesis

A good understanding of the pathogenesis of a disease is fundamental to a full grasp of the clinical features of the disease and its logical management. There is almost a universal tendency to blame one or two factors as causative factor(s) in the development of CRVO, but association does not necessarily mean there is a cause-and-effect relationship. Available evidence strongly suggests that the pathogenesis of CRVO, like many other ocular vascular occlusive disorders, is a multifactorial process. It seems that some risk factors predispose an individual or an eye to CRVO (predisposing risk factors), while others act as the final insult and produce clinically evident disease (precipitating risk factor(s)). Only when an eye and an individual have the critical number of risk factors required for the development of CRVO, does the CRVO develop. This must explain why bilateral CRVO is rare. Once this basic concept of multifactorial causation is understood, one can attach appropriate significance to the various risk factors. The various risk factors for CRVO may be divided into the following three categories:

Local. Two local factors are particularly important:

1. The central retinal vein and central retinal artery lie in the center of the optic nerve, surrounded by a fibrous tissue envelope (**Figure 1**). In elderly persons, sclerotic changes in the central retinal artery and the fibrous tissue envelope compress the thin-walled central retinal vein, resulting in narrowing of its lumen. This produces circulatory stasis. According to Virchow's triad, slowing down of the blood stream causes stagnation thrombosis.

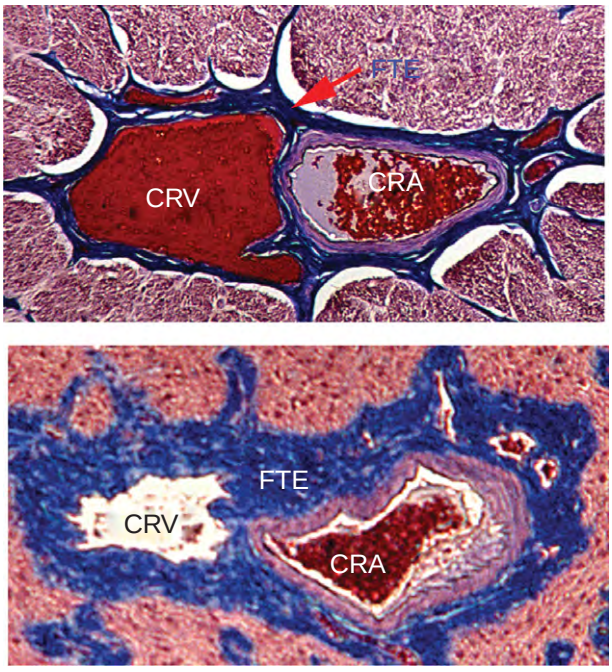

Figure 1 Histological sections (Masson's trichrome staining) showing the central retinal vessels and surrounding fibrous tissue envelope, as seen in a transverse section of the central part of the retrolaminar region of the optic nerve, in a normal rhesus monkey (above) and in a rhesus monkey with experimental arterial hypertension, atheroselerosis, and glaucoma (below). CRA, Central retinal artery; CRV, central retinal vein; FTE, fibrous tissue envelope.

2. It is well established that CRVO is significantly more common in patients with raised intraocular pressure (IOP) and glaucoma.

Systemic. A significant association of CRVO has been reported with arterial hypertension, diabetes mellitus, cardiovascular disease, atherosclerosis, and thyroid disease.

Hematological. The literature is full of reports of hematological abnormalities in CRVO. The author recently critically reviewed the literature dealing with these and found no definite pattern – often the negative findings outweighed the positive ones. The idea of hematologic factors playing a role in CRVO is essentially based on the assumption that those hematological disorders, which play a role in development of systemic venous thrombosis (e.g., deep vein thrombosis), must also do so in CRVO. All the available evidence, however, indicates that the hematologic risk factor responsible for major systemic venous thrombosis occurs only sporadically in CRVO. Furthermore, CRVO is extremely rare in patients with systemic venous thrombosis. Moreover, the presence of a particular hematologic disorder in a patient does not necessarily mean it has a cause-and-effect relationship with CRVO. In view of this, there is no particular reason for conducting a detailed hematological investigation in all patients with CRVO.

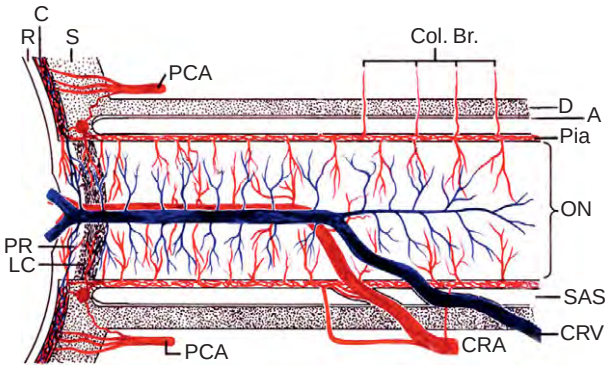

Figure 2 Schematic representation of blood supply of the optic nerve. A, arachnoid; C, choroid; CRA, central retinal artery; Col. Br., collateral branches from other orbital arteries to the optic nerve; CRV, central retinal vein; D, dura; LC, lamina cribrosa; ON, optic nerve; PCA, posterior ciliary artery; PR, prelaminar region; R, retina; S, sclera; SAS, subarachnoid space. Adapted from Hayreh, S. S. (1974). *Transactions – American Academy of Ophthalmology and Otolaryngology* 78: OP240–OP254, with permission from American Academy of Ophthalmology.

Site of Occlusion in CRVO

Based on histopathological studies, there is a widespread misconception that the site of occlusion in CRVO is invariably at the lamina cribrosa. However, all the available anatomical, experimental, and clinical evidence (particularly fluorescein fundus angiography) shows that the actual site of occlusion in the central retinal vein is typically in the optic nerve, at a variable distance posterior to the lamina cribrosa, and not at the lamina cribrosa (Figure 2). The farther back the site of occlusion, the more collaterals are available, and the less severe is the retinal venous stasis. Thus, in nonischemic CRVO the site of occlusion most likely is farther back in the optic nerve, whereas in ischemic CRVO it is closer to the lamina cribrosa.

Demographic Characteristics

CRVO is more common in middle-aged and elderly persons, and patients with ischemic CRVO tend to be older than those with nonischemic CRVO. Contrary to the prevalent impression, CRVO is not at all rare in young persons, and the incidence in persons under the age of 45 years has been reported as high as 18%. Thus, no age is immune. In our series of 620 consecutive CRVO cases, 81% were nonischemic and 19% ischemic CRVO. The Kaplan–Meier estimate of the cumulative proportion of eyes that developed nonischemic CRVO in the fellow eye is about 6% within 1 year and 7% within 5 years from onset in the first eye; for ischemic CRVO it is 5.6% at 2.8 years.

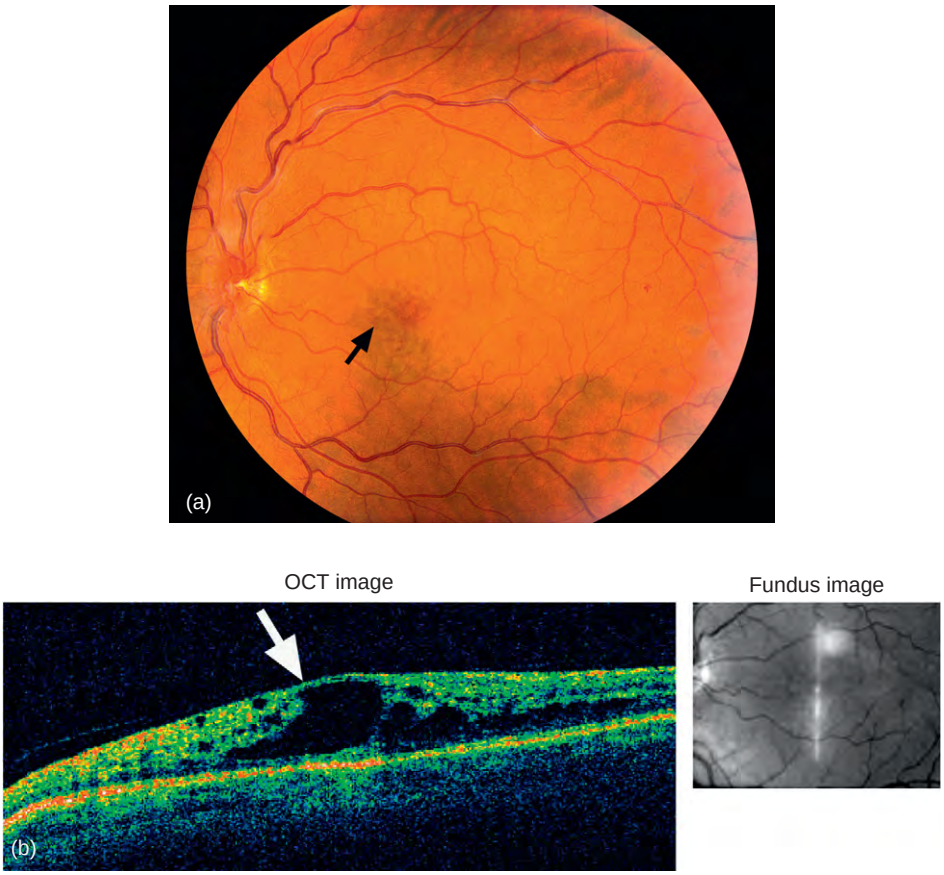

Figure 3 Fundus photograph (a) and OCT (b) of a nonischemic CRVO eye with resolution of retinopathy, except for the cystoid macular edema (arrow).

Clinical Features

With regard to symptoms, patients with nonischemic CRVO may have no symptoms and it may be detected as an incidental finding on a routine ophthalmic examination. Retinal venous stasis with mild retinal hemorrhages *per se* is asymptomatic. Occasionally there may be a history of episodes of transient visual blurring before constant visual deterioration. Almost invariably, it becomes symptomatic only when there is involvement of the foveal region by development of macular edema (**Figures 3** and **4**) and rarely by hemorrhages. Therefore, the most common complaint is gradual development of central visual blurring, usually more marked on waking up in the morning, improving to a variable extent after a few hours or in the afternoon. In ischemic CRVO, on the other hand, there is always marked deterioration of vision.

While the diagnosis of CRVO is not difficult because of its classical clinical features (**Figures 5** and **6**), the main problem is differentiation of nonischemic from ischemic CRVO, which is crucial for the correct management of CRVO. This is because nonischemic CRVO is a comparatively benign condition, with permanent central

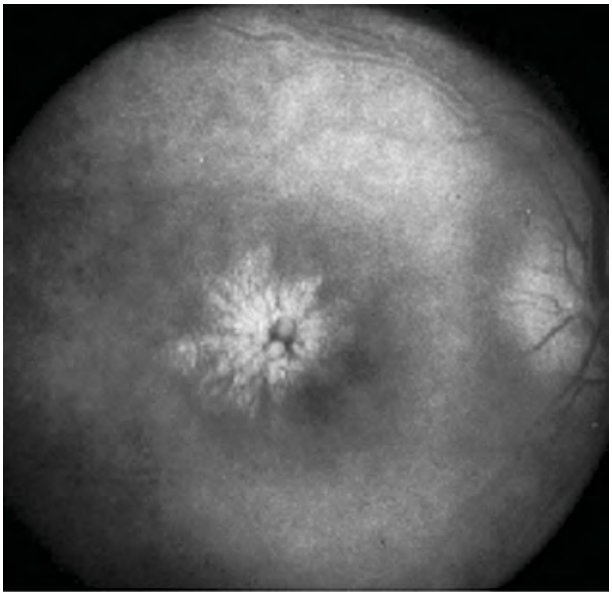

Figure 4 Late phase of fluorescein fundus angiogram of an eye with nonischemic CRVO showing classical petaloid pattern of cystoid macular edema.

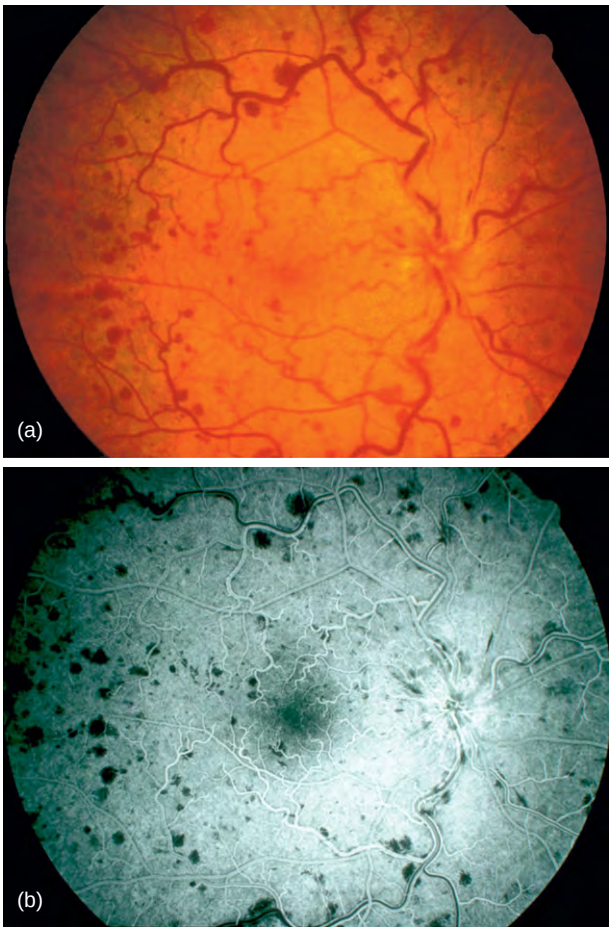

Figure 5 Fundus photograph (a) and fluorescein fundus angiogram showing intact retinal capillary network (b) of an eye with nonischemic CRVO. Reproduced from Hayreh, S. S. (1994). *Indian Journal Ophthalmology* 42: 109–132.

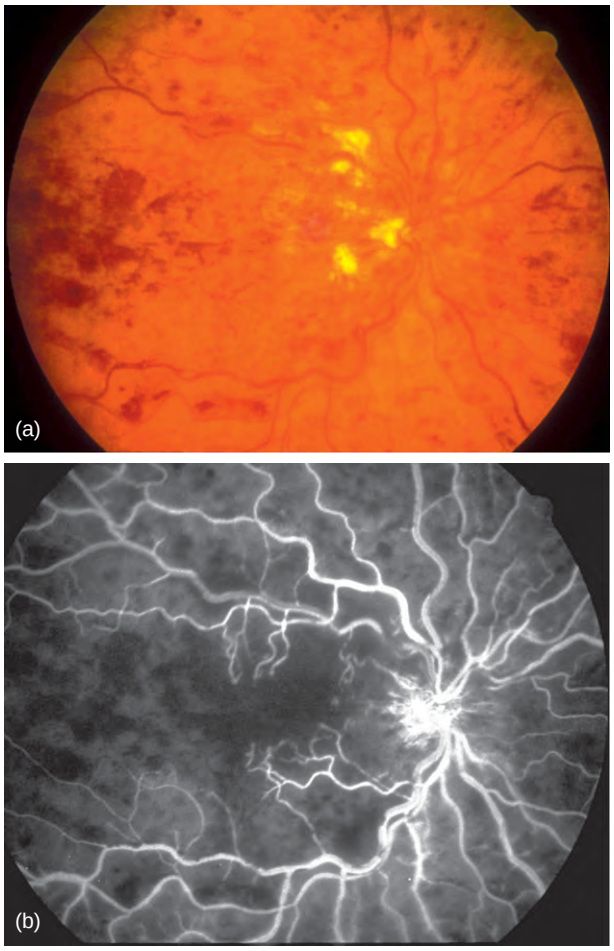

Figure 6 Fundus photograph (a) and fluorescein fundus angiogram showing complete nonperfusion of retinal capillary network (b) of an eye with ischemic CRVO. Reproduced from Hayreh et al. (1983). Ocular neovascularization with retinal vascular occlusion III. Incidence of ocular neovascularization with retinal vein occlusion. *Ophthalmology* 90: 488–506.

scotoma as the major complication in some eyes, but no ocular neovascularization (NV). In sharp contrast to this, ischemic CRVO is a blinding disease, with high risk of development of anterior segment NV, particularly neovascular glaucoma, which often results in blindness or even loss of the eye. Thus, the two types of CRVO can be compared to benign and malignant tumors.

Differentiation of Ischemic from Nonischemic CRVO

Ophthalmologists have almost universally used ophthalmoscopic and fluorescein angiographic appearances to evaluate and manage CRVO and to differentiate ischemic from nonischemic CRVO. However, these two morphological tests have much lower sensitivity and specificity to differentiate the two types of CRVO compared to the four functional tests – visual acuity, peripheral visual fields plotted with a Goldmann perimeter, relative afferent pupillary defect, and electroretinography. Table 1 gives sensitivity and specificity of various functional tests to differentiate ischemic from nonischemic CRVO.

On fluorescein fundus angiography, to differentiate ischemic from nonischemic CRVO, the presence of a 10 disk area or more retinal capillary obliteration has been regarded as the gold standard in practically all the reported studies, but there are several serious problems with this criterion, including the following:

1. During the early, acute stages of CRVO, to provide reliable information on retinal capillary obliteration, angiography has many serious limitations, including extensive retinal hemorrhages, poor-quality angiograms, inability to perform angiography for a variety of reasons, the time lag of several weeks after the onset of CRVO before retinal capillary obliteration is visible, and other limitations. A study showed that fluorescein angiography provided reliable information at best in only

50–60% of cases during the early, acute phase, which is clinically unsatisfactory for early management.
2. Most importantly, a criterion of a 10 disk area or more of retinal capillary obliteration has been widely advocated as the definitive yardstick for diagnosis of ischemic CRVO. However, this is an invalid criterion to differentiate nonischemic from ischemic CRVO. A multicenter study showed that eyes with <30 disk diameters of nonperfusion and no other risk factor are at low risk for iris/angle NV (i.e., ischemic CRVO), 'whereas eyes with 75 disk diameters or more are at highest risk'.

As regards ophthalmoscopy, there is a marked overlap between the two types of CRVO and virtually a continuous evolution of ophthalmoscopic lesions (i.e., retinal hemorrhages, venous dilatation, and cotton-wool spots, etc.; **Figures 5(a)** and **6(a)**), which makes it hard to use this to differentiate the two types of CRVO.

A study showed that to differentiate the two types of CRVO, the overall order of reliability of various tests is as follows:

1. *Relative afferent pupillary defect*. In unilateral CRVO, when the fellow eye is normal.
2. *Electroretinography*. This is the next best test and it can be done even when the fellow eye is not normal, as in bilateral CRVO.
3. *Relative afferent pupillary defect combined with electroretinography*. This proved to be the most reliable (in 97%).
4. *Peripheral visual fields plotted with a Goldmann perimeter*. This is next in order and better than visual acuity. Since central scotoma is present in all CRVO eyes, that does not help in differentiation.
5. *Visual acuity*. This is also helpful in many cases.
6. *Fluorescein angiography*. This proved to be much worse than any of the functional tests in early stages.
7. *Ophthalmoscopy*. This is the least reliable and most misleading parameter of all.

Table 1 Sensitive and specify of various functions tests to differentiate ischemic from nonischemic CRVO

Functional test		*Sensitivity*	*Specificity*
Visual acuity	20/400 or less	91%	88%
Peripheral visual fields	No I-2e	97%	73%
	Defective V-4e	100%	100%
Relative afferent pupillary defect	≥0.9 log units	80%	97%
Electroretinography	b-wave amplitude <60%	80%	80%

From Hayreh, S. S., Klugman, M. R., Beri, M., Kimura, A. E., and Podhajsky, P. (1990). Differentiation of ischemic from non-ischemic central retinal vein occlusion during the early acute phase. *Graefe's Archive for Clinical and Experimental Ophthalmology* 228: 201–217.

Thus, we can conclude that no single test has 100% sensitivity and specificity to differentiate the two types of CRVO during the early, acute phase, such that no single test can be considered a gold standard; however, combined information from all the six tests is almost always reliable. The four functional tests overall are much superior to the two morphologic tests.

Course of CRVO

Both types of CRVO run a self-limited course, taking from a few weeks to many years for the retinopathy to resolve. In the meantime, some of these eyes can develop various complications, including those discussed below.

Complications

The main complications of the two types of CRVO are as follows:

1. *Macular edema*. This is the most common complication in both types of CRVO (**Figures 3** and **4**). However, it does not affect eyes with mild nonischemic CRVO. Chronic macular edema later on may produce cystoid macular degeneration (**Figure 3(a)**), macular pigmentary degeneration (very much resembling age-related macular degeneration; **Figure 7**), and/or epiretinal membrane – all resulting in central scotoma.
2. *Ocular NV*. This is the most dreaded complication of CRVO and a complication of ischemic CRVO alone. It is extremely important to note that ocular NV is almost never seen in nonischemic CRVO, unless it is associated with diabetic retinopathy or ocular ischemia.

The cumulative probability of developing various types of ocular NV in ischemic CRVO is shown

Figure 7 Fundus photograph of an eye with resolved nonischemic CRVO, showing macular pigmentary degeneration and retinociliary collaterals on the optic disk, as the permanent, residual changes.

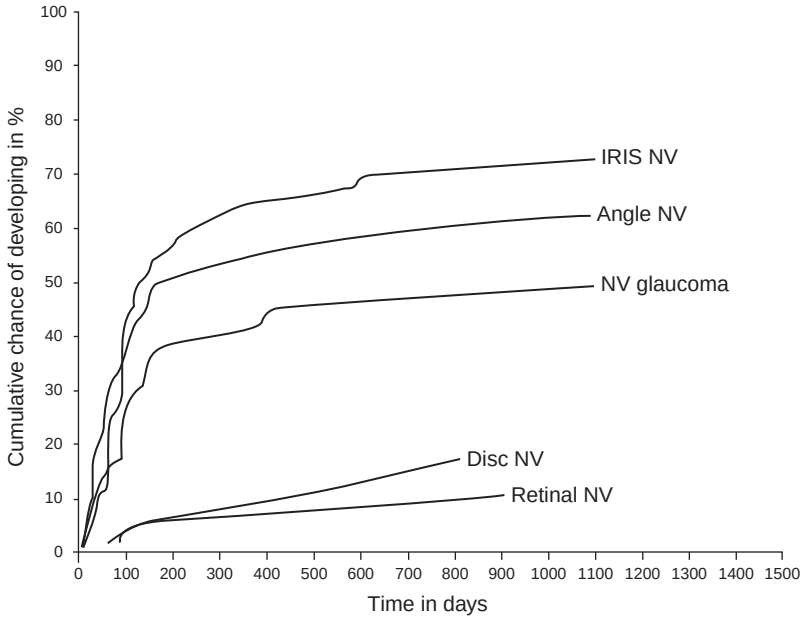

Figure 8 A graphic representation of cumulative chances (in %) of developing various types of ocular neovascularization in ischemic CRVO in relation to time from onset of the disease (in days).

graphically in Figure 8, which provides five very important pieces of information for management of CRVO:

a. Not every eye fulfilling the criteria given above for ischemic CRVO develops ocular NV.
b. When ocular NV does develop, the most common site is the anterior segment, much less frequently the posterior segment.
c. The greatest risk of developing anterior segment NV is during the first 7–8 months, after which the risk falls dramatically, to minimal. The old concept of 100-day glaucoma has no validity.
d. The maximum risk of developing neovascular glaucoma is about 50% – not 100%, as often stated.
e. About one-third of eyes with iris NV and about one-quarter of eyes with both iris and angle NV, contrary to the prevalent impression, never progress to develop neovascular glaucoma.

In order to place the overall incidence of ocular NV, particularly of neovascular glaucoma in CRVO, in true perspective, it is essential to point out two important facts:

i. ischemic CRVO constitutes only one-fifth of all CRVO cases (see above);
ii. neovascular glaucoma, the most dreaded complication of CRVO, is seen at the maximum in about 50% of ischemic CRVO cases only.

This means that the overall incidence of neovascular glaucoma in all CRVO cases is no more than 10% at the most – a key fact in any consideration of the management of CRVO.

3. *Vitreous hemorrhage.* In CRVO, this may be either secondary to retinal/optic disk NV or due to rupture of the retinal blood through the internal limiting membrane, particularly in eyes with many subinternal limiting membrane hemorrhages (Figures 9–11). Therefore, it is important to be aware that the presence of vitreous hemorrhages in CRVO does not always mean that there is retinal/disk NV.

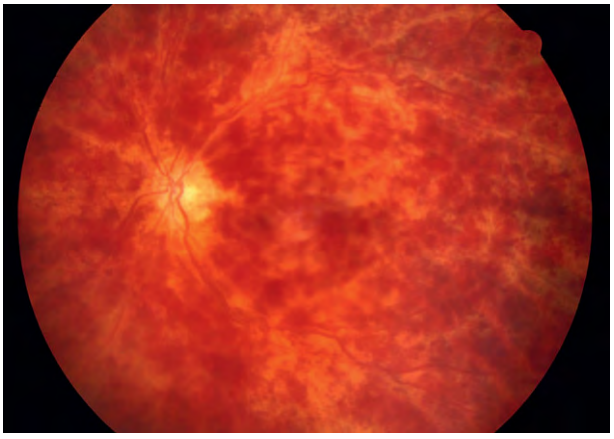

Figure 9 Fundus photograph of an eye with nonischemic CRVO in a patient on aspirin, showing extensive retinal hemorrhages.

4. *Cilioretinal artery occlusion.* The major cause of serious visual loss in nonischemic CRVO is the development of associated transient occlusion of a cilioretinal artery due to hemodynamic block and not due to any thrombosis in the artery (Figures 12 and 13). This is particularly so when the artery supplies a large sector of the retina (Figure 13) or supplies the entire maculopapillar bundle (resulting in a large absolute centrocecal defect).

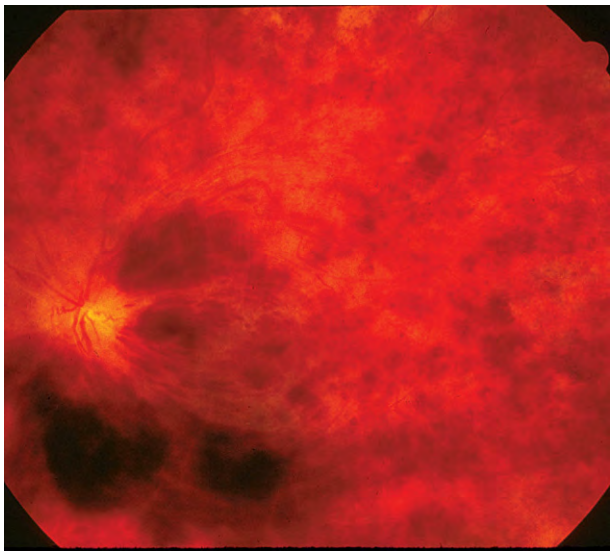

Figure 10 Fundus photograph of an eye with nonischemic CRVO in a patient on anticoagulant therapy, showing extensive retinal hemorrhages. Reproduced from Hayreh, S. S. (2006). *Retina* 26: S51–S62, with permission from Wolters Kluwer.

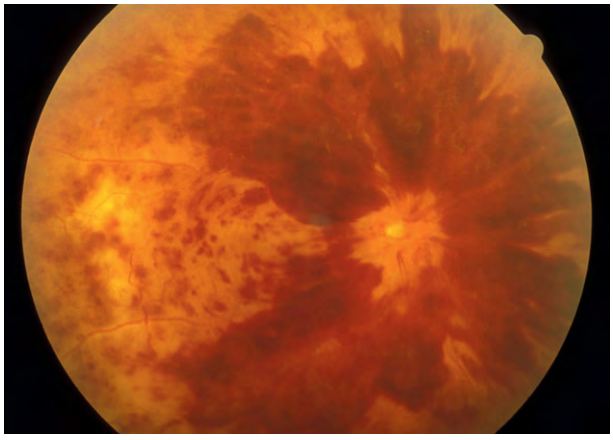

Figure 11 Fundus photograph of an eye with ischemic CRVO in a patient on anticoagulant therapy, showing extensive preretinal hemorrhages.

5. *Conversion of nonischemic CRVO to ischemic CRVO.* Figure 14, based on study of 620 consecutive CRVO eyes, shows Kaplan–Meier survival curves for cumulative probability of conversion of nonischemic CRVO to the ischemic type. This change can happen either overnight or gradually.

Management of CRVO

In the management of CRVO, the first, most crucial step is to determine whether one is dealing with nonischemic or ischemic CRVO because of their very different nature, prognosis, visual outcome, and management. Lack of such differentiation has resulted in major controversies on CRVO.

Figure 12 Fundus photograph of an eye with nonischemic CRVO and retinal infarct in a narrow strip below the foveola due to associated cilioretinal artery occlusion. Reproduced from Hayreh, S. S., Fraterrigo, L., and Jonas, J. (2008). Central retinal vein occlusion associated with cilioretinal artery occlusion. *Retina* 28: 581–594, with permission from Wolters Kluwer.

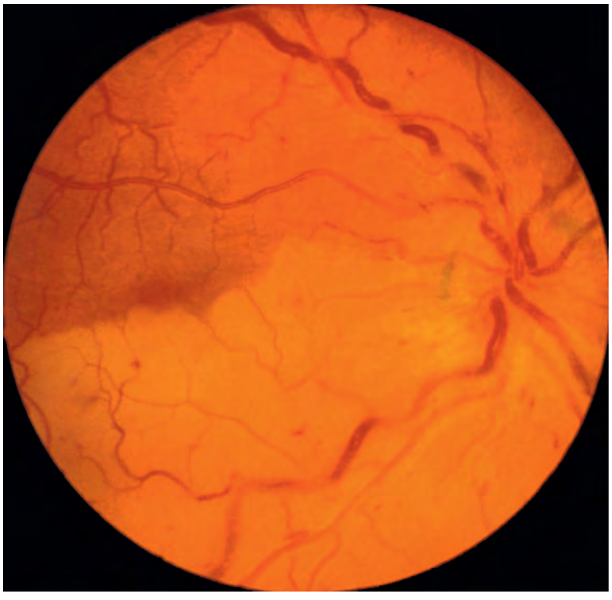

Figure 13 Fundus photograph of an eye with nonischemic CRVO and retinal infarct involving most of the lower half of the retina due to associated cilioretinal artery occlusion. Reproduced from Hayreh, S. S., Fraterrigo, L., and Jonas, J. (2008). Central retinal vein occlusion associated with cilioretinal artery occlusion. *Retina* 28: 581–594, with permission from Wolters Kluwer.

Over the years, many treatments have been advocated enthusiastically and success claimed. A review of the treatment options, which have been championed from time to time, reveals that they vary from the logical to the totally absurd. The most important consideration when evaluating any proposed therapy for any disease is

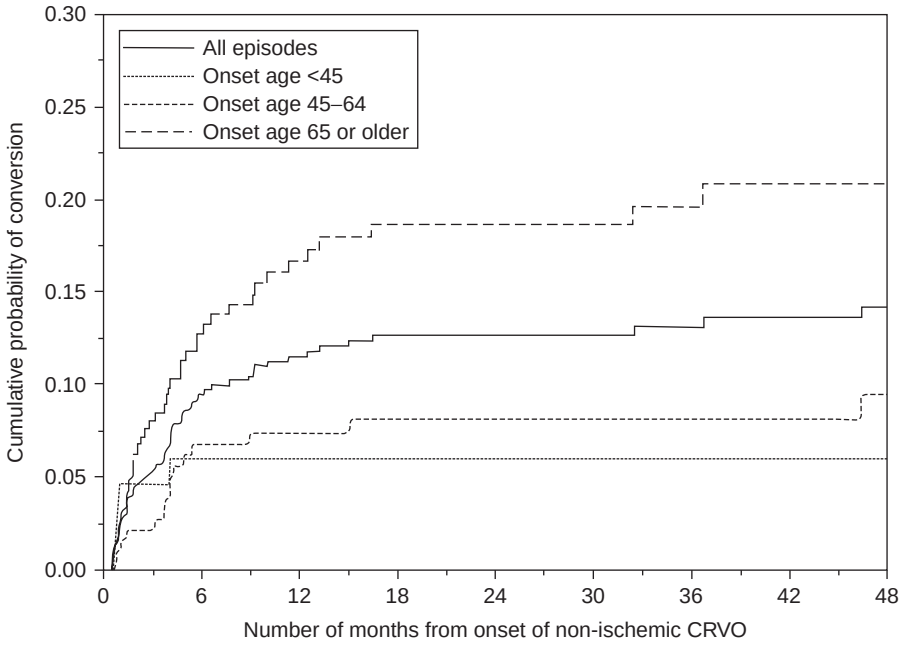

Figure 14 Kaplan–Meier survival curve for cumulative probability of conversion of nonischemic central retinal vein occlusion to ischemic type. Vertical axis gives cumulative probability of the conversion. Horizontal axis gives number of months from onset of nonischemic central retinal vein occlusion. Reproduced from Hayreh, S. S., et al. (1994). *American Journal of Ophthalmology* 117: 429–441.

to determine whether it is based on incontrovertible scientific facts and rationale. Treatments without such a logical foundation prove not only useless but also sometimes harmful. Most of the reported studies have been based on retrospective collection of information or on limited personal experience and, therefore, have a variety of limitations which make it hard to evaluate the claimed benefits; the limitations include lumping together of central and branch retinal vein occlusion, no differentiation of ischemic and nonischemic CRVO or use of invalid criteria to do so, therapies having no scientific validity, flawed study designs, and personal biases. All the proposed therapies must then be carefully scrutinized.

The main treatments advocated for CRVO can be divided into three categories, namely medical, surgical, and panretinal photocoagulation (PRP), which are discussed below.

Medical Treatments

These include anticoagulants, aspirin or other antiplatelet agents, ocular hypotensive therapy, hemodilution, systemic or intravitreal corticosteroids, intravitreal anti-VEGF (VEGF, vascular endothelial growth factor) drugs, systemic acetazolamide, and antihypertensive therapy. Of these, either aspirin or anticoagulants have been most widely used, based on the impression that a treatment which is beneficial for systemic venous thrombosis is also good for CRVO; however, the two conditions are totally different etiologically and pathogenetically. Neither anticoagulants nor aspirin has any scientific rationale in the management of CRVO. They increase retinal hemorrhages (**Figures 9–11, and 15**), thereby adversely influencing the visual outcome. Moreover, patients already on those drugs for other reasons do develop CRVO, indicating that they do not prevent an eye from developing CRVO. The so-called blood-and-thunder or tomato-ketchup fundus appearance described in CRVO is usually an iatrogenic phenomenon resulting from the use of aspirin or anticoagulants; it is not usually seen in regular CRVO. There is no scientific rationale for the commonly used ocular hypotensive therapy in CRVO eyes with normal IOP; however, if the fellow uninvolved eye has ocular hypertension or glaucoma (which is common), that eye must be treated to reduce the chances of its developing CRVO – thus, it is mostly the wrong eye (i.e., with CRVO) which is being treated. Recently, intravitreal corticosteroids and intravitreal anti-VEGF drugs have been widely advocated, primarily to manage macular edema; however, it is important to stress that the treatment with these agents is simply helping to reduce or eliminate macular edema transiently to prevent long-term permanent macular changes (**Figures 3 and 7**); it is not a cure for the CRVO, which has to take its own natural course. Moreover, both drugs require repeated intravitreal injections to maintain effectiveness and can have some side effects. As regards the rest of treatment modalities, there is not much scientifically valid evidence of beneficial effects.

Surgical or Invasive Treatments

These include (1) surgical decompression of the central retinal vein, (2) fibrinolytic therapy, and (3) laser-induced

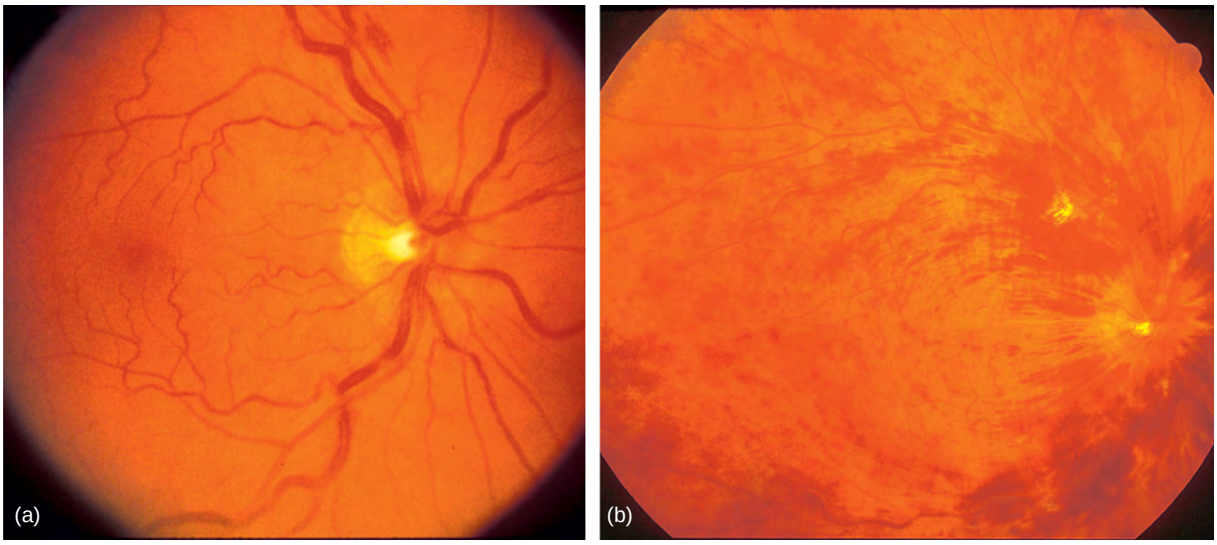

Figure 15 Fundus photographs of a 36-year-old man, who had nonischemic CRVO. When first seen by his ophthalmologist, he had a visual acuity of 20/20 and the fundus showed some peripheral retinal hemorrhages and a rare one posteriorly (a). The ophthalmologist started him on aspirin, and at next visit he had extensive hemorrhages all over (b). On follow-up, his visual acuity progressively deteriorated to finally 20/200. Reproduced from Hayreh, S. S. (2006). *Retina* 26: S51–S62, with permission from Wolters Kluwer.

chorioretinal venous anastomosis for treatment of nonischemic CRVO, which are detailed below:

1. *Surgical decompression of central retinal vein.* It has been claimed that a procedure called radial optic neurotomy, in which a radial cut in the optic nerve head, from the vitreous side, extending all the way down to the lamina cribrosa and adjacent sclera, is beneficial. This procedure not only has no scientific rationale but also can actually be deleterious – it involves cutting thousands of optic nerve fibers, which results in visual loss in the distribution of the cut nerve fibers.
2. *Fibrinolytic therapy.* Currently, the most widely promoted procedure of this type is vitrectomy with branch retinal vein cannulation and infusion of tissue plasminogen activator (t-PA). This procedure lacks scientific rationale and can be associated with complications; beneficial claims made for it seem unwarranted.
3. *Laser-induced chorioretinal venous anastomosis for treatment of nonischemic CRVO.* This procedure has many immediate and late complications, which heavily outweigh any dubious benefits. Therefore, it is not a safe and effective mode of treatment for a condition which has a fairly good outcome if simply left alone (see below).

Panretinal Photocoagulation

Currently, PRP is almost universally considered the treatment of choice in CRVO to prevent development of ocular NV, and macular grid photocoagulation for the management of macular edema. The rationale for usefulness of PRP in CRVO is based primarily on its beneficial effect seen in proliferative diabetic retinopathy.

1. *Macular grid photocoagulation for macular edema.* A multicenter clinical trial showed no difference between treated and untreated eyes in visual acuity at any point during the follow-up period. This indicated that there is no role for this treatment in CRVO.
2. *PRP for prevention of ocular NV.* The theoretical justification for PRP in ischemic CRVO is to prevent development of ocular NV and associated blinding complications of neovascular glaucoma and/or vitreous hemorrhage. As discussed above, ocular NV and neovascular glaucoma are seen only in ischemic CRVO. Since nonischemic CRVO does not develop these complications, there is absolutely no indication or justification for PRP in nonischemic CRVO.

Two large prospective studies have been conducted to evaluate the role of PRP in ischemic CRVO. The first study, based on 123 eyes with ischemic CRVO (47 had PRP and 76 no PRP), showed no statistically significant difference between the two groups in the incidence of development of angle NV, neovascular glaucoma, retinal and/or optic disk NV, or vitreous hemorrhage, or in visual acuity. What it did show was that the PRP group suffered a statistically significant ($p \leq 0.03$) greater loss of peripheral visual fields than the nonlaser group (**Figure 16**).

The second study investigated the role of PRP in ischemic CRVO by a multicenter clinical trial in 181 eyes (90 had immediate prophylactic PRP, and 91 no PRP). The purpose of that study was twofold – first to determine whether prophylactic PRP prevents development of iris and angle NV, and second whether PRP prevents progression of iris/angle NV to neovascular glaucoma. In answer to the first question, the study

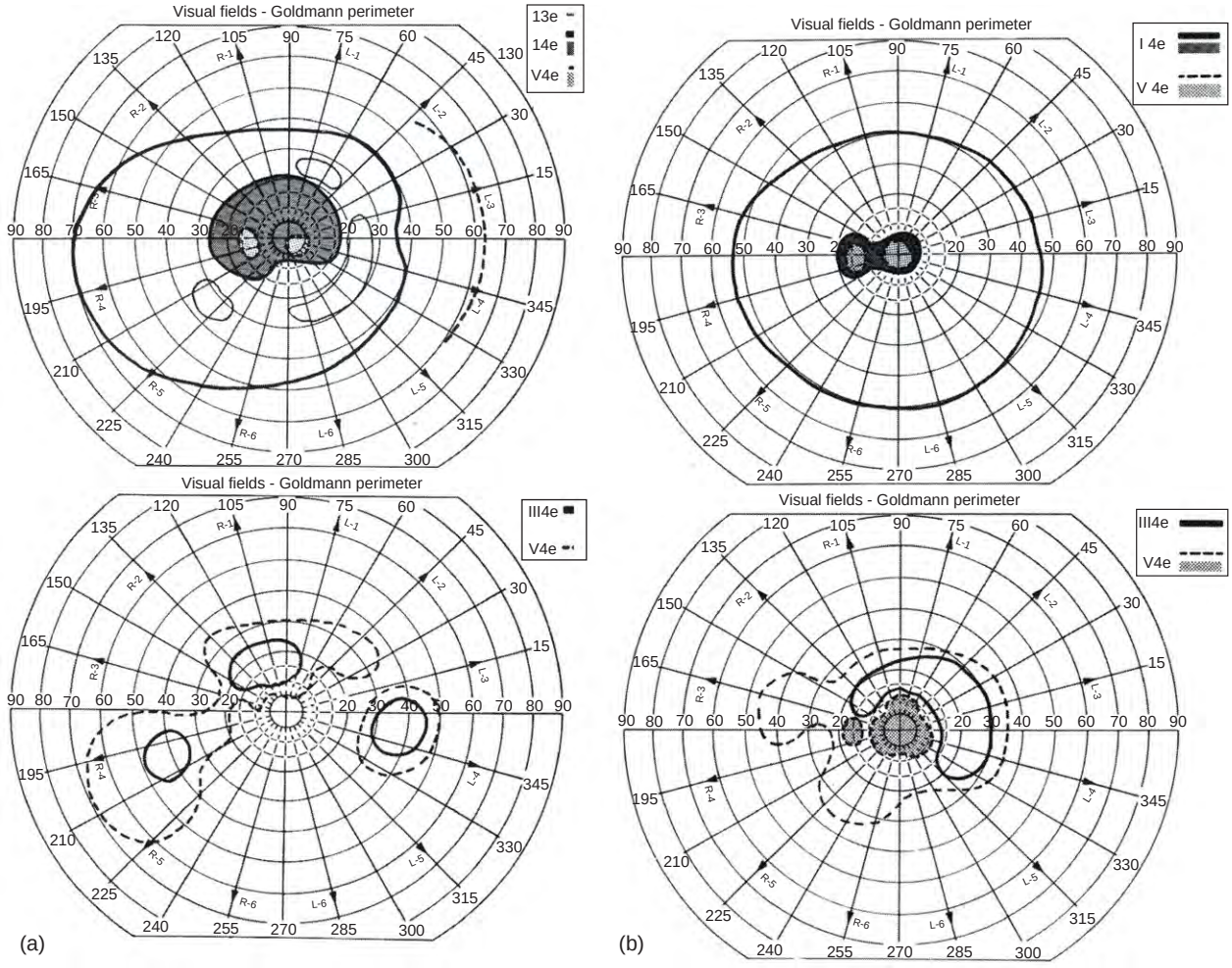

Figure 16 Visual fields, plotted with a Goldmann perimeter, of two left eyes (a, b) with ischemic CRVO, before (top) and after (bottom) panretinal photocoagulation. In both eyes, before photocoagulation (top) the peripheral fields were normal with I4e and V4e isopters, but after photocoagulation (bottom) the peripheral fields developed marked constriction and deterioration. Reproduced from Hayreh, S. S., Klugman, M. R., Beri, M., Kimura, A. E., and Podhajsky, P. (1990). Differentiation of ischemic from non-ischemic central retinal vein occlusion during the early acute phase. *Graefe's Archive for Clinical and Experimental Ophthalmology* 228: 201–217.

reported that "prophylactic PRP does not totally prevent" development of iris/angle NV; its recommendation was not to do that. As for the second aspect of the study, the authors recommended "careful observation with frequent follow-up examinations in the early months (including undilated slit-lamp examination of the iris and gonioscopy) and prompt PRP of eyes in which 2'clock iris/angle neovascularization develops." The most important feature of any study is its design, because that can determine its conclusions and their validity. This multicenter study unfortunately had flaws in its study design, which raised serious issues about the validity of its conclusions. There were three major flaws with the design of this study;

1. there was poor differentiation of ischemic and nonischemic CRVO, so that their treated and untreated groups had mixtures of both types of CRVO, instead of only ischemic CRVO (PRP is indicated only for ischemic CRVO);
2. all eyes that developed 2'clock iris/angle NV were treated so that there was no control group to determine whether there was any difference in progression of iris/angle NV to neovascular glaucoma in treated versus the untreated eyes; and
3. no visual fields were plotted to evaluate the side effects and complications of PRP in CRVO.

The first study, as mentioned above, showed that following PRP, the large central scotoma combined with severe loss of peripheral visual fields might virtually blind the eye (**Figure 16**). It is unfortunate, that this multicenter study, in spite of all these serious flaws, has become the gold standard for treatment of CRVO.

In conclusion, as is quite evident from the brief discussion above, there is no scientifically valid proof so far that

PRP is safe and effective in prevention or management of neovascular glaucoma in ischemic CRVO.

Primary Factor Responsible for Blindness in Ischemic CRVO with Neovascular Glaucoma

The most important consideration in the management of neovascular glaucoma seen in ischemic CRVO is high IOP, which is the primary factor causing marked loss of vision or even blindness in the vast majority of these eyes, by producing glaucomatous optic neuropathy and anterior segment changes. Therefore, if neovascular glaucoma develops (the maximum risk of that is 50%; Figure 8) and the IOP is controlled satisfactorily by any means, the eye can maintain a reasonably good peripheral visual field once the retinopathy burns itself out in due course; the peripheral visual field constitutes a very important component of our visual function, because our navigational capacity depends essentially on that. As the retinopathy regresses, the stimulus for NV diminishes, resulting in spontaneous regression of NV – a fact too often overlooked.

Overall Conclusions About Advocated Treatments for CRVO

It is well known that 'a disease which has no treatment has many treatments' – each advocated enthusiastically for a while and then found to be not only no better than the natural history of the disease or sometimes actually harmful. CRVO has become a graveyard of such therapies, but, given that they were not backed by sound science, it is not surprising that there is so far no treatment for CRVO that has stood the test of time for safety, efficacy. and long-term beneficial and curative effect. It is unfortunate when enthusiastic claims made for different modes of treatment give desperate patients false hope, cost them so much, not only in money but also in trouble, unnecessary pain and disappointment, and, sometimes, do them more harm than good. Currently, these desperate patients shop for treatment via the Internet and are often misled because not all the information on the Internet is peer reviewed. In this review, we have challenged some of the conventional wisdom in the management of CRVO – that is never popular. To advocate watchful waiting rather than action is even more unpopular. We can only hope that science, logic, and common sense will prevail in the end.

Natural History of Visual Outcome in CRVO

The outcome of all advocated treatments has to be compared with the natural history of a disease, so that natural recovery is not attributed to the beneficial effect of a mode of treatment. Recently, the natural history of visual outcome was reported in a prospective study of 214 untreated consecutive patients with nonischemic CRVO – in 155 of them the retinopathy and macular edema had resolved completely during follow-up and 59 eyes still had macular edema at the last visit. This study was based on evaluation of both visual acuity and visual fields plotted with a Goldmann perimeter – visual acuity provides information about the function of the fovea only and not of the entire retina, while visual fields provide information about the function of the entire retina involved by CRVO. Table 2 gives the findings on visual acuity and permanent central scotoma in all the 214 eyes as well as in 155 eyes with completely resolved retinopathy. Peripheral visual fields were perfectly normal in both the groups all along. Among the 59 eyes that still had macular edema, resolution of macular edema would improve the visual acuity and central visual fields in due course. Thus, the natural history of visual outcome in nonischemic CRVO is much better than the results of any of the treatments advocated so far. By contrast, in ischemic CRVO, during the initial stages, the ganglion cells in the macular retina are irreversibly damaged by ischemia → a permanent central scotoma → little chance of improvement of visual acuity. Almost all eyes with ischemic CRVO initially have normal peripheral visual fields.

Table 2 Visual acuity in 214 eyes with nonischemic CRVO – in 155 of them retinopathy had resolved completely and 59 eyes still had macular edema

	All eyes (214 eyes)	*Resolved eyes (155 eyes)*
Visual acuity		
20/20–20/25	50%	65%
20/30–20/40	14%	12%
20/50–20/70	11%	7%
20/80–20/100	4%	3%
20/200	12%	6%
20/400–CF[a]	10%	7%
Central scotoma		
None	56%	68%
Small size	34%	26%
Moderate size	5%	3%
Large size	1%	1%

[a]Mainly due to cataract, age-related macular degeneration, etc. but not due to CRVO.
From *Retina* 2007 27: 514–517.

Investigations of CRVO Patients

Finally, a commonly asked question is: What systemic and hematologic investigations need to be done in patients with CRVO? A voluminous and confusing literature exists on systemic and hematologic disorders in CRVO. Our study of 612 patients with CRVO showed that, apart from a routine medical evaluation, the vast majority of

patients with CRVO need not undergo an extensive and expensive workup for systemic diseases. As regards hematological evaluation, there is no good reason why all patients with CRVO should be subjected to the costly, exhaustive special hematologic and hypercoagulability investigations usually done in patients with spontaneous major systemic venous thrombosis – unless, of course, there is some clear indication. The routine, inexpensive hematologic evaluation is the one required by CRVO patients.

See also: Ischemic Optic Neuropathy; Physiological Anatomy of the Choroidal Vasculature; Physiological Anatomy of the Retinal Vasculature.

Further Reading

Hayreh, S. S. (1983). Classification of central retinal vein occlusion. *Ophthalmology* 90: 458–474.

Hayreh, S. S. (1996). The CVOS Group M and N Reports. *Ophthalmology* 103: 350–352.

Hayreh, S. S. (2002). *Radial optic neurotomy for central retinal vein occlusion. Retina* 22: 374–377; 827.

Hayreh, S. S. (2003). Management of central retinal vein occlusion. *Ophthalmologica* 217: 167–188.

Hayreh, S. S. (2005). Prevalent misconceptions about acute retinal vascular occlusive disorders. *Progress in Retinal and Eye Research* 24: 493–519.

Hayreh, S. S., Fraterrigo, L., and Jonas, J. (2008). Central retinal vein occlusion associated with cilioretinal artery occlusion. *Retina* 28: 581–594.

Hayreh, S. S., Klugman, M. R., Beri, M., Kimura, A. E., and Podhajsky, P. (1990). Differentiation of ischemic from non-ischemic central retinal vein occlusion during the early acute phase. *Graefe's Archive for Clinical and Experimental Ophthalmology* 228: 201–217.

Hayreh, S. S., Klugman, M. R., Podhajsky, P., Servais, G. E., and Perkins, E. S. (1990). Argon laser panretinal photocoagulation in ischemic central retinal vein occlusion – A 10-year prospective study. *Graefe's Archive for Clinical and Experimental Ophthalmology* 228: 281–296.

Hayreh, S. S., Rojas, P., Podhajsky, P., Montague, P., and Woolson, R. F. (1983). Ocular neovascularization with retinal vascular occlusion III. Incidence of ocular neovascularization with retinal vein occlusion. *Ophthalmology* 90: 488–506.

Hayreh, S. S., Zimmerman, M. B., Beri, M., and Podhajsky, P. A. (2004). Intraocular pressure abnormalities associated with central and hemi-central retinal vein occlusion. *Ophthalmology* 111: 133–141.

Hayreh, S. S., Zimmerman, M. B., McCarthy, M. J., and Podhajsky, P. (2001). Systemic diseases associated with various types of retinal vein occlusion. *American Journal of Ophthalmology* 131: 61–77.

Hayreh, S. S., Zimmerman, M. B., and Podhajsky, P. (1994). Incidence of various types of retinal vein occlusion and their recurrence and demographic characteristics. *American Journal of Ophthalmology* 117: 429–441.

Hayreh, S. S., Zimmerman, M. B., and Podhajsky, P. A. (2002). Hematologic abnormalities associated with various types of retinal vein occlusion. *Graefe's Archive for Clinical and Experimental Ophthalmology* 240: 180–196.

Ingerslev, J. (1999). Thrombophilia: A feature of importance in retinal vein thrombosis? *Acta Ophthalmologica* 77: 619–621.

The Central Retinal Vein Occlusion Group (1995). *A randomized clinical trial of early panretinal photocoagulation for ischemic central vein occlusion – the central vein occlusion study group N report. Ophthalmology* 102: 1434–1444.

The Central Retinal Vein Occlusion Group (1995). Evaluation of grid pattern photocoagulation for macular edema in central vein occlusion – the central vein occlusion study group M report. *Ophthalmology* 102: 1425–1433.

The Eye Disease Case-Control Study Group (1996). Risk factors for central retinal vein occlusion. *Archives of Ophthalmology* 114: 545–554.

Chick Metabolism in the Chick Retina

P M Iuvone, Emory University School of Medicine, Atlanta, GA, USA

Glossary

Basic helix–loop–helix-Per-ARNT-Sim (bHLH-PAS) domain transcription factors – A family of transcription factors that heterodimerize and bind to E box enhancer elements in gene promoters. The family includes the clock gene products CLOCK, neuronal PAS domain protein 2 (NPAS2), and brain and muscle aryl hydrocarbon receptor nuclear translocator 1 (BMAL1), as well as the arylhydrocarbon nuclear receptor and the hypoxia-inducible factors.

Circadian rhythms – Changes in biological processes that occur on a daily basis; they are driven by autonomous circadian clocks; these rhythms provide selective advantage to organisms by allowing them to anticipate temporal changes in their environment.

Clock-controlled genes – Genes that are regulated by circadian oscillators via clock gene transcription factors; the proteins encoded by clock-controlled genes are rhythmically expressed and generate rhythms of physiology.

Clock genes – Genes that encode proteins that form the molecular basis of circadian oscillators; most clock gene proteins are transcription factors.

Scotopic vision – Vision in dim light that is mediated by rod photoreceptors and rod bipolar cell pathways.

Zeitgeber time – Time of day relative to the light–dark cycle; light onset corresponds to ZT0.

Introduction

The chick retina has been used extensively to study ocular circadian rhythms. It displays particularly robust rhythms of clock gene expression, clock-controlled gene expression, and several biochemical and physiological clock outputs. In addition, embryonic chick retinal cells can be cultured, and they maintain light responsiveness and circadian rhythm generation *in vitro*. These cell cultures facilitate pharmacological and molecular studies of clock signaling pathways.

Clock Gene Expression

The current model for the molecular basis of circadian clocks involves transcriptional–translational feedback loops that are comprised of highly conserved clock genes and the proteins that they encode (**Figure 1**). The clock gene proteins are characterized as positive and negative elements, based on their transcriptional activity. The positive elements include basic helix–loop–helix–PAS-domain (bHLH-PAS) transcription factors that heterodimerize and bind to circadian E box enhancer elements in promoters of other clock genes and clock-controlled genes. These positive elements include brain and muscle aryl hydrocarbon receptor nuclear translocator 1 (BMAL1; also called ARNTL, MOP3) and CLOCK. The BMAL1 heterodimerizes with CLOCK and the dimerized transcription factors stimulate the transcription of the genes encoding the negative elements, the cryptochromes (CRY1 and CRY2) and periods (PER1, PER2, and PER3). The CRY and PER proteins are imported into the nucleus and inhibit transactivation of their own promoters by BMAL1:CLOCK. In some clocks, neuronal PAS domain protein 2 (NPAS2, also called MOP4) can substitute for CLOCK and form active heterodimers with BMAL1. A second feedback loop involves E-box-mediated transcriptional activation of the orphan retinoic-acid-related receptor family genes, *Rev-erbα* and *Rora*; the protein products of these genes contribute to the rhythmic regulation of *Bmal1* gene transcription. These feedback loops, coupled with a variety of post translational modifications, generate daily rhythms of gene expression that ultimately generate physiological circadian rhythms.

Most of the clock gene transcripts identified in mammalian circadian clocks have been identified in the chick retina and in cultured chick photoreceptors, and the regulation of their expression has been analyzed (**Figures 2 and 3**). Of the genes encoding the positive elements of the oscillator, *Bmal1* and *Npas2* transcripts show robust daily rhythms under light–dark cycles or in constant (24 h day^{-1}) darkness (**Figure 2**). These circadian rhythms peak near the time of subjective dusk (~ZT12) *in vivo* and *in vitro*. In contrast, *Clock* mRNA appears to be constitutively expressed in dark–dark (DD). Transcripts encoding the negative elements, the cryptochrome and period proteins, also show rhythmic expression (**Figure 3(a)** and **3(b)**). The *Cry1* mRNA peaks in the middle of the day (~ZT8) *in vivo* and in photoreceptor cultures. *In vivo*, the most robust rhythms of *Cry1* mRNA expression are observed in the ganglion cell and photoreceptor cell layers. The *Cry2* mRNA is also expressed in retina, but analyses of whole retina mRNA suggest that it is not rhythmically expressed. The *Per2* mRNA expression is maximal in the early morning, while *Per3* transcript level appears maximal late in the night.

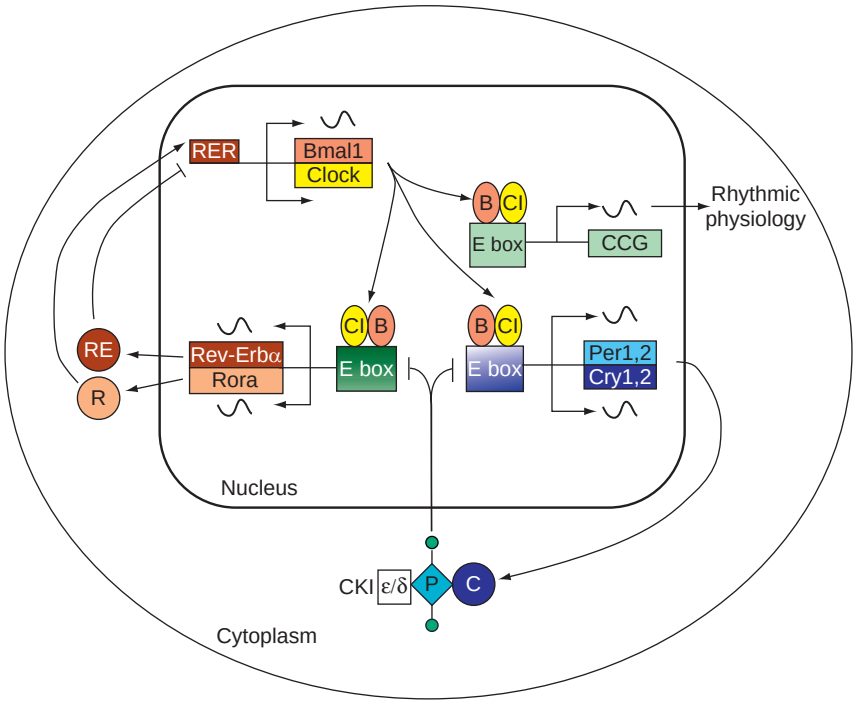

Figure 1 Circadian clockwork mechanism. Circadian clocks in a wide range of organisms are composed of two interdependent transcription–translation feedback loops that drive the periodic rhythms in the mRNA and protein levels of the clock components. In mammalian SCN, the first loop involves two bHLH-PAS-containing transcription factors, CLOCK (Cl) and BMAL1 (B). These transcription factors heterodimerize and activate the rhythmic transcription of three *period* genes (*Per1-Per3*, with *Per1* and *Per2* being critical to the circadian clock) and two *cryptochrome* genes (*Cry1* and *Cry2*). The PER (P) and CRY (C) proteins complex with casein kinase 1 δ and ε (CKIδ/ε), which phosphorylates PER. The resulting complex inhibits CLOCK/BMAL1-mediated transcription of *period* and *cryptochrome* genes, thus providing the negative feedback loop. The second loop involves CLOCK/BMAL1 driven rhythmic transcription of *Rev-erbα* and *Rora*, members of the retinoic acid-related orphan nuclear receptor family. The phase of *Rora* expression closely resembles those of *Per1* and *Per2*, and is opposite in phase with *Rev-erbα*. The resultant REV-ERBα and RORa proteins (RE and R, respectively) compete for the same promoter element, RRE (Rev-erb/Ror element) and drive the rhythm in *Bmal1* transcription. CLOCK/BMAL1 heterodimers also bind to circadian E-boxes in clock-controlled genes (CCGs), providing an output from the clock that drives rhythmic physiology. Adapted from Iuvone, P. M., Tosini, G., Pozdeyev, N., et al. (2005). Circadian clocks, clock networks, arylalkylamine N-acetyltransferase, and melatonin in the retina. *Progress in Retinal and Eye Research* 24: 433–456, with permission from Elsevier.

Thus far, *Per1* has not been identified in the chick retina, and the gene may be missing from the chicken genome. In addition to oscillating in a clock-dependent manner, *Per2* and *Cry1* are rapidly induced by light exposure (**Figure 3(c)** and **3(d)**). It is generally thought that this induction is a mechanism for circadian clock entrainment by light.

The rhythmic and light-regulated expression of circadian clock genes in the chick retina, particularly in cultured retinal cells, provides conclusive evidence that the retina contains autonomous circadian oscillators that can function independently of oscillators in the brain and pineal gland. Nevertheless, in the intact organism, retinal, pineal, and brain clocks are thought to interact to regulate physiology.

Circadian Regulation of Cyclic AMP in Retina

Cyclic AMP is a ubiquitous second messenger molecule that regulates multiple aspects of cellular metabolism and function. Effects of cyclic AMP are mediated by activation of cyclic AMP-dependent protein kinase (PKA), which phosphorylates proteins to regulate their function or activity. In so doing, cyclic AMP regulates intermediary metabolism, neurotransmission, and gene expression. Cyclic AMP can also affect cellular function by regulating cyclic nucleotide-gated channels or activating Epac, a cyclic AMP-dependent Rap GTP exchange factor. The Rap is a guanine nucleotide-binding protein of the Ras family.

In chick photoreceptor cell cultures, cyclic AMP levels are regulated by light and circadian clocks. Photoreceptor cyclic AMP levels are high in darkness and reduced by light exposure. Thus, when cells are exposed to a daily light–dark cycle, cyclic AMP fluctuates as a daily rhythm with high levels at night in darkness and low levels during the daytime in light (**Figure 4**). Exposure to light at night rapidly reduces cyclic AMP. The daily rhythm of cyclic AMP persists, albeit with reduced amplitude, when cells are transferred from a light–dark cycle to constant darkness. Thus, the combined effects of illumination and

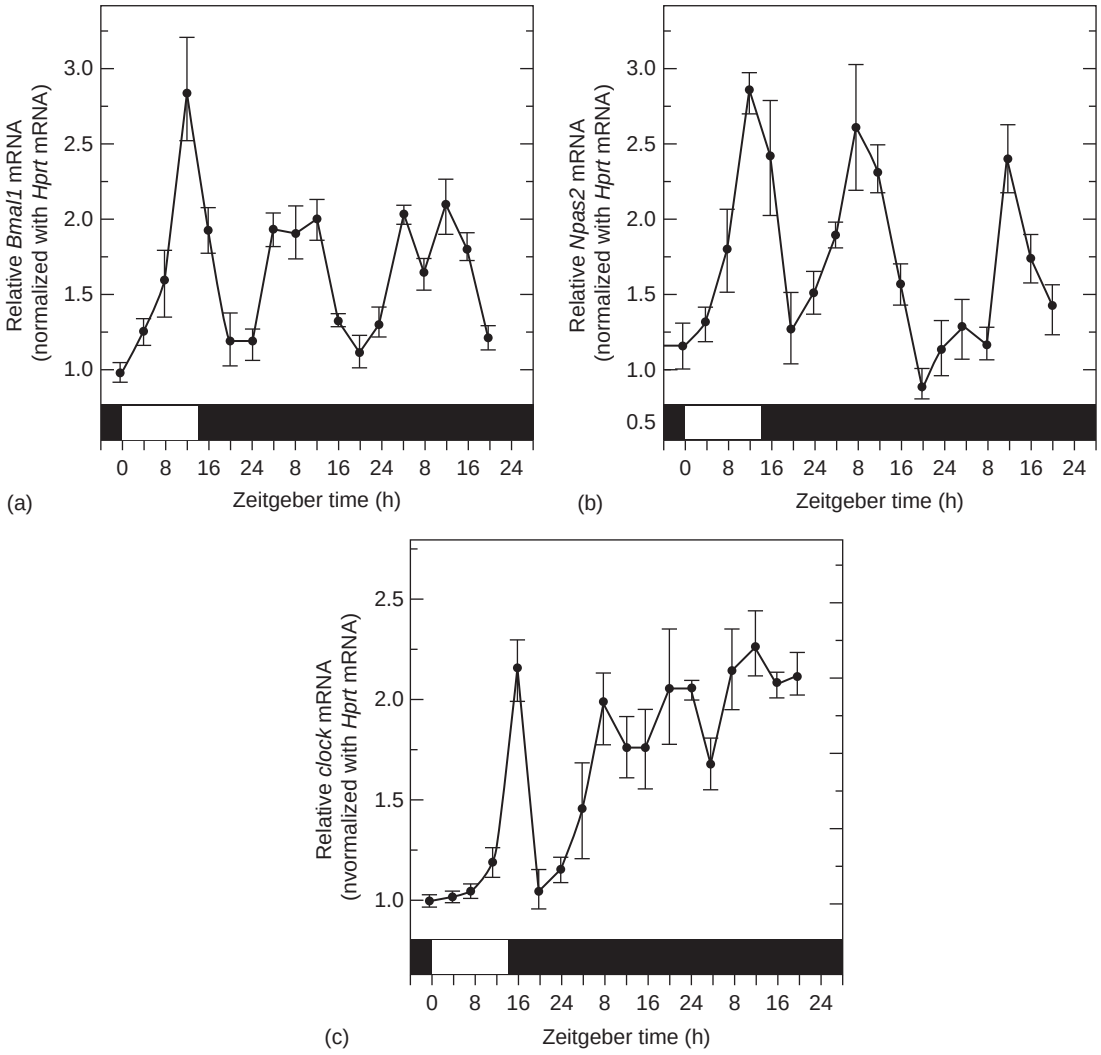

Figure 2 Temporal expression of positive modulators of the circadian clockwork system. Relative mRNA levels of *Bmal1* (a) and *Npas2* (b) in photoreceptor-enriched retinal cell cultures collected at the indicated Zeitgeber times (ZT) in light–dark (LD) and dark–dark (DD). Each data point represents clock gene transcripts normalized to hypoxanthine-guanine phosphoribosyl transferase (*Hprt*) mRNA and expressed relative to the lowest values in LD. The open horizontal bar at the X-axis represents times of light exposure; the black bars represent times of darkness. Analysis of variance (ANOVA) indicated significant rhythms of *Bmal1* and *Npas2* transcripts in LD and DD, with highest levels in the late day and early night. (c) *Clock* mRNA showed significantly higher values during the night (ZT 16) than during the day in LD; transcript levels increased on the first day of DD but there were no significant rhythms on DD1 or DD2. Reproduced from Chaurasia, S. S., Pozdeyev, N., Haque, R., et al. (2006). Circadian clockwork machinery in neural retina: Evidence for the presence of functional clock components in photoreceptor-enriched chick retinal cell cultures. *Molecular Vision* 12: 215–223, Copyright Molecular Vision 2006.

circadian influences interact to generate the daily rhythm of cyclic AMP.

The regulation of cyclic AMP formation in chick photoreceptor cells is Ca^{2+}-dependent, at least in part. Depolarization of the plasma membrane with high concentrations of extracellular K^+ stimulates cyclic AMP formation. This effect requires Ca^{2+} influx through L-type voltage-gated Ca^{2+} channels. The plasma membrane of photoreceptors is partially depolarized in darkness and is hyperpolarized by light. Thus, the dark–light difference in cyclic AMP formation in photoreceptors is likely due to high Ca^{2+} conductance in darkness and decreased Ca^{2+}conductance following light exposure, due to closure of the voltage-gated channels. Accordingly, the circadian fluctuation in cyclic AMP levels is eliminated by nitrendipine, an L-type Ca^{2+} channel blocker.

Cyclic AMP is synthesized from ATP by adenylyl cyclase. There are 10 isoforms of adenylyl cyclase that are regulated by multiple mechanisms. The findings described above indicate that photoreceptor cyclic AMP levels may be regulated by a Ca^{2+}/calmodulin-stimulated cyclase. The type 1 and type 8 adenylyl cyclases are both stimulated by Ca^{2+}/calmodulin and are both expressed in the chick retina. There is a circadian rhythm in the expression of

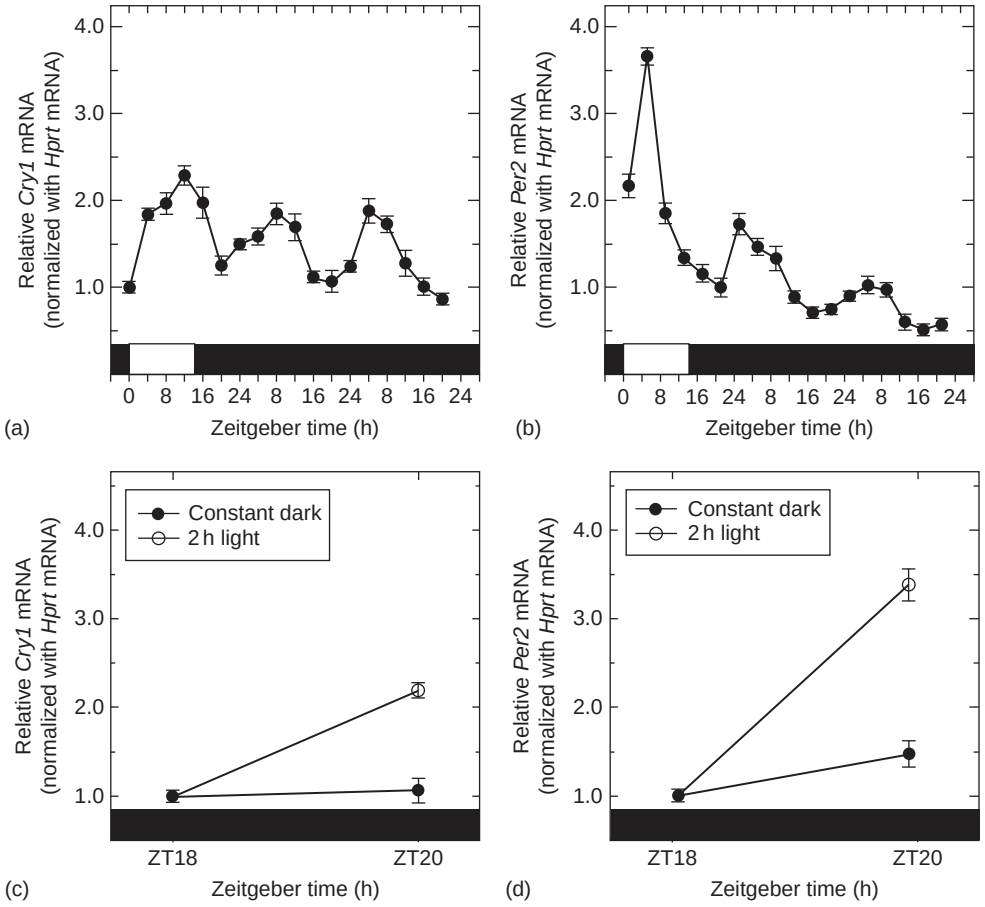

Figure 3 Temporal expression of negative modulators of the circadian clockwork system. Circadian profiles of *Cry1* (a) and *Per2* (b) transcripts in the photoreceptor-enriched retinal cell cultures collected at the indicated Zeitgeber time (ZT) in light–dark (LD) and dark–dark (DD). Each data point represents clock gene transcripts normalized to *Hprt* mRNA, expressed relative to the lowest values in LD. Acute light exposure at night induces *Cry1* (c) and *Per2* (d) mRNA expression. On day 9 *in vitro* (DIV9) cells were kept in constant darkness until ZT 18, when one group of cells was collected. Another group of cells remained in darkness for an additional 2 h (solid symbol), while a third group of cells was exposed to light for 2 h prior to cell harvesting (open symbol). Exposure to light significantly increased *Cry1*and *Per2* transcript levels. Reproduced from Chaurasia, S. S., Pozdeyev, N., Haque, R., et al. (2006). Circadian clockwork machinery in neural retina: Evidence for the presence of functional clock components in photoreceptor-enriched chick retinal cell cultures. *Molecular Vision* 12: 215–223, Copyright Molecular Vision 2006.

Adcy1, the transcript that encodes the type 1 adenylyl cyclase, in photoreceptor cell cultures and in the chick retina *in vivo*. In addition, there is a circadian rhythm in Ca^{2+}/calmodulin-stimulated adenylyl cyclase activity in membranes prepared from photoreceptor cell cultures, with high activity at night. Thus, the circadian regulation of cyclic AMP is due to clock-controlled expression of Ca^{2+}/calmodulin-stimulated adenylyl cyclase. The mammalian *Adcy1* gene contains an E-box in its promoter that can be activated by BMAL1:CLOCK heterodimers, and a similar mechanism may contribute to the circadian regulation of *Adcy1* expression in chick photoreceptor cells. However, this hypothesis has not yet been tested directly in the chick. The circadian rhythm of cyclic AMP formation may also be influenced by the clock-controlled expression and activity of the L-type Ca^{2+} channels in photoreceptors.

Circadian Regulation of Melatonin Biosynthesis

Melatonin is a neurohormone that is synthesized in the retinal photoreceptor cells and in the pineal gland. Melatonin synthesis in retinas of most vertebrate species, including chicken, is regulated in a circadian fashion, with high levels at night in darkness. Melatonin functions in the retina to optimize nighttime visual function. Like cyclic AMP formation, melatonin levels are regulated by both illumination and circadian clocks.

The key regulatory enzyme in melatonin biosynthesis is arylalkylamine N-acetyltransferase (AANAT). In chicken retina, AANAT activity undergoes a robust circadian rhythm with peak activity at night (**Figure 5**). Exposure to light at night causes a rapid decline in AANAT activity

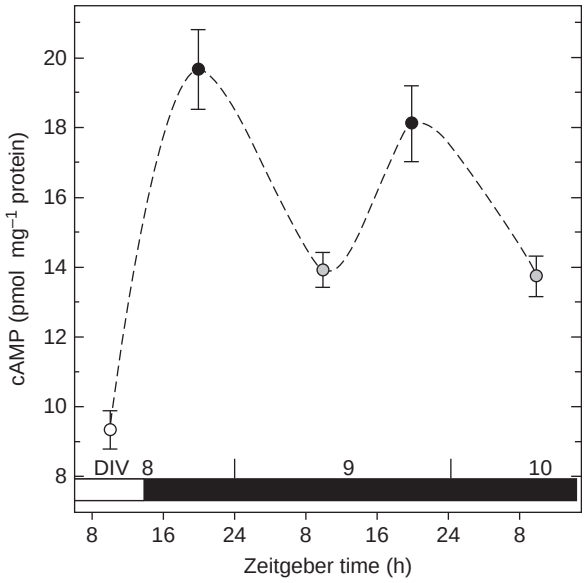

Figure 4 Circadian fluctuation of intracellular cAMP level. Cells were prepared from embryonic neural retinas and incubated for 8 days under LD. Illumination was switched from LD to DD before expected onset of light at the beginning of day 9 *in vitro* (DIV 9). White symbols represent cAMP level at Zeitgeber time (ZT) 10 in light; black symbols represent ZT 20 in darkness; gray symbols represent subjective day, ZT 10, in darkness. The horizontal white and black bars above the *x*-axis represent times of light and darkness, respectively. Level of cAMP was significantly higher at night than during the day in LD on DIV 8 and this fluctuation persisted in DD on DIV 9 and DIV 10. Reproduced from Ivanova, T. N. and Iuvone, P. M. (2003). Circadian rhythm and photic control of cAMP level in chick retinal cell cultures: A mechanism for coupling the circadian oscillator to the melatonin-synthesizing enzyme, arylalkylamine N-acetyltransferase, in photoreceptor cells. *Brain Research* 991: 96–103, with permission from Elsevier.

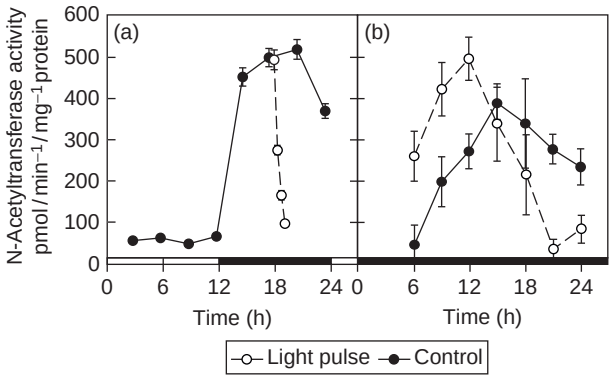

Figure 5 Daily rhythm of retinal AANAT activity: effects of light. (a) AANAT activity fluctuates during the 12 h light–12 h dark cycle (filled circles). Unexpected light exposure at night (open circles) rapidly inhibits activity. (b) AANAT activity in constant (24 h day^{-1}) darkness. The activity rhythm persists on the second day of constant darkness (filled circles). The rhythm is phase advanced by a 6 h light pulse from 18 to 24 h 2 days prior to sampling in constant darkness (open circles). Filled bars on the *x*-axis represent darkness; open bars represent light. Activity was measured in retinal homogenates of 2-week old chickens. Reproduced from Iuvone, P. M. and Alonso-Gómez, A. L. (1998). Melatonin in the vertebrate retina. In: Christen Y., Doly, M., and Droy-Lefaix, M. -T. (eds.) *Retine, Luminiere, et Radiations,* vol. 9, pp. 49–62. Paris: Irvinn; and Iuvone, P. M., Tosini, G., Pozdeyev, N., et al. (2005). Circadian clocks, clock networks, arylalkylamine N-acetyltransferase, and melatonin in the retina. *Progress in Retinal and Eye Research* 24: 433–456, with permission from Elsevier.

($t^{1/2} \approx 20$ min), to insure that significant melatonin synthesis occurs in darkness only. Chicken AANAT activity is regulated by transcriptional and post-translational mechanisms (**Figure 6**). The retina displays daily rhythms of *Aanat* mRNA and AANAT protein in chickens exposed to a light–dark cycle or constant darkness. Levels of transcript, protein, enzyme activity, and melatonin all peak at night. The proximal promoter of the chicken *Aanat* gene contains a circadian E-box that can be activated by either BMAL1:CLOCK or BMAL1:NPAS2 heterodimers, and it is generally thought that this directly couples the circadian clock to the rhythmic expression of *Aanat*. In addition, the chicken *Aanat* 5′-flanking region contains cyclic AMP response elements. Thus, the circadian rhythm of cyclic AMP may also contribute to the rhythm of *Aanat* mRNA.

The AANAT protein is regulated by PKA-dependent phosphorylation and proteasomal degradation (**Figure 6**). The AANAT contains two consensus PKA phosphorylation sites. When cyclic AMP levels are high at night, AANAT is phosphorylated. Phospho-AANAT binds to 14-3-3 proteins, which are ubiquitous signaling proteins involved in multiple cellular functions. The interaction of 14-3-3 with AANAT increases the affinity of the enzyme for its substrate, increasing catalytic activity. Exposure to light at night causes a very rapid decrease in AANAT activity and protein level ($t^{1/2} \approx 20$ min) without any initial change of *Aanat* mRNA (**Figure 6**). The decrease of AANAT is accompanied by a similarly rapid decline in melatonin levels, insuring that melatonin only functions in darkness. The decrease of protein and activity results from the light-induced decrease of cyclic AMP levels, resulting in dephosphorylation of AANAT, unbinding of 14-3-3, and rapid proteolytic degradation of the enzyme. The degradation can be blocked by proteasome inhibitors, indicating that this is a proteasome-dependent event.

During the daytime, multiple mechanisms cooperate to keep melatonin biosynthesis at a minimum (**Figure 6**). Low levels of cyclic AMP appear to play key roles in these mechanisms. The *Aanat* transcript levels are low, presumably due to reduced cyclic AMP-directed transcriptional activation and suppression by Cry1 of E-box-mediated transactivation (**Figure 6**). In addition, the low levels of cyclic AMP during the daytime, especially in light, favor the dephosphorylated state of the AANAT protein, resulting in its rapid degradation by proteasomes.

The majority of AANAT in the chick retina is expressed at night in photoreceptor cells. However, there is some

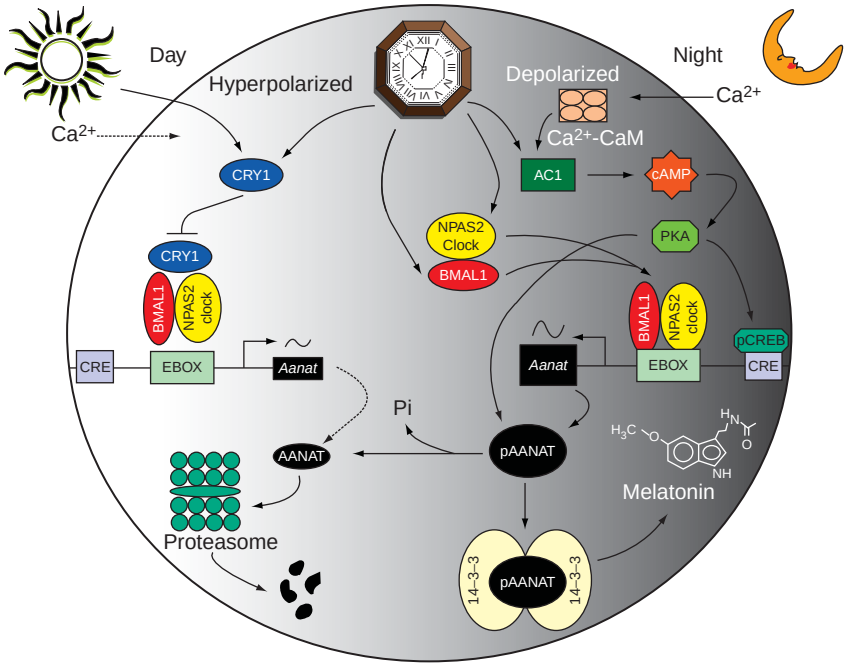

Figure 6 Model for circadian clock- and light-regulated melatonin biosynthesis in photoreceptor cells (see text for detailed description of the model). The left side of the figure depicts processes occurring in light while the right side shows processes occurring at night in darkness. Abbreviations: AANAT, arylalkylamine N-acetyltransferase; AC1, type 1 Ca^{2+}/calmodulin-stimulated adenylyl cyclase; CaM, calmodulin; cAMP, cyclic adenosine 3′,5′-monophosphate; CRE, cAMP-responsive element; pAANAT, phosphorylated AANAT; pCREB, phosphorylated cAMP response element-binding protein; PKA, cAMP-dependent protein kinase, with permission from Elsevier.

evidence that small amounts of AANAT may be expressed in ganglion cells during the daytime. The role of ganglion cell-derived AANAT is not known.

Other Rhythms of Gene Expression and Metabolism in the Chick Retina

Circadian clocks regulate phospholipid metabolism in the chick retina. Daily rhythms of phospholipid labeling with either ^{32}P or [^{3}H]glycerol have been observed in chicks kept on a light–dark cycle or in constant darkness. The ^{32}P labeling of total phospholipids in photoreceptors and ganglion cells peaks in the late night. The major phospholipid labeled under these conditions is phosphotidylinositol. In contrast, labeling with [^{3}H]glycerol peaks midday, with phosphatidylcholine as the major labeled species.

Melanopsin (Opn4) is a photopigment first discovered in *Xenopus* melanocytes, where it mediates photic regulation of melanin pigment aggregation. Subsequent cloning of orthologous melanopsin genes revealed that it is expressed in mammalian retina exclusively in a small subset of ganglion cells that are intrinsically photosensitive. These ganglion cells project to the suprachiasmatic nucleus (SCN) of the hypothalamus, the inferior olivary nucleus, and other brain regions involved in nonimage forming vision. The intrinsically photosensitive ganglion cells mediate the pupillary light reflex and photic entrainment of the circadian oscillator in the SCN.

In contrast to mammals, chickens express two melanopsin genes, designated *Opn4x* and *Opn4m* because of their sequence homology to the *Xenopus* and mammalian melanopsin genes, respectively. The *Opn4x* and *Opn4m* transcripts are more widely distributed than their mammalian counterpart. Chicken melanopsin transcripts are found in a subpopulation of cells in the ganglion cell layer, and also in photoreceptors, retinal pigment epithelium (RPE) cells, inner nuclear layer (INL) cells, the pineal gland, and areas of the brain known to contain deep brain photoreceptors. The *Opn4x* is rhythmically expressed in the chicken retina in light–dark cycles and in constant darkness. Patterns of rhythmicity differ among retinal layers; *Opn4x* peaks in the morning in RPE and INL cells, but at night in photoreceptors. Similar to the retinal photoreceptors, *Opn4x* also peaks at night in chicken pinealocytes, which are directly photosensitive and contain a circadian clock that is entrained by light. The regulation and localization of *Opn4* is consistent with the hypothesis that this novel photopigment plays a role in circadian regulation in the retina and pineal gland.

Iodopsin is the photopigment of red-sensitive cone photoreceptors of avian species. Iodopsin mRNA levels fluctuate as a circadian rhythm in retinal photoreceptors *in vivo* and *in vitro*, in cultured photoreceptors, and in

retinal explants. The rate of transcription of the iodopsin gene peaks late in the subjective day in constant darkness, ~3 h before the beginning of the subjective night, and mRNA levels peak early in the subjective night. The functional significance of the circadian rhythm of iodopsin mRNA is yet to be determined.

Ion channels in chicken cone photoreceptors are also subject to circadian regulation. There is a circadian rhythm in the affinity of the cone cyclic nucleotide-gated channel for cGMP, with highest affinity during the subjective night. In addition, L-type Ca^{2+} channels are regulated in a circadian fashion. The Ca^{2+} currents and immunoreactivity for α1C and α1D calcium channel subunits are greater at night than during the day. There is also a rhythm of α1D mRNA level. More details on rhythms of ion channels can be found elsewhere in this encyclopedia.

Conclusion

The chick retina is a remarkably rhythmic tissue, with robust circadian control of gene expression, metabolism, physiology, and melatonin synthesis. Most attention has been paid thus far to photoreceptor rhythms, but inner retinal neurons also express clock genes and are likely to be subject to circadian control. The ability to generate retinal cell cultures, which maintain their circadian properties and can be manipulated pharmacologically and genetically, suggests that the chick retina will continue to be a valuable model system for exploring the circadian organization of the retina.

Acknowledgments

The author is grateful to the past and present members of his laboratory, especially Rashidul Haque, Nikita Pozdeyev, Shyam Chaurasia, and Tamara Ivanova, and to David Klein and the members of his laboratory, who contributed greatly to the body of knowledge contained within this article. The author also thanks Gianluca Tosini for his collaborative contributions and for critical comments and suggestions on the article. Research in the author's laboratory is funded by the National Institutes of Health EY004864 and EY06360, and by Research to Prevent Blindness.

See also: The Circadian Clock in the Retina Regulates Rod and Cone Pathways; Circadian Photoreception; Circadian Regulation of Ion Channels in Photoreceptors; Circadian Rhythms in the Fly's Visual System; Fish Retinomotor Movements; *Limulus* Eyes and Their Circadian Regulation; Neurotransmitters and Receptors: Dopamine; Neurotransmitters and Receptors: Melatonin Receptors.

Further Reading

Bailey, M. J., Beremand, P. D., Hammer, R., et al. (2004). Transcriptional profiling of circadian patterns of mRNA expression in the chick retina. *Journal of Biological Chemistry* 279: 52247–52254.

Bellingham, J., Chaurasia, S. S., Melyan, Z., et al. (2006). Evolution of melanopsin photoreceptors: Discovery and characterization of a new melanopsin in nonmammalian vertebrates. *PLoS Biology* 4: e254.

Bailey, M. J., Chong, N. W., Xiong, J., and Cassone, V. M. (2002). Chickens' Cry2: Molecular analysis of an avian cryptochrome in retinal and pineal photoreceptors. *FEBS Letters* 513: 169–174.

Bernard, M., Iuvone, P. M., Cassone, V. M., et al. (1997). Avian melatonin synthesis: Photic and circadian regulation of serotonin *N*-acetyltransferase mRNA in the chicken pineal gland and retina. *Journal of Neurochemistry* 68: 213–224.

Chaurasia, S. S., Haque, R., Pozdeyev, N., Jackson, C. R., and Iuvone, P. M. (2006). Temporal coupling of cyclic AMP and Ca/calmodulin-stimulated adenylyl cyclase to the circadian clock in chick retinal photoreceptor cells. *Journal of Neurochemistry* 99: 1142–1150.

Chaurasia, S. S., Pozdeyev, N., Haque, R., et al. (2006). Circadian clockwork machinery in neural retina: Evidence for the presence of functional clock components in photoreceptor-enriched chick retinal cell cultures. *Molecular Vision* 12: 215–223.

Chaurasia, S. S., Rollag, M. D., Jiang, G., et al. (2005). Molecular cloning, localization and circadian expression of chicken melanopsin (Opn4): Differential regulation of expression in pineal and retinal cell types. *Journal of Neurochemistry* 92: 158–170.

Chong, N. W., Bernard, M., and Klein, D. C. (2000). Characterization of the chicken serotonin N-acetyltransferase gene. Activation via clock gene heterodimer/E box interaction. *Journal of Biological Chemistry* 275: 32991–32998.

Chong, N. W., Chaurasia, S. S., Haque, R., Klein, D. C., and Iuvone, P. M. (2003). Temporal-spatial characterization of chicken clock genes: Circadian expression in retina, pineal gland, and peripheral tissues. *Journal of Neurochemistry* 85: 851–860.

Garbarino-Pico, E., Carpentieri, A. R., Contin, M. A., et al. (2004). Retinal ganglion cells are autonomous circadian oscillators synthesizing N-acetylserotonin during the day. *Journal of Biological Chemistry* 279: 51172–51181.

Guido, M. E., Pico, E. G., and Caputto, B. L. (2001). Circadian regulation of phospholipid metabolism in retinal photoreceptors and ganglion cells. *Journal of Neurochemistry* 76: 835–845.

Hamm, H. E. and Menaker, M. (1980). Retinal rhythms in chicks – circadian variation in melatonin and serotonin N-acetyltransferase. *Proceedings of the National Academy of Sciences of the United States of America* 77: 4998–5002.

Haque, R., Chaurasia, S. S., Wessel, J. H., III, and Iuvone, P. M. (2002). Dual regulation of cryptochrome 1 mRNA expression in chicken retina by light and circadian oscillators. *NeuroReport* 13: 2247–2251.

Iuvone, P. M. and Alonso-Gómez, A. L. (1998). Melatonin in the vertebrate retina. In: Christen, Y., Doly, M., and Droy-Lefaix, M.-T. (eds.) *Retine, Luminiere, et Radiations,* vol. 9, pp. 49–62. Paris: Irvinn.

Iuvone, P. M., Brown, A. D., Haque, R., et al. (2002). Retinal melatonin production: Role of proteasomal proteolysis in circadian and photic control of arylalkylamine N-acetyltransferase. *Investigative Ophthalmology and Visual Science* 43: 564–572.

Ivanova, T. N. and Iuvone, P. M. (2003). Circadian rhythm and photic control of cAMP level in chick retinal cell cultures: A mechanism for coupling the circadian oscillator to the melatonin-synthesizing enzyme, arylalkylamine N-acetyltransferase, in photoreceptor cells. *Brain Research* 991: 96–103.

Iuvone, P. M., Tosini, G., Pozdeyev, N., et al. (2005). Circadian clocks, clock networks, arylalkylamine N-acetyltransferase, and melatonin in the retina. *Progress in Retinal and Eye Research* 24: 433–456.

Pierce, M. E., Sheshberadaran, H., Zhang, Z., et al. (1993). Circadian regulation of iodopsin gene expression in embryonic photoreceptors in retinal cell culture. *Neuron* 10: 579–584.

Pozdeyev, N., Taylor, C., Haque, R., et al. (2006). Photic regulation of arylalkylamine N-acetyltransferase binding to 14-3-3 proteins in retinal photoreceptor cells. *Journal of Neuroscience* 26: 9153–9161.

Choroidal Neovascularization

M R Kesen and S W Cousins, Duke Eye Center, Durham, NC, USA

Glossary

Age-related macular degeneration (AMD) – An eye disease with its onset usually after age 60 that progressively destroys the macula, the central portion of the retina.
Angiomatous – Relating to a tumor consisting of a mass of blood vessels.
Brusch's membrane – The inner layer of the choroid, separating it from the pigmentary layer of the retina.
Choriocapillaris – The capillaries forming the inner vascular layer of the choroid.
Choriocapillaris pillars – Lateral walls of the choriocapillaris.
Choroid – The layer of the eye containing blood vessels that furnish nourishment to the other parts of the eye, especially the retina.
Leukostasis – Increased blood viscosity and tendency to clotting.
Subretinal space – An area below the retina.
Telangiectatic – Small dilated blood vessels.

Choroidal Neovascularization

Choroidal neovascularization (CNV) is the growth of pathologic new blood vessels originating from the choriocapillaris invading into the subretinal pigment epithelium (subRPE) and/or the subretinal space. In the early stages of CNV formation, these vessels are capillary-like, lacking the structural integrity of mature vessels causing them to leak plasma or blood. Components of CNV often mature into more organized vessels with features of arteries and veins, and CNV can ultimately evolve into fibrovascular scar tissue.

CNV is known to occur in many ophthalmic diseases. However, it is the most important sequella of age-related macular degeneration (AMD), causing the neovascular form of AMD (NVAMD). In developed countries, NVAMD is the leading cause of blindness in people older than 50 years of age.

Clinical Detection of CNV

Clinically, CNV is detected in patients who complain of blurred and distorted vision, often caused by leakage of plasma from the CNV into or under the overlying neurosensory retina. Because of the optical clarity of the ocular media, the retina can be directly observed by clinicians. Upon examination, eyes with CNV exhibit evidence of leakage such as retinal edema, subretinal fluid, or hemorrhage (**Figure 1(a)** and **1(b)**). If they are not leaking, CNV can sometimes be observed as circular gray or reddish structures under the retina (**Figure 2(a)**). However, in most cases, nonleaking CNV is not directly visible. In some cases, untreated CNV evolves into fibrovascular membranes, called disciform scars.

Clinical imaging technologies have greatly contributed to our understanding of CNV pathobiology and are utilized to enhance detection of CNV. Fluorescein angiography (intravenous injection of a fluorescent dye which can be photographed as it transits through the retina and CNV) is the standard diagnostic technology to confirm the presence of CNV. In classic CNV, fluorescein angiography often reveals CNV to manifest well-defined margins with homogeneous leakage of dye (**Figure 2(b)**). Yet, most cases of CNV are occult, demonstrating less well-defined margins with irregular leakage. Originally, an association was assumed between the fluorescein angiographic appearance and the anatomic location or the growth pattern of CNV. It was presumed that classic CNV was located subretinally, external to the retinal pigment epithelium (RPE) and occult CNV was located external to the RPE within Bruchs membrane. However, data from the Submacular Surgery Trials (SST) research group indicated a lack of correlation between fluorescein angiography pattern and anatomic localization of the CNV.

In the past decade, newer imaging technologies have revealed that the morphologic manifestation of pathologic new vessels in NVAMD (and presumably other diseases with CNV) is much more diverse than traditionally described using fluorescein angiography. Another angiographic imaging technology employs indocyanine green (ICG) dye, allowing visualization of the morphology and the flow of the choroidal vasculature. Dynamic (or video) ICG angiography demonstrates that most CNV is a complex of three components, including an intrachoroidal feeder artery, a subretinal or subRPE capillary network, and an intrachoroidal draining vein (**Figure 2(c)**).

By ICG angiography, CNV appears to manifest a spectrum of morphology ranging from capillary pattern to branching arteriolar pattern. Capillary pattern CNVs are composed mostly of capillaries with minimal arterioles and short, small-caliber feeder arteries. Branching arteriolar pattern CNVs are composed of long, large-caliber

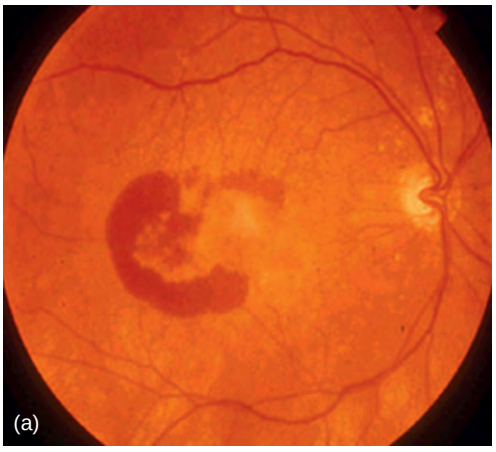

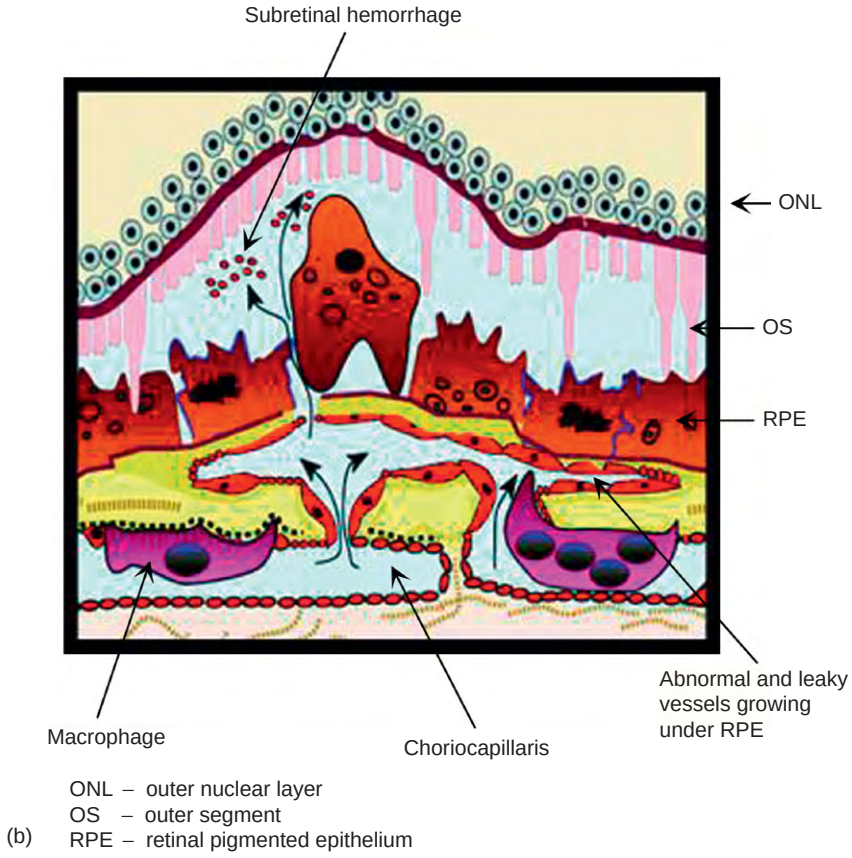

Figure 1 (a) The color fundus photograph demonstrates subfoveal choroidal neovascular membrane with surrounding subretinal hemorrhage. (b) Schematic diagram demonstrates the choroidal neovascular membrane located beneath the retinal pigment epithelium causing leakage of fluid or blood. Arrow indicate direction of fluid and blood leakage.

feeder arteries, many branching arterioles, and minimal capillary morphology (**Figure 3(a)–3(d)**). Mixed pattern CNV demonstrates feature of both extremes. Presumably, all CNVs initially begin as capillary pattern, then progress through a process of remodeling whereby small capillaries obtain a sheath of pericytes which stabilize the incipient new vessel. In some cases, the new vessels become surrounded by vascular smooth muscle and collagen, thus becoming arteriolarized. Hypothetically, the variability among CNV morphology is due to differences in the degree and extent of remodeling. One emerging hypothesis is that capillary-dominated CNVs are exquisitely responsive to anti-vascular endothelial growth factor (anti-VEGF) treatment, whereas branching arteriolar CNV with large feeder vessels are less responsive or even resistant to anti-VEGF therapy.

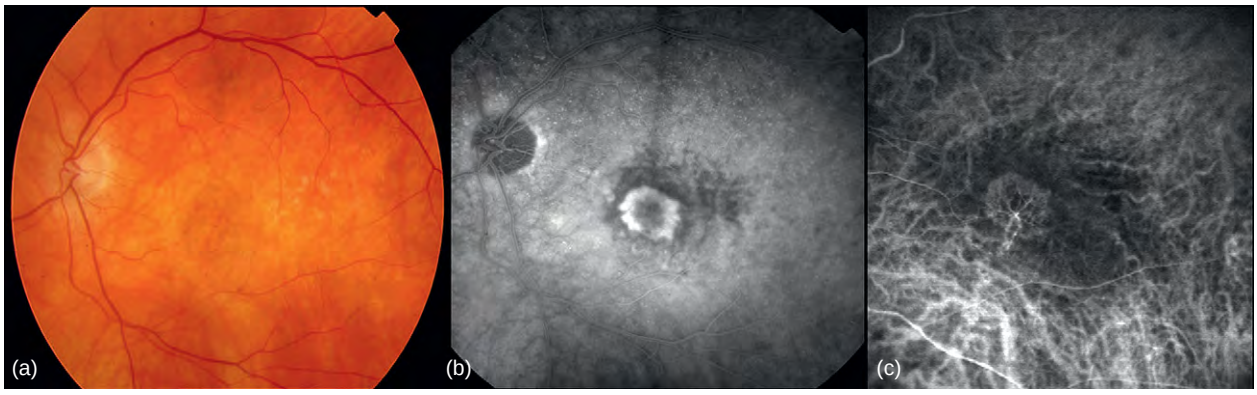

Figure 2 (a) The color fundus photograph demonstrates subtle gray discoloration of the retina due to underlying choroidal neovascular membrane. (b) Late phase fluorescein angiogram shows area of hyperfluorescence corresponding to classic choroidal neovascular membrane with progressive leakage of dye resulting in blurring of the margins. (c) Dynamic indocyanine green angiogram reveals branching vascular network composed of afferent arteriole, capillaries, and draining venule.

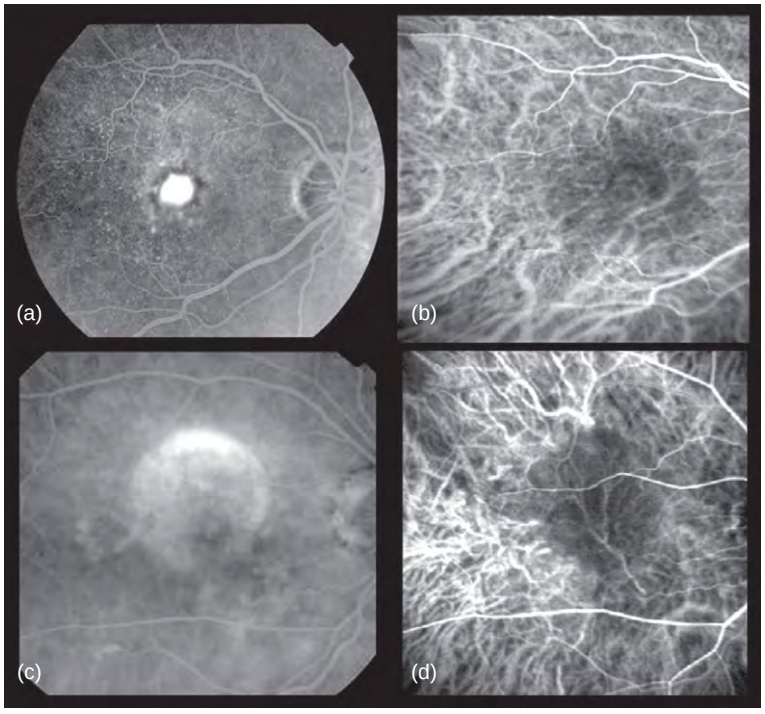

Figure 3 (a) Late arteriovenous phase angiogram shows bright hyperfluorescence corresponding to choroidal neovascular membrane. (b) Dynamic indocyanine angiogram reveals neovascular membrane composed of capillaries with minimal branching arterioles or venules. (c) Venous phase angiogram shows a well-demarcated area of hyperfluorescence corresponding to pigment epithelium detachment with pooling of dye. (d) Dynamic indocyanine angiogram reveals long, large-caliber choroidal feeder vessel perfusing many branching arterioles extending into the pigment epithelium detachment. Minimal capillary structure is observed.

Another imaging technology, called optical coherence tomography (OCT), is a high-resolution, cross-sectional imaging technique that enables visualization of tissue structures up to 2 mm below the surface of the retina. The projected light is reflected back from intraocular structures based upon their distance, thickness, and reflectivity. OCT has become the most commonly used imaging modality in diagnosis and management of patients with AMD since it can demonstrate retinal edema, subretinal fluid, pigment epithelial detachments, and, in some cases, the CNV itself (**Figure 4**). Being the preferred technique to assess treatment response, OCT plays a critical role in guiding the management of patients with AMD.

Histopathology of CNV

Histopathology of CNV has been performed by two types of analyses: evaluation of postmortem specimens within

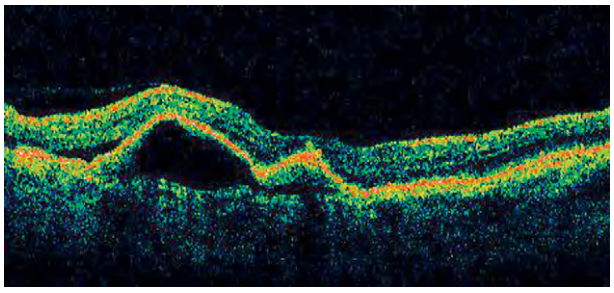

Figure 4 Optical coherence tomography (OCT) image demonstrates pigment epithelial detachments with overlying subretinal fluid.

intact eyes or after removal of CNV as part of a surgical procedure. Postmortem analysis demonstrates that CNV exhibits a wide morphological spectrum. Some cases demonstrate that endothelial-lined capillary tubes are within Bruch's membrane or under the retina. Most cases show that CNV demonstrates more complex morphology, with additional cellular components including RPE cells, pericytes, myofibroblasts, and inflammatory cells. Many cases also demonstrate extensive extracellular matrix deposition and fibrosis. Unfortunately, minimal information is available for the histopathology of the initial stages of CNV formation.

Analysis of the choroid in postmortem specimens has also revealed significant changes, including loss of choriocapillaris surface area, changes in large vascular architecture, increased extracellular matrix, and thickening of the choriocapillaris pillars. Additionally, intrachoroidal vascular changes with polypoidal-like outpouchings of some of the choroidal vessels have been observed.

Analyses of surgically excised CNV during submacular surgery have allowed examination of CNV at an earlier stage in the course of the disease than in postmortem eyes. Histopathology of many early CNV is dominated by macrophage infiltration in addition to the other cellular components (endothelial-lined channels, pericytes, RPE cells) and extracellular matrix. Some examples of surgically excised CNV demonstrate more fibrosis and myofibroblasts with minimal inflammation. In general, Grossniklaus and colleagues have suggested that CNVs in postmortem eyes appear to be more fibrotic than surgically excised CNV, implying that cellular morphology evolves from inflammatory active to inflammatory inactive stages.

Animal Models of CNV

No ideal animal exists for CNV or NVAMD. In current experimental models, CNV is induced by disruption of the Bruch's membrane/RPE complex using laser (argon, krypton, diode), by injections of growth factors, and by genetic manipulations (transgenic or gene transfer) to overexpress angiogenic growth factors. At present, the few models of spontaneous CNV in animals are not reproducible enough to lend themselves to robust scientific analysis.

Laser-induced CNV

Placement of a small laser injury to the outer retina and choroid reliably induces CNV in rodents and subhuman primates. Some believe that a physical hole in Bruch's membrane is necessary. Others believe that thermal injury to the choroid and Bruch's membrane without physical disruption is adequate to trigger CNV, and the model represents a response to injury. Nevertheless, laser injury does not mimic the (unknown) natural stimulus for spontaneous neovascularization in humans. In spite of the artificial trigger, the model does accurately mimic many of the subsequent mechanisms for neovascularization and has predicted therapeutic response to drugs that have been validated in human studies.

The model is triggered by local inflammation at the laser site. Within 3–5 days, authentic pathologic neovascularization occurs. The initial lesion appears to be an invasion of fibrocytes and endothelial cells. Macrophages are prominent at all stages of development. Within a week of development, cell types within the growing vessels include endothelial cells, mesenchymal subtypes (pericytes, myofibroblasts, and smooth muscle cells), macrophages, RPE cells, CD34 cells, and bone-marrow-derived progenitor cells. Numerous growth factors are expressed within the growing CNV, including angiogenic factors, inflammatory cytokines, integrins, and connective tissue growth factor. Among agents that prevent the development of CNV include VEGF inhibitors, anti-inflammatory agents, and integrin antagonists. Recently, agents that block platelet-derived growth factor (PDGF) – important growth factor for mesencyhmal cells – have shown to cause regression of established laser-induced CNV.

Growth factor models

Overexpression of angiogenic growth factors in the outer retina can also induce CNV, but the interpretation of the pathobiology is surprisingly complex. A detailed review is beyond the scope of this article. Briefly, subretinal injection using adenoviral vector containing VEGF-164 causing RPE transduction and overexpression of VEGF induces robust CNV in rodents. Interestingly, transgenic overexpression of VEGF using choroid- or photoreceptor-specific promoters failed to induce CNV without additional injury by subretinal injection, suggesting another stimulus (inflammation or injury) is necessary to trigger CNV. Subretinal injection of pellets or spheres impregnated with basic fibroblast growth factor or other angiogenic factors could also induce CNV in rabbits and primates.

Pathobiology of CNV

Several theories regarding the pathogenesis of CNV have been proposed including RPE dysfunction, changes in choroid, changes in Bruch's membrane, oxidative stress, genetics, ocular perfusion abnormalities, inflammation, and ischemia.

Angiogenesis

Angiogenesis is the growth of new blood vessels originating from preexisting network of blood vessels. Angiogenesis plays a major role in normal vascular development and in wound healing (during which new vessels form, then regress). Angiogenesis has been proven to contribute significantly to the formation of pathologic new vessels in CNV and NVAMD.

Vascular endothelial growth factor

It is now well established that VEGF plays a key role as a stimulator in the neovascular forms of AMD. VEGF, a homodimeric glycoprotein of approximately 45 kDa, is a very potent vascular endothelial cell mitogen that stimulates proliferation, migration, and proteolytic activity of endothelial cells. VEGF is also a potent mediator of increased vascular permeability. Its additional functions include retinal leukostasis and neuroprotection. Three receptor tyrosine kinases have been identified for VEGF: VEGF receptor 1 (VEGFR1) has both positive and negative angiogenic effects; VEGFR2 is the primary mediator of the mitogenic, angiogenic, and vascular permeability effects of VEGF-A, and VEGFR3 mediates the angiogenic effects on lymphatic vessels.

The VEGF gene family is comprised of VEGF-A, -B, -C, -D, and placental growth factor (PlGF). VEGF-A has the strongest association with angiogenesis and is the target of most current anti-VEGF treatments. Nine major VEGF-A isoforms with varying heparin-binding capabilities and tissue distribution have been identified to date: 121, 145, 148, 162, 165, 165b, 183, 189, and 206. These isoforms are produced by alternative exon splicing of the VEGF-A gene. VEGF-165 has been shown to be the most abundant isoform and has a vital role in angiogenesis.

VEGF is essential for normal and abnormal angiogenesis. Deficiency of VEGF expression in the RPE results in the absence of choroid. VEGF is induced by hypoxia in RPE cells and is secreted from the basal side of these cells toward the choroid. High levels of VEGF receptors KDR and flt-4 are found on the choriocapillaris endothelium facing the RPE layer.

The strong evidence supporting its critical role in CNV has made VEGF an optimal target for the treatment of NVAMD. Ranibizumab, a humanized antibody fragment against all isoforms of VEGF, has been developed and proven to be efficacious. Data from two pivotal phase III clinical trials – MARINA (Minimally Classic/Occult Trial of the Anti-VEGF Antibody Ranibizumab in the Treatment of Neovascular AMD) and ANCHOR (Anti-VEGF Antibody for the Treatment of Predominantly Classic CNV in AMD) – led to the approval of Food and Drug Administration (FDA) of Ranibizumab in June 2006 for the treatment of all forms of NVAMD.

Other angiogenic factors

Although VEGF has the primary role in the development of CNV, it likely does so in concert with other growth factors including transforming growth factor-β (TGF-β), aFGF, and bFGF. Other cytokines including the integrins, angiopoetins, and matrix metalloproteinase (MMP) inhibitors may also play an important role. Activation of endothelial cells from the subjacent choriocapillaris results in the production of various degradatory enzymes, such as MMP-2 and -9, allowing them to invade Bruch's membrane and the subretinal space. Both MMP-2 and -9 are activated by VEGF and facilitate the spread of proliferating endothelial cells by digesting the extracellular matrix.

Natural inhibitors of angiogenesis

Endogenous inhibitors include endostatin, and pigment epithelium-derived factor (PEDF), both of which were demonstrated to be significantly reduced in Bruch's membrane in eyes with AMD. Thrombospondin 1, a 450-kDa glycoprotein, contributes to the regulation by functioning both as a stimulator and an inhibitor with its ability to bind to different matrix proteins and cell-surface receptors.

Inflammation Inflammation is typically divided into antigen-specific immunity (T cells, B cells, and antibody-mediated reactions) and innate immunity (neutrophils, macrophages, and amplification cascades, such as cytokines and complement). Although a role for specific immunity has not been excluded, a major role for innate immunity is emerging in the pathogenesis of CNV. Space does not permit a thorough review, but brief mention will be made of two key inflammatory components: monocytes/macrophages and complement.

Monocytes and macrophages Monocytes (the circulating cells) and macrophages (tissue infiltrating equivalent) represent 5% of the circulating white blood cell population. Macrophages are recruited into tissues for the purposes of scavenging, repair, and defense. In the process, they can impart either beneficial effects (like removing deposits and repairing extracellular matrices) or harmful ones (like bystander damage to healthy tissue or neovascularization). As mentioned above, macrophages are numerous in many examples of human CNV. In most experimental models of CNV, macrophages are positive regulators of increased severity of pathologic neovascularization, although some

investigators have identified an anti-angiogenic subtype of macrophages. Macrophages can be induced to synthesize and release pro-angiogenic factors, including VEGF, PDGF, tumor necrosis factor-alpha, prostaglandin E2, and others. Conversely, VEGF is a moderately potent chemotactic factor to recruit and stimulate macrophages into tissues. In addition to their role in angiogenesis, macrophages may contribute to bystander damage in the retina. Numerous macrophage-like cells can be observed in the neurosensory retina overlying CNV in animal models and in human specimens. Presumably, these cells may be releasing factors that promote neuronal injury and decreased vision. Patients with circulating monocytes in the blood that express high levels of pro-angiogenic factor mRNA are more likely to have CNV. Macrophages are attractive targets for therapy. Antimacrophage drugs that are under investigation include those that block macrophage-derived pro-angiogenic cytokines, block cell adhesion molecules (especially integrin alpha 5, beta 1, necessary for monocytes to adhere to vessel surfaces and enter into tissues), block cyclo-oxygenase and block macrophage retention within the CNV or retina.

Complement Complement is a series of over 30 proteins, produced by the liver and secreted into the blood, that serve as an amplification cascade for host defense. Complement activation is triggered by one of three distinct processes (immune complexes, lectin pathway, or alternative pathway) to activate a sequential cascade of interrelated proenzyme intermediates, whose main goal is to produce three types of effector molecules: C3b (coats structures to promote phagocytosis), anaphylatoxins (C3a, C5a, promotes chemotaxis of macrophages and neutrophils), and membrane attack complex (creates pores in cell membranes promoting activation or death). Recently, genetic variations in various complement molecules have been associated with AMD, especially polymorphism in CFH (a negative regulator of activation of the alternative pathway). C3, C3b, and other complement fragments have been demonstrated in specimens of human CNV. In experimental CNV, genetic knock-out or drug inhibition of complement, C3aR, and C5aR significantly diminish CNV formation. It is assumed that C5a may directly activate endothelial cells, or may serve to recruit macrophages into CNV to potentiate neovascularization. Accordingly, complement inhibitors are in clinical trial for the treatment of CNV, including inhibitors of C3, C5, and C5aR.

Vasculogenesis Postnatal or adult vasculogenesis is the contribution of circulating bone-marrow-derived vascular progenitor cells to the repair of normal vessels or the formation of pathologic new vessels. Adult animals maintain a reservoir of stem cells in the bone marrow that may enter the circulation, become recruited into tissues, and differentiate into mature cell types that contribute to healthy repair in regenerating organs. A subset of these marrow cells has been shown to exist in humans and animals that specifically contribute to vascular repair, including both endothelial cells and mesenchymal subtypes (pericytes, myofibroblasts, vascular smooth muscle). Although this field is in its infancy, postnatal vasculogenesis has been shown to contribute to both endothelial and mesenchymal subsets in experimental CNV in several animal models. These cells can be positive or negative regulators of CNV severity, depending on prior environmental exposure of the bone marrow stem cells. Vascular progenitor cells can be identified in the blood of patients with AMD, and certain subsets may identify those with more severe pathology or worse therapeutic outcomes. If confirmed, identification of these cells may be useful as a biomarker for worse outcome and blocking their recruitment may be a therapeutic target.

Therapy of CNV

Prior to 1970, no effective therapy for CNV was available. Upon the recognition of the vascular character of CNV, thermal laser ablation of the CNV lesion as defined by the area of classic leakage on fluorescein angiography was introduced as therapy. The effectiveness of thermal laser as superior to the natural history was validated by several randomized controlled trials, and laser remained the standard of care until the twenty-first century. Photodynamic therapy (PDT) with the photosensitizing agent verteporfin was introduced in early 2000. After intravenous infusion of verteporfin, low energy red-laser light directed at the CNV was used to photoactivate verteporfin into a thrombotic agent, which caused occlusion of the CNV. PDT with verteporfin was proven superior for the treatment of classic CNV, but remained controversial for other subtypes.

Upon the realization that VEGF was the major factor driving angiogenesis and vascular permeability, several companies developed inhibitors of VEGF that could be administered by direct injection into the vitreous cavity of the eye. The first of these to become approved and clinically available was pegaptanib, a synthetic RNA aptamer which specifically bound extracellular VEGF-165 isoform. Although superior to PDT and standard of care, the therapeutic effect on vision and leakage control was modest. Subsequently, two pan-VEGF (i.e., blocking all isoforms) antibody-based inhibitors were introduced. Bevacizumab, a full-length antibody, was developed for intravenous inhibition of VEGF in cancer treatment. Ranibizumab, closely related to the Fab fragment of bevacizumab, was developed for intraocular injection. In 2005, ranibizumab's effectiveness was validated in two landmark clinical trials which showed that monthly injections resulted in outstanding leakage control, stabilization of CNV growth, and improved vision in 30–40% of patients with classic or occult CNV. However, effectivity

requires once a month injection for at least 2 years, and less frequent regimens have not produced the same magnitude of positive outcomes. Subsequently, intravitreal injection of the full-length antibody, bevacizumab, has also been adopted by clinicians but without validation by a randomized controlled trial.

Other interesting agents are currently in clinical trial. Several target VEGF, including VEGF trap (a fusion protein between Fc heavy chain and VEGF receptor that blocks extracellular VEGF), bevasirinib (RNA interference, selectively targeting VEGF mRNA), and several small molecule drugs that inhibit VEGF receptor signaling (the so-called receptor tyrosine kinase inhibitors). Drugs targeting other molecular targets are also in trial, including inibitors of complement, integrins, and PDGF.

Variants of Pathologic Neovascularization in NVAMD

Over the past decade, the spectrum of neovascular AMD has been expanded beyond classic and occult CNV. Identification of additional variants, especially polypoidal choroidal vasculopathy (PCV) and retinal angiomatous proliferation (RAP), has suggested that the pathobiology and treatment of neovascular AMD is a more complex than suggested by the previous review.

Polypoidal choroidal vasculopathy

PCV is a form of intrachoroidal neovascularization that accounts for up to 50% of NVAMD in Asians and may be underdiagnosed in Caucasians. PCV is characterized by large-caliber feeder vessels perfusing intrachoroidal branching arteriolar networks which terminate in one or more intrachoroidal polypoidal structures rather than typical subretinal capillaries of CNV (**Figure 5(a)–5(d)**). Clinical features include orange–red subretinal nodules corresponding to dilated, polyp-like lesions associated with hemorrhagic or serous pigment epithelial detachments, retinal edema, or subretinal hemorrhage. PCV most commonly occurs in the peripapillary and macular regions. ICG angiography is required for diagnosis and visualization of PCV.

The pathobiology of PCV is debated, especially whether it is a distinct disorder from CNV or a disease of similar biology but with different vascular morphology. Anectdotal cases illustrate examples of eyes with PCV

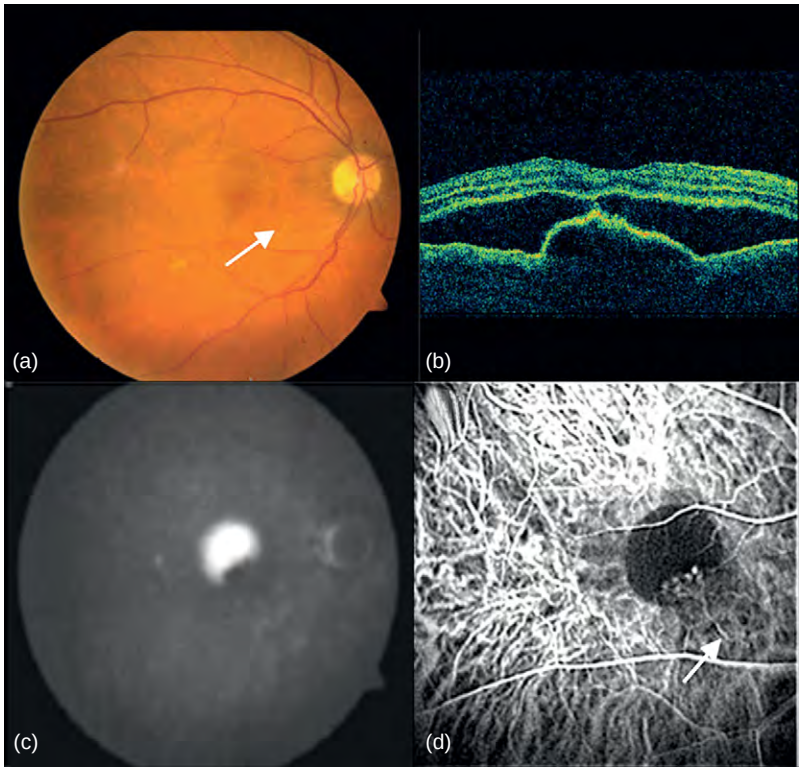

Figure 5 (a) A color fundus photograph shows pigment epithelial detachment and faintly visible feeder vessel extending into the detachment as pointed by the arrow. (b) Optical coherence tomography image shows pigment epithelial detachment with overlying subretinal fluid. (c) Late venous phase fluorescein angiogram shows an area of hyperfluorescence due to pooling of dye into the pigment epithelial detachment. The angiogram fails to show any details of the choroidal neovascular membrane. (d) Dynamic ICG angiogram demonstrates a long afferent arteriole perfusing terminal polypoidal structures consistent with classification as polypoidal choroidal vasculopathy as indicated by the arrow.

that later develop CNV, and vice versa. Histopathology demonstrates thin-walled, saccular polypoidal vessels that were initially regarded as being of venular origin. However, some excised specimens demonstrate the presence of both large choroidal arterioles and venules. Light microscopy demonstrated disruption of inner elastic layer and arteriolosclerotic changes of the blood vessels, and in some cases, the branching arterioles are associated with pericyte-like cells.

The natural history and treatment of PCV is not well established. Anecdotal reports suggest that about half of cases demonstrate deterioration of vision in spite of treatment and that anti-VEGF therapy is less effective than for traditional CNV. The efficacy and safety of PDT seems promising in small studies, but this treatment combined with anti-VEGF therapy must be investigated in future randomized clinical trials.

Retinal angiomatous proliferation

RAP is another recently recognized but common variant of NVAMD that is characterized by the formation of pathologic new vessels within the retina that secondarily invade into the subretinal space or into the choroid. The incidence of RAP variant of NVAMD is unknown, since it requires the use of ICG angiography for definitive diagnosis. Anecdotal reports suggest that at least 15% of the newly diagnosed patients with NVAMD manifest RAP. This variant may be less common in Asians.

High speed ICG angiography offers best visualization of the RAP lesion, particularly for localizing the retinal feeding arterioles and draining venules (**Figure 6(a)–6(e)**). Clinically, stage I RAP lesions present with intraretinal neovascularization with telangiectatic retinal capillaries and small angiomatous structures perfused by the retinal circulation. Stage II RAP lesions extend the new vessel complex into the subretinal space to form subretinal neovascularization often associated with a serous PED. Most stage II RAP lesions are also perfused by retinal arterioles and drained by retinal venules. In these cases, focal closure of the retinal feeding arteriole by thermal laser leads to loss of flow into the RAP lesion and disappearance of hemorrhage, retinal edema, and PED. In stage III RAP,

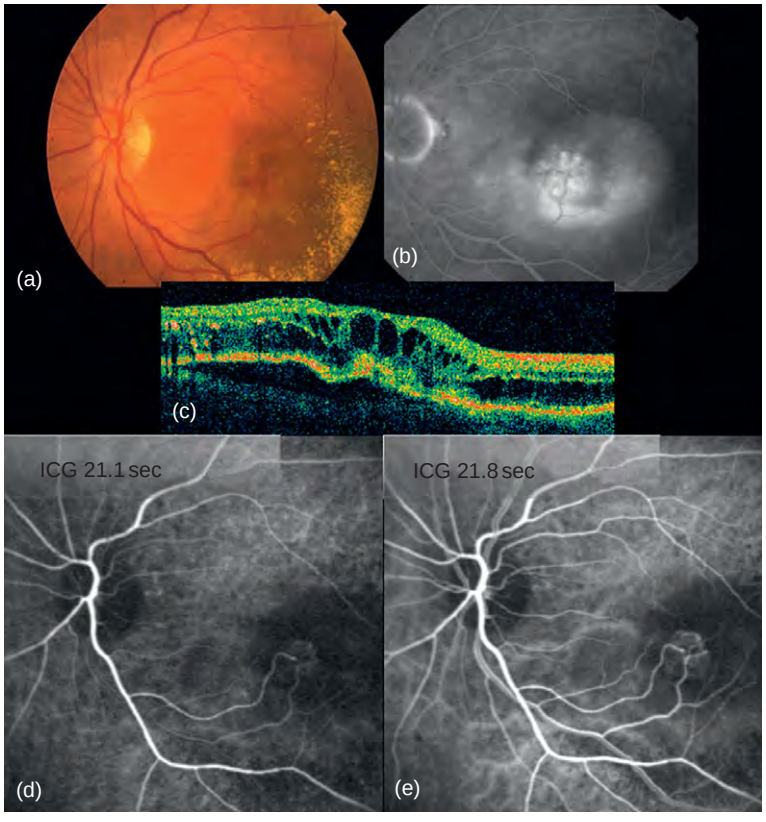

Figure 6 (a) A color fundus photograph shows pigment epithelial detachment associated with intraretinal hemorrhages and extensive exudates temporal to the detachment. (b) Late arteriovenous phase angiogram demonstrates an area of hyperfluorescence corresponding to the pigment epithelial detachment, however, fails to reveal details of the choroidal neovascular membrane to allow for proper classification. (c) Optical coherence tomography image demonstrates serous pigment epithelial detachment with cystic thickening of the overlying retina. Areas of intraretinal hemorrhage appear as hyperreflective spots. (d, e) Dynamic angiogram clearly demonstrates the details of the subretinal neovascular membrane including the afferent arteriole derived from the retinal artery, capillary network, and the draining venule merging with the retinal vein, consistent with classification of the lesion as stage II RAP lesion.

retinal–choroidal anastomosis (RCA) is formed through a break in RPE, often associated with an underlying choroidal neovascular membrane with both choroidal and retinal perfusion. Late stage III RAP lesions develop large fibrotic scars. The transition between purely retinal perfusion (stage I–II RAP) into choroidal perfusion (early stage III RAP) can be difficult to determine clinically.

As with PCV, the pathobiology of RAP is unknown. The histopathological findings in stage II cases demonstrate intraretinal neovascularization without any evidence of CNV. Stage III cases demonstrate both CNV and chorio–retinal anastomosis. RAP responds well to anti-VEGF therapy, suggesting that the underlying pathobiology is strongly mediated by VEGF. Identification of the cellular source of VEGF in RAP (i.e., retinal, RPE, or choroidal) to explain the origination of new vessel growth in the retina as differentiated from choroidal origin in typical CNV remains speculative.

Prior to the advent of anti-VEGF therapy, many treatments for RAP were tried, however, with variable results. Fortunately, anti-VEGF agents effectively control leakage, but rapid recurrences necessitate frequent injections. Focal thermal laser treatment of the afferent arteriole and extrafoveal angioma has been demonstrated to be effective as salvage therapy for recurrences. Advanced forms of the disease involving a vascularized RPE detachment and RCA are unlikely to respond well to any form of current treatment.

Future Directions

Our knowledge base regarding the pathobiology of CNV is expanding as new generation imaging modalities become available and provide us with further anatomical details allowing recognition of the variety in morphology of these lesions. A vast amount of research is focused on learning various aspects of AMD. Although we have come a long way in understanding and treating AMD, considerable amount of work remains to fully understand the pathogenesis, recognize different types, and tailor the therapy based upon special characteristics of each of these lesions to optimize the prognosis in these patients. Areas that especially require additional study include the role of VEGF isoform contribution to healthy choroid and CNV, role of complement and macrophage inflammation, role of endothelial and mesenchymal subtypes in vasculogenesis, predictive biomarker development, and clarification of pathobiology of NVAMD variants, especially PCV and RAP. Combination of comparison of imaging technologies, genotyping studies, and biomarker studies in the context of therapeutic trials will clarify some of these issues.

See also: Angiogenesis in Inflammation; Angiogenesis in Response to Hypoxia; Angiogenesis in Wound Healing; Dry Eye: An Immune-Based Inflammation; Injury and Repair: Neovascularization; Innate Immunity and Angiogenesis; Physiological Anatomy of the Choroidal Vasculature; Retinal Pigment Epithelial–Choroid Interactions; Stability and Functional Integrity of New Blood Vessels; The Vascular Stem Cell.

Further Reading

Ciardella, A. P., Donsoff, I. M., Huang, S. J., Costa, D. L., and Yanuzzi, L. A. (2004). Polypoidal choroidal vasculopathy. *Survey of Ophthalmology* 49: 25–37.

Cousins, S. W., Csaky, K. G., and Espinosa-Heidmann, D. G. (2005). Macular degeneration. In: *Clinical Strategies for Diagnosis and Treatment of AMD: Implications from Research*, pp. 167–191. Berlin: Springer.

Csaky, K. G. and Cousins, S. W. (2007). Immunology of age-related macular degeneration. In: Jennifer, I. and Lim, M. D. (eds.) *Age-Related Macular Degeneration,* 2nd edn., pp. 11–33. Boca Raton, FL: CRC Press.

Fukushima, I., McLeod, D. S., and Lutty, G. A. (1997). Intrachoroidal microvascular abnormality: A previously unrecognized form of choroidal neovascularization. *American Journal of Ophthalmology* 124: 473–487.

Green, W. R. (1999). Histopathology of age-related macular degeneration. *Molecular Vision* 5: 27.

Grossniklaus, H. E. and Green, W. R. (2004). Choroidal neovascularization. *American Journal of Ophthalmology* 137: 496–503.

Grossniklaus, H. E., Ling, J. X., Wallace, T. M., et al. (2002). Macrophage and retinal pigment epithelium expression of angiogenic cytokines in choroidal neovascularization. *Molecular Vision* 8: 119–126.

Lutty, G., Grunwald, J., Maiji, A. B., Uyama, M., and Yoneya, S. (1999). Changes in choriocapillaris and retinal pigment epithelium in age-related macular degeneration. *Molecular Vision* 5: 35.

Chromatic Function of the Cone

D H Foster, University of Manchester, Manchester, UK

Glossary

CIE, Commission Internationale de l'Eclairage – The CIE is an independent, nonprofit organization responsible for the international coordination of lighting-related technical standards, including colorimetry standards.
Color-matching functions – Functions of wavelength λ that describe the amounts of three fixed primary lights which, when mixed, match a monochromatic light of wavelength λ of constant radiant power. The amounts may be negative. The color-matching functions obtained with any two different sets of primaries are related by a linear transformation. Particular sets of color-matching functions have been standardized by the CIE.
Fundamental spectral sensitivities – The color-matching functions corresponding to the spectral sensitivities of the three cone types, measured at the cornea. The spectral sensitivities may be normalized so that the maximum is unity or according to the nominal population densities of the cone types.
Heterochromatic flicker photometry – The adjustment of the radiant power of one of two spatially coextensive lights presented in alternating sequence at a temporal frequency such that there is a unique value of the radiant power where the sensation of flicker is minimum; that is, with a higher or lower radiant power, the sensation of flicker becomes greater.
Luminous efficiency function V_λ – The inverse of the radiant power of a monochromatic stimulus of wavelength λ that produces a luminous sensation equivalent to that of a monochromatic stimulus of fixed wavelength λ_0. The units and λ_0 may be chosen so that the maximum of this function is unity. It is also known as the relative luminous efficiency or relative luminosity function.
Optical density – Absorbance; see spectral absorbance.
Radiant power and quantum units – Radiant power is measured in watts but it is sometimes more appropriate to measure it in quanta s^{-1}. Sensitivities may be expressed as the logarithm to the base 10 of the reciprocal of the radiant power required to reach a criterion level of performance.
Spectral absorbance $A(\lambda)$ – Logarithm to the base 10 of the reciprocal of the spectral transmittance, $\tau(\lambda)$; that is, $A(\lambda) = -\log_{10} \tau(\lambda)$. It depends on the path length. If l is the path length and $a(\lambda)$ is the spectral absorptivity, then, for a homogeneous isotropic absorbing medium, $A(\lambda) = la(\lambda)$ (Lambert's law).
Spectral absorptance $\alpha(\lambda)$ – Ratio of the spectral radiant flux absorbed by a layer to the spectral radiant flux entering the layer. If $\tau(\lambda)$ is the spectral transmittance, then $\alpha(\lambda) = 1-\tau(\lambda)$. The value of $\alpha(\lambda)$ depends on the length or thickness of the layer. For a homogeneous isotropic absorbing medium, $\alpha(\lambda) = 1-\tau(\lambda) = 1-10^{-la(\lambda)}$, where l is the path length and $a(\lambda)$ is the spectral absorptivity. Changes in the concentration of a photopigment have the same effect as changes in path length.
Spectral absorptivity $a(\lambda)$ – Spectral absorbance of a layer of unit thickness. Absorptivity is a characteristic of the medium, that is, the photopigment. Its numerical value depends on the unit of length.
Spectral sensitivity – The inverse of the radiant power of a monochromatic stimulus of wavelength λ that produces a criterion response equal to that of a monochromatic stimulus of fixed wavelength λ_0. The units and λ_0 may be chosen so that the maximum of this function is unity. In specifications by the CIE, the lower limit of the wavelength range is generally 360–400 nm and the upper limit is generally 760–830 nm, but smaller ranges may be used. The spectral sensitivity of a cone is essentially the normalized spectral absorptance of its photopigment (discounting any geometrical factors, e.g., cone waveguide properties).
Spectral transmittance $\tau(\lambda)$ – Ratio of the spectral radiant flux leaving a layer to the spectral radiant flux entering the layer. The value of $\tau(\lambda)$ depends on the path length.
Unique hues – Hues that are judged to be unmixed. They form mutually exclusive pairs, so that no light can appear to contain both red and green or both blue and yellow.
Wavenumber – The reciprocal of wavelength, usually in cm^{-1}.

Introduction

Normal human color vision is governed by three types of retinal cone photoreceptors sensitive to light over

different, but overlapping, regions of the spectrum and conventionally designated long-, medium-, and short-wavelength-sensitive (L, M, and S). Because the intensity and spectral properties of light cannot be distinguished once it has been absorbed (the principle of univariance), chromatic information is obtained by comparing the outputs of these different cone types. Signals from L, M, and S cones converge via excitatory and inhibitory pathways onto subsets of anatomically distinct ganglion-cell populations, which then project to the lateral geniculate nucleus, and thence to the higher cortical areas. The aim of this article is to provide an overview of how the cones contribute to chromatic function and how that contribution is modified by prereceptoral filtering and postreceptoral processing within the eye.

Photopigments and Phototransduction

The photopigment in the outer segment of the cone consists of two covalently linked parts, a protein called opsin and a chromophore based on retinal, an aldehyde of vitamin A. It is the latter that provides light sensitivity by isomerizing from 11-*cis* to all-*trans* forms. This leads to the activation of a guanine nucleotide-binding protein (G-protein), transducin, and a cascade of molecular events that result in a change in the rate of neurotransmitter release from the receptor to other neurons in the retina. In the course of the cascade, the signal provided by photon absorption is greatly amplified.

The wavelength λ_{max} of maximum absorption of the pigment (see the section entitled 'Cone Spectral Sensitivities') depends on the particular amino acid sequence of the opsin and its relationship to the chromophore. The L and M pigments are members of an ancestral medium/long-wavelength-sensitive class of vertebrate pigments. These two pigments have a high degree of homology, and the majority of the difference in λ_{max} arises at just a few amino acid sites. A common polymorphism of the L and M pigments, in which alanine is substituted for serine at codon 180, can create shifts in λ_{max} of several nanometers.

The S pigment is a member of a distinct ancestral ultravoilet (UV)-sensitive class of vertebrate pigments. Its spectral tuning is different from that of the L and M pigments, and the shift in λ_{max} from UV to the violet of normal human S cones arises from amino acid replacements at multiple tuning sites.

Fundamental Spectral Sensitivities

The spectral sensitivities of the cones, *in vivo*, have been estimated by many different methods. Historically, the most important method is based on psychophysical color-matching, in which a mixture of three fixed primary lights is matched against a monochromatic light of variable wavelength and constant radiant power. These data form the basis of the system of colorimetry standardized by the Commission Internationale de l'Eclairage (CIE). In the normal trichromatic eye, such color-matching functions yield a family of spectral sensitivities that are a linear transformation of the unknown cone spectral sensitivities. This transformation is not unique in that it varies with the choice of primaries, but data obtained from dichromatic and sometimes monochromatic observers, who have, respectively, only two and one of the three normal cone types, provide good estimates of these so-called fundamental spectral sensitivities.

Figure 1 shows one set of normalized L-, M-, and S-cone fundamental spectra, with wavelengths λ_{max} of maximum sensitivity of *c.* 570, 543, and 442 nm. These estimates represent corneal cone spectral sensitivities, as color matching necessarily involves the spectral transmission properties of the ocular media (see the section entitled 'Prereceptoral Attenuation'). Several such sets of fundamentals have been derived, based on different sets of color-matching functions and different assumptions about cone sensitivity and prereceptoral absorption.

Other psychophysical methods of estimation involve selectively chromatically adapting the three cone types by a background light and measuring the spectral sensitivity of the most sensitive color mechanism at or near its threshold level of response, a technique associated primarily with W. S. Stiles (see the subsection entitled 'Isolating Cone Responses: Selective Chromatic Adaptation'). Psychophysical methods have the advantage that sensitivity can be determined over a range of two to five decades

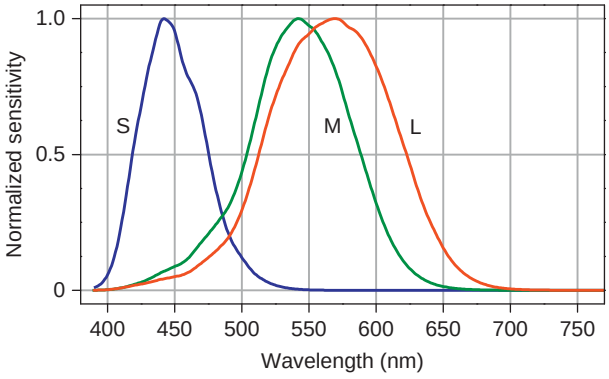

Figure 1 Fundamental spectral sensitivities of the long-, medium-, and short-wavelength-sensitive (L, M, and S) cones. Data are normalized to a maximum of unity on a radiance scale and are based on the 2° data of Table 2 of Stockman, A. and Sharpe, L. T. (2000). The spectral sensitivities of the middle- and long-wavelength-sensitive cones derived from measurements in observers of known genotype. *Vision Research* 40: 1711–1737; modified from the mean 10° color-matching functions of Stiles, W. S. and Burch, J. M. (1959). N.P.L. colour-matching investigation: Final Report (1958). *Optica Acta* 6: 1–26.

(i.e. 2–5 log units), although with normal trichromats, chromatic adaptation cannot generally isolate the response of a single cone type throughout the spectrum.

Nonpsychophysical but noninvasive methods of *in vivo* estimation include retinal densitometry (i.e., fundus spectral reflectometry) and electroretinography. In retinal densitometry, differences in reflectance of the fundus are measured, at various wavelengths, before and after selectively bleaching the cone pigments. The method is limited by its low signal-to-noise ratio and the need to distinguish between signals from L and M cones. It is also difficult to obtain signals reliably from S cones. In electroretinography, the summed electrical response of the retina to a flickering light is measured with a corneal electrode. This method provides a much larger dynamic range, of several log units, along with a good signal-to-noise ratio, but, as with retinal densitometry, signals from L and M cones need to be separated. Both techniques are best applied to well-characterized dichromats.

Prereceptoral Attenuation

The spectrum of the incident light reaching the cones is modified by two prereceptoral filters. The first is the lens (and cornea). In the young eye, the lens appears colorless, but, with increasing age, it becomes yellow, partly as a result of light scatter and absorption, which produce large transmission losses at short wavelengths (**Figure 2**). Even within the same age group, however, the size of the loss at 400 nm may vary over 1 log unit. Another important factor in the changing appearance of the lens is the accumulation of a particular fluorogen, which leads to increased lens fluorescence.

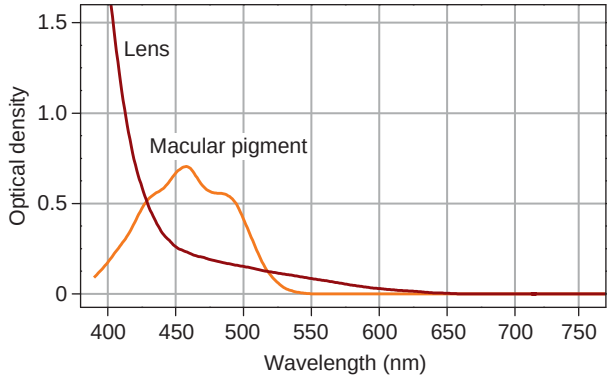

Figure 2 Variation of the optical density of the lens and of the macular pigment with wavelength. Data are from Table 2 of Stockman, A. and Sharpe, L. T. (2000). The spectral sensitivities of the middle- and long-wavelength-sensitive cones derived from measurements in observers of known genotype. *Vision Research* 40: 1711–1737; based on van Norren, D. and Vos, J. J. (1974). Spectral transmission of human ocular media. *Vision Research* 14: 1237–1244; and on Bone, R. A., Landrum, J. T., and Cains, A. (1992). Optical density spectra of the macular pigment *in vivo* and *in vitro*. *Vision Research* 32: 105–110. Plotted values are means over observers. Macular-pigment densities have been doubled for clarity.

The second prereceptoral filter is a nonphotosensitive yellow pigment, usually referred to as the macular pigment. Its maximum absorption is at *c.* 460 nm (**Figure 2**). It is a carotenoid consisting of two xanthophylls, lutein and zeaxanthin, whose densities decline with increasing eccentricity, with zeaxanthin concentrated only in the fovea.

The optical density of macular pigment can be quantified, *in vivo*, by heterochromatic flicker photometry and by Raman spectroscopy, in which argon laser light is used to excite the xanthophylls. Values of the optical density at the fovea vary markedly across individuals, from >1.0 to almost zero, with a mean of *c.* 0.6. Some of the hypothesized benefits of the macular pigment include protection from the damaging effects of short-wavelength light, reducing the effects of longitudinal chromatic aberration and glare, and protection against reactive oxygen species.

In addition to the lens and macular pigment, there is another important factor modifying the effective spectral sensitivity of the cones, namely, self-screening by the photopigment, which acts to broaden its absorption spectrum. If at wavelength λ the spectral absorptivity is $a(\lambda)$ and the path length is l, then the spectral absorptance $\alpha(\lambda)$ is given by $1-10^{-la(\lambda)}$. Therefore, increasing l (or equivalently the concentration of the pigment) has a proportionally larger effect at values of λ where $\alpha(\lambda)$ is small than at values where it is large.

Cone Spectral Sensitivities

Estimates of cone spectral sensitivities can be obtained from corneal spectral sensitivities, that is, the fundamental spectra of **Figure 1**, by eliminating the estimated effects of prereceptoral losses (see the section entitled 'Prereceptoral Attenuation'). **Figure 3** shows the results. The normalized L-, M-, and S-cone spectral sensitivities have wavelengths λ_{max} of maximum sensitivity of *c.* 559, 530, and 421 nm, respectively. Comparing these spectra with corneal spectra (**Figure 1**) reveals the influence of prereceptoral filtering in shifting λ_{max} toward longer wavelengths, especially for S cones, where the increase in λ_{max} is *c.* 20 nm.

In vitro methods of estimating cone spectral sensitivities include recording from single cone outer segments with a suction microelectrode, direct microspectrophotometry of intact receptor outer segments, and differential spectrophotometry of recombinant cone pigments produced in tissue-culture cells. Microelectrode recordings take advantage of the amplification of the signal provided by the phototransduction cascade and so can provide sensitivities over 5–6 log units, but spectrophotometry, as with *in vivo* reflectance measurements, is limited by

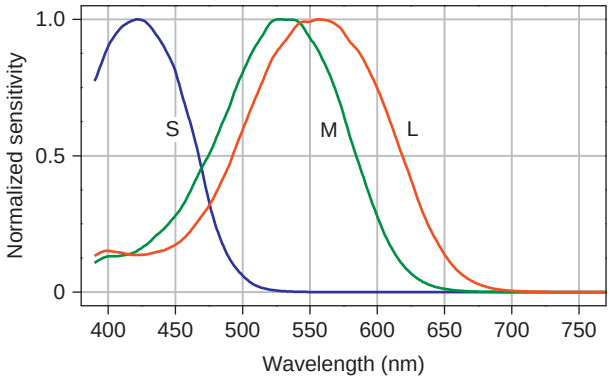

Figure 3 Spectral sensitivities of the long-, medium-, and short-wavelength-sensitive (L, M, and S) cones derived from mean L-, M-, and S-cone fundamental spectra (Figure 1). Data are normalized to a maximum of unity on a radiance scale and are based on Table 2 of Stockman, A. and Sharpe, L. T. (2000). The spectral sensitivities of the middle- and long-wavelength-sensitive cones derived from measurements in observers of known genotype. *Vision Research* 40: 1711–1737.

its low signal-to-noise ratio, providing sensitivities over only 1 or 1–2 log units. All *in vitro* methods are constrained by the nonphysiological nature of the illumination (and sometimes by the method of specimen preparation and recording). Notwithstanding the differences in experimental methodology and analysis, there is broad agreement in the values of λ_{max} (Table 1).

Template for Cone Spectral Sensitivity

The response of a cone is determined by the number of photons it absorbs: the spectral sensitivity describes the probability of that absorption at each frequency ν, which is invariant of the medium, unlike wavelength λ. The main absorption band of mammalian visual pigments is the α band (the β and other bands at progressively shorter wavelengths have less influence because of absorption in the ocular media). Despite the differences in λ_{max} of the L, M, and S pigments, plotting cone spectral sensitivity or spectral absorbance against the normalized frequency, that is, ν/ν_{max}, where ν_{max} is the frequency of maximum sensitivity, yields closely similar dependencies, as illustrated by the data in Figure 4 for suction microelectrode recordings from monkey cones (symbols).

These dependencies may be fitted empirically by a polynomial or other smooth function of normalized frequency (Figure 4, curve). This function may then be used as a template or nomogram and applied to sample data that are noisy or of limited range, allowing, for example, more accurate estimates of λ_{max}, as was done with the entries in Table 1. Templates are best obtained separately for sensitivities on logarithmic and linear ordinates, for the weighting of the fits is different and the templates are therefore not exact logarithmic transforms of each other (the data in Table 1 were based on both kinds of templates).

Table 1 Estimated wavelengths λ_{max} of maximum sensitivity of long-, medium-, and short-wavelength-sensitive cones and cone pigments from *in vivo* and *in vitro* measurements in humans and primates

Method	λ_{max} *(nm)*		
	L	*M*	*S*
Psychophysics[a]	559	530	421
Suction microelectrode recording from primate cones[b]	561	531	430
Microspectrophotometry of excised human cones[c]	558	531	419
Recombinant human cone pigments[d]	558	530	425

[a]Stockman, A. and Sharpe, L. T. (2000). The spectral sensitivities of the middle- and long-wavelength-sensitive cones derived from measurements in observers of known genotype. *Vision Research* 40: 1711–1737.
[b]Baylor, D. A., Nunn, B. J., and Schnapf, J. L. (1987). Spectral sensitivity of cones of the monkey *Macaca fascicularis*. *Journal of Physiology – London* 390: 145–160.
[c]Dartnall, H. J. A., Bowmaker, J. K., and Mollon, J. D. (1983). Human visual pigments: Microspectrophotometric results from the eyes of seven persons. *Proceedings of the Royal Society of London, Series B: Biological Sciences* 220: 115–130.
[d]Merbs, S. L. and Nathans, J. (1992). Absorption spectra of human cone pigments. *Nature* 356: 433–435; Oprian, D. D., Asenjo, A. B., Lee, N., and Pelletier, S. L. (1991). Design, chemical synthesis, and expression of genes for the three human color vision pigments. *Biochemistry* 30: 11367–11372.

Cone Gains and von Kries Scaling

The chromatic function of the cones is determined by not only their spectral sensitivities but also their relative gains. The effect of the spectrum of the prevailing light on those gains is summarized by the coefficient rule of von Kries, which refers to the idea that the sensitivity of each cone type depends only on activity in that cone type. Thus, if the radiant power in the light is biased toward long wavelengths, then the gain of the L cones is reduced in proportion to that bias. In fact, the evidence from microelectrode recordings in the retina of primates suggests that although substantial and independent chromatic adaptation does takes place among the three cone types, it is not complete. Adaptation also takes place at postreceptoral levels (see the section entitled 'Postreceptoral Spectra'). Even so, to a first-order approximation, von Kries scaling achieves a normalization of cone responses over a wide range of illumination conditions before bleaching dominates.

Isolating Cone Responses

The experimental investigation of chromatic function sometimes requires the selective stimulation of a particular cone type. There are two general methods for achieving this *in vivo*: one employs selective adaptation either by

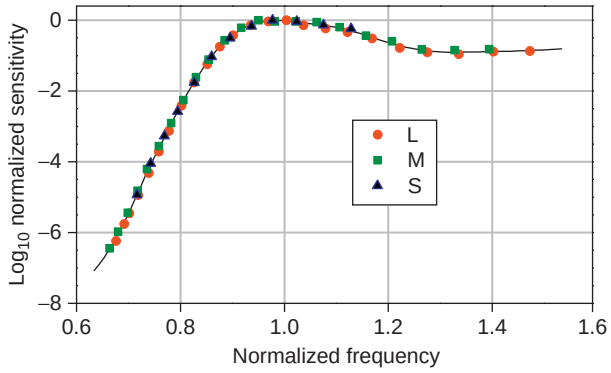

Figure 4 Spectral sensitivities of long-, medium-, and short-wavelength-sensitive (L, M, and S) monkey cones measured by suction microelectrode. Log mean absorbance, normalized to a maximum of zero (i.e., unity on a linear scale), is plotted against normalized frequency ν/ν_{max} for each cone type. Data are from Table 1 of Baylor, D. A., Nunn, B. J., and Schnapf, J. L. (1987). Spectral sensitivity of cones of the monkey *Macaca fascicularis*. *Journal of Physiology – London* 390: 145–160. The smooth curve is a locally weighted polynomial regression.

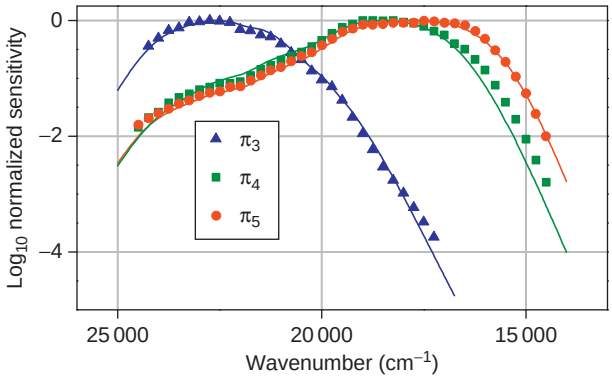

Figure 5 Stiles' background-field spectral sensitivities of the mechanisms π_3, π_4, and π_5 (symbols). Log mean sensitivity, normalized to a maximum of zero on a log quantum scale (i.e., unity on a linear scale), is plotted against wavenumber (proportional to frequency). The corresponding mean S-, M-, and L-cone fundamental spectral sensitivities, in the same units, are also shown (curves). Data are based on Table 2 (7.4.3) of Wyszecki, G. and Stiles, W. S. (1982). Color science: Concepts and methods, quantitative data and formulae. New York: John Wiley & Sons and on Table 2 of Stockman, A. and Sharpe, L. T. (2000). The spectral sensitivities of the middle- and long-wavelength-sensitive cones derived from measurements in observers of known genotype. *Vision Research* 40: 1711–1737.

a steady or temporally modulated background field so that only the chosen cone type mediates detection; the other constrains changes in the stimulus so that they are invisible to all but the chosen cone type.

Selective Chromatic Adaptation

The two-color threshold method of Stiles is based on the properties of the increment-threshold function. The minimum detectable radiance (the increment threshold) of a small test flash of wavelength λ is measured as a function of the radiance of a large steady background field of wavelength μ. The resulting monotonically increasing, threshold-versus-radiance (t.v.r.) curve may have more than one branch, but, over a limited range, each branch typically retains its shape while undergoing a vertical displacement with a change in λ (yielding a test spectral sensitivity) or a horizontal displacement with a change in μ (yielding a background-field spectral sensitivity). Provided certain assumptions hold, the test spectral sensitivity should coincide with the background-field spectral sensitivity, where both are defined. The assumptions are that the mechanisms underlying the t.v.r. curves – Stiles' π mechanisms – act independently of each other; that the observed t.v.r. curve depends only on the smallest increment threshold of the mechanisms available; and that each mechanism has a well-defined spectral sensitivity.

Figure 5 shows background-field spectral sensitivities for three mechanisms, π_3, π_4, and π_5 (symbols) superimposed on the corresponding S-, M-, and L-cone fundamental spectra (curves) (see the section entitled 'Fundamental Spectral Sensitivities').

The π mechanisms cannot represent individual cone activity, for there are too many of them: three S mechanisms (π_1, π_2, and π_3), two M mechanisms (π_4 and π_4'), and two L mechanisms (π_5 and π_5'), depending on the conditions of measurement. In addition to their multiplicity, there is evidence of nonadditivity, that is, the effect of a background field consisting of two monochromatic lights is different from the sum of the effects of the two lights alone. Yet, as Figure 5 shows, π_3, π_4, and π_5 approach quite closely the corresponding cone fundamentals.

The mechanisms defined by the t.v.r. curves depend, of course, on where in the visual pathway the threshold for detection is determined. With an appropriate choice of the spatial and temporal properties of the test flash and the background field, it is possible to obtain both test and background-field spectra that appear to mainly represent not cone responses but opponent combinations of cone responses (see the subsection entitled 'Postreceptoral Spectra: Cone Opponency').

Silent Substitution

The principle of silent substitution is illustrated in Figure 6. At a particular criterion response level, here 0.9 of maximum (other levels might be chosen), there are two wavelengths, 543 nm and 594 nm, at which the L-cone sensitivities are equal (red crosses). The alternation of two monochromatic, equal-radiance lights at these two wavelengths is therefore invisible to L cones but visible to M cones, for the M-cone sensitivity at 543 nm is more

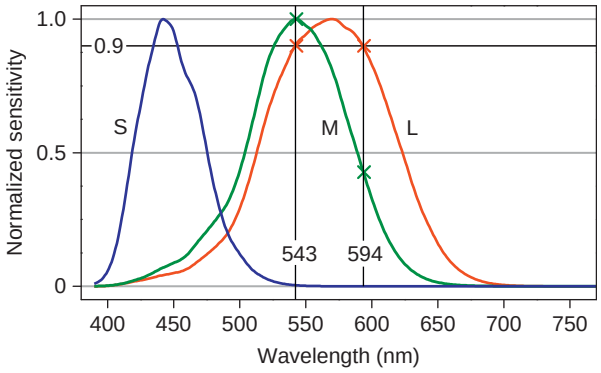

Figure 6 Silent substitution. Responses at 543 and 594 nm are the same for L cones (red crosses) but different for M cones (green crosses). Data are normalized cone fundamental spectra (Fig. 1).

than twice that at 594 nm (green crosses). At these two wavelengths, the S-cone sensitivity is vanishingly small and can be ignored. The same technique may be applied to M and S cones.

Unlike selective chromatic adaptation, the isolation achieved by silent substitution is a second-order one: it is not the stimulus but its alternation that is silent. Nevertheless, the method may be used to determine the spectral sensitivity of the isolated cone class (here the M cones); and even when the spectral sensitivity of the silenced class (the L cones) is known only approximately, it may still, in principle, be applied in an iterative way.

Rod Intrusion

The rod photoreceptors of the retina are not normally associated with chromatic function. But with large stimulus fields of low-to-moderate luminance, color vision can be influenced by rod activity, which biases the apparent hue and diminishes the saturation of extrafoveal stimuli. Even for foveal stimuli of just 1° visual angle, some rod involvement may be detected. Under daylight conditions, however, rod intrusion in color matches is small and is likely to be negligible above 100 cd m^{-2}.

Spatial Densities

The numbers of the three cone types are neither constant over individuals nor uniform across the retina. These variations have different implications for chromatic and luminance function.

Individual Variations

The relative frequencies of the different cone types, as proportions of the total number of cones, have been estimated across individuals by indirect psychophysical methods and by more direct methods, both *in vivo* and *in vitro*. The most important psychophysical method models the photopic luminous efficiency function obtained by heterochromatic flicker photometry as a linear sum of signals from L and M cones, under the working assumptions that the contribution of each is weighted by its numerosity and that the spectral sensitivity of each is known. Direct *in vivo* methods include retinal densitometry, electroretinographic flicker photometry, and high-resolution adaptive-optics imaging combined with retinal densitometry. Results from flicker photometry correlate with those from electroretinographic methods. *In vitro* methods include microspectrophometry with single cones, immunocytochemical labeling of small retinal patches, and analysis of L and M opsin messenger RNA in homogenized retinal patches.

It is clear that the relative frequency of S cones is fairly constant over individuals, *c.* 5–6% for a patch of retina at 1° eccentricity. For L and M cones, it is their ratio that is normally specified, and, although a working value of 1.5:1 or 2:1 is often assumed in modeling their contributions to the luminous efficiency function, the actual ratio varies greatly from individual to individual, from *c.* 0.7:1 to 12:1, by direct measurement, and over a somewhat larger range by indirect measurement. This variation may reflect the different evolutionary and developmental histories of the S-cone and L- and M-cone pathways.

Retinal Distributions

That the three cone types have different distributions across the retina has been long known from psychophysical measurements of, for example, increment threshold and grating acuity with cone-specific stimuli. These findings have been confirmed and extended by some of the techniques mentioned in the preceding subsection.

The spatial density of L and M cones is greatest in the central fovea and it declines steadily with increasing retinal eccentricity. By contrast, the spatial density of S cones is zero in the central *c.* 20 arcmin of the fovea (0.1 mm); it increases to a maximum at *c.* 1° eccentricity, and then declines again. Because the decrease in S-cone density is less rapid than that of the other cone types, the relative frequency of S cones, as a proportion of the total number of cones at each eccentricity, increases slowly with eccentricity and levels off at *c.* 5° or a little more.

In the fovea, there seems to be little evidence for other than a random distribution of S cones and L and M cones, although occasional departures in the direction of a more regular S-cone distribution and some clumping of L and M cones have been observed. In the periphery, there are more systematic departures from randomness in the distributions of both S cones and L and M cones. The purpose of the cone-rich rim of the ora serrata is unknown.

Eccentricity and Chromatic Function

The absence of S cones in the center of the fovea accounts for the perceptual phenomenon of small-field tritanopia: for sufficiently small fields, color vision is dichromatic, so that just two fixed primary lights are needed to match an arbitrary test light (see the section entitled 'Fundamental Spectral Sensitivities'). The size of the tritanopic zone varies across individuals, and it may be absent in some.

The consequences of individual variation in L:M cone ratios are largely confined to luminance function. For chromatic function, the variation may be counterbalanced by changes in gain associated with excitatory and inhibitory inputs. In judgments of a perceptually unique yellow, in which the wavelength of a monochromatic light is adjusted so that it appears neither red nor green and which might be expected to reveal an imbalance between L and M cone inputs, the variation in the selected wavelength seems not to be attributable to ratio differences. One factor contributing to the stability of unique hues may be a form of chromatic adaptation to the spectrum of the environment.

For the individual eye, there are marked variations in chromatic function with retinal eccentricity. Thus, in general terms, color-matching performance with a small field, of the order of 1° extent, diminishes with increasing distance from the fovea, tending to dichromacy at 25–30° and to monochromacy at 40–50°. More specific changes are revealed by psychophysical measurements of hue and saturation and of chromatic contrast sensitivity with eccentricity. The latter is quantified by the detectability of a stimulus modulated along a red–green or blue–yellow color axis, defined with respect to stimuli specific for L, M, or S cones (i.e., an L vs. M axis and an S vs. L + M axis). The size of the stimulus is usually increased with eccentricity for optimum response. For red–green modulation, contrast sensitivity is high at the fovea and then declines rapidly with eccentricity, falling to zero at 25–30°, whereas for blue–yellow modulation, contrast sensitivity is much flatter and declines only slowly with eccentricity, and at a rate similar to that for luminance modulation. Since luminance contrast sensitivity is determined by the same cone signals as red–green contrast sensitivity, the decline in the latter with eccentricity is presumably due to changes in chromatic coding rather than in L and M cone densities (see the subsection entitled 'Postreceptoral Spectra: Cone Opponency').

Postreceptoral Spectra

Cone Opponency

Spectral sensitivity at postreceptoral levels is modified by antagonistic interactions between signals from the different cone types. This cone opponency – also occasionally called color opponency – is not the same as the red–green and blue–yellow color opponency identified in some perceptual experiments where the poles of the reference axes correspond to the unique hues, red, green, blue, and yellow.

The detailed organization of cone opponency has been difficult to characterize unambiguously, and retinal connectivity is not as specific as has sometimes been assumed. Thus, there is anatomical evidence of random, nonselective connectivity of L and M cones to ganglion-cell receptive fields, and physiological evidence of both randomness and selectivity. Nevertheless, because the response of a ganglion cell is determined by a weighted sum of its excitatory and inhibitory inputs, the nature of the connectivity has less effect on the spectral characteristics of cone-opponent responses than the weights associated with the inputs. Figure 7 shows theoretical cone-opponent spectra (curves) from simple linear combinations of cone signals of the form $S - k(M + L)$ in the left panel, $M - kL$ in the middle panel, and $L - kM$ in the right panel, where the amount of inhibition is indicated by the weight constant k (the assumption of linearity is not essential).

With $k = 0.4$, the wavelength λ_{max} of maximum sensitivity for the $L - kM$ spectrum shifts from 570 to 589 nm, a difference of 19 nm, whereas for the $M - kL$ spectrum, λ_{max} shifts from 543 to 539 nm, that is, just 4 nm, and for the $S - k(M + L)$ spectrum, there is no shift at all. With larger k, both $L - kM$ and $M - kL$ spectra become more narrowed. Combined with a shift in λ_{max}, the effect is sometimes described as spectral sharpening.

These changes in spectral shape are similar to those observed in microelectrode recordings in primate retina and psychophysically in both test and background-field spectral sensitivities (see the subsection entitled 'Isolating Cone Responses: Selective Chromatic Adaptation') obtained under conditions designed to isolate cone-opponent activity. Examples of background-field cone-opponent spectra are also shown in Figure 7 (symbols). Notice that the asymmetries in the shifts of λ_{max} do not themselves require asymmetric weighting of cone signals nor do they imply asymmetric $L - kM$ and $M - kL$ responses.

As already observed (see the subsection entitled 'Spatial Densities: Eccentricity and Chromatic Function'), red–green and blue–yellow contrast sensitivity varies with retinal eccentricity, but there is evidence that the opponent weights revealed in those measurements remain constant with retinal location up to *c.* 10° eccentricity. Beyond that, differences emerge in the L versus M and M versus L responses.

It is at present unclear how these kinds of cone-opponent activity relate to the perceptual color opponency of unique hues.

Advantages of Cone Opponency

Along with providing information about the spectral content of a stimulus, cone opponency has two other

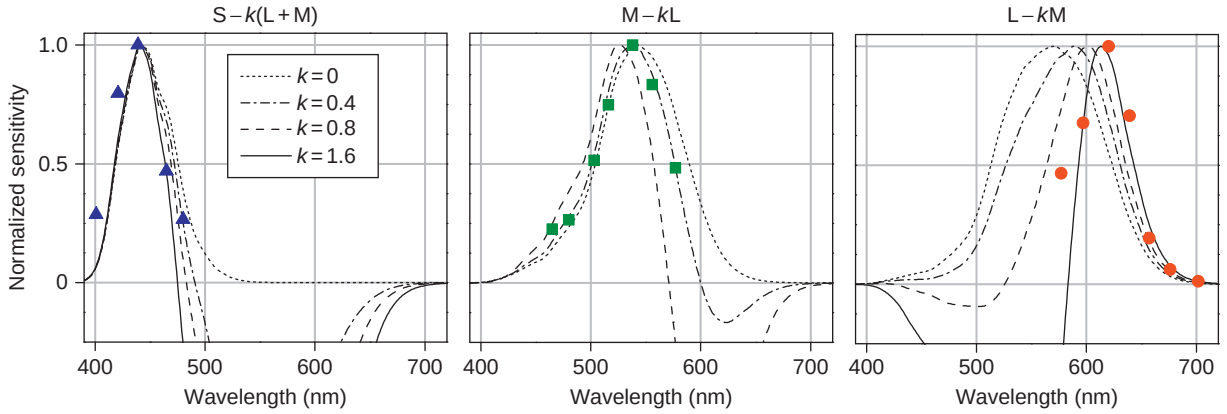

Figure 7 Theoretical and observed cone-opponent spectral sensitivities. Each set of curves represents spectra of the form S − *k*(M + L) (left panel), M − *k*L (middle panel), and L − *k*M (right panel), normalized to a maximum of unity on a radiance scale, with values of the weight constant *k* indicated (for *k* = 1.6, the function M − *k*L is mainly negative). Normalized L-, M-, and S-cone fundamental spectra were taken from Table 2 of Stockman, A. and Sharpe, L. T. (2000). The spectral sensitivities of the middle- and long-wavelength-sensitive cones derived from measurements in observers of known genotype. *Vision Research* 40: 1711–1737. The symbols show psychophysical background-field spectra obtained under conditions intended to isolate cone-opponent function, and are means calculated from Figure 1(a)–(c) of Foster, D. H. and Snelgar, R. S. (1983). Test and field spectral sensitivities of colour mechanisms obtained on small white backgrounds: Action of unitary opponent-colour processes? *Vision Research* 23: 787–797.

advantages. First, it reduces information redundancy. Because of the close overlap in the L- and M-cone spectral sensitivities, their responses are highly correlated. But spectrally sharpened L − *k*M and M − *k*L combinations provide greater independence and more efficient coding for neural transmission. Second, with chromatic adaptation at a cone-opponent level and not just at a receptoral level (see the subsection entitled 'Cone Spectral Sensitivities: Cone Gains and von Kries Scaling'), it is possible to compensate more completely for any bias in the spectrum of the prevailing light. This may be achieved by von Kries scaling, but of cone-opponent responses rather than cone responses.

See also: Color Blindness: Inherited; Photopic, Mesopic and Scotopic Vision and Changes in Visual Performance; Phototransduction: Phototransduction in Cones; Rod and Cone Photoreceptor Cells: Inner and Outer Segments.

Further Reading

Baylor, D. A., Nunn, B. J., and Schnapf, J. L. (1987). Spectral sensitivity of cones of the monkey *Macaca fascicularis*. *Journal of Physiology – London* 390: 145–160. The smooth curve is a locally weighted polynomial regression.

Bone, R. A., Landrum, J. T., and Cains, A. (1992). Optical density spectra of the macular pigment *in vivo* and *in vitro*. *Vision Research* 32: 105–110.

Bowmaker, J. K. (2008). Evolution of vertebrate visual pigments. *Vision Research* 48: 2022–2041.

Buzás, P., Blessing, E. M., Szmajda, B. A., and Martin, P. R. (2006). Specificity of M and L cone inputs to receptive fields in the parvocellular pathway: Random wiring with functional bias. *Journal of Neuroscience* 26: 11148–11161.

Crook, J. M., Lee, B. B., Tigwell, D. A., and Valberg, A. (1987). Thresholds to chromatic spots of cells in the macaque geniculate nucleus as compared to detection sensitivity in man. *Journal of Physiology – London* 392: 193–211.

Curcio, C. A., Allen, K. A., Sloan, K. R., et al. (1991). Distribution and morphology of human cone photoreceptors stained with anti-blue opsin. *Journal of Comparative Neurology* 312: 610–624.

Dacey, D. M. and Packer, O. S. (2003). Colour coding in the primate retina: Diverse cell types and cone-specific circuitry. *Current Opinion in Neurobiology* 13: 421–427.

Dartnall, H. J. A., Bowmaker, J. K., and Mollon, J. D. (1983). Human visual pigments: Microspectrophotometric results from the eyes of seven persons. *Proceedings of the Royal Society of London, Series B: Biological Sciences* 220: 115–130.

Foster, D. H. and Snelgar, R. S. (1983). Test and field spectral sensitivities of colour mechanisms obtained on small white backgrounds: Action of unitary opponent-colour processes? *Vision Research* 23: 787–797.

Hofer, H., Carroll, J., Neitz, J., Neitz, M., and Williams, D. R. (2005). Organization of the human trichromatic cone mosaic. *Journal of Neuroscience* 25: 9669–9679.

Lee, B. B., Dacey, D. M., Smith, V. C., and Pokorny, J. (1999). Horizontal cells reveal cone type-specific adaptation in primate retina. *Proceedings of the National Academy of Sciences of the United States of America* 96: 14611–14616.

Mansfield, R. J. W. (1985). Primate photopigments and cone mechanisms. In: Fein, A. and Levine, J. S. (eds.) *The Visual System*, pp. 89–106. New York: Liss.

Merbs, S. L. and Nathans, J. (1992). Absorption spectra of human cone pigments. *Nature* 356: 433–435.

Nickle, B. and Robinson, P. R. (2007). The opsins of the vertebrate retina: Insights from structural, biochemical, and evolutionary studies. *Cellular and Molecular Life Sciences* 64: 2917–2932.

Oprian, D. D., Asenjo, A. B., Lee, N., and Pelletier, S. L. (1991). Design, chemical synthesis, and expression of genes for the three human color vision pigments. *Biochemistry* 30: 11367–11372.

Sakurai, M. and Mullen, K. T. (2006). Cone weights for the two cone-opponent systems in peripheral vision and asymmetries of cone contrast sensitivity. *Vision Research* 46: 4346–4354.

Sperling, H. G. and Harwerth, R. S. (1971). Red–green cone interactions in the increment-threshold spectral sensitivity of primates. *Science* 172: 180–184.

Stiles, W. S. and Burch, J. M. (1959). N.P.L. colour-matching investigation: Final Report (1958). *Optica Acta* 6: 1–26.

Stockman, A. and Sharpe, L. T. (2000). The spectral sensitivities of the middle- and long-wavelength-sensitive cones derived from measurements in observers of known genotype. *Vision Research* 40: 1711–1737.

Stockman, A., Sharpe, L. T., Merbs, S., and Nathans, J. (2000). Spectral sensitivities of human cone visual pigments determined *in vivo* and *in vitro*. *Methods in Enzymology.*

Part B: Vertebrate Phototransduction and the Visual Cycle 316: 626–650.

Stromeyer, C. F., III, Lee, J., and Eskew, R. T., Jr (1992). Peripheral chromatic sensitivity for flashes: A post-receptoral red–green asymmetry. *Vision Research* 32: 1865–1873.

van Norren, D. and Vos, J. J. (1974). Spectral transmission of human ocular media. *Vision Research* 14: 1237–1244.

Ciliary Blood Flow and its Role for Aqueous Humor Formation

J W Kiel, University of Texas Health Science Center at San Antonio, San Antonio, TX, USA
H A Reitsamer, Paracelsus Medical University, Salzburg, Austria

Glossary

Diffusion – The movement of molecules down a concentration gradient.
Hydrostatic pressure – The pressure (force per unit area) in a liquid.
Oncotic pressure – The hydrostatic pressure needed to stop the movement of water due to a protein concentration gradient.
Osmosis – The movement of water down its concentration gradient. For example, water will move across a semipermeable membrane from a compartment with a low sodium concentration (high water concentration) to a compartment with a high sodium concentration (low water concentration).
Osmotic pressure – The hydrostatic pressure needed to stop the movement of water due to a solute concentration gradient.
Pseudofacility – The decrease in aqueous production that can occur when intraocular pressure is elevated during tonography and can cause falsely high measurements of outflow facility.
Starling equilibrium – The sum of hydrostatic and oncotic pressures across a vessel wall.
Ultrafiltration – The passive movement of fluid out of a blood vessel due to a net positive gradient of hydrostatic and oncotic pressures across the vessel wall.

Introduction

Aqueous humor is the clear liquid in the posterior and anterior chambers of the eye. It is produced by the ciliary processes, flows through the posterior chamber, then between the iris and lens through the pupil into the anterior chamber, and then leaves the eye through the trabecular and uveoscleral outflow pathways. The flow of aqueous humor serves two vital functions – it is the surrogate vascular system for the cornea and lens, delivering nutrients and removing metabolic waste for these avascular tissues, and it generates the intraocular pressure (IOP), which maintains the shape of the eye and sets the venous pressure for the intraocular circulations.

Figure 1 shows a schematic overview of aqueous production. Aqueous humor is formed in the ciliary processes in the pars plicata region of the anterior uvea by the translocation of fluid and solute across the pigmented epithelial (PE) and nonpigmented epithelial (NPE) layers, the epithelial bilayer that comprises the primary blood–aqueous barrier. Aqueous production occurs in three steps: (1) convective delivery of the aqueous components and metabolic fuels through the ciliary circulation, (2) ultrafiltration and diffusion from the capillaries into the stroma driven by the oncotic pressure, hydrostatic pressure, and concentration gradients, and (3) ionic transport into the basolateral spaces between the NPE cells, followed by water movement down the resultant osmotic gradient into the posterior chamber. Once formed, the aqueous composition is modified as it travels through the posterior and anterior chambers by metabolic exchange with the tissues it contacts – the lens, iris, and cornea.

Ciliary Circulation

The circulation of the ciliary processes is derived from branches off the major arterial circle of the iris, which is fed by the long posterior ciliary arteries and anastomotic connections from the anterior ciliary arteries. In humans, the vasculature of the ciliary processes divides into three zones. The first zone is at the anterior base of the processes and consists of arterioles and capillaries that drain into a venular system separate from the other zones. This zone is the boundary between the nonfenestrated capillaries of the iris and the fenestrated capillaries of the ciliary processes. The fenestrations in the ciliary capillaries permit passage of protein into the stroma which establishes an oncotic pressure that is important in aqueous production. The second zone also originates at the anterior base but extends more anteriorly into the processes and then drains into marginal venules running along the inner edge of the processes that coalesce into a venous segment that travels posteriorly into the pars plana and the vortex veins. The third zone supplies the posterior portion of the major processes and the minor processes.

Because of its inaccessible location and complexity, our knowledge of ciliary hemodynamics is somewhat limited. However, the plasma clearance of ascorbate is high in the ciliary processes, and the typical values for the aqueous-to-plasma ascorbate ratio (26.5) and aqueous production (2.75 $\mu l\,min^{-1}$) in humans provide a rough estimate of ciliary plasma flow at 73 $\mu l\,min^{-1}$, or a blood flow of 133 $\mu l\,min^{-1}$ assuming a normal hematocrit. Microsphere measurements in anesthetized monkeys indicate a slightly lower ciliary

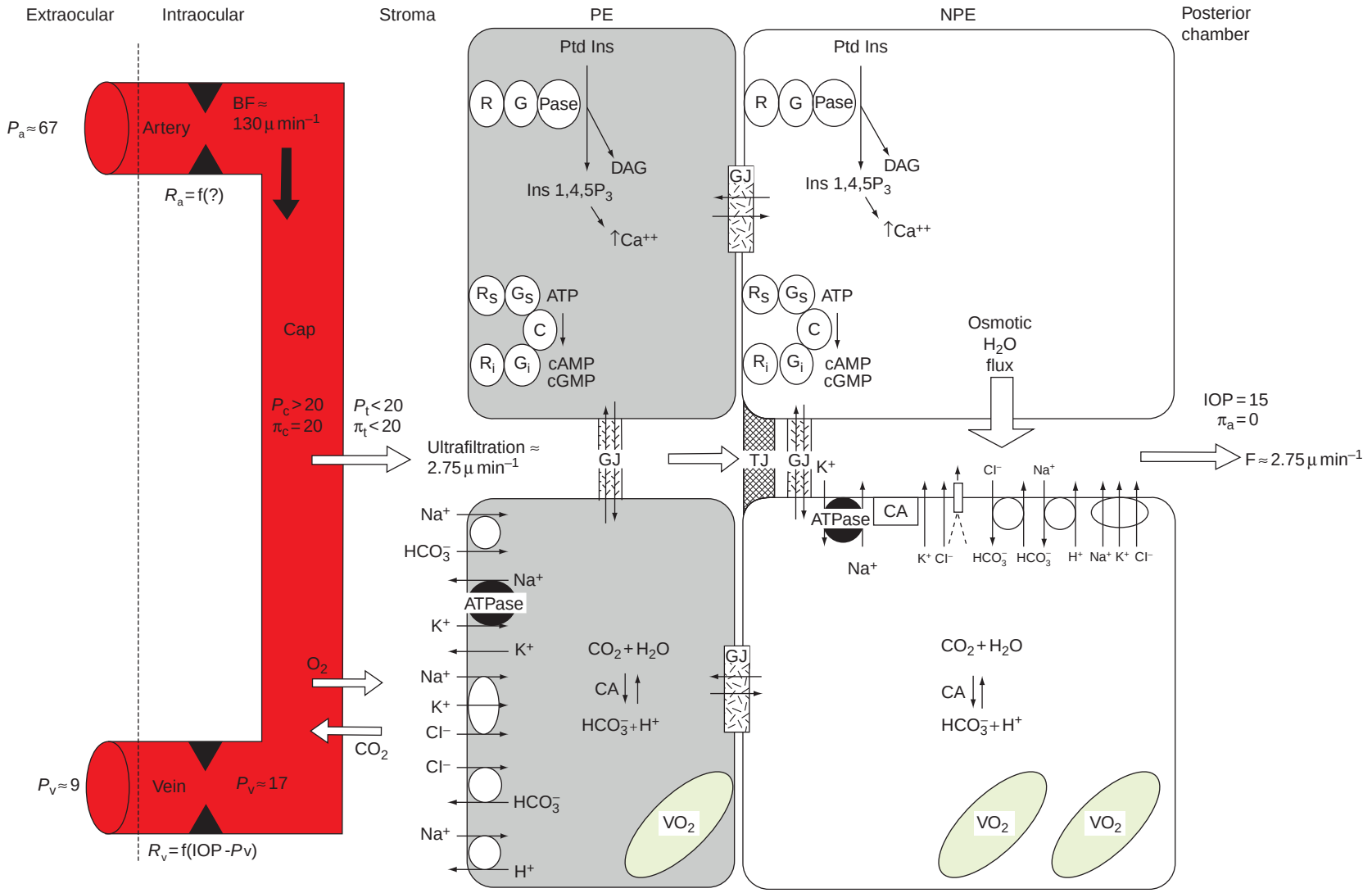

Figure 1 Overview of aqueous formation. Open circles with arrows: transporters/cotransporters/antiporters; arrows: movement via ionic channels or diffusion. P_a, extraocular arterial pressure; R_a, ciliary arterial resistance; BF, ciliary blood flow; P_c, ciliary capillary pressure; πc, capillary plasma oncotic pressure; P_t, stromal tissue hydrostatic pressure; πt, stromal tissue oncotic pressure; P_v, ciliary venous pressure; R_v, ciliary venous resistance; VO_2, mitochondrial oxygen consumption; πa, aqueous oncotic pressure; F, aqueous flow; Ptd Ins, phosphatydalinositol; Ins 1;4;5 P3, inositol trisphosphate (second messenger for Ca^{++} release); DAG, diacylglycerol (second messenger for protein kinase C activation); Pase, phosphoinositidase; G, G-protein complex; R, receptor; C, adenylate cyclase; Gs, stimulatory G-protein complex; Gi, inhibitory G-protein complex; Rs, stimulatory receptor; Ri, inhibitory receptor; GJ, gap junction; TJ, tight junction; ATPase, Na/K ATPase. Adapted from Kiel, J. W. (1998). Physiology of the intraocular pressure. In: Feher, J. (ed) *Pathophysiology of the Eye 4 Glaucoma*. Budapest: Academiai Kiado.

blood flow at 89 µl min^{-1}. Direct measurements of ciliary arterial pressure have not been made, but a reasonable estimate for arterial pressure just outside the eye is 67 mmHg for humans in an upright position with a normal mean arterial pressure (MAP) of 100 mmHg. Episcleral venous pressure is approximately 9 mmHg in humans. However, the venous pressure inside the eye is set by the IOP, and in animals it is 1–2 mmHg higher than the IOP. Capillary pressure is similarly IOP dependent, and approximately 8 mmHg higher than the IOP in the rabbit choriocapillaris. Assuming that ciliary hemodynamics are similar in humans, the ciliary capillary and venous pressures should be approximately 23 and 17 mmHg, respectively, at a normal IOP of 15 mmHg.

Ultrafiltration

The permeability of the ciliary capillaries permits the passage of water, ions, and relatively large molecules into the stroma. The larger molecules move by diffusion down their respective concentration gradients, while the movement of water and dissolved solutes occurs by ultrafiltration, which is driven by the hydrostatic and oncotic pressure gradients across the capillary wall as defined by the Starling equation:

$$\text{Flux} = Kf[(P_c - P_t) - \sigma(\pi_p - \pi_t)] \quad [1]$$

Here, the flux is the fluid movement, Kf is the capillary filtration coefficient, P_c and P_t are the capillary and tissue hydrostatic pressures, σ is the protein reflection coefficient (an index of protein permeability), and π_p and π_t are the plasma and tissue oncotic pressures.

The dynamics of the Starling equilibrium in the ciliary processes are poorly understood. However, values for some of the Starling variables are known, and reasonable estimates can be deduced for the others. At steady state, the flux out of the capillaries must equal the rate of fluid movement into the posterior chamber plus any fluid exiting the ciliary processes through the supraciliary space. Thus, the normal rate of aqueous formation in humans of 2.75 µl min^{-1} provides an estimate of the minimum rate of ultrafiltration. The normal value for π_p is 20 mmHg. In rabbits, the stromal protein concentration is approximately 75% of that in plasma. Assuming that the same ratio holds for humans, the estimated π_t is 17 mmHg. Based on the net filtration of albumin and gamma globulin, σ is approximately 0.96. A reasonable estimate for P_t is 15 mmHg, since P_t should equal or slightly exceed the IOP.

The more difficult Starling variables to estimate are P_c and Kf. As mentioned earlier, P_c in the choriocapillaris is approximately 8 mmHg higher than the IOP, suggesting a ciliary P_c estimate of 23 mmHg at a normal IOP. The ciliary capillary Kf is unknown, but if the values for the other variables are correct, the graphic analysis in **Figure 2** (left) indicates that the Kf would need to be at least 0.48 µl min^{-1}mmHg^{-1} to provide a flux of 2.75 µl min^{-1}. The Kf for the whole eye is 0.3 µl min^{-1} mmHg^{-1}. Alternatively, lower Kf values would provide sufficient ultrafiltration if P_c were higher than 23 mmHg.

The role of ultrafiltration in aqueous formation is permissive rather than active; aqueous could not be formed if the fluid were not provided. However, although arguments to the contrary have been made, ultrafiltration appears to contribute little to the movement of fluid from the stroma into the posterior chamber. This is clear from the analysis of the capillary-to-aqueous Starling forces shown in **Figure 2** (right). For this analysis, the aqueous oncotic pressure is zero and σ is 1 since the ciliary nonpigmented epithelium is normally impermeable to protein. Consequently, the P_c would have to exceed 35 mmHg to generate a net movement of fluid from capillary to aqueous by ultrafiltration. Since P_c is likely less than 35 mmHg, the Starling forces favor reabsorption of fluid from the aqueous back into the ciliary processes.

The analysis in **Figure 2** is useful for estimating the minimal values of Kf and P_c consistent with normal steady-state ocular conditions. However, because the analysis holds the other variables constant, it fails to accurately predict the flux behavior in response to a change in Kf or P_c. Specifically, if P_c increases so that ultrafiltration exceeds

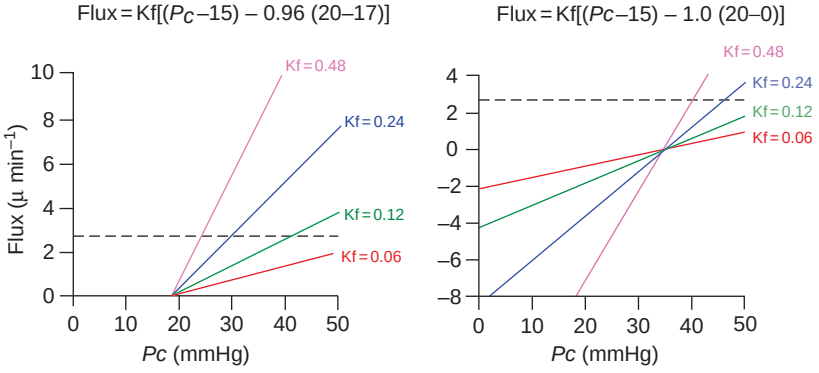

Figure 2 Graphic analysis of the Starling forces for fluid movement from capillary to stroma (left) and from capillary to aqueous (right). Adapted from Kiel, J. W. (1998). Physiology of the intraocular pressure. In: Feher, J. (ed) *Pathophysiology of the Eye 4 Glaucoma*. Budapest: Academiai Kiado.

aqueous formation, the fluid volume in the stroma increases, thereby raising P_t and lowering π_t until the flux re-equilibrates with aqueous formation.

Conversely, if P_c decreases so that ultrafiltration falls below aqueous production, the loss of stromal fluid volume decreases P_t and raises π_t until ultrafiltration and aqueous formation are again equal. It should be noted that the equilibrium of the Starling forces obscures the true value of Kf, which may be much higher than the minimum value needed to support a particular rate of aqueous formation, and that a higher Kf would also tend to preserve ultrafiltration if P_c falls. Nonetheless, if P_c falls below some critical level, aqueous production will become limited by the reduced rate of ultrafiltration. Autoregulation of ciliary blood flow may help maintain P_c during moderate reductions in MAP, but further reductions in MAP will cause P_c to fall. In monkeys, aqueous production starts to decline when the MAP falls below 70–90 mmHg.

In contrast to the effects of arterial pressure on the Starling forces, the effect of IOP is more difficult to assess. IOP elevation reduces aqueous formation by approximately 0.02–0.06 $\mu l\ min^{-1}\ mmHg^{-1}$, and this effect has been attributed to the Starling equilibrium, that is, raising the IOP increases P_t, which reduces the hydrostatic pressure gradient for ultrafiltration from the capillaries. A problem with this explanation is that raising the IOP should cause a similar increase in P_c due to the Starling resistor effect on the intraocular veins. If the hyrdostatic gradient is not altered appreciably, it seems unlikely that the reduction in aqueous production is due to a change in capillary ultrafiltration. Alternative explanations include increased fluid loss through the supraciliary space and sclera, or blood-flow-dependent changes in epithelial metabolism. Regardless of the underlying mechanism, an IOP-dependent decrease in aqueous formation (also known as pseudofacility) is a potential source of error in tonographic measurements of outflow facility.

Active Secretion

The transciliary Starling gradients and the significant plasma-to-aqueous concentration differences for certain solutes and macromolecules indicate the presence of a permeability barrier within the ciliary epithelia, and that a mechanism other than ultrafiltration is responsible for the majority of the fluid entry into the posterior chamber. The available evidence indicates that the majority of the barrier arises from the tight junctions between adjacent NPE cells, and that active secretion of Na^+ and other ions into the basolateral spaces between NPE cells establishes the osmotic gradient responsible for fluid movement across the barrier.

The ciliary epithelia consist of an outer layer of PE cells and an inner layer of NPE cells. The PE and NPE cells are arranged apex to apex, a unique organization caused by the embryonic invagination of the optic cup. The PE is the anterior continuation of the retinal pigment epithelium and its basal surface is separated from the stroma by a basement membrane contiguous with Bruch's membrane. The NPE is the anterior continuation of the retina and its basal surface is separated from the posterior chamber by an extension of the retinal internal limiting membrane.

The proximity of the layers and the complex array of intercellular connections within and between layers suggest that the bilayer behaves as a syncytium, although it is as yet poorly understood. The numerous gap junctions may provide sites of rapid intercellular communication. In addition, the channels seen in electron micrographs of PE and NPE apical surfaces provide another potential route of communication. Moreover, electrical coupling between the PE and NPE has also been reported.

The PE basement membrane and the gap junctions between PE cells do not impede the movement of protein or tracers, such as horseradish peroxidase, rather it is the tight junctions at the apical surface of adjacent NPE cells that constitutes the transciliary barrier. The other component of the blood–aqueous barrier is the absence of fenestrations and the low permeability of the iris capillaries, the other potential site for appreciable blood–aqueous exchange.

The barrier formed by the NPE cells and their tight junctions has a low hydraulic conductivity (i.e., 0.0071 $\mu l\ min^{-1}\ mmHg^{-1}$ from stroma to aqueous) that must be overcome for fluid to reach the posterior chamber. This is thought to occur by means of a standing osmotic gradient established in the lateral intercellular channels beyond the NPE tight junctions. The osmotic gradient is generated by the active transport of solute into the intercellular channels, with the highest solute transport occurring nearest to the tight junctions. This results in fluid flux from the NPE cells and across the tight junctions so that the fluid leaving the channels and entering the posterior chamber is either isoosmotic or slightly hyperosmotic relative to plasma.

Na^+ is one of the principal ions responsible for generating the osmotic gradient in the intercellular channels, and the basolateral membrane adjacent to the tight junctions has a high concentration of the membrane-bound sodium–potassium–adenosine triphosphate (Na/K-ATP) ase enzyme complex needed to provide the transport. The operation of the Na/K-ATPase requires the expenditure of metabolic energy and, as would be expected, perturbations that disrupt ATP production or utilization also decrease aqueous formation. The PE and NPE cells appear similar in their aerobic and anaerobic ability, but the NPE cells are more active with a higher rate of oxygen consumption. Although both cell types can increase their glycolytic activity if oxygen or substrate is unavailable, glycolysis alone cannot fully support normal rates of Na^+ transport.

Another significant contributor to the fluid flux into the intercellular channels is HCO_3^- and the enzyme carbonic anhydrase. The enzyme is present in high concentration in the basolateral membrane and in the cytosol, and

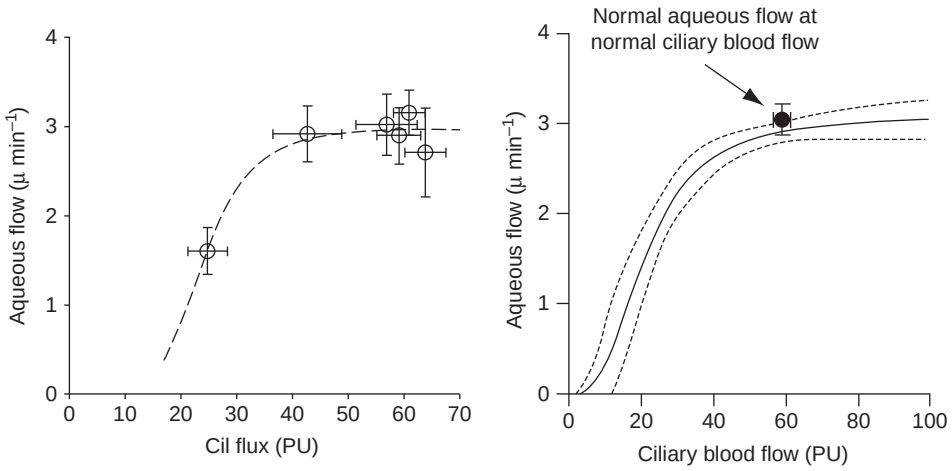

Figure 3 Relationship between ciliary blood flow and aqueous flow in anesthetized rabbits. (Left) Original relationship based on 43 experiments. (Right) Revised relationship based on additional experiments. The open circle is the average baseline value at spontaneous ciliary blood flow and aqueous flow. Aqueous flow is relatively blood flow independent until ciliary blood flow decreases below ≈75% of baseline when aqueous flow becomes blood flow dependent. Adapted from Reitsamer, H. A. and Kiel, J. W. (2003). The relationship between ciliary blood flow and aqueous production in rabbits. *Investigative Ophthalmolology and Visual Science* 44: 3967–3971; Kiel, J. W. and Reitsamer, H. A. (2006). The relationship between ciliary blood flow and aqueous production: Does it play a role in glaucoma therapy? *Journal of Glaucoma* 15: 172–181; and Reitsamer, H. A. and Kiel, J. W. (2008). Effects of circulatory events on aqueous humor inflow and intraocular pressure. In: Civan, M. M. (ed). *The Eye's Aqueous Humor. From Secretion to Glaucoma*, pp. 273–300, San Diego: Academic Press.

acetazolamide and other carbonic anhydrase inhibitors significantly inhibit aqueous formation. In addition to the Na/K ATPase and carbonic anhydrase contributions to aqueous formation, a variety of other transport systems have been identified as shown in **Figure 1**. Also shown are corresponding transport systems present in the PE basal membrane. In both locations, some of these may be important in aqueous formation, while others may not, and continued research is needed to clarify their separate roles.

The orchestration of the various transport systems is modulated by the neurohumoral milieu of the ciliary process and the receptor distributions in the different cell types. One primary common pathway in this complex regulatory system is the adenylate cyclase receptor complex generating the intracellular second messenger, cyclic adenosine monophosphate (cAMP), since changes in aqueous formation are typically associated with changes in cAMP. Growing evidence indicates that nitric oxide and cyclic guanosine monophosphate (cGMP) may also play a regulatory role. Another regulatory candidate is the phosphoinositidase receptor complex. When activated, this system hydrolyzes phosphatidylinositol 4,5 P2 to yield the second messengers, inositol 1,4,5 trisphosphate (Ins1,4,5P3) and diacylglycerol (DAG). Ins1,4,5P3 mobilizes intracellular Ca^{2+} by stimulating release of internal Ca^{2+} stores and promoting extracellular Ca^{2+} entry. DAG activates protein kinase C. The phosphoinositidase system has been identified in both PE and NPE cell types, both of which undergo spontaneous and agonist-evoked changes in intracellular Ca^{2+}.

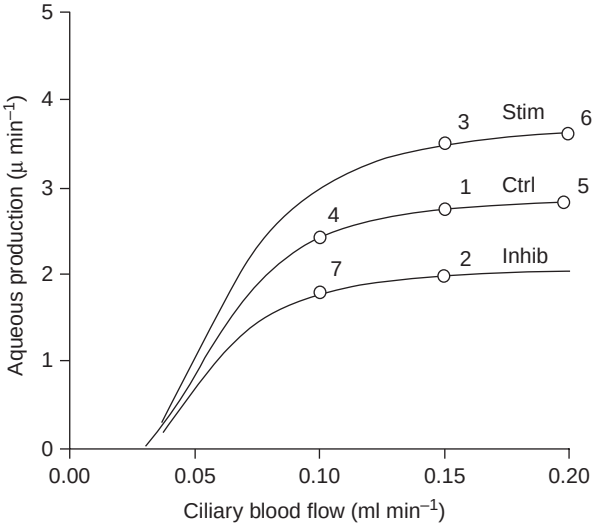

Figure 4 Hypothetical curves for aqueous production vs. ciliary blood flow under stimulated, control, and inhibited conditions. Points show: 1: control production and blood flow; 2: inhibited production without change in blood flow; 3: stimulated production without change in blood flow; 4: ciliary vasoconstriction with flow-dependent decrease in production; 5: ciliary vasodilation with small flow-dependent increase in production; 6: stimulated production with metabolic-dependent vasodilation; 7: inhibited production with metabolic-dependent vasoconstriction. From Reitsamer, H. A. and Kiel, J. W. (2008). Effects of circulatory events on aqueous humor inflow and intraocular pressure. In: Civan, M. M. (ed) *The Eye's Aqueous Humor: From Secretion to Glaucoma*, pp. 273–300, San Diego: Academic Press.

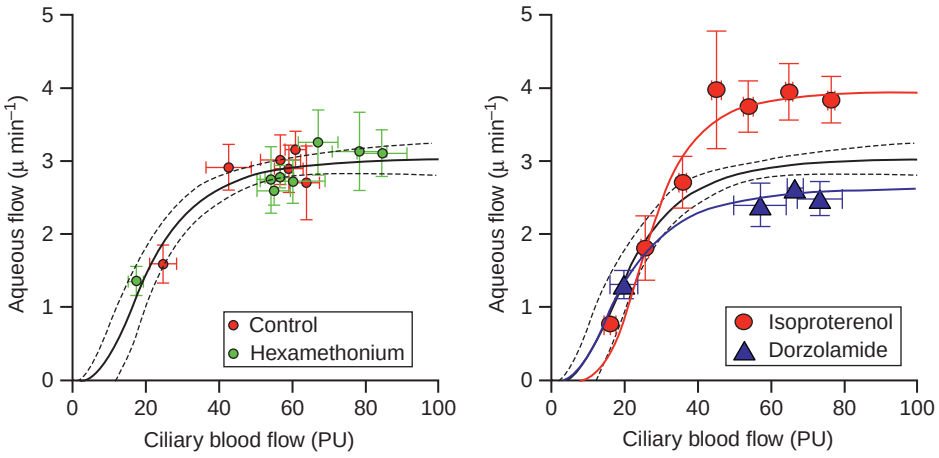

Figure 5 Rabbit aqueous flow responses to varying ciliary blood flow by mechanical manipulation of blood pressure under control conditions and after ganglionic blockade (left) and during secretory stimulation with isoproterenol and inhibition with dorzolamide (right). *In vivo* results support model predictions in **Figure 4**. Data from Reitsamer, H. A. et al. (2009). Effects of Dorzolamide on choroidal blood flow, ciliary blood flow, and aqueous production in rabbits. *Investigative Ophthalmology and Visual Science* 50: 2301–2307, and authors' unpublished results.

Relationship between Ciliary Blood Flow and Aqueous Production

From the preceding section it is evident that aqueous formation is dependent on ciliary blood flow; however, it should be noted that ciliary blood flow and aqueous production are difficult to measure, and little was known about the relationship between them until recently. The information in the following section is based on ciliary blood flow measurements by fiber-optic-based laser Doppler flowmetry (LDF) that gives readings in arbitrary perfusion units (PUs), and fluorophotometry that uses the rate of disappearance from the cornea and anterior chamber of fluorescein applied to the cornea to calculate the rate of aqueous flow through the anterior chamber.

To determine the relationship between ciliary blood flow and aqueous production, it is necessary to vary ciliary blood flow and measure the resulting effect on aqueous flow. Ideally, only ciliary blood flow should be varied (i.e., neurohumoral input to the eye, the ocular perfusion pressure, and blood flow through the other ocular circulations should all be constant), but this is impossible. Instead, ciliary blood flow has been varied by mechanically holding blood pressure at different levels (80, 70, 55, and 40 mmHg) in anesthetized rabbits. The results of the initial study are shown in **Figure 3** (left); the relationship between ciliary blood flow and aqueous flow based on additional experiments are also shown (right).

The graphs in **Figure 3** show that when ciliary blood flow is increased above its normal level, aqueous flow is relatively unchanged. This is also true for reductions in ciliary blood flow of ≈25%, but further reductions cause proportional decreases in aqueous flow. In other words, there is a critical level of ciliary blood flow below which aqueous flow is blood flow dependent; above that critical level, aqueous flow is independent of ciliary blood flow. A similar relationship occurs in the gastric mucosa, where acid secretion is blood flow independent until mucosal blood flow is reduced below a critical level, whereupon it becomes blood flow dependent. In addition, secretory stimulants in the stomach shift the relationship upward, whereas secretory inhibitors shift the relationship downward. Ciliary secretion behaves similarly, giving rise to the following hypotheses: (1) aqueous production requires an

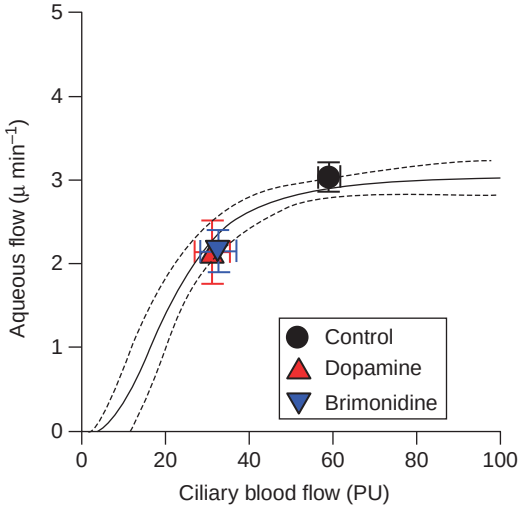

Figure 6 Vasoconstrictors decrease ciliary blood flow below the critical point and decrease aqueous flow indirectly. Data from Reitsamer, H. A. and Kiel, J. W. (2002). Effects of dopamine on ciliary blood flow, aqueous production, and intraocular pressure in rabbits. *Investigative Ophthalmology and Visual Science* 43: 2697–2703; and Reitsamer, H. A. Posey, M. and Kiel, J. W. (2006). Effects of a topical α2 adrenergic agonist on ciliary blood flow and aqueous production in rabbits. *Experimental Eye Research* 86: 405–415.

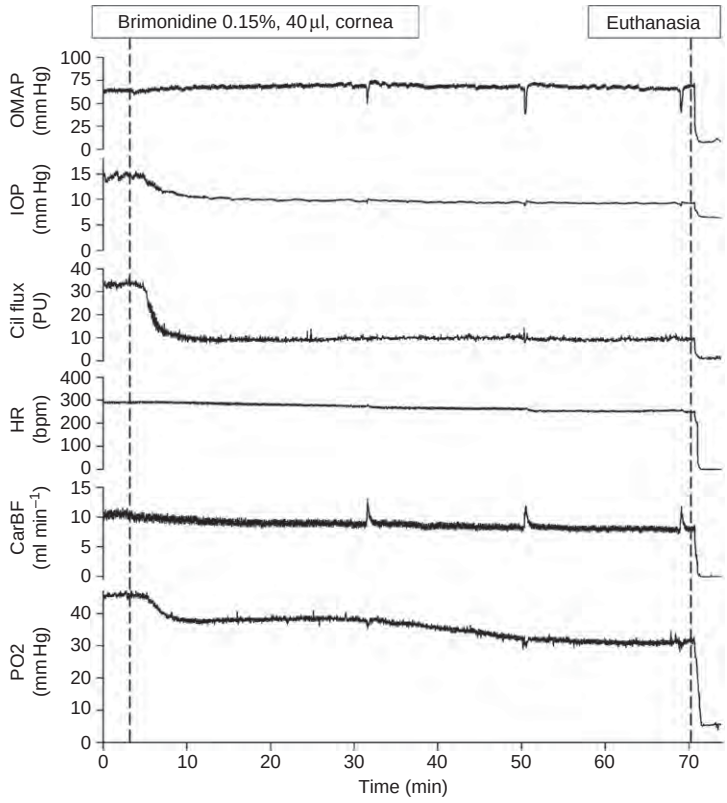

Figure 7 Effect of brimonidine-induced decrease in ciliary blood flow on ciliary PO_2. Representative trace showing ciliary PO_2 response to topical brimonidine and rapid decline in ciliary PO_2 upon cessation of ciliary perfusion at death. Decrease in ciliary PO_2 indicates increased oxygen extraction rather than decreased oxygen consumption. Cil Flux, ciliary blood flow; HR, heart rate; CarBF, carotid blood flow; PO_2, partial pressure of oxygen next to ciliary body). Reproduced from Reitsamer, H. A., Posey, M., and Kiel, J. W. (2006). Effects of a topical α2 adrenergic agonist on ciliary blood flow and aqueous production in rabbits. *Experimental Eye Research* 86: 405–415, with permission from Elsevier.

adequate supply of oxygen and nutrients delivered by the ciliary circulation, (2) the neurohumoral milieu of the ciliary processes determines the level of secretory stimulation so that the rate of aqueous production at a given ciliary blood flow can be stimulated or inhibited pharmacologically, and (3) the autoregulatory mechanisms governing ciliary blood flow are modulated by endogenous neurohumoral factors and that ciliary autoregulation can be overridden by the administration of exogenous vasoactive compounds or large changes in perfusion pressure.

These hypotheses are illustrated in **Figure 4**. The figure has three curves generated by a mathematical model with aqueous production plotted as a function of ciliary blood flow: a control curve for a normal level of secretory stimulation (Ctrl), a curve for a state of heightened secretory stimulation (Stim), and a curve for an inhibited secretory state (Inhib). Point #1 on the control curve occurs at a normal ciliary blood flow (150 $\mu l\,min^{-1}$) and aqueous production (2.75 $\mu l\,min^{-1}$). A drug that acts directly on the active secretion by the epithelial cells (e.g., by changing intracellular cAMP) can decrease (point #2) or increase (point #3) production without changing ciliary blood flow. In this scenario, imposing large changes in perfusion pressure sufficient to overcome ciliary autoregulation will define the stimulated and inhibited curves. Alternatively, a drug that causes ciliary vasoconstriction (point #4) or vasodilation (point #5) without altering the stimulus for secretion can nonetheless decrease or slightly increase production. In this case, imposing large changes in perfusion pressure will generate the normal curve and reveal that the drug had no direct effect on secretion. A third scenario is that ciliary autoregulation is linked to metabolism so that a drug that stimulates secretion will cause a concomitant vasodilation (point #6), while a drug that inhibits secretion will cause a vasoconstriction (point #7). In this case, varying the perfusion pressure will reveal that the system has shifted to a new level of secretory stimulation rather than the effect being due simply to a change in blood flow. Some drugs will affect both secretion and vascular tone, and in this case varying the perfusion pressure will help to discern the relative contributions to the overall effect on production.

Figure 5 shows results in the rabbit similar to the model predictions. Eliminating neural circulatory control by ganglionic blockade with hexamethonium permits a wider range of ciliary blood flow with perfusion pressure manipulation, but does not alter the relation between ciliary blood flow and aqueous flow. (Note that aqueous

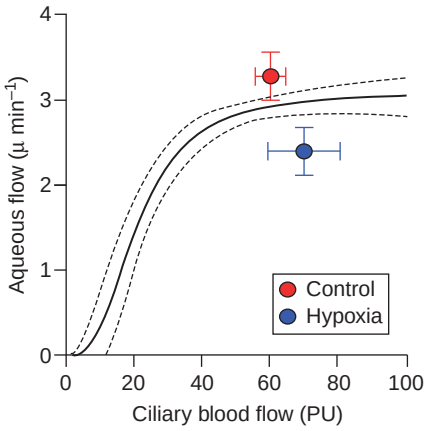

Figure 8 Effect of hypoxia on ciliary blood flow and aqueous flow. Lowering the percent saturation of hemoglobin with oxygen from 95% to 75% decreases aqueous flow without changing ciliary blood flow or the delivery of other nutrients and washout of metabolites. Adapted from Reitsamer, H. A. and Kiel, J. W. (2008). Effects of circulatory events on aqueous humor inflow and intraocular pressure. In: Civan, M. M. (ed) *The Eye's Aqueous Humor: From Secretion to Glaucoma*, pp. 273–300, San Diego: Academic Press.

flow is normal in Horner's patients, adrenalectomized patients, and atropine-administered primates.) Consistent with the model prediction, stimulating aqueous production with a subpressor dose of isoproterenol (0.02 μg min^{-1} kg^{-1}, intravenous (i.v.) infusion) shifts the relationship upward, while inhibiting aqueous production with topical dorzolamide (2%, 50 μl) shifts the relationship downward. The latter findings indicate that isoproterenol and dorzolamide exert direct effects of the ciliary epithelium. By contrast, ciliary vasoconstrictors, such as dopamine (300 μg kg^{-1} min^{-1}, iv) or brimonidine (0.15%, topical), decrease aqueous flow to the same extent as mechanically decreasing ciliary blood flow, indicating their effect on aqueous production is indirect (Figure 6).

A key question for the role of ciliary blood flow in aqueous production is what is provided by the ciliary blood flow. It provides oxygen and nutrients to the ciliary epithelia and removes metabolic waste. It is unclear which of these is critical; however, oxygen is a reasonable candidate because the ionic transport systems responsible for the osmotic gradient that produces aqueous utilize oxidative metabolism for energy and they largely stop functioning when insufficient oxygen is provided, despite the availability of other substrates. If ciliary blood flow is raised above the critical level, oxygen extraction decreases and the excess simply passes through in the venous effluent. However, if blood flow is reduced below the critical level, even maximum oxygen extraction cannot provide sufficient high-energy substrates (e.g., ATP) to drive ionic transport, and therefore aqueous production decreases. In support of oxygen as the critical factor, the change in the partial pressure of oxygen (PO_2) adjacent to the ciliary body in the rabbit decreases with ciliary blood flow in response to topical brimonidine (Figure 7). The decrease in PO_2 indicates increased oxygen extraction rather than the decreased oxygen consumption that would be consistent with secretory inhibition.

Additional evidence that oxygen is the critical factor delivered in ciliary blood flow is shown in Figure 8. In this experiment, anesthetized rabbits (n = 12) were respired with a mixture of room air and nitrogen sufficient to lower their percent hemoglobin saturation with oxygen to 75%. Ciliary blood flow increased slightly but not significantly, yet aqueous flow decreased by 22%. In this situation, the delivery of other nutrients and removal of metabolic waste remained constant and only oxygen delivery was reduced. Thus, it appears that oxygen is indeed a critical factor delivered in ciliary blood flow.

Acknowledgments

This work was supported by NIH EY09702 (JWK), a Research to Prevent Blindness Lew R Wasserman Merit Award (JWK), Austrian FWF J1866-MED (HAR), the van Heuven endowment (JWK), and an unrestricted grant from Research to Prevent Blindness, Inc.

See also: Control of Aqueous Humor Flow; Ion transport in the Ciliary Epithelium; Neuroendocrine Properties of the Ciliary Epithelium; Pharmacology of Aqueous Humor Formation; The Role of the Ciliary Body in Aqueous Humor Dynamics. Structural Aspects.

Further Reading

Barany, E. H. (1963). A mathematical formulation of intraocular pressure as dependent on secretion, ultrafiltration, bulk outflow, and osmotic reabsorption of fluid Investigative. *Ophthalmology* 2: 584–590.

Brubaker, R. F. (1991). Flow of aqueous humor in humans. *Investigative Ophthalmology and Visual Science* 32: 3145–3166.

Gabelt, B. T. and Kaufman, P. L. (2003). Aqueous humor hydrodynamics. In: Kaufman, P. L. and Alm, A. (eds.) *Adler's Physiology of the Eye: Clinical Application,* 10th edn., pp. 237–289. St. Louis, MO: Mosby.

Kiel, J. W. and Reitsamer, H. A. (2006). The relationship between ciliary blood flow and aqueous production: does it play a role in glaucoma therapy? *Journal of Glaucoma* 15: 172–181.

Kiel, J. W., Reitsamer, H. A., Walker, J. S., and Kiel, F. W. (2001). Effects of nitric oxide synthase inhibition on ciliary blood flow, aqueous production and intraocular pressure. *Experimental Eye Research* 73: 355–364.

Linner, E. (1950). A method for determining the rate of plasma flow through the secretory part of the ciliary body. *Acta Physiologica Scandinavia* 22: 83–86.

Moses, R. A. (1987). Intraocular pressure. In: Moses, R. A. and Hart, W. M. (eds.) *Adler's Physiology of the Eye: Clinical Application,* 7th edn., pp. 223–245. St. Louis, MO: Mosby.

Moses, R. A., Grodzki, W. J., and Carras, P. L. (1985). Pseudofacility: Where did it go? *Archives of Ophthalmology* 103: 1653–1655.

Reitsamer, H. A. and Kiel, J. W. (2003). The relationship between ciliary blood flow and aqueous production in rabbits. *Investigative Ophthalmology and Visual Science* 44: 3967–3971.

Rohen, J. W. and Funk, R. H. W. (1994). Vasculature of the anterior eye segment. *Progress in Retinal and Eye Research* 13: 653–685.

Shepherd, A. P. and Öberg, P. (1990). *Laser Doppler Blood Flowmetry.* Norwell, MA: Kluwer Academic Publishers.

Circadian Photoreception

I Provencio, University of Virginia, Charlottesville, VA, USA

Glossary

Circadian rhythm – An endogenously generated biological rhythm with a period of about 24 h.
ipRGC – The term stands for intrinsically photosensitive retinal ganglion cell, which is a small subset of retinal ganglion cells that are rendered light sensitive because they express melanopsin, implicated in nonvisual photoresponses.
Melanopsin – The opsin-based photopigment of intrinsically photosensitive RGCs.
Nonvisual photoresponses – Physiological or behavioral responses to light that do not require the formation of images. Circadian photoentrainment is an example of a nonvisual photoresponse.
Photoentrainment – The synchronization of circadian rhythms to the daily light:dark cycle.

Introduction

Circadian rhythms are biological rhythms that exhibit a period of about 24 h (Latin, *circa* around + *dies* day). They persist in an environment devoid of time cues (*Zeitgebers*; German, *Zeit* time + *Geber* giver). This persistence of rhythmicity in constant conditions indicates the presence of an internal circadian clock. Circadian clocks are ubiquitous, existing in organisms ranging from cyanobacteria to humans. In metazoans, many tissues are capable of autonomous circadian rhythmicity, however, the phases of such rhythms tend to be orchestrated by a master pacemaker. In mammals, this master circadian pacemaker resides in the hypothalamic suprachiasmatic nuclei (SCN), two bilateral structures that straddle the midline immediately dorsal to the optic chiasm and are separated from each other by the third ventricle. The SCN coordinate the phases of multiple oscillators located in peripheral tissues, including heart, liver, and lung. The intergeniculate leaflet (IGL) of the lateral geniculate complex is also considered a component of the circadian system and receives input from both of the eyes. The IGL has been proposed to function in assessing ambient illumination levels.

While the periods of circadian rhythms are about 24 h, rarely are they exactly 24 h. Similar to a timepiece that runs too slowly or too quickly, the utility of a circadian clock is dependent on occasional resetting of its phase. The primary resetting agent for most circadian systems is light. Daily fluctuation in ambient irradiance resulting from the Earth's rotation about its axis is the most predictable diurnally variable feature of the environment. Organisms have evolved photoreceptive mechanisms to communicate this most reliable of *Zeitgebers*, the day:night cycle, to the circadian machinery so that circadian phase can be synchronized (entrained) with the astronomical day.

The SCN receives retinal input via the retinohypothalamic tract which is comprised of the myelinated axons of retinal ganglion cells (RGCs) (**Figure 1**). The response of the SCN to phase-shifting stimuli varies throughout the course of the circadian day and is phase-dependent (**Figure 2**). For photic stimuli, illumination during an animal's early subjective night results in a phase delay of the circadian clock as measured through the recording of circadian locomotor activity rhythms. By contrast, light pulses administered during the late subjective night cause activity rhythms to be phase advanced. Illumination during the subjective day has a negligible effect on circadian phase. In addition to this phase dependence, the magnitude of the light-induced phase shifts also varies as a function of the duration, intensity, and wavelength composition (color) of the light pulse. Conclusive identification of the photoreceptors that mediate circadian phase shifting has been wrought with problems but significant strides have been made recently.

Nonvisual Photoreception

Nonmammalian vertebrates possess numerous extraocular photoreceptors, some of which are necessary to shift the phase of the circadian system, so it is in proper phase alignment with the day:night cycle. Amphibians, for example, have photoreceptors in the pineal gland, the frontal organ, paraventricular zones of the brain, iris, and skin, in addition to the classical rod and cone photoreceptors of the retina. By contrast, all mammalian photoreception is restricted to the eyes.

One notable exception was a report in humans claiming that blue-light illumination of the popliteal region behind the knee caused shifts in the phase of salivary melatonin and temperature rhythms. This surprising result, which suggested the presence of extraocular photoreception in the mammals, inspired others to investigate the possibility of extraocular photoreception in other animal models. One group found no effect of direct sunlight on bilaterally

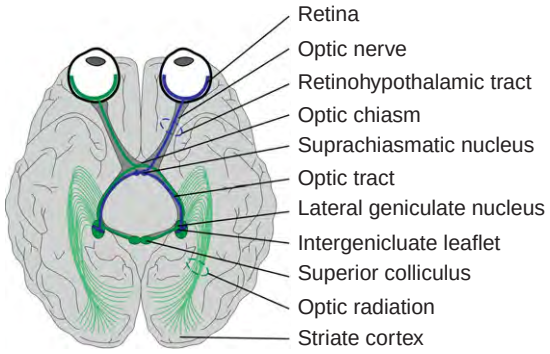

Figure 1 Retinal projections to the visual and circadian systems. Projections to the visual system are shown in green and those to the circadian system are shown in blue.

enucleated golden hamsters whose backs were shaved to maximize skin exposure. In these animals, locomotor circadian rhythms and levels of pineal melatonin were unperturbed by sunlight exposure during the animals' subjective night. Intact control animals, however, showed dramatic phase shifts in activity rhythms and suppression of pineal melatonin levels. Several other groups using human subjects failed to replicate the initial observation in humans indicating that some uncontrolled, nonphotic aspect of the experimental paradigm in the original study caused the observed effects on the circadian system. It is now widely accepted that the anatomical site of mammalian photoreception is exclusively ocular.

Physiological responses to light may be classified as visual or nonvisual. The responses that require the construction of images are considered visual, while those responses that simply require detection of changes in irradiance, such as circadian photoentrainment, may be considered nonvisual. The mammalian retina, the primary focus of this article, subserves both visual and nonvisual photoreception.

Due to the anatomical accessibility of the eye and the profound quality-of-life deficits experienced by the blind, the retina has been one of the most intensely studied tissues. Additionally, the laminar organization of the retina has made it an exquisite model for understanding basic concepts of development and neural communication. Retinal cytoarchitecture has been extensively described for more than 150 years. In fact, the rod and cone cells were postulated to be the light-sensing elements of the retina, as early as the mid-1850s by the German anatomist and physiologist Heinrich Müller.

In view of this long history of study, it was reasonable to suspect that rods and cones mediated both visual and nonvisual photoreception because no other classes of photoreceptors were known to exist in the mammalian eye. However, several lines of evidence suggested the existence of a class of ocular photoreceptor that was neither rod nor cone. In 1927, Clyde Keeler recognized that blind mice lacking photoreceptor cells continued to exhibit a pupillary light reflex, although this response was slower and less sensitive than that of fully sighted mice. Seventy-four years later, it was confirmed that the pupillary light reflex does indeed persist in blind mice and is maximally sensitive to blue wavelengths. Phase shifting of the circadian clock in response to light pulses is also maintained in mice homozygous for the retinal degeneration 1 allele ($Pde6b^{rd1/rd1}$), resulting in the loss of rods and cones. Similar to the pupillary response, light-induced circadian phase shifting in these visually blind mice exhibits a peak spectral sensitivity in the blue wavelengths. Finally, elevated nighttime levels of serum melatonin can be acutely suppressed by blue light presented to the eyes.

All of these blue-sensitive responses exhibit a peak spectral sensitivity in the 460–480 nm wavelength range, a domain of the electromagnetic spectrum that does not coincide with the peak sensitivity of known rod and cone photopigments of the human or murine retina. Since photoreceptors are defined by their photopigments, which in turn dictate their spectral sensitivity, a common strategy for identifying new photoreceptors is to identify new photopigments which should eventually point to the identification of a new photoreceptor class. The accumulating evidence for novel photoreceptors that mediate nonvisual responses to light led to the discovery of many new opsin-based photopigments. First among these was pinopsin, which was originally identified in the pineal gland of chicken and whose function remains unknown, but most likely plays a role in the photoregulation of melatonin synthesis. Very ancient opsin (VA-opsin), parapinopsin, and parietopsin were subsequently identified in the eye, parapineal, and parietal eye, respectively, of nonmammalian vertebrates. Based on an inspection of completed genomes, it is unlikely that mammalian homologs of these opsins exist.

However, within the last decade new opsins were indeed revealed in the mammals, none of which were localized to rods or cones. Peropsin and retinal G-protein-coupled receptor (RGR) opsin are expressed in the retinal pigment epithelium and are likely to function as accessory photoisomerases which use photic energy to convert all-*trans*-retinoids to their respective 11-*cis* isomers. 11-*cis*-Retinal is the requisite chromophore of all vertebrate signaling opsins. Encephalopsin was originally identified only in the brain and spinal cord of mouse, sites not known to be inherently photoreceptive. A subsequent study claimed the presence of encephalopsin message in the eye, however, the role of encephalopsin in the central nervous system remains unknown. Opn5 is another opsin predicted to exist within the mammalian eye based on the presence of messenger ribonucleic acid (mRNA), although a translated gene product remains to be discovered (**Table 1**).

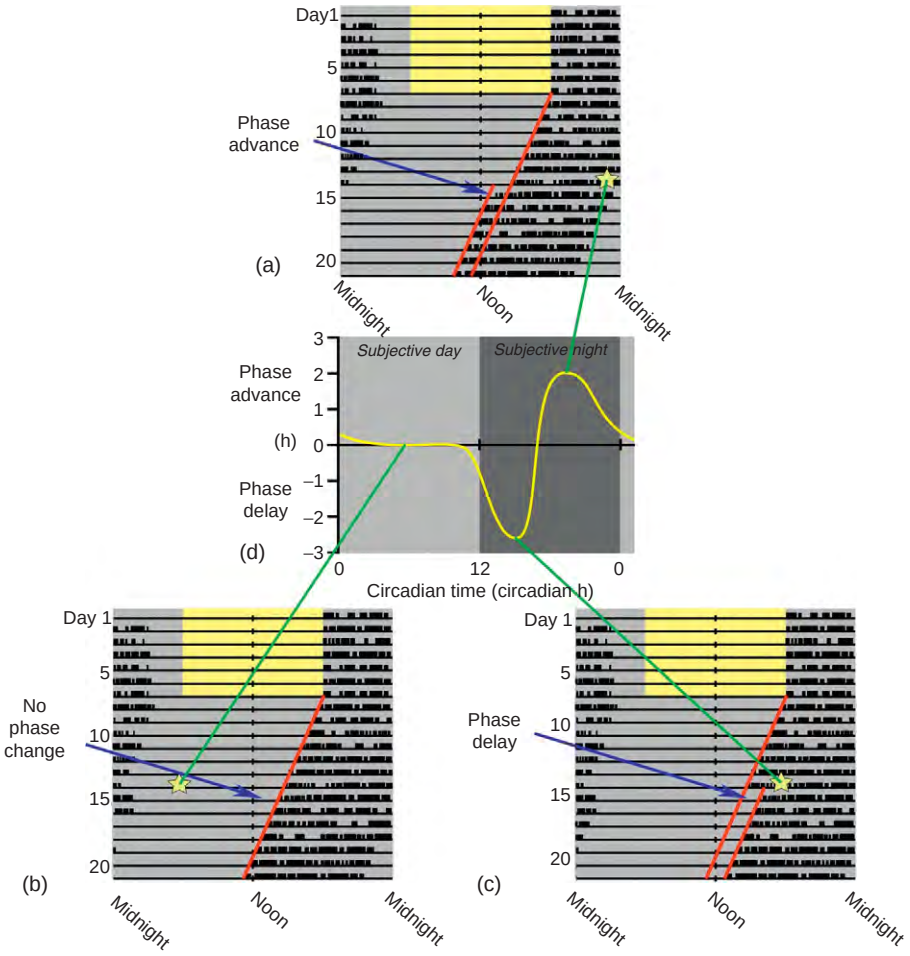

Figure 2 Phase response curve. Actograms (a, b, c) of daily activity obtained in running wheel cages containing a single mouse. Each horizontal line represents one day. Line thickenings indicate bouts of activity. Animals are maintained in a 12-h light:12-h dark cycle for the first week (gray background, dark; yellow background, light) and then maintained in constant darkness for the remainder of the experiment (gray background). After approximately 1 week in constant darkness, a standardized light pulse is administered (star symbol) and the phase shift of the onsets of activity on the days following the pulse are determined. The magnitude and direction (delay or advance) of the phase shift in response to a standardized light pulse varies as a function of the circadian phase of the circadian cycle during which the pulse is given. This relationship can be plotted as a phase:response curve (d). In general, light exposure during the early subjective night elicits phase delays, while illumination during the late subjective night causes phase advances. Pulses administered during the subjective day do not shift the clock.

Melanopsin and the Mammalian ipRGC

Among the nonvisual opsins, melanopsin has been the most extensively studied photopigment. It is expressed in a small subset of RGCs that project to sites in the brain not involved in the formation of images. Originally cloned from the photosensitive dermal melanophores of *Xenopus laevis*, homologs were subsequently identified in chicken and other nonmammalian vertebrates. A second melanopsin gene was recognized in the chicken genome and is also present in other vertebrate classes. However, based on chromosome synteny, it is clear that one of these two genes has been lost in mammals.

In the nonmammalian vertebrates, melanopsin is expressed in the retina and extraretinal tissues, including the iris, brain, pineal, and skin. Many of these sites had been shown previously to be inherently light sensitive, although the photopigments mediating the sensitivity were unidentified. Unlike the broad anatomical distribution observed in nonmammalian vertebrates, in mammals, melanopsin expression is restricted to less than 2% of the RGCs. Notably, extraretinal expression has not been observed in any mammal.

Pituitary adenylyl cyclase-activating peptide and glutamate are coexpressed within the melanopsin-containing cells. Melanopsin is what confers photosensitivity upon these intrinsically photosensitive retinal ganglion cells (ipRGCs). Loss of melanopsin renders these cells nonresponsive to light.

Murine ipRGCs elaborate two or three primary dendrites which bifurcate within 50 μm of the perikaryon. The

Table 1 Nonvisual opsins of mammals

Opsin	*Gene name*	*Tissue distribution*	*Putative function*
Peropsin	*rrh*	rpe	Photoisomerase
Retinal G protein-coupled receptor	*rgr*	rpe	Photoisomerase
Melanopsin	*opn4*	Retina	Nonvisual photoreception
gpr136/ neuropsin	*opn5*	Eye, brain, testis, and spinal cord	Unknown
Encephalopsin/ panopsin	*opn3*	Brain, testis	Unknown

dendrites ramify within the S1 (OFF layer) or S5 (ON layer) sublaminae of the inner plexiform layer. A small fraction of ipRGCs may have dendrites arborizing in both S1 and S5. Dendrites are studded with varicosities giving a rosary bead appearance. Melanopsin protein is found throughout the plasma membrane of the cell body, the segment of the axon contained within the eye, and the dendritic arbor. Arbors are sparse, regularly tiled across the retina with substantial overlap, and rather large, having mean field diameters of around 450 μm in mice and 600 μm in rats. The receptive field of ipRGCs corresponds to the dimension of the dendritic field, indicating that the entire arbor is capable of initiating phototransduction. Membrane density of melanopsin is about 10 000-fold lower than that of rods and cones. This is largely attributable to the lack of a specialized light harvesting organelle in ipRGCs comparable to the photopigment-dense outer segments of rods and cones. This relative paucity of photopigment in ipRGCs results in a very low photon-capture efficiency, thereby rendering this system effective only in very bright irradiances. Nevertheless, ipRGCs, similar to rods, can signal the absorption of single photons. The spectral sensitivity of dark-adapted melanopsin peaks in the blue wavelengths and coincides with the action spectra of many of the nonvisual responses previously described, including circadian photoentrainment and the pupillary light reflex of visually blind mice that lack rods and cones.

A comparison of the melanopsin peptide sequence against known opsins indicates that it more closely resembles the rhabdomeric opsins of invertebrates rather than the ciliary opsins of vertebrates. Not surprisingly, melanopsin employs a phototransduction cascade more similar to that of insect rhabdomeres rather than vertebrate outer segments. Illuminated amphibian melanophores darken and exhibit a light-stimulated increase in inositol trisphosphate and protein kinase C (PKC)-dependent phosphorylation. Presumably, these effects are mediated by a melanopsin-initiated cascade because overexpression of melanopsin hypersensitizes melanophores to light. Inhibition of phospholipase C (PLC), PKC, or chelation of intracellular calcium blocks melanophore darkening suggesting that this light-initiated response must activate a phosphoinositide signaling cascade. Heterologous expression of melanopsin in HEK293 cells renders them light sensitive and leads to a light-dependent increase in intracellular calcium and depolarization of membrane potential. Depolarization can be blocked by pharmacologic inhibitors of the $G\alpha_{(q/11)}$ subunit of guanine nucleotide-binding protein or PLC. These lines of evidence again suggest that light-activated melanopsin triggers a phosphoinositide signaling cascade similar to that of rhabdomeric photoreceptors. These same transduction components are found within ipRGCs and are critical for eliciting photoresponses. Furthermore, responses to light can be elicited in excised, inside-out patches of ipRGC membrane indicating that the critical signaling molecules are closely associated or are within the plasma membrane. A hallmark of rhabdomeric opsins is the formation of a stable red-shifted metastate in response to illumination. Whether melanopsin forms such a state remains equivocal, although some dark-adapted responses to blue light appear to be primed by preexposure to red light, which presumably photoconverts a red-sensitive metastate back to the blue-sensitive dark-adapted state. The general similarity to rhabdomeric signaling indicates that ipRGCs and invertebrate photoreceptors may have shared a common evolutionary ancestor.

ipRGCs project to central sites not associated with vision but implicated in regulating different forms of nonvisual photophysiology. For example, the SCN of the hypothalamus, the site of the primary circadian pacemaker, receives a robust input from ipRGCs. By contrast, the classical, nonphotosensitive RGCs provide minimal innervation to the SCN. Photoreceptor-mediated effects on the circadian axis occur exclusively through ipRGCs, suggesting that classical retinal rod and cone circuits impinge upon ipRGCs at the inner plexiform layer. Other principle central targets of ipRGCs include the IGL, the olivary pretectal nucleus, and the lateral habenula. The subparaventricular zone, the ventrolateral preoptic nucleus, and the ventral lateral geniculate nucleus are secondary, less intensely innervated targets.

Functions of ipRGCs

The role of ipRGCs in mediating nonvisual responses to light has been largely elucidated through the use of genetic mouse models. Mice null for melanopsin exhibit rather modest phenotypes. The magnitude of light-induced phase shifts of circadian locomotor activity rhythms is attenuated in melanopsin knock-out mice to about 40% of that observed in wild-type sibling controls (**Figure 3(a)**). The lengthening of circadian period observed in wild-type

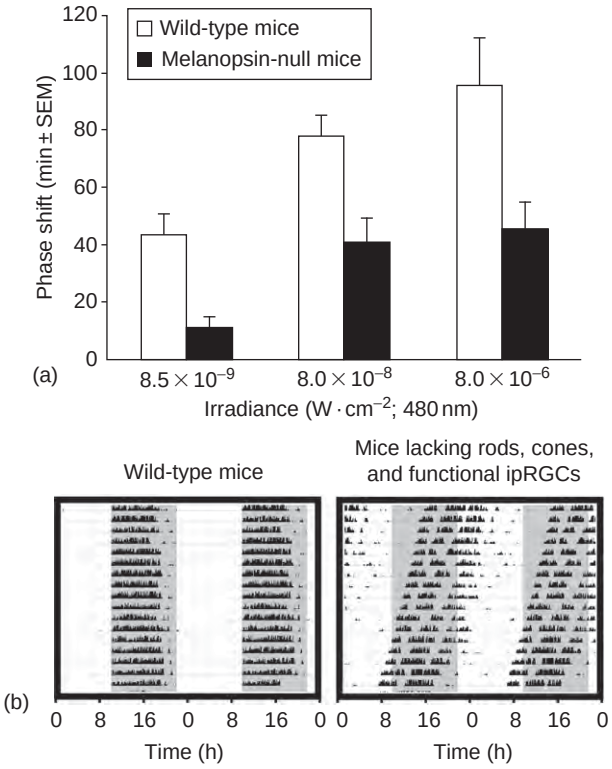

Figure 3 Circadian responses to light in retinal mutants. (a) Irradiance-dependent circadian phase shifting in wild-type and melanopsin-null mice. Mice lacking melanopsin were deficient in light-induced circadian phase shifting at all irradiances tested. (b) Melanopsin-null mice also lacking rods and cones fail to show synchronization (entrainment) of circadian locomotor activity to the light:dark cycle; white is the time that lights are on. Actograms are double plotted (i.e., horizontal lines correspond to 48 h) and darkness is indicated by a gray background. By contrast, the wild-type mouse is well entrained.

mice that are maintained in constant light is also diminished in melanopsin knockout mice. However, entrainment to standard light:dark cycles appears to be unaffected in mice lacking melanopsin. Other nonvisual responses such as the pupillary light response, the acute inhibition of activity by light (masking), and the suppression of the melatonin biosynthetic pathway are unaffected in melanopsin knockout mice. Interestingly, many of these same responses show no deficits in murine genetic models lacking rods and cones. Combined, these results suggest some level of redundancy between the rod/cone system and ipRGCs. To test this possibility, melanopsin-null mice have been crossed with mice either lacking functional rods and cones or lacking rods and cones all together. These animals exhibit no responses to light (**Figure 3(b)**). Essentially, they behave as though they have been bilaterally enucleated.

Many of the retinorecipient structures such as the SCN that mediate nonvisual responses to light receive negligible, if any, input from rod and cone pathways. However, melanopsin-knockout mice with light-insensitive ipRGCs continue to exhibit some degree of light-driven nonvisual responses. This raises the possibility that in addition to their inherent photoreceptive capacity, ipRGCs may also serve to convey light signals initially detected by rods and/or cones to brain sites such as the SCN. Indeed, specific ablation of ipRGCs mimics the previously mentioned results obtained in animals lacking functional rods, cones, and ipRGCs. These results indicate that ipRGCs, while intrinsically light sensitive, also transmit information generated by the classical photoreceptors.

Apart from its role in entraining circadian rhythms, the eye is a circadian oscillator itself. This was first demonstrated in the isolated eyes of gastropods, which show a circadian rhythm in the firing frequency of compound action potentials. Shedding of disks from the distal tips of rods is also circadian and persists in isolated amphibian and mammalian eyes whose optic nerves have been severed. Teleost eyes exhibit circadian rhythms in retinomotor movements of photoreceptors and the migration of melanosomes within cells of the retinal pigment epithelium. Syntheses of melatonin and dopamine are perhaps the best-studied circadian outputs of the eye. These amines are synthesized in antiphase; melatonin levels peak in the night and dopamine levels peak during the day. This phase relationship is maintained in constant darkness indicating that these rhythms are indeed circadian. However, in the absence of melatonin, dopamine is only acutely synthesized in response to light and is no longer produced in a circadian fashion.

Determining which ocular cell types harbor the circadian clock has proved to be difficult. Isolated amphibian eyecups continue to produce melatonin rhythmically, even when the vast majority of inner retinal neurons are lesioned. These findings suggest that the photoreceptors contain a competent clock and the biosynthetic machinery to make melatonin. Additionally, action spectral analyses in the amphibian retina implicate the principal green-sensitive rods as critical to the acute light-mediated regulation of ocular melatonin synthesis. Whether these cells are the actual site of the amphibian retinal clock remains to be determined.

The mammalian eye also contains a circadian clock. Cultured hamster retinas maintained in constant darkness produce melatonin rhythmically with a period near 24 h. Retinas from *tau* hamsters whose period of locomotor rhythms are significantly shorter than those of wild-types also exhibit rhythms in retinal melatonin with periods that parallel the shortened activity cycles. Importantly, these rhythms can be reset by pulses of light demonstrating that similar to the amphibian eye, the mammalian eye is an autonomous circadian system with a circadian pacemaker that drives a measurable output, which can be reset if it comes out of phase with the light:dark cycle.

In summary, the mammalian eye has a dual function. Similar to the ear which supplies auditory and vestibular

input to the brain, the eye provides visual input for the formation and interpretation of images and nonvisual input for the regulation of a myriad of light-regulated physiology such as the entrainment of circadian rhythms. The primary central circadian pacemaker within the SCN is entrained by light, the most reliable of external, daily time cues. The photoreceptors mediating photoentrainment include the classical photoreceptors (rods and/or cones), known primarily for their role in vision, and unique RGCs, which are inherently light sensitive because they express the photopigment melanopsin. The relative insensitivity of ipRGCs suggests that the classical photoreceptors mediate photoentrainment at low light levels, while ipRGCs are responsible for entraining the SCN at higher irradiances. However, even at low light levels, photoreceptive signals transmitted through rod or cone pathways reach sites of the brain involved in nonvisual photoresponses via the ipRGCs.

The presence of an ocular photoreceptive system that is anatomically distinct from the rods and cones raises the possibility that individuals suffering from blindness due to photoreceptor loss may retain a full healthy complement of ipRGCs. Some blind individuals do indeed lack cognitive vision but maintain an ability to regulate pineal melatonin and remain synchronized to the prevailing day:night cycle. The high incidence of ocular infection in the blind drives many clinicians to replace the eyes with prosthetics. Care should be taken to consider the anatomical source of blindness. Those suffering from photoreceptor-derived or cortical blindness may develop circadian-based maladies upon removal of the eyes, thereby exacerbating an already diminished quality of life.

See also: The Circadian Clock in the Retina Regulates Rod and Cone Pathways; Circadian Regulation of Ion Channels in Photoreceptors; The Evolution of Opsins; Microvillar and Ciliary Photoreceptors in Molluskan Eyes; The Photoreceptor Outer Segment as a Sensory Cilium; Phototransduction: Inactivation in Rods; Phototransduction: Phototransduction in Rods; Rod and Cone Photoreceptor Cells: Inner and Outer Segments.

Further Reading

Berson, D. M. (2007). Phototransduction in ganglion-cell photoreceptors. *Pflugers Archiv* 454: 849–855.

Berson, D. M., Dunn, F. A., and Takao, M. (2002). Phototransduction by retinal ganglion cells that set the circadian clock. *Science* 295: 1070–1073.

Cahill, G. M. and Besharse, J. C. (1993). Circadian clock functions localized in xenopus retinal photoreceptors. *Neuron* 10: 573–577.

Campbell, S. S. and Murphy, P. J. (1998). Extraocular circadian phototransduction in humans. *Science* 279: 396–399.

Czeisler, C. A., Shanahan, T. L., Klerman, E. B., et al. (1995). Suppression of melatonin secretion in some blind patients by exposure to bright light. *New England Journal of Medicine* 332: 6–11.

Do, M. T., Kang, S. H., Xue, T., et al. (2009). Photon capture and signalling by melanopsin retinal ganglion cells. *Nature* 457: 281–287.

Graham, D. M., Wong, K. Y., Shapiro, P., et al. (2008). Melanopsin ganglion cells use a membrane-associated rhabdomeric phototransduction cascade. *Journal of Neurophysiology* 99: 2522–2532.

Guler, A. D., Ecker, J. L., Lall, G. S., et al. (2008). Melanopsin cells are the principal conduits for rod–cone input to non-image-forming vision. *Nature* 453: 102–105.

Hattar, S., Liao, H. W., Takao, M., Berson, D. M., and Yau, K. W. (2002). Melanopsin-containing retinal ganglion cells: Architecture, projections, and intrinsic photosensitivity. *Science* 295: 1065–1070.

Keeler, C. E. (1927). Iris movements in blind mice. *American Journal of Physiology* 81: 107–112.

Kumbalasiri, T. and Provencio, I. (2005). Melanopsin and other novel mammalian opsins. *Experimental Eye Research* 81: 368–375.

Provencio, I. (2007). Melanopsin cells. In: Hoy, R. R., Shepherd, G. M., Basbaum, A. I., Kaneko, A., and Westheimer, G. (eds.) *The Senses: A Comprehensive Reference.* Oxford: Elsevier.

Tosini, G. and Menaker, M. (1996). Circadian rhythms in cultured mammalian retina. *Science* 272: 419–421.

Wright, K. P. Jr. and Czeisler, C. A. (2002). Absence of circadian phase resetting in response to bright light behind the knees. *Science* 297: 571.

Circadian Regulation of Ion Channels in Photoreceptors

G Y-P Ko, K Jian, L Shi, and M L Ko, Texas A&M University, College Station, TX, USA

Glossary

Circadian oscillator – A system that generates self-sustained oscillations or rhythms of about 24 h. Current models include self-sustained transcription and translation feedback loops that operate at the cellular level to provide outputs that are circadian in nature.

Cyclic GMP-gated cation channels (CNGCs) – The nonselective cation channels that are activated through direct binding of cyclic nucleotides onto the channel proteins. In general, cyclic-nucleotide gated channels are heterotetrameric complexes consisting of two or three different subunits (α, β, and γ), with important channel properties determined by the subunit composition.

ENSLI amacrine cells – A class of retinal amacrine cells that release the peptide, somatostatin. These cells get their name because they are immunoreactive for enkephalin, neurotensin, and somatostatin (ENSI, enkephalin-, neurotensin-, and somatostatin-like immunoreactive).

L-type voltage-gated calcium channels (L-VGCCs) – The membrane channels that mediate a voltage-dependent and depolarization-induced calcium influx. They regulate diverse biological processes such as contraction, secretion, neurotransmission, differentiation, and gene expression in many different cell types. The L-VGCCs are composed of a pore-forming α1-subunit and the auxiliary β-, $\alpha 2\delta$-, and γ-subunits. They can be blocked by divalent cations (e.g., cobalt) and organic L-VGCC antagonists, including dihydropyridines, phenylalkylamines, and benzothiazepines.

Retinoschisis – An X-linked retinal dystrophy that features disorganization of retinal cell layers, disruption of the synaptic structures and neurotransmission between photoreceptors and bipolar cells, and progressive degeneration of rod and cone photoreceptor cells. Retinoschisis results from mutations in retinoschisin.

Circadian Oscillators Regulate the Functions of the Visual System

Circadian oscillators are biological clocks that exist in almost all living organisms on the earth from bacteria to humans, with persistent rhythmic periods close to 24 h (*circa dian*) even in the absence of external timing cues. The circadian oscillators coordinate rhythmic changes in biochemistry, physiology, and behavior of living organisms, so that organisms can be synchronized with the 24-h oscillations of the external environment. The molecular nature of circadian oscillators varies from species to species. A generalized model for the generation of circadian rhythm involves the transcription, translation, and feedback of clock genes and their own transcriptional products. It is composed of two interlocking transcription–translation feedback loops as well as post-translational modulations. Collectively, these components comprise the core oscillator or the circadian oscillator. Visual systems have to detect images despite large daily changes in ambient illumination between day and night, and intrinsic circadian oscillators in the retina provide such a mechanism for visual systems to initiate more sustained adaptive changes throughout the course of the day. The retina is a heterogeneous tissue with multiple cell types organized in several cell layers. Early studies of circadian regulation in *Xenopus* and chicken retinas indicated that retinal circadian clocks are mainly located in the photoreceptors. Later research revealed that there are multiple oscillators present in various retinal cells in a species-dependent manner. The overall circadian regulation of the retina relies on the synaptic circuitry and feedback modulation among different retinal oscillators, so that the retina is able to anticipate and adapt to sustained daily illumination changes as well as acute light/dark adaptation.

Circadian Regulation of Photoreceptors

The circadian oscillators in photoreceptors are endogenous and able to function independently in the absence of other retinal inputs. These photoreceptor oscillators lead to morphological, physiological, biochemical, and molecular changes that ultimately regulate photoreceptor function and physiology in a circadian fashion. In vertebrate rod photoreceptors, outer segment shedding and renewal is a continuous process, but its rate is under circadian control. In some teleosts and anurans, the

inner segments of rod and cone photoreceptors undergo contraction and elongation (i.e., retinomotor movement) in response to changes in ambient illumination as well as in the circadian cycles. While cones remain in a contracted state during the day, rods contract at night. Photoreceptors form specialized ribbon synapses with secondary neurons such as horizontal or bipolar cells. The numbers and ultrastructures of synaptic ribbons in both photoreceptors and bipolar cells undertake changes in relation to the time of day and light intensities. In avians, amphibians, reptiles, and other lower vertebrate species, melatonin is synthesized and secreted from photoreceptors at night, while its synthesis is inhibited by light. The transcription of arylalkylamine N-acetyltransferase (AANAT), the melatonin synthesis enzyme, is under circadian control. While the synthesis and release of dopamine from retinal amacrine cells shows light-driven and circadian fluctuations, the circadian nature of dopamine is dependent on the melatonin rhythm. In addition to the circadian oscillator genes, several photoreceptor-specific genes, ion channels, and enzyme activities are also under circadian control that ultimately contribute to the circadian regulation of photoreceptor physiology and function.

Ion Channels in Photoreceptors

Ion channels are macromolecular pores that allow charged ions to move across cell membranes and contribute to the excitability of neurons and muscles. Electrical signals are generated and modulated as different types of channels open and close in response to neurotransmitters, hormones, membrane potential changes, mechanical forces, and other agents. There are two major classes of ion channels: voltage-gated and ligand-gated ion channels. Voltage-gated ion channels open or close their pores in response to membrane potential changes. Ligand-gated ion channels gate ion movements and generate electrical signals in response to specific chemicals such as neurotransmitters or cyclic nucleotides. Vertebrate photoreceptors are highly polarized, so the distribution of ion channels on the plasma membrane is spatially compartmentalized. The outer segment membrane contains cyclic guanosine monophosphate (cGMP)-gated ion channels that are closed by light, whereas the inner segment and the synaptic terminal are furnished with at least six different ion channels. These six ion channels include:

1. hyperpolarization-activated and cyclic-nucleotide-modulated cation channels;
2. L-type voltage-gated calcium channels (L-VGCCs);
3. calcium-activated potassium (K_{Ca}) channels;
4. noninactivating voltage-gated potassium channels;
5. calcium-activated chloride channels; and
6. cGMP-gated ion channels.

Thus far, cGMP-gated ion channels and L-VGCCs have been studied the most rigorously, especially with regard to their gating properties and physiological functions in photoreceptors. Both ion channels are under circadian control. In the following sections, the circadian regulation of cGMP-gated ion channels and L-VGCCs are reviewed in detail.

Circadian Regulation of cGMP-gated Cation Channels

Cyclic GMP-gated cation channels (CNGCs) are nonselective cation channels that belong to the family of cyclic-nucleotide-gated channels. In general, cyclic-nucleotide-gated channels are heterotetrameric complexes consisting of two or three different subunits (α, β, and γ), with important channel properties determined by the subunit composition. Activation of these channels is through direct binding of cyclic nucleotides onto the channel proteins. The CNGCs of rods and cones have structurally similar but distinct α- and β-subunits. Rods contain CNGCα1-subunits that are more sensitive to calcium-induced inhibitions, while cones contain CNGCα3-subunits that are not as sensitive to calcium. In the vertebrate retina, phototransduction is mediated by a G-protein-coupled cascade that results in changes in the gating of CNGCs in the outer segments of rods and cones. Light initiates a fall in intracellular cGMP as the end point of a G-protein-mediated phototransduction cascade, resulting in closure of CNGCs, reduced cation influx, and membrane hyperpolarization. In the dark, the intracellular cGMP concentration is relatively high. This causes tonic activation of these channels and a steady transmembrane influx of sodium (Na^+) and calcium (Ca^{2+}) ions. Therefore, CNGCs carry the photoreceptor dark current and serve essential roles in the light-dependent changes in photoreceptor membrane potential and subsequent neural processing.

In chick cone photoreceptors, the apparent affinity of CNGCs for their activating ligand is under circadian regulation. There is roughly a twofold change in the apparent affinity of CNGCs for cGMP throughout the course of a day, with the affinity substantially higher at night than during the day even in constant darkness. Such changes in channel affinities can be expected to occur especially at the lower range of cGMP concentrations ($\leq$7 μM in the dark) that are within the photoreceptor physiological range. Other biophysical features of the gating of CNGCs, such as unitary conductance, numbers of cGMP-binding sites on the channels, density of channels in the plasma membrane, and the maximum current amplitudes do not vary as a function of the time of day.

The ion channel gating properties of photoreceptor CNGCs can be modulated by multiple processes, including direct phosphorylation or dephosphorylation of the

channel subunits and the binding of Ca^{2+}/calmodulin or related molecules. Dephosphorylation of CNGCs on serine/threonine residues or tyrosine residues causes an increase in the apparent affinity of CNGCs for their activating ligand. Binding of Ca^{2+}/calmodulin or phosphorylation of CNGCs causes these channels to shift to a lower affinity state for cGMP. The clock regulation of cone CNGCs entails a post-translational modification of the channel molecules. More specifically, it is the circadian rhythmicity of tyrosine phosphorylation that underlies the circadian modulation of cone CNGC affinity to its ligand. Inhibition of tyrosine kinases during the day increases the apparent affinity of CNGCs for cGMP, whereas inhibition of tyrosine phosphatases at night produces the opposite effect. While the protein expression and phosphorylation of the channel pore-forming CNGCα3-subunits remain constant throughout the course of the day, tyrosine phosphorylation of an auxiliary subunit (probably the β-subunit, ~85 kDa) displays a circadian rhythm. During the daytime, tyrosine phosphorylation on this 85-kDa protein is twice as high as at night. Therefore, circadian rhythmicity of tyrosine phosphorylation on the 85-kDa auxiliary subunit of cone CNGCs provides one of the final steps in the circadian regulation of CNGCs.

The CNGCs in photoreceptors are essential components of visual phototransduction cascades. As such, it is possible that they also play a role in the light entrainment of the circadian oscillators in photoreceptors. As the gating of CNGCs is under circadian control in cone photoreceptors, these channels represent a potential example of an entity that is both an input to and an output from the circadian oscillator. Roenneberg and Merrow have presented models of circadian oscillator systems in which pathways that lead to entrainment of the core oscillators (i.e., the circadian inputs) can themselves be regulated by the oscillators (i.e., they are also components of circadian outputs). One feature of these models is that they contain additional feedback loops that can markedly enhance the stability of the overall oscillator system. Therefore, the circadian regulation of CNGCs in retinal photoreceptors represents an adaptation to enhance the stability of the circadian oscillators in photoreceptors.

Signaling Pathways Leading to the Circadian Regulation of CNGCs

Even though the connection from the molecular oscillator to the regulation of CNGC affinity rhythm is still not completely understood, the small guanosine triphosphate (GTP)ase Ras and mitogen-activated protein kinase (MAPK) signaling pathway and calcium-calmodulin kinase II (CaMKII) are involved as circadian outputs to regulate CNGC rhythms. The activities of Ras and MAPK are themselves under circadian control and oscillate concurrently with the CNGC affinity rhythm. The activity of CaMKII also displays a circadian rhythm, but it runs antiphase to the MAPK rhythm, and CaMKII is a downstream target of MAPK. Perturbation of the activities of Ras, MAPK, or CaMKII causes phase-dependent changes in the gating properties of CNGCs. Furthermore, this Ras–MAPK–CaMKII pathway serves as part of a common circadian output pathway to regulate other molecules in photoreceptors (see **Figure 1**). However, neither MAPK nor CaMKII directly phosphorylates CNGCs in a circadian fashion. It is their downstream targets leading to tyrosine phosphorylation on the auxiliary subunit of CNGCs that ultimately govern the circadian regulation of CNGC gating properties.

The expression and activation of adenylate cyclase in the retina are under circadian control, and the cyclic adenosine monophosphate (cAMP) content in retinal photoreceptors is maximal at night. In avian retinas, this cAMP rhythm not only drives the rhythm of melatonin synthesis and secretion, but it also serves as part of the circadian output and leads to MAPK activation and modulation of the CNGC affinity rhythm. Besides serving as a circadian output to regulate ion channels, cAMP can stimulate retinomotor movements. In *Xenopus* retina, cAMP signaling resets circadian oscillators within photoreceptors. Hence, the second messenger, cAMP, may well serve as part of both input and output pathways in photoreceptors.

Circadian Phase-Dependent Modulation of Cone CNGCs by Dopamine

While circadian rhythms can occur in retinal photoreceptors cultured in the absence of other functional cell types, multiple cell types contribute to the overall circadian control of the intact retina. In avian retina, melatonin inhibits the release of dopamine from a subpopulation of amacrine cells. Consequently, retinal melatonin and dopamine are in antiphasic circadian cycles. As a result, dopamine functions as a feedback signal from the inner retina that refines and modulates circadian control mechanisms within the photoreceptors. Dopamine evokes a phase-dependent modulation of CNGC affinity rhythm in chick cone photoreceptors that is through the activation of the D2 family of dopamine receptors. Exposure to dopamine or D2 agonists causes a significant decrease in the apparent affinity of CNGCs at night but has no effect on CNGCs during the day. It is well established that D2 receptors are pertussis-toxin-sensitive G-protein-coupled receptors that mediate inhibition of adenylate cyclase and cause a decrease of cAMP formation in the retina. However, the phase-dependent modulation of

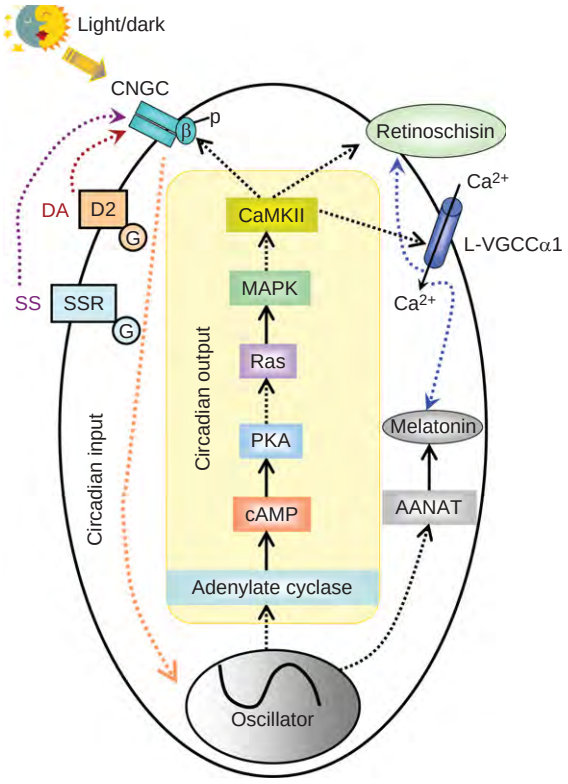

Figure 1 This model illustrates the circadian rhythm in retina cone photoreceptors. Light and dark (day and night) signals from the environment enter the photoreceptor through cGMP-gated cation channels, since cGMP-gated cation channels are essential in phototransduction for light detection. The light/dark signals through the circadian input pathway entrain the photoreceptor core oscillator that cause the photoreceptor to be in sync with the environment. From the core oscillator through the circadian output, the activities of different molecules, including cGMP-gated ion channels, L-type voltage-gated ion channels, and retinoschisin are under circadian regulation. This circadian output is composed of a series of signaling pathways. The circadian regulation of CNGCs in retinal photoreceptors represents an adaptation to enhance the stability of retinal circadian oscillators. It demonstrates a model that Roenneberg and Merrow have presented, in which the elements that lead to entrainment of the core oscillators (e.g., cGMP-gated cation channels) can themselves be regulated by the oscillators. One feature of this model is that it contains additional feedback loops that can markedly enhance the stability of the overall oscillator system at the cellular level (photoreceptors only) and maybe at the retinal network level (the retinal oscillators). The circadian phase-dependent regulation of cGMP-gated cation channels by dopamine and somatostatin is represented by brown and purple dotted arrows, respectively. The black dotted arrows indicate that there are multiple steps currently not known, while the solid arrows represent known signaling. Blue dotted arrows represent that the secretion of melatonin and retinoschisin is under the control of L-type voltage-gated calcium channels. AANAT, arylalkylamine N-acetyltransferase; Ca^{2+}, calcium ion; CaMKII, calcium-calmodulin kinase II; CNGC, cGMP-gated cation channel; DA, dopamine; D2, dopamine D2 receptor; G, G protein; L-VGCCα1, L-type voltage-gated calcium channel α1-subunit; SS, somatostatin; SSR, somatostatin receptor.

CNGCs in cone photoreceptors by dopamine does not involve pertussis-toxin-sensitive G protein or cAMP signaling, since exposure to cAMP or pertussis toxin does not reverse the phase-dependent modulation of dopamine on CNGCs. This circadian modulation of cone CNGCs by dopamine is partially through the MAPK–CaMKII signaling pathway.

Modulation of Cone CNGCs by Somatostatin

Somatostatin is released from a class of amacrine cells that are immunoreactive for enkephalin, neurotensin, and somatostatin, and thus are called ENSLI (enkephalin-, neurotensin-, and somatostatin-like immunoreactive) amacrine cells. There are two forms of somatostatin: somatostatin-14 (SS-14) with 14 amino acids and somatostatin-28 (SS-28) with 28 amino acids, and both forms are released from ENSLI cells. The release of somatostatin from the ENSLI cells is under circadian control, which is high at night and low during the day in mammalian retinas, and this rhythm is concurrent with the activities of these cells with a high sustained rate of activity in the dark and a low sustained rate of activity in the light. The five somatostatin receptors (referred to as Sst1–Sst5) are guanine nucleotide binding protein (G-protein)-coupled receptors. While all five subtypes of somatostatin receptors are expressed in mammalian retina, only Sst2–Sst5 are present in the chick retina. Both SS-14 and SS-28 modulate cone CNGC sensitivity to cGMP that depend on circadian phase and immediate history of illumination. Both SS-14 and SS-28 decrease CNGC sensitivity to cGMP at night, which are similar to the action of dopamine via the D2 receptor and resistant to pertussis toxin. In addition, SS-28, but not SS-14, evokes a transient increase in CNGC affinity to cGMP only during the early part of the day in cone photoreceptors that have been exposed to light for 1–2 h. This transient effect by SS-28 is mediated by pertussis-toxin-sensitive G-protein-coupled receptors and activation of phospholipase C and protein kinase C signaling cascades. Therefore, somatostatin modulation of retinal cones may serve to reinforce circadian processes intrinsic to the photoreceptors, and may also contribute to more rapid adaptive responses to changes in ambient illumination.

Circadian Regulation of L-VGCCs

L-VGCCs mediate a voltage-dependent and depolarization-induced calcium influx and regulate diverse biological processes, such as contraction, secretion, neurotransmission, differentiation, and gene expression in many different cell types. The L-VGCCs are composed of a pore-forming α1-subunit and the auxiliary β-, $\alpha 2\delta$-, and γ-subunits, and

they can be blocked by divalent cations (e.g., cobalt) and organic L-VGCC antagonists, including dihydropyridines, phenylalkylamines, and benzothiazepines. The α1-subunit serves as a voltage sensor to detect voltage changes across the plasma membrane, and it also controls the pore size to allow selective divalent cations to pass through. Mammalian α1-subunits are encoded by at least 10 distinct genes, and α1C, α1D, and α1F (also known as $Ca_v1.2$, $Ca_v1.3$, and $Ca_v1.4$, respectively) are expressed in the retina photoreceptors. Photoreceptors are nonspiking neurons, and they release glutamate continuously in the dark as a result of depolarization-evoked activation of L-VGCCs.

Circadian regulation of L-VGCCs has been observed in goldfish retinal bipolar cells, chick cone photoreceptors, and other nonretinal neurons. In both retinal cases, the average maximum current amplitudes of L-VGCCs are significantly larger at midnight than at midday. The activation voltages that elicit L-VGCC currents (i.e., current–voltage relationship) and the channel gating kinetics do not change throughout the course of a day. In chick retinas, the main factor contributing to the circadian regulation of L-VGCC current amplitudes is the expression of functional L-VGCCα1-subunits, and both messenger RNA (mRNA) levels and protein expression of VGCCα1D are rhythmic. The Ras–MAPK–CaMKII signaling pathway (**Figure 1**) serves as part of the circadian output to regulate L-VGCCs as well as CNGCs as described above. However, the varying maximum amplitudes of the L-VGCC currents is in stark contrast to the CNGC maximum currents, which remain constant throughout the day, and which instead exhibit changes in gating properties.

One major functional significance of the L-VGCC rhythm is the circadian control of melatonin release. In nonmammalian vertebrates, melatonin is synthesized and secreted from retinal photoreceptors and is under circadian control. Inhibition of L-VGCCs with dihydropyridines blocks the synthesis and release of melatonin. Another physiological aspect of the L-VGCC rhythm is the circadian control of retinoschisin secretion. Retinoschisin is a 224-amino-acid protein secreted mainly by retinal photoreceptors and bipolar cells. Retinoschisin is distributed throughout the retina but is mainly concentrated around outer and inner segments of photoreceptors and both retinal plexiform layers. Mutations in the retinoschisin gene (*RS1*) cause X-linked retinoschisis, a retinal dystrophy that features disorganization of retinal cell layers, disruption of the synaptic structures and neurotransmission between photoreceptors and bipolar cells, and progressive degeneration of rod and cone photoreceptor cells. Hence, retinoschisin is believed to play an important role in the development and maintenance of retinal cytoarchitecture. In chick retinas, the mRNA level and protein expression of retinoschisin are under circadian control, and the secretion of retinoschisin is higher at night than during the day. Inhibition of L-VGCCs with dihydropyridines dampens the circadian rhythm of retinoschisin secretion where only nighttime secretion is affected. Therefore, the circadian control of L-VGCCs has a profound impact in regulation of photoreceptor physiology and synaptic transmission.

Circadian Regulation of Other Photoreceptor Ion Channels: Potassium Channels (K^+ Channels)

Potassium (K^+) channels are the most diverse ion channels with more than 100 genes of the pore-forming α-subunits identified to date. They can dampen membrane excitability and set the resting membrane potentials in neurons. According to their genetic homology and functional characteristics, there are four major families of K^+ channels: voltage-gated K^+ channels, Ca^{2+}-activated K^+ channels, inward rectifier K^+ channels, and leak K^+ channels. In photoreceptors, the dark inward current through CNGCs in the outer segment is balanced by a K^+ outward current in the inner segment, and this K^+ outward current is mainly carried out by the voltage-gated K^+ channels. The major subtypes of voltage-gated K^+ channels present in photoreceptors are delayed-rectifier K^+ channels (Kv1.2, 1.3, and 2.1) and A-type transient K^+ channels (Kv4.2). The Ca^{2+}-activated K^+ channels and outward-rectifying noninactivating K^+ channels (Kv10.2; *eag*2) are also found in photoreceptors.

Thus far, the reports on circadian regulation of K^+ channels have been limited to invertebrate studies. In *Aplysia* retinal pacemaker neurons (not photoreceptors), there is a robust circadian rhythm of potassium currents carried by voltage-gated K^+ channels (I_{KV}), while A-type K^+ currents and Ca^{2+}-activated K^+ currents remain constant throughout the day. When I_{KV} peaks during the late night (predawn), the compound action potential firing frequencies reaches its nadir. The circadian rhythm of I_{KV} contributes to the circadian control of the frequency of compound action potentials in pacemaker neurons. The basal retinal neurons in the eye of the mollusk *Bulla gouldiana* express a circadian rhythm in optic nerve impulses. It is the circadian regulation of I_{KV}, but not other outward K^+ channels, that drive the daily fluctuations in membrane conductance and membrane potential of these neurons.

Conclusion

The circadian oscillators in the retina play important roles in the regulation of retinal physiology and function, including sensitivity to light, neurotransmitter release, gene expression, morphological changes at the synaptic terminals, metabolism (as pH changes), and rod–cone dominance. The photoreceptor components of

electroretinograms (ERGs), the electrophysiological recordings of retinal physiology, recorded from humans as well as animals, show daily rhythms. The circadian oscillators in photoreceptors are endogenous, and they can function independently without other retinal inputs. These circadian oscillators regulate retinomotor movement, outer segment disk shedding and membrane renewal, morphological changes at synaptic ribbons, gene expression, a delayed rectifier potassium current, the affinity of cGMP-gated ion channels, the L-type voltage-gated Ca^{2+} channel currents, and the activities of MAPK and CaMKII, among other photoreceptor activities. Photoreceptors are more sensitive to intense light damage during the subjective night than during the subjective day, even in animals that have been maintained in constant darkness for several days after circadian light–dark cycle entrainment. Several retinal degenerative diseases are associated with dampened or abnormal circadian rhythms in ERGs. In the Royal College of Surgeons rats, the first known animal model with inherited retinal degeneration, the diurnal changes in the c-wave of the ERGs are dampened prior to the beginning of retinal degeneration from postnatal day 17 to 24. Mutations in human cone–rod homeobox (CRX) are associated with retinal diseases, including cone–rod dystrophy-2, retinitis pigmentosa, and Leber congenital amaurosis, which all lead to blindness. In a mouse model of CRX mutation, the circadian rhythmicity of the ERG is abolished, and the mutant mice are not able to be entrained by light–dark cycles. The synthesis and release of dopamine from retinal amacrine cells is also under circadian control, and disruption of the circadian rhythmicity of dopamine synthesis causes a glaucoma-like disorder in quails. Fain and Lisman have proposed that circadian oscillators may provide a common pathway mediating several forms of retinal degeneration. Therefore, dysfunctions of circadian oscillators in the retina contribute to some forms of retinal degeneration, which in many instances may lead to blindness.

See also: Chick Metabolism in the Chick Retina; The Circadian Clock in the Retina Regulates Rod and Cone Pathways; Circadian Rhythms in the Fly's Visual System; Fish Retinomotor Movements; *Limulus* Eyes and Their Circadian Regulation; Neurotransmitters and Receptors: Dopamine; The Photoreceptor Outer Segment as a Sensory Cilium.

Further Reading

Barnes, S. and Jacklet, J. W. (1997). Ionic currents of isolated retinal pacemaker neurons: Projected daily phase differences and selective enhancement by a phase-shifting neurotransmitter. *Journal of Neurophysiology* 77: 3075–3084.

Barnes, S. and Kelly, M. E. (2002). Calcium channels at the photoreceptor synapse. *Advances in Experimental Medicine and Biology* 514: 465–476.

Chae, K. S., Ko, G. Y., and Dryer, S. E. (2007). Tyrosine phosphorylation of cGMP-gated ion channels is under circadian control in chick retina photoreceptors. *Investigative Ophthalmology and Visual Science* 48: 901–906.

Chen, S. K., Ko, G. Y., and Dryer, S. E. (2007). Somatostatin peptides produce multiple effects on gating properties of native cone photoreceptor cGMP-gated channels that depend on circadian phase and previous illumination. *Journal of Neuroscience* 27: 12168–12175.

Green, C. B. and Besharse, J. C. (2004). Retinal circadian clocks and control of retinal physiology. *Journal of Biological Rhythms* 19: 91–102.

Kaupp, U. B. and Seifert, R. (2002). Cyclic nucleotide-gated ion channels. *Physiological Reviews* 82: 769–824.

Ko, G. Y., Ko, M. L., and Dryer, S. E. (2001). Circadian regulation of cGMP-gated cationic channels of chick retinal cones. Erk MAP Kinase and Ca2+/calmodulin-dependent protein kinase II. *Neuron* 29: 255–266.

Ko, G. Y., Ko, M. L., and Dryer, S. E. (2003). Circadian phase-dependent modulation of cGMP-gated channels of cone photoreceptors by dopamine and D2 agonist. *Journal of Neuroscience* 23: 3145–3153.

Ko, G. Y., Ko, M. L., and Dryer, S. E. (2004). Circadian regulation of cGMP-gated channels of vertebrate cone photoreceptors: Role of cAMP and Ras. *Journal of Neuroscience* 24: 1296–1304.

Ko, M. L., Liu, Y., Dryer, S. E., and Ko, G. Y. (2007). The expression of L-type voltage-gated calcium channels in retinal photoreceptors is under circadian control. *Journal of Neurochemistry* 103: 784–792.

Ko, M. L., Liu, Y., Shi, L., Trump, D., and Ko, G. Y. (2008). Circadian regulation of retinoschisin in the chick retina. *Investigative Ophthalmology and Visual Science* 49: 1615–1621.

Michel, S., Manivannan, K., Zaritsky, J. J., and Block, G. D. (1999). A delayed rectifier current is modulated by the circadian pacemaker in Bulla. *Journal of Biological Rhythms* 14: 141–150.

Molday, R. S. and Kaupp, U. B. (2000). Ion channels of vertebrate photoreceptors. In: Stravenga, D. G., Degrip, W. J., and Pugh, E. N., Jr. (eds.) *Molecular Mechanisms in Visual Transduction,* 1st edn., pp. 143–182. Amsterdam: Elsevier Science.

Pugh, E. N., Jr. and Lamb, T. D. (2000). Phototransduction in vertebrate rods and cones: Molecular mechanisms of amplification, recovery and light adaptation. In: Stravenga, D. G., Degrip, W. J., and Pugh, E. N., Jr. (eds.) *Molecular Mechanisms in Visual Transduction,* 1st edn., pp. 183–255. Amsterdam: Elsevier Science.

Tosini, G., Pozdeyev, N., Sakamoto, K., and Iuvone, P. M. (2008). The circadian clock system in the mammalian retina. *BioEssays* 30: 624–633.

Circadian Rhythms in the Fly's Visual System

E Pyza, Jagiellonian University, Kraków, Poland

Glossary

Circadian clock – A cell-autonomous, cyclical autoregulatory molecular mechanism, involving genes – clock genes and their proteins that generate circadian molecular oscillations.
Clock genes – The cyclically, with a cycle about a day, expressed genes engaged in molecular mechanism of circadian clock.
Cryptochrome – A blue-light absorbing protein, which contains a flavin-binding domain and functions as a circadian photoreceptor and an element of the molecular clock in the central and peripheral clocks of *Drosophila*, respectively. In the mammalian circadian clock, cryptochromes are the core clock elements.
Electroretinogram – A record of electric activity of cells, measured by inserting an electrode into the eye.
Entrainment – The synchronization of circadian oscillations of the clock to the external daily changes of day and night or to other cyclically changing environmental cues.
Green fluorescent protein (GFP) – A green-light-emitting protein originally found in *Aquorea victoria* and used, after insertion of its gene in transgenic animals, as a reporter of selected proteins and cell types.
Pigment-dispersing hormones – A family of peptides that regulates migration of pigment granules in the crustaceans' eye and in chromatofores of their body surface and also plays the role of neurotransmitters in circadian systems of crustaceans and insects. In insects, these peptides are called pigment-dispersing factors.
Rhabdomere – A light-absorbing part of the compound eye photoreceptor.
Subjective day – A part of the circadian cycle under constant darkness (DD) or in continuous light (LL) in which previously, in the day/night cycle (LD), was the day.
Subjective night – A part of the circadian cycle under constant darkness (DD) or in continuous light (LL) in which previously, in the day/night cycle (LD), was the night.
Zeitgeber time – A time of the 24-h day/night cycle in the environment measured in hours. Usually ZT0 means the beginning of the day.

The Fly's Visual System

The visual system is a major sensory system for flies and includes the large compound eyes, the ocelli – simple eyes located on the vertex of the head and the optic lobes of the brain. The compound eyes are image-forming eyes, while the ocelli play a role in orientation. In addition to the photoreceptors in the compound eyes and ocelli, light stimuli can be received by extraocular photoreceptors and deep brain photoreceptors.

The most external layer of the compound eye is the retina, which overlies three optic neuropils of the optic lobe: lamina, medulla, and lobula (**Figures 1(a)** and **1(b)**). In flies, the lobula is divided into the lobula and the lobula plate. The retina of the compound eye is composed of many single units called ommatidia whose number depends on the size of the eye. In the housefly *Musca domestica*, the compound eye is composed of 3000 ommatidia, while the fruit fly, *Drosophila melanogaster*, has about 800 ommatidia in each eye. Each ommatidium is composed of eight photoreceptors and six of them, R1–R6, terminate in the first optic neuropil or lamina. The other two photoreceptors, R7 and R8, have axons that bypass the lamina and terminate in the medulla. The light-sensitive pigment in the R1–R6 is the blue-sensitive rhodopsin Rh1, while the visual pigments in R7 and R8 are ultraviolet (UV)-sensitive: Rh3, Rh4, or Rh5.

The lamina also has a modular structure and is composed of cylindrical modules called cartridges (**Figures 1(c)**, **1(d)** and **2**). Each cartridge contains 12 cell types and is surrounded by three epithelial glial cells. Elements of the cartridge include the terminals of photoreceptors R1–R6, the axons and dendrites of the lamina monopolar cells L1–L5, amacrine cell processes, processes of cells located in the medulla, and processes of tangential neurons with cell bodies located in other parts of the brain. The structure and synaptic contacts of the medulla have not been as extensively studied as in the lamina; however,

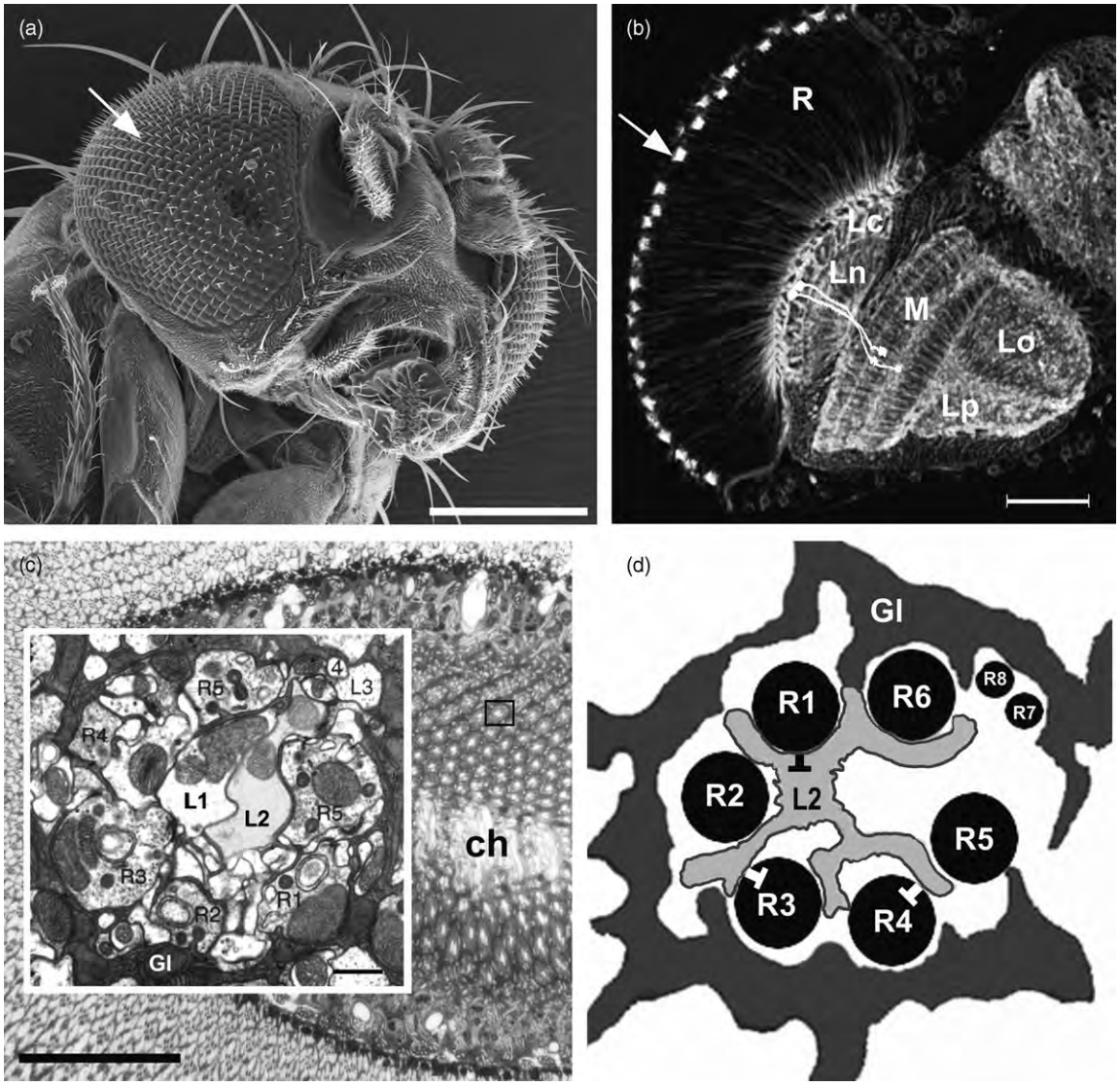

Figure 1 The visual system of *Drosophila melanogaster*. (a) Scanning electron micrograph of the head and compound eye of *Drosophila* viewed from the right side. The fly's compound eye is composed of hexagonally arranged units/facets called ommatidia. Arrow denotes the surface of the compound eye. Scale bar = 200 μm. (b) The structure of the compound eye and optic lobe in horizontal section as revealed by immunostaining with an antibody against α-tubulin. The ommatidial array of photoreceptors in the retina (R) innervates the first of a series of neuropils, the lamina (Ln), where the first-order interneurons, L1 and L2 monopolar cells (marked in white) have their cell bodies and axons. L1 and L2 axons terminate in the second optic neuropil or medulla (M). Lc, lamina cortex; Ln, lamina neuropil; M, medulla; Lo, lobula; Lp, lobula plate. Arrow indicates the surface of the eye. Scale bar = 50 μm. (c) The structure of the lamina in cross section. The lamina is composed of cylindrical modules called cartridges (the region enclosed in a small box), which comprise the same cell types and constitute synaptic units of this neuropil. ch, chiasma. Scale bar = 20 μm. Inset: EM micrograph showing the magnification of a single cartridge with the profiles of L1 and L2 monopolar cells at its axis and the surrounding photoreceptors (R1–R6) and glial cells (Gl). L3: monopolar cell L3; 4: monopolar cell L4. Scale bar = 1 μm. (d) Schematic representation of the lamina cartridge in cross section with the positions of photoreceptors axons (R1–R-8), and the axon of L2 monopolar cell (L2), as well as presynaptic elements (T-bars) of synaptic contacts that are formed between these cell types; tetrad synapses (white T-bars) and feedback synapses (black T-bar). Gl, epithelial glia that surround each cartridge. Reproduced from Pyza, E. and Górska-Andrzejak, J. (2008). External and internal inputs affecting plasticity of dendrites and axons of the fly's neurons. *Acta Neurobiologiae Experimentalis* 68: 322–333.

the medulla is known to consist of columns each of which contains 35 cells. The lobula and the lobula plate are centers for processing motion information, and they contain, among others, 10 individually identifiable vertical system neurons that respond to visual wide-field motions of arbitrary patterns.

The function of the retina is to receive photic and visual information, transduce this information into receptor

potentials, then transmit the information to the lamina by regulating the release of the neurotransmitter histamine at synaptic contacts called tetrad synapses. At these tetrad synapses, photoreceptors R1–R6 contact two large monopolar cells (LMCs), L1 and L2, the major output neurons of lamellar cartridges, and two other postsynaptic elements which may include processes of amacrine cells, epithelial glial cells, and L3 monopolar cell (**Figure 2**). L2 also forms feedback synapses back onto the photoreceptor terminals.

The Fly's Circadian System

Circadian rhythms are self-sustaining oscillations with a period of about 24 h that are maintained in constant conditions, such as constant darkness (DD). These rhythms are not only entrained to the external day/night cycle primarily by light, but they also can be entrained by other environmental cues. The eyes of flies and of other insect species provide light input to the circadian system which controls circadian rhythms in behavior and in physiological and biochemical processes, including those within the visual system. The circadian system in flies is composed of a central clock (pacemaker) located in the brain as well as peripheral clocks located in many tissues throughout the body. All circadian rhythms in the body are synchronized to each other and maintain the organism's homeostasis in time. As will be described in greater detail below, the circadian system controls structural changes within the lamina of the visual system and the numbers of specific synapse, and these changes are correlated with the animal's locomotor activity rhythm.

In *D. melanogaster*, clock genes are expressed in approximately 100 neurons in the brain belonging to seven groups on each side of the brain: small and large ventral

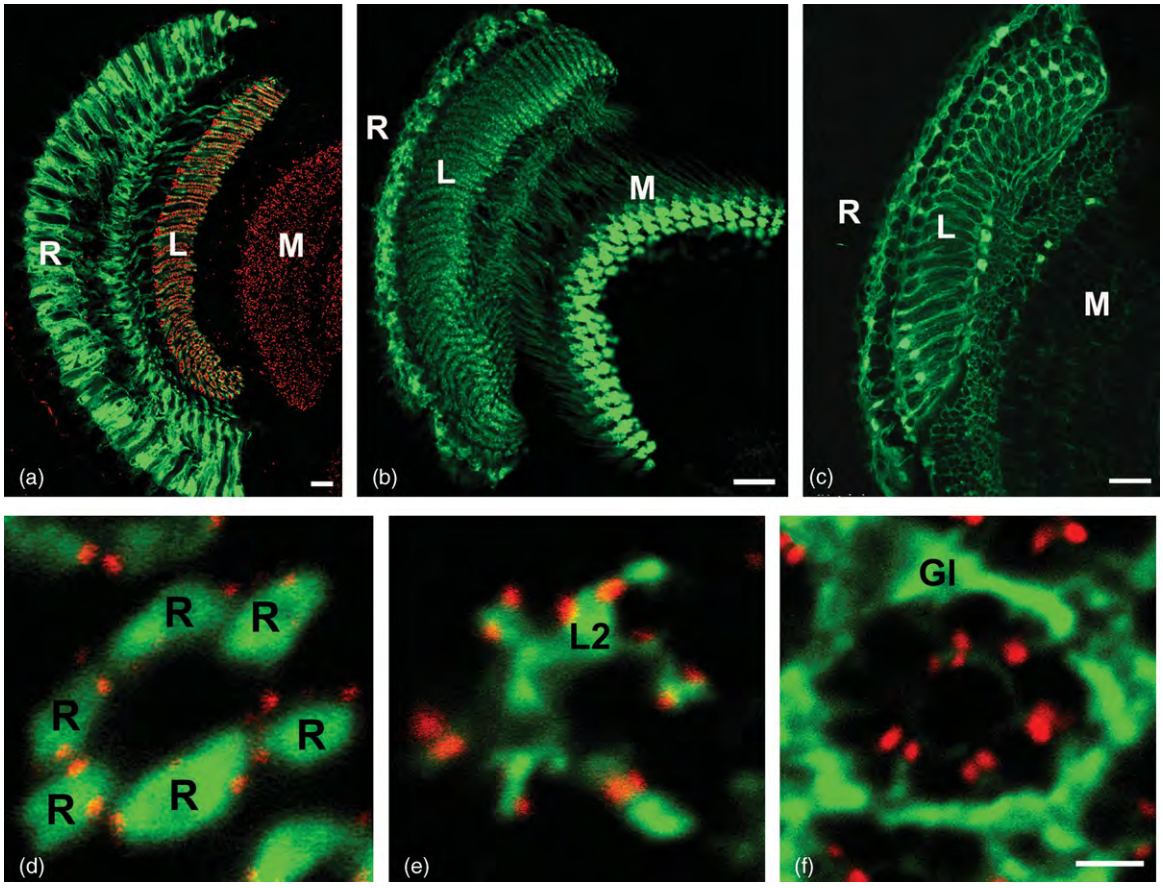

Figure 2 (a–c) Confocal images of frontal cryostat sections through the retina and optic lobes of lines of *Drosophila* showing targeted expression of green fluorescent protein (GFP) (green) in photoreceptors, L2 monopolar cell, and epithelial glial cells, respectively. The section shown in (a) was also immunolabeled with a monoclonal antibody specific for the presynaptic protein Bruchpilot (red). R, retina; L, lamina; M, medulla. Scale bar = 20 μm. (d–f) Cross sections of the lamina cartridges of the GFP (green)-expressing transgenic flies described above. Sections were also immunostained for the presynaptic protein Bruchpilot (red). R: axons of photoreceptors; L2: axon of L2 monopolar cell; Gl: processes of epithelial glial cells. Scale bar = 1 μm. Reproduced from Pyza, E. and Górska-Andrzejak, J. (2008). External and internal inputs affecting plasticity of dendrites and axons of the fly's neurons. *Acta Neurobiologiae Experimentalis* 68: 322–333.

lateral neurons (s-LN_vs and l-LN_vs), dorsal lateral neurons (LN_ds), lateral posterior neurons (LPNs), and three groups of dorsal neurons (DN_1, DN_2, and DN_3). These cell groups constitute the main circadian pacemaker. Four of five s-LN_vs and four l-LN_vs express the neuropeptide pigment-dispersing factor (PDF), the only output neurotransmitter of the circadian system known so far. Peripheral clocks, distributed throughout the animal, generate circadian rhythms in peripheral organs, including antennae, Malpighian tubules, testes, and the retina photoreceptor cells. In contrast to the pacemaker neurons, in which the circadian oscillations of clock gene expression are self-sustained for many days in DD, oscillations in the peripheral clocks decline after several cycles in DD. Thus, the molecular mechanisms underlying central and peripheral clocks may be different.

Circadian clocks are cell autonomous, and a cell is said to contain a circadian clock if it expresses clock genes, those that show circadian expression and control the expression of a large population of other genes (so-called clock-controlled genes). In clock cells, clock genes and their proteins form transcriptional/translational negative- and positive-feedback loops that are the molecular basis of circadian clocks. Much of our understanding of molecular clocks comes from studies of *D. melanogaster*, and our ideas about how these molecular clocks are regulated and entrained continue to be refined. A basic model is presented below and in **Figure 3**.

In central pacemaker clock cells, two cyclically expressed core clock genes are *period* (*per*) and *timeless* (*tim*). When their proteins PERIOD (PER) and TIMELESS (TIM) accumulate in cytoplasm, they form heterodimers and enter the nucleus. In the nucleus, they bind to heterodimers of the transcription factors CLOCK(CLK)/CYCLE(CYC) encoded by *Clock* (*Clk*) and *cycle* (*cyc*) genes, respectively, and PER, and possibly TIM, repress their own transcription. This is the negative-feedback loop of the molecular clock. CLK/CYC also control the cyclical expression of two other core clock genes, *vrille* (*vri*) and *Par domain protein* 1ε (*Pdp*1ε) and their protein products, VRI and Pdp1ε, respectively, regulate the transcription of *clk*. VRI represses the transcription of *Clk* while Pdp1ε enhances it. The increase in *clk* transcription is a positive-feedback loop of the molecular clock. The level of PER and the transition of PER and TIM from the cytoplasm to the nucleus is controlled by phosphorylation so that the transcriptional feedback occurs at a particular time of the day.

Light entrainment of the molecular clock in central pacemaker neurons depends on an intracellular blue-light-photosensitive protein CRYPTOCHROME (CRY). CRY is involved in the light-dependent degradation of TIM. When the light is on, TIM does not accumulate in the cytoplasm, the negative-feedback loop that represses *per* and *tim* transcription is delayed and, as a result, the phase of the clock will be delayed. However, if TIM is degraded, while it is in the nucleus, the repression of CLK/CYC will be removed early, the transcription of *per* and *tim* will be advanced and the phase of the clock will be advanced.

The molecular mechanism in the peripheral clocks is also based on *per* and *tim* cyclical expression; however, in peripheral clocks, CRY may be a central element of the molecular mechanism in addition to its role as a circadian photoreceptor involved in the light entrainment of the molecular clock. It has been suggested that in peripheral clocks of *D. melanogaster*, CRY is a transcriptional repressor playing a role similar to that of CRY proteins (mCRY1 and mCRY2) in mammalian molecular clocks.

Similar circadian systems – consisting of many circadian clocks that are based on a transcriptional/translational feedback loop model – are probably present in other insect species. However, some aspects of the molecular mechanism of the clock may differ in even closely related dipteran species. For example, in *Lucilia cuprina*, the PER expression pattern is similar to that of *D. melanogaster*, but in the housefly, *M. domestica*, PER isolated from the whole head does not cycle.

As was described above, light is the major environmental cue that entrains the central pacemaker to the day/night cycle. The light input to the central pacemaker is complex, and the fly's compound eyes are not the only source. Ocelli photoreceptors, the extraocular photoreceptors known as the Hofbauer–Buchner (H–B) eyelet, and the intracellular blue-light-photosensitive protein CRYPTOCHROME (CRY), which is present in most cells harboring molecular circadian clocks, also provide light input. The H–B eyelet consists of four photoreceptors located between the retina and medulla. These photoreceptors contact the small LN_vs pacemaker neurons and synchronize the molecular rhythms in these neurons. The small LN_vs, in turn, synchronize the animal's behavioral rhythms by the rhythmic release of PDF. Since the pacemaker comprises several groups of neurons, each group may be important for producing circadian rhythms in different cells, tissues, and systems, and receive light inputs from different photoreceptors.

The visual system receives circadian input from pacemakers; however, it is still unknown which group or groups of pacemaker neurons send the circadian input to the visual system. In addition, the visual system possesses peripheral clocks in the retina photoreceptor cells.

Circadian Rhythms in the Retina of the Compound Eye

Most arthropods, including insects, show daily changes in the structure of photoreceptors manifested by changes in the size of the rhabdomere, the photosensitive part of photoreceptors. Moreover, daily changes in screening pigment movements have been documented in many

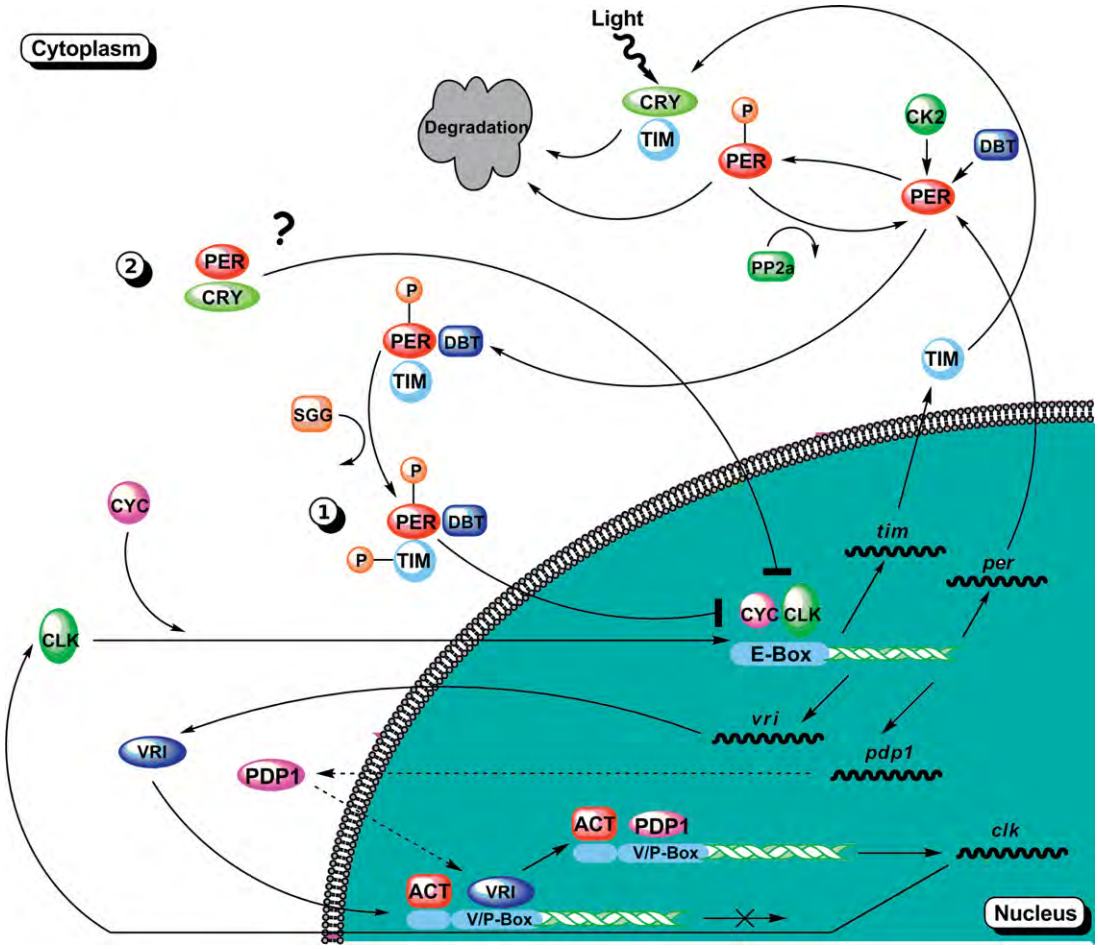

Figure 3 Molecular mechanisms of circadian clocks in *Drosophila*. 1. Current model of the circadian clock operating in the pacemaker neurons in the brain. In this model *period* (*per*) and *timeless* (*tim*) clock genes are cyclically expressed at the end of day and at the beginning of night. Later during the night, PER and TIM proteins accumulate in the cytoplasm and PER is phosphorylated by DOUBLETIME (DBT) and possibly by casein kinase CK2. The phosphorylation leads to PER degradation if TIM does not bind to PER forming PER/TIM heterodimers. PER is also stabilized by PP2a, which dephosphorylates PER. In the heterodimers PER/TIM, TIM is phosphorylated by SHAGGY (SGG) and PER is bound to DBT which enables PER and TIM to be transported to the nucleus. In the nucleus, PER and, possibly, also TIM inhibit transcription factors CYCLE (CYC) and CLOCK (CLK), which as heterodimers repress transcription of *per* and *tim*. Repression of *per* and *tim* transcription by their own proteins constitutes a negative-feedback loop of the molecular clock. CYC/CLK heterodimers also control cyclical expression of *vrille* (*vri*) and *pdp*1ε which proteins affect transcription of *clk* by competing for binding to *clk* promotor. PDP1ε stimulates, while VRI inhibits *clk* expression. The increase in *clk* transcription is a positive loop of the molecular clock. Transcription of *clk* can also be activated by a clock-independent activator, ACT. In this model, CRYPTOCHROM (CRY) protein is a clock photoreceptor. During the day, CRY is activated by light and binds TIM leading to TIM degradation. After TIM degradation PER cannot form heterodimers with TIM in the cytoplasm and be transported to the nucleus. In result, the clock is delayed in phase. When light stimulates the degradation of TIM while TIM is in the nucleus, the repression of *per* and *tim* transcription by PER/TIM is removed and the molecular clock advances in phase. 2. A possible mechanism of circadian clock functioning in peripheral clocks and in a clock controlling circadian rhythms in the visual system. In this model, PER forms heterodimers with CRY which are transported to the nucleus where CRY represses the transcription of *per* and *tim*.

insect and crustaceans species. The most pronounced structural changes in photoreceptors, regulated by a circadian clock, have been described in the horseshoe crab *Limulus polyphemus*. In contrast to crustaceans, locusts, praying mantis, and mosquitoes, the cross-sectional area of rhabdomeres in the retina photoreceptors of flies shows no (*L. cuprina*) or only little (*D. melanogaster*) change during the day and night cycle.

However, in many species, including flies, diurnal rhythms have been detected in the amplitude of the electrical activity of the eye recorded with the electroretinogram (ERG). The ERG originates from both the retina and the lamina L1 and L2 monopolar cells and measures changes in eye sensitivity. In *D. melanogaster*, cyclical changes are observed in both the amplitude of the ERG and the level of visual pigment in photoreceptors as measured by microspectrophotometry. When *D. melanogaster* is maintained under normal LD conditions, the ERG-measured sensitivity and the concentration of visual pigment in photoreceptors are highest during the night. Then about 8 h before

lights-on, the sensitivity begins to decline and, about 2 h after lights-on, the level of visual pigment in the eye starts to decrease. The sensitivity and the level of visual pigment continue to decrease until 4 h after the onset of the light. In white-eye *D. melanogaster* mutants, the level of visual pigment recovers 2–4 h later. The observations that changes in ERG sensitivity and visual pigment levels anticipate changes in illumination, and that these cyclic changes are maintained in DD conditions indicate both processes are under circadian control.

In the blowfly *Calliphora vicina*, a diurnal insect, three ERG components have been studied under LD and DD conditions; one component called the sustained negative potential originates at least partly from the retina photoreceptors, and two others, ON and OFF transients, originate from the lamina monopolar cells. The lamina transients exhibit circadian oscillations and increase during the subjective night in DD. The negative potential that originates from the retina changes in antiphase with the transients and becomes smaller during the subjective night, indicating that the retina and the lamina components of ERG seem to be regulated by two different circadian clocks. In the cockroach *Leucophaea maderae*, a nocturnal insect, the opposite changes to those recorded in the blowfly have been observed, and the negative potential of ERG in this species exhibits the highest amplitude during the subjective night. The changes in the ERG observed in these two different species indicate that the photoreceptor activity is correlated with the animal's pattern of locomotor activity. This activity is higher during the day than at night in diurnal insects and higher at night in nocturnal insects.

In addition to regulating the content of visual pigment in insect photoreceptors, circadian clocks may regulate phototransduction by controlling the expression of some genes such as the one that encodes a transient receptor potential channel involved in this process.

Much evidence indicates that retinal photoreceptors are themselves peripheral clocks. They show daily changes in the abundance of the clock protein PER that are maintained in DD conditions and they express other clock genes, including *cry*. As in the pacemaker neurons in the brain, the abundance of PER in the photoreceptors is highest at the end of the night. In photoreceptors, however, PER decays faster during the day than in the *per*-expressing neurons in the brain. The rhythmic changes in PER immunostaining in the photoreceptors are also affected by *per* mutations. For example, in flies expressing the per^{s} mutation, in which the period of circadian locomotor activity is shorter (19 h) than 24 h, PER in photoreceptors appears earlier than in wild-type flies. Evidence that the circadian clocks in retinal photoreceptors are cell autonomous comes from experiments that used transgenic *D. melanogaster* in which PER was expressed only in photoreceptors. In these animals, cyclic PER expression was observed in photoreceptors in DD condition, even though no PER expression was detected elsewhere in the animal and the animals were otherwise arrhythmic. Although the retinal photoreceptors possess autonomous circadian clocks, it is unknown to what extent these clocks control the rhythms observed in photoreceptors. Again, it is unknown if the clocks in the fly's retina impact the rhythms in cells that are postsynaptic to the photoreceptors.

Circadian Rhythms in the First Visual Neuropil (Lamina)

Although structural changes in the photoreceptor cell bodies of flies are not dramatic, striking circadian rhythms have been detected in the lamina of the fly's visual system. Here, the number of synaptic contacts, the morphology of two visual interneurons, and the number of some organelles in the photoreceptor terminals change during the LD and DD conditions. These rhythms are examples of plasticity in the nervous system regulated by a circadian clock, and they may serve to gate the flow of information through the visual system to correlate with the animal's locomotor activity.

Since clock gene expression has not been detected in the lamina neurons, circadian rhythms observed in the lamina must be driven by circadian pacemaker neurons located in the brain and/or clocks present in the retina photoreceptors. These rhythms may also be maintained by clock-gene-expressing glial cells distributed between neurons and other glial cells in the optic neuropils.

Circadian Plasticity of Synaptic Contacts

In the lamina of the housefly *M. domestica*, cyclic changes have been found in the frequency of two types of synaptic contacts: tetrad presynaptic profiles or the so-called T-bars, and feedback synapses (**Figure 1(d)**). In the housefly, which is a diurnal species, the number of tetrad presynaptic profiles is highest at the beginning of the day when the flies also show the highest locomotor activity. In contrast to the tetrads, the number of feedback synapses peak at the beginning of the night. The oscillations in the number of feedback synapses are maintained in DD and are not affected by light. Therefore, they are clearly controlled by circadian clocks. By contrast, the number of tetrad synapses does not significantly change in DD, but increases after a 1-h light pulse presented during the subjective day or subjective night in DD. This could be interpreted to mean that the number of tetrad synapses is controlled by light, not by circadian clocks. However, studies with *D. melanogaster* suggest that circadian clocks are important regulators of the number of tetrad synapses.

In *D. melanogaster*, daily oscillations have been found in the abundance of a scaffolding protein of the T-bar ribbon in presynaptic tetrad synapses, the BRP protein encoded by the *Bruchpilot* gene (**Figure 2**). As in the housefly, the number of presynaptic sites immunoreactive to BRP and the abundance of the protein in the lamina are highest at the beginning of the day. This rhythm was not detected in DD, but it was also absent in cyclic light in the arrhythmic *per* null mutant. Taken together, these observations indicate that although the daily rhythm in the formation of T-bar presynaptic tetrads depends on light, signals from circadian clocks are also required.

Circadian Plasticity of Second-Order Neurons and Glial Cells

The daily oscillations in the frequency of photoreceptor tetrad synapses are correlated with morphological changes in the L1 and L2 monopolar cells of the lamina. In the housefly, both cells swell at the beginning of the day and shrink during the night, and this rhythm is maintained in DD and also in LL, a condition that disrupts circadian rhythms in behavior, causing animals to become arrhythmic. Examination of the morphology of the entire L2 cells in transgenic *D. melanogaster*, in which green fluorescent protein (GFP) was expressed specifically in L2 cells (**Figures 2(b) and 2(e)**), has shown that circadian changes occur in the girth of axons and in the length of dendrites extending from these axons (**Figure 4**). The daily pattern of morphological changes of the L2 is slightly different in males than in females. Circadian changes also occur in the size of L2 nuclei but not in their cell bodies (**Figure 4**).

Changes in the size of monopolar cell axons are correlated with the pattern of the locomotor activity of fly species. In typically diurnal species such as *M. domestica* and *C. vicina*, L1 and L2 monopolar cell axons are largest at the beginning of the day when flies show highest locomotor activity. The sizes of these axons can be further increased, by 20–30%, when insects are additionally stimulated to fly intensively. In *D. melanogaster* the daily pattern of changes in sizes of L1 and L2 axons is different. Under LD, *D. melanogaster* has two peaks in locomotor activity, one in the morning and a second one in the evening, and in this species, the L1 and L2 cell axons enlarge twice during the day, in the morning and in the evening. Changes in size of L1 and L2 monopolar cell axons are offset by changes in size of the surrounding epithelial glial cells, which shrink during the day and swell during the night. Changes in the girth of L1 and L2 interneuron axons seem to be correlated with the perimeter of their dendritic trees. Studies of transgenic

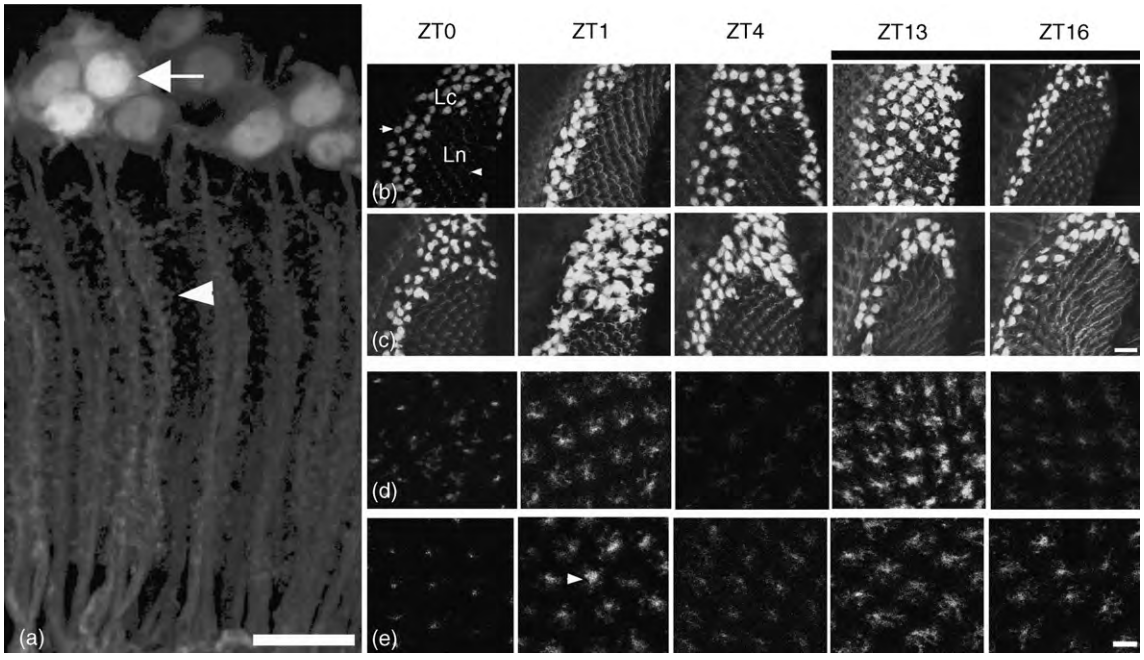

Figure 4 Daily changes in morphology of L2 monopolar cell in the lamina of transgenic *D. melanogaster* expressing GFP in the L2 cells (21D-GAL4/UAS-S65T-GFP). (a) Confocal image showing the structure of L2 monopolar cells in the lamina. GFP expression labels nuclei of the somata (arrow) in the lamina cortex, as well as axons and dendrites (arrowhead) in the neuropil. Scale bar = 10 μm. (b, c) Daily changes (ZT0-ZT16, ZT0: the beginning of the day. ZT 13: the beginning of the night, dark bar) in the size of L2 cell nuclei in males (b) and females (c). The cross-sectional area of the nuclei appears to be largest 1 h after lights-on (ZT1, females) and 4 h after lights-on (ZT4, males) and smallest in the middle of the night (ZT16, females and males). Scale bar = 20 μm. (d, e) Differences in morphology of the dendritic tree of L2 in males (d) and females (e). The cross-sectional area of L2 monopolar cell axons is larger at ZT1 and ZT13 than in other time points in both males and females. Scale bar = 5 μm. Reproduced from Pyza, E. and Górska-Andrzejak, J. (2008). External and internal inputs affecting plasticity of dendrites and axons of the fly's neurons. *Acta Neurobiologiae Experimentalis* 68: 322–333.

D. melanogaster, in which GFP is expressed specifically in L2 monopolar cells, revealed that the L2 dendrites postsynaptic to tetrad synapses are longest at the beginning of the day. This rhythm is absent in arrhythmic *per* null mutant flies (per^0), and its pattern is changed from wild-type in mutant flies harboring a mutation in the CRY protein (cry^b). These findings indicate that circadian plasticity of the L2 cells depends on cyclical expression of *per* and involves *cry* in maintaining the phase of the rhythm.

In contrast to L1 and L2 monopolar cells, photoreceptor terminals in the lamina do not change their girth. It is unknown, however, if other monopolar cells in the lamina show similar morphological circadian changes.

Circadian Rhythms in Organelles inside Photoreceptor Terminals

Although photoreceptor terminals in the lamina do not show circadian changes in their size, circadian structural changes have been detected in some organelles inside the terminals. For example, in the housefly, there is a vertical migration of pigment granules into and out of photoreceptor terminals. Radial movements of screening pigment within the cell bodies of photoreceptors R1–R6 are well documented. These movements are driven by light. Pigment granules move horizontally toward the rhabdomeres during light adaptation and away from the rhabdomeres during dark adaptation providing an important pupillary mechanism. However, the vertical migration of pigment granules in the housefly photoreceptors appears regulated by a circadian clock. Fewer pigment granules are present in photoreceptor terminals during the day compared to the night. This rhythm is maintained in DD, thereby indicating its endogenous, circadian regulation. These vertical movements of pigment granules may play a role in light adaptation providing more pigment granules to the photoreceptor cell bodies during the day.

Other organelles in the housefly photoreceptor cell terminals are formed from the invaginations of neighboring cells in the lamina: from other photoreceptor terminals and glial cells. Among these two types of invaginations, only the number of inter-receptor invaginations changes during the subjective day and subjective night in DD, and the number is greatest at the end of the subjective night. These organelles are rare in the photoreceptor terminals in flies reared in LD conditions, but increase in dark-reared flies. Their functions remain to be discovered.

Neurotransmitter Regulation of Circadian Rhythms in the Visual System

The lamina is invaded by several sets of wide-field tangential neurons with processes directed at right angles to the lamellar cartridges; thus, they are appropriately suited for the global regulation of visual processing. In the housefly's lamina, the most numerous of these processes are immunoreactive for serotonin (5-hydroxytryptamine, 5-HT). They originate from two giant ventral protocerebral neurons called LBO5-HT that project ipsi- and contralaterally to the optic lobes. Another group of processes is immunoreactive for PDF and originates from the LNvs. Still other processes are immunoreactive for the neuropeptide Phe-Met-Arg-Phe-NH_2 (FMRFamide). The neurotransmitter chemistry of remaining processes remains to be identified.

Processes of LBO5-HT neurons are also present in the lamina of *D. melanogaster*, but in this species, processes of other wide-field neurons, including PDH-immunoreactive processes, arborize in the distal medulla and only a few reach the lamina. Since the paracrine release of both biogenic amines and neuropeptides has been reported, neuromodulators released in the medulla may reach targets in the lamina of the fruit fly through volume transmission.

Among neurotransmitters detected in the lamina and the medulla, 5-HT has been found to influence both photoreceptors and L1 and L2 monopolar cells. 5HT modulates potassium channels in the photoreceptors of *D. melanogaster*, and in photoreceptors of locust, a diurnal modulation of potassium channel function can be mimicked by application of 5-HT. In the lamina of the housefly, 5-HT has robust effects on the structure of L1 and L2 cells, but the effects are not the same on both cells. Injections of 5-HT into the housefly's medulla increase the diameter of L1 but not L2 monopolar cell axons. However, when 5-HT and other biogenic amines are depleted from the lamina by injecting the drug reserpine, there is a decrease in the girth of the L2 axon but not in the axon of the L1 cell. This suggests that 5-HT influences the diameter of both L1 and L2 axons, but that the effects observed depend on its concentration.

Injections of other neurotransmitters into the medulla also affect L1 and L2 axon sizes, but their effects are less significant than that of 5-HT. PDF injections induce a small increase of both cells, while FMRFamide had the opposite effect. PDF applications also have an effect on the screening pigment granules in the photoreceptor terminals. Injections of histamine, a neurotransmitter released from photoreceptor terminals, increase the size of L1 but not L2 processes, while injections of either glutamate or gamma aminobutyric acid (GABA) decrease L1 and L2 axons. The effects of glutamate and GABA mimic the changes in L1 and L2 processes seen during the night under LD conditions and during the subjective night in flies held in constant darkness. Glutamate is a transmitter candidate for the L1 and L2 cells and amacrine cells of the lamina, and GABA is detected in cells that project from the medulla into the lamina. GABA injections also decreased the number of feedback synapses from L2 onto photoreceptors.

Larval Visual System

Circadian rhythms in the visual system exist not only in adult flies but also in larvae. The larval visual system, Bolwig's organ (BO) is located on both sides of the head and consists of 12 photoreceptors expressing either Rh-5 or Rh-6. All these photoreceptors project to the LNs of the larval circadian system, which includes four neurons on each side of the fruit fly's larval brain. The BO photoreceptors do not express clock genes, so they are not circadian oscillators like the retina photoreceptors; instead, the BO photoreceptors receive circadian information from the LNs as do other target neurons. The circadian input from the LNs seems to control sensitivity of the larval visual system since the *per* and *tim* null mutants are relatively insensitive to light, while mutations in the positive clock elements, *Clk* and *cyc*, increase the light sensitivity of larvae. In *D. melanogaster* larvae, the circadian clock regulates the light-avoidance behavior and visual sensitivity. Both are high at the end of the subjective night and low at the end of subjective day in DD conditions.

The BO photoreceptors survive metamorphosis, and in the adult fly, Rh6-expressing photoreceptors correspond to the extraocular photoreceptors of the H–B eyelet. In larvae and in adults these structures play an active, if subsidiary, role in the entrainment of circadian rhythms. In larvae, light is transmitted from the BO to the LNs where light-induced degradation of TIM is essential for the larval circadian clock entrainment. Moreover, when BO is eliminated, the LN dendrite structure is altered indicating direct interactions between the larval visual system and the larval circadian system. The larval optic nerve is also required for the development of a serotonergic arborization originating in the central brain and for the development of the dendritic tree of the circadian pacemaker neurons – the small LN_vs. The larval optic nerve and adult extraocular photoreceptors sequentially associate with the small LN_vs during *D. melanogaster* brain development.

Circadian Circuits in the Fly's Visual System

In flies, circadian rhythms in the visual system are correlated to the circadian rhythm in locomotor activity. This indicates that circadian oscillators, both central and peripheral, must communicate with each other, but the underlying circuitry is largely unknown. The circadian rhythms in the retina seem to depend mostly on the peripheral clocks inside the photoreceptors, although pacemaker neurons could impact rhythms in the retina by controlling the number of feedback synapses from L2 onto photoreceptor terminals. As it was described above, these synapses show robust circadian changes. However, it is unclear if the rhythms in the lamina, and probably in the other optic neuropils, are regulated only by the LNs or by both the photoreceptor's clocks and the LNs. It is also unknown if the dorsal neurons, DN_1–DN_3, have any effects on the circadian rhythms in the visual system.

In the housefly, severing the optic lobe from the rest of the brain abolishes circadian changes in the sizes of the L1 and L2 monopolar cell axons. This suggests that circadian information is transmitted to lamina monopolar cells from central pacemaker neurons by neurotransmitters. So far, the only neurotransmitter identified in the pacemaker neurons is PDF, which is present in the LNvs of *D. melanogaster* and in a similar set of neurons in *M. domestica*. In the housefly, this peptide is cyclically released from PDF varicosities in a paracrine fashion. In this species, the circadian changes of PDF varicosity sizes have been observed in LD and DD, and the daily release of PDF from the dense-core vesicles of PDF-immunoreactive processes have been detected. If PDF, which has been detected in dense arborizations in the medulla of all fly species studied and clearly in the lamina of larger flies, transmits circadian information from the LNvs, then PDF receptors should be present in neurons in this part of the visual system. However, PDF receptors have not been detected in the distal part of the medulla or in the lamina, but in the proximal medulla and in the lobula. In *D. melanogaster*, however, the processes of PDF-immunoreactive l-LN_vs terminate in the distal medulla next to *per*-expressing glial cells, which may intermediate between the pacemaker neurons and neurons in the lamina cartridges showing circadian plasticity. Thus, glial cells in the optic lobe might be the third player in the regulation of circadian rhythms in the visual system. In the lamina, the epithelial glial cells change their sizes, decreasing during the day and increasing during the night, completely opposite to the neurons. Disrupting glial metabolism and closing gap-junction channels in the lamina have an effect on L1 and L2 monopolar cell sizes and their circadian morphological plasticity.

The Role of Circadian Clocks in the Visual System

The autonomous circadian oscillators located in retina photoreceptors, and clocks in the pacemaker neurons and in glial cells of the optic lobe, provide a circadian gating of visual information. This gating changes during the day and night and differs between diurnal and nocturnal animals. The activity of the visual system is the highest during the day in diurnal species and during the night in nocturnal species. Furthermore, this pattern correlates with the pattern of locomotor activity in each species. Because of the circadian gating of visual information, light stimuli received during the night in diurnal species

do not disrupt its daily rhythm of activity and the daily pattern of animal behavior, but light stimuli can shift the phase of these rhythms. On the other hand, stressful conditions in the environment and a temporary increase in locomotor activity can result in an increase of the flow of information through the visual system, but only when this stimulation is correlated with the active period of the daily rest (sleep)/activity rhythm. Locomotor stimulation, however, may also shift the phase of the rhythm.

In addition to the gating visual information, the circadian system allows an organism to predict daily changes in the environment, and to prepare the visual and other sensory systems for a proper reception of sensory stimuli and efficient transmission of sensory information. The circadian clocks in the photoreceptors control the reception of light stimuli, while the transmission of sensory information is controlled by clocks in several types of cells, including the retina photoreceptors, the pacemaker neurons, and glial cells. These properties of the circadian and visual systems are typical not only for flies but also for other animals.

See also: Chick Metabolism in the Chick Retina; The Circadian Clock in the Retina Regulates Rod and Cone Pathways; Circadian Regulation of Ion Channels in Photoreceptors; Fish Retinomotor Movements; Genetic Dissection of Invertebrate Phototransduction; *Limulus* Eyes and Their Circadian Regulation; Retinal Degeneration through the Eye of the Fly.

Further Reading

Battelle, B. A. (2002). Circadian efferent input to *Limulus* eyes: Anatomy, circuitry, and impact. *Microscopy Research and Techniques* 15: 345–355.

Collins, B. and Blau, J. (2007). Even a stopped clock tells the right time twice a day: Circadian timekeeping in *Drosophila*. *Pflügers Archives – European Journal of Physiology* 454: 857–867.

Hall, J. (2003). Genetics and molecular biology of rhythms in *Drosophila* and other insects. *Advances in Genetics* 48: 1–280.

Hardie, R. C. (2001). Phototranduction in *Drosophila melanogaster. Journal of Experimental Biology* 204: 3403–3409.

Hardin, P. E., Krishnan, B., Houl, J. H., et al. (2003). Central and peripheral circadian oscillators in *Drosophila*. In: Chadwick, D. J. and Goode, J. A. (eds.) *Novartis Foundation Symposia 253: Molecular Clock and Light Signalling*, pp. 140–150. Hoboken, NJ: Wiley.

Marrone, D. F., Boutillier, J. C., and Petit, T. L. (2005). Morphological plasticity of the synapse. Interaction of structure and function. In: Stanton, P. K., Bramham, C., and Scharfman, H. E. (eds.) *Synaptic Plasticity of Transsynaptic Signaling*, pp. 495–518. New York: Springer.

Meinertzhagen, I. A. and Pyza, E. (1999). Neurotransmitter regulation of circadian structural changes in the fly's visual system. *Microscopy Research and Techniques* 45: 96–105.

Meinertzhagen, I. A. and Sorra, K. E. (2001). Synaptic organization in the fly's optic lamina: Few cells, many synapses and divergent microcircuits. In: Kolb, H., Ripps, H., and Wu, S. (eds.) *Progress in Brain Research*, vol. 131, pp. 53–69. Amsterdam: Elsevier Science.

Pyza, E. (2001). Cellular circadian rhythms in the fly's visual system. In: Denlinger, D. L., Giebultowicz, J., and Saunders, D. S. (eds.) *Insect Timing: Circadian Rhythmicity to Seasonality*, pp. 55–68. Amsterdam: Elsevier Science.

Pyza, E. (2002). Dynamic structural changes of synaptic contacts in the visual system of insects. *Microscopy Research and Techniques* 58: 335–344.

Pyza, E. and Górska-Andrzejak, J. (2008). External and internal inputs affecting plasticity of dendrites and axons of the fly's neurons. *Acta Neurobiologiae Experimentalis* 68: 322–333.

Sehgal, A. (ed.) (2004). *Molecular Biology of Circadian Rhythms*. Hoboken, NJ: Wiley.

Tosini, G., Pozdeyev, N., Sakamoto, K., and Iuvone, P. M. (2008). The circadian clock system in the mammalian retina. *BioEssays* 30: 624–633.

Townes-Anderson, E. and Zhang, N. (2006). Synaptic plasticity and structural remodeling of rod and cone cells. In: Pinaud, R., Tremere, L. A., and De Weerd, P. (eds.) *Plasticity in the Visual System: From Genes to Circuits*, pp. 13–32. New York: Springer.

Relevant Websites

http://flybase.org – FlyBase: A Database of Drosophila and Genomes.
http://flybrain.neurobio.arizona.edu – Flybrain: An Online Atlas and Database of the *Drosophila* Nervous System.

Color Blindness: Acquired

D M Tait and J Carroll, Medical College of Wisconsin, Milwaukee, WI, USA

Glossary

Blue–yellow (tritan) defect – A color-vision deficiency in which colors along the blue–yellow axis are difficult to distinguish from one another and sensitivity to blue light is decreased. This is typically caused by a defect in the short-wavelength-sensitive cone photoreceptor pathway. The word tritanopia derives from the Greek *tritos*, meaning third, alluding to the defect being associated with the third of the three primary colors (blue) + *anopia*, meaning blindness.

Deuteranopia – A type of red–green defect in which the middle-wavelength-sensitive photopigment is nonfunctional, leading to decreased hue discrimination and a tendency to confuse reds and greens. Derives from the Greek *deuteros*, meaning second, alluding to the defect being associated with the second of the three primary colors (green) and *anopia*, meaning blindness.

Monochromacy – A complete lack of ability to distinguish colors.

Photopigment – A light-sensitive protein in the photoreceptors (rods and cones) that undergoes a conformational change when absorbing light and initiates the process of visual transduction.

Protanopia – A type of red–green defect in which the long-wavelength-sensitive photopigment is nonfunctional, leading to a loss of sensitivity to red light and a tendency to confuse reds and greens. Derives from the Greek *protos*, meaning first, alluding to the defect being associated with the first of the three primary colors (red) and *anopia*, meaning blindness.

Trichromacy – The fundamental ability to see in full color, based on the possession of three types of cone photoreceptor. The formal proposal of this theory to explain human color vision is credited to Thomas Young.

Introduction

"He *knew* the colors of everything, with an extraordinary exactness (he could give not only the names but the numbers of colors as these were listed in a Pantone chart of hues he had used for many years). He could identify the green of Van Gogh's billiard table in this way unhesitatingly. He knew all the colors in his favorite paintings, but could no longer see them, either when he looked or in his mind's eye. Perhaps he knew them, now, only by verbal memory." Oliver W. Sacks describes the 'Case of the colorblind painter' in his book *An Anthropologist on Mars* where after a car accident a painter tragically lost all ability to experience color.

While many color-vision deficiencies are inherited and present from birth (congenital), they may also be acquired, as in the case of the colorblind painter described above. Acquired defects, as the name implies, indicate a disruption in color discrimination as a consequence of a traumatic event, such as exposure to toxins, a cortical injury, or the defect may accompany an ocular disease. In most cases, the color-vision defect can be thought of as secondary because the causative event often has more serious consequences for the individual.

Classifying Acquired Color Blindness

Normal color vision relies on the presence of three spectrally distinct cone photoreceptor types in the retina, where the spectral sensitivity of the cone cell is determined by the photopigment it contains (short-, middle-, or long-wavelength sensitive; S, M, or L, respectively). Inherited disruptions in color discrimination are normally classified according to which of the cone photopigment classes is functionally disrupted or absent altogether. A defect in the S photopigment produces a tritan defect, corresponding to a loss along the blue–yellow axis, whereas defects in the M and L pigments produce a deutan or protan defect, respectively, though both correspond to a loss along the red–green axis of color vision. Consequently, in inherited defects there is a 1:1 relationship between the affected cone type and the perceptual deficit. However, acquired defects are far more complex and thus must be categorized not by the type of photoreceptor affected, but rather as a variable loss along a particular color axis: blue–yellow axis, red–green axis, or a nonspecific loss of color vision. The dimensionality of these losses can be appreciated by looking at **Figure 1** which illustrates the red–green and blue–yellow axes of color vision.

In addition to classifying the perceptual problems associated with acquired defects, they can be categorized based on the mechanism of the defect: absorption, alteration, and reduction. Absorption defects affect the absorption of a

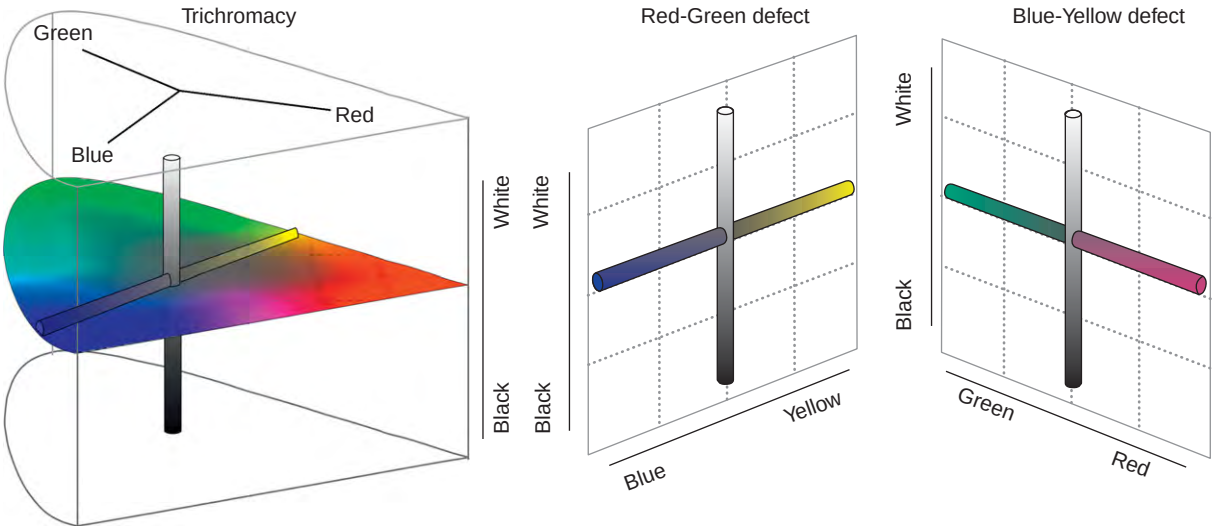

Figure 1 The geometric reduction of color discrimination that accompanies color-vision defects. Possession of three types of cone photopigment makes trichromatic color vision possible. In this case, there is good color discrimination along three distinct axes (black–white, red–green, and blue–yellow) and each discriminable hue (of which there are over 2 million) has a unique combination of activity along each of these axes (left). Acquired color-vision defects can typically be characterized by a loss along the blue–yellow or red–green axis. In red–green defects (middle), color vision is reduced to only the black–white and blue–yellow axes, reducing the dimensionality of color vision (c. 10 000 discriminable hues). Blue–yellow defects (right) show the same reduction in dimensionality. However, the residual color discrimination exists along the red–green and black–white axes. Modified from Neitz, J., Carroll, J., and Neitz, M. (2001). Color vision: Almost reason enough for having eyes. *Optics and Photonics News*, January 2001, pp. 26–33.

particular hue due to deposits affecting the lens or cornea. For example, the normal aging process introduces a yellowing of the lens of the eye, causing a selective absorption defect in discrimination in the blue–yellow axis of color vision. An alteration defect is one that shifts normal color perception and normally reflects a destruction of the macular cones. A reduction defect occurs typically as a result of diseases of the optic nerve and causes perceptive reduction of saturation within colors along the red–green axis as well as a more mild blue–yellow reduction.

Discriminating Acquired from Inherited Color Blindness

There are a number of key differences between inherited and acquired defects. Acquired defects are often difficult to classify because combined, and sometimes subtle, defects often occur. While congenital color-vision deficiencies are typically stable throughout life and both eyes are equally affected, acquired deficits may change in severity over time, and they are more likely to be asymmetric. Furthermore, acquired defects are predominantly tritan, have an equal incidence in males and females, and are typically accompanied by a reduction in visual acuity. Erroneously, color-vision defects are often thought of as being exclusively inherited. However, acquired defects are even more common, with 5% of the population being affected. Table 1 provides a complete comparison of acquired and inherited defects.

Table 1 General differences between acquired and inherited color-vision defects

Acquired color-vision defects	*Inherited color-vision defects*
Acquired after birth	Present at birth
May progress with age	Stable throughout life span
Combined defects may occur making diagnosis difficult	Precise diagnosis of a given type (protan, deutan, tritan)
Monocular deficiencies can occur	Both eyes are equally affected
Visual acuity is often reduced	Visual acuity is unaffected (except in achromatopsia and blue-cone monochromacy)
Predominantly tritan deficiencies	Predominantly red–green deficiencies
Equal incidence in males and females	Higher incidence in males
Frequency (1 in 20 individuals)	Frequency (1 in 12 males affected with red–green defect)

Clinically, there are a number of tests used to diagnose color-vision defects (acquired or inherited). While genetic tests are obviously the definitive approach for characterizing inherited disorders, the diagnosis of acquired color-vision defects relies on the patients' performance on psychophysical tests of color vision. Perhaps the most

widely used are pseudoisochromatic plate tests. These plates contain a field of dots that vary in luminance, and embedded within the dots is a number or other shapes differing in chromaticity from the background. For normal trichromats, this shape will be distinguishable from the background. However, depending on the design of the plate, the shape may blend into the background or a different shape may appear altogether for the color-deficient observer. Different plates are used to test for defects along the primary color axes (red–green and blue–yellow). Another type of test is an arrangement test in which the patient orders materials in a specific hue or saturation order. The stimulus is prearranged in a random order and subjects are instructed to arrange the stimuli according to color. Correct arrangement of the various color samples requires not only normal color vision, but also good discriminative ability. Finally, the gold standard in assessing color vision is color matching. By asking the patient to match either a monochromatic yellow test light to a mixture of red and green primaries (Rayleigh match) or a cyan/yellow test mixture to a blue/green primary mixture (Moreland match), one can detect even the most mild red/green or blue/yellow defect, respectively.

Conditions Resulting in an Acquired Color-Vision Defect

Ocular Diseases

The most common acquired color-vision deficiencies arise from various diseases which can impact the eye in a number of ways. Such diseases include progressive cone dystrophies, retinal pigment epithelium (RPE) dystrophies, ocular media opacities, and impairments that affect the retinal neurons (ganglion cells). As a group, these deficiencies can be characterized by an abnormal cone electroretinogram (ERG), reduced visual acuity, central visual-field loss, and/or light sensitivity (photophobia). The age of onset, severity of color-vision defect, and rate of progression can vary widely among different diseases. A few of the most common diseases are discussed below. As an aside, the color-vision defect is often the least of these patients' worries; nonetheless, it is affiliated with the disease (which itself may be an inherited condition) and can sometimes contribute to the diagnosis.

Age-related macular degeneration

Age-related macular degeneration (AMD) is the leading cause of blindness in the developed world. As such, it also represents the most prevalent form of acquired color-vision deficiency. Although this disease has two forms (wet and dry), both involve a degeneration of the photoreceptors in the central retina (macula). It is in this area where acuity and color vision are at their best, so it comes as no surprise that individuals with AMD suffer deficits in both. In the slower-progressing dry form of AMD, yellow deposits called drusen develop underneath the macula. As these drusen negatively affect the health of the RPE, which is required for normal function of the photoreceptors, a loss of vision slowly results. In the fast-progressing wet AMD, tiny blood vessels begin to grow behind the retina toward the macula. Bleeding, leaking, and scarring occur from these fragile blood vessels, eventually causing irreversible damage to the retina and rapid vision loss. Color vision becomes progressively distorted as the disease progresses and more photoreceptors are functionally compromised, but this does not usually contribute to the differential diagnosis.

Glaucoma

The term glaucoma represents a group of diseases of the optic nerve characterized by a loss of retinal ganglion cells with a corresponding loss of some or most of the fibers of the optic nerve. In this disease, constriction of the visual field occurs slowly over time, and may not be recognized until the impairment is quite severe, with as many as 60% of the retinal ganglion cells degenerating before a perceptual consequence is detected. Worldwide, glaucoma is the second leading cause of blindness, and interestingly the deterioration in color vision of these patients has been proposed as a predictor of significant visual-field loss. Field loss arises from diffuse changes in the neural retina, supporting the idea that acquired color deficiency in glaucoma is caused by damage to the neural pathway rather than the retinal photoreceptors. Despite these patients having a normal S-cone ERG, acquired tritanopia (with severity paralleling the visual-field loss) is often found. This tritan deficiency is consistent with other optic nerve diseases, which suggests that the S-cones themselves remain intact, but that postreceptoral mechanisms involved in the transmission of blue–yellow color discrimination must be selectively disrupted.

Retinitis pigmentosa

Retinitis pigmentosa (RP) is a hereditary retinal dystrophy in which abnormalities of the rods, or the RPE of the retina, lead to progressive visual loss. Affected individuals first experience night blindness and defective dark adaptation, followed by reduction in peripheral vision (tunnel vision), and often a loss of central vision late in the course of the disease. There is good evidence that the progressive degeneration of the rods leads to the secondary loss of cones, likely as a result of reduced rod-derived cone viability factors. Disruptions in color discrimination can occur as the cones degenerate, and these individuals can exhibit a severe tritan defect or occasionally pseudoprotanomaly (a mild red–green defect). Most RP sufferers eventually go blind, therefore again the color-vision defect is of relatively minor importance to the individual.

Cataract

An age-related cataract is an impairment of the crystalline lens of the eye in which the lens hardens, becomes opaque, and yellows. A normal lens selectively absorbs short-wavelength light, however, both normal aging and the development of cataracts enhance this effect and causes problems discriminating in the blue–green portion of the spectrum. This condition is known as xanthopsia and refers to an abundance of yellow which dominates the visual scene. Patients who have cataract surgery in which their natural lens is removed and replaced with a clear plastic lens often experience cyanopsia – or a blue-dominated visual scene. This cyanopsia results because the brain compensates the perceptual yellow tint caused by the cataract by adding a blue tint to the visual scene, and when the yellow lens is removed it takes the brain time to renormalize to the new chromatic input. The mild-blue perception after cataract removal may persist for weeks or even months but normal color vision gradually returns, highlighting the significant chromatic plasticity of the adult visual system.

Diabetic retinopathy

Diabetic retinopathy is an ocular manifestation of the systemic disease, diabetes, occurring when the disease is left untreated. Elevated blood sugar levels present in diabetics can induce changes in the retinal blood vessels severe enough to impact patients' vision. The swelling and growth of new vessels in the eye can cause these vessels to bleed, cloud vision, and destroy the retina by failing to supply adequate oxygen and meet the metabolic needs of the photoreceptors. Visual disturbances begin with a blur, but the pattern of vision loss in these patients is often diffuse, irregular, and achromatic, reducing visual perception to shades of gray interrupted by large blank patches.

Optic neuritis

Optic neuritis is an inflammation of the optic nerve which can cause partial or complete vision loss. These patients report sensitivity to light (photophobia), pain with eye movements, and a degradation of color vision. Direct axonal damage may also play a role in nerve destruction in many cases. The loss of color vision starts as an abnormal dimming, and apparent increased noise in the visual images, which then progresses to a general dimming or loss of color discrimination and blurring across the entire visual field. In many cases, only one eye is affected and patients are not aware of the loss of color vision until the doctor asks them to close or cover the healthy eye. Typically, these defects are similar to a deutan defect (a form of red–green defect), but with additional reduction in sensitivity to the shorter wavelengths. Nearly half of all patients with multiple sclerosis (MS) will develop an episode of optic neuritis, and up to one-third of the time optic neuritis is the presenting sign of MS. This stems from inflammation of the optic nerve, as a result of the degeneration of the myelin sheath surrounding it. MS patients may suffer periodic attacks of optic neuritis, which increase in severity, leading to a permanent loss of color vision.

Cortical Defects

Another way in which one can acquire a color-vision deficiency is through a cortical insult. Cortical defects result from a head injury, stroke, or neurodegenerative disease. Unlike other forms of acquired color-vision deficiencies, those arising from cortical defects are often unilateral, impacting one-half of the brain, and in turn only one part of the visual field, although full-field defects can occur. Injuries impacting color vision typically result from damage to either V2 (prestriate cortex), or V4 – the areas of the brain responsible for processing color information; however, uncertainty remains about precisely which cortical loci (if any) are responsible. As cortical damage is rarely localized to a small section of the brain, there are often other behavioral deficits resulting from the injury, making it difficult to interpret individual cases and generalize about an individual's symptoms.

Cerebral achromatopsia

One famous case of cerebral achromatopsia is that of the colorblind painter discussed in the introduction of this article. It is presumed that the painter's acquired monochromacy was due to cortical injury caused either by damage to the visual cerebral cortex during an automobile accident, or by a stroke affecting one of the visual areas. As V2 and V4 are among the most metabolically active areas of the cerebral cortex, they are among the first to suffer from the effects of reduced oxygen delivery, and may therefore be affected in the case of a stroke. In this case, color disturbances occur very rapidly and may precede other symptoms. The resulting loss of color vision may occur as a total loss (complete achromatopsia), or as a partial loss affecting only one-half of the visual field (hemiachromatopsia). Unlike degenerative disorders with the same perceptual appearance, in central achromatopsia, the retina is not damaged so acuity typically remains unchanged. This finding illustrates how different cortical areas can serve discrete aspects of vision.

Neurodegenerative diseases

Parkinson's disease (PD) is a disease that impairs cognitive, motor, and sensory function through the progressive loss of dopaminergic neurons, and a few studies have reported abnormal color vision in these patients. Dopamine

deficiency is believed to alter retinal visual processing primarily by changing the receptive field properties of ganglion cells. The S-cone photoreceptors are sparse in the retina and are believed to have elevated susceptibility to retinal damage caused by progressive loss of the dopaminergic cells in the retina. This is certainly the case in retinal detachments where S-cone defects predominate. Consequently, those who have cited color-discrimination problems in patients with PD identified a tritan axis of confusion. There is debate on this, however, because most standard methods of testing color vision require the patient to make motor movements, which can provide an additional disadvantage and confounding variable for PD patients.

Another neurodegenerative disease, Alzheimer's disease, also has implications for color vision. The cortical atrophy which causes the hallmark dementia associated with this disease causes not only degeneration of the visual areas of the brain (gray matter), but may also induce optic nerve degeneration. As the disease progresses, patients' vision tends to decline from a mild tritan color-vision deficiency into complete achromatopsia.

Toxin-Induced Defects

In addition to the internal defects that cause color-vision abnormalities, there are numerous environmental factors that can alter color perception. Multiple therapeutic drugs have been reported to produce color-vision deficiencies in patients. While most of these occurrences have been documented as a result of toxic levels of the prescribed drugs, some can occur even at recommended dosages, though most side effects are transient. Many studies have found altered color perception in workers occupationally exposed to chemicals as well. A possible mechanism for these toxin-induced defects may be related to the direct effect of the chemicals on cone function, and/or an interference with neurotransmitter signaling.

Digitalis

The digitalis family of drugs (digoxin and digitoxin) is typically prescribed to control congestive heart failure as well as certain cardiac arrhythmias. Several retinal cells (i.e., photoreceptors, Müller's cells, and retinal pigment epithelial cells) express digitalis-sensitive isoforms of sodium–potassium adenosine triphosphate (ATP)ase, and inhibition of these pumps by digitalis is associated with alterations in electrical-response properties of the retina. Clinical ERG and *in vitro* cell studies have shown that toxic levels of digoxin lead to rod and cone dysfunction, with cones being affected to a greater extent. Patients experiencing disturbances of color vision while taking these drugs usually exhibit a red–green defect in which objects are covered with a reddish haze and sometimes exhibit symptoms similar to optic neuritis. Fortunately, color vision tends to recover after the drug is withdrawn. It has been speculated that the prevalent use of yellow in Vincent Van Gogh's work may be due to the use of digitalis, used at the time for its euphoric effects and as a treatment for epilepsy.

PDE5 inhibitors

Phosphodiesterase (PDE) inhibitors, including Viagra (sildenafil), Levitra (vardenafil), and Cialis (tadalafil), are used to treat erectile dysfunction by selectively inhibiting cyclic guanosine monophosphate (cGMP)-phosphodiesterase type 5 (PDE5), present in all vascular tissue, which leads to vasodilation. It also exerts an inhibitory action against PDE6, the phosphodiesterase isoform present in rod and cone photoreceptors, though the inhibition efficacy is only about 1/10 of that for PDE5. PDE6 is a key player in the phototransduction cascade, catalyzing the hydrolysis of cGMP in response to absorption of light by the photopigment molecule. This results in a reduction in cGMP, which results in a closing of the cyclic-nucleotide-gated ion channels and thus a hyperpolarization of the cell. As such, PDE5 inhibitors can interfere with this process and lead to transient changes in rod and cone outer segment function, and the retinal effects may include impaired blue–green color discrimination and decreased rod- and cone-driven ERG amplitudes. At high doses of PDE5 inhibitors, patients have reported a blue tinge to vision, increased apparent brightness of lights, and blurred vision, although some studies report no effects on vision. Color-vision disruptions that were experienced were transient, and no consistent pattern has emerged to suggest any long-term effect of PDE5 inhibitors on the retina or other ocular structures.

Chloroquine

This drug is used in the treatment and prevention of malaria and more recently has gained use as an immune system suppressant prescribed in autoimmune disorders such as rheumatoid arthritis and lupus erythematosus. The color-vision impairment from chloroquine is a consequence of the fact that it is a melanotropic compound with an affinity for pigmented, melanin-containing structures; this naturally results in accumulation of the drug in the highly pigmented RPE. Both the dose and duration of chloroquine treatment impact the level of toxicity because the compound remains in the retina for several years, even after treatment has been discontinued. A tritan defect is most common, but as toxicity increases, a protan-like red–green defect can also manifest. Unfortunately, this is one of the few cases in which withdrawal of the drug is typically insufficient to prevent further damage.

Ethambutol

Ethambutol is a drug prescribed in combination as a treatment for tuberculosis. It has been found to induce a secondary color-discrimination disturbance which shifts the threshold for wavelength discrimination without a change

in absolute sensitivity, resulting in color-discrimination errors along the red–green axis. There is evidence that it may disrupt the morphology of the cone pedicle – disturbing the transmission of signals from the cone photoreceptors to their postreceptoral contacts (horizontal and bipolar cells). This disturbance is most profound for low-intensity stimuli. These effects can occur after either a lengthy therapy at a low dosage, or a short therapy at high doses. The color defect is similar to a deutan-like red–green defect, but with a reduction in sensitivity to the shorter wavelengths as well. Unlike many other acquired defects, in this case, impairments in color discrimination can be useful for detection of toxicity, thus color vision should be monitored in patients undergoing regular treatment for tuberculosis. Generally, color vision improves gradually after withdrawal of the drug; yet, in some cases color vision is permanently impaired.

Vitamin A deficiency

Common in developing countries, and associated with alcoholism and metabolic storage diseases in developed countries, vitamin A deficiency is a very preventable cause of acquired color-vision deficiency. This essential vitamin is required for regeneration of the visual pigments of both rods and cones in the retina. A deficit in vitamin A initially causes night blindness and, if left untreated, will contribute to complete blindness by making the cornea very dry and damaging the retina and cornea. In the more mild forms, tritan deficiencies occur, and transition to a general loss of hue discrimination. Approximately 400 000 children in developing countries go blind each year due to a deficiency in vitamin A. If reached before the onset of blindness, recovery can be shown following oral or injectable doses of the vitamin.

Exposure to metals and chemicals

Multiple studies have examined the color perception in groups of workers exposed to high levels of metallic mercury. Surprisingly, a dose-related loss of color vision is demonstrated even at presumed safe levels of mercury exposure. Although the mechanism of mercury's impact on the visual system is not fully understood, it seems to be localized to the retina because traces of mercury have been reported in the optic nerve, RPE, inner plexiform layer, vessel walls, and ganglion cells. Color-vision deficiencies revolve mainly around the blue–yellow axis, but may show some nonspecific losses. As with most of the other toxins, this effect seems to be reversible if individuals are removed from toxic exposure.

An additional collection of chemicals used in plastic, rubber, and viscose rayon manufacturing plants, rotogravure printing industries, as well as dry-cleaning facilities have similarly been implicated in reversible color-vision deficiencies. These chemicals include styrene, perchloroethylene (PCE), toluene, carbon disulfide, and n-hexane.

Conclusion

The range of acquired color-vision deficiencies is broad in both type and severity; some affect ocular structure directly while others perturb the neural pathways responsible for color vision, some are preventable and/or reversible while others are merely an indicator of a more serious condition. Despite their diverse etiology and manifestation, these defects can have a significant impact on the individual, for unlike those born with a color-vision deficiency, acquired sufferers know, and in most cases can remember, what they are lacking perceptually. Returning to the case of the colorblind painter gives those of us who are color normal a small taste of the devastating psychological effect of an acquired color-vision deficiency: "The wrongness of everything was disturbing, even disgusting, and applied to every circumstance of daily life."

See also: Color Blindness: Inherited; The Colorful Visual World of Butterflies; Cone Photoreceptor Cells: Soma and Synapse; Phototransduction: Adaptation in Cones; Phototransduction: Inactivation in Cones; Phototransduction: Phototransduction in Cones; Polarized-Light Vision in Land and Aquatic Animals; Primary Photoreceptor Degenerations: Retinitis Pigmentosa; Primary Photoreceptor Degenerations: Terminology; Rod and Cone Photoreceptor Cells: Outer-Segment Membrane Renewal; Secondary Photoreceptor Degenerations: Age-Related Macular Degeneration.

Further Reading

Birch, J. (1993). *Diagnosis of Defective Colour Vision.* New York: Oxford University Press.

Cowey, A. and Heywood, C. A. (1995). There's more to colour than meets the eye. *Behavioural Brain Research* 71: 89–100.

Gegenfurtner, K. R. and Sharpe, L. T. (1999). *Color Vision: From Genes to Perception.* New York: Cambridge University Press.

Heywood, C. A. and Kentridge, R. W. (2003). Achromatopsia, color vision, and cortex. *Neurological Clinics of North America* 21: 483–500.

Iregren, A., Andersson, M., and Nylen, P. (2002). Color vision and occupational chemical exposures: I. An overview of tests and effects. *NeuroToxicology* 23: 719–733.

Jackson, G. R. and Owsley, C. (2003). Visual dysfunction, neurodegenerative diseases, and aging. *Neurologic Clinics of North America* 21: 709–728.

Lamb, T. D. and Pugh, E. N., Jr. (2006). Phototransduction, dark adaptation, and rhodopsin regeneration: The proctor lecture. *Investigative Ophthalmology and Visual Science* 47(12): 5137–5152.

Pokorny, J. (1979). *Congenital and Acquired Color Vision Defects.* New York: Grune and Stratton.

Pokorny, J. and Smith, V. C. (1986). Eye disease and color vision defects. *Vision Research* 26: 1573–1584.

Sacks, O. W. (1995). *An Anthropologist on Mars.* New York: Random House.

Zeki, S. (1990). A century of cerebral achromatopsia. *Brain* 113: 1721–1777.

Color Blindness: Inherited

J Carroll and D M Tait, Medical College of Wisconsin, Milwaukee, WI, USA

Glossary

Blue–yellow defect – A color-vision deficiency in which blue and yellow are difficult to distinguish from one another. In inherited defects, this is typically caused by a defect in the short-wavelength-sensitive photoreceptor.
Dichromacy – A color-vision deficiency in which only two primaries are required to perfectly match a monochromatic light. In this deficiency, one of the three types of photopigments is functionally absent so color vision is reduced to only two dimensions.
Monochromacy – A complete lack of ability to distinguish colors caused by defects in the morphology or function of the cones.
Photopigment – A light-sensitive protein in the photoreceptors (rods and cones) that undergoes a conformational change when absorbing light and initiates the process of visual transduction.
Red–green defect – A color-vision deficiency in which red and green are difficult to distinguish from one another. There are two inherited forms of this defect: Deutan, which is caused by a defect in the medium-wavelength-sensitive photoreceptor, and protan, which is caused by a defect in the long-wavelength-sensitive photoreceptor.
Trichromacy – The fundamental ability to see in full color, based on the ability to match a monochromatic light by using a mixture of any three primaries. This ability requires the possession of three distinct classes of photoreceptors.

Introduction

Beyond the occasional spousal argument over the color of a shirt or tie, a significant number of people are born with a defect in their ability to perceive and discriminate colors. While the existence of deficiencies in color discrimination had been appreciated for some time, it was the famous chemist John Dalton who gave the most well-known analytical description of the condition in 1798. This was due to the fact that he himself suffered from a color-vision defect: "Reflecting on these facts, I was led to conjecture that one of the humors of my eye must be a transparent, but colored, medium, so constituted as to absorb red and green rays principally, because I obtain no proper ideas of these in the solar spectrum; and to transmit blue and other colours more perfectly." While Dalton did not accurately identify the biological basis of his color-vision deficiency, he articulately described it, and thus the term Daltonism is now synonymous with color-vision deficiencies.

Photoreceptor Basis of Human Color Vision

Humans with normal color vision can discriminate some 2 million hues. The retinal substrate for this exquisite color vision is the cone photoreceptor mosaic. While the highly sensitive rods outnumber cones nearly 20:1 and subserve vision at low (scotopic) light levels, it is the cones that underlie the majority of our visual experience at high light levels (photopic), including high spatial acuity and color vision.

There are three subclasses of cone photoreceptor, each having a distinct spectral sensitivity (**Figure 1**). The spectral sensitivity of the photopigment simply reflects the probability of it absorbing a photon of light, and is determined by the particular photopigment present in the cone cell. Photopigments (and their associated cones) are classified according to the region of the visible spectrum they are most sensitive to – either short-, middle- or long-wavelength sensitive (abbreviated S, M, and L). All humans with normal color vision have the same S-cone pigment, with peak absorption around 417 nm. The M-cone pigment varies slightly among individuals, with an average peak of about 530 nm. There is widespread variation in the peak sensitivity of the L-cone pigment among humans with normal color vision, though there are two main variants that peak at 555 and 559 nm, respectively. Trichromatic color vision is afforded by the presence of one cone type from each of these three spectral classes, and these cone types appear to be randomly arranged within the cone mosaic (**Figure 1**). While the human retina contains nearly 100 million photoreceptors, only about 5 million of them are cones, and of the cones, about 95% are of the L/M type. If the function of one or more of the cone classes is disrupted or absent, the result is a compromised ability to make chromatic discriminations, that is, a color-vision deficiency.

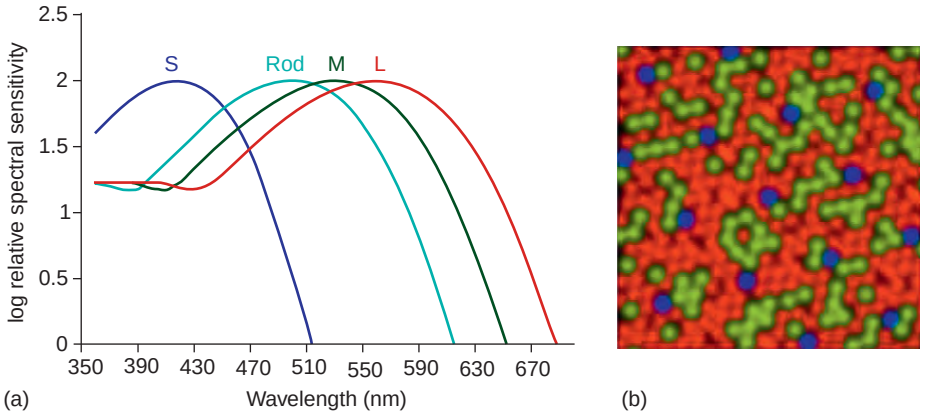

Figure 1 Photopigment basis for trichromatic color vision. (a) Photopigment absorption spectra. The human photopigments have different, but overlapping, spectral sensitivities. The cone photopigments, which dominate our photopic (daytime) vision, are named based on the region of maximal absorption in the visible spectrum – short-(S), middle-(M), or long-wavelength sensitive (L). Rods serve scotopic vision and are maximally sensitive at about 500 nm. (b) Simulation of the organization of the L (red), M (green), and S (blue) cones within the cone photoreceptor mosaic. Note the relative paucity of S cones in the mosaic, and the random arrangement of the L and M cones, with L cones outnumbering M cones by about 2:1 in individuals with normal color vision, though this is variable.

Genetic Basis of Human Color Vision

All inherited color-vision defects are associated with disruptions in the expression of normal cone photopigments. Human photopigments differ only in their opsin (protein) component, though they share the same chromophore, 11-*cis*-retinal. At the protein level the L and M pigments are about 96% homologous, though they show only 43% identity with the S pigment, while human rhodopsin (the opsin found in rods) is about 41% homologous with any of the cone opsins. Each of the human cone opsins is encoded by a different gene. The gene encoding rhodopsin is 5.0-kb long and found on chromosome 3, while the gene encoding the S opsin is located on chromosome 7 and is 3.2-kb long. The rhodopsin and S-opsin genes each have four introns and five exons, and as a result of their autosomal location, humans normally have two copies of each of these genes. In contrast, the L/M gene(s) are located on the X chromosome. While most mammals have only a single L/M gene on the X chromosome, most Old World primates (including humans) possess both L and M genes. In primates that have both the L and M genes on a single X chromosome, they are located in a tandem array near the end of the long arm of the X chromosome (Xq28), and a locus-control region (LCR) enables exclusive expression of one gene from the array in a given cone photoreceptor cell.

The location of the L/M gene array and their high homology allow for frequent unequal homologous crossovers (intermixing of the genes). During meiosis, this can occur between the genes (intergenic crossover) or within the genes (intragenic crossover) between two parental X chromosomes. Such recombination events are responsible for the observed variation in L/M gene number on the X chromosome (humans with normal color vision can have between two and nine genes in this array). In addition, genes with hybrid L and M sequences are produced from intragenic crossover events. These hybrid genes encode photopigments that have spectral sensitivities intermediate of the normal L- and normal M-cone photopigments. The combined variability in gene number and gene sequence means that in a group of 100 males, the probability that any two will have identical L/M arrays is less than 2%. Interestingly, there is no normal variation in the S-pigment gene.

As mentioned previously, there is a great deal of variability in the L and M photopigments. In fact, of the 364 amino acids there are 18 residues where differences have been identified between and among the L and M photopigments (positions 65, 111, 116, 153, 171, 174, 178, 180, 230, 233, 236, 274, 275, 277, 279, 285, 298, and 309; see **Figure 2(a)**). Positions 274, 275, 277, 279, 285, 298, and 309 co-segregate and can be used to identify a pigment as either L or M. This is because these amino acids, in particular the substitutions at positions 277 and 285, are responsible for generating the majority of the spectral separation between the L and M pigment classes. L genes specify tyrosine and threonine at positions 277 and 285, respectively, whereas M genes specify phenylalanine and alanine at these same positions, resulting in a shift in peak sensitivity toward shorter wavelengths of approximately 24 nm. Substitutions at the other amino acid positions can produce more subtle spectral shifts, driving the spectral variations within the L and M classes. The most common, a serine/alanine dimorphism at position 180, shifts the maximum absorption (λ_{max}) by about 3–7 nm, though the amino acid identity at other polymorphic positions can influence the magnitude of this shift.

This genetic variation can have a measurable impact on color vision. For example, among normal trichromats, the

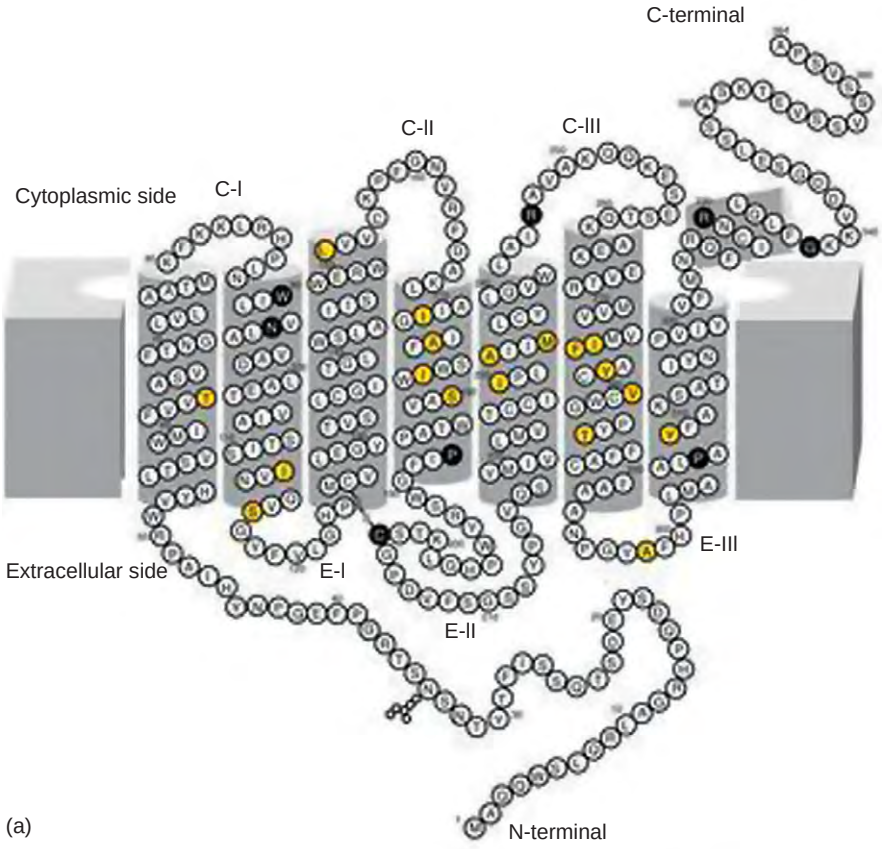

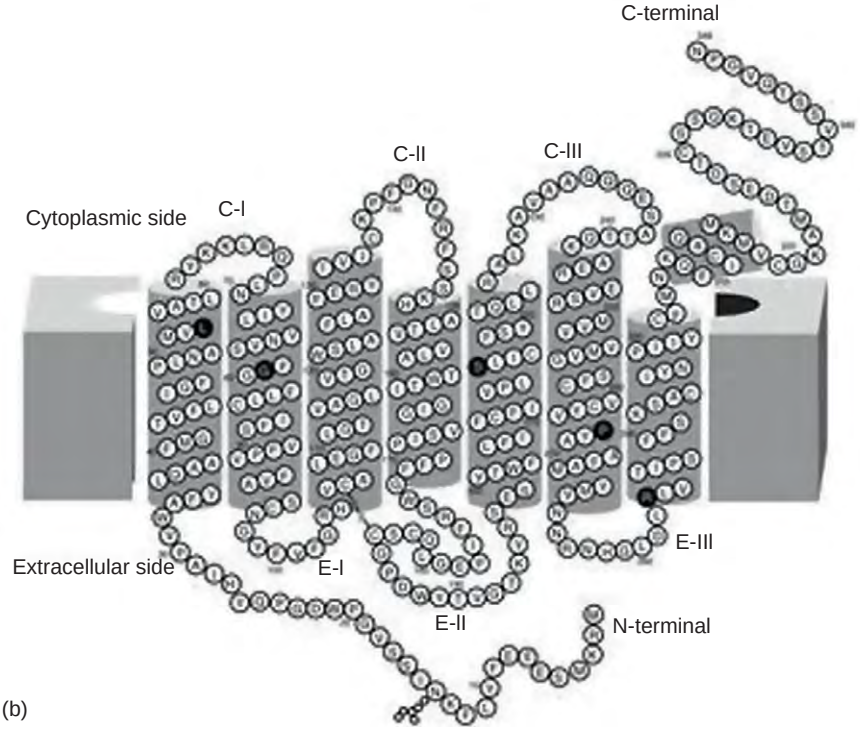

Figure 2 Two-dimensional models of the human cone opsins. (a) L/M opsin. Each circle represents a single amino acid, with mutations associated with the loss of L- or M-pigment function shown as filled black circles. Filled yellow circles represent the dimorphic sites that can differ between the L and M pigments. A number of these sites have been shown to be involved in the spectral tuning of the pigments (see text). The amino acid identities at all 18 dimorphic sites are those of the presumed primordial L opsin. (b) S opsin. Each circle represents a single amino acid. The five mutation sites associated with inherited tritan color-vision deficiency are indicated by black circles.

variation in spectral sensitivity within the L and M pigment classes can be readily observed on color-matching performance. In the Rayleigh match, an individual is asked to determine the mixture of a red and green primary needed to exactly match a monochromatic yellow light. Variability in color-matching behavior had long been recognized, but only in the last 20 years has it been directly linked to the variability in the L and M photopigments, and thus the L/M gene array.

Red–Green Color-Vision Deficiencies

Besides inducing subtle alterations in performance on laboratory color-vision tests, the genetic mechanisms that give rise to variability in the L/M-gene array can induce significant defects in color discrimination. Disruptions in normal L/M-photopigment expression result in an inherited form of color-vision deficiency that affects the red–green (L/M cone) system. Among individuals of Western European ancestry, about 8% of males have a red–green color-vision defect. The incidence is significantly lower among Africans and Asians, as well as smaller isolated populations such as Fijian Islanders and the Inuit. These defects are associated with the L/M array on the X chromosome and are inherited as X-linked recessive traits, so the incidence in females is much lower (approximately 0.4%). Nonetheless, approximately 15% of females are heterozygous carriers of a red–green color-vision defect. It has been suggested that there may be a heterozygous advantage for female carriers, as given the variability with the L and M spectral classes, these women can have four spectrally distinct cone types, providing the photoreceptor basis for tetrachromatic color vision.

The genetic causes of inherited red–green color-vision deficiency fall into two main categories. The most common cause is a rearrangement of the L/M genes resulting either in the deletion of all but one L or M pigment gene, or in the production of a gene array in which the first two genes encode a pigment of the same spectral class (i.e., L/L or M/M). Even though the L/M array can contain more than two genes, it is believed that only the first two genes in the array are expressed. The second general cause involves the introduction of a mutation in either the first or the second gene in the array, rendering the expressed pigment nonfunctional. The most prevalent inactivating mutation, accounting for nearly 10% of red–green dichromacy, results in the substitution of arginine for cysteine at position 203 (C203R) in the L/M opsin molecule. Mutating the corresponding cysteine residue in human rhodopsin (position 187) causes autosomal dominant retinitis pigmentosa (RP). This cysteine residue forms an essential disulfide bond and is highly conserved among all G-protein-coupled receptors. Mutant photopigments do not fold properly, and are retained in the endoplasmic reticulum and not targeted to the cone outer segment membrane. As such, L/M cones expressing this mutant pigment are nonfunctional, and individuals harboring this mutation base their color vision on an S cone and a single L- or M-cone type (rendering them dichromatic).

In the case where the first two genes encode pigments from the same spectral class, they can have either the same spectral sensitivity or slightly different spectral sensitivity (owing to the fact that there is variation within the L and M pigment classes). If the first two genes encode pigments with identical spectral sensitivities, the individual again bases their color vision on an S cone and a single L- or M-cone type and will be dichromatic. However, if the first two genes encode pigments with different spectral sensitivities (though from the same spectral class, L or M), the individual is technically trichromatic, in that they have three different cone types. However, since the spectral separation between their two types of L (or M) pigment is not as great as the separation between L and M, their discrimination is not normal. Thus, these individuals are known as anomalous trichromats. The standard L and M photopigments differ in their peak spectral sensitivity by nearly 30 nm. In anomalous trichromats with multiple L (or M) pigments, the λ_{max} may be separated by as few as 2 nm or as many as 10–12 nm, where the degree of spectral separation depends on the identity of the amino acids at sites 65, 111, 116, 153, 171, 174, 178, 180, 230, 233, and 236 within the L/M pigment (**Figure 2(a)**). In general, the further apart the pigments, the better the discrimination; in some cases, the deficiency is so mild that the individual is unaware of it until genetic and/or behavioral testing. Likewise, as the λ_{max} of the pigments gets closer together, the discrimination worsens, with the most severe individuals behaving nearly like dichromats.

The red/green defects can be separated based on the (1) dimensionality of the residual color vision (dichromat or anomalous trichromat) and (2) spectral subtype of the remaining cone (protan or deutan). **Figure 3** shows the different spectral sensitivity curves that underlie the different forms of red/green color-vision deficiency.

Individuals with an absence of L-cone function are said to have a protan defect. Protanopes are dichromats who possess an S pigment and an M pigment. Protanomalous trichromats possess a normal S pigment and two spectrally distinct M pigments. Perceptually, the absence of a cone type can have differing effects. Individuals with a protan defect are less sensitive to light in the long-wavelength (red) portion of the spectrum. Therefore, the brightness of red, orange, and yellow are reduced compared with a normal observer. Furthermore, they may have problems in distinguishing red from green, as well as difficulties differentiating a red hue from black.

Individuals with an absence of M-cone function are said to have a deutan defect. A deuteranope possesses an

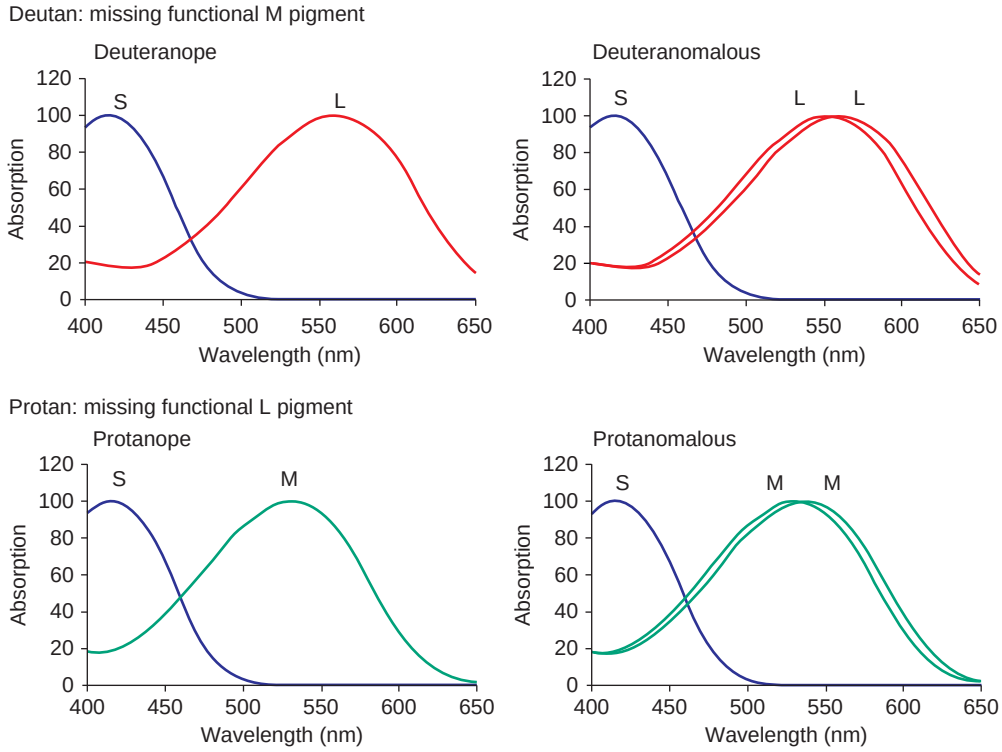

Figure 3 Photopigments underlying defective red–green color vision. Red–green color-deficient individuals are missing either all members of the M class or all members of the L class of pigment. Dichromats have only one pigment in the L/M region of the spectrum, whereas trichromats have two pigments in the L/M region of the spectrum. The degree of color-vision deficiency in persons with anomalous trichromacy depends on the magnitude of the spectral difference between their pigment subtypes. Deuteranopes and deuteranomalous trichromats have no functional M pigment, though deuteranomals have two slightly different L pigments. Likewise, protanopes and protanomalous trichromats have no functional L pigment, though protanomals have two slightly different M pigments.

S pigment and an L pigment, whereas deuteranomalous trichromats possess an S pigment and two spectrally distinct L pigments. Deuteranomalous defects are by far the most prevalent of any of the congenital color-vision defects, affecting nearly 5% of men. Individuals with deutan defects exhibit a reduction of sensitivity to colors in the green region of the spectrum, though the decrease in sensitivity is less pronounced than the long-wavelength depression in protans due to the manner in which the spectral sensitivities overlap (**Figure 1**). Deutans suffer similar hue-discrimination problems as the protans, but without the long-wavelength dimming. These discrimination errors are exploited in the design of color-vision tests; however, the real-world consequences of having certain red–green deficiency can be minimal. The perceptual consequences of having various color-vision defects are simulated in **Figure 4**. Interestingly, there is evidence that individuals with red–green defects may actually have an advantage when viewing camouflage, which is designed to blend into the environment, but this is done assuming a trichromatic visual system.

While the red–green color-vision defects can be behaviorally classified according to the cone subtype that is nonfunctional, the structural basis of the defects has been unclear. Recent work using high-resolution, *in vivo* imaging of the human retina has shown that while conceptually one can think of a deutan retina containing only S and L cones, and a protan retina containing only S and M cones, the residual cone mosaic in red–green-deficient individuals can vary dramatically, depending on the genetic cause of the defect. Shown in **Figure 5** are images of the cone mosaic from a normal trichromat and an individual with a red–green defect caused by an inactivating mutation in his M gene. Each circle is a single cone photoreceptor, and the dark spaces in the red–green-deficient retina represent cones that have degenerated or that are morphologically compromised. Thus, some individuals will have normal numbers of cones (though only two, instead of three types), while some will be structurally missing an entire cone class. The impact on vision in general is not yet known, and the genetic heterogeneity within the red–green defects remains to be reconciled with the mosaic phenotype.

Tritan Color-Vision Deficiencies

Tritan defects are an inherited autosomal dominant abnormality of S-cone function. These defects occur in

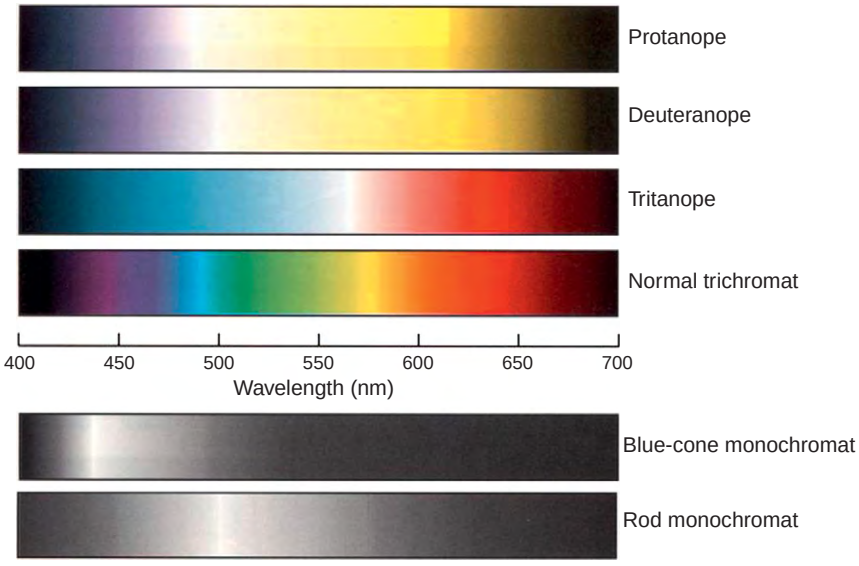

Figure 4 Perceptual consequences of inherited color-vision defects. Shown is a computer simulation of the color spectrum as it would appear to a protanope, deuteranope, tritanope, and normal trichromat. Each color-vision deficiency shows greatly reduced chromatic discrimination compared to that of a normal trichromat. The bottom two panels reveal the perceptual consequences of monochromacy on the appearance of the spectrum for a blue-cone monochromat and rod monochromat. Reproduced from Gegenfurtner, K. R. and Sharpe, L. T. (1999). *Color Vision: From Genes to Perception*. New York: Cambridge University Press, with permission of Cambridge University Press.

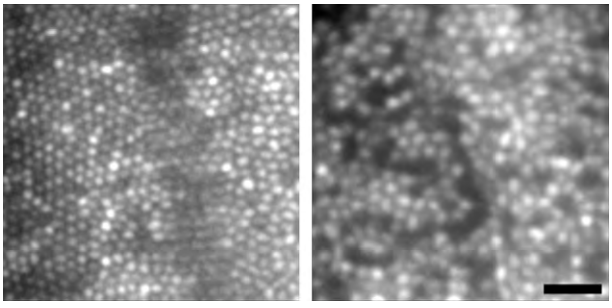

Figure 5 High-resolution images of the living retina obtained with adaptive optics. On the left is a retinal image from a patient with normal vision, at an eccentricity of approximately 1° temporal to fixation. Each circular structure is an individual cone photoreceptor. On the right is an image from a patient who is red–green color blind. Visible are numerous holes where cones have either died or degenerated, due to a mutation in one of the genes responsible for normal color vision. Despite the loss of nearly 33% of his functioning cones, this person has normal visual acuity. Scale bar = 20 μm.

both males and females with equal frequency and are believed to be rare, affecting as few as 1 in 10 000 people. As the S-pigment gene is on chromosome 7 and humans are diploid, each S-cone photoreceptor expresses the S-cone pigment genes from both copies of chromosome 7. Consequently, a defect in one S-pigment gene can be sufficient to cause tritanopia, just as a mutation in one rhodopsin gene is sufficient to cause RP, a retinal degeneration that involves the degeneration of the rod photoreceptors. Unlike the red–green defects, there is no genetic/pigment basis for a tritanomalous defect, as there is no spectral variation among functional S-cone pigments.

This disorder exhibits incomplete penetrance, meaning that individuals with the same underlying mutation manifest different degrees of color-vision impairment, even within a sibship. Mutations in the S-cone-opsin gene, which encodes the protein component of the S-cone photopigment, have been identified and they give rise to five different single amino acid substitutions that have only been found in affected individuals but not in unaffected control subjects (**Figure 2(b)**). Each substitution occurs at an amino acid position that lies in one of the transmembrane alpha helices, and is predicted to interfere with folding, processing, or stability of the encoded opsin. For example, one of the identified mutations corresponds to an amino acid position at which a substitution in the rod pigment, rhodopsin, causes autosomal dominant RP.

A fundamental difference between S cones and L/M cones is the potential for dominant negative interactions between normal and mutant opsins. This is because each S cone expresses both autosomal copies of the S-opsin gene, whereas L and M cones each only express one gene from the L/M array on the X chromosome. Rod photoreceptors also express a rhodopsin gene from two autosomes, and for rhodopsin mutations underlying autosomal dominant RP, dominant negative interactions lead to the death of the photoreceptors and ultimately the degeneration of the retina. Curiously, tritan defects have not been reported to cause progressive retinal degeneration and are only slightly

more rare than adRP; however, it has been suggested that the relative paucity of S cones compared to rods in the normal retina may be responsible for the absence of more general retinal degeneration. Nevertheless, the structural homology between the S-cone opsin and rhodopsin, taken together with the similar molecular mechanisms underlying the defects, suggest that S cones themselves degenerate in autosomal dominant tritan defects.

Blue-Cone Monochromacy

Blue-cone monochromacy (BCM) is a condition where both L- and M-cone function is absent. This disorder affects approximately 1 in 100 000 individuals. Since L and M cones comprise about 95% of the total cone population, these individuals have a rather severe visual impairment, including photophobia (light sensitivity), poor acuity, minimally detectable electroretinogram (ERG) responses, and diminished color discrimination. Any residual color vision in these individuals must be based solely on the S cones and rods. This means that under most conditions, they are monochromatic, though under mesopic (dim light; between photopic and scotopic levels) conditions they may gain some additional discrimination capacity.

As with the red–green defects, there are two main genetic causes of BCM, sometimes referred to as one-step or two-step mutations, though both lead to the absence of functional L and M cones. One-step mutations involve a deletion of essential *cis*-regulatory DNA elements needed for normal expression of the pigment genes. Two-step mutations involve a deletion of all but one of the X-chromosome visual pigment genes. This would normally confer red–green dichromacy (see above), but the one remaining gene contains a missense mutation. Due to the X-linked nature of the condition, female carriers are spared from a full manifestation of the associated defects, but they can show abnormal cone function on the ERG. One-step and two-step conditions may have important phenotypic differences in terms of the architecture of the cone mosaic in carriers. For the one-step mutations, the absence of an essential enhancer means that the cone photoreceptors cannot transcribe an opsin gene from the affected X chromosome. In contrast, for the two-step condition, there is a completely functional gene but the encoded opsin has a deleterious amino acid substitution, and the photoreceptor is expected to produce the mutant opsin. Depending on the nature of the mutation, it may either reduce or abolish proper folding of the encoded protein, or the gene may be transcribed but the message may be immediately targeted for degradation, and these may in turn ultimately affect the viability of the cone or its neighboring cells. While both conditions will likely compromise the viability of the cone, they may do so over different timescales.

Achromatopsia

Complete achromatopsia (i.e., rod monochromacy) is a congenital vision disorder in which all cone function is absent or severely diminished. It is typically characterized by an absolute lack of color discrimination, photophobia, reduced acuity, visual nystagmus, and a nondetectable cone ERG. Previously, exploration of this disease was limited to findings from histological and anatomical review and there was a debate surrounding whether the cones were absent, malformed, or merely minimally present. Recent work using *in vivo* cellular imaging, together with improved measures of cone function, suggest that not all achromats have the same cellular deficit, though in all cases their perception is dominated by the rod system and vision at normal light levels can be difficult if not impossible.

Rod monochromacy affects up to 1 in 30 000 people, and results from mutations in one of two components of the cone phototransduction cascade – transducin or the cyclic-nucleotide-gated (CNG) channel. Mutations in CNG alpha 3 (CNGA3) and CNG beta 3 (CNGB3), which encode the α- and β-subunit of the CNG channel, respectively, are by far the most common genetic cause of rod monochromacy, accounting for about 60–80% of the cases. A relatively small number of patients (~5%) have a mutation in the GNAT2 gene, which encodes the α-subunit of the cone G-protein transducin. The current theory is that the genetic heterogeneity underlies the observed phenotypic variability in patients with this disease, and this likely explains the previous discrepancies in histological reports. However, a systematic linkage of genotype and phenotype has not been done. Recently, a gene therapy approach has been used to restore cone function in dog and mouse models of the disease; however, one would predict that the degree of remaining cone structure would be a predictor of whether a particular human achromat could benefit from similar therapeutic intervention.

Conclusion

Inherited color-vision deficiencies range from mild difficulties discerning pale hues from gray to quite severe issues differentiating even the most saturated hues, and while most of these deficiencies are often categorized by the general misnomer color blindness, the defects are in fact quite different from one another and rarely indicate a condition in which the patient is truly blind to color. There is enormous genetic variation in all inherited color-vision defects, and it is becoming clear that this variation has consequences for the visual system that reach far beyond subtle differences in color perception/discrimination.

See also: The Colorful Visual World of Butterflies; Cone Photoreceptor Cells: Soma and Synapse; Phototransduction: Adaptation in Cones; Phototransduction: Inactivation in Cones; Phototransduction: Phototransduction in Cones; Polarized-Light Vision in Land and Aquatic Animals; Primary Photoreceptor Degenerations: Retinitis Pigmentosa; Primary Photoreceptor Degenerations: Terminology; Rod and Cone Photoreceptor Cells: Outer-Segment Membrane Renewal.

Further Reading

Birch, J. (1993). *Diagnosis of Defective Colour Vision*. New York: Oxford University Press.

Carroll, J., Choi, S. S., and Williams, D. R. (2008). *In vivo* imaging of the photoreceptor mosaic of a rod monochromat. *Vision Research* 48: 2564–2568.

Cruz-Coke, R. (1970). *Color Blindness: An Evolutionary Approach*. Springfield, IL: Charles C Thomas.

Dalton, J. (1798). Extraordinary facts relating to the vision of colours: With observations. *Memoirs of the Literary and Philosophical Society of Manchester* 5: 28–45.

Gegenfurtner, K. R. and Sharpe, L. T. (1999). *Color Vision: From Genes to Perception*. New York: Cambridge University Press.

Hess, R. F., Sharpe, L. T., and Nordby, K. (1990). *Night Vision: Basic, Clinical, and Applied Aspects*. New York: Cambridge University Press.

Mollon, J. D. (2003). The origins of modern color science. In: Shevell, S. K. (eds.) *The Science of Color*, 2nd edn., pp. 1–39. New York: Elsevier.

Nathans, J., Piantanida, T. P., Eddy, R. L., Shows, T. B., and Hogness, D. S. (1986). Molecular genetics of inherited variation in human color vision. *Science* 232(4747): 203–210.

Pokorny, J. (1979). *Congenital and Acquired Color Vision Defects*. New York: Grune and Stratton.

Sharpe, L. T., Stockman, A., Jägle, H., et al. (1998). Red, green, and red–green hybrid pigments in the human retina: Correlations between deduced protein sequences and psychophysically measured spectral sensitivities. *Journal of Neuroscience* 18(23): 10053–10069.

Concept of Angiogenic Privilege

B Regenfuss and C Cursiefen, Friedrich-Alexander University Erlangen-Nuernberg, Erlangen, Germany

Glossary

Angioblast – Mesenchymal tissue that differentiates into blood cells and vascular endothelium.
Angiogenesis – Formation of new blood vessels by outgrowth from preexisting vessels.
Intussusception – Formation of new blood vessels by splitting of existing vasculature.
Keratoplasty – Corneal transplantation.
Vasculogenesis – *De novo* blood-vessel formation from endothelial progenitor cells.

Introduction: Angiogenesis and Lymphangiogenesis

(Hem)angiogenesis describes the process of new blood-vessel formation by outgrowth from preexisting vessels. Accordingly, lymphangiogenesis means the formation of lymphatic vessels from preexisting ones. Both processes are precisely regulated and play an essential role in physiological and pathophysiological events in the organism.

In the context of the eye, pathological new blood and lymphatic vessels are associated with numerous disorders reducing visual acuity.

New blood-vessel formation in the organism is achieved either by angiogenesis or by vasculogenesis. Both processes can be distinguished from each other and strongly differ in the way the vessels arise. Vasculogenesis occurs mainly during embryogenesis and implies *de novo* blood-vessel formation by endothelial progenitor cells. During embryonic development, angioblasts, a subset of mesodermal cells, differentiate into endothelial cells and form the early vascular plexus. After establishing the primary vascular plexus, new blood vessels can be generated through angiogenesis that means by sprouting from preexisting blood vessels or by intussusception (nonsprouting angiogenesis). Angiogenesis and vasculogenesis normally occur during embryonic development. For the vascularization of the central nervous system (CNS) and the kidneys, angiogenesis seems to be the more important process. Following birth, most blood vessels remain in a quiescent state except for the once in the hair cycle, in the female reproductive system and during wound healing. In the case of unregulated angiogenesis, however, neovascularization can occur in the adult organism and usually is associated with diseases such as arthritis, tumors, or corneal and retinal disorders.

During early development of the retina, which is embryologically derived from the diencephalon, vasculogenesis and angiogenesis take place. In 1970, Ashton first described the mechanism of vasculogenesis for blood vessel formation in the retina of the human embryo. He proposed that primitive mesenchymal cells, after invading the retina, differentiate into endothelial cells, thereby, forming a capillary network. Nowadays there is evidence that vasculogenesis and angiogenesis both are responsible for the vascular development of the human fetal retina. Hughes and colleagues suggest a mechanism where vasculogenesis pioneers the establishment of a rudimentary vascular plexus, whereas angiogenesis provides further expansion of the vascular network and cares for increasing vessel density. Considering the fact that the retina is a highly metabolic active tissue both mechanisms complement one another and contribute to meet the metabolic requirements of the developing retina. The developed retina is a highly vascularized tissue that shows a dual blood supply. The inner layer of the retina is supported by the centralis retinae artery, originating from the arteria ophthalmica. The outer layer – especially the receptors – receive blood from the arteriae chorioideae.

In general, the eye is an efficiently vascularized organ and shows a significantly higher blood circulation compared to other organs with the same volume; however, there are exceptions at the anterior pole of the eye being completely devoid of blood and lymph vessels. Whereas posterior structures like the retina, as mentioned earlier, show a strongly branched blood-vessel network, the sclera is relatively low vascularized and the adjacent cornea and the vitreous even are devoid of blood and lymphatic vessels. Keeping up corneal avascularity comprises an active process and needs the balance between angiogenic and anti-angiogenic factors. In this process, the cornea maintains the transparency even under inflammatory or other pro-angiogenic conditions by different molecular mechanisms which are not completely elucidated to date. This ability is called the corneal angiogenic privilege.

Corneal Angiogenic Privilege

Corneal Avascularity

The corneal angiogenic privilege normally prevents the ingrowths of new vessels in the cornea even under

inflammatory or angiogenic conditions, thus maintaining corneal transparency and preventing loss of vision. A study with corneas from stillborn patients showed that this privilege is already present during intrauterine development at least from gestational age of 17 weeks. Contrary to the conjunctiva, in which blood and lymphatic vessels are detectable, no vessels are found in the cornea. This leads to the presumption that due to an early expression of anti-angiogenic and anti-lymphangiogenic factors, the cornea is primarily devoid of blood and lymphatic vessels and not as a result of regression of already existing vessels. The occurrence of neovascularization by angiogenic activity is initiated by a disbalance of angiogenic and anti-angiogenic factors caused by upregulating angiogenic molecules as well as by downregulating angiogenesis-inhibiting molecules. Interestingly, homozygote TSP-1 or TSP-2-knockout mice and even TSP-1/2-knockout mice showed no spontaneous corneal angiogenesis. The deficiency of an important anti-angiogenic factor like TSP-1 or TSP-2 does not result in a breakdown of the angiogenic privilege. This leads to the conclusion that at least during embryonic development the angiogenic privilege seems to be redundantly regulated by several anti-angiogenic factors. However, secondary to severe inflammation and several other diseases the angiogenic privilege can be overcome and an initial parallel outgrowth of blood and lymphatic vessels occurs.

Several factors comprising angiogenic and anti-angiogenic molecules, the cornea itself, and adjacent structures like the limbus are known to be involved in affecting the angiogenic privilege (see **Figure 1**). Deprivation of the angiogenic privilege can lead to corneal neovascularization and, in consequence, loss of vision.

Angiogenic and Anti-Angiogenic Molecules Involved in Corneal Neovascularization

Numerous angiogenic and anti-angiogenic molecules have been identified in the cornea over the last years. Angiogenic molecules include vascular endothelial growth factors (VEGFs), basic fibroblast growth factors (bFGFs), and matrix metalloproteinases (MMPs). Angiostatin, endostatin, thrombospondins, and pigment epithelium-derived factor (PEDF) are some of the anti-angiogenic molecules detected in the cornea.

The regulation of angiogenesis is due to the interaction of pro-angiogenic molecules and angiogenesis inhibitors, where tilting the balance toward pro-angiogenic factors can lead to neovascularization. Lymphangiogenesis seems to proceed in a similar way as angiogenesis, and can be activated in the adult during inflammation, immune responses, or malignant processes.

Stimuli like hypoxia, for example, in the context of wound healing, can also trigger the induction of hemangiogenesis via hypoxia-inducible transcription factor (HIF), a key transcriptional regulator for VEGF-A. In contrast, lymphangiogenic VEGF-C cannot be upregulated by hypoxia but only by proinflammatory cytokines.

Vascular endothelial growth factors

The VEGF growth factor family currently consists of five members, VEGF/VEGF-A, PIGF, VEGF-B, VEGF-C, and VEGF-D. The growth factors are recognized by different VEGF receptors, namely VEGFR-1, VEGFR-2, and VEGFR-3. VEGF-A originally isolated from a human histiocytic lymphoma cell line U937 is secreted

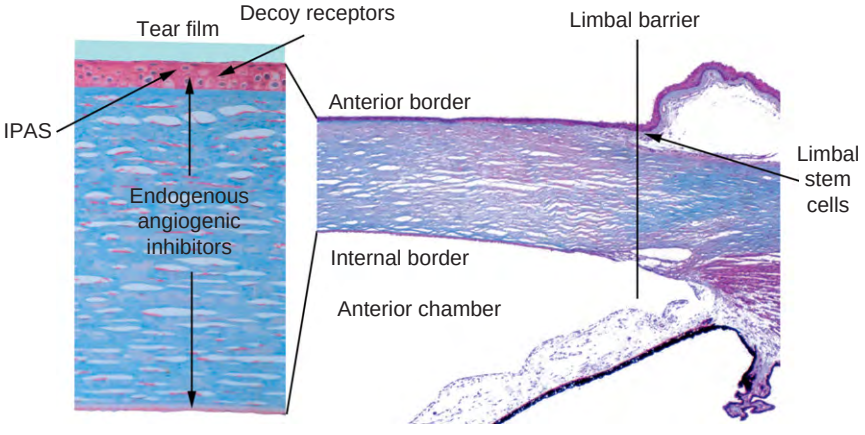

Figure 1 Several strategies are used by the normal cornea to maintain corneal avascularity (corneal angiogenic privilege): The cornea possesses several defense lines against invading vessels: an anterior border at the epithelial basement membrane, an internal border at Descemet's membrane, and the limbal barrier beneath the limbal epithelial stem cell niche. Several mechanisms contribute to maintain the angiogenic privilege of the cornea: (a) endogenous inhibitors of angiogenesis, (b) decoy receptors neutralizing angiogenic growth factors, (c) anti-angiogenic stem cells, and (d) anti-hypoxia-driven-angiogenesis agents. © M. Vogler.

in five different isoforms, generated by alternative splicing: $VEGF_{115}$, $VEGF_{121}$, $VEGF_{165}$, $VEGF_{189}$, and $VEGF_{206}$.

Vascular endothelial growth factor

VEGF-A shows numerous activities such as inducing endothelial cell proliferation and migration, proteolytic activity, and stimulating microvascular leakage – all of them promoting angiogenesis. VEGF-A mediates its function through receptors VEGFR-1 and VEGFR-2. Additionally, VEGF-A was reported to promote angiogenesis via an indirect pathway by upregulating NRP1, a neuronal receptor that has recently been shown to act as an isoform-specific receptor for $VEGF_{165}$.

VEGF-A can be released during hypoxia, in inflammatory situations, and during glucose deficiency. It was shown that the expression of VEGF-A is upregulated in inflamed and vascularized human corneas. In conclusion, VEGF-A seems to play an important role in inducing wound and inflammation-related corneal neovascularization. This was confirmed by the fact that corneal neovascularization could be suppressed after implantation of VEGF-A neutralizing antibodies in the corneal stroma of rats and rabbits. Whereas early data proposed that VEGF stimulates selectively hemangiogenesis but not lymhangiogenesis, recent data also suggest an (indirect) lymphangiogenic role: endogenous VEGF can promote lymphangiogenesisvia the recruitment of bone marrow-derived macrophages, releasing lymphangiogenic growth factors such as VEGF-C and -D. This broadens the impact of VEGF-A, not only for pathological hemangiogenesis, but also for lymphangiogenesis – at least in context of inflammation-induced neovascularization. A specific role for VEGF-A in the regulation of lymphangiogenesis was also described for primary tumors. The tumors were shown to overexpress VEGF-A, thereby inducing sentinel lymph node lymphangiogenesis. In a mouse model of delayed-type hypersensitivity (DTH), lymphangiogenesis was promoted by VEGF-A that was produced in the inflamed tissue.

In addition, genetic variety, that is, single-nucleotide polymorphisms in the gene coding for VEGF-A, is associated with eye diseases like neovascular age-related macular degeneration and diabetic retinopathy.

VEGF-C and VEGF-D

VEGF-C and VEGF-D are the main growth factors for lymphangiogenesis and both mediate their function by binding to receptors VEGFR-2 and VEGFR-3, present on endothelial cells. VEGF-C stimulates migration of cultured endothelial cells *in vitro* and increases – in its fully processed form – vascular permeability, migration, and proliferation of endothelial cells. Recently, the decisive role for VEGF-C during lymphangiogenic development was demonstrated in a study where homozygote as well as heterozygote VEGF-C-lacking mice were shown to have severe defects in the formation of lymphatic vessels. A study undertaken to analyze VEGF-C and its role in corneal neovascularization suggests VEGF-C to induce corneal lymphangiogenesis by binding to its cognate receptor VEGFR3 on lymphatic vessels in the conjunctiva. Inflammatory cells invading the cornea were identified as the main source of VEGF-C that was strongly upregulated 3 days following the injury. Besides its role as classic lymphangiogenic growth factor, VEGF-C was reported to induce angiogenesis *in vivo*. VEGF-D also can act as a potent angiogenic factor, controlled by the nuclear oncogene c-fos and thus playing an important role in tumor invasion and tumor cell growth.

Basic fibroblast growth factor

Another important pro-angiogenic molecule – the basic fibroblast growth factor (bFGF/ FGF-2) – belongs to the FGF family. bFGF and acidic FGF (aFGF) expression has been demonstrated immunohistochemically in the outer retina of rat and mouse. bFGF was analyzed in several corneal neovascularization models and was recently demonstrated to induce angiogenesis as well as lymphangiogenesis *in vivo* in a mouse model corneal micropocket assay. Lymphangiogenesis was mediated by bFGF in an indirect way via VEGFR3 and was suppressed after inhibition of VEGFR3 signaling with anti-VEGFR3 antibodies.

Both factors, bFGF and aFGF, were detectable in retinal pigment epithelial cells from choroidal neovascular membranes from human subjects with age-related macular degeneration (AMD), whereas there was only little immunoreactivity for the growth factors in retinal pigmented epithelial (RPE) cells from healthy eyes. This suggests an important role for aFGF and bFGF in the development of choroidal neovascularization. bFGF might play an indirect role in initiation of neovascularization and interacts with the VEGF signal-transduction pathways. This is supported by the fact that bFGF was found to be colocalized with VEGF in cells of epiretinal and choroidal neovascular membranes, suggesting that more than one growth factor may contribute to pathological angiogenesis. In favor for that theory is that mice with a disruption of the bFGF-coding gene can still develop choroidal neovascularization.

Recently, bFGF was thought to take a role in progression and survival of retinoblastoma, a tumor producing significant amounts of bFGF. The differential production and response to isoforms of bFGF reveal bFGF as a growth factor influencing pathogenesis and chemoresistence of retinoblastoma.

Inhibitory PAS (Per/Arnt/Sim) domain protein

As mentioned earlier, the upregulation of angiogenic molecules like VEGF-A and angiopoietin-4 (Ang-4)

during hypoxia is mediated by hypoxia-inducible transcription factor-1 (HIF-1) and can induce an angiogenic response. Interestingly, hypoxic conditions in the cornea appearing, for example, during overnight closure of the eye, do not induce corneal neovascularization, indicating the presence of factors suppressing hypoxia-induced angiogenesis. However, prolonged contact lens use has been associated with corneal angiogenesis and hypoxia has been implicated in this process. IPAS, a basic helix–loop–helix (bHLH)/PAS protein, expressed in mouse corneal epithelium, was suggested as a negative regulator of HIF-mediated control of gene expression: only low levels of IPAS mRNA were detectable in primary cultures of mouse corneal cells under normoxic conditions, whereas under hypoxic conditions IPAS mRNA expression was upregulated. Following transfection of primary corneal cells with an IPAS antisense vector, VEGF mRNA expression – under normoxic and hypoxic conditions – was upregulated. Furthermore, *in vivo* experiments with mouse corneas containing pellets with IPAS antisense oligonucleotides showed a significantly induced neovascularization compared to the eyes treated with the IPAS sense oligonucleotide.

Cornea and Corneal Epithelium

Consistent with the assumption of a redundantly organized angiogenic privilege, numerous endogenous anti-angiogenic factors in the cornea are described to be implicated in the regulation of angiogenesis.

Years ago, the corneal epithelium itself was found to have angiogenic activity. In 1978, Eliason reported data from an *in vivo* system suggesting corneal epithelium as a source for an unknown vasostimulating substance. *In vitro* experiments from Eliason and Elliott also showed a stimulating effect of corneal epithelial homogenate and epithelial-conditioned medium on the proliferation of cultured rabbit vascular endothelial cells. Recent research attributes corneal epithelium an anti-angiogenic function: an intact corneal epithelium can suppress inflammation and corneal neovascularization in the graft following orthotopic transplantation in mice. Secondly, mice with de-epithelialized corneas have significantly increased recruitment of CD45+ inflammatory cells and an increased neovascular response compared to mice with an intact epithelium. One potent mechanism for an anti-angiogenic function of corneal epithelium is the ectopic constitutive expression of VEGFR-3 on normal human corneal epithelial cells. VEGFR-3 can act as a decoy receptor to bind VEGF-C, thus functioning as a sink for the angiogenic molecules and inhibiting inflammation induced corneal hemangiogenesis and lymphangiogenesis. A similar task fulfils the soluble form of VEGFR-1 – expressed in the cornea – where it can neutralize VEGF-A.

Limbal Barrier Function

The border between sclera/conjunctiva and the transparent cornea, the limbus, is of great importance for angiogenesis: the loops and arcades of conjunctival capillaries as well as the lymphatic capillaries end in the limbal region. Corneal neovascularization, however, arises in the limbal area from preexisting pericorneal vessels (hemangiogenesis as well as lymphangiogenesis).

Stem cells, required for corneal epithelial cell proliferation and differentiation, are located in the basal epithelium at the corneoscleral limbus. They were described to act as a barrier between conjunctival and corneal epithelium and as important for corneal wound healing. In normal situations, the limbal stem cells prevent conjunctival epithelial cells from migrating to the ocular surface thereby inhibiting corneal neovascularization. This limbal-barrier concept may contribute to the maintenance of the angiogenic privilege. The theory is supported by the observation of conjunctivalization of the corneal surface with subsequent vascularization in situations of loss or malfunction of the stem cells.

Angiogenic Privilege and Immune Privilege

Ingrowth of blood and lymphatic vessels into the cornea is incompatible with good vision. Visual acuity is impaired not only by vascularization itself, but also by secondary changes such as lipid keratopathy, corneal edema, or bleeding into the cornea, thereby reducing corneal clarity and transparency. As mentioned earlier, actively maintaining the avascularity even under inflammatory or other angiogenic conditions is ensured by the angiogenic privilege. It contributes, at least partly, to the occurrence of the prolonged graft survival of corneal allografts, called the immune privilege of the eye. The phenomenon of the immune-privileged site was first proposed by Medawar, in 1948, and has built a foundation for numerous research. Nowadays, ocular immune privilege is commonly seen as the fact that vulnerable organs or tissues are protected from pathogens without an immunogenic inflammation that would permanently damage those tissues and/or would lead to a loss of specialized functions.

An immune response after transplantation in so-called low-risk eyes can only be noticed in around 10%, although under normal circumstances there is no HLA matching and only a topical, but no systemic, immunosuppression. In contrast, immune reactions in high-risk eyes with preceding corneal inflammation or neovascularization occur in over 50%. The pathologically vascularized recipient bed prior to corneal transplantation (i.e., penetrating keratoplasty), therefore, lowers the outcome of corneal transplantation and is an important risk factor for subsequent immune reactions.

Immune responses are primarily mediated by corneal lymphatic vessels which form the afferent arc of the immune response. Via the lymphatic vessels invading antigen-presenting cells (APCs; dendritic cells from the graft or host) and antigenic material from the graft can be transported via conjunctival lymph vessels to the regional lymph nodes. The draining cervical lymph nodes were shown to be critically involved in promoting alloimmunity and allograft rejection. Following surgical removal of the cervical lymph nodes and following orthotopic corneal transplantation of fully mismatched high-risk allografts, over 90% of the hosts accepted the allograft.

The importance of the lymphatic vessels, being the afferent arc of the immune response, offers new therapeutic opportunities for improving graft survival. Interfering with this pathway might restore the immune privileged status of the eye and ensures prolonged graft survival in low- and high-risk eyes. Early studies have shown that induction of donor-specific anterior chamber-associated immune deviation (ACAID) – manifestation of the ocular immune-privilege induced prolonged graft survival in high-risk eyes of C57BL/6 mice. Recently, it was shown that Integrin a5-blockade could significantly block the outgrowth of lymphatic vessels in the cornea. The angiostatic drug bevacizumab, a recombinant humanized monoclonal antibody against VEGF-A, inhibits corneal hemangiogenesis and lymphangiogenesis *in vitro* and *in vivo*. Furthermore, inhibition of corneal hemangiogenesis and lymphangiogenesis by a molecular VEGF-A trap leads to improved long-term graft survival. In addition to the inhibition of inflammatory lymphangiogenesis, alternative strategies like induction of regression of established lymphatic vessels in prevascularized corneas and influencing the recruitment of APCs could be possible methods for corneal anti-lymphangiogenic treatment. Recently, it was shown that even hemangiogenesis and lymphangiogenesis occurring following transplantation increase the risk for graft rejection after high-risk corneal transplantation.

See also: Avascularity of the Cornea; Corneal Angiogenesis; The Immunological Aspects of Aqueous Humor Turnover.

Further Reading

Azar, D. T. (2006). Corneal angiogenic privilege: Angiogenic and antiangiogenic factors in corneal avascularity, vasculogenesis, and wound healing (an American Ophthalmological Society thesis). *Transactions of the American Ophthalmological Society* 104: 264–302.

Cebulla, C., Jockovich, M. E., Pina, Y., et al. (2008). Basic fibroblast growth factor impact on retinoblastoma progression and survival. *Investigative Ophthalmology and Visual Science* 49(12): 5215–5221.

Chang, J. H., Gabison, E. E., Kato, T., and Azar, D. T. (2001). Corneal neovascularization. *Current Opinion in Ophthalmology* 12: 242–249.

Churchill, A. J., Carter, J. G., Ramsden, C., et al. (2008). VEGF polymorphisms are associated with severity of diabetic retinopathy. *Investigative Ophthalmology and Visual Science* 49: 3611–3616.

Cursiefen, C. (2007). Immune privilege and angiogenic privilege of the cornea. *Chemical Immunology and Allergy* 92: 50–57.

Cursiefen, C., Chen, L., Dana, M. R., and Streilein, J. W. (2003a). Corneal lymphangiogenesis: Evidence, mechanisms, and implications for corneal transplant immunology. *Cornea* 22: 273–281.

Cursiefen, C., Seitz, B., Dana, M. R., and Streilein, J. W. (2003b). Angiogenesis and lymphangiogenesis in the cornea. Pathogenesis, clinical implications and treatment options. *Ophthalmologe* 100: 292–299.

Folkman, J. and Shing, Y. (1992). Angiogenesis. *Journal of Biological Chemistry* 267: 10931–10934.

Hori, J. and Niederkorn, J. Y. (2007). Immunogenicity and immune privilege of corneal allografts. *Chemical Immunology and Allergy* 92: 290–299.

Makino, Y., Cao, R., Svensson, K., et al. (2001). Inhibitory PAS domain protein is a negative regulator of hypoxia-inducible gene expression. *Nature* 414: 550–554.

Niederkorn, J. Y. (1999). The immune privilege of corneal allografts. *Transplantation* 67: 1503–1508.

Niederkorn, J. Y. (2007). Immune mechanisms of corneal allograft rejection. *Current Eye Research* 32: 1005–1016.

Shweiki, D., Itin, A., Soffer, D., and Keshet, E. (1992). Vascular endothelial growth factor induced by hypoxia may mediate hypoxia-initiated angiogenesis. *Nature* 359: 843–845.

Streilein, J. W. (2003a). Ocular immune privilege: The eye takes a dim but practical view of immunity and inflammation. *Journal of Leukocyte Biology* 74: 179–185.

Streilein, J. W. (2003b). Ocular immune privilege: Therapeutic opportunities from an experiment of nature. *Nature Reviews Immunology* 3: 879–889.

Cone Photoreceptor Cells: Soma and Synapse

R G Smith, University of Pennsylvania, Philadelphia, PA, USA

Glossary

Cascade – A sequence of biochemical reactions that process a neural signal.
Connexin – A molecule comprising a gap junction that sits in a neuron's membrane and can join with a connexin from another neuron to create a large nonspecific pore that conducts ions and small molecules.
Ephaptic – Electrical conduction across a synapse between neurons without the mediation of a neurotransmitter.
Henle fiber – The long axon of a foveal cone that extends laterally to terminate outside of the fovea.
Invagination – A permanent infolding of a cell's external membrane, associated in photoreceptors with their synaptic ribbons, and containing fine dendritic processes of bipolar and horizontal cells.
Invert – In a postsynaptic cascade, to convert a rising signal into a falling signal.
Low-pass filter – A filter that removes high frequencies and passes low frequencies.
Mesopic – The 3-log unit range of background illuminance in which rod and cone signals temporally sum in cones and the cone bipolar pathway.
Microtubule – A small tubule composed of the protein tubulin, often found as arrays in neural axons, involved in transport of cellular components.
Pedicle – The cone terminal, with a foot-like flat base, which contains synaptic ribbons.
Ribbon – A presynaptic structure that collects vesicles of neurotransmitter for release.
Telodendria – Fine axonal processes extending laterally from the base of the cone terminal, which contact neighboring rod and cone terminals.
Triad – A synapse in the cone terminal that contacts dendritic processes of two horizontal cells and a bipolar cell.

Introduction

The cone photoreceptor is responsible for vision in daylight and provides color vision for most vertebrates. The cone is specialized to compress the large range of environmental illumination into a neural signal that can be processed by bipolar and ganglion cells in the retina and passed to the brain. The cone soma and synapse support this compression by several mechanisms located in its biophysical properties and at its ribbon synapse. In addition, cones perform spatial filtering because their terminals are electrically coupled to their neighbors and to the surrounding rods through gap junctions.

Structure

Morphology and Topology

The cone is a specialized neuron consisting of an outer segment, inner segment and soma, axon, and axon terminal (Figure 1). The biochemical pathways responsible for transducing light into an electrical signal are contained in the outer segment. The electrical signal passes to the inner segment where it is processed by voltage-gated channels. The inner segment is contiguous with the soma but they lie in distinct retinal layers separated by the external limiting membrane. The cone soma lies in the upper row of the outer nuclear layer. For most mammalian cones, the soma is larger in diameter (~5 μm) than the outer segment. It contains the nucleus which holds the cell's DNA, necessary for development and to maintain the cell's biochemical machinery. Many mammalian species have ~20-fold more rods than cones, so the remainder of the outer nuclear layer consists of several layers of rod somas. Cones of most species (and outside the fovea in primate) are spaced semirandomly with a nearest-neighbor distance that varies from ~5 μm in central retina or the visual streak (e.g., cat, rabbit, and guinea pig) to ~15 μm in peripheral retina, and are surrounded by rods.

Axon and Terminal

The cone axon carries the electrical signal from the soma to the axon terminal. The axon varies in length depending on the species and eccentricity (distance from central retina) of the photoreceptor. In foveal cones near the center of the primate eye, cone axons extend up to 400–600 μm laterally to allow the outer segments to be packed tightly together in the foveal pit and the axon terminals to be given adequate space outside the fovea to make their synaptic connections with other neurons. These long axons are termed Henle fibers, and the layer containing the horizontally projecting axon fibers is termed Henle's layer. In other mammals, the cone axon

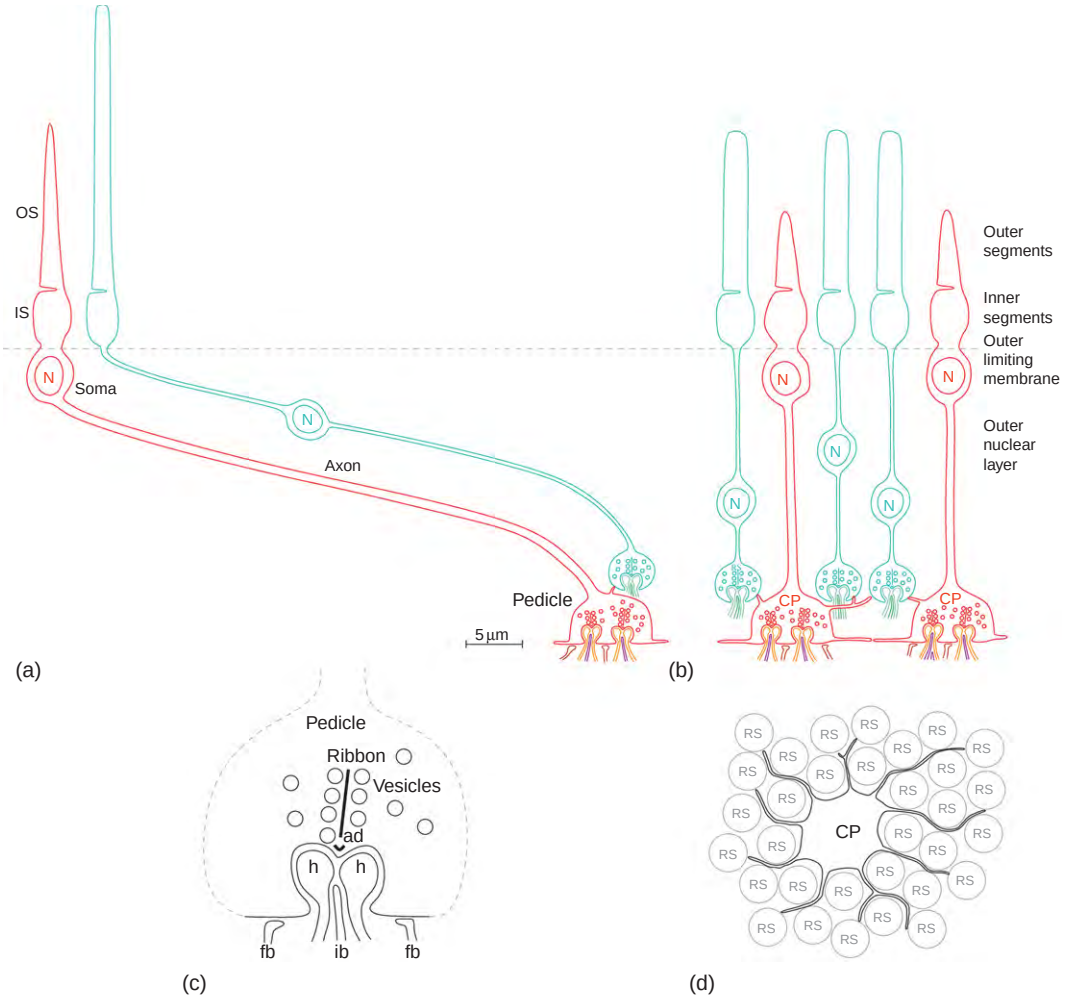

Figure 1 Morphology and topology of the cone. (a) Primate cone with its outer segment in parafovea, showing the lateral extension of the axon which allows the axon terminal sufficient space to make its synaptic connections. A few rods (gray) exist in the parafovea and their axons also extend laterally. Primate foveal cones extend farther, up to 600 µm. (b) In most mammals and in distal primate retina, cones extend vertically interspersed between rods (gray). The cone pedicles are interconnected by gap junctions between basal processes. (c) The cone ribbon synapse sits at the apex of an invagination into the basal surface of the cone pedicle. Attached to the ribbon are two rows of vesicles that contain glutamate. The vesicles are released at the active zone near the arciform density (ad). Two horizontal cell processes (h) and one or more invaginating ON bipolar cell dendrites (ib) extend into the pedicle to receive glutamate from vesicles released from the ribbon. Flat OFF bipolar cell dendrites (fb) contact the cone pedicle outside the invagination, and are thought to receive glutamate that diffuses from several nearby ribbons. (d) Tangential view of a cone pedicle (CP) surrounded by rod spherules (RS, gray). Telodendria extend from each cone pedicle to contact all the surrounding rods and cones with gap junctions.

extends vertically: in cat, the cone axon typically extends ~50 µm in the outer nuclear layer traversing 6–10 layers of rod somas, and in guinea pig, the axon is shorter, typically 10–25 µm. Typically, cone axons are 1–2 µm in diameter, interspersed between rod somas (35 µm dia.) and rod axons (0.4 µm dia.). The fourfold greater diameter of cone axons suggests a functional interpretation, because space in the outer nuclear layer is limited. One possibility is that the faster cone response might require a larger diameter in a long axon to transmit the cone's higher frequency response. This was tested with a computational model, and a thin diameter in a long axon was found sufficient, also consistent with the maintenance of the difference in diameter between cone and rod axons even where they are shorter. Another possibility is related to the axon terminal: the cone terminal has ~20-fold more synaptic contacts than the rod, and its cross-sectional area is ~16-fold greater. Both rod and cone axons are filled with microtubules, which are essential for transporting synaptic proteins from the nucleus, so the larger diameter of the cone axon may be a consequence of its need to perform more synaptic maintenance. The cone axon terminal is typically ~5 µm in diameter, and is flat on its basal surface (toward the ganglion cells); hence, it looks

like a foot and is commonly called a pedicle. The pedicles of adjacent cones align to form a flat plane which lies near the upper edge of the outer plexiform layer.

Synapse

The cone makes chemical synaptic contacts onto ~10 types of bipolar cell and two types of horizontal cell (HA and HB in cat and rabbit; H1and H2 in primate) at its axon terminal. The synapse releases glutamate via packets of membrane called synaptic vesicles, which are small (~30–50 nm) organelles created by endocytosis from the cell's external membrane. The vesicles diffuse freely around the cytoplasm while they are being filled with glutamate by transporters. The presynaptic machinery in the terminal contains several dense structures known as ribbons because in cross section they are thin and extend vertically away from the cell's membrane. The active zone, where vesicles are released from the ribbon onto the external membrane, is defined by a trough-shaped band called the arciform density, which contains structural proteins for anchoring the ribbon to the cell membrane and the calcium channels responsible for triggering release. The ribbon allows high continuous release rates, for it collects several rows of vesicles and tethers them for release, to provide a larger readily releasable pool. The mechanism for vesicle release is complex, containing several dozen proteins, and its details are not yet understood, but it is initiated by calcium ions binding to a receptor protein which causes a vesicle to fuse with the external membrane and release its contents into extracellular space. To fuse with the external membrane, the vesicle must be docked near membrane calcium channels at the base of the ribbon. However, there is some evidence for compound fusion, where vesicles fuse with and release into nearby docked vesicles. After release, the vesicle membrane is recycled with a specialized mechanism involving the protein clathrin which coats an invaginating bit of external membrane with a buckyball-type structure and pinches it off as a cytoplasmic vesicle.

Invagination and Triad

The cone's ribbon synapse is located at the apex of an extension of extracellular space into the bottom surface of the cone terminal, called an invagination, where fine processes of horizontal and bipolar cells extend to form postsynaptic specializations. Each invagination holds two horizontal cell dendritic processes which emanate from different horizontal cells, and one fine dendritic process of an ON bipolar cell. The horizontal cell processes swell up inside the invagination on either side of the bipolar dendrite. Together, the ribbon and postsynaptic processes are called 'a triad'. The function of the invagination is unknown but it has been suggested to limit diffusion of the neurotransmitter released by the cone or by horizontal cells for negative feedback. The cone terminal contains 20–50 ribbons, each in a separate invagination, so there are several dozen triads. Off-bipolar cells also contact the cone terminal. Some with alpha-amino-3-hydroxy-5-methyl-4-isoxazolepropionic acid (AMPA) receptors invaginate the cone near the ON bipolar process, and others with kainate receptors contact the base of the pedicle at the so-called flat or basal contacts which lack associated presynaptic vesicles. The flat contacts are located in the space between the invaginations, allowing them to sense the release from several ribbons.

Biophysical Properties

The inner segment and axon terminal of photoreceptors contain several membrane-bound ion channels, including K_v, K_{Cn}, BK, and L-type Ca^{2+}. The K_v channels of the inner segment are activated by depolarization, providing an outward current to balance the inward dark current through the light-modulated cyclic guanosine monophosphate (cGMP)-gated channels of the outer segment. These K^+ channels provide an adaptational influence, opposing the dark signal, and indirectly opposing the light signal by deactivating with hyperpolarization. The K_{Cn} channels, underlying the I_h current, provide a delayed depolarization when activated by hyperpolarization, and calcium-activated potassium channels (BK) help to maintain the resting potential near −40 mV. These are adaptational effects that tend to limit the hyperpolarization from bright light and depolarization in the dark. The cone terminal's L-type Ca^{2+} channels ($Ca_v1.4$) uniquely include alpha 1D subunits and may have special gating properties. In addition, the terminal contains a calcium-activated chloride current ($I_{Cl(Ca)}$) and calcium-induced calcium release (CICR). Calcium is highly regulated in the terminal, with internal buffering and plasma membrane transporters (protein misfolding cyclic amplifications (PMCAs)), because calcium is the trigger for vesicle release. Calcium is highly compartmentalized at the terminal because calcium in the outer and inner segments and soma performs other cellular functions. In the terminal, ryanodine receptors and IP_3 receptors modulate calcium release from internal stores. Voltage-gated sodium channels have been identified in primate cones, possibly to help amplify the cone signal along its axon. The cone terminal contains several transporters with special functions. A proton pump in the vesicles acidifies them so that protons are released along with the glutamate. The protons bind to the local calcium channels to block calcium entry, and thus regulate release. Several transporter proteins carry glutamate, including at least two isoforms that are inserted into the membrane of vesicles to load them with glutamate. A glutamate transporter sitting in the external membrane of the pedicle is important for uptake

of glutamate from the extracellular space. The light response of postsynaptic cells depends on a reduction in glutamate, but when the transporter is blocked pharmacologically the postsynaptic light response is greatly reduced. This implies that the triad synapse is protected to some extent against diffusion by the cone pedicle's invagination.

Gap Junctions

Cone axon terminals are coupled by gap junctions which carry electrical signals and small molecules directly from each cone to its neighbors. Each gap junction comprises connexin molecules which can form a conductive pore when they are aligned in the membrane of both coupled neurons. The gap junctions are located on telodendria which are basal processes that emanate from the cone terminals to make contact with the neighbors. The cone gap junctions are punctate, that is, they comprise just a few connexin molecules. The connexin has been identified as Cx36. In addition, a cone's telodendria contact all the surrounding rods with punctate gap junctions. The cone side of the rod-cone gap junction also comprises Cx36, but the identity of the rod-specific connexin molecule is not known. In foveal cones, because their terminals are all located outside the fovea, some of the telodendria extend several hundred micrometers around the perimeter of the fovea to make contact with the neighboring cones, whose axons have extended in the opposite direction from central fovea.

Morphological Implications of Spectral Sensitivity

The cones of most vertebrates exist in several types that differ in their spectral sensitivity. Until recently, it was difficult to distinguish cone spectral type based on morphology, but antibodies are now available to specifically stain the outer segments by spectral type. Direct imaging is now able to routinely determine the spectral type. The inner segments of birds and some species of reptiles and mammals contain oil droplets which filter out some wavelengths, to narrow the outer segment's sensitivity and improve the ability for color discrimination. The primate S-cone, sensitive to short wavelengths, is smaller and its terminal makes fewer contacts, so it is distinguishable from middle (M)- and long (L)-wavelength-sensitive cones. In addition, the M- and L-type cones can be distinguished by the number and location of their synaptic connections with bipolar cells. The M- and L-cones are electrically coupled by gap junctions, which blur their spectral sensitivity. The coupling is a reasonable compromise because the coupling increases their contrast sensitivity and the spectral blurring effect is moderate due to the similarity of the M- and L-type spectral sensitivities. The M- and L-type cones are located randomly in bunches of similar type, which along with the indiscriminate coupling may improve contrast sensitivity without causing much blurring of color. The S-type cone is not coupled strongly to its M- and L-type neighbors, apparently because its spectral sensitivity is farther from the M- and L-type curves.

Function

Adaptation and Predictive Coding

The role of the cone photoreceptor in daylight is crucial because it is the first step in the visual pathway. The cone's task is to transduce and relay information in the visual environment relevant to an organism's survival. A major problem faced by the cone is that daylight varies over 5 log units, but a synaptic signal is only able to vary only over 1–2 log units. The problem is one of dynamic range and also of noise because dynamic range limits the maximum signal, and noise limits the minimum discriminable signal. The amount of information available is related to the maximum signal divided by the minimum, that is, the number of distinguishable levels. Since cone transduction is noisy and the ribbon synapse is also noisy, to maximize the amount of information the cone must remove all irrelevant information and selectively transmit the most important signal components with high sensitivity. One way the cone deals with this problem is by removing information about the background level by adaptation. This is accomplished first in the outer segment. In addition, the cone has several more adaptational mechanisms: modulation of the light-evoked signal by voltage-gated channels in the inner segment and terminal, gain reduction at the ribbon synapse, and regulation of its neurotransmitter release by negative feedback. To preserve information about fine temporal detail, the adaptational mechanisms must be slow, and to preserve spatial detail, the adaptational mechanisms must be wide. The theory for such adaptational mechanisms is called predictive coding, in which a temporally slow or spatially wide average signal is subtracted from a photoreceptor. Thus, the cone ribbon synapse carries a signal that is optimally adapted in time and also in space.

Synaptic Transfer Function

Upon depolarization, the ribbon synapse releases glutamate with a nonlinear transfer function, which is controlled by the voltage sensitivity of the L-type calcium channel. The mechanism for release is linearly modulated by calcium because glutamate release is proportional to the terminal's local calcium concentration. Release is maximal in the dark when the cone is depolarized, and minimal in bright light when the cone is hyperpolarized

(Figure 2). Due to the nonlinear release function, the synaptic gain for small light increments is also maximal in the dark, and minimal in the light. Thus, the synaptic gain is adaptive, that is, it tends to oppose the light-evoked signal and reduce contrast gain in bright light. Negative feedback tends to oppose this effect, that is, it reduces the change in synaptic gain due to a change in background level. Glutamate released by the cone binds to the postsynaptic metabotropic glutamate receptor 6 (mGluR6) receptor to activate a second-messenger cascade which inverts and low-pass filters the signal in the bipolar cell. Glutamate also diffuses out of the invagination to bind to kainate receptors at the tips of off-bipolar cells.

Rate of Vesicle Release

A major source of noise for the cone signal is the random release of vesicles by the ribbon. Although the details of the release mechanism are not known, it is thought to be stochastic (noisy), similar to a modulated Poisson distribution, for which the standard deviation is equal to the square root of the mean. There is also some evidence for more regular release. Protons released along with the vesicle's packet of glutamate bind to the local calcium channels which may generate a short refractory period, allowing release to be more regular. The cone synapse is thought to release vesicles at 100–200 s^{-1} per active zone in the dark, but in bright sunlight the rate is reduced to $<10\,s^{-1}$ per active zone. The ability of a ribbon synapse to transmit information about contrast, even with a high release rate, is extremely limited: at a Poisson rate of 200 ves s^{-1}, contrast threshold for a 100 ms response would be ~0.2. Therefore to increase sensitivity, several ribbons transmit the same cone signal in parallel. With 20 ribbons, the total release rate is $\sim 2000\,s^{-1}$, for which the contrast threshold would be 0.07. Each bipolar cell contacts several (4–8) ribbons per cone, and bipolar cells (except foveal midget bipolars) normally contact several (4–6) cones, so a bipolar cell integrates signals from one to several dozen cone ribbons.

Electrical Coupling

The gap junctions between cone terminals function as a spatial filter, averaging cone signals to remove noise, and removing high spatial frequencies. The effect is to enlarge the cone receptive field beyond the effect of optical blur. Adjacent L- and M-cones in primate are electrically coupled by gap junctions, which blur to some extent their ability to support color discrimination, implying that their action to reduce noise provides a benefit to luminance contrast discrimination. S-cones are uncoupled to the other types, probably because their spectral sensitivity is so different that it would suffer out of proportion to the potential increase in contrast sensitivity. Cone coupling is paradoxical to some extent because in a linear system which collects cone signals, for example, convergence to a large ganglion cell's dendritic tree, gap junctions would

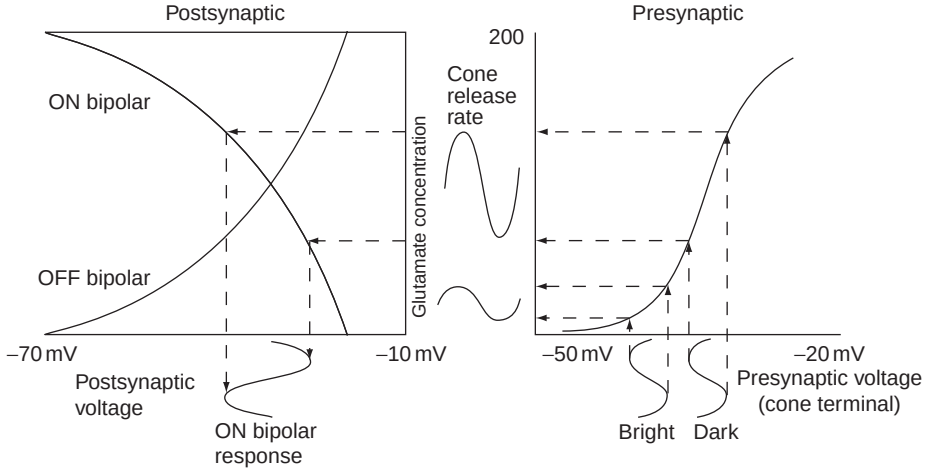

Figure 2 Transfer function of cone ribbon synapse. At right, presynaptic ribbon release function, showing two signals in the cone terminal, one more hyperpolarized (bright), and the other more depolarized (dark). The brighter signal releases less glutamate and has lower release gain because the release function is nonlinear. The fraction of modulated release is higher for the hyperpolarized (bright) signal than for the depolarized (dark) signal because the maintained release rate is lower in bright light. However, the system must compromise to set a relatively high release rate. At left, the postsynaptic transfer function from glutamate binding to voltage in the ON bipolar response is inverted. For the relatively high release of the dark signal, the ON and OFF bipolar responses are similar in amplitude and degree of saturation. The presynaptic release rate must be maintained relatively high to keep the postsynaptic signals symmetrical; if the release rate were lower, the OFF bipolar signal would decrease and the ON bipolar signal would saturate. Negative feedback maintains the cone ribbons' relatively high maintained release rate to optimize the signal/noise ratio in both ON and OFF bipolar cells.

provide no benefit. However, the cones apparently benefit from the reduction of noise before their signal passes through the ribbon synapse which is to some extent nonlinear. The gap junctions coupling a cone to its neighboring rods allow rod signals at mesopic backgrounds, where a rod temporally sums several photon signals, to pass to cones to be transmitted through the cone pathway to ganglion cells. Since cones are 30–100-fold less sensitive than rods, this rod–cone coupling represents a form of adaptation for the cone pathway.

Negative Feedback

Adaptation from spatially pooled horizontal cell feedback at the cone triad is important for retinal signal processing. Glutamate released by the cone ribbon synapse binds to AMPA receptors on the horizontal cell dendrite to depolarize it, and in turn the horizontal cell provides negative feedback to control the release of glutamate by the cone. The negative feedback contributes to an antagonistic surround in bipolar cells and in all other postsynaptic neurons. In some species (e.g., turtles, fish, and putatively in some mammals), horizontal cells receive spectrally specific signals from cones and therefore their negative feedback contributes to cone color opponency. The mechanism for the negative feedback from horizontal cells is not known but several candidates are currently being studied. Horizontal cells synthesize γ-aminobutyric acid (GABA) and release it through a transporter working in reverse, and in some species (e.g., turtle, fish, salamander, and frog), GABAergic feedback has been found in the cone terminal. Horizontal cells also generate a feed-forward surround signal in both on- and off-bipolar cells, which have $GABA_A$ receptors in their dendrites. The effect is to generate a stronger surround signal in the bipolar cell, allowing it to more tightly control its release of neurotransmitter. However, standard GABA-receptor blockers do not affect the surround in most species. Some evidence suggests that feedback may be provided through release of protons in the invagination, because when pH buffers, such as 4-(2-hydroxyethyl)-1-piperazineethanesulfonic acid (HEPES) are applied via the perfusion bath *in vitro*, they block horizontal cell feedback proportionate to their buffering capacity. A third possibility is that the feedback is ephaptic (electrical). The pH and ephaptic theories describe a feedback signal that directly modulates the cone terminal's calcium current. One benefit of all these putative feedback mechanisms is their freedom from noise that would occur with vesicular release. Feedback is necessary to control neurotransmitter release, but it has one problem, that if too strong it can cause instability from delays in the feedback loop. Oscillations can be evoked by flashed full-field stimuli with a dark mask over the horizontal cell recording site. The dark depolarizes the cone, increasing gain in the feedback loop, which tends to generate oscillations. Other adaptational mechanisms such as K^+ channels can generate similar resonances related to the delay in their response.

Theory of Ephaptic Feedback

The proposed ephaptic feedback modulates the cone pedicle's calcium channels by controlling the polarization of the external surface of the membrane inside the invagination. When a horizontal cell is hyperpolarized by a remote light (i.e., without modulating local glutamate release), the current that flows from extracellular space into its dendritic tips is increased. The increase in current causes a voltage drop inside the invagination, which shifts the voltage at the external membrane surface more negative. As both surfaces of the membrane have been shifted negative, the calcium channel senses a depolarization (lack of polarization) and thus opens further, which opposes the original light signal. The opposite effect occurs when a cone terminal is hyperpolarized by light but the horizontal cell is not. Light reduces glutamate release, which closes the horizontal cell's glutamate-gated (AMPA) channels, decreasing the current flow into the dendritic tip, which shifts the external cone membrane more positive, causing the calcium channel to sense a greater hyperpolarization, which comprises net positive feedback. However, the horizontal cell dendritic tips contain hemichannel gap junctions (connexins) which are not gated by glutamate but shunt the glutamate-gated channels. Their effect is to reduce positive feedback and to enhance negative feedback. One potential problem for the theory is that the hemichannels reduce the light response, and because their conductance is less than the AMPA receptor channels one imagines they should not cause a robust effect. However, the theory is supported by strong evidence, for example, the hemichannels can be blocked by carbenoxolone which reduces the negative feedback, and the same result occurs in knockout animals in which the hemichannels are removed. The relative magnitude of the positive and negative ephaptic feedback effects depend on several factors, including the conductances and the location of the underlying channels. The amount of voltage drop at the external membrane surface depends on the geometry of the current path through extracellular space in the invagination. A robust feedback signal, for example, the typical 5–10 mV shift seen in the calcium current in the cone pedicle, would require a relatively high resistance, and therefore the mechanism is currently controversial. Although the ephaptic theory has not generally been accepted by the field, it can explain

some of the phenomena given as evidence for pH feedback. HEPES buffer is known to acidify neurons, and hemichannels are known to be modulated by internal pH, which is consistent with the well-known effect of HEPES to block the cone surround. An advantage of ephaptic feedback is its short delay, reducing the tendency for instability. A further merit to the ephaptic theory is that it provides a functional role for the invagination, to generate the extracellular voltage shift. Putatively, then, the invagination creates a specialized local environment for the triad synapse, to limit chemical and/or electrical diffusion.

Bandpass Adaptation Filter

The cone terminal comprises a spatiotemporal filter consisting of a low-pass filter from electrical coupling between cones, and a high-pass filter from horizontal cell negative feedback. The signal in horizontal cells is low pass in space because they are large and well coupled: their receptive fields can be ~10-fold larger than their dendritic field. The feedback signal in some species has two components, the faster (pH or ephaptic) modulation of the calcium current, and a slower GABAergic component. Therefore, the horizontal cell signal, when it modulates the cone synaptic release, can be characterized as a subtraction of a low-pass filter, effectively making the cone synapse a high-pass filter. The overall effect of electrical coupling and negative feedback is to generate a band-pass filter at the cone terminal. The filter removes spatial and temporal frequencies that transmit less information, improving the performance of the visual pathway which utilizes noisy synapses for transmission.

Conclusion

The cone photoreceptor plays a crucial role in vertebrate vision because it is responsible for transducing fast changes in contrast while ignoring the background light level. To improve its sensitivity over 5 log units of background illumination, the cone contains several mechanisms for adaptation, originating in the transduction cascade, in its biophysical properties, and in the ribbon synapse. The ribbon is part of a complex local circuit called the triad that combines adaptation with spatial filtering. The triad maximizes the amount of information that can be transmitted through noisy synapses over a wide range of environmental light levels.

Acknowledgment

This work was supported by NEI grant EY016607.

See also: Phototransduction: Adaptation in Cones.

Further Reading

Copenhagen, D. R. (2004). Excitation in retina: The flow, filtering, and molecules of visual signaling in the glutamatergic pathways from photoreceptors to ganglion cells. In: Chalupa, L. M. and Werner, J. S. (eds.) *The Visual Neurosciences,* 2 vols, pp. 234–259. Cambridge, MA: MIT Press.

DeVries, S. H., Li, W., and Saszik, S. (2006). Parallel processing in two transmitter microenvironments at the cone photoreceptor synapse. *Neuron* 50: 735–748.

Gaal, L., Roska, B., Picaud, S. A., et al. (1998). Postsynaptic response kinetics are controlled by a glutamate transporter at cone photoreceptors. *Journal of Neurophysiology* 79: 190–196.

Heidelberger, R., Thoreson, W. B., and Witkovsky, P. (2005). Synaptic transmission at retinal ribbon synapses. *Progress in Retinal and Eye Research* 24: 682–720.

Hsu, A., Smith, R. G., Buchsbaum, G., and Sterling, P. (2000). Cost of cone coupling to trichromacy in primate fovea. *Journal of the Optical Society of America A: Optics, Image Science and Vision* 17: 635–640.

Hsu, A., Tsukamoto, Y., Smith, R. G., and Sterling, P. (1998). Functional architecture of primate cone and rod axons. *Vision Research* 38: 2539–2549.

Massey, S. (2008). Circuit functions of gap junction coupling in the mammalian retina. In: Basbaum, A. I., Kaneko, A., Shepherd, G., and Westheimer, G. (eds.) *The Senses: A Comprehensive Reference.* Vol. 1, pp. 457–471. San Diego: Elsevier.

Rodieck, R. W. (1998). *The First Steps in Seeing*. Sunderland, MA: Sinauer Associates.

Smith, R. G. (2003). Retina. In: Arbib, M. A. (ed.) *The Handbook of Brain Theory and Neural Networks,* 2nd edn., pp. 11–23. Cambridge, MA: MIT Press.

Smith, R. G. (2008). Contribution of horizontal cells. In: Basbaum, A. I., Kaneko, A., Shepherd, G., and Westheimer, G. (eds.) *The Senses: A Comprehensive Reference.* Vol. 1, pp. 341–349. San Diego: Elsevier.

Smith, R. G., Freed, M. A., and Sterling, P. (1986). Microcircuitry of the dark-adapted cat retina: Functional architecture of the rod–cone network. *Journal of Neuroscience* 6: 3505–3517.

Sterling, P. and Matthews, G. (2005). Structure and function of ribbon synapses. *Trends in Neuroscience* 28: 20–29.

Thoreson, W. B. (2007). Kinetics of synaptic transmission at ribbon synapses of rods and cones. *Molecular Neurobiology* 36: 205–223.

Tsukamoto, Y., Masarachia, P., Schein, S. J., and Sterling, P. (1992). Gap junctions between the pedicles of macaque foveal cones. *Vision Research* 32: 1809–1815.

van Hateren, J. H. (2007). A model of spatiotemporal signal processing by primate cones and horizontal cells. *Journal of Vision* 7: 3.

Congenital Cranial Dysinnervation Disorders

T M Bosley, D T Oystreck and K K Abu-Amero, Ophthalmology Department, King Saud University, Riyadh, Saudi Arabia

Glossary

ABDS (Athabascan brainstem dysgenesis syndrome) – A syndrome found in American Indians that is also caused by homozygous *HOXA1* mutations, but usually with more severe symptoms than BSAS, including primary hypoventilation in childhood, cerebral cortical ischemic injury, and mental retardation.

BSAS (Bosley–Salih–Alorainy syndrome) – An autosomal recessive syndrome including variable bilateral DRS type 3 (sometimes with complete horizontal gaze restriction bilaterally), deafness due to absence of the hearing apparatus in the petrous bones, cerebrovascular and cardiac malformations, and autism, caused by homozygous mutations in *HOXA1*.

CFEOM (congenital fibrosis of the extraocular muscles) – A group of congenital, nonprogressive strabismus disorders that may be sporadic, familial, or teratogenic.

CFEOM1 – An autosomal dominant congenital bilateral ptosis with globes infraducted bilaterally and unable to elevate even to primary gaze; in general, ocular motility is restricted bilaterally in an asymmetric fashion in all directions; sometimes associated with DRS; caused by heterozygous mutations in *KIF21A*.

CFEOM2 – An autosomal recessive congenital bilateral ptosis with a large exotropia and complete inability to adduct, elevate, or depress either globe, often with partial restriction of abduction bilaterally as well; associated with unreactive pupils; caused by homozygous mutations in *PHOX2A*.

CFEOM3 – An autosomal recessive congenital bilateral ptosis and asymmetrically restricted ocular motility similar to CFEOM1, but in general less severe so that globes can be elevated to primary position; associated with heterozygous mutations in *KIF21A*, a locus at 16q24.2–q24.3, and other heterozygous mutations.

DRRS (Duane radial ray syndrome) – Also known as Okihiro syndrome, this is an autosomal dominant syndrome marked by DRS together with forearm and hand anomalies and variable expression of cardiac, renal, hearing, and vertebral anomalies; caused by heterozygous mutations in *SALL4*.

DRS (Duane retraction syndrome) – A congenital horizontal ocular motility disturbance, usually unilateral but occasionally bilateral, defined largely by the presence of retraction of the globe and narrowing of the palpebral fissure on adduction; usually described as types 1, 2, and 3; most often sporadic but familial in 5–10%.

HGPPS (Horizontal gaze palsy and progressive scoliosis) – An autosomal recessive disorder marked by congenital absent or almost absent horizontal gaze (not caused by DRS) and severe, progressive scoliosis typically beginning in early childhood; caused by homozygous mutations in *ROBO3*.

Moebius syndrome – A congenital neurologic disorder marked by unilateral or bilateral facial weakness, often with horizontal ocular motility restriction, usually in abduction.

Introduction

Early Concepts and Nomenclature

The concept of congenital fibrosis of the extraocular muscles (CFEOM) was created to include strabismus disorders that were congenital and nonprogressive with active limitation and/or passive restriction of globe movement. These disorders were commonly associated with fibrous changes in extraocular muscles that were obvious to ophthalmologic surgeons trying to correct the strabismus that was frequently associated. The most common CFEOM pattern was a horizontal retraction syndrome (now typically called Duane retraction syndrome (DRS)) involving the medial and/or lateral recti muscles. Pediatric ophthalmologists knew for years that extraocular muscles of patients with DRS were frequently tight and fibrotic, sometimes with posterior insertions into the globe or anomalous fibrous bands to the globe and other orbital structures. These observations led to the concept that many individuals with congenital ocular motility disorders suffered from an abnormality in the development of extraocular muscles. Thus, the original CFEOM concept focused on abnormal muscle development.

Many CFEOM problems seemed sporadic, but others were clearly familial. CFEOM was initially categorized into

five groups based on the putative muscles involved: (1) typical and atypical horizontal retraction syndrome (presumably involving medial and/or lateral recti, now commonly called DRS), (2) strabismus fixus (involving medial and/or lateral recti), (3) vertical retraction syndromes (involving superior and/or inferior recti), (4) superior oblique tendon sheath syndromes (possibly involving inferior and superior oblique muscles, now commonly called Brown syndrome), and (5) general fibrosis syndromes (involving three or more of the extraocular muscles). Defined broadly, the concept of the congenital fibrosis syndromes includes CFEOM, Duane syndrome, Moebius syndrome, and certain other sporadic and hereditary disorders of ocular motility.

It is now well recognized that some of these syndromes affect muscles and somatic structures not directly related to vision. Perhaps the best recognized of these is the Moebius syndrome, which has been defined in a variety of ways, but which is now typically recognized as the association of unilateral or bilateral facial weakness with horizontal gaze restriction, commonly with at least an abduction defect.

In addition, it became clear after hundreds of publications, that other, less common, sometimes familial, congenital ocular motility disturbances also existed. These were particularly vexing problems, clinically because of technical difficulties dealing with ptosis and fibrotic muscles, and theoretically because of enormous variability from patient to patient. At times, CFEOM was also found in association with deformities of the limbs (including limb hypoplasia, polydactyly, hypoplastic or absent radius and thumb, and other anomalies), skull hypoplasia and asymmetry, cleft palate, Klippel–Feil anomaly, scoliosis, spina bifida, and anomalies of the vertebra, ribs, and scapulae. Associations were also described with nystagmus, ptosis, microphthalmos, colobomas, iris heterochromia, congenital cataracts, congenital ear anomalies, and sensorineural deafness. Clearly, this was a complex field, and initially, only descriptive, phenotypic reports were possible.

Information regarding the possible etiology of a number of CFEOM disorders gradually became available shortly after the concept was initially proposed. In 1932, Phillips first reported the absence at autopsy of the sixth cranial nerves on both sides in a child operated for DRS. Since then, at least four additional autopsy reports have described the absence of the sixth cranial nerves in patients with DRS. Electrical studies of extraocular muscles documented anomalous firing of the lateral recti on attempted adduction, and DRS also occurs in the setting of other conditions with anomalous axonal guidance. Brainstem abnormalities have been found at autopsy in a number of patients with Moebius syndrome. These and many other reports began to point toward a possible neurologic etiology of at least some patients previously described as having CFEOM.

The concept of congenital fibrosis of extraocular muscles has a 50-year history and has become well entrenched in ophthalmologic textbooks. During this time, hundreds of reports described unusual congenital abnormalities of ocular motility, the lids, and the face, occasionally also associated with other dysmorphic changes of the skull and body. Through this time, the suspicion lingered that these congenital strabismus syndromes might in some way contain clues regarding the much more common comitant esotropia and exotropia. These comitant ocular motility abnormalities are commonly not present at birth, but appear within the first months of life. They are not associated with fibrosis of the extraocular muscles, and surgical correction (when necessary) is more easily performed. More importantly, they are much more common, occurring in as many as 1–5% of Americans and Europeans. The hope still persists that understanding the uncommon occurrence of congenital noncomitant strabismus may tell us something important about the development of the human ocular motility apparatus and ways to avoid or more easily ameliorate the visual and cosmetic effects that occur when that developmental process goes awry.

The Concept of Congenital Cranial Dysinnervation Disorders

In October 2002, a multidisciplinary group of clinicians and scientists met in Naarden, The Netherlands, under the auspices of the European Neuromuscular Center (ENMC). The meeting was extraordinarily timely because the power of modern genetics was just beginning to yield important results with regard to some variants of CFEOM. At that time, the responsible genes had been identified for CFEOM type 2 (*PHOX2A*) and DRS with radial ray anomalies (*SALL4*), and considerable clinical and radiological data had been obtained regarding other CFEOM syndromes. In every case, the available clinical, radiologic, and genetic data pointed toward a neurogenic etiology rather than a myopathic one. Therefore, the ENMC group suggested that the term congenital fibrosis of the extraocular muscles was likely inaccurate because it specifically identified the extraocular muscles as the unifying cause of these ocular motility abnormalities. They proposed the alternative concept of congenital cranial dysinnervation disorders (CCDDs) to focus attention on abnormalities of innervation of extraocular and facial muscles together with dysinnervation by nearby nerves when the correct nerve failed to innervate a developing muscle or muscle group. The subsequent years have seen a rapid elaboration of knowledge regarding the genetic etiology of a number of syndromes included under the concept of CCDDs (**Table 1**). However, the conceptual grouping remains large, and there are likely many additional genetic and teratogenic syndromes that are yet to be identified and characterized.

Current Genetically Defined CCDDs

Congenital Fibrosis of the Extraocular Muscles Type 1 (CFEOM1; MIM #135700)

This is the most common of the genetic CFEOM phenotypes. It is defined by the presence of congenital bilateral ptosis and bilateral, frequently asymmetric, ocular motility limitation. By the current definition of the syndrome, the globes bilaterally must be infraducted and unable to reach primary position. Upgaze is severely restricted, while horizontal and downgaze is variably restricted (Figure 1). These patients commonly have positive forced ductions and misdirected eye movements such as synergistic convergence on attempted upgaze, but they are rarely noted to have retraction of the globe unless DRS coexists. Neuropathology has suggested a defect of at least the superior division of the oculomotor nerve.

Detailed orbital magnetic resonance imaging (MRI) neuroimaging in CFEOM1 patients showed profound atrophy of the levator and superior rectus muscles, and all the remaining extraocular muscles had reduced size of varying degrees. The orbital motor nerves were absent, hypoplastic, or misdirected in most patients. Intracranial imaging revealed hypoplastic oculomotor and abducens nerves in appropriately imaged subjects. Optic nerve size was reduced 30–40% in cross section, but no patient reported a visual problem or had an afferent pupillary defect.

CFEOM1 is an autosomal-dominant syndrome present worldwide that is caused by heterozygous mutations in *KIF21A*. The *KIF21A* gene encodes a kinesin microtubule-associated motor protein that is associated with anterograde organelle transport in neuronal cells. The corresponding protein is neuronally expressed and is important in axonal maintenance. All mutations detected thus far in this gene are located in the stalk domain of the *KIF21A* protein, which links the active motor domain to the tail domain. These mutations may affect some of the structural components of the protein and thus limit its function.

Congenital Fibrosis of the Extraocular Muscles Type 2 (CFEOM2; MIM #602078)

Patients with CFEOM2 have bilateral ptosis and a large angle exotropia with severely limited horizontal and vertical eye movements. The disorder looks like bilateral oculomotor nerve palsies with no adduction, elevation, or depression on both sides and with incomplete abduction (Figure 2). Pupils are variable in size and shape and unreactive to light even though they react correctly to pupillary pharmacologic agents. High-resolution MRI documented absence of the oculomotor nerves bilaterally in all appropriately studied patients, but the remainder of the brain appeared grossly normal.

CFEOM2 is an autosomal-recessive genetic disorder caused by homozygous mutations in the gene *PHOX2A*. *PHOX2A* is a homeodomain transcription factor that regulates the expression of tyrosine hydroxylase and

Table 1 Current genetic classification of CCDDs

Type	*OMIM*	*Inheritance*	*Gene*	*Locus*
CFEOM1	#135700	Autosomal dominant	*KIF21A*	12q12
CFEOM2	#602078	Autosomal recessive	*ARIXIPHOX2A*	11q13.1
CFEOM3	%600638	Autosomal dominant	*KIF21A*	12q12
			unknown	16q24.2–q24.3
			unknown	13q12
HGPPS	#607313	Autosomal recessive	*ROBO3*	11Q24.2
HOXA1 Spectrum	#601536	Autosomal recessive	*HOXA1*	7p15.3
DRRS	#607323	Autosomal dominant	*SALL4*	20q13.13–13.2
DURS2	#604356	Autosomal dominant	*CHN1*	2q31
DURS1	%126800	Sporadic/autosomal dominant	unknown	8q13
			unknown	8q12.2–q21.2

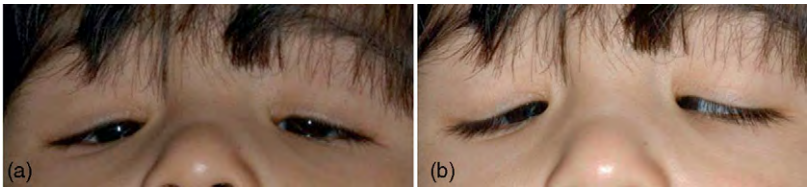

Figure 1 CFEOM1 phenotype. (a) bilateral ptosis with a characteristic chin-up head posture. Eyes are straight in downgaze but both globes are fixed in an infraducted position and are unable to elevate to midline; (b) attempted upgaze results in marked bilateral adduction.

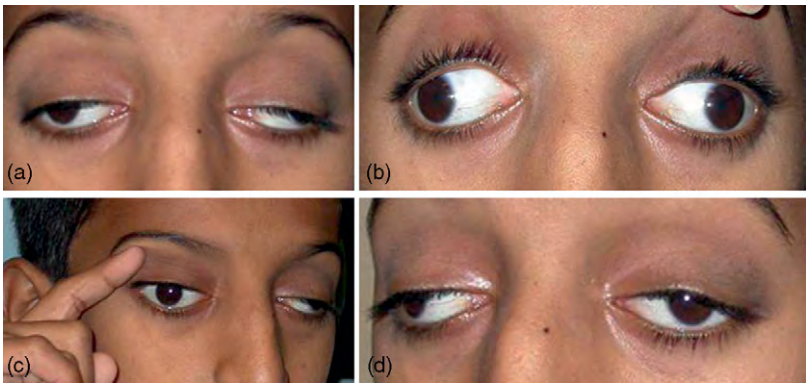

Figure 2 CFEOM2 phenotype. (a) primary position showing bilateral ptosis with brow effort trying to clear visual axis; (b) primary position with lids held showing both globes fixed in abducted positions with neither eye able to fixate in a straight ahead position. Anomalous horizontal head position is adopted to fixate with either eye. (c) the right eye is fixed in abduction requiring a marked head turn to the left. Brow effort cannot clear the right visual axis, requiring manual lid elevation to see. Chin elevation to avoid ptosis cannot be utilized because of the absence of downgaze; and (d) marked head turn to the right to fixate with left eye where adequate lid elevation from brow effort is achieved.

dopamine β-hydroxylase, two catecholaminergic biosynthetic enzymes essential for the differentiation and maintenance of the noradrenergic neurotransmitter phenotype. The encoded protein plays a central role in the development of the autonomic nervous system and has also been shown to regulate transcription of the α3 nicotinic acetylcholine receptor gene. *PHOX2A* is mainly expressed in the nervous system and specifically in the developing oculomotor and trochlear nerve nuclei, supporting the hypothesis that CFEOM2 results from maldevelopment of the oculomotor and trochlear nerves.

Congenital Fibrosis of the Extraocular Muscles Type 3 (CEOM3; MIM #600638)

This is another CCDD in which patients have bilateral ptosis and bilateral, typically asymmetric, restriction of ocular motility in all directions of both eyes (OU). This congenital ocular motility syndrome looks very similar to CFEOM1, although generally without the complete restriction of upgaze that is a diagnostic feature of CFEOM1 (**Figures 3** and **4**).

Inheritance is autosomal dominant with incomplete penetrance and variable expressivity. This phenotype may be caused by mutations in several different genes, including *KIF21A* at times. CFEOM3 has been mapped to 16q24.2–q24.3 in several pedigrees, and analysis of chromosomal translocation t(2;13)(q37.3;q12.11) detected in a three-generation family with clinical features typical of CFEOM3 has helped in mapping a fourth locus. It seems quite possible that each of the genes involved in this syndrome may have a role similar to *KIF21A* in directing growing cranial nerves to a correct termination in the extraocular muscles.

Horizontal Gaze Palsy and Progressive Scoliosis (HGPPS; MIM #607313)

This disorder was first described in English literature by Dretakis because he recognized the severe associated scoliosis. Neurologically, the syndrome is marked by complete or almost complete bilateral horizontal gaze restriction with full vertical gaze (**Figure 5**), variable convergence, variable congenital nystagmus, rare and mild vertical oculomotor imbalance, and normal lids except for asynchronous blinking. These patients are generally intellectually normal. Neuroimaging revealed intact abducens nerves bilaterally but deep anterior and posterior clefts in the medulla and low pons, a large fourth ventricle (**Figure 6**), and no evidence of corticospinal tract or superior cerebellar peduncle decussation.

HGPPS is an autosomal recessive syndrome caused by homozygous mutations in *ROBO3*. *ROBO3* mutations likely disturb brainstem morphogenesis by failing to promote decussation of long motor and sensory tracts in the pons and medulla. Impaired decussation of pontine horizontal gaze pathways in the pontine paramedian reticular formation could explain the absence of horizontal eye movements and, to some extent, the small size of the pons on neuroimaging. Mutation of the *ROBO3* gene may disturb decussation in the spinal cord as well as the brainstem (as happens in the mouse), even though the human spinal cord appears normal on neuroimaging, preventing equalization of tone in the paraspinous muscles on the two sides of the spine. Such a tone asymmetry might well lead to scoliosis over time as the spine is bent and twisted by the action of asymmetric forces. Most of the mutations in *ROBO3* are homozygous mutations reported in consanguineous families, but some are compound heterozygous mutations found in nonconsanguineous families.

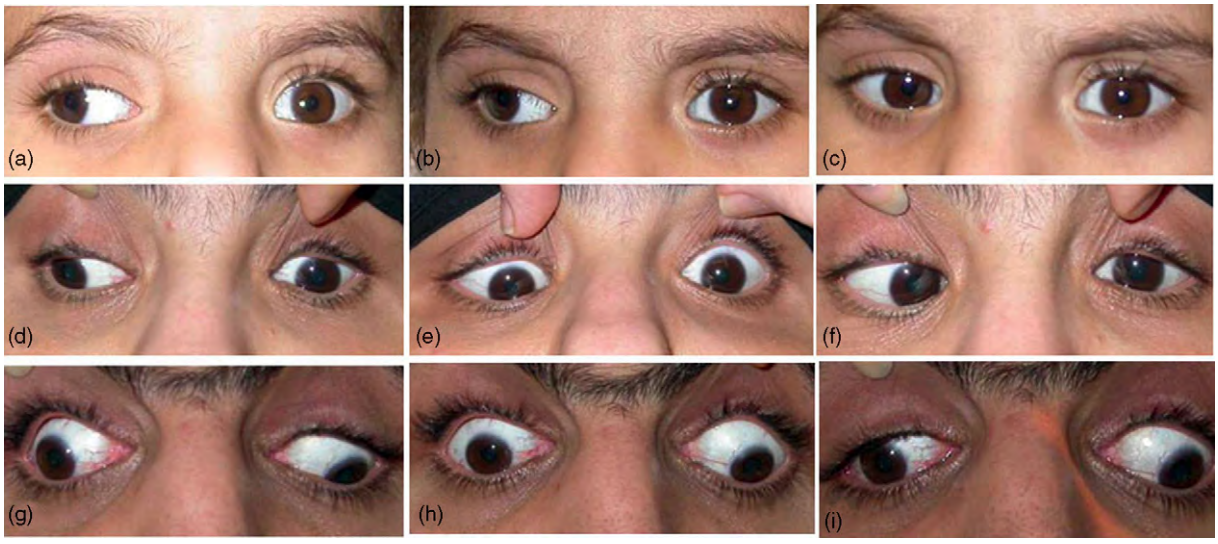

Figure 3 Phenotypic heterogeneity in CFEOM3 – horizontal eye movements. Images (b), (e), and (h) are in primary position, while images (a), (d), and (g) are right gaze, and images (c), (f), and (i) are left gaze. Example subject 1 (images (a), (b), and (c)) has unilateral absence of horizontal movement in the left eye. Interestingly, the preferred eye in primary position is the left eye, resulting in a marked secondary exotropia of the right eye. Example subject 2 (images (d), (e), and (f)) also has a unilateral absence of horizontal eye movements in the left eye together with bilaterally infraducted globes and an esotropia. There is globe retraction on the left with attempted right gaze. Example subject 3 (images (g), (h), and (i)) is the brother of subject 2. He also has bilaterally infraducted globes, but has a marked exotropia and complete absence of adduction. He retains some abduction of each eye and develops synergistic divergence of the left eye during attempted right gaze (g).

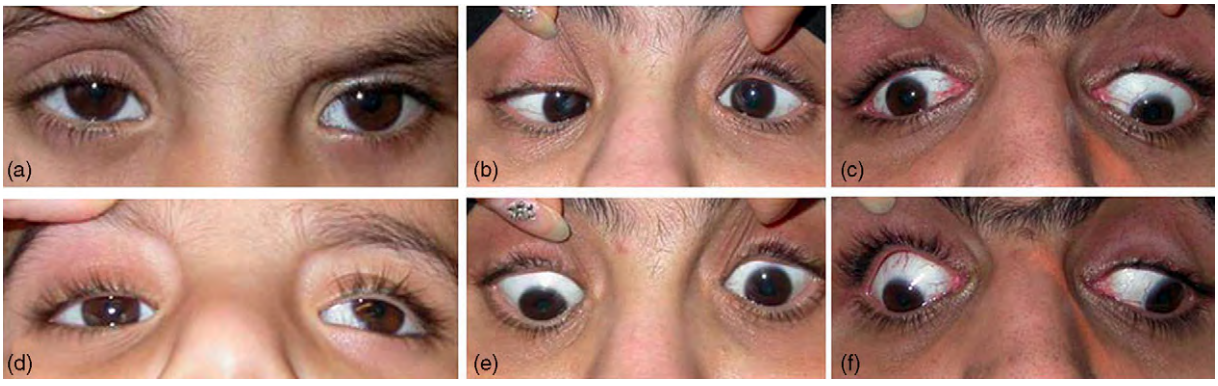

Figure 4 Phenotypic heterogeneity in CFEOM3 – vertical eye movements. Images (a), (b), and (c) are of upgaze, and images (d), (e), and (f) are of downgaze in the same three subjects seen in **Figure 3**. Example subject 1 (images (a) and (d)) has unilateral absence of vertical movement in the left eye. Example subject 2 (images (b) and (e)) has bilateral absence of upgaze with synergistic convergence during attempted movement. Only slight downward movement could be achieved in each eye from the already infraducted position of the eyes. In example subject 3 (images (c) and (f)), elevation is absent bilaterally, and he lacks the synergistic convergence movement evident in his sister. However, right globe retraction is present during attempted downgaze.

The *HOXA1* Spectrum (BSAS and ABDS; MIM #601536)

In 2003, several consanguineous families in Saudi Arabia were found to have a previously unreported syndrome consisting most notably of deafness, bilateral DRS type 3 (**Figure 7**), and cerebrovascular malformations without other obvious central nervous system abnormalities. Careful neuroimaging revealed absence of the abducens nerve bilaterally and almost completely absent development of the hearing and vestibular apparatus in the petrous bone. Several of the patients were autistic. This disorder was termed the Bosley–Salih–Alorainy syndrome (BSAS) after the clinicians who initially recognized the syndrome.

Genome wide screen revealed homozygous mutations in *HOXA1* that presumably cause an early and profound disturbance of brainstem development, probably including loss of rhombomere 5 similar to that found in the knockout mouse model. The Athabascan brainstem dysgenesis syndrome (ABDS) in Native Americans had similar characteristics, and after the gene responsible for BSAS

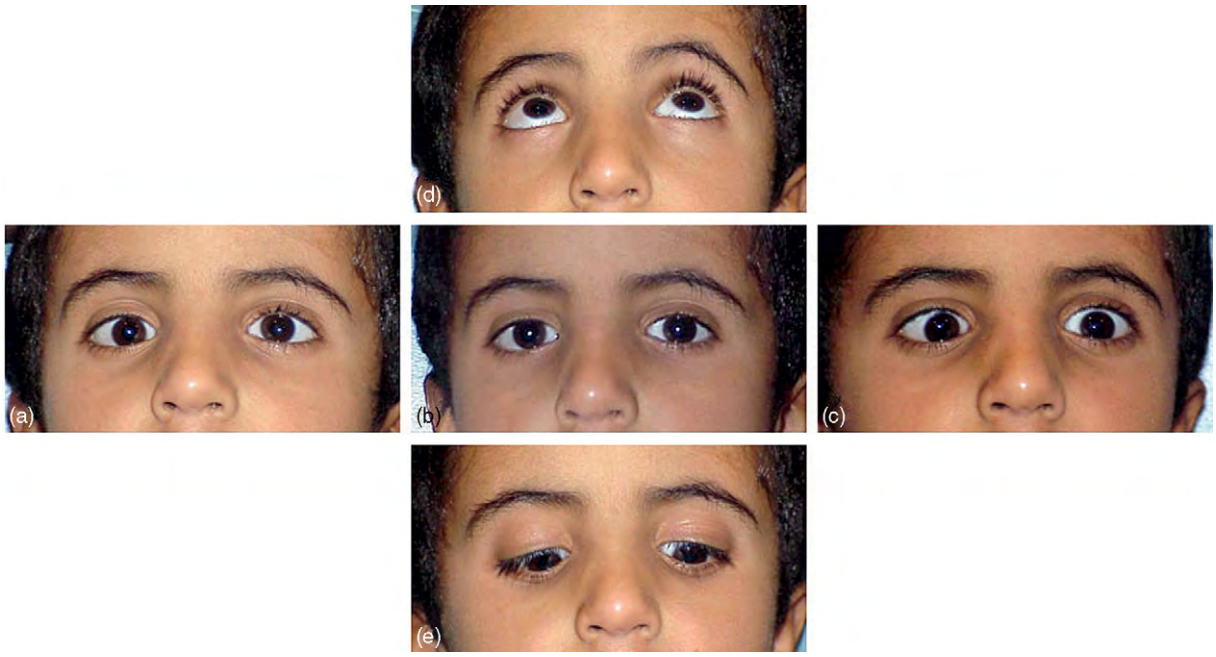

Figure 5 Ocular motility in HGPPS. Image (b) is primary gaze. Images (a) and (c) show that attempted right and left gaze, respectively, are severely limited. Images (d) and (e) show that upgaze and downgaze, respectively, are full.

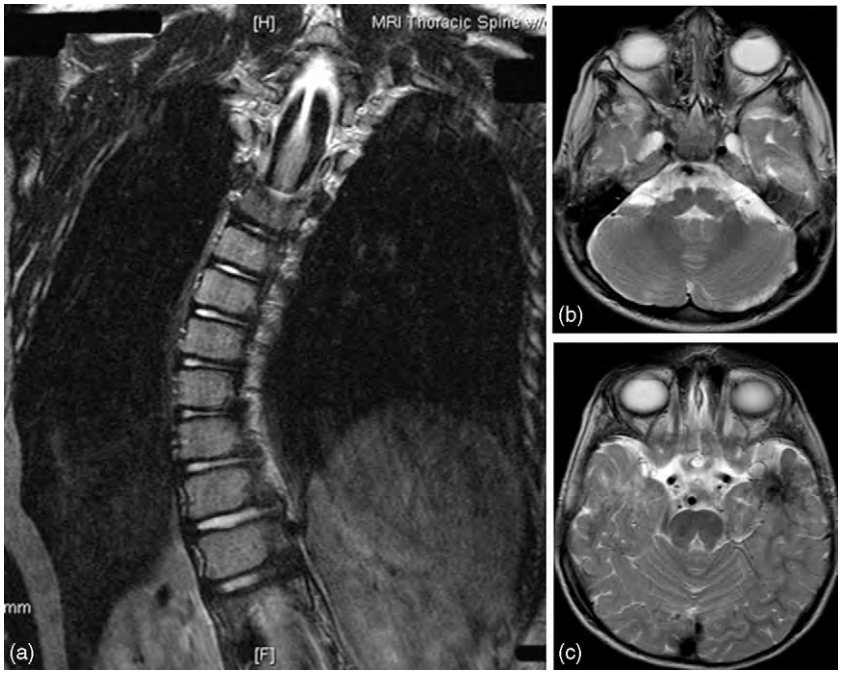

Figure 6 MRI in HGPPS. Image (a) is a coronal image through the thoracic spine showing severe scoliosis concave right. Image (b) is a transverse image through the medulla, where the brainstem is small and indented by both an anterior and posterior cleft. The fourth ventricle is large. Image (c) is a transverse image through the pons, where the brainstem is smaller than normal with a deep posterior cleft.

was identified, ABDS also was found to be due to homozygous mutations in *HOXA1*.

The Saudi population and the Native American population quite likely provide substantially different genetic substrates on which *HOXA1* mutations act, and these genetic differences alone may explain the fact that ABDS tends to be clinically more severe than BSAS. However, it is also noteworthy that Native Americans often exhibit symptoms

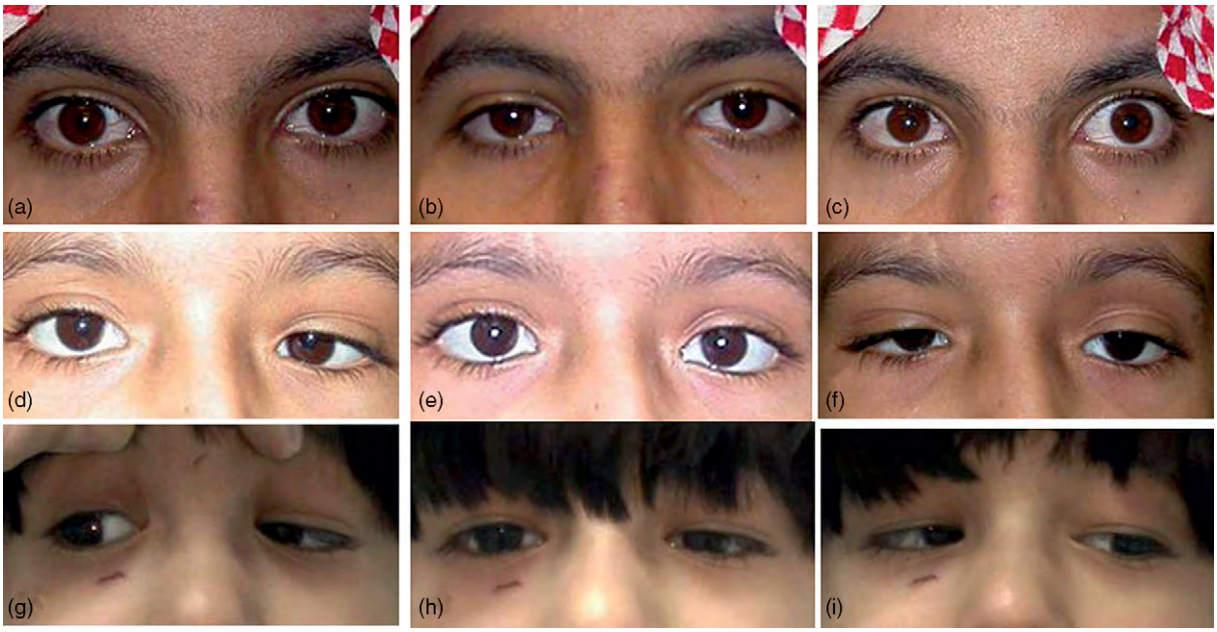

Figure 7 Ocular motility in the *HOXA1* spectrum. Images (a), (b), and (c) are from example subject 1, while images (d), (e), and (f) are from example subject 2, and images (g), (h), and (i) are from example subject 3. Images (b), (e), and (h) are in primary gaze; images (a), (d), and (g) are right gaze; and images (c), (f), and (i) are left gaze. Example subject 1 has very little horizontal movement and this could be termed horizontal gaze palsy. Example subject 2 has classic bilateral DRS type 3 with no abduction in both eyes (OU), restricted adduction OU, and retraction of the adducting globe, associated with narrowing of the palpebral fissures. Example subject 3 has full ocular motility OU despite having homozygous *HOXA1* mutations. Vertical gaze was full in all three. These three patients illustrate the variability of ocular motility in the *HOXA1* spectrum.

of primary hypoventilation during infancy and cortical ischemic injury when older, possibly because they are frequently born at a considerably higher altitude than Saudi patients. The current suggestion is that there exists a *HOXA1* spectrum of disorders that is made up of BSAS and ABDS and consists of variable horizontal gaze restriction (usually due to bilateral DRS type 3), deafness, cerebrovascular and cardiovascular maldevelopment, and cognitive disturbances ranging from autism to diffuse cortical ischemic injury.

Duane Retraction Syndrome (DRS)

DRS is the most common of all CCDD ocular motility patterns. It is characterized most commonly by limited or absent abduction and full adduction marked by retraction of the globe and narrowing of the palpebral fissure. This ocular motility pattern is called DRS type 1 and is generally sporadic, unilateral, and more common in females than in males. DRS type 2 consists of full abduction with limited adduction, also with globe retraction and narrowing of the palpebral fissure on adduction. DRS type 3 is similar to DRS type 1 except that adduction (as well as abduction) is limited to some extent (Figure 8).

Up to 10% of cases may be familial, including obvious autosomal-dominant inheritance in some families. At times, DRS may be found in other congenital ocular motility syndromes like Moebius syndrome, CFEOM1, and the *HOXA1* spectrum, and on occasion it may be associated with other developmental problems.

Recent neuroimaging studies provide evidence supporting abducens nerve abnormalities and anomalous innervation in DRS. DRS can be differentiated by MRI from congenital abducens nerve palsy because lateral rectus atrophy is found in chronic cases of abducens nerve palsy but not in DRS. The lateral rectus in DRS may be spared denervation atrophy as a result of anomalous innervation from branches of the oculomotor nerve. Several imaging studies in sporadic DRS involving types 1, 2, and 3 have reported either absence or hypoplasia of the abducens nerve.

Monogenetic autosomal-dominant syndromes in which DRS is prominent include Duane-radial ray syndrome (DRRS) and familial dominant DRS (DURS2-DRS).

Duane-Radial Ray Syndrome (DRRS or Okihiro syndrome; MIM #607323)

This syndrome is characterized by DRS with forearm and/or hand anomalies and variable expression of cardiac, renal, hearing, and vertebral anomalies. This genetic syndrome also includes absent or small abducens nerves with normal-appearing oculomotor and optic nerves. DRRS is caused by mutations in the *SALL4* gene, which is thought to be involved in the patterning of several embryonic structures such as limbs, abducens nerve, and heart.

Figure 8 Ocular motility variants in DRS. Images (a), (b), and (c) are from example subject 1, while images (d), (e), and (f) are from example subject 2, and images (g), (h), and (i) are from example subject 3. Images (b), (e), and (h) are in primary gaze; images (a), (d), and (g) are right gaze; and images (c), (f), and (i) are left gaze. Example subject 1 has DRS type 1 OD with an upshoot of that eye together with globe retraction and fissure narrowing on adduction. Example subject 2 has bilateral DRS type 1 with retraction of the adducting globe bilaterally together with narrowing of the palpebral fissure. Example subject 3 had a left DRS type 3 with limitation of both right and left gaze with the left eye together with globe retraction and narrowed palpebral fissure on adduction.

Duane Retraction Syndrome (DURS2-DRS; MIM #604356)

Individuals with DURS2-DRS can have isolated unilateral Duane syndrome but more commonly have bilateral involvement and associated vertical movement anomalies. Neuroimaging studies have demonstrated absent or hypoplastic abducens nerves and, in some cases, hypoplastic oculomotor nerves or muscles innervated by the oculomotor nerve. The causative gene has recently been identified as *CHN1*, which is thought to participate in ocular motor axon path finding, particularly involving the abducens nerve and to a certain extent the oculomotor nerve.

Discussion

The CCDDs provide an excellent example of the power of current genetic techniques to advance our understanding of certain complex clinical disorders. This heterogeneous amalgam of congenital ocular motility disorders coalesced 50 years ago around the concept of undefined abnormalities in the development of extraocular muscles. Subsequent anatomic, neuroradiologic, and genetic information has largely left in place the clinical grouping, but replaced the central concept with one of developmental abnormalities in ocular motility mechanisms in the brainstem, peripheral cranial nerves, and orbit that are neurogenic in origin. This group of disorders proved very difficult to classify by clinical criteria alone, but much more progress has been made since it has become possible to study groups of genetically homogenous individuals.

There appear to be at least three pathways by which congenital abnormalities in the human ocular motility system occur in these patients with genetically defined disorders (Table 1). The first involves the failure of cranial nerve nuclei to develop normally. Perhaps the best current example of this mechanism is the *HOXA1* clinical spectrum in which abducens nerve nuclei fail to develop as part of the loss of rhombomere 5 during development in the absence of a normal *HOX* cascade. The second mechanism involves genetic defects that lead to abnormal axonal transport of molecules necessary for normal guidance of developing peripheral neurons to the correct extraocular muscles and possibly for the normal functional development of these muscles. The best current example of this mechanism is CFEOM1 with mutations in *KIF21A* causing abnormalities in axonal transport and leading to loss of ocular motor axons and possibly abnormal termination of all peripheral nerves within the orbits. CFEOM3 is a clinically similar disorder but genetically heterogeneous, implying that other genes may play similar roles in orbital innervation. The third mechanism occurs with abnormalities in the development of upper motor neurons in the brainstem, sometimes with associated lower motor neuron abnormalities as well. The best-understood current example of this mechanism would

be individuals with HGPPS who have mutations in *ROBO3* resulting in the loss of decussation of a number of developing brainstem neural pathways, including those in the pontine paramedian reticular formation responsible for horizontal gaze.

Today, we can finally define at least some CCDD syndromes by the responsible gene as we build a montage of genes acting during development of the brainstem and orbits (**Table 1**). We now have some idea about what can go wrong in the setting of certain specific mutations, and by inductive reasoning, what role these genes play in the development of the normal human efferent visual system. Curiously, an intensive evaluation of the CCDD group has not yet yielded any implication that genes responsible for the development of the extraocular muscles themselves are involved. Rather, anatomic abnormalities in extraocular muscles noted in this group of disorders seem to be secondary to denervation and dysinnervation. Further study, of course, may change this situation.

Thus far, we have no complete explanation for the variability within each genetically defined disorder. At times, it is clear that individuals with identical mutations of the same gene nevertheless have a somewhat different phenotype, as described with mutations of *KIF21A*, *ROBO3*, and *HOXA1*. It is now clear that a single genetic abnormality can result in a fairly broad range of phenotypic presentations. For example, *KIF21A* mutations can cause CFEOM1 or CFEOM3, both of which may present with variable, bilateral ocular motility restriction and may occur with or without DRS. Likewise, *HOXA1* mutations cause deafness in most, but not all, affected individuals, autism in some, and a range of cardiovascular and cerebrovascular malformations in all individuals who have been studied appropriately.

It also seems clear now, even within this limited set of genetic syndromes, that different mutated genes can result, at least in part, in the same phenotype. DRS, for example, occurs with heterozygous mutations of *KIF21A* and *SALL4* and homozygous mutations of *HOXA1*. The cause of DRS is relatively well understood in each setting. *HOXA1* mutations probably result in the loss of rhombomere 5, including the absence of abducens nucleus development. In contrast, *KIF21A* mutations cause abnormalities in directing the abducens nerve successfully to the ipsilateral lateral rectus muscle. The diagnostic feature of globe retraction on attempted adduction is probably the result of lateral rectus denervation by the abducens nerve and dysinnervation by a nearby branch of the oculomotor nerve.

Some variants of DRS are associated with somatic mutations involving the face, neck, ears, and extremities. Such an association is understandable in the setting of *HOXA1* mutations, given that *HOXA1* is the first gene in the *HOX* cascade that is responsible for the development of orientation and certain major anatomic features of the early fetus. In fact, it is somewhat surprising that *HOXA1* mutations result in such a relatively benign syndrome given the role of *HOXA1* at the beginning of the *HOX* cascade. However, consanguineous families with *HOXA1* homozygous mutations have a greater than normal spontaneous abortion rate, implying that the result of these mutations may not always be benign.

The role of *HOXA1* is complex because it seems that this gene is not expressed in the petrous bone, and yet the petrous bone fails to elaborate the bony hearing and vestibular structures in most individuals with homozygous *HOXA1* mutations. It seems likely that abnormal development of the petrous bone results from the absence of appropriate developmental signals from abnormal neuroectoderm and brainstem nearby. The cause of cerebrovascular and cardiovascular abnormalities in patients with *HOXA1* mutations seems somewhat more straightforward because *HOXA1* may actually be active in the early development of the vascular system. The *HOXA1* clinical spectrum resembles early thalidomide poisoning, bringing up the possibility that thalidomide interferes with the early *HOX* cascade. Thus, genetic knowledge of these uncommon congenital ocular motility syndromes can increase our understanding of teratogenic phenomena as well.

HGPPS brings up further considerations regarding development during childhood. The ocular motility abnormalities of HGPPS are congenital. However, the severe scoliosis associated with the syndrome is not present at birth; rather, it begins in early childhood and progresses rapidly. *ROBO3* activity has not been documented to date in the developing spine. A direct effect of this gene's activity remains possible, but an alternative explanation is that the tone of the powerful paraspinous muscles is asymmetric in affected individuals because the absence of *ROBO3* prevents decussation of fibers in the brainstem and/or spinal cord important for equalization of paraspinous muscle tone. The action of gravity across the spine would conceivably result in accelerating scoliosis once a mild bend or torque occurs in the spine. Whatever the actual mechanism, it is possible that better understanding of the scoliosis that occurs with *ROBO3* mutations will aid in understanding other early scoliosis syndromes and even the fairly common sporadic scoliosis in pubescent females.

Patients with homozygous *ROBO3* mutations lack decussation of the major corticospinal tracts and medial lemniscus sensory tracts, an unanticipated and truly profound neuroanatomic abnormality. Curiously, these individuals in general are intellectually normal, implying that these major motor and sensory tracts find the correct termination, permitting grossly normal cortical activity despite being in the wrong hemisphere. The implication of this observation is that these developing fiber tracts respond to direction signals sequentially, with a response (or lack of it) to one signal potentially having little or no effect on the response to the next signal.

It is obvious that development of the human brainstem and development of the human efferent visual system do

not depend exclusively on the few genes identified in the CCDD syndromes discussed here. It is quite likely, therefore, that more autosomal dominant and recessive clinical syndromes are yet to be identified under the CCDD rubric. Indeed, there have been many reports over the last 50 years of unusual congenital ocular motility syndromes that were clearly familial, and some of these are surely genetic in origin. The power of current genetics may finally permit us to identify the responsible genes.

See also: Abnormal Eye Movements due to Disease of the Extraocular Muscles and Their Innervation; Cranial Nerves and Autonomic Innervation in the Orbit; Extraocular Muscles: Extraocular Muscle Anatomy; Extraocular Muscles: Functional Assessment in the Clinic.

Further Reading

Al-Baradie, R., Yamada, K., St Hilaire, C., et al. (2002). Duane radial ray syndrome (Okihiro syndrome) maps to 20q13 and results from mutations in SALL4, a new member of the SAL family. *American Journal of Human Genetics* 71: 1195–1199.

Bosley, T. M., Alorainy, I. A., Salih, M. A., et al. (2008). The clinical spectrum of homozygous HOXA1 mutations. *American Journal of Medical Genetics A* 146: 1235–1240.

Bosley, T. M., Oystreck, D. T., Robertson, R. L., et al. (2006). Neurological features of congenital fibrosis of the extraocular muscles type 2 with mutations in PHOX2A. *Brain* 129: 2363–2374.

Bosley, T. M., Salih, M. A., Jen, J. C., et al. (2005). Neurologic features of horizontal gaze palsy and progressive scoliosis with mutations in ROBO3. *Neurology* 64: 1196–1203.

Demer, J. L., Clark, R. A., Lim, K. H., and Engle, E. C. (2007a). Magnetic resonance imaging evidence for widespread orbital dysinnervation in dominant Duane's retraction syndrome linked to the DURS2 locus. *Investigative Ophthalmology and Visual Science* 48: 194–202.

Doherty, E. J., Macy, M. E., Wang, S. M., et al. (1999). CFEOM3: A new extraocular congenital fibrosis syndrome that maps to 16q24.2–q24.3. *Investigative Ophthalmology and Visual Science* 40: 1687–1694.

Dretakis, E. K. and Kondoyannis, P. N. (1974). Congenital scoliosis associated with encephalopathy in five children of two families. *Journal of Bone and Joint Surgery. American Volume* 56: 1747–1750.

Gutowski, N. J. (2000). Duane's syndrome. *European Journal of Neurology* 7: 145–149.

Gutowski, N. J., Bosley, T. M., and Engle, E. C. (2003). 110th ENMC International Workshop: The congenital cranial dysinnervation disorders (CCDDs). Naarden, The Netherlands, 25–27 October, 2002. *Neuromuscular Disorders* 13: 573–578.

Harley, R. D., Rodrigues, M. M., and Crawford, J. S. (1978). Congenital fibrosis of the extraocular muscles. *Transactions of the American Ophthalmological Society* 76: 197–226.

Jen, J. C., Chan, W. M., Bosley, T. M., et al. (2004). Mutations in a human ROBO gene disrupt hindbrain axon pathway crossing and morphogenesis. *Science* 304: 1509–1513.

Miyake, N., Chilton, J., Psatha, M., et al. (2008). Human CHN1 mutations hyperactivate alpha2-chimaerin and cause Duane's retraction syndrome. *Science* 321: 839–843.

Nakano, M., Yamada, K., Fain, J., et al. (2001). Homozygous mutations in ARIX(PHOX2A) result in congenital fibrosis of the extraocular muscles type 2. *Nature Genetics* 29: 315–320.

Tischfield, M. A., Bosley, T. M., Salih, M. A., et al. (2005). Homozygous HOXA1 mutations disrupt human brainstem, inner ear, cardiovascular and cognitive development. *Nature Genetics* 37: 1035–1037.

Yamada, K., Andrews, C., Chan, W. M., et al. (2003). Heterozygous mutations of the kinesin KIF21A in congenital fibrosis of the extraocular muscles type 1 (CFEOM1). *Nature Genetics* 35: 318–321.

Conjunctiva Immune Surveillance

E Knop, Charité – Universitätsmedizin Berlin, Berlin, Germany
N Knop, Hannover Medical School, Hannover, Germany

Glossary

Conjunctiva-associated lymphoid tissue (CALT) – It is the physiological protective mucosal immune tissue of the conjunctiva. It consists of lymphoid cells and accessory cells inside the mucosal tissue and can be divided into the epithelial and underlying connective tissue (lamina propria) compartments. It is arranged as a diffuse lymphoid effector tissue along the whole extension of the conjunctiva and has interspersed organized lymphoid follicles for afferent antigen uptake and effector cell generation.

Dendric cells (DCs) – They are a special class of professional antigen-presenting cells (**APC**, together with macrophages and B-cells). They take up external antigens, degrade them into small fragments (epitopes), present them on MHC-class-II to T-helper cells, and hence, induce immune reactions. Depending on their maturation status which is influenced by the presence of inflammatory signals, they modulate between the inductions of tolerance versus inflammation. They also link the unspecific innate to the induced specific immune system and are hence key modulators of the immune reaction.

Eye-associated lymphoid tissue (EALT) – This tissue summarizes all the lymphoid tissues of the extended mucosal ocular surface, that is, of ocular surface proper (conjunctiva and cornea) along with its mucosal adnexa (the lacrimal-drainage-associated lymphoid tissue, LDALT, and the lymphoid cells inside the lacrimal gland). EALT is in line with the mucosal immune system in other parts of the body (e.g., gut-associated lymphoid tissue (GALT) in the gut and bronchus-associated lymphoid tissue (BALT) in the airways).

High endothelial venules (HEVs) – Specialized postcapillary venules that have an endothelium of bright roundish cells compared to the ordinary flat dense ones. They are located in lymphoid tissues and have tissue-specific adhesion molecules (vascular addressins) on the cell surface that specifically interact with homing receptors on circulating lymphocytes in order to maintain a regulated immigration of lymphocytes into the tissue.

Human leukocyte antigen (HLA) – A system of the major histocompatibility complex (⇒ MHC) in humans. It contains of a number of genes and their respective encoded proteins (that can act as antigens). The term HLA is frequently used to describe immunological self and nonself in the context of transplant rejection.

Intercellular adhesion molecule 1 (ICAM-1) – An adhesion molecule (CD54 according to the immunological cluster of differentiation, CD, nomenclature) mainly on vascular endothelial cells which is upregulated in inflammation and promotes the increased immigration of leukocytes, that carry corresponding integrin receptors, into the tissue.

Membraneous cells (M-cells) – Also called microfolded cells, they are a special type of cells in the modified epithelium overlying organized lymphoid follicles, the so-called follicle-associated epithelium (FAE). Their name refers to the fact that they have a different, usually smooth, surface ultrastructure compared to the ordinary epithelial cells. They form cellular pockets populated by groups of leukocytes which are separated from the lumen by a thin luminal cytoplasmic sheet. M-cells actively transcytose luminal antigens for uptake by the leukocytes and their subsequent presentation to and activation of T- and B-cells in order to generate antigen-specific effector cells.

Major histocompatibility complex (MHC) – It is differentiated mainly into class-I and class-II. Their encoded proteins on the surface of cells perform the presentation of protein antigen fragments (epitopes) to immune cells. MHC-class-I is found on all nucleated cells and presents antigens produced inside the cell (either own or viral proteins after infection) to cytotoxic CD8 lymphocytes and natural killer cells. MHC-class-II, in contrast, occurs physiologically only on specialized antigen-presenting cells and presents foreign antigens to the CD4 receptor of T-helper cells. In inflammation, it can be upregulated by other cells.

Lipopolysaccharide (LPS) – A component of the outer cell membrane of the wall of Gram-negative bacteria that acts as an endotoxine. The presence of LPS, that is detected for example, by toll-like receptors, signals the pathogenic nature of antigens to the immune system and elicits a strong inflammatory reaction.

Tolerance – Immune tolerance is a status in which the immune system is in a state of nonreactivity to an antigen in order to prevent inflammatory tissue-destructive reactions. Tolerance is actively generated and directed not only against the bodies' own cellular self-antigens but also against nonpathogenic external antigens. If tolerance fails, autoimmunological disease or allergy may occur. Tolerance is the default mode of the mucosal immune system, including CALT and EALT, in order to preserve tissue integrity.

Conjunctival Morphology and Function Are Closely Interacting for Immune Surveillance

Epithelial Defense Mechanisms

Epithelial morphology and function

The conjunctiva is a moist mucous organ that consists of a surface epithelium and an underlying loose connective tissue (lamina propria), separated by the epithelial basement membrane. The epithelium of the human conjunctiva has, in contrast to small rodents (e.g., rat and mouse), a stratified nonsquamous morphology and consists of two to three cell layers of cubical cells in most parts. It becomes multilayered and assumes prismatic morphology at the fornix whereas it tends to become squamous toward the limbus (**Figure 1(a)** and **1(b)**). Interspersed mucus-secreting goblet cells occur inside the epithelium as single cells or in small groups as well as intraepithelial lymphocytes (IELs) that reside mainly in the basal layers (**Figure 2(b)** and **Figure 3(a)**) as well as dendritic cells (DCs), that have long narrow extensions, for uptake of antigens from the surface. The conjunctival epithelial surface is covered by small cytoplasmic protrusions (microvilli and microplicae) with a well-developed surface coat of filamentous projections (glycocalyx) that form a meshwork (**Figure 1(c)** and **Figure 2(a)**).

Epithelial Immune Surveillance Takes Care of Environmental Antigens

Physical and physicochemical barriers keep antigens outside

The structure of the conjunctival epithelium already contributes to basic protective mechanisms which can be considered as part of the innate defense. Epithelial cells are mechanically connected by desmosomes and have an apical belt of intercellular junctions including tight junctions that seal the intercellular space and limit the passive para-cellular leakage of antigens in and out of the tissue (**Figure 2(a)**). This physical cellular barrier is supplemented by the physicochemical barrier of the epithelial mucins, that consist of cell membrane-spanning mucins (glycocalyx) produced by the ordinary epithelial cells and of soluble mucins secreted by the goblet cells which mix with the aqueous phase. Together they form a layer in the range of few micrometers thickness, that is, a sticky gel to which microbes adhere and can hence be cleared by the constant renewal of the preocular tear film. Soluble protective factors, including secretory immunoglobin A (SIgA), are fixed to the mucin layer in order to make it an almost impenetrable and lethal barrier to antigens and in particular to microbes.

Figure 1 Structure of the human conjunctival epithelium. (a) The epithelium of the human conjunctiva is stratified cuboidal in most regions and assumes more layers with prismatic surface cells toward the fornix. Interspersed goblet cells (BZ) release mucus (M) tufts onto the surface. (b) Goblet cells contain densely packed mucin granules and a flat or triangular nucleus. They may be slightly inclined if located in the relatively flat bulbar epithelium close to the limbus. The surface of the conjunctival epithelial cells shows numerous microprotrusions that result in a rough surface in low-magnification transmission electron microscopy. (c) In higher enlargement, microvilli (MV) and microplicae (MP) are seen which have a dense glycocalyx of fine molecular antennae (arrows) that project into the lumen and form a meshwork, as better seen in cross section (inset, ×2). Reproduced from Knop, E. and Brewitt, H. (1992). *Morphology of the Conjunctival Epithelium in Spectacle and Contact Lens Wearers – A Light and Electron Microscopic Study*. Contactologia, Stuttgart: Enke Verlag.

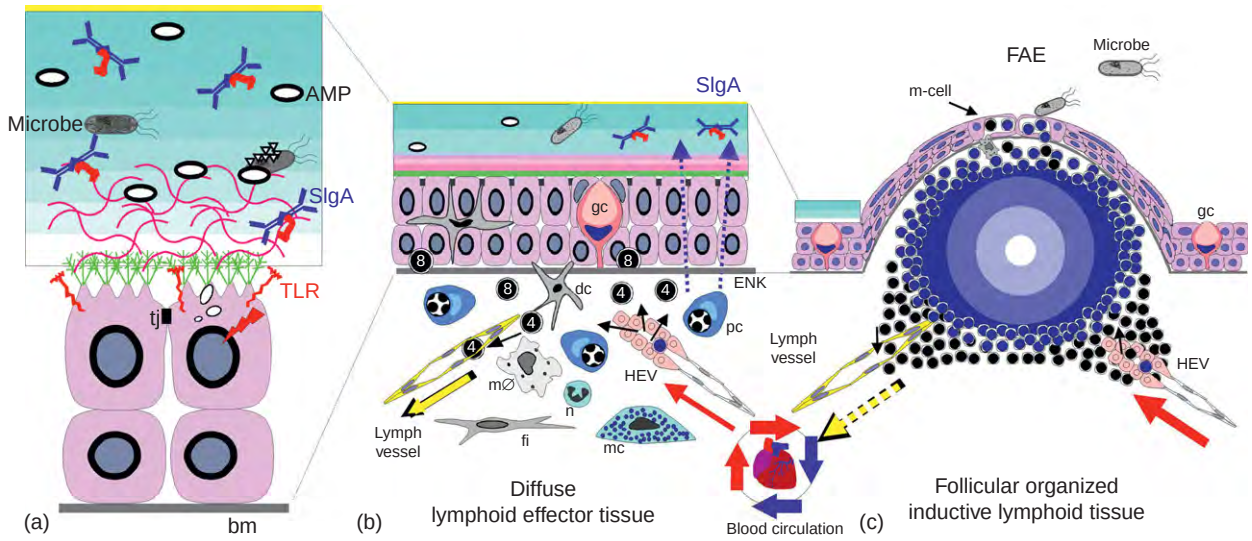

Figure 2 Defense systems of the human conjunctiva. (a) The conjunctival epithelium has an array of defense systems consisting of the integrity of the surface epithelial cells (provided with pattern recognition receptors, TLR) that are sealed by apical tight junctions (tj), of the attached mucin layer that is enforced by adhering antimicrobial proteins and peptides (AMPs) including specific secretory IgA (SIgA) and of the overlying tear film (shaded blue) that contains similar protective molecules and provides a washing effect. (b) A diffuse effector tissue is formed by lymphoid cells of the specific adaptive immune system and by innate cells such as macrophages (mø), mast cells (mc), neutrophilic granulocytes (n), and dendritic cells (dc). They functionally interact with stromal fibrocytes (fi). Lymphoid cells consist of $CD4^+$ and $CD8^+$ T-cells (black circles) that constitute intraepithelial and lamina propria lymphocytes. Differentiated B-cells (plasma cells (pc), large blue) produce dimeric IgA, which is transported through the epithelium as SIgA. (c) Interspersed solitary lymphoid follicles consist of B-cells (small blue circles), frequently have a bright germinal center due to cell proliferation, have an apical follicle-associated epithelium (FAE) with M-cells for antigen transport but without goblet cells (gc) and have para-follicular T-cell (small black circles) zones with lymph vessels (yellow) and high endothelial venules (HEVs); small arrows indicate the direction of cell migration. The mechanisms for conjunctival immune surveillance are explained topographically in this figure from the epithelium (a) over the diffusely interspersed effector cells (b) toward the organized lymphoid follicles that generate the effector cells (c). Functionally, it is reverse because the effector cells generated in lymphoid follicles after antigen uptake and presentation recirculate via the blood circulation (symbol of heart and blood flow between (c) and (b)) to and migrate into the diffuse effector sites to exert their protective function by cell contact or by soluble mediators. The drawing is not to scale.

The mechanical washing effect of the tear film wipes away antigens and detritus

The tear film is an important functional component of the ocular surface mucosal protection system. Apart from providing the necessary moisture, the constant flow of tears over the ocular surface and in particular, over the cornea, together with the wiping effect of the lid margin with every blink, provides a constant mechanical washing. This discharges antigens and removes dust and cell detritus. Other parts of the ocular surface along the retropalpebral tear film are not so rapidly cleared so that antigens can stay in longer contact with the epithelium. Therefore, the tear film contains a large number of antimicrobial factors that contribute more specifically to the innate immune defense.

Epithelial innate immune defense factors

The innate immune system uses pattern-related receptors (PRRs) that mainly detect conserved pathogen-associated molecular patterns (PAMPs) but also host antigens from destroyed cells. It reacts via effectors, which consist of soluble antimicrobial proteins and peptides (AMPs) which bind to the microbial cell wall in order to destroy it or which interfere with the microbial metabolism. The innate immune system also employs production of soluble mediators, such as inflammatory cytokines and chemotactic cytokines (chemokines) that functionally couple the innate and adaptive immune answer.

PRRs on epithelial cells provide an external alarm system

As soon as microbial antigens have breached the physicochemical barrier, they get in touch with epithelial PRRs (**Figure 2(a)**, the most prominent of which is presently the diverse family of toll-like receptors (TLRs). Binding of their ligands causes activation of the host cell via a MyD88-dependent signaling pathway that activates a nuclear transcription factor, nuclear factor kappa B (NFκB), and results in production of inflammatory cytokines such as interleukin 6 (IL-6), interferon gamma (IFN-γ), or tumor necrosis factor alpha (TNF-α). Subsequently, these induce the production of chemokines, adhesion molecules, and inducible AMP. Altogether this represents an inflammatory cascade with activation, first

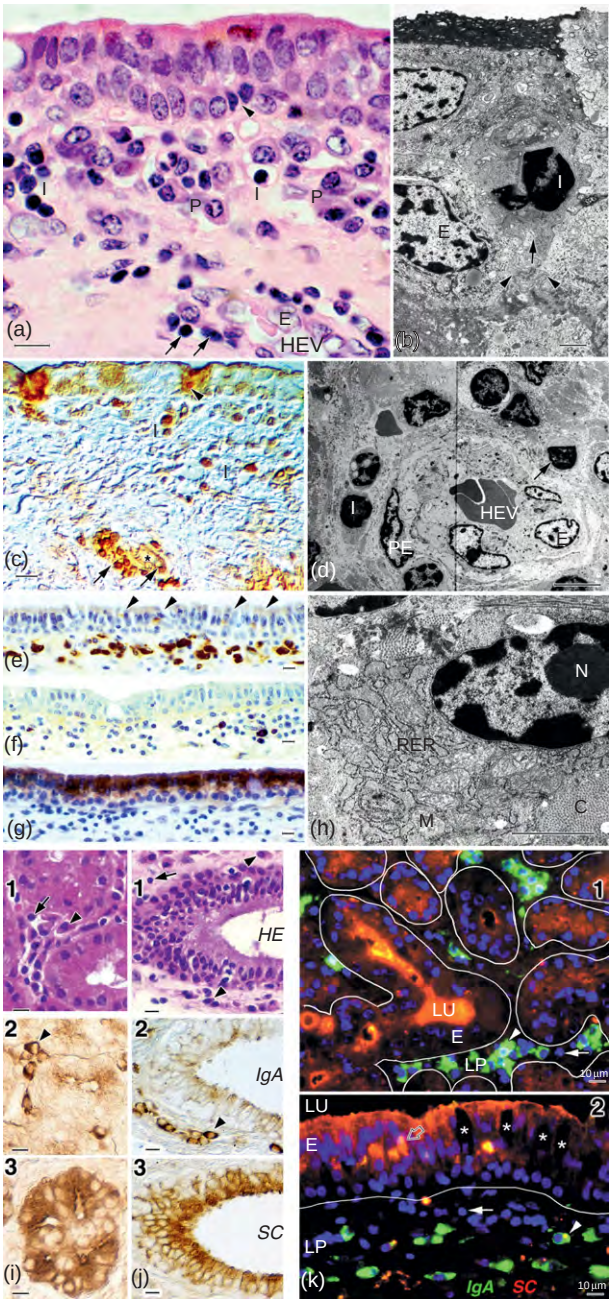

Figure 3 Characteristics of diffuse CALT. (a) Tarso-orbital conjunctiva. Plasma cells (P) and lymphocytes (l) form a diffuse lymphoid cell layer in the lamina propria covered by an epithelium with intraepithelial lymphocytes (arrowhead). A high endothelial venule (HEV) underneath has typical roundish endothelial cells (E) and contains lymphocytes within and around the wall (arrows). (b) TEM shows an intraepithelial lymphocyte (l) between epithelial cells (E) on the basement membrane (arrowheads). (c) Immunostaining indicates T-cells inside the epithelium (arrowhead), in the lymphoid layer (l) and around or in the wall (arrows) of a HEV (asterisk). (d) Ultrastructurally, a HEV shows large bright endothelial cells (E), a contractile pericyte layer (PE), and adjacent (l) or intramural (arrow) lymphocytes. (e) The vast majority of plasma cells in the lymphoid layer are IgA positive as also deposits in the epithelium (arrowheads), while IgM (f) is rare. (g) The epithelium is positive for the transporter SC. (h) A plasma cell lying in the loose collageneous (C) tissue has extended rough endoplasmic reticulum (RER), mitochondria (M), large nucleolus (N), and radial heterochromatin; (b, d, h: bar = 1 µm; a, c, e–g: bar = 10 µm). (i (1–3)) Lacrimal gland, LG, with lymphocytes (arrow), and plasma cells (arrowead) between the roundish acini. (2) IgA is found strongly in plasma cells and as weaker patchy staining in acinar epithelial cells, which more strongly express SC (3). (j (1–3)) Excretory lacrimal ducts that connect the LG to the conjunctiva have similar characteristics but in the epithelium IgA (2) and SC (3) are mainly expressed in the luminal layer (j) the duct has two cell layers but appears wider to the left due to oblique plane of section. (k (1,2)) Multiple-fluorescent staining for IgA (green), SC (red), and cell nuclei (blue) shows that the components of the secretory immune system are similarly arranged in the LG (1) and the conjunctiva (2, here orbital zone); bm level indicated by fine lines. IgA-positive plasma cells are diffusely interspersed in the LP of both tissues; in the LG frequently in groups. Epithelium (E) shows strong staining for SC;

of the epithelial cells and later also of lamina propria leukocytes and vascular endothelial cells. It induces leukocyte recruitment into the epithelium and their immigration from the blood stream into the tissue.

The normal conjunctival epithelium expresses a number of different TLRs, similar to the cornea. TLR1, 2, 3, 5, and 6 were found in all conjunctival and limbal epithelial cell samples, TLR4 and 9 only inconstantly, but not TLR7, 8, and 10. TLR2 may only occur upon stimulation by IFN-γ and bacterial cell wall extract, for example, in patients with ocular allergy. This results in upregulation of inflammatory markers, such as the intercellular adhesion molecule 1 (ICAM-1), human leukocyte antigen (HLA), TNF-α, and IL-8, in a dose-dependent manner. Bacterial-specific TLRs are of interest in ocular allergy because colonization by bacteria is common there. The activation of TLRs represents an important co-factor in ocular allergy and their blockade can significantly inhibit release of inflammatory mediators which may turn out as a promising new therapy option for ocular allergy.

The conjunctival epithelium secretes diverse AMPs

The spectrum of epithelial derived AMPs is distinct for cornea and conjunctiva but overlapping. Conjunctival epithelium produces not only the human β-defensins (hBD)-1,2,3 and further AMPs such as liver-expressed antimicrobial peptides (LEAPs) 1 and 2 and cathelicidin (LL-37) but also macrophage inflammatory protein 3alpha (MIP-3α) and thymosin beta 4 (Tβ-4). Some of the AMPs are constitutively produced, whereas others are inducible. hBD-2 is induced by inflammatory cytokines in ocular surface inflammation and by presence of bacterial LPS, while hBD3 is induced by infection and LL-37 by epithelial wounding. Conjunctival AMPs such as LL-37 are active against bacterial (*Pseudomonas aeruginosa*, *Staphylococcus aureus*, *Staphylococcus epidermidis*) and viral (Herpes simplex virus 1, adenovirus) infection. They can act as multifunctional factors in wound healing and signaling pathways. Interestingly, the antimicrobial activity of some of these AMPs (e.g., hBD-1, hBD-2, and Tbeta-4) is almost completely inhibited in the presence of tear fluid. This may indicate that not all epithelial AMPs are produced in order to act as tear film factors but rather play a major role for local protection inside the conjunctival epithelium itself. Apart from AMPs, there is a plethora of other protective proteins. AMPs continue downstream in the lacrimal drainage system.

Conventional antibacterial factors are surprisingly versatile defense tools

Even the 'old fashioned' established antimicrobial proteins in the tear film, such as lysozyme and lactoferrin, have surprising newly detected functions. Apart from being bactericidal, either by lysis of components in the Gram-positive bacterial cell wall (lysozyme) or by interfering with their iron metabolism (lactoferrin), they are also antifungal and antiviral. Through the absorption of the strongly inflammatory bacterial endotoxin lipopolysaccharide (LPS), which is a surface molecule on Gram-negative bacteria, they also act anti-inflammatory. They have further anti-inflammatory functions by their influence on antigen-presenting cells (APCs) and hence appear as key elements in host defense that link innate and adaptive immunity.

Conjunctival Lamina Propria: Morphology and Function of the Diffuse Mucosal Immune System

Diffusely arranged lymphoid and innate cells contribute to conjunctival immune surveillance

The lamina propria contains bone-marrow-derived cells and vessels of different types. Apart from capillaries and lymph vessels, specialized high endothelial venules (HEVs) occur. Vessels serve for the supply with nutrition and discharge of metabolites, for hormonal regulation of the tissue, and also for the migration of immune cells. Lymphocytes, together with accessory leukocyte populations (macrophages, granulocytes, mast cells, and DCs), form a diffuse lymphoid tissue (**Figure 3(a)**) which is regarded mainly as an effector site of CALT although antigen uptake via DCs can also occur here to a certain extent. The diffuse lymphoid tissue is located in the vast majority of the surface, except for the solitary lymphoid follicles. The thickness of this cell layer depends on the location along the conjunctiva, shows a certain topographical variation, and is frequently only one to two cells wide, which may be a reason why these cells have often been overlooked in the past. It also shows a certain interindividual variation that may depend on the immune status of the person. IEL also functionally belong to the diffuse effector cells (**Figure 3(b)**).

Different subtypes of lymphocytes occur in the conjunctiva

Diffuse conjunctival lymphocytes are mainly $CD3^+$ T-cells (**Figure 3(c)**) (whereas $CD20^+$ B-cells are largely restricted to the solitary lymphoid follicles). They are activated ($CD45Ro^+$, $CD25^+$) and express the human

goblet cells (asterisks) are negative for SC. Mixed color indicating both proteins (=SIgA) is seen in the tubuloacinar lumina (LU) of the LG and frequently delineates the luminal cell surface. (a–h) Adapted from Knop, N. and Knop, E. (2000). Conjunctiva-associated lymphoid tissue in the human eye. *Investigative Ophthalmology and Visual Science* 41: 1270–1279. (i–k) Knop, E., Knop, N., and Claus, P. (2008). Local production of secretory IgA in the eye-associated lymphoid tissue (EALT) of the normal human ocular surface. *Investigative Ophthalmology and Visual Science* 49: 2322–2329.

mucosa lymphocyte antigen (HML-1, integrin αEβ7) which substantiates the integration of CALT into the mucosal immune system. In the epithelium $CD8^+$, cytotoxic/suppressor cells prevail that have been proposed to act mainly in the suppressor mode and may hence provide a component of the immune tolerance at the ocular surface. Lamina propria lymphocytes, in contrast, consist of equal or prevailing amounts of $CD4^+$ T-helper (Th) cells compared to $CD8^+$ T-cells. All known types of T-cells exist in CALT and their immune regulation is considered below (see the section titled 'Mechanisms of conjunctival immune regulation'). Plasma cells (see the section titled 'The conjunctiva contributes actively to the secretory immune system') account for about 20% of the conjunctival leukocytes in histology but their absolute number is in the range (2/3) of those in the lacrimal gland that was long regarded as the sole source of tear film SIgA. Conjunctival lymphocytes are even more abundant. This supports the concept that the conjunctiva considerably contributes to its own specific defense and it very well supports the recognition of a diffuse CALT along the whole extension of the human conjunctiva in tissue whole mounts.

The conjunctiva contributes actively to the secretory immune system

Specific soluble antigen-receptors (immunoglobulins, Ig) produced by local mucosal differentiated B-lymphocytes (plasma cells) and transported through the overlying epithelium constitute the secretory immune system. This is a major mucosal defense mechanism and is also present in the conjunctiva. Mucosal Ig mainly consist of polymeric (p)IgA that also forms the predominant Ig in the tear film, besides small amounts of the other polymeric Ig (IgM) and trace amounts of IgG. During eye closure, overnight IgA is the predominant protein in the closed eye tear film, but only recently the components of the conjunctival secretory immune system could be consistently verified by immunohistochemistry and polymerase-chain reaction.

Local conjunctival plasma cells produce mainly the anti-inflammatory IgA

The vast majority of conjunctival plasma cells produce IgA and hence stain positive for it in immunohistochemistry (**Figure 3(e)**). IgM, which performs the initial acute secretory immune answer, is rarely observed (**Figure 3(f)**) and hence indicates that the physiological conjunctival diffuse lymphoid cells do not reflect any kind of reaction to an acute insult. The epithelial transporter molecule for both of them (pIgR, represented by its extracellular domain secretory component, SC) is strongly expressed throughout the human conjunctival epithelium (**Figure 3(g)**). After transport, SC remains linked to pIgA which together constitute secretory IgA (SIgA). Conjunctival plasma cells show a typical ultrastructure in transmission electron microscopy (**Figure 3(h)**).

IgA-positive plasma cells in the lamina propria and SC in the overlying epithelium are continuously expressed from the lacrimal gland (**Figure 3(i)** 1–3) along its excretory ducts (**Figure 3(j)** 1–3) into the conjunctiva and further within the lacrimal drainage system. In multifluorescent immune staining, the secretory immune system of the lacrimal gland and the conjunctiva show the same characteristics (**Figure 3(k)** 1,2).

SIgA performs diverse protective and antiinflammatory functions at the ocular surface

SIgA is deposited onto the epithelial surface and into the tear film (**Figure 2(a)**). It contributes to the binding of specific antigens and to their immobilization and discharge. It binds to the surface of microbes and viruses and thereby limits their binding to and entrance into the tissue. It binds and thereby neutralizes bacterial toxins such as LPS. SIgA antibodies occur naturally to the physiological commensal ocular flora and are induced by the presence of pathological microbes, such as *Acanthamoeba* and *Pseudomonas*.

IgA does not only exert immune functions at the luminal ocular surface but also locally inside the tissue. IgA has a low complement-binding activity and hence acts in an antiinflammatory fashion. Bound antigens are opsonized to phagocytes which facilitates microbe uptake and destruction. IgA can bind to pathogens that have already penetrated into the tissue including intracellular viral particles. During the vectorial transport of pIgA toward the lumen, the bound pathogens are cleared from the tissue. IgA-bound antigens have an antiinflammatory effect on signaling networks and immune regulation inside the tissue by induction of the tolerogenic cytokines TGF-β and IL-10 and by limiting the activation of DC.

Lamina Propria Leukocytes Provide Immediate Innate Response against Invading Pathogens and can Orchestrate an Inflammatory Reaction

Apart from the lymphocytes, various other types of bone-marrow-derived leukocytes exist in the diffuse conjunctival effector tissue that are all not purely pathogenic, but exert important protective immune functions. Macrophages are reportedly frequent in immunohistochemistry but less obvious in conventional histology (**Figure 3(a)**). Phagocytes, such as macrophages, granulocytes, and DCs, can engulf and devour the invader but in addition, they act in different ways. Macrophages mainly destroy pathogens by internal digestion but are also capable to present epitopes of the pathogen on the MHC-class-II molecule (MHC-II) to $CD4^+$ T helper-cells for their subsequent activation. DCs digest pathogens mainly for this purpose. Granulocytes, also known as polymorphonuclear (PMN) cells, are usually the first cells that arrive at the site of acute defense reactions.

Protective functions of conjunctival lamina propria leukocytes

Neutrophile granulocytes are regularly observed in the normal human conjunctiva. They account for about 5% of the leukocytes and occur massively in the closed-eye tear film. In addition to their phagocytic capacity, they secrete several soluble factors such as antimicrobial proteins (e.g., lactoferrin, alpha-defensins, and cathelicidin) for immediate destruction of microbes. Furthermore, they secrete proteases (e.g., cathepsins, gelatinase, and neutrophile elastase) that lead to digestion of the extracellular matrix in order to provide space for accommodating the plethora of cells necessary to mount an effective inflammatory response. Eosinophile granulocytes are reportedly not observed in a normal conjunctiva but immigrate in parasitic infection. They produce chemokines and cytokines (e.g., RANTES [CCL5], TGF-β, TNF-α) for the activation and recruitment of other leukocytes including T-cells, as found in ocular allergy. Mast cells, apart from their potential physiological function, are mainly known for their inflammatory activity during IgE-mediated allergic disease where they release a variety of vasoactive mediators (e.g., histamine and heparin) and Th1 and Th2 cytokines (IL-4, IL-5, IL-6, and TNF-α) that can orchestrate an inflammatory response.

HEVs Provide the Regulated Immigration of Bone-Marrow-Derived Cells into the Tissue

The bone-marrow-derived cells that populate the conjunctiva all arrive here via the blood stream. Most of them stay here but lymphocytes, after being primed, and DCs, after antigen uptake, can also leave the tissue again via lymphatics. Although lymphocytes can emigrate through ordinary capillaries and venules, they do so with higher efficiency through conjunctival HEV via their tissue-specific adhesion molecules (lymphocyte homing molecules) that interact with vascular endothelial addressins. HEVs occur particularly in the para-follicular T-cell areas of lymphoid follicles (**Figure 2(c)**) but they are also found in the diffuse lymphoid effector tissue of the conjunctiva. Emigrated T-cells are frequently observed around HEV (**Figures 3(c)** and **3(d)**). Conjunctival HEVs are a normal component of the lymphoid tissue and they have a characteristic ultrastructure similar to that in other mucosal organs.

Conjunctival Lymphoid Follicles Have a Typical Morphology and Function

Solitary organized lymphoid follicles are interspersed into the diffuse effector tissue along the conjunctiva. They are relatively flat due to the limited space in the narrow conjunctival lamina propria but still show typical follicular characteristics. They consist of accumulations of B-cells (**Figure 4(a)**). The overlying epithelium changes its morphology toward the apex into a follicle-associated epithelium (FAE) by losing the goblet cells, by assuming a flat cell shape (**Figures 4(a)–4(c)**), and by a rarefied expression of SC (**Figure 4(c)**). Groups of lymphocytes, including $CD20^+$ B-cells (**Figure 4(a)**) and $CD3^+$ T-cells, occur inside the epithelium and are separated from the lumen just by a very narrow epithelial lining. Altogether, this is a conspicuous sign for the presence of specialized M-cells that form intraepithelial pockets populated by lymphoid cells. M-cells serve for the uptake and transport of luminal antigens toward the lymphoid cells in the pocket that can detect the antigen and present it to naive lymphocytes. The typical morphology of conjunctival M-cells and their antigen transport have been verified in a number of animal species, including guinea pig, turkey, chicken, rabbit, dog, and monkey. It has been shown that CALT is able, for example, to induce a tolerance against retinal antigens upon their topical conjunctival instillation.

The number of lymphoid follicles in elderly humans is relatively low (about 10 follicles per eye) with an average diameter of about 0.25 mm. Their small size again offers an explanation for the fact that CALT has frequently been overlooked in the past. They are more frequent in the upper conjunctiva than in the lower one (**Figure 5(a)**) and show a bilateral symmetry. In younger individuals, however, lymphoid follicles are more frequent and before puberty they occur in every person. Therefore, CALT follicles show a similar involution with age as observed for other locations of the mucosal immune system in general. Mucosal lymphoid B-cell follicles and their associated para-follicular T-cell zones (**Figure 2(c)**) serve for the generation of B- and T-effector lymphocytes, respectively (**Figure 7**).

The Topographical Distribution of CALT is in the Right Place to Assist Corneal Immune Surveillance

If the distribution of CALT is used to draw a topographical map (**Figure 5(b)**), it corresponds to the position of the cornea during eye closure. CALT in the tarso-orbital regions of the palpebral conjunctiva is then in the right position to support the immune protection of the cornea, which itself is largely devoid of lymphoid cells and other leukocytes. CALT may act during blinking as an immunological windscreen wiper and during sleep as an immunological cushion that covers the cornea (**Figure 5(c)**).

CALT can provide the cornea with innate and specific antibacterial peptides and proteins including SIgA that are not produced there. This concerns the usual daytime setting when the conjunctiva regularly glides over the cornea and wipes it clean. Even more so, CALT may be

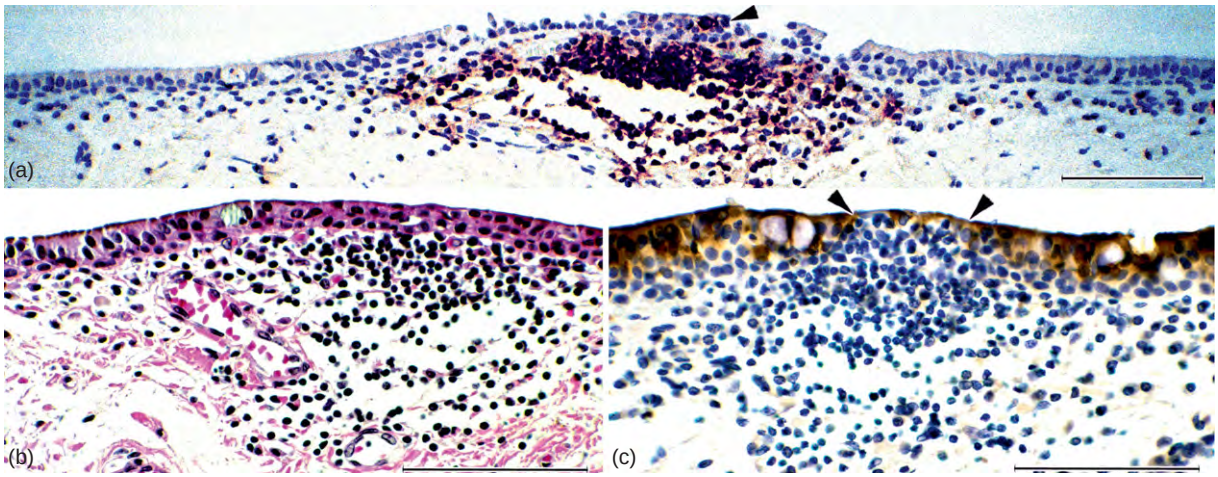

Figure 4 Characteristics of follicular CALT. (a) Even smaller lenticular lymphocyte accumulations are primarily composed of B-cells in immunostaining (brown dots). Over the apex, the overlying epithelium becomes flatter ((b), this follicle is not exactly met at the apex) and changes into a follicle-associated epithelium (FAE, between arrowheads in (c)), where goblet cells are absent, immunostaining for secretory component is rarefied (c) and numerous intraepithelial lymphocytes (IEL) are present in groups, suspicious for M-cells. The IEL are arranged in groups, including B-cells (arrowhead in (a)). Immunostaining for $CD20^+$ B-cells (a) and the IgA-transporter SC (c) of a small, almost flat, follicular accumulation that appears homogeneous, apart from disintegration at the location of the former germinal center, in HE staining (b); size bar in all figures = 100 μm. From Knop, N. and Knop, E. (2000). Conjunctiva-associated lymphoid tissue in the human eye. *Investigative Ophthalmology and Visual Science* 41: 1270–1279.

relevant during nighttime when the eye is closed. Then, an upregulated level of proinflammatory factors from PMN cells is obtained as a temporary approach in order to dampen the growth of the entrapped microorganisms that enjoy a comfortable environment without disturbance. Due to the intimate contact, CALT can also detect corneal antigens and generate respective effectors.

CALT is a Part of the Complete Eye-Associated Lymphoid Tissue

The conjunctival mucosa is, at the temporal and nasal side (**Figure 6**), anatomically continuous, through the lacrimal excretory ducts, with the lacrimal gland and through the lacrimal canaliculi with the lacrimal drainage system, respectively.

The histology clearly shows that a continuous mucosal immune system is also present from the periacinar tissue of the lacrimal gland throughout the conjunctiva into the lacrimal drainage system, that is, along the extended ocular surface. Together, this constitutes an eye-associated lymphoid tissue (EALT) and CALT is the regional part of it at the ocular surface proper (**Figure 6**).

EALT is an undividable anatomical and functional unit and its different parts support each other in function. EALT is in line with the other parts of the mucosal immune system of the body, such as gut-associated lymphoid tissue (GALT) in the gut or bronchus-associated lymphoid tissue (BALT) in the bronchi. Therefore, primed effector cells from EALT can be distributed by the regulated recirculation of lymphocytes (**Figure 2(b)** and **(c)**) within the mucosal immune system in order to repopulate the ocular surface mucosal tissues and other mucosa-associated lymphoid tissue (MALT) locations and in return, EALT can also share effector cells from other organs.

Mechanisms of Conjunctival Immune regulation

CALT Is Physiologically Biased to Tolerogenic, Anti-Inflammatory Responses

The mucosal immune regulation including CALT is maintained via the mode of antigen presentation by APC, on their MHC-class-II, to the T-cell-receptor (TCR) of naïve $CD4^+$ T-cells (To) and influenced by additional signals such as co-stimulatory molecules and the prevailing cytokine milieu within the tissue. This leads to the generation of different types of $CD4^+$ Th cells which produce characteristic cytokine patterns and have different functions (**Figure 7**). Due to the prevalence of nonpathogenic antigens and the delicate tissue construction, CALT is biased toward anti-inflammatory immune answers. Tolerance is also necessary in order to avoid autoimmune reactions against own tissue constituents by self-reactive T-cells.

Normally, CALT favors Th2 cells under the influence of cytokines such as IL-4. These interact with B-cells and produce cytokines (e.g., IL-4, IL-5, and IL-13) that promote B-cell Ig iso-type class switch to IgA and their differentiation into IgA-secreting plasma cell precursors

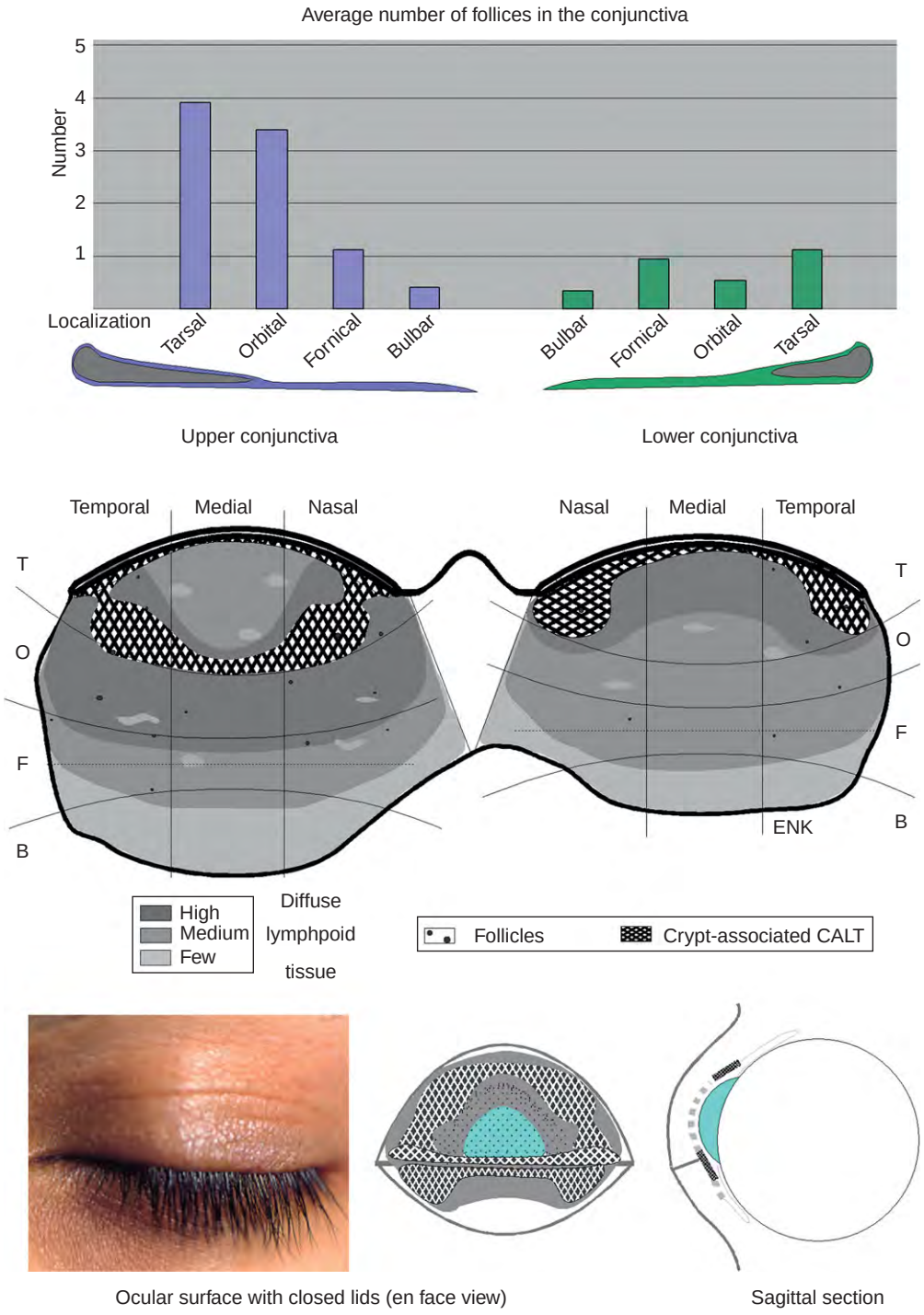

Figure 5 Topography of CALT – in the right position to assist corneal immune protection. (a) Morphometrical analysis of lymphoid follicles in the different zones (tarsal, orbital, fornical, bulbar) of upper (left) and lower (right) human conjunctiva, in a flat preparation of a tissue whole mount, shows a main expression in the tarso-orbital zones. More follicles are present in the upper lid and the average total number of CALT follicles in an elderly population is about 10 follicles per eye. (b) The topographical distribution of lymphoid follicles is the same as that of the diffuse lymphoid effector tissue in which they are interspersed, as seen in a topographical map of CALT in a complete flat whole mount of a human conjunctiva with the lid margin to the top and the nasal zone in the middle. The map differentiates the previously mentioned zones (T, O, F, B) as well as temporal, medial, and nasal locations. Increasing density of diffuse lymphoid cells is indicated as increased shades of gray. Hatched lines indicate the location of conjunctival crypts of Stieda that are associated with CALT. (c) If the topographical distribution of CALT is projected onto the bulbar surface in a closed lid situation, it is obvious that CALT covers the cornea as seen in frontal en face view (middle) and sagittal section (right). The central portion is covered by the tarsal crypts of Henle (open circles in middle figure) that are associated with CALT but not indicated in the topographical map in (b). From Knop, E. and Knop, N. (2003) *Eye-Associated Lymphoid Tissue* (*EALT*) *is Continuously Spread Throughout the Ocular Surface from the Lacrimal Gland to the Lacrimal Drainage System*. Der Ophthalmologe, Heidelberg: Springer.

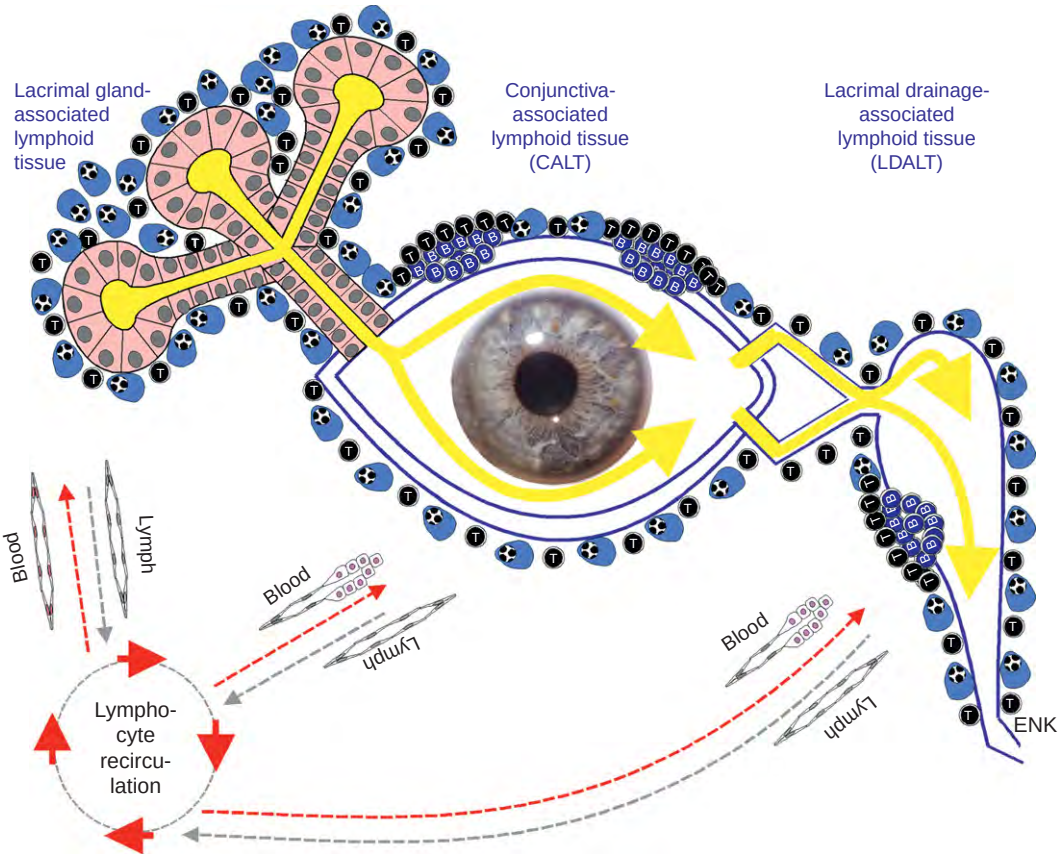

Figure 6 Eye-associated lymphoid tissue (EALT). Eye-associated lymphoid tissue integrates the continuous mucosal immune system of the conjunctiva (CALT) and its mucosal adnexa, composed of the lacrimal gland and lacrimal drainage system, which together form the extended functional ocular surface. The ocular tissues belong together embryologically and functionally. They are connected by the flow of tears (yellow arrows) which lets them share protective immune factors as well as antigens and they are furthermore connected by the regulated recirculation of lymphoid cells in the body via efferent lymph vessels and blood vessels. Lymphoid cells enter the tissues via blood vessels, including high endothelial venules (represented by roundish endothelial cells), and leave them via lymphatics. EALT is continuous throughout these organs in the form of a diffuse lymphoid effector tissue composed of T-lymphocytes (represented by black cells in the drawing) and plasma cells (represented by large blue cells) together with accessory leukocytes (not indicated here, compare **Figure 2(b)**). Inductive sites, in the form of lymphoid follicles, composed of B-cells (small blue cells) with adjacent para-follicular T-cell areas (compare **Figure 2(c)**), are present in CALT and LDALT. They serve for the uptake and presentation of antigens and for the subsequent generation of respective effector cells specific for the ocular surface relevant antigens. Not only the effector cells generated in EALT, but also those from other mucosal sites, can, after recirculation in the lymph and blood system, populate the diffuse lymphoid effector tissue that is present along the whole extended ocular surface including the large mucosa-associated gland (lacrimal gland). Adapted from Knop, E. and Knop, N. (2007). Anatomy and immunology of the ocular surface. In: Niederkorn, J. Y. and Kaplan, H. J. (eds.) *Immune Response and the Eye. Chemical Immunology and Allergy*. Basel: Karger Verlag.

and mature plasma cells as observed in the conjunctiva. Under the influence of mainly IL-6, the well-known inflammatory Th1 cells are formed that produce inflammatory cytokines such as IFN-γ and TNF-α which have the physiological function to activate cells, in particular phagocytes, to destroy intracellular pathogens. If inflammatory cytokines and other danger signals, such as bacterial LPS or components of dead cells occur in the tissue, they can bind to TLRs and mediate the secretion of excess inflammatory cytokines that skew CALT toward inflammatory immune answers. The antagonistic action of Th1 and Th2 cells led to the construction of the Th1–Th2 paradigm for explanation of immune regulation and phenomena at the ocular surface. In recent years, however, other anti-inflammatory (regulatory T-cells, Treg) and inflammatory (Th17 cells) were also observed which indicated that immune regulation is more complex (**Figure 7**) and needs further investigation.

Deregulation of EALT Is a Central Component of Inflammatory Ocular Surface Disease

Various stress mechanisms, for example, mechanical alteration, hyperosmolar tears or exposure to inflammatory cytokines can pathologically activate the ocular surface epithelium that responds by secretion of (further) inflammatory cytokines and proteases (such as matrix-metalloproteinase, MMP) and upregulates surface

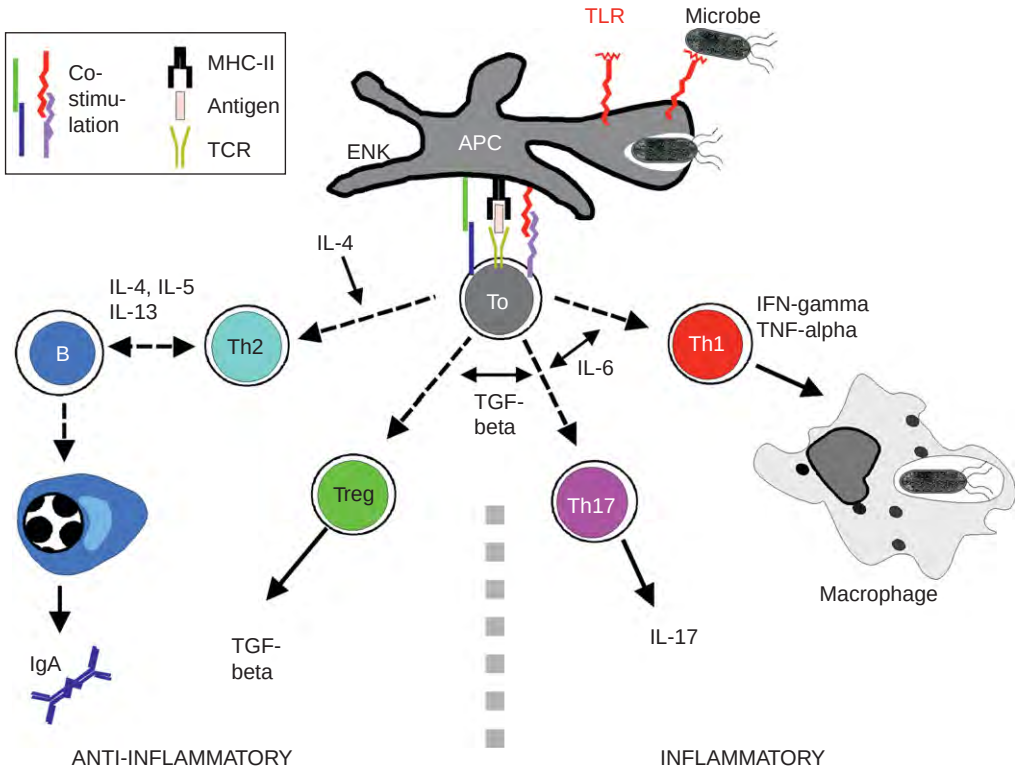

Figure 7 Generation of T- and B-effector cells in CALT. Immune regulation in CALT is governed via the presentation of antigens by antigen-presenting cells (APC) on their MHC-class-II (MHC-II) to the T-cell-receptor (TCR) of naive $CD4^+$ T-cells (To), and assisted and modulated by co-stimulatory molecules. This is influenced (indicated by uninterrupted arrows) by cytokines (interleukins, IL) and by microbial antigens that are recognized, for example, by TLR. This leads to the generation (interrupted arrows) of different types of $CD4^+$ T-helper cells (Th) that produce characteristic cytokine patterns and perform different functions. CALT is naturally biased toward anti-inflammatory immune answers. It favors the generation of Th2 that promote B-cells to differentiate into IgA secreting plasma cells. It also favors Treg that produce anti-inflammatory TGF-beta. Binding of microbial antigens to TLR and presence of IL-6 represents danger signals to the immune system and induces inflammatory immune answers via Th17 and Th1, the latter of which normally assist phagocytic cells to clear intracellular pathogens.

markers, such as ICAM-1 and MHC-class-II. This promotes an inflammatory process and through MCH-class-II the epithelial cells acquire the potential for presentation of antigens, including self-antigens, to resident conjunctival T-cells (**Figure 8(a)**) that can induce a loss of natural conjunctival immune tolerance.

Similar events are also shown for the acinar epithelial cells in inflammatory disease of the lacrimal gland where diverse perturbations result in altered intracellular protein traffic, alter the lacrimal acinar cell autoantigenic spectra, and upregulate MHC-class-II. This results in a loss of tolerance to own cell constituents, such as the M3 receptor with a subsequent autoimmune process. This again indicates that the natural tolerogenic bias can be lost in inflammatory disease and may be the underlying reason for a self-perpetuating inflammatory process at the ocular surface and its associated gland.

In fact, in inflammatory ocular surface diseases such as dry eye disease, autoreactive T-cells are generated that are specific to ocular surface tissue. They can be transferred and lead to destruction of the same ocular tissues in a naive recipient that has never experienced the pathological condition. Respective Tregs can prevent the tissue destruction and offer therapeutic potentials.

In addition, wounding can allow the entry of nonpathogenic antigens into the tissue and their presentation to T- and B-cells, as observed in ocular allergy. Downstream effects are the activation of conjunctival vascular endothelial cells that upregulate adhesion molecules (such as ICAM-1, VCAM-1, or E-selectin) with subsequent recruitment of further leukocytes from the vascular compartment and the activation of bystander cells including stromal fibroblasts. They contribute to the accumulation of MMPs that lead to tissue degradation. Altogether, this constitutes an immune-mediated conjunctival inflammatory process (**Figure 8(a)**), that can be compared with events in other mucosal organs, for example, in inflammatory bowel disease, and is based on a deregulation of the physiologically protective CALT and perpetuated by several vicious circles.

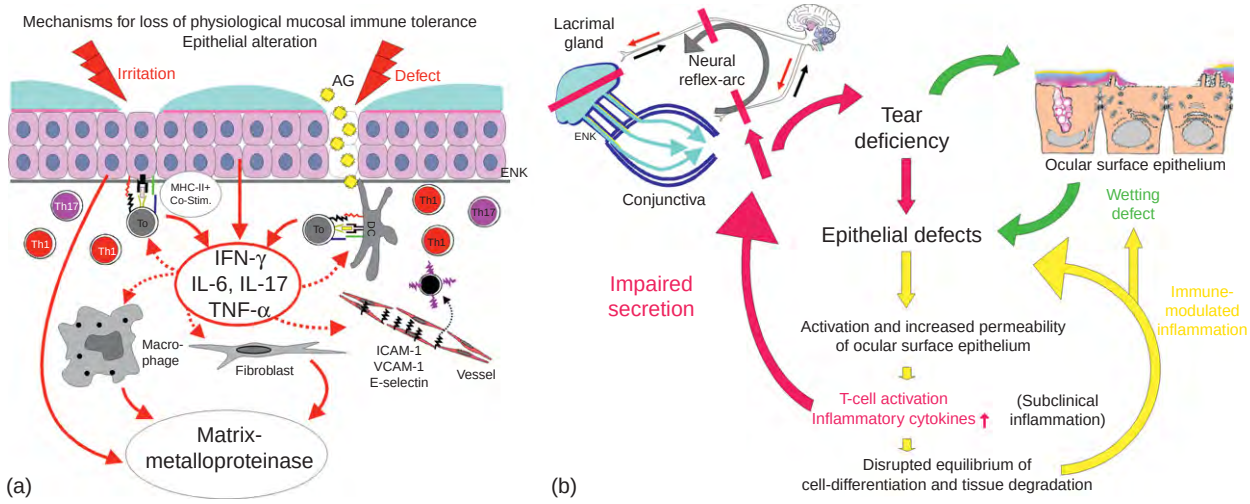

Figure 8 Deregulation of CALT determines immune-mediated inflammatory ocular surface disease. (a) Compromised integrity leads to loss of mucosal immunological tolerance and to immune-mediated inflammation. Irritation of the surface epithelium, for example, by tear film (light blue) defects, its infection or its wounding results in activation of the epithelial cells. These may respond by secretion of inflammatory cytokines and proteases (such as matrix-metalloproteinase, MMP) and by expression of the antigen-presenting molecule MHC-class-II (MHC-II) resulting in potential presentation of self-antigens to resident conjunctival T-cells. Wounding with physical defects can, in addition, allow the entry of nonpathogenic antigens into the tissue and their presentation in the context of inflammatory cytokines as observed in ocular allergy. As described for immune-regulation (**Figure 7**) this represents danger signals that contribute to a further accumulation of inflammatory cytokines in the tissue and to the generation of inflammatory, potentially autoreactive, types of T-cells. All of which is shown in inflammatory ocular surface disease. Downstream effects are the activation of vascular endothelial cells that upregulate adhesion molecules with subsequent recruitment of further leukocytes from the vascular compartment and the activation of bystander cells, including stromal cells (fibroblasts). They contribute to the accumulation of MMPs that lead to tissue degradation which all together constitutes an immune-mediated conjunctival mucosal inflammatory process that is based on a deregulation of the physiologically protective CALT. (b) Immune-mediated inflammation is a core mechanism that results in several vicious circles in the pathogenesis and propagation of ocular surface disease. An immune-mediated inflammation represents an important common factor in the vicious circles of ocular surface disease, including the dry eye syndrome and ocular allergy, which is first subclinical but tends to amplify if it is not limited. Tear film deficiency results in epithelial defects and these in turn are an important primary factor for onset of an immune-mediated inflammatory conjunctival process that tends to self-propagation via several vicious circles. These include disturbance of afferent innervation resulting in impaired secretion with further tear film deficiency and increase of epithelial damage and in impairment of mature ocular surface differentiation (leading to squamous metaplasia) that results in wetting defects and amplification of epithelial destruction. (a) From Knop E. and Knop N. (2005). *Influence of the Eye-associated Lymphoid Tissue* (*EALT*) *on Inflammatory Ocular Surface Disease*. The Ocular Surface, Ethis Communications. (b) Adapted from Knop E. et al. (2003). *Dry Eye Disease as a Complex Dysregulation of the Functional Anatomy of the Ocular Surface. New Impulses to Understanding Dry Eye Disease*. Der Ophthalmologe, Heidelberg: Springer.

See also: Adaptive Immune System and the Eye: Mucosal Immunity; Corneal Epithelium: Response to Infection; Defense Mechanisms of Tears and Ocular Surface; Dry Eye: An Immune-Based Inflammation; Immunopathogenesis of Onchocerciasis (River Blindness); Molecular and Cellular Mechanisms in Allergic Conjunctivitis; Pathogenesis of Fungal Keratitis; Tear Drainage.

Further Reading

Argueso, P. and Gipson, I. K. (2001). Epithelial mucins of the ocular surface: Structure, biosynthesis and function. *Experimental Eye Research* 73: 281–289.

Brandtzaeg, P. and Pabst, R. (2004). Let's go mucosal: Communication on slippery ground. *Trends in Immunology* 25: 570–577.

Chodosh, J., Nordquist, R. E., and Kennedy, R. C. (1998). Comparative anatomy of mammalian conjunctival lymphoid tissue: A putative mucosal immune site. *Developmental and Comparative Immunology* 22: 621–630.

Dua, H. S., Gomes, J. A., Jindal, V. K., et al. (1994). Mucosa specific lymphocytes in the human conjunctiva, corneoscleral limbus and lacrimal gland. *Current Eye Research* 13: 87–93.

Hingorani, M., Metz, D., and Lightman, S. L. (1997). Characterisation of the normal conjunctival leukocyte population. *Experimental Eye Research* 64: 905–912.

Knop, E. and Brewitt, H. (1992). Morphology of the conjunctival epithelium in spectacle and contact lens wearers – a light and electron microscopic study. *Contactologia* 14: 108–120.

Knop, N. and Knop, E. (2000). Conjunctiva-associated lymphoid tissue in the human eye. *Investigative Ophthalmology and Visual Science* 41: 1270–1279.

Knop, E. and Knop, N. (2003). Eye-associated lymphoid tissue (EALT) is continuously spread throughout the ocular surface from the lacrimal gland to the lacrimal drainage system. *Ophthalmologe* 100(11): 929–942.

Knop, E. and Knop, N. (2005). Influence of the eye-associated lymphoid tissue (EALT) on inflammatory ocular surface disease. *Ocular Surface* 3(4): S180–S186.

Knop, E. and Knop, N. (2005). The role of eye-associated lymphoid tissue in corneal immune protection. *Journal Anatomy* 206: 271–285.

Knop, N. and Knop, E. (2005). Ultrastructural anatomy of CALT follicles in the rabbit reveals characteristics of M-cells, germinal centers and high endothelial venules. *Journal of Anatomy* 207: 409–426.

Knop, E. and Knop, N. (2007). Anatomy and immunology of the ocular surface. In: Niederkorn, J. Y. and Kaplan, H. J. (eds.) *Immune Response and the Eye. Chemical Immunology and Allergy,* vol. 92, pp. 36–49. Basel: Karger Verlag.

Knop, E., Knop, N., and Brewitt, H. (2003). Dry eye disease as a complex dysregulation of the functional anatomy of the ocular surface. New impulses to understanding dry eye disease. *Ophthalmologe* 100: 917–928.

Knop, E., Knop, N., and Claus, P. (2008). Local production of secretory IgA in the eye-associated lymphoid tissue (EALT) of the normal human ocular surface. *Investigative Ophthalmology and Visual Science* 49: 2322–2329.

Liu, H., Meagher, C. K., Moore, C. P., and Phillips, T. E. (2005). M cells in the follicle-associated epithelium of the rabbit conjunctiva preferentially bind and translocate latex beads. *Investigative Ophthalmology and Visual Science* 46: 4217–4223.

McDermott, A. M., Perez, V., Huang, A. J., et al. (2005). Pathways of corneal and ocular surface inflammation: A perspective from the cullen symposium. *Ocular Surface* 3: S131–S138.

Mircheff, A. K., Wang, Y., Jean, Mde S., et al. (2005). Mucosal immunity and self-tolerance in the ocular surface system. *Ocular Surface* 3: 182–192.

Pflugfelder, S. C. and Stern, M. E. (2007). Future directions in therapeutic interventions for conjunctival inflammatory disorders. *Current Opinion in Allergy and Clinical Immunology* 7: 450–453.

Sack, R. A., Beaton, A., Sathe, S., et al. (2000). Towards a closed eye model of the pre-ocular tear layer. *Progress in Retinal and Eye Research* 19: 649–668.

Sullivan, D. A. (1999). Ocular mucosal immunity. In: Ogra, P. L., Mestecky, J., Lamm, M. E., et al. (eds.) *Handbook of Mucosal Immunology,* 2nd edn., pp. 1241–1281.

Conjunctival Goblet Cells

R R Hodges and D A Dartt, Schepens Eye Research Institute, Boston, MA, USA

Glossary

Dry eye – A multifactorial disorder of the tear film characterized by either decreased tear production or increased tear evaporation.
Glycosylation – The process by which a carbohydrate is added to protein.
Goblet cells – Specialized epithelial cells that secrete mucins.
Mucins – Large, highly glycosylated proteins.
Signal transduction – The process by which a cell converts a signal or stimulus from outside the cell into a functional change.

Goblet cells are columnar epithelial cells that synthesize and secrete mucins, for example, the gel-forming mucin MUC5AC. These cells were originally termed goblet cells because of their distinctive goblet-like shape (Figure 1). The basal portion is narrow and shaped like the stem of a goblet containing the nucleus and organelles, while the apical portion of the cell is shaped like a cup due to the presence of numerous secretory granules. Goblet cells are found in all wet-surfaced epithelia such as the respiratory, gastrointestinal, and reproductive tracts, and the conjunctiva and are surrounded by stratified squamous epithelial cells. Goblet cells of the respiratory, gastrointestinal, and reproductive tracts have been extensively studied with regard to secretion and proliferation in healthy and diseased states. Conjunctival goblet cells have not been studied as extensively, but much information is available. The purpose of this article is to examine the current knowledge of conjunctival goblet cells.

Goblet Cell Development

In humans, conjunctival goblet cells begin to appear in the eighth to ninth week of gestation in the region of the lid margin. By the 11th to 12th week, mature goblet cells can be seen containing secretory granules in the palpebral conjunctiva. Goblet cells appear in the bulbar conjunctiva around the 20th week. In the developing chick, goblet cells appear 2 days after hatching in the fornix and 3 days after hatching in the palpebral and bulbar conjunctivae. In rats, messenger ribonucleic acid (mRNA) expression for the conjunctival goblet cell-specific mucin, MUC5AC, first appears 1 day after birth, before eyelid opening. This expression was detected in cells in the fornix region. By day 13 (before eyelid opening), a few round-shaped cells in the fornix expressed cytokeratin 7 (a cytokeratin expressed in goblet cells of adult rats) and were positive for alcian blue/periodic acid Schiff's (AB/PAS) reagent, a stain that that binds to sialomucins synthesized and secreted by the goblet cells. These cells also bind Ulex europaeus agglutinin I (UEA-I), which is a lectin that binds specific glycoprotein moieties present in adult goblet cells of the rat. In humans, the lectin Helix pomatia agglutinin (HPA) specifically binds to the goblet cell secretory products. On day 17, single and small clusters of these cells were seen distributed in the fornix and palpebral regions. Goblet cell clusters were seen by day 60. In addition to the appearance of the secretory product, by day 17, immunofluorescence microscopy showed nerves surrounding the basolateral portion of goblet cell clusters and the muscarinic receptor subtypes M_2 and M_3 and β_1- and β_2-adrenergic receptors were located on the goblet cells. The presence of nerves and neurotransmitter receptors on goblet cells around the time of eyelid opening (12–15 days after birth) implies that mucin secretion is regulated as the eyes open (Figure 2).

There is considerable evidence that stem cells of the conjunctival epithelium, including goblet cells, are distinct from the stem cells of the cornea. This is despite the fact that conjunctival cells can, in the case of a corneal wound involving the limbus, rapidly migrate over the wound and eventually form an epithelium similar to the normal cornea that does not contain goblet cells. However, when bulbar, fornical, and palphebral conjunctivae were grown separately, each with 3T3 feeder cells, they did not express the cornea-specific cytokeratin pair of K3/K12. In addition, when cultured conjunctival cells were injected into athymic mice, the epithelial cyst formed contained epithelial and goblet cells. Given these data, it is thought that conjunctival stem cells are different from stem cells of the cornea.

It is well established that corneal stem cells reside in the limbus, the area between the cornea and bulbar conjunctiva. The location of conjunctival stem cells is not as clear. In the mouse and rabbit, it is believed that the stem cells reside in the fornix based on the fact that slow-cycling cells are clustered in the fornix, and these cells do not incorporate tritiated thymidine or bromodeoxyuradine that label dividing cells. In addition, cells in the fornix have the highest rate of proliferation *in vitro*.

Cells grown from the bulbar conjunctiva and fornix had the same proliferative capacity as cells grown from

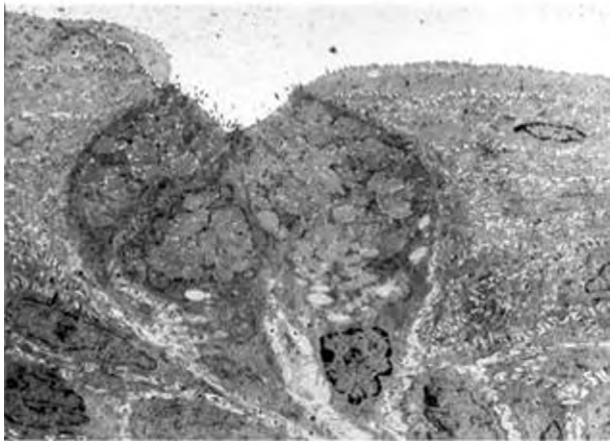

Figure 1 An electron micrograph of rat conjunctival goblet cells. Numerous secretory vesicles can be seen in the apical portion of the cells, while nuclei can be seen in the apical portion. Magnification ×6000. Reprinted from Dartt, D. A. Regulation of mucin and fluid secretion by conjunctival epithelial cells. *Progress in Retinal and Eye Research* 21: 555–576. With kind permission of Elsevier.

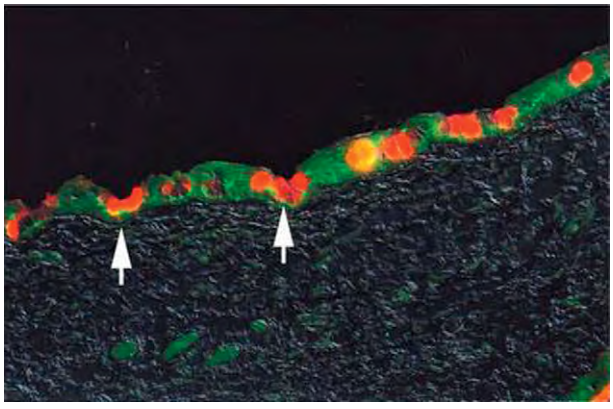

Figure 2 Co-localization of the M3 muscarinic receptor with goblet cells from the developing rat conjunctiva. Sections from a 17-day-old rat conjunctiva were incubated with an antibody against M3 muscarinic receptor (shown in green) and the lectin UEA-I conjugated to rhodamine (shown in red) which is specific for rat goblet cells. Goblet cells were visualized with differential interference contrast microscopy. Arrows indicate the presence of M3 muscarinic receptor subjacent to the secretory vesicles (shown in red). Magnification ×200.

the corneal limbus. Cells from all areas of the fornix and bulbar conjunctiva were capable of undergoing 80–100 cell divisions before reaching senescence, similar to limbal cells. Interestingly, goblet cells were present during the entire life span of the cultures of fornix and bulbar conjunctivae and the number of goblet cells increased during cultivation of the cell cultures. As goblet cells were present during the entire culture time, it seems likely that conjunctival stem cells are bipotent, that is, capable of differentiating into either goblet or stratified squamous cells. It is not known what causes the stem cell to differentiate into either cell type. Possible explanations include genetic programming as it was demonstrated that conjunctival cells with high proliferative capacity differentiate into goblet cells at specific times in their cell cycle of duplication. The first goblet cells appear after a cell has achieved 45–50 doublings and, subsequently, another 10–20 doublings before senescence occurs. It is also possible that environmental effectors such as cytokines or growth factors play a role in the differentiation of a goblet cell.

The number of goblet cells in the adult conjunctiva varies depending upon the location in the conjunctiva and species. For example, in the rabbit: (1) the tarsal conjunctiva contains the highest number of goblet cells while the bulbar conjunctiva contains the least, (2) the goblet cells of the tarsal conjunctiva were larger than those present in the bulbar conjunctiva, and (3) conjunctival goblet cells appeared as single cells interspersed throughout the stratified squamous epithelial cells. In contrast, in the rat: (1) the fornix contained the most goblet cells while very few were seen in the bulbar and limbal conjunctivae and (2) goblet cells appear as clusters with as many as 10 goblet cells present in some clusters in the fornix (**Figure 3**). Goblet cells in the human conjunctiva tend to appear as single cells (**Figure 4**), similar to the rabbit, though in certain areas, the density of goblet cells is high enough such that they appear to be clustered. The highest goblet cell density in human conjunctiva is in the inferior palpebral conjunctiva. It has been proposed that clusters of goblet cells, such as those that occur in rats, arise from the fact that goblet cells divide several times before senescence giving rise to the clusters. In contrast, in species such as rabbit and human, where goblet cells occur as single cells in the conjunctiva, differentiation into goblet cells occurs after the cell has undergone terminal differentiation.

Function of Conjunctival Goblet Cells

The tear film is a thin layer of fluid that covers the ocular surface. Tears are secreted in response to decreased humidity, bright light, mechanical stimulation, bacterial and viral pathogens, and other environmental factors. The tear film is a stratified fluid layer consisting of three layers: (1) the outermost, which is a lipid layer secreted by meibomian glands of the upper and lower eyelids and is thought to be a barrier to evaporation; (2) the middle, which is an aqueous layer secreted essentially by the main and accessory lacrimal glands and contains water, electrolytes, and proteins such as growth factors and antibacterial proteins necessary for the health of the ocular surface; and (3) the innermost, which is a mucin layer, containing mucins that are not only secreted mainly by the conjunctival goblet cells, but also the stratified squamous cells of the cornea and conjunctiva. The mucin layer moves freely over the ocular surface toward the nasolacrimal

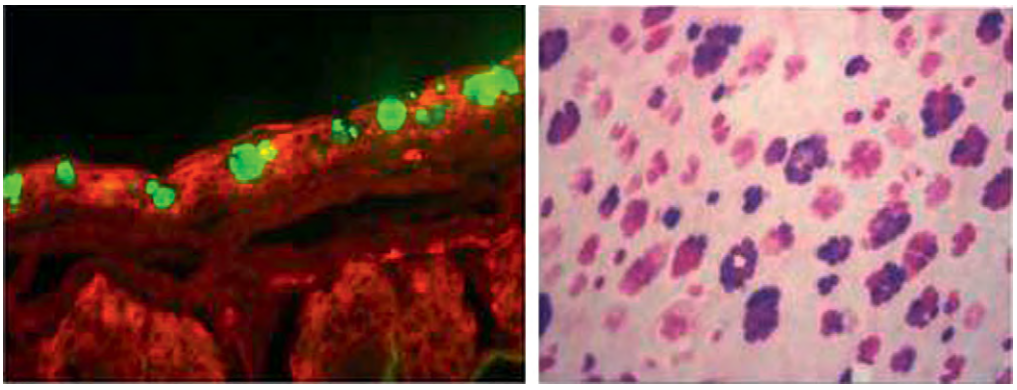

Figure 3 Goblet cell clusters in rat conjunctiva. Rat conjunctival sections were incubated with the EGF receptor (shown in red) the lectin UEA-I conjugated to fluorescein isothiocyanate (FITC; shown in green) which is specific for rat goblet cells (left). Flat mounts of rat conjunctiva were prepared and stained with AB/PAS (right). Goblet cells appear as pink-to-purple cells. These micrographs indicate the clusters of goblet cells in rat conjunctiva. Magnification ×200.

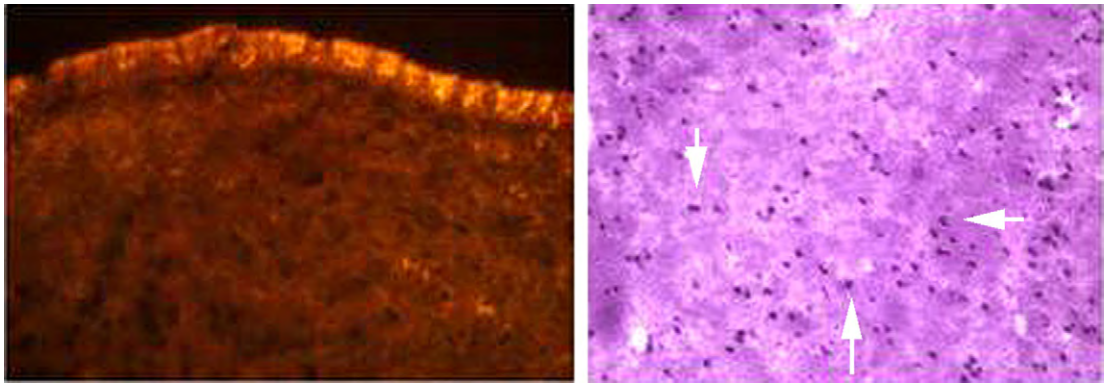

Figure 4 Goblet cell in human conjunctiva. Human conjunctival sections were incubated with an antibody specific to cytokeratin 7 (shown in red) which is specific for goblet cells (left). Impression cytology samples of human conjunctiva were prepared and stained with AB/PAS (right). Arrows indicate goblet cells. These micrographs indicate that goblet cells occur as single cells. Magnification ×200.

duct with the blink providing the mechanism of movement. As it moves, it traps debris and pathogens.

The function of conjunctival goblet cells is to synthesize and secrete mucins onto the ocular surface. Mucins are large, highly glycosylated proteins containing tandem repeats of amino acids that are rich in serine and threonine. Owing to the large amount of glycosylation, mucins are highly negatively charged molecules that are believed to be a barrier to pathogens. The glycosylation moieties are quickly hydrated upon exiting the cell, causing them to swell. Thus, mucins provide lubrication, water retention, and a barrier to infectious agents. Members of the mucin family can be subdivided based on whether they are secreted from the cell (secretory) or remain associated with the plasma membrane (membrane associated). While other members of the mucin family, namely MUC1, MUC2, MUC4, and MUC16, are present in the conjunctiva, only the gel-forming, secretory mucin MUC5AC has been identified in conjunctival goblet cells.

MUC5AC is a large gel-forming mucin that is closely related to the other gel-forming mucins MUC2, MUC5B, and MUC6. It contains four cysteine-rich domains (D domains), a tandom repeat region that can be duplicated 17–124 times, as well as a cysteine knot along with an additional cysteine region. The D domains, based on their large number of cysteines, form disulfide bridges with other MUC5AC molecules to form a large gel-like association of mucin molecules (**Figure 5**).

Control of Goblet Cell Proliferation and Mucin Secretion

It is vital for the mucin in the tear film be of sufficient quantity and quality. The quantity of mucin depends on the: (1) number of goblet cells present (proliferation or differentation), (2) amount of mucin synthesized and

stored in secretory granules, (3) rate of mucin secretion, and (4) rate of mucin degradation. There are no studies on the rate of mucin synthesis or mucin degradation.

Goblet Cell Proliferation

With the development of a method to culture conjunctival goblet cells, studies of goblet cell proliferation are now underway. One important stimulus of goblet cell proliferation is the epidermal growth factor (EGF) family as measured by both a cell proliferation assay kit and by immunoflouresence microscopy using the an antibody against Ki-67, a protein known to be present in cells that have entered the cell cycle. EGF, transforming growth factor α (TGFα), heparin-binding EGF (HB-EGF), and heregulin are present in rat conjunctiva as well as cultured rat goblet cells as determined by reverse transcriptase polymerase chain reaction (RT-PCR), Western blot analysis, and immunofluorescence microscopy. EGF, TGFα, and HB-EGF increased goblet cell proliferation through activation of the EGF receptor. There are four types of EGF receptors, namely ErbB1 (the EGF receptor), ErbB2 (HER), ErbB3, and ErbB4. Each receptor binds to specific members of the EGF family. Activated EGF receptors form homo- or heterodimers and then recruit adaptor molecules including Shc/Grb2, phosphoinositide-3 kinase (PI-3K), phospholipase C (PLC)γ, p38 mitogen-activated protein kinase (MAPK), and c-jun NH (2)-terminal kinase (JNK). Each of these kinases initiates a cascade of kinases leading to a cellular response. The downstream kinase activated by Shc/Grb2 is the extracellular-related kinase 1/2 (ERK1/2); the downstream kinase activated by PI-3K is AKT; the downstream kinase activated by PLCγ is protein kinase C (PKC); and the downstream kinase activated by JNK is c-jun (**Figure 6**).

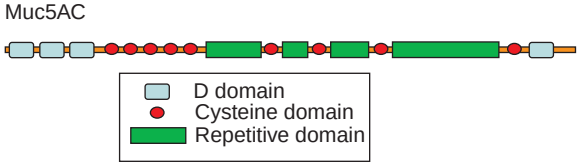

Figure 5 A schematic of MUC5AC.

Further investigation of the role of ERK in EGF-stimulated conjunctival goblet cell proliferation demonstrated that EGF increased the number of cells expressing ERK in their nucleus in a biphasic manner. Under basal conditions, ERK is present in the cytosol. Upon stimulation, ERK translocates to the nucleus where it phosphorylates proteins necessary for proliferation. The first, major peak occurs 1 min after the addition of EGF to cultured rat goblet cells. The number of goblet cells with ERK present in the nucleus returned to basal levels before increasing again approximately 18 h after the addition of EGF. The second peak corresponded with the appearance

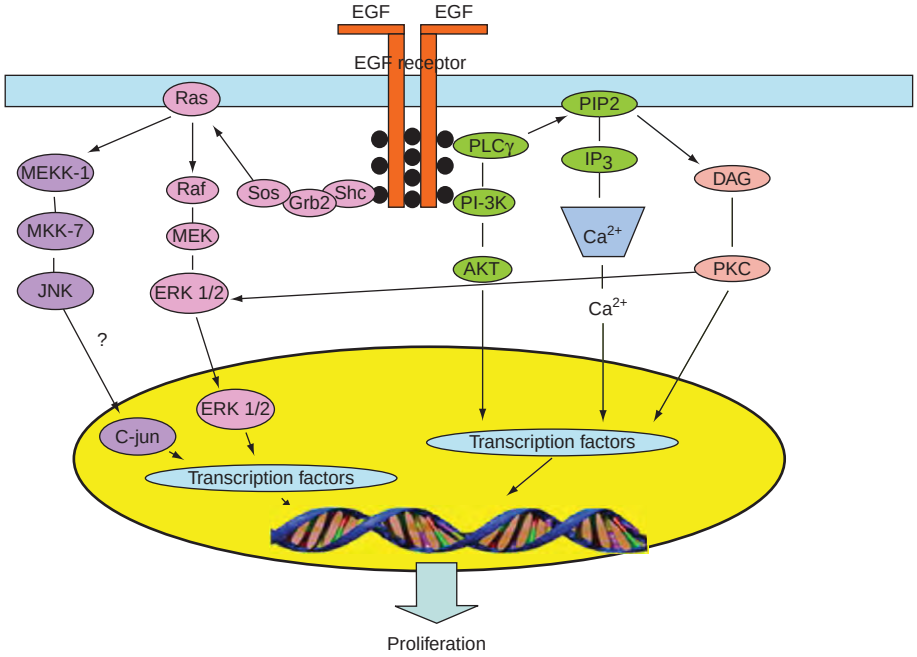

Figure 6 A schematic representation of the EGF pathway leading to goblet cell proliferation. EGF receptor dimerizes upon EGF binding, recruiting the adaptor molecules leading to cell proliferation. PI-3K, phosphoinositide-3 kinase; PLCγ, phospholipase Cγ; JNK, c-Jun NH (2)-terminal kinase; ERK1/2, extracellular-related kinase 1/2; PKC, protein kinase C; PIP2, phosphatidylinositol bisphosphate; IP_3, inositol trisphosphate; DAG, diacylglycerol; PKC, protein kinase C; MEK, mitogen-activated kinase kinase; MEKK-1, mitogen-activated kinase kinase-1; MKK-7, mitogen activated kinase kinase-7.

of Ki-67, indicating that goblet cells were starting to proliferate. The ERK inhibitor U0126, added 20 min prior to EGF, inhibited both peaks of the translocation of ERK as well as goblet cell proliferation. Interestingly, inhibition of the second peak of ERK translocation with U0126 also prevented EGF-stimulated proliferation. In addition to the activation of ERK, EGF also activates PKC isoforms -α and -ε to, in turn, stimulate proliferation.

Most proliferation studies to date have been performed on cultured goblet cells from rat. Several studies have examined the proliferation of human goblet cells in comparison to rat cells, and demonstrated that human goblet cells respond similarly to EGF. For example, EGF stimulates human goblet cell proliferation in a similar time- and concentration dependency. In both cell types, EGF activates ERK and PKC to stimulate proliferation. Due to the difficulty of obtaining a human conjunctiva and culturing human goblet cells, rat goblet cells are an excellent model for studying human goblet cell proliferation.

Goblet Cell Mucin Secretion

Goblet cell secretion occurs through an apocrine mechanism. In this mechanism, most or all the secretory vesicles fuse with one another upon stimulation and subsequently with the apical membrane releasing the mucin into the extracellular space. Therefore, the amount of mucin released is dependent upon the number of cells responding to a given stimulus. A strong stimulus would involve responses from more goblet cells than a weak stimulus. Taking advantage of this property, conjunctival samples can be treated with histochemical stains that recognize mucins in goblet cells, and the number of goblet cells can be counted. A decrease in the number of goblet cells would indicate an increase in secretion.

Another method to measure conjunctival goblet cell secretion is based on the fact that the lectins UEA-I and HPA bind to specific carbohydrate residues found in MUC5AC, depending on the species. The amount of secreted mucin can be determined by an enzyme-linked lectin assay (ELLA) and Western blot or dot-blot analyses.

Using the histochemical method of staining for mucins in a conjunctival button, it was demonstrated, for the first time, that goblet cell mucin secretion is neurally mediated, as a wound to the central cornea induced goblet cell mucin secretion. Sensory nerves in the cornea were activated by the wound causing a neural reflex arc in which the parasympathetic nerves that surround the goblet cells released their neurotransmitters to stimulate mucin secretion.

These results were confirmed when parasympathetic nerves containing the neuropeptide vasoactive intestinal peptide (VIP) were demonstrated to be present in the conjunctiva surrounding the goblet cells subjacent to the secretory granules. Addition of exogenous VIP or the cholinergic agonist carbachol (an analog of the parasympathetic neurotransmitter acetylcholine) stimulated goblet cell secretion. Other compounds which have been shown to stimulate conjunctival mucin secretion include activators of the purninergic receptor subtype $P2Y_2$, such as ATP, UTP, and INS365, the neurotrophins nerve growth factor, and bone-derived neurotrophic factor, and the drug OPC-12759, an antigastric ulcer drug. Interestingly, no sympathetic neurotransmitter has been shown to stimulate goblet cell secretion despite the presence of the receptors for these neurotransmitters on goblet cells.

The signal transduction pathways utilized by cholinergic agonists have been well studied. Cholinergic agonists bind to M2 and M3 muscarinic receptors which are present on conjunctival goblet cells. Classically, these receptors activate PLC, which hydrolyzes phosphatidylinositol-bisphosphate into 1,4,5-inositol trisphosphate (IP_3) and diacylglycerol (DAG) (**Figure 7**). IP_3 induces the release of Ca^{2+} from the endoplasmic reticulum into the cytosol. It is not known if this occurs in goblet cells; however, what is known is that an increase in intracellular Ca^{2+} alone is sufficient to cause mucin secretion from conjunctival goblet cells. Calcium can also activate Ca^{2+}-/calmodulin-dependent protein kinase. However, inhibitors of Ca^{2+}/calmodulin protein kinase do not have any effect on cholinergic agonist-stimulated mucin secretion.

DAG is a phospholipid activator that along with Ca^{2+} activates PKC. Though a direct role for PKC involvement in conjunctival goblet cell mucin secretion has not been demonstrated, activators of PKC (phorbol esters) do stimulate secretion.

In addition to the Ca^{2+} pathway, cholinergic agonists in goblet cells activate a second pathway leading to protein secretion. This pathway involves the transactivation of the EGF receptor through the stimulation of the focal adhesion kinase Pyk2. Pyk2, in turn, activates the nonreceptor tyrosine kinase p60Src. Pyk2 and p60Src are activated in goblet cells by Ca^{2+} and PKC as the addition of either a calcium ionophore or a phorbol ester increases phosphorylation (activation) of Pyk2 and p60Src and the use of PKC inhibitors inhibits cholinergic agonist-stimulated Pyk2 and p60Src phosphorylation (**Figure 7**). This again implies that PKC plays a vital role in conjunctival goblet cell secretion. The Pyk2/p60Src complex then transactivates the EGF receptor, recruiting the adaptor molecules Shc, Grb2, and the Ras guanine nucleotide exchange factor Sos. Sos binds to and activates the low molecular weight guanosine triphosphate (GTP)ase, Ras, causing the exchange of guanosine diphosphate (GDP) for GTP to activate Ras. Ras initiates another kinase cascade of Raf (also known as MAPK kinase kinase), mitogen-activated kinase kinase (MEK) (MAPK kinase), and ERK 1/2 (p44/p42 MAPK). Upon stimulation by cholinergic agonists, ERK activates proteins in the cytosol, leading to secretion. Inhibition of ERK inhibits cholinergic agonist-stimulated mucin secretion (**Figure 7**).

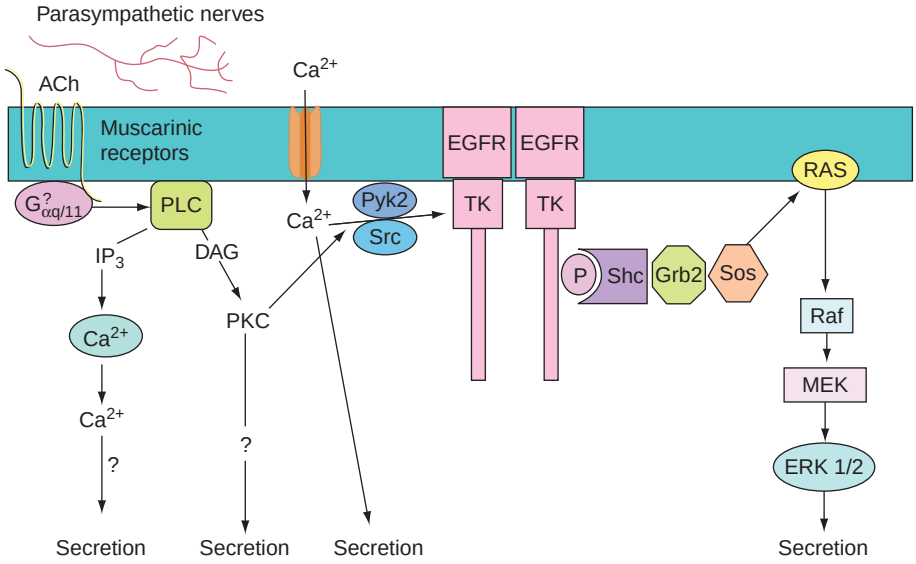

Figure 7 A schematic representation of the cholinergic pathway leading to goblet cell mucin secretion. Muscarinic receptors activate phospholipase C (PLC) to generate the production of inositol trisphosphate (IP_3), which releases intracellular Ca^{2+} and diacylglycerol (DAG), which activates protein kinase C (PKC). The EGF receptor (EGFR) is transactivated leading to the activation of Ras, Raf, mitogen-activated kinase kinase (MEK), and ERK 1/2.

In contrast, when ERK is activated by exogenous EGF, ERK 1/2 translocates to the nucleus where it stimulates proliferation.

The signaling pathways of the other compounds that stimulate mucin secretion are not well studied. Receptors for VIP (VPAC1 and VPAC2) are present on goblet cells both *in vivo* and *in vitro*. It is not known if exogenous VIP (which causes mucin secretion) acts through these receptors. As it is well established in other tissues that VIP increases the intracellular cyclic adenosine monophosphate (cAMP) concentration as well as the intracellular $[Ca^{2+}]$, it is likely that a similar mechanism occurs in goblet cells.

It is not know if the EGF family stimulates mucin secretion. As these growth factors activate ERK, which plays an important role in both secretion and proliferation, it is likely that they do. It is interesting that many of the same proteins and kinases are used by EGF to stimulate proliferation and by cholinergic agonists to stimulate mucin secretion. ERK1/2 is known to phosphorylate over 100 proteins. In order to confer specificity, ERK1/2, as is the case for many signaling molecules, is organized through the use of scaffold proteins. These proteins bind to two or more components of a signaling pathway in close proximity to assist with their interactions. Scaffolding proteins also target signaling molecules to particular areas of the cell in order to phosphorylate specific substrates. They can prevent cross talk between pathways. As the scaffolding proteins are also regulated, their stability can affect the duration of the signal. Several different scaffolding proteins have been identified in mammalian cells including kinase suppressor of Ras, MEK partner-1, Morg1, IQGAP1, and β-arrestins 1 and 2. Not surprisingly, scaffolding proteins are required for the translocation of ERK1/2 to the nucleus and other proteins are responsible for maintaining ERK1/2 in the cytosol. In fact, ERK1/2 translocation to the nucleus requires phosphorylation by MEK, which causes conformational changes in ERK1/2, allowing for the formation of ERK dimers. This dimerization facilitates the translocation of phosphorylated ERK1/2 into the nucleus. In contrast, PEA-15, a small phosphoprotein, has been shown to anchor ERK1/2 in the cytosol.

Clinical Implications of Mucin Deficiency on the Ocular Surface

The presence of goblet cells in the conjunctiva is of great importance to the health of the ocular surface. Dry eye, which is characterized by a deficient tear film or excessive evaporation, is a multifactorial disorder that causes damage to the ocular surface. One characteristic of dry eye is a decrease in the number of mucin-containing goblet cells. All *in vivo* studies to date identify goblet cells by their secretory product, either by staining with AB/PAS or by the presence of MUC5AC within the cell, and should be termed filled goblet cells. Thus, a decrease in the number of filled goblet cells in the conjunctival tissue indicates that goblet cells have secreted. Under chronic conditions, the decrease in filled goblet cells could indicate repeated stimulation such that mucin synthesis is unable to keep pace with secretion or indicate a loss of goblet cells through either a decrease in goblet cell proliferation,

dedifferentiation, or an increase in goblet cell death. It is difficult to know whether the loss of goblet cells is a cause of the disease or a result of it. Indeed, the mechanism by which goblet cells are lost from the conjunctiva has not been studied. In animal models of dry eye, proteins involved in apoptosis have been shown to be upregulated in conjunctival epithelial cells, though the effects on the goblet cells themselves were not clear. The loss of goblet cells in dry eye patients warrants further examination.

The presence or absence of conjunctival goblet cells has been examined in different types of dry eye. These have been described below.

Sjögren Syndrome

Sjögren syndrome is an autoimmune disease characterized by profound lymphocytic infiltration of the lacrimal and salivary glands, resulting in dry eye and dry mouth. It is not known whether the changes seen in the conjunctiva are a result of the autoimmune disease itself or as a result of the change in tears due to lacrimal gland destruction. Though the changes in the conjunctiva are relatively mild compared to the destruction of the lacrimal glands, there is a decrease in the number of mucin-containing goblet cells in patients with Sjögren syndrome, as determined by histochemical staining methods. In addition, the amount of MUC5AC mRNA is decreased in patients with Sjögren syndrome and the amount of MUC5AC detected in tears of these patients is also decreased.

Vitamin A Deficiency

Vitamin A is vital for the health of the ocular surface as it is essential for the development of goblet cells in the conjunctiva. Vitamin A deficiency has been shown to cause keratinization and squamous metaplasia of the conjunctiva. The lack of goblet cells in the conjunctiva in vitamin-A-deficient patients has been documented through the use of impression cytology and histochemical staining methods. It has also been demonstrated that in vitamin-A-deficient rats, not only were there no mucin-containing goblet cells, but the mRNA for MUC5AC and MUC5AC protein also disappeared 20 weeks after the initiation of a vitamin-A-deficient diet. Reintroduction of vitamin A into the diet has been shown to increase the number of conjunctival mucin-containing goblet cells.

Topical Preservatives

Preservatives, such as benzalkonium chloride, are often found in artificial tears and medications such as those used to treat glaucoma and anti-inflammatory medications. These patients often report the signs and symptoms of dry eye. Benzalkonium chloride has been shown to decrease the number of mucin-containing goblet cells present in the conjunctiva.

Ocular Cicatrical Pemphigoid

Mucous membrane pemphigoid is an autoimmune disease that is characterized by blisters in the mucous membranes of the body including the mouth, nose, trachea, and conjunctiva. When the conjunctiva is involved, it is known as ocular cicatrical pemphigoid (OCP). This condition causes chronic conjunctivitis and, eventually, complete keratinization of the conjunctiva, resulting in severe dry eye. It has been observed that the mucin-containing goblet cell number is reduced in the later stages of the disease, likely as a result of the keratinization. Interestingly, it has been shown that the expression of a specific glycosyltransferase present exclusively in goblet cells in normal human conjunctiva is altered in late stages of OCP. This enzyme, which is responsible for the glycosylation of mucins, is expressed in stratified squamous cells in areas of the conjunctiva that were nonkeritinized in OCP patients, and, as the disease progressed, the expression disappeared.

Laser *In Situ* Keratomileusis

Patients undergoing laser *in situ* keratomileusis (LASIK) often experience dry eye symptoms. These symptoms are usually temporary, but can develop into chronic dry eye. It is known that the number of mucin-containing goblet cells decreases significantly within 1 week postsurgery, but returns to preoperative levels by 3 months after surgery.

Diseases and disorders of goblet cells are a result not only of mucous underproduction, but also of mucous overproduction.

Ocular Allergies

The symptoms of allergic conjunctivitis include mucus production, ocular itching, foreign-body sensation, tearing, hyperemia, chemosis, and lid edema. Traditionally, allergic eye disease has been classified into: seasonal allergic conjunctivitis (SAC), perennial allergic conjunctivitis (PAC), vernal keratoconjunctivitis (VKC), atopic keratoconjunctivitis (AKC), and contact-lens-induced papillary conjunctivitis (CLPC). Each of the five categories of allergic conjunctivitis has a distinct pathology. In SAC and PAC, conjunctival inflammation is mild and of short duration. In VKC and AKC, conjunctival inflammation has an unclear history of exposure to allergen, is more severe, and lasts longer than SAC and PAC.

A common symptom of allergic conjunctivitis in the human is alteration in mucus production. One hypothesis as to how mucous production is altered in allergic conjunctivitis is that activation of sensory nerves in the cornea

and conjunctiva, manifested by itchiness, foreign-body sensation, and increased tearing, could occur. This, in turn, could activate the efferent parasympathetic and sympathetic nerves that surround conjunctival goblet cells to release the neurotransmitters acetylcholine and VIP, which are known to stimulate conjunctival goblet cell secretion. When goblet cells secrete, all secretory granules are released at once. Under these chronic conditions, the decrease in filled goblet cells could indicate repeated stimulation with mucin synthesis unable to keep pace with secretion. In support of this, a decrease in filled conjunctival goblet cells in VKC and AKC patients, respectively, compared to control subjects, has been noted. In addition, the amount of MUC5AC RNA in the conjunctiva was decreased in AKC and VKC patients versus control. The excess mucus seen on the conjunctiva in individuals with VKC is a stringy mucus and does not necessarily represent goblet cell MUC5AC, but could be stratified squamous cell membrane-spanning mucins, poorly hydrated mucins, or mutated mucin variations. Additional study of the role of goblet cell mucin secretion in different types of ocular allergy is warranted.

Results from animal models of allergic conjunctivitis, which most closely mimics SAC and PAC, found that the number of filled goblet cells decreased for 6 h after the final allergen challenge. Over 48 h, the number of filled goblet cells returned toward control values, indicating that goblet cell mucin secretion increased during delayed hypersensitivity, but that goblet cells refilled after allergen removal. MUC5AC RNA was also depleted by the final challenge and recovered at 6 h, indicating that the delayed hypersensitivity depletes MUC5AC RNA; however, it recovers quickly to begin synthesizing MUC5AC to refill the goblet cells.

Summary

Much information has been gathered regarding the role of conjunctival goblet cells in the health of the ocular surface. Goblet cell proliferation, mucin synthesis, and secretion control the amount of mucin present on the ocular surface. These processes are regulated as growth factors increase proliferation and neural stimulation causes mucin secretion. However, many questions remain. Are the three processes that regulate mucin amount coordinated so that one stimulus activates all three? While some of the intracellular pathways leading to proliferation or secretion are known, it is not known if these pathways are altered in diseases. The life span of a conjunctival goblet cell as well as the mechanisms by which goblet cells are lost in disorders of the tear film are unknown. It is also not known if goblet cells are able to secrete mucins multiple times, perhaps refilling secretory granules, in response to either a sustained signal or multiple stimuli. Further research into these questions may lead to the development of treatments for many of the ocular surface diseases.

See also: Defense Mechanisms of Tears and Ocular Surface; Ocular Mucins; Overview of Electrolyte and Fluid Transport Across the Conjunctiva.

Further Reading

Dartt, D. A. (2004). Control of mucin production by ocular surface epithelial cells. *Experimental Eye Research* 78: 173–185.

Gipson, I. K. and Argueso, P. (2003). Role of mucins in the function of the corneal and conjunctival Epithelia. *International Review of Cytology* 231: 2–49.

Gipson, I. K., Hori, Y., and Argueso, P. (2004). Character of ocular surface mucins and their alteration in dry eye disease. *Ocular Surgery* 2: 131–148.

International Dry Eye Workshop (2007). The definition and classification of dry eye disease. Report of the definition and classification subcommittee of the International Dry Eye Workshop (2007). *Ocular Surgery* 5: 75–92.

Lavker, R. and Sun, T-T. (2003). Epithelial stem cells: The eye provides a vision. *Eye* 17: 937–942.

Pellegrini, G., Golisano, O., Paterna, P., et al. (1999). Location and clonal analysis of stem cells and their differentiated progeny in the human ocular surface. *Journal of Cell Biology* 145: 769–782.

Ramos, J. W. (2008) The regulation of extracellular signal-regulated kinase (ERK) in mammalian cells. *International Journal of Biochemistry and Cell Biology*, 40: 2707–2719.

Rios, J. D., Forde, K., Diebold, Y., et al. (2000). Development of conjunctival goblet cells and their neuroreceptor subtype expression. *Investigative Ophthalmology and Visual Science* 41: 2127–2137.

Sellheyer, K. and Spitznas, M. (1988). Ultrastructural observation on the development of the human conjunctival epithelium. *Graefe's Archive of Clinical and Experimental Ophthalmology* 226: 489–499.

Shapiro, M. S., Friend, J., and Thoft, R. A. (1981). Corneal re-epithelialization from the conjunctiva. *Investigative Ophthalmology and Visual Science* 21: 135–142.

Shatos, M. A., Rios, J. D., Tepavcevic, V., Kanno, H., Hodges, R. R., and Dartt, D. A. (2001). Isolation, characterization, and propagation of rat conjunctival goblet cells in vitro. *Investigative Ophthalmology and Visual Science* 42: 1455–1464.

Contact Lenses

N Carnt and Y Wu, Institute for Eye Research, Sydney, NSW, Australia
F Stapleton, University of New South Wales, Sydney, NSW, Australia

Glossary

Contact lens-induced papillary conjunctivitis (CLPC) – Enlarged papillae accompanied by redness of the upper palpebral conjunctiva. Symptoms include discomfort, itching, mucous discharge, and foreign body sensation.
Corneal infiltrates – Corneal inflammatory response which appears as single or multiple, focal or diffuse lesions in the corneal stroma.
Endothelial polymegethism – Variation in the size of the endothelial cells of the cornea as a result of disturbed metabolism.
HEMA – Hydroxyethylmethacrylate monomer forming the basis of many soft contact lens material polymers.
Hypermetropia – Also known as farsightedness, it is a defect of vision caused by an imperfection in the eye (often when the eyeball is too short or when the lens cannot become round enough), causing difficulty focusing on near objects.
Lens-induced chronic hypoxia – Corneal oxygen deprivation that results from contact lenses that greatly impede oxygen diffusion to the cornea. Chronic hypoxia may cause changes in corneal structure and neovascularization.
Multipurpose solutions (MPSs) – Solution for cleaning, rinsing, disinfecting, and storing your contact lenses.
Myopia – The ability to see close objects more clearly than distant objects. Myopia can be caused by a longer-than-normal eyeball or by any condition that prevents light rays from focusing on the retina.
Orthokeratology – The practice of reshaping the cornea by wearing specially designed rigid contact lenses. These lenses are usually worn only during sleep and they reshape the front surface of the eye, correcting the refractive error and allowing clear vision.
PMMA – Polymethylmethacrylate material used for oxygen impermeable hard contact lenses.
RGP – Rigid gas permeable materials used for oxygen permeable hard contact lenses.
Superior epithelial arcuate lesions (SEALs) – Whitish, opalescent lesions, located adjacent or at the superior limbus, caused predominantly by a mechanical interaction between the (usually) silicone hydrogel or hydrogel contact lens, the eyelid, and the superior peripheral cornea.

Introduction

Contact lenses provide a safe and reversible means of refractive error correction; lenses are currently worn by 150 million individuals worldwide. Contact lenses have many optical, sporting, cosmetic, therapeutic, and vocational advantages over conventional spectacles. The vast majority of wearers use contact lenses for the correction of simple low refractive errors but other applications include presbyopia, astigmatism, high refractive error, and other medical, cosmetic, or therapeutic indications.

Given their close association with the ocular surface, contact lens wear may have an impact on ocular surface anatomy and physiology and they may be associated with adverse effects, including ocular surface infection or inflammation. The impact of contact lens wear varies with lens type, mode of wear, indication for lens wear, and with wearer factors including demographics, hygiene, compliance, and behavior factors.

Types of Contact Lenses

Hard lenses, made from polymethylmethacrylate (PMMA), were first available in 1934 and soft lenses during the 1960s. Lens materials have evolved since with the advent of gas permeable rigid materials and more recently silicone hydrogel materials. An ideal material and lens design would maintain normal ocular surface physiology, have a low rate of complications, provide vision correction, and be comfortable during wear (**Table 1** and **Figures 1–6**).

Probably the most exciting recent innovation in the field has been the introduction of silicone hydrogel materials. The high oxygen permeability of these new silicone-based products has limited the effects of hypoxia and largely eliminated a range of physiological complications such as corneal edema, microcysts, corneal vascularization, endothelial polymegethism, overwear syndrome, and corneal exhaustion.

Lenses may be worn on a daily wear basis, where they are removed, cleaned and disinfected overnight, and reinserted the following day. Daily lens use is the most common modality prescribed. Complication rates are generally lowest with this wear modality; however, conditions associated with toxic or allergic responses to lens care products occur more commonly with daily lens use. Daily disposable contact lenses (lenses worn once during the day and discarded on removal) have eliminated many

Table 1 Contact lens types and materials

CL type	*Material*	*Comments*	*Illustration*
Rigid corneal contact lenses	PMMA: polymethylmethacrylate	• Readily machined and polished • Impermeable to oxygen • Average lens diameter range 7–12 mm	**Figure 1**
	RGP: rigid gas permeable (fluoro-siloxane acrylates, perfluoroethers)	• Higher oxygen permeability compared with PMMA • Average corneal lens diameter range 9–12 mm	**Figure 1**
	Orthokeratology lenses: generally highly oxygen permeable rigid gas permeable materials	• Overnight use of orthokeratology lenses reshapes the cornea to reduce the refractive error with overnight use • Larger diameter lenses with an oblate profile used to reduce myopic refractive errors	**Figure 2**
Soft contact lenses	Hydrogel: hydroxyethylmethacrylate (HEMA), with other monomers, such as vinyl pyrollidone, vinyl chloride, methacrylic acid and others, added to alter ionicity and water content of the material	• Flexible polymers which conform to the shape of the cornea and limbus • Average lens diameter 13–15 mm • Water content of polymer determines oxygen permeability	**Figure 3**
	Silicone hydrogel: silicone incorporated into a diverse group of hydrogel monomers. Wettability is enhanced by either surface treatment or by the incorporation of soluble polymers within the bulk material	• Higher oxygen permeability than hydrogel contact lenses, consequently less corneal hypoxia • Lens design similar to hydrogel contact lenses • Generally stiffer modulus than hydrogel contact lenses	**Figure 3**
Other contact lenses	Hybrid Hard/soft combination	• An RGP center with a soft hydrogel or silicone hydrogel periphery • Useful in fitting irregular corneas	**Figure 4**
	Scleral/semiscleral/mini-scleral lenses	• Scleral lenses use the sclera rather than the cornea as the bearing surface • Consequently a range of abnormal corneal topographies may be fitted • The overall diameter ranges from 16 mm (miniscleral) to 24 mm (full scleral) and lenses are made in RGP materials	**Figures 5** and **6**

Adapted from Fonn, D., Reyes, M., Terry R., and Williams L. (2000) *The IACLE Contact Lens Course*, 1st edn., vols. 2 and 8. Sydney: The International Association of Contact Lens Educators.

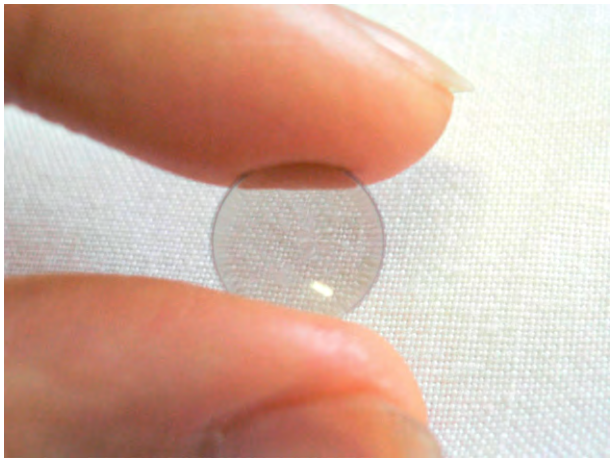

Figure 1 Rigid contact lens of 9.5 mm diameter.

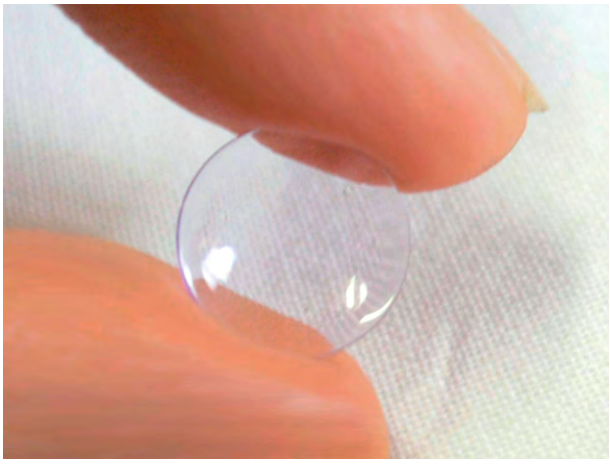

Figure 2 Orthokeratology contact lens.

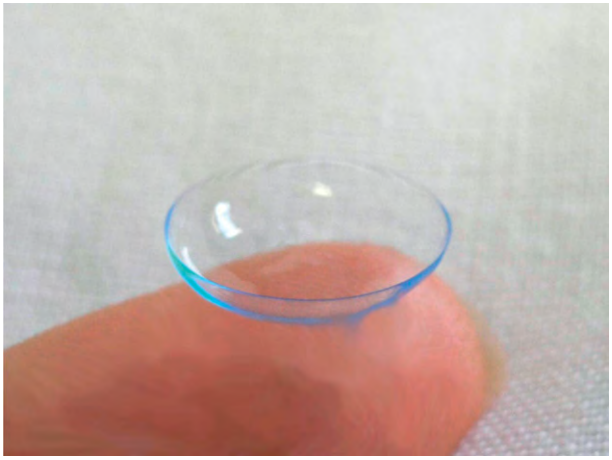

Figure 3 Hydrogel lens of 14 mm diameter.

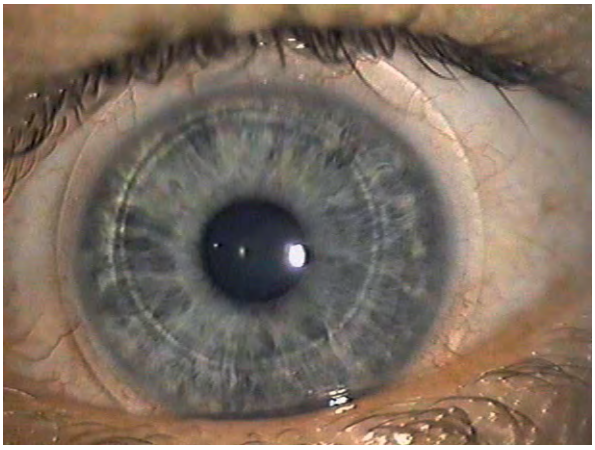

Figure 4 Hybrid lens on eye.

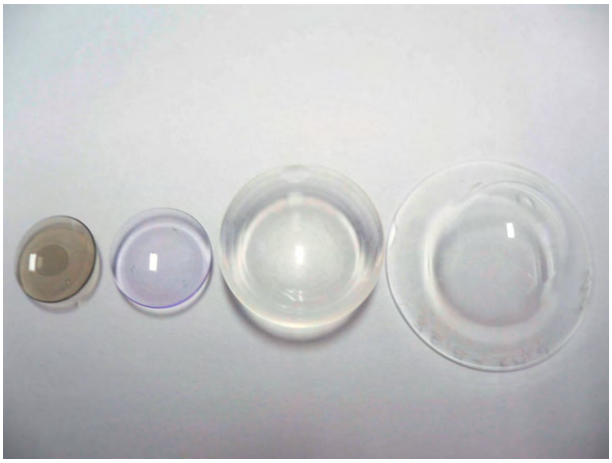

Figure 5 Rigid lenses from left to right: corneal RGP; orthokeratology RGP, mini-scleral, full scleral.

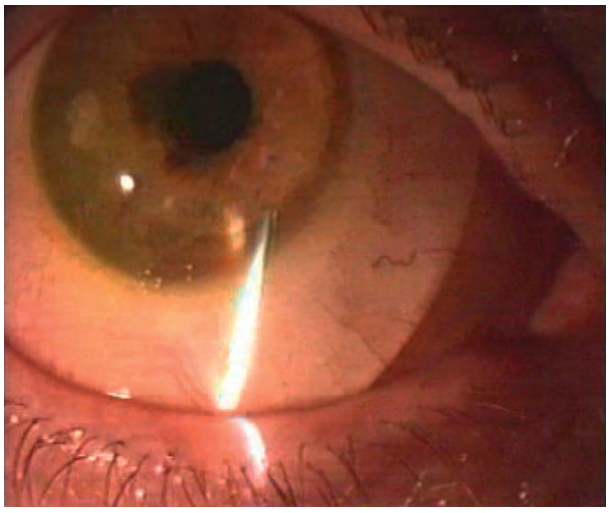

Figure 6 Full scleral contact lens on eye.

complications related to care solution use and those due to inadequate contact lens or storage case hygiene. A proportion of daily lens users (13–23%) report occasional unscheduled overnight use of lenses of up to one night per week. Certain lenses may be prescribed for overnight use, where they are worn continuously for up to 30 consecutive nights.

How Contact Lens Wear Affects the Ocular Surface

Hydrogel and silicone hydrogel contact lenses are on average 2–3 mm larger than the cornea and overlay the limbus and surrounding bulbar conjunctiva, consequently contact lenses interact directly with the corneal, limbal, bulbar, and tarsal conjunctival epithelia, and with the tear film. Their impact on the ocular surface can be characterized as follows.

Effects of Contact Lens Wear on the Corneal and Limbal Epithelium

Lens-induced chronic hypoxia can lead to changes in the corneal epithelium such as thinning, lower oxygen uptake rates, and increased microcysts. In addition, limbal hyperemia is increased and encroachment of blood vessels into the corneal stroma can occur. The smaller diameter of rigid lenses results in less interaction between the lens and limbal or conjunctival epithelium, generally less corneal hypoxia and greater tear exchange compared with soft contact lenses.

Epithelial microcysts are one of the more obvious clinical markers of hypoxia, appearing as small, irregular dots in retro illumination of the cornea with a slit lamp biomicroscope at high magnification. They are comprised of degenerated cellular material and are most often seen after 3 months of extended wear of low oxygen transmissible

lenses. They are transitory, exhibiting a spike in numbers approximately 1 month after hypoxic stress is removed and returning to normal within 3 months.

All contact lenses slow the corneal epithelial cell renewal cycle by slowing epithelial cell proliferation and migration and lowering the exfoliation rate. At the limbus, stem cells continually provide new basal corneal epithelial cells, where the rate of production increases during ocular surface damage. Recurrent erosion, chronic inflammation, and blood vessel growth onto the cornea (vascularization) can occur as a result of compromise to the limbal stem cells. Basal epithelial cells produced from slow cycling stem cells replicate and migrate horizontally, differentiating upward, before undergoing either apoptosis (programmed cell death) or necrosis and exfoliation into the precorneal tear film. Soft contact lens wear, in particular, lens-related hypoxia, has been reported as a possible cause of limbal stem cell damage. To a lesser extent contact lenses may have a mechanical effect on the limbal stem cells, which are protected somewhat due to their location at the level of the basal epithelium.

Alteration of the Lens: Cornea Resurfacing Mechanism

The precorneal tear film maintains the normal optical, lubrication, and defence functions of the ocular surface. Wear of a contact lens may destabilize the tear film by compartmentalizing the tear film into prelens and postlens regions, by changing the tear film structure and components and by reducing tear exchange.

Compared with the normal precorneal tear film, the prelens tear film is thinner, less stable, and exhibits higher evaporation. The increased evaporation rate is thought to be related to a thinner lipid layer which is more prone to contamination. A thinner lipid layer, lens dehydration, and an unstable tear film can lead to corneal epithelial dessication.

All contact lenses inhibit normal tear exchange by trapping debris, toxins, antigens, and microorganisms beneath the lens and interfering with the normal resurfacing action of blinking. Increasing the retention time of metabolic debris, toxins, or antigens at the ocular surface has been implicated in the development of inflammatory conditions. The rate of tear exchange varies with lens type, material and wearer characteristics. For example, rigid gas permeable (RGP) contact lenses allow more rapid tear exchange than hydrogel or silicone hydrogel lenses and are associated with a lower rate of inflammatory complications compared to soft lens wear.

Adverse Events

Inflammation

Corneal inflammation occurs relatively often in contact lens wear, affecting 7% of wearers. The risk of inflammation varies with different lens materials and wear modalities. The severity of inflammation varies and several systems have been used to characterize and classify corneal inflammation. Contact lens-related corneal inflammation is characterized by white blood cells, usually polymorphonuclear leukocytes, invading the cornea stroma (infiltrates). The infiltrates appear as small, usually round, opaque lesions (focal) or dispersed in a haze (diffuse). Usually limbal and bulbar redness accompanies the infiltrates. Epithelial damage can be present. Inflammation can be as a result of mechanical trauma but more often results from toxic reactions to bacteria. In the closed eye environment, bacterial toxin concentration behind the lens as well as compromise to the normal lid-tear resurfacing and alteration of tear defence proteins may lead to more frequent inflammation in extended compared to daily wear.

Contact lens-induced papillary conjunctivitis (CLPC) is an inflammatory reaction of the upper palpebral conjunctiva, caused by mechanical trauma and/or allergic response to the lens or deposits on the surface of the lens. It is the most common contact lens-related adverse event that leads to discontinuation of lens wear. Clinically, it presents as raised papillae, which comprise lymphocytes and plasma surrounding central blood vessels and associated hyperemia. There are two forms of CLPC, one that involves the entire upper palpebral area (generalized) and the other a small cluster (localized). CLPC is more frequent in soft than rigid lenses, and more common in extended compared to daily wear. The generalized form is more common in softer, hydrogel lenses which attract more protein deposits; this form likely represents a hypersensitivity (both type I and type IV) response, whereas localized disease is more likely to be found with the stiffer silicone hydrogel lenses and is thought to be related to mechanical trauma.

Infection

Corneal infection is a rare but severe complication of contact lens wear, affecting 4 per 10, 000 wearers per year, with higher rates (20 per 10, 000) per year in overnight lens use. These estimates have remained remarkably consistent over a 20-year period, despite advances in contact lens materials, wear modalities, and care system technologies. Permanent vision loss occurs in 6 per 100, 000 wearers per year or in 10–15% of cases of infection. Lower rates of severe keratitis and vision loss have been reported with daily disposable contact lens use. A poorer disease outcome is strongly associated with recovery of an environmental pathogen and a delay in receiving appropriate treatment.

Unlike corneal infections in noncontact lens wearers, *Pseudomonas aeruginosa* is the most common pathogen associated with contact lens-related disease, accounting for 50–60% of culture proven cases. More recently, environmental organisms such as *Acanthamoeba* and the fungi

Fusarium have been associated with outbreaks of disease, particularly disease linked with the use of specific multipurpose solutions (MPSs). In the case of *Acanthamoeba keratitis*, strong links with contaminated water have been identified.

Mechanical effects

Contact lenses can cause mechanical effects on the cornea due to their physical presence. For soft contact lenses, superior epithelial arcuate corneal lesions (SEALs), white heaped lesions occurring adjacent to and concentric with the superior limbus are thought to be due to a combination of tight upper-lid pressure, stiffness of the lens material, poor surface, and tight fitting of soft lenses. These are usually associated with foreign body and discomfort symptoms and resolve with interruption to lens wear within 1 week. Erosions, a full thickness epithelial loss, appear as a plug of epithelium that has been lifted off the cornea. Resolution is rapid and often results in clumping of the epithelial cells as healing takes place. Care must be taken to observe good hygiene and not patch the lesion, as the break in the epithelium renders the cornea more prone to infection. Sometimes prophylactic antibiotic therapy is used. Symptoms can be quite painful and can be eased by use of ocular lubricants. For RGP lenses, the most common mechanical effect is abrasion due to debris trapped behind the contact lens. Corneal abrasions are more commonly seen with rigid lenses compared with soft. Often the patient is symptomatic despite quite spectacular appearances; resolution is rapid, usually within a day or two. Abrasions can also occur due to fingernail injuries on removal of lenses.

Current Hot Topics in Contact Lens Research

Contact Lens Care Products

MPSs dominate the CL care market and are used by 99% of soft lens wearers. In recent years, the industry has been focused on comfort and convenience for the wearer, formulating new preservatives and incorporating comfort additives into care products.

Corneal staining (visualization of damaged epithelial cells by instillation of sodium fluorescein) is the most reliable clinical way to assess corneal integrity. Solution-related corneal staining has been reported from a 2-h provocative test and over 3 months of lens wear with a range of lens and solution combinations. Performance has not been predictable in terms of solution preservative or across different silicone hydrogel lens types, likely due to the more complicated lens chemistry compared to hydrogel lenses. Solution-related corneal staining has been associated with decreased comfort and increased risk of low-grade inflammatory events. MPSs have been associated with decreased epithelial barrier function and increased susceptibility to bacterial binding; however, no evidence to date shows that solution-related staining is a risk factor for infection. Further exploration of the mechanisms and implications of short- and long-term corneal staining is underway.

Corneal Infection

Other than overnight wear of contact lenses, a range of hygiene, compliance, and demographic factors have been consistently associated with disease. In contemporary lens wearers these include increasing the degree of lens use in daily wear, poor-storage case hygiene, smoking, Internet purchase, less than 6 months wear experience, and socioeconomic class. Further study is directed toward exploration of new risk factors, particularly establishing the impact of wearer risk behavior such as internet purchase: evaluation of specific hygiene practice such as rub and rinse and establishing the impact of second generation silicone hydrogel lens materials on the risk of infection. Ongoing surveillance enables monitoring of disease outbreaks and new or unusual causative organisms.

In corneal infection associated particularly with daily wear of contact lenses, the storage case has been identified as the source of organisms. This has resulted in the uptake of antimicrobial technologies, such as silver, into contact lens storage cases to limit microbial adhesion and colonization of the contact lens storage case. Early reports indicate some reduction in levels of certain microorganisms, but the long-term impact of these technologies in clinical use has not yet been established.

Orthokeratology

Orthokeratology is a nonsurgical approach to temporarily correct or eliminate refractive error through rigid lens wear to reversibly change the curvature of the cornea. More recent approaches include using specially designed rigid contact lenses worn overnight to enable clear vision without lens wear during the daytime. In the case of myopia correction, a reverse-geometry lens with a base curve flatter than the peripheral curve of the back surface is worn. The reduction in myopia occurs through central corneal epithelial thinning. While these effects are reversible there is discussion whether the impact of orthokeratology lenses on the corneal epithelium increases the risk of corneal infection. Ongoing studies endeavor to optimize the refractive effects both in myopia and hypermetropia, to understand the mechanisms in epithelial thinning and to establish whether orthokeratology can be used to permanently reduce or eliminate refractive error or to prevent myopia progression.

Summary

A range of materials and wear modalities are available in contemporary contact lens practice to correct a wide range of refractive errors, potentially to slow or prevent refractive error development and to meet other medical or cosmetic requirements. Contact lenses interact closely with the ocular surface and all lenses, to a lesser or greater degree, will impact on the conjunctiva, lid, cornea, and tear film physiology. While the majority of their effects and complications are reversible and nonsevere, corneal infection remains the most severe response which can potentially result in vision loss due to scarring and perforation. Safe contact lens wear requires awareness by wearers to ensure that their eyes "Feel good, see well and look good" at all times. In the rare event of corneal infection, morbidity can be limited by prompt treatment by the practitioner. Recent outbreaks of corneal infection caused by unusual environmental organisms have resulted in the industry demanding more appropriate care solution testing for licensing purposes, and improved guidelines and recommendations for contact lens wearers. Research into the impact of care solutions on the ocular surface, optimization of orthokeratology, eludication of new risk factors for corneal infection, and ongoing disease surveillance will better inform practitioners and wearers and result in improved outcomes for contact lens wearers.

See also: Corneal Epithelium: Response to Infection; Corneal Epithelium: Transport and Permeability; Immunopathogenesis of Pseudomonas Keratitis; Inflammation of the Conjunctiva; Tear Film Overview.

Further Reading

Carnt, N., Jalbert, I., Stretton, S., Naduvilath, T., and Papas, E. (2007). Solution toxicity in soft contact lens daily wear is associated with corneal inflammation. *Optometry and Vision Science* 84: 309–315.

Dart, J. K. G., Radford, C. F., Minassian, D., Verma, S., and Stapleton, F. (2008). Risk factors for microbial keratitis with contemporary contact lenses: A case-control study. *Ophthalmology* 115: 1647–1654. e1643.

Fon, D., Reyers, M., Terry, R., and Williams, L. (2000). *The IACLE Contact Lens Course*, 1st edn., vols. 2 and 8. Sydney: The International Association of Contact Lens Educators.

Holden, B. A., Sweeney, D. F., Vannas, A., Nilsson, K. T., and Efron, N. (1985). Effects of long-term extended contact lens wear on the human cornea. *Investigative Ophthalmology and Visual Science* 26: 1489–1501.

Keay, L., Edwards, K., Naduvilath, T., Forde, K., and Stapleton, F. (2006). Factors affecting the morbidity of contact lens related microbial keratitis: A population study. *Investigative Ophthalmology and Visual Science* 47: 4302–4308.

Keay, L., Jalbert, I., Sweeney, D. F., and Holden, B. A. (2001). Microcysts: Clinical significance and differential diagnosis. *Optometry (St Louis, MO)* 72: 452–460.

Li, S. L., Ladage, P. M., Yamamoto, T., et al. (2003). Effects of contact lens care solutions on surface exfoliation and bacterial binding to corneal epithelial cells. *Eye Contact Lens* 29: 27–30.

O'Hare, N., Stapleton, F., Naduvilath, T., et al. (2003). Interaction between the contact lens and the ocular surface in the aetiology of superior epithelial arcuate lesions. *Advances in Experimental Medicine and Biology* 506: 973–980.

Ren, D. H., Petroll, W. M., Jester, J. V., and Cavanagh, H. D. (1999). The effect of rigid gas permeable contact lens wear on proliferation of rabbit corneal and conjunctival epithelial cells. *CLAO Journal* 25: 136–141.

Stapleton, F., Keay, L., Jalbert, I., and Cole, N. (2007). The epidemiology of contact lens related infiltrates. *Optometry and Vision Science* 84: 257–272.

Stapleton, F., Keay, L., Edwards, K., et al. (2008). The incidence of contact lens related microbial keratitis. *Ophthalmology* 115: 1655–1662.

Swarbrick, H. A. (2006). Orthokeratology review and update. *Clinical and Experimental Optometry* 89: 124–143.

Sweeney, D. F., Jalbert, I., Covey, M., et al. (2003). Clinical characterisation of corneal infiltrative events observed with soft contact lens wear. *Cornea* 22: 435–442.

Thai, L. C., Tomlinson, A., and Doane, M. G. (2004). Effect of contact lens materials on tear physiology. *Optometry and Vision Science* 81: 194–204.

Truong, T., Wofford, L., and Lin, M. (2005). Effects of lens-care solutions on corneal epithelial barrier function. *Optometry and Vision Science* 82: E-Abstract 055009.

Vermeltfoort, P. B. J., Hooymans, J. M. M., Busscher, H. J., and van der Mei, H. C. (2008). Bacterial transmission from lens storage cases to contact lenses – effects of lens care solutions and silver impregnation of cases. *Journal of Biomedical Materials Research* 87B(1): 237–243.

Contrast Sensitivity

P Bex, Schepens Eye Research Institute, Boston, MA, USA

Glossary

Channels – The groups of visual sensors that are selective for a narrow range of image spatial or temporal structure.
Contrast constancy – At high contrasts, apparent contrast is relatively independent of the parameters that strongly influence contrast-detection threshold.
Contrast-detection threshold – The statistical contrast boundary below which contrast is too low for an image to be detected reliably and above which contrast is high enough for frequent image detection. Often defined as the contrast that produces 75% correct target identifications in forced-choice paradigms.
Contrast sensitivity – The reciprocal of contrast-detection threshold that also represents the transition between visible and invisible images.
Critical flicker frequency – The highest flicker rate of a full contrast image that can be detected reliably.
Forced-choice paradigms – Robust behavioral method used to measure detection or discrimination thresholds. Observers are forced to select between two or more intervals, of which only one contains a target.
Fourier analysis – Analytical method that calculates the simple sine-wave components whose linear sum forms a given complex image.
Resolution limit – The highest spatial frequency of a full contrast image that can be detected reliably.
Spatial frequency – The number of image cycles that fall within a given spatial distance, typically 1° of visual angle.
Temporal frequency – The number of image cycles that fall within 1 s.
Wavelets/gabors – A local filter that is the point-wise product of a two-dimensional (2D) spatial sine wave and a 2D Gaussian envelope.

Most people are familiar with image brightness and contrast from their controls on computer and television displays. The brightness control adjusts the mean luminance of the display uniformly, in order that the intensity of every point in the image increases when brightness is increased or decreases when brightness is reduced. The contrast control adjusts the difference between the lightest and darkest areas of the image. Increasing contrast makes areas that are below mean luminance darker and areas that are above mean luminance lighter, without changing the mean value. Decreasing contrast draws all values toward the mean, thus making the whole image fainter, similar to viewing the image through fog.

Figure 1 illustrates the effect of changing the contrast of a sine-wave striped pattern (the reasons for using a sine-wave pattern are described below). The top panel shows images of gratings whose contrast increases from 12.5% on the left to 100% on the right. The mean luminance of each image is the same. The traces in the bottom row plot luminance versus position for a horizontal slice through each image.

Contrast-Detection Threshold

A powerful measure of visual sensitivity can be obtained by finding the minimum contrast that is necessary for an image to be detected. This minimum contrast is referred to as contrast-detection threshold (C_{thresh}) and it is important because it defines the transition at which an image moves from invisible to visible. One method to estimate C_{thresh} might be to allow a subject to adjust the contrast until an image is just visible. However, this method is highly subjective and large differences in individual criteria for just visible make this measure unreliable.

Psychophysical Assessment of Vision

To overcome these problems, most researchers employ forced-choice procedures that require an observer to identify which of two or more intervals (the more the better) contain the target. An example of a four-alternative forced-choice (4AFC) detection task is shown in Figure 2(a). In this case, a computer presents a target in one of four positions at random around a central fixation point. The observer's task is to fixate the central dot and to indicate the location of the target, usually by pressing a computer button. Targets that are below C_{thresh} (sub-threshold) are rarely detected, whereas targets that are above C_{thresh} (supra-threshold) are usually detected. Contrast-detection thresholds are therefore probabilistic and are defined as the contrast at which they are correctly detected midway between chance and perfect performance.

It is difficult to cheat on forced-choice methods or to change criteria – the target is either seen, in which case its position is correctly identified, or it is not seen, in which

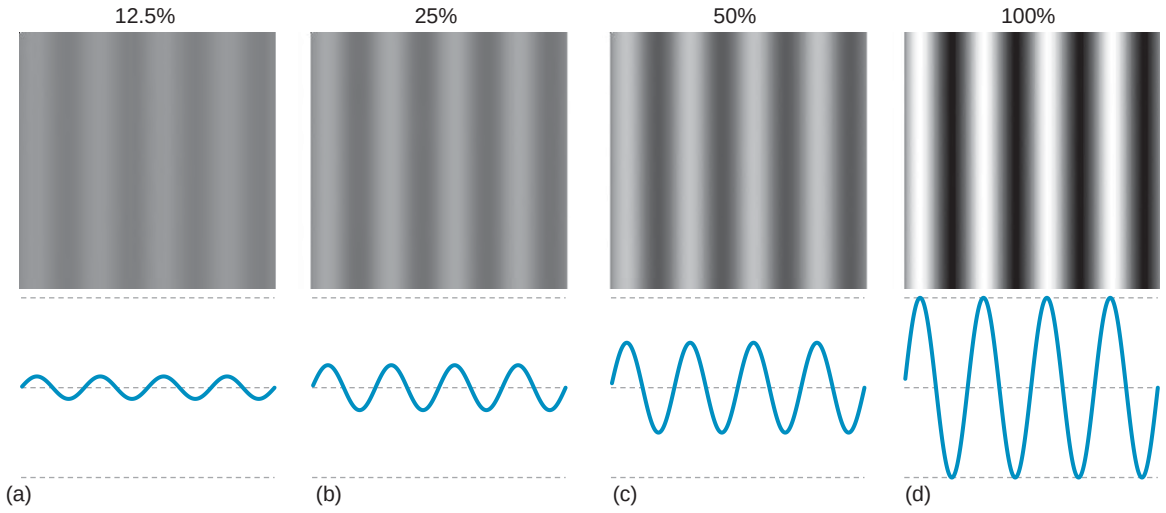

Figure 1 Image contrast. The top row shows the appearance of two-dimensional (2D) sine-grating patterns that are routinely used in vision research. The contrast of the sine grating increases from left (12.5%) to right (100%) as shown by the caption. The bottom row plots a horizontal section through each image and shows that contrast changes the luminance range separately from mean luminance.

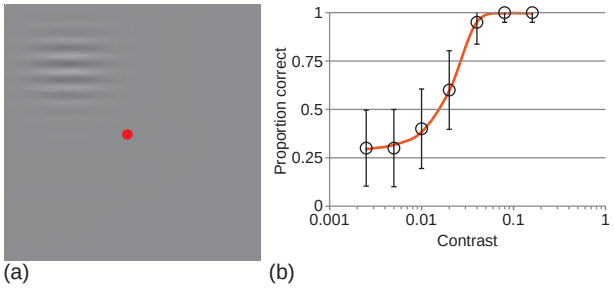

Figure 2 Contrast detection. (a) Example of a four-alternative forced-choice (4 AFC) task. The observer is required to fixate the central dot and to indicate whether the target appeared top left, top right, bottom left, or bottom right. The target contrast is adjusted by computer to a level that produces 75% correct detection. (b) A typical psychometric function. Circles show the proportion of trials the target was detected (ordinate) as a function of the target contrast (abscissa). Error bars show ±1 standard deviation. The curve shows the best-fitting cumulative normal function, from which the interpolated 75% correct point is taken as contrast-detection threshold.

case the subject is forced to guess. Notice that when guessing, the subject is still correct sometimes (25% if there are four alternatives, 33% if there are three, or 50% if there are two, etc.), as shown in the frequency of seeing curve in **Figure 2(b)**, where, at low contrasts, performance is 25% correct. The data have been fit with a curve known as a psychometric function, in this case a cumulative Gaussian:

$$Y = g + (1 - g)^{*}\mathrm{erf}(z/\mathrm{sqrt}(2))/2$$

where $z = (X - \mu)/\sigma$; g is the guess rate (0.25 in a 4AFC experiment). The mid-point (μ) of the psychometric function is often taken as C_{thresh} – for a 2AFC task, this is 75% correct. In the example shown, the observer achieved 75% correct at approximately 2.5% contrast. The slope (σ) can be used to infer how easily nearby contrasts can be discriminated from one another – a shallow slope means that a large contrast difference is required to achieve a given change in performance, whereas a steep slope means that a small change in the stimulus produces a large change in performance.

Spatial Frequency Channels

Based on behavioral observations in humans and single unit recordings in mammalian visual systems, researchers discovered around half a century ago that the visual system analyses images at a series of relatively narrow spatial scales and orientations known as channels. Thus, fine and coarse image details are encoded separately and Fourier analysis can be used to study the image structure that is encoded by different visual processing channels. Fourier analysis computes the sum of basic sine waves whose linear sum produces the image. To illustrate the representations of an image that are available at different spatial scales, **Figure 3(a)** shows a typical image, together with its coarse (**Figure 3(b)**) and fine (**Figure 3(c)**) spatial structure.

Visually responsive neurons in primary visual cortex, the first cortical projection from the retina through the lateral geniculate nucleus of the thalamus, respond to images only within a limited area of the visual field, known as the classical receptive field, and are selective for a limited range of spatial frequencies and orientations. These receptive fields are now routinely modeled as Gabor or wavelet functions, defined as:

Figure 3 Spatial frequency in real images. (a) An image of Albert Einstein's face is encoded at a range of spatial scales, from (b) coarse – low spatial frequency to (c) fine – high spatial frequency.

$$G(x, y, \lambda, \varphi, \sigma, \gamma) = \exp\left(-\frac{x'^2 + \gamma^2 y'^2}{2\sigma^2}\right)\sin\left(2\pi\frac{x'}{\lambda} + \varphi\right)$$

where $x' = x\cos\theta + y\sin\theta$ and $y' = -x\sin\theta + y\cos\theta$, λ represents the wavelength, θ the orientation, and ψ the phase of the sine-wave component. For the Gaussian window, σ is the standard deviation and γ is the spatial aspect ratio. Examples of Gabors are illustrated in **Figure 4**. On the top row, spatial frequency increases from left to right and all Gabors are of the same orientation 0° and contrast. On the bottom row, spatial frequency is fixed, but orientation is 45°, 90°, or 135° (from left to right). The visual system encodes image structure with a bank of such wavelet filters that represent the retinal image through patch-wise local analysis.

Figure 5 provides compelling demonstrations that our visual system employs a set of spatial frequency and orientation-selective channels. These demonstrations show that after prolonged viewing of a particular pattern (termed adaptation) the appearance of other patterns can be altered (termed an aftereffect). In these demonstrations, adapting to a pattern of one spatial frequency or orientation produces a loss in sensitivity in the channel that responds most to that pattern, but little change in channels tuned to other spatial frequencies or orientations. This localized loss in sensitivity produces a relative shift in the responses of our visual channels that cause us to experience changes in the appearance of the image.

These observations have led to the widespread use of sine-wave grating patterns in basic and clinical vision research. In order to derive a measure of vision that reflects the sensitivity across our set of visual channels and to reflect the fact that functional vision requires us to detect and interact with objects of various sizes, contrast-detection thresholds are measured for gratings of a range of bar widths, expressed as spatial frequency or the number of grating cycles per unit distance. **Figure 4** illustrates Gabors of differing spatial frequency; however, the size of one grating cycle on the retina depends on the distance

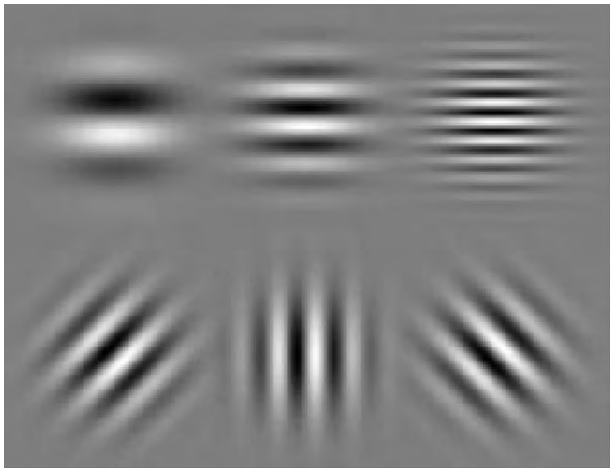

Figure 4 Gabor (wavelets) of differing spatial frequency and orientation. Top row: spatial frequency increases from left to right, orientation is fixed at 0°. Bottom row: Orientation increases from left to right: 45°, 90°, and 135°, spatial frequency is fixed.

from which it is viewed. Therefore, image sizes are usually calculated in terms of visual angle, which specifies the retinal image size. **Figure 6** shows how visual angle is calculated and its relationship to image size and viewing distance. A convenient rule is that 1 cm viewed from 57 cm subtends a visual angle of 1° and roughly corresponds to a finger nail viewed at arm's length.

Contrast Sensitivity Function

Many researchers have shown that for sine-grating patterns, C_{thresh} strongly depends on spatial frequency. This fundamental observation is demonstrated in the classic image shown in **Figure 7**. Spatial frequency increases from left to right and contrast increases from top to bottom, so that contrast is constant across any horizontal line. Contrast-detection thresholds can be visualized on this figure as the imaginary curve along

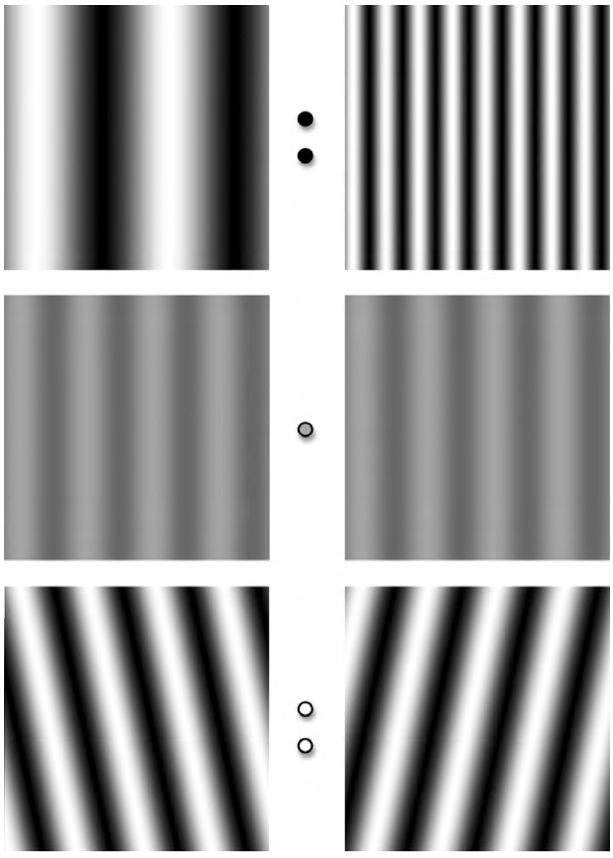

Figure 5 Demonstration of spatial frequency- and orientation-selective aftereffects. First note that when you fixate the centre gray dot, the gratings in the middle row are of the same spatial frequency and orientation. Next, look back and forth between the black dots in the top row for around 10 s. Now, when you look at the center gray dot, the grating on the left appears to be of higher spatial frequency than the grating on the right. Next, look back and forth between the white dots in the bottom row for around 10 s. Now, when you look at the center gray dot, the grating on the left appears tilted counterclockwise, while the grating on the right appears tilted clockwise. These aftereffects are robust even though you know that the gratings in the middle row are the same. These demonstrations provide compelling evidence that visual processing involves channels that are narrowly tuned for spatial frequency and orientation.

which the grating changes from invisible (toward the top of the figure) to visible (toward the bottom of the figure). Most people report that the function peaks somewhere near the middle of the figure. Notice that the peak shifts as you move the figure closer or further away. This demonstrates the importance of visual angle rather than physical image size. Note that the highest spatial frequency that can be detected at maximum contrast is given by the rightmost point on a contrast sensitivity function (CSF). This is referred to as the resolution limit and is a quick and convenient method of assessing visual sensitivity than measuring the entire CSF.

When measured with forced-choice procedures, (**Figure 2**) contrast-detection thresholds are lowest for gratings around 2–5 cycles per degree of visual angle (c deg^{-1}). By convention, the inverse of C_{thresh} ($1/C_{\text{thresh}}$) is usually reported and is termed contrast sensitivity. The rationale for the use of contrast sensitivity over contrast-detection threshold is most likely because the shape of the CSF is the same as that of the underlying modulation transfer function of the system. The circles in **Figure 8** show the author's contrast sensitivity as a function of spatial frequency measured with a forced-choice procedure. Error bars show 95% confidence intervals. The data have been fit (green curve) with the outputs of a set of spatial frequency channels shown by the colored curves. The channels are log spaced in spatial frequency (with peaks at 0.5, 1, 2, 4, 8, 16, or 32 c deg^{-1}) and have the same bandwidth (1.4 octaves). The summed outputs of the set of filters provide a good fit to the data and this channel-based system is now a widely accepted model of early visual processing.

The spatial frequency aftereffect shown in **Figure 5** is easily explained with this channel-based model. Adapting to one spatial frequency reduces the responses of the channel that is most sensitive to that spatial frequency, but has little effect on the responses of other channels. When a different spatial frequency is subsequently viewed, the overall activity across the channels is shifted away from the adapted channel. This shift in the population response produces a shift in apparent spatial frequency away from the adapting frequency. An analogous model explains the shifts in orientation in the lower row of **Figure 5**, except that orientation-selective channels are adapted rather than spatial-frequency-selective channels.

The CSF is highly dependent on the mean luminance of the display on which it is measured. This can easily be experienced by viewing **Figure 7** with a pair of dark sunglasses (possibly two pairs), which moves the curve down (reducing sensitivity) and shifts the peak to lower spatial frequencies. The data in **Figure 8** were collected on a standard computer monitor that has a mean luminance of 50 cd m^{-2} (candelas per square meter). Photopic, mesopic, and scotopic vision and changes in visual performance show that sensitivity to high spatial frequencies increases with mean luminance. This property is important because CSFs are routinely measured on relatively dim displays (e.g., 50–100 cd m^{-2}) in the laboratory and in the clinic; however, the luminance of the real world is typically much greater. For example, the luminance of a cloudy sky is around 35 000 cd m^{-2}, suggesting that standard experimental conditions may underestimate sensitivity to fine spatial structure.

Temporal Contrast Sensitivity

In addition to a dependence on spatial frequency, contrast sensitivity also depends strongly on temporal frequency. **Figure 1** illustrates spatial variation in luminance, but

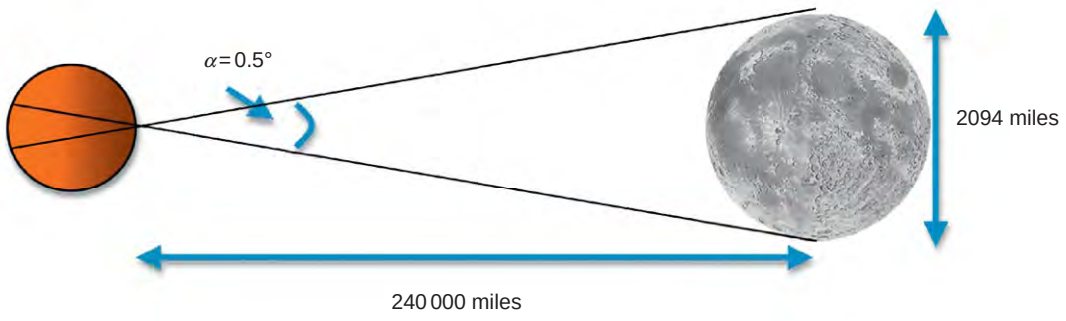

Figure 6 Visual angle and viewing distance. The angular size of an object is calculated as 2*tan((0.5*h)/d), where h is the height of the object and d is the distance from which it is viewed. The example, which is not to scale, shows the angular size subtended by the moon is 0.5°. For comparison, the nail of the average index finger viewed at arm's length subtends 1°.

Figure 7 Illustration of the contrast sensitivity function (CSF). Spatial frequency increases from left to right, contrast increases from top to bottom. The contrast along any horizontal line is fixed. Different spatial frequencies become visible at different contrasts and define an imaginary curve that separates seen from unseen structure. Notice that if you move the image closer to your eye, the peak moves to the right and if you move it further away, the peak moves to the left. This demonstrates that contrast sensitivity depends on retinal not physical image size. If you wear one or two pairs of dark sunglasses, the curve shifts down and the peaks moves left, which demonstrates the dependence of the CSF on mean luminance.

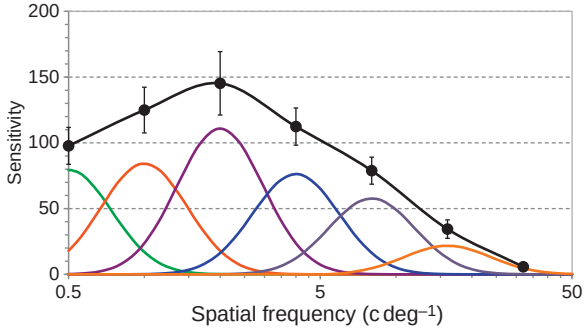

Figure 8 Spatial contrast sensitivity. Circles show contrast sensitivity (the reciprocal of contrast-detection threshold) for sine gratings of a range of spatial frequencies. Sensitivity peaks at around 2 c deg^{-1} under the conditions employed here and decreases at lower or higher spatial frequencies. The black curve is the summed sensitivity of the set of log-scaled channels shown by the colored curves and provides a good fit to the data.

imagine instead that the x-axis represents time, rather than space. Now the figure illustrates flicker. Flicker frequency can be varied in the same way as spatial frequency is varied in **Figures 3 and 7**. The circles in **Figure 9** show how the author's contrast sensitivity varies as a function of temporal frequency for a 2 c deg^{-1} grating pattern. Sensitivity peaks around 5 Hz, at the mean luminance used here (50 cd m^{-2}) and decreases at lower or higher temporal frequencies. These data are well fit (black curve) by a model with only two temporal channels, compared with the multiple channels that support spatial contrast sensitivity. One channel (red curve) is low-pass or sustained and is most sensitive to structure that is stationary or slowly changing over time. The second channel (blue curve) is band-pass or transient and is most sensitive to structure that changes at around 5 Hz.

The spatial resolution limit falls steadily with distance from the fovea, an effect that can be experienced by viewing **Figure 7** while fixating away from the center of the image. As you fixate further away, the threshold curve moves further down the figure and its peak shifts further to the left. Unlike spatial resolution, temporal resolution (the highest flicker rate that can be detected at any contrast, often called critical flicker fusion frequency)

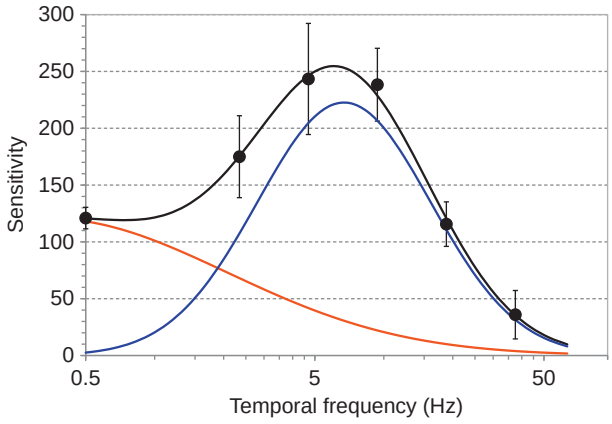

Figure 9 Temporal contrast sensitivity. Circles show contrast sensitivity (the reciprocal of contrast-detection threshold) for sine gratings of a range of temporal frequencies. The black curve is the summed sensitivity of the two log-scaled channels shown by the red and blue curves. The red curve has peak sensitivity at low temporal frequencies – that is, static images – and is termed a sustained channel. The blue curve has peak sensitivity around 6 Hz and is termed a transient channel.

increases moderately with distance from the fovea. This explains why older, 60-Hz computer displays can sometimes be seen to flicker when seen in the peripheral visual field, but not when viewed directly. Just as spatial contrast sensitivity depends on luminance, so does temporal contrast sensitivity. A 35-mm film is generally recorded at 24 frames per second, a refresh rate that could be easily detected at moderate light levels, as can be seen from Figure 9. For this reason, movie theaters are generally dark because sensitivity to high flicker rates is poor under those conditions. In addition, the visible 24-Hz image update rate is masked by flashing the illuminant at 48 Hz, so each frame is flashed twice.

At supra-threshold contrasts, apparent contrast is relatively independent of spatial or temporal frequency, a phenomenon termed contrast constancy.Contrast constancy can be experienced in Figure 7 – while the transition between visible and invisible gratings has a curved shape, toward the bottom of the figure, the gratings appear to have similar contrast regardless of spatial frequency. This has important implications for image enhancement, which should therefore target only image components that are below their C_{thresh}.

See also: Acuity; Anatomically Separate Rod and Cone Signaling Pathways; Anti-Angiogenic Properties of Vitreous; Chromatic Function of the Cone; Information Processing: Contrast Sensitivity; Information Processing: Direction Sensitivity; Information Processing in the Retina; Information Processing: Retinal Adaptation; Photopic, Mesopic and Scotopic Vision and Changes in Visual Performance.

Further Reading

Bracewell, R. (1999). *The Fourier Transform and Its Applications*, 3rd edn. London: McGraw-Hill.

Campbell, F. W. and Robson, J. G. (1968). Application of Fourier analysis to the visibility of gratings. *Journal of Physiology* 197: 551–566.

Field, D. J. and Tolhurst, D. J. (1986). The structure and symmetry of simple-cell receptive-field profiles in the cat's visual cortex. *Proceedings of the Royal Society of London. Series B. Biological Sciences* 228(1253): 379–400.

Georgeson, M. A. (1990). Over the limit: Encoding contrast above threshold in human vision. In: Kulikowski, J. J. (ed.) *Limits of Vision*, pp. 106–119. London: Erlbaum.

Hubel, D. H. and Wiesel, T. N. (1959). Receptive fields of single neurones in the cat's striate cortex. *Journal of Physiology* 148: 574–591.

Kelly, D. H. (1961). Visual responses to time-dependent stimuli. 1. Amplitude sensitivity measurements. *Journal of the Optical Society of America. A, Optics, Image Science, and Vision* 51: 422–429.

Kulikowski, J. J. and Tolhurst, D. J. (1973). Psychophysical evidence for sustained and transient detectors in human vision. *Journal of Physiology* 232(1): 149–162.

Landis, C. (1954). Determinants of the critical flicker-fusion threshold. *Physiological Reviews* 34(2): 259–286.

O'Shea, R. P. (1991). Thumb's rule tested: Visual angle of thumb's width is about 2 deg. *Perception* 20(3): 415–418.

Rovamo, J., Virsu, V., Laurinen, P., and Hyvarinen, L. (1982). Resolution of gratings oriented along and across meridians in peripheral vision. *Investigative Ophthalmology and Visual Science* 23: 666–670.

Control of Aqueous Humor Flow

J W McLaren, Mayo Clinic, Rochester, MN, USA

Glossary

Circadian rhythm – The repeated physiologic rhythm having an association with the 24-h period of the Sun.
Diurnal – Taking place during the day. In this article, we assume that normal alert wakefulness takes place during the day.
Nocturnal – Taking place at night. In this article, sleep is assumed to take place at night.
Ocular fluorophotometry – The measurement of fluorescence in the eye. For determination of aqueous humor flow rate, fluorescence originates from the dye fluorescein.
Ocular fluorophotometer – A device used to measure fluorescence in the living eye.

The Significance of Aqueous Humor Flow

The cornea and crystalline lens must be oxygenated, provided nutrition, and provided disposal of waste without the benefit of a direct blood supply; blood vessels that would serve this purpose as they do in other tissues of the body would interfere with light and degrade the image on the retina. This circulatory function is served by a unique local system, the aqueous humor circulation (**Figure 1**). Aqueous humor is secreted by the ciliary body, it flows through the posterior chamber between the posterior surface of the iris and the anterior surface of the crystalline lens, and enters the anterior chamber through the pupil. Convection and eye movements mix this warmer aqueous humor with the slightly cooler aqueous humor in the anterior chamber and provide flow across the endothelial surface of the cornea. Aqueous humor flows out of the eye at the perimeter of the anterior chamber through the trabecular meshwork and, through a parallel path, it percolates into the uveoscleral tissue. The continuous flow of aqueous humor brings nutrients to the crystalline lens and the cornea, it removes metabolites and waste, it prevents the accumulation of debris in the anterior chamber, and it mediates inflammatory responses to protect the eye from invasion by foreign substances and organisms. The cornea receives most of the oxygen it needs directly from the air, because it is thin enough for oxygen to diffuse through its entire thickness.

Continuous aqueous humor flow is also the source of intraocular pressure. The trabecular meshwork is not a simple open drain, but resists movement of fluid. This resistance requires a pressure difference to move aqueous humor out through the trabecular meshwork into Schlemm's canal, and into collector channels and episcleral veins, a pressure that bears on the sclera and inflates the eye. Intraocular pressure is related to flow rate as described by the Goldmann equation:

$$IOP = \frac{F - F_u}{C} + P_e \qquad [1]$$

where F is aqueous humor production rate, F_u is the rate of aqueous humor loss through the uveoscleral path and does not contribute to intraocular pressure, C is outflow facility (the inverse of resistance), and P_e is the pressure in the episcleral veins. Notice that aqueous flow through the trabecular meshwork contributes to the intraocular pressure above episcleral venous pressure.

When the resistance to outflow increases chronically (outflow facility, C, decreases), intraocular pressure increases. Chronic ocular hypertension is a primary risk factor for glaucoma. Ocular hypertension has been associated with decreased outflow facility, but not with hypersecretion of aqueous humor. To date, the only practical therapy for treating glaucoma is reduction of intraocular pressure. This can be accomplished by reducing the resistance to outflow at the trabecular meshwork, increasing the amount of aqueous humor that bypasses the trabecular meshwork through the uveoscleral path, or by reducing the production of aqueous humor by the ciliary body, and all of these approaches are used therapeutically. Studies of aqueous humor flow have assisted with the understanding of the mechanism of action of ocular hypotensive agents and have clarified certain aspects of the physiology and natural variation of aqueous humor formation in normal and diseased eyes.

Measuring Aqueous Humor Flow

Aqueous humor flow has been measured noninvasively in the living human eye since the early 1950s and the methods used today are in principle similar to these early methods. The rate of aqueous humor flow is usually determined indirectly from the rate of disappearance from the anterior chamber and cornea of the fluorescent tracer fluorescein, a nontoxic, fluorescent disclosing agent. This technique has allowed investigators to study

aqueous humor flow in humans under a variety of conditions, in a number of pathologic states, and under the influence of a wide variety of pharmacologic agents.

A high concentration of fluorescein (2–10%) is instilled in the conjunctival *cul-de-sac*, and after a brief time for the dye to penetrate the corneal epithelium, excess is rinsed from the eye and eyelids. A small amount of fluorescein (typically 200–500 ng) crosses the corneal epithelium and enters the stroma, and from here it passes through the corneal endothelium into the anterior chamber. In the anterior chamber, fluorescein mixes with aqueous humor. It is slowly diluted as unstained aqueous humor enters the anterior chamber through the pupil, and aqueous humor with fluorescein leaves the eye through the outflow pathways.

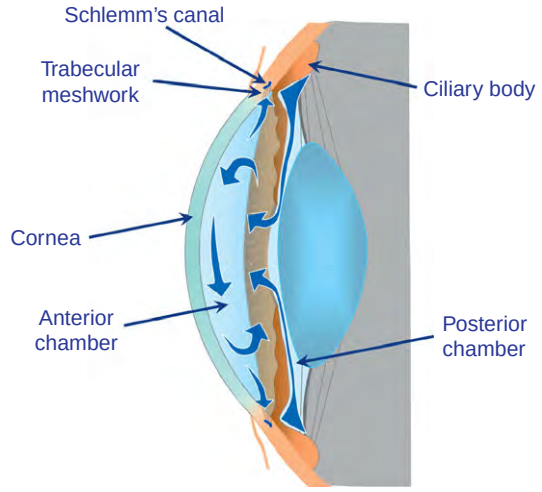

Figure 1 Circulation of aqueous humor. Aqueous humor is secreted into the posterior chamber by the ciliary body. It flows between the iris and lens, enters the anterior chamber though the pupil, and is mixed in the anterior chamber by convection and eye movements. Aqueous humor leaves the eye through the trabecular meshwork and the uveoscleral tissues at the angle between the iris and cornea.

Once the fluorescein is uniformly distributed in the stroma, its concentration is measured in the cornea and anterior chamber by fluorophotometry at the beginning and end of several intervals (**Figure 2**). The mean flow rate during each interval is calculated from the rate of loss of fluorescein from the eye between measurements:

$$flow = \frac{-\Delta m_t}{\overline{C}_a \Delta t} - d \qquad [2]$$

where Δm_t is the change in total mass of fluorescein in the cornea and anterior chamber on interval Δt, $\overline{C}_a$ is the average concentration of fluorescein in the anterior chamber during the interval, and d is the flow equivalent to loss of fluorescein by diffusion directly into vessels, but not by bulk flow of aqueous humor. Typically, the total mass of fluorescein is determined as the sum of the mass in the anterior chamber and cornea:

$$m_t = v_c C_c + v_a C_a \qquad [3]$$

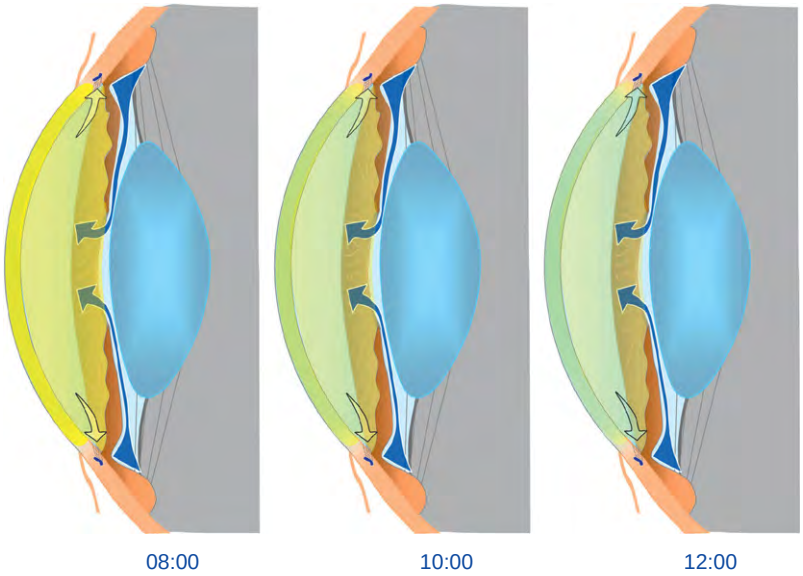

Figure 2 Aqueous humor flow rate is determined from the dilution of the fluorescent dye fluorescein. Fluorescein is instilled topically and a small amount enters the cornea. From the corneal stroma, it crosses the corneal endothelium and mixes with aqueous humor. As aqueous humor flows through the anterior chamber it carries fluorescein out of the eye, and by measuring the rate of fluorescein loss from the eye, we can determine the aqueous humor flow rate. Typically, fluorescein in the cornea and anterior chamber is measured at 1- or 2-h intervals. Adapted from Brubaker, R. F. (1998). Clinical measurements of aqueous dynamics: Implications for addressing glaucoma. In: Civan, M. M. (ed.) *The Eye's Aqueous Humor. From Secretion to Glaucoma*, pp. 233–284. San Diego, CA: Academic Press, with permission from Elsevier.

where v_c and v_a are the volumes of the cornea and anterior chamber, respectively, and C_c, and C_a are the concentrations of fluorescein in the cornea and anterior chamber, respectively.

What is the Aqueous Humor Flow Rate?

The Normal Eye

In normal eyes of men and women, mean aqueous humor flow through the anterior chamber during hours of wakefulness has typically been 2.2 –3.1 µl min^{-1}, depending on the study. Flow rate in a population is normally-distributed with a standard deviation of about 0.8 µl min^{-1} (**Figure 3**). This provides an efficient circulation; for persons with an average anterior chamber volume of 185 µl, aqueous humor production represents approximately 1.2% of the anterior chamber volume per minute. At this rate the fluid in the anterior chamber and any solutes or contaminants, have a half-life of 43 min. For fluorescein, a substance that fills the anterior chamber and corneal stroma, the half-life in these combined compartments is approximately 4 h.

Aqueous Humor Flow is not Affected by Elevated or Decreased Intraocular Pressure

Few, if any, conditions (other than sleep, as discussed later is this chapter) affect aqueous humor production. The ability of the ciliary body to change flow rate in response to changes in intraocular pressure has been examined in a variety of conditions. In an interesting experiment to test the dependence of flow on intraocular pressure, Dr. Keith Carlson suspended volunteers (including the author) upside down by their feet for 30-min intervals alternating with 30 min in an upright position, and measured aqueous humor flow from fluorescein concentrations at the beginning and end of each interval. Inversion increased central and episcleral venous pressure and raised intraocular pressure by an average of 11.2 mmHg. The intraocular pressure increase was not, however, associated with a compensatory change in aqueous humor production. In this and other experiments, the rate of aqueous flow appeared to be independent of transient changes in intraocular pressure, in a moderate range of pressures. If, of course, intraocular pressure were increased so high that blood flow to the ciliary body were compromised, this relationship would likely change. Measurements of flow rate in patients with glaucoma and other disorders have shown that aqueous humor production also does not change to compensate for chronic ocular hypertension or hypotension.

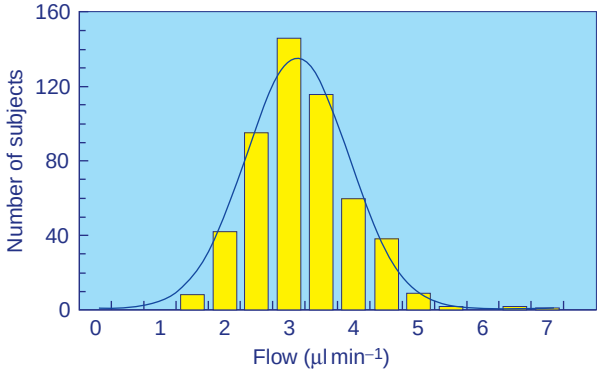

Figure 3 Distribution of aqueous humor flow in 519 subjects during the morning. Mean flow rate was normally distributed (solid line) with a mean of 3.0 ± 0.8 µl min^{-1}. Adapted from Brubaker, R. F. (1998). Clinical measurements of aqueous dynamics: Implications for addressing glaucoma. In: Civan, M. M. (ed.) *The Eye's Aqueous Humor. From Secretion to Glaucoma*, pp. 233–284. San Diego, CA: Academic Press, with permission from Elsevier.

Aqueous Humor Flow Decreases Slowly with Age

Aqueous humor formation gradually slows with age by about 4% per decade of life. One might expect this decrease to diminish the efficiency of the circulatory function, but the reduction in flow is accompanied by a reduction in the volume of the anterior chamber by approximately 14–24 µl per decade. The smaller anterior chamber requires less flow to maintain the same clearance. From age 20 to 80 years, aqueous humor flow rate decreases by approximately 25%, while anterior chamber volume decreases by 40%, and this combined change provides a 20% faster turnover rate of aqueous humor over a lifetime.

Aqueous Humor Flow Changes Dramatically during Sleep

Under most conditions, aqueous humor flow rate varies little from the flow rate during the day while subjects are alert and untreated. Sleep is an exception; during sleep, the rate of aqueous flow diminishes to approximately half the rate during wakefulness (**Figure 4**). This daily rhythm is driven by an internal circadian rhythm of the body and not simply by the environmental and postural conditions at night. It is partly preserved during a single episode of sleep deprivation and is not affected by ambient light at night or a supine position during the day while awake.

The strongest evidence for an origin of this circadian rhythm points to β-adrenergic stimulation during the day driving flow rate up during hours of wakefulness, and lack of this stimulation during sleep, allowing flow rate to diminish. During sleep, circulating catecholamines, including epinephrine, decrease. If a high blood concentration of epinephrine is artificially maintained during sleep, flow rate does not decrease as much as it normally would during sleep. Timolol, which blocks β-adrenergic receptors, suppresses flow during the day to rates that are similar to those

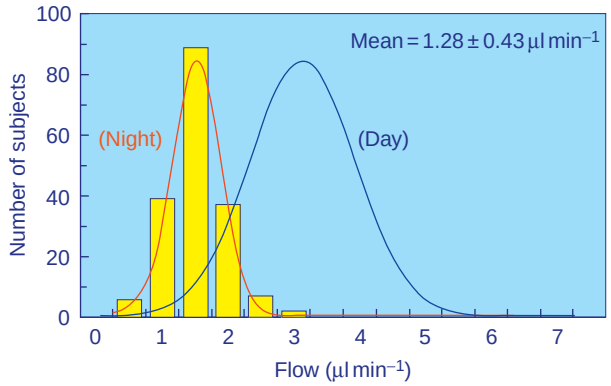

Figure 4 Distribution of aqueous humor flow in 180 subjects during sleep. Mean flow rate decreased to approximately half of the rate during the day. The Gaussian curve to show the distribution of flow in the morning was normalized to the nighttime curve for comparison. Adapted from Brubaker, R. F. (1998). Clinical measurements of aqueous dynamics: Implications for addressing glaucoma. In: Civan, M. M. (ed.) *The Eye's Aqueous Humor. From Secretion to Glaucoma*, pp. 233–284. San Diego, CA: Academic Press, with permission from Elsevier.

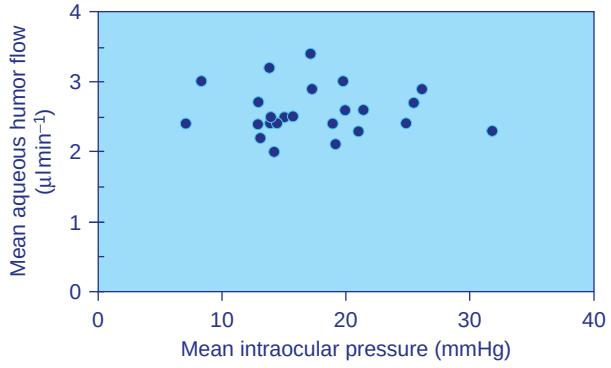

Figure 5 Mean aqueous humor flow was not correlated with mean intraocular pressure in 20 published studies of aqueous humor flow in pathologic conditions. Adapted from McLaren, J. W. (2009). Measurement of aqueous humor flow. *Experimental Eye Research*, 88: 641–647, with permission from Elsevier.

during sleep. However, if timolol is administered just before sleep, it does not suppress flow rate any further than the normal rate during sleep. Other ocular hypotensive agents that do not interact with the β-adrenergic system but reduce flow rate through other receptors do not suppress the circadian rhythm, although they diminish the magnitude of flow changes from wake to sleep.

The circadian variation of epinephrine activity seems to be at least partially responsible for modulating aqueous humor flow during a circadian day, although the control by epinephrine is far from simple. For example, the circadian rhythm of flow persists even in patients who have low circulating catecholamines because of adrenalectomy. Epinephrine supplied by sympathetic nerve activity also does not seem to drive the rhythm entirely; flow rate is normal in patients with sympathetic denervation. So far no single factor has been identified that would provide a comprehensive and sufficient explanation for the origin of the circadian rhythm of aqueous humor flow.

Flow in Abnormal Eyes

Aqueous humor flow has been studied in a number of systemic and ocular conditions, including chronic open-angle glaucoma, low-tension glaucoma, ocular hypertension, exfoliation syndrome, pigment dispersion, Horner's syndrome, Fuchs' dystrophy, myotonic dystrophy, diabetes mellitus, cystic fibrosis, and carotid stenosis. These studies reported a range of mean intraocular pressures from 7 to 32 mmHg. Remarkably, aqueous humor flow rate was largely unaffected by most of these conditions (**Figure 5**). Mean daytime flow rate ranged from 2.1 µl min^{-1} to 3.4 µl min^{-1}, and was not correlated with mean intraocular pressure. Patients with diabetes mellitus may be an exception; in a few studies, flow rates in diabetic patients were somewhat lower than normal, although their intraocular pressures were normal. In these conditions, aqueous flow certainly does not vary to the extent that would be regarded as clinically significant and is independent of intraocular pressure across the range of pressures experienced by most patients. Stated another way, the intraocular pressure does not appear to be regulated or stabilized by compensatory changes in aqueous humor flow in abnormal as well as in normal eyes. We do not know, however, if flow would change if intraocular pressure increased or decreased to extremes that would compromise blood flow or deflate the eye.

Pharmacologic Agents and Hormones

With a few exceptions, most pharmacologic agents and hormones have no measurable stimulatory effect on flow. Pharmacologic agents with β-adrenergic agonist activity are an exception, and these can, under some conditions, increase the rate of aqueous humor flow during the day by a small amount, typically, 15%. They are particularly effective when given at night when intrinsic concentrations of circulating and neuronal catecholamines are low. Other agents, notably those used as ocular hypotensives, suppress aqueous humor formation, and these fall into three categories: β-adrenergic antagonists, α_2-adrenergic agonists, and carbonic anhydrase inhibitors. Some of these agents are clinically relevant and their study has contributed to our knowledge of the physiologic properties of aqueous humor production.

β-Adrenergic Antagonists

The ocular hypotensive activity of systemically and topically administered propranolol, a β-adrenergic antagonist,

has been known since the 1960s. Timolol, another β-adrenergic antagonist and ocular hypotensive agent, was discovered shortly thereafter and developed for clinical use. Soon after the first clinical use of timolol, fluorophotometry was used to show that it lowered intraocular pressure by suppressing aqueous humor production by as much as 50%. Other β-adrenergic antagonists, such as betaxolol, a β_2-selective antagonist, and levobunolol, reduce intraocular pressure in a similar way, by suppressing aqueous humor flow.

β-Adrenergic antagonists affect aqueous humor flow differently, depending on whether they are administered during the day or during the night. The effects of β-adrenergic antagonists on aqueous humor flow were all originally studied during the daytime, when human subjects were awake and active. In contrast, at night during sleep, when flow is normally low, these drugs have no measurable effect on flow rate. The only exception is when flow is artificially stimulated by epinephrine at night during sleep; timolol can suppress the epinephrine-stimulated flow. The differential activity of β-adrenergic antagonists suggest that the circadian rhythm in aqueous flow is driven by an endogenous hormonal agent that can be blocked when the agent is high, during waking hours; however, because it is not present during sleep, it cannot be blocked during sleep. The best candidate for this agent is circulating epinephrine, from adrenal or neural sources. However, evidence for epinephrine being the sole driver of the circadian rhythm is circumstantial, and other hormonal agents, such as corticosteroids, may play a role in the behavior of this system.

α_2-Adrenergic Agonists

In the 1960s, clonidine was the first selective α-adrenergic agonist discovered to reduce intraocular pressure after systemic administration. It was later found to suppress aqueous humor flow by 21%, enough to explain the hypotensive effect. A derivative of clonidine, para-aminoclonidine (apraclonidine, aplonidine), was developed for topical application and also decreased aqueous humor flow by about 30%.

Apraclonidine and timolol suppress aqueous humor production by about the same amount in normal volunteers. These drugs when acutely administered together are not additive. In contrast to timolol, apraclonidine suppresses flow during sleep. Although these two classes of drug may have common features, the pathways to suppression of flow are not identical.

Carbonic Anhydrase Inhibitors

Systemic administration of acetazolamide has been associated with a reduction of intraocular pressure since the early 1950s, and this reduction is also associated with a reduction of aqueous humor flow. Systemic carbonic anhydrase inhibitors affect carbonic anhydrase activity all over the body and have many side effects. Two topically applied carbonic anhydrase inhibitors, dorzolamide and brinzolamide, were developed to reduce these side effects. These drugs, which minimized the systemic dose, also reduced aqueous humor flow, although to a somewhat lesser degree than did systemic carbonic anhydrase inhibitors. Both systemic and topical carbonic anhydrase inhibitors also reduce aqueous humor production during sleep, topical to a somewhat lesser extent than systemic.

Other Classes of Drugs and Hormones

Several other classes of pharmacologic agents that reduce intraocular pressure have shown little suppression of aqueous humor flow, if any. Epinephrine provided a weak stimulation of flow during the day in some studies and had no effect or a mild suppression of flow in others. Stimulatory effects were typically less than 15%, an increase that could be considered clinically unimportant. Other β-adrenergic selective agonists also stimulate aqueous humor flow weakly, and these include salbutamol, isoproterenol, terbutaline, and ibopamine. When β-adrenergic agonists are administered during sleep, they stimulate flow by a greater amount than they do during the day, although they do not stimulate flow to the daytime rate. These agents likely bind receptors that have low endogenous stimulation at night, and therefore are associated with reduced aqueous humor production during sleep, but are strongly stimulated during the day.

Cholinergic agonists and antagonists minimally affect aqueous humor flow. Pilocarpine, a cholinergic agonist that has been used to decrease pressure by opening the outflow pathways, may stimulate flow rate slightly, although not all studies agreed. Scopolamine, an anticholinergic usually administered transdermally through a patch, has no effect on flow.

Prostaglandins and their analogs are an important therapeutic agent to treat increased intraocular pressure. These drugs seem to enhance outflow of aqueous humor through uveoscleral pathways, removing flow from the trabecular pathway. These drugs, including prostaglandin $F_{2\alpha}$-isopropyl ester, bimatoprost, latanoprost, and travoprost, lower intraocular pressure without suppressing aqueous formation. In fact, some studies have indicated a small, clinically insignificant increase in flow rate.

Several hormones have also been studied to see if their circadian rhythms might drive the circadian rhythm in flow, either by administrating the hormones when they are normally at low concentrations in the blood or by measuring flow rate in patients who lack the hormone because of a clinical condition. Melatonin, norepinephrine, antidiuretic hormone, and hormones of pregnancy all have no direct effect on aqueous humor flow that could explain the circadian rhythm. Only epinephrine stimulates flow at night (when it is normally absent) by enough that could

explain the diurnal rise in aqueous flow. Other hormones, such as corticosteroids, may enhance the effects of epinephrine, although details of their role in adjusting the circadian rhythm are unknown.

Control of Aqueous Humor Production, the Basis of Pharmacologic Manipulation of Intraocular Pressure

Aqueous humor is secreted by 70–90 ciliary processes that extend into the posterior chamber (Figure 6). A bilayer of epithelium separates the stroma of each process from the aqueous humor and has a layer of pigmented and a layer of nonpigmented cells. The pigmented epithelium lies on the surface of the ciliary stroma, while the nonpigmented epithelium contacts the aqueous humor in the posterior chamber. The apical surfaces of the two cell types contact each other and their basolateral surfaces face the ciliary stroma (pigmented epithelium) or the aqueous humor (nonpigmented epithelium). These two layers of cells behave as a functional syncytium; gap junctions between their apical surfaces provide the structural basis of intracellular communication and movement of water and various ions. A small amount of aqueous humor is formed by ultrafiltration across this layer, but most is formed when this bilayer epithelium transfers solute between the ciliary process stroma and aqueous humor to create osmotic pressure that draws water passively along its chemical gradient into the posterior chamber.

The primary solutes that determine the rate of aqueous humor formation are sodium, potassium, and bicarbonate ions. This is a simplification; chloride movement is also important and several ion exchange proteins play a role in ionic balance and rates of ion and water movement. Sodium transfer is mediated by the enzyme sodium–potassium adenosine triphosphatase (Na,K-ATPase), which moves three sodium ions out of the nonpigmented cell and two potassium ions into the cell against their respective electrochemical gradients, at the expense of energy in the form of ATP. Bicarbonate ions move down their electrochemical gradient into the posterior chamber through a carrier molecule. In the nonpigmented epithelium, carbon dioxide and water react to form bicarbonate, and this reaction is catalyzed by carbonic anhydrase. This reaction is reversible, depending on the pH and the concentrations of bicarbonate and carbon dioxide. The transfer of sodium and potassium and the catalysis of bicarbonate are dynamic and determine the rate of aqueous humor production. As concentrations of solute increase on the aqueous humor side of nonpigmented cell membrane, water is drawn by osmotic pressure to form aqueous humor.

Figure 6 Ciliary processes. Approximately 70–90 ciliary processes extend into the posterior chamber and secrete aqueous humor. In this view from behind the iris, the crystalline lens has been removed, the posterior surface of the iris is visible at the bottom, and the cut edge of the sclera is visible at the top. Each of these processes is lined with a layer of pigmented and nonpigmented epithelium, with the nonpigmented epithelium in contact with the aqueous humor.

The activity of Na,K-ATPase and the movement of sodium and potassium are linked to adrenergic receptors on the nonpigmented ciliary epithelium through adenylate cyclase and an internal messenger system. As activity of adenylate cyclase is stimulated, activity of the Na,K-ATPase increases and aqueous humor production increases. Two broad classes of adrenergic receptors are linked to adenylate cyclase and have opposite effects: stimulation of β-adrenergic receptors increases adenylate cyclase activity and aqueous humor secretion, whereas stimulation of α_2-adrenergic activity suppresses adenylate cyclase activity and reduces aqueous humor secretion.

Intracellular carbonic anhydrase catalyzes the formation of bicarbonate somewhat independently of the Na,K-ATPase system, although this is a simplification. Rates of both reactions are determined by the availability of substrate, cellular pH, and other ionic composition, and may be interdependent. As bicarbonate concentration increases, bicarbonate moves across the cell membrane down its electrochemical difference into the aqueous humor. This transfer is dependent on carrier molecules that likely involve movement of other ions, and rates may be dependent on concentration and movement of these ions.

This model is consistent with our observations of circadian rhythms and pharmacologic manipulation of aqueous humor production. During sleep, when β-adrenergic activity is low, Na,K-ATPase activity is unstimulated and is also low. Aqueous humor is produced at a low rate (Figure 7). On awakening and becoming active, circulating and neural catecholamine activity increases and binds β-adrenergic receptors in the ciliary body, stimulating Na,K-ATPase and increasing aqueous humor production to rates observed during wakefulness (Figure 8). The daily rise and fall of β-adrenergic activity likely drives the circadian rise and fall of aqueous humor flow.

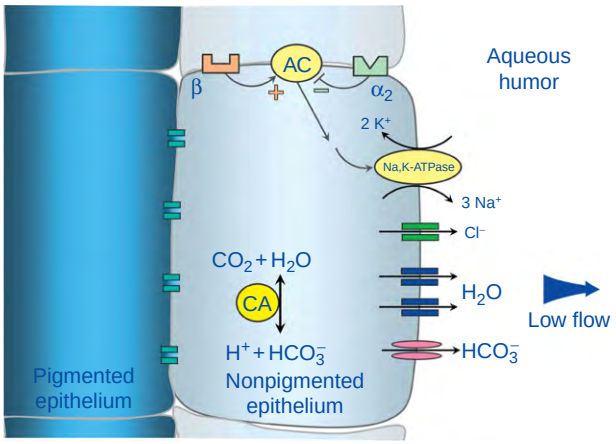

Figure 7 Basal secretion of aqueous humor. In the unstimulated state, sodium is transferred in and potassium is removed from the aqueous humor by a Na,K-ATPase. This process requires energy in the form of ATP. Bicarbonate is produced in the cell by the catalysis of water and carbon dioxide and moves into the aqueous humor through a carrier protein that likely involves co-transport of another ion. The increased concentration of sodium and bicarbonate draws water osmotically through water channels in the cell membrane (aquaporin-1) to form aqueous humor. Chloride likely transfers into the aqueous humor through a chloride channel to maintain electrochemical neutrality.

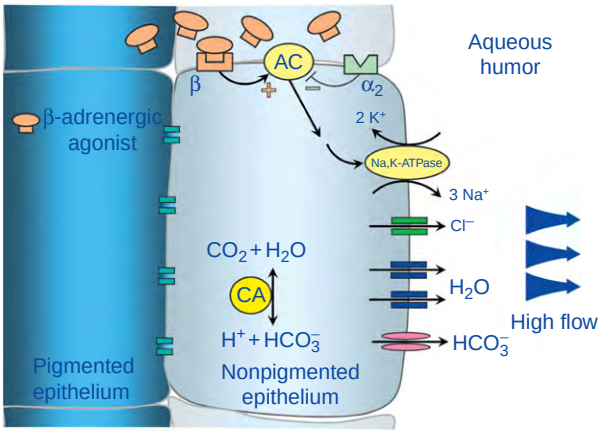

Figure 8 Flow is stimulated during the day by β-adrenergic activity. The activity of Na,K-ATPase, and the rate of sodium movement into the aqueous humor, is linked to adenylate cyclase through several steps. Adenylate cyclase is linked to two classes of receptors on the cell membrane, α_2-adrenergic and β-adrenergic receptors, that have opposite effects. When the β-adrenergic receptors bind transmitter, the linkage stimulates adenylate cyclase activity, which stimulates the Na,K-ATPase and increases aqueous flow. This is the normal state during the day when circulating and neural catecholamine concentrations are high.

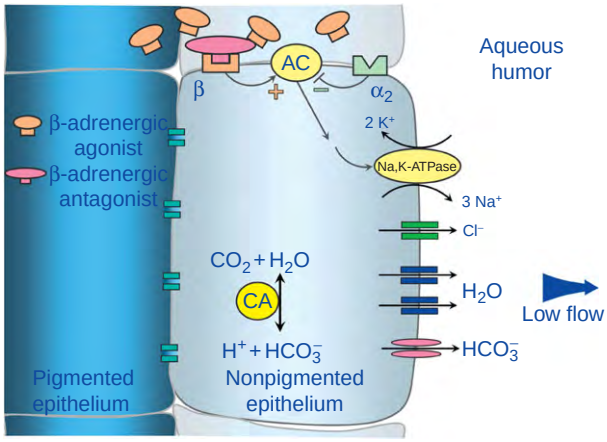

Figure 9 β-Adrenergic antagonists block β receptors and prevent the stimulation of adenylate cyclase. Flow rate decreases to approximately what it is during sleep when there is no intrinsic β-adrenergic stimulation.

The circadian variation in β-adrenergic stimulation of aqueous humor production provides an explanation of why β-adrenergic antagonists reduce flow during the day but not at night (**Figure 9**). During the daytime, when flow is high because of endogenous β-adrenergic activity, drugs such as timolol or betaxolol block the β-adrenergic receptors, and flow rate returns to its basal rate. These β-adrenergic inhibitors administered at night, when β-adrenergic activity is normally low, cannot suppress flow further because flow is not stimulated and there is no β-adrenergic activity to block. When epinephrine is given at night, it binds β-adrenergic receptors and stimulates aqueous humor flow. However, when β-adrenergic agonists are given during the day, they only poorly stimulate flow because most of the β-adrenergic receptors are already stimulated.

Apraclonidine and other α_2-adrenergic agonists decrease flow during the day by actively suppressing Na, K-ATPase through the adenylate cyclase messenger system (**Figure 10**). This pathway is also active at night, although flow does not decrease as much as it does during the day with α_2-adrenergic stimulation.

The transfer of bicarbonate into the posterior chamber is determined by the rate of catalysis of bicarbonate by carbonic anhydrase. Drugs that inhibit carbonic anhydrase, such as acetazolamide, dorzolamide, or brinzolamide, slow down the formation of bicarbonate, and the reduced movement of bicarbonate into the posterior chamber reduces water movement and aqueous humor production. (**Figure 11**) Suppression of carbonic anhydrase reduces aqueous humor production during the day, when flow rate is normally high, and is also effective at night.

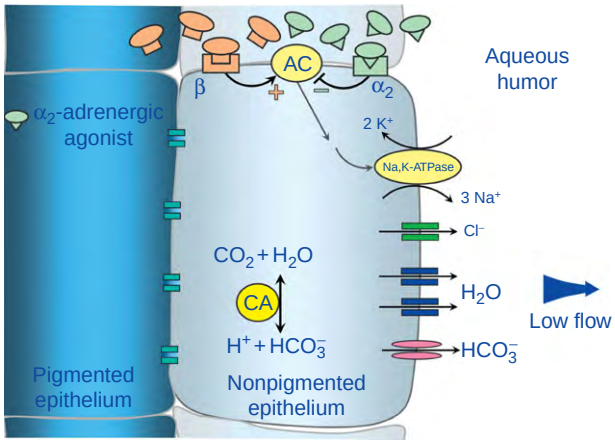

Figure 10 Adenylate cyclase is linked through a suppressive path to α_2-adrenergic receptors. Drugs with α_2-adrenergic activity bind these receptors and suppress activity of adenylate cyclase, and the reduced Na,K-ATPase activity reduces aqueous humor production.

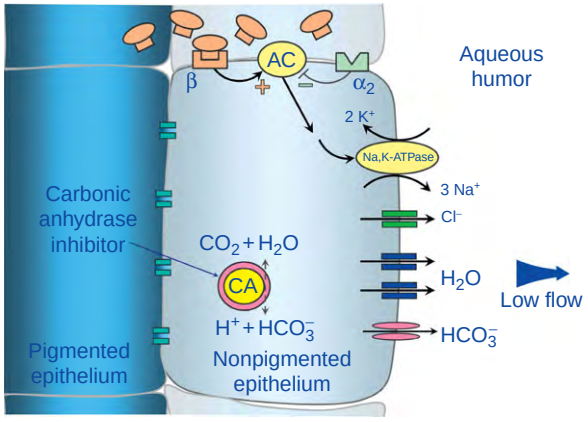

Figure 11 Movement of bicarbonate across the nonpigmented cell membrane is also responsible for a portion of aqueous humor production, and, as in other cells in the body, the reaction that produces bicarbonate is catalyzed by carbonic anhydrase. Drugs that inhibit carbonic anhydrase, such as dorzolamide or brinzolamide, reduce the production of bicarbonate in the cell and its movement into the aqueous humor, and aqueous humor flow decreases.

Summary

Much has been learned about aqueous humor dynamics and ocular hypotensive medications since aqueous humor flow was first measured over 50 years ago. Whereas aqueous humor production decreases slowly through life, it is unaffected by most afflictions and diseases. It varies greatly with the circadian cycle. During the morning, aqueous humor flow rate is the greatest and is about 3.0 µl min^{-1}, while at night during sleep, it drops to about half of this rate. The rate of aqueous humor production is determined by the activity of two enzymes, Na,K-ATPase and carbonic anhydrase, in the nonpigmented ciliary epithelium, and pharmacologic manipulation of these enzymes can reduce flow rate to treat ocular hypertension. Aqueous humor flow can be suppressed by β-adrenergic antagonists, which block β-adrenergic stimulation of Na,K-ATPase. This class of drugs has no effect at night when intrinsic β-adrenergic stimulation is minimal. The system is actively suppressed by α_2-adrenergic agonists, and these drugs also suppress flow rate at night. Carbonic anhydrase inhibitors reduce aqueous humor production by reducing the production and transfer of bicarbonate into the posterior chamber. Only drugs with β-adrenergic activity can stimulate flow, and then only poorly during the day when endogenous β-adrenergic stimulation is high. These drugs can increase flow rate during sleep, when natural β-adrenergic activity is low, but not to the extent that flow increases during the day. Our knowledge of fundamental dynamics and control of production and circulation of aqueous humor has provided a basis for understanding and developing better pharmacologic and surgical treatments of glaucoma.

See also: Biomechanics of Aqueous Humor Outflow Resistance; Ciliary Blood Flow and its Role for Aqueous Humor Formation; Ion transport in the Ciliary Epithelium; Pharmacology of Aqueous Humor Formation; The Role of the Ciliary Body in Aqueous Humor Dynamics. Structural Aspects.

Further Reading

Brubaker, R. F. (1991). Flow of aqueous humor in humans (The Friedenwald lecture). *Investigative Ophthalmology and Visual Science* 32: 3145–3166.

Brubaker, R. F. (1998). Clinical measurements of aqueous dynamics: Implications for addressing glaucoma. In: Civan, M. M. (ed.) *The Eye's Aqueous Humor. From Secretion to Glaucoma*, pp. 233–284. San Diego, CA: Academic Press.

Brubaker, R. F., Maurice, D. M., and McLaren, J. W. (1990). Fluorophotometry of the anterior segment. In: Masters, B. R. (ed.) *Noninvasive Diagnostic Techniques in Ophthalmology*, pp. 248–280. New York: Springer.

Carlson, K. H., McLaren, J. W., Topper, J. E., and Brubaker, R. F. (1987). Effect of body position on intraocular pressure and aqueous

flow. *Investigative Ophthalmology and Visual Science* 28: 1346–1352.

Civan, M. M. (ed.) (1998). *The Eye's Aqueous Humor. From Secretion to Glaucoma.* San Diego, CA: Academic Press.

Maren, T. H. (1994). Biochemistry of aqueous humor inflow. In Podos, S. M. and Yanoff, M. (eds.) and Kaufman, P. L. and Mittag, T. W. (associate eds.) *Textbook of Ophthalmology, Vol. 7: Glaucoma*, pp. 1.35–1.46. London: Mosby.

McLaren, J. W. (2009). Measurement of aqueous humor flow. *Experimental Eye Research* 88: 641–647.

Nilson, S. F. E. and Bill, A. (1994). Physiology and neurophysiology of aqueous humor inflow and outflow. In: Podos, S. M. and Yanoff, M. (eds.) and Kaufman, P. L. and Mitag, T. W. (associate eds.) *Textbook of Ophthalmology, Vol. 7: Glaucoma*, pp. 1.17–1.34. London: Mosby.

Wang, Y-L., Hayashi, M., Yablonski, M. E., and Toris, C. B. (2002). Effects of multiple dosing of epinephrine on aqueous humor dynamics in human eyes. *Journal of Ocular Pharmacology and Therapeutics* 18: 53–63.

Coordinating Division and Differentiation in Retinal Development

R Bremner and M Pacal, University of Toronto, Toronto, ON, Canada

Glossary

Cell birth – For the purposes of this article, cell birth is the activation of a new transcriptional program that is never seen in retinal progenitor cells (RPCs), but is limited to differentiating retinal transitional cell (RTCs). This definition excludes cell-cycle exit because, as discussed in this article, differentiating RTCs can be generated independent of exit. In normal cells, the timing of cell birth is usually measured by briefly labeling replicating DNA with bromodeoxyuridine (BrdU) or tritiated thymidine (^{3}H-thymidine) and then, days/weeks later, counting intensely labeled cells which, by definition, exited the cell cycle soon after the label was introduced. This tool is useless in mutants where cell birth occurs in the absence of cell-cycle exit. In that case, birth must be noted when it occurs using markers induced in differentiating RTCs that are never present in RPCs (e.g., Nrl in newborn rods).

Cell-cycle rate – It reflects the rate of cell expansion, which correlates with cell-cycle length.

Competence – This activity influences the ability of RPCs to generate certain cell types. It is permissive, but not instructive in that it creates potential, but it is not sufficient to force cell birth on its own. The competence of RPCs changes throughout development. Early RPCs are competent to produce ganglion, horizontal, amacrine, and cone cells, while late RPCs produce bipolar and Müller cells. Rods are generated throughout, but predominantly are a mid–late-born cell type.

Exit – Normally, cell birth is closely coupled to cell-cycle exit and ensures that a newborn RTC remains post mitotic until and after it becomes a terminally differentiated cell.

G0 – Cells can be driven out of G1 into reversible G0 by serum starvation or contact inhibition, or into irreversible G0 by terminal differentiation or senescence.

G1, S, G2, and M – Most cell cycles have four phases: S phase is when DNA is synthesized; M phase is when cells undergo mitosis to generate two offspring (often termed daughters); G1 and G2 are gaps between M and S or S and M, respectively.

Interkinetic nuclear migration (INM) – Cellular processes connect the RPC to the apical (also called outer or ventricular) and basal (also called inner or vitreal) surfaces of the retina. RPC nuclei move as they traverse the cell cycle. M-phase nuclei are located at the apical surface, then move more basally to go through G1 and start S, then finish S migrating back to the apical side, and go through G2 just before they reach the end of that journey.

Mitogen – Extracellular factor that induces cell division.

R – The restriction point in G1, beyond which a cell will continue into S phase even if mitogens are withdrawn.

Retinal progenitor cell (RPC) – A dividing cell in the normal developing retina.

Retinal transition cell (RTC) – Also termed precursor. These are newborn differentiating cells. They are distinguished from RPCs by a novel transcriptome that includes many mRNAs/proteins that are never detected in RPCs. Normally, RTCs are post mitotic. However, failure to exit does not prevent induction of the RTC transcriptome. Birth (induction of the differentiation program) and exit can be uncoupled and are, therefore, viewed as separate in this article.

Introduction

Cell division is driven by extrinsic mitogens that influence the intrinsic core cell-cycle machinery. Extrinsic factors can also influence the decision to exit and differentiate during development. In the retina, the earliest born cells are ganglion neurons (**Figure 1**) and these cells secrete factors that have crucial roles in influencing division and fate, such as Sonic Hedgehog. Beyond this stage, however, although many factors can influence division and fate, it is not clear whether they actually do so *in vivo*. Dissociated, well-separated, individual retinal progenitor cells (RPCs) can generate clones of cells that resemble clones *in vivo* in both size and composition, except for ganglion cells which do not survive *in vitro*. These data suggest that apart from ganglion cell births, much of retinal development is intrinsically programmed and thus, apart from a general requirement for mitogens, extrinsic factors may not play a major role in determining whether RPCs divide or exit. Further, we have introduced a few of the basic issues around cell-cycle regulation, discuss the role of some

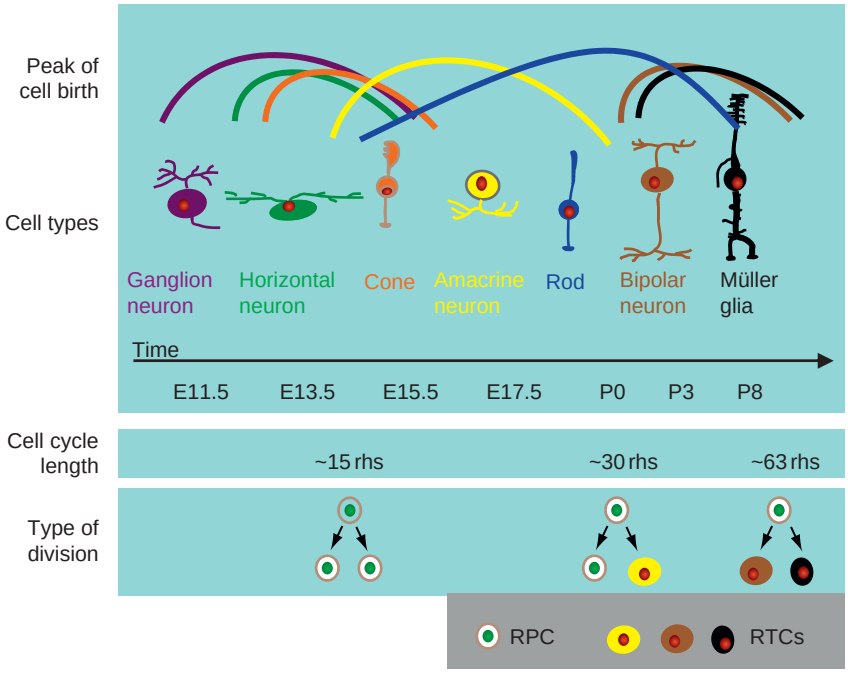

Figure 1 Retinal histogenesis. The upper schematic shows approximate time periods (E, embryonic; P, postnatal) of genesis for each of the seven major murine retinal cell types. The lower-half depicts when symmetric production of two RPCs gradually switches to symmetric production of two differentiating RTCs. This switch is matched by an increase in cell-cycle length. Dividing RPCs are depicted with white cytoplasm and green nuclei. Postmitotic differentiating RTCs are depicted with red nuclei and colored cytoplasm.

key cell-cycle regulators in retinal development, and finish with a discussion as to how RPC expansion versus neurogenesis is coordinated through the Notch pathway.

A Few Basics of Cell-Cycle Regulation

Extracellular positive (mitogenic) and inhibitory cues are sensed in cells through fluctuating levels of cyclins. These proteins are required to activate cyclin-dependent kinases (Cdks). Cyclin D-Cdk4/6 complexes form in G1, cyclin E-Cdk2 complexes act at G1-S, cyclin A-Cdk2 complexes drive S, and cyclin B-Cdk1 complexes drive M. However, these complexes may act in other phases and show considerable functional redundancy. Treatment of resting cells with mitogens induces *Cyclin D1* transcription through Ras–Raf–Erk-mediated activation of the immediate early gene Ap1 (Ap1/Ets). Glycogen synthase kinase 3 beta (Gsk3β)-mediated Thr phosphorylation of cyclin D reduces its stability and nuclear localization. Mitogens also activate the Ras–Pi3k–Akt pathway which phosphorylates and inactivates Gsk3β, doubling cyclin D1 half-life and promoting nuclear translocation. Cyclin D-Cdk4/6 complexes phosphorylate retinoblastoma (Rb) proteins on multiple sites. The cyclin D-Cdk4/6 complex also titrates the Cip/Kip family of Cdk2 inhibitors (CKI), discussed further below.

Rb inhibits division in two major ways (Figure 2). First, it binds the activating E2f transcription factors (E2f1, 2, and 3a). These are inducer genes that positively regulate the cell cycle (e.g., cyclins E and A) and other genes that are necessary for the nuts and bolts of DNA replication (e.g., PCNA, RRM1). Rb binds and quenches E2f activity, and recruits silencing cofactors to permanently shut down genes in terminally differentiating or senescent cells. Rb also binds E2f3b and E2f4, whereas its relatives p107 (Rbl1) and p130 (Rbl2) preferentially bind E2f4 and 5 – which are thought to be repressive E2fs that primarily mediate inactivation of target genes (although E2f3b can mimic some functions of E2f3a). However, p107/p130 can partner with activating E2fs if E2f4 is missing. E2fs 6–8 do not bind the Rb family of pocket proteins, but inhibit transcription by recruiting other co-repressors. The extent to which E2f target-gene induction involves direct activation (mediated by activator E2fs) versus derepression (loss of Rb pocket proteins from repressor E2fs) is not completely resolved.

Second, Rb – but not p107/p130 – binds the Cdh1 subunit of anaphase-promoting complex or cyclosome (APC/C) (Figure 2). APC/C ubiquitin ligase degrades securin and cyclins to permit passage through and escape from M phase, but in G1 it degrades Skp2 – part of another E3 ubiquitin ligase (SCF^{Skp2}) that degrades Cip/Kip CKIs to promote Cdk2 activity. Rb binds Skp2,

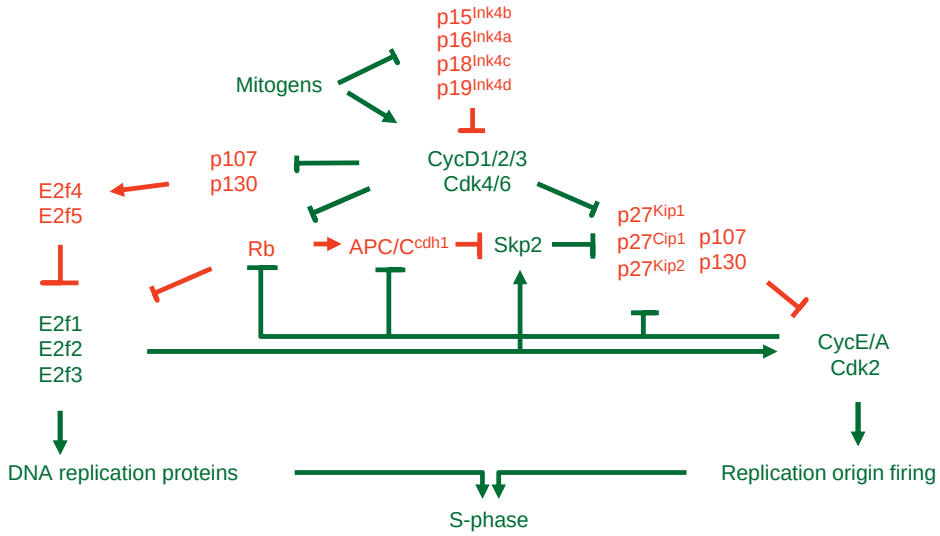

Figure 2 Some Key Regulators of G1/S transition. The two major axes of G1/S inhibition are the Rb–E2f and the Cip/Kip–Cdk2 axes. Mitogens stimulate division by inhibiting INK4a CKIs (e.g., $p19^{Ink4d}$) and increasing CycD levels. Activated Cdk4/6 phosphorylates and inhibits the Rb family. D-Cdk4/6 complexes also sequester Cip/Kip CKIs (e.g., p27). Active Rb binds and inhibits gene transactivation by E2f1-3. p107/130 form repressor complexes with E2f4/5 that target the same genes as E2f1-3. On the other axis, Cip/Kip CKIs bind and inhibit Cdk2 complexes. P107 and p130 – unlike Rb – can bind and inhibit Cdk2 complexes. There are also feed-forward and feedback links between the Rb–E2f and Cip/Kip–Cdk2 axes. Feed-forward effects include blockade of Skp2-mediated degradation of p27 by Rb-Cdh1, and E2f-mediated induction of CycE/A. Feedback effects include inhibition of Rb by Cdk2 (thus further activating both E2fs and Skp2). Positive regulators are in red, negative are in green. The figure does not, by any means, include all regulators and links.

presenting it for destruction to APC/C, thus preventing degradation of Cip/Kip CKIs and blocking Cdk2 action.

Rb phosphorylation weakens binding to E2f, resulting in induction of cyclin E, Cdk2 activation, further Rb phosphorylation, and induction of cyclin A – a sequential process that is necessary for cell-cycle progression. Cyclin D function is dispensable in Rb-deficient cells, but cyclin E is required for division even in the absence of Rb, indicating it has other targets. Indeed, independent of Cdk2 activation, cyclin E promotes loading of MCM proteins onto origins of replication, and E-Cdk2 phosphorylates this complex to trigger DNA replication. Cyclin E overexpression can drive the cell cycle even when E2f activity is blocked. Apart from unleasing E2f, Rb phosphorylation also releases it from both Skp2 and Cdh1 – thus activating Cdk2 by a second route (**Figure 2**). This positive-feedback loop allows cells to pass R and enter S; indeed, E2f1 behaves as a bistable switch to drive this irreversible transition.

Distinct CKI families bind and inhibit cyclin-Cdks (**Figure 2**). The Ink4 family, which includes $p16^{Ink4a}$, $p15^{Ink4b}$, $p18^{Ink4c}$, and $p19^{Ink4d}$ (encoded by *Cdkn2a/b/c/d*, respectively), inhibits Cdk4/6. Ink4 CKIs act upstream of Rb-E2f and need Rb plus p107 or p130, and E2f4 or E2f5 to block division. The Cip/Kip family of CKIs, which includes $p21^{Cip1}$, $p27^{Kip1}$, and $p57^{Kip2}$ (encoded by *Cdkn1a/b/c*, respectively), inhibit cyclin A/E-Cdk2 and cyclin B-Cdk1 and can act downstream of Rb. Notably, p107 and p130, but not Rb, also function as CKIs that inhibit Cdk2 activity as potently as $p21^{Cip1}$ (**Figure 2**). In the complete absence of the Rb family, mouse embryo fibroblasts (MEFs) lack a G1 restriction point, and progress even if mitogens are withdrawn, but these cells arrest at G2 due to the combined action of Cip/Kip CKIs and p53 tumor suppressor.

Inhibitory mitogens – such as transforming growth factor-beta (TGFβ), block cyclin D induction or inhibit its activity by inducing the expression of Ink4 CKIs. TGFβ also inhibits cell-cycle progression by triggering nuclear translocation of an E2F4/E2f5–p107–Smad3 complex that associates with Smad4 protein, and then binds and silences the c-*Myc* promoter through a Smad-E2f element.

In summary (**Figure 2**), Rb and Cip/Kip CKIs cooperatively inhibit division by constraining E2f- and Cdk2-mediated induction of S-phase gene transcription and replication origin firing, respectively. Rb and $p27^{Kip1}$ cross-talk positively by promoting Skp2 degradation and blocking Rb phosphorylation, respectively. Mitogen-activated cyclin-Cdks sequentially phosphorylate Rb, cyclin D-Cdk4/6 sequesters Cip/Kip CKIs, and Skp2, freed of Rb, stimulates CKI degradation, all of which leads to activation of E2f and Cdk2. E2f and Cdk2 cross-talk positively by inducing cyclins and phosphorylating Rb, respectively, This dual axis triggers the production and/or activation of the components needed for DNA replication.

Cyclins and Cdks in Retinal Development

RPCs express higher levels of cyclin D1 than any other embryonic tissue (Figure 3). D1 absence causes severe retinal hypocellularity. Downregulation/inhibition of D1 during differentiation is important since ectopic expression in differentiating photoreceptors prevents normal cell-cycle exit, mimicking the effect of pocket protein loss. The large induction in $p27^{Kip1}$ protein translation in newborn retinal neurons likely dwarfs any remaining D1-Cdk4/6 in these cells. D1 loss reduces RPC division beyond E16.5 but not earlier, suggesting that the earliest phase of RPC expansion is D1-independent. This delayed requirement for D1 may reflect the gradual increase in Rb and p107 expression in RPCs during development. Consistent with the role of D cyclins in inactivating Rb and sequestering CKIs (see above), the *D1*-null retina has hypophosphorylated Rb, no cyclin E–Cdk2 activity, and hypocellularity is rescued when $p27^{Kip1}$ is also missing. A cyclin $D1^{KE}$ point mutant binds but fails to activate Cdk4/6 and partially rescues the *D1*-null retina. Like normal D1-Cdk, $D1^{KE}$-Cdk complexes sequester $p27^{Kip1}$, and consequently both Cdk2 activity and Rb phosphorylation are increased in $D1^{KE}$ versus *D1*-null retinas.

The D family has two other members – D2 and D3. The defect in *D1*-null mice is rescued in mice expressing

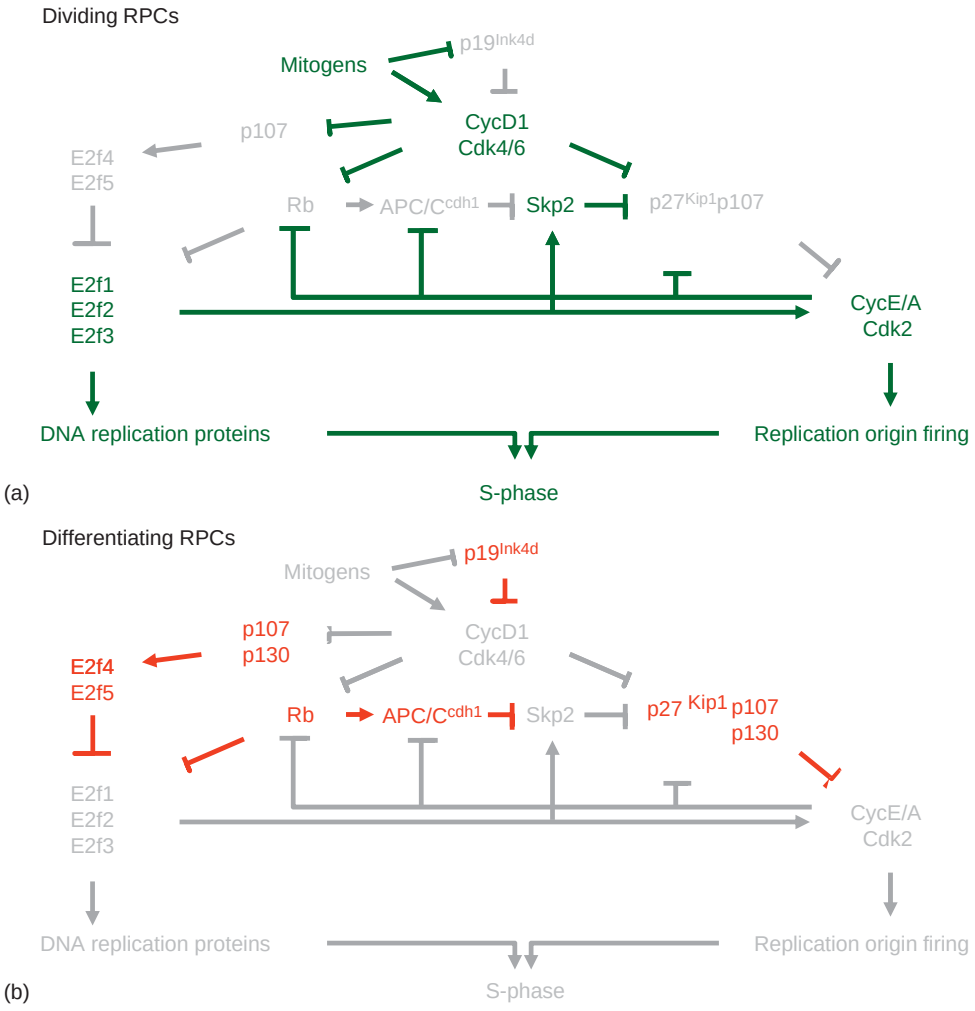

Figure 3 Cell-cycle regulation in RPCs versus differentiating RTCs. (a) In dividing RPCs, extremely high levels of CycD1 activate Cdk4/6 and maintain Rb and p107 in an inactive phosphorylated state and sequester $p27^{Kip1}$. The latter is also efficiently degraded, presumably due to high levels of Skp2. Inactive pocket proteins leave the activating E2fs free to induce transcription of genes required for DNA replication and CycE/A that activate Cdk2. $p27^{Kip1}$ absence leaves CycE/-Cdk2 free to fire DNA origins and further inhibit negative cell-cycle regulators (e.g., Rb, $p27^{Kip1}$). (b) In differentiating RTCs, both $p19^{Ink4d}$ and $p27^{Kip1}$ proteins are induced and inhibit Cyc–Cdk complex activity. Cyclin expression is downregulated. Pocket proteins are activated by dephosphorylation and quench E2f activity. p107/p130 act in other cells to form repressor complexes with E2f4/5, although whether this is the case in the retina has not been shown explicitly. Rb may facilitate $p27^{Kip1}$ stability by bringing Skp2 into contact with APC/C. However, in human retina, there is only brief overlap in Rb and $p27^{Kip1}$ expression in differentiating neurons. The picture is more complex than depicted.

D2 from the *D1* locus, so they are interchangeable in this regard. Normally, however, D2 is not expressed in the retina and while D3 is expressed in Müller glia, it is present at very low levels in RPCs. There is no induction of D2 or D3 in *D1*-null retinas and *D1/D2*- or *D1/D3*-null retinas do not show a more severe phenotype than the *D1* knockout (KO). The loss of $p27^{Kip1}$ in *D1*-null retinas also does not affect *D2* and *D3* expression. Triple-null mice survive to ~E15 and, consistent with the idea that D cyclins are not required for early RPC division the early triple-null retina also appears wild-type (WT).

The cyclin E family consists of E1 (formerly E) and E2, and both are expressed in retina. Apart from a spermatogenesis defect in *E2*-null males, *E1*- and *E2*-null mice are normal. $E1^{-/-};E2^{-/-}$ mice die around mid-gestation (~E10) due to defective endoreduplication (repeated S with no M-phase) in trophoblasts, and thus a defective placenta. By using tetraploid WT blastocysts, which form a normal placenta but do not contribute to the embryo proper – $E1^{-/-};E2^{-/-}$ embryonic stem (ES) cells injected into these blastocysts could, in about half the cases, generate a normal embryo that, like WT ES cells in this approach, survive to birth. Half of $E1^{-/-};E2^{-/-}$ embryos die with cardiac defects, all megakaryocytes (like trophoblasts) show defective endoreduplication, and while MEFs could divide normally, they were unable to exit quiescence. Importantly, no neural phenotypes were reported in $E1^{-/-};E2^{-/-}$ embryos, suggesting that cyclin E functions are redundant in RPCs, perhaps due to the combined actions of cyclins D1 and A.

Remarkably, knocking in cyclin *E1* to the *D1* locus partially rescues the cyclin *D1*-null retinal phenotype with retinal thickness reaching ~75% WT. Rb phosphorylation is only slightly higher than in the *D1* KO, suggesting that low levels of Rb phosphorylation are sufficient to permit RPC division. Indeed, cyclin E can override a cell-cycle block induced by overexpressing a mutated version of Rb lacking most of its phosphorylation sites. The Cdk-independent role of cyclin E in loading DNA-replication origins may be important in this context.

Like cyclins, there is also considerable redundancy among Cdks. Although $Cdk4^{-/-}$ mice are 20% smaller at birth, show pancreatic islet cell hypotrophy, and null MEFs divide more slowly due to elevated $p27^{Kip1}$, there are no obvious retinal defects. Apart from a mild hematopoietic defect $Cdk6^{-/-}$ mice are normal, and *Cdk4/6* redundancy in RPCs remains to be addressed since double-null mice die after E14.5. Cdk3 is rarely mentioned as it is defective in many mice and is thus dispensable. *Cdk2*-null mice appear normal except for a defect in meiosis, and deleting *Cdk2* does not affect fibroblast division. *Cdk2/4/6* triple-null mice die around E12.5 and retinal explant studies have not been attempted. The latter study also shows that Cdk1 (also called Cdc2) – the most ancient cell-cycle kinase best known for its role at G2/M in mammals – can substitute for other kinases to mediate much of the proliferation needed for embryogenesis. Moreover, it is required for the first division following fertilization. A conditional allele will be needed to study its role in later stages, including RPC expansion.

In summary, cyclin D1 promotes RPC division both by phosphorylating Rb proteins and sequesterating $p27^{Kip1}$, although early RPC expansion appears cyclin D-independent. E cyclins, Cdk4/6, or Cdk2 each seem redundant, but further studies are required to tease apart overlapping cyclin and Cdk roles and to determine if Cdk1 is essential for RPC division.

The Rb Family in Retinal Development

Rb is the tumor suppressor mutated in the familial cancer retinoblastoma. Rb and p107 pocket proteins are present in mouse and human RPCs as well as in postmitotic retinal transition cells (RTCs), whereas p130 seems to be confined to the latter. As expected, Rb loss triggers extra division. However, Rb and p107 seem to be inactive in RPCs as removing Rb or both Rb and p107 in mouse retina does not affect the number of M-phase or visual system homeobox 2 ($Vsx2^{+}$, also called Chx10) RPCs. Inactivation of Rb in RPCs may be due to the extremely high levels of cyclin D1 and, as noted above, Rb is hypophosphorylated in *D1*-null retinas. The logical explanation for Rb expression in RPCs may be that it is poised to act rapidly in newborn RTCs once D1 levels drop (**Figure 3**). Rb is also important for arresting division following DNA damage, which could also be employed in RPCs. Nevertheless, the irrelevance of Rb in controlling normal RPC division is a hard pill to swallow in view of multiple *in vitro* overexpression experiments implying that Rb tempers the expansion of all dividing cells. Yet Rb-null ES cells divide normally, and Rb-null embryos are not enlarged despite minimal apoptosis, and the same is true of p107/p130-null embryos, and there is not much compensation in either case. Moreover, Rb loss does not impact much of *Xenopus* embryonic development, again implying that it is already inactive.

Instead of tempering expansion, Rb is employed mainly to promote permanent cell-cycle exit, such as in terminally differentiating (**Figures 3** and **4**) or senescing cells, or to execute arrest in DNA-damaged cells. Thus, in contrast to the undetectable effect of *Rb* loss in RPCs, there is a dramatic effect in differentiating RTCs (**Figure 4**). RTCs missing Rb, or Rb and one or more of its relatives, divide ectopically. Some cell types choose apoptosis to defend the tissue from cancer, which is E2f1-dependent, but p53-independent. Indeed, most defects in the Rb-null retina are rescued in the *Rb/E2f1*-null retina, except for a notable cell-cycle and cell-death-independent differentiation defect in a subset of amacrine interneurons that is caused by E2f3a. Intriguingly, Rb repression of E2f3 is also

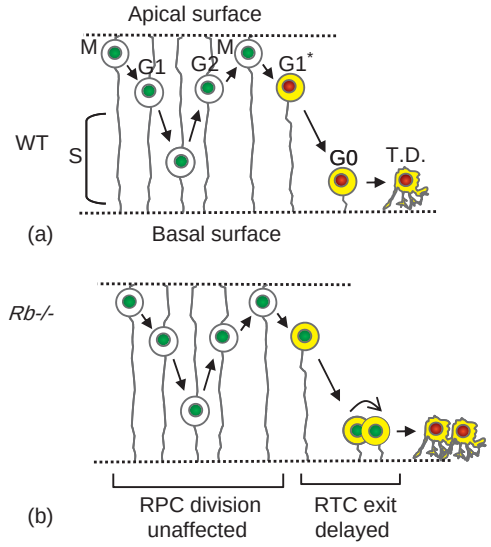

Figure 4 Uncoupling cell birth and cell-cycle exit. (a) In the WT retina, the RPC nucleus/cell body changes position as the cell progresses through the cell cycle. This process is termed interkinetic nuclear migration (INM). Following cell birth, the apical process begins to retract as the newborn RTC moves to its final destination and undergoes terminal differentiation (TD) Green and red nuclei depict whether the cell is dividing or post mitotic, respectively. Yellow cytoplasm indicates induction of a distinct transcriptome in the RTC. (b) In the absence of Rb, RPC division is unaffected, but differentiating RTCs divide ectopically (note green, instead of red, nucleus). However, the birth transcriptome (yellow cytoplasm) is activated. The response of different RTCs to Rb loss is cell-type specific. Some (as depicted here) survive, terminally differentiate and exit division via Rb-independent means. During ectopic division, these cells are at risk for neoplastic transformation (not shown). Other cell types (e.g., ganglion cells) escape transformation by undergoing apoptosis (not shown).

important to ensure proper migration of forebrain neurons against independent of cell cycle/apoptosis activities. Amacrine cells are one of a subset that survive loss of Rb proteins, and most escape tumorigenesis not by death, but by Rb-independent cell-cycle escape (**Figure 4**). However, rare *Rb/p107*-null or *Rb/p130*-null amacrine cells – likely through post-pocket protein events that override this arrest – can form sporadic retinoblastoma. Human retinoblastoma does not require p107 or p130 loss, likely reflecting broader expression of these proteins in other species. Intriguingly, long-term ectopic division of differentiating cells in fly tissues also requires disruption of multiple cell-cycle regulators. Ectopically dividing murine horizontal cells are also resistant to apoptosis, but they are better protected against transformation and require loss of *Rb*, *p130*, and one allele of *p107* to form tumors. Natural resistance to apoptosis is an attractive feature for a cancer cell-of-origin, especially one like retinoblastoma that requires fewer rate-limiting events than adult cancers. Several post-Rb events have been identified in human retinoblastoma and likely facilitate progression past a benign retinoma state, which ends in senescence.

In summary, pocket proteins apparently do not regulate the cell cycle in normal RPCs, but are poised to act in differentiating RTCs where Rb is required to quench E2f1 activity (**Figures 3** and **4**). p107 and p130, although nonessential, act as backups when Rb is removed. The CKIs $p19^{Ink4d}$ and $p27^{Kip1}$ may play an important role in activating Rb proteins in differentiating RTCs (**Figure 3**). Pocket protein loss creates a dangerous state where ectopically dividing RTCs risk neoplastic transformation. This risk is countered in some cells by apoptosis and others by Rb-independent means of cell-cycle exit.

Ink4 CKIs and $p19^{Arf}$ in Retinal Development

Cdkn1c encoding $p18^{Ink4c}$ is expressed weakly in the embryonic NBL, but is dispenable for retinal development. *Cdkn2b*, which encodes $p15^{Ink4b}$, lies adjacent to *Cdkn2a*, which encodes two transcripts that have distinct first, but shared downstream, exons and encode $p16^{Ink4a}$ and the p53-activating protein $p19^{Arf}$ ($p14^{ARF}$ in humans) from different reading frames. $p15^{Ink4b}$ expression has not been reported in the retina and, while deleting both *Cdkn2b/2a* loci (which removes all three proteins) renders mice extremely susceptible to tumorigenesis, eye defects in addition to those seen in *Cdkn2a* or *p19*^{Arf}-null mice were not described. $p19^{Arf}$ is expressed in embryonic vitreal pericytes where it represses platelet-derived growth factor receptor beta (PDGFRB) expression independent of double minute 2 (MDM2) or p53, limiting expansion of these endothelial support cells, thus its absence triggers abnormal expansion and severe defects in the adult eye. As expected, *Cdkn2a*-null mice, lacking both $p16^{Ink4a}$ and $p19^{Arf}$, also have this defect, but no obvious retinal defects – consistent with the absence of these proteins in RPCs. The fourth Ink4 protein – $p19^{Ink4d}$ – is encoded by *Cdkn2d*. Its expression pattern is consistent with a role in facilitating cell-cycle exit (**Figure 3**) and, indeed, null mice show abnormal division followed by elevated apoptosis. The defects may be a milder version of those seen in the absence of Rb or following overexpression of E2f1 or cyclin D1 in differentiating retinal neurons.

Cip/Kip CKIs in Retinal Development

Some $p21^{Cip}$ – encoded by *Cdkn1a* – is expressed in the WT retina, which increases in the absence of *Rb*, implying a context-specific role in retinal cell-cycle control. $p21^{Cip}$ absence alone does not affect retinal development, so it would be interesting to know its effect when combined with Rb loss.

In the embryonic retina, a few cells express $p57^{Kip2}$ (e.g., 3%, E14.5) and its loss triggers extra division, which

may reflect extra RPCs and/or ectopically dividing RTCs; the latter fits the observation that $p57^{Kip2}$ is expressed in late G1 or G0. Expression ceases around P0, and is reactivated in a subset of postmitotic amacrine cells, consistent with a role for $p57^{Kip2}$ in differentiation.

The most influential Cip/Kip CKI in the retina is $p27^{Kip1}$ (**Figure 3**), as suggested by its broader expression pattern in mouse and human retina (e.g., ~50%, E14.5). $p27^{Kip1}$ mRNA is high in mouse RPCs and low in differentiating RTCs but vice versa for protein, implying that rapid translation and mRNA degradation parallels differentiation. In human RTCs, $p27^{Kip1}$ expression seems, in general, to precede Rb protein expression, suggesting that a dual wave of inhibitors is employed to shut division down. $p27^{Kip1}$ is detected at G2 in RPCs, earlier than $p57^{Kip2}$, consistent with an early role in promoting cell-cycle exit in newborn RTCs. The *Cdkn1b*-null retina has excess dividing cells at least until P10, which could reflect extra RPCs and/or ectopically dividing differentiating RTCs.

Some adult $p27^{Kip1}$-deficient retinas contain focal hyperplastic lesions, possibly due to reactive gliosis. These lesions are more severe when the *Cdkn1b* gene is replaced by an altered protein ($p27^{CK-}$) that cannot bind cyclin–Cdk complexes. $p27^{+/CK-}$ mice do not get retinoblastoma, but do develop lung tumors. The increased phenotypic severity in $p27^{+/CK-}$ mice relative to $p27^{Kip1}$-null mice reveals that $p27^{Kip1}$, when freed from cyclin–Cdks, has a dominant disruptive function. This activity may relate to the cytoplasmic role of $p27^{Kip1}$ in regulating the Rho-Rock signaling pathway which, intriguingly, is also targeted by $p21^{Cip}$ and $p57^{Kip2}$. $p27^{Kip1}$ has other cytoplasmic activities such as binding the microtubule regulator stathmin. $p21^{Cip}$ and 27^{Kip} are distributed between the cytoplasm and nucleus in mouse retina.

Cell-cycle defects in the $p19^{Ink4d}$- or $p27^{Kip1}$-deficient retinas are enhanced when both are missing, consistent with cooperative Rb activation and Cdk inactivation to promote cell-cycle exit. Apoptosis and dysplasia are also more severe. As in the $Rb^{-/-}$ retina, deleting p53 does not rescue apoptosis, yet surprisingly it does reverse the dysplasia.

E2Fs in Retinal Development

Multiple E2f mRNAs have been detected in the retina, and protein expression has been confirmed for E2f1 as well as both a and b isoforms of E2f3. Deleting *E2f1* slows RPC division approximately twofold, whereas *E2f3* loss has no effect, suggesting redundancy. The superior role for E2f1 in RPCs differs from that in MEFs where E2f3 is more important. As noted above, E2f1 drives ectopic division in differentiating $Rb^{-/-}$ RTCs and transgenic E2f1 expression in photoreceptors also impairs cell-cycle exit. E2f3a perturbs differentiation in some $Rb^{-/-}$ amacrine cells, which is similar to its effect in the $Rb^{-/-}$ forebrain. E2f4 loss affects Shh expression in the telencephalon, but its role in the retina, similar to other E2fs, awaits further study.

Separating Rate, Birth, and Exit

The above discussion summarizes how cell-cycle regulators affect RPC expansion and RTC cell-cycle exit. We now turn to how the factors that promote cell birth influence the cell-cycle machinery. At this point, we encourage the reader to review the glossary definition of the terms competence, interkinetic nuclear migration (INM), cell birth, and exit. To facilitate discussion of the model below, we emphasize that birth and exit are viewed as separate activities that are temporally coupled. Birth is the new transcriptional program activated in a differentiating cell that defines its identity, and exit is the cessation of division.

Distance from Notch Predicts Birth

As already described, RPC nuclei undergo INM. Live imaging studies in zebrafish have indicated that nuclei that migrate deeper into the basal layer are more likely to generate a differentiating RTC when they return to the apical surface and undergo mitosis. These data raise the possibility that to achieve birth, nuclei must escape from a diffusable inhibitory signal. An attractive candidate is the antineurogenic factor Notch (**Figure 5**). Activated Notch is cleaved, releasing its intracellular domain (Nicd), which binds recombination signal-binding protein (Rbpj, also called Cbf1, Suh, Igkrb, Kbf2). Rbpj activates expression of hairy and enhancer of split (Hes) proteins, which are basic helix-loop-helix (bHLH) transcriptional repressors that block expression of proneurogenic genes. In line with the speculative model in **Figure 5**, Notch is more abundant at the apical side, but there is conflicting literature on whether the diffusable cleaved Nicd fragment or its gene targets (e.g., the Hes proteins) are more abundant/active in apically located nuclei. The Baier/Link groups found that antibodies to Nicd labeled apically located fish RPCs. Using live imaging, this group also found that a fluorescent protein expressed from the Nicd-inducible *her4* promoter was more abundant in RPCs with more apically located nuclei. However, the Reh group finds that Nicd is lowest in the apically located nuclei in the mouse retina, and both the Reh group and the Kageyama group report higher levels of Hes1 in progenitors when their nuclei are located at the basal side of the neuroepithelium in mouse and chick retina and mouse cortex (using highly destabilized Hes1 reporters). Given the highly transient

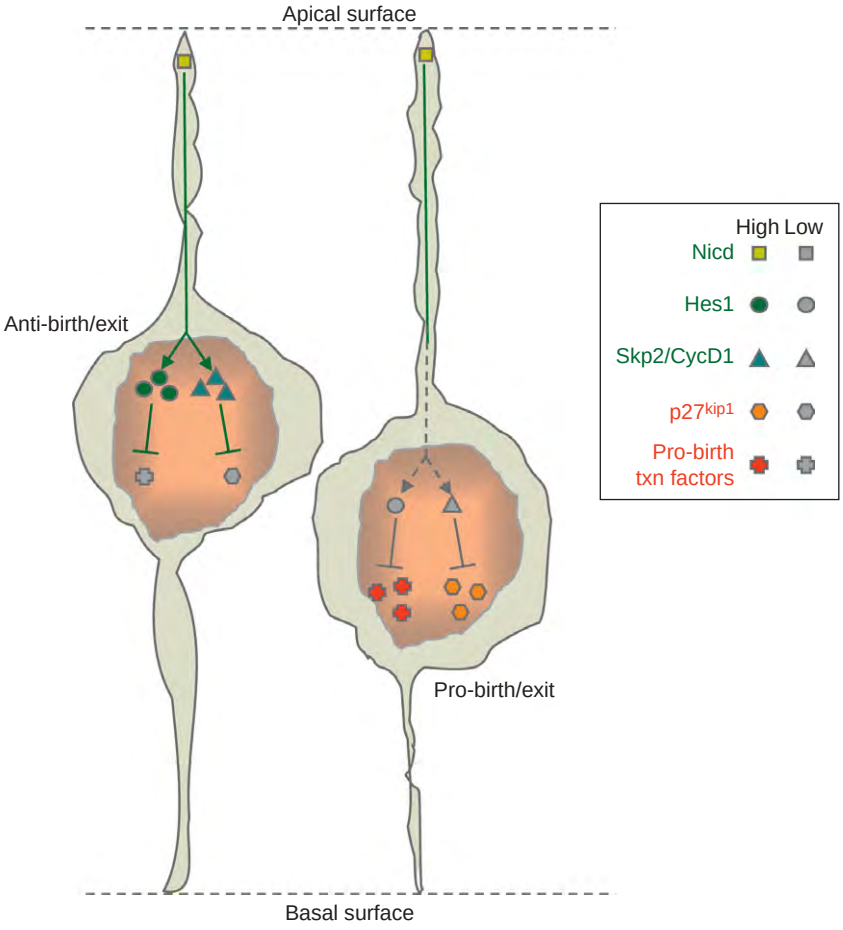

Figure 5 Notch and INM control birth/exit pathways. This Nicd gradient model is based on data from zebrafish studies, but is still controversial (see text for details). In addition, the link between Nicd and Skp2/cyclin D1 induction has been shown in other cell types but not, as yet, RPCs. In this speculative model, the RPC nucleus on the left migrates less basally than the RPC nucleus on the right. As a result, the former is under control of the apical gradient of Notch signaling mediated by the cleaved diffusable Nicd, which drives transcription of Hes1 (green) as well as Skp2 and Cyclin D1 (blue) which counter-expression of neurogenic bHLH factors and inhibit $p27^{Kip1}$, respectively. On the contrary, the nucleus that migrates deeper is less affected by Nicd because it has to diffuse further (dotted gray arrows), and the reduced levels of Hes1 and Skp2/CycD1 permit induction of pro-birth bHLH factors (red) and stabilization of $p27^{Kip1}$ (orange).

nature of Notch signaling, it will be important to use highly destabilized reporters, like those used in cortex by Kageyama's group, for future studies in retina, to better characterize cell-cycle-dependent changes in Notch signaling. Genetic studies prove that Notch is antineurogenic, so it will be important to deduce exactly how it achieves this end.

Genetic analysis in fish shows that, whether or not Nicd/Hes gradients are involved, INM plays a key role in determining birth. In dynactin-1 (mok) mutants, it was found that RPC nuclei migrated deeper (thus appearing to escape Notch signaling) and generated more early-born ganglion cells. The mechanisms that control INM distance are unclear, but both actin- and microtubule-based motors have been implicated. Notably, RPCs are in S-phase when they approach the basal side and neurogenic bHLH genes are induced in S-phase. Moreover, transplant experiments indicate that both cortical and retinal progenitors can change fate during this period. Together, these data build a model in which nuclei destined to undergo birth are moved a sufficient distance from the apical surface to escape influence of the Notch pathway, thus permitting induction of neurogenic factors required to activate the birth program.

Birth Does Not Require Exit

Birth and cell-cycle exit are intimately linked, so it is tempting to conclude they must be interdependent (birth needs exit). There is also a model proposing that slowing cell-cycle rate in the last division might also be critical to facilitating birth. Below, we summarize evidence for and against these issues.

In support of the notion that rate reduction favors birth, progenitor cell-cycle length increases with the gradual transition to symmetric production of two RTCs. In zebra fish, the average cell-cycle length does not predict birth, but, of two sibling RPCs, the one with the longer cycle is more likely to differentiate following M-phase. Moreover, amounts of the Cdk-inhibitor drug olomoucine that slow, but do not stop, division are sufficient to trigger premature neurogenesis in the telencephalon. In support of the idea that birth requires exit, the two are temporally coupled and $p27^{Kip1}$ induction occurs in the last G2 just prior to RTC birth. Moreover, overexpression of this CKI induces early birth.

The above data are not totally conclusive. Correlations do not distinguish consequence from cause. A longer final cycle in sibling RPCs might reflect deeper migration of the neurogenic partner trying to escape Notch. Olomoucine has targets other than Cdks and importantly, mutations in *E2f1*, *cyclin D1*, or *Vsx2* that lengthen cell cycle by specific genetic means do not cause a switch to early-born cell types. Thus, whether lengthening the cell cycle is necessary for birth remains moot.

What about exit, is it required for birth? Notch-pathway defects trigger both birth and exit, but this is also a correlation that does not distinguish whether they are interdependent or can be uncoupled. Genetic evidence supports the latter since neurogenesis in the retina, forebrain, cerebellum, and inner ear goes ahead in the absence of Rb and differentiating neurons divide ectopically. As discussed earlier, a subset of ectopically dividing neurons eventually undergo apoptosis, while others survive and exit independent of Rb, and these are the source of sporadic retinoblastoma. However, clearly, birth occurs despite these downstream defects. As with Rb loss, there is also not a shift to late-born cells in retinas lacking $p27^{Kip1}$ and/or $p19^{Ink4.}$ The interphotoreceptor retinoid-binding protein (IRBP) promoter is activated just before photoreceptors are born, yet its use to overexpress cyclin D1 or E2f1 does not prevent initiation of the birth program, and the resulting photoreceptors divide ectopically. CKI overexpression assays suggest that exit can drive birth, yet do not prove that this is the physiologically relevant or necessary route. Indeed, arresting division with hydroxyurea or aphidicolin in *Xenopus* embryos does not disrupt most central nervous system (CNS) differentiation, indicating that arrest *per se* is not neurogenic. Perhaps, CKIs induce early birth by affecting a process other than exit, and, indeed, a mutated version of $p27^{Kip1}$ incapable of binding and inhibiting Cdks induces neurogenesis through interaction and stabilization of neurogenin 2 (Neurog2 or Ngn2). Alternatively, active cell-cycle components may maintain expression and/or activity of Notch-pathway components and downregulation of the cell cycle would thus block Notch signaling, an intriguing possibility given that E2f regulates the expression of Hes family members.

In summary, while birth and exit are closely coupled, exit is not necessary for birth. They are both induced following escape from Notch-pathway signals, but in an apparently parallel rather than interdependent fashion.

Mechanisms Linking Birth to Exit

Despite functional independence, birth and exit are coupled temporally, which makes sense given that a single pathway, Notch, is so central in coordinating them both. It is well established that Notch downregulation leads to induction of neurogenic transcription factors through alleviation of Hes1-mediated repression. But how is Notch connected to cell-cycle exit? Hes1 also represses expression of $p27^{Kip1}$ mRNA, but in mouse retina $p27^{Kip1}$ protein induction during cell birth is regulated at a posttranscriptional level. There are many ways in which $p27^{Kip1}$ translation and stability are regulated, yet the specific approach used in the retina is unclear. Activated Notch can induce Skp2 through the same mechanism it uses to activate Hes1 expression and, as noted earlier, Skp2 promotes $p27^{kip1}$ ubiquitin-mediated degradation (**Figure 2**). Forkhead transcription factors can promote $p27^{Kip1}$ stability by downregulating a proteosome subunit. Notch loss downregulates Vsx2 and Tlx4, and both are required for high cyclin D1 and low $p27^{Kip1}$ levels, although the details are unclear. The intracellular cleaved domain of Notch can directly activate the cyclin D1 promoter, so this mechanism might be employed in the retina. Cyclin D1 downregulation likely ensures activation of Rb protein in newborn neurons. $p19^{Ink4d}$ induction would also facilitate this event, but – although it is regulated at both transcriptional and posttranscriptional levels – the mechanisms used in retinal cells are unclear. Once Rb is activated, it shuts down E2f, and the most critical target is E2f1 since removing the latter rescues all ectopic division and apoptosis in the Rb-null retina.

Conclusion

Birth and exit are coordinately regulated through escape from Notch signaling, which may involve a distance-dependent mechanism that relies on polarity signals and INM. It is unclear exactly how the decision to evade Notch is made. Despite their temporal proximity birth is not dependent on exit. The factors that activate the new transcriptional program can be induced independent of signals necessary to shut off division and neurons attempt to develop as they divide ectopically. Failure to couple birth to exit can lead to retinoblastoma, underscoring the importance of maintaining tight coupling. To avoid this catastrophe, some neurons undergo apoptosis, but others adopt Rb-independent means of exiting, which provides a window of time during which neoplastic clones may

evolve. Well-known cell-cycle regulators are downregulated and activated to ensure exit parallels birth, and many of these events are posttranscriptional. Exactly how evading Notch triggers these events in the retina remains to be resolved, although there are clues from work in other cell types.

Acknowledgments

We are grateful to Valerie Wallace, Tom Reh, and Brian Link for comments. Research on retinal development in the Bremner lab is funded by the Canadian Institute for Health Research (CIHR) and the Foundation Fighting Blindness. M. Pacal is supported by a Vision Science Research Program fellowship from the University of Toronto.

See also: Coordinating Division and Differentiation in Retinal Development; Embryology and Early Patterning; Eye-Field Transcription Factors; Histogenesis, Cell Fate, and Signaling Factors; Intraretinal Circuit Formation; Photoreceptor Development: Early Steps/Fate; Retinal Histogenesis.

Further Reading

Baye, L. M. and Link, B. A. (2008). Nuclear migration during retinal development. *Brain Research* 1192: 29–36.

Besson, A., Dowdy, S. F., and Roberts, J. M. (2008). CDK inhibitors: Cell cycle regulators and beyond. *Developmental Cell* 14: 159–169.

Burkhart, D. L. and Sage, J. (2008). Cellular mechanisms of tumour suppression by the retinoblastoma gene. *Nature Reviews. Cancer* 8: 671–682.

Buttitta, L. A. and Edgar, B. A. (2007). Mechanisms controlling cell cycle exit upon terminal differentiation. *Current Opinion in Cell Biology* 19: 697–704.

Cayouette, M., Barres, B. A., and Raff, M. (2003). Importance of intrinsic mechanisms in cell fate decisions in the developing rat retina. *Neuron* 40: 897–904.

Cayouette, M., Poggi, L., and Harris, W. A. (2006). Lineage in the vertebrate retina. *Trends in Neuroscience* 29: 563–570.

Chen, D., Opavsky, R., Pacal, M., et al. (2007). Rb-mediated neuronal differentiation through cell-cycle-independent regulation of E2f3a. *PLoS Biology* 5: e179.

Del Bene, F., Wehman, A. M., Link, B. A., and Baier, H. (2008). Regulation of neurogenesis by interkinetic nuclear migration through an apical-basal notch gradient. *Cell* 134: 1055–1065.

Farkas, L. M. and Huttner, W. B. (2008). The cell biology of neural stem and progenitor cells and its significance for their proliferation versus differentiation during mammalian brain development. *Current Opinion in Cell Biology* 20: 707–715.

Gotz, M. and Huttner, W. B. (2005). The cell biology of neurogenesis. *Nature Reviews. Molecular Cell Biology* 6: 777–788.

Kageyama, R., Ohtsuka, T., Shimojo, H., and Imayoshi, I. (2008b). Dynamic Notch signaling in neural progenitor cells and a revised view of lateral inhibition. *Nature Neuroscience* 11: 1247–1251.

Levine, E. M. and Green, E. S. (2004). Cell-intrinsic regulators of proliferation in vertebrate retinal progenitors. *Seminars in Cell and Developmental Biology* 15: 63–74.

Malumbres, M. and Barbacid, M. (2009). Cell cycle, CDKs and cancer: A changing paradigm. *Nature Reviews. Cancer* 9: 153–166.

Nelson, B. R., Hartman, B. H., Georgi, S. A., Lan, M. S., and Reh, T. A. (2007). Transient inactivation of Notch signaling synchronizes differentiation of neural progenitor cells. *Developmental Biology* 304: 479–498.

Pacal, M. and Bremner, R. (2006). Insights from animal models on the origins and progression of retinoblastoma. *Current Molecular Medicine* 6: 759–781.

Shimojo, H., Ohtsuka, T., and Kageyama, R. (2008). Oscillations in notch signaling regulate aintenance of neural progenitors. *Neuron* 58: 52–64.

van den Heuvel, S. and Dyson, N. J. (2008). Conserved functions of the pRB and E2F families. *Nature Reviews. Molecular Cell Biology* 9: 713–724.

Wallace, V. A. (2008). Proliferative and cell fate effects of Hedgehog signaling in the vertebrate retina. *Brain Research* 1192: 61–75.

Cornea Overview

P Asbell and D Brocks, Mount Sinai Hospital, Department of Ophthalmology, New York, NY, USA

Glossary

Conductive keratoplasty (CK) – Refractive surgery that uses heat from radio waves to shrink the collagen in the cornea. It is useful for patients with hyperopia and presbyopia.
Dry eye syndrome (DES) – Lack of quantity or quality of tears that lubricate the ocular surface.
Disodium ethylenediaminetetraacetic acid (EDTA) – Chemical that chelates calcium.
Descemet's stripping automated endothelial keratoplasty (DSAEK) – Surgical procedure where the Descement's basement membrane and endothelium of the host are removed and replaced with a thin posterior donor cornea lenticule in its place.
Hyperopia – Disorder of vision where the eye focuses images behind the retina instead of on it so that distant objects can be seen better than near objects.
Lamellar keratoplasty (LK) – Replacement of damaged or diseased anterior corneal stroma and Bowman's membrane with donor material.
Laser *in situ* keratomileusis (LASIK) – Refractive surgery that uses a laser to reshape the cornea.
Laser subepithelial keratomileusis (LASEK) – Refractive surgery that uses a laser to reshape the anterior cornea.
Laser thermokeratoplasty (LTK) – Refractive surgery using a mid-infrared laser shrinks the collagen of the corneal periphery.
Penetrating keratoplasty (PK) – Corneal transplant using the entire cornea from a donor.
Photorefractive keratectomy (PRK) – Refractive surgery where the corneal epithelium is removed and the stroma reshaped.
Phototherapeutic keratectomy (PTK) – Procedure where the corneal epithelium is removed and an excimer laser is used to smooth the surface of the cornea.
Radial keratotomy (RK) – Refractive surgery in which radial incisions are made in the cornea from the pupil to cornea.
Scheimpflug imaging – It measures central corneal thickness and anterior chamber depth.

Anatomy of the Layers

The cornea, often referred to as the window of the eye, is covered by the precorneal tear film, and provides a smooth, transparent medium for light rays to pass through. The average cornea measures approximately 12 mm horizontally and 11 mm vertically and seamlessly joins with the opacified sclera at its periphery. The normal cornea has five layers (epithelium, Bowman's membrane, stroma, Descemet's membrane, and endothelium), and has an approximate average central thickness of 540 μm.

Epithelium

The corneal epithelium is composed of approximately 5–6 rows of stratified squamous epithelial cells. It is these cells in this configuration, along with the overlying tear film that help create the smooth, clear surface. The tight junctions between epithelial cells help to prevent the penetration of microbes and fluid into the corneal stroma.

Epithelial cells are continuously being created by the basal limbal stem cells. New cells slowly migrate to the corneal surface where devitalized cells are lost and washed away in the tear film. The entire process takes approximately 2 weeks.

Epithelial Basement Membrane

Posterior to the epithelium of the cornea is the proteinacous epithelial basement membrane. Although only an ≈50-nm thick membrane, the importance of this layer to maintaining a compact, clear, thin anterior corneal surface is obvious when dysfunction occurs, such as in map-dot-fingerprint dystrophy (corneal epithelial basement membrane dystrophy). The thickened basement membrane present in this condition can be visualized on slit-lamp examination and it is the dysfunction of this layer that often leads to recurrent corneal erosions.

Bowman's Membrane

Beneath the epithelial basement membrane lies the acellular Bowman's membrane. This membrane marks the transition from the epithelium to the cornea stroma.

Stroma

A majority of the cornea (approximately 90% of the full corneal thickness) is the stroma. The stroma is composed of a mixture of lamellae of collagen fibrils, proteoglycans, and keratocytes. The collagen and proteoglycans are produced by the keratocytes, which are dispersed throughout the stoma. The arrangement of collagen fibrils in the stroma plays an important role in maintaining corneal transparency.

Descemet's Membrane

The endothelial basement membrane is termed Descement's membrane. This basement membrane is continually laid down throughout life by the corneal endothelium and is approximately 4-µm thick at birth and approximately 12-µm thick in adulthood. Descemet's membrane is firmly attached to the endothelium by hemidesmosomes (Figure 1).

Endothelium

The corneal endothelium is only a single cell-layer thick. These hexagonal cells are of vital importance to maintaining the clarity of the cornea. The endothelial cells lie adjacent to the anterior chamber and work to help maintain the relative dehydrated state of the cornea. The electrolyte pump of the endothelial cells creates an osmotic gradient that draws fluid from the stromal tissue.

Unlike the corneal epithelium, the endothelium is not replaced by limbal stem cells when damaged. The average person is born with approximately 3500 cells mm^{-2}, which declines to approximately 2500 cells mm^{-2} in the eighth decade of life. When endothelial cells are lost or lose functionality, adjacent endothelial cells must enlarge or change shape to attempt to maintain deturgescence. Once a significant portion of endothelial cells are damaged or not functioning properly, corneal edema ensues. The loss of endothelial function can be evaluated by slit-lamp exam, corneal thickness measurements, or through visualization with confocal microscopy, where the number, size, and shape of endothelial cells can be evaluated (Figure 2).

Function

The cornea performs vital functions as a protective barrier and as an optically clear media.

Protective Barrier

The corneal tear film is of vital importance to protecting the eye from invading pathogens. However, in addition to the tear film, it is the tight junctions between the posterior epithelial cells that act as the final barrier in preventing the entrance of microbes into the corneal stroma. This barrier also acts to prevent the inflow of excessive fluid to the stoma from the outside environment.

Transparency

There are three main attributes of the cornea that allow the tissue to maintain its transparency.

First, the water content of the cornea tissue must be maintained at approximately 78%. This water content is dependent on both the epithelial and endothelial cells. The epithelium functions as the physical anterior barrier to the influx of excessive fluid into the corneal stroma. The endothelium is not only a posterior physical barrier to the influx of fluid into the corneal stroma but also uses its sodium–potassium pump to create an osmotic gradient that draws water out of the corneal stroma.

Second, it is the compact arrangement and concentration of collagen, keratocytes, and extracellular matrix within the stroma that limits the scattering of light passing through the tissue.

Third, the lack of blood vessels in the cornea allows the light rays that pass through the clear tissue to not be

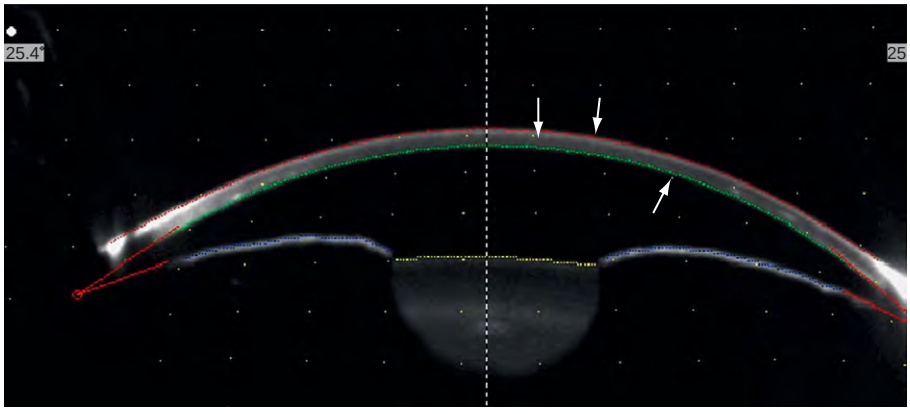

Figure 1 Layers of the cornea as visualized by Scheimpflug imaging. Yellow arrow indicates epithelium, pink arrow indicates stroma, and white arrow indicates endothelium.

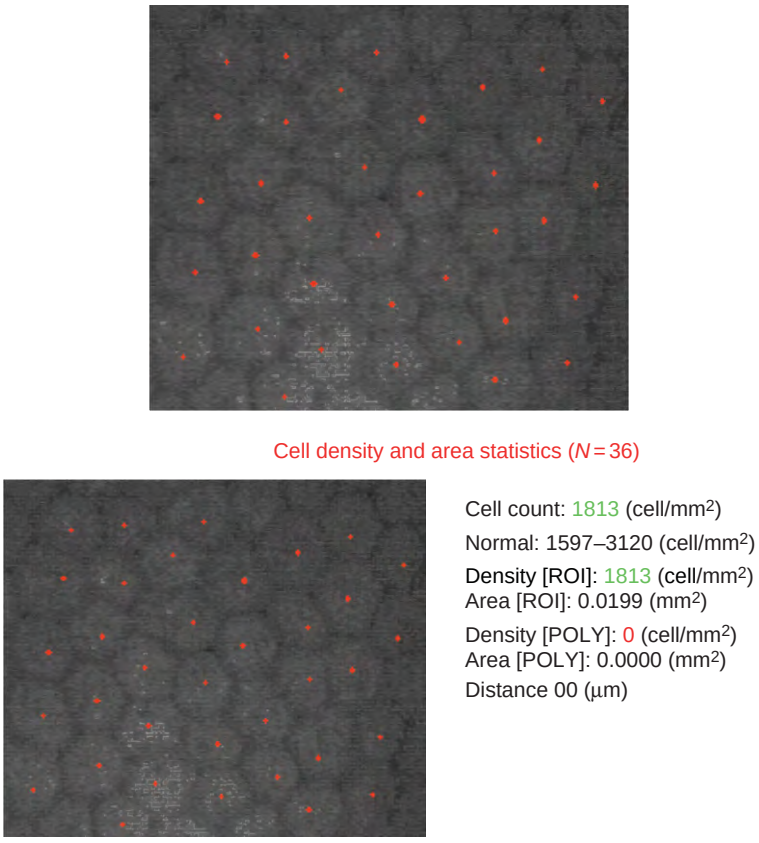

Figure 2 Endothelial cells and cell count as measured by confocal microscopy.

obscured, refracted, or diffracted in any way by blood vessels. The lack of blood vessels also limits the effect that egress or ingress of fluid into or out of the blood vessels could have on corneal deturgescence (Figure 3).

Disease Processes

The disease processes affecting the cornea are extensive. The following review is not meant as an exhaustive list, but rather as an introduction to many of the more commonly observed or discussed pathologies in clinical practice. The use of slit-lamp biomicroscopy to clearly identify which corneal layers are affected by the disease process is of vital importance to the corneal surgeon when choosing among the available medical and surgical treatment options.

Epithelial Disease

Epithelial staining patterns

The use of vital dyes is required to discern the disease process affecting the corneal epithelium. These dyes include fluorescein, rose bengal, and lissamine green. Fluorescein will stain areas with an epithelial defect, while rose bengal and lissamine green will stain areas of devitalized epithelium.

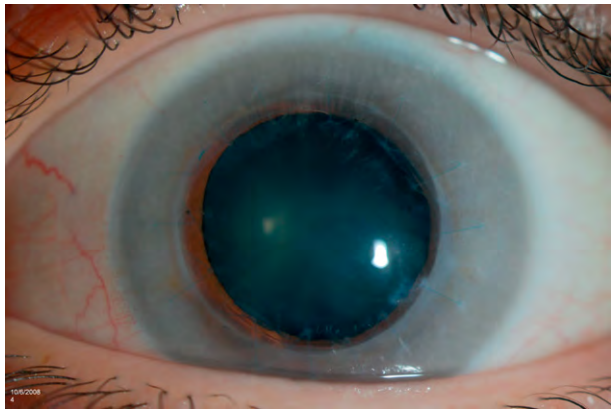

Figure 3 Loss of corneal transparency from a mucopolysaccharidosis. The peripheral cornea remains opacified, while the central cornea is transparent following a penetrating keratoplasty.

By analyzing the staining pattern on the corneal surface, the possible etiology of the disease process (Figure 4) may become apparent (Table 1).

Epithelial iron deposition

Often, the deposition of iron can be visualized on slit-lamp examination of the corneal epithelium. The deposition of

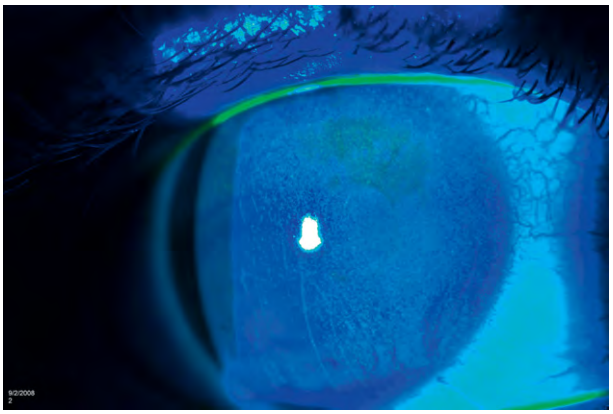

Figure 4 Diffuse damage to the corneal epithelium following the accumulation of environmental debris beneath the upper eyelid. Fluorescein was applied topically to show the epithelial defect (arrow).

Table 1 Examples of staining patterns associated with corneal pathology

Diagnosis	*Staining pattern*
Herpes Simplex Virus keratitis	Dendritic
Medication toxicity	Punctate inferior/inferonasal
Exposure keratitis	Punctate inferior
Superior limbic keratoconjunctivitis	Punctate superior
Superior palpebral conjunctiva foreign body	Vertical linear
Dry eye syndrome	Diffuse punctate, with filaments when severe

iron is believed to be related to the uneven distribution of the tear film over the corneal surface in these areas (Table 2).

Band keratopathy

Deposition of calcium in the epithelium and calcification of Bowman's membrane is termed band keratopathy. Of unknown etiology, this process tends to occur in eyes with significant chronic disease. It has also been seen in patients with elevated serum calcium levels, such as occurs with hyperparathyroidism.

Chemical/thermal burns

Significant chemical or thermal burns of the corneal epithelium can result in not only diffuse epithelial damage, but also damage to limbal stem cells, perhaps limiting the capacity of the epithelium to heal. These cases may require further surgical intervention, such as limbal stem cell transplant.

Medication toxicity

Topical and systemic medications and preservatives used in topical medications are an important cause of induced epithelial changes.

Table 2 Iron deposition in the corneal epithelium

Iron line name	*Iron line location*
Hudson-Stahli line	Horizontal line in lower third of cornea
Stocker's line	At edge of pterygium
Ferry's line	At edge of glaucoma filtering bleb
Fleischer's ring	Around keratoconus cone

The commonly used eyedrop preservative benzalkonium (BAK), non-steroidal anti-inflammatory eyedrops, trifluridine, proparacaine, and tetracaine are a few examples of medications that can result in nonhealing epithelial defects. Usually, if identified early enough and if without infection, the induced punctate epithelial defects will rapidly heal. However, if left unchecked and continued use of such medications occurs, corneal melt and even perforation can occur.

Deposition of material in the epithelium can occur with certain eyedrops and systemic medication. For example, the use of amiodarone can result in a whorl-like deposition of material. This is not an indication for stopping the medication, as it generally does not affect vision in any manner. Ciprofloxacin, when given topically, can result in a deposition of white crystals in epithelial defects. This can have visual symptoms, and, therefore, the medication should be stopped and replaced with an alternative antibiotic.

Thygeson's punctate keratitis

The presence of round central punctate white opacities without corneal edema is the hallmark presentation of Thygeson's punctate keratitis. The etiology of this disease is unknown. Patients generally present complaining of a significant foreign-body sensation and may have decreased vision if subepithelial haze is present. While usually controlled by steroid or cyclosporin topical treatment, this entity commonly recurs.

Subepithelial Disease

Epithelial basement membrane dystrophy

Also known as Cogan's dystrophy and map-dot-fingerprint dystrophy, this disease is characterized by areas of thickened epithelial basement membrane appearing as grey epithelial patches or lines along with microcystic epithelial changes appearing as epithelial dots. Although usually asymptomatic, the disease can result in recurrent corneal erosion which is frequently difficult to treat and requires medical or possibly even surgical intervention.

Subepithelial infiltrates

Following infection with adenovirus resulting in epidemic keratoconjunctivitis, patients may experience persistent haze in their vision. This may be related to persistent subepithelial infiltrates in the visual axis. These infiltrates

may improve with time. Although treatment with topical steroid may clear the infiltrates rapidly, they routinely reappear once steroid treatment is discontinued. A very slow taper is advocated in these situations. Overall, avoidance of topical steroids as primary treatment is recommended due to this issue of steroid dependence.

Stromal Disease

Infection

A variety of infections can result in significant damage to the corneal tissue. The pathogens include bacterial, viral, fungal, and parasitic microbes.

Differentiating between bacterial corneal ulcers on examination can be quite difficult. A broad-spectrum antibiotic is generally initially prescribed until further information is obtained from corneal cultures. The more common bacterial pathogens include staphylococcus, streptococcus, and pseudomonas, but cultures must be used to rule out the more rare bacterial organisms such as *Bacillus*, *Corynebacterium*, *Actinomyces*, and *Neisseria*. While most bacteria require an epithelial defect of some degree to allow bacteria to enter the corneal tissue, it is important to note *Neisseria* can penetrate through intact epithelium (**Figure 5**).

Herpes simplex virus is of significant importance to consider when evaluating a patient with infectious keratitis. While the characteristic dendritic appearance of the herpes virus moving along corneal nerves makes it fairly obvious to diagnose in these situations, the sometimes atypical appearing stromal infiltrates may require a culture to identify the causative organism.

Fungal corneal ulcers, though more rare than bacterial ulcers, recently had a resurgence possibly related to contaminated contact lens solution. The corneal infiltrates tend to have a feathery appearance along their edges and do not respond to antibiotics. Sending fungal cultures at the same time as bacterial cultures is key to avoid late diagnosis of these infections.

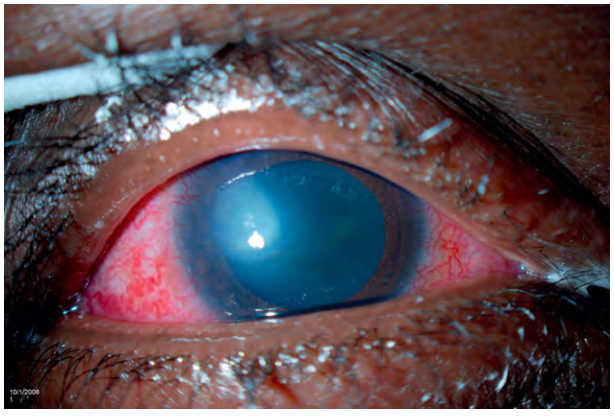

Figure 5 Infectious keratitis with diffuse conjunctival injection (dilated blood vessels), corneal edema, and a dense corneal infiltrate (arrow).

Even more rare are parasitic corneal ulcers, such as acanthameoba. Acanthameoba ulcers are most often seen in patients with a history of contact lens wear who frequently have a recent history of swimming. Generally these ulcers are more painful than they appear they should be. Initial appearance on slit-lamp examination can mimic Herpes keratitis, and these ulcers are often initially misdiagnosed as such. Later in the course of the disease a ring infiltrate can present, sometimes mimicking the corneal pattern seen in topical anesthetic abuse. The acanthameoba parasites can be difficult to culture and may require corneal biopsy for diagnosis. Sometimes, it is also possible to visualize the parasitic cysts on confocal microscopy.

Dystrophies

Stromal corneal dystrophies are rare, yet important, inherited corneal diseases to identify. There are three main types of stromal corneal dystrophies, including granular, macular, and lattice dystrophy. **Table 3** reviews the inheritance patterns, material deposited, and appropriate stain to visualize the material on pathologic specimen.

Degenerations

Corneal degenerations encompass a large category of corneal disease, which includes such more common processes as keratoconus, pellucid marginal degeneration, and arcus senilis.

Keratoconus has an unclear etiology, but pathological specimens reveal degeneration of the corneal stroma, Descemet's membrane breaks, and damage to Bowman's membrane. Clinically, progressive steepening and thinning of the central cornea can be seen, which eventually can create a cornea too irregular for even hard contact lens wear. Other corneal changes that may be visualized include an iron line around the area of corneal steepening (Fleischer's ring), stress lines on the posterior cornea (Vogt's striae), a scissoring reflex on retinoscopy, or areas of corneal opacification and edema from ruptures of Descemet's membrane (acute hydrops). These changes may be seen on slit-lamp examination; however, it may be necessary to employ computerized tomography or topography to diagnose early keratoconic (forme fruste) changes. Patients with advanced degeneration can consider either intrastromal ring segments or corneal transplantation (**Figure 6**).

Table 3 Stromal dystrophies

	Inheritance	*Material deposited*	*Stain*
Granular	Autosomal dominant	Hyaline	Masson trichrome
Macular	Autosomal recessive	Mucopolysaccharide	Alcian blue
Lattice	Autosomal dominant	Amyloid	Congo red

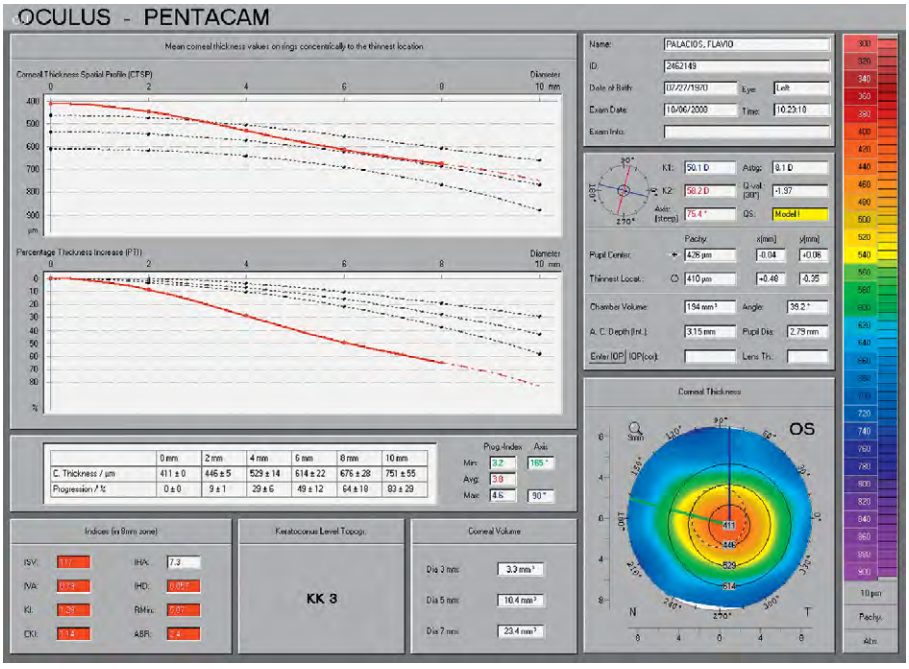

Figure 6 Corneal tomography revealing a central corneal elevation with corneal thinning in a pattern strongly suggestive of keratoconus. Color scale on right indicates thickness where purple is thickest and red is thinnest.

Pellucid marginal degeneration has a similar disease process as keratoconus; however, while the cornea in keratoconus is thinnest at the steepest location, the cornea in pellucid marginal degeneration is thinnest just below the steepest location, which is often near the inferior limbus. Similar pathologic changes can be seen and similar surgical interventions can be considered.

Arcus senilis is a peripheral corneal degeneration that is quite common in those 50 years of age or older. When examined pathologically, the white ring seen peripherally consists of lipid deposits. This can be a sign of systemic hyperlipidemia in those younger than 50 years of age or can be a sign of carotid stenosis in those with asymmetric arcus senilis.

Descemet's copper deposition

The deposition of copper in Decesmet's membrane can sometimes be seen in Wilson's disease. This often difficult to diagnose disease of copper transport, which leads to copper deposition in the liver and brain, can sometimes be diagnosed quickly at the slit-lamp examination with visualization of the green–brown deposition of copper in the posterior cornea (Kayser–Fleischer ring).

Endothelial Disease

Fuchs' dystrophy

Fuchs' dystrophy is characterized by dysfunction of corneal endothelial cells. Wart-like excrescences are deposited by the endothelium into Descemet's membrane, which can be visualized on slit-lamp examination and on confocal microscopy. Confocal microscopy can also reveal the change in size (polymegathism) and change in shape (pleomorphism) of the dysfunctional endothelial cells. As the endothelium becomes further damaged, corneal edema worsens and may require medical treatment with hypertonic eyedrops and, eventually, even surgical intervention with cornea transplantation to improve visual acuity.

Pseudophakic bullous keratopathy

During phacoemulsification of the lens, significant stress can be placed on the corneal endothelium, either mechanically with intraocular instruments, or through transfer of energy in the form of ultrasound. These processes can result in loss of endothelial cells, with resultant increased pleomorphism and polymegathism in an attempt to maintain corneal deturgescence. When too much endothelial damage has occurred, persistent corneal edema may present postoperatively and may worsen with time. These patients may require medical intervention with hypertonic eyedrops or, eventually, may require cornea transplantation.

Surgery

Once a thorough corneal examination is completed, a proposed medical or surgical intervention can be planned. To understand which surgical options are available, slit-lamp biomicroscopy must be used to accurately identify the layers of the cornea affected by the disease process.

The answer to this question will guide the physician to determine which of a vast array of surgical procedures could be undertaken.

The grand scope of the surgical treatment of corneal disease cannot be covered, in full, in this article. A brief overview of some of the more frequently used interventions will be reviewed.

Surgical Intervention of Epithelial Disease

Amniotic membrane graft

Amniotic membranes have many applications in ocular surgery. For nonhealing or slowly healing epithelial defects, this tissue can be sutured in place over the anterior surface of the cornea, where it helps protect against further corneal degradation and promotes epithelial healing. The amniotic membrane provides a matrix on which new cells can grow, helps prevent excessive inflammation, and aids in preventing corneal scarring and neovascularization.

Conjunctival flap

For poorly healing or nonhealing damage to the corneal surface, a conjunctival flap is an option. A partial or complete (Gunderson) flap can be dissected to cover the affected area, depending on the peripheral or central location of the corneal damage. Any patients with an active corneal process, such as infectious keratitis, are not good candidates for a conjunctival flap as it will not only interfere with appropriate treatment measures, but will also obscure the surgeon's view when attempting to examine the affected tissue.

Corneal glue

Cyanoacrylate tissue adhesive can be used to adhere small corneal perforations or severely thinned corneal tissue. Areas of perforated cornea from infection, trauma, postoperative wound leaks, or other etiologies can be treated with cynanoacrylate adhesive, which can at least temporarily renew the integrity of the globe.

Disodium ethylenediaminetetraacetic acid chelation

Band keratopathy can present as a dense deposition of calcium hydroxyapetite in the visual axis. Following removal of the corneal epithelium, the anterior corneal calcium deposition can be removed by soaking the affected tissue in disodium EDTA, and scraping away the residual calcium with an ophthalmic blade. Patching or bandage contact lens must be placed until the epithelium heals adequately (Figure 7).

Limbal stem cell transplant

Poorly healing epithelial defects may be a result of damaged epithelial limbal stem cells. When enough damage has occurred to these stem cells, vascularization of the corneal surface ensues. This can result from a variety of conditions such as infections, chemical burns, or post operatively. If the disease is unilateral, a stem cell autograft can be attempted from the fellow eye. If both eyes are affected, an allograft from donor tissue must be used, leading to a poorer prognosis and the necessity to systemically immunosuppress the patient postoperatively.

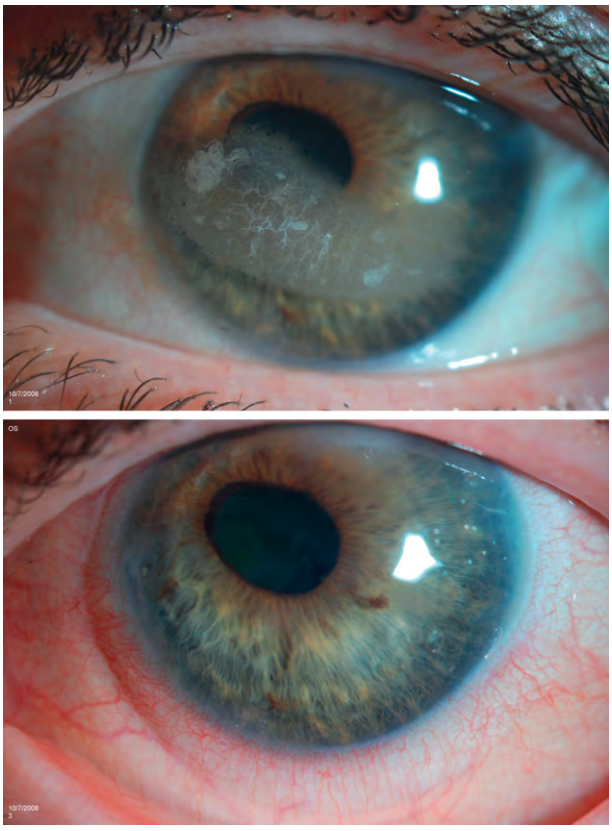

Figure 7 Pre- (top) and postoperative (bottom) band keratopathy following disodium-EDTA chelation. Notice the white calcium hydroxypatite in the top photograph.

Phototherapeutic keratectomy

Phototherapeutic keratectomy (excimer laser) can be used to remove diseased tissue in the anterior cornea, such as deposits associated with anterior corneal dystrophies or anterior corneal scars. Although typically no significant refractive change is induced, with the removal of more tissue, the risk of corneal flattening inducing hyperopia increases. Postoperative scarring can occur, and many advocate the use of topical mitomycin C intraoperatively to decrease the risk of scarring.

Pterygium excision

Pterygium refers to a benign growth of the conjunctiva. A pterygium commonly grows from the nasal side of the sclera and is associated with ultraviolet-light exposure.

The most successful technique for pterygium excision has been under much debate for many years. The options of leaving behind a bare sclera, using a conjunctival autograft, rotational graft, or amniotic membrane graft are all under current use. The debate centers around the question of which technique results in the lowest frequency of recurrence. The gold standard seems to be pterygium excision with conjunctival autograft, despite several ongoing studies reviewing the newer option of using the amniotic membrane graft.

Stromal puncture

The epithelial disease of anterior basement membrane dystrophy often leads to chronic recurrent corneal erosions. In an effort to create better adherence of the epithelium to its basement membrane and stroma, stromal puncture is attempted, usually with a 25-gauge needle inserted into the anterior stroma. Most commonly, this procedure is undertaken in affected areas outside of the visual axis and only in those patients that have failed medical therapy with lubrication and hypertonic solutions such as sodium chloride, which are also used to try to create a more firm adherence between the anterior cornea layers.

Tarsorrhaphy

Tarsorrhaphy is a surgical procedure in which the eyelids are sutured together to protect the cornea. A temporary or permanent tarsorrhaphy can be one of the most important options in the corneal surgeons armamentarium. Particularly helpful in creating a more hospitable environment for epithelial healing, this process can be used to promote epithelial healing in instances such as post operatively following penetrating keratoplasty (PK), neurotrophic epithelial defects, Bells palsy, or chemical burns. A newer option – using botulinum toxin A to create a temporary tarsorrhaphy – is currently being studied as an alternative, which perhaps affords similar protection to a sutured tarsorrhapy while allowing for easier slit-lamp examination.

Surgical Intervention of Stromal Disease

Anterior lamellar keratoplasty

Anterior corneal scars or deposits can be treated with an anterior lamellar keratoplasty. Rather than replacing a full-thickness corneal button as is accomplished in a PK, a partial-thickness trephination or dissection is accomplished to remove only the anterior diseased tissue without performing any manipulation of the posterior endothelial layer. This is an especially important option in young patients with excellent endothelial cell counts and morphology, but whose vision is obstructed by stromal opacities.

Penetrating keratoplasty

Unlike lamellar keratoplasty, a PK involves the full-thickness removal of diseased corneal tissue from the host and replacement of all layers of corneal tissue with a donor cadaveric corneal button. The procedural technique has evolved over the past 100 years, resulting in the high success rate that is now enjoyed by the thousands of patients that undergo full-thickness corneal transplantations each year (**Figure 8**). Topical immunosuppression, usually with prednisolone acetate 1%, is generally a long-term necessity to prevent rejection. Irregular astigmatism generally requires suture manipulation or hard contact lens placement post operatively to attain the best-corrected visual acuity.

Corneal biopsy

For those patients with unusual corneal processes without clear diagnosis despite corneal culture or scrapings, corneal biopsy is the next option. Removing a small anterior portion of corneal tissue from the periphery affords a tissue sample for further pathological examination.

Corneal laceration repair

With the advent of the 10-0 nylon suture, the ability of the corneal surgeon to repair the integrity of the globe following penetrating corneal injury improved significantly. Ensuring the absence of vitreous or iris incarceration in the wound, that the wound edges are well apposed, and that the wound is watertight are of vital importance. Fulfilling these objectives as soon as possible after the penetrating injury occurs will hopefully help to promote healing and lower the risk of endophthalmitis (vision-threatening inflammation of the internal ocular tissues).

Refractive surgery

Since its introduction, the field of corneal refractive surgery has grown exponentially. Earlier procedures, such as

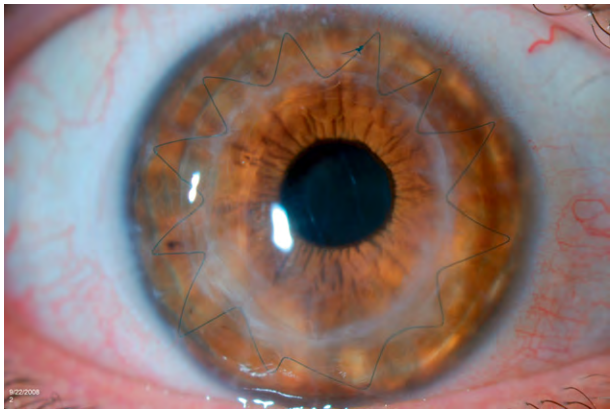

Figure 8 One-year status post penetrating keratoplasty. A single 10-0 prolene running suture remains.

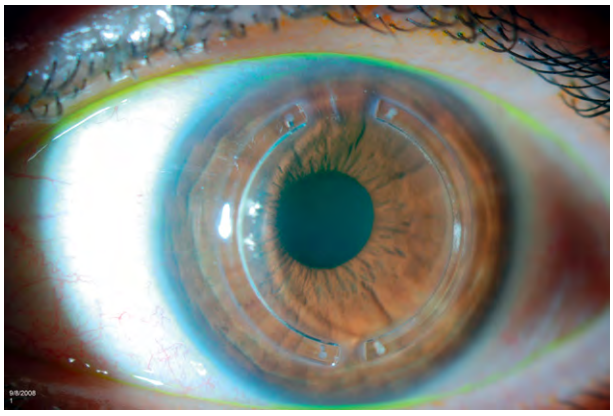

Figure 9 Status post intrastromal ring-segment implantation.

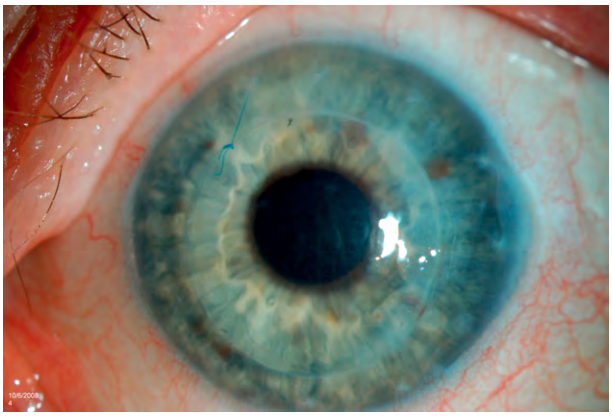

Figure 10 Status post Descemet's Stripping Automated Endothelial Keratoplasty. Notice the clear cornea.

radial keratotomy (RK) and laser thermokeratoplasty (LTK) – which have since fallen out of favor – provided important knowledge and insight into the manipulation of corneal tissue. The current options include procedures such as laser *in situ* keratomileusis (LASIK), photorefractive keratectomy (PRK), laser subepithelial keratomileusis (LASEK), conductive keratoplasty (CK), and intrastromal ring segments. The goal of these procedures is usually to remove the need for corrective lenses in all, or most, distance and/or near-daily situations. A thorough review of the importance of appropriate patient selection, preoperative evaluations, individual surgical options, the risks and benefits of each procedure, and the appropriate postoperative care is beyond the scope of this article (**Figure 9**).

Prosthetic keratoplasty

For those patients with extensive corneal neovascularization, severe damage to limbal stem cells, or who have failed prior PKs, the prosthetic keratoplasty is available (i.e., Boston type 1 keratoprosthesis). Although the technology has evolved substantially over the last 10 years, the keratoprosthesis generally still requires glaucoma surgical management concomitantly and is not appropriate for those patients requiring straightforward PK without a history of such issues as significant corneal vascularization or repeat PK failures.

Surgical Intervention of Endothelial Disease

The surgical manipulation and replacement of diseased corneal endothelium has taken substantial strides forward in recent years. After going through several generations of endothelial surgery with disappointing results, the ophthalmology community has arrived at the more promising current technique of Descement's Stripping Automated Endothelial Keratoplasty (DASEK).

Descements Stripping Automated Endothelial Keratoplasty

The most common diseases resulting in endothelial dysfunction are Fuchs' dystrophy and pseudophakic bullous keratopathy. Although it has been well understood for quite some time that corneal edema in these situations was a result of dysfunctional corneal endothelium, until recently, a full-thickness (penetrating) keratoplasty was the sole viable option. The well-documented time-consuming process of helping these patients obtain their best corrected visual acuity following PK could not be avoided. Now, however, with the advent of the DSAEK procedure, the corneal surgeon can carefully dissect off the Descement's basement membrane and endothelium of the host, and replace a thin posterior donor cornea lenticule in its place (**Figure 10**). Early studies suggest that, when successful, this process results in faster healing, less induced postoperative astigmatism, and patients reach their best-corrected visual acuity faster when compared to PK.

See also: Adaptive Immune System and the Eye: Mucosal Immunity; Artificial Cornea; Blinking Mechanisms; Contact Lenses; Corneal Dystrophies; Corneal Endothelium: Overview; Corneal Epithelium: Cell Biology and Basic Science; Corneal Epithelium: Response to Infection; Corneal Epithelium: Transport and Permeability; Corneal Imaging: Clinical; Corneal Nerves: Anatomy; Corneal Nerves: Function; Corneal Scars; The Corneal Stroma; Drug Delivery to Cornea and Conjunctiva: Esterase- and Protease-Directed Prodrug Design; Gene Therapy for the Cornea, Conjunctiva, and Lacrimal Gland; Imaging of the Cornea; Knock-Out Mice Models: Cornea, Conjunctiva, Eyelids and Lacrimal Gland; Lids: Anatomy, Pathophysiology, Mucocutaneous Junction; Refractive Surgery and Inlays; Regulation of Corneal Endothelial Cell Proliferation; Regulation of Corneal Endothelial Function; Stem Cells of the Ocular Surface;

Tear Film; Tear Film Overview; The Surgical Treatment for Corneal Epithelial Stem Cell Deficiency, Corneal Epithelial Defect, and Peripheral Corneal Ulcer.

Further Reading

Ang, L., Chua, K., and Tan, D. (2007). Current concepts and techniques in pterygium treatment. *Current Opinion in Ophthalmology* 18: 308–313.

Bahar, I., Kaiserman, I., McAllum, P., et al. (2008). Comparison of posterior lamellar keratoplasty techniques to penetrating keratoplasty. *Ophthalmology* 115: 1525–1533.

Beebe, D. (2008). Maintaining transparency: A review of the developmental physiology and pathophysiology of two avascular tissues. *Seminars in Cell and Developmental Biology* 19: 125–133.

Cauchi, P., Ang, G., Azuara-Blanco, A., et al. (2008). A systematic literature review of surgical interventions for limbal stem cell deficiency in humans. *American Journal of Ophthalmology* 146: 251–259.

Dua, H. and Azuara-Blanco, A. (2000). Limbal stem cells of the corneal epithelium. *Survey of Ophthalmology* 44: 415–425.

Gomes, J., Romano, A., Santos, M., et al. (2005). Amniotic membrane use in ophthalmology. *Current Opinion in Ophthalmology* 16: 233–240.

Hersh, P., Brint, S., Maloney, R., et al. (1998). Photorefractive keratectomy versus laser *in situ* keratomileusis for moderate to high myopia. *Ophthalmology* 105: 1512–1523.

Ma, J., Graney, J., and Dohlman, C. (2005). Repeat penetrating keratoplasty versus the Boston keratoprosthesis in graft failure. *International Ophthalmology Clinics* 45: 49–59.

Meek, K., Dennis, S., and Khan, S. (2003). Changes in the refractive index of the stroma and its extrafibrillar matrix when the cornea swells. *Biophysical Journal* 85: 2205–2212.

Meek, K., Leonard, D. W., Connon, C. J., et al. (2003). Transparency, swelling and scarring in the corneal stroma. *Eye* 17: 927–936.

McCarey, B., Edelhauser, H., and Lynn, M. (2008). Review of corneal endothelial specular microscopy for FDA clinical trials of refractive procedures, surgical devices and new intraocular drugs and solutions. *Cornea* 27: 1–16.

Suh, L., Yoo, S., Deobhakta, B. S., et al. (2008). Complications of descemet's stripping with automated endothelial keratoplasty. *Ophthalmology* 115: 1517–1524.

Sutphin, J. (ed.) (2007). *Basic and Clinical Science Course. External Disease and Cornea.* San Francisco, CA: American Academy of Ophthalmology.

Trattler, W. and Barnes, S. (2008). Current trends in advanced surface ablation. *Current Opinion in Ophthalmology* 19: 330–334.

Yanoff, M. and Duker, J. (2004). Ophthalmology. St. Louis, MO: Mosby.

Corneal Angiogenesis

M S Cortina and D T Azar, University of Illinois at Chicago, Chicago, IL, USA

Glossary

Angiogenesis – The formation of new vessels from preexisting vascular structures.
Allograft – The tissue taken from one person for transplantation into another.
Autograft – The tissue transplanted from one part of the body to another part of the same individual.
Chemotaxis – The movement of neutrophils toward bacteria or an area of tissue damage.
Conjunctival metaplasia – An abnormal epithelial differentiation represented by a spectrum of skin-like changes of conjunctival epithelium.
Corneal extracellular matrix – The tissue that provides structural support to the cells in the cornea.
Corneal pannus – The fibrovascular connective tissue that proliferates in the anterior layers of the peripheral cornea in inflammatory corneal disease.
Growth factor – A naturally occurring protein capable of stimulating cellular growth, proliferation, and differentiation.
Hypercapnia – High levels of carbon dioxide.
Hypoxia – Oxygen deficiency.
Limbal stem cell deficiency – The loss of stem cells in the limbus (ring around the base of the cornea which supports health of the corneal epithelium).
Matrix metalloproteinases (MMPs) – The zinc-dependent endopeptidases capable of degrading all kinds of extracellular matrix proteins; they can also process bioactive molecules.
Penetrating keratoplasty (PK) – The procedure in which a full-thickness button of cornea is removed from the recipient and replaced with a similar-sized or larger button of tissue from a donor.
Vasculogenesis – The formation of new blood vessels from bone-marrow-derived angioblasts that occurs mainly during embryogenesis.

Introduction

Under homeostatic conditions, the cornea is avascular, which is critical for corneal light transmission and proper optical performance. Corneal avascularity is maintained by tightly controlled biological anti-angiogenic events that counterbalance the effects of pro-angiogenic factors in the cornea. Under pathological conditions, the balance may be shifted toward angiogenesis, leading to the formation of new blood vessels and lymphatic channels. New blood vessel formation or corneal neovascularization (NV) is a sight-threatening condition usually associated with inflammatory or infectious disorders. It is a major contributor to the loss of corneal transparency. The presence of corneal NV, in turn, elevates the risk of graft rejection and decreases the success of penetrating keratoplasty (PK).

Angiogenesis

Angiogenesis is the main process of blood vessel formation in nonembryonic tissue. It involves the formation of new vessels from preexisting vascular structures and is the primary mechanism underlying corneal NV. New blood vessels also form during vasculogenesis, which is the formation of new blood vessels from bone-marrow-derived angioblasts and occurs mainly during embryogenesis.

Angiogenesis is a complex process that starts with vasodilation of existing vessels and an increase in vascular permeability. This leads to extravasation of plasma proteins (such as fibrin), growth factors, and inflammatory mediators. The accumulation of plasma proteins in the surrounding tissue provides a supporting structure for subsequent endothelial cell (EC) migration. The combined presence of growth factors and inflammatory mediators stimulates the degradation of the extracellular matrix (ECM), making room for EC migration as well as releasing angiogenic factors anchored in the matrix. The newly released angiogenic factors then continue to activate ECs, which migrate from preexisting vessels and form sprouting tubes.

The avascularity of the cornea dictates that nutrients for this tissue be obtained from adjacent tissues. The three major sources of nutrients are tear film, aqueous humor, and the pericorneal capillary plexus at the limbus. This plexus nourishes the peripheral cornea and is derived from ciliary arteries, which are branches of the ophthalmic artery. These vessels do not normally enter the cornea. However, new blood vessels may sprout from capillaries and venules of the pericorneal plexus under pathological conditions, leading to corneal NV.

Etiology and Epidemiology of Corneal NV

Although the exact incidence of corneal NV is not known, it was estimated that this condition affects 1.4 million

patients in the United States annually and that 20% of corneal buttons obtained during PK show evidence of NV. The causes of corneal NV include immune, inflammatory, infectious, degenerative, and traumatic disorders. Corneal infections are the most common worldwide causes of corneal NV leading to vision loss. A classic example is trachoma, an infectious disease characterized by the formation of a superior pannus, which can extend to the central cornea and is often associated with corneal scarring, opacification, and loss of visual acuity. The incidence of trachoma in the US is low; however, this condition remains a major cause of blindness in other parts of the world (**Figure 1**).

Corneal NV is also commonly associated with other severe bacterial and viral infections. The herpes virus family (primarily herpes simplex and herpes zoster viruses) is the primary cause of keratitis-induced NV in transplant buttons. In herpes-simplex-induced stromal keratitis, NV is essential for the pathogenesis of keratitis, and inhibition of angiogenesis can reduce the formation of corneal lesions.

Although infections account for many US cases of corneal NV, the most common cause of corneal NV in the US is the use of contact lenses. In this case, hypoxia and hypercapnia are thought to be associated with the induction of NV (**Table 1**).

The incidence of corneal NV after PK can be as high as 40% at 6–9 months after surgery. The prognosis of transplanting grafts into heavily vascularized corneas is poor. Graft failure has been reported to contribute to >30% of the histopathological diagnoses obtained from vascularized corneal buttons. Risk factors for corneal NV after PK in patients without active inflammation, previous corneal NV, or persistent epithelial defects include suture knots buried in the host stroma, active blepharitis, and a large recipient bed.

Figure 1 Salzman's nodular degeneration with associated superficial corneal neovascularization.

Immune disorders also contribute to corneal NV (**Figure 2**). These disorders can result in significant vision loss and include ocular pemphigoid, rosacea, atopic keratoconjunctivitis, and Stevens–Johnson syndrome. The incidence of corneal NV among patients with these disorders can be considerable. Long-term follow-up of patients with atopic keratoconjunctivitis, for example, revealed that the rate of corneal NV was as high as 60% during the disease course.

Limbal stem cell deficiency, which may occur following trauma and chemical burns, is another cause of corneal NV. It may be also associated with aniridia and autoimmune disorders. Limbal stem cell deficiency produces not only corneal NV, but also corneal inflammation and conjunctivalization of the corneal epithelium. The restoration of corneal avascularity after successful limbal stem cell transplantation underscores the importance of the anti-angiogenic and anti-inflammatory activity of normal corneal epithelial cells.

Clinical Manifestations

Corneal NV can be classified as pannus or stromal NV. In the former, fibrovascular tissue is visible between the epithelium and Bowman layer. Inflammatory pannus is associated with prominent leukocyte infiltration and disruption of Bowman's layer. In contrast, degenerative pannus is characterized by fewer inflammatory cells, an intact Bowman's layer, and regression of the vascular component that leaves a layer of fibrous tissue. Stromal NV, located posterior to Bowman's layer, is more commonly seen in the anterior two-third of the stroma. In herpetic and syphilitic interstitial keratitis, deep stromal vessels (and ghost vessels in the late quiescent stages) are seen just anterior to Descemet's membrane (**Figure 3**).

Visual acuity is reduced by corneal NV. Reduced visual acuity may be secondary to multiple factors. For example, opacity caused by circulating blood cells may interfere with visual acuity. Acuity may also be reduced by irregular architecture of vascular walls, a feature that induces higher-order aberrations. Other effects contributing to diminished visual acuity may include alteration in the spacing of stroma collagen fibers, fluid leakage, edema and lipid deposition in the surrounding tissue, and corneal surface irregularities (**Figure 4**).

Mechanisms Underlying the Maintenance of Corneal Avascularity

Several mechanisms have been proposed to contribute to corneal avascularity. These include:

Table 1 Causes of corneal neovascularization

Inflammatory disorders	*Infectious keratitis*	*Degenerative/congenital*	*Traumatic/iatrogenic*
Ocular pemphigoid	Herpes simplex	Pterygium	Contact lens wear
Atopic conjunctivitis	Herpes zoster	Terrien marginal	Alkali burns
Rosacea	Pseudomonas	degeneration	Ulceration
Graft rejection	Chlamydia	Aniridia	Iatrogenic
Lyell's syndrome	Syphilis	Degenerative pannus	Stem cell deficiency
Stevens–Johnson	Candida		
syndrome	Fusarium		
Graft vs. host disease	Aspergillus		
	Onchocerciasis		

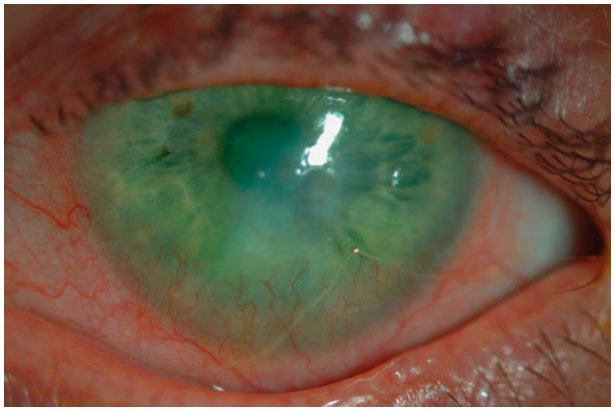

Figure 2 Corneal neovascularization and infectious keratitis in a patient with underlying severe dry eye syndrome secondary to rheumatoid arthritis.

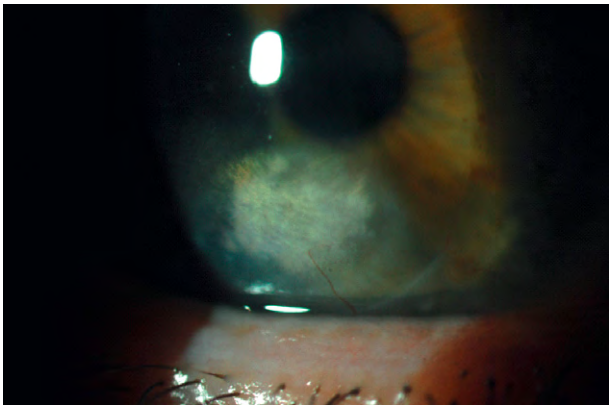

Figure 4 Lipid deposition secondary to corneal neovascularization. Note relative small vessel crossing the host-graft junction responsible for significant lipid deposit.

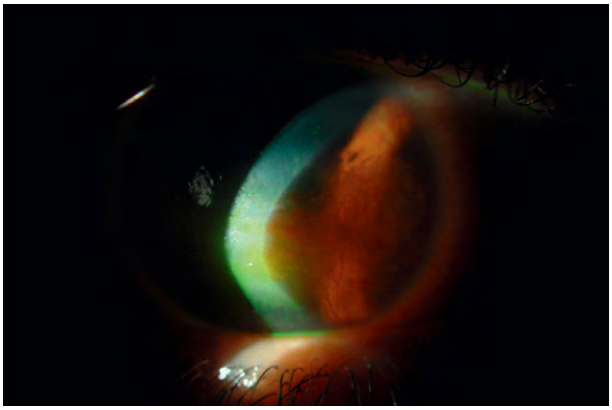

Figure 3 Superficial and deep stromal neovascularization in a patient with neurotrophic cornea.

1. *Corneal dehydration resulting in tightly packed collagen lamellae.* The relationship between corneal NV and corneal edema was first reported in 1949 by Cogan, who postulated that the distention and bursting of the vessels preceding formation of the capillary sprouts were due to a decrease in external pressure that reduced vessel wall support. However, subsequent studies showed that corneal edema alone is not sufficient to trigger corneal NV.
2. *The angiostatic nature of corneal epithelial cells.* Blood vessels are known to be capable of growing into corneas in the absence of epithelium. Early research suggested that corneal epithelial cells are a source of angiogenic factors. More recent studies suggest that the corneal epithelium has an anti-angiogenic effect. The presence of soluble vascular endothelial growth factor (VEGF) receptors 1 and 3, and other naturally occurring anti-angiogenic factors, in the corneal epithelium contributes to its angiostatic nature.
3. *The immune privilege of the cornea.* The mechanisms underlying corneal immune privilege include low expression of major histocompatibility complex (MHC) antigens on corneal cells, expression of Fas ligand by the cornea, a relative paucity of mature antigen-presenting cells, and the presence of immunomodulatory molecules in the anterior chamber. Importantly, this state can be reversed by inflammation, and such reversal may contribute to vascularization. For example, polymorphonuclear leukocytes have the potential to initiate corneal NV through

the release of chemical mediators. Accordingly, there is a clear association between corneal inflammation and NV. Nevertheless, corneal NV may occur in the absence of inflammation.

4. *Low corneal temperature, extensive innervation, and movement of the aqueous humor across the cornea.* The roles of these factors in the maintenance of corneal avascularity are currently unclear.
5. *The barrier function of limbal cells.* The limbus is thought to prevent corneal NV by acting as a barrier to conjunctival growth over the cornea. This barrier function may be attributable to the ability of limbal stem cells to replenish the corneal epithelium, thus preventing invasion of conjunctival epithelium and avoiding NV. This hypothesis has been used to account for corneal NV following experimental limbal damage and stem cell dysfunction. It is also one of the explanations for corneal pannus observed in aniridia. This hypothesized barrier function of limbal cells supports the use of limbal stem cell transplantation as a definitive treatment for ocular-surface disorders. However, a physical barrier may not completely explain corneal avascularity.
6. *Low levels of angiogenic factors and active production of potent anti-angiogenic factors in the cornea during homeostasis.*
7. *Active production of potent anti-angiogenic factors.* Although the five previously mentioned factors likely contribute to maintenance of corneal avascularity, available evidence supports this as the main mechanism responsible for maintaining corneal avascularity.

Table 2 Factors involved in the regulation of angiogenesis

Angiogenic factors	*Anti-angiogenic factors*
Fibroblast growth factor (FGF)	Endostatin
Vascular endothelial growth factor (VEGF)	Angiostatin
Placenta growth factor (PGF)	Prolactin
Transforming growth factor-α (TGF-α)	Matrix metalloproteinases (MMPs)
Transforming growth factor-β (TGF-β)	Tissue inhibitor of MMPs (TIMPs)
Insulin-like growth factor (IGF)	Thrombospondin
Leptin	Arresten
Integrins (αvβ3)	Canstatin
Platelet-derived growth factors (PDGF)	Tumstatin
Matrix metalloproteinases (MMPs)	Pigment-epithelium-derived factor (PEDF)
Angiogenin	Tumor necrosis factor α (TNF-α)
Hepatocyte growth factor-scatter factor (HGF-SF)	Interleukin-4 (IL-4)
Tumor necrosis factor-α (TNF-α)	Interleukin-13 (IL-13)
Connective tissue growth factor (CTGF)	Fibulin
Interleukin-8 (IL-8)	Endoperellin
Monocyte chemoattractant protein-1 (MCP-1)	Antithrombin
Platelet-activating factor (PAF)	Plasminogen activator inhibitor (PAI)
	Vasostatin
	Neostatin-7

Corneal Angiogenic Privilege: The Balance between Angiogenesis and Anti-Angiogenesis

Multiple local and systemic signals are responsible for regulating growth and regression of new blood vessels. These signals include cyclic adenosine monophosphate (cAMP), steroid hormones, protein kinase C (PKC) agonists, polypeptide growth factors, oxygen, free radicals, glucose, cobalt, and iron. In the cornea, the tight equilibrium between these pro- and anti-angiogenic signals may be disrupted under pathological conditions. Ultimately, this may tip the balance toward an upregulation of pro-angiogenic factors or a downregulation of anti-angiogenic factors, in either case leading to corneal NV (**Table 2**).

When the cornea is injured, wound healing often occurs in the absence of NV. This is the case for most adequately treated corneal infections. Healing after corneal surgery is also usually avascular. Corneal wound healing involves four phases. In the first phase, keratocytes near the area of epithelial debridement undergo apoptosis. In the second phase, adjacent keratocytes proliferate to repopulate the wound within 24–48 h after wounding. These keratocytes transform into fibroblasts and migrate into the wound area. This process may take up to a week and is not accompanied by corneal NV. In the third phase, fibroblasts may transform into myofibroblasts. This occurs in laser-inflicted wounds lacking Bowman's layer and in incisional wounds. Myofibroblasts may take up to a month to become apparent. Corneal NV is also absent in this phase of wound healing. The fourth and final phase involves stromal remodeling and is dependent on the original wound. When wound healing is accompanied by ECM turnover, angiogenesis in granulation tissue is usually observed.

Some of the molecules that regulate angiogenesis are discussed below.

Angiogenic Molecules

Vascular endothelial growth factor

VEGF is a dimeric 46-kDa glycoprotein. This growth factor stimulates angiogenesis by increasing EC proliferation, migration, proteolytic activity, and capillary tube formation. It also significantly increases vascular permeability. The VEGF family includes VEGF-A, -B, -C, -D, placenta growth factor (PlGF), and the viral VEGF

homolog VEGF-E. VEGF-B promotes nonangiogenic tumor progression, while VEGF-C and -D participate in angiogenesis and lymphangiogenesis. VEGF-A also participates in angiogenesis and increases vascular permeability.

Five isoforms of VEGF-A (VEGF115, 121, 165, 189, and 206) can be generated by alternative splicing of the same gene. The longer isoforms (VEGF189 and 206) are matrix-bound, whereas the shorter isoforms (VEGF121 and 165) are freely diffusible. These VEGF isoforms produce different actions when secreted. For example, all isoforms increase in vascular permeability, but only VEGF121 and VEGF165 have mitogenic activity. VEGF121 has greater angiogenic activity than VEGF165 or VEGF189. On the other hand, VEGF165 is more potent than VEGF121 in induction of inflammation, intercellular adhesion molecule-1 (ICAM-1) expression in ECs, and chemotaxis of monocytes. This suggests that alternate splicing of VEGF messenger RNA (mRNA) can be regulated to achieve a range of physiologic actions.

The VEGF family members act through binding to high-affinity receptor tyrosine kinases. Two high-affinity receptor tyrosine kinases have been identified for VEGF-A: VEGFR-1 (fms-like tyrosine kinase-1 or Flt-1) and VEGFR-2 (kinase insert domain-containing receptor or KDR). VEGFR-3 (fms-like tyrosine kinase-4 or Flt-4) serves as a high-affinity receptor for VEGF-C and -D. Both VEGFR-1 and -2 are expressed primarily in vascular ECs, while VEGFR-3 is predominantly expressed in lymphatic ECs. VEGF-B binds to VEGFR-1 and has mild mitogenic activity. In contrast, binding of VEGF-D and -C to VEGFR-3 regulates the growth and differentiation of blood vessels and lymphatic endothelium.

VEGF is produced by macrophages, T cells, astrocytes, pericytes, fibroblasts, retinal pigment epithelial cells, and smooth muscle cells. In addition, VEGF is expressed in all three cellular layers of the cornea. It is highly expressed in vascular ECs of limbal vessels and in new stromal vessels. Under inflammatory conditions, VEGF expression is increased in epithelial and vascular ECs, particularly near macrophage infiltrates and fibroblasts in corneal scars. Following corneal cautery, VEGF165 and 189 mRNA is increased at 48 h and returns to baseline by day 7. Immunohistochemistry has revealed that VEGF is initially expressed in neutrophils and later expressed in macrophages, demonstrating that VEGF production by leukocytes is associated with corneal NV. In addition, VEGF concentration is significantly increased in vascularized corneas as compared to normal corneas. In limbal-deficiency-induced corneal NV, VEGF mRNA and protein are induced after injury and are both temporally and spatially correlated with inflammation and NV. VEGF is not only induced during NV, but is also required for corneal angiogenesis. The indispensable role of VEGF in angiogenesis is shown by the finding that stromal implantation of anti-VEGF antibodies inhibits NV in a rat model. Conversely, implantation of a Hydron pellet containing VEGF into the stroma induces severe corneal NV without significant inflammation.

The effects of VEGF in the cornea are not limited to NV, as this growth factor has also been shown to regulate goblet cell migration. Studies analyzing the correlation between cornea NV and conjunctivalization showed that VEGFR-1 is present in the conjunctiva-like epithelium covering the cornea as well as in goblet cells, invading leukocytes, and the corneal vasculature. Inhibition of VEGF activity inhibited not only corneal NV, but also goblet cell density, suggesting that VEGF may promote goblet cell migration.

Evidence suggests that VEGF also participates in corneal lymphangiogenesis. Corneal lymphangiogenesis may contribute to graft sensitization and rejection, following high-risk keratoplasty of vascularized corneas. VEGF-C binds to VEFGR-3 and induces lymphatic growth in the cornea. Interestingly, inhibition of lymphatic growth is observed after administration of a VEGF trap that neutralizes VEGF-A, but not VEGF-C or -D. This could be explained by the chemotactic effect on macrophages that release VEGF-C in inflamed corneas observed with VEGF-A. Thus, VEGF-A amplifies signals essential for lymphatic growth. In general, corneal lymphangiogenesis seems to correlate well with the degree of corneal hemangiogenesis.

Recent studies have shown that VEGF, although present in the cornea, does not promote angiogenesis under normal conditions. VEGF-A found in corneal tissue is mostly bound to an alternative spliced secreted isoform of VEGFR-1 (sflt-1), which acts as a trap for secreted VEGF-A and in this way contributes to maintenance of corneal avascularity. In addition, VEGFR-3 is expressed in endothelial as well as epithelial cells in the cornea. When VEGF-C and -D bind to endothelial VEGFR-3, they stimulate proangiogenic signaling. In contrast, VEGFR-3 expressed by corneal epithelium acts as a decoy receptor sequestering VEGF but yet rendering it available when an angiogenic response is needed to enhance the immune defense. This VEGFR-3 sink system is a potent mechanism that inhibits inflammatory-induced angiogenesis.

Basic fibroblast growth factor

Basic fibroblast growth factor (bFGF) is another potent angiogenic factor. It is a member of the fibroblast growth factor (FGF) family, which includes 23 heparin-binding peptides widely expressed during cell differentiation, angiogenesis, mitogenesis, and wound healing. bFGF functions are mediated by the receptors FGFR-1, -2, -3, and-4. FGF recptor-1 (FGFR-1) is expressed in normal corneal epithelium, while bFGF is upregulated following injury. It is also upregulated following co-culture of corneal epithelial cells with vascular EC and keratocytes. The affinity of bFGF for its receptor differs according to the extent of

maturation of new vessels. This may be due to varying expression of heparan sulfate proteoglycans and highlights the role of ECM proteins in the regulation of corneal angiogenesis.

Matrix metalloproteinases

The matrix metalloproteinases (MMPs) constitute a multigene family of zinc-binding proteolytic enzymes that participate in ECM remodeling. Many of the growth factors that modulate angiogenesis also influence MMP expression. These growth factors include VEGF, FGF-2, and tumor necrosis factor-alpha (TNF-α). Vascular ECs respond by secreting proteolytic enzymes that degrade the ECM to facilitate migration and differentiation of ECs. The MMPs that have identified in the cornea are collagenases I and II (MMP-1 and -13), stromelysin (MMP-3), matrilysin (MMP-7), membrane-type MMP (MT-MMP-14), and gelatinases A and B (MMP-2 and -9). Both MMP-2 and MMP-9 are proteolytically activated primarily by MT1-MMP during capillary formation. Several reports suggest that these MMPs participate in vascular invasion by directly degrading the matrix or releasing matrix-bound cytokines and growth factors. Accordingly, inhibition of MMP-9 activity in the cornea decreases angiogenesis. However, given their ability to degrade ECM, MMPs exhibit a dual action in angiogenesis. For example, MMP-2 activation may release anti-angiogenic fragments, allow the production of potent angiostatic factors, or facilitate angiogenesis.

Lipid mediators

One of the initial events that occurs after corneal injury is the release of arachidonic acid. In the corneal epithelium, arachidonic acid is then metabolized by cyclooxygenase (COX) to generate eicosanoids (such as 12- and 15-HETE), lipoxin A4 (LXA4), and prostaglandins. 12(S)-HETE is a powerful angiogenic factor, and COX inhibitors have been shown to reduce corneal angiogenesis in animal models. Platelet-activating factor is another potent lipid mediator released from the cell membrane after corneal injury. It contributes to corneal NV by increasing expression of VEGF, MMP-9, and urokinase plasminogen activator (uPA), all of which subsequently stimulate vascular EC migration.

Anti-Angiogenic Molecules

Angiostatin

Angiostatin results from the cleavage of plasminogen. Several MMPs can cleave plasminogen to generate angiostatin-like molecules. The inhibitory effect of angiostatin on vascular ECs may be due to inhibition of adenosine triphosphate (ATP) synthesis in these cells, an effect that decreases EC migration and proliferation. Angiostatin binds to integrin alpha-v beta-3 ($\alpha v\beta 3$) and affects angiogenesis as well as developmental NV. It also induces vascular EC apoptosis mainly in areas of NV.

All three layers of the cornea are able to synthesize plasminogen and angiostatin. Tears collected after overnight eye closure contain a significant amount of angiostatin-related molecules known to have anti-angiogenic properties. This has also been shown in tears of contact lens-bearing patients, suggesting that these molecules play a role in preventing NV under hypoxic conditions. Corneal NV occurs following injection of anti-angiostatin antibodies into corneas having undergone post-excimer laser keratectomy. This supports the idea that plasminogen and angiostatin are important for the maintenance of corneal avascularity.

Endostatin and neostatins

Endostatin is a 20-kDa proteolytic fragment of collagen XVIII that exhibits anti-angiogenic activity. It was originally discovered as an angiogenic inhibitor purified from conditioned media of murine hemangioendothelioma cells. Endostatin inhibits bFGF-induced corneal NV as well as VEGF-induced vascular EC migration and proliferation. Collagen XVIII is localized mainly in the corneal vascular and epithelial basement membrane. Smaller fragments of collagen XVIII, known as Neostatins -7 and -14, are generated by the enzymatic activity of MMPs -7 and -14, respectively. They have potent anti-angiogenic and anti-lymphangiogenic properties. Local production of endostatin and Neostatins -7 and -14 may occur during wound healing. Endostatin is Food and Drug Administration (FDA)-approved for the treatment of cancer-related NV.

Pigment-epithelial-derived factor

Pigment-epithelial-derived factor (PEDF) is a potent anti-angiogenic and neurotrophic factor that is found in multiple eye tissues including the cornea. In contrast to VEGF, which is induced under low oxygen conditions, PEDF expression is suppressed during hypoxia. PEDF induces EC apoptosis. It also has antipermeability and anti-inflammatory activity that counterbalances VEGF actions. Studies have shown that PEDF-blocking antibodies induce corneal NV when implanted into the stroma and that recombinant PEDF inhibits bFGF-induced corneal NV. These findings are consistent with an essential role for PEDF in maintaining the avascularity of ocular tissues. Given its effectiveness at countering VEGF activity, PEDF may be a good pharmacological inhibitor of angiogenesis.

Arresten, canstatin, and tumstatin

Arresten is a 26-kDa protein derived from the non-collagenous (NCl) domain of the type IV collagen $\alpha 1$ chain. This molecule has been shown to inhibit bFGF-stimulated proliferation, migration, and tube formation of

cultured ECs. It also inhibits NV *in vivo*. Canstatin is a 24-kDa fragment of the type IV collagen α-chain. It also inhibits EC proliferation and tube formation. The mechanism of action appears to involve phosphoinositide 3-kinase/protein kinase B (PI3K/Akt) inhibition and depends on signaling events transduced through membrane-death receptors. Tumstatin, a 28-kDa fragment of the type IV collagen α3 chain, also has anti-angiogenic activity.

Therapy

Identifying and adequately treating the underlying cause of corneal NV is critical. Therapies for corneal NV may range from antimicrobial therapy for infectious keratitis to systemic immunosuppression for autoimmune diseases such as ocular cicatricial pemphigoid. Some of the established and investigational medical and surgical treatments for corneal NV are discussed below.

Medical Treatments

Anti-inflammatory compounds, such as steroids, have a long history of use for the suppression of inflammation and associated angiogenesis. The anti-angiogenic effects of steroid treatment are likely secondary to their anti-inflammatory actions and include inhibition of chemotaxis and cytokine synthesis. Steroids have also been shown to inhibit vascular EC proliferation and migration. Unfortunately, the side effects of these compounds make long-term administration difficult in some patients. Moreover, their role in corneal NV that is not associated with inflammation is limited.

Advances in our understanding of the mechanisms underlying ocular NV has led to the identification of new pharmacologic targets. Given the key role of VEGF in NV of the eye, attention has been directed to developing drugs that will counteract the activity of this factor. Bevacizumab is an anti-VEGF antibody that binds to all VEGF isoforms. This molecule inhibits VEGF-receptor interactions and in this way, blocks all VEGF actions. It is currently approved by the FDA to treat metastatic colorectal cancer. It has also been tested for the treatment of wet (neovascular) age-related macular degeneration (AMD). Ranibizumab is another anti-VEGF antibody that has been approved for use in the eye to treat wet AMD. Bevacizumab treatment of corneal NV has gained popularity since the successful use of this molecule to treat choroidal NV. Subconjunctival injection as well as topical application of this molecule has also been used with promising results to treat herpes simplex virus (HSV) keratitis, recurrent pterygia, rejection of corneal grafts, and Stevens–Johnson syndrome. However, data on these treatments are limited, and adverse effects such as loss of epithelial integrity and progression of thinning have been reported in a small number of patients. Further investigation is required to establish efficacy, adequate dosing, and safety in the different clinical scenarios that present with corneal NV.

Other forms of anti-VEGF therapy are currently undergoing clinical trials. One example is VEGF TRAP, a high-affinity VEGF antagonist designed to bind and neutralize VEGF in the circulation and within tissues. It binds to all isoforms of VEGF and to placental growth factor, which is a related pro-angiogenic factor. SIRNA-027, another anti-VEGF therapy, is a short interferon RNA designed to downregulate VEGFR-1 expression. PKC412 is an orally administered tyrosine kinase inhibitor that binds to the intracellular, enzymatically active domain of the VEGF receptor and prevents phosphorylation and activation of the VEGF signaling cascade. Some of these compounds may be available for use in the near future.

Surgical Treatment

One surgical approach for the treatment of corneal NV is laser therapy. The use of laser photocoagulation with a 577-nm yellow dye for the treatment of established corneal NV has been investigated. The effectiveness of this technique has been tested in clinically significant corneal NV resistant to medical therapy both before and after PK. Some reduction of corneal NV can be achieved; however, the benefit of laser photocoagulation prior to high-risk keratoplasty is unclear, and this technique does not appear to be useful for treating extensive corneal NV.

An alternative to laser occlusion is fine-needle diathermy. This procedure is easy to perform, requiring only a 10-0 nylon suture and a unipolar diathermy unit. It produces occlusion of 50–100% of corneal NV and has been show to moderately benefit visual acuity in a series of 17 patients.

Photodynamic therapy is currently used to treat choroidal NV. In this technique, a photo-sensitizer selectively accumulates in new vessels and is subsequently activated by a laser beam. This technique is currently under investigation in animal models of corneal NV.

Finally, in some cases, conjunctival, limbal, or amniotic membrane transplantation may be required to restore the ocular surface. Conjunctival autograft and allograft transplantation have been shown to decrease corneal NV. Amniotic membrane has anti-angiogenic properties as well. Limbal autograft transplantation has been successful in cases of stem cell deficiency and conjunctival metaplasia. This technique not only treats the stem cell deficiency and decreases the angiogenic stimulus from chronic ulceration, but also directly inhibits vascular ECs.

No ideal treatment is currently available for corneal NV. However, significant progress in the understanding of corneal angiogenesis has opened a new field of investigation that may lead to the development of novel therapeutic agents for the treatment of this condition.

See also: Angiogenesis in the Eye; Angiogenesis in Wound Healing; Concept of Angiogenic Privilege.

Further Reading

Ambati, B. K., Nozaki, M., Singh, N., et al. (2006). Corneal avascularity is due to soluble VEGF receptor-1. *Nature* 443: 993–997.

Azar, D. (2006). Corneal angiogenic privilege: Angiogenic and antiangiogenic factors in corneal avascularity, vasculogenesis, and wound healing. *Transactions of the American Ophthalmological Society* 104: 264–302.

Chang, J. H., Gabison, E. E., Kato, T., and Azar, D. T. (2001). Corneal neovascularization. *Current Opinion in Ophthalmology* 12: 242–249.

Cursiefen, C., Chen, L., Saint-Geniez, M., et al. (2006). Nonvascular VEGF receptor 3 expression by corneal epithelium maintains avascularity and vision. *Proceedings of the National Academy of Sciences of the United States of America* 103: 11405–11410.

Dorrel, M., Uusitalo-Jarvinen, H., Aguilar, E., and Friedlander, M. (2006). Ocular neovascularization: Basic mechanisms and therapeutic advances. *Survey of Ophthalmology* 52: 3–19.

Ma, D. H., Chen, J. K., Zhang, F., et al. (2006). Regulation of corneal angiogenesis in limbal stem cell deficiency. *Progress in Retinal and Eye Research* 25: 563–590.

Zhang, S. X. and Ma, J. X. (2007). Ocular neovascularization: implication of endogenous angiogenic inhibitors and potential therapy. *Progress in Retinal and Eye Research* 26: 1–37.

Corneal Dystrophies

B H Feldman, Philadelphia Eye Associates, Philadelphia, PA, USA
N A Afshari, Duke University Medical Center, Durham, NC, USA

Glossary

Amyloid – Insoluble, fibrous, and primarily extracellular protein aggregates exhibiting beta-sheet structures that are deposited in many local and systemic diseases.
Anterior synechia – A pathological condition where the iris adheres to the cornea.
Corectopia – An iris defect involving displacement of the pupil from its normal position.
Corneal dystrophy – A bilateral inherited disorder of noninflammatory, progressive corneal disease.
Corneal guttata – Wart-like excrescences of Descemet's membrane that are associated with Fuchs' corneal dystrophy.
Lamellar keratoplasty – A partial thickness corneal transplant of either the anterior or posterior corneal layers.
Penetrating keratoplasty – Full thickness corneal transplant.
Phototherapeutic keratectomy – A surgical procedure in which the epithelium is removed and then an excimer laser is used to ablate abnormal anterior stromal tissue.
Recurrent erosion – A syndrome of repeated epithelial defects due to abnormal adhesion of the epithelial basement membrane.

Introduction

The corneal dystrophies are a group of noninflammatory, inherited, and bilateral disorders characterized by pathognomonic patterns of corneal deposition and morphological changes. These heterogeneous dystrophies are defined by their clinical characteristics, histological findings, and genetics. Traditionally, they have also been grouped anatomically into three categories of anterior, stromal, and posterior dystrophies. The anterior dystrophies affect the epithelium, epithelial basement membrane (EBM), or Bowman's layer. The stromal dystrophies primarily affect the stroma, but may extend into the anterior corneal layers and may rarely affect Descemet's membrane and the endothelium. The posterior dystrophies are primarily disorders of endothelial cells and the posterior portion of Descemet's membrane. They may also alter the structure of the stroma and anterior cornea.

There is a wide variation in the type and degree of symptoms caused by the corneal dystrophies. Progressive accumulation of tissue deposits can lead to vision loss from corneal opacification and astigmatism. Disruption of normal cell function can lead to abnormal epithelial adhesion with resultant painful recurrent epithelial erosions or loss of endothelial cell activity with resultant corneal edema. Several of the dystrophies are associated with vision-threatening ocular or systemic manifestations. Together, corneal dystrophies are the primary indications for approximately 10–15% of the corneal transplantations performed in the United States each year.

Anterior Dystrophies

Epithelial and EBM Dystrophies

EBM Dystrophy

Also known by the descriptive term, map-dot-fingerprint (MDF) dystrophy, or the eponym, Cogan's dystrophy, EBM dystrophy (EBMD) is arguably the most common dystrophy, found in approximately 5% of the adult population, with a slight preponderance of women. While in rare instances an autosomal dominant inheritance pattern has been identified, in the vast majority of cases this disease is sporadic, making its designation as a corneal dystrophy controversial.

On examination, several patterns of basement membrane and epithelial involvement can be observed, including dots or microcysts, map lines, and fingerprint lines. These abnormalities may fluctuate over time but are rarely progressive.

The most common symptoms of EBMD are recurrent erosions and blurred vision. The recurrent erosions arise because of poor epithelial adhesion to the underlying basement membrane. These erosions may be triggered by the lid trauma caused by an innocuous blink and are most often noted upon eye opening in the morning – with pain sometimes – waking the patient from sleep. The pain, foreign body sensation, and blurring associated with the erosions typically last only several minutes, but for some may be prolonged and severe. In addition to these transient symptoms, the surface changes from EBMD in the visual axis may lead to irregular astigmatism and adversely affect a patient's best-corrected visual acuity.

Recurrent erosions are managed acutely with lubricants, bandage contact lenses, patching, and prophylactic antibiotics. Medical options for prophylaxis against these recurrent erosions begin with aggressive lubrication and an

emphasis on the use of bedtime ointments to avoid epithelial dehydration which can potentiate poor epithelial adhesion. Additionally, it is beneficial to address co-existing ocular surface diseases such as blepharitis, and the use of oral tetracyclines may inhibit epithelial breakdown. Similarly, anti-inflammatory agents such as topical steroids may inhibit this breakdown, but the long-term use of these agents should be dealt with caution. If recurrent erosions persist despite medical interventions, epithelial adhesion can be improved through mechanical disruption with subsequent healing through debridement with diamond burr polishing, stromal needle puncture, or Nd:YAG laser puncture. For large or recurrent lesions in the visual axis, excimer laser phototherapeutic keratectomy may be preferred to avoid scarring due to other techniques.

Microscopic examination of EBMD reveals a thickened epithelial layer with a thickened or redundant basement membrane that has extended into the epithelium in either linear propagations or sheets, representing the map and fingerprint lines, respectively. The dots are microcysts formed by these abnormal extensions of basement membrane that have entrapped degenerated epithelial cells.

Meesman's

This rare anterior dystrophy is an autosomal dominant disorder characterized by the development of intraepithelial vesicles in the central cornea that appear as early as in the first few years of life. Over time, there is progressive involvement of the mid-peripheral cornea and an increase in the number and density of vesicles. As the disease progresses, vision may slowly deteriorate and the eye may become irritated as the intraepithelial vesicles rupture. In contrast to EBMD, recurrent erosions are uncommon in this dystrophy. While most patients are asymptomatic, those who have ocular irritation from ruptured vesicles are treated with lubricants or soft contact lenses to manage these microerosions.

The pathologic changes in the epithelium are thickening of the basement membrane and the formation of small epithelial cysts containing a material composed of degenerated keratin with cytoplasmic and nuclear debris, known as peculiar substance. Consistent with the epithelial nature of this dystrophy, Meesman's lesions are known to recur in cornea transplants as the host epithelium repopulates the surface of the donor button.

Genetic analysis has elicited responsible mutations in two genes (KRT3 and KRT 12) on chromosomes 12q13 and 17q12, respectively, which code for two corneal keratins (k3 and k12).

Bowman's Layer Dystrophies

Reis-Buckler's

Also known as corneal dystrophy of Bowman's type 1 (CDB-1) and granular dystrophy type III (GD-3), this is an autosomal dominant dystrophy that is marked by geographic opacification of Bowman's layer, beginning as fine granular deposits that evolve into confluent opacities over time. Reis-Buckler's arises during childhood or adolescence and often leads to frequent recurrent erosions and marked, progressive visual loss (Figure 1). The recurrent erosions can be managed in a manner similar to in EBMD, but the progression of opacification may necessitate extensive excimer laser phototherapuetic keratectomy. Despite initial clearing of the visual axis, these patients often have recurrence of opacities requiring additional treatment.

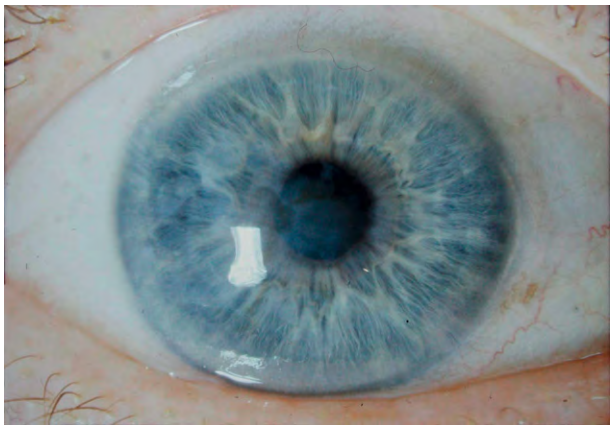

Figure 1 External photograph of Reis-Buckler's dystrophy (corneal dystrophy of Bowman's type 1 or granular dystrophy type 3) demonstrating geographic opacification of Bowman's layer.

Histological examination demonstrates that the normally acellular collagenous Bowman's is disrupted, noncontiguous, or absent and is replaced with fibrocellular tissues. The opacities in Bowman's layer are band-shaped, granular, and stain red with Masson's trichrome. Similar to other granular dystrophies, these lesions appear as rod-shaped bodies under electron microscopy.

Multiple mutations of the human transforming growth factor inducible gene (TGFBI) – previously known by the misnomer, keratoepithelin – on chromosome 5q31 may lead to the Reis-Buckler's phenotype. The most common mutations are Arg124 or Arg555 which are both thought to affect the solubility and stability of the TGFBI protein.

Thiel-Behnke

Initially classified as a variant of Reis-Buckler's, Thiel-Behnke, or corneal dystrophy of Bowman's type 2 (CDB-2), at times is similar in its clinical appearance but is always distinct in its histological and electron microscopic appearance. Also autosomal dominantly inherited, Thiel-Behnke has a slightly later onset of recurrent erosions, typically in the second decade of life, and vision loss is more slowly progressive. At the slit lamp, this dystrophy typically appears as honeycombed-shaped subepithelial

opacities. It can be managed similarly to Reis-Buckler's and recurrence after keratectomy is infrequent.

Examination of pathologic specimens reveals only weakly positive Masson's trichome staining, in contrast to the strongly positive staining of Reis-Buckler's. The pathognomonic features are the 8–10 nm curly fibers identified by electron microscopy.

Similar to Reis-Buckler's, this dystrophy is sometimes linked to the TGFBI gene. However, there is genotypic heterogenicity for Thiel-Behnke as evidenced by the discovery that mutations on chromosome 10q23-q24 can also lead to this phenotype.

Stromal Dystrophies

Lattice

There are three major types of lattice dystrophy and all are unified by the appearance of lattice lines on slit-lamp examination and amyloid deposition on histological examination.

Lattice type 1. In type 1 lattice, or Biber–Haab–Dimmer corneal dystrophy, amyloid is deposited in the cornea but is not found elsewhere in the body. It can vary in its appearance, and there is often progression from round, ovoid and white, or small, filamentous, and refractile anterior stromal lesions to more nodular, threadlike, and thicker linear lesions that extend into deep stroma (**Figure 2(a)**). Initially, the stroma between lesions remains clear, but over time these spaces opacify and assume a ground-glass appearance. The limbus is typically spared. Signs of lattice dystrophy most often appear in early childhood, but symptoms of surface erosions, irregular astigmatism, and vision loss usually begin in the second or third decades of life.

Recurrent erosions can be frequent and can be managed as described previously. Some authors believe that phototherapeutic keratectomy should be avoided (as well as laser-assisted *in situ* keratomileusis (LASIK) and photorefractive keratectomy (PRK)) because excimer laser, within the UV light spectrum, may trigger activation of TGFB and exacerbate this condition. For severe vision loss due to opacification, penetrating and lamellar keratoplasty may be warranted. Recurrence may occur in these grafts but presents differently than the primary lesions.

Specimens are positive for amyloid and stain with Congo red, periodic acid-Schiff's reagent (PAS), Masson's trichrome, and thioflavine-T fluorochrome, and are metachromatic with crystal violet (**Figure 2(b)**). As with all amyloid, they demonstrate apple-green birefringence under polarized light.

Lattice type 2. Type 2 lattice, also known as Meretoja's, familial, or Finnish amyloidosis syndrome, is characterized by both systemic and corneal amyloid deposition. Typically seen in families of Finnish, European, or Japanese origin, it is usually asymptomatic until early adulthood.

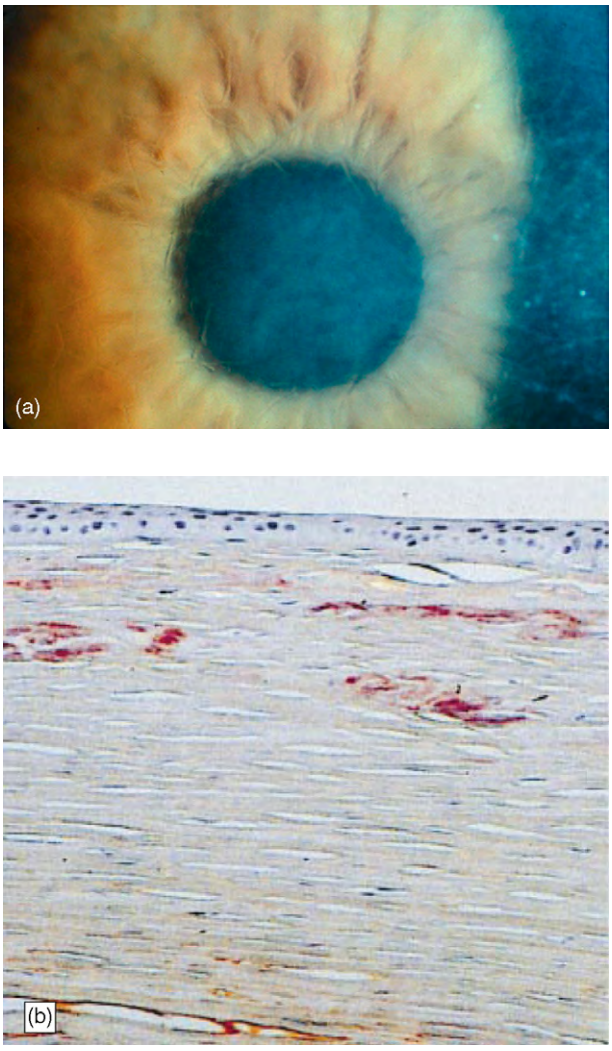

Figure 2 (a) Slit-lamp photograph of lattice type 1 dystrophy. Arrow indicates amyloid deposition. (b) Congo red stain of cornea in lattice type 1 demonstrating amyloid deposition. Afshari, N. A., Mullally, J. E., Afshari, M. A. et al. (2001). Survey of patients with granular, lattice, avellino, and Reis-Bücklers corneal dystrophies for mutations in the BIGH3 and gelsolin genes. *Archives of Ophthalmology* 119: 16–22. © 2001 American Medical Association. All rights reserved.

Corneal slit-lamp examination shows more peripheral deposits, with fewer and finer lattice lines, and a primarily sub-Bowman's location of deposition.

Patients begin to experience corneal changes in the third decade of life, but symptoms of reduced corneal sensation and frequent recurrent erosions are uncommon until the fifth decade. Overall, the visual prognosis is better than in type 1 with many patients not developing visual loss until late in the course of disease. While there is a decreased severity of corneal disease, the systemic manifestations can be serious and include dry, itchy skin, intermittent proteinuria, and cardiac abnormalities. Patients may develop severe mask-like facial paresis (loss of facial

muscle motor function), blepharochalasis (inflammation of eyelid), protruding lips, and pendulous ears from amyloid deposition and secondary muscular dysfunction.

Unique among the lattice dystrophies, type 2 does not arise from a mutation in the TGFBI gene. Instead, it has been linked to a dominant mutation of the gelsolin gene on 9q32–34 that encodes an amyloid precursor.

Lattice types 3 and 3a. Type 3 lattice is the least severe and has an autosomal recessive pattern of inheritance. The lattice lines in type 3 are thicker and ropier in appearance, and later in onset. Vision is often not affected until the sixth or seventh decade of life, and recurrent erosions are rare. Like type 1, type 3 is associated with a defect in the TGFBI gene. Type 3a is similar in presentation to type 3 but follows an autosomal dominant inheritance pattern.

Granular

Granular type 1

The most common of the stromal dystrophies, granular dystrophy is named for its typical appearance as crumb-like, discrete, grainy opacities in the anterior stroma. Initially, these opacities are fine dots or lines and with time they assume their more characteristic appearance of anterior stromal drops, rings, or crumbs with intervening clear spaces. As the dystrophy progresses, the lesions coalesce and extend into deeper stroma, and the intervening spaces take on a ground-glass appearance. The lesions rarely extend to the limbus (**Figure 3**). Symptoms of vision loss do not usually occur until the fifth decade. Despite the anterior location of the dystrophy, recurrent erosions are rare. There are exceptions to this mild course, and some variants of the disease cause earlier and more severe vision loss.

For patients with severe vision loss, management options include superficial keratectomy, phototherapeutic keratectomy, and lamellar or full thickness keratoplasty depending on the depth of involvement. Recurrence may occur even in full thickness grafts necessitating repeat procedures. With recurrence, the lesions may appear similar to primary disease or may consist of subepithelial lesions emanating from the graft periphery.

The pathology of granular type 1 shows eosinophilic, rod-shaped, trapezoidal hyaline deposits in the stroma that are bright red on Masson's trichome and weakly PAS positive. On electron microscopy, the amorphous material appears rod or trapezoidal in shape.

Granular dystrophy type 1 is also due to a defect in the TGFBI gene and at least two causative mutations have been identified.

Granular type 2

Previously known as Avellino dystrophy (because the initial reports were of families from Avellino, Italy) this variant of granular dystrophy is characterized both by granular deposits and lattice lines or stellate deposits. Early lesions are often ring-like and anterior and can appear similar to type 1 granular lesions. As the disease progresses, deeper lesions appear and the lattice-like

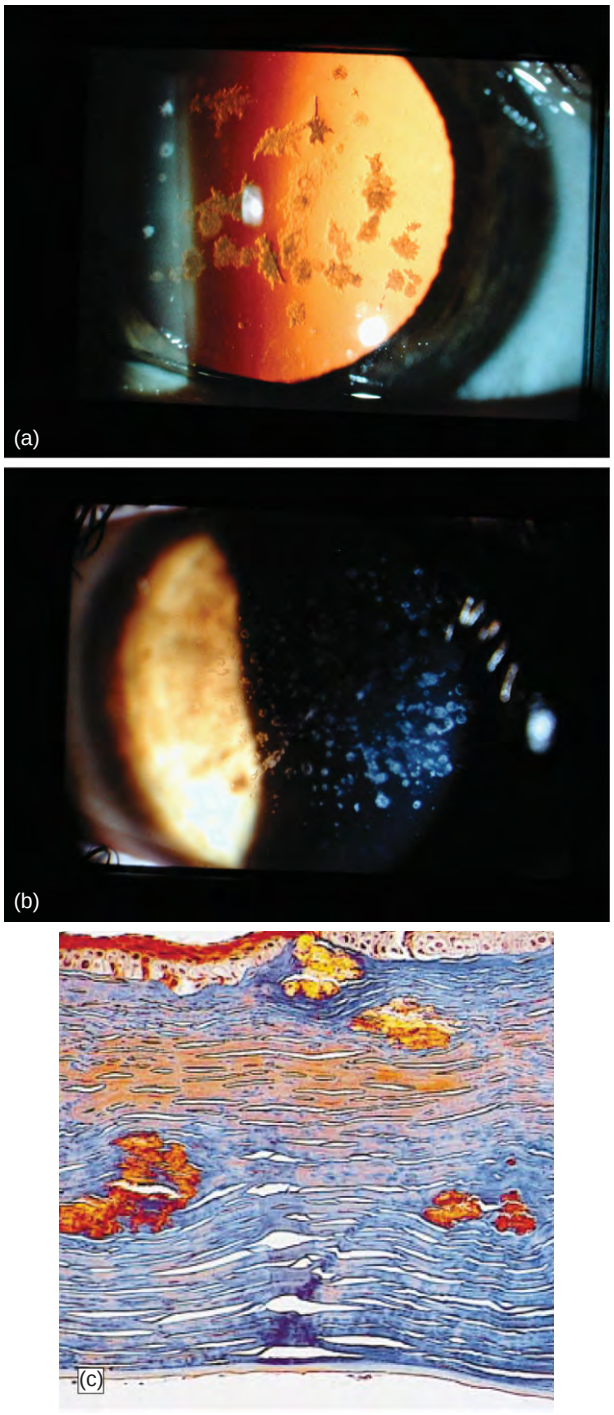

Figure 3 Slit-lamp photographs of mild (a) and moderate (b) granular type 1 corneal dystrophy. (c) Masson's trichrome staining of hyaline deposits in granular dystrophy. Afshari, N. A., Mullally, J. E., Afshari, M. A. et al. (2001). Survey of patients with granular, lattice, avellino, and Reis-Bücklers corneal dystrophies for mutations in the BIGH3 and gelsolin genes. *Archives of Ophthalmology* 119: 16–22.

lesions are observed. With progression, the intervening clear spaces between lesions assume a hazy appearance.

Symptoms may be more severe and the onset earlier than in type 1 granular dystrophy. Many patients experience vision loss by adolescence, but vision rarely drops below the 20/70 level. Recurrent erosions and related ocular discomfort occur in a minority of patients, but more frequently than in type 1 granular patients.

Not every patient displays clinical evidence of both granular and lattice lesions, but on histologic examination these patients uniformly demonstrate both hyaline and amyloid deposits, the distinguishing pathologic findings of the two respective diseases.

As both granular and lattice dystrophies can arise from dominant TGFBI gene defects, it is not surprising that TGFBI mutations have been found to be responsible for this dystrophy which displays characteristics of both diseases. The autosomal dominant inheritance of type 2 granular dystrophy has a high penetrance, but phenotypic expressivity is quite variable between family members.

Macular

The least common of three major stromal dystrophies, the autosomal recessive Macular dystrophy is also the most severe. Its clinical appearance is unique, seen at the slit-lamp as diffuse, cloudy, gray–white lesions that begin superficially and centrally and then spread downward and outward. By late adolescence, these lesions may progress to involve the entire cornea from limbus to limbus and from anterior stroma to the endothelium. Anteriorly protruding nodules may cause highly irregular astigmatism, and Descemet's membrane involvement may produce corneal guttata.

Vision loss can begin in the first decade of life and may be severe by the third decade. Recurrent erosions are more frequent and may also begin at an early age. Due to photophobia, many patients seek treatment with tinted lenses, phototherapeutic keratectomy, or lamellar and penetrating keratoplasty. Unfortunately, recurrence is common and may lead to significant vision loss even in penetrating keratoplasty recipients. This recurrence most often begins in the periphery near the graft–host junction, and has been found to be more common in smaller-sized grafts.

The key histopathologic finding of Macular dystrophy is glycosaminoglycan accumulation. This accumulation may occur both intracellularly and extracellularly and is found between stromal lamellae, subepithelially, and within keratocytes and endothelial cells. The deposits stain with Alcian blue, colloidal iron, metachromatic dyes, and PAS. The cornea may have decreased overall thickness with a thinned or absent Descemet's membrane and an epithelium that is stretched thin over anterior stromal deposits.

Unique in its autosomal recessive inheritance, Macular dystrophy is linked to various mutations on chromosome 16q2 and the CHST6 gene that encodes enzymes of keratan sulfate synthesis. This keratan sulfate defect is systemic and the varied expression of keratan sulfate in serum and cornea has led to the classification of several types of Macular dystrophy. In type 1, keratan sulfate is completely undetectable in the cornea and serum. In type 1a, the only detectable keratan sulfate is found within keratocytes, and in type 2 corneal keratan sulfate is present but levels are diminished.

Rare Stromal Dystrophies

Gelatinous drop-like dystrophy

Presenting in the first decade of life with photophobia, foreign body sensation and decreased vision, this autosomal recessive dystrophy, also known as familial subepithelial amyloidosis, resembles band keratopathy. The opacities are subepithelial and anterior stromal, and may, over time, assume a mulberry-like gelatinous appearance. Keratectomy and keratoplasty may be performed with variable success due to recurrence.

This dystrophy is linked to mutations in the M1S1 gene on chromosome 1p31. These defects lead to the accumulation of amyloid from a truncated surface glycoprotein.

Schnyder's crystalline dystrophy

Also known as Scandinavian dystrophy due to a reported cohort of patients in central Massachussets of Scandinavian origin, this autosomal dominant dystrophy occurs within the first year of life as central, crystalline, anterior stromal lesions that are either discoid, ring-like, or geographic in distribution. A significant minority may have a noncrystalline form which occurs later in life. As the lesions progress, they involve more posterior stroma. By the third decade a prominent arcus lipoides is seen, and by age 40 most patients have full thickness corneal opacities. While there is no correlation between this disease and elevated serum cholesterol, patients' lipid and cholesterol levels should be checked as early arcus, before age 50, and can be an indicator of hyperlipidemia. Important diseases in the differential diagnosis of central crystalline corneal deposits should also be ruled out and these include Bietti's corneoretinal dystrophy, cystinosis, and dysproteinemias such as multiple myeloma.

Pain is infrequent because many of these patients develop decreased corneal sensation. Vision loss is the most common presentation and may be treated with lamellar or penetrating keratoplasty. Histologic examination of the corneal buttons reveal that the crystals are composed of cholesterol and lipid and the pathogenesis is believed to involve a defect in local lipid metabolism or

transport. The genetic defect has been linked to chromosome 1p.

Central cloudy dystrophy

First described by Francois, this autosomal dominant or, rarely, sporadic dystrophy appears as bilaterally symmetric central and deep stromal cloudy, gray–white, ill-defined, snowflake-like lesions. The appearance is similar to posterior crocodile shagreen, and, similarly, is rarely symptomatic.

Congenital hereditary stromal dystrophy

This dystrophy, which is often static or slowly progressive, has been described in several families and occurs at birth as a diffusely hazy cornea of normal thickness. The lesions are diffuse, bilateral, small, and located primarily in the anterior stroma. This generalized opacification may lead to profound vision loss and early penetrating keratoplasty may be warranted to prevent amblyopia.

The pathogenesis involves disorganization of corneal lamellae with randomly arranged collagen fibrils and loss of corneal transparency. The inheritance pattern is autosomal dominant and a defect has been identified in the decorin gene that encodes a dermatan sulfate proteoglycan.

Posterior amorphous dystrophy

Remarkable for central stromal thinning without ectasia or astigmatism, this autosomal dominant dystrophy begins in childhood and slowly progresses. It is characterized by bilateral gray sheets in the deep stroma extending to the limbus. The stroma may thin to about 300μm, but vision is only mildly affected.

In addition to stromal thinning, histologic examination demonstrates a thick collagenous layer posterior to Descemet's membrane as well as relative absence of stromal keratocytes. The endothelium is unaffected.

Fleck dystrophy

Fleck dystrophy is usually discovered as an incidental finding, because it is asymptomatic in the majority of patients (recurrent erosions can rarely occur). It is autosomal dominant, may be present at birth or arise in infancy, and is rarely progressive. On slit-lamp examination, small white flecks can be seen in all stromal layers and represent swollen keratocytes with cytoplasmic vesicles due to membrane-bound vacuoles of lipid and mucopolysaccharide. On electron microscopy, flecks stain with oil-red O.

A causative mutation on chromosme 2q35 in the PIP5K3 gene has been identified. This gene codes for an enzyme involved in post-Golgi vesicle processing of protein and lipids.

Posterior Dystrophies

Fuchs' Endothelial

By far the most common corneal dystrophy to lead to corneal transplantation, Fuchs' is an autosomal dominant dystrophy that directly involves Descemet's membrane and the endothelium, and may indirectly impact all layers of the cornea. The classic lesion of Fuchs' is the central guttae, but a controversial nonguttate form has been described. Over time, the guttata spread peripherally and coalesce. Descemet's may assume a thickened, grayish, irregular appearance, and this may eventually mask the guttata. If corneal edema develops, it begins posteriorly as evidenced by Descemet's and deep-stromal wrinkles. As the corneal edema progresses, the stroma thickens and microcystic epithelial edema can usually be appreciated by the time the cornea thickness has increased by 100 μm. Later in the course of the disease, the cornea takes on a ground-glass appearance (**Figure 4**).

Fuchs' guttata are 2.5 times more likely to develop in women than men, and women are nearly 6 times more likely to develop Fuchs' corneal edema. Symptoms of blurring are often first seen in during the morning hours because the cornea swells overnight due to decreased evaporation and the increased hypotonicity of the tear film. Some patients find relief from hypertonic solutions, decreasing intraocular pressure, or by facilitating tear evaporation with external devices such as blow dryers. Recurrent erosions often occur in advanced cases due to edema-induced anterior basement membrane-like lesions and ruptured epithelial bullae. Repeat epithelial defects may lead to fibrous scarring and neovascularization. These epithelial lesions may be managed with bandage contact lenses. As mentioned previously, many patients require management with penetrating or endothelial keratoplasty, especially after other intraocular surgeries which may lead to further loss of endothelial cell viability.

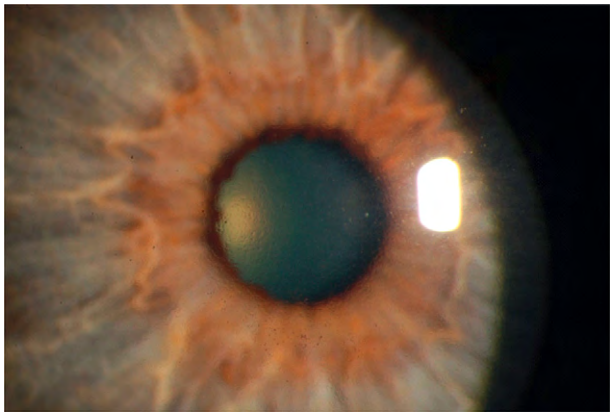

Figure 4 Slit-lamp photograph of Fuch's dystrophy.

The pathology of Fuchs' is well characterized and primarily consists of changes in endothelial cell architecture and number, and abnormalities of posterior Descemet's membrane. The number of endothelial cells decreases while the remaining cells show an increase in size, a less hexagonal and more irregular shape, and an eccentricity of cellular nuclei. This can be seen *in vivo* with specular microscopy as a decreased endothelial cell density, polymegathism, and cellular polymorphism. On electron microscopy the cells look more fibroblastic with an increase in rough endoplasmic reticulum, lysosomes, vacuoles, and cytoplasmic filaments. The posterior nonbanded zone of Descemet's membrane is thinner than normal, on an average less than 2 μm compared to 8 μm in a normal adult population. An abnormal PAS-positive posterior collagenous layer significantly increases the overall thickness of Descemet's to 2–3 times that of normal corneas, and this layer is contiguous with guttae that jut out posteriorly, thinning the overlying endothelial cells and pushing their nuclei aside into the intervening valleys. With corneal edema, the corneal lamellae thicken, and histologically this is evidenced by a decrease in artifactual clefting.

The genetic defects leading to Fuchs' are numerous and the identified mutations have been linked to chromosome 1p32-1p34, as well as chromosomes 7, 15, 17, and X.

Posterior Polymorphous Membrane

Typically beginning in the second or third decade of life, this autosomal dominant dystrophy of Descemet's and the endothelium is named for the diversity of clinical findings seen on slit-lamp examination. The hallmark lesions are posterior vesicles, and these may be accompanied by bands or by diffuse opacities in 50% and 10% of the cases, respectively. The vesicles, misleadingly, look like transparent cysts of Descemet's membrane. The bands, if present, are usually horizontal, have scalloped edges, and most commonly occur along the inferior paracentral cornea. The bands can be distinguished from tears or folds of Descemet's because they lack tapered edges. Diffuse opacities range in size from 500 to 2000 μM, have a peau d'orange texture and are associated with adjacent posterior stromal haziness. As in Fuchs', guttata may be seen and corneal edema can develop. Rarely, this dystrophy is associated with corneal steepening or ectasia.

For the majority of patients the dystrophy causes no symptoms, is nonprogressive and may be picked up incidentally in the second or third decade of life. However, there is a wide spectrum of disease severity and some cases are vision threatening. In fact, severe corneal edema and clouding may be present at birth or early childhood, and this dystrophy needs to be considered in the differential diagnosis of congenital corneal clouding. While most cases are bilateral, there may be a marked degree of asymmetry in its presentation. In addition to corneal symptoms, patients may develop high intraocular pressure as a result of the peripheral anterior synechiae.

For patients with corneal decompensation, penetrating keratoplasty has been the treatment of choice. The success rate of keratoplasty is much higher for patients without significant broad preoperative synechiae or high pressure, and may be extremely low for patients with these problems. Recurrence after keratoplasty may occur in the form of a retrocorneal membrane. The pressure elevations associated with this dystrophy are difficult to manage medically or surgically.

The pathologic findings demonstrate layered-endothelial cells that have assumed epithelial characteristics such as microvilli and rapid growth in culture, and stain with epithelial cell markers such as cytokeratin (CK), pancytokeratin, and CK7 (a glandular epithelial marker). Descemet's membane is irregular with a typically normal anterior-banded zone but an absent or markedly abnormal posterior nonbanded zone. Much of the posterior zone is replaced by heterogenous collagenous components that comprise a 15–25-μM-thick posterior collagenous layer. Posterior synechiae may be found in up to a quarter of patients, and may be accompanied by iris defects including atrophy and corectopia.

On specular microscopy, the various posterior polymorphous lesions can be further examined. The vesicles appear as well-demarcated dark round areas with lighter ridges and dots. The bands have shallow hills and valleys composed of confluent vesicles, and the diffuse lesions are well-demarcated reflective areas with enlarged, pleomorphic, indistinct endothelial cells that are surrounded by more normal appearing endothelial cells.

At least two different loci are associated with posterior polymorphous dystrophy and they are found on chromosomes 20q11 and 1p34.3–p32. The resultant defects may affect the production of type VIII collagen, the predominant component of the anterior-banded zone.

Congenital Hereditary Endothelial Dystrophy

Present at birth or in the early postnatal period, this dystrophy is bilateral, symmetric, and diffuse, with corneal haze spanning from limbus to limbus. The cornea is very thick – 2–3 times normal – and there are no other associated anterior segment defects. Rarely, this corneal edema begins later in infancy or early childhood. Treatment consists of early keratoplasty.

Examination of the excised corneal buttons reveals reduction, absence, or degeneration of endothelial cells and diffuse corneal edema. As in all posterior dystrophies, there is an abnormal posterior nonbanded zone which merges into a posterior collagenous layer.

Inheritance is most often autosomal recessive and linked to chromsome 20p13, but rarely may be inherited as a dominant trait on chromosome 20p11.2–q11.2.

See also: Corneal Endothelium: Overview; Corneal Epithelium: Cell Biology and Basic Science; Corneal Epithelium: Transport and Permeability; Corneal Epithelium: Wound Healing Junctions, Attachment to Stroma Receptors, Matrix Metalloproteinases, Intracellular Communications; Corneal Imaging: Clinical; Corneal Scars; The Corneal Stroma; Cornea Overview; Imaging of the Cornea; Regulation of Corneal Endothelial Cell Proliferation; Regulation of Corneal Endothelial Function.

Further Reading

Afshari, N. A., Mullally, J. E., Afshari, M. A., et al. (2001). Survey of patients with granular, lattice, avellino, and Reis-Bücklers corneal dystrophies for mutations in the BIGH3 and gelsolin genes. *Archives of Ophthalmology* 119: 16–22.

Afshari, N. A., Li, Y. J., Pericak-Vance, M. A., et al. (2009). Genome wide linkage scan in Fuchs endothelial corneal dystrophy. *Investigative Ophthalmology and Visual Science* 50: 1093–1097.

Bron, A. J. (2000). Genetics of the corneal dystrophies: What we have learned in the past twenty-five years. *Cornea* 19: 699–711.

Dinh, R., Rapuano, C. J., Cohen, E. J., et al. (1999). Recurrence of corneal dystrophy after excimer laser phototherapeutic keratectomy. *Ophthalmology* 106: 1490–1497.

Holland, E. J., Daya, S. M., Stone, E. M., et al. (1992). Avellino corneal dystrophy: Clinical manifestations and natural history. *Ophthalmology* 99: 1564–1568.

Kang, P. C., Klintworth, G. K., Kim, T., et al. (2005). Trends in the indications for penetrating keratoplasty, 1980–2001. *Cornea* 24: 801–803.

Krachmer, J. H., Mannis, M. J., and Holland, E. J. (2005). *Cornea*, 2nd edn. Philadelphia, PA: Elselvier Mosby.

Kanski, J. J. (2003). *Clinical Ophthalmology: A Systematic Approach*, 5th edn. Edinburgh: Butterworth Heinemannn.

Stone, E. M., Mathers, W. D., Rosenwasser, G. O., et al. (1994). Three autosomal dominant corneal dystrophies map to chromosome 5q. *Nature Genetics* 6: 46–51.

Vasilliki, P. and Colby, K. (2008). Genetics of anterior and stromal corneal dystrophies. *Seminars in Ophthalmomlogy* 23: 9–17.

Yanofff, M. and Duker, J. S. (2004). *Ophthalmology*, 2nd edn. St. Louis, MO: Mosby.

Relevant Websites

http://www.emedicine.com – eMedicine: Ophthalmology Article.
http://www.nei.nih.gov – Facts about the Cornea and Corneal Disease (NEI Health Information).
http://www.cornealdystrophyfoundation.org – The Corneal Dystrophy Foundation.

Corneal Endothelium: Overview

D R Whikehart, The University of Alabama at Birmingham, Birmingham, AL, USA

Glossary

Autosomal dominant – The property of inheritance of a disease or trait from a single parent.
Chamber angle – This is the natural angle formed at the junction of the posterior limbus (at the trabecular meshwork), the ciliary body, and the iris.
Glycosaminoglycan – A general term for any sugar polymer of alternating sugars and aminosugars (aka a GAG).
Homeobox protein – A protein that is concerned with the embryological development of a multicellular organism. It is synthesized by a homeobox gene.
Keratocyte – A cell type found in the corneal stroma that makes and maintains collagens and glycosaminoglycans (aka a stromal cell).
Knock-out mouse – A genetically engineered mouse in which one or more specific genes have been made nonfunctional.
Schlemm's canal – A vessel behind the trabecular meshwork through which the aqueous fluid of the eye can drain into the venous system.
Stem cell – A primitive cell that has not differentiated into a functional cell of a multicellular organism.
Trabecular beam – A portion of the trabecular meshwork of the posterior limbus that consists of a rod of largely collagen material. When assembled in its typical complex pattern, trabecular beams offer resistance to the outflow of the aqueous fluid.
Transient amplifying cell – A cell in the process of differentiation from a stem cell as a functioning cell.

Anatomy

General Description

The corneal endothelium consists of a monolayer of polygonal cells, primarily hexagonal in shape, such that each has dimensions of 18–20 μm (width) by 5 μm (thickness). These cells produce a predominately collagenous product known as Descemet's membrane that is sandwiched between the anterior basal side of the endothelial cells and the posterior layer of the stroma. Descemet's membrane is a basement membrane that may act as a cushion for endothelial cell trauma and, in general, such basement membranes have been assigned roles associated with cell adhesion, migration, differentiation, and signal transduction. However, the exact roles of this membrane are presently unknown. Endothelial cells continually synthesize Descemet's membrane throughout life. On the posterior apical side, endothelial cells make direct contact with the anterior aqueous fluid in the anterior chamber. This pH neutral fluid (pH 7.4) is virtually absent in serum proteins and lipids, but contains nourishing glucose, antioxidants, and a variety of cytokines. At the boundary of the endothelium, endothelial cells are joined to a limbus whose transitional area is composed of cells that may contain precursor stem cells for the endothelium. The circular diameter of the corneal endothelium is approximately 11.7 mm in the adult. As with the remainder of the cornea, there are normally no blood vessels in this tissue. Although the anterior cornea does possess nerve endings, none are found in the endothelium (see **Figures 1–3**).

Cell-to-Cell Junctions

Corneal endothelial cells number about 3000 mm^{-2} in healthy, young adults and slowly decrease in number with age. The cells have a well-defined nucleus and their cytoplasm is packed with mitochondria necessitated by a high-energy requirement for the cells to act as a fluid pump. The cells also have a well-developed Golgi apparatus associated with the production of extracellular proteins needed for the assembly of Descemet's membrane. The cell-to-cell junctions are somewhat tortuous and interdigitated, a form that helps to keep the cells together. The cellular membranes at these junctions are held together with well-described joining proteins, of which one assembled complex has been called a zonula occludens (tight junction). However, there is still a controversy about whether or not this is a true zonula occludens. The reason for this is that the channel joining adjacent endothelial cells must allow both sodium and water to flow into the anterior chamber. This junctional form has been described to be more focal or point-like than that of the true riveted tight junctions of a zonula occludens. Gap junctions have also been shown to exist between the cells for the purpose of transporting small molecules between each cell. Additionally, adhesion junctions to strengthen cell-to-cell fastening can be found there. The membranes facing the anterior chamber have a number of microvilli, typical of many endothelial cell types. However, no roles for the microvilli in these cells have been described (see **Figures 3** and **4**).

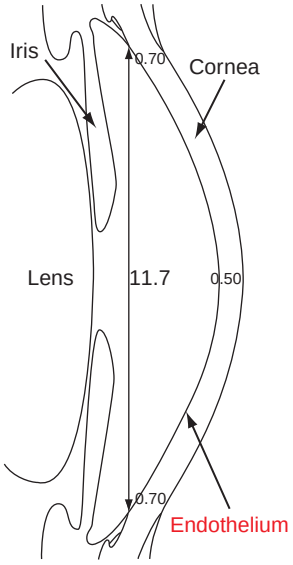

Figure 1 Overview of the anterior segment of the eye showing the cornea with the endothelium labeled in red. Numbers within the cornea are the cross-sectional dimensions in millimeters. The vertical line with the number represents the approximate diameter of an adult cornea in millimeters. Modified from Hogan, M. J., Alvarado, J. A., and Weddell, J. E. (1971). *Histology of the Human Eye*, p. 61. Philadelphia, PA: Saunders.

Figure 2 Cross-section of the human cornea. a, epithelium; b, Bowman's membrane; c, stroma; d, Descemet's membrane; e, endothelium. Adapted from Hogan, M. J., Alvarado, J. A., and Weddell, J. E. (1971). *Histology of the Human Eye,* p. 65. Philadelphia, PA: Saunders.

Embryology

Initial Development

It has been known for a long time that the corneal endothelium originates from neural crest, stem cells. These

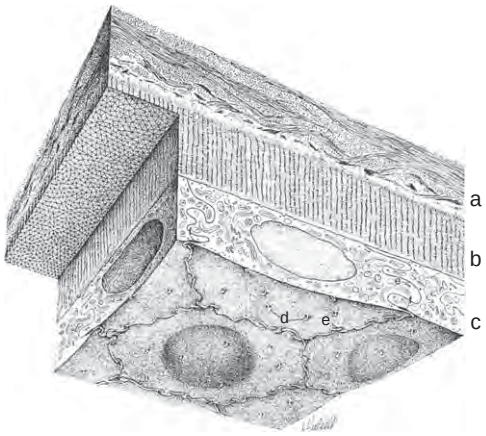

Figure 3 Three-dimensional, representational sketch of the corneal endothelium (c) with attached Descemet's membrane (b) and posterior stroma (a). Endothelial cell microvilli are shown at (d). Intercellular channels are indicated at (e) while quasi-tight junctions occur at (f). Adapted from Hogan, M. J., Alvarado, J. A., and Weddell, J. E. (1971). *Histology of the Human Eye,* p. 101. Philadelphia, PA: Saunders.

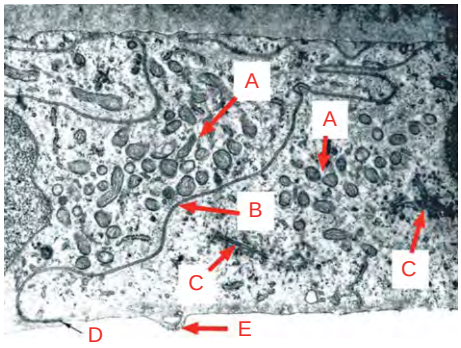

Figure 4 Cross-section of human corneal endothelial cells. The large population of mitochondria are evident at (A) while an intercellular channel may be seen at (B). Two Golgi apparatus are pointed out at (C). The intercellular channel, labeled at (B) is shown to empty out at the aqueous chamber at (D). At (E) can be seen a microvillus. Modified from Hogan, M. J., Alvarado, J. A., and Weddell, J. E. (1971). *Histology of the Human Eye,* p. 103. Philadelphia, PA: Saunders.

cells migrate from folds of the neural ectoderm at weeks 4–5 of embryonic development. This is illustrated in Figures 5–7. Since the developing embryo is relatively small and neural crest cells are localized along each section of the neural folds, from which they detach, migration is not very distant for each group of cells. In eye development, optic sulci (the primordial eyes) appear as shallow pits along the neural plate at week 4. These sulci begin to protrude outward as hollow optic vesicles from the proencephalon or forebrain of the neural plate. At just over 30 days, a wave of mesenchymal cells (in this case, neural crest cells) migrates over the optic cup into the space between the anterior surface of the lens and the surface ectoderm (corneal epithelium). These cells will become

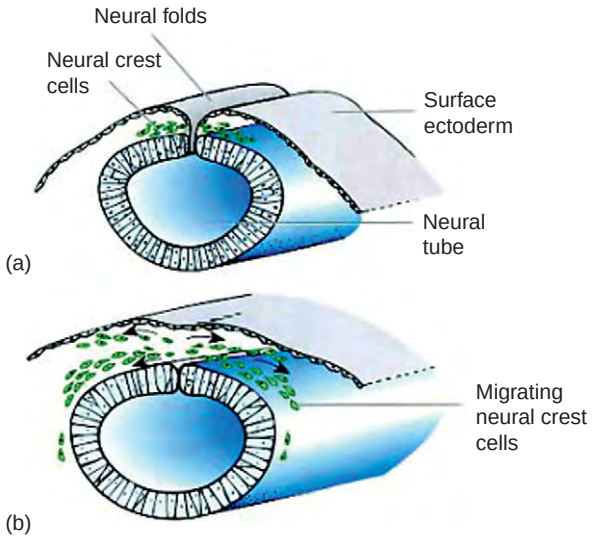

Figure 5 The developing neural folds and neural tube. As the neural folds move away from the neural tube (a and b), neural crest cells break away from the neural fold tissue (a) and begin their migration (b) to specific developing tissues. Modified from Forrester, J. V., Dick, A. D., McMenamin, P. G., and Roberts, F. (2008). *The Eye. Basic Science in Practice,* 3rd edn., p. 111. Edinburgh: Saunders.

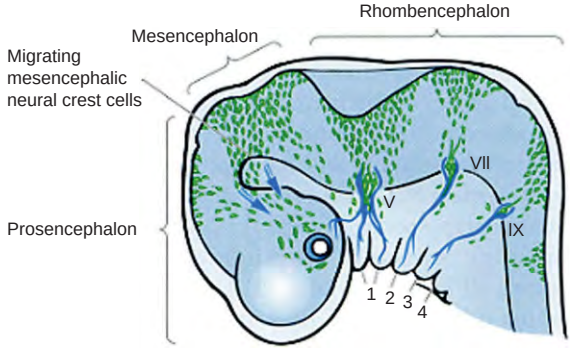

Figure 6 Migration pathways of neural crest cells. Neural crest cells are shown in green. The neural crest cells migrating to the eye originate primarily from the proencephalon (developing forebrain and brainstem) and the mesencephalon (developing midbrain). Migration is shown by dark blue arrows. Adapted from Forrester, J. V., Dick, A. D., McMenamin, P. G., and Roberts, F. (2008). *The Eye. Basic Science in Practice*, 3rd edn., p. 119. Edinburgh: Saunders.

the corneal endothelium. A second wave of mesenchymal cells (also neural crest cells) migrates around day 49 and places itself between the endothelium and epithelium. These cells are destined to become the keratocytes of the corneal stroma. Based on mouse model studies, it appears that those neural crest cells that will define the corneal endothelium at first remain in contact with the anterior lens and flatten out into a monolayer of cells. Then, the lens detaches from the endothelial monolayer to provide space for an anterior chamber where the aqueous fluid may enter (**Figures 8** and **9**). During this process, a third wave of neural crest cells migrates to the angle between the posterior cornea (endothelium) and the anterior edge of the optic cup (**Figure 10**). These cells eventually develop into the ciliary body and the iris.

During this development, the tissues anterior to the chamber angle between the anterior eye cup and the endothelium becomes occupied by a mass of mesenchymal (neural crest) cells that remain, at first, undifferentiated. These cells develop into flat endothelial-like cells that bring about the trabecular beams (trabecular meshwork) and, separately, Schlemm's canal cells. Some of the stellate cells, between the trabecular beams and the endothelial lining of Schlemm's canal, appear to remain undifferentiated. Evidence to support this is seen in a number of stem cell markers in this area which change with wounding (**Figure 11**). This is an important observation as it suggests the retention of stem cells in a niche for the replacement of cells in the posterior limbus and for the corneal endothelium. The point is made again that evidence strongly suggests that nearly all the mesenchymal cells that invade these areas of the anterior segment are neural crest in origin.

Role of Transcription Factors

Molecular biological mechanisms that control the overall development of the anterior segment remain incompletely described. This is also true for the corneal endothelium. What is known can explain some developmental effects. It is understood, for example, that inductive signals from the lens are partly responsible for endothelial cell differentiation. Defects in three lens genes that produce the homeobox proteins – MAF, FOXE3, and PITX3 – result in the inability of the lens to separate from the cornea (**Figure 12**).) Homeobox proteins assemble in a specific binding area of DNA to signal a specific RNA synthesis. They are required to bind to DNA in a set order for synthesis to begin. The three genes mentioned are concerned with producing genetic transcription factors that cause the synthesis of proteins necessary for lens–cornea separation. Other genetic abnormalities may also occur in the mesenchymal (stem) cells themselves that cause corneal development. In the endothelium itself, mutations in the genes PITX2, FOXC1, and PAX6, for example, are known to prevent satisfactory, functional corneal development. Normally, these genes produce the transcription factors for protein synthesis related to such development. PAX6, in particular, is required for making signaling molecules that cause transport of neural crest cells into the eye as well as the phenotypical development of the corneal endothelium itself. In addition, the amounts and origins of PAX6 proteins appear to be critical for the sequence signaling of corneal development. One signaling molecule that may be produced as a result of DNA binding of such transcription factors is transforming

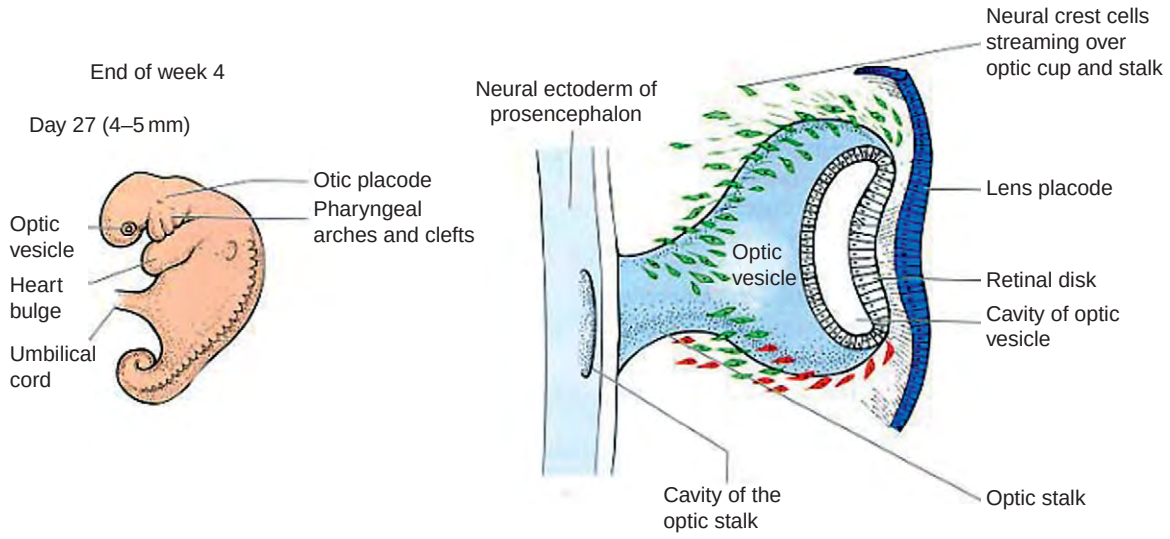

Figure 7 Cell migration pattern to the eye cup at the end of the 4th week. Neural crest cells are shown in green. Mesodermal cells are shown in red. Adapted from Forrester, J. V., Dick, A. D., McMenamin, P. G., and Roberts, F. (2008). *The Eye. Basic Science in Practice,* 3rd edn., p. 112. Edinburgh: Saunders.

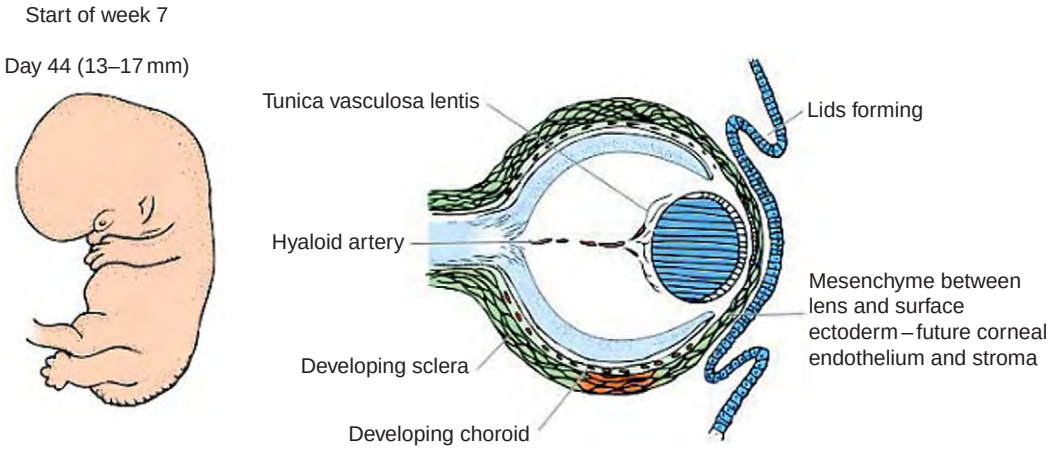

Figure 8 Established neural crest cells in the eye at the beginning of the 7th week. Neural crest cells are shown in green and include the future corneal endothelium and stroma. Adapted from Forrester, J. V., Dick, A. D., McMenamin, P. G., and Roberts, F. (2008). *The Eye. Basic Science in Practice*, 3rd edn., p. 113. Edinburgh: Saunders.

growth factor, beta 2 (TGF-β2). In TGF-β2 knock-out mice, that cannot produce this protein due to a lack of PAX6, the corneal endothelium is completely absent. It is also known that the overexpression of TGF-β1 (a related molecule using similar receptors) results in an absent endothelium. So, the case is made that these controlling proteins must be present in specific amounts and at the right time sequence to allow proper corneal endothelial cell development to occur.

Biochemistry and Metabolism

Glucose and Energy Metabolism

The corneal endothelium is a cell type that is required to have large outputs of energy to maintain the process of deturgescence (discussed in the section entitled 'Proteins synthesized for external transport'). In this regard, corneal endothelial cells maintain a high amount of adenosine triphosphate (ATP)-producing mitochondria as well as a defined Golgi apparatus for the complete synthesis, retention, and export of proteins. In studies of comparative carbohydrate metabolism, it has been shown that the amount of aerobic glycolysis (glucose breakdown to produce ATP) is 3 times higher than it is in the cells of the corneal epithelium and stromal keratocytes. Compared to the cells of the lens, corneal endothelial cells use aerobic glycolysis at better than 6 times the amount used by the lens. On a per cell basis, it is even estimated that corneal endothelial cells produce more ATP energy than individual cells of the ciliary body by 40%. Only cells of the retina exceed the cells of the corneal endothelium in

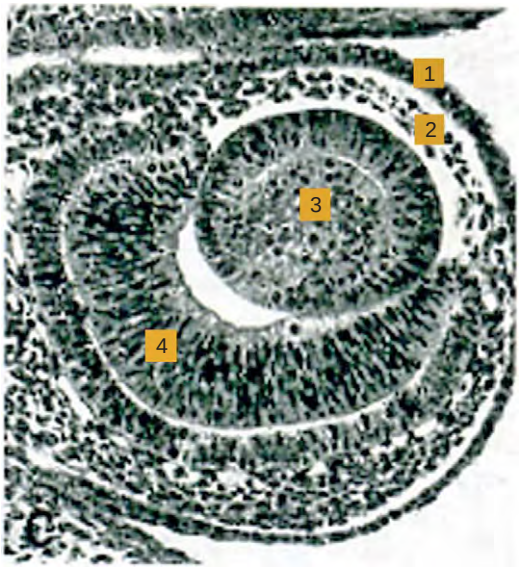

Figure 9 A developing eye of a human fetus past 6 weeks. 1. the outer cornea (epithelium). 2. coalescing stem cells forming the endothelium and keratocytes. 3. the developing lens. 4. the inner layer of the retina. Modified from Forrester, J. V., Dick, A. D., McMenamin, P. G., and Roberts, F. (2008). *The Eye. Basic Science in Practice*, 3rd edn., p. 115. Edinburgh: Saunders.

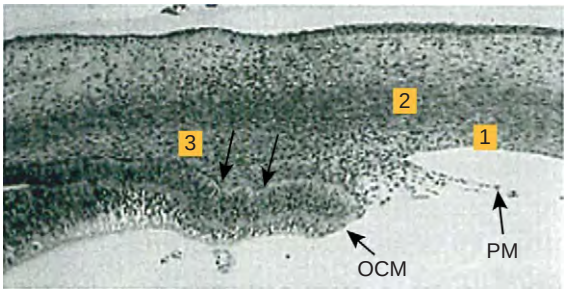

Figure 10 Development of tissues at the angle of the posterior limbus at 12 weeks. The figure shows the pupillary membrane (PM) beginning to form the optic cup margin (OCM) and indentation caused by vascular mesenchyme (double arrows). At (1) are the corneal endothelium (1st wave of neural crest cells); (2) the forming keratocytes (2nd wave of neural crest cells) and collagen; and (3) possible 3rd wave of invading neural crest cells to form the trabecular meshwork. Modified from Forrester, J. V., Dick, A. D., McMenamin, P. G., and Roberts, F. (2008). *The Eye. Basic Science in Practice*, 3rd edn., p. 131. Edinburgh: Saunders.

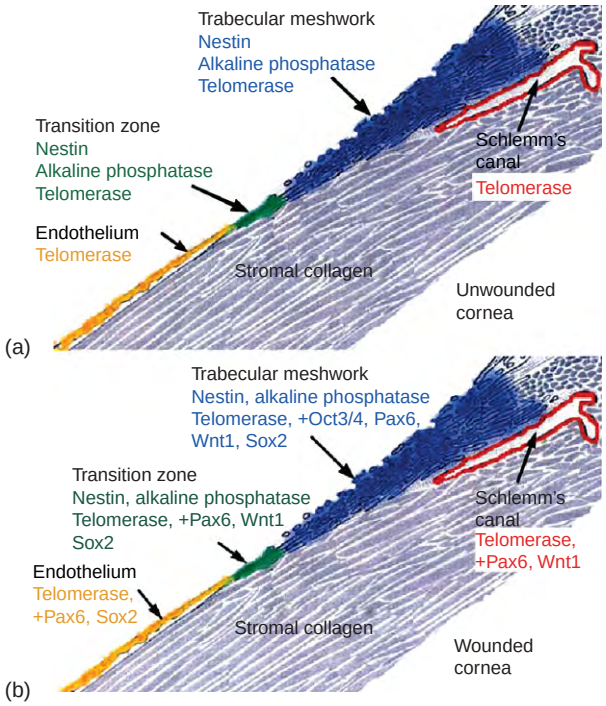

Figure 11 Stem cell and transient amplifying cell staining patterns at the peripheral corneal endothelium, transition zone, and trabecular meshwork of the posterior limbus in adult humans. Unwounded tissue is shown at (a) while wounded tissue is shown at (b). Tissues were stained with the following stem cell marker proteins: nestin, alkaline phosphatase, Wnt1, and Oct3/4. Tissues were stained with the following marker for both stem cells and transient amplifying cells: telomerase. Wounded tissues were stained with the following cell differentiation markers: Pax-6 and Sox2. Adapted from McGowan S. L., Edelhauser, H. F., Pfister, R. R., and Whikehart, D. R. (2007). Stem cell markers in the human posterior limbus and corneal endothelium of unwounded and wounded corneas. *Molecular Vision* 13: 1984–2000. http://www.molvis.org/molvis/v13/a224/.

metabolic energy produced. Although direct evidence is scarce, it seems that corneal endothelial cells are not insulin dependent and, therefore, are not starved of glucose in diabetes. On the contrary, it is perplexing that glycation of sodium, potassium-ATPase (Na, K-ATPase) does not cause an inhibition of the enzyme in the diabetic.

Cell Division and Replenishment

The lack of any ready, apparent replication of endothelial cells has been an ongoing problem when cell replacement might be required. In general, the population of these cells decline with age, but usually there remain sufficient numbers of cells at an advanced age to maintain corneal clarity. This has not seemed to be the case with wounding, trauma, and other dramatic forms of endothelial cell loss. Studies of the cell cycle in endothelial cell have indicated that the cells tend to remain in the G_1 phase (perhaps even the G_o temporary exit of cell division). This could be due to such factors as simple cell-to-cell contact inhibition or the presence of the TGF-β2 protein found in the aqueous humor. Departure from the G_1 stage toward replication can be artificially induced with the E2F2 transcription factor since the E2F2 protein is known to bring cells into the S-phase of the cell cycle. Cells that have been transformed either with the SV40 large T-antigen or with the E6/E7 human papilloma virus can also act to initiate replication. The SV-40 and E6/E7 proteins inactivate the activity of retinoblastoma (Rb) and p53 cell cycle suppressor proteins by interacting with

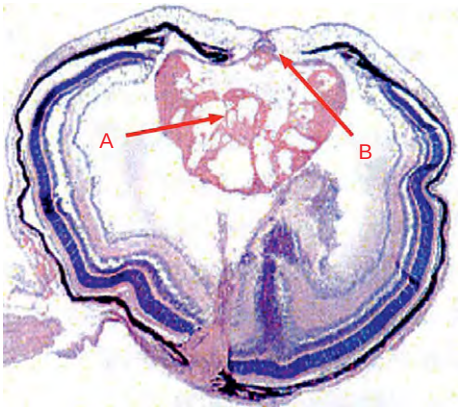

Figure 12 Cross-section of Foxe3$^{-/-}$(deficient) mouse eye showing small lens (A) and persistent attachment of lens to cornea (B). Adapted with permission from Medina-Martinez, O. and Jamrich M. (2007). Foxe view of lens development and disease. *Development* 134: 1455–1463.

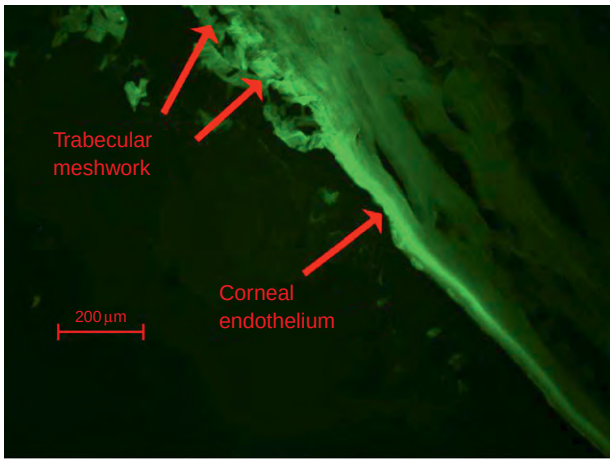

Figure 13 BrdU fluorescence shown in the peripheral corneal endothelium and trabecular meshwork 48 h after a mechanical wound to the endothelium. Adapted from Whikehart, D. R., Parikh, C. H., Vaughn, A. V., Mishler, K., and Edelhauser, H. F. (2005). Evidence suggesting the existence of stem cells for the human corneal endothelium. *Molecular Vision* 11: 816–824. http://www.molvis.org/molvis/v11/a97/.

them and allowing the E2F2 transcription factor to initiate the cell cycle. These are not the usual cell processes, however, and the lack of normal cell division remains unresolved. There is evidence, however, that endothelial cells are replaced *in vivo*. Studies have pointed to the existence of stem cells in the posterior limbus just beyond the boundary of the corneal endothelium (**Figure 11**). Initially, some investigators noted a higher than usual density of corneal endothelial cells that exist at the endothelial periphery. This suggested that replacement cells or germinating cells were present in this area. Later, stem cells were identified in the posterior limbus. This has been shown by labeling with stem cell markers such as Nestin and Oct3/4 in the limbus and the subsequent appearance of repair or developmental proteins such as PAX6 and Wnt1 in the limbus and the peripheral endothelium following wounding. The appearance of the transient amplifying cell marker telomerase in these areas strongly points to the possibility that stem cells, resident in the posterior limbus, give rise to new corneal endothelial cells. In fact, BrdU studies have confirmed the generation of new cells from the posterior limbus into the peripheral endothelium after wounding (**Figure 13**). This is analogous to what occurs in the corneal epithelium, but at a significantly lower rate of reproduction.

Cytokines and Immune Privilege

The existence of cytokines, generated by the lens and other cells adjacent to the anterior chamber in the aqueous fluid, suggests that the endothelium may be influenced by its neighboring tissues. Cytokines are a broad mixture of polypeptides or proteins that are able to communicate a signal to a cell to initiate some change or response from the cell. In fact, the distinction between a cytokine and a local hormone is considered moot by many. Cytokines were originally associated only with immune functions. An example of a cytokine that has both immune and nonimmune effects is the TGF-β, pointed out earlier. In the eye, TGF-β is known to modulate cell migration, proliferation, death, development, tissue repair, and many pathological processes as well. Generally, however, this cytokine is responsible for extracellular matrix production and the suppression of cell proliferation. There are three isoforms of TGF-β. Of the three, TGF-β2 is the predominant cytokine that is found in the aqueous fluid bathing the endothelium. The presence of TGF-β2 is essential to the cornea since its absence results in a failure of the endothelium to develop (see **Figure 14**).

Immune privilege in the eye is a process in which the eye protects itself from undesirable immune characteristics, such as inflammation, as a device to preserve vision. For the anterior segment, that means the ability of light to pass through its tissues unimpeded. Immune privilege is the summation of many complex molecular and cellular mechanisms whose operation, as a whole, remains incompletely understood. It is also the process by which corneal transplants are more likely to be free of immune reactions than transplants in other parts of the body. In an immune-privileged site, such as the corneal endothelium, active processes are set in motion to suppress immune reactions when an antigen enters the site. The aqueous humor is responsible for this action since it contains the necessary suppression cytokines that are released by cells bordering the anterior chamber. TGF-β2, in addition to its roles mentioned previously, inhibits T-cell activation and differentiation that are necessary to initiate inflammation.

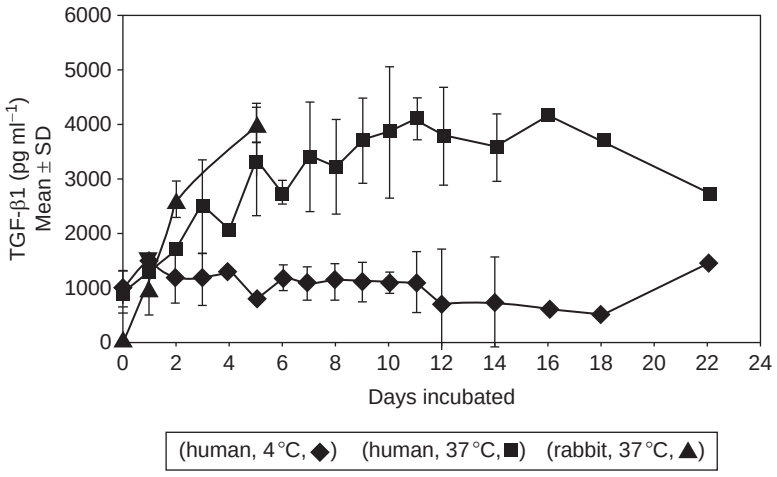

Figure 14 Levels of TGF-β1 in fluids bathing an excised cornea following mechanical wounding. At 37°C, it is seen that the levels of the cytokine, produced by the cornea, are increased as a mechanism to limit cell division about 48 h after wounding. Adapted from Whikehart, D. R., Parikh, C. H., Vaughn, A. V., Mishler, K., and Edelhauser, H. F. (2005). Evidence suggesting the existence of stem cells for the human corneal endothelium. *Molecular Vision* 11: 816–824. http://www.molvis.org/molvis/v11/a97/.

Other examples of cytokines that contribute to immune privilege are: α-melanocyte stimulating hormone, vasoactive stimulating peptide, calcitonin gene-related peptide, and somatostatin. A more recent finding has been the discovery of another cytokine: cluster of differentiation 95 ligand (CD95L) at immune-privileged sites. CD95L acts as a death signal that triggers apoptosis (programmed cell death) in CD95 sensitive T cells. The membrane protein form of CD95L, expressed on corneal endothelial cell membranes, has been shown to be important for the preservation of orthoptically placed corneal grafts and it does this by interacting with these T cells.

Some contradictions in the understanding of immune suppression also exist. For example, it is not understood how the soluble versus membrane forms of CD95 function and why the CD95L form is important for graft acceptance. In addition, many of the cells that surround the anterior chamber have receptors for tumor necrosis factor-α. This cytokine, unfortunately, plays an important role in intraocular inflammation (endotoxin-induced uveitis) when it occurs.

Proteins Synthesized for External Transport

In human corneas, there are known anatomical subdivisions found in Descemet's membrane: an anterior, banded zone and a nonbanded, amorphous zone (**Figure 15**). The banded zone is formed before birth while the amorphous zone is continuously synthesized during life. Four principal proteins have been found to constitute Descemet's membrane in both zones: collagens type IV and VIII as well as laminin and fibronectin. All are considered to be synthesized by corneal endothelial cells throughout the lifetime of an individual. However, recent suggestions

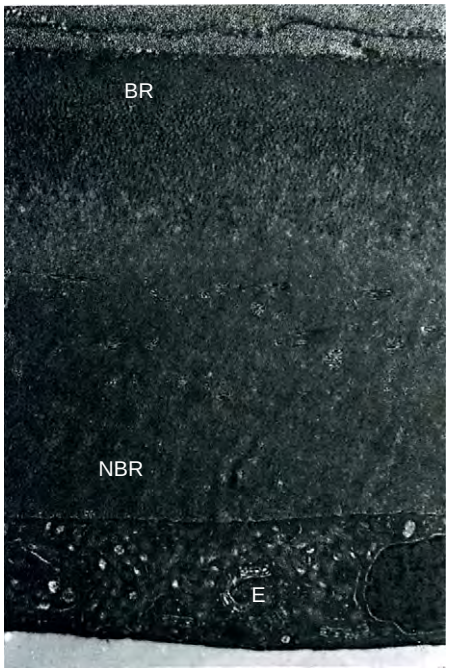

Figure 15 The banded (BR) and nonbanded (NBR) regions of Descemet's membrane. The BR is formed before birth while the NBR is made continuously throughout life. E, the endothelium. ×7000. Adapted from Forrester, J. V., Dick, A. D., McMenamin, P. G., and Roberts, F. (2008). *The Eye. Basic Science in Practice*, 3rd edn., p. 21. Edinburgh: Saunders.

contend that some evidence points to the posterior keratocytes as sources for some of this synthetic work. Collagen type IV was originally considered to be the principal collagen of Descemet's membrane. It is described as the main structural protein of all basement membranes. The α-1–α-6 chains are found in Descemet's membrane facing the stromal and endothelial sides of the membrane in both

infants and adults. Type VIII collagen is a short nonfibrillar protein that may determine cell phenotype. In the infant, it is found on the endothelial face of the membrane, whereas it occurs on the stromal face of the membrane in the adult. Laminin is a noncollagenous glycoprotein that binds to other proteins to form sheets. Its association with type IV collagen in basement membranes is well known. Laminin occurs on the stromal and endothelial faces of infants, but it is not found on the stromal face of adult Descemet's membrane. Fibronectin is a high-molecular-weight protein that can bind to membrane receptor proteins as well as collagen. It is involved in cell adhesion. Fibronectin only occurs on the stromal face of Descemet's membrane in both infants and adults. Mucin-1 (MUC-1), a cell surface protein that has largely been considered to be present on the surface of the corneal epithelium, has also been found to be synthesized by the endothelium and transported to its apical surface. Its function there would be as an interfacing protein to the aqueous fluid.

The Role of the Corneal Endothelium in Deturgescence

Introduction

The average human cornea in the adult is maintained at a thickness of 500 μm in the center to about 700 μm at the periphery (Figure 1). Keeping these parameters stable is important for corneal clarity. Deturgescence is the physiological process of maintaining such a clear cornea. The process is active and continuous. Two forces are at work during deturgescence. In one process, the cornea swells and tends to become cloudy. Due to the large volume of negatively charged glycosaminoglycans (GAGs) bound to the proteoglycans in the cornea, there is a constant influx of cations into the stroma from fluids outside of this tissue. These cations are accompanied by water as an osmotic compensation and bring about corneal swelling. The stroma is composed of layers of collagenous lamellae with each collagen strand separated from its neighbor by an aquous space. Disruption of the geometric regularity in the aqueous spaces that contain the GAGs brings about a loss in the mutual interference of light that is refracted through the cornea. This results in the beginning of a loss of clarity which can continue through progressive degrees of opacity (cloudiness). If unchecked, this process would result in functional blindness. In the second process of deturgescence, excess water is actively transferred out of the stroma by the corneal endothelium into the aqueous fluid of the anterior chamber. The corneal epithelium takes on a rather passive role in this process by acting more as a barrier to water flow. Early experiments demonstrated the existence of this active process to be predominately in the endothelium. This was accomplished by the selective removal of corneal outer layers to determine which side (epithelium or endothelium) was involved in pumping out water. A metabolic component was shown to exist when the deturgescent process was compared in experimental corneas at cold versus physiological temperatures (Figure 16).

The Biochemistry of Active Deturgescence

Active deturgescence is considered to occur as the result of the catalytic activity of two enzymes: sodium, potassium-stimulated adenosine triphosphatase (Na, K-ATPase) and bicarbonate-stimultated adenosine triphosphatase ($^{-}HCO_3$-ATPase). Na, K-ATPase resides in the basolateral membranes of corneal endothelial cells in sufficient quantities to ensure significant pumping activity.

As an enzyme, Na, K-ATPase exists with a minimal structure of four polypeptide chains of which two (the α-chains) are catalytic and two (the β-chains) are structural stabilizers in the cell membrane. In carrying out pumping activity, the enzyme is energized by the hydrolysis of ATP to adenosine diphosphate (ADP) in which energy, contained in the released inorganic phosphate group, is transferred to an α-subunit. This energy provides for the kinetic transfer of two potassium ions into an endothelial cell while three sodium ions are virtually, simultaneously moved to the cell exterior. The result is the net movement of one cation outside the cell (Figure 17). The osmotic consequence of this is the simultaneous flow of water into the anterior chamber either directly or through the channels that lie between endothelial cells. Water therefore flows osmotically, due to ion transfer, through endothelial cells by means of proteins known as aquaporins.

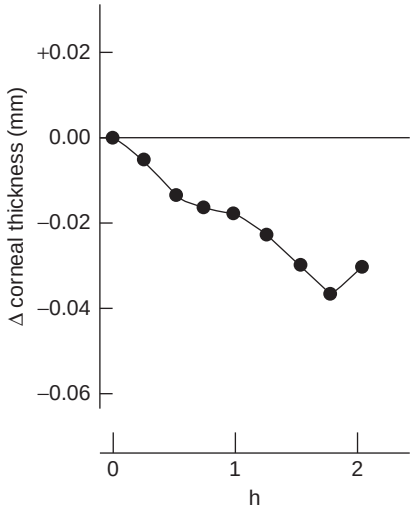

Figure 16 A temperature-reversal experiment in which a cornea is previously allowed to swell in the cold and then demonstrated to decrease in thickness when placed at room temperature for 2 h. From Dr. Henry Edelhauser.

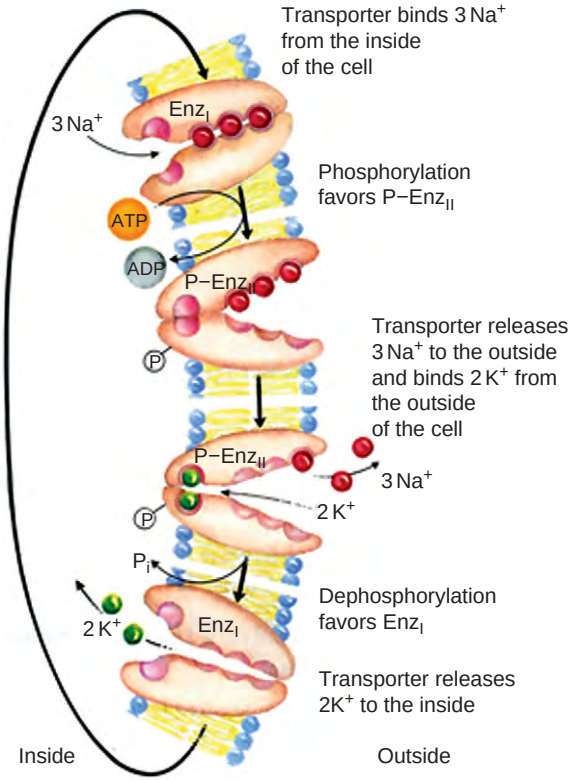

Figure 17 A postulated mechanism for the two α-subunits of Na, K-ATPase. The mechanism (beginning at the top of the figure) is initiated with the cytosolic binding of three sodium cations, followed by ATP hydrolysis, sodium external transport, two potassium cation external binding, potassium internal transport, and release. The cycle is then repeated. Adapted from Nelson, D. L. and Cox, M. M. (2005). *Lehninger. Principles of Biochemistry*, 4th edn., p. 399. New York: Freeman.

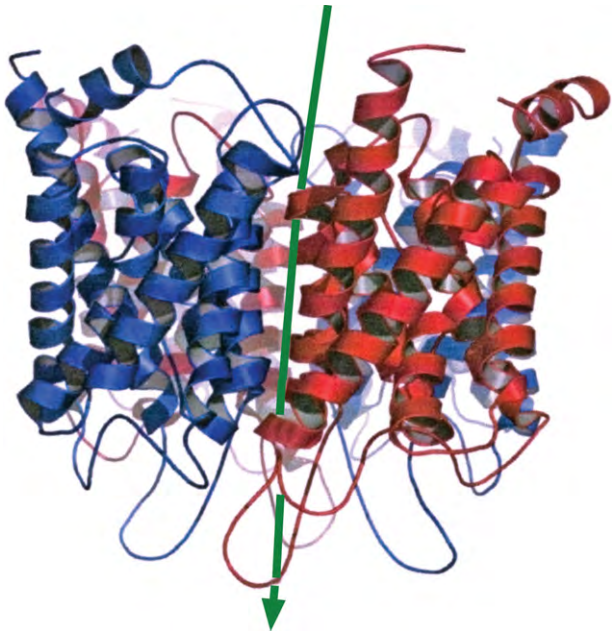

Figure 18 Aquaporin-1 consists of four polypeptide chains (shown here in red and blue). The channel for water that they form is shown as a green arrow. Modified from Wikipedia/Aquaporin.

The water transport protein in the cornea is known as aquaporin-1 (AQP-1; Figure 18).

Bicarbonate-ATPase has a role that is more difficult to define, but which has been considered by some to be supportive of the role of Na, K-ATPase. Evidence indicates that the enzyme has a molecular weight similar to the α-subunit of Na, K-ATPase. Part of the difficulty in understanding how or why this enzyme functions lies in the fact that it is resident in mitochondria rather than in plasma membranes. The enzyme functions, just as Na, K-ATPase, by obtaining energy from ATP hydrolysis and is, therefore, also a P-type ATPase. The energy incorporated into the enzyme causes it to transfer anions across membranes that include chloride as well as bicarbonate. In the literature, there has been considerable confusion about whether this enzyme is primarily a chloride or a bicarbonate transporting enzyme *in situ* in the corneal endothelium. Experimentally, it seems that either anion may be substituted for the other or that bicarbonate may be required to stimulate the transport of chloride. The importance of bicarbonate cannot be denied as, experimentally, a decrease in bicarbonate, and the use of carbonic anhydrase inhibitors clearly shows a loss of deturgescence. Carbonic anhydrase converts water and carbon dioxide into bicarbonate and a proton. At this point, whether chloride or bicarbonate is of prime importance is unclear.

The Physiological Control of Active Deturgescence

It is evident that moving a net amount of cations from the corneal endothelium (via Na, K-ATPase) to the anterior chamber will result in transferring water from the endothelium to the aqueous to maintain an osmotic balance. This activity serves to remove excess water from the stroma (via aquaporin transport through the corneal endothelium) while water leaks back into the stroma simultaneously. Normally, the concentration of Na^+ ions is higher in the anterior chamber than in the stroma, so the activity of Na, K-ATPase is required to push Na^+ ions against the gradient of the anterior chamber. The two processes (pump and leak) operate in a fashion analogous to water leaking into a basement while it is being removed by a sump pump at the same time. Since Na, K-ATPase requires a substantial supply of ATP as an energy source from mitochondria, it can be speculated that the membrane potential and pH of that organelle requires that the potential and pH stability be well maintained. To what degree the operation of a $^-HCO_3$-ATPase in the mitochondria contributes to these phenomena is unknown.

There remain other physiological observations that challenge further investigation of the pump-leak hypothesis of deturgescence. For example, do the aquaporins (AQP-1 in the endothelium and AQP-5 in the epithelium) play more than a passive role in deturgescence? What function might TRPV4 (an osmolar-sensing protein in the epithelium) play in regulating stromal volume?

Genetic Diseases of the Corneal Endothelium

Fuchs' Endothelial Dystrophy

This disease is considered to be the result of an autosomal dominant disorder. It is a true disease of the corneal endothelium rather than one that originates from another area of the cornea (Figure 19). It was first described in 1910. There are two forms of the disease: early onset (mutations associated with chromosomes 13 and 18) and late onset (perhaps found on chromosome 1 or at other locations). The early onset form is associated with a mutation of the COL8A2 gene which synthesizes collagen VIII, a major collagen of Descemet's membrane. The exact identity of the gene defect in the late onset form has been proposed to be SLC4A11, a gene that causes the synthesis of a transport protein in endothelial cells. Both forms of the disease manifest themselves initially in the formation of guttae (gutattae) or buttons on the endothelium. Later development of the condition occurs with the formation of edema or swelling in the posterior stroma. The edema spreads anteriorly and leads to the development of corneal cloudiness. The stroma may take on the appearance of ground glass as the disease progresses. This disease progresses slowly and is more common in females than in males. Effective treatment is a penetrating keratoplasty (corneal transplant).

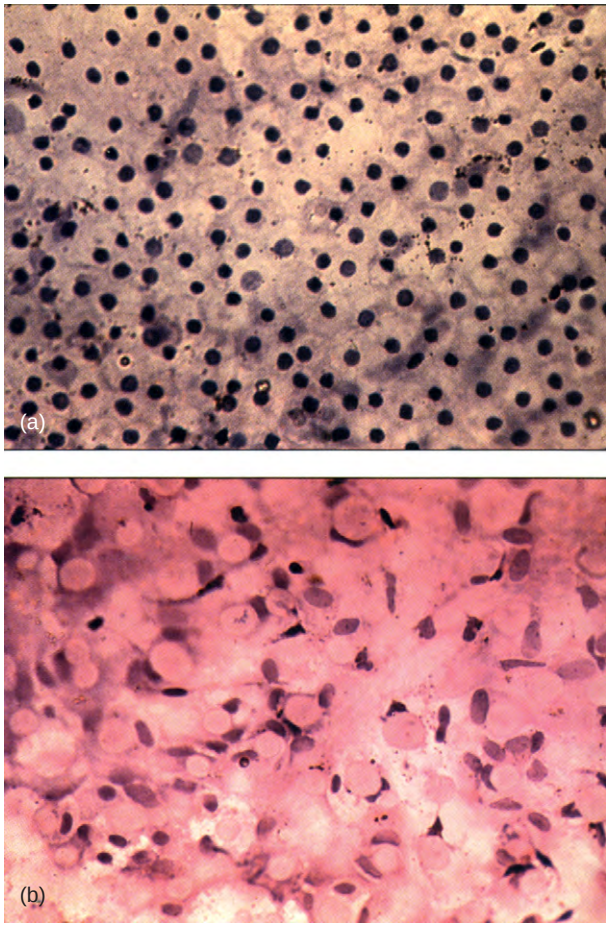

Figure 19 Endothelial cell layers as viewed from the posterior side of the cornea: (a) is a normal endothelium showing a regular pattern of polygonal cells and (b) is an example of moderately advanced Fuch's dystrophy. It shows a marked decrease in cell numbers, abnormal nuclei, and cell displacement by guttatae from Descemet's membrane. Adapted from Kratchmer, J. H., *et al.* (eds.) (2005). *The Cornea*, 2nd edn., vol. 1, p. 942. Philadelphia, PA: Elsevier.

Related Posterior Membrane Dystrophies

Two dystrophies that have some similarities to Fuch's dystrophy are posterior polymorphous dystrophy (PPMD) and congenital hereditary endothelial dystrophy (CHED). PPMD has been associated with four gene mutations on chromosomes 10 and 20 that affect the synthesis of collagens IV and VIII. In PPMD, there are differences in the effects on Descemet's membrane and the corneal endothelium versus the effects that occur in Fuchs' dystrophy. The nonbanded zone of Descemet's membrane becomes absent or minimal while the endothelial cells can take on the appearance of epithelial cells. PPMD patients are often asymptomatic, but those receiving penetrating keratoplasties sometimes develop increased intraocular pressure associated with iris attachments (synechiae). By contrast in CHED, the genetic abnormalities have been associated with one or more gene mutations only on chromosome 20. There is a decided loss of endothelial cells rather than a thinning of cells as occurs with Fuchs' dystrophy. The outcome of penetrating keratoplasty for CHED patients is mixed.

See also: Regulation of Corneal Endothelial Cell Proliferation; Regulation of Corneal Endothelial Function.

Further Reading

Cveki, A. and Tamm, E. R. (2004). Anterior eye development and ocular mesenchyme: New insights form mouse models and human diseases. *BioEssays* 26: 374–386.

Forrester, J. V., Dick, A. D., McMenamin, P. G., and Roberts, F. (2008). *The Eye. Basic Sciences in Practice*, 3rd edn. Edinburgh: Saunders/Elsevier.

Gerencher, G. A. and Zhang, J. (2003). Chloride ATPase pumps in nature: Do they exist? *Biological Reviews* 78: 197–218.
Hogan, M. J., Alvarado, J. A., and Weddell, J. E. (1971). *Histology of the Human Eye*. Philadelphia, PA: Saunders.
Krachmer, J. H., Mannis, M. J., and Holland, E. J. (eds.) (2005). *Cornea,* 2nd edn., vol. 1, Philadelphia, PA: Mosby/Elsevier.
Kratchmer, J. H., Mannis, M. J., and Holland, E. J. (eds.) (2005). *The Cornea*, 2nd edn., vol. 1, p. 942. Philadelphia, PA: Elsevier.
McCarey, B. E., Edelhauser, H. F., and Lynn, M. J. (2008). Review of corneal endothelial specular microscopy for FDA trials of refractive procedures, surgical devices, and new intraocular drugs and solutions. *Cornea* 27: 1–16.
McGowan, S. L., Edelhauser, H. F., Pfister, R. R., and Whikehart, D. R. (2007). Stem cell markers in the human posterior limbus and corneal endothelium of unwounded and wounded corneas. *Molecular Vision* 13: 1984–2000.
Medina-Martinez, O. and Jamrich, M. (2007). Foxe view of lens development and disease. *Development* 134: 1455–1463.
Mimura, T. and Joyce, N. C. (2006). Replication competence and senescence in central and peripheral human corneal endothelium. *Investigative Ophthalmology and Visual Science* 47: 1387–1396.
Streilein, J. W. and Stein-Streilein, J. (2000). Does innate immune privilege exist? *Journal of Leukocyte Biology* 67: 479–486.
Verkman, A. S. (2005). Aquaporins in endothelia. *Kidney International* 69: 1120–1123.
Vithana, E. N., Morgan, P. E., Ramprasad, V., *et al.* (2008). SLC4A11 mutations in Fuchs endothelial corneal dystrophy. *Human Molecular Genetics* 17: 656–666.
Whikehart, D. R. (2003). *Biochemistry of the Eye*, 2nd edn. Philadelphia, PA: Butterworth-Heinemann/Elsevier.
Whikehart, D. R., Parikh, C. H., Vaughn, A. V., Mishler, K., and Edelhauser, H. F. (2005). Evidence suggesting the existence of stem cells for the human corneal endothelium. *Molecular Vision* 11: 816–824.
Wilson, S. E., Weng, J., Blair, S., He, Y. G., and Lloyd, S. (1995). Expression of E6/E7 or SV40 large T antigen-coding oncogenes in human corneal endothelial cells indicates regulated high-proliferative capacity. *Investigative Ophthalmology and Visual Science* 36: 32–40.
Zhu, C., Rawe, I., and Joyce, N. C. (2008). Differential protein expression in human corneal endothelial cells cultured from young and older donors. *Molecular Vision* 14: 1805–1814.

Relevant Websites

http://www.eyesite.org – Diagrams and a video on corneal endothelial transplantation, The Eyesite.
http://dev.biologists.org – The Company of Biologists Ltd: Development. (This on-line paper reports about the deleterious effects of either TGFα or EGF on corneal endothelial development in a transgenic mouse.).

Corneal Epithelium: Cell Biology and Basic Science

M A Stepp, The George Washington University Medical Center, Washington, DC, USA

Glossary

Adhesion complex – The term used to refer to the different components of the cell: substrate junction that is present at the basal aspect of the stratified squamous epithelial tissues of the body, including the skin and the cornea. The adhesion complex includes not only the hemidesmosomes that contain $\alpha 6\beta 4$ integrin and collagen XVII, but also the inner hemidesmosomal plaque that contains plectin and BPA230, the anchoring filaments that are made of laminin 332, the anchoring fibers and the adhesions plaques that both contain collagen type VII. This structure forms during development and must partially or completely disassemble during wound healing and tissue regeneration and then reassemble after healing is complete. If the adhesion complex fails to form due to mutations in one of its components, blistering of the epithelial sheets covering the skin and cornea occurs.

Basement membrane zone – Sheets of epithelial cells that form the outer surfaces of the body are separated from their underlying mesechymal cells by basement membranes. Basement membranes are composed of the network-forming collagen type IV, the heparan sulfate proteoglycan perlecan, and several different types of laminins. The basement membrane zone consists of the basal plasma membrane surface of the basal epithelial cells, the hemidesmosomes, and the basement membrane itself. At the EM level, it consists of the inner and outer plaques of the hemidesmosomes, the lamina lucida, and the lamina densa.

Defensins – These are small cysteine-rich cationic proteins first characterized in leukocytes in 1985. The name was chosen because these proteins have antibacterial, antifungi, and antiviral activity. They consist of 18–45 amino acids including six (in vertebrates) to eight conserved cysteine residues. They bind to proteins on the surfaces of pathogens and form much of the basis of what immunologists call the innate defense system. Human tears have at least 4 different defensins and their presence in the tears is regulated during the healing of corneal wounds.

Glycocalyx – This term means sugar coat and in the cornea it refers to the thin film of sugar-containing material at the apical surface of the apical cells on the cornea. The primary molecules that make up the glycocalyx in the cornea are called mucins. There are several different types of mucins, some secreted and some cell-surface bound, on the healthy, wet ocular surface. The mucins of the glycocalyx help the tear film to spread over the ocular surface.

Integrins – A family of glycoproteins that function as heterodimers to mediate both cell:matrix interaction and cellular signaling. Integrins are integral membrane single pass proteins whose cytoplasmic domains bind to elements of the cytoskeleton including actin for most of the integrins and intermediate filaments for $\alpha 6\beta 4$. Their extracellular domains bind to extracellular matrix proteins including collagens, fibronectin, and laminins. Integrins are considered mechanotransducers of forces from outside cells and tissues to the cytoskeleton to allow cells to change shape during development and wound healing.

Niche – From the old French word *nichier* meaning to nest, this term is usually used to refer to the site where adult stem cells reside. In the cornea, the niche is believed to be located at the palisades of Vogt at the corneoscleral junction. Stem cell niches consist of both specialized extracellular matrix molecules that the stem cells adhere to as well as other cell types that play supportive roles by expressing cell:cell adhesion proteins and/or growth factors that act to maintain the stem cells within the niche and inhibit their differentiation.

Refractive surgery – This term refers to surgical procedures developed to improve the refractive state of the eye and decrease dependence of the patient on glasses or contact lenses. The major forms of refractive surgery are laser-assisted *in situ* keratomileusis and photorefractive keratectomy. According to the American Society of Cataract and Refractive Surgery, more than 900 000 refractive procedures were performed in the US in 2005.

The Corneal Epithelium Has Vital Functions in Vision

The corneal epithelium is a transparent covering that allows light entry into the eye. It is the outermost

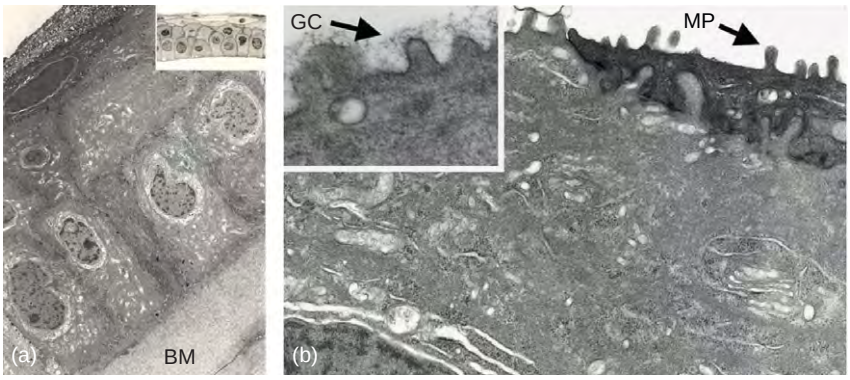

Figure 1 The surface epithelium of the cornea is specialized for light transmission and spreading of the tear film. (a) Transmission electron micrograph of the human corneal epithelium; a lower magnification image is in the inset. There are 3–5 cell layers and both apical and basal surfaces are flat and shear to minimize refraction of light. (b) The apical surface of the corneal epithelium has projections called microplicae. When shown at higher magnification as in the inset, the glycocalyx is seen covering the microplicae. The mucin proteins in the glycocalyx are hydrophilic and bind water which helps the tear film spread over the ocular surface. (a, b) Reproduced from Gipson, I. K. (1994). Anatomy of the conjunctiva, cornea, and limbus. In: Smolin and Thoft (eds.) *The Cornea: Scientific Foundations and Clinical Practice*, 3rd edn., Chapter 1, p. 8. New York: Little Brown and Company, with permission from I. K. Gipson.

layer of the cornea and is comprised of three to five anatomically distinct layers of stratified squamous nonkeratinizing epithelial cells (**Figure 1(a)**). It protects the inner neuronal tissues of the retina from microbial invasion and prevents water loss from the corneal stroma.

When light waves hit the curved corneal surface and pass from the air to an aqueous medium, they are bent. This refraction of light waves focuses the light on the fovea of the retina. The crystalline lens is less powerful than the cornea at bending light waves because the light waves are already in an aqueous environment when they pass from the cornea to the lens. Although the lens does refract light, the differences in the refractive indices of the corneal stroma, the aqueous humor, and the lens are small compared to the difference in refractive index between air and the tear film at the corneal surface. Thus the cornea is the major refractive surface of the eye. Because of its significant impact on the refraction of light, changes in the curvature of the cornea alter the position where light focuses on the retina. This property of the cornea has lead to the development of procedures to alter corneal curvature to reduce or eliminate refractive errors such as myopia and astigmatism. One of the most popular of these procedures worldwide is refractive surgery using laser-assisted *in situ* keratomileusis (LASIK) which involves cutting a flap of tissue at the front of the cornea through the epithelium and stroma, removing or ablating tissue from the stroma using an excimer laser, and repositioning the flap of tissue. LASIK patients will experience an immediate improvement in their sight; as a result, millions of these procedures are performed. It remains to be determined whether or not there will be long term consequences for people who have had LASIK or other corneal refractive procedures as their corneas age and for this reason basic researchers in the field of corneal wound healing are concerned over the popularity of this procedure.

The Apical Squames Possess Specializations to Promote Tear Film Spreading

The apical-most epithelial surface of the cornea has flattened cells called squames. The apical surfaces of these cells have protrusions called microplicae (**Figure 1(b)**). These are specialized structures that facilitate the spreading of the tear film. The microplicae have bound to them the glycocalyx that contains the membrane-associated mucins and other glycoproteins whose functions include facilitating tear film spread. The outermost layer of the tear film is a layer of lipid molecules that increases the stability of the tear film and prevents tear evaporation. The tear film itself has several functions. It prevents the eyelids from adhering to the corneal epithelium. It is the medium through which carbon dioxide, a product of corneal metabolism, is exchanged for oxygen from the air. In addition, it contains small molecules called defensins that inhibit the growth of microbial agents. When the corneal epithelium is injured, the concentration of these defensins in tears increases transiently and then, after the wound is closed, decreases back to the levels before wounding. These data suggest that defensins play important roles in protecting the cornea from infection especially after the epithelial barrier is disrupted during wound healing. Underneath the superficial apical layer are two to three layers of cells often referred to as wing cells by corneal biologists. The final layer that sits on the basement membrane is called the basal cell layer.

The Epithelial Basal Cells Adhere to the Underlying Basement Membrane via tight Adhesive Junctions called Hemidesmosomes

The corneal basal cells maintain the tight association of the epithelium with the basement membrane through specialized adhesion junctions called hemidesmosomes. A schematic representation of the adhesion complex, including the hemidesmosomes, is shown in **Figure 2(a)** and a transmission electron micrograph is shown in **Figure 2(b)**. The hemidesomosomes form a tight rivet holding the epithelial cells on to the basement membrane and anterior stroma. Unlike adherens junctions and focal adhesions, hemidesmosomes utilize intermediate filaments rather than actin to stabilize cell adhesion and maintain cell:matrix adhesions. Hemidesmosomes must disassemble when the corneal epithelium is injured to permit the sheet of epithelial cells to move. The failure of the hemidesmosomes to disassemble during wound healing can lead to delayed wound closure, and failure to reassemble after migration is complete can lead to corneal epithelial erosions. The molecules that are present within hemidesmosomes that mediate these events are beginning to be characterized. α6β4 integrin acts as the primary mechanotransducer of forces from the basal cells to the extracellular matrix molecule laminin 332 in the basement membrane. In addition, a membrane-associated collagen, collagen XVII/BPA180, is also important for the stability of these structures. The function of these integral membrane molecules within the hemidesmosome is to associate with laminin 332, which makes up the anchoring filaments and type VII collagen that makes up the anchoring fibers. The anchoring filaments are found in the basement membrane and the anchoring fibers in the anterior corneal stroma. Thus, the hemidesmosomes are an essential part of an adhesion complex that distributes sheering forces from the cell surface to deep within the stroma. This adhesion complex includes the intra- and extracellular aspects of the hemidesmosomal plaque at the plasma membrane as well as the anchoring filaments and anchoring fibers.

The need for rapid mobilization of the corneal epithelial cells after a corneal wound combined with the sheerness of the corneal epithelial basement membrane forced a compromise during evolution: the basal surfaces of the corneal basal cells are more exposed to sheering forces from the environment compared to the basal surfaces of the basal cells in skin. The enfolding and ridges in the epidermis result in a basement membrane surface area that is increased in the basal keratinocytes relative to their lateral and apical surfaces. This provides increased protection from debridement of the epidermis. Because of the sheerness of the corneal epithelial basement membrane, it is more prone to recurrent epithelial erosions compared to the skin. However, this sheer surface also permits the corneal epithelial sheet to migrate rapidly and thereby minimizes dessication of the cornea and allows wounds to close quickly to minimize infections.

While the cells that make up the corneal epithelial basal cell layer are the most proliferative of all the corneal epithelial layers, research has shown that the cornea epithelial basal cell layer does not contain the corneal epithelial stem cells (CESCs). If the CESCs were primarily located in the central cornea, they would be exposed to the DNA-damaging affects of ultraviolet light, and, lacking pigment to absorb light energy, would sustain irreversible mutations. To maintain the corneal epithelium throughout life,

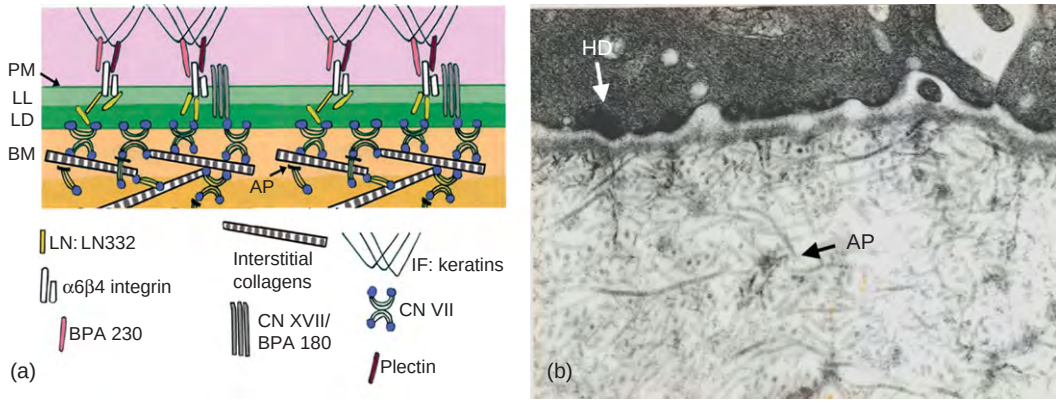

Figure 2 The adhesion complex maintains the tight adhesion of the corneal epithelium to the underlying basement membrane and Bowman's layer and is shown schematically in (a) and by transmission electron micrograph in (b). It consists of the inner plaque with keratins, plectin, and BPA230, hemidesmosomes (HD) at the plasma membrane (PM) containing α6β4 integrin and type XVII collagen (CN)/BPA180, anchoring filaments at the basement membrane zone and Bowman's layer containing laminin LN332, and the anchoring fibers and adhesion plaques (AP) containing type VII collagen. The lamina lucida (LL) and lamina densa (LD) contain type IV collagen (light green) and perlecan (dark green), respectively, in addition to numerous other proteins and proteoglycans. Type VII collagen indirectly links the intermediate filaments of the cytoskeleton to the interstitial collagens of the anterior lamellae of the corneal stroma. Adapted from Gipson, I. K. (1994). Anatomy of the conjunctiva, cornea, and limbus. In: Smolin and Thoft (eds.) *The Cornea: Scientific Foundations and Clinical Practice*, 3rd edn., Chapter 1, p. 10. New York: Little Brown and company, with permission from I. K. Gipson.

mammals maintain an epithelial stem cell population at the periphery of the cornea at an area called the corneoscleral junction or limbus. At this location, the CESCs are adjacent to a rich environment, often called a niche, which includes both melanocytes that produce melanin and absorb excess light to protect the stem cells from DNA damage, and blood vessels that release growth factors as well as immune cells. The idea that the limbus is a unique and distinct environment is supported by the fact that the composition of the basement membrane beneath the limbal basal cells is unique. It has different relative ratios of collagens and laminins compared to either the conjunctival or corneal basement membrane. Data characterizing the microanatomical relationships among the cells that make up the limbal niche are shown schematically in **Figure 3(a)**. Different integrin heterodimers have been studied as potential markers for the CESCs. **Figures 3(b)** and **3(c)** show the localization of integrins in the human and mouse limbus respectively. One integrin, $\alpha 9\beta 1$, is only expressed in the unwounded adult cornea at the limbus; detailed studies in the mouse using bromodeoxyuridine to study label retaining cells have shown that $\alpha 9\beta 1$ is not expressed on the stem cells themselves but is expressed on the cells that are the immediate progeny of the stem cells, which have been called transit amplifying cells. The CESCs have been shown to express high levels of $\alpha 6\beta 4$- and $\beta 1$-family integrins.

The Palisades of Vogt

The palisades of Vogt were first described over 90 years ago but were named by Vogt in 1921. They can be seen at the corneal periphery at the limbus by a clinician using an ophthalmoscope as shown in **Figures 4(a)–(c)**. A scanning electron micrograph of the palisades of Vogt is shown in **Figure 4(d)**. The palisades of Vogt consist of ridges of stromal tissue covered by epithelial cells. After noting their loss during progression of certain corneal disease states, recent studies have shown that the palisades of Vogt become increasingly less prominent as the cornea ages and disappear entirely in patients with conditions that are associated with CESC deficiency.

As discussed above and shown in **Figure 3**, the CESCs reside in the corneoscleral junction. These adult stem cells are small and relatively undifferentiated. Recently, *in vivo* confocal micrographs taken of human corneas as a function of age from 10- to 80-year olds show that the epithelial cells within the palisades of Vogt are smaller than those of the central cornea, that the palisades disappear with aging, and that the sizes of the corneal epithelial cells get larger as the palisades get smaller and disappear. These data are consistent with the hypothesis that the CESCs are located within the palisades of Vogt and that the aging cornea displays a progressive reduction in both the palisades and the stem-like cells that reside there. While palisades of Vogt have not been reported in non-human corneas, it is likely that similar structures are present but are not as morphologically distinct as those in the young human cornea.

Bowman's Layer Is an Acellular Zone Located Immediately under the Corneal Epithelial Basement Membrane

Bowman's layer is usually considered the second of the five layers of the cornea. It is a specialized acellular layer immediately beneath the epithelial basal cell basement membrane; in humans it is 12–18-μm thick and it begins at the corneoscleral junction. It is composed of an amorphous collection of collagen fibers intertwined with a rich collection of fine sensory nerve axons that mostly run parallel to the corneal surface. First observed in the chicken cornea, anatomically distinct Bowman's layers have been widely reported to be present only in avian, primate, and cat corneas. It can be seen in **Figure 1(a)**. Rabbits and mice were thought to lack a Bowman's layer. More recent studies suggest that Bowman's layers are found in mammalian, avian, and even fish corneas, but their thickness and composition vary significantly. The function of Bowman's layer has remained controversial primarily because there are no true markers for Bowman's layer and the lack of consensus regarding which species possess true Bowman's layers; a better understanding of what constitutes a Bowman's layer is necessary before its function can be determined. The most likely function for Bowman's layer is to enhance corneal strength and/or integrity perhaps by providing a mesh-like environment through which the thicker more uniform anterior stromal collagen lamellae insert into the type VII collagen containing adhesion complex. This insertion would link and stabilize the corneal epithelial basal cell adhesion complex in the anterior corneal stroma. A secondary function for Bowman's could be to facilitate nerve innervation of the ocular surface by providing a space through which axons can move during development.

The Collagen- and Proteoglycan-Rich Corneal Stroma with Its Stromal Cells, Descemet's Membrane, and the Corneal Endothelial Cells are all Vital to the Health of the Cornea

The third layer of the cornea is the stroma; it is transparent, compact, and fibrous and serves as a structural support. The clarity of the corneal stroma is due to the regularity of the diameter of the various collagen fibers that comprise it and the packing and specialized arrangement of these sheets, called lamellae, relative to one another. The collagen fiber spacing within and between lamellae is regulated by

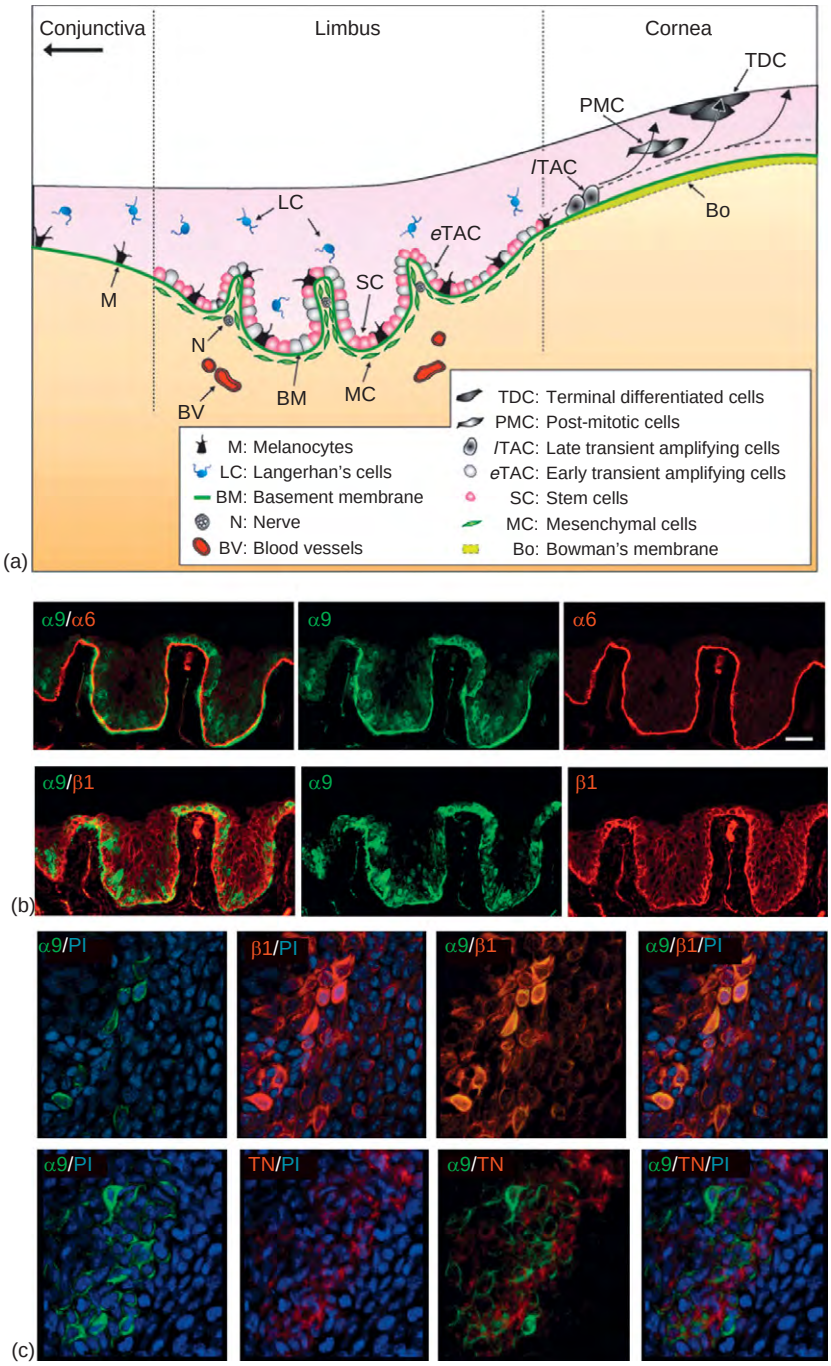

Figure 3 The CESCs are present within the limbus at the palisades of Vogt where the epithelial cells show distinctive integrin expression profiles. The schematic representation in (a) summarizes our knowledge on the different cell types reported to be involved in maintaining the stem cell niche at the limbus. (b) Cross sections through the human limbus showing the palisades of Vogt and stained (1) for α9 integrin, which is a marker for cells arising directly from division of the CESCs, and for α6 integrin, a component of the hemidesmosomes that stains the basement membrane zone at the limbus; or (2) for α9 integrin and β1 integrin, an integrin shown to be expressed at high levels on the CESCs. α9 integrin is present in subsets of the basal cells present at both apical and basal sites along the ridges. (c) En face images taken from whole flat mounted mouse corneas stained with antibodies to reveal the localization of α9 and β1 integrin or stained to reveal the localization of α9 integrin and tenascin-C, an extracellular matrix molecule present only at the limbus of the unwounded mouse cornea; nuclei have been stained with the nuclear marker DAPI. Note that there are many more β1 positive cells than α9 positive cells and that tenascin-C and α9 integrin do not appear to co-localize but rather tenascin-C is found beneath the cells that are α9 integrin positive. The magnification bar in (b) equals 25 μm and the magnification bar in (c) equals 5 μm. (a) Adapted from Li, W., Hayashida, Y., Chen, Y. T., and Tseng, S. C. (2007). Niche regulation of corneal epithelial stem cells at the limbus. *Cell Research* 17: 26–36, with permission from Scheffer C. G. Tseng (c) Adapted from Stepp, M. A. and Zieske, J. D. (2005). The corneal epithelial stem cell niche. *Ocular Surface* 3: 15–26.

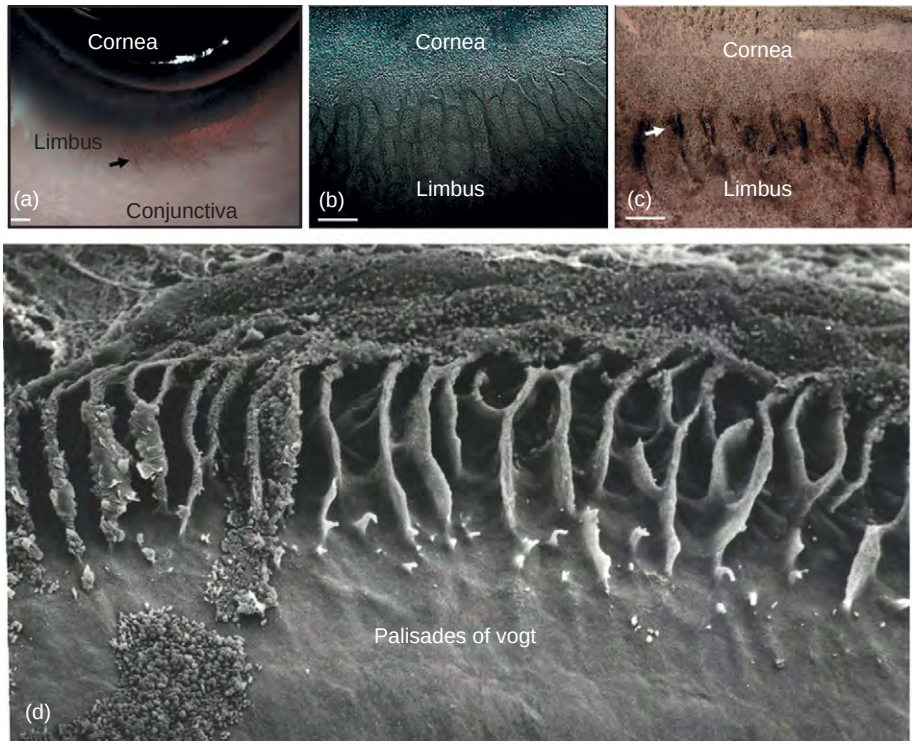

Figure 4 The palisades of Vogt are undulating pigmented ridges of tissue at the periphery of the cornea at a region called the corneoscleral junction or limbus. (a–c) The ridges of the palisades can be seen *in vivo* on the ocular surface (a). They can also be seen on sheets of human corneal epithelium removed with dispase from less pigmented (b) and more pigmented eyes (c). The fact that the corneal epithelial sheets contain pigment suggests that melanocytes are present intermixed with the epithelial cells at the limbus. (d) The palisades of Vogt are revealed in detail in this scanning electron micrograph of the de-epithelialized ocular surface. (a–c) Adapted from Li, W., Hayashida, Y., Chen, Y. T., and Tseng, S. C. (2007). Niche regulation of corneal epithelial stem cells at the limbus. *Cell Research* 17: 26–36, with permission from Scheffer C. G. Tseng. (d) Adapted from Gipson, I. K. (1989). The epithelial basement membrane zone of the limbus. *Eye* 3: 132–140, with permission from I. K. Gipson.

proteoglycans, including lumican, decorin, and bilycan. The proteoglycans bind and organize water molecules and constrain the spacing of the collagen fibers. The cells that produce and maintain the collagens and proteoglycans of the stromal matrix are mesenchymal cells of neural crest origin and are frequently referred to as corneal keratocytes. During wound healing, these cells become activated to become myofibroblasts and they function to facilitate wound closure.

Between the stroma and the corneal endothelial cells there is a specialized homogenous basement membrane known as Descemet's membrane. The single layers of flattened cells that make up the corneal endothelium are primarily responsible for secreting the extracellular matrix proteins that make up Descemet's membrane. They are absolutely essential for a healthy cornea. The corneal endothelial cells have numerous channel proteins in their plasma membrane that pump ions and excess water in and out of the cornea to maintain its hydration state. The clarity of the corneal stroma is readily lost if the stroma begins to dry out or desiccate. Dessication disrupts the organization of the collagen molecules by removing the ordered water molecules associated with the proteoglycans. The endothelial cells also pump nutrients from the aqueous humor into the corneal stroma. Nutrients diffuse across Descemet's membrane and then passively diffuse outward to nourish the corneal stromal and epithelial cells. Because the cornea is avascular, it requires the corneal endothelial cells to provide its nourishment. It is likely that Descemet's membrane acts as a sponge to trap nutrients delivered by the corneal endothelial cells. This would provide a sustained release of those nutrients to the rest of the cornea. In the healthy cornea, the corneal endothelial cells are more metabolically active compared to the corneal epithelium and corneal stromal cells. The generation of nutrient and ion gradients is energy dependent and these cells are constantly synthesizing channel and ion pump proteins. In contrast, in the unwounded cornea, the corneal stromal cells and the corneal epithelial cells are fairly quiescent and primarily utilize glycolysis to generate energy.

The Avascular Cornea

The healthy central cornea is avascular to permit light to fall on the retina without distortion; blood and

lymphatic vessels are present only at the corneal periphery at the limbus. Developing a better understanding of the mechanisms underlying the maintenance corneal avascularity is of extreme importance to cell biologists and many excellent studies have made progress in this area. We now know that the avascular status of the healthy cornea is maintained by the production by the corneal epithelial and stromal cells of several antiangiogenic factors, including angiostatin and endostatin. After corneal injury, corneal cells transiently produce angiogenic factors such as basic fibroblast growth factor and vascular endothelial growth factor (VEGF) disrupting the normal balance of pro- and anti-angiogenic factors and allowing for the ingrowth of blood vessels from the limbus. After healing is complete, these transient vessels undergo pruning and the avascular nature of the cornea is restored. However, prolonged inflammation or recurrent epithelial erosions can compromise corneal avascularity.

The clarity of the cornea and its accessibility has given rise to several widely used assays to assess the mechanisms underlying angiogenesis. One is called the corneal pocket assay. This assay has been used by researchers to identify factors that inhibit new blood vessel growth primarily as a tool to learn how to inhibit the growth of tumor cells in various different types of cancer. A small pellet is inserted into an incision made on the cornea surface. If the pellet contains pro-angiogenic growth factors such as FGF or VEGF, blood vessels will sprout from the limbus and grow toward the pellet. The number of vessels that form and the speed with which they move toward the pellet can be quantified, and drugs that inhibit or enhance angiogenesis can be tested. A second procedure used for similar types of studies of angiogenesis involves placing a suture on the cornea. If the suture is placed at a regular distance from the limbus then the ingrowth of vessels from the limbal vasculature can be measured and the ability of various drugs to enhance or inhibit angiogenesis can also be assessed.

See also: Artificial Cornea; Conjunctival Goblet Cells; Contact Lenses; Corneal Dystrophies; Corneal Endothelium: Overview; Corneal Epithelium: Response to Infection; Corneal Epithelium: Transport and Permeability; Corneal Epithelium: Wound Healing Junctions, Attachment to Stroma Receptors, Matrix Metalloproteinases, Intracellular Communications; Corneal Imaging: Clinical; Corneal Nerves: Anatomy; Corneal Nerves: Function; Corneal Scars; The Corneal Stroma; Cornea Overview; Defense Mechanisms of Tears and Ocular Surface; Dry Eye: An Immune-Based Inflammation; Imaging of the Cornea; Ocular Mucins; Refractive Surgery and Inlays; Regulation of Corneal Endothelial Cell Proliferation; Regulation of Corneal Endothelial Function; Stem Cells of the Ocular Surface; The Surgical Treatment for Corneal Epithelial Stem Cell Deficiency, Corneal Epithelial Defect, and Peripheral Corneal Ulcer; Tear Film Overview.

Further Reading

Argüeso, P., Balaram, M., Spurr-Michaud, S., et al. (2002). Decreased levels of the goblet cell mucin MUC5AC in tears of patients with Sjögren syndrome. *Investigative Ophthalmology and Visual Science* 43: 1004–1011.

Dupps, W. J., Jr. and Wilson, S. E. (2006). Biomechanics and wound healing in the cornea. *Experimental Eye Research* 83: 709–720.

Gipson, I. K. (2007). The ocular surface: The challenge to enable and protect vision: The Friedenwald lecture. *Investigative Ophthalmology and Visual. Science* 48: 4390–4398.

Li, W., Hayashida, Y., Chen, Y. T., and Tseng, S. C. (2007). Niche regulation of corneal epithelial stem cells at the limbus. *Cell Research* 17: 26–36.

Müller, L. J., Marfurt, C. F., Kruse, F., and Tervo, T. M. (2003). Corneal nerves: Structure, contents and function. *Experimental Eye Research* 76: 521–542.

Pajoohesh-Ganji, A., Pal-Ghosh, S., Simmens, S. J., and Stepp, M. A. (2006). Integrins in slow-cycling corneal epithelial cells at the limbus in the mouse. *Stem Cells* 24: 1075–1086.

Ruberti, J. W. and Zieske, J. D. (2008). Prelude to corneal tissue engineering – gaining control of collagen organization. *Progress in Retinal and Eye Research* 27: 549–577.

Sakimoto, T., Rosenblatt, M. I., and Azar, D. T. (2006). Laser eye surgery for refractive errors. *Lancet* 367: 1432–1447.

Stepp, M. A. (2006). Corneal integrins and their functions. *Experimental Eye Research* 83: 3–15.

Stepp, M. A. and Zieske, J. D. (2005). The corneal epithelial stem cell niche. *Ocular Surface* 3: 15–26.

Taneri, S., Zieske, J. D., and Azar, D. T. (2005). Evolution, techniques, clinical outcomes, and pathophysiology of LASEK: Review of the literature. *Survey of Ophthalmology* 49: 576–602.

Wilson, S. E., Chaurasia, S. S., and Medeiros, F. W. (2007). Apoptosis in the initiation, modulation and termination of the corneal wound healing response. *Experimental Eye Research* 85: 305–311.

Corneal Epithelium: Response to Infection

Elizabeth A Szliter-Berger and L D Hazlett, Wayne State University School of Medicine, Detroit, MI, USA

Glossary

Caspases – Humans express 11 different cysteine-aspartic acid proteases classified as either initiator or effector caspases, which play essential roles in apoptosis, necrosis, and inflammation.
CD44 – A type I transmembrane glycoprotein that regulates conformational changes of integrin heterodimers and their ability to microcluster and anchor to the actin cytoskeleton.
Desmosomes – A junctional complex of adhesion molecules and linking proteins in the plasma membrane for cell-to-cell adhesion and contributes to the structural integrity through linkage of keratin cytoskeletal filaments of adjoining cells.
Epidermal growth factor (EGF) – Expressed by corneal epithelial and stromal cells, it promotes cell migration and the attachment of corneal epithelial cells to fibronectin.
Hemidesmosomes – Integral membrane protein complexes of integrin hetrodimers in the basal cell plasma membrane anchoring cells to the extracellular matrix.
Langerhans cells – Unique subset of dendritic cells located in mucosal stratified squamous epithelium and skin epidermis; as professional antigen-presenting cells, they express toll-like receptors (TLRs) as well as C-type lectin receptors.
Melanocytes – Pigment-producing cells located within the uvea of the eye.
Nuclear factor-kappa B (NF-κB) – A protein complex that functions as a transcription factor; NF-κB is found in almost all animal cell types and is involved in cellular responses to stimuli such as stress, cytokines, free radicals, ultraviolet irradiation, and bacterial or viral antigens.
Pathogen-associated molecular patterns (PAMPs) – Small, highly conserved molecular motifs present in bacteria, yeast, or viruses but not in mammalian cells and induce inflammatory signaling via interaction with receptors families, such as TLRs.
Tritiated thymidine-labeling – Technique used to label cells actively undergoing DNA synthesis; it estimates the proportion of S-phase cells in a cell population.
Trophic – It refers to a nutrition-derived function.
Zonula occludens – Also known as tight junctions, these structures are primarily composed of occludins and claudins to form a virtual impermeable barrier between adjacent cell membranes.

Introduction

Basic Structure and Function

The corneal epithelium is a remarkably proficient tissue that combines structure and function to serve as the major refractive component of the eye and maintain ocular surface integrity; yet provide a critical barrier protecting the visual axis from the external environment. The corneal epithelium is the outermost layer of the cornea and is comprised of stratified, nonkeratinized, nonsecretory, squamous epithelial cells, intermixed with Langerhans' cells and occasional dendritic melanocytes. This tissue layer is a highly organized structure that is avascular and almost perfectly transparent in order to preserve the optical properties of the cornea. It is 5–7 cell layers thick and contains three cell types (posterior to anterior): basal cells, wing cells, and superficial cells. The deepest layer is comprised of cuboidal basal cells. This single cell layer of progenitor cells undergoes mitosis at a rate of 10–15% per day, followed by intermediate differentiation of daughter cells into one to three layers of wing cells as they migrate toward the surface. Superficial to wing cells is a three- to four-cell thick layer of terminally differentiated squamous cells. These cells constantly degenerate and desquamate from the corneal surface in a continuous cycle of shedding of superficial cells and proliferation of cells in the basal layer resulting in complete renewal of the epithelium every 7 days, as has been demonstrated by mitotic rate measurements in basal cells and by tracking the migration of tritiated thymidine-labeled cells to the ocular surface. This regenerative process is further maintained by a constant renewal of basal cells from the limbal epithelium via stem cells located in the limbus that differentiate into basal cells, followed by centripetal migration into the cornea. Although the corneal epithelium is constructed as a highly effective, semipermeable membrane on the ocular surface,

it is also well equipped to participate in the host response to invading pathogens and infection as described in greater detail below.

Corneal Infection

The corneal epithelium, similar to other mucosal epithelial linings in the body, constitutes the eye's first line of defense against microbial pathogens. The cornea has an immune-privileged status, which includes features such as avascularity of the cornea and dearth of antigen-presenting cells (APCs) in the central region of the cornea in order to protect the visual axis. Although resident dendritic cells or Langerhans cells, known for their global antigen-presenting properties, are present in the corneal periphery, they can readily be recruited into the central cornea when necessary. In addition, the corneal epithelium plays an active role in host defense against invading pathogens. Cells of the corneal epithelium: (1) recognize pathogens and their by-products and, as a result, (2) respond through expression and secretion of a network of proinflammatory cytokines and chemokines that recruit inflammatory cells into the cornea, (3) secrete antimicrobial products, and (4) promote wound healing and restoration of tissue homeostasis.

Keratitis is a condition of corneal inflammation, which can be caused by a number of bacterial, viral, and fungal pathogens. Clinically, it is associated with symptoms such as redness, tearing, reduced visual clarity, corneal discharge, and severe pain. Bacterial keratitis is the leading cause of corneal infection. Staphylococci are the most commonly occurring organisms in bacterial conjunctivitis and keratitis, including *Staphylococcus* (*S.*) *aureus*, *S. pneumoniae, S. intermedius,* and α-hemolytic streptococcus. *Pseudomonas aeruginosa* (*P. aeruginosa*) is most frequently encountered in keratitis cases associated with extended contact lens wear and constitute 19–42% of bacterial keratitis cases. Other bacteria known to cause keratitis include *Escherichia coli* and *Morganella morganii*. Common pathogens associated with viral keratitis include, yet are not limited to, herpes simplex virus (HSV) and adenovirus. HSV infection is the most common cause of corneal blindness in the United States at present time. Approximately 400, 000 people in the United States have been infected with ocular herpes and 50, 000 initial and recurring cases of HSV keratitis are diagnosed annually. *Fusarium, Aspergillus* (both filamentary fungi), and *Candida albicans* (a yeast) constitute those fungi associated with the majority of fungal keratitis cases. Sterile keratitis also incites an immune response from the corneal epithelium; however, instead of bacteria adhering to and invading the ocular surface (requisite for bacterial keratitis), the epithelium responds to the presence of bacterial endotoxin (lipopolysaccharide or LPS). Sterile keratitis can also occur when bacteria colonize contact lenses and subsequently, release endotoxin onto the corneal surface, a condition known as CLARE or contact lens-induced acute red eye.

The effects of both the invading pathogen on corneal tissue and the host immune response to the pathogen lead to many structural alterations that are otherwise essential to maintaining transparency of the cornea and, as a result, directly compromise visual acuity. As such, components of the corneal epithelium have evolved to respond to infection and these are described in greater detail below.

TLRs and TLR-Related Molecules

Toll-like receptors (TLRs) are evolutionarily conserved type I transmembrane protein receptors that are expressed by corneal epithelial cells (as well as inflammatory cells) and function to respond to pathogens as the corneal epithelium's first line of defense. These receptors initiate innate immunity and are essential for host defense against infection. TLRs recognize a broad spectrum of pathogen-associated molecular patterns (PAMPs), ranging from LPS (predominately recognized by TLR4), flagellin (TLR5), peptidoglycan (TLR2), single- or double-stranded RNA (TLR3,-7,-8), and unmethylated CpG DNA (TLR9). TLRs signal through several adaptor molecules, including the common adaptor protein myeloid differentiation factor (MyD)88 and MD-2; however, the reader is referred to Further Reading section for more information.

It has been proposed that corneal epithelial cells play a central role in regulation of inflammatory responses by expression of functional TLRs and adaptor molecules. Epithelial cells are thought to intrinsically respond to the presence of pathogens through TLR recognition of PAMPs. Of the 13 TLRs identified to date, human corneal epithelial cells have been shown to express TLR-1,-2,-4,-5,-6, and -9 either intercellularly or at the cell surface (and has yet to be fully elucidated). TLRs primarily associate as homodimers, with exceptions for TLR-1,-2, and -6, which form heterodimers. Upon recognition of PAMPs expressed by invading pathogens on the ocular surface, TLRs produce downstream signaling events which induce translocation of nuclear factor kappa B (NF-κB), a major transcription factor of numerous genes important in both innate and acquired immune responses. These genes include proinflammatory cytokines and chemokines, leading to activation of adhesion molecules, and subsequently resulting in macrophage and polymorphonuclear neutrophilic leukocyte (PMN) recruitment into the

cornea. Antimicrobial peptide expression by corneal epithelial cells is induced by TLR activation, as well. Although there is a common pathway for TLR activation (the myeloid differentiation protein–IL-1 receptor-associated kinase–tumor necrosis factor receptor-associated kinase (MyD88–IRAK–TRAF) pathway), individual TLRs most likely activate different, alternative, signaling pathways as well, and these remain under investigation (IL, interleukin).

Cytokines/Chemokines

The immune response of the corneal epithelium utilizes a variety of different substances to mount an attack upon organisms invading the ocular surface. Cytokines and chemokines are produced and endogenously released by corneal epithelial cells to directly and indirectly recruit and activate immune cells of both innate and adaptive immunity. Gram-negative bacterial endotoxin such as LPS, for example, elicit production of endogenous proinflammatory cytokines such as tumor necrosis factor (TNF)-α, interleukin (IL)-6, and IL-1. Protein levels for both IL-1α and IL-1β have been shown to be constitutively expressed in the normal human cornea. It has further been demonstrated that upon rupture of the epithelial cell membrane by infectious agents or trauma, IL-1α is passively released, contributing to increased vascular permeability, macrophage and lymphocyte infiltration and activation, angiogenesis, as well as regulatory effects on corneal fibroblasts. If left unchecked, these events would destroy the cornea; however, the epithelium also secretes both soluble and membrane-bound forms of IL-1RII, a receptor and natural antagonist of IL-1 in order to modulate the effects of this potent proinflammatory cytokine and consequently preserve visual function.

In addition to IL-1, *in vitro* studies using primary human corneal epithelial cells (HCECs) and telomerase-immortalized HCECs have revealed expression and secretion of IL-6, IL-8, and TNF-α following either *P. aeruginosa* or HSV-1 challenge. TNF-α is a major proinflammatory mediator that is known to promote apoptosis, inflammation, and regulate immune cells. IL-6 is both a pro- and anti-inflammatory cytokine that can potentiate the inflammatory response, yet also modulate inflammation through its inhibitory effects on TNF-α and IL-1, while activating IL-1 receptor antagonist and IL-10. IL-8 is a chemokine that is secreted by the epithelium under stress and functions as a strong chemoattractant for neutrophils (PMN); MIP-3α, also released by corneal epithelial cells after infection, promotes directed migration of leukocytes, such as immature dendritic cells and effector T cells. TGF-α,-β1, and -β2 are expressed also by corneal epithelial cells and contribute to re-epithelization, an essential step in resuming normal corneal function after infection. TGF-β1, in particular, is a potent anti-inflammatory cytokine that modulates lymphocyte activation and promotes wound healing; regarding the cornea, it is further known to promote proliferation and lamellar differentiation of corneal epithelial cells via keratocyte-mediated stimulation.

Antimicrobial Molecules

The corneal epithelium also employs the action of small (100 amino acids or less), positively charged (arginine- and lysine-rich) molecules known as antimicrobial peptides to further assist in combating invading pathogens. Over 500 naturally occurring antimicrobial peptides have been identified in mammals. Typically these molecules are cationic polypeptides that disrupt bacterial membranes through charge interactions and hydrophobic amino acids. Many antimicrobial peptides and their microbicidal effects are induced locally by inflammatory stimuli at the site of infection and act synergistically with other anti-inflammatory mechanisms (cytokines, inflammatory cells) in defending against microbial pathogenesis. Of the four distinct structural classes of antimicrobial molecules, recent studies have shown that corneal epithelial cells secrete peptides from the defensin and cathelicidin families, which are thought to help protect the eye through broad spectrum activity against microorganisms including Gram-positive and -negative bacteria, fungi, and certain enveloped viruses. These molecules and their roles in preventing microbial invasion and managing infection are discussed in greater detail below.

β-Defensins

The defensins include α- and β-defensin subfamilies, all of which are characterized by a β-sheet-rich fold and three disulfide bridges. A third class of θ-defensins has been recently identified in rhesus macaque leukocytes. Although θ-defensin mRNA is detectable in humans, these transcripts contain a premature stop codon preventing translation of functional protein. Leukocytes (PMN) and various types of epithelial cells have been shown to express both α- and β-defensins; however, the corneal epithelium has been demonstrated to produce and secrete only members of the β-defensin subfamily.

Human β-defensins (hBDs) include 28 members, of which three have been associated with the corneal epithelium. Human β-defensin-1 (hBD-1) is constitutively expressed by corneal epithelial cells; while studies have shown that hBD-2 is induced by bacterial infection and bacterial products such as lipoprotein and lipotechoic acid, and is mediated by TLR2. In addition, cytokines TNF-α and IL-1 upregulate hBD-2 expression by corneal epithelial cells. Expression of hBD-3 is more variable,

whereby some studies have indicated solely constitutive expression by corneal epithelial cells; and others have demonstrated inducible expression by TNF-α and interferon-gamma (IFN-γ). Regardless, hBD-3 was shown by McDermott and colleagues to exert most potent antibacterial activity against *S. epidermidis*, *S. aureus,* and *P. aeruginosa* using *in vitro* antimicrobial assays, followed by hBD-2; while hBD-1 showed moderate activity against *Pseudomonas*, but no activity against *Staphylococcus* strains. *In vivo*, it was recently demonstrated that murine (m) BD2, but not mBD1, was protective in the *P. aeruginosa*-infected mouse cornea. The importance of these antimicrobial peptides has been demonstrated by knocking out the mouse β-defensin-1 gene, which led to less effective clearance of *Haemophilus influenzae* from the lung and increased colonization of *Staphylococcus* in the bladder.

Cathelicidins

Of the numerous members of the cathelicidin family, only LL-37 has been described in humans. Cathelicidins express a highly conserved cathelin domain and a less conserved, more variable antimicrobial region. LL-37, as its name suggests, is a 37-amino acid linear peptide expressed by inflammatory/immune cells and epithelial tissue. It is derived by cleavage of the precursor, human cationic antimicrobial protein 18 (hCAP18) and appears to function as both an antibacterial peptide and immunomodulator. Low expression levels of LL-37 are detected constitutively and subsequently upregulated following injury, infection, and exposure to IL-1β, as well as heat-killed *P. aeruginosa.* Regarding antimicrobial properties, LL-37 is thought to function in a similar manner to that described for defensins and work synergistically with corneal epithelial proteins such as defensins, lactoferrin, and lysozyme (latter two present in tear film). LL-37 is able to bind and neutralize LPS and lipotechoic acid, thus reducing the inflammatory response associated with these molecules. In addition to eradicating ocular pathogens, studies have demonstrated that LL-37 enhances the innate and adaptive immune response in the corneal epithelium through modulation of cytokine/chemokine expression. Using an *in vitro* stimulation assay, LL-37 was shown to induce production of IL-1β, IL-6, IL-8, and TNF-α by human corneal epithelial cells. Furthermore, this molecule promotes wound repair through enhanced cell migration, including fibronectin-induced migration by stimulating corneal epithelial cells.

In addition to microbicidal activities of β-defensins and LL-37, these molecules also wield effects over immune cells and influence wound healing. They have been demonstrated to recruit and activate immune cells through the induction of cytokine and chemokine production by epithelial cells, which further actuate the cellular components of the immune response to corneal infection. Regarding postinfection, both hBD-2 and LL-37 have been shown to be upregulated in an *in vitro* organ culture model of corneal epithelial wound healing suggesting roles for corneal epithelial cell migration and proliferation.

Complement System

The complement system also contributes to the first line of innate immune defense against corneal infection. This critical system is composed of a series of effector and regulatory proteins that sequentially activate one another to generate biologically active molecules, such as opsonins and chemotaxins. The complement system is continuously activated at low levels in the eye under normal conditions, as supported by detection of soluble and membrane-associated complement regulatory proteins (e.g., rsCD59), which are also strongly expressed in the corneal epithelium for tight regulation of aberrant activation. Components of complement are also more heavily distributed in the peripheral versus the central cornea, potentially due to the diffusion of complement molecules from corneal limbal vessels. In response to infection activation of complement can occur via both the classical and alternate pathways.

Secretory IgA

Although this molecule is not essential in ocular defense, secretory IgA (sIgA) does play a major role in the prevention of some corneal infections, including *Pseudomonas* and *Acanthamoeba.* In fact, over 75% of the general population contain anti-*P. aeruginosa*-specific IgAs in their tear film. sIgA protects the corneal epithelium by accumulating in the ocular mucin layer and displays an antigen–antibody clearance function. Aggregated sIgA opsonizes bacteria for PMN phagocytosis and processing via recognition by sIgA receptors expressed on the immune cell surface. IL-8, which is secreted by corneal epithelial cells during infection, further enhances the ability of sIgA to induce release of reactive oxygen species by PMN.

Adhesion Molecules

Under normal conditions, integrity of the corneal epithelium depends upon a number of factors, including adhesion molecules. Corneal epithelial cells are interdigitated, particularly in the middle layers, and largely interconnected by desmosomes. Basal cells are firmly attached to the basement membrane, neighboring basal cells and overlying wing cells via hemidesmosomes. Tight junctional complexes, or zonula occludens, found only between superficial cells are

of great importance regarding the barrier function of the corneal epithelium. As such, superficial cells form a highly effective, semipermeable membrane on the corneal surface. Not only does the tight junctional barrier prevent decreases in net fluid transport out from the stroma, but it also prevents corneal penetration by pathogens. In addition, gap junctions connect the cells of all layers of the corneal epithelium and function as communication conduits between cells. These tight anatomical arrangements with virtual absence of intercellular spaces contribute to the remarkable transparency of the epithelium, but have deleterious effects when breached after infection (or wounding) and must be restored forthwith in order to restore/preserve visual function.

Upon infection of the corneal epithelium, breakdown of tight junctional integrity occurs due to the loss or disruption of the outermost layers of the epithelium by invading pathogens. This results in a collapse of cell membrane permeability and selectivity, in addition to creating an unrestricted portal for further pathogen intrusion into the cornea until the corneal epithelium and its adhesion molecules are regenerated. Additional adhesion molecules such as selectins, intercellular adhesion molecule-1 (ICAM-1) and vascular cell adhesion molecule-1 (VCAM-1), are modified after infection due to the secretion of epithelial-derived cytokines, such as TNF-α. As a result, these barriers are further breached to allow the transmigration of inflammatory cells into the injured or infected tissue site. Recruitment of activated leukocytes to sites of infection is essential to the function of both inflammation and innate immunity. However, the extent of leukocyte recruitment contributes largely to the intensity of the inflammatory response, and if this is not well balanced it can result in considerable tissue damage. However, the corneal epithelium does play an active role in regenerating and repairing itself after infection.

CD44 is among the molecules that corneal epithelial cells express to mediate wound healing after infection. This molecule is thought to be involved in cell–cell interactions that provide adhesive strength for the epithelial sheet and in cell–matrix interactions that occur during cell migration and the re-epithelialization process. Basal cells of the corneal epithelium have been demonstrated to secrete APLP2, an amyloid precursor-like protein that is suggested to influence reorganization of the extracellular matrix and dynamic cell–matrix adhesion during re-epithelialization. It has been demonstrated that the corneal epithelium (as well as stromal and endothelial cells) produces and secretes epithelial growth factor (EGF), which is thought to promote cell migration and mitosis of epithelial cells. Corneal epithelial cells then resume expression of molecules such as connexins 45/43 and $\alpha 6\beta 4$ integrin, which participate in the formation of gap junctions and hemidesmosomes/desmosomes, respectively, thus restoring homeostasis of an intact corneal epithelium.

Neuropeptides

Innervation of the Corneal Epithelium

The cornea is among the most densely innervated tissues in the body. In regards to the corneal epithelium, the subbasal epithelial nerve plexus originates from the ophthalmic division of the trigeminal nerve via the anterior ciliary nerves and provides innervation to the basal epithelial cell layer and terminates within the superficial epithelial layers. These nerve fibers are predominately sensory (most classified as nociceptors) and serve a protective role, typically responding to mechanical, thermal, and chemical stimuli. They are stimulated during corneal abrasions and ulcers, and are extremely painful. It is estimated that single corneal sensory neurons support approximately 200 and 3000 individual nerve endings in the mouse and rabbit, respectively, demonstrating the high density of innervation in the corneal epithelium. Corneal nerves in the epithelium have a trophic function, as well. In addition, neuropeptides have been associated with corneal nerves and include: substance P (SP), calcitonin gene-related peptide (CGRP) and vasoactive intestinal peptide (VIP), pituitary adenylate cyclase activating peptide (PACAP), and neuropeptide Y (NPY) among others. Nerve damage can lead to transient or chronic neurotrophic deficits following infection of the corneal epithelium. Corneal denervation also significantly impairs the ability of the corneal epithelium to heal itself and predisposes newly healed corneas to periodic, spontaneous epithelial erosions. Although the nerves coursing through the human corneal epithelium are known to produce a variety of neuropeptides, the following sections focus on the importance of two of these molecules: SP and VIP.

Substance P

SP is an 11-amino acid neuropeptide that is largely associated with proinflammatory events during corneal infection, including upregulation of TLR4 and TLR9 mRNA and of cytokines/chemokines IL-1β, TNF-α, IFN-γ, and MIP-2 as demonstrated in a murine model of *P. aeruginosa*-induced keratitis. Physiologically relevant concentrations of SP are present in the normal human (and mouse) cornea and corneal epithelial cells express the NK1 receptor, which is the major physiological receptor for SP. The neuropeptide also has been associated with wound healing properties and together with insulin-like growth factor-1 (IGF-1) has been demonstrated to have a stimulatory effect on corneal epithelial cell migration, adhesion, and wound closure.

Vasoactive intestinal peptide

VIP is a 28-amino acid neuropeptide that exerts immunomodulatory properties in the cornea following infection.

It has been demonstrated in a murine model of *P. aeruginosa*-induced ocular infection that VIP downregulates the production of several proinflammatory cytokines, including: TNF-α, IL-1, IL-6, IL-12, and IFN-γ, while stimulating the production of anti-inflammatory cytokines IL-1 receptor antagonist, IL-10, and TGF-β. Macrophage and PMN activation was also shown to be influenced by the presence of VIP. Studies in the mouse further support a role for VIP in wound healing and restoration of immune homeostasis in the cornea; however, it has yet to be determined the extent of which is carried out by the epithelium versus stroma.

Thymosin-β4

As previously stated, after eradication of the invading pathogen, the corneal epithelium must heal and promptly resume normal activity. Thymosin (T)β-4 is a 43-amino acid protein produced by corneal epithelial cells that contributes to the resurfacing of the epithelium and regeneration of cell adhesion molecules to reconstitute the epithelial barrier. Studies have shown that Tβ-4 levels are increased in murine corneas during re-epithelialization and also significantly enhance the migration of human corneal epithelial cells through upregulation of molecules associated with cell migration, including laminin-5 and matrix metalloproteinase 1 (MMP-1). Furthermore, Tβ-4 modulates corneal cytokine production in an anti-inflammatory manner by downregulating levels of MIP-2 and TNF-α, as demonstrated in the murine cornea. Tβ-4 has been demonstrated to inhibit apoptosis of human corneal epithelial cells through inhibition of caspases and suppression of Bcl-2 (an antiapoptotic factor) release from mitochondria. Lastly, this molecule has been demonstrated to modulate matrix metalloproteinase expression and prevent PMN infiltration in an alkali injured mouse cornea model, further supporting a key role for Tβ-4 in the repair and remodeling of the injured cornea.

Conclusion

The cornea generates approximately 80% of the eye's refractive power; therefore, it is imperative that the corneal epithelium possess the ability to effectively and appropriately activate an innate immune response when pathogens are encountered on the ocular surface. The protective mechanisms employed by the epithelium have evolved to balance recognition and elimination of pathogens while limiting corneal damage and preserving the visual axis. In order to do so, the corneal epithelium is able to recognize invading organisms through TLR signaling, generate a network of cytokines and chemokines to recruit and activate host inflammatory cells, produce antimicrobial molecules, and provide activation signals to the complement system, all of which coalesce into an effective and efficient immune response as depicted schematically in **Figure 1**. The corneal epithelium also possesses the ability to regenerate itself and promote wound healing through expression and secretion of adhesion molecules and Tβ-4; this process is enhanced by the presence of corneal nerve fibers that release neuropeptides such as SP and VIP, molecules that further contribute to the healing process and restoration of tissue homeostasis.

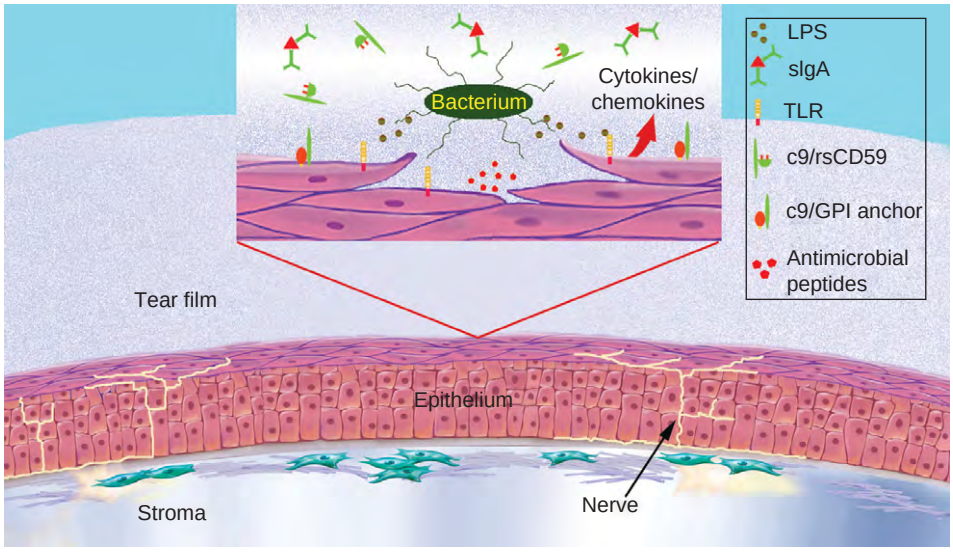

Figure 1 The corneal epithelium also possesses the ability to regenerate itself and promote wound healing through expression and secretion of adhesion molecules and Tβ-4; this process is enhanced by the presence of corneal nerve fibers that release neuropeptides such as SP and VIP, molecules that further contribute to the healing process and restoration of tissue homeostasis.

See also: Immunopathogenesis of Pseudomonas Keratitis.

Further Reading

Akpek, E. K. and Gottsch, J. D. (2003). Immune defense at the ocular surface. *Eye* 17: 949–956.

Bora, N. S., Jha, P., and Bora, P. S. (2008). The role of complement in ocular pathology. *Seminars in Immunopathology* 30: 85–90.

Dohlman, C. H. (1971). The function of the corneal epithelium in health and disease. *Investigative Ophthalmology* 10(6): 383–407.

Edelhauser, H. F. and Ubels, J. L. (2003). *Adler's Physiology of the Eye: The Cornea and the Sclera.* St. Louis, MO: Mosby.

Ganz, T. (2003). Defensins: Antimicrobial peptides of innate immunity. *Nature Reviews Immunology* 3: 710–720.

Kumar, A., Zhang, J., and Yu, F. X. (2006). Toll-like receptor 2-mediated expression of β-defensins-2 in human corneal epithelial cells. *Microbes and Infection* 8: 380–389.

Lu, L., Reinach, P. S., and Kao, W. W. (2001). Corneal epithelial wound healing. *Experimental Biology and Medicine* 226(7): 653–664.

McDermott, A. M. (2004). Defensins and other antimicrobial peptides at the ocular surface. *Ocular Surface* 2(4): 229–247.

McDermott, A. M. (2007). Ocular surface expression and *in vitro* activity of antimicrobial peptides. *Current Eye Research* 32(7–8): 595–609.

Muller, L. J., Marfurt, C. F., Kruse, F., and Tervo, T. M. (2003). Corneal nerves: Structure, contents and function. *Experimental Eye Research* 76(5): 521–542.

Sack, R. A., Nunes, I., Beaton, A., and Morris, C. (2001). Host-defense mechanism of the ocular surfaces. *Bioscience Reports* 21(4): 463–480.

Sosne, G., Qiu, P., and Kurpakus-Wheater, M. (2007). Thymosin β-4 and the eye: I can see clearly now the pain is gone. *Annals of the New York Academy of Science* 1112: 114–122.

Szliter, E. A., Lighvani, S., Barrett, R. P., and Hazlett, L. D. (2007). Vasoactive intestinal peptide balances pro- and anti-inflammatory cytokines in the *Pseudomonas aeruginosa*-infected cornea and protects against corneal perforation. *Journal of Immunology* 178(2): 1105–1114.

Uematsu, S. and Akira, S. (2008). *Handbook of Experimental Pharmacology: Toll-like Receptors (TLRs) and Innate Immunity: Toll-Like Receptors (TLRs) and Their Ligands.* Berlin: Springer.

Wilson, S. E., Liu, J. J., and Mohan, R. R. (1999). Stromal–epithelial interactions in the cornea. *Progress in Retinal and Eye Research* 18 (3): 293–309.

Zhang, J., Wu, X., and Yu, F. X. (2005). Inflammatory responses of corneal epithelial cells to *Pseudomonas aeruginosa* infection. *Current Eye Research* 30: 527–534.

Relevant Websites

http://www.nei.nih.gov – Facts about the Cornea and Corneal Disease, National Eye Institute.

http://www.revoptom.com – Handbook of Ocular Disease Management: Cornea.

Corneal Epithelium: Transport and Permeability

P S Reinach, The State University of New York, New York, NY, USA
F Zhang, The State University of New York, New York, NY, USA
J E Capó-Aponte, U.S. Army Aeromedical Research Laboratory (USAARL), Fort Rucker, AL, USA

Glossary

Barrier – Protein-containing formations between cells in the more superficial layers of the corneal epithelium to prevent infiltration of pathogens into the underlying stroma.
Deturgescence – Physiological state of corneal hydration required for optimal transparency.
Electrochemical equilibrium – Membrane voltage and intracellular ionic activity at which there is no net flux of a specific ion across a membrane.
Net flux – Algebraic difference between unidirectional ionic fluxes across a membrane, which is indicative of active ion-transport activity.
Transient receptor potential protein – Membrane proteins in a superfamily of 27 different genes that arrange themselves in tetrameric configurations to form plasma membrane channels, which can be activated by a large variety of stimuli.

Introduction

Corneal epithelial ion transport and permeability underlie the ability of this tissue to maintain corneal transparency. In this article, we describe how different types of receptors modulate through second messenger-signaling control of ion transporter function and cell membrane permeability. Figure 1 depicts a schematic summarizing the current picture of ion transporters and channels mediating control of cornea epithelial renewal and tissue transparency. To provide insight into the outcome of dysregulation of transporter activity and permeability, we discuss strategies that may circumvent these pathophysiological consequences.

The cornea provides about 75% of the total refractive power required for normal vision. This function depends on the ability of the cornea to remain transparent. The corneal epithelial layer undergoes continuous renewal every 14–28 days. This process preserves its integrity and assures that the cornea is protected from environmental pathogenic infiltration. Such protection is provided by tight junctional continuity forming a moderately high resistance barrier between neighboring cells. This resistance is essentially only selectively permeable to low-molecular-weight ionic species. As the epithelial top layers continuously undergo terminal differentiation followed by being sloughed off, the maintenance of tight junctional integrity is critical for the corneal epithelial to provide its barrier function. Any disruption of upper cell layer apposition that is not rapidly repaired through wound healing renders the cornea vulnerable to infection, swelling, and opacification leading to losses in visual acuity. Losses in tissue transparency occur since swelling of the corneal ground substance leads to disruption of extracellular matrix organization and an irregular corneal surface. These changes cause impinging light to be reflected or scattered, instead of being refracted. Therefore, studies directed toward understanding how the corneal undergoes continuous renewal are relevant for delineating strategies to restore corneal transparency in a clinical setting.

Corneal Hydration Control and Transparency

In humans, the cornea is approximately 500–550 μm thick and is composed of three layers: epithelium, stroma, and endothelium. These tissues have different embryonic origin. Corneal thickness is dependent on the hydration state of the stromal ground substance, whose physiochemical properties cause continuous fluid imbibition. Excessive fluid uptake by the stromal ground substance lying between collagen lamellae results in corneal swelling and opacity.

The stromal ground substance continuously imbibes fluid from the tears and the aqueous humor in the anterior chamber facing the endothelium. This imbibing process is equivalent to a negative pressure of approximately −60 mmHg. In order for this suction effect not to lead to excessive swelling, it is essential that the corneal epithelium, in concert, with the underlying endothelial layer mediate osmotically coupled water flow outward from the stroma through net ion transport. The endothelial layer facing the anterior chamber provides most of the dehydrating function whereas the epithelial layer contribution is relatively minor. In other words, epithelial layer-mediated net fluid transport toward the tears from the stroma appears to play a fine-tuning role in maintaining a state of corneal hydration commensurate with normal vision. Nevertheless, under stimulated conditions, the rabbit epithelial layer can provide up to 25% of the total

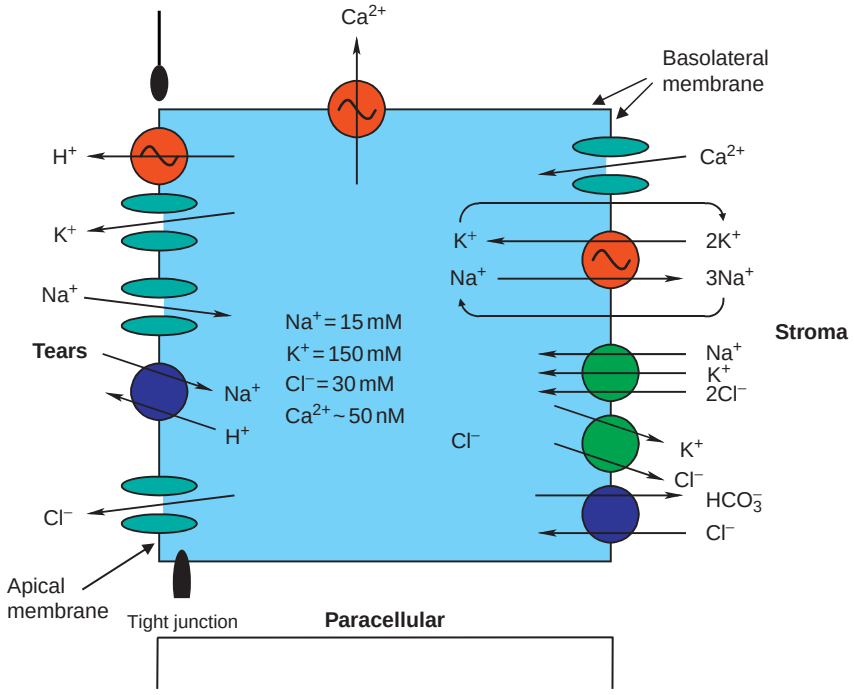

Figure 1 Current model describing ion transporters and channels in corneal epithelium: Arrow heads point in directions of net fluxes. At the tear-side facing apical membrane, there is a Na^+:H^+ exchanger and a conductive pathway for net Cl^- and K^+ efflux. There is also Na^+ entry at this membrane. At the stromal and paracellular sides is the basolateral membrane. It has a K^+ efflux pathway along with the Na^+–K^+ pump coupled to an electroneutral Na^+:K^+:2Cl^- cotransporter. A Cl^-:HCO_3^- electroneutral cotransporter and a Ca^{2+} channel reflective of different subtypes are shown. A K^+:Cl^- cotransporter is also indicated.

dehydrating function. However, if the epithelial layer integrity is damaged, fluid leakage from the tears cannot be compensated by the dehydrating function of the innermost endothelial layer. In this case, the stroma will continuously swell. Therefore, epithelial wound healing through cell proliferation, migration, and tight junction renewal is crucial for maintaining the corneal barrier function.

Importance of Transport Mechanisms to Epithelial Function

The corneal epithelial electrical resistance is dependent on the intactness of its tight junctions forming appositions in the upper layers of the epithelial functional syncytium. In order to provide an effective barrier function, the electrical resistance of the corneal epithelium has to be relatively high (i.e., at least 1 kΩ cm^2). In addition, the ability of the epithelium to mediate net ion transport from the stroma into the tears is dependent on tight junctional resistance. If the resistance falls due to injury, there is a corresponding decrease in net ion transport, resulting in compromise of the barrier function followed by a decline in osmotically coupled fluid flow toward the tears.

In all species studied, the corneal epithelial layer elicits secondary active chloride (Cl^-) transport from the stroma to the tears whereas net sodium (Na^+) transport occurs in the opposite direction, from the tears to the stroma. There is variability in the magnitude of active Na^+ transport due to differences in the Na^+ permselectivity of the tear-side-facing apical membrane. In rabbits and humans, the relative Na^+ and Cl^- permeabilities are similar to one another whereas in the amphibian this membrane is essentially Cl^- permselective. There is large variability among different species with regard to the ratio between tear-directed Cl^- transport and stroma-directed Na^+ transport. In the rabbit and human, this ratio under baseline conditions is about 50%, whereas in the amphibian (i.e., toad and bullfrog) it is at least 90%. Despite such differences, osmotically coupled fluid flow across this layer has been identified both in the isolated rabbit and amphibian cornea suggesting that net Cl^- fluxes toward the tears exceed stroma-directed Na^+ fluxes.

Corneal transparency is dependent on net influx and efflux of inorganic and organic osmolytes. For example, amino acid uptake mechanisms have been identified in this tissue. By definition, an active uptake mechanism depends on metabolic energy generated by aerobic and anaerobic metabolism. Its metabolic dependence is evident, since exposure to metabolic inhibitors results in

corneal swelling and the development of opacification. These changes occur because corneal deturgescence (i.e., physiological hydration state) and maintenance of epithelial health are dependent on the ability of this tissue to: (1) elicit osmolyte and drug extrusion against opposing electrochemical gradients and (2) accumulate organic substrates to levels above those in the extracellular bathing solution. This array of very different transport functions are performed by transporters of distinct ionic and substrate selectivity.

Primary and Secondary Ionic Transport Mechanisms

The corneal epithelial cells express both primary and secondary ionic transport mechanisms. As in all epithelial cells, Na^+:K^+ ATPase expression occurs along the basolateral membrane facing the stroma and the paracellular pathway between the neighboring epithelial cells. This transport mechanism is primary since its ATPase activity directly elicits electrogenic Na^+ extrusion into the stromal and paracellular media. Such efflux is coupled to intracellular K^+ accumulation above its predicted electrochemical value. On the other hand, secondary ionic transporter function is driven by the Na^+ and K^+ electrochemical gradients established by Na^+:K^+ ATPase activity. In all species, there is Na^+:K^+:$2Cl^-$ co-transport activity in the basolateral membrane, which is reflective of secondary active ion transport function. This cotransporter functions to accumulate intracellular Cl^- to levels above its predicted electrochemical values. Net Cl^- transport into the tears occurs as a consequence of its efflux by electrodiffusion across the tear-side facing essentially Cl^- permselective apical membrane. In order to maintain charge neutrality, Na^+ moves in parallel as a counter ion through the paracellular pathway.

Another primary active ion transporter identified in the corneal epithelium is the H^+ pump. Its activity in combination with two different types of cotransporters is required for mediating regulation of intracellular pH. These cotransporters are Cl^-:HCO_3^- and Na^+:H^+ antiporters whose transport directionality is determined by the electrochemical gradients of the involved ions. Specifically, the Cl^-:HCO_3^- antiport will drive HCO_3^- out of the cell, provided there is sufficient carbonic anhydrase activity to raise intracellular bicarbonate levels above those in the external medium. Under such conditions, Cl^- will be taken up from the stroma into the cell interior in exchange for bicarbonate efflux into the external medium. In this scenario, intracellular pH falls resulting in increases in the activity of two different alkalinizing mechanisms: Na^+:H^+ antiport activity in combination with H^+ pump ATPase activity. The Na^+:H^+ antiport can provide an alkalinizing function if the Na^+:K^+ pump activity is sufficient to establish a steep enough Na^+ gradient between the external milieu and the intracellular compartment to exchange H^+ from the cell interior for downhill Na^+ movement into the cell interior.

Cl^- efflux out of the epithelial cells across the apical membrane is dependent on membrane voltage electronegativity relative to the bathing solution. Numerous studies have shown that the intracellular membrane voltage is about -50 mV. This value is dictated to a large extent by the activity of the electrogenic Na^+:K^+ pump and the relative K^+ permeability of the basolateral membrane. The electrogenic Na^+:K^+ exchange pump contributes since its pump Na^+:K^+ stoichiometry exceeds a value of 1. In other words, with each pump cycle, more Na^+ ions are extruded than K^+ ions are taken up into the cell interior from the stroma. In any case, due to the activity of the Na^+:K^+ pump, Cl^- is accumulated into the epithelial cells above its predicted electrochemical equilibrium value. In turn, K^+ diffuses downward and outward, essentially across the basolateral rather than the apical membrane since the former barrier has a much higher K^+ permselectivity. This downward movement of K^+ establishes a negative membrane voltage which is dependent on the activity of the Na^+:K^+ pump and the relative basolateral membrane K^+ permeability. Another factor affecting the level to which K^+ is elevated above electrochemical equilibrium is the tightness of coupling between the Na^+:K^+:$2Cl^-$ cotransporter and the Na^+:K^+ pump. Stimulation of the Na^+:K^+:$2Cl^-$ cotransporter may occur as a consequence of increases in Na^+:K^+ pump activity leading to enhancement of intracellular K^+ accumulation. A rise in K^+ can then be compensated for by a rise in basolateral K^+ membrane permeability, which will increase outward directed K^+ efflux and the membrane voltage electronegativity. This chain of events will stimulate net Cl^- efflux from the stroma into the tears since the driving force for Cl^- efflux into the tears, across the highly Cl^- permselective apical membrane, is the magnitude of the membrane voltage electronegativity.

Therefore, it is through the concerted activity of the aforementioned transport mechanisms, along with appropriate regulation of the cell-limiting membranes, that the corneal epithelium can elicit net Cl^- transport from the stroma toward the tears and regulate its intracellular pH within bounds that are required for the maintenance of anterior ocular surface health.

Coupling of Ionic Transport Mechanisms to Stromal Deturgescence

It is commonly thought that the driving force for fluid transport out from the stroma across the epithelial cells into the tears is local osmosis. The fact that the corneal epithelium elicits net Cl^- transport into the tears suggests

that this ionic flux may be sufficient to account for the magnitude of outward-directed fluid transport. This expectation has been proven to be correct since, under open circuit conditions, net Cl^-transport is commensurate with measured isotonic fluid transport. The dependence of transepithelial fluid transport into the tears on net Cl^- transport was validated by showing that drugs which either stimulate or inhibit net Cl^- transport have corresponding effects on fluid transport.

The fact that there is a coupling between fluid and net Cl^- transport prompted investigators to probe for receptor-mediated control of net Cl^- transport since corneal epithelial health is dependent on innervation of this tissue. This dependence suggests that neurotransmitter release from nerve endings mediate – through receptor stimulation – responses supportive of corneal epithelial functions. Such a notion was validated by showing that loss of neural input results in impaired corneal epithelial regeneration and recurrent erosion. Accordingly, it has also been shown that the corneal epithelium expresses receptor subtypes responsive to adrenergic and cholinergic agonists released from sympathetic and parasympathetic branches of the autonomic nervous system. Other studies indicated that stimulation of these receptors elicit regulation of corneal epithelial renewal, ion transport activity, transparency, and fluid transport.

The regulation of cell volume by the aforementioned ionic transport mechanisms underlies the ability of the corneal epithelium to elicit net fluid transport from the stroma into the tears. It is possible that fluid transport is dependent on serial repetitive swelling and shrinking of cell volume. In this way, swelling occurs as a result of initial stimulation of net osmolyte uptake. Such rises occur in response to increases in Na^+:K^+ pump activity leading to rises in sodium chloride (NaCl) and potassium chloride (KCl) uptake through the Na^+:K^+:$2Cl^-$ cotransporter. As a consequence of an increase in osmolyte uptake, fluid flow into the cells increases. Subsequently, the epithelial cell volume decreases as a result of stimulation of ionic efflux (i.e., KCl) into the tears. The swelling response is referred to as regulatory volume increase (RVI) due to increases in NaCl and KCl uptake. Subsequent shrinkage occurs as a consequence of RVI and is dependent on increases in KCl efflux leading to osmotically coupled fluid loss. This cell shrinkage is known as regulatory volume decrease (RVD). Therefore, fluid transport is tightly regulated by alternating stimulation and inhibition of osmolyte uptake and efflux into the corneal epithelium. How such tight and time-dependent control of these different transport mechanisms is mediated is unknown. It may be dependent on the ability of different receptor types to elicit – through a variety of second messenger pathways – rapid changes in the activities of these ion transporters mediating alternating RVI and RVD responses.

In addition to mediating fluid transport under isotonic conditions as a possible result of differential activation and inhibition of ion-transport activity and membrane permeability, RVD and RVI responses can be induced through variations in bathing solution osmolarity similar to those encountered in daily living and those identified in some types of dry eye disease. In order for cell volume regulatory responses to change fluid transport rates and thereby maintain corneal homeostasis, despite being exposed to an environmental hypertonic or hypotonic challenge, it is also necessary to have a coordinated regulation of ion transporters and parallel cell membrane permeability. Such regulation occurs through receptor-mediated events that can modulate ion transporter rates to either increase or decrease net ionic influx or efflux from corneal epithelial cells. These receptors elicit control of ion transporter function and cell permeability through second messengers that either concomitantly increase or inhibit ion transport rates through stimulation or inhibition of active ion transporter, cotransporters, and cell membrane permeability.

Such coordinated control is required for the maintenance of corneal transparency since they underlie RVD and RVI responses driving fluid out of stroma into the tears. Depending on the type of osmotic challenge, these responses sustain corneal epithelial barrier function. However, in individuals afflicted with dry eye disease, one problem is compromise of barrier function leading to stromal infection. Even though, in these patients, there may be activation of a RVI response due to chronic exposure to hypertonic tears, it may not be adequate to restore isotonic cell volume resulting in disruption of barrier function. This suggestion has prompted a host of studies over the last 30 years that are focused on characterizing receptor-mediated regulation of corneal epithelial active ion transport underlying regulatory volume responses. Their results have pointed investigators in directions that may lead to the identification of novel strategies for improving the rates of corneal epithelial renewal as well as restoring its transparency and refractive properties following an injury.

Other Transport Mechanisms

The limited corneal epithelial layer permeability presents a formidable barrier to solute and drug permeation into the ocular interior. This hindrance has prompted efforts to probe for the expression of transporters that could facilitate their uptake into the eye. A number of different transporters were identified that can elicit this effect. They include a carnitine/organic cation transporter and a sodium-dependent amino acid transporter. On the other hand, rather than identifying a drug-influx mechanism,

a multi-drug-resistant (MDR)-1 efflux mechanism has been described. Such an efflux process does not promote drug uptake into the ocular interior if they are substrates for the MDR-1 pumps. Therefore, improving drug delivery into the ocular interior is in most cases focused on increasing their hydrophobicity so that they can more readily permeate by membrane diffusion. One example of such an improvement is exemplified by rendering epinephrine more lipid soluble through its derivatization with a lipid. An alternative is to inhibit MDR-1-elicited drug efflux. However, none of the currently used inhibitors have adequate selectivity for this purpose.

Receptor-Mediated Control of Corneal Epithelial Ionic Transport Functions

Adrenergic subtype (α_1, α_2, and β), serotonergic, and cholinergic receptor-linked functions have been identified in the corneal epithelium. Adrenergic receptors mediate their control of ionic transport and membrane permselectivity through second messenger pathways involving increases in intracellular Ca^{2+} and modulation of adenylate cyclase activity. Such variations change either the basolateral or apical membrane permeabilities resulting in modulation of active Cl^- transport through changes in the intracellular potential difference. For example, β-adrenergic receptor stimulation has a corresponding effect on net Cl^- transport by enhancing K^+ basolateral membrane permselectivity as well as increasing Cl^- electrodiffusion across the apical membrane into the tears. Less is known about the signaling pathways eliciting cholinergic and serotonergic receptor control of net ion transport.

The corneal epithelium and accessory anterior ocular tissues express a host of cytokines that are critical to the maintenance of corneal epithelial functions. In particular, cytokine expression is critical for inducing control of cell proliferation, migration, and terminal differentiation. Their importance has become self-evident from studies on the mechanisms of corneal epithelial wound healing induced by injury. Numerous cytokine expression levels are upregulated to hasten corneal epithelial wound healing through stimulation of cell migration and proliferation. Such a realization has heightened the interest in determining the mechanisms of regulation of cell-signaling pathways linking their cognate receptor activation to these responses. It is believed that these studies will identify potential drug targets to improve in a clinical setting the outcome of injury-induced corneal wound healing.

Active ion transporters and membrane channels underlying receptor activation are components of a myriad of cell signaling pathways that mediate cytokine receptor control of epithelial renewal. One of the most potent and efficacious mitogens hastening corneal epithelial renewal is epidermal growth factor (EGF). This mitogen induces increases in cell proliferation and migration through stimulation of different ion-transport mechanisms, ionic permeabilities, and receptor-linked channels. They include increases in the activity of the basolateral membrane localized Na^+:K^+:$2Cl^-$ cotransporter resulting from stimulation of plasma membrane Ca^{2+} influx and activation of the mitogen-activated protein kinase (MAPK) superfamily. The increase in Ca^{2+} influx through a Ca^{2+} channel is dependent on EGF receptor (EGFR)-induced stimulation of membrane-associated phospholipase C (PLC) followed by hydrolysis of a phosphoinositide to induce Ca^{2+} release from an intracellular Ca^{2+} store. Another ionic influx affected by EGFR stimulation is K^+ efflux through the basolateral membrane. In addition, mitogenic responses to EGF require that during cell-cycle progression cell volume is modulated to accommodate increases in the parent cell of genomic content prior to cell division. Such modulation is, in part, dependent on changes in K^+:Cl^- cotransporter expression and activity. Another example of a cytokine whose induced effects are dependent on modulation of channel activity is the tumor necrosis factor-alpha (TNFα).

Cell-Volume Control and Epithelial Renewal

Epithelial renewal is a dynamic process that is dependent on tight regulation of cell volume. Prior to cell division, volume expansion of a parent cell is required to accommodate doubling of the nuclear and cytoplasmic components in preparation for their equal distribution into daughter cells. Similarly, changes in cell volume are requisite for cell migration, as this process involves repeated and coordinated leading-edge cytoplasmic volume extension, along with retraction at the opposite pole. As modulation of ion-transport activity and membrane permeability underlie changes in cell volume, cytokine-induced control of renewal is, therefore, dependent upon modulation of ionic influx and efflux. Such control requires that there is synchronized release of specific cytokines that alter ion transport at appropriate times during the cell cycle. Numerous cytokines mediate the required regulation for error-free proliferation and migration. Therefore, cytokine receptor control of ion transport activity is of critical importance in the maintenance of corneal epithelial renewal, transparency, and its refractive properties.

Ca^{2+} Channel and Pump Activity

Receptor-induced Ca^{2+} signaling contributes to the regulation of net Cl^- transport and proliferation of corneal epithelial cells. In order for Ca^{2+} to link receptor activation to these responses, its intracellular concentration must be regulated at sub-micromolar levels.

Such regulation occurs through different types of Ca^{2+}/Mg^{2+}-ATPase plasma membrane and endoplasmic reticulum transporters and channels. The plasma membrane pump counterpart is selectively stimulated by

calmodulin, whereas one type of channel in this domain is activated as a direct consequence of emptying of intracellular Ca^{2+} stores. This channel is formed by a tetrameric configuration of transient receptor potential (TRP) protein subunits. Each of the different types of TRP channels identified in the corneal epithelium is activated by different stimuli. Currently, three different types are expressed and studied in corneal epithelial cells. Even though their activation leads in all cases to increases in plasma membrane Ca^{2+} influx, the types of responses elicited are very different from one another. The four identified types are TRPC4, TRPV1, TRPV4, and TRPM8. In human cornea epithelial cells, TRPC4 is activated during exposure to EGF. TRPV1 is stimulated by an agonist contained in an extract of red peppers (capsaicin) leading to increases in proinflammatory cytokine expression. TRPV4 is activated by a decreased bathing-solution osmolarity and elicits a RVD response. On the other hand, TRPM8 is temperature sensitive. The Ca^{2+} signaling role attributable to activation of each of these three different TRP isoforms is dependent on the ability of endoplasmic reticulum Ca^{2+} transporters to rapidly take up into intracellular stores the Ca^{2+} that has flowed in through these different plasma membrane TRP channels. Otherwise, a sustained rise in intracellular Ca^{2+} concentration may be cytotoxic. The importance of Ca^{2+} signaling in mediating receptor control of corneal epithelial renewal and transparency suggests that its modulation by drugs is of potential value in a clinical setting.

K^+, Cl^-, and Na^+ Channels

Modulation of K^+ channel activity is essential for mediating different responses associated with corneal epithelial function. For example, changes on K^+ channel activity mediate EGF-induced mitogenic responses, ultraviolet (UV) light-induced apoptosis, and adrenoceptor-induced increases in net Cl^- transport. In these cells, there is expression of Ca^{2+}-dependent and inwardly rectifying K^+ channels. Even though activation of these different K^+ channels types induces intracellular K^+ losses, the responses are very different from one another. Additional studies are required to understand how their activation leads to such disparate responses.

Chloride channel activity modulation occurs in response to adrenergic receptor-induced increases intracellular Ca^{2+} concentration and rises in intracellular cyclic adenosine monophosphate (cAMP) levels. Corneal epithelial cells express cystic fibrosis transmembrane regulator (CFTR) channels that are stimulated by rises in cAMP and underlie stimulation of net Cl^- transport. They also express a Cl^- channel designated as ClC-3 and their activation is suggested to underlie a regulatory volume response mediating shrinkage during exposure to a hypotonic challenge.

There is some evidence for the expression of tetrodotoxin-blockable Na^+ channels in corneal epithelial cells. The functional importance of such activity is unclear since their activation only occurs at membrane voltages far less negative than those described in corneal epithelial cells.

Summary

Ion transporter and membrane permeability regulation are essential to the maintenance of corneal epithelial health. Such control is essential for mediating responses that are required for corneal epithelial renewal and the maintenance of corneal transparency. The corneal epithelial cells express both primary and secondary ionic transport mechanisms whose regulation occurs through receptor activation. These ion transporters in concert with changes in membrane permeability underlie: (1) osmotically coupled fluid flow; (2) cell-volume regulation; (3) intracellular pH regulation; and (4) Ca^{2+} signaling. Such control assures that epithelial renewal maintains barrier function and the fine-tuning contribution capability of the corneal epithelium to elicit adequate fluid egress from the cornea for sustaining tissue transparency. Additional studies are warranted to identify novel drug targets in the signaling pathways mediating receptor control of ion transporter and channels. This endeavor will possibly identify improved techniques for restoring corneal epithelial function subsequent to injury.

See also: Corneal Epithelium: Response to Infection; Dry Eye: An Immune-Based Inflammation; Stem Cells of the Ocular Surface; The Surgical Treatment for Corneal Epithelial Stem Cell Deficiency, Corneal Epithelial Defect, and Peripheral Corneal Ulcer; Tear Film Overview.

Further Reading

Al-Nakkash, L., Iserovich, P., Coca-Prados, M., Yang, H., and Reinach, P. S. (2004). Functional and molecular characterization of a volume-activated chloride channel in rabbit corneal epithelial cells. *Journal of Membrane Biology* 201: 41–49.

Al-Nakkash, L. and Reinach, P. S. (2001). Activation of a CFTR-mediated chloride current in a rabbit corneal epithelial cell line. *Investigative Ophthalmology and Vision Science* 42: 2364–2370.

Bildin, V. N., Yang, H., Crook, R. B., Fischbarg, J., and Reinach, P. S. (2000). Adaptation by corneal epithelial cells to chronic hypertonic stress depends on upregulation of Na:K:2Cl cotransporter gene and protein expression and ion transport activity. *Journal of Membrane Biology* 177: 41–50.

Candia, O. A. and Alvarez, L. J. (2008). Fluid transport phenomena in ocular epithelia. *Progress in Retinal and Eye Research* 27: 197–212.

Capó-Aponte, J. E., Wang, Z., Bildin, V. N., Pokorny, K. S., and Reinach, P. S. (2007). Fate of hypertonicity-stressed corneal epithelial cells depends on differential MAPK activation and p38MAPK/Na-K-2Cl cotransporter1 interaction. *Experimental Eye Research* 84: 361–372.

Lu, L. (2006). Stress-induced corneal epithelial apoptosis mediated by K^+ channel activation. *Progress in Retinal Eye Research* 25: 515–538.

Lu, L., Reinach, P. S., and Kao, W. W. (2001). Corneal epithelial wound healing. *Experimental Biology and Medicine* 226: 653–664.

Pan, Z., Yang, H., Mergler, S., et al. (2008). Dependence of regulatory volume decrease on transient receptor potential vanilloid 4 (TRPV4) expression in human corneal epithelial cells. *Cell Calcium* 44: 374–385.

Reinach, P. S., Capó-Aponte, J. E., Mergler, S., and Pokorny, K. S. (2008). Roles of corneal epithelial ion transport mechanisms in mediating responses to cytokines and osmotic stress. In: Tombran-Tink, J. and Barnstable, C. J. (eds.) *Ocular Transporters: In Ophthalmic Diseases and Drug Delivery, Series Ophthalmology Research*, pp. 17–46. Totowa, NJ: Humana Press.

Reinach, P. S., Holmberg, N., and Chiesa, R. (1991). Identification of calmodulin-sensitive Ca^{2+}-transporting ATPase in the plasma membrane of bovine corneal epithelial cell. *Biochimica et Biophysica Acta* 1068: 1–8.

Wolosin, J. M. and Candia, O. A. (1987). Cl^- secretagogues increase basolateral K^+ conductance of frog corneal epithelium. *American Journal of Physiology* 253: C555–C560.

Wu, X., Yang, H., Iserovich, P., Fischbarg, J., and Reinach, P. S. (1997). Regulatory volume decrease by SV40-transformed rabbit corneal epithelial cells requires ryanodine-sensitive Ca^{2+}-induced Ca^{2+} release. *Journal of Membrane Biology* 158: 127–136.

Yang, H., Mergler, S., Sun, X., et al. (2005). TRPC4 knockdown suppresses epidermal growth factor-induced store-operated channel activation and growth in human corneal epithelial cells. *Journal of Biological Chemistry* 280: 32230–32237.

Yang, H., Sun, X., Wang, Z., et al. (2003). EGF stimulates growth by enhancing capacitative calcium entry in corneal epithelial cells. *Journal of Membrane Biology* 194: 47–58.

Zhang, F., Yang, H., Wang, Z., et al. (2007). Transient receptor potential vanilloid 1 activation induces inflammatory cytokine release in corneal epithelium through MAPK signaling. *Journal of Cellular Physiology* 213: 730–739.

Corneal Epithelium: Wound Healing Junctions, Attachment to Stroma Receptors, Matrix Metalloproteinases, Intracellular Communications

G M Gordon and M E Fini, University of Southern California, Los Angeles, CA, USA

Glossary

Apoptosis – The most common form of physiological (as opposed to pathological) cell death. Apoptosis is an active process requiring metabolic activity by the dying cell; often characterized by shrinkage of the cell, cleavage of the DNA into fragments that give a so-called laddering pattern on gels and by condensation and margination of chromatin.
Cytoskeleton – General term for the internal components of animal cells which give them structural strength and motility: plant cells and bacteria use an extracellular cell wall instead. The major components of cytoskeleton are the microfilaments (of actin), microtubules (of tubulin), and intermediate filament systems in cells.
Diabetic retinopathy – Damage to the retina caused by diabetes mellitus.
Dystrophic epidermolysis bullosa – A rare disorder caused by a mutation in the keratin gene and is characterized by the presence of extremely fragile skin and recurrent blister formation.
Filopodia – A thin protrusion from a cell, usually supported by microfilaments; may be functionally the linear equivalent of the leading lamella.
Idiopathetic pulmonary fibrosis – A chronic, progressive interstitial lung disease with an unknown cause.
Phagocytosis – Uptake of particulate material by a cell (endocytosis).
Phenotype – The characteristics displayed by an organism under a particular set of environmental factors, regardless of the actual genotype of the organism.
Recurrent corneal erosion – A disorder of the eye characterized by failure of the epithelial cells to attach to the basement membrane.

Corneal Epithelial Wound Healing: Introduction

The main function of the cornea is to prevent infectious invasion and to retain a smooth, optically clear surface to transmit light into the retina. The cornea has evolved a complex wound healing process for dealing with any insults to this tissue. The overall goal of corneal wound healing, as in most healing processes, is to repair the damaged tissue to resemble the unwounded tissue as closely as possible. In the cornea, this is especially important, as a failure to recapitulate an unwounded state can lead to visual impairments and a lower quality of life. The process of corneal wound healing is multifaceted involving many cell bound and secreted factors which work together to induce large-scale gene expression and phenotypic alterations in order to coordinate cell migration, proliferation, and survival rates for optimum regeneration and restoration of tissue function. While the process of corneal epithelial wound healing is well understood on the macro-molecular level (as will be discussed), there remain many micromolecular aspects to be elucidated if we are to completely understand this process.

Corneal Epithelial Wound Healing: Phases of Wound Healing Process

The corneal epithelial wound healing process can be described as having three overlapping phases: the lag phase, the migration phase, and the proliferation/restratification phase (**Figure 1**). The lag phase occurs immediately following any disruption of the corneal epithelium such as a scratch or puncture. During this phase, polymorphonuclear (PMN) cells from the tear fluid clear damaged and necrotic tissue from the wound area by phagocytosis, resulting in a microscopic enlargement of the wound area. These PMN cells generally disappear shortly after complete resurfacing of the wound by the epithelial cells though they can persist in cases of infection. Concurrently, a provisional matrix composed mainly of fibrin and fibronectin is secreted by the epithelial cells and the lacrimal gland and is laid down over the wound area. The provisional matrix acts as a substrate for migrating epithelial cells as well as an activator of integrin receptors on the cell surface to keep intact intracellular migration signals, mediated by the small GTPase proteins Rho and ROCK.

Also, during this phase, the epithelial cells must prepare themselves for the migratory phase. For cells proximal to the wound edge, this includes a dramatic alteration

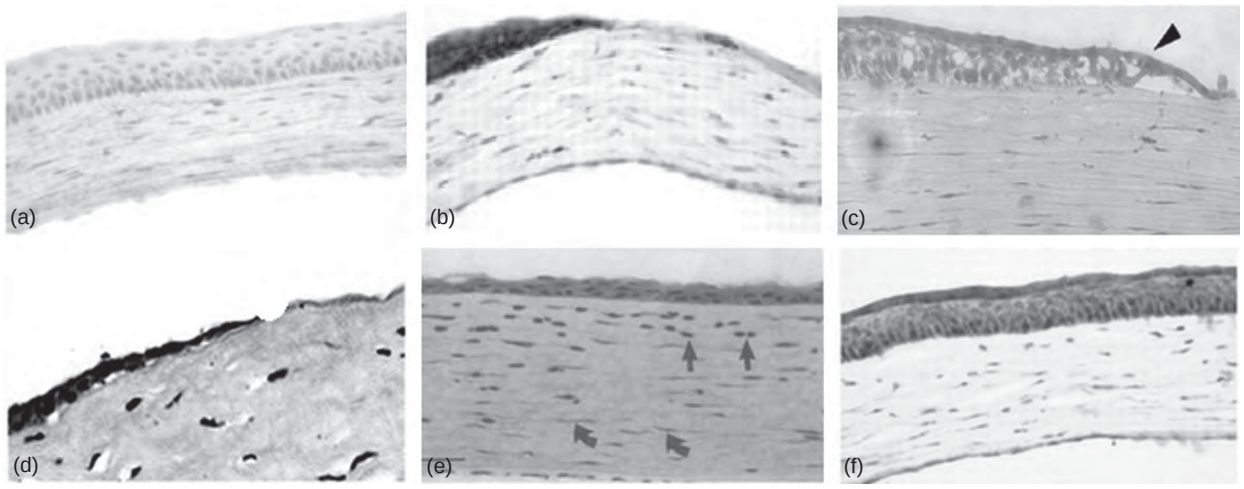

Figure 1 The stages of corneal epithelial wound healing. Histological examination of corneal resurfacing. (a) The unwounded cornea. (b) 1 h after removal of the corneal epithelium without penetrating the basement membrane cells at the wound margin have begun to alter their morphology and gene expression in preparation for migration. (c) 8 h and (d) 18 h after wounding, epithelial cells have begun to migrate over the provisional matrix. Note that there is a monolayer of migrating cells; the spacing between the cells and the basement membrane in (c) is an artifact of the sectioning process. (e) 24 h after wounding, cells have completely resurfaced the wound and begin the third phase: proliferation/restratification. By 7 days out (f), the corneal layers are repopulated and the ocular surface resembles the unwounded cornea. Arrowhead in (c) indicates leading edge; arrows in (e) indicate inflammatory cells. Curved arrows in (e) indicate fibroblasts.

in their gene expression profile including a secession of proliferation, and an alteration in cytokine and protease secretion, an alteration of the cytoskeleton including formation of lamellapodia and fillipodia, and an alteration of cell–cell and cell–matrix adhesions. Cells farther from the wound continue to proliferate to replace cells that enter into migratory phase. Additionally, during this phase, loss of superficial keratocytes due to apoptosis can be observed directly beneath the wound even when the basement membrane (BM) remains intact immediately following wounding. In a nonpenetrating wound, these stromal keratocytes are slowly replaced by proliferation of the surviving keratocytes without fibroblast activation or myofibroblast differentiation. In penetrating wounds, secreted factors induce fibroblast activation and proliferation and myofibroblast differentiation of the remaining keratocytes as will be discussed.

The second phase of corneal wound healing is the migratory phase. It is important that the wound resurfaces quickly, as prolonged or chronic wound healing scenarios may lead to degradation of the BM due to an increased proteolytic profile. This may in turn lead to ulceration of the underlying stroma, activation of the keratocytes into myofibroblasts, scarring, and possible visual impairments. The migratory phase is characterized by the centripetal migration of a continuous monolayer of nondividing corneal epithelial cells (CECs) over the wound and usually lasts between 24 and 36 h depending on the size of the wound and animal species. Cells at the wound edge flatten out and migrate while those more distal to the wound are induced to proliferate to replace the migratory cells. Cell migration rates vary by species, with rabbit CECs migrating at around 64 mm day^{-1} and mouse CECs at around 17 mm day^{-1}. During this phase, epithelial cells must be anchored enough to the underlying provisional matrix so that they are not removed casually (blinking, rubbing, etc.), but if the attachments are too strong, the cells will be unable to migrate. Laminin-5 has been implicated as a major determinant in the adhesion of epithelial cells to the underlying matrix. In the unwounded cornea, processed laminin-5 is present and helps hemidesmosomes in epithelial cells adhere strongly to the collagen VII anchoring fibrils. However, following wounding, the presence of the processed form becomes secondary to that of the unprocessed form which is not bound by cells as strongly. Unprocessed laminin-5 is deposited in the provisional matrix and, along with other provisional matrix components such as fibronectin, promotes the migration of epithelial cells rather than stationary adherence.

It has been proposed that epithelial cell migration is driven by an adhesion/deadhesion cycle that is regulated by two things: (1) a careful ratio of adherence molecules for attachment and proteolytic enzymes that degrade these attachments and (2) intracellular extension and contractile signals that alter the actin cytoskeleton morphology. Migratory cells first extend lamellapodia and fillopodia forward and form temporary focal adhesion complexes with the provisional matrix. Focal adhesions at the tail end of the cell are removed by a combination of proteolytic enzymes that cleave the complex and

intracellular contractile mechanisms that rip the trailing focal adhesions from the underlying stratum, sometimes even leaving part of the cell membrane behind. This cycle allows the cells to loosely adhere to the underlying matrix so that they can move due to contraction and reformation of the actin cytoskeleton.

The third phase of corneal wound healing is the proliferation/restratification phase. During this phase, the basal cells which have just finished the migratory phase and were kept in a nondividing state begin to proliferate once more in order to repopulate then differentiate and restratify the corneal epithelial layers and smooth out any irregularities in the BM. Also during this phase, the epithelial basement membrane (EBM) is reformed (in penetrating or large debridement wounds), the provisional matrix is broken down, and permanent attachments are reformed between the basal epithelial cells and the EBM. In nonpenetrating wounds, this phase is usually accomplished within a few weeks. In penetrating wounds, remodeling of the ECM may persist for months and even years after the insult, and may never completely regenerate.

Corneal Nerves

The cornea is one of the most densely innervated tissues of the body and corneal nerves have been shown to play a significant role in the maintenance of the cornea and in various corneal diseases. There are three networks of corneal nerves that enter the stroma and innervate the mid-stromal, bowman's layer, and epithelial layers. Regeneration of epithelial nerves has been shown to depend on the type of insult sustained. For example, reinnervation of the epithelial layer is much faster following laser ablation of the epithelium versus manual debridement and reinnervation density correlates with renewed corneal sensitivity. Following penetrating wounds, as in a laser-assisted in situ keratomileusis (LASIK) procedure, nerve bundles in the Bowmans layer and stromal flap (those that were severed) disappear completely. Within the first 6 months, nerves first reinnervate the stromal flap, then the Bowman's layer. A cycle of regeneration has been observed where the number of nerves is brought back to normal levels by 2 years post-LASIK, then reduced significantly by 3 years out though the reason and mechanism of this loss remains unknown. Nerve densities in the stroma below the wound remain unchanged following wounding.

Although there is much greater complexity involved in penetrating wound healing scenarios, including the drastic alteration of the stromal keratocyte phenotype with the possibility of permanent scarring, the overall phases of the penetrating corneal wound healing (i.e., lag, migration, and proliferation/restratification) is similar to those of the nonpenetrating process. Important additional differences include cell invasion from limbal blood vessels, the greater cytokine expression profile, and the much longer time frame for remodeling of the wound microenvironment due to the greater scale of remodeling that must take place in the stroma in order to maintain the optimal arrangement for light transmission.

Corneal Epithelial Wound Healing: Cell–Cell and Cell–Matrix Junctions

Cell–cell and cell–matrix junctions are critical components of both unwounded and wounded cell environments and every tissue in the body has a unique profile. Along with secreted factors, these junctions are responsible for all the possible signaling triggers that can alter gene expression and affect cell phenotype, function, and survival. Additionally, these junctions in combination with cellular cytoskeletons give a tissue its structure and help define function. Following wounding, some of these junctions must be broken down while others must be formed to allow cells to migrate while still others must remain to retain as much of a barrier to the outside environment and ensure a cohesive, coordinated sheet of cells resurfaces the wound rather than cells migrating individually. There are four known types of cell–cell interactions: gap junctions, tight junctions, adherins junctions, and desmosomes.

Cell–Cell Junctions: Gap Junctions

Gap junctions are formed by connexins which are homo- or heterohexameric proteins that form on the lateral side of cells and can form both homo- and heterotypic interactions with each other in order to connect the cytoplasm of two neighboring cells between an intercellular space. Gap junctions allow the passage of low-molecular-weight proteins (water, ions, secondary messengers, electrical impulses, and low-molecular-weight ($<$1 kDa) metabolites and nutrients) to pass freely from one cell to another, allowing cells to communicate quickly with each other in order to coordinate such physiological processes as development and regeneration.

Connexins(cxs) are named according to their molecular weight; thus, connxin43 is a 43-kDa protein. Multiple connexins have been observed in the cornea by studying various mammalian species (**Table 1**). Connexin 43 is the most well-documented connexin in the corneal epithelium and it is found primarily in the basal epithelial cells with expression decreasing progressively toward the superficial layers. Other connexins such as cxs26, 30, 31.1, 37, and 50 have been observed with spatially distinct patterns in the unwounded cornea. No connexins have been detected in migrating CECs following wounding though gap junctions in cells distal to the wound remain; thus, gap junctions in cells proximal to the wound are broken down during the lag phase and expression is downregulated throughout the

Table 1 Cell–cell junctions in the unwounded and wounded cornea

	Unwounded	*Wounded*
Gap Jxns		
C×26	X	
C×30	X	
C×30.3		
C×31		
C×31.1	X	
C×31.9		
C×32		
C×36		
C×37	X	
c×40		
C×40.1		
C×43	X	
C×45		
C×46		
C×47		
C×50	X	
C×58		
C×62		
Tight Jxns	X	X
Adherens Jxns	X	X
Desmosomes	X	

migration phase. Following resurfacing, gap junction reformation correlates with the reappearance of laminin-1 in the EBM. Expression of connexin43 has been attributed to Rho, but not ROCK signaling. The functional significance of the loss of gap junctions in migrating cells has yet to be determined.

Cell–Cell Junctions: Tight Junctions

Tight junctions are homeotypic interactions by transmembrane protein structures which link the actin cytoskeleton of neighboring cells and act like cellular gaskets. These structures are composed mainly of claudin occludin and junctional adhesion molecule A (JAMA) and have several purposes: they link neighboring cells, separate proteins in the apical cell membrane from those in the basal–lateral, and they prevent their passage of ions and other small molecules from penetrating between neighboring cells, thus contributing to corneal deturgesence. In the cornea, tight junctions have been detected in the superficial and wing cells. Early work in the field had found that tight junctions were reduced at the wound margin following wounding but reformed quickly behind the migrating front of epithelia. However, more recently, it has been shown that these junctions persist following corneal epithelial ablation with no significant alteration in expression. This newer finding correlates well with an older finding that showed a component of the tight junction complex, ZO-1, is upregulated following removal of superficial CECs. While there is no direct evidence yet, retention of tight junctions presumably helps ensure the integrity of the corneal surface as much as possible and helps to keep cells migrating together as a cohesive sheet.

Cell–Cell Junctions: Adherins Junctions

Adherins junctions are also found on the lateral side of cells and keep neighboring cells firmly attached to each other by anchoring to the actin cytoskeleton. Adherins junctions in the cornea are formed by homeotypic dimers of transmembrane E-cadherin molecules which bind each other in the intercellular space. E-cadherin is calcium dependent and is anchored intracellularly to the actin cytoskeleton by vinculin and α- and β-catenin molecules. E-cadherin-containing adherins junctions have been found throughout the cornea epithelium, and wounding does not seem to affect the expression or distribution of these junctions. Similar to tight junctions, adherins junctions may be retained in order to keep cells migrating together as a cohesive sheet, though again, direct proof is still lacking.

Cell–Cell Junctions: Desmosomes

The final type of cell–cell junction is the desmosome. Desmosomes are similar to adherins junctions in that they both function to keep neighboring cells attached to each other and they are both composed of molecules from the cadherin family. However, unlike adherins junctions which are composed of the cadherin family member E-cadherin, desmosomes are composed mainly of the caherin family members desmoglein and desmocollin. Also, while the adherins junction is anchored to the actin cytoskeleton, desmosomes are anchored by desmoplakin, plakoglobin, and plakophillin to the intermediate filament (IF), or cytokeratin, cytoskeleton. Interestingly, unlike adherins junctions, desmosomes do alter their expression pattern following wounding. It has been found that similar to connexin43, desmoglein is downregulated in migrating CECs, and this downregulation persists until resurfacing is complete and laminin-1 reappears below the epithelial cells. Like gap junctions, the functional significance of the loss of desmosomes in migrating cells has yet to be determined, though it may be necessary for the morphological changes needed for migration.

Cell–Matrix Junctions: Hemidesmosomes and Adhesion Complexes

In addition to cell–cell interactions, cell–matrix interactions are also critical components of tissue function and structure in normal, wounded, and diseased tissue, and a lack of adherence to an underlying matrix may result in apoptosis by ceratin cell types (such as epithelia) and a separation of the dermal and epidermal layers. Cells can be connected to an underlying extracellular matrix by

adhesions that are anchored intracellularly to either the actin or IF cytoskeleton, both of which utilize integrins to form these anchors.

Integrins are not only structural proteins which affect cell attachment, but they are also potent signaling molecules that can affect cell proliferation, migration, and survival properties. Intergins form heterodimers of an α- and β-chain and the different combination of chains determines the extracellular binding partner; some have only one substrate while others have multiple substrates with differing binding kinetics. In mammals, there are 19 known α-chains and 9 known β-chains which can assemble into about 25 distinct integrins. Integrins α2β1, α3β1, α6β1, α9β1, αvβ1, αvβ5, αvβ6, and α6β4 have all been localized to the corneal epithelium with the strongest expression being found in the basal epithelial cells and getting progressively weaker as the cells get closer to being sloughed off into the tear fluid. This progressive loss of integrins ensures that cells that migrate away from the basal epithelium proliferate less and provide a less adhesive surface for microbial adherence and infection of the corneal surface.

Hemidesmosomes are present at the basal membrane of unwounded basal epithelial cells and are composed of the α6β4 integrin as well as adaptor proteins for linking this protein to the IF cytoskeleton. In the unwounded cornea, hemidesmosomes are tightly bound to anchoring fibers composed of collagen VII which pass perpendicular through the BM then make a 90° turn and wrap around collagen III bundles. Following wounding, hemidesmosomes are broken down and are no longer detectable for 70–200 μm outside the wound area in order to allow cells to begin the migratory phase. Although the hemidesmosomes are absent, α6β4 integrin expression is actually increased during resurfacing, though these integrins are no longer associated with hemidesmosomes but instead form focal adhesion complexes (discussed earlier) which now connect the components of the underlying provisional matrix such as unprocessed laminin-5 with the actin cytoskeleton. In penetrating wounds, reformation of the basal lamina and hemidesmosome complexes occurs concurrently in about 6–8 weeks, though studies in monkeys have shown that reformation of the anchoring fibrils may take as long as 18 months to reform. All of these time frames are approximations and can be affected by variables such as the size of the wound, the age and species of the subject, and if there are any complicating factors such as infection or genetic abnormalities.

Secreted Factors Involved in Corneal Epithelial Wound Healing

Along with cell–cell and cell–matrix junctions, secreted factors such as cytokines, growth factors, and proteases are also responsible for regulating normal tissue maintenance and wound healing properties. Cytokines and growth factors are small molecules that can bind and activate their cognate cell surface receptors. These activated receptors then transduce the signal to the nucleus via various intracellular signaling pathways such as the mitogen-activated protein kinase (MAPK), Smad, and nuclear factor kappa-light-chain-enhancer of activated B cells (NF-κB) pathways. However, signaling is not necessarily linear and cross-talk between the pathways can and often does occur.

In other epithelia of the body, these factors are usually secreted by platelets or other cell types that enter a wound from the blood stream. The cornea, however, is an avascular tissue and thus all signals must come from either the tear fluid or the epithelial and stromal cells themselves. Corneal epithelial and stromal cells have been shown to secrete a host of cytokines and growth factors. Transcriptional analysis of primary corneal epithelial cultures has found insulin-like growth factor (IGF), epidermal growth factor (EGF), transforming growth factor (TGF)-α, b-fibroblast growth factor (FGF), TGF-β1, TGF-β2; in addition, all of their cognate receptors are expressed by both corneal epithelial and stromal cells, though to varying degrees, and may act via both autocrine and paracrine mechanisms. Some other important factors have more specific localization patterns and generally act via paracrine signaling. For example, both keratinocyte growth factor (KGF) and hepatocyte growth factor (HGF) are only expressed by stromal keratocytes though their cognate receptors are much more preferentially expressed by epithelial cells, while platelet-derived growth factor (PDGF)-bb is expressed by epithelial cells and its cognate receptor is only expressed in stromal cells. The inflammatory cytokines interleukin (IL)-1α and IL-1β are only expressed by epithelial cells in the unwounded state, but their cognate receptor is present on both epithelial and stromal cells. However, stimulation of keratocytes by IL-1 as occurs during penetrating wounds can induce an autocrine feedback loop; thus, keratocytes can express IL-1. Furthermore, this IL-1 feedback loop also induces other secreted factors such as HGF and KGF expression by keratocytes.

Cytokines can induce gene expression changes that can alter the proliferation, migration, and survival properties of a cell. For example, it has been shown that KGF and EGF can induce CEC proliferation. Also, while neither EGF, PDGF-bb, IL-1, nor TNF-α alone can induce epithelial cell migration, when combined with fibronectin as a substrate, these factors can all significantly speed up migration rates as compared to fibronectin alone. This further emphasizes the complex and combinatorial signaling that controls corneal epithelia wound healing. The role of the TGF-β family in epithelial migration is controversial with some labs showing that it enhances epithelial migration rates, and others finding that it slows down resurfacing rates. Further studies must be done to reconcile these seemingly opposite results.

Matrix Metalloproteinases

Matrix metalloproteinases (MMPs) are a family of structurally related zinc-dependent proteases with overlapping substrate specificities. MMPs are known regulators and effectors of many cellular processes, including tumor progression, development, and epithelial wound healing as well as normal tissue maintenance. The MMP family consists of over 20 members whose substrates have come to include all extracellular membrane proteins as well as many cell surface proteins (i.e., cadherins, heparin-binding EGF (HB-EGF), etc.) and secreted proteins (i.e., TGF-β, IL-1, TNF-α, etc.) which can be both activated and degraded by MMPs. Thus, MMPs can affect gene expression by alterating intracellular (nuclear) signaling by cleavage of cell–cell and cell–matrix interactions as well as by altering the active cytokine and growth factor microenvironment. Due to their broad substrate specificity and potent proteolytic activity, MMPs must be tightly controlled, and are regulated at the transcriptional and posttranslational levels. MMPs can be either secreted or membrane bound and contain a propeptide at their N-terminal that must be removed before they can become proteolytically active.

MMPs are critical components of the wound healing process, as global MMP inhibition by pharmacological agents results in a failure to resurface a wound. Similarly, an overexpression of MMPs is also involved in many epithelial disorders such as idiopathic pulmonary fibrosis in the lung, dystrophic epidermolysis bullosa in the skin, and diabetic retinopathy and recurrent corneal erosion in the eye. Therefore, a precise level of MMP expression is necessary for normal tissue maintenance and optimal wound repair.

In the unwounded cornea, most MMPs are expressed at basal or undetectable levels, except for MMP-7 and -14 which are expressed constitutively. Following removal of the epithelium, several MMPs are upregulated and various family members take on a distinct localization pattern, though the expression patterns of MMP-7 and -14 do not change significantly. MMP-9 is the most well-studied family member and is strongly upregulated at the very tip of the migrating epithelial cells. MMP-10 becomes upregulated by all migratory cells, and MMP-13 expression is upregulated by cells throughout the wound area and in the periphery of the wound. MMP-12 mRNA upregulation has also been detected in the peripheral cells, but this upregulation has not been detected for the actual protein. Penetration of the EBM induces expression of more MMPs such as MMP-2, -3, and possibly -8 which are used to remodel the stromal compartment.

Following resurfacing of nonpenetrating wounds, MMP levels are generally decreased, though MMP-9 expression persists and spreads distally from the wound closure with the timing of its expression correlating with degradation of the provisional matrix. This correlation has been confirmed using MMP-9 knockout (KO) mice which are unable to degrade the fibrin in the provisional matrix which remains as a corneal haze. However, a recent study in human eyes has found that people displaying uncomplicated LASIK surgeries (penetrating wound) may, up to 7 years later, still have EBM irregularities around the wound edges that lead to stromal–epithelial contact causing MMP expression and indicating a continuing wound healing process.

While MMP-9 is critical for overall corneal wound regeneration, it is not critical for corneal re-epithelialization, and in fact acts to slow the rate of re-epithelialization. Other MMPs, however, are critical for corneal resurfacing as global inhibition of MMPs retards resurfacing. However, which specific MMPs are necessary, what their substrates are, and why these MMPs are necessary is still unknown. These questions are especially difficult to answer because loss of an MMP, as in a knockout or knockdown model, can be compensated for by other MMPs due to the overlapping substrate specificities as indicated by the low number of MMP KO mice displaying drastically different phenotypes.

Corneal Epithelial Wound Healing: Conclusion

While the corneal epithelial wound healing process shares some similar properties with skin, lung, and gut epithelial wound healing, there are important differences. For example, whereas skin epithelia can heal by a scarring or vascularization process, the corneal wound healing process must minimize these parameters in order to retain optimal visual clarity. Formation of scar tissue on the molecular level means the accumulation of α-smooth muscle actin-containing fibroblasts also known as granular tissue myofibroblasts that form the fibrous tissue in the early scar before the secretion and formation of the older collagen scar tissue. As the central cornea is an avascular tissue, formation of α-smooth muscle actin expressing cells is initially derived solely from stromal keratocytes. Stromal keratocytes are induced to differentiate into α-smooth muscle actin expressing cells by secreted factors expressed by the CECs and present in the tear fluid such as TGF-β. In the unwounded eye, the EBM binds TGF-β and acts as a physical barrier to prevent the stromal keratocytes from being activated. Over a remodeling period of weeks, months, or even years, myofibroblasts can slowly disappear from a wound site via an unknown mechanism, possibly apoptosis. This disappearance is by no means guaranteed and even if it does occur, it may or may not improve visual acuity depending on whether or not a collagenous scar tissue has formed.

The severity of the wound response is correlated with the severity of the wound; wounds that do not penetrate the EBM tend to regenerate completely, whereas wounds

that do penetrate the EBM tend to induce myofibroblast differentiation, require much longer to heal, and may never quite regain the original architecture. Thus, the most important factor involved in corneal wound healing is whether or not the EBM has been disrupted. While penetration of the BM is arguably the most important factor in corneal wound healing, it is by no means the only determining factor; the size of the wound, the age of the subject, and the causative agent are also important factors. Additionally, any defect in the tear fluid composition or integrity may further impair the wound healing process. All of these factors can affect the cellular microenvironment by alteration of cell adhesion molecules (CAM) and secreted factors which both coordinate and drive the wound healing process.

See also: Corneal Epithelium: Transport and Permeability; Corneal Nerves: Anatomy; Refractive Surgery and Inlays.

Further Reading

Fini, M. E., Cook, J. R., and Mohan, R. (1998). Proteolytic mechanisms in corneal ulceration and repair. *Archives of Dermatological Research* 290(supplement): S12–S23.

Fini, M. E. and Stramer, B. M. (2005). How the cornea heals: Cornea-specific repair mechanisms affecting surgical outcomes. *Cornea* 24 (8 supplement): S2–S11.

Gipson, I. K., Spurr-Michaud, S. J., and Tisdale, A. S. (1988). Hemidesmosomes and anchoring fibril collagen appear synchronously during development and wound healing. *Developmental Biology* 126(2): 253–262.

Imanishi, J., Kamiyama, K., Iguchi, I., et al. (2000). Growth factors: Importance in wound healing and maintenance of transparency of the cornea. *Progress in Retinal and Eye Research* 19(1): 113–129.

Li, D. Q. and Tseng, C. G. (1995). Three patterns of cytokine expression potentially involved in epithelial–fibroblast interactions of human ocular surface. *Journal of Cell Physiology* 163(1): 61–79.

Lu, L., Reinach, P. S., and Kao, W. W.-Y. (2001). Corneal epithelial wound healing. *Experimental Biology and Medicine (Maywood)* 226(7): 653–664.

Mohan, R., Chintala, S. K., Jung, J. C., et al. (2002). Matrix metalloproteinase gelatinase B (MMP-9) coordinates and effects epithelial regeneration. *Journal of Biological Chemistry* 277(3): 2065–2072.

Schultz, G. S., White, M., Mitchell, R., et al. (1987). Epithelial wound healing enhanced by transforming growth factor-alpha and vaccinia growth factor. *Science* 235(4786): 350–352.

Sivak, J. M. and Fini, M. E. (2002). MMPs in the eye: Emerging roles for matrix metalloproteinases in ocular physiology. *Progress in Retinal and Eye Research* 21(1): 1–14.

Steele, C. (1999). Corneal wound healing: A review. Part I. *Optometry Today* 24: 28–32.

Stepp, M. A. (2006). Corneal integrins and their functions. *Experimental Eye Research* 83(1): 3–15.

Stepp, M. A., Spurr-Michaud, S., and Gipson, I. K. (1993). Integrins in the wounded and unwounded stratified squamous epithelium of the cornea. *Investigative Ophthalmology and Visual Science* 34(5): 1829–1844.

Stramer, B. M., Zieske, J. D., Jung, J. C., Austin, J. S., and Fini, M. E. (2003). Molecular mechanisms controlling the fibrotic repair phenotype in cornea: Implications for surgical outcomes. *Investigative Ophthalmology and Visual Science* 44(10): 4237–4246.

Suzuki, K., Saito, J., Yanai, R., et al. (2003). Cell–matrix and cell–cell interactions during corneal epithelial wound healing. *Progress in Retinal and Eye Research* 22(2): 113–133.

Zieske, J. D. (2001). Extracellular matrix and wound healing. *Current Opinion in Ophthalmology* 12(4): 237–241.

Corneal Imaging: Clinical

S Garg and R F Steinert, University of California, Irvine, Irvine, CA, USA

Glossary

Confocal – Noncontact imaging modality based on the principle that light passed through an aperture and focused by an objective lens onto an area of interest.

Optical coherence tomography (OCT) – Noncontact imaging modality in which back-reflected light or backscattered infrared light from internal tissue microstructure is analyzed to achieve two or three-dimensional cross-sectional tomographic images of optical reflectivity.

Phototherapeutic keratectomy (PTK) – Surgery using a laser to treat various ocular disorders by removing tissue from the cornea.

Introduction

Assessment of anterior segment structures is an integral part of the ophthalmic evaluation. Clinical techniques for examining the human cornea *in vivo* have greatly expanded over the last several decades. The clinician's armamentarium includes slit lamp biomicroscopy, specular microscopy of the endothelium, computed corneal topography, high-frequency ultrasound, anterior segment optical coherence topography (OCT), and confocal microscopy. Advanced anterior segment imaging is a routine part of the anterior segment physicians' practice. Confocal microscopic evaluation of the cornea *in vivo* began in the late 1980s. The invention of OCT in the early 1990s initially centered on retinal imaging and was subsequently modified for anterior segment applications.

In the clinical setting, confocal microscopy and anterior segment OCT are noninvasive devices that allows for examination of normal and diseased corneas and anterior segment structures such as the angle, iris, and lens, aiding in both routine patient care and in managing complex pathology.

Confocal Microscopy

Historical Overview

Marvin Minsky invented the confocal microscope in 1955. His novel invention imaged tissue parallel to its surface. Traditionally, images of the tissue were oriented perpendicular to their surface. Minsky exploited the pinhole effect to accomplish his goal. He proposed that both the illumination (condenser) and observation (objective) systems could be focused on a single point (both have common focal points, and thus the name confocal). Using a pinhole eliminates unwanted optical artifacts from light reflected above and below the tissue of interest, improving image quality. However, this increased resolution comes at a cost of a small field of view. A full field of view is accomplished by scanning. In 1968, the first tandem scanning confocal microscope (TSCM) was developed. This improvement used a rotating Nipkow disk to simultaneously scan multiple points on a stationary specimen. In 1985, the confocal was first used to describe imaging of human corneas *ex vivo* and rabbit corneas *in vivo*. Around the same time of development of the TSCM, Svishchev introduced the scanning two-sided mirror confocal microscope. This was later modified by Thaer to enable real-time scanning, the precursor to the modern slit scanning confocal microscope (SSCM).

Current commercially available confocal microscopes include the Confoscan 4 (Nidek Technologies, Gamagori, Japan), Confoscan P4 (Tomey Corporation, Cambridge, MA, USA), Microphthal (Helmut Hund, Wetzlar, Germany), and the Heidelberg Retina Tomograpy II Rostock Cornea Module (Heidelberg Engineering, GmBH, Germany).

How it Works

Confocal microscopy is based on the principle that light passed through an aperture and focused by an objective lens onto an area of interest. The reflected light is then focused by a second objective lens through a second aperture to eliminate out of focus light. The ability of the system to discriminate light that is outside the focal plane results in images of higher *X*-, *Y*-, and *Z*-axis resolutions. The drawback is a small field of view (**Figure 1**). Moving the confocal system (scanning) over the stationary specimen allows for larger fields of view. The *Z*-axis resolution of the confocal microscope permits the dynamic scanning capability of the instrument, allowing *in vivo* corneal imaging without the need for stains or dyes. With computerized three-dimensional reconstruction, this technology has improved lateral and axial resolution to 1–6 and 4–15 μm, respectively, and increased magnification up to 600×. Image quality is affected by image contrast, the light source, the scanning method, the path of light in the cornea, and the optics of the objective.

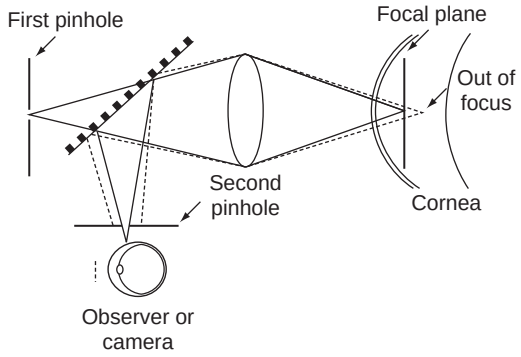

Figure 1 Schematic of the optical principles of confocal microscopy. White light that passes through the first pinhole is focused on the focal plane in the cornea by the condensing lens. Returning light is diverted through the objective lens and a conjugate exit pinhole and reaches the observer or camera. Scattered out of focus light from below or above the focal plane (broken lines) is greatly limited by the pinholes and does not reach the observation system. Reprinted with permission from BJO.

Image separation (depth) is recorded by the movement of the objective between images. Water immersion objective lenses of high numerical apertures are typically used, as they eliminate surface reflections and provide good depth resolution. This requires a short working distance. In clinical practice, subject preparation for the scan is of great importance. Topical anesthesia, patient counseling of the short working distance, bright illumination, and use of coupling agents all aid in capturing useful images. Maintaining a perpendicular orientation to the corneal surface is necessary to avoid oblique sectioning.

Clinical Applications

The normal cornea

The normal human cornea consists of five layers: epithelium, Bowman's layer, stroma, Descemet's membrane, and endothelium. All of these layers, with the exception of Descemet's membrane, can be imaged by confocal microscopy. It is important to note that the more a cellular component reflects light, the brighter the image will appear on a confocal scan.

From front to back, the corneal epithelium is composed of superficial, wing, and basal cells, with a normal thickness of approximately 50 μm. In the superficial layers, cells appear flat and polygonal with hyperreflective nuclei. Wing cells appear uniform in shape and size with dark nuclei. These cells are generally larger than basal cells, but smaller than superficial cells. The basal cells are smaller, more uniform in size, and have bright borders and highly reflective cell nuclei (**Figures 2** and **3**).

Between the basal epithelium and Bowman's layer are corneal nerves that appear as beaded, well-defined linear branching structures with homogeneous reflectivity (**Figure 4**).

Bowman's layer appears as an amorphous homogenous layer in the normal cornea. It is acellular, with randomly

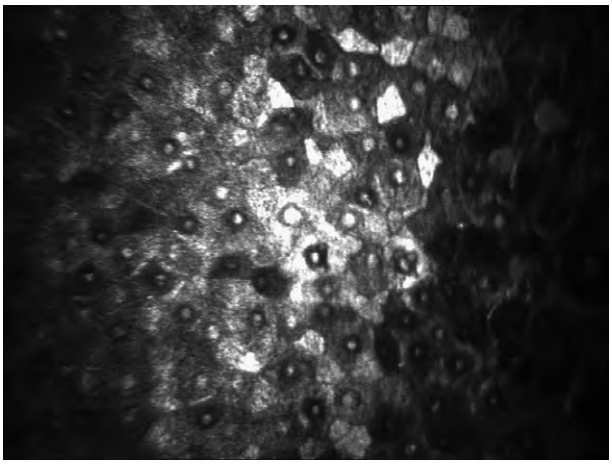

Figure 2 Superficial epithelium.

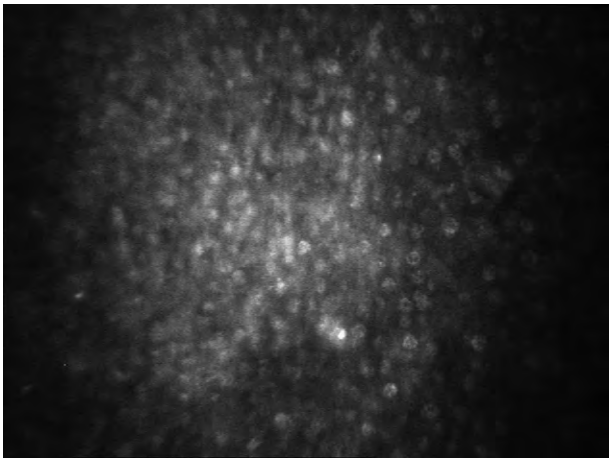

Figure 3 Basal epithelium.

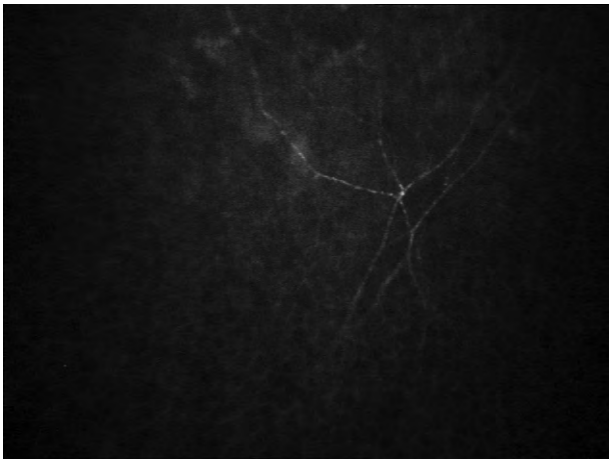

Figure 4 Basal nerve plexus.

dispersed collagen fibrils. On confocal microscopy, Bowman's layer is imaged poorly without the aid of anatomical landmarks such as the highly reflective subbasal nerve plexus due to an average thickness of only 15 µm.

In the corneal stroma, which typically is about 500-µm thick, keratocyte nuclei appear hyperreflective against a dark background. Confocal images exhibit poor reflectivity of stromal keratocyte cytoplasm, cell boundaries, and collagen substance. In the anterior stroma keratocyte nuclei appear as distinct, bright, and oval-round in random orientation. In the mid-stroma, keratocytes exhibit a more regular oval shape transitioning to elongated spindle-shaped as the scan approaches the posterior stroma. Additionally, hyperreflective nerve fibers are sporadically seen coursing within the anterior and mid-stroma, but they are absent in the posterior stroma (**Figures 5** and **6**).

Descemet's membrane thickens throughout life. It is the basement membrane of the inner layer of endothelial cells. Because of the lack of cellularity and thinness, it is poorly captured by confocal microscopy.

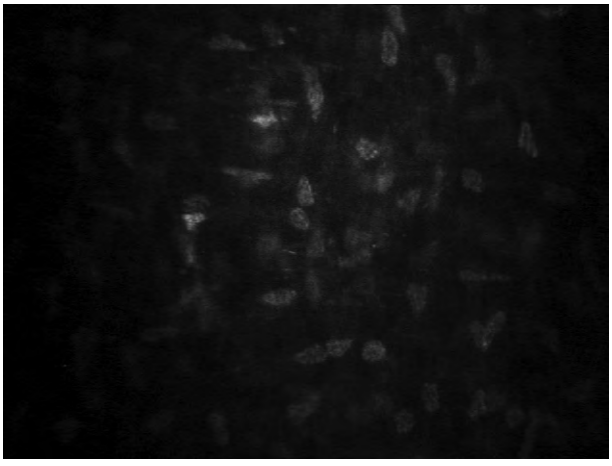

Figure 5 Anterior stroma.

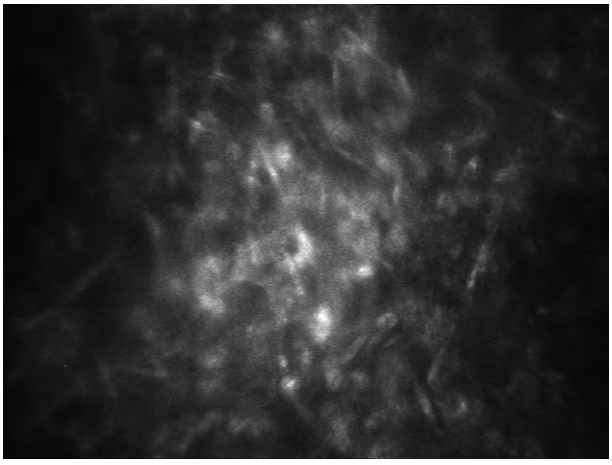

Figure 6 Deep stroma.

Corneal endothelial cells are single layered, normally characterized by a regular hexagonal hyperreflective cell body, void of nuclei, and surrounded by hyporeflective borders (**Figure 7**).

Pachymetry

Confocal microscopy can be used to determine corneal thickness through a function known as confocal microscopy through focusing (CMTF) on the TSCM. This is accomplished by focusing in the *Z*-axis and determining the amount of light backscattering which in turn is plotted as an intensity profile curve. The differences in scattering of the various corneal layers allows for determination of each layer's location. Overall, this method for determination of corneal thickness offers good repeatability, especially for determination of thin layers such as the epithelium and Bowman's membrane. Nontandem models such as the Nidek Confoscan 4 utilize a contact ring at the limbus.

Applications in Pathology

The treatment of infectious keratitis can be challenging. The golden standard for diagnosis of infectious keratitis is light microscopic examination and culture of corneal scrapings. However, confocal microscopy is a very useful tool in helping with diagnostic quandaries. Confocal microscopy is particularly helpful when *Acanthamoeba* or fungal elements are suspects as etiologies. Bacteria (2 µm) can theoretically be visualized; however, given their small size (near the typical resolution for confocal microscopy), clinical distinction is not possible. Fungal infections generally image as hyperreflective, elongated, filaments, or budding yeasts (**Figures 8** and **9**). In its cystic form, *Acanthamoeba* appears as a highly reflective, round, or ovoid double-wall structure with a diameter of 10–25 µm (**Figure 10**). Radial keratoneuritis may appear as irregularly enlarged nerve fibers.

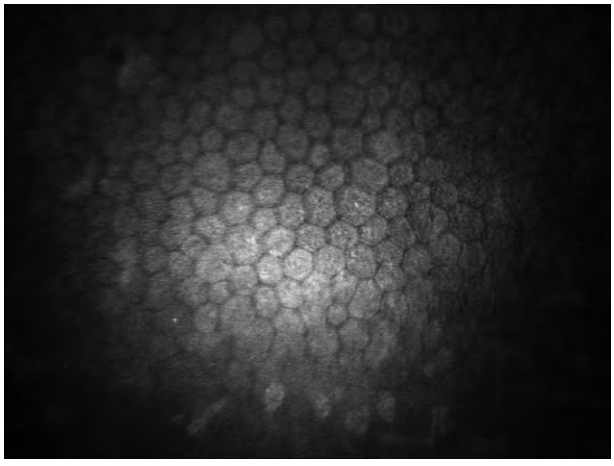

Figure 7 Endothelium.

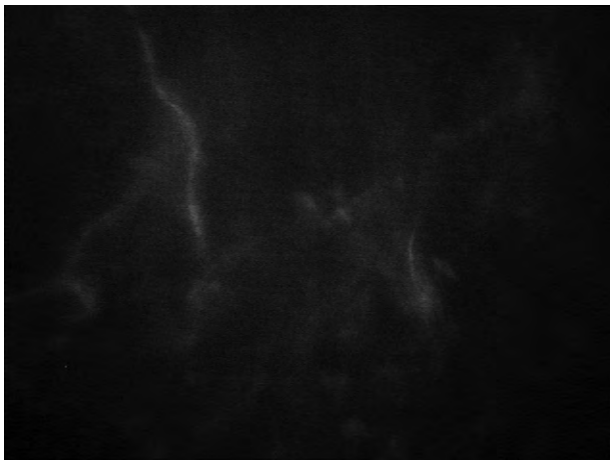

Figure 8 *Fusarium* keratitis.

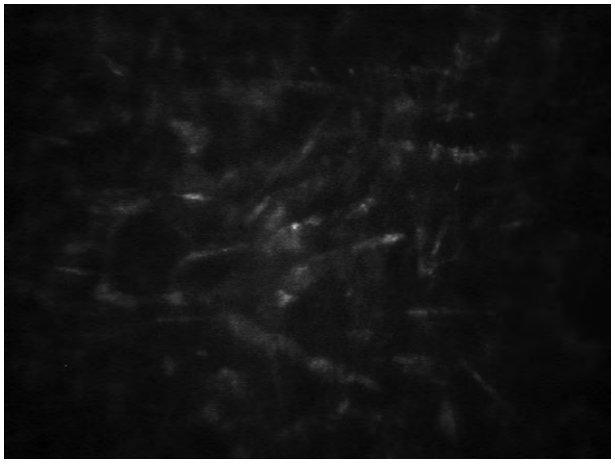

Figure 9 *Fusarium* keratitis.

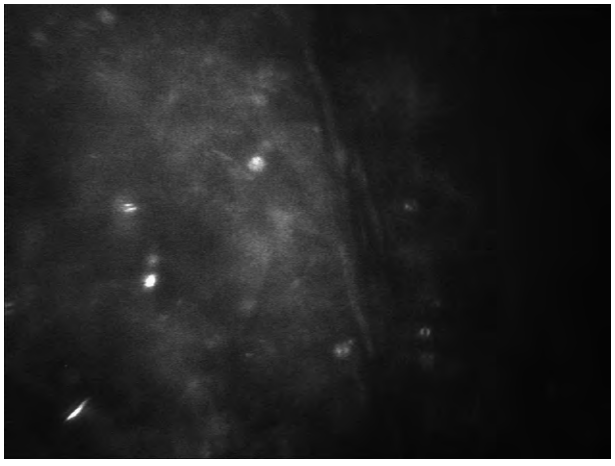

Figure 10 *Acanthaeomba*.

Other applications

Confocal microscopy has also been used to research and clinically evaluate the effects of refractive surgery on the cornea, evaluation of corneal deposits and stromal dystrophies, endothelial pathology, as well as evaluation of corneal ectatic disorders (**Figures 11** and **12**).

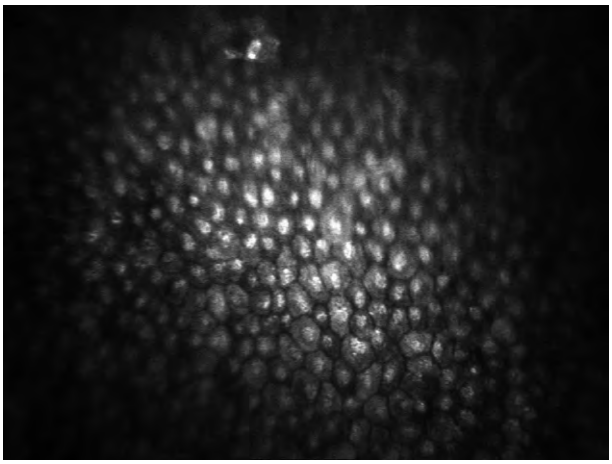

Figure 11 Iridocorneal endothelial syndrome (ICE). Note the epithelial-like endothelial cells with hyperreflective nuclei, which is characteristic of ICE syndrome in which the endothelium grows across the angle and iris. Notice irregular rows and shape of the endothelial cells.

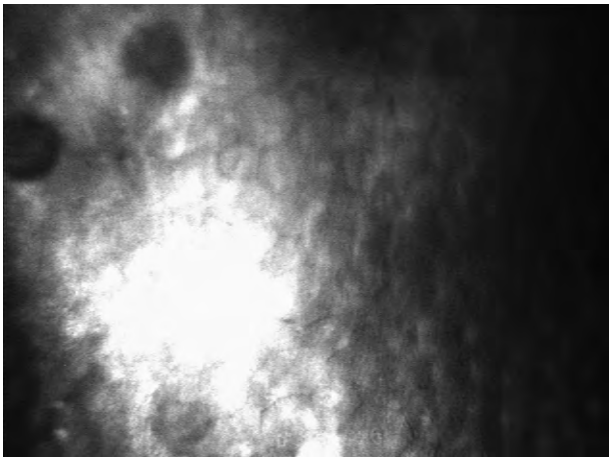

Figure 12 Posterior polymorphous membranous dystrophy (PPMD). Note the hyporeflective vesicular changes which are characteristic of PPMD in which the endothelium has areas of large and irregularly shaped cells.

Anterior Segment OCT

Historical Overview

David Huang and colleagues developed OCT in the early 1990s. Joseph Izatt and colleagues first demonstrated corneal and anterior segment OCT in 1994. Over the next decade, the majority of developments in OCT technology focused on retinal imaging. The use of longer wavelengths, telecentric transverse scanning, and very high-speed axial scanning with a grating-based rapid scanning optical delay (RSOD) mechanism in the

reference arm allowed for improved imaging of the anterior segment. In October 2005, the Food and Drug Administration in the United States approved the Zeiss Visante anterior segment OCT, the first commercially available OCT device designed for the anterior segment.

How it Works

Anterior segment OST (AS-OCT) is a noncontact imaging technique based on Michelson low coherence inferometry. In conventional interferometry with long coherence length (laser interferometry), interference of light occurs over a distance of meters. In OCT, this interference is shortened to a distance of micrometers. Light in an OCT system is broken into two arms – a sample arm (containing the item of interest) and a reference arm (usually a mirror). The combination of reflected light from the sample arm and reference light from the reference arm gives rise to an interference pattern, but only if light from both arms have traveled the same optical distance (same meaning a difference of less than a coherence length). By scanning the mirror in the reference arm, a reflectivity profile of the sample can be obtained (time domain OCT). Areas of the sample that reflect with greater intensity will create greater interference than areas that do not. Any light that is outside the short coherence length will not interfere. This reflectivity profile, called an A-scan, contains information about the spatial dimensions and location of structures within the item of interest (**Figure 13**). This is analogous to B-scan ultrasonography; however, OCT uses light as compared to sound waves. OCT was initially used for retinal evaluation, where images are optimized with an 820-nm light. AS-OCT evolved from retinal OCT. For the Visante AS-OCT, Zeiss uses a longer wavelength (1310 nm) that allows for greater penetration through tissues that scatter light intensely such as the sclera and limbus, which in turn permits visualization of anterior segment structures such as the angle, ciliary body, and ciliary sulcus. Approximately 90% of the 1310-nm light is absorbed prior to reaching the retina allowing for the AS OCT to be used as a higher power than retinal OCT. This results in real-time imaging and decreased motion artifacts. Currently, there are three commercially available anterior segment OCT devices: the Visante OCT (Visante OCT, Carl Zeiss Meditech Inc, Dublin, CA, USA), the Slit Lamp OCT (SL-OCT, Heidelberg Engineering GmbH, Heidelberg, Germany), and the Optovue (RTVue with Cornea-Anterior Module, Freemont, CA, USA). The Visante OCT provides high-resolution corneal scans, anterior segment scans (anterior-chamber depth, anterior-chamber angle, angle-to-angle distance), and pachymetry maps. It is reported to have an axial resolution of 18 µm and a transverse resolution of 60 µm. The SL-OCT is essentially a slit lamp biomicroscope-mounted OCT device allowing similar

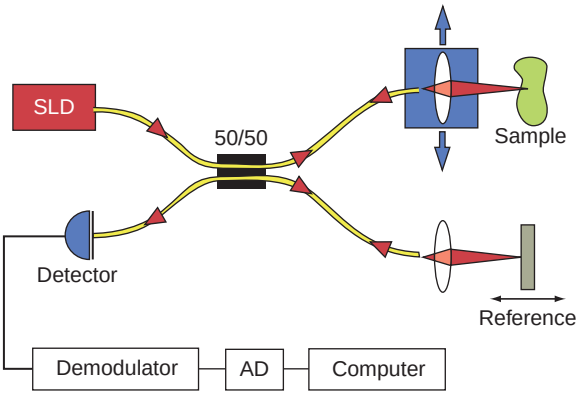

Figure 13 Schematics of the basic fiber-optic OCT system. Light from a superluminescent diode (SLD) is launched into a single mode-optical fiber. The light is equally split at the coupler into the sample and reference arms. Sample and reference reflections are recombined at the coupler and the interference pattern is converted to an electrical signal by the detector. The signal is demodulated and converted from analog to digital (AD) form for computer signal and image processing. To scan the reflections from various depths in the sample, the reference mirror is scanned over the equivalent range of delay. This produces a scan of sample reflectivity versus depth, also called an axial scan. From Steinert, R. E. and Huang, D. (2008). *Anterior Segment Optical Coherence Tomography.* Thorofare, NJ: SLACK Incorporated. Reprinted with permission from SLACK Incorporated.

measurements as the Visante OCT. The potential advantage of the SL-OCT is its attachment to the biomicroscope. The SL-OCT has a reported axial resolution of 25 µm and a transverse resolution of 20–100 µm. The speed of acquisition is 4–8 frame s^{-1} for the Visante OCT and 1 frame s^{-1} for the SL-OCT. The Optovue OCT employs an interchangeable lens system for anterior-segment images. Its principal advantage is the use of spectral domain OCT technology, with a substantially higher resolution. However, scans are limited in width, so only a portion of the cornea can be imaged at one time, and the retina-optimized wavelength does not allow useful imaging of the angle.

Clinical Applications

Anterior segment OCT is a powerful tool for the clinician. It can be used to measure corneal thickness, pachymetry maps, total corneal power, corneal backscatter, angle configuration, anterior-segment tumors, anterior-segment depth, lens vault, corneal opacities, and corneal refractive implants. The following discussion pertains to applications of the Visante OCT.

Keratoconus is a bilateral corneal ectasia characterized by progressive thinning and inferior protrusion. Diagnosis of this and other ectasias (e.g., pellucid marginal degeneration) is critical when evaluating patients for possible refractive surgery. Form fruste keratoconus is subclinical and can often be difficult to diagnose. Anterior segment OCT is a valuable tool in evaluating these patients

to aid in proper diagnosis. As both the Orbscan and Pentacam are based on slit-scanning principles, they tend to underestimate corneal thickness in keratoconic eyes. OCT has a higher resolution as compared to these other imaging modalities and therefore accurately maps the corneal thickness of normal, postoperative, and opacified corneas. The pachymetry map allows for accurate pachymetry readings over broad areas of the cornea allowing for detection of subclinical thinning suggestive of corneal ectatic disorders (**Figures 14** and **15**).

The Visante OCT can obtain high-resolution images of the cornea. The flap tool measures laser-assisted *in situ* keratomileusis (LASIK) flap thickness and residual stromal bed (RSB) in up to seven locations. This application allows for evaluation of LASIK flaps in uncomplicated and ectatic cases. RSB measurements are invaluable in providing

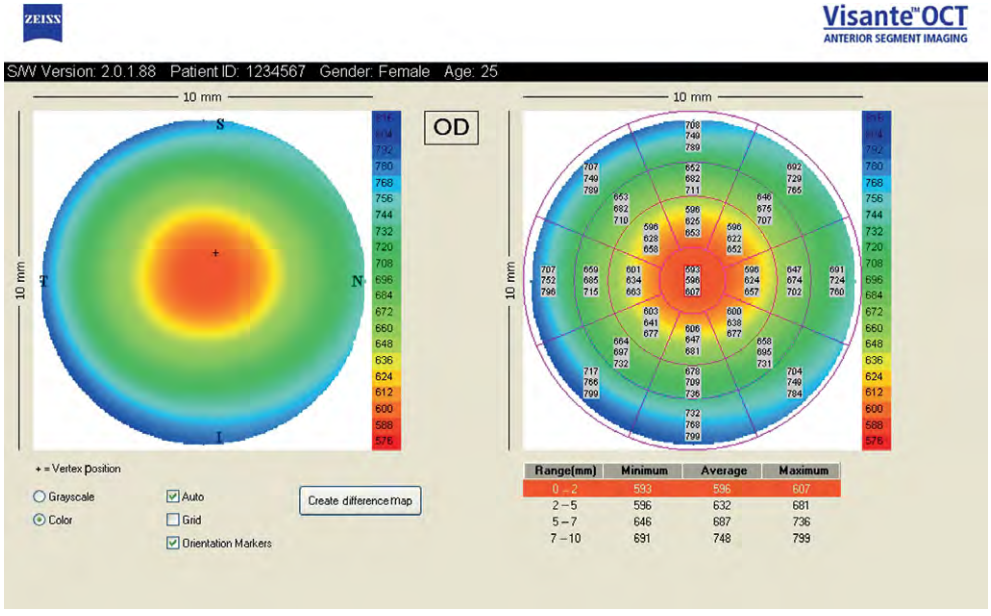

Figure 14 Normal visante OCT pachymetry map. The visante OCT allows for a global pachymetry map represented by numerical values and a corresponding color gradient. The cooler colors represent thicker pachymetry values and the warmer colors represent thinner pachymetry values.

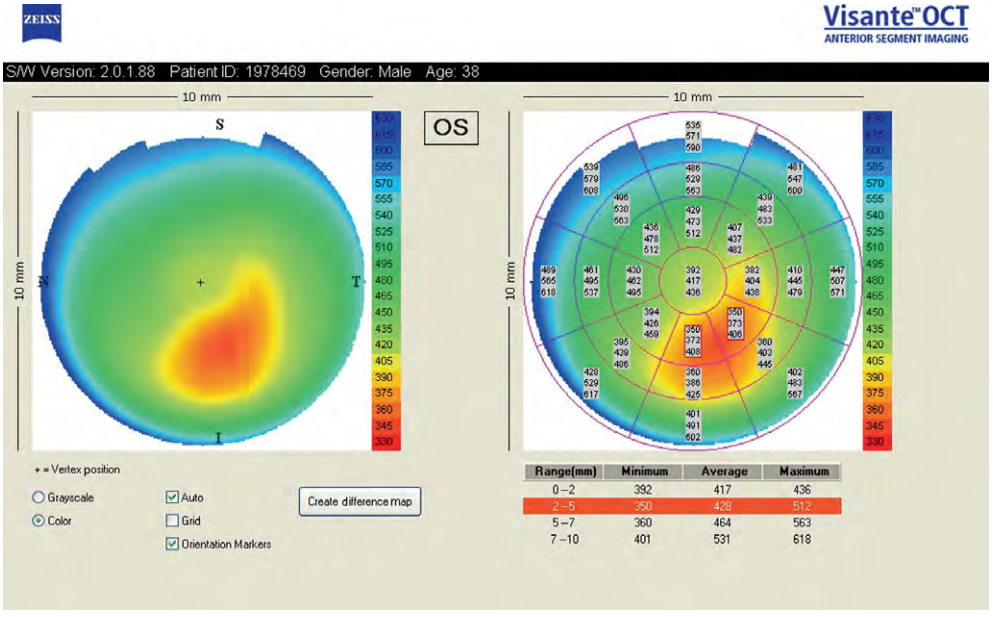

Figure 15 Visante pachymetry map in a patient with keratoconus. Note the infero-temporal thinning represented by the warmer orange-red.

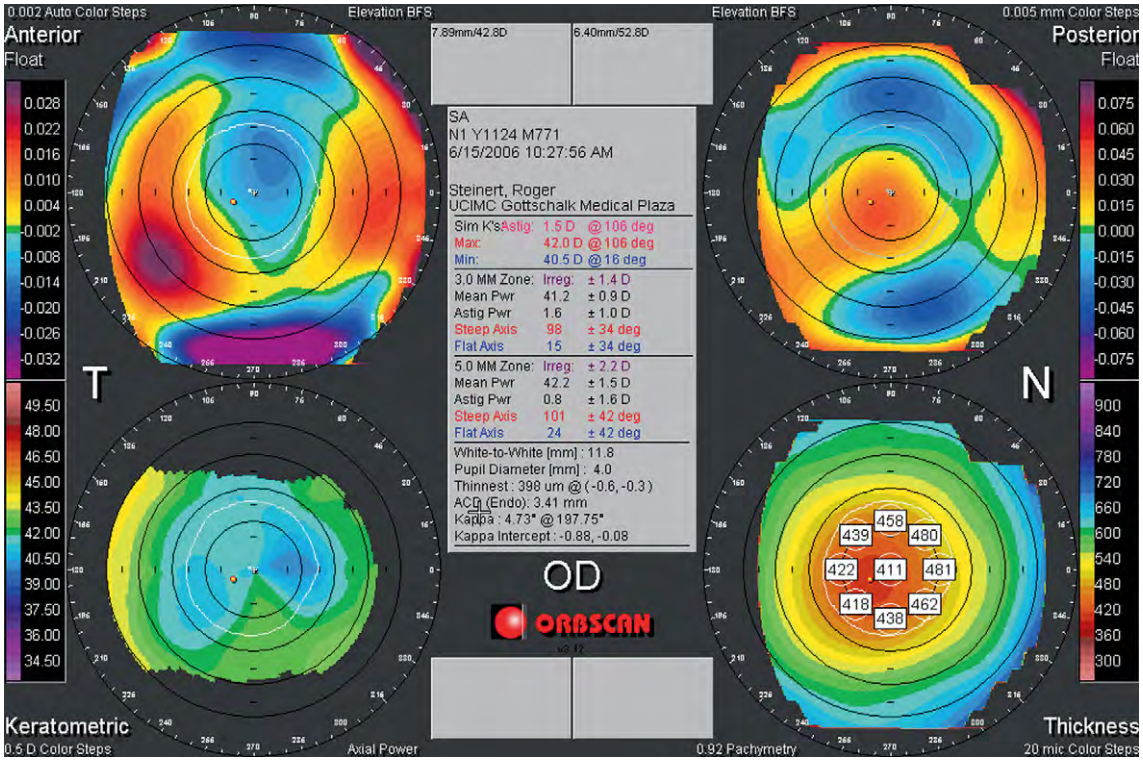

(a)

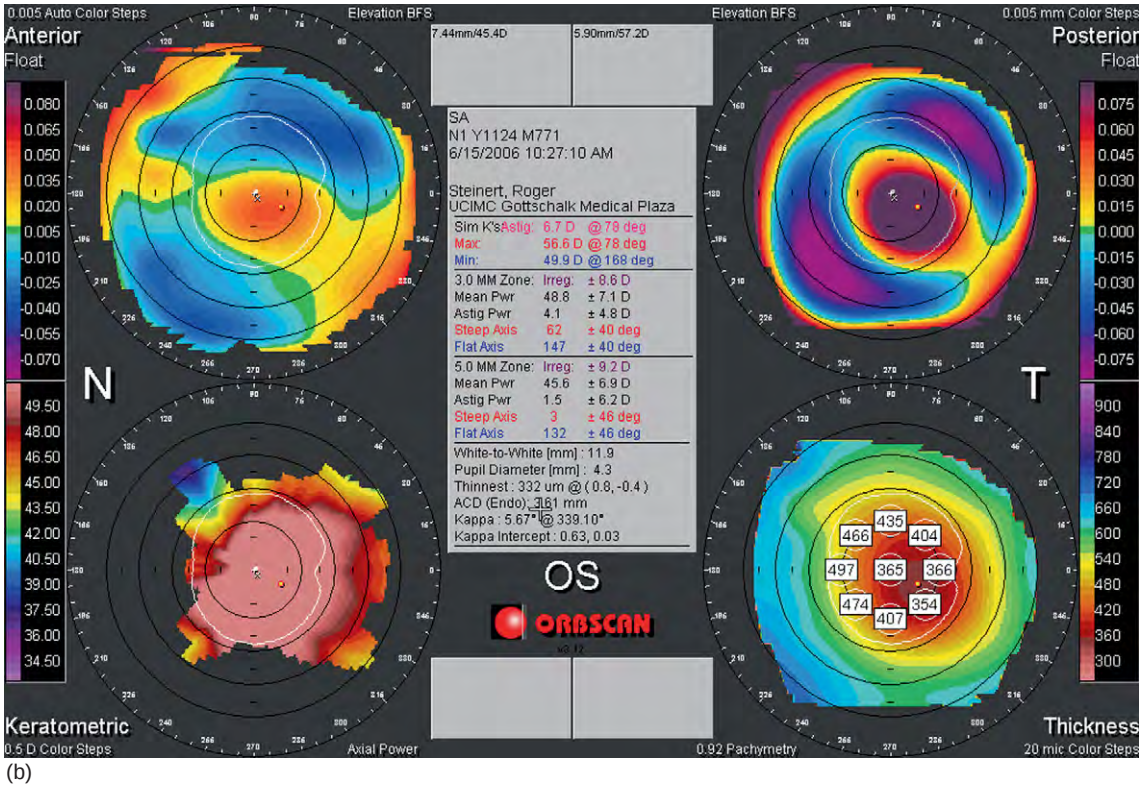

(b)

Figure 16 Continued

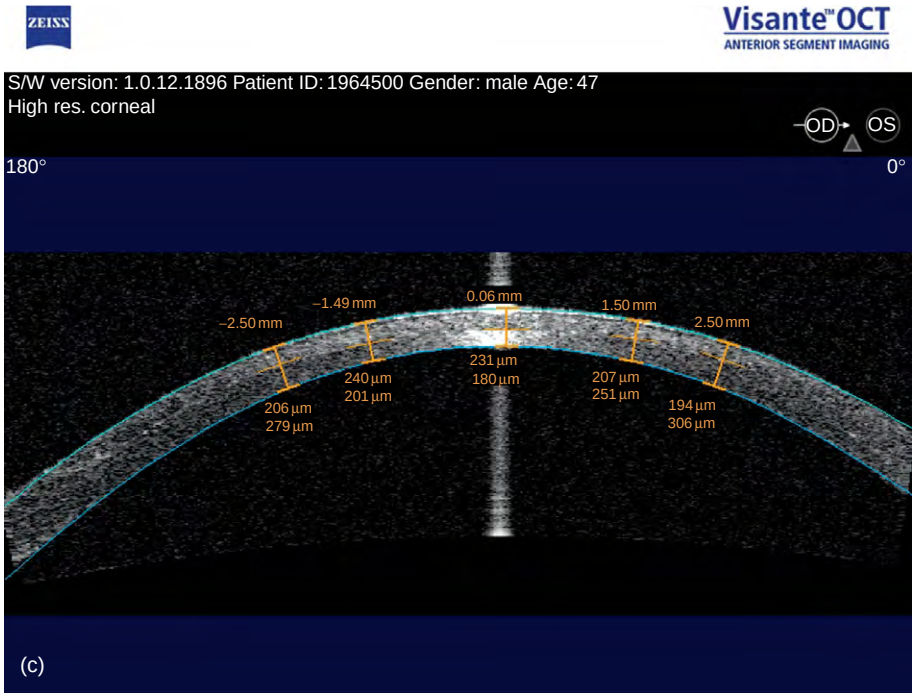

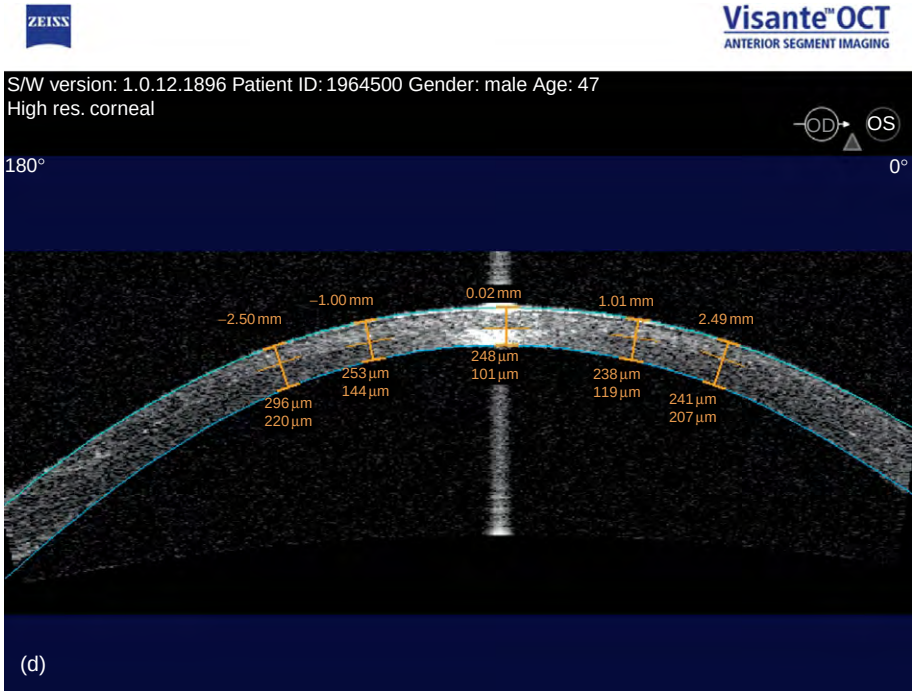

Figure 16 Forty-seven-year-old male with a history of bilateral conventional LASIK, with subsequent wave front-guided enhancements. (a) Corneal topography of the right eye with mild irregularity noted on the anterior float. (b) Corneal topography of the left eye with marked steepening on the keratometric map, anterior irregularity, and abnormal posterior curvature consistent with postrefractive ectasia. (c) OCT of the right cornea with thick flap and thin residual stromal bed. The number anterior to the epithelium represents the location from the apex in millimeters, the first number on the endothelial aspect represents the thickness from the horizontal line anteriorly (i.e., the flap thickness), the second number on the endothelial aspect represents thickness from the horizontal line posteriorly (i.e., the residual stromal bed). (d) OCT of the left cornea with thick flap and very thin residual stromal bed. Note that centrally the flap measures 248 µm and the residual stromal bed only 101 µm. From Steinert, R. E. and Huang, D. (2008). *Anterior Segment Optical Coherence Tomography.* Thorofare, NJ: SLACK Incorporated. Reprinted with permission from SLACK Incorporated.

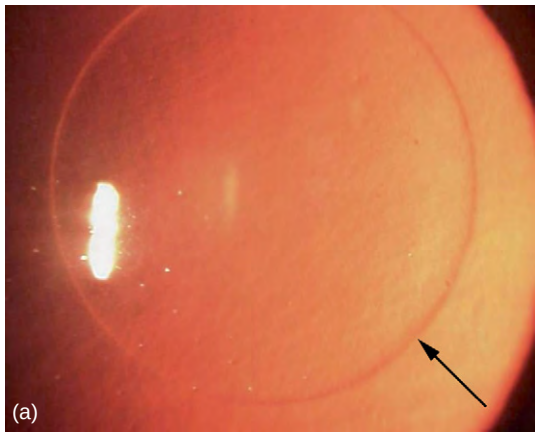

Figure 17 Continued

information regarding the potential safety of performing an enhancement when lifting the flap. Additionally, the flap tool can be useful when evaluating a patient with post-LASIK keraecastia (**Figure 16(a)–16(d)**). Likewise, OCT is useful in evaluations of refractive corneal inlays and intacs intracorneal ring segments (**Figures 17(a)–17(c) and 18**).

Assessment of the depth of corneal ulcers is another valuable application of AS-OCT. Involved tissue appears hyperintense on OCT images. The clinician is able to follow the progression of keratitis by imaging the depth of involvement, the density of the infiltrate, and evaluating for possible corneal thinning (**Figures 19(a)–19(e)** and **20(a)–20(e)**). Penetrating (full thickness) and lamellar (partial thickness) corneal transplantation has been the focus of several technologic and surgical advancements over the past several years. The development of posterior lamellar keratoplasty (Descemet stripping endothelial keratoplasty, or DSEK), and femtosecond laser-enabled keratoplasty have dramatically changed corneal transplantation techniques. AS-OCT evaluation of these patients pre- and postoperatively is helpful in surgical planning and clinical follow-up (**Figures 21–23**).

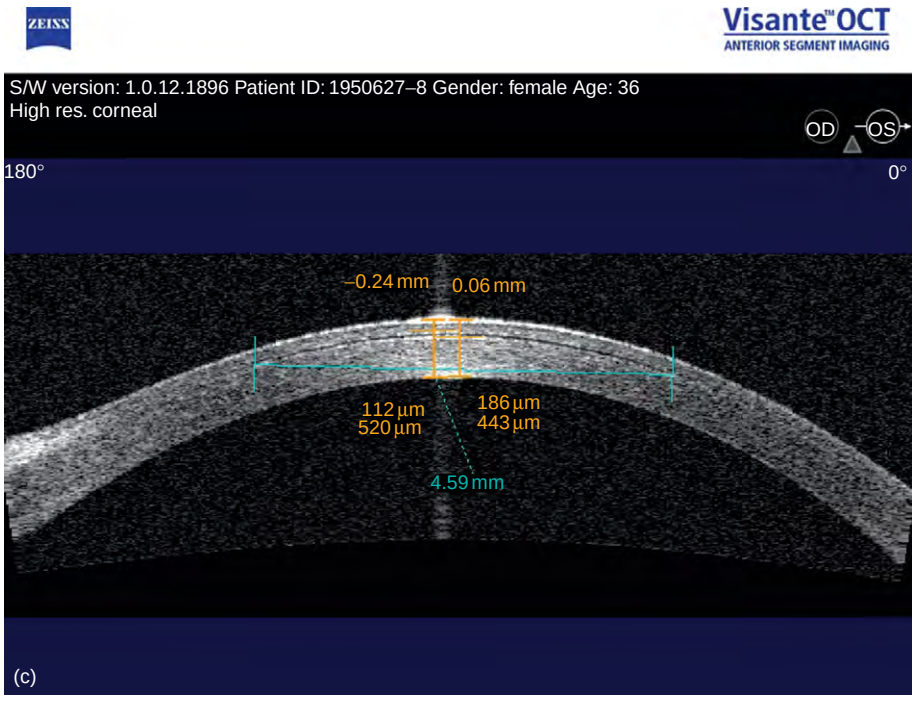

Figure 17 Fifty-two-year-old female with revision optics 5-mm corneal inlay. (a) Slit lamp photo. Note edge of inlay highlighted by black arrow. (b) Visualization of implant which appears dark on OCT highlighted by white arrow. (c) Flap tool used to measure inlay thickness and implant size. The yellow bars represent the flap tool indicating the depth of the inlay, and the blue bars represent the width of the inlay. From Steinert, R. E. and Huang, D. (2008). *Anterior Segment Optical Coherence Tomography.* Thorofare, NJ: SLACK Incorporated. Reprinted with permission from SLACK Incorporated.

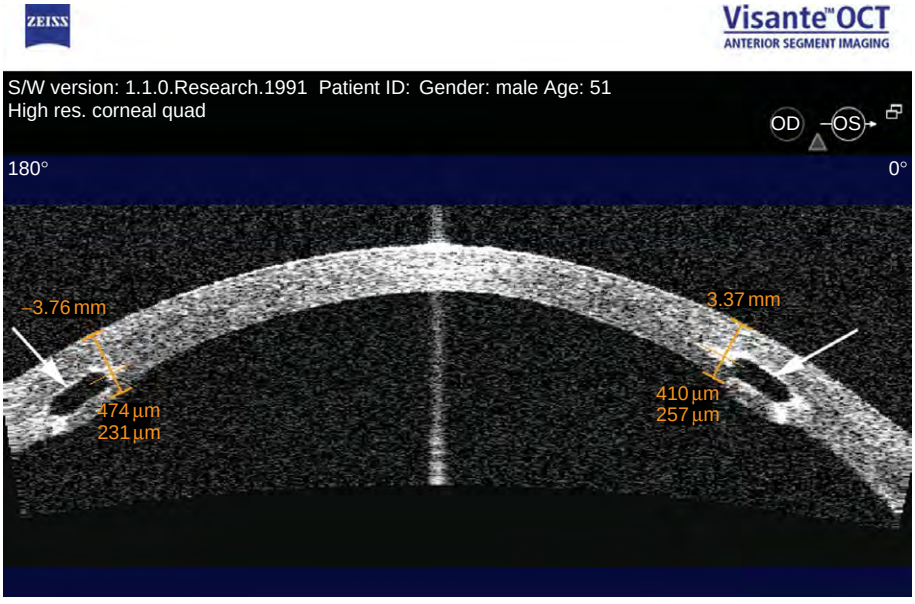

Figure 18 Use of flap tool to measure intacs depth. The intacs is highlighted by the white arrow and the yellow bars represent the flap tool. From Steinert, R. E. and Huang, D. (2008). *Anterior Segment Optical Coherence Tomography.* Thorofare, NJ: SLACK Incorporated. Reprinted with permission from SLACK Incorporated.

Accurate measurement of corneal opacities is another clinical application of AS-OCT. Compared to ultrasonic pachymetry, ultrasound imaging, optical pachymetry, confocal microscopy, and optical low-coherence reflectometry, OCT has been shown to accurately map pachymetry in both normal and opacified corneas. This accuracy aids in clinical decision making with respect to ablative treatments such as phototherapeutic keratectomy, mechanical scraping and peeling, or their combination.

Peripheral corneal pathologies, such as peripheral corneal and scleral melts, are also amenable to OCT scans. The longer wavelength (1310 nm) allows for full thickness imaging of the cornea and sclera through overlying opacities such as infiltrate, pannus (flap of tissue), and calcium plaques. Measurement of the depth of involvement and thickness of remaining tissue is useful for clinical and surgical planning (**Figure 24(a)–24(c)**).

Beyond corneal applications, AS-OCT can also be utilized for glaucoma evaluations. Determination of angle configuration, visualization of normal angle structures (**Figure 25(a)–25(c)**), iris configuration (pupillary block configuration, pre- and postiridotomy (procedure to create a hole in the iris to enhance the drainage passages blocked by a portion of the iris), plateau iris configuration, pre- and postiridoplasty, a surgical procedure where the position of the peripheral iris is changed), and evaluation of peripheral anterior synechiae closure (condition where the peripheral iris adheres to the cornea) (**Figure 26(a)–26(c)**) are among the many applications of AS-OCT pertaining to glaucoma.

Conclusion

Confocal microscopy and optical coherence tomography imaging allow clinicians and researchers to evaluate the structure of the cornea and anterior segment at levels beyond slit lamp biomicroscopy. Each technology has its own advantages and drawbacks, with their applications generally complementing each other. Quantitative and qualitative measures of normal and pathologic states greatly improve the clinician's ability to follow and treat.

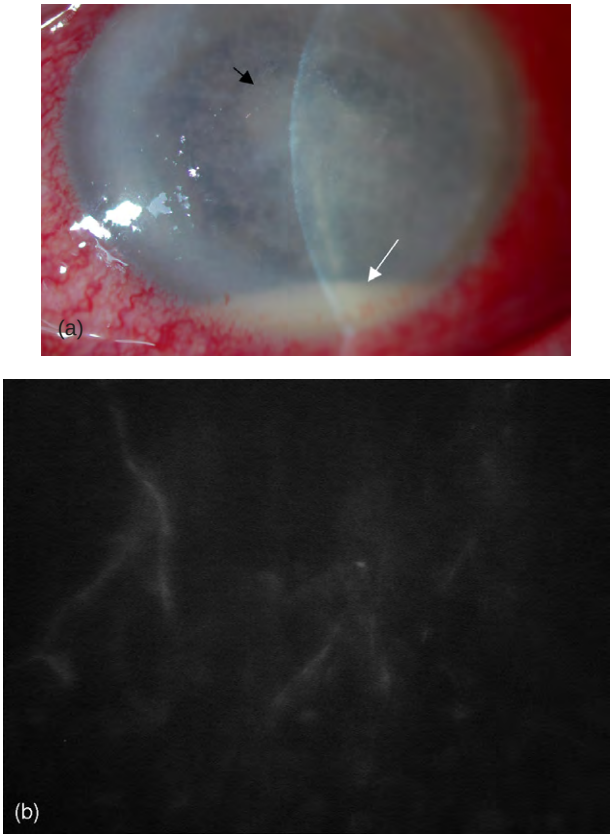

Figure 19 Continued

Figure 19 Continued

Figure 19 Fifty-eight-year-old male with misdiagnosed *Fusarium* keratitis. (a) Moderately dense full-thickness central corneal infiltrate (black arrow) and small hypopyon (white arrow). (b) Confocal microscopy shows multiple linear structures with branching at 45°, consistent with *Fusarium* species (later culture proven). (c–e) OCT showed a remarkable funnel of fibrin (white arrow) from the base of the ulcer to the pupil. From Steinert, R. E. and Huang, D. (2008). *Anterior Segment Optical Coherence Tomography*. Thorofare, NJ: SLACK Incorporated. Reprinted with permission from SLACK Incorporated.

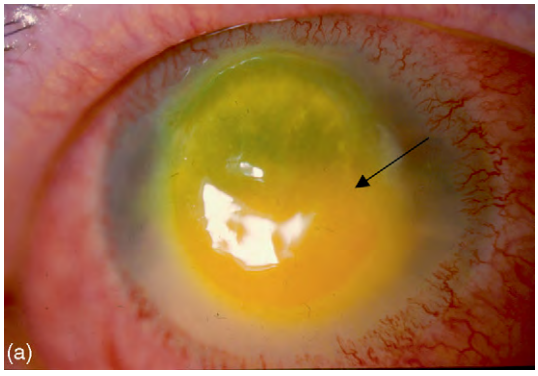

Figure 20 Continued

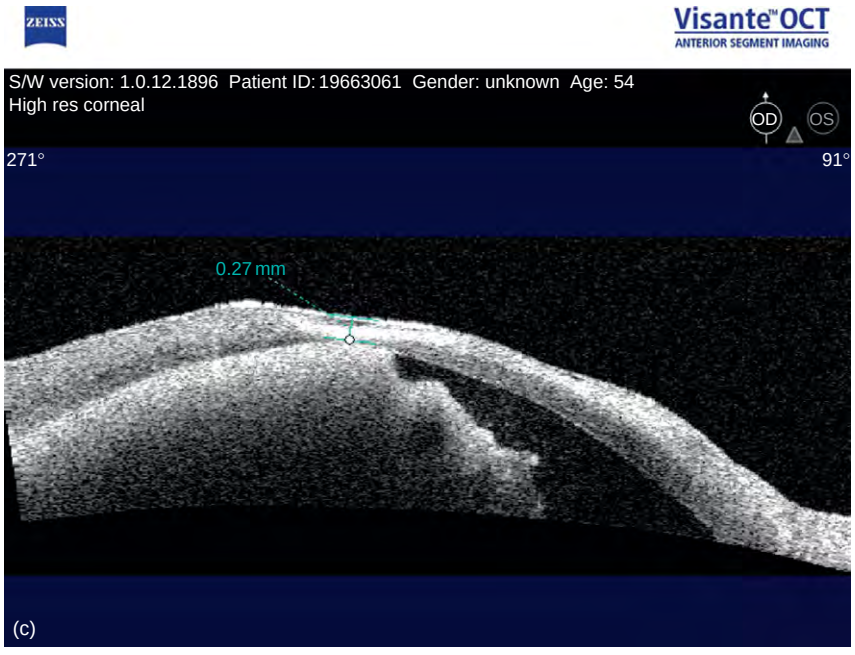

Figure 20 Continued

Figure 20 Fifty-four-year-old female with severe infectious keratitis. Gram stain of the corneal scrapings showed gram-negative rods, and cultures were positive for *Pseudomonas*. (a) Large infiltrate with large hypopyon. (b) Vertical orientation of OCT shows 60–70% anterior chamber hypopyon. Note white arrow representing interface between cornea (anterior) and hypopyon (posterior). (c) Significant stromal thinning with 270 μm shown by caliper tool (blue bar). Note that normal corneal thickness is about 540 μm. (d) The patient was admitted and treated aggressively; 1 week later, the thinning was nonprogressive. (e) Over a 2-month period, the area of corneal thinning gradually improved to nearly normal thickness and the anterior chamber hypopyon regressed as shown in this high-resolution corneal quadrant image. Each image represents a corneal section through a particular axis which is shown above the image. From Steinert, R. E. and Huang, D. (2008). *Anterior Segment Optical Coherence Tomography.* Thorofare, NJ: SLACK Incorporated. Reprinted with permission from SLACK Incorporated.

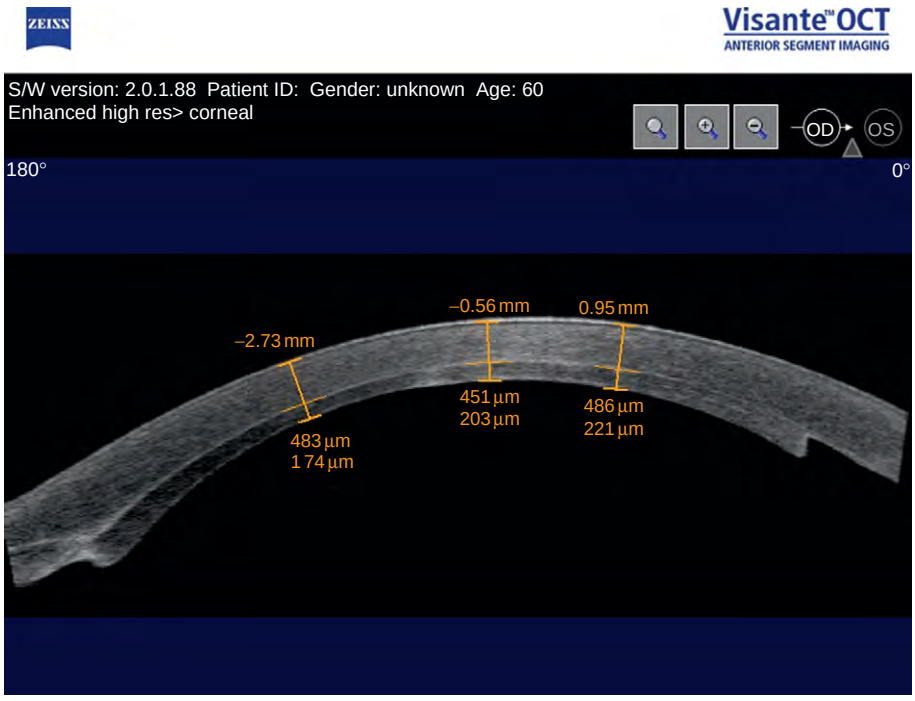

Figure 21 DSEK (note attached graft with flap tool showing thickness of DSEK lenticule and compact overlying stroma).

Figure 22 Dislocated DSEK (note fluid cleft in interface (white arrow) and relative thickness of overlying stroma and DSEK lenticule).

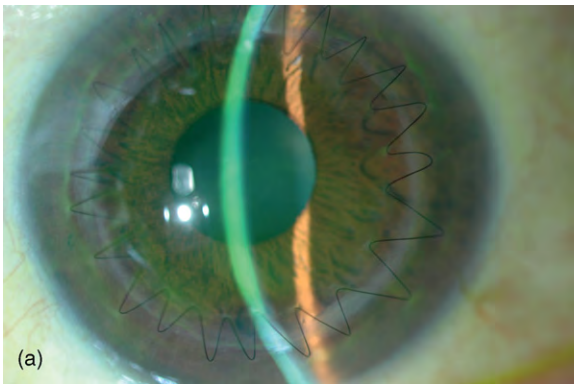

Figure 23 Continued

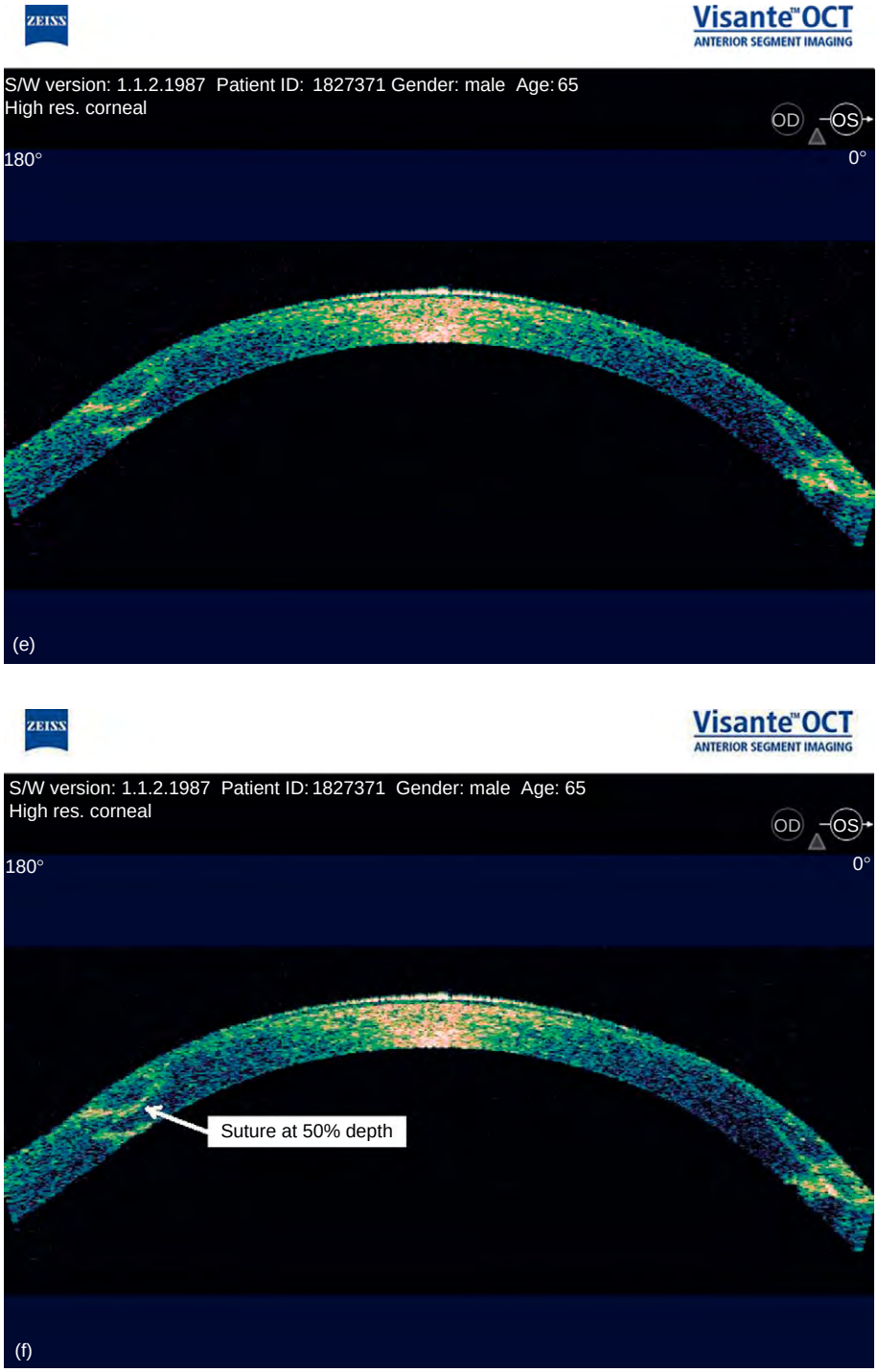

Figure 23 Zig-zag shaped PKP femtosecond laser incisions. (a) Slit lamp photo showing well-aligned incision with smooth transition from donor to host. (b) Angled anterior incision is clearly visible (black arrow). (c) OCT at 1 month postoperatively shows excellent alignment of donor and host, both at the anterior and posterior surfaces (white arrows). (d) OCT at 3 months shows higher signal return at incision indicating stronger wound healing as compared to postop month one. (e) The rainbow color image highlights the zig-zag incision. (f) Suture depth is noted at 50% depth with perfect posterior tissue alignment and apposition. From Steinert, R. E. and Huang, D. (2008). *Anterior Segment Optical Coherence Tomography.* Thorofare, NJ: SLACK Incorporated. Reprinted with permission from SLACK Incorporated.

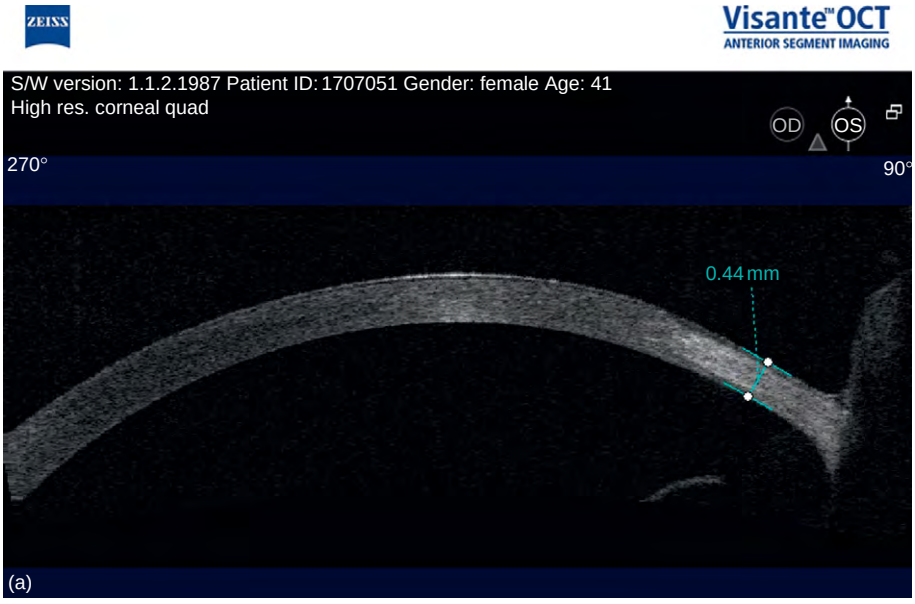

Figure 24 Continued

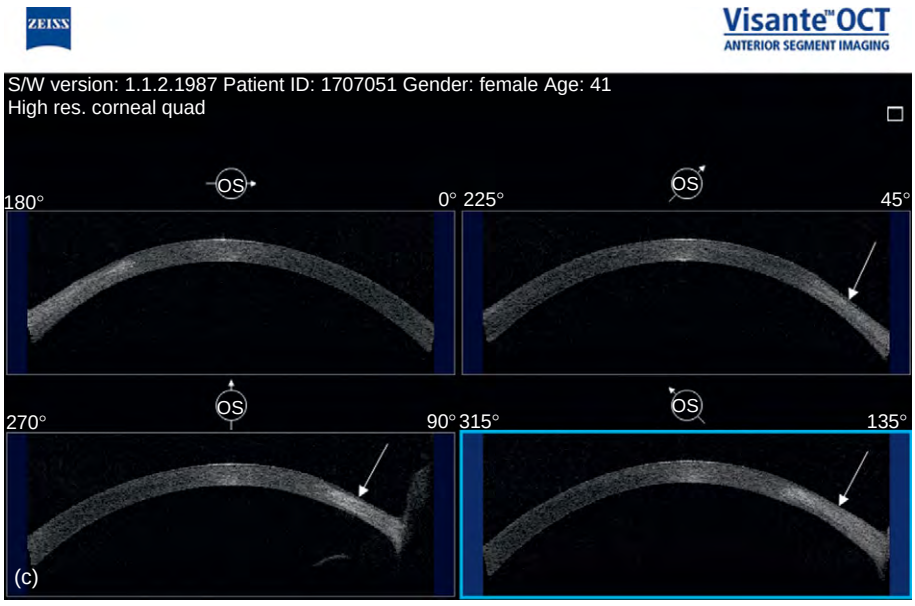

Figure 24 Forty-one-year-old patient with a corneal melt. (a) Left eye showing superior corneal thinning (vertical orientation) as shown by the caliper tool (blue bar). Normal corneal thickness is about 540 μm. (b) Left eye showing supero-temporal thinning (oblique orientation). (c) Corneal quad scan of left eye showing a generalized superior corneal thinning (white arrows).

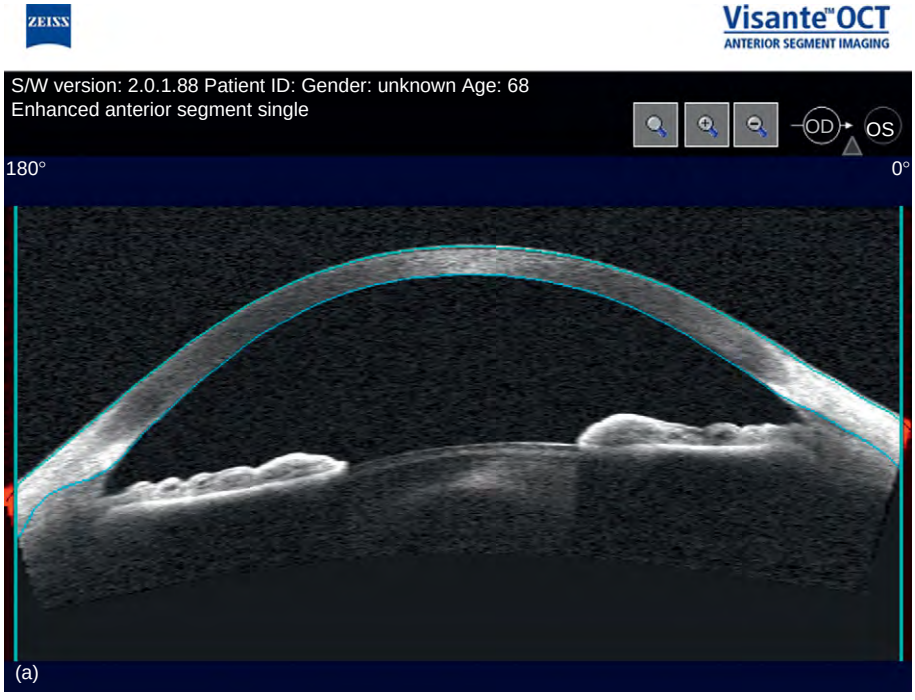

Figure 25 Continued

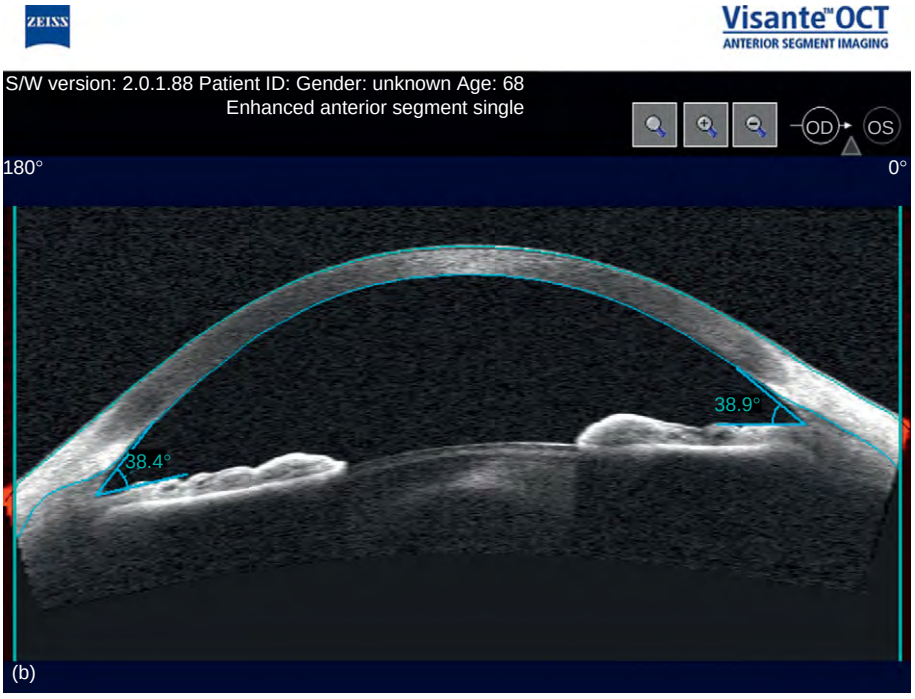

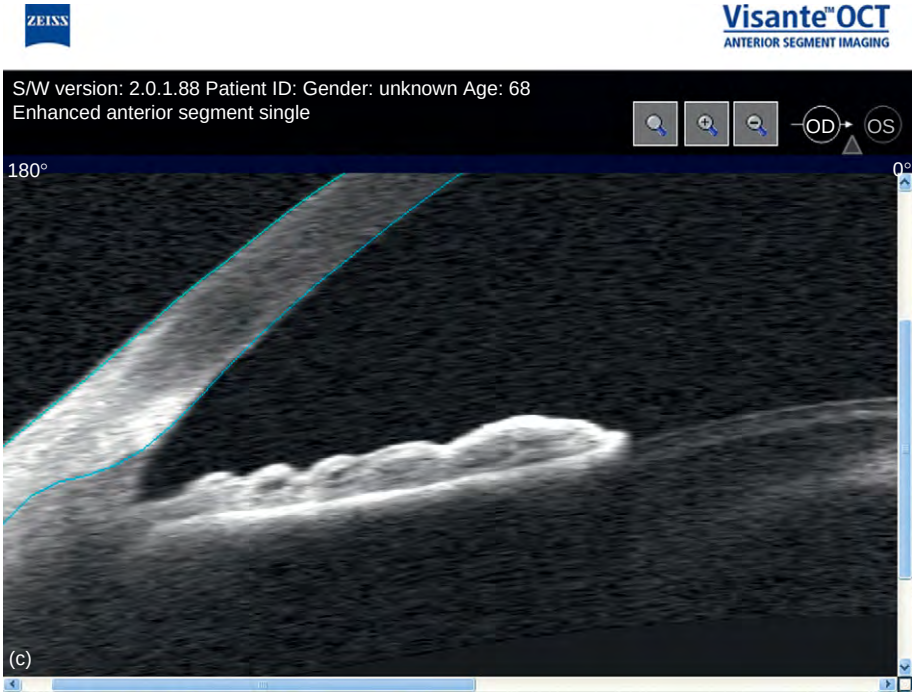

Figure 25 Sixty-eight-year-old male with normal angle configuration. (a) Horizontal meridian scan showing open angles. (b) Horizontal meridian scan with angle degree markers. (c) High resolution of angle at 180°.

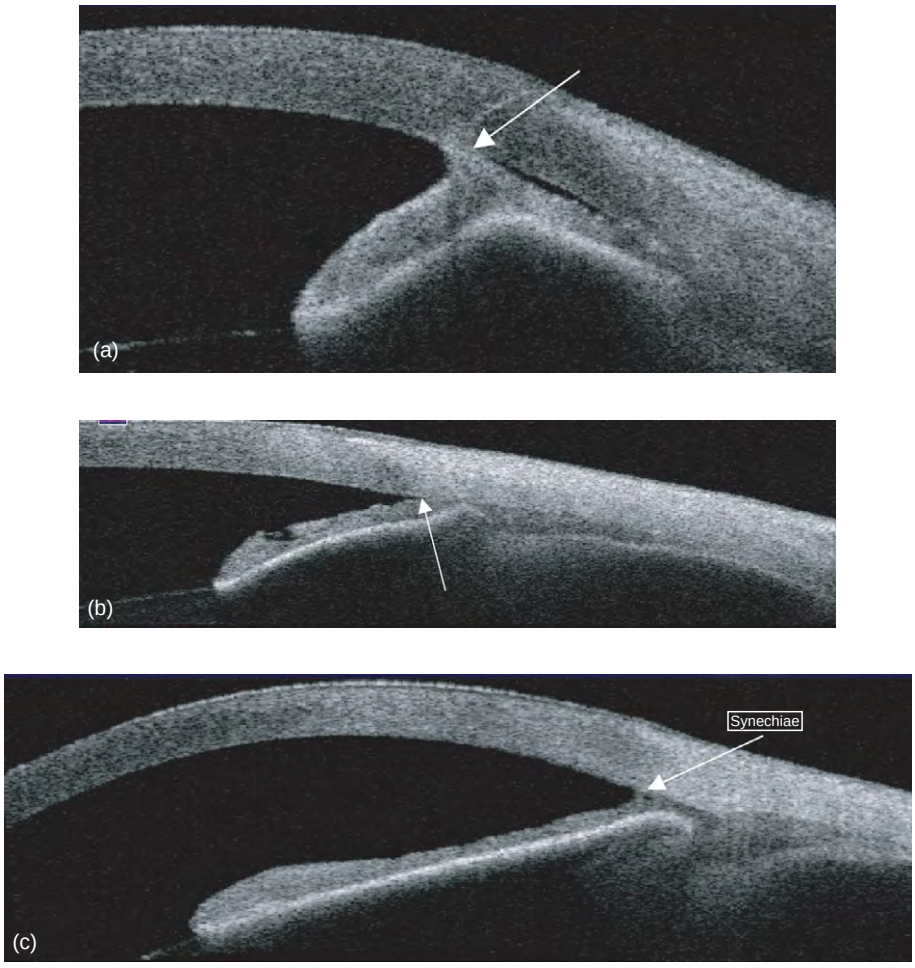

Figure 26 (a–c) Peripheral anterior synechiae (white arrows). From Steinert, R. E. and Huang, D. (2008). *Anterior Segment Optical Coherence Tomography.* Thorofare, NJ: SLACK Incorporated. Reprinted with permission from SLACK Incorporated.

See also: Penetrating Keratoplasty; Refractive Surgery.

Further Reading

Chiou, A. G., Kaufman, S. C., Kaufman, H. E., et al. (2006). Clinical confocal microscopy. *Survey of Ophthalmology* 51: 482–500.

Dhaliwal, J. S., Kaufman, S. C., and Chiou, A. G. (2007). Current applications of clinical confocal microscopy. *Current Opinion in Ophthalmology* 18: 300–307.

Jalbert, I., Stapleton, F., Papas, E., et al. (2003). *In vivo* confocal microscopy of the human cornea. *British Journal Ophthalmology* 87: 225–236.

Kaufman, S. C. and Kaufman, H. E. (2006). How has confocal helped us in refractive surgery? *Current Opinion in Ophthalmology* 17: 380–388.

Konstantopoulous, A., Hossain, P., and Anderson, D. F. (2007). Recent advances in ophthalmic anterior segment imaging: A new era for ophthalmic surgery? *British Journal of Ophthalmology* 91: 551–557.

Lim, L. S., Aung, H. T., and Tan, D. T. (2008). Corneal imaging with anterior segment optical coherence tomography for lamellar keratoplasty procedures. *American Journal of Ophthalmology* 145: 81–90.

Patel, D. V. and McGhee, C. N. (2007). Contemporary *in vivo* confocal microscopy of the living human cornea using white light and laser scanning techniques: A major review. *Clinical Experiment Ophthalmology* 35: 71–88.

Schallhorn, J. M., Tang, M., Song, J. C., et al. (2008). Optical coherence tomography of clear corneal incisions for cataract surgery. *Journal of Cataract and Refractive Surgery* 34: 1561–1565.

Steinert, R. F. and Huang, D. (2008). *Anterior Segment Optical Coherence Tomography.* Thorofare, NJ: SLACK.

Corneal Nerves: Anatomy

C F Marfurt, Indiana University School of Medicine – Northwest, Gary, IN, USA

Glossary

Chemotropic guidance – A process whereby a chemical substance, usually secreted by some target cell, attracts growing axons.
Cochet–Bonnet esthesiometer – A hand-held instrument that uses the pressure transmitted by a nylon monofilament of known diameter and variable length to measure the mechanical sensitivity of the cornea.
Iridectomy – A surgical procedure that removes a small piece of the iris, most often for treatment of closed-angle glaucoma or melanoma of the iris.
Laser-assisted *in situ* keratomileusis (LASIK) – A form of refractive laser eye surgery designed to change the shape of the cornea.
Neurite – Any cytoplasmic extension from a neuron; the term is used frequently to describe developing or regenerating axons that have not yet attained their mature adult form.
Neurotrophic epitheliopathy – The minor degenerative changes of the corneal epithelium caused by damage or functional impairment of the corneal innervation, especially as occurs after LASIK surgery.
Neurotrophic keratitis – A serious degenerative condition of the cornea, affecting especially the corneal epithelium, caused by impairment of the corneal sensory innervation. It often manifests as corneal epithelial defects, ulceration, melting, and diminished wound healing.
Phacoemulsification – A procedure in which a cataractous lens is broken up (emulsified) by ultrasound and aspirated from the eye; an intraocular lens is then inserted.
Receptive field – The area of the cornea (or other body part) supplied by a single sensory nerve fiber.
Trabeculectomy – A surgical procedure that removes part of the trabeculum of the eye in order to facilitate drainage of aqueous humor. It is performed for the relief of increased intraocular pressure associated with glaucoma.
Trophic substances – The molecules that promote the growth, differentiation, and survival of specific cell populations.

Origins of Corneal Nerves

The cornea is richly supplied by sensory neurons located in the ophthalmic region of the trigeminal ganglion (Figure 1). Although the entire sensory innervation of the mammalian cornea is derived from a relatively small number (~50–450) of neurons, each neuron supports as many as 200–3000 individual corneal nerve endings. The sensory nerves reach the eye through the nasociliary branch of the ophthalmic nerve. In humans, the nasociliary nerve branches typically into two long ciliary nerves, one nasal and the other temporal, which course directly to the posterior pole of the eye, and a communicating branch carrying sensory fibers to the ciliary ganglion. Five to ten short ciliary nerves, carrying a mixture of sensory and autonomic fibers, emerge from the anterior pole of the ciliary ganglion and together with the long ciliary nerves pierce the posterior globe in the vicinity of the optic nerve. After penetrating the sclera, the nerves enter the suprachoroidal space and course anteriorly toward the cornea. While in transit to the anterior eye segment, the fibers branch repeatedly and eventually form a series of prominent, evenly spaced nerve bundles that approach the corneoscleral limbus uniformly from all directions.

Some mammalian corneas also receive a modest sympathetic innervation from the superior cervical ganglion; however, the existence and magnitude of this contribution vary widely among species. In rabbits and cats, corneal sympathetic nerves may constitute as much as 10–15% of the total corneal innervation, while in humans and other primates corneal sympathetic fibers are exceedingly rare or absent. A very sparse parasympathetic innervation has been reported in rat and cat corneas; however, the meager nature of this innervation and its absence from most mammalian corneas suggest that they are likely of little physiologic significance.

Architecture of the Corneal Innervation

Limbal Plexus

Prior to entering the cornea, the nerve bundles traverse the limbus and contribute fibers to the limbal, or pericorneal plexus, a dense, ring-like meshwork of nerve fibers that completely surrounds the peripheral cornea. The three-dimensional structure of the limbal plexus varies considerably in anatomical complexity according to species and contains complex mixtures of sensory, sympathetic, and parasympathetic nerves. Most limbal

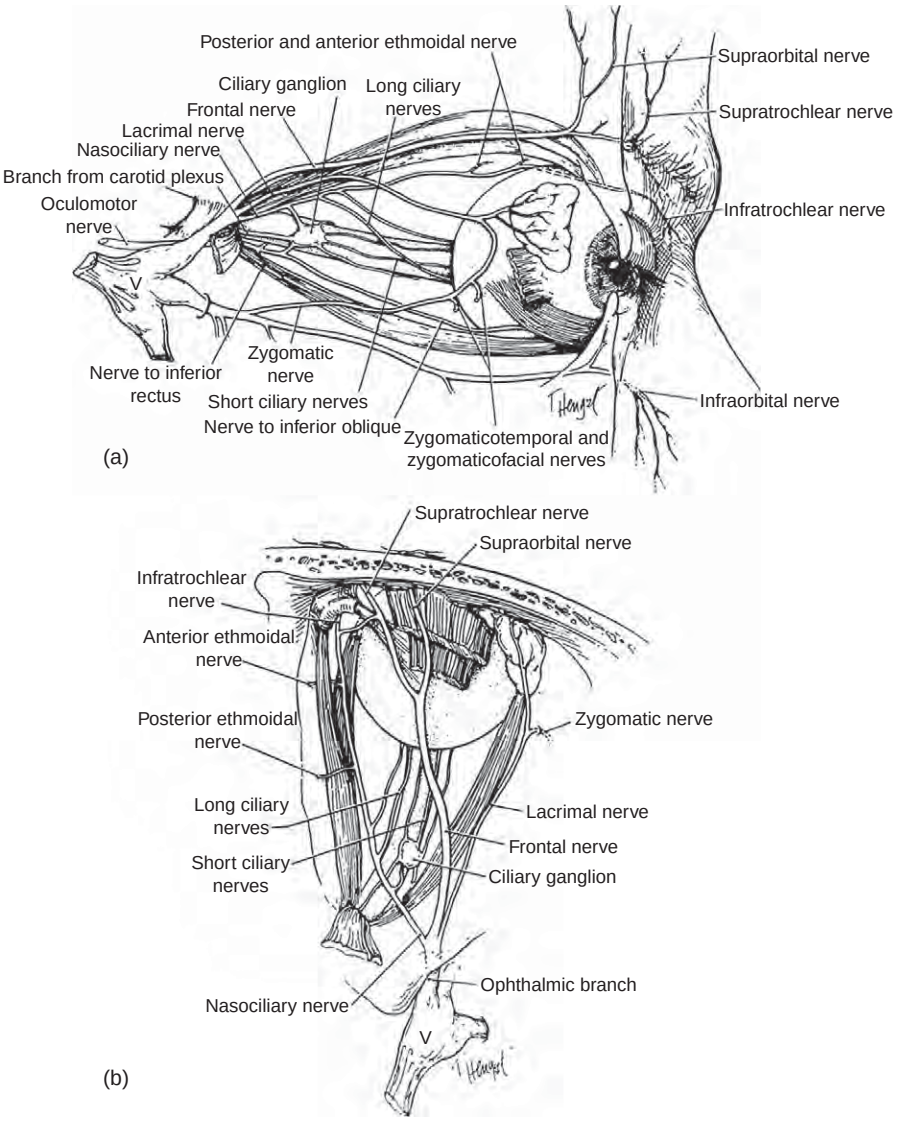

Figure 1 The branches of the ophthalmic division of the trigeminal nerve as seen from the lateral side (a) and from above (b). Sensory nerves to the cornea travel mainly in the nasociliary nerve and its ocular branches, the long and short ciliary nerves. Reproduced from figure 25-5 in Liu, G. T. (2004). The trigeminal nerve and its central connections. In: Miller, N. R. and Newman, N. J. (eds.). *Walsh and Hoyt's Clinical Neuro-Ophthalmology*, vol. 2, pp. 1233–1274. New York: Lippincott, Williams and Wilkins with permission from Lippincott, Williams and Wilkins.

nerves supply functional innervation to the limbal vasculature; however, occasional fibers travel through the limbal stroma unrelated to blood vessels and may provide sensory or autonomic innervation to resident cells.

Stromal and Subepithelial Plexuses

Most nerves enter the peripheral cornea in a series of radially directed major stromal nerve bundles, each containing as many as several dozen axons, arranged at regular intervals around the limbal circumference. On average, 60–80 major stromal nerves supply innervation to the human cornea, while 12–20 bundles supply rabbit, cat, and dog corneas. Additional numbers of smaller nerve fascicles enter the peripheral cornea slightly superficial to the main stromal bundles and provide limited innervation to the perilimbal and peripheral cornea. At their point of entry in the peripheral cornea, most corneal nerves are unmyelinated C-fibers; however, perhaps as many as 30% are finely myelinated A-delta fibers that shed their myelin sheaths within a millimeter or so after entering the cornea. The axons then continue into the stroma as flattened, ribbon-like fascicles surrounded only by Schwann cell cytoplasm and basal lamina.

Soon after entering the peripheral cornea, the major stromal bundles branch repeatedly to form elaborate, tree-like arbors whose distal branches anastomose extensively with neighboring branches to form a dense anterior stromal plexus. The plexus occupies approximately the anterior 25–50% of the corneal stroma, depending on the species, and consists of complex admixtures of seemingly randomly organized small and medium-sized nerve bundles and individual axons with straight, curvilinear, and tortuous trajectories. The plexus becomes increasingly denser and anatomically complex in the anterior direction. The most superficial layer of the anterior stromal plexus in humans and other large mammals is especially dense and is referred to as the subepithelial plexus (SEP). In contrast, the posterior half of the corneal stroma and the endothelium are, with rare exceptions, devoid of nerve fibers.

A small but indeterminate number of nerve fibers in the anterior stromal and SEPs appear to terminate in the stroma, usually as slightly bulbous terminal swellings or free nerve endings. At the electron microscopic level, the stromal fibers and their terminals resemble morphologically free nerve endings found in the corneal epithelium, suggesting that stromal nerve endings may subserve undetermined sensory transduction functions. Some stromal fibers form intimate relationships with keratocytes and are occasionally enwrapped in keratocyte cytoplasmic extensions that may provide a morphological substrate for reciprocal functional interactions.

Individual stromal axons entering at the corneoscleral limbus may travel as much as three-quarters of the way across the cornea before ending and, as a result of repetitive branching, possess receptive fields that range in size from less than 1 mm^2 to as much as 50 or more square millimeters and may cover up to 20% or more of the corneal surface. The receptive fields are generally round, oval, or wedge-shaped in outline and often extend several millimeters beyond the cornea onto the adjacent limbus and bulbar conjunctiva. The large sizes and extensive overlap between adjacent receptive fields, coupled with convergent mechanisms in the central nervous system, explain why stimulation of the corneal surface is poorly localized.

Subbasal Nerve Plexus

The subbasal nerve plexus comprises the densest part of the corneal innervation and is so-named because the nerves that comprise this plexus travel in the subnuclear part of the basal epithelium or between the basal epithelial cells and their basal laminae. Estimates of subbasal nerve fiber density in the central human cornea are expressed conventionally as the total length of all nerve fibers and branches per square millimeter, and range from 15–27 mm mm^{-2} (by *in vivo* confocal microscopy) to 40–55 mm mm^{-2} (by immunohistochemical staining of corneal whole mounts).

Approximately 400–500 widely spaced stromal nerves penetrate Bowman's membrane, mainly in the peripheral and intermediate cornea, to give origin to the human subbasal plexus. Additional subbasal nerves enter the peripheral cornea directly from the limbal plexus. Relatively few stromal nerves penetrate Bowman's membrane in the central 2 mm of the human cornea; hence, the latter region receives most of its epithelial innervation from long subbasal nerves that invade the central cornea from more peripheral origins.

Immediately after penetrating Bowman's membrane, each stromal nerve bends at a 90° angle and branches simultaneously into 2–20 thinner nerve fascicles termed subbasal nerves. Subbasal nerves course in the horizontal plane, roughly parallel to one another and to the epithelial basal lamina, for 1–2 mm in rats and up to 6 mm or more in humans. The neuroanatomical structure thus formed by a stromal axon branching into multiple, parallel subbasal daughter fibers is termed an epithelial leash, a unique, two-dimensional sensory nerve specialization found only in the cornea (**Figure 2**). At the electron microscopic level, human subbasal nerves average 1.5 μm in diameter and may contain up to 40 individual unmyelinated axons (**Figure 3**). Immediately upon entering the basal epithelium, the axons shed their Schwann cell investments and continue as naked axon cylinders. Subbasal nerves in adjacent leashes interconnect frequently with one another. As a result, the boundaries between individual leashes are soon lost and a composite subbasal nerve plexus is formed.

When viewed in its entirety, the subbasal nerve plexus forms a gentle spiral or whorl-like pattern on the curved corneal surface (**Figure 4**). The center of the spiral, often called the vortex, is located in human corneas approximately 2–3 mm inferior and nasal to the corneal apex. As a consequence of this arrangement, subbasal nerves in the superior and apical human cornea are oriented vertically, whereas subbasal nerves in other corneal regions may be oriented horizontally or obliquely, consistent with their geographical locations within the whorl-like plexus. The mechanisms that govern the formation and maintenance of this spiral-like pattern remain uncertain; however, it has been established that basal epithelial cells and subbasal nerves migrate centripetally in tandem. According to one theory, basal epithelial cells derived from stem cells in the corneoscleral limbus migrate centripetally in a whorl-like fashion toward the corneal apex in response to chemotrophic guidance, electromagnetic cues, and population pressures; the subbasal nerves, occupying cytoplasmic invaginations or narrow intercellular spaces between adjacent columns of migrating cells, are pulled along and undergo compensatory horizontal elongation. Alternatively, subbasal nerves may develop whorl-like,

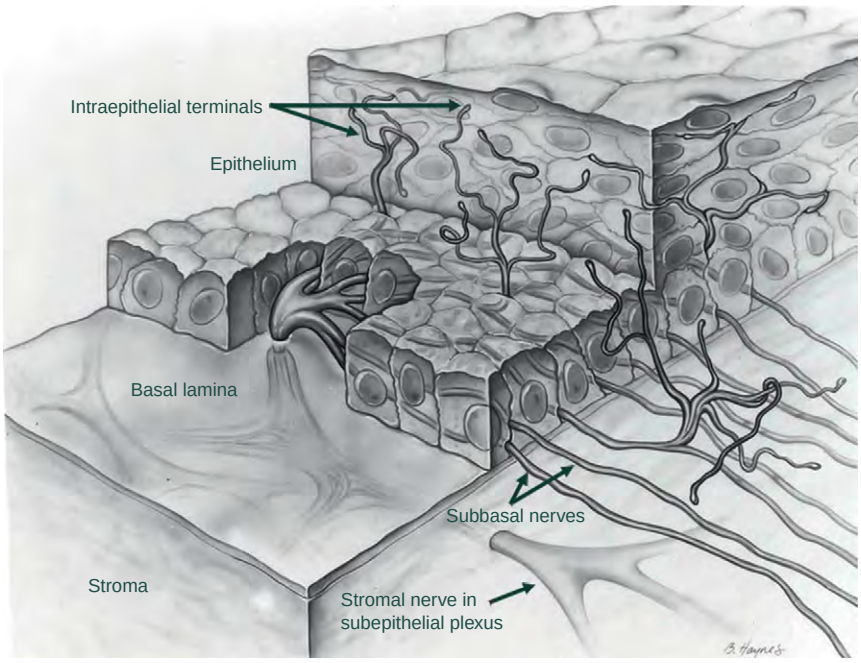

Figure 2 Innervation of the rabbit corneal epithelium. Stromal nerves penetrate the basal lamina and branch into a leash-like assemblage of horizontally oriented fibers called subbbasal nerves; the latter nerves give rise to a profusion of intraepithelial terminals. Modified from figure 6 in Rozsa, A. J. and Beuerman, R. W. (1982). Density and organization of free nerve endings in the corneal epithelium of the rabbit. *Pain* 14: 105–120. With kind permission from International Association for the Study of Pain.

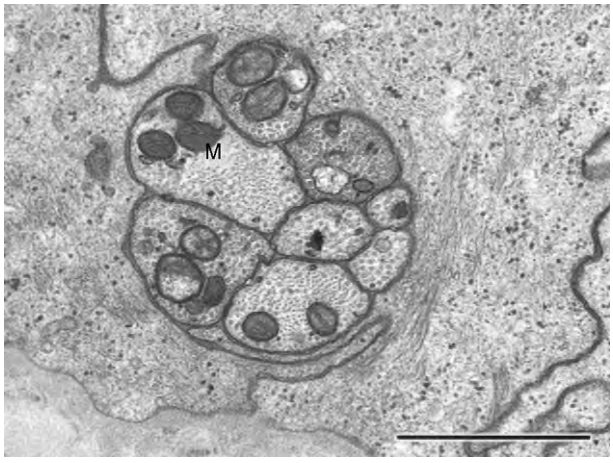

Figure 3 Electron micrograph of a subbasal nerve from a human cornea. The nerve, cut in cross section, contains eight individual unmyelinated axons. M, mitochondria. Calibration bar is 1 μm. Reproduced from figure 5c in Muller, L. J., et al. (2003). Corneal nerves: Structure, contents and function. *Experimental Eye Research* 76: 521–542. With kind permission from Elsevier.

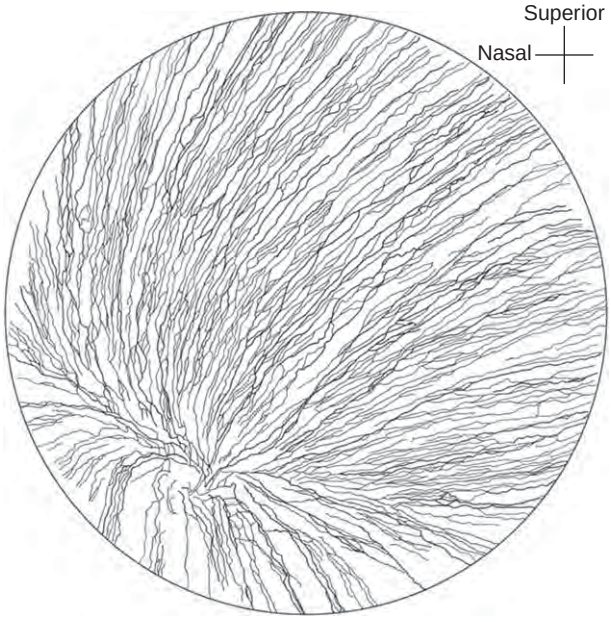

Figure 4 Architecture of the subbasal nerve plexus in the human cornea. The area illustrated is 6.5 mm in diameter and centered on the corneal apex. Subbasal nerves converge in a gentle, whorl-like pattern on a region approximately 2–3 mm inferonasal to the corneal apex known as the vortex.

curvilinear orientations independent of epithelial cell dynamics and may, in turn, provide a structural scaffold that patterns and directs epithelial cell migration.

Intraepithelial Nerve Terminals

As the subbasal nerves course horizontally through the basal epithelium, they give rise to a profusion of thin, occasionally beaded terminal axons that ascend vertically or obliquely, often with a modest amount of additional branching, into the more superficial epithelial layers before ending (**Figure 5**). In some mammalian corneas,

additional epithelial nerves originate as single axons directly from the SEP. The end of each intraepithelial fiber is tipped by a conspicuous, bulbous terminal expansion. At the ultrastructural level, these expansions contain abundant small clear vesicles, varying numbers of large dense-cored vesicles, mitochondria, glycogen particles, neurofilaments, and neurotubules. Morphologically, they resemble nociceptor nerve endings described in other tissues. The neurochemical content of the small clear vesicles is uncertain but may include excitatory amino acids, while the large, dense-cored vesicles likely contain substance P (SP), calcitonin gene-related peptide (CGRP), and/or other neuropeptides.

The terminals are located throughout all layers of the corneal epithelium but are especially numerous in the basal and wing cell layers. Some terminals may extend to within a few microns of the corneal surface. The epithelial cell membranes facing the nerve terminals often demonstrate numerous invaginations and, in many cases, the epithelial cell cytoplasm totally surrounds the nerve ending. The intimate morphological relationship thus formed between nerve terminal and epithelial cell does not constitute a true synapse, but may nevertheless provide a favorable environment for the exchange of diffusible substances and receptor-mediated interactions. The intimate contacts may also allow nerve endings to sense osmotic changes in epithelial cell shape and volume brought about by dessication of the ocular surface. When osmotic stimulation reaches threshold, the nerve fibers fire and activate brainstem circuits that promote reflex tear production and blinking in an effort to maintain the physiologic integrity of the ocular surface.

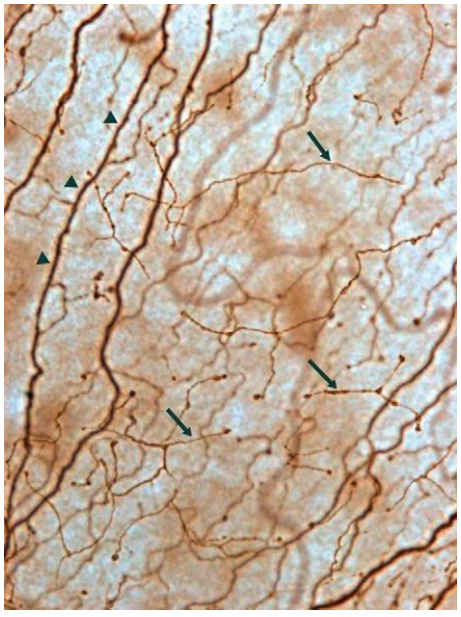

Figure 5 Intraepithelial nerve terminals (arrows) in the human corneal epithelium stained by neurotubulin immunohistochemistry. Arrowheads, subbasal nerve.

The innervation density of the corneal epithelium is probably the highest of any surface epithelium, and the central corneal epithelium of humans and rabbits contains approximately 5000–8000 nerve terminals per square millimeter. Both nerve terminal density and corneal sensitivity are greatest in the central cornea and decrease progressively in the peripheral direction. The richness of the corneal epithelial innervation provides a nociceptive detection system of unparalleled sensitivity and it is hypothesized that injuries to individual epithelial cells may be sufficient to trigger pain perception. Both corneal sensitivity and nerve density decrease progressively as a function of age and may contribute to the pathogenesis of dry eye disease in some elderly patients.

Corneal Nerve Neurochemistry

Corneal sensory nerves help maintain a healthy ocular surface by activating brainstem circuits that stimulate reflex tear production and blinking, and by releasing trophic substances, including numerous neuropeptides, which promote corneal epithelial physiologic renewal and wound repair. Corneal nerves contain, in varying proportions, the same neuropeptides that are expressed in other ocular nerves. Each corneal fiber population (sensory, sympathetic, and parasympathetic) maintains a distinctive phenotypic signature; however, the chemical coding is complex and most fibers likely express combinations of neuropeptides rather than individual markers. To date, 12 different neuropeptides have been detected by radioimmunoassay or immunohistochemistry in the mammalian cornea.

Corneal sensory nerves may contain one or more of six different neuropeptides. Two of these peptides, CGRP and SP, are found in especially high percentages of corneal nerves and remain the most studied and well characterized of the corneal peptidergic nerves (**Figure 6**).

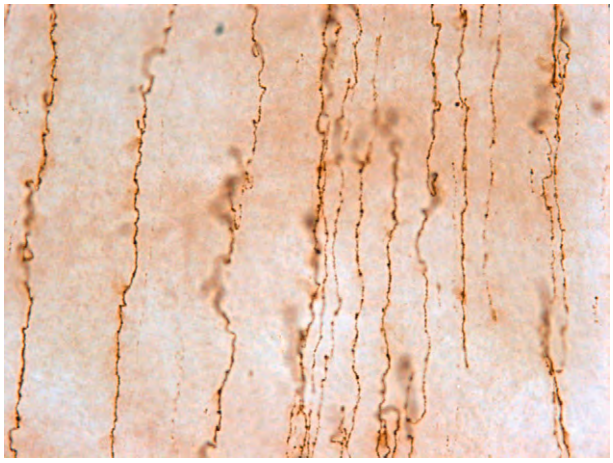

Figure 6 Calcitonin gene-related peptide (CGRP)-immunoreactive subbasal nerves in the rat corneal epithelium.

CGRP and SP are expressed in approximately 30–60% and 10–20% of corneal sensory nerves, respectively, and have been found in all mammalian corneas investigated to date. The vast majority of nerves that contains CGRP also contain SP and the two peptides probably co-localize in the same vesicles. Other neuropeptides expressed in more limited numbers of corneal sensory nerves include: neurokinin A (a member of the tachykinin family) secretoneurin (a member of the chromogranin/secretogranin family), pituitary adenylate cyclase-activating peptide (PACAP, a member of the vasoactive intestinal polypeptide (VIP)-glucagon-secretin super family), and galanin. The extent to which these peptides coexist with CGRP and SP or represent distinct populations of corneal sensory nerves remains to be determined.

Despite the richness of the corneal peptidergic innervation, it does not fully account for the known density of the corneal sensory innervation and it is therefore likely that many corneal sensory nerves do not express neuropeptides. Immunohistochemical investigations of rat corneal sensory nerves suggest that up to 40% of rodent corneal nerves do not express known neuropeptides. Most of the so-called nonpeptidergic nerves express a cell-surface glycoconjugate that binds the plant isolectin *Bandaireae simplicifolia* IB4 and contain the enzyme, fluoride-resistant acid phosphatase (FRAP). The neurotransmitters expressed by this prominent population of corneal IB4-positive nerves remain to be determined; however, excitatory amino acids such as aspartame and glutamate, or unknown neuropeptides that remain to be characterized, are likely candidates.

Corneal autonomic nerves, which constitute in most species only a small percentage of corneal nerve fibers, are also neurochemically diverse. Corneal sympathetic nerves express (in addition to noradrenalin) serotonin and neuropeptide Y (NPY), while corneal parasympathetic nerves express VIP, met-enkephalin, NPY, and galanin.

Functional roles of most neuropeptides in the mammalian cornea remain unclear and knowledge of their physiological roles has not kept pace with the results of immunohistochemical analyses. An important exception to this statement is SP, which exerts essential trophic functions on the corneal epithelium. SP receptors are present on corneal and limbal epithelial cells and it is thought that, under resting physiologic conditions, SP released from corneal sensory nerve terminals promotes corneal epithelial maintenance and physiological renewal by activating cellular pathways that stimulate epithelial cell proliferation, migration, and adhesion. In addition, topical application of SP has been reported to accelerate the rate of corneal epithelial wound healing in both experimental animal models and clinical patients with persistent corneal epithelial defects. Damage to corneal sensory nerves by surgery or trauma deprives the corneal epithelium of SP and other essential nerve-derived trophic substances and is associated with a variety of ocular surface disorders, including dry eye disease, epitheliopathy, and neurotrophic keratitis.

Even less is known of the functional roles of the cornea's limited autonomic innervation. In animal models, corneal sympathetic nerves act through adrenergic mechanisms to modulate corneal epithelial cell ion transport processes, epithelial cell proliferation and mitosis, and cell migration during epithelial wound healing. In the corneoscleral limbus, NPY augments the vasoconstrictor effects of noradrenalin and exerts strong angiogenic effects.

Corneal Nerve Remodeling

Corneal subbasal nerves and their intraepithelial terminals are dynamic structures that undergo morphological rearrangements continuously under normal physiologic conditions. Time-lapse, *in vivo* confocal microscopic examination of living human eyes reveals that subbasal nerves slide centripetally in tandem with their neighboring basal epithelial cells at rates of 10–20 $\mu m\, day^{-1}$ and that this nerve elongation occurs through the addition of new nerve material near the site of nerve penetration at Bowman's membrane. As subbasal nerves cannot elongate indefinitely, it is hypothesized that the distal nerve segments eventually degenerate or slough into the tear film. Intraepithelial nerve terminals also undergo continuous remodeling through combinations of long-term, nerve-directed reconfigurations and passive, short-term reorganization in response to outward migrations of differentiating epithelial cells.

Corneal Nerve Regeneration after Ocular Surgery

Corneal nerves are transected during a variety of corneal and anterior-segment surgical procedures, including refractive surgery, perlimbal incisions performed for cataract surgery, iridectomy and trabeculectomy, and penetrating keratoplasty (PK; corneal transplantation). Corneal nerves depend for their survival on axoplasmic transport of essential substances from their parent nerve cell bodies in the trigeminal ganglion; thus, surgical procedures that interrupt corneal nerve fibers cause rapid degeneration of the distal axons, decreased corneal sensitivity, and compromised functional integrity of the ocular surface.

Corneal nerves are capable of regeneration; however, it is a slow, imperfect process and the regeneration that takes place after most corneal surgeries is characterized by reduced nerve density, alterations in nerve architecture, and diminished corneal sensitivity. The more proximally the nerves are cut, the more delayed and incomplete the regeneration process will be. Thus, surgical disruption of

the subbasal and subepithelial nerve plexuses produce, in general, less serious and more short-term damage to the corneal innervation than do deep or penetrating incisions that affect major stromal nerve bundles.

Refractive Surgery

In laser-assisted *in situ* keratomileusis (LASIK), a mechanical or femtosecond laser microkeratome is used to create a circular flap of corneal epithelium and superficial stroma with a hinge at one end; the flap is then folded back and an excimer laser is used to remove several tens of microns of stroma from beneath the flap. The microtome severs subbasal and subepithelial nerves all around the flap margin except at the hinge, and the excimer laser destroys additional nerves in the anterior stromal bed. Regenerating nerve fibers emerge first as neurites from the subbasal plexus at the hinge and, to a lesser extent, elsewhere around the flap margin, followed by a second generation of neurites originating from the transected stromal nerve trunks. Abnormal proteoglycans present at the LASIK scar interface between the stromal bed and the overlying flap are postulated to impede successful reinnervation from the anterior stromal plexus. Regeneration is slow and incomplete, with subbasal and stromal nerve densities returning to less than half of preoperative levels by 12 months after LASIK and failing to reach preoperative levels even 3–5 years later. In addition, the architecture and morphology of the regenerated subbasal nerve plexus are often abnormal. Long-term studies are needed to determine whether subbasal nerve density will eventually return to pre-LASIK levels.

Although corneal reinnervation after LASIK surgery is incomplete, the corneal sensitivity, as determined by Cochet–Bonnet esthesiometry, in most cases returns to preoperative levels by 6–12 months and the short-term clinical outcome in most patients is excellent. Most patients experience a decrease in corneal sensitivity and mild-to-moderate dry eye after LASIK surgery that lasts for only a few days; however, approximately 5% of LASIK patients suffer long-term dry eye symptoms that may be related at least in part to impaired corneal reinnervation and interruption of the neural circuits that drive reflex tear production. Some patients with chronic dry eye after LASIK experience persistent and aberrant pain sensations that likely reflect sensitization and altered responsiveness of the immature, regenerating nerves.

In photorefractive keratectomy (PRK), the corneal epithelium is removed and an excimer laser is used to ablate the most anterior portion of the corneal stroma. Nerve regeneration and recovery of corneal sensitivity under these conditions, in which a flap is not cut in the cornea, reportedly occurs more quickly than following LASIK surgery; nevertheless, subbasal nerve density, architecture, and corneal sensitivity remain depressed for up to 1–2 years postoperatively.

Cataract Surgery

Penetrating perilimbal incisions, such as those performed for cataract surgery, are curvilinear incisions that are a few millimeters in length, which transect small numbers of major stromal nerve trunks near their sites of entry into the cornea. Neural regeneration proceeds slowly through a combination of nerve regrowth and collateral sprouting from adjacent, uninjured stromal nerves. The success of nerve regeneration varies from individual to individual; some nerve trunks fail to regenerate and, the ones that do regenerate, often contain diminished numbers of axons or form tangled masses of disorganized nerves in previously denervated areas of the stroma. Since the advent of phacoemulsification, the incision sizes used in cataract surgery have decreased steadily to as little as 1 mm and the risk of significant injury to the corneal innervation has been minimized.

Penetrating Keratoplasty

PK requires a full-thickness, 360° corneal incision that cuts all corneal nerves and results in complete denervation of the transplanted cornea. Nerve regeneration proceeds from the peripheral recipient cornea into the donor cornea very slowly and, even many years later, the innervation density of the grafted tissue remains far less than that of the host, peripheral cornea (**Figure 7**). Stromal nerves, in particular, regenerate very poorly after PK, perhaps because when the graft is introduced Schwann cell channels in the donor cornea are misaligned with the stromal nerve stumps in the host cornea. This contrasts to the perlimbal incisions used in cataract surgery, where nerve trunks and Schwann cell channels on opposing sides of the incision remain closely aligned. The limited nerve regeneration that does take place following PK derives mostly from small numbers of subbasal nerve fibers that elongate through epithelial bridges at the graft margin to enter directly into the donor basal epithelium. Many of the regenerated subbasal nerves are shorter than normal and exhibit atypical orientations and morphologies. Even several decades after surgery, median subbasal nerve density and corneal sensitivity in clear grafts remain significantly reduced compared to healthy corneas, and in about one-half of cases no subbasal nerves are visible by routine *in vivo* confocal microscopy. The return of sensation to the donor tissue is highly variable and, in many cases, hypoesthesia persists for many years after initial surgery. Fortunately, a return to normal innervation levels is not necessary for corneal clarity. Transplanted corneas can have severe nerve deficits and hypoesthesia for many years but remain clear; nevertheless, it is theorized that the impaired sensory innervation after PK may contribute to the relatively high frequency of epithelial complications observed after this procedure.

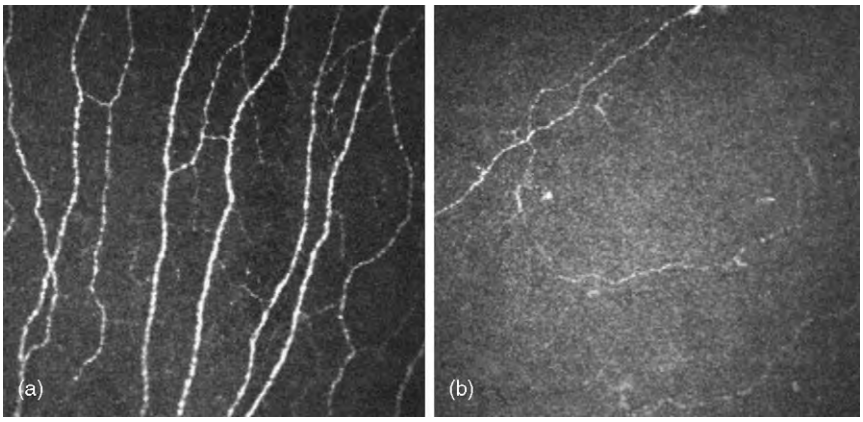

Figure 7 Subbasal nerve fibers in human corneas as demonstrated by *in vivo* confocal microscopy. (a) Normal subbasal nerves in a control subject. (b) Decreased subbasal nerve fiber density after penetrating keratoplasty. Reproduced from figure 1 in Niederer, R. L., et al. (2007). Corneal innervation and cellular changes after corneal transplantation: An *in vivo* confocal microscopy study. *Investigative Ophthalmology and Visual Science* 48: 621–626. With kind permission from Investigative Ophthalmology and Visual Science (IOVS).

Mechanisms of Nerve Regrowth

The mechanisms that stimulate and direct neurite outgrowth from injured and intact areas of the corneal innervation following local nerve injury are incompletely understood and, in most cases, these mechanisms are unable to restore the corneal innervation completely to its preoperative density, architecture, and sensory function. Growth factors expressed by corneal epithelial cells and released at the wound site following injury may play important roles. Nerve growth factor (NGF), a small protein that promotes the growth, survival, and maintenance of peripheral sensory nerve fibers, is constitutively expressed in corneal epithelial cells and is upregulated after epithelial wounding. Topical NGF administration stimulates corneal nerve regeneration and recovery of corneal sensitivity after PRK and LASIK in rabbits, and promotes healing of neurotrophic ulcers in clinical patients. Development of additional molecules that promote regeneration of injured nerves and restore the functional integrity of the ocular surface after corneal surgery is needed.

See also: Corneal Nerves: Function; Cornea Overview; Cranial Nerves and Autonomic Innervation in the Orbit; Refractive Surgery; Refractive Surgery and Inlays.

Further Reading

Auran, J. D., Koester, C. J., Kleiman, N. J., et al. (1995). Scanning slit confocal microscopic observation of cell morphology and movement within the normal human anterior cornea. *Ophthalmology* 102: 33–41.

Calvillo, M. P., McLaren, J. W., Hodge, D. O., and Bourne, W. M. (2004). Corneal reinnervation after LASIK: Prospective 3-year longitudinal study. *Investigative Ophthalmology and Visual Science* 45: 3991–3996.

deLeeuw, M. A. and Chan, K. Y. (1989). Corneal nerve regeneration. Correlation between morphology and restoration of sensitivity. *Investigative Ophthalmology and Visual Science* 30: 1980–1990.

Jones, M. A. and Marfurt, C. F. (1998). Peptidergic innervation of the rat cornea. *Experimental Eye Research* 66: 421–435.

Marfurt, C. F. (2000). Nervous control of the cornea. In: Burnstock, G. and Sillito, A. (eds.) *Nervous Control of the Eye*, pp. 41–92. Amsterdam: Harwood Academic Publishers.

Marfurt, C. F. (2009). Peptidergic innervation of the cornea: Anatomical and functional considerations. In: Troger, J. and Kieselbach, G. (eds.) *Neuropeptides in the Eye*, pp. 22–37. Trivandrum, India: Research Signpost.

Müller, L. J., Pels, L., and Vrensen, G. F. J. M. (1996). Ultrastructural organization of human corneal nerves. *Investigative Ophthalmology and Visual Science* 37: 476–488.

Müller, L. J., Marfurt, C. F., Kruse, F., and Tervo, T. (2003). Corneal nerves: Structure, contents, and function. *Experimental Eye Research* 76: 521–542.

Niederer, R. L, Perumal, D., Sherwin, T., and McGhee, C. (2007). Corneal innervation and cellular changes after corneal transplantation: An *in vivo* confocal microscopy study. *Investigative Ophthalmology and Visual Science* 48: 621–626.

Oliveira-Soto, L. and Efron, N. (2001). Morphology of corneal nerves using confocal microscopy. *Cornea* 20: 374–384.

Patel, D. V. and McGhee, C. (2005). Mapping of the normal human corneal sub-basal nerve plexus by *in vivo* laser scanning confocal microscopy. *Investigative Ophthalmology and Visual Science* 46: 4485–4488.

Patel, D. V. and McGhee, N. J. (2009) *In vivo* confocal microscopy of human corneal nerves in health, in ocular and systemic disease, and following corneal surgery: A review. *British Journal of Ophthalmology* 93: 853–860.

Rózsa, A. J. and Beuerman, R. W. (1982). Density and organization of free nerve endings in the corneal epithelium of the rabbit. *Pain* 14: 105–120.

Tervo, T., Vannas, A., Tervo, K., and Holden, B. A. (1985). Histochemical evidence of limited reinnervation of human corneal grafts. *Acta Ophthalmologica* 63: 207–214.

Zander, E. and Weddell, G. (1951). Observations of the innervation of the cornea. *Journal of Anatomy* 85: 68–99.

Corneal Nerves: Function

C Belmonte, Instituto de Neurociencias de Alicante, Universidad Miguel Hernández-Consejo Superior de Investigaciones Científicas, San Juan de Alicante, Spain

Glossary

Dysesthesias – Unpleasant abnormal sensations, spontaneous or evoked, such as burning, dryness, itching, electric shock, and pins and needles caused by the lesions of the peripheral or central nervous system.
Ectopic activity – The abnormal generation of propagated nerve impulses in areas of the sensory neuron membrane that are normally not spontaneously excitable, often generated by peripheral sensory axons or cell bodies of injured sensory ganglion neurons.
Ion channels – Pore-forming proteins located in the cell membrane of all living cells that selectively regulate the flow of ions (cations or anions) into and out of the cell. The ion channel switches between open and closed when the protein undergoes a conformational change, helping to establish and control a voltage gradient (membrane potential) across the plasma membrane.
Nerve impulse – The electrical signal conducted along the axon of neurons by which information is conveyed within the nervous system.
Neuropathic pain – Pain of pathological origin resulting of the abnormal functioning of the peripheral and/or central neural pathways involved in the detection of noxious stimuli.
Sensory afferents – Peripheral branches of sensory neurons located in the dorsal root or trigeminal ganglia that innervate body tissues and carry sensory information to the brain. When covered with a myelin sheath (myelinated or A fibers), they conduct nerve impulses at rapid speeds (over 3 m s^{-1}), while unmyelinated (or C) fibers lack the myelin sheath and have conduction velocities below 2 m s^{-1}.
Sensory receptors – The terminal portion of peripheral sensory axons specialized in the transduction of physical or chemical forces into a discharge of short-lasting (≈1 ms) membrane depolarizations, referred to as nerve impulses, which travel rapidly along the axon.
Signal transduction pathways – The binding of extracellular signaling molecules (or ligands) to cell-surface receptors triggers ordered sequences of biochemical reactions carried out by enzymes activated by second messengers that finally result in a cellular event as, for instance, the opening or closing of specific ion channels.

The cornea is innervated by different functional types of sensory afferent fibers that are selectively activated by physical and chemical stimuli. They give rise to conscious sensations of variable quality that are referred to the eye and/or the periocular region.

The cell bodies of corneal sensory afferents, most of which are of small or medium size, are located in the ipsilateral trigeminal ganglion and reach the cornea through the ciliary nerves. Sensory axons enter the cornea grouped into a variable number of radially oriented nerve bundles that branch extensively and form the sub-basal plexus below the basal epithelial cells. From this plexus, naked single fibers ascend vertically between the epithelial cells ending at variable depths. Immunocytochemical staining of the cell soma and axons of ocular sensory neurons reveals the presence of neuropeptides, principally substance P (SP) and calcitonin gene-related peptide (CGRP). Neuropeptides participate in neurogenic inflammation and promote corneal healing and/or maintenance of epithelial integrity either alone or in combination with growth factors.

Functional Properties of Corneal Sensory Receptors

Functional studies of corneal sensory fibers have been performed recording electrophysiologically in single corneal nerve fibers nerve impulses evoked by physical and chemical stimuli applied to the corneal surface. The majority of corneal sensory nerve fibers, about 70%, are polymodal nociceptors (Figure 1). They are activated by near-noxious mechanical energy, heat, chemical irritants, and by a large variety of endogenous chemical mediators released by damaged corneal tissue, resident inflammatory cells, or those which leak from vessels in the periphery of the cornea (the limbus). Some of the polymodal nociceptor fibers belong to the group of thin myelinated (A-delta) nerve fibers, but most of them are unmylelinated C fibers. Polymodal nociceptors respond to their natural stimuli with a continuous, irregular discharge of nerve impulses that persist as long as the stimulus is maintained. They have a firing frequency roughly proportional to the intensity of the stimulating force. Therefore, the impulse discharge of polymodal nociceptors not only signals the presence of a noxious stimulus, but also encodes its intensity and duration in a certain degree. Corneal polymodal nociceptors have a mechanical threshold slightly lower than mechanonociceptors

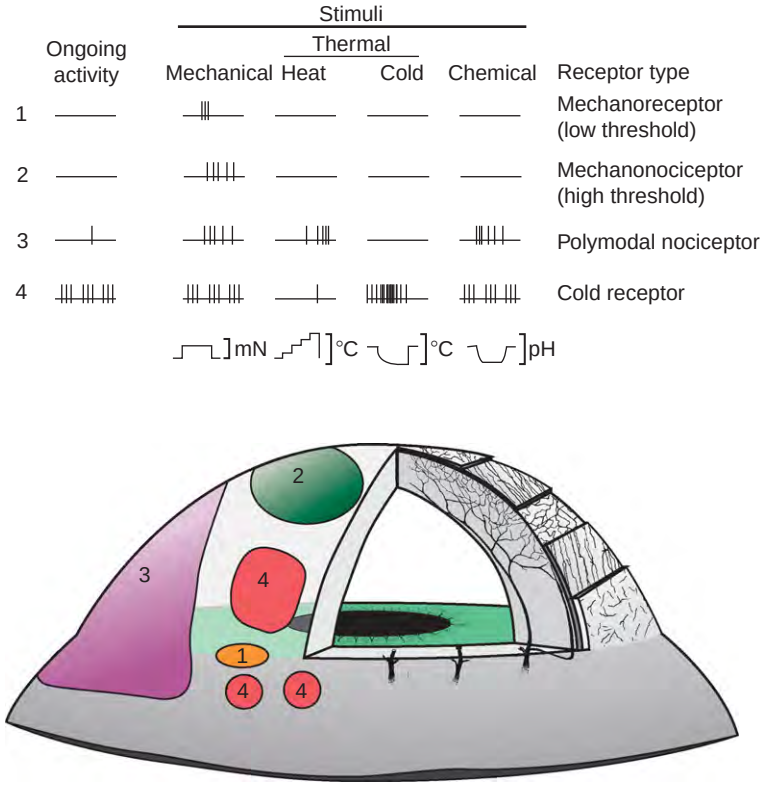

Figure 1 Schematic representation of the types of sensory receptors found in the cornea. In the upper part of the figure, the presence of ongoing activity at rest and the discharge of nerve impulses to the different modalities of stimuli have been displayed for each functional type of corneal sensory receptor type. The shape and time course of the stimulus applied are represented in the lower line. In the lower part of the figure, a scheme of the anterior segment of the eye shows the location and size of the receptor areas of the different types of receptors presented in the upper part of the figure. Modified from Belmonte, C., Aracil, A., Acosta, M. C., Luna, C., and Gallar, J. (2004). Nerves and sensations from the eye surface. *Ocular Surface* 2: 29–34.

(**Figure 2B(a)**) and, when stimulated with heat, they begin to fire at temperatures over 39–40 °C (**Figure 2B(b)**). A fraction of polymodal fibers (*c.* 50%) also increase their firing rate when the corneal temperature is reduced below 29 °C. Many chemical agents known to excite polymodal nociceptors of other territories also activate ocular nociceptors. Acidic solutions (of pH 5.0–6.5), or gas jets containing increasing concentrations of CO_2 (that in contact with the aqueous corneal surface forms carbonic acid and drops the local pH), evoke an impulse discharge in corneal polymodal nociceptors (**Figure 2B(c)**). Polymodal nociceptors are likely the origin of unpleasant sensations evoked by near-noxious and injurious chemical, thermal, and mechanical stimuli acting on the cornea.

Approximately 15–20% of the axons innervating the cornea (all thin myelinated) respond only to mechanical forces in the order of magnitude close to that required to damage corneal epithelial cells. Accordingly, they belong to the mechanonociceptor type (**Figure 2A**). Fibers of this class of receptor fire only one or a few nerve impulses in response to brief or sustained indentations of the corneal surface and, often, also when the stimulus is removed. Thus, they are phasic sensory receptors that signal the presence of the stimulus and, in a very limited degree, its intensity and duration. The threshold force required to activate mechanonociceptors is apparently low (*c.* 0.6 mN), far below the force that activates mechanonociceptor fibers in the skin. However, this intensity might be sufficient to damage unkeratinized corneal epithelium. Mechanonociceptors in the cornea are probably responsible for the acute, sharp sensation of pain produced by touching the corneal surface. The after-sensations of pain elicited by noxious stimuli are probably explained by the more sustained activity exhibited by polymodal nociceptors.

Another category of corneal nerve fibers that represents 10–15% of the total population is cold-sensitive thermal receptors. These are A-delta and C fibers that discharge spontaneously at rest and increase their firing rate when the normal temperature of the corneal surface (*c.* 33 °C) is reduced while they are transiently silenced upon warming. They also increase their firing rate as soon as the temperature of the cornea drops because of evaporation at the corneal surface, application of cold solutions,

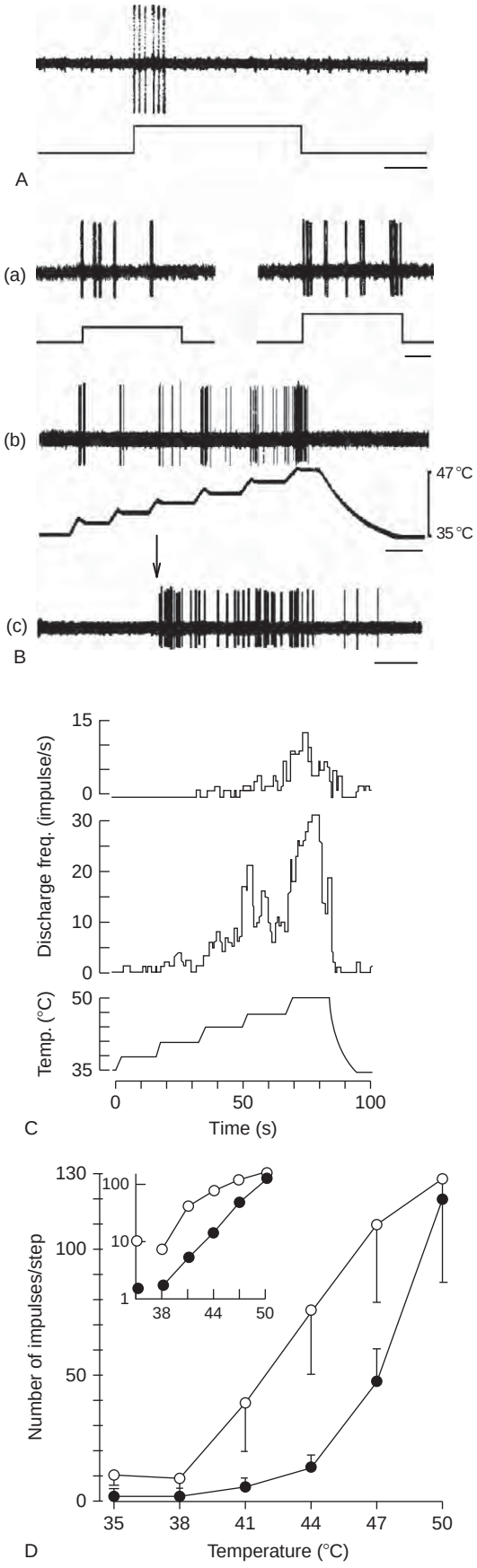

or blowing of cold air on the cornea. Cold receptor fibers are able to detect and encode as a change in impulse frequency and small temperature variations of 0.1 °C or less, thus allowing for the perception of decreases in corneal temperature as a conscious sensation of innocuous cooling.

Finally, it has been suggested that the cornea possesses mechanically insensitive, silent nociceptors, that is, nerve terminals that are not activated by mechanical or thermal stimuli when the tissue is intact, but, in the case of local inflammation, become responsive to these exogenous stimuli as well as to a variety of endogenous chemicals. Although the experimental evidence for their presence in the cornea is only indirect, they have been identified in virtually all other somatic tissues. Thus, it seems likely that such nociceptors also exist in the cornea. **Figure 1** presents a schematic diagram of the firing response to mechanical, thermal, and chemical stimuli of the various functional types of sensory endings identified electrophysiologically in the cornea.

The detection of stimuli by corneal receptor terminals, as occurs with sensory receptors of other tissues of the body, depends on membrane signaling proteins which convert the stimulus energy into a conformational change, leading to an alteration in ionic permeability and an electrical depolarization of the membrane of the nerve terminal, the generator potential. This potential change in the peripheral nerve endings gives rise to propagated nerve impulses in more proximal portions of the axon which travel centripetally to the brain. In nociceptors,

Figure 2 A and B: Impulse response to different stimulus modalities of corneal sensory fibers. A: Transient discharge evoked in a mechanonociceptor fiber by a sustained mechanical indentation. B: Response of a polymodal nociceptor fiber to (a) mechanical indentations of increasing amplitude (80 and 150 μm); (b) stepwise heating of the corneal surface from 34 to 47°C; and (c) application of a drop of 10-mM acetic acid to the corneal surface. In all cases, upper traces depict the nerve impulse recordings and lower traces the stimulus waveform; time scales: A and B(a) = 1 s; B(b) = 15 s; and B(c) = 0.5 s. C and D: Sensitization to heat of corneal polymodal nociceptors. C: Peristimulus histograms of a corneal unit showing the first (upper) and second (lower) response to two identical stepwise heatings separated by 3 min. Each bar indicates the number of impulses evoked per second and the lower trace shows the stimulus waveform. E: Mean stimulus response relation of eight corneal units in response to the first (filled circles) and the second (open circles) stepwise heating. Each point represents the mean number of impulses evoked at the temperature indicated in the abscissa. The bars indicate the standard error of mean. A and B reproduced from Belmonte, C. Gallar, J. The primary nociceptive neuron: A nerve cell with many functions. In: Rowe M. J. (ed.) Somatosensory processing: From single neuron to brain imaging. Sydney, NSW: Harwood Academic Publishers. C and D reproduced from Belmonte, C. and Giraldez, F. (1981). Responses of cat corneal sensory receptors to mechanical and thermal stimulation. *Journal of Physiology* 321: 355–368.

most transduction molecules are ion channels that are directly gated by the stimulus or open by intracellular messenger systems that can, in turn, be activated by a variety of membrane proteins.

Several classes of ion channels have been associated with the transduction of the various forms of energy and the production of the generator potential at nociceptor nerve terminals. A channel protein named transient receptor potential type vanilloid 1 (TRPV1) receptor, a nonselective cation channel with pronounced permeability for Ca^{2+} ions, is the main molecular substrate for the ability of polymodal nociceptors to respond to acid, heat, certain irritant chemicals, and inflammatory mediators. Another ion channel of the same family – transient receptor potential cation channel, subfamily A, member 1 (TRPA1) – also exhibits a prominent sensitivity to pungent chemicals. Thus, these channels serve as molecular integrators for multiple types of stimuli. The nature of the molecular entities involved in the transduction of mechanical forces at nociceptor endings is still uncertain. Stretch-activated ion channels have been identified in the membrane of mammalian sensory neurons. Extracellular matrix attachments have been proposed as the mechanism involved in the transmission of external mechanical forces to the neuronal surface and, subsequently, to ion channels activated or inactivated by stretch. Finally, TRPM8 and leak K^+ channels have been suggested as cold sensors in cold thermoreceptor corneal fibers. The depolarization of sensory nerve terminals in the cornea secondary to ion channel opening has a variable duration. In the case of rapidly adapting corneal mechanosensory endings, only one or few nerve impulses are generated. Thus, they serve primarily to signal the presence of a stimulus. Polymodal nociceptors and cold receptors encode the intensity and the time course of the stimulus in their firing rate and duration. They therefore provide information to the brain on both the modality and the characteristics of the stimulus (**Figure 1**).

Response of Corneal Receptors to Local Inflammation

One of the most prominent features of polymodal nociceptors is that sustained or repetitive stimulation tends to augment their response to new noxious stimuli. This phenomenon, referred to as sensitization, is also present in corneal nociceptors. Sensitization is characterized by a reduction of the impulse firing threshold such that impulse discharges are now evoked by intensities of the stimulus within the innocuous range. Moreover, noxious stimuli elicit a stronger and more sustained impulse discharge. Finally, sensitized corneal nociceptors often develop an irregular, low-frequency ongoing activity of nerve impulses in the absence of stimulation (**Figures 2D** and **2E**). This spontaneous activity, coupled with the enhanced responsiveness to stimulating forces, is the peripheral substrate of the augmented pain sensitivity and the presence of pain sensation in the absence of stimulus, exhibited by injured and/or inflamed corneas.

The sensitization of corneal nociceptors occurs as a result of the local release by injury of a large variety of inflammatory mediators from damaged cells and from resident and invasive cells of the immune system. Endogenous chemicals include H^+ and K^+ ions, adenosine and adenosine triphosphate (ATP), serotonin, histamine, platelet-activating factor, bradykinin, prostaglandins, leukotrienes, tromboxanes, interleukins, tumor-necrosis factor, and nerve growth factor (NGF). These mediators are responsible for local inflammatory reactions in the cornea and conjunctiva (vasodilatation, plasma extravasation, and cell migration), and act on membrane channels and receptor proteins at corneal nociceptor nerve endings, provoking short-term changes in their opening probability. TRPV1 and TRPA1 channels at the membrane of polymodal nociceptors are direct or indirect targets for many of the inflammatory mediators released upon corneal injury. The enhanced ion flow and increased membrane excitability resulting of ion channel activation create the augmented impulse firing and reduced threshold that characterize the process of sensitization of injured corneal nerve terminals (**Figures 2D** and **2E**). Inflammatory mediators use different signaling pathways to exert their effects on channel activity. For instance, prostaglandin E2, ATP, and adenosine or 5-hydroxytryptamine (5-HT) activate the protein kinase A (PKA) signaling pathway, whereas other mediators such as bradykinin act on protein kinase C to produce sensitization. The sensitization of corneal nociceptors develops within minutes of an acute corneal injury and normally fades when inflammation subsides. Long-lasting corneal inflammation, as occurs, for instance, in chronic dry eye, may produce more permanent changes in nociceptive terminals, including modified expression of the existing receptor molecules and expression of new ones possibly mediated by growth factors, in particular NGF.

The nerve impulses evoked by noxious stimuli in corneal nociceptors not only travel centripetally to the brain, but also invade antidromically other nonstimulated peripheral branches of the parent axon, causing the release of neuropeptides contained into their peripheral endings. CGRP and SP released by depolarized nociceptor endings contribute to local inflammatory responses and amplify the proinflammatory effect of other endogenous mediators. This neurogenic inflammation mediated by the sensory nerves affects noninjured areas of the cornea and conjunctiva and explains the extension of inflammation to distant, intact tissues (conjunctiva, iris, and ciliary body) following a limited corneal lesion.

Effects of Injury on Corneal Nerves

After ocular surgery, accidental trauma, and nerve injury secondary to certain ocular or systemic diseases, corneal sensory nerves may become damaged at different points of their trajectory. It is well established that peripheral axotomy changes the morphology and functional properties of nerve fibers projecting to the cornea substantially. Denervated areas are invaded by outgrowths of adjacent noninjured nerve fibers and sprouts of the injured axons. Some of terminal stumps of severed axons are entrapped by scar tissue and form microneuromas. The expression of genes that encode ion channels (in particular sodium and potassium channels) and receptor proteins by primary sensory neurons is also modified by peripheral nerve injury. This alters nerve excitability and favors the development of ectopic discharges and abnormal responsiveness in damaged neurons, giving rise to peripheral neuropathic pain.

Sensitivity of the Intact Cornea

Clinical exploration of the sensitivity of the cornea or conjunctiva to mechanical stimulation is normally performed by gently touching the ocular surface with a wisp of cotton, and observing the blink reflex or comparing the subjective sensation with that evoked in the fellow eye. A more quantitative approach is obtained using a calibrated hair of variable length (the Cochet–Bonnet esthesiometer). The Belmonte noncontact gas esthesiometer uses an air jet of adjustable flow and temperature that contains CO_2 in a variable concentration to reduce local pH, which allows separate mechanical, thermal, or chemical stimulation applied to a restricted area of the cornea or the conjunctiva. Using these procedures, changes in normal corneal sensitivity in relation to age, sex, pregnancy, iris color, and use of contact lenses; pathological changes associated to ocular surgery; corneal pathologies such as herpes virus infections, keratitis, iritis, uveitis, and glaucoma; or systemic diseases such as fibromyalgia or diabetes have been detected in multiple clinical and experimental studies.

Studies with the Belmonte esthesiometer have determined that the quality of the sensation evoked from the intact cornea and conjunctiva depends on the modality of the stimulus applied. Furthermore, electrophysiological recordings of nerve impulse activity in experimental animals applying mechanical, thermal, and acidic stimuli to the cornea with the Belmonte esthesiometer showed that each of them excited, in a variable degree, the various functional subpopulations of corneal nerve fibers. In humans, the sensations produced by suprathreshold mechanical, chemical, and heat stimulation of the cornea possessed, in each case, a distinct quality that allowed the psychophysical identification of the stimulus modality, but always included a component of irritation. In contrast, the application of cold pulses to a corneal spot that moderately decreased (1–3 °C) the local temperature evoked almost exclusively an innocuous cooling sensation, which acquired an additional component of irritation when more pronounced temperature reductions were applied. The psychophysical characteristics of sensations evoked by stimulation of the bulbar conjunctiva are quite similar to those of the cornea, except that sensitivity was comparatively lower and light mechanical stimuli were felt as nonirritating.

Sensitivity of the Injured Cornea

Following surgical procedures for cataract removal, retinal detachment, and glaucoma, and particularly after surgery performed to correct refractive defects (radial keratotomy, photorefractive keratectomy, laser *in situ* keratomileusis, and keratoplasty), nerves directed to the cornea are usually damaged in a degree that, for photorefractive surgery, depends on the extent of the corneal lesion. Severed nerves start to regenerate soon after injury, but only a part of them succeed in penetrating the injured corneal tissue, and corneal innervation remains disorganized and reduced in number, months and even years after surgery. In parallel with the morphological changes, functional alterations have been described. Axotomized corneal neurons and nerve fibers innervating the injured cornea exhibit an altered threshold to their natural stimuli and abnormal responsiveness to mechanical, chemical, and thermal stimuli.

As a result of the disturbances in peripheral innervation, corneal sensitivity to mechanical stimulation is impaired, with a remarkable increase in threshold of the denervated areas that takes months to recover, and may never return to normal values. Transplanted corneas or implanted lenticules in epikeratophakia remain totally anesthetic for years, or recover, at best, a very limited mechanical sensitivity usually restricted to the periphery of the transplant. After laser-assisted *in situ* keratomileusis (LASIK) surgery, corneal sensitivity to mechanical and chemical stimulation measured with the Belmonte esthesiometer remained significantly below control 3 and 6 months post-LASIK, becoming close to normal only 2 years postsurgery. However, at that time, a few patients with deep photo ablations presented severe sensory impairments.

In parallel with the hypoesthesia just described, spontaneous pain sensations and dysesthesias may appear following refractive surgery. The lower sensitivity of the cornea to external corneal stimulation is explained by the reduced number and the altered threshold of corneal

sensory nerve fibers after surgery. The additional development of unpleasant dryness sensations and/or pain referred to the eye in some patients is attributable to the spontaneous firing and abnormal responsiveness of some of the injured corneal nerve fibers that were unable to fully recover their transducing capacities and exhibit abnormal excitability after injury. These disturbances seem to affect mainly polymodal nociceptor and cold corneal nerve fibers. Thus, these two functional subpopulations of corneal nerves appear to be the main peripheral source of abnormal sensations following corneal surgery.

See also: Corneal Nerves: Anatomy.

Further Reading

Belmonte, C. (2007). Eye dryness sensations after refractive surgery. Impaired tear secretion or 'phantom' cornea? *Journal of Refractive Surgery* 23: 598–602.

Belmonte, C., Acosta, M. C., and Gallar, J. (2004). Neural basis of sensation in intact and injured corneas. *Experimental Eye Research* 78: 513–525.

Belmonte, C. and Tervo, T. T. (2005). Pain in and around the eye. In: McMahon, S. and Koltzenburg, M. (eds.) *Wall and Melzack's Textbook of Pain,* 5th edn., pp. 887–901. London: Elsevier.

Belmonte, C. and Viana, F. (2007). Transduction and encoding of noxious stimuli. In: Schmidt, R. F. and Willis, W. (eds.) *Encyclopedia of Pain,* vol. 3, pp. 2515–2528. Berlin: Springer.

Müller, L. J., Marfurt, C. F., Kruse, F., and Tervo, T. M. (2003). Corneal nerves: Structure, contents and function. *Experimental Eye Research* 76: 521–542.

Corneal Scars

D G Dawson, Emory University School of Medicine, Atlanta, GA, USA

Glossary

Corticosteroid – A class of steroid hormones that are produced in the adrenal cortex and are involved in a wide range of physiologic systems, such as the stress response, the immune response, regulation of inflammation, carbohydrate metabolism, protein catabolism, blood electrolyte levels, and behavior. In wound healing, its primary role is in suppressing the immune response and reducing the release of inflammatory cell mediators.

Epikeratome laser-assisted *in situ* keratomileusis (EpiLASIK) – An anterior surface ablative refractive surgical procedure that uses a unique epikeratome (a microkeratome with a blunt, oscillating blade) to mechanically separate the epithelium from the Bowman's layer and stroma, while suction is applied, to make a hinged epithelial flap, similar to a traditional LASIK flap. Unlike LASIK, no sharp blades or intrastromal cuts are made. It is most similar to LASEK, but no alcohol is required.

Extracellular matrix (ECM) – Any material produced by cells and secreted into the surrounding medium, but it usually is applied to the noncellular portion of living tissues. It typically is classified as basement membrane or interstitial ECM.

Fibrosis – Formation of excessive fibrotic scar tissue in an organ or specific tissue of the body.

Hypertrophic scar – An abnormal, excessively large fibrotic scar due to a pathologic reparative wound-healing response, where the scar is raised above the surrounding adjacent normal tissue, but it does not grow beyond the boundaries of the original wound. It often regresses in size and improves in appearance over a few years after.

Keloid – An abnormal, excessively large fibrotic scar due to a pathologic reparative fibrotic wound-repair response, where the scar extends beyond the boundaries of the original wound in addition to being raised above the surrounding adjacent normal tissue. It is a more severe degree of pathologic scarring than a hypertrophic scar because it can carry on growing indefinitely into a large, benign growth that can present a significant cosmetic issue to the individual.

Laser-assisted subepithelial keratomileusis (LASEK) – An anterior surface ablative refractive surgical procedure that reshapes the cornea to correct refractive errors of the eye and is basically a modified form of photorefractive keratectomy (PRK). With LASEK, instead of removing or excising the epithelium completely as in PRK, the surgeon cuts a round semi-circular area of epithelium with a fine-bladed instrument called a trephine. A dilute alcohol solution is then applied to loosen the cut epithelium inside the semi-circle where it attaches to Bowman's layer and then the surgeon gently lifts and folds back the hinged loosened epithelial flap, exposing the underlying Bowman's layer and corneal stroma for the excimer laser treatment.

Mitomycin C (MMC) – Mitomycins are a family of aziridine-containing natural products isolated from the soil fungus, *Streptomyces caespitosus*. One of these compounds, MMC, finds use as a chemotherapeutic agent or as a scar-reducing agent by virtue of its potent DNA cross-linking.

Myofibroblast – An epithelial-, endothelial-, or mesenchymal-derived cell (e.g., keratocyte) that acquires morphological and biochemical features of smooth muscle cells, including the expression of alpha-smooth muscle actin (α-SMA). It can contract by using the actin smooth muscle filament complex, which can help speed up wound repair by contracting the edges of the wound and enhancing ECM deposition compared to that of simply an activated fibroblast. It has been suggested that in several fibrotic diseases (e.g., liver cirrhosis, kidney fibrosis, retroperitoneal fibrosis, corneal fibrotic scarring) that persistence of myofibroblasts and chronic wound contracture leads to a long-term fibrotic scar.

Platelet-derived growth factor (PDGF) – A family of growth factors (GFs) involved in stimulating fibrotic wound repair and angiogenesis. Three PDGF isomers are found in humans: PDGF-AA, PDGF-AB, and PDGF-BB. In wound healing, its primary cellular source is platelets, which degranulate and release PDGF-AB. This initiates a fibrotic repair response by chemotactic and proliferative effects on fibroblasts and inflammatory cells.

Regeneration – Regrowth of a damaged organ or tissue so that the original structure and function are restored back to normal.

Transforming growth factor-beta (TGF-β) – A family of cytokine proteins that are expressed by almost all mammalian cells in three isoforms (TGF-β1, TGF-β2, and TGF-β3), which have different functions in wound healing. All three TGF-β isoforms play major roles in wound healing including chemotaxis

(signaling migration of macrophages, monocytes, fibroblasts, and neutrophils), fibroblast proliferation, collagen production, and angiogenesis. They act on target cells to generate a specific molecular signaling response by binding to cell surface TGF-β receptors, types RI, RII, and RIII, which then initiates activation of several intracellular signaling pathways. All three TGF-β isoforms are secreted from cells as a large (125–160 kDa) latent TGF-β complex (LL-TGF-β complex), composed of an active TGF-β dimer, a latency-associated peptide (LAP), and one of four possible isoforms of the latent TGF-β-binding protein (LTBP). Overall, the LL-TGF-β complex covalently binds with high affinity to ECM, such as fibronectin, through its specific LTBP domain to create storage pools of latent TGF-β, whereas the free active TGF-β dimer binds to TGF-β cell receptors or creates more storage pools by binding to the core protein portion of dermatan sulfate and heparin sulfate protoglycans (PGs) in the ECM.

Introduction

Tissue or organs of mammalian embryos and fetuses up to the first-half of gestation heal through scar-free regenerative wound healing, whereas tissues in late gestation fetuses up to elderly adults heal more slowly (inversely related to postnatal age) and less efficiently through scar-forming fibrotic wound healing. At the microscopic level, a fibrotic scar is basically defined as disorganized extracellular matrix (ECM) containing repair mesenchymal cell phenotypes as opposed to regenerative or uninjured normal tissue, which have normal ECM architecture containing quiescent mesenchymal cell phenotypes, or tissue fibrosis, which has disorganized ECM containing quiescent mesenchymal cell phenotypes. At the macroscopic level, a fibrotic scar leaves a mark or cicatrix on the skin or tissue after injury, often leading to an alternation in function or cosmesis, whereas tissue fibrosis leaves an inconspicuous mark and regenerative tissue leaves flawless tissue restoration. Thus, fibrotic scarring represents reparation failure to complete tissue fibrosis and both represent failures to achieve true tissue regeneration. Research studies on prenatal embryos and fetuses suggest that the mechanisms involved in the regenerative response are intrinsic to the tissue itself and are not caused by the sterile prenatal environment in the womb. The evolutionary reason for the transition from the scar-free regenerative response to the scar-forming fibrotic repair response in higher mammals, such as humans, is that such a variation helped an individual live longer to reproduce and take care of their young (i.e., natural selection). The fibrotic repair response results in rapid inflammatory cell recruitment and subsequent wound contracture and filling of space, which can be organ or life saving. The main disadvantages of the fibrotic repair response are that it commonly results in the reconstitution of semi-functioning tissue or can fill the tissue with a cosmetically displeasing scar. In modern times, the result of this evolutionary mismatch is that a fibrotic scar can occur from even minor injury (e.g., sterile, simple surgical incision with suturing).

In humans, tissue fibrosis or fibrotic scarring occurs after almost any type of injury to any tissue in the adult human body, including the eye. One exception is injury in which ectodermal cells alone are damaged (e.g., first-degree burns, corneal abrasion, skin abrasion) and heal through scar-free cellular regeneration without any long-term fibrotic effects to the underlying interstitial mesenchymal cells. In fact, in certain cases where the context of the injury and the molecular signaling pathways invoked are shifted toward embryonic mechanisms, scar-free tissue regeneration may still occur as opposed to fibrotic scarring. Thus, tissue fibrosis or fibrotic scarring is not inevitable. For example, if oral mucosa (e.g., gums, palate, and inner cheek) is superficially damaged, complete regeneration occurs. Other examples include complete regeneration of the liver even if up to two-thirds of the liver is removed or complete regeneration of the skin in specific injury contexts, such as a pin-prick, a hypodermic needle stick, or multiple needle insertions (tattooing). In contrast, fibrotic scarring results from penetrating stab incision into the liver or various more severe injuries to the skin, such as: (1) a larger incision than a needle stick, (2) an excision, (3) suturing a wound closed with pro-inflammatory material (cat gut suture), and (4) leaving sutures in place too long or with incorrect tension. These examples illustrate the plasticity of the two wound-healing responses, fibrosis and regeneration. Differences between the desired responses (regeneration or secondarily minimal to mild tissue fibrosis) and the less desired responses (nonhealing wounds or excessive fibrotic scarring) are subtle, but fundamentally come down to three variables: (1) the molecular signaling pathways invoked, (2) the targeted responding cells, and (3) the context and degree in which the targeted responding cells are stimulated.

Central to our understanding of the pathogenesis of tissue regeneration versus fibrotic scarring (and tissue fibrosis) has been the identification of several cytokines and growth factors (GFs) involved in initiating and/or regulating the ongoing wound-healing responses. The relationship between these cytokines and GFs and their predicted cellular responses is now only being partially understood. As such, it is currently known that cytokines and GFs, their associated target cell surface receptors, and their molecular signaling pathways play a significant role

in directing cellular behavior and/or phenotype in normal, diseased, and wound-healing states. Currently, the cytokine best known to play the most crucial role in mediating either tissue regeneration or fibrotic scarring is transforming growth factor-beta (TGF-β). Three isoforms of TGF-β have been identified in mammals, TGF-β1, β2, and β3, all having major roles in wound healing. Studies comparing embryonic tissue regeneration versus adult fibrotic scarring have identified a variety of differences in their intrinsic cellular levels of expression and release. TGF-β3 elicits a regenerative response, whereas both TGF-β1 and TGF-β2 elicit a fibrotic-repair response. There are other notable disparities between the TGF β isoforms (Table 1). TGF-β is secreted extracellularly in a latent or inactive pro-peptide form, consisting of a 25 kDa disulfide-linked homodimeric TGF-β peptide, also known as the active form, that is bound to a latency-associated peptide (LAP), which itself is bound to a specific latent TGF-β-binding protein (LTBP). This 125–160 kDa TGF-β complex is known as a large latent TGF-β (LL-TGF-β) complex. It binds covalently to ECM (e.g., fibronectin) through its LTBP domain to create storage reservoirs of latent TGF-β. During wound healing or inflammation, proteolytic enzymatic cleavage (e.g., tissue plasminogen activator (TPA), plasmin, matrix metalloproteinases (MMPs), or cathepsin) or nonproteolytic dissociation (e.g., low pH, reactive oxygen species) of the active TGF-β dimer occurs from the LL-TGF-β complex, leading to TGF-β activation. Active TGF-β isoform dimer binding to its targeted cell surface receptor(s) leads to a cascade of intracellular signaling pathways, including a Smad pathway as well as other pathways, each resulting in a cell-specific set of responses.

Table 1 Comparison of embryonic and adult wound healing characteristics

Wound healing characteristics	*Embryo/fetus*	*Adult*
Fluid environment	Present	Absent
Sterile environment	Present	Absent
Oxygen tension	Lesser	Greater
Temperature	Warmer	Cooler
Speed of epithelialization/ wound closure	Faster	Slower
Fibroblast migration/ proliferation	Faster	Slower
Fibroblast cellularity	Greater	Lesser
Myofibroblastic differentiation	Absent	Present
Extracellular matrix deposition	Faster	Slower
Extracellular matrix architecture	Normal	Disorganized
Tensile wound strength	Normal	Reduced
Inflammation		
Immune system	Immature	Mature
Inflammatory response	Sparse	Great
Neutrophil transmigration	Absent	Present
Platelets/degranulation	Absent	Present
Cytokine profile the fibroblasts		
TGF-β1 and β2	Low	High
TGF-β3	High	Low
FGF	High	Low
PDGF	Absent	High
Angiogenesis	Lesser	Greater
Wound healing response	Tissue regeneration	Fibrotic scarring

Data from Ferguson, M. W. J. and O'Kane, S. (2004). Scar-free healing: From embryonic mechanisms to adult therapeutic intervention. *Philosophical Transactions of the Royal Society, London B* 359: 839–850.

In general, TGF-β/receptor-mediated intracellular signaling pathways stimulate the production of various ECM proteins and inhibit ECM degrading enzymes (increases inhibitors of MMPs and decreases expression of MMPs), although exceptions to these principles abound. TGF-β also modulates cellular functions such as apoptosis, motility, mitosis, and differentiation or transdifferentiation into new cellular phenotypes. With wound healing, the various cytokine or GF cascades sometimes result in overlapping specific cellular responses that are not completely well understood. For mesenchymal fibrocytes (e.g., keratocytes), this set of responses includes fibrocyte migration and proliferation and subsequent differentiation into a metabolically activated repair cell type known as a fibroblast. Fibroblast cellular behavior results in the synthesis and deposition of a provisional fibronectin matrix comprised of ECM adhesion molecules (fibronectin), ECM space-filling molecules (hyaluronic acid), and ECM signaling molecules (tenascin). The next step is the conversion to early mature ECM, comprised of collagen fibrils, sulfated protoglycans (PGs), and possibly epithelial- or endothelial-derived surface basement membranes (BMs). Under appropriate conditions, such as prolonged or excessive TGF-β exposure, some fibroblasts differentiate into another repair phenotype known as a myofibroblast, which is the central cellular mediators of the fibrotic repair response (Figure 1). Myofibroblasts originate by differentiation from fibrocytes or activated fibroblasts or by transdifferentiation, also known as metaplasia, from epithelial, endothelial, or local smooth muscle cells that are associated with blood vessels (Figure 1). Morphologically, myofibroblasts are larger than activated fibroblasts and uniquely express alpha-smooth muscle actin (α-SMA), an important morphologic marker identifying this cell type using immunohistochemistry techniques. Myofibroblasts are highly contractile repair cells that promote wound closure and contraction. Functionally, myofibroblasts also express and secrete greater amounts of cytokines and GFs, synthesize and deposit greater amounts of ECM, and have stronger and more focal ECM cell surface adhesion receptor sites compared to activated fibroblasts. Myofibroblasts first appear in the stroma directly under the epithelium and

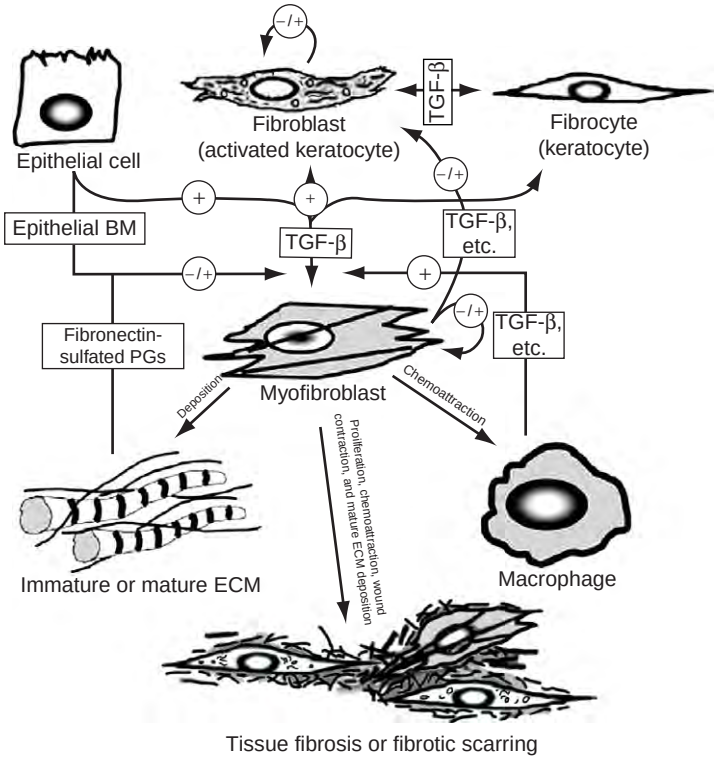

Figure 1 TGF-β is the main cytokine player and the myofibroblast is the main cellular player in the fibrotic repair response. A myofibroblast is derived from a fibroblast, an epithelial cell, a fibrocyte (bone-marrow derived cell?), or many other cell types, and it exerts a central role in cellular reconstitution, inflammation, and extracellular matrix (ECM) deposition in the pathogenesis of tissue fibrosis. Specific cell–cell interactions and ECM–cell interactions further modulate myofibroblast cell behavior. + = amplifying factor. − = suppressing factor.

then their domain advances to progressively deeper levels. Myofibroblast-mediated ECM deposition occurs in an orderly sequence from immature (primitive) to mature (fibrotic) stages: first fibronectin and other noncollagenous provisional ECM proteins (hyaluronic acid, tenascin, etc.), then collagen type III, and lastly collagen type I and sulfated PGs (e.g., decorin, lumican, biglycan). As the scar matures, most of the provisional ECM components are replaced by collagen fibrils (type I >> type III) and sulfated PGs. As judged by collagen fibril diameter and density, ECM usually first reconstitutes to the most mature and most fibrotic stage in the portion of the wound just under the epithelium and then it advances progressively to deeper levels. Additionally, during the evolution of maturation, the hypercellularity and hypervascularity decreases due to apoptosis and tensile strength increases due to increased maturity acquired collagen fibril cross-linking. The mechanism of late disappearance of myofibroblasts is uncertain, but probably is due to a combination of apoptosis and dedifferentiation of cells back to quiescent fibrocytes.

In humans, fibrotic scarring commonly causes major medical problems in a variety of tissues. In the eye, fibrotic scarring causes visual impairment or even blindness. In the peripheral and central nervous systems, glial scarring prevents neuronal reconnections and hence blocks reparative attempts at restoring normal neuronal function. In gastrointestinal and reproductive organs, strictures and adhesions can give rise to serious or life-threatening conditions, such as infertility, bowel obstruction, or chronic pain. In ligaments and tendons, fibrotic scarring restricts motility and decreases strength. Additionally, if the fibrotic repair response is incomplete, becomes excessive, or fails to appropriately terminate, pathologic wound healing occurs resulting in unhealed wounds, hypertrophic scars, or keloid scars, respectively. Overexpression and release of pro-fibrotic TGF-β1 and β2 cytokines, upregulation of TGF-β receptors RI and RII, and/or the formation of a positive, autoinducible feedback loop have been suggested as the primary reasons for excessive fibrotic scarring in hypertrophic or keloid scars. The potential for TGF-β autoinduction is usually self-limited in nonpathologic fibrotic repair responses through a negative feedback loop that terminates further TGF-β expression and release from that cell. In adult humans, the degree of fibrotic scarring versus tissue regeneration or tissue fibrosis depends on the following five factors: tissue site, sex, race, age, and magnitude and contamination of the wound. For tissue site, the gums, liver, and skin can either regenerate or scar, depending on the context of the injury. Most other tissues or organs in the body just repair themselves through tissue fibrosis or

fibrotic scarring, which is body site dependent. The deltoid, sternum, and conjunctiva scar more than the face, abdomen, legs, and cornea. Concerning sex, fertile females scar more than postmenopausal females and all males as estrogen has a major stimulatory effect on the fibrotic repair response. For race, darker pigmented individuals scar more than less pigmented individuals. Concerning age, young people in their teens and 20s scar more than infants and children, who have an immature immune response, and both heal better than older individuals, whose inflammatory response becomes sluggish and less effective with age and whose mesenchymal cells become senescent. Finally, the magnitude of injury and wound contamination alter the wound-healing response as larger, more inflamed, more contaminated wounds scar more than smaller, uncontaminated wounds.

Ocular Wound Healing

The ocular fibrotic wound-repair response is quite similar to that seen in other tissues in the human body. In the eye, fibrotic scarring most commonly occurs in the conjunctiva, cornea, iris, lens, retina, and choroid (**Figure 2**). In vascularized ocular tissues, like the conjunctiva, iris, choroid, or even the cornea or retina after having chronic ocular disease, fibrovascular scars are basically granulation tissue. Scars normally develop in response to vascular stromal injury whereby serum plasma or blood leaks into the wound resulting in a clot. This initiates a fibrovascular repair response predominantly through a platelet-derived growth factor (PDGF)-mediated platelet degranulation signaling pathway resulting in massive release of PDGF into the wound along with some TGF-β release. However, the eye also has several avascular transparent tissues (e.g., cornea, lens, vitreous, and portions of the retina) that also can repair themselves through fibrosis, albeit through four less intense TGF-β-mediated signaling pathways.

TGF-β-mediated wound healing occurs because TGF-β and its associated receptors are constitutively expressed in the normal state by almost all cells residing in or on ocular tissues. The external ocular surface has other factors to additionally consider in that it is bathed in a tear film composed of lacrimal gland secretions that are rich in latent TGF-β1. Similarly, internal intraocular structures are bathed in aqueous humor composed of ciliary and lens epithelial secretions that are rich in latent TGF-β2. Latent TGF-β2 is thought to be one of the principal factors promoting the normal naive immune status of intraocular tissues, including the cornea, due to its ability to maintain resident tissue immune cells in an immature state. Secondarily, latent TGF-β2 has a direct immunosuppressive effect whereby it inhibits immune cell proliferation and inflammatory cell cytokine and GF release. At the concentration levels found in the normal aqueous humor, latent TGF-β2 is also thought to participate in the inhibition of angiogenesis into transparent parts

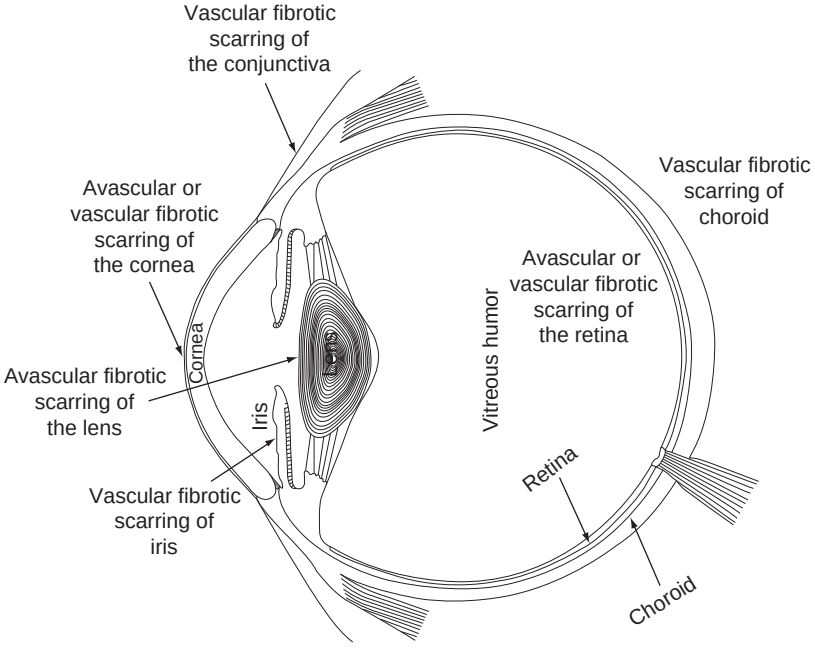

Figure 2 After injury, tissue fibrosis or fibrotic scarring occurs in the cornea, conjunctiva, iris, lens, retina, or choroid. The origin of the mesenchymal repair cell types (activated fibroblasts, myofibroblasts) in each case is either from local fibrocytes (keratocytes, subconjunctival fibrocytes), local epithelial cells (lens epithelium, retinal pigment epithelium), local endothelial cells (corneal endothelium), or local smooth muscle cells that are associated with blood vessels (iris, choroid). The lens undergoes only avascular fibrotic scarring, while conjunctiva, iris, and choroid only undergo fibrovascular granulation tissue scarring; the cornea and retina can undergo both, depending on whether preexisting corneal or retinal disease is present or on the context and severity of the initial injury.

of the eye, although a primary role for latent TGF-β2 in preventing vascularization in the cornea remains controversial. In various ocular diseases or after injury, TGF-β release and subsequent extracellular activation usually initiates a fibrotic repair response. The TGF-β-mediated fibrotic repair response can lead to significant visual impairment. TGF-β can cause overcorrection, undercorrection, or regression of refractive effect leading to refractive instability. TGF-β can also cause loss of refractive function by inducing irregular astigmatism or it can cause loss of transparency by inducing corneal haze, cataract, capsular fibrosis, or vitreous opacification. Tractional distortion of ocular structures, such as proliferative vitreoretinopathy, or other ocular complications, such as wound dehiscence, epithelial ingrowth, infection, hypotony (low intraocular pressure), epiretinal membranes, or retinal detachment, can also be caused by TGF-β . Thus, this molecule is a subject of intense research. Avascular transparent tissue fibrosis or fibrotic scarring in the cornea, lens, and retina is perhaps even more intriguing to researchers since it provides a unique opportunity to directly examine the cell biology during wound healing caused by the four TGF-β-mediated signaling pathways in isolation from the PDGF-mediated platelet degranulation signaling pathway.

Corneal Wound Healing

Although corneal neovascularization resulting from chronic ocular disease, such as corneal infection or chemical injury, may lead to a fibrovascular repair response (**Figure 3**, far-right), this type of repair response will not be focused on in this article. Instead, this article will strictly focus on the avascular corneal fibrotic repair response (**Figure 3**, middle). In the latter repair response, all cases have in common early inflammation that is minimally present up to 2 weeks after injury and maximally present up to 1 month after injury, at least some transient myofibroblast differentiation that is minimally present up to 4–6 months after injury and maximally present long-term, and the long-term presence of disorganized collagenous ECM (**Figure 4**).

Cell–Cell Communication

Cytokines and GFs

Corneal wound healing is an exceedingly complex process mediated by autocrine (affecting the same cell), juxtacrine (affecting adjacent similar cell types), or, most commonly, paracrine (affecting other adjacent cell types) cell–cell interactions involving cytokines and GFs produced by epithelial, stromal keratocyte, endothelial, immune, lacrimal gland, and corneal nerve cells (**Figure 4**). The paracrine interactions usually affect cells at most 50–75 μm from one another, while the other modes of interactions operate over shorter distances. The earliest event involves cell-mediated release of several cytokines and GFs by directly injured resident tissue cells or secretion by resident tissue cells just adjacent to the injury site and their subsequent extracellular activation. In the normal, uninjured state, the participating cytokines and GFs are expressed constitutively and stored intracellularly by the corneal epithelium, corneal nerves, keratoctyes, and corneal endothelium. These cytokines play a vital role in the maintenance of normal corneal health, structure, and function as some are secreted in a limited controlled fashion, mostly in the latent or inactive form. The adjacent tear film produced by the lacrimal gland and other ocular surface epithelia and the aqueous humor produced by ciliary and lens epithelial cells' secretions are another rich source of cytokines and GFs in the normal, uninjured state since these fluids supply various nutrients to the avascular cornea that otherwise would not be available. After wounding activates this direct resident tissue injury-induced

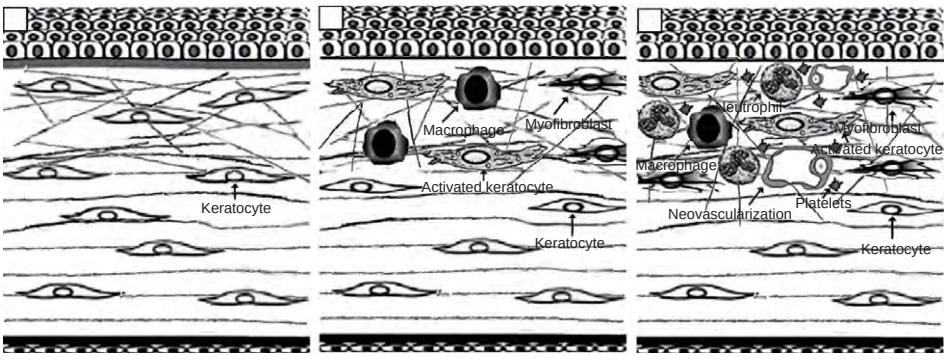

Figure 3 Schematic diagrams demonstrating the histology of the cornea during the active wound-healing phase, approximately 1 week after injury when re-epithelization has just been completed and epithelial thickness restored, in normal uninjured cornea (far-left), avascular fibrotic scarring (middle), and fibrovascular granulation tissue scarring (far-right). If these wounds eventually reach the conclusion of the remodeling phase (not shown), the middle illustration would end up with corneal tissue fibrosis or fibrotic scarring, whereas the far-right illustration would end up with fibrovascular corneal scarring.

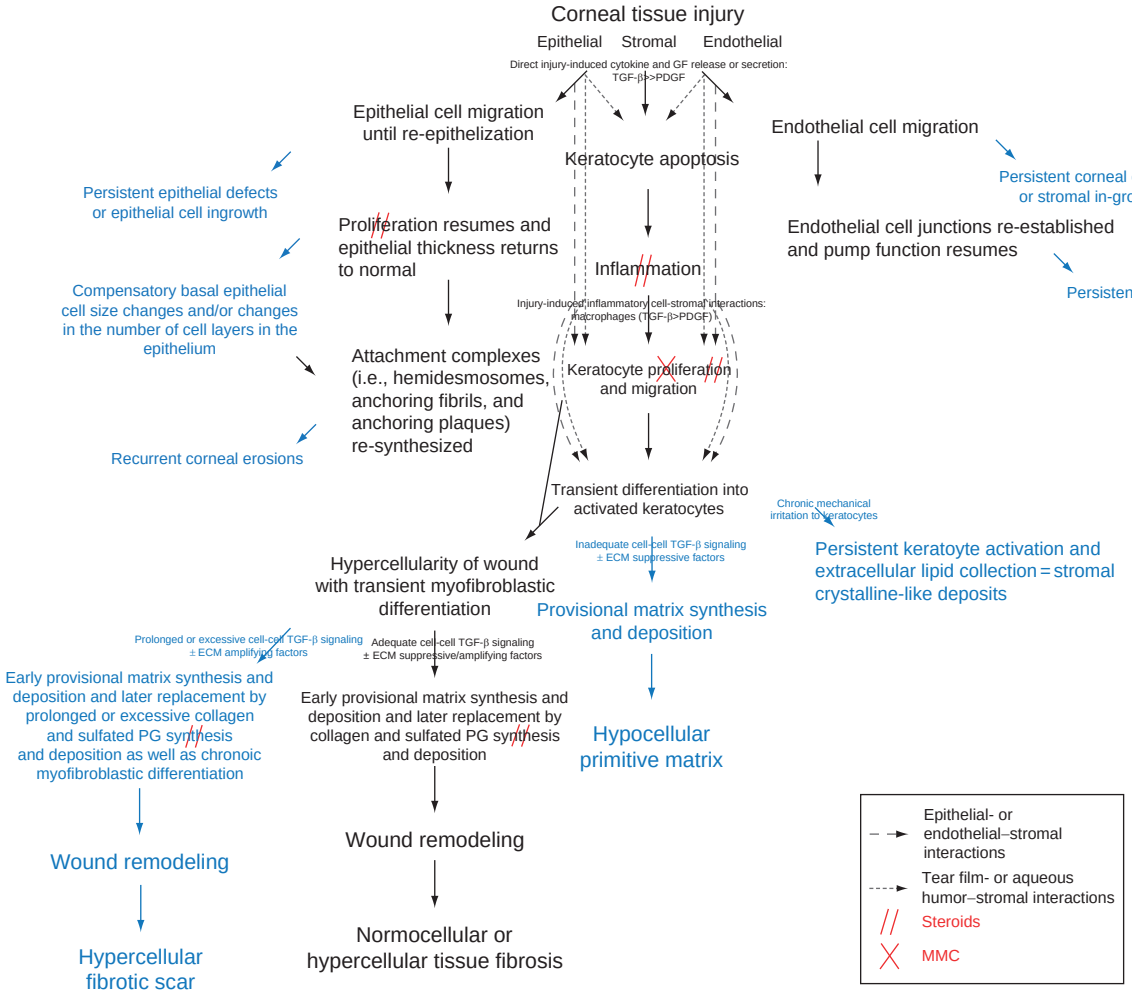

Figure 4 Diagram of normal corneal wound-healing pathways in black and abnormal or pathologic healing pathways in blue. Depending on the context of the injury and the molecular signaling pathways invoked, three types of long-term corneal stromal scars are possible: hypocellular primitive matrix, normocellular-to-hypercellular tissue fibrosis, and hypercellular fibrotic scars. The most functionally optimal type is that of normocellular-to-hypercellular tissue fibrosis as it is macroscopically transparent, yet still somewhat strong in tensile strength (~30%). Imbalances in the fibrotic repair response result in the other two stromal scar types. An incomplete fibrotic repair response results in a hypocellular primitive matrix scar, which is transparent, but very weak in tensile strength (~2–3%). An excessive, nonpathologic fibrotic repair response results in a hypercellular fibrotic scar, which is hazy, yet the strongest in tensile strength (~40%). Note that complete tissue regeneration is not possible in the *in vivo* adult human cornea, but if it could be manipulated to occur it would be the best option since it would be both transparent and back to normal tensile strength (100%). Topical corticosteroid drops suppress (i.e., decreases inflammation and blunts the intensity of some remaining wound-healing steps) the wound-healing pathways in both the epithelium and stroma (stroma > epithelium), while single intraoperatively applied mitomycin C (MMC) appears to block only the stromal wound-healing pathway by preventing keratocyte proliferation. Adapted from Dawson, D. G., Edelhauser, H. F., and Grossniklaus, H. E. (2005). Long-term histopathologic findings in human corneal wounds after refractive surgical procedures. *American Journal of Ophthalmology* 139: 168–178.

cytokine and GF cascade, supplemental exposure to additional cytokines and GFs may occur by four dynamic signaling pathways (**Figure 4**): epithelial– or endothelial–stromal interactions, inflammatory cell–stromal interactions, tear film– or aqueous humor–stromal interactions, and keratocyte mechanotransduction.

The major pertinent cytokines and GFs studied to date in regard to corneal wound healing include connective tissue growth factor (CTGF), epithelial growth factor (EGF), fibroblast growth factor (FGF), interleukin-1 (IL-1), nerve growth factor (NGF), PDGF, TGF-α, TGF-β, tumor necrosis factor-alpha (TNF-α), and vascular endothelial growth factor (VEGF). Currently, TGF-β is thought to be the most important one of this group in regard to stimulating a fibrotic repair response. The major resident cellular source of TGF-βs in the normal, uninjured cornea is the epithelium, which primarily expresses TGF-β2, while keratocytes and endothelial cells express only a little TGF-β1. No TGF-β3 expression has been found in the adult human cornea.

Resident cell surface TGF-β receptor sites are most numerous on keratocytes, while epithelial and endothelial cells have very little. After injury, increased expression of both TGF-β1 and -β2 and their associated receptors occurs, with TGF-β2 predominating in epithelial–stromal interactions (stroma within 75 μm from the epithelium) and TGF-β1 predominating in endothelial–stromal interactions (stroma within 75 μm from the endothelium). In contrast, stromal injury more than 75 μm from either surface invokes only slightly increased TGF-β1 expression and, most importantly, receives no paracrine supplementation from epithelial– or endothelial–stromal interactions.

Although the normal tear film contains high concentrations of latent TGF-β1, immediately following corneal epithelial injury, stimulation of the corneal nerve-lacrimal gland reflex arc causes hypersecretion of tears and increased secretion of several pro-fibrotic cytokines and GFs, such as PDGF-BB, NGF, and additional TGF-β1, all of which are normally stored intracellularly in lacrimal gland cells. The higher amounts of latent TGF-β1 as well as the newly secreted PDGF-BB and NGF are then activated by plasmin or MMPs, which are both released or secreted by injured or healing corneal epithelial cells into the wound. This corneal nerve-lacrimal gland reflex arc secretion and protease release usually returns to baseline levels within 7 days of epithelial defect closure; hence it is a transient event.

Other cytokines or GFs from the group listed above have intriguing complementary or antagonizing effects to TGF-β's pro-fibrotic effects. As discussed in the ocular fibrovascular repair response section, PDGF's pro-fibrotic effects are almost identical to TGF-β's pro-fibrotic effects. In the normal, uninjured cornea, small amounts of PDGF-BB are produced by the corneal epithelium that reacts with its receptors, which are most highly concentrated in the keratocytes of the stroma and the corneal endothelium. Also, a limited amount of PDGF-BB is secreted by macrophages and lacrimal gland cells. After epithelial injury, the expression, release, and activation of PDGF-BB increases in parallel to that of TGF-β. NGF, a trophic neuropeptide important in maintaining corneal epithelial health, is another GF that is complementary to TGF-β's pro-fibrotic effects as NGF is known to directly stimulate myofibroblastic transformation, but without the proliferative or ECM deposition effects of TGF-β. CTGF is also complementary to TGF-β as it too stimulates tissue fibrosis. However, CTGF is only potently expressed when stimulated by TGF-β, suggesting CTCF mediates several downstream actions of TGF-β. Thus, CTGF may be more important in chronic stages of fibrotic scarring as opposed to initiation or early regulation of the fibrotic repair response. Alternatively, CTGF may just synergize with TGF-β's pro-fibrotic effects since CTGF binds to TGF-β and potentiates TGF-β binding to TGF-β type II receptors. In contrast, TNF-α directly antagonizes TGF-β's pro-fibrotic effects by inhibiting the TGF-β/Smad pathway. This direct antifibrotic effect may seem counterintuitive since TNF-α is one of the major pro-inflammatory cytokines of the cornea. As can be appreciated, a correct combination and temporal sequencing of the various cytokines and GFs is required for proper healing to occur. Imbalances can result in incomplete wound repair, such as (1) persistent epithelial defects and corneal ulceration or melting, or (2) excessive pathological tissue fibrosis, such as stromal outgrowth, fibrodegenerative pannus formation, stromal ingrowth, or retrocorneal membrane formation.

TGF-β signaling pathways

Both historical clinical anecdotal observations and recent experimental investigations have suggested that epithelial–stromal interactions are the primary mediator of the avascular fibrotic repair response in the cornea. Thus, epithelial cell-derived substances substitute for those produced by platelets in the skin and other vascular tissues. The cornea consists of three cellular layers consisting of epithelium, interstitial stroma with interspersed keratocytes, and endothelium and two acellular layers consisting of an epithelial BM/Bowman's layer complex and an endothelial Descemet's membrane. Although Bowman's layer is not re-formed if damaged, both BM layers are re-formed if damaged because they are produced by epithelial or endothelial cells. Both acellular layers seem to function clinically as physiological barriers to separate the three cellular layers from direct contact or communication with one another to maintain normal corneal homeostasis. Disruption of the epithelial BM/Bowman layer complex induces maximal epithelial–stromal interactions that are intense enough even in a minimal injury state to cause a fibrotic repair response. This is seen clinically with bullous keratopathy – a pathological condition in which small blisters (vesicles or bullae) are formed in the corneal epithelium due to endothelial dysfunction, at the host–graft interface after penetrating keratoplasty (aka full-thickness corneal transplantation; a surgical procedure where a damaged or diseased cornea is replaced by full-thickness donated corneal tissue), or with Bowman's layer breaks (a degenerative disorder of the cornea in which structural changes cause it to thin and change in shape resulting an outward bulging of the tissue) as a subepithelial fibrotic scar, stromal outgrowth, or fibrodegenerative pannus formation (fibrocollagen connective tissue that proliferates in the anterior layers of the cornea in degenerative corneal disease). In some cases of bullous keratopathy, there may even be an no obvious microscopic full-thickness Bowman's layer break, but rather just separation of the of epithelium and its associated BM from Bowman's layer due to severe epithelial edema causing subepithelial bullae or blisters. In this extreme example of epithelial–stromal interactions, the keratocytes apparently migrate through trigeminal nerve fiber perforation sites found in Bowman's layer to the

subepithelial space created by the edema, where they undergo a fibrotic repair response. Separation or breaks in Descemet's membrane provide a similar trigger for causing a fibrotic repair response in the posterior cornea through endothelial–stromal interactions. For example, with penetrating corneal injury or breaks in Descemet's membrane, whether caused by trauma, disease (keratoconus), or surgery, endothelial–stromal interactions stimulate fibrotic scarring resulting in a supraendothelial fibrotic scar, stromal ingrowth, or retrocorneal membrane formation, depending on the degree of apposition of the broken Descemet's membrane wound margins. Therefore, current evidence suggests that the main TGF-β pro-fibrotic signaling pathway to block or suppress to prevent or reduce the chance for fibrotic scarring is that of direct epithelial–stromal or endothelial–stromal interactions.

Three other TGF-β pro-fibrotic signaling pathways are also present in the cornea and can initiate an avascular fibrotic repair response, but more often they just sustain the response already initiated by epithelial- or endothelial–stromal interactions. As already discussed earlier, a robust inflammatory cell response is part of a normal or nonpathologic fibrotic repair response. However, along with the advantages of stimulating an immediate innate immune response and thus preventing or at the very least lowering the risk for infection, leukocytes also secrete many pro-fibrotic cytokines and GFs, such as TGF-β and, to a lesser extent, PDGF. These pro-fibrotic factors are disadvantageous because they cause keratocytes in the corneal wound to undergo a higher degree of tissue fibrosis, which can lead to chronic nonpathologic scarring or even pathologic scarring. Usually after sterile clean injury, the inflammatory response in the avascular cornea is quite mild compared to that of the skin or other vascular tissues. However, dirty injuries or wounds complicated by infection or with preexisting immune-related disease may make the inflammatory response so massive that it becomes the primary pro-fibrotic signaling pathway resulting in varying degrees of severe corneal scarring. Another TGF-β pro-fibrotic signaling pathway was already discussed in the the section entitled 'Cytokines and GFs' when discussing the epithelial cell injury-induced corneal nerve-lacrimal gland reflex arc. These tear film–stromal interactions are usually transient (<7 days) and minor in comparison to the two already discussed. However, with persistent epithelial defects or chronic corneal ulceration, tear film–stromal interactions may become of paramount importance in causing fibrotic scarring in addition to the chronic increased release of epithelial cell-derived cytokines at the peripheral edge of the epithelial defect. The aqueous humor may have a similar role with posterior stromal injury. Finally, the fourth TGF-β pro-fibrotic signaling pathway involves keratocyte mechanotransduction interactions. Historically, wound tension has been known for years to promote a higher degree of fibrotic scarring. This mechanotransduction pathway was confirmed experimentally using cell culture experiments where mechanical strain on fibroblasts increased pro-fibrotic TGF-β1 expression, upregulated TGF-β receptors RI and RII, and markedly increased collagen expression. Findings by other researchers indicate that fibrocyte (e.g., keratocyte) cell surface integrins, which form cell–ECM adhesions, can act as strain gauges to external mechanical stress, triggering both direct intracellular signaling pathways or indirect release of paracrine cytokine and GFs factors, which stimulates the fibroblastic phenotype and augments ECM synthesis and deposition.

Cell–ECM Communication

Suppressing or amplifying factors

The ECM, through intrinsic binding and storage properties or cellular receptor-mediated adhesive properties, collaborates with cytokines and GFs in regulating cell behavior and phenotype through bidirectional cytokine and GF–ECM and cell–ECM interactions. In the latter, ECM adhesion and surface characteristics influence cellular behavior through interaction with cell surface receptors.

Clinical anecdotal observation supports the contention that having an intact corneal BM usually prevents fibrotic repair phenotypes from forming in the stroma and return of the BM usually correlates with loss of the fibrotic repair phenotype. Apparently, an intact epithelial BM or Descemet's membrane is the key factor in suppressing direct maximal epithelial- or endothelial–stromal interactions from taking place in the normal, uninjured state by binding and storing the soluble LL-TGF-β complex. Thus, epitheial BM or Descemet's membrane act as passive diffusion barriers to epithelial- or endothelial-derived latent TGF-β, respectively, and they ultimately regulate the bioavailability of TGF-β to the underlying or overlying corneal stroma. BMs are composed mainly of collagen type IV, entactin/nidogen, different laminins, and heparan and chondroitin sulfate PGs. The LL-TGF-β complex binding and storage property of BMs is likely related to heparin binding mechanisms intrinsic to the heparin sulfate PGs found in BMs, which bind to the soluble LL-TGF-β complex through either LTBP-1 or -3 domains. Fibronectin, which is found in the provisional matrix, also has LL-TGF-β complex binding and storage properties similar to that of BMs. Some sulfated PGs in the corneal stroma, like decorin, can even bind to the active dimer form of TGF-β through their core proteins; thus, additionally antagonizing the biological affects of TGF-β. BM-bound heparin sulfate PGs may have a similar function through their core proteins too.

With injury, corneal BM barriers are breached so that normal maximal epithelial- or endothelial–stroma interactions take place in addition to the acute wound-healing cascade already started by direct resident tissue injury itself. For example, with combined superficial epithelial

and stromal injury (photorefractive keratectomy (PRK), sterile corneal ulceration), this stromal wounding response is clearly seen clinically as it frequently stimulates excessive subepithelial fibrotic scarring resulting in prolonged or even permanent subepithelial haze. Apparently, removal of the epithelial BM directly exposes anterior stromal keratocytes to maximal pro-fibrotic effects of TGF-β released by the injured epithelial cells or found in the neurally stimulated tear film. Moreover, after injury, return of an intact epithelial BM suppresses normal epithelial cell-derived TGF-β2 intracellular expression and, more importantly, binds the TGF-β2 extracellularly secreted from epithelial cells. Thus, epithelial and presumably endothelial BMs represent an efficient ECM antifibrotic mechanism that goes slightly beyond just simple barrier function. However, this ECM antifibrotic mechanism is not foolproof since chronic subepithelial haze still persists long-term or episodic subepithelial haze still exacerbates after ultraviolet light overexposure, despite having an intact epithelial BM. This persistent haze seems to be best explained by TGF-β signaling pathways that work only in the stroma, such as mechanotransduction or inflammatory cell TGF-β signaling pathways, respectively. These two TGF-β signaling pathways can act directly on activated keratocytes and/or myofibroblasts in the stroma without having to send cytokines or GFs through a BM. Regarding the latter UV light example, quiescent or regressed myofibroblasts in a subepithelial fibrotic scar may have long-term upregulated TGF-β receptor sites densities, making them hypersensitive to any TGF-β, whether caused by inflammation or late resident cell injury. This may then lead to an autocrine positive feedback loop of more TGF-β production from a single myofibroblast or from a paracrine positive feedback loop due to macrophage infiltration and further TGF-β release.

Corneal cell–ECM interactions are an area that needs further study. Other disciplines have already shown that cells adhere to the ECM usually through their cell surface receptors (e.g., integrins, cell surface proteoglycans). For example, cell–ECM adhesion by integrins receptors regulates cellular homeostasis in multiple ways, including regulation through direct and indirect connections to the actin cytoskeleton, growth factor receptors, and intracellular signal transduction cascades. Integrins also sense mechanical strain arising from the ECM, thereby converting these stimuli to downstream signals modulating cell behavior. Disruption of this connection to the ECM has deleterious effects on cell survival, sometimes leading to a specific type of programmed cell death called anoikis. Anoikis is defined as apoptosis that is induced by inadequate or inappropriate cell–ECM interactions. Another direct extension of this cell–ECM interaction theme is clinical anecdotal reports and experimental animal research studies in which injury-induced stromal surface irregularity, also known as irregular surface nanotopography, results in increased TGF-β expression and a higher degree of corneal fibrotic scarring. Although irregular surface nanotopography is known to alter cell adhesion and positional information to the surface cells, such as epithelium and endothelium, it remains to be proven whether this pathway directly leads to myofibroblastic transformation since incomplete return of an intact epithelial BM has been reported as another possible cause.

Bone marrow-derived stem cells

Bone marrow-derived immune cells have been recently been detected in the corneal stroma and they may also participate in TGF-β molecular signaling pathways, especially the histiocytes (tissue macrophages). The relative contribution and importance of bone marrow-derived stem cells to regenerative or fibrotic repair responses needs to be explored further. Because of their extraordinary plasticity and their ability to secrete embryonic cytokines and GFs that promote tissue regeneration over fibrotic repair, bone marrow-derived stem cells are being explored as restorative cellular therapy in preclinical trials for myocardial infarction, neurodegenerative disorders, and osteogenesis imperfecta. However, some bone marrow-derived cells, or their progeny, may reside for prolonged periods in the stroma and could make an as yet unknown contribution to the wound-healing process.

Cellular responses

After injury-mediated induction of the TGF-β/receptor molecular signaling pathway, keratocytes undergo a series of repair phenotypic and behavioral changes that are temporally and spatially regulated during the corneal wound-repair process. Keratocytes are neural crest-derived mesenchymal cells that are sandwiched between collagenous lamellae forming a closed, highly organized syncytium. Keratocytes communicate with one another through gap junctions present on their long dendritic processes. The adult human corneal stroma has approximately 2.4 million keratocytes that occupy approximately 10% of the stromal volume. In postnatal life, they remain in the corneal stroma as modified fibrocytes, where they inconspicuously maintain the ECM of the corneal stroma. Depending on the type of injury and the molecular signaling invoked, keratocytes can be stimulated to undergo cell death (apoptosis) or transform to become a migratory keratocyte, an activated keratocyte, or a myofibroblast. Within minutes after injury, exposure to cytokines and GFs, such as IL-1 and TNF-α, found in the neurally stimulated tear film or released from injured epithelial cells is thought to lead to keratocyte apoptosis. The phenotypic transition (actin-cytoskeleton rearrangement) from a keratocyte to a migratory keratocyte appears to be initiated by loss of gap junction contact and possibly loss of keratocyte ion channels. Behaviorally, migratory keratocytes serve to reconstitute the cellularity of the tissue by once again re-forming a large intercommunicating network of keratocytes. The phenotypic transition

from a keratocyte to an activated keratocyte and then possibly to a myofibroblast depends on the TGF-β ligand/receptor occupancy rate and the duration of this occupancy rate. The myofibroblast phenotype may also require synergistic PDGF co-stimulation. Behaviorally, activated keratocytes promote provisional fibronectin ECM synthesis and deposition, while myofibroblasts promote mature collagenous fibrotic ECM synthesis and deposition. It has been postulated that at least partial ECM regeneration may still be possible *in vivo* since an adult keratocyte stem cell subpopulation has been discovered near the limbus. These progenitor cells express the ocular development gene *Pax6*, which is an embryonic marker not expressed by resident stromal keratocytes. Overall, it has been suggested that variations in these two repair phenotypes (activated keratocyte and myofibroblast), especially the degree and duration of myofibroblast differentiation, ultimately determine the final clinical outcome of the wound-healing process, resulting in either primitive, incomplete wound repair, acceptable tissue fibrosis, or excessive fibrotic scarring.

Three Phases of Corneal Wound Healing

Classically, corneal wound healing is typically divided into three overlapping phases (**Figure 5**): (1) inflammatory phase – cytokine release and amplified expression, keratocyte apoptosis, and inflammation; (2) active wound-healing phase – epithelial cell migration, proliferation, and regeneration, keratocyte migration and proliferation, keratocyte metabolic activation and eventual quiescence, myofibroblast development, ECM synthesis and deposition (immature primitive scar formation with or without transition to early mature fibrotic scar formation); and (3) remodeling phase – decrease in cellular density, persistence or disappearance of myofibroblasts, persistence or disappearance of primitive scar, and collagen fibril re-organization/remodeling (mature fibrotic scar formation).

Inflammatory phase (lasts up to 2–4 weeks after injury)

As described earlier, after injury, damaged resident cells in the cornea release or adjacent surviving cells secrete a variety of cytokines and GFs into the wound. As the local concentration of these cytokines and GFs increases and these compounds are converted to their active form, one of the first morphologically observable changes in the corneal stroma following injury is a 50–75 μm zone of keratocyte apoptosis surrounding the actual direct injury site. This is followed by a subsequent transient influx of mixed acute and chronic inflammatory cells. Keratocyte apoptosis usually peaks at approximately 4 h after injury, but may still occur minimally up until approximately 1 week after the initial insult. After the initial peak of keratocyte apoptosis, an increased proportion of cells die

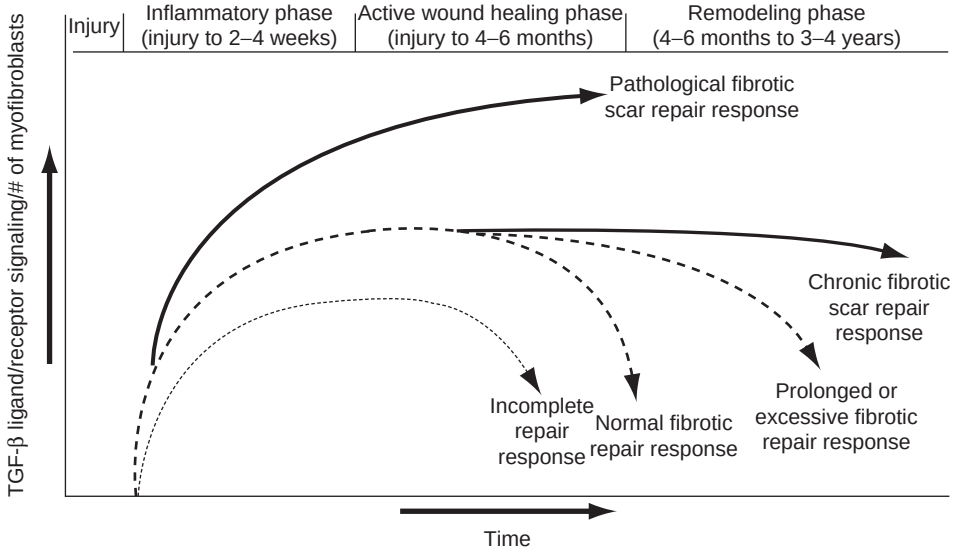

Figure 5 Representative line graph of a normal fibrotic repair response (dashed black line) in the cornea that results in tissue fibrosis (long-term fibrotic ECM, transient (<6 months) myofibroblast differentiation) at the end of the active wound-healing phase. If the transient myofibroblastic diffentiation extends into the remodeling phase, but eventually goes away, it still is considered a normal fibrotic repair response, albeit prolonged or excessive. If myofibroblastic differentiation is chronic (persistent or long-term), it is considered a fibrotic scar (solid black line). In comparison, representation plots for incomplete (dotted black line) or pathologic (thickest solid black line) fibrotic repair responses are shown. In normal corneal wound healing, myofibroblastic differentiation and ECM synthesis and deposition are both TGF-β dependent processes, which are appropriately terminated through negative regulatory mechanisms during the active wound-healing phase. However, prolonged or excessive TGF-β production occurs through four possible signaling pathways that may result in excessive tissue fibrosis, fibrotic scarring, or pathologic fibrosis. In comparison, incomplete TGF-β production results in primitive or provisional fibronectin matrix deposition long-term wound healing.

through necrosis. Within 8 h of injury, neutrophils are attracted to the wound site by chemokines and these inflammatory cells function by killing microbes and even host resident cells with their secretion of free radicals. Neutrophils serve no direct role in amplifying or suppressing the fibrotic repair response through its secreted cytokines or GFs, but may indirectly amplify it by damaging more resident tissue cells. Within 24 h of injury, monocytes are attracted to the wound site where they differentiate into macrophages, which serve to degrade and remove dead or damaged cells and ECM. Keratocytes and epithelial-derived proteases and collagenases help macrophages in this degradation and removal process. Macrophages also directly amplify the fibrotic repair response through secretion of pro-fibrotic TGF-β 1 and some PDGF, which can potentially result in a paracrine positive feedback loop, if intense enough. Finally, within 3 days of injury, lymphocytes enter the wound, where they secrete antifibrotic cytokines and GFs. Overall, this direct injury-mediated innate inflammatory response typically adds more pro-fibrotic cytokines and GFs to the original direct resident tissue injury-mediated cytokine and GF cascade. The innate inflammatory response amplifies the cascade of events already taking place, commonly resulting in additional keratocyte proliferation and migration, further keratocyte differentiation to one of the various fibrotic repair phenotypes including the myofibroblastic stage. Thus, inflammation has both positive and negative consequences of preventing infection and amplifying the fibrotic repair response, respectively.

Active wound-healing phase (lasts up to 4–6 months after injury)

Proliferation and migration of residual surviving keratocytes begins 12–24 h after injury to reconstitute the cellularity of the injured area and typically continues for only several days after injury. The migrating keratoctyes are spindle-shaped in appearance and highly motile. Subsequently, migratory keratocytes differentiate into a metabolically activated repair phenotype called an activated keratocyte. Within 1–2 weeks after injury, myofibroblasts first begin to appear in the stromal wound under the epithelium and then develop in the deeper stroma down to a depth of approximately 50–75 μm. Myofibroblasts are a fibrotic repair phenotype characterized by significant deposition of a disorganized collagenous ECM, significant hypercellularity, and extensive wound contraction. An important physical characteristic of myofibroblasts in the cornea is their reduced transparency relative to other cell types in the corneal stroma, which may be due to a loss of soluble cytoplasmic corneal crystallins in combination with assembly of insoluble actin stress fiber bundles.

Remodeling phase (occurs from 4–6 months to 3–4 years after injury)

During the remodeling phase, corneal cellularity in the repair tissue decreases closer to normal because of the disappearance or persistence of residual keratocytes or myofibroblasts. The stromal cells also revert back to a more normal nonfibrotic reparative phenotype as actin stress fibril bundles disappear and TGF-β receptor site density gets closer to baseline. The ECM reorganizes closer to normal as collagen fibrils become larger in diameter, more regular, more orderly in arrangement, richer in collagens type I molecules, less rich in type III molecules, and more cross-linked. In addition, any residual hyaluronic acid in the provisional ECM is replaced by more mature, sulfated PGs. The remodeling phase is the dominant process guiding the early mature scar to complete the maturation process. As such, this phase may be considered more or less a functional improvement phase. After remodeling, corneal scars gain increased tensile strength, have less haze and less wound contracture, and are more cosmetically pleasing with a reduction in size and improvement in structure.. During the remodeling phase, the collagen fibril turnover rate is still higher than normal, most likely due to ongoing MMP activity. Unfortunately, if only an immature provisional fibronectin ECM is present after completion of the active wound-healing phase, then the remodeling phase is incapable of making the transition from the immature provisional matrix to the mature collagenous ECM and a provisional fibronectin matrix remains permanently in the corneal stroma.

Termination of the fibrotic repair response (about 3–4 years after injury)

In humans, the long-term result of corneal wounding is the production of a hypercellular fibrotic scar (i.e., chronically hazy fibrotic scar) or a normocellular-to-hypercellular tissue fibrosis (i.e., transparent fibrotic tissue) in wound regions where epithelial– and endothelial–stromal interactions took place and a hypocellular primitive matrix (i.e., transparent immature provisional fibronectin ECM) in wound regions where keratocyte injury pathways took place in the absence of other supplemental healing responses (**Figure 4**). These three long-term histological tissue repair types have functional differences as the hypercellular fibrotic scar is strong (tensile strength approximately 40% of normal), but clinically hazy because of persistent myofibroblasts present in the repair tissue long-term. In contrast, the hypocellular primitive matrix is transparent, but it is very weak in tensile strength since it is composed of very little collagen fibrils (tensile strength approximately 2–3% of normal). Normocellular-to-hypercellular tissue fibrosis more or less is a hybrid of the two just described as it is macroscopically transparent and somewhat strong (tensile strength approximately 30% of normal). An additional variable to consider in this scheme

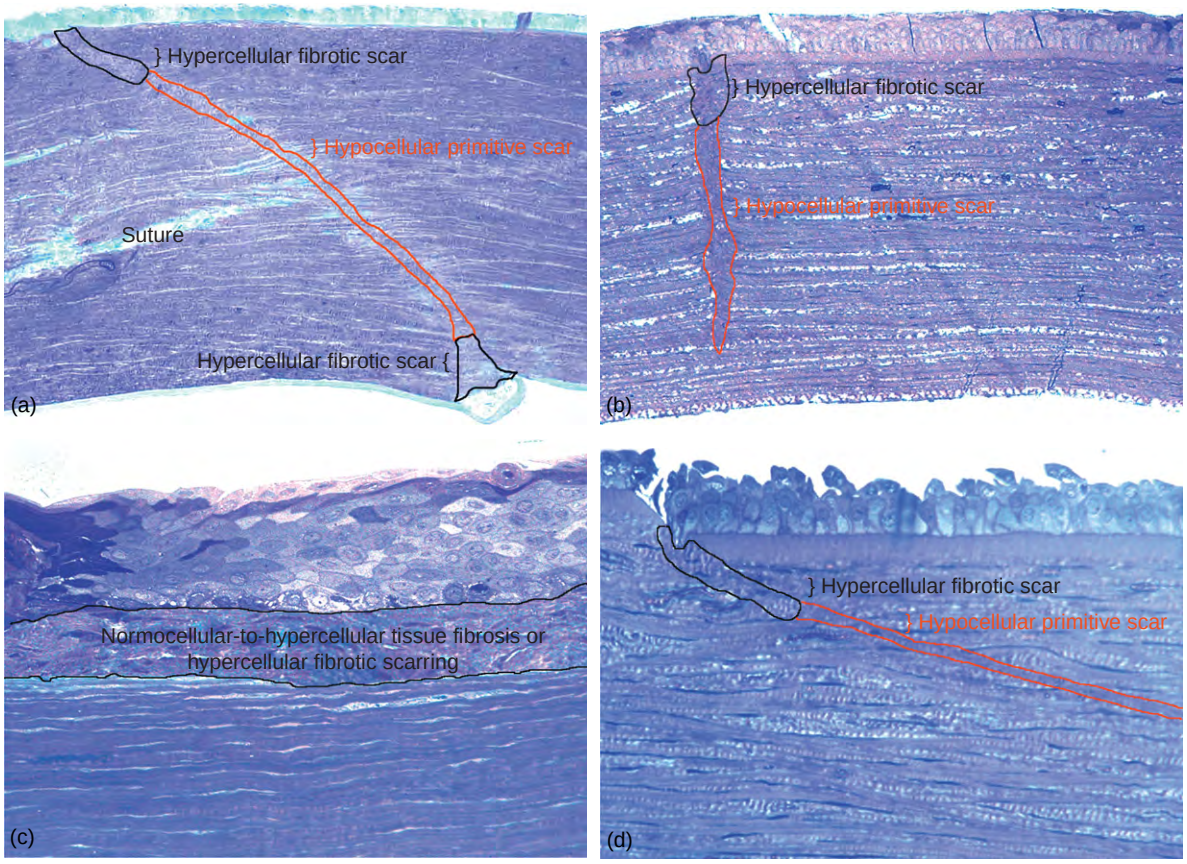

Figure 6 Long-term histologic findings of corneas that had undergone sutured, temporal, clear-corneal cataract extraction surgery (a), astigmatic keratotomy (b), photorefractive keratectomy (c), and laser-assisted *in situ* keratomileusis (d). All corneas shown are greater than 4 years after surgery and, technically, they have completed the remodeling phase and have terminated the fibrotic repair response (toluidine blue 15X for a, 25X for b, and 100X for c and d). Adapted from Dawson, D. G., Edelhauser, H. F., and Grossniklaus, H. E. (2005). Long-term histopathologic findings in human corneal wounds after refractive surgical procedures. *American Journal of Ophthalmology* 139: 168–178.

is the fact that more precisely realigned wounds, such as sutured and unsutured wounds with minimal gaping and no epithelial cell plugging, heal better than poorly aligned wounds, such as wounds with wide wound gaping; epithelial plugging; or incarceration of Bowman's layer, Descemet's membrane, or uvea (Figure 6).

Modulation of Scarring

Currently Available Scar-Reducing Therapies

Corneal fibrotic scars remain difficult to cure. Thus, the best approach is prevention. At present, there is no pharmacologic agent or surgical procedure that is universally effective in ameliorating fibrotic scarring. The best strategy currently entails a polytherapeutic empirical approach involving short-term (approximately 1–3 months in duration) topical corticosteroids, a single intraoperative local application of mitomycin C (MMC), and possibly several alternative or emerging options (Table 2). The

Table 2 Mechanism of action of scar-reducing agents

Agent	*Mechanism*
Corticosteroids	Inhibition of inflammatory response Possible inhibition of keratocyte proliferation and collagen synthesis
Chemotherapeutic agent (MMC)	Inhibition of keratocyte proliferation Promotes keratocyte and myofibroblastic apoptosis
Amniotic membrane	Suppression of epithelial-stromal interactions Potent anti-fibrotic, anti-inflammatory, and anti-angiogenic properties
Exogenous TGF-β3 supplementation	Partially shifts the fibrotic repair response over to the scar-free regenerative response
Anti-TGF-β1 and β2 agents	Decreased myofibroblast differentiation and collagen synthesis
Gene therapy	Gene transfer of TGF-β antagonists (e.g., fibromodulin) or blockers of TGF-β signaling (e.g., truncated TGF-β receptor II)

easiest way to understand the place that a drug is located in the range of possible treatment options is to consider the TGF-β signaling pathway or the wound-healing phase that the compounds act on.

Corticosteroids reduce scar formation primarily by suppressing the TGF-β-mediated inflammatory cell–stromal interactions and, secondarily, by possibly depressing steps in the active wound-healing phase, such as inhibition of fibroblast proliferation and diminished collagen synthesis. Regarding the fibroblasts, a previous study demonstrated that corticosteroids have a direct antiproliferative effect on ocular fibroblasts by altering the intracellular activity and expression of multiple genes that participate in fibrotic scar formation, including inhibition of TGF-β1, TGF-β2, and collagen expression. Thus, it should not be surprising that corticosteroids affect stromal wound healing to a greater degree than epithelial wound healing. Unfortunately, in randomized, placebo controlled, prospective clinical trials, corticosteroids produced no clinically significant long-term effects on either haze or refractive regression due to fibrotic scarring compared to placebo, but were definitely associated with a few unwanted side effects (high intraocular pressure and posterior subcapsular cataract formation). Thus, the role of steroids in the prevention of fibrotic scarring remains limited. Moreover, in view of their side-effect profile, steroids clearly would be unacceptable for long-term use in scar prevention and should be strictly used short-term (about 1–3 months from injury). Overall, corticosteroids will likely be used most effectively in future scar-reducing protocols as part of a polytherapeutic strategy since inflammation is just one of the four TGF-β signaling pathways involved in the avascular fibrotic repair response. When used, however, the timing of corticosteroid administration is crucial as the best results occur if used within hours of injury before neutrophils and profibrotic macrophages enter the wound. Once the injury-induced inflammatory response is initiated in the wound, it is somewhat self-amplifying, making it quite difficult to immediately suppress the response with corticosteroids.

The mechanism by which MMC prevents or reduces fibrotic scar formation has not been fully elucidated. It appears to work by inhibiting cell proliferation due to its potent alkylating chemotherapeutic effect by cross-linking DNA after metabolic activation by way of reduction. This effect is downstream from the initiating pro-fibrotic events in the four TGF-β-mediated signaling pathways of the cornea. Thus, MMC may affect all the four pathways, at least acutely while it remains in the tissue at therapeutic concentrations. MMC is potent because it affects cells in all phases of the cell cycle. In high concentration, MMC also is known to promote direct keratoctye and myofibroblast apoptosis in the inflammatory phase via free radical injury, which may be another mechanism by which it works. MMC combined with low-dose corticosteroids is the conventional treatment approach used today for corneal fibrotic scar prevention in high-risk cases. This combination is also used in the treatment of corneal fibrotic scars after additional maneuvers are performed to remove as much of the scar tissue as possible by surgical debridement (e.g., phototherapeutic keratectomy (PTK) before direct MMC local application).

An alternative or supplementary scar-reducing treatment is that of using fresh or cryopreserved amniotic membrane (AM) allografts to cover treated areas of exposed injured corneal stroma to prevent fibrotic scarring. Human fetal AM is composed of three layers: a cuboidal to columnar epithelial monolayer, a 200–300-nm thick BM, and an avascular stroma. This membrane suppresses the inflammatory and active wound-healing phases of the fibrotic repair response. Intact AM–BM suppresses epithelial–stromal interactions since the stroma has intrinsic antifibrotic, anti-inflammatory, and antiangiogenic properties, presumably due to cytokine and GF binding to sulfated PGs in the AM stroma. AM also aids in re-epithelization due to its epithelial surface and its BM, which contains cell adhesion molecules, such as fibronectin. The primary disadvantages of AM are its expensive cost and increased surgical time. Thus, AM is used more often for severe corneal and/or limbal stem cell disease rather than repair of simple corneal wounds.

Newer advanced surface ablation techniques, such as laser subepithelial keratectomy (LASEK) or epikeratome laser-assisted *in situ* keratomileusis (EpiLASIK), modify the PRK surgical technique using natural means to suppress direct epithelial–stromal interactions. For example, in LASEK surgery, the replaced epithelial flap retains as much intact epithelial BM as possible, which serves to bind and store direct injury-induced epithelial-derived TGF-β. Thus, LASEK ingeniously takes advantage of natural antifibrotic cytokine and GF–ECM interactions to reduce the degree of fibrosis. EpiLASIK goes one step further in that the epithelial flap retains much healthier, living corneal epithelium as well as an intact epithelial BM. Thus, EpiLASIK additionally blunts pro-fibrotic tear film–stromal interactions by natural means since a healthy, viable superficial squamous epithelial layer containing zonula occludens tight junctions serves as a physical barrier to direct stromal exposure to cytokines and GFs factors in the tear film.

Emerging Scar-Reducing Therapies

Extensive research has been performed to elucidate the fibrotic repair response, particularly in the skin, with the long-term goal of iatrogenically manipulating this response toward obtaining a clinical advantage. Recent molecular therapeutic investigations have concentrated on inhibiting myofibroblast differentiation by targeting TGF-β. A promising strategy currently being evaluated

in phase-I and-II clinical trials in the skin entails manipulating the ratio of the three TGF-β isoforms in the wound in favor of TGF-β3. Three independent, randomized, placebo controlled, prospective clinical trials have shown that exogenous TGF-β3 supplementary treatment resulted in clinically significant scar prevention or reduction with primary and multiple secondary endpoints in the skin. Inhibition of TGF-β1 and β2 binding to their associated receptors with topical anti-TGF-β antibodies has also been shown to reduce myofibroblastic differentiation, ECM deposition, and cell haze induced by PRK in animal models. By subtly altering the ratio of cytokines or GFs present in the wound during corneal wound healing, it is ultimately hoped that one day postnatal wounds could be induced to heal like embryonic wounds through tissue regeneration. An important caveat to these molecular therapies is that the timing of the application of these agents is critical, usually with the best results occurring if used immediately after injury or, at the very least, within 48 h of injury.

There have been a few published studies, limited to animal models, using gene therapy for scar reduction. To date, fibroblasts have been used as the primary targets. Further investigation into the role of gene therapy for scar reduction is still needed since the practical use of such an approach is not presently feasible.

Other possible emerging fibrotic scar-reducing therapies include systemically administered minocycline antibiotics, which significantly reduce the severity of hypertrophic scarring in a rabbit ear scar model. The mechanism by which minocycline reduces scar formation in this model remains unanswered, but the most plausible mechanism involves inhibition of MMPs resulting in the inhibition of fibroblast migration. Anti-intracellular Smad signaling pathway agents are another promising possibility.

Conclusion

Significant advances have been made in understanding the mechanisms controlling the adult fibrotic wound-repair response in comparison to the embryonic scar-free regenerative response. Discovery of four TGF-β signaling pathways and the central role of myofibroblasts in corneal wound healing have been crucial to this end. Currently, the most effective corneal scar-reducing therapies involve a rather crude polytherapeutic empirical strategy of management involving short-term topical steroids and single intraoperative MMC application. Hopefully, in the near future, the recent advances in understanding the molecular and cell biology of fibrotic wound repair can translate into the development and clinical use of more promising agents, such as molecular, gene, or stem cell therapies. The capability to successfully manipulate the fibrotic repair process in the cornea *in vivo* offers many tantalizing prospects from preventing blindness from corneal scarring to obtaining 20/8 perfect vision with optimal corneal wound healing after keratorefractive surgery to perfect tissue regeneration due to converting the adult fibrotic repair response back to an embryonic scar-free regenerative response to the possibility of restoring vision through tissue engineering of a human healthy cornea for replacement purposes.

Acknowledgments

This work was supported in part by NIH Grants P30 EY06360 (Departmental Core Grant), T32EY07092 (DGD), R01EY00933 (HFE), and Research to Prevent Blindness, Inc., New York, New York.

See also: Corneal Endothelium: Overview; Corneal Epithelium: Wound Healing Junctions, Attachment to Stroma Receptors, Matrix Metalloproteinases, Intracellular Communications; The Corneal Stroma; Cornea Overview; Refractive Surgery and Inlays; Regulation of Corneal Endothelial Cell Proliferation; Regulation of Corneal Endothelial Function; The Surgical Treatment for Corneal Epithelial Stem Cell Deficiency, Corneal Epithelial Defect, and Peripheral Corneal Ulcer.

Further Reading

Dahlmann, A. H., Mireskandari, K., Cambrey, A. D., et al. (2005). Current and future prospects for the prevention of ocular fibrosis. *Ophthalmology Clinics of North America* 539–559.

Ferguson, M. W. J. and O'Kane, S. (2004). Scar-free healing: From embryonic mechanisms to adult therapeutic intervention. *Philosophical Transactions of the Royal Society B: Biological Sciences* 359: 839–850.

Fini, M. E., Stramer, B. M., Fini, M. E., and Stramer, B. M. (2005). How the cornea heals: Cornea-specific repair mechanisms affecting surgical outcomes. *Cornea* 24(8 supplement): S2–S11.

Gabison, E. E., Huet, E., Baudouin, C., and Mensashi, S. (2009). Direct epithelial–stromal interaction in corneal wound healing: Role of EMMPRIN/CD147 in MMPs induction and beyond. *Progress in Retinal Eye Research* 28(1): 19–33.

Klenkler, B., Sheardown, H., Jones, L., et al. (2007). Growth factors in the tear film: Role in tissue maintenance, wound healing, and ocular pathology. *Ocular Surface* 5(3): 228–239.

Klenkler, B., Sheardown, H., Klenkler, B., and Sheardown, H. (2004). Growth factors in the anterior segment: Role in tissue maintenance, wound healing and ocular pathology. *Experimental Eye Research* 79(5): 677–688.

LaGier, A. J., Yoo, S. H., Alfonso, E. C., et al. (2007). Inhibition of human corneal epithelial production of fibrotic mediator TGF-beta2 by basement membrane-like extracellular matrix. *Investigative Ophthalmology and Visual Science* 48(3): 1061–1071.

Netto, M. V., Mohan, R. R., Ambrosio, R., Jr, et al. (2005). Wound healing in the cornea: A review of refractive surgery complications and new prospects for therapy. *Cornea* 24(5): 509–522.

Obata, H., Tsuru, T., Obata, H., and Tsuru, T. (2007). Corneal wound healing from the perspective of keratoplasty specimens with special

reference to the function of the Bowman layer and Descemet membrane. *Cornea* 26(9 supplement 1): S82–S89.
Peled, Z., Liu, W., Levinson, H., et al. (2000). Cellular strain upregulated profibrotic growth factors and collagen gene expression. *Surgical Forum* 51: 591–593.
Saika, S., Yamanaka, O., Sumioka, T., et al. (2008). Fibrotic disorders in the eye: Targets of gene therapy. *Progress in Retinal and Eye Research* 27: 177–196.
Stramer, B. M., Mori, R., and Martin, P. (2007). The inflammation–fibrosis link? A Jekyll and Hyde role for blood cells during wound repair. *Journal of Investigative Dermatology* 127: 1009–1017.
Stramer, B. M., Zieske, J. D., Jung, J. C., et al. (2003). Molecular mechanisms controlling the fibrotic repair phenotype in cornea: Implications for surgical outcomes. *Investigative Ophthalmology and Visual Science* 44(10): 4237–4246.
Wilson, S. E., Liu, J. J., and Mohan, R. R. (1999). Stromal–epithelial interactions in the cornea. *Progress in Retinal and Eye Research* 18(3): 293–309.

Cortical Cataract

R Michael, Institut Universitari Barraquer, Barcelona, Spain

Glossary

Lens cortex – The part of the crystalline lens surrounding the nucleus and bound anteriorly by the epithelium and posteriorly by the capsule.
Lens equator – The border of the crystalline lens where the anterior and posterior parts meet. The zonular fibers, which hold the crystalline lens in place, are connected at the lens equator; also, the part of the lens farthest from the optical axis.
Lens nucleus – The core of the crystalline lens, surrounded by the cortex.
Refractive index – The ratio of the speed of light in a vacuum to the speed of light in a given material. According to Snell's law, the refractive index is also the ratio of the sine of the angle of incidence to the sine of the angle of refraction. The refractive index indicates the extent to which a light beam is deflected when passing from a vacuum into a given material.

Definition

Cataract is the clinical term for reduced visual function resulting from optical disturbances in the crystalline lens. These optical disturbances absorb and scatter light. Reduced lens transparency and scattered light induces straylight on the retina. The word itself is of Greek origin and means cascading water or waterfall. Its use in ophthalmology probably alludes to the white appearance of running water or the blurred view from behind a waterfall. Cataracts differ greatly in density, color, shape, size, and location inside the crystalline lens. Cortical cataract defines a cataract located in the lens cortex or periphery. The other two main subdivisions by location are nuclear cataract and posterior subcapsular cataract.

Morphology

The first changes to arise in the transparent lens cortex are small, spot- or star-like opacities measuring several micrometers in diameter (**Figures 1(a)** and **1(e)**). On the cellular level, they probably correspond to membrane-bound bodies or multilamellar bodies (**Figure 2(d)**) frequently found in the lens cortex inside or between otherwise normal lens fiber cells. More advanced changes include radial and circular shades (**Figures 1(b)** and **(f)**). These are located in the equatorial and pre-equatorial regions of the lens, close to the border between the lens cortex and lens nucleus (**Figure 1 (j)**). Radial and circular shades are often in close proximity (**Figure 1(f)**). Radial shades are usually diffuse and extend between the layers of lens fiber cells of the lens equator in a half circle in the anterior and posterior direction (**Figure 1(j)**). Radial shades consist of restricted parts of a small group of fibers in the deep cortex. The affected lens fiber cells are filled with medium-to-large globular elements (**Figure 2(e)**). The circular shades are well delineated and line-like (**Figure 2(c)**). They originate as fractures of a large group of fibers in the deep equatorial cortex, perpendicular to the course of the fibers. The fractured surfaces are slightly swollen, but the membranes on both sides of the fracture have normal ultrastructure (**Figure 2(f)**).

The most prominent cortical opacities are peripheral band-like and spoke-like opacities, which share a basic morphology despite wide variations in shape and severity (**Figures 1(c), 1(d), 1(g), 1(h), 1(k),** and **1(l)**). They have been referred to in the literature as wedge-shaped fiber opacities, spoke-shaped opacities, cuneiform opacities, water clefts, and supranuclear opacities. The development of these opacities probably starts in the anterior and posterior pre-equatorial zones. The first signs might be small numbers of opaque fiber bundles (**Figure 1(k)**), which develop into larger opaque areas and extend toward the lens pole and lens equator, finally progressing to thicker and denser opacities (**Figure 1(l)**) covering the entire equatorial and pre-equatorial zones and sometimes extending into the pupillary area. There is significant variability in the anterior and posterior extensions of the opacities (**Figures 1(c), 1(d), 1(k),** and **1(l)**). Scanning electron microscopy revealed small and large groups of cortical fibers with broken ends in the pre-equatorial zone at a depth corresponding to the cortical/nuclear interface (**Figures 3(e)** and **3(f)**). The portions of these fibers posterior and/or anterior to the breaks appeared folded and undulated, while both the deeper nuclear and more superficial neighboring cortical fibers exhibited normal structure and architecture. The sealed ends of the broken fibers might explain why these fibers remain arranged regularly and mutually connected despite their breaks; the sealed ends might also explain the lack of involvement of neighboring fibers. This is consistent with, and may in part explain, the generally slow progression of cortical opacities. Fluorescence microscopy (**Figures 3(h)** and **3(j)**)

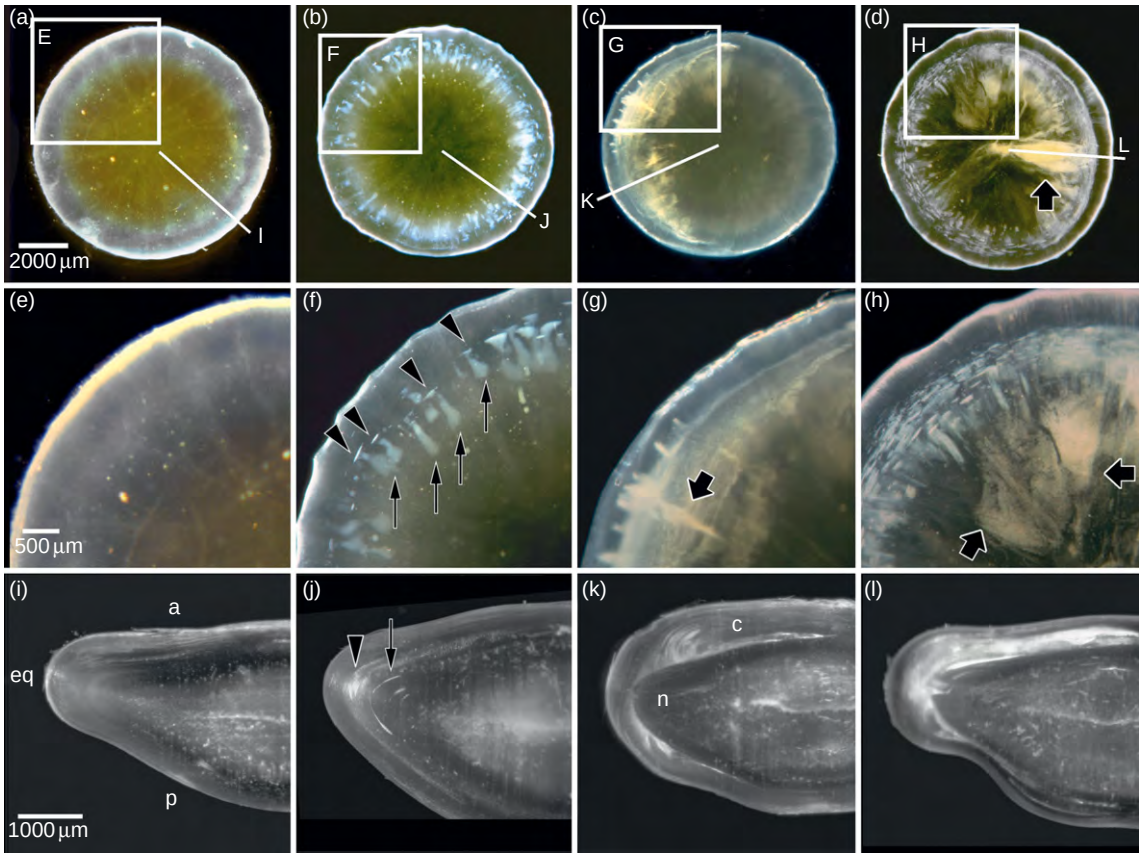

Figure 1 Panel of dark-field micrographs of aged human donor lenses (a–d). The boxed areas are magnified below (e–h). Except for nuclear coloration, a transparent lens with small, spot- or star-like opacities (a, e), a lens with radial shades (arrows) and circular shades (arrow heads) (b, f), a lens with peripheral, band-like and spoke-like opacities (bold arrows) (c, g), and a lens with mixed types of cortical opacities (d, h). Below are dark-field micrographs of slices cut in the axial plane of the fixed donor lenses (i–l); the lens equator (eq) and the anterior (a) and posterior (p) poles are indicated (l). The cutting plane is indicated by a white line in (a)–(d). In addition to some irregular scattering due to imperfect slicing, the central nuclear parts of the slices are free of opacification. The opacities extend in the anterior (a) and posterior (p) directions (j–l. Except for the spokes (bold arrows) (c, g), the opacities are outside the pupillary space and will not have seriously influenced vision (without regard to nuclear opacity). Adapted from Michael, R., Barraquer, R. I., Willekens, B., van Marle, J., and Vrensen, G. F. (2008). Morphology of age-related cuneiform cortical cataracts: The case for mechanical stress. *Vision Research* 48(4): 626–634, with permission from Elsevier.

supports the results of scanning electron microscopy studies demonstrating broken, folding, and undulating fibers in this border region as well as the presence, between the aberrant fibers, of small and large spaces that appear filled with fluid. This is in line with the clinical description of water clefts associated with cortical opacities.

Optical Effects

The transparency of the crystalline lens depends on the regular organization of its cells and proteins. This regularity must be maintained on the molecular level of the proteins, on the protein concentration level inside the lens fiber cells, and on the tissue level between the lens fiber cells.

At the molecular level, the short-range, liquid- or glass-like order of the protein molecules is required for lens transparency. At this level, the dimensions are shorter than the wavelength of light because the size of the protein molecules is less than 10 nm. Higher protein concentration in the cells indicates denser packing of the protein molecules, resulting in higher short-range order and less light scattering.

At the cellular level, local variations in the refractive index are the principal physical cause of light scattering. Here, the dimensions are greater than the wavelength of light. The average refractive index of living cells depends mostly on protein concentration. A typical mammalian cell has an average protein content of 18%, corresponding to a refractive index of about 1.37. The protein concentration in the center of the human lens is about 32%, with a refractive index of about 1.41. The main components of cell membranes are phospholipids, cholesterol, and membrane-spanning proteins and usually have a much higher refractive index than the proteins in the cytoplasm. The refractive index of membranes is about 1.48. When variations in

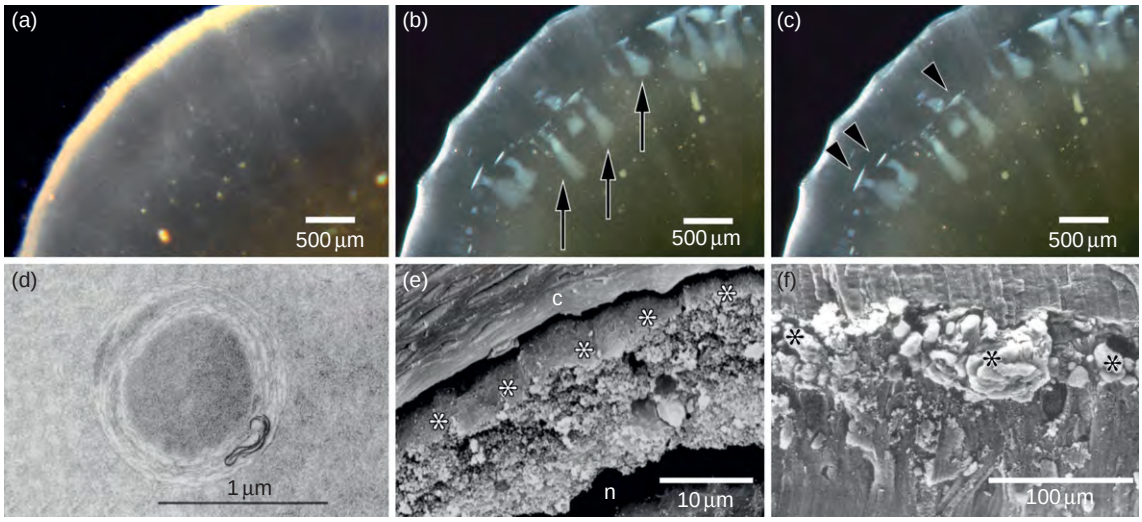

Figure 2 Dark-field micrographs of aged human donor lenses, illustrating small, spot- or star-like opacities (a) and radial (b) and circular shades (c). Multilamellar body, as frequently found in human lenses with early cortical opacities (d). Scanning electron microscopy cross section of a fractured radial shade (e); disturbed lens material is formed by lens fibers with aberrant membranes (asterisks) and are filled with globular material. Scanning electron microscopy of a circular shade (f) showing swelling of the broken parts (asterisk) and the disturbance of the lens fiber cells. (a–c, e) Adapted from Michael, R., Barraquer, R. I., Willekens, B., van Marle, J., and Vrensen, G. F. (2008). Morphology of age-related cuneiform cortical cataracts: The case for mechanical stress. *Vision Research* 48(4): 626–634. (f) Reprinted from Vrensen, G. and Willekens, B. (1990). Biomicroscopy and scanning electron microscopy of early opacities in the aging human lens. *Investigative Ophthalmology and Visual Science* 31(8): 1582–1591, with permission from Investigative Ophthalmology and Visual Science. (d) Reprinted from Vrensen, G., Kappelhof, J., and Willekens, B. (1990). Morphology of the aging human lens. II. Ultrastructure of clear lenses. *Lens and Eye Toxicity Research* 7(1): 1–30, with permission from Marcel Dekker.

the refractive index are random, light will scatter in all directions. However, if there is a high degree of orderliness, destructive interference of locally scattered light will occur, and this will result in less total light scattering.

Membrane-bound bodies disturb the regular refractive index distribution of the protein-filled lens fiber cells and therefore scatter light; they are visible as small, spot- or star-like opacities (**Figures 2(a)** and **2(d)**). The globular material found at the location of the radial and circular shades (**Figures 2(e)** and **2(f)**) probably reflects variations in the protein concentration. This, along with the abnormal membranes at this location, induces light scattering (**Figures 2(b)** and **2(c)**). In the lens cortex, high spatial order in the lens fiber lattice (**Figures 3(d)** and **3(g)**) is required to compensate for light scattering caused by fluctuations in the refractive index between membranes and cytoplasm. This results in a relatively transparent lens cortex (**Figure 3(a)**). When this spatial order is disturbed (**Figures 3(e), 3(f), 3(h),** and **3(j)**), light is scattered, and the peripheral band- and spoke-like opacities become visible (**Figures 3(b)** and **3(c)**).

Impact on Vision

The location of the opacities and pupil size determine whether opacities affect vision. In daylight, the pupil diameter is small, about 3 mm. Small, spot- or star-like opacities and radial and circular shades, which are usually located outside this central area, do not affect vision (**Figures 1(a)** and **1(b)**). The same holds for peripheral band-like opacities (**Figure 1(c)**). Some spoke-like opacities (**Figure 1(d)**), however, extend into the pupillary area and will affect vision. At night, the pupil diameter increases to about 5–8 mm. Under these conditions, some radial and circular shades and peripheral, band-like opacities affect vision.

Optical disturbances reduce lens transparency and scatter light. This directly reduces visual acuity and contrast sensitivity because less light reaches the retina. Furthermore, the scattered light induces straylight on the retina, resulting in visual glare and halo effects around bright light sources at night when the pupil diameter is wide. Glare further reduces contrast in a visual scene.

Some cortical cataracts can induce changes in astigmatism. This probably results from localized refractive index changes along spoke-like opacities within the pupillary area.

Prevalence

Clinical observations have shown that the normal aging of the human lens, in the absence of disease, is accompanied by an increase in the overall light scattering of the lens. Up to age 40, light scattering remains rather

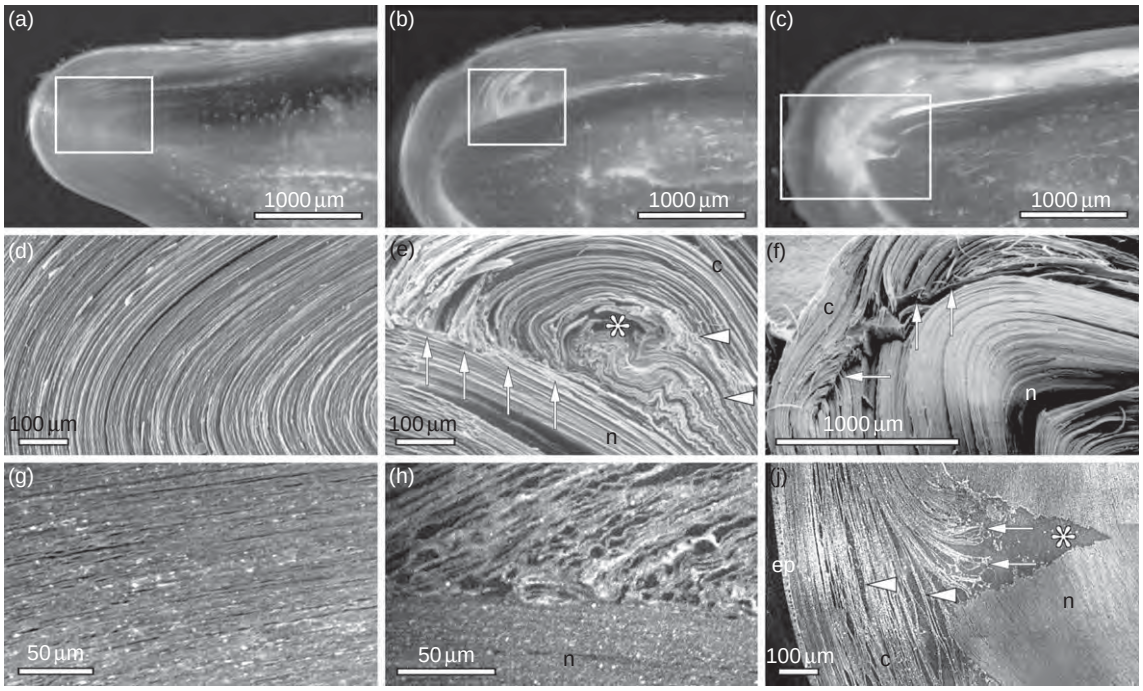

Figure 3 Fiber organization in a lens without cortical cataract (a) and in two cases of cortical opacities (boxed areas in (b) and (c)), as visualized by scanning electron microscopy (d, f) and fluorescence histology (g, h, and j). (e) Shows that fibers at the border zone between the nuclear and cortical lens regions are broken (arrows) and that the broken ends are directed against the nuclear fibers, which maintain regular, uninterrupted organization. Further, note the curled (asterisk) and folded (arrowheads) fibers in the region adjoining the broken fibers. Fluorescence histology of this type of opacification (h) shows the oblique orientation of the broken fibers on the regularly organized nuclear fibers. The dark regions in the fluorescence micrograph indicate the presence of spaces likely filled with fluid. The scanning electron microscopy micrograph of (f) shows broken fibers at several places (arrows) in the border zone between the cortex and nucleus. The nuclear fibers are regularly organized, as are the more superficial cortical fibers bridging the break zone. The fluorescence micrograph (j) shows the nuclear fibers and the most superficial fibers, which are regularly organized. The fibers between these layers are partly separated by water lakes (arrowheads). Some are broken (arrows), and there is a large triangular region (asterisk) (cf. (f)) free of fibers, most likely filled with fluid. ep, epithelium; n, nuclear side; c, cortical side. Reprinted from Michael, R., Barraquer, R. I., Willekens, B., van Marle, J., and Vrensen, G. F. (2008). Morphology of age-related cuneiform cortical cataracts: The case for mechanical stress. *Vision Research* 48(4): 626–634, with permission from Elsevier.

constant, thereafter increasing exponentially with age. Epidemiological studies have shown that, in developed countries, cortical cataract is by far the most prevalent age-related cataract, more common than nuclear cataract. However, since cortical cataracts may affect vision less often than nuclear cataracts, they may less often lead to cataract surgery.

The prevalence of radial and circular shades is age related, radial shades occurring earlier than circular shades. These are quite common, with a prevalence of approximately 20% at age 45 and about 75% above age 75. Peripheral band- and spoke-like opacities, which occupy more than 5% of the lens area, have a prevalence of about 5% at age 45, increasing to 30–50% after age 75.

Cortical cataracts can be restricted to either a sector or a quadrant (**Figure 1(c)**) or found around the entire circumference of the lens (**Figure 1(d)**); their extent is not directly related to age. Segmental cortical cataract is more prevalent in the lower nasal quadrant of the lens.

Causes

Unaltered transparency of the crystalline lens requires proper protein synthesis and the maintenance of equilibrium between water content, molecular compounds, and other constituents of the lens. Chemical agents and factors that disturb the equilibrium induce cataract. Such factors include metabolic disorders, certain drugs, different types of radiation, ocular inflammation, and physical injury. Age also plays an important role in cataract formation, as do nutrition, genetic factors, and race. Therefore, cataract is seen as an age-related, multifactorial disease.

Alterations and damage to the crystalline lens accumulates throughout life because there is no cell shedding. Lens cells developed before and after birth must remain transparent until old age. Any damage to these cells over the years will accumulate. Free radicals may play an important role in the damage process.

Exposure to ultraviolet radiation (UVR) is a major risk factor for cortical cataract. Several epidemiological studies

have demonstrated this by correlating the individual UVR dose from solar exposure with the incidence of cortical cataract. UVR-B (wavelengths between 280 and 315 nm) particularly correlates with cortical cataract formation. Shorter UVR wavelengths are completely absorbed by the cornea and do not reach the lens, while longer wavelengths are transmitted by the lens and therefore are less damaging. The common finding that cortical cataract appears more frequently in the lower nasal quadrant of the lens may indicate a role for sunlight in its etiology. The eye's exposure to the sun usually takes place from above and from the lateral side because the nose has a shadowing effect. Hence, solar radiation from above is focused on the lower quadrants of the lens, while radiation from the lateral side is focused on the nasal quadrants. There are a few reported cases in which people who received significant UVR doses from artificial sources subsequently developed cortical cataract that could be correlated with that exposure.

A relationship also seems to exist between cortical cataract and mechanical stress on the lens. During accommodation, the lens changes its shape by deforming its nucleus. With the onset of presbyopia, the elasticity of the nucleus decreases, and the lens no longer changes shape, although the ciliary muscle continues pulling on the lens, by way of the zonular fibers. This induces mechanical stress at the cortex–nucleus border zone, which might induce cortical cataract. The lens area under mechanical stress might become more vulnerable to environmental factors, such as ocular UVR exposure and nutrition.

Epidemiological studies suggest that some metabolic diseases, such as diabetes, vascular disease, hormonal factors in women, and corticosteroid intake, can induce cortical cataract. These studies have also shown that vitamin and antioxidant intake can delay nuclear cataracts, but the effect is not significant for cortical cataracts. Only the intake of polyunsaturated fats was associated with reduced prevalence of cortical cataract.

There might be racial factors for the development of cortical cataract, but they are often confounded by environmental factors, so there is no conclusive epidemiological data. Twin studies estimated the heritability of cortical cataract at about 50%, while the influence of individual environment is 35%, and age 15%.

See also: Accommodation; Contrast Sensitivity; Nuclear Cataract; Posterior Subcapsular and Anterior Polar Cataract; Presbyopia; Pupil.

Further Reading

Brown, N. P. P. and Bron, A. J. (1996). *Lens Disorders a Clinical Manual of Cataract Diagnosis*. Oxford: Butterworth-Heinemann.

Maisel, H. (ed.) (1985). *The Ocular Lens, Structure, Function and Pathology.* New York: Marcel Dekker.

Michael, R., Barraquer, R. I., Willekens, B., van Marle, J., and Vrensen, G. F. (2008). Morphology of age-related cuneiform cortical cataracts: The case for mechanical stress. *Vision Research* 48(4): 626–634.

Michael, R., van Marle, J., Vrensen, G. F., and van den Berg, T. J. (2003). Changes in the refractive index of lens fibre membranes during maturation – impact on lens transparency. *Experimental Eye Research* 77(1): 93–99.

Michael, R., Vrensen, G. F., van Marle, J., Löfgren, S., and Söderberg, P. G. (2000). Repair in the rat lens after threshold ultraviolet radiation injury. *Investigative Ophthalmology and Visual Science* 41(1): 204–212.

Oyster, C. W. (1999). *The Human Eye: Structure and Function*. Sunderland: Sinauer.

Vrensen, G. and Willekens, B. (1990). Biomicroscopy and scanning electron microscopy of early opacities in the aging human lens. *Investigative Ophthalmology and Visual Science* 31(8): 1582–1591.

Vrensen, G., Kappelhof, J., and Willekens, B. (1990). Morphology of the aging human lens. II. Ultrastructure of clear lenses. *Lens and Eye Toxicity Research* 7(1): 1–30.

Cranial Nerves and Autonomic Innervation in the Orbit

B C Anderson and L K McLoon, University of Minnesota, Minneapolis, MN, USA

Glossary

Abducens nerve – A general motor efferent which provides motor innervation to the lateral rectus muscle in the orbit. This nerve is often referred to as cranial nerve VI (CNVI).

Autonomic nervous system – This consists of motor nerve fibers that provide involuntary control of viscera, including smooth muscle, specialized conducting cells of heart muscle, as well as secretion in glandular cells. It consists of two divisions, a parasympathetic division and a sympathetic division.

Ciliary ganglion – A collection of neuronal cell bodies that give rise to the postganglionic parasympathetic nerve fibers that will innervate the ciliary and sphincter muscles of the eye. These are important for accommodation for near vision and for pupil closure in response to bright light.

Oculomotor nerve – A general motor efferent which provides motor innervation to the levator palpebrae superioris, superior rectus, medial rectus, inferior rectus, and inferior oblique muscles within the orbit. Additionally, it carries the preganglionic visceral efferents from the accessory oculomotor nucleus toward the ciliary ganglion. This nerve is often referred to as cranial nerve III (CNIII).

Parasympathetic nervous system – This consists of visceral motor nerves whose cells bodies of origin are located in craniosacral regions of the central nervous system. Four cranial nerves have parasympathetic components: oculomotor (CNIII), facial (CNVII), glossopharyngeal (CNIX), and vagus (CNX). Sacral levels S2–S4 also contain neurons that form nerve fibers which bring parasympathetic innervation to pelvic viscera.

Sympathetic nervous system – This consists of visceral motor nerves whose cell bodies of origin are located in the thoracic and upper lumbar regions of the spinal cord. The preganglionic nerve fibers exit in the spinal nerve, form white rami communicans which project into the sympathetic chain on each side of the vertebral column. The sympathetic chain runs the full length of the vertebral column, from the cervical to the sacral region. Within the sympathetic chain are sympathetic chain ganglia where the preganglionic nerve fibers synapse with postganglionic neurons. The postganglionic nerve fibers exit the sympathetic chain using gray rami communicans. These sympathetic nerve fibers join nearby nerves and blood vessels, which in turn carry them to all parts of the body.

Trigeminal nerve – This has three very large sensory roots and a small motor root. The sensory roots provide general somatic afferents to the face and the scalp anterior to the mid-auricular line and to a variety of structures within the head. This nerve is often referred to as cranial nerve V (CNV). There are three divisions of the trigeminal nerve: (1) the ophthalmic division, or V1, is sensory only and is the main sensory nerve of the orbit and the skin of the upper eyelid, forehead, and anterior half of the scalp; (2) the maxillary division, or V2, also is sensory only and provides sensory innervation to areas of the nasopharynx, parts of the nasal and oral cavities, as well as skin of the face lateral and inferior to the orbit; and (3) the mandibular division, or V3, has a sensory and a motor root. The mandibular division provides sensory innervation to parts of the oral cavity as well as to specific areas of the facial skin, including the mandibular region. The motor root innervates the muscles of mastication, as well as several other small muscles of the head.

Trochlear nerve – A general motor efferent which provides motor innervation to the superior oblique muscle in the orbit. This nerve is often referred to as cranial nerve IV (CNIV).

Weighted magnetic resonance imaging (MRI) – The signals from tissues of different densities create a difference in contrast and relaxation times (e.g., T1 and T2) and thus in the strength of the nuclear magnetic resonance signal that is produced in an MRI scanner. In a T_1-weighted MRI, the white matter appears white, the gray matter, containing the neurons, appears gray, and the cerebrospinal fluid appears dark. In a T_2-weighted image, the contrasts are reversed.

Complex Innervation Patterns Are Present in the Orbit

The paths of nerves found within the orbit are extremely complex, particularly when one considers the relatively small volume of each orbit. Knowledge of these patterns

of innervation is important for understanding both normal function, as well as impaired function when there is injury or disease affecting the nerve pathways. In addition, understanding the pattern of innervation can minimize injury during intraorbital surgical and/or injection procedures.

The orbit contains portions of five cranial nerves: the optic nerve or cranial nerve II, the oculomotor nerve or cranial nerve III, the trochlear nerve or cranial nerve IV, the ophthalmic division (VI) and the maxillary division (V2) which are both branches of the trigeminal nerve or cranial nerve V, and the abducens nerve or cranial nerve VI. In addition, the orbit receives autonomic nervous system innervation, and thus contains nerves that carry parasympathetic and sympathetic innervation to a number of structures. Each of these nerve pathways is described individually.

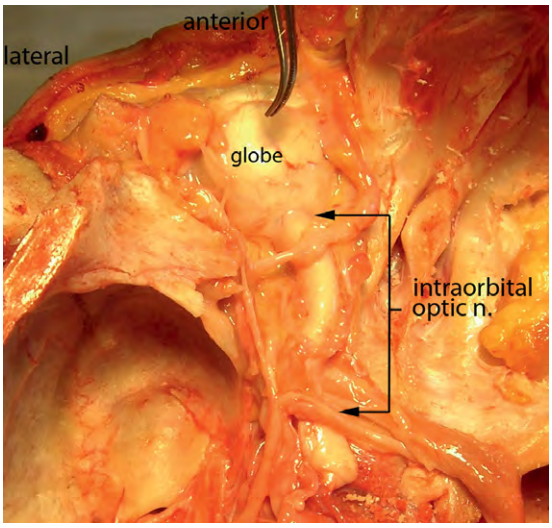

Figure 1 Superior view of the orbital contents in a human cadaver. The frontal bone that forms the orbital roof has been removed, as have the overlying levator palpebrae superioris and superior rectus muscles. The forceps tips are pointing to the globe, and the full extent of the optic nerve can be seen (indicated by the bracket between the two arrows). Note the S shape of the optic nerve, caused by the fact that the optic nerve is longer than the anterior to posterior length of the bony orbit.

Sensory Nerves

The Optic Nerve or Cranial Nerve II

The optic nerve is a special sensory nerve that carries information from the visual world to the brain. Embryologically, the optic nerve is derived from an outgrowth of the forebrain; therefore, it is part of the central nervous system (CNS) and is composed of CNS fiber tracts. It is surrounded by all the meningeal layers of the brain and has a subarachnoid space that contains cerebrospinal fluid. There are four parts to the optic nerve: intraocular or optic nerve head, intraorbital, interosseus, and intracranial. The optic nerve is formed as axons of the retinal ganglion cells exit the retina through the optic disc. This intraocular portion is approximately 1 mm in length and consists of unmyelinated ganglion cell axons. The intraorbital portion of the optic nerve contains mainly myelinated optic axons. The length of the optic nerve is greater than the distance from the optic nerve head to its entry into the optic foramen. The intraorbital portion of the nerve is approximately 30 mm long, while the distance from the posterior globe to the optic foramen is only 20 mm long (Figure 1). This generally gives the optic nerve an S shape within the orbit, and it is hypothesized that this extra length allows free movement of the globe without injuring the optic nerve. The optic nerve leaves the bony orbit via the optic foramen located within the lesser wing of the sphenoid bone. It travels through the optic canal and enters the intracranial space before joining with the contralateral optic nerve to form the optic chiasm.

Trigeminal Nerve or Cranial Nerve V

The trigeminal nerve is responsible for carrying general sensory information from the entire face, including the orbit and eyelids, to the brain. The cell bodies of origin of the sensory components of this large nerve are found in the trigeminal ganglion located in a cavity within layers of dura near the apex of the petrous portion of the temporal bone (Figure 2). Medial to the ganglion is the posterior cavernous sinus and the internal carotid artery. The human trigeminal ganglion contains approximately 27 000 sensory neurons. The central projections carry general sensory information to the sensory trigeminal nerve nuclei, which extend the whole length of the midbrain and medulla. There are three distinct nuclei from rostral to caudal: the mesencephalic nucleus involved in proprioception, the chief sensory nucleus involved in two-point touch discrimination, and the spinal trigeminal nucleus which mainly receives touch, pain, and temperature information. Three large divisions emanate from the trigeminal ganglion, each of which runs in a distinctly different direction and distributes to different parts of the face. These afferent branches are named for the region to which they form corrections: the ophthalmic division, often referred to as V1; the maxillary division, often referred to as V2; and the mandibular division, often referred to as V3 (Figure 2). Only the ophthalmic and maxillary divisions of the trigeminal nerve have branches within the orbit, and these are discussed individually.

Ophthalmic Division of the Trigeminal Nerve

The ophthalmic division is considered the first branch of the trigeminal nerve as it is the superior-most branch of the trigeminal nerve (Figure 2). It conveys general

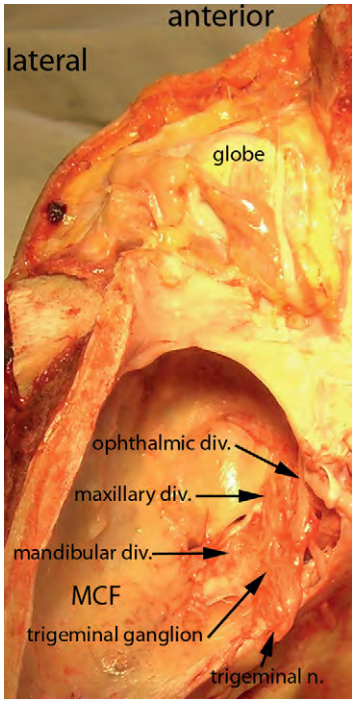

Figure 2 Superior view of the orbital contents and the middle cranial fossa (MCF) in a human. The trigeminal nerve and ganglion are visible on the medial wall of the middle cranial fossa after removal of the overlying dura mater. The three divisions can be seen each running toward their appropriate cranial foramina. The ophthalmic division of the trigeminal nerve is the most superior branch and enters the orbit through the superior orbital fissure (not seen). The maxillary nerve courses almost horizontally and leaves the middle cranial fossa through the foramen rotundum (not seen) to enter the pterygopalatine fossa. The mandibular division courses inferiorly through the foramen ovale (not seen) to enter the infratemporal fossa.

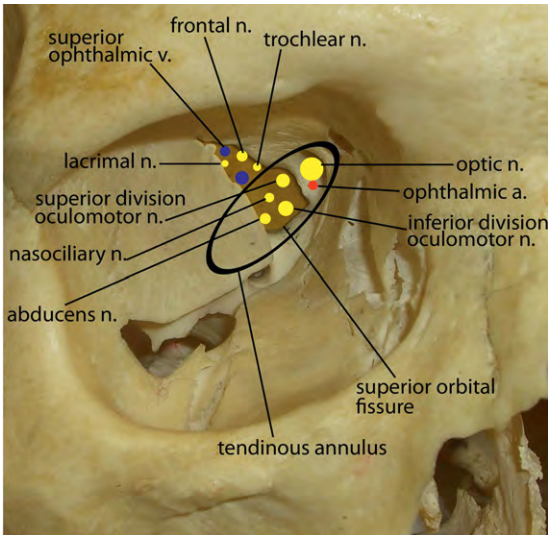

Figure 3 Photograph of the bony orbit in a dry skull from the anterior view. Medial is to the right and superior is at the top. The large opening between the greater and lesser wings of the sphenoid bone in the posterior of the orbit is the superior orbital fissure. Medial to the superior orbital fissure is the optic foramen, formed within the lesser wing of the sphenoid bone. There is a tendinous annulus at the posterior of the orbit, attaching to orbital bones medially and laterally. The rectus muscles take their origin from this connective tissue structure. The tendinous annulus separates the nerves entering the orbit into two groups: those that enter (1) superior to the annulus and (2) within the annular ring. A large number of nerves and veins pass through the superior orbital fissure superior to the annulus. From superior to inferior they are the superior ophthalmic veins, although these can be quite variable (blue circles); the frontal and lacrimal nerves which are branches of the ophthalmic division of the trigeminal nerve; and the trochlear nerve which innervates the superior oblique muscle. A large number of nerves enter the orbit within the annulus, and these are often referred to as intraconal. The optic nerve (yellow circle) and ophthalmic artery (red circle) enter the orbit through the optic foramen. The superior division of the oculomotor nerve, which innervates the superior rectus and levator palpebrae superioris muscles, and the inferior division of the oculomotor nerve, which innervates the medial rectus, the inferior rectus, and the inferior oblique muscles, pass through the superior orbital fissure. The nasociliary nerve, the third branch of the ophthalmic division of the trigeminal nerve, also enters via the superior orbital fissure. The final structure which enters the orbit within the annulus is the abducens nerve, which innervates the lateral rectus muscle.

sensory afferents that subserve pain, touch, and temperature sensitivity to the brain. As a sensory nerve, it is important to remember that the nerve branch consists of sensory afferents, with the information traveling into the brain. However, it makes the most sense to describe the complex branching pattern of the ophthalmic division of the trigeminal nerve starting from the apex of the orbit and working peripherally.

Separate branches of the ophthalmic division of the trigeminal nerve pass through the superior orbital fissure, as they do not coalesce into a single division until within the wall of the cavernous sinus intracranially. The superior orbital fissure is located between the lesser and greater wings of the sphenoid bone, and three distinct branches of the ophthalmic division of CNV can be seen traversing through this foramen (**Figure 3**).

Lacrimal nerve

The most superior and laterally placed is the smallest branch, the lacrimal nerve (**Figure 4**). The lacrimal nerve enters the orbit via the superior orbital fissure, outside the tendinous annulus formed by the origins of four extraocular muscles at the apex of the bony orbit (**Figure 3**). The nerve courses on the superior aspect of the lateral rectus muscle to enter the lacrimal gland. Prior to entry into the lacrimal gland, it receives a communicating branch from the zygomatic nerve which carries secretomotor innervation from the parasympathetic nervous system. The lacrimal nerve terminates on the conjunctiva and skin of the lateral part of the upper lid where it receives general sensory information.

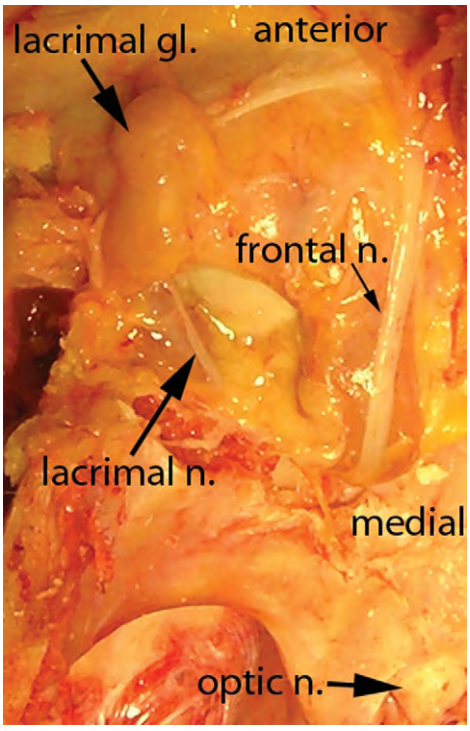

Figure 4 Superior view of the human orbital contents. The frontal bone that forms the roof of the orbit has been removed, as has the periorbita, a dense connective tissue that is the periosteal layer that lines the orbit. The most superior structures are visible. The lacrimal gland is located in the superior lateral part of the orbit. The superior-most structures are the frontal and lacrimal nerves, which are branches of the ophthalmic division of the trigeminal nerve. Just inferior to the frontal nerve is the levator palpebrae superioris muscle, which inserts into the eyelid skin to raise the eyelid.

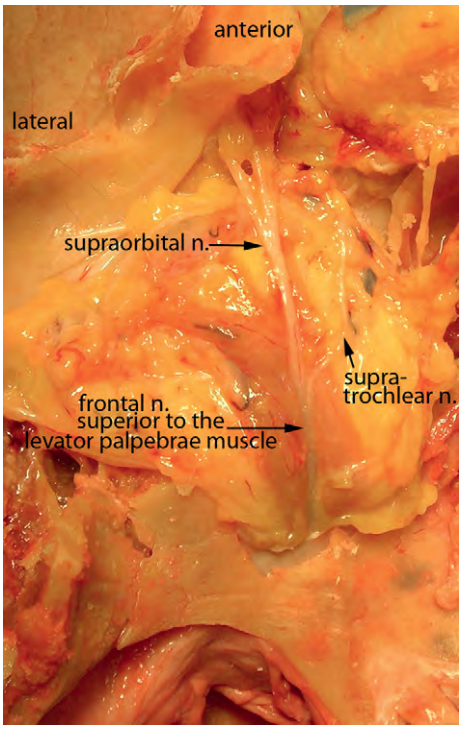

Figure 5 Superior view of the human orbital contents. The frontal bone that forms the roof of the orbit has been removed, as has the periorbita, a dense connective tissue that is the periosteal layer that lines the orbit. The most superior structures are visible. In this specimen, the frontal nerve can be seen forming its two terminal branches, the supraorbital and supratrochlear nerves. These exit the orbit anteriorly and provide sensory innervation to the upper eyelid, forehead and scalp.

Frontal nerve

The frontal nerve is the largest of the sensory branches of the ophthalmic division of the trigeminal nerve, entering the orbit within the uppermost part of the superior orbital fissure outside the tendinous annulus (**Figure 3**). It runs anteriorly between the periorbita, the dense connective tissue covering the orbital bones, and the levator palpebrae superioris muscle (**Figure 5**). Variably along its length, it divides into two terminal branches, the supratrochlear and supraorbital nerves (**Figure 5**). The small supratrochlear nerve runs superior to the trochlea, a cartilaginous structure attached superiomedially to the bony orbit, and exits the orbit anteriorly to supply the skin of the medial forehead, upper eyelid, and conjunctiva. The supraorbital branch is larger and continues anteriorly on the superior surface of the levator to exit the orbit through the supraorbital foramen or notch to provide sensory innervation to the conjunctiva and skin of the upper eyelid, forehead, and scalp anterior to the midauricular line. The supraorbital notch is located in the frontal bone which forms the superior orbital margin and is located approximately 31 mm from the midline bilaterally.

Nasociliary nerve

The nasociliary nerve passes through the superior orbital fissure between the two branches of the oculomotor nerve, running within the tendinous annulus (**Figure 3**). The course of this nerve in the orbit is particularly long and complicated (**Figure 6**). In the majority of cases, the nasociliary nerve turns medially and courses with the ophthalmic artery superior to the optic nerve, but deep to the superior rectus muscle. As it continues anteriorly, its path runs between the superior oblique and medial rectus muscles and in the process gives off five branches: sensory root of the ciliary ganglion, long ciliary nerves, posterior ethmoidal nerve, anterior ethmoidal nerve, and infratrochlear nerve.

Sensory root of the ciliary ganglion

These branches carry sensory information through the ciliary ganglion without synapsing. They run in both the short and long ciliary nerves, which pierce the sclera when they reach the globe. The sensory nerves here are very thin and vary between 5 and 12 mm in length.

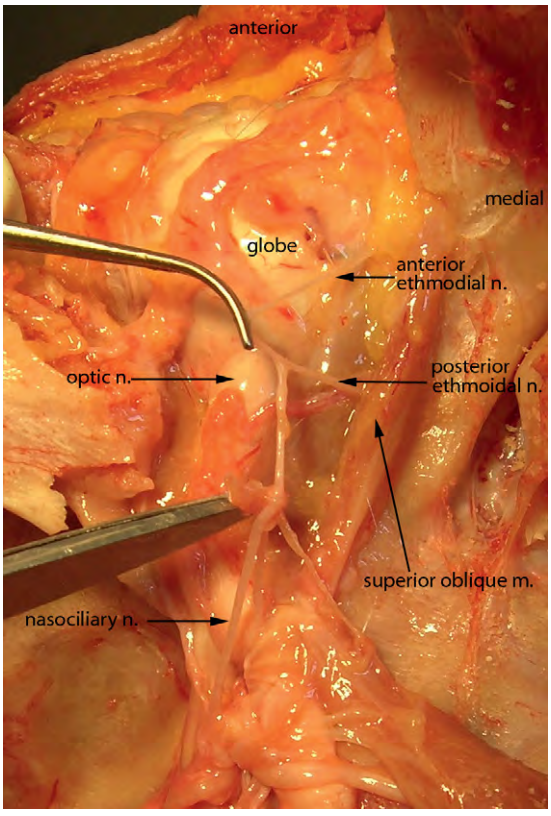

Figure 6 Deep dissection of the human orbit from the superior view. The levator palpebrae superioris and superior rectus muscles have been removed and the frontal nerve reflected. This allows the visualization of the nasociliary nerve, a branch of the ophthalmic division of the trigeminal nerve (note that the bony orbit posteriorly has been dissected open). The nasociliary nerve enters the orbit superior and lateral to the optic nerve, but rapidly moves medially and anteriorly where two sets of branches emerge: the posterior and the anterior ethmoidal nerves (lifted by the scissor tips and blunt probe). These enter the ethmoid air cells, which are part of the nasal sinuses in the mid-region of the head.

Long ciliary nerves

These nerves vary in number, although commonly there are two or three. These nerves course toward the globe, pierce the sclera, and extend anteriorly to provide sensory innervation to the iris, ciliary muscles, and cornea (Figure 7).

Posterior ethmoidal nerve

This is a small and variable branch that emerges off the nasociliary nerve and runs medially between the superior oblique and medial rectus muscles (Figure 6). It terminates in the sphenoid and posterior ethmoid sinuses, providing sensory innervation to these regions.

Anterior ethmoidal nerve

The anterior ethmoidal nerve runs anteriorly between the superior oblique and medial rectus muscles (Figure 6). It exits the orbit with the anterior ethmoidal artery through

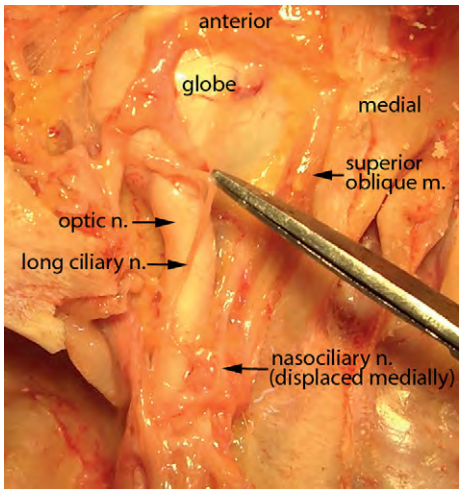

Figure 7 A deep dissection of the orbit seen from the superior view. The long ciliary nerves can be seen coursing between the nasociliary nerve, a branch of the ophthalmic division of the trigeminal nerve, and the globe (lifted at scissor tip). While this is largely carrying sensory information from the globe, recent studies have demonstrated that autonomic system nerves course in this structure.

the anterior ethmoidal canal, which is located between the ethmoid and frontal bones. It carries sensory innervation from the anterior and middle ethmoidal air cells as well as from the frontal sinus. The anterior ethmoidal nerve terminates by dividing to form internal and external nasal nerves, and the latter supplies the skin of the dorsum of the nose.

Infratrochlear nerve

This is the termination of the nasociliary nerve on the face, where it provides sensory innervation of the medial canthal area, the root of the nose, and the lacrimal sac and canaliculi. If this nerve is absent, the supratrochlear or anterior ethmoidal nerves provide the sensory innervation for these areas.

Maxillary Division of the Trigeminal Nerve

The maxillary division is considered the second branch of the trigeminal nerve, and similar to the ophthalmic division of CNV, it brings sensory information into the CNS via nerves whose cell bodies are located in the trigeminal ganglion. The maxillary division enters the pterygopalatine fossa via the foramen rotundum (Figure 2). It continues to course anteriorly and enters the inferior orbital fissure on the floor of the orbit within the maxillary bone. Within the fissure, two branches are formed: the zygomatic and infraorbital nerves. Only these two nerves, of the many branches of the maxillary division, are germane to a discussion of innervation within the orbit.

Zygomatic nerve

The zygomatic nerve emerges from the inferior orbital fissure and courses superiorly on the lateral orbital wall. Current dogma indicates that postganglionic parasympathetic fibers from the facial nerve (CNVII) run in this nerve, branch off in the lateral orbit, and enter the lacrimal nerve to provide secretomotor innervation to the lacrimal gland. Recent studies in nonhuman primates and humans indicate, however, that the parasympathetic nerves run directly to the lacrimal gland as 5–10 separate rami lacrimales (**Figure 8**). This is discussed in further detail in the section on the autonomic nervous system.

The zygomatic nerve divides into two terminal branches, the zygomaticotemporal and the zygomaticofacial, both of which supply skin over the temporal and buccal regions of the face, respectively.

Infraorbital nerve

This is the very large terminal branch of the maxillary nerve, which runs first in the inferior orbital fissure, then in the inferior orbital grove and canal to emerge on the face through the infraorbital foramen (**Figure 9**). This foramen is approximately 10 mm from the inferior orbital margin formed by the maxillary bone. This nerve provides sensory innervation to a large area of the face from the upper lip to the lower eyelid. Specific palpebral branches supply the skin and conjunctiva of the lower eyelid.

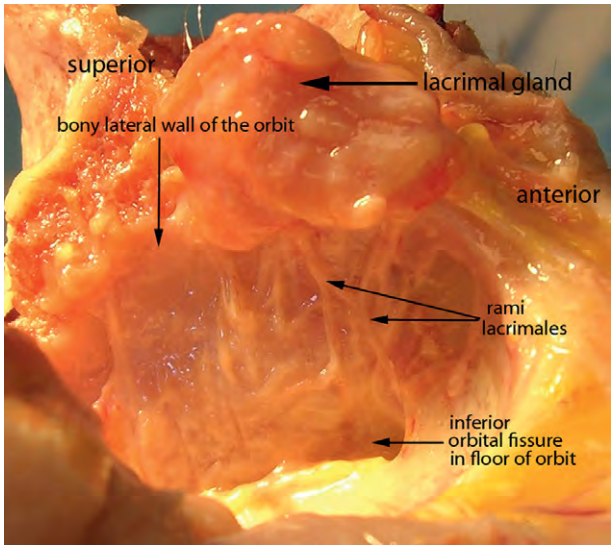

Figure 8 A view of the lateral wall of the orbit with the bony roof and all the orbital contents removed. This allows visualization of parasympathetic nerves coursing in a superior direction from the inferior orbital fissure on the bony orbit floor toward the lacrimal gland. These carry parasympathetic secretomotor postganglionic innervation to the lacrimal gland.

Motor Nerves

The Oculomotor Nerve or Cranial Nerve III

The oculomotor nerve provides motor innervation to the levator palpebrae superioris, the superior, medial and inferior rectus muscles, and the inferior oblique muscle. All these muscles insert directly onto the globe and move the eye within the orbit. In addition, as discussed in the section on autonomic innervation, the oculomotor nerve carries the parasympathetic preganglionic axons that synapses in the ciliary ganglion, and whose postganglionic axons innervate the pupillary sphincter and ciliary muscles of the eye.

The oculomotor neurons within the brainstem that give rise to the oculomotor nerve have a complex organization. The oculomotor nucleus is found at the level of the mesencephalon, ventral to the cerebral aqueduct. It extends from the posterior floor of the fourth ventricle to the trochlear nucleus. Generally, the oculomotor nucleus contains a midline dorsal nucleus and two lateral nuclei. Using a variety of tract-tracing techniques, it has been shown that the oculomotor nucleus is organized in a muscle-specific manner, with specific groups of neurons innervating single extraocular muscles. In addition, the muscles can receive ipsilateral, contralateral, or bilateral innervation. Each superior rectus muscle is innervated by contralateral oculomotor neurons located medially within the paired lateral nuclei. Each medial rectus is innervated by ipsilateral oculomotor neurons found in the inferior-most part of the paired lateral nuclei. Each inferior rectus muscle is innervated by ipsilateral oculomotor neurons located in the superior-most part of each of the paired lateral nuclei. The inferior oblique is innervated ipsilaterally by neurons located in the middle and lateral portion of the paired

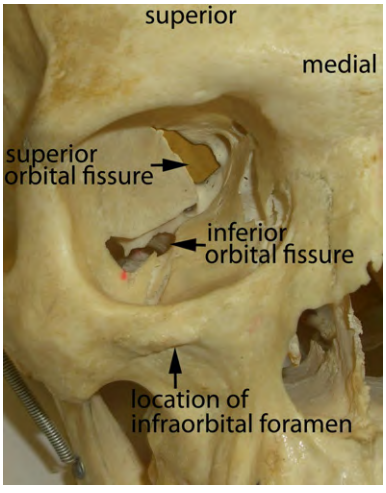

Figure 9 An anterior view of the orbit on a dry skull. Foramina, or openings in the bone, can be seen. The superior orbital fissure is found at the orbital apex. The inferior orbital fissure is found on the orbital floor. The optic foramen is found on the superior-medial wall.

lateral nuclei. Only the levator palpebrae superioris muscle receives bilateral innervation from the single dorsal caudal nucleus located in the midline. All the nerve fibers from these various topographically organized nuclei join together within the brainstem, and after running through the red nucleus and cerebral peduncle, exit the brainstem on its ventral surface in the interpeduncular fossa. In their cisternal location, they pass between the posterior cerebral and superior cerebellar arteries, and course anteriorly, deep to the posterior communicating artery. The intracranial course is on average 25 mm long before the nerves enter into the dural border of the lateral cavernous sinus at the level of the posterior clinoid process (**Figure 10**). The oculomotor nerve enters the orbit through the superior orbital fissure, where it divides into a superior and an inferior division and enters the tendinous annulus (**Figure 3**). The diameter of the oculomotor nerve, as it enters the superior orbital fissure, is on average 2.1 mm, while the superior and the inferior divisions are 1.6 and 1.9 mm in diameter, respectively. The superior division innervates the superior rectus and levator palpebrae superioris muscles; the nerve enters the conal surface of the superior rectus muscle (**Figure 11**), and nerve fibers continue to the levator by either piercing through the superior rectus muscle or passing on its lateral border. The inferior division innervates the medial rectus, the inferior rectus, and the inferior oblique muscles. To reach these muscles, the inferior division of the oculomotor nerve runs medially and inferiorly, dividing into three branches (**Figure 12**). One branch enters the medial rectus muscle and the second branch enters the inferior rectus muscle, both on their conal surfaces; a third branch courses anteriorly along the lateral border of the inferior rectus muscle and pierces the inferior oblique at the point where it crosses the inferior rectus muscle. All the oculomotor nerve branches enter the muscles between the middle and posterior 1/3 of each muscle. In the majority of cases, the branch to the inferior oblique gives rise to nerves that carry parasympathetic axons to the ciliary ganglion. This is discussed in the section on autonomic nervous system.

The course of the oculomotor nerve is easily seen using standard magnetic resonance imaging (MRI) techniques, both intracerebrally and intraorbitally.

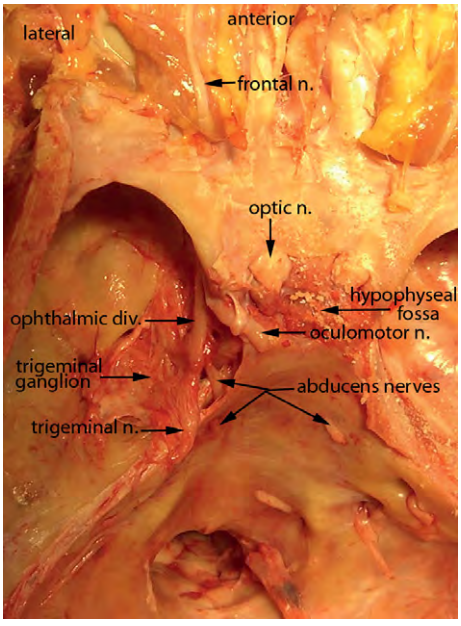

Figure 10 Superior view of the floor of the cranium. The orbital contents can be seen anteriorly. Four of the five cranial nerves can be seen. On the medial wall of the middle cranial fossa, the three divisions of the trigeminal nerve can be seen coursing from the anterior border of the trigeminal ganglion. The ophthalmic division can be seen coursing in the direction of the orbit. The oculomotor nerve can be seen crossing superior to the sella turcica of the sphenoid bone (which houses the pituitary gland in the hypophyseal fossa). The abducens nerve can be seen diving through the dura and coursing on the medial side of the trigeminal ganglion. The large foramen seen at the bottom of the photograph is the foramen magnum, where the spinal cord joins the medulla oblongata of the brain. The optic nerve can also be seen as it enters the optic canal.

The Trochlear Nerve or Cranial Nerve IV

The trochlear nerve provides innervation to one skeletal muscle only, the superior oblique. The motor neurons that form the trochlear nerve are located in the trochlear

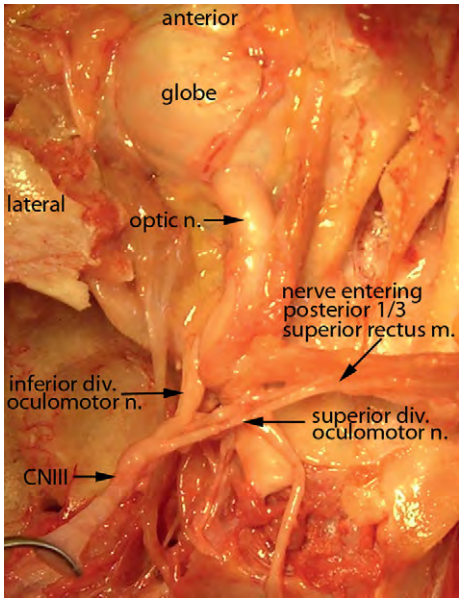

Figure 11 A deep dissection of the orbit from the superior view of the orbit. The optic nerve can be seen exiting the globe. The two divisions of the oculomotor nerve are dissected. The superior division is seen entering the superior rectus/levator palpebrae superioris muscles. The inferior division dives deep to the optic nerve on its way to innervate the medial and inferior rectus, and inferior oblique muscles. (Forceps is holding the cut proximal end of the oculomotor nerve.)

nucleus, which is located at the caudal end of the oculomotor nucleus at the level of the inferior colliculus. The nerve fibers run dorsally and slightly caudally, decussate (cross the midline), and emerge on the dorsal surface of the brainstem caudal to the inferior colliculus. This means that each trochlear nucleus innervates the contralateral superior oblique muscle within the orbit. However, a number of studies in various species unequivocally demonstrate that up to 5% of the superior oblique muscle innervation originates in the ipsilateral trochlear nucleus; this means that there is a small bilateral component to the innervation of the superior oblique muscle.

The course of the trochlear nerve is long, with an intracranial course of 60 mm. It also has the smallest cross-sectional diameter, averaging between 0.75 and 1 mm. The trochlear nerve courses on the lateral side of the midbrain running anteriorly to enter the cavernous sinus. Prior to entering the sinus wall, in 90% of specimens examined, the trochlear nerve is associated with the superior cerebellar artery, which usually runs superior to the nerve. Upon entering the cavernous sinus, the oculomotor nerve is medial and superior to the trochlear nerve and, more anteriorly, the oculomotor nerve ends up inferior and lateral to the trochlear nerve. The ophthalmic division of the trigeminal nerve consistently runs inferior to the trochlear nerve. Interestingly, in over 25% of trochlear nerves examined, there were nerves interconnecting V1 and trochlear nerves, presumably carrying general sensory information from the superior oblique muscle. The mean length of the intracavernous portion of the trochlear nerve is 26.8 mm.

The trochlear nerve enters the orbit through the superior orbital fissure in its most superior-lateral part, entering superior to the tendinous annulus (**Figure 3**). In this location its diameter is approximately 1.18 mm. Within the orbit, the trochlear nerve runs anteriorly and medially, with only periosteum separating the nerve from the sphenoid bone. The trochlear nerve terminates within the posterior half of the superior oblique muscle (**Figure 13**); in 76% of the orbits it ends in the medial aspect of the muscle and in the remaining 24% it ends in the superior aspect of the muscle. Generally, the total length of the trochlear nerve in the orbit is approximately 25 mm. Nerve branches first enter the muscle 17.25 mm from the muscle origin. Branches continue to dive into the muscle surface for an additional 7 mm.

Due to its small diameter, the trochlear nerve is difficult to image consistently using normal T1-weighted MRI, although T2-weighted fast spin-echo or T2-weighted

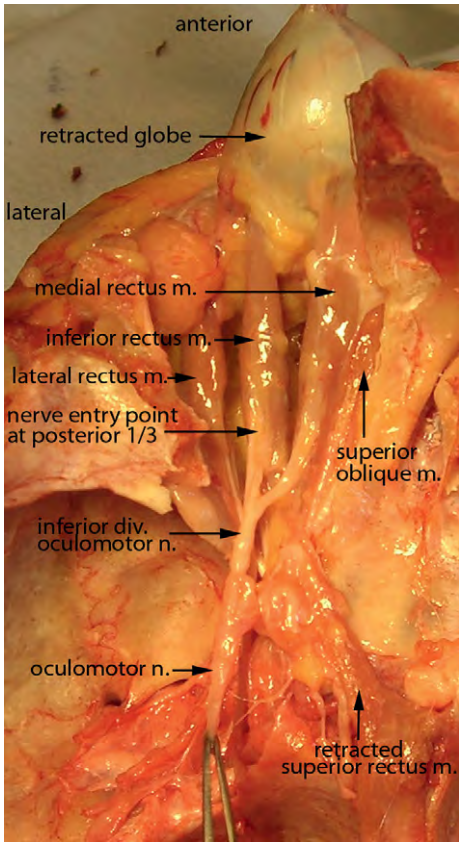

Figure 12 Superior view of a deep dissection of the human orbit. The globe has been retracted so we can see its inferior surface. This allows visualization of the lateral, the inferior, and the medial rectus muscles. The inferior division of the oculomotor nerve can be seen coursing directly into the posterior 1/3 of the inferior and medial rectus muscles. (Forceps is holding the cut proximal end of the oculomotor nerve. The lacrimal gland is covering the anterior portion of the lateral rectus muscle.)

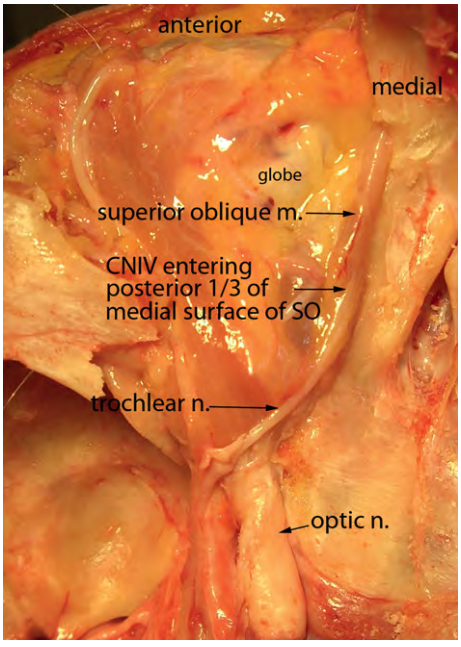

Figure 13 Superior view of a superficial dissection of the human orbit. The trochlear nerve is dissected to its entry point into the posterior 1/3 of the medial surface of the superior oblique muscle. The globe is obscured by orbital fat and the superiorly located muscles.

three-dimensional sequences, such as 3D-CISS, were able to visualize the trochlear nerve in up to 95% of patients examined.

The Abducens Nerve or Cranial Nerve VI

The abducens nerve provides motor innervation to only one extraocular muscle in humans, the ipsilateral lateral rectus muscle. While CNVI innervates the retrobulbar muscle in animals such as rats and rabbits, nonhuman primates and humans do not have a retrobulbar muscle. The motor nucleus for the abducens nerve lies inferior to the floor of the fourth ventricle. Nerve fibers leave the nucleus and run anteriorly, laterally, and caudally through the pons, emerging in the medullary–pontine sulcus, a groove between the medulla and the pons. In this location the nerve is intracisternal, deep to the pons. The nerve is in close proximity to the anterior inferior cerebellar artery, and in approximately 80% of dissected human cadavers, the artery is inferior to the nerve. The nerve courses over the lateral edge of the dorsum sellae, pierces the dura of the clivus, runs in a canal formed by the petrosphenoidal ligament superiorly and a bony ridge in the petrous ridge of the temporal bone (Dorello's canal), and passes through the inferior petrosal sinus as it courses anteriorly, lateral to the petrous part of the temporal bone. It crosses superior to the petrous ridge and deep to the petrosphenoidal ligament, lateral to the bend of the internal carotid artery. Unlike CNIII, CNIV, and CNV1, the abducens nerve does not sit within the wall of the cavernous sinus; it floats free within the cavernous sinus, where it is medial to the trigeminal ganglion (**Figure 10**). The total length of the intracranial abducens nerve is on average 53 mm in adults.

The abducens nerve enters the orbit through the superior orbital fissure within the tendinous annulus (**Figure 3**). In this location its mean diameter is 1.54 mm, and it is found lateral to both branches of the oculomotor nerve and inferior to the nasociliary nerve and the superior branch of CNIII. It rapidly gains the medial surface of the lateral rectus muscle, splits into three to four branches, and enters the muscle within the posterior 1/3 of its length (**Figure 14**). The intraconal length of the abducens nerve is about 5 mm.

In contrast to the trochlear nerve, the abducens nerve, from its exit at the brainstem to its entry into the lateral rectus muscle, can be visualized using MRI.

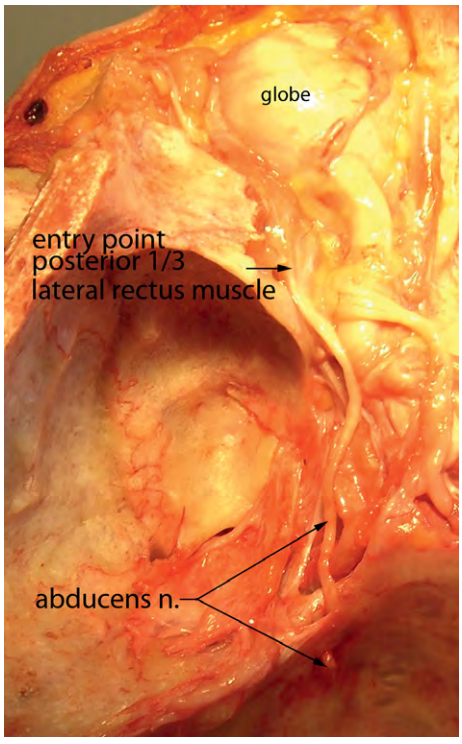

Figure 14 Superior view of the floor of the cranial fossa in a human cadaver. The abducens nerve was dissected from its entry into the dura, through the cavernous sinus on the lateral side of the sella turcica (medial to the trigeminal ganglion). It enters the orbit through the superior orbital fissure (lesser sphenoid bone has been removed to open the fissure), and its entry into the posterior 1/3 of the lateral rectus muscle is visible.

Autonomic Nervous System Contributions to Orbital Innervation

The autonomic nervous system is ubiquitously located throughout the body and is responsible for controlling involuntary structures, including smooth muscle, the conducting cells of the heart, and glandular secretion. The autonomic nervous system is divided into two systems: the sympathetic and the parasympathetic nervous systems. As a rule, these two parts of the autonomic nervous system have opposing functions. Simplistically speaking, the sympathetic nervous system helps the body respond to stress, such as increasing blood flow to the muscles in preparation for activity. The parasympathetic nervous system, in general, actively promotes normal bodily functions at rest, such as increasing blood flow to the intestines and aiding in peristalsis.

The main anatomical differences of the two parts of the autonomic nervous system are based on the location of the preganglionic neuronal cell bodies and what nerves conduct their axons to the periphery. Each autonomic circuit consists of a two-neuron chain. In general, the sympathetic nervous system has short preganglionic nerves and long postganglionic nerves. The opposite is true of the parasympathetic nervous system, where the preganglionic nerves are long and the postganglionic nerves are short. The preganglionic sympathetic neuronal cell bodies are located in the thoracic and upper lumbar regions of the spinal cord, while the preganglionic parasympathetic neuronal cell bodies are located in specific brainstem nuclei as well as in lower sacral levels of the spinal cord.

Parasympathetic Innervation in the Orbit

As is typical of parasympathetic innervation, the nerve fibers originate in specific brainstem nuclei. The axonal paths of these parasympathetic nerves within the orbit are extremely complex. Four of the twelve cranial nerves have parasympathetic components (CNIII, CNVII, CNIX, and CNX). Of these, both the oculomotor (CNIII) and facial (CNVII) nerves send parasympathetic innervation into the orbit. The preganglionic neuronal cell bodies are located in brain nuclei, while the postganglionic cell bodies are located in peripherally located ganglia.

Parasympathetic innervation within the oculomotor nerve

The accessory oculomotor nucleus is the site of origin of the preganglionic nerve fibers that enter the orbit with the oculomotor nerve. This nucleus is located both rostral and dorsal to the oculomotor nucleus. Its nerve fibers run into and travel along with the superior aspect of the ipsilateral oculomotor nerve. Within the orbit, these preganglionic parasympathetic nerve fibers run with the inferior division of the oculomotor nerve, and eventually extend nerve branches to the ciliary ganglion. The ciliary ganglion is located on the lateral side of the optic nerve close to the orbital apex. It is between 1 and 3 mm in diameter. In approximately 8% of the orbits, the ciliary ganglion is located directly on either the inferior division of the oculomotor nerve or the nerve to the inferior oblique muscle. In addition, many authors have described accessory ciliary ganglia as well as scattered ganglion cell neurons within the ciliary nerves themselves. We use the term ciliary ganglion to encompass all three of these ganglion locations.

Within the ciliary ganglion are postganglionic neuronal cell bodies that receive synapses from the preganglionic nerve fibers. The postganglionic nerve fibers, for the most part, travel within the short ciliary nerves and enter the sclera on the temporal side of the globe. These nerves innervate the ciliary muscles and iris sphincter muscles; roughly 95% go to the ciliary muscles and 5% innervate the sphincter muscles. Thus, this parasympathetic innervation is responsible for pupil constriction in response to light as well as for accommodation needed for near vision.

It should also be noted that experimental evidence demonstrates that intraocular parasympathetic projections also can arise from the pterygopalatine ganglion. These fibers arrive in the orbit by either (1) joining the retro-orbital plexus and then traveling anteriorly to the globe with the ciliary artery, long ciliary nerve, short ciliary nerve, and/or within the optic nerve sheath, or (2) they travel retrogradely with the ethmoidal or infratrochlear nerves and join the long ciliary nerves to enter the globe.

An additional source of parasympathetic innervation to the globe itself is supported by the fact that removal of the ciliary ganglion only reduces the cholinergic nerve fibers within the cornea, iris, and choroid by 60%.

Parasympathetic innervation to the lacrimal gland

The brainstem neurons, which every basic anatomy textbook describes as giving rise to the parasympathetic secretomotor nerve fibers of the lacrimal gland, are found within the ventral subgroup of neurons in the superior salivatory nucleus located between the root of the facial nerve and the superior olive nuclei. The preganglionic parasympathetic secretomotor fibers exit the brainstem within the intermediate root of the facial nerve. The intermediate root joins the motor root of the facial nerve and exits the cranium through the internal acoustic meatus. Within the temporal bone, the parasympathetic fibers exit the facial nerve at the geniculum and leave the temporal bone as the greater petrosal nerve. This nerve courses anteriorly, crosses the middle cranial fossa, and enters the pterygoid canal where it is joined by the deep petrosal nerve, which brings sympathetic nerve fibers that ascended from the superior cervical ganglion by running on the internal carotid artery. These two nerve branches unite and form the nerve of the pterygoid canal (formerly called the vidian nerve). The nerve of the pterygoid canal courses to the pterygopalatine ganglion, which is associated with V2 within the pterygopalatine fossa. Here in the pterygopalatine ganglion, the preganglionic parasympathetic nerve fibers synapse with neurons that will form the postganglionic nerve fibers. These secretomotor fibers have been described as coursing with the zygomatic nerve, which runs on the floor and lateral wall of the orbit. Eventually, a nerve root anastamosis with the lacrimal nerve forms and carries the postganglionic secretomotor fibers that originated in CNVII to the lacrimal gland. A number of scientists question this pathway, as it is extremely complex and the anastamosis between the zygomatic and lacrimal nerve is often nonexistent. In addition, section of the connecting ramus between the zygomatic and lacrimal nerves does not reduce lacrimation.

Recent studies using modern tract-tracing techniques have demonstrated that, in fact, there is a direct pathway from the pterygopalatine ganglion to the lacrimal gland via a retro-orbital autonomic plexus. In humans and in the nonhuman primates, 5–10 rami can be traced directly from the pterygopalatine ganglion to the retro-orbital nerve plexus, and rami from this plexus are easily traced directly to the lacrimal gland. In other studies, nerve rami were followed that passed directly from the pterygopalatine ganglion to the lacrimal gland. These studies demonstrate that, contrary to current dogma, pterygopalatine

postganglionic parasympathetic efferents course to the lacrimal gland without using branches of the maxillary (zygomatic branch) nerve as a route.

Sympathetic Innervation in the Orbit

The sympathetic innervation of the body is extremely ubiquitous. It has long been understood that preganglionic sympathetic neuronal cell bodies are located in the intermediolateral portion of the spinal cord at the thoracic and upper lumbar levels. The sympathetic nerve fibers exit the spinal cord in the ventral root and branch off as white rami communicans to join the sympathetic chain running on the lateral sides of the vertebral bodies. First-order central sympathetic fibers arise from the posterolateral hypothalamus and descend to terminate in the intermediolateral cell column of the spinal cord at the level of C8–T2. Second-order preganglionic pupillomotor fibers exit the spinal cord at the level of T1 and ascend in the cervical sympathetic chain which is found on the lateral sides of the cervical vertebrae. The fibers synapse in the superior cervical ganglion at the level of the bifurcation of the common carotid artery (C3–C4). After the postganglionic fibers leave the superior cervical ganglion, the pupillomotor fibers ascend along the internal carotid artery and enter the cavernous sinus. Some axons leave the carotid plexus to join the abducens nerve (CNVI) in the cavernous sinus and enter the orbit through the superior orbital fissure along with the ophthalmic branch of the trigeminal nerve (V1). These axons course toward the globe in the long ciliary nerves, which innervate the iris dilator and superior and inferior tarsal muscles within the upper and lower eyelids, respectively. In addition, these sympathetic nerves control the diameter of all vasculature.

The standard view that the only route of entry of sympathetic nerve fibers into the orbit is the ophthalmic artery, a branch of the internal carotid artery that enters the orbit through the orbital foramen, has been challenged in recent years. A large proportion of the sympathetic innervation does enter the orbit hitchhiking on the ophthalmic artery and traveling along its branches within the orbit. However, with the use of specific enzymatic labeling methods, the sympathetic nerve routes within the orbit have turned out to be much more numerous and complex than previously described in standard anatomy textbooks. Sympathetic nerves now are known to enter the orbit by a significant number of other routes, including the first and second divisions of the trigeminal nerve (the ophthalmic and maxillary nerves) as they enter the orbit through the superior orbital fissure. All branches of the ophthalmic division of the trigeminal nerve within the orbit contain sympathetic nerve fibers. Sympathetic nerves from these sensory branches of the trigeminal nerve join and travel within the extraocular motor nerves in the posterior orbit. The smooth muscles that open the eyelid and the superior and inferior tarsal muscles receive their sympathetic innervation from terminal branches of the lacrimal nerves and the infratrochlear branch of the nasociliary nerve. Sympathetic nerve fibers from the nasociliary nerve also run directly through the ciliary ganglion without synapsing and travel distally toward the sclera in long ciliary nerves. Sympathetic innervation also has been seen in the short ciliary nerves by some authors, although there appears to be some variability in this pathway. Within the sclera, the sympathetic nerves reach the iris dilator muscle, the ciliary body, and the trabecular meshwork anteriorly. Injury to these nerves anywhere along their pathway results in Horner's syndrome, which refers to a constellation of signs produced when sympathetic innervation to the eye is interrupted. This results in moderate ptosis due to denervation of the superior tarsal muscle, slight elevation of the lower lid due to denervation of the inferior tarsal muscle, a muscle analogous to the superior tarsal muscle in the upper lid, as well as miosis and dilation lag, that is, pupillary dilation is slowed in the affected pupil.

The zygomatic branch of the maxillary division of the trigeminal nerve carries sympathetic nerve fibers; thus, sympathetic innervation is carried to the lacrimal gland within both the zygomatic and lacrimal nerves. This innervation not only controls vascular diameter, but also directly innervates the secretory acini within the gland. In addition, sympathetic nerve fibers have been demonstrated to enter the orbit within the optic nerve, trochlear nerve, and abducens nerve, again contrary to what has been believed historically.

In summary, the postganglionic sympathetic fibers appear to be distributed to and course in all cranial nerves entering the orbit, as well as within more distal branches. While a large number enter the orbit with the ophthalmic artery as traditionally described, the ophthalmic division of the trigeminal nerve provides a major route for entry of sympathetic fibers into the human orbit.

Acknowledgements

This work was supported by EY15313 and EY11375 from the National Eye Institute, the Minnesota Medical Foundation, the Minnesota Lions and Lionesses, Research to Prevent Blindness (RPB) Lew Wasserman Mid-Career Development Award (LKM) and an unrestricted grant to the Department of Ophthalmology from RPB.

See also: Congenital Cranial Dysinnervation Disorders; Extraocular Muscles: Extraocular Muscle Anatomy; Extraocular Muscles: Extraocular Muscle Involvement in Disease; Extraocular Muscles: Functional Assessment in the Clinic; Eyelid Anatomy and the Pathophysiology of Blinking; Imaging of the Orbit.

Further Reading

Bron, A. J., Tripathi, R. C., and Tripathi, B. J. (1997). *Wolff's Anatomy of the Eye and Orbit*, 8th edn. London: Chapman and Hall Medical.

Büttner-Ennever, J. A. (2005). The extraocular motor nuclei: Organization and functional neuroanatomy. *Progress in Brain Research* 151: 95–125.

Cavallotti, C., Frati, A., Sagnelli, P., and Pescosolido, N. (2005). Re-evaluation and quantification of the different sources of nerve fibers supplying the rat eye. *Journal of Anatomy* 206: 217–224.

Doxanas, M. T. and Anderson, R. L. (1984). *Clinical Orbital Anatomy*. Baltimore, MA: Williams and Wilkins.

Ettl, A. and Salomonowitz, E. (2004). Visualization of the oculomotor cranial nerves by magnetic resonance imaging. *Strabismus* 12: 85–96.

Iaconetta, G., Fusco, M., Cavallo, L. M., et al. (2007) The abducens nerve: Microanatomic and endoscopic study. *Operative Neurosurgery* ONS7–ONS14.

Oikawa, S., Kawagishi, K., Yokouchi, K., Fukushima, N., and Moriizumi, T. (2004). Immunohistochemical determination of the sympathetic pathway in the orbit via the cranial nerves in humans. *Journal of Neurosurgery* 101: 1037–1044.

Ruskell, G. L. (2004). Distribution of pterygopalatine ganglion efferents to the lacrimal gland in man. *Experimental Eye Research* 78: 329–335.

Thakker, M. M., Huang, J., Possin, D. E., et al. (2008). Human orbital sympathetic nerve pathways. *Ophthalmic Plastic and Reconstructive Surgery* 24: 360–366.

Villain, M., Segnarbieux, F., Bonnel, F., Aubry, I., and Arnaud, B. (1993). The trochlear nerve: Anatomy by microdissection. *Surgical-Radiologic Anatomy* 15: 169–173.

D

Defense Mechanisms of Tears and Ocular Surface

A M McDermott, University of Houston, Houston, TX, USA

Glossary

Antigen-presenting cell – Bone-marrow-derived cell that ingests antigen and presents it to T lymphocytes to trigger adaptive immune response.
Antimicrobial peptide – Small protein, typically cationic, with broad spectrum antimicrobial activity.
Pattern recognition receptor – Cell surface or intracellular protein receptor that binds conserved motifs (pathogen-associated molecular patterns) on microorganisms.
Siderophore – Iron chelating compound secreted by bacteria and fungi to facilitate uptake of this essential nutrient.

Introduction

The ocular surface is composed of the epithelia of the cornea, limbus, and conjunctiva, the anatomy and physiology of which are discussed in detail elsewhere in this encyclopedia. The tear film coats the epithelia and is a complex structure composed of an outer anterior-most lipid component that prevents evaporation, an aqueous component that has ions, soluble mucins, enzymes, and a range of other proteins and closest to the epithelial surface is a thick mucus, primarily composed of the gel-forming mucin MUC5AC. Together, the ocular surface epithelia and tears: (1) create a formidable barrier that helps prevent microbial attachment in the first place, (2) bombard organisms with a plethora of chemicals to stop them dead in their tracks (or at least stop them proliferating), and (3) provide a detection system such that when an organism actually manages to circumvent the primary innate defenses, adaptive immunity can be activated to provide further help to eliminate the offending organism.

The defense mechanisms are remarkably effective, as despite constant exposure to the external environment and frequent interaction with unwashed fingertips, the ocular surface rarely succumbs to infection. Generally only when there is physical disruption of the epithelial barrier such as occurs with contact lens wear or injury do the defenses encounter serious challenge and infections become a significant cause of morbidity. Infection can affect both the cornea (infectious keratitis) and conjunctiva (infectious conjunctivitis), but is most serious when the cornea is involved as this structure provides the majority of the refracting power of the eye and loss of visual acuity or even blindness may be the consequence. Given appropriate circumstances, a range of organisms can infect the ocular surface. The most common bacterial species are *Pseudomonas aeruginosa*, *Serratia marcescens*, *Staphylococcus aureus*, *Staphylococcus epidermidis*, and *Streptococcus pneumoniae*. Herpes simplex virus is the most common viral culprit. Fungal infection is less common than bacterial or viral infection, but is on the rise, with the most frequently isolated species in the USA being *Aspergillus*, *Candida*, and *Fusarium*. Some of the ocular surface and tear defenses that help prevent these infections are depicted in Figure 1 using the corneal epithelium as a model.

Defense Mechanisms of Tears

Tears provide both physical/mechanical and chemical defense to the ocular surface. The act of blinking moves tears toward the puncta and into the lacrimal sac, thus helping to wash away any potential pathogens before they have had time to interact with and invade the ocular surface epithelial cells. Furthermore, reflex tearing increases tear volume which helps to rapidly dilute harmful substances released by invading pathogens.

Chemical entities with antimicrobial properties present in tears primarily originate from lacrimal and accessory gland secretions and the ocular surface epithelial

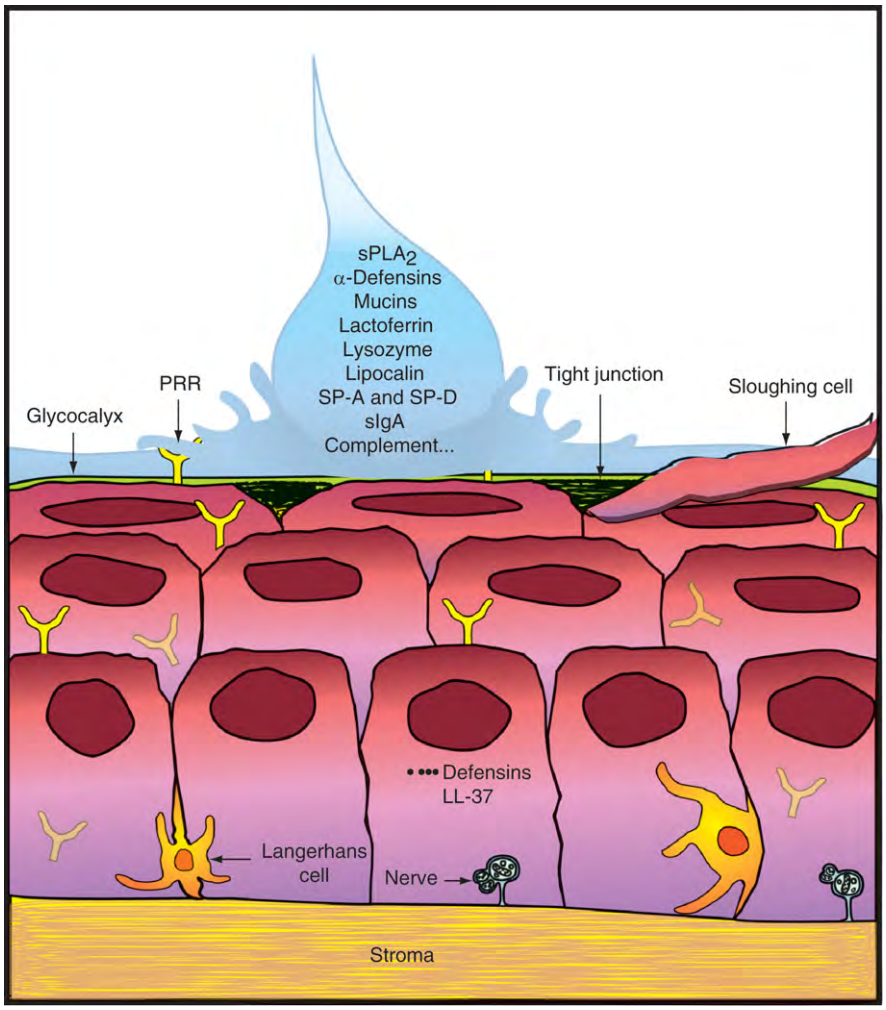

Figure 1 Summary of defense mechanisms of tears and ocular surface. Schematic diagram of some of the various defenses used by tears and ocular surface epithelia to prevent infection (additional ones are discussed in the text). The corneal epithelium is depicted (note not all cell layers are shown) but as described in the text similar mechanisms are used by conjunctival epithelial cells. PRR, pattern recognition receptor (e.g., TLRs); SP-A, surfactant protein-A; SP-D, surfactant protein-D; sIgA, secretory IgA; $sPLA_2$, secretory phospholipase A_2.

cells. Other components include serum exudates and secreted products of neutrophils and other infiltrating cells. Several tear film components have been identified that have direct antimicrobial activity or which can otherwise limit pathogen entry and growth. The first identified was lysozyme which was shown to kill Gram-positive bacteria by Alexander Fleming (of penicillin fame) in 1922. This enzyme accounts for 20–40% of total tear protein and has the ability to catalyze the hydrolysis of 1,4-beta-linkages between *N*-acetylmuramic acid and *N*-acetyl-D-glucosamine in the peptidoglycan backbone of bacterial cell walls. It is also able to cleave chitodextrins in fungal cell walls. The compromised cell wall is then no longer able to maintain a stable osmotic environment and lysis of the organism ensues. Secretory phospholipase A_2 ($sPLA_2$) has been identified as the major tear protein active against Gram-positive bacteria, although it has no activity against Gram-negatives in the normal ionic environment of tears and notably is some 50-fold less abundant in tears than lysozyme. Secretory PLA_2 hydrolyzes the *sn*-2-fatty acyl moiety from phospholipids, in particular, phosphatidylglycerol, which is abundant on bacterial cell membranes.

Other tear fluid components showing direct microbial killing include the cationic antimicrobial peptides (AMP; see the section entitled 'Defense mechanisms of the ocular surface epithelia') and the α-defensins human neutrophil peptide (HNP) 1, 2, and 3. As implicated by their names these peptides are produced by neutrophils and while present in only low concentrations under normal circumstances their level in tears rises after ocular surface injury. As depicted in **Figure 2**, these positively charged peptides exert their activity by interacting electrostatically with the negatively charged microbial cell membrane and form pores or otherwise disrupt the membrane

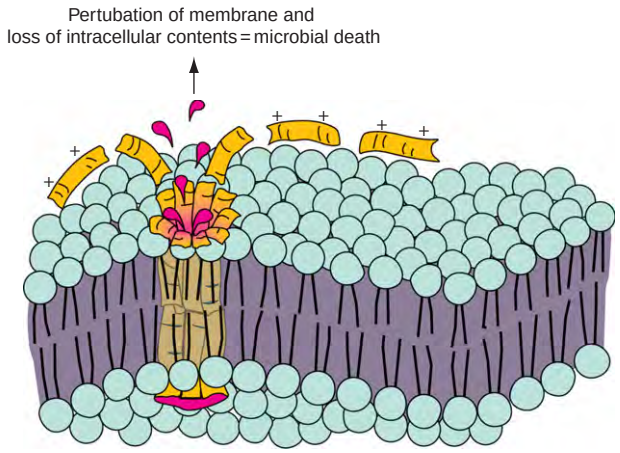

Figure 2 Mechanism of action of antimicrobial peptides. Positively charged peptides (shown in yellow) such as defensins and cathelicidin (LL-37) interact with negatively charged microbial membranes leading to disruption of the membrane, and possibly transient or stable pore formation, which results in leakage of intracellular contents, disturbance of metabolism, and death of the organism.

leading to disturbances of respiration and metabolism, leakage of cell contents, and eventual death of the organism. A lytic effect of these peptides is also possible. Betalysin and secretory leukocyte protease inhibitor (SLPI) are other examples of cationic proteins found in tears, which also interact with bacterial cell membranes and cause cell lysis. SLPI, which comes from lacrimal gland and ocular surface epithelial cells, has a defensin-like domain that confers antimicrobial activity and is also a potent inhibitor of neutrophil elastase. Thus, SLPI can both help prevent infection and protect host cells from the damaging effects of neutrophil enzymes. Elafin is another protein, which exerts similar dual functionality. Histatins, which are small histidine-rich AMPs with antifungal activity, have also been detected in the tears.

A number of tear components limit bacterial growth rather than actually killing the invading organism. Lactoferrin represents some 21% of the total reflex tear protein and has a high capacity to bind divalent cations including iron, thus depriving many bacteria of this essential nutrient for growth. Furthermore, a highly basic sequence at the N-terminus (referred to as lactoferricin) allows lactoferrin to act as a cationic detergent and disrupt the cell membrane of some organisms. Tear lipocalin represents approximately 25% of the reflex tear proteins and was recently shown to be capable of binding siderophores produced by a range of bacteria and fungi. Siderophores are chelating compounds that transport iron into microorganisms. Thus, like lactoferrin, lipocalin exerts a bacteriostatic effect by interfering with the ability of pathogens to take up iron.

The tear film also contains members of the collectin family of C-type lectins, surfactant proteins (SP)-A and -D. Collectins bind to carbohydrates on the surface of various microorganisms and to receptors on phagocytic cells, which in turn promotes their phagocytic activity. SP-A and SP-D are produced by lacrimal gland cells and also corneal and conjunctival epithelial cells. SP-D is known to exert growth inhibitory effects on some Gram-negative bacteria, to promote pathogen phagocytosis by mononuclear cells and through an interaction with lipopolysaccharide (LPS), which is present on the outer membrane of Gram-negative bacteria, can inhibit bacterial adhesion to target cells. SP-D inhibits corneal epithelial cell invasion by *P. aeruginosa* (a Gram-negative pathogen that commonly causes ulcers in contact lens wearers), possibly via an LPS-dependent mechanism.

Secretory IgA (sIgA) is the predominant immunoglobulin in the tear film. This antibody is of great importance as it facilitates removal of pathogens right at the point of entry at the ocular surface. sIgA is not a particularly efficient activator of complement (important for preventing unwanted inflammation) or a good opsonin (although neutrophils do have receptors for sIgA which when engaged could trigger phagocytosis). The major effector mechanism of sIgA is neutralization, which prevents attachment to host cells. sIgA can also bind to lectin-like adhesin molecules on pathogens causing them to aggregate and trapping them within the tear film. sIgA is produced by plasma cells (terminally differentiated B lymphocytes) residing in the lacrimal gland and in specialized areas of the conjunctiva referred to as conjunctival-associated lymphoid tissue. sIgA binds to specific receptors on lacrimal gland acinar cells, conjunctival epithelial cells, and is taken up by endocytosis, and then traverses the cell by transcytosis. This antibody is then released into the tears attached to a protein called secretory component, a fragment of the receptor to which the antibody was bound during its passage through the cells. Secretory component stabilizes the antibody and masks proteolytic sites so conferring resistance to host and pathogen proteases.

Low levels of functionally active complement and complement regulatory proteins have also been detected in tears. An overview of the complement pathway is presented in **Figure 3**. The relative amounts of different components, namely abundant C3 and factor B, but less C1q, suggest that activation via the alternative pathway (i.e., spontaneous hydrolysis of C3) is the predominant mechanism. Possible sources of the various complement components are leakage of plasma through the conjunctival vessels during sleep, infiltrating neutrophils, and local synthesis by corneal and conjunctival epithelial cells. Activation of the complement pathway generates fragments involved in acute inflammatory responses, fragments that act as opsonins which facilitate target recognition by neutrophils and results in the formation of membrane attack complexes that can lyse pathogens

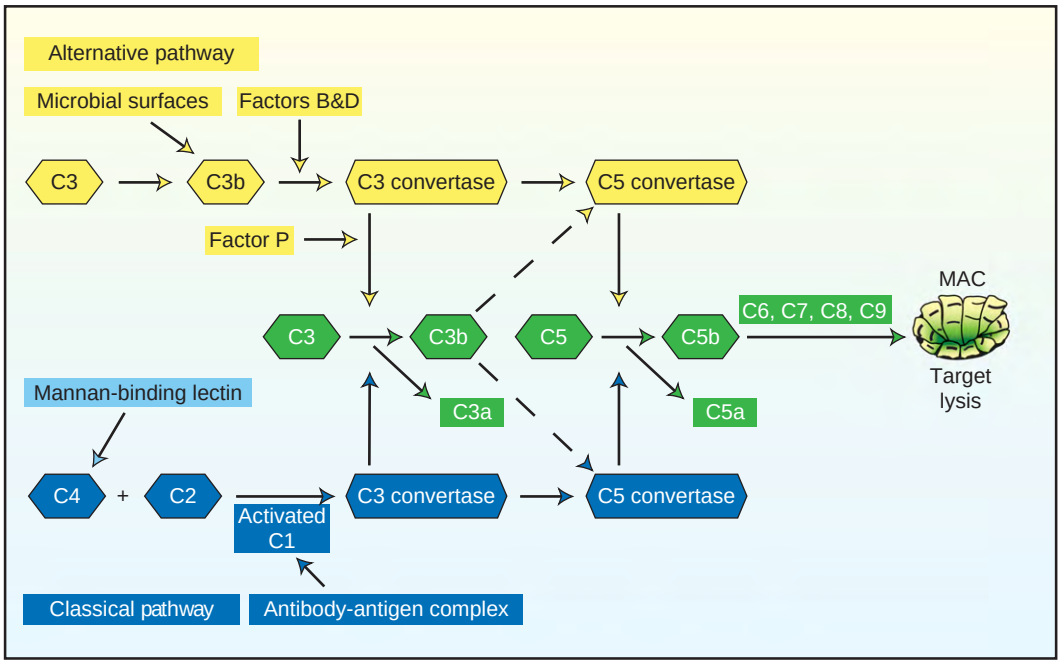

Figure 3 Overview of the complement pathway. The major components of the three known pathways (classical (blue), alternative (yellow) and mannan-binding lectin (light blue)) that lead to activation of complement are shown. In tears the primary pathway is believed to be the alternative pathway but, as can been seen, regardless of the mechanism of activation the outcome is the same (green), i.e., production of intermediaries with enzymatic activity (the convertases), generation of inflammatory mediators such as C3a and C5a and of opsonins such as C5b which bind to pathogen surfaces to facilitate their recognition by phagocytes. The final product of the pathway is the membrane attack complex (MAC) in which several complement components come together to form pores on a pathogen surface leading to lysis and death of the pathogen.

(and host cells). The complement pathway is believed to be most active when the eyes are closed (see comments below on closed-eye tears). To prevent unnecessary activation and hence tissue damage, the complement pathway is regulated by a number of factors. This pathway is inhibited by molecules such as lactoferrin and vitronectin both of which are present in the tears and CD55 (decay accelerating factor) as well as CD59 which are membrane-bound molecules expressed by corneal and conjunctival epithelial cells.

In immediate apposition to the superficial epithelial cells is a blanket of mucus, composed primarily of the gel-forming mucin MUC5AC which is secreted by goblet cells in the conjunctiva in response to parasympathetic stimulation. This blanket interacts with the glycocalyx coating the superficial cells. Membrane spanning mucins MUC 1, 4, and 16 produced by the epithelial cells are important components of the glycocalyx and can be cleaved from the cell surface and released into the tear film. Mucins are known to help prevent bacteria from reaching epithelial surfaces. This function has been attributed to a number of mechanisms, for example, mucin can bind and trap the bacteria, which are then effectively removed from the ocular surface by blinking. It should be noted, however, that the ability to interact with mucins varies widely among different organisms. There is also evidence that sIgA and positively charged proteins such as lysozyme and SLPI accumulate in the mucous blanket, thus providing a reservoir of antimicrobial agents. Therefore, mucins may trap microbes, which are then killed by accumulated antimicrobials or aggregated by sIgA and then cleared by blinking.

Thus, tears are equipped with a plethora of chemical entities capable of neutralizing invading pathogens. While many tear components have independent antimicrobial effects, several are thought to cooperate in a synergistic fashion to yield maximal effect. For example, sequestering of cations by lactoferrin destabilizes the cell wall of Gram-negative bacteria making the peptidoglycan layer more accessible to cleavage by lysozyme. Also, it should be brought to the reader's attention that the composition of the tears changes during sleep. Open-eye and reflex tears have primarily lysozyme, lactoferrin, lipocalin, and sIgA, whereas closed-eye tears have increased amounts of sIgA (up to 80% of total tear protein), complement components, and of serum-derived proteins. There is also a large influx of neutrophils within 2–3 h of eye closure, which provides additional defense factors in the guise of AMPs and reactive oxygen species, for example. Overall, these changes appear to represent a shift to a subclinical state of inflammation, which is believed to be necessary to protect the ocular surface from invasion by entrapped pathogens while the lids are closed. There is also an increase in proteins such as SLPI and elafin, which have potent

antiprotease activity, and vitronectin, which inhibits complement, which serve to protect the ocular surface cells in this proinflammatory environment.

Defense Mechanisms of the Ocular Surface Epithelia

Mechanical/Physical Defenses

The outermost superficial epithelial cells are bound by tight junctions, which effectively seal two cells together forming a barrier against free diffusion of fluids, electrolytes, and macromolecules as well as microorganisms and their secreted products. Tight junctions are also important in establishing and maintaining cell polarity. Polarized cells are characterized by differences in the composition and distribution of proteins and other surface molecules between apical and basolateral surfaces. This arrangement is maintained by the aforementioned tight junctions that segregate the domains and targeted delivery that sends the molecules to their correct location. Disruption of polarity, such as occurs with corneal epithelial cells migrating to recover an injured area, has been shown to increase susceptibility to infection. This may be the result of a number of factors, for example, host cell receptors with which pathogens interact may be more abundant on basolateral surfaces. Also, loss of polarity disrupts the apical mucin-containing glycocalyx, which normally helps restrict bacterial attachment.

Another important feature contributing to defense is the constant turnover of the ocular surface epithelial cells. Both corneal and conjunctival epithelia have a population of strategically located stem cells that provide new cells to replace those being shed into the tear film. In the absence of a penetrating injury, infection begins in the most superficial epithelial layers and so through the constant renewal of cells, outer infected cells may be sloughed off before there is time for the infection to spread to the lower epithelial layers.

Pathogen Recognition

While the tear film acts to prevent pathogens from reaching the ocular surface epithelial cells in the first place, it is very important that the cells have a system to recognize the presence of invading organisms if they do happen to conquer the outer defenses. Host cell proteins that mediate pathogen recognition are often referred to as pathogen recognition receptors (PRRs) and they recognize pathogen-associated molecular patterns present on bacteria, viruses, and fungi. The primary PRRs on epithelial cells are toll-like receptors (TLRs). These are type I transmembrane glycoproteins, which have an extracellular leucine-rich domain and a cytoplasmic domain homologous to the signaling domain of the interleukin (IL)-1 receptor.

Of the 10 functional human TLRs that have been identified all have been reported to be expressed by corneal and conjunctival epithelial cells. **Figure 4** shows a simplified diagram of the distribution of TLRs, their ligands, and signaling pathways. TLR1, 2, 4, 5, 6, and 10 are typically located at the cell surface. TLR2 forms heterodimers with TLR1 and with TLR6 and so can recognize a large variety of microbial products. For example, TLR2/6 heterodimers recognize lipoteichoic acid from Gram-positive bacteria and TLR2/1 heterodimers recognize triacyl lipoprotein/peptides of bacterial cell walls. TLR4 forms a complex with MD2 (also known as lymphocyte antigen 96) and cluster of differentiation 14 (CD14) protein and recognizes LPS from Gram-negative bacteria, while TLR5 recognizes flagellin, a component of bacterial flagella. TLR10, the ligand for which is unknown, is able to dimerize with TLR1 and TLR2. TLR3, 7, 8, and 9 are (typically) all located intracellularly, on endosomal membranes and recognize nucleic acids. TLR3 recognizes double-stranded RNA, a by-product of the replication of some viruses, whereas TLR7 and 8 recognize viral single-stranded RNA. TLR9 responds to unmethylated cytosine–phosphate–guanosine dinucleotide motifs found in both bacterial and viral DNA. Thus, by interacting with specific pathogen-derived molecules TLRs can detect the presence of a wide range of organisms, including those that replicate intracellularly.

The engagement of TLRs with their specific microbial ligand results in activation of intracellular signaling pathways, leading to a variety of functional changes in the ocular surface epithelial cells. The latter include production of inflammatory cytokines such as IL-6 and chemokines such as IL-8 that will attract neutrophils for phagocytosis and AMPs such as human β-defensin-2 that can directly kill invading pathogens (see the section entitled 'Antimicrobial peptides').

It is important that members of the normal ocular flora do not trigger TLR activation and hence cause unwanted inflammatory reactions at the ocular surface. To this end, it has been observed that flagellin from pathogenic, but not from nonpathogenic bacteria, can activate TLR5 in corneal epithelial cells. Expression of TLR5 (and possibly TLR4) appears to be restricted to basal and wing cells suggesting that TLR5 will only be activated when there is a breach in the corneal epithelium. Also, rather than being surface bound, TLR4 may be expressed intracellularly and so would not be available.

Evidence for the expression of another class of PRRs, the cytoplasmic nucleotide-binding and oligomerization domain (NOD) proteins, has yet to be investigated for the human ocular surface. However, mouse anterior eye tissue expressed both NOD1 (which recognizes meso-DAP, a component of peptidoglycan in Gram-negative organisms) and NOD2 (which recognizes muramyl dipeptide found in both Gram-positive and -negative bacteria).

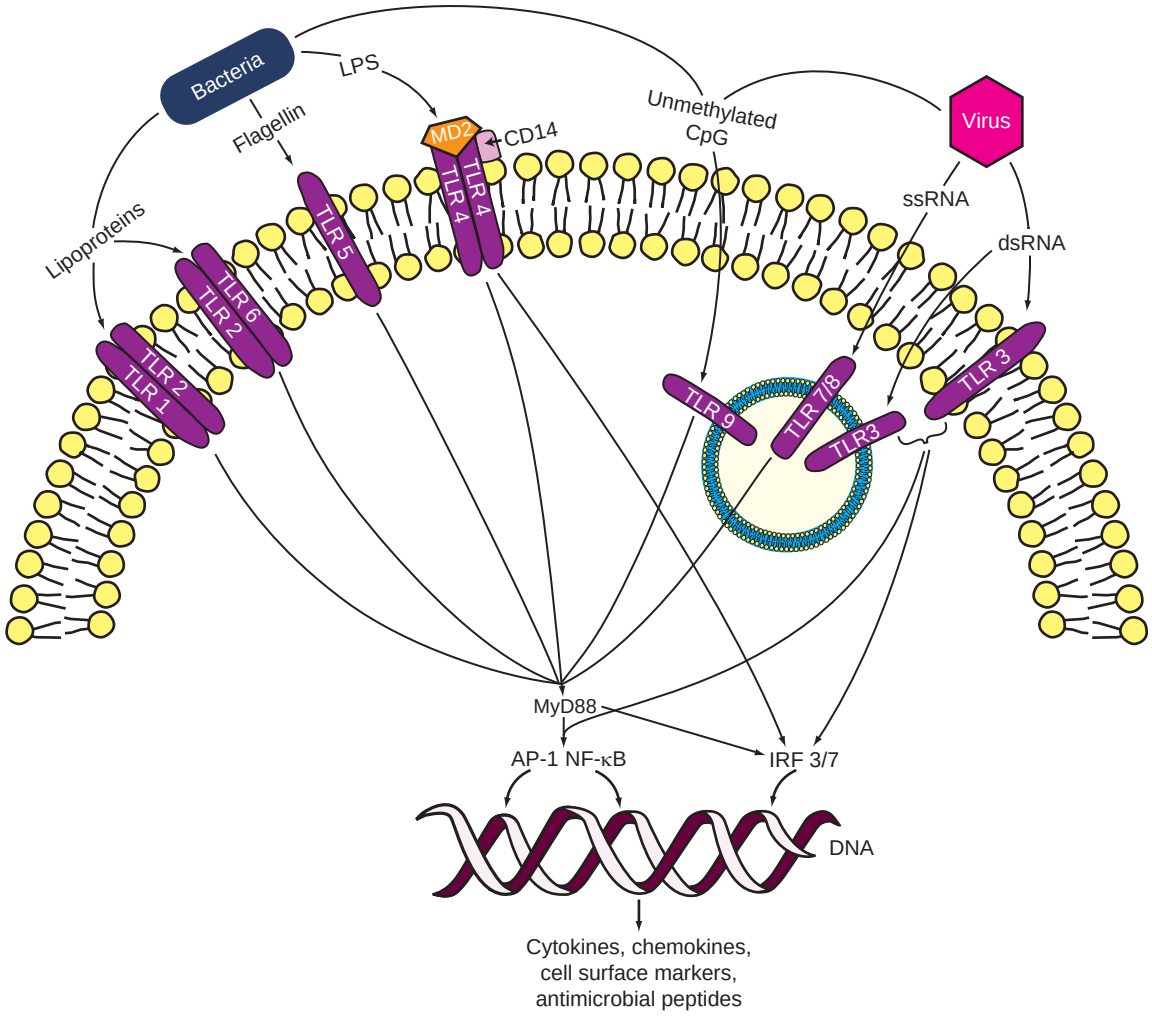

Figure 4 Toll-like receptor activation. The major TLRs expressed by ocular surface epithelial cells and their known bacterial and viral ligands are shown. For clarity the details of the several signaling pathways that lead to transcription factor activation and gene transcription have been omitted. LPS, lipopolysaccharide; CpG, cytosine–phosphate–guanosine dinucleotide; ssRNA, single stranded RNA, dsRNA, double stranded RNA, MyD88, myeloid differentiation protein 88; IRF 3/7, interferon regulatory factor 3/7; AP-1, activating protein-1; NF-κB, nuclear factor κB.

Antimicrobial Peptides

AMPs are small peptides, most less than 50 amino acids, that are amphipathic and typically carry an overall positive charge (+2 or greater) due to a relative excess of amino acids such as arginine and lysine. These peptides show a broad spectrum of antimicrobial activity and many have additional effects on mammalian cell behavior.

The two major categories of mammalian AMPs are the defensins and cathelicidins. Human defensins are characterized by the presence of six cysteine residues that interact to form three disulfide bonds (the specific pattern of connectivity gives rise to two classes referred to as α and β). Both corneal and conjunctival epithelial cells express at least three β-defensins (hBDs). hBD-1 and hBD-3 are constitutively expressed, whereas the expression of hBD-2 is variable, being expressed by normal tissue only occasionally. Ocular surface hBD-2 expression is known to be inducible by exposure to both Gram-negative and -positive bacteria and bacterial products such as LPS, peptidoglycan, and lipoproteins. This upregulation is chiefly mediated via the activation of TLRs such as TLR2. In a recent study, expression of a novel beta defensin gene DEFB 109 was detected in the ocular surface epithelia, and interestingly its expression was decreased in inflammation and infection. As noted earlier, α-defensins HNP-1 through -3 are produced by neutrophils and are present in the normal tear film. They can also be detected in the cornea and conjunctiva when neutrophils infiltrate in response to a specific stimulus.

The cathelicidins have a highly conserved N-terminal cathelin domain and a variable antimicrobial domain. Only one, LL-37, is expressed in humans. LL-37 is expressed by both corneal and conjunctival epithelial cells and its expression is increased in response to corneal epithelial injury

and bacterial challenge with *P. aeruginosa* and *S. aureus*. LL-37 is also a major component of neutrophil granules; thus, its ocular surface levels are expected to rise in situations leading to infiltration of these and other inflammatory cells.

While defensins and LL-37 represent the main AMPs present at the ocular surface, others have been reported including liver expressed AMP-1 and -2, statherin, CCL28 and CXCL-1 (two of many antimicrobial cytokines), MIP3α, and thymosin β-4. However, as most of these molecules have other recognized functions, it is unlikely that antimicrobial effects are the major facet of their action at the ocular surface.

The primary site of AMP action is the microbial cell membrane, electrostatic disruption of which leads to permeabilization, loss of essential intracellular components, and death (see **Figure 2**). However, intracellular targets may also be utilized leading to inhibition of protein, peptidoglycan, and nucleic acid synthesis and interference with the activity of bacterial heat-shock proteins. Epithelial β-defensins and LL-37 are effective against common ocular surface bacterial pathogens *in vitro* with hBD-3 and LL-37 showing the broadest spectrum and most potent activity. Animal studies have revealed that experimental infection with *P. aeruginosa* in genetically modified mice unable to express cathelicidin causes much more severe disease and corneal damage than in normal wild-type mice, thus showing that AMPs are important for ocular surface defense *in vivo*.

In addition to exerting direct antimicrobial effects, AMPs have other properties that help protect against pathogens and their destructive actions. For example, LL-37 is known to bind and neutralize LPS. The latter is a product from Gram-negative bacteria and through activating TLR4 induces an inflammatory response and likely mediates much of the ocular surface damage that results from infections with pathogens such as *P. aeruginosa*. Thus, LL-37 may have a role in dampening LPS-mediated ocular surface inflammation and damage. Also, both defensins and LL-37 have been shown to be chemotactic for a variety of immune and inflammatory cells, including lymphocytes, monocytes, and immature dendritic cells thus may help draw these cells to a site of infection. AMPs also stimulate inflammatory and immune cell cytokine production, which in turn can modulate cellular functions. Additionally, hBD-3 has been shown to activate dendritic cells, raising the possibility that corneal/conjunctival epithelial hBD-3 may be able to activate epithelial Langerhans cells and stromal dendritic cells which in turn may initiate an adaptive immune response.

Other Contributions to Ocular Surface Epithelial Defense

As noted earlier, the outermost superficial cells of both the cornea and conjunctiva are coated in a matrix of carbohydrate referred to as the glycocalyx. By projecting from the epithelial cell surface, membrane spanning mucins MUC 1, 4, and 16 of the glycocalyx physically prevent pathogens from reaching the cell membrane. Also, some organisms are repulsed by negatively charged glycosaminoglycans present on the mucin.

The ocular surface epithelial cells also produce a variety of cytokines and chemokines that are important in protection from microbial invasion. IL-1 is an important cytokine released in response to trauma and injury and among a plethora of activities serves to regulate production of other molecules such as IL-6, growth regulated oncogene (GRO)-α, -β, -γ, TNF-α, and IL-8, which in turn modulate inflammatory and immune cell infiltration and activation.

Dispersed between the epithelial cells of the cornea and conjunctiva are bone-marrow-derived dendritic cells called Langerhans cells. These cells are highly potent antigen-presenting cells which capture antigen and when mature present it to T lymphocytes in nearby secondary lymphoid tissues so activating adaptive immunity. The Langerhans cells are typically found between basal epithelial cells and in the cornea their density is lowest in the central region and gradually increases toward the periphery. Also, most cells in central cornea appear to be small immature cells. In the periphery, larger mature major histocompatibility complex class II (MHC II) expressing cells with prominent dendritic processes are observed. Overall Langerhans cells perform a surveillance function, screening their environment for pathogens that have breached the defenses of the tear film and the epithelial barrier. If successful in their search they then activate adaptive immunity to help eliminate the invader.

Sensory nerves, which are particularly abundant in the cornea, also provide an important contribution to ocular surface defense. When triggered nerves induce the production of reflex tears, which, by virtue of their increased volume, help wash pathogens from the ocular surface and dilute out their toxic products. Release of neuropeptides such as substance P from the nerve termini may also affect epithelial cell cytokine production that, as noted above, may modulate other aspects of host defense.

The presence of a complement of nonpathogenic organisms also assists in preventing infection. Such commensals deplete the tears of nutrients, occupy attachment sites so preventing binding of pathogens, and produce bacteriocins that kill members of nonrelated species.

Concluding Remarks

In summary, the ocular surface and tears possess a wide range of chemicals and physical attributes that help prevent infection. Such redundancy is commonplace in biological systems, but is particularly important at the ocular surface where the inability to control and eliminate

an infection can have dire consequences for visual function. Having multiple protective mechanisms is also necessary as pathogens are very adept at developing strategies to circumvent host defenses. While countering one specific mechanism is relatively easily achieved, developing multiple strategies is rather more challenging.

Acknowledgments

The author acknowledges grant support from NIH, NSF, and the State of Texas for her work on ocular surface antimicrobial peptides and thanks Kimberly Thompson of the University of Houston College of Optometry audio-visual department for drawing the figures.

See also: Antigen-Presenting Cells in the Eye and Ocular Surface; Conjunctiva Immune Surveillance; Corneal Epithelium: Cell Biology and Basic Science; Corneal Nerves: Anatomy; Corneal Nerves: Function; Immunopathogenesis of HSV Keratitis; Immunopathogenesis of Pseudomonas Keratitis; Overview of Electrolyte and Fluid Transport Across the Conjunctiva; Pathogenesis of Fungal Keratitis; Tear Film Overview.

Further Reading

Chen, G., Shaw, M. H., Kim, Y. G., and Nunez, G. (2009). Nod-like receptors: Role in innate immunity and inflammatory disease. *Annual Review of Pathology* 4: 365–398.

Evans, D. J., McNamara, N. A., and Fleiszig, S. M. J. (2007). Life at the front: Dissecting bacterial–host interactions at the ocular surface. *Ocular Surface* 5: 213–227.

Flanagan, J. L. and Willcox, M. D. P. (2009). Role of lactoferrin in the tear film. *Biochimie* 91: 35–43.

Fleming, A. (1922). On a remarkable bacteriolytic element found in tissues and secretions. *Proceedings of the Royal Society Series B* 93: 306–317.

Gupta, G. and Surolia, A. (2007). Collectins: Sentinels of innate immunity. *BioEssays* 29: 452–464.

Hamrah, P. and Dana, M. R. (2007). Corneal antigen-presenting cells. *Chemical Immunology and Allergy* 92: 58–70.

Hazlett, L. D. (2007). Bacterial infections of the cornea (*Pseudomonas aeruginosa*). *Chemical Immunology and Allergy* 92: 185–194.

McDermott, A. M. (2009). The role of antimicrobial peptides at the ocular surface. *Ophthalmic Research* 41: 60–75.

Paulsen, F. P. and Berry, M. S. (2006). Mucins and TFF peptides of the tear film and lacrimal apparatus. *Progress in Histochemistry and Cytochemistry* 41: 1–53.

Sack, R. A., Nunes, I., Beaton, A., and Morris, C. (2001). Host-defense mechanisms of the ocular surfaces. *Bioscience Reports* 21: 463–480.

Shafer, W. M. (ed.) (2006). *Antimicrobial Peptides and Human Disease.* Berlin: Springer.

Yu, F.-S. X. and Hazlett, L. D. (2006). Toll-like receptors and the eye. *Investigative Ophthalmology and Visual Science* 47: 1255–1263.

Development of the Retinal Vasculature

T Chan-Ling, University of Sydney, Sydney, NSW, Australia

Glossary

Angiogenesis – The growth of new blood vessels through the process of budding from existing vessels. Angiogenesis occurs in response to a stimulus such as hypoxia.
Inner plexus – The network of superficial blood vessels that lies on the inner surface of the retina.
Mural cells – Includes pericytes and smooth muscle cells. These cells surround the endothelial cell tubes and contribute to the formation of stable vessels.
Outer plexus – The deeper network of blood vessels that lies at the junction of the inner nuclear layer and the outer plexiform layer of the retina. This layer of vessels forms by budding from the inner plexus, and consists entirely of capillaries.
Pericytes – Mesenchymal cells that are associated with small vessels. These cells are critical for vessel stability and for the formation of the blood–retinal barrier.
Vasculogenesis – The process of vessel formation through the organization of vascular precursor cells into chords and vessels. Vasculogenesis proceeds in the absence of stimuli such as VEGF.

Introduction

The development of the vascular network of the human retina follows a very specific topography and series of events, producing a network of vessels that precisely meets the metabolic demands of the healthy adult retina. Disruption of this process can lead to the under- or overproduction of vessels and/or the formation of vessels with pathological characteristics, including a breakdown of the blood–retina barrier (BRB) and inappropriate pericyte ensheathment leading to vessel instability. In this article, we describe the process through which the vasculature develops, and the intrinsic and extrinsic signals that control its formation.

An Overview of Human Adult Retinal Vasculature

The retina has the highest metabolic demand of any tissue in the body. The conflicting requirements of sufficient blood supply and minimal interference with the light path to the photoreceptors are met by two vascular supplies: inherent intraretinal vessels supply the inner two-thirds of the retina, and the choroidal vasculature supplies the outer third of the retina.

The vasculature of the adult retina enters and exits through the optic disk (**Figure 1(a)**). As shown in the fundus photo (**Figure 1(b)**), four main artery/vein pairs supply the human retina. These vessels are termed the superior nasal, inferior nasal, superior temporal, and inferior temporal branches of the central retinal artery and vein. Smaller arterioles branch off these four main arteries, whereas terminal branches bifurcate toward the peripheral retina. The fovea, a region of the retina that contains the highest density of photoreceptors, remains avascular throughout development and in the adult retina. The inner plexus ramifies in the ganglion cell and nerve fiber layers. Some of these vessels dive down through the inner plexiform and inner nuclear layers to form the outer, or deep, plexus at the junction of the inner nuclear and outer plexiform layers of the retina (**Figure 1(c)**). Vessels in the inner plexus cover the spectrum from arterioles and venules to capillaries and postcapillary venules, whereas vessels in the outer plexus are mainly capillary in size. Both vascular layers reach almost to the edge of the adult retina, leaving an avascular rim that is thin enough to be adequately oxygenated through diffusion from the choroid. A third intraretinal vascular network, the radial peri-papillary capillaries (RPCs), forms a limited plexus in the nerve fiber layer around the optic disk. The RPCs radiate out from the optic nerve head (ONH) and supply the thick nerve fiber bundles where they exit the retina.

Figure 1(d) is a schematic representation of central nervous system (CNS)/microvascular interface, as would be found typically in the human retina. CNS vessels are characterized by tight junctions between adjacent vascular endothelial cells; the tight junctions are responsible for creating the BRB. Outside the endothelial cell layer lays the basal lamina, which is laid down by endothelial cells and pericytes. This layer is composed predominantly of collagen IV, fibronectin, and laminin. Pericytes are located within the basal lamina, between the vascular endothelial cells and the astrocytic endfeet that form the glia limitans, or glial limiting membrane. In addition to astrocytes, ultrastructural evidence suggests that the glia limitans also includes perivascular cells and microglia.

Vasculature of the Primordial Retina

During embryonic development, the retina forms as an extension of the diencephalon. The rudimentary structures

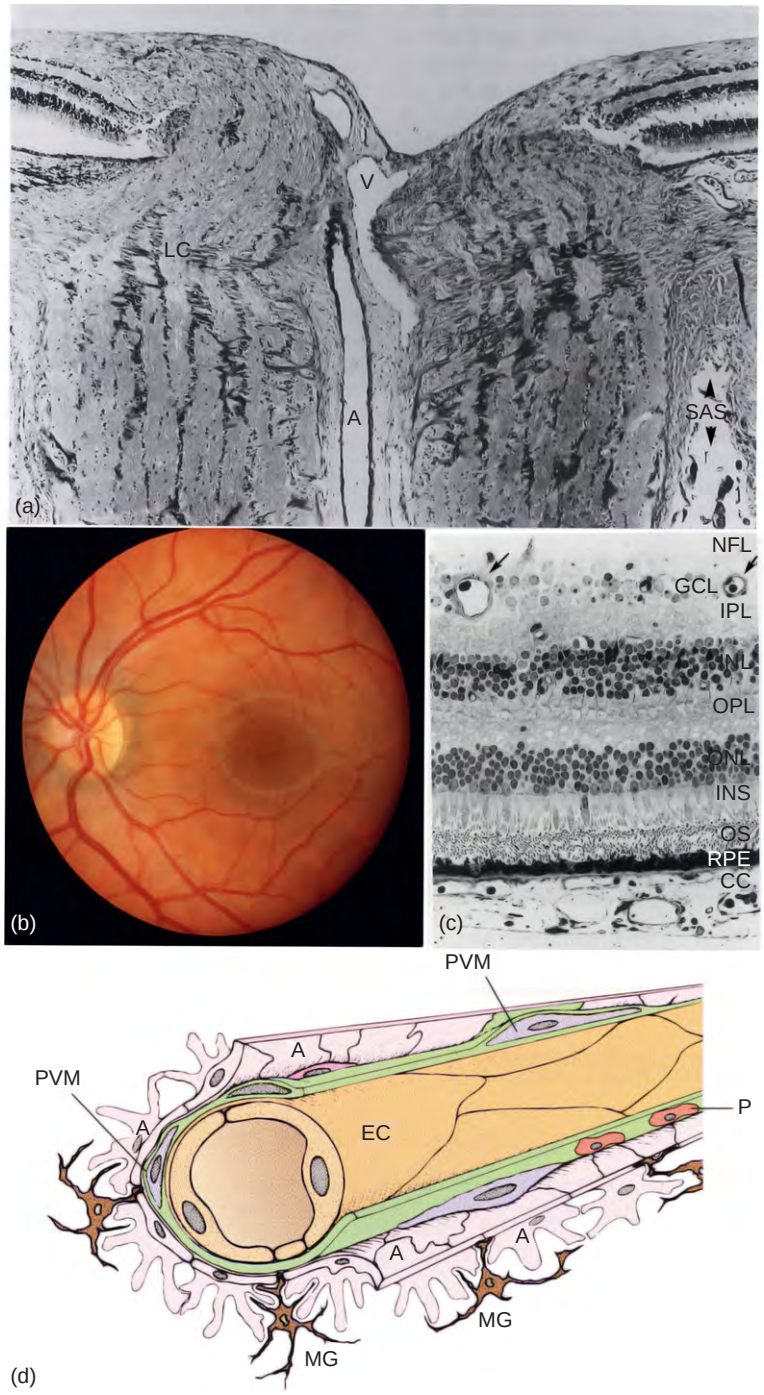

Figure 1 Structure of the adult retina. (a) Cross-section of the adult retina through the optic nerve. Shown are a vein (V), artery (A), lamina cribrosa (LC), and subarachnoid space (SAS). Forrester, J. V., Dick, A. D., McMenamin, P. G., and Lee, W. R. (2002). *The Eye: Basic Sciences in Practice*, 2nd edn. London: Elsevier. (b) Wide-field photograph of the normal human fundus. Visible are the four main artery/vein pairs, extending out from the optic nerve in a four-lobed pattern. Reproduced from Ms. Christine Craigie, Sydney Australia. (c) Low magnification micrograph of the human retina. Starting with the inner retina at the top of the image, visible are the nerve fiber layer (NFL), the ganglion cell layer (GCL), the inner plexiform, and inner nuclear layers (IPL/INL), the outer plexiform and outer nuclear layers (OPL/ONL), the photoreceptor inner segments (INS) and outer segments (OS), the retinal pigmented epithelium (RPE), and the choroid (CC). The arrows point to vessels of the inner (superficial) plexus. From Forrester, J. V., Dick, A. D., McMenamin, P. G., and Lee, W. R. (2002). *The Eye: Basic Sciences in Practice*. London: Elsevier. (d) Schematic diagram illustrating the components of a retinal (brain) vessel wall. From the vascular lumen outwards, shown are endothelial cells (EC; in pale orange), basal lamina (including collagen IV, fibronectin and laminin; in green), pericytes (P; in red), astrocytes (A; in lavender), perivascular cells (PVM; light blue), and perivascular microglia (MG; brown). McMenamin, P. G. and Forrester, J. V. (1999). In: Lotze, M. T. and Thompson, A. W. (eds.) *Dendritic Cells in the Eye*. London: Academic Press.

of the eye are distinguishable by 4–5 weeks gestation (WG). At the earliest stages in development, the primordial lens and retinal tissues are oxygenated through the hyaloid vasculature, a vascular network that begins as an artery entering the eye through the optic nerve (the central hyaloid artery), splits into hyaloid vessels as it continues forward through the vitreous and around the developing lens, and exits at the front of the eye. This vascular network is present early in human embryonic development and regresses as the retinal vasculature forms and is able to meet the increasing metabolic demands of the eye. Typically, the hyaloid vasculature has totally regressed by the ninth month of gestation.

Formation of the Human Retinal Vasculature Takes Place Through Vasculogenesis and Angiogenesis

Blood vessels can be formed by one of two distinct mechanisms. Vasculogenesis is the *de novo* formation of vessels by the aggregation of endothelial precursor cells. Vessels develop from vascular precursor cells (VPCs) that aggregate into solid vascular cords, which then become patent and differentiate to form primitive endothelial tubes. Formation of vessels by angiogenesis occurs through budding from existing vessels; this process takes place through proliferation of vascular endothelial cells and serves to vascularize neighboring tissues. The process of angiogenesis is driven by signals that are produced in response to hypoxia, including vascular endothelial growth factor$_{165}$ (VEGF$_{165}$), whereas the process of vasculogenesis is independent of hypoxia.

Vasculogenesis: Vascular formation through transformation from VPCs

The first event in the development of the retinal vasculature is the *de novo* formation of vessels by vasculogenesis. This stage, detectable in the human retina before 12 WG, initiates with the migration of spindle-shaped cells of mesenchymal origin from the ONH. The individual cells can be Nissl stained and express CD39, vascular endothelial growth factor receptor 2 (VEGFR2), and ADPase, an ecto-enzyme found on the luminal surface of endothelial cells in the adult retinal vasculature. The VPCs migrate outward from the optic disk, as shown in **Figure 2(a)**.

Patent vessels form through the transformation of solid vascular chords. The VPCs localize to the inner surface of the retina, between nerve fiber bundles, and orient their longitudinal axes along the direction of migration. The population of VPCs proliferates and differentiates to form a primordial vascular bed centered on the optic disk (**Figure 2(b)**). As early as 14–15 WG, vascular chords begin to coalesce on the surface of the retina behind the wave of spindle cells, beginning in the region proximal to the ONH and progressing outward (**Figure 2(c)** and **2(e)**). **Figure 2(d)** shows the transition from vascular chords and the discrete spindle cells located more peripherally.

Vascular chords begin to establish themselves as vessels that express CD34 and support blood flow as early as 18 WG (**Figure 2(f)**). These first primordial vessels formed through vasculogenesis are typically radial, have uniform diameter and have low capillary density (**Figure 3(a)**). The formation of primitive vessels lags behind the leading edge of VPCs by a distance of at least 1 mm. Vasculogenesis and the formation of the primordial vessel architecture is complete by 21 WG, at which point spindle cells are no longer detectable in the retina (**Figure 3(b)**).

Spindle cells (and the formation of cords and vessels behind the leading edge of spindle cells) migrate outward from the optic disk in a four-lobed pattern, as seen in **Figure 3(b)**. The lobes extend the farthest in the temporal and superior directions, and they correspond to the future location of the four major artery–vein pairs in the adult retina (**Figure 1(b)**). The lobes curve around the region of the incipient fovea, leaving this area free of spindle cells and vascular cords. The fovea and perifoveal region remains avascular through 25 WG.

Although vasculogenesis is responsible for the primordial vessels that form in the inner two-thirds of the developing retina, this primitive network with its low capillary density is very inefficient in meeting the metabolic demands of the underlying retinal tissue. As a result, the remaining vessels in the retina form through the process of angiogenesis, which is driven by physiological levels of hypoxia. Angiogenesis is responsible for the increasing vascular density in the central retina (**Figure 3(c)**), vessel formation on the inner surface (the inner plexus) of the peripheral retina, and the formation of the outer, deep plexus and the radial RPCs near the ONH.

Angiogenesis. Angiogenesis in the retina is driven by physiological hypoxia, which occurs as a result of the increasing synaptic activity in the retinal tissues. As the retina thickens and the cell layers start to differentiate and become active, the tissue becomes hypoxic. In response to hypoxia, the astrocytes in the nerve fiber and ganglion cell layers (GCLs) express VEGF$_{165}$, which in turn stimulates endothelial cell growth. Once these vessels become patent and can direct blood flow, the demand for oxygen is met and local VEGF expression decreases. It is important to note that the physiologic levels of hypoxia are too low to damage the surrounding tissue, but are sufficient to signal the need for increased oxygen supply to the tissue.

Inner plexus: Angiogenic filopodial extension is mediated by an astrocytic template and basal lamina components. As with vasculogenesis of the retina, formation of the superficial vascular plexus through angiogenesis begins in the region around the optic disk and spreads outward toward the periphery. As early as 17–18 WG, an exuberant network of broad capillaries starts to grow out from the primary

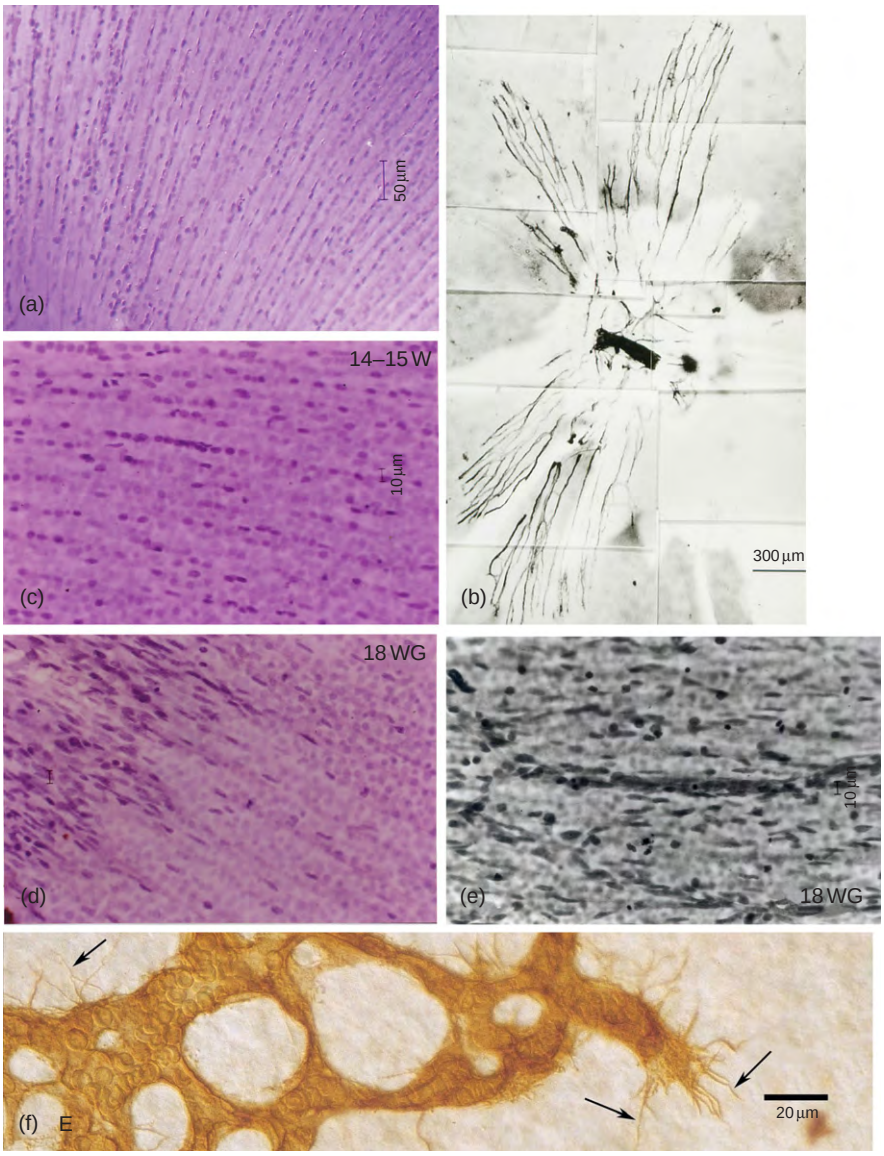

Figure 2 Formation of the early retinal vasculature. (a) Nissl-stained retinal whole mount of a 14–15 WG human fetal retina, immediately peripheral to the optic nerve head. Large numbers of spindle cells are visible, streaming from the optic nerve head. These cells were concentrated between nerve fiber bundles. (b) Immunohistochemical analysis of $CD34^+$ vessels in a human fetal retina whole mount, 15 WG. (c) Nissl-stained retinal whole mount of a 14–15 WG human fetal retina, showing the alignment of vascular precursor cells, the first evidence of chord formation prior to the development of patent vessels. (d) Nissl-stained retinal whole mount of an 18 WG human fetal retina. Visible is the leading edge of migration of the spindle-shaped vascular precursor cells. Vascular chords are visible behind the leading edge. (e) A newly-formed solid chord of cells forming a vessel in a human fetal retina at 18 WG. From Hughes, S., Yang, H., and Chan-Ling, T. (2000). Vascularization of the human fetal retina: Roles of vasculogenesis and angiogenesis. *Investigative Ophthalmology and Visual Science* 41: 1217–1228. Copyright Association for Research in Vision and Ophthalmology. (f) CD34+ vessels in a human retina, 18 WG. Note the red blood cells in the patent vessels and the filopodial extensions (arrows) in the region of new vessel growth. From Chan-Ling, T., McLeod, D. S., Hughes, S., et al. (2004). Astrocyte-endothelial cell relationships during retinal vascular development. *Investigative Ophthalmology and Visual Science* 45: 2020–2030. Copyright Association for Research in Vision and Ophthalmology.

vasculature, filling the area that lies between the primordial vessels (**Figure 3(d)**). Between 18 and 30 WG, the sprouting of new vessels is led by the filopodia of endothelial tip cells (**Figures 3(e)** and **4(b)**). These filopodia orient along the net-like framework that has been set up by astrocytes in the wake of the leading edge of APCs, initially producing a capillary bed that closely follows the structure and organization of the astrocyte scaffold (**Figure 4(a)** and **4(c)**). Although endothelial tip cells serve to orient the growth of the capillary network, the tip cells themselves do not divide. Instead, rapid cell growth occurs at the level of the trailing stalk cell (**Figure 4(b)**).

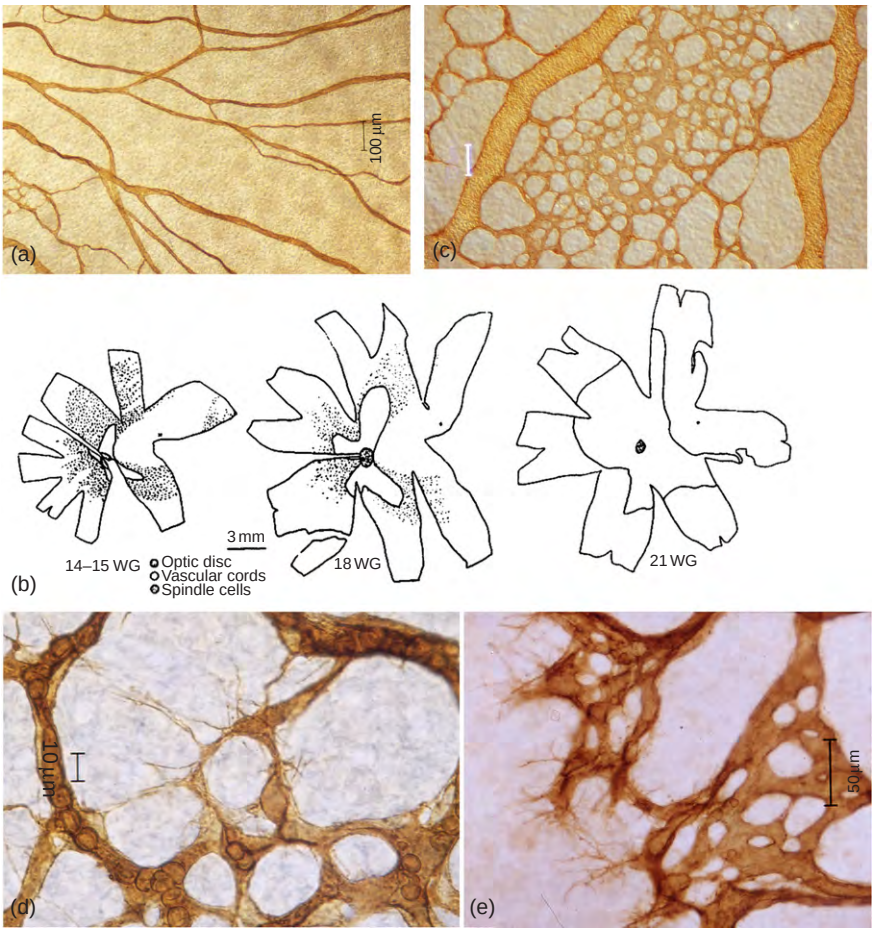

Figure 3 Vascularization of the human fetal retina. (a) Immunohistochemical analysis of $CD34^+$ vessels in the central retina at 18 WG. These near-radial vessels all extend predominantly radially from the optic disk. (b) Topographical maps of the outer limits of spindle cells and vascular chords in the human fetal retina at 14–15, 18, and 21 WG. (c) $CD34^+$ vessels in a human fetal retina at 21 WG. Note the extensive capillary network that has formed in the space between the major vessels. (d) $CD34^+$ vasculature in a human fetal retina at 26 WG. Vessel development follows the extension of numerous filopodia. Capillary sprouting (angiogenesis) is responsible for increasing capillary density in central retina. (e) $CD34^+$ vasculature in a region of filopodial extension at the leading edge of patent vessel formation in a human fetal retina at 25 WG. Red blood cells evident in the vessel lumen in the vessels just central to the region of filopodial extension demonstrate that these vessels are patent. From Hughes, S., Yang, H., and Chan-Ling, T. (2000). Vascularization of the human fetal retina: Roles of vasculogenesis and angiogenesis. *Investigative Ophthalmology and Visual Science* 41: 1217–1228. Copyright Association for Research in Vision and Ophthalmology.

In the human fetal retina, Pax-2 expression is limited to cells of the astrocyte lineage. Glial fibrillary acidic protein (GFAP) is expressed in mature astrocytes. $Pax\text{-}2^+/GFAP^-$ astrocyte precursor cells (APCs) can be detected at the ONH around 12 WG. This population of cells appears at a slightly later time than the VPCs, and can readily be distinguished from VPCs by their rounded shape and by the expression of Pax-2. Like the VPCs, the APCs migrate outward from the optic disk. The leading edge of APCs is immediately peripheral to the leading edge of vessel formation, preceding the region of vessel formation by no more than 120 µm (**Figure 4(c)**). Beginning at 18 WG, astrocytes loosely ensheath the newly formed vessels, where they play a role in the induction of the BRB. APCs migrate outward from the optic disk behind the spindle cells. Similar to the spindle cells, they also remain excluded from the incipient fovea as they migrate outward. VPCs (and the primordial vasculature formed from these cells) are limited to the inner two-thirds of the retina (**Figures 2(b)** and **3(b)**) but APCs continue to migrate toward the peripheral retina. As they mature, APCs begin to express GFAP. The $Pax\text{-}2^+/GFAP^+$ astrocyte cells reach the edge of the retina around 26 WG.

In addition to driving the formation of capillaries in the space between the primitive vascular network, angiogenesis also controls the peripheral spread of vessels beyond the inner two-thirds of the retina. The growth of vessels in this region closely follows the central-to-peripheral migration of astrocytes. **Figure 4(c)** and **4(d)** show the relationship between patent vessel formation, APCs, and differentiated astrocytes. Again, the increasing metabolic demands of the maturing tissues lead to hypoxia and the

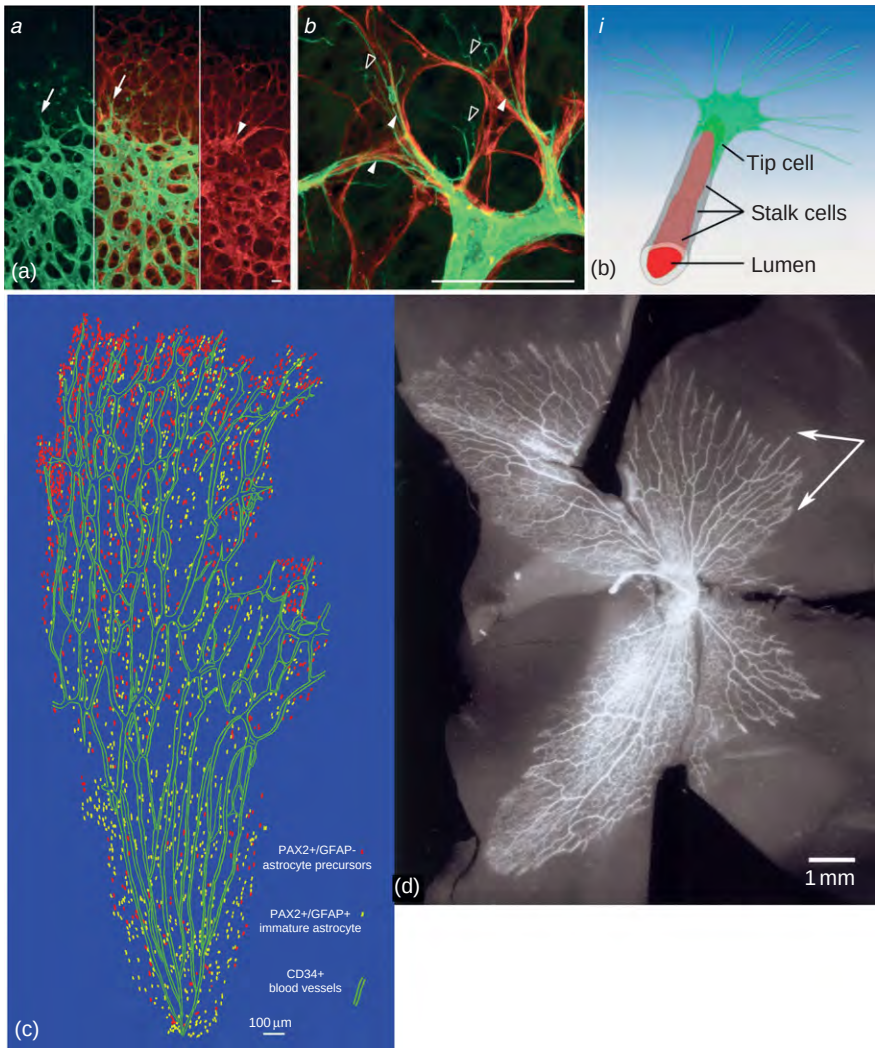

Figure 4 Angiogenesis and association of the developing vasculature with an astrocytic scaffold. (a) Low magnification (3 panels on the left) and high magnification (right panel) of an early postnatal mouse retinal whole mount, showing the overlap between the vascular plexus (isolectin, green) and astrocytic scaffold (GFAP; red) during development. (b) An illustration of endothelial tip cells, stalk cells and lumen. From Gerhardt, H., Gloding, M., Fruttinger, M., et al. (2003). VEGF guides angiogenic sprouting utilizing endothelial tip cell filopodia. *Journal of Cell Biology* 161: 1163–1177. (c) Developmental map of a 14-WG retina. Red: $Pax2^{+}/GFAP^{-}$ APCs; yellow: $Pax2^{+}/GFAP^{+}$ immature astrocytes; green: $CD34^{+}$ blood vessels. At this stage, $Pax2^{+}/GFAP^{-}$ APCs extend in advance of the leading edge of $CD34^{+}$ blood vessels by a small margin. At the midretina and near the optic nerve head, most cells are $Pax2^{+}/GFAP^{+}$ immature astrocytes, and $CD34^{+}$ vessels are clearly evident. (d) ADPase vasculature in a retinal wholemount from a human fetus at 16 WG. Note the four well-defined vascular arcades. From Chan-Ling, T., McLeod, D. S., Hughes, S., et al. (2004). Astrocyte-endothelial cell relationships during retinal vascular development. *Investigative Ophthalmology and Visual Science* 45: 2020–2030. Copyright Association for Research in Vision and Ophthalmology.

production of VEGF by the network of astrocytes that has formed on the surface of the retina; the dense capillary mesh forms along the astrocyte scaffold. Conversely, the endothelium may also influence astrocytic differentiation, as vascular endothelial cells have been shown to induce the expression of GFAP in APCs.

Outer plexus: Angiogenic growth is driven by neuronal maturation. The outer or deep layer of vessels also forms by the process of angiogenesis. Beginning around 25–26 WG, the superficial vessels start to bud and grow radially down from the inner plexus of the retina (**Figure 5**). At the junction of the inner nuclear layer and the outer plexiform layer, the vessels start to ramify among the two layers. This stage in fetal development coincides with the peak period of eye opening, when the visually evoked potential, indicative of a functional visual pathway and photoreceptor activity, is first detectable in the human infant. The radial growth of these descenders is not preceded by either VPCs or APCs. VEGF expression in this region correlates with the soma of Müller cells, suggesting

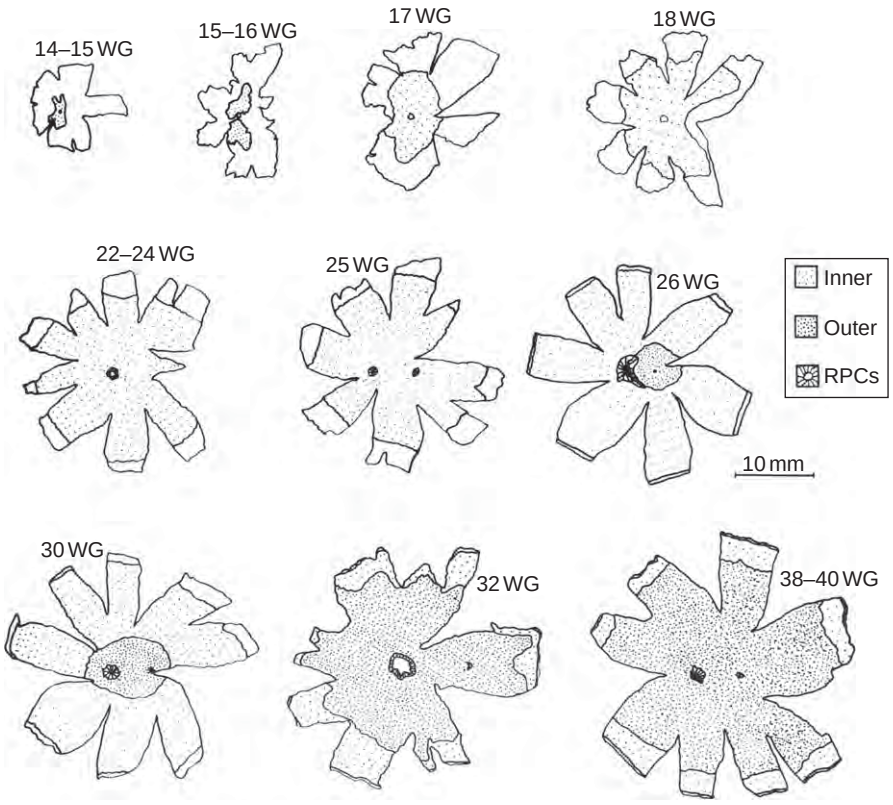

Figure 5 Outer limits of the inner and outer plexuses and the RPCs during development of the human fetal retina. Shown are representative maps of human vascular development from 14–40 weeks gestation. From Hughes, S., Yang, H., and Chan-Ling, T. (2000). Vascularization of the human fetal retina: Roles of vasculogenesis and angiogenesis. *Investigative Ophthalmology and Visual Science* 41: 1217–1228. Copyright Association for Research in Vision and Ophthalmology.

that these cells produce the VEGF that stimulates and guides endothelial cell growth in the outer vascular plexus.

Unlike the inner plexus, the formation of the outer plexus is centered around the fovea. Formation of the outer plexus exactly matches the pattern of maturation of the neuronal retina, suggesting that increased metabolic demands from active neurons produce local, physiological hypoxia and drive the growth of vessels to these tissues (**Figure 5**). In this region, the vasculature is limited to capillary-sized vessels; larger vessels are not found in the outer plexus.

Foveal and perifoveal region. The vasculature of the inner plexus surrounds, but does not enter, the fovea; the fovea is supported by the outer plexus alone. The area of greatest cone density in the retina lies in the center of the avascular area, in a region called the fovea centralis (**Figure 6(a)–6(c)**). The absence of surface vessels in this region allows for maximal light penetration with minimal shadowing of the densely packed cones. The fovea itself, an oval of 500 – 600 μm in diameter, remains completely avascular through 25 WG (**Figure 6(d)**). The developmental cues that direct this aspect of retinal vascularization are not well understood, but recent evidence suggests that the developing fovea expresses antiangiogenic factors including pigment epithelium derived factor (PEDF), natriuretic peptide precursor B, and collagen type IVα2.

More recently, it has been shown that expression of Eph-A6 directs vascularization in the fovea and perifoveal region. Immunohistochemistry from fetal primate retinas suggests that a gradient of Eph-A6 is centered at the fovea. This gradient, which is highest at the inner GCL and lowest near the inner plexiform layer, serves to repel astrocytes and angiogenesis from the inner layer of the retina toward the inner plexiform layer, where the vessels are found in the primate fovea. Because the incipient fovea lacks an astrocytic scaffold to set up the framework for vascularization, the pattern of formation of vessels in the outer plexus of the fovea and perifoveal region is different from that of the capillary networks in the inner plexus. As shown in **Figure 6(e)**, from the time they are formed, the vessels are much more regular in their size and spacing than are newly formed capillary networks elsewhere in the retina (**Figure 6(f)**).

Radial peri-papillary capillaries. The third vascular plexus of the retina, the RPCs, begins to form around 21 WG (**Figure 5**). These capillary-sized vessels typically extend radially from the ONH (**Figures 5** and **7(a)**) and cover a small rim surrounding the optic papilla (ONH); for this

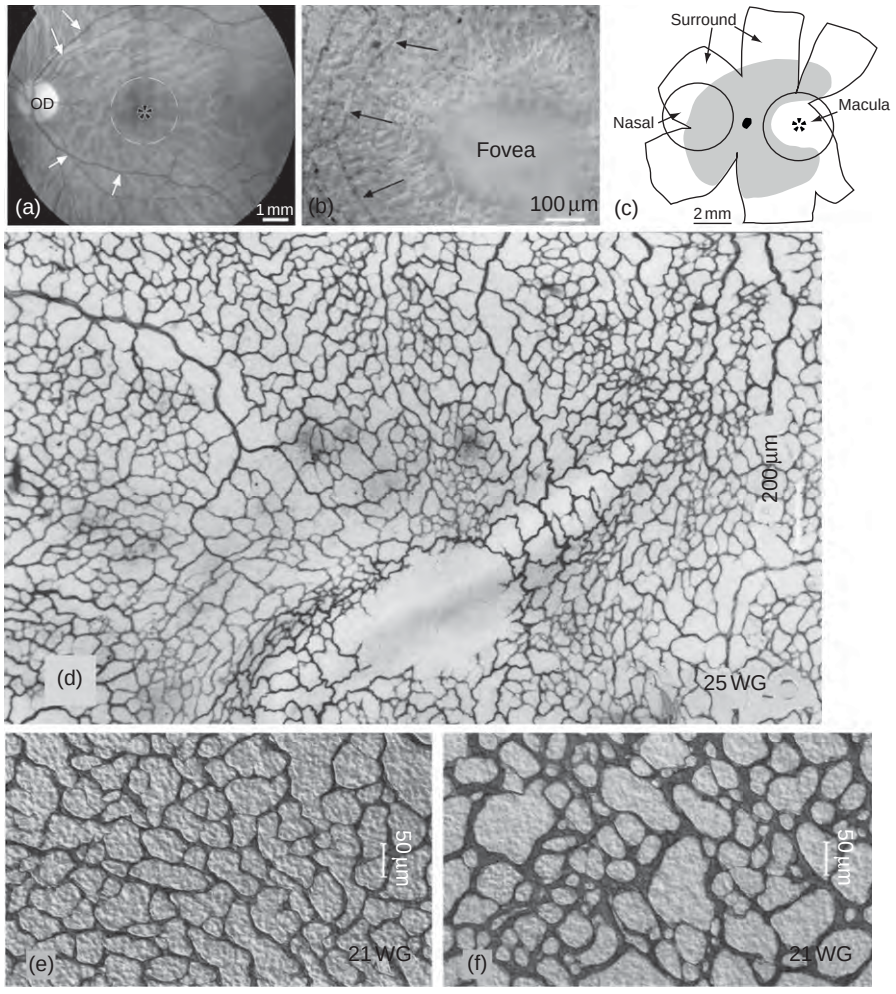

Figure 6 Vascularization in the foveal and perifoveal region. (a) Fundus of the adult human retina. Shown are the optic disk (OD), the macula (broken circle), and the fovea centralis (asterisk). (b) High magnification image of a flatmount of a human fovea. Note the vessels near the fovea (arrows); no vessels are seen on the surface of the fovea. (c) Diagram of a human fetal retina flatmount at 19 WG, showing the vascularized region (gray shading), the macula (circle), and the fovea (asterisk). Note how the region of vascularization curves around the fovea and does not enter. Reproduced from Kozulin, P., Natoli, R., O'Brien, K. M. B., Madigan, M. C., and Provis, J. M. (2009). Differential expression of anti-angiogenic factors and guidance genes in the developing macula. *Molecular Vision* 15: 45–59. (d) Immunohistochemical analysis of $CD34^+$ vessels in a human fetal retina at 25 WG. Visible is the foveal region, showing the absence of blood vessels. (e) and (f) Immunohistochemical analysis of $CD34^+$ vessels in a human fetal retina at 25 WG. Region adjacent to (e) ir distant from (f) the fovea. Note the finer caliber and more regular meshwork of the vasculature in the perifoveal region. From Hughes, S., Yang, H., and Chan-Ling, T. (2000). Vascularization of the human fetal retina: Roles of vasculogenesis and angiogenesis. *Investigative Ophthalmology and Visual Science* 41: 1217–1228. Copyright Association for Research in Vision and Ophthalmology.

reason, they have been given the name RPCs. These vessels extend from the inner vasculature to supply the nerve fiber layer near the ONH (**Figures 5** and **7(b)**). The RPCs form a very limited plexus, extending no further than 1 mm from the ONH throughout human fetal development (**Figure 5**). As with other retinal vessels that are formed through angiogenesis, the timing and extent of RPC formation suggests that it is driven by hypoxia-mediated VEGF resulting from increased metabolic demands of the underlying tissues. Their superficial location and lack of mural cell ensheathment, leading to a thin vascular wall, makes RPCs particularly prone to hypoxia resulting from raised intraocular pressure in glaucoma (the ischemic model of glaucoma susceptibility).

Lack of Involvement of VEGF in Early Stages of Vascularization

Although retinal angiogenesis is driven by hypoxia-induced VEGF expression, vasculogenesis in the human retina is independent of metabolic demand and hypoxia-induced VEGF expression. Most of the vessels formed by vascularization develop prior to the expression of VEGF. By 18 WG, the inner plexus covers more than half of the

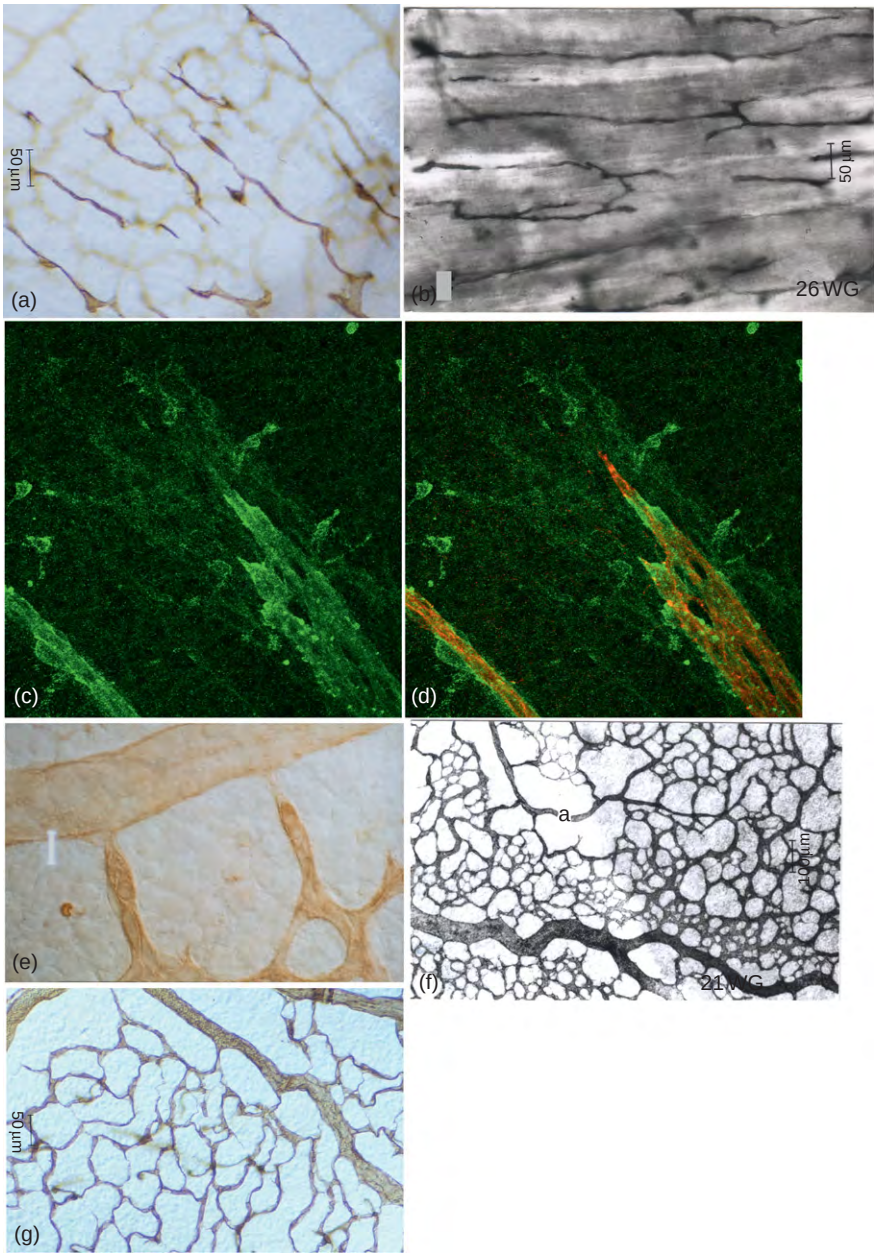

Figure 7 Later stages in the development of human retinal vasculature. (a) and (b) Radial peri-papillary capillaries in the region of the optic nerve head at 25 (a) and 26 (b) WG. These vessels were located superficially, were of fine caliber and extended radially from the optic nerve head. From Hughes, S., Yang, H., and Chan-Ling, T. (2000). Vascularization of the human fetal retina: Roles of vasculogenesis and angiogenesis. *Investigative Ophthalmology and Visual Science* 41: 1217–1228. Copyright Association for Research in Vision and Ophthalmology. (c) and (d) Newly formed capillaries at the leading edge of patent vessel formation in an 18 WG human retina are already closely ensheathed by $NG2^+$ pericytes. Personal observations. (c) Shows NG2 immunolabeling whereas (d) shows co-localization of both NG2 and Cd34 in the same field of view. (e)–(g) Vascular remodeling of capillary beds in the inner plexus. Vessels retract, leaving behind a fine meshwork of capillaries. Formation of the capillary-free zone around arteries (f and g) is visible by 21 WG. (e) From Hughes, S. and Chan-Ling, T. (2000). Roles of endothelial cell migration and apoptosis in vascular remodeling during development of the central nervous system. *Microcirculation* 7: 317–333. (f) From Hughes, S., Yang, H., and Chan-Ling, T. (2000). Vascularization of the human fetal retina: Roles of vasculogenesis and angiogenesis. *Investigative Ophthalmology and Visual Science* 41: 1217–1228. Copyright Association for Research in Vision and Ophthalmology. (g) Personal observations.

retinal area. However, VEGF mRNA is not detectable in the human retina until 20 WG. Formation of the inner plexus is well underway by 14–15 WG, prior to the differentiation of most retinal neurons. Finally, the development of the inner plexus is centered at the optic disk, whereas neuronal maturation is centered at the fovea. In contrast, development of the outer plexus by angiogenesis is centered on the fovea.

Angiogenic and anti-angiogenic factors

Retinal angiogenesis is controlled by a balance of pro-angiogenic and antiangiogenic factors. VEGF is a pro-angiogenic factor that has several forms: VEGFA (there are four isoforms, including $VEGFA_{165}$), VEGFB, VEGFC, and VEGFD. There are at least three VEGF receptors: VEGFR1, 2, and 3. VEGFA is not only a pro-angiogenic factor, but it also has protective functions. Further, it prevents vessel regression and appears to stabilize the mature vasculature, rendering mature vessels resistant to fluctuations in tissue oxygen levels. VEGFA also has a protective effect in the maintenance and function of the neuronal and Muller cells of the retina. VEGFR3 is required for normal retinal vascular development and is upregulated during VEGFA-induced angiogenesis. Its ligand, VEGFC, can cause blood vessel enlargement and tortuosity, and *in vitro* has a synergistic effect on angiogenesis with VEGFA.

Anti-angiogenic factors in the retina include PEDF and vascular endothelial growth inhibitor (VEGI). PEDF is synthesized by cells of the retinal pigment epithelium (RPE), and is present in the developing embryonic and adult human RPE, choroid, and retina. In the human, it is unclear as to how the expression of PEDF relates to the developing vasculature. VEGF stimulates PEDF expression by RPE cells but suppresses PEDF expression by Müller cells. VEGI inhibits endothelial cell proliferation and causes the apoptosis of proliferating endothelial cells. It is expressed by endothelial cells and is thought to play a role in the maintenance of a quiescent adult vasculature. Little is known about VEGI expression in ocular tissues. $VEGI_{192}$ may not be expressed during retinal and choroidal vessel formation but instead may be expressed by the endothelial cells of the quiescent adult vasculature, and may be associated with mural cell maturation. The relative expression of pro- and antiangiogenic growth factors ultimately determines whether neovascularization takes place once a stable quiescent vascular plexus is reached in young adulthood.

Cell–Cell Interactions in the Formation of the Human Retinal Vasculature

Müller cell–endothelial cell interactions

Along with astrocytes, Müller cells are found surrounding the vessels of the inner plexus of the retina, and are thought to be involved in the establishment of the BRB. However, astrocytes are not found in the deeper plexus of the retina; these vessels are ensheathed solely by Müller cells. The existence of an intact BRB and the presence of tight junction proteins in the deep plexus suggest that in this layer of vasculature, Müller cells are capable of inducing the formation and maintenance of barrier properties.

Pericyte–endothelial cell interactions: Vessel stability

Pericytes are another integral component of the mature retinal vasculature. These cells are found within the basal lamina that ensheaths capillary-sized vessels, and play a role in vessel stabilization, control of blood flow, and possibly in modulating vascular permeability and maintenance of the BRB. Pericyte density in the retina is the highest of any tissue, and these cells are also the first to be lost in diabetic retinopathy. Although immature pericytes associate with newly formed retinal vessels (**Figure 7(c)** and **7(d)**), the presence of these immature mural cells does not prevent vessel regression. However, mature vessels that are ensheathed by mature pericytes are quite stable and resistant to $VEGF_{165}$ withdrawal, suggesting that pericytes must be mature and fully differentiated to contribute to vessel stability. A reciprocal relationship exists between endothelial cells and pericytes; whereas pericytes express $VEGF_{165}$ and contribute to vessel stability, retinal endothelial cells express PDGFB, which induces recruitment and proliferation of pericytes.

Pericytes and smooth muscle cells constitute the mural cells, an important component in the maturation and stabilization of vessels. Mural cells are recruited to ensheath immature endothelial tubes by the localized expression of platelet-derived growth factor (PDGF). The inappropriate expression of PDGF interferes with the recruitment of mural cells and leads to abnormal retinal vascular remodeling. More specifically, the endothelial tube must be ensheathed by three components for a new vessel to become patent and stable: mural cells, a basal lamina, and astrocytes. Without any one of these components, vessels are leaky and unstable. Although the presence of immature pericytes along vessels does not protect these vessels from hyperoxia-induced regression, a mature vasculature with mature mural cells, astrocytes, and basal lamina is stable and resistant to the effects of hyperoxia. It appears that the extent of desmin expression by pericytes ensheathing immature vessels imparts upon its associated vascular segment vascular stability.

Vascular Remodeling

With the formation of an exuberant capillary plexus (**Figure 3(c)**) coupled with decreased metabolic demand as endothelial cell growth slows, the newly vascularized region becomes hyperoxic. Hyperoxia in turn leads to vascular remodeling, a paring back of the new vascular network to more precisely meet the metabolic needs of the underlying retina. Remodeling of the vascular network of the retina includes two processes: coalescence of smaller vessels into larger vessels and the retraction of endothelial cells from vessels that are pruned back (**Figure 7(e)**), followed by redeployment of most of these cells to areas where the vascular network is actively

forming. Most noticeably, capillaries retract near the arteries, forming a capillary-free space in this region (**Figures 6(d)** and **7(f)**). Although some apoptosis is evident in the retracting vessels, cell death is not the main mechanism for vessel retraction. As the vascular network is remodeled and the metabolic demands of the tissue stabilize, the capillary network becomes very well organized and regular in appearance (**Figure 7(g)**). The process of vascular remodeling occurs over an extended period of time during human embryonic development.

Vascularization and the Health of the Eye

Interruptions to the normal cellular and molecular mechanisms of retinal vascular formation/function can lead to blindness. In infants, retinopathy of prematurity (ROP) develops when premature delivery and supplemental oxygen exposes an infant's developing retina to elevated oxygen levels. This hyperoxygenation of the retina leads to a loss of the normal molecular cues that drives vessel formation such that when the infant is returned to room air, the rate of retinal vascularization is significantly delayed relative to neuronal maturation. A subsequent return to normoxic conditions generates retinal hypoxia that exceeds the normal physiologic levels, triggering the formation of leaky, tortuous vessels. This abnormal vasculature can lead to intraretinal hemorrhage and partial or complete retinal detachment.

In adults, the effects of tissue hypoxia and hyperglycemia can be seen in diabetic retinopathy. In this disease, the physiologic processes of diabetes prevent the retinal vasculature from meeting the metabolic demands of the active retina and generate locally high levels of hypoxia, in addition to the damaging effects of prolonged hyperglycemia. This retinal hypoxia stimulates angiogenesis in the context of a mature, fully developed retinal vasculature. Subsequent retinal neovascularization produces tortuous, fragile vessels over the surface of the retina. These vessels often leak fluid into the vitreous and can cause macular edema. In addition, the development of fibrous tissue in association with these vessels can lead to traction retinal detachments or vitreous hemorrhages.

Conclusions

The human retina is vascularized by a combination of two mechanisms: vasculogenesis and angiogenesis. Vasculogenesis is responsible for the formation of the earliest vessels of the inner plexus, starting at the ONH and reaching the inner two-thirds of the retina. Between that boundary and the inner periphery of the retina, in the space between these early vessels, reaching down to the outer plexus, under the fovea and over the nerve bundles at the optic nerve, the process of angiogenesis drives the formation of the remaining vasculature. The formation of these vessels is controlled by physiological hypoxia – a level of hypoxia that is well tolerated by the tissue but is insufficient to cause tissue damage. Physiological hypoxia is sufficient to stimulate VEGF production (mediated by hypoxia inducible factor-1α (HIF-1α)) by astrocytes and Müller cells and to direct endothelial growth where it is needed. Once this proliferation of new vessels becomes patent and directs blood flow to the developing retinal tissues, a modest level of hyperoxia then orchestrates vascular remodeling and retraction, a process that is still ongoing in a full-term neonate. The balance between physiological hypoxia and hyperoxia, vessel growth and vessel retraction, leads to the formation of a vasculature that precisely meets the metabolic demands of the human retina.

See also: Orbital Vascular Anatomy; Pericytes and Microvascular Remodeling: Regulation of Retinal Angiogenesis; Physiological Anatomy of the Retinal Vasculature; Stability and Functional Integrity of New Blood Vessels; The Vascular Stem Cell.

Further Reading

Adamis, A. P., Aiello, L. P., and D'Amato, R. A. (1999). Angiogenesis and ophthalmic disease. *Angiogenesis* 3: 9–14.

Chan-Ling, T. (2006a). Glial, neuronal and vascular interactions in the mammalian retina. *Progress in Retinal and Eye Research* 13: 357–389.

Chan-Ling, T. (2006b). The blood retinal interface: Similarities and contrasts with the blood–brain interface. In: Dermietzel, R., Spray, D. C., and Nedergaard, M. (eds.) *Blood–Brain Barriers – From Ontogeny to Artificial Interfaces*, pp. 701–724. Weinheim: Wiley-VCH.

Chan-Ling, T., Gock, B., and Stone, J. (1995). The effect of oxygen on vasoformative cell division. *Investigative Ophthalmology and Visual Science* 36: 1201–1212.

Chan-Ling, T., Halasz, P., and Stone, J. (1990). Development of retinal vasculature in the cat: Processes and mechanisms. *Current Eye Research* 9: 459–476.

Chan-Ling, T., McLeod, D. S., Hughes, S., et al. (2004). Astrocyte-endothelial cell relationships during retinal vascular development. *Investigative Ophthalmology and Visual Science* 45: 2020–2030.

Dorrell, M. I., Aguilar, E., and Friedlander, M. (2002). Retinal vascular development is mediated by endothelial filopodia, a preexisting astrocytic template and specific R-cadherin adhesion. *Investigative Ophthalmology and Visual Science* 43: 3500–3510.

Dorrell, M. I. and Friedlander, M. (2006). Mechanisms of endothelial cell guidance and vascular patterning in the developing mouse retina. *Progress in Retinal and Eye Research* 25: 277–295.

Flynn, J. T. and Chan-Ling, T. (2006). Retinopathy of prematurity: Two distinct mechanisms that underlie Zone 1 and Zone 2 disease. *American Journal of Ophthalmology* 142: 46–59.

Fruttinger, M. (2007). Development of the retinal vasculature. *Angiogenesis* 10: 77–88.

Gerhardt, H., Gloding, M., Fruttinger, M., et al. (2003). VEGF guides angiogenic sprouting utilizing endothelial tip cell filopodia. *Journal of Cell Biology* 161: 1163–1177.

Hughes, S. and Chan-Ling, T. (2000a). Roles of endothelial cell migration and apoptosis in vascular remodeling during development of the central nervous system. *Microcirculation* 7: 317–333.

Hughes, S., Yang, H., and Chan-Ling, T. (2000b). Vascularization of the human fetal retina: Roles of vasculogenesis and angiogenesis. *Investigative Ophthalmology and Visual Science* 41: 1217–1228.

Kozulin, P., Natoli, R., Madigan, M. C., O'Brien, K. M. B., and Provis, J. M. (2009). Gradients of *Eph-A6* expression in primate retina suggest a role in definition of the foveal avascular area. *Molecular Vision* 15: 2649–2662.

Kozulin, P., Natoli, R., O'Brien, K. M. B., Madigan, M. C., and Provis, J. M. (2009). Differential expression of anti-angiogenic factors and guidance genes in the developing macula. *Molecular Vision* 15: 45–59.

Lutty, G. A., Chan-Ling, T., Phelps, D. L., et al. (2006). *Proceedings of the Third International Symposium on Retinopathy of Prematurity*: An update on ROP from the lab to the nursery (November 2003, Anaheim, California). *Molecular Vision* 12: 532–580.

Stone, J., Itin, A., Alon, T., et al. (1995). Development of retinal vasculature is mediated by hypoxia-induced vascular endothelial growth factor (VEGF) expression by neuroglia. *Journal of Neuroscience* 15: 4738–4747.

Developmental Anatomy of the Retinal and Choroidal Vasculature

B Anand-Apte and J G Hollyfield, Cleveland Clinic, Cleveland, OH, USA

Glossary

Angiogenesis – The formation of new blood vessels from preexisting ones, generally by sprouting.
Central retinal artery – A branch of the ophthalmic artery that enters the eye via the optic nerve.
Choriocapillaris – An exceptionally dense capillary bed that nourishes the posterior choroid up to the level of the equator of the eye.
Circle of Zinn – An annular artery surrounding the optic nerve. Its branches contribute to the pial circulation, the optic nerve at the level of the lamina cribrosa and to the nerve fiber layer of the optic disk.
Fenestrae – The circular openings in the choriocapillaris facing Bruch's membrane that measure approximately 800 Å. The fenestrae of the choriocapillaries have a diaphragm covering.
Posterior ciliary arteries – The branches of the ophthalmic artery that form the blood supply to the choroid.
Vasculogenesis – The formation of new blood vessels through *de novo* formation of new endothelial cells.
Vortex veins – The venous collecting vessels draining the choroid, ciliary body, and iris.

Choroidal Vascular Network

Embryology

At the fourth week of gestation in humans (5-mm stage), the undifferentiated mesoderm surrounding the optic cup begins to differentiate and form endothelial cells adjacent to the retinal pigment epithelium (RPE). These early vessels are the precursors of the choriocapillaris, which ultimately envelop the exterior surface of the optic cup. Concurrently, the hyaloid artery branches from the primitive dorsal ophthalmic artery and passes along the embryonic (choroidal) fissure to enter the optic cup. Shortly thereafter, the condensation of the mesoderm occurs at the site of future choroidal and scleral stroma with the gradual onset of pigmentation in the outer neuroepeithelial layer of the optic cup, the RPE. By the fifth week of development (8–10-mm stage), the RPE becomes more melanized and the vascular plexus extends along the entire exterior surface of the cup from the posterior pole to the optic cup rim. By the sixth week (12–17-mm stage), the choriocapillary network begins to develop a basal lamina. This, together with the basement membrane of the RPE, forms the initial boundaries of Bruch's membrane separating the neural retina from the choroid. Concomitantly, rudimentary vortex veins develop in all four quadrants of the eye. Except for the two basal lamina (of the RPE and choriocapillaris), the only other component of Bruch's membrane at this stage is a collagenous central core. The choroidal capillary network becomes almost completely organized by the eighth week (25–30-mm stage) with connections to the short posterior ciliary arteries. By the eleventh week (50–60-mm stage), the posterior ciliary arteries show extensive branching throughout the choroid. It is only following the third and fourth months of gestation that most of the choroidal vasculature matures.

While the molecular mechanisms regulating choroidal development have not been fully defined, it is largely accepted that the presence of differentiated RPE and its secretion of growth factors, such as vascular endothelial growth factor (VEGF) and fibroblast growth factor 9 (FGF-9), are critical for the physiological development and differentiation of the choroidal vascular network.

Gross Anatomy

Almost the entire blood supply of the eye comes from the choroidal vessels, which originate from the ophthalmic arteries. The left and right ophthalmic arteries arise as the first major branch of the internal carotid, usually where the latter break through the dura to exit the cavernous sinus. In some individuals (around 10%), the ophthalmic artery arises within the cavernous sinus, while in others (around 4%), it arises from the middle meningeal artery, a branch of the external carotid.

The ophthalmic artery shows a wide variation in the branching pattern as it approaches the eye. The posterior ciliary arteries, which form the blood supply to the choroid, and the central retinal artery, which enters the eye via the optic nerve, are branches of the ophthalmic artery (**Figure 1**). Other branches of the ophthalmic artery supply the lacrimal gland, extraocular muscles, and lids.

The choroid (also referred to as the posterior uveal tract) is vascularized by two separate arterial systems: (1) the short posterior ciliary arteries, which supply the posterior choroid and (2) the long posterior ciliary arteries, which supply the anterior portion of the choroid (as well as the iris and ciliary body).

Approximately 16–20 short posterior ciliary arteries penetrate the sclera in a circular pattern surrounding the optic nerve, with the distance between these vessels and the nasal side of the nerve being closer than that on the temporal side. These arteries anastomose within the sclera to form the circle of Zinn, an annular artery surrounding the optic nerve (**Figures 1** and **2**). The branches from the circle of Zinn contribute to the pial circulation, the optic nerve at the level of the lamina cribrosa, and the nerve fiber layer of the optic disk. Other branches from the circle of Zinn along with direct branches from the short posterior ciliary arteries enter the choroid to provide the arterial blood supply to the posterior uveal track. These arteries divide rapidly to terminate in the choriocapillaris, an exceptionally dense capillary bed that nourishes the posterior choroid up to the level of the equator of the eye.

The two long posterior ciliary arteries penetrate the sclera on either side of the optic nerve near the level of the horizontal meridian of the eye. The temporal long posterior ciliary artery enters the sclera approximately 3.9 mm from the temporal border of the optic nerve while the nasal long posterior ciliary artery enters approximately 3.4 mm from the nasal border of the optic nerve. Additional long posterior ciliary arteries are present that course farther toward the anterior segment before penetrating the sclera, usually more anterior than the entry of the temporal and nasal long posterior ciliary arteries. The long posterior ciliary arteries course through the suprachoroid, begin to branch just anterior to the equator, and contribute to the circulation of the iris and ciliary body. Just anterior to the equator, some branches of these vessels course down into the choroid and branch to terminate in the choriocapillaris from the ora serrata back to the equator of the eye.

In general, the larger diameter arteries of the choroid are found most proximal to the sclera, in an area referred to as the lamina fusca. These arteries continue to branch and ultimately form the extensive choriocapillaris adjacent to the acellular Bruch's membrane located on the basal side of the RPE (**Figure 3**). The capillary network of the choriocapillaris is approximately 3–18 μm in diameter and oval shaped in the posterior eye, becoming gradually wider and longer as it moves toward the equatorial region (approximately 6–36 μm wide by 36–400 μm long). The network becomes irregular in the peripheral third of the choroid owing to the entrance and exit of arterioles and venules. Compared to capillaries in other organs, the choriocapillary lumen are significantly larger, with a diameter of nearly 20 μm in the macular region and 18–50 μm in the periphery. A network of collagen fibrils surrounds the choriocapillaris and provides a structural supportive framework.

From the choriocapillaris, venous collecting vessels emerge that ultimately exit the eye through the vortex veins (**Figure 1**). In addition to the choroid, the vortex veins also drain the ciliary body and iris circulation. The number of vortex veins is variable, with at least one per

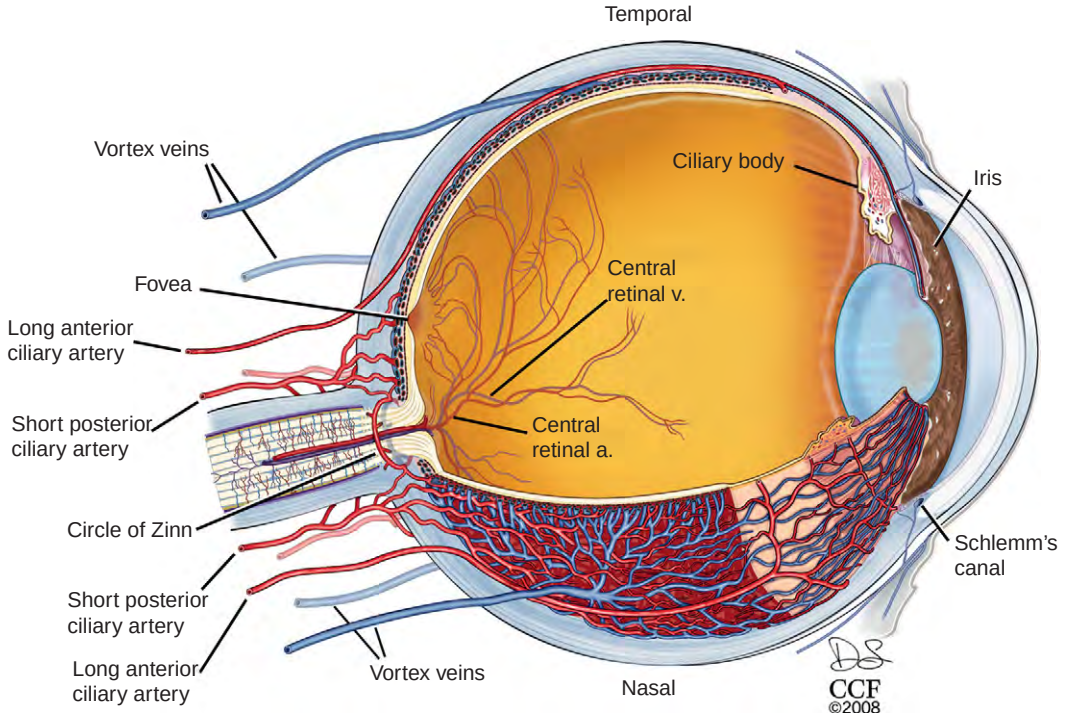

Figure 1 A cutaway drawing of the human eye showing the major blood vessels supplying the retina choroid and anterior segment. The view is from a superior position over the left eye and the horizontal section passes through both the optic nerve and the fovea. Drawing by Dave Schumick.

eye quadrant; however, the total number per eye is usually seven, with more found on the nasal side than are found temporally. The vortex veins usually exit the sclera at the equator or up to 6 mm posterior to this location after forming an ampulla near the internal sclera. The venous branches that open into the anterior and posterior regions of the vortex venular network are oriented along the meridian and are mostly straight, while those joining on the lateral and medial sides have a circular orientation. The vortex veins, in turn, empty into the superior and

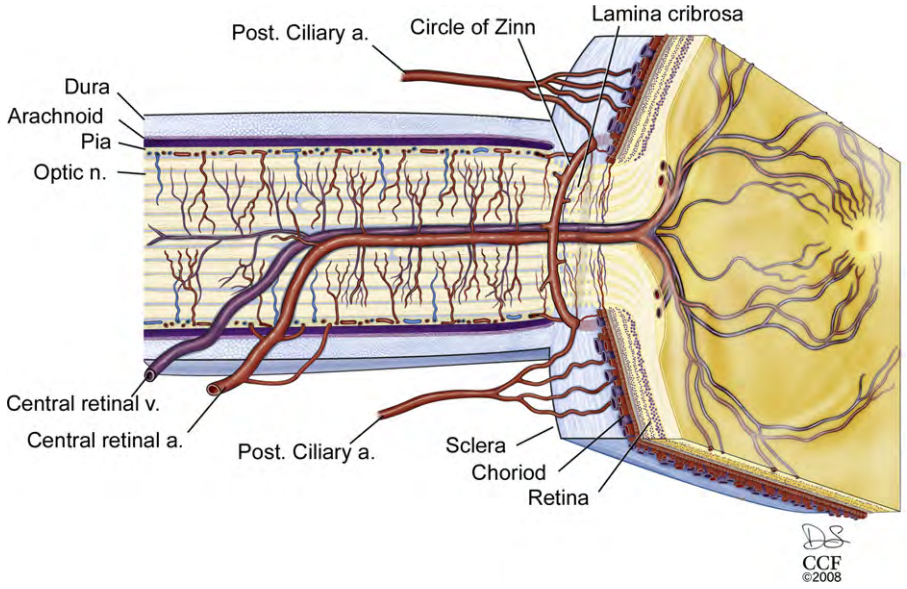

Figure 2 A cutaway drawing along the superior–inferior axis of a left human eye through the optic nerve, showing details of the vascular supply in this location. The fovea is present on the right side of the drawing at the center of the termination of the central retinal vessels. Drawing by Dave Schumick.

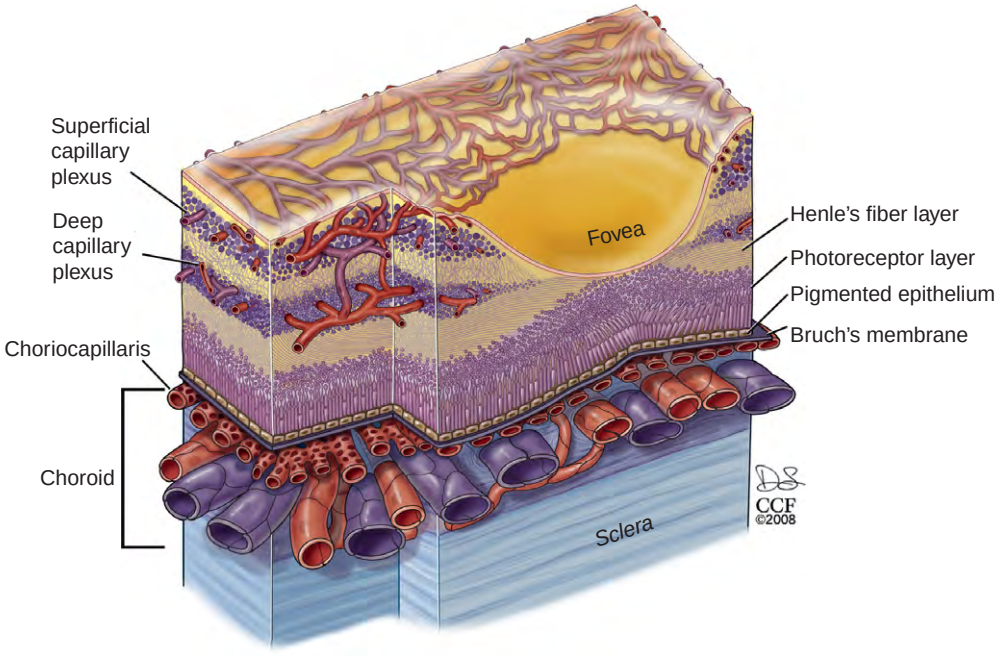

Figure 3 A diagram showing details of the retinal and choroidal vasculature and changes that occur at the level of the human fovea. The branches from the central retinal circulation form two distinct capillary plexi within the ganglion cell layer (the superficial capillary plexus) and in the inner nuclear layer (the deep capillary plexus). These two vascular plexi end as the ganglion cell and inner nuclear layer disappear in the foveal slope. The choroid contains a dense vascular network terminating with the fenestrated choriocapillaris adjacent to Bruch's membrane. Drawing by Dave Schumick.

inferior ophthalmic veins, which leave the orbit and enter the cavernous sinus.

Physiology

The primary function of the choroid vasculature is to provide nutrients and oxygen to the outer retina. The loss of the choriocapillaris, as occurs in central areolar choroidal sclerosis, results in atrophy of the overlying retina. The choriocapillary network is unique in that it lies in a single plane below Bruch's membrane. Normal choroidal circulation occurs when both choroidal arterial and venous pressures are above 15–20 mm of Hg, which is the normal physiological intraocular pressure. In addition, since the blood flow rate through the choroid is relatively high compared to other tissues and is regulated by the arterial vessel diameter, it causes relatively lower amounts of oxygen to be extracted from each milliliter of blood.

The wall of the choriocapillaris facing Bruch's membrane is fenestrated with circular openings (fenestrae) measuring approximately 800 Å. The fenestrae of the choriocapillaries are unique in that they have a diaphragm covering them, unlike those seen in the renal glomerulus. These fenestrae allow easy movement of large macromolecules into the extracapillary compartment. Fluid and macromolecules escaping from these leaky vessels percolate through Bruch's membrane and have access to the basal side of the RPE. The passive movement of fluid and macromolecules from this leaky circulation is blocked from reaching the subretinal space (interphotoreceptor matrix) by zonula occludens junctions that form a continuous belt-like barrier near the apical border of the RPE. Thus, the RPE is able to block the passive movement of the large molecules and fluid from the choroid, allowing the RPE to function as the outer portion of the blood retinal barrier.

Pathology

The exudative (wet form) of age-related macular degeneration (AMD) is characterized by an abnormal proliferation of the choriocapillaris with occasional invasion through Bruch's membrane into the subretinal space. Leakage of the fluid and/or blood often leads to retinal or RPE detachment and loss of central vision. VEGF, basic fibroblast growth factor (bFGF), and pigment epithelial-derived growth factor (PEDF) have been postulated to play a role in the development of choroidal neovascularization (CNV). Some studies have suggested that the thickening of Bruch's membrane that occurs with age and in AMD could result in decreased permeability. The survival factors for the choriocapillaris, such as VEGF, which are secreted basally from the RPE, could remain sequestered in Bruch's membrane and be unable to reach the endothelial cells of the choriocapillaris. This could potentially lead to atrophy of the choriocapillaris that is seen in dry AMD and may be the initiating event for local hypoxia, and upregulation of VEGF and CNV. Myopia is the second most common cause of CNV. Presumed ocular histoplasmosis syndrome, multiple white dot syndrome, multifocal choroiditis, punctate inner choroidopathy, birdshot chorioretinopathy, and the healing phase of choroidal ruptures are the other causes of CNV.

Hyaloid Vascular Network

Embryology

During the first gestational month, the posterior compartment of the globe contains the primary vitreous comprised of a fibrillary meshwork of ectodermal origin and vascular structures of mesodermal origin. At the 5-mm stage, the primitive dorsal ophthalmic artery sprouts off the hyaloid artery, which passes through the embryonic choroidal fissure and branches within the cavity of the primary optic vesicle. Behind the lens vesicle, some of the branches make contact with the posterior side of the developing lens (capsula perilenticularis fibrosa), while others follow the margin of the cup and form anastomoses with confluent sinuses to form an annular vessel. The arborization of the hyaloid artery forms a dense capillary network around the posterior lens capsule (tunica vasculosa lentis, TVL) and surrounding the lens equator. In addition, capillary branches are given off that course throughout the vitreous (vasa hyaloidea propria). The capsulopupillary vessels anastomose with the annular vessel around the rim of the optic cup and connect to the choroidal vasculature through which venous drainage occurs. By the sixth week (17–18-mm embryo), the annular vessel sends loops forward and centrally over the anterior lens surface. By the end of the third month, the anterior portion of the TVL is replaced by the pupillary membrane, which is supplied via loops from the branches of the long posterior ciliary arteries and the major arterial circle. The development of the hyaloid vasculature is almost complete at the ninth week (40 mm) stage. The venous drainage from the vessels of the anterior lens capsule and, subsequently, from the pupillary membrane and from the capsulopupillary vessels occurs through vessels that assemble into a network in the region where the ciliary body will eventually form and will anastomose and feed into the venules of the choroid.

Normally, the hyaloid vascular system begins to regress during the second month of gestation. This process begins with atrophy of the vasa hyaloidea propria, followed by the capillaries of the TVL, and, finally, the hyaloid artery (by the end of the third month). The occlusion of the regressing capillaries by macrophages appears to be a critical step for atrophy to occur. As the vascular structures regress, the primary vitreous retracts, and collagen fibers and a ground substance of hyaluronic acid are produced, forming a

secondary vitreous. By the fifth to the sixth month of gestation, the posterior compartment is primarily composed of the secondary vitreous, and the primary vitreous is reduced to a small, central structure, the Cloquet canal, which is a thin, S-shaped structure that extends from the disk to the posterior surface of the lens.

Physiology

The hyaloid vascular system apparently supplies the nutritive requirements of both the lens and the developing retina before the acquisition of the retinal vasculature. The localization of VEGF in the TVL and papillary membrane may be responsible for fenestrae being present only in the hyaloid capillaries facing the lens. The hypoxia-inducible factor and VEGF have been postulated to play a role in the development and regression of the hyaloid. Other factors that have a part to play in regression are Wnt receptor (Lrp5), Frizzled-4, collagen-18, Arf, Ang2, and BMP-4.

Pathology

Persistent hyperplastic primary vitreous occurs owing to the failure of the hyaloid vasculature to completely regress. The TVL, the anterior extension of the primary vitreous, is comprised of a layer of vascular channels originating from the hyaloid artery, the vasa hyaloidea propria, and the anterior ciliary vessels. The anterior part of this system is supplied by the ciliary system and the posterior part by the hyaloid artery and its branches. The posterior system usually regresses completely by the seventh month of gestation, while the anterior part follows by the eighth month. Two clinical forms of persistent hyperplastic primary vitreous have been identified based on the vascular system that fails to regress: (1) persistent TVL that mainly affects the anterior segment and is now termed anterior hyperplastic primary vitreous and (2) posterior hyperplastic primary vitreous. The hallmark of posterior hyperplastic primary vitreous is the presence of a retinal fold. The lens is usually clear, but may form a cataract over time if the membranous vessels grow forward to enter the lens through the posterior capsule. Other complications include secondary angle-closure glaucoma, microophthalmia, vitreous membranes, tractional retinal detachment at the posterior pole, and a hypoplastic (underdeveloped) or dysplastic (disorganized) optic nerve head. Patients with the anterior hyperplastic primary vitreous often have the best prognosis for visual recovery. The posterior pole is usually normal, with no evidence of a retinal fold or abnormalities in the optic nerve or macula. Patients characteristically present with the appearance of a whitish mass behind the lens (leukokoria) early in life. Occasionally, elongated ciliary processes are present and the eye is microphthalmic. Intralenticular hemorrhage can occur if the fibrovascular membrane invades the lens. Other complications include secondary angle-closure glaucoma, strabismus, and coloboma iridis.

Retinal Vascular Network

Embryology

Until the fourth month of gestation, the retina remains avascular as the hyaloid vasculature provides the nutrients to the developing retina. At the fourth month (100-mm stage), the primitive vascular mesenchyme cells near the hyaloid artery invade the nerve fiber layer. At later stages in development, the hyaloid artery regresses back to this point, which marks the posterior origin of the retinal circulation. In the fourth month of gestation, the first retinal vessels appear when solid endothelial cords sprout from the optic nerve head to form a primitive central retinal arterial system. By the sixth month, these vessels start developing a faint lumen that occasionally contains a red blood cell. At this time, the vessels extend 1–2 mm from the optic disk and continue to migrate outward extending to the ora serrata nasally and to the equator temporally by the seventh to eighth month. Pericytes or mural cells are conspicuously absent from the vessels at this time and do not appear until 2 months after birth. The retinal vasculature achieves the adult pattern by the fifth month after birth. The relative roles of angiogenesis versus vasculogenesis in the development of the retinal vascular network are still controversial. However, it is generally accepted that VEGF secreted in a temporal and spatial pattern by microglia and astrocytes plays a critical role in the development of the superficial and deep layers of the retinal vasculature. Platelet-derived growth factor (PDGF) produced by the neuronal cells induces the proliferation and differentiation of astrocytes, which respond to the hypoxic environment by secreting VEGF. These cells establish a gradient of VEGF and a track for endothelial cells to follow. The hypoxia-inducible factor has been shown to be critical in the hypoxia-induced regulation of retinal vascular development. VEGF isoforms have been shown to perform highly specific functions during developmental retinal neovascularization.

Gross Anatomy

Usually, the only arterial blood supply to the inner retina is from the central retinal artery that runs along the inferior margin of the optic nerve sheath and enters the eye at the level of the optic nerve head (**Figure 2**). Within the optic nerve, the artery divides to form two major trunks and each of these divides again to form the superior nasal and temporal and the inferior nasal and temporal arteries that supply the four quadrants of the retina. The retinal venous branches are distributed in a relatively similar pattern. The major arterial and venous branches and the successive divisions of the retinal vasculature are present in the

nerve fiber layer close to the internal limiting membrane. The retinal arterial circulation in the human eye is a terminal system with no arteriovenous anastomoses or communication with other arterial systems. Thus, the blood supply to a specific retinal quadrant comes exclusively from the specific retinal artery and vein that supply that quadrant. Any blockage in blood supply therefore results in infarction. As the large arteries extend within the retina toward the periphery, they divide to form arteries with progressively smaller diameters until they reach the ora serrata where they return and are continuous as a venous drainage system. The retinal arteries branch either dichotomously or at right angles to the original vessel. The arteries and venules generated from the retinal arteries and veins form an extensive capillary network in the inner retina as far as the external border of the inner nuclear layer. Arteriovenous crossings occur more often in the upper temporal quadrants with the vein usually lying deeper than the artery at these crossings.

Branches from the central retinal vessels dive deep into the retina forming two distinct capillary beds, one in the ganglion cell layer (superficial capillary plexus) and the other in the inner nuclear layer (deep capillary plexus). Normally, no blood vessels from the central retinal arteries extend into the outer plexiform layer (**Figure 3**). Thus, the photoreceptor layer of the retina is free of the blood vessels supplied by the central retinal artery. The choriocapillaris provides the blood supply to photoreceptors. Since the fovea contains only photoreceptors, this cone-rich area is free of any branches from the central retinal vessels (**Figure 3**).

In some individuals (18%), a cilioretinal artery derived from the short posterior ciliary artery (from the choroid vasculature) enters the retina around the termination of Bruch's membrane, usually on the temporal side of the optic nerve, and courses toward the fovea, where it ends in a capillary bed and contributes to the retinal vasculature. In approximately 15% of eyes with a cilioretinal artery, the branches supply the macula exclusively, whereas in other individuals, they can nourish the macular region and regions of the upper or lower temporal retina.

Physiology

The rate of blood flow through the retinal circulation is approximately 1.6–1.7 ml g^{-1} of retina with a mean circulation time of approximately 4.7 s. The flow rate through the retinal vessels is significantly slower than that through the choroidal vasculature.

The arteries around the optic nerve are approximately 100 μm in diameter with 18-μm-thick walls. These decrease in diameter in the branched arteries located in the deeper retina to around 15 μm. The walls of the retinal arteries have the characteristics of other small muscular arteries and are composed of a single layer of endothelial cells: a subendothelial elastica, a media of smooth muscle cells, a poorly demarcated external elastic lamina, and an adventitia comprised of collagen fibrils. Near the optic disk, the arterial wall has five to seven layers of smooth muscle cells, which gradually decrease to two or three layers at the equator and to one or two layers at the periphery. These vessels continue to have the characteristics of arteries, and not arterioles, up to the periphery. The retinal arteries lose their internal elastic lamina soon after they bifurcate at the optic disk. This renders them immune from developing temporal arteritis and distinguishes them from muscular arteries of the same size in other tissues. As a compensatory mechanism, the retinal arteries have a thicker muscularis, which allows increased constriction in response to pressure and or chemical stimuli.

The major branches of the central vein close to the optic disk have a lumen of nearly 200 μm with a thin wall made up of a single layer of endothelial cells having a thin basement membrane (0.1 μm), which is continuous with the adjacent media comprised predominantly of elastic fibers, a few muscle cells, and a thin adventitia. The larger veins in the posterior wall have three to four layers of muscle cells in the media. As the retinal veins move peripherally from the optic disk, they lose the muscle cells, which are replaced by pericytes. The lack of smooth muscle cells in the venular vessel wall results in a loss of a rigid structural framework for the vessels, resulting in shape changes under conditions of sluggish blood flow (e.g., diabetes mellitus) or increased blood viscosity (polycythemia), or with increased venous pressure (papilledema or orbital compressive syndromes).

The retinal capillary network is spread throughout the retina, diffusely distributed between the arterial and venous systems. There are three specific areas of the retina that are devoid of capillaries. The capillary network extends as far peripherally as the retinal arteries and veins up to 1.5 mm from the posterior edge of the troughs of the ora serrata (ora bays), leaving the ora serrata ridges (ora teeth) without any retinal circulation. The 400-μm-wide capillary-free region centered around the fovea is another area lacking retinal capillaries. Finally, the retina adjacent to the major arteries and some veins lacks a capillary bed.

The retinal capillary wall is comprised of the endothelial cells, basement membrane, and intramural pericytes. The retinal capillary lumen is extremely small (3.5–6 μm in diameter), requiring the circulating red blood cells to undergo contortions to pass through. Unlike the choriocapillaris, the endothelial cells of retinal capillaries are not fenestrated. The edges of endothelial cells show interdigitation and are joined by the zona occludens at their lumenal surface. The endothelial cells of the retinal arteries are linked by tight junctions, which prevent the movement of large molecules in or out of the retinal vessels. These tight junctions, in concert with the Muller

cells and astrocytes, establish the blood–retinal barrier that prevents the passage of plasma proteins and other macromolecules in or out of the capillary system. The pericytes (also called mural cells) are embedded within the basal lamina of the retinal capillary endothelium. The pericytes are believed to play an important role in the stabilization of the retinal capillary vasculature.

Pathology

Diabetic retinopathy (maculopathy) is the leading cause of vision loss in patients with type 2 diabetes and is characterized by the hyperpermeability of retinal blood vessels, with subsequent formation of macular edema and hard exudates. Early changes in the retinal vasculature include thickening of the basement membrane, loss of pericytes, formation of microaneurysms, and increased permeability. It is generally hypothesized that these changes lead to the dysfunction of the retinal vessels, loss of vessel perfusion, hypoxia, induction of retinal VEGF expression, and pathological neovascularization as seen in proliferative diabetic retinopathy. In severe cases, retinal detachment can occur as a result of traction caused by fibrous membrane formation. Laser photocoagulation and VEGF-blocking agents are currently being used as therapeutic approaches for this disease.

Retinopathy of prematurity is a potentially blinding disorder affecting premature infants weighing 1250 g or less and with a gestational age of less than 31 weeks. This disease is characterized by abnormal retinal vascularization and can be classified into several stages ranging from mild (stage I), with mildly abnormal vessel growth, to severe (stage V), with severely abnormal vessel growth and a completely detached retina. The pathophysiology of this disease has been extensively studied and several factors have been implicated. The premature birth of an infant before the retinal vasculature has extended to the periphery results in stoppage of the normal blood vessel growth that is driven by the hypoxia-mediated expression of VEGF. This is compounded by the oxygen therapy given to alleviate the respiratory distress, which reduces VEGF expression leading to vaso-obliteration. Once the infant is taken off oxygen, there is a relative hypoxia, upregulation of VEGF, and florid abnormal neovascularization.

See also: Angiogenesis in Inflammation; Angiogenesis in Response to Hypoxia; Angiogenesis in the Eye; Angiogenesis in Wound Healing; Blood–Retinal Barrier; Development of the Retinal Vasculature; Vessel Regression.

Further Reading

Hogan, M. J., Alvarado, J. A., and Weddell, J. (1971). *Histology of the human eye.* Philadelphia, PA: W.B. Saunders.

Jakobiec, F. A. (1982). *Ocular anatomy, embryology and teratology.* Philadelphia, PA: Harper and Row.

Saint-Geniez, M. and D'Amore, P. A. (2004). Development and pathology of the hyaloid, choroidal and retinal vasculature. *International Journal of Developmental Biology* 48: 1045–1058.

Wolff, E. (1933). *The anatomy of the eye and orbit.* Philadelphia, PA: P. Blakiston's and Co.

Differentiation and Morphogenesis of Extraocular Muscles

D M Noden, Cornell University, Ithaca, NY, USA

Glossary

Mesenchyme – Embryonic cells with a fibroblast-like appearance, surrounded by extracellular matrix, lacking tight junctions with their neighbors, and often capable of undergoing extensive migratory movements. These can be of several different embryonic origins, and include cells that will contribute to many lineages.

Morphogenesis – It includes those processes that establish the correct locations and three-dimensional organization of tissues and organs. This includes the proper positioning of extraocular muscles around the globe and their attachments to the sclera and orbital skeleton.

Myoblasts – Mitotically active cells committed to the skeletal muscle lineage but not yet expressing muscle-specific proteins such as desmin and myosins, which generally are not evident until after myoblasts fuse to form multinucleated myofibers.

Myotome – The several regions of each somite that contain progenitors of skeletal muscle progenitors.

Neural crest – Mesenchymal cells that are derived from neural fold tissues and that move peripherally along well-delineated pathways to form neurons and glia of the peripheral nervous system and, in the head region, the connective tissues of the midface and branchial regions.

Paraxial mesoderm – Early embryonic cells that are located beside and beneath the developing brain and spinal cord, and include the precursors of most skeletal muscles.

Introduction

Muscles that move and stabilize the eye have been highly conserved during vertebrate evolution. While a few remarkable adaptations have occurred, such as co-opting of the dorsal (superior) oblique muscle to generate protective heating for the brain in some fishes, these muscles have retained an anatomical organization linking axes of the body and the eye that arose hundreds of millions of years ago.

Considering their ancient status, it is logical to assume that the early development of extraocular muscles would similarly be well conserved among different species, and therefore amenable to comparative analyses that supplant the absence of direct examination in mammals, including humans. However, compared to trunk and limb muscles, our understanding of the origins of ocular muscles and the mechanisms that initiate then maintain their development is at best fragmentary.

Myogenesis of skeletal muscles is a lengthy process, with several parameters continuing to be function-dependent throughout the life of an animal. Primary myogenesis spans the period during which populations of myoblasts – committed, mitotically active muscle progenitors – arise, emigrate to their sites of differentiation, fuse to form multinucleated innervated myofibers, and establish intimate connections with connective tissues. This population forms a scaffolding, including the delineation of global and orbital domains, within which secondary myogenesis occurs. During secondary myogenesis stages, previously sequestered latent myoblasts are activated to proliferate and differentiate, forming more than 90% of the myofibers present in mature muscles and generating region-specific specialized fiber types that in most species are present before or soon after birth.

Origins of Extraocular Muscles

Striated (skeletal) muscles throughout the body arise within paraxial mesoderm, which is located in close apposition to the embryonic brain and spinal cord. Exceptions to this are the avian striated ciliary muscle that is of neural crest origin, and possibly the striated muscles of the esophageal wall; however, both of these are involuntary. Among voluntary muscles, some of the more ventrally located branchial muscles arise from lateral mesoderm that is contiguous with paraxial mesoderm.

Many early accounts of head myogenesis placed the embryonic origin of some eye muscles, especially the lateral rectus, in the same category as branchial (pharyngeal) arch muscles, and ascribed both to a lateral mesoderm origin. These claims were based on the sites at which muscle condensations are first grossly evident in the embryo. However, with the advent of mapping methods and assays for early muscle-specific gene expression patterns, separate and distinct sites of origin for all eye muscles within preotic (i.e., located rostral, in front of the developing inner ear) paraxial mesoderm was confirmed (Figure 1).

The sites of origin of extraocular muscles parallel the sites of emergence of the three cranial motor nerves that

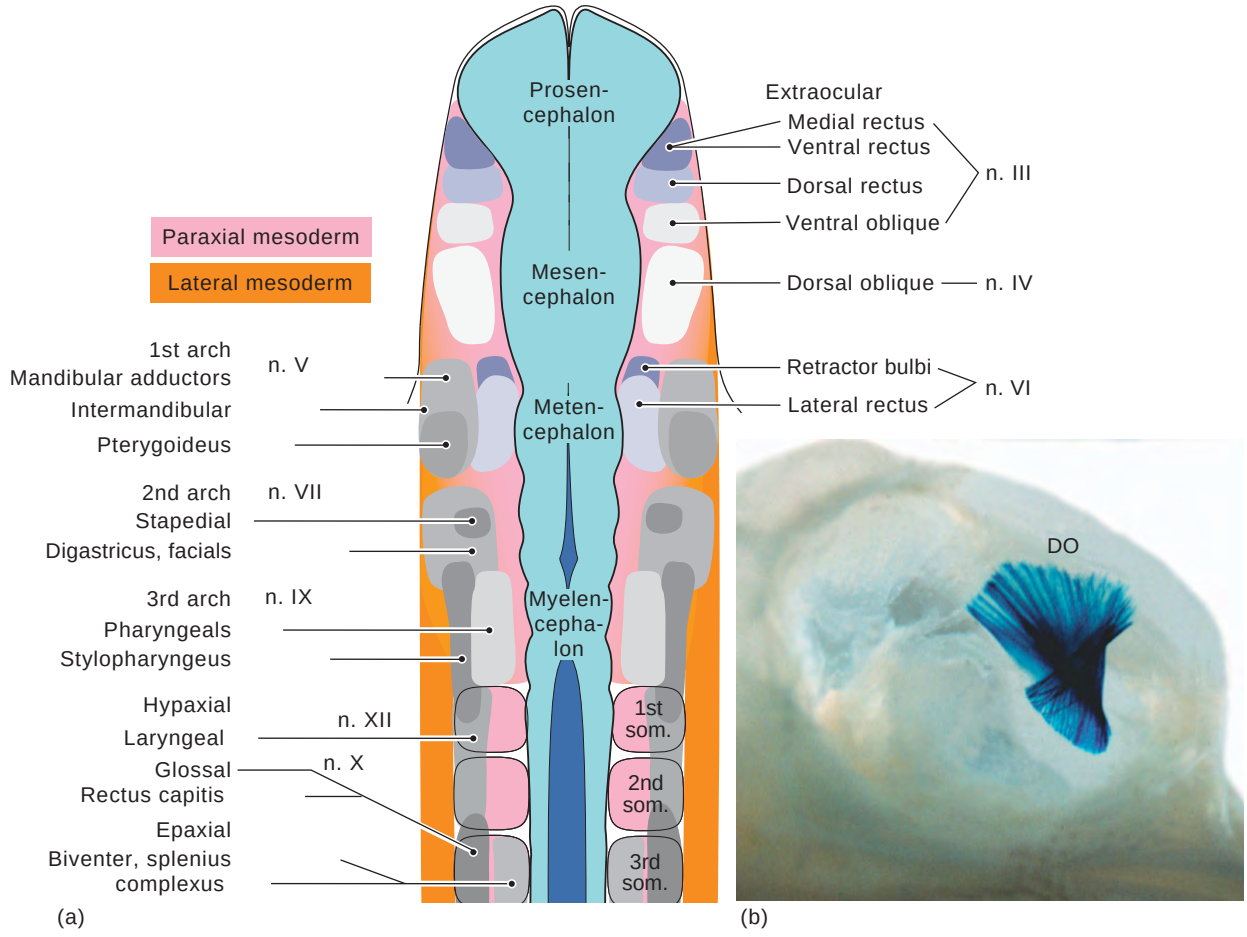

Figure 1 Sites of origin of craniofacial striated muscles in avian embryos. Panel (a) shows, in dorsal view, the locations of each muscle primordia within paraxial and lateral mesoderm. Panel (b) illustrates one mapping method used in avian embryos, wherein a small bolus of replication-incompetent retrovirus injected into early mesoderm and the embryo harvested 2 weeks later and stained for the appropriate reporter gene, in this case a bacterial galactosidase. In this embryo, in which the eye has been removed to reveal underlying tissues, only the dorsal (superior) oblique muscle was labeled.

innervate them. However, in contrast to axial and branchial muscles, sites of myogenesis are not congruent with locations of motor nerve emergence. Indeed, each of these cranial nerves needs to elongate considerably through peripheral tissues before initial contacts with target muscles are established. Some axons, such as those of the abducens nerve, must extend longitudinally beneath the brain to reach their target lateral rectus muscles, while others, such as the oculomotor nerve fibers, project perpendicular to the floor of the brain before decussating to approach their several target muscles.

In extant vertebrates, head paraxial mesoderm constitutes a sparse population of mesenchymal cells (Figure 2). This contrasts with the situation in the neck and trunk regions, where paraxial mesoderm first forms somites, which are segmentally arranged, cuboidal aggregates of epithelial cells. As each somite matures, it becomes delineated into distinct myogenic (myotome) and connective tissue-forming (sclerotome) regions. The most cranial somite is located beside the hindbrain, immediately caudal to the otic vesicle, and paraxial mesoderm rostral to this site fails to form epithelial tissues and lacks overt evidence of segmentation.

Head paraxial mesoderm is present adjacent to the prospective eye-forming regions of the rostral neural plate, but is largely displaced caudally as the optic vesicles emerge and expand lateral to the diencephalon. In the midline just in front of the notochord, this population of loose paraxial mesoderm cells is contiguous with a sparse and species-variable population of prechordal mesenchymal cells. Mapping experiments in avian embryos have shown that prechordal mesoderm contributes to the genesis of extraocular muscles innervated by the oculomotor nerve (Figure 3), but it is not known whether this contribution is exclusive of or supplementary to that of paraxial mesoderm. It is not known if the same occurs in mammalian embryos.

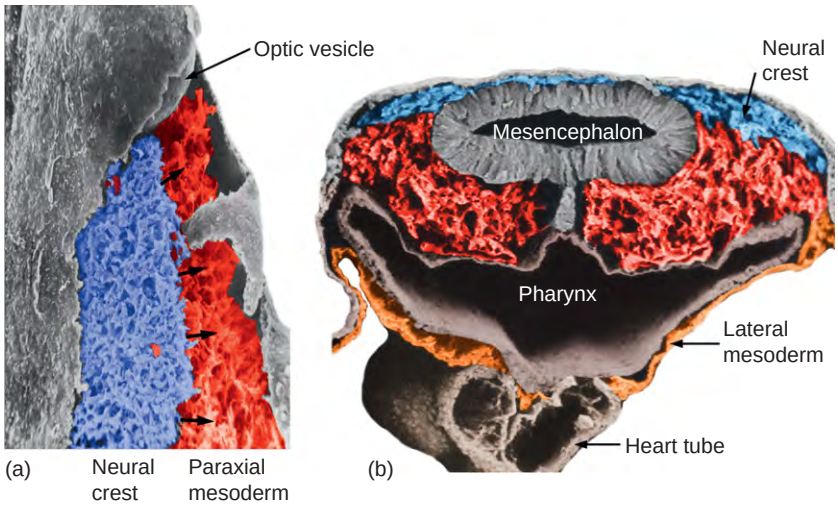

Figure 2 Colorized scanning electron micrographs showing the early relations of neural crest (blue) to mesodermal (red) populations in dorsal (a) and transverse (b) views. Small arrows indicate the direction of movement of the neural crest cells.

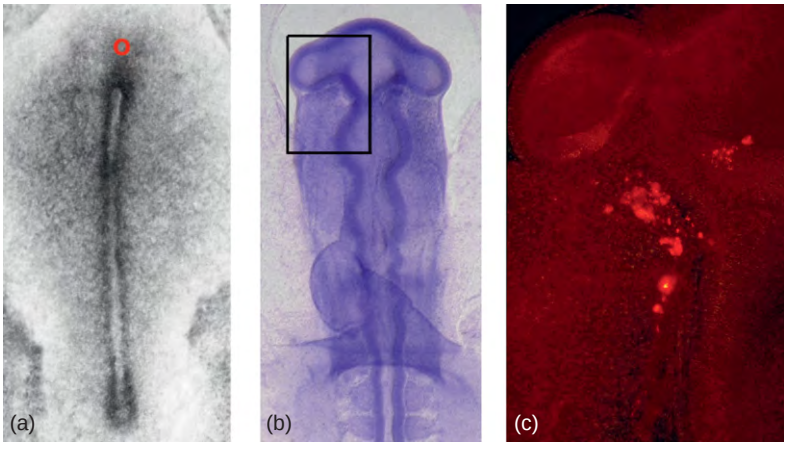

Figure 3 Contributions of prechordal mesoderm to developing extraocular muscles is shown by labeling their precursors at stage 4–5 (early gastrulation) with DiI, a fluorescent membrane-binding tag (site 'o' in (a)), and fixing the embryos over a day later((b), stage 12, ventral view). Labeled cells in (c) are within the eye muscle-forming region of paraxial mesoderm.

Determination of Eye Muscle Precursors

Head paraxial mesoderm contains progenitors for many tissues in addition to skeletal muscle. These include cartilages and bones associated with the braincase, loose connective tissues such as meninges and adipocytes, and endothelial cells. In contrast to somites, wherein these progenitor populations are largely segregated, it appears based on mapping studies that these diverse precursors are either intermingled or contiguous in head mesoderm.

The significance of this lies in the problem of generating diverse lineages. Somite cells are held in fixed positions relative to the dorsal and ventral parts of the adjacent neural tube (hindbrain and spinal cord) and overlying surface epithelium, all of which provide combinations of positive and negative regulators of early myogenesis and skeletogenesis.

A further complication – and one essential for the development of all craniofacial musculoskeletal systems – is the presence of a large, later-arising population of mesenchymal cells called the neural crest (Figure 2). Derived from neural folds either during (mammals) or shortly following (birds) closure of the cephalic neural tube (brain), these cells acquire a mesenchymal phenotype and quickly move peripherally, mostly atop underlying paraxial mesoderm.

Neural crest cells from the rostral midbrain level move rostrally and caudally around the optic stalk and posterior part of the optic vesicle, then spread outwardly as the vesicle is transformed into the optic cup. After delineation of the lens from the lens placode, crest cells secondarily invade the space created anterior to the lens and establish the posterior epithelium (endothelium) and stromal populations of the cornea.

In the trunk, members of the *wnt* family of growth factors are secreted by surface ectoderm and provide essential positive stimuli for muscle differentiation. The same are released by head surface epithelium, but here their effects are to retard myogenesis of branchial muscles. Arriving neural crest cells separates branchial muscle progenitors from the source of these negative effects and, augmented by the release of additional myogenesis-promoting factors, allows myogenesis to progress.

The extent to which eye muscle progenitors follow a similar scenario is unclear. Some extraocular precursors, particularly the lateral rectus progenitors, are embedded deep within paraxial mesoderm and are therefore quite distant from both surface ectoderm and, at early stages, neural crest cells. This deep location places the lateral rectus precursors close to the neural epithelium at the level of the future metencephalon (pons).

Several experiments have established that this location provides essential cues for lateral rectus formation. When newly formed trunk paraxial mesoderm cells were excised, before they had formed somites, then grafted into the head, in place of prospective lateral rectus mesoderm cells, the transplanted cells formed a muscle that expressed molecular markers unique to the lateral rectus and established proper anatomical connections with the braincase and sclera. Small changes in the location of the implants resulted in grafted cells contributing to the dorsal oblique or branchial arch musculature. Thus, the sites within head paraxial mesoderm at which each muscle primordium forms and is specified as to its identity are highly localized.

Placing a barrier between the brain and paraxial mesoderm at this region does not prevent myogenesis, but the developing muscle cells lack molecular features that define their specific identity. Together, these experiments suggest that a rich tableau of local signals is necessary for early eye muscle differentiation, with both general myogenic and individual eye muscle-specific components.

Molecular Signatures and Muscle Differentiation

All skeletal myoblasts use members of a closely related set of muscle-specific transcription factors to promote and coordinate their differentiation. Two of these, *myf5* and *myoD,* are cross-activating regulators that are among the earliest muscle-specific genes expressed. The upstream regulatory components of these genes are body region- and muscle group-specific, and serve to integrate the diverse micro-environments surrounding each muscle group with a highly shared set of outcomes, for example, activation of genes for desmin, myosins, muscle-specific actins, and junctional receptors.

Expression of *myf5* then *myoD* genes in eye muscle precursors generally is slightly later than expression in trunk axial muscles, but is simultaneous with that of branchial muscles (**Figure 4**). Expression of these regulatory genes coincides with the onset of aggregation of most muscle precursors (**Figure 5**), although it is not known whether these aggregates represent the totality of muscle precursors or only a subset of primary myoblasts.

By these criteria, extraocular muscles appear similar to other head and also to trunk and appendicular muscles. However, as additional features of trunk and head myogenic regulatory networks have been identified, the number of differences has exceeded the similarities, and a heretofore underlying complexity has been revealed (**Table 1**). This area of investigation is rapidly expanding, and rather than detail each gene currently described, a few examples of categories of differences among muscle groups will be presented.

Pax3 is a regulatory gene expressed in axial and appendicular muscle precursors, and null mutations of this transcription factor (e.g., *Splotch* mutation) result in severe depletion of trunk muscles. However, it is not expressed in head muscle precursors, and null mutations have no discernable effect on branchial or extraocular muscles. Another pronounced difference is in the hepatocyte growth factor (HGF) – cMet growth factor-receptor complex, which is functionally required for the correct dissemination and differentiation of appendicular and tongue muscle precursors. Again, this pathway has no known role in eye and branchial myogenesis, even though HGF is expressed in and around the precursors of branchial arch, lateral rectus, and both oblique muscles.

The latter example further illustrates the considerable heterogeneity among extraocular muscles. The lateral rectus is particularly enigmatic, being the only head muscle that expresses the ubiquitous trunk paraxial mesoderm marker *paraxis*, and together with the dorsal oblique, the transcription factor *lbx1*, which is present in trunk hypaxial (thoracic and abdominal wall) muscle precursors.

A further complexity arises from the often-changing patterns of gene expression during the early stages of head paraxial mesoderm development. The transcription factor *pitx2*, which is a key mid-level participant in the integrated formation of left-right asymmetry for the heart and mid-gut, is initially expressed symmetrically and ubiquitously throughout head paraxial mesoderm (**Figure 6**). However, a day later, during early myogenesis stages, its expression becomes more restricted but includes the first branchial arch, lateral rectus, and both oblique muscles in addition to periocular neural crest cells. Another regulatory gene, *Tbx1*, which is located in the region of chromosome 22 wherein deletions cause the DiGeorge syndrome, is similarly expressed over a wide domain of mesoderm (and pharyngeal endoderm) before becoming restricted to branchial arch and the lateral rectus muscles.

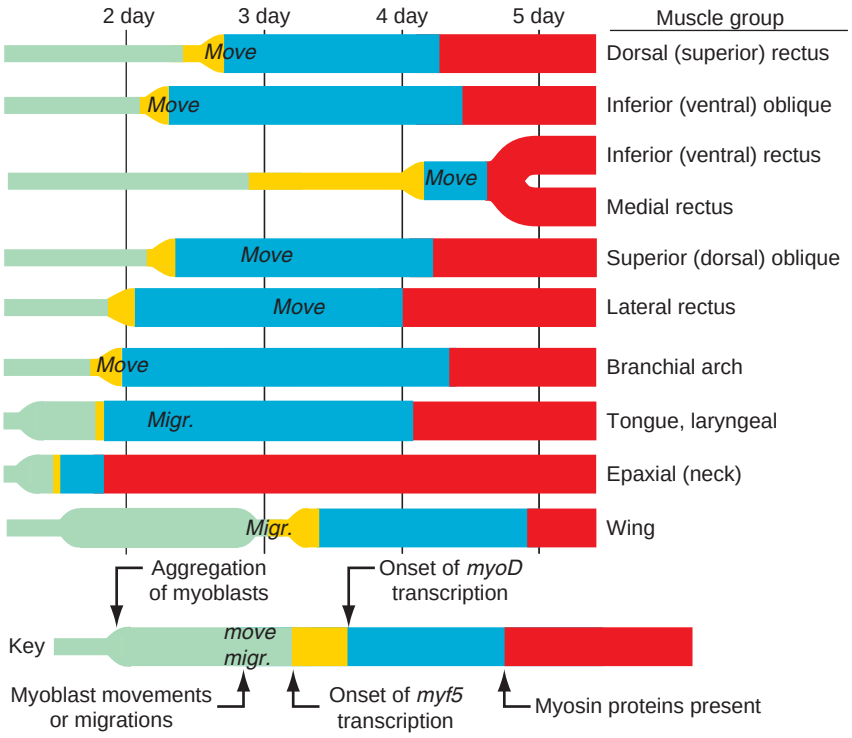

Figure 4 Timetable of gene activation in extraocular and other head and trunk muscles. The most consistent difference between trunk and head muscles is that the latter show a prolonged delay between the onset of *myoD* expression and the synthesis of muscle-specific proteins.

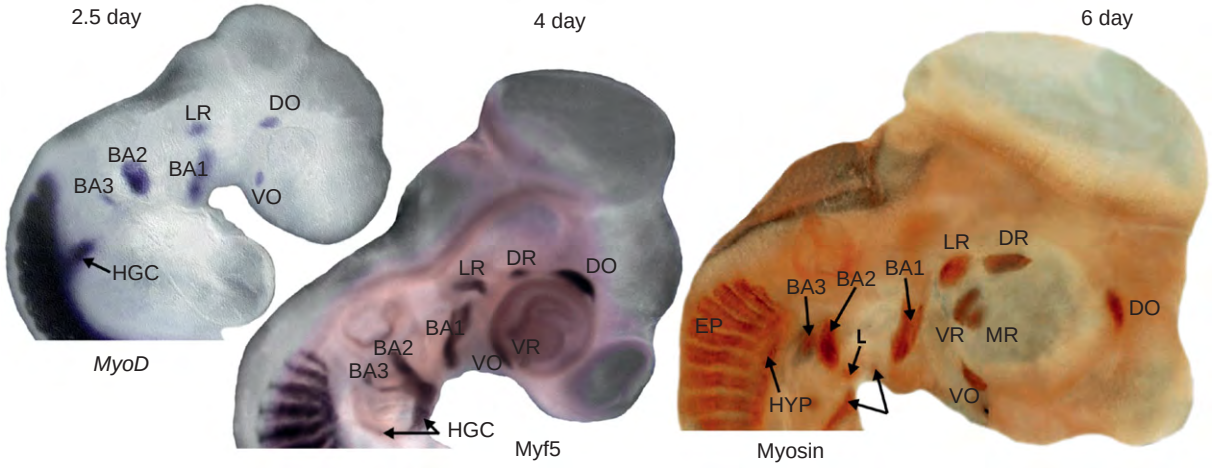

Figure 5 Early differentiation and morphogenesis of head muscles in chick embryos. BA1, 2, 3, branchial arches; DO, dorsal oblique; DR, dorsal rectus; Ep, epaxial muscle precursors; Hyp, hypaxial precursors, HGC, hypoglossal cord that forms tongue muscles; LR, MR, VR, lateral, medial and ventral rectus muscles; VO, ventral oblique.

At present the significance of these spatially and temporally dynamic expression patterns is unknown. It is possible that early expressions presage the later focal appearance of certain muscles, but it is equally plausible that each of these genes has multiple and distinct functions associated with each stage.

As extraocular muscles mature, they exhibit a progression of fiber types, evidenced by changes in the myosin isoforms and related contractile and energy metabolism proteins expressed. Emergence of these complex patterns requires a series of interactions among developing myofibers, surrounding connective tissues, and innervation. In the avian embryo, the primary myofibers of most extraocular muscles express embryonic slow myosin isoforms. However, one muscle, the quadratus nictitans, which is homologous to retractor bulbi muscles and is innervated

Table 1 Summary of myogenic regulatory networks of head and trunk

Expression sites	*Genes*	*Trunk*	*Limb and tongue*	*Branchial*	*EOMs*
All muscle	*myf5, myoD*	+	+	+	+
Trunk only	*noggin, ptc1*	+	−	−	−
	pax3, c-met	+	+	−	−
	barx2	+	+	+	+
Trunk and Head	*lbx1*	+	+	−	LR, DO
	paraxis	+	+	−	LR
	pitx2	+	+	−	+
	tbx1	−	(+)	+	LR
Head only	*en2*	−	−	BA1	−
	pod1	−	−	+	+
	hgf	−	−	BA1	DO, VO
	myoR	−	−	+	DO, VO, L1

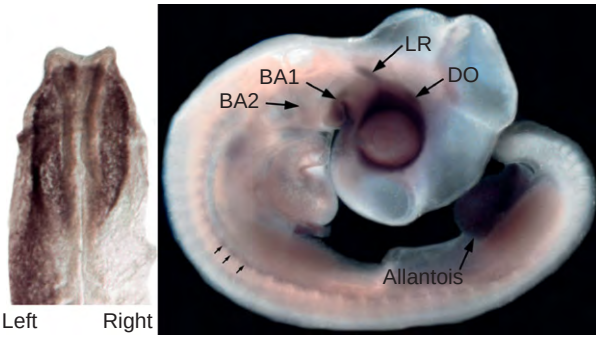

Figure 6 At stage 8 ((a), dorsal view) *Pitx2* is expressed symmetrically throughout head paraxial (and lateral) mesoderm populations, but only on the left within trunk mesoderm. By stage 21 ((b), 4 days) it is restricted to a subset of eye muscles, the first and second branchial arch muscle masses, and periocular mesenchyme.

by the accessory abducens nerve, the myofibers are either completely fast myosin expressing, as in the quail embryo, or mixed, as in the chick embryo (**Figure 7**). To explore the basis for these distinct, species-specific patterns, periocular neural crest cells of the chick were replaced with comparable populations from a quail embryo. The quadratus muscle in these chimeric embryos exhibits the quail donor phenotype (**Figure 7**), indicating that initial differentiation of fiber types requires interactions among myofibers and encompassing connective tissues.

Muscle Morphogenesis

Except for muscles that remain closely associated with the vertebral column and skull, all muscle progenitors leave their sites of origin in paraxial mesoderm and disperse into peripheral tissues. Body wall muscles do so together with sclerotome-derived connective tissue precursors, and maintaining these close spatial relations is essential for the morphogenesis of thoracic and abdominal muscles. For appendicular myogenesis, lateral myotome-derived cells move in sequential waves of primary and secondary myoblasts into nearby limb buds, where they form longitudinal bands of future dorsal and ventral groups before segregating into individual muscles. In the hindlimbs, some of these undergo secondary dispersal to form muscles of the perineal region.

Branchial muscles are comparable to body wall muscles in that they initially exhibit a constant juxtaposition with the precursors of their connective tissues, which in the head are all derived from neural crest cells, and also with the motor nerves that innervate them. This maintained registration permits continuous exchange of signals among all three components during all stages of muscle differentiation and morphogenesis.

This constant contiguity has most dramatically been demonstrated for the trapezius muscle, whose precursors arise among caudal branchial arch mesodermal populations and secondarily shift caudally to attach to the scapula. Mapping studies in both bird and mouse embryos revealed that the neural crest-derived connective tissues move with, and perhaps somewhat in advance of, these myoblasts and indeed contribute to the scapula. This recapitulates an ancestral condition in which the forelimb girdle articulated with the back of the skull, as is still present in fish.

Again, however, the extraocular muscles exhibit a developmental scenario unlike any other muscles. As illustrated in **Figures 5** and **8**, these muscle precursors move towards, then around, the equatorial region of the developing eye to assume their definitive locations. During this process, each muscle leaves the company of surrounding mesoderm cells and becomes fully encompassed by neural crest cells, which secondarily penetrate the muscle mass and form internal (e.g., endomysium) as well as surrounding (perimysium, fascia, and tendon) connective tissues.

These periocular crest cells need not have originated at the same axial level as the muscles. For example, the lateral rectus muscle, the neural crest cells that will form

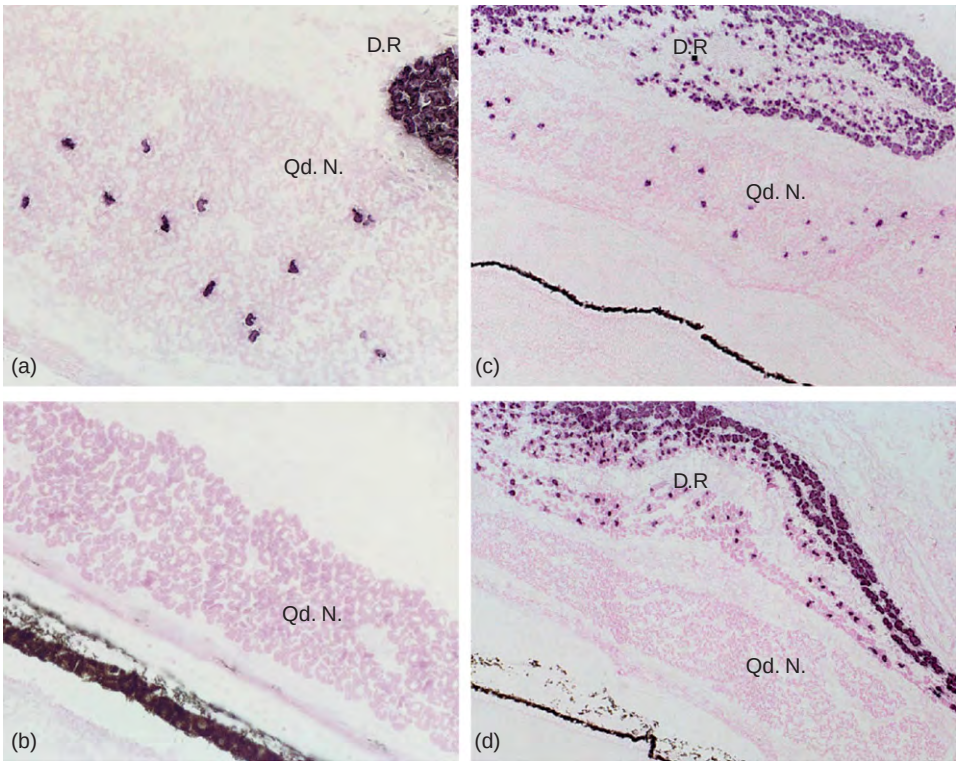

Figure 7 Fiber-type determination in the quadratus nictitans (Qd. N.) muscle. (a, b) Sections through this muscle in chick and quail embryos processed with antibodies to slow myosin isoforms. The quail Qd. N. lacks slow fibers, whereas in the chick both fast and slow fibers are present. (c) A control embryo in which chick neural crest cells were transplanted into a chick host, and the Qd. N. developed normally. However, when quail crest cells were grafted into a chick host embryo (d), the exclusive fast donor phenotype resulted.

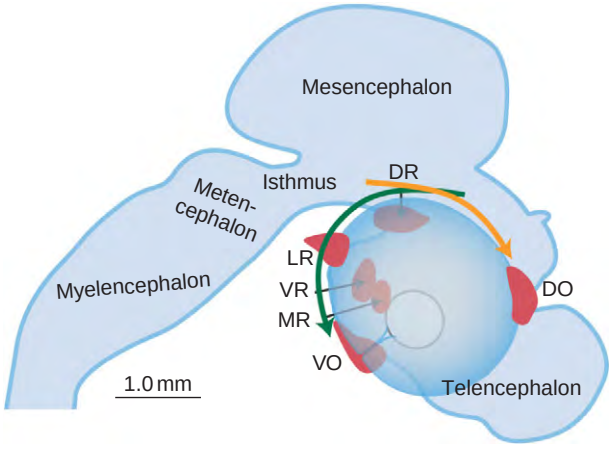

Figure 8 The movements of the dorsal (yellow arrow) and ventral (green arrow) oblique muscles from their sites of origin to their terminal locations along the equatorial zone of the globe.

its connective tissues, and the abducens nerve that innervates it originate at three separate axial levels. Indeed, these primordia do not become intimately associated until each has independently approached the periocular environment. This negates the possibility of prolonged interactions among contiguous progenitor populations, as occurs for branchial musculoskeletal systems.

The mechanisms by which aggregates of extraocular muscle primordia change both absolute and relative positions remain enigmatic. There is no precedence elsewhere in the embryo for condensations of cells moving actively through surrounding tissues. However, several lines of evidence support a model based on passive displacement of eye muscle primordia. As was shown in **Figure 2**, the interface between neural crest and myogenic paraxial mesoderm is initially a flat plane. Changes in the relative positions of the eye due to flexures and differential growth of the brain and expansion of the optic cup introduce distortions in this plane, but the extent to which this might affect individual eye muscles has been difficult to define.

In screening for a wide range of gene expression patterns, several were found that coincided with the patterns of movements taken by some extraocular muscles (**Figure 9**). These reveal a set of localized distortions of the neural crest-mesoderm interface. Finger-like projections of paraxial mesoderm expand dorsally and caudally around the optic cup, becoming interdigitated with periocular neural crest populations and passively bringing the dorsal and ventral oblique muscle primordia to their definitive

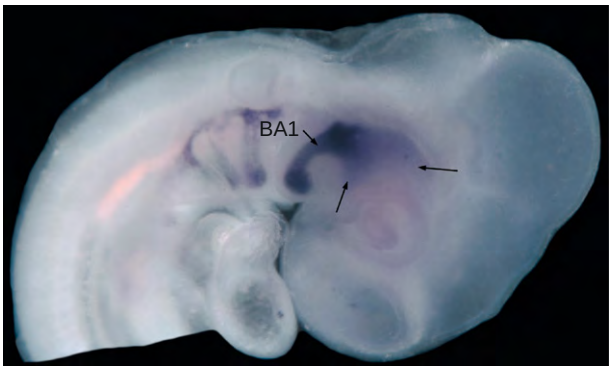

Figure 9 Lateral view of a 3.5-day chick embryo showing the sites of expression of the *MyoR* gene. Note the finger-like projections (arrows) extending dorsal and caudal to the optic vesicle, along the sites at which the dorsal and ventral oblique are expanding.

locations. Subsequently, crest cells close behind each of these muscle primordia, creating the appearance of an island of myoblasts/myofibers amid a sea of crest cells. How these focal distortions are established is unknown. The cell surface adhesion molecule semaphorin 3A is expressed by mesodermal cells in these projections, but its role in not known.

Summary

The early stages of extraocular muscle formation are well described but poorly understood mechanistically. They arise at discrete sites within unsegmented head paraxial mesoderm then launch into developmental programs that share some features with trunk and branchial muscles but are largely and surprisingly unique. Passive distortions of the mesoderm-neural crest interface bring these muscle primordia to their definitive locations around the ocular globe, where they become surrounded then infused by connective-tissue forming neural crest cells, which largely direct both the gross and microscopic differentiation of these muscles.

See also: Congenital Cranial Dysinnervation Disorders; Extraocular Muscles: Extraocular Muscle Anatomy; Extraocular Muscles: Extraocular Muscle Involvement in Disease.

Further Reading

Borue, X. and Noden, D. M. (2004). Normal and aberrant craniofacial myogenesis by grafted trunk somitic and segmental plate mesoderm. *Development* 131: 3967–3980.

Bryson-Richardson, R. J. and Currie, P. D. (2008). The genetics of vertebrate myogenesis. *Nature Reviews Genetics* 9: 632–646.

Evans, D. J. R. and Noden, D. M. (2006). Spatial relations between avian craniofacial neural crest and paraxial mesoderm cells. *Developmental Dynamics* 235: 1310–1325.

Grenier, J., Teillet, M. A., Grifone, R., Kelly, R. G., and Duprez, D. (2009). Relationship between neural crest cells and cranial mesoderm during head muscle development. *PLoS ONE* 4: e4381.

Marcucio, R. M. and Noden, D. M. (1999). Myotube heterogeneity in developing chick craniofacial skeletal muscles. *Developmental Dynamics* 214: 178–194.

Noden, D. M. and Francis-West, P. (2006). The differentiation and morphogenesis of craniofacial muscles. *Developmental Dynamics* 235: 1194–1218.

Noden, D. M., Marcucio, R. M., Borycki, A-G., and Emerson, C. P., Jr. (1999). Differentiation of avian craniofacial muscles. I. Patterns of early regulatory gene expression and myosin heavy chain synthesis. *Developmental Dynamics* 216: 96–112.

Noden, D. M. and Schneider, R. A. (2006). Neural crest cells and the community of plan for craniofacial development: Historical debates and current perspectives. In: Saint-Jeannet, J. P. (ed.) *Neural Crest Induction and Differentiation*, pp. 1–23. Boston, MA: Landes Bioscience and Springer Science Media.

Tzahor, E. (2009). Heart and craniofacial muscle development: A new developmental theme of distinct myogenic fields. *Developmental Biology* 327: 273–276.

Yoshida, T., Vivatbutsiri, P., Morriss-Kay, G., Saga, Y., and Iseki, S. (2008). Cell lineage in mammalian craniofacial mesenchyme. *Mechanisms of Development* 125: 797–808.

Drug Delivery to Cornea and Conjunctiva: Esterase- and Protease-Directed Prodrug Design

R S Talluri, S Hariharan, P K Karla, and A K Mitra, University of Missouri–Kansas City, Kansas City, MO, USA

Glossary

Amidases – The enzymes that catalyze the cleavage of carbon–nitrogen bonds in amides.
Bioreversion – The conversion of a prodrug to an active form.
Esterases – The enzymes that catalyze the hydrolysis of an ester into its alcohol and acid.
Peptidases – The enzymes that catalyze the hydrolysis of peptides into amino acids.
Prodrug – The drugs designed to be inactive until *in vivo* activation generates the active form of the drug.
Transporter – The protein that translocates materials in biological systems resulting from expenditure of metabolic energy.

Topical Ocular Drug Delivery

Topical drug delivery is the most acceptable form of treatment for the diseases affecting the anterior segment such as corneal epithelial and stromal keratitis, glaucoma, conjunctivitis, dry eye syndrome, iritis, uveitis, and blepharitis. The structure of the eye is shown in **Figure 1**. Topically applied drugs can reach the intraocular tissues either by corneal and/or noncorneal (conjunctival–scleral) pathway(s). Drugs traversing the corneal pathway should permeate through the corneal epithelium and stroma which are rate-limiting barriers for hydrophilic and lipophilic molecules, respectively. Conjunctival absorption could result in higher drug concentrations in the anterior as well posterior chambers depending on the mechanism of absorption. Conjunctival–scleral pathway is favored for the treatment of diseases in the posterior segment, as it can bypass the anterior chamber and thus permit direct access to intraocular tissues like sclera retina and vitreous humor. However, nasolacrimal drainage, tear dilution, as well as the outer conjunctiva and cornea, act as barriers to drug absorption. As a result, therapeutic concentrations in intraocular tissues following topical administration are difficult to achieve and about 1–5% of topically instilled dose reaches the anterior segment of the eye. Moreover, a larger fraction of the applied drug is eliminated from the precorneal area within 5 min, through drainage across nasolacrimal duct into the systemic circulation. Fifty percent of the normal human tear film is replaced every 2–20 min. Such a high tear-turnover rate also reduces the drug-residence time in precorneal and conjunctival areas. Therefore, rapid tear-film drainage can also impede the drug absorption following topical administration. Topically administered agents have a low probability of reaching the posterior segment in significant amounts, as passage through the corneal and conjunctival epithelia, aqueous humor, and lens is required to reach the retina.

Various strategies have been investigated in order to improve the corneal and conjunctival absorption of drugs instilled topically. Prodrug approach is one of the most promising and effective strategies currently being investigated for ophthalmic drug delivery. Exploring the inherent drug metabolism capability of ocular tissues is one of the important aspects of prodrug design. In this strategy, the drug molecule is modified chemically by attaching it to a promoiety to improve the physicochemical characteristics, such that higher drug absorption into the tissues can be achieved.

Prodrugs are designed to be therapeutically inactive until *in vivo* activation to generate the parent drug. The compounds are synthesized by linking an appropriate chemical moiety to the parent drug, usually linking by an ester or an amide bond. Upon absorption into the tissue, the prodrug will be subjected to enzymatic hydrolysis (bioreversion by esterases/peptidases) to release the active parent drug (**Figure 2**). The rate of bioreversion depends upon various factors, including affinity of the prodrug linkage toward hydrolyzing enzyme(s), the capacity and turnover rate of the enzyme, etc. The enzymes responsible for hydrolysis of prodrugs are present ubiquitously in all biological fluids and tissues. For example, esterases are expressed throughout the body and can be utilized in the hydrolysis of an ester functional group. In ocular tissues, the esterase activity has been found to be the highest in iris-ciliary body followed by the cornea and the aqueous humor. Among ocular esterases, butyrylcholinesterase (BuChE) constitutes the major proportion compared to acetylcholinesterase (AChE) – except in the corneal epithelium of albino rabbits. Drugs and prodrugs containing ester linkages can undergo varying extents of esterase-mediated hydrolysis while permeating the cornea/conjunctiva and upon entering into the aqueous humor, iris, and ciliary body. Proteases or peptidases are primarily responsible for hydrolysis of amide linkage in

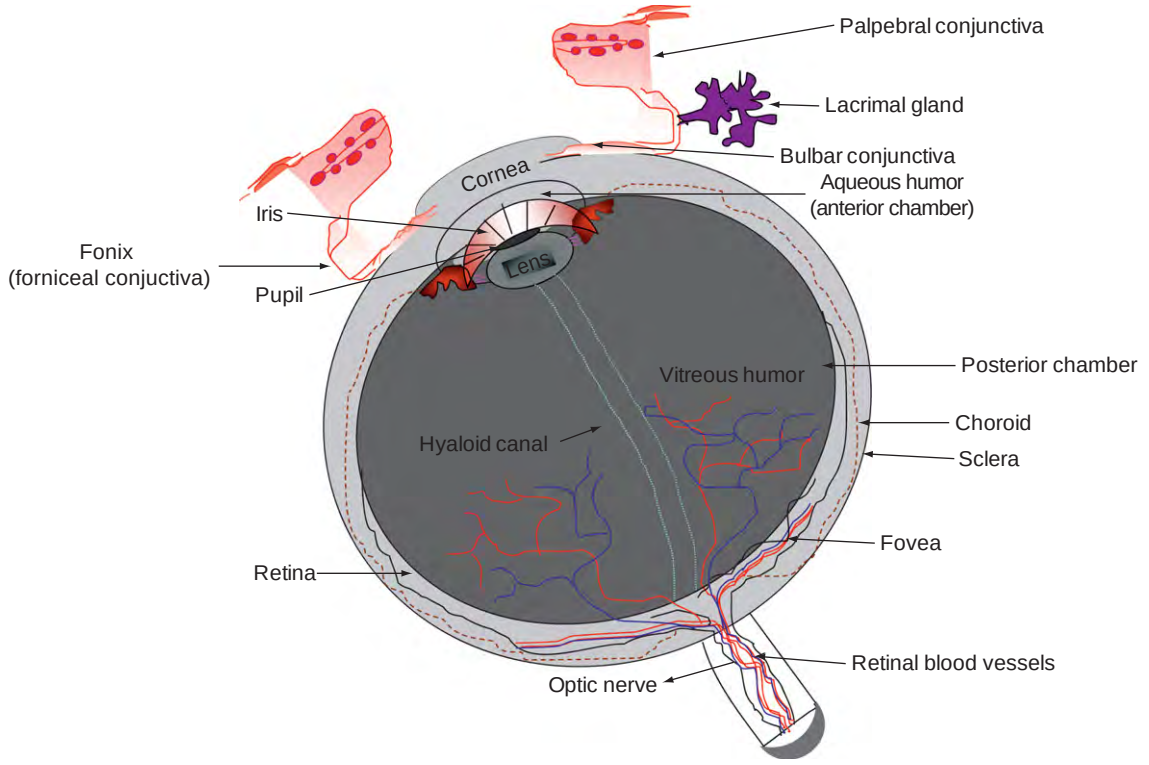

Figure 1 Cross-sectional view of the eye. From Hosoya, K., Lee, V. H., and Kim, K. J. (2005). Roles of the conjunctiva in ocular drug delivery: A review of conjunctival transport mechanisms and their regulation. *European Journal of Pharmaceutics and Biopharmaceutics* 60: 227–240.

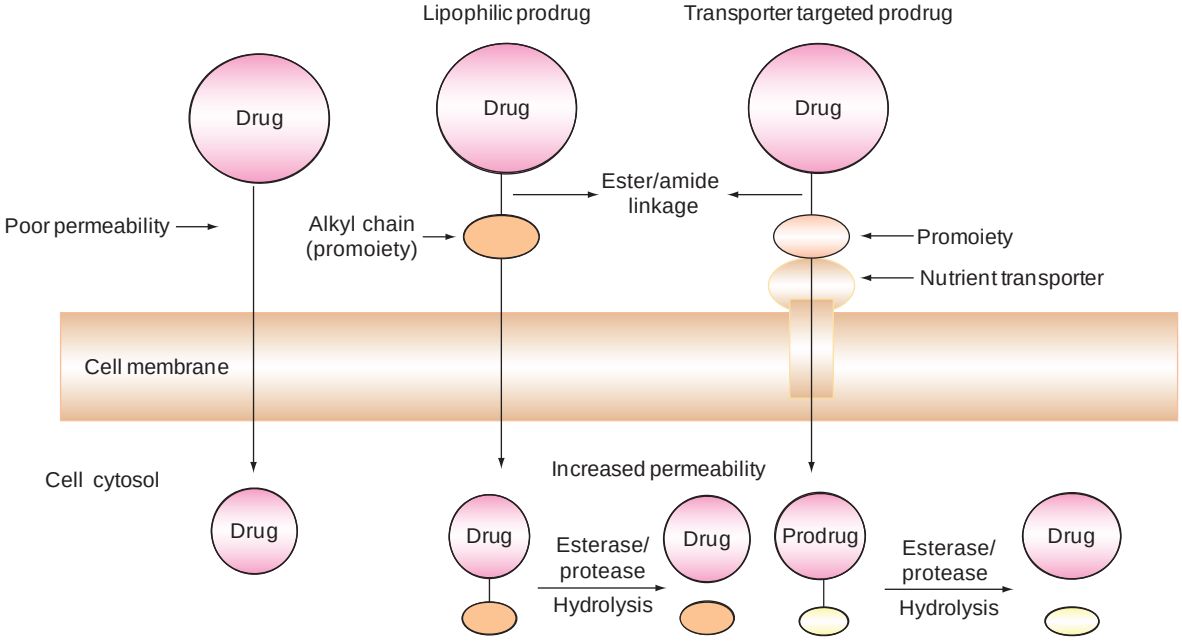

Figure 2 Schematic: Lipophilic and transporter targeted prodrug design.

peptides or peptide-based prodrugs. These enzymes are classified as either 'endo-' or 'exo-' depending on whether they cleave internal or external peptide bonds. The aminopeptidase activity is the highest in the corneal epithelium and iris-ciliary body followed by conjunctiva and corneal stroma.

Kashi and colleagues have shown that aminopeptidases, dipeptidyl peptidase, and dipeptidyl carboxylpeptidase are

involved in hydrolysis of enkhaphilins in rabbit ocular-tissue homogenates including conjunctiva, corneal stroma, iris ciliary body, lens, and tears.

Prodrugs targeted toward membrane transporters expressed on the epithelial cells are perhaps the most exciting of all the current drug-delivery strategies. Epithelial cells express various nutrient transporters and receptors on their membrane surface. Analogs or prodrugs targeted toward these transporters can significantly enhance the absorption of poorly permeating therapeutic agents. Such prodrugs are recognized by membrane transporters as natural substrates and are translocated across the epithelial membranes. Once inside the cell, the conjugate will release the parent drug by enzymatic hydrolysis (**Figure 2**). Various nutrient transporters are expressed on the cornea and conjunctiva. Their utility in drug delivery will be discussed in subsequent sections.

Role of Cornea in Topical Drug Delivery

Cornea is the outermost avascular and transparent dome-shaped structure of the eye. It consists of five layers (in the direction from anterior to posterior): epithelium, Bowman's layer, stroma, Descemet's membrane, and corneal endothelium (**Figure 3**). The lipoidal corneal epithelium is comprised of five to six layers of tightly adherent columnar cells with tight-junction proteins called zonulae occludens – acting as a major barrier to hydrophilic drugs. On the other hand, the stroma – which is comprised of 90% water – lies directly beneath the corneal epithelium and acts as a rate-limiting barrier to lipophilic drugs. Thus, even if a molecule is sufficiently lipophilic to rapidly cross the epithelium, penetration through the stroma is still rate limiting. In addition, the physicochemical properties of the drug itself limit its permeability across the cornea. More recently, the expression of multidrug resistance proteins such as the P-glycoprotein (P-gp) and multidrug-resistance-associated proteins (MRPs) has been reported on rabbit and human corneal epithelium. They have gained attention lately, since majority of the drug molecules applied topically have been categorized as substrates to one or more of these efflux pumps. In fact, P-gp and MRP-2- localized on the rabbit corneal epithelium can act as a barrier to *in vivo* drug absorption through cornea.

Lipophilic prodrug derivatization has been considered as a viable strategy to enhance transcorneal permeation of ocular therapeutic agents. High octanol/water coefficient of these prodrugs can facilitate permeation across the corneal epithelium. The water-laden stroma, in turn, does not act as a barrier to the regenerated hydrophilic parent drug – thereby enhancing the overall permeability of the prodrug across cornea. Esterase activity has been reported to be the highest in iris-ciliary body followed by cornea and the aqueous humor. Even though high levels of esterases are reported in the iris-ciliary body, the activity in the cornea is highly relevant since cornea acts as a major permeation pathway to these lipophilic ester prodrugs. Bulk of esterase-mediated hydrolysis takes place in the corneal epithelium where the esterase activity is about 2 times to that of stroma and endothelium.

Lipophilic ester prodrug design has been employed for a variety of ocular therapeutic agents, which suffer from poor ocular absorption. Esterification of prostaglandin $F_{2\alpha}$

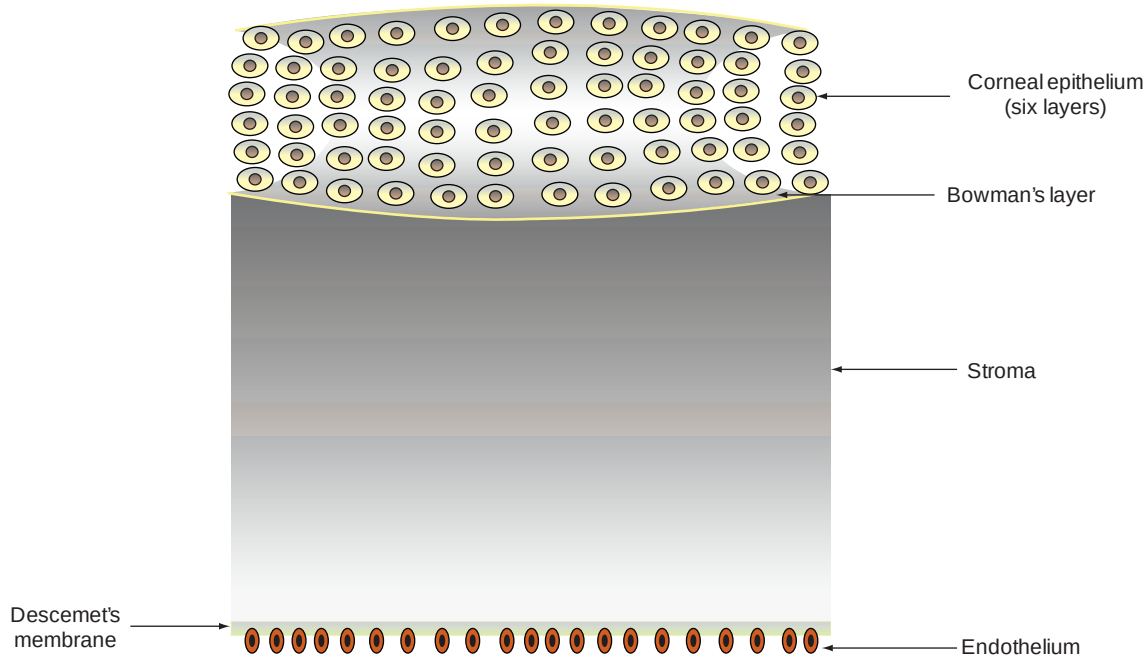

Figure 3 Structure of cornea.

($PGF_{2\alpha}$) analogs which exhibit higher potency than $PGF_{2\alpha}$ have resulted in blockbuster drugs such as bimatoprost, travoprost, latanoprost, and isopropyl unoprostone. Travoprost, latanoprost, and isopropyl unoprostone are isopropyl esters of $PGF_{2\alpha}$ analogs, whereas bimatoprost is an ethyl amide prodrug (**Figure 4**). The free acid form of all the above prodrugs has shown poor permeability across cornea, thus obviating the need for lipophilic ester prodrug design. Such strategy is particularly applicable to β-blockers such as timolol – widely used in the treatment of glaucoma – which suffers from high incidence of cardiovascular and respiratory side effects due to systemic absorption of the topically administered dose. Lipophilic prodrug derivatization of timolol to acetyl, propionyl, and butyryl ester prodrugs resulted in corneal permeabilities 2–3 times higher than timolol. Moreover, the enhanced corneal permeation leads to a four- to sixfold increase in the aqueous humor concentrations. Better corneal permeation and high aqueous humor concentration of lipophilic ester prodrugs of timolol consequently resulted in a twofold reduction in the topical dose. Reduced dose can, in turn, decrease the concentration in the systemic circulation, thereby reducing the incidence of cardiovascular and respiratory side effects.

The lipophilic ester prodrug design has been extended to antiviral agents such as acyclovir (ACV) and ganciclovir (GCV). These are highly potent against Herpes simplex virus (HSV). Currently available therapy for HSV keratitis involves the use of a 1%-trifluorothymidine (TFT) solution. However, long-term treatment with TFT raises potential concerns due to its high cytotoxicity. ACV is a potent candidate effective against HSV which is available as a 3% ophthalmic ointment. However, due to various problems associated with the use of ointments in the eye, it has not been approved in the United States. Ocular bioavailability of these compounds is extremely limited because of poor corneal permeability. Corneal permeability coefficients increase with increasing lipophilicity for monoester prodrugs of GCV, with the optimal prodrug form having three or four carbon atoms in the side chain. The apparent permeability (P_{app}) of the valerate-ester prodrug of GCV was sixfold higher than the parent drug GCV, across the cornea. Acylation of ACV also led to improved corneal permeation of the parent drug. There is a linear relationship between the corneal permeability coefficient and the octanol/water partition coefficient with a positive slope, except for ACV isobutyrate – which displayed an anomalously low corneal permeability despite improved lipophilicity. The anomaly with branched alkyl side chain could be explained due to enhanced stability of these prodrugs toward esterases present in the corneal epithelium. The branched side chain offers steric hindrance for enzyme accessibility. The concept has been proven where the stability of homologous series of oxprenolol esters increases with increasing carbon chain length of the side chain. It has been shown that hydrolysis rates are moderate for *O*-propionyl, *O*-butyryl, and *O*-valeryl prodrugs of oxprenolol, with *O*-acetyl-oxprenolol being highly unstable and *O*-pivaloyl-oxprenolol being highly stable (**Table 1**). Again, the steric hindrance offered by the bulky tertiary butyl group in the pivaloyl derivative has been cited as the primary reason for superior enzymatic stability. However, all of these prodrugs described above are highly lipophilic and possesses very low aqueous solubility to be formulated into aqueous drops for topical administration. Reports indicate that the aqueous solubility of the lipophilic ester prodrugs decrease with increasing carbon side-chain length. Low aqueous solubility has been considered as a major drawback for formulating these lipophilic ester prodrugs into eyedrops. Thus, for a compound to be effective topically and to be formulated into eyedrops, it must possess sufficient hydrophilicity and at the same time exhibit sufficient permeability across the cornea to reach therapeutic levels.

Recently, transporter-targeted prodrug approach has received significant attention and a number of membrane transporters have been discovered in various ocular tissues such as the cornea, conjunctiva, and retina. These transporters are involved in the translocation of essential nutrients and xenobiotics across biological membranes. Ocular transporters include carriers for peptides, amino acids, glucose, lactate, and nucleosides/nucleobases and are primarily localized on the corneal epithelium, corneal endothelium, retinal pigmented epithelium (RPE), and retinal capillary endothelium. Prodrugs or analogs designed to target these transporters can significantly enhance the absorption of poorly permeating parent drug. Both solubility and the desired membrane permeability can be achieved by proper selection of the promoiety. Such prodrugs are recognized by the membrane transporters as substrates and are translocated across the epithelia. Subsequently, the prodrugs are enzymatically cleaved to release the parent drug and free ligand which in most cases is a nutrient and nontoxic.

Of late, such transporter-targeted prodrug design has been applied to the antiviral drugs ACV and GCV. The existence of an oligopeptide transport system (PEPT1) on the rabbit corneal epithelium has been demonstrated which can transport peptidomimetic prodrugs of acyclovir. Permeation of valine-ester prodrug of acyclovir (L-Val-ACV) across the cornea has been found to be much higher than that of the parent drug ACV (**Table 2**). The transport of L-Val-ACV is saturable at higher concentrations, pH dependent, and competitively inhibited by other known PEPT1 substrates indicating its translocation by PEPT1 present on the cornea. This result prompted the investigators to synthesize a series of water-soluble dipeptide prodrugs of acyclovir targeting the peptide transport system on the cornea to improve the ocular bioavailability.

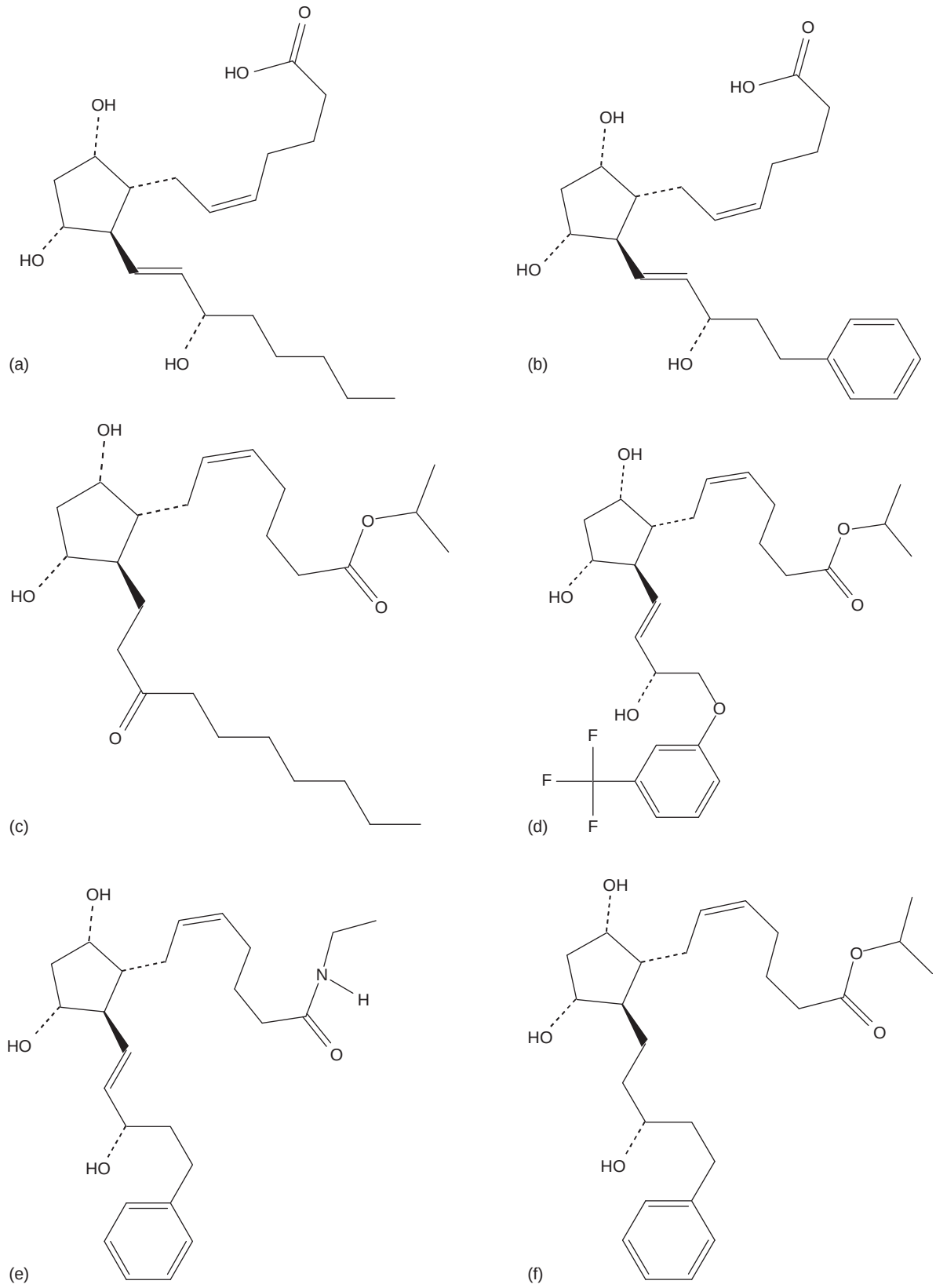

Figure 4 Chemical structures: (a) $PGF_{2\alpha}$, (b) 17-phenyl-$PGF_{2\alpha}$, (c) isopropyl unoprostone, (d) travoprost, (e) bimatoprost, and (f) latanoprost.

Table 1 Half-life values for a homologous series of oxprenolol (*O*) esters in 0.05 M phosphate buffer (pH 7.4), 30% human plasma, aqueous humor, and corneal extract at 37 °C (data taken from Geraldine, C. and Jordan M. 1998)

	Half-life ($t_{1/2}$, min)			
Ester	*Buffer (pH 7.4)*	*Human plasma 30%*	*Aqueous humor*	*Corneal extract*
O-acetyl	9.1	4.3	6.1	9.6
O-propionyl	10.4	6.4	14.6	11.3
O-butyryl	19.1	12.8	18.3	13.0
O-valeryl	21.1	16.2	19.6	16.4
O-pivaloyl	2035.5	263.2	687.8	375.5

Table 2 Permeability of dipeptide prodrugs of ACV across freshly excised rabbit cornea

Drug	*P_{app} ($\times 10^6$ cm s^{-1})*
ACV	4.24 ± 1.41[a]
VACV	12.1 ± 0.44*
VVACV	9.91 ± 2.40*
GVACV	12.4 ± 1.42*
YVACV	7.19 ± 1.38*
VYACV	8.34 ± 1.12*

[a]Control

All values are expressed as mean ± SD. Statistically significant difference between control and test is represented by * ($p < 0.05$). ACV, acyclovir; VACV, val-acyclovir; VVACV, val-val-acyclovir; GVACV, gly-val-acyclovir; YVACV, tyr-val-acyclovir; VYACV, val-tyr-acyclovir.

Data from Anand, B. S., Nashed, Y. E., and Mitra, A. K. (2003). Novel dipeptide prodrugs of acyclovir for ocular herpes infections: Bioreversion, antiviral activity and transport across rabbit cornea. *Current Eye Research* 26: 151-163, with permission from Taylor & Francis.

The structures of ACV, valine-based amino acid ester of ACV (VACV), and valine- and glycine-based dipeptide conjugate of acyclovir – valine–valine–acyclovir (VVACV) and glycine–valine–acyclovir (GVACV) are shown in **Figure 5**. VACV is found to be hydrolyzed primarily by esterases to release ACV, whereas VVACV is hydrolyzed initially by aminopeptidases to release VACV, which is further acted upon by esterases to release ACV (**Figure 6**). Direct conversion of VVACV to ACV appears to be minimal. These prodrugs exhibited excellent solution stability and solubility allowing formulation into suitable eyedrops. All dipeptide prodrugs of ACV exhibited enhanced transcorneal permeability resulting in higher ocular bioavailability in rabbits, with GVACV being the highly permeable prodrug (**Table 2**). The prodrugs also exhibit higher antiviral efficacy against HSV epithelial keratitis and stromal keratitis and are less cytotoxic and more effective than trifluorothymidine (TFT) – a current drug of choice.

In addition to peptide transporters, even amino acid transporters such as ASCT1 (Na^+-dependent neutral amino acid transporter) and $B^{0,+}$ (Na^+-dependent neutral and cationic amino acid transporter) have been explored for ocular delivery of ACV. A series of amino acid ester prodrugs including alanine-ACV, serine-ACV, isoleucine-ACV, γ-glutamate-ACV, and valine-ACV were synthesized and evaluated by Katragadda and colleagues for *in vivo* corneal absorption against the parent drug, ACV. Results showed that the amino acid-ester prodrug, serine-ACV – owing to its enhanced stability – exhibited higher area under the curve, C_{max} and C_{last} values, in comparison to ACV and seemed to be a promising candidate for the treatment of ocular HSV infections. Gunda and colleagues have applied similar chemical derivatization to GCV – an acyclic guanosine analog. GCV has shown to exhibit excellent antiviral activity against the herpes viruses but suffers from poor corneal permeability due to its hydrophilicity. Hence, in order to enhance the corneal permeability and ocular bio availability, dipeptide monoester prodrugs of GCV targeting the peptide transporter on the corneal epithelium were synthesized. Among the synthesized prodrugs, tyrosine–valine–GCV and valine–valine–GCV, exhibited significantly higher transcorneal permeability *ex vivo* and *in vivo* leading to higher ocular bioavailability when compared to GCV.

Role of Conjunctiva in Ocular Drug Delivery

Conjunctiva is a transparent, highly vascularized mucous membrane that covers the sclera and lines the inner surfaces of eyelids. It covers almost 80% of exposed ocular surface and is comprised of many small blood vessels and tiny secretory glands. These glands produce tear film that lubricates and protects the eye during its movement in the socket. Three different types of conjunctival membranes have been identified based on its location. Palpebral or tarsal conjunctiva is the one lining the eyelids. Bulbar or ocular conjunctiva is a semipermeable and colorless membrane covering the eyeball, over the sclera. Fornix conjunctiva is where the inner part of the eyelids and the eyeball meet. It is loose and flexible, allowing free movement of the lids and eyeball. The tissue consists of pseudostratified columnar epithelium rich in goblet cells and it contains ductules of main lachrymal gland, accessory lachrymal glands, and lymphoid follicles. The space between the palpebral and bulbar conjunctiva is called the conjunctival *cul-de-sac*. Conjunctiva is typically composed of two layers, an outer epithelium and underlying

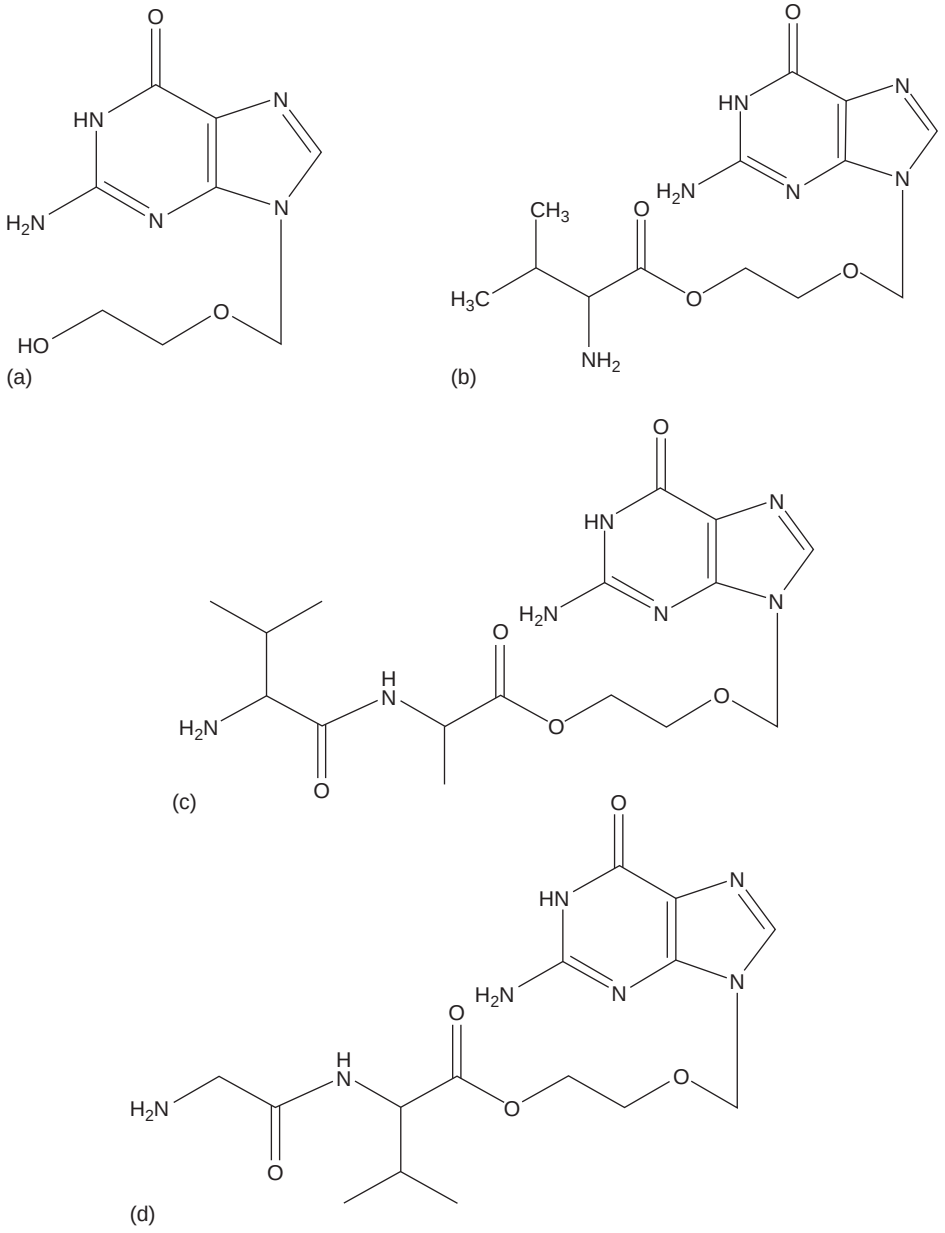

Figure 5 Chemical structures: (a) acyclovir, (b) valine–acyclovir, (c) valine–valine–acyclovir, and (d) glycine–valine–acyclovir.

stroma. The epithelium consists of 5–15 layers of stratified epithelial cells and is covered with microvilli. The stroma loosely attaches to the underlying sclera. It contains all the lymphatics and blood vessels.

The larger surface area and pore density coupled with expression of various nutrient transporters listed in the subsequent sections makes the conjunctiva more amenable for topical drug delivery. The surface area of the conjunctiva is almost 9 and 17 times larger than that of cornea in rabbits and humans, respectively. Compared to cornea, the paracellular pore size as well as the pore density in conjunctiva is larger. Due to such increased pore size and density small peptides and oligonucleotides can permeate across conjunctival pores. However, for hydrophilic drugs instilled topically, the lipophilic conjunctival epithelium acts as rate-limiting barrier for drug absorption. In addition, an external enzymatic barrier in the conjunctival epithelium – specifically the proteases – restricts the penetration of peptide drugs like enkephalins, substance P, and insulin. One of the major disadvantages associated with conjunctival absorption following topical administration is drainage of drug molecules by conjunctival blood vessels into the systemic circulation. Moreover, it has been shown that the conjunctiva expresses efflux transporters including P-gp on the apical side of conjunctival epithelium. These can limit the absorption of several

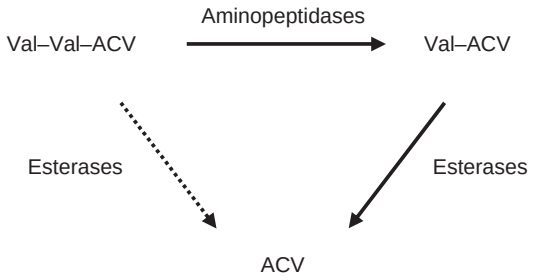

Figure 6 Metabolic pathway of valine–valine–acyclovir (VVACV) to valine-based amino acid ester of acyclovir (VACV) and acyclovir (ACV). From Anand, B. S., Nashed, Y. E., and Mitra, A. K. (2003). Novel dipeptide prodrugs of acyclovir for ocular herpes infections: Bioreversion, antiviral activity and transport across rabbit cornea. *Current Eye Research* 26: 151–163, with permission from Taylor & Francis.

fluoroquinolones such as levofloxacin, gatifloxacin, and grepafloxacin instilled topically. Thus, improving the drug absorption across conjunctiva is one of the major challenges needed to be overcome. Based on the target tissue, conjunctival drug delivery can be divided into subconjunctival and transconjunctival delivery.

Transconjunctival Pathway

In this route, agents can be targeted toward the conjunctiva for treatment of local conjunctival infection as well as other anterior chamber diseases such as dry eye syndrome and glaucoma. Transconjunctival absorption could also result in higher concentrations in posterior ocular tissues through conjunctival–scleral pathway. However, subconjunctival pathway is widely exploited to deliver drugs to posterior ocular segment.

Hydrophilic molecules can permeate through paracellular pathway between epithelial cells through the tight junctions. However, their penetration will be extremely low due to the small surface area of paracellular pathway compared to transcellular route. Transconjunctival drug penetration can be enhanced by increasing the lipophilicity of the drug molecule through chemical modification, mostly as prodrugs or analogs. Propranolol – with a log partition coefficient between octanol and water (log P) of 3.21 – is absorbed through cornea and conjunctiva up to tenfold greater than a hydrophilic drug of similar size, for example, sotalol with a log P of −0.62.

Prodrug strategy has not been exploited in conjunctiva as extensively as in cornea. As discussed earlier, *in vivo* activation of the prodrug is very essential for the success of this approach. As ester and amide linkages are widely utilized in prodrug design, it is important to know the activities of esterases and amidases in conjunctiva. As mentioned before, esterase and aminopeptidase activity has been reported in conjunctiva along with the cornea and iris-ciliary body. These play a role in hydrolysis of ester and amide bases prodrugs in the conjunctiva. The peptidases can also hydrolyze short-chain, biologically active peptides such as methionine and leucine enkephalins. There is good number of studies demonstrating esterases/amidases targeted prodrug approach to enhance drug absorption across conjunctiva. A few of them are discussed below.

PGs can lower intraocular pressure (IOP) in open-angle glaucoma. However, due to the low permeability of $PGF_{2\alpha}$ across the cornea, a relatively high concentration of $PGF_{2\alpha}$ is necessary for effective IOP reduction. This can result in conjunctival hyperemia, ocular discomfort, headaches, and other side effects. Chen and colleagues have evaluated lipophilic $PGF_{2\alpha}$ ester prodrugs for improving the permeability of $PGF_{2\alpha}$ following topical administration. A series of lipophilic esters such as $PGF_{2\alpha}$ 1-isopropyl, 1, 11-lactone, 15-acetyl, 15-pivaloyl, 15-valeryl, and 11, 15-dipivaloyl esters have been evaluated for transport and bioreversion in rabbit cornea, conjunctiva, and iris-ciliary body (**Figure 7**). All of the prodrugs penetrated the rabbit cornea and conjunctiva faster than $PGF_{2\alpha}$ except the 15-acetyl ester prodrug, which is equally permeable as $PGF_{2\alpha}$ across conjunctiva. However, a direct relationship is not observed between the degree of apparent permeability and prodrug lipophilicity. The two most lipophilic prodrugs – the 15-valeryl and 11, 15-dipivaloyl esters – were less permeable in the cornea and conjunctiva than other prodrugs with comparatively lower lipophilicity. The high permeabilities of 1-isopropyl ester and 1, 11-lactone is attributed to their state of ionization at the site of absorption where they exist more in unionized form. The prodrug 1, 11-lactone hydrolyzed at a slower rate in the ocular tissues probably due to the intracyclic ester linkage. The bulky pivaloyl group in 15-pivaloyl prodrug rendered it enzymatically more stable than the 1-isopropyl and other 15-monoester prodrugs. Bulky moiety (steric hindrance) might have impeded access of esterases to hydrolyze the pivaloyl ester linkage. Similarly, the prodrug with two pivaloyl groups – 11, 15-dipivaloyl prodrug – is much more stable as expected. Thus, the size and structural branching of the promoiety can influence enzymatic hydrolysis of prodrugs which, in turn, can further determine the permeability across tissues.

Corticosteroids find applications in the treatment of uveitis and postsurgical inflammation. However, these drugs can cause significant adverse effects such as increase in IOP, cataract, and herpetic reactivation. Dexamethasone (DX) is the one drug mostly indicated for ocular corticosteroid treatment. Several lipophilic esters of dexamethasone prodrugs have been evaluated for their ocular permeability and bioreversion in bovine conjunctival epithelial cell line (BCEC) and isolated rabbit cornea (**Figure 8**). This study is mainly aimed at selecting an optimum prodrug that improves the delivery of dexamethasone to the target tissue with minimum permeation across other

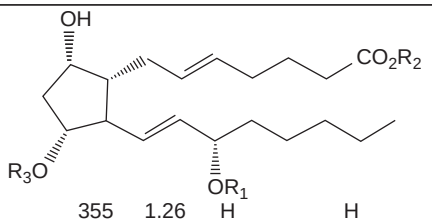

compound	MW[a]	log P[b]	R_1(C-15)	R_2(C-1)	R_3(C-11)
$PGF_{2\alpha}$	355	1.26	H	H	H
15-Acetyl ester	396	2.16	CH_3CO	H	H
1-Isopropyl ester	396	2.50	H	$CH_2(CH_3)_2$	H
1,11-Lactone	337	2.61			

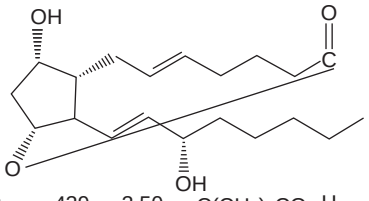

15-Pivaloyl ester	439	3.50	$C(CH_3)_3CO$	H	H
15-Valeryl ester	439	3.75	C_4H_9CO	H	H
11,15-Dipivaloyl ester	523	5.0	$C(CH_3)_3CO$	H	$C(CH_3)_3CO$

[a]Molecular weight. [b]Log *P* was determined from the Pomona Med. Chem. Software system or measured by HPLC.

Figure 7 Chemical structures of $PGF_{2\alpha}$ and its prodrugs. From Chien, D. S., Tang-Liu, D. D., and Woodward, D. F. (1997). Ocular penetration and bioconversion of prostaglandin F2alpha prodrugs in rabbit cornea and conjunctiva. *Journal of Pharmaceutical Sciences* 86: 1180–1186, with permission from John Wiley & Sons, Inc.

Dexamethasone (DX) ester	Abbreviation
21-sodium phosphate	DSP
21- metasulfobenzoate	DSB
21-acetate	DAC
17-propionate	DPR 17
21-propionate	DPR
21-butyrate	DBU
21-valerate	DVA
21-palmitate	DPALM

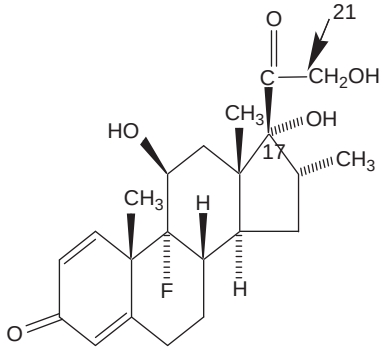

Figure 8 Dexamethasone esters and their abbreviations. From Civiale, C., Bucaria F., Piazza S., et al. (2004). Ocular permeability screening of dexamethasone esters through combined cellular and tissue systems. *Journal of Ocular Pharmacology and Therapeutics* 20: 75–84, with permission from JOPT.

ocular tissues to reduce adverse effects. The permeability of these dexamethasone prodrugs correlated well with their lipophilicity until a maximum value is reached, which corresponded to dexamethasone butyrate (log $P = 3.95$). DSP and DSB prodrugs are hydrophilic and thus do not permeate across BCEC as expected. Other prodrugs exhibited higher permeability with increase in lipophilicity till DBU, after which it started to plateau as observed with DVA (**Figure 9**). A similar trend has been observed across the cornea with exceptions at the extreme ends of log *P* values (DSP and DVA) which has been attributed to the rate of hydrolysis of prodrugs in corneal tissue and BCEC an epithelial layer. DVA being highly lipophilic gets absorbed into corneal epithelium and its further permeation is limited by hydrophilic corneal stroma unless it is hydrolyzed to relatively more hydrophilic dexamethasone. However, the hydrolysis of DVA to dexamethasone is very poor in cornea, confining the prodrug in the corneal epithelium (**Table 3**). This may be optimum for delivery of dexamethasone to cornea, where the prodrug in the corneal epithelium can hydrolyze slowly and sustain the release. Thus, it reduces the drug concentrations in aqueous humor and other intraocular tissues minimizing its side effects. Unlike in BCEC,

DSP has been found to hydrolyze rapidly in the cornea creating a concentration gradient for higher absorption into cornea. DBU is the prodrug that is completely hydrolyzed both in BCEC and cornea and also has tremendously improved the permeability of dexamethasone. This may be more suitable prodrug to deliver dexamethasone to other intraocular tissues. These studies clearly show that both the promoiety as well as the ability of the prodrug to get hydrolyzed are important in designing an optimum prodrug in ocular drug delivery.

A series of alkyl, cycloalkyl, and aryl ester prodrugs of timolol has been evaluated to examine the effect of enzymatic lability of prodrugs on corneal and conjunctival penetration of timolol. Straight-chain alkyl and the unsubstituted cycloalkyl esters hydrolyzed more rapidly than their corresponding branched-chain and substituted analogs as well as the aryl esters. This might be due to free accessibility of the ester linkage to esterases in straight-chain alkyl esters. The slower hydrolysis of branched chain alkyl esters might be due to steric hindrance to hydrolyzing enzymes. As expected, the esters with enzymatically labile straight-chain alkyl chains penetrated the cornea and conjunctiva at faster rates than the esters with branched alkyl chains that are less labile toward enzymatic hydrolysis. Thus, this study has shown that the rate of enzymatic hydrolysis can highly influence the corneal/conjunctival absorption of prodrugs.

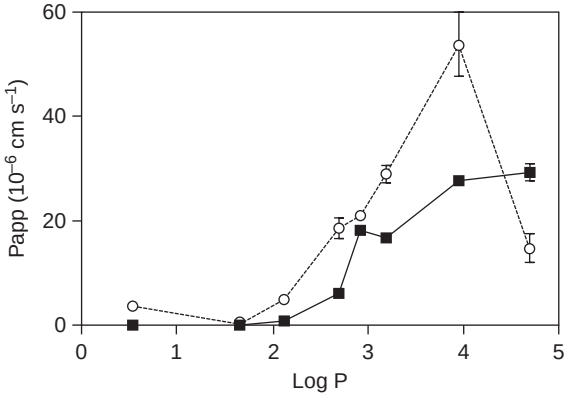

Figure 9 Permeability rates of dexamethasone esters through BCEC (filled squares) and excised cornea (empty circles) versus log *P*. Left to right, 21-sodium phosphate ester (DSP), 21-metasulfobenzoate ester (DSB), dexamethasone (DX), 17-propionate ester (DPR17), 21-acetate ester (DAC), 21-propionate ester (DPR), 21-butyrae ester (DBU), and 21-valerate (DVA). From Civiale, C., Bucaria F., Piazza S., et al. (2004). Ocular permeability screening of dexamethasone esters through combined cellular and tissue systems. *Journal of Ocular Pharmacology and Therapeutics* 20: 75–84, with permission from JOPT.

Carrier-mediated transport represents an area of growing interest to pharmaceutical scientists. These transport systems play an important role in absorbing nutrients as well as their mimetic drugs. Transporter-targeted prodrug delivery can be an effective strategy to improve the permeability of poorly absorbed drugs, as conjunctiva has been shown to express various transporters for nutrients such as amino acid, peptides, L-lactate, and nucleosides. These transporters can be utilized for improved drug absorption across the conjunctiva. However, such a strategy has not been explored to a large extent.

Functionally active sodium-dependent, carrier-mediated, monocarboxylate transport system has been reported on the mucosal or tear-side of the rabbit conjunctival epithelium. It has been shown to recognize and translocate nonsteroidal anti-inflammatory drugs (NSAIDs) and fluoroquinolone antibiotics administered topically. The conjunctiva expresses Na^+-glucose transporter (SGLT1) on the mucosal side and a sodium-dependent nucleoside transporter has been characterized that can be targeted by nucleoside mimetic antivirals on conjunctiva. Various amino acid-transporter systems including L-lysine and $B^{0,+}$ are present on the apical side of rabbit conjunctiva. Among various transporters exploited for drug delivery, peptide transporters (PEPT1 and 2) have become

Table 3 Transport of dexamethasone and its esters across BCEC and rabbit cornea

		In vitro		*Ex vivo*	
Steroid	*Log P*	P_{app} ($\times 10^6$ cm s^{-1})	*Conv. to DX (%)*	P_{app} ($\times 10^6$ cm s^{-1})	*Conv. to DX (%)*
DX	2.12	1.08 0.17	-	5.06 1.01	-
DSP	0.54	< 0.02	0	3.87 0.62	100
DSB	1.65	< 0.02	0	0.51 0.23	42
DAC	2.92	18.2 1.11	90	21.1 1.17	100
DPR17	2.69	6.29 0.22	100	18.6 4.94	100
DPR	3.19	16.8 2.17	61	29.1 3.70	100
DBU	3.95	27.8 1.64	99	53.8 13.8	100
DVA	4.70	29.4 5.4	99	14.8 6.65	21

DX, Dexamethasone; DSP, 21-sodium phosphate ester; DSB, 21-metasulfobenzoate ester; DAC, 21-acetate ester; DPR17, 17-propionate ester; DPR, 21-propionate ester; DBU, 21-butyrae ester; DVA, 21-valerate.
Data from Civiale, C., Bucaria, F., Piazza, S., et al. (2004). Ocular permeability screening of dexamethasone esters through combined cellular and tissue systems. *Journal of Ocular Pharmacology and Therapeutics* 20: 75-84, with permission from JOPT.

popular due to their high capacity and wide substrate specificity. These play an important role in the translocation of di- and tripeptides and peptidomimetic drugs across various tissues. A proton-coupled dipeptide transporter process has been reported to be present on pigmented rabbit conjunctiva. A proton-coupled, saturable, and temperature-dependent uptake of a dipeptide on rabbit conjunctival epithelial cells (RCEC) was reported. However, the expression level of the dipeptide transporters seems to be rather low in conjunctiva. Overall, the presence of a variety of influx transporters on the conjunctiva offers an immense potential for targeted delivery after topical prodrug administration.

Subconjunctival Delivery

This approach of drug delivery is more popular and safer and less invasive than intravitreal injection. Moreover, it offers the potential advantage of localized, sustained delivery in the treatment of ocular diseases affecting the posterior segment such as age-related macular degeneration (AMD) and diabetic retinopathy. As this route can circumvent both the corneal and conjunctival barriers, it has immense potential for delivery of both small molecules and macromolecular drugs to posterior ocular tissues including choroid and retina. Moreover, sclera is much more permeable than conjunctiva. Drug delivery by this route exploits the large surface area, easy accessibility, and relatively high permeability of sclera. By this route, sustained intraocular therapeutic drug concentrations can be achieved without surgical implantation of controlled-release drug-delivery implant in the vitreous humor or by repeated intravitreal/periocular injections. In this regard, a subconjunctival injection of drug-loaded nanoparticulate system offers potential alternative. These systems can release the drug in a sustained manner as well as achieve higher drug concentrations in the target tissues. Drug-loaded nanoparticulate systems prepared with biodegradable polymers have been widely used in sustaining the drug release. Nanoparticles are usually taken up into the cell by endocytosis which will significantly enhance the uptake of nanoparticles into the targeted cells. Moreover, receptor-mediated endocytosis have attracted attention due to high capacity and targeting feasibility. Expression of various receptors by RPE will enable this strategy to be successfully applied for subconjunctival administration of receptor-targeted nanoparticles. In this strategy, a promoiety is conjugated to the polymer, which is used to prepare these nanoparticles. It is also ensured that these targeting promoieties are present on the surface of nanoparticles, such that it is recognized by a specific receptor present on the RPE and undergo receptor-mediated endocytosis. Thus, drug loaded nanoparticles improve drug absorption into RPE, enable targeting, and sustain the release for prolonged periods of time.

In addition to this, a sustained drug release can also be achieved by dispersing the drug/prodrug in a thermosensitive gelling polymer. These are the polymers that are liquids at room temperature and gels at body temperature. Drug/prodrug can be mixed homogenously in the polymer solution and injected subconjunctivally. Upon injection, the polymer solution gels and sustains the release of drug. The drug loading and release can be optimized to maintain therapeutic concentrations for prolonged periods of time.

Conclusion

Prodrugs have proven to be an effective strategy for drug delivery to the anterior segment. Several examples of successfully marketed ophthalmic prodrugs including dipivalyl ester of epinephrine (dipivephrine) are available. In addition, ester prodrugs of PGF2α analogs such as bimatoprost, travoprost, and latanoprost are highly effective. However, the application of this strategy to a particular drug molecule depends upon its chemical structure. The drug molecule needs to have a specific functional group such as carboxyl/hydroxyl/amine group to facilitate the conversion to an ester or amide-based prodrug. Despite this, a significant amount of research needs to be performed to examine the feasibility of extending the prodrug strategy to deliver macromolecular drugs like proteins and antibodies which have been highly effective in treatment of various ocular diseases, especially the AMD.

See also: Cornea Overview; Corneal Angiogenesis; Corneal Endothelium: Overview; Corneal Epithelium: Transport and Permeability; The Corneal Stroma; Drug Delivery to Cornea and Conjunctiva: Esterase- and Protease-Directed Prodrug Design; Overview of Electrolyte and Fluid Transport Across the Conjunctiva.

Further Reading

Anand, B. S., Nashed, Y. E., and Mitra, A. K. (2003). Novel dipeptide prodrugs of acyclovir for ocular herpes infections: Bioreversion, antiviral activity and transport across rabbit cornea. *Current Eye Research* 26: 151–163.

Chang, S. C., Bundgaard, H., Buur, A., and Lee, V. H. (1987). Improved corneal penetration of timolol by prodrugs as a means to reduce systemic drug load. *Investigative Ophthalmology and Visual Science* 28: 487–491.

Chien, D. S., Sasaki, H., Bundgaard, H., Buur, A., and Lee, V. H. (1991). Role of enzymatic lability in the corneal and conjunctival penetration of timolol ester prodrugs in the pigmented rabbit. *Pharmaceutical Research* 8: 728–733.

Chien, D. S., Tang-Lio, D. D., and Woodward, D. F (1997). Ocular penetration and bioconversion of prostaglandin F2alpha prodrugs in rabbit cornea and conjunctiva. *Journal of Pharmaceutical Sciences* 86: 1108–1186.

Civiale, C., Bucaria, F., Piazza, S., et al. (2004). Ocular permeability screening of dexamethasone esters through combined cellular and tissue systems. *Journal of Ocular Pharmacology and Therapeutics* 20: 75–84.

Geraldine, C. and Jordan, M. (1998). How an increase in the carbon chain length of the ester moiety affects the stability of a homologous series of oxprenolol esters in the presence of biological enzymes. *Journal of Pharmaceutical Sciences* 87: 880–885.

Gunda, S., Hariharan, S., and Mitra, A. K. (2006). Corneal absorption and anterior chamber pharmacokinetics of dipeptide monoester prodrugs of ganciclovir (GCV): *In vivo* comparative evaluation of these prodrugs with Val-GCV and GCV in rabbits. *Journal of Ocular Pharmacology and Therapeutics* 22: 465–476.

Horibe, Y., Hosoya, K., Kim, K. J., and Lee, V. H. (1998). Carrier-mediated transport of monocarboxylate drugs in the pigmented rabbit conjunctiva. *Investigative Ophthalmology and Visual Science* 39: 1436–1443.

Hosoya, K., Lee, V. H., and Kim, K. J. (2005). Roles of the conjunctiva in ocular drug delivery: A review of conjunctival transport mechanisms and their regulation. *European Journal of Pharmaceutics and Biopharmaceutics* 60: 227–240.

Hughes, P. M. and Mitra, A. K. (1993). Effect of acylation on the ocular disposition of acyclovir. II: Corneal permeability and anti-HSV 1 activity of 2′-esters in rabbit epithelial keratitis. *Journal of Ocular Pharmacology* 9: 299–309.

Kashi, S. D. and Lee, V. H. (1986). Hydrolysis of enkaphilins in homogenates of anterior segment tissues of the albino rabbit eye. *Investigative Ophthalmology and Visual Science* 27: 1300–1303.

Katragadda, S., Gunda, S., Hariharan, S., and Mitra, A. K. (2008). Ocular pharmacokinetics of acyclovir amino acid ester prodrugs in the anterior chamber: Evaluation of their utility in treating ocular HSV infections. *International Journal of Pharmaceutics* 359: 15–24.

Lee, V. H. (1983). Esterase activities in adult rabbit eyes. *Journal of Pharmaceutical Sciences* 72: 239–244.

Stratford, R. E., Jr. and Lee, V. H. (1985). Ocular aminopeptidase activity and distribution in the albino rabbit. *Current Eye Research* 4: 995–999.

Tirucherai, G. S., Dias, C., and Mitra, A. K. (2002). Corneal permeation of ganciclovir: Mechanism of ganciclovir permeation enhancement by acyl ester prodrug design. *Journal of Ocular Pharmacology and Therapeutics* 18: 535–548.

Dry Eye: An Immune-Based Inflammation

M E Stern, Allergan Inc, Irvine, CA, USA
S C Pflugfelder, Baylor College of Medicine, Houston, TX, USA

Glossary

Autoimmunity – An immune response of an organism against any of its own tissues, cells, or cellular components. Diseases, such as rheumatoid arthritis, systemic lupus erythematosus, multiple sclerosis, and dry eye are considered autoimmune based.
CD4+ T cells – T helper cells (T_h), a subgroup of lymphocytes that play an important role in establishing and maximizing the capacity of the immune response against invading extracellular pathogens, for example, bacteria and parasites. The CD4+ T cells bearing T-cell receptors that recognize self-antigen, that is, autoantigen, contribute to the immunopathogenesis of several autoimmune diseases, for example, rheumatoid arthritis, multiple sclerosis, and dry eye.
Dry eye – An ocular surface immune-based inflammatory disease resulting from an unstable tear film composition mediated by dysfunction of a complex Lacrimal Function Unit (LFU: cornea, conjunctiva, lacrimal glands, and meibomian glands), which causes damage to the interpalpebral ocular surface and is associated with symptoms of ocular discomfort. Dry eye is also known as lacrimal keratoconjunctivtis (LKC) and most recently, dysfunctional tear syndrome (DTS).
Desiccating stress (DS) – Following exposure to DS in low humidity (<40%) mice display similar clinical and histopathological features to human patients with dry eye, including rapid and coordinated upregulation of proinflammatory cytokines, decreased tear production and goblet cell number, surface epithelial apoptosis, and increased cellular infiltration, for example, CD4+ T cells into the LFU.
Goblet cells – Glandular simple columnar conjunctival epithelial cells that function to secrete mucus.
Lacrimal glands – Glands located in the upper, distal portion of the orbit of each eye that secrete the aqueous layer of the tear film.
Lacrimal function unit (LFU) – The lacrimal functional unit is composed of the lacrimal glands (both main and accessory), the ocular surface (cornea, conjunctiva, goblet cells, and meibomian glands), and the interconnecting innervation that coordinates afferent (ocular surface to the brain) and efferent (brain to the ocular surface tissues and associated glands) signals. The LFU is responsible for maintaining the quantity and quality of the tear fluid.
Meibomian glands – Sebaceous glands at the rim of the eyelids responsible for the supply of sebum, an oily substance that prevents evaporation of the eye's tear film.
MHC class II (major histocompatability complex class II) – This is responsible for presenting antigen fragments to T helper cells by binding exclusively to the T-cell receptor present of the surface of CD4+ T cells. The MHC class II is involved in presentation of antigen derived from extracellular pathogens, thus providing specificity for the generation of adaptive immunity. The MHC class II molecules bearing self-antigen (autoantigen) may trigger activation of autoreactive CD4+ T cells and autoimmunity.

Defining the Problem

Epidemiology of Dry Eye

In 1993 the National Eye Institute (NEI)/Industry workshop formally defined dry eye as a "disorder of the tear film due to tear deficiency or excessive evaporation, which causes damage to the interpalpebral ocular surface and is associated with symptoms of discomfort." Recently, we and others proposed a more comprehensive definition of dry eye based on the increasing evidence demonstrating that ocular surface immune-based inflammation and ocular surface epithelial diseases result from dysfunction of a complex Lacrimal Function Unit (LFU) and the resultant unstable tear film. To provide guidelines for selection of treatment, the Delphi panel of experts coined the term dysfunctional tear syndrome (DTS) based on symptoms and signs (not tests) of dry eye disease.

Dry eye is a highly prevalent condition and one of the leading causes of visits to ophthalmologists and optometrists in the United States. Epidemiologic studies have reported that dry eye affects up to 11% of people 30–60 years of age and 15% of those 65 years of age or older. As many as 12 million Americans have moderate to severe dry eye and this number is likely to increase as the population ages. Dry eye affects 0.1–33% of the worldwide population; the wide range of variability is dictated by the study and diagnostic criteria used.

Dry Eye Syndrome in Peri- and Post-menopausal Women

Dry eye is more common in women than men (2:1) and the incidence increases with age. The role of sex hormones in dry eye has been reported in several studies. For example, data from 36 995 female health professionals ranging from age 49 to 89 years old (estimated at least 3.2 million (or 7.8%) women aged 50 years and older) suffer from dry eye disease in the US. The incidence appears to be higher among older women (9.8%, $\geq$75 years) than women under 50 years of age (5.7%). The incidence of clinically significant rosacea is also higher among aging females and occurs in approximately 30% of menopausal women. In fact, it is predicted that up to 75% of peri-menopausal women with facial rosacea will develop ocular involvement.

Estrogen may have detrimental effects on the tear film and could influence the development of dry eye; although the ratio between estrogens and androgens may be a better indicator. It was reported that women who receive hormone replacement therapy, especially with unopposed estrogen therapy, have an increased risk of developing dry eye disease. On the other hand, androgen deficiency and/or imbalance in estrogen–androgen levels are also associated with dry eye. Along these lines, androgen deficiency as seen in Sjögren syndrome and Sjögren's syndrome keratoconjunctivitis sicca (KCS) occurs almost exclusively in women. Furthermore, women who suffer from premature ovarian failure lack both estrogens and androgens and exhibit more ocular surface damage and dry eye-related symptoms than age-matched controls.

Patients on Anti-androgen Therapy

Androgenic hormones play an important role in supporting the secretory immune function of the lacrimal glands and meibomian glands. The meibomian glands are the main androgen target organs on the ocular surface. Androgen deficiency that may occur during menopause, aging in both sexes, autoimmune disorders (e.g., Sjögren's syndrome, Systemic Lupus Erythematosus, rheumatoid arthritis, RA), complete androgen insensitivity syndrome (i.e., women with dysfunctional androgen receptors, congenital androgen insensitivity syndrome), and the use of anti-androgen medications (e.g., for prostatic cancer or hypertrophy) is associated with meibomian gland dysfunction, tear film instability, and a significant increase in dry eye signs and symptoms. Studies showed that anti-androgen treatment is paralleled by significant changes in the fatty acid profiles of neutral lipid fractions in meibomian gland secretions. Conversely, treatment with androgens has been reported to alleviate dry eye conditions and stimulate tear flow in Sjögren's syndrome patients.

Clinical Features of Dry Eye

Chronic Pain

Ocular surface neuropathy in dry eye

Ocular surface pain and discomfort in severe sicca disease may partially result from the well-documented neuropathy associated with Sjögren's syndrome, which is categorized with the neuropathies associated with connective tissue disease. Indeed, clinical evidence has shown that peripheral sensory neuropathy may be an important presenting sign for Sjögren's patients. In accordance, ocular surface discomfort is often the initial motivation for dry eye patients to visit the ophthalmologist. In affected individuals, ganglioside-specific antibodies are found in peripheral nerves, dorsal root ganglia, and dorsal roots, and inflammatory cells are localized within the ganglia. Although the trigeminal system has not been studied in as much detail, the ocular surface discomfort of dry eye may be a form of sensory neuropathy; however, this theory requires confirmation. Small diameter myelinated and unmyelinated axons in the cornea are potential targets for peripheral nerve disorders, and inflammatory cells infiltrating the ocular surface are well documented in dry eye. These cells, in combination with ganglioside-specific antibodies and other neural proteins, could cause local degeneration of small diameter axons and axon terminals. Cranial neuropathies may be more common in Sjögren's syndrome than is currently recognized, and the dysthesias associated with the cornea may indicate an inflammatory neuropathy within the trigeminal system.

Comorbidities

Patients with lacrimal keratoconjunctivitis (LKC) typically experience ocular discomfort. The most common symptoms include scratchiness, grittiness, foreign body sensation, burning, and itching; these symptoms are exacerbated by prolonged visual activity (e.g., viewing a video display terminal) and environmental stresses, such as low humidity and air drafts. The LKC patients often complain of blurred and fluctuating vision that stimulates increased blink frequency, an unconscious response to clear the visual field. Together, these symptoms contribute to severe ocular fatigue and many patients report that they are unable to read or concentrate for more than a few minutes at a time.

Also, LKC can cause considerable ocular morbidity. The thinned and unstable precorneal tear layer and the altered corneal epithelial barrier function that accompany LKC are major risk factors for sterile keratolysis (loss of uppermost layer of cells in cornea) and microbial keratitis (infection of the cornea). Severe and recurrent corneal ulceration mediated by LKC can ultimately lead to reduced vision, blindness, and in severe cases, loss of the eye.

Pre-existing LKC is an important cause of complications following corneal surgery. Complications include

penetrating keratoplasty and LASIK, and may lead to decreased vision, pain, epithelial and stromal wound healing problems, haze, ulceration, and predisposition to microbial infections. Surgical amputation of the corneal sensory nerves that drive glandular secretion, a direct consequence of LASIK and other refractive procedures, negatively impacts the integrated ocular surface secretory gland functional unit. This exacerbates pre-existing LKC and most likely results in new cases of dry eye.

Quality of Life Impact

The LKC symptoms significantly impact quality of life documented by utility scores. Utility scores quantify how many years a subject would give up from the end of his/her life in exchange for avoiding a particular malady. Utility scores for dry eye were found to be similar to those from patients with angina. The chronic and unremitting nature of dry eye syndrome can lead to despair, depression, decreased productivity, and in some cases permanent job disability. The physical and psychological impact of LKC symptoms is similar to that experienced by patients with other chronic regional pain syndromes, such as those affecting the lower back.

How We Secrete Normal Tears

The Lacrimal Functional Unit

The ophthalmic pathology seen in Sjögren's syndrome and chronic dry eye surrounds an immune-based inflammatory disruption of the LFU (**Figure 1**). The LFU is composed of the ocular surface (cornea, conjunctiva, conjunctival blood vessels), the lacrimal glands (main and accessory (Wolfring and Krauss)), and the interconnecting innervations (V, VII). This tear secreting reflex is also modulated by hormonal and immune factors. The role of the LFU is to secrete a precise tear film composition that maintains a homeostatic environment around the epithelial cells of the ocular surface.

The general role of the LFU in homeostasis and disease

The purpose of the tightly controlled ocular surface environment is to preserve corneal clarity and vision. The main and accessory lacrimal glands, the corneal limbus, and the meibomian glands provide the vital supportive function to protect the sensitive epithelial surfaces of the conjunctival and corneal tissues from environmental injury that results in pain and decreased visual acuity. The

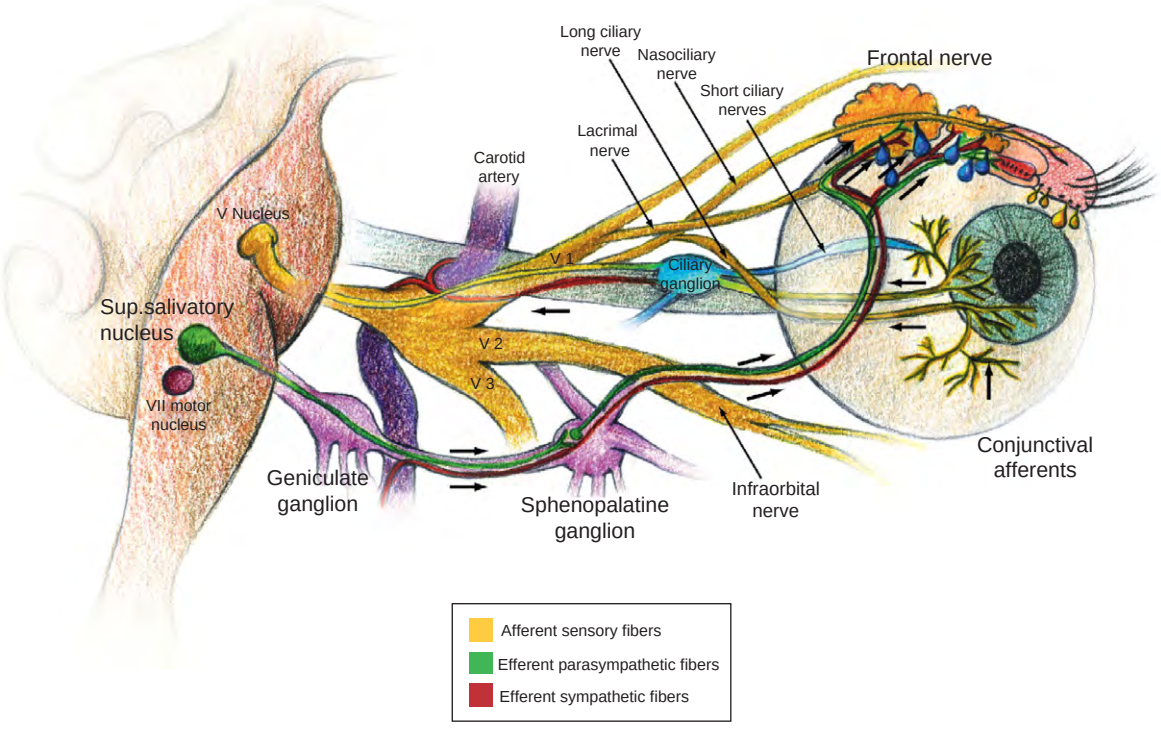

Figure 1 The lacrimal functional unit. Subconscious stimulation of the free nerve endings within the cornea generates afferent nerve impulses through the ophthalmic branch of the Trigeminal Nerve (V) to the midbrain (pons). The afferent signals are integrated in the midbrain and then travel via the efferent branch through the pterygopalatine ganglion, terminating in the main and accessory (Wolfring and Krause) lacrimal glands. Evidence suggests that this pathway also controls secretion from meibomian glands and conjunctival goblet cells. Proper function of the LFU supports homeostasis on the ocular surface by controlling secretion of the three major tear film components (mucin, aqueous, and lipid) to maintain the optimal quantity and quality of tear fluid; however, dysfunction of the LFU may lead to altered tear film composition and dry eye disease.

function of the LFU is to control secretion of tear constituents that help sustain a stable, anti-infective, and epithelial supportive tear layer essential for optimal optical performance. Signals emanating from ocular surface sensory nerves supply continuous input into the CNS that tells the brain what changes are occurring within the ocular surface milieu. The brain then sends signals to the specialized support tissues, for example, lacrimal and meibomian glands that are programmed to secrete the optimal tear quantity and composition.

The process by which normal tears are secreted is initiated following corneal nerve stimulation. The process occurs unconsciously and in response to many stimuli; however, environmentally induced dry spot formation is thought to be among the most common. Out of necessity for survival, evolution has shaped the cornea to become the most densely sensory nerve innervated epithelial surface in the body. Conduction of pain originates from myelinated and unmyelinated nerves that terminate in the cornea, limbus, and conjunctival epithelium. Neural receptors in the cornea are free nerve endings that terminate in all of the corneal epithelial layers and are protected from direct irritation by zonula occludens and the tear mucin gel. Afferent (ocular surface to the brain) nerve traffic through the ophthalmic branch of the Trigeminal Nerve (V) enters the central nervous system in the area of the pons (midbrain) and the para spinal sympathetic tract. These signals are integrated with cortical and other inputs and are then transmitted to the efferent (brain to ocular surface tissues and associated glands) secretomotor impulses resulting in secretion of the homeostatic tear-film components.

Tear secretion by the lacrimal gland also occurs in response to neural stimulation. The acini, ducts, and blood vessels of the lacrimal gland are innervated by parasympathetic, sympathetic, and sensory nerves. The initial signal originates from the parasympathetic cholinergic nerves via acetylcholine release, which then binds to M_3 muscarinic acetycholine receptors on the basolateral cell membrane of secretory epithelia. At the same time, vasoactive intestinal peptide (VIP) binds to VIPergic receptors, and norepinephrine, a sympathetic neurotransmitter binds to α_1- and β-adrenergic receptors. Neural innervation of the accessory lacrimal glands has also been reported and fibers positive for CGRP and substance P are associated with secretory tubules, interlobular and excretory ducts, and blood vessels. However, the degree of neural influence over accessory lacrimal glands is still being elucidated.

Sensory, sympathetic, and parasympathetic neuropeptides are present in the ocular surface tissues and associated glands. Conjunctival goblet cells have a secretory response to the parasympathetic cholinergic muscarinic output from the pterygopalatine ganglion. Goblet cells express M_3-muscarinic receptors on their membranes. The M_1 and M_2 receptors are located throughout the conjunctiva. The presence of α_{1A}- and β_3-adrenergic receptors on conjunctival goblet cells suggests the presence of sympathetic innervation. In addition, transmission electron microscopy of meibomian glands revealed the presence of unmyelinated axons with granular and agranular vesicles. Substance P- and CGRP-positive axons have also been identified, but their function is uncertain, as these neurological peptides would be expected to conduct information into, rather than away from, the CNS. It is predicted that parasympathetic fibers innervating the meibomian glands are indeed present at higher levels. Parasympathetic neurotransmitters neuropeptide Y and VIP have been found around the meibomian glands, as well as tyrosine hydroxylase in sympathetic axons, implicating that both types of autonomic nerves may play an important role in stimulating lipid secretion onto the ocular surface.

Patients with LKC commonly complain of constant corneal sensations normally described as a gritty, sandy, or itchy. These complaints are usually accompanied with a pathophysiological state that indicates a chronic state of inflammation and a disadvantageous change in tear film composition. Infiltrating inflammatory cells within the ocular surface tissues have been reported in dry eye. These inflammatory cells, in addition to ganglioside-specific antibodies and other neural proteins, may result in regional degeneration of small diameter axons and their terminals. Chronic dysfunction of the LFU results in a shift toward inflammation and persistent psychological distress.

Events on the Ocular Surface

Environmental Impact on the Ocular Surface

The immune response is designed to defend against stress and/or microbial assaults on the ocular surface and paradoxically may also contribute to autoimmunity. Along these lines, regulatory mechanisms have evolved to modulate the afferent and efferent arms of the immune response to preserve tissue and limit activation of autoreactive lymphocytes following acute inflammation. The afferent events leading to cellular immunity include antigen processing and presentation by ocular surface antigen presenting cells (APCs) and migration of these cells to the draining lymph nodes. Afferent immune processes are modulated by a wide variety of anti-inflammatory factors that include cellular, for example, T regulatory cells (Tregs), and diffusible factors, for example, transforming growth factor beta (TGF-β) and interleukin (IL)-1 receptor antagonist, that favor protective immunity without breaking self-tolerance. The afferent arm of the immune response dictates the efferent response, the phase involved with antigen driven homing of primed and targeted lymphocytes to tissue-specific inflammatory sites. The efferent response is initiated in the secondary lymphoid organs and amplified on the ocular surface via

cell-to-cell interactions between lymphocytes and APCs; activation and differentiation of lymphocytes and migration to the ocular surface is tightly regulated to control the efferent immune response. Indeed, immunoregulation on the ocular surface is the result of the coordinated effort between a wide variety of immune players. However, when these mechanisms are compromised the ocular surface may become susceptible to chronic and/or autoimmune-mediated ocular disease, such is the case with dry eye.

Afferent arm of the immune response: immunoregulation

Redundant mechanisms regulate the afferent immune response to guard against activation and infiltration of autoreactive lymphocytes to the ocular surface tissues. For instance, there is a predominance of intraepithelial lymphocytes, for example, CD4+/CD8+Tregs and gamma delta T cells in the normal conjunctival epithelium; these cells are thought to harbor immunoregulatory functions similar to those found in other mucosal tissues, such as the intestine. The conjunctiva and cornea are also covered by mucin, which forms a barrier, guarding against unwarranted infiltration of inflammatory cells into the epithelium. Furthermore, the cornea lacks lymphatic and blood vessels, mature APCs, and resident T cells, thereby reducing the incidence of chronic inflammation and bystander cell damage on ocular surface following an acute inflammatory insult.

The tear fluid also contains high concentrations of soluble immunoregulatory factors that help maintain homeostasis before, during, and after environmental challenge. For example, androgenic hormones provide an immunosuppressive umbrella to help protect the secretory function of the lacrimal and the meibomian glands. In addition, the corneal epithelium expresses vascular endothelial growth factor (VEGF) receptors that function in part to sequester soluble VEGF, which ultimately reduces the stimulus for neovascularization after ocular surface challenge. Neurotrophic factors produced by the limbal corneal epithelia, such as glial cell line-derived neurotrophic factor (GDNF) also appear to have immunoregulatory activity. Transforming growth factor beta (TGF-β), a cytokine that can inhibit the function of APCs and effector T-cell proliferation, is secreted by goblet cells and is found in high levels within the tear fluid. Indeed, the presence of TGF-β may bias conjunctival APCs to activate Tregs instead of effector T cells, thereby preventing the activation/infiltration of autoreactive T cells. In addition, interleukin 1 receptor antagonist (IL-1RA) mutes the effects of the potent proinflammatory cytokine IL-1. The action of tissue inhibitor of matrix metalloproteinase (TIMP-1) inhibits matrix metalloproteinases (MMPs), which play a dominant role in promoting immune cell infiltration into ocular surface tissues during inflammation.

Efferent arm of the immune response: immunoregulation

The efferent arm of the immune response includes several mechanisms to prevent spurious activation and infiltration of autoreactive lymphocytes to the ocular surface during acute inflammation. It is critically important that the immune response is sufficient to eliminate the current threat, and then tempered to avoid chronic inflammation and tissue destruction. Similar to the afferent arm, recent studies have shown that the efferent arm of the immune response is also regulated by the concerted effort of Tregs, anti-inflammatory cytokines, and other factors vital for preventing autoimmunity.

Activation and differentiation of CD4+ and CD8+ Tregs in the secondary lymphoid organs are critical for limiting bystander tissue damage and maintaining self-tolerance and are emerging as important efferent immune modulators in the eye. Indeed, CD4+ Tregs present in C57BL/6 mice decrease clinical and histopathological disease in a mouse model of dry eye, which are exacerbated when mice are depleted of CD4+CD25+FoxP3+ Tregs. In addition, *in vitro* expanded CD4+CD25+Foxp3+ Tregs mute ocular surface inflammation in a Th1-mediated adoptive transfer model of dry eye disease. These data suggest that CD4+CD25+ Tregs present in the secondary lymphoid organs and ocular surface tissues inhibit the pathogenic effect of autoreactive effector T cells in an effort to maintain homeostasis.

Restricted homing of effector T cells from the regional lymphoid organs to the ocular surface also facilitates immunoregulation following acute insult. For example, the programmed death ligand-1 (PD-L1) has been implicated in protecting the ocular surface from unwanted T cell infiltration and tissue injury. The PDL-1 is a negative regulator of T-cell activation; the interaction between PDL-1 and the PD-1 receptor (expressed on activated T cells) inhibits lymphocyte proliferation and cytokine secretion. Furthermore, PD-1-deficient mice develop spontaneous autoimmunity. The PDL-1 is expressed constitutively on the ocular surface and is upregulated in both human cell lines stimulated with proinflammatory cytokines and in patients with ocular inflammation. In a mouse model of corneal allograft transplantation, PDL-1 was shown to promote apoptosis of the infiltrating CD4+ and CD8+ T cells that was associated with sustained corneal allograft survival. By contrast, PDL-1 blockade resulted in increased lymphocyte infiltration within the ocular surface tissues and enhanced allograft rejection.

Exactly where and how CD4+ and CD8+ Tregs exert their regulatory affects is a current area of intense research. Activation and differentiation of antigen-specific Tregs is mediated by interaction with APCs within the lymphoid organs and is influenced by the local cytokine milieu. It is clear that CD4+ Tregs are involved in suppressing inflammation on the ocular surface; however, the underlying

mechanisms driving activation and differentiation of these cells are currently unknown. Following ocular surface insults, it is suspected that Tregs function to suppress inflammation by dampening T-cell priming in the lymphoid organs, and inhibit T-cell effector function within inflamed ocular surface tissues. The immunosuppressive properties of Tregs are likely to occur by cell contact-dependent, for example, Treg:APC and/or Treg:T cell, and cell contact-independent mechanisms, that is, anti-inflammatory cytokine production. One possibility is that CD4+ Tregs temper the inflammatory response on the ocular surface by secreting TGF-β and IL-10, which may bias APC-mediated activation and differentiation of other regulatory lymphocytes in the lymphoid tissue and/or decrease Th1-mediated inflammation locally within ocular surface tissues.

Afferent arm of the immune response during autoimmune-based inflammation

During dry eye the afferent arm of the immune response is initiated following environmental stress-mediated desiccation and/or increased tear osmolarity (**Figure 2**). The initial response disrupts the protective barrier by promoting proteolysis of tight junction proteins and alters the pattern of epithelial differentiation towards squamous metaplasia and decreased mucus production. Osmotic stress activates signaling pathways in a variety of cell types, including the ocular surface epithelia. Exposure to increased osmolarity *in vivo* or *in vitro* activates mitogen-activated protein kinase (MAPK) pathways, including p38 and c-Jun N-terminal kinases, and nuclear factor (NF)-κB in the ocular surface epithelia; desiccating and osmotic

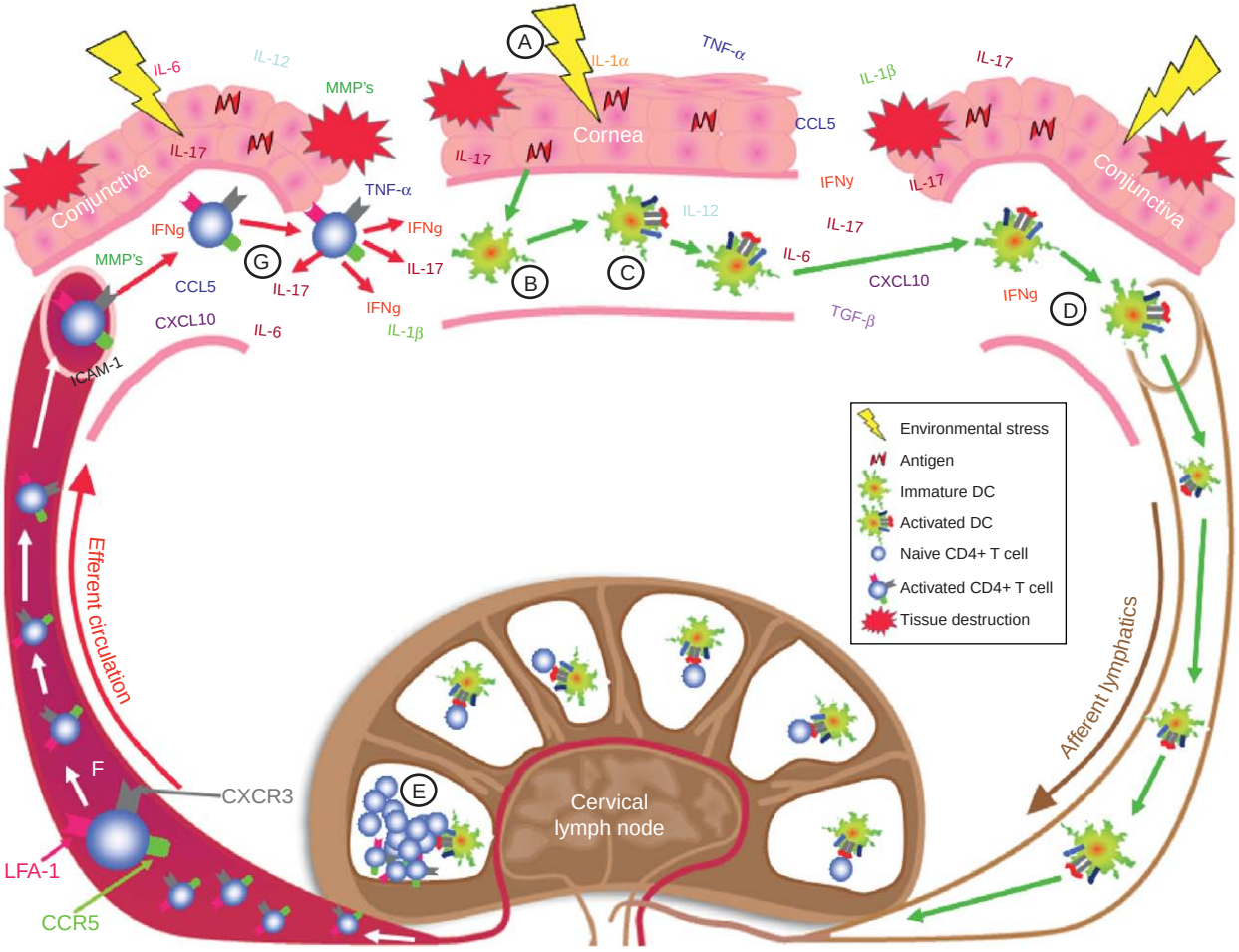

Figure 2 Autoimmune cycle of chronic inflammation during the immunopathogenesis of dry eye disease. Afferent arm of the immune response: (a) An environmental stimulus initiates acute inflammation on the ocular surface stimulating upregulation of proinflammatory cytokines (e.g., TNF-α, IL-1α and IL-1β), matrix metalloproteinases (MMPs), adhesion molecules (e.g., ICAM-1), and chemokines (e.g., CCL5 and CXCL10) within the conjunctival and corneal epithelium that act in concert to perpetuate the immune response; (b) Antigen presenting cells (e.g., dendritic cells) process autoantigen and (c) following activation, (d) traffic to the draining cervical lymph nodes (CLNs) via the afferent lymphatics, where they (e) present antigen to autoreactive CD4+ T cells. Efferent arm of the immune response: (f) Activated CD4+ T cells bearing specific adhesion molecules and chemokine receptors (e.g., CCR5 and CXCR3) migrate specifically to the ocular surface tissues (conjunctiva and cornea are shown), including the meibomian and lacrimal glands where they infiltrate the tissue and (g) release proinflammatory cytokines (IFN-γ and IL-17) that promote chronic inflammation and tissue destruction.

stress-mediated MAPK activation stimulates corneal epithelial cells to produce of a variety of proinflammatory mediators. In addition, the altered barrier facilitates diffusion of soluble inflammatory factors into the epithelium and stroma and inflammatory cell infiltration into the ocular surface tissues.

Exposure to desiccating stress (DS) initiates ocular surface epithelial cells to release proinflammatory cytokines and chemokines (e.g., IL-1β, TNF-α, IFN-γ, IL-8, CXCL10, MMP-1, -3, -9, -10, and -13). For instance, IFN-γ upregulates the adhesion molecule ICAM-1 expression within the epithelium, stromal fibroblasts and vascular endothelium, and increases vascular permeability in animal models and patients with non-Sjögren's or Sjögren's syndrome-mediated dry eye. Indeed, effector CD4+ T cells express high levels of lymphocyte function-associated antigen 1 (LFA-1), the cognate binding partner to ICAM-1. The upregulation of adhesion molecules on T cells and endothelial cells coupled with increased vascular permeability results in peripheral immune cell infiltration. The IL-1α and IL-1β levels are also elevated in the tears and conjunctiva from Sjögren's syndrome-associated tear deficiency patients and in a mouse model of dry eye. The IL-1 also induces upregulation of adhesion molecules localized on endothelial cells and stimulates expression of chemokines, which act in concert to facilitate leukocyte infiltration. The TGF-β-dependent suppression of DC activation is also compromised as TGF-β2-secreting conjunctival goblet cells undergo apoptosis during the immunopathogenesis of dry eye. Along these lines, IL-1 and TNF-α also activate immature APCs in the cornea and conjunctiva, which results in increased expression of MHC class II antigens, co-stimulatory molecules, VEGFr3, and CCR7. These molecules act together to coordinate APC migration to the draining lymph nodes and activation of effector T cells that drive the efferent arm of the immune response.

Efferent arm of the immune response during autoimmune-based inflammation

The efferent arm of the immune response is mediated by autoreactive T cells that (1) are activated within secondary lymphoid tissue via cell-to-cell contact with ocular surface-derived APCs, (2) are targeted to ocular surface tissues by acquisition of trafficking molecules and chemokine receptors, and (3) compromise the integrity of the ocular surface and contribute to prolonged inflammation (**Figure 2**). During the immunopathogenesis of dry eye, activation of autoreactive CD4+ T cells is thought to be driven within secondary lymphoid tissue by ocular surface-derived dendritic cells bearing self-antigen presented in the context of MHC class II. This theory is well supported by animal studies demonstrating that CD4+ T cells from the cervical lymph nodes of dry eye mice specifically home to the ocular surface tissue and mediate dry eye disease when adoptively transferred to athymic nude recipient mice. Importantly, DS-specific CD4+ T cells are not detected in any other tissues indicating that these cells are targeted to the ocular surface during activation within the secondary lymphoid organs.

Tissue-specific targeting of autoreactive T cells occurs within secondary lymphoid organs and is dictated by interactions between adhesion molecules and chemokine receptors that bind and respond to ligands expressed locally within inflamed tissues. Expression of LFA-1 on the T cells from patients with non-Sjögren's or Sjögren's syndrome-mediated dry eye and high-level ICAM-1 expression within ocular surface tissues of these patients suggest that LFA-1:ICAM-1 binding contributes to T-cell infiltration. Chemokine receptor signaling also appears to contribute to efferent homing of autoreactive T cells during dry eye disease. Elevated expression of the chemokine receptors CCR5 and CXCR3 and the chemokine ligands, CCL3, CCL4, CCL5, CXCL9, and CXCL10 has been detected within the cornea and conjunctiva of dry eye mice. In addition, CCR5 is also expressed on cells within conjunctival epithelium of patients with dry eye and CCL5 and CXCL10 are upregulated in human conjunctival epithelium cells in response to cytokine stimulation. These results suggest that the CCL5:CCR5 and CXCL9/CXCL10:CXCR3 signaling axes play a role in T-cell trafficking during dry eye disease.

The T-cell infiltration compromises the integrity of the ocular surface and drives chronic autoimmune-mediated inflammation. In the mouse model of dry eye, accumulation of CD4+ T cells within ocular surface tissues correlates with increased cytokine production (e.g., IFN-γ, IL-1β, TNF-α, and MMP-9), epithelial cell apoptosis, and decreased goblet cell density, tear production, and turnover. The presence of T cells in human dry eye patients also correlates with similar pathology. Indeed, CD4+ T cells are a prominent source of IFN-γ, which can induce expression of a variety of proinflammatory factors, including trafficking molecules, such as ICAM-1, CCL5, and CXCL10, and the pro-apoptotic proteins, Fas-FasL. These factors may contribute to chronic inflammation on the ocular surface by attracting infiltrating T cells and macrophages and perpetuate bystander tissue damage, including epithelial cell apoptosis and nerve damage. The IFN-γ was also shown to activate a cornified envelope precursor and genes involved in conjunctival epithelial differentiation, implicating CD4+ T cells as mediators of epithelial cell abnormalities and keratinization of the ocular surface. The CD4+ T cell accumulation is also associated with increased levels of IFN-γ in the tears of dry eye mice and is inversely related to goblet cell density and conjunctival squamous metaplasia. Furthermore, exogenous administration of IFN-γ to IFN-γ-deficient mice results in goblet cell loss. These findings suggest that CD4+ T-cell-derived IFN-γ is a major

component of chronic inflammation, epithelial cell metaplasia, and tissue destruction observed during dry eye. Emerging evidence demonstrating (1) the presence of Th17-specific CD4+ T cells within the draining cervical lymph nodes of mice with experimental dry eye and (2) high-level expression of IL-6 and IL-17 in experimental dry eye and human patients suggests that in addition to IFN-γ-producing Th1 cells, IL-17-producing Th17 cells also play a pivotal role in the underlying immunopathogenesis of dry eye.

Past, Future, and Current Therapies

Artificial Tears

Individuals with aqueous tear deficiency have decreased tear film stability and diminished tear volume. There are several therapeutic options for these patients. Artificial tears, applied topically to the ocular surface, are polymer-based. The type of polymer used determines the artificial tear viscosity, retention time, and adhesion to the ocular surface. For example, artificial tears containing hyaluronic acid exhibit non-Newtonian properties and relatively long retention times. Other types of polymers used in different artificial tears include cellulose esters (increases tear viscosity), polyvinyl alcohol (provides optimal wetting), povidone (superior wetting), and carbomers (longer retention times). There are tear gels made with polyacrylic acid that provide greater retention times than artificial tears. Some formulations add a lipid component, such as castor oil, that helps to prevent evaporation. Many tears contain electrolytes and buffers to help normalize the tear pH. Artificial tears offer provisional relief of eye irritation but do not reverse conjunctival squamous metaplasia. Preservatives in artificial tears such as benzalkonium chloride can induce ocular surface epithelial toxicity if frequently applied on patients with low tear turnover or individuals that have punctual occlusion. Preservative-free artificial tears may be a consideration for patients using artificial tears more than four times per day. Artificial tears provide a palliative therapy to dry eye patients, but do not prevent the underlying cause of disease. Inflammation!

Corticosteroids

Dry eye is an immune-based inflammatory disease. Chronic dry eye requires topical treatment with therapies designed to manage inflammation. Corticosteroids effectively block multiple inflammatory pathways including proinflammatory cytokine and chemokine secretion, synthesis of matrix metalloproteinases and prostaglandins, and cell adhesion molecule expression. Activated steroid receptors bind to DNA and control gene expression and impede transcriptional regulators (AP-1 and NFκB) of proinflammatory genes. Topical corticosteroid use, while effective, is normally prescribed for short-term use (up to 4 weeks) due to the plethora of potential side effects including glaucoma, cataracts, and ocular infection. Topical non-preserved methylprednisolone (1%) treatment of 15 Sjögren's syndrome patients three times daily for 2 weeks followed by punctual occlusion resulted in moderate to complete relief of disease symptoms.

Cyclosporine

Restasis (topical CsA, 0.5%) is the only FDA-approved therapeutic for dry eye syndrome. A fungal-derived peptide, CsA, inhibits nuclear translocation of cytoplasmic transcription factors that are necessary for T-cell activation and the production of pro-inflammatory cytokines. The CsA was first identified as therapy for dry eye in dogs with spontaneous keratoconjunctivitis sicca. In human dry eye patients, treatment with topical CsA reduced conjunctival cellular infiltration, IL-6 levels, and increased conjunctival goblet cell numbers. In two 6-month independent FDA Phase III clinical trials CsA treatment resulted in a significant ($p \leq 0.05$) improvement in corneal fluorescein staining and anesthetized Schirmer test values in patients treated with CsA (0.05 or 0.1%) compared to patients treated with vehicle alone. There was no indication of a dose-dependent effect with a safety profile of 0.05% and 0.1%. Moreover, patients did not show any serious adverse effects other than occasional burning and stinging. In addition, CsA also increased tear production in patients. There were no detectable levels of CsA in the blood of patients treated with CsA for 12 months, suggesting that topical CsA does not reach high enough levels to impact the systemic immune response. In addition to the clinical improvement in CsA-treated patients, there was also a marked decrease in expression of HLA-DR and IL-6 by conjunctival epithelial cells. Infiltration of CD3+, CD4+, and CD8+ T cells was also decreased in the conjunctiva of patients treated with CsA, but increased in those treated with vehicle alone.

Mucin Secretagogues

Secretagogues induce tear production by the lacrimal glands and the ocular surface epithelia. Pilocarpine and cevimeline are cholinergic agonists approved for oral administration. Patients taking Pilocarpine 5 mg four times daily reported a significantly greater overall improvement in ocular problems. Patients taking cevimeline had improvement in ocular irritation symptoms and aqueous tear production. A potential future secretagogue, Diquafosol tetrasodium, is an agonist for the P2Y2 receptor. Small molecule tyrosine kinase receptor agonists that induce mucin MUC5AC secretion from conjunctival goblet cells have also been developed.

Tetracyclines

Tetracyclines, traditionally used as antibiotics, have been reported to have a number of anti-inflammatory properties including inhibition of proinflammatory cytokines, MMP production, and nitric oxide production. On the ocular surface, tetracyclines reduce human corneal epithelial production of IL-1 and MMPs, preserving the ocular surface epithelial barrier, and blocking the activation of destructive cytokines.

See also: Adaptive Immune System and the Eye: Mucosal Immunity; Conjunctiva Immune Surveillance; Conjunctival Goblet Cells; Defense Mechanisms of Tears and Ocular Surface; Lacrimal Gland Hormone Regulation; Lacrimal Gland Overview; Lacrimal Gland Signaling: Neural; Meibomian Glands and Lipid Layer; Ocular Mucins; Overview of Electrolyte and Fluid Transport Across the Conjunctiva; Tear Film; Tear Film Overview.

Further Reading

Lam, H., Bleiden, L., de Paiva, C. S., et al. (2009). Tear cytokine profiles in dysfunctional tear syndrome. *American Journal of Ophthalmology* 147(2): 198–205.

Niederkorn, J. Y., Stern, M. E., Pflugfelder, S. C., et al. (2006). Desiccating stress induces T cell-mediated Sjögren's syndrome-like lacrimal keratoconjunctivitis. *Journal of Immunology* 176(7): 3950–3957.

Siemasko, K. F., Gao, J., Calder, V. L., et al. (2008). *In vitro* expanded CD4+CD25+Foxp3+ regulatory T cells maintain a normal phenotype and suppress immune-mediated ocular surface inflammation. *Investigative Ophthalmology and Visual Science* 49(12): 5434–5440.

Stern, M. E., Beuerman, R., and Pflugfelder, S. C. (2009). *Dry Eye and the Ocular Surface*. New York: Marcel Dekker.

Dynamic Immunoregulatory Processes that Sustain Immune Privilege in the Eye

J Y Niederkorn, University of Texas Southwestern Medical Center, Dallas, TX, USA

Glossary

ACAID (anterior chamber-associated immune deviation) – A dynamic antigen-specific downregulation of T-cell-mediated immunity that is elicited when antigens are introduced into the anterior chamber of the eye. ACAID is believed to be a mechanism to maintain homeostasis in the eye and reduce the likelihood of T-cell-dependent inflammation in response to noninfectious, nominal antigens that enter the eye. ACAID is also believed to be induced by orthotopic corneal allografts and promotes their survival.

Alloantigens – Histocompatibility antigens that provoke immune rejection of organ transplants. These include both major histocompatibility complex antigens and antigens encoded by a wide diversity of minor histocompatibility genes.

Delayed-type hypersensitivity – The T-cell- and immune-mediated inflammation that contributes to resistance to intracellular pathogens but also carries a heavy burden of collateral damage to innocent bystander tissues.

TGF-β (transforming growth factor-β) – A cytokine that is produced by many cells and has pleiotropic effects on the immune system. TGF-β is present in the anterior chamber of the eye and is crucial for altering the behavior of ocular antigen-presenting cells within the eye such that they induce ACAID.

T_{regs} (T regulatory cells) – These are T lymphocytes that can be induced in multiple ways and suppress T-cell-dependent immune processes. Introducing antigens into the anterior chamber or the vitreous cavity of the eye elicits the generation of T regulatory cells.

VCAID (vitreous cavity-associated immune deviation) – Antigens introduced into the vitreous cavity or into the subretinal space elicit an immune deviation that is indistinguishable from ACAID and is characterized by antigen-specific suppression of T-cell-dependent inflammation.

Introduction

The immune privilege of the eye was recognized over a century ago by the Dutch ophthalmologist van Dooremaal, who introduced a variety of foreign bodies and tissues into the eyes of animals as a means of studying cataractogenesis, and, in the process, unwittingly discovered the prolonged survival of mouse skin grafts placed in the anterior chamber (AC) of the dog eye. Evidence suggesting that tissue grafts might also enjoy prolonged survival in the eyes of humans surfaced when the first successful corneal transplant in a human subject was reported in 1905, a landmark event that occurred over 60 years before antirejection drugs were used in the first human heart transplant. In the 1940s, experimental pathologists transplanted human tumor cells into the AC of the rabbit eye as a bioassay for determining the malignancy of biopsy specimens. We now know that the survival of such tumor implants in the AC of the rabbit eye was not a property of malignant cells *per se*, but like the survival of corneal transplants, was a manifestation of ocular immune privilege. It was not until the early 1950s that the preeminent immunologist and Nobel Laureate, Sir Peter Medawar, recognized the significance of the prolonged survival of skin grafts placed into the eye and the brain and coined the term "immune privilege." Although the concept of ocular immune privilege is widely recognized, it is frequently misunderstood or over-simplified. There are two common misconceptions of ocular immune privilege. The first misconception is that corneal transplants are universally exempt from immune rejection. While it is true that corneal allografts benefit from immune privilege and enjoy a high success rate compared to other categories of transplants, they can undergo immune rejection and, in some cases, the rejection cannot be prevented, even with potent immunosuppressive drugs. The second misconception is that ocular immune privilege is due to the absence of lymph vessels draining the interior of the eye, which would sequester antigens in the eye and deny them access to regional lymph nodes where they would elicit an immune response. Although there are no anatomically detectable patent lymphatics draining the interior of the eye, antigens and cells placed into the AC do in fact reach

the cervical lymph nodes in rodents. Thus, other explanations are needed to account for ocular immune privilege.

Important clues as to the possible underlying mechanisms for ocular immune privilege surfaced in the mid-1970s in seminal studies from J. Wayne Streilein and colleagues, who demonstrated that introducing antigens into the AC elicited a deviation in the systemic immune responses resulting in the suppression of T-cell-mediated immunity. This anterior chamber-associated immune deviation (ACAID) is characterized by the antigen-specific suppression of Th1 immune responses, such as delayed-type hypersensitivity (DTH), and Th2-based inflammation, such as experimental allergic asthma in mice. Although antigens introduced into the AC suppress Th1- and Th2-based immune inflammation, other immune elements are preserved. Noncomplement fixing antibodies are generated, while complement-fixing antibody production is silenced. Initial studies demonstrated that the induction of ACAID was associated with the production of IL-10, which at the time was considered a Th2 cytokine, and the suppression of the Th1 cytokine, interferon-γ (IFN-γ). This led some to conclude that ACAID was simply the preferential cross regulation of Th1 immune response by Th2 cytokines. However, further analysis revealed that ACAID also suppressed Th2-based inflammatory responses and that ACAID did not require the participation of a key Th2 cytokine, IL-4.

Not only does ACAID suppress classical Th1 immune responses, but it also mitigates Th2-mediated allergic inflammatory lung disease. ACAID also deviates antibody responses by preserving the production of noncomplement-fixing antibodies while blocking the generation of complement-fixing antibodies. This reduces the likelihood of immune inflammation, which is precipitated by activation of the complement cascade. Once activated by complement-fixing antibodies, the complement cascade spins off pro-inflammatory molecules that stimulate granulocytic inflammation. Thus, ACAID suppresses both Th1- and Th2-based inflammation and the generation of complement-fixing antibodies and thereby reduces the likelihood that antigens entering the eye will elicit immune inflammation that could injure tissues in the eye that possess little or no regenerative properties.

Induction of ACAID

Studies conducted over the past 30 years have shed light on the molecular and cellular basis of ACAID and have revealed the remarkable complexity of this systemic immunoregulatory phenomenon. The eye, thymus, spleen, and sympathetic nervous system are required for the induction of ACAID. Chemical sympathectomy prior to AC injection of antigen or removal of any of these organs within 3 days of AC injection prevents the induction of ACAID, and in many cases, allows the development of robust Th1 immune responses, such as DTH.

Ocular Phase of ACAID

The induction of ACAID begins when antigens enter the AC. The eye is an active participant in the induction of ACAID, as enucleation of the eye within 3 days of AC injection not only prevents the induction of ACAID, but also results in active immunization and development of DTH to the antigens that were introduced into the AC. It is widely believed that within the eye, antigen is captured by $F4/80^+$ macrophages, which under the influence of TGF-β (which is present in the aqueous humor), are imprinted to produce IL-10 while simultaneously extinguishing IL-12 production. The preferential production of IL-10 by ocular macrophages is crucial for the induction of ACAID, as macrophages from IL-10 knockout mice are incapable of inducing ACAID. TGF-β also stimulates ocular macrophages to produce macrophage inflammatory protein-2 (MIP-2), which is a potent chemokine that is pivotal in the splenic phase of ACAID (see below).

Thymic Phase of ACAID

Within 72 h of antigen entering the eye, $F4/80^+$ ocular macrophages capture antigen and migrate to the thymus. Within the thymus, they evoke the generation of $CD4^-$, $CD8^-$, and $NK1.1^+$ T cells (NKT cells), which then emerge from the thymus and enter the bloodstream where they migrate to the spleen. Other $F4/80^+$ ocular macrophages are believed to migrate directly from the eye to the spleen. Both populations of $F4/80^+$ ocular macrophages contribute to the generation of $CD4^+$ and $CD8^+$ T regulatory cells (T_{regs}) within the spleen.

Splenic Phase of ACAID

After entering the spleen, $F4/80^+$ ocular macrophages secrete MIP-2, which attracts $CD4^+$ NKT cells. The NKT cells in turn interact with the ocular macrophages and secrete the chemokine, RANTES, which recruits other cells into the marginal zone of the spleen. Within the marginal zone, $F4/80^+$ ocular macrophages, NKT cells, B cells, and $CD4^+$ T cells, in the presence of the third component of complement, collaborate to generate $CD8^+$ T_{regs}. The $CD8^+$ T_{regs} are the end-stage effector cells of ACAID that inhibit Th1- and Th2-based immune-mediated inflammation and promote corneal allograft survival.

Sympathetic Nervous System and ACAID

All three organs involved in the induction of ACAID – eye, spleen, and thymus – possess dense sympathetic innervations. Many immune responses are influenced by

the sympathetic nervous system, including ACAID. Animals subjected to chemical sympathectomy prior to AC injection of antigen fail to develop ACAID. It is not clear at what level the sympathetic nervous system exerts its effect, but it appears that it is not at the ocular phase, as chemical sympathectomy does not affect the generation of $F4/80^+$ ocular macrophages. Thus, the induction and expression of ACAID are remarkably complex and require the active participation of multiple organs and organ systems including the circulatory system, sympathetic nervous system, thymus, spleen, and eye (**Figure 1**).

ACAID T Regulatory Cells

Two phenotypically and functionally distinct populations of T_{regs} are induced in ACAID. $CD4^+$ T_{regs} inhibit the induction of T-cell-mediated immune responses, but do not suppress T-cell effector responses, such as DTH. Thus, $CD4^+$ ACAID T_{regs} act at the afferent arm of the immune response and prevent the initiation of immune responses, but have no effect if an immune response has already been initiated. $CD4^+$ afferent T_{regs} are also needed for the generation of $CD8^+$ T_{regs} that suppress immune responses at the effector stage. $CD8^+$ T_{regs} are the end-stage regulatory cells of ACAID that block effector immune responses, such as DTH, even if the host has been previously immunized and is capable of mounting a robust DTH response. Both the $CD4^+$ afferent T_{regs} and the $CD8^+$ efferent T_{regs} are antigen-specific. It is not clear how the $CD8^+$ ACAID T_{regs} suppress DTH and other T-cell immune effector responses, but evidence to date indicates that these T_{regs} do not lyse immune cells via a perforin-dependent mechanism or induce apoptosis by Fas/FasL interactions. Interestingly, $CD8^+$ efferent T_{regs} express IFN-γ receptors and require IFN-γ to exert their suppressive properties. However, the precise molecular mechanisms whereby $CD8^+$ efferent T_{regs} produce their effects remain to be elucidated. Although two distinct T_{reg} populations have been detected in ACAID (i.e., $CD4^+$ and $CD8^+$), it is possible that other T_{regs} might also participate

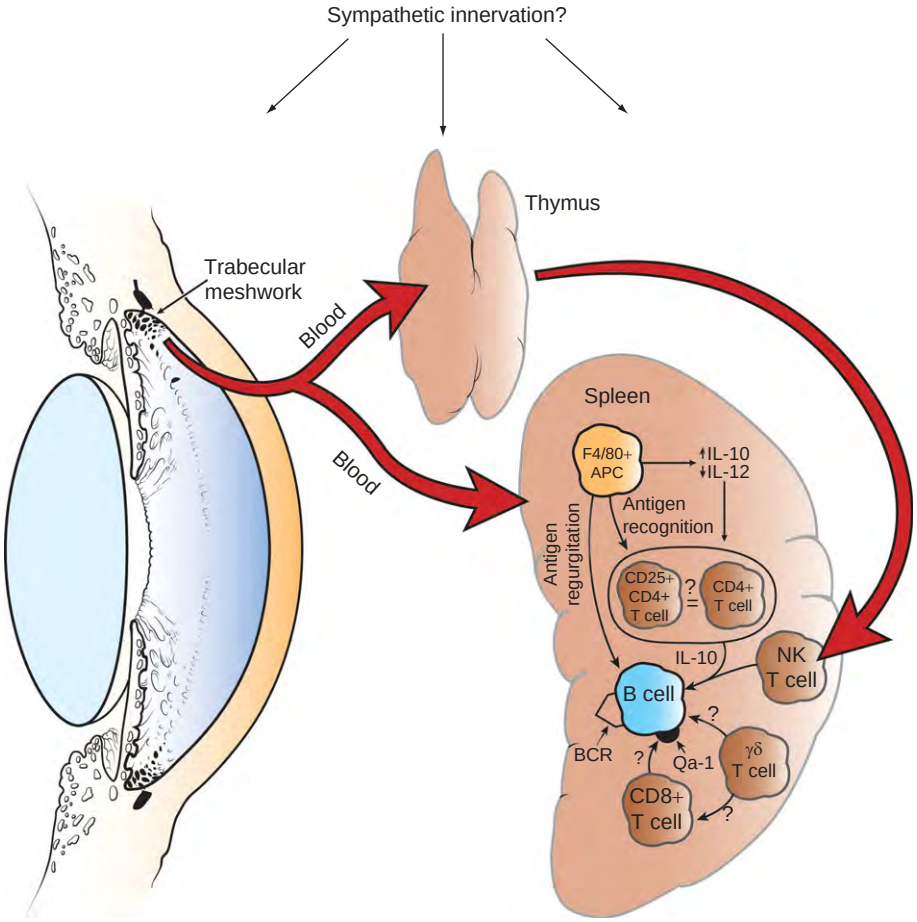

Figure 1 Organ systems and immune cells involved in the induction of ACAID. Removal of the eye, thymus, or spleen within 72 h of AC injection prevents the induction of ACAID. Chemical sympathectomy prior to AC injection of antigen also prevents the induction of ACAID. BCR, B-cell receptor. Reproduced from Niederkorn, J. Y. (2006). See no evil, hear no evil, do no evil: The lessons of immune privilege. *Nature Immunology* 7: 354–359, with permission from Nature Publishing Group.

in the induction and expression of ACAID. Although, most, if not all, of the studies performed to date have examined T_{regs} in the spleens of mice with ACAID, it is entirely possible that T_{regs} may also be present in lymph nodes, such as the cervical and submandibular lymph nodes.

What is the Relevance of ACAID?

One might argue that ACAID and immune privilege create an immunological blind spot that renders the eye potentially vulnerable to infectious agents. However, the eye and the brain are part of the central nervous system and possess very limited regenerative properties. Thus, limiting the immunological options to viral or bacterial infections is desirable for the preservation of vision. DTH is crucial for controlling intracellular pathogens, while activation of the complement cascade is an important mechanism for clearing bacterial infections. However, DTH and complement elicit granulocytic inflammation. Granulocytes produce a potpourri of reactive oxygen species and proteases that are notorious for producing extensive collateral damage to innocent bystander tissues. If unrestrained, such inflammation would produce extensive necrosis of ocular tissues leading to blindness. Thus, suppressing DTH and the complement cascade has a clear benefit for preserving the functional integrity of the visual apparatus.

The eye is also at risk from other T-cell-mediated immune responses, such as cytotoxic T lymphocyte (CTL)-mediated immunity. During virus infections, viral antigens are displayed on major histocompatibility complex (MHC) class I molecules of the virus-infected cells. The MHC class I/viral antigen complex serves as a docking station for CTL, which kill the virus-infected cells, and thus, eliminate the viral invaders. Although this is a highly efficient mechanism for controlling virus infections in most parts of the body, it would be devastating in the eye. However, CTL responses are suppressed as a consequence of ACAID. Interestingly, corneal endothelial cells and cells of the retina do not express the critical MHC class I molecules that are necessary for recognition and elimination of virus-infected cells by CTL. Thus, the active downregulation of CTL responses to ocular antigens combined with the absence of MHC class I molecules shield ocular cells from CTL-mediated injury. The preferential production of noncomplement fixing antiviral antibodies provides a level of protection by neutralizing viral particles without activating the complement cascade and provoking granulocytic inflammation.

Although ACAID seems to be an adaptation to prevent unwitting immune-mediated injury to ocular tissues, it may also benefit the corneal transplant recipient. Animal studies have shown that hosts bearing successful long-term orthotopic corneal allografts display an immune deviation that is reminiscent of ACAID. Moreover, AC injection of donor cells prior to transplantation results in a dramatic enhancement of corneal allograft survival in rodent models of penetrating keratoplasty.

Vitreous Cavity-Associated Immune Deviation

Immune privilege is not restricted to the AC, but appears to be equally expressed in the vitreous cavity and in the subretinal space. Although less is known about the immune privilege in the poster segment of the eye, it is clear that antigens introduced into the vitreous cavity elicit an immune deviation that appears to be identical to ACAID and has been termed vitreous cavity-associated immune deviation (VCAID).

Ocular Regulatory Cells Induced *In Situ*

The aqueous humor contains a myriad of anti-inflammatory and immunosuppressive molecules. Iris and ciliary body (I/CB) cells line a major portion of the AC and secrete constituents of the aqueous humor. I/CB cells not only secrete immunosuppressive and anti-inflammatory molecules such as TGF-β, but they also have the capacity to suppress T-cell proliferation and the secretion of pro-inflammatory cytokines, such as IFN-γ, by cell contact-dependent mechanisms, which are independent of soluble anti-inflammatory molecules such as TGF-β, IL-10, and tumor necrosis factor-α (TNF-α). I/CB cells are strategically located at sites where T cells can enter the eye and, thus, are positioned to exert their influence by inhibiting T-cell proliferation and production of IFN-γ shortly after T cells enter the eye.

Alpha-melanocyte-stimulating hormone (α-MSH) is one of the numerous immunosuppressive constituents of the aqueous humor. In addition to suppressing the production of pro-inflammatory cytokines, α-MSH stimulates T cells to produce anti-inflammatory cytokines such as TGF-β. Moreover, α-MSH converts Th1 cells into $CD4^+$, $CD25^+$ T_{regs}, which suppress DTH and mitigate experimental autoimmune uveitis (EAU).

The induction of ACAID requires penetration of the eye (i.e., antigen injection via a needle) in order to introduce antigens into the AC. AC injections, even if performed in the least possible traumatic manner, elicit the local production of pro-inflammatory cytokines including TNF-α. Thus, ACAID can be envisioned as a form of immune tolerance induced by antigens entering the AC as a consequence of perforating injuries to the eye. However, the eye may need to regulate immune responses to endogenous ocular antigens. During ontogeny, some structures in the eye are isolated from the immune system and

Table 1 Ocular-induced regulatory cells

Induction	*Antigen pecificity*	*Organs involved in induction*	*Regulatory cell phenotype*
ACAID	Yes	Eye, spleen, thymus, sympathetic nervous system	$CD4^+$; $CD8^+$; $CD4^+CD25^+$
VCAID	Yes	Eye	ND
I/CB	No	Iris and ciliary body	I/CB cells
Endogenous retinal neoantigens	Yes	Retina	ND
EAU[a]	Yes	Retina/uveal tract	$CD4^+$
α-MSH[b]	Yes	AC and retina	$CD4^+$

[a]T regulatory cells that develop following resolution of EAU.
[b]Alpha-melanocyte stimulating hormone-induced regulatory cells induced *in situ* in the AC or in the retina.
ND, not determined.

express tissue-specific antigens that, under some circumstances, can initiate an immune response. This has led some to suspect that ACAID and VCAID might be fail-safe mechanisms that generate T_{regs}, which prevent immune responses to tissue-specific ocular antigens (e.g., lens crystallins and retinal antigens). Studies using transgenic mice have demonstrated that novel neoantigens engineered to be exclusively expressed in the retina induce the development of T_{regs} that suppress DTH responses, yet are significantly different from the T_{regs} induced by AC injection of antigens. Thus, endogenous ocular antigens arising *in situ* in an intact eye can elicit the generation of T_{regs}, which presumably maintain immune homeostasis in the eye and serve as buffers against autoimmune inflammation, although through mechanisms that are likely distinct from ACAID and VCAID.

Conclusions

Ocular immune privilege is the product of multiple anatomical and physiological properties of the eye. The blood–eye barrier restricts entry of inflammatory and immune cells into the eye. Moreover, once in the eye, cells of the immune system encounter a milieu that is rich with soluble immunosuppressive and anti-inflammatory molecules. Cells lining the interior of the eye are decorated with membrane-bound molecules such as FasL, programmed death ligand-1 (PD-L1), and tumor necrosis factor-related apoptosis-inducing ligand, each of which can induce apoptosis of activated T cells. In addition, the limited expression of MHC complex molecules on the corneal endothelium and the retina render these cells invisible to CTL.

Immune privilege is also maintained by dynamic immunoregulatory processes that are initiated when antigens are introduced into the eye by injection, corneal transplantation, or endogenous ocular antigens. Each of these dynamic immunoregulatory processes relies on T_{regs} that act to either prevent the induction or expression of immune processes that inflict injury on tissues with little or no regenerative properties, while preserving immune effector mechanisms that provide protection against pathogens without damaging innocent bystander cells in the eye (Table 1). As stated over two decades ago by the preeminent ocular immunologist J. Wayne Streilein, the eye and the immune system are engaged in "a dangerous compromise." This compromise protects the eye from unwitting immune-mediated injury at the risk of being vulnerable to ocular infections and perhaps blindness. The reader's capacity to read through the articles in this encyclopedia is a testament to the success of this compromise.

See also: Adaptive Immune System and the Eye: T Cell-Mediated Immunity; Antigen-Presenting Cells in the Eye and Ocular Surface; Immunosuppressive and Anti-Inflammatory Molecules that Maintain Immune Privilege of the Eye; Role of Complement in Ocular Immune Response.

Further Reading

Ashour, H. M. and Niederkorn, J. Y. (2006). Peripheral tolerance via the anterior chamber of the eye: Role of B cells in MHC class I and II antigen presentation. *Journal of Immunology* 176: 5950–5956.
Caspi, R. R. (2006). Ocular autoimmunity: The price of privilege? *Immunological Reviews* 213: 23–35.
Cone, R. E., Li, X., Sharafieh, R., O'Rourke, J., and Vella, A. T. (2006). The suppression of delayed-type hypersensitivity by $CD8_+$ regulatory T cells requires IFN-γ. *Immunology* 120: 112–119.
Faunce, D. E., Sonoda, K. H., and Stein-Streilein, J. (2001). MIP-2 recruits NKT cells to the spleen during tolerance induction. *Journal of Immunology* 166: 313–321.
Faunce, D. E. and Stein-Streilein, J. (2002). NKT cell-derived RANTES recruits APCs and $CD8_+$ T cells to the spleen during the generation of regulatory T cells in tolerance. *Journal of Immunology* 169: 31–38.
Li, X., Taylor, S., Zegarelli, B., et al. (2004). The induction of splenic suppressor T cells through an immune-privileged site requires an intact sympathetic nervous system. *Journal of Neuroimmunology* 153: 40–49.
McKenna, K. C. and Kapp, J. A. (2004). Ocular immune privilege and CTL tolerance. *Immunologic Research* 29: 103–112.

Niederkorn, J. Y. (2006). Anterior chamber-associated immune deviation and its impact on corneal allograft survival. *Current Opinion in Organ Transplantation* 11: 360–365.

Niederkorn, J. Y. (2006). See no evil, hear no evil, do no evil: The lessons of immune privilege. *Nature Immunology* 7: 354–359.

Niederkorn, J. Y. and Wang, S. (2005). Immune privilege of the eye and fetus: Parallel universes? *Transplantation* 80: 1139–1144.

Skelsey, M. E., Mellon, J., and Niederkorn, J. Y. (2001). Gamma delta T cells are needed for ocular immune privilege and corneal graft survival. *Journal of Immunology* 166: 4327–4333.

Stein-Streilein, J. (2003). Invariant NKT cells as initiators, licensors, and facilitators of the adaptive immune response. *Journal of Experimental Medicine* 198: 1779–1783.

E

Embryology and Early Patterning

P Bovolenta and R Marco-Ferreres, Instituto Cajal (CSIC) and CIBER de Enfermedades Raras (CIBERER), Madrid, Spain
I Conte, Telethon Institute of Genetics and Medicine (TIGEM), Naples, Italy

Glossary

Agenesis – Failure of an organ to develop during embryonic growth and development.
Anophthalmia – Absence of the eye as a result of a congenital malformation during development.
Coloboma – Congenital malformation due to failure of fusion of optic fissure.
Hyperplasia – Abnormal increase in cell proliferation within an organ or tissue due to the disregulation of cell-cycle control mechanisms.
Induction – Change in cell fate resulting from an external signal (inducer). This signal secreted by a group of cells instructs target cells to acquire specific properties.
Invagination – Morphogenetic process leading to the coordinated inward folding of a cell layer forming a pocket on the surface.
Mesenchyme – Embryonic mesodermal connective tissue composed of loosely packed unspecialized cells characterized by the ability to migrate into other tissues.
Phenotype – Expression of a specific trait based on genetic and environmental influences.
Prosencephalon – Anterior-most division of the developing vertebrate brain (forebrain) that further subdivides into the telencephalon and the diencephalon.

Embryology

Eye development starts at late gastrula stages with the specification of retinal precursor cells within the eye field in the anterior neural plate. At this stage, retinal progenitor cells occupy a medial position and are surrounded rostrally and laterally by telencephalic precursors and caudally and medially by cells that will form the diencephalon. During neurulation, coordinated rearrangement of the cells that form each of these presumptive regions results in a new cell organization, whereby retinal progenitor cells now become laterally positioned. *In vivo* monitoring of retinal progenitor cell movement has shown that, at least in fish, dorsal diencephalic cells – positioned caudally to the eye field – move inward and forward, displacing prospective eye and optic stalk tissue forward and then sidewise. At the same time, laterally positioned telencephalic precursors fold toward the midline leaving retinal precursors cells to the side of the neural tube (Figure 1). As these movements happen, the cells of the left and right eye, which were initially intermingled, segregate in their respective domains forming two visible optic vesicles.

At the present time, it is not clear whether similar morphogenetic movements occur in other vertebrate species. In mammals, for instance, these early events might be slightly different as the first visible sign of eye formation are two small depressions (optic pits) in the anterior neural tube, which appear well before folding of the tube occurs.

Independent of these initial differences, in all vertebrates the optic vesicles are formed by a single pseudostratified neuroepithelium that is surrounded by cephalic mesenchyme, including migrating neural crest cells, and limited at the most distal tip by the surface ectoderm. The cells that compose the optic vesicle neuroepithelium are initially morphologically and molecularly indistinguishable but reach their final complexity through a series of inductive and morphogenetic events that, in part, depend on their interaction with the surrounding tissues. The extension of thick cytoplasmic processes emanating from the basal surface of both optic vesicle and ectodermal cells establishes cell-to-cell contact and initiates a series of temporally correlated structural changes in both structures. A fibrillar extracellular matrix (ECM) builds up between the neuroectoderm and the ectoderm,

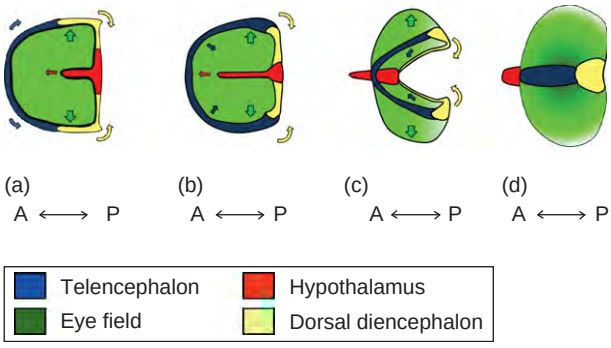

Figure 1 Optic vesicle morphogenesis in zebrafish. (a) The eye field (in green) in the anterior neural plate is surrounded anteriorly and peripherally by telencephalic precursors (blue), posteriorly by the dorsal diencephalon (light yellow) and medially by cells that will form the hypothalamus (red). (b, c) The hypothalamic and dorsal diencephalic precursors move forward beneath the eye field displacing it to the front and laterally. The lateral edges of the neural plate fold toward the midline. (c, d) The lateral telencephalon cells meet at the dorsal midline, leaving two optic vesicles at the side. Adapted from Egland, S. J., Blanchard, G. B., Mahadevan, L., and Adams, R. J. (2006). A dynamic fate map of the forebrain shows how vertebrate eyes form and explains two causes of cyclopia. *Development* 133: 4613–4617.

favoring strong adhesion, while the ectoderm immediately adjacent to the optic vesicle thickens forming the lens placode (**Figure 2**).

Once formed, the lens placode and the adjacent optic vesicle begin a coordinated invagination to form the lens pit and the optic cup. ECM-mediated adhesion between the two tissues is important for coordinating morphogenetic movements. In addition, some of its components, such as laminin and fibronectin, may participate in lens cell differentiation, which occurs concomitantly. As a result, the lens pit deepens and gradually assumes a spherical shape that finally breaks away from the ectoderm forming the lens vesicle. A spatio-temporally restricted massive apoptosis contributes to this separation. Thereafter, the lens vesicle undergoes an asymmetric differentiation acquiring a characteristic polarity: cells located in the most proximal region (facing the neuroepithelium) elongate to form the primary lens fibers, whereas those in the most distal portion (facing the ectoderm) form a cuboidal monolayer known as the anterior lens epithelium.

Concomitant with lens formation, the optic neuroepithelium undergoes a series of rearrangements that culminates with the formation of a bi-layered optic cup (**Figure 2(c)** and **2(c′)**). The distal inner layer will give rise to the future neural retina (NR), while the distal outer layer to the retinal pigmented epithelium (RPE), which acquires specialized epithelial characteristics. The proximal ventral region forms the optic stalk, from which the optic nerve derives. The transition zone between the future retina and the RPE forms the ciliary margin (CM), or periphery of the retina. Despite its neural origin, the CM differentiates into non-neural structures: the proximal part into the ciliary epithelium while the distal part becomes the iris. In fish and amphibians, the CM harbors bona fide stem cells, which continue to proliferate throughout life to increase the eye size. Cells with stem-like properties also appear to be present in the CM of birds and mammalian eyes. These cells, however, are quiescent in physiological conditions.

Although there are common features in the way the optic cup is formed among vertebrates, differences do exist. In fish and amphibians, the optic vesicles, which develop as flat wing-like protrusions, undergo a process of cavitation, rotation, and invagination that shifts cells that were originally in a ventral position to the medial layer, from which the RPE progenitors derive. These progenitors stretch over the prospective NR, occupying the dorsal aspect of the optic cup. In mammals and birds instead, the optic vesicle neuroepithelium undergoes two simultaneous foldings (**Figure 2(b)**): (1) the spherical vesicle becomes concave outward, resembling the bowl of a spoon where the optic stalk is the handle and (2) at the same time, the ventral portion of the entire vesicle folds inward giving rise to the groove of the optic (choroid) fissure. Differential growth rates are associated with these events. In the future RPE as well as in the CM, the proliferation rate is quite slow in comparison to that of the perspective NR. There are also differences along the dorso-ventral axis, with an initial higher proliferation rate in the ventral part, which enables the formation of the optic fissure.

The optic fissure can be divided into two adjoining parts – the retinal fissure and the optic groove – which derive from the progressive invagination of the ventral surface of the optic vesicle and stalk, respectively. The transition between the retinal fissure and the optic groove dictates the position where the optic disk, or blind spot of the retina, will form. This structure, a real interface between the optic stalk and the retina, enables the entrance of surrounding mesenchymal cells into the developing eye chamber, which will form the hyaloid artery, the main blood supply for the eye. At the same time, it allows the egression of retinal axons from the eye cup.

As a last step in the formation of a complete optic cup, its dorsal portion begins to proliferate more rapidly enabling the shallow bowl to become deeper, while its lateral edges meet ventrally across the optic fissure. The eye rudiment now has the appearance of a hemispheric cup where the RPE completely surrounds the NR. The sealing of the optic fissure completes these morphogenetic events (**Figure 2(c)** and **2(c′)**). Although this is a poorly understood process, in humans the fusion usually begins in the middle portion of the fissure and extends anteriorly and posteriorly.

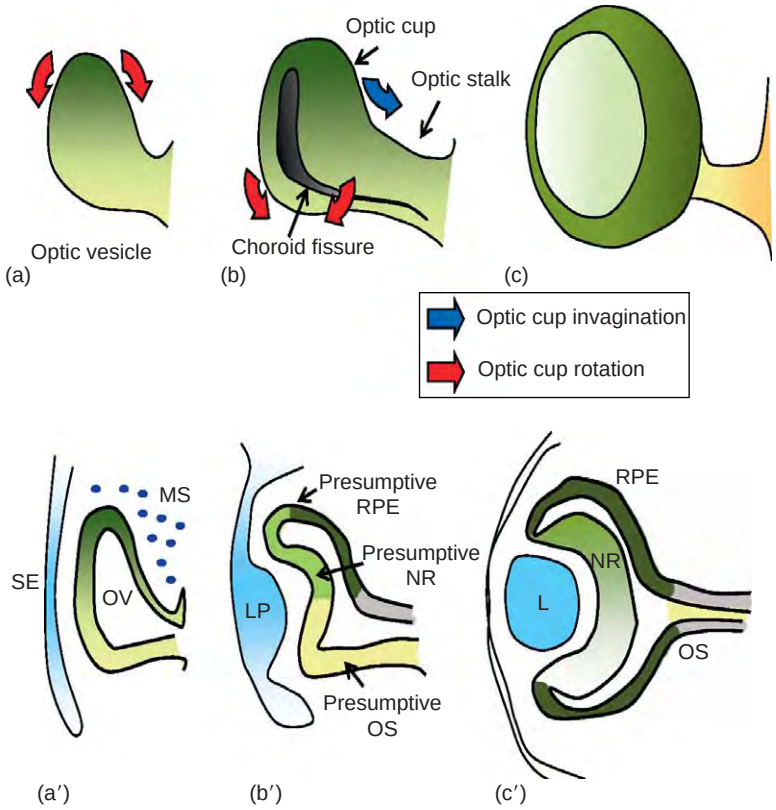

Figure 2 Schematic representation of initial eye morphogenesis. (a) The optic vesicle appears as a protrusion of the anterior neural tube. (b) Folding of the distal and ventral neuroepithelium generates the optic cup and the optic (choroids) fissure. (c) The optic fissure seals and a spherical eye cup forms. (a′) The optic vesicle neuroepithelium is composed of the cells that are morphologically and molecularly indistinguishable. (b′) As the vesicle folds, the dorsal neuroepithelium specifies as presumptive RPE (dark green), the distal region as presumptive neural retina (light green), while the ventral portion as optic stalk (light yellow). The surface ectoderm thickens forming the lens placode (blue). (c′) Complete folding of the vesicle results in an optic cup, where the RPE completely surrounds the neural retina. L, lens; LV, lens vesicle; MS, mesenchyme; NR, neural retina; OS, optic stalk; OV, optic vesicle; RPE, retinal pigment epithelium; SE, surface ectoderm.

Table 1 Summary of extracellular molecules and transcription factors implicated in early eye development

Events in eye development	*Secreted molecules*	*Transcription factors*
Proximo-distal patterning of OV	Shh, nodal	Pax2, Pax6, Vax1
Specification of NR and RPE	FGF, TGFβ; Activin/BMPs	Chx10, Six3, Six6, Lhx2, Pax6, Mitf, Otx1, Otx2
Dorso-ventral patterning of the optic cup	BMP4, BMP7, Shh, RA, ventroptin, noggin	Pax6, Pax2, Vax, Tbx5

Shh, Sonic hedgehog; FGFs, Fibroblast grow factors; BMPs, bone morphogenetic proteins; RA, retinoic acid.

Early Patterning

The morphogenetic movements and the tissue interactions described above are orchestrated by specific genetic programs coordinated by cell-signaling mechanisms – inductive signals – and regulated by the activity of a relatively small number of transcription factors (see **Table 1**). Many of the genes involved in the specification of the eye field, including retinal homeobox (Rx), paired box 6 (Pax6), hairy enhancer of split 1 (Hes1), orthodenticle homolog 2 (Otx2), LIM homeobox 2 (Lhx2), and SIX homeobox 3 (Six3), are also involved in the early patterning events that convert eye-field cells into the structures that compose the optic cup (**Figure 3(a′)**). However, changes in the expression levels, as well as combinatorial interaction with other factors, diversify the activity of these genes enabling the progressive acquisition of different fates and functions. As mentioned above, cells that compose the optic vesicle are initially morphologically and molecularly undistinguishable and, therefore, are all potentially competent to originate the NR, the optic stalk, or RPE. Information, in the form of signaling molecules, derived from the surrounding tissues and the neuroepithelium itself modulates and restricts the expression of different transcription factors to a specific

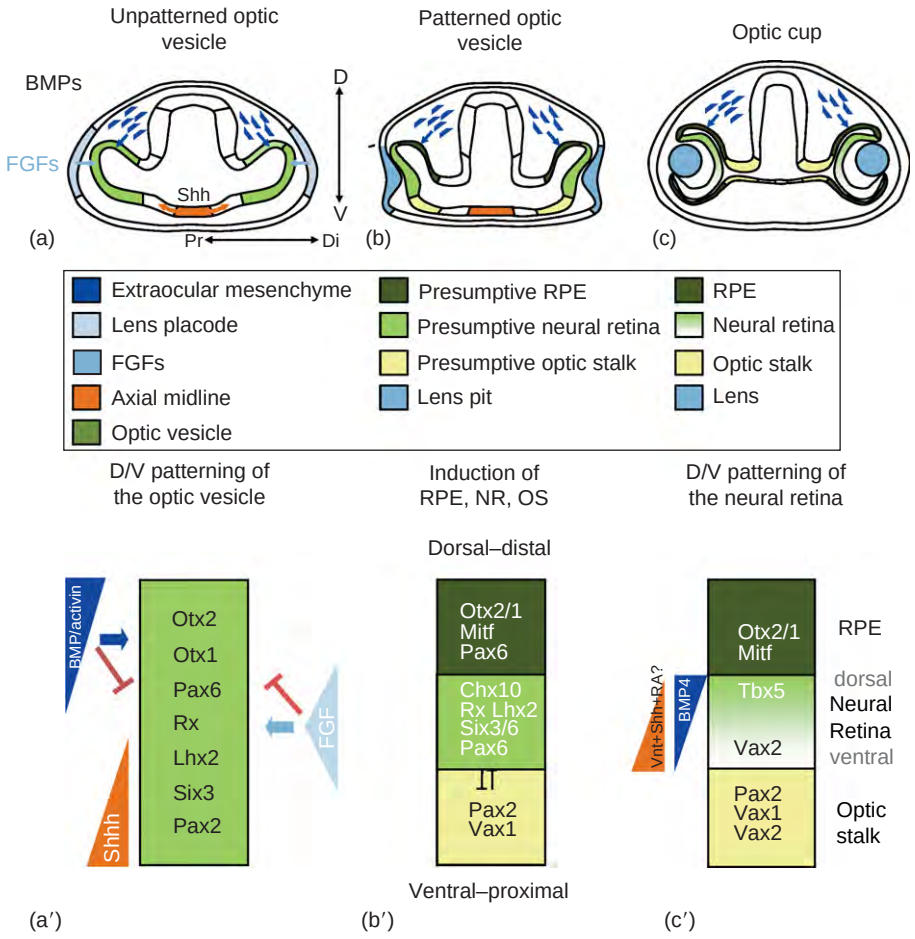

Figure 3 Distribution of inductive signals and transcription factors involved in early patterning of the eye. Progressive tissue specification during the transition from unpatterned (a) to patterned optic vesicle (b) and optic cup (c) where the different colors represent the distinct territories. In (a′)–(c′) color bar graphs represent the distribution of molecular components implicated in the patterning of the optic vesicle into optic cup. In (a) and (a′) all the neuroepithelial cells are indistinguishable (light green) and express a common set of transcription factors. Shh signaling from the axial midline is required for the specification of the proximo-ventral optic stalk (orange in (b) and (b′)). TGFβ-like signals from the extraocular mesenchyme promote RPE character (dark green in (b) and (b′)), whereas FGF signals from the lens placode repress RPE and activate neural retina identity (light green in (b) and (b′)). During optic cup formation the graded distribution of BMP4 dorsally and ventroptin, possibly together with RA and Shh, in the ventral side establish the dorso-ventral polarity of the neural retina (shaded green in (c) and (c′)). Shh, Sonic hedgehog; FGFs, fibroblast growth factors; BMPs, bone morphogenetic proteins; RA, retinoic acid; Vnt, ventroptin.

domain of the vesicle, initiating its patterning along the proximo-distal and dorso-ventral axis.

Proximo-Distal Patterning of the Optic Vesicle

The optic vesicles are bulges of the neural tube and thus their subdivision is often described according to a proximal–distal axis. In this view, future optic stalk precursors occupy a proximal location, while distal cells constitute the NR and RPE precursors (**Figure 3(b)**).

Proximo-ventral cells of the optic stalk are generated under the influence of signaling molecules, emanating from the axial ventral midline, including Sonic hedgehog (Shh) and nodal, a member of the transforming growth factor-beta (TGFβ) family (**Figure 3(b)**). Mutations in these genes cause severe anterior neural tube defects that include the formation of a single midline (cyclopic) eye, lacking optic stalk tissue. The phenotype is the result of Shh-mediated regulation of the spatial expression of Pax6 and Pax2 – two homeobox transcription factors of the paired type – which normally demarcate the distal and proximal optic primordium, respectively (**Figure 3(b′)**). Indeed, overexpression of Shh causes the expansion of the Pax2 domain at the expense of the Pax6-positive tissue, while the opposite occurs in absence of Shh. A similar dependence on Shh signaling has also been observed for the expression of Vax genes, other homeobox transcription factors involved in optic stalk generation.

Targeted inactivation of Pax2 or Vax1 in mice results in severe optic nerve abnormalities, consistent with a role

for these genes in proximal eye development. The phenotype of these mice is characterized by the presence of coloboma of the ventral optic fissure, and, in the case of Pax2, an extension of the RPE into the optic nerve region. In contraposition, the Pax6 gene is necessary for the formation of the distal vesicle, including the lens tissue. Mutations in this gene impair both lens and optic vesicle formation, ultimately causing anophthalmia. In these mice, the only remnant of the eye primordium has optic stalk characteristics. Conditional inactivation of Pax6 at different time points of eye development, however, has highlighted additional functions for this gene both in NR and RPE development (see below).

In summary, acquisition of the ventral optic stalk phenotype depends on the Shh-dependent expression of transcription factors that impose ventral character to optic vesicle precursors. The establishment of a precise boundary between the presumptive optic stalk and the distal optic vesicle may result from the reciprocal transcriptional repression between Pax6 and Pax2 (**Figure 3(b′)**).

Specification of the RPE and NR

Extracellular signals, derived from the surface ectoderm in contact with the prospective NR or from the periocular mesenchyme surrounding the presumptive RPE, pattern the distal optic vesicle (**Figure 3(a)**).

Removal of the surface ectoderm induces prospective NR cells to acquire the characteristics of RPE cells. This is because the ectoderm secretes high levels of two members of the fibroblast growth factor (FGF) family of signaling molecules – FGF1 and FGF2 – while the prospective retina expresses the FGF receptor 1. The addition of either one of the two factors is sufficient to rescue NR formation after ectoderm removal. On the contrary, exposure of the presumptive RPE to FGF confers to the cells NR properties. Therefore, FGF signaling normally activates NR specification but inhibits RPE formation. The future retina itself expresses other FGFs, such as FGF3, FGF8, FGF9, and FGF15, which may contribute to maintain the properties of the retina, but are not sufficient to induce them, since addition of these FGFs cannot rescue the phenotype caused by surface ectoderm removal.

The activity of the FGF is complemented by other signals, originating from the dorsal extraocular mesenchyme, which have opposite effects on the specification of these territories. Members of the TGFβ superfamily of signaling molecules, such as activins or the related bone morphogenetic proteins (BMP) – Bmp4 and Bmp7 – are expressed in the surrounding mesenchyme and/or the presumptive RPE itself. Interference with the activity of these molecules prevents RPE development and induces NR-specific genes, whereas their addition activates RPE characteristics in the entire vesicle.

Thus, TGFβ/BMP and FGF signaling act antagonistically on the specification of RPE and NR precursors. Directly or indirectly, their activity seems to impinge upon the expression of specific transcriptional regulators, such as *Caenorhabditis elegans* homeo domain 10 (Chx10) and Otx2 or microphthalmia-associated transcription factor (Mitf), the function of which is instrumental to the acquisition of either RPE or NR identities. Indeed, FGF signaling activates the expression of Chx10 in the retina but represses that of Otx2 and Mitf in the RPE, while opposite results have been observed with manipulations of TGFβ/BMP signaling.

Besides those mentioned above, a number of additional transcription factors are also specifically expressed in the presumptive neural retina and RPE (**Figure 3(b′)**). Currently, it is not clear how many of them are really needed to impose tissue specificity. The paired-like homeobox gene Chx10 (also known as Vsx1) is possibly the best candidate to impose a neural retina character to the naive optic vesicle cells (**Figure 3(b′)**). The onset of Chx10 expression is restricted to the presumptive NR domain and mutations in the human or mouse gene lead to microphthalmia, cataracts, and abnormal iris development. The expression of two members of the Six family of homeobox transcription factors, Six3 and Six6, initially expressed in the entire vesicle, is also soon restricted to the prospective NR. The overexpression of these factors in fish embryos causes retinal hyperplasia and ectopic formation of retinal-like tissue. In mice, genetic inactivation of Six3 leads to complete loss of the forebrain, while that of Six6 impairs retinal proliferation and differentiation. It is, therefore, still unclear whether the two genes are essential pieces of the genetic program that establishes NR identity. Nevertheless, overexpression of either one of them in the RPE cells leads to the acquisition of a NR phenotype, suggesting that their function is at least incompatible with the acquisition of the RPE character.

Similarly to Six3, the expression of Lhx2 becomes restricted to the prospective NR. Mice deficient in Lhx2 function are characterized by anophthalmia, like that observed in mice mutants for the Pax6 gene. Although the two genes seem to act independently, both are required during the period of close contact between the surface ectoderm and optic vesicle. Whether this implies that their activity participates in the specification of the NR domain still needs to be established.

The function of at least four transcription factors – Otx1, Otx2, Mitf, and Pax6 – is at the core of the transcriptional network required to establish the RPE character. Functional inactivation of either Mitf or Otx1 and Otx2 genes (bHLH and homeo-domain-containing transcription factors, respectively) impairs RPE differentiation. On the contrary, retinal cells transfected with either Otx or Mitf genes acquire a RPE phenotype and accumulate granules of pigment. Although it is unclear whether Otx and Mitf

act in a feedback loop or in parallel, they synergize in the activation of melanogenic gene expression, including tyrosinase or the tyrosinase-related protein 2. Although Pax6 expression in the prospective RPE is transient, its function – possibly together with that of Pax2 – seems necessary to initiate Mitf expression. Indeed, Pax6 binds directly to the Mitf promoter and in embryos deficient in both Pax2 and Pax6 optic vesicles are small and composed of Mitf-negative cells that instead co-express Otx2 and the NR marker, Chx10.

As in the case of the proximo-distal patterning of the optic vesicle, subdivision of the distal vesicle in the NR and RPE is reinforced by reciprocal repression of transcription factors. Mitf is expressed ectopically in the neuroretina of Chx10-deficient mice, driving cells toward an RPE-like identity. Conversely, misexpression of Chx10 in the developing RPE caused downregulation of Mitf with a consequent loss of pigment, strongly suggesting an antagonistic interaction between Chx10 and Mitf.

Chx10 function also appears to be required to establish a boundary between central and peripheral retina, the CM. In Chx10 null mutants, in fact, peripheral structures, including the ciliary body, are abnormally expanded. Similar expansions are also observed upon stabilization of β-catenin, a key effector of canonical wingless pathway (Wnt) signaling. In addition, ectopic expression of Wnt ligand induces abnormal expression of CM markers, such as Otx1 and msh homeobox 1 (Msx1), in the central retina. This suggests that canonical Wnt signaling plays a crucial role in establishing a difference between central and peripheral retina, imposing identity to the ciliary body and iris.

Dorso-Ventral Patterning of the Optic Cup

As mentioned above, the transition between the optic vesicle and the optic cup establishes a new position for most of the optic vesicle precursors. Once this rearrangement is accomplished, the optic cup undergoes a new wave of polarization along the dorso-ventral axis.

A gradient of BMP signaling is primarily responsible for this new pattern (**Figure 3(c)** and **(c′)**). Bmp4 is expressed in the dorsal retina of most vertebrate species analyzed. Mis-expression of Bmp4 in the ventral portion of the optic cup suppresses the expression of Pax2 and Vax and activates that of Tbx5, a transcription factor of the T-box class normally expressed only in the dorsal portion of the optic cup. The counterbalance for this dorsalizing activity is ventroptin, a BMP signaling antagonist expressed in the ventral optic cup. Forced expression of ventroptin in the dorsal cup decreases Bmp4 expression and expands that of Vax genes. Thus, the ventral character of the optic cup seems to depend on the inhibition of Bmp4-mediated dorsalizing activity.

Structures that are typical of the ventral optic cup – such as the optic fissure, the hyaloid artery, and the pecten (a vascular-like structure in birds) – also depend on BMP signaling, although this may be due to actions of other members of the family. Overexpression of the BMP antagonist noggin in the chick ventral optic cup alters its development and induces ectopic expression of optic stalk markers in the region of the ventral retina and RPE. Furthermore, in Bmp7 null mice the optic fissure does not form. Retinoic acid (RA) is an additional signal that may be involved in establishing the ventral optic cup identity, although its precise functions are controversial. Enzymes involved in the synthesis and degradation of RA as well as RA receptors are expressed in the eye with complex and polarized patterns. RA treatment upregulates Pax2 expression in the eye of zebrafish embryos, while deprivation of vitamin A during embryogenesis, inactivation of RA receptors, or inhibition of RA synthesis all lead to embryos with defects in the ventral retina. Despite this, embryos deficient in Raldh1, Raldh2, and Raldh3, genes coding for RA-synthesis enzymes, develop an optic cup with a normal dorso-ventral patterning, questioning the relevance of RA in this process.

Equally unclear is whether Shh signaling contributes to impose a ventral character to the optic cup. Although Shh is needed to control the initial expression of Pax2 and Vax genes in the optic vesicle, its forced dorsal expression at slightly later stages of development does not ventralize the dorsal optic cup, although BMP4 expression is downregulated. Defects are, instead, observed in the optic disk and the NR, where Shh causes activation of Otx2 expression and pigmentation. Conversely, interference with Shh signaling perturbs Otx2 expression and pigment formation in the ventral RPE, which loses its characteristics. Thus, Shh signaling may have a more specific function in the specification of the ventral RPE cells as well as of those that compose the optic fissure.

Independent of the signaling mechanism, the transcriptional control of dorso-ventral polarization of the optic cup depends largely on the activity of Tbx5 in the dorsal portion of the cup and Vax genes in the ventral part. Overexpression of Tbx5 causes dorsalization of the optic cup while overexpression of Vax leads to its ventralization. Pax6 seems to regulate the expression of both genes but in opposite directions establishing an intermediate zone that separate the two domains.

The significance of a dorso-ventral polarity in the NR at this stage and, thus, of the function of Tbx5 and Vax genes might be tightly linked to the establishment of the proper spatial order of the retino-tectal projections through the regulation of the expression of members of the ephrin (Eph) family of receptor tyrosine kinases and their ephrin ligands, which are axon-guidance cues essential for target recognition of RGC axons.

Conclusions

Early eye patterning in vertebrates is controlled by an evolutionary conserved genetic program, although initial morphogenetic events may vary from species to species. This program is regulated by the interplay among a number of signaling pathways and transcription factors. The information available at present represents an important backbone that needs to be extended for full understanding of eye development. *In vivo* imaging of eye morphogenesis as well as additional characterization of the involved genetic networks may help to understand the causes of inborn eye malformation such as anophthalmia, microphthalmia, and coloboma.

See also: Developmental Anatomy of the Retinal and Choroidal Vasculature; Eye-Field Transcription Factors; Histogenesis, Cell Fate, and Signaling Factors; Photoreceptor Development: Early Steps/Fate; Retinal Histogenesis; Zebrafish: Retinal Development and Regeneration.

Further Reading

Adler, R. and Canto-Soler, M. V. (2007). Molecular mechanisms of optic vesicle development: Complexities, ambiguities and controversies. *Developmental Biology* 305: 1–13.

Barishak, Y. R. (2001). *Embryology of the Eye and Its Adnexa.* Basel: Karger.

Chow, R. L. and Lang, R. A. (2001). Early eye development in vertebrates. *Annual Review of Cell and Developmental Biology* 17: 255–296.

Egland, S. J., Blanchard, G. B., Mahadevan, L., and Adams, R. J. (2006). A dynamic fate map of the forebrain shows how vertebrate eyes form and explains two causes of cyclopia. *Development* 133: 4613–4617.

Fitzpatrick, D. R. and van Heyningen, V. (2005). Developmental eye disorders. *Current Opinion in Genetics and Development* 15: 348–353.

Lupo, G., Harris, W. A., and Lewis, K. E. (2006). Mechanisms of ventral patterning in the vertebrate nervous system. *Nature Reviews Neuroscience* 7: 103–114.

Martinez-Morales, J. R., Rodrigo, I., and Bovolenta, P. (2004). Eye development: A view from the retina pigmented epithelium. *BioEssays* 26: 766–777.

Rembold, M., Loosli, F., Adams, R. J., and Wittbrodt, J. (2006). Individual cell migration serves as the driving force for optic vesicle evagination. *Science* 313: 1130–1134.

Relevant Website

http://www.med.unc.edu – University of North Carolina at Chapel Hill, School of Medicine: Eye Development.

Extraocular Muscles: Extraocular Muscle Anatomy

L K McLoon, University of Minnesota, Minneapolis, MN, USA
S P Christiansen, Boston University, Boston, MA, USA

Glossary

Abducens nerve (CNVI) – The cranial motor nerve which controls contraction of the lateral rectus muscle.
Aponeurosis – A large flat and dense connective tissue layer which anchors a muscle to its origin or insertion.
Excyclotorsion – An outward rotation of the upper pole of the vertical midpoint of each eye.
Incyclotorsion – An inward rotation of the upper pole of the vertical midpoint of each eye.
Myosin heavy chain (MyHC) isoforms – The major contractile protein in muscle is myosin, which in turn is composed of two heavy and four light chains. MyHC isoforms are responsible for the shortening velocity of muscle fibers during muscle contraction.
Oculomotor nerve (CNIII) – The cranial motor nerve which controls contraction of the levator palpebrae superioris muscle, the inferior, medial, and superior rectus muscles, as well as the inferior oblique muscle. It also contains parasympathetic preganglionic axons that are destined for the ciliary body and iris sphincter muscles of the eye.
Ora serrata – The junction between the neurosensory retina and the ciliary body.
Satellite cells – Myogenic precursor cells that reside between the sarcolemma of the muscle fiber and its surrounding basal lamina. They are responsible for myofiber repair and regeneration after injury or in disease.
Strabismus – A disorder characterized by altered tonus or restrictive disease of the extraocular muscles resulting in loss of conjugate binocular vision.
Trochlear nerve (CNIV) – The cranial motor nerve which controls contraction of the superior oblique muscle.

The extraocular muscles (EOMs) have an extremely complex anatomy, both at the gross anatomical and histological levels. The main function of the EOM is to move the eyes in the orbit such that the eyes can be precisely positioned to allow focusing of the visual world on corresponding regions of each retina. Within each bony orbit the EOM includes four rectus muscles (superior, lateral, inferior, and medial) and two oblique muscles (superior and inferior; Figure 1). A seventh skeletal muscle within the human orbit is the levator palpebrae superioris (LPS) muscle. It is the superior-most muscle in the orbit directly inferior to the frontal bone forming the orbital roof. The levator lies directly inferior to the periorbita and inserts via a large aponeurosis into the eyelid skin. The descriptions of the EOM will be primarily based on human muscles for ease of presentation. The general characteristics of size, shape, fiber type, and the like are similar for all EOM in principle, although they vary in detail for each specific animal that has been examined.

Gross Anatomy of the EOM within the Orbit

The four rectus muscles originate from the apex of the bony orbit by a common tendinous annulus (of Zinn). The tendinous annulus attaches to the greater and lesser wings of the sphenoid bone as well as to the periosteum, the dense connective tissue lining the orbit. The annulus crosses over the inferior portion of the superior orbital fissure and runs superior and medial to the optic foramen (Figure 2). The superior (Figure 3) and medial rectus muscles arise from the superior part of this annulus, while the inferior and lateral rectus muscles arise from its inferior part. These muscles are all surrounded by a connective tissue capsule called Tenon's capsule and are described as forming the muscle cone. The superior oblique (SO) muscle originates from the periosteum slightly superior and medial to the tendinous annulus. The inferior oblique (IO) muscle is the only EOM that does not arise from the orbital apex, but rather originates from the lateral border of the lacrimal fossa, which is anterior and nasal within the orbit.

The rectus muscles run anteriorly to insert on the sclera on the anterior pole of the globe, at a location superficial to the ora serrata. The lateral and medial rectus muscles in human adults are approximately 41 mm in length. The superior rectus (SR) is the longest, averaging 42 mm, while the inferior rectus is the shortest averaging 40 mm. The insertions of the muscles onto the globe vary in their distance from the corneal limbus, with the SR furthest and the medial rectus closest. According to a study by Fuchs in 1884 on cadaver eyes, the distance from the limbus of rectus muscle insertions onto the globe

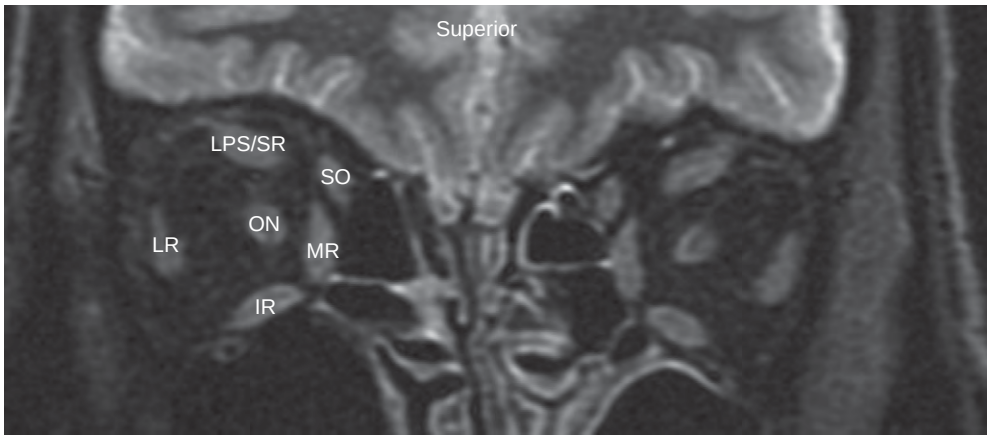

Figure 1 Magnetic resonance imaging view of the orbit in cross section. LPS/SR: levator palpebrae superioris and superior rectus muscles. SO, superior oblique muscle; MR, medial rectus muscle; IR, inferior rectus muscle; LR, lateral rectus muscle; ON, optic nerve. MRI generously provided by Dr. Michael S. Lee at the University of Minnesota.

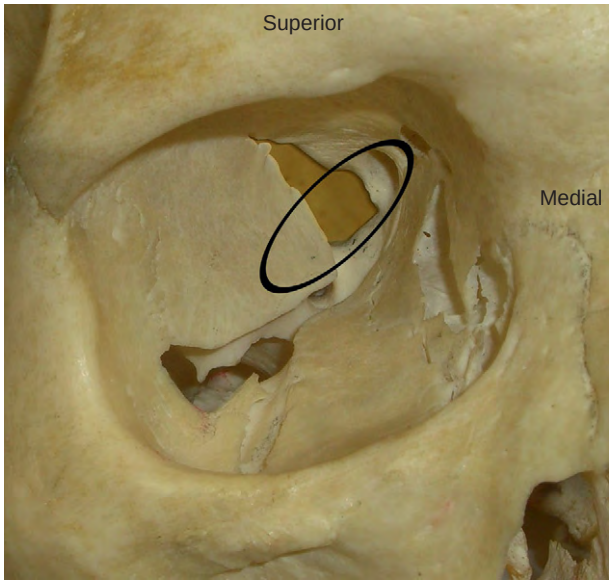

Figure 2 Bony orbit with the tendinous annulus indicated in the orbital apex by the black oval. It encloses the optic foramen superiorly and crosses the inferior portion of the superior orbital fissure.

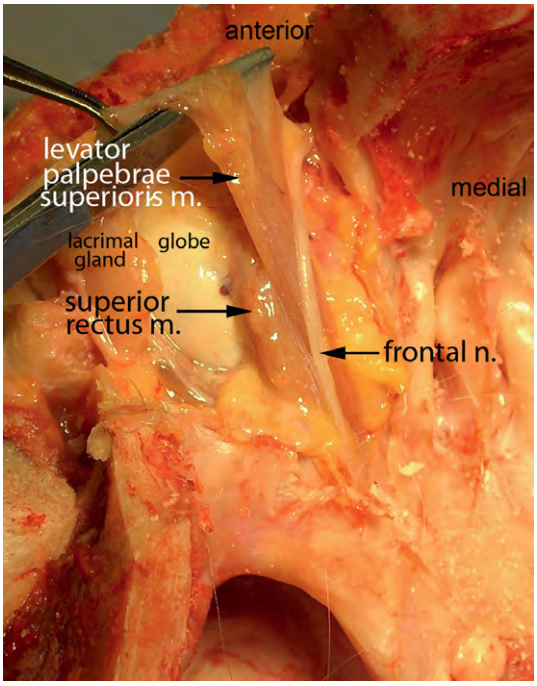

Figure 3 Dissection of the human orbit from the superior view with the orbital bony roof and the periorbita removed. The most superficial structure is the frontal nerve. Directly inferior to the frontal nerve is the levator palpebrae superioris (LPS, elevated by scissor tips). Inferior to the LPS is the superior rectus muscle.

decreases as one progresses sequentially in the following order: SR at 7.7 mm, lateral rectus at 6.9 mm, inferior rectus at 6.5 mm, and medial rectus at 5.5 mm. However, when measured *in vivo* during strabismus surgery the distances were shorter for all muscles: SR at 6.7 mm, lateral rectus at 6.2 mm, inferior rectus at 5.89 mm, and medial rectus at 4.5 mm. The insertions typically are circumferential to the limbus. However, wide variations in obliquity and regularity of the insertions are common, both from patient to patient and from muscle to muscle, even in the same eye. These differences are important in the context of planning surgery on the EOM for treatment of eye motility disorders, such as strabismus. Recent studies convincingly show that the distance from muscle insertion to the limbus has a high inter-individual variability, and there appears to be no correlation between insertional distance and the amount of deviation in strabismus patients.

The lateral rectus is innervated by the abducens nerve (CNVI) on its intraconal or deep surface (Figure 4). The SR muscle is innervated on its intraconal surface by the superior division of the oculomotor nerve (CNIII), while the inferior and medial rectus muscles and the IO muscles

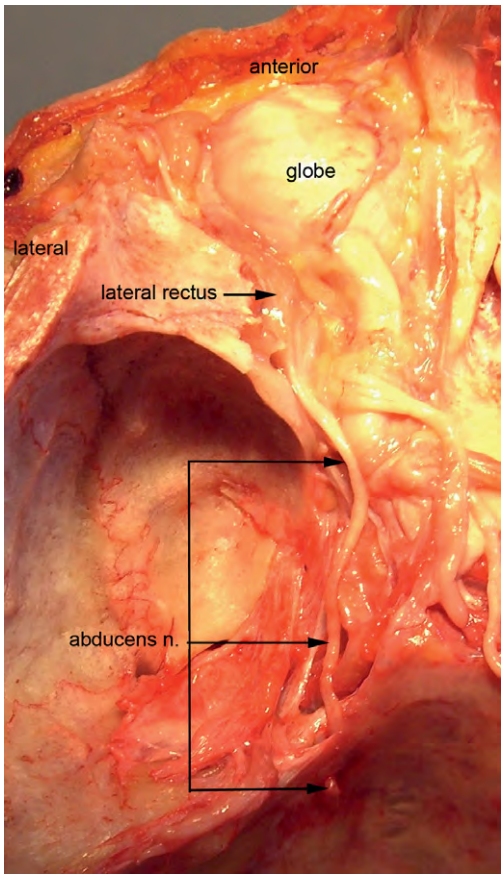

Figure 4 Dissection of the human orbit from the superior view. The bony roof, periorbita, levator palpebrae superioris, and superior rectus muscles are removed. The abducens nerve can be traced from where it pieces the dura in the posterior cranial fossa, through the superior orbital fissure, which has been opened in this dissection, to where it enters the lateral rectus muscle which it innervates.

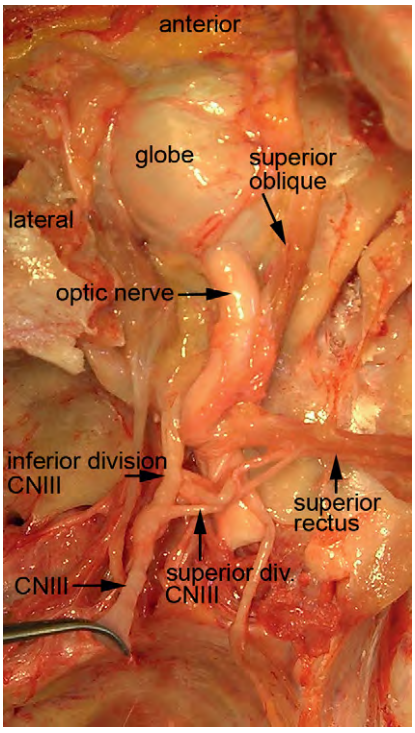

Figure 5 Deep orbital dissection from the superior view. The levator palpebrae superioris and superior rectus muscles are reflected medially to allow visualization of the superior and inferior divisions of the oculomotor nerve (CNIII).

are innervated by the inferior division of CNIII (Figure 5). All the cranial motor nerves except for the trochlear nerve (CNIV) enter the muscles intraconally, and all the motor nerves enter at approximately one-third of the muscle's length from the orbital apex (Figure 6). The six EOMs control the position of the eye in the orbit while orbital fat and fascia constrain the paths of the muscles within the orbit.

The two horizontal rectus muscles of each eye are agonist–antagonist pairs with relatively straightforward function; the medial rectus adducts the eye and the lateral rectus abducts it (Figure 7). By contrast, the SO and the IO muscles and the two vertical rectus muscles have far more complex functions. The primary direction of movement caused by the superior and inferior rectus muscles is elevation and depression, respectively. However, due to the shape of the bony orbit and their sites of origin and insertion, the vertical recti have secondary and tertiary actions that are torsional and horizontal, respectively. The SR, for example, is a secondary incyclorotator, moving the superior pole of the eye toward the nose; its tertiary function is adduction. The inferior rectus muscle, by contrast, is also a secondary excyclorotator, but similar to the SR is a tertiary adductor (Figure 8). Thus, the SR, if acting unopposed, would elevate, adduct and incyclotort the eye such that the eye would be looking up and in. The inferior rectus, if acting unopposed, would depress, adduct, and excyclotort the eye such that the eye would be looking down and in. The superior and IO muscles have a similarly complex cyclovertical functions. The primary action of these two muscles is rotation or torsion, but due to the angle which they take in the orbit toward their insertion on the sclera, they will also elevate (IO) or depress (SO) the eye; both abduct the eye. The remarkable balance and integrity of the ocular motor plant becomes evident when one considers that to look straight superiorly without moving the head, both the IO (a primary excyclorotator, secondary elevator, and tertiary abductor) and the SR (a primary elevator, secondary incyclorotator, and tertiary adductor) coordinately contract. The same is true for the inferior rectus and SO muscles moving the eye straight inferiorly.

The SO muscle is the thinnest, roundest, and longest of the EOM. The muscle runs 32 mm along the border of the medial wall and roof of the orbit, and 10–15 mm from the orbital margin it becomes tendinous and passes through

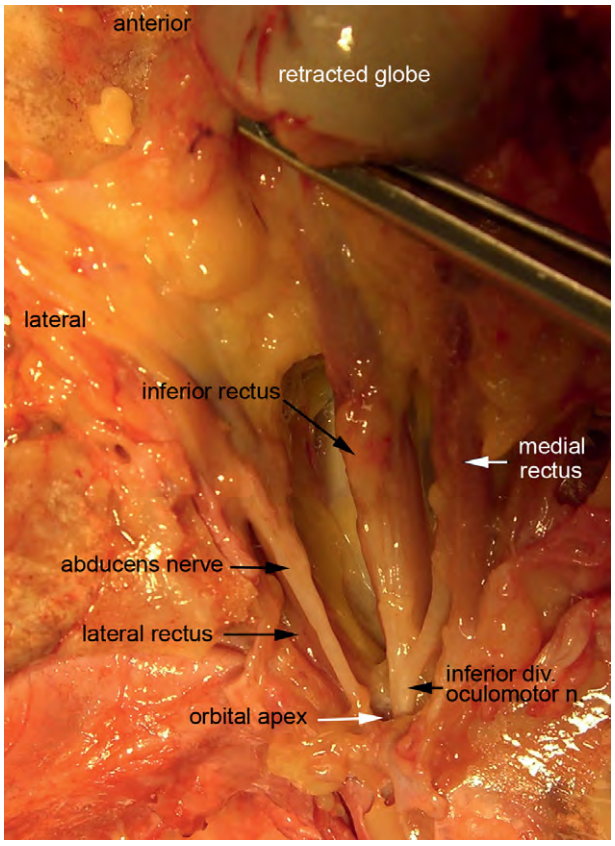

Figure 6 Deep orbital dissection from the superior view. The lateral, inferior, and medial rectus muscles are clearly visible, as are the nerves entering each muscle. The globe has been retracted anteriorly (by scissors).

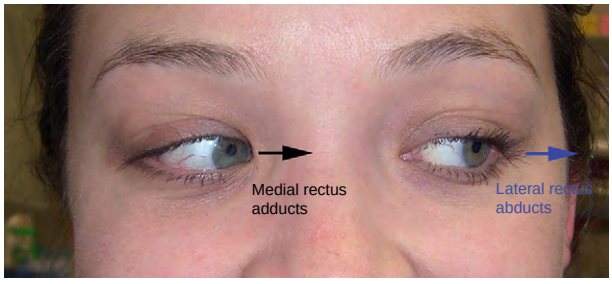

Figure 7 The lateral rectus (LR) and medial rectus (MR) muscles move the eyes in the horizontal plane. The MR adducts the eye, moving the eye toward the midline. The LR abducts the eye, moving the eye away from the midline. These muscles are antagonists; they have opposite functions.

Figure 8 The primary role of the superior rectus (SR) muscles is to elevate the eye; however, they have a secondary role in adducting the eye. The primary role of the inferior oblique (IO) muscles is to extort the eye, rotating the eye upward (elevation) and outward (abduction).

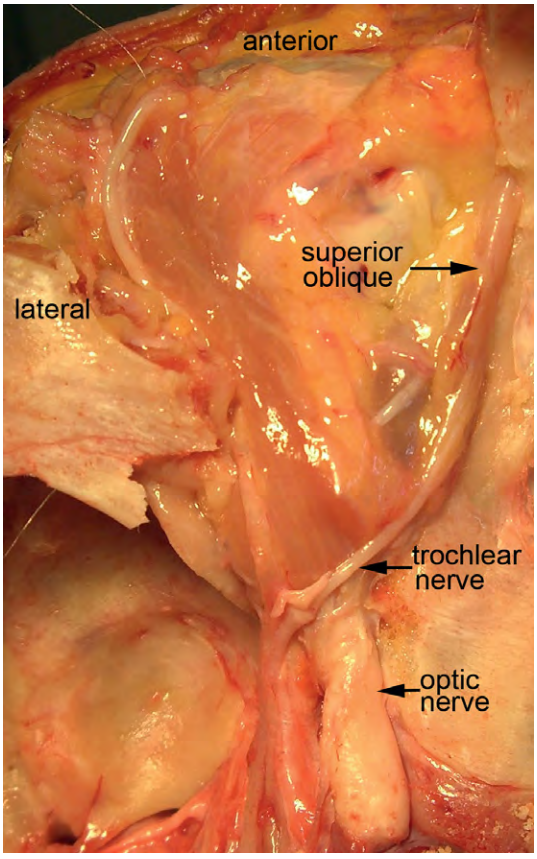

Figure 9 The superior oblique muscle can be seen along the medial wall of the orbit. The trochlear nerve (CNIV) is seen coursing along the muscle's superior surface and enters into the posterior 1/3 of the muscle on its medial side.

a fibro-fascial structure called the trochlea, located anteriomedially under the orbital roof. The trochlea changes the orientation of the muscle, becoming the functional origin of this muscle. The tendon of the SO courses deep to the SR muscle to insert into the sclera laterally on the posterior pole of the globe. The position of the SO tendon insertion, posterior and temporal to the center of rotation of the globe, explains the complex cyclovertical function of the muscle. The trochlear nerve (CNIV) innervates this muscle, coursing first on the muscle's superior side, and finally entering the muscle superiomedially at about the proximal one-third of the muscle's length (**Figure 9**).

The IO muscle is approximately 37 mm in length and travels in a similar orientation to the reflected tendon of the SO distal to the trochlea. The muscle runs inferior to

the inferior rectus muscle and inserts into the sclera of the posterior pole on the lateral side of globe. The insertion is relatively close to the macula of the retina. The IO is innervated by the inferior division of the oculomotor nerve (CNIII) on its superior surface with the nerves entering the muscle at approximately the posterior one-third.

Histological Anatomy of the EOMs

Overall Organization

The EOMs have a complex anatomical organization at the microscopic level. These muscles differ from those in the limbs and body in that the muscle fibers themselves have extremely small cross-sectional areas, with an average in human EOM of $340 \pm 200\,\mu m^2$ (**Figure 10**). In addition, there is a great deal of variability in the myofiber cross-sectional areas; this heterogeneity is quite striking. In cross-section, two distinct layers can be seen in all six EOMs, the orbital and the global layers. The orbital layer faces the bony orbit and is composed of myofibers with extremely small cross-sectional areas, with a mean of $260 \pm 160\,\mu m^2$. The global layer faces the globe, and the myofibers are markedly bigger than those in the orbital layer with a mean of $440 \pm 200\,\mu m^2$. However, they are still very small compared to body and limb skeletal muscle myofibers, which typically range from 3500 to $4000\,\mu m^2$ in the human soleus muscle, as an example.

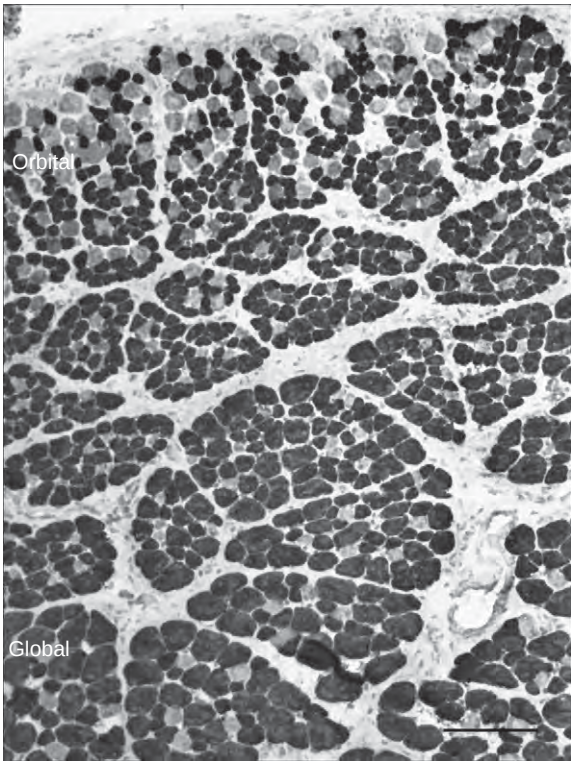

Figure 10 A cross section of the medial rectus muscle from a Rhesus monkey immunostained for the presence of the fast myosin heavy chain (MyHC) isoform, which labels all forms of the fast MyHC. The orbital layer is composed of myofibers with extremely small cross-sectional areas, while myofibers in the global layer are somewhat larger. Bar is 50 μm.

The total number of myofibers found within each of the six EOMs varies significantly. When measured in the mid-belly region of the muscles, the numbers of myofibers in the orbital layer in human EOM range from 7400 to 14 600 and in the global layer the numbers range from 8000 to 16 400 myofibers. This variation in myofiber number is seen in other species where the fiber number has been examined, although the range varies significantly from human. For example, monkey EOMs have approximately half the number of myofibers compared to human EOM. In addition, total myofiber number decreases along the length of each muscle as the insertions are approached. This variation in fiber number is due to the fact that the majority of myofibers within the EOM does not run tendon to tendon, as has been shown by a number of investigators. This can be demonstrated quite easily by serially sectioning muscles and following individual myofibers in consecutive sections (**Figure 11**). This is also supported by electrophysiological evidence demonstrating that the force produced by stimulating two separate motor unit groups individually is often more than the force produced by stimulating both motor groups simultaneously. This nonlinearity, or loss of force in summated motor units, is postulated to be caused by the lateral dissipation of force due to myofibers that do not reach the tendon ends.

Innervation

Most skeletal muscles receive their motor nerve innervation in approximately the middle, and the neuromuscular junctions form a single endplate zone. Neuromuscular junctions are a pentomer composed of four distinct subunits: α (2), β, γ, and δ. During maturation, the γ subunit is replaced with an ε subunit, forming the adult acetylcholine receptor. In contrast to limb skeletal muscle, the EOM maintains a subpopulation of neuromuscular junctions with the immature subunit configuration.

While the vast majority of EOM muscle fibers is fast-twitch fibers and receive a typical *en plaque* type of neuromuscular junction somewhere along their length, the EOM also contains two types of multiply innervated myofibers. These account for approximately 10% of the fibers in the global and orbital layers. In the global layer, these multiply innervated myofibers contain slow-tonic myosin and appear to be innervated by small *en grappe* endplates along their length. These *en grappe* neuromuscular junctions retain the γ subunit of the acetylcholine receptor, rather

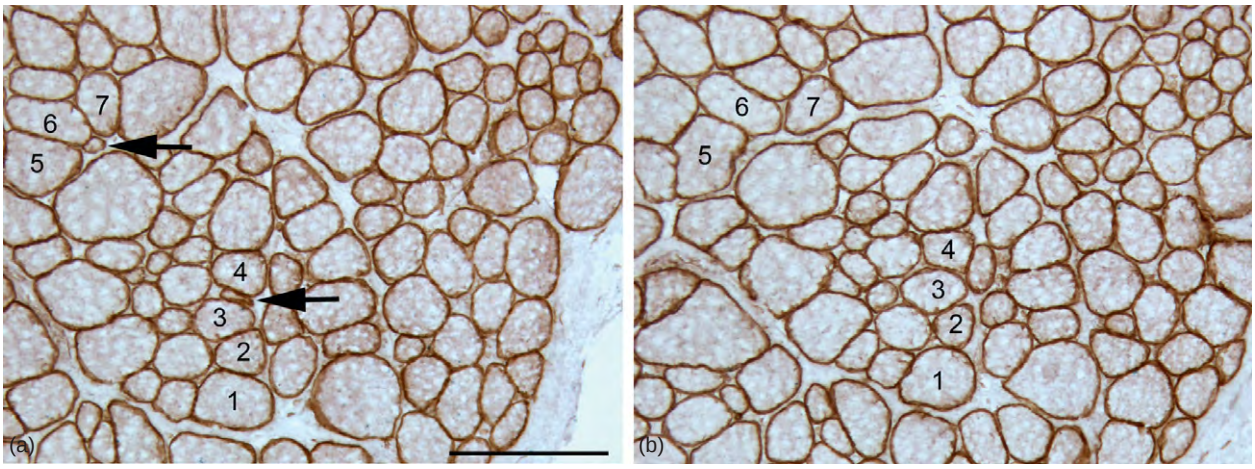

Figure 11 Two serial sections from a normal rabbit superior rectus muscle. Several sets of muscle fibers in cross section are numerically identified. (a) Note two small myofibers present in this section, one to the right of group 5, 6, and 7 (black arrow), and one between fibers 3 and 4 (black arrow). (b) Note that in a section 20 μm from the section in (a) that those two small fiber ends have ended and thus are no longer present in the cross-section. Muscle sections immunostained to visualize dystrophin on the sarcolemma. Bar is 40 μm.

than the ε subunit of the mature neuromuscular junction. There are reports in the literature that the *en plaque* endings in mammalian EOM can also express the immature γ subunit of the acetylcholine receptor. This type of multiply innervated myofiber develops a slow-graded or tonic tension when the nerves are stimulated. The orbital layer has a second type of multiply innervated myofiber. These fibers have a neuromuscular junction in the central one-third of their length with typical *en plaque* structure. In addition, however, there are multiple *en grappe* endings at the myofiber ends. Thus, the central region displays fast-twitch properties with nerve stimulation while the fiber ends display slow-tonic contractile properties.

As a result of fibers that do not run the origin-to-insertion length of the muscles and the presence of neuromuscular junctions on fiber ends, neuromuscular junctions are found throughout the length of the EOM. This has important implications for pharmacologic and surgical manipulations of the muscles in the treatment of eye motility disorders such as strabismus and nystagmus.

Skeletal Muscle Fiber Types

From a physiological perspective, the EOMs have extremely fast contractile properties, produce low levels of force, and are relatively fatigue resistant. These properties are conferred on muscle fibers by their expression of specific contractile proteins such as the myosin heavy chain isoforms (MyHC), as well as differences in cellular organelles such as mitochondria and other cellular metabolic pathways. One unusual aspect of EOM histology is the expression, within and between these two layers, of a complex pattern of MyHC expression.

Myosin Isoform Complexity in the EOM

Skeletal muscle fibers in body and limb muscles have generally been described as fast, expressing MyHC type IIa, IIb (nonhuman), and/or IIx/d, or slow, expressing MyHC type 1. However, this fiber type organization breaks down in the EOM, as was described by Mayr in 1971. On average, only 16% of the myofibers within the orbital layer are positive for the slow MyHC (MYH7), while 14% of the myofibers in the global layer are positive for slow MyHC. Thus, the vast majority of myofibers expresses the fast MyHC2a isoform (MYH2) which is responsible for the extremely fast contractile properties of the EOM. However, the EOMs express, in total, at least eight distinct MyHC isoforms: 2a, 2x/d, 1 (β-cardiac), developmental (embryonic), neonatal (perinatal), α-cardiac, slow-tonic, and EOM-specific. If serial sections of individual myofibers are examined immunohistochemically, it quickly becomes evident that single myofibers express more than one isoform (**Figure 12**). In the Kjellgren et al. study of adult human EOMs, single fibers immunostained for the slow or MyHC type 1 isoform can co-express either or both slow-tonic MyHC and α-cardiac MyHC. If just the slow myofibers are considered, they can express:

1. only MyHC type 1,
2. only slow-tonic,
3. only α-cardiac,
4. only EOM-specific,
5. MyHC type1 and slow-tonic,
6. MyHC type 1 and α-cardiac,
7. myosin type 1 and EOM-specific,
8. slow-tonic and α-cardiac,
9. slow-tonic and EOM-specific,

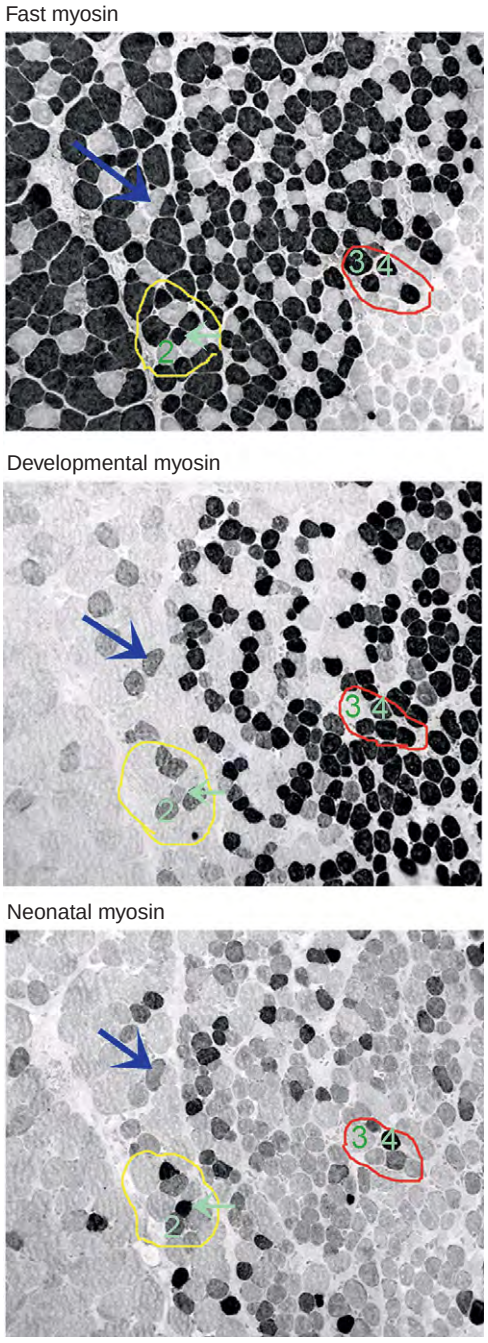

Figure 12 Three serially cut cross sections from a region of a rabbit lateral rectus muscle approaching the anterior 1/3 of the muscle. They have been immunostained for fast, developmental, and neonatal myosin heavy chain (MyHC) isoforms. One group of muscle fibers has been circled in yellow with two fibers identified by a light-green arrow and a fiber numbered 2. Note that the fiber indicated by the green arrow is positive for fast and neonatal MyHC but negative for developmental MyHC. Note that fiber 2 is negative for fast MyHC but positive for developmental and neonatal MyHC. A second group of muscle fibers has been circled in red with two fibers identified as fiber 3 and 4. Fiber 3 is positive for fast MyHC but negative for both developmental and neonatal MyHC, while fiber 4 is positive for all three of these isoforms. The fiber indicated by the large blue arrow is negative for fast MyHC, but positive for both developmental and neonatal MyHC.

10. α-cardiac and EOM-specific,
11. slow type 1, slow-tonic, and α-cardiac,
12. slow type 1, slow-tonic, and EOM-specific,
13. slow-tonic, α-cardiac, and EOM-specific, or
14. all four isoforms (**Figure 13**).

These combinations may result in 14 types of fibers. It is also known that embryonic (developmental) and neonatal-specific MyHC isoforms are also expressed by some of these fibers as well. The same complexity is seen with the myofibers positive for the fast MYHC type 2A. Single fibers can also express one of one or more of these isoforms: developmental, neonatal, EOM-specific, and 2x/d. These types of myofibers are referred to as hybrid fibers, and they can be seen, albeit to a lesser extent, in other muscles such as the diaphragm. Even when only MyHC expression characteristics are considered, the high degree of individual myofiber polymorphism seen in the collective data from many laboratories strongly supports the view that there is a continuum of myofiber types within the EOM. In some ways, trying to fit the EOM into the classical fiber typing scheme is misleading, as it does not deal effectively with the hybrid and mismatched fibers.

This complexity has significant ramifications for muscle function. MyHC isoforms control muscle-shortening velocity, and it has been proposed that this type of polymorphism allows for fine-tuned control over a wide range of forces, velocities, and fatigue properties. From a teleological perspective, these coexpression patterns would allow the EOM to contract at high velocities but with minimal fatigue, a characteristic that is important for muscles that are continually functioning in order to maintain fixation of gaze on the fovea in an infinite number of eye positions. Additionally, studies have shown that the EOMs show rapid alterations in MyHC isoform expression in response to stretch, alterations in hormones, botulinum toxin treatment, denervation, and the like.

Nonuniform Expression of MyHC Isoforms along the Muscle Length

Immunohistological examination of cross-sections taken from the tendon ends and the middle region of an EOM shows that the overall percentages of specific MyHC isoforms change dramatically depending on the location along the muscle length (**Figure 14**). For example, in a study of rat EOM, within the orbital layer the mid-belly region expresses EOM-specific MyHC but this isoform is completely excluded from the tendon ends where the embryonic (developmental) MyHC isoform is present. This is seen even at the level of single isolated myofibers, where the fiber ends express neonatal MyHC and the mid-region of the same myofiber expresses fast MyHC. This type of non-uniform expression of MyHC along the length of single fibers also is seen in the intrafusal muscle

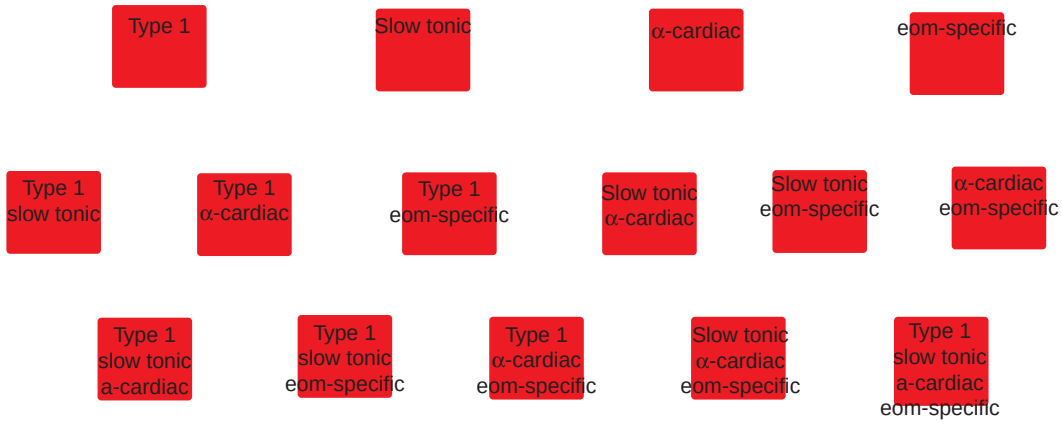

Figure 13 Diagrammatic representation of possible co-expression patterns when four myosin heavy chain isoforms are considered. Each red rectangle represents a single myofiber. Based on Kjellgren, D., Thornell, L. E., Andersen, J., and Pedrosa-Domellof, F. (2003). Myosin heavy chain isoforms in human extraocular muscles. *Investigative Ophthalmology and Visual Sciences* 44: 1419–1425.

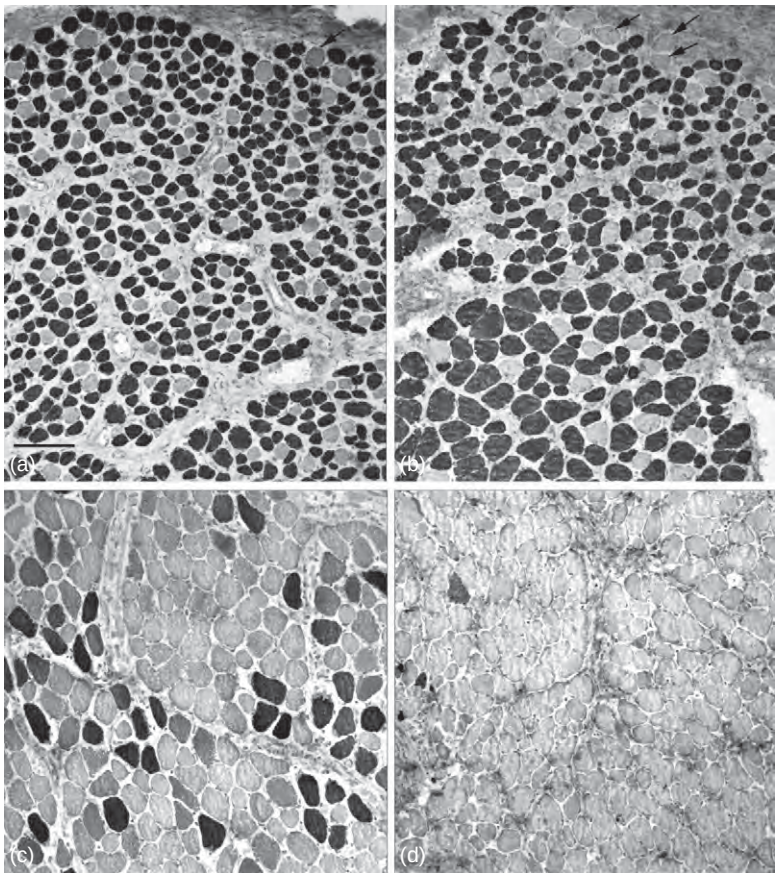

Figure 14 Cross section from a single superior rectus muscle of an adult monkey taken from the orbital (a, b) and global (c, d) regions of the mid-region of the muscle (a, c) and the tendon end (b, d) immunostained for fast myosin heavy chain isoform (MyHC) (a, b) and neonatal MyHC (c, d). The orbital region is at the top of the photomicrographs in (a) and (b). Note that the orbital layer is thicker in (a), but that the individual myofibers have a smaller cross-sectional area in the mid-region compared to the tendon end. Additionally, there are more fast-negative fibers in the tendon region of the orbital layer. In the global layer, the mid-region has 20% of its myofibers positive for the neonatal MyHC, while the tendon end is almost devoid of this isoform. Bars is 50 μm.

fibers found in muscle spindles, another specialized myofiber structure. Using single myofiber reconstructions to localize neonatal MyHC isoform expression in single fibers, myofibers are found that are neonatal MyHC-positive from fiber tip to fiber tip, but it is more common to find single myofibers with variable percentages of the total fiber length expressing this isoform, including fibers where the expression is discontinuous. It is emerging that these types of hybrid fibers are present in other craniofacial muscles, such as jaw and laryngeal muscles.

In limb and body skeletal muscles, innervation, neuromuscular activity, exercise (use/disuse), mechanical loading or unloading, hormones, and aging all cause adaptive changes in contractile properties and metabolic profiles. This supports the view that expression of contractile proteins within muscle fibers is extremely dynamic and possesses an incredible adaptability to meet the physiological demands placed upon them. EOMs are constantly active and appear to represent the far end of a continuum of skeletal muscle types relative to their ability to react and adapt to changing functional needs. As the MyHC controls shortening velocity, this MyHC polymorphism would result in a gradation of function within populations of single myofibers. In other words, a continuum of force and movement would be possible, as the contractile properties of each myofiber would reflect its particular subset of contractile proteins. An example of this is shown in Figure 15, where force was determined using a single fiber preparation and the MyHC content was analyzed for each single fiber using polyacrylamide gel separation. As can be seen, fibers that produce the same amount of force can have significantly different MyHC isoform expression patterns.

While it has not been demonstrated specifically within EOM myofibers, it is a well-known characteristic of multinucleated myofibers that each myonucleus controls the expression of proteins in what is called its myonuclear domain. An elegant study by the Hardeman laboratory showed that transcription occurs in pulses within individual myonuclei, and the activities of single nuclei are not in sync with each other. Each nucleus, and thus each myonuclear domain, is individually controlled, and protein synthesis is a dynamic process that is altered at the local level to respond to the particular stress or strain.

The advantage conferred by this complexity within populations of individual EOM myofibers can be hypothesized as an adaptation to the functional needs of eye movements in maintaining binocular vision and highly coordinated vergence movements, where a continuum of contraction forces and speeds would be required. Functionally, the complex MyHC co-expression patterns, and their presumed continuous modulation, would allow finely tuned control over these movements, as the kinetics of the EOM would cover a wide range of eye positions and velocities.

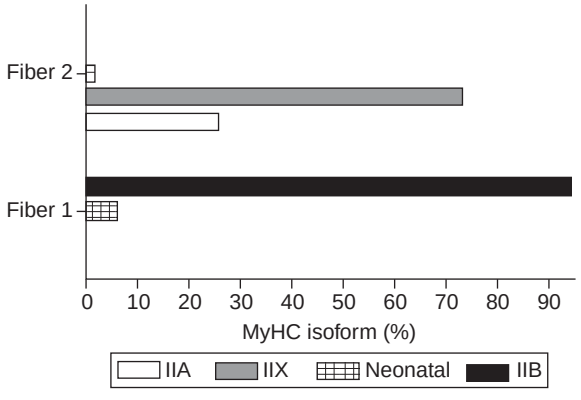

Figure 15 Relative percentages of four myosin heavy chain isoforms from two single-skinned myofibers with the same shortening velocity of 9.4 fiber lengths per second as determined using single-skinned fiber physiology in the EOM of rabbits. Note that fiber 1 has three isoforms expressed, and it contains type IIX as its main isoform, while fiber 2 has only two isoforms expressed, and IIB is the isoform with the greatest amount of expression.

Other Molecules Heterogeneously Expressed

The heterogeneity of individual myofibers is made even more complex not only by differences in other contractile proteins, such as myosin light chains and troponin, but also by other metabolic differences. Of the molecules that have been specifically examined, the EOM often has patterns of expression not seen in limb muscle. For example, myosin-binding protein C has three isoforms. Despite the fact that the vast majority of myofibers within human EOM is positive for fast MyHC, the EOM does not express the fast form of myosin-binding protein C. Recent work showed that, in contrast to limb skeletal muscles, high levels of glycolytic and oxidative pathways coexist within single myofibers in the EOM. This molecular mismatch would provide these very active muscles with both fatigue resistance and fast contractile properties.

Continuous Remodeling in Normal Adult EOM

Early studies by Moss and LeBlond demonstrated that the myonuclei within mature, multinucleated myofibers are postmitotic. However, muscle has regenerative capacity that resides in myogenic precursor cells called satellite cells, and these cells become activated, divide, and are responsible for muscle repair and/or regeneration of new fibers in disease and after injury. The EOM in normal adult mammals maintain an elevated number of satellite cells throughout life (Figure 16), which divide and integrate continuously into apparently normal muscle fibers. Concomitantly with nuclear addition, apoptosis of individual myonuclei is seen with apparent segmental cytoplasmic remodeling. The factors that control this process are

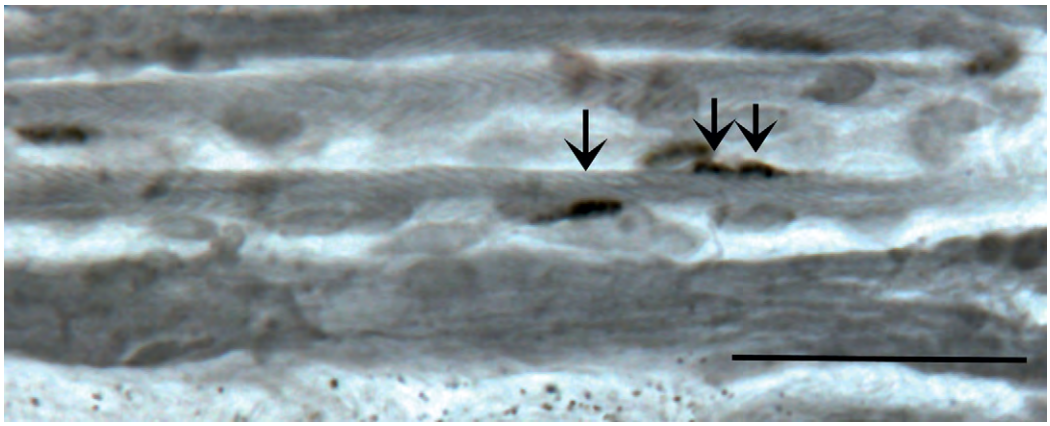

Figure 16 Several longitudinally sectioned myofibers from the inferior oblique muscle of a human cadaver donor. Note three satellite cells positive for Pax-7, a marker of all satellite cells. Two satellite cells in close proximity to each other is a common observation in the extraocular muscles.

unknown, but this process represents another dynamic physiological property of the EOM that would allow continuous adaptation of single fiber functional properties in response to physiological needs. The existence of ongoing remodeling in normal adult EOM suggests that there may be ways to modulate this process *in vivo* to alter muscle size, force, or response to injury or disease. In particular, it suggests new hypotheses to explain the preferential sparing or involvement of the EOM in skeletal muscle disease.

Acknowledgments

This work was supported by EY15313 and EY11375 from the National Eye Institute, the Minnesota Medical Foundation, the Minnesota Lions and Lionesses, Research to Prevent Blindness (RPB) Lew Wasserman Mid-Career Development Award (LKM), and an unrestricted grant to the Department of Ophthalmology from RPB.

See also: Extraocular Muscles: Extraocular Muscle Involvement in Disease; Extraocular Muscles: Extraocular Muscle Metabolism; Extraocular Muscles: Functional Assessment in the Clinic; Eyelid Anatomy and the Pathophysiology of Blinking; Orbital Bony Anatomy and Orbital Fractures.

Further Reading

Asmussen, G., Punkt, K., Bartsch, B., and Soukup, T. (2008). Specific metabolic properties of rat oculorotatory extraocular muscles can be linked to their low force requirements. *Investigative Ophthalmology and Visual Sciences* 49: 4865–4871.

Caiozzo, V. J., Baker, M. J., Huang, K., et al. (2003). Single-fiber myosin heavy chain polymorphism: How many patterns and what proportions? *American Journal of Physiology – Regulatory, Integrative and Comparative Physiology* 285: R570–R580.

Harrison, A. R., Anderson, B. C., Thompson, L. V., and McLoon, L. K. (2007). Myofiber length and three-dimensional localization of NMJs in normal and botulinum toxin-treated adult extraocular muscles. *Investigative Ophthalmology and Visual Sciences* 48: 3594–3601.

Jacoby, J., Chiarandini, D. J., and Stefani, E. (1989). Electrical properties of multiply innervated fibers in the orbital layer of rat extraocular muscles. *Journal of Neurophysiology* 61: 116–125.

Kallestad, K. M. and McLoon, L. K. (2008). Myogenic precursor cells in the extraocular muscles. In Low, W. C. and Verfaillie, C. M. (eds.) *Stem Cells and Regenerative Medicine.* Hackensack, NJ: World Scientific.

Kaminski, H. J., Kusner, L. L., and Block, C. H. (1996). Expression of acetylcholine receptor isoforms at extraocular muscle endplates. *Investigative Ophthalmology and Visual Sciences* 37: 345–351.

Kjellgren, D., Thornell, L. E., Andersen, J., and Pedrosa-Domellof, F. (2003). Myosin heavy chain isoforms in human extraocular muscles. *Investigative Ophthalmology and Visual Sciences* 44: 1419–1425.

Li, Z. B., Rossmanith, G. H., and Hoh, J. F. Y. (2000). Cross-bridge kinetics of rabbit single extraocular and limb muscle fibers. *Investigative Ophthalmology and Visual Sciences* 41: 3770–3774.

Mayr, R. (1971). Structure and distribution of fiber types in the external eye muscles of the rat. *Tissue and Cell* 3: 433–462.

McLoon, L. K., Rowe, J., Wirtschafter, J. D., and McCormick, K. M. (2004). Continuous myofiber remodeling in uninjured extraocular myofibers: Myonuclear turnover and evidence for apoptosis. *Muscle and Nerve* 29: 707–715.

Shall, M. S., Dimitrova, D. M., and Goldberg, S. J. (2003). Extraocular motor unit and whole-muscle contractile properties in the squirrel monkey. Summation of forces and fiber morphology. *Experimental Brain Research* 151: 338–345.

Stephenson, G. M. M. (2001). Hybrid skeletal muscle fibers: A rare or common phenomenon? *Clinical and Experimental Pharmacology and Physiology* 28: 692–702.

Extraocular Muscles: Extraocular Muscle Involvement in Disease

F Pedrosa-Domellöf, Umeå University, Umeå, Sweden

Glossary

Amyotrophic lateral sclerosis (ALS) – A progressive neurodegenerative disease where the motor neurons degenerate, resulting in loss of voluntary control over movement.
Arreflexia – The absence of a reflex, usually due to nerve damage.
Ataxia – A brain disease of the cerebellum and associated brain areas that affects the ability to make coordinated movements.
Duchenne muscular dystrophy – An X-chromosome-linked disease caused by a mutation in the gene for dystrophin; a protein important for structural stability of muscle fibers. It is characterized by progressive muscle degeneration, resulting in loss of mobility and death.
Juvenile spinal muscular atrophy – A slowly progressive disease characterized by proximal muscle weaknesses and wasting, beginning in childhood. It is due to the death of the motor neurons in the spinal cord.
Miller Fisher syndrome – A rare nerve disease related to Guillain–Barré syndrome, characterized by abnormal muscle coordination, paralysis of eye muscles, and loss of tendon reflexes.
Myasthenia gravis – An autoimmune disease characterized by weakness of the skeletal muscles.
Ophthalmoplegia – A condition where one or more of the extraocular muscles are weak or paralyzed, resulting in abnormal eye movements.
Poliomyelitis – A disease caused by an acute viral infection, which can cause motor neuron degeneration. This results in muscle weakness and flaccid paralysis.

Introduction

The extraocular muscles (EOMs), defined as the superior, lateral, inferior, and medial rectus and the superior and inferior oblique muscles, are the most fascinating muscles in the human body because of their complex structural and physiological characteristics adapted to meet the motility requirements of fovea-based binocular vision and, in particular, their unique responses to disease.

At one extreme of the spectrum, the EOMs are able to remain intact in devastating neuromuscular diseases affecting all other muscles in the body, such as the muscle dystrophies and motor neuron disease. At the other extreme, they are the only or the preferential muscles to be involved in myasthenia gravis (MG), mitochondrial myopathies (MMs), oculopharyngeal muscular dystrophy, thyroid-associated orbitopathy, and the Miller Fisher syndrome.

The EOMs are considered to be a separate muscle allotype, that is, a separate class of muscles with intrinsically different properties that differ significantly from those of the other two allotypes, that is, limb and masticatory muscles. A large body of data collected so far strongly defines the EOMs as a unique class of muscles at the structural, cellular, molecular, and gene level, suggesting that the special behavior of these muscles in disease most likely reflects their unique identity in all respects and that further studies are needed to understand the mechanisms determining their response in disease. On the other hand, deeper knowledge of the mechanisms involved in the selective sparing of the EOMs may provide the groundwork for further advances toward breakthrough therapies for devastating neuromuscular diseases with lethal outcomes.

The EOMs Are Selectively Spared in Muscular Dystrophies

Muscle fiber integrity is dependent on a functionally intact connection between the extracellular matrix molecules on the cell surface, a number of transmembrane proteins, and the complex cytoskeleton inside the cell. Of particular importance are laminin 211 (merosin), the sarcoglycans, and caveolin-3, which are all members of the so-called dystrophin-associated protein complex and dystrophin itself; a gene defect in any of these components gives rise to a muscular dystrophy.

Duchenne muscular dystrophy (DMD) is the most well-studied form of human dystrophy, and a large number of mutations and deletions in the dystrophin gene have been reported. The dystrophin molecule is a part of the cytoskeleton located under the sarcolemma. The muscles of patients with DMD undergo a successive process of fiber degeneration and regeneration and, with time, show increased amounts of connective tissue and fatty replacement. Clinically, there is progressive muscle weakness and wasting starting in childhood, loss of ambulation at

an early age, and precocious death due to respiratory complications and respiratory failure.

The EOMs are clinically and microscopically spared in patients with DMD and in several relevant animal models of dystrophies, including the mdx mouse (Figure 1) and cmdx dog, the γ- or δ-sarcoglycan-deficient mouse, and the merosin-deficient mouse. The reasons for the selective sparing of the EOMs in these dystrophies are not fully understood, with the exception of merosin-deficient congenital muscle dystrophy. It is noteworthy that in animal models, the true EOMs are unaffected, whereas the retractor bulbi and the levator palpebrae muscles are not spared.

The EOM fibers of the mdx mouse express utrophin extrasynaptically, suggesting that this cytoskeletal protein may compensate for the lack of dystrophin. However, approximately half of the fibers are still spared in the EOMs of mice lacking both dystrophin and utrophin, indicating that other mechanisms are also of importance for the selective sparing of these muscles in DMD. Very small fiber size and small loads to work against, as well as an enhanced capacity to regulate calcium homeostasis, may protect the EOMs against mechanical stress and allow for the maintenance of fiber integrity even in the case of absent dystrophin or a defective dystrophin-associated protein complex.

The human and mouse adult EOM fibers co-express α-4, α-5, and β-2 laminin chains on the surface of the extrasynaptic sarcolemma in addition to the α-2 and β-1 laminin chains found on all adult skeletal muscle fibers. This indicates the possible coexistence of laminins 411, 421, 511, and 521 in the EOMs in addition to laminin 211 and 221. The α-4 chain of laminin is normally expressed in all skeletal muscle fibers during development and is later downregulated in the limb muscle. The presence of these additional laminin isoforms in the basal lamina of normal adult human EOM fibers is most likely the mechanism behind the selective sparing of the EOMs in merosin-deficient congenital muscle dystrophy. This hypothesis has been confirmed in the dy^{3k}/dy^{3k} mice, which completely lack the α-2 laminin chain and develop the corresponding muscle dystrophy, but their EOMs are spared.

Using markers of satellite cell activation validated in other skeletal muscles and experiments using bromodeoxyuridine (brdU) labeling, data from human, monkey, rabbit, and mouse indicate that the EOMs normally have a significant population of activated satellite cells resulting in a continuous myonuclear addition to individual muscle fibers in the absence of injury or disease. Thereby, the EOMs appear to normally have an ongoing remodeling process that is likely to be advantageous in disease situations such as the muscular dystrophies. Microarray data revealed increased expression of genes related to growth, development, and regeneration in the EOMs in comparison to the limb muscles, supporting the concept of increased regenerative capacity as an important factor for the selective sparing of the EOMs in disease.

The EOMs Are Spared in Motor Neuron Disease

Motor neuron disease such as amyotrophic lateral sclerosis (ALS), juvenile spinal muscular atrophy, and poliomyelitis generally do not involve the EOMs, or at least do not affect the EOMs to the same degree as the limb, trunk, and other cranial muscles. Abnormal ocular motility in ALS patients may be (1) due to supranuclear or extrapyramidal dysfunction and (2) underestimated due to the more dramatic consequences of the other denervation symptoms, such as loss of ambulation or swallowing difficulties.

Recent data indicate that the EOMs in the terminal stage of ALS are not completely spared, although they are remarkably well preserved compared to the limb muscles (Figure 2). We have found signs of ongoing denervation,

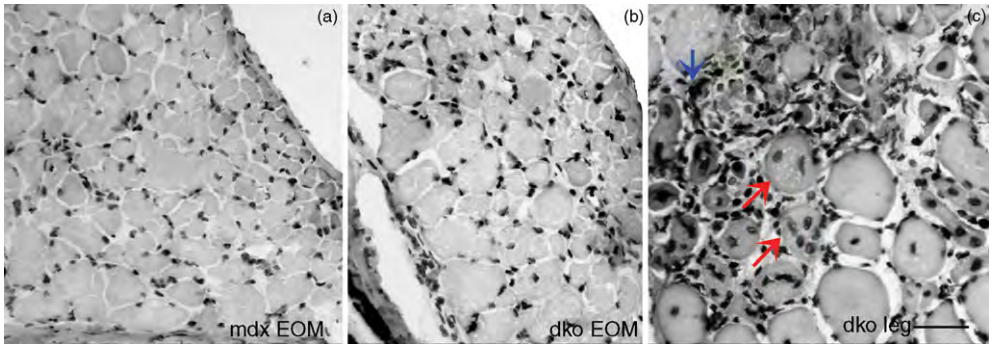

Figure 1 Extraocular muscles (EOMs) of two mouse models of Duchenne muscle dystrophy (mdx mouse in (a) and double knockout for dystrophin and utrophin (dko) in (b) show normal morphology, in strong contrast to the dystrophic leg muscle shown in (c)). Red arrows show muscle cells with centrally placed nuclei, indicating ongoing regeneration and the blue arrow shows the presence of infiltrating nonmuscle cells. Section stained to visualize all nuclei. Bar is 20 μm. Courtesy of Dr. Linda McLoon, University of Minnesota.

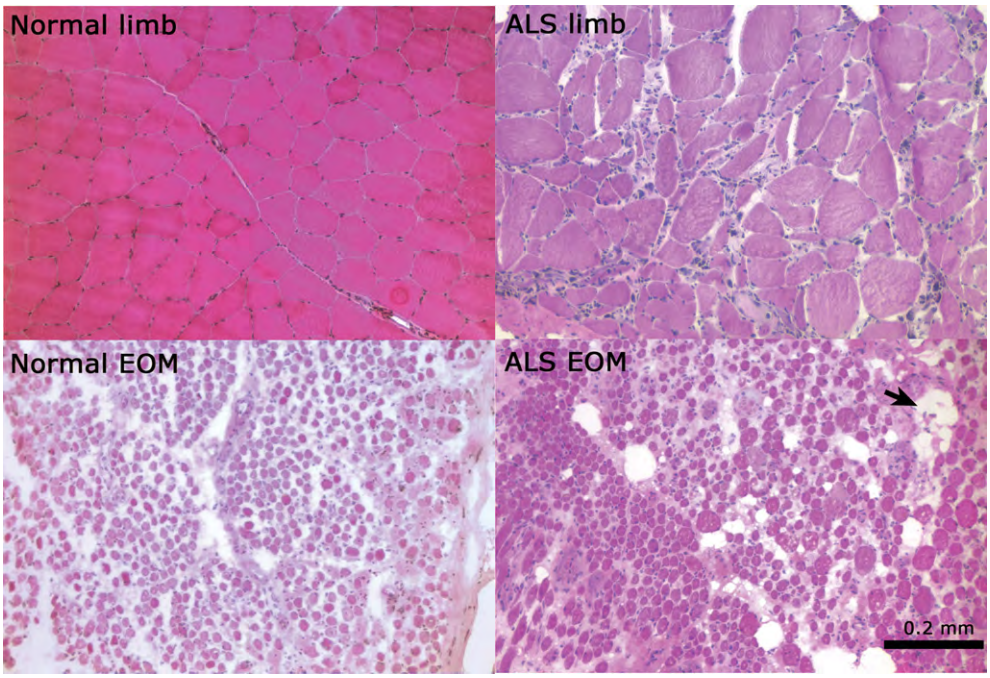

Figure 2 Limb and extraocular muscle (EOM) samples from normal subjects and from patients with amyotrophic lateral sclerosis (ALS). In the terminal phase of ALS, the EOMs are not truly spared and show wide variation in fiber size and some areas of fatty replacement (the arrow and white areas in the lower right panel).

regeneration, and overuse of some fibers in the EOMs collected at autopsy from both familial and sporadic forms of ALS.

Differences in calcium-binding protein composition between the spinal motor neurons and those supplying the EOMs have been reported and may be an important factor determining the different susceptibility of the EOMs in ALS.

The EOMs Are Selectively Affected in the Miller Fisher Syndrome

The Miller Fisher syndrome is a milder form of the Guillain–Barré syndrome, characterized by the clinical triad of ophthalmoplegia, ataxia, and arreflexia as well as the presence of autoantibodies against GQ1b gangliosides. Autoantibodies against other structurally similar gangliosides may also be present, and a mechanism of molecular mimicry has been proposed, whereby these autoantibodies are postulated to arise following a variety of intestinal and respiratory infections, such as by *Campylobacter jejuni*. A complement-mediated inflammatory reaction at the neuromuscular junction, where the gangliosides reside outside of the blood–nerve barrier, is responsible for the muscular paralysis.

Recent data clearly show differences in ganglioside composition between the EOM and limb muscle synapses (Figure 3), providing a molecular basis for the paralysis of the EOMs in this syndrome. The fact that the EOMs have the highest capillary density reported for any human muscle may be a very important factor facilitating the access of the circulating ganglioside autoantibodies to the neuromuscular junctions of the eye muscles.

The EOMs Are Frequently Involved in Myasthenia Gravis

MG is a chronic autoimmune disorder affecting the neuromuscular junctions of skeletal muscles and causing muscle fatigue and weakness. The EOMs and the levator palpebrae muscle are almost invariably involved, and they are often the first muscles to be affected. The EOMs and the levator palpebrae muscle can, in fact, be the only muscles to be affected, and the disease is then referred to as ocular myasthenia. Untreated and over time, the majority of patients with ocular myasthenia will progress toward the generalized form.

Typical symptoms of MG and ocular myasthenia are diplopia (double vision) and ptosis (drooping of the upper eyelid) that vary in intensity over time and improve after rest or cooling down (see below, ice-pack test).

Autoantibodies against acetylcholine receptors are highly specific for MG, but may be absent in patients with ocular myasthenia. False positive detection of autoantibodies against acetylcholine receptors occurs, however, in a number of autoimmune disorders, such as

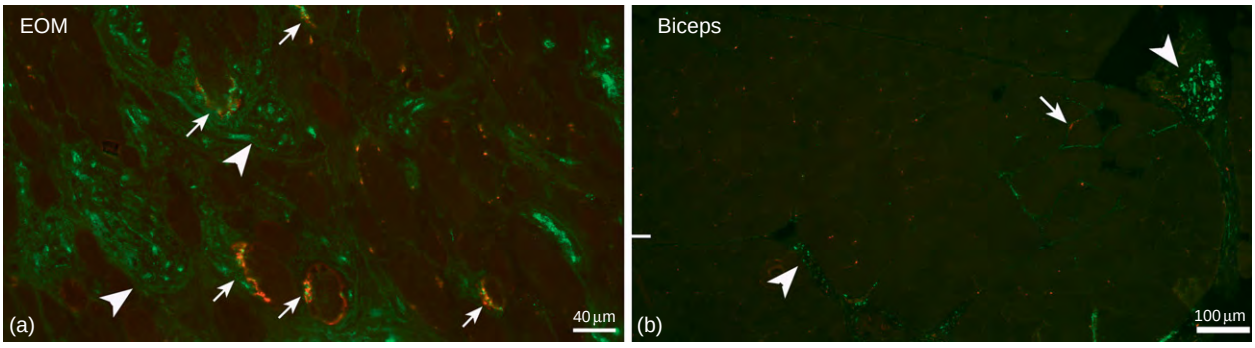

Figure 3 Human extraocular (EOM) (a) and biceps brachii muscle sections (b) immunostained with an antibody against GQ1b/GT1a ganglioside (green). Neuromuscular junctions were labeled by rhodamine-conjugated α-bungarotoxin (red; yellow where there is co-localization with the ganglioside staining). Massive staining with anti-GQ1b/GT1a ganglioside is shown at neuromuscular junctions (arrows) around the EOM fibers and in the nerves (arrow heads) (a), whereas there is very scarce staining in limb muscles (b).

systemic lupus erythematosus, rheumatoid arthritis, liver disease, and thyroid-associated ophthalmopathy, as well as in ALS.

Tests aimed at increasing the concentration of acetylcholine at the synaptic cleft typically reveal improvement of muscle function in myasthenic patients, with less ptosis or better function in a paretic (weak, with partial paralysis) EOM, and therefore are very useful diagnostic tools. These tests are done either by intravenous administration of edrophonium chloride (a rapid-acting reversible inhibitor of acetylcholinesterase) under careful monitoring, by cooling of the ptotic eyelid with an ice pack for 2–5 min, or by letting the patient close the eyelids for 5 min. The amount of ptosis, measured in millimeters as the distance between the upper and the lower eyelid margins, is carefully measured before and after the test, for comparison.

Electrophysiologically, MG is characterized by a reduction in the so-called safety factor, that is, the normal difference between the actual endplate potential and the action potential threshold needed to depolarize the muscle cell. In other words, in MG, there is a loss of the normal overcapacity of the endplate potential and, with stress, the endplate potential is not enough to generate an action potential. In the EOMs, the safety factor is normally low or absent, and the firing frequencies required for the saccades can be up to 4 times those recorded in limb muscles. Moreover, force generation in the multiinnervated, slow-tonic fibers is solely dependent on the endplate potentials, as no action potential generation occurs. These special properties of the EOMs partly explain their early involvement in MG, as reductions in endplate potentials due to the loss of acetylcholine receptors will have immediate consequences.

Morphologically, MG is characterized by a loss of synaptic folds and acetylcholine receptors due to autoantibody-triggered and complement-mediated lesions of the neuromuscular junctions. The molecular basis for the preferential involvement of the EOMs in MG is not fully understood, but it is apparently not necessarily related to the presence of autoantibodies against the acetylcholine receptor. The γ subunit of the acetylcholine receptor is found in multiply innervated fibers of the EOMs, but not in other adult muscles, especially not in the levator palpebrae, a muscle which is as likely to be involved in MG or ocular myasthenia as are the true EOMs. Furthermore, although antibodies against the acetylcholine receptor γ subunit have been detected in MG patients, there seems to be a lack of correlation between the presence of these antibodies and the involvement of the EOMs and levator palpebrae. Because ocular myasthenia tends to be accompanied by lower levels or the lack of autoantibodies against the acetylcholine receptor, it has been proposed that the low expression in the EOMs of decay accelerating factor, important to moderate the complement cascade involved in the destruction of the neuromuscular junction, may be an important factor making these muscles more susceptible.

Although our understanding of MG and ocular myasthenia has steadily increased over the past years, more research is needed to understand these two forms of the disease at the molecular level and thereafter be able to devise better therapeutic strategies.

The EOMs Are Frequently Involved in Mitochondrial Myopathies

Mitochondrial disorders are a large and heterogeneous group of diseases caused by impaired oxidative phosphorylation and, consequently, compromised mitochondrial energy output. Due to the contribution of both the nuclear and the mitochondrial genomes to the synthesis of the respiratory chain elements and the possible coexistence of normal and mutated mitochondrial DNA in the same cell, the genetic basis of these diseases is rather complex. A number of mitochondrial disorders have a myopathy component, and these, in turn, typically show EOM involvement.

Chronic progressive external ophthalmoplegia (CPEO) is the most common mitochondrial disorder affecting muscles. It is a slowly progressing MM that primarily affects the EOMs. It usually has a late, albeit varying, age of onset and insidious progression of ptosis followed by EOM weakness, leading to severe restriction of ocular motility. In some cases, downward gaze may be preserved until late stages of the disease. Weakness of the orbicularis oculi muscle may also be a feature of CPEO, and ptosis and ocular motility restriction can show different courses of development. The ophthalmoplegia is often rather symmetric and compensated for by head movements, so that the patients do not necessarily experience diplopia or functional impairment due to limited ocular motility. There is indication that the symmetry of the ophthalmoplegia may reflect supranuclear involvement, rather than being solely due to EOM dysfunction. Proximal muscle weakness, muscle wasting, and exercise intolerance are also typical features of CPEO.

CPEO can result from both single and multiple deletions and from point mutations of mitochondrial DNA; approximately 15% of cases are autosomal dominant, and in rare cases autosomal recessive inheritance has been reported. Mutations in the ADP/ATP translocator ANT-1 (adenosine diphosphate/adenosine triphosphate translocator ANT-1), a nuclear-encoded mitochondrial protein, have been detected in patients with an autosomal form of CPEO. Pathological changes have been reported in the EOMs of mice lacking this protein, even though there was no evidence of ocular motor or functional abnormalities in these animals.

Additionally, there are more severe forms of MM that involve the eye muscles. Patients with the Kearns–Sayre syndrome have CPEO combined with short stature, pigmentary retinal degeneration, cardiomyopathy, cardiac conduction block at an early age, ataxia, and neuropathy. External ophthalmoplegia occurs in approximately 13% of patients with a syndrome comprising MM and encephalopathy, lactate acidosis, and stroke-like episodes, so-called MELAS. These patients also have short stature and muscle weakness, and their clinical course is dominated by the stroke-like episodes and seizures. The EOMs are also involved in a very rare mitochondrial syndrome characterized by sensory ataxic neuropathy, dysarthria (difficult speech articulation), and ophthalmoplegia, described with the acronym SANDO, and is considered to be a variant of autosomal dominant CPEO. External ophthalmoplegia may also be part of other mitochondrial disorders, such as myoclonus, epilepsy, myopathy with ragged-red fibers (MERRF), mitochondrial neurogastrointestinal encephalomyopathy (MNGIE), and a condition characterized by neuropathy, ataxia, and retinopathia pigmentosa (NARP).

A skeletal muscle biopsy, showing ragged-red fibers and abnormal mitochondrial morphology and/or enzymatic activity, and genetic analysis for mitochondrial DNA mutations are helpful in the diagnosis of MM. An extremely high mitochondrial content and high oxidative enzyme activity are hallmarks of the EOMs and, in part, the reason why these muscles are so susceptible to MMs. However, our understanding of the cellular and molecular basis for the involvement of the EOMs in some mitochondrial disorders, but not in others, where defective oxidation–phosphorylation coupling is a common denominator, is very rudimentary. The development of animal models of CPEO, such as the recently reported mouse lacking ANT-1, a nuclear-encoded mitochondrial protein implicated in an autosomal form of CPEO, may help to advance this quest.

The EOMs Are Involved in Oculopharyngeal Dystrophy

Oculopharyngeal muscular dystrophy is a late-onset dystrophy, typically starting in the fifth or sixth decade of life, and is manifested clinically by the presence of ptosis and subsequently includes swallowing difficulties. With time, both the EOMs and other muscles, including the tongue and the masticatory muscles, are also affected. Diplopia may eventually occur, and there is impairment of ocular motility, although not a total external ophthalmoplegia. Typically, it is an autosomal dominant disease, but recessive inheritance and sporadic cases have also been reported. The genetic defect consists of short $(GCG)_{8–13}$ expansions in the nuclear poly(A)-binding protein 1 (PABPN1) gene (chromosome 14q11.1), causing polyalanine tract expansions. The molecular mechanisms behind muscle dystrophy due to these expansions are not yet fully understood.

Miscellaneous

There are numerous case reports of EOM involvement or sparing in a wide array of systemic disorders. While the EOMs are very rarely the site of primary tumors (e.g., rhabdomyosarcomas, granular cell tumors, and liposarcomas), non-Hodgkin T-cell lymphomas have been reported in these muscles. The EOMs may also be the site of solitary metastasis from primary tumors of the breast, lung, and skin.

Involvement of the EOMs, with detectable contrast enhancement in computed and in magnetic resonance tomography, has been reported in a case of Behcet's syndrome with orbital inflammation. Behcet's syndrome is a multisystem vasculitis, clinically characterized by uveitis, with recurrent oral and genital ulcers. At least one case of primary systemic amyloidosis with initial involvement of an EOM has been reported. Polymyositis may have extensive EOM involvement, although the EOMs are often spared in dermatomyositis.

EOM involvement has been documented to occur during or after systemic infectious diseases. For example, acute onset, noncomitant strabismus with documented thickening of the EOMs has been reported following streptococcal infection of the upper airways. Cysticercosis, infection with the tapeworm *Taenia solium*, may involve the EOMs, in addition to the skeletal muscles, and the globe itself. The cysts may be painful, cause diplopia, and even require surgical removal.

In summary, the EOMs show complex patterns of disease involvement and disease sparing. While some evidence for the causes of these differential propensities for or sparing from pathology exists, most are not well understood. This is an area of active research, as understanding the mechanism for the differential disease susceptibility of the EOMs may help elucidate potential approaches for the treatment of these largely devastating skeletal muscle diseases.

See also: Congenital Cranial Dysinnervation Disorders; Extraocular Muscles: Extraocular Muscle Anatomy; Extraocular Muscles: Extraocular Muscle Metabolism; Extraocular Muscles: Functional Assessment in the Clinic; Thyroid Eye Disease.

Further Reading

Andrade, F. H., Porter, J. D., and Kaminsky, H. J. (2000). Eye muscle sparing by the muscular dystrophies: Lessons to be learned? *Microscopy Research and Technique* 48: 92–203.

Kusner, L. L., Puwanant, A., and Kaminsky, H. J. (2006). Ocular myasthenia: Diagnosis, treatment and pathogenesis. *Neurologist* 12: 231–239.

Liu, J. X., Willison, H. J., and Pedrosa-Domellof, F. (2009). Immunolocalisation of GQ1b and related gangliosides in human extraocular neuromuscular junctions and muscle spindles. *Investigative Ophthalmology and Visual Science* 50: 3226–3232.

Muntoni, F. and Voit, T. (2004). The congenital muscular dystrophies in 2004: A century of exciting progress. *Neuromuscular Disorders* 14: 635–649.

O'Hanlon, G. M., Bullens, R. W. M., Plomp, J. J., and Willison, H. J. (2002). Complex gangliosides as autoantibody targets at the neuromuscular junction in Miller Fisher syndrome: A current perspective. *Neurochemical Research* 27: 697–709.

Schoser, B. G. H. and Pongratz, D. (2006). Extraocular mitochondrial myopathies and their differential diagnosis. *Strabismus* 14: 107–113.

Spencer, R. F. and Porter, J. D. (2006). Biological organization of the extraocular muscles. *Progress in Brain Research* 151: 43–80.

Zeviani, M. and Di Donato, S. (2004). Mitochondrial disorders. *Brain* 127: 2153–2172.

Extraocular Muscles: Extraocular Muscle Metabolism

F H Andrade, University of Kentucky Medical Center, Lexington, KY, USA

Glossary

Adenine nucleotide translocator – An inner mitochondrial protein that exchanges adenosine diphosphate (ADP) and adenosine triphosphate (ATP) between the mitochondrial matrix and the cytoplasm. It is also known as the ADP/ATP translocator.

Chronic progressive external ophthalmoplegia – A syndrome characterized by progressive inability or difficulty to move the eyes and elevate the eyelids. It is a common manifestation of some mitochondrial diseases.

Electron transport chain – The set of mitochondrial protein complexes that couples the oxidation of electron donors (such as NADH) to the reduction of electron acceptors (such as oxygen) in order to produce ATP.

Gene expression profiling – The measurement of the activity (or expression) of large numbers of genes simultaneously.

Glycolysis – The metabolic pathway that converts glucose to pyruvate, with a net result of 2 ATP and 2 NADH.

M line – A dark band or line seen in the center of the sarcomeres, using electron microscopy.

NADH – Nicotinamide adenine dinucleotide (NAD^+) and its reduced form NADH are coenzymes involved in oxidation/reduction reactions as electron acceptors and donors.

Oxidative phosphorylation – The metabolic pathway that uses the energy released during the oxidation of nutrients to produce ATP.

The extraocular muscles exhibit the greatest diversity among mammalian skeletal muscles, a likely consequence of the varied functional requirements imposed by the ocular motor system. Extraocular muscle fibers differ from typical limb and respiratory skeletal muscles in mitochondrial content, innervation/contractile patterns, contractile protein isoforms, hormone receptors, cell surface markers, and a variety of other cell and molecular properties that may relate to their unique functions. The divergence from the skeletal muscle stereotype is further exemplified by the fact that extraocular muscles do not conform to traditional fiber type classifications, which are based primarily on myosin isoform expression. The most accepted fiber-type classification scheme for extraocular muscles includes six fiber types based upon: (1) distribution into orbital and global layers, (2) innervation status, single versus multiple nerve contacts per fiber, and (3) mitochondrial/oxidative enzyme content. **Figure 1** shows representative micrographs of extensor digitorum longus (EDL, which is a predominantly type IIB fiber – fast, fatigable – limb skeletal muscle), diaphragm (mixed fiber type, fatigue-resistant respiratory muscle), and the extraocular muscle from rats. EDL is recruited sporadically and diaphragm is constantly active as is the extraocular muscle. Despite the wide difference in activity, EDL and diaphragm sections are mostly indistinguishable. For sure, there are important biochemical differences between the two muscles that reflect their specific adaptations to their respective activation patterns. However, the divergent requirements of EDL and diaphragm motor systems are met with fairly stereotypical muscle fibers, as evident from the micrographs. In contrast, the extraocular muscle fibers are very different: small round fibers with prominent mitochondria, suggestive of atypical contractile and metabolic properties. This article outlines newly identified unique aspects of extraocular muscle metabolism and how they may correspond to contractile function.

Insights from Gene Expression Profiling

The fast and constant contractions of the extraocular muscles necessitate well-developed energy supply systems. It might be expected *a priori* that these muscles would upregulate all the main energy-supply metabolic pathways, from glycolysis to mitochondrial metabolism. Surprisingly, this may only apply to mitochondrial content, which is the highest reported in mammalian skeletal muscles. Studies comparing the gene expression profile of extraocular and limb muscles found that genes coding for key enzymes of glycogen synthesis and breakdown were repressed in the extraocular muscles. Glycogen content in the extraocular muscles is correspondingly reduced. These findings indicate that the extraocular muscles are seemingly less dependent on stored glycogen as a metabolic fuel than other skeletal muscles. They also suggest that the extraocular muscles rely, instead, on constant transport of blood-borne glucose and fatty acids through their extensive microvascular network. Interestingly, the expression of the lactate dehydrogenase (LDH) isoform that preferentially oxidizes lactate to pyruvate is increased

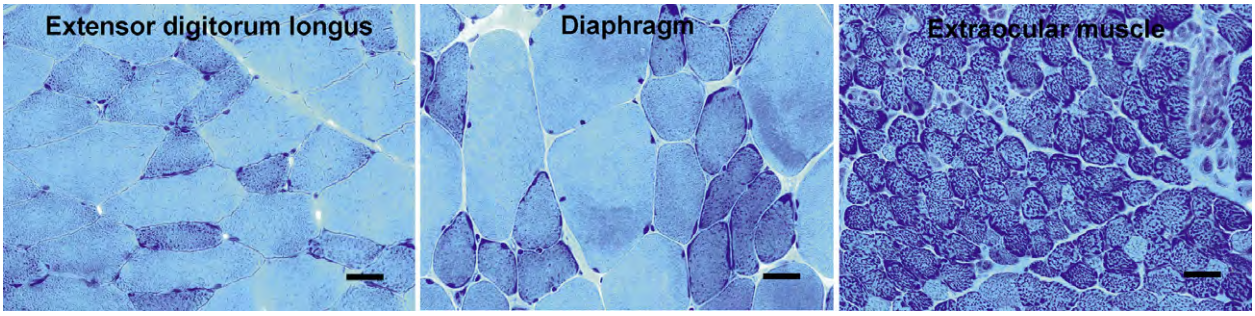

Figure 1 The extraocular muscles are not typical skeletal muscles. The figure shows representative micrographs of limb (left, extensor digitorum longus), respiratory (middle, diaphragm), and extraocular (right) muscle sections stained with Gomori's trichrome. This technique stains mitochondria (and sarcoplasmic reticulum) a darker reddish-blue. Despite the differences in functional profiles (occasionally active limb muscle vs. constantly active diaphragm), notice the similarity in fiber size and shape: large polygonal muscle fibers with peripheral myonuclei (left and middle panels). Some fibers have darker cytosolic staining indicating higher mitochondrial content. In contrast, the extraocular muscle shows significantly smaller fibers with clumpy cytosolic and subsarcolemmal staining due to abundant mitochondria (right panel). Scale bars = 25 μm.

in the extraocular muscles, compared to typical skeletal muscles, and that may allow them to use lactate as a fuel for aerobic pathways. The importance of these alternative metabolic pathways is now being tested in extraocular muscles.

Lactate: An Oxidizable Substrate for the Extraocular Muscle

In limb skeletal muscles, glycogen breakdown drives glycolysis only during brief bursts of intense activity (Figure 2). In most muscles, metabolic demand during moderate activity is met by aerobic (mitochondrial) pathways. During periods of sustained peak activity, when mitochondrial capacity is exceeded in skeletal muscle, lactate is the end product of glycolysis in a reaction that reduces pyruvate at the expense of NADH and is catalyzed by LDH. For this and other reasons, increased production and accumulation of lactic acid during exercise has been associated with muscle fatigue. However, cells can also use the LDH reaction in the reverse direction from lactate oxidation to pyruvate, and lactate then goes on to become a substrate for aerobic metabolism. As mentioned above, the expression of the LDH isoform that preferentially oxidizes lactate to pyruvate is higher in the extraocular muscles. Combined with their high aerobic capacity, this reaction would allow the extraocular muscles to use lactate as a metabolic substrate. Cinnamate, a blocker of lactate transport, alone or in combination with exogenous lactate can be used to evaluate the role of lactate on fatigue resistance. Cinnamate accelerates fatigue in the extraocular muscles significantly: treated muscles lose their ability to generate force at a faster rate than untreated extraocular muscles. Conversely, cinnamate treatment does not affect the endurance or residual force of limb muscles. Replacing glucose with exogenous lactate increases limb-muscle fatigability but has no effect on the extraocular muscles. However, the extraocular muscles fatigue faster when exposed to exogenous lactate combined with cinnamate treatment. These results indicate that LDH oxidation of lactate to pyruvate seems to be an important source of metabolic substrate for aerobic metabolism in the extraocular muscles. This conclusion is a significant deviation from the traditional view of lactate as a final waste product of glycolysis; increased lactate production and accumulation during vigorous contractile activity is typically associated with fatigue. Muscle fatigue is a complex phenomenon: substrate depletion, metabolite accumulation, and ionic imbalances are some of the factors that combine to reversibly impair contractile function. In the particular case of the extraocular muscles, lactate can be used via the LDH reaction as an additional substrate source for aerobic metabolism, a concept developed recently for other aerobic muscles and one that also applies to the nervous system.

Creatine Kinase, the Missing ATP Buffer in the Extraocular Muscle

Skeletal muscles and other tissues with fluctuating metabolic needs rely on the creatine–phosphocreatine system to buffer intracellular ATP concentration: creatine kinase (CK) catalyzes the reversible transfer of the phosphoryl group from phosphocreatine to ADP in order to maintain constant ATP levels. Cellular CK activity is due to a family of oligomeric enzymes: two cytosolic, ubiquitous brain-type CK-B and muscle-type CK-M, and two mitochondrial isoforms, ubiquitous mitochondrial CK (uCK) and sarcomeric mitochondrial CK (sCK). In differentiated skeletal muscle, CK-MM and sCK are the predominant isoforms. In fast-twitch muscles, most CK activity is due to the CK-MM isoform, some of which is found

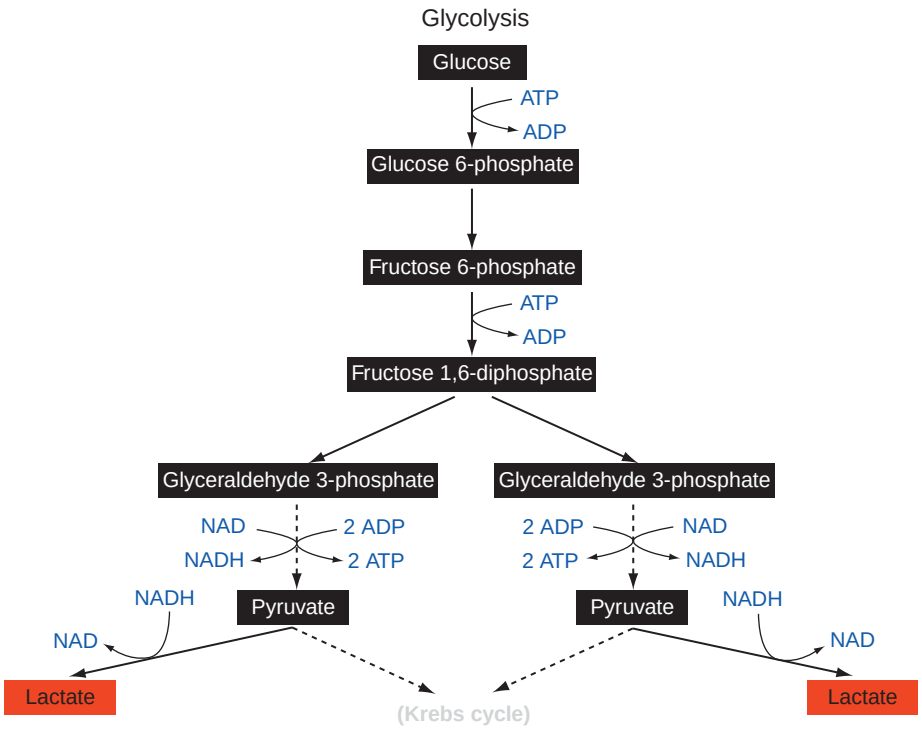

Figure 2 Glycolysis, the anaerobic breakdown of glucose. The figure presents a diagram showing the sequence of steps in glycolysis, from glucose to pyruvate. The end product, pyruvate, may move on to the Krebs cycle (inside the mitochondria) to continue substrate oxidation, or it may be reduced to lactate in the reaction catalyzed by LDH that restores NAD. Dashed arrows represent omitted steps.

associated with the sarcomeric M line, the sarcoplasmic reticulum, and T-tubules. This arrangement couples the CK-dependent ATP-buffering system to the cellular sites with the highest ATPase activity, and is needed for normal contractile function. Given the predicted need for ATP buffering in the extraocular muscles, we proposed that (1) CK isoform expression and activity in rat extraocular muscles would be higher and (2) the resistance of these muscles to fatigue would depend on CK activity. Instead, we found that messenger ribonucleic acid (mRNA) and protein levels for all (cytosolic and mitochondrial) CK isoforms are lower in the extraocular muscles than in limb muscles. The muscle-enriched isoforms, CK-M and sCK, are less abundant in extraocular muscle, despite the fact that the extraocular muscles have a higher mitochondrial content than limb muscles. Total CK activity is also correspondingly decreased in the extraocular muscles. Moreover, cytoskeletal components of the sarcomeric M line, where a significant fraction of cytosolic CK activity is found, are downregulated in the extraocular muscles as was initially suggested by gene expression profiling. To explore the role of CK activity on muscle function, the CK inhibitor 2,4-dinitro-1-fluorobenzene (DNFB) was used during an *in vitro* fatigue protocol. Treatment with DFNB accelerates the development of fatigue in limb muscle, but has no detectable effect on the extraocular muscles. These data support the conclusion that CK activity is not an important ATP buffer in the extraocular muscles. The myokinase reaction ($2\ ADP \rightarrow ATP + AMP$), catalyzed by adenylate kinase (AK), serves as an additional ATP-buffering system in skeletal muscle. While total AK activity is similar in extraocular and limb muscles, the mRNA content for two putative mitochondrial AK isoforms (AK3 and AK4) is over 13-fold more abundant in the extraocular muscles. This suggests that the relative lack of CK in the extraocular muscles may be compensated by upregulation of selected AK isoforms.

Mitochondrial Content in the Extraocular Muscles

Aerobic capacity is typically measured by mitochondrial volume density (percentage of muscle fiber volume occupied by mitochondria). In general, mitochondrial volume density is well matched to the metabolic needs of skeletal muscle and it scales almost linearly with maximal oxygen uptake among muscles and across mammalian species. In other words, the consensus is that changes in the oxidative (aerobic) capacity of mammalian skeletal muscles are met by corresponding increases or decreases in mitochondrial volume density. Since the mitochondrial content and the

activity of respiratory complexes and enzymes of mitochondrial metabolic pathways change in parallel, enzymatic activities are used as indices of mitochondrial content and aerobic capacity. Highly aerobic muscle groups in mammals have abundant capillaries and elevated mitochondrial volume density. The extraocular muscles have, arguably, the highest mitochondrial content of all mammalian skeletal muscles. However, the mechanism responsible for maintaining mitochondrial abundance in the extraocular muscles remains unclear. We have identified a number of transcription factors that influence mitochondrial biogenesis and that are upregulated in the extraocular muscles. Surprisingly, these factors are different from the mitochondrial biogenesis program initiated in response to endurance training.

Mitochondria as Calcium Sinks in the Extraocular Muscle

The fast-contracting extraocular muscles rely on tight regulation of free cytosolic calcium concentration ($[Ca^{2+}]_i$). In principle, the extraocular muscles have the profile of very efficient calcium handling capacity: extensive and well-developed sarcoplasmic reticulum and the expression of fast calcium ATPase isoforms. Moreover, the extraocular muscles contain parvalbumin, a low-weight calcium-binding protein that serves as a temporary buffer to accelerate the removal of calcium off its binding sites on the myofilaments and facilitates muscle relaxation. Other investigators have already shown that the kinetics of calcium flux into mitochondria are fast enough to influence very rapid events such as neurotransmitter release from motor nerve terminals. The specific inhibition of mitochondrial calcium transport slows the relaxation of mitochondria-rich skeletal muscles. We recently reported that the magnitude and speed of calcium uptake by mitochondria are sufficient to influence contractile function. This property of the extraocular muscles appears to serve at least two complementary functions. First, it couples metabolic supply to demand because higher mitochondrial calcium stimulates enzymes that control substrate oxidation: pyruvate dehydrogenase, 2-oxoglutarate dehydrogenase, isocitrate dehydrogenase, and glycerol 3-phosphate dehydrogenase. The combined activity of these enzymes sustains a high $NADH/NAD^+$ level and maximizes oxidative phosphorylation and ATP production. Second, by limiting the $[Ca^{2+}]_i$ increase during contractions in response to submaximal stimulation frequencies, mitochondria widen the dynamic range of the extraocular muscles. In other words, the capacity of the extraocular muscles to produce force is spread over a wider stimulation frequency range, increasing the fine control of the effector arm of the ocular motor system.

Are Extraocular Muscle Mitochondria Different?

The adenine nucleotide transporter 1 (*Ant1*) gene encodes an inner mitochondrial membrane protein that transports ADP into mitochondria and ATP from mitochondria to the cytosol. Mutations within *Ant1* have been shown to produce a syndrome of chronic progressive external ophthalmoplegia (CPEO) in humans. *Ant1* knockout ($Ant1^{-/-}$) mice develop cardiomyopathy and severe exercise intolerance. Despite this dramatic phenotype, the extraocular muscles are mostly unaffected. Histologically, the extraocular muscles from $Ant1^{-/-}$ mice present a relatively mild mitochondrial myopathy. There are no measurable ocular motor abnormalities in $Ant1^{-/-}$ mice, and their peak eye velocities overlap with those measured in control mice. Moreover, their extraocular muscles do not show evidence of increased fatigability. In addition, the extraocular muscles have higher levels of *Ant2* mRNA compared to the limb muscles. *Ant2* is a nonskeletal muscle isoform previously described in the heart. Its presence in the extraocular muscles may explain the lack of effects of *Ant1* loss, and it was the first documented difference between extraocular muscle and limb muscle mitochondria.

The ability of muscles to perform aerobic work depends on their mitochondrial volume density, with the assumption that the composition of these organelles is fairly constant across muscle types and mammalian species. One of these components is the electron transport chain, a series of multimeric complexes (complexes I–IV, plus the ATP synthase which is sometimes called complex V) in the inner mitochondrial membrane responsible for most of the aerobic ATP generation (**Figure 3**). Recently, we found that the extraocular muscle mitochondria have lower content or lower activity of some enzyme complexes of the electron transport system, causing them to respire at slower rates. This is puzzling given that the extraocular muscles are constantly active and aerobic capacity was predicted to be elevated, given their high mitochondrial content. These findings are not explained by differences in the ultrastructure of extraocular muscle mitochondria: the surface area of their inner membrane is comparable to values reported for other skeletal muscle. Furthermore, the differences are not generalized or systematic: complex II content and activity, and complex III content are similar in mitochondria from triceps surae (a limb skeletal muscle) and extraocular muscle. Complexes I and IV give a more puzzling result: their activities are lower, but their content is higher in the extraocular muscle mitochondria. These are multimeric protein complexes, and differential expression of isoforms of some subunits has been described in skeletal muscle and other tissues.

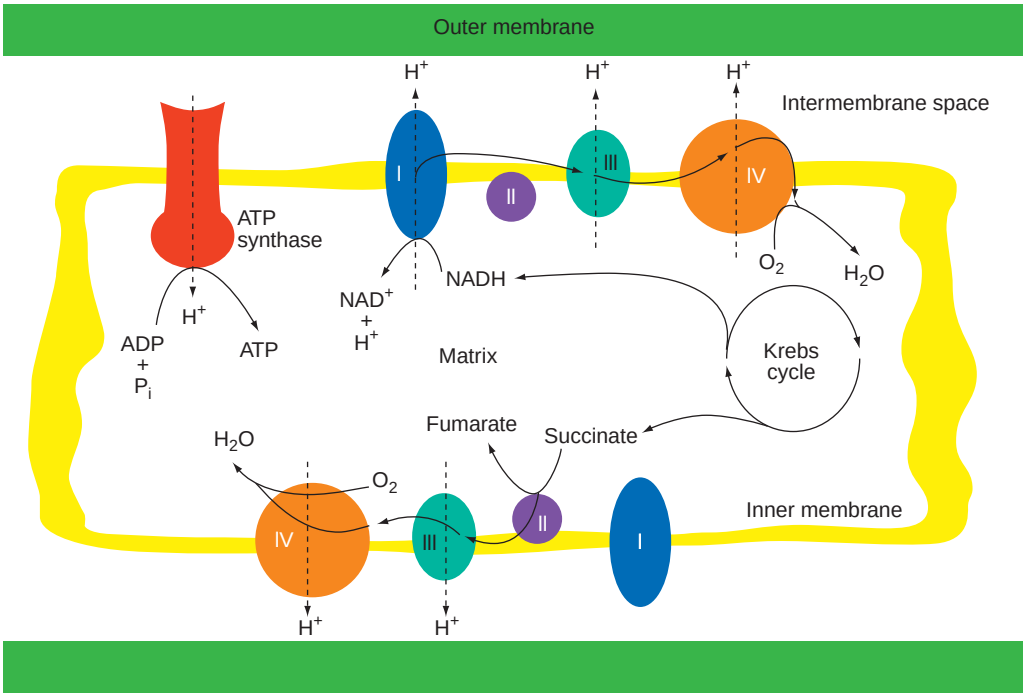

Figure 3 Mitochondrial electron transport chain and ATP synthase. The figure presents a drawing showing the oxidative phosphorylation steps that couple the final substrate oxidation to the reduction of oxygen to water, pumping hydrogen ions (protons, H^+) from the mitochondrial matrix to the intermembrane space. The substrates for this chain are NADH or succinate, shown here as originating from the Krebs cycle. Complex I (NADH dehydrogenase) oxidizes NADH and transfers the electrons to complex III, which in turn transfers the electrons to complex IV (cytochrome c oxidase). The latter is the complex that reduces oxygen to water. Complex II (succinate dehydrogenase) is not an H^+ pump; it funnels electrons from succinate to complex III, and then complex IV. The ATP synthase (complex V) is driven by the trans-inner membrane electrochemical potential generated by the movement of H^+ to the intermembrane space.

Therefore, the content of some electron transport chain complexes (I, IV, and V) and the subunit composition of some others (I and IV) may not be the same in the extraocular muscles compared to limb muscles. This demonstrates that the metabolic divergence between extraocular and limb muscles includes major differences in the composition and basic function of their respective mitochondrial populations. Intrinsic differences in mitochondrial structure and function may explain the susceptibility of the extraocular muscles to some hereditary and acquired mitochondrial myopathies such as CPEO and related syndromes. For example, the extraocular muscles present the most severe age-dependent loss of mitochondrial respiratory complex activity among muscles. There is a significant increase in the number of fibers with cytochrome c oxidase defects in the extraocular muscles of humans and other primates, even when compared to other highly aerobic muscles such as the diaphragm and heart. This can be at least partially explained by mitochondrial DNA mutations, presumably due to reactive oxygen species generated during mitochondrial respiration or present as part of a more generalized cellular oxidative stress.

Matching Mitochondrial Capacity to Contractile Function

The primary role of mitochondria is to generate ATP. Recent studies lead to an obvious question: How do extraocular muscles sustain their contractile function with mitochondria that respire half as fast as mitochondria from other muscles? The content of respiratory complexes is one parameter behind tissue variations in mitochondrial respiration, although some argue that it is not particularly relevant for metabolic control. Under experimental conditions, mitochondrial respiration in the skeletal muscle and heart is regulated at the level of the respiratory chain, while in the liver, kidney, and brain it is controlled mainly at the phosphorylation level by ATP synthase (complex V) and phosphate carrier. That may not be the case *in vivo*, where different parameters such as cellular steady state, the energy demand, and the energy supply of the tissue may also regulate mitochondrial respiration. In the case of the extraocular muscles, allosteric regulation of respiratory complexes may combine with changing metabolite concentrations to maintain mitochondrial respiration closer to its theoretical maximum.

For example, a mechanism to enhance energy production in the extraocular muscle is mitochondrial calcium influx during contractile activity in order to activate enzyme systems that exert strong control on substrate oxidation, as mentioned above.

Matching Energy Supply to Demand

Initially inspired by morphological characteristics and gene-expression-profiling results, a more global perspective of extraocular muscle metabolism is beginning to emerge. First, glycogen content is low and the glycogenolysis pathway seems to be downregulated in the extraocular muscles. Second, CK activity and content, including the mitochondrial isoform, are lower in the extraocular muscles, indicating that phosphocreatine may be a less important temporal and spatial ATP buffer in these muscles. In other words, mitochondrial ATP production may be sufficiently high and close to cellular sinks as to obviate the need for an energy buffer. Third, the extraocular muscles can use lactate as an oxidizable substrate due to the presence of a LDH isoform that catalyzes the conversion of lactate to pyruvate that then goes to the Krebs cycle. Finally, the mitochondrial population in extraocular muscles appears to respond to a different biogenesis program, and exhibits atypical functional characteristics that may influence the contractile activity of these muscles significantly.

Acknowledgements

The author's work in this field is supported by the National Eye Institute (grant R01 EY012998).

See also: Extraocular Muscles: Extraocular Muscle Anatomy.

Further Reading

Andrade, F. H. and McMullen, C. A. (2006). Lactate is a metabolic substrate that sustains extraocular muscle function. *Pflügers Archiv-European Journal of Physiology* 452: 102–108.

Andrade, F. H., McMullen, C. A., and Rumbaut, R. E. (2005). Mitochondria are fast Ca^{2+} sinks in rat extraocular muscle: A novel regulatory influence on contractile function and metabolism. *Investigative Ophthalmology and Visual Science* 46: 4541–4547.

McMullen, C. A., Hayeß, K., and Andrade, F. H. (2005). Fatigue resistance of rat extraocular muscles does not depend on creatine kinase activity. *BMC Physiology* 5: 12.

Porter, J. D., Khanna, S., Kaminski, H. J., et al. (2001). Extraocular muscle is defined by a fundamentally distinct gene expression profile. *Proceedings of the National Academy of Sciences of the Unites States of America* 98: 12062–12067.

Spencer, R. F. and Porter, J. D. (2006). Biological organization of the extraocular muscles. *Progress in Brain Research* 151: 43–80.

Yin, H., Stahl, J. S., Andrade, F. H., et al. (2005). Eliminating the Ant1 isoform produces a mouse with CPEO pathology but normal ocular motility. *Investigative Ophthalmology and Visual Science* 46: 4555–4562.

Extraocular Muscles: Functional Assessment in the Clinic

S P Christiansen, Boston University School of Medicine, Boston, MA, USA
L K McLoon, University of Minnesota, Minneapolis, MN, USA

Glossary

Binocular vision – The simultaneous perception by both eyes of two slightly disparate images of the same target on corresponding retinal elements resulting in a single three-dimensional image.
Cover test – The use of an ocular occluder over one eye or alternately occluding the eyes, either alone or in conjunction with prisms, to detect the presence of an ocular deviation and to measure its magnitude.
Diplopia – Double vision caused by a misalignment of the eyes resulting from the same image stimulating noncorresponding retinal elements in the two eyes.
Esotropia – A form of strabismus where there is a nasal-ward deviation of the nonfixing eye.
Exotropia – A form of strabismus where there is a temporal deviation of the nonfixing eye.
Phoria – This is a latent misalignment of the eyes kept under control by fusional mechanisms and is contrasted with a tropia which is a manifest constant or intermittent deviation of the eyes. A phoria can be seen only when fixation is interrupted, as during a cover test.
Recession surgery – In recession surgery, the overacting extraocular muscle is surgically removed from the sclera and resutured in a more posterior location on the globe. The goal is to decrease the rotational effect of muscle contraction.
Resection surgery – In resection surgery, the underacting extraocular muscle is surgically removed from the sclera, a portion of the insertional end is removed, and the remaining, now shorter, muscle is resutured to its original insertional site on the globe. The goal is to increase the rotational effect of muscle contraction.
Strabismus – A latent or manifest misalignment of the eyes.
Tropia – A manifest misalignment of the visual axes of both eyes.

Normal Eye Movements

There are six extraocular muscles responsible for eye movement within each orbit. These muscles are innervated by cranial nerves III (superior rectus, medial rectus, inferior rectus, and inferior oblique), IV (superior oblique), and VI (lateral rectus). The medial rectus muscles are primarily responsible for adduction, pulling the eyes toward the nose. The lateral rectus muscles are responsible for abduction, pulling the eyes temporally. These horizontal movements are the most straightforward of the six extraocular muscles. The remaining four are cyclovertical muscles and have more complex function related to the fact that forward-oriented eyes are housed in laterally directed orbits. This means that the midline of these muscles does not consistently lie over the center of rotation of the globe in any position of gaze.

If examined from the superior view, the bony medial orbital walls are parallel to each other and are in the sagittal plane. The lateral walls, however, are at a 45° angle from the plane of the medial walls. Since all but the inferior oblique muscles take their origin from the orbital apex, contraction of the superior and inferior rectus and superior oblique muscles will have a rotational or torsional component. The same is true for the inferior oblique, which originates from the anterior and inferior nasal orbital wall and courses posteriorly and laterally to insert onto the globe inferior to the belly of the inferior rectus muscle. The direction of contraction of the inferior oblique muscle thus also results in both a torsional and vertical movement of the eye. The function of the individual extraocular muscles has been more extensively covered elsewhere in this encyclopedia. To summarize, however, the superior rectus muscle and the inferior oblique muscles are the principal elevators of the eye while the inferior rectus muscle and superior oblique muscle are the principal depressors of the eye. The incyclotorters of the eye are the superior oblique and the superior rectus while the excyclotorters are the inferior oblique and the inferior rectus muscles. Each of the cyclovertical muscles also has minor horizontal function. It is important to recognize that the vertical or torsional component of each of the cyclovertical muscles changes depending on whether the eye is held in adduction or abduction.

There are two basic kinds of eye movements: saccade and pursuit. Saccades are rapid and subserve fast changes in fixation. They are generated by a pulse-step pattern of innervation from the brainstem. An estimate of saccadic velocity can be gained by clinical observation alone, often with the use of an optokinetic nystagmus (OKN) drum or flag that the examiner uses to drive repeated changes in fixation, first in one direction and then in another.

RSR	LIO	RSR	LSR	RIO	LSR
RLR	LMR			RMR	LLR
RIR	LSO	RIR	LIR	RSO	LIR

(b)

Figure 1 (a) Composite photographs showing a subject displaying the nine cardinal positions of gaze and (b) Chart showing the principal yoked muscles from the right (pink) and left (green) eyes responsible for movement of the eyes into the nine cardinal positions of gaze.

A decrease in saccadic velocity can be seen in patients with extraocular muscle palsy. Pursuit movements are slower, and are driven by smooth following movements in response to a target moved slowly before the patient. There should be no lag or saccadic interlude during pursuit movements.

Gaze refers to movement of both eyes together. Gaze is conjugate if both eyes move the same amount, at the same speed, and in the same direction. Thus, in right gaze, both eyes look to the right and reach the intended target at the same time. Gaze is disconjugate if both eyes move in opposite directions or there is substantial failure of one eye to reach the target. Therefore, convergence and divergence movements are disconjugate. Ductions are movements of one eye examined under monocular viewing conditions. For example, we refer to adduction as a nasalward movement of an eye when the other eye is covered, eliminating any binocular adjustment in eye position. In contrast, versions are movements of both eyes examined under binocular viewing conditions. Dextroversion is movement of both eyes to the right; levoversion is movement of the eyes to the left. Version testing is helpful for assessing over- or under-action of a muscle compared to its yoked muscle in the other eye.

As conjugate gaze position shifts, yoked muscles contract in response to gaze-evoked increases in innervational frequency (**Figures 1(a) and 1(b)**). However, innervation to the antagonist muscles is inhibited. Therefore, for gaze right, the right lateral and the left medial muscles contract, but the right medial and left lateral rectus muscles are innervationally inactive. Because the eyes must move in an accurate, balanced, and coordinated fashion when gaze position is changed, complex central nervous system control mechanisms are required. Input from the frontal and parietal cortex and from the cerebellum is routed through a neural integrator in the brainstem whose function and control is still being investigated. Feedback from the afferent visual system and from proprioceptive input from the extraocular muscles modulates innervational tone to all the extraocular muscles and is important for long-term calibration of eye movements.

Ocular Motility Assessment in the Clinic

When an individual is looking straight ahead, in what is called primary gaze, a light falling on the eyes from a distance will be perceived by an examiner as a corneal reflex or reflection in approximately the same position in the pupil of each eye (**Figure 1(a)**, central photograph). If the eyes are not aligned, there will be a nasal, temporal, or vertical offset of the corneal reflex in one eye compared to the other eye. The amount of offset of the reflex can be estimated subjectively by the examiner or measured with prisms. Care must be taken in the patient who has a very small degree of misalignment as these tests are not sensitive enough to detect it.

To confirm normal alignment of the eyes, a cover test is performed. If there is no refixation movement of either eye

when the other eye is covered, the alignment of the eyes is considered orthotropic. This does not imply, however, that the eyes are normally aligned since latent misalignment of the eyes may be controlled by fusional mechanisms that can be remarkably robust. To determine if an individual's eyes are normally aligned, an alternate cover test is performed. Here, the eyes are alternately occluded. If no refixation movement of the eye under cover occurs when the cover is moved to the other eye, then the individual is considered to have normal eye alignment and is deemed orthophoric. The alternate cover test can be used in all the cardinal positions of gaze to determine if changes in gaze position result in any misalignment. If refixation movement is detected with alternate cover testing, then prisms may be used with the cover test to measure the magnitude of the misalignment. A convergent misalignment of the eyes is called esotropia; divergent misalignment is called exotropia; and vertical misalignment is called hypertropia.

In addition to alignment testing, an examiner performs certain sensory tests to determine the quality of binocular function. These tests detect the presence of normal or abnormal retinal correspondence, the presence of suppression or diplopia, even if not subjectively present, the quality of stereoacuity if present, and the presence of torsion. The nature of this text does not allow an in-depth review of such testing, but it is useful to document, as binocular function is an important aspect of normal visual experience, and is critical to the assessment of outcomes after treatment for strabismus.

Children with strabismus typically do not experience diplopia unless the onset of misalignment has been rapid as might be seen in an acute CN VI palsy due to increased intracranial pressure or due to a brain tumor. More often, children with strabismus suppress the nonfixing eye, an adaptive mechanism that obviates diplopia, but places the child at risk for the development of amblyopia, a nonorganic loss of vision that may be permanent if not treated during the child's period of visual plasticity. Therefore, during the examination of children being evaluated for strabismus, careful assessment of visual acuity is essential.

During a motility examination, all patients should be carefully observed for the presence of nystagmus (rhythmic to and-fro movements of the eyes), muscle weakness (paresis), muscle restriction, or binocular-gaze deficits along with abnormal head posturing, head nodding, or other adaptive mechanisms that may arise as a result of an abnormal ocular motor condition.

Clinical Treatment for Primary Eye Motility Disorders

Once strabismus has been diagnosed, then a decision must be made regarding how to treat it. In children, glasses are an important consideration. Children with esotropia who are hyperopic (far-sighted) will often have an accommodative component to their strabismus. Control of accommodation by correcting the hyperopia may eliminate or reduce the angle of esotropia. Glasses are occasionally used in children with exotropia as well. Certainly, if a child has a significant refractive error, glasses will be required to optimize acuity.

A child with strabismus and amblyopia will likely be given treatment for the amblyopia which may include occlusion therapy or optical penalization with atropine drops. Treatment of amblyopia is usually recommended before more definitive treatment of the strabismus is undertaken. Other nonsurgical treatments for strabismus include prisms, if the angle of misalignment is small or, in less common scenarios, exercises such as convergence training.

When a decision has been made to proceed with surgery, there are several available options. Typical incisional surgery addresses the misalignment mechanically. If a muscle is overacting, then it is weakened. This is usually done by recession surgery in which the muscle insertion on the sclera is transected and then attached with sutures more posteriorly on the globe. This decreases the mechanical advantage of the muscle by reducing the arc of contact of the muscle on the globe. By contrast, if a muscle is underacting relative to its antagonist, then the muscle insertion is resected. In this surgery, a portion of the insertion is removed and the shortened muscle is reattached to the original muscle insertion on the sclera. This surgery works by shortening the tether length of the muscle and increasing its mechanical advantage relative to its antagonist. The amount of recession or resection is titrated to the angle of the strabismus with larger amounts of surgery for larger angles of misalignment. There are numerous variations on this theme, and the literature is full of unique means of weakening or strengthening muscles. In certain situations, such as when a muscle is significantly paralyzed, healthy muscle insertions may be transposed to approximate the insertion of the paralyzed muscle to assist its function. Sometimes, this is done in conjunction with botulinum toxin injection into the antagonist muscle to weaken it and to improve the rotation of the globe in the direction of the paralyzed muscle.

Botulinum toxin A has heralded the beginning of a new era in strabismus surgery. First introduced into clinical use in the early 1980s by Dr. Alan Scott at Smith-Kettlewell in San Francisco, botulinum toxin weakens muscle by chemical denervation of the muscle. Release of the neurotransmitter, acetylcholine, into the synaptic cleft of neuromuscular junctions (NMJs) of treated skeletal muscle (including extraocular muscle) is blocked. This temporary paralysis of the synapses of the NMJs results in a spread of NMJ sites across the surface of the muscle. Treatment effect is maximal for approximately 6 weeks and then begins to diminish as the terminal nerves regrow and form new NMJs. Ultimately, there is a return of

function at the sites of the original NMJs and retraction of the sprouted nerves. Treatment effect is essentially void by 3 months postinjection.

Botulinum injection has been used by some clinicians for the treatment of infantile and childhood forms of strabismus, especially esotropia, but its use has not been widely adopted because of the frequent need for reinjections, especially for larger angles of misalignment. However, pharmacologic treatment of strabismus is attractive because of decreased operative times required for injection compared with typical incisional surgery, decreased scarring, and preserved biomechanical relationships of the muscle, and orbital soft tissues. In the recent literature, there have been a number of reports of the use of new candidate drugs for both weakening and strengthening extraocular muscle in experimental animals. Although much research is still needed, the era of drug treatment for strabismus is dawning, and heralds the possibility of both reducing the short-term risks of strabismus surgery and improving the long-term outcomes of our interventions.

Acknowledgments

This work was supported by EY15313 and EY11375 from the National Eye Institute, the Minnesota Medical Foundation, the Minnesota Lions and Lionesses, Research to Prevent Blindness (RPB) Lew Wasserman Mid-Career Development Award (LKM), and an unrestricted grant to the Department of Ophthalmology from RPB.

See also: Abnormal Eye Movements due to Disease of the Extraocular Muscles and Their Innervation; Congenital Cranial Dysinnervation Disorders; Extraocular Muscles: Extraocular Muscle Anatomy; Extraocular Muscles: Extraocular Muscle Involvement in Disease; Extraocular Muscles: Extraocular Muscle Metabolism; Imaging of the Orbit; Orbital Bony Anatomy and Orbital Fractures; Orbital Soft Tissue Biomechanics.

Further Reading

Anderson, B., Christiansen, S. P., and McLoon, L. K. (2008). Myogenic growth factors can decrease extraocular muscle force generation: A potential biological approach to the treatment of strabismus. *Investigative Ophthalmology and Visual Science* 49: 221–229.

Leigh, R. J. and Zee, D. S. (1999). *The Neurology of Eye Movements*, 3rd edn. New York: Oxford University Press.

McLoon, L. K., Anderson, B., and Christiansen, S. P. (2006). Sustained release of insulin growth factor-I results in stronger extraocular muscle. *Journal of the American Association of Pediatric Ophthalmology and Strabismus* 10: 424–429.

McLoon, L. K. and Christiansen, S. P. (2005). Pharmacological approaches for the treatment of strabismus. *Drugs of the Future* 30: 319–327.

Wong, A. (2008). *Eye Movement Disorders*. New York: Oxford University Press.

Extraocular Muscles: Proprioception and Proprioceptors

R Blumer, Medical University of Vienna, Vienna, Austria

Glossary

Choline acetyltransferase – The enzyme responsible for the synthesis of the neurotransmitter acetylcholine, causing the transfer of acetate to choline.
Choline transporter – These recapture choline from the synaptic cleft after acetylcholine release and degradation. This process is critical for new acetylcholine synthesis at the synapse.
Golgi tendon organ – A proprioceptive organ that provides information to the brain about changes in muscle tension. In contrast to muscle spindles, these are in series with muscle fibers, interwoven with the collagen in the muscle tendon. Tension on the tendon caused by muscle contraction activates these proprioceptors.
Muscle spindles – Proprioceptive organs that provide the brain with information about changes in muscle length and are organized in parallel with the skeletal muscle fibers. They contain modified muscle fibers called intrafusal fibers, in contrast with the muscle fibers themselves, which are called extrafusal fibers. They have a complex structure; they are surrounded by a connective tissue capsule, and contain several types of modified myofibers within them. They are innervated by sensory afferents.
Myotendinous cylinders or palisade endings – Proprioceptive organs found at the myotendinous junction consisting of dense axonal branching which invests the tips of single muscle fibers. These are unique to the extraocular muscles. The nerves establish synaptic contacts with both collagen fibrils and muscles fibers at the myotendinous junction. The function of these structures is unknown.
Proprioception – The sense that provides information about the location of various parts of the body in relation to each other and in relation to the space.
Proprioceptors – Sensory receptors which are found in muscles and tendons that bring sense of body position to the brain.
Vesicular acetylcholine transporter – A membrane protein which is necessary for the uptake of acetylcholine into synaptic vesicles.

Proprioception

Proprioception refers to a sense that provides information about the location of various parts of the body in relation to each other and in relation to space. It is of practical importance for activities in everyday life and allows a person to use the foot pedal of a car properly while driving or to learn to walk in darkness. Moreover, sportsmen use specific training devices to sharpen their proprioceptive sense. Proprioceptive signals come from specialized sensory nerve endings called proprioceptors that occur throughout skeletal muscle. Typical proprioceptors in skeletal muscle are muscle spindles and Golgi tendon organs which constantly transmit information to the brain. In this way the brain knows, at any given time, the spatial position of our body parts.

The eyes are the most mobile organs of the body, and vision is useful only if the brain knows the position of the eyes in the orbit. By knowing where the eyes are pointing, the brain is aware of the position of objects in the surrounding space: if objects are leftwards, straight ahead, or rightwards. Several studies indicate that the brain has access to proprioceptive information from the extraocular muscles (EOMs). Specifically, neuronal tracing experiments have demonstrated projections from the EOM to various peripheral and central nervous system structures, including the trigeminal ganglion, the mesencephalic trigeminal nucleus, the superior colliculus, the vestibular nuclei, and the cerebellum. A recent physiology experiment showed that the primary somatosensory cortex, which receives proprioceptive input from all other skeletal muscles, also receives signals from EOM. This new finding completes the somatotopic representation of the body in the primary somatosensory cortex which, thus far, had lacked a map of the eye muscles.

Indication that there is proprioceptive input from the EOM has also come from psychophysical investigations. Patients suffering from strabismus were tested after surgery, and it was detected that they had deficits in spatial perception. These results were interpreted to mean that the surgical intervention has damaged the proprioceptors at the myotendinous junction resulting in a loss of eye position signals.

Despite this evidence for EOM proprioception, there are also counterarguments. Specifically, no stretch reflex has been observed in the EOM of monkey. By cutting the ophthalmic nerve, which is supposed to carry the afferent fibers from EOM, deficits in eye movements would be

expected. However, findings indicate that deafferentation does not affect ocular alignment or eye movements, including saccades and smooth pursuit. Such observations led scientists to doubt whether EOM proprioception really exists. Instead, it has been hypothesized that the motor command that is sent to the EOMs is copied, called efference copy, and this copy provides the necessary information for the brain to be aware of the eye's position.

If there is sensory feedback from EOM, the eye muscles should have proprioceptors. In the last century, the EOMs of several mammalian species and man have been screened for muscle spindles and Golgi tendon organs. Interestingly, the endowment with classical proprioceptors varies widely among the species, and there are even some species that do not have proprioceptors at all. In view of these interspecies variations, it is not clear where the source of EOM proprioception lies. By searching for alternative sensory organs in the EOMs, palisade endings (also called myotendinous cylinders) have been detected, and so far, palisade endings have been observed in each species investigated. In the following section, we discuss EOM proprioceptors, including muscle spindles, Golgi tendon organs, and palisade endings. We give an overview about the occurrence, distribution, number, and structure of these organs and speculate about their putative function. Recent studies have focused on the molecular characteristics of palisade endings, and we also refer to these findings.

Muscle Spindles

Occurrence, Distribution, and Number of Muscle Spindles

Muscle spindles are regularly observed in the EOMs of even-toed ungulates (sheep, cow, camel, goat, and pig) and in the EOMs of primates (monkey and man). In other animal species, including fellidae (cat), rodents (rat and guinea pig), odd-toed ungulates (horse), and lagomorphs (rabbit), muscle spindles have not been found (Table 1).

In the EOMs of even-toed ungulates, muscle spindles are uniformly distributed throughout the entire muscle length. The number of muscle spindles is remarkably high, and counts per muscle yield between 146 and 333 muscle spindles in pig; between 100 and 181 muscle spindles in camel; and more than 200 muscle spindles in cow. In man the distribution of muscle spindles exhibits differences when compared with that in even-toed ungulates. Specifically, muscle spindles are located predominantly in the proximal and distal parts of the EOM, and each muscle has a spindle-free zone approximately in the middle. The number of human EOM spindles varies between 13 and 42. Only in the inferior oblique muscle has a lower number of muscle spindles been counted (3–7). The density of human EOM spindles is comparable to that of muscle spindles in finely controlled skeletal muscle such as the hand lumbrical and deep dorsal neck muscles. In monkey (rhesus monkey and cynomolgus monkey), very few muscle spindles (2–6) have been observed in some EOMs, and none in the others.

Table 1 Occurrence of muscle spindles, Golgi tendon organs, and palisade endings in the extraocular muscles of man and mammals

Species	*Muscle spindles*	*Golgi tendon organs*	*Palisade endings*
Man	+	−	
Monkey	+	−	+
Fellidae	−	−	+
Even-toed ungulates	+	+	+[a]
Odd-toed ungulates	−	−	[b]
Lagomorphs	−	−	+
Rodents	−	−	+

[a]So far, palisade endings have only been demonstrated in sheep.
[b]So far not analyzed for palisade endings.

Structure of Muscle Spindles

Muscle spindles in the EOMs of even-toed ungulates conform in their structure with those in other skeletal muscles. The muscle spindles have a fusiform shape with a wide central region (equatorial region) and two narrow polar regions. Muscle spindles are ensheathed by a capsule consisting of several layers of perineural cells. The capsule space is filled with a viscous fluid containing acidic mucopolysaccharides. Inside the capsule two types of intrafusal muscle fibers (nuclear chain fibers and nuclear bag fibers) can be distinguished, which both exhibit modifications concerning their myonuclei in the spindle's equatorial region. Nuclear chain fibers have a single row of centrally arranged nuclei, whereas nuclear bag fibers show an accumulation of nuclei. In the muscle spindle's equatorial region, a large tissue-free space (periaxial space) separates the intrafusal muscle fibers from the capsule.

Muscle spindles in the EOMs of even-toed ungulates receive a double innervation from sensory and motor nerve fibers. In the equatorial region, both types of intrafusal muscle fibers are endowed with sensory nerve endings (annulospiral sensory endings) which are wrapped spirally around the muscle fibers. Whether a second type of sensory nerve ending (flower-spray ending) that is common in other mammalian skeletal muscle spindles is also present in ungulate EOM spindles is unclear. Fine structural analyses have shown that sensory nerve terminals contain mitochondria and a few clear vesicles. The synaptic cleft separating the nerve terminal from the muscle fiber surface is free from a basal lamina. At the muscle spindle's pole, intrafusal muscle fibers receive motor terminals. Motor terminals contain mitochondria

and dense aggregations of clear vesicles, and the synaptic cleft is filled with a basal lamina.

Muscle spindles in EOM of primates exhibit structural differences when compared with those in even-toed ungulates. Specifically, in most muscle spindles of monkey and man the periaxial space exhibits little or no expansion. Only in human infants have some muscle spindles with a wide periaxial space been observed. Thorough analyses of the intrafusal fiber composition have been done in human EOM spindles. The findings indicate that human EOM spindles contain nuclear chain fibers but most of them lack nuclear bag fibers. Only 2% of the spindles contain nuclear bag fibers and, when present, the bag region is poorly developed with only two nuclei lying side by side. In addition to nuclear chain fibers, anomalous muscle fibers are also regularly observed in human EOM spindles. Anomalous muscle fibers exhibit no nuclear modification in the spindle's equatorial region and are indistinguishable from muscle fibers outside the spindle. The unique morphology of human EOM spindles was initially described in aged persons (67–83 years old) and later was confirmed in infants (**Figure 1(a)**).

The innervation pattern of primate EOM spindles has only been analyzed in humans. In human EOM spindles, sensory nerve endings have been observed on nuclear chain and, when present, on nuclear bag fibers, but only 7% of the anomalous fibers are endowed with sensory nerve terminals. In their fine structure, sensory nerve terminals in human EOM spindles do not differ from sensory nerve terminals in EOM spindles of even-toed ungulates. At the muscle spindle's pole, intrafusal muscle fibers are equipped with motor terminals. Motor terminals in human EOM spindles are identical in their structure with those in EOM spindles of even-toed ungulates (**Figure 1(b)**).

Function of Muscle Spindles

Muscle spindles in mammalian skeletal muscle are stretch receptors which register changes in muscle length. Indications that muscle spindles in the EOMs of even-toed ungulates are capable of monitoring muscle length have come from electrophysiological investigations. Specifically, in goat and sheep the EOMs were stretched and afferent signals were recorded in the sensory trigeminal ganglion. Recorded signals exhibited characteristics that are the same as muscle spindles in other skeletal muscles.

There is controversy whether muscle spindles in human EOMs are functional. Due to their unusual morphology, some authors suppose that human EOM muscle spindles are not functional. On the other hand, muscle spindles in human EOMs are numerous, and their nerve terminals exhibit a normal morphology. This is why other authors suggest that human EOM spindles are functional, and their unusual morphology might indicate special functional properties. In particular, as most human EOM muscle spindles lack nuclear bag fibers, muscle spindles might have a predominantly static function and monitor the degree of muscle stretch rather than the contraction velocity of muscle fibers.

Golgi Tendon Organs

Occurrence, Distribution, and Number of Golgi Tendon Organs

Golgi tendon organs are exclusively found in the EOMs of even-toed ungulates (pig, sheep, camel, and cow). They have not been found in other mammals and man. In even-toed ungulates, Golgi tendon organs are distributed throughout the proximal and distal EOM tendons, their number always being higher in the distal tendons (**Table 1**). The number of Golgi tendon organs per muscle has been counted to be

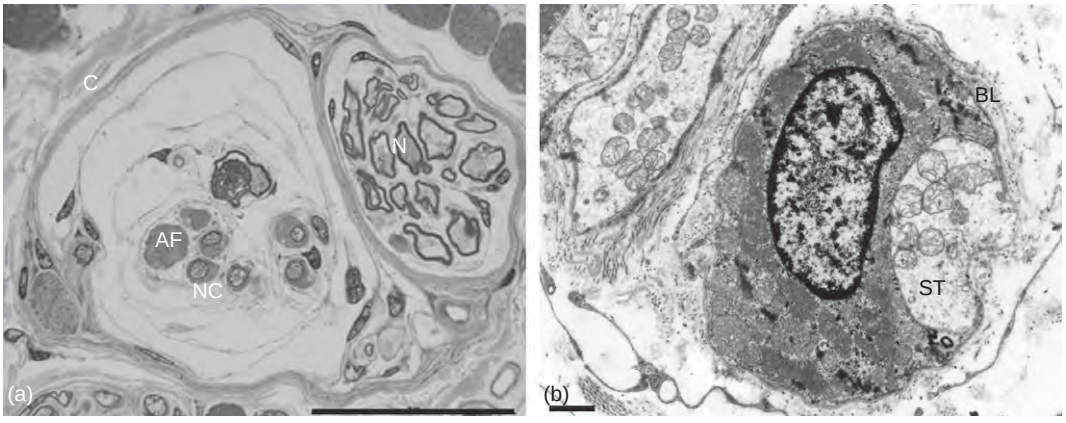

Figure 1 (a) Semi-thin cross section through an extraocular muscle spindle of a 2-year-old human infant and (b) ultra-thin cross section through a nuclear chain fiber. (a) The muscle spindle contains six nuclear chain fibers (NF) and one anomalous fiber (AF). The anomalous fiber is indistinguishable from muscle fibers outside the spindle. N, nerve and C, capsule. Scale bar = 100 μm. (b) Nuclear chain fiber (NF) with a sensory nerve terminal (ST). BL, basal lamina. Scale bar = 1 μm.

46–128 and 30–90 in pig and camel, respectively. In both species, Golgi tendon organs are more frequent in the rectus EOMs than in the oblique EOMs.

Structure of Golgi Tendon Organs

Golgi tendon organs in EOMs of even-toed ungulates exhibit a fusiform shape and are enclosed by a capsule of perineural cells. The capsule space is filled with a viscous fluid containing acidic mucopolysaccharides. The main component of the Golgi tendon organs are collagen bundles that pass through the organ. At one end of the organ the collagen fascicles are attached to muscle fibers, and at the other end the fascicles merge with the tendon of the muscle. Many Golgi tendon organs contain only collagen bundles, but there are others which contain both collagen bundles and muscle fibers. Such intracapsular muscle fibers penetrate the Golgi tendon organ at one end and either terminate in collagen bundles or, more rarely, pass through the tendon organ. All Golgi tendon organs in the EOMs of even-toed ungulates exhibit a wide space in the central region that separates the collagen bundles and muscle fibers, if present, from the capsule (**Figure 2(a)**).

Each Golgi tendon organ is innervated by a single sensory nerve fiber. The nerve fiber penetrates the capsule at various points. Inside the organ, the axon divides into several preterminal branches which finally establish nerve terminals that contact the surrounding collagen fibrils. Nerve terminals are only partly covered with Schwann cells, and at the area of contact only a basal lamina lies between the nerve terminal and the neighboring collagen. Nerve terminals contain mitochondria and a few clear vesicles (**Figure 2(b)**).

With the exception of intracapsular muscle fibers and a more pronounced capsule space in the central region, Golgi tendon organs in even-toed ungulates share the structural features of Golgi tendon organs found in other mammalian skeletal muscles.

Function of Golgi Tendon Organs

Golgi tendon organs in mammalian skeletal muscle are sensitive to muscle contraction. During muscle fiber contraction collagen bundles are stretched, and the nerve terminals within the collagen are deformed, thereby generating a receptor potential. Golgi tendon organs in EOMs of ungulates are supposed to function analogously and register muscle fiber contraction. Muscle fibers passing through Golgi tendon organs are supposed to regulate the sensitivity of the organ.

Palisade Endings

Occurrence, Distribution, and Number of Palisade Endings

Palisade endings (myotendinous cylinders) are sensory end organs that are unique to EOMs. So far, palisade endings have been found in the EOMs of almost all species investigated, including fellidae (cat), lagomorphs (rabbit), even-toed ungulates (sheep), rodentia (rat), and primates (monkey and man). These organs are located at the distal and proximal myotendinous junctions. Palisade endings are plentiful in the EOMs of monkey and cat (**Table 1**). In the distal myotendon of a monkey medial rectus 350 palisade endings have been counted, and in a

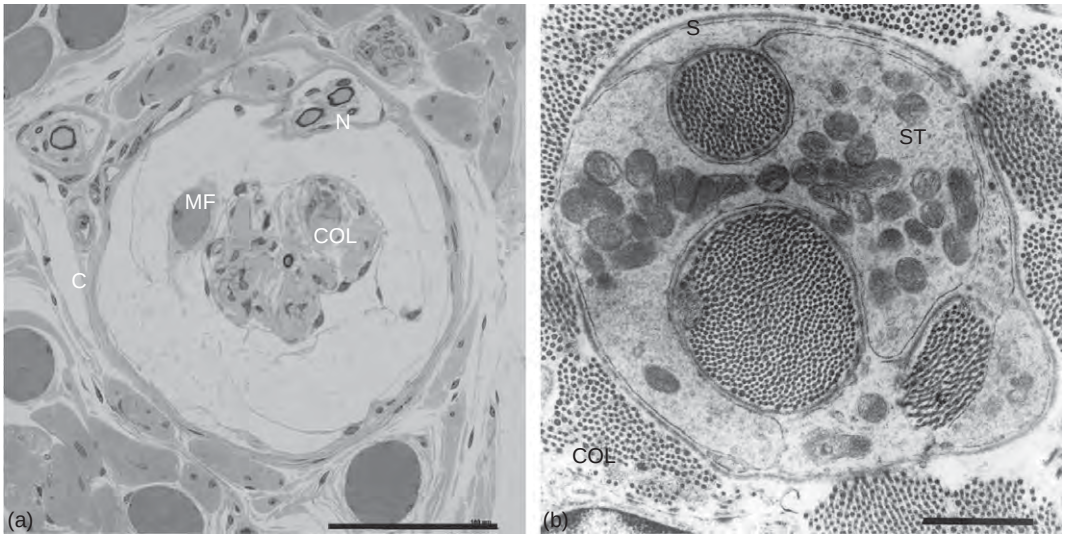

Figure 2 (a) Semi-thin cross section through a Golgi tendon organ of a calf extraocular muscle and (b) ultrathin section through a sensory nerve terminal. (a) The Golgi tendon organ is ensheathed by a capsule (C) and contains collagen bundles (COL) and one muscle fiber (MF). Nerve fiber (N). Scale bar = 100 μm. (b) A sensory nerve terminal (ST) which is partly ensheathed by Schwann cells (S) contacts the surrounding collagen bundles (COL). Scale bar = 1 μm.

cat medial rectus 94. A smaller number of this EOM-specific organ have been found in the distal EOM myotendons of rat (27) and human (20–30).

Structure of Palisade Endings

Innervation for the palisade endings arises from nerve fibers that come from the muscle and extend into the tendon. Within the tendon, the nerve fibers make a 180° loop and return to the muscle. At the muscle–tendon junction, the returning axons divide into preterminal branches. Preterminal axons establish nerve terminals around the muscle fiber tips which have the appearance of a palisade fence (**Figure 3**), which is also the reason why this formation is called a palisade ending. The whole palisade complex is ensheathed by a capsule of fibroblasts.

Palisade ending is exclusively associated with the multiply innervated muscle fibers of the global (inner) layer of the EOMs. Such muscle fibers have several motor contacts along their length, and with respect to contraction they exhibit nontwitch characteristics. The multiply innervated muscle fibers have a unique innervation from small motoneurons located outside the borders of the main EOM nuclei.

The fine structure of palisade endings was initially analyzed in cat and monkey and later in sheep, rabbit, and man. It was observed that the majority of palisade nerve terminals contact the collagen fibrils of the tendon, and only a few of them contact the muscle fiber tip. Nerve terminals contacting the collagen fibrils are only partly enwrapped with Schwann cells, and at the area of contact with the collagen only a basal lamina covers the nerve terminals. Such neurotendinous contacts contain dense aggregations of clear vesicles and mitochondria. Palisade nerve terminals contacting the muscle fiber are free from a basal lamina in the synaptic cleft, thereby resembling sensory nerve terminals on intrafusal fibers of muscle spindles. Identical to neurotendinous contacts, neuromuscular contacts contain mitochondria and a large number of clear vesicles. Interestingly, in palisade endings of man and monkey, neuromuscular contacts have a basal lamina in the synaptic cleft which is a feature of motor terminals. Palisade endings in rabbits and rats are an exception. In both species, the palisade endings lack neurotendinous contacts and neuromuscular contacts are present exclusively.

Molecular Characteristics of Palisade Endings

In cat and monkey, it has been recently demonstrated that palisade endings have a cholinergic phenotype. Utilizing immunohistochemistry, palisade endings have been labeled with all commercially available cholinergic markers, including antibodies against choline transporter (ChT), choline acetyltransferase (ChAT), and vesicular acetyl choline transporter (VAChT), as well as α-bungarotoxin. In the nervous system, ChT is used for the uptake of choline, ChAT is the synthesizing enzyme of acetylcholine, and VAChT is used to transport acetylcholine into the synaptic vesicles. α-Bungarotoxin is a snake venom that binds to nicotinic acetylcholine receptors, and this neurotoxin is widely used to detect motor terminals in skeletal muscle.

In cat and monkey, it has been shown that the nerve fibers supplying palisade endings are ChAT immunoreactive. The palisade complexes, including palisade nerve terminals, are ChAT positive as well. In monkey, it also has been demonstrated that palisade nerve terminals exhibit ChT/VAChT immunoreactivity, and neuromuscular contacts, when present, exhibit α-bungarotoxin binding. Finally, in some cases it has been detected that nerve fibers supplying palisade endings establish α-bungarotoxin-positive neuromuscular contacts outside the palisade complex (**Figure 3(b)**).

Function of Palisade Endings

So far, physiological studies on palisade ending are missing, and their function remains speculative. Indication that palisade endings are sensory organs comes from morphological studies and a single neuronal tracing experiment. Specifically, morphological studies show that palisade endings have nerve terminals contacting the tendon, and nerve terminals in apposition to collagen are arguably sensory. Palisade nerve terminals contacting

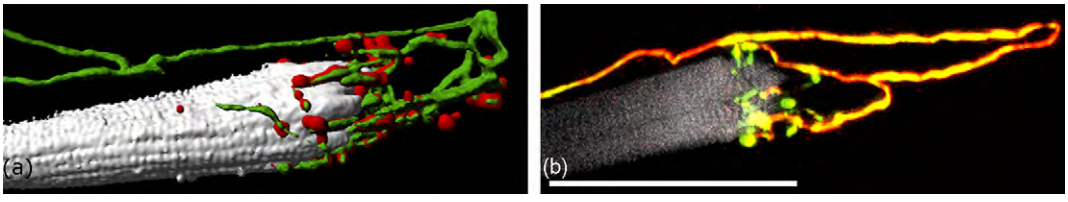

Figure 3 Palisade endings: (a) three-dimensional reconstruction of a palisade ending and (b) palisade ending labeled with anti-neurofilament (general marker for nerve fibers) and anti-ChAT (marker for cholinergic nerve fibers). Muscle fibers are counterstained with phalloidin. The tendon is not labeled and is continuous with the muscle fiber tip to the right. (a) A nerve fiber (green) coming from the muscle extends into the tendon and turns back to establish nerve terminals (red) around a muscle fiber tip. The muscle fiber is white. (b) This shows a nerve fiber forming a palisade ending. The nerve fiber and the palisade ending are positive for neurofilament (red) and ChAT (green). Muscle fiber (white). Scale bar = 100 μm.

the muscle fibers lack a basal lamina in the synaptic cleft which is common with sensory nerve terminals in muscle spindles. Moreover, by injecting neuronal tracer into the sensory trigeminal ganglion, structures resembling palisade endings have been labeled. Palisade endings lie in series to the multiply innervated muscle fibers of the global (inner) EOM layer, and it is supposed that palisade endings register contraction of such muscle fibers.

Although a consensus exists that palisade endings are sensory, there are other findings which favor a motor role for palisade endings. In particular, immunohistochemical studies have demonstrated that palisade endings are cholinergic, a feature common with motor nerve terminals. Nerve fibers forming palisade endings also establish motor neuromuscular contacts outside the palisade complex. In a nerve degeneration experiment a lesion of the oculomotor nucleus was performed and, in addition to the expected loss of motor terminals, the palisade endings degenerate as well. The functional significance of palisade endings with a motor nature is difficult to predict. In particular, it is unclear what effect cholinergic neurotendinous contacts would have on the surrounding collagen. At the moment the function of palisade endings is still a matter of discussion, and for clarification physiological studies are highly warranted.

See also: Cranial Nerves and Autonomic Innervation in the Orbit.

Further Reading

Billig, I., Buisseret, D. C., and Buisseret, P. (1997). Identification of nerve endings in cat extraocular muscles. *The Anatomical Record* 248: 566–575.

Blumer, R., Konakci, K. Z., Brugger, P. C., et al. (2003). Muscle spindles and Golgi tendon organs in bovine calf extraocular muscle studied by means of double-fluorescent labeling, electron microscopy, and three-dimensional reconstruction. *Experimental Eye Research* 77: 447–462.

Blumer, R., Lukas, J. R., Aigner, M., et al. (1999). Fine structural analysis of extraocular muscle spindles of a two-year-old human infant. *Investigative Ophthalmology and Visual Science* 40: 55–64.

Blumer, R., Wasicky, R., Brugger, P. C., et al. (2001). Number, distribution and morphological particularities of encapsulated proprioceptors in pig extraocular muscle. *Investigative Ophthalmology and Visual Science* 42: 3085–3094.

Blumer, R., Wasicky, R., and Lukas, J. R. (2001). Presence and structure of innervated myotendinous cylinders in rabbit extraocular muscle. *Experimental Eye Research* 73: 787–796.

Buisseret, P. (1995). Influence of extraocular muscle proprioception on vision. *Physiological Reviews* 75: 323–338.

Buttner, E. J. A., Konakci, K. Z., and Blumer, R. (2005). Sensory control of extraocular muscles. *Progress in Brain Research* 15(1): 81–93.

Donaldson, I. M. L. (2000). The functions of proprioceptors of the eye muscles. *Philosophical Transactions of the Royal Society of London* 355: 1685–1754.

Konakci, K. Z., Streicher, J., Hoetzenecker, W., et al. (2005). Molecular characteristics suggest an effector function of palisade endings. *Investigative Ophthalmology and Visual Science* 46: 155–165.

Konakci, K. Z., Streicher, J., Hoetzenecker, W., et al. (2005). Palisade endings in extraocular muscles of the monkey are immunoreactive for choline acetyltransferase and vesicular acetylcholine transporter. *Investigative Ophthalmology and Visual Science* 46: 4548–4554.

Lukas, J. R., Aigner, M., Blumer, R., Heinzl, H., and Mayr, R. (1994). Number and distribution of neuromuscular spindles in human extraocular muscles. *Investigative Ophthalmology and Visual Science* 35: 4317–4327.

Lukas, J. R., Blumer, R., Denk, M., et al. (2000). Innervated myotendinous cylinders in human extraocular muscle. *Investigative Ophthalmology and Visual Science* 41: 2422–2431.

Ruskell, G. L. (1989). The fine structure of human extraocular muscle spindles and their potential proprioceptive capacity. *Journal of Anatomy* 167: 199–214.

Ruskell, G. L. (1990). Golgi tendon organs in the proximal tendon of sheep extraocular muscle. *The Anatomical Record* 227: 25–31.

Ruskell, G. L. (1999). Extraocular muscle proprioceptors and proprioception. *Progress in Retinal and Eye Research* 18: 269–291.

Eye-Field Transcription Factors

M E Zuber, SUNY Upstate Medical University, Syracuse, NY, USA

Glossary

Aniridia – Congenital condition resulting in the underdevelopment or lack of an iris.
Anophthalmia – Congenital absence of one or both eyes.
Ectopic eye – An eye that has formed in an abnormal location (an additional eye).
Eye field – A region of the anterior neural plate of vertebrate embryos that is fated to generate the eyes.
Gene homology – Two genes are homologous if they are derived from the same gene in a common ancestor.
Hypomorphic mutant – A mutation in which the altered gene product has reduced activity or in which the wild-type gene product is expressed at a reduced level.
Iris – Colored portion of the eye surrounding the pupil.
Microphthalmia – Congenital defect resulting in small eyes.
Retina – Light-sensing part inside the inner layer of the eye. The vertebrate retina consists of seven major cell classes.

Discovery and Structural Features of Eye-Field Transcription Factors

Pax6

Vertebrate Pax6 (paired box gene 6) was identified, in 1991, in mouse and humans as a member of a multigene family of paired-box-containing (Pax) genes. Small-eye (Sey) mutant mice were found to have mutations in the Pax6 gene predicted to interrupt gene function. The *Drosophila melanogaster* (fly) mutant eyeless (ey) was subsequently shown to be homologous to vertebrate Pax6. Remarkably, the mouse Pax6 was shown to functionally rescue the eyeless phenotype in flies, demonstrating functional conservation of Pax6 from flies to mammals. Pax transcription factors contain a paired domain and either a partial or complete (as in the case of Pax6) homeodomain (see **Figure 1** and **Table 1** for EFTF structure and characteristics). In addition, Pax6 contains a proline–serine–threonine-rich (PST-rich) C-terminus. The paired domain is an approximately 126-residue DNA-binding domain originally described in the *Drosophila* gene of the same name. Two distinct DNA-binding domains are present in the paired-type domain in the form of N-terminal and C-terminal subdomains. Alternative splicing of the Pax6 gene results in alternate isoforms with distinct DNA-binding activities with functional consequences. The 60-residue homeodomain forms a helix-turn-helix structure at the carboxy-terminal end that also binds DNA. As with the paired domain, an altered homeodomain can result in developmental defects. The PST-rich region acts as a trans-activating domain with binding sites for other proteins such as transcriptional coregulators. Pax6 mutants that truncate the C-terminal-half of the protein remove the PST-rich region, retain their DNA-binding capacity, but act dominantly to repress normal Pax6 function.

Six3

The first Six (Sine oculis homeobox) family member was identified in 1994 as the gene altered in the *Drosophila* mutant *sine oculis* (*so*), the most striking phenotype of which is the lack of eyes. Vertebrate Six3 (*sine oculis* homeobox homolog 3) was first identified in mouse in 1995 and shown to share significant amino-acid homology with *so*. Members of the Six family of homeobox transcription factors are characterized by two conserved domains – the Six domain (SD) followed by a more carboxy-terminal homeodomain (HD). The Six domain is typically 115 residues and is required for protein–protein interactions between Six genes and their binding partners. The homeodomain is a 60-residue DNA-binding domain (as described above). Both the SD and HD are required for normal function of the protein. The more recent identification of additional *Drosophila* Six family members also demonstrated vertebrate Six3 (and section titled 'Six6') share greater sequence homology with fly *Optix* than its namesake *sine oculis*. Based on sequence homology, intron–exon boundries, and the proteins with which they form complexes, Six family members are divided into three subfamilies. Six3 and Six6 have been assigned to the Six3/6 subfamily.

Six6

A second Six gene structurally related to Six3 was identified, in 1998, in zebrafish, chicken, and mouse as Six6 (*sine oculis* homeobox homolog 6) and Optx2 (optic six gene 2). Among the family of Six genes, Six6 shares greatest sequence homology and expression pattern with Six3,

suggesting they may have arisen via gene duplication. Despite their similarities, Six6 and Six3 can be easily distinguished at the amino-acid level. The most highly divergent regions lie at the amino- and carboxy-terminals to the Six and homeodomains. In particular, the region of Six6 amino-terminal to the Six domain is dramatically smaller than the corresponding region of Six3. For example, only nine residues are present at the amino-terminal to the Six domain in mouse Six6, while 88 residues are present in the Six3 protein.

Rax

Vertebrate Rax (retina and anterior neural fold homeobox) was identified, in 1997, by three independent groups in Xenopus, mouse, and zebrafish, and is shown to be expressed in the developing eyes and required for normal mouse eye formation. Rax – like Pax6 – is classified as a member of the paired homeobox class of transcription factors. In contrast to Pax6, however, Rax contains a paired-like homeodomain, but no paired domain. Within the amino-terminal, Rax contains an octapeptide motif consistent with this homeobox gene subfamily. In the carboxy-terminal, a 15-residue region present in other paired-like genes termed the paired tail or OAR (otp, aristaless, and rax) domain is also conserved. Finally, the sequence carboxy-terminal to the paired-like homeodomain is PST-rich. These regions (octapeptide, OAR, and PST-rich) may function as transactivation domains.

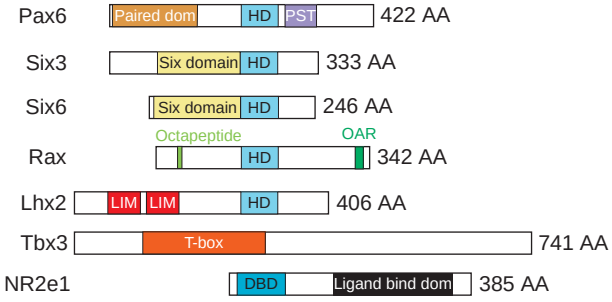

Figure 1 Schematic illustrating the location of structural domains in the mouse eye-field transcription factors. The EFTFs – with the exception of the Six genes Six3 and Six6 – have distinct domain structures and are members of different transcription-factor families. Five of the seven bind DNA targets via a homeobox domain (HD). While Tbx3 (via the T-box) and Nr2e1 bind DNA through DNA-binding domains (DBDs) specific to their transcription factor family. Each EFTF also contains protein motifs that allow it to complex with other proteins. These protein–protein interactions serve to facilitate (or sometimes block) the ability of the transcription factor to bind its DNA targets. Co-regulatory proteins that bind to these regions can serve as co-activators or co-repressors to increase or decrease, respectively, the rate of expression from a target gene. Courtesy of Andrea Viczian.

Lhx2

First identified in rat as LH-2 (LIM Hox gene 2) in 1993, vertebrate Lhx2 (LIM homeobox-2) is a member of a large LIM-domain (Lin 11, Isl-1, Mec-3)-containing family of genes with diverse structure and biological functions. Mouse Lhx2 was subsequently shown to be required for normal eye formation. The LIM domain (two of which are found in Lhx2) is a cysteine- and histidine-rich zinc-finger motif involved in protein–protein interactions. The LIM domains of Lhx2 protein are located in the amino-terminal region and followed by a carboxy-terminal, highly conserved, DNA-binding homeodomain. There is little evidence that LIM domains of the LHX class can bind DNA directly, but may regulate DNA binding of the protein via interactions with other proteins.

Tbx3

Vertebrate Tbx3 was identified, in 1994, in mouse as a member of a large gene family characterized by a shared T-box protein motif. Mutation of the founding member of this family caused truncated tails in mice and was shorthand named T for short-tail. Once the gene was identified, the DNA-binding region of the T protein (which is 180–190 residues and can be located at any position in the protein) was subsequently named the T-box. The more than 50 T-box family members identified have been classed into five subfamilies. Tbx3 is a member of the Tbx2 subfamily that includes Tbx2-5 and is most similar to Tbx2.

Nr2e1

Vertebrate NR2E1 (nuclear receptor subfamily 2, group E, member 1) was originally identified in 1994 as Tlx,

Table 1 Names and the null phenotypes of EFTF homologs

EFTF	*TF family*	*Fly homoloq*	*Vertebrate alias(es)*	*Eye phenotype of mouse null*
Pax6	Paired homeobox	eyeless, twin of eyeless	AN2, WAGR	small or no eyes
Six3	Six homeobox	sine oculls/optix	Holoproencephaly 2 (HPE2)	lack of anterior brain (no eyes)
Six6	Six homeobox	sine oculis/optix	Optx2, Six9	small eyes
Rax	Paired-like homeobox	DRx	Rx	no eyes
Lhx2	LIM homeobox	apterous	LH-2	no eyes
Tbx3	T-box	optomotor blind	ET, XHL, UMS	embryonic lethal (eye normal)
NR2E1	Nuclear receptor type	tailless	XTll, Tlx	degenerated retina

a unique vertebrate nuclear receptor with structural homology to the previously described fly gene, *tailless* (*tll*). Tll was classified as a member of the steroid receptor superfamily of proteins. Nr2e1 (and tll) are orphan nuclear receptors, implying – although their protein sequence predicts a hormone-binding domain – the hormone ligand that binds to it has not been identified. The NR2E1 DNA and ligand-binding domains are located in the amino- and carboxy-terminal regions of the protein, respectively. NR2e1 shares the highest similarity with tll in these regions. *In vitro* DNA-binding assays, and misexpression of vertebrate Nr2e1 in the fly shows that the vertebrate and fly proteins share similar target-gene specificity, which is unique among the nuclear receptor superfamily.

The EFTFs are Expressed during and are Required for Normal Eye Formation

Transplantation experiments performed in the beginning of the last century demonstrated that the amphibian eye field (originally called the eye anlagen or, sometimes, eye primordia) is located in the neural plate. Removing the anterior portion of the neural plate resulted in the creation of eyeless animals. When this same region was transplanted to the belly-wall or grown in culture, a histologically normal eye would form. These remarkably simple experiments clearly demonstrated that the eye primordia is specified in embryos at the neural plate stage, and that all the genes required to initiate eye formation were being expressed in the tissue at that time. Subsequent, detailed mapping experiments using more modern tools precisely defined the location and shape of the eye field as a single crescent of cells spanning the breadth of the early anterior neural plate.

During embryonic development, eye and brain formation are tightly coordinated. Neural induction results in an early neural plate with a propensity to form anterior structures (including the eyes). This early neural plate is subsequently patterned in response to diffusible molecules that help to form the different brain regions (the forebrain, midbrain, and hindbrain). The signaling systems known to regulate this patterning include the wingless (Wnts), fibroblast growth factors (FGFs), bone morphogenetic proteins (BMPs), Nodals, and retinoic acid. Inactivation or modification of any one of these signaling systems can result in abnormal eye formation. These abnormalities are often coincident with changes in the expression of the EFTFs. These effects may sometimes be indirect, however, as some of these molecules are required for neural induction and not directly responsible for the formation of the eye field. Nevertheless, EFTF expression can be regulated by these signaling systems. For example, cultured embryonic stem cells treated with BMP, Wnt, and/or Nodal antagonists express EFTFs and are directed to a retinal progenitor lineage. Precise control of the Wnt signaling system appears to be critical for patterning of the forebrain – the brain region in which the eye field and ultimately the eyes form. Disrupting Wnt activity by modifying the ligand or its signaling cascade can have dramatic effects on eye formation. Either too much or too little Wnt activity can lead to abnormal eye formation. The evidence suggests that a precise Wnt gradient is required to pattern and appropriately position the eye field within the forebrain.

The location and timing of eye-field specification in the anterior neural plate is synchronized with the expression of the EFTFs. The expression patterns of the individual genes are distinct and extend to other regions of the neural plate and beyond. However, all are to some extent expressed in the eye field in one or more species. For example, the expression pattern of the frog (*Xenopus laevis*) EFTFs overlap in the eye field during and immediately following its specification (**Figure 2**). The EFTFs of other species have similar patterns of coordinated expression. At neural plate stages, for example, Pax6, Rax, Six3, and Six6 are also observed in a single band of expression in chicken, zebrafish, and mouse embryos.

The single band of EFTFs expressing eye-field cells generates both eyes. Since all vertebrate embryos have a pair of eyes organized symmetrically across the body midline, the single eye field described above must be split into two lateral eye primordia. Infrequently, this separation does not take place due to environmental toxins or genetic mutations. This results in cyclopia, the formation of one large midline eye. One toxin long known to induce cyclopia is 11-deoxyjervine (also known as cyclopamine). A US Department of Agriculture study, in the 1950s, showed that pregnant ewes feeding on corn lily (a naturally occurring source of cyclopamine) bore one-eyed lambs (**Figure 3**). More recent studies have demonstrated that diffusible factors secreted by cells near the eye field regulate its splitting. Signaling pathways regulated by the ligands hedgehog and nodal converge and are required for eye-field separation. Hedgehog represses the EFTF Pax6 and since hedgehog is normally expressed underneath the eye field midline, it is likely that hedgehog expression is required for normal eye-field separation and the formation of two eyes (**Figure 3**). Consistent with this interpretation, humans, mice, and fish lacking functional nodal or hedgehog signaling are cyclopic. Interestingly, the action of cyclopamine also appears to be through the hedgehog signaling pathway. Cyclopamine regulates the activity of Smoothened, the receptor for the hedgehog ligand.

Evidence that the EFTFs are required for normal eye formation is abundant. The most extensively studied of the EFTFs, Pax6, was originally identified as the gene mutated in the small eye (Sey) mouse which, when

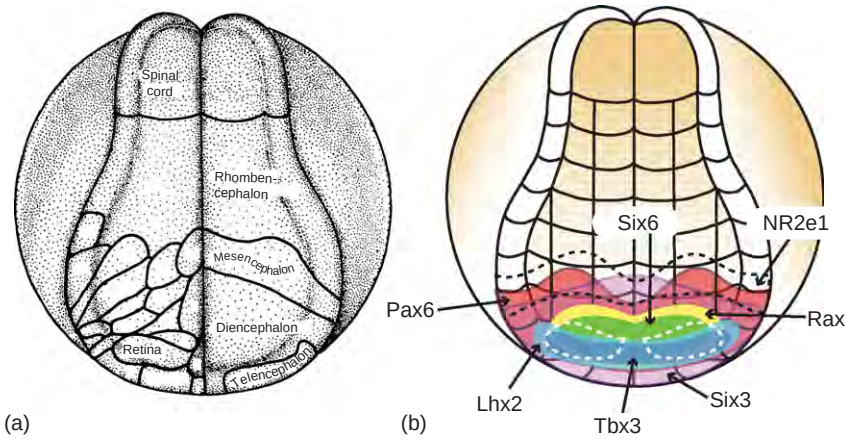

Figure 2 Schematic diagrams of stage 15 *Xenopus laevis* embryos. (a) Fate-map illustrating the areas of the neural plate that will eventually form the major brain regions. (b) Expression patterns of the frog eye-field transcription factors. The approximate location of the eye field is outlined in white. No two EFTFs have identical expression patterns, yet all (but Nr2e1) are expressed in the eye field. Nr2e1 is expressed posterior to the eye field proper at stage 15. However, only a few hours later, its expression overlaps that of the other EFTFs in the eye primordia. Courtesy of Andrea Viczian.

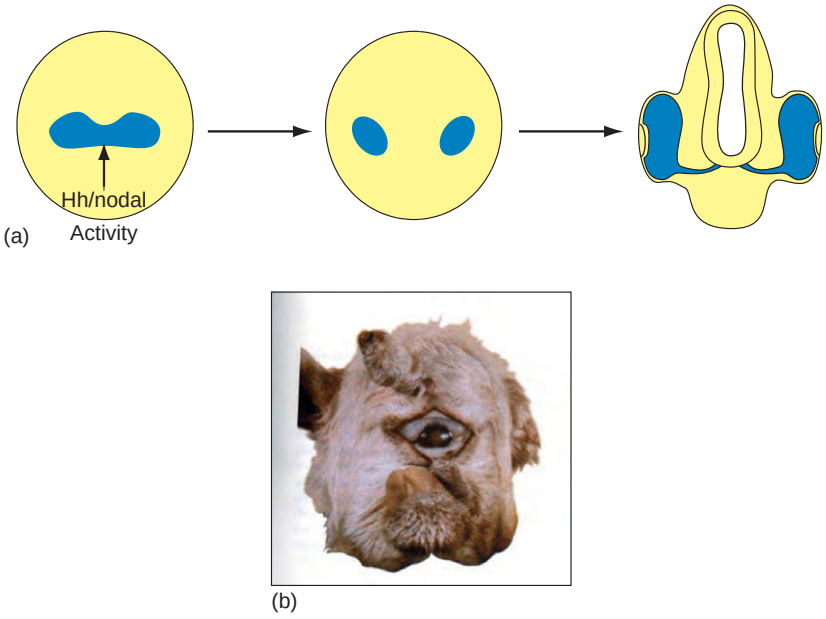

Figure 3 Generation of two eyes from a single eye field. (a) The single eye-field spans the entire anterior neural plate. For two eyes to form, this single EFTF-expressing domain must be split into the two (left and right) eye primordia. Cells posterior to and underlying the midline are required for this process. Signaling via the hedgehog (Hh) and nodal systems are thought to repress midline eye-field fate. (b) When these signaling systems are abnormal, eye-field separation does not take place and a single midline eye forms. The mother of this lamb fed on corn lily while pregnant. Cyclopamine made by corn lily blocks hedgehog signaling with dramatic effects. Courtesy of L. James, USDA Poison Plant Laboratory.

homozygous, lacks eyes. A large number of null and hypomorphic mutant alleles have been generated – with variable eye phenotypes including lens/cornea fusion, microphthalmia, cataracts, and anophthalmia. Flies with a mutant version of the *Drosophila* homolog of Pax6 (eyeless) also lack eyes, while frog eye development can be arrested using a function-blocking (dominant negative) version of Pax6. As with Pax6, functional inactivation of Six3, Six6, Rax, Lhx2, and Nr2e1 results in flies, frogs, fish, and/or rodents with abnormal or no eyes.

Mutation of human EFTFs also results in abnormalities affecting the eyes. Pax6 mutations result in aniridia, microphthalmia, and Peters' anomaly – in which patients have cornea and iris abnormalities. Anophthalmia and microophthalmia have also been attributed to mutations in the human Six6 and Rax genes. Six3 mutation results in

holoprosencephaly, a failure of the forebrain to divide properly into the two hemispheres. Holoprosencephaly is, in most cases, fatal. In less severe cases, facial deformities affecting the eyes are observed.

The EFTFs Form a Self-Sustaining Feedback Network

As described briefly above, many of the vertebrate EFTFs were originally identified as *Drosophila* genes required for fly eye formation or that have fly homologs. In some instances, the vertebrate versions can functionally restore the corresponding fly mutant or induce ectopic eyes in the fly. For example, mis-expression of mouse eyes absent (eya) and Pax6 in flies can induce ectopic eye development and rescue eye formation in loss-of-function mutants. Based on its remarkable evolutionary conservation, requirement for normal eye formation in multiple species, and the ability of mammalian Pax6 homologs to induce ectopic fly eyes, ey/Pax6 was originally hailed as a potential master regulator of eye formation. In initial models, eyeless was placed atop a hierarchy of genes that drove eye formation in the eye portion of the eye-antennal imaginal disk complex. However, a much more complex set of interactions has emerged. The genes twin-of-eyeless (toy), *sine oculis* (*so*), optix, eyes absent (eya), dachshund (dac), eye gone (eyg), and twin-of-eyegone (toe) are all required for fly eye formation. Individually or in combinations, these genes can also induce ectopic eyes, sometimes in the absence of eyeless. For instance, both toy and optix can induce ectopic eyes via an *ey*-independent mechanism. In the fly, a model has developed in which the retinal determination genes described above behave as a network with both hierarchical components and regulatory feedback loops.

In recent years, it has been discovered that an analogous – but by no means identical – transcription factor network may also be at work during vertebrate eye formation. As described above, fly retinal determination genes have the ability to induce ectopic eyes. Similarly, some EFTFs can induce ectopic retinal tissue and lenses in vertebrates. For example, in the frog, ectopic expression of Pax6 leads to the formation of ectopic eye-like structures. Lineage-tracing experiments show that the lens, retina, and retinal pigment epithelium of these eyes all arose in response to Pax6. Molecular markers confirmed the presence of some retinal cell types in the induced eyes. In a similar manner, ectopic expression of either fish or mouse Six3 promotes the formation of ectopic lens and retina cells. Remarkably, Six3 mis-expression was also reported to promote the formation of ectopic tissues with an optic vesicle-like structure in the hindbrain–midbrain region of developing mouse embryos. Experiments performed in fish and frogs also show that Rax homologs can induce eye tissues. The mechanisms by which individual EFTFs induce the formation of eye tissue are still unclear. Dosage is important. In the case of frog Six6, relatively low doses stimulate the proliferation of eye-field cells, dramatically increasing the size of the eye field and eventually resulting in the growth of eyes nearly twice their normal size. At higher doses, ectopic eyes form in the rostral brain, suggesting that tissue which would normally form midbrain is respecified to form retina.

A likely mechanism is the ability of the vertebrate EFTFs to induce each other's expression. Pax6, Six3, Rax, and Six6 activate each other's expression, while inactivation of each, sometimes, reduces the expression of the others. When high doses of Six6 or Six3 sufficient to drive ectopic eye formation are injected into frog or fish embryos, the expression of genes normally present in the rostral brain is lost, while Pax6 and Rax are induced in their place. When eye-inducing levels of Pax6 are injected into frogs, ectopic expression of Rax and Six3 are detected. Some of these EFTF interactions are direct – that is, they involve one transcription factor binding to and activating the regulatory sequences of another. For instance, experiments using *in vitro* and transgenic approaches in mouse have demonstrated that Pax6 and Six3 bind directly to regulatory sequences in each other's gene. In addition to regulating each other's expression, both Pax6 and Six3 induce their own expression in developing embryos. Not all the inductive effects of the EFTFs on one another's expression are direct. For example, in $Pax6^{-/-}$ mice, early expression of Rax, Six3, and Lhx2 is unaffected. Similarly, Pax6, Six3, and Rax expression are normal in the small-eyed $Six6^{-/-}$ mouse. Intervening, yet-to-be-discovered signaling cascades remain to be identified. Nevertheless, these results demonstrated that EFTFs form a genetic network that has been partially conserved during evolution, which, in the anterior neural plate of vertebrate embryos, is required for eye primordia formation.

The Coordinated Expression of EFTFs is Sufficient for Eye Formation

As described above, the EFTFs are coordinately expressed in the eye of multiple species during its formation and they can regulate each other's expression. There is clear evidence from experiments with the retinal determination genes in flies that they can act coordinately, forming protein–protein interactions to activate downstream targets necessary for ectopic eye formation. For example, *Drosophila sine oculis* physically interacts with eyes absent through the Six domain, and, together, they can induce ectopic compound-eye formation. Vertebrate EFTFs have also been shown to act synergistically. In frogs, mis-expression of Six6 dramatically increases eye

size by stimulating the proliferation of eye-field cells. In contrast, Pax6 alone has no effect on eye size. However, when co-expressed in the eye field of developing frogs, Pax6 potentiates the effect of Six6 on eye enlargement. Recent evidence also suggests that Pax6 and Lhx2 act synergistically by binding to and regulating Six6 expression. As in fly, functional interactions have also been detected among the vertebrate EFTFs. *In vitro* and *in vivo* assays show Rax physically associates with and can enhance the Pax6-mediated transactivation of a minimal promoter. Pax6 can also associate with Six3 and Lhx2 *in vitro*. Dach is the mouse homolog of the eye-inducing fly gene dachshund. Six6 physically associates with Dach and, together, they regulate mouse retinal cell proliferation by co-repressing the cyclin-dependent kinase inhibitor p27Kip1. Peculiarly, while fly dachshund mutants lack eyes, mouse Dach – which is expressed in developing eyes – does not appear to be required for mouse eye formation.

Together, these observations lead to the proposal that, in vertebrates – as in the *Drosophila* compound eye – specification might be driven by the coordinated expression of the EFTFs. This model was tested in vertebrates by co-expressing the EFTFs in developing *Xenopus* embryos. Coordinated expression of the EFTFs Tbx3, Rax, Pax6, Six3, Nr2e1, and Six6 with the anterior neural patterning gene Otx2 was found to be sufficient to induce ectopic eye fields and eye structures (**Figure 4**). In contrast to ectopic retinal tissues induced by individual EFTFs, cocktail-induced eyes were generated at a higher frequency, were larger, and develop outside the nervous system at various locations on the body including the belly. EFTF cocktail subsets and inductive analysis has also been used to begin to characterize the network of interactions between vertebrate EFTFs in frogs and generate a working model for the interactions required for eye-field specification. In the model, coordinated expression of the EFTFs specifies the eye field within the presumptive forebrain (**Figure 5**). These results suggested the vertebrate EFTFs redirect noneye cells to an eye-field-like fate since their coordinate mis-expression induced eyes.

To some extent, the model outlined for frog eye-field specification is consistent with results generated using targeted knockout of mouse EFTFs (**Table 1**). In the frog model, Rax is predicted to be upstream of Pax6. Consistent with this order, $Rax^{-/-}$ mice lack normal Pax6 expression in the optic primordia, while Rax expression is unaffected in the $Pax6^{-/-}$ mice. Neither Six6 nor

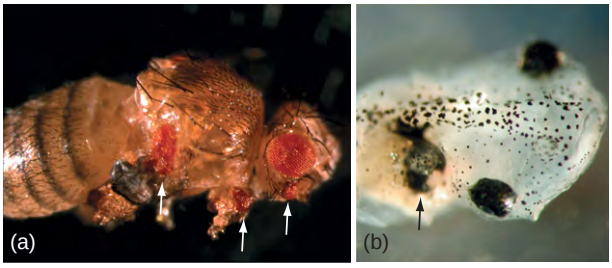

Figure 4 Ectopic Fly and Frog eyes can be generated by misexpression of the Eye Field Transcription Factors. (a) Ectopic eyes (red, white arrows) form on the wing, leg and antennae in response to the misexpression of the *Drosophila eyeless* (*ey*) gene. (b) Similarly, misexpression of a cocktail of vertebrate EFTFs including the frog *Pax6* (a homolog of *Drosophila ey*), *Tbx3*, *Rax*, *Six3*, *Nr2e1, Six6,* and *Otx2* induces the formation of extra frog eyes (white arrow). Fly and images courtesy of Donghui Yang-Zhou (F. Pignoni laboratory) and Andrea Viczian, respectively.

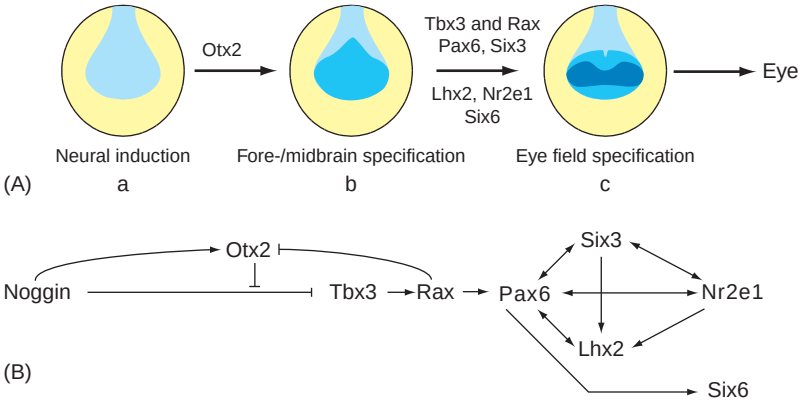

Figure 5 Simplistic model of eye field specification in the anterior neural plate of the frog embryo. (A) The initial neural plate (lightly shaded in a) is patterned to form fate-restricted areas. Otx2 expression is required for patterning of the early fore- and midbrain (b). Finally, the EFTFs form a self-sustaining feedback network that specifies the eye field (darkly shaded in c). (B) Neural induction (initiated by factors including noggin) results in an only partially patterned neural plate. Neural patterning genes like Otx2 then specify different neural regions. The early-expressed EFTFs Tbx3, Rax, Pax6, Six3, and Lhx2 act coordinately to specify the eye field. Although not required for the initial specification of the eye field, evidence suggests Nr2e1 and Six6 play later roles in eye formation. Arrows and bars indicate the induction and repression of target gene expression, respectively. Evidence for some, but not all, aspects of this predicted network are found in other species. Illustration courtesy of Andrea Viczian.

Nr2e1 are required for the initial specification of the eye field in frog. Six6$^{-/-}$ mice have normal (although small) eyes and Nr2e1$^{-/-}$ mice do not develop retinal defects until 3 weeks after birth. In mouse as well as frog, altering Six6 levels does not effect Pax6, Six3, or Rax expression.

Despite these similarities, inconsistencies and clear differences exist between the networks driving eye formation in vertebrates. In the frog model, Tbx3 is positioned upstream of Rax and is required for early eye formation. Although Tbx3$^{-/-}$ mice die as embryos, there are no obvious early eye abnormalities. Mutation of Rx3 (one of three Rax genes in fish) results in eyeless fish. Directly contradicting the frog model, Tbx3 expression is lost in the developing retina. These differences may be species specific or result from the use of different analytical methods. Additional work is needed to more clearly define the genetic interactions among these genes and their role in specification of the vertebrate eye field.

Conclusions

Experiments first performed over a century ago established that the eyes form from the most anterior region of the vertebrate neural plate. However, only recently have genes responsible for eye-field specification been identified. Using multiple techniques and model systems, researchers have identified a network of transcription factors that are required and, in some cases, sufficient for eye formation. In spite of recent work, the functional relationships among the EFTFs are still not clear. In addition to understanding how these gene products regulate each other's expression, future work is also needed to determine the upstream regulators and downstream targets of the EFTFs.

See also: Coordinating Division and Differentiation in Retinal Development; Embryology and Early Patterning; Histogenesis, Cell Fate, and Signaling Factors; Retinal Histogenesis; Zebrafish: Retinal Development and Regeneration.

Further Reading

Chow, R. L. and Lang, R. A. (2001). Early eye development in vertebrates. *Annual Review of Cell Developmental Biology* 17: 255–296.

Donner, A. L. and Maas, R. L. (2004). Conservation and non-conservation of genetic pathways in eye specification. *International Journal of Developmental Biology* 48: 743–753.

Hanson, I. M. (2001). Mammalian homologues of the Drosophila eye specification genes. *Seminars in Cell and Developmental Biology* 12: 475–484.

Kumar, J. P. (2001). Signalling pathways in Drosophila and vertebrate retinal development. *Nature Reviews Genetics* 2: 846–857.

Kumar, J. P. (2008). The molecular circuitry governing retinal determination. *Biochimica et Biophysica Acta* 1789(4): 306–314.

Pappu, K. S. and Mardon, G. (2004). Geneti control of retinal specification and determination in Drosophila. *International Journal of Developmental Biology* 48: 913–924.

Zaghloul, N. A., Yan, B., and Moody, S. A. (2005). Step-wise specification of retinal stem cells during normal embryogenesis. *Biology of the Cell* 97: 321–337.

Zuber, M. E., Gestri, G., Viczian, A. S., Barsacchi, G., and Harris, W. A. (2003). Specification of the vertebrate eye by a network of eye field transcription factors. *Development* 130: 5155–5167.

Zuber, M. E. and Harris, W. A. (2006). Formation of the eye field. In: Sernagor, E., Eglen, S., Harris, W., and Wong, R. (eds.) *Retinal Development*, pp. 8–29. Cambridge: Cambridge University Press.

Eyelid Anatomy and the Pathophysiology of Blinking

C Evinger, SUNY Stony Brook, Stony Brook, NY, USA

Glossary

Blepharospasm – A dystonic muscle contraction disorder characterized by forceful, bilateral, and uncontrolled closure of the eyelids.
Hemifacial spasm – A muscle contraction disorder characterized by forceful uncontrolled contraction of the facial muscles on one side of the face.
Levator palpebrae superioris muscle – A skeletal muscle innervated by cranial motor nerve 3 whose primary function is elevation of the upper eyelid.
Müller's muscle – A smooth muscle that runs from the inferior surface of the tendon of the levator palpebrae superioris to insert into the tarsal plate. It receives sympathetic nervous system innervation.
Omnipause neurons – Part of the brainstem neural circuit that controls saccades. These neurons fire during fixation and cease firing before and during saccadic movements. Stimulation of omnipause neurons interrupts saccades.
Orbicularis oculi muscle – A circumferential muscle of facial expression innervated by the facial nerve that lies just deep to the skin within both eyelids as well as the surrounding bones of the orbital margin. Its main function is closure of the eyelid.
Paresis – Partial paralysis of a skeletal muscle resulting in muscle weakness.
Retractor bulbi muscle – Skeletal muscles innervated by cranial nerve 6 whose function is to retract the eyeball into the orbit causing movement of the nictitating membrane over the surface of the eye.
Saccades – Rapid eye movements that redirect the line of sight so that the image of interest falls on the fovea of the retina.
Vergence – The coordinated movements of both eyes in opposite directions in order to maintain binocular vision.

Organization of the Eyelid System

To understand the neural control of eyelids, the basis of neurological diseases affecting eyelid control, and how the eyelids protect the eye, think about the evolutionary origins of eyelids. For fish, a class of vertebrates without eyelids, eye protection primarily requires avoiding objects hitting and damaging the cornea. To avoid objects hitting the eyeball, fish retract their eyes into the orbit by co-contracting their extraocular muscles. Thus, cornea protection was initially linked to neural circuits whose primary goal was to move the eye. When vertebrates moved onto the land, the development of eyelids was a critical step in reducing the dehydrating effects of air on the cornea. Although goblet cells, lacrimal and meibomian glands produce the fluids to coat the corneal surface, it is blinking of the eyelid that spreads the tears to restore the tear film, which maintains corneal hydration. In addition, blinking removes small objects from the surface of the eye and provides some protection from objects getting into the eye. Although blinking is essential for maintaining the cornea, lid closure has the undesirable side effect of blocking vision. Thus, an eyelid control system must generate blinks that minimally disrupt vision while adequately protecting the cornea. The nervous system deals with this constraint by developing fast eyelid closure and opening without carefully controlling absolute eyelid position. The other restriction on the nervous system's management of the eyelids is that they must move synchronously with vertical eye movements to avoid blocking vision. Overcoming this problem requires the nervous system to control eyelid position accurately. The eyelid control system accomplishes this feat by linking itself to the eye movement system. The melding of the eyelid system with the eye movement system reveals itself first in the anatomical organization of the eyelids.

Only four forces act on the upper eyelid (**Figures 1(a)** and **2**). (1) The phasically active orbicularis oculi (OO) muscle actively closes the eyelid. The ipsilateral facial (VII) nucleus innervates the OO muscle. (2) The tonically active levator palpebrae superioris (LP) muscle actively elevates the upper eyelid. LP innervation arises from the oculomotor (III) nucleus. (3) Raising the eyelid stretches the superior transverse (Whitnall's) ligament and the lateral and medial canthal tendons to create a passive downward force. Thus, the lowest energy state for the eyelid is closed. (4) Müller's smooth muscle (**Figure 2**), which bridges the belly and the tendon of the LP, raises the eyelid approximately 1.5 mm with sympathetic activation. Post-ganglionic nerves from the superior cervical ganglion innervate Müller's muscle. The interaction between the first three forces (OO, LP, and passive downward forces) enables

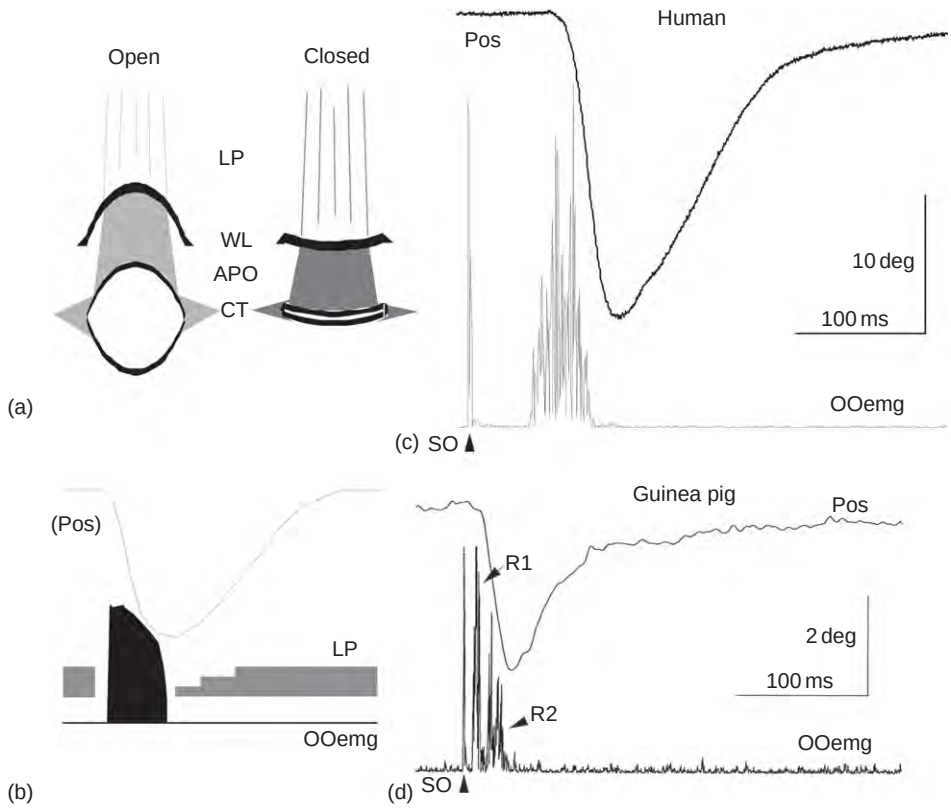

Figure 1 Forces acting on the eyelid and mammalian blinking. (a) Opening the eye stretches the levator palpebrae (LP) aponeurosis (APO), the superior transverse ligament (Whitnall's ligament, WL), and the medial and lateral canthal tendons (CT) to create passive downward forces. The lowest energy state for the eyelid system is closed. (b) Lid (Pos) lowering during a blink results from a transient relaxation of the LP followed by a phasic activation of the orbicularis oculi (OO) muscle. Raising the eyelid occurs as the LP resumes its tonic activity following the completion of OO activity. Gray indicates LP activity and black indicates OO activity. (c, d) Individual examples of a reflex blink evoked by stimulation of the supraorbital branch of the trigeminal nerve (SO ▲) for a human (c) and a guinea pig (d). R1 is the short latency response and R2 is the long latency response seen after nerve stimulation. Abbreviations: OOemg, orbicularis oculi EMG; Pos, upper eyelid position.

the eyelids to blink rapidly yet accurately match the vertical position of the eyeball.

The characteristic rapid eyelid closure of a blink followed by lid opening at approximately half the speed of lid closure follows directly from the anatomical organization of the eyelid (**Figures 1(b)–1(d)**). A blink begins with relaxation of the tonically active LP muscle. LP relaxation releases the passive downward forces to initiate lid closure. The phasically active OO muscle discharge combines with the passive downward forces to lower the eyelid rapidly. As the OO muscle relaxes, the LP muscle slowly resumes its tonic discharge. This LP contraction raises the upper eyelid. Eyelid elevation is slower than lid closure because the LP muscle must work against the passive downward forces. The point at which the tonically active LP force matches the passive downward force created by tendon and ligament stretching determines final lid position. This anatomical organization is conserved so that the pattern of blinking is similar among mammals (**Figures 1(c)** and **1(d)**).

In contrast to the interactions between the OO and LP muscles and passive downward forces with blinking, the coordination of eyelid motion with vertical eye movement arises from the antagonistic interactions between the LP muscle and the passive downward forces. The linkage with eye movements occurs because the LP behaves like the superior rectus muscle, which rotates the eye upward. Embryologically, the LP muscle arises from the superior rectus muscle, and LP motor neurons are always adjacent to superior rectus motor neurons in the oculomotor nucleus. LP and superior rectus motor neurons exhibit similar patterns of activity except during a blink. The tonic firing frequency of superior rectus and LP motor neurons correlates with vertical eye position. With an upward saccadic eye movement, superior rectus and LP motor neurons generate a burst of action potentials followed by an increased tonic firing frequency that holds the eye in the new elevated position. A downward saccade results from a cessation of tonic activity followed by a lower frequency tonic discharge to hold the eye in the

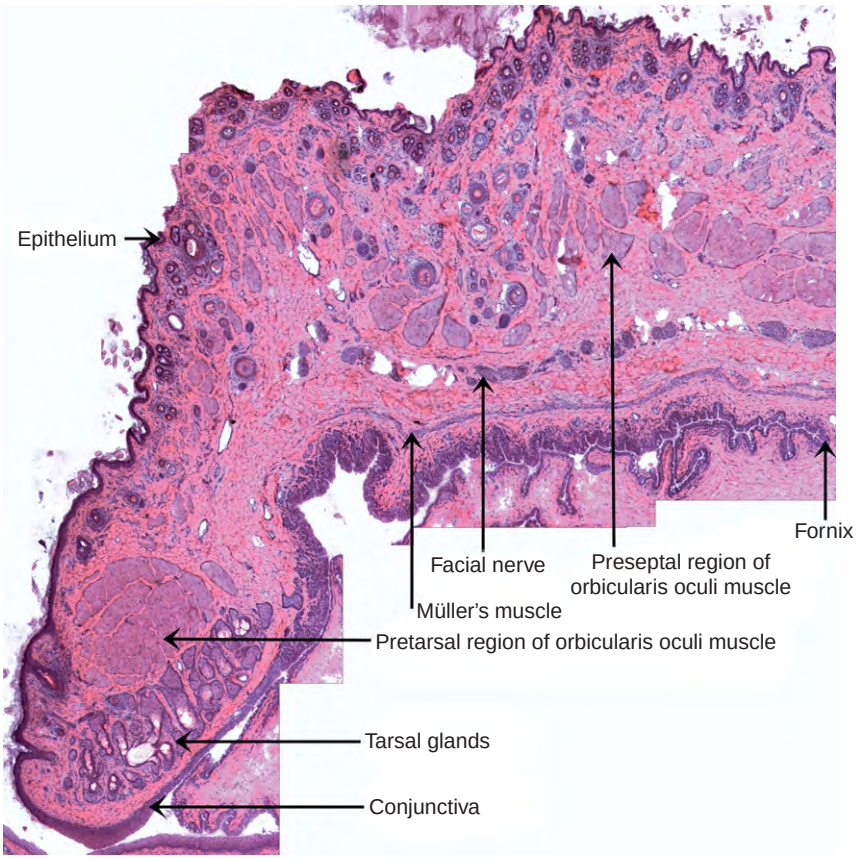

Figure 2 Montage of a sagittal section of the eyelid from an adult rabbit stained with hematoxylin and eosin. Courtesy of Dr. Linda K. McLoon.

depressed position. When the LP motor neurons transiently cease discharging during a downward saccadic eye movement, unopposed passive downward forces lower the eyelid. When the LP motor neuron resumes its activity at a lower tonic firing frequency, the new balance point between passive downward forces and active upward LP muscle force establishes the final eyelid position. With an upward eye movement, the increased LP motor neuron firing frequency pulls the eyelid upward until the LP muscle and passive downward forces match. Although it seems counter-intuitive that passive downward forces rather than the OO muscle act as the antagonist to the LP muscle with eye movements, it is clear that the OO does not participate in eyelid movement with vertical saccades. For example, individuals with OO denervation created by seventh nerve palsy exhibit nearly normal saccadic lid movements with vertical saccadic eye movements, but abnormally slow blinks.

Further evidence of the evolutionary linkage of blinking with the oculomotor system is that blinks frequently occur with saccadic eye movements. These gaze-evoked blinks most commonly accompany large saccades to visual targets that do not have a strong behavioral significance. The advantage of combining blinks with saccades is that visual suppression occurs during both blinks and saccades. A gaze-evoked blink refreshes the tear film, but does not produce more loss of vision than the saccadic eye movement. The evolutionary linkage also appears in the eye movements associated with blinking, blink-evoked eye movements. When looking straight ahead, there is an adducting and downward rotation of the eye with each blink. Nevertheless, the state of the eyelid system determines the trajectory of blink-evoked eye movements. These movements exhibit an upward trajectory in both eyes and are smaller than normal in individuals with a unilateral seventh nerve palsy. Eyeball retraction is also a component of these blink-evoked eye movements. For mammals, the eyeball retraction with blinking results from extraocular muscle co-contraction and contraction of the retractor bulbi muscle. This accessory extraocular muscle is innervated by motor neurons in the accessory abducens nucleus that send their axons to the orbit as part of the VIth nerve. Extraocular muscle co-contraction with blinking in mammals appears to reflect the evolutionary origins of the eyelid control system from eye retraction of fish. Despite blink-evoked eye movements accompanying all blinks, neither gaze-evoked nor reflex blinks occurring with a saccade prevent the eye from achieving its desired endpoint. With a simultaneous blink and saccade, the eyes follow a complex trajectory instead of the nearly straight path of a saccadic eye movement alone. This complex

trajectory results in a significantly slower saccade than when the saccade occurs alone.

The linkage between blinking and saccadic eye movements indicates that blinking interacts with the brainstem circuits that generate saccadic eye movements. This interaction is apparent when reflex blinks increase the speed of saccadic eye movements in individuals with abnormally slow saccades, initiate saccade oscillations, and alter the speed of vergence eye movements where the eyes are moving in opposite directions. The neurophysiological mechanism that may underlie these effects is the activity of omnipause neurons, which control fixation, and are associated with reflex blinks. Tonically active omnipause neurons gate saccadic eye movements. Omnipause neurons cease discharging immediately before and during all saccadic eye movements and reflex blinks. Microstimulation of omnipause neurons blocks reflex blinks as well as saccadic eye movements. The evolutionary origins of eyelid control functionally intertwine blinking and saccadic eye movements so that blinks frequently occur with saccadic eye movements, blinking modifies the trajectory of eye movements, and blinking and saccadic eye movements utilize some of the same brainstem neuronal circuits.

Modifiability of the Blink System

In order to respond to challenges to the eyelid's protective function, the neural control of blinking exhibits significant adaptive plasticity. The most common challenge to the protective function of blinking is the development of dry eye. Cornea irritation created by tear film inadequacy rapidly initiates several changes. First, the trigeminal system becomes more excitable, so that a given blink-evoking stimulus elicits a bigger blink than before cornea irritation. In addition to increased blink excitability, the trigeminal reflex blink circuit begins to 'oscillate' in response to a blink-evoking stimulus (**Figure 3**). In this condition, a single stimulus evokes a reflex blink followed by blink oscillations, one or more additional large blinks. Blink oscillations occur at a constant interblink interval. These modifications compensate for dry eye in at least two ways. The reduced threshold for evoking a blink produces more frequent blinking so that blinks can occur before significant disruptions of the tear film. The larger blinks increase the amount of meibum released over the tear film. Increasing the thickness of the oily meibum layer superficial to the aqueous layer reduces aqueous evaporation. Disruptions of these normally adaptive mechanisms may underlie neurological disorders involving the eyelids, benign essential blepharospasm (BEB) and hemifacial spasm (HFS).

We have an outline of the neural basis for these adaptive modifications of the blink reflex initiated by eye irritation. The adaptive changes occur in trigeminal blink circuits, but not at OO motor neurons or reticular neurons receiving bilateral trigeminal inputs. If just one eye experiences irritation, stimulating the ophthalmic branch of the trigeminal nerve on the irritated side elicits adaptive blink modifications in both eyelids. Stimulating the contralateral trigeminal nerve associated with the unaffected eye, however, elicits normal, unadapted blinks in both eyes. Consistent with this result, spinal trigeminal neurons in the corneal-evoked blink circuit discharge before blink oscillations, and this discharge correlates with the pattern of OO activity producing the blink oscillation. Although the adaptive processes clearly involve the trigeminal system, the cerebellum is also essential for blink adaptation. Blink-related neurons in the cerebellum are active with blink adaptation, and lesioning the cerebellum blocks this form of motor learning. A hypothesis for the function of this brainstem–cerebellum circuit is that the cerebellum recognizes an error signal produced by eye irritation and then initiates modifications in spinal trigeminal blink circuits to compensate for the eye irritation. These adaptive modifications in the trigeminal blink circuits may involve long-term potentiation (LTP)- and long-term depression (LTD)-like processes.

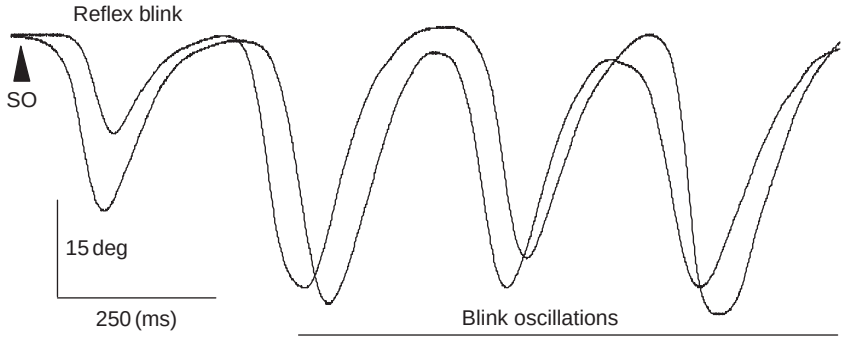

Figure 3 Stimulating the supraorbital branch of the trigeminal nerve (SO ▲) evokes a reflex blink followed by additional blinks with a constant interblink interval, blink oscillations. Each upper eyelid position trace is a record from a single trial from an individual with dry eye.

As discussed in the next section, the cerebellum appears to be an important element in creating the symptoms of dystonic movement disorders such as BEB.

Benign Essential Blepharospasm and Hemifacial Spasm

BEB is a focal dystonia characterized by involuntary bilateral spasms of lid closure, trigeminal reflex blink hyperexcitablity, and photophobia (i.e., excessive sensitivity to light). BEB frequently begins with a complaint of ocular discomfort. The available evidence indicates that BEB arises from the confluence of a predisposing and a precipitating factor. Although the predisposing factor has not been identified, the genetic basis for other forms of dystonia suggests that the predisposing factor for BEB is genetic. The precipitating factor appears to be ocular irritation. Consistent with eye irritation as the precipitating factor is that BEB characteristics appear to be an exaggeration of the normally adaptive response to dry eye. For most individuals, the spasms of lid closure in BEB are rapid, repetitive contractions of the OO muscle. This spasm pattern is equivalent to shortening the interblink interval of the blink oscillations developed in response to dry eye (**Figure 3**). BEB patients exhibit trigeminal reflex blink hyperexcitability. One adaptive response to dry eye is to elevate trigeminal reflex blink excitability, although this increase accompanying dry eye is not as profound as occurs with BEB. The trigeminal hyperexcitability with BEB is sufficient to explain the photophobia. Consistent with the exaggeration of dry eye hypothesis, photophobia is present with dry eye although the light sensitivity is not as debilitating as with BEB. Thus, the exaggerated dry eye hypothesis proposes that BEB begins with the onset of dry eye or significant eye irritation. The nervous system initiates blink modifications to compensate for this irritation, but the genetic predisposition prevents the nervous system from recognizing that the adaptive changes corrected the ocular irritation. The nervous system responds by further increasing these adaptive modifications until the normally compensatory mechanisms becomes so maladaptive as to create the BEB syndrome.

Although genetic modifications probably create the predisposing environment for BEB, the genetics underlying this focal dystonia are not yet clear. Most investigators argue that there is an autosomal dominant transmission with reduced penetrance in BEB. One challenge to linking genetics to specific types of dystonia, however, is that individuals with the same genetic mutation may exhibit very different forms of dystonia. For example, individuals with the DYT1 mutation responsible for the most common form of generalized dystonia may exhibit generalized dystonia, focal dystonia, or may be asymptomatic. Individuals with generalized dystonia, focal dystonia, and asymptomatic DYT1 carriers all exhibit a similar pattern of abnormal brain activity. Positron emission tomography (PET) and functional magnetic resonance imaging (fMRI) scans reveal hyperactivity in the basal ganglia, primary motor cortex, supplementary motor area, putamen, thalamus, and cerebellum. In patients with BEB, these areas are also active, but the focus of abnormal activity is in the brainstem and cerebellum. Abnormal cerebellar activity with BEB supports the hypothesis that abnormal blink adaptation involving the cerebellum is critical in the development of BEB. Consistent with the hypothesis that a genetic predisposing factor affects adaptation or motor learning, individuals with BEB exhibit exaggerated LTP-like plasticity of blink circuits relative to normal subjects.

There are two clear examples in which exaggeration of the adaptive processes initiated by eye irritation or dry eye leads to BEB. A small number of individuals with Bell's palsy develop blepharospasm. The ocular irritation produced by incomplete eye closure, the precipitating factor, initiates unabated modifications that produce the BEB syndrome. As predicted by the exaggerated dry eye hypothesis, implanting gold weights in the paretic (weakened) eyelid, enabling nearly complete closure of the paretic eyelid, reduces eye irritation and allows a resolution of BEB signs. Combining predisposing and precipitating factors can also create a BEB-like syndrome in rats. In this model, a chemical lesion reducing approximately 30% of the dopamine neurons in the substantia nigra pars compacta elevates the excitability of the trigeminal blink reflex circuits. This increased trigeminal excitability acts as the predisposing factor. Transient eye irritation produced by crushing a facial nerve branch providing a portion of the OO innervation acts as the precipitating factor. The reduced eyelid mobility created by this procedure causes eye irritation that initiates adaptive blink modifications. Although the eye irritation resolves following nerve regrowth, rats continue to exhibit spasms of lid closure caused by repetitive bursts of OO activity and hyperexcitable trigeminal reflex blinks. Thus, the evidence indicates that BEB occurs in individuals genetically predisposed to the disorder who experience a precipitating condition, ocular irritation. The ocular irritation initiates a series of normally adaptive modifications. In the presence of the predisposing condition which creates an abnormal environment for motor learning, these modifications become exaggerated to create the signs of BEB.

HFS begins as spontaneous, unilateral spasms of eyelid closure. Over a period of weeks to months, the spasms expand to include the rest of the facial muscles on that side of the face. Another characteristic of HFS is synkinesis in which there is an involuntary activation of multiple muscles that normally do not act together. An example of synkinesis is that stimulating the supraorbital branch of the trigeminal nerve would strongly activate the mentalis muscle, as well as the OO, in HFS patients. Unlike BEB,

HFS is unilateral and involves most of the ipsilateral facial muscles in addition to the OO. There is strong evidence, however, that HFS also arises from a combination of predisposing and precipitating factors that disrupt normal motor learning.

The accepted precipitating factor for HFS is arterial compression at the root entry zone of the facial nerve. The most common blood vessels affecting the facial nerve in HFS are the anterior inferior cerebellar artery, the posterior inferior cerebellar artery, or the vertebral artery. Microsurgical decompression of the facial nerve typically reduces or eliminates the spasms and synkinesis of HFS so that spasms disappear in 64% and synkinesis in 53% of HFS patients within the first week following surgery. After 2–8 months, 90% of patients are spasm or synkinesis free. If arterial compression of the facial nerve alone is responsible for these signs of HFS, however, then decompression surgery should eliminate the spasms and synkinesis in less than 2–8 months. To understand the basis for this delay, it is important to consider what neural modifications might occur in response to pulsatile arterial compression of the facial nerve. A strong argument that facial nerve compression alone is insufficient to cause HFS is that 15–25% of the population exhibits arterial compression of the facial nerve, but do not develop HFS. This observation shows that HFS requires a predisposing factor as well as the precipitating factor, arterial compression of the facial nerve.

Pulsatile arterial compression of the facial nerve can generate many modifications in brainstem neural circuits. Compression injury to motor neuron axons effectively weakens facial muscles, which initiates adaptive modifications. Repetitive antidromic activation of facial motor neurons by pulsatile compression of axons can alter facial motor neuron excitability or motor neuron excitability may increase because of facial motor neuron axotomy, severing the facial nerve fibers. Repetitive orthodromic activation of facial muscles by pulsatile compression of motor neuron axons can lead to a reorganization of sensory trigeminal circuits. Simultaneous orthodromic (electrical impulses traveling in the normal direction) activation of muscles that normally do not act together, for example, mentalis and OO, causes trigeminal primary afferent sensory signals from mentalis and OO muscle contraction to reach second-order trigeminal neurons synchronously. This abnormal pairing of sensory inputs can restructure trigeminal receptive fields so that the second-order trigeminal neurons respond strongly to inputs from both mentalis and OO activity instead of weakly to one and strongly to the other. Pulsatile activation of the facial nerve can also augment reflex circuit excitability because of synchronous activation of circuit elements. Second-order trigeminal neurons receiving synchronous afferent inputs innervate facial motor neurons that are already depolarized by antidromic activation. This activity pattern can strengthen trigeminal inputs onto facial motor neurons in a spike timing-dependent plasticity-like manner.

It is clear that pulsatile activation of the facial nerve can produce blink modifications, but these changes should not cause HFS by themselves. The eyelid system normally modifies itself so as to perform appropriately in the face of changes in the motor system or sensory inputs. For example, creating unexpectedly large blinks by adding weights to the upper eyelids initiates a rapid reduction in the trigeminal drive onto OO motor neurons. Similarly, chronic, repetitive facial nerve stimulation, such as occurs with pulsatile facial nerve compression, reduces blink amplitude. Thus, pulsatile facial nerve compression is insufficient to cause spasms of lid closure because the blink system will modify itself to prevent spasms of lid closure. The significant number of humans not experiencing HFS, but exhibiting arterial compression of the facial nerve, further supports this interpretation. These observations indicate that HFS, like BEB, requires a predisposing factor to develop spasms. Like BEB, an autosomal-dominant genetic mutation with low penetrance may provide the predisposing condition, which disrupts normally adaptive processes to create a pathological condition.

See also: Cranial Nerves and Autonomic Innervation in the Orbit.

Further Reading

Bour, L. J., Aramideh, M., and de Visser, B. W. (2000). Neurophysiological aspects of eye and eyelid movements during blinking in humans. *Journal of Neurophysiology* 83: 166–176.

Evinger, C., Manning, K. A., and Sibony, P. A. (1991). Eyelid movements. Mechanisms and normal data. *Investigative Ophthalmology and Visual Science* 32: 387–400.

Fukuda, H., Ishikawa, M., and Okumura, R. (2003). Demonstration of neurovascular compression in trigeminal neuralgia and hemifacial spasm with magnetic resonance imaging: Comparison with surgical findings in 60 consecutive cases. *Surgical Neurology* 59: 93–99; discussion 99–100.

Manning, K. A. and Evinger, C. (1986). Different forms of blinks and their two-stage control. *Experimental Brain Research* 64: 579–588.

Nielsen, V. K. and Jannetta, P. J. (1984). Pathophysiology of hemifacial spasm: III. Effects of facial nerve decompression. *Neurology* 34: 891–897.

Rambold, H., Sprenger, A., and Helmchen, C. (2002). Effects of voluntary blinks on saccades, vergence eye movements, and saccade–vergence interactions in humans. *Journal of Neurophysiology* 88: 1220–1233.

Sibony, P. A. and Evinger, C. (1998). Normal and abnormal eyelid function. In: Miller, N. R. and Newman, N. J. (eds.) *Walsh and Hoyt's Clinical Neuro-Ophthalmology,* vol. 1, pp. 1509–1594. Baltimore, MD: Williams and Wilkins.

Sparks, D. L. (2002). The brainstem control of saccadic eye movements. *Nature Reviews Neuroscience* 3: 952–964.

VanderWerf, F., Brassinga, P., Reits, D., Aramideh, M., and Ongerboer de Visser, B. (2003). Eyelid movements: Behavioral studies of blinking in humans under different stimulus conditions. *Journal of Neurophysiology* 89: 2784–2796.

VanderWerf, F., Reits, D., Smit, A. E., and Metselaar, M. (2007). Blink recovery in patients with Bell's palsy: A neurophysiological and behavioral longitudinal study. *Investigative Ophthalmology and Visual Science* 48: 203–213.

Fish Retinomotor Movements*

B Burnside, University of California, Berkeley, Berkeley, CA, USA
C King-Smith, Saint Joseph's University, Philadelphia, PA, USA

Glossary

Calycal processes – The microvillus-like projections extending from the distal end of the photoreceptor inner segment ellipsoid to form a chalice-like support around the base of the outer segment.
Ciliary axoneme – The cytoskeletal scaffold of the photoreceptor outer segment, which is composed of nine microtubule doublets that extend from the basal body lying at the distal end of the photoreceptor ellipsoid.
Cyclic adenosine monophosphate (cAMP) – A nucleotide that is generated from adenosine triphosphate (ATP) in response to hormonal stimulation of cell surface receptors coupled to adenyl cyclase. cAMP acts as a signaling molecule by activating A-kinase; it is hydrolyzed to AMP by a phosphodiesterase.
Cytochalasin D – A drug that inhibits polymerization of actin monomers into actin filaments, and thus inhibits actin-dependent motility.
Dynein – A member of a family of large motor proteins that undergo ATP-dependent movement along microtubules toward the microtubule's slow-growing (minus) end.
Ellipsoid – The mitochondria-rich distal region of the photoreceptor inner segment between the myoid and the outer segment.
K_d – Dissociation constant, measure of the tendency of a complex to dissociate.
Kinesin – A member of a family of motor proteins that undergo ATP-dependent movement along microtubules toward the microtubule's fast-growing (plus) end.
Myoid – The neck-like region of the photoreceptor inner segment between the nucleus and the ellipsoid, so called because it elongates and contracts in lower vertebrates.
Polymerase chain reaction (PCR) – The technique for amplifying specific regions of DNA by multiple cycles of DNA polymerization, each followed by a brief heat treatment to separate complementary strands.
Sodium/potassium adenosine triphosphatase (Na^+/K^+ ATPase) – The sodium pump, transmembrane carrier protein found in the plasma membrane of most animal cells, which pumps Na^+ out of and K^+ into the cell, using the energy derived from ATP hydrolysis.

Nature and Occurrence

In fish, photoreceptors and retinal pigment epithelium (RPE) undergo retinomotor movements in response to changes in ambient light conditions and to circadian signals. Retinomotor movements include elongation and contraction of the myoid regions of rod and cone photoreceptors and migration of melanin pigment granules (melanosomes) within long apical projections of the RPE (**Figure 1**). In light, cone outer segments are positioned first in line to absorb incoming light and rod outer segments are buried in the dispersed shielding pigment granules of the RPE. In the dark, rods are positioned first in line and RPE pigment granules are aggregated, fully exposing the rod outer segments. Thus, the retina's entire light capture area is rod-dominated at night and cone-dominated in the day.

Cone length changes range from 15 to 80 μm; while rod length changes are generally more modest. Since rates of elongation and contraction are in the range of 1–4 μm min^{-1}, transitions between light-adapted and dark-adapted positions are slow, requiring as much as 60 min in some species. This slowness may explain why mammals evolved the more agile strategy of pupillary dilation for light adaptation.

As these dramatic morphological changes can be easily detected in light micrographs of sectioned retinas, many early studies of retinal morphology were focused on the properties and species distribution of retinomotor movements. After Kühne's initial paper in 1856, the late eighteenth and early nineteenth century produced a huge literature describing retinomotor movements in various vertebrate groups. Retinomotor movements are modest or nonexistent in mammals, urodeles, and reptiles, more robust and widespread in anurans and birds, and most extensive and widely distributed in fishes with duplex retinas. In the pure cone retinas of early fish larvae and in the pure rod retinas of benthic fishes, retinomotor movements are absent.

Retinomotor movements are regulated not only by light but also by an endogenous circadian rhythm. In animals maintained in constant darkness (DD), retinomotor movements persist at expected dawn and dusk. In constant illumination, the cycles of retinomotor movements are suppressed. Circadian cone retinomotor movements have been observed in most fish species studied;

*Adapted from Burnside, B. and King-Smith, C. (2009). Retinomotor movements. In: Squire, L. R. (ed.) *Encyclopedia of Neuroscience.* Oxford: Academic Press.

circadian rod and RPE retinomotor movements are considerably less common. In all species studied to date, cones have been found to contract to their light-adaptive position in anticipation of expected dawn. Thus, for fish in natural environments, a circadian signal, rather than light onset, is the natural trigger for light-adaptive retinomotor movements.

Mechanisms of Force Production for Retinomotor Movements

Many of the earliest studies of retinomotor movement grappled with whether retinomotor movements required energy or represented passive accommodations to other forces. More recent studies using isolated cells have demonstrated that rod, cone, and RPE retinomotor movements can each occur in the absence of other cell types; even in photoreceptor fragments consisting of inner/outer segments only. Thus, force production for photoreceptor elongation and contraction and for pigment migration appears to be locally autonomous for each cell type.

Force Production for Photoreceptor Elongation and Contraction

In photoreceptors, retinomotor movements are effected by cell shape change. Photoreceptors elongate and contract by changing the length of the photoreceptor inner segment, that is, the part of the photoreceptor between the photopigment-bearing outer segment and the junctional complexes of the outer limiting membrane, where photoreceptors are attached by adherens junctions to supportive Müller cells. The motile portions of photoreceptors protrude into the subretinal space between retina and RPE, where they interdigitate with the long apical projections of the RPE cells (**Figure 1**). The interphotoreceptor matrix filling the subretinal space thus lubricates, or at least permits, the shear produced by rods and cones moving in opposite directions. The photoreceptor inner segment is comprised of the distal ellipsoid, containing a mass of aggregated mitochondria, and the more proximal myoid, so named for its ability to undergo retinomotor contraction. Retinomotor shape change is primarily mediated by change in myoid length (**Figures 2** and **3**).

In most vertebrate cells, force production for cell shape change is generated by actin filaments or microtubles, or both. Rods and cones are highly asymmetric cells with highly polarized and paraxially aligned actin and microtubule cytoskeletons (**Figures 2** and **3**). From the distal end of the inner segment, microvillus-like calycal processes extend up around the base of the outer segment. Paraxial bundles of highly cross-linked actin filaments form the cores of the calycal processes, continue through the peripheral cytoplasm of the ellipsoid, and then splay

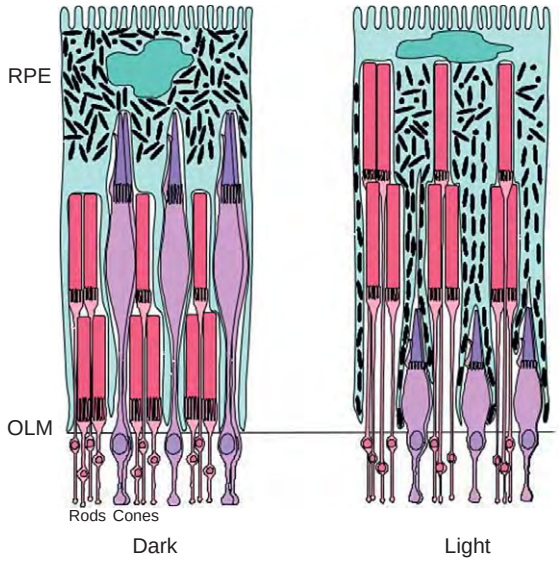

Figure 1 Retinomotor positions of rods, cones, and RPE pigment granules in light- and dark-adapted fish retinas. In dark-adapted retinas, cone myoids (purple) are long, rod myoids (pink) are short, and pigment granules (black) are aggregated to the base of the RPE cell. In light-adapted retinas, cone myoids (purple) are short, rod myoids (pink) are long, and pigment granules (black) have migrated into the long, interdigitating apical projections of the RPE. RPE, retinal pigment epithelium; OLM, outer limiting membrane.

out into a less tightly cross-linked, but still longitudinally oriented, actin filament array in the photoreceptor myoid. The calycal, ellipsoid, and myoid actin filaments are polarized and uniformly oriented with their fast-growing (plus) ends toward the outer segment. Since each type of myosin motor can walk in only one direction along an actin filament, the polarity of actin filaments determines the vector of force production for actin-based motility. Thus, a plus-end-directed myosin motor would walk along a photoreceptor inner segment actin bundle toward the outer segment, while a minus-end-directed motor would walk toward the nucleus. Of the more than 18 classes of myosins, only the class VI myosins have been found to be minus-end-directed motors. All other classes are plus-end directed. Myosins IIA, IIIA, IIIB, VI, VIIA, and IXB have all been shown to be present in fish photoreceptor inner segments. Thus, both plus- and minus-end-directed motors are present in or near the regions of elongation and contraction.

The microtubule cytoskeleton of the photoreceptor consists of two functionally distinct microtubule populations with different properties: the highly stable $(9+0)$ ciliary axoneme of the outer segment, and the more labile paraxially aligned cytoplasmic microtubules of the photoreceptor cell body. Relatively parallel microtubules populate the sleeve of cytoplasm surrounding the mitochondrial mass in the ellipsoid and extend throughout the myoid and axon. As with actin, microtubule polarity and the orientation of the microtubules within a cell play

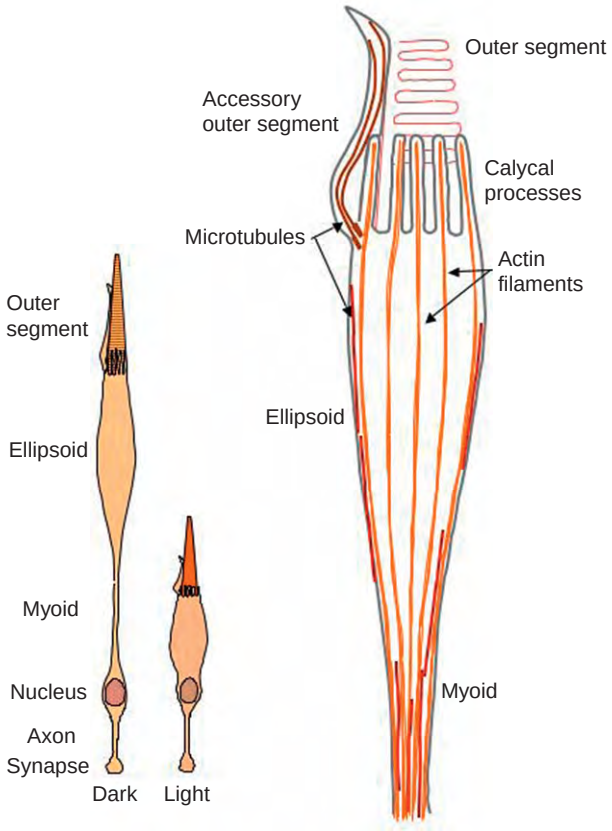

Figure 2 Schematic illustration of teleost cone retinomotor cell shape change and cytoskeleton. Retinomotor length change is mediated primarily by the cone's myoid region. Paraxially aligned actin filaments form the core bundles of cone calycal processes and course through the peripheral ellipsoid and the myoid. Cones possess two populations of microtubules: the axonemal microtubules of the accessory outer segment and the cytoplasmic microtubules of the ellipsoid, myoid, and axon.

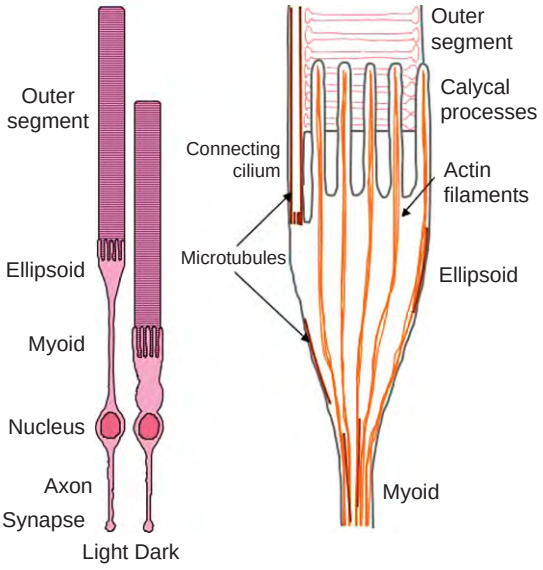

Figure 3 Schematic illustration of teleost rod retinomotor cell shape change and cytoskeleton. Retinomotor length change is mediated primarily by the rod's myoid region. Paraxially aligned actin filaments form the core bundles of rod calycal processes, and course through the peripheral ellipsoid and the myoid. Rods possess two populations of microtubules: the axonemal microtubules of the connecting cilium and outer segment and the cytoplasmic microtubules of the ellipsoid, myoid, and axon.

critical roles in microtubule-based motility. Dynein motors move toward the microtubule minus end and most kinesins move toward the plus end. Both cytoplasmic dynein and kinesin II are found in photoreceptor inner segments. The polarity of the inner segment and axonal microtubules is uniform, with virtually all microtubules oriented with minus ends toward the outer segment. Thus, in a photoreceptor, a minus-end-directed microtubule motor, like dynein, would walk toward the outer segment, while a plus-end-directed microtubule motor, like kinesin, would walk toward the synapse.

Cytoskeletal inhibitors have been used to identify the roles of microtubules and actin filaments in teleost rod and cone retinomotor movements. In cones, dark-adaptive myoid elongation is microtubule dependent (and actin independent), while light-adaptive cone myoid contraction is actin dependent (and microtubule independent). The mechanisms of both microtubule-based elongation and actin-dependent cone myoid contraction are not established. Myosin IIA, a cytoplasmic myosin capable of forming bipolar filaments, is concentrated in the myoids of trout and bass cones, suggesting that muscle-like sliding filaments of actin and myosin might be responsible for cone contraction. Since isolated cone inner/outer segment fragments undergo myoid contraction *in vitro*, it is clear that force production and regulatory machinery necessary for contraction both reside within the inner segment.

In rods, myoid elongation and contraction are both actin dependent and microtubule independent, although microtubules are present in the rod ellipsoid and myoid. Studies using the actin inhibitor cytochalasin D indicate that inhibition of elongation is produced at concentrations so low that actin assembly is blocked but preexisting actin filaments are not disrupted, suggesting that force production for rod elongation depends upon actin assembly. Since quantitative assessment of F-actin indicates that there is no net actin assembly in elongating rod inner outer segments, actin polymerization at the minus ends of filaments must be coupled with depolymerization at filament plus ends. The mechanism of rod contraction is less well studied. Since rod inner–outer segment fragments can both elongate and shorten in culture, it is clear that all necessary machinery is resident in the myoid/ellipsoid (Figure 3).

The RPE Cytoskeleton and Force Production for Pigment Granule Dispersion and Aggregation

Light-induced dispersion of melanin pigment granules (melanosomes) out into the apical projections of fish

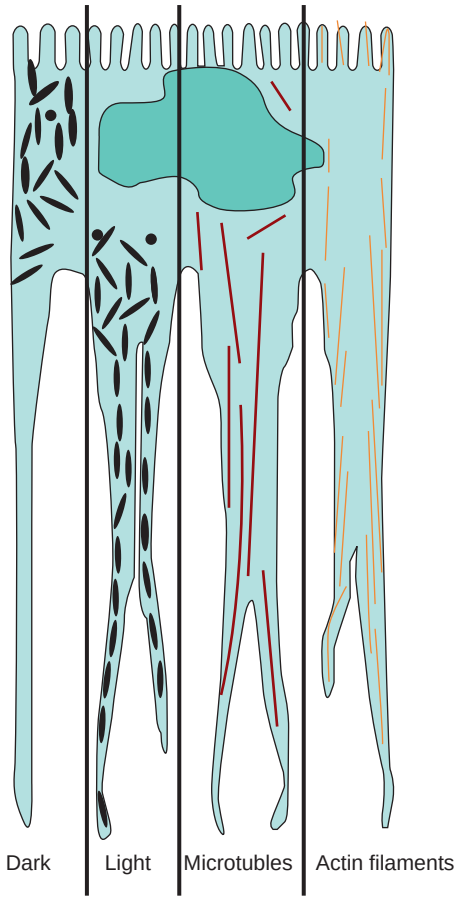

Figure 4 Schematic illustration of teleost RPE retinomotor pigment migration and cytoskeleton. Pigment granules aggregate into the cell body in the dark and disperse into apical RPE projections in the light. Both microtubules and actin filaments are found in the cell body and the apical projections.

RPE cells and dark-induced aggregation of granules back into the RPE cell body results from translocation of individual pigment granules within apical projections of the RPE cells, not from extension and retraction of the apical projections themselves. Apical projections extend from the RPE cell apical surface out into the subretinal space where they interdigitate with photoreceptor inner and outer segments. Thus, when the membrane-bound pigment granules are dispersed, they shield and protect rod outer segments from full bleach in bright light. RPE apical projections may be up to 100 μm long in some fish species and they remain extended throughout the light and dark phases of pigment granule migration.

Apical projections of fish RPE cells contain both actin filaments and microtubules. Microtubule disruption by intraocular injection of inhibitors *in vivo* blocks motility of pigment granules both in the cell body and in the apical projections; this finding would suggest that melanosome movement is microtubule dependent. However, when inhibitor studies are carried out using dissociated RPE cells in culture, microtubule disruption has no effect on melanosome aggregation or dispersion. Presumably, this discrepancy results from the need for microtubules to provide structural support for apical projections, *in vivo*, or to maintain patent tracks or pathways through which pigment granules can move. In isolated cells, on the other hand, the attachment of the projections to the substrate likely keeps projections intact enough to permit pigment granule translocation. Isolated cell studies therefore suggest that microtubules are needed for the structural integrity of RPE apical projections, but the forces that actually power pigment granule translocation are microtubule independent.

In contrast, if the actin cytoskeleton is disrupted by cytochalasin D in dissociated RPE cells, both aggregation and dispersion of pigment granules are reversibly blocked, and maintenance of full aggregation or full dispersion is compromised. Thus, actin filaments are necessary and sufficient for both aggregation and dispersion. The actin dependence of pigment granule translocation in RPE cells suggests that myosin motor proteins are likely to play a role in force production. Polymerase chain reaction (PCR) screens of fish RPE have identified 11 distinct myosins expressed in RPE. Immunocytochemistry with antibodies to four of these myosins indicated that the fish RPE has abundant levels of myosins IIIA, VI, and IXb, and lower levels of myosin VIIa. Myosin VIIa has been immunolocalized on pigment granules in RPE of humans, rodents, and fish, and defective localization of pigment granules to the RPE apical projections in mice with a mutant myosin VIIA gene has been reported. *In vitro* motility assays have shown that isolated teleost RPE pigment granules do support plus-end-directed, actin-dependent motility.

A role for nonmuscle myosin II in RPE pigment granule movement has been implicated in studies using the myosin II inhibitor, blebbistatin, which partially blocked pigment granule aggregation in isolated sunfish RPE cells, but did not affect dispersion. Similarly, inhibitors of Rho guanosine triphosphate (GTP)-binding protein-activated kinase (ROCK), which is involved in myosin II activity, also blocked aggregation. These results suggest myosin II may contribute to pigment granule aggregation, possibly by contracting an actin network with which pigment granules are associated. Myosin IIa was identified in striped bass RPE by PCR amplification of a complementary DNA (cDNA) library.

Intracellular Regulation of Retinomotor Movements: The Role of Cyclic Adenosine Monophosphate

Numerous experimental observations demonstrate that cyclic adenosine monophosphate (cAMP) plays a critical role in the regulation of retinomotor movements in both photoreceptors and RPE. Studies using both intraocular

injections *in vivo* and isolated retinas in culture have shown that a variety of treatments that elevate cAMP (but not cyclic guanosine monophosphate (cGMP)) produce retinomotor movements characteristic of darkness (night). Similar effects were obtained *in vitro* using isolated RPE cells, permeabilized cones, and isolated photoreceptor fragments (inner/outer segments), suggesting that increased cytoplasmic cAMP has a local and direct effect of triggering dark-adaptive retinomotor movements in each cell type. These findings are consistent with many other reports showing that elevated cAMP levels in the dark are a general feature of diurnal and circadian signaling cycles in vertebrate photoreceptors. For example, light and circadian control of photoreceptor melatonin release is closely correlated with changes in intracellular cAMP levels in photoreceptors.

Since inhibitors of cAMP-dependent kinase (protein kinase A (PKA)) block dark-adaptive retinomotor movements in both isolated cone and rod fragments and in intact retinas, it seems likely that cAMP regulates the photoreceptor cytoskeleton via protein phosphorylation. cAMP triggers elongation in detergent-permeabilized cone models, further suggesting that PKA and its targets are detergent-insoluble, and thus likely to be physically associated with the cytoskeleton (or pigment granules). Pharmacological studies of rod inner–outer segment fragments suggest that PKA phosphorylation is enhanced in darkness and that dephosphorylation is required for light-induced elongation (**Figures 5** and **6**).

Regulation of Photoreceptor Retinomotor Movements by Paracrine Messenger

Dopamine

A role for paracrine signaling in light regulation of retinomotor movements is implicated by spectral sensitivity studies of cone retinomotor movements *in vivo*. The action spectrum for light-adaptive cone and RPE retinomotor movements most closely fits the absorption curve of the rod photopigment, suggesting that in cones and RPE, retinomotor movements are not directly triggered by light but are activated indirectly through a rod-mediated pathway. Two experimental observations demonstrate that the

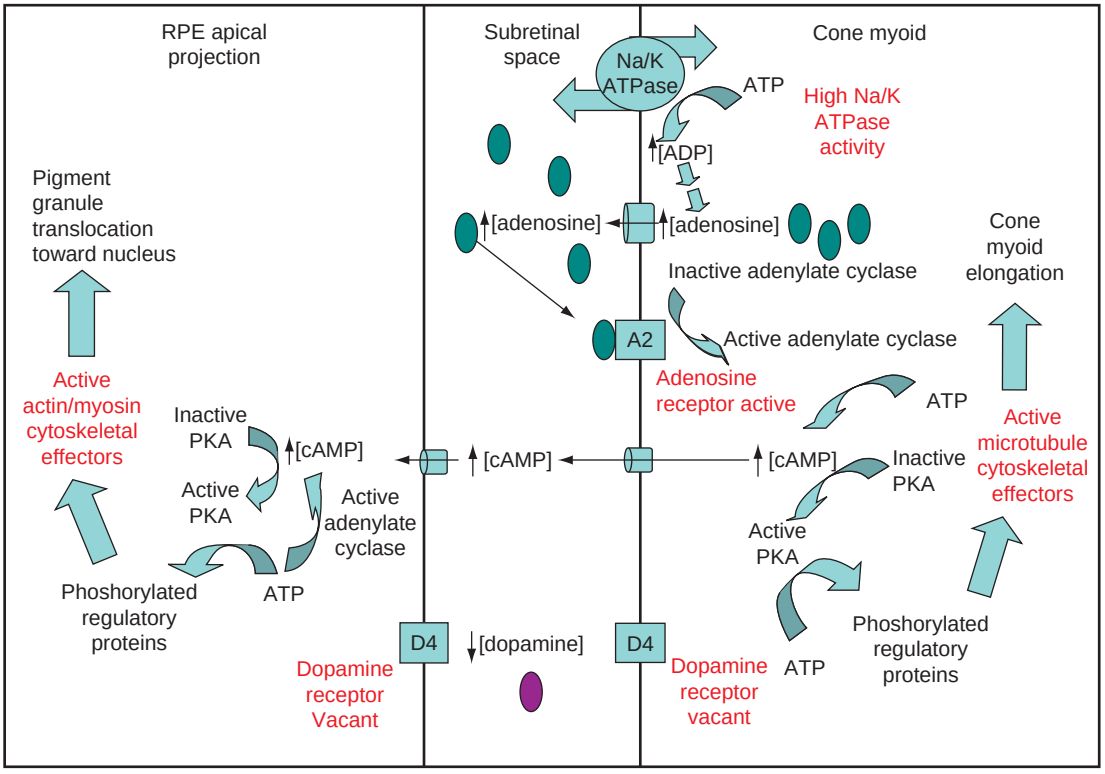

Figure 5 Model of first- and second-messenger signaling in teleost RPE, subretinal space, and cone myoid in darkness. The elevated dark activity of the cone Na/K ATPase elevates cytoplasmic adenosine, which exits through adenosine transporters to the subretinal space. Elevated extracellular adenosine enhances intracellular cAMP level via A2 receptors in cones but not in RPE. Extracellular dopamine levels are low. Elevated cone cytoplasmic cAMP triggers phosphorylation of regulatory proteins that activate microtubule-mediated cone elongation. Cone cytoplasmic cAMP also exits to the subretinal space through organic ion transporters in the cone plasma membrane. From the subretinal space cAMP enters the RPE cell through organic ion transporters, thereby elevating cAMP levels in the RPE cytoplasm and stimulating phosphorylation of regulatory proteins that activate actin-filament-mediated pigment aggregation.

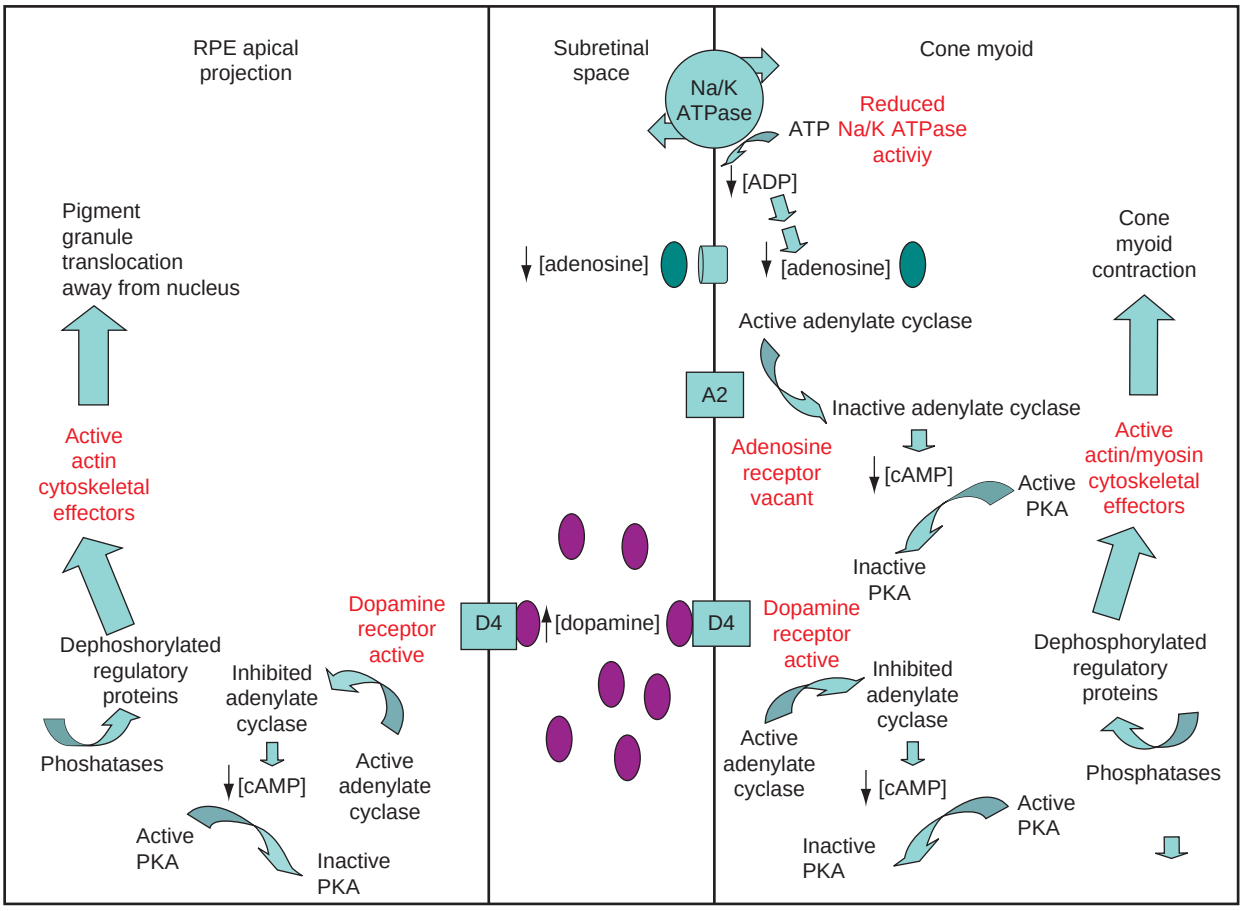

Figure 6 Model of first- and second-messenger signaling in teleost RPE, subretinal space, and cone myoid in the light. Reduced activity of the cone Na/K ATPase in the light reduces adenosine levels in the cone cytoplasm and subretinal space, thus decreasing cAMP production by cone A2 receptors. Increased dopamine release from interplexiform cells in the light produces elevated dopamine levels in the subretinal space. Dopamine activates D4 receptors on the cones and the RPE cells, thereby inhibiting adenylate cyclase and reducing intracellular cAMP in both cell types. Dephosphorylation of cytoskeletal regulatory proteins in cones inactivates microtubule-mediated cone elongation and triggers actin-filament-mediated contraction. Simultaneously, dephosphorylation of cytoskeletal regulatory proteins in RPE activates actin-filament-mediated pigment granule dispersion.

neuromodulator dopamine is a key player in this rod-mediated pathway:

1. intraocularly injected dopamine triggers light-adaptive cone contraction and RPE pigment granule dispersion in animals maintained in the dark, and
2. dopamine antagonists block light-induced cone contraction and RPE pigment granule dispersion in animals moved from darkness to light.

Further evidence that dopamine plays a central role in paracrine regulation of cone retinomotor movements is provided by pharmacological studies using intraocular injection *in vivo*, isolated retinas in culture, and isolated cone inner–outer segment fragments *in vitro*. In each of these preparations, light and/or dopamine promote cone contraction, whereas darkness and/or the adenylate cyclase stimulator, forskolin, promote cone elongation. Pharmacological profiles indicate that dopamine is acting through D4-like or other D2 family dopamine receptors. This class of dopamine receptors causes inhibition of adenylate cyclase and, thus, would be expected to lower cone cytoplasmic cAMP levels, consistent with observations that experimentally increasing cAMP produces dark-adaptive movements.

The ability of light and dopamine to regulate retinomotor movement in isolated cone inner–outer segment fragments indicates that these agents can act directly on cones. Thus, light can trigger cone contraction in isolated cones, even though action spectra indicate that *in vivo* light acts through a rod-mediated pathway. These studies also indicate that D4 dopamine receptors are present on cone inner and/or outer segments. In teleost retinas, the source of dopamine is the interplexiform cell. Since projections of this inner retinal cell extend only into the outer plexiform layer, released dopamine would have to diffuse over tens of microns to reach receptors on the inner

segments *in vivo*. The very high affinity of D4 receptors (dissociation constant (K_d) in the nM range) may facilitate this paracrine mode of signaling.

Light is much more effective than dopamine in triggering myoid elongation in rod fragments, and light and circadian regulation of rod movement was unaffected by treatment with 6-hydroxydopamine, which kills dopaminergic interplexiform cells. Light activation of myoid elongation in rod inner–outer segment fragments *in vitro* requires relatively high light intensities (20% bleach). The photoreceptive mechanism responsible for this activation can apparently count photons accurately for light pulse durations up to at least 10 min, suggesting that the critical factor in light activation of rod elongation is quantum catch, rather than duration of the light stimulus. Similar high-intensity thresholds and photon counting have been reported to mediate entrainment of circadian rhythms in several species.

The observation that dopamine plays a role in circadian as well as light regulation of cone retinomotor movement is suggested by results obtained by intraocular injection of dopamine agonists and antagonists in animals maintained in DD. Cone myoid contraction can be induced at midnight by intraocular injection of dopamine or D4 receptor agonists. Partially contracted cones of DD animals at subjective midday can be induced to contract fully by intraocular injection of dopamine or D4 agonists, or to elongate by injection of the D4/D2 family antagonists. The predawn cone contraction observed in DD animals in response to circadian signals can be completely eliminated by intraocular injection of the D4/D2 antagonist shortly before the expected time of light onset. These observations suggest that circadian regulation of cone myoid length is mediated by endogenous dopamine, acting through D4/D2 family receptors.

Consistent with these findings, retinal dopamine release is higher in the light than in the dark, and dopamine release is higher in subjective day than in subjective night in DD in many species. These diurnal and circadian cycles of dopamine release are inversely correlated with diurnal and circadian cycles of cAMP and protein phosphorylation levels in photoreceptors. Recent findings suggest that dopaminergic amacrine cells contain an autonomous circadian clock that drives dopamine release and metabolism. Although dopamine plays a critical role in regulating fish retinomotor movements, it is nonetheless unlikely to be the sole circadian regulator, since both light-induced and circadian cone movements persist (at reduced amplitude) in fish retinas after lesion of interplexiform cells by 6-hydroxydopamine.

Adenosine

This neuromodulator has an opposite effect to that of dopamine on cone retinomotor movements. In isolated cone inner–outer segment fragments, adenosine A2 receptor agonists activate and A2 antagonists inhibit cone myoid elongation. Since A2 receptors are positively coupled to adenylate cyclase, adenosine effects on cone fragments are consistent with observations that elevating cAMP triggers dark-adaptive retinomotor movements. These findings indicate that A2 receptors must be present on cone inner (and/or outer) segments. Since cones elongate at subjective dusk in fish maintained in DD, and since adenosine stimulates cone elongation, adenosine could provide an endogenous circadian signal for expected dark onset in addition to the decrease in dopamine release occurring at that time.

Adenosine effects on cone movements could be a local effect, reflecting photoreceptor metabolic activity. Since an adenosine transporter is present in photoreceptors, increases in adenosine in photoreceptor inner segments are likely to be accompanied by an increase in adenosine level in the subretinal space. The increased sodium/potassium adenosine triphosphatase (Na^+/K^+-ATPase) activity in photoreceptor inner segments occurring in darkness is likely to be accompanied by an increase in intracellular adenosine levels, and consequently, increased release of adenosine into the subretinal space. The binding of released adenosine to photoreceptor A2 receptors might then enhance dark adaptation of the photoreceptors by stimulating adenylate cyclase, thereby reinforcing the dark signal. Other studies have shown that adenosine triphosphate (ATP) is released across the apical membrane of the RPE into the subretinal space in response to various triggers. This ATP is dephosphorylated into adenosine by extracellular enzymes (ectoenzymes) on the RPE apical membrane. Regulation of adenosine release and ectoenzme activity in response to light signals could also alter the balance of purines in subretinal space and, thus, influence retinomotor movements in cones.

Regulation of Retinomotor Movements in RPE Cells by Paracrine Messengers

RPE pigment migration in frogs has an action spectrum most closely resembling that of the rod photopigment. These observations suggest that for RPE, as for cones, a rod-mediated pathway triggers light-adaptive retinomotor movement. Pigment position is not affected by light in isolated sheets of teleost RPE, further demonstrating that light acts indirectly through a photoreceptor-mediated, paracrine pathway.

In isolated sheets of teleost RPE in culture, dopamine and D2 family agonists induce pigment granule dispersion, while treatments that elevate cAMP induce pigment granule aggregation. In isolated RPE cells aggregated in cAMP, pigment dispersion is induced by microinjection of PKA inhibitors, suggesting that continuous phosphorylation of PKA targets is required to maintain the aggregated state. Since aggregation can also be induced by the phosphatase inhibitor okadaic acid, it seems likely that PKA

and phosphatases are simultaneously active in RPE cells, and that their relative activities are altered by light and dark signals from the retina.

Surprisingly, underivatized cAMP is just as effective as membrane-permeant cAMP analogs at activating pigment granule aggregation in isolated RPE sheets. Washout of exogenous cAMP induces dispersion. This cAMP directly enters the RPE cell through organic ion transporters is suggested by observations that ATP and adenosine are ineffective at triggering aggregation and that organic ion transport inhibitors block cAMP – but not forskolin-induced pigment aggregation. Recently, it has been shown that isolated RPE takes up cAMP in a saturable manner. Thus, it seems clear that cAMP from the subretinal space can actually enter RPE cells through organic ion channels to activate pigment aggregation. These findings indicate that an increase in cAMP in the subretinal space in the dark would activate pigment granule aggregation in RPE cells. cAMP efflux has been shown to be associated with increased intracellular cAMP accumulation in many cell types, including pinealocytes. Thus, diurnal cycles of cAMP levels in retinal photoreceptors might be expected to produce increased cAMP efflux into the subretinal space at night. This extracellular cAMP in the subretinal space could then function as a retina-to-RPE signal for darkness.

cAMP and intracellular calcium often interact in cellular signaling pathways, either antagonistically or synergistically. Pigment granule migration is regulated by calcium in several types of dermal chromatophores. However, increasing extracellular or intracellular calcium has no effect on pigment granule position in either aggregated or dispersed isolated RPE cells. Furthermore, intracellular calcium levels are unaffected when RPE pigment granule motility is triggered by cAMP or cAMP washout. These findings suggest that RPE pigment granule movements are regulated directly by cAMP, that is, by phosphorylation and dephosphorylation of PKA targets, and that calcium does not act downstream of cAMP in the regulatory process.

Carbachol (an acetylcholine analog) triggers dispersion in isolated fish RPE. The carbachol receptor acts through a pathway commonly linked to calcium mobilization and carbachol-induced pigment granule dispersion is blocked by the calcium chelator 1,2-bis(*o*-aminophenoxy) ethane-*N,N,N′,N′*-tetraacetic acid (BAPTA), suggesting that a rise in intracellular calcium plays a role upstream of cAMP in carbachol-induced dispersion.

Functions and Significance of Retinomotor Movements

What role retinomotor movements play in retinal function has been a topic of inquiry and speculation for more than a century. Direct experimental demonstration that retinomotor movements affect vision has been difficult to achieve, primarily because of the difficulty in interfering with retinomotor movements without compromising other aspects of retinal function. Nevertheless, several likely functions for retinomotor movements have been suggested. Occurring generally in species that lack pupillary movements, rod and RPE retinomotor movements provide an alternative mechanism to pupillary movements for shielding rods from full bleach in bright light while permitting optimal exposure for dim-light vision. Repositioning the rod and cone photoreceptors likewise provides an efficient mechanism for optimizing space by positioning the rods first in line to detect light at the focal plane across the entire retinal surface under dim-light conditions, and then moving cones to this position for bright-light vision. These movements permit the entire retinal surface to be used alternately for rod and cone vision. Some have noted that each photoreceptor type is elongated when it is expected to be silent, and suggested that the cable properties of the elongated myoid might contribute to attenuation of the signal from outer segment to synapse. The great morphological variation in retinomotor movements perhaps reflects the optimization of one or the other of these functions in different species.

Summary

Although retinomotor movements are most pronounced in lower vertebrates, their study contributes to a broader understanding of diurnal and circadian regulation of photoreceptor and RPE physiology. Retinomotor movements provide excellent models for investigating the roles of cytoskeletal elements in cell shape change and intracellular transport. Studies of retinomotor movements have called attention to the importance of cyclic changes in intracellular cAMP levels in the diurnal and circadian regulation of other aspects of photoreceptor physiology and metabolism. The recognition that light induction of cone and RPE movements depends on a rod-mediated paracrine pathway has contributed to recognition of the role that dopamine plays in light and circadian signaling. Since retinomotor movements exhibit properties of light and circadian regulation, characteristic of many other aspects of retinal physiology, they provide excellent experimental models for understanding light and circadian-regulatory processes.

See also: Chick Metabolism in the Chick Retina; The Circadian Clock in the Retina Regulates Rod and Cone Pathways; Circadian Regulation of Ion Channels in Photoreceptors; *Limulus* Eyes and Their Circadian Regulation; Neurotransmitters and Receptors: Dopamine.

Further Reading

Ali, M. A. (1975). Retinomotor responses. In: Ali, M. A. (ed.) *Vision in Fishes*, pp. 313–355. New York: Plenum Press.

Arey, L. B. (1915). The occurrence and significance of photomechanical changes in the vertebrate retina – a historical survey. *Journal of Comparative Neurology* 25: 535–554.

Back, I., Donner, K. O., and Reuter, T. (1965). The screening effect of the pigment epithelium on the retinal rods in the frog. *Vision Research* 5: 101–111.

Blaxter, J. H. S. (1975). The eyes of larval fish. In: Ali, M. A. (ed.) *Vision in Fishes*, pp. 427–443. New York: Plenum Press.

Burnside, B. (1988). Photoreceptor contraction and extension: Calcium and cAMP regulation of microtubule- and actin-dependent changes in cell shape. In: Lasek, R. J. (ed.) *Intrinsic Determinants of Neuronal Cell Form*, pp. 323–359. New York: Alan R. Liss.

Burnside, B. (2001). Light and circadian regulation of retinomotor movement. *Progress in Brain Research* 131: 477–485.

Burnside, B. and Dearry, A. (1986). Cell motility in the retina. In: Alder, R. and Farber, D. B. (eds.) *The Retina*, Part 1, pp. 151–206. New York: Academic Press.

Burnside, B. and King-Smith, C. (2009). Retinomotor movements. In: Squire, L. R. (ed.) *Encyclopedia of Neuroscience.* Oxford: Academic Press. http://www.sciencedirect.com/science/referenceworks/9780080450469 (accessed July 2009).

Burnside, B. and Nagle, B. (1983). Retinomotor movements of photoreceptors and retinal pigment epithelium: Mechanisms and regulation. *Progress in Retinal Research* 2: 67–109.

Dearry, A. and Burnside, B. (1989). Regulation of cell motility in teleost retinal photoreceptors and pigment epithelium by dopaminergic D2 Receptors. In: Redburn, D. and Morales, H. P. (eds.) *Extracellular and Intracellular Messengers in the Vertebrate Retina*, pp. 229–256. New York: Alan R. Liss.

Douglas, R. H. (1982). The function of photomechanical movements in the retina of the rainbow trout (*Salmo gairdneri*). *Journal of Experimental Biology* 96: 389–403.

McNeil, E. L., Tacelosky, D., Basciano, P., et al. (2004). Actin-dependent motility of melanosomes from fish retinal pigment epithelial (RPE) cells investigated using *in vitro* motility assays. *Cell Motility and the Cytoskeleton* 58: 71–82.

Pozdeyev, N., Tosini, G., Li, L., et al. (2008). Dopamine modulates diurnal and circadian rhythms of protein phosphorylation in photoreceptor cells of mouse retina. *European Journal of Neuroscience* 27: 2691–2700.

Wagner, H. J., Kirsch, M., and Douglas, R. H. (1992). Light dependent and endogenous circadian control of adaptation in teleost retinae. In: Ali, M. A. (ed.) *Rhythms in Fishes*, pp. 255–292. New York: Plenum Press.

Formation and Regression of the Primary Vitreous and Hyaloid Vascular System

S Rao, Cincinnati Children's Hospital Medical Center, Cincinnati, OH, USA
R A Lang, University of Cincinnati, Cincinnati, OH, USA

Glossary

Angiogenesis – The process of forming new blood vessels from existing blood vessels.
Choroid fissure – A transient opening on the ventral side of the optic cup which provides an entry site for newly forming blood vessels and an exit for newly born retinal axons. Failure of the choroid fissure to close during eye development results in ocular colobomas.
Laser capture microdissection (LCM) – A method for isolating pure cells of interest from specific microscopic regions of tissues or tissue sections.
Lymphangiogenesis – The formation of lymphatic vessels from preexisting lymphatic vessels.
Norrie disease (ND) – An inherited disorder that leads to blindness at birth or soon after, hearing loss, and developmental delay. Mutations in the NDP gene on the X chromosome cause Norrie disease.
Osteoporosis-pseudoglioma syndrome (OPGG) – An autosomal recessive disorder that affects vision and bones. Individuals suffering from this disease exhibit characteristic eye lesions very early in childhood followed by bone fractures that occur later in childhood due to low bone density.
Persistent fetal vasculature (PFV) – Used to be known as persistent hyperplastic primary vitreous (PHPV), it is a congenital developmental anomaly of the eye that results due to the failure of the fetal primary vitreous and hyaloid vasculature to regress.
Pupillary membrane (PM), tunica vasculosa lentis (TVL), and vasa hyaloidia propria (VHP or hyaloid vessels) – The three temporary embryonic vasculatures that provide nutrition to the developing eye. In humans, this vasculature regresses in the third trimester, while in rodents it occurs postnatally.
Retrolental mass – A fibrous mass posterior to the lens and is very commonly observed in many ocular anomalies.

The Anatomy of the Temporary Ocular Vessels

In the developing eye of mammals, there are three connected but anatomically distinct embryonic vascular networks called the pupillary membrane (PM), tunica vasculosa lentis (TVL), and vasa hyaloidia propria (VHP or hyaloid vessels) (Figure 1). These vascular networks have a nutritive function and provide the molecular building blocks as well as the oxygen required for rapid growth of the eye during its developmental phases. These vascular networks are also temporary. In humans, they regress in the third trimester and in rodents, during the first few weeks after birth.

Although a number of species have embryonic ocular vessels, their developmentally scheduled regression appears to be a unique feature of mammals and is presumably an adaptation to allow light transmission from the cornea, through the lens, and to the retina. In humans, congenital defects such as osteoporosis pseudoglioma, and persistent fetal vasculature (PFV) where the hyaloid vessels fail to regress, results in a serious vision deficit. Perhaps this means that in species where embryonic ocular vessels are retained, such as the zebrafish, they may diminish the quality of images formed on the retina.

For the most part, studies of development and regression of the ocular vessel networks have been performed in rodents. Thus, besides occasional reference to other species, this article refers to developmental mechanisms that have been revealed in the mouse and rat. It is highly likely that these same mechanisms apply to humans also.

Development of the Hyaloid Vessels

The hyaloid vessels can first be observed in the mouse eye at about embryonic day (E) 10.5 (Figure 2). At this stage, the surface ectoderm of the embryo has just invaginated to form the lens pit. Lens pit development occurs in coordination with formation of the optic cup which in turn requires invagination of the optic cup along the ventral midline to form the ventral choroidal fissure. The hyaloid artery that is the origin of the hyaloid vessels is engulfed

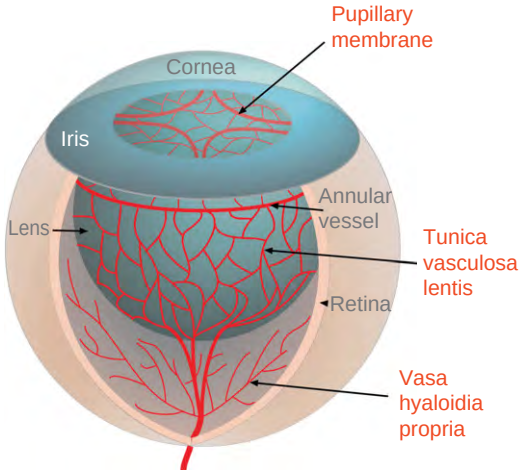

Figure 1 The temporary vessels of the rodent eye. This schematic shows the major components of the temporary vascular networks including the pupillary membrane, the annular vessel, the tunica vasculosa lentis, and the vasa hyaloidia propria (hyaloid vessels). The hyaloid vessels lie against the vitreal face of the retina, and the tunica vasculosa lentis and pupillary membrane against the posterior and anterior hemispheres, respectively, of the lens.

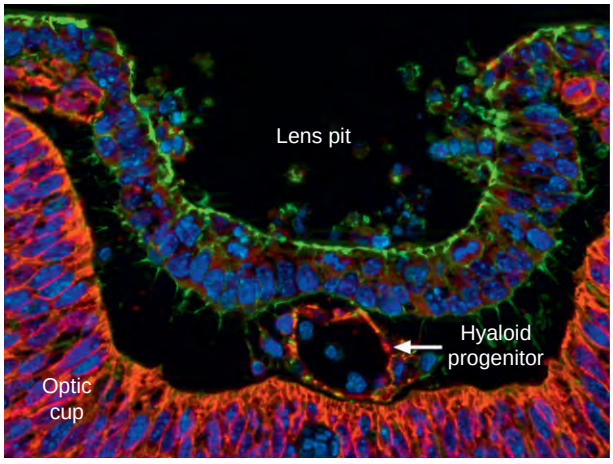

Figure 2 The hyaloid artery at embryonic day 10.5 in the mouse. This micrograph shows the hyaloid progenitor lying between the epithelia of the presumptive lens and retina. Nuclei are labeled blue and filamentous actin is green. The red labeling is junctional β-catenin that can be observed in optic cup and hyaloid artery but not in presumptive lens because this particular example is a mutant conditional for *β-catenin* deletion in the lens lineage.

into the central axis of the eye as the ventral choroidal fissure wraps around it. After this complex morphogenesis, the head of the hyaloid artery is located between the epithelia of the lens pit and presumptive retina (Figure 2).

The presumptive hyaloid vasculature is not a mature network with a hierarchy of vessel sizes but appears more like a vascular sinus. Over the period of E10.5 to E18.5 (the day of birth in the mouse) this early vascular structure changes to appear more like a vascular plexus and then finally into the hierarchical form of a mature structure. As this is occurring, vessels expand from the hyaloid artery over the posterior surface of the developing lens and anterior surface of the developing retina to form the TVL and hyaloid vessels, respectively (Figure 1). While there is a likelihood that this vessel expansion is mediated by the process of angiogenesis (growth of new vessels from existing ones), this has not been directly documented.

Establishment of the PM occurs after the lens vesicle has separated from the surface ectoderm at E12.5. At this time, vessels within the ocular mesenchyme can extend across the anterior eye underneath the presumptive corneal epithelium. As the layers of cornea are formed by successive migrations of neural crest-derived mesenchyme, the PM vessels are displaced toward the lens and ultimately lie in direct contact with the extracellular matrix of the lens capsule that overlies the lens epithelium. After birth, in the mouse, the vessels of the PM are incorporated into the structure of the iris diaphragm as it migrates into the anterior chamber.

As the embryonic ocular vessels develop, they form connections that allow blood flow. As its name would imply, the hyaloid artery directs blood flow into the eye. Blood flowing through the hyaloid artery continues to flow in an anterior direction through the hyaloid vessels and TVL until it reaches the annular vessel. The annular vessel runs in a ring around the lens anterior to the lens equator just underneath the ciliary process and iris (Figure 1). In turn, the annular vessel makes connections with arcades of the PM that extend along the anterior lens posteriorly and underneath the developing iris. The pattern of blood flow in the PM is a little more complex. It has two opposing quadrants in which arterioles direct flow from the iris into the PM. In the two alternating opposing quadrants, venules direct flow from the PM into the iridal vasculature.

Development of the TVL and PM Is Dependent on VEGF Signaling

Vascular endothelial growth factor A (VEGFA) is a key regulator of physiological and pathological angiogenesis and is a member of a larger family of signaling ligands that have a variety of effects on different cell types. Three conventional tyrosine kinase receptors belong to the VEGFA receptor family but only receptors 1 and 2 mediate signaling by VEGFA (Figure 3). The VEGFR2 (aka Flk1) is expressed on vascular endothelial cells (VECs) and is the major mediator of the angiogenic, survival-enhancing, and mitogenic effects of VEGFA. The biology of VEGFR1 (aka Flt1) is more complex as it may act as a VEGFA-sequestering decoy receptor (Figure 3) that prevents VEGFR2 signaling and is expressed on other cell types. The VEGFR1 activation in VECs can result in the

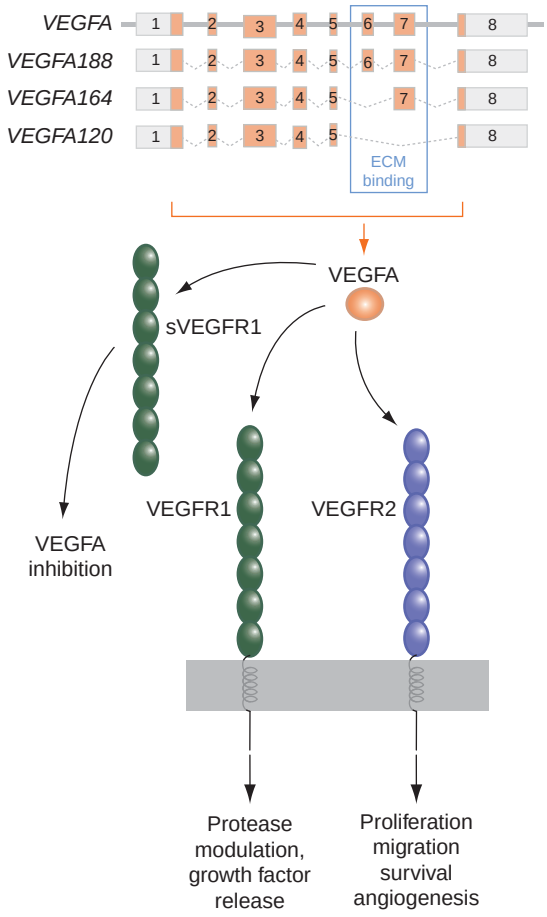

Figure 3 The VEGFA isoforms and receptor signaling. The *VEGFA* gene is shown schematically on the top line as exonic regions that are noncoding (gray) and coding (orange). The mouse isoforms VEGFA188, VEGFA164, and VEGFA120 are the result of alternative splicing patterns for exons 6 and 7 that encode extracellular matrix (ECM) binding domains. The VEGFA isoforms can signal through VEGFR1 (green) or VEGFR2 (blue) that comprise seven extracellular Ig domains and a cytoplasmic tyrosine kinase domain. The VEGRF2 is primarily responsible for the proliferation, migration, and survival responses that constitute angiogenesis. The VEGFR1 signaling can elicit protease modulation responses and can act as a VEGFA inhibitor when it is cleaved from the cell surface into a soluble form.

release of growth factors and matrix metalloproteinases that may be important for VEC migration during angiogenesis and vascular remodeling.

Mouse mutants of VEGFA and VEGFR1 and 2 have defects in development and regression of the ocular vessel networks. In work performed by the Beebe group, conditional deletion of *VEGFA* from the developing lens results in a failure of development of the TVL and the PM, the vessel networks that reside on the surface of the lens. When coupled with studies showing that ECM-binding isoforms of VEGFA are expressed in the lens, this has suggested that VEGFA associates with the matrix of the lens capsule as a way of stimulating angiogenesis locally. Interestingly, *VEGFA* deletion from the developing lens does not obviously affect development of the hyaloid vessels. It is most likely that a retinal source of VEGFA is critical for their development.

Through alternative splicing, VEGFA can form a number of isoforms that are named according to the number of amino acids present (**Figure 3**). These isoforms have distinct characteristics. The VEGF188 incorporates exons 6 and 7 that both encode ECM-binding domains and this binds strongly to the matrix. The VEGF164 incorporates only exon 7 and so is more freely diffusible. The VEGF120 incorporates neither exons 6 nor 7 and is the most freely diffusible. Thus, VEGFA isoforms have a range of biological characteristics.

The D'Amoré group has shown that these three VEGFA isoforms have biological significance for ocular vessel development. In mice that produce only VEGF165, both retinal angiogenesis and regression of the PM, TVL, and hyaloid vessels are normal indicating that this isoform is sufficient for all these processes. Mice that produce only VEGF188 have largely normal retinal angiogenesis (with the exception of a reduced number of arterioles) but have a hyaloid vessel persistence. Similarly, mice that produce only VEGF120 have both a severe retinal angiogenesis defect and persistent hyaloid vessels.

Regression of the Temporary Ocular Vessels Is Macrophage Dependent

Researchers have long wondered about the function of the resident population of ocular macrophages (**Figure 4**), sometimes known as hyalocytes. They may have multiple functions, including perhaps being precursors for retinal microglia, but were more recently shown to be required for regression of the temporary ocular vessels. This was demonstrated by the Lang group using a macrophage-specific diphtheria toxin-expressing transgene and the *PU.1* mutant mouse that shows a complete absence of mature tissue macrophages. In the *PU.1* mutant, all the temporary ocular vessel structures persist suggesting a common regression mechanism. The analysis performed has shown that macrophages are necessary for VEC apoptosis, which is the driving force behind programmed vascular regression. It has also been shown that injected bone-marrow macrophages can restore the regression process in the *PU.1* mutant. This demonstrated that macrophages are sufficient for programmed vascular regression. The suggestion that VEC apoptosis and programmed vascular regression were macrophage-dependent was initially quite controversial but has now generally been accepted. This notion is also very much supported by analysis indicating that in *Caenorhabditis elegans*, the apoptotic cell recognition machinery of phagocytes acts as a backup pathway for actively induced target cell death. Together, these data suggest metazoan conservation of phagocyte-induced cell death.

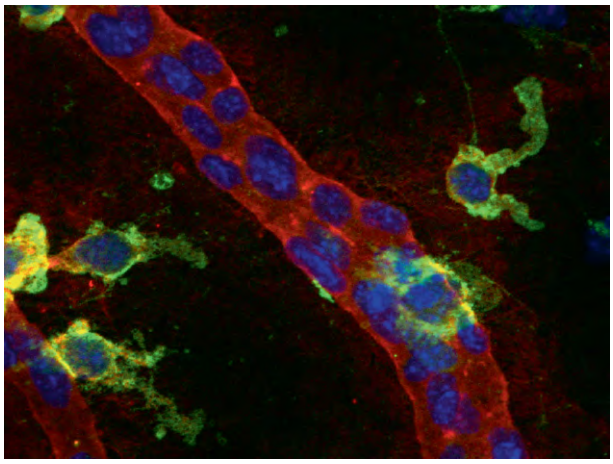

Figure 4 Resident macrophages associated with the hyaloid vessels. Macrophages (yellow-green) are labeled with F4/80 antibody. They associate closely with laminin-labeled capillaries (red). Nuclei are labeled blue.

The Wnt Signaling Pathway

There are a number of possible pathways downstream of Wnt receptor complexes. Since the canonical pathway is critical for hyaloid regression, only this branch is mentioned here. The canonical Wnt signaling pathway has been a major focus of attention because it is critical in embryonic development and tumorigenesis. The signaling system is complex but well characterized (**Figure 5**). There is a family of 18 known Wnt ligands that are lipid modified and therefore poorly soluble. For this reason, it is most likely that the Wnt signaling action occurs upon cell–cell contact. Optimal Wnt signaling requires two transmembrane components, the Frizzled family receptors and the Drosophila arrow-related coreceptors Lrp5 or Lrp6. In the mouse, there are nine Frizzled-related receptors. The Lrp5 and Lrp6 are part of a larger class of receptors related to the low-density lipoprotein receptor, but only Lrp5 and Lrp6 are closely related to arrow, the *Drosophila* Wnt signaling coreceptor.

Engagement of a Frizzled/Lrp5/6 complex by a Wnt ligand results in the activation of Disheveled (Dvl) and, in turn, suppression of the activity of the glycogen synthase kinase-3β (GSK3β), axin, APC complex. In the absence of Wnt ligands, GSK3β phosphorylates β-catenin and causes its degradation via the tumor suppressor gene product APC and the proteasome. When Dvl suppresses GSK3β, β-catenin is stabilized, binds to the TCF/Lef transcription factors, and regulates the target genes. There is a large set of genes known to be directly regulated at the transcriptional level by the canonical Wnt pathway (http://www.stanford.edu/~rnusse/wntwindow.html) and presumably some of these participate in hyaloid regression.

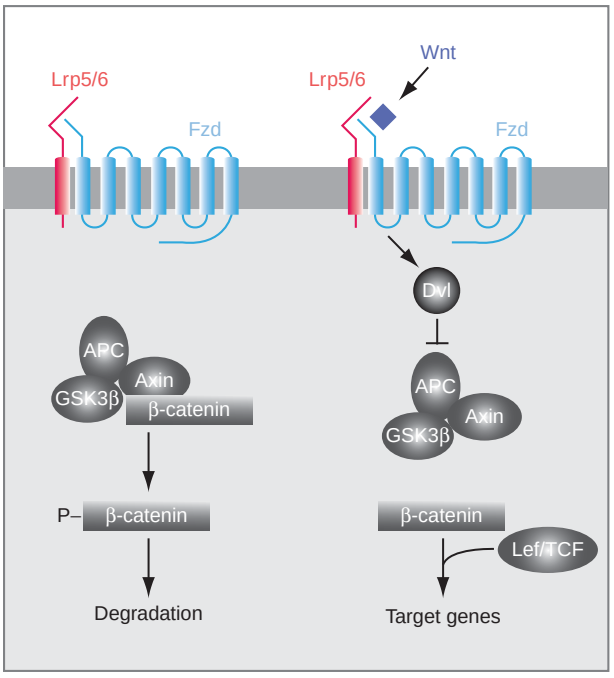

Figure 5 The canonical Wnt signaling system. In the absence of a Wnt ligand, a complex consisting of APC, axin, and GSK3β causes the phosphorylation-mediated degradation of β-catenin. In the presence of a Wnt ligand, Disheveled (Dvl) is activated by the receptor complex and suppresses the APC–axin–GSK3β complex allowing β-catenin to stabilize. In turn, β-catenin associates with transcription factors of the Lef/TCF family and regulates target gene transcription.

Wnt7b Is a Macrophage Ligand Critical for Hyaloid Vessel Regression

The hyaloid vessel persistence characteristic of the human syndrome osteoporosis pseudoglioma is caused by a mutation in the Wnt pathway coreceptor Lrp5. This prompted the Lang group to examine involvement of the Wnt pathway in regulating hyaloid regression. Examination of hyaloid vessel structures in the *lacz* expressing Wnt reporter mouse TOPGAL showed that hyaloid VECs were Wnt-responsive. Reduced numbers of Wnt-responsive VECs in *PU.1* mutant mice suggested that macrophages might be a source of Wnt ligands and this was born out with expression studies performed on hyaloid macrophages isolated by laser capture micro-dissection. Among the Wnt ligands expressed, Wnt7b was an interesting candidate because it was expressed in hyaloid but not in cultured macrophages. Analysis of Wnt7b mutant mice revealed hyaloid vessel persistence. Furthermore, when injected into the eye, wild-type but not *Wnt7b* mutant macrophages could rescue the failure of regression in the *PU.1* mutant. Thus, Wnt7b is a macrophage Wnt ligand critical for hyaloid regression.

The Angiopoietin and Wnt Pathways Integrate to Regulate Hyaloid Regression

The discovery of the Tie2 receptor, a conventional receptor tyrosine kinase expressed in VECs, led directly to identification of the angiopoietin family of Tie2 ligands. Angiopoietin 1 and 2 have been well characterized experimentally. Angiopoietin 1 (Ang1) is an agonist of the signaling pathway and among other responses can promote cell survival through the PI3 Kinase-Akt signaling axis. The function of Ang2 is context-dependent. In some settings (like lymphangiogenesis) it is an agonist of the angiopoietin pathway. In other settings (the hyaloid vessels) it is an antagonist and thus promotes cell death.

The Ang2 mutant mice, like the Wnt pathway mutants, show a failure of hyaloid vessel regression and this prompted an investigation of mechanisms of Wnt–angiopoietin pathway integaration. Several mechanisms were revealed. First, both pathways influenced the cell cycle behavior of hyaloid VECs (**Figure 6**). As might be expected given direct targets like *myc*, the Wnt pathway promotes cell cycle entry. In doing so, the Wnt pathway sensitizes VECs to the effects of Ang2 in suppressing survival signaling and promoting cell death in G1 phase of the cell cycle. Second, the angiopoietin pathway stabilizes β-catenin through signaling mechanisms that are incompletely understood. This means that both the conventional Wnt pathway and the angiopoietin pathway converge on β-catenin and regulate cell cycle entry. Finally, Ang2 (probably produced by pericytes) is required for the expression of Wnt7b in macrophages (**Figure 6**). This configuration of signaling interactions means that Ang2 has two functions; suppression of cell survival and, via macrophage Wnt7b expression, an alternative pathway to promote cell cycle entry. This signaling pattern is also a means to ensure that when cell death occurs, the macrophage and its phagocytic disposal capability are on hand.

Fzd4 and Norrin in Hyaloid Regression

Norrie disease is an inherited disorder in which blindness is the major feature. The Norrie disease protein (Ndp) – also called Norrin – was recently shown by the Nathans group to be an unconventional ligand for the receptor Fzd4 and that Norrin activated the canonical Wnt signaling pathway. The phenotypes of the Fzd4 and Ndp mutant mice are similar and include defective retinal angiogenesis and persistence of the hyaloid vessels – both being reasons for blindness. Currently, it is unclear how this information can be integrated with the macrophage-dependent hyaloid regression mechanisms described above. There may be local effects of Fzd4 and Norrin that cause hyaloid persistence but it is equally possible that the hyaloid and retinal vessels interact hemodynamically to influence regression and angiogenesis respectively.

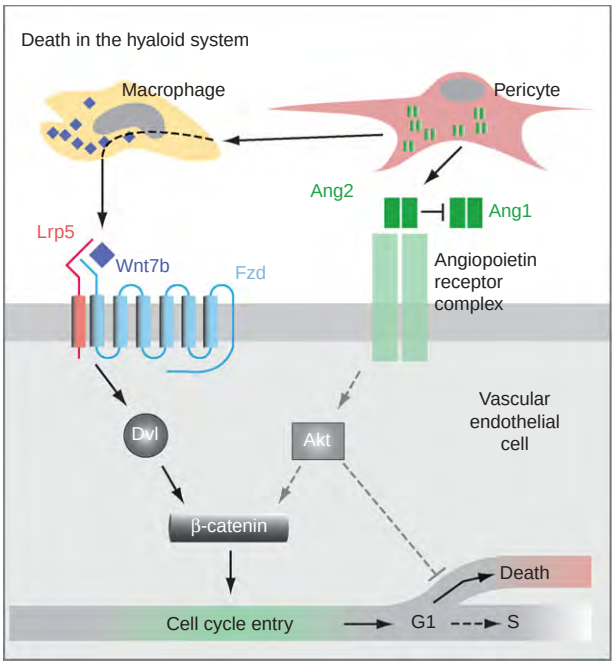

Figure 6 A model for regulation of VEC death in the hyaloid system. Hyaloid VECs will die when Ang2 promotes cell death via suppression of Akt and cell cycle entry by upregulating Wnt7b in macrophages. In the absence of survival signals the cycling hyaloid VECs will undergo apoptosis in the G1 phase of the cell cycle. Adapted from Rao, S., Lobov, I. B., Vallance, J. E., et al. (2007). Obligatory participation of macrophages in an angiopoietin 2-mediated cell death switch. *Development* 134: 4449–4458.

Collagen 18 and Endostatin in Hyaloid Regression

Endostatin was originally isolated as an inhibitor of angiogenesis and was proposed as an antitumor therapeutic agent. It was shown to be a proteolytic cleavage product of collagen 18. While the therapeutic potential of endostatin has not thus far been realized, the collagen 18 mutant mouse, in which no endostatin production is possible, does have a defect in hyaloid regression. This interesting observation from the Olsen group indicated that collagen 18, and perhaps endostatin, promote vessel regression and is consistent with the originally identified anti-angiogenic activity of endostatin.

The mechanism of action of collagen 18 in hyaloid regression is currently unclear but there are several possibilities. First, since collagen 18 is normally a component of hyaloid vessel basal lamina, it may be involved in regulating the macrophage–endothelial cell interaction. Presumably, given the hyaloid vessel persistence of the mutant mouse, collagen 18 would normally promote the interaction and thus facilitate regression. An alternative, or perhaps an additional mechanism, may be modulation of the Wnt pathway signaling by the collagen 18 fragment endostatin. As work from the Sokol group has suggested

that endostatin is an inhibitor of Wnt signaling, it is possible that like a defective Wnt pathway, the Wnt pathway activation predicted for the collagen 18/endostatin mutant might also perturb the hyaloid regression.

The Arf Tumor Suppressor and PHPV

Persistent hyperplastic primary vitreous (PHPV) is an ocular developmental defect in which the hyaloid vasculature within the vitreous overgrows and fails to regress. The disease is most often detected in infants as a fibrovascular, retrolental mass that in severe cases causes retinal detachment. The Skapek group has identified a good model of PHPV in mice mutant for the Arf tumor suppressor.

The *Arf* gene encodes $p19^{Arf}$, a nuclear protein that can complex with Mdm2 and thus influence activity of the p53 tumor suppressor. In addition, $p19^{Arf}$ has p53-independent effects. Since Arf mutant mice, unlike p53 mutants, reliably show a PHPV-like phenotype, it is likely that the p53-independent effects are responsible. In Arf mutant mice, PDGFRβ expressing cells with the characteristics of vascular mural cells populate the vitreous and envelop the hyaloid vessels to form the retrolental mass. In a revealing experiment it was shown that mutation of the *PDGFR*β gene can rescue the PHPV defect of the Arf mutant mice. Furthermore, through mechanisms that are not currently defined, p19Arf normally suppresses the PDGFRβ and in the Arf mutant, an overly sensitive signaling pathway leads to greater recruitment of mural cells. This is consistent with the general role of the PDGFRβ signaling system in recruitment of vascular mural cells by PDGFB-expressing VECs. The hyaloid vessel hyperplasia of *TGF β* mutant mice also suggests that this pathway will be involved in regulating development of the hyaloid system. In the Arf and TGFβ2 mutant models, early developmental perturbation of hyaloid vessel development is the primary defect and hyaloid vessel persistence, likely a secondary consequence. This contrasts with the Wnt and angiopoietin models described above where there are no detectable defects in hyaloid vessel development but there are major consequences for hyaloid regression.

Future Directions

The temporary vascular networks of the eye have so far served as an excellent model system to understand the mechanisms of vascular regression. This is clearly of interest to developmental and vascular biologists and with the involvement of macrophages, also to those interested in this versatile cell type. In studying these vascular networks, the greatest payoff may be when these mechanisms are applied to disease systems where antivascular therapy is advantageous. An important outstanding question is whether the Wnt ligands produced by macrophages have a role in regulating the vascularity – and therefore the progression – of tumors. Thus, it may be that the ocular vessels can provide the basis for future antitumor therapies of novel design. An additional challenge will be the work that allows us to understand how vascular regression pathways are integrated. While some progress has been made, more sophisticated methods of analysis will be required to understand, for example, the influence of VEGF signaling on the Wnt pathway or the influence of collagen 18 on Wnt signaling.

See also: Hyalocytes.

Further Reading

Ferrara, N., Gerber, H. P., and LeCouter, J. (2003). The biology of VEGF and its receptors. *Nature Medicine* 9: 669–676.

Fukai, N., Eklund, L., Marneros, A. G., et al. (2002). Lack of collagen XVIII/endostatin results in eye abnormalities. *EMBO Journal* 21: 1535–1544.

Garcia, C. M., Shui, Y. B., Kamath, M., et al. (2009). The function of VEGF-A in lens development: Formation of the hyaloid capillary network and protection against transient nuclear cataracts. *Experimental Eye Research* 88(2): 270–276.

Lang, R. A. and Bishop, M. J. (1993). Macrophages are required for cell death and tissue remodeling in the developing mouse eye. *Cell* 74: 453–462.

Lobov, I. B., Rao, S., Carroll, T. J., et al. (2005). WNT7b mediates macrophage-induced programmed cell death in patterning of the vasculature. *Nature* 437: 417–421.

Ohlmann, A. V., Adamek, E., Ohlmann, A., and Lutjen-Drecoll, E. (2004). Norrie gene product is necessary for regression of hyaloid vessels. *Investigative Ophthalmology and Visual Science* 45: 2384–2390.

Rao, S., Lobov, I. B., Vallance, J. E., et al. (2007). Obligatory participation of macrophages in an angiopoietin 2-mediated cell death switch. *Development* 134: 4449–4458.

Stalmans, I., Ng, Y. S., Rohan, R., et al. (2002). Arteriolar and venular patterning in retinas of mice selectively expressing VEGF isoforms. *Journal of Clinical Investigation* 109: 327–336.

Thornton, J. D., Swanson, D. J., Mary, M. N., et al. (2007). Persistent hyperplastic primary vitreous due to somatic mosaic deletion of the arf tumor suppressor. *Investigative Ophthalmology and Visual Science* 48: 491–499.

Xu, Q., Wang, Y., Dabdoub, A., et al. (2004). Vascular development in the retina and inner ear: Control by Norrin and Frizzled-4, a high-affinity ligand-receptor pair. *Cell* 116: 883–895.

Functional Morphology of the Trabecular Meshwork*

E R Tamm, University of Regensburg, Regensburg, Germany

Glossary

Inner-wall region – Comprised of the inner-wall endothelium of Schlemm's canal, its basement membrane, and the adjacent juxtacanalicular tissue. It is the site of resistance in the trabecular meshwork outflow pathways.

Juxtacanalicular tissue – The outermost part of the trabecular meshwork that lies directly adjacent to Schlemm's canal. It does not form lamellae, but represents a loose connective tissue. An alternative term is cribriform meshwork.

Mechanosensor – The terminal of an afferent nerve ending that is in contact with fibrillar components of the extracellular matrix and measures stress or strain in those. An alternative term is mechanoreceptor.

Myofibroblast – A resident cell in some connective tissues that shows structural and functional characteristics of both fibroblasts and smooth muscle cells, and appears to be an intermediate form of those.

Schlemm's canal – A circular vascular tube that lies in the scleral sulcus, a circular groove on the inner aspect of the corneoscleral limbus. It is part of the trabecular outflow pathways. The inner aspects of Schlemm's canal are in contact with the juxtacanalicular tissue.

Scleral spur – A wedge-shaped circular ridge protruding from the sclera posterior to Schlemm's canal.

Trabecular meshwork – A porous, filter-like tissue in the irido-corneal angle consisting of connective tissue strands (trabecular beams or lamellae) that attach to one another and are covered by cells.

Introduction

The major drainage structures for aqueous humor (AH) are the conventional or trabecular outflow pathways, which are comprised of the trabecular meshwork (made up by the uveal and corneoscleral meshworks), the juxtacanalicular connective tissue (JCT), the endothelial lining of Schlemm's canal (SC), the collecting channels, and the aqueous veins. When AH has passed through the trabecular outflow pathways, it drains into the episcleral venous system. In addition, there is an unconventional or uveoscleral outflow route which is open to AH at the chamber angle in the region of the anterior insertion of the ciliary muscle, since there is no complete endothelial or epithelial layer that covers the anterior surface of the ciliary body. The trabecular meshwork (TM) outflow pathways are critical in providing resistance to AH outflow. Intraocular pressure (IOP) builds up in response to this resistance until it is high enough to allow flow of AH across the TM into SC. AH passes through the TM as bulk flow driven by the pressure gradient, and active transport is not involved as neither metabolic poisons nor temperature affects AH flow across the TM. At steady-state IOP, fluid flow rate across the trabecular outflow resistance equals the rate of aqueous production by the ciliary body. Outflow resistance in the TM outflow pathways increases with age and primary open-angle glaucoma (POAG). This article reviews the functional morphology of the TM outflow pathways.

The TM Outflow Pathways

The tissue structures of the TM outflow pathways are embedded in the internal scleral sulcus, a circular groove on the inner aspect of the sclera in region of the corneoscleral limbus. The scleral sulcus extends from the peripheral edge of Descemet's membrane to the scleral spur, a wedge-shaped circular ridge protruding from the inner sclera (**Figure 1(a)**). SC, a circular, vascular-like collecting channel, lies in the outer portion of the scleral sulcus, while the TM occupies most of its inner aspects (**Figure 1(a)**).

The TM is formed by connective tissue beams or lamellae that have a core of collagenous and elastic fibers, and are covered by flat cells which rest on a basal lamina. The beams attach to one another in several layers and form a porous filter-like structure. Anteriorly, the trabecular beams are attached near the end of Descemet's membrane (Schwalbe's line) and extend posteriorly to the stroma of the ciliary body and iris at their junction, and to the scleral spur (**Figure 1(a)**). As SC is shorter in anterior–posterior direction than the TM, a filtering portion of the TM can be differentiated from a nonfiltering

*An adaptation and extension of Tamm, E. R. (2009). The trabecular meshwork outflow pathways: Structural and functional aspects. *Experimental Eye Research* 88: 648–655. http://www.sciencedirect.com/science/journal/00144835.

portion which has no SC next to its external aspect (**Figure 1(a)**). Those cells of the nonfiltering portion of the TM, which reside close to the attachment of the TM at Schwalbe's line, differ in structure from that of the TM proper. There is some evidence that this region serves as a niche for cells with adult stem cell-/progenitor cell-like properties that are capable of dividing and repopulating the filtering part of the TM after injury.

The TM consists of three regions that differ in structure: the inner uveal meshwork, the deeper corneoscleral meshwork, and the JCT or cribriform region that is localized directly adjacent to the inner-wall endothelium of SC (**Figure 1(b)**). The uveal meshwork, which originates from the anterior aspect of the ciliary body, consists of one to three layers of trabecular beams or lamellae (**Figure 1(b)**). The corneoscleral meshwork forms 8–15 trabecular layers, which are thicker than those of the uveal TM and originate from the scleral spur (**Figure 1(b)**). The JCT, which is localized directly to the endothelial lining of SC, is the smallest part of the TM with a thickness of only 2–20 μm. It does not form trabecular lamellae or connective tissue beams, but rather represents a typical loose connective tissue with two to five layers of scattered cells that are embedded in a loosely arranged fibrillar extracellular matrix (ECM) (**Figures 1(b)** and **2(a)**).

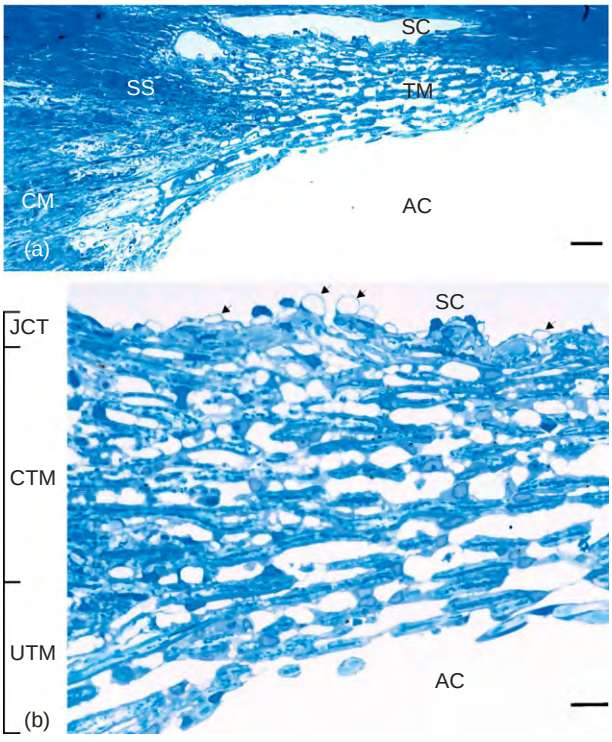

Figure 1 Light micrograph of a meridional section through the trabecular meshwork. (b) is a magnification of (a). Arrows in (b) point to giant vacuoles in the inner-wall endothelium of SC. Magnification bar = 20 μm (a), 5 μm (b). SC, Schlemm's canal; TM, trabecular meshwork; SS, scleral spur; CM, ciliary muscle; AC, anterior chamber; JCT, juxtacanalicular tissue; CTM, corneoscleral trabecular meshwork; UTM, uveal trabecular meshwork. From Tamm, E. R. (2009). The trabecular meshwork outflow pathways: Structural and functional aspects. *Experimental Eye Research* 88: 648–655.

The Trabecular Lamellae

Each lamella or beam of the uveal or corneoscleral TM contains densely packed collagen and elastic fibers. The collagen fibers are mostly collagens type I and III. The elastic fibers, which localize to the core of the beams (**Figure 2(b)**), differ in their ultrastructure from those in other parts of the body, as they contain considerable amounts of electron-dense material. TM elastic fibers are surrounded by a sheath that thickens with age and

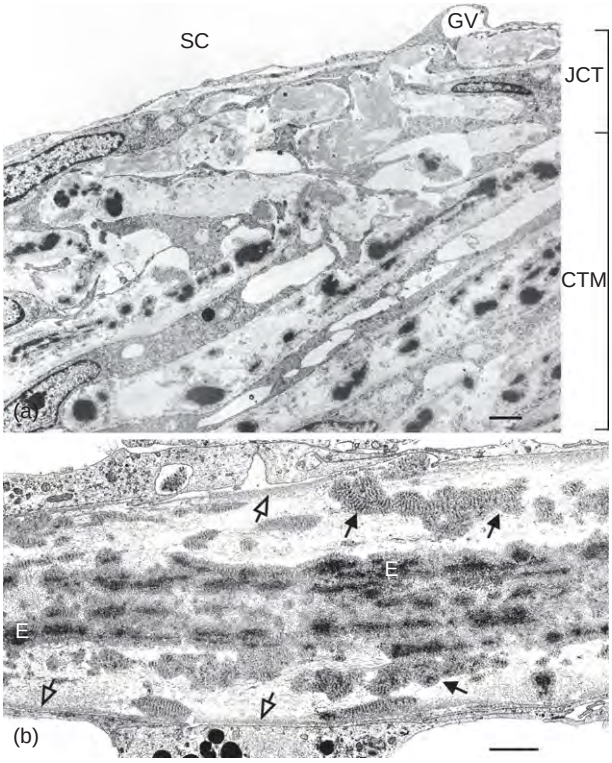

Figure 2 Electron micrographs of the trabecular meshwork. (a) Cells and extracellular fibrils in the juxtacanalicular tissue (JCT) are arranged in an irregularly network in contrast to the more regular structure of the beams in the corneoscleral trabecular meshwork (CTM). (b) Ultrastructure of a corneoscleral trabecular meshwork beam. The core of the beam contains elastic fibers (E) that are surrounded by banded sheath material. Open arrows denote the basal lamina of the trabecular meshwork cells, while solid arrows point to aggregates of long-spacing collagen in the cortical region of the beam. The beam is completely covered by flat trabecular meshwork cells. SC, Schlemm's canal; GV, giant vacuole. Magnification bar = 2 μm. From Tamm, E. R. (2009). The trabecular meshwork outflow pathways: Structural and functional aspects. *Experimental Eye Research* 88: 648–655.

that may show an 80–120-nm periodicity. Clumps of similar material and periodicity have been referred to as long-spacing collagen and are found in the cortical zone of the beams, between the elastic fiber core and basal lamina of the TM cells (**Figure 2(b)**). Fine fibrils that enter the aggregates of long-spacing collagen have been shown to label with antibodies against collagen type VI. The cells covering the TM beams reside on a basal lamina that is rich in collagen type IV and laminin (**Figure 2(b)**). A three-dimensional network is established by TM cells that bridge intertrabecular spaces to cover two adjacent beams. TM cells are capable of phagocytosis and may contain pigment particles, and these particles in TM cells probably derive from the iris and their phagocytosis by TM cells may be part of an important self-cleaning mechanism of the trabecular filter. TM regions that contain a high number of pigmented cells appear to be preferentially localized adjacent to collector channels, suggesting preferential AH flow pathways in the TM.

The Juxtacanalicular Tissue

TM cells in the JCT are surrounded by fibrillar elements of the ECM to form a loose connective tissue. As JCT cells and ECM fibrils are arranged in an irregular network (in contrast to the more regular structure of the beams in the inner parts of the TM), some authors prefer the term cribriform meshwork. The cells in the JCT form long processes by which they attach to one other, to ECM fibrils or to the cells of the endothelial lining of SC (**Figure 2(a)**). The spaces between JCT cells and ECM fibers serve as pathway for AH and contain a ground substance consisting of various proteoglycans and hyaluronan. The extent to which this ground substance fills the spaces between cells and fibrillar ECM is not clear as proteoglycans are not readily retained during processing of tissue for conventional electron microscopy. Recent studies using quick-freeze/deep-etch methodology visualized considerably more ECM in the JCT compared to that seen by conventional electron microscopy.

A characteristic structural element of the JCT is a network of elastic fibers (cribriform plexus), which is arranged tangentially to the SC endothelial lining. The elastic fibers of the cribriform plexus show ultrastructural characteristics similar to those in the trabecular beams as they consist of an electron-dense core and a sheath of banded material. The molecular nature of the sheath material has not been identified, but there is evidence that collagen type VI and fibronectin are associated with it. Fibers of the cribriform plexus connect with the SC inner-wall endothelium through either their sheath material or fine fibrils that emerge from it (**Figure 3(a)**). Fibronectin-based cell–matrix connections appear to be very important for the adhesion of SC endothelial cells to the fibrillar ECM

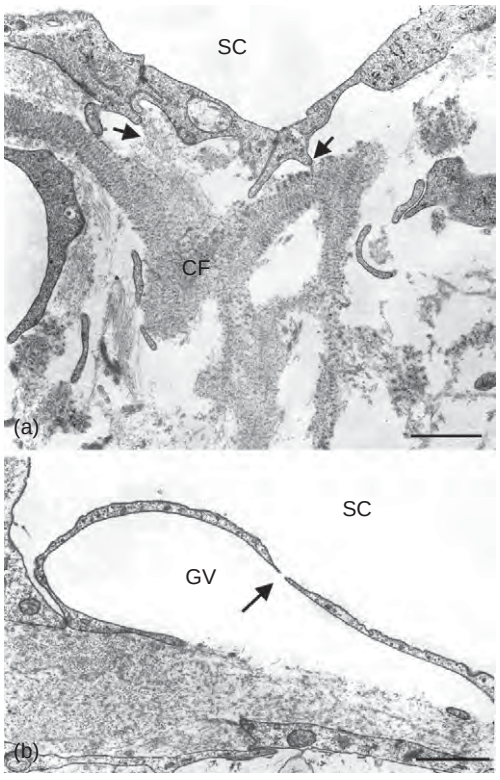

Figure 3 Electron microscopy of the SC inner-wall region. (a) Connecting fibers (CF) in the juxtacanalicular tissue, which emerge from the cribriform elastic plexus, connect the plexus with the inner-wall endothelium of Schlemm's canal (SC). The connection with the inner-wall endothelium is made through either the banded sheath material of the fibers or fine fibrils that emerge from it (solid arrows). (b) A giant vacuole in the inner wall of SC forms an intracellular pore (arrow). Magnification bar = 1 μm. From Tamm, E. R. (2009). The trabecular meshwork outflow pathways: Structural and functional aspects. *Experimental Eye Research* 88: 648–655.

of the JCT, as treatment of perfused anterior segment organ cultures with the integrin/syndecan-binding domain of fibronectin, called the heparin II (Hep II) domain, leads to a focal detachment of SC endothelium from the JCT, and to a significant increase in outflow facility.

The ECM in the JCT does not only contain structural elements, but also matricellular proteins such as thrombospondin-1 and SPARC. Matricellular proteins are secreted ECM proteins that influence cell function by modulating cell–matrix interactions. Another important component of the JCT ECM is myocilin, one of the most highly expressed molecules in the TM. Myocilin has been shown to associate with fibrillar elements of the JCT ECM, but its biochemical function is largely unclear.

Synthesis and degradation of ECM molecules in the JCT is under control of autocrine and paracrine growth factors, such as transforming growth factor beta 2 (TGF-β2), connective tissue growth factor (CTGF), bone morphogenetic protein 7 (BMP7), and BMP4. In addition, glucocorticoids and prostaglandin derivatives appear to modulate

ECM turnover in the JCT. A characteristic structural change in the eyes of patients with POAG and steroid-induced glaucoma is an increase in fibrillar ECM in the JCT.

Because of their high porosity, the uveal and corneoscleral parts of the TM do not provide a significant resistance to AH outflow. Support for this comes from experimental studies, which show that cutting through the inner parts of the TM does not affect outflow facility, and from theoretical calculations using Poiseuille's law. In contrast, there is considerable evidence that normal AH outflow resistance resides in the inner-wall region of SC, which is formed by the JCT and SC inner-wall endothelium. As of today, there is active debate and research regarding the specific role of SC inner-wall endothelium and/or JCT for the formation of resistance in the TM outflow pathways.

Schlemm's Canal

A characteristic aspect of the SC inner-wall endothelium is the formation of cellular outpouchings (the so-called giant vacuoles) in response to the pressure gradient associated with AH flow (**Figure 3(b)**). Endothelial cells of the SC inner wall rest on an incomplete basal lamina and considerable areas of their basal cell membrane are not supported by ECM, but are in direct contact with the open spaces of the JCT and AH flow. Giant vacuoles form when AH pushes against the basal side of SC cells, and are often associated with intracellular pores that have diameters from 0.1 to 2 μm. In addition to intracellular pores, paracellular pores have been observed, which usually have diameters comparable to that of intracellular pores, but are less common in most eyes. Paracellular pores are very likely the morphological correlate for paracellular flow through SC endothelium, which has been described in perfusion studies using cathionized ferritin. The junctional complexes between SC cells contain tight junctions and very likely restrict paracellular flow. Inner-wall pores allow passage of microparticles 200–500 nm in size. In their 1972 work, Bill and Svedbergh calculated the hydraulic conductivity and the flow resistance generated by inner-wall pores and concluded that the inner-wall endothelium could not generate more than 10% of total TM outflow resistance. More recent experiments indicate that the number of intracellular pores increases with the amount of fixative perfused through the TM outflow pathways and with the postmortem time of the enucleated donor eye, strongly indicating that the total number of pores identified by electron microscopy in fixed tissues is likely considerably smaller than that in the living eye. The number of paracellular pores was not affected by the amount of fixative or postmortem time, but increased with increasing fixation pressure. As fixation conditions can influence the apparent pore density in the inner-wall endothelium significantly, the conclusion reached previously that pores contribute only 10% of die aqueous outflow resistance, may require reevaluation. Nevertheless, it appears to be reasonable to assume that not all intracellular pores are artifacts, since the SC inner-wall endothelium has one of the highest hydraulic conductivities in the body, comparable only to that of fenestrated endothelia.

The molecular processes that contribute to or cause formation of intracellular pores in SC inner-wall endothelium are largely unknown. Small minipores that are covered by a diaphragm (**Figure 4**) may be involved. Diaphragmed minipores (DMPs) have similar ultrastructural characteristics as those forming the fenestrae of fenestrated capillaries, for example, in ciliary body or choroid. These are regularly found in SC inner-wall endothelium, but are considerably rarer than the fenestrae in fenestrated epithelia. In their 1995 work, Bill and Maepea hypothesized that DMPs represent an early stage in pore formation. The thin diaphragm, which in blood vessels is probably supported by the basal lamina, has no such support in the inner-wall cells and so may tend to burst.

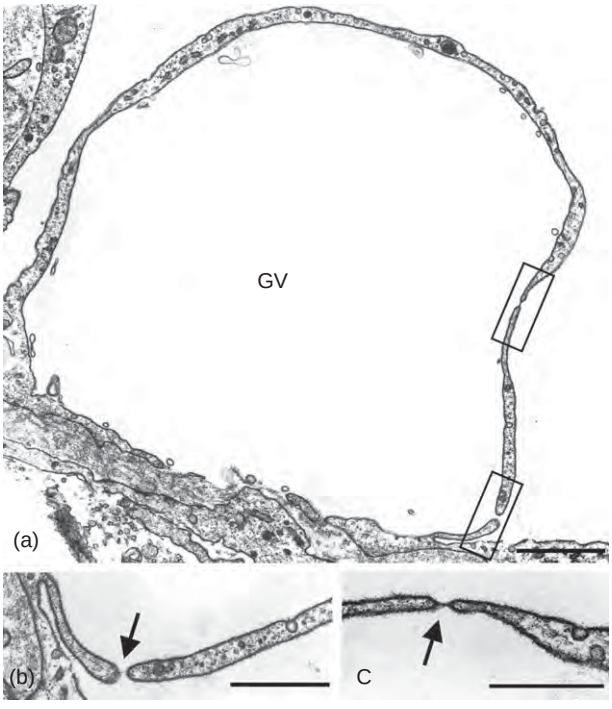

Figure 4 Electron microscopy of an inner-wall giant vacuole (GV) that forms two intracellular pores (boxed areas in (a)). Both boxed areas are shown in (b) and (c) at higher magnification. While the pore in (b) is largely open and only covered by very fine filamentous material, the pore in (c) is covered by a diaphragm (arrow). Magnification bar = 1 μm (a), 0.5 μm (b), 0.5 μm (c). From Tamm, E. R. (2009). The trabecular meshwork outflow pathways: Structural and functional aspects. *Experimental Eye Research* 88: 648–655.

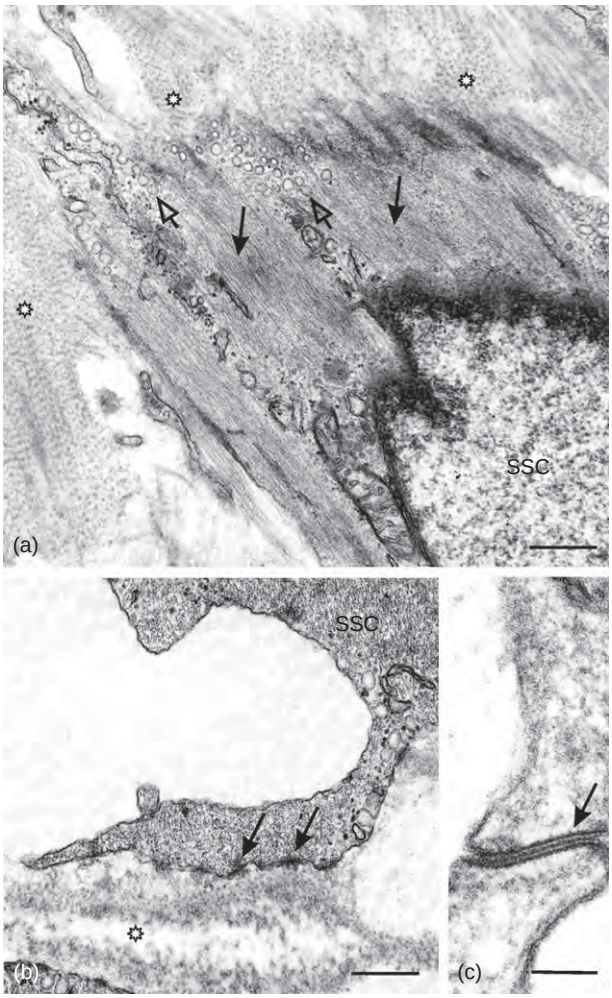

Figure 5 Electron microscopy of scleral spur cells. (a) Scleral spur cells (SSC) are in close contact with banded sheath material (asterisks) of elastic fibers. The cytoplasm of the cells is filled with abundant 6–7-nm-thin (actin) filaments which run parallel to the long axis of the cells (solid arrows). The cell membrane shows numerous membrane bound caveolae (open arrows). (b) Scleral spur cells may form long processes to contact the elastic fibers (asterisk) in the scleral spur. In region of contact, dense bands (arrows) are formed at the cell membrane of the scleral spur cell. (c) Scleral spur cells are connected by gap junctions (arrow). Magnification bar = 1 μm (a, b); 125 nm (c). From Tamm, E., Flügel, C., Stefani, F. H., and Rohen, J. W. (1992). Contractile cells in the human scleral spur. *Experimental Eye Research* 54: 531–543.

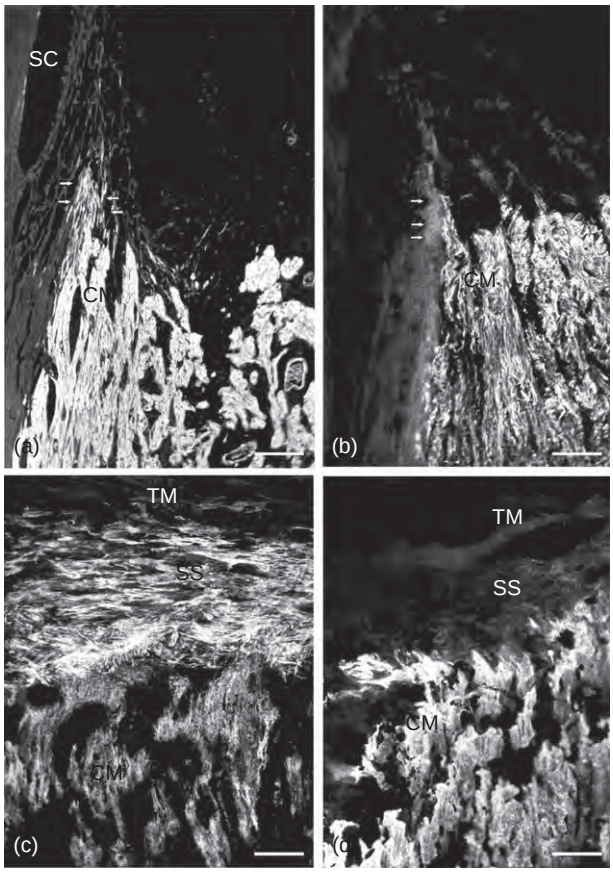

Figure 6 Meridional (a, b) and tangential sections (c, d) through ciliary muscle (CM), scleral spur (SS), and trabecular meshwork (TM) stained with antibodies against α-smooth muscle actin (a, c) or desmin (b, d). (a) Ciliary muscle cells and vascular smooth muscle cells stain positively with antibodies against α-smooth muscle actin. Arrows indicate the scleral spur, where all cells show intense immunoreactivity for α-smooth muscle actin. (b) Immunostaining with antibodies against desmin. Ciliary muscle cells stain brightly positive, whereas the scleral spur is not labeled for desmin. (c) Tangential section of scleral spur, trabecular meshwork, and ciliary muscle. Positively stained cells oriented in a circular direction are seen throughout the entire spur tissue. While ciliary muscle cells also stain positive, no staining is seen in the trabecular meshwork. (d) Tangential section of scleral spur and ciliary muscle after staining for desmin. The plane of the section is the same as in (c). Ciliary muscle cells stain brightly positive, whereas the cells of the scleral spur remain unstained. Magnification bar = 30 μm. From Tamm, E., Flügel, C., Stefani, F. H., and Rohen, J. W. (1992). Contractile cells in the human scleral spur. *Experimental Eye Research* 54: 531–543.

Contractile Influence on Trabecular Outflow

The muscle bundles of the ciliary muscle form tendons in region of their anterior insertion, which attach to the scleral spur or are continuous with the ECM of the TM. Because of the structural connections between ciliary muscle, scleral spur, and TM, contraction of the ciliary muscle pulls the spur posteriorly and/or widens the trabecular spaces, thereby inducing changes in TM geometry that lead to a reduction in outflow resistance.

In addition to ciliary muscle cells, there is another contractile cell population in this area, which very likely affects the TM tone. The resident cells within the scleral spur contain numerous actin filaments (**Figure 5(a)**), stain with antibodies against α-smooth muscle (SM) actin (**Figures 6(a) and 6(c)**), and generally express a myofibroblast-like phenotype. α-SM actin is an actin isoform that is typically expressed in vascular SM cells and myofibroblasts, cells that are present in healing

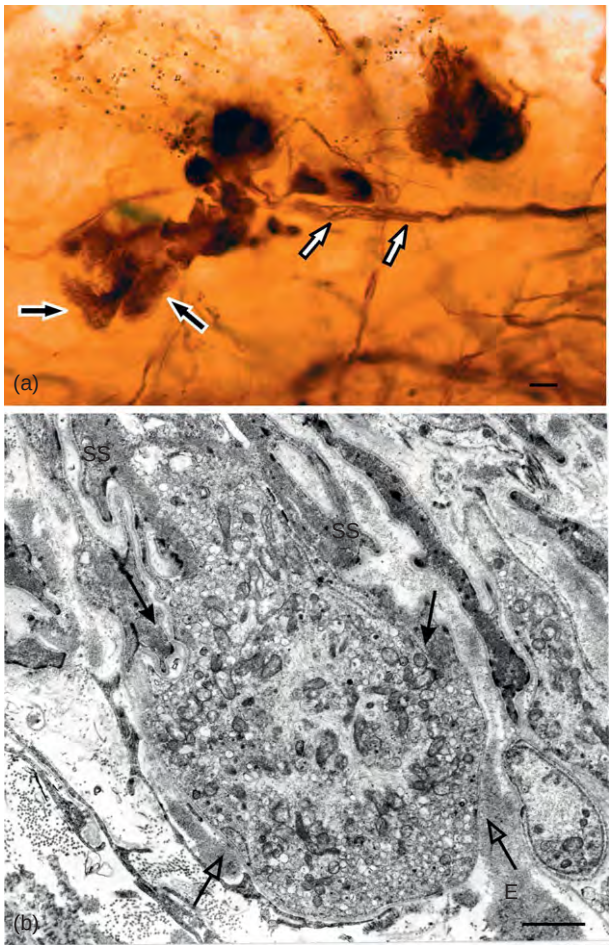

Figure 7 Mechanosensors in the scleral spur. (a) Whole mount of the scleral spur stained with antibodies against neurofilament proteins. Axons are labeled that terminate as bulb or club-shaped structures (arrows). (b) Electron micrograph of a mechanoreceptive nerve terminal in the scleral spur. The terminal is a bulb or club shaped and contains numerous neurofilaments, mitochondria, and vesicles of different sizes. The elastic fibers of the scleral spur (E, open arrows), and the scleral spur cells (solid arrows) are in close proximity to the terminal. Magnification bar = 10 μm (a), 1 μm (b). From Tamm, E. R. (2009). The trabecular meshwork outflow pathways. Functional morphology and surgical aspects. In Shaarawy, T. M., Sherwood, M. B., Hitchings, R. A., and Crowston, J. G. (eds.) *Glaucoma*, vol. II, pp. 31–44. Philadelphia, PA: Saunders.

wounds and scars. In contrast to the ciliary muscle cells that attach to the spur, scleral spur cells are circumferentially oriented (**Figure 6(c)**), and do not stain for desmin, the intermediate filament that is characteristic for ciliary muscle cells (**Figures 6(b)** and **6(d)**).

Scleral spur cells are innervated, coupled to each other by gap junctions (**Figure 5(c)**), and form tendon-like contacts with the elastic fibers within the scleral spur and their nonelastic sheath material (**Figures 5(a)** and **5(b)**). Since scleral spur elastic fibers are directly continuous with the elastic fibers in the TM beams and the cribriform plexus in the JCT, changes in scleral spur cell tone are likely to modulate outflow resistance by altering the architecture of the TM outflow pathways. In addition to scleral spur cells, some scattered cells in the TM proper have also been shown to express α-SM actin. The expression of α-SM actin induced by TGF-β1 has been shown to substantially enhance cell traction force in myofibroblasts, a scenario that might be also true for TM cells where TGF-β1 has similar effects on the expression of α-SM actin. There is experimental evidence that TM cells influence the hydraulic conductivity of the inner-wall region and outflow resistance by actively changing cell shape and altering the geometry of the outflow pathways. An increase in TM cell tone is correlated with an increase in outflow resistance.

Throughout the entire circumference of the scleral spur, club-shaped nerve endings are found, which derive from myelinated axons (**Figure 7(a)**). The ultrastructure of the nerve endings is very similar to that of mechanosensors in other parts of the body (**Figure 7(b)**).

The cell membrane of the nerve endings is in direct contact with the elastic fibers of the scleral spur. The contact between nerve terminal and connective tissue fibers is a very characteristic feature of mechanosensors, as it is required to measure the tone of the extracellular fibers. The mechanosensors of the scleral spur may act as proprioreceptive tendon organs for the ciliary muscle, or modulate the tone of the scleral spur cells. Alternatively, scleral spur mechanosensors could perform a baroreceptor-like function in response to changes in IOP. Indeed, physiological studies indicate that such sensors might exist, as sensory discharges have been recorded in experimental animals in response to changes in IOP.

Acknowledgment

This work was supported by DFG Research Unit 1075 (TP 5).

See also: The Biology of Schlemm's Canal; Biomechanics of Aqueous Humor Outflow Resistance; The Fibrillar Extracellular Matrix of the Trabecular Meshwork; Myocilin; Role of Proteoglycans in the Trabecular Meshwork; Structural Changes in the Trabecular Meshwork with Primary Open Angle Glaucoma.

Further Reading

Acott, T. S. and Kelley, M. J. (2008). Extracellular matrix in the trabecular meshwork. *Experimental Eye Research* 86: 543–561.

Bill, A. and Mäepea, O. (1995). Mechanisms and routes of aqueous humor drainage. In: Albert, D. M. and Jakobiec, F. A. (eds.) *Principles and Practice of Ophthalmology, Vol. I: Basic Sciences*, pp. 206–226. Philadelphia, PA: WB Saunders.

Bron, A. J., Tripathi, R. C., and Tripathi, B. J. (1997). Anterior chamber and drainage angle. In: Bron, A. J., Tripathi, R. C., and Tripathi, B. J. (eds.) *Wolff's Anatomy of the Eye and Orbit*, pp. 279–307. London: Chapman and Hall Medical.

Epstein, D. L. and Rohen, J. W. (1991). Morphology of the trabecular meshwork and inner-wall endothelium after cationized ferritin perfusion in the monkey eye. *Investigative Ophthalmology and Visual Science* 32: 160–171.

Ethier, C. R. (2002). The inner wall of Schlemm's canal. *Experimental Eye Research* 74: 161–172.

Ethier, C. R., Coloma, F. M., Sit, A. J., and Johnson, M. (1998). Two pore types in the inner-wall endothelium of Schlemm's canal. *Investigative Ophthalmology and Visual Science* 39: 2041–2048.

Fuchshofer, R. and Tamm, E. R. (2009). Modulation of extracellular matrix turnover in the trabecular meshwork. *Experimental Eye Research* 88: 683–688.

Gong, H., Ruberti, J., Overby, D., Johnson, M., and Freddo, T. F. (2002). A new view of the human trabecular meshwork using quick-freeze, deep-etch electron microscopy. *Experimental Eye Research* 75: 347–358.

Johnson, M. (2006). What controls aqueous humour outflow resistance? *Experimental Eye Research* 82: 545–557.

Johnson, M., Chan, D., Read, A. T., et al. (2002). The pore density in the inner wall endothelium of Schlemm's canal of glaucomatous eyes. *Investigative Ophthalmology and Visual Science* 43: 2950–2955.

Lütjen-Drecoll, E. (1999). Functional morphology of the trabecular meshwork in primate eyes. *Progress in Retinal and Eye Research* 18: 91–119.

Rohen, J. W., Futa, R., and Lütjen-Drecoll, E. (1981). The fine structure of the cribriform meshwork in normal and glaucomatous eyes as seen in tangential sections. *Investigative Ophthalmology and Visual Science* 21: 574–585.

Rohen, J. W., Lütjen, E., and Bárány, E. H. (1967). The relation between the ciliary muscle and the trabecular meshwork and its importance for the effect of miotics on aqueous outflow resistance. A study in two contrasting monkey species, *macaca irus* and *cercopithecus aethiops*. *Albrecht von Graefe's Archive for Clinical and Experimental Ophthalmology* 172: 23–47.

Sit, A. J., Coloma, F. M., Ethier, C. R., and Johnson, M. (1997). Factors affecting the pores of the inner wall endothelium of Schlemm's canal. *Investigative Ophthalmology and Visual Science* 38: 1517–1525.

Tamm, E., Flügel, C., Stefani, F. H., and Rohen, J. W. (1992). Contractile cells in the human scleral spur. *Experimental Eye Research* 54: 531–543.

Tamm, E. R. (2009). The trabecular meshwork outflow pathways: Structural and functional aspects. *Experimental Eye Research* 88: 648–655.

Tamm, E. R. (2009). The trabecular meshwork outflow pathways. Functional morphology and surgical aspects. In: Shaarawy, T. M., Sherwood, M. B., Hitchings, R. A., and Crowston, J. G. (eds.) *Glaucoma,* vol. II, pp. 31–44. Philadelphia, PA: Saunders.

Tamm, E. R., Flügel, C., Stefani, F. H., and Lütjen-Drecoll, E. (1994). Nerve endings with structural characteristics of mechanoreceptors in the human scleral spur. *Investigative Ophthalmology and Visual Science* 35: 1157–1166.

Tamm, E. R. and Lütjen-Drecoll, E. (1996). Ciliary body. *Microscopy Research and Technique* 33: 390–439.

Tian, B., Gabelt, B. T., Geiger, B., and Kaufman, P. L. (2008). The role of the actomyosin system in regulating trabecular fluid outflow. *Experimental Eye Research* 88: 713–717.

Wiederholt, M., Thieme, H., and Stumpff, F. (2000). The regulation of trabecular meshwork and ciliary muscle contractility. *Progress in Retinal and Eye Research* 19: 271–295.

Fundamentals of Stereopsis

L M Wilcox, York University, Toronto, ON, Canada
J M Harris, University of St. Andrews, St. Andrews, UK

Glossary

Binocular disparity – The positional differences between two retinal images generated at any instance by the two eyes. The brain uses this information to extract an estimate of the depth of an object or point.
Horopter – The set of points having zero binocular disparity that represent an arc passing through the fixation point.
Stereoacuity – The smallest binocular disparity that can reliably be discriminated.
Spatial frequency – A mathematical term describing the amount of detail in a scene and any scene can be broken down into a set of constituent sinuosoidal waveforms of different frequencies.
Stereoscope – Instrument invented by Wheatstone in 1838, which uses a pair of mirrors set at right angles to focus pictures separately to the two eyes as stereograms.

Defining Stereopsis

Stereopsis is a powerful cue to depth that arises as a consequence of having two eyes that are laterally offset in the head. This means that each eye receives a slightly different image of the world, a fact one can easily confirm by holding a finger in front of the face, and looking at it with each eye in turn. The two retinal images generated at any instant are identical in most respects, except for a positional shift which makes it appear that the finger is jumping back and forth as one changes the viewing eye. This positional difference is illustrated in **Figure 1**, which shows a cluster of grapes as a stereo pair (one image for each eye, photographs taken from each eye's viewpoint). Notice that the upper grape of the central group of three occludes part of the background on the left (right-eye image) that is visible on the right (left-eye image).

These differences in image position are known as binocular disparity, and this is the information the brain uses to extract an estimate of the depth of an object or point, relative to where the observer is fixating. This disparity may also be thought of as the angular difference between a pair of points on the retinas. The geometry is straightforward as illustrated in **Figure 2**.

Figure 2 shows two eyes fixating point F, so it stimulates the fovea, while point P is further away from the observer. Relative binocular disparity, η, is defined as the angle subtended at the eyes by one point (ω) minus the angle subtended by the other point (θ):

$$\eta = \omega - \theta \qquad [1]$$

This equation can be re-expressed in terms of distances, rather than angles. Notice that

$$\tan\left(\frac{\omega}{2}\right) = \frac{\text{io}d}{2d} \text{ and } \tan\left(\frac{\theta}{2}\right) = \frac{\text{io}d}{2(d+\Delta d)} \qquad [2]$$

Next, if we assume that the viewing distance, d, is large relative to the distance between F and P, Δd, then we can assume that $\tan(\omega/2) \approx (\omega/2)$, $\tan(\theta/2) \approx (\theta/2)$, and $d \approx d + \Delta d$, where the angles are expressed in radians. Equations [1] and [2] can then be rearranged to reduce approximately to

$$\eta \approx \frac{\text{io}d\Delta d}{d^2} \qquad [3]$$

In this example, point P lies beyond the fixation point F. However, the computation of binocular disparity is the same for an object in front of the fixation point. Points in space with images that fall on corresponding points on the two retinas have zero disparity and are said to lie along the horopter (**Figure 3**).

In **Figure 3**, points F, L, and M have zero binocular disparity and lie on the horopter, while points P and C do not lie on the horopter and therefore do have binocular disparity. Point P lies beyond the fixation point and therefore its lines of sight do not cross in front of the horopter; it is said to have uncrossed disparity. The lines of sight for point C do cross in front of the fixation point, and therefore have crossed disparity. Points with zero disparity are fused by the visual system such that we perceive a single image. However, points still appear fused as long as the disparity does not exceed a certain limit, which is known as Panum's fusional area. Panum's fusional area is illustrated in **Figure 4** as the shaded zone on either side of the horopter. Even though points within the fusional area are seen as one, their disparity creates an impression of depth. Points with a disparity greater than the fusion limit appear double or diplopic and we see that, up to a certain limit, diplopic points also produce a percept of depth.

From the geometry outlined here, it is clear that the critical information for stereopsis is the distance of an object relative to the fixation point, not relative to the

Figure 1 A stereoscopic image pair taken with two cameras. Right eye view on the left, left eye view on the right. To view, cross your eyes, until the two squares align, and focus on the middle image. Courtesy of Zeb Hodge, as posted on Flickr.

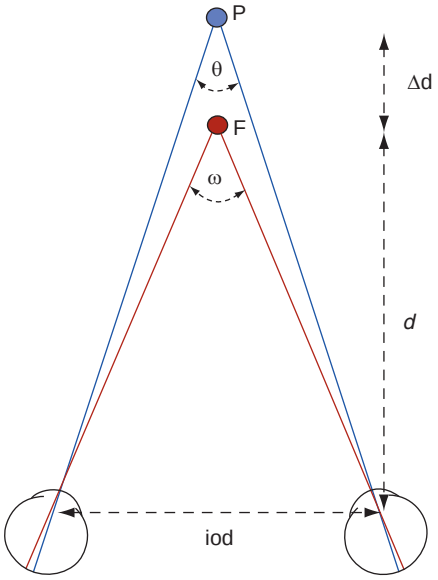

Figure 2 The geometry of binocular disparity. The two eyes view a point P while fixating point F, at distance *d* from the observer. The distance between F and P is given by Δd and the interocular distance is iod. Angles ω and θ give the angular subtense of points F and P, respectively.

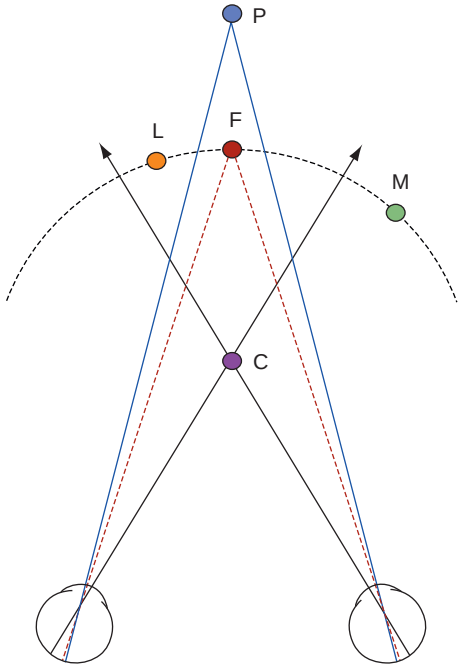

Figure 3 The horopter and crossed vs. uncrossed disparities. The horopter is the set of points having zero binocular disparity, given by the dotted arc passing through the fixation point, F. In this example, L and M lie on the horopter while P (with uncrossed disparity) and C (with crossed disparity) do not.

observer. Thus, in Figure 3, point C has a larger disparity than P (though of opposite sign), even though C is closer to the observer. There is an extensive literature on the concept of the horopter, and the coordinate systems for binocular stereopsis. Ian Howard and Brian Rogers provide a more complete account in their excellent review of binocular vision and stereopsis.

Stereograms and Binocular Viewing

The study of binocular vision has a long history extending back to Euclid's *Optics*, written in 300 BC, and in the neglected writings of Alhazen (AD 965–1040). However, it was only 150 years ago when Sir Charles Wheatstone discovered the link between the geometry of binocular vision and depth perception. Wheatstone invented the stereoscope which uses a pair of mirrors set at right angles to present pictures separately to the two eyes (stereograms). When pictures of the same object or scene taken from different vantage points are viewed in the stereoscope, the observer obtains a compelling view of space and volume (Figure 5).

Wheatstone's invention of the stereoscope inaugurated the empirical study of stereoscopic vision. While considerable research has since been devoted to this topic, the

study of how binocular information is extracted by the brain, and then interpreted to provide an extremely precise estimate of relative depth, remains a fascinating puzzle. In the remainder of this article we review how stereopsis is currently assessed, when it excels and fails, and describe the neural mechanisms that support it.

Classic Stereograms

There are two main types of stereoscopic stimuli used by researchers today. What have traditionally been referred to as local stimuli consist of isolated single targets presented relative to a reference point or frame. Much like the examples used by Wheatstone in his original paper, the monocular form, or structure, of the stimulus is obvious, although the direction of the disparity and depth relationships may not be. Even simpler line patterns (**Figure 6**) have often been used by scientists to investigate the fundamental properties of human stereopsis.

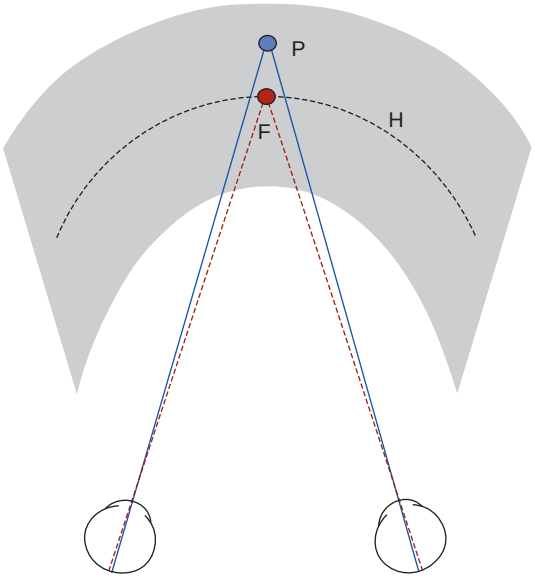

Figure 4 Panum's fusional area is illustrated here in gray. Within this region (exaggerated here for purpose of exposition) points such as P, which lie off the horopter, H, have binocular disparity but are seen as single and in depth relative to the fixation point, F.

Random-Dot Stereograms

In the early 1960s, while working at Bell Laboratories, Bela Julesz created computer-generated random-dot stereograms (RDSs), stimuli that were to have far-reaching effects on the study of stereopsis. To generate an RDS, a pattern of random elements is produced and duplicated to provide a pair of images, one for each eye. A selected region of elements is shifted in equal and opposite directions in the two patterns. This procedure overwrites elements on one side, and leaves empty spaces on the other, in both images. The empty spaces are then filled with samples of the random pattern. When viewed in a stereoscope, the shifted region appears to float (or recede) in depth, by an amount proportional to the size of the lateral shift (**Figure 7**). Julesz used the RDS to highlight the problem of how the human visual system correctly matches the images in the two eyes, an issue which became known as the binocular correspondence problem. Julesz's RDS took this problem to its extreme by providing hundreds of identical dots in the two eyes, any of which could be matched with any other dot when viewed stereoscopically.

Julesz and others suggested that the brain's strategy to solve this problem is to correlate small regions of the retinal images to identify corresponding areas. Julesz noted that the correlated area would have to scale in size with the amount of disparity in the image (called the size-disparity correlation). While there is still some debate as to how the size of the required correlation region can be estimated prior to knowing the binocular

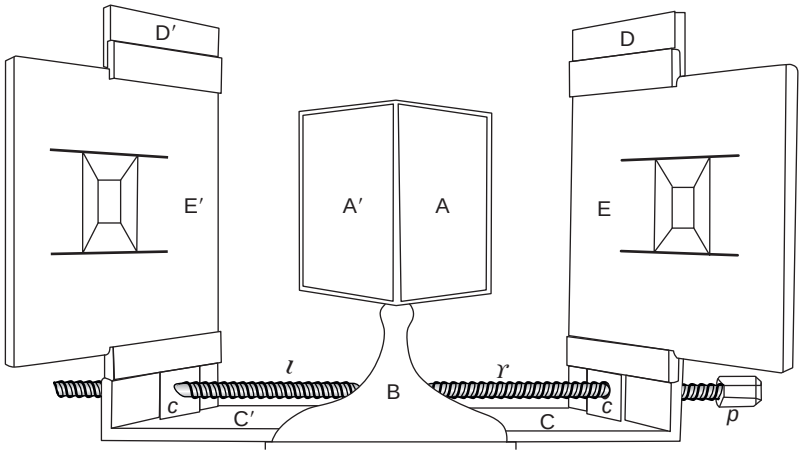

Figure 5 Wheatstone's diagram of his stereoscope as published in 1838. A′ and A are mirrors, which reflect images of the stereo pair (E′, E) separately to the two eyes. The same principle is used in laboratories today.

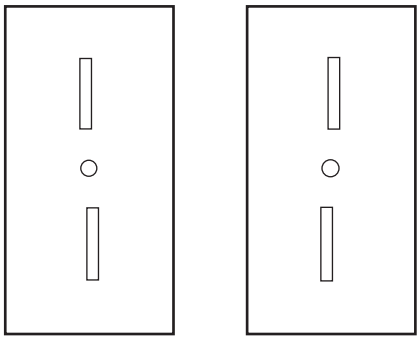

Figure 6 A simple line stereogram. By cross-fusing (left image to right eye, right image to left eye) the two dark frames and the central dot, the relative depth of the unfilled bars become apparent. The upper bar should appear closer to the observer than the central dot and frame, while the lower bar should appear further away.

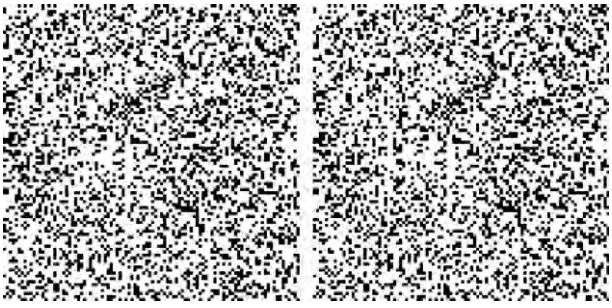

Figure 7 A random-dot stereogram image similar to that presented by Julez in 1964. By cross-fusing this stereo pair, one can observe a central square region displaced in depth in front of the surrounding region.

disparity, this approach remains the first step for many computational models of stereopsis. The concurrent introduction of the RDS and growth of the field of computational vision was responsible for new directions in the study and computational modeling of stereopsis as exemplified by David Marr.

Although Julesz's demonstrations prove that we solve the correspondence problem, other work has shown that we do not appear to use each element in the display as an independent depth sample. Julie Harris and Andrew Parker measured the efficiency of stereopsis by adding binocular disparity noise to a stereogram and comparing human depth judgments with those of an ideal detector that correctly extracted the disparity of each element. Human efficiency was very low, particularly when observers viewed displays with jagged, rather than smooth, depth profiles. This suggests that although we experience highly stable percepts of scenes in depth, only a small proportion of the available disparity information is actually used.

Prior to Julesz's introduction of the RDS, Gestalt psychologists believed that the percept of depth in stereograms followed the internal creation of two forms, or Gestalten, that then resulted in a percept of depth. Julesz recognized immediately that since no coherent monocular form is visible in either of the random-dot images prior to fusion into a cyclopean percept, his stereograms provide strong proof against the Gestalt interpretation of stereopsis. To summarize, there are several important consequences in the introduction of RDSs to vision science including:

1. The robust depth percepts obtained from RDSs suggest that there must be a neural mechanism which is able to resolve the ambiguous matches inherent in binocularly camouflaged stimuli, without relying on higher level interpretation of form.
2. The RDSs lead to the creation of simple, easy to apply, clinical tests of stereopsis in which monocular form or disparities could not be used instead of stereoscopic depth.
3. The ambiguous nature of RDSs highlighted the correspondence problem, and the need to understand the constraints on binocular matching, which gave rise to computational models of stereopsis.

The Empirical Study of Stereopsis: Thresholds and Upper Limits

Stereoacuity

Stereoacuity is defined as the smallest binocular disparity that can reliably be discriminated. While fixating a reference stimulus, the observer indicates if a target stimulus is closer or further away from the fixation stimulus. Several different psychophysical procedures may be used, but in all the disparity of the target is varied so the experimenter can assess the stereothreshold (typically defined as 75% correct). Under ideal conditions, the stereoacuity threshold tends to range from 2 to 6 s of arc, less than the width of a human hair held at an arm's length. Ideal stimuli are of high contrast, with sharp edges, and viewed at approximately an arm's length; however, the following variables dramatically influence stereoacuity.

Contrast

It is well established that stereoacuity for luminance-defined stimuli depends on stimulus contrast, or the relative intensity of dark and light regions in an image. Stereoscopic thresholds increase substantially at very low contrasts (near the contrast threshold for stereopsis) but this effect plateaus at higher contrasts where the stimuli are clearly visible. At high contrasts, stereoacuity is influenced more by the interocular contrast ratio than the overall binocular contrast, an effect that is also contingent on the spatial frequency content of the stimulus.

Spatial frequency/size

Spatial frequency is a mathematical term describing the amount of detail in a scene and, formally, any scene can be

divided into a set of constituent sinuosoidal waveforms of different frequencies. A high-frequency sinusoid is one with lots of narrow stripes, whereas a low-frequency sinusoid has only a few broad stripes. Much of the research on human stereopsis in the later part of the twentieth century has been based by a model of visual processing as a form of linear systems analysis, proposed by Fergus Campbell and John Robson in 1968. Thus, the receptive fields of cortical neurons were often discussed in terms of their preferred spatial frequency, and it was widely held that the visual system processed information through a series of spatial frequency-tuned channels. In accordance with this, there have been numerous psychophysical investigations of stereoacuity as a function of the frequency of sinusoidal luminance variations. Experiments have shown that stereoacuity improves with increasing spatial frequency in periodic (striped) stimuli up to 2.4 cycles per degree (c/deg), at which point performance flattens. However, in studies in which the stimulus size was scaled with changing frequency, improvements were found up to 5 c/deg.

Modulation frequency

While luminance-defined spatial frequency may be important for many visual functions, stereopsis has another dimension, and it stands to reason that there may be detectors that are tuned to the depth modulation frequency of a scene. For example, an egg provides a smooth change in disparity and contains a low modulation frequency, while a leafy tree contains many regions of rapidly changing disparity and therefore a high modulation frequency. Christopher Tyler created RDS patterns that contained random luminance variations but, when fused, appeared to modulate smoothly in depth. The frequency of the modulation could be manipulated, and stereoacuity measured, to provide an estimate of a modulation frequency transfer function (MTF) for disparity, independent of luminance frequency. The data from such cyclopean patterns show much lower peak sensitivity than reported for luminance frequency, near 0.4 c/deg.

Duration

Stereoacuity for luminance-defined stimuli shows a clear dependence on exposure duration, with thresholds improving with increasing duration up to a full second. As we observe from the next section, this dependence on viewing time is specific to luminance-defined stimuli such as bars, or dots, presented at small disparities. Investigators have suggested that such performance reflects the operation of a slow, sustained stereoscopic mechanism, which responds best to small disparities.

Configuration

An often-overlooked attribute that influences disparity processing is the configuration of the parts of the stereogram. Consider the work of Suzanne McKee, who showed in 1983 that stereoacuity for a pair of thin vertical lines was dramatically altered by the addition of two horizontal lines to form a box. As shown in **Figure 8** below, even the addition of a single line connecting the vertical lines, results in a large threshold increase. In all cases the observer is asked to judge the relative depth of the two vertical lines. In **Figure 8(a)**, the lines are unattached and thresholds are low. The addition of a single connecting horizontal line in **Figure 8(b)** increases thresholds by a factor of 4. The addition of two horizontal lines forming closed **Figures 8(c)** and **8(d)** further degrade performance. As shown in **Figure 8(e)**, the horizontal connectors need to only imply a cohesive figure to cause a doubling of the threshold.

Such effects are difficult to account for based on low-level information alone. Instead, it appears that even though the original disparity signal is present in the box configuration, the stereoscopic system is unable to make use of it with the same precision because the two parts now belong to a single figure. There is other evidence of mid-level configural effects on perceived depth via stereopsis, for instance, the perception of shape in biological motion figures influences observers' ability to discriminate the length of body parts as they receded in depth. These phenomena show that the perceptual grouping of parts into a whole can degrade our ability to make simple depth discrimination judgments, and demonstrate that the extraction of binocular disparity is the first stage of a complex process that extracts the depth and shape of objects around us.

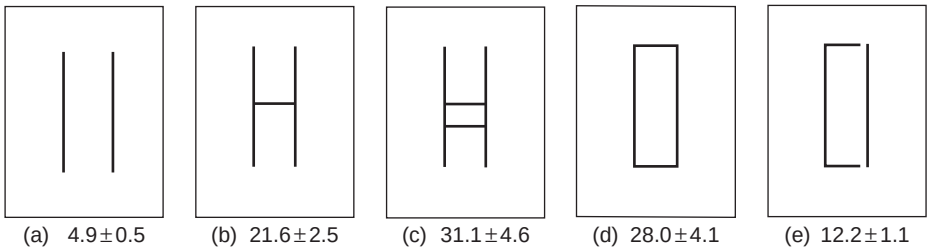

Figure 8 Stimuli adapted from, and thresholds (in seconds of arc) reported by Suzanne McKee in 1983. In each instance the two vertical lines are displaced in depth to assess stereoacuity and are identical in all conditions (a–e).

Stereopsis at Large Disparities

As described above (**Figure 4**), the stereoscopic system processes disparity information over a wide range of disparities at which, depending on the nature of the stimulus, the image may appear either fused or diplopic. On the horopter there is no binocular disparity between a point and the fixation location, therefore the point is perceived as equidistant with fixation. As disparity is increased, the point is perceived at different locations in depth relative to fixation, with perceived depth increasing with increasing disparity. Within Panum's fusional area, the disparate object appears single, fused, and in depth. At some point, as disparity continues to increase, fusion will be lost and the object will become diplopic or doubled. Surprisingly, as Kenneth Ogle documented in 1952, the percept of relative depth is not lost at the diplopia point. Instead, there remains a compelling sense of depth over a large range of disparities until, for very large disparities, the now diplopic object appears to return to the fixation plane. The disparity at which the percept of depth is lost is called the upper disparity limit. Ogle categorized the high-resolution range of disparities, which provides good relative depth information, as patent stereopsis; this range of disparities extends beyond the fusion limit. At some point, as disparity is increased, the quality of the depth percept changes and we are no longer able to judge the amount of depth, but simply have a sensation of the direction of the depth offset. Ogle named this latter range as qualitative stereopsis.

Spatial frequency/size

We have not included specific disparity estimates at which the upper limit for stereopsis occurs, for research has shown that this limit (D_{max}) depends critically upon the size of the stimulus, with larger D_{max} obtained for wider stimuli. Laurie Wilcox and Robert Hess demonstrated that for Gabor stimuli (a luminance sinusoid enveloped by a Gaussian distribution), the size of the Gaussian envelope is the only attribute that influences D_{max}; changing the center spatial frequency of the Gabors (the width of the stripes in the pattern) has no effect on the upper limit. They concluded that depth percepts from diplopic targets are mediated by the second-order, or envelope-based system, which is insensitive to the luminance-defined detail within a stimulus.

Duration

High-resolution stereoacuity judgments for edges and lines improve with increasing viewing time. Quite a different pattern of results is emerging for stimuli that access a more coarse stereoscopic mechanism (second order or qualitative stereopsis). In such cases, it appears that the stereoscopic system is more transient and, so as proposed by Mark Edwards and colleagues, operates best when the viewing time is brief, less than 200 ms. Recent work has shown that for this type of stimulus, increasing the viewing time over 50 ms results in no improvement in performance; but results in, if anything, performance decline.

Similarity

There is evidence suggesting that depth percepts for diplopic stimuli are robust to large interocular stimulus differences. Donald Mitchell and Gerald Westheimer used diplopic stereopairs containing, for example, a circle in one eye and a cross in the other and measured depth discrimination. Similar resilience of stereopsis to the dissimilarity of the stimuli in the two eyes has been reported by a number of investigators, who have shown that depth perception for large disparities is not significantly influenced by interocular differences in contrast, or orientation.

The Mechanisms of Fine and Coarse Disparity Processing

As is evident from the preceding sections, there are some substantial differences in the processing of fine- and large-scale disparity information, particularly when the large disparities are outside the fusion range. There have been a number of attempts to capture these differences and use them to categorize stereopsis. For instance, Ogle argued that the range of disparities that can be used to make quantitative depth estimates involve patent stereopsis, and the binocular disparities that give rise to a more vague percept of depth involve qualitative stereopsis. Importantly, Ogle's limits are contingent on the scale of the line stimuli used to make the measurements, so they will change as stimulus size is varied. The sustained or transient stereopsis distinction mentioned above appears to be based solely on the temporal properties of stimuli. However, the link between the transient process and large disparities suggests the existence of separate coarse and fine mechanisms that have different temporal properties. This proposal is consistent with the series of experiments by Wilcox and Hess describing first- and second-order stereoscopic mechanisms. The current consensus is that stereopsis has a high-resolution system that is sensitive to luminance changes in an image. This is the classic stereoscopic mechanism studied since Wheatstone's invention of the stereoscope. The second-order system is sensitive to contrast variation, and so is able to abstract over the fine detail in an image to provide a disparity signal for an object as a whole. This mechanism is most similar to Ogle's qualitative stereopsis, and is likely responsible for many of the puzzling results in the literature of stereopsis from dissimilar stimuli.

The Depth of Moving Objects

The details of stereoscopic vision described up to this point have been restricted to static stereoscopic images. However, very often in the natural world objects are in motion, and we must determine their positions in the world as they move in depth. When an object moves in depth, its binocular disparity changes with respect to the stationary background. In principle, the mechanisms that underlie binocular disparity processing could be used to detect motion in depth, if the change in depth is then monitored across time. But there is another potential source of binocular visual information. When a point moves directly toward an observer, the retinal image of that point moves over the left retina in a leftwards direction and moves rightwards on the right retina. If the visual systems were to first use monocular motion-sensitive mechanisms to detect the motion, and then use a binocular mechanism to compare those motion signals, motion in depth could be detected without the explicit use of disparity detectors. Using a dynamic random-dot stereogram (DRDS) that contains no consistent monocular motion information, Julesz showed that the former information, from changing binocular disparity, supports the perception of motion in depth. More recently, visual stimuli have been designed to isolate the motion information. In a time-correlated random-dot stereogram (TCRDS), each eye views consistent leftwards or rightwards motion but, point for point, there is no consistent binocular disparity information. As discussed by Harris and colleagues in their recent review of this topic, currently there is much debate in the literature about which source of information is used, and when. Motion in depth does appear to be perceived in a TCRDS, at least for some observers, yet thresholds for detecting the minimum amount of motion in depth are not improved by the addition of consistent motions to a DRDS stimulus. Further, there is a correlation between static stereoacuity and acuity for motion in depth, suggesting a crucial role for disparity detectors. A very small number of studies have demonstrated that some observers, who cannot see changing disparity in a DRDS (some with misaligned eyes, and some with no history of ocular problems), can instead use the motion information provided by a TCRDS. This suggests that there may be two separable binocular mechanisms for detecting motion in depth: one that relies on changing disparity and another that uses monocular motion signals. It appears that, when present, the changing disparity information is the default signal used by most observers.

The Neural Basis of Stereopsis

Nonhuman Animal Studies

Our understanding of the neural basis of stereopsis has grown exponentially since David Hubel and Torsten Wiesel's Nobel-prize winning work in the 1960s and Horace Barlow's studies of disparity selective neurons in 1967. These investigators were the first to record responses of binocular neurons in the cat visual cortex, and laid the foundation for subsequent work on the neural underpinnings of stereopsis. Subsequently, Gian Poggio and David Ferster showed that disparity-tuned neurons exist in cortical areas V1 and V2 of the monkey and that further, they could be classified according to their response properties as tuned excitatory, tuned inhibitory, and near and far. Tuned neurons have response properties consistent with high-resolution depth judgments, while the near and far cells provide a more coarse disparity signal, and respond over a larger range of disparities. The link between neural disparity detectors, and the percept of depth was firmly established when Blake and Hirsch conducted experiments in which cats were raised with alternating monocular deprivation. They showed that:

1. Binocularly deprived cats, while visually normal on monocular tasks, had no stereopsis. This makes the link between perception and the cortical effects of deprivation.
2. Animals that viewed the world monocularly alone did not develop binocular neurons; hence simultaneous binocular input is critical to the normal development of binocular neurons.

Based on such deprivation experiments, it is clear that disparity detectors are the basis for perception of depth through stereopsis. Electrophysiological studies from the late 1970s onward have revealed much about the neural coding of stereopsis. For instance, Bruce Cumming and Andrew Parker have demonstrated that neurons in primary visual cortex respond to anticorrelated RDS patterns, that is, RDSs with a zero-disparity region defined by identical dots in the two eyes surrounding a region of elements that have the opposite contrast (black vs. white) in the two eyes. Human observers do not see consistent depth in the anticorrelated region, but some V1 neurons respond reliably to these stimuli. This suggests that the primary visual cortex codes disparity but this signal is not sufficient to support our perception of depth. However, cells in the V2 area are specifically sensitive to correlated RDSs. Recent electrophysiological experiments strongly indicate that extrastriate cortical areas (beyond V1) respond to different patterns of binocular disparity. For example, investigators have shown that disparity tuning is a dominant attribute of medial temporal (MT) neurons, which traditionally have been cast as motion-sensitive units. In a recent study, Takanori Uka and Greg DeAngelis used electrical stimulation of neurons in monkey MT region to bias their near or far response to a stereoscopic stimulus. Note that, this result was obtained for coarse disparity-tuned neurons, but not for fine. In the inferotemporal cortex (IT), which is well known for its role in coding

faces and complex forms, researchers have identified neurons that respond to the three-dimensional (3D) shape (i.e., convex vs. concave) of disparity-defined surfaces. There is ongoing debate regarding the implications of the widespread presence of disparity selectivity throughout cerebral cortex. One possibility is that disparity processing occurs for different purposes along separate pathways in the visual system. Along the dorsal pathway, which includes MT, there may be specialization for coarse disparity processing, which is useful for the guidance of vergence eye movements. Along the ventral pathway, which involves V2 and IT, higher-resolution disparity signals are combined to provide precise estimates of shape and location. This proposal is the focus of much of the ongoing electrophysiological research on stereopsis.

Brain Imaging in Humans

Human functional magnetic resonance imaging (fMRI) experiments have mirrored electrophysiological studies in showing that stereoscopic stimuli activate most, if not all, of the visual areas of the cerebral cortex. The important factors in isolating specific regions are, not surprisingly, the nature of the stimulus (e.g., correlated vs. anticorrelated RDS patterns) and the task. For example, in the first systematic fMRI study of the cortical areas involved in human stereopsis, Benjamin Backus and colleagues found elevated activity in area V3A when observers were asked to make depth discrimination judgments, instead of passively viewing stereoscopic stimuli. In the past 10 years, fMRI research on human stereopsis has flourished, and for the most part appears to map well onto the electrophysiological data. The field of fMRI is advancing, and investigations of stereopsis are moving from identification of where it occurs to how it occurs. For instance, Andrew Welchman and colleagues recently used fMRI to examine the visual areas in which stereoscopic information is combined with other depth cues, and how the combination process is reflected in the variance of the scanning signal.

Conclusion

Since Wheatstone's introduction of the stereoscope in 1838, we have all enjoyed stereograms of one form or another. From the impressive large-format three-dimensional (3D) movies shown in IMAX theaters to the Magic Eye books, there is a quality of magic in the experience of depth from stereopsis. Scientists too have that sense of wonder that the simple physical fact of having two simultaneous views of the world results in such a vivid sense of the space between and taken up by objects in the world. Our goal is to understand how the brain achieves this feat. Although we are making considerable progress, several questions remain unanswered, including: What types of neural pathways are responsible for stereopsis? How is stereoscopic information integrated with other cues to depth? How does the stereoscopic system represent extended surfaces in depth?

See also: Amblyopia; Binocular Vergence Eye Movements and the Near Response.

Further Reading

Arditi, A. (1986). Binocular vision. In: Boff, K., Kaufman, L., and Thomas, J. (eds.) *Handbook of Perception and Human Performance.* New York: Wiley.

Howard, I. P. and Rogers, B. J. (2002). *Seeing in Depth,* Vol. 2. Toronto, ON: I. Porteous Press.

Julesz, B. (1971). *Foundations of Cyclopean Perception* (reprinted in 2006). Boston, MA: MIT Press.

Marr, D. (1982). *Vision*. New York: W.H. Freeman.

Regan, D. M. (ed.) (1991). *Binocular Vision (Vision and Visual Dysfunction)* Vol. 9. Boca Raton, FL: CRC Press.

Sacks, O. (2006). Stereo Sue. *The New Yorker* June 19: 64–73.

Von Noorden, G. and Campos, E. (2002). *Binocular Vision and Ocular Motility*. St. Louis, MO: Mosby.

G

GABA Receptors in the Retina

S Yazulla, Stony Brook University, Stony Brook, NY, USA

Glossary

Disinhibition – A synaptic interaction in which the inhibitory input to a neuron is itself inhibited, thereby relieving the neuron of inhibitory control.
Endocannabinoids – Natural chemicals in the body whose actions on metabotropic cannabinoid receptors are mimicked by the active component of marijuana.
Ionotropic receptors – Membrane proteins that, when activated by specific ligands, directly alter membrane conductance.
IPSC – Inhibitory post synaptic current counteracts excitatory input to a neuron, for example by hyperpolarization or induction of a shunt current.
Metabotropic receptors – Membrane proteins that, when activated by specific ligands, indirectly alter a wide variety of cellular properties through G-protein-coupled enzyme cascades.

Introduction

Gamma-aminobutyric acid (GABA) is the major inhibitory amino acid transmitter in the retina. It is overwhelmingly represented in lateral inhibition, being most prominent in one class of horizontal cell and in numerous subtypes of amacrine cell. GABAergic transmission requires the synthesizing enzyme glutamic acid decarboxylase (GAD) and the degradative enzyme GABA transaminase (GABA-T) that may or may not be found in the same cells. The physiological actions of GABA are effected by receptors that may be broadly defined as proteins that bind to and respond to the presence of GABA. Under this scheme, there are three functional types of GABA receptor: (1) a vesicular transporter that concentrates cytoplasmic GABA into synaptic vesicles, (2) a membrane transporter that translocates GABA from the extracellular space into glia or neurons, and (3) plasma membrane receptors that mediate the cell's response to synaptically released GABA. This article highlights the properties and functions of these major types of the GABA receptor. Numerous sources on the history, physiology, and molecular biology of these receptor types are provided. Table 1 illustrates the major types of the GABA receptor with representative agonists, antagonists, and most common cellular locations in the outer plexiform layer (OPL) and inner plexiform layer (IPL). The pharmacology of GABA transporters (GATs) is less well developed than it is for the synaptic receptors and continues to be an area of intensive research.

Vesicular Transporters

Cytoplasmic GABA is concentrated into synaptic vesicles by a vesicular inhibitory amino acid transporter (VIAAT) that uses H^+-antiport activity to drive the uptake of GABA or glycine into synaptic vesicles. VIAAT is the only member of the solute carrier 32 (SLC32) family of H^+-coupled amino acid transporters; it is not related to the vesicular transporters for glutamate, monoamines, or acetylcholine. VIAAT, referred to as the vesicular GAT (VGAT), when applied to GABAergic neurons, is essential for the vesicular release of GABA and glycine. The existence of a common vesicular transporter for GABA and glycine is consistent with reports of a small percentage of amacrine cells that co-localize and likely release both GABA and glycine.

VIAAT was localized by immunohistochemistry (IHC) in zebrafish, mouse, rat, cat, and human retinas. In the inner retina, synaptic boutons throughout all layers of the IPL contain VIAAT immunoreactivity (IR), consistent with data showing that virtually all amacrine cells in the retina are either GABAergic or glycinergic. Data from salamander, cat, and human suggest the existence of

Table 1 GABA receptor types, agonists, antagonists, and localization in the retina

Synaptic receptors		*Agonist*	*Antagonist*	*Location OPL*	*Location IPL*
	$GABA_A$	Muscimol	Bicuculline	Cones	Amacrine cells
		Isoguavacine	Picrotoxin	Horizontal cells	Cone bipolar cells
		THIP	SR 95531	Bipolar cells	Ganglion cells
		TACA			Mueller's Cells
	α1–3,5$\beta\gamma$2 subunits	Benzodiazapines	Flumazenil	Horizontal cells	Amacrine and ganglion cells
	$GABA_B$	(R)-Baclofen	CGP 35348		Presynatic amacrine
		SKF 9751	SCH 50911		Postsynaptic ganglion
	$GABA_C$	TACA	Picrotoxin	Cones	Rod bipolar cells (mammals)
		CACA (partial)	Isoguavacine		Mixed bipolar cells (fish)
		Muscimol (partial)	TPMPA		
Transporter (plasma)		Uptake substrate	Uptake inhibitor		
	GAT-1	GABA	Cl 966		Amacrine cells (major)
			NO 711		Mueller's cells (minor)
			(R)-tiagabine		
			SKF 89976A		
	GAT-2	GABA	EF1502	Horizontal cells (fish)	
		β-Alanine	Nipecotic Acid		
	GAT-3	GABA	Nipecotic Acid	Horizontal cells (fish)	Mueller's cells
		β-Alanine	(S)-SNAP 5114		
	BGT-1	GABA	(S)-SNAP 5114		
		Betaine			
Transporter (vesicular)	VIAAT (VGAT)	GABA	Vigabatrin	Horizontal cells	Amacrine cells
			Nipecotic Acid		Bipolar cells (subset)

This listing is representative and not meant to be exhaustive regarding GABA receptor pharmacology. The most common sites for localization are listed to provide a general framework. Species-specific exceptions are listed in the text.

subpopulations of bipolar cells that likely release both GABA and glutamate. For example, certain OFF cone bipolar cells in the cat retina contain not only VIAAT-IR and GAD65-IR, but also vesicular glutamate transporter-IR (VGLUT-IR). In the outer retina, VIAAT-IR is present in horizontal cell dendrites in zebrafish, mouse, rat, and human. The presence of $GABA_A$ receptors on the photoreceptor terminals of some mammals supports the notion that GABA is synaptically released in the OPL. VIAAT-IR in the OPL most likely includes not only the horizontal cell dendrites, but also the boutons of GABAergic and glycinergic interplexiform cells. These processes, however, have a relatively low density and are unlikely to be confused with the more numerous horizontal cell dendrites. Electron microscopy shows that VIAAT-immunoreactive horizontal cell dendrites innervate rods and cones in mouse and rat, suggesting that A-type and B-type horizontal cells of the mammalian retina are capable of vesicular GABA release. In fish horizontal cells, the subcellular localization of VIAAT-IR has not been determined by electron microscopy; there are no data to indicate whether VIAAT-IR is restricted to the H1 GABAergic horizontal cells, innervating only cones, or distributed among all four types, innervating both rods and cones.

In the outer retina of mammals and nonmammals, the classification of neurons as GABAergic can be difficult. The presence of VIAAT alone does not necessarily indicate the presence of GABA for vesicular release. Other indicators, such as the presence of glutamate decarboxylase (GAD), the enzyme that catalyzes decarboxylation of glutamate to form GABA, or GABA uptake, are needed to support a GABAergic identity. For example, in most nonmammalian species, VIAAT-positive horizontal cell dendrites do not contain synaptic vesicles or synaptic specializations. Rather, a sodium-dependent GAT appears to facilitate GABA release from horizontal cells. To complicate matters further, the presence of GABA or GAD in an outer retinal neuron does not necessarily stipulate that GABA is synaptically released. For example, although GAD-IR and GABA-IR have been found in cone terminals in primate, lizard, and toad retinas, VIAAT-IR has not been localized to photoreceptor terminals in any species. Lastly, although horizontal cells of some mammals

contain VIAAT-IR, GABA-IR, and GAD-IR, neither GABA uptake nor GATs have been described in the horizontal cells of any mammal.

Plasma Membrane Transporters

GATs are members of the SLC6 family that belongs to the Na^+/Cl^--dependent neurotransmitter transporter superfamily. GATs are arranged in 12 transmembrane domains. Molecular cloning studies identified three subtypes of high-affinity GAT (GAT-1, GAT-2, and GAT-3) and one lower-affinity betaine/glycine transporter that also transports GABA (BGT-1). GATs are responsible for the clearance of GABA from the extracellular space and, conceivably, could be present on the presynaptic neuron, postsynaptic neuron, or surrounding glia. In general, GAT-1 is present in neurons of the inner retina, GAT-3 in Müller's cells, and GAT-2 in the retinal pigmented epithelium (RPE) and ciliary epithelium of the mammalian retina (Figure 1). Overall, there is excellent agreement in the cellular distributions of ^{3}H-GABA uptake, GABA-T, which degrades GABA, and GATs in amacrine cells across species. However, in regard to horizontal cells and Müller's cells, there are notable species differences and inconsistencies.

Neuronal Localization

In a wide variety of mammals and nonmammals, from humans to teleost fish, GAT-1 is the predominant GAT/type in amacrine cells, displaced amacrine cells, and interplexiform cells. This distribution is consistent with the patterns of GAD-IR, GABA-IR, and ^{3}H-GABA uptake. Mammalian Müller's cells are labeled intensely with GAT-3 and, to a lesser extent, by GAT-1, consistent with observations that Müller's cells contain high levels of GABA-T and are the initial site for ^{3}H-GABA uptake. For the most part, nonmammalian Müller's cells neither take up ^{3}H-GABA nor display GAD-IR or GABA-IR. One exception is the skate retina, in which Müller's cells express GAT-1 and GAT-3, display a GAT current, and take up ^{3}H-GABA. Another exception is the salmon retina, in which Müller's cells have GABA-IR, but do not contain GAT-1. Cultured chick Müller's cells contain GAT-1 and GAT-3, while bullfrog Müller's cells contain GAT-1 and GAT-2 and display a GAT current. The implication of these findings in chick and bullfrog is not clear, given the absence of supporting evidence from ^{3}H-GABA uptake or GABA-T immunohistochemical studies. Given the high density of GAT on chick and bullfrog Müller's cells, including the end feet at the inner margin of the retina, it is surprising that ^{3}H-GABA uptake has never been demonstrated in Müller's cells of these species, regardless of how the ^{3}H-GABA was administered.

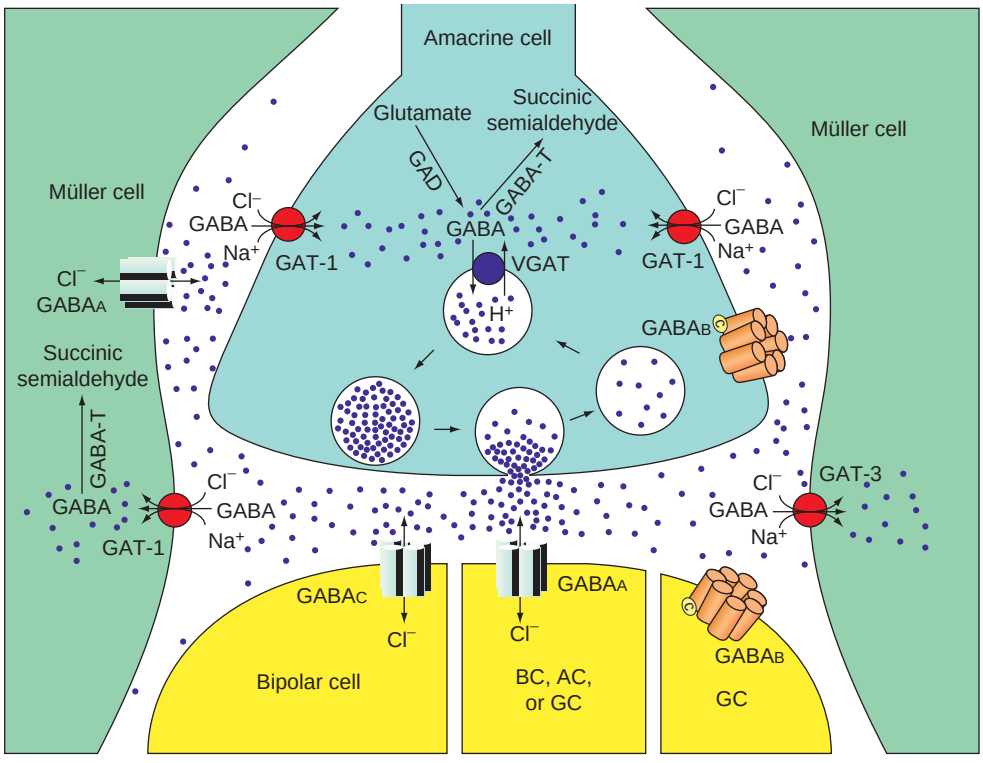

Figure 1 Schematic representation of GABA metabolism, receptor type, and localization in the inner retina. Receptor and transporter types have been placed in the most common locations. See text for details and listing of species-specific exceptions. GAD, glutamic acid decarboxylase; GABA-T, GABA transaminase; AC, amacrine cell; BC, bipolar cell; GC, ganglion cell.

Although horizontal cells in many mammals contain GABA-IR and GAD-IR, they do not take up ^{3}H-GABA. As would be expected, GATs have not been localized to any mammalian horizontal cells. The evidence for a class of GABAergic horizontal cell is overwhelming for nonmammals. Horizontal cells of fish, amphibians, birds, and reptiles take up ^{3}H-GABA with great avidity. GAT-1, present in the inner retina, has not been localized to horizontal cells of any species. Studies on the localization of GAT-2 and GAT-3 in nonmammalian horizontal cells are sporadic, with studies usually focusing on one or the other. Exceptions are goldfish and zebrafish in which GAT-2 and GAT-3 were localized to a subtype of the cone horizontal cell, the H1 luminosity type. GAT-3 was not found in horizontal cells of skate, salamander, or bullfrog. GAT-2, absent in bullfrog horizontal cells, was not studied in skate, salamander, or salmon.

Except for goldfish and zebrafish, the lack of horizontal cell labeling by GAT in other nonmammals could be due to the general use of antibodies against the C-terminus of rat GAT-2 and GAT-3. There is a strong homology in the GAT amino acid sequence in the animal kingdom. Torpedo GAT-3 shows a 77% identical amino acid sequence with the mammalian GAT-3. Immunoblots of the goldfish brain with GAT-3 show a band between 60 and 75 kDa, consistent with the expected weight of 71 kDa. However, regardless of the overall homology or the sequence homology at the C-terminus, the site of antibody production is more critical in determining the validity of the labeling. Except for fish, the negative finding of GAT-2 and GAT-3 on horizontal cells in nonmammals has not been resolved. A curiosity is that ^{3}H-muscimol, a $GABA_A$ agonist, is transported avidly by amacrine cells in mammals and nonmammals, but not to any great extent by horizontal cells in any species, including fish and bird. This is a further indication of the difference in the type of GAT present on amacrine cells and nonmammalian horizontal cells.

A small percentage (~10%) of bipolar cells in some retinas may be GABAergic. In salamander, the vast majority of bipolar cells that contain GAT-1-IR also contain GABA-IR, as well as VGAT and GAD. Two types of OFF bipolar cell in zebrafish contain GABA and likely correspond to the OFF bipolar cells that display a GAT current. However, in primate retina, the variable reports of GABA-IR in bipolar cells are not supported by data localizing GAD, GAT-1, GAT-2, GAT-3, or GABA-T. These findings are significant because of the possibility that some bipolar cells release GABA and glutamate as neurotransmitters.

A GABA/taurine transporter was identified in bullfrog at the apical surface of the RPE. It was suggested that the RPE could take over the clearance of GABA released from horizontal cells in the distal retina of nonmammals because there are no reports that Müller's cells transport ^{3}H-GABA. Despite the reports of GATs in bullfrog Müller's cells, this seems to be an attractive idea that would be supported by the demonstration of GABA-T localization and GABA-T activity in the nonmammalian RPE.

Function

The major function of the GATs is to clear GABA from the extracellular space to either re-enter the vesicular pool or enter the tricarboxylic acid cycle after GABA-T action (**Figure 1**). There are at least three other consequences of the transporter activity. The first is that GABA transport is electrogenic with two Na^{2+}, one Cl^-, and one GABA per cycle, resulting in one-net inward positive charge. The depolarization that accompanies GABA uptake could modulate neuronal excitability by triggering Ca^{2+} influx and the subsequent release of Ca^{2+} from intracellular stores. For example, a nonsubstrate blocker of GABA transport (NO-711) reduced cellular edema, presumably by blocking the ionic influx that accompanies GABA uptake. This strategy has proven useful in treating seizures and could apply to protecting retinal ganglion cells following ischemia or an excitotoxic release of glutamate from bipolar cells. As a second consequence of transporter activity, neuronal depolarization or a breakdown of the Na^+/Cl^-/GABA gradient can cause the GATs to operate in the reverse direction, thus releasing GABA. For example, an excitotoxic assault on the chick retina increases extracellular GABA by reversal of the GAT. This calcium-independent GABA release has been suggested to be the normal mode of release in horizontal cells, glia, and, perhaps, in starburst amacrine cells. This form of GABA release does not require adenosine triphosphate (ATP), except to maintain the ionic gradients. Third, the activity of GATs can limit the spillover of GABA in the extracellular space and regulate inhibition. This has been shown in the inner retina, in which inhibition of GATs by NO-711 enhances the light-evoked inhibitory postsynaptic currents (IPSCs) at $GABA_C$ receptors on bipolar cells, but has no effect on $GABA_A$ receptors on ganglion cells. The difference in response is due to the observation that $GABA_A$ receptors desensitize, whereas $GABA_C$ receptors do not. Thus, the GAT selectively modulated the transmission of signals from bipolar cells to ganglion cells. In all these cases, the effect of GAT activity is to regulate excitability.

Synaptic Receptors

There are three general classes of synaptic GABA receptors: two ionotropic and one metabotropic. These are differentiated by ligand-binding affinities and molecular-cloning techniques. $GABA_A$ receptors are heteropentameric structures that form a chloride channel using structurally related subunits α1–6, β1–4, γ1–3, δ, ε, and π. The most common pentamers are composed of $\alpha\beta\gamma$ subunits, with δ often substituting for γ. The subunit composition determines receptor pharmacology and kinetics.

For example, $GABA_A$ receptors mediate the effects of benzodiazepines (BDZ), and the γ subunit is necessary for BZD sensitivity, while the type of α subunit determines BZD affinity. The β subunit affects channel properties and BZD efficacy. Substitution of an α4 or α6 subunit for an α1 subunit eliminates BZD sensitivity as does substitution of the δ subunit for a γ subunit. $GABA_A$ receptors are blocked by bicuculline, the nonselective chloride channel blocker, picrotoxin, and can be modulated allosterically by barbiturates, BZDs, ethanol, and steroids. The action of the $GABA_A$ receptor tends to be phasic. The ionotropic $GABA_C$ receptor also is a chloride channel that is composed mostly of homoligomeric ρ subunits (ρ_1, ρ_2, and ρ_3). $GABA_C$ receptors are insensitive to bicuculline, more sensitive to GABA than $GABA_A$ receptors, and can also be blocked by picrotoxin. $GABA_C$ receptors do not desensitize; therefore, their effect is tonic. Metabotropic $GABA_B$ receptors are guanine nucleotide-binding protein-coupled receptors and regulate potassium or calcium channels. $GABA_B$ receptors are activated by baclofen, antagonized by phaclofen, insensitive to bicuculline and picrotoxin blockade, and less sensitive to GABA than $GABA_A$ receptors.

Photoreceptors

The source of GABA in the OPL of nonmammals is a type of horizontal cell, so-called H1 or luminosity cells. In mammals, GABA can be released from a type of interplexiform cell as well as from horizontal cells. $GABA_A$ receptors were localized to the OPL by *in vitro* autoradiography (ARG) of ^3H muscimol binding, $GABA_A$ receptor subunit-specific IHC, and single-cell electrophysiology. ^3H-BZD-binding sites were localized by *in vitro* ARG in the OPL of rat, monkey, and human, but were not present in the OPL of fish, salamander, or bird. There is evidence for $GABA_A$ receptors on rod terminals in goldfish and rat, and on the cone terminals in goldfish, tiger salamander, bullfrog, turtle, chicken, rat, mouse, pig, and cat. Most evidence shows β2/3 subunits on photoreceptor terminals. Data for α subunits are inconsistent, with negative results from *in situ* hybridization and positive results with IHC. In contrast to the localization of γ1 and γ2 subunits to salamander cone terminals by IHC, negative results with ^3H-BZD binding indicate an absence of γ subunits. This discrepancy could be due either to the nonspecific nature of IHC using antibodies that are not against salamander γ subunits or to low sensitivity of *in vitro* ARG using photoaffinity labeling of BZD ligands.

GABA-induced responses in cones of all species are reduced by bicuculline, indicating $GABA_A$ receptors. In addition, there is a component of GABA-induced responses in mammalian (pig and mouse) cones that is resistant to bicuculline, but sensitive to antagonists of $GABA_C$ receptors, indicating participation of $GABA_A$ and $GABA_C$ receptors. $GABA_C$ receptors have not been identified on photoreceptors in nonmammals as yet. In mouse, both $GABA_A$ and $GABA_C$ components of the response to GABA are potentiated by pentobarbital, suggesting heteromeric channels of $GABA_C$ ρ1 and $GABA_A$ receptor subunits. In bullfrog, $GABA_B$ receptors contribute to the GABA response along with $GABA_A$ receptors. GABAergic negative feedback onto cones is well established and involves a suppression of presynaptic Ca^{2+} currents. The function of GABA feedback onto photoreceptors is still controversial; it may have limited participation in the formation of the cone receptive field surround. More likely, the modulation of voltage-gated Ca^{2+} currents could set the gain at the cone synapse to maintain sensitivity to changing light conditions. The nondesensitizing nature of $GABA_C$ receptors on mammalian cones may compensate for the lower level of GABA release that is available from horizontal cells and interplexiform cells in the OPL of mammals compared to the high GABA content of H1 horizontal cells in nonmammals.

Horizontal Cells

The information regarding GABA receptors on horizontal cells is based primarily on data obtained with electrophysiology and, to a lesser extent, on immunohistochemical evidence. In addition, there is considerable species variability. $GABA_A$ and $GABA_B$ receptors have been localized by IHC on horizontal cells of some mammals and nonmammals, while $GABA_C$ receptors have been localized to horizontal cells of perch and goldfish. $GABA_B$ receptor-mediated responses have not been reported for horizontal cells in any species. $GABA_A$ responses have been recorded from horizontal cells in catfish, salamander, mouse, rabbit, and cat, while $GABA_C$ responses are prominent in horizontal cells in fish (goldfish, perch, and catfish) and salamander. Skate and zebrafish horizontal cells reportedly show neither $GABA_A$ nor $GABA_C$ responses. In goldfish, $GABA_A$ responses are present in isolated chromaticity horizontal cells, while $GABA_C$ responses are present in the cell body and axon terminal of the GABAergic H1 horizontal cells. In contrast, in perch, $GABA_C$ responses are restricted to the rod horizontal cells. The $GABA_A$ response in isolated mouse horizontal cells is enhanced by the BZD, diazepam, and pentobarbital, consistent with the localization of ^3H-BZD-binding sites in the mammalian OPL by ARG. $GABA_C$ receptor-mediated responses of GABAergic horizontal cells are complicated by the presence of the electrogenic GAT current. H1 horizontal cells release GABA at some steady rate under ambient illumination. They are depolarized by decrements in light intensity, resulting in increased GABA release by the transporter. During the hyperpolarizing response to light onset, the reuptake of GABA will depolarize the horizontal cells, reducing the light response and establishing a

positive-feedback loop that allows for further GABA release from the H1 horizontal cells. In turn, the released GABA, via $GABA_A$ receptors, will depolarize the other cone and rod horizontal cells. In addition, the $GABA_C$ response shows a run-up with repetitive application of GABA, further depolarizing the horizontal cells. However, $GABA_A$ and $GABA_C$ receptors are suppressed by Zn^{2+} that is co-released with glutamate. This dampening effect by Zn^{2+} is especially important to downregulate the tonic $GABA_C$ response.

Bipolar Cells

Bipolar cells form functionally diverse groups that are differentiated on the bases of rod and cone input as well as ON or OFF response. On anatomical grounds, bipolar cells can receive GABAergic input from horizontal cells and interplexiform cells in the OPL and from a multitude of amacrine cell types in the IPL. Species differences among mammals and nonmammals and the effects of dissociation techniques on GABA receptors have resulted in considerable variability in the data. However, $GABA_A$ receptors are generally more prominent on dendrites in the OPL and the ratio of $GABA_A$ to $GABA_C$ receptors on axon terminals in the IPL is high for cone bipolar cells and low for rod bipolar cells. In mammals, IR to $GABA_A$ receptors ($\alpha1$, $\beta2/3$, and $\gamma2$) and the $GABA_C$ ρ subunit is present at nonoverlapping, extrasynaptic sites on the dendrites of rod and cone bipolar cells. The contribution of $GABA_A$ and $GABA_C$ receptors to GABA-evoked IPSCs is balanced in dendrites of isolated mouse rod bipolar cells, whereas, in the ferret retinal slice, $GABA_A$ receptors overwhelmingly dominate the response to GABA puffed at dendrites in all types of the bipolar cell. Dendrites of bipolar cells are insensitive to GABA in salamander and display $GABA_A$ properties in goldfish and $GABA_C$ properties in zebrafish. In bullfrog, all bipolar cells show $GABA_A$ and $GABA_C$ sensitivity at dendrites, though $GABA_A$ receptors dominated, particularly for on bipolar cells.

In the IPL, GABA-evoked IPSCs are carried mostly by tonic $GABA_C$ receptors in rod bipolar cells and by phasic $GABA_A$ receptors in cone bipolar cells (**Figure 1**). This difference in GABA receptor type likely corresponds to the rapid kinetics of the photopic pathway and slower kinetics of the scotopic pathway. This is illustrated in the ferret retina in which activation of $GABA_C$ receptors more effectively inhibits the output to AII and A17 amacrine cells than $GABA_A$ receptors. When co-expressed ON bipolar cell axons, $GABA_A$ and $GABA_C$ receptors are differentially distributed. For example, in the ON mixed rod/cone bipolar cell of goldfish, $GABA_C$ receptors are clustered at the distal (vitreal) margin of the terminal, while $GABA_A$ receptors are more proximal to the cell body, near the connecting axon. Unlike the photoreceptors, there is a very high density of GABA receptors on glutamatergic bipolar cell terminals. Zn^{2+}, likely to be co-released with glutamate, suppresses the amplitude of responses mediated by $GABA_C$ receptors more so than $GABA_A$ receptors. The effects of zinc on the kinetics of $GABA_A$ receptors are variable and likely due to differences in $GABA_A$ subunit composition. The hyperpolarizing effect of GABA on all bipolar cells strongly inhibits glutamate release. This powerful inhibition is buffered by Zn^{2+} and other endogenous modulators including dopamine, neuropeptides, and endocannabinoids that control the transmission of signals to amacrine and ganglion cells.

Amacrine Cells and Ganglion Cells

At least two-thirds of the amacrine cells in all species utilize GABA as the primary neurotransmitter; GABAergic amacrine cells have additional secondary transmitters including acetylcholine, glycine, dopamine, and a wide selection of neuropeptides. Their processes are present in all layers of the IPL and they make extensive feedback contact with bipolar cells, serial contacts with other amacrine cells, and feed-forward contacts with ganglion cells. This makes for an inordinately complicated series of nested inhibitory circuits. In all species, $GABA_A$ receptors are expressed postsynaptically on amacrine cells and ganglion cells. $GABA_B$ receptors are located presynaptically on amacrine cells and postsynaptically on ganglion cells (**Figure 1**). $GABA_C$ receptors are found on ganglion cells in salamander, but apparently not in other species, and only rarely on amacrine cells. $GABA_A$ receptors on subtypes of GABA-receptive amacrine and ganglion cells are characterized by specific subunit compositions. Cholinergic amacrine cells are the only retinal neurons shown, as yet, to express the δ subunit, the presence of which should eliminate BZD sensitivity. The various α subunits aggregate at different synaptic sites. For example, the $\alpha2$ subunit is found on cholinergic amacrine cells, while the $\alpha4$ subunit is found on ganglion cells. Also, for the most part, $GABA_A$ receptors in the inner retina are enhanced by barbiturates and BZDs, indicating the presence of the γ subunit. In general, the effect of $GABA_A$ stimulation of amacrine cells is to suppress the transient component of the light response. The application of GABA tends to suppress the spontaneous activity and light responses of ganglion cells without having a great effect on the center-surround organization. However, $GABA_A$ antagonists abolish directional and orientation selectivity in ganglion cells, presumably by interacting with $GABA_A$ receptors on bipolar cells and other amacrine cells.

In general, the activation of $GABA_B$ receptors on amacrine cells and ganglion cells makes the light response more transient and reduces spike frequency in ganglion cells. In rabbit retina, baclofen facilitates the light-evoked release of ACh. $GABA_B$ receptors are found at limited but discrete locations on the dendrites of starburst and other

types of amacrine cells. A feedback circuit involving the disinhibition of glycine onto starburst amacrine cells could account for the facilitatory effect of baclofen. GABAergic modulation of ganglion cell activity involves a complicated interaction of the subtypes of $GABA_A$, $GABA_C$, and $GABA_B$ receptors that are present ON bipolar and amacrine cells and act on chloride channels and a variety of calcium channels. While $GABA_A$ influence is rapid in onset and offset and likely participates in phasic inhibition, $GABA_B$ and $GABA_C$ influences are slower and likely participate in tonic inhibition. As $GABA_B$ receptors are less sensitive to GABA than $GABA_A$ or $GABA_C$ receptors, their influence may be more prominent during excessive GABA release that could occur with intense stimulation or excitotoxic release of glutamate from bipolar cells.

Müller's Cells

In addition to expressing GATs, Müller's cells in skate, baboon, and human express $GABA_A$ receptors (**Figure 1**). GABA-evoked currents in skate and human Müller's cells show $GABA_A$ pharmacology, including enhancement by Zn^{2+} and, in human, enhancement by barbiturates and BZDs. In human, the $GABA_A$ response is depolarizing and sensitivity is higher at the endfoot, soma, and sclerad margin. The efflux of Cl^- in response to $GABA_A$ activation on Müller's cells could have a variety of consequences. For example, it could regulate extracellular Cl^- homeostasis following Cl^- influx into neuronal $GABA_A$ and $GABA_C$ receptors. It could also accelerate the clearance of extracellular GABA by stimulating uptake, which requires cotransport of Na^+ and Cl^-. This latter function could be critical given data in mouse showing that $GABA_A$ activation could play a role in ganglion cell death following oxidative stress. In rabbit, Müller's cells synthesize and release the diazepam-binding inhibitor (acyl coenzyme A-binding protein, ACBP) in response to protein kinase A activation, mimicking intense neuronal activity. ACBP binds to an α subunit to reduce the Cl^- current, and hence, the level of inhibition. The reduction of Cl^- influx could reduce the osmotic entry of water into neurons, thereby preventing cell swelling. Thus, in mammals at least, Müller's cells that extend across the thickness of the retina play a major role in regulating neuronal GABAergic transmission, with the additional consequence of maintaining extracellular ionic and osmotic balance.

See also: Glutamate Receptors in Retina; Information Processing: Amacrine Cells; Information Processing: Bipolar Cells; Information Processing: Ganglion Cells; Information Processing: Horizontal Cells; Neurotransmitters and Receptors: Dopamine.

Further Reading

Brecha, N. C. (1992). Expression of $GABA_A$ receptors in the vertebrate retina. In: Mize, R. R., Marc, R. E., and Sillito, A. M. (eds.) *Progress in Brain Research*, vol. 90, pp. 3–28. New York: Elsevier Science.

Cueva, J. G., Haverkamp, S., Reimer, R. J., et al. (2002). Vesicular γ-aminobutyric acid transporter expression in amacrine and horizontal cells. *Journal of Comparative Neurology* 445: 227–237.

Gasnier, B. (2004). The SLC32 transporter, a key protein for the synaptic release of inhibitory amino acids. *Pflugers Archiv European Journal of Physiology* 447: 756–759.

Jellali, A., Stussi-Garaud, C., Gasnier, B., et al. (2002). Cellular localization of the vesicular inhibitory amino acid transporter in the mouse and human retina. *Journal of Comparative Neurology* 449: 76–87.

Nelson, H. (1998). The family of Na^{2+}/Cl^- neurotransmitter transporters. *Journal of Neurochemistry* 71: 1785–1803.

Olsen, R. W. and Sieghart, W. (2009). $GABA_A$ receptors: Subtypes provide diversity of function and pharmacology. *Neuropharmacology* 56: 141–148.

Raiteri, M. (2008). Presynaptic metabotropic glutamate and $GABA_B$ receptors. *Handbook of Experimental Pharmacology* 184: 373–407.

Schwartz, E. A. (2002). Transport-mediated synapses in the retina. *Physiological Reviews* 82: 875–891.

Wässle, H., Koulen, P., Brandstätter, J. H., Fletcher, E. L., and Becker, C. M. (1998). Glycine and GABA receptors in the mammalian retina. *Vision Research* 38: 1411–1430.

Yang, X-L. (2004). Characterization of receptors for glutamate and GABA in retinal neurons. *Progress in Neurobiology* 2004: 127–150.

Yazulla, S. (1986). GABAergic mechanisms in the retina. *Progress in Retinal Research* 5: 1–52.

Relevant Website

http://webvision.med.utah.edu – John Moran Eye Center, University of Utah, Webvision. The Organization of the Retina and Visual System.

Ganglion Cell Development: Early Steps/Fate

N L Brown, Cincinnati Children's Research Foundation, Cincinnati, OH, USA

Glossary

Atonal – Basic helix–loop–helix transcription factors involved in development. Atoh7, also called Ath5, is important in ganglion cell development.
Basic helix–loop–helix (bHLH) – A basic protein–DNA and helix–loop–helix protein–protein interaction domain found in some transcription factors.
Ganglion cell layer (GCL) – The innermost retinal cell layer, which contains retinal ganglion cell bodies and, in many vertebrates, displaced amacrine interneurons.
POU-domain transcription factors – A large group of transcription factors containing a bipartite DNA-binding domain called a POU domain.
Retinal progenitor cell (RPC) – A developing retinal cell that undergoes mitotic cell division to produce cells that can differentiate into retinal neurons or glia.
Transitional cell – A retinal progenitor cell that is newly postmitotic, but not yet differentiated as a particular retinal neuron or glial cell type.

Retinal Ganglion Cell Formation

Ganglion cells are the first neurons generated by retinal progenitor cells (RPCs) in the developing optic cup. Retinal ganglion cells (RGCs) differentiate first in all vertebrates. In birds and mammals, retinal neurogenesis begins in the center of the cup with the cell cycle exit of a group of RPCs near the optic stalk. Many, but not all, early neurons differentiate as RGCs. From this initiation zone, RGC genesis spreads outward to the periphery of the optic cup. However, in zebrafish, retinal neuron formation initiates in the ventral, nasal cup and propagates around the circumference of the eye as a wave. Ganglion cell layer (GCL) formation is the initial step of optic cup lamination, which results in a mature retina organized into three cell layers (outer nuclear layer, inner nuclear layer, and GCL) separated by two synaptic layers (outer and inner plexiform layers).

Over the past 15 years, considerable progress has been made toward understanding of how mitotically active RPCs choose the RGC fate, terminally differentiate as RGC neurons, extend their axons, and establish synaptic connections in the brain. Yet, this gene network remains incomplete, with more work needed to define RGC formation in molecular terms. Within the hierarchy, both intrinsic transcription factors and extrinsic signaling pathways provide integrated regulation of progenitor development into an RGC. While this article emphasizes intrinsic regulation of RGC fate specification, a short description of extrinsic signaling pathways known to regulate RGC development is also included.

Atoh7/Ath5 Function is Critical for RGC Development

The onset of retinal neurogenesis in a subset of optic cup RPCs is characterized by the activation of the basic helix–loop–helix (bHLH) transcription factor Atoh7/Ath5. The bHLH factors regulate many characteristics of retinal neuron formation. The encoded proteins contain both a basic DNA-binding and helix–loop–helix protein dimerization domains. These factors are expressed by RPCs, in which one or more cells ultimately becomes a neuron. Atoh7/Ath5 occupies a critical node in the RGC gene hierarchy, since zebrafish or mouse mutants lacking the gene have a profound to total loss of RGC differentiation and abnormal optic nerve formation. Adult mutant animals are viable, but have no optic nerves or chiasmata. Overexpression of frog and chick Ath5 during retinal development induces ectopic RGCs, but mammalian Atoh7 does not seem to have this ability. This difference correlates with the observation that, in the mouse retina, Atoh7-expressing cells (the Atoh7 retinal lineage) give rise to all seven major classes of retinal neurons and glia in the adult retina, and do not strictly produce RGCs. This indicates that Atoh7 function is needed to acquire the potential to become an RGC, but is insufficient to commit a cell to this fate. During embryonic retinal neurogenesis, the Atoh7 lineage is hypothesized to predominantly give rise to RGCs, but after the peak of RGC genesis, Atoh7-expressing cells are better able to adopt other retinal fates. This change in developmental ability is presumably due to input from signals secreted by differentiated RGCs and possibly other (non-Atoh7) retinal lineages. Such signals may either promote the adoption of non-RGC retinal neuron or glial fates, block RGC fates, or both.

One role for Atoh7 in the mouse retina is to facilitate cell cycle exit, since mutant cells appear to stall at a cell cycle checkpoint, unable to either resume mitosis or differentiate as RGCs. Eventually, these cells erroneously adopt the last retinal fate, that of Müller glia. Mouse

retinal cells expressing Atoh7 fit the definition of transitional cells, because they are nonmitotic, migratory RPCs that commit to a particular fate, but remain undifferentiated when they express Atoh7. Atoh7+ cells co-express the cyclin kinase inhibitor Cdkn1b/$p27^{Kip1}$, which has multiple functions, including promoting exit from mitosis of cells at the G_1/G_0 checkpoint. Without Atoh7, the percentage of Cdkn1b+ cells fluctuates in both number and arrangement during the peak of RGC genesis. However, questions remain about the relationship between Atoh7 and Cdkn1b. Does mouse Atoh7 directly regulate the activation of Cdkn1b, or do Atoh7 and Cdkn1b act cooperatively to drive RPCs out of mitosis? The latter possibility has been proposed for frog Ath5 and cyclin-dependent kinase inhibitor xic1 (p27Xic1), although it is unclear whether this represents protein–protein interactions, coordinate regulation of shared downstream genes, or cross-regulation. Alternatively, the shifts in mammalian cyclin-dependent kinase inhibitor 1B ($p27^{Kip1}$) expression in Atoh7 mutant eyes may be correlative, but not indicative, of either type of interaction. Since cyclin-dependent kinase inhibitor 1B (Cdkn1b) transcription, translation, and protein stability are independently regulated during development, distinguishing among these possibilities will require further in-depth analyses.

Integrated Regulation of Atoh7/Ath5 Retinal Expression

Many proneural bHLH genes autoregulate their expression, including fruit fly atonal and mouse Atoh1, the most closely related bHLH factors to Atoh7. However, multiple lines of evidence show that Atoh7/Ath5 does not regulate its own expression. Atoh7/Ath5 appears in the optic cup slightly ahead of other proneural bHLH factors and has a very dynamic expression pattern first detectable in a subset of transitional cells that give rise to the earliest retinal neurons. Therefore, determining which transcription factors and signal transduction pathways directly influence Atoh7/Ath5 expression is essential for comprehending how broadly acting factors regulate the precise spatiotemporal patterns of retinal neurons. Among the early optic cup transcription factors, only Pax6 has been shown to directly activate retinal expression of Atoh7/Ath5 via binding to its highly conserved enhancer. Because Atoh7/Ath5 expression initiates in a subset of Pax6-expressing cells, other factors must simultaneously restrict Atoh7/Ath5 expression to newly postmitotic transition cells (**Figure 1**). Another equally important aspect of Atoh7/Ath5 regulation is its turnover, since Atoh7 mRNA disappears abruptly from transitional cells at their entry into the GCL. Therefore, repression is just as important as initial activation for the proper regulation of Atoh7/Ath5 (**Figure 1**).

There are several factors that genetically suppress Atoh7/Ath5 expression, including hairy and enhancer of split 1 (Hes1), neurogenic differentiation 1 (Neurod1), and neurogenic differentiation 4 (Neurod4/Ath3). Because Hes1 is a transcriptional repressor, it is not surprising that it blocks Atoh7 expression. Hes1 similarly suppresses the expression of other retinal proneural bHLH factors like neurogenin 2 (Neurog2) and achaete-scute complex homolog 1 (Ascl1). In the absence of Hes1, Atoh7, Neurog2, and Ascl1 are each prematurely activated in the mouse optic cup. Although Hes1 regulates the overall

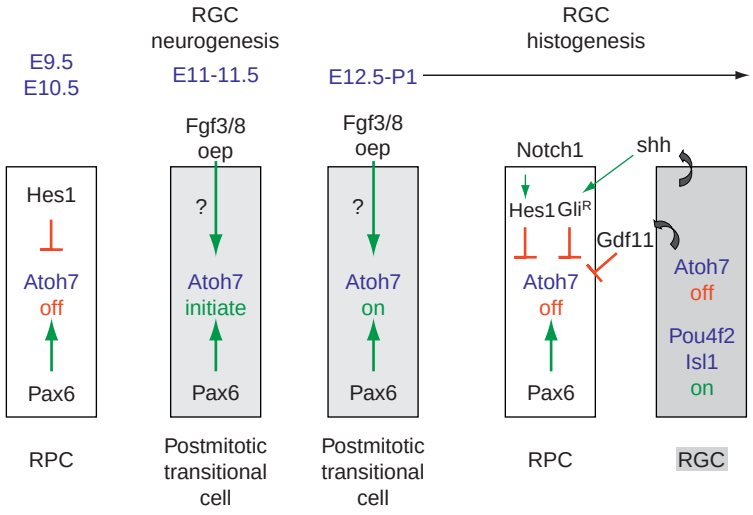

Figure 1 Regulation of Atoh7/Ath5 in postmitotic retinal progenitors. Combinatorial regulatory input for Atoh7/Ath5 transcription in the optic cup. Paired box gene 6 (Pax6) provides cells with the competence to express Atoh7, but Hes1 prevents activation from occurring prematurely. When Hes1 is downregulated, localized Fgf signaling triggers a subset of RPCs to express Atoh7. Retinal cells adopting the RGC fate express Atoh7 for a relatively short time, after which multiple signaling pathways (Notch, Shh, and/or Gdf11) abruptly shut off Atoh7, particularly as differentiating RGCs enter the GCL. Mature RGCs control their own number by secreting Shh and Gdf11, which block Atoh7 expression.

timing of neurogenesis, other regulatory inputs control the precise onset of each proneural bHLH gene. The timing function of Hes1 reflects its role as a downstream effector of Notch signaling, although not all Hes1 functions are Notch dependent. Other factors that suppress Atoh7 expression are Neurod1 and Neurod4, which do so synergistically. Embryonic mouse retinas that are mutant for both genes have expanded Atoh7 expression and a dramatic increase in RGCs, along with a profound loss of amacrine neurons. Thus, Neurod1 and Neurod4 repress Atoh7 expression (directly or indirectly) in RPCs that normally give rise to amacrine cells.

Multiple extrinsic signals influence vertebrate Atoh7/Ath5 expression, particularly for RGC formation. These include fibroblast growth factor 3 (Fgf3), fibroblast growth factor 8 (Fgf8), one eyed pinhead/nodal-like (oep/nodal-like), notch homolog 1 (Notch1), growth differentiation factor 11 (Gdf11), and sonic hedghog (Shh) signaling pathways (**Figure 1**). As shown in the zebrafish and chick retina, Fgf and oep signaling are required for Ath5 activation, while Notch (chick, frog, mouse), Gdf11 (mouse), and Shh (zebrafish, chick, mouse) each suppresses Atoh7/Ath5 expression. Intriguingly, chick Fgf3 and Fgf8 are both expressed in the central optic cup, just prior to the onset of retinal neurogenesis and Fgf protein-coated beads induce Ath5 expression. Although no role during early mouse retinal development has been reported for the orthologous genes, the secretion of stimulatory signals from the central optic cup (Fgf3 or 8) and/or optic stalk (Fgf8 and oep) would be sufficient to explain the onset of Atoh7/Ath5 expression in a restricted retinal domain. By contrast, the extrinsic pathways that negatively regulate Atoh7/Ath5 expression emanate from two distinct sources, RPCs and RGCs. The Notch pathway functions in multiple and complex ways during neurogenesis, but its classic role is to transduce a competitive signal between two adjacent progenitors, in which one cell (expressing more ligand) laterally inhibits the other (expressing more receptor) from differentiating. Therefore, Notch+ cells remain proliferative by suppressing neuron promoting factors like Atoh7. The other two signals, Gdf11 and Shh, are made and secreted by differentiated RGCs to provide negative feedback regulation to RPCs so that the number of neurons is not drastically overproduced. But, to date none of these pathways have been shown to directly activate or repress Atoh7/Ath5 transcription.

Atoh7/Ath5 Activates Pou4f/Brn3 Expression in RGCs

Atoh7/Ath5 activation of Pou4f/Brn3b expression is the principal molecular pathway directing RGC specification and differentiation. Studies in the chick, frog, and mouse eye all suggest that this activation is direct, although definitive biochemical assays have not yet been performed. In the mouse optic cup, Atoh7 and Pou4f2 expression are 90% overlapping, with Atoh7 appearing slightly earlier than Pou4f2 in cells completing their final mitosis, migrating toward the GCL, and differentiating (**Figure 2**). Importantly, Atoh7 is abruptly turned off as nascent RGCs enter the GCL, while Pou4f2 expression is maintained by mature RGCs, even into adulthood.

The Pou4f/Brn subfamily of POU-domain transcription factors is comprised of Pou4f1/Brn3a, Pou4f2/Brn3b, and Pou4f3/Brn3c. Each of these genes acts as key regulators of sensory neuron development, particularly projection neurons. But, each POU-domain factor is required by different kinds of projection neurons. Although a particular class of projection neuron can express all three Pou4f factors, the one that is activated first performs the critical functions. For example, in the retina, all three factors are present in overlapping subsets of differentiated RGCs, but Pou4f2/Brn3b expression initiates expression

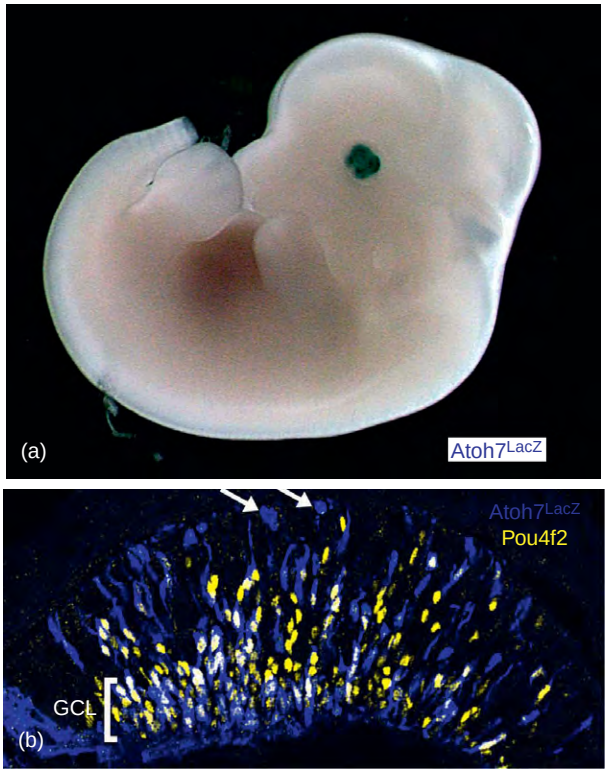

Figure 2 Atoh7 and Pou4f2 expression during RGC development. (a) E11.5 Atoh7$^{LacZ/+}$ embryo expressing β-galactosidase in the optic cup (detected through a chromagenic reaction that turns cells in the eye blue). (b) Anti-β-galactosidase (which detects cells with Atoh7^{LacZ} expression) and anti-Pou4f2 double immunofluorescent staining of E13.5 central optic cup section. Arrows point to Atoh7-expressing cells completing mitosis, which then migrate to the GCL. During migration, these cells initiate Pou4f2 expression (in yellow). Atoh7/Pou4f2 co-expressing cells are in white. Pou4f2 activates downstream target genes for RGC differentiation, axon outgrowth/guidance or survival. The bacterial β-galactosidase has a long half-life in mouse tissues, thus is present in mature RGCs, while endogenous Atoh7 is absent from the GCL (bracket).

about 2 days ahead of the others. The loss of either Pou4f1/Brn3a or Pou4f3/Brn3c has no effect on RGC development, although trigeminal and dorsal root ganglia critically require Pou4f1, and cochlear and vestibular neurons need Pou4f3. However, Pou4f2/Brn3b is a key regulator of RGC development, and mutant adult eyes have extremely thin optic nerves lacking 70% of the RGCs. In contrast to Atoh7 mutants, Pou4f2 mutants have differentiated RGCs that extend axons through the optic nerve, but subsequently fail to innervate the correct regions of the brain and die because these cells lack a critical survival factor. Although Pou4f1 and Pou4f3 seem dispensable for retinal development, they act redundantly with Pou4f2. Pou4f1−/−;Pou4f2−/− and Pou4f3−/−;Pou4f2−/− double mutants have a more profound loss of RGCs than Pou4f2 single mutants. Moreover, overexpression of individual Pou4f genes in chick RPCs demonstrated that each is fully capable of inducing RGCs. Finally, Pou4f3 rescues the loss of Pou4f2 in retinal explant cultures; and targeted replacement of Pou4f1 into the Pou4f2 locus restores RGC development and survival.

Pou4f2 regulates two distinct molecular pathways during RGC development. In the first, Pou4f2 turns on unknown downstream genes within the earliest differentiating RGCs. This subset of RGCs can develop as if Pou4f2 independent, because in Pou4f2 mutants Pou4f1 and Pou4f3 expression rescues them. The second, Pou4f2-dependent pathway produces the bulk of RGCs at later embryonic ages. Here, Pou4f2 regulates a distinct set of downstream genes from those found in the earliest RGCs, including the transcription factors distal-less homeobox 1 and 2 (Dlx1 and Dlx2). When Pou4f2 function is removed from the mouse optic cup, the early RGCs persist, due to Pou4f1 and Pou4f3 compensation. However, the larger, Pou4f2-dependent RGC population cannot complete neuronal differentiation, correctly innervate the brain or express survival factors. This results in mutant eyes with abnormally thin optic nerves. Interestingly, these circumstances point to the Pou4f2 mutant mouse as an excellent system in which to study optic nerve regeneration. For instance, could *ex vivo* cultured (and introduced) RPCs, or early differentiating RGCs, use the Pou4f2 mutant reduced optic nerve, as a substrate for projecting their axons to the correct regions of the brain? Or, could Pou4f1 and Pou4f3 expression be manipulated (activated or derepressed) within the second, later group of developing RGCs to rescue their outgrowth and survival defects?

Pou4f2/Brn3b Controls Numerous RGC Processes

Multiple studies indicate that Pou4f2 is strictly a transcriptional activator, with numerous potential downstream target genes. The list of identified downstream genes includes Pou4f2 itself (autoregulation), Pou4f1 (cross-regulation), the transcription factor eomesodermin homolog (Eomes), the anti-apoptosis factor B-cell lymphoma-2 associated protein (Bcl2), the signaling molecule Shh and multiple cytoplasmic or cell surface proteins, including actin-binding LIM protein 1 (Ablim1), which participate in axon outgrowth, guidance, or vesicular trafficking at synapses. Among these Eomes, Ablim1, and Shh are described here as examples that highlight the diverse set of genes that Pou4f2 directly or indirectly regulates in nascent RGCs. First, Eomes is a transcription factor with a T-box DNA-binding protein motif. During the period of maximal Pou4f2 embryonic expression, Pou4f2 directly activates Eomes transcription in differentiated RGCs. Eomes is also expressed by a subset of inner nuclear retinal cells, potentially amacrine cells, but the role of this factor in the inner nuclear layer remains unexplored. When Eomes function was removed during retinal development, mutant mice have thinner than normal optic nerves, which reflect a postnatal loss of RGCs. Although initial RGC development does not require Eomes activity, myelination of RGC nerve fibers does, and this defect causes elevated RGC death in Eomes mutants. This myelination defect is very similar to the one that has been described for Pou4f2 mutant mice.

Pou4f2 function is also necessary for the proper expression of proteins that direct neurite outgrowth, axon guidance, and neuronal function at synapses. One such gene is Ablim1, encoding an actin-binding protein, with a LIM protein–protein interaction domain. Misexpression of a mutant form of Ablim1 during chick optic nerve development causes RGC axon guidance defects. But paradoxically, Ablim1 mutant mice have no retinal or optic nerve defects. This implies that Ablim1 acts redundantly with another molecule during RGC axon outgrowth. Because there are two other Ablim genes in mammals, future studies are needed to test the role of these genes, singly and in combination with each other and Ablim1, to understand if Pou4f2 regulation of Ablim expression is sufficient to explain the RGC axon guidance defects of Pou4f2 mutant mice. Finally, the search for additional genes regulated by Pou4f2 uncovered the secreted signaling molecule Shh.

Islet1 Acts Parallel to Pou4f2 During RGC Development

Although Atoh7 activation of Pou4f2 deploys an important molecular mechanism for generating RGCs, other factors also act at this same step in the genetic hierarchy of RGC. These genes, which largely encode transcription factors, require Atoh7/Ath5, but not Pou4f2, for their activation. There are several possibilities for how these additional factors act during RGC genesis. They may

regulate a separate set of target genes, cross-regulate or interact with Pou4f2 and its downstream targets, or both. Several candidates that appear to act parallel with Pou4f2 are lim-homeodomain protein 1, Islet1 (Isl1), transducin-like enhancer of split 1 homolog (Tle1), and myelin transcription factor (Myt1). At present only Isl1 is known to function during RGC formation, and retinal-specific deletion of Isl1 results in adult mice lacking 95% of RGCs. This profound loss is more like the Atoh7 phenotype than it is to that of Pou4f2, with the main difference being the developmental age when RGCs are affected. The Isl1 transcription factor contains both a protein–protein interaction LIM-domain and a DNA-binding homeo-domain. Isl1 function is not only important during development in multiple tissues, like the spinal cord and pancreas, but also for cholinergic amacrine and bipolar neuron genesis in the retina. In optic cups devoid of Isl1 function, RGCs are specified and differentiate on schedule, including activating expression of Pou4f2 and other differentiation markers. But by birth, most RGCs down-regulate Pou4f2 expression and then rapidly die. Closer examination of Isl1 mutant RGCs showed both aberrant axon projections and reduced Ablim1 expression, reminiscent of Pou4f2 mutants. Importantly, Pou4f2 and Isl1 act synergistically to control the activation of shared downstream genes, like Pou4f2, Pou4f1, and Shh. Thus, more work is needed to determine which genes Isl1 and Pou4f2 regulate in common versus those controlled by one factor or the other. Since presumably Tle1 and Myt1 also regulate similar processes during RGC formation, working out the combinatorial code of which transcription factors regulate each downstream gene is still needed.

Conclusion

As the genetic hierarchy of RGC development is deciphered, these studies draw us increasingly closer to understanding the sequence of steps for directing RPCs out of the cell cycle to differentiate as RGCs, and how these neurons make appropriate connections in the brain.

See also: Coordinating Division and Differentiation in Retinal Development; Embryology and Early Patterning; Eye-Field Transcription Factors; Histogenesis, Cell Fate, and Signaling Factors; Information Processing: Ganglion Cells; Intraretinal Circuit Formation; Photoreceptor Development: Early Steps/Fate; Retinal Histogenesis.

Further Reading

Brown, N. L., Patel, S., Brzezinski, J., and Glaser, T. (2001). Math5 is required for retinal ganglion cell and optic nerve formation. *Development* 128: 2497–2508.

Erkman, L., Yates, P. A., McLaughlin, T., et al. (2000). A POU domain transcription factor-dependent program regulates axon pathfinding in the vertebrate visual system. *Neuron* 28: 779–792.

Hatakeyama, J. and Kageyama, R. (2004). Retinal cell fate determination and bHLH factors. *Seminars in Cell and Developmental Biology* 15: 83–89.

Kanekar, S., Perron, M., Dorsky, R., et al. (1997). *Xath5* participates in a network of bHLH genes in the developing *Xenopus* retina. *Neuron* 19: 981–994.

Kay, J. N., Finger-Baier, K. C., Roeser, T., Staub, W., and Baier, H. (2001). Retinal ganglion cell genesis requires lakritz, a zebrafish atonal homolog. *Neuron* 30: 725–736.

Livesey, F. J. and Cepko, C. L. (2001). Vertebrate neural cell-fate determination: Lessons from the retina. *Nature Review Neuroscience* 2: 109–118.

Marquardt, T. (2003). Transcriptional control of neuronal diversification in the retina. *Progress in Retinal and Eye Research* 22: 567–577.

Mu, X., Fu, X., Beremand, P. D., Thomas, T. L., and Klein, W. H. (2008). Gene regulation logic in retinal ganglion cell development: Isl1 defines a critical branch distinct from but overlapping with Pou4f2. *Proceedings of the National Academy of Sciences of the United States of America* 105: 6942–6947.

Pan, L., Deng, M., Xie, X., and Gan, L. (2008). ISL1 and BRN3B co-regulate the differentiation of murine retinal ganglion cells. *Development* 135: 1981–1990.

Rapaport, D. H. (2006). Retinal neurogenesis. In: Sernagor, E., Eglen, S., Harris, B., and Wong, R. (eds.) *Retinal Development*, pp. 30–58. New York: Cambridge University Press.

Wang, S. W., Kim, B. S., Ding, K., et al. (2001). Requirement for Math5 in the development of retinal ganglion cells. *Genes and Development* 15: 24–29.

Gene Therapy for the Cornea, Conjunctiva, and Lacrimal Gland

A Sharma, A Ghosh, and C Siddappa, University of Missouri–Columbia, Columbia, MO, USA
R R Mohan, University of Missouri–Columbia, Columbia, MO, USA

Glossary

Alloantigen – An antigen that is the part of an animal's self-recognition system. The common alloantigens are the major histocompatibility complex and red blood cells.
Astigmatism – The inability of the eye to focus sharp image on the retina due to the irregular shape of the cornea or lens.
Capsid – The protein shell that surrounds genetic material of the virus.
Corneal graft or penetrating keratoplasty – The replacement of the central diseased cornea with a healthy donor cornea. This process is also called corneal transplantation.
Corneal neovascularization – The ingrowth of new blood vessels from limbal plexuses toward clear cornea.
Corneal scarring or haze – The loss of corneal transparency and appearance of scar because of injury or abnormal wound healing.
Corneal stroma – The tissue between the epithelium and endothelium of the cornea. It constitutes approximately 90% of corneal thickness and comprises collagens, keratocytes, and extracellular matrix.
CRE-adenovirus vector – An adenovirus vector generated with the helper vector that has a packaging sequence flanked by Cre/*lox*-P system using human embryonic kidney 293 cells stably transfected with Cre recombinase. This results in selective deletion of packaging sequence from helper virus.
Dominant-negative mutant construct – A plasmid encoding for a mutant protein that competes with wild-type (normal) protein within the same cell to inhibit its function.
Enhanced green fluorescent protein (EGFP) – A 27-kDa protein isolated from jelly fish. It fluoresces green when exposed to blue light and is commonly used as a marker for gene transfer studies.
Hyperopia – A term used to define eye defect in which near objects appear blurred because images are focused on the back of the retina instead of on the retina. This medical condition is also known as far- or long-sightedness.
Keratitis – The inflammation in the cornea causing pain and discomfort.
Myopia – A term used to define eye defect in which distant objects appear blurred because images are focused in front of the retina instead of on the retina. It is also called near- or short-sightedness.
Orthotopic graft/transplant – The transplantation or grafting of tissue at its normal position in the body.
Reporter/marker gene – The gene(s) used to track and/or quantify levels of gene delivery in the cell. The common reporter genes are green fluorescent protein, beta galactosidase, etc.
Serotype – A characteristic set of antigens used to distinguish closely related virus strains.
Sonoporation – A technique used to produce small pores temporarily in the cell membrane using ultrasonic waves for introducing RNA, DNA, or small drugs into the cells.
Vector – Virus or nonviral materials used as a vehicle for carrying genes into the cells.

Introduction

Gene therapy is an attractive approach to treat ocular surface diseases and disorders (Table 1). Recent reports of improved visual function in adult patients with Leber's congenital amaurosis with gene therapy attest the potential of this form of molecular medicine to cure eye disease and prevent blindness. The front of the eye, commonly referred as ocular surface, primarily consists of the tear film, cornea, and conjunctiva. The lids, tears, and lacrimal glands are also considered integral parts of the ocular surface, as they spread tears and protect the eye. Nearly all ocular surface diseases entail an abnormality in the cornea. Consequently, more research has been performed to develop gene therapy approaches for the cornea compared to other ocular surface constituents. This article provides an overview of ocular surface gene transfer studies performed by us and many other investigators.

Corneal Gene Therapy Methods

Cornea is an attractive target for gene therapy because of its accessibility, immune-privileged status, and ability to be monitored visually. Gene transfer research in the

Table 1 Genes used for gene therapy of the ocular surface

	Gene	*Vector*	*Mode of transfection*	*Effect on resolution of disease process*
Cornea				
Graft rejection	Cytotoxic T-lymphocyte-associated antigen 4 (CTLA-4)	Adenovirus	Topical application	+/−
	CTLA-4	Adenovirus	IV injection	+
	CTLA-4	Adenovirus	IP injection	+
	CTLA-4	Minimalistic immunolistic immunologically defined gene expression vector	Gene gun	+/−
	Inducible T-cell co-stimulator (ICOS)	Adenovirus	IP injection	−
	Interleukin (IL) 10 antagonist	Adenovirus	Organ culture	+ in ovine − in rat
	Interleukin 12 antagonist	Adenovirus	Organ culture	+ in ovine − in rat
	Interleukin 4	Adenovirus	Organ culture	−
Wound healing	Soluble type II transforming growth factor (TGF)β receptor	Adenovirus	IM injection	+
	Decorin	Adeno-associated virus	Organ culture	+
	Tissue plasminogen activator	Plasmid	Electroporation in the anterior chamber	+
Alkali burns	SMAD 7	Adenovirus	Topical application	+
	Bone morphogenic protein 7	Adenovirus	Topical application	+
	Peroxisome proliferator-activated receptor(PPAR)-γ	Adenovirus	Topical application	+
Scarring or haze	Herpes simplex virus (HSV) thymidine kinase	Retrovirus	Topical application	+
	Dominant-negative cyclin G1	Retrovirus	Topical application	+
Neovascularization	Vascular endothelial growth factor receptor FLT-1	Plasmid	Intrastromal injection	+
	Vascular endothelial growth factor receptor FLT-1	Adenovirus	Injection into anterior chamber	+

	Vascular endothelial growth factor receptor FLT-1	Adeno-associated virus	Subconjunctival injection	+
	FLT23K	Plasmid	Intrastromal injection	+
	FLT24K	Plasmid	Intrastromal injection	+
	Endostatin/kringle-5 domain of plasminogen fusion protein	Lentivirus	*In vitro*	+
	Kringle 5 plasminogen	Electroporation	Organ culture	+
	Angiostation	Adeno-associated virus	Organ culture	+
	IL12	Plasmid	Topical application or intrastromal injection	+
	IL 10	Plasmid	Topical application or intrastromal injection	+
Dystrophies	β-Glucuronidase	Adenovirus	Injected into anterior chamber or intrastromal injection	+
Disorders				
Increase immunity against HSV-induced ocular keratitis	HSV-1 glycoprotein D, B1	Plasmid	Topically, subconjunctival, IP, or IM injection	+
Herpes keratitis	IL2, 4, 10, interferon, tumor necrosis factor	Plasmid	Topical application	−
Lacrimal gland				
Sjögren syndrome	IL10	Adenovirus	Injected into lacrimal gland	+
	TNF	Adenovirus	Injected into lacrimal gland	+
Conjunctiva				
Wound healing	Dominant-negative p38MAPK	Adenovirus	Topical application	+
	SMAD 7	Adenovirus	Topical application	+
	PPARγ	Adenovirus	Topical application	+

cornea primarily focuses on developing therapeutic modalities for common clinical problems such as corneal neovascularization, graft rejection, corneal scarring, and wound healing. The scope of developing novel interventional gene therapy strategies has been markedly enhanced because of an increased understanding of the molecular mechanisms and pathogenesis of corneal diseases. Multiple vectors, techniques, and strategies have been utilized to deliver foreign genes in the cornea. Employing *in vitro*, *ex vivo*, and *in vivo* models, the efficiency of numerous viral and plasmid vectors to deliver genes in the ocular surface tissues has been evaluated. Among viral vectors, adenovirus, adeno-associated virus (AAV), retrovirus, and lentivirus vectors were found to efficiently introduce genes in the cornea. However, none of these vectors is ideal, and each had its own pros and cons.

Viral Vectors

Adenovirus and retrovirus vectors provided short-term transgene expression in the mouse and rabbit cornea with moderate-to-severe inflammatory response. These vectors also transduced corneal and conjunctival epithelium efficiently in human cornea but failed to deliver genes in rat, rabbit, and sheep corneal epithelium. Interestingly, adenovirus vector showed the best transduction efficiency for corneal endothelial cells when compared to the vectors developed from equine immunodeficiency virus, lentivirus, or bacculovirus. Nonetheless, both adenovirus and retrovirus vectors are of limited use for corneal gene therapy because of their inability to transduce nondividing cells, low transduction efficiency for corneal cells, and propensity to induce immune reactions. AAV and disabled lentivirus vectors can transduce nondividing cells and provide long-term transgene expression, thus offering good alternatives for delivering genes into keratocytes and endothelium of the cornea. However, limited studies have been performed to evaluate the utility of these vectors for corneal gene therapy. We, for the first time, showed selective transgene delivery into keratocytes of the rabbit cornea *in vivo* with AAV2 vector using a lamellar flap technique. Figure 1 shows the levels and locations of β-galactosidase (β-gal) reporter gene expression in the rabbit cornea. This study also revealed that direct contact of vector to stroma is critical for introducing therapeutic genes into rabbit keratocytes *in vivo*. Our subsequent studies with AAV serotypes 2 and 5 showed that AAV vectors provide long-term transgene expression in the mouse and rabbit stroma *in vivo*. The mouse eyes continued to express enhanced green fluorescent protein (EGFP) in the corneal stroma for 10 months, without showing any significant side effects (Figure 2).

In recent years, several hybrid AAV vectors have been engineered using the genome of AAV serotype 2 and capsid protein of AAV serotypes 1–9 for gene therapy. The newly produced hybrid AAV vectors have shown improved trangene delivery in many tissues including the eye. However, besides the AAV2/5 vector, transduction efficiency of other newly developed hybrid AAV vectors for the cornea has not been investigated. Recently, our laboratory tested the transduction efficiency of AAV2/6, AAV2/8, and AAV2/9 vectors for the human corneal fibroblasts and epithelial cells *in vitro* and for mouse cornea *in vivo*. The results showed that the tested hybrid AAV vectors are more efficient when compared to nonhybrid AAV2 serotypes for each corneal cell type. Figure 3 demonstrates the levels of transgene delivery in human corneal epithelium (a) and human corneal fibroblast (b) delivered with AAV2/6 vector. The analysis of AAV2/6, AAV2/8, and AAV2/9 gene transfer data revealed that AAV2/6 vector is the most efficient among the three tested vectors for human corneal fibroblasts and epithelial cells *in vitro*. Although AAV vectors are efficient and safe for delivering genes in the cornea, unfortunately they are incapable of transporting large genes (>1.8 kb).

Disabled lentivirus vectors have been used to deliver large genes to all three major cells of the human cornea *in vitro* and to mouse corneal endothelium *in vivo*. In addition, transgene delivered with lentivirus vectors showed long-term expression. Our research team noted efficient EGFP gene delivery into keratocytes of the mouse cornea *in vivo* with lentivirus vector that was applied to the mouse stroma for 2 min after removal of

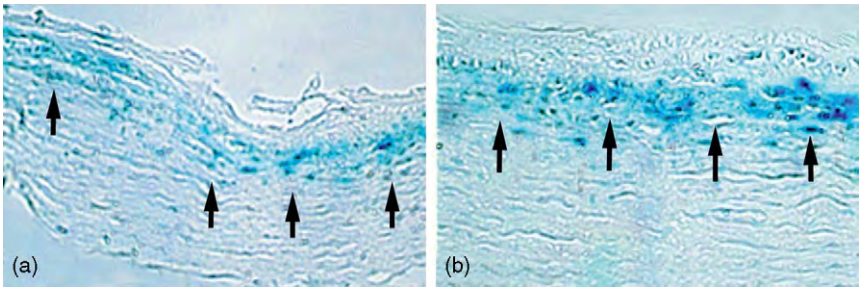

Figure 1 AAV-mediated targeted transgene delivery into keratocytes of the rabbit cornea *in vivo* using lamellar flap technique. The AAV2 vector was topically applied on the stromal bed after making corneal flap with microkeratome. Significant levels of transgene delivery in the rabbit stroma at day 3 and day 10, respectively, are shown in (a) and (b).

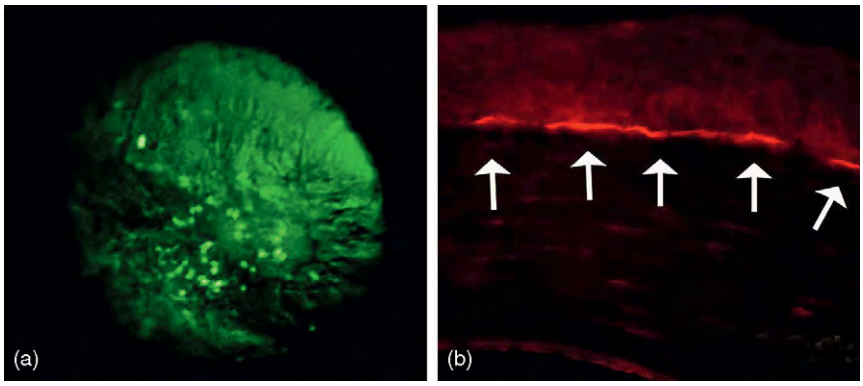

Figure 2 AAV-mediated transgene transduction into keratocytes of the mouse cornea *in vivo* observed at 10 months. Representative stereomicrograph of the cornea surface (a) and tissue section (b) images demonstrate detection of high levels of fluorescent GFP reporter gene expression in the mouse cornea *in vivo* delivered into mouse keratocytes with AAV5 vector applied topically.

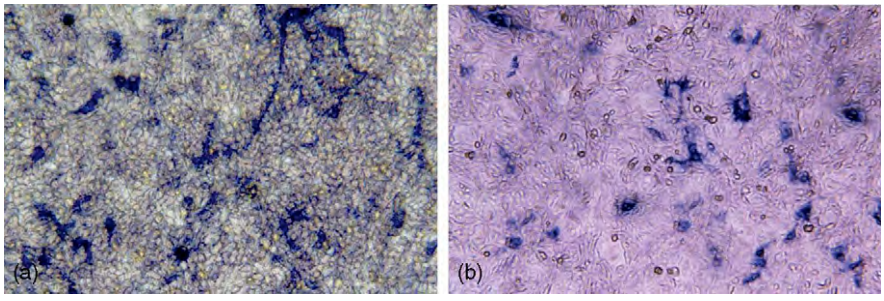

Figure 3 Efficient transduction of cultured human corneal epithelial (a) and fibroblast (b) cells by the AAV2/6 hybrid vector detected 40 h after vector treatment. The transduction efficiency of AAV2/6, AAV2/8, and AAV2/9 vectors to transduce human corneal epithelial and fibroblast cells was compared. AAV2/6 vector showed the highest transduction efficiency for tested corneal cultures. Transduced cells expressing human placental alkaline phosphatase reporter gene are stained blue.

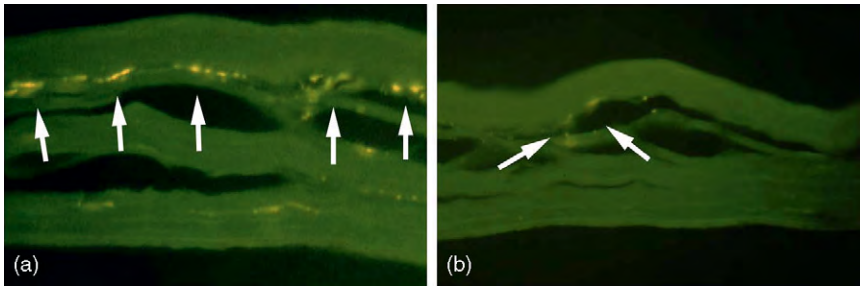

Figure 4 Lentivirus-mediated transgene delivery in the mouse cornea *in vivo* noted after 6 weeks of vector application. Two microliters of lentivirus titer was either topically applied for 2 min or microinjected in the cornea using a glass needle. Transgene delivery in the rabbit stroma noted at 2 weeks in the tissue sections of the cornea, shown in (a) and (b), which received vector through topical application (a) or microinjection (b) techniques.

epithelium. Figure 4 shows the quantity and distribution of transgene in the mouse cornea with lentivirus vector administered in the stroma topically or through microinjection technique. Detection of distinctly different levels and locations of transgene in the cornea supports our hypothesis that gene delivery in the cornea is regulated by both vector and vector-delivery techniques and not by the vector alone. No serious cytotoxicity or side effects have been reported with the AAV- or lentivirus-mediated gene delivery, suggesting that these vectors may be suitable for gene therapy treatments for patients. However, safety remains a major concern for using lentivirus vectors because of their origin from human immunodeficiency virus.

Nonviral Vectors

Contrary to viral vectors, nonviral vectors are nontoxic, nonpathogenic, and nonimmunogenic, and can deliver large genes. Additionally, their production is simple and

cost effective. Various surgical, mechanical, electrical, or chemical approaches were used to administer plasmid DNA in the cornea *in vitro*, *ex vivo*, and *in vivo*. Intrastromal injection of plasmid DNA encoding reporter, vascular endothelial growth factor, or interleukin-1 receptor antagonist successfully delivered transgene into the mouse cornea. A major advantage of this method over viral technology was that it provided rapid transgene expression in the mouse cornea *in vivo*. Transgene expression was detected as early as 1h after administration, with a peak occurring in 12–24 h. Furthermore, the plasmid-injected corneas remained clear and free of inflammation. Plasmid applied during stromal hydration and filtration bleb surgeries delivered genes in rabbit corneas, *in vivo*.

Techniques using electric current plasmid DNA delivery in corneal epithelium, keratocytes, and endothelium have been reported. Electrical current up to 200 V cm^{-1} did not cause trauma, edema, or inflammation in the cornea but introduced only low levels of transgene. Higher electrical current increased transgene delivery but was associated with substantial corneal damage.

Firing of DNA- or RNA-coated gold microparticles on the cornea with a gene gun introduced transgene in the corneal epithelium. However, gene-gun-mediated gene delivery was limited to epithelium and was associated with corneal damage.

Lipids and polymers have been used frequently to deliver genes in corneal cells *in vitro* but provide inadequate levels of transgene in the cornea *in vivo*. Low transfection efficiency and short-term transgene expression are among the major challenges of nonviral gene therapy that need to be addressed. Use of nanoparticles as vectors has great potential for improving nonviral gene transfer.

Use of Gene Therapy to Treat Corneal Diseases

Corneal Graft Rejection

Many gene therapy studies for prevention of corneal graft rejection have focused on the use of cytotoxic T-lymphocyte-associated antigen-4 conjugated to human immunoglobulin G (IgG) heavy chain (CTLA-4 Ig). The rationale for this therapy is based on the fact that helper T-cell activation primarily involves the interaction between T-cell receptor/cluster of differentiation 3 (CD3) and the alloantigen/major histocompatibility complex II (MHCII) of the antigen-presenting cells (APCs). An additional, essential stimulus for T-cell activation is provided by the interaction between co-stimulatory molecules, such as APC B7 antigens, and the CD28 molecule of T cells. T-cell activation can be prevented by blocking this interaction with administration of chimeric protein, CTLA-4 Ig. Multiple studies have evaluated the efficiency of CTLA-4 Ig gene therapy to control corneal graft rejection. The CTLA-4 Ig gene therapy was delivered to the donor rat corneas with adenovirus prior to transplantation topically or after transplantation by a single intravenous or intraperitoneal injection. Topical application of adenovirus expressing CTLA-4 Ig had a marginal effect on preventing graft rejection, whereas systemic administration markedly prolonged graft survival. In another study, minimalistic immunologically defined gene expression (MIDGE) vector encoding for CTLA-4 was delivered in the corneal epithelial cells with a gene gun 10 days after orthotopic corneal transplantation. A marginal beneficial effect of CTLA-4 expression was noted for graft survival in the tested model. However, a subsequent study of MIDGE-mediated CTLA-4 gene transfer in mice demonstrated significant prolongation of graft survival when gene therapy was delivered 1 day before corneal transplantation. Contrary to the encouraging CTLA-4 gene transfer studies, the results have been disappointing when other co-stimulatory pathways of T-cell activation are inhibited. Adenovirus-mediated ICOS, which is an inducible co-stimulatory receptor expressed by activated T cells, *ex vivo* or systemic gene therapy did not result in a significant prolongation of corneal graft survival.

Cytokines play an important role in corneal graft survival and rejection. Consistently elevated levels of proinflammatory cytokines, such as Th (T-helper cell) type 1, have been detected in the corneal tissues and aqueous humor of eyes with graft rejection. Th type 2 cytokines, such as interleukin (IL)-10 and IL-4, exert inhibitory effects on Th1 cytokines. The effects of elevation of anti-inflammatory Th type 2 cytokines or inhibition of proinflammatory Th type 1 cytokines on graft survival have been the focus of many gene therapy studies. Significantly increased corneal graft survival, from 18–20 days to 45–55 days, was observed in ovine donor corneas transduced with adenovirus-expressing IL-10 or IL-12 antagonist. On the other hand, adenovirus-mediated IL-10 or IL-12 antagonist gene therapy did not prevent corneal transplant rejection in a rat model. This disparity in results could be due to differences in the kinetics of graft rejection in the two animal species. Interestingly, IL-4 gene therapy was found to be ineffective in both the species.

Corneal Wound Healing

Wound healing plays important role in maintaining corneal transparency and normal visual function. Injury to the cornea is known to trigger unregulated wound-healing response that can lead to scar formation and loss of vision. Multiple growth factors and cytokines have been shown to regulate wound healing in the cornea. Out of many cytokines influencing corneal wound healing, transforming growth factor beta (TGFβ) has been shown to play a central role in corneal wound healing, myofibroblast generation, and haze development. Soluble

type II TGFβ receptor binds TGFβ and blocks its biological activity. Soluble type II TGFβ receptor gene therapy has been shown to reduce corneal opacification in corneal injury model. A single intramuscular injection of recombinant adenovirus encoding for soluble type II TGFβ receptor in the mouse eye prevented corneal edema, angiogenesis, inflammatory cell infiltration, and deposition of extracellular matrix in the cornea. High levels of soluble TGFβ receptor were detected in the serum and corneal fluid of treated animals for 10 days but several side effects were also observed. This study demonstrated the potential application of gene therapy to treat corneal disorders but several issues such as safety, immunological reaction, etc., associated with adenovirus-based gene therapy still need to be resolved.

AAV-mediated gene therapy may address some of these issues. Our laboratory, for the first time, demonstrated efficient transgene delivery into keratocytes of the normal and diseased (hazy and neovascularized) rabbit corneas *in vivo* with AAV2 and AAV5 vectors. The tested AAV vectors showed high levels and long-term transgene expression (over 4 months) in the rabbit corneas. Our ongoing gene transfer experiments include evaluation of AAV-mediated decorin gene therapy to control corneal scarring and angiogenesis. Decorin is a small leucine-rich proteoglycan and blocks biological activity of TGFβ. Our *in vitro* studies revealed that decorin gene delivery into rabbit and human keratocytes significantly reduces TGFβ-driven transdifferentiation of keratocyte to myofibroblasts. This transformation is believed to cause corneal haze *in vivo*.

Employing nonviral gene transfer approach, the role of fibrin deposition on corneal transparency was also studied in laser-induced fibrin clot formation model *in vivo*. Administration of plasmid-DNA-expressing tissue plasminogen activator gene through electroporation in the anterior chamber of the eye markedly reduced extracellular matrix deposition in treated eyes. The beneficial effects lasted for 4 days.

Corneal Alkali Burn

Alkali burn injury to the cornea is a serious clinical problem that often leads to permanent visual loss due to ulceration, scarring, and/or neovascularization. A gene therapy approach has been used to treat corneal alkali burn by targeting modulation of TGFβ super family genes using adenovirus vectors. Mothers against decapentaplegic homolog 7 (Smad7) is well documented to inhibit TGFβ signaling. Topical application of Cre-adenovirus encoding for Smad7 effectively prevented alkali-induced corneal scaring. Bone morphogenic protein-7 (BMP7) is another member of TGFβ super family and has been shown to antagonize the effects of TGFβ. Adenovirus-mediated BMP7gene transfer in the cornea has been shown to accelerate re-epithelilization of corneal surface and suppress myofibroblast generation, monocytes/macrophages infiltration and macrophage chemoattractant protein-1 (MCP-1), and TGFβ and collagen expression in the corneal stroma in alkali-induced corneal injury mouse model. However, BMP7 gene therapy was ineffective to suppress stromal neovascularization. Another study reported that topical application of Cre-adenoviral vector encoding for peroxisome proliferator-activated receptor-gamma (PPARγ) reduced inflammatory and fibrogenic responses in the alkali burn mouse cornea. Adenovirus-mediated PPARγ overexpression inhibited growth factors and upregulation of matrix metalloproteinases, monocytes/macrophages infiltration, and myofibroblasts production in healing cornea *in vivo*. Further, accelerated re-epithelization and basement membrane reconstruction was observed in mouse cornea overexpressing PPARγ gene.

Corneal Scarring or Haze

Corneal scarring is primarily caused by injury or infections to the eye. It is also a common side effect of the photorefractive keratectomy (PRK) surgery, particularly in patients undergoing high myopia correction. The PRK surgery is frequently used worldwide to treat myopia, hyperopia, and astigmatism. Accumulating evidences suggest that corneal scarring occur due to abnormal wound healing, deposition of disorganized extracellular matrix, keratocyte activation, and transdifferentiation of keratocytes to fibroblasts and myofibroblasts. Gene therapy offers a unique approach for intercepting the molecular events involved in the development of corneal haze. Blockade of keratocyte proliferation is an attractive approach for controlling corneal haze *in vivo*. Rabbit corneas transduced with retroviral vector encoding for herpes simplex virus (HSV) thymidine kinase gene after keratectomy, followed by topical application of ganciclovir, showed significant inhibition of laser-induced corneal haze. Another approach that has been tested to control corneal haze is the blockade of cyclins and cyclin-dependent kinases that play an active role in controlling cell division. Again using a retroviral vector, a dominant-negative mutant construct for cyclin G1 was delivered in the rabbit cornea after transepithelial phototherapeutic keratectomy surgery. Analysis of corneal tissues showed that dominant-negative cyclin G1 delivery decreased extracellular matrix production and markedly reduced the development of corneal haze in tested rabbit model. Apoptosis of activated keratocytes by the delivered dominant-negative cyclin is believed to be a mechanism for the decrease in corneal haze appearance. As noted above, we have also shown the potential of decorin gene therapy to inhibit corneal haze using an *in vitro* model.

Corneal Neovascularization

Corneal insults, such as infection, degenerative disease, chemical damage, mechanical/surgical injury, and immunologic disease, can cause corneal neovascularization (CNV) that affects about 1.4 million Americans each year. Multiple lines of evidence suggest that cytokine vascular endothelial growth factor (VEGF) plays a key role in CNV development. Various gene therapy strategies have been developed and examined to suppress VEGF-induced corneal angiogenesis using experimental models. Intrastromal injection of plasmid encoding a soluble form of the VEGF receptors Flt-1, which neutralizes VEGF, significantly inhibited CNV in the mouse eye. Similar inhibition of CNV was demonstrated by sFlt1 gene transfer with adenovirus and AAV. In a novel approach for controlling CNV with gene therapy, plasmids encoding for Flt23K or Flt24K peptide (VEGF-binding domains of sFlt-1) coupled with endoplasmic reticulum-retaining peptide have been developed. These peptides are not secreted outside the cell and therefore are capable of neutralizing intracellular VEGF. Intrastromal injection of these plasmids in mouse eye inhibited CNV by as much as 50% in the experimental models of corneal angiogenesis. Recently, these scientists reported CNV reduction up to 40% in the mouse cornea after delivering Flt23K gene with albumin nanoparticles.

Gene therapy has also been evaluated in a corneal transplant rabbit model to study the effect of gene transfer of a fusion protein. These rabbit corneas were transduced *ex vivo* with lentiviral vector encoding for endostatin and kringle-5 domain of plasminogen fusion protein. Endostatin is an anti-angiogenic peptide derived from type XVIII collagen, and Kringle 5 domain of plasminogen is a specific inhibitor for endothelial cell proliferation derived from the proteolytic fragment of human plasminogen. The endostatin-kringle-5 fusion protein effectively inhibited allogenic transplantation-induced neovascularization. Delivering kringle-5-plasminogen gene through electroporation was also demonstrated to be effective in reducing CNV in a rat model. Angiostatin is another potent, recently identified anti-angiogenic agent. AAV vectors encoding angiostatin gene effectively reduced alkali-induced CNV in rat corneas. In another study, mouse corneas transfected with plasmid encoding for IL12 or IL10, using topical application or intrastromal techniques, showed marked suppression of CNV. Interestingly, a careful review of the literature reveals that few gene transfer studies of CNV in experimental disease models have reported, discussed, or investigated the side effects or downsides of the gene transfer methods that were investigated.

Corneal Dystrophies

In the past decade, several genes and gene mutations, such as BIGH3, TGFβ1, gelsolin, and CHTS6 have been identified to cause granular, lattice, Avellino, and/or Reis–Bücklers corneal dystrophies. However, a paucity of experimental models for evaluating the usefulness of gene therapy to cure genetic corneal dystrophies remains a major obstacle to the development of therapeutic interventions for these vision-threatening disorders. Very few gene transfer studies using corneal buttons collected from patients or rodent models have been performed to evaluate the efficacy of gene therapy in corneal dystrophies. Gene therapy approaches can be used as a tool for creating animal models of corneal dystrophies by overexpressing aberrant proteins in the cornea.

Mucopolysaccharidosis is a group of metabolic disorders characterized by deficiency of lysosomal enzymes needed to degrade glycosaminoglycans. This disorder causes corneal abnormalities, including the loss of corneal transparency. Delivering human beta-glucuronidase gene in the cornea induced significant clearance of corneal clouding in mouse model of type VII mucopolysaccharidosis. The adenovirus vector encoding human beta-glucuronidase gene was injected in the anterior chamber or intrastromal region to deliver transgene in the eye. A rapid clearance of lysososmal-storage vesicles in keratocytes and clearing of the cornea were observed.

Other Corneal Disorders

HSV keratitis is a leading cause of infectious blindness. Developing vaccination using gene transfer approaches have been the focus of several studies. Most of these studies used plasmid DNA encoding for HSV-1 glycoproteins, such as glycoprotein (g) D, gB1, or a cocktail of glycoproteins in an effort to increase immunity against HSV-induced ocular keratitis. The plasmids were administered in test animals through either topical application, or subconjunctival, intramuscular, or intraperitoneal injection. The intramuscular route of administration has been found to confer total protection against HSV keratitis, whereas topical application and subconjunctival administration prevented stromal keratitis but not the epithelial keratitis. In another study, enhancement of gD glycoprotein was observed when it was administered in combination with IL-2. Conversely, many investigators have reported limited success in controlling herpes keratitis with gene therapy, as a topical application of naked plasmid vector encoding for cytokines, such as IL2, IL4, IL10, interferon (IFN), or tumor necrosis factor (TNF) alpha, demonstrated very little or no benefit. Nonetheless, cytokine gene therapy has been shown to inhibit corneal lesion severity if used 3 days prior to HSV infection. Clinically, such treatment may be beneficial for preventing primary HSV keratitis.

Lacrimal Gland Gene Therapy

Lacrimal glands produce tears and tear proteins which lubricate, and supply nutrition and protection to ocular

surface tissues. Several autoimmue disorders such as Sjögren syndrome, rheumatoid arthritis, systemic lupus erythematosus, and uveitis affect lacrimal gland function and result in dry eye syndrome. This syndrome affects about 4% people in the United States. Unlike conventional therapy that demands repeated lubricant application, gene therapy could potentially require just one treatment. Genes delivered to lacrimal glands can modulate tear composition and flow rate. Initial studies tested the efficacy of vaccinia, herpes, and adenovirus vectors for delivering genes in lacrimal gland using *ex vivo* rat lacrimal gland. Vaccinia viral vector showed highest transgene delivery followed by adenovirus and herpes viral vector. Histological examination of tissues revealed that vaccinia vector delivered transgene in the lacrimal duct cells and acini, whereas adenovirus vector mainly transduced myoepithelial cells surrounding the lacrimal acini. Cellular degradation response was also noted with adenovirus vector, possibly due to vector's toxicity. Subsequent studies showed IL-10 and TNF inhibitor gene delivery in cultured rabbit lacrimal gland epithelial cells by the adenovirus. *In vivo* studies examined the efficacy of these cytokines-based gene therapy for Sjögren syndrome, using a rabbit model of dacryoadenitis. The prophylactic adenovirus-mediated IL-10 gene delivery resulted in protection against lacrimal gland immunopathology, ocular surface disease, and decrease in tear production. On the other hand, adenovirus-mediated TNF inhibitor gene delivery increased basal tear production and its stability, and reduced corneal surface defects and intensity of immune cell infiltration in lacrimal gland.

Adenovirus-mediated gene delivery has also been utilized to investigate cellular and physiological functions of the lacrimal gland. Examples include investigation of androgens in the pathophysiology of Sjögren syndrome and the role of dyneins, protein kinases, and cytoskeletal proteins in the secretory functions of the lacrimal gland. Besides adenovirus, not many other viral vectors have been evaluated for lacrimal gland gene delivery *in vivo*. Retroviral vectors expressing the E6 and E7 genes of the human papillomavirus have been employed to generate immortalized lacrimal gland epithelial cell lines for laboratory studies.

Conjunctiva Gene Therapy

A handful of gene transfer studies have been performed for the conjunctiva. Recently, transfection efficiency of hyaluronic acid–chitosan nanoparticles to deliver genes in human conjuctival cells has been examined. These nanoparticles were found to be nontoxic to the conjuctival cells and exhibited moderate transfection efficiency (15%) for the conjunctiva. Topical application of these nanoparticles to the rabbit eye demonstrated a successful delivery of reporter gene into conjunctival epithelium. Sonoporation (application of sound waves), following subconjuctival injection in the eye, delivered considerable levels of EGFP in the rat conjunctiva.

Among viral vectors, adenovirus has been most widely investigated for transgene delivery in the conjunctiva. Modulation of wound healing and prevention of scarring in the conjunctiva has been the primary focus of conjunctival gene therapy studies. As in corneal injury, TGFβ has been shown to play a critical role in conjunctiva wound healing and scarring. Activation of p38 mitogen-activated protein (MAP) kinase is one of the key signaling pathways activated by TGFβ Adenovirus-mediated delivery of p38 MAPkinase suppressed myofibroblast generation and decreased messenger RNA (mRNA) expression of connective tissue growth factor (CTGF) and monocyte/macrophage chemoattractant protein-1 (MCP-1) in the mouse model of conjunctival injury. The protective effects of Smad7 gene transfer on conjunctival fibrosis have also been reported using a mouse model. Cultured subconjunctival fibroblasts transduced with adenoviral vector expressing Smad7 inhibited type-I collagen, α smooth muscle actin, and CTGF, whereas topical application of adenoviral vector expressing Smad7 gene prevented macrophage invasion and decreased VEGF and α smooth muscle actin levels in conjunctival fibroblasts *in vivo*. More recently, adenovirus-mediated PPARγ gene transfer was found to be protective against conjunctival fibrosis. PPARγ overexpression suppressed expression of type I collagen, fibronectin, and CTGF in cultured human conjunctival fibroblasts both at mRNA or protein level. *In vivo* experiments showed that PPARγ gene delivery significantly decreased monocyte/macrophage invasion, myofibroblast generation, and blocked upregulation of cytokines/growth factors, collagen I, and α2 mRNA in the healing conjunctiva.

In summary, many studies have demonstrated the ability of gene therapy to treat ocular surface diseases and improve visual function. Numerous vectors, techniques, and strategies have been identified for establishing novel gene therapy modalities to treat ocular surface disorders. Although the proof-of-principle experiments validated the potential and promise of gene therapy for ocular surface disorders, several obstacles remain to be cleared before gene therapy clinical trials for these diseases are instituted.

Acknowledgments

The work is supported by the RO1EY17294 (RRM) grant from the National Eye Institute, National Institutes of Health, Bethesda, Maryland, USA and a grant from the Research to Prevent Blindness, New York, USA.

See also: Angiogenesis in the Eye; Conjunctival Goblet Cells; Corneal Dystrophies; Corneal Epithelium: Cell Biology and Basic Science; Corneal Epithelium: Response to Infection; The Corneal Stroma; Cornea Overview; Defense Mechanisms of Tears and Ocular Surface; Drug Delivery to Cornea and Conjunctiva: Esterase- and Protease-Directed Prodrug Design; Imaging of the Cornea; Lacrimal Gland Hormone Regulation; Lacrimal Gland Overview; Lacrimal Gland Signaling: Neural; Overview of Electrolyte and Fluid Transport Across the Conjunctiva.

Further Reading

Bainbridge, J. W., Tan, M. H., and Ali, R. R. (2006). Gene therapy progress and prospects: the eye. *Gene Therapy* 13: 1191–1197.

Buch, P. K., Bainbridge, J. W., and Ali, R. R. (2008). AAV-mediated gene therapy for retinal disorders: From mouse to man. *Gene Therapy* 15: 849–857.

Jun, A. S. and Larkin, D. F. (2003). Prospects for gene therapy in corneal disease. *Eye* 17: 906–911.

Klausner, E. A., Peer, D., Chapman, R. L., Multack, R. F., and Andurkar, S. V. (2007). Corneal gene therapy. *Journal of Controlled Release* 124: 107–133.

Mohan, R. R., Schultz, G. S., Hong, J. W., Mohan, R. R., and Wilson, S. E. (2003). Gene transfer into rabbit keratocytes using AAV and lipid-mediated plasmid DNA vectors with a lamellar flap for stromal access. *Experimental Eye Research* 76: 373–383.

Mohan, R. R., Sharma, A., Netto, M. V., Sinha, S., and Wilson, S. E. (2005). Gene therapy in the cornea. *Progress in Retinal and Eye Research* 24: 537–559.

Saika, S., Yamanaka, O., Sumioka, T., et al. (2008). Fibrotic disorders in the eye: Targets of gene therapy. *Progress in Retinal and Eye Research* 27: 177–196.

Selvam, S., Thomas, P. B., Hamm-Alvarez, S. F., et al. (2006). Current status of gene delivery and gene therapy in lacrimal gland using viral vectors. *Advanced Drug Delivery Reviews* 58: 1243–1257.

Williams, K. A., Jessup, C. F., and Coster, D. J. (2004). Gene therapy approaches to prolonging corneal allograft survival. *Expert Opinion on Biological Therapy* 4: 1059–1071.

Genetic Dissection of Invertebrate Phototransduction

B Katz and B Minke, Hebrew University, Jerusalem, Israel

Glossary

Electroretinogram (ERG) – *In vivo* extracellular recording of the voltage response to light of the entire retina.

G protein – Guanine nucleotide-binding protein, a ubiquitous biological switch that is turned on by receptor-activation-induced exchange of bound guanosine diphosphate (GDP) with cytoplasmic guanosine triphosphate (GTP) and turned off by hydrolysis of the bound GTP.

Phosphoinositide (PI) signaling – Also designated as inositol-lipid signaling, it is a ubiquitous enzymatic cascade that uses phospholipids or their products for signaling.

Phospholipase C (PLC) – A superficial membrane-bound enzyme that hydrolyzes a minor plasma membrane phospholipid, phosphatidylinositol-4,5-bisphosphate (PIP_2), and produces two messengers: inositol 1,4,5-trisphosphate ($InsP_3$) and diacylglycerol (DAG).

Photochemical cycle – A multistep process that begins by absorption of a photon by the light-sensitive receptor, rhodopsin, which undergoes multiple modifications and ends by the regeneration of the original molecule.

Phototransduction – The process by which absorption of photons by light-sensitive receptors lead to production of electrical signal comprehensive to the nervous system.

Prolonged depolarizing afterpotential (PDA) – The light-induced electrical signal that continues in the dark long after light is turned off, produced in invertebrate photoreceptor cells. The PDA phenomenon has been widely exploited to screen for visual defective *Drosophila* mutants.

Rhabdomere – The photosensitive organelle of *Drosophila* photoreceptors which is composed of tightly packed microvilli.

Transient receptor potential (TRP) channels – A family of cation channel proteins that mediate a large variety of physical stimuli such as light, temperature, and chemical compounds.

Phototransduction is a process by which light is converted into electrical signals understood by the central nervous system. Initial studies of invertebrate phototransduction used *Balanus* and *Limulus* as the preparations of choice, due to their extremely large photoreceptor cells and the assumption that they constitute a simplified model system that represents phototransduction in general. However, later studies revealed that although both invertebrate and vertebrate photoreceptors use rhodopsin (R) as a receptor and a G (guanine nucleotide-binding)-protein-coupled signaling cascade to produce the electrical response to light; the rest of their enzymatic cascade of vision is entirely different. Phototransduction in vertebrate rods and cones uses cyclic guanosine monophosphate (cGMP) phosphodiesterase as an effector enzyme and cGMP-gated ion channels as its target. In contrast, phototransduction in the microvillar photoreceptors of invertebrates (photoreceptors in which the photosensitive organelle is composed of microvilli – the rhabdomere) uses a phosphoinositide (PI) signaling cascade, which is characterized by phospholipase C (PLC) as the effector enzyme and, at least in *Drosophila*, the TRP channels as its target. Nevertheless, phototransduction in invertebrate microvillar photoreceptors has become a model system for investigating inositol-lipid signaling and its role in TRP channel regulation and activation. The great advantage of using invertebrate microvillar photoreceptors is the accessibility of the preparation, the ease of light stimulation, the robust expression of key molecular components, and most importantly, the ability to apply the power of molecular genetics. The latter feature is mainly attributed to *Drosophila melanogaster* as a preferred preparation.

Although the phototransduction cascade of invertebrate microvillar photoreceptors is clearly different from that of vertebrate rods and cones, it may be similar to that in the intrinsically photosensitive retinal ganglion cells (RGCs) in vertebrates. The light-sensitive RGCs contain the visual pigment melanopsin and provide photic input to the circadian pacemaker of the master circadian clock. Both *Drosophila* photoreceptors and the light-sensitive RGCs are characterized by a bi-stable R that initiates a phototranduction cascade with TRP channels as the final target. It is now widely accepted that the detailed knowledge that has been obtained through studies of *Drosophila* photoreceptors constitute guidelines for research of the melanopsin-containing RGCs, and that a striking commonality has been found in both cell types.

Extensive genetic studies of the fruit fly, *D. melanogaster*, initiated at the turn of the twentieth century, by the Nobel prize laureate, Thomas Hunt Morgan, and greatly advanced by many other laboratories, has established the *Drosophila* as an extremely useful experimental model for genetic

dissection of complex biological processes. The relatively small size of the *Drosophila* genome, ease of growth, rapid generation time, and high fecundity make this system ideally suited for screening large numbers of mutagenized individual flies for defects in virtually any phenotypically observable or measurable trait. The creation of balancer chromosomes – containing dominant markers and multiple inversions – which prevent recombination with the native chromosomes, allows any mutation – once recognized – to be rapidly isolated and maintained. Importantly, germ line transformation, using P-element transposition, combined with the availability of tissue-specific promoters, allows the introduction of cloned genes into specific cells of the organism. This provides a way to study *in vitro* modified gene products in their native cellular environment. These powerful molecular genetic tools, combined with the available genome sequence, allow screening for mutants defective in critical molecules, while devoid of *a priori* assumptions. Indeed, this methodology has produced large numbers of mutants defective in novel proteins the existence of which would have been difficult to otherwise predict. The following sections emphasize the unique contribution of the research in *Drosophila* photoreceptors, which has led to the discovery of novel molecules and processes important not only for phototransduction but also for many other biological mechanisms (**Figure 1**).

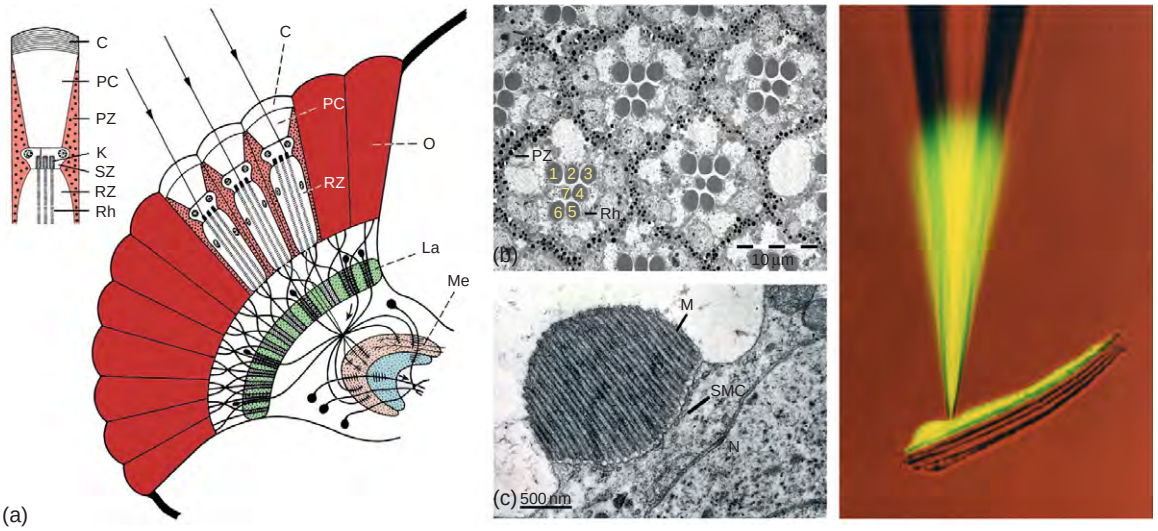

Figure 1 The morphology of the compound eye. The *Drosophila* compound eyes are made up of ~800 repeat and well-organized units termed ommatidia ((a) and (b)). The ommatidium consists of 20 cells, eight of which are the photoreceptor cells (RZ; (a)). (b) and (c) show an electron microscopic (EM) cross section of ommatidia and a rhabdomere (Rh) at the upper region of the photoreceptors, respectively. (d) shows an isolated ommatidium in which one photoreceptor cell is marked by a yellow fluorescent dye introduced by a patch pipette. Each ommatidium contains a dioptric apparatus composed of transparent chitinous cuticle, which forms the cornea (C;(a)) and an extracellular fluid-filled cavity, called the pseudocone (PC; (a)). The floor of the cavity is formed by four Semper cells (SZ; (a)) and the walls by primary pigment cells (PZ; (a) red and (b)), which together circle the pseudocone, shielding the photoreceptor from light coming from adjacent ommatidia. Below this rigid structure of the optical apparatus lie eight photoreceptor cells (RZ; (a), (b), and (d)). The photoreceptor cells are highly polarized epithelial cells, having a specialized compartment known as the rhabdomere (Rh; (a), (b), and (c)), consisting of a stack of ~30 000–50 000 microvilli (M; (c)) each ~2-μm long and ~60 nm in diameter. The transduction machinery is arrayed in these tightly dense structures, while the nucleus (N; (c)) and cellular organelles, such as submicrovillar cisternae (SMC; (c)), reside at the cell body. These highly ordered rhabdomeres form wave-guides that have been widely exploited for optical methods. The eight photoreceptors can be divided into two functional groups according to their position, spectral specificity and axonal projection. The R1–R6 cells (marked 1–6 in (b)) represent the major class of photoreceptors in the retina and are involved in image formation and motion detection. These cells have peripherally located rhabdomeres extending from the basal to the apical side of the retina where they terminate in a rhabdomere cap (K; (a)). They express a single opsin called Rh1, which when combined with 11-*cis* 3-hydroxy retinal, forms a blue-absorbing rhodopsin (R) or orange-absorbing metarhodopsin (M). The R1–6 cells (b) project their axons to the first optic lobe, the lamina (La; (a) green). The second group consists of two cells in the center of each ommatidium termed, R7 (marked 7 in (b)) and R8 (not shown) each spanning only half of the retina in length. The R7 rhabdomere is located distally in the retina and expresses one of two opsins, Rh3 or Rh4, characterized by a UV-absorbing R and blue-absorbing M. The R8 rhabdomere is located proximally in the retina, beneath the R7 rhabdomere (not shown) and expresses one of three opsins – Rh3, Rh5, or Rh6 – characterized by a UV, blue, or green-absorbing R, respectively. The R7 and R8 cells project their axons to the second optic lobe, the medulla (Me; (a) pink). On the basis of opsin expression in the R7 and R8 cells, three ommatidia subtypes can be distinguished. The R7 and R8 cells in ommatidia residing in the dorsal rim area both express Rh3 opsin. The 'pale' ommatidia subtype express Rh3 in R7 cells and Rh5 in R8 cells and constitute ~30% of the total ommatidia, while the 'yellow' ommatidia subtype express Rh4 in R7 cells and Rh6 in R8 cells and constitute ~70% of the total ommatidia. The central cells R7/8 function in color vision and detection of polarized light. This intriguing repeated structure has been a major scientific preparation for research of various aspects of retinal-cell differentiation and development. (a) Modified from Kirschfeld, 1967 and (b) modified from Minke and Selinger, 1996.

The *Drosophila* Phototransduction Cascade

Genetic Screens for Mutants Defective in Phototransduction Proteins

A genetic screen is a procedure to identify and select mutated individuals that possess a phenotype with a specific malfunction in a specific trait. This method requires a large number of mutated individuals, usually obtained by the use of mutagens or by random DNA insertions (transposons) and a simple, but powerful, isolation procedure. Additionally, this method requires genetic tools to isolate and maintain the stability of the mutation through generations. These requirements make *Drosophila* an ideal organism for genetic screens. Wide genetic screens targeting the two autosomes (II and III) and the X chromosome of *Drosophila*, have produced many mutants with identified phenotypes linked specifically to genes involved in visual behavior or photoreceptor cell function. These screens used defects in a number of visual functions such as optomotor response, phototaxis, and electrophysiological response to light. The isolation of mutants, specifically defective in the visual transduction pathway initially made use of the electroretinogam (ERG), which measures the electrical activity of the eye at the corneal level (**Figure 1(a)**). However, the ERG methodology failed to isolate the large numbers of mutants expected from a multistep and complex process such as the phototransduction cascade. The main reasons for this failure are that the phototransduction proteins are highly abundant and the upper limit in the depolarization signal is reached even when only a small fraction of the signaling molecules are excited. Therefore, mutations causing even a significant reduction in concentration or subtle malfunction of the phototransduction components could not be identified by this method. This necessitated the employment of a more sensitive, and yet simple, method for isolation of mutants.

In order to find mutants that are specifically affected in the phototransduction cascade and to identify those with subtle phenotypes, Pak and colleagues employed the electrical phenomenon devised by Hillman Hochstein and Minke designated prolonged depolarizing afterpotential (PDA; **Figure 2(a)**, upper trace). This method is based on a large net photoconversion of R to its dark stable photoproduct metarhodopsin (M) with a minimal conversion back to R (**Figure 3**), which brings the capacity of the phototransduction process to its upper limit. PDA is achieved in the fly by genetically removing the red screening pigment (**Figure 1(a)**) and by applying blue light, which is preferentially absorbed by the R state of the Rh1 photopigment. Rh1 is the photopigment expressed in photoreceptors R1–R6 in the *Drosophila* eye (**Figure 1(a)** and **(b)**). A large net photoconversion of R to M (**Figure 3**) prevents phototransduction termination at the photopigment level. As a result, excitation is sustained long after the light is turned off, and the PDA-producing cells are unable to respond further (termed inactivation, **Figure 2(a)**, upper trace). Subsequently, application of orange light reconverts the activated M back to R and terminates the sustained excitation after the light is turned off. Since the PDA tests the maximal capacity of the photoreceptor cell to maintain excitation for an extended period and is strictly dependent on the presence of high concentrations of R and other signaling molecules, it detects even minor defects in R biogenesis, or exhaustion of critical signaling molecules. Thus, defects in the PDA easily reveal deficiencies in the concentration of phototransduction components. Indeed, the PDA screen yielded a plethora of novel and interesting visual mutants. One group of PDA mutants exhibited a loss in several features of the PDA. They were termed *nina* mutants, which stands for neither inactivation nor afterpotential (**Figure 2(a)**, lower trace). Most *nina* mutants were caused by reduced levels of R. The second group of PDA mutants lost the ability to produce the voltage response associated with the PDA, but were still inactivated by strong blue light and the inactivation could be relieved by orange light (**Figure 2(a)**, middle trace). These mutants, consisting of seven allelic groups, are termed *inaA–G*, which stand for inactivation but no afterpotential (no PDA-voltage response). The *ina* mutants were found to have normal R levels but are deficient in proteins associated with the function of the TRP channel. The *nina* and *ina* mutants have led to the identification of most of the crucial components of *Drosophila* phototransduction, many of which are novel proteins of general importance for many cells and tissues.

The Photochemical Cycle and the Mechanism Underlying Termination of M Activity

The *ninaE* mutant, having reduced Rh1 opsin levels, was isolated by Pak and colleagues using the PDA screen. R belongs to the super family of seven transmembrane G-protein-coupled receptors. It is activated by the absorption of a photon that isomerizes the chromophore (11-*cis* 3-hydroxy retinal), resulting in a conformational change of the opsin molecule and production of the physiologically active M state of the photopigment. To ensure high sensitivity, high temporal resolution, and low dark noise of the photoresponse, the active M has to be quickly inactivated and recycled (**Figure 3**). The latter requirement is achieved, in invertebrates, by two means: the absorption of an additional photon by the dark stable M – which photoconverts M back to R – or by a multistep photochemical cycle (**Figure 3**). The termination of vertebrate M activity is a two-step process initiated by M phosphorylation, followed by the binding of the protein arrestin (ARR) to phosphorylated M. Invertebrate M also undergoes

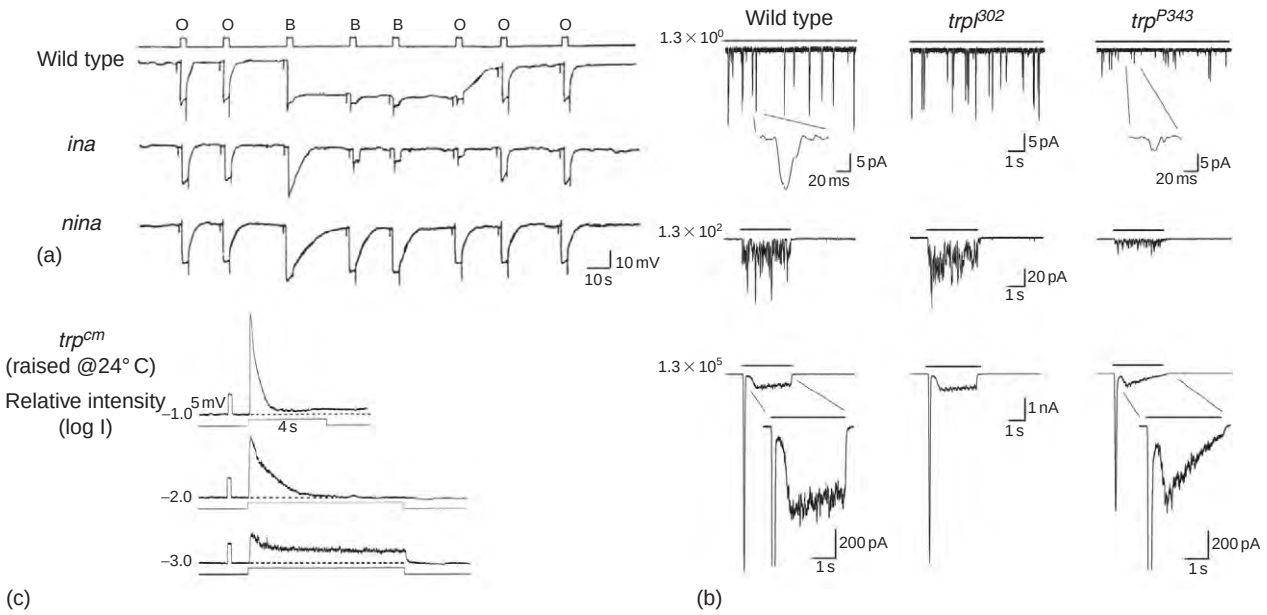

Figure 2 The electrophysiological responses to light of *Drosophila.* (a) The prolonged depolarization afterpotential (PDA) response of wild-type *Drosophila* and its modifications in the *nina* and *ina* mutants: Upper trace: ERG recordings from a wild-type fly in response to a series of intense blue (B, Schott, BG 28 broad-band filter) and orange (O, Schott OG 590 edge filter) light pulses used for induction and suppression of the PDA. This paradigm included two intense orange light pulses followed by an intense blue light pulse which converted ~80% of the Rh1 photopigment from R to M and resulted in prolonged corneal negative response that continued in the dark. Two additional intense blue lights elicited small responses that originated from the central cells (R7 and 8) in which PDA was not induced, due to their UV-absorption spectra, while the R1–6 cells were nonresponsive (inactivated) due to maximal activation of the channels. The following orange light suppressed the PDA after light is turned off. Middle trace: The paradigm of the upper trace was repeated in an *ina* mutant. In contrast to wild type, the response to the intense blue light declined to baseline. However, the R1–6 cells remained inactivated and additional blue lights elicited responses only in R7 and 8 cells while the following orange light removed the inactivation and allowed recovery of the R1–6 cells response to light. Bottom trace: The paradigm of the upper traces was repeated in a *nina* mutant. The first blue light elicited a short PDA that quickly declined to baseline and additional blue lights elicited responses in all photoreceptor cells and allowed additional activation of R1–6 cells by orange lights. (b) (Top) Whole-cell patch-clamp recordings (clamped at −70 mV) from photoreceptor cells of wild-type (WT, left column), $trpl^{302}$ mutant, expressing only the TRP channels (middle) and trp^{P343} mutant, expressing only the TRPL channels (right). Quantum bumps are elicited in response to very dim orange light (1.3 effective photons s^{-1}). The inset shows single bumps in faster time scale of WT fly and the trp^{P343} mutant. The bump amplitudes in the trp^{P343} mutant are significantly smaller than in WT or the $trpl^{302}$ mutant. Middle: In response to 100-fold more intense light, the bumps sum up to produce a noisy light induced current (LIC, note the change in scale). Bottom: A further increase of 1000-fold in the light intensity induced a large response with an initial fast transient that declined to a small steady-state response, due to fast Ca^{2+}-dependent light adaptation in both WT and the $trpl^{302}$ mutant. In the trp^{P343} mutant, the steady-state response declined to baseline during light. The inset shows amplified responses where the initial transient is off scale (note the change in scale). (c) Intracellular recordings from the trp^{CM} mutant, raised at 24 °C, in which the TRP channels are not functional. Responses to increasing intensities of orange light pulses are shown. The response to dim light (bottom trace) showed a sustained response during light. In contrast, the responses to medium and intense orange lights declined to baseline during illumination, showing the typical transient receptor potential of the *trp* mutant. (a) Modified from Pak, 1979.

light-dependent phosphorylation (**Figure 3**; Mpp), but this process is not required for response termination. This was demonstrated in experiments which showed that two *Drosophila* transgenic mutants, P[$Rh1^{\Delta 356}$] and P[$Rh1^{S\ to\ A}$], expressing Rs that lack the putative phosphorylation sites exhibit normal inactivation and ARR binding. However, as in the photoreceptors of vertebrates, the binding of ARR to M in *Drosophila* photoreceptors inactivates M (**Figure 3**). *Drosophila* has two protein homologs to the vertebrate ARR, both undergo light-dependent phosphorylation: the 49-kDa ARR (ARR2) and the 39-kDa ARR (ARR1). The phosphorylation of ARR2 is evident at dim light, while phosphorylation of ARR1 requires stronger light intensities. Both arrestins are phosphorylated by a Ca^{2+}-calmodulin-dependent protein kinase II (CaMK II). ARR phosphorylation is required for the dissociation of ARR from the phosphorylated M (Mpp) upon photoconversion and for preventing endocytotic internalization of the ARR2–Mpp complex (**Figure 3**).

Based on an understanding of the photochemical cycle, Minke and Selinger explained the PDA phenomenon as follows: cellular ARR2 is present at a concentration which is insufficient to inactivate all the M generated by a large net photoconversion of R to M, leaving an excess of M persistently active in the dark. This explanation easily accounts for the elimination of the PDA response by mutations or by carotenoid deprivation which reduce the cellular level of R. It also accounts for the need to

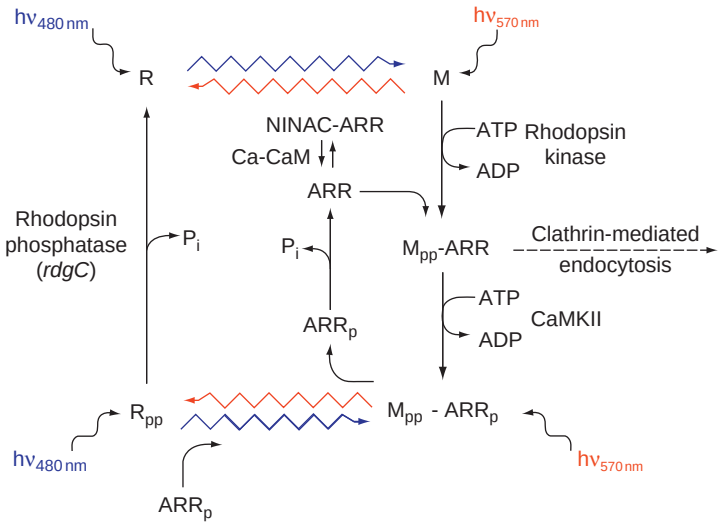

Figure 3 The photochemical cycle: the turn-on and turn-off of the photopigment. The arrestin (ARR) family of proteins play a key role in regulating the activity of G-protein-coupled receptors (GPCR). In *Drosophila,* two protein homologs of vertebrate arrestin exist. Both undergo light-dependent phosphorylation by Ca^{2+} calmodulin-dependent kinase (CaMK II), as shown by Matsumoto and colleagues. Their binding is essential for M inactivation. The study, which clarified the regulatory role of ARR2 was initiated by Selinger, Minke, and colleagues, using *in vitro* assays of ARR2 and M, in *Drosophila* and *Musca* eyes. They showed that upon photoconversion of R to M by illuminating with blue light (wavy blue arrow), the fly ARR2 was found predominantly in the membrane fraction, while photoconversion of phosphorylated M (Mpp) back to phosphorylated R (Rpp), by illuminating with orange light (wavy red arrow), resulted in the detection of ARR2 in the supernatant fraction (cytosol). ARR1 on the other hand always remains membrane bound (not shown). These studies indicated that the functional role of ARR2 binding to M is to terminate its activity. Binding of ARR2 also protects the phosphorylated metarhodopsin (Mpp) from phosphatase activity. Only upon photoregeneration of Mpp to Rpp, is ARR2 released and the phosphorylated rhodopsin (Rpp) is exposed to phosphatase activity by rhodopsin phosphatase (encoded by the *rdgC* gene discovered by O'Tousa and colleagues). These combined actions are crucial for preventing reinitiation of phototransduction in the dark as the reversible binding of ARR2 directs the protein phosphatase only toward the inactive Rpp. Subsequent studies by Dolph and colleagues and by Ranganathan and colleagues revealed that both CaMKII-dependent phosphorylation of ARR2 at Ser366 and the photoconversion of Mpp are required to release phosphorylated ARR2. They, furthermore, showed that the phosphorylation of ARR2 is required for its dissociation from Mpp upon photoconversion and that ARR2 phosphorylation prevents endocytotic internalization of the ARR2–Mpp complex. Montell and colleagues showed that ARR2 binds to myosin III kinase (NINAC). Recent studies by Hardie and colleagues suggest that, under low Ca^{2+} conditions, ARR2 is prevented from rapid binding to M because it is sequestered by NINAC. Ca^{2+} influx acting via CaM, during light (Ca-CaM), rapidly releases ARR2 and allows its binding to M and consequently, M inactivation.

photoconvert large net amounts of R to M to elicit the PDA response. Electrophysiological analysis performed by Zuker and colleagues on strong ARR2 (*arr2*) and ARR1 (*arr1*) mutant alleles revealed a set of phenotypes consistent with the stoichiometric requirement of ARR binding for M inactivation *in vivo*. In their study, they showed that a significant reduction in ARR2 levels leads to abnormally slow termination of light-activated currents and production of a PDA in mutants with low R levels.

Coupling of Photoexcited R to Inositol Phospholipid Hydrolysis

Light-Activated Gq Protein

It has been well established in photoreceptors of several invertebrate species that photoexcited R activates a heterotrimeric G protein. The first experiments, conducted on fly photoreceptors, were carried out by Minke and Stephenson who showed that when pharmacological agents known to activate G proteins were applied to photoreceptors in the dark, they mimicked the light-dependent activation of the photoreceptor cells. Later studies used genetic screens, which resulted in the isolation of two genes encoding visual specific G-protein subunits. These genes – *dgq* and *gβe* – encode, respectively, the alpha and beta subunits of the guanine nucleotide-binding G protein ($G_q\alpha$ and $G_q\beta$). The *Drosophila* eye-specific $G_q\alpha$ ($DG_q\alpha$), cloned by Hyde and colleagues, showed ~75% identity to mouse $G_q\alpha$ known to activate PLC. The most direct demonstration that $DG_q\alpha$ participates in the phototransduction cascade came from studies of mutants defective in $DG_q\alpha$ which showed highly reduced sensitivity to light. In the $G\alpha q^1$ mutant – isolated by Scott, Zuker, and colleagues – $DG_q\alpha$ protein levels are reduced to ~1%, while $G_q\beta$, PLC, and R protein levels are virtually normal. The $G\alpha q^1$ mutant exhibits an ~1000-fold reduced sensitivity to light and slow response termination, thus strongly suggesting that there is no parallel pathway mediated by another G protein. Manipulations of the $DG_q\alpha$ protein level by the inducible heat-shock promoter made it possible to show a strong correlation between the

sensitivity to light and $DG_q\alpha$ protein levels, further establishing its major role in *Drosophila* phototransduction.

The eye-specific $G_q\beta$ ($G_q\beta_e$) shares 50% amino acid identity with other Gβ homolog proteins. Analysis of mutants, isolated by Zuker and colleagues, which are defective in $G_q\beta_e$ ($G\beta_e^1$ and $G\beta_e^2$), showed a greatly (~100-fold) decreased sensitivity and slow response termination. Studies conducted by Selinger, Minke, and colleagues revealed that $DG_q\alpha$ is dependent on $G_q\beta\gamma$ for both membrane attachment and targeting to the rhabdomere, suggesting that the decreased light sensitivity of these mutants may result from the mislocalization of the $DG_q\alpha$ subunit. Previous studies showed that the attachment of $DG_q\alpha$ to $G_q\beta\gamma$ prevents spontaneous guanosine diphosphate and guanosine triphosphate (GDP–GTP) exchange. Analysis of Selinger, Minke, and colleagues of the stoichiometry between the $DG_q\alpha$ and $G_q\beta$ subunits revealed a twofold excess of $G_q\beta$ over $DG_q\alpha$. Genetic elimination of the $G_q\beta$ excess led to spontaneous activation of the visual cascade in the dark, demonstrating that $G_q\beta$ excess is essential for the suppression of dark electrical activity produced by spontaneous GDP–GTP exchange of $DG_q\alpha$.

Light-Activated PLC

Evidence for a light-dependent activation of PLC by $G_q\alpha$ in fly photoreceptors came from combined biochemical and electrophysiological experiments. These experiments were conducted by Selinger, Minke, and colleagues, in membrane preparations and intact *Musca* and *Drosophila* eyes. The eye membrane preparations responded to illumination with a $G_q\alpha$-dependent accumulation of inositol-1,4,5-trisphosphate ($InsP_3$) and inositol-bisphosphate ($InsP_2$), derived from phosphatidylinositol-4,5-bisphosphate (PIP_2) hydrolysis by PLC (**Figure 4**, lower panel). However, genetic elimination of the single $InsP_3$ receptor, performed by Zuker and colleagues and by Hardie and colleagues, had no effect on light excitation, thus putting in question the role of $InsP_3$ in phototransduction.

The key evidence for the participation of PLC in visual excitation of the fly was provided by Pak and colleagues, who isolated and analyzed the PLC gene of *Drosophila*, designated no receptor potential A (*norpA*). The *norpA* mutant has long been a strong candidate for a transduction defective mutant because of its drastically reduced receptor potential. The *norpA* gene encodes a β-class PLC that is predominately expressed in the rhabdomeres (**Figure 4**) and has extensive amino acid homology to a PLC extracted from bovine brain. Transgenic *Drosophila* carrying the *norpA* gene on a null *norpA* background rescued the transformant flies from all the physiological, biochemical, and morphological defects associated with the *norpA* mutants. The *norpA* mutant thus provides essential evidence for the critical role of inositol-lipid signaling in phototransduction, by showing that no excitation takes place in the absence of functional PLC. However, the events required for light excitation downstream of PLC activation remain unresolved.

The TRP Channels

The *trp* Mutant and the Discovery of the TRP Channel

A spontaneously occurring *Drosophila* mutant (isolated by Cosens and Manning), showing a decline in the receptor potential to baseline during prolonged illumination, was designated transient receptor potential (*trp*) by Minke and colleagues (**Figure 2(b) and (c)**). Minke and Selinger suggested that the *trp* gene encodes a Ca^{2+} channel/transporter mainly because application of the Ca^{2+} channel blocker La^{3+} to wild-type photoreceptors mimicked the *trp* phenotype. Subsequently, the cloning of the *trp* locus by Montell and Rubin revealed a novel membrane protein with a sequence of a channel. The available sequence of the *trp* gene led, several years later, to the discovery of mammalian TRPs and the TRP superfamily. However, the significance of the *trp* sequence – as a gene encoding a putative channel protein – was only first appreciated after a *trp* homolog, *trp-like* (*trpl*), was cloned by Kelly and colleagues. They used a screen for calmodulin-binding proteins and found a transmembrane (TM) protein. A comparison of its TM domain to that of voltage-gated Ca^{2+} channels and the TRP protein led to the conclusion that this protein is a putative channel protein with large identity to TRP (**Figure 5**). Strong evidence supporting the notion that TRP is the major light-activated channel came from a comparative patch-clamp study of isolated ommatidia (**Figure 1(d)**) of wild-type and the *trp* mutant conducted by Hardie and Minke. The use of Ca^{2+} indicator dyes and Ca^{2+}-selective microelectrodes, by Minke and colleagues, directly demonstrated that the TRP channel is the major route for Ca^{2+} entry into the photoreceptor cell. The final evidence showing that TRP and TRP-like protein (TRPL) are the light-activated channels came from the isolation of a null mutant of the *trpl* gene, by Zuker and colleagues, who demonstrated that the double mutant, *trpl;trp*, is blind. The notion that the *trp* gene encodes a Ca^{2+} channel has been recently confirmed by Hardie and colleagues by using a mutant with a point mutation at the suspected pore region of the channel, altering its Ca^{2+} permeability properties (**Figure 5**, D621 at the pore region of TRP channel).

Biophysical Properties of the TRP Channel

The *Drosophila* light-sensitive channels – TRP and TRPL – could be studied separately by utilizing the $trpl^{302}$ and trp^{P343} null mutants, respectively. The channels are permeable to a

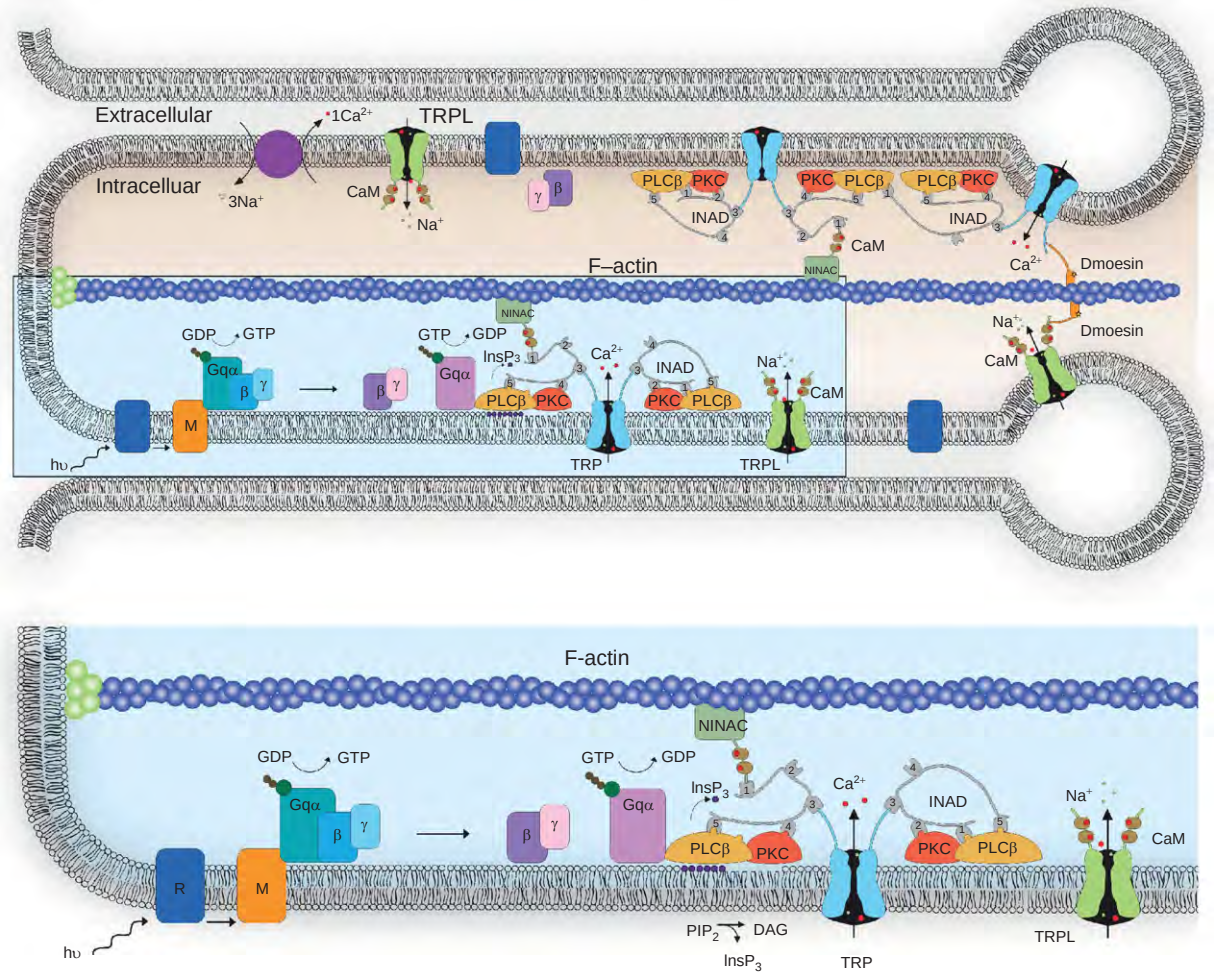

Figure 4 The phosphoinositide cascade of vision. The signaling proteins of the phototransduction cascade are tightly assembled in the microvillar structure (upper panel). The upper panel emphasizes the link of the signaling proteins to the actin cytoskeleton (F-actin) via two proteins: Dmoesin that binds the TRP and TRPL channels, at the base of the microvilli to F-actin and NINAC that associates INAD to F-actin. The only protein that diffuses during the phototransduction cascade is Gqα. The lower panel highlights the molecular components that directly participate in the phototransduction cascade. The numbers on the INAD indicate the various PDZ domains. Upon absorption of a photon, R (encoded by the *ninaE* gene, lower panel) is converted into the active state of the photopigment, M. This, leads to the activation of heterotrimeric G protein (G_q) by promoting the GDP to GTP exchange. In turn, this leads to activation of phospholipase Cβ (PLCβ, encoded by the *norpA* gene), which hydrolyzes the minor phospholipid, PIP_2 into the soluble $InsP_3$ and the membrane-bound diacylglycerol (DAG). Subsequently, two classes of light-sensitive channels, the TRP and TRPL, open by a still unknown mechanism. PLC also promotes hydrolysis of the bound GTP, resulting in $G_q\alpha$ bound to GDP and this ensures the termination of $G_q\alpha$ activity. The TRP and TRPL channel openings lead to elevation of calcium ions extruded by the Ca^{2+}/Na^+ exchanger CALX (violet circle, upper panel). Elevation of DAG and Ca^{2+} promote eye-specific protein kinase C (PKC, encoded by the *inaC* gene) activity, which regulates channel activity. PLC, PKC, NINAC (encoded by the *ninaC* gene), and the TRP ion channel form a supramolecular complex with the scaffolding protein INAD (encoded by the *inaD* gene). Recent studies by Minke and colleagues have shown a light- and phosphorylation-dependent dynamic association of Dmoesin to the *Drosophila* TRP and TRPL channels involved in rhabdomere maintenance. Dmoesin belongs to the ezrin–radixin–moesin (ERM) protein family, which is known to regulate actin–plasma membrane interactions in a signal-dependent manner. Dmoesin is localized to the base of the microvilli in adult *Drosophila* and its function is still unknown.

variety of monovalent and divalent ions including Na^+, K^+, Ca^{2+}, and Mg^{2+} and even to large organic cations such as tris(hydroxymethyl)aminomethane (TRIS) and tetraethylammonium (TEA). The reversal potential of the light-induced current (LIC) shows a marked dependence on extracellular Ca^{2+} indicating a high permeability for this ion. Hardie and colleagues measured the permeability ratios for a variety of divalent and monovalent ions determined under bi-ionic conditions and confirmed a high Ca^{2+} permeability of $\sim 57{:}1 = Ca^{2+}{:}Cs^+$ in the *trpl* mutant and $\sim 4.3{:}1 = Ca^{2+}{:}Cs^+$ for the *trp* mutant.

The TRP and TRPL channels show voltage-dependent conductance during illumination. An early study by Hardie and Mojet revealed that the light response can

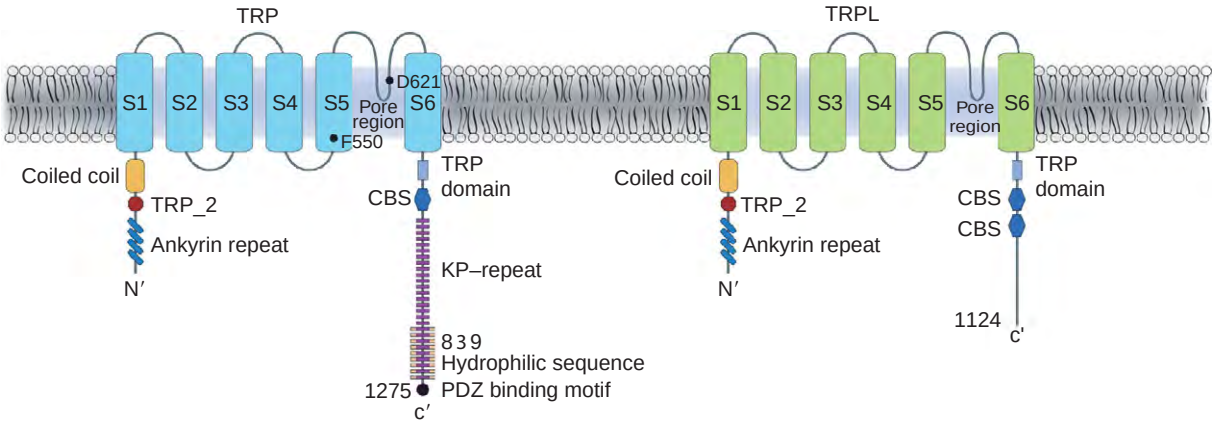

Figure 5 Structural features of the *Drosophila* TRP and TRPL channels. The *trp* and *trpl* genes encode a 1275- and 1124-amino acid membrane protein, respectively, which are presented schematically. The TRP channels share overall 40% amino acid sequence identity with TRPL and a greater similarity (~70%) in the putative transmembrane regions but little homology (~17%) in the C-terminal. The transmembrane domain (TM) of TRP and TRPL channels shows significant identity of ~40% with the TM of vertebrate voltage-gated Ca^{2+} channels; all contain six TM helices and a pore loop between S5 and S6. The S5 pore loop and S6 region are likely the pore-forming region of TRP, as evidenced by a study of Hardie and colleagues. They replaced Asp^{621} (D621) with glycine or asparagine and the mutated TRP channel showed reduced Ca^{2+} permeability. Voltage-gated Ca^{2+} channels are formed by a single peptide and contain charged residues in the putative S4 helix, believed to form the voltage sensor. TRP and TRPL channels, on the other hand, assemble by four peptides as homo- or hetromultimeres and do not contain charged residues in S4. While the gating mechanism of the TRP and TRPL channels is unclear, a study conducted by Yoon, Pak, Minke, and colleagues showed that the substitution of Phe^{550} (F550) to isoleucine in S5 of the TRP channel (in the mutant fly trp^{P365}) forms a constitutively active channel leading to extremely fast light-independent retinal degeneration. The TRPL channel was originally identified as a calmodulin (CaM)-binding protein and contains two CaM-binding sites (CBS) in the C-terminal of the channel. One of these is unconventional in the sense that it can bind CaM in the absence of Ca^{2+}. The C-terminus fragment of the TRP sequence also has been reported to bind CaM in a Ca^{2+}-dependent manner. Both channels have a designated TRP domain located adjacent to the S6 with a EWKFAR motif found in many members of the TRP family. At the C-terminal region of the TRP there is a proline-rich sequence with 27 KP repeats, which overlap with a multiple repeat sequence, DKDKKP(G/A)D termed 8 × 9. Such proline-rich motifs occur widely and are predicted to form a structure involved in binding interactions with other proteins, including cytoskeletal elements such as actin. This region is unique to TRP and has not been found in any other member of the TRP family. The last 14 amino acids in the C-terminal of TRP are essential for the binding of INAD (see **Figures 4** and **7**) and form a PDZ binding domain. At the C-terminal, between the CBS and the KP-repeat domains, there is an unmarked sequence with low homology to a proline, glutamic acid, serine, and threonine (PEST) sequence commonly found in CaM-binding proteins and which is believed to be a target for rapid degradation by the Ca^{2+}-dependent protease calpain. The N-terminal regions of the TRP and TRPL proteins contain four ankyrin repeats and a coiled-coil domain. Both domains are believed to mediate protein–protein interactions. The N-terminal regions also contain a TRP_2 domain with unknown function, predicted recently as involved in lipid-binding and trafficking.

be blocked by physiological concentrations of Mg^{2+} ions. The block mainly influenced the TRP channel and affected its voltage dependence. Detailed analysis by Parnas, Katz, and Minke described the voltage dependence of heterologously expressed TRPL in S2 cells and of the native TRPL channel, using the *Drosophila trp*-null mutant. These studies indicated that the voltage dependence of the TRPL channel is not an intrinsic property, as is thought for other members of the TRP family, but arises from divalent open-channel block that can be removed by depolarization. The open-channel block by divalent cations is thought to play a role in improving the signal-to-noise ratio of the response to intense light and may function in light adaptation and response termination.

A comparison with voltage-gated K^+ channels and cyclic nucleotide-gated (CNG) channels, postulates that both TRP and TRPL are assembled as tetrameric channels, thus raising the question whether they assemble as homomultimers or as heteromultimers. Since both null *trp* and *trpl* mutants respond to light, each can clearly function without the other. However, a study by Montell and colleagues – based on heterologous coexpression studies and coimmunoprecipitation – led to the suggestion that the TRP and TRPL channels can assemble into heteromultimers. Detailed measurements of biophysical properties performed by Hardie and colleagues, questioned this conclusion since they found that the wild-type conductance could be quantitatively accounted for by the sum of the conductances determined in the *trp* and *trpl* mutants. In addition, Paulsen, Huber, Minke, and colleagues have demonstrated that the TRPL, but not the TRP, channel reversibly translocates from the rhabdomere to the cell body upon illumination, further implying that TRP and TRPL do not form heteromultimeres.

Lipids Activate the Light-Sensitive Channels in the Dark

The activation of PLC results in the hydrolysis of PIP_2 into DAG (Figures 4 and 6) and $InsP_3$. The pathway which recycles DAG back to PIP_2 – the PI pathway – has emerged to be most important for activation of the TRP and TRPL channels. The most familiar action of DAG is to activate the classical protein kinase C (PKC) synergistically with Ca^{2+}. However, mutations in the eye-specific PKC (PKC, *inaC*; Figures 4 and 7) lead to defects in response termination with no apparent effects on activation. A second role for DAG in *Drosophila* photoreceptors is to act as a precursor for regeneration of PIP_2 via conversion to phosphatidic acid (PA) by DAG kinase (DGK, *rdgA*; Figure 6). Mutations in DGK (*rdgA*) lead to a severe form of light-independent degeneration. Other mutations in the PI pathway – the CDP–diacylglycerol synthase (CDP–DAG Syntase, *cds*; Figure 6) and the PI transfer protein (PITP, *rdgB*; Figure 6), also lead to severe forms of light-dependent degeneration. The degeneration phenotype – assumed to be caused by toxic increase in cellular Ca^{2+} due to constitutive activity of the TRP channels – suggested a possible involvement of the PI pathway in channel activation. Accordingly, a hypothesis has been put forward whereby DAG acts as an intracellular messenger leading directly to TRP and TRPL channel activation (see below). However, application of DAG to isolated *Drosophila* ommatidia did not activate the channels.

DAG is also a precursor for the formation of polyunsaturated fatty acids (PUFAs) via DAG lipase (Figure 6). Studies conducted by Hardie and colleagues showed that application of PUFAs to isolated *Drosophila* ommatidia, as well as to recombinant TRPL channels expressed in *Drosophila* S2 cells, reversibly activated the TRP and TRPL channels. Moreover, they showed that, in the *rdgA* mutant, TRP and TRPL channels are constitutively active, while elimination of TRP by a mutation (in the double-mutant

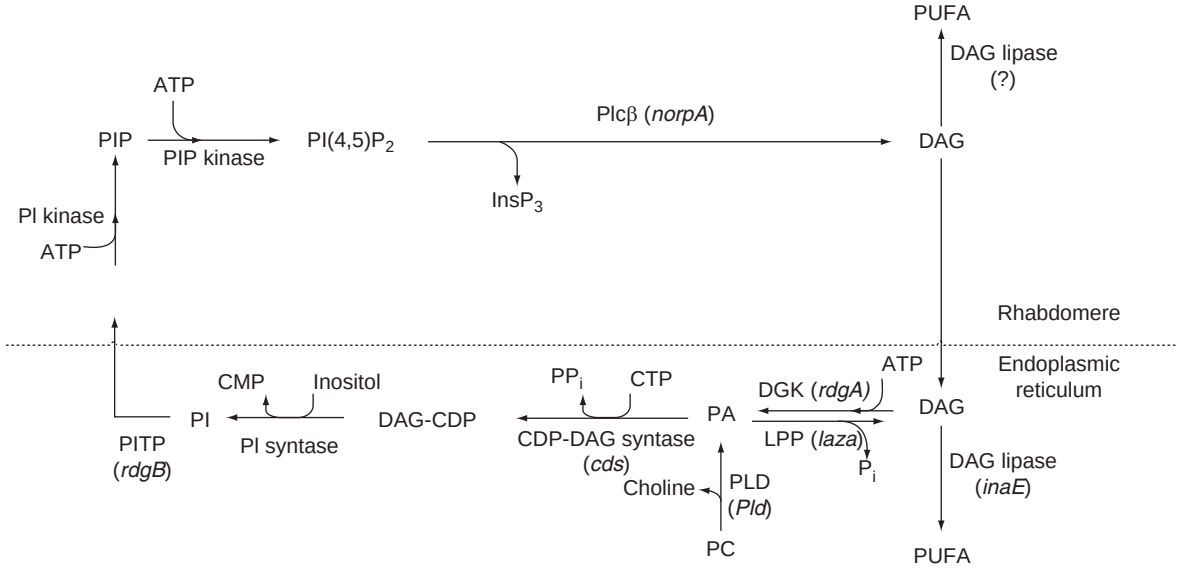

Figure 6 The inositol lipid cycle. In the phototransduction cascade, light triggers the activation of phospholipase Cβ (PLCβ). This catalyzes hydrolysis of the membrane phospholipid phosphatidylinositol-4,5-bisphosphate (PIP_2) into water-soluble inositol-1,4,5-trisphosphate ($InsP_3$) and membrane-bound diacylglycerol (DAG). The continuous functionality of the photoreceptors during illumination is maintained by rapid regeneration of PIP_2 in a cyclic enzymatic pathway (the PI pathway). DAG is transported by endocytosis to the endoplasmic reticulum (submicrovillar cisternae (SMC)) and inactivated by phosphorylation into phosphatidic acid (PA) via DAG kinase (DGK, encoded by the *rdgA* gene and cloned and localized by Hotta and colleagues) and to CDP–DAG via CDP–DAG syntase (encoded by the *cds* gene and cloned by Zuker and colleagues). PA can be converted back to DAG by lipid phosphate phosphohydrolase (LPP; also designated phosphatidic acid phosphatase (PAP)) encoded by *laza* (cloned by Raghu and colleagues and by Montell and colleagues). PA is also produced from phosphatidyl choline (PC) by phospholipase D (PLD, encoded by *Pld).* DAG is also hydrolyzed by DAG lipase (encoded by *inaE*) into polyunsaturated fatty acids (PUFA). This DAG lipase was predominantly localized outside the rhabdomeres, putting in question the participation of PUFA in channel activation *in vivo*. Subsequently, CDP–DAG is converted into phosphatidyl inositol (PI), which is transferred back to the microvillar membrane, by the PI transfer protein (PITP; encoded by the *rdgB* gene and cloned by Hyde, O'Tousa, and colleagues). Both RDGA and RDGB proteins have been immunolocalized to the SMC of the smooth endoplasmic reticulum at the base of the rhabdomere (Figure 1(c)). PIP and PIP_2 are produced at the microvillar membrane by PI kinase and PIP kinase, respectively. The SMC in *Drosophila* has been proposed to posses Ca^{2+} stores endowed with $InsP_3$ receptors ($InsP_3R$). Genetic elimination of the single $InsP_3R$ did not produce any phenotype, suggesting that Ca^{2+} release from stores does not participate in the production of the response to light. It is important to realize that the PI-recycling enzymes – which are essential for continuous production of PIP_2 and hence for the maintained light response – are localized at the SMC. Therefore, the function of the SMC as a lipid-supplying organelle and its role in phototransduction should be further explored.

rdgA;trp), partially rescued the degeneration. The authors suggested a hypothesis in which the elimination of DAG kinase – by the *rdgA* mutation – leads to accumulation of DAG and hence of PUFAs. According to this model, a still undemonstrated accumulation of DAG or PUFAs – acting as messengers of excitation – constitutively activate the TRP and TRPL channels, which in turn leads to a toxic increase in cellular Ca^{2+} and thereby degeneration. Recently, Pak and colleagues identified the *inaE* gene as encoding a homolog of mammalian *sn-1* type DAG lipase and showed that it is expressed predominantly in the cell body of *Drosophila* photoreceptors. Mutant flies expressing low levels of the *inaE* gene product have an abnormal light response, while the activation of the light-sensitive channels was not prevented. Thus, the participation of DAG or PUFAs in TRP and TRPL activation *in vivo* needs further exploration.

It is important to realize that PLC activation, which converts PIP_2 – a charged molecule containing a large hydrophilic head-group – into DAG, which is devoid of the hydrophilic head-group, may cause major changes in lipid packing and lipid-channel interactions. It is, therefore, possible that neither PIP_2 hydrolysis nor DAG production affect the TRP and TRPL channel as second messengers but rather act as modifiers of membrane lipid-channel interactions. This may, in turn, act as a possible mechanism of channel activation.

Organization in a Supramolecular Signaling Complex via the Scaffold Protein Inactivation No Afterpotential D

An important step toward understanding *Drosophila* phototransduction has been achieved by the finding that some of the key elements of the phototransduction cascade are incorporated into supramolecular signaling complexes via a scaffold protein, inactivation no afterpotential D (INAD; **Figure 7**). The INAD protein was discovered by a PDA screen of defective *Drosophila* mutants (*inaD*). The first-discovered *inaD* mutant – the $InaD^{P215}$ – was isolated by Pak and colleagues and subsequently was cloned and sequenced by Shieh and Zhu. Studies in *Calliphora* by Paulsen Huber and colleagues have shown that INAD binds not only TRP but also PLC (NORPA) and PKC (INAC). The interaction of INAD with TRP, NORPA, and INAC was later confirmed in *Drosophila*. It was further found by Zuker, Tsunoda, and colleagues that *inaD* is a scaffold protein, which consists of five ~90-amino acid protein-interaction motifs called postsynaptic density protein (PSD95), *Drosophila* disc large tumor suppressor (DlgA), and zonula occludens-1 protein (zo-1) (PDZ) domains. These domains are recognized as protein modules which bind to a diversity of signaling, cell-adhesion, and cytoskeletal proteins by specific binding to target sequences typically, though not always, in the final three residues of the C-terminal. The PDZ domains of INAD bind to the signaling molecules as follows: PDZ1 and PDZ5 bind PLC, PDZ2 or PDZ4 bind PKC, and PDZ3 binds TRP. This binding pattern is still in debate due to several contradictory reports. On the other hand, TRPL appears not to be a member of the complex, since unlike INAC, NORPA and TRP it remains strictly localized to the rhabdomeral microvilli in the $inaD^{1}$-null mutant isolated by Zuker, Tsunoda, and colleagues. Several studies by Montell and colleagues have suggested that, in addition to PLC, PKC, and TRP, other signaling molecules such as calmodulin, R, TRPL, and neither inactivation nor afterpotential C (NINAC) bind to the INAD-signaling complex. Such binding, however, must be dynamic. Biochemical studies by Huber, Paulsen, and colleagues conducted in *Calliphora* have revealed that both INAD and TRP are targets for phosphorylation by the nearby PKC. Accordingly, the association of TRP into transduction complexes may be related to increasing the speed and efficiency of transduction events as reflected by the proximity of TRP to its upstream activator, PLC, and its possible regulator, PKC.

TRP plays a major role in localizing the entire INAD multimolecular complex. Association between TRP and INAD is essential for correct localization of the complex in the rhabdomeres. This conclusion was derived by Tsunoda, Zuker, and colleague and by Montell and colleagues using *Drosophila* mutants in which the signaling proteins which constitute the INAD complex were removed genetically, and by deletions of the specific binding domains which bind TRP to INAD. These experiments show that INAD is correctly localized to the rhabdomeres in *inaC* mutants (where PKC is missing) and in *norpA* mutants (where PLC is missing), but severely mislocalized in null *trp* mutants. This indicates that TRP, but not PLC or PKC, is essential for localization of the signaling complex to the rhabdomere. To demonstrate that specific interaction of INAD with TRP is required for the rhabdomeric localization of the complex, the binding site at the C-terminal of TRP was removed or the three conserved residues in PDZ3 – which are expected to disrupt the interaction between PDZ domains and their targets – were modified. As predicted, both TRP and INAD were mislocalized in these mutants. The study of the above mutants was also used to show that TRP and INAD do not depend on each other to be targeted to the rhabdomeres; thus, INAD–TRP interaction is not required for targeting but for anchoring of the signaling complex. Additional experiments on TRP and INAD further show that INAD has other functions in addition to anchoring the signaling complex. One important function is to preassemble the proteins of the signaling complex. Another important function, at least for the case of PLC, is to prevent degradation of the unbound signaling protein.

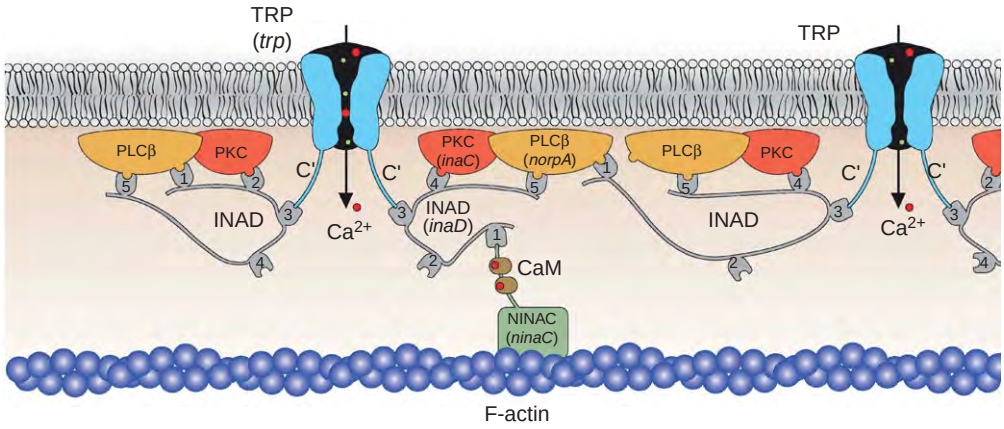

Figure 7 The INAD-signaling complex. The INAD is a 674-amino acid-scaffold protein with homology to cytoskeleton-associated proteins, which include PSD-95 (implicated in clustering of *N*-methyl-D-aspartate (NMDA) receptors and K^+ channels), *Drosophila discs large*, and the epithelial tight-junction protein ZO-1. These proteins all include a variable number of so-called PDZ domains – now recognized as protein modules – which anchor a variety of receptors, ion channels, and other signaling molecules, by specific binding to target sequences. The TRP protein anchors the INAD complex adjacent to the plasma membrane while the disruption of the interaction between these two proteins does not influence the target of either protein in pupae, while disrupting their retention at adulthood. The INAD sequence contained five consensus PDZ domains and identified specific interactions between PKC and PDZ2 or PDZ4, TRP and PDZ3, PLC with PDZ1 and PDZ5 and NINAC with PDZ1. This binding pattern is still in debate due to several contradictory reports. It was also reported that the INAD contains a Ca^{2+}-calmodulin-binding site which may be involved in its regulation. Several authors have commented that the close association of elements of the transduction cascade may be essential for the rapid response kinetics, which characterizes *Drosophila* phototransduction, by minimizing or eliminating diffusional delays. The slow response termination in $InaD^{P215}$ mutant (disrupting INAD–TRP interaction) also leads to speculation that one function of the INAD complex is to target Ca^{2+} influx via the TRP channels directly to PKC, which appears to be required for Ca^{2+}-dependent inactivation of the light response. It is also speculated that PLC activity may be regulated by TRP-mediated Ca^{2+} influx. With regard to activation, any *norpA* or *inaD* mutation which prevents association of PLC and INAD leads to severe defects in excitation. This can be explained by a large reduction of PLC in the microvillar membranes, which would be expected to be essential for normal phototransduction in any model. Interestingly, the specific dissociation of TRP from the INAD complex in the $inaD^{P215}$ mutant, leads to very minor, if any, defect in excitation, except in older flies where TRP levels begin to decline. Nevertheless, several authors have speculated that the INAD complex may provide a mechanism for direct gating of the light-sensitive channels by protein–protein interactions. At present, the only functional roles of INAD, as determined experimentally, are to protect its binding proteins from mislocalization and degradation. These functions are important for maintaining the specific stoichiometry among the signaling proteins (see the section titled 'The photoreceptor cells are sensitive to single photons').

A recent study by Ranganathan and colleagues has suggested that the binding of signaling proteins to INAD may be a dynamic process that allows additional levels of phototransduction regulation. Their study showed that two crystal structural states of the isolated INAD PDZ5 domain differ mainly by the formation of a disulfide bond. This conformational change has a light-dependent dynamic that was demonstrated by the use of transgenic *Drosophila* flies expressing the INAD with a point mutation that disrupts the formation of the disulfide bond. They proposed a model in which PKC phosphorylation of INAD at a still-unknown site promotes a light-dependent conformational change of PDZ5 which distorts its binding site for PLC and thus regulates phototransduction.

The Photoreceptor Cells Are Sensitive to Single Photons

Dim-light stimulation induces discrete voltage (or current) fluctuations in most invertebrate species, which are called quantum bumps (**Figure 2(b)**). Each bump is assumed to be evoked by the absorption of a single photon and these bumps sum up to produce the macroscopic response to more intense lights (**Figure 2(b)**). The bumps vary significantly in latency, time course, and amplitude, even when the stimulus conditions are identical. Bump generation is a stochastic process described by Poisson statistics whereby each effectively absorbed photon elicits only one bump. However, in at least three *Drosophila* mutants (*cam*, *ninaC*, and *arr2*) absorption of a single photon elicits a train of bumps with a rather fixed interval. This phenomenon is explained by a failure of M molecules to be inactivated in these mutants (**Figure 3**) and the existence of a positive and negative feedback and a refractory period in the bump-generating mechanism. The single-photon-single-bump relationship requires that each step in the cascade includes not only an efficient turn-on mechanism, but also an equally effective turn-off mechanism. The functional advantage is the production of a very sensitive photon counter with a fast transient response, very well suited for both the sensitivity and the

temporal resolution required by the visual system. The requirement for efficient turn-off mechanisms is revealed when either M (see above) or PLC fail to inactivate and lead to continuous production of bumps long after light is turned off. Cook, Minke, and colleagues demonstrated that *Drosophila* PLC functions as a GTPase-activating protein (GAP). PLC thus terminates its own activity by accelerating the GTPase activity of the $G_q\alpha$ protein thereby causing the dissociation of $G_q\alpha$ from its target, the PLC (**Figure 4**). The inactivation of the G-protein by its target PLC ensures that each activated G-protein activates only one PLC and thus produces only one bump. It also ensures that every activated G-protein will eventually encounter a PLC molecule and thereby produce a bump. The accurate stoichiometry between PLC and G-protein molecules in the rhabdomere of wild-type flies is maintained by the binding of PLC to the scaffold protein INAD (**Figure 7**). This accurate stoichiometry ensures instantaneous inactivation of all activated G-proteins, when light is turned off, and fast response termination. However, in *norpA* or *inaD* mutants, in which the PLC level is reduced, excessive numbers of active $G_q\alpha$ proteins – relative to scarce PLC molecules – leads to continuous production of bumps in the dark until the last $G_q\alpha$-GTP encounters a PLC and is thereby inactivated by the GAP activity of PLC. This remarkable mechanism makes the photoreceptor cell a photon counter and ensures the high temporal and light-intensity resolutions of the response to light.

Conclusions

Drosophila photoreceptors use the ubiquitous inositol-lipid signaling for phototransduction with TRP channels as its target. While mammalian TRP channels are also modulated by the PI cascade and are activated by a large variety of stimuli, the physiological function and mechanism of activation is not entirely clear. In contrast, the physiological function of the *Drosophila* TRP channels as light-activated channels is well established, as well as the requirement of PLC for their activation. It is, therefore, important to direct future efforts toward investigating the activation mechanism of the various TRP channels in the native cells. Genetic tools seem to be especially suitable for such investigation. The similar structural features of the pore domain in all members of TRP channels and the involvement of PLC in their activation/modulation suggest that, in principle, they may share a common mechanism of activation. Thus, studies of *Drosophila* TRP channels is important for the understanding of this diverse and important family of channel proteins.

See also: Circadian Photoreception; Microvillar and Ciliary Photoreceptors in Molluskan Eyes; Phototransduction: Inactivation in Cones; Phototransduction in *Limulus* Photoreceptors; Phototransduction: Inactivation in Rods; Phototransduction: Phototransduction in Cones; Phototransduction: Phototransduction in Rods; Phototransduction: Rhodopsin.

Further Reading

Bloomquist, B. T., Shortridge, R. D., Schneuwly, S., et al. (1998). Isolation of a putative phospholipase C gene of *Drosophila*, *norpA*, and its role in phototransduction. *Cell* 54: 723–733.

Byk, T., Bar-Yaacov, M., Doza, Y. N., Minke, B., and Selinger, Z. (1993). Regulatory arrestin cycle secures the fidelity and maintenance of the fly photoreceptor cell. *Proceedings of the National Academy of Sciences of the United States of America* 90: 1907–1911.

Chyb, S., Raghu, P., and Hardie, R. C. (1999). Polyunsaturated fatty acids activate the *Drosophila* light-sensitive channels TRP and TRPL. *Nature* 397: 255–259.

Cook, B., Bar-Yaacov, M., Cohen Ben-Ami, H., et al. (2000). Phospholipase C and termination of G-protein-mediated signalling *in vivo*. *Nature Cell Biology* 2: 296–301.

Devary, O., Heichal, O., Blumenfeld, A., et al. (1987). Coupling of photoexcited rhodopsin to inositol phospholipid hydrolysis in fly photoreceptors. *Proceedings of the National Academy of Sciences of the United States of America* 84: 6939–6943.

Hardie, R. C. and Minke, B. (1992). The *trp* gene is essential for a light-activated Ca^{2+} channel in *Drosophila* photoreceptors. *Neuron* 8: 643–651.

Hardie, R. C. and Postma, M. (2008). *Phototransduction in Microvillar Photoreceptors of Drosophila and Other Invertebrates. The Senses: A Comprehensive Reference* vol. 1. Vision I, pp. 77–130. San Diego, CA: Academic Press.

Huber, A., Sander, P., Gobert, A., et al. (1996). The transient receptor potential protein (Trp), a putative store-operated Ca^{2+} channel essential for phosphoinositide-mediated photoreception, forms a signaling complex with NorpA, InaC and InaD. *EMBO Journal* 15: 7036–7045.

Minke, B. and Cook, B. (2002). TRP channel proteins and signal transduction. *Physiological Review* 82: 429–472.

Montell, C. and Rubin, G. M. (1989). Molecular characterization of the *Drosophila trp* locus: A putative integral membrane protein required for phototransduction. *Neuron* 2: 1313–1323.

Phillips, A. M., Bull, A., and Kelly, L. E. (1992). Identification of a *Drosophila* gene encoding a calmodulin-binding protein with homology to the *trp* phototransduction gene. *Neuron* 8: 631–642.

Scott, K., Becker, A., Sun, Y., Hardy, R., and Zuker, C. (1995). Gq alpha protein function *in vivo*: Genetic dissection of its role in photoreceptor cell physiology. *Neuron* 15: 919–927.

Tsunoda, S., Sierralta, J., Sun, Y., et al. (1997). A multivalent PDZ-domain protein assembles signalling complexes in a G-protein-coupled cascade. *Nature* 388: 243–249.

Vihtelic, T. S., Hyde, D. R., and O'Tousa, J. E. (1991). Isolation and characterization of the *Drosophila* retinal degeneration B (*rdgB*) gene. *Genetics* 127(4): 761–768.

Yamada, T., Takeuchi, Y., Komori, N., et al. (1990). A 49-kilodalton phosphoprotein in the *Drosophila* photoreceptor is an arrestin homolog. *Science* 248: 483–486.

Relevant Website

http://flybase.org – Flybase: Detailed information on all Drosophila Genes.

Genetics of Age-Related Cataract

A Shiels, Washington University School of Medicine, St. Louis, MO, USA
J F Hejtmancik, National Institutes of Health, Bethesda, MD, USA

Glossary

Association – A tendency for two characters (e.g., disease phenotypes, genetic variants or alleles) to occur together at nonrandom frequencies.
Epidemiology – The study of disease epidemics aimed at discovering the cause(s).
Genome – The complete set of different DNA molecules of an organism, cell or subcellular organelle (e.g., mitochondria). Humans have 25 different DNA molecules, the mitochondrial DNA molecule, and the 24 chromosome DNA molecules (22 autosomes plus 2 sex chromosomes, X and Y).
Genotype – The genetic composition of an organism, either overall or at a specific chromosomal location or locus, as distinct from its phenotype.
Linkage – The tendency of characters (disease phenotypes, genetic variants or alleles) located on the same chromosome to be inherited together, or co-segregate, in a family.
Phenotype – The physical appearance of an organism, tissue, or cell as distinct from its genotype.

Introduction

Clouding of the eye lens, or cataract, is a common symptom of aging (>50 years), and age-related or senile cataract is a leading cause of visual impairment. The World Health Organization estimates that, despite recent advances in its surgical treatment, age-related cataract still accounts for 40–50% of global blindness, and with continued growth and aging of the world's population; the prevalence of age-related cataract is projected to double. In the United States alone, age-related cataract afflicts more than 22 million Americans over age 40 (~17% of this age range), and by age 80 over 50% have cataract. Currently, about 1.5 million cataract surgeries are performed annually and age-related cataract surgery represents a major healthcare expense. It has been estimated that delaying the onset of age-related cataract by 10 years would decrease the demand for surgery by about 45%.

Despite the prevalence of age-related cataract in humans and many domestic animals, the underlying molecular pathology is poorly understood. Epidemiological studies indicate that age-related cataract is a multifactorial disease involving complex interactions between environmental risk factors (e.g., cigarette smoking status and ultraviolet sunlight exposure), and significant genetic risk factors. The discovery of these genetic factors is at an early stage, and here we outline recent progress in the molecular genetics of age-related cataract.

Age-Related Cataract Phenotypes

Clinical classification of age-related cataract is largely based on the location, size, shape, density, and color of opacities when visualized in the lens by slit-lamp examination (Figure 1). Defined by lens location, age-related cataract may be divided into three pure subtypes referred to as nuclear cataract, cortical cataract, and posterior subcapsular cataract. Nuclear cataract, often associated with a brown discoloration, affects the central core of the lens and is prevalent in most white populations and indigenous populations from Africa, India, and Southern China, whereas, cortical cataract, which usually appears as wedge-shaped opacities, affecting the outer cortex of the lens is more common in Icelandic, African-American, and certain East Asian populations. Posterior subcapsular cataract, which usually appears as a granular deposit or plaque-like opacity, is confined to the back of the lens, lying just beneath the capsule or basement membrane that envelopes the lens mass, and represents the least prevalent type in all populations studied. Pure types of age-related cataract can be further graded for severity according to their size and density by evaluation of lens photographs taken with a slit-lamp camera (Figure 1). In practice, however, age-related opacities often occur in combination (i.e., mixed nuclear and cortical with or without posterior sub-capsular) and may eventually progress to total opacification of the lens.

Genetic Epidemiology of Age-Related Cataracts

Increasing epidemiological evidence, which is primarily based on statistical analyses, points to the importance of genetic factors in the pathogenesis of age-related cataract. However, as compared to inherited forms of congenital or childhood cataract, age-related cataract by definition has a late age of onset, so that multi-generation families with age-related cataract tend not to be readily

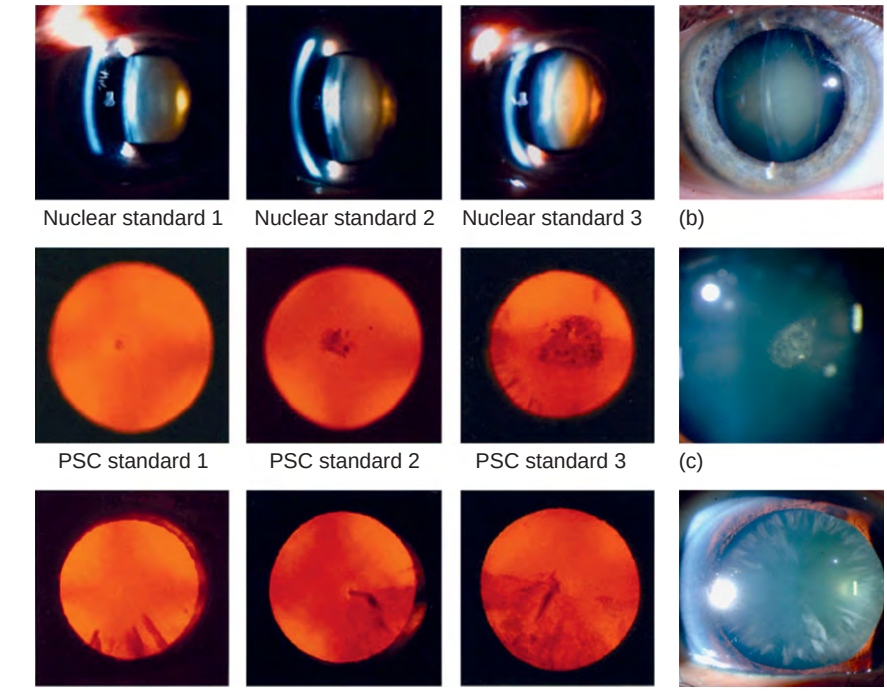

Figure 1 Three main types of age-related cataracts. (a) The age-related eye disease study (AREDS) system for classifying cataracts from photographs. (b) Nuclear cataracts. (c) Posterior subcapsular cataracts. (d) Cortical cataracts. Courtesy of Dr. M. Datiles III and the National Eye Institute AREDS.

available. This necessitates the study of either, siblings, twins and parent-offspring trios, or genetically unrelated case-control cohorts of affected and unaffected individuals. Initially, studies of affected sibling-pairs revealed that a positive family history was strongly correlated with age-related nuclear and posterior subcapsular cataract (more thanthreefold increased risk), consistent with clustering of lens opacities within families due to genetic or environmental factors. Subsequently, affected sib-pair and twin studies indicated that genetic factors may directly account for 14–48% of the heritability for age-related nuclear cataract, and 24–75% of the heritability for age-related cortical cataract. However, the molecular identity of such genetic risk factors cannot be resolved by purely statistics-based approaches.

Genes Associated with Age-Related Cataract

In contrast to inherited congenital or childhood forms of cataracts, relatively few genes have been unambiguously associated with risk of age-related cataracts (Table 1). Several studies have taken a candidate gene approach in which genes are selected for investigation based on their known biological function and/or suspected dysfunction. Polymorphisms in the genes coding for the antioxidant enzymes known as glutathione-S-transferases (GSTs) have been variously associated with age-related cataract in different populations. Homozygous deletion of the GSTM1 gene (i.e., the null genotype) has been implicated in risk of age-related cataract in Japanese, Chinese, Iranian, and Turkish populations; however, no such association was replicated in Italian or Chinese populations. Notably, in the Iranian and Turkish studies the association of the GSTM1-null genotype was restricted to females, and in the latter study combination of the GSTM1-null and GSTT1-positive genotypes was associated with nuclear cataract in females. Conversely, the GSTM1-positive genotype, either alone or in combination with the GSTP1*A allele, was identified as a possible risk factor for age-related cortical cataract in an Estonian population. Thus, the association of GSTM1 with age-related cataract remains controversial.

The Osaka variant of the gene for galactokinase-1 (GALK1), which catalyzes the first step in galactose metabolism to glucose, has been detected at increased frequency (~7%) in a Japanese cohort with age-related cataract. This heterozygous protein coding variation involves an amino acid substitution (Ala198Val) that results in reduced stability of the variant enzyme and mild galactokinase deficiency equivalent to about 20% of normal levels. The Osaka variant was also present in Koreans (frequency 2.8%) but had a lower incidence in Chinese, and was not detected in blacks and whites from the United States or in a North Italian cohort with

Table 1 Summary of genes or loci associated with age-related cataracts

Chromosome	*Gene/locus*	*Protein function*	*Associated variant*	*Cataract type*	*Population*
1p36	*EPHA2*	Cell Signaling	rs11260867 rs7543472	Cortical Cortical/nuclear	Italian
1p36.3	*MTHFR*	Folate Metabolism	677C/C 1298A/A	Mixed	Estonian
1p13	*GSTM1*	Antioxidant Metabolism	Null Null Null Positive	? Nuclear (♀) Nuclear/mixed (♀) Cortical	Japanese Iranian Turkish Estonian
6p12-6q12	ARCC1	?	?	Cortical	Beaver Dam, WI
14q32.3	*KLC1*	Microtubule Motor Activity	rs8702	All types	Estonian
16q21	*HSF4*	Transcription Factor	Gln61Arg	Cortical	Chinese
17q24	*GALK1*	Glucose Metabolism	Ala198Val	?	Japanese Korean
19q13.3	*ERCC2/XPD*	DNA Repair	Lys751GLn	Cortical	Turkish

age-related cataract. These observations suggest that the genetic contribution to age-related cataract might vary in different populations. Interestingly, severe homozygous mutations in the GALK1 gene are usually associated with classic autosomal recessive galactokinase-1 deficiency and isolated congenital cataracts as a result of galactitol (a sugar alcohol) accumulation in the lens. These findings show that different variations in the GALK1 gene can contribute to both congenital and age-related forms of cataract – a principle that is also borne out by an increased incidence of pre-senile cataract in individuals (age range 20–55 years) heterozygous for GALK1 deficiency.

Sequence variations in the gene for heat-shock transcription factor-4 (HSF4) have been associated with age-related cortical cataract in a Chinese population. HSF4 regulates the expression of several heat shock proteins, including the abundant lens protein alphaB-crystallin, in response to elevated temperature and other stress stimuli such as photo-oxidation. Mutations affecting the protein coding regions, or exons, of the HSF4 gene have been shown to underlie autosomal dominant and autosomal recessive forms of familial cataract. Several of the HSF4 variants associated with age-related cataract were found within intervening sequences or introns, which are located between the protein coding exons of the gene. Other variants found within exons only resulted in silent changes that did not alter the amino acid composition of HSF4. However, two of the coding variants resulted in amino acid substitutions (Gln61Arg and Arg116His) that were predicted to impair the DNA binding activity of HSF4. Interestingly, one of the coding variants (Arg116His) was also found in two control subjects suggesting that it should be excluded as a risk variant for age-related cataract. However, both control subjects were aged in their mid-40s and may have been pre-symptomatic for age-related cataract. These studies highlight the necessity for acquiring well matched (age and gender, etc.) cases and controls for association studies of age-related cataract.

In addition to the arbitrary testing of candidate genes for association with age-related cataract, the first systematic scan of the human genome using linkage analysis of affected families and sibling-pairs, has recently mapped a number of major and minor susceptibility loci for age-related cortical cataract in whites from the United States. The most statistically significant loci were found on chromosome 6 (6p12-q12), and the short arm of chromosome 1 (1p36), with up to ten potential loci on eight other chromosomes. The disease interval on chromosome 6 spanned the centromere and contained a large number of positional-candidate genes (about 260) for age-related cataract; however, the identity of the susceptibility gene remains to be determined. The disease interval on chromosome 1p also contained a large number of positional-candidate genes (about 400). However, this region also appeared to overlap loci for inherited forms of childhood cataract that were associated with mutations in the gene coding for Eph-receptor type-A2 (EPHA2), which functions in the ephrin cell signaling and guidance pathway. Subsequent candidate gene association analysis identified single nucleotide polymorphisms (SNPs) in the EPHA2 region of chromosome 1 that were associated with age-related cortical cataract in an Italian population, further suggesting that EPHA2 variants may underlie both inherited and age-related forms of cataract.

Summary and Future Prospects

Beyond aging and certain environmental risk factors for age-related cataract, it is increasingly clear that genetic

risk factors are involved in this common multifactorial disease; however, their identity remains uncertain. The association of GST gene variants with age-related cataract, albeit inconsistent, supports the general belief that variants of genes that function in antioxidant metabolism, especially to combat photo-oxidative stress, are likely to be involved in age-related cataract. The association of GALK1, HSF4, and EPHA2 gene variants with age-related cataract further raises the likelihood that genes underlying inherited forms of cataract also contribute to age-related cataract. In addition, variants of several other genes involved in diverse biological functions have been tentatively implicated in age-related cataract; including those mediating estrogen metabolism, systemic inflammation, DNA repair, folate metabolism, and kinesin motor transport. Further replication and validation studies of these genes, coupled with functional expression studies of their variant proteins, will be required to substantiate their role in age-related cataractogenesis. However, it is likely that all of the currently implicated genes will account for a relatively small percentage of the genetic risk for age-related cataract.

In the future, family-based linkage studies and case-control association studies will continue to identify, test, and validate candidate genes for age-related cataract. In addition, the advent of whole genome sequencing techniques capable of deciphering genetic variation in large numbers of individuals will provide powerful insights regarding the molecular genetic basis of age-related cataract. Ultimately, a molecular genetic understanding of age-related cataract may aid the design of targeted drugs to help treat and manage cataract, thereby reducing the need for surgery, and permit better evaluation of environmental risk factors in order to promote lifestyle interventions (e.g., diet) that help to delay or even prevent cataract onset.

Acknowledgments

We thank Dr. M. Datiles III and the National Eye Institute AREDS for generously sharing the images.

See also: Genetics of Congenital Cataract.

Further Reading

Andersson, M. E., Zetterberg, M., Tasa, G., et al. (2007). Variability in the kinesin light chain 1 gene may influence risk of age-related cataract. *Molecular Vision* 13: 993–996.

Asbell, P. A., Dualan, I., Mindel, J., et al. (2005). Age-related cataract. *Lancet* 365: 599–609.

Güven, M., Unal, M., Sarici, A., et al. (2007). Glutathione-S-transferase M1 and T1 genetic polymorphisms and the risk of cataract development: A study in the Turkish population. *Current Eye Research* 32: 447–454.

Hejtmancik, J. F. and Kantorow, M. (2004). Molecular genetics of age-related cataract. *Experimental Eye Research* 79: 3–9.

Iyengar, S. K., Klein, B. E., Klein, R., et al. (2004). Identification of a major locus for age-related cortical cataract on chromosome 6p12-q12 in the Beaver Dam Eye Study. *Proceedings of the National Academy of Sciences of the United States of America* 101: 14485–14490.

Klein, B. E., Klein, R., Lee, K. E., Knudtson, M. D., and Tsai, M. Y. (2006). Markers of inflammation, vascular endothelial dysfunction, and age-related cataract. *American Journal of Ophthalmology* 141: 116–122.

Lee, S. M., Tseng, L. M., Li, A. F., et al. (2004). Polymorphism of estrogen metabolism genes and cataract. *Medical Hypotheses* 63: 494–497.

McCarty, C. A. and Taylor, H. R. (2001). The genetics of cataract. *Investigative Ophthalmology and Visual Science* 42: 1677–1678.

Okano, Y., Asada, M., Fujimoto, A., et al. (2001). A genetic factor for age-related cataract: Identification and characterization of a novel galactokinase variant, ''Osaka,'' in Asians. *American Journal of Human Genetics* 68: 1036–1042.

Shi, Y., Shi, X., Jin, Y., et al. (2008). Mutation screening of HSF4 in 150 age-related cataract patients. *Molecular Vision* 14: 1850–1855.

Shiels, A., Bennett, T. M., Knopf, H. L., et al. (2008). The EPHA2 gene is associated with cataracts linked to chromosome 1p. *Molecular Vision* 14: 2042–2055.

Sperduto, R. D., Clemons, T. E., Lindblad, A. S., and Ferris, F. L., III (2008). Age-Related Eye Disease Study Research Group. Cataract classification using serial examinations in the age-related eye disease study: Age-related eye disease study report no. 24. *American Journal of Ophthalmology* 145: 504–508.

Unal, M., Güven, M., Batar, B., et al. (2007). Polymorphisms of DNA repair genes XPD and XRCC1 and risk of cataract development. *Experimental Eye Research* 85: 328–334.

Zetterberg, M., Tasa, G., Prince, J. A., et al. (2005). Methylenetetrahydrofolate reductase genetic polymorphisms in patients with cataract. *American Journal of Ophthalmology* 140: 932–934.

Zhang, T., Hua, R., Xiao, W., et al. (2009). Mutations of the EPHA2 receptor tyrosine kinase gene cause autosomal dominant congenital cataract. *Human Mutation*.

Relevant Websites

http://www.nei.nih.gov – National Eye Institute (NEI) of the United States.
http://www.preventblindness.org – Prevent Blindness America.
http://www.who.int – World Health organization (WHO).

Genetics of Congenital Cataract

A Shiels, Washington University School of Medicine, St. Louis, MO, USA
J F Hejtmancik, National Eye Institute, Bethesda, MD, USA

Published by Elsevier Ltd.

Glossary

Anterior segment of eye – The front part of the eyeball including the sclera, conjunctiva, cornea, anterior chamber, iris, and lens.
Genotype – The genetic makeup of an organism with reference to a single trait, a set of traits, or an entire complex of traits.
Lens crystallin – The structural proteins of the eye lens that contribute to transparency by providing a constant refractive index.
Mendelian – In accord with Gregor Mendel's laws including independent assortment. A Mendelian trait is one that is controlled by a single locus in either a dominant or recessive fashion.
Phenotype – The physical appearance of an organism or part of an organism as distinguished from its genetic makeup.
Transcription factor – A protein that binds to specific parts of DNA using DNA-binding domains and controls the transfer (or transcription) of genetic information from DNA to RNA.

Introduction

Definition

The human lens is derived from surface ectoderm that begins to thicken and forms the lens placode, then invaginates toward the developing optic cup to form the lens pit. The lens pit closes, and the resulting lens vesicle is pinched off from surface ectoderm. The resulting lens can first be detected at 3–4 weeks of gestation. Cells along the posterior layer of the optic vesicle elongate to fill the vesicle by the seventh week of development and become primary fiber cells. These eventually become the embryonic lens nucleus (the central nonnucleated fiber cells). The remaining cells become the cuboidal anterior epithelium, some of which divide and differentiate to become secondary fibers. Fiber cells make up the bulk of the lens. Layers of nucleated cortical fiber cells form highly ordered concentric shells around the nonnucleated central fiber cells which make up the lens nucleus. The ends of the more peripheral fiber cells abut in branched anterior and posterior sutures (**Figure 1**).

Cataract can be defined as any opacity of the crystalline lens. Lens opacity results when the refractive index of the lens varies significantly over distances approximating the wavelength of the transmitted light. Changes in either lens cell structure or lens protein constituents or both can cause variation in the refractive index sufficient to cause opacity. The cellular architecture of the fiber cells and, particularly, their sutures is important for light transmission and lens transparency. There is little extracellular space between the fiber cells, which have many interdigitations. Cataracts can be associated with breakdown of the lens microarchitecture, including vacuole formation, cell dysplasia or degradation, or death. High-molecular-weight protein aggregates, roughly 1000 Å or more in size can also result in light scattering and opacity. The short-range ordered packing of the crystallins, which make up over 90% of soluble lens proteins, is important for the maintenance of lens transparency, as are the support systems that keep the lens in a reduced state under osmotic and ionic equilibrium.

Cataract can be defined by age at onset. A congenital or infantile cataract is visible within the first year of life. A juvenile cataract appears within the first decade of life, and a presenile cataract occurs before the age of 45 years. The boundaries between different types of cataract are approximate. Moreover, subtle cataracts might not be seen for years after they occur, especially if they are asymptomatic. The age of onset of a cataract does not necessarily indicate its etiology. Congenital cataracts may be hereditary or secondary to a prenatal infection (e.g., rubella), and cataracts associated with a systemic or genetic disease such as retinitis pigmentosa may not occur until the second or third decade.

It seems likely that when mutations in crystallins or other lens proteins are sufficient in and of themselves to cause protein aggregation they usually result in congenital cataract, while if they merely increase susceptibility to environmental insults, such as light, hyperglycemia, or oxidative damage, they might contribute to age-related cataract. Thus, hereditary congenital cataracts tend to be inherited in a Mendelian fashion with high penetrance, making them significantly more amenable to genetic and biochemical study.

Overview

Between 8.3% and 25% of congenital cataracts are estimated to be inherited, depending to some extent on the

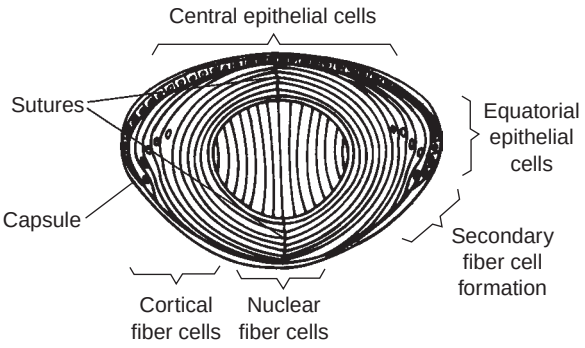

Figure 1 Simplified structure of the adult lens.

population studied. Inherited cataracts may involve the lens alone, or may be associated with other ocular anomalies including microphthalmia (abnormally small eyes), aniridia (underdevelopment of the iris), and other anterior chamber developmental anomalies. For example, mutations in the transcription factors PITX3 or FOXC1 can cause cataracts associated with anterior segment mesenchymal dysgenesis (heterogeneous group of complex diseases including aniridia). Cataracts may also be part of multisystem genetic disorders such as chromosome abnormalities, Lowe syndrome, or neurofibromatosis type 2. In some cases, this distinction is blurred. Inherited cataracts may be isolated and mild in some individuals and associated with additional findings in others, as in the developmental abnormality anterior segment mesenchymal dysgenesis including corneal opacification and optic nerve atrophy resulting from abnormalities in the PITX3 gene 6. The most frequent inheritance pattern for Mendelian cataracts is autosomal dominant, although they can also be inherited as autosomal recessive or X-linked traits. It is difficult to derive phenotype–genotype relationships for congenital cataracts.

Phenotypically identical cataracts can result from mutations at different genetic loci and may have different inheritance patterns. Conversely, phenotypically variable cataracts can be found in a single large family. The most common classification system which has been developed based on the anatomic location and morphologic appearance of the opacity is that of Merin. In this system, polar opacities involve either the anterior or posterior pole of the lens and may include the posterior subcapsular lens cortex (PSC) extending to the lens capsule. Zonular cataracts include specific regions of the lens and include nuclear cataracts, which affect the fetal or embryonic lens nucleus and lamellar cataracts. Nuclear lamellar cataracts tend to affect lens fibers that are formed at the same time, resulting in a shell-like opacity. Zonular cataracts can also be characterized as dense or pulverulent (dusty appearing), and can be accompanied by arcuate opacities extending into the lens cortex, called cortical riders. Sutural cataracts, also called stellate, affect the sutural regions of the fetal nucleus, at which the ends of the lens fiber cells converge. Cerulean cataracts, also called blue-dot cataracts, have numerous small bluish opacities in the lens cortex and nucleus. Finally, membranous or capsular cataracts can result from resorption of lens proteins after capsular rupture, often from a traumatized or severely dysfunctional lens. In addition, there are a number of morphologically distinctive types of cataract such as the ant egg cataract and corraliform cataracts that are not well described by the above system. Total (mature or complete) cataracts can often occur as the end result of a process that began as one of the above cataract types, and capsular or membranous cataracts can result from resorption of lens proteins after capsular rupture (**Figure 2**).

Most mutant genes responsible for congenital cataracts have been identified by a combination of linkage analysis and screening candidate genes for mutations. Linkage analysis, a powerful tool to sort out the different genetic loci which can cause human cataracts, localizes mutant genes causing inherited cataracts to a specific chromosomal region by comparing their inheritance patterns to those of known genetic markers. Usually candidate genes in this region are sequenced in order of the perceived likelihood of their involvement. New analytical approaches, using homozygosity mapping methods to identify genomic regions identical by descent, promise to be increasingly useful in studying rare autosomal recessive cataracts from isolated populations.

Genetic Causes of Congenital Cataract

Isolated Congenital Cataract

Currently there are about 41 genetic loci to which isolated or primary cataracts have been mapped (**Table 1**), although the number is constantly increasing. Of these, eight are associated with additional abnormalities, primarily in the anterior chamber of the eye. Two notable exceptions are cataracts associated with the αB-crystallin gene, mutations in which can cause either isolated cataracts or cataracts associated with myopathy, and the ferritin light chain gene, which causes the hyperferritinemia-cataract syndrome (**Table 1**). With the exception of heat-shock transcription factor 4 (HSF4), most inherited cataracts caused by mutations in growth or transcription factors can be associated with extralenticular abnormalities. In some cases including some connexin 50, αA-, and γD-crystallin mutations, inherited congenital cataracts are associated with microcornea and even microphthalmia, although this may represent early severe disruption of the lens with consequent effects on anterior chamber and eye development.

Of the mapped isolated congenital or infantile cataract loci, over 25 have been associated with mutations in specific genes. Of the cataract families for whom the mutant gene is known, about 40% have mutations in crystallins,

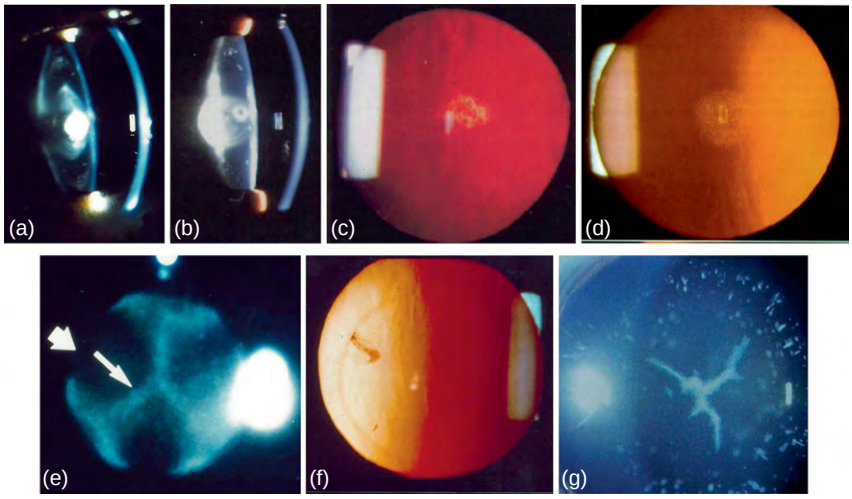

Figure 2 Examples of various types of cataract: (a) anterior polar cataract, (b) posterior polar cataract, (c) posterior subcapsular cataract, (d) pulverulent nuclear cataract, (e) sutural cataract showing the outline of the lens nucleus (broad arrow) and the sutural opacity (narrow arrow), (f) nuclear lamellar cataract with a cortical rider at 10 o'clock, and (g) cerulean (blue dot) cataract also showing a sutural opacity.

Table 1 Summary of genes and loci for inherited cataracts

Chromosome	*Gene/locus*	*Inheritance*	*No. of mutations*	*OMIM no.*
1p	CCV	AD	?	115665
	CTPP1	AD	?	116600
	FOXE3	AD	1	601094
1q	GJA8	AD, AR	16	600897
2q	CRYGC	AD	3	123680
	CRYGD	AD	10	123690
3q	BFSP2	AD	2	603212
	CRYGS	AD	1	123730
6p	GCNT2	AR	4	600429
9q	CAAR	AR	?	605749
10q	SLC16A12	AD	1	611910
	PITX3	AD	3	602669
11q	CRYAB	AD	4	123590
12q	MIP	AD	5	154050
13q	GJA3	AD	14	121015
14q	CTPP5	AD	?	610634
15q	CCSSO	AD	?	605728
16p	TMEM114	AD	3	611579
16q	HSF4	AD, AR	8	602438
	MAF	AD	4	177075
17p	CTAA2	AD	?	601202
17q	CRYBA3/A1	AD	3	123610
	GALK1	AR	>20	604313
19q	FTL	AD	>20	134790
	LIM2	AR	2	154045
20p	BFSP1	AR	1	603307
20q	CHMP4B	AD	2	610897
21q	CRYAA	AD, AR	9	123580
22q	CRYBB1	AD, AR	5	600929
	CRYBB2	AD	3	123620
	CRYBB3	AR	1	123630
	CRYBA4	AD	2	123631
Xp	CCT	XL	?	302200
	NHS	XL	15	302350

about 17% have mutations in connexins, with the remainder largely split between the genes for transcription factors (including HSF4, NHS, macrophage activating factor (MAF), VSX2, PITX3, and eyes absent homolog 1 (EYA1), 20%), aquaporin-0 (AQP0, MIP, 3%), and beaded filament structural protein-2 (BFSP2, 3%). The remaining represents mutations in a group of other unrelated genes (5%) or are currently unknown (19%).

Phenotype–Genotype Correlations

Overall, it is difficult to draw phenotype–genotype correlations for congenital cataracts. However, the limited experience available suggests some rules of thumb, as described below. However, inheritance of the same mutation in different families or even the same mutation within the same family can result in radically different cataract morphologies and severities. This suggests that additional genes or environmental factors might modify the expression of the primary mutation associated with the cataracts. Conversely, cataracts with similar or identical clinical presentations can result from mutations in quite different genes, perhaps reflecting the limited spectrum of responses of the lens cells to a variety of insults.

Specific Genes Implicated in Congenital Cataracts

α-Crystallins

In addition to being of clinical interest, examination of the genes implicated in congenital cataracts and the resultant lens pathology provide insight into those biological pathways important for lens transparency. Mutations in the αA-crystallin gene have been implicated in both autosomal recessive and dominant cataracts. The autosomal recessive cataracts are associated with a chain-termination mutation near the beginning of the protein, which would be expected to cause loss of function of the mutant protein without affecting protein synthesized from the normal gene. The viewpoint that heterozygotes have clear lenses suggests that half the normal levels of α-crystallin provide sufficient chaperone-like activity and structural crystallin packing to establish and maintain lens transparency. Autosomal dominant cataracts result from nonconservative missense mutations in the αA-crystallin gene. These presumably cause cataracts by the mutant αA-crystallin protein exerting a deleterious effect that actively damages the lens cell or its constituent proteins, or inhibits the function of the remaining normal α-crystallin, rather than acting through loss of chaperone or structural function as the recessive cataract appears to do.

The αA- and αB-crystallins are found in the lens associated together into large multimeric complexes and function similarly *in vitro* as chaperones. This might suggest that mutations in αB-crystallin would behave similarly to those in αA-crystallin, at least in the lens. However, the first human mutation reported in αB-crystallin, a missense mutation that reduces αB-crystallin chaperone activity dramatically and causes aggregation and precipitation of the protein under stress, was associated with desmin-related myopathy and only discrete cataracts. The myopathy associated with this mutation is probably related to the expression of αB-crystallin, but not αA-crystallin, in muscle cells. In these cells αA-crystallin, binds and presumably stabilizes desmin. Similarly, an αB-crystallin knockout mouse exhibits myopathy without cataracts, confirming that αB-crystallin is necessary for normal myocyte function. However, a deletion in the αB-crystallin gene resulting in a frameshift and expression of an aberrant 184-aminoacid protein causes autosomal dominant cataracts in the absence of myopathy. This is consistent with the dominant αA-crystallin-associated cataract in which the aberrant protein is likely to have a toxic effect on the lens cells. Both αA- and αB-crystallin mutations tend to be associated with nuclear or nuclear lamellar or on occasion posterior polar cataracts.

βγ-Crystallins

Most mutations described in the βγ-crystallins would be expected to cause major abnormalities in the protein structure, presumably resulting in an unstable protein. This then precipitates from solution and serves as a nidus for additional protein denaturation and precipitation, perhaps in some cases as an amyloid-type fibril. This process overcomes the chaperone activity of the α-crystallins and results in cataract formation. The specific mutations include missense mutations, insertions changing the reading frame and causing expression of aberrant peptides with premature termination, and splice. Although phenotypes can vary significantly, mutations in γ-crystallins tend to produce nuclear or nuclear lamellar cataracts, consistent with their high level of expression in the lens nucleus. The cataract phenotypes reported with mutations in the β-crystallins is somewhat more varied, ranging in different families and even individuals within families from zonular pulverulent with or without involvement of the sutures to cerulean cataracts. These cataracts can also be progressive in nature. This variability emphasizes the importance of modifying genes or perhaps random developmental events in the phenotypic expression of these mutations. In contrast to those mutations that produce unstable proteins, two mutations in γD-crystallin have been shown not to alter the protein fold, but rather to alter the surface characteristics of the protein, lowering the solubility and enhancing the crystal nucleation rate so that they precipitate out of solution, in at least one case actually forming crystals in the lens. Similarly, a third mutation, the protein also maintains a normal protein fold, but is susceptible to thiol-mediated

aggregation. Thus, βγ-crystallins need not undergo denaturation or other major changes in their protein folds to cause cataracts.

Feritin Light Chain

In the hyperferritinemia-cataract syndrome, cataracts are associated with hyperferritinemia without iron overload. The ferritin L iron-responsive element, a stem-loop structure in the 5′-untranslated region of the ferritin messenger RNA (mRNA) normally binds a cytoplasmic protein, the iron regulatory protein, which then inhibits translation of ferritin mRNA. Mutations in this structure and overexpression of ferritin by loss of translational control result in ferritin L (light chain) levels in the lens increasing to levels approaching those of a crystallin. This results in crystallization of ferritin in the lens, similar to that described above for certain γD-crystallin mutations, and the appearance of breadcrumb-like opacities in the cortex and nucleus. Both of these emphasize the necessity for crystallins or other proteins to be exceptionally soluble to be expressed at such high levels in the lens without causing dysfunction.

Connexins

The avascular lens depends on gap junctions with their constituent proteins connexins 46 and 50 are for nutrition and intercellular communication, and mutations in either gene often result in nuclear or nuclear lamellar cataracts. At least one cataract-associated mutation in the connexin 50 gene has been shown to result in a connexin that fails to form functional gap-junctional channels with incorporation of even a single mutant protein molecule into a gap-junction-inhibiting channel function. Two mutations in connexin 46 also fail to form intercellular channels; however, these mutant connexins are not able to participate in gap-junction formation at all, indicating that inhibition of channel function by products of the normal gene is not necessary for cataract formation. Mutations in connexin 50 can also be associated with microcornea.

Membrane Proteins

In addition to connexins, a diverse group of other membrane proteins has been associated with early-onset cataracts. Lamellar, sutural, and polymorphic cataracts, often progressive, have been associated with mutations in the aquaporin-0 gene (AQP0, MIP), which codes for a water channel that represents the most abundant intrinsic membrane protein in the lens. Two missense mutations have been shown to act by interfering with normal trafficking of AQP0 to the plasma membrane and thus with water-channel activity. In addition, both mutant proteins appear to interfere with water-channel activity by normal AQP0, consistent with a dominant-negative mechanism for the autosomal dominant inheritance of the cataracts. Mutations in LIM2, the second most abundant intrinsic membrane protein of the lens fiber cells, have been described as causing either presenile cortical and nuclear sutural cataracts or severe congenital total autosomal recessive congenital cataracts. Similarly, mutations in TMEM114, a transmembrane protein homolog of LIM2, have been associated with congenital lamellar cataracts, and mutation of the gene for a solute transporter protein (SLC16A12) has been associated with juvenile cataracts, microcornea, and renal glucosuria. Finally, mutations in the gene for a charged multivesicular body protein (CHMP4B), a membrane-associated component of the endosome sorting complex, has been linked with autosomal dominant posterior polar cataracts.

Beaded Filament-Specific Proteins

Beaded filaments are a type of intermediate filament unique to the lens fiber cells in which they replace vimentin filaments in the epithelial and elongating cortical cells. They are made up of BFSP1 (also called CP115 or filensin) and BFSP2 (also called CP49 or phakinin), highly divergent intermediate filament proteins that combine in the presence of α-crystallin to form the appropriate beaded structure. Cataracts associated with mutations in BFSP2 are often nuclear with a sutural component and progressive in nature, consistent with fiber-cell-specific expression of the beaded filament proteins. In contrast, a family with a frameshift mutation in BFSP1 shows fluffy and cystic cortical cataracts requiring surgery in early childhood.

Transcription Factors

Mutations in a number of transcription factors can also cause congenital cataracts. HSF4 is a member of the HSF family, members of which regulate expression of heat-shock proteins, including lens αB-crystallin, in response to elevated temperature and other stress stimuli (e.g., oxidation). Mutations in HSF4 have been associated with both autosomal dominant and recessive cataracts. The dominant cataracts tend to present in early childhood are described as total, lamellar, or stellate with an anterior polar component, including the historically important Marner cataract. Recessive cataracts tend to have a congenital or early childhood onset and range in severity from nuclear with some cortical involvement to total lens opacities. Interestingly, the dominant mutations in HSF4 lie within the α-helical DNA-binding domain, whereas the recessive mutations lie outside this highly conserved functional domain. Mutations in many other growth factors tend to be associated with extralenticular findings, including anterior segment mesenchymal dysgenesis (ASMD). Mutations in FOXE3 and PITX3 have been associated with ASMD and cataracts. EYA1 has been associated with ASMD and

cataracts as well as BOR, central corneal opacity, and Peter anomaly. Mutations in VSX2 have been associated with cataracts and microphthalmia, inferior iris coloboma, and absence of papillary apertures, and mutations in MAF with cataracts, microcornea, and iris coloboma. Finally, mutations in NHS are usually associated with total congenital cataracts with the dental anomalies and dysmorphic features that make up the Nance Horan syndrome.

Enzymes

Two genes for enzymes involved in diverse aspects of carbohydrate metabolism have been associated with autosomal recessive forms of congenital cataracts. Mutations in GALK1, which encodes the first enzyme in galactose metabolism, underlie galactokinase-deficiency cataracts, which may be treated by dietary, rather than surgical, intervention. Second, homozygous mutations in the gene for glucosaminyl (*N*-acetyl) transferase-2 (*GCNT2*), a blood group (Ii) glycosylation enzyme, result in persistence of the fetal I-antigen on red blood cells. This failure to synthesize the adult I-antigen has been associated with congenital cataracts in Asian and Arab families.

Current State of Knowledge and Future

While the eye lens is appealing as a relatively simple system with only epithelial and fiber cells, both derived from one progenitor cell type, it is still a remarkably complex tissue. This is reflected by the large number of genes which, when mutated, can cause cataract. While it has been estimated that there are 30 autosomal dominant congenital cataract loci in man, the number of currently identified loci is well past that figure. This in part reflects the complex systems required to maintain lens transparency over the lifetime of an organism. However, not all proteins necessary for lens transparency are common causes of cataracts in all populations. For example, while some studies suggest that crystallin and connexin mutations, the two most frequently found groups of mutant genes in families reported to date, account for as much as 75% of familial childhood cataracts in a European population, others in Indian and Australian populations suggest that the figure might be much lower. It seems likely that each population might have its own set of genes responsible for congenital cataracts, and that at least some largely remain to be delineated.

See also: Genetics of Age-Related Cataract.

Further Reading

Amaya, L., Taylor, D., Russell-Eggitt, I., Nischal, K. K., and Lengyel, D. (2003). The morphology and natural history of childhood cataracts. *Survey of Ophthalmology* 48: 125–144.

Benedek, G. B. (1971). Theory of transparency of the eye. *Applied Optics* 10: 459–473.

Francis, P. J., Berry, V., Bhattacharya, S. S., and Moore, A. T. (2000). The genetics of childhood cataract. *Journal of Medical Genetics* 37: 481–488.

Graw, J. (2004). Congenital hereditary cataracts. *International Journal of Developmental Biology* 48: 1031–1044.

Haargaard, B., Wohlfahrt, J., Fledelius, H. C., Rosenberg, T., and Melbye, M. (2004). A nationwide Danish study of 1027 cases of congenital/infantile cataracts: Etiological and clinical classifications. *Ophthalmology* 111: 2292–2298.

Hejtmancik, J. F., Kaiser-Kupfer, M. I., and Piatigorsky, J. (2003). Molecular biology and inherited disorders of the eye lens. In: Scriver, C. R., Beaudet, A. L., Valle, D., Sly, W. S., Childs, B., Kinzler, K. W., and Vogelstein, B. (eds.) *The Metabolic and Molecular Basis of Inherited Disease,* 9th edn., pp. 6033–6062. New York: McGraw Hill.

Merin, S. (1991). Inherited cataracts. In: Merin, S. (ed.) *Inherited Eye Diseases*, pp. 86–120. New York: Marcel Dekker.

Shiels, A. and Hejtmancik, J. F. (2007). Genetic origins of cataract. *Archives of Ophthalmology* 125: 165–173.

Relevant Websites

http://www.dsi.univ-paris5.fr – GENATLAS (Université René Descartes, Paris).

http://www.ncbi.nlm.nih.gov – Online Mendelian Inheritance in man (OMIM).

http://www.ncbi.nlm.nih.gov – National Center for Biotechnology Information (NCBI).

http://www.genome.ucsc.edu – UCSC Genome Bioinformatics.

Glutamate Receptors in Retina

M M Slaughter, University at Buffalo School of Medicine, Buffalo, NY, USA

Glossary

Alpha-amino-3-hydroxy-5-methyl-4-isoxazolepropionic acid (AMPA) – A ligand for ionotropic glutamate receptors mediating fast synaptic transmission. AMPA is also used as the name of the receptor.
D-2-Amino-5-phosphonovalerate (D-AP5) – An antagonist at NMDA glutamate receptors.
D-(-)-2-Amino-7-phosphonoheptanoic acid (D-AP7) – An antagonist at NMDA glutamate receptors.
(5R,10S)-(-)-5-Methyl-10,11-dihydro-5H-dibenzo [a,d]cylc ohepten-5,10-imine maleate (MK801) – A noncompetitive antagonist at NMDA-type glutamate receptors.
Glutamate receptors (GluRs) – The receptors that bind and respond to the excitatory amino acid transmitter, L-glutamate. They fall under two classes called ionotropic and metabotropic. Ionotropic receptors are composed of multiple subunits and are named after pharmacological agents (NMDA, kainate, AMPA) that activate them. Metabotropic receptors are generally guanine-nucleotide-binding protein (G-protein)-coupled receptors.
Metabotropic glutamate receptors (mGluRs) – The glutamate receptors that act through an indirect or metabotropic mechanism. They are members of the class of guanine-nucleotide-binding protein (G-protein)-coupled receptors.
***N*-methyl-D-aspartic acid (NMDA)** – An agonist binding to ionotropic glutamate receptors. The receptors themselves are generally referred to as NMDA receptors.
(RS)-α-Cyclopropyl-4-phosphonophenylglycine (CPPG) – An antagonist of group III metabotropic glutamate receptors in the retina.
6-Cyano-7-nitroquinoxaline-2,3-dione (CNQX) – An antagonist of AMPA and kainate glutamate receptors.
6,7-Dinitroquinoxaline-2,3-dione (DNQX) – An antagonist of AMPA and kainate glutamate receptors.
2-Amino-4 phosphonobutyric acid (APB, AP4) – The selective agonist for group III metabotropic glutamate receptors in the retina.
(2S)-2-Amino-2-[(1S,2S)-2-carboxycycloprop-1-yl]-3-(xan th-9-yl) propanoic acid (LY341495) – An antagonist for group III metabotropic glutamate receptors in the retina.
2,3-Dioxo-6-nitro-1,2,3,4-tetrahydrobenzo[f] quinoxaline-7-sulfonamide (NBQX) – An antagonist of AMPA and kainate glutamate receptors.

Glutamate Pathways

Glutamate serves as the primary excitatory neurotransmitter in both plexiform layers of the retina. Rods and cones release glutamate, which activates postsynaptic, metabotropic receptors on the ON bipolar cells and alpha-amino-3-hydroxy-5-methyl-4-isoxazolepropionic acid (AMPA)/kainic acid (KA) ionotropic receptors on horizontal and OFF bipolar cells. In turn, both ON and OFF bipolar cells release glutamate, which excites amacrine and ganglion cells by activating AMPA/KA and *N*-methyl-D-aspartic acid (NMDA) receptors. Finally, ganglion cells also use glutamate to excite neurons in visual centers throughout the brain. Thus, glutamate mediates the entire straight-line synaptic circuit in retina. In addition, there are metabotropic glutamate receptors that modulate voltage-activated calcium channels at each of these synapses, generally serving to suppress transmitter release.

The retina has exemplified a number of unique features of glutamate receptors. These include the exclusive utilization of metabotropic receptors to form a sign-inverting synapse, the complexity of desensitization in signal coding, the direct control of neurotransmitter release by ionotropic glutamate receptors, and information encoding by glutamate receptor subtypes.

Glutamate Receptor Pharmacology

Retina possesses AMPA, kainate, NMDA, as well as several metabotropic glutamate receptors. The first three, ionotropic receptors, are tetramers. The AMPA receptors are made from four glutamate receptor subunits (GluR1–4), with additional variability added by splice variants. The kainate (KA) receptors are formed from GluR5–7 and KA1&2 subunits. The NMDA receptors contain NR1, NR2, and NR3 subunits, again with variations. Eight metabotropic glutamate receptors have been identified and divided into three groups based on sequence homology. They likely exist as dimers.

One means of separating receptors is the use of pharmacological agents. This works best for NMDA receptors, where its namesake (*N*-methyl-D-aspartate) is a very selective agonist, and there are reasonably selective and potent antagonists such as D-AP5, D-AP7, and MK-801. AMPA and kainate receptors are difficult to separate. For example, kainate is actually a better agonist at AMPA receptors than is AMPA, because it does not desensitize the receptor as much. There are a number of antagonists that block AMPA/kainate receptors selectively, not affecting NMDA receptors, such as 6-cyano-7-nitroquinoxaline-2,3-dione (CNQX), 2,3-dihydroxy-6-nitro-7-sulfamoyl-benzo[f] quinoxaline-2,3-dione (NBQX), and 6,7-dinitroquinoxaline-2,3-dione (DNQX). However, these antagonists do not discriminate between AMPA and kainate receptors. Sometimes agents that block desensitization are used to distinguish between KA and AMPA receptors, notably cyclothiazide, which reduces AMPAR desensitization.

Among the metabotropic receptors, there is a very good selective agonist for group III receptors (L-AP4, also called 2-amino-4 phosphonobutyric acid (APB)), which is important in retina. There are also several reasonable antagonists, including (RS)-α-cyclopropyl-4-phosphonophenylglycine (CPPG) and LY341495. There are selective agonists and antagonists for the groups I and II as well, but they are not as effective.

Glutamate Receptors in Distal Retina

The glutamate receptors postsynaptic to photoreceptors present an instructive example of information processing by receptor specialization. The ON and OFF bipolar cells read the output of photoreceptors but respond oppositely. The OFF bipolar and horizontal cells use ionotropic AMPA and kainate receptors to follow the voltage polarity of photoreceptors. However, the ON bipolar cells utilize metabotropic glutamate receptors to produce a sign-inverting synapse. In each case, receptor desensitization produces tonic and phasic responses.

The ON Bipolar Cell Metabotropic Glutamate Receptor

Metabotropic glutamate receptors are omnipresent in retina. The most striking member is the mGluR6 metabotropic receptor, which is exclusively localized at ON bipolar cell dendrites and inverts the polarity of photoreceptor light responses. The ON pathway in vision, conveyed by half the visual pathways throughout the brain, originates at this synaptic receptor. The mGluR6 is selectively activated by 2-amino-4-phosphonobutyrate (APB, AP4) and is linked to a pertussis-toxin-sensitive G-protein cascade. L-AP4 activates all of the group III metabotropic receptors, found in many retinal neurons. However, its effect in eliminating light responses of ON bipolar cells is so prominent, and its effects at other group III receptors so subtle, that it is used as a selective agonist for the ON bipolar synapse. The activation of the mGluR6 activates guanine-nucleotide-binding proteins (G proteins) of the Go type, leading to closure of cationic channels and hyperpolariztion of ON bipolar cells. This is analogous to the effect of rhodopsin activation in photoreceptors, which initially led to the erroneous assumption that the transduction mechanisms were similar. Instead, cyclic guanosine monophosphate (cGMP) potentiates the postsynaptic response to light and may be particularly important in the detection of responses to dim light. Calcium has the opposite effect: by activating calcineurin, it reduces postsynaptic responses to light (the removal of glutamate). Consequently, ON bipolar cell light responses have a peak and then a plateau phase due to the negative effect of calcium influx during the light response. There are two types of ON bipolar cell: one in which the plateau phase is about half the peak response and another type in which the plateau is only about 10% of the peak. Furthermore, these two types of bipolar cells can be correlated with sustained and transient ganglion cells, respectively. Thus, the rate and extent of desensitization of the mGluR6 pathway account for the transient and sustained pathways throughout the ON system.

Fish ON bipolar cell dendrites possess an APB-sensitive metabotropic receptor and a glutamate transporter that gates a chloride channel. The former produces a glutamate-induced hyperpolarization due to a conductance decrease in a cationic channel, while the latter induces a conductance increase in a chloride channel. Rods relay information through metabotropic receptors, while cones utilize the transporter channel.

The OFF Bipolar Cell AMPA and Kainate Receptors

AMPA receptors dominate the dendritic synapses of OFF bipolar and horizontal cells, with a smaller contribution from kainate receptors. Curiously, NMDA receptors are absent. Kainate and AMPA receptors generally desensitize rapidly, an apparent paradox at a synapse with tonic transmitter release. One explanation is that a specific synaptic release site is used so infrequently that desensitized receptors can fully recover before they are likely to be recruited again. However, it has also been found that subtypes of OFF bipolar cell have glutamate receptors with widely differing desensitization rates, indicating that desensitization can be an important information mechanism in labeled lines of the OFF pathway.

In the all-cone ground squirrel retina, there are three types of OFF bipolar cell and each has a distinct AMPA or kainate receptor with discrete desensitization properties. The time course of desensitization filters the photoreceptor

signal both by truncating the response to glutamate during desensitization and by reducing the responsiveness to ensuing glutamate inputs. This is postulated to prevent receptor saturation and ensure that the OFF bipolar cells can follow the full dynamic range of the cones.

In an additional layer of processing, the AMPA-containing and kainate-containing OFF bipolar cells sense very different glutamate levels. One type of OFF bipolar cell sends its dendrites into the synaptic invagination and responds to high concentrations of glutamate with a rapidly desensitizing AMPA receptor that produces transient responses. The dendrites of a second bipolar cell type are at basal synapses further from the glutamate release site, detect smaller and more gradually changing levels of glutamate, and produce sustained responses through activation of kainate receptors.

Glutamatergic Feedback to Photoreceptors

Photoreceptor presynaptic output can be suppressed by glutamate acting on either metabotropic receptors or transporter-associated channels. These receptors may mediate autoreceptor negative feedback or lateral inhibition from other photoreceptors. Metabotropic group II receptors suppress the output of both rods and cones. The mGluR8, a member of the group III family, has also been found in photoreceptor terminals where it suppresses calcium currents, a mechanism to reduce photoreceptor output.

In addition, glutamate activates a transporter in salamander rods and cones. This transporter protein contains a chloride channel so that it can perform the dual functions of an ionic channel and an amino acid carrier. From noise analysis in cones the single-channel conductance is very low (0.7 pS) and opens briefly (mean openings are 2 ms), yet high glutamate levels shut the terminal and suppress calcium influx in cones.

These two feedback systems may mediate different pathways. They likely have different glutamate sensitivities; metabotropic receptors respond to low micromolar concentrations, while the transporter is active when glutamate levels approach millimolar concentrations.

Modulation of Glutamate Receptors

Postsynaptic ionotropic glutamate receptors in distal retina can be modulated by two mechanisms. One is suppression by zinc, which is apparently released by photoreceptors. The AMPA receptors in horizontal cells are suppressed by zinc, although the physiological impact is unclear because the half maximal inhibitory concentration (IC_{50}) is several hundred micromolar. The other mechanism is enhancement by dopamine, an interplexiform cell or paracrine transmitter that activates sites throughout the distal retina. In fish horizontal cells, dopamine slows the desensitization of AMPA receptors. Single-channel recording in perch horizontal cells shows that dopamine increases receptor current by increasing the opening rate and decreasing the closing rate. In salamander, dopamine increases the glutamate current in OFF bipolar cells by almost 50%, acting through D1 receptors to increase cyclic adenosine monophosphate (cAMP). In Xenopus horizontal cells, which apparently possess only one type of GluR, the AMPA and glutamate currents were small and transient under photopic conditions, larger and more sustained in dark-adapted retina. In contrast, the responses to kainate were largest in light-adapted retina and potentiated by D1 dopamine agonists. The suggestion is that even though one receptor population is used, the receptors at rod and cone synapses are differentially modulated.

Glutamate Receptors in Inner Retina

Similar to the photoreceptors, bipolar cells are capable of tonic glutamate release. The postsynaptic amacrine and ganglion cells possess AMPA, kainate, and also NMDA receptors. There are also pre- and postsynaptic metabotropic glutamate receptors. The synaptic input to ganglion cells is mediated predominantly by AMPA receptors; kainate receptors may be more relevant in at least some types of amacrine cells. There are a number of interesting aspects to the glutamate receptors at these synapses. One is the appearance of NMDA receptors, which play no role in the outer retina. Another is the placement of different receptors on each side of a single ribbon synapse, an exquisite refinement of the receptor specialization observed in the distal retina. Then, there is the continued importance of receptor desensitization in the shaping of transiently responding amacrine and ganglion cells.

The Mystery of the NMDA Receptors

The NMDA-type glutamate receptors are present in amacrine and ganglion cells, where exogenous application of NMDA agonists is as stimulatory as AMPA/KA agonists. Ganglion cells are particularly sensitive. In rabbit, it is estimated that 87% of ganglion cells and 58% of amacrine cells are excited by NMDA. Strangely, synaptically driven NMDA receptors are difficult to detect. Spontaneous miniature synaptic events stimulate AMPA, but not NMDA currents. The relative effectiveness of weak competitive antagonists suggest that NMDA receptors are exposed to lower concentrations of synaptic glutamate, consistent with NMDA receptors being further from presynaptic release sites than AMPA receptors. Often, inhibition has to be blocked using gamma aminobutyric acid (GABA) and glycine receptor antagonists, before prominent synaptic NMDA currents are evident. Under these conditions, some studies indicate that NMDA receptors can linearize the synaptic response since they are larger at

depolarized potentials (due to removal of magnesium block), where diminished driving force has reduced the AMPA/KA currents. In addition, in the presence of GABA and glycine receptor antagonists, transient excitatory postsynaptic currents (EPSCs) in salamander ganglion cells can be separated into an early AMPA receptor current and delayed, longer-duration NMDA receptor current.

The NMDA receptor is a tetramer that is activated by the simultaneous binding of two glutamate molecules and two glycine molecules. In some parts of the central nervous system, D-serine replaces glycine as the essential coagonist. This seems to be the case in retina, where experiments using D-serine degradative enzymes reduce the endogenous activation of NMDA receptors, which may eventually explain the disparity between the large number of NMDA receptors and the small endogenous activation, if receptor activation may be dependent not on glutamate release but on D-serine levels. A major potential source of D-serine is glial cells, leading to speculation that glia cells can control synaptic transmission.

Glutamate Receptor Diversity at the Synapse

One feature of retinal glutamatergic synapses is the diverse yet discrete receptor distribution at a single synapse. This theme starts in the distal retina. Photoreceptor glutamate activates metabotropic receptors on ON bipolar cells and different types of ionotropic receptors at different types of OFF bipolar cells. In salamander retina, the dendrites of rod-dominant OFF bipolar cells have AMPA receptors with larger conductances and slower rates of desensitization than the corresponding cone-dominant OFF bipolar cells. In rat rods and cones, the GluR6/7 kainate receptors are found in horizontal cells postsynaptic to rods and cones, but in only one of the two horizontal cell processes that enter each invagination. This theme is repeated in the inner plexiform layer (IPL). Rod bipolar cells synapse onto AII, S1, and S2 amacrine cells. Only the AIIs have GluR2/3 or 4 subunits, while only the S1 has delta1/2 subunits. Thus, the three postsynaptic amacrine cells can respond differently to the same glutamate signal. Even at a single synaptic dyad, the subunit expressed at one side is different from that expressed on the other. The KA receptor subunits are found postsynaptic to rod and cone bipolar cells, but generally only one of the two postsynaptic elements at the dyad possesses a particular kainate receptor subunit. Remarkably, mGluR feedback may be just as specialized. The mGluR7 receptors are bipolar cell autoreceptors likely to mediate negative-feedback regulation of glutamate release. They are found only on one side of the dyad, presumably allowing separate control of glutamate release on each side of this single ribbon synapse. In addition, kainate GluR6/7 receptors are postsynaptic to bipolar cells, but not at the ribbon synapse dyads. Based on several studies, it seems likely that kainate receptors are on amacrine but not on ganglion cells. Furthermore, receptor expression occurs in sublayers within the IPL. For example, in primate retina, although GluR2,2/3, and 4 are concentrated throughout the IPL, NR2A subunits are found in two bands at the center of the IPL.

This receptor diversity in the IPL is linked to release. In salamander retina, spontaneous events can be separated into release of single vesicles or multiple vesicles that stimulate fast-activating AMPA receptors and other release sites where there are clusters of vesicles released, which more slowly activate either AMPA or NMDA receptors.

Calcium-Permeable AMPA Receptors

Although the NMDA-type glutamate receptor is noted for its unusually high calcium permeability, the earliest evidence that AMPA receptors could also pass high levels of calcium came from the retina. Two intriguing ramifications are the direct control of transmitter release and the long-term modulation at a synapse. A central dogma of neurophysiology is that voltage-gated calcium channels allow for the increase in internal calcium that initiates vesicle fusion. However, there is a circuit in retina where this is not necessary. Bipolar cells activate AMPA receptors on A17, the amacrine cell, leading to a direct influx of calcium. This stimulates GABA transmitter release and inhibitory feedback to the bipolar cell. This type of regulation has a number of unique potential properties, such as voltage-independent transmitter release that is localized to a specific synaptic location rather than controlled by electrical spread throughout the neuron.

Receptor Desensitization

It is well established that kainate and AMPA receptors exhibit rapid desensitization, while NMDA receptors do not. The AMPA desensitization found at the bipolar to ganglion cell synapse makes the responses of some ganglion cells more phasic than that of the bipolar cells that drive them. This is of particular relevance in retina because ganglion cells can be divided into tonic and phasic light responders, carrying different components of the decomposed image. It has been suggested that the transient responses are formed by AMPA receptor desensitization in ganglion cells. However, this is likely to be a supplementary mechanism, with the primary formation of this dichotomy occurring in distal (outer) retina.

Pre- and Postsynaptic Metabotropic Glutamate Receptors

In bipolar cell terminals, the group III metabotropic receptors suppress glutamate output. As might be expected, this

feedback is minor or absent during weak light stimulation, but becomes saturating under strong light stimulation. Experimental evidence indicates that one function of this feedback is to extend the dynamic range at the synapse by requiring a stronger stimulus before the synapse becomes saturated.

Postsynaptically, ganglion cells possess a plethora of metabotropic receptors that act to suppress calcium channels. This is unrelated to transmitter release (unless ganglion cells are presynaptic within the retina) but these receptors may be important in regulating calcium-activated potassium channels that are found in most, if not all, ganglion cells. Thus, activation of mGluRs will facilitate excitatory responses in ganglion cells.

See also: GABA Receptors in the Retina; Information Processing: Amacrine Cells; Information Processing: Bipolar Cells; Information Processing in the Retina; Neurotransmitters and Receptors: Dopamine; Physiology of Photoreceptor Synapses and Other Ribbon Synapses; The Role of Acetylcholine and its Receptors in Retinal Processing.

Further Reading

Awatramani, G. B. and Slaughter, M. M. (2000). Origin of transient and sustained responses in ganglion cells of the retina. *Journal of Neuroscience* 20: 7087–7095.

Brandstatter, J. H. (2002). Glutamate receptors in the retina: The molecular substrate for visual signal processing. *Current Eye Research* 25: 327–331.

Chavez, A. E., Singer, J. H., and Diamond, J. S. (2006). Fast neurotransmitter release triggered by Ca influx through AMPA-type glutamate receptors. *Nature* 443: 705–758.

DeVries, S. H., Li, W., and Saszik, S. (2006). Parallel processing in two transmitter microenvironments at the cone photoreceptor synapse. *Neuron* 50: 735–748.

Grunert, U., Lin, B., and Martin, P. R. (2003). Glutamate receptors at bipolar synapses in the inner plexiform layer of primate retina: Light microscopic analysis. *Journal of Comparative Neurology* 466(1): 136–147.

Lukasiewicz, P. D., Lawrence, J. E., and Valentino, T. L. (1995). Desensitizing glutamate receptors shape excitatory synaptic inputs to tiger salamander retinal ganglion cells. *Journal of Neuroscience* 15: 6189–6199.

Massey, S. C. and Redburn, D. A. (1987). Transmitter circuits in the vertebrate retina. *Progress in Neurobiology* 28: 55–96.

Miller, R. F. and Slaughter, M. M. (1986). Excitatory amino acid receptors of the retina: Diversity of subtypes and conductance mechanisms. *TINS* 9: 211–218.

Mittman, S., Taylor, W. R., and Copenhagen, D. R. (1990). Concomitant activation of two types of glutamate receptor mediates excitation of salamander retinal ganglion cells. *Journal of Physiology* 428: 175–197.

Palmer, M. J., Taschenberger, H., Hull, C., Tremere, L., and von Gersdorff, H. (2003). Synaptic activation of presynaptic glutamate transporter currents in nerve terminals. *Journal of Neuroscience* 23: 4831–4841.

Rabl, K., Bryson, E. J., and Thoreson, W. B. (2003). Activation of glutamate transporters in rods inhibits presynaptic calcium currents. *Visual Neuroscience* 20: 557–566.

Wu, S. M. and Maple, B. R. (1998). Amino acid neurotransmitters in the retina: A functional overview. *Vision Research* 38: 1371–1384.

Relevant Websites

http://www.bris.ac.uk – University of Bristol.
http://webvision.med.utah.edu – WEBVISION: The Organization of the Retina and the Visual System.

H

Hemangiogenesis versus Lymphangiogenesis

A Kaipainen, University of Calgary, Calgary, AB, Canada
D R Bielenberg, Harvard Medical School, Boston, MA, USA

Glossary

Angioblast – A mesodermal cell committed to the endothelial lineage; primitive endothelial cell.
E9.5 – It denotes embryonic day 9.5 or 9.5 days following fertilization; total gestation in a mouse requires 18–20 days depending on the strain.
Hemangioblast – A stem cell that can give rise to cells of both the endothelial lineage and the hematopoietic lineage.
Hemangiogenesis – It is also called angiogenesis – widely used as a general term to mean the growth of blood vessels yet more exactly means the sprouting of a capillary to form new capillaries.
Lymphangiogenesis – The growth of new lymphatic vessels by sprouting or the enlarging of existing vessels due to proliferation.
Vasculogenesis – The formation of *de novo* blood vessels by the assembly of angioblasts.

Hemangiogenesis

Overview

All cells in the body require oxygen and nutrients to survive. Therefore, all tissues in the body are vascularized (with a few exceptions: cartilage, cornea, lens, epidermis); and nearly every cell is located within the diffusion distance of oxygen (100–150 μm) from a capillary. In a developing embryo, new blood vessels are needed to supply oxygen and nutrients to the newly developing organs and tissues; therefore, it is not surprising that the vascular system is one of the first organ to develop. In fact, endothelial cells, the cells that line blood vessels, provide trophic cues during organ morphogenesis and help to guide organogenesis.

Vasculogenesis, the *de novo* formation of blood vessels, is the process responsible for the first vessels in life. This process occurs via the aggregation and assembly of angioblasts, endothelial cell precursors, to form a primitive vascular plexus. This plexus is then remodeled by a process called hemangiogenesis (or angiogenesis) that consists of the pruning of some vessels and the sprouting and growth of other vessels. Vasculogenesis occurs primarily during development, whereas hemangiogenesis can be induced throughout life. The development of the vascular system consists of a series of interrelated steps, including commitment of mesodermal cells toward the endothelial lineage or the formation of angioblasts, the alignment of angioblasts into cords, the formation of lumens within these cords, and the organization into functional channels.

Angioblasts

Endothelial cells and circulating hematopoietic cells share a close relationship in proximity, locality, and ancestry as their precursor cells, angioblasts and hemangioblasts, share a common lineage. Hemangioblasts are pluripotent cells that can give rise to cells of both the endothelial lineage and the hematopoietic lineage. Angioblasts originate from mesodermal cells and express two key markers: vascular endothelial growth factor receptor-2 (VEGFR2, also called Flk1) and a basic helix–loop–helix transcription factor called Tal1/Scl. As angioblasts differentiate into endothelial cells, they lose expression of Tal1 but VEGFR2 expression remains. The new endothelial cells begin to express platelet endothelial cell adhesion molecule-1 (PECAM-1, also called CD31), CD34, vascular endothelial (VE)-cadherin, and later the angiopoietin receptor, Tie2. A specialized subset of endothelial cells derived from angioblasts has hemogenic potential indicating that these endothelial cells can spawn hematopoietic cells.

Vasculogenesis

Vasculogenesis refers to the *in situ* differentiation of mesodermal cells (angioblasts) into endothelial cells and the subsequent morphogenesis and organization into a vascular plexus. This vascular development process depends upon both intrinsic (pre-patterned) criteria as well as extrinsic responses to stimuli. Vasculogenesis occurs in two spatially and temporally distinct phases within the embryo: (1) the formation of the extra-embryonic vessels and (2) the formation of intra-embryonic vessels. Intra- and extra-embryonic vessels are derived from different cell populations. First, yolk sac angioblasts, a subset of Brachyury-positive cells expressing VEGFR2, migrate out from the posterior primitive streak (mice E6.5–8.0) into the extra-embryonic yolk sac and coalesce into blood islands. These angiogblasts migrate, aggregate, expand, and differentiate to form a labyrinth of small vessels. These cords of endothelial cells form tight cell–cell connections followed by the formation of an internal lumen.

The second wave of endothelial cell differentiation occurs inside the embryo together with the formation of the endocardium from progenitor cells (mice E7.3). At the same time as the heart is developing, intra-embryonic angioblasts migrate out from the lateral plate mesoderm to the midline, coalesce, and differentiate to form the dorsal aorta (mice E7.6) just ventral to the notochord. The angioblasts also form the posterial cardinal vein ventral to the aorta. The dorsal aorta and the cardinal vein are formed directly without an intermediate plexus phase. Between E8.0 and E8.5 in mice (end of third week of development in humans), a rudimentary circulatory system is completed. With the first heartbeat, the vascular channels become perfused for the first time. From E8.5 (mice), the vitelline vein is first seen to transport nutrients from the yolk sac out into the embryo.

Angiogenesis

Secondary vessels are formed via the angiogenic process. Hemangiogenesis (also called angiogenesis) is widely used as a general term to describe the growth of blood vessels yet more exactly defines the sprouting of a capillary from a preexisting one. The first new sprouts form the intersegmental (intersomitic) vessels (which align dorsoventrally at the myotomal boundary between the somites) and the parachordal vessels (which align longitudinally at either side of the notochord).

During the angiogenic phase, the plexus composed of endothelial cells gradually expands by means of sprouting, proliferation, pruning, apoptosis, and remodeling into a network of hierarchical vessels consisting of larger vessels branching into smaller ones. Very early in this process, the endothelial cells already have acquired an arterial or venous specification, suggesting that the fate is genetically programmed and not determined solely by external factors such as hemodynamic forces. The Notch family of factors drives arterial differentiation, whereas the transcription factor, COUP-TFII, drives the venous genetic program. The heart pumps oxygenated blood into arteries, the largest vessels, which branch into smaller vessels called arterioles, which ramify into smaller vessels called capillaries. Capillaries exchange oxygen and nutrients between the blood and the surrounding tissues. Then they return the (usually de-oxygenated) blood back toward the heart via larger vessels called venules to still larger vessels called veins. During the final steps of maturation, vessels recruit smooth muscle cells called pericytes to surround and stabilize the vessel. Pericytes provide strength and help to regulate perfusion.

Lymphangiogenesis

Structure and Function of the Lymphatic System

The lymphatic system forms a one-way route, carrying lymph from the periphery of tissues through the thoracic duct or the right lymphatic duct into the venous blood. These two main lymphatic ducts are connected with the venous system at the junction of the left internal jugular vein and the left subclavian vein and at the veins of the right jugulo-subclavian confluence, respectively. However, other potential lymphaticovenous communications (e.g., iliac and renal areas) may become functional when lymphatic pressure rises or in a pathological situation.

Beyond its main function, the drainage of extravasated tissue fluid back to the venous circulation, the lymphatic system serves several other functions which include transport for immune defense and absorption of lipids from the intestine. Nearly all vascularized tissues, except the central nervous system (CNS), are invested with lymphatic vessels. The CNS lacks lymphatics since it has a blood-neural barrier that is less permeable than other tissues and is immune-privileged. In the eye, lymph drainage is present in the conjunctiva, sclera, and choriocapillaris, while there is no lymph drainage for the anterior chamber, vitreous cavity, subretinal space, or cornea.

In the peripheral tissues, lymphatic vessels and blood vessels are found in close proximity, yet the two systems never intermix (**Figure 1**). Lymphatic functions are reflected in the particular structure of the lymphatic vessels. A main characteristic is the discontinuity of the basement membrane at the interface between the lymphatic endothelium and the surrounding connective tissue that facilitates active fluid transport. In some tissues, including intestine, lung, and skin, lymphatic vessels completely lack a basement membrane. A second major characteristic is the tight connection of the lymphatic endothelial cells (LECs) to the surrounding matrix through anchoring filaments (AFs). It has been proposed

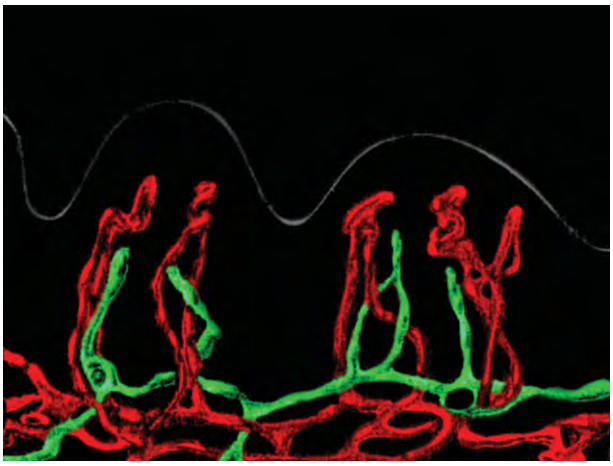

Figure 1 Schematic depicting the blood vascular system (red color) and the lymphatic system (green color) in the skin. Notice that the two systems are closely aligned but never mix. The blood vascular system is a closed circulatory system, with arteries leading to capillary loops (shown close to the epidermis) and draining to veins. The lymphatic capillaries are blind-ended, finger-like projections that begin near the epidermis and drain into larger collecting lymphatic vessels.

Table 1 Differences between the vascular and lymphatic systems

Blood vessels	*Lymphatic vessels*
Circular system	Unidirectional system
Artery → capillary → vein	Capillary → collector → TD → vein
Formed E6.5–9.5 (mice)	Sprout from vein at E9.5–12.5 (mice)
Capillaries have BM	Capillaries have discontinuous or lack BM
SMC may surround capillaries	Capillaries lack SMC
No anchoring filaments	Capillaries have anchoring filaments
Flow is dictated by heart beat	Flow is dictated by interstitial pressure
No valves in capillaries	Capillaries have valves
Blood inside the vessels	Lymph inside the vessels
Contain all the hematopoietic cells	Contain immune cells and no RBC
Retina has blood vessels	Retina lacks lymphatic vessels

BM, basement membrane; RBC, red blood cells; SMC, smooth muscle cells; TD, thoracic duct.

that tissue expansion due to excess interstitial fluid tightens the AFs, which pull on the lymphatic capillaries, thereby creating gaps between the LEC to increase the intake of fluid. A third characteristic of the lymphatic vessels is that valves in the vessel wall are already present at the level of capillaries, unlike in the venous blood system where they are found only in venules and larger vessels. These valves ensure unidirectional flow of the lymphatic fluid, which starts in the blind-ended capillaries. Furthermore, LECs are significantly larger than the blood endothelial cells; this enables elongation of the cells to accommodate the tissue stretch (see **Table 1** for a list of differences between lymphatic vessels and blood vessels).

Short Historical Perspective on Studying the Lymphatic System

The discovery of the lymphatic system was based upon intestinal absorption of fat particles, which color lymphatic capillaries white and stand out from the red-colored blood capillaries. Although Hippocrates described lymph nodes and termed lymphatic fluid as white blood in the fifth century BC, it was not until 1622, when Gasparo Aselli, an Italian anatomist and surgeon, provided a more accurate description of the lymphatic system. However, it took three more centuries before any detailed investigations were performed on the developmental origin of the lymphatic system. At the turn of the twentieth century, three different theories of the formation of the lymphatic system were proposed. These theories were based on studies from serial sections of fixed tissues or on ink injections into the lymphatic system. Florence Sabin hypothesized that the lymphatic system originates from the venous system as sprouts (lymph sacs) growing in a centrifugal manner. Huntington and Kampmeier proposed that lymphatics are derived from mesenchymal cells that grow in a centripetal manner. According to a third theory, the lymphatic system is in part derived from the venous endothelium and in part, notably at the periphery, through mesenchymal differentiation.

Lymphangiogenesis in Development

Modern molecular biological analysis predominantly supports Sabin's theory. She demonstrated that lymphatic vessel development is initiated by budding of six lymphatic sacs from the venous endothelium. These include the paired jugular lymph sacs, the paired posterior iliac lymph sacs, the retroperitoneal sac, and the cisterna chili, which are localized at sites where large veins merge and are separated from veins with valves. The lymphatic vessels grow radially outward from these lymph sacs as continuous channels into the periphery. In humans, the lymphatic system starts to develop at gestational day 35, when the jugular lymph sacs begin to bud. By gestational day 56, the primitive lymphatic system, which includes all six lymph sacs, is complete.

The first molecular clues supporting Sabin's theory came from Alitalo and co-workers in 1995 who reported the first gene whose expression pattern is highly specific for lymphatic tissue: *VEGFR3*. VEGFR3, a member of the VEGF receptor family, which also comprises VEGFR1 and -2, is expressed already at E7.5 (mice) in the

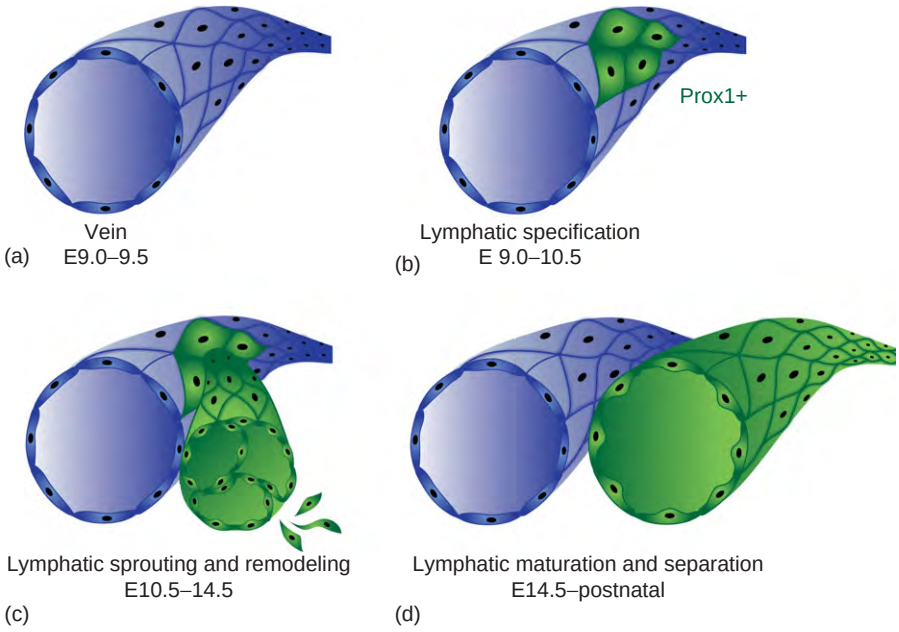

Figure 2 The formation of the lymphatic system during development in mice.(a) The first lymphatic vessel sprouts from the cardinal vein. (b) A subset of venous endothelial cells express Prox1. (c) Prox1 induces lymphatic-associated genes necessary for migration of lymphatic endothelial cells. (d) Lymphatic vessel remodeling and maturation results in separate venous and lymphatic vessels.

endothelium of the cardinal vein and between developing somites and in angioblasts of the head mesenchyme. At approximately E14.5 (mice), its expression becomes restricted predominantly to the lymphatic endothelium. One possible trigger for the downregulation of *VEGFR3* in blood endothelium is the interaction of the endothelium with smooth muscle cells.

More recently, Guillermo Oliver has proposed a four-stage model for the differentiation of the lymphatic vasculature: (1) lymphatic competence, (2) lymphatic bias, (3) lymphatic specification, and (4) LEC differentiation (**Figure 2**). He defines LEC competence (stage 1) as an autonomous ability of a venous endothelium to respond to one or more specific lymphatic-inducing signal(s), which is controlled by a developmental timer. Studies, performed in mice at E9.0–E9.5, suggest that the earliest indication that differentiation has started is the random expression of lymphatic vessel endothelial hyaluronan receptor 1 (LYVE1) in some of the endothelial cells of the anterior cardinal vein. However, LYVE1 is not a competence factor as *LYVE1*-deficient embryos lack any obvious lymphatic phenotype.

The fate of the LEC is determined during bias (stage 2). On one side of the anterior cardinal vein shortly after cells start expressing LYVE1 a subpopulation of venous endothelial cells starts expressing the transcription factor, prospero-related homeobox-1 gene, *Prox1* (**Figure 2(b)**). Expression of Prox1 in the venous endothelial cells is necessary and sufficient to drive lymphatic cell differentiation. However, signals that switch on Prox1 expression are not known.

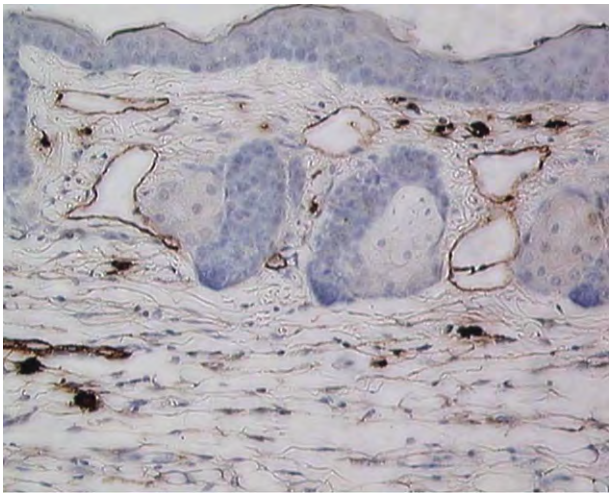

Figure 3 Lymphatic vessels in the skin. Immunohistochemistry using anti-podoplanin antibodies reveals lymphatic vessels (brown color) near the murine epidermis. The section is counterstained with hematoxylin. Notice the large lumens and presence of valves in the lymphatic capillaries.

During specification (stage 3) the cells differentiate into the desired phenotype independently from their regional environment. Once the cells express Prox1, they begin to express, in a stepwise manner, other lymphatic markers, such as neuropilin-2 and podoplanin (**Figure 3**). Concomitantly, they lose the expression of blood endothelial cell markers, such as CD34 and laminin. In the final stage of LEC differentiation (stage 4), first the lymphatic sacs and then the mature vessel network is

formed. In order to form lymphatic sacs, Prox1-positive cells have to migrate. This process requires VEGFC, a ligand for VEGFR3, expression by stromal cells. Thus, mice deficient for *VEGFC* fail to form primary lymph sacs. VEGF-C driven early sprouting and migration of LEC is modified by another ligand for VEGFR3, VEGF-D. Unlike blood capillaries, which sprout during angiogenesis at right angles from the original capillary, lymphatic capillaries sprout at a more acute angle to the vein or subsequent lymphatic vessel (**Figure 2(c)**).

Molecular studies have demonstrated that at E14.5, mouse embryos that are deficient for cytoplasmic signaling proteins Syk, SLP76, or phospholipase-Cγ2 (PLCγ2) exhibit backflow of blood into lymphatic sacs and vessels. This deficiency indicates that at the sites of budding, the valves did not develop, and/or that the anastomoses did not close. Syk, SLP76, and PLCγ2 are only expressed on hematopoietic cells, and the underlying mechanism for the defect seen in embryos lacking these factors is still unclear. However, a noncell autonomous mechanism is possible. In this model, these three genes stimulate a nonendothelial cell (e.g., a hematopoietic stem cell) to secrete factors that activate developmental processes in lymphatic endothelium that are needed for the separation of blood and lymphatic vessels. Alternatively, a cell autonomous mechanism is also possible in which Syk, SLP76, or PLCγ2 are transiently expressed in hematopoietic stem cells which can differentiate into lymphatic endothelial precursor cells.

Several genes involved in lymphatic vessel maturation and patterning have now been identified. A forkhead transcription factor, FOXC2, is required for the establishment of the pericyte- and smooth muscle cell (SMC)-free lymphatic capillaries, a process thought to happen through a specific repression of PDGFBB in lymphatic vessels. In addition, FOXC2 is important in lymphatic vessel patterning and in the genesis of valves in the collecting lymphatic vessels. Neuronal guidance molecules, such as ephrinB2 and neuropilin-2, are also involved. Mice lacking the carboxy-terminal PDZ domain in the ephrinB2 receptor display hyperplastic collecting lymphatics, lack luminal valves, and fail to remodel their primary lymphatic capillary plexus. Similarly, neuropilin2-mutant mice have a reduced number of lymphatic capillaries in the gut, dermis, heart, and lung. *In vitro* experiments show that Semaphorin 3F (SEMA3F), a ligand of neuropilin-2, repels LECs, suggesting that guidance molecules also regulate lymphatic vessel patterning in a similar manner as has been shown for the vascular system.

Defects in the lymphatic system have been found in various gene knock-out mouse strains. *Angiopoietin-2*-deficient mice develop large vessels with irregular edges and capillaries with abnormal patterning. Mice deficient in *podoplanin*, a mucin-type transmembrane glycoprotein (**Figure 3**), have dilated and disorganized intestinal and skin lymphatics, yet the subserosal lymphatic capillaries appear normal. Lymphatic vessels are filled with blood in mice deficient for *Fiaf* (fasting-induced adipose factor), while *Elk3*-(ETS-domain protein), *Integrin α9*-, *Prox1*-, *VEGFC*-, and *Ang2*-null mice have chylous ascites, and mutated *ephrinB2* mice have a chylothorax.

During the last 15 years immense progress has been made in understanding the mechanisms of lymphatic vessel development, notably the identification of genes that are essential for normal development, yet open questions remain, among which the most salient are: what are the signals that switch on expression of Prox1, a key trigger of LEC differentiation in the venous endothelium? Do mammals have lymphatic precursor cells capable of differentiating into LEC? And what controls the budding and separation of lymph sacs from the venous system?

Corneal Lymphangiogenesis

In adults, physiological lymphangiogenesis is an important component of normal wound healing as well as estrus and ovulation in the female reproductive tract. Pathological lymphangiogenesis can occur during lymphedema, lymphatic malformations, inflammatory diseases, and tumor metastasis. In the eye, the healthy cornea is devoid of both blood and lymphatic vessels. Therefore, corneal lymphangiogenesis, secondary to keratitis, graft rejection, limbal insufficiency, and chemical burns, is an undesirable process. On the other hand, because of its avascularity, the cornea displays an excellent in vivo model system to determine mechanisms of lymphangiogenesis. Indeed, several groups have established corneal lymphangiogenesis models to determine growth factor responses, test inhibitory factors, and study tumor lymphatic vessels. Cursiefen, Dana, and Streilein have established several models to determine the mechanisms involved in corneal lymphangiogenesis during corneal inflammatory processes and graft rejection.

Folkman and his coworkers have established a corneal lymphangiogenesis assay, which has allowed investigators to demonstrate that (1) lymphangiogenesis can occur, against existing dogma, without preexisting angiogenesis; (2) a pleotropic growth factor, fibroblast growth factor 2 (FGF2), can stimulate only lymphangiogenesis; and most importantly (3) this assay can identify factors that can inhibit lymphatic vessel growth. It is noteworthy that in this assay, while an 80ng-pellet of FGF2, which is routinely used in corneal angiogenesis assay, stimulates both angiogenesis and lymphangiogenesis, a 12.5ng FGF2-pellet only stimulated lymphatic vessel growth by inducing the production of VEGF-C and-D in corneal keratinocytes. FGF2-driven lymphangiogenesis could be inhibited with systemic administration of soluble receptors, sVEGFR2 or sVEGFR3, via adenoviruses or by neutralizing antibodies to these

receptors, as well as with the small molecule COX-2 inhibitors, rofecoxib and celecoxib.

A variety of modifications of the corneal lymphangiogenesis assays now exist which provide a powerful tool, not only to investigate diseases of the cornea and to evaluate possible therapies, but also to determine the more general mechanisms of lymphangiogenesis involved in, for example, tumor metastasis.

Summary

Hemangiogenesis and lymphangiogenesis are two important processes that occur early in development just before and during organogenesis. The development of the circulatory system allows nutrients and oxygen to be delivered in the blood throughout the body to all organs and tissues. The lymphatic system returns the fluid that leaks into the interstitial space back to the blood vascular system. Both systems are necessary for normal tissue homeostasis. Lymphatic vessels differ from blood vessels in many aspects, including their structure, function, expression of growth factor receptors, and response to ligands or cytokines. Hemangiogenesis and lymphangiogenesis are rare in the adult, but do occur during physiological processes such as wound healing and ovulation/menstruation. Pathological processes such as tumor progression also induce neovascularization to support the growing tumor cells with oxygen and nutrients. Likewise, these tumor vessels are leaky and result in increased interstitial pressure and lymphangiogenesis.

Acknowledgments

This work was funded in part by the National Cancer Institute (CA118732) and the National Eye Institute (EY018347).

See also: Angiogenesis in the Eye; Avascularity of the Cornea; The Corneal Stroma; Stability and Functional Integrity of New Blood Vessels; The Vascular Stem Cell.

Further Reading

Alitalo, K., Tammela, T., and Petrova, T. V. (2005). Lymphangiogenesis in development and human disease. *Nature* 438: 946–953.

Barnes, C., Christison-Lagay, E., Huang, S., and Kaipainen, A. (2008). Development of the vascular system. In: Epstein, C. J., Erickson, R. P., and Wynshaw-Boris, A. (eds.) *Inborn Errors of Development: The Molecular Basis of Clinical Disorders of Morphogenesis*, 2nd edn., pp. 130–149. New York: Oxford University Press.

Chang, L., Kaipainen, A., and Folkman, J. (2002). Lymphangiogenesis new mechanisms. *Annals of the New York Academy of Sciences* 979: 111–119.

Coultas, L., Chawengsaksophak, K., and Rossant, J. (2005). Endothelial cells and VEGF in vascular development. *Nature* 438: 937–945.

Cursifien, C., Chen, L., Dana, M. R., and Streilein, J. W. (2003). Corneal lymphangiogenesis. Evidence, mechanisms, and implications for corneal transplant immunology. *Cornea* 22: 273–281.

Oliver, G. (2004). Lymphatic vasculature development. *Nature Reviews Immunology* 4: 35–45.

Oliver, G. and Detmar, M. (2002). The rediscovery of the lymphatic system: Old and new insights into the development and biological function of the lymphatic vasculature. *Genes and Development* 16(7): 773–783.

Sabin, F. R. (1902). On the origin of the lymphatic system from the veins and the development of the lymph hearts and thoracic duct in the pig. *American Journal of Anatomy* 1: 367–391.

Zwaans, B. M. and Bielenberg, D. R. (2007). Potential therapeutic strategies for lymphatic metastasis. *Microvascular Research* 74(2–3): 145–158.

Hereditary Vitreoretinopathies

S Meredith and M Snead, Cambridge University Hospitals NHS Foundation Trust, Cambridge, UK

Glossary

Dominant negative effect – An altered gene product is produced that interacts with, and prevents the normal functioning of, the normal protein that is present.
Haploinsufficiency – A mutation resulting in a single copy of the normal gene is present so that only 50% of normal protein is produced, which is not enough for normal function.
OMIM – An online compendium of human genes and genetic phenotypes derived from the Mendelian Inheritance in Man (MIM) database.
Phenotype – The observable characteristics of an organism which are dependent on both genetic and environmental factors.
Pseudoexotropia – The appearance of a divergent squint when both eyes are fixing on the fovea measurable as a large angle kappa.

Introduction

The inherited vitreoretinopathies are collectively characterized by abnormalities in vitreous development and architecture. Since the development of the primary, secondary, and tertiary vitreous is largely complete by the first trimester, abnormalities of vitreous phenotype are present at birth, providing a useful and often pathognomonic diagnostic hallmark. In addition however, it is important to remember that the congenital anomalies of gel development and architecture will not be exempt from the more generalized age-related biochemical and structural changes.

Classification of the Hereditary Vitreoretinopathies

There have been significant, recent advances in both the clinical and molecular genetic analysis of the inherited vitreoretinopathies. Classification on clinical grounds (Table 1) is a helpful and convenient way to approach the investigation and diagnosis of the hereditary vitreoretinopathies. Four principal categories are currently recognized as follows: vitreoretinopathies that are associated with (1) skeletal abnormalities, (2) retinal dysfunction, (3) retinal vascular abnormalities, and (4) corneal guttata. Other varieties of inherited vitreoretinopathies do not fit easily into any of these subgroups and it is inevitable that a classification will be expanded as further clinical and molecular genetic heterogeneity is resolved.

Clinical Features of the Hereditary Vitreoretinopathies

The clinical features in each of the individual hereditary vitreoretinopathies are summarized in Table 2. Of the clinical features, the vitreous is the only category in which an abnormality has been universally described in the disorders collectively known as the hereditary vitreoretinopathies.

Vitreoretinopathies Associated with Skeletal Abnormalities

Stickler syndrome (OMIM #108300, #604841, and #184840)

The Stickler syndromes are a group of interrelated dominantly inherited disorders of collagen connective tissue which results in an abnormal vitreous embryology and a variable degree of orofacial abnormality, deafness, and arthropathy. Unlike some other hereditary arthro-ophthalmopathies, patients with Stickler syndrome have normal stature. In many patients with Stickler syndrome, systemic features may not be immediately obvious and the diagnosis of Stickler syndrome depends primarily on the recognition of characteristic congenital vitreous changes.

Stickler syndrome is the most common hereditary vitreoretinopathy. The majority of patients with Stickler syndrome have type 1 Stickler syndrome, which is part of the spectrum of type II collagen disorders. The type II collagenopathies, including type 1 Stickler syndrome, are characterized by a membranous vitreous appearance on biomicroscopy (Figure 1). Type 2 Stickler syndrome refers to Stickler syndrome associated with defects of type XI collagen and has a different vitreous appearance described as beaded or fibrillar (Figure 2). More recently, a recessive form of Stickler syndrome associated with mutations in a gene coding for type IX collagen has been described.

Table 1 Clinical classification of the hereditary vitreoretinopathies

	Syndrome		*OMIM classification*
Vitreoretinopathies associated with skeletal abnormalities			
1.	Stickler syndrome	Type 1	#108300
		Type 2	#604841
			#184840
2.	Kniest dysplasia		#156550
3.	Sponyloepiphyseal dysplasia congenital (SEDC)		#183900
4.	Marshall syndrome		#154780
5.	Knobloch syndrome		#267750
6.	Marfan syndrome		#154700
Vitreoretinopathies associated with progressive retinal dysfunction			
7.	Wagner syndrome		#143200
8.	Goldmann–Favre syndrome/Enhanced S-cone dystrophy		#268100
Vitreoretinopathies associated with abnormal retinal vasculature			
9.	Familial exudative vitreoretinopathy (FEVR)		#133780
			#601813
			#305390
10.	Autosomal dominant vitreoretinochoroidopathy (ADVIRC)		#193220
Vitreoretinopathy associated with corneal changes			
11.	Snowflake vitreoretinal degeneration		#193230

Weissenbacher–Zweymuller syndrome is sometimes included in the classification of the hereditary vitreoretinopathies. This syndrome is not associated with a vitreoretinopathy. The ocular features are hypertelorism, refractive errors, and strabismus. It results from mutations in the COL11A2 gene which is not expressed in the eye and is therefore not considered further in this article.

In contrast to the developmental myopia in the general population, myopia in Stickler syndrome is typically congenital, of high degree, and nonprogressive. It is important to remember that although the disorder is associated with congenital megalophthalmos, up to 20% of patients are not refractively myopic due to associated cornea plana.

Stickler syndrome is associated with a high risk of retinal detachment. The lifetime risk of retinal detachment is probably approaching 80% in type 1 Stickler syndrome, the majority of which is bilateral frequently as a result of a giant retinal tear at the pars plana (**Figures 3(a)** and **3(b)**). Other ocular findings are radial paravascular lattice, congenital quadrantic lamellar cataract (**Figure 4**), and early-onset nuclear sclerosis.

Orofacial abnormalities are common in Stickler syndrome and, even in the absence of a history of a cleft palate, it is important to examine the oral cavity for evidence of a submucous cleft or high-arch palate (**Figure 5**). Conductive hearing loss is an acknowledged association with any midline cleft via associated eustachian tube dysfunction, but the audiometry in Stickler syndrome will often reveal an additional high-tone (4000 Hz) sensorineural deficit as a result of associated developmental abnormalities of the cochlea.

Both collagen type II alpha 1 (COL2A1) and collagen type XI alpha 1 (COL11A1) are expressed in cartilage accounting for the combined ocular and skeletal manifestations in Stickler syndrome. The arthropathy typically manifests as joint laxity and hypermobility from an early age and a premature degenerative osteoarthropathy by the third to fourth decade, characteristically affecting the lumbosacral spine, hips, and knees.

The majority of patients with Stickler syndrome will exhibit both vitreoretinal and systemic involvement. A smaller but important subgroup presents with a predominantly ocular, or ocular-only, phenotype as a result of a mutation which is preferentially expressed in ocular tissues. Ophthalmologists have a key role to play in recognition and diagnosis of this important subgroup who are otherwise frequently undiagnosed until retinal detachment occurs.

Other more severe chondrodysplasias result from dominant negative changes within the type II collagen triple helix and include kniest dysplasia, spondyloepiphyseal dysplasia congenita (SEDC), and dominant spondylo-epi-metaphyseal dysplasia (SEMD). Similar to Stickler syndrome, these disorders present with congenital vitreous abnormalities, retinal detachment, deafness, and midline clefting, but with more pronounced arthropathy than Stickler syndrome and disproportionate (rhizomelic) limb shortening.

Kniest dysplasia (OMIM #156550)

Kniest dysplasia is an autosomal dominant vitreoretinopathy associated with skeletal dysplasia presenting with shortening of the trunk and limbs (**Figure 6**). The vitreous is congenitally abnormal and associated with megalophthalmos, cleft palate, and midfacial hypoplasia. Both conductive and sensorineural hearing loss are common and the joints display characteristic enlargement, particularly of the proximal interphalangeal joints, with the fingers appearing long and knobbly (**Figure 7**).

Spondyloepiphyseal dysplasia congenital (OMIM #183900)

SEDC is an autosomal dominant vitreoretinopathy presenting at birth with shortening of the trunk and thereafter progressively disproportionate (proximal) limb shortening, with the hands and feet appearing relatively normal in contrast to Kniest dysplasia, and flattening of the midface (**Figure 8**). The chest is barrel shaped with associated kyphosis and increased lumbar lordosis. The ocular phenotype is very similar to Stickler syndrome with congenital megalophthalmos and a type 1 (membranous) vitreous anomaly.

Marshall syndrome (OMIM #154780)

There is some uncertainty as to whether or not the Stickler and Marshall syndromes are clinically separate entities.

Table 2 Clinical features of the hereditary vitreoretinopathies

	Description of the clinical features								
Name of the syndrome	*Refractive error*	*Cornea*	*Lens*	*Vitreous*	*Retina*	*ERG*	*Optic disk*	*Other ocular features*	*Systemic features*
Vitreoretinopathies associated with skeletal abnormalities									
Stickler syndrome	Congenital nonprogressive myopia		Quadrantic lamellar or early-onset nuclear sclerosis	Membranous or beaded vitreous anomaly	Giant retinal tears, retinal detachment, and radial perivascular lattice degeneration		Myopic/ peri-papillary change	Megal-ophthalmos	Midfacial hypoplasia, cleft palate, joint hypermobility, arthropathy, and sensorineural deafness
Kniest dysplasia	Myopia			Membranous vitreous anomaly				Megal-ophthalmos	Shortening of trunk and limbs, midfacial hypoplasia, cleft palate, and hearing loss
SEDC	Myopia			Membranous vitreous anomaly				Megal-ophthalmos	Shortening of trunk and disproportionate proximal limb shortening, kyphosis, lumbar lordosis, and barrel-shaped chest
Marshall syndrome	Myopia		Congenital or juvenile cataracts	Syneresis				Ocular hypertelorism	Spondyloepiphyseal abnormalities, short stature, flat midface, cleft palate, sensorineural deafness, ectodermal dysplasia with hypotrichosis and hypohidrosis , dental structure abnormalities, calvarial thickening, and falx cerebri calcification
Knobloch	High myopia		Subluxated, cataract	Degenerative	Retinal detachment, macular degeneration				Occipital encephalocele, lung hypoplasia, cardiac dextroversion, flat nasal bridge, midface hypoplasia, joint hyperextensibility, unusual palmer crease, and unilateral duplicated renal collecting system
Marfan syndrome	Myopia	Cornea plana	Ectopia lentis, early nuclear sclerosis	Vitreous degeneration	Retinal detachment			Increased globe length, hypoplastic iris, and glaucoma	Increased height, scoliosis, lumbar lordosis, joint laxity, narrow high-arched palate, anterior chest deformity, mitral valve prolapse, mitral and aortic regurgitation, and dilatation of aortic root
Vitreoretinopathies associated with progressive retinal dysfunction									
Wagner syndrome/ erosive vitreoretinopathy	Myopic		Early-onset cataract	Syneresis and condensation, membranes	Chorioretinal atrophy, tractional and rhegmatogenous retinal detachment, and retinal pigment epithelial change	Subnormal		Ectopic fovea with pseudoexotropia, and hemeralopia	

Continued

Table 2 Continued

	Description of the clinical features								
Name of the syndrome	*Refractive error*	*Cornea*	*Lens*	*Vitreous*	*Retina*	*ERG*	*Optic disk*	*Other ocular features*	*Systemic features*
Goldmann–Favre syndrome/ enhanced S-cone dystrophy			Cortical lens opacities	Liquefaction and fibrillar changes	Equatorial chorioretinal atrophy and pigment clumping, peripheral and macular schisis, and diffuse vascular leakage	Dysfunctional cone mechanism			
Vitreoretinopathies associated with abnormal retinal vascularization									
FEVR				Peripheral 'snowflake' vitreous changes	Avascularity of peripheral retina, retinal exudates, retinal traction			Macular pucker, tractional and exudative detachment	
ADVIRC		Micro cornea	Congenital cataract	Fibrillar condensation	Circumferential hyperpigmented band, punctuate white opacities, choroidal atrophy, retinal neovascularization, posterior staphyloma	EOG abnormal at level of RPE		Nano-ophthalmos, and closed-angle glaucoma	
Vitreoretinopathy associated with corneal changes									
Snowflake vitreoretinal degeneration		Corneal guttata	Cataract in young adulthood	Fibrillar degeneration with thickened cortical vitreous	Peripheral retinal abnormalities (small, shiny, snowflake like), sheathing and obliteration of retinal vessels		Waxy pallor		

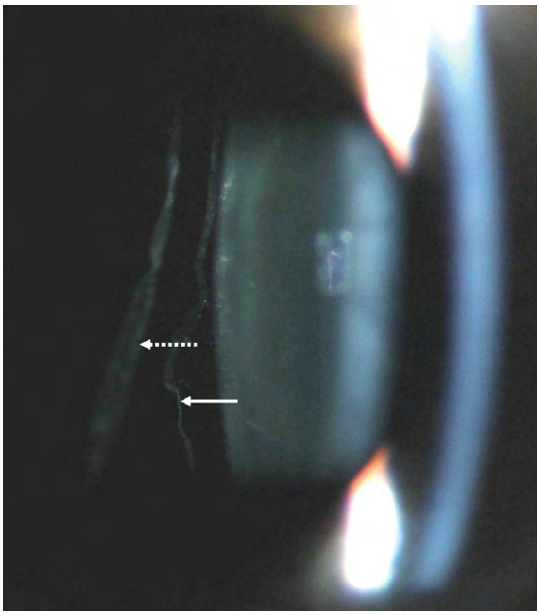

Figure 1 Membranous vitreous phenotype in type 1 Stickler syndrome. Dotted line indicates detached posterior hyaloid membrane; solid line indicates the type 1 membranous anomaly.

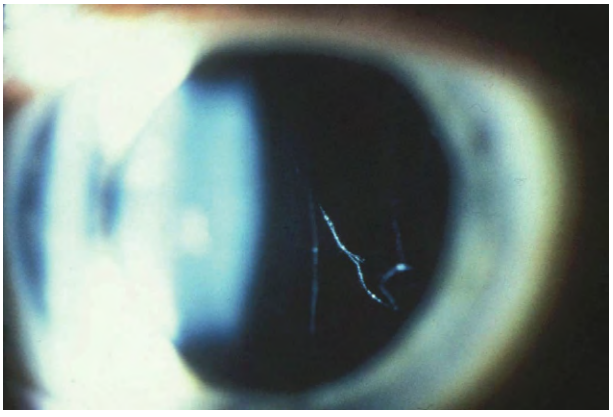

Figure 2 Beaded vitreous phenotype in type 2 Stickler.

Many features are shared such as midfacial hypoplasia, spondyloepiphyseal abnormalities, cleft palate, and sensorineural hearing loss, but patients with Marshall syndrome are reported to also have ectodermal dysplasia with hypertrichosis and hypohyidrosis, calvarial thickening, and ocular hypertelorism. The term Marshall–Stickler syndrome has been used but is potentially confusing and best avoided until Marshall syndrome is better characterized on clinical and molecular genetic grounds.

Knobloch syndrome (OMIM #267750)

Knobloch syndrome has been molecularly characterized and results from a mutation in the gene coding for type XVIII collagen. It has a more extensive systemic phenotype than Stickler or Marshall syndrome with developmental abnormalities described in several major systems of the body, including lung hypoplasia, cardiac dextroversion, and renal abnormalities as well as the ocular features of a degenerative vitreous appearance, high myopia, and retinal degeneration with retinal detachment. The distinguishing clinical feature of Knobloch syndrome is the presence of an occipital encephalocele.

Marfan syndrome (OMIM #154700)

Marfan syndrome is an autosomal dominant connective tissue disorder associated with an abnormal vitreous appearance, myopic astigmatism, and characteristic skeletal features of increased height with disproportionately long limbs and digits, scoliosis and lumbar lordosis, joint laxity, narrow, high-arched palate, and anterior chest deformity (**Figure 9**). Ectopia lentis (with the lens typically dislocated superior and temporally; **Figure 10**) is the ocular major Ghent criterion for the diagnosis of Marfan syndrome. Retinal detachment, myopia, increased globe length, cornea plana, hypoplastic iris, glaucoma, and early nuclear sclerotic cataract are all minor criteria. Marfan syndrome has cardiovascular manifestations of mitral valve prolapse,

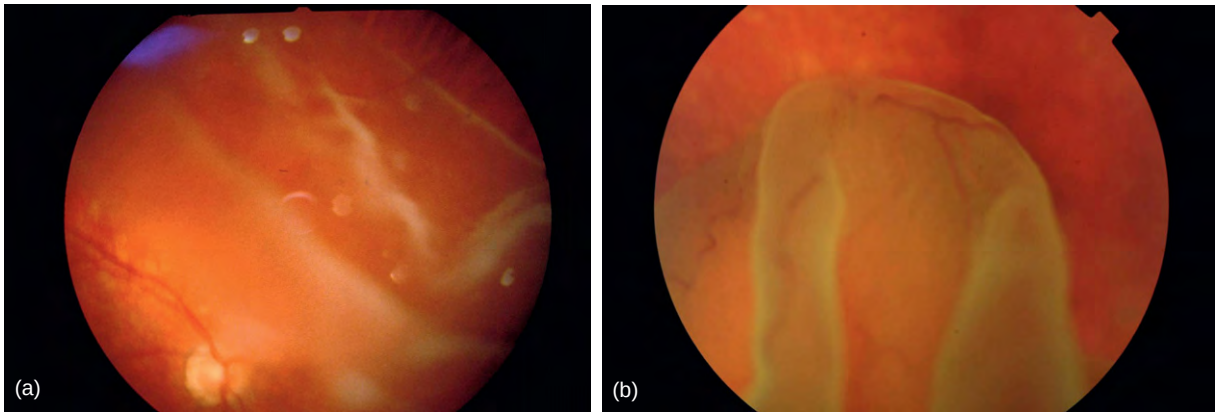

Figure 3 (a) Giant retinal tear characteristic of the retinal break seen in Stickler syndrome. (b) Retinal detachment caused by a giant retinal tear.

mitral regurgitation, dilation of the aortic root, and aortic regurgitation, with aneurysm of the aorta and aortic dissection being major life-threatening complications.

Vitreoretinopathies Associated with Progressive Retinal Dysfunction

The remaining hereditary vitreoretinopathies described in this article are purely ocular disorders. Those that are associated with retinal dysfunction – Wagner syndrome, erosive vitreoretinopathy, Goldmann–Favre syndrome, and enhanced S-cone syndrome (ESCS) – all have measurable electrophysiological changes of the retina demonstrated by recording a subnormal electroretinogram (ERG).

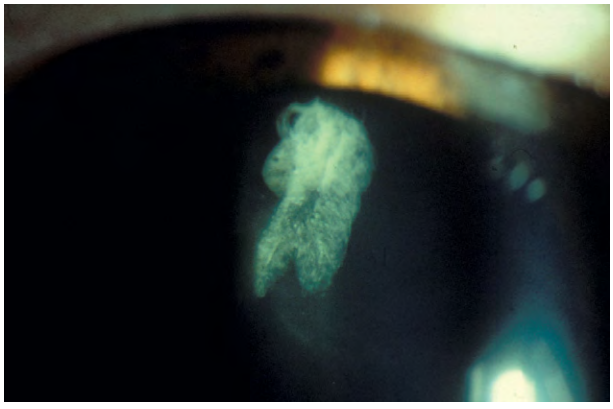

Figure 4 Congenital, quadrantic, lamellar cataract seen in both type 1 and type 2 Stickler syndrome.

Wagner syndrome (OMIM #143200)

The most striking finding in Wagner syndrome is the thickening and incomplete separation of the posterior hyaloid membrane, which tends to occur in a circular band and is variously described as a veil, sheets, or ropes. A large range of chorioretinal abnormalities have been described with the typical finding being chorioretinal atrophy with pigment migration into the retina (**Figure 11**). Electroretinographic responses are progressively subnormal (**Figure 12**) and visual-field testing demonstrates ring scotomas with eventual loss of central visual acuity. The chorioretinal pathology results in gradual progressive visual loss in the absence of retinal detachment, and has a progressive course. There is an association with early-onset cataract and mild myopia. Wagner syndrome is also associated with large angle kappas indicative of an ectopic fovea (**Figure 13**).

Prognosis in Wagner syndrome is poor with progressive visual loss. The risk of rhegmatogenous retinal detachment with Wagner syndrome is higher than that of the normal population, but the incidence does not appear to be as high as that seen in the Stickler syndromes.

The term Jansen syndrome has been used to describe a hereditary vitreoretinopathy but the clinical features reported are consistent with Wagner syndrome and linkage has been demonstrated in the original family to the same area as the causative gene in Wagner syndrome. The syndrome referred to as erosive vitreoretinopathy is reported to be associated with vitreous changes, hemeralopia with accompanying grossly reduced rod and cone responses, progressive chorioretinal atrophic changes, and combined traction-rhegmatogenous retinal detachments. Affected family members also had large angle kappas.

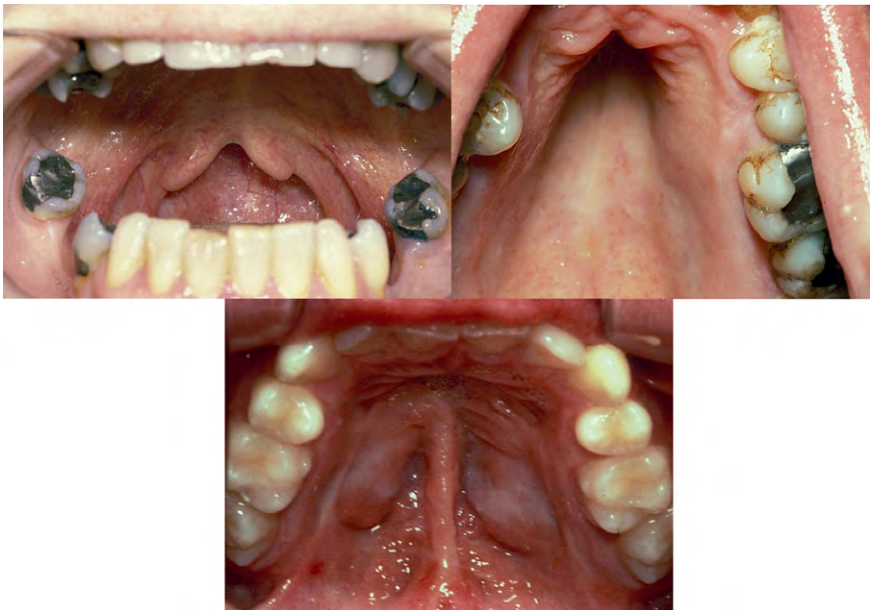

Figure 5 Bifid uvula and high-arch palate in Stickler syndrome.

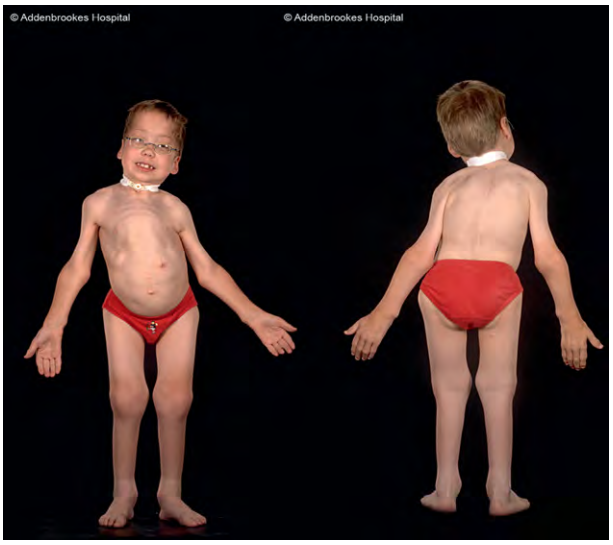

Figure 6 Kniest dysplasia demonstrating shortening of trunk and limbs.

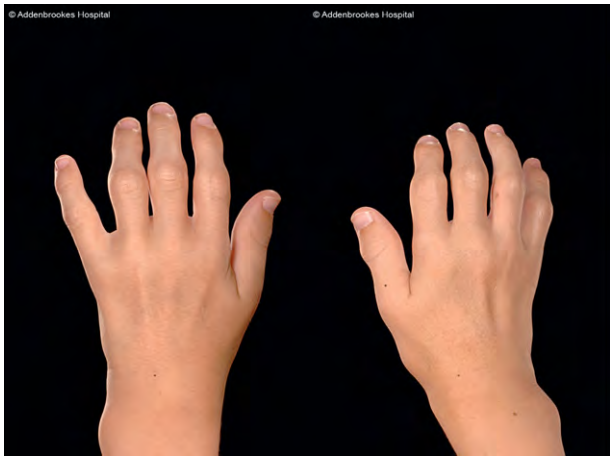

Figure 7 Interphalangeal dysplasia in Kniest dysplasia.

Mutations in the same gene that cause Wagner syndrome have been implicated in erosive vitreoretinopathy. It is likely both Jansen syndrome and erosive vitreoretinopathy are phenotypic variants of Wagner syndrome.

Goldmann–Favre syndrome/enhanced S-cone dystrophy (OMIM #268100)

Patients with Goldmann–Favre syndrome have liquefaction and fibrillar changes of the vitreous, night blindness, equatorial chorioretinal atrophy and pigment clumping, peripheral and macular schisis, cortical lens opacities, rod–cone dysfunction, and diffuse vascular leakage on fluorescein angiography. Goldmann–Favre syndrome is inherited as an autosomal recessive disorder and is now known to be caused by a mutation in the same gene that causes ESCS (the NR2E3 gene). ESCS is the only inherited retinal disease

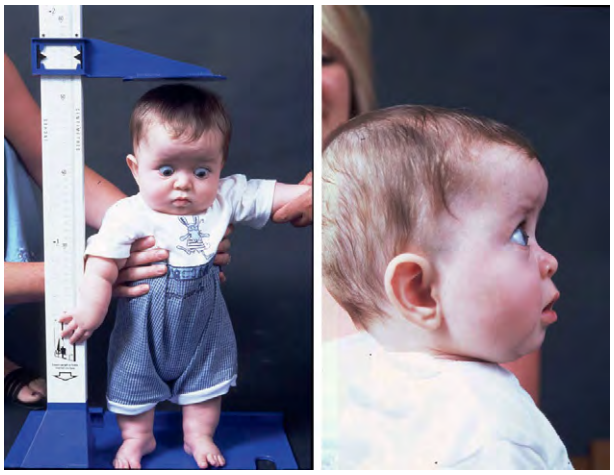

Figure 8 Spondyloepiphyseal dysplasia congenital demonstrating short stature and flattening of the midface.

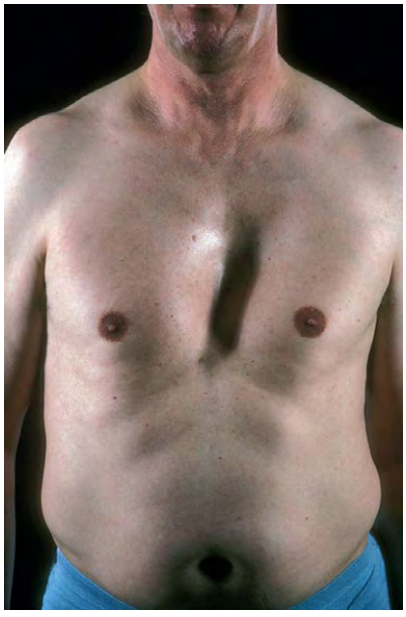

Figure 9 Pectus excavatum in Marfan syndrome.

which exhibits a gain in photoreceptor function, with patients showing enhanced sensitivity to blue (short wavelength) light, with night blindness and loss of sensitivity to long and medium wavelengths. The ERG findings in this group of disorders demonstrate undetectable rod-isolated responses and reduced combined rod–cone responses.

Vitreoretinopathies Associated with Abnormal Retinal Vasculature

The clinical feature on ocular examination of the hereditary vitreoretinopathies in this category is an abnormal

vascular pattern on the retina. This is demonstrated in more subtle cases using fluorescein angiographic studies.

Familial exudative vitreoretinopathy (OMIM #133780, #601813, and #305390)

The primary pathological process in familial exudative vitreoretinopathy (FEVR) is believed to be a premature arrest of retinal angiogenesis and vascular differentiation resulting in incomplete vascularization of the peripheral retina. The failure to vascularize the retina is the unifying feature seen in all affected individuals but, by itself, is usually asymptomatic. Secondary changes include neovascularization, retinal exudates, peripheral snowflake vitreous changes, and retinal traction. Epiretinal traction from vitreous and retinal surface membrane is the usual cause of retinal detachment and severe retinal distortion is a common finding resulting in retinal folds and tractional or combined tractional and rhegmatogenous retinal detachment (Figure 14). The prognosis is highly variable with some individuals blind by age 10 and others (sometimes within the same family) asymptomatic throughout adult life. The eye with the milder phenotype may have only a small avascular area, visible only on fluorescein angiography.

Figure 10 Ectopia lentis with dislocation of the lens superiorly in Marfan syndrome.

Autosomal dominant vitreochoroidopathy (OMIM #193220)

Autosomal dominant vitreochoroidopathy (ADVIRC) is characterized by vitreous liquefaction with or without peripheral vitreal condensations. Peripheral pigmentary changes typically occur at the equatorial region with a discrete posterior boundary associated with diffuse retinal vascular leakage, cystoid macular edema, and early-onset cataract. The peripheral pigmented band extends from the ora serrata to the equator for 360° of the retina. Other ocular associations are vitreous cells and condensation, puntate opacities in the retina, choroidal atrophy, and early nuclear sclerosis. The ERG responses are normal although the electroculogram (EOG) has been shown to be abnormal in ADVIRC.

Vitreoretinopathy Associated with Corneal Changes

The remaining category contains only one hereditary vitreoretinopathy called snowflake vitreoretinal degeneration named after the retinal appearance.

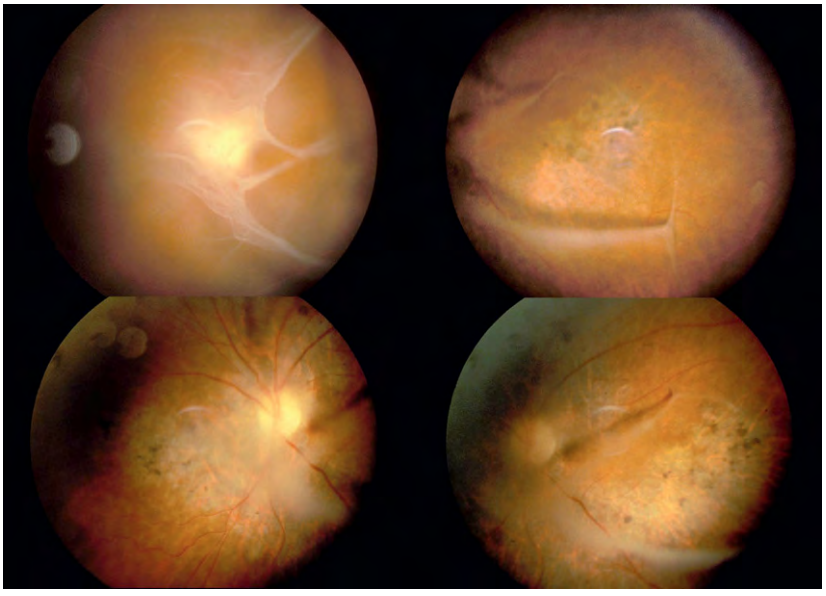

Figure 11 Fundal images showing vitreous condensations and chorioretinal atrophy characteristic of Wagner syndrome.

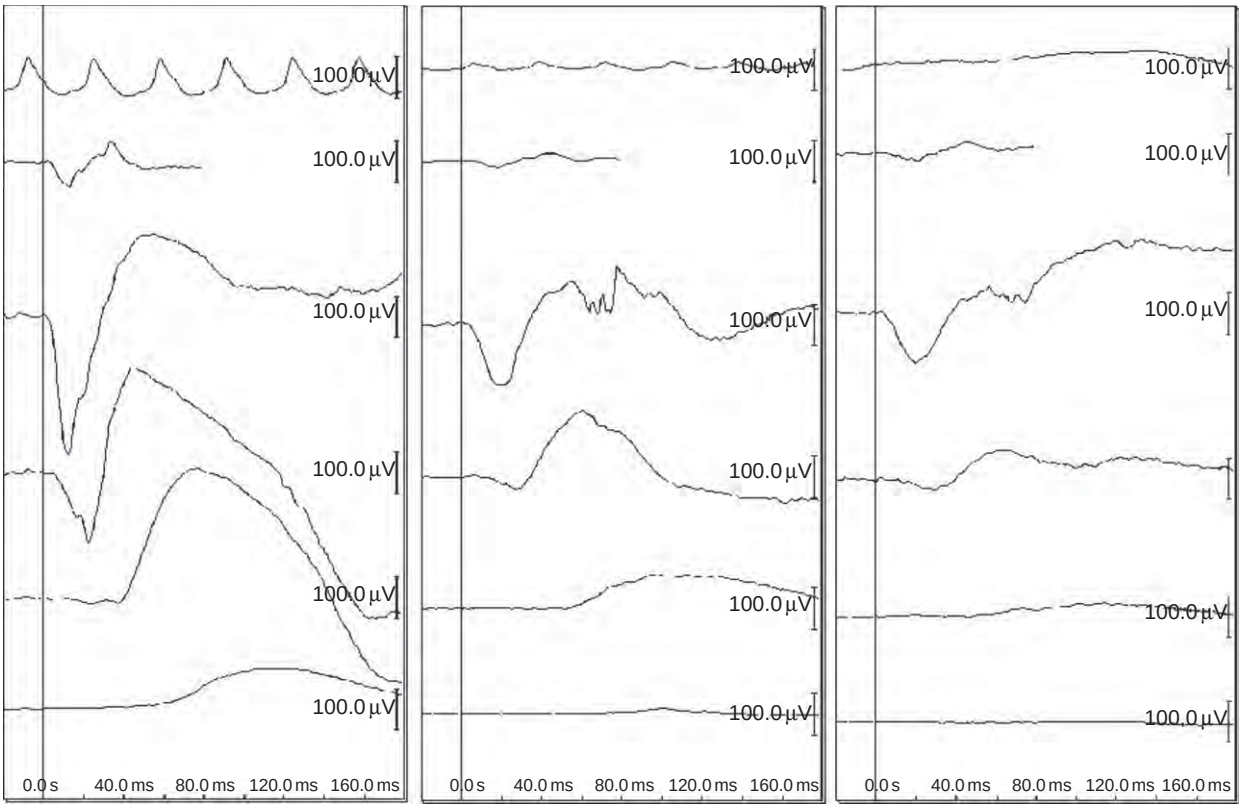

Figure 12 Rod and cone electroretinograms. (a) Representative normal responses, (b) responses from the left eye of a patient with Wagner syndrome aged 55, and (c) responses from the left eye of the daughter aged 19 who had inherited Wagner syndrome. The top two traces are light-adapted cone responses to 30-Hz flicker and to a bright flash; lower four traces are dark-adapted rod and mixed rod–cone responses to a range of stimulus intensities from dim (bottom) to bright (fourth from bottom).

Snowflake vitreoretinal degeneration (OMIM #193230)

The pathognomic feature of snowflake vitreoretinal degeneration is the association with corneal guttata. Disk pallor is also a key feature of snowflake vitreoretinal degeneration not described in any of the other hereditary vitreoretinopathies. The vitreous has a fibrillar appearance. The snowflake-like opacities in the retina are small and may not be immediately obvious. Minor vascular abnormalities of small retinal vessels have been described in snowflake vitreoretinal degeneration.

Molecular Genetics of the Hereditary Vitreoretinopathies

The classification in Table 1 correlates with genotype. Table 3 lists the causative genes that have been identified to date in the hereditary vitreoretinopathies with the protein affected (Table 3).

Mutations in genes coding for the structural components of vitreous result in a hereditary vitreoretinopathy. In common with connective tissues in other parts of the body, vitreous is composed of an extracellular matrix with relatively few cells and the arrangement of the collagenous proteins, along with the high water content, maintains transparency. Vitreous collagen fibrils are heterotypic and have a core of type II and V/XI collagen, with type IX collagen on the surface. Mutations in genes coding for chains which comprise these three types of collagen result in the most common hereditary vitreoretinopathy, Stickler syndrome.

The majority of patients with Stickler syndrome have type 1 Stickler syndrome which is part of the spectrum of type II collagen disorders along with Kniest dysplasia and SEDC. Most have premature termination mutations of the COL2A1 gene and are characterized by a membranous vitreous appearance on biomicroscopy. Other pedigrees exhibit a different beaded vitreous phenotype and are associated with mutations in one of the genes coding for type V/XI collagen (COL11A1). Type 1 Stickler syndrome, in the majority of cases, results from haploinsufficiency from nonsense-mediated decay through point mutations or frameshifts, whereas type 2 Stickler syndrome results from dominant negative mutations.

Collagen types II and IX are expressed in both vitreous and cartilage, so Stickler syndrome is characterized by an

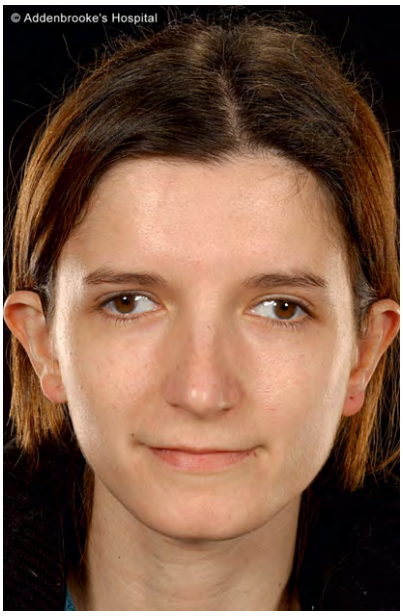

Figure 13 Pseudoexotropia in Wagner syndrome.

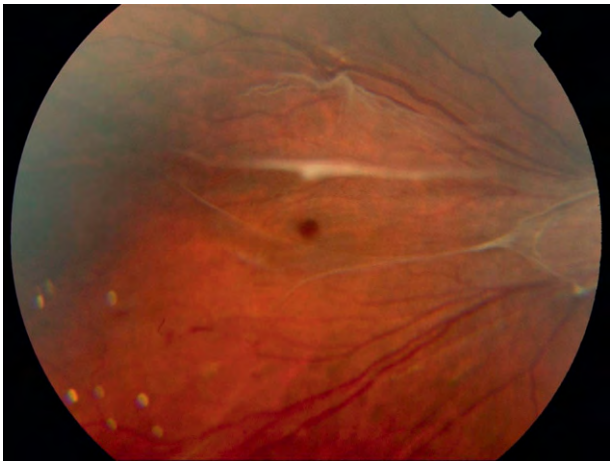

Figure 14 Retinal folds seen in familial exudative vitreoretinopathy.

ocular and skeletal phenotype. Cartilage also contains type XI collagen, which is similar to the type V/XI collagen of vitreous and they share the α1(XI) chain that is encoded by COL11A1; so mutations in this gene have an ocular and skeletal phenotype. A subgroup of Stickler syndrome, designated predominantly ocular, or ocular-only, has been shown to result from mutations of COL2A1 which are preferentially expressed in ocular tissues. Exon 2 of COL2A1 is spliced out of cartilage type II collagen and therefore mutations in exon 2 have a normal skeletal phenotype while displaying the characteristic ocular features of Stickler syndrome. Prior to detailed understanding of the molecular genetics of Stickler syndrome, the existence of patients demonstrating ocular features without systemic findings was a source of confusion between Stickler syndrome and other vitreoretinal degenerative conditions without systemic involvement.

Fibrillins are one of the main constituents of extracellular microfibrils and these provide structural support in many tissues. Mutations in FBN1, encoding for fibrillin 1, are the major cause of Marfan syndrome. Mutations in a second gene, transforming growth factor beta receptor II (TGFBR2), have been found in patients fulfilling the clinical criteria for Marfan syndrome, but the mechanism for this remains to be clarified.

Wagner syndrome is a further example of a hereditary vitreoretinopathy which results from a mutation in a gene coding for a structural protein in the vitreous. CSPG2 encodes the core protein of a chondroitin sulfate proteoglycan called versican. Versican binds hyaluronan and therefore may contribute to the structure of the vitreous. Versican undergoes alternative splicing and several splice variants have been identified in the eye. All causative mutations to date affect the splicing of exon 7 of the CSPG2 gene which represents one of two glycosaminoglycan attachment sites. In Wagner syndrome there is an altered appearance to the vitreous, and progressive retinal dysfunction and hemeralopia even in the absence of retinal detachment, suggesting that versican has additional roles to being a structural component of the vitreous.

FEVR is also genetically heterogenous. All the causative genes to date in FEVR code for proteins involved in the Wnt signaling pathway. Frizzled homolog 4 (Drosophila) (FZD4) is a presumptive Wnt receptor, lipoprotein-receptor-related protein 5 (LRP5) can transduce Wnt signaling *in vitro*, and Norrie disease (Pseudoglioma) (NDP) encodes for norrin. Norrin is present in extracellular matrices and is thought to act as a ligand-receptor pair with FZD4. Although unrelated to Wnts, norrin may act on the Wnt signaling pathway through the frizzled receptor. Wnt receptors are implicated in retinal neovascularization. NDP mutations can also cause Norrie disease (characterized by incomplete retinal vascularization along with more extensive retinal degenerative changes, microphthalmia, and progressive mental disorder).

In general, the molecular genetics of the hereditary vitreoretinopathies demonstrate how mutations of key genes involved in ocular development and structure can result in different phenotypes. Goldmann–Favre syndrome is allelic with enhanced S-cone dystrophy (ESCD). The responsible gene encodes a retinal nuclear receptor involved in signaling pathways. ADVIRC is allelic with Best's macular dystrophy and results from mutations in the VMD2 gene encoding a transmembrane chloride channel. Snowflake vitreoretinal dystrophy is caused by a mutation in a gene encoding a different transmembrane channel.

Of the hereditary vitreoretinopathies associated with skeletal abnormalities, the majority are inherited as an autosomal dominant trait. The exceptions are Stickler

Table 3 Causative genes identified to date and the protein affected in the hereditary vitreoretinopathies

Vitreoretinopathy	*OMIM number*	*Causative gene*	*Affected protein*	*First reference*
Stickler syndrome	#108300	COL2A1	Type II collagen	Ahmad et al. (1991)
	#604841	COL11A1	Type XI collagen	Richards et al. (1996)
	#108300	COL9A1	Type IX collagen	van Camp et al. (2006)
Kniest dysplasia	#156550	COL2A1	Type II collagen	Winterpacht et al. (1993)
SEDC	#183900	COL2A1	Type II collagen	Tiller et al. (1995)
Knobloch syndrome	#267750	COL18A1	Type XVIII collagen	Sertie et al. (2000)
Marfan syndrome	#154700	FBN1	Fibrillin	Dietz et al. (1991)
		TGFBR2	Transmembrane receptor	Boileau et al. (1993)
Wagner syndrome	#143200	CSPG2	Chondroitin sulfate proteoglycan	Miyamoto et al. (2005)
Goldmann–Favre syndrome	#268100	NR2E3	Retinal nuclear receptor	Sharon et al. (2003)
FEVR	#133780	FZD4	Wnt receptor	Robitaille et al. (2002)
	#601813	LRP5	Wnt receptor	Toomes et al. (2004)
	#305390	NDP	Wnt receptor ligand	Fullwood et al. (1993)
ADVIRC	#193220	VMD2	Bestrophin	Yardley et al. (2004)
Snowflake vitreoretinopathy	#193230	KCNJ13	K^+ transporter	Hejtmancik et al. (2008)

syndrome specifically associated with COL9A1 mutations, and Knobloch syndrome, both of which have an autosomal recessive pattern of inheritance. Wagner syndrome/erosive vitreoretinopathy is inherited in an autosomal dominant pattern. Favre–Goldmann syndrome/ESCD is autosomal recessive. Vitreoretinopathies associated with abnormal retinal vascularization are again inherited as autosomal dominant traits for the majority with the one exception being an X-linked form of FEVR. Snowflake vitreoretinal dystrophy is autosomal dominant.

See also: Molecular Composition of the Vitreous and Aging Changes; Rhegmatogenous Retinal Detachment; Secondary Photoreceptor Degenerations; Vitreous Anatomy, Aging, and Anomalous Posterior Vitreous Detachment.

Further Reading

Ahmad, N. N., Ala-kokko, L. A., Knowlton, R. G., et al. (1991). Stop codon in the procollagen II (COL2A1) in a family with Stickler syndrome (arthro-ophthalmopathy). *Proceedings of the National Academy of Sciences of the United States of America* 88: 6624–6627.

Boileau, C., Jondeau, G., Babron, M-C., et al. (1993). Autosomal dominant Marfan-like connective-tissue disorder with aortic dilation and skeletal anomalies not linked to the fibrillin gene. *American Journal of Human Genetics* 53: 46–54.

Dietz, H. C., Cutting, G. R., Pyeritz, R. E., et al. (1991). Marfan syndrome caused by a recurrent *de novo* missense mutation in the fibrillin gene. *Nature* 352: 337–339.

Fullwood, P., Jones, J., Bundey, S., et al. (1993). X-linked exudative vitreoretinopathy: Clinical features and genetic linkage analysis. *British Journal of Ophthalmology* 77: 168–170.

Hejtmancik, J. F., Jiao, X., Li, A., et al. (2008). Mutations in KCNJ13 cause autosomal-dominant snowflake vitreoretinal degeneration. *American Journal of Human Genetics* 82(1): 174–180.

Miyamoto, T., Inoue, H., Sakamoto, Y., et al. (2005). Identification of a novel splice site mutation of the CSPG2 gene in a Japanese family with Wagner syndrome. *Investigative Ophthalmology and Visual Science* 46: 2726–2735.

Richards, A. J., Yates, J. R. W., Williams, R., et al. (1996). A family with stickler syndrome type 2 has a mutation in the COL11A1 gene resulting in the substitution of glycine 97 by valine in alpha1(XI) collagen. *Human Molecular Genetics* 5(9): 1339–1343.

Robitaille, J., MacDonald, M. L., Kaykas, A., et al. (2002). Mutant frizzled-4 disrupts retinal angiogenesis in familial exudative vitreoretinopathy. *Nature Genetics* 32(2): 326–330.

Ryan, S. J., Hinton, D. R., Schachat, A. P., and Wilkensen, P. (eds.) (2006). *Retina,* 4th edn. Philadelphia, PA: Elsevier.

Sertie, A. L., Sossi, V., Camargo, A. A., et al. (2000). Collagen XVIII, containing an endogenous inhibitor of angiogenesis and tumor growth factor, plays a critical role in the maintenance of retinal structure and in neural tube closure (Knobloch syndrome). *Human Molecular Genetics* 9: 2051–2058.

Sharon, D., Sandberg, M. A., Caruso, R. C., Berson, E. L., and Dryja, T. P. (2003). Shared mutations in NR2E3 in enhanced S-cone syndrome, Goldmann–Favre syndrome, and many cases of clumped pigmentary retinal degeneration. *Archives of Ophthalmology* 121(9): 1316–1323.

Taylor, D. and Hoyt, C. S. (eds.) (2005). *Pediatric Ophthalmology and Strabismus,* 3rd edn. Philadelphia, PA: Elsevier.

Tiller, G. E., Weis, M. A., Polumbo, P. A., et al. (1995). An RNA-splicing mutation (G+5IVS20) in the type II collagen gene (COL2A1) in a family with spondyloepiphyseal dysplasia congenital. *American Journal of Human Genetics* 56(2): 388–395.

Toomes, C., Bottomley, H. M., Jackson, R. M., et al. (2004). Mutations in LRP5 or FZD4 underlie the common familial exudative vitreretinopathy locus on chromosome 11q. *American Journal of Human Genetics* 74(4): 721–730.

Van Camp, G., Snoeckx, R. L., Hilgert, N., et al. (2006). A new autosomal recessive form of stickler syndrome is caused by a mutation in the COL9A1 gene. *American Journal of Human Genetics* 79(3): 449–457.

Winterpacht, A., Hilbert, M., Schwarze, U., et al. (1993). Kniest and Stickler dysplasia phenotypes caused by collagen type II gene (COL2A1) defect. *Nature Genetics* 3(4): 323–326.

Yardley, J., Leroy, B. P., Hart-Holden, N., et al. (2004). Mutations of VMD2 splicing regulators cause nanophthalmos and autosomal dominant vitreoretinochoroidopathy (ADVIRC). *Investigative Ophthalmology and Visual Science* 45(10): 3683–3689.

Relevant Website

http://www.ncbi.nlm.nih.gov – National Center for Biotechnology Information, Online Mendelian Inheritance in Man.

Histogenesis, Cell Fate, and Signaling Factors

M Cwinn, B McNeill, A Ha, and V A Wallace, Ottawa Hospital Research Institute, Ottawa, ON, Canada

Glossary

Cell extrinsic signaling – It refers to the activation of a biological pathway within a particular cell by an extracellular factor such as a hormone and morphogen.

Cell intrinsic signaling – It refers to the activation of a biological pathway within a particular cell by a factor that is produced by that cell and is not secreted, such as a transcription factor.

Differentiation – The process whereby a less-specialized cell, such as a progenitor, becomes a specialized cell type. In general, a cell undergoing a differentiation program will exit the cell cycle and become restricted in the number of lineages it can adopt.

Lineage commitment/fate specification – The process whereby cell intrinsic and extrinsic cues will direct a progenitor cell toward differentiating into a specific cell lineage or cell type.

Multipotency – The ability of a particular progenitor cell to give rise to a limited number of different cell lineages.

Retinal progenitor cell (RPC) – An undifferentiated, proliferating, multipotent cell located in the neuroblast layer of the developing retina. RPCs are competent to give rise to the six neural and one glial cell types found in the mature retina; however, as retinal development proceeds, the competence of an RPC becomes restricted. The undifferentiated state, proliferative capacity, and multipotency of RPCs is controlled by both cell extrinsic and intrinsic signaling factors.

Introduction

The six different types of neurons and the one glial cell type in the adult vertebrate retina are generated in a conserved temporal sequence from a pool of multipotential retinal progenitors cells (RPCs). Retinal ganglion cells (GCs), cone photoreceptors, horizontal cells, and half of the amacrine neurons are born during the embryonic period, while the remaining amacrine neurons, bipolar neurons, and Müller glia are born in the postnatal period. Rod photoreceptors are generated throughout histogenesis. To explain the temporal sequence of neuron generation from multipotential progenitors, a competence model has been proposed in which RPCs progress irreversibly through a series of stages where they are competent to generate a limited number of cell types. Because, depending upon the species, retinal histogenesis occurs over several days to weeks, factors that influence proliferation, timing of differentiation, as well as cell fate will impact this program. The role of transcription factors in lineage specification of RPCs is well established and a growing body of evidence also implicates a role for intercellular signaling in this process. Here, we review the impact of major developmental signaling pathways such as Hedgehog, Wnt, Notch, transforming growth factor-β (TGF-β), and retinoic acid (RA) on the histogenic program in the vertebrate retina.

Notch

The notch pathway is an evolutionarily conserved intercellular signaling mechanism that regulates numerous cellular programs. Activation of notch signaling is initiated through interaction of the notch extracellular domain on the surface of one cell with the DSL ligands (Delta, Serrate, and Lag2) on the surface of a neighboring cell (**Figure 1**). Upon binding to the DSL ligand, notch is cleaved by the γ-secretase complex releasing the notch intracellular domain (NICD). NICD translocates to the nucleus where it interacts with C-promoter binding factor 1/suppressor of hairless/longevity assurance gene 1 (CSL) complex and converts it from a transcriptional repressor to an activator. In the absence of notch signaling, CSL recruits corepressor proteins to form a transcriptional repressor complex, which inhibits target gene expression. The association of NICD with CSL displaces corepressors and recruits coactivators which results in transcriptional activation of basic helix–loop–helix (bHLH) transcription factors such as hairy and enhancer of split 1 and 5(Hes1 and Hes5).

Findings from early studies on the role of notch signaling in the retina suggest that one of its major functions is in controlling the timing of cell cycle exit and maintenance of the retinal progenitor pool. For example, in the frog, fish, rat, chick, and mouse retina the level of notch signaling is inversely proportional to the rate of cell cycle exit and neuronal differentiation. Similar to its actions in other regions of the central nervous system (CNS), the antidifferentiation effects of notch activity in the retina are associated with inhibition of proneural bHLH gene

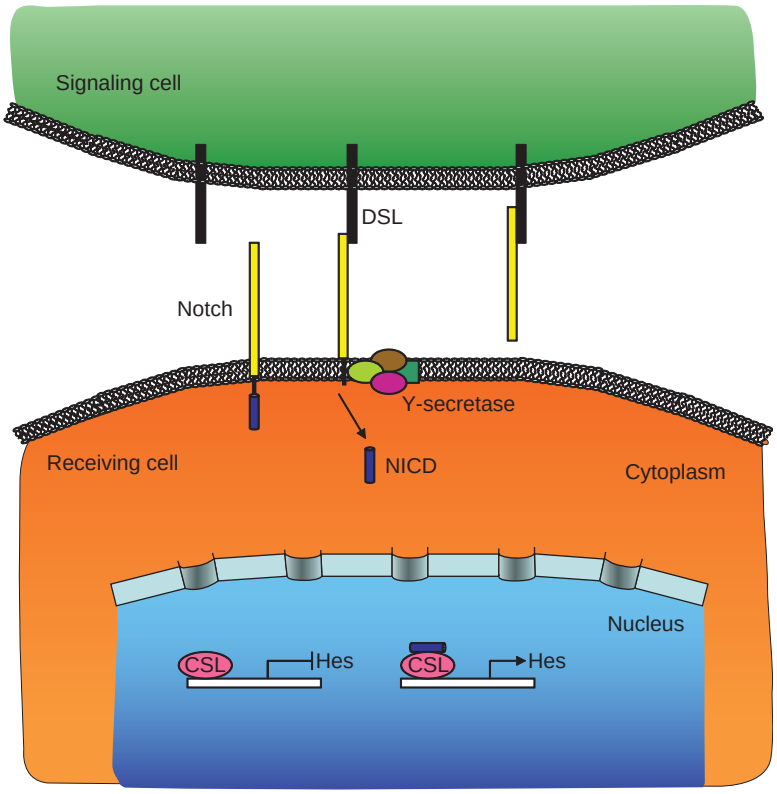

Figure 1 The notch signaling pathway. Ligand binding to the notch receptor leads to a γ-secretase-mediated proteolytic cleavage resulting in the release of the notch intracellular domain (NICD). NICD is able to enter the nucleus and associate with CSL (CBF1, Su(H), Lag1) resulting in transcription activation of target genes such as Hes genes.

expression. While notch activity does not appear to influence the temporal competence of retinal, it has been implicated in cell fate selection. Notch pathway inactivation at early stages of retinal development results in the preferential production of GC or cone photoreceptors and increased notch signaling or expression of its downstream effectors, Hes1 and Hes5, at later stages of retinal development promotes Müller glial cell development. If notch signaling maintains RPCs in cycle, it follows that notch signaling has to be reduced for RPCs to differentiation. Recent work in zebrafish suggests that regional differences in the localization of notch ligands contribute to the variability in notch signaling levels in the retinal neuroepithelium, thereby promoting the balance between cell cycle reentry and exit.

The Wnt Pathway

Wnt signaling has been shown to regulate a number of cellular processes, including differentiation, proliferation, polarity, and migration. Wnt molecules are lipid-modified secreted glycoproteins and 21 vertebrate Wnt homologs have been identified to date. Wnt binding to frizzled (Fzd) receptors and low-density lipoprotein-related receptor 5/6 (Lrp5/6) coreceptors induces the activation of the cytoplasmic phosphoprotein disheveled (Dsh). Three distinct signaling pathways have been described that function downstream of Dsh activation: canonical, planar cell polarity (PCP), and the Wnt/calcium pathway (**Figure 2**). The canonical Wnt pathway, the best characterized of the three, functions to regulate the stability and transcriptional activity of β-catenin. In the absence of Wnt signaling, β-catenin is phosphorylated and targeted for proteosome-dependent degradation by the axin/adenomatous polyposis coli (APC)/glycogen synthase kinase-3β (GSK-3β) destruction complex. Wnt signaling inhibits the activity of the degradation complex, which allows stabilized β-catenin to translocate to the nucleus where it interacts with T-cell factor (TCF)/lymphoid enhancing binding factor (LEF) transcription factors to regulate target gene expression. In the PCP pathway, which is involved in cell and tissue polarity, Rho GTPases are activated leading to alterations in the cytoskeleton. Finally, the Wnt/calcium pathway stimulates the release of intracellular calcium and activates protein kinase C and calcium/calmodulin-dependent protein kinase II to regulate cell fate and movement.

Gene expression profiling has revealed the expression of a number of Wnt pathway components, including Wnt ligands and Fzd receptors in the developing retina.

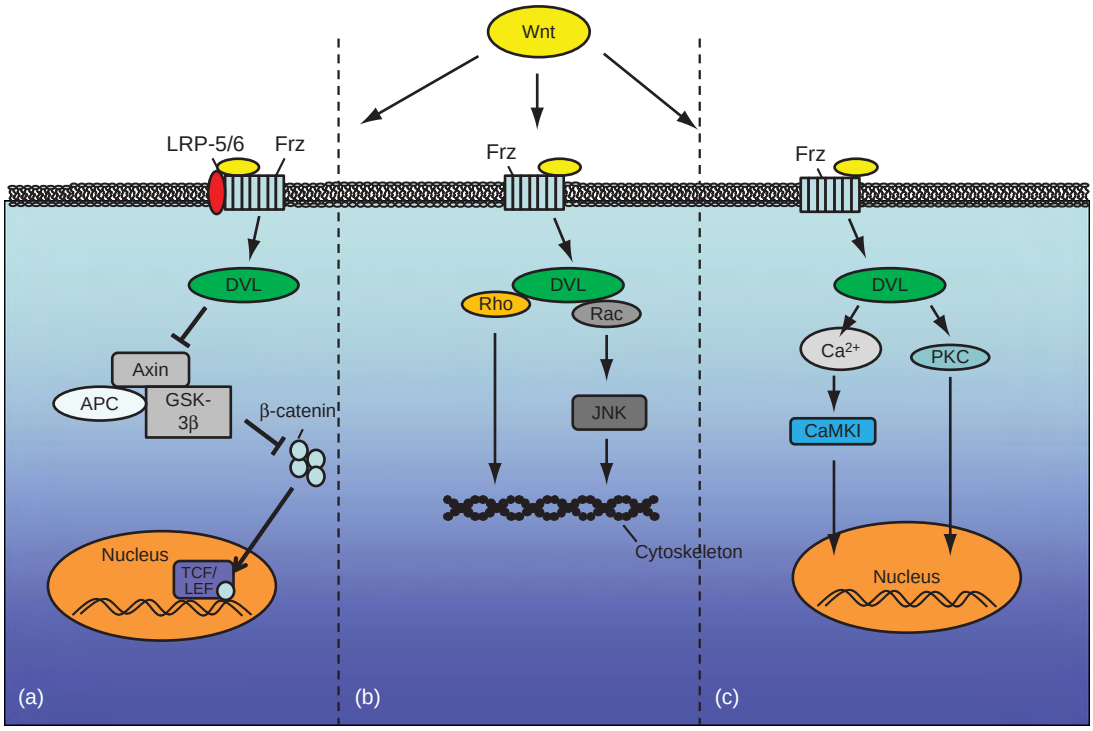

Figure 2 Wnt signaling pathway. Wnt signaling is initiated with the binding of a Wnt protein to its transmembrane receptor frizzled (Frz), leading to activation of one of three main branches of the Wnt signaling pathway. (a) Canonical signaling pathway, where the inhibition of the Axin/APC/GSK-3β destruction complex leads to an accumulation of β-catenin that is able to translocate into the nucleus and regulate transcription. (b) Planar cell polarity (PCP) pathway, where activation of Rho GTPases, Rho, and Rac results in changes to the cytoskeleton. (c) Wnt or calcium pathway, where an increase in intracellular calcium activates protein kinase C (PCK) and calcium or calmodulin-dependent protein kinase II (CaMKII) to regulate cell fate and movement.

The analysis of TCF/LEF transgenic Wnt reporter mice suggests that canonical Wnt signaling is active during eye development. Numerous studies published in recent years on chick, fish, frog, and mammals have implicated Wnt activity in retinal field establishment, retinal regeneration, and lens development. The role of Wnt signaling in retinal histogenesis is more controversial. In the frog, Fzd5 signaling through β-catenin is required for the induction of *Sex determining Y-box 2* (*Sox2*) expression and retinal neurogenesis. In the mouse and chick, however, canonical Wnt pathway activation suppresses neurogenesis and neuronal differentiation. The function of Fzd5 and β-catenin in retinal development is not conserved, as retinal cell specification and proliferation are normal in knockout mice for these genes, although β-catenin is required for lamination and cell adhesion in the retina. Moreover, the effect of Wnt/β-catenin on proliferation appears to be context and species dependent. Increased canonical Wnt signaling promotes proliferation in the frog and fish retina as well as at the marginal zone in the chick retina, but it inhibits proliferation in peripheral regions of the mouse and chick retina. One common theme that has emerged from these studies is the effect of Wnt/β-catenin signaling at the peripheral region of the developing eyecup. In mouse and chick, Wnt/β-catenin promotes the acquisition of peripheral eyecup fates, including the ciliary marginal zone, ciliary body, and iris. Thus, the conservation of Wnt/β-catenin signaling in eye development might be at the level of the localization of the signal, rather than its developmental outcome.

The Hedgehog Signaling Pathway

Members of the Hedgehog (Hh) protein family are secreted signaling molecules that mediate patterning and growth in a number of tissues and organs during embryonic development. In mammals, there are three members of the hedgehog family: Sonic Hedgehog (Shh), Desert Hedgehog, and Indian Hedgehog. The biologically active amino-terminal fragment of Hh proteins is generated by autoproteolytic cleavage of the precursor protein, which is catalyzed by residues in the carboxy terminal domain of the precursor protein. Fully processed Hh-N is lipid modified with palmitate at the amino terminus and cholesterol at the carboxy terminus. For simplicity, we will refer to fully processed Shh-N as Shh. The Hh signaling cascade is initiated by Hh binding to its receptor, the 12-pass transmembrane protein, Patched (Ptc), and subsequent derepression of Smoothened (Smo), a seven-transmembrane domain

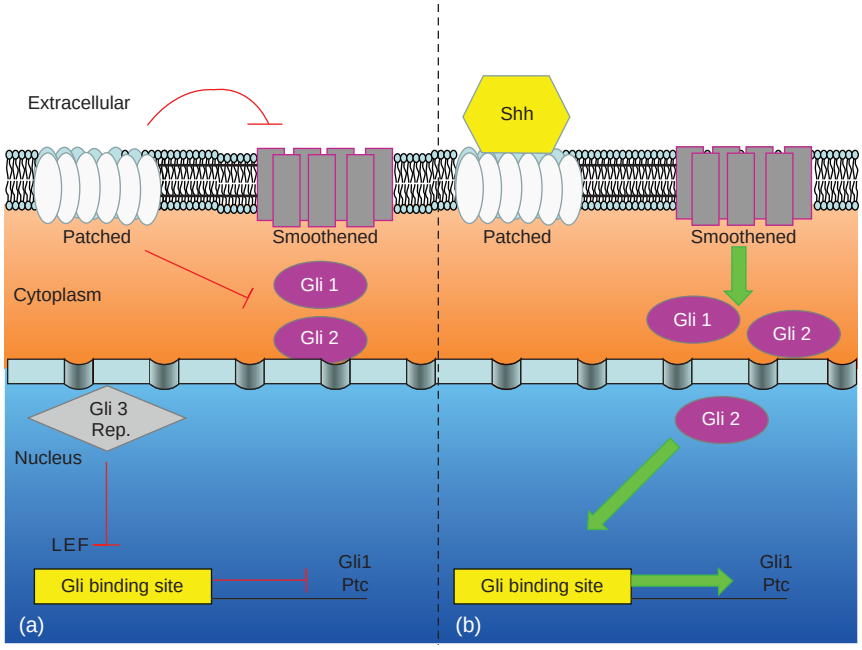

Figure 3 The hedgehog signaling pathway. (a) In the absence of Shh ligand, Patched (Ptc) represses Smoothened (Smo), leading to the inactivation of the Shh pathway. In this scenario, Gli3 repressor can also bind Gli consensus motifs to further repress hedgehog pathway activity. (b) The binding of Shh to Ptc derepresses Smo. The signaling cascade then converges on the Gli1 and Gli2 transcription factors that translocate into the nucleus to induce the transcription of target genes, such as Gli1 and Ptc.

receptor that mediates signal transduction leading to target gene activation (**Figure 3**). The signaling cascade converges on the activity of the *Gli* transcription factors, which regulate target gene expression, in part, through binding to conserved sequences in the promoters and enhancers of these genes. In vertebrates, there are three *Gli* proteins: *Gli1, Gli2*, and *Gli3*. *Gli1* and *Ptc* are direct targets of the Hh signaling pathway and the presence of mRNA for these genes indicates regions of active Hh signaling in tissues.

Retinal expression of Hh pathway components has been described in a number of vertebrate species. Several lines of evidence indicate that Shh expression in GCs is the primary mediator of Hh signaling during retinal development. The timing of Shh and Gli induction in GCs and RPCs, respectively, mirrors the central to peripheral wave of GC differentiation. GCs and Shh are required for Gli induction in RPCs, as GC ablation in explant culture or through conditional endotoxin expression abrogates *Gli1* expression, as does conditional inactivation of *Shh* in the retina. In the adult murine retina, *Shh* is also expressed in the inner nuclear layer most likely in amacrine neurons and *Ptc* is expressed in Müller glia; however, the functional significance of Hh pathway expression at this stage is not known.

Shh signaling has been shown to play a critical role in the histogenic program of RPC in a number of vertebrate species. Shh functions as a mitogen for RPCs, thereby regulating the total cell number in the retina. The mitogenic effect of Hh signaling in this context is mediated, in part, through its effects on the kinetics of the cell cycle and the regulation of G1 and G2 cell cycle genes. Shh signaling also exerts species-dependent effects on the timing of cell cycle exit of RPCs. In the mouse, Hh is required to maintain RPC in the cell cycle, possibly by regulating expression of Hes1, an antidifferentiation bHLH transcription factor. Conversely, in zebrafish, Hh signaling is required for driving cell cycle exit, in part through the induction of p57, a cyclin-dependent kinase inhibitor. These Hh-dependent effects on cell cycle exit are associated with alterations in retinal histogenesis, as loss of Hh signaling in both species results in a deficit in late born retinal cell types. Shh signaling also exerts cell cycle-independent effects on GC development. Gain and loss of function studies in chick and mouse have demonstrated a requirement for Shh in negatively regulating GC development, thereby providing a mechanism by which GC control their number by feedback inhibition.

These studies on Hh signaling in the retina highlight the importance of GC-derived signals on the histogenic program in the retina and they also show how impacting the cell cycle and timing of differentiation contribute toward the establishment of the correct balance of retinal cell types.

Transforming Growth Factor-β

The TGF-β superfamily of signaling molecules is comprised of a number of subgroups, including the TGF-β,

the bone morphogenic protein (BMP), and the growth and differentiation factor (GDF) subgroups. The TGF-β family members are involved in a variety of different developmental processes, including proliferation, migration, and cell death. Classical TGF-β signaling (**Figure 4**) involves ligand binding to a heteromeric receptor complex consisting of two type I and type II receptors that results in the activation and dimerization of homolog of mothers against Dpp (Smad) transcription factors, which then translocate into the nucleus where they interact with a number of cofactors to regulate target gene transcription. Signaling through different receptor combinations and Smad coactivators/corepressors allows members of the TGF-β superfamily to induce a multitude of cell-type and context-specific outputs. In the context of the retina, members of the TFG-β superfamily have been implicated in several aspects of retinal histogenesis including, the regulation of programmed cell death (PCD), progenitor proliferation, and patterning.

TGF-β signaling proteins (TGF-β1, -β2, and -β3) are important for the regulation of PCD, proliferation, and cell fate determination. Single TGF-β2 or double TGF-β2, and TGF-β3 null mice exhibit retinal hypercellularity likely as a consequence of reduced PCD during retinal development. TGF-β1 may also play a role in PCD as explants from early postnatal mice exhibit increased PCD in the presence of TGF-β1. In the early postnatal retina, TGF-β2 is the most abundantly expressed TGF-β family subtype, and it has been implicated in the induction of mitotic senescence of retinal progenitor cells and Müller glia. In addition to controlling PCD and proliferation, TGF-β2 plays a role in cell fate determination, as it negatively regulates amacrine cell genesis.

Studies to date have implicated BMP4 and BMP7 in early eye formation, retinal patterning, and retinal cell survival. The majority of BMP4 null embryos die prior to the stage of eye development; however, the cohort that survives to later stages fail to form a lens and some exhibit malformed optic vesicles. Consistent with a role for BMP4 signaling in eye development, mutations in BMP4 are associated with eye abnormalities in humans, the most severe being anopthalmia. Within the retina proper, BMP4 plays a role in the patterning of the retina by regulating transcription factors required for dorsal retina identity. Interestingly, BMP4 gene dosage is important for normal eye development, as haploinsufficiency for BMP4 in mice is associated with eye defects, such as a reduction in the number of ganglion and inner nuclear cells. BMP7 dosage is also important for eye development as gain and loss of function for BMP7 is associated with apoptosis in the retina and microopthalmia and anophthalmia. BMP signaling is also important for the specification of peripheral eye fates, such as the ciliary body. BMP4 and BMP7 are expressed in the ciliary margin, the distal part of the eye cup, and BMP signaling is required to maintain this structure, as it differentiates into neurons in the presence of ectopically expressed Noggin, a soluble BMP antagonist.

Studies employing mice that are conditionally null for type 1 BMP receptors have provided further evidence in support of a general role for BMP signaling in retinal

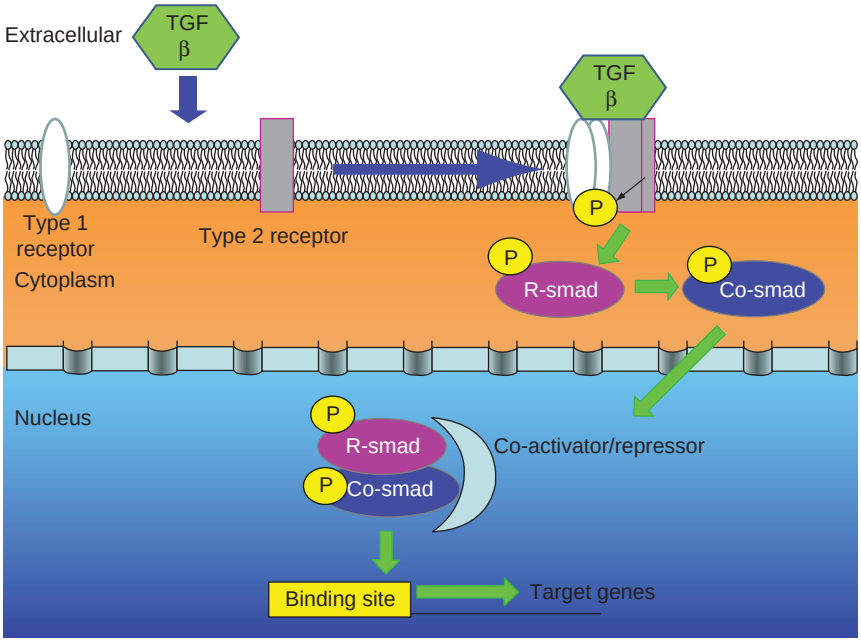

Figure 4 The TGF-β signaling pathway. The TGF-β signaling molecule binds to the heteromeric receptor complex consisting of type-1 and type-2 receptors, resulting in the phosphorylation of the type-1 receptor. This leads to the phosphorylation of a receptor Smad (R-Smad) which then dimerizes with a common-Smad (Co-Smad). The Smad complex then translocates to the nucleus where it can associate with a variety of coactivators or corepressors and modulate gene expression.

development. Two type I BMP receptors, BMPR-Ia and BMPR-Ib, are expressed in the retina. Deletion of either BMP-Ia or BMP-Ib alone does not have a drastic phenotype, likely due to compensatory functions of the two receptors. However, compound BMPR-1a$^{-/-}$BMPR-1b$^{+/-}$ mutant mice have dorsal retina patterning defects and mice null for both genes initially develop an eye structure but the retina undergoes extensive apoptosis and the mice are anopthalmic or microopthalmic at birth. Thus, the effects of BMPR-I deletions further demonstrate the roles of BMP's in eye development and patterning as well as cell survival and confirm the requirement for correct BMP dosage during eye development.

Although it is evident that TGF-β signaling is crucial for retinal development, the functions of other TGF-β family members in retinal development and histogenesis are still being uncovered. For example, GDF-11 has recently been shown negatively regulate ganglion cell genesis by controlling the time that RPCs are competent to produce this cell type. Thus, in GDF-11 null mice, an increase in RGCs occurs at the expense of amacrine cells and photoreceptors. Although it is not as defined as in the murine retina, some of the effects of TGF-β signaling in retinal development may also be conserved in other vertebrate species. For example, TGF-β and BMP signaling molecules are expressed in the chick and frog retina. In the chick, both TGF-β and BMP4 may play a role in mediating PCD.

Signaling Molecules and Photoreceptor Development

Cell extrinsic factors have also been implicated in rod photoreceptor development. Rods are highly specialized sensory neurons that have a complex morphology that is essential for their light-capturing function. Rod differentiation is a protracted process, in that there is a considerable lag between the cell cycle exit of rod precursors and the expression of end stage markers of the phototransduction cascade, including rhodopsin. Thus, differences in rhodopsin expression can be a consequence of altered cell specification or differentiation. To distinguish between these two possibilities, it is important to determine whether the signaling pathway under investigation exerts its effects on dividing or postmitotic cells and to assay early stage markers of rod development.

RA is a vitamin A derivative that regulates a number of aspects of development. RA enters the nucleus where it binds to RA receptor (RAR) heterodimers to regulate context-specific target gene expression (Figure 5). RA is synthesized by RPCs, differentiated neurons in the retina as well as the RPE in the adult eye. At early stages in ocular development, RA signaling plays an important role in regulating the growth of the ventral optic cup. RA signaling has also been shown to promote photoreceptor

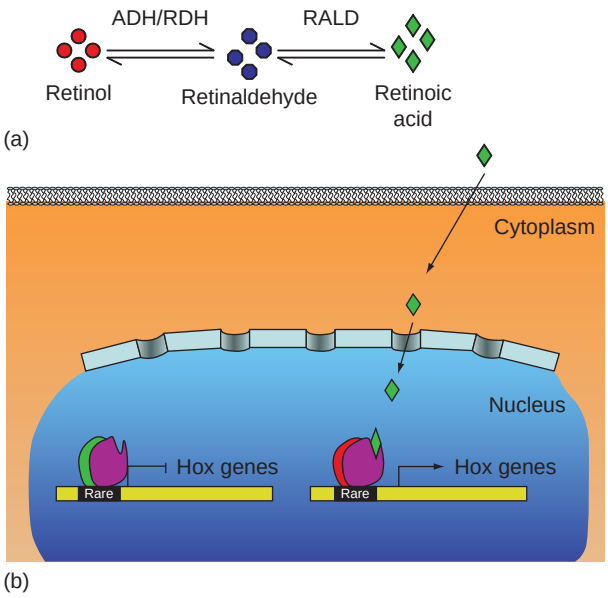

Figure 5 The retinoic acid (RA) pathway. (a) The metabolic pathway for the synthesis of RA from vitamin A. RA is synthesized through a series of oxidation reactions beginning with the oxidation of vitamin A (retinol) to retinal by aldehyde dehydrogenases (ADHs) and/or by retinol dehydrogenase (RDHs). Retinaldehyde dehydrogenase (RALD) converts retinal to RA. RA is able to enter the nucleus and bind to RAR/RXR heterodimers at RARE sites leading to transcriptional activation.

development in several vertebrate species. Whether RA mediates these effects by acting at the stages of rod specification or differentiation is more controversial. There is evidence that RA functions at the level of dividing progenitor cells to promote rod development. Conversely, RA has been shown in other studies to promote rhodopsin expression in postmitotic cells, and perturbation of RA signaling is associated with reduced or delayed rhodopsin expression rather than photoreceptor specification. Consistent with a role in differentiation, RA has been shown to regulate a number of photoreceptor-specific genes, including *arrestin*, *Cone rod homeobox* (*Crx*), and *Neural retina leucine zipper* (*Nrl*). Additional photoreceptor promoting molecules include taurine, an amino acid, that promotes the differentiation of postmitotic rod-precursor cells, b2-laminin and, depending on the context, fibroblast growth factor 2 (FGF2). Differential effects of Hh signaling on photoreceptor development have also been reported, with some studies finding positive effects of Hh signaling on rod development and others reporting an inhibitory effect.

In contrast, epidermal growth factor (EGF) has been reported to inhibit rod development. EGF might mediate this suppressive effect at the level of rod specification, as increased EGFR signaling in RPCs promotes Müller cell development at the expense of rods; however, a role for EGF signaling in rod development *in vivo* has not been established. Ciliary neurotropic factor (CNTF) exerts

pleiotropic effects on neurons and glia in the developing and adult nervous system. In the retina, it exerts opposite effects on the development of postmitotic rod precursors in the rodent and chick. In rodents it is a powerful inhibitor of rod differentiation, whereas in chick it promotes rod development. The timing of CNTF receptor downregulation in rod precursors is coincident with the induction of rhodopsin expression. Thus, in conjunction with other extrinsic cues, CNTF signaling may coordinate the timing of final photoreceptor maturation with the development of other retinal components.

Conclusion

A primary theme that emerges from this overview of notch, Wnt, Hh, and TGF-β signaling in retinal histogenesis is the function of these pathways in controlling patterning, proliferation, and cell survival and to a more limited extent, cell fate. Key questions remain regarding the downstream events controlled by these pathways and how they converge on the cell intrinsic processes that regulate cell fate, competence, and the cell cycle machinery. Addressing these issues will lead to a deeper understanding of neurogenesis in general and will be beneficial in the development of techniques to manipulate stem cells for therapeutic applications.

See also: Coordinating Division and Differentiation in Retinal Development; Embryology and Early Patterning; Eye-Field Transcription Factors; Injury and Repair: Stem Cells and Transplantation; Retinal Histogenesis.

Further Reading

Campo-Paysaa, F., Marletaz, F., Laudet, V., and Schubert, M. (2008). Retinoic acid signaling in development: Tissue-specific functions and evolutionary origins. *Genesis* 46: 640–656.

Ingham, P. W. and McMahon, A. P. (2001). Hedgehog signaling in animal development: Paradigms and principles. *Genes and Development* 15: 3059–3087.

Lad, E. M., Cheshier, S. H., and Kalani, M. Y. S. (2008). Wnt signaling in retinal development and disease. *Stem Cells and Development* 18(1): 7–16.

Levine, E. M., Fuhrmann, S., and Reh, T. A. (2000). Soluble factors and the development of rod photoreceptors. *Cellular and Molecular Life Sciences* 57: 224–234.

Lillien, L. (1995). Changes in retinal cell fate induced by overexpression of EGF receptor. *Nature* 377: 158–162.

Livesey, F. J. and Cepko, C. L. (2001). Vertebrate neural cell-fate determination: Lessons from the retina. *Nature Reviews Neuroscience* 2: 109–118.

Logan, C. Y. and Nusse, R. (2004). The Wnt signaling pathway in development and disease. *Annual Review of Cell and Developmental Biology* 20: 781–810.

Mann, R. K. and Beachy, P. A. (2004). Novel lipid modifications of secreted protein signals. *Annual Review of Biochemistry* 73: 891–923.

Massague, J. and Gomis, R. R. (2006). The logic of TGFbeta signaling. *FEBS Letters* 580: 2811–2820.

Ohsawa, R. and Kageyama, R. (2008). Regulation of retinal cell fate specification by multiple transcription factors. *Brain Research* 1192: 90–98.

Ross, S. and Hill, C. S. (2008). How the smads regulate transcription. *International Journal of Biochemistry and Cell Biology* 40: 383–408.

Schmierer, B. and Hill, C. S. (2007). TGFbeta-SMAD signal transduction: Molecular specificity and functional flexibility. *Nature Reviews Molecular Cell Biology* 8: 970–982.

Selkoe, D. and Kopan, R. (2003). Notch and Presenilin: Regulated intramembrane proteolysis links development and degeneration. *Annual Review of Neuroscience* 26: 565–597.

Wallace, V. A. (2008). Proliferative and cell fate effects of hedgehog signaling in the vertebrate retina. *Brain Research* 1192: 61–75.

Hyalocytes

T Kita, Y Hata, and T Ishibashi, Kyushu University, Fukuoka, Japan

Glossary

Autocrine – One of three fundamental types (with paracrine and endocrine) of cellular regulation by intercellular diffusible factors, where the diffusible factor exerts a regulatory influence primarily on the same cell that secreted it.
Epitope – A small site on an antigen where an antibody binds via its variable region.
Green fluorescent protein (GFP) – A protein from jellyfish. The GFP converts blue light (activation light) to green light (emission light). It has been widely used as a report protein because of its ability to label living cells.
Isoforms – The different forms of a protein that may be produced from different genes, or from the same gene by alternative splicing.
Paracrine – One of three fundamental types (with autocrine and endocrine) of cellular regulation by intercellular diffusible factors, where the diffusible factor exerts a regulatory influence primarily on cells in the immediate area of the cell that secreted it.
Transgenic mouse – A mouse which carries experimentally introduced DNA in its genome. Linear DNA is injected into a fertilized embryo at the pronuclear stage and may be incorporated into the genome. Injected embryos are implanted into a foster mother. Progenitors are screened for transgene in their genome.

Existence and Distribution of Hyalocytes

The vitreous body makes up the greatest volume of the eye. The body is a clear, jellylike substance composed mainly of water and delicate collagenous network associated with hyaluronic acid. The vitreous not only offers support to the structures within the eye but also helps maintain the transparency of the media.

The embryonic vitreous contains relatively numerous cells, the number of which gradually decreases, and only a small number of cells are in the vitreous cavity in the adult eyes under physiological conditions. In 1840, Hannover first described cells in the vitreous body of the eye. The term hyalocytes was introduced in 1959 by Balazs in order to define a homogeneous population of cells in the cortical layer of the vitreous body of various animal species. Hyalocytes are on average 50 μm from the inner surface of the retina entangled within the collagen fibrils in the vitreous cortex (**Figure 1(a)–1(d)**). The average number of hyalocytes in human cortical and basal vitreous is about 150 per mm^2 and in pig or bovine eyes is reported to be around 100 per mm^2. It has been noted that the hyalocytes are arranged in tree-like branching patterns, following the course of the retinal vessels (**Figure 2**).

Morphological Characteristics of Hyalocytes

Morphological studies using both light and electron microscopes demonstrate that the shape of hyalocytes varies from oval to spindle or stellate, and that hyalocytes possess lysosomes, mitochondria, ribosomes, and micropinocytotic vesicles with numerous microvilli on their surface, indicating that hyalocytes are morphologically very similar to the so-called macrophages. Therefore, hyalocytes are considered to belong to the monocyte/macrophage lineage (**Figure 1(b)**).

From immunocytochemical analyses, hyalocytes possess antigenic determinants that react with antibodies directed against CD45 (leukocyte common antigen), CD64 (Fc receptor I), CD11a (leukocyte-function antigen-1), histocompatibility complex (MHC) class II antigens, and S100 protein. The presence of CD45, which is selectively expressed by all hematopoietic cells, excluding mature erythroid cells, and CD11a, which is present on virtually all leukocytes, strongly suggests that hyalocytes are derived from a leukocytic cell lineage. In addition, Fc receptor I is the particular IgG receptor which is expressed constitutively only by monocytes and tissue macrophages. The expression of MHC class II antigens and S100 protein, although not unique to the monocyte/macrophage lineage, is consistent with this cellular origin.

Although hyalocytes do not react with CD11b, CD11c, or CD14, these antigenic determinants are variably expressed by tissue macrophages. They differ from other cells of the mononuclear phagocytic system in that they lack immunocytochemically detectable CD68 antigen, an epitope that is highly expressed by peripheral blood monocytes and macrophages of virtually all tissues. Furthermore, antigens that are typically associated with epithelial cells (cytokeratin and epithelial membrane antigen), fibroblasts (prolyl 4-hydroxylase and vimentin), endothelial cells (CD31 and von Willebrand factor), neuroglial cells

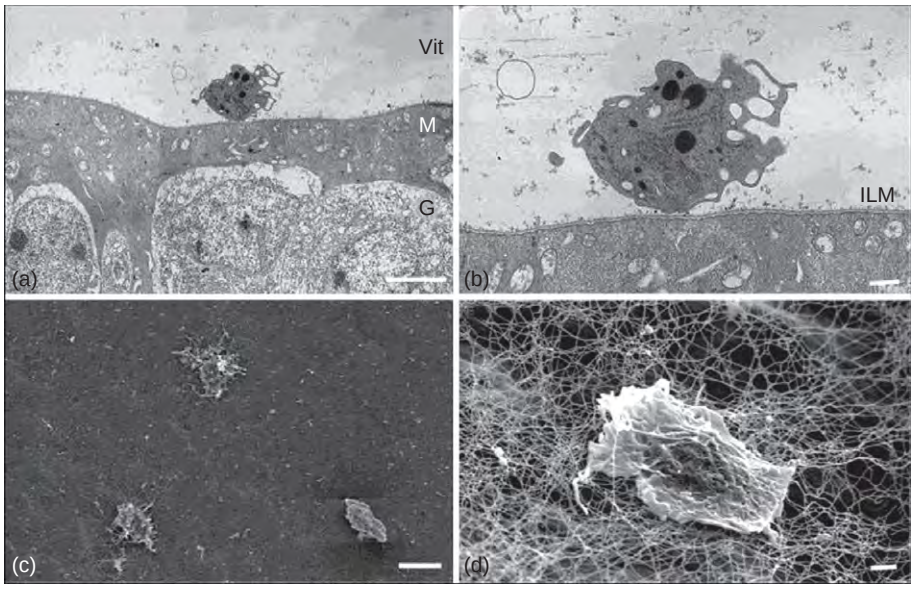

Figure 1 The morphological characteristics and the distribution of hyalocytes in the vitreoretinal interface: (a) Transmission electron micrograph shows a hyalocyte in the vitreous cavity close to the retina. (b) Higher magnification shows that hyalocytes are completely free from but close to the inner limiting membrane (ILM) of the retina. The hyalocyte possesses lysosome-like granules, mitochondria, and micropinocytotic vesicles, features characteristic of cells of the macrophage lineage. (c) Scanning electron micrograph showing free hyalocytes in the vitreous cortex that are very close to the retina, which lies in the background of the image. (d) A higher magnification view showing that the cell is entangled in a collagen fibril network in the vitreous cortex, a few protuberances can be observed at the cell surface. (Original magnification a, 62 600x, bar 5 μm; b, 66 000x, bar 1 μm; c, 61 100x, bar 10 μm; d, 64 300x, bar = 1 μm). Qiao, H., Hisatomi, T., Sonoda, K. H. *et al.* (2005). The characterization of hyalocytes: The origin, phenotype, and turnover. *British Journal of Ophthalmology* 89: 513–517, with permission from BMJ Publishing Group.

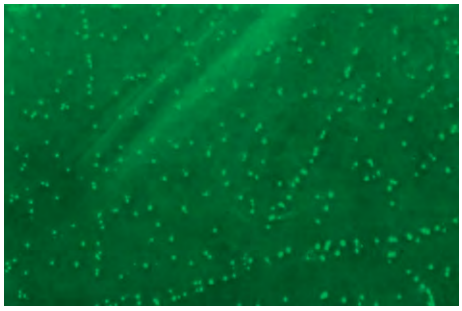

Figure 2 Hyalocytes in the extracted vitreous. The hyalocytes were present mainly on the vitreous gel surface and arranged in branching patterns that are thought to follow the patterns of blood vessels in the retina.

(glial fibrillary acidic protein: GFAP), neuronal cells (neuron-specific enolase) and RPE cells, and Muller cells (cellular retinaldehyde binding protein) are not present on hyalocytes.

In addition, other immunophenotypic analysis demonstrated that most (90%) of the hyalocytes are positive against ED2 antibody, which recognizes membrane and cytoplasmic antigens of tissue macrophages, and a few (15%) hyalocytes were positive against ED1 antibody, which recognizes an antigen in monocytes and in most macrophages, free and fixed. Only 5% of hyalocytes showed both ED1 and ED2 positive staining. Antibodies directed against ED1, bearing the characteristic phenotype of monocyte derived macrophages, only label a small proportion of hyalocytes. Antibodies directed against ED2 typically associated with hyalocytes, illustrate that vitreous hyalocytes have the characteristic phenotype of tissue macrophages.

Origin of Hyalocytes

Numerous theories regarding the origin of the vitreous hyalocytes, including derivation from neuroglia of the retina, mesenchymal cells of the retinal vasculature, or cells of the hyaloid system, have been proposed. However, evidence to date suggests that hyalocytes belong to the monocyte/macrophage lineage; thus the recent popular concept about their origin has proposed that hyalocytes originate from blood monocytes.

To confirm the origin of the hyalocytes we created chimeric mice by transplanting the bone marrow cells from enhanced green fluorescent protein (GFP) mice into them. In these chimeric mice, the hyalocytes were GFP negative immediately after transplantation of bone marrow cells. However, more than 60% of total vitreous hyalocytes were replaced within 4 months and approximately 90% within 7 months under physiological conditions, suggesting that bone marrow derived cells differentiate into hyalocytes and turn over even under physiological conditions.

The large number of bone marrow derived cells lining in the vitreous cavity suggests that they might contribute to the maintenance of homeostasis within the vitreous cavity.

Role of Hyalocytes During Development

One interesting example of tissue regression occurs during development of the eye, where arcades of the hyaloid capillary network (called the vasa hyaloidia propria) disappear from the vitreous between 5 and 7 days after birth and other branches (called the tunica vasculosa lentis) between 7 and 21 days after birth in the mouse eye. Histological studies have shown that the embryonic vitreous contains relatively numerous hyalocytes, which are closely associated with the hyaloid vasculature prior to and during the phase of remodeling. The two transient ocular structures, the hyaloid vasculature and the pupillary membrane, which normally regress according to a defined developmental timetable, are found to persist in macrophage ablation transgenic mice. Hyalocytes are associated with the loss of capillary integrity, leakage of erythrocytes into the vitreal compartment, and phagocytosis of the apoptotic endothelium. It has also been reported that hyalocytes are directly responsible for the endothelial cell death in the system. Furthermore, it has been reported that hyalocytes secrete some antiangiogenic factors. Those experiments provide direct evidence for the active involvement of macrophages in developmentally programmed tissue remodeling and identify hyaloid vessels and pupillary membrane in the eye as targets of macrophage-mediated remodeling, and suggest that hyalocytes actively elicit targeted cell death during development of the mouse eye.

In addition, it has been suggested that hyalocytes contribute toward the formation of the extracellular matrix of the vitreous. However, recent experiments have shown that the major source is the nonpigmented ciliary epithelium, so if they do make a contribution, it is likely to be minor.

Role of Hyalocytes Under Physiological Conditions

Hyalocytes are thought to function as resident macrophages of the vitreous cavity under physiological conditions. Phagocytic activity of hyalocytes has been confirmed experimentally by the injection of foreign substances into the vitreous and in experiments with cultured hyalocytes. Thus, hyalocytes are thought to be active in maintaining the vitreous cavity as an avascular and transparent tissue.

Hyalocytes also show fibrinolytic activity. The platelet-derived growth factor (PDGF) enhances the expression of urokinase-type plasminogen activator (uPA) by hyalocytes and stimulates the (uPA)-plasmin activity. This activity was demonstrated *in vitro* where plated fibrin was shown to be lysed using fibrin zymographic analysis. In the vitreous cavity, the humoral element circulates poorly because of the gelatinous structure of the vitreous. Therefore, a vitreous hemorrhage tends to remain in the cavity for a long time. The fibrinous material not only affects the visual acuity because it is opaque, but the fibrinous membranes on the retinal surface can also function as a scaffold for infiltrating cells, resulting in fibrous membrane formation and tractional retinal detachment through its cicatricial contraction. It is thus reasonable to suggest that hyalocytes digest the fibrinous material in the vitreous cavity as a physiological function, thus indicating that one of the physiological properties of these cells is to maintain vitreous transparency.

In addition, hyalocytes are also assumed to be involved in ocular immune privilege, which serves the purpose of limiting the extent of immune responses that can lead to intraocular inflammation. After antigen inoculation into the vitreous cavity, antigen-specific delayed type hypersensitivity responses are impaired. The form of systemic tolerance was similar to anterior chamber-associated immune deviation (ACAID) and named vitreous cavity-associated immune deviation (VCAID). Hyalocytes, which are also F4/80 positive, are presumed to function as antigen-presenting cells (APCs) responsible for mediating VCAID, which could also serve to maintain vitreous transparency.

Functional Properties of Hyalocytes in Vitreoretinal Interface Diseases

Proliferative Diabetic Retinopathy and Proliferative Vitreoretinopathy

Proliferative diabetic retinopathy (PDR) and proliferative vitreoretinopathy (PVR) still remain common causes of severe vision loss or blindness in spite of the dramatic development of vitreoretinal surgery. The PDR and PVR cause tractional retinal detachment due to the formation of contractile preretinal fibrous membranes as a result of excessive wound healing under the pathological conditions. Previous studies revealed that various types of ocular cells, such as retinal pigment epithelial cells (RPEs) which contribute especially to the pathogenesis of PVR, glial cells, vascular endothelial cells, myofibroblast-like cells of unknown origin, and hyalocytes, organize into the proliferative membranes. Specifically, in human diabetic eyes the hyalocytes have a different shape compared with those in normal eyes, and their numbers appear to be increased. Hyalocytes may participate in the initiation and progression of PDR and PVR through the formation of proliferative membranes and subsequent cicatricial contraction.

Formation of proliferative membranes

The formation of proliferative membrane is characterized by the proliferation and migration of cells, and the excessive synthesis and deposition of extracellular matrix (ECM) proteins. This tissue repair process is regulated by a number of polypeptides including cytokines and growth factors. Growth factors such as PDGF, HGF (hepatocyte growth factor), and MCP-1 (monocyte chemoattractant protein-1) regulate the proliferation and migration of the cells. The PDGF stimulates the proliferation of hyalocytes through p44/p42 MAPK, PI3 kinase, and p38 MAPK, and promotes migration of hyalocytes through PI3 kinase and p38 MAPK, but not p44/p42 MAPK. In addition, TGF-β (transforming growth factor-β), which is overexpressed in the vitreous and proliferative membranes in those diseases, is involved in the production of extracellular matrix proteins such as collagen and fibronectin by various types of cells. Also in hyalocytes, TGF-β promotes the expression of fibronectin, which is one of the major extracellular matrix proteins observed in the epiretinal proliferative membranes. Furthermore, TGF-β stimulates the expression of its downstream mediator, CTGF (connective tissue growth factor) by hyalocytes via activation of Smad signaling, which is mediated through Rho/Rho kinase (ROCK) pathway and at least partially through p38 MAPK. Various types of vitreoretinal cells other than hyalocytes, such as RPEs, Muller cells, and retinal endothelial cells can also be sources of CTGF, with CTGF stimulating cell growth and extracellular matrix synthesis by hyalocytes and RPEs. Therefore, hyalocytes could modulate the formation of proliferative fibrous membranes along with other neighboring cells, in both an autocrine and paracrine manner. In addition, CTGF stimulates the expression of the angiogenic factor VEGF (vascular endothelial growth factor) by hyalocytes and RPEs, so hyalocytes might have a paracrine angiogenic effect on retinal endothelial cells leading to retinal neovascularization.

Cicatricial contraction of the proliferative membrane

Cicatricial contraction of the preretinal proliferative membranes causes tractional retinal detachment, which leads to photoreceptor apoptosis and ultimately to permanent visual loss. Hyalocytes are incorporated into the proliferative membranes and get contractile properties in response to various contractile promoting factors, the expression of which are enhanced in PDR or PVR vitreous and proliferative membranes. Recent investigations have revealed some of the responsible growth factors and their cellular mechanisms in hyalocytes, thereby suggesting potential pharmacologic strategies for the management of these conditions.

Human vitreous samples collected from PDR or PVR patients significantly enhanced the contraction of hyalocyte-containing collagen gels, an established *in vitro* cicatricial contraction model, compared with vitreous from patients with nonproliferative diseases such as macular hole and rhegmatogenous retinal detachment. In addition, PDR/PVR-induced collagen gel contraction is dramatically but incompletely suppressed by TGF-β blockade. Furthermore, contraction of hyalocyte-containing collagen gels strongly correlates with the concentration of activated TGF-β2 in the vitreous.

In addition, PDR/PVR vitreous enhances α-smooth muscle actin (α-SMA) expression and phosphorylation of myosin light chain (MLC) in hyalocytes and RPEs, both of which were dramatically suppressed by TGF-β blockade. Overexpression of α-SMA indicates transdifferenciation of hyalocytes and RPEs into myofibroblasts, and phosphorylation of MLC is associated with actin–myosin interaction to form stress fibers and contractile rings, facilitating cell contraction and motility. Therefore, PDR/PVR vitreous may exert their contractile property by furthering myofibroblastic transdifferentiation and MLC phosphorylation in target cells such as hyalocytes. Furthermore, the results single out TGF-β as one of the main factors responsible for the procontractile property of PDR/PVR vitreous. Certainly, recombinant TGF-β2, the predominant isoform of three TGF-β isoforms (TGF-β1, 2, and 3) in the posterior segment of the eye, remarkably stimulates the contraction of hyalocyte-embedded collagen gels, and enhances α-SMA expression and MLC phosphorylation by hyalocytes. However, as TGF-β blockade does not abolish the procontractile property of PDR/PVR vitreous, other factors such as PDGF, IGF-1 (insulin-like growth factor-1), and endothelins may also significantly contribute to the cicatricial contraction of the proliferative membrane, albeit to a lesser extent than TGF-β.

Rho-kinase (ROCK), a target protein of Rho, regulates MLC phosphorylation both directly and via inactivation of the MLC phosphatase. Fasudil, a potent and selective ROCK inhibitor, abolished the PDR/PVR-induced hyalocyte-containing collagen gel contraction as well as contraction induced by recombinant TGF-β2. Fasudil almost completely suppressed MLC phosphorylation by hyalocytes, which is a common downstream mediator of various contractile growth factors including TGF-β, PDGF, IGF-1, and endothelins. In addition, while PDR/PVR-induced α-SMA expression by hyalocytes was unaffected by fasudil, α-SMA organization, which modulates the contractile property of myofibroblastic cells, was effectively disrupted. This suggests that fasudil might diminish the contractile property of proliferative membranes, which are supposed to be at least partly composed of transdifferentiated hyalocytes, by abolishing MLC phosphorylation and perturbing α-SMA organization (**Figure 3**).

Hyalocytes play a crucial role in the formation and contraction of proliferative membrane in response to growth factors overexpressed in eyes with proliferative vitreoretinal diseases such as PDR and PVR (although RPEs play a central role in PVR complicating rhegmatogenous retinal

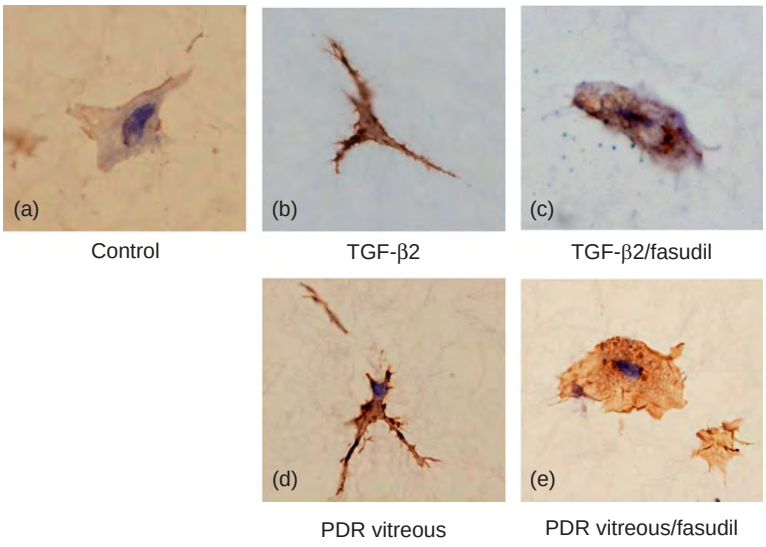

Figure 3 Immunocytochemical analysis of α-SMA (*brown*) in hyalocytes embedded in collagen gels. Representative micrographs, showing hyalocyte-containing collagen gels that were treated with: (a) control (DMEM), (b) recombinant TGF-β2, (c) recombinant TGF-β2 with fasudil (20 μM), (d) PDR vitreous, and (e) PDR vitreous with fasudil (20 μM). The TGF-β2 and PDR vitreous treatment increase α-SMA expression. Fasudil disrupted α-SMA organization without affecting its expression.

detachment), and ROCK inhibition might become a therapeutic strategy in the management of these diseased states.

Idiopathic Epiretinal Membrane and Macular Hole

Idiopathic epiretinal membrane (iERM) are preretinal fibrotic lesions containing various cell types that are located on the inner retinal surface and cause mild to moderate visual disturbance or metamorphopsia.

In 1978, Machemer first showed that iERMs could be removed using vitrectomy techniques. Since then, there have been several ultrastructural and histopathologic studies of iERM specimens removed during vitreous surgery. Those studies have demonstrated that four types of cells are observed in the simple ERMs including (1) fibrocyte-like cells, (2) macrophages, (3) myofibroblast-like cells, and (4) glial cells; the fibroblast-like cells and macrophages are thought to be hyalocytes.

Regarding the pathogenesis of ERM formation, older theories hypothesized that posterior vitreous detachment (PVD) could result in dehiscences in the internal limiting membrane and subsequent glial cell migration and process extension onto the retinal surface then causes ERM formation. However, this hypothesis has never been confirmed histologically.

It has been shown that PVD may leave a portion of posterior vitreous cortex attached to the macular area, and even in the absence of PVD, a premacular liquefied pocket is often present in adult eyes as a result of age-related vitreous liquefaction, the vitreous cortex then forms the posterior wall of the premacular liquefied pocket. This premacular vitreous cortex may play a key role in the development of iERMs. In addition, it has been suggested that when anomalous PVD results in vitreoschisis this process may contribute to the formation of iERMs.

A recent immunohistochemical study has demonstrated that iERMs contain both GFAP immunopositive cells and α-SMA immunopositive cells, but no double positive cells were observed. The α-SMA immunopositive cells were located mainly at the contracted foci of ERMs. On the other hand, GFAP immunopositive cells were present at the periphery of ERMs. In line with previous reports, α-SMA positive myofibroblast-like cells are thought to be the main contributors to the membrane contraction similar to PDR and PVR.

In vitro studies showed that the diameter of hyalocyte-containing collagen gels decreased and there was α-SMA overexpression in the presence of TGF-β2 or vitreous from patients with iERM, which was almost completely abolished by anti-TGF-β2 antibody. By contrast, cultured human astrocytes had no apparent contractile properties of collagen gels in the presence of TGF-β2 and TGF-β2 has little effect on human astrocytes and did not cause myofibroblastic transdifferentiation. The TGF-β2 is constitutively expressed to some level and it is expressed in iERM specimens, so hyalocytes may be the primary component of the contracted ERM foci since they abound in the posterior hyaloid and they undergo myofibroblastic transdifferentiation and have contractile properties in the presence of TGF-β. Therefore, the premacular vitreous cortex containing hyalocytes might cause ERM formation. Once the ERM contracts, it may cause dehiscence in the

internal limiting membrane with subsequent glial cell process extension or migration onto the retinal surface. That could provide an explanation as to why glial cells are observed only at the periphery of ERMs.

Several histological studies examining postmortem cases of macular hole have noted a high incidence of epiretinal membranes, which contain macrophages, fibrocyte-like cells, glial cells, and myofibroblast-like cells. Therefore the histological appearance is very similar to that of iERMs. These thin, delicate, hypocellular preretinal membranes were associated with most lamellar and full-thickness macular holes. Thus, epiretinal membranes are also considered to play an important role in the pathogenesis of macular hole formation. In addition, myofibroblastic differentiation has been observed in epiretinal membranes associated with idiopathic macular holes, which suggested that contraction of these cells is at least partly responsible for formation and enlargement of macular holes. The similarities between epiretinal membranes associated with idiopathic macular holes and simple iERMs indicate a common pathogenesis of these two entities. In addition, because these membranes result from cellular proliferation, migration, and myofibroblastic transdifferentiation resulting in membrane contraction, they share many features in common with PDR and PVR, so these diseases might be interpreted as quiet PVR.

One of the recent hypotheses underlying these diseases is the unifying concept of anomalous PVD. Collapse of the liquefied vitreous body without sufficient dehiscence at the vitreoretinal interface can induce vitreoschisis, a split within the posterior vitreous cortex, leaving the outermost layer of the posterior vitreous cortex attached to the macula. If anomalous PVD is an important event in macular hole formation and ERMs, there must be some other factors to account for the dissimilar clinical and topographic features of the two conditions. The ERM tissues are reported to be hypercellular, whereas the tissue surrounding macular holes is hypocellular in composition. Sebag has hypothesized that the difference could be due to the level at which vitreoschisis splitting occurs during anomalous PVD; if vitreoschisis occurs anterior to the hyalocytes then the residual membrane is hypercellular, but if it is posterior to the hyalocytes the membranes are hypocellular and this results in macular hole formation.

Conclusion and Perspective

Accumulating studies are clarifying the important roles of hyalocytes in the pathogenesis of various vitreoretinal interface diseases, along with their contribution to the maintenance of vitreous transparency. The careful removal of posterior vitreal cortex containing hyalocytes during vitreoretinal surgery, in combination with surgical adjuvants such as triamcinolone acetonide, is thought to result in an improvement of the outcome. Further understanding of the role of hyalocytes in the pathogenesis of vitreoretinal interface diseases might contribute to better management of the diseases by both surgical and/or pharmacological treatment.

See also: Cellular Origin, Formation and Turnover of the Vitreous; Formation and Regression of the Primary Vitreous and Hyaloid Vascular System; Proliferative Vitreoretinopathy; Vitreous Anatomy, Aging, and Anomalous Posterior Vitreous Detachment.

Further Reading

Grabner, G., Blotz, G., and Forster, O. (1980). Macrophage-like properties of human hyalocytes. *Investigative Ophthalmology and Visual Science* 19: 333–340.

Hamburg, A. (1959). Some investigations on the cells on the vitreous body. *Ophthalmologica* 138: 81–107.

Kampik, A., Kenyon, K. R., Michels, R. G., Green, W. R., and de la Cruz, Z. C. (1981). Epiretinal and vitreous membranes. Comparative study of 56 cases. *Archives of Ophthalmology* 99: 1445–1454.

Kita, T., Hata, Y., Arita, R., et al. (2008). Role of TGF-β in proliferative vitreoretinal diseases and ROCK as a therapeutic target. *Proceedings of the National Academy of Sciences of the United States of America* 105: 17504–17509.

Kita, T., Hata, Y., Kano, K., et al. (2007). Transforming growth factor-β 2 and connective tissue growth factor in proliferative vitreoretinal diseases: Possible involvement of hyalocytes and therapeutic potential of Rho kinase inhibitor. *Diabetes* 56: 231–238.

Kita, T., Hata, Y., Miura, M., et al. (2007). Functional characteristics of connective tissue growth factor on vitreoretinal cells. *Diabetes* 56: 1421–1428.

Kishi, S. and Shimizu, K. (1994). Oval defect in detached posterior hyaloid membrane in idiopathic preretinal macular fibrosis. *American Journal of Ophthalmology* 118: 451–456.

Kohno, R., Hata, Y., Kawahara, S., et al. (2009). Possible contribution of hyalocytes to idiopathic epiretinal membrane formation and its contraction. *British Journal of Ophthalmology* 93: 1020–1026.

Noda, Y., Hata, Y., Hisatomi, T., et al. (2004). Functional properties of hyalocytes under PDGF-rich conditions. *Investigative Ophthalmology and Visual Science* 45: 2107–2114.

Lang, R. A. and Bishop, J. M. (1993). Macrophages are required for cell death and tissue remodelling in the developing mouse eye. *Cell* 74: 453–462.

Lazarus, H. S. and Hageman, G. S. (1994). *In situ* characterization of the human hyalocyte. *Archives of Ophthalmology* 112: 1356–1362.

Qiao, H., Hisatomi, T., Sonoda, K. H., et al. (2005). The characterization of hyalocytes: The origin, phenotype, and turnover. *British Journal of Ophthalmology* 89: 513–517.

Sebag, J., Gupta, P., Rosen, R. R., Garcia, P., and Sadun, A. A. (2007). Macular holes and macular pucker: The role of vitreoschisis as imaged by optical coherence tomography/scanning laser ophthalmoscopy. *Transactions of the American Ophthalmological Society* 105: 121–129.

Sonoda, K.-H., Sakamoto, T., Qiao, H., et al. (2005). The analysis of systemic tolerance elicited antigen inoculation into the vitreous cavity: Vitreous cavity-associated immune deviation. *Immunology* 116: 390–399.

Hyperopia

E Harb, New England College of Optometry, Boston, MA, USA

Glossary

Accommodation – Increase in optical power by the eye in order to maintain a clear image (focus) as objects are moved closer. It occurs through a process of ciliary muscle contraction and zonular relaxation that causes the elastic-like lens to round up and increase its optical power. Natural loss of accommodation with increasing age is called presbyopia.
Amblyopia – Decreased vision in one or both eyes due to an amblyogenic factor (e.g., refraction, strabismus, and cataract) without detectable anatomic damage in the eye or visual pathways.
Asthenopia – Vague eye discomfort arising from use of the eyes; it may consist of eyestrain, headache, and/or brow ache. It may be related to uncorrected refractive error or poor fusional amplitudes.
Astigmatism – Optical defect in which refractive power is not uniform in all directions (meridians). Light rays entering the eye are bent unequally by different meridians that prevent formation of a sharp image focus on the retina.
Convergence – Inward movement of both eyes toward each other, usually in an effort to maintain single binocular vision as an object approaches.
Cycloplegic – An agent (typically eye drops) that paralyzes the accommodation system of the crystalline lens to eliminate variability in retinoscopy or refraction measures.
Emmetropization – An active growth process in which the eye grows toward a refractive error of plano.
Esotropia – Eye misalignment in which an eye deviates inward (toward nose) while the other fixates normally.
Strabismus – Eye misalignment caused by extraocular muscle imbalance: one fovea is not directed at the same object as the other.

Definition and Classifications of Hyperopia

Hyperopia, also termed hypermetropia or farsightedness, is a common refractive error in children and adults. In a hyperopic eye, parallel rays of light entering the eye reach a focal point behind the plane of the retina, while accommodation is in a relaxed state. Hyperopia can produce variable symptoms, depending on the magnitude of hyperopia, the age of the individual, the status of the accommodative and convergence systems, and the demands placed on the visual system (distance vs. near). Individuals with uncorrected hyperopia may experience symptoms such as blurred vision, asthenopia, accommodative/binocular dysfunction, amblyopia, and/or strabismus.

The vast majority of cases of hyperopia are of a physiological nature. In terms of physiological optics, hyperopia occurs when the axial length of the eye is shorter than the refracting components the eye requires for light to focus precisely on the photoreceptor layer of the retina. Hyperopia may result in combination with or isolation from a relatively flat corneal curvature, insufficient crystalline lens power, increased lens thickness, short axial length, or variance of the normal separation of the optical components of the eye relative to each other. Astigmatism, the most common refractive error, is often present in conjunction with hyperopia. High hyperopia is associated with high levels of astigmatism, suggesting a breakdown in the process of emmetropization that results in a component-type refractive error. Hereditary factors are probably responsible for most cases of refractive error, including physiologic hyperopia, with environment playing some role in influencing the development and degree of the error.

The American Optometric Association Clinical Practice Guideline has outlined the classifications for hyperopia in the following ways:

1. Hyperopia can be classified on the basis of structure and function. These three classifications are based solely on the structure of the eye:
   - simple hyperopia, due to normal biological variation, can be of axial or refractive etiology;
   - pathological hyperopia is caused by abnormal ocular anatomy due to mal-development, ocular disease, or trauma; and
   - functional hyperopia results from paralysis of accommodation.
2. Clinically, hyperopia may also be categorized based on degree of the refractive error. The magnitude of hyperopia can be classified in the following three ways:
   - low hyperopia consists of an error of +2.00 diopters (D) or less;

- moderate hyperopia includes a range of error from +2.25 to +5.00 D;
- high hyperopia consists of an error over +5.00 D.

3. An additional classification may be based upon the outcome of noncycloplegic and cycloplegic (1.0% cycloplentolate) refractions and takes the patient's accommodative system in consideration:
   - manifest hyperopia, the amount of refractive error that is detected by noncycloplegic refraction;
   - latent hyperopia, the amount of refractive error that is detected only by cycloplegia, can be overcome by accommodation under noncycloplegic conditions.

The sum of latent and manifest hyperopia is equal to the magnitude of hyperopia.

Active accommodation mitigates some or all of hyperopia's adverse effects on vision. The impact of accommodation is highly dependent on age, the amount of hyperopia and astigmatism, the status of the accommodative and vergence systems, and the demands placed upon the visual system. Latent hyperopia is typically overcome in the young patient by the action of accommodation, but may not be sustainable for long periods of time under conditions of visual stress. Signs and symptoms such as blurred vision, asthenopia, accommodative and binocular dysfunction, and strabismus may develop. These signs and symptoms occur more readily and to a greater degree in manifest hyperopia. In general, younger individuals with lower degrees of hyperopia and moderate visual demands are less adversely affected than older individuals, who have higher degrees of hyperopia and more demanding visual needs.

Pathological hyperopia is a rarer type of hyperopia, is typically greater in magnitude, and may be due to several etiologies: mal-development of the eye during the prenatal or early postnatal period, a variety of corneal or lenticular changes, aphakia, chorioretinal or orbital inflammation or neoplasms, neurological- or pharmacological-based etiologies, micro- or nan-ophthalmia, anterior segment malformations, and acquired disorders. A number of congenital and/or genetic developmental disabilities and syndromes are also associated with high hyperopia.

Prevalence

Although it is difficult to discuss the prevalence of hyperopia due to variations in its definition by researchers (e.g., with or without cycloplegia, spherical equivalent, and least hyperopic meridian), the prevalence of hyperopia is age related. Most full-term infants are mildly hyperopic (approximately +2.00 D), while premature infants and those of low birth weight tend to be either less hyperopic or myopic (approximately +0.24 D). The prevalence of refractive error among full-term infants has a normal bell-shaped distribution (see **Figure 1**). Up to 9% of 6–9-months-old infants have hyperopia greater than +3.25 D, but this prevalence decreases to 3.6% in the 1-year-old population. Over the next 10–15 years of life, there is a further decrease in the prevalence of hyperopia and an increase in the frequency of myopia. With the development of presbyopia, latent hyperopia becomes manifest, contributing to an apparent increase in the prevalence of hyperopia.

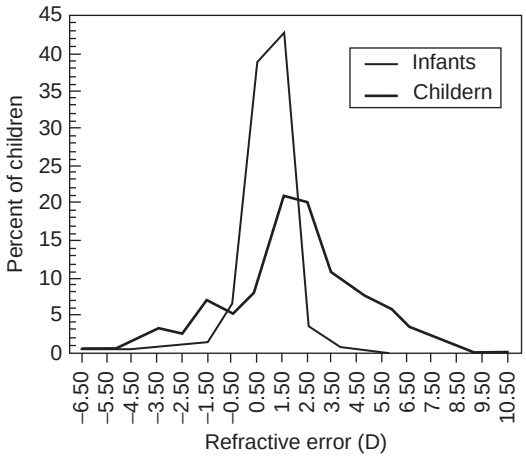

Figure 1 Comparison of refractive error distributions between newborns and children illustrates a shift away from hyperopia during the emmetropization process. Reprinted from Cotter, S. A. (2007). Management of childhood hyperopia: A pediatric optometrist's perspective. *Optometry and Vision Science* 84(2): 103–109.

Normal Time Course of Hyperopia

Emmetropization results in a gradual decrease in the level of hyperopia in most patients (see **Figure 2**), but in patients who have high degrees of hyperopia the change occurs more rapidly. However, infants with high hyperopia are more likely to remain significantly hyperopic throughout childhood. These infants may also have an increased incidence of against-the-rule astigmatism, which appears to further decrease the reduction in hyperopia during emmetropization compared to hyperopic infants without significant astigmatism.

During the school years, there is a slow but continued decreasing trend in the incidence and the magnitude of hyperopia, except in patients with high hyperopia, whose refractive error is more likely to remain relatively unchanged. During the years of presbyopia development, latent hyperopia may become manifest requiring the implementation of both distance and near correction, yet in older individuals (>75 years of age) a myopic refractive shift may ensue likely due to crystalline lens changes.

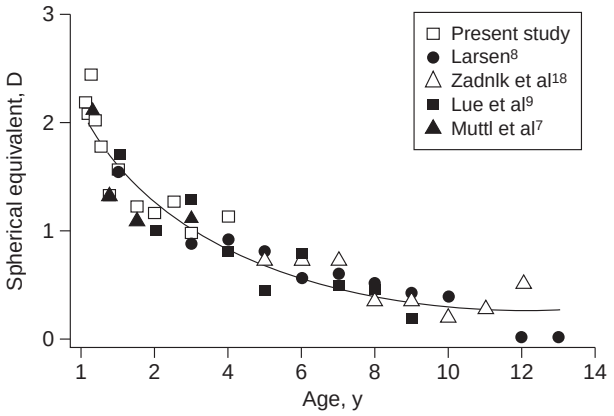

Figure 2 Mean spherical equivalent refractive errors, as reported by several studies, plotted by age. A smooth curve (single exponential function) was plotted to illustrate the change in refractive error with age. Reprinted from Mayer, L., Hansen, R., Moore, B., Kim, S., and Fulton, A. (2001) Cycloplegic refractions in healthy children aged 1 to 48 months. *Archives of Ophthalmology* 119: 1625–1628.

Clinical Presentations of Hyperopia

Young persons with hyperopia generally have sufficient levels of accommodation to maintain clear vision without producing asthenopia symptoms. However, when the level of hyperopia is too great or the accommodative reserves are insufficient due to age or fatigue, blurred vision and asthenopia may develop. Presbyopia brings an increase in absolute hyperopia, causing blur, especially at near. The influence of accommodation on the vergence system also plays a role in the presence or absence of symptoms in patients with hyperopia. Individuals with esophoria and inadequate negative fusional vergence ability are frequently symptomatic and may become esotropic as a result of the uncorrected hyperopia.

Among the signs and symptoms of hyperopia are red or tearing eyes, squinting and facial contortions while reading, ocular fatigue or asthenopia, frequent blinking, constant or intermittent blurred vision, focusing problems, decreased binocularity and eye–hand coordination, and difficulty with or aversion to reading. The presence and severity of these symptoms varies widely. Some young patients with hyperopia, including those with moderate and high hyperopia, may be relatively free of signs and symptoms.

Early detection of hyperopia may help prevent the complications of strabismus and amblyopia in young children. In older children, uncorrected hyperopia may affect learning abilities and in individuals of any age, it can contribute to ocular discomfort and visual inefficiency.

Risks of Uncorrected Hyperopia

The major complications of moderate and high physiologic hyperopia in children are amblyopia and strabismus. Infants with moderate to high hyperopia (>+3.50 D) are up to 13 times more likely to develop strabismus by 4 years of age if left uncorrected, and they are 6 times more likely to have reduced visual acuity than infants with low hyperopia or emmetropia. Children who had significant hyperopia during infancy are much more likely to develop amblyopia and strabismus by 4 years of age. The presence of anisometropic hyperopia further increases the risk of strabismus and amblyopia, especially if found beyond 3 years of age. The American Optometric Association has published guidelines stating that levels greater than 1.00 D of hyperopic anisometropia and 5.00 D of isometropic hyperopia are amblyogenic.

Early detection and treatment of hyperopia may reduce the incidence and severity of consequential amblyopia and strabismus and is a major justification for universal vision evaluation of young children.

Importance of Early Detection of Significant Hyperopia

Atkinson and colleagues showed that uncorrected hyperopia (>3.5 D in one meridian) might contribute to poor motor and cognitive development in younger children (9 months to 5.5 years) and/or learning problems in some older children. The precise mechanism of this relationship is unclear, but optical blur, accommodative and binocular dysfunction, and fatigue all appear to play roles. In fact, uncorrected infant hyperopia has been associated with mild delays in visuo-cognitive and visuo-motor development, but has appeared to reach the level of their emmetropic counterparts after 6 weeks of full time hyperopic spectacle wear in 3–5-year-olds. The substantial number of school-age children and young adults who have uncorrected significant hyperopia is evidence of the potential impact of this learning-related vision problem and the need for early detection screening programs.

Examination Techniques of Hyperopia

Optical correction should be based on both static (normal accommodation) and cycloplegic (e.g., 1% cyclopentolate) retinoscopy, accommodative and binocular assessment, and AC/A (accommodative convergence/accommodation) ratio. The correction should then be modified as needed to facilitate binocularity and compliance. Plus-power spherical or sphero-cylindrical lenses are prescribed to shift the focus of light from behind the eye to a point on the retina. Accommodation plays an important role in determining the prescription. Some older patients with hyperopia do not initially tolerate the full correction indicated by the manifest refraction, and many patients with latent hyperopia do not tolerate the full correction of hyperopia indicated under cycloplegia.

However, young children with accommodative esotropia and hyperopia generally require only a short period of adaptation to tolerate full optical correction. Patients with latent hyperopia who prove intolerant to the use of full or partial hyperopic correction may benefit from initially wearing the correction only for near viewing; or alternatively, trial use of a short-acting cycloplegic agent may enhance acceptance of the optical correction. Patients with absolute hyperopia are more likely to accept nearly the full correction, because they typically experience immediate improvement in visual acuity.

Management of Hyperopia

The specific elements of treatment (e.g., final spectacle prescription) should be tailored to individual patient needs. Among the factors to consider when planning treatment and management strategies are: the magnitude of the hyperopia (under dry and cycloplegic conditions), the presence of astigmatism and/or anisometropia, the patient's age, the presence of an associated esotropia and/or amblyopia, the status of the accommodative and convergence systems, the demands placed on the visual system, and any symptoms.

Among several available treatments for hyperopia-related symptoms, optical correction of the refractive error with spectacles and contact lenses is the most commonly used modality. Newer high-index lens materials and aspheric lens designs have reduced the thickness and weight of high plus-power lenses, increasing wear ability and patient acceptance. Spectacles, especially those with lenses of polycarbonate material, provide protection against trauma to the eye and orbital area and are imperative in children.

Soft or rigid contact lenses are an excellent alternative for some patients. Contact lenses not only provide better cosmesis and compliance, but they reduce aniseikonia in persons with anisometropia, improving binocularity. Multifocal or monovision contact lenses may be considered for patients who require additional near correction, but resist the use of multifocal spectacles because of their appearance. Patients who wear contact lenses are at increased risk for ocular complications due to corneal hypoxia, mechanical irritation, or infection; but nevertheless, improved vision makes contact lens wear a valuable treatment option for compliant patients.

Vision therapy and modification of the patient's habits and environment can be important in achieving definitive long-term remediation of symptoms. Such modifications include, but are not limited to, improved lighting, longer near working distances, using better-quality-printed material, taking frequent breaks when reading or working on a computer for sustained periods of time. These modifications all work to reduce the accommodative demand placed on the patient and can allow, irrespective of spectacle wear, the patient to perform their daily near activities with less symptoms.

Several refractive surgery techniques to correct hyperopia are under development. The major procedures currently being studied as possible therapies for hyperopia are – Holmium: YAG laser thermal keratoplasty, automated lamellar keratoplasty, spiral hexagonal keratotomy, excimer laser, and clear lens extraction with intraocular lens implantation. The American Academy of Ophthalmology has recently reviewed 36 research articles studying the efficacy and safety of refractive surgery for hyperopia and found that the surgery provides an effective and safe correction for lower ranges of hyperopia ($<$3.00 D). Although still considered to be investigative on a long-term treatment basis, laser-assisted *in situ* keratomileusis (LASIK) is Food and Drug Administration (FDA) approved for hyperopia up to +6.00 D.

There is no universal approach to the treatment of hyperopia. The goals of treatment are to reduce accommodative demand and to provide clear, comfortable vision and normal binocularity at all distances. It is not simply determination of the lens power required to focus light onto the retina, but a complex approach encompassing the patient's visual needs, magnitude of accommodation, coexisting amblyopia and/or strabismus, and sensitivity. The following are specific management strategies appropriate for different age groups and conditions as outlined by the American Optometric Association's Clinical Guidelines for Hyperopia.

Young children (birth–10 years of age) with low to moderate hyperopia, but without strabismus, amblyopia, or other significant vision problems, usually require no treatment. However, even occasional evidence of decreased visual acuity, binocular anomalies, or functional vision problems may signal the need for treatment. Whereas the effects of uncorrected hyperopia may manifest as visual perceptual dysfunction, reading difficulties, or failure in school, any child with hyperopia who is experiencing learning or other school difficulties needs careful assessment and may require treatment.

In most young hyperopic children, the process of emmetropization leads to a gradual reduction in the degree of hyperopia by 5–10 years of age. Some children do not go through this process, however. They remain significantly hyperopic and at increased risk for developing strabismus and amblyopia. Patients under age 5 who have hyperopia over 3.25 D appear to benefit from early optical correction to reduce the risk for strabismus and amblyopia. Clinical pediatric studies suggest that partial hyperopic prescriptions do not impede infants' emmetropization by 36 months.

Optical correction of hyperopia should generally be prescribed for young children who have moderate to high hyperopia. However, there are many differences in

prescribing patterns within and between pediatric optometrists and ophthalmologists. Lyons and colleagues surveyed pediatric optometrists and ophthalmologists prescribing thresholds for hyperopia in 2-year-olds and found that 65% of pediatric optometrists used +3.0 D of bilateral asymptomatic hyperopia as their threshold for prescribing and 25% used +5.0 D, while pediatric ophthalmologists had less conservative thresholds with 66% using +5.0 D and 25% using +3.0 D. It should also be prescribed, along with other interventions (e.g., occlusion or active vision therapy), for all young patients with actual or suspected amblyopia or strabismus. Optical correction may be deferred for some patients with moderate hyperopia, but such patients should be considered at risk and re-examined periodically.

Careful follow-up is essential, and frequent lens changes may be needed. It is not unusual for a significant increase in hyperopia to occur after optical correction has been worn for even a short time, due to the manifestation of latent hyperopia. It is also important to continually monitor for the presence of an esotropia during all follow-up visits. When compliance proves difficult, the clinician may encourage acceptance of the prescribed treatment by using cycloplegic agents to blur uncorrected vision. Contact lenses may be a good alternative for patients who do not comply with prescriptions for spectacle wear, especially those with anisometropia, high hyperopia with or without nystagmus, and hyperopia with accommodative esotropia.

Special consideration should be given to several specific categories of problems in young children who have significant hyperopia. Prior to the onset of accommodative esotropia, which usually becomes evident at about 2–3 years of age, few children exhibit obvious signs of ocular problems, with the exception of intermittent esotropia in children who are ill or very tired. Early screening for refractive error usually detects hyperopia, but due to the relative infrequency of refractive screening, many children with underlying moderate to high hyperopia go undetected until the appearance of frank strabismus. Appropriate treatment includes the use of either single vision or multifocal spectacles depending on the patient's binocular and accommodative status. Concurrent amblyopia, when present, may be treated by patching and active vision therapy.

Less commonly, young children with bilateral high hyperopia develop isoametropic amblyopia due to the resulting constant state of severely blurred vision. Such patients may have an associated esotropia, or conversely, may not manifest esotropia because they make no attempt to accommodate. Optical correction of this condition is indicated in order to prevent or treat the associated amblyopia and/or strabismus; however, careful monitoring is warranted a previously nonexistent esotropia may present itself following correction. Partial correction may inadvertently stimulate accommodative esotropia, because the patient now has good reason to attempt to overcome the remaining uncorrected hyperopia. Treatment to improve vision in the child with amblyopia may take a few years, but improvement is usually possible with full time spectacle wear and/or patching or pharmacological penalization.

Many persons between the ages of 10 and 40 years who have low hyperopia require no correction because they have no symptoms. Ample accommodative reserves shelter them from visual problems related to their hyperopia. Under increased visual stress, such persons may develop symptoms that require correction. Wearing prescribed lenses with low amounts of plus power usually alleviates the problem. Patients with moderate degrees of hyperopia are more likely to require at least part-time correction, especially those who have significant near demands or have accommodative or binocular anomalies. Accommodative or binocular dysfunction associated with uncorrected low to moderate hyperopia may be treated by optical correction or vision therapy. Vision therapy may be instituted initially or after optical correction in patients who have significant binocular vision problems. The effects of visual habits and environment play an increasing role in determining the need for and characteristics of treatment.

By the age of 30–35 years, most previously asymptomatic, uncorrected hyperopic patients begin to experience blur at near and visual discomfort under strenuous visual demand. Facultative hyperopia can no longer be sustained comfortably due to decreasing accommodative amplitudes. Latent hyperopia should be suspected when symptoms occur in conjunction with lower amplitude of accommodation than expected for the patient's age. Cycloplegic retinoscopy can help identify this latent component. By the mid-1930s, accommodation takes noticeably longer while facility decreases, causing associated visual problems in many hyperopic persons previously free of symptoms. A prescription for the distance manifest (noncycloplegic) refraction for the patient to wear as needed (i.e., part time at near) often suffices. The patient may require additional correction with increasing age and visual demands at near. Before prescribing a permanent pair of spectacles, the optometrist may lend the patient a pair of spectacles (i.e., over-the-counter reading glasses) to demonstrate the potential benefits of optical correction of latent hyperopia.

With the onset of presbyopia (loss of accommodation), maintaining focus at near becomes progressively more difficult, especially in poor illumination. Prescribing an optical correction for most or all of the distance manifest refraction, along with a near addition, can greatly improve vision and comfort. Hyperopia equal to or greater than +1.00 D to +1.50 D generally requires full-time distance correction, with a near addition for patients over about

age 45. As facultative hyperopia becomes absolute, more plus power at distance is required. Progressive multifocal lenses enable clear focusing at a range of finite distances. A monovision, bifocal, or multifocal contact lens prescription is an option in some patients.

Physiological hyperopia is not progressive. Therefore, the prognosis, which can be given at diagnosis, is generally excellent, except for those patients with both hyperopia and amblyopia or strabismus, for whom it is less certain. Appropriate optical correction almost always leads to clear and comfortable single binocular vision. Younger children who have significant hyperopia associated with amblyopia, strabismus, or anisometropia require intensive follow-up and treatment for their more complex problems, starting as early as 3–6 months of age. The timing of periodic preventive optometric care for uncomplicated hyperopia depends on the patient's age and circumstances. For children with hyperopia, follow-up may be required as often as every 3–6 months depending on the concern for strabismus and/or amblyopia, while for asymptomatic adults, every 1 or 2 years is generally sufficient.

The underlying cause, rather than hyperopia itself, is the chief concern in patients with pathologic hyperopia. Because the causes of pathologic hyperopia are both uncommon and diverse, general statements concerning treatment must be limited to the need to correct the hyperopia in the best manner possible, depending on the underlying etiology. Conditions of a developmental or anatomic nature are rarely progressive. When useful vision is thought to be obtainable, the treatment of hyperopia resulting from nonprogressive conditions is similar to that for physiologic hyperopia. Patients with pathological hyperopia require treatment of their underlying conditions and, when indicated, referral to another eye care provider for special services. All patients treated for hyperopia with persistent symptoms require additional follow-up care to remediate their problem.

Conclusion

Hyperopia is a common refractive disorder that has a close association with other consequential disorders, namely amblyopia and strabismus, especially in children. This makes hyperopia a greater risk factor for more permanent vision loss than myopia. In addition, it appears that uncorrected hyperopia has a detrimental effect on a child's learning and development. Therefore, the early diagnosis and treatment of significant hyperopia and its consequences can prevent a significant amount of visual disability in the general population. Because hyperopia is usually not readily apparent, preventive examination of all young children is essential. Although there is no clear consensus on the prescribing practices for hyperopia, clinicians must examine the visual needs and binocular system of each patient to best determine their final treatment plan. Periodic eye examinations are needed thereafter to help ensure the provision of treatment appropriate to the changing visual needs of the hyperopic patient.

See also: Abnormal Eye Movements due to Disease of the Extraocular Muscles and Their Innervation; Amblyopia.

Further Reading

AOA Consensus Panel on Care of the Patient with Hyperopia (1997). American Optometric Association Clinical Practice Guidelines: Hyperopia. http://www.aoa.org/documents/CPG-16.pdf (accessed Jun. 2009).

Atkinson, J., Anker, S., Nardini, M., et al. (2002). Infant vision screening predicts failures on motor and cognitive tests up to school age. *Strabismus* 10(3): 187–198.

Atkinson, J., Braddick, O., Nardini, M., and Anker, S. (2007). Infant hyperopia: Detection, distribution, changes and correlates – outcomes from the Cambridge infant screening programs. *Optometry and Vision Science* 84(2): 84–96.

Atkinson, J., Nardini, M., Anker, S., Braddick, O., Hughes, C., and Rae, S. (2005). Refractive errors in infancy predict reduced performance on the movement assessment battery for children at 3½ and 5½ years. *Developmental Medicine and Child Neurology* 47: 243–251.

Cotter, S. A. (2007). Management of childhood hyperopia: A pediatric optometrist's perspective. *Optometry and Vision Science* 84(2): 103–109.

Donahue, S. P. (2007). Prescribing spectacles in children: A pediatric ophthalmologist's approach. *Optometry and Vision Science* 84(2): 110–114.

Guzowski, M., Wang, J. J., Rochtchina, E., Rose, K. A., and Mitchell, P. (2003). Five-year refractive changes in an older population: The blue mountains eye study. *Ophthalmology* 110(7): 1364–1370.

Lee, K. E., Klein, B. E. K., Klein, R., and Wong, T. Y. (2002). Changes in refraction over 10 years in an adult population: The beaver dam eye study. *Investigative Ophthalmology and Visual Science* 43(8): 2566–2571.

Lyons, S. A., Jones, L. A., Walline, J. J., et al. (2004). A survey of clinical prescribing philosophies for hyperopia. *Optometry and Vision Science* 81(4): 233–237.

Mayer, L., Hansen, R., Moore, B., Kim, S., and Fulton, A. (2001). Cycloplegic refractions in healthy children aged 1 to 48 months. *Archives of Ophthalmology* 119: 1625–1628.

Varley, G. A., Huang, D., Rapuano, C. J., et al. (2004). LASIK for hyperopia, hyperopic astigmatism, and mixed astigmatism: A report by the American Academy of Ophthalmology. *Ophthalmology* 111(8): 1604–1617.

Imaging of the Cornea

S C Kaufman, M Fung, D Raja, and N Kramarevsky, University of Minnesota, Minneapolis, MN, USA

Glossary

Chemosis – Swelling of the iris due to swelling of the bulbar conjunctiva.
Corneal verticillata – Congenital whorl-like opacities in the cornea.
DSAEK – Descemet's Stripping Automated Endothelial Keratoplasty, a form of keratoplasty which involves the removal of the host's central Descemet's membrane and corneal endothelium, which is subsequently replaced with a disc shaped graft of donor corneal stroma, Descemet's membrane and endothelium.
Follicles – Lymphoid tissue in the conjunctival stroma.
Fuchs' dystrophy – A common adult-onset form of corneal dystrophy with autosomal dominant inheritance. In this disease, the endothelial cells in the cornea gradually deteriorate.
Guttae – Drop-like.
Keratic precipitates – Fibrous deposits on the posterior surface of the cornea, usually associated with uveitis.
Laser-assisted *in situ* keratomileusis (LASIK) – Refractive surgery to correct myopia, hyperopia, and astigmatism.
Lattice dystrophy – Hereditary corneal dystrophy in which there is an accumulation of amyloid deposits throughout the middle and anterior stroma of the cornea.
Lenticle – Relating to the lens.
Pappillas – Small projection of tissue commonly triggered by constant irritation of the conjunctiva by contact lenses.
Pachymetry – Measurement of the thickness of the cornea.
Pigment dispersion syndrome (PDS) – Condition when the iris pigment epithelium and the lens come into contact. This leads to mechanical disruption of the iris resulting in release of pigment granules into the posterior chamber, which follows the flow of aqueous into the anterior chamber angle. The pigment can block the aqueous outflow resulting in elevated intraocular pressure with possible damage to the optic nerve.
Posterior polymorphous dystrophy – Disease involving metaplasia and overgrowth of corneal endothelial cells.
Pseudoexfoliation syndrome – Characterized by flakes of granular material at the pupillary margin of the iris and throughout the inner surface of the anterior chamber. It is also associated with secondary open-angle glaucoma.
Pseudophakic bullous keratopathy – Corneal edema occurring following cataract extraction.
Sclerotic scatter – Biomicroscope illumination that scatters light throughout the cornea.
Subluxation – Partial dislocation of an organ.

Slit-Lamp Biomicroscopy

The slit-lamp biomicroscope is a versatile device that is the primary diagnostic instrument used during the clinical examination of the cornea and the external structures of the eye and adenexa. It has two primary components mounted on a common axis – the slit illuminator and the biomicroscope. The slit-beam-illumination unit is essentially a projector with a light beam that is adjustable in height, width, direction, and intensity. The examiner can create a sharply focused narrow slit beam which can illuminate and isolate fine detail in otherwise translucent tissue. The biomicroscope component is a binocular Galilean telescope that can produce excellent resolution at multiple magnifications. A headrest stabilizes the patient, and adjustable oculars allow the examiner to focus a stereoscopic image.

The biomicroscope and the illuminator are arranged to be parfocal (focus on the same plane) and isocentric (the slit beam is centered in the field of view), which is necessary for its function. This essential setup allows for both direct illumination and – with shifting of the alignment – indirect illumination.

During diffuse illumination, the light beam is broadened to its largest aperture and kept at both low magnification and reduced intensity. The illuminator is directed at the eye from an oblique angle and rotated through its arc of travel from side to side. When the light is applied tangentially, surface changes are enhanced and dimensionalized through the effect of creating highlights and shadows. Subtle alterations from normal topography become more clearly noticeable. Direct illumination can highlight conjunctival changes such as chemosis, follicles, and papillae and can further direct the examiner's exam.

Broad-beam illumination can help the examiner visualize opaque lesions that may reflect or absorb light. This technique can be invaluable in evaluating the anterior segment structures from the cornea to the iris. When no abnormalities are seen with this technique, other forms of illumination should be explored.

Narrow-beam illumination allows the examiner to evaluate transparent tissues such as the cornea and lens through virtual cross-sections. When used under high magnification, the principal layers of the corneal can be distinguished clearly with great precision. In addition, a narrow beam can be used to identify the presence of anterior chamber cell and flare. Cell and flare is best seen against the background of the dark pupil with an intense but shortened slit light beam.

Specular reflections represent the normal light reflexes that bounce off of an ocular surface. These reflections actually correspond to the mirrored reflections from the light source itself. The most important application of specular reflection is in the evaluation of the corneal endothelium. This involves arming the slit beam at an angle of 40–60° from the viewing arm and using a short slit. Then, the specular reflection of the light bulb's filament is identified on the tear film. Adjacent to this area (on the side away from the light source), the less bright endothelial reflection can be viewed. Moving the biomicroscope slightly forward will bring the endothelial cellular detail into focus. A magnification of 25× to 40× is usually needed to obtain a clear view of the endothelial mosaic. Cell density and morphology can be evaluated; guttae and keratitis precipitates will appear as nonreflective dark areas.

Indirect illumination can provide unique information. In this method of illumination, the light beam is directed to an area adjacent to the area needing to be examined. Under higher magnification powers, the light beam may need to be decentered from the normal isocentric position. The area being evaluated is seen via retro-illumination from the deeper layers. This method is highly effective for observing detail in areas that are deep to more anterior lesions which may prevent light from penetrating through. For example, an embedded foreign body that is obscured by tissue reaction can be better mapped out through proximal illumination.

Sclerotic scatter takes advantage of the optical phenomenon total internal reflection seen in the cornea. The examiner should direct a de-centered – but intense – light beam at the corneoscleral junction. In a normal cornea the light is only seen where it intersects and reflects the sclera. A ring of light around the limbus is seen, but the cornea will remain dark against an essentially dark background. In an abnormal cornea, the light that is reflected at the sclera will illuminate an abnormality. Thus, abnormalities can be seen in totality and be better recognized as part of a broader disease pattern (e.g., corneal verticillata).

Retro-illumination of the iris combines both direct illumination and indirect retro-illumination to reveal different details about the area being examined. When the light beam is directed tangentially toward the cornea, direct retro-illumination from the iris can reveal opaque corneal lesions. In contrast, the areas adjacent to the light beam can reveal subtle refractile changes of lower density in the cornea, through indirect retro-illumination from the iris. The interface against both light and dark backgrounds is what shapes the light to reveal details through retro-illumination. Examples of corneal pathology which are best revealed through retro-illumination from the iris include folds in Descemet's membrane, and the linear stromal corneal changes in Lattice dystrophy. Retro-illumination from the fundus reflects light from the retinal pigment epithelium through the pupil to reveal changes in the cornea, lens, and anterior vitreous. A well-dilated pupil will achieve the most effect because light will not be scattered from the iris. In contrast to sclerotic scatter where abnormalities are best seen against a dark background, this technique uses brightfield illumination to reveal pathology. Lenticular changes, such as posterior subcapsular cataracts or subluxation, can be clearly visualized against the color reflected from the retinal pigmented epithelium. Retro-illumination of the iris and lens can reveal iris defects seen in glaucomatous diseases such as pigment-dispersion syndrome and pseudoexfoliaiton syndrome.

Specular Microscopy

Specular microscopy was developed by David Maurice in 1968. This device was used to examine the corneal endothelium, *ex vivo,* in the laboratory. This first microscope had an effective magnification of 500×, but was not practical for clinical use. In 1975, Bourne, Kaufman, and Lange developed clinical specular microscopes. Specular reflections arise from light which is reflected from the interfaces of materials with different indices of refraction. This occurs when the angle of incidence is equal to the angle of reflection. Thus, the difference between the index of refraction between the corneal endothelium

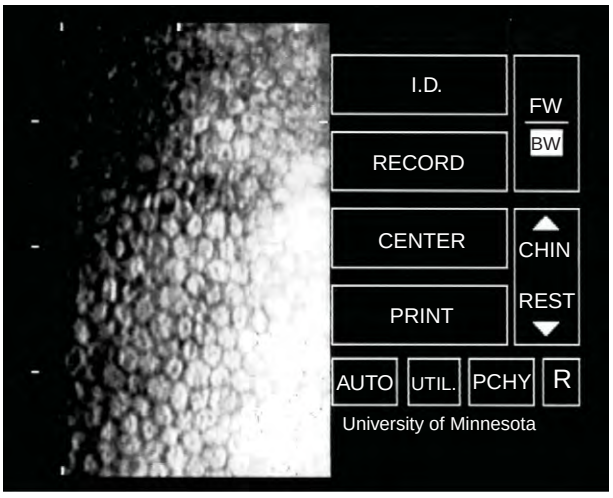

Figure 1 The specular photomicrograph shows a typical image from a noncontact specular microscope. From the information in this image, a cell count can be obtained and the degree of polymegathism and pleomorphism can be assessed.

and the aqueous produces a specular reflection. Many types of specular microscopes exist, which can be divided into contact and non-contact, and clinical (horizontal) and upright (which is used by eyebanks). Other types of specular microscopes are capable of visualizing other layers within the cornea.

The advent of the specular microscope allowed the ophthalmologist direct observation of the corneal endothelium in patients with Fuchs' dystrophy, posterior polymorphous dystrophy, psuedophakic bullous keratopathy, and other disorders of the corneal endothelium (**Figure 1**). If the cornea is significantly edematous, the specular reflection can be masked – which prohibits the visualization of the corneal endothelium. Specular microscopy is also used by eye banks to examine the corneal endothelium of donor corneas. The endothelial cell counts – which are reported as cells per square millimeter – are used to determine the suitability and health of the transplant tissue. Corneal endothelial cells typically demonstrate a hexagonal shape. A deviation from the normal hexagonal endothelial mosiac is termed pleomorphism. Although the size of corneal endothelial cells may vary slightly, in a healthy cornea, the cells should be similar in size. When there is great variablity in cell size, this is termed polymegathism.

Confocal Microscopy

Confocal microscopy employs a point source of light, which is focused on a thin section of the specimen. The confocal point detector is used to collect the resulting reflected signal. The use of a pinhole light source and its conjugate pinhole detector trades field of view for enhanced resolution by eliminating light which is reflected from structures above and below the focal plan under observation. A full field of view must be obtained by scanning many regions of the specimen. This can be achieved by rotating discs that contain multiple conjugate point detectors-pinhole light sources that allow for even scanning of the tissue. Other confocal systems use a slit beam which scans the specimen with a mechano-optical mirror system. White-light or a laser can be used at the light source. These systems are respectively termed white light confocal microscopes or laser scanning confocal microscopes.

The confocal microscope examines the cornea in coronally oriented sections versus the typical sagittal sections that are common to most histological tissue preparations (**Figure 2**). The corneal epithelium appears as a large cellular mosaic with bright, hyper-reflective central nuclei (**Figure 2(a)**). The basal epithelium consists of smaller cells and, generally, does not exhibit visible nuclei (**Figure 2(b)**). The corneal stroma appears as a collection of hyper-reflective, bean-shaped keratocyte nucei (**Figure 2(d)** and **2(e)**). The dendritic-appearing cell bodies of the keratocytes are only visible when the keratocytes are active. Corneal nerves can be seen passing through the stroma (**Figure 2(c)**). The deeper corneal nerves are large compared to the subepithelial nerve plexus, which resembles a fine filamentous membrane (**Figure 2(e)**). The corneal endothelium appears next (**Figure 2(f)**). Because the confocal microscope is able to eliminate aberrant light, corneal edema rarely obscures the corneal endothelium – unlike in the specular microscope.

Images that are obtained during confocal microscopy are native video; individual still-frames can be captured, as well as video. The images can be stored digitally or on video tape. Because of the ability to scan through the cornea and other tissues, video images can be particularly informative. Furthermore, the images are typically registered by *z*-axis location (depth within the cornea or other tissue). Thus, three-dimensional (3D) reconstructions can be produced which reveal *ex vivo* histopathology – like those depicting sections of the cornea.

The advantages of confocal microscopy are as follows: (1) the resolution can be better than the resolution obtained with the conventional light microscopy, allowing for imaging of the epithelial surface, stroma, nerves, and endothelium (2) high-resolution images can be obtained *in vivo* without the need for staining or processing of the cornea.

The clinical applications of confocal microscopy include the identification of corneal infectious agents, including bacteria, fungi, and *Acanthamoeba*. It has been used in clinical research to assess the effect of corneal wound-healing responses after refractive surgery and to characterize corneal dystrophies (**Figure 3**). Because the device can measure in the *z*-axis, it can be used to determine the depth of structures within the cornea, such as the thickness of the laser-assisted *in situ* keratomileusis (LASIK) flap or the residual bed, and the depth of corneal scars. These devices may also be useful in diagnosing neoplasia of the cornea and conjunctiva.

Ultrasound Biomicroscopy

High-frequency ultrasound biomicroscopy (UBM) produces high-resolution images of the anterior segment. Cross-sectional images of the eye are produced using a frequency range of 25–100 MHz. Resolution ranges from 20 to 100 μm. Higher frequencies provide higher resolution but the signal is increasingly attenuated, thereby limiting penetration of the signal. Newer technology can amplify the returning signal based on the depth of the structure under examination. The transducer has also evolved. An arc transducer follows the curvature of the cornea and permits the visualization of the entire cornea and anterior segment. The analog signal is digitized and can be used to construct a 3D-representation of the anterior segment. The required use of a water bath – as a fluid coupler – may limit the applicability of the UBM.

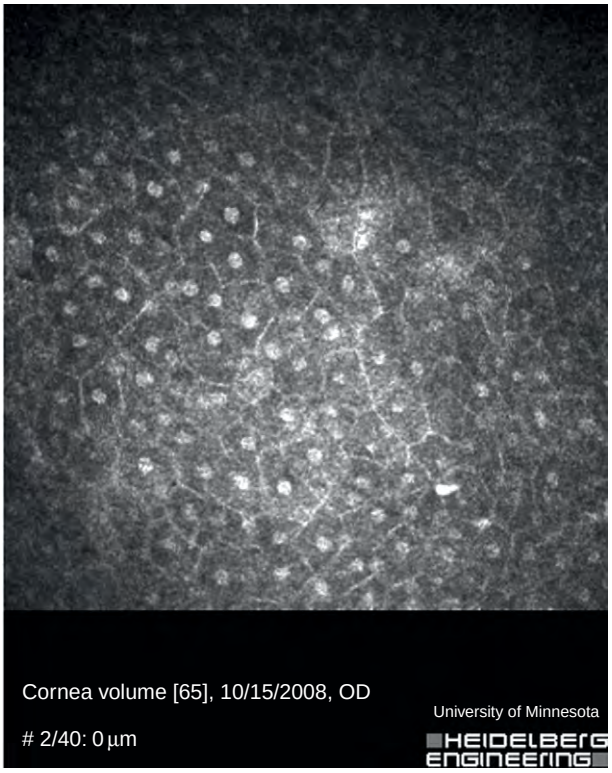

(a)

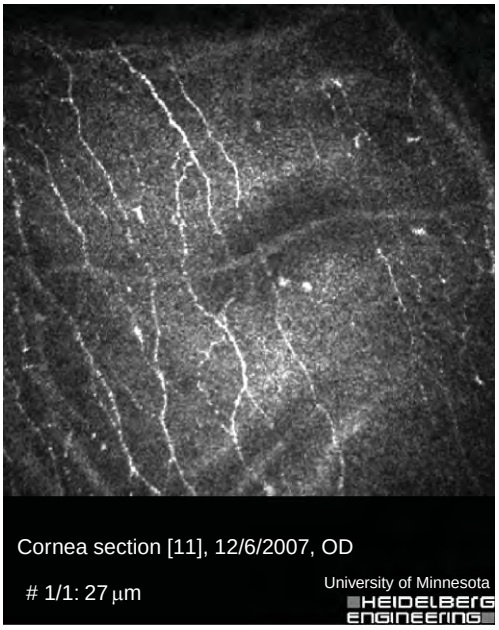

(c)

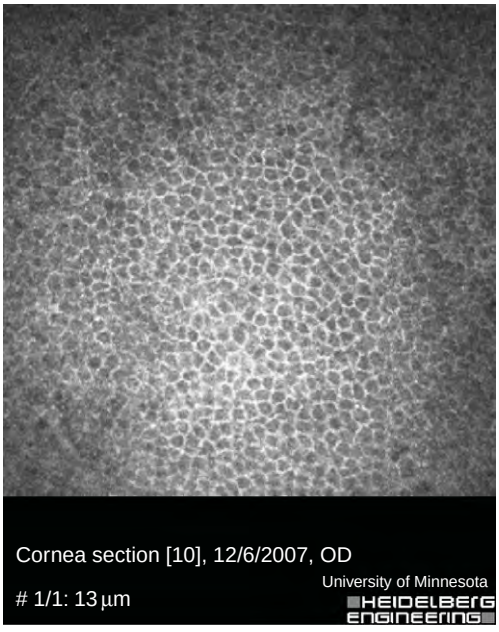

(b)

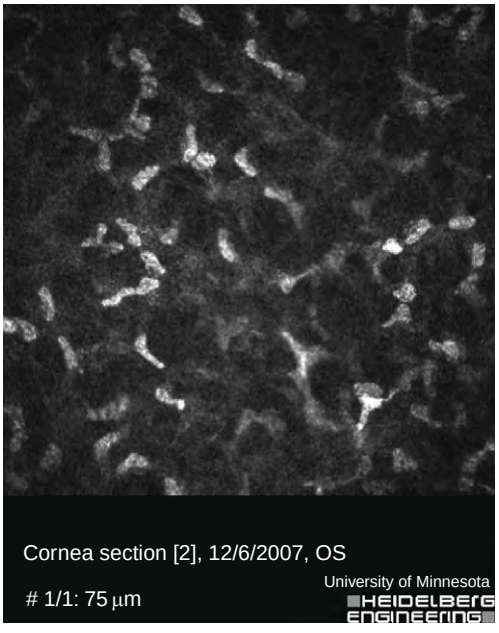

(d)

Figure 2 (Continued)

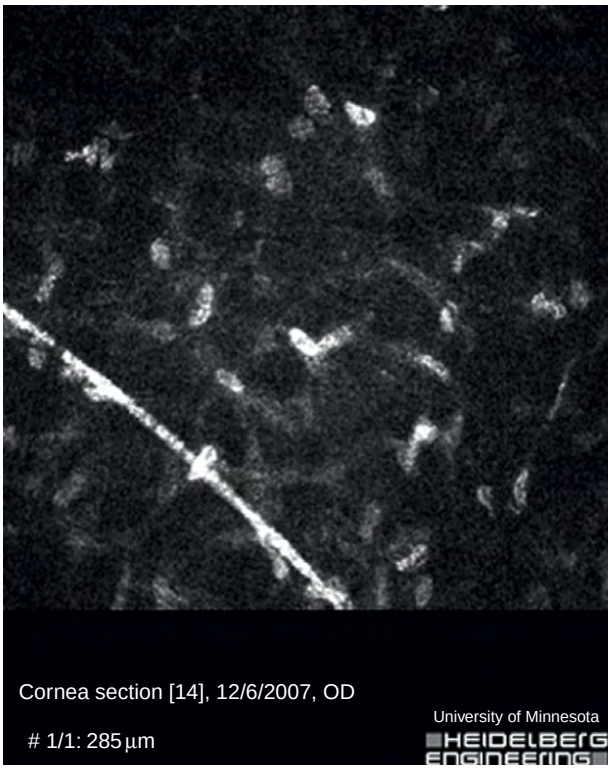

(e)

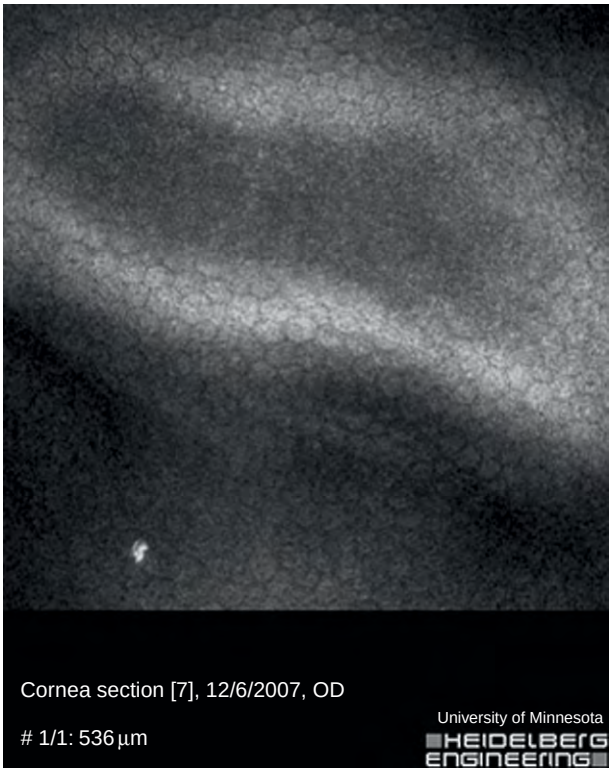

(f)

Figure 2 Confocal microscopy permits the examination of each layer of the cornea. (a) The superficial corneal epithelium appears as a cellular mosaic of nucleated cells. (b) The basal corneal epithelial cells are smaller than the more superficial layers of epithelium. (c) Just below the corneal epithelium lies the subbasal nerve layer. This fine meshwork of corneal nerves is responsible for the exquisite sensitivity of the cornea. (d) Confocal images of the anterior corneal stroma reveal the nuclei of the keratocytes. Contrasting the density of the anterior stromal keratocyte nuclei with the keratocyte density in (e), demonstrates that there is a greater density of keratocytes in the anterior stroma. (e) This confocal image of deep corneal stroma reveals a field of keratocyte nuclei and a corneal nerve (hyper-reflective linear structure). (f) The hexagonal mosaic of the corneal endothelium is seen with the confocal microscope.

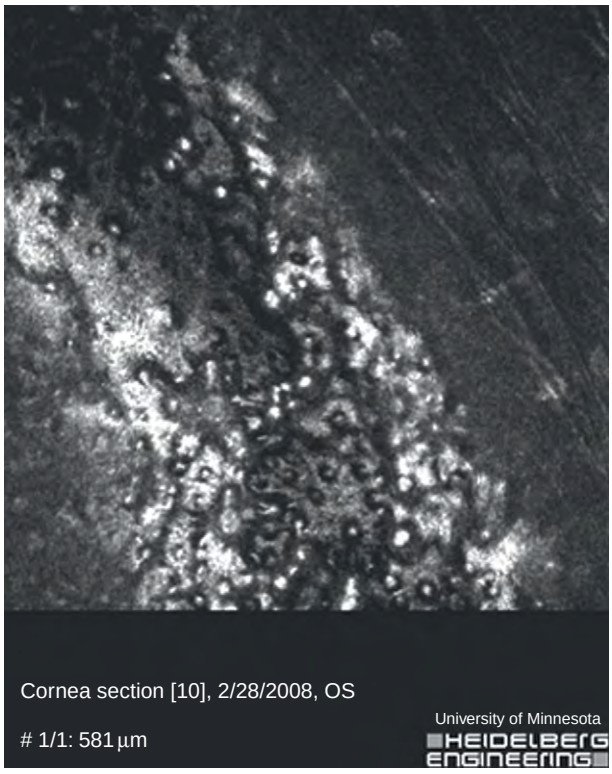

Figure 3 A confocal micrograph of the corneal endothelium of a patient with Fuchs' dystrophy. The scant number of corneal endothelial cells is evident.

UBM is used to examine many pathological conditions of the cornea, ocular adnexa, tumors of the anterior segment, intraocular lens, and diseases of the sclera. Because the UBM can image intraocular structures, it can be used to view intraocular cysts, narrow anterior chamber angle, and intraocular foreign bodies.

Anterior Segment Optical Coherence Tomography

Anterior segment optical coherence tomography (OCT) is an imaging technique that can provide detailed *in vivo* visualization of the anterior chamber. This noninvasive, noncontact device uses OCT to produce direct cross-sectional images that can be measured and used for diagnostic purposes.

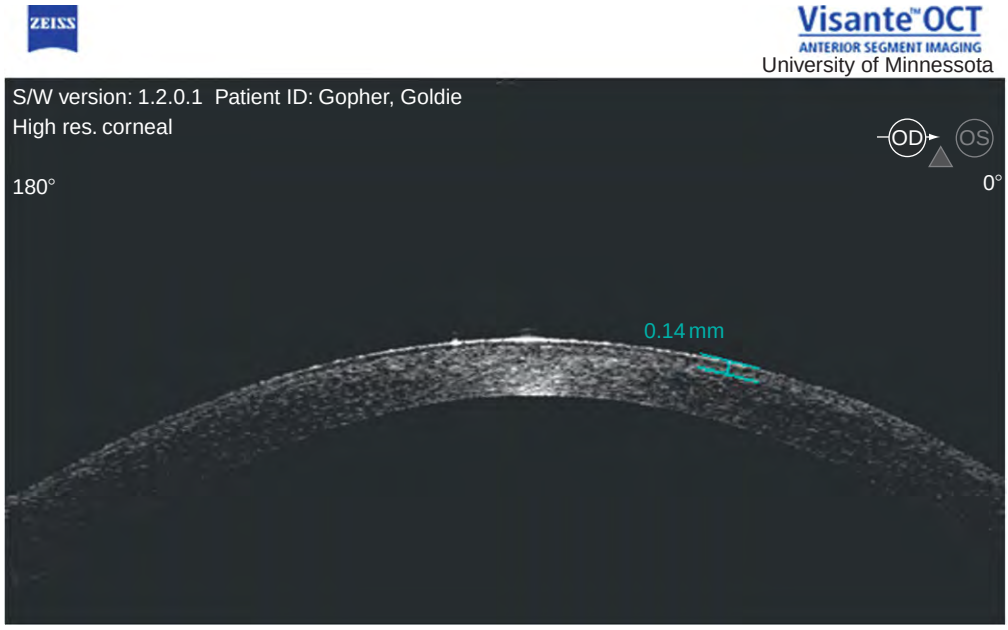

Figure 4 An OCT of the cornea of a LASIK patient. The blue caliper demonstrates the measurement of the thickness of the LASIK flap.

Using low coherence tomography, the light is set along two different optical paths: a sample path into the eye and a reference path of the interferometer. The light source is a 1310-nm superluminescent light-emitting diode (SLD). The light returning from the sample and reference paths are then combined at the photo-detector. The strength of the return signal is a measure of the reflectance of a small volume of tissue. Varying the optical lengths of the reference paths at each of the scanning points determines the axial depth of the tissue signal. By moving the scanning spot across the eye, multiple A-scans align to form a two-dimensional image.

There are many versatile uses of this device in assessing the anterior segment. The anterior chamber dimensions (depth, diameter, etc.) can accurately be measured. The iris and pupil – as well as the crystalline, pseudophakic, and refractive lens implants – can also be evaluated. A highly detailed evaluation of the angle structures can be assessed as well. *In vivo* measurements of the cornea can be evaluated in aid of surgical and refractive procedures as well as in diagnosing pathological processes. The device can measure post-LASIK corneal flap and residual stromal bed thickness, as well as produce full-thickness pachymetry maps which can assist both in refractive and glaucoma surgical planning (Figure 4). With the growing number of Descemet's Stripping Automated Endothelial Keratoplasty (DSAEK) surgeries being performed, this tool has found an additional role in post-surgical lenticle-placement evaluation.

Despite its numerous uses, using light as its medium limits its penetration into the eye. For example, ciliary body tumors cannot always be adequately visualized. In addition, image quality can be greatly reduced when imaging dense corneal opacities.

Acknowledgments

We would like to acknowledge the support of Research to Prevent Blindness and the Minnesota Lions Club.

See also: Corneal Dystrophies; Corneal Endothelium: Overview; Corneal Epithelium: Cell Biology and Basic Science; Corneal Nerves: Anatomy; Corneal Scars; The Corneal Stroma; Ocular Mucins; Optical Coherence Tomography; Overview of Electrolyte and Fluid Transport Across the Conjunctiva; Refractive Surgery and Inlays; The Surgical Treatment for Corneal Epithelial Stem Cell Deficiency, Corneal Epithelial Defect, and Peripheral Corneal Ulcer.

Further Reading

Chiou, A. G., Beuerman, R. W., Kaufman, S. C., and Kaufman, H. E. (1999). Confocal microscopy in lattice corneal dystrophy. *Graefe's Archive for Clinical and Experimental Ophthalmology* 237: 697–701.

Chiou, A. G., Kaufman, S. C., Beuerman, R. W., Maitchouk, D., and Kaufman, H. E. (1999). Confocal microscopy in posterior polymorphous corneal dystrophy. *International Journal of Ophthalmology* 213: 211–213.

Dhaliwal, J. S., Kaufman, S. C., and Chiou, A. G. (2007). Current applications of clinical confocal microscopy. *Current Opinion in Ophthalmology* 18: 300–307.

Kaufman, S. C., Musch, D. C., Belin, M. W., Cohen, E. J., Meisler, D. M., Reinhart, W. J., Udell, I. J., and Van Meter, W. S. (2004). Confocal microscopy: A report by the American Academy of Ophthalmology. *Ophthalmology* 111(2): 396–406. (Review.)

Ledford, J. and Sanders, V. (2006). *The Slit Lamp Primer,* 2nd edn. New York: Slack Inc.

Ramos, J. L., Li, Y., and Huang, D. (2009). Clinical and research applications of anterior segment optical coherence tomography – a review. *Clinical and Experimental Ophthalmology* 37(1): 81–89.

Wylegała, E., Teper, S., Nowińska, A. K., Milka, M., and Dobrowolski, D. (2009). Anterior segment imaging: Fourier-domain optical coherence tomography versus time-domain optical coherence tomography. *Journal of Cataract and Refractive Surgery* 35(8): 1410–1414.

Imaging of the Orbit

R A Zaldívar, M S Lee, and A R Harrison, University of Minnesota, Minneapolis, MN, USA

Glossary

Angiography – A method for imaging blood vessels that uses the injection of a radioopaque dye that outlines and facilitates their visualization on X-ray images.

Computed tomography (CT) – An imaging method where a large series of X-rays, taken in two dimensions, is computer-processed to result in the generation of a three-dimensional body image around a single axis of rotation. It is also called computed axial tomography, or CAT scan.

Magnetic resonance imaging (MRI) – An imaging method that uses powerful magnetic fields to align specific molecules in the body, such as the hydrogen in water, to produce high contrast images of the soft tissues in the body.

Imaging of the orbit and periorbital regions has revolutionized the way in which diseases of the orbit are managed both pre-operatively, intra-operatively, and post-operatively. The various imaging modalities that have been developed allow us to adequately plan pre-operatively for surgical intervention, including performing three-dimensional reconstruction. Intra-operative imaging can be used to assess our anatomic location or whether an intra-operative treatment has had its effect, as with vascular lesions. Once a diagnosis is made, monitoring the condition of the patient with the use of imaging further augments our clinical assessment. The rapid pace in which orbital imaging technology has developed also allows it be accessible throughout the country.

Computed Tomography

In the early 1970s, the use of computers allowed radiologists to visualize differences in densities among tissues and structures; this first method of computer-processed imaging became known as computed tomography (CT). In the 1980s and 1990s, the technology continued to improve and became the principal modality for orbital imaging as it is effective and cost efficient. Today we use a 64-slice CT scanner that combines speed, resolution, and processing, allowing complex image processing. These new scanners allow for axial and coronal imaging without the need to reposition the patient and can acquire the images in as little as 5 s with resolution up to 0.4 mm. The speed of the image acquisition also allows for rapid imaging in the pediatric patient often with little or no anesthesia. The use of computers to re-process the images, without quality degradation, eliminates additional radiation exposure from the second acquisition plane.

All aspects of the orbit can be analyzed via CT and has become the screening examination of choice by most orbital specialists. In particular, the changes of the orbital bone either by trauma or by compression (lysis or erosion) are better appreciated than by any other imaging modality. Various aspects of bony changes can be seen with CT, that is, compact and spongy layers in fibrous dysplasia (**Figure 1**) or the compact bone layer in meningioma (**Figure 2**). Bony changes secondary to trauma are also well visualized using both the coronal and axial planes of section. The coronal sections are especially useful in evaluating orbital floor fractures. If there is a complex fracture or need for craniofacial reconstruction, use of three-dimensional CT reconstruction may aid in conceptualization of orbital bone changes and in preparation for surgery (**Figure 3**).

From anterior to posterior, the soft tissues of the orbit and the periorbital structures, including most orbital pathology, can be evaluated efficiently with CT. Periorbital imaging, specifically of the eyelids, is primarily performed in conjunction with orbital imaging when there is suspicion of orbital cellulitis (**Figure 4**). In conjunction with the clinical exam, the integrity of the eye can be evaluated in situations of trauma (**Figure 5**). Computed tomography is also an excellent modality to evaluate the extraocular muscles. One or more muscles can be affected either by infectious, inflammatory, vascular, or neoplastic processes. Myositis, either due to infection or inflammation, appears as an enlargement of the involved extraocular muscle. The muscle tendon may be thickened in up to 50% of patients with inflammatory orbital pseudotumor, in contrast with thyroid eye disease in which the muscle insertions are generally spared (**Figure 6**). An important periorbital structure to evaluate during orbital imaging with CT is the optic nerve. The course of the optic nerve can be tracked with both axial and coronal planes of section. These two views are critical in evaluating the optic nerve for tumors (e.g., gliomas and meningiomas) and compression or stretch as in thyroid eye disease and intraconal tumors. Although CT images of the optic nerve do provide excellent imaging, when available we prefer magnetic resonance imaging for optic nerve disease (see the following section).

Figure 1 Fibrous dysplasia with thickened sclerotic bone of the right sphenoid. Note the ground glass appearance and destruction of the ethmoid sinus.

Figure 2 Optic nerve meningioma. Note enhancement of the optic nerve sheath on the right.

The morphology and pathology of orbital and periorbital structures are quickly and effectively viewed by today's modern CT scanners; however, when certain soft tissues and vascular lesions need to be assessed, other modalities, such as magnetic resonance imaging (MRI) and angiography, provide the clinician with important additional information.

Figure 3 T1 MRI, Coronal view of orbit posterior to globe. Note the bright signal of the orbital fat.

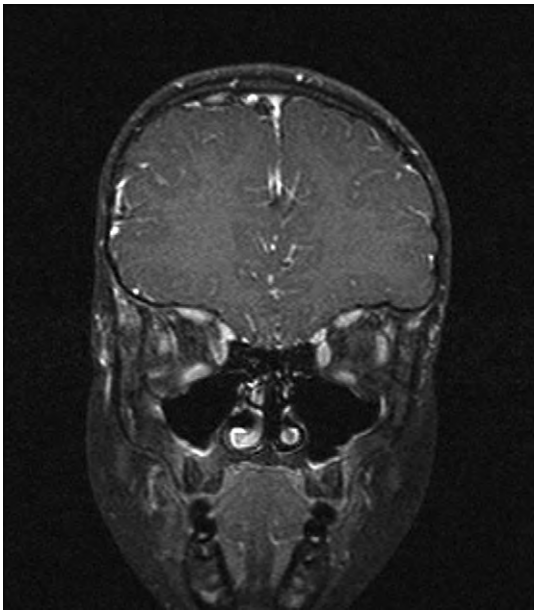

Figure 4 T2 MRI, coronal view of orbit posterior to globe. Note bright signal of the CSF around the optic nerve and nasal mucosa.

Magnetic Resonance Imaging

MRI is a noninvasive imaging technique that does not expose the patient to ionizing radiation. An image is created when a tissue containing hydrogen atoms is placed in a magnetic field and excited by a radiofrequency. The nuclei undergo an alignment that emits a radiofrequency. This radiofrequency can be captured and processed to produce the image. The quality of the images produced by MRI studies is determined by the magnet potency, signal to noise ratio, field of view, pixel size, slice

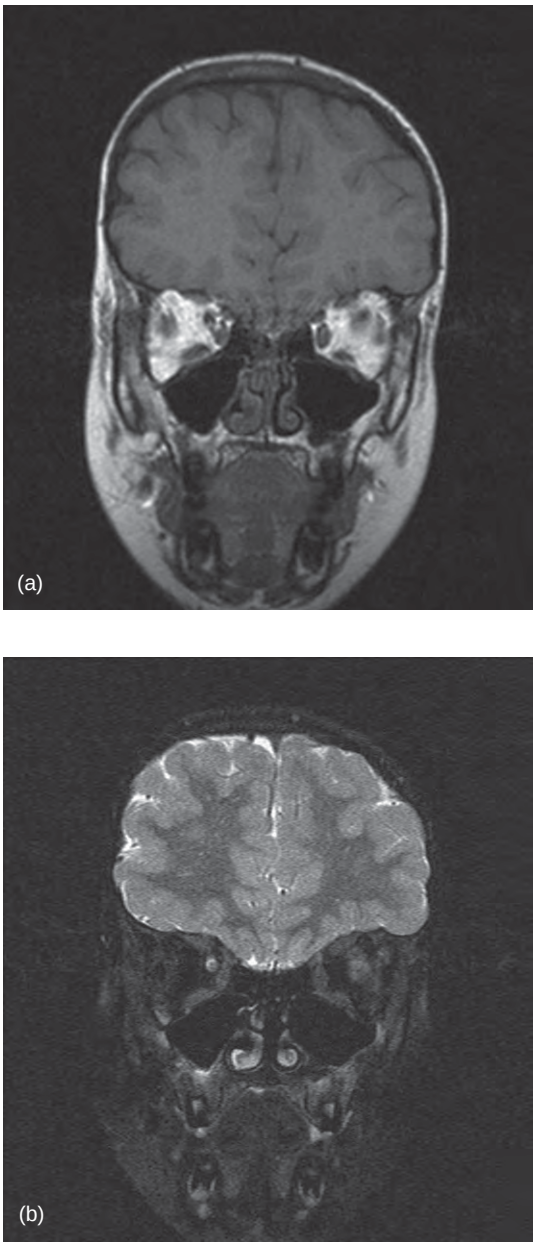

Figure 5 (a) Three-dimensional reconstruction of the face following orbital trauma. This may assist in pre-operative planning for reconstructive surgery. (b) Left orbital subperiosteal abscess secondary to ethmoid sinusitis. Note the enhancment of the thickened periorbita.

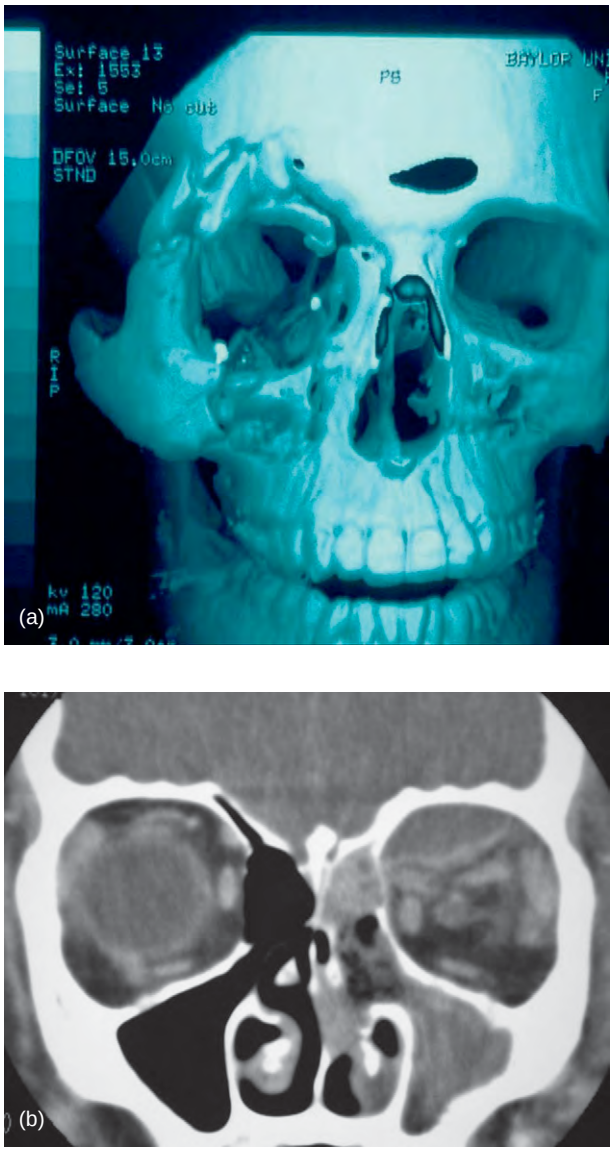

Figure 6 (a) Right ruptured globe. Note the tenting of the globe and intraocular hemorrhage. (b) Right eye ruptured globe. The pupil is peaked temporally secondary to prolapse of uvea.

thickness, and pulse sequences. The use of intravenous gadolinium helps to enhance vascularized lesions and provide additional information.

Based on the time it takes the hydrogen atoms in the tissue to realign, two images can be formed: T1 (longitudinal relaxation time) or T2 (transverse relaxation time). These two views help in differentiating various lesions. T1-weighted images generally offer the best anatomic detail of the orbit and require less acquisition time, therefore reducing the potential for motion artifact. However, the orbital fat in T1 images produces a bright signal that requires fat suppression (Figures 7 and 8). T2-weighted images can differentiate methemoglobin from melanin. As an example, this is useful in differentiating melanotic lesions from hemorrhage. The T1 and T2 image types produce different signal intensities for different tissues in the body. Most lesions seen on T1 MRI images of the orbit are dark except for fat, lipoma, liposarcoma, mucus as seen in mermaid cysts and mucoceles, and melanin.

Advantages of MRI over CT include: no ionizing radiation, excellent soft tissue resolution of the orbit and cavernous sinus, multiplanar imaging, and the ability to perform noninvasive arteriography. However, the disadvantages include: poor bony detail, longer scan times,

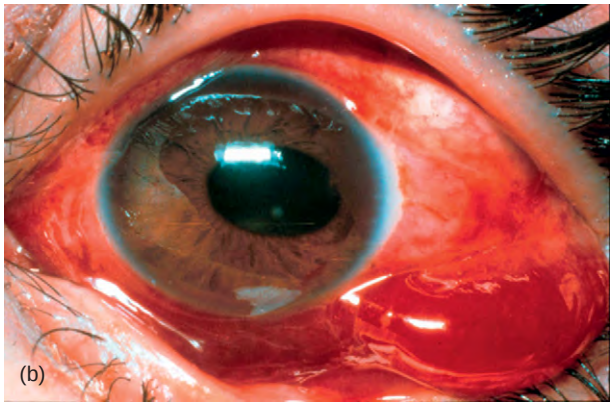

Figure 7 (a) Classical myopathy of thyroid eye disease. Note the enlarged medial recti with sparing of the muscle insertions. (b) Left lateral rectus orbital myositis. Differentiated from myopathy of thyroid eye diease in that the muscle insertions are involved.

images sensitive to motion artifact, difficulties for claustrophobic patients, contraindications for patients with ferromagnetic metallic foreign bodies, aneurysm clips, and pacemakers, as well as cost.

Specific indications for obtaining an MRI include demyelinating disease such as optic neuritis and multiple sclerosis, neurogenic tumors such as gliomas and meningiomas, visualization of lesions of the orbital apex or

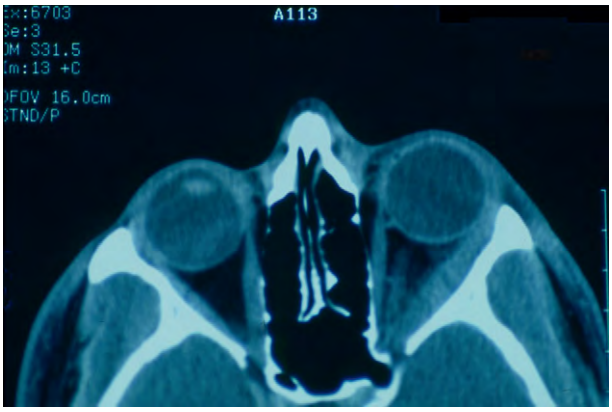

Figure 8 Pre-gadolinum T1-fat suppressed MRI, coronal view of orbit posterior to globe. Note the enhancment of the nasal mucosa.

cavernous sinus, optic nerve lesions, tissue specific signals such as for blood, lipid, mucus and melanin, and wooden or other less dense foreign bodies.

Angiography

Both venography and arteriography angiography were the original modalities used to study vascular lesions. However, because of the risk involved with these procedures and the development of other imaging techniques, there has been a decline in their use in the evaluation of orbital lesions. Some of these techniques include magnetic resonance angiography which allows for noninvasive visualization of large and medium-sized vessels of the arterial system but do not provide the detail seen in angiography.

See also: Optic Nerve: Optic Neuritis; Orbital Bony Anatomy and Orbital Fractures; Orbital Masses and Tumors; Orbital Soft Tissue Biomechanics; Orbital Vascular Anatomy; Thyroid Eye Disease.

Further Reading

Aviv, R. I. and Casselman, J. (2005). Orbital imaging: Part 1. Normal anatomy. *Clinical Radiology* 60: 279–287.

Aviv, R. I. and Miszkiel, K. (2005). Orbital imaging: Part 2. Intraorbital pathology. *Clinical Radiology* 60: 288–307.

Immunobiology of *Acanthamoeba* Keratitis

J Y Niederkorn, University of Texas Southwestern Medical Center, Dallas, TX, USA

Glossary

Clodronate – Drug that preferentially kills macrophages, but has no known deleterious effects on other cells of the innate or adaptive immune responses.

Interferon-γ (IFN-γ) – Cytokine produced by T cells that activates macrophages and enhances their capacity to kill *Acanthamoeba* trophozoites.

Mannose-binding protein (MBP) – Lectin receptor that is expressed on *Acanthamoeba* trophozoites and facilitates their adherence to mannosylated proteins that are expressed on corneal epithelial cells.

Major histocompatibility complex (MHC) class-I antigens – Antigens that allow cytotoxic T lymphocytes to recognize and kill cells infected with viruses and some protozoal parasites.

Mannose-induced protease 133 (MIP-133) – The 133-kDa protease that is induced when *Acanthamoeba* trophozoites engage mannose in the cell walls of bacteria or upon mannosylated proteins on corneal epithelial cells. This protease facilitates invasion of *Acanthamoeba* trophozoites by degrading basement membranes and it also induces apoptosis of corneal cells.

Mucosal immunity – Immune responses that are primarily in the form of secretory immunoglobulin A (IgA) antibodies, which preferentially accumulate in the milk, tears, and in mucosal secretions. This form of T-cell-dependent immunity acts primarily to prevent pathogens from entering the body via mucosal surfaces and rarely directly kills microorganisms.

Trophozoite – Amoebic phase of *Acanthamoeba* spp. *Acanthamoeba* spp. can exist as either dormant cysts or as the active trophozoite (amoebic) phase. Unlike cysts, trophozoites are invasive, produce pathogenic proteases, and directly kill host cells by apoptosis and direct cytolysis.

Introduction

Acanthamoeba spp. are the causative agents for *Acanthamoeba* keratitis (AK) and can be isolated from virtually any terrestrial, aquatic, and marine environment. Viable *Acanthamoeba* spp. have even been isolated from eyewash stations, bottled water, and contact lens cases of asymptomatic contact lens wearers. *Acanthamoeba* can exist either as a dormant cyst or as the active amoebic stage called the trophozoite. Trophozoites are the active vegetative stage that normally exist as free-living amoebae and feed on bacteria and fungi. Trophozoites are approximately the size of a leukocyte (10–25 μm) and are readily identified by their spiny pseudopodia that give them a sea urchin-like appearance. *Acanthamoeba* cysts are the dormant stage and are approximately half the size of the trophozoite. The cyst wall is comprised primarily of protein and cellulose. Interestingly, the latter molecule is not normally found in animals, but is restricted to members of the plant kingdom including bacteria and fungi. The cyst is remarkably resistant to environmental agents and can remain viable even after 20 years of storage at room temperature or following treatment with over 250 000 rads of gamma irradiation or doses of ultraviolet B (UVB) irradiation that are known to kill every category of mammalian cells. Although AK is believed to be caused by corneal infections produced by trophozoites adhering to contact lenses, cysts can also adhere to contact lenses, and, under certain circumstances, can produce corneal infections in experimental animals. Cysts can persist in corneal tissue for up to 31 months following antiamoebic treatment and may be the underlying cause for recrudescence in patients, especially those who receive corneal transplants to restore the vision lost as a consequence of AK. Corticosteroids are often used to extinguish the inflammation that is provoked in AK. However, corticosteroids have been shown to induce cysts to excyst and transform into infectious trophozoites. Moreover, corticosteroids activate trophozoites and render them more pathogenic and invasive. Thus, corticosteroid treatment may unwittingly exacerbate AK and contribute to the recrudescence that has been reported in AK patients who are treated with topical corticosteroids to prevent immune rejection of their corneal transplants.

In spite of the ubiquitous distribution of *Acanthamoeba* spp. in the environment and widespread contact lens wear, AK is remarkably rare. Moreover, environmental exposure to *Acanthamoeba* spp. is commonplace; up to 100% of the normal individuals with no history of AK possess serum antibodies to *Acanthamoeba* antigens, suggesting previous environmental exposure to *Acanthamoeba* spp. Viable *Acanthamoebae* can be isolated from the contact lens cases of individuals with no symptoms or history of AK. Collectively, these findings suggest that a large portion of the population is exposed to *Acanthamoeba* spp. and

may express some degree of immunity against corneal *Acanthamoeba* infection. This proposition begs the obvious question as to which immune component provides protection and how does it do it.

Anatomical and Physiological Barriers to Corneal Infections with *Acanthamoeba*

Clinicians have long suspected that contact lenses served as vectors for transmitting *Acanthamoeba* trophozoites to the corneal surface, and that antecedent injury to the corneal surface created epithelial defects that permitted trophozoites to gain a foothold in the cornea. Less than one-third of the cases of AK involve both eyes, even though contact lens wearers typically store their lenses in the same contact lens case, use the same contact lens solutions, and use the same finger for inserting their contact lenses. If a preexisting corneal epithelial barrier defect were not necessary, one would expect that the overwhelming majority of AK cases would be bilateral. Studies in animal models of AK confirm the importance of preexisting corneal epithelial defects in the development of AK that is produced by applying *Acanthamoeba*-laden contact lenses to the abraded corneal surface. However, other animal studies have shown that breaching the intact corneal epithelium by direct injection of trophozoites into the corneal stroma produces AK. Thus, the intact corneal epithelium provides a barrier for preventing the establishment of ocular infections with *Acanthamoeba* trophozoites.

In addition to the physical barrier provided by an intact corneal epithelium, the ocular surface is bathed in tears, which contain multiple factors that inhibit trophozoite binding and cytopathic effects. Although never formally proven, it is suspected that the shear forces produced by the blinking eyelid interfere with trophozoite adherence to the corneal epithelium and reduce the likelihood of the trophozoites gaining a foothold in the cornea.

Innate Immune System and Resistance to *Acanthamoeba* Infections

The immune system is divided into two functionally distinct components: (1) the innate immune apparatus – which is characterized by its nimble response, but lack of antigen specificity – and (2) the adaptive immune apparatus – which, although slower in its response, provides long-lasting immunity and memory. Elements of the innate immune apparatus are the first responders via their detection of pathogen-associated molecular patterns (PAMPS) that are widely and promiscuously expressed by many microorganisms. By utilizing PAMPS, macrophages and neutrophils are able to rapidly identify invading microorganisms and mount an initial response that restrains the infectious agents, thereby providing much-needed time for the development of the adaptive immune response.

Role of Macrophages in the Resistance to *Acanthamoeba* Infections

In vitro studies have demonstrated that macrophages are capable of killing *Acanthamoeba* trophozoites. Moreover, depletion of periocular macrophages by subconjunctival injection of liposomes containing the macrophagicidal drug clodronate results in a dramatic exacerbation of AK in experimental animals. Likewise, *in vitro* or *in vivo* exposure to liposomes containing interferon-γ (IFN-γ) activates macrophages, increases their capacity to kill *Acanthamoeba* trophozoites, and mitigates AK in experimental animals. In animal models, AK is a self-limiting disease that resolves in 4–5 weeks. However, depletion of conjunctival macrophages results in progressive AK that does not resolve and mimics the human counterpart. The extraordinarily low incidence of AK is not commensurate with the enormous number of contact lens wearers and the ubiquitous distribution of *Acanthamoeba* spp. This suggests that the presence of an additional risk factor is involved in the development of AK. It is tempting to speculate that patients who develop AK represent a small population of individuals who have underlying deficiencies in their conjunctival macrophage population or altered macrophage function.

Role of Neutrophils in the Resistance to *Acanthamoeba* Infections

The neutrophil is another constituent of the innate immune system that plays an important role in the resistance and resolution of AK. Neutrophils are consistently found in AK lesions – both in patients and in experimental animals. Neutrophils are highly effective in detecting the presence of both trophozoites and cysts. They kill both cysts and trophozoites in a myeloperoxidase-dependent manner. Blocking chemotactic responses of conjunctival neutrophils or depleting neutrophils with anti-neutrophilic antiserum results in progressive AK. Likewise, intracorneal injection of macrophage inflammatory protein-2 (MIP-2) – a potent chemoattractant for neutrophils – results in a swift infiltration of neutrophils into the central cornea and in an accelerated resolution of AK in experimental animals.

Ocular *Acanthamoeba* infections rarely progress beyond the cornea and are not known to produce endophthalmitis. Only three reports in the literature suggest that *Acanthamoeba* infections of the cornea progress to the posterior segment of the eye and involve the choroid or retina. Moreover, only one publication provides histopathological documentation of *Acanthamoeba* cysts in the posterior segment of the eye in a single AK patient. Moreover, the patient in this study had received four

separate corneal transplants in the affected eye. Likewise, more than 16 years of experience with both the pig and Chinese hamster models of AK has failed to produce any evidence of *Acanthamoeba* infections progressing posterior from the cornea or involving the uveal tract or retina. *In vitro* studies have shown that trophozoites can penetrate Descemet's membrane and are, theoretically, capable of entering the anterior chamber. Further studies showed that intraocular injection of 1 million trophozoites into the anterior chamber of the eye in Chinese hamsters did not produce intraocular infection. A swift neutrophilic infiltrate eliminated the injected trophozoites without inflicting collateral damage to the intraocular tissues.

Humoral Factors of the Innate Immune System that Affect Resistance to *Acanthamoeba* Infections

Tears contain a potpourri of antimicrobial factors that protect the ocular surface from pathogenic insults. Among these are lysozyme, lactoferrin, and complement components. Lysozyme is active against Gram-negative bacteria and some fungi, but is ineffective against Gram-positive bacteria. By contrast, lactoferrin and transferrin are effective in controlling Gram-positive bacteria. Complement is present in tears and can be activated by the alternate pathway via bacterial products or by the classical pathway by antibodies. Thus, the complement system straddles the innate and adaptive immune systems. Complement appears to have little or no effect in controlling AK, as pathogenic *Acanthamoeba* spp. express complement-regulatory proteins – including decay-accelerating factor – which disable the complement system. Tears and milk also contain a factor that inhibits trophozoite adherence and cytolysis of corneal cells. Interestingly, the factor in both milk and tears is not an Ig. The milk-borne factor is >100 kDa and is inactivated by proteinase K, indicating that it is a protein. The two major proteins in milk – α1-antitrypsin and α1-antichemytrypsin – are not the milk-borne factors, as neither of these proteins blocks trophozoite adherence or cytolytic activity.

Thus, both humoral and cellular elements of the innate immune system can contribute to the resistance to AK (**Table 1**).

Adaptive Immune System and Resistance to *Acanthamoeba* Infections

Elements of the innate immune system serve as the first responders to pathogens and are characterized by capacity to act immediately in response to microbial infections. However, the innate immune system acting alone cannot clear all microbial infections. Unlike the innate immune system, the adaptive immune apparatus needs a jump start to generate its effector elements, but – once engaged – is crucial for the recovery from microbial infections and the establishment of immunity to future infections. The innate and adaptive immune systems do not function in isolation, but communicate with each other in a coordinated immune response. Macrophages and dendritic cells present antigens to T and B cells, which process is facilitated by another innate immune system component – complement. T and B cells have the capacity to generate an endless array of antigen receptors that, when confronted with antigens expressed on antigen-presenting cells, culminates in the generation of antibodies and T cells that possess exquisite specificity and are used by antibodies to identify and kill bacteria and neutralize viruses. T cells utilize their antigen receptors and CD8 surface molecules to identify and kill virus-infected cells. The adaptive immune system is characterized by its exquisite specificity and memory. The efficacy of preventive immunization relies entirely on the capacity of the vaccine to activate crucial elements of the adaptive immune system. One has to look no further than the biology of acquired immune deficiency syndrome (AIDS) to recognize the importance of the adaptive immune system. With few exceptions, recovery and survival from microbial infections is contingent upon the effective activation of the adaptive immune system. However, AK is a notable exception to this rule.

There is no evidence to date that patients with AIDS have an increased incidence of AK, suggesting that a disabled adaptive immune system does not increase the susceptibility to corneal infections with *Acanthamoeba* even though *Acanthamoeba* spp. express antigens that are capable of activating the adaptive immune system. Fifty to one hundred percent of the individuals with no past history of AK possess serum and tear antibodies specific for *Acanthamoeba* antigens – indicating that *Acanthamoeba* antigens can

Table 1 Elements of the innate immune system that control ocular *Acanthamoeba* infections

Component	*Function*	*Evidence for role in protection*
Neutrophils	Kill trophozoites	Treatment with anti-neutrophil serum exacerbates AK; stimulating neutrophil infiltration into the cornea mitigates AK; neutrophils kill trophozoites *in vitro*.
Macrophages	Kill trophozoites	Depletion of conjunctival macrophages exacerbates AK; activating conjunctival macrophages mitigates AK; macrophages kill trophozoites *in vitro*.
Nonimmunoglobulin tear-borne factor	Prevents trophozoite adherence to cornea	*In vitro* assays demonstrate that tears from normal animals block adherence of trophozoites to corneal cells and prevent trophozoite-mediated cytolysis of corneal cells.

activate the adaptive immune system and that exposure to these antigens is remarkably widespread. The T-cell arm of the adaptive immune system is also activated by *Acanthamoeba* antigens, as 50% of the normal population with no known history of AK demonstrate T-cell lymphoproliferative responses to *Acanthamoeba* antigens. In spite of this, patients whose initial AK has been brought under control with antimicrobial therapy can experience recrudescence. This suggests that even if the adaptive immune system has been activated, it is ineffectual in controlling AK. This impression has been confirmed in animal models of AK. Both in Chinese hamsters and pigs, subcutaneous immunization with *Acanthamoeba* antigens elicits robust IgG antibody and T-cell responses, yet fails to protect the animals against ocular challenge with *Acanthamoeba* trophozoites. Moreover, resolution of AK does not render animals resistant to second ocular infections with trophozoites; repeat ocular *Acanthamoeba* infections are as severe as the primary infections.

Role of the Mucosal Immune System in Resistance to AK

On first blush, it would appear that the adaptive immune system is utterly incapable of preventing or resolving AK. However, animal studies and serological studies on human AK patients suggest that secretory IgA antibodies in the tears may prevent initial corneal *Acanthamoeba* infections. It is widely accepted that corneal infection with *Acanthamoeba* spp. begins when trophozoites adhere to mannosylated proteins on the corneal epithelium. Mannosylated proteins appear to be key ligands for trophozoite attachment – which is facilitated by the expression of a 136-kDa mannose-binding protein (MBP) that is expressed on the trophozoite cell membrane. Mannose expression on the corneal epithelium is dramatically upregulated by contact lens wear or by mild trauma to the ocular surface. In addition to promoting the adhesion of trophozoites, mannose stimulates the trophozoites to secrete a 133-kDa pathogenic protease (mannose-induced protease-133 (MIP-133)), which facilitates trophozoite invasion and cytolysis of corneal cells. Upregulation of mannosylated protein expression on the corneal epithelium is crucial for the establishment of AK. However, blocking the interaction between mannosylated glycoproteins on the corneal epithelium and the MBP on the trophozoite cell membrane is an effective strategy for preventing AK. Immunization through mucosal surfaces such as the gastrointestinal tract preferentially stimulates the generation of secretory IgA antibodies that appear in the tears and in mucosal secretions. Animals immunized orally with the *Acanthamoeba* MBP develop secretory IgA antibodies in the tears, which prevent the development of AK. Secretory IgA antibodies block the adhesion of *Acanthamoeba* trophozoites to corneal epithelial cells, and thereby, disrupt the first key step in the pathogenic cascade of AK. Anti-MBP secretory IgA antibodies are not toxic to trophozoites, even in the presence of complement and are ineffectual if they are generated after a corneal infection had been established. Thus, IgA antibodies in the tears are the only known component of the adaptive immune system that has an effect on the development of AK (**Table 2**).

Evading the Adaptive Immune Response

Exposure to *Acanthamoeba* antigens is commonplace as evidenced by the high incidence of serum antibodies and T-cell responses to *Acanthamoeba* antigens in individuals with no previous history of *Acanthamoeba* infections. In experimental animals, subcutaneous and intramuscular immunization with *Acanthamoeba* antigens elicits high titers of IgG antibodies and T-cell activation, yet fails to protect against AK. Although the adaptive immune

Table 2 Role of adaptive immunity in preventing ocular acanthamoeba infections

Immune element	*Role in AK*	*Evidence for effect*
Serum IgG	None	Animals and humans with anti-*Acanthamoeba* IgG antibodies can develop AC. Anti-*Acanthamoeba* antiserum fails to kill trophozoites *in vitro*, even in the presence of complement.
Delayed-type hypersensitivity	None	Subcutaneous immunization with *Acanthamoeba* antigens induces robust delayed-type hypersensitivity to *Acanthamoeba* but fails to prevent or mitigate AK.
Complement	None	Trophozoites resist complement-mediated lysis due to their expression of complement decay accelerating factor.
Cytotoxic T lymphocytes	None	Trophozoites are extracellular pathogens that do not express the crucial major histocompatibility complex class I restricting elements that are necessary for cytotoxic T lymphocyte function.
Secretory IgA	Prevents initial corneal infection	Mucosal immunization with surface antigens expressed on trophozoites induces production of secretory IgA in the tears; anti-*Acanthamoeba* IgA prevents trophozoite adherence to corneal cells and prevents trophozoite-mediated cytolysis of corneal cells; passive transfer of IgA monoclonal antibody against *Acanthamoeba* surface eptiotpes protects animals against ocular *Acanthamoeba* infections.

system is capable of eliminating a wide range of microbial agents, it is ineffectual in preventing corneal infections with *Acanthamoeba* or recrudescence of previous corneal infections. *Acanthamoeba* spp. employ at least three strategies to evade immune elimination: (1) inactivating immune effector elements; (2) escaping detection by cytotoxic T lymphocytes; and (3) forming dormant cysts that escape immune detection (**Table 3**). *Acanthamoeba* trophozoites can activate the complement cascade via the alternate pathway or by the direct pathway by complement-fixing IgG antibodies that recognize surface determinants on the trophozoite cell membrane. Complement components are present in the tears and at the ocular surface, yet trophozoites escape complement-mediated cytolysis – both *in vitro* and *in vivo*. The ability of trophozoites to elude the ravages of complement is ostensibly due to their expression of complement-regulatory proteins (i.e., decay-accelerating factor) – which disable the complement cascade. Complement-regulatory proteins are also present on the corneal epithelium and may further interfere with complement-mediated cytolysis of trophozoites at the ocular surface.

Trophozoites secrete a variety of proteases that are known to degrade Igs, including secretory IgA antibodies in the tears. The importance of this evasive strategy is limited, as IgA antibodies in the tears can prevent the initial establishment of *Acanthamoeba* infections of the cornea.

Acanthamoeba trophozoites are extracellular pathogens and thus, escape detection and elimination by cytotoxic T lymphocytes – which are only able to kill intracellular pathogens whose antigens are presented on host cells that are expressing major histocompatibility complex (MHC) class-I molecules.

Table 3 *Acanthamoeba* immune escape mechanisms

Factor or mechanism	*Potential effect in Acanthamoeba keratitis*
Secretion of serine proteases	Degrade immunoglobulins; induce apoptosis of leukocytes
Complement decay accelerating factor	Inactivate complement and disable complement-fixing antibodies
Encystment	Escape detection by inflammatory and immune cells; resistant to phagocytosis by non-activated macrophages; weakly immunogenic; do not produce chemoattractants for leukocytes
Immune privilege of cornea	Corneal infections fail to elicit IgG antibody or delayed-type hypersensitivity responses to *Acanthamoeba* antigens
Extracellular infection	Trophozoites are extracellular pathogens and do not reside in host cells that express MHC class I antigens. Thus, they escape recognition and attack by cytotoxic T lymphocytes

Protozoal parasites have the capacity to encyst and, thereby, escape immune detection and elimination. *Acanthamoeba* spp. are one of the few protozoal parasites of humans that form cysts in tissues. Although most intestinal protozoal parasites can encyst, the cysts reside transiently within the lumen of the large intestine and are typically eliminated in the feces. *Toxoplasma gondii* can encyst within mammalian cells and not in extracellular sites. *Acanthamoeba* cysts occur in tissue and have been reported to persist in corneal tissue for up to 31 months. *Acanthamoeba* cysts are remarkably resistant to a variety of agents and can remain viable for decades. Moreover, *Acanthamoeba* cysts are poor immunogens, have only weak chemoattractive properties, and often reside in an immune-privileged site (i.e., the cornea), thereby enhancing their ability to escape immune detection.

Anti-Disease Vaccine for AK

Effector elements of the adaptive immune system appear to be incapable of killing or inactivating *Acanthamoeba* trophozoites. Thus, immunotherapeutic strategies are limited to two potential targets: (1) preventing the initial adherence of trophozoites to the corneal surface, or (2) inactivating the trophozoite-borne pathogenic molecules that damage the cornea. As stated earlier, secretory IgA antibodies directed against the cell-membrane molecules on the trophozoite can prevent the establishment of corneal infections by blocking the adherence of trophozoites to the corneal epithelium, but only if the antibodies are present in the tears when trophozoites are first introduced to the corneal surface. IgA antibodies are unable to alter the course of disease once the trophozoites have gained a foothold in the cornea.

Trophozoites elaborate a variety of proteases that produce extensive cytolysis and apoptosis of corneal cells, degradation of basement membranes, and melting of the stroma. One of the most important trophozoite-borne proteases is a 133-kDa serine protease – MIP-133 – which is secreted in response to trophozoites binding to mannosylated glycoproteins on the corneal epithelium. Mucosal immunization with MIP-133 elicits the generation of secretory IgA antibodies that inhibit the cytolysis of corneal cells and neutralize the enzymatic degradation of stromal proteins. Hosts mucosally immunized with MIP-133 have much milder disease compared to controls. An attractive feature of eliciting mucosal immunity against a pathogenic molecule is that the ocular surface is bathed in tears containing neutralizing antibodies which are continuously replenished. An anti-disease vaccine could be implemented at the time AK is diagnosed and used in combination with conventional anti-*Acanthamoeba* chemotherapy.

Conclusions

The immunobiology of AK is puzzling. *Acanthamoeba* spp. are free-living amoebae that can be found in virtually any environmental niche, yet rarely cause disease. Environmental exposure to *Acanthamoeba* spp. is commonplace and results in the activation of the adaptive immune response as evidenced by the high percentage of individuals who display antibody and T-cell responses to *Acanthamoeba* antigens. The low incidence of AK combined with the high frequencies of anti-*Acanthamoeba* antibody and T-cell immunity suggest that the adaptive immune response protects against corneal infection with *Acanthamoeba* spp. However, animal studies suggest otherwise and indicate that – with the exception of secretory IgA antibodies – the adaptive immune system is incapable of preventing or controlling *Acanthamoeba* infections. By contrast, the innate immune apparatus appears to control ocular *Acanthamoeba* infections.

This article offers the following theory to explain the immunobiology of AK. Environmental exposure to *Acanthamoeba* spp. is common and occurs via mucosal surfaces by breathing airborne *Acanthamoebae* that can readily be isolated from heating and cooling vents or by ingestion of *Acanthamoebae* that are found in a variety of vegetables and fruits. Most environmental isolates of *Acanthamoeba* spp. are nonpathogenic, but are immunogenic. The presence of anti-*Acanthamoeba* IgA antibodies in the tears protects against ocular infection, especially in individuals without corneal epithelial defects. Occasionally, *Acanthamoeba* trophozoites will reach the ocular surface and escape detection by IgA antibodies in the tears, but are eliminated by neutrophils and macrophages. The small number of individuals who develop AK might have underlying deficiencies in their tear antibody titers or in their periocular neutrophil and macrophage repertoire. Such immunological blind spots might account for corneal *Acanthamoeba* infections. This theory remains to be confirmed, but is consistent with results from animal studies and with clinical findings from AK patients.

See also: Adaptive Immune System and the Eye: Mucosal Immunity; Adaptive Immune System and the Eye: T Cell-Mediated Immunity; Innate Immune System and the Eye; Role of Complement in Ocular Immune Response.

Further Reading

Clarke, D. W. and Niederkorn, J. Y. (2006). The immunobiology of *Acanthamoeba* keratitis. *Microbes and Infection* 8: 1400–1405.

Clarke, D. W. and Niederkorn, J. Y. (2006). The pathophysiology of *Acanthamoeba* keratitis. *Trends in Parasitology* 22: 175–180.

Khan, N. A. (2003). Pathogenesis of *Acanthamoeba* infections. *Microbial Pathogenesis* 34: 277–285.

Khan, N. A. (2006). *Acanthamoeba*: Biology and increasing importance in human health. *FEMS Microbiology Reviews* 30: 564–595.

Kumar, R. and Lloyd, D. (2002). Recent advances in the treatment of *Acanthamoeba* keratitis. *Clinical Infectious Diseases* 35: 434–441.

Leher, H., Silvany, R., Alizadeh, H., Huang, J., and Niederkorn, J. Y. (1998). Mannose induces the release of cytopathic factors from *Acanthamoeba castellanii*. *Infection and Immunity* 66: 5–10.

Leher, H., Zaragoza, F., Taherzadeh, S., Alizadeh, H., and Niederkorn, J. Y. (1999). Monoclonal IgA antibodies protect against *Acanthamoeba* keratitis. *Experimental Eye Research* 69: 75–84.

Li, L. and Sun, X. (2008). Impaired innate immunity of ocular surface is the key bridge between extended contact lens wearing and occurrence of *Acanthamoeba* keratitis. *Medical Hypotheses* 70: 260–264.

Marciano-Cabral, F. and Cabral, G. (2003). *Acanthamoeba* spp. as agents of disease in humans. *Clinical Microbiology Reviews* 16: 273–307.

McClellan, K., Howard, K., Niederkorn, J., and Alizadeh, H. (2001). The effect of corticosteroid on *Acanthamoeba* cysts and trophozoites. *Invesigative Ophthalmology and Visual Science* 42: 2885–2893.

Niederkorn, J. Y., Alizadeh, H., Leher, H., and McCulley, J. P. (1999). The pathogenesis of *Acanthamoeba* keratitis. *Microbes and Infection* 1: 437–443.

Immunobiology of Age-Related Macular Degeneration

R L Ufret-Vincenty, University of Texas Southwestern Medical Center at Dallas, Dallas, TX, USA

Glossary

Adaptive immune system – An arm of the immune system that recognizes and responds to specific antigens. It is composed mainly of lymphocytes (T cells and B cells) and antigen-presenting cells that present antigen to T cells. B cells produce antibodies, which recognize antigens with high specificity. One of the properties of the adaptive immune system is immunological memory, which enables the body to respond in a faster and stronger manner to an antigen that is encountered a second time.

Drusen – The deposits of extracellular material lying between the basement membrane of retinal pigment epithelium (RPE) cells and the inner collagenous zone of Bruch's membrane. Drusen are readily visible as yellowish deposits lying deep to the retina. They vary in size and shape and may have a crystalline appearance due to calcification. They are often the earliest clinical sign of AMD.

Innate immune system – It comprises the cells and molecules that defend the host from infection by other organisms, in a nonspecific manner.
The components of the innate (nonadaptive, non-antigen-specific) system recognize pathogens in a generic way. The innate immune system does not confer memory (long-lasting and enhanced immune responses). Components of the innate immune system include the complement system, and cells such as natural killer cells, mast cells, eosinophils, basophils, macrophages, and neutrophils.

M2 macrophages – Macrophages are cells that phagocytose (engulf and digest) cellular debris and pathogens. They can then stimulate or modulate lymphocytes and other immune cells. In a simplified scheme, macrophages can be sub-classified into M1 and M2. M1 macrophages are microbicidal and inflammatory, while M2 macrophages are immunomodulators. Among other things, M2 polarization is induced by interleukin-4, interleukin-10, interleukin-13, immune complexes, and glucocorticoid hormones. M2 macrophages express high levels of legumain (an endopeptidase) and this molecule can be used as a phenotypical marker for polarization. Macrophage polarization has been shown to be reversible.

Neoantigen – A newly acquired and expressed antigen that elicits an immune response. Examples include the antigens present in cells infected by viruses, those on tumor cells, or those induced by damage of normal molecules during tissue injury (e.g., oxidative damage to normal proteins).

Opsonization – A process by which a molecule (opsonin) enhances the binding of immune system cells to an antigen or cell surface, for example, by coating the negatively charged molecules on a cell membrane. This helps in the process of phagocytosis. Examples of opsonins are antibodies and complement molecules.

Single nucleotide polymorphism (SNP) – A type of mutation or allelic variant of a gene in which the DNA sequence differs only in a single nucleotide.

Vascular endothelial growth factor (VEGF) – A critical regulator of both physiological and pathological angiogenesis. It is involved in pathologic ocular neovascularization as seen in proliferative diabetic retinopathy, retinopathy of prematurity, and AMD. VEGF also promotes vascular permeability. It is strongly upregulated by hypoxia.

Epidemiology and Clinical Findings of Age-Related Macular Degeneration

Approximately 1.75 million Americans have advanced age-related macular degeneration (AMD). In fact, an estimated 30% of the population older than 75 years of age has some degree of macular degeneration. AMD is classified into a dry or non-neovascular form and a wet or neovascular form. About 12% of patients with AMD end up having advanced disease (neovascular AMD or central geographic atrophy (GA)). Presentations of dry AMD include drusen and a wide range of abnormalities of the retinal pigment epithelium (RPE), going from focal areas of hypopigmentation and hyperpigmentation, to the more advanced GA. Several studies have shown that self-reported quality-of-life scores for patients with choroidal neovascularization (CNV) secondary to AMD are worse than those reported by patients with acquired immune deficiency syndrome (AIDS; receiving treatment) and chronic obstructive pulmonary disease. Moreover, the levels of anxiety and depression were comparable. Genetic factors, smoking, and increased body mass index seem to have the highest impact on the likelihood of progression of AMD.

Despite recent advances in the treatment of CNV, clinical outcomes remain suboptimal. Furthermore, there is still no effective therapy for atrophic AMD. The Age-Related Eye Disease Study (AREDS) demonstrated that using high doses of certain vitamins and minerals (15 mg of β-carotene, 500 mg of vitamin C, 400 IU of vitamin E, 80 mg of zinc oxide, and 2 mg of cupric oxide) leads to a 25–30% reduction in the risk of development of advanced AMD. These vitamins and minerals mostly act as antioxidants. Their efficacy, combined with the observation that smoking is a significant risk factor for AMD, suggests an important role of oxidative damage in the early stages of macular degeneration. Current therapies for neovascular AMD include laser photocoagulation, photodynamic therapy, and anti-VEGF (VEGF, vascular endothelial growth factor) agents. All of these attempt to close or cause regression of the already-formed neovascular membranes. Although the newer anti-VEGF agents such as bevacizumab (Avastin) and ranibizumab (Lucentis) can lead to an average improvement in vision of up to two lines from the time of the detection of the neovascularization, this still means a significant loss in vision for many patients. The goal of newer therapeutic modalities should be to stop the process that leads to atrophy of the RPE and retina or to the formation of neovascularization before irreversible damage has occurred. This, of course, requires a better understanding of the pathogenetic mechanisms involved in the early stages of disease. Most experts now suspect that the immune system plays an important, although poorly understood, role in those early events.

The Immune System in AMD

Multiple lines of evidence imply a role of the immune system in AMD, including the presence of chronic inflammatory cells in retinal lesions and antiretinal antibodies in the serum of AMD patients. Macrophages, lymphocytes, and mast cells have been detected in CNV membranes and near ruptures of Bruch's membrane in eye specimens from AMD patients. In addition, AMD patients seem to have increased systemic levels of the inflammatory markers C-reactive protein (CRP) and interleukin-6 (IL-6). Yet, it is debated whether the immune system plays a role in initiating or exacerbating the disease, or if these findings are a response to the retinal damage.

The early stages of AMD are characterized by accumulation of debris (altered proteins and lipids) underneath the RPE. Recent literature suggests that an immune reaction to this debris may promote more tissue damage and/or a neovascular response. Both the innate and the antigen-specific arms of the immune system can cause local damage to RPE cells, Bruch's membrane, and the choriocapillaris, leading to either the atrophic or neovascular forms of AMD.

Histopathology of Drusen

For the last four decades there has been a debate surrounding the mechanism for the formation of drusen. However, whether drusen form from fragments of RPE cells, from abnormal material secreted by dysfunctional RPE cells, or whether some components come from the choriocapillaris, the composition of drusen gives us important information about the pathogenesis of AMD.

During the last decade Hageman, Anderson, Johnson, Penfold, and others have contributed a great deal to our knowledge of drusen composition by extensive histopathological analysis of human AMD specimens obtained within the first few hours of death. They have performed light microscopy, confocal microscopy, electron microscopy, and immunostaining in hundreds of specimens; and have also evaluated the levels of mRNA expression of inflammatory mediators in the RPE and choroid. From these studies they have identified a large number of molecules found in drusen, many of which are in some way related to inflammation:

1. acute-phase reactant proteins such as CRP;
2. inflammatory mediators such as serum amyloid P;
3. potential activators of the complement cascade, including nuclear fragments/nucleic acids, membrane-bound vesicles, mitochondria, modified lipids, cholesterol, and microfibrillar debris;
4. complement components such as C3 and its fragments, C5, and the membrane attack complex (C5b-9); and
5. complement regulatory proteins including vitronectin, clusterin, membrane cofactor protein (CD46), complement receptor 1, and complement factor H (CFH).

Role of Macrophages

Some studies have suggested that macrophages may play a protective role in AMD, while others suggest that they promote disease progression. Some investigators have suggested that macrophages promote CNV formation. They have shown in the mouse laser-injury model of CNV that depletion of macrophages diminishes the size of the CNV lesions. They have also shown that neovascular AMD patients tend to have higher levels of expression of tumor necrosis factor (TNF)-α in their circulating monocytes than controls. TNF-α is considered a marker for monocyte activation. Others propose that macrophages have a role in preventing AMD. Mice deficient in monocyte chemoattractact protein-1 (also known as CCL-2) or its receptor can develop CNV in old age, suggesting that impaired macrophage recruitment in these mice is responsible for decreased clearance of proinflammatory mediators, such as C5 and IgG, from the sub-RPE tissues, resulting in an increased risk for CNV. This idea is very attractive, but other groups have had difficulty reproducing the results. Mouse studies

using the laser model of CNV have shown that IL-10 inhibits recruitment of macrophages into CNV lesions, but this leads to increased CNV size, suggesting that macrophages are antiangiogenic. Additional animal studies propose that senescence may cause a shift in the ocular microenvironment (including higher IL-10 levels) that makes it more proangiogenic; and that microenvironment, in turn, alters the polarization of macrophages toward an M2 phenotype which is unable to regulate angiogenesis. Thus, young macrophages appear to have an antiangiogenic role, while aging M2 macrophages change toward a proangiogenic phenotype. This could explain the different results obtained by different groups using the mouse laser model. Although it is still too early to determine if these conclusions apply to a noninjury model of CNV or to human AMD, the idea that "not all macrophages are made equal" and under different conditions may have opposing roles in AMD is very attractive.

Adaptive Immune System

The potential role of the innate arm of the immune system in AMD is further explored under the topic of genetics. The adaptive arm of the immune system is composed primarily of T cells and B cells. Although T and B cells have been identified in human AMD lesions, it is still not known whether they play causal roles in AMD versus being epiphenomena. Some investigators suggest that these T and B cells may be responding to subretinal neoantigens. Proteome analysis of the Bruch's membrane of AMD patients demonstrates higher levels of lipid–protein adducts derived from oxidative damage when compared to controls. These carboxyethyl pyrrole (CEP)–protein adducts are generated by the cross-linking of oxidized lipids and proteins. It has been proposed that the CEP–protein adducts may serve as neoantigens triggering an antigen-specific immune response in the subretinal/sub-RPE tissues that could promote the development of AMD. Moreover, immunization of mice with CEP-adducted mouse serum albumin led to an immune response and the formation of drusen and GA-like lesions in some animals.

Infectious Agents

Several mechanisms have been proposed by which infectious agents may promote the development of AMD. Molecular mimicry occurs when a microbial antigen resembles a self-antigen (in AMD it could be molecules on RPE cells or Bruch's membrane) so much that the immune system attacks the self-antigen while trying to eradicate the intended microbial antigen. By-stander injury refers to injury to self-tissues caused by the immune system as it tries to attack a microbial organism in close proximity. Finally, the infection can directly injure the host tissues. It is not clear if in AMD any of these mechanisms can be invoked.

In 2005, the Nobel prize in medicine was awarded for the work associating *Helicobacter pylori* with gastritis and peptic ulcer disease. Several epidemiological studies have found that *Chlamydia pneumoniae* (serology) may be associated to atherosclerosis, a disease that has several risk factors in common with AMD. Moreover, recent findings indicate that patients with AMD may be more likely to have higher anti-*C. pneumoniae* antibody levels than matched controls. There was also an association with pathology specimens of surgically excised choroidal neovascular membranes. Two other studies in Japan and Australia confirmed the serological association. Other studies could not reproduce these results, but instead found an association between high anti-CMV antibody levels and neovascular AMD. Critics comment that these are mere statistical associations and not proof of causality. Furthermore, they may be the result of unintentionally biased statistical analyses. Finally, the numbers included in the studies were often low. In the case of *Chlamydia* and atherosclerosis, clinical studies found that antibiotics did not alter the risk for vascular events. This could mean that *Chlamydia* is merely a commensal organism that thrives on atheromatous plaques without causing the disease; or it could mean that *Chlamydia* triggers the disease, but is not needed for disease progression. The same reasoning applies to AMD. One potential hypothesis is that *Chlamydia* or other organisms could cause a chronic low-grade infection at the deep retina/RPE/choriocapillaris level, and that in susceptible individuals (e.g., those with the at-risk variant of complement factor H) this could lead to chronic low-grade inflammation and the formation of drusen or CNV. It is difficult to prove this hypothesis due to the lack of good experimental models. However, we expect further research may shed light on this.

Genetics of AMD and Evidence for a Role of Inflammation in the Pathogenesis of AMD

Mutations may account for up to 70% of the population-attributable risk for AMD. Specific single nucleotide polymorphisms (SNPs) that increase the risk for AMD have been identified in several genetic loci. Two of these loci are particularly interesting since they have been reproduced by different research groups and in different populations. The first locus is in chromosome 1q32 (regulator of complement activation or RCA locus), which includes the gene for complement factor H. Several SNPs that appear to be statistically associated with the development of AMD have been identified within this locus. The most consistent association has been with a polymorphism that causes a substitution of a tyrosine for a histidine at amino acid position 402 in complement factor H (CFH Y402H).

However, several other polymorphisms, including CFH I62V and some intronic SNPs, have also been found to be associated to AMD by different groups. Within the same locus 1q32, a deletion affecting factor-H-related genes (CFHR1 and CFHR3) may decrease the risk of AMD, perhaps by decreasing the competition with factor H for the binding of C3.

The second locus of interest involves a region of chromosome 10q26 containing three genes PLEKHA, LOC387715/ARMS2, and HTRA1. The strongest associations in this locus have been with SNPs in the hypothetical gene LOC387715 and in the promoter region for HTRA1.

A third, and perhaps less common association, involves a locus in chromosome 6p21. Mutations affecting complement factors B and C2 in this region have been shown to alter the risk for AMD.

It is difficult to determine if there is a causal relationship between all these SNPs and AMD phenotypes. The best rationale for causality is for the Y402H mutation. Complement factor H (CFH or Cfh) is a key regulator of the alternative complement pathway. A point mutation that leads to a histidine, instead of a tyrosine at amino acid position 402 of CFH (Y402H), increases the risk of AMD by sevenfold in homozygotes. Moreover, this histidine variant of CFH appears to make AMD patients resistant to therapy with anti-VEGF agents. Despite the eagerness of the pharmaceutical industry to dive into this field, our knowledge of the mechanisms explaining this increase in risk for disease and decrease in susceptibility to therapy is in its infancy. One hypothesis is that normally CRP opsonizes subretinal debris and helps macrophages clear this debris in a noninflammatory fashion. For this to work, CFH has to bind CRP, preventing CRP from fully activating the complement cascade. The at-risk variant of CFH (402H) has a reduced affinity for CRP, which may lead to reduced binding of CFH to CRP in the subretinal debris. Thus, the full complement cascade would be activated by CRP, resulting in a vicious cycle of accumulation of debris and CRP, activation of complement, and tissue damage. In support, one study demonstrated that individuals homozygous for the at-risk variant of CFH have elevated levels of CRP in the choroid. Moreover, 402 YY patients receiving a liver transplant from 402 HH donors quickly developed drusen. Nevertheless, some investigators suggest that the Y402H mutation may not be pathogenic; that it may simply be in linkage disequilibrium with a yet-unidentified pathogenic mutation. It is essential to determine if Y402H has causal relevance in AMD.

It is more difficult to explain causality for the 10q26 SNPs: LOC387715 is still considered a hypothetical gene since the protein it codes for has not been unequivocally identified. HTRA1 is a serine protease and it has been proposed that it may be involved in the facilitation of penetration of Bruch's membrane by neovascular fronds. Unfortunately, many of the identified SNPs are in regions of high linkage disequilibrium. In other words, it may be that the identified SNPs are not directly responsible for the disease, or that they are simply strongly associated with other mutations which are the direct culprits for the pathological events leading to AMD.

A large group of investigators from several institutions have recently published a single report showing an association between a mutation in the gene for toll-like receptor 3 (TLR3) and the development of GA using three separate case-control series. SNP rs3775291 in TLR3 seemed to offer mild-to-moderate protection against GA. It has no effect on drusen or CNV formation. Toll-like receptors are a class of membrane-spanning receptors that recognize structurally conserved molecules derived from microbes and play a critical role in innate immunity. TLR3, in particular, is expressed on dendritic cells and B lymphocytes and recognizes double-stranded RNA (dsRNA, usually from viruses). The hypothesis is that dsRNA from infecting viruses may trigger apoptosis of RPE cells through activation of TLR3. The SNP in question causes a reduction in TLR3-mediated cell death. If this hypothesis is correct, it not only implies a role for infectious agents in inducing AMD, but also raises concern for RPE damage with the new small interfering RNA (siRNA) investigational drugs (which are also small double-stranded RNA molecules). However, an earlier study was not able to find any association between the same SNP in TLR3 and AMD.

Mouse Models of AMD

Several groups have recently demonstrated that, despite the obvious anatomical differences with humans (lack of a macula), mice can develop drusen and CNV similar to those seen in clinical AMD. Some of the most interesting models will be discussed here.

One study examined mice deficient in either chemokine ligand 2 (CCL2) or chemokine receptor 2 (CCR2). The findings were discussed earlier. Investigators at the National Eye Institute have generated mice that are deficient in both chemokine receptors CCL2 and CX3CR1. These mice develop drusen-like and pigmentary changes by 6 weeks of age, and 15% of them develop CNV as early as 12 weeks of age. It should be noted that, at least in CX3CR1-deficient mice (not deficient in CCL2), another group in France has shown that the drusen-like lesions seen clinically are histopathologically different from drusen seen in AMD and consist of lipid-bloated subretinal microglial cells rather than subretinal pigment epithelium deposits. Both CCL2 and CX3CR1 are involved in the recruitment of microglia and monocytes into tissues. Monocytes can then further differentiate into macrophages and dendritic cells. Somewhat counter-intuitively, the CCL2/CX3CR1-deficient mice have increased numbers of macrophages and microglia in the subretinal space and retinal lesions. Some investigators suggest that an alternative pathway for monocyte recruitment involving the upregulation of CCL5 is

responsible for this finding. They also suggest that CX3CR1-deficient microglia may behave abnormally and produce local tissue injury. Furthermore, these mice have increased complement activation and retinal autoantibodies in their retinas. It is still not clear the mechanism by which these mice develop the AMD-like changes and if these mechanisms are relevant to human AMD. An association between two mutations in CX3CR1 and AMD has been reported. However, these mutations have not been identified in genome-wide scans and other studies. Further studies will be required to determine if mutations in CX3CR1 and/or CCL2 are truly involved in the pathogenesis of human AMD. In the meantime, it is clear from these studies that the migration and function of macrophages, microglia, and dendritic cells may lead to features similar to those seen in AMD and may, under certain circumstances or in certain subgroups of patients, have pathophysiologic relevance.

The effect of apolipoprotein (ApoE) variants on AMD pathogenesis has been examined in mice. It was shown that the eyes of aged, targeted replacement mice expressing human apoE4 and maintained on a high-fat and cholesterol diet develop diffuse sub-RPE deposits, drusenoid deposits, thickened Bruch's membrane, and RPE pigmentary abnormalities. Close to 20% of the mice also developed CNV. Multiple genetic studies have given mixed results regarding the clinical relevance of ApoE variants and/or mutations.

Studies in superoxide dismutase 1 (SOD1)-deficient mice show that they develop drusen and CNV at an old age. This suggests that the increased oxidative stress in the retina leads to tissue injury and accumulation of debris. It should be noted that more recent work suggests that the yellow deposits seen clinically in these animals may not be drusen, but collections of lipid-laden macrophages. Moreover, there is no genetic evidence for an association between SOD1 and AMD.

Summary

The pathogenesis of AMD is complex and clearly involves genetic and environmental risk factors. At least three genes have been identified to be strongly correlated to the disease. However, it is likely that many others have an impact in the disease for some subpopulations of patients. A very simplified diagram on the pathogenesis of AMD is included in Figure 1. Note that the potential roles of neither the 10q26 locus and the TLR3 mutation nor the antibodies and T cells have been included.

Based on the genetic, histopathologic, serologic, and animal model data, it is clear that the immune system has a significant role in the development of AMD. However, we are still far from determining the exact mechanisms by which it affects the clinical course of the disease. In fact,

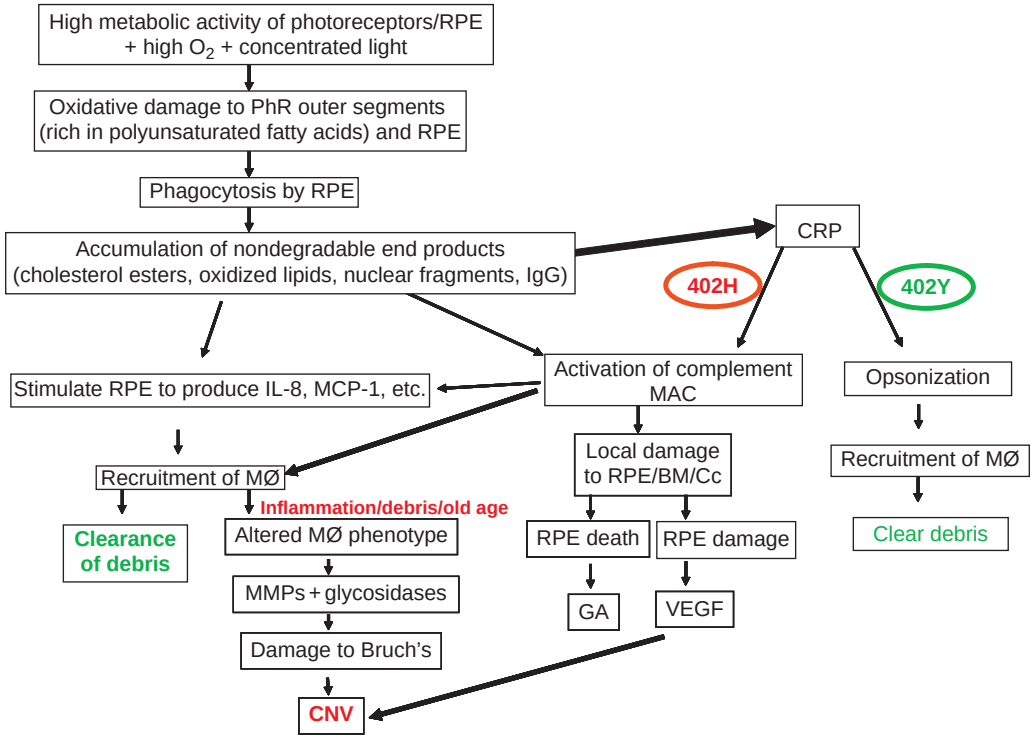

Figure 1 Proposed simplified pathogenesis of AMD. BM, Bruch's membrane; Cc, choriocapillaris; CNV, choroidal neovascularization; CRP, c-reactive protein; GA, geographic atrophy; IgG, immunoglobulin G; IL-8, interleukin 8; MAC, membrane attack complex; MCP-1, monocyte chemoattractant protein 1; MMPs, matrix metalloproteinases; MØ, macrophage; O_2, oxygen; PhR, photoreceptor; RPE, retinal pigment epithelium; VEGF, vascular endothelial growth factor; 402H, histidine-402 variant of complement factor H; 402Y, tyrosine-402 variant of complement factor H.

although the strongest incriminating data available point to the complement system and macrophages, it is not clear if the adaptive immune system (T cells, B cells, and antibodies) is also important.

The pharmaceutical industry, at present, has a great impetus to develop new therapeutic agents for AMD based on controlling inflammation. Several agents that block complement components 3 or 5 or factor B are in preclinical or early clinical trials. Furthermore, the effect of anti-inflammatory agents, in combination with anti-VEGF agents, is being studied. Yet, given our limited knowledge, the approach is far from ideal. Better animal models of AMD (based on genetic and environmental risk factors known to be important in AMD) would help us improve our understanding of the early steps in the pathogenesis of the disease, and perhaps allow us to identify new therapeutic targets and test new drugs.

See also: Adaptive Immune System and the Eye: Mucosal Immunity; Adaptive Immune System and the Eye: T Cell-Mediated Immunity; Role of Complement in Ocular Immune Response.

Further Reading

Bressler, N. M., Bressler, S. B., and Fine, S. L. (2006). Neovascular (exudative) age-related macular degeneration. In Schachat, A. P. and Ryan, S. J. (eds.) *The Retina,* 4th edn., pp 1075–1114. Philadelphia, PA: Elsevier.

Bressler, S. B., Bressler, N. M., Sarks, S. H., and Sarks, J. P. (2006). Age-related macular degeneration: Nonneovascular early, AMD, intermediate AMD, and geographic atrophy. In Schachat, A. P. and Ryan, S. J. (eds.) *The Retina,* 4th edn., pp 1041–1074. Philadelphia, PA: Elsevier.

Edwards, A. O. and Malek, G. (2007). Molecular genetics of AMD and current animal models. *Angiogenesis* 10(2): 119–132.

Gehrs, K. M., Anderson, D. H., Johnson, L. V., and Hageman, G. S. (2006). Age-related macular degeneration – emerging pathogenetic and therapeutic concepts. *Annals of Medicine* 38(7): 450–471.

Haddad, S., Chen, C. A., Santangelo, S. L., and Seddon, J. M. (2006). The genetics of age-related macular degeneration: A review of progress to date. *Survey of Ophthalmology* 51(4): 316–363.

Nussenblatt, R. B. and Ferris, F. 3rd (2007). Age-related macular degeneration and the immune response: Implications for therapy. *American Journal of Ophthalmology* 144(4): 618–626.

Patel, M. and Chan, C. C. (2008). Immunopathological aspects of age-related macular degeneration. *Seminars in Immunopathology* 30(2): 97–110.

Immunobiology of Uveal Melanoma

M J Jager, Leiden University Medical Centre, Leiden, The Netherlands
J Y Niederkorn, University of Texas Southwestern Medical Center, Dallas, TX, USA

Glossary

Adaptive immune responses – Immune responses that require priming, participation of T lymphocytes, and are characterized by antigen specificity and memory.
Antigen-presenting cells (APCs) – These cells may either stimulate or inhibit T-cell-mediated immune responses.
Complement regulatory proteins (CRPs) – Cell membrane-bound and secreted molecules that disable the complement cascade and thereby inhibit the efficacy of complement-fixing anti-tumor antibodies.
Human leukocyte antigen (HLA) – Necessary for target cell recognition by (NK) and T cells.
Innate immune response – Immune responses that are T-lymphocyte-independent, lack antigen specificity, and do not express memory. Innate immune elements include granulocytes, macrophages, NK cells (see below), and the complement system. Innate immune elements are the first responders and do not require priming to produce their effects.
Melanoma antigen-encoding gene (MAGE) – Proteins encoded by MAGE are expressed on skin and uveal melanomas and are potential immunogens for eliciting anti-tumor immunity.
Natural killer (NK) cells – Lymphocytes that spontaneously kill tumor cells that do not express human leukocyte antigen (HLA) class I molecules.
Uvea – Ocular tissue composed of the iris, ciliary body, and choroid.
Uveal melanoma – Most common intraocular tumor in adults; originates from neural crest precursors.

Introduction

Different types of tumors may arise in the eye, but the most common primary malignant ocular tumors are retinoblastoma in children and uveal melanoma in adults. While there are many treatments for the intraocular tumors, metastases are more difficult to manage. Cutaneous melanoma has been a target for many types of immunotherapy, and as cutaneous and uveal melanoma share many characteristics, one might expect a similar situation with regard to uveal melanoma. However, with sporadic exceptions, immunotherapy for uveal melanoma metastases has as yet not been successful. Uveal melanoma seems to be able to escape immune responses irrespective of the manner in which the immune system is triggered. While immunotherapy of metastases does not seem to be effective, there are many indications that the innate immune system influences the tumor's behavior. Macrophages are associated with increased malignancy by their mechanism of influencing the development of blood vessels in the tumor. Natural killer (NK) cells may play a role during the migration of metastatic cells through the blood and their residence in the liver. As many uveal melanoma patients die from liver metastases, it is clear that the immune system is not effectively recognizing and eliminating disseminated uveal melanoma cells. Some of the most important mechanisms involved in immune surveillance and the tumor's response against them will be discussed in this article.

Survival

Uveal melanoma is the most frequent intraocular tumor in adults. Death from this tumor usually results from the development of liver metastases. Indeed, approximately 90% of uveal melanoma patients have liver metastases at the time of death. An important characteristic of uveal melanoma is the time between recognition of the primary tumor and the first sign of metastases. Metastases are rarely found when the intraocular tumor is first diagnosed, but up to one-third of patients may develop clinically recognizable metastases during the 3 years thereafter (**Figure 1**). Although there are many effective therapies for managing primary uveal melanomas, there are no therapeutic modalities that have been proven to be effective in the treatment of liver metastases. Indeed, the 5-year survival rate for uveal melanoma patients has not improved in the past 30 years. Potential new approaches include transfer of uveal melanoma-specific T cells and induction of strong T-cell responses by using newly developed vaccines. Uveal melanomas are antigenic, and, in theory, they should be accessible to anti-tumor immune responses. However, the tumors originally reside in the eye, which provides an immunologically privileged environment that inhibits both the induction and expression of many forms of immunity. Both the innate and adaptive

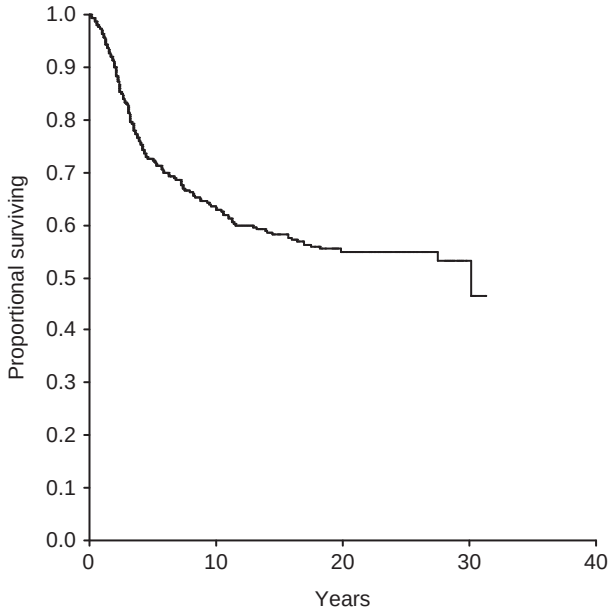

Figure 1 Long-term survival of patients who underwent enucleation for a uveal melanoma.

immune responses are impaired within the eye. Moreover, mounting evidence suggests that uveal melanoma cells have adopted many of the strategies that the eye utilizes to promote immune privilege and disarm destructive immune responses.

Anti-Tumor Immune Responses

T-Cell Immunity

The immune system may function in different locations: in the primary intraocular tumor, during the transportation of tumor cells through the blood, and at the site of the metastases.

With regard to the intraocular tumor, several studies have reported the presence of CD4+ and CD8+ T cells in the tumor, although the degree of T-cell infiltration varies among tumors. At least one out of five uveal melanomas contains significant numbers of infiltrating lymphocytes, which can be analyzed for their cell-surface characteristics. Most infiltrating cells are T cells, with many more CD8+ suppressor/cytotoxic T cells than CD4+ helper T cells. Infiltrating T cells often express human leukocyte antigen DR-1 (HLA-DR), while T helper cells often express receptors for cytokines such as interleukin (IL)-2R, most of the T suppressor/cytotoxic cells do not. This would limit the capacity to stimulate the expansion of cytotoxic T lymphocytes (CTLs) with IL-2. In addition, many tumors contain macrophages. However, there is a paucity of NK cells in primary uveal melanomas. Interestingly, there is evidence that the presence of tumor-infiltrating lymphocytes is associated with a poor prognosis in uveal melanoma, which is the opposite of what has been reported with cutaneous melanoma. It is clear, however, that the presence of tumor-infiltrating macrophages is associated with a poor prognosis both in uveal and cutaneous melanomas.

Antigen Expression

The expression of anti-tumor immunity is affected by the expression of two molecules on the tumor cell membrane: HLA class I molecules and melanoma-specific antigens. HLA class I molecules act as docking stations for the CTLs and also provide the grooves into which tumor-specific peptides are presented for cognate recognition by CTLs. HLA class II molecules can also function as restricting elements that present tumor antigens to CD4+ T cells, which exert their anti-tumor activity by elaborating cytokines such as tumor-necrosis factor alpha (TNF-α), which is toxic to the tumor cells, and other cytokines such as interferon-γ (IFN-γ), which activates elements of the innate immune system (e.g., macrophages and NK cells). Several studies on tumor-containing eyes have analyzed the presence of target molecules on uveal melanoma cells. Immunohistochemical approaches with monoclonal antibodies directed against cutaneous melanoma-associated antigens demonstrated the expression of many immunological epitopes on uveal melanoma cells. Potential T-cell targets that are expressed on uveal melanoma cells include the melanoma-associated antigens S-100 (a protein found in brain cells that cross-reacts with melanoma and melanocytes), HMB45 (which is specific for the melanosomal gp100 protein), tyrosinase, tyrosinase-related protein (Tyrp1), and Melan-A/Mart 1. In addition, MC1R, the receptor for α-melanocyte-stimulating hormone, is present on almost all primary uveal melanomas and all metastases tested so far. Uveal melanoma also expresses melanoma-specific antigens from the melanoma antigen-encoding gene (MAGE) family. These findings indicate that specific T cells should be able to lyse uveal melanoma cells, assuming that the melanoma cells co-express the proper HLA antigens.

Effect of HLA Expression on the Progression of Uveal Melanomas

Different studies have demonstrated that uveal melanoma can express HLA class I and II molecules, but often at low expression levels. In general, HLA expression as detected by monoclonal antibodies is usually high on primary tumors and cell lines, and can be further upregulated by exposure to IFN-γ. In cell lines derived from uveal melanoma, loss of one or both B alleles has been observed; loss of one HLA-A or one HLA-B gene leads to homozygosity for the HLA area on chromosome 6.

HLA-A2 and-A3 are usually highly expressed on histological sections of primary tumors, while the HLA-Bw4 and Bw6 antigens are only weakly expressed. These observations indicate that selective loss or downregulation of HLA class I expression may occur and this may provide a selective advantage to the tumor for avoiding immune-mediated destruction by CTLs. Interestingly, HLA class I antigens are highly expressed on liver metastases, which may be an effective mechanism for evading NK-cell-mediated surveillance in the liver, which contains one of the highest concentrations of NK cells of any organ in the body (see below).

NK Cells

In vitro studies using a battery of human uveal melanoma cell lines have demonstrated that uveal melanomas are vulnerable to NK cell-mediated cytolysis. Studies in mice have shown that metastasis of ocular melanoma cells is inhibited by NK cells, as disruption of NK-cell function in mice produces a sharp increase in the formation of liver metastases. The susceptibility of tumor cells to NK-cell-mediated cytolysis is influenced by the expression of major histocompatibility complex (MHC; HLA in humans and H-2 in mice) class I molecules on the surface of the tumor cells. As discussed earlier, MHC class I molecules serve as docking stations for CTLs and are absolutely necessary for CTL-mediated cytolysis of target cells. However, many tumors downregulate MHC class I molecules to escape cytolysis by tumor-specific CTLs. By contrast, the absence of MHC class I molecules provokes cytolysis by NK cells, which are programmed to kill any cell lacking MHC class I molecules. Thus, the absence of MHC class I molecules would seem to render uveal melanomas vulnerable to NK-cell-mediated destruction. However, the fluids in the eye contain macrophage-migration-inhibitory factor (MIF) and transforming growth factor-β (TGF-β) which profoundly suppress NK-cell-mediated cytolysis. Uveal melanomas most frequently metastasize to the liver, which contains one of the highest concentrations of NK cells of any organ in the body. Thus, uveal melanoma metastases would seemingly be vulnerable to NK-cell-mediated clearance in the liver. However, there is evidence that uveal melanoma cells undergo a selection process that favors the emergence of NK-resistant subpopulations in the liver. Melanoma cells isolated from a primary uveal melanoma and liver metastases in the same patient have revealed that the expression of MHC class I molecules was 10-fold higher in liver metastases compared to the primary tumor. The elevated expression of MHC class I dramatically reduces the vulnerability of the melanoma metastases to NK-cell-mediated clearance in the liver.

That NK cells may play a role during the metastatic spreading itself is supported by retrospective studies on archival specimens from human uveal melanoma patients; tumor sections were examined for the expression of the HLA-A and-B loci using monoclonal antibody HCA2 for HLA-A and HC10 for HLA-B. Of the 30 tumors, only 12 expressed HLA-A and seven HLA-B on more than 25% of their cells. A high expression of HLA-B was associated with the presence of epithelioid cells, which is a bad prognostic sign. Indeed, high HLA class I expression on the primary intraocular tumor was associated with significantly poorer survival. By contrast, uveal melanomas with low HLA class I expression – which are considered good NK-cell targets – were associated with excellent survival. Thus, primary uveal melanomas contain subpopulations of cells that express low amounts of MHC class I and are vulnerable to NK-cell-mediated cytolysis. However, NK cells would not have been able to attack the primary tumor, as soluble factors in the aqueous humor – such as MIF and TGF-β – block NK activity within the eye.

Immune Escape Mechanisms

A similar condition might apply to elements of the adaptive immune system such as CTL. As discussed earlier, many uveal melanomas express melanoma-associated antigens and tumor-specific antigens along with the relevant MHC class I molecules that present these antigens to CTLs; despite this, tumor-infiltrating T cells isolated from these eyes fail to express significant cytolysis of the tumor cells when examined *in vitro*. A variety of factors present in the aqueous humor are known to inhibit T-cell activity. Thus, the function of tumor-infiltrating CTLs might be suppressed in the ocular tumor in the same manner that occurs with tumor-infiltraing NK cells.

As stated above, many uveal melanoma cells express tumor-specific antigens and appropriate MHC class I molecules that should render them vulnerable to immune elimination by CTLs. Likewise, a significant number of uveal melanoma cells are susceptible to NK-cell-mediated cytolysis *in vitro*, yet uveal melanoma metastases that have escaped from the eye will thrive in the liver – which expresses the highest concentration of NK cells of any organ in the body. These two observations suggest that uveal melanoma cells have the capacity to escape immune surveillance by both the adaptive and innate immune systems. A growing body of evidence suggests that uveal melanomas escape immunological attack by adopting some of the same strategies that support immune privilege in the eye.

Indoleamine 2,3 Dioxygenase

T cells require tryptophan for clonal expansion and proliferation, and in the absence of tryptophan, T cells perish. The enzyme indoleamine 2,3-dioxygenase (IDO) catabolizes the degradation of tryptophan, and accordingly, upregulation

of IDO results in rapid depletion of this necessary amino acid. Although tryptophan is not vital for NK-cell survival, IDO inhibits the cytolytic activity of NK cells. Thus, IDO impairs the expression of both the adaptive and innate immune responses. IDO can be upregulated by proinflammatory signals such as IFN-γ. IDO is produced in the eye and is believed to contribute to the immune privilege in the anterior chamber. Uveal melanoma cells do not constitutively produce IDO; however, when exposed to the T-cell cytokine IFN-γ, uveal melanoma cells produce significant quantities of IDO. Thus, uveal melanomas have the capacity to produce an immune privileged environment once they perceive the presence of an immune response (i.e., T-cell- and NK-cell-derived IFN-γ). Whether this is an effective strategy utilized by uveal melanomas to evade T-cell immunity remains to be determined, but is an intriguing possibility.

Programmed Death-1 Ligand

The cells lining the interior of the eye are decorated with a variety of cell membrane-bound molecules that protect the eye from inflammation by inducing apoptosis of infiltrating T cells. Among these cell membrane molecules is programmed death-1 ligand (PD-L1), which is a transmembrane glycoprotein belonging to the B7 family. Its receptor, programmed death-1 (PD-1) is expressed on thymocytes, mature T cells, and myeloid cells, and interaction of PD-L1 with its receptor leads to downregulation of T-cell proliferation and apoptosis. PD-L1/PD-1 interactions are important in regulating T-cell-mediated immune responses and for preserving immune privilege in the eye. Corneal allografts express PD-L1, which is crucial for their survival, as blocking PD-L1/PD-1 interactions culminates in a steep increase in the incidence and tempo of corneal allograft rejection. PD-L1 is also expressed on human uveal melanoma cells and may serve a similar role in the evasion of T-cell attack. Similar to IDO, PD-L1 expression is upregulated by the T-cell and NK-cell cytokine IFN-γ. The induced expression of PD-L1 is believed to contribute to the uveal melanoma cell's capacity to elude attack by T cells and NK cells. When activated T cells are exposed to PD-L1-expressing uveal melanoma cells, they downregulate their production of IFN-γ and TNF-α – two potent cytokines involved in the immune surveillance of many tumors. Thus, T-cell- and NK-cell-derived factors (e.g., IFN-γ) appear to alert uveal melanomas of the presence of activated T cells and NK cells and prompt intraocular tumors to upregulate the expression of immunoevasive molecules such as PD-L1 and IDO.

Complement Regulatory Proteins

The complement system is a complex array of serum proteins with enzyme-like activity, which are activated in a cascade-like fashion resulting in the generation of a membrane-attack complex that perforates bacterial and mammalian cell walls and induces osmotic lysis. Activation of complement also generates a variety of chemoattractants that induce the migration and activation of granulocytes. The complement cascade can be activated by the classical pathway when antibodies bind to their cognate antigens on the surface of bacterial or mammalian cells. Complement can also be activated by bacterial products in the absence of antibodies, which is referred to as the alternative pathway. Since the complement cascade can be activated by specific antibodies or by bacteria, it straddles the adaptive and innate immune systems. The complement membrane-attack complex is an effective mechanism for destroying bacteria and mammalian cells, including some tumor cells. However, complement activation stimulates robust granulocytic inflammation, which could inflict injury to ocular tissues. The eye is protected against the unwitting activation of the complement cascade through its expression of complement regulatory proteins (CRPs), which act as buffers to dampen the deleterious effects of complement activation. CRPs can occur as soluble molecules within the aqueous humor or as cell membrane molecules on the surface of intraocular cells. CRPs restrain the untoward effects of complement and protect the eye from immune-mediated injury. Studies in rats have shown that animals with deleted CRP genes suffer severe spontaneous complement-dependent ocular inflammation. Uveal melanomas express CRPs and have been found to be highly resistant to complement-mediated cytolysis initiated by complement-fixing antibodies. Thus, uveal melanomas have adopted yet one more of the strategies employed by the eye to foster immune privilege and have used it to evade immune destruction.

Resistance to Perforin-Mediated Cytolysis

As mentioned previously, treatment with IFN-γ stimulates expression of HLA class I on uveal melanoma cells. The effect has been determined in several uveal melanoma cell lines, and in all cases, expression of HLA class I was sensitive to upregulation by incubation with IFN-γ. As CTLs lyse tumor cells following recognition of the specific peptide presented by an HLA class I molecule, one might expect that tumor cells would undergo extensive cytolysis after incubation with IFN-γ. However, this does not occur. Uveal melanoma cells exposed to IFN-γ resist CTL-mediated lysis. This protection develops when uveal melanoma cells are incubated with either IFN-γ or TNF-α, both of which upregulate HLA class I expression. CTLs utilize a variety of molecules to kill their target cells. These include Fas ligand (FasL), TNF-related apoptosis-inducing ligand (TRAIL), cytokines such as TNF-α, and the direct deposition of cytolytic granules (i.e., perforin) onto the cell membrane of the target cells. Although uveal

melanoma cells are sensitive to perforin-mediated cytolysis, they become resistant following exposure to IFN-γ. This represents one more example of how uveal melanomas seem to perceive the presence of a potentially injurious immune response and respond by elaborating molecules that disable immune effector mechanisms.

Overcoming the Immune Privilege of Uveal Melanomas

Although uveal melanomas reside within an immunologically privileged site and incorporate a variety of novel mechanisms to create their own independent form of immune privilege, there are promising immunotherapeutic strategies on the horizon. A particularly interesting new approach is to create designer tumor vaccines using engineered HLA class II-matched uveal melanoma cells selected from a bank of uveal melanoma cell lines that express different HLA class II haplotypes, which can be matched with the prospective patient. These HLA class II-matched uveal melanoma vaccines can be engineered to express co-stimulatory molecules so that they act as surrogate APCs to stimulate melanoma-specific, MHC class II-dependent, CD4+ T-cell-mediated immune responses. As HLA class II alleles are not as polymorphic as the MHC class I alleles, a relatively small set of cell lines with the most common HLA class II antigens would be sufficient for use in tailoring vaccines for individual patients. These vaccines can be applied early after identifying patients with a high risk of metastases. The designer vaccine approach, although risky, is worth pursuing considering the conspicuous absence of any proven therapeutic modality for treating uveal melanoma metastases and the stagnation in the 5-year survival rate for uveal melanoma patients.

Conclusion

Although uveal melanomas express many of the relevant target and accessory molecules needed to provoke and succumb to an effective immune response, they also possess an array of molecules that allow them to evade immune effector elements. Many of these molecules are the same ones that endow the eye with immune privilege. These molecules not only protect the primary intraocular tumor from immune attack, but also shield uveal melanoma metastases from the immune effector mechanisms that greet them when they enter the liver. The goal for the tumor immunologist is to gain a better understanding of immune privilege of the eye and its tumors and, in so doing, design immunotherapeutic strategies that abrogate immune privilege and unleash the full potential of the immune system to rid both the eye and the liver of uveal melanoma cells.

See also: Adaptive Immune System and the Eye: T Cell-Mediated Immunity; Dynamic Immunoregulatory Processes that Sustain Immune Privilege in the Eye; Immunosuppressive and Anti-Inflammatory Molecules that Maintain Immune Privilege of the Eye; Innate Immune System and the Eye; Role of Complement in Ocular Immune Response.

Further Reading

Apte, R. S. and Niederkorn, J. Y. (1995). Efect of a putative suppressor factor in the aqueous humor on natural killer activity *in vitro*. *Investigative Ophthalmology and Visual Science* 36S: 144.

Blom, D.-J. R., Luyten, G. P. M., Mooy, C., et al. (1997). Human Leukocyte antigen class I expression: Marker of poor prognosis in uveal melanoma. *Investigative Ophthalmology and Visual Science* 38: 1865–1872.

Bosch, J. J., Thompson, J. A., Srivastava, M. K., et al. (2007). MHC class II-transduced tumor cells originating in the immune-privileged eye prime and boost CD4 T lymphocytes that cross-react with primary and metastatic uveal melanoma cells. *Cancer Research* 67: 4499–4506.

Chen, P. W., Mellon, J. K., Mayhew, E., et al. (2007). Uveal melanoma expression of indoleamine 2,3-deoxygenase: Establishment of an immune privileged environment by tryptophan depletion. *Experimental Eye Research* 85: 617–625.

Cousins, S. W., McCabe, M. M., Danielpour, D., and Streilein, J. W. (1991). Identification of transforming growth factor beta as an immuno-suppressive factor in aqueous humor. *Investigative Ophthalmology and Visual Science* 32: 2201–2211.

de Waard-Siebinga, I., Houbiers, J. G. A., Hilders, C. G. J. M., De Wolff-Rouendaal, D., and Jager, M. J. (1996). Differential expression of HLA-A and -B alleles on uveal melanoma as determined by immunohistology. *Ocular Immunology and Inflammation* 4: 1–14.

Goslings, W. R. O., Blom, D. J. R., De Waard-Siebinga, I., et al. (1996). Membrane-bound regulators of complement activation in uveal melanoma. *Investigative Ophthalmology and Visual Science* 37: 1884–1891.

Hallermalm, K., Seki, K., De Geer, A., et al. (2008). Modulation of the tumor cell phenotype by IFN-γ results in resistance by uveal melanoma cells to granule-mediated lysis by cytotoxic lymphocytes. *Journal of Immunology* 180: 3766–3774.

Hurks, H. M. H., Metzelaar-Blok, J. A. W., Mulder, A., Claas, F. H. J., and Jager, M. J. (2000). High frequency of allele-specific down-regulation of HLA class I expression in uveal melanoma cell lines. *International Journal of Cancer* 85: 697–702.

Ksander, B. R., Rubsamen, P. E., Olsen, K. R., Cousins, C. W., and Streilein, J. W. (1991). Studies on tumor-infiltrating lymphocytes from a choroidal melanoma. *Investigative Ophthalmology and Visual Science* 32: 3198–3208.

Lopez, M. N., Pereda, C., Ramirez, M., et al. (2007). Melanocortin 1 receptor is expressed by uveal malignant melanoma and can be considered a new target for diagnosis and immunotherapy. *Investigative Ophthalmology and Visual Science* 48: 1219–1227.

Ma, D., Luyten, G. P. M., Luider, T. M., and Niederkorn, J. Y. (1995). Relationship between natural killer cell susceptibility and metastasis of human uveal melanoma cells in a murine model. *Investigative Ophthalmology and Visual Science* 36: 435–441.

Natali, P. G., Bigotti, A., Nicotra, M. R., et al. (1989). Analysis of the antigenic profile of uveal melanoma lesions with anti-cutaneous melanoma-associated antigen and anti-HLA monoclonal antibodies. *Cancer Research* 49: 1269–1274.

Verbik, D. J., Murray, T. G., Tran, J. M., and Ksander, B. R. (1997). Melanomas that develop within the eye inhibit lymphocyte proliferation. *International Journal of Cancer* 73: 470–478.

Yang, W., Chen, P. W., Li, H., Alizadeh, H., and Niederkorn, J. Y. (2008). PD-L1: PD-1 interaction contributes to the functional suppression of T cell responses to human uveal melanoma cell *in vitro*. *Investigative Ophthalmology and Visual Science* 49: 2518–2525.

Immunopathogenesis of Experimental Uveitic Diseases

R R Caspi, National Institutes of Health, Bethesda, MD, USA

Published by Elsevier Ltd.

Glossary

Antibodies (Abs) – Also called immunoglobulins, these protein molecules are produced by differentiated B cells (i.e., plasma cells) and are secreted into the serum. Antibodies bind to antigens and can either neutralize pathogens or activate the complement cascade. The latter process generates membrane-attack complexes that pierce the cell walls and membranes of bacteria leading to bacterial cell death.

Antigens (Ags) – High-molecular-weight proteins that are recognized by the adaptive immune system as foreign and as a result, antigens induce immune responses that culminate in protective immunity or in some cases, autoimmune diseases.

Autoimmune regulator (AIRE) – A gene that causes the expression of a wide selection of organ-specific proteins in the thymus. The expression of organ-specific antigens in the thymus reduces the risk of the unwitting generation of autoimmunity by promoting the deletion of autoreactive T cells by the process of negative selection.

Antigen-presenting cells (APCs) – Dendritic cells, macrophages, and B cells that process antigens and present them to T lymphocytes. This is the first step in the generation of an adaptive immune response.

Complete Freund's adjuvant (CFA) – A mixture of mineral oil, alum, and killed *Mycobacterium*. Antigens mixed with CFA elicit potent adaptive immune responses.

Experimental autoimmune anterior uveitis (EAAU) – An animal model of uveitis of the anterior segment of the eye. Melanin-associated antigens mixed with CFA induce uveitis of the anterior segment in rodents.

Experimental autoimmune uveitis (EAU) – An animal model of posterior segment uveitis is elicited when rodents are immunized with interphotoreceptor-binding peptide (IRBP) or retinal S-antigen (S-Ag) emulsified in CFA. The inflammation is usually progressive and destroys the retina. This model most closely resembles sympathetic ophthalmia.

Experimental melanin-induced uveitis (EMIU) – A model of uveitis that closely resembles EAAU.

Hemagglutinin (HA) – A transgene of this influenza virus antigen, has been expressed in the retinas of experimental mice as a means of developing a novel model of uveitis.

Hen egg lysozyme (HEL) – The transgene of HEL has been expressed in the retinas of experimental mice as a means of developing a novel model of uveitis.

Human lymphocyte antigens (HLAs) – Also called major histocompatibility complex antigens, these class I HLA antigens are expressed on virtually all nucleated cells in the body and are used as platforms to present endogenous antigens to the immune system.

Pertussis toxin (PTX) – This is used to breach the blood–retina barrier and thereby facilitate the full expression of EAU and other autoimmune diseases in rodents.

T cell receptor (TCR) – The heterodimer molecule that is expressed on the surface of T cells and displays exquisite specificity in recognizing a specific antigen. Each TCR binds to a very limited range of antigens. Antigens binding to the TCR in the presence of co-stimulatory molecules expressed on APC activate a signaling cascade that leads to activation and clonal expansion of specific T-cell populations.

Transgenic (Tg) – Introducing a specific gene into a cell or an animal's genome is a means of studying the gene's specific function or the effect of overexpression of a specific gene.

Uveitis: The Disease and Its Experimental Models

The eye is an immunologically privileged organ, which translates to an ability to protect itself from day-to-day inflammatory insults using a variety of passive and active mechanisms. Of the rather short list of organs considered immunologically privileged (eye, brain, ovary, testis, the pregnant uterus and – of all things – the hamster cheek pouch), the eye is arguably the most privileged. Although immune privilege undoubtedly serves to protect the visual axis from damage resulting from overzealous immune responses to random environmental stimuli, the eye is subject to autoimmune uveitis. Autoimmune uveitis,

which has no known infectious etiology, can accompany one of a number of systemic diseases affecting a range of organs, or can be a stand-alone disease in which the eye is the only target. Ankylosing spondylitis, Behçet's disease, systemic sarcoidosis (SS), and Vogt–Koyanagi–Harada disease (VKH) are examples of the former, whereas Fuchs heterochromic cyclitis, birdshot retinochoroidopathy (BR), and sympathetic ophthalmia (SO) are examples of the latter. Autoimmune uveitis can be either anterior (Fuchs heterochromic cyclitis or uveitis accompanying ankylosing spondylitis), or mainly posterior, as in Behçet's disease, VKH, SS, BR, and SO. Due to the ocular anatomy, it is the posterior uveitides that are particularly likely to affect the photoreceptor cells and damage vision. Uveitic diseases of an autoimmune nature have been estimated to cause about 10% of severe visual handicap in the US.

Uveitis patients often exhibit lymphocyte and antibody responses to antigens present in the eye, supporting the autoimmune nature of the disease. Although it is unclear whether these responses are the cause or represent an epiphenomenon resulting from autoimmunization to tissue-breakdown products, they are believed to fuel progression of the disease. The etiologic causes of uveitis are unclear, with the exception of SO, which is precipitated by ocular trauma to one eye that is followed by inflammation in the nontraumatized, or sympathizing, eye. It is thought that antigens (Ags) released from the traumatized eye find their way into the draining lymph node and elicit systemic immunity. An accompanying infection may provide an adjuvant effect. In uveitic disease that cannot be linked to a trauma, it is believed that lymphocytes capable of recognizing retinal Ags are primed in the periphery by a cross-reactive microbial stimulus. Animal models of uveitis based on immunization of laboratory animals with retinal Ags in complete Freund's adjuvant (CFA) seek to duplicate this condition.

The objective limitations and ethical issues inherent in human studies have made animal models of uveitis an invaluable tool for dissecting the basic mechanisms in pathogenesis of the disease. As no animal model can reproduce the full complexity of the human disease, it is necessary to develop and use a variety of models to represent different aspects and diverse clinical/immunological manifestations of uveitis. The longest used and by far the best-explored model is experimental autoimmune uveitis (EAU), which is induced by active immunization with one of a number of retinal Ags in complete Freund's adjuvant. Although EAU can be elicited in a variety of species and with a variety of antigens, the model in rats induced with retinal arrestin (retinal soluble Ag, S-Ag) and the model in mice induced with the interphotoreceptor retinoid-binding protein (IRBP) have gained the widest acceptance. Quantitative histological scores can be assigned with a fair degree of precision based on fundus examination or histopathological appearance (**Figure 1**). The mouse model in particular has been extremely useful

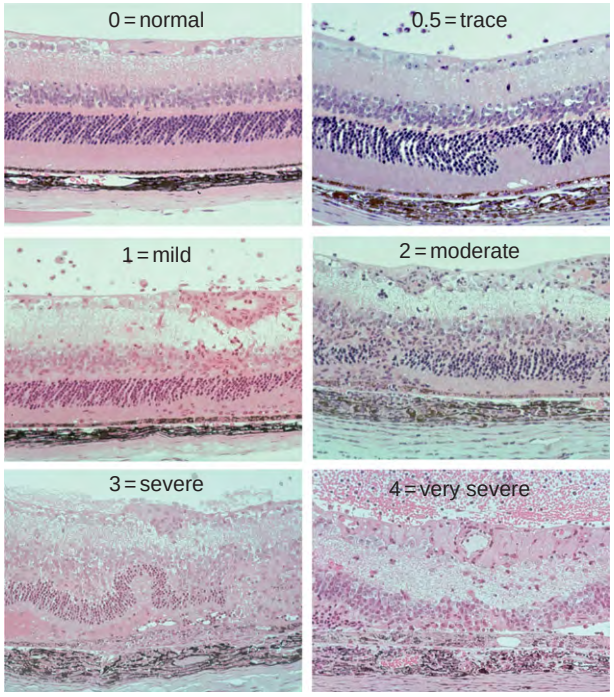

Figure 1 EAU histopathology of eyes collected from B10.RIII mice 21 days after uveitogenic immunization with IRBP, representing a range of disease scores. Eyes were processed and embedded in methacrylate. Sections 4–6 μm in thickness were stained with hematoxylin and eosin and photographed at ×400 magnification. Reprinted from Cortes, L.M., Mattapallil, M.J., Phyllis B. Silver, P.B. (2008). Repertoire analysis and new pathogenic epitopes of IRBP in C57BL/6 (H-2^b) and B10.RIII (H-2^r) mice. *Investigative Ophthalmology and Visual Science* 49: 1946–1956. Note: Clinical scoring by fundus appearance is depicted and described in the reference cited as Xu et al. (2008).

for dissecting basic cellular and molecular mechanisms of the disease. Over the years, the mouse model has seen a proliferation of variants on the EAU theme as to mode of induction and antigenic target, which have allowed investigators to address specific questions (**Table 1**).

Particular models and their attributes are mentioned further on, in conjunction with the immunopathogenic mechanisms to which they pertain, but it is of interest to mention here a model of EAU that develops in HLA class II transgenic (Tg) mice, in which the mouse MHC class II molecules have been replaced with the human counterparts. HLA-DR3 (DRB1*0301), –DR4 (DRB1*0401), –DQ6 (DQB1*0601), or –DQ8 (DQB1*0302). Tg mice present and respond to antigenic epitopes that would be recognized by humans bearing these class II molecules. Unlike the wild-type (WT) parental mice that are resistant to S-Ag induced EAU, the HLA Tg mice develop disease when immunized with S-Ag. Importantly, HLA DR3 mice responded immunologically and developed EAU when immunized with defined S-Ag peptides, among them peptide N (residues LPLLANNRERRGIALDGKIKHE) that is known to elicit lymphocyte responses in uveitis

Table 1 Models of autoimmune uveitis

#	*Type of model*	*Examples of models*	*Comments*
1	Active immunization with an ocular antigen emulsified in complete Freund's adjuvant (CFA)	Experimental autoimmune uveitis (EAU) induced in B10.RIII or C57BL/6 mice with IRBP, or in HLA-Tg mice with S–Ag. Anterior uveitis induced by immunization of rats with melanin components (EAAU; EMIU – see glossary). Other Ags, or their peptide fragments, can be used	Mycobacteria in CFA provide innate danger signals that polarize autoimmune lymphocytes toward the Th1 and Th17 lineages. Pertussis toxin (PTX) as additional adjuvant is needed in less susceptible strains
2	Infusion of Ag-pulsed mature dendritic cells	EAU variant induced in B10.RIII mice by injection of splenic DC elicited with Flt3L, matured *in vitro* and pulsed with IRBP (pp. 161–180)	Requires 2 injections of DC and pertussis toxin. Less severe than #1 and appears mostly dependent on Th1 cells
3	Mice transgenic for a TCR that recognizes a retinal Ag	Spontaneous EAU-like uveitis in IRBP TCR Tg mice	High frequency of TCR Tg cells
4	Tg mice expressing a neo-Ag in the retina bred to mice expressing, or adoptively transferred with, T cells bearing the specific TCR. Conceptually meant to mimic #3.	Uveitis in mice transgenic for hen egg lysozyme (HEL) or betagalactosidase (β-gal) on a retinaspecific promoter. A variant is *in vivo* retrovirally induced expression of influenza hemagglutinin (HA) in the retina and adoptive transfer of activated T cells specific for HA	May be spontaneous in some double-Tg mice. This may at least in part depend on the frequency and affinity of the transgenic TCR
5	Disrupted negative selection of T cells in the thymus	Spontaneous uveitis in AIRE$^{-/-}$ mice directed at IRBP, spontaneous uveitis in nude mice implanted with embryonic rat thymus	Higher frequency and higher affinity of cells bearing TCRs to IRBP

patients. HLA Tg mice may thus help to define the antigenic regions involved in human disease, and thus may be important for devising antigen-specific therapies for human uveitis.

Central Tolerance: Retina-Specific Antigens and the Thymus

As is discussed later, susceptibility to uveitis is affected by the frequency of pathogenic T cells on the one hand, and natural regulatory T cells on the other hand. Both are controlled by the thymic selection process, which leads to establishment of central tolerance. Many tissue-specific antigens, including retinal Ags such as S-Ag, IRBP, and S100, are expressed ectopically in the thymus under control of the transcription factor, autoimmune regulator (AIRE). Other Ags are imported from outside the thymus and presented on bone-marrow-derived Ag-presenting cells. These self-Ags actively select the developing T-cell repertoire by eliminating or anergizing (i.e., rendering unresponsive) T cells with high affinity to self-antigens that could mediate autoimmunity and sparing T cells with low affinity to self, which will mediate host defense. The level of thymic expression of the retina-specific Ags S-Ag and IRBP was shown to be inversely correlated with susceptibility of the particular strain of mice or rats to uveitis induced with these Ags, suggesting that a quantitatively higher expression of these molecules more efficiently deletes autoreactive cells. Qualitative and quantitative changes in the autoreactive repertoire to IRBP have subsequently been demonstrated to occur in IRBP gene knockout (KO) versus WT mice and to be directly related to presence of IRBP in the thymus.

These data raised the notion that precursor frequency of retinal Ag-specific cells is an important factor in setting the threshold of EAU susceptibility. Direct experimental support for this notion comes from observations that gene-manipulated mice that have deficient thymic selection of IRBP-specific cells, and consequently sport an expanded T-cell repertoire to IRBP, are more susceptible to EAU, or even develop spontaneous EAU-like disease. Three such examples can be cited: (1) thymectomized, immunoablated, and bone-marrow-reconstituted WT mice that receive thymi from IRBP-deficient mice (forced to re-select their T-cell repertoire on the IRBP-deficient thymus) respond to IRBP epitopes that are not recognized by WT mice, and are extremely susceptible to EAU induced with IRBP; (2) mice that were made deficient in the AIRE molecule, which controls ectopic expression of tissue Ags in the thymus, develop multiorgan autoimmunity, including antiretinal antibodies, cellular responses to IRBP, and a spontaneous EAU-like uveitis directed at IRBP. Interestingly, although thymic selection to S-Ag and other retinal Ags controlled by AIRE is also compromised, IRBP is the only antigen recognized by these mice as pathogenic; and (3) nude mice grafted with a neonatal thymus develop a spontaneous autoimmune disease that

resembles the AIRE deficiency disease, and exhibit an immune response directed against photoreceptors with specificity to IRBP, but not S-Ag. Data obtained using human thymic tissue from immunologically normal patients undergoing open-heart surgery suggest that thymic control of repertoires specific to retinal Ags may also hold true for humans.

In addition to deleting high-affinity autoreactive T cells, the thymus also positively selects T cells with intermediate affinity that is slightly below the threshold for negative selection. Instead of being deleted, these cells are rendered unresponsive (i.e., anergized) acquire regulatory function, and exit into the periphery as natural regulatory T cells. Studies with IRBP KO mice demonstrated that selection of IRBP-specific natural T-regulatory cells requires endogenous expression of IRBP (see ahead).

Peripheral Tolerance and the Double-Edged Sword of Immune Privilege

The process of negative selection is not 100% efficient, and some autoreactive T cells escape deletion and exit into the periphery. Such escapees are subject to peripheral tolerance, which follows encounter with tissue Ags under non-inflammatory conditions (in the absence of co-stimulation). However, Ags residing in the healthy eye are sequestered behind an efficient blood–retina barrier and are not freely accessible to recirculating lymphocytes. This hinders peripheral tolerance and leaves a population of circulating retina-specific T lymphocytes that are ignorant, but not tolerant, and are able to be triggered by a chance encounter with their nominal or a cross reactive Ag (**Figure 2**).

The notion that retinal Ags are in fact functionally sequestered from the immune system has recently been debated. On the one hand, there is the phenomenon known as anterior-chamber-associated immune deviation (ACAID) in which Ags injected into the anterior chamber of the eye are not ignored, but rather induce a deviant type of immunity that includes a generation of Ag-specific regulatory cells that suppress cell-mediated immune responses. However, one must be careful when extrapolating from these data to Ags residing in the healthy eye, since ACAID by necessity involves perturbation of the ocular integrity. On the other hand, experiments using HEL transgenically expressed in the retina demonstrated

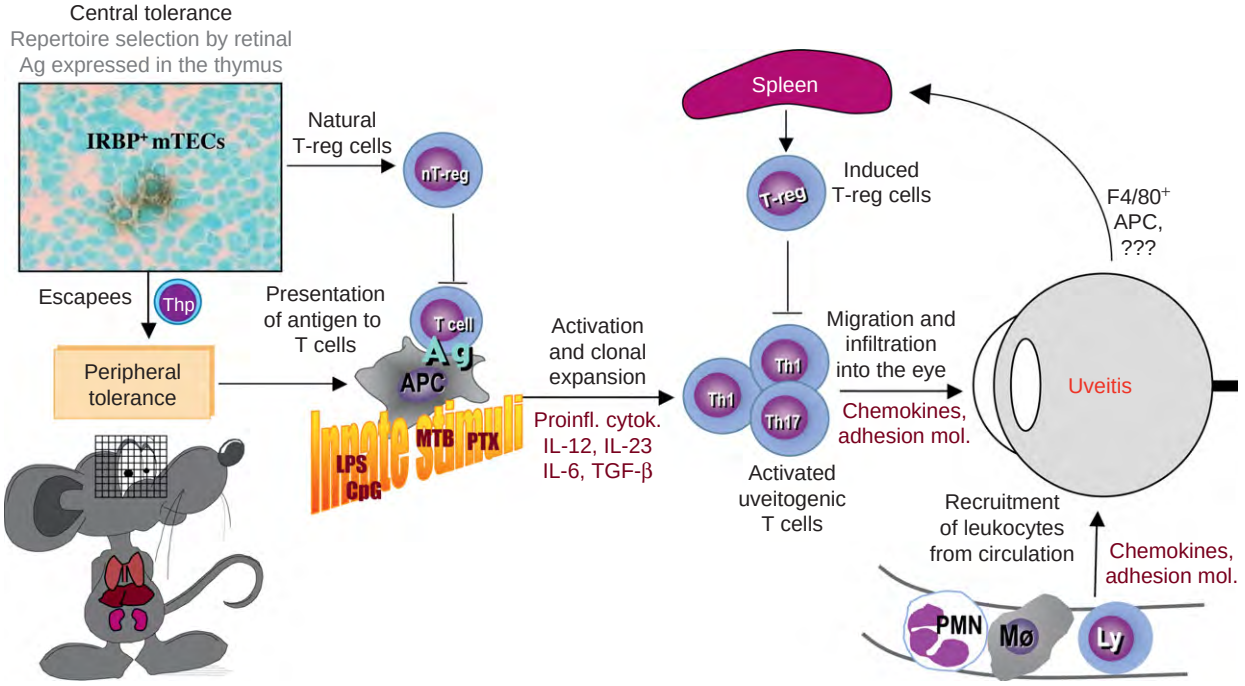

Figure 2 Critical checkpoints in pathogenesis of uveitis, based on data from animal models of EAU. Autoreactive T cells that failed to be deleted in the thymus have limited access to retinal Ags due to their relative sequestration from the immune system, which hinders peripheral tolerance. Despite the presence of natural T regulatory cells, such nontolerant thymic escapees may get primed by exposure to retinal or cross-reactive microbial Ag, and in the appropriate milieu differentiate to Th1 or Th17 effector lymphocytes that reach the eye, recognize their Ag *in situ*, and recruit inflammatory leukocytes from the circulation. T regulatory cells that are induced during and as a result of the disease process ultimately control the pathogenic effector cells and downregulate inflammation. Ag, antigen; APC, Ag-presenting cells; Mol, molecules; Proinfl, proinflammatory; Cytok, cytokines; LPS, lipopolysaccharide (bacterial endotoxin); MTB, mycobacterium tuberculosis; PTX, pertussis toxin; CpG, cytosine and guanidine separated by a phosphate (bacterial DNA motif); mTEC, thymic medullary epithelial cells; T-reg, T regulatory cells; nT-reg, natural T-reg; Th, T helper; Thp, Th precursor. Adapted from Caspi, R. R. (2006). Ocular autoimmunity: The price of privilege? *Immunological Reviews* 213: 23–35.

that peripheral tolerance to Ags expressed in the eye is low compared to Ags residing in nonprivileged tissues such as the pancreas, even though their thymic expression is similar. In keeping with this, forced expression of retinal Ags outside the eye results in enhanced tolerance, and in resistance to uveitis, support the notion that peripheral tolerance to ocular Ags can be improved. Recent data suggest that retinal expression of a novel, nonmammalian transgene (β-galactosidase) may generate some level of peripheral tolerance, but it is too low to alter susceptibility of these mice to EAU induced with β-galactosidase. On the whole, these studies lead to the conclusion that peripheral tolerance to Ags residing in the intact eye, while perhaps not entirely absent, is relatively limited.

Effector T Cells in Uveitis: Activation and Activity

As peripheral tolerance to retinal Ags is inefficient, autoreactive cells persist in the periphery in the nontolerized state. Accidental exposure to a retinal Ag released as a result of trauma or to a microbial agent can activate these naive T cells and induce them to differentiate into mature effector T cells that orchestrate tissue damage by producing proinflammatory cytokines and chemokines. This process is strongly promoted by innate endogenous and exogenous adjuvant co-stimulatory danger signals provided by tissue breakdown and/or microbial products. Strong danger signals also appear to overcome the threshold of resistance afforded by naturally occurring T regulatory cells (nTregs) and under some circumstances may temporarily inactivate them. In keeping with this, immunization of experimental animals for induction of EAU requires delivery of the retinal antigen in CFA, which contains heat-killed mycobacteria. Without them, disease is not induced and the effector T cells differentiate toward a nonpathogenic or a regulatory phenotype.

Activated retina-specific effector T cells are necessary and sufficient to elicit EAU when transferred from diseased donors to healthy recipients. Antibodies in hyperimmune serum by themselves are insufficient to initiate disease. Due to their molecular size, they are unable to penetrate the blood–retinal barrier. However, if the blood–retinal barrier is breached by uveitogenic T cells, serum antibodies enter the eye and result in an exacerbation of EAU scores. A considerable body of evidence has accumulated over the years to support an association between EAU and T helper 1 (Th1) effector T cells, whose hallmark cytokine is interferon-gamma (IFN-γ). However, recent findings in other autoimmune disease models identified a new effector cell phenotype involved in autoimmune inflammation; it was named Th17 after its hallmark cytokine, interleukin-17 (IL-17). Th1 and Th17 cells differentiate from the same naive precursor under different sets of conditions: Th1 cells are induced in the presence of the cytokine IL-12 and express the lineage-specific factor T-bet, whereas TGF-β and IL-6 drive commitment to the Th17 lineage, which is maintained by IL-23, and these cells express the lineage-specific transcription factor RORγt. Findings showing that interference with induction or with function the Th17 lineage abrogates induction of the classical autoimmune disease models such as experimental autoimmune encephalomyelitis (EAE, a model for multiple sclerosis), and collagen-induced arthritis (CIA, a model of rheumatoid arthritis), led investigators to propose that Th17 and not Th1 is the major pathogenic effector in autoimmune inflammation, and that Th1 has a minor role, if any.

Th17 cells indeed appear to have a critical role in EAU induced with IRBP immunization in CFA. In contrast to neutralization of systemic IFN-γ, neutralization of IL-17 prevents and reverses EAU in this model. Furthermore, Th17 cells are able to act as stand-alone effectors in the absence of Th1cells. Not only do IFN-γ KO mice develop severe EAU, but T cells from IFN-γ KO mice polarized toward the Th17 phenotype induce EAU in unimmunized IFN-γ KO recipients which do not have a Th1 response. Conversely, however, IL-17 KO mice develop EAU and polarized Th1 cells induce ocular pathology without participation of host-derived IL-17, showing that Th1 cells can also be stand-alone uveitogenic effectors. Finally, in the recently developed EAU model induced with Ag-pulsed mature dendritic cells (DCs) there seems to be a requirement for a generation of IFN-γ producing effector T cells, as IFN-γ KO mice fail to develop EAU when injected with uveitogenic DC that induce EAU in WT mice. It thus appears that ocular autoimmunity can be driven by either a Th17 or a Th1 effector response. Extrapolating from the CFA–EAU and the DC–EAU models, the effector type that is destined to predominate in a given situation is affected by the conditions of disease induction. Presentation of Ag in the context of mycobacteria (included in CFA) by diverse APC present in the lymph node (LN) appear to promote a dominant Th17 response, whereas Ag presented by DC matured *in vitro* with LPS and anti-CD40 as a single APC type promotes a Th1 response.

It is important to keep in mind that human uveitis is clinically heterogeneous even though the patients may respond to the same retinal Ag(s). Both Th1 and more recently the Th17 response has been associated with uveitic diseases. It is conceivable that the CFA and the DC-induced EAU models, which differ immunologically as well as clinically despite having been induced with the same Ag in genetically identical mice, could shed light on this heterogeneity of human uveitis. The initial eliciting event(s) connected to human uveitis are largely unknown, but if the animal models are in any way representative, the conditions prevailing at the time of Ag exposure could determine the subsequent course of disease.

Regardless of the Th1 or Th17 phenotype, the uveitogenic effector T cells that have been primed in the periphery travel through the circulation and extravasate into tissues, seemingly at random. A number of studies based on tracking the migration of labeled uveitogenic lymphocytes infused into naive recipients revealed that only a very few of the infused cells actually reach the eye, about 150 cells out of 10 million (= 0.0015%). Since half a million uveitogenic T cells are sufficient to cause EAU, this translates to 7–10 cells per retina. Cytokines, chemokines, and other soluble mediators released by these initial infiltrating cells upon recognition of their Ag in the tissue, trigger a complex process of activation of the ocular resident cells and the vascular endothelium, breakdown of the blood–retinal barrier and recruitment of inflammatory leukocytes, including neutrophils, monocytes, and nonspecific T cells, that are the final mediators of tissue damage (**Figure 2**). Each of these cell types apparently provides an essential function, as depletion of any one of them lowers EAU susceptibility.

Th1 and Th17 cells recruit different populations of inflammatory leukocytes by producing different sets of cytokines and eliciting different sets of chemokines. Th17 cells are known to preferentially attract neutrophils, whereas Th1 cells preferentially attract mononuclear cells, and this is in fact reflected in the composition of the inflammatory infiltrate in eyes of mice with EAU induced by adoptive transfer of Th1- or Th17-polarized uveitogenic cell populations, Paradoxically, however, the dominant ocular infiltrate in CFA-induced EAU, which is Th17 dependent, is mainly mononuclear, whereas the infiltrate in the Th1-dependent DC-induced EAU is predominantly polymorphonuclear. This suggests that the intraocular microenvironment is only partly determined by the systemically dominant effector T cell type and underscores the complexity of *in vivo* systems.

Regulatory T Cells and Uveitis

Tregs control induction and progression of immune responses. Two major categories of Tregs have been described: natural and induced. Natural Tregs (nTregs) were initially discovered as a result of the 3-day neonatal thymectomy model, in which mice whose thymus is removed 3 days after birth develop a variety of organ-specific autoimmune diseases, including oophoritis, gastritis, and thyroiditis. It was subsequently found that nTregs are generated in the thymus by positive selection on ectopically expressed self-Ags, in parallel to negative selection of high-affinity autoreactive effector T cells. nTregs are believed to originate from precursor T cells with intermediate affinity T-cell receptors (TCRs), just below the borderline of negative selection. Instead of being deleted, they become anergic and acquire regulatory function. They are typically $CD4^+CD25^+$ and express the Treg-lineage-specific transcription factor FoxP3.

Although spontaneous uveitis has not been reported as one of the autoimmune manifestations in the 3-day thymectomy model, nTregs appear to be important in controlling responses to retinal Ags. Depletion of natural Tregs by treatment with anti-CD25 antibodies (Abs) prior to immunization with a uveitogenic dose of IRBP greatly exacerbates EAU scores and associated immunological responses and permits EAU to develop in normally resistant mouse strains such as BALB/c. This demonstrates the role of nTregs in raising the threshold of susceptibility to EAU. Thymic generation of IRBP-specific nTregs is dependent on endogenous expression of IRBP, as they are absent in $IRBP^{-/-}$ mice.

When regulation by nTregs is insufficient and priming of functional retina-specific effector T cells occurs, exposure to Ag induces Tregs *de novo* from peripheral T cells. The distinction between natural and induced Tregs blurs in immunized animals, as both share FoxP3 expression and surface markers, although some induced Tregs are $CD8^+$. As part of its immune-privileged status, the eye is capable of inducing Tregs through a variety of methods, both local and systemic. Two examples of systemic induction of eye-related Tregs are: (1) the ACAID phenomenon discussed above, which when induced with IRBP can prevent and reverse EAU and (2) postrecovery regulatory T cells, whose induction is dependent on the presence of the eye and does not occur in enucleated animals immunized as for induction of EAU. Although induced Tregs come into play as a result of damage already sustained by the eye, they can limit further development of disease and ameliorate its re-induction.

During EAU, $FoxP3^+$ Tregs accumulate in the eye, reaching 20% of $CD4^+$ T cells in the eye 5 weeks after uveitogenic immunization, and this increase parallels resolution of disease. Data from IRBP TCR Tg mice demonstrate that the fraction of IRBP-specific Tregs (detectable by their specific TCRs) in the $FoxP3^+$ population is enriched in the eye fourfold to fivefold compared to the submandibular (eye draining) and other lymph nodes. It is not known whether this reflects preferential retention, proliferation, or conversion of non-Treg cells to Tregs within the eye; however, the ocular microenvironment has the potential to promote local induction of Tregs. Ocular resident cells including Müller cells and ocular pigmented epithelial cells are inhibitory to T cells. Ocular pigmented epithelia (though not Müller cells) may convert T cells to Tregs upon contact. Furthermore, the ocular fluids contain TGF-β, α-MSH, and other factors that can directly inhibit T-cell activation and function, and/or convert them to regulatory cells. Although these data are quite compelling, they represent mostly *in vitro* observations and it is still unclear how much of a role these phenomena have *in vivo* in controlling uveitis.

Treg defects have been reported in some human autoimmune diseases, such as multiple sclerosis and type-1 diabetes. The importance of Tregs in controlling human uveitic disease is not well understood, but patients with uveitis associated with VKH disease have been noted to have reduced Treg function. In contrast to human uveitis, which tends to be chronic, EAU in rodent models tends to be monophasic. This may conceivably be due to Treg defects in predisposed human patients, which are not found in the common strains of laboratory rodents, in which uveitis must be induced with the aid of strong immunization regimens. This notion is supported by findings showing that weak Treg activity may contribute to recurrent versus monophasic uveitis in the rat EAU model.

Non-Treg Cells in Regulation of Uveitis

To complete the picture, it is important to keep in mind that cells and processes other than the classical natural and induced T regulatory cells may also regulate uveitis. Inhibition of T-cell activation and function by ocular resident cells, at least *in vitro*, has already been mentioned. At the systemic level, non-Treg cells able to produce cytokines also may regulate disease. Natural killer T (NKT) cells rapidly produce cytokines upon engagement of their TCR, including IFN-γ, IL-4, and more recently they were also demonstrated to produce IL-17. Mice immunized for EAU and concurrently treated with the glycolipid α̃GalCer, which is a ligand for the invariant NKT TCR, develop reduced disease scores. Interestingly, among analogs that elicit different amounts of IFN-γ versus IL-4 from NKT cells, the most protective analog was the one that elicited the highest levels of IFN-γ. Protection was associated with reduced adaptive IL-17 and IFN-γ responses to IRBP. Concurrent treatment with a neutralizing IFN-γ Ab reversed protection and restored adaptive IFN-γ and IL-17 responses, demonstrating the role of IFN-γ in this process. This is reminiscent of data showing that injection of IL-12 at the time of immunization had a protective IFN-γ-dependent effect, and was shown to be associated with apoptotic elimination of newly primed effector T cells. Thus, unlike locally produced IFN-γ which enhances pathology by inducing a broad spectrum of proinflammatory mediators, elevated systemic levels of IFN-γ at the time of priming, restrain development of adaptive immunity. Endogenous ligands that bind to the NKT cell invariant TCR might trigger them to regulate EAU. These data help to reconcile the apparent paradox that lack of IFN-γ (through genetic or treatment-induced deficiency) results in higher EAU scores in the IRBP–CFA model.

See also: Dynamic Immunoregulatory Processes that Sustain Immune Privilege in the Eye; Immunosuppressive and Anti-Inflammatory Molecules that Maintain Immune Privilege of the Eye.

Further Reading

Agarwal, R. K. and Caspi, R. R. (2004). Rodent models of experimental autoimmune uveitis. *Methods in Molecular Medicine* 102: 395–419.

Avichezer, D., Grajewski, R. S., Chan, C. C., et al. (2003). An immunologically privileged retinal antigen elicits tolerance: Major role for central selection mechanisms. *Journal of Experimental Medicine* 198: 1665–1676.

Caspi, R. R. (2006). Ocular autoimmunity: The price of privilege? *Immunological Reviews* 213: 23–35.

Egwuagu, C. E., Charukamnoetkanok, P., and Gery, I. (1997). Thymic expression of autoantigens correlates with resistance to autoimmune disease. *Journal of Immunology* 159: 3109–3112.

Grajewski, R. S., Silver, P. B., Agarwal, R. K., et al. (2006). Endogenous IRBP can be dispensable for generation of natural $CD4^+CD25^+$ T-regs that protect from IRBP-induced retinal autoimmunity. *Journal of Experimental Medicine* 203: 851–856.

Kyewski, B. and Klein, L. (2006). A central role for central tolerance. *Annual Review of Immunology* 24: 571–606.

Lambe, T., Leung, J. C., Ferry, H., et al. (2007). Limited peripheral T cell anergy predisposes to retinal autoimmunity. *Journal of Immunology* 178: 4276–4283.

Luger, D., Silver, P. B., Tang, J., et al. (2008). Either a Th17 or a Th1 effector response can drive autoimmunity: Conditions of disease induction affect dominant effector category. *Journal of Experimental Medicine* 205: 799–810.

Nussenblatt, R. B. and Whitcup, S. M. (2004). *Uveitis: Fundamentals and Clinical Practice,* 3rd edn. Philadelphia, PA: Mosby (Elsevier).

Prendergast, R. A., Iliff, C. E., Coskuncan, N. M., et al. (1998). T cell traffic and the inflammatory response in experimental autoimmune uveoretinitis. *Investigative Ophthalmology and Visual Science* 39: 754–762.

Shevach, E. M., DiPaolo, R. A., Andersson, J., et al. (2006). The lifestyle of naturally occurring $CD4^+$ $CD25^+$ $Foxp3^+$ regulatory T cells. *Immunological Reviews* 212: 60–73.

Stein-Streilein, J. and Taylor, A. W. (2007). An eye's view of T regulatory cells. *Journal of Leukocyte Biology* 81: 593–598.

Tang, J., Zhu, W., Silver, P. B., et al. (2007). Autoimmune uveitis elicited with antigen-pulsed dendritic cells has a distinct clinical signature and is driven by unique effector mechanisms: Initial encounter with autoantigen defines disease phenotype. *Journal of Immunology* 178: 5578–5587.

Xu, H., Koch, P., Chen, M., et al. (2008). A clinical grading system for retinal inflammation in the chronic model of experimental autoimmune uveoretinitis using digital fundus images. *Experimental Eye Research* 87: 319–326.

Immunopathogenesis of HSV Keratitis

K Buela, G Frank, J Knicklebein, and R Hendricks, University of Pittsburgh School of Medicine, Pittsburgh, PA, USA

Glossary

Anterograde axonal transport – Transport through the cytoplasm of axons from the neuron cell body or soma towards the synapse.
Chemokine – A combined form of the words chemotactic (able to attract cells) and cytokines. Chemokines are a family of low-molecular-weight chemotactic cytokines that attract and activate leukocytes at sites of infection and inflammation.
Cytokine – A large and diverse family of intercellular molecular messengers that, like hormones, transmit information from one cell to another. The term is often used to denote polypeptides with immunomodulatory activity.
HSV-1 latency – The retention of a complete viral genome for extended periods without production of infectious virions.
Immunosurveillance – The continuous monitoring function of the immune system whereby it recognizes and reacts against aberrant cells arising within the body.
Regulatory T cells – Specialized subpopulation of T cells that act to suppress activation of the immune system and thereby maintain immune system homeostasis and tolerance to self-antigens.
Retrograde axonal transport – The transport of vesicles from the synaptic region of an axon toward the cell body or soma.
T cells – A population of lymphocytes that derive from bone marrow precursors, mature in the thymus, and play a central role in cell-mediated immunity.
Trigeminal ganglia – The ganglia that house the cell bodies of primary afferent neurons innervating the head and neck.
Virion – A mature infectious virus particle existing outside a cell.

Natural History of Herpes Stromal Keratitis

Although herpes stromal keratitis (HSK) has been studied in a variety of animal models, much of our current knowledge regarding the immunopathogenesis of HSK has derived from murine models due to the plethora of immunologic reagents available to dissect the immune response in mice. Strain differences in susceptibility to HSK have been noted with A/J>Balb/c>C57BL/6. With most strains of HSV-1, corneal infection requires surface abrasion to facilitate entry of the virus into corneal epithelial cells. An epithelial lesion then forms as a result of virus replication in and destruction of epithelial cells. The lesions are transient, resolving by 4 days post infection (dpi), with eradication of replicating HSV-1 by 7–8 dpi. Healing of the lesions is aided by the rapid turnover of corneal epithelial cells.

Eradication of Replicating HSV-1 from the Corneal Epithelium

Viral clearance appears to be largely a function of the innate immune system, consistent with the rapid kinetics of virus elimination. Evidence suggests a role for neutrophils, natural killer (NK) cells, and γδ T cells in the eradication of replicating virus from the cornea. These cells are attracted to and activated within the cornea as a result of the release of cytokines, including cyclooxygenase 2, prostaglandin E2, type 1 interferon, interleukin (IL)-1, IL-6, IL-17, granulocyte macrophage colony stimulating factor (GM-CSF), and tumor necrosis factor (TNF); and chemokines including CXCL10 (IP-10), CXCL9 (MIG), CXCL2 (MIP-2), and CCL3 (MIP-1α). The production of these cytokines and chemokines appears to be initiated by ligation of toll-like receptors (TLRs), especially TLR2 and TLR9, and in response to cytokines including IL-17, IL-6, and interferon-gamma (IFN-γ). The initial neutrophilic infiltrate peaks in HSV-1 infected mouse corneas around 4 dpi, and declines between 6 and 8 dpi, coincident with the peak and decline of viral titers in the mouse cornea.

The adaptive immune system appears to play a less significant role in the initial clearance of HSV-1 from the infected cornea following primary infection. However, it is noteworthy that severe combined immune-deficient (SCID) mice that lack an adaptive immune system do not fully eradicate replicating virus from the cornea. Accordingly, activated CD4 T cells have been detected within the infected cornea by 3 dpi, although their role in inhibiting HSV-1 replication within the cornea has not been established. It is possible, and indeed likely that the failure of SCID mice to eradicate replicating HSV-1 from the cornea during primary infection results from their inability to fully establish and maintain viral latency in the trigeminal

ganglion. Replicating virus in the trigeminal ganglion could then be transported back to and shed into the cornea, perpetuating the corneal infection. The role of T cells in clearing virus from the corneal epithelium following reactivation has not been studied. Antibodies also appear to play an important role in the clearance of HSV-1 from the cornea during both primary and recurrent disease.

HSV-1 Colonization of Sensory Ganglia

During the course of virus replication in epithelia of the cornea, oral, or nasal passages of mice, the virus gains access to the termini of sensory neurons and is transported to neuronal nuclei in trigeminal ganglia. There it replicates briefly and then establishes a latent infection that is characterized by retention of a functional viral genome without production of infectious virions. Evidence suggests that control of acute HSV-1 replication and establishment of latency in trigeminal ganglia is mediated largely by an innate response of macrophages and NK cells mediated by TNFα, IFN-γ, and nitric oxide. However, complete eradication of replicating virus requires reinforcement by $CD8^+$ T cells and γδ T cells. Latently infected neurons within the ophthalmic branch of trigeminal ganglia then serve as a source of virus for recurrent corneal disease. HSV-specific $CD8^+$ T cells then remain in the trigeminal ganglion in close apposition to infected neurons for the life of the mouse. These $CD8^+$ T cells express a persistent activation phenotype and have been shown to inhibit HSV-1 reactivation from latency both *in vivo* and in *ex vivo* ganglionic cultures. A similar association of activated $CD8^+$ T cells with latently infected neurons has also been established in human ganglia. Moreover, psychological stress, which is associated with recurrent herpetic disease in humans, causes a transient compromise of the function of ganglionic $CD8^+$ T cells and HSV-1 reactivation from latency in trigeminal ganglia of mice. These findings suggest that maintenance of HSV-1 latency and prevention of recurrent shedding of virus at mucosal surfaces such as the cornea requires constant immunosurveillance by $CD8^+$ T cells.

Herpes Stromal Keratitis

Following resolution of the epithelial lesion, corneal clarity is reestablished in mice. However, by 7–10 dpi corneal opacity develops accompanied by ingrowth of blood vessels into the normally avascular cornea, and massive leukocytic infiltration. These are manifestations of HSK, which in mice progresses from a non-necrotizing form with little epithelial involvement to severe necrotizing keratitis in which stromal inflammation gives rise to epithelial necrosis. The necrotizing form represents about 7% of human HSK, with 88% exhibiting the non-necrotizing form, and 5% exhibiting a mixture of both forms. It is not clear if the reduced incidence of necrotizing HSK in humans relative to mice is due to medical management of inflammation in human corneas or a reflection of fundamentally different pathogenic mechanisms in most human cases of HSK.

T Cells in HSK

Early studies revealed that HSK failed to develop in athymic nude mice that lacked T cells, but could be reconstituted in these mice by T-cell adoptive transfer. The $CD4^+$ T cell population appears to be the predominant mediator of HSK in most mouse models, with $CD8^+$ T cells tending to reduce disease severity. However, $CD8^+$ T cells can also mediate a milder and more transient form of HSK when mice are deficient in $CD4^+$ T cells or infected with certain strains of HSV-1. Human corneas with HSK contain both $CD4^+$ and $CD8^+$ T cells that are specific for HSV antigens, though the relative contribution of these cells in the progression or resolution of HSK cannot be evaluated. Recently, a population of $CD4^+$ T cells referred to as natural T regulatory cells (nTregs) that co express CD25 and the forkhead/winged-helix transcriptional regulator, FoxP3 were shown to moderate the severity of HSK. The fact that these nTregs maintain the capacity to regulate HSK when expanded *in vitro* and adoptively transferred into infected mice offers a potentially useful therapeutic modality.

Cytokines and Their Role in HSK

Cytokines provide a means of communication among leukocytes and between leukocytes and parenchymal cells at sites of infection and/or antigen deposition. Under optimal conditions cytokines orchestrate an immunoinflammatory response that eliminates a pathogen with minimal damage to host tissue. In HSK resolution of the immunoinflammatory lesions in the cornea is accompanied by scar tissue formation. This trade-off of strength for clarity is unacceptable in a tissue within the visual axis. Moreover, the fact that in both mice and humans HSK can develop in the absence of replicating virus in the cornea renders HSK a purely immunopathological process. Thus, regulating the production and/or function of the cytokines that orchestrate HSK would reduce tissue damage without compromising protection of the host.

Most studies in the murine models have implicated the Th1 cytokines as playing a primary role in the pathogenesis of HSK. The prototypic Th1 cytokine, IFN-γ, aids neutrophil extravasation into the cornea at least in part through upregulation of platelet/endothelial cell adhesion molecule 1 (PECAM-1, CD31) on local vasculature. Th1 cells also produce IL-2 that has been shown to directly or indirectly regulate the migration of neutrophils into the central cornea during HSK. The Th1-associated cytokine

IL-12 also contributes to HSK development, presumably through its capacity to regulate IFN-γ production. The cytokine IL-6 also plays a central role in orchestrating HSK in part through its ability to induce the neutrophil chemokine MIP-2 (CXCL2).

Recently, the functional repertoire of $CD4^+$ T cells was expanded to include Th17 cells. The IL-17 cytokine family represents the signature cytokines of Th17 cells, and is now implicated in a variety of inflammatory processes and autoimmune diseases. IL-17 is produced in both human and mouse corneas during HSK. Both human and mouse keratocytes express receptors for IL-17, and engagement of this receptor induces their production of neutrophil chemotactic factors as well as GM-CSF. The chemotactic factors attract neutrophils into the cornea while GM-CSF activates them and maintains their viability. Recent studies support a role for IL-17 in neutrophilic infiltration during the early stages of HSK. The requirement for IL-17 is transient and presumably superseded by Th1 cytokines as HSK progresses.

Regulating the production or blocking the function of the Th1 and Th17 cytokines offer potential therapeutic benefit in preventing the progression of HSK. In addition, the Th1/Th2/Treg cytokine IL-10 has a proven capacity to ameliorate HSK. The general anti-inflammatory properties include inhibition of the production and function of IFN-γ.

Antigen-Presenting Cells in HSK

Antigen-presenting cell (APC) refers to the ability of certain cells, including macrophages, dendritic cells, and B lymphocytes to take up, process, and present antigenic peptides to naive $CD4^+$ T cells in the context of major histocompatibility complex class II (MHC class II) and co-stimulatory molecules. The once prevalent view that the normal cornea is devoid of these specialized cells has now been dispelled by several recent histological studies of mouse and human corneas. Dendritic cells (DCs) are present in the basal layer of the corneal epithelium and macrophages are present throughout the corneal stroma, with the density of both cell types gradually diminishing from the peripheral to the central cornea.

During HSV-1 infection of the corneal epithelium, the resident DCs are reinforced by immigrants from the limbus. Studies employing ultraviolet irradiation to diminish DCs or cautery to increase their presence in the cornea prior to HSV-1 infection suggested a role for these cells in directly or indirectly inducing a delayed-type hypersensitivity response in lymphoid organs. Since DCs exhibit transient survival following HSV-1 infection, it is likely that either noninfected corneal DCs acquire viral antigens from corneal epithelial cells for direct presentation to T cells in the lymph nodes, or infected corneal DCs travel to the lymph nodes where they are phagocytosed by resident DCs and viral antigens are cross-presented to T cells. The DC depletion studies also suggested an important role for corneal DC in presenting HSV-1 antigens to $CD4^+$ T cells upon infiltration of the infected cornea. This is consistent with the observation that $CD4^+$ T cells induce a second and more profound infiltration of DC into the cornea at the time of onset of HSK. It should be noted, however, that the method of DC depletion employed in these early studies was not specific, and the role of DC and DC subpopulations in the efferent and afferent limbs of the $CD4^+$ T cell response in HSK awaits confirmation in studies employing specific depletion strategies now available.

Although many cell types can be induced to express MHC class II antigens, professional APCs are uniquely able to co-express the co-stimulatory molecules that are required for the activation of naive and, in many cases, effector $CD4^+$ T cells. In a mouse model of HSK, blocking the interaction of the ligands B7-1 (CD86) and B7-2 (CD80) on APCs with the co-stimulatory molecule CD28 on $CD4^+$ T cells locally within the cornea inhibited the HSK progression. In contrast, ligation of the inhibitory receptor program death 1 (PD-1) by its ligand B7-H1 (CD274) appears to inhibit HSK progression, though it is not clear if this effect is exerted in the cornea or lymphoid organs. HSK progression was not influenced by blocking the interaction of the APC activating receptor OX40 by its T-cell ligand OX40L (CD154). These studies suggest that local inhibition of co-stimulatory molecule or augmentation of inhibitory molecule signaling in $CD4^+$ T cells might hold therapeutic potential in the management of HSK.

Chemokine Involvement in HSK

Chemokines are chemotactic cytokines that activate and direct the migration of leukocytes into sites of inflammation. Chemokines not only orchestrate the innate immune response that eradicates replicating HSV-1 from the cornea (see above), but also have a central role in regulating HSK. Defining the role of chemokines in inflammatory processes is complicated by the fact that they are pleiotropic, have overlapping functions, share receptors, and can bind to multiple receptors. Not surprisingly, studies of their involvement in HSK, have in some cases, produced conflicting results. While IP-10 (CXCL10) and MCP-1 (CCL2) appear to be important for directing $CD4^+$ T cells into the cornea, IP-10 might also inhibit neovascularization (see below). The chemokine CCL20, expressed by HSV-1-infected corneal epithelial cells and corneal keratocytes when stimulated by IL-1β and TNFα, appears to be involved in DC infiltration during both epithelial lesions and the secondary infiltration during HSK development. The chemoattractants MIP-2 (CXCL2), MIP-1α (CCL3), and RANTES (CCL5) have all been implicated in guiding neutrophils into the cornea

during HSK. A variety of neutralizing antibodies, and peptide and nonpeptide inhibitors of these chemokines have been developed and might have therapeutic potential in managing HSK, though their successful use will likely be complicated by the redundant nature of the chemokines.

Angiogenesis in HSV-1 Stromal Keratitis

Neovascularization of the normally avascular cornea appears to be a requisite step in the development of severe HSK in mice. Both vascular endothelial growth factor (VEGF) and matrix metalloproteinase (MMP)-9 have an important role in the neovascularization of corneas with HSK. Production of these factors is induced by IL-1, IL-6, and MIP-2. Corneal cell production of soluble VEGF receptors prevents vascularization of the cornea during steady state. Clearly, the capacity of the soluble VEGF receptor to neutralize VEGF and prevent its binding to VEGF receptors on the limbal vascularture is overwhelmed by the amount of VEGF produced in HSV-1 infected corneas. Neovascularization provides enhanced corneal access of blood-borne leukocytes that mediate HSK, and blocking neovascularization effectively prevents HSK progression. Based on the established roles for vascularization and VEGF in mouse models of HSK, and the prominent presence of corneal vessels in necrotizing keratitis in humans, therapeutic approaches geared toward blocking vascularization hold great promise in the management of HSK.

Models of HSK Pathogenesis

Despite extensive advances in our understanding of the pathogenesis of HSK in mice, one of the most basic questions (viz., what stimulates the $CD4^+$ T cells that mediate HSK) remains unanswered. Three models of CD4+ T-cell activation in HSV-1 infected corneas have been advanced and supported by experimental data. These include: (1) bystander activation by the cytokine milieu present in the cornea, (2) autoimmunity to corneal tissue resulting from molecular mimicry by viral proteins, and (3) virus-specific activation.

The concept that bystander activation of $CD4^+$ T cells mediated by the cytokine milieu within the infected cornea is sufficient to induce HSK was proposed based on findings in mice whose T cells all express transgenic T-cell receptors (TCRs) specific for ovalbumin (ova). When the corneas of these mice were infected with HSV-1, they developed HSK that was mediated by ova-specific $CD4^+$ T cells. However, these mice failed to control HSV-1 replication in the cornea, and succumbed to infection early during HSK development. Indeed, when HSV-1 replication was controlled in the corneas of these with kinetics similar to that of immunologically normal mice, the mice failed to develop HSK. Thus, in immunologically normal mice (and presumably people) bystander activation of $CD4^+$ T cells might contribute to, but is not itself sufficient for, the development of HSK.

Other studies incorporating BALB/c mice that are congenic for the IgH locus concluded that HSK develops as a result of an autoaggressive attack of $CD4^+$ T cells on corneal tissue. This autoimmune response was induced by a peptide contained in the viral UL6 protein that mimicked a sequence in a corneal protein and in the Ig heavy chain of one of the congenic strains. The BALB/c strain that expressed the mimicked peptide in its Ig heavy chains did not respond to the peptide due to clonal deletion, and were highly resistant to HSK. In contrast, the congenic strain that failed to express the UL6-mimicked peptide in its Ig heavy chain generated a response to UL6 that cross-reacted with a corneal protein. The authors concluded from these findings that HSK is an autoimmune disease arising from antigenic mimicry by the HSV-1 UL6 protein. Unfortunately, these intriguing findings were not reproduced in subsequent studies by another group, and no UL-6-specific or cornea-specific $CD4^+$ T cells have been isolated from mouse or human corneas with HSK. Thus, the involvement of autoimmunity in HSK remains uncertain.

A third possibility is that reactivity of HSV-specific $CD4^+$ T cells to HSV antigens within the cornea triggers HSK. This hypothesis is consistent with the fact that HSV-1-specific $CD4^+$ T cells have been isolated from both human and murine corneas at varying stages of keratitis. Further support for this concept came from a study in which partial tolerization of $CD4^+$ T cells to HSV-1 antigens was associated with reduced severity of HSK. However, no studies to date have established a clear role for HSV-1-specific $CD4^+$ T cells in directly mediating HSK. Based on the available data, it is likely that the initiation of HSK results from stimulation of HSV-specific $CD4^+$ T cells in the cornea, while bystander activation might contribute to the progression and chronicity of the inflammation.

Epidemiology and Pathogenesis of Human HSK

Clinically, ocular HSV-1 infection remains a significant cause of visual impairment worldwide. In developed nations, there are approximately 8.4–13.2 new ocular HSV-1 infections per 100 000 person-years with an overall incidence, including recurrences, of 20.7–31.5 episodes per 100 000 person-years. Perhaps the most serious manifestation of ocular HSV-1 infection is the potentially blinding HSK, which accounts for only 2% of initial HSV-1 ocular presentations but represents 20–61% of recurrent disease.

Multiple forms of HSK exist and no classification system is universally accepted (here we use a classification system described by Liesegang). HSK commonly presents as a non-necrotizing or immune form, but can also present as the rarer but more serious necrotizing form. Based on limited data, it appears that both the necrotizing and immune presentations of human HSK share the features of neovascularization and leukocytic infiltration seen in the mouse model. Since HSK in the mouse progresses from disease resembling immune HSK to disease resembling necrotizing HSK, it is reasonable to propose that the two forms represent a continuum rather than distinct pathologies. However, there are important differences between the human and mouse HSK, including the fact that HSK rarely leads to corneal perforation in humans, while perforation is a frequent occurrence in the mouse model. Moreover, human HSK is often associated with replicating HSV-1 in the cornea and overlying epithelial lesions, whereas replicating HSV-1 is typically eradicated from the mouse cornea prior to the onset of HSK.

Management of Human HSV Stromal Keratitis and Implications on Pathogenesis

Management of HSK is complicated by the fact that the cells that are responsible for eliminating the virus also contribute to immunopathology in the cornea. Treating the inflammation alone can significantly exacerbate viral replication. In contrast, treating with antivirals alone can lead to uncontrolled inflammatory damage to the cornea. The current standard of care for both non-necrotizing and necrotizing HSV stromal keratitis includes topical corticosteroids and topical antivirals. Corticosteroids are used to diminish the immunopathological component of stromal disease, while the antivirals prevent further viral replication. However, corticosteroids applied to the ocular surface can lead to adverse side effects including development of cataracts or glaucoma. A less well-studied treatment option for patients suffering from HSV stromal keratitis is topical cyclosporin A (CsA) in addition to topical antivirals. Several small noncontrolled trials in humans with HSK suggested that treatment with CsA may be beneficial in cases resistant to corticosteroids. Additionally, studies using murine models of HSK revealed that CsA effectively reduced stromal inflammation and haze in a dose-dependent manner. Similar to corticosteroids, CsA also functions to dampen the immune system. CsA blocks transcriptional activation of CD4+ T-cell pathways necessary for production of inflammatory cytokines, such as IL-2 and IFN-γ. Furthermore, CsA inhibits corneal neovascularization in murine models of HSK.

Successful medical treatment of human HSK has important implications concerning the theories of HSK pathogenesis. CsA functions to inhibit TCR-induced calcineurin signaling that leads to production of inflammatory cytokines, such as IL-2. Therefore, effective treatment of HSK with CsA implicates TCR signaling, favoring $CD4^+$ T-cell activation by viral or autoantigens, but not by cytokines.

Studies in mice emphasize an important role for neovascularization in HSK progression. Mouse studies also implicate VEGF as a critical regulator of vascularization associated with HSK. The current availability of therapeutic agents such as Avastin and Leucentis that inhibit vascularization by blocking VEGF offers the potential for exciting new treatment alternatives.

Acknowledgments

The authors would like to thank Kira Lathrop, MAMS, for technical assistance within this article.

See also: Adaptive Immune System and the Eye: T Cell-Mediated Immunity; Angiogenesis in Inflammation; Antigen-Presenting Cells in the Eye and Ocular Surface; Avascularity of the Cornea; Corneal Epithelium: Response to Infection; Immunopathogenesis of Pseudomonas Keratitis.

Further Reading

Biswas, P. S. and Rouse, B. T. (2005). Early events in HSV keratitis – setting the stage for a blinding disease. *Microbes and Infection* 7: 799–810.

Lepisto, A. J., Frank, G. M., and Hendricks, R. L. (2007). How herpes simplex virus type 1 rescinds corneal privilege. In: Niederkorn, J. Y. and Kaplan, H. J. (eds.) *Immune Response and the Eye,* vol. 92, pp. 203–212. Karger: Basel.

Liesegang, T. J. (1999). Classification of herpes simplex virus keratitis and anterior uveitis. *Cornea* 18: 127–146.

Metcalf, J. F., Hamilton, D. S., and Reichert, R. W. (1979). Herpetic keratitis in athymic (nude) mice. *Infection and Immunity* 26: 1164–1171.

Sheridan, B. S., Knickelbein, J. E., and Hendricks, R. L. (2007). CD8 T cells and latent herpes simplex virus type 1: Keeping the peace in sensory ganglia. *Expert Opinion on Biological Therapy* 7: 1323–1331.

Immunopathogenesis of Onchocerciasis (River Blindness)

E Pearlman, Case Western Reserve University, Cleveland, OH, USA
K Gentil, University of Bonn, Bonn, Germany

Glossary

Microfilariae – First stage (L1) larvae of filarial nematodes including *Onchocera volvulus*, the causative agent of river blindness.
TLR (toll-like receptor) – A family of surface and endosomal receptors that are expressed on mammalian cells, including the cornea. These receptors recognize microbial products and transmit cell signals that culminate in the elaboration of chemokines and cytokines.
Wolbachia – Obligate intracellular bacteria that exist as endosymbionts in filarial nematodes including *Onchocerca volvulus*.

Onchocerciasis (river blindness) remains endemic in a number of sub-Saharan African countries and has foci in Yemen and in Latin America. Most recent (2006) estimates indicate that there are 37 million individuals infected with *Onchocerca volvulus*. The life cycle of all filarial nematodes includes transmission through insect vectors, with *Simulium* blackflies transmitting *O. volvulus*. First stage larvae (microfilariae, L1) are ingested during a blood meal and migrate through the insect gut, thorax and into the salivary gland having undergone two molts to the third-stage larvae (L3). Infective L3 enter the mammalian host during a second insect blood meal, where they develop to L4 stage and then adult males and females. Adult male and female worms live for over 10 years in subcutaneous tissues, producing millions of microfilariae over their lifespan. Microfilariae can survive for over 1 year in the skin, and can enter the anterior and porterior segments of the eye. While alive, microfilariae appear to cause minimal damage, and individuals can be very heavily infected; however, when the larvae die either by natural attrition or following chemotherapy, the host immune response causes acute and chronic tissue damage, with severe onchodermatitis in the skin, visual impairment, and blindness. **Figure 1** shows examples of sclerosing keratitis and of cellular infiltration and vascularization in the corneal stroma of an infected individual in west Africa.

The Role of Endosymbiotic *Wolbachia* Bacteria in Onchocerciasis

Intracytoplasmic *Rickettsia*-like bacteria were first described in filarial nematodes in 1977, and later identified as *Wolbachia pipientis*. Although 75% of insect species and a number of crustaceans harbor *Wolbachia* as endosymbionts, filarial nematodes are the only group of parasitic worms that are infected, most likely because they are the only nematode group with an obligate insect host. In filarial nematodes, *Wolbachia* are detected with in cells in the hypodermis and uterus, in immature microfilariae in the uterus, and in mature microfilariae in the skin and cornea. The bacteria are most numerous in the mammalian host compared with the insect stage, and appear to have an essential, though poorly understood, role in nematode embryogenesis. Antibiotic (Doxycycline) treatment of filaria-infected individuals effectively sterilizes the adult females, reducing overall microfilaria numbers in the skin and blocking disease transmission.

Role of *Wolbachia* in Pathogenesis – Evidence from Infected Individuals

The role of *Wolbachia* in the pathogenesis of filarial disease has been implicated from observations made after antifilarial therapy. Elevated *Wolbachia* DNA and even intact *Wolbachia* are detected in the blood, and are associated with the proinflammatory cytokines seen in patients with post-treatment side effects such as fever, edema, and headache. Using quantitative PCR for *Wolbachia* surface protein (WSP) gene, which is present as a single copy per organism, the number of bacteria per worm was found to be similar in all insect stages of *B. malayi*. However, within 7 days in the mammalian host, bacteria numbers increased 600-fold and showed a high ratio of *Wolbachia*/nematode DNA in L4 larvae, indicating rapid bacterial replication within the worms. This *Wolbachia* load is maintained in adult males, but increases in females during embryogenesis. *Wolbachia* are therefore a target for antibiotic treatment, and patients given a course of doxycyline in addition to annual ivermectin treatment have reduced systemic microfilariae, and significantly fewer adult worm number in subcutaneous nodules. *Wolbachia* appear to mediate recruitment of neutrophils, as the number of neutrophils in nodules from doxycycline-treated individuals is greatly reduced compared with untreated individuals. An additional line of evidence for a role for *Wolbachia* in the pathogenesis of onchocerciasis relates to earlier studies showing that two strains of *O. volvulus* that differ in virulence exist in West Africa based on DNA probes using a noncoding repeat sequence, and the strain

Figure 1 Ocular onchocerciasis. (a) Blind individual in endemic region of Cote D'Ivoire, West Africa, 1999, with both corneas opaque as a result of infection with *Onchocerca volvulus* (photograph by Eric Pearlman); (b) sclerosing keratitis, showing central region of corneal opacification and neovascularization (with permission from Dr Hugh Taylor); (c) corneal section showing intact microfilariae (arrow) in the corneal stroma. Blood vessels (V) and cellular infiltrate are also visible (from Armed Forces Institute of Pathology).

shown to cause more severe ocular disease has significantly higher *Wolbachia* loads compared with the second, less virulent strain, indicating a correlation between virulence and *Wolbachia* in ocular onchocerciasis.

Taken together, these findings strongly support the notion of an important role for *Wolbachia* in the proinflammatory response and pathogenesis of onchocerciasis.

The Role of *Wolbachia* in the Pathogenesis of ocular onchocerciasis – Lessons from the Murine Model of *O. volvulus*/*Wolbachia* Keratitis

Microfilariae invade both the anterior and the posterior segments of the eye. In the latter case, they cause uveitis and chorioretinitis, resulting in loss of vision; therefore, although *Onchocerca* keratitis is more frequent and more readily detectable, corneal transplants are not conducted as the patients generally also have posterior segment disease. Because eyes from human cases of onchocerciasis are not available, the host response to *Onchocerca* has been examined in the skin of infected individuals. As such, *Onchocerca* infected individuals show microfilariae in the dermis surrounded by neutrophils, eosinophils, or macrophages. The likely explanation is that neutrophils surround recently dead and degenerating worms in the skin, whereas macrophages and eosinophils migrate to the site at later time points. Our findings in a murine model of *Onchocerca* keratitis shows that neutrophils surround microfilariae in the cornea within 24 h and immunogold labeling of the major *Wolbachia* surface protein shows neutrophils in close proximity to *Wolbachia* (Figure 2). Using this mouse model of *O. volvulus* keratitis in which filaria/*Wolbachia* extracts are injected into the corneal stroma, St. Andre and colleagues demonstrated that endosymbiotic *Wolbachia* bacteria are essential for the pathogenesis of *O. volvulus* keratitis as: (1) *O. volvulus* from individuals depleted of *Wolbachia* by antibiotic treatment do not induce corneal inflammation; (2) related filarial species containing *Wolbachia* induce keratitis in contrast to filarial species lacking *Wolbachia*; and (3) isolated *Wolbachia* induce neutrophil recruitment to the corneal stroma.

Wolbachia and TLRs in the Cornea

TLRs are surface and endosomal receptors that are expressed in the cornea and respond to microbial products such as lipopolysaccharide (TLR4) and lipoproteins (TLR2). TLR2 forms heterodimers with TLR1 or TLR6 to initiate signaling through adaptor molecules and induce nuclear factor kappa B (NFκB) translocation to the nucleus, and results in production of pro-inflammatory and chemotactic cytokines. Our findings using gene knock-out mice clearly demonstrate that either *O. volvulus* extracts

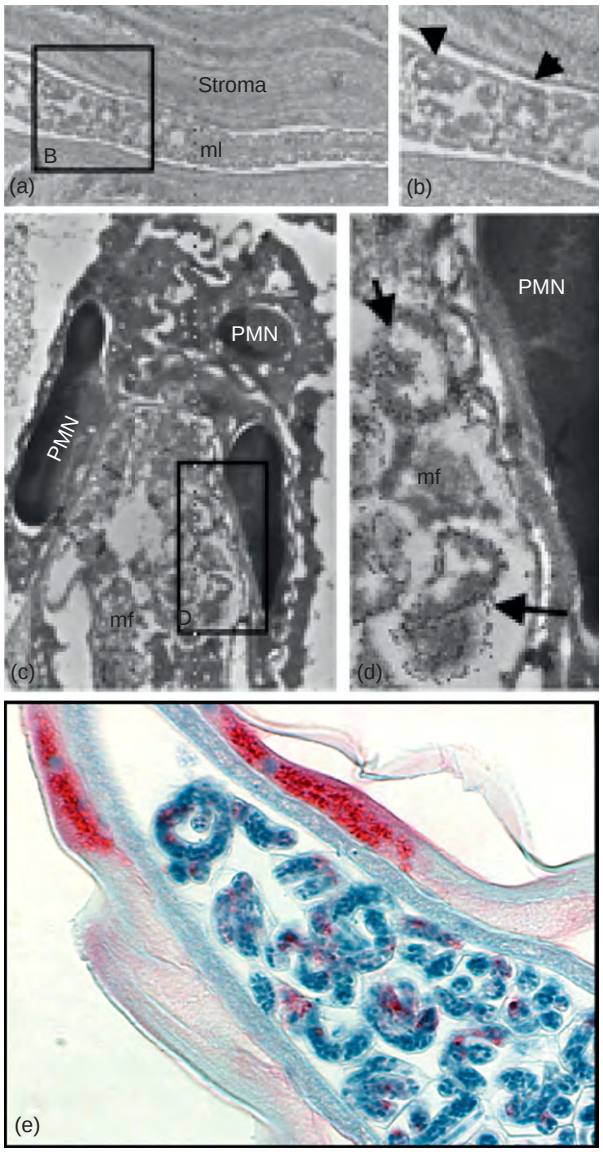

Figure 2 Presence of endosymbiotic *Wolbachia* bacteria in microfilaria and adult female worms. C57BL/6 mice were injected into the corneal stroma with microfilariae, corneas were removed after 4 h or 18 h and thin sections were immunostained with anti-*Wolbachia* Surface Protein (WSP) and visualized with IgG conjugated to 15 nm gold particles. Sections were counterstained with uranyl acetate and lead citrate, and examined by electron microscopy. (a, b) 4 h after injection. WSP was clearly detected inside microfilariae in the corneal stroma (arrows). Mf: microfilariae. (c, d) 18 h after injection microfilariae containing *Wolbachia* were surrounded by neutrophils (PMN). WSP labeled with gold particles (arrows) are present in the microfilariae adjacent to the neutrophils. Magnifications: (a) ×4800; (b) ×8400; (c) ×5300; (d) ×16 000. Reprinted with permission from Gillette-Ferguson, I., Hise, A. G., McGarry, H. F., et al. (2004). *Wolbachia*-induced neutrophil activation in a mouse model of ocular onchocerciasis (river blindness). *Infection and Immunity* 72: 5687. (e) Longitudinal section of adult female *Brugia malayi* immunostained with anti-WSP showing WSP positive microfilariae in the uterus (magnification ×400). Reprinted from Science; photomicrograph by Amy Hise.

containing *Wolbachia*, or isolated *Wolbachia* bacteria selectively activate TLR2 and TLR6, and adaptor molecules MyD88 and Mal. **Figure 3** shows that corneal inflammation (neutrophil infiltration and increased corneal haze) is entirely dependent on activating TLR2. Moreover, studies using chimeric mice have shown that TLR2 expressed on bone-marrow-derived cells have an important role in provoking corneal inflammation.

Taken together, findings from our group and others indicate that *Wolbachia* induces TLR2 activation in resident macrophages in the corneal stroma, and produce pro-inflammatory cytokines and CXC chemokines, which mediate neutrophil recruitment from peripheral, limbal vessels into the corneal stroma. Neutrophil responses to *Wolbachia* are also dependent on TLR2/MyD88, which mediate cytokine production by these cells, and may contribute to degranulation and secretion of reactive oxygen species and matrix metalloproteinases, resulting in cell death and loss of corneal clarity.

In chronically infected, untreated individuals, there is also an ongoing adaptive immune response, due to repeated invasion of microfilariae into the corneal stroma, and prolonged worm degeneration and release of *Wolbachia*. Infiltrating eosinophils and macrophages also contribute to tissue damage, manifesting as corneal opacification, loss of vision, and blindness. We found that a third role for the TLR2 is filaria/*Wolbachia* activation of dendritic cells and T-cell production of IFN-γ but not IL-4 or IL-5. IFN-γ also has an indirect role in enhancing pro-inflammatory and chemotactic cytokine production, thereby increasing neutrophil recruitment to the corneal stroma (**Figure 4**). Together, these findings demonstrate that TLR2 governs the host response to *Wolbachia* at several levels, including systemic and corneal responses, and may be a target for blocking corneal inflammation.

Identification of a *Wolbachia* TLR2/TLR6 Ligand

The TLR2/TLR6 heterodimer is activated by diacylated lipoproteins. To identify possible *Wolbachia* lipoproteins that activate TLR2/TLR6, Taylor and colleagues searched the lipoprotein databases, and identified *Brugia malayi Wolbachia* peptidoglycan-associated lipoprotein PAL (wBmPAL). Synthetic diacylated wBmPAL was shown to selectively induce IFN-γ production, to induce systemic TNF-α in a murine model of lymphatic filariasis, and to induce corneal inflammation in a TLR2/TLR6–dependent manner. These data indicate that the interaction between these (and likely other) lipoproteins and TLR2/6 in the cornea is essential for the development of *O. volvulus* keratitis.

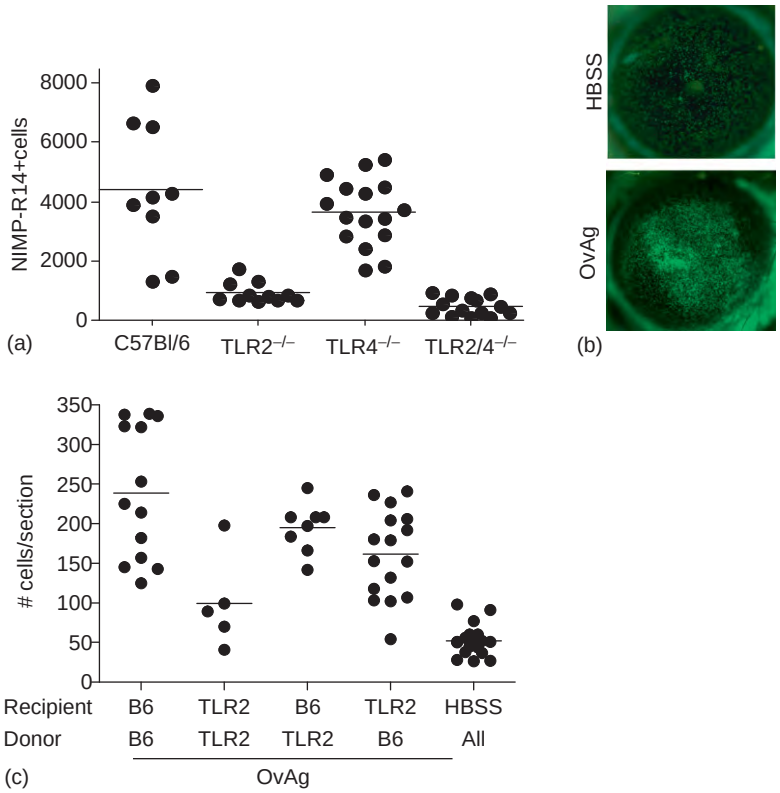

Figure 3 *O. volvulus* /*Wolbachia* keratitis is dependent on TLR2. *O. volvulus* extract containing *Wolbachia* (OvAg) was injected into the corneal stroma of C57BL/6, TLR2$^{-/-}$, TLR4$^{-/-}$ and TLR2/4$^{-/-}$ mice. After 18 h, mice were sacrificed and corneas were examined as described. (a) Single cell suspension was prepared from the corneal stroma, and total neutrophils were detected by flow cytometry using MAb NIMP-R14. (b, c) Bone marrow cells from donor C57BL/6 / eGFP+ and TLR2$^{-/-}$ mice were used to reconstitute sublethally irradiated recipient C57BL/6 or TLR2$^{-/-}$ mice. After 2 weeks, chimeric mice were injected intrastromally with *O. volvulus* extract (OvAg) or saline (HBSS), and 18 h later, 5 μm corneal sections were examined by fluorescence microscopy. Corneal sections were examined for neutrophils by immunohistochemistry. (b) Representative corneas from irradiated C57BL/6 mice reconstituted with C57BL/6 / eGFP+ bone marrow cells. After 2 weeks, mice were either untreated (naive), or examined 24 h after injection with either saline (HBSS) or *O. volvulus* extract (OvAg). (c) Total neutrophils per corneal section. Data points represent individual corneas; these data points are combined from three repeat experiments. Reprinted from Gillette-Ferguson, I., Daehnel, K., Hise, A. G., et al. (2007). Toll-like receptor 2 regulates CXC chemokine production and neutrophil recruitment to the cornea in Onchocerca volvulus/*Wolbachia*-induced keratitis. *Infection and Immunity* 75: 5908–5915.

Conclusion

River blindness appears to be mostly under control due to mass distribution of ivermectin (Mectizan), which kills microfilariae and has led to reduced prevalence of disease. Recent studies targeting *Wolbachia* for antibiotic treatment now demonstrate that doxycycline can also be used to treat infected individuals. This is not only a paradigm shift in treating filarial-infected individuals, but given the risk for ivermectin resistance, also provides a critical second approach to treatment, although this is still at the clinical trial stage. The Bill and Melinda Gates Foundation recently provided funds to develop novel antibiotics as an adjunct treatment for river blindness and lymphatic filariasis, and are described in the anti-*Wolbachia* website. Overall, the increased understanding of the pathogenesis of this disease and targeting *Wolbachia* in particular bring these devastating diseases closer to being controlled.

Acknowledgments

We gratefully acknowledge the contribution of our colleagues in these studies, including Illona Gillette-Ferguson, Amy Hise, Achim Hoerauf and Mark Taylor. This work was supported by NIH grants EY10320 and EY11373, by the Research to Prevent Blindness Foundation and the Ohio Lions Eye Research Foundation.

See also: Immunopathogenesis of Onchocerciasis (River Blindness); Innate Immune System and the Eye; Pathogenesis of Fungal Keratitis.

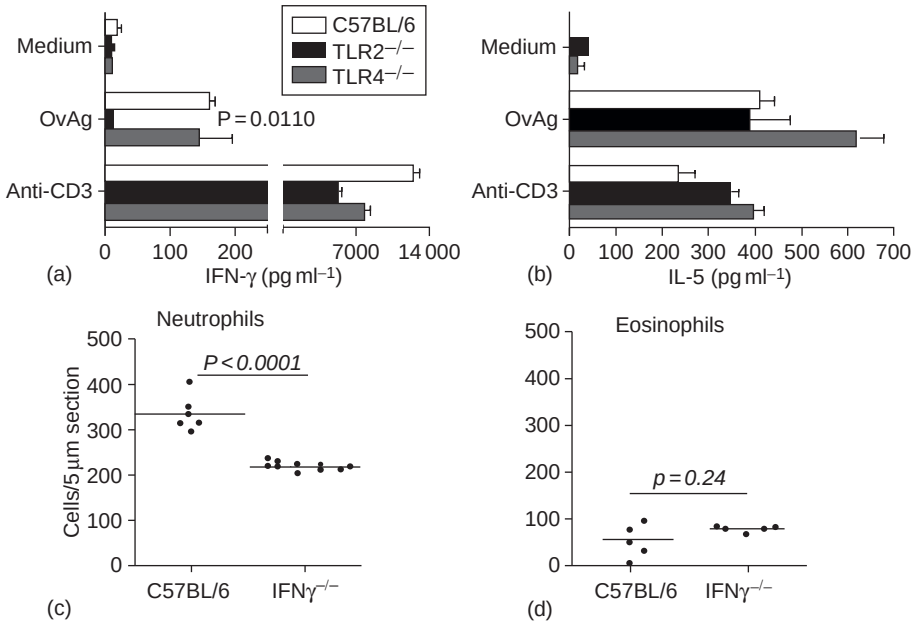

Figure 4 IFN-γ production is dependent on TLR2 and regulates neutrophil recruitment to the corneal stroma. (a, b) Mice were immunized three times with soluble *O. volvulus* extract containing *Wolbachia* (OvAg). After the final immunization, mice were sacrificed and spleens removed for *in vitro* recall response with soluble OvAg. As a positive control, splenocytes were incubated with stimulatory anti-CD3. Cytokine production by splenocytes after 72 h of culture was measured by ELISA. Note TLR2-dependent IFN-γ, but not IL-5 production. (c, d) C57BL/6 and IFNγ$^{-/-}$ mice were immunized 3 times subcutaneously with OvAg, and injected into the corneal stroma with OvAg. After 24 h, 5 μm corneal sections were immunostained for neutrophils or eosinophils, and the number of positive cells in the corneal stroma was assessed by fluorescence microscopy. Each data point represents an individual cornea, and the experiment was repeated 3 times. Note IFN-γ-dependent recruitment of neutrophils, but not eosinophils to the cornea. (a, b) Daehnel, K., Gillette-Ferguson, I., Hise, A. G., et al. (2007). Filaria/*Wolbachia* activation of dendritic cells and development of Th1-associated responses is dependent on Toll-like receptor 2 in a mouse model of ocular onchocerciasis (river blindness). *Parasite Immunology* 29: 455–465. (c, d) Gentil, K. and Pearlman, E. (2009). IFN-γ and IL-1R1 regulate neutrophil recruitment to the corneal stroma in a murine model of *Onchocerca volvulus* keratitis (river blindness). *Infection and Immunity* 77(4): 1606–1612.

Further Reading

Boatin, B. A. and Richards, F. O., Jr. (2006). Control of onchocerciasis. *Advances in Parasitology* 61: 349–394.

Brattig, N. W. (2004). Pathogenesis and host responses in human onchocerciasis: Impact of Onchocerca filariae and *Wolbachia* endobacteria. *Microbes and Infection/Institut Pasteur* 6: 113–128.

Daehnel, K., Gillette-Ferguson, I., Hise, A. G., et al. (2007). Filaria/*Wolbachia* activation of dendritic cells and development of Th1-associated responses is dependent on Toll-like receptor 2 in a mouse model of ocular onchocerciasis (river blindness). *Parasite Immunology* 29: 455–465.

Gentil, K. and Pearlman, E. (2009). IFN-γ and IL-1R1 regulate neutrophil recruitment to the corneal stroma in a murine model of *Onchocerca volvulus* keratitis (river blindness). *Infection and Immunity* 77(4): 1606–1612.

Gillette-Ferguson, I., Daehnel, K., Hise, A. G., et al. (2007). Toll-like receptor 2 regulates CXC chemokine production and neutrophil recruitment to the cornea in Onchocerca volvulus/*Wolbachia*-induced keratitis. *Infection and Immunity* 75: 5908–5915.

Gillette-Ferguson, I., Hise, A. G., McGarry, H. F., et al. (2004). *Wolbachia*-induced neutrophil activation in a mouse model of ocular onchocerciasis (river blindness). *Infection and Immunity* 72: 5687–5692.

Higazi, T. B., Filiano, A., Katholi, C. R., et al. (2005). *Wolbachia* endosymbiont levels in severe and mild strains of *Onchocerca volvulus*. *Molecular and Biochemical Parasitology* 141: 109–112.

Hise, A. G., Daehnel, K., Gillette-Ferguson, I., et al. (2007). Innate immune responses to endosymbiotic *Wolbachia* bacteria in *Brugia malayi* and *Onchocerca volvulus* are dependent on TLR2, TLR6, MyD88, and Mal, but not TLR4, TRIF, or TRAM. *Journal of Immunology* 178: 1068–1076.

Hoerauf, A. (2008). Filariasis: New drugs and new opportunities for lymphatic filariasis and onchocerciasis. *Current Opinion in Infectious Diseases* 21: 673–681.

Hoerauf, A., Mand, S., Adjei, O., Fleischer, B., and Buttner, D. W. (2001). Depletion of *Wolbachia* endobacteria in *Onchocerca volvulus* by doxycycline and microfilaridermia after ivermectin treatment. *Lancet* 357: 1415–1416.

Pearlman, E., Johnson, A., Adhikary, G., et al. (2008). Toll-like receptors at the ocular surface. *Ocular Surface* 6: 108–116.

Saint Andre, A., Blackwell, N. M., Hall, L. R., et al. (2002). The role of endosymbiotic *Wolbachia* bacteria in the pathogenesis of river blindness. *Science* 295: 1892–1895.

Taylor, M. J., Bandi, C., and Hoerauf, A. (2005). *Wolbachia* bacterial endosymbionts of filarial nematodes. *Advances in Parasitology* 60: 245–284.

Turner, J., Langley, R. S., Johnston, K. L., et al. (2009). Filarial *Wolbachia* lipoprotein stimulates innate and adaptive inflammatory responses through TLR2 and TLR6 and induce disease manifestations of lymphatic filariasis and river blindness. *Journal of Biological Chemistry* 284: 22364–22378.

Relevant Websites

http://www.a-wol.net – A-WOL – Anti-Wolbachia Consortium.

Immunopathogenesis of Pseudomonas Keratitis

L D Hazlett, Wayne State University School of Medicine, Detroit, MI, USA

Glossary

Akt1 – Also known as Akt or protein kinase B, it is an important molecule in mammalian cellular signaling and inhibits apoptotic processes.
Eicosanoids – Signaling molecules made by oxygenation of 20-carbon essential fatty acids. There are four families of eicosanoids: the prostaglandins, prostacyclins, thromboxanes, and the leukotrienes.
IRF1 (interferon regulatory factor 1) – A member of the interferon regulatory transcription factor family. IRF1 serves as an activator of interferons alpha and beta transcription, and in mouse it has been shown to be required for double-stranded RNA induction of these genes. IRF1 also functions as a transcription activator of genes induced by interferons alpha, beta, and gamma. Further, IRF1 has been shown to play roles in regulating apoptosis and tumor-suppression.
Keratitis – A condition in which the cornea becomes inflamed. The condition is often marked by moderate to intense pain and usually involves impaired eyesight.
LPS (lipopolysaccharide, endotoxin) – Major outer membrane component of Gram-negative bacteria comprising a lipid A core (endotoxin) and polysaccharide of varying length and composition. Toll-like receptor 4 (TLR4) and MD2 (myeloid differentiation 2) bind to the lipid A moiety.
MAPK (mitogen-activated protein kinase) – Serine/threonine-specific protein kinases that respond to extracellular stimuli (mitogens) and regulate various cellular activities, such as gene expression, mitosis, differentiation, and cell survival/apoptosis.
Matrix metalloproteinase-9 (MMP-9) – Gelatinase B, 92 kDa gelatinase, 92 kDa type IV collagenase is a biological enzyme. Proteins of the MMP family are involved in the breakdown of extracellular matrix in normal physiological processes, as well as in disease processes. Most matrix metalloproteinases (MMPs) are secreted as inactive pro-proteins which are activated when cleaved by extracellular proteinases. The enzyme encoded by this gene degrades type IV and V collagens.
NF-κB (nuclear factor-kappa B) – A protein complex that is a transcription factor. NF-κB is found in almost all animal cell types and is involved in cellular responses to stimuli such as stress, cytokines, free radicals, ultraviolet irradiation, and bacterial or viral antigens.
Peroxynitrite – An anion, with the formula $ONOO^-$, it is an unstable valence isomer of nitrate, NO_3^-, which has the same formula but a different structure. Although peroxynitrous acid is highly reactive, its conjugate base, peroxynitrite is stable in basic solution.
SIGIRR (single immunoglobulin interleukin 1 receptor (IL-1R)-related protein) – An inhibitory member of this receptor superfamily. SIGIRR seems to temper cellular activation by IL-1, LPS, and probably other activators of receptors in the TLR–IL-1R superfamily, such that the biological outcome will be the result of a balance between activation by a receptor and dampening by SIGIRR. SIGIRR therefore acts as a brake on the TLR system, which may be essential for regulating the detrimental effects of innate immunity, as occurs in sepsis and chronic inflammation.
siRNA (short interfering RNA or silencing RNA) – A class of 20–25 nucleotide-long double-stranded RNA molecules that play a variety of roles in biology. Most notably, siRNA is involved in the RNA interference pathway, where it interferes with the expression of a specific gene.
T helper (Th) 1 (e.g., predominant IL-12 and interferon gamma production) and Th2 (predominant IL-4, 5, 10, 13) response – Response involving effector T cells that play an important role in establishing and maximizing the capabilities of the immune system.

Introduction

In the United States, microbial keratitis is frequently associated with complications resulting from use of extended wear contact lenses with an incidence of about 30 000 cases annually. The cost of treatment is estimated at between $15 and $30 million, representing a considerable medical and economic impact. Of the bacterial organisms able to induce keratitis, *Pseudomonas aeruginosa* remains an important Gram-negative pathogen. The bacteria is often referred to as opportunistic, as it is capable of inducing keratitis not only in extended wear contact lens users, but

also in more tropical climates, and in patients that are either debilitated or hospitalized. Most of the complications of bacterial keratitis are structural alterations of the cornea, but other sight-threatening problems include development of secondary glaucoma and cataract. These consequences are largely caused by the host's inflammatory response, but the influence of bacterial toxins, exoproducts, and toxicity from antibiotic treatment cannot be overlooked. There is also a recent increase in the incidence of reported antibiotic resistant strains and failure of an initially promising treatment using antimicrobial peptides to manage keratitis, suggesting that better understanding of the pathogenic mechanisms of disease induction by this pathogen will be critical to development of improved therapeutic strategies.

P. aeruginosa, like most other microorganisms, typically requires surface injury to permit corneal invasion. Because it has few nutritional requirements, it can adapt to a variety of ecological conditions and niches, such as preserved ophthalmic solutions and the hospital environment. Pseudomonal and other Gram-negative bacterial infections often present as a rapidly progressing, suppurative stromal infiltrate with a marked mucopurulent exudate. Yellowish coagulative necrosis surrounded by inflammatory epithelial edema is distinctive and stromal ulceration can lead to stromal tissue destruction and vision loss. A ring infiltrate may appear in the surrounding paracentral cornea and hypopyon (a dense inflammatory coagulum) is usually present; in addition, descemetocele (ulcer penetrated through cornea) formation or corneal perforation are not uncommon. Animal models of bacterial keratitis continue to be of value in the study of this disease and are produced by topical bacterial application after abrading the epithelium, by intrastromal inoculation, or by placing a contaminated suture or contact lens on the cornea. These approaches and models have led to increased understanding of the mechanisms of corneal inflammation and innate immunity that are operative in bacterial keratitis.

Bacterial eradication by neutrophils (PMN) involves phagocytosis, lysosomal degranulation and bacterial killing within the acidic lysosomal compartment of the cell. Phagocytosis and intracellular degranulation by PMN also involve oxidative attack, production of toxic oxygen metabolites, triggering of the respiratory burst, biosynthesis of superoxide anions, and other oxidizing agents such as hydrogen peroxide and formation of peroxynitrite. Phagocytic secretion and lysis result in release of extracellular lysosomal enzymes, including, but not limited to, elastase, collagenase and myeloperoxidase (MPO). These enzymes and the oxygen-derived free radicals cause stromal destruction by breaking down collagen, digesting glycosaminoglycans, and disrupting stromal keratocytes. Nitric oxide (NO) also mediates vasodilation and can be important in bacterial killing as well as in bystander tissue damage. These and other substances released from activated PMN and other inflammatory cells (e.g., macrophages, Mϕ) contribute to stromal necrosis and corneal edema during bacterial disease. Bacterial endotoxin and exotoxins also stimulate Mϕ to release biologically active substances including, but not limited to, interleukin (IL)-1, IL-6, and tumor necrosis factor (TNF)-α, cytokines that synergize to elicit inflammatory events. Selected cytokines, certain eicosanoids, and other molecular mediators are also involved in ulceration and angiogenesis during bacterial keratitis.

Maintenance of leukocyte recruitment during inflammation requires intercellular communication between infiltrating leukocytes, the epithelium, neuropeptides such as substance P (SP) and vasoactive intestinal peptide (VIP), vascular endothelium, and resident stromal cells. These events are mediated by generation of early response cytokines (e.g., IL-1), the expression of adhesion molecules such as intercellular adhesion molecule-1, and the production of chemotactic cytokines and chemokines.

PMN, Cytokines, and Chemokines

If leukocytes such as PMN persist within the cornea, destructive pathology ensues, including stromal scarring and perforation, potentially requiring corneal transplantation. PMN infiltration into inflamed tissue is controlled largely by local production of inflammatory mediators. In the mouse, two members of the CXC family of chemokines, MIP-2 (functional homolog of human IL-8) and KC, are potent chemoattractants and activators of PMN. In corneal infections, MIP-2 has been shown to be the major chemokine that attracts PMN into the *P. aeruginosa* infected cornea and persistence of PMN in the cornea of susceptible (cornea perforates) C57BL/6 versus resistant BALB/c (no corneal perforation) mice (Table 1) was found to correlate with higher MIP-2 chemokine levels (both mRNA and protein). IL-1, produced by Mϕ, monocytes, and resident corneal cells also influences PMN infiltration into tissues. When tested, IL-1α and β (mRNA and protein) were elevated in the infected cornea of C57BL/6 over BALB/c mice. Furthermore, after infection, MMP-9 was shown to upregulate chemotactic cytokines/chemokines (IL-1β and MIP-2), contribute to degradation of collagen IV, and overall, enhanced *P. aeruginosa* keratitis. In contrast, neutralization of IL-1β in infected C57BL/6 mice reduced

Table 1 Response to *P. aeruginosa* corneal infection in mice

C57BL/6 (B6)	*BALB/c*
Th1 responder	Th2 responder
Corneal perforation	Corneal healing
IFN-γ, IL-12	IFN-γ, IL-10

disease severity, evidenced by reduction of PMN in cornea (MPO assay), decreased bacterial load, and decreased levels of MIP-2 at both the mRNA and protein levels. The use of caspase 1 (enzyme that processes IL-1β to generate the mature cytokine) inhibitor treatment in C57BL/6 mice confirmed these data, even when inhibitor treatment was initiated 18 h after disease onset. In addition, improvement was augmented when the caspase 1 inhibitor was given after infection together with the antibiotic ciprofloxacin. A live attenuated *P. aeruginosa* vaccine also has been tested and found to elicit outer membrane protein-specific active and passive protection against corneal infection.

T Cells and IL-12

The role of other cells, such as T cells in *P. aeruginosa* corneal infection, was first studied in inbred C57BL/6 wild type and cytotoxic, CD8(+) T deficient, β2 microglobulin knockout mice (on the C57BL/6 background). Corneas of both groups of mice perforated by 7 days post-infection (p.i.) and histopathology was similar, with infiltration of PMN within 24 h p.i. In contrast, corneas of wild-type mice antibody depleted of helper, CD4(+) T cells and infected with *P. aeruginosa* did not perforate at 7 days p.i., versus mice depleted of CD8(+) T cells or treated with an irrelevant antibody. Antibody neutralization of IFN-γ before infecting C57BL/6 mice also prevented corneal perforation and was associated with a lower delayed type hypersensitivity response when compared with C57BL/6 mice similarly treated with an irrelevant antibody. These data support that a CD4(+) T cell T helper type 1 (Th1) dominant response following *P. aeruginosa* infection is associated with genetic susceptibility and corneal perforation in C57BL/6 mice and provided the first evidence that CD4(+) T cells are important in development of severe keratitis and eventual corneal perforation. In addition, use of gene array studies confirmed a Th1 versus Th2 bias of C57BL/6 versus BALB/c mice to infection with *Pseudomonas*. Other studies investigated whether IL-12 (IL-12 p40) was associated with IFN-γ production and the susceptibility response of C57BL/6 mice after *P. aeruginosa* challenge. IL-12 p40 knockout mice (C57BL/6 background) versus wild-type mice were tested to examine disease progression in endogenous absence of the cytokine. When tested, both groups of mice were susceptible to corneal challenge with *P. aeruginosa* and corneal perforation was observed at 5–7 days p.i. Semi-quantitative reverse transcription polymerase chain reaction (RT-PCR) and enzyme-linked immunosorbent assay analyses confirmed that IL-12 p40 message and protein levels were elevated after infection in the wild type over the expected absence of IL-12 p40 in the knockout mouse cornea. Immunostaining for IL-12 in wild-type C57BL/6 mice revealed that stromal PMN were at least one source of the cytokine.

IL-18 and IFN-γ

The role of IL-18 and IFN-γ production in the resistance response of the predominantly Th2 responding BALB/c mouse was also tested. Semi-quantitative RT-PCR detected IFN-γ mRNA expression levels in the cornea of infected mice at 1–7 days p.i. Cytokine levels were significantly upregulated when compared with control, uninfected normal mouse corneas. Using RT-PCR, IL-18 mRNA expression was detected constitutively in the normal, uninfected cornea, but levels were significantly elevated 1–7 days p.i. To test whether IL-18 regulated IFN-γ production, BALB/c mice were injected with an anti-IL-18 monoclonal antibody. Treatment decreased corneal IFN-γ mRNA levels and both bacterial load and disease severity increased when compared to immunoglobulin G injected control mice. Data provided evidence that IL-18 is critical to the resistance response of BALB/c mice by induction of IFN-γ and that IFN-γ is required for bacterial killing/stasis in the cornea. Another separate study showed that the killing effect of IFN-γ was indirect, through regulation of NO levels in the infected cornea.

IFN-γ and SP

Further study of the resistance response in BALB/c mice examined the role of the pro-inflammatory neuropeptide, SP in IFN-γ production. This study provided evidence that natural killer (NK) cells were required to produce IFN-γ; that the cells expressed the neurokinin-1 receptor (NK1R, the major SP receptor); and that they directly and tightly regulated IFN-γ production through SP interaction with this receptor, suggesting a unique link between the nervous system and development of innate immunity in the cornea. On the other hand, a disparate distribution of SP in the infected cornea of susceptible C57BL/6 (higher levels) versus resistant BALB/c (lower levels) mice also has been documented and blocking the interaction of SP with its major receptor (NK1R) in C57BL/6 mice improved disease outcome, supporting a role for SP in development of the susceptible phenotype after *P. aeruginosa* corneal infection. Thus, the amount of SP and its interaction with available NK1R sites after infection contributes either to resistance or susceptibility, and appears an important component of keratitis outcome in these murine models.

Neuropeptides

SP

In this regard, SP involvement in the pathophysiology of inflammatory disease generally has been evidenced by aberrant levels of SP and SP containing nerve fibers,

as well as NK1R, in diseased tissues. SP has been shown to elicit cytokine secretion (IL-2, IL-4, IL-10, and IFN-γ) from mouse T cells. In addition, it was demonstrated that human bronchial epithelial cells produce IL-6, IL-8, and TNF-α after SP treatment. SP-induced cytokine production and secretion by leukocytes, including T cells, Mϕ, and dendritic cells leads to the release of a number of inflammatory mediators such as additional cytokines, oxygen radicals, arachidonic acid derivatives, and histamine, all of which further amplify the inflammatory response.

VIP

Recent studies have also provided ample evidence for another neuropeptide, VIP, functioning as a potent endogenous anti-inflammatory molecule affecting the immune response antithetically when compared to SP. VIP regulates inflammatory mediators via several transduction pathways and transcription factors essential for gene activation, such as nuclear factor-kappa B, interferon regulatory factor-1 (IRF-1), mitogen-activated protein kinase (MAPK), and cAMP response element. VIP downregulates the production of several pro-inflammatory cytokines, including: TNF-α, IL-1, IL-6, IL-12, and IFN-γ, while stimulating production of anti-inflammatory cytokines IL-10, IL-1 receptor (R) antagonist, and TGF-β. Investigation of the effect of VIP in a murine endotoxin challenge model showed that after treatment with VIP, levels of TNF-α and IL-6 in serum and peritoneal fluid were reduced by almost 50%. Regarding the eye, VIP treatment converted the susceptible phenotype (corneal perforation) to resistant (no perforation) in a mouse model of *P. aeruginosa*-induced infection via downregulation of pro-inflammatory mediators, upregulation of anti-inflammatory molecules, and modulation of host inflammatory cell activation. Thus VIP, a 28-amino-acid peptide, delivered by several types of neurons to immune organs and lymphoid tissues in the heart, gastrointestinal tract, lungs, kidney, cornea and skin, is anti-inflammatory. In fact, evidence indicated a differential response to VIP between infected BALB/c (more) and C57BL/6 (less) mice, due to disparate VIPR1 expression by Mϕ (which can be induced in a dose-dependent manner by VIP itself). Mϕ are known to play a key role in regulating/balancing pro- and anti-inflammatory activity in the resistant (BALB/c) and susceptible, C57BL/6 murine models; therefore, evidence that VIP influences the functional behavior of these cells further supports a more salient role for this neuropeptide in regulating the inflammatory response.

TLR

Mouse eye infection models have also been used to study the role of Toll receptors in disease. The Toll family of receptors, conserved throughout evolution from flies to humans, is central in initiating innate immune responses. This family of receptors, composed of trans-membrane molecules, links the extracellular compartment where contact and recognition of microbial pathogens occurs and the intracellular compartment, where signaling cascades leading to cellular responses are initiated. Gene array data showed that the expression of TLRs and related molecules including CD14, soluble IL-1 receptor antagonist, TLR-6, and IL-18R-accessory-protein were significantly elevated in susceptible (C57BL/6) versus resistant (BALB/c) mice following challenge with *P. aeruginosa*. In another model system involving induction of sterile keratitis, when C3H/HeJ (Toll-like receptor 4, TLR4, point mutation) versus control mice were treated with lipopolysaccharide (LPS) from *P. aeruginosa,* a significant increase in stromal thickness and haze was seen in the cornea of TLR4 sufficient control, but not in TLR4 deficient mutant mice. The severity of disease coincided with PMN stromal infiltration, indicating that TLR4 signaling enhances corneal disease. In contrast, in a bacterial keratitis model, TLR4 mRNA expression was markedly increased in the cornea of resistant BALB/c mice after bacterial infection. These data led to testing corneas from TLR4-deficient and wild-type control (BALB/c) mice after challenge with live *P. aeruginosa* to determine the role of TLR4 in bacterial keratitis. Given that TLR4 deficiency was suggested to be protective in sterile keratitis, we might predict that corneas of TLR4-deficient mice would be less susceptible and exhibit a decreased inflammatory response to bacterial infection. In marked contrast, TLR4-deficient versus control mice exhibited significantly increased inflammation and corneal perforation instead of healing after infection. Furthermore, data from clinical score, slit lamp, and histopathology confirmed that TLR4-deficient versus wild-type control mice exhibited significantly increased corneal disease with more opacity and more severe stromal swelling and destruction. In addition, bacterial load (more than 10-fold higher) and PMN recruitment (MPO activity) were markedly upregulated in the infected cornea of TLR4-deficient versus TLR4-sufficient control mice. The data provide strong evidence that TLR4 is required for the resistance response of BALB/c mice to *P. aeruginosa* challenge and, unlike the sterile keratitis model, TLR4 is required for disease resolution in bacterial keratitis.

Overall, it appears conflicting that TLR4 is critical in the pathology of corneal disease in sterile keratitis, while it is protective in bacterial keratitis and required for host resistance. In fact, these data illustrate the characteristic double-edge sword activity of TLR4 activation. On the one hand, in the keratitis model, TLR4 recognized LPS, a component of *P. aeruginosa,* and initiated an innate immune response that was important for bacterial clearance. TLR4 deficiency impaired bacterial clearance, led

to overgrowth of bacteria, an overwhelming PMN infiltrate and excessive pro-inflammatory cytokine production. This in turn contributed to corneal destruction and perforation. In the sterile keratitis model, activation of LPS-TLR4 signaling in TLR4 sufficient mice, lead to pro-inflammatory cytokine production and PMN infiltration, increased stromal thickness and contributed to haze production which increased, albeit transiently, corneal perturbation when compared with TLR4 mutant mice.

Negative regulators of TLR are also of importance and recent evidence showed that one of them, single immunoglobulin IL-1R related molecule is differentially expressed in BALB/c (resistant) versus C57BL/6 (susceptible) mice. This Toll receptor is critical in resistance to *P. aeruginosa* infection in BALB/c mice, functioning to downregulate type 1 immunity and negatively regulating sustained IL-1 and TLR4 signaling. siRNA treatment to knockdown TLR9 was also found to influence the outcome of bacterial keratitis, and lead to reduced inflammation, but with the unwanted effect of decreased bacterial killing.

Apoptosis

Delay in apoptosis in bacterial keratitis, as evidenced by terminal deoxynucleotidyl transferase dUTP nick end labeling (TUNEL) staining, also contributes to corneal perforation in C57BL/6 mice. Consistent with this finding, Bcl-2, an anti-apoptotic gene, was significantly upregulated in C57BL/6 mouse cornea at 18 h p.i., suggesting that the delayed onset of apoptosis in C57BL/6 mouse cornea may be, in part, due to upregulation and signaling of this gene. These data are also consistent with previous studies showing that over-expression of Bcl-2 reduces lymphocyte apoptosis in *P. aeruginosa*-induced pneumonia.

In the process of apoptosis, execution of cells largely depends on proteolytic cleavage and activation of caspase 3. In this regard, BALB/c versus C57BL/6 mouse cornea expressed more intense staining for activated caspase 3 at 1 day p.i. compared to the delayed peak intensity in C57BL/6 mice. The two mouse groups were also disparate for expression of caspase 9, with significantly more mRNA expression in BALB/c over C57BL/6 mice. Although only hypothetical, these data suggest that different pathways of apoptosis may be operative in the infected cornea of the two groups of mice. Our studies, using a combination of TUNEL and immunostaining, as well as PMN depletion, also provided evidence that the corneal apoptotic cells identified in both groups of mice were predominantly PMN and confirmed that apoptosis of these cells is delayed in C57BL/6 mice. We hypothesize that earlier apoptosis of PMN in resistant BALB/c mice is consistent with effective elimination of invading bacteria, while inducing minimal tissue damage due to unresolved and persistent inflammation.

Neuropeptides

The balance between apoptosis and cell survival, as well as the tissue milieu and timing of apoptosis, is critical in immune defense. In this regard, the neuropeptide SP, mentioned above, is a potent anti-apoptotic regulator and can exacerbate inflammation.

SP has been shown to stimulate phosphorylation of the anti-apoptotic molecule Akt in colonic mucosa both *in vivo* and *in vitro*, preventing apoptosis in humans with colitis. In another *in vitro* study, SP induced p53, Bcl-2, and NO expression in peritoneal Mϕ, blocking apoptotic signals. SP delays spontaneous apoptosis of PMN in a dose-dependent fashion by its interaction with the NK1R *in vitro*, and this effect could be inhibited by application of the NK1R antagonist GR82334.

In this regard, C57BL/6 mice treated with another NK1R antagonist, Spantide I, showed significantly improved disease outcome and an earlier onset of apoptosis, similar to the pattern observed in naturally resistant BALB/c mice. Consistent with earlier onset of apoptosis, mRNA expression of caspase 3 was also significantly upregulated earlier in the cornea of Spantide I, versus control treated animals. The data suggest that the protective mechanism of Spantide I treatment in C57BL/6 mice involves induction of earlier PMN apoptosis in the infected cornea, with less bystander tissue damage. Whether in C57BL/6 mice, the effects of Spantide I are directly mediated via the PMN or indirectly through Mϕ regulation of PMN also required resolution. Clodronate depletion of Mϕ with or without Spantide I treatment revealed that in the absence of the Mϕ, apoptosis was reduced/absent in the cornea. To further explore the role of this cell in susceptibility and resistance, Mϕ from both groups of mice (C57BL/6 and BALB/c) were incubated in the presence of SP together with LPS or with LPS alone. Significantly fewer apoptotic cells were detected in cells from C57BL/6 mice in the presence of SP and LPS versus LPS alone, while the same combined treatment (SP and LPS) did not decrease the number of LPS induced apoptotic Mϕ from BALB/c mice. To determine the mechanism for the disparate response to SP treatment between Mϕ from the two mouse groups, expression levels of the NK1R were comparatively tested. Although cells from both groups expressed the receptor, with a slightly weaker signal in BALB/c cells, after LPS stimulation, mRNA expression for the NK1R was only detected in cells from C57BL/6 mice. These data suggest that the possible mechanism for the absence of the anti-apoptotic effects observed in BALB/c Mϕ after SP treatment may involve a low level of NK1R expression on the cells and possible rapid depletion of the receptor upon LPS stimulation. In this regard, VIPR1, the major receptor for the neuropeptide VIP, was also reported to be expressed disparately in Mϕ from C57BL/6 (less) versus BALB/c (more) mice.

Figure 1 *P. aeruginosa* infection in Marmoset monkey model.

Mϕ also may provide distinct activation signals for Th1/Th2 differentiation. In this regard, others have reported that *Leishmania major* infected Mϕ enhanced the proliferation and IL-4 secretion of Th2 T cells, but inhibited the response of Th1 T cells. When testing for this possibility, we detected that Mϕ from C57BL/6 mice expressed significantly more IL-12, while BALB/c Mϕ expressed more IL-10 after LPS stimulation. IL-10 appears protective in the BALB/c infected cornea, as after subconjunctival injection of clodronate-containing liposomes to deplete these cells, higher levels of IFN-γ and lower levels of IL-10 were detected and resistant mice were converted to the susceptible phenotype. It was also reported that VIP treated C57BL/6 mice showed improved disease outcome and increased IL-10 expression after *P. aeruginosa* corneal infection. Furthermore, the data suggest that SP, which acts in an anti-apoptotic manner toward activated C57BL/6 mouse Mϕ, may also enhance an IL-12 driven, Th1 type immune response and thus further contribute to the susceptibility of this mouse strain to *P. aeruginosa* infection.

New Animal Model

Without doubt, experimental animal models of bacterial infection with *P. aeruginosa* have provided us with important insights into mechanisms underlying ocular infection and inflammation and our understanding of the effector and regulatory mechanisms involved in disease continues to grow. However, our understanding and knowledge of the precise mechanisms operative in human cases of keratitis (sterile and infectious) remains much more limited. In this regard, development of a new primate model of keratitis would be a timely and important translational approach to facilitate eventual human application of what has been learned in rodent and other species. The Marmoset monkey, with 98% homology to the human genome, provides such a model. Initial studies have been undertaken in the monkey and show that with scarification of the cornea (similar to that done in the mouse), infection can be initiated and progresses similar to the human pattern. A photograph of the new animal model is provided in Figure 1. This model will allow us to explore treatment paradigms that have been efficacious in the mouse and other rodent species and may more quickly result in clinical trial of successful candidates.

See also: Corneal Epithelium: Response to Infection.

Further Reading

Delgado, M., Pozo, D., and Ganea, D. (2004). The significance of vasoactive intestinal peptide in immunomodulation. *Pharmacological Reviews* 56(2): 249–290.

DeVane, L. The fibromyalgia community, substance P: A new era, a new role. http://fmscommunity.org/subp.htm (accessed June 2009).

Dinarello, C. A. (2005). Blocking IL-1 in systemic inflammation. *Journal of Experimental Medicine* 201(9): 1355–1359.

Ferguson, T. A. and Griffith, T. S. (2007). The role of Fas ligand and TNF-related apoptosis-inducing ligand (TRAIL) in the ocular immune response. *Chemical Immunology and Allergy* 92: 140–154.

Harrison, S. and Geppetti, P. (2001). Substance P. *International Journal of Biochemistry and Cell Biology* 33(6): 555–576.

Hazlett, L. D. (2004). Corneal response to *Pseudomonas aeruginosa* infection. *Progress in Retinal and Eye Research* 23(1): 1–30.

Janeway, C. A., Jr. and Medzhitov, R. (2002). Innate immune recognition. *Annual Review of Immunology* 20: 197–216.

Kernacki, K. A., Barrett, R. P., Hobden, J. A., and Hazlett, L. D. (2000). Macrophage inflammatory protein-2 is a mediator of polymorphonuclear neutrophil influx in ocular bacterial infection. *Journal of Immunology* 164(2): 1037–1045.

Lighvani, S., Huang, X., Trivedi, P. P., Swanborg, R. H., and Hazlett, L. D. (2005). Substance P regulates natural killer cell interferon-gamma production and resistance to *Pseudomonas aeruginosa* infection. *European Journal of Immunology* 35(5): 1567–1575.

McClellan, S. A., Huang, X., Barrett, R. P., van Rooijen, N., and Hazlett, L. D. (2003). Macrophages restrict *Pseudomonas aeruginosa* growth, regulate polymorphonuclear neutrophil influx, and balance pro- and anti-inflammatory cytokines in BALB/c mice. *Journal of Immunology* 170(10): 5219–5227.

Meek, B., Speijer, D., de Jong, P. T., de Smet, M. D., and Peek, R. (2003). The ocular humoral immune response in health and disease. *Progress in Retinal and Eye Research* 22(3): 391–415.

Rudner, X. L., Kernacki, K. A., Barrett, R. P., and Hazlett, L. D. (2000). Prolonged elevation of IL-1 in *Pseudomonas aeruginosa* ocular infection regulates macrophage-inflammatory protein-2 production, polymorphonuclear neutrophil persistence, and corneal perforation. *Journal of Immunology* 164(12): 6576–6582.

Strand, F. L. (1999). *Neuropeptides: Regulators of Physiological Processes.* Cambridge, MA: MIT Press.

Substance P: A modulator of inflammation. (1998). http://www.woongbee.com/Cytokine/Cytokine%20bulletin/Spring%201998/spring1998-3.htm (accessed June 2009).

Szliter, E. A., Lighvani, S., Barrett, R. P., and Hazlett, L. D. (2007). Vasoactive intestinal peptide balances pro- and anti-inflammatory cytokines in the *Pseudomonas aeruginosa*-infected cornea and protects against corneal perforation. *Journal of Immunology* 178(2): 1105–1114.

Taylor, P. R., Martinez-Pomares, L., Stacey, M., et al. (2005). Macrophage receptors and immune recognition. *Annual Review of Immunology* 23: 901–944.

Todar, K. (2008). *Todar's Online Textbook of Bacteriology: Immune Defense against Bacterial Pathogens: Innate Immunity*. http://textbookofbacteriology.net/innate.html (accessed June 2009).

Winkler, J. D. (ed.) (1999). *Apoptosis and Inflammation.* Basel: Birkhauser Verlag.

Relevant Websites

http://www.diseasesdatabase.com – Diseases Database Ver 1.8; Medical lists and links Diseases Database, Vasoactive Intestinal Peptide.

http://www.macrophages.com – Macrophages.com.
http://users.rcn.com – RCN Corporation: Apoptosis.
http://users.rcn.com – RCN Corporation: Innate Immunity.
http://www.ResearchApoptosis.com – Research Apoptosis.

Immunosuppressive and Anti-Inflammatory Molecules that Maintain Immune Privilege of the Eye

A W Taylor, Schepens Eye Research Institute, Boston, MA, USA

Glossary

Adaptive Immunity – The part of the immune system utilizing T cells and B cells that adapt to specifically target, eliminate, and prevent pathogenic infections. Through adaptive immunity, immunological memory is established to further adapt immunity to mount stronger responses each time the pathogen is encountered.

Immune homeostasis – The state of immunity in a stable, unperturbed tissue environment.

Immune privilege – The immune status of the ocular microenvironment that has evolutionally adapted itself to prevent the induction of excess inflammation, thereby protecting its delicate structures from the damages of inflammation. It is also defined as any tissue site, such as the brain and eye, which affords survival of incompatible grafts without immunosuppressive therapy.

Innate immunity – A more primitive defensive mechanism against infecting pathogens. The activation of innate immunity is through pathogen-associated molecules that bind specific recognition receptors on innate immune cells. Innate immunity is associated with phagocytosis, complement activation, and infiltration of neutrophils and macrophages.

Neuropeptides – The low-molecular-weight proteins that are found in, and released from, centrally derived neurons; however, their production is not limited to neurons. They are produced by cells of endocrine glands, immune cells, and cells that make up immune-privileged tissue microenvironments.

Immunosuppression and Anti-Inflammatory Activity in Aqueous Humor

The immune-privileged microenvironment of the eye suppresses the induction of inflammation. One of the most dominant mechanisms of this suppression, by which the immune-privileged eye prevents induction of inflammatory immunity, is the manipulation of the functionality of immune cells that enter the ocular microenvironment. A well-characterized set of neuropeptides that targets specific immune cells and their activities mediates this manipulation. The result of this immunosuppression and immunoregulation is the induction of immune cells that are not only prevented from expressing proinflammatory functionalities, but also regulate other immune cells. The regulatory activity itself is not unique; it occurs at the resolution of immune responses and is part of the mechanisms that prevent the induction of autoimmunity. These are the mechanisms of immune homeostasis that tailor the immune response, and prevent uncontrolled immunity. What is unique is that within the ocular microenvironment these mechanisms are constantly active, and are mediated by constitutively present soluble factors that provide the eye with its unique form of immune homeostasis.

Over the past two decades, we have come to understand that the ocular microenvironment is rich with immunosuppressive molecules that influence the activity of immune cells. Many of these molecules are found in the aqueous humor. The first indication that soluble mediators in the eye manipulate the function of immune cells was the finding that aqueous-humor-treated macrophages process and present antigen in a manner that promotes activation of suppressor T cells. This activity is associated with a phenomenon of systemic antigen-specific immunosuppression induced by placing an antigen into the anterior chamber of the eye. This phenomenon is called anterior-chamber-associated immune deviation (ACAID), which may be responsible for the highly successful acceptance of corneal grafts, and may be important in the survival of ocular stem cell and retinal transplants.

Macrophages and dendritic cells stimulated with bacterial products that activate innate immune-mediated inflammation fail to mediate inflammation when they are treated with aqueous humor. The expected promotion of macrophages and dendritic-cell-antigen-presenting cell functionality to promote proinflammatory T-cell activation are also suppressed by aqueous humor treatment. Moreover, aqueous-humor-treated macrophages and dendritic cells produce anti-inflammatory cytokines, and present antigens in a manner that promotes immune regulation. Therefore, resident ocular macrophages and dendritic cells, while still able to respond to infectious agents and unhealthy cells, are inhibited from mediating an inflammatory response. It is not completely understood how aqueous humor manipulates the functionality of macrophages. It is possible that ocular resident macrophages function perfectly well in

clearing and defending the ocular microenvironment from a pathogen, but cannot recruit other immune cells to help control the infection through inflammation, or to mediate an effective wound response.

T cells treated with aqueous humor are inhibited in proliferation, cytotoxic activity, and production of proinflammatory cytokines. The $CD4^+$ T cells treated with aqueous humor are not only suppressed in their production of the proinflammatory cytokine interferon-gamma (IFN-γ), but they also produce the regulatory cytokine, transforming growth factor-beta (TGF-β). This change in cytokine production is associated with a change in T-cell functionality from inflammatory to regulatory. The resistance of the ocular microenvironment to the activation of inflammation mediated by T cells is seen when T cells that mediate delayed-type hypersensitivity are placed into the anterior chamber of the eye along with antigen and antigen-presenting cells. These T cells normally mediate inflammation if injected into the skin, a conventional immune site, with their antigen and antigen-presenting cells; however, in the anterior chamber, the T cells do not mediate inflammation. In addition, treating the T cells *in vitro* with aqueous humor and then transferring them into the skin fails to produce inflammation. Moreover, aqueous-humor-treated T cells function as regulatory T cells that can suppress the activation of other hypersensitivity-mediating T cells. Therefore, the constitutive immunoregulation and immunosuppressive soluble factors of aqueous humor prevent the activation of inflammatory immunity while turning the immune response onto itself to further regulate the immune response within the immune-privileged ocular microenvironment.

There is an ever-growing list of identified factors in aqueous humor that have the potential to suppresses and regulate immunity (**Table 1**). Neuropeptides form a major group of these factors and most of these factors are found throughout the eye, suggesting that they regulate immunity in all tissue sites of the ocular microenvironment. The factors important for the regulation of T-cell activation and innate immunity in aqueous humor are TGF-β, alpha-melanocyte-stimulating hormone (α-MSH), calcitonin-gene-related peptide (CGRP), somatostatin (SOM), and vasoactive intestinal peptide (VIP) (**Figure 1**). Other factors, such as Fas ligand (FasL), maybe important in eliminating activated T cells within the ocular microenvironment, and factors such as macrophage migration inhibitory factor (MIF), and complement inhibitors are important in the regulation of innate immunity. In addition to neuropeptides, the retina produces thrombospondin-1 (TSP-1), and pigment epithelium-derived factor (PEDF), which influence the activation and regulation of immunity. It is the collective activity of these molecules within an intact blood–ocular barrier that maintain the unique immune homeostasis of the ocular microenvironment, a process called immune privilege.

Table 1 Immunoregulating and immunosuppressive factors of ocular immune privilege

Immune response	*Regulation*	*Factors*
Innate immune-mediated inflammation[a]	Suppression	α-MSH, CGRP, PEDF, MIF, CRP[e]
Adaptive immune-mediated inflammation		
APC[b]	Suppression	α-MSH, CGRP, VIP, TGF-β2
T cell[c]	Suppression	TGF-β2, α-MSH, VIP, SOM, FasL
Regulatory immunity		
ACAIDogenic APC[d]	Induce	TGF-β2, TSP-1
Treg cells	Induce	α-MSH, TGF-β2, SOM

[a]Production of proinflammatory cytokines and antimicrobial molecules induced by bacterial products or by interleukin-1 and tumor necrosis factor.
[b]Assayed for APC activation of hypersensitivity-mediating T cells.
[c]Assayed for antigen-stimulated T-cell production of proinflammatory cytokines, proliferation, cytotoxic activity, and survival.
[d]Assayed in an adoptive transfer of treated APC for induction of immune deviation.
[e]Complement regulatory proteins.

The Immunoregulatory and Immunosuppressive Factors of The Immune-Privileged Eye

Transforming Growth Factor-Beta

TGF-β was the first identified immunosuppressive factor in aqueous humor. While it is common to discuss TGF-β in a generic manner, the most interesting aspect of the TGF-β produced in the eye is that a single isoform, TGF-β2, is the dominant form found in aqueous humor, with very little of the other forms of TGF-β being present in the aqueous humor. The dominant expression of TGF-β2 over the other isoforms of TGF-β is a common feature of neurological tissues. The significance of expressing TGF-β2 over the other isoforms of TGF-β is not known. In addition, TGF-β is normally expressed in a latent form, requiring activation by other enzymes or binding proteins. It is through TGF-β2 that aqueous humor induces ACAID-mediating antigen-presenting cells (APCs). Treating macrophages *in vitro* with TGF-β2 induces the characteristics of the aqueous-humor-induced and the *in-vivo*-induced ACAID APCs. When exposed to TGF-β2, the macrophages increase their expression of the surface marker F4/80, and have reduced expression of co-receptors needed in T-cell activation. The macrophages express anti-inflammatory cytokines of interleukin-10 (IL-10) and activated TGF-β. The activated TGF-β production by the macrophages is probably associated with an

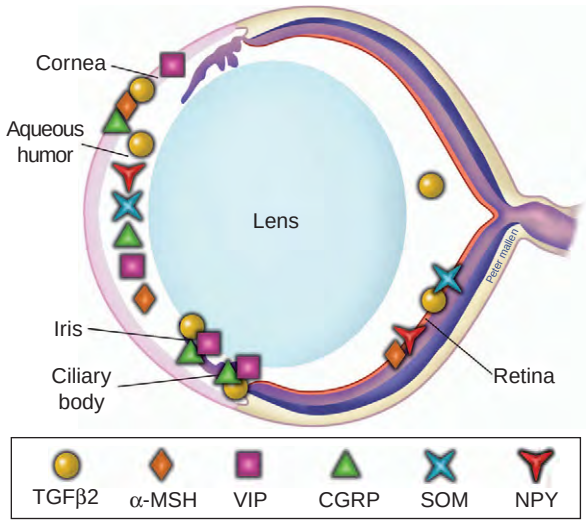

Figure 1 Distribution of soluble immunomodulating proteins in the eye. TGF-β, transforming growth factor-beta; α-MSH, alpha-melanocyte-stimulating hormone; VIP, vasoactive intestinal peptide; CGRP, calcitonin-gene-related peptide; SOM, somatostatin; NPY, neuropeptide Y. Adapted from Taylor, A. W. (2009). Neuropeptides, aqueous humor, and ocular immune privilege. In: Troger, J., Kieselbach, G., and Bechrakis, N. (eds.) *Neuropeptides in the Eye*, pp. 79–91. Research Signpost, Kerala, India.

autocrine pathway involving TSP-1. This induction of ACAID-inducing APCs is not limited to the anterior chamber and aqueous humor. Injecting antigen into the retina induces a similar immune deviation involving TGF-β and TSP-1 as well. While the phenomenon of ACAID is an antigen-specific systemic immunosuppression initiated by ACAIDogenic APCs that migrate to the spleen, it is not clear how these APCs may function within the ocular microenvironment. Macrophages or dendritic cells that take up residence with the ocular microenvironment will likely be exposed to some level of activated TGF-β2, and as a result, they express low levels of molecules that promote T-cell action, and simultaneously produce anti-inflammatory cytokines. There is evidence to support this hypothesis. Expression of antigen-presenting molecules within the ocular microenvironment is rarely detected. However, the expression of anti-inflammatory cytokines, such as IL-10, has not been found in abundance in normal aqueous humor. This suggests that while the presentation of antigen by resident APCs in the eye is impaired by TGF-β, other functionalities induced by TGF-β *in vitro* may not occur within the ocular microenvironment. Some of the suppression of T-cell activation by aqueous humor may involve TGF-β2; however, neutralization of TGF-β2 in aqueous humor does not eliminate all of the T-cell suppression by aqueous humor. Aqueous-humor-treated T cells function as regulatory T cells, which produce TGF-β and suppress the action of other T cells. Therefore, it appears that one of the effects of TGF-β2 in the ocular microenvironment is the suppression of antigen presentation that promotes inflammatory T-cell activation. If there is activation, it results in the generation of immune cells that produce additional TGF-β that further promotes immune privilege.

Alpha-Melanocyte-Stimulating Hormone

The neuropeptide α-MSH is a 13-amino-acid-long neuropeptide that is derived from sequential endoproteolytic cleavage and post-translational modifications of the protein proopiomelanocortin (POMC) hormone. Originally described for its melanin-inducing activity in frogs, α-MSH has a fundamental role in modulating inflammatory responses. Injections of α-MSH suppress systemic inflammatory responses to endotoxin, and proinflammatory cytokines such as IL-1 and tumor necrosis factor (TNF). Its anti-inflammatory activity is greatest on macrophages, dendritic cells, and neutrophils where it can suppress the induction of reactive oxygen intermediates, nitric oxide, proinflammatory cytokine production, and immune cell migration. It also enhances its own receptor expression and production in macrophages, which in turn, promotes an anti-inflammatory autocrine loop. α-MSH also induces IL-10 production by macrophages and dendritic cells. The anti-inflammatory activity of aqueous humor resembles the anti-inflammatory activity of α-MSH. α-MSH is constitutively present in the aqueous humor in pg ml^{-1} amounts that are highly anti-inflammatory. In aqueous humor, α-MSH has two roles: it suppresses proinflammatory cytokine production by endotoxin-stimulated macrophages and it induces regulatory activity in T cells. While α-MSH suppresses proinflammatory cytokine production, it does not affect antigen presentation other than causing the APCs to present antigen in a manner that does not promote inflammatory T-cell activation. α-MSH-treated macrophages that are stimulated with endotoxin have their intracellular signaling pathway from endotoxin-bound receptors blocked by α-MSH treatment. Thus, instead of a classically activated macrophage producing proinflammatory cytokines and anti-microbial molecules, it produces anti-inflammatory cytokines. This suggests that the ocular microenvironment has a pathway to clear microbial molecules or pathogens without inducing an inflammatory response. Whether this is an effective process is yet to be confirmed.

The effect of aqueous humor α-MSH on T cells is profound. It is possible to change an antigen-specific proinflammatory T-cell response to an antigen-specific regulatory T-cell response by treating T cells with aqueous humor or with α-MSH. In this process, TGF-β2 helps in promoting α-MSH induction of regulatory activity in T cells. Flow cytometric analysis of the α-MSH-treated T cells has shown that they express the regulatory T-cell marker CD25 and that this activity is limited to $CD4^+$

T cells. Unlike other types of regulatory T cells, TGF-β is the only cytokine that appears to be produced by these α-MSH-induced regulatory T cells. Such regulatory T cells can be generated *in vitro* and used in adoptive transfer experiments to show that they require antigen specificity to activate their suppressive functionality. When their antigen specificity is for retinal autoantigens, they can be used to suppress autoimmune uveitis, and promote retinal allograft survival. Recently, it has been reported that mice that naturally recovered from autoimmune uveitis produce regulatory $CD4^+$ T cells that are specific for retinal autoantigens. Importantly, such $CD4^+$ T-regulatory cells are not detected in mice that do not require the receptor for α-MSH on their T cells. There are four α-MSH receptors that are differentially expressed on immune cells. For T cells, it is the melanocortin 5 receptor (MC5r) that is required for α-MSH to induce regulatory T-cell activity. Interestingly, the retinas of post-experimental autoimmune uveitis (EAU) mice, which do not express MC5r, are severely damaged with losses in photoreceptors. This severe damage is not seen in normal post-EAU mouse retinas. The retina itself also expresses MC5r, and there is evidence that the melanocortin family of proteins is needed for normal ocular development. This suggests that α-MSH, which is produced by several layers of cells in the retina, is important for healthy retinal development, survival, and immune privilege. It has been proposed that immune privilege is an evolutionary adaptation to protect the eye from inflammation, and α-MSH may be one these adaptations of a molecule originally used for other purposes, but now has the added role of being immunosuppressive and immunoregulatory.

Other Neuropeptides

Three neuropeptides were examined for their presence, and a possible role in aqueous humor immunosuppression because they are found in the neurons that innervate the anterior chamber and some are produced by neural cells of the retina. SOM, CGRP, and VIPs are constitutively present in aqueous humor in ng ml^{-1} amounts, are expressed in the retina, and target different cells of the immune response.

While SOM is found in aqueous humor, its presence was not required for aqueous-humor-mediated immunosuppression. We discovered that SOM induced α-MSH production in T cells that in turn caused the T cells to become regulatory T cells. Therefore, SOM contributes to immune privilege by further promoting production of anti-inflammatory and immunoregulating factors by immune cells. There are some contradictory findings regarding the role of SOM in the retina. A protein produced by a retinal pigment epithelial (RPE) cell called PEDF was found to suppress the induction of inflammatory activity in macrophages. However, this suppression was countered by SOM. Activating macrophages by treatment with RPE-derived factors results in enhanced nitric oxide production, yet the macrophages continue to produce anti-inflammatory cytokines. The meaning for this contradictory finding is not clear. It is possible that macrophages are alternatively activated within the retina and possibly in other tissue sites of the ocular microenvironment.

The role of VIP in immune privilege still remains a bit of a mystery. This neuropeptide is in aqueous humor, and it suppresses the activation and proliferation of T cells; however, it does not induce regulatory T cells. The suppression of T-cell proliferation by VIP is only 50%, and there is some speculation that selected populations of T cells are responsive to VIP. Therefore, it is possible that whole aqueous humor selectively expands a subpopulation of T cells that is not responsive to VIP. Maybe these are the regulatory T cells. VIP receptors are present on macrophages, but there is nothing known about the role of aqueous humor VIP on antigen presentation, and on inflammatory activity of macrophages. One problem is that it is not clear whether VIP exists in the ocular microenvironment as a whole molecule or as immunoreactive functional peptide. It is possible that in aqueous humor, or in other regions of the ocular microenvironment, different types of VIP fragments are present and affect different target cells and have different effects on immunity. Whether it is a whole polypeptide or a fragmented peptide, VIP is a contributing factor to the immunosuppression seen within the immune-privileged eye.

Unlike the other neuropeptides in aqueous humor, GCRP does not target T cells, but instead, influences macrophage activity. Most mature T cells are unresponsive to CGRP. The CGRP in aqueous humor suppresses nitric oxide generation by macrophages that have been stimulated with endotoxin and IFN-γ. Neutralization of CGRP activity in aqueous humor also eliminates aqueous-humor-mediated suppression of nitric oxide production by inflammatory macrophages. The concentration of CGRP in healthy aqueous humor is 20-fold less than its concentration in uveitic aqueous humor. At the higher concentration found in uveitic eyes, CGRP has no effect on inflammatory macrophage function. This suggests that in normal conditions, there is a specifically maintained concentration of CGRP for immunosuppression. Studies on CGRP in aqueous humor have brought to light several issues about the homeostatic environment of the immune-privileged ocular microenvironment. The immune-privileged ocular microenvironment needs to not only maintain a constitutive level of a specific set of factors, but also must maintain them at physiological and functional concentrations.

Other Molecules

There are several publications that individually describe the immunosuppressive activity of proteins that are not

always considered immunosuppressive. Two that have already been discussed above, PEDF acting as an anti-inflammatory cytokine, and TSP-1 being important in TGF-β activation and in the process of ACAID, are usually considered anti-angiogenic factors. Their regulation of angiogenesis may be their main function within the eye, but may have evolved like α-MSH, also to function as an immunoregulatory factor. The inflammatory cytokine, macrophage MIF, was considered an important molecule produced by activated T cells to keep macrophages migrating from sites of inflammation. In the eye it has been found to be constitutively expressed in aqueous humor and has a role in preventing natural killer (NK) cells from killing cells not expressing major histocompatibility complex (MHC) antigens. Transformed and injured cells express altered or reduced MHC class I antigens on their surface, and NK cells see this as signal to kill the cell. Since MHC class I molecules are expressed at low levels within the ocular microenvironment, the presence of MIF protects these cells from NK cell attack. The regulation of NK cells and inflammatory macrophages is part of the ocular microenvironment that controls innate immunity. Another component of innate immunity is the complement cascade pathways that release protein fragments that induce migration and activation of immune cells, vascular leakage, and cellular lysis. There are constitutively expressed inhibitors of complement within the eye. In aqueous humor, there are two inhibitors that prevent activation of the alternative complement pathway. Although complement inhibitors are present in the eye, there is evidence that complement activation maybe occurring at a low level that might be necessary to maintain normal aqueous flow.

Finally, there is the expression of FasL, a membrane-bound immunosuppressive molecule that is expressed by cells throughout the ocular microenvironment. When FasL binds to Fas, a molecule on activated immune cells, it triggers programmed cell death. It has been suggested that it is a major contributor to immune privilege and is necessary for graft survival within the ocular microenvironment. However, its expression has not explained the finding that FasL expression can induce neutrophil activation and destruction of corneal grafts. Recently, there is some evidence that FasL exists as a soluble molecule in aqueous humor, and that soluble FasL may block neutrophil activation, and act as an immunosuppressive molecule. This could mean that the balance between soluble FasL and membrane-bound FasL is what is important for maintaining immune privilege in the eye. In addition, surviving allografts of other tissues when engineered to express FasL promote induction of graft-specific regulatory T cells. While expression of FasL may keep activated immune cells at bay, it could be a selective element within ocular microenvironment promoting activation of regulatory immune cells.

Application of the Lessons of Immune Privilege

The rapidly expanding discoveries of the mechanisms of immune privilege demonstrate that within the ocular microenvironment are active processes for suppressing inflammatory immunity, promulgating alternative activation of immune cells, and mediating regulatory immunity are present. Many of these mechanisms are normally found at various phases of a conventional immune response, especially in the resolution phase, and it appears that the responsiveness of the immune cells to the ocular immunosuppressive and immunoregulating mechanisms is the same whether the cells are taken from the eye or from other tissues. Therefore, it is becoming clear that such mechanisms of ocular immune privilege can be imposed onto immunity to prevent, cure, and establish or reestablish immune tolerance in various hypersensitivity responses, autoimmune diseases, and prevent allograft rejection in tissues other than just the eye. The mechanisms of ACAID and α-MSH-mediated suppression of immunity have been used to demonstrate the potential of applying the lessons of ocular immune privilege as a therapy.

The therapeutic approaches for both mechanisms are direct applications that in some ways are personalized therapies tailored to the disease and the patient. The ACAID therapy involves the use of patient's monocytes, which are treated *ex vivo* with TGF-β and antigen and reinfused into the same patient. The α-MSH therapy involves either injecting the neuropeptide into the tissue site or collecting the patients' own immune cells and treating them *ex vivo* with α-MSH while they are restimulated with autoantigen. The feasibility of these therapeutic approaches has been demonstrated using rodent models of autoimmune diseases, allografts, and hypersensitivity. The therapeutic utilization of the mechanisms of ocular immune privilege is in its infancy, and has a strong potential in being a new direction in immunotherapy.

Conclusion

Starting with the first experimental description of ocular immune privilege by Medawar in the 1940s, the understanding of the mechanisms of immune privilege has grown. Along with this understanding is a change in the concept of immune privilege. At first, immune privilege was viewed as an interesting experimental phenomenon that was explained by the unique anatomical features of the ocular microenvironment, which include the anterior chamber's lack of direct lymphatic drainage and the presence of an ocular–blood barrier. These passive mechanisms suggested that the immune system was ignorant of the presence of antigen within the eye. However, today we

know that the immune system perceives antigen placed into the eye, but it is the active engagement with the ocular microenvironment that regulates and controls immunity within the eye and systemically to the intraocular antigen. This active engagement is mediated by soluble immunoregulatory and immunosuppressive factors and neuropeptides. Our discovery and understanding of the mechanisms of ocular immune privilege will not only lead to potentially new immunotherapeutic approaches, but may also reveal the mechanisms of how the immune system regulates itself.

See also: Adaptive Immune System and the Eye: T Cell-Mediated Immunity; Antigen-Presenting Cells in the Eye and Ocular Surface; Ciliary Blood Flow and its Role for Aqueous Humor Formation; Immunobiology of Uveal Melanoma; The Immunological Aspects of Aqueous Humor Turnover; Injury and Repair Responses: Retinal Detachment; Innate Immune System and the Eye; Neuropeptides: Function; Neuropeptides: Localization.

Further Reading

Apte, R. S., Sinha, D., Mayhew, E., Wistow, G. J., and Niederkorn, J. Y. (1998). Cutting edge: Role of macrophage migration inhibitory factor in inhibiting NK cell activity and preserving immune privilege. *Journal of Immunology* 160: 5693–5696.

Cousins, S. W., McCabe, M. M., Danielpour, D., and Streilein, J. W. (1991). Identification of transforming growth factor-beta as an immunosuppressive factor in aqueous humor. *Investigative Ophthalmology and Visual Science* 32: 33–43.

Granstein, R., Staszewski, R., Knisely, T., et al. (1990). Aqueous humor contains transforming growth factor-b and a small (<3500 daltons) inhibitor of thymocyte proliferation. *Journal of Immunology* 144: 3021–3027.

Griffith, T. S., Brunner, T., Fletcher, S. M., Green, D. R., and Ferguson, T. A. (1995). Fas ligand-induced apoptosis as a mechanism of immune privilege. *Science* 270: 1189–1192.

Han, D., Tian, Y., Zhang, M., Zhou, Z., and Lu, J. (2007). Prevention and treatment of experimental autoimmune encephalomyelitis with recombinant adeno-associated virus-mediated alpha-melanocyte-stimulating hormone-transduced PLP139-151-specific T cells. *Gene Therapy* 14: 383–395.

Ng, T. F., Kitaichi, N., and Taylor, A. W. (2007). *In vitro* generated autoimmune regulatory T cells enhance intravitreous allogeneic retinal graft survival. *Investigative Ophthalmology and Visual Science* 48: 5112–5117.

Nishida, T., Miyata, S., Itoh, Y., et al. (2004). Anti-inflammatory effects of alpha-melanocyte-stimulating hormone against rat endotoxin-induced uveitis and the time course of inflammatory agents in aqueous humor. *International Immunopharmacology* 4: 1059–1066.

Taylor, A. W. (2003). Modulation of regulatory T cell immunity by the neuropeptide alpha-melanocyte stimulating hormone. *Cellular and Molecular Biology (Noisy-le-grand)* 49: 143–149.

Taylor, A. W. (2007). Ocular immunosuppressive microenvironment. *Chemical Immunology and Allergy* 92: 71–85.

Taylor, A. W., Streilein, J. W., and Cousins, S. W. (1992). Identification of alpha-melanocyte stimulating hormone as a potential immunosuppressive factor in aqueous humor. *Current Eye Research* 11: 1199–1206.

Taylor, A. W., Streilein, J. W., and Cousins, S. W. (1994). Immunoreactive vasoactive intestinal peptide contributes to the immunosuppressive activity of normal aqueous humor. *Journal of Immunology* 153: 1080–1086.

Taylor, A. W. and Yee, D. G. (2003). Somatostatin is an immunosuppressive factor in aqueous humor. *Investigative Ophthalmology and Visual Science* 44: 2644–2649.

Taylor, A. W., Yee, D. G., and Streilein, J. W. (1998). Suppression of nitric oxide generated by inflammatory macrophages by calcitonin gene-related peptide in aqueous humor. *Investigative Ophthalmology and Visual Science* 39: 1372–1378.

Wilbanks, G. A. and Streilein, J. W. (1992). Fluids from immune privileged sites endow macrophages with the capacity to induce antigen-specific immune deviation via a mechanism involving transforming growth factor-beta. *European Journal of Immunology* 22: 1031–1036.

Zhang-Hoover, J. and Stein-Streilein, J. (2007). Therapies based on principles of ocular immune privilege. *Chemical Immunology and Allergy* 92: 317–327.

Inflammation of the Conjunctiva

T Nishida, Yamaguchi University Graduate School of Medicine, Yamaguchi, Japan

Glossary

Cell-adhesion molecule – Cell-adhesion molecules are cell surface proteins, usually glycoproteins, that mediate cell–cell adhesion. They play important roles in the assembly and maintenance of tissues, wound healing, morphogenic cellular movements, cell migration, and metastasis. Intercellular adhesion molecule-1 (ICAM-1) functions in leukocyte adhesion and inflammation. Its expression is induced in various cell types by interferon-γ (IFN-γ), and it mediates interactions with neutrophils in inflamed tissue. Vascular cell-adhesion molecule-1 (VCAM-1) is presented on the surface of various cell types, including endothelial cells, tissue macrophages, fibroblasts, and dendritic cells. Its expression is induced by cytokines, and it plays a key role in the recruitment of eosinophils to sites of inflammation.

Collagenase (microbial) – Microbial collagenase is a metalloproteinase produced by bacteria that degrades helical regions of native collagen to yield small protein fragments. The preferred cleavage site is immediately upstream of the glycine residue in the sequence – proline–X–glycine–proline – where X is any amino acid. Six forms (or two classes) of microbial collagenase have been isolated from *Clostridium histolyticum*; these proteins are immunologically cross-reactive but possess different amino acid sequences and different specificities. Other variants have been isolated from *Bacillus cereus, Empedobacter collagenolyticum, Pseudomonas marinoglutinosa*, and species of *Vibrio* and *Streptomyces*.

Helper T cell – Helper T cells constitute a specific subpopulation of $CD4^+$ T cells that provides help to other cells of the immune system in mounting an immune response either through direct cell–cell interaction or the secretion of cytokines. They are also referred to as effector T cells. Several distinct subtypes of helper T cells, designated Th1, Th2, Th3, and Th17, have been identified.

Matrix metalloproteinase – Matrix metalloproteinases (MMPs) constitute an important family of enzymes that regulate composition of the extracellular matrix. They are synthesized as inactive precursor proteins that consist of propeptide, catalytic, and hemopexin domains; proteolytic removal of the propeptide domain results in MMP activation. MMPs are zinc-dependent endopeptidases that cleave one or several constituents of the extracellular matrix as well as nonmatrix proteins, and they play an important role in cleaving fibrillar collagen types I, II, and III into characteristic three-fourths and one-fourth fragments. Some MMPs are associated with the cell membrane, either through a transmembrane domain or through glycosylphosphatidylinositol anchor; such MMPs may act within the pericellular environment to influence cell migration. MMP-1, MMP-8, and MMP-13 are also known as collagenase 1, collagenase 2 (neutrophil collagenase), and collagenase 3, respectively.

Th1 cytokine – Th1 cytokines include interleukin (IL)-2, IFN-γ, IL-12, and tumor necrosis factor-β. They are secreted by Th1 cells and play an important role in cell-mediated immunity and chronic inflammation. In general, Th1 responses are stimulated by intracellular pathogens, including viruses as well as certain mycobacteria, yeasts, and parasitic protozoans.

Th2 cytokine – Th2 cytokines include IL-4, IL-5, IL-6, IL-10, and IL-13. They are secreted by Th2 cells and play a key role in the initiation of allergic responses. Th2 responses are also elicited by free-living bacteria and other parasites.

Inflammation

Inflammation is a biological response of the living body to injury or other harmful insults including microbial pathogens, allergens, and physical or chemical agents. It serves to protect the body and is the precursor to wound healing. Classical signs and symptoms of inflammation include redness, swelling, heat, pain, and loss of tissue function. Thus, although inflammatory reactions are well regulated to maintain homeostasis of the body and to promote wound repair, they may result in bodily discomfort. In some instances, however, excessive inflammation may result in tissue damage. Classically, inflammation has been considered to begin with a reaction of vascular tissue that renders vessels permeable to blood cells at the site of injury, resulting in the extravasation of such cells. Recent advances in immunology and molecular cell biology have revealed the mechanisms of inflammation at the level of cellular

interactions and molecular networks. Allergens and infection by pathogens are the major pathological triggers for inflammation at the ocular surface.

The Conjunctiva and Cornea

The ocular surface is composed of the cornea, conjunctiva, lacrimal glands, and associated lid structures. Both the conjunctiva and the cornea are derived from the embryonic epidermis, and they are separated from each other by tear fluid. External insults to the ocular surface evoke different types of inflammatory reactions in the conjunctiva and the cornea that are related to the anatomic differences and physiological roles of these two structures as well as to their connection via tear fluid (Figure 1).

The conjunctiva is a semitransparent membrane that covers the surface of the eye from the back surface of the eyelids to the edge of the transparent cornea. It serves as a barrier at the surface of the eyeball and helps to protect against the invasion of biological, chemical, or physical agents without interrupting the free movement of the eyeball. The surface of the conjunctiva is covered by multiple layers of epithelial cells. The conjunctival epithelium is a relatively inefficient barrier, however, with the result that pathogens, allergens, and biologically active substances readily penetrate into the stroma of the conjunctiva. The conjunctival stroma consists of conjunctival fibroblasts, loosely packed collagen fibers, a vascular system, and abundant immune cells. The triggering of an inflammatory reaction by pathogens or allergens results in enlargement of the blood vessels of the conjunctiva and consequent increased blood flow (hyperemia). The associated increase in the permeability of the conjunctival vascular system leads to leakage of liquid components and to the development of conjunctival edema. It also allows the infiltration of blood cells into the conjunctival stroma and the consequent activation of conjunctival fibroblasts.

Like the conjunctiva, the cornea faces the external environment. However, unlike the conjunctiva, the cornea is transparent, and its surface must be maintained smooth for the proper transmission of light into the eye. The anatomic structure of the cornea is relatively simple compared with that of the conjunctiva. Its surface is also covered by multiple layers of epithelial cells, but the corneal epithelium provides a much tighter barrier than does the conjunctival epithelium. In the absence of any loss or dysfunction of its component cells, the corneal epithelium prevents the entry of pathogens and allergens into the corneal stroma. The cornea does not contain a vascular system. Although a small number of immune cells such as Langerhans cells, stromal dendritic cells, and macrophages are present in the cornea, its major cellular components are epithelial cells, stromal keratocytes (corneal fibroblasts), and endothelial cells. Both the conjunctiva and the cornea are innervated by the ophthalmic branch of the trigeminal nerve, but the cornea is the most sensitive tissue at the ocular surface, and indeed maybe in the entire body, as a result of the high density of sensory nerve endings in the corneal epithelium.

Tear Fluid: A Reservoir of Inflammatory Cells and Modulators

Tear fluid functions as a lubricant between the tarsal conjunctiva and the surface of the cornea and serves to

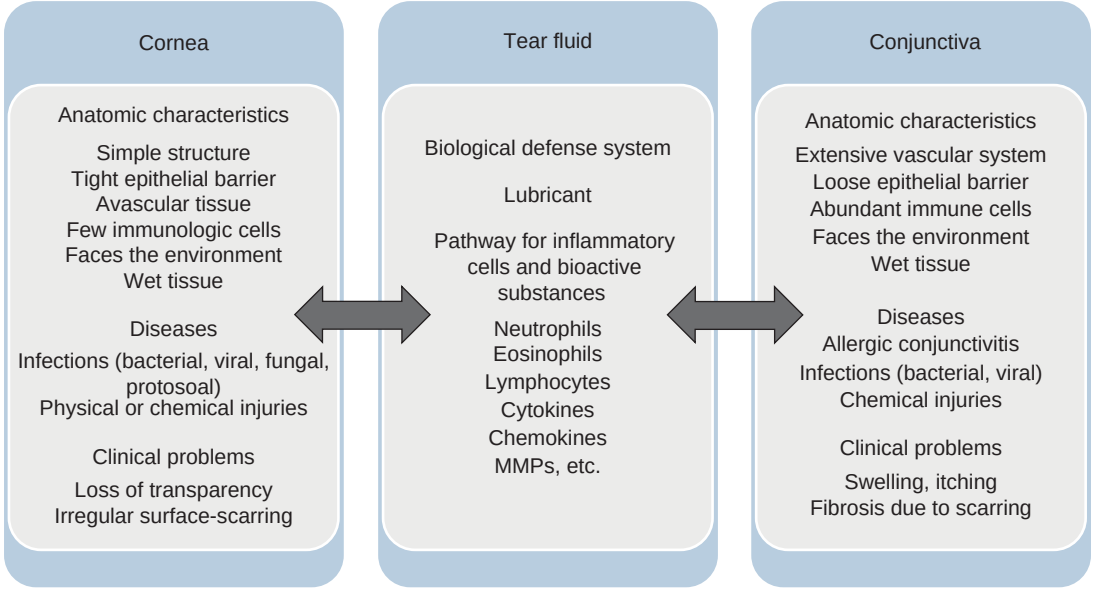

Figure 1 Cornea–tear fluid–conjunctiva axis in ocular surface inflammation. MMP, matrix metalloproteinase.

maintain the ocular surface wet. It is also important for ensuring the generation of a clear image on the retina. Moreover, it contributes to the biological defense system of the ocular surface, containing immunoglobulin, lactoferrin, lysozyme, and other protective proteins. With regard to inflammation at the ocular surface, tear fluid provides a pathway for the movement of inflammatory cells – such as neutrophils, eosinophils, and lymphocytes – between the conjunctiva and the cornea. It also serves as a reservoir of various inflammatory cytokines, chemokines, and growth factors as well as of nutrients and oxygen. Collagen-metabolizing enzymes such as matrix metalloproteinases (MMPs) are present in the tear fluid of individuals with certain ocular inflammatory conditions.

Allergic Reactions in the Conjunctiva

The conjunctiva is a common site for allergic reactions (Figure 2). Clinical characteristics of conjunctival allergic disease include hyperemia, edema, the formation of papillary discharge, the development of corneal epithelial disorders, and, in some patients, corneal ulcer. Hyperemia and edema result from dilation and an increase in the permeability of the vascular system in the conjunctiva. Conjunctival fibroblasts are responsible for the formation of papillae. Mechanical injury caused by papillae as well as the effects of inflammatory cytokines, such as interleukin (IL)-4, IL-13, and tumor necrosis factor-alpha (TNF-α), are responsible for discharge and damage to the corneal epithelium. Disruption of corneal epithelial barrier-function results in the spread of inflammation to the cornea and the development of various types of corneal epithelial disorders. Corneal fibroblasts contribute to the pathology of corneal ulceration. The primary cells that mediate allergic reactions at the ocular surface include mast cells, vascular endothelial cells, eosinophils, T helper 2 (Th2) cells, and conjunctival fibroblasts, with corneal epithelial cells and corneal fibroblasts also contributing in some cases.

Certain allergens that enter tear fluid from the environment are solubilized by the fluid and penetrate through the loose barrier provided by the conjunctival epithelium into the conjunctival stroma. In the stroma, the allergens trigger the secretion of histamine and inflammatory cytokines, such as IL-4, IL-13, TNF-α from mast cells, and IL-3 and IL-5 from Th2 cells. Histamine acts on the vascular endothelium to increase vessel

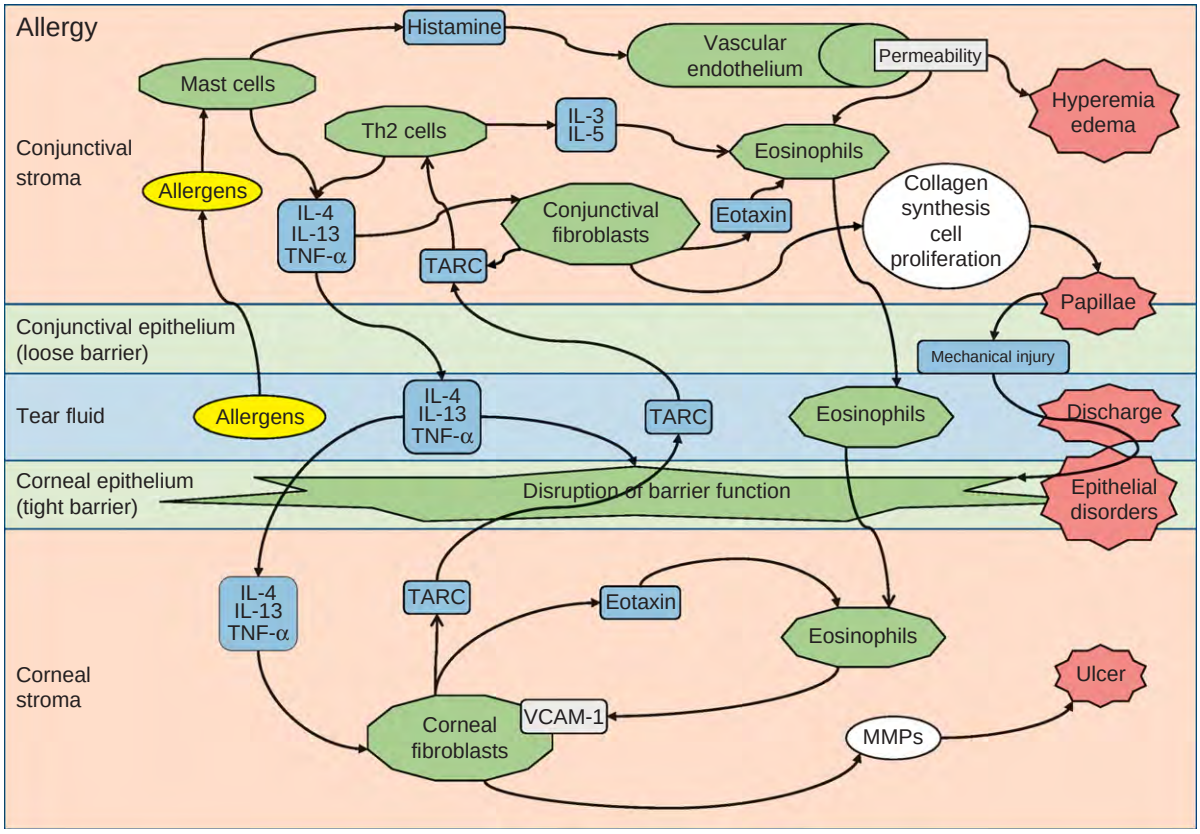

Figure 2 Clinical characteristics of allergic reactions in the conjunctiva and the cornea. IL, interleukin; MMP, matrix metalloproteinase; Th2, T helper 2 cell; TARC, thymus and activation-regulated chemokine; TNF-α, tumor necrosis factor alpha; VCAM, vascular cell-adhesion molecule.

permeability and induce vessel enlargement, resulting in conjunctival hyperemia and edema. IL-4, IL-13, and TNF-α – released by mast cells – activate conjunctival fibroblasts and trigger their secretion of the chemokines eotaxin and thymus and activation-regulated chemokine (TARC). Eotaxin attracts eosinophils to the interstitial space, and the extravasated eosinophils are then activated by IL-3 and IL-5 released by Th2 cells. TARC attracts Th2 cells into the interstitial space, and these cells then serve as an additional source of IL-4, IL-13, and TNF-α. Exposure of conjunctival fibroblasts to IL-4, IL-13, and TNF-α also stimulates the synthesis of collagen and cell proliferation – effects that give rise to the formation of papillae. The protrusive shape of the papillae results in mechanical injury of both conjunctival and corneal epithelia; such injury together with the effects of IL-4, IL-13, and TNF-α that enter tear fluid from the conjunctiva lead to disruption of the barrier function of the corneal epithelium and to discharge. Eosinophils that enter tear fluid from the conjunctiva are then able to penetrate into the corneal stroma. IL-4, IL-13, and TNF-α also enter the corneal stroma from tear fluid and activate corneal fibroblasts to express TARC, eotaxin, and vascular cell-adhesion molecule-1 (VCAM-1) – a cell-adhesion molecule for eosinophils. The activated corneal fibroblasts also produce MMPs, which degrade collagen of the extracellular matrix in the corneal stroma, resulting in corneal ulceration. TARC released from corneal fibroblasts passes through tear fluid into the conjunctival stroma, where it further promotes the secretion of IL-4, IL-13, and TNF-α by Th2 cells in a vicious cycle. This scenario thus reveals that, although immune cells such as mast cells, Th2 cells, and eosinophils play a prominent role in allergic disorders at the ocular surface, resident fibroblasts in both the conjunctiva and cornea also contribute to the inflammatory process.

Infection of the Conjunctiva or Cornea

The clinical characteristics of infection at the ocular surface include swelling, hyperemia at the conjunctiva, discharge, and epithelial defects and ulceration in the cornea. As with allergic reactions, the reactions of the conjunctiva and cornea to infection differ (**Figure 3**). The vascular system of the conjunctiva ensures a robust immune response to infection in this tissue, with conjunctivitis being a relatively mild clinical condition. However, the cornea is avascular and possesses few immune cells, with the result that corneal infection is more serious and may become sight threatening.

If a pathogen survives the biological defense system in tear fluid, it readily penetrates the conjunctival epithelium and triggers the dilation and permeabilization of conjunctival blood vessels, resulting in swelling and hyperemia. Neutrophils and Th1 cells enter the conjunctival stroma from the bloodstream and serve as the second line of defense against pathogens. Both neutrophils and Th1 cells secrete IL-1, with Th1 cells also secreting interferon-γ (IFN-γ). These cells and cytokines may be sufficient to inactivate the pathogen and limit the inflammatory response to the conjunctiva. However, pathogens also act on conjunctival epithelial cells to trigger the secretion of IL-8, IL-6, and TNF-α. These cytokines together with IL-1 and IFN-γ can enter tear fluid and, in the presence of damage to the corneal epithelium, may penetrate into the corneal stroma and activate corneal fibroblasts.

The tight barrier provided by the corneal epithelium normally prevents the entry of pathogens into the cornea. However, corneal epithelial injury can result in pathogen penetration into the corneal stroma. Pathogen-associated various factors such as lipopolysaccharide (LPS) of Gram-negative bacteria and peptidoglycan (PGN) of Gram-positive bacteria are recognized by toll-like receptors (TLRs) on the surface of corneal fibroblasts and trigger the production of IL-8 and the expression of intercellular adhesion molecule-1 (ICAM-1) by these cells. IL-8, IL-6, TNF-α, IFN-γ, and IL-1 that enter the corneal stroma via tear fluid also induce IL-8 production by corneal fibroblasts. IL-8 then attracts neutrophils exuded (extravasated) from conjunctival blood vessels into the corneal stroma, and these cells interact with corneal fibroblasts via ICAM-1. IL-1 released from neutrophils further stimulates corneal fibroblasts.

Corneal infection is associated with the production of two types of collagen-degrading enzymes: collagenase released from the pathogen and MMPs released from corneal fibroblasts. These enzymes destroy stromal collagen, eventually resulting in the development of corneal ulcer. Collagen destruction by MMPs released from activated corneal fibroblasts may continue even if the pathogen has been killed by antimicrobial treatment. Neutrophils were originally thought to destroy stromal collagen, but these cells were subsequently found to promote the production of MMPs by corneal fibroblasts rather than to degrade the collagen themselves. As with ocular allergy, corneal fibroblasts thus play a key role in the progression of the inflammatory response to corneal infection.

Tear Fluid as a Diagnostic Indicator of Inflammation

The measurement of inflammatory cytokines or chemokines and the cellular components of tear fluid provides clinically important information on inflammation at the ocular surface. The presence of eosinophils in tear fluid thus confirms a diagnosis of allergic inflammation,

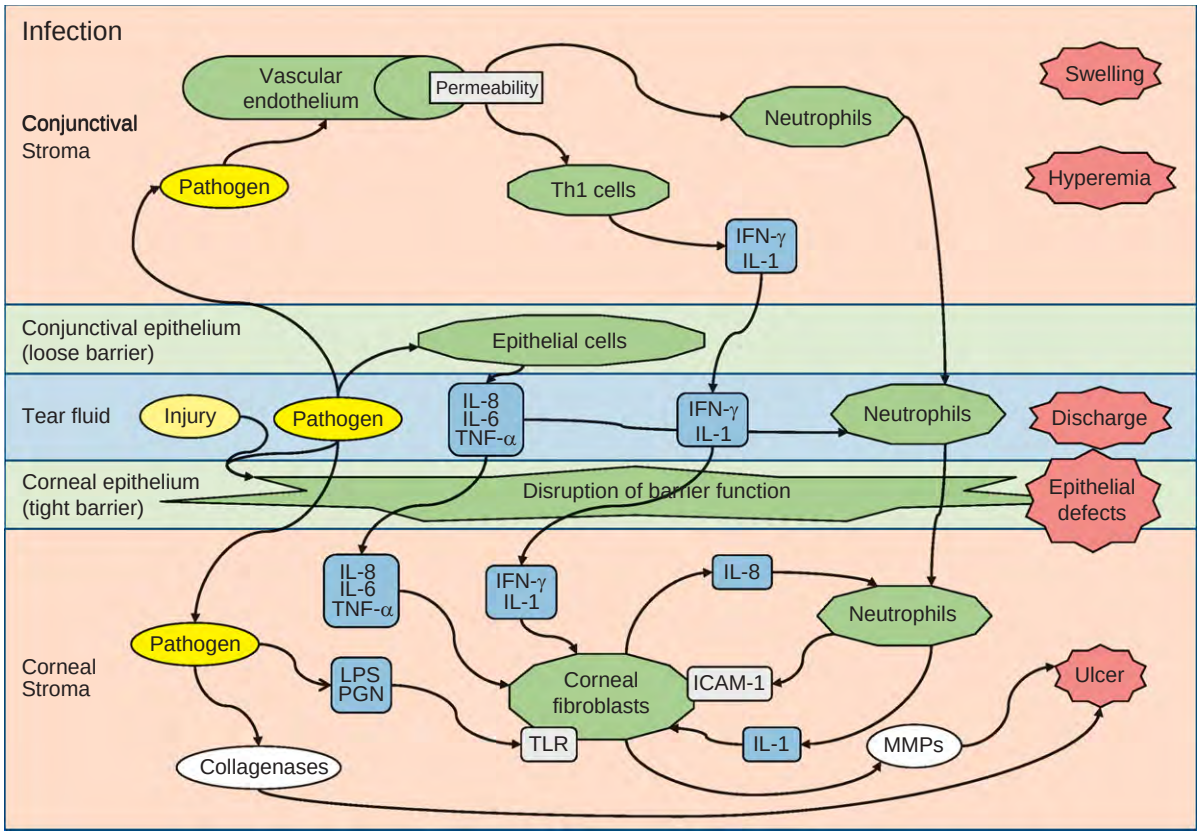

Figure 3 Clinical characteristics of infection in the cornea and conjunctiva. ICAM, intracellular adhesion molecule; IFN-γ, interferon-gamma; IL, interleukin; LPS, lipopolysaccharide; MMP, matrix metalloproteinase; PGN, peptidoglycan; Th2, T helper 2 cell; TARC, thymus and activation-regulated chemokine; TLR, toll-like receptor; TNF-α, tumor necrosis factor alpha.

whereas the presence of neutrophils is indicative of infectious inflammation.

In addition to being of diagnostic value, the condition of the tear fluid can affect the progression of ocular surface inflammation. In individuals with dry eye, for example, the decrease in tear secretion and small volume of tear fluid may result in concentration of inflammatory cells and proteins. The condition of tear fluid should thus be taken into account in the treatment of patients with ocular surface inflammation.

Connection of the Conjunctiva and Cornea via Tear Fluid

The surfaces of both the conjunctiva and the cornea are covered by epithelial cells. However, the biological responses of these two tissues to allergens or to pathogens differ markedly. The conjunctiva has a prominent vascular system and contains abundant immune cells, whereas the cornea is transparent and avascular and contains few immune cells. These anatomic differences between the conjunctiva and cornea are reflected in the types of inflammatory condition that affect them. The conjunctiva is the principal target tissue for allergic reactions at the ocular surface, whereas the cornea is the main target for microbial infection or injury. The vascular system of the conjunctiva serves as a key source of immune cells in each of these conditions. The cornea is also affected by inflammatory reactions that occur in the conjunctiva, with the tear fluid that covers the surface of both the conjunctiva and the cornea serving as a conduit for the exchange of immune cells, cytokines, chemokines, and growth factors.

The concept of inflammation was first described more than 2000 years ago as redness and swelling with heat and pain by Celsus. In the nineteenth century, the concept of loss of tissue function associated with inflammation was recognized. Recent advances in cell and molecular biology have revealed the cytokine and chemokine network that underlies inflammation. However, the availability of effective anti-inflammatory drugs other than steroids remains limited. Nonsteroidal antiallergic drugs have been developed and are effective for the treatment of allergic conjunctivitis. Nonsteroidal anti-inflammatory drugs (NSAIDs) are also effective in ameliorating inflammatory reactions. However, anti-inflammatory agents that halt tissue destruction

are needed. Further characterization of the bidirectional regulation of conjunctival and corneal resident cells via cytokines and chemokines, as well as immune cells, released into tear fluid may provide a basis for the development of new drugs effective for the treatment of inflammation at the ocular surface.

See also: Adaptive Immune System and the Eye: Mucosal Immunity; Adaptive Immune System and the Eye: T Cell-Mediated Immunity; Angiogenesis in the Eye; Antigen-Presenting Cells in the Eye and Ocular Surface; Conjunctiva Immune Surveillance; Conjunctival Goblet Cells; Defense Mechanisms of Tears and Ocular Surface; Dry Eye: An Immune-Based Inflammation; Immunopathogenesis of Pseudomonas Keratitis; Molecular and Cellular Mechanisms in Allergic Conjunctivitis; Ocular Mucins; Overview of Electrolyte and Fluid Transport Across the Conjunctiva; Tear Film Overview.

Further Reading

Hazlett, L. D. (2005). Role of innate and adaptive immunity in the pathogenesis of keratitis. *Ocular Immunology and Inflammation* 13: 133–138.

Kolaczkowska, E., Chadzinska, M., and Plytyez, B. (2008). Basic concepts of inflammation – from pioneer studies until now. In: Romano, G. T. (ed.) *Inflammation Research Perspectives*, pp. 113–168. New York: Nova Science Publishers.

Kumagai, N., Fukuda, K., Fujitsu, Y., Yamamoto, K., and Nishida, T. (2006). Role of structural cells of the cornea and conjunctiva in the pathogenesis of vernal keratoconjunctivitis. *Progress in Retinal and Eye Research* 25: 165–187.

Kumar, V., Abbas, A. K., Fausto, N., and Mitchell, R. N. (2007). *Robbins Basic Pathology,* 8th edn., pp. 31–58. Philadelphia, PA: Saunders-Elsevier.

Ley, K. (2001). History of inflammation research. In: Ley, K. (ed.) *Physiology of Inflammation*, pp. 1–10. New York: Oxford University Press.

Pearlman, E., Johnson, A., Adhikary, G., et al. (2008). Toll-like receptors at the ocular surface. *Ocular Surface* 6: 108–116.

Tuli, S. S., Schultz, G. S., and Downer, D. M. (2007). Science and strategy for preventing and managing corneal ulceration. *Ocular Surface* 5: 23–39.

Information Processing in the Retina

F S Werblin, UC Berkeley, Berkeley, CA, USA

Glossary

Directional sensitive ganglion cell – Ganglion cells that are particularly sensitive to movement of an image in a specific direction across the retina.
Local edge detector (LED) – A ganglion cell that appears to be unique in that it is activated by a local edge at the center of its receptive field, and suppressed by edges in the surround.
OFF pathway – Retinal circuitry within the retina responding at the offset of light.
ON pathway – Retinal circuitry within the retina responding at the onset of light.
Starburst amacrine cell – Retinal amacrine cells with a large and symmetrical dendritic arbor that uses both actylcholine and gamma aminobutyric acid. These cells play an important role in directional selectivity.

Introduction

The retina creates a dozen different representations of the visual world, each embodied at a separate sublayer of the inner plexiform layer, and carried by a separate class of ganglion cell. These representations are not just enhanced edges, but are often also complex space–time abstractions of the visual world. The early studies of Barlow; Maturana, Lettvin, McCulloch, and Pitts; and Campbell and Robson suggested that the optic nerve contains information carried by a number of different channels, each formed as a result of sophisticated neural computations. In the frog, for example, the retinal output contains the trigger features that guide the frog's behavior, including detectors for flys, edges, dimming, and contrast. As Barlow points out, the activity of individual neurons is not just a reflection of thought processes, but these activities are also thought processes. Therefore, what are these processes and how are they formed through neural interactions in the retina?

Over the last 40 years, visual neuroscientists have attempted to understand retinal function from a variety of perspectives. What is the nature of the representations of the visual world formed by the retina? Through what neural processes are these representations formed? Answering these questions requires a merging of information from a variety of different disciplines. Retinal anatomists have defined both the morphology and the conductivity between retinal neurons at the light electron microscope levels. Retinal electrophysiologists have defined the response properties of each class of retinal neurons. Retinal circuitry has been analyzed, aided in great measure by pharmacological studies where specific synaptic pathways have been defined for the use of receptor agonists and antagonists. A number of general principles of organization and function have been gleaned from these studies.

For example, as predicted by Horace Barlow and later verified through experiment, most retinal neurons operate in a spikeless mode, whereby membrane potential and synaptic transmission are continuous and graded. Furthermore, under most ambient conditions, most graded-potential retinal neurons operate at or near the midpoint of their response range, capable of signaling both increments and decrements. Embedded in a complex circuitry including feedback, most neurons are constantly active, talking to each other with a continuous stream of activity. The presentation of visual stimuli offsets this ambient state, generating at least a dozen different space–time patterns of neural activity at the retinal output that correspond to, and represent, the visual input.

The Outer Retina, Gain and Level Adjustment

One of the first steps in retinal processing performs the operations that match the response range of retinal neurons to the light input, setting the dynamic range. A significant amount of neural housekeeping is required to maintain the retina in a steady-state condition such that most neurons are operating near their mid-potential range. This set point control is achieved through a series of processes known as adaptation. Adaptation to luminance maintains the photoreceptors at an ambient potential level that varies little with the overall luminance state, over very many orders of magnitude. This is accomplished because cone gain decreases as ambient luminance increases. It is as though the cones put on sunglasses as the brightness of the environment increases. This adaptation is an inherent part of the transduction machinery, mediated at the outer segments of photoreceptors. Much more about the process of adaptation can be found in elsewhere in the encyclopedia.

Bifurcation of the Visual Pathways into ON and OFF streams

The pathway from cones to bipolar cells bifurcates at the bipolar dendrites into the ON and OFF streams of activity. Activity is initiated in OFF bipolars via ionotropic glutamate receptors in the bipolar dendrites; therefore, OFF bipolars polarize in phase with the photoreceptors. Activity is initiated in the ON bipolar dendrites via metabotropic receptors such that ON bipolar cells polarize out of phase with the photoreceptors. Both bipolar types drive ganglion cells via α-amino-3-hydroxyl-5-methyl-4-isoxazole-propionate (AMPA), kainate, and *N*-methyl-D-aspartic acid (NMDA) receptors; therefore, all ganglion cells respond in phase with their bipolar cell inputs. These differential streams are carried to different strata of the inner retina with most of the OFF streams in regions that are distal to the ON streams. These ON and OFF streams are then carried through many synapses in the visual system and can also be measured at the visual cortex. A sketch of the retinal pathways from cones to the ON and OFF bipolars, to the ON and OFF ganglion cells, is shown in Figure 1. More about bipolar cells can be found elsewhere in the encyclopedia.

Horizontal Cell Synaptic Interactions

The pathway from cones to bipolar cells is intersected by horizontal cells. Cones drive the horizontal cells, but horizontal cells are strongly electrically coupled; therefore, the neural image carried by horizontal cells is blurred. The coupled network of horizontal cells feeds forward to bipolar cells via *gamma aminobutyric acid* (GABA)ergic synapse. ON and OFF bipolar cells respond with opposite polarities to light; therefore, horizontal cells must polarize the ON and OFF bipolar cells in opposite directions: GABA depolarizes ON bipolar cells and hyperpolarizes OFF bipolar cells because the chloride concentrations, and therefore the reversal potentials for GABA input, are different in the two bipolar cell types. Horizontal cells also feed back to cones, but the feedback mechanism from horizontal cells to cones remains controversial. Feedback may be mediated by an electrical synaptic feedback, by GABA, or it might be controlled by pH. Experiments in different animals under different conditions have led to these diverse theories. The circuitry is shown in Figure 2, added to the ON–OFF streams shown above. The role of GABA in horizontal cells is described elsewhere in the encyclopedia.

Horizontal Cells and Local Gain Control

Feedback from horizontal cells to cones provides a form of local adaptation or gain control so that local bright spots do not saturate neural activity the way they might in a conventional camera where the level of light arriving at the sensor is controlled by aperture size. Local gain control is achieved by the electrical coupled horizontal cells network whose blurred image is subtracted from the sharper image carried by the cones and bipolar cells. This subtraction normalizes activity across the retina with respect to the blurred activity of horizontal cells. The subtraction has two major results: the neural representation of edges is

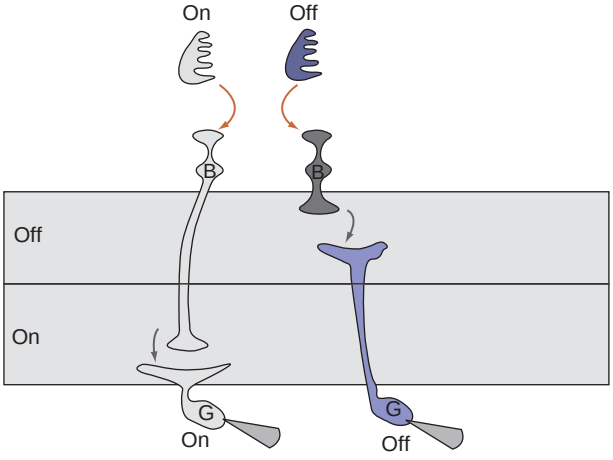

Figure 1 General glutamatergic pathways in the retina from photoreceptors (top) to bipolar cells (B) to ganglion cells. ON and OFF pathways are initiated at the dendrites of the bipolar cells (B, orange arrows). ON and OFF ganglion cells (G) are driven by their respective ON and OFF bipolar cells (black arrows). OFF activity is located in the distal half of the outer plexiform layer, while ON activity is located in the proximal half.

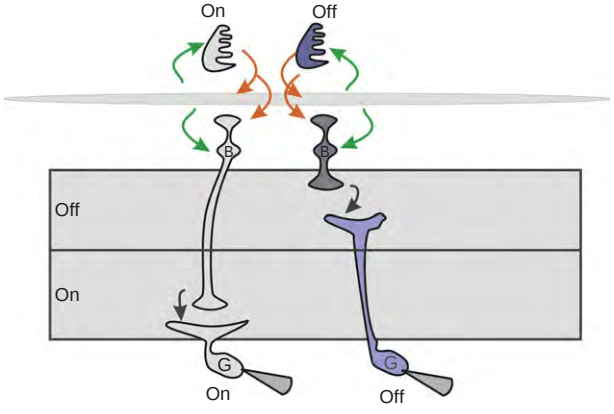

Figure 2 Horizontal cell feedback and feedforward added to the circuitry. Orange arrows represent glutamate pathways from cones to ON and OFF bipolar cells and to horizontal cells. Green arrows represent inhibitory pathways that mediate the horizontal-mediated antagonistic surround. The synaptic mechanism underlying this feedback pathway is still not fully understood. This feedback pathway is also implicated in local gain control. GABA is also thought to be fed forward to both bipolar cell types.

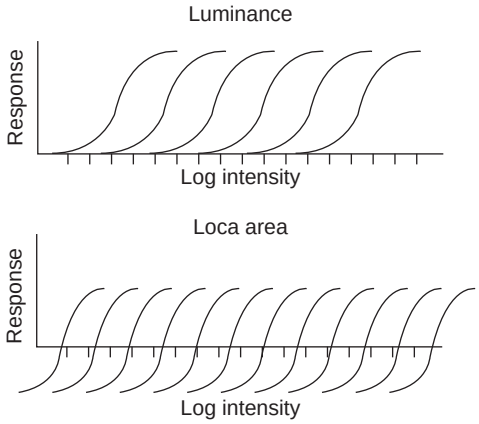

Figure 3 Luminance and local gain changes. Upper traces: gain changes at the photoreceptors shift the intensity–response curves along the log intensity axis; as ambient illumination increases, the transduction gain is reduced. Lower traces: local adaptation mediated by horizontal cell feedback subtracts the luminance level from the cone-to-bipolar signal, leaving mainly the contrast signal.

sharpened by the subtraction, resulting in the presence of Mach bands. Put differently, broadly distributed luminance changes are lost, subtracted from the cone to bipolar patterns by the blurred horizontal cell image. The neural image that remains after this subtraction is primarily related to local contrast. It is the local contrast image that is then brought to the inner retina at the synaptic terminals of the ON and OFF bipolar cells. A family of adaption curves is shown in Figure 3.

Interactions at the Inner Retina: Contrast Gain

The local gain-controlled neural image, brought to the inner retina, is subject to an additional adjustment by contrast gain control, that constrains signal magnitude so that postsynaptic neurons operate within their dynamic range. Contrast gain control is mediated by at least two mechanisms. Amacrine cell feedback to bipolar cells is thought to contribute to contrast gain control. In addition, a more significant mechanism, still not well understood, but likely located at the bipolar cell terminals, has been shown to increase contrast gain at low temporal contrast and to decrease gain at high temporal contrast. Contrast gain control is described elsewhere in the encyclopedia.

To summarize, there are three main gain control systems in the retina: luminance gain at the outer segments, local luminance gain at the horizontal cell system, and contrast gain control. These systems, taken together, allow the retina to detect dim objects at low contrast or bright objects at high contrast, with all neurons operating near their optimal gain and never saturating.

General Organizational Principles

Lateral Interactions are Concatenated

The results of an interaction that takes place early in visual processing are carried through and appear at later stages of processing. As an example, antagonistic lateral interactions at the outer retina, mediated by horizontal cell feedback and feedforward, form an initial antagonistic center-surround receptive field interaction. These concentric fields are first formed at the cone terminals, mediated by feedback from horizontal cells; however, this activity is read out by both the ON and OFF bipolar cell types. Therefore, bipolars, similar to cones, show concentric antagonistic receptive fields. Part of the antagonistic surround measured at ganglion cells derives from the interactions between cones and horizontal cells at the outer retina and carried to the ganglion cells via the bipolar cells. Additional antagonistic components are added through interactions at the inner retina, mediated by amacrine cells, and then measured in ganglion cells. Therefore, ganglion cells carry the results of lateral antagonism at the outer retina superimposed upon additional forms of lateral interaction formed at the inner retina. Ganglion cells can contain as many as five different lateral antagonistic components.

Mutual Antagonism is a Form of Amplification

Once again, lateral antagonism at the outer retina serves as an example of mutual antagonism because adjacent retinal regions, via horizontal cells antagonize, are mutually antagonistic. This mutual antagonism amplifies and generates the familiar Mach bands which enhance the neural image of edges in the visual world. As described later, the mutual antagonism between motion-detecting starburst amacrine cells amplifies directional differences. There are many other forms of mutual antagonism in the retina operating in different domains, and each of these serves to amplify the quality represented in that domain.

Redundant Feedforward and Feedback Interactions

As shown above, the lateral antagonistic signal that is fed back to cones is also fed forward to both ON and OFF bipolar cells. In many cases of retinal interaction, the GABAergic signal that is fed back to bipolar cells by amacrine cells is also fed forward to ganglion cells as shown in Figure 4.

Interaction between the Two Complementary Visual Streams in the Visual System

The ON and OFF pathways do not remain independent, but interact at every neural level in the retina and continue to interact at each of the higher visual centers. This interaction between the ON and OFF pathways, called

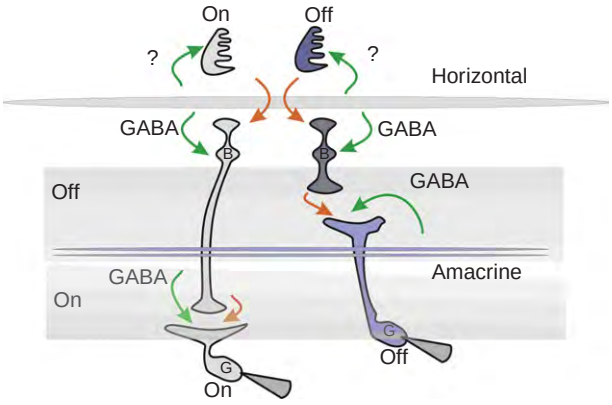

Figure 4 GABAergic amacrine cell feedback and feedforward can provide an additional lateral antagonistic interaction, generating an additional receptive field surround superimposed upon the feedback and feed-forward interactions mediated by horizontal cells at the outer retina.

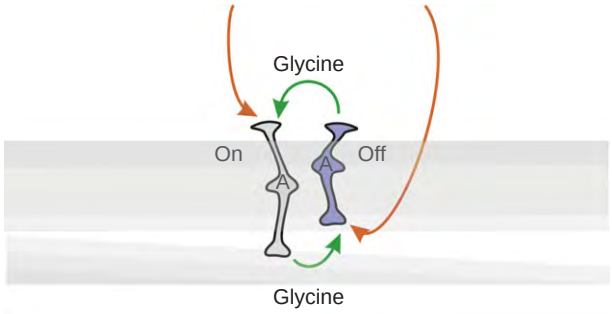

Figure 5 Crossover circuitry isolated. The ON system inhibits the OFF system, and the OFF system inhibits the ON system by way of glycinergic amacrine cells that span the ON–OFF sublaminae. This interaction compensates for the nonlinearities introduced by synaptic transmission. The interaction is found in most bipolar, amacrine, and ganglion cells.

crossover inhibition, is mediated by glycinergic amacrine cells, and serves to relinearize signals that have been distorted by nonlinear transmission at synapses. It is necessary to provide this circuitry compensation at each stage of processing to maintain a linear signal stream because if a nonlinear signal is filtered, linearity can never be reconstructed. In the transistor world, analog signal processing design requires interactions between the equivalent of ON and OFF circuitry to compensate for the rectifying nonlinearities inherent in transistors.

The circuitry underlying crossover inhibition involves ON amacrine cells feeding the OFF pathway, and OFF amacrine cells feeding the ON pathway. The circuit module representing this crossover activity is shown in Figure 5.

The crossover circuitry is superimposed upon and intersects the glutamate pathways and the GABAergic inhibitory pathways. The overall circuitry is summarized in Figure 6. More on amacrine cells can be found in elsewhere in the encyclopedia.

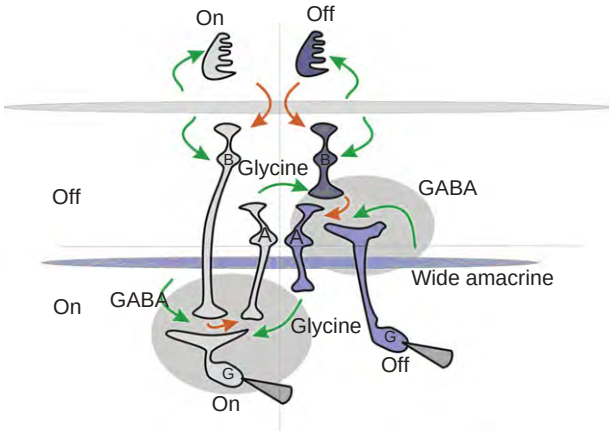

Figure 6 Generalized retinal circuit including horizontal cells, lateral amacrine cells, and vertical amacrine cells. This general circuit includes feedback and feed-forward horizontal cell interactions, feed-forward and feedback GABAergic amacrine cell interactions, and ON to OFF as well as OFF to ON crossover circuitry. Each of these five interactions can generate a different antagonistic receptive field surround for ganglion cells.

This is a summary of a basic retinal design. It accounts for most of the general activity measured in bipolar, amacrine, and ganglion cells. In almost all cases, the inhibition carried by the vertical amacrine cell elements is mediated by glycine, while inhibition carried by the laterally oriented amacrine cells is mediated by GABA. These general circuitry rules underlie a more specific circuitry that generates the physiological behavior of each ganglion cell type. This additional circuitry has been described for a few ganglion cells. In each case, special variations to the basic circuitry endows these cell types with their specific characteristics. More on neurotransmitters and receptors can be found elsewhere in the encyclopedia.

Inner Retinal Processing: Circuitry for Feature Extraction

Having solved both the housekeeping problems related to adaptation to luminance contrast and the nonlinearity problem introduced by synaptic transmission through appropriate crossover circuitry, the stage is set for the real work of the retina, which is creating the appropriate representations of the visual world. Most of the interesting interactions take place at the inner plexiform layer that is itself a multilayered and exquisitely organized structure. There appear to be about 10 strata in every retina species that has been studied. The strata are defined by the 10 levels at which the dendrites of different ganglion cell types ramify. Remarkably, there also appear to be about 10 different types of bipolar cells, and the axon terminals of each of these bipolar cell types also terminate roughly in the same 10 strata as a ganglion cell dendrites. To a first rough approximation, it appears that each

ganglion cell type receives input from a separate bipolar cell type as shown in Figure 7. However, a close look at the bipolar terminals shows that they are often more diffusely distributed, and there are ganglion cells with multistratified dendritic arborizations. Physiologically, the connections must be more diffuse because most ganglion cells ramify in either the ON or the OFF sublamina; however, most ganglion cells appear to receive both ON and OFF inputs (although activity tends to be dominated by either ON or OFF excitation).

Although the excitatory pathway from photoreceptors to bipolars to ganglion cells appears to be relatively straightforward, there exists a bewildering array of amacrine cells that generate a variety of interactions at the inner plexiform layer. Amacrine cells come in many diverse morphologies, and there appear to be approximately 30 different types. Functional properties of these amacrine cells can be thought of at three different levels of refinement: (1) there are two major morphological classes of amacrine cells identified by their vertical versus lateral orientation in the retina, (2) there are circuitries involving amacrine cells that mediate specific functions, and (3) there are amacrine cells that possess unique physiological properties. Each level of functionality is described below.

Amacrine Cell Morphological Types

The majority of amacrine cells falls into one of two general classes. One consists of narrowly ramifying vertically oriented amacrine cells that span the ON and OFF sublamina. This class contains and releases glycine as its inhibitory transmitter. These amacrine cells appear to be strategically located to carry information from the ON to the OFF and the OFF to be ON sublamina, and are probably the key players in mediating crossover inhibition described earlier. The other major class of amacrine cell consists of widely ramifying, but monostratified, amacrine cells, each stratifying in a separate sublamina. These amacrine cells contain and release GABA as their inhibitory transmitter and may be responsible for various forms of lateral inhibition mediated at the inner retina. In some cases, this lateral inhibition is mutual and when this is the case, it serves as an amplifier of the visual quality carried by that specific form of inhibition.

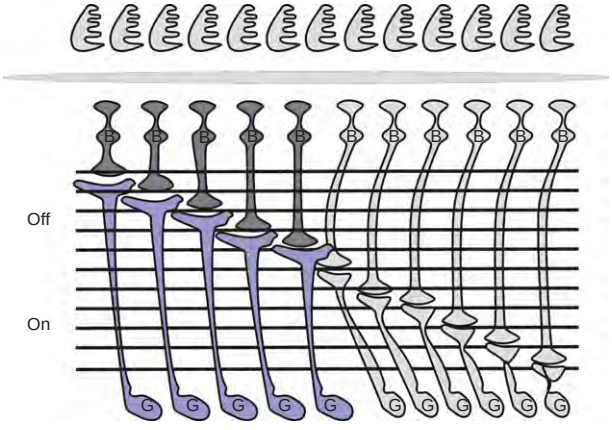

Figure 7 Schematic of the layering of the inner plexiform layer (IPL). Each of the 10 bipolar cell types sends its axon terminal to a distinct region of the IPL, approximately a single substratum of the IPL. Each of the ganglion cell types sends its dendrites to a distinct substratum. Roughly speaking, each bipolar cell type is associated with a unique ganglion cell type. This description is only approximate. In fact, some ganglion cell dendritic fields are bistratified, such as the direction selective (DS) cells, and the axon terminals of some bipolar cells are more diffuse.

Specific Ganglion Cell Circuitries

Directional selectivity

There are a few amacrine cells that have now been identified with very specific personalities. For example, starburst amacrine cells, named for the characteristic starburst pattern of their processes, span about 200 μm. Starburst cells contain and release both GABA and acetylcholine. They are the key elements in the organization of directional selectivity in the retina. A large population of starburst amacrine cells is associated with each directionally selective (DS) ganglion cell, and neighboring DS ganglion cells likely share many starburst amacrine cells. Starburst cells are inherently DS, generating more release for centrifugal movement. One likely mechanism involves calcium-initiated calcium release, but this remains an area of intense exploration. Release occurs along the outer one-third of the starburst processes. These processes not only release GABA, but are also GABA sensitive. This creates a mutual inhibition between starburst cells that acts to amplify directional motion sensitivity as shown in Figure 8. Starburst cells inhibit the DS cells asymmetrically, with stronger inhibition arriving from the null side than from the preferred side. These three mechanisms, inherent directional selectivity in the starburst cells themselves, mutual antagonistic interaction between neighboring starburst cells, and asymmetrical inhibition acting both pre- and postsynaptically at the ganglion and bipolar cells endow the DS cell with some of its directional properties as shown in Figure 9. More on DS circuitry can be found elsewhere in the encyclopedia.

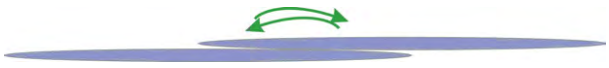

Figure 8 Mutual inhibition between starburst amacrine cells amplifies the directional properties of the starburst network. Here, two starburst amacrine cells, themselves directionally selective, are mutually inhibitory (green arrows). In the circuit of this figure, the right starburst cell supplies inhibition to the ganglion cell for movement in the null direction from right to left. The right starburst cell is turned off by the left starburst cell for movement from left to right.

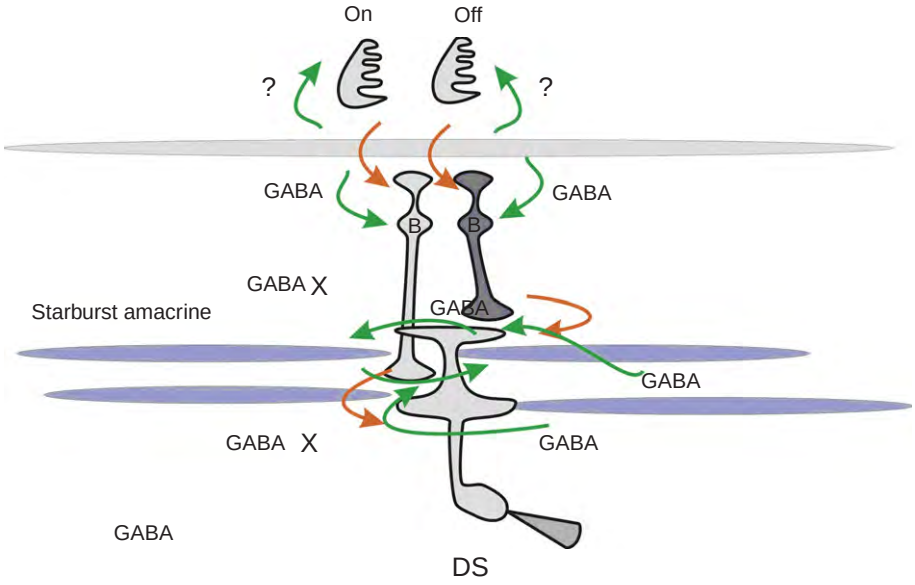

Figure 9 Pathways underlying the behavior of the directionally selective (DS) ganglion cell. Starburst amacrine cells (light blue), themselves directionally selective, are mutually inhibitory. They inhibit by feeding back to bipolar cells and forward to ganglion cells. Both feedback and feed-forward inhibition are asymmetric: they are stronger on the null side than on the preferred side, thereby endowing the DS ganglion cell with directional properties.

The circuitry puzzle regarding the DS cells is far from solved; however, the general organizational rules listed above still apply. The lateral inhibitory interneuron is GABAergic, following the GABA rule for laterally oriented cells.

Functions of AII Amacrine Cells

AII amacrine cells serve a very specific function to transcribe signals in the rod bipolar cells to both the ON and OFF cone pathways. The circuitry underlying this function is now well defined. AII amacrine cells are driven by rod bipolar cells that respond at ON. The AIIs are electrically coupled to cone bipolars, and make glycinergic synaptic contact with the OFF pathway. Recently, the AII amacrine cells have been shown to serve other functions. For example, the AII amacrine cells appear to be the key elements in providing glycinergic inhibition to the so-called looming detectors and in alpha cells, both described elsewhere in the encyclopedia (Figure 10).

There are numerous other examples of special purpose circuitry that utilize laterally oriented amacrine cell interneurons. The polyaxonal amacrine cells are thought to mediate saccadic suppression. In other cases, the same cell type has been implicated in mediating object motion sensitivity. It is likely that other amacrine cell types also serve specific functions, but their properties have not yet been identified.

At about the time that Levick was characterizing the DS ganglion cell, he also described another ganglion cell

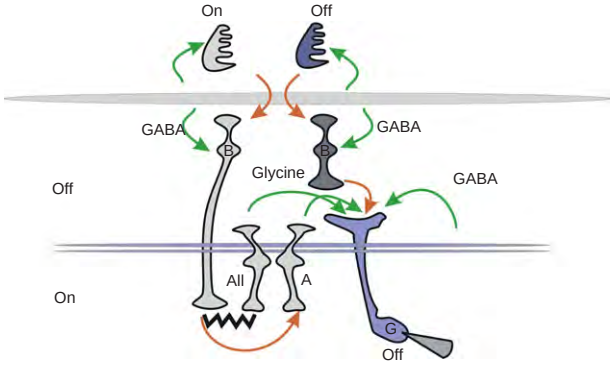

Figure 10 Pathways underlying the behavior of the alpha cell/looming detector. This ganglion cell appears to respond to a dark target at its receptive field center that increases in size, much like an approaching predator. It appears to receive glycinergic inhibition from two types of local amacrine cells: input from an AII amacrine cell that is electrically coupled to ON bipolar cells, and input from another amacrine cell class that receives excitatory glutamate input from ON bipolar cells.

that he termed the local edge detector (LED). This cell appears to be unique in that it was activated by a local edge at the center of its receptive field, and that activity was suppressed by edges in the surround. Van Wyk, Taylor, and Vaney have recently gone on to characterize some of the special temporal properties of this neuron. It receives excitation and also glycinergic inhibition at both ON and OFF, and is inhibited by edge stimuli presented at the surround via a GABAergic lateral pathway. Both inhibitory components follow the general rule of vertical glycinergic and lateral GABAergic activity as

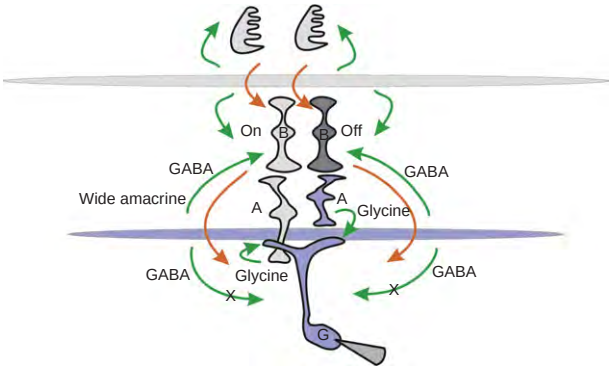

Figure 11 Pathways underlying the response properties of the local edge detector. This cell responds to subreceptive field detail at its receptive field center, most likely from the bipolar cells that drive it. It also receives local ON and OFF inhibition that is glycinergic (green arrows), as well as broad-field inhibition (green arrows) that is GABAergic and also responsive to fine detail. In this cell type, GABA is only fed back, not fed forward.

shown in Figure 11. The role of this neuron in the overall scheme of vision remains obscure, but it is likely involved in high-resolution, slow temporal response activity.

See also: GABA Receptors in the Retina; Glutamate Receptors in Retina; Information Processing: Amacrine Cells; Information Processing: Bipolar Cells; Information Processing: Contrast Sensitivity; Information Processing: Direction Sensitivity; Information Processing: Ganglion Cells; Information Processing: Retinal Adaptation; The Role of Acetylcholine and its Receptors in Retinal Processing.

Further Reading

Barlow, H. B. (1953). Summation and inhibition in the frog's retina. *Journal of Physiology* 119: 69–88.

Beaudoin, D. L., Borghuis, B. G., and Demb, J. B. (2007). Cellular basis for contrast gain control over the receptive field center of mammalian retinal ganglion cells. *Journal of Neuroscience* 27: 2636–2645.

Demb, J. B. (2008). Functional circuitry of visual adaptation in the retina. *Journal of Physiology* 586: 4377–4384.

Fried, S. I., Munch, T. A., and Werblin, F. S. (2002). Mechanisms and circuitry underlying directional selectivity in the retina. *Nature* 420: 411–414.

Fried, S. I., Munch, T. A., and Werblin, F. S. (2005). Directional selectivity is formed at multiple levels by laterally offset inhibition in the rabbit retina. *Neuron* 46: 117–127.

Hsueh, H. A., Molnar, A., and Werblin, F. S. (2008). Amacrine to amacrine cell inhibition in the rabbit retina. *Journal of Neurophysiology* 100(4): 2077–2088.

Lee, S. and Zhou, Z. J. (2006). The synaptic mechanism of direction selectivity in distal processes of starburst amacrine cells. *Neuron* 51: 787–799.

Levick, W. R. (1965). Receptive fields of rabbit retinal ganglion cells. *American Journal of Optometry and Archives of American Academy of Optometry* 42: 337–343.

Maturana, H. R., Lettvin, J. Y., McCulloch, W. S., and Pitts, W. H. (1960). Anatomy and physiology of vision in the frog (*Rana pipiens*). *Journal of General Physiology* 43(supplement 6): 129–175.

Molnar, A. and Werblin, F. (2007). Inhibitory feedback shapes bipolar cell responses in the rabbit retina. *Journal of Neurophysiology* 98: 3423–3435.

Roska, B., Molnar, A., and Werblin, F. S. (2006). Parallel processing in retinal ganglion cells: How integration of space-time patterns of excitation and inhibition form the spiking output. *Journal of Neurophysiology* 95: 3810–3822.

van Wyk, M., Taylor, W. R., and Vaney, D. I. (2006). Local edge detectors: A substrate for fine spatial vision at low temporal frequencies in rabbit retina. *Journal of Neuroscience* 26: 13250–13263.

Werblin, F. S. and Dowling, J. E. (1969). Organization of the retina of the mudpuppy, *Necturus maculosus*. II. Intracellular recording. *Journal of Neurophysiology* 32: 339–355.

Information Processing: Amacrine Cells

R E Marc, University of Utah, Salt Lake City, UT, USA

Glossary

Buffer – A device that collects signals from a source and distributes them to targets without taxing the limited capacity of the source.
Dendrodendritic synapses – Unique synaptic motifs where both pre- and postsynaptic assemblies coexist on the same neuronal dendrite rather than segregating into dendrites and axons, respectively; they are the fundamental modes for biological feedback in sensory pathways.
Directional selectivity – The ability of a neuron to preferentially spike in response to stimuli originating from a given visual quadrant, but not others.
Feedback – The use of a portion of an output signal as an additional upstream input to modify the amplification in a network. Negative feedback reduces the gain and noise and improves the frequency response (spatial, temporal, or spectral). Positive feedback can be used to further tune the frequency response or generate resonance.
Feed forward – The use of a portion of an output signal as an additional parallel input to a downstream target. Negative feed forward selectively improves the frequency response (spatial, temporal, or spectral), but has little benefit on system noise or stability. Positive feed forward can be used to further amplify the effect of a signal.
Gain – The ratio of output and input amplitudes for a system, typically specified logarithmically as decibels of power [10 log (Pout/Pin)] or squared voltage [20 log (V^2out/V^2in)].
Nested feedback – The use of a portion of the feedback signal on the feedback process itself, allowing the effect of feedback to be more precisely tuned.
Sign-conserving synapses – Postsynaptic events mediated by receptors whose activation generates the same polarity of signal as the presynaptic terminal, that is, typically, a-amino-3-hydroxy-5-methyl-4-isoxazolepropionic acid, *N*-methyl D-aspartate, and nicotinic acetylcholine receptors.
Sign-inverting synapses – Postsynaptic events mediated by receptors whose activation generates the opposite polarity of signal as the presynaptic terminal, that is, typically, gamma aminobutyric acid and glycine.
Transfer function – The output of a given cell or device relative to its input, usually expressed as gain versus temporal or spatial frequency.

Amacrine Cells

Amacrine cells (ACs) and axonal cells (AxCs) are multipolar neurons that shape the ganglion cell (GC) function. While two to four classes of horizontal cells (HCs) provide lateral signal processing in the outer plexiform layer, ACs and AxCs are the most diverse neuronal group of any brain region, with over 30 classes in mammals and even more in highly visual nonmammalians, such as cyprinid fishes, where over 70 AC classes have been documented.

AC Classification, Form, and Patterns

The neural retina is composed of three superclasses of cells: (1) sensory neuroepithelial cells (photoreceptors and bipolar cells (BCs)); (2) multipolar neurons (ACs, AxCs, and GCs); and (3) gliaform neurons (HCs). Retinal multipolar neurons are further divisible into projection neurons (GCs and AxCs) and *bona fide* local circuit neurons, the ACs. This is an important distinction. The definition of the term amacrine refers to lacking an axon and ACs are neurons that mix presynaptic and postsynaptic specializations on their dendrites. These dendrodendritic specializations make them homologous to the anaxonic granule cells (GrCs) of the olfactory bulb (**Figure 1**). Both ACs and GrCs are inhibitory neurons that provide in-channel and cross-channel feedback. Conversely, GCs are classical projection neurons with exclusively postsynaptic retinal dendrites and presynaptic axon terminal ramifications in the central nervous system (CNS). The AxC group is a collection of diverse, nonamacrine retinal neurons that are similar to GCs in having distinct dendritic arbors and one or more long intraretinal axons. The AxC group includes polyaxonal cells in mammals and avians, certain dopaminergic neurons, and interplexiform cells. Interestingly, topologically similar AxCs in the olfactory bulb are the periglomerular cells and some of them are also dopaminergic.

Different kinds of ACs form two large superclasses with shared features: lateral and vertical ACs. Lateral ACs are precisely stratified in a single or a few layers of

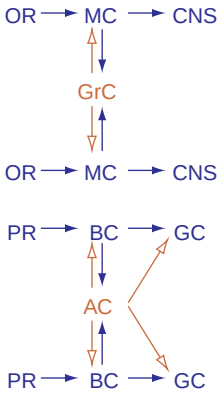

Figure 1 Signal processing in the olfactory bulb (top) and retina (bottom). Glutamatergic sensory neurons such as olfactory receptors (OR) and photoreceptors (PR) directly drive glutamatergic target neurons in the afferent chain, that is, olfactory mitral cells (MC) and retinal bipolar cells (BC), respectively. MCs and BCs then target the next glutamatergic elements as well as sets of inhibitory GABAergic local circuit neurons: olfactory granule cells (GrC) and retinal amacrine cells (AC). Both these neurons provide local inhibitory feedback onto their source neurons. ACs also provide inhibitory feed forward onto ganglion cells (GC) in the chain. Blue elements are glutamatergic. Red elements are GABAergic.

the inner plexiform layer, and spread their dendrites laterally either in a narrow to wide span as needed for their function; most of them release γ aminobutyrate (γ ACs). Vertical ACs distribute their dendrites across several levels of the inner plexiform layer, mostly in narrow and medium spans; most of them are glycinergic (gly ACs). **Figure 2** illustrates three very different structural patterns of vertebrate ACs. Radiate γ ACs (**Figure 2(a)**) are cone BC-driven pyriform cells with a single, thick proximal dendrite that descends to a given level of the inner plexiform layer and then generates nearly 50 dendrites that each radiates unbranched through the retina at one level for up to 0.5 mm. It exists in both on and off varieties, each branching extensively in a narrow band of the inner plexiform layer as a sparse field of processes. Similar cells are present in most vertebrates, but are incompletely studied. Another lateral cell is the widely studied starburst γ AC (**Figures 2(a)** and **2(b)**). It exists in both on and off varieties, each branching extensively in a narrow band of the inner plexiform layer as a dense field of processes. In nonmammalians with thick inner plexiform layers, it is a pyriform cell; however, in most mammals, it is a multipolar cell. Mammalian rod gly ACs exemplify the vertical phenotype (**Figures 2(a)–2(c)**), with deeply branching arboreal dendrites that collect signals from rod BCs in the proximal inner plexiform layer, mid-inner plexiform layer gap junctions with on-cone BCs, and both inputs and outputs onto off BCs from lobular dendrites in the distal inner plexiform layer. As these cells illustrate, the inner plexiform layer is laminated according to cone BC type (**Figure 2(c)**), with off cells terminating in the distal

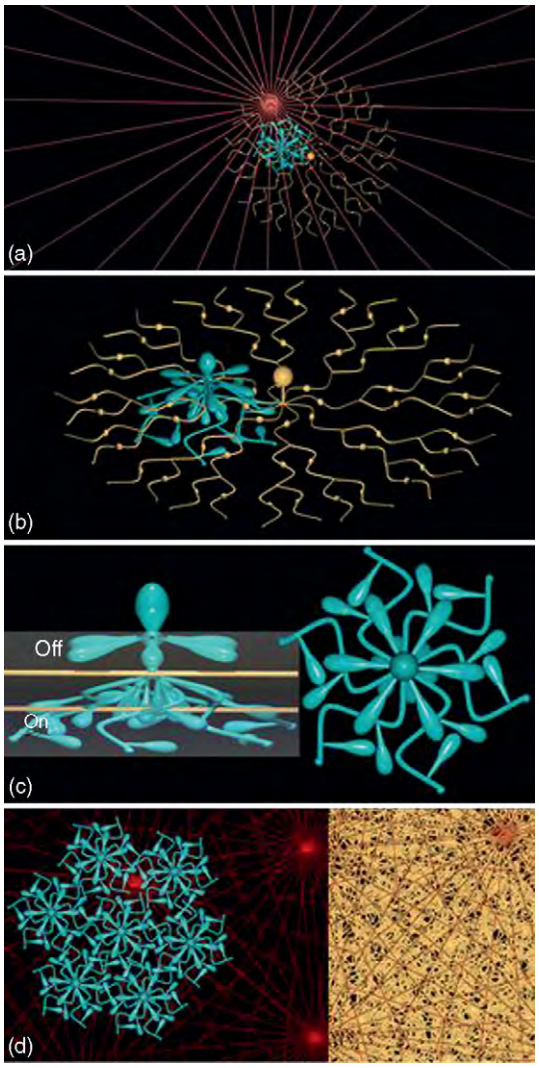

Figure 2 Schematic shapes and patterns of three canonical varieties of retinal ACs. (a) Top view of two lateral ACs and one vertical AC. Red: an off radiate γ AC from goldfish retina, with a wide-field, monostratified nonbranching dendritic arbor over 0.5 mm in diameter. These cells appear to be present in all vertebrates. Yellow: a goldfish off-starburst γ AC with a medium, monostratified, bifurcating, wavy arbor approximately 0.2 mm in diameter. Starburst cells are found in all vertebrates. In species with thick inner plexiform layers, they are pyriform with a single proximal dendrite; in those with thin inner plexiform layers (mammals), they are multipolar. Cyan: a mammalian vertical gly AC with a small, multistratified arbor nearly 0.05 mm in diameter. (b) Oblique view of the starburst γ AC and gly rod ACs showing that the starburst cell captures more synaptic space, but is laminated between the distal and proximal dendrites of the gly rod AC. (c) Vertical and top views of the gly rod AC. Immediately beneath the soma are several large lobular dendrites that contact off BCs. Deep in the inner plexiform layer are arboreal dendrites that capture rod BC inputs at their tips and, as they ascend through the inner plexiform layer, make gap junctions with cone BCs. The inner plexiform layer is divided into on and off layers exemplified by the yellow starburst AC dendritic bands. (d) Coverage patterns of ACs. The red radiate γ ACs are sparse and have coverage factors (CF) of approximately 4–6. The yellow starburst ACs are more frequent and have CF >100 and capture a great fraction of the synaptic space in a thin stratum of the inner plexiform layer. The cyan rod gly ACs are densely packed but have CF ≈ 1.

part and on cells in the proximal part. The AC processes fill the inner plexiform layer from the AC layer to the GC layer. The on- and off-starburst ACs indicate the positions of two fine on- and off-sublayers and exemplify the lateral motif of a large cohort of γ ACs. The gly rod ACs exemplify the vertical motif, bridging both on and off layers and transporting scotopic information in the on → off direction.

AC branching is quantified in many ways. The fractal box dimension (D) summarizes how effectively a dendritic pattern captures the synaptic space in a plane. $D = 1$ for a line and $D = 2$ for a complete plane. For radiate cells, $D \approx 1.2$ (low capture efficiency), while it approaches 1.5 for starburst cells (very high capture efficiency). In biological terms, radiate cells rigidly cover space, but not synapses, and contact inputs stochastically as they traverse wide swaths of the image. Conversely, starburst cells aggressively capture many synapses, rather than space, with curving dendrites. Thus, these cells will have very different signal-processing functions. Most ACs are distributed in coverings, which is one of the three types of two-dimensional (2D) cell patterns. The other two are packings (photoreceptors) and tilings (GCs). Patterns are partly defined by the extent of overlap that exists between members of a cell group (the coverage factor, CF) and how evenly the geometric centers of the cell fields are distributed over space (the conformity ratio, CR). Packings such as blue cones have CF < 1 and CRs ≈ 3 (weakly orderly) in mammals to >15 (crystalline) in fishes. GCs tile, with CFs ≈ 1 and CRs ≈ 3. Coverings shown by ACs have CF >1–100, indicating that for some ACs, dendritic fields of over 100 cells overlap a single point in the image plane, implying an intense synaptic control of signaling in that zone. Most CRs for ACs range from 1 to 4 in mammals. Using our examples from above (**Figure 2(d)**), radiate cells have CF $\approx$ 4–6 (center-to-center spacing) and form a sparse, but orderly, synaptic mesh over the retina. Starburst cells have CF ≈ 60 or more and densely pack the synaptic space. Narrow-field glycinergic ACs have CF ≈ 1 and act as nonspatial intercalary amplifiers or cross-channel controllers (discussed below).

AC Synapses and Neurochemistry

Almost all ACs are driven by BCs at ribbon synapses, decoding that glutamatergic input with a-amino-3-hydroxy-5-methyl-4-isoxazolepropionic acid (AMPA) receptors. ACs driven by rod BCs almost exclusively use AMPA-receptor-mediated currents, while most of those driven by cone BCs amplify and sustain the initial AMPA-driven currents with *N*-methyl D-aspartate (NMDA) receptors. Most native AMPA receptors are heteromers (some homomers may exist) of two or more of four known glutamate receptor (GluR) subunits: GluR1, GluR2, GluR3, and GluR4. There is no required stoichiometry; however, receptors with a mixture of GluR2 and GluR3 subunits are common in the brain and retina. There are post-translational modifications that change receptor conductances, kinetics, and glutamate sensitivity. The most important of these is the *gluR2* messenger ribonucleic acid (mRNA) pre-editing of a codon that converts a pore-lining neutral Q residue to a cationic R residue. Almost all mature GluR2 subunits are edited.The expressing of a GluR2 subunit has four important actions regardless of its partners: (1) it nearly abolishes the AMPA receptor Ca^{2+} permeability; (2) it decreases the channel conductance twofold or more; (3) it linearizes the I–V relation; and (4) it eliminates the GluR1 subunit phosphorylation-dependent increases in receptor conductance. Thus, ACs can express a range of sensitivities to glutamate. The most glutamate-sensitive neuron in the retina is the starburst AC population. Similarly, ACs express different levels and kinds of NMDA receptors, resulting in a broad spectrum of response attributes.

The outputs of ACs are conventional synapses targeting BCs, ACs, and GCs. Thus, ACs are positioned to powerfully shape all signal flow through the retina. However, there is a key difference in the high tonic vesicle fusion rate synapses of photoreceptor and BC ribbon synapses and the transient vesicle fusion of ACs. As a result, ACs act as temporal filters and signal through bursts of apparently precisely timed inhibitory transmitters. The presynaptic vesicle pools of ACs are generally very small, with tens to hundreds of vesicles, rather than the pools of thousands harbored by BCs. Thus, the actions of ACs are both swift and subtle. This is unlike the strong tonic influence of HCs as shown below.

Of the approximately 30 classes of ACs described for mammals, half to two-thirds of the classes are GABAergic and release GABA via small to large patches of vesicles at conventional synapses. Most of the remaining cells are narrow-field glycinergic cells. These two fast classical inhibitory transmitters act largely by opening anion-permeant channels that, in most cases, generate hyperpolarizing inward chloride currents. The purpose of the two kinds of anion channel transmitters is additivity: they do not occlude each other's receptors either by desensitization or by subadditivity, as in the cases of side-by-side GABA receptor patches.

The targets of GABAergic ACs decode GABA signals with either ionotropic GABAA or GABAC receptors (which modulate anion conductances) or metabotropic GABAB receptors that modulate K^+ conductances, or the operating range of voltage-gated Ca^{2+} channels. The difference between GABAA and GABAC receptors is similar to the difference between fast AMPA receptors and slower, more sustained NMDA receptors. GABAA receptors are heteromeric pentamers of GABA receptor subunits. Though they can have large anion conductances, they tend to desensitize quickly and act transiently. GCs and ACs predominantly express GABAA receptors. Ionotropic

GABAC receptors are homomeric assemblies of ρ subunits and are, arguably, a subset of the GABAA receptor group. When activated by GABA, GABAC receptor conductances are smaller, but more sustained, and they are more GABA sensitive. These receptors are primarily expressed by BCs. Since both ionotropic GABA and glycine receptor types activate chloride conductances, their efficacies can vary with the membrane potential of the target cell and the chloride gradient. Another mechanism that mediates the inhibition is shunting inhibition, where large conductance increases diminish the space and time constants of small dendrites. This inhibition is independent of the postsynaptic voltage and the chloride gradient and is most effective on small processes far from the major dendrites of a cell.

GABAB receptors are also highly effective regardless of membrane potential. They are guanine nucleotide binding protein coupled receptors (GPCRs) that either increase the voltage threshold of synaptic Ca^{2+} channels or the conductance of K^+ channels, strongly hyperpolarizing the cells (both slowing synaptic release). The former effect seems more prominent on BC axon terminals and the latter in GC dendrites or somas. Each mechanism can inhibit synaptic signaling in target processes with different timing and efficacy. However, the synaptic gain of such signaling is generally low and is often lesser than 1. Thus, individual GABAergic or glycinergic synapses are rather weak, and stimulus-dependent synchronicity is required for strong effects.

Several additional neuroactive signals associated with GABAergic ACs are co-transmitters: acetylcholine (ACh), certain catecholes, serotonin in nonmammalians, several peptides, and nitric oxide (NO). The differential regulation (if any) of GABA and ACh, catecholamine, serotonin, or peptide release is poorly understood. Glutamate may also be an excitatory AC co-transmitter for glycinergic ACs that express vGlut3, a vesicular glutamate transporter. Further, the roles of peptides and monoamines in information processing *per se* are also not completely clear, though some data suggest that peptides such as somatostatin may improve signal-to-noise ratios through an unknown mechanism.

ACs and Signal-Processing Fundamentals

ACs are components of small network submotifs (stereotyped aggregates of cell processes and synapses) that carry out analog signal-processing operations, including filtering (spatial, temporal, and spectral), gain control, signal–noise separation, signal buffering, and feature definition. Feedback is an essential control process in all amplification systems. Sign-inverting feedback (**Figure 3(a)**) is the primary mechanism by which most of these operations are effected in biology and electronics, and its essential nature is the addition of a scaled, inverted copy of the output of an amplification stage back to that stage. Every system has an input–output response R that, for simple time-invariant linear systems, can be expressed as a transfer function of stimulus frequency $G(s)$, where G is the system gain and s is frequency. This is often referred to as the open-loop gain and has a shape similar to that in **Figure 3**. As inputs become faster (higher frequency), the gain begins to fall off. In a moving transient world, we would prefer to have the best gain at a higher frequency and negative feedback as the mechanism. The electronic negative-feedback amplifier was invented by Harold Stephen Black of Bell Laboratories in 1927, and the biological one by evolution some 3 billion years BP. By providing an inverted signal with transfer function $H(s)$ to the input, R changes from $G(s)$ to $G(s)/[G(s)H(s)+1]$. For $H(s) \geq 1$, the shape of the response function changes based on the shape of $H(s)$. If $H(s)$ is a slow, tonic response, then by depressing slow frequencies more than fast ones, R feedback has an improved frequency response. Similarly, feedback can reduce noise. Negative feedforward is also common biologically and can be even more potent in shaping outputs than feedback, although it is not as effective for frequency response or noise control.

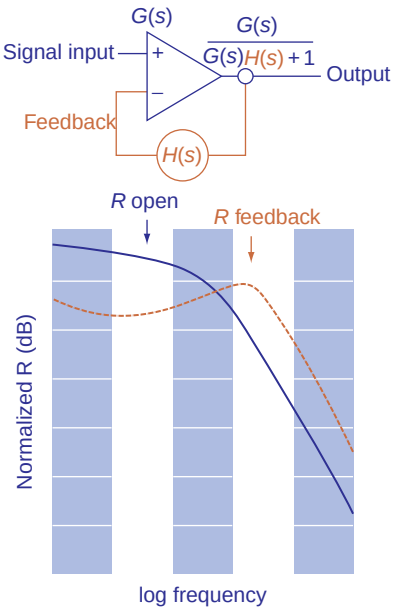

Figure 3 The basic principles of feedback. Top: an operational amplifier feedback circuit with an open loop sign-conserving transfer function $G(s)$ and part of the output fed back to the sign-inverting input, the transfer function $H(s)$, and net output transfer of $G(s)/[G(s)H(s)+1]$. Bottom: the effect of feedback on a given amplifier's performance. With no feedback, the response R as a function of frequency slowly rolls off. With feedback, the normalized peak response is at a higher frequency.

We can consider the retina as having only two amplification stages: (1) photoreceptors → BCs and (2) BCs → GCs (**Figure 4**). Every stage of feed-forward gain also requires feedback or feed-forward control, whether made of silicon or cells. In the retina, an amplification stage is a

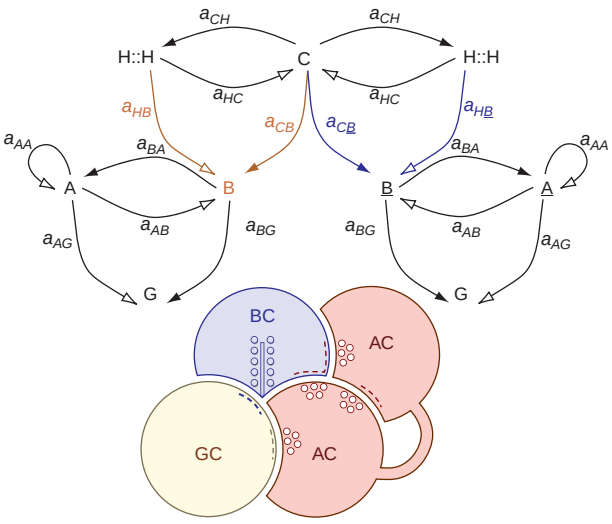

Figure 4 The basic connectivity of ACs. Top: the stages of amplification in the retina flowing from cones (C) to BCs (B) to GCs (G). Cones provide lateral excitatory signals to coupled sheets of HCs (H::H) which, in turn, provide lateral feedback to cones and lateral feed forward to BCs. Cone signals bifurcate, generating sign-conserving responses in off BCs (B) and sign-inverting responses in on BCs (B̲). Similarly, any feed-forward HC signals must also bifurcate to generate sign-inverting signals in off BCs and anomalous sign-conserving signals in on BCs. BC signals bifurcate and drive both ACs and GCs with sign-conserving mechanisms. ACs have the most complex topology, with feedback signals to BCs, feed-forward signals to GCs, and nested feed-forward/feedback by re-entrant loops. Every pairwise signal transfer has a transfer function, for example, B → A has transfer a_{BA}. Bottom: the topology of AC signaling at the BC → GC synapse. BCs provide a fast glutamatergic ribbon synapse input to ACs and GCs via AMPA receptors (blue dashes). ACs provide small conventional synapse GABA inhibition at predominantly ionotropic GABA receptors (red dashes) on ACs, BCs, and GCs.

small collection of properly connected excitatory and inhibitory synapses. Each synapse is itself a bicellular amplifier that encodes a presynaptic input voltage as a time-varying neurochemical signal, and postsynaptically decodes it as a direct current via ionotropic receptors or an indirect current or response modulation (e.g., intracellular Ca^{2+} release), typically through G-protein-coupled receptors (GPCRs). Excitatory synapses typically have amplifications or gains >>1, while inhibitory synapses typically have gains <1. ACs are the key feedback and feed-forward devices of the inner plexiform layer and their spatial distributions shape the nature of their interactions with BCs and GCs.

In detail, there are three primary submotifs that can strongly shape how ACs are involved in signal processing (Figure 4). The first is the classical reciprocal feedback synapse BCΔAC, wherein a signal from a BC ribbon onto an AC process is directly antagonized by an AC, typically a γ AC. This signaling pathway increases the frequency response and stabilizes the gain of the BC itself. The second is the parallel classical feed-forward synapse chains BC1 G and BC1 AC G where the AC synapse antagonizes the BC excitation directly in the GC. However, as any BC noise has already been amplified by the BC1 G synapse, feed forward is ineffective in improving the signal-to-noise ratio. However, it is very effective in generating stimulus-specific lateral signals in GCs. The third submotif is the AC AC synapse. While extremely common, the kind of signal processing associated with this submotif is poorly understood. In its most concrete form, homotypic or even autotypic AC synapses appear to be a fundamental attribute of the reciprocal feedback system by adding a loop known as nested feedback: BC□AC□. This process is reminiscent of nested transconductance amplifiers where stages of looped self-inverting signals are used to tune up the amplifier, endowing it with better, high-frequency performance and giving it a wider bandwidth. Nested AC feedback may do the same.

Examples of AC Networks

There are almost no AC systems whose complete range of functions is completely understood, largely owing to their diversity and the difficulty of obtaining large physiological samples. Four generic mammalian AC networks and signal processing functions that are of particular interest are outlined here.

γ ACs of the Rod Pathway

γ ACs of the rod pathway mediate temporal processing, gain control, and noise suppression. Extensive anatomy, ultrastructure, physiology, and pharmacology reveal the serotonin-accumulating (S1/S2) γ ACs of the mammalian retina to be archetypal in-channel feedback devices. The mammalian rod pathway is unique among vertebrates (as far as is known) in using two cycles through BC amplification (Figure 5). All the outputs of the rod BC target ACs of two major classes: γ ACs that engage in feedback and gly ACs that engage in re-entrant feed forward to pass rod signals through the cone on and off channels. Every BC displays γ feedback synapses, which suggests that the narrowly stratified medium-to-wide field γ AC is a standard motif component. Rod BCs display clear GABAC-mediated inhibition and the S1/S2 γ ACs that provide feedback are strongly AMPA driven, on-center ACs. This simple feedback circuit will provide the BC with better temporal response, as scotopic light gets brighter, and improve signal-to-noise performance. Though the mammalian retina contains no serotonin, it is likely that the indoleamine-transporting S1/S2 cells are descendants of the nonmammalian serotoninergic/γ (S γ AC) system, which forms feedback synapses with both off and on mixed rod-cone BCs. The disappearance of serotonin signaling is clearly a recent evolutionary event, but the

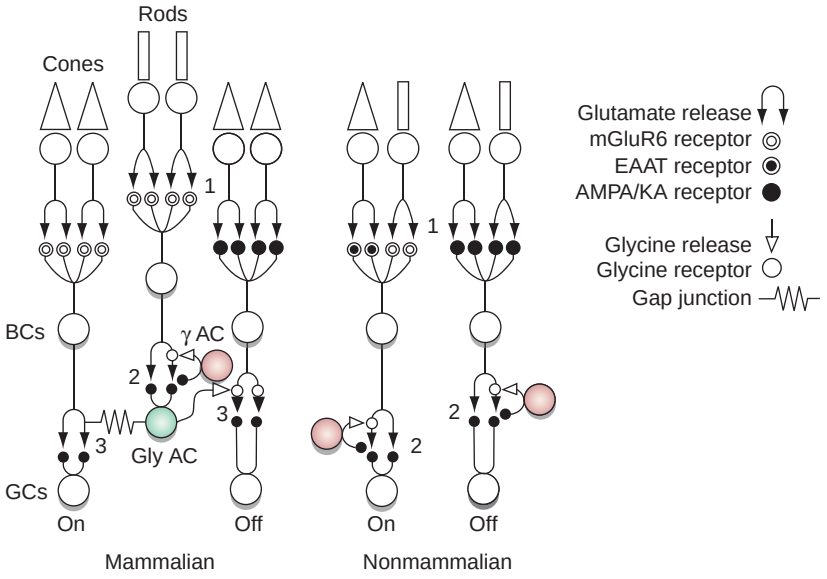

Figure 5 A comparison of rod and cone convergence onto GCs in mammalian and nonmammalian retinas. Nonmammalians use conventional mixed rod-cone BCs with direct input onto GCs and classical GABAergic feedback. Mammals predominantly exploit a rod BC that drives an intermediate stage of gain via the gly rod AC, which re-enters the cone pathways at the inner plexiform layer. The gly rod AC rives the off-BC pathway with sign-inverting glycine receptors and the on-BC pathway with gap junctions. Similar to nonmammalians, the γ rod AC provides BC feedback.

association of this simple BCΔAC network with rod BC pathways is clearly ancient.

Gly ACs of the Rod Pathway

Gly ACs of the rod pathway mediate cross-channel feed-forward buffering. In electronics, a buffer is an element interposed between two device stages to provide improved transfer. Buffers are often used to fan out input signals to several different outputs while isolating the input stage from the output loads. The gly rod AC represents an evolutionary buffer to further amplify the rod signal and distribute it in a low-noise manner. All vertebrates send rod signals to the CNS via GCs that also carry cone signals. There is no private rod pathway to the brain, though almost all species have private pure cone photopic channels (e.g., the primate foveal midget pathway). Nonmammalians combine the rod and cone pathways at the first synapse in the outer plexiform layer by converging on mixed rod-cone BCs. This chain involves two high-gain ribbon synapses: rod → mixed BC → GC. Mammalians combine rod and cone pathways by fanning out from a pure rod BC pathway back into cone pathways via two scotopic motifs in the inner plexiform layer:

1. rod → rod BC → gly rod AC :: ON cone BC → GC and
2. rod → rod BC → gly rod AC → OFF cone BC → GC.

This circuit is more complex as there are two photopic motifs:

1. cone → OFF cone BC → gly rod AC and
2. cone → ON cone BC :: gly rod AC.

There are also γ AC → gly AC inputs of unknown provenance. Physiologically, dark-adapted rod ACs have strong transient AMPA-like depolarizations, while light-adapted cells have more sustained, small depolarizations. In what manner all of the inputs are regulated remains unknown.

Small γ ACs of the Primate Midget BC → GC Pathway

These cells may mediate the red–green (R–G) color opponent pathway. These ACs receive direct input from midget BCs of either the on or off pathways and provide reciprocal feedback as well as feed forward to a small patch of midget GC dendrites. Midget GCs apparently connect almost exclusively to cones that express the long-wave system (LWS) pigment gene: either LWS VP 560 nm (R) or LWS VP 530 nm (G) cones. By extension, midget BCs exist as R and G forms. Ultrastructural data suggest that each AC collects signals from several midget BCs and is presynaptic to each. This suggests that there is no R–G chromatic selectivity in the AC surround and that a midget-pathway AC has no mechanism to sort BC chromatic type. This sets the stage for one of the longest running controversies in primate vision. Are midget CG receptive fields truly center/surround (C/S) pure opponent [+R/–G, –R/+G, +G/–R, and –G/+R] or are they a collection of cells with a weighted distribution of

surrounds that range from predominantly R or G or a mixture of R+G or yellow (Y) signals? A purely theoretical model has been proffered that involves glyc ACs as nulling tools to remove the inappropriate signal, making the surround appear pure. In any case, the appearance of small, spectrally pure antagonistic surrounds is inconsistent with large yellow-dominated HC surrounds observed in blue on-center GCs. How that signal disappears from R and G cone BCs remains a mystery in the face of strong evidence of coneΔHC feedback.

γ ACs of the Directionally Selective GC pathway

γ ACs mediate feature detection in the directionally selective (DS) GC pathway. The best-known feature detection event in the retina is the dependence of mammalian DS GC signaling on ionotropic GABA receptors. DS GCs exist in both on and on–off varieties; however, the qualitative feature of their signaling is similar. DS GCs have two response modes: (1) when a stimulus spot approaches the cell from the excitatory side, the cell fires, excited by both cone BC glutamate release activating AMPA receptors and starburst AC ACh activating nicotinic ACh receptors. Similar to the rod gly AC, starburst ACs provide the afferent flow with another burst of gain: cone → cone BC → starburst AC → GC. As starburst ACs are one of the most glutamate-sensitive cells in the retina, this makes DS cells exceptionally responsive. (2) When a stimulus spot approaches the cell from the null side, firing is inhibited by a GABAergic mechanism, possibly a γ AC or AxC (see below) with an eccentric output field so that it receives excitation long before the DS GC does. The blockade of ionotropic GABAA receptors converts the DS GC into a highly excitable cell with no directional bias. It has been found that starburst ACs themselves have a directional bias in that stimuli starting at the tips of the dendrites tend to hyperpolarize and those starting dead center and moving away tend to depolarize; in addition, some authors argue that this is sufficient to build a DS network. However, given the CF of the starburst ACs (>100) compared to that of the DS GCs (≈1), the geometric requirements for this seem difficult to achieve. It is possible, even probable, that an additional γ AC or AxC is involved, as shown in **Figure 6**.

Axonal Cells

A subset of retinal neurons are the axonal or polyaxonal cells, which includes one of the dopaminergic neurons of the mammalian retina. Many are clearly GABAergic, while others, such as the dopaminergic neuron, may be dual glutamate/dopamine neurons. The essential feature of AxCs is the axon: a long–range output device that enables these neurons to send signals to regions substantially displaced from the soma and dendritic arbor. AxCs (including dopamine neurons) show either on or on–off responses. In nonmammalian retinas, object motion-selective (OMS) cells achieve their feature detection via polyaxonal γ AxCs. This raises the question of whether the mammalian DS GC uses the same strategy.

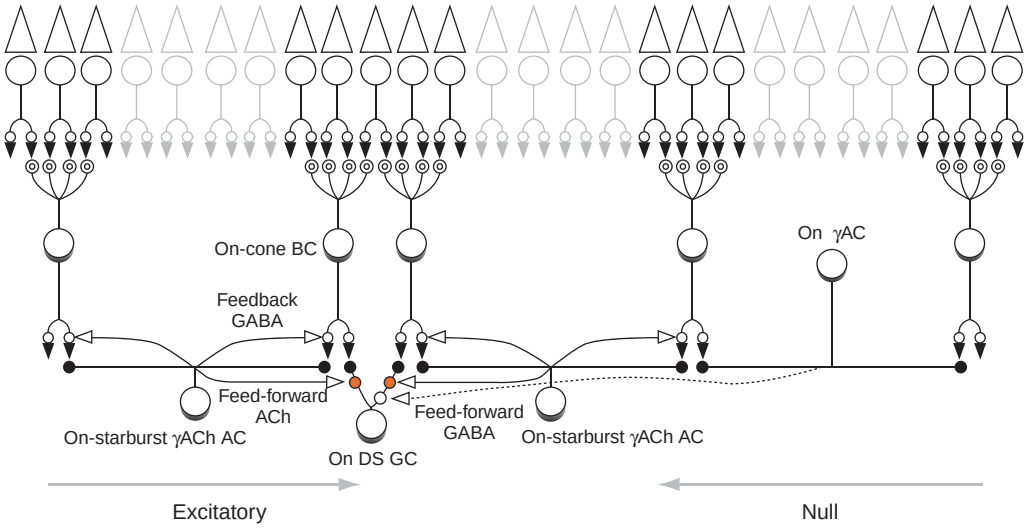

Figure 6 One topology for the generic on directionally selective (DS) pathway. The on DS GC receives glutamatergic excitation directly from on-cone BCs (black arrows and dots) and cholinergic feed-forward excitation (red dots) from local patches of starburst ACs. The starburst ACs also provide GABAergic feedback to BCs (open arrows and dots). While some argue that the starburst alone can generate directional surrounds for DS GCs, the symmetry of starburst AC fields makes this a challenging model. Similar to object motion sensitive (OMS) GCs, it is also possible that a γ polyaxonal AxC provides asymmetric inhibition for targets approaching from the null direction.

ACs and Disease

Over the past 5 years, it has become evident that, similar to the CNS, the retina undergoes extensive remodeling in response to sensory deafferentation effected by retinal degenerations, especially the retinitis pigmentosas. ACs are especially active components of remodeling, often sprouting new dendrites and participating in anomalous synaptic structures known as microneuromas. In addition, similar to other retinal neurons, they can be induced to relocate to ectopic somatic clusters loci (either to the distal retinal margin or GC layer) via anomalous migration columns. The most resilient cells of all, they are the last to die as the retina is slowly depleted of neurons. In fact, ACs may be a key component of neural survival in the remnant retina by providing a periodic source of neural activity in the absence of photoreceptors.

See also: GABA Receptors in the Retina; Glutamate Receptors in Retina; Information Processing: Amacrine Cells; Information Processing: Bipolar Cells; Information Processing: Contrast Sensitivity; Information Processing: Direction Sensitivity; Information Processing: Ganglion Cells; Information Processing: Horizontal Cells; Information Processing in the Retina; Injury and Repair: Retinal Remodeling; Morphology of Interneurons: Amacrine Cells; Morphology of Interneurons: Bipolar Cells; Morphology of Interneurons: Interplexiform Cells; Neuropeptides: Function; Neuropeptides: Localization; Neurotransmitters and Receptors: Dopamine; Retinal Cannabinoids; The Role of Acetylcholine and its Receptors in Retinal Processing.

Further Reading

Baccus, S. A., Olveczky, B. P., Manu, M., and Meister, M. (2008). A retinal circuit that computes object motion. *Journal of Neuroscience* 28: 6807–6817.

Famiglietti, E. V., Jr. (1983). On and off pathways through amacrine cells in mammalian retina: The synaptic connections of ''starburst'' amacrine cells. *Vision Research* 23: 1265–1279.

Kittila, C. A. and Massey, S. C. (1997). Pharmacology of directionally selective ganglion cells in the rabbit retina. *Journal of Neurophysiology* 77: 675–689.

MacNeil, M. A., Heussy, J. K., Dacheux, R. F., Raviola, E., and Masland, R. H. (1999). The shapes and numbers of amacrine cells: Matching of photofilled with Golgi-stained cells in the rabbit retina and comparison with other mammalian species. *Journal of Comparative Neurology* 413: 305–326.

Marc, R. E. (1999). Kainate activation of horizontal, bipolar, amacrine, and ganglion cells in the rabbit retina. *Journal of Comparative Neurology* 407: 65–76.

Marc, R. E. (2004). Retinal neurotransmitters. In: Chalupa, L. and Werner, J. (eds.) *The Visual Neurosciences,* vol. 1, pp. 315–330. Cambridge, MA: MIT Press.

Marc, R. E. (2008). Functional neuroanatomy of the retina. In: Albert, D. M. and Miller, J. W (eds.) *Albert & Jakobiec's Principles and Practice of Ophthalmology,* 3rd edn, pp. 1565–1592. Philadelphia, PA: Saunders Elsevier.

Slaughter, M. M. (2004). Inhibition in the retina. In: Chalupa, L. and Werner, J. (eds.) *The Visual Neurosciences,* vol. 1, pp. 355–368. Cambridge, MA: MIT Press.

Tauchi, M. and Masland, R. H. (1984). The shape and arrangement of the cholinergic neurons in the rabbit retina. *Proceedings of the Royal Society of London B* 223: 101–119.

Vaney, D. I. (1990). The mosaic of amacrine cells in the mammalian retina. In: Chader, J. and Osborne, N. (eds.) *Progress in Retinal Research*, pp. 49–100. New York: Pergamon.

Vaney, D. I. (2004). Retinal amacrine cells. In: Chalupa, L. and Werner, J. (eds.) *The Visual Neurosciences,* vol. 1, pp. 395–409. Cambridge, MA: MIT Press.

Völgyi, B., Xin, D., Amarillo, Y., and Bloomfield, S. A. (2001). Morphology and physiology of the polyaxonal amacrine cells in the rabbit retina. *Journal of Comparative Neurology* 440: 109–125.

Wilson, M. and Vaney, D. I. (2008). Amacrine cells. In: Masland, R. H. and Albright, T. (eds.) *The Senses: A comprehensive reference*, pp. 361–367. Amsterdam: Elsevier.

Zhang, J., Jung, C. S., and Slaughter, M. M. (1984). Serial inhibitory synapses in retina. *Visual Neuroscience* 14: 553–563.

Zhang, J., Li, W., Trexler, E. B., and Massey, S. C. (2002). Confocal analysis of reciprocal feedback at rod bipolar terminals in the rabbit retina. *Journal of Neuroscience* 22: 10871–10882.

Information Processing: Bipolar Cells

S M Wu, Baylor College of Medicine, Houston, TX, USA

Glossary

Center-surround antagonistic receptive field (CSARF) – A receptive field of a visual neuron whose light response to light falling on the center region is of the opposite polarity (or spike increment/decrement) to the response to light falling on the surrounding regions of the cell's receptive field.

Depolarizing (ON-center) bipolar cell (DBC) – A bipolar cell exhibiting a depolarizing voltage response to light falling on the center region of its receptive field and a hyperpolarizing voltage response to light on its receptive field surround region.

Distal and proximal retina – In a retinal cross section, the distal retina refers to the photoreceptor side of the retina and the proximal retina refers to the ganglion cell side.

Feedback synapse – A synapse made from a higher-order neuron to a lower-order neuron, such as synapses made from horizontal cells to cones and from amacrine cells to bipolar cell axon terminals.

Hyperpolarizing (OFF-center) bipolar cell (HBC) – A bipolar cell exhibiting a hyperpolarizing voltage response to light falling on the center region of its receptive field and a depolarizing voltage response to light on its receptive field surround region.

Metabotropic glutamate receptor 6 (mGluR6) – A metabotropic glutamate receptor coupled with a second-messenger cascade found in DBC dendrites. It results in closure of cation channels in DBCs when bound with glutamate or its agonist L-2-amino-4-phosphonobutyrate (LAP4).

Rod bipolar cell – A bipolar cell whose light-evoked cation current is mediated primarily by rod synaptic inputs. In mammals, only rod DBCs have been identified.

Bipolar cells (BCs) are second-order neurons in the retina whose somas are located in the distal half of the inner nuclear layer (INL) (except for the displaced BCs found in some species whose somas are located in the outer nuclear layer (ONL)). BC dendrites branch in the outer plexiform layer (OPL) and make synaptic contacts with rod spherules, cone pedicles, and horizontal cell (HC) dendrites. Each BC bears an axon projecting to the inner plexiform layer (IPL) with terminals ramifying in different patterns at different sublaminae of the IPL. Based on their rod/cone contacts and axon terminal ramification patterns, BCs have been classified morphologically into several types. In mammals, one type of rod BC and 9 to 10 types of cone BCs have been identified (**Figure 1**). In fish, small BCs make synaptic contacts exclusively with cones and large BCs make contacts with both rods and cones, and in turtle, 11 morphological types of BCs have been found, with some contacting only cones and others contacting only rods. BCs in amphibian retinas contact both rods and cones, but some are clearly rod dominated where others are cone dominated.

BCs are the first neurons along the visual pathway that exhibit the center-surround antagonistic receptive field (CSARF) organization, the basic code for spatial information processing in the visual system. Light falling directly on the BC receptive field center region elicits voltage responses of the opposite polarity to the responses elicited by light falling on the surrounding regions of the BC's receptive field. BCs may be ON center with OFF surrounds (named ON-center BCs or depolarizing BCs (DBCs)), or OFF center with ON surrounds (named OFF-center BCs or hyperpolarizing BCs (HBCs)). The center input of BCs is mediated by rod and cone photoreceptors, which make chemical synapses on BC dendrites. BC receptive field centers are often found to be larger than their dendritic fields, suggesting that these cells may be electrically coupled. The surround input to BCs is mediated by interneurons that carry signals laterally from the surround region to the central region of the BCs' receptive field. These interneurons include HCs in the outer retina and amacrine cells (ACs) in the inner retina. HCs mediate BC surround responses through HC–cone–BC feedback synaptic pathways and/or HC–BC feed-forward (electrical or chemical) synapses, whereas ACs mediate BC surrounds through chemical synapses made on BC axon terminals in the IPL.

By using the whole-cell or microelectrode recording techniques in conjunction with fluorescent dye filling method, it has been shown that light response characteristics of various types of BCs are closely correlated with their axon terminal morphology. For example, it has been found in many species that axon terminals of DBCs ramify in the proximal half (sublamina B) of the IPL, whereas those of the HBCs ramify in the distal half (sublamina A) of the IPL. Axon terminals of rod BCs in mammalian retinas end near the proximal margin of the IPL, and axon terminals of cone BCs ramify in more central regions of the IPL. This agrees with the patterns of BC axon terminal stratification

in the salamander: axon terminals of rod-dominated BCs ramify at the two margins of the IPL, whereas those of cone-dominated BCs ramify at central regions of the IPL. Additionally, despite the anatomical finding that mammalian rod and cone BCs make segregated synaptic contacts with rods and cones, it has been recently shown that some mammalian BCs exhibit mixed rod/cone responses similar to most BCs in lower vertebrates. Furthermore, although rod HBCs were not identified by earlier mammalian anatomical studies, recent physiological evidence suggests that they may exist at least in some mammals.

Based on studies of BC physiological properties in various species, it is reasonable to propose that vertebrate retinas have six major functional types of BCs: the rod (or rod dominated), cone (or cone dominated), and mixed (rod/cone) depolarizing and hyperpolarizing BCs (DBC_R, DBC_C, DBC_M, HBC_R, HBC_C, and HBC_M). Each carries a characteristic set of light response attributes and projects them to the inner retina through axons that terminate at segregated regions (strata) of the IPL. Such stratum-by-stratum projection of light response attributes is exemplified by a large-scale voltage-clamp study of the salamander BC responses and morphology. This study reveals several rules for the function–morphology relationships of retinal BCs: (1) Cells with axon terminals in strata 1–5 (sublamina A) are HBCs (with outward light-evoked cation currents (ΔI_C)) and those in strata 6–10 (sublamina B) are DBCs (with inward ΔI_C). This agrees with the sublamina A/B rule observed in many vertebrate species (see, e.g., **Figure 1**, in which the IPL is divided into five sublaminae instead of 10). (2) Cells with axon terminals in strata 1, 2, and 10 are rod dominated, those in strata 4–8 are cone dominated, and

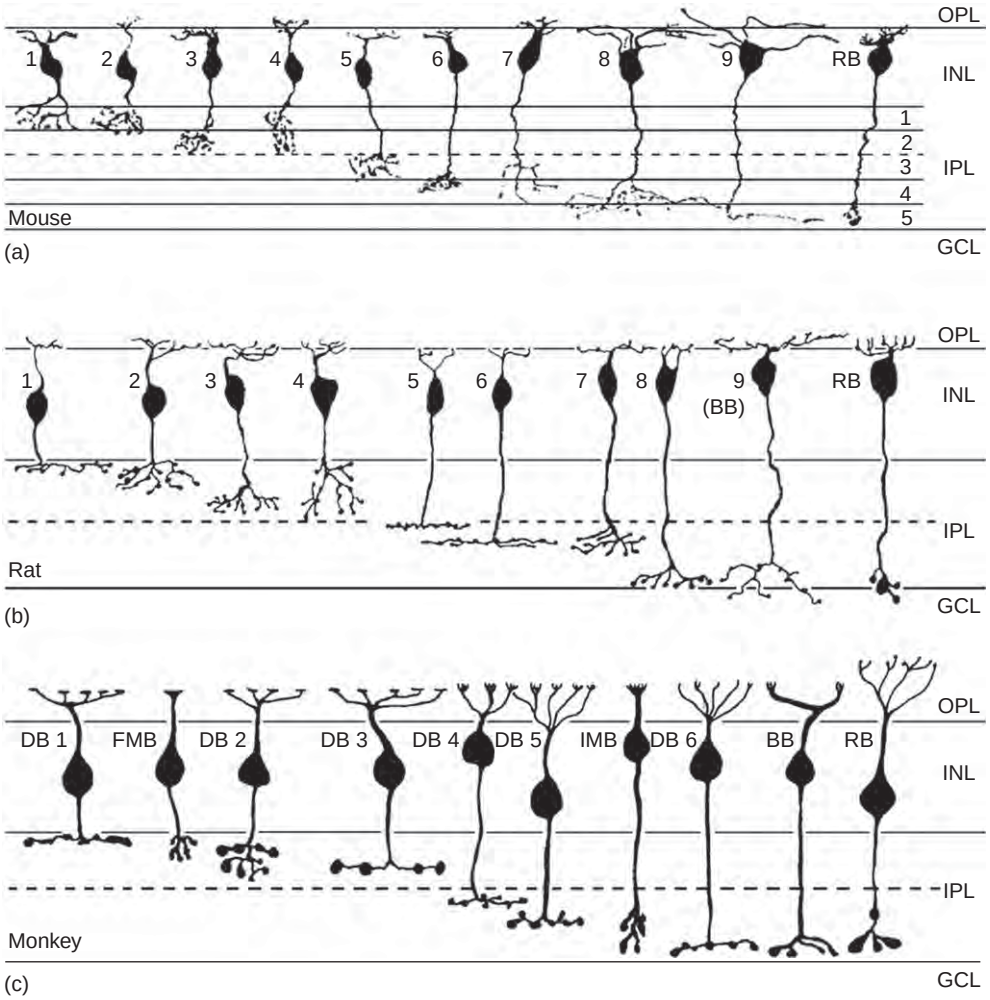

Figure 1 Schematic diagram of various types of bipolar cells in the mouse (a), rat (b), and monkey (c) retinas. Bipolar-cell images are derived from confocal images (a) or drawings (b) of Lucifer yellow/neurobiotin-injected cells, or drawings of Golgi-stained retinas (c). Inner plexiform layer (IPL) in this figure is divided into five sublaminae and IPL in the salamander retina (**Figures 2** and **3**) is divided into 10 sublaminae. OPL, outer plexiform layer; INL, inner nuclear layer; GCL, ganglion cell layer. From Ghosh, K. K., Bujan, S., Haverkamp, S., Feigenspan, A., and Wassle, H. (2004). Types of bipolar cells in the mouse retina. ***Journal of Comparative Neurology* 469: 70–82.**

those in strata 3 and 9 exhibit mixed rod/cone dominance. (3) Light-evoked ΔI_C at light onset in rod-dominated HBCs and DBCs are sustained, that of the cone-dominated HBCs exhibit a smaller sustained outward current followed by a transient inward current at the light offset, and that of the cone-dominated DBCs exhibit a sustained inward current followed by a small transient off outward current. (4) ΔI_{Cl} (light-evoked chloride currents) in rod-dominated BCs are sustained ON currents, whereas those in cone-dominated BCs are transient ON–OFF currents. ΔI_{Cl} in all BCs are outward, and thus they are synergistic to ΔI_C in HBCs and antagonistic to ΔI_C in DBCs. (5) BCs with axon terminals stratified in multiple strata exhibit *combined* light response properties of the narrowly monostratified cells in the same strata. (6) BCs with pyramidally branching or globular axons exhibit light response properties very similar to those of narrowly monostratified cells whose axon terminals stratified in the same stratum as the axon terminal endings of the pyramidally branching or globular cells.

In addition to projecting signals to various strata of the IPL, where ACs and ganglion cells (GCs) gather their inputs, BCs with various light response attributes have different CSARF organizations. **Figure 2** shows the morphology, patterns of dye coupling, light responses, CSARF properties, and membrane resistance changes associated with the center and surround voltage responses of the six functional types of BCs (HBC_R, HBC_M, HBC_C, DBC_C, DBC_M, and DBC_R) in the tiger salamander retina. These results suggest that the center and surround responses of various types of BCs in the retina are mediated by heterogeneous synaptic circuitry. The BC receptive field center diameters (RFCDs) vary with the relative rod/cone input: RFCD is larger in DBCs with stronger cone input, and it is larger in HBCs with stronger rod input. RFCD also correlates with the degree of dye coupling: BCs with larger RFCD are more strongly dye coupled with neighboring cells of the same type, suggesting that BC–BC coupling significantly contributes to the BC receptive field center.

BC center inputs are mediated by glutamatergic synapses. In darkness, glutamate is released from rod and cone photoreceptors, and it closes cation channels in DBCs and opens cation channels in HBCs. Postsynaptic responses of DBCs are mediated by metabotropic (metabotropic glutamate receptor 6 (mGluR6), L-2-amino-4-phosphonobutyrate (L-AP4)-sensitive) receptors coupled with a second-messenger cascade. In fish, the cone-to-DBC synaptic signal is mediated by a glutamate-activated chloride current that is suppressed by light and thus results in a membrane depolarization. Postsynaptic responses of HBCs are mediated by ionotropic receptors, and recent studies have shown that different subtypes of ionotropic glutamate receptors may be used by different types of HBCs in mediating rod/cone and transient/sustained signals.

Membrane resistance measurements in **Figure 2(e)** demonstrate that the center responses of all HBCs are associated with a resistance increase and the center responses of all DBCs are accompanied with a resistance decrease. This is consistent with the notion that glutamate released from rods and cones in darkness opens α-amino-3-hydroxyl-5-methyl-4-isoxazole-propionate (AMPA)/kainate receptor-mediated cation channels in HBCs and closes mGluR6-receptor-mediated cation channels in DBCs. Center light stimuli hyperpolarize rods and cones, suppress glutamate release, and result in a resistance increase (close ion channels) in HBCs and a resistance decrease (open ion channels) in DBCs.

Figure 3 is a schematic representation of the possible and unlikely synaptic pathways underlying surround inputs of various types of BCs, based on the surround response polarity and accompanying resistance changes shown in **Figure 2**. These results suggest that the HC–cone–BC feedback synapses may contribute to the surround responses of all six types of BCs. The negative HC–cone feedback synapses (pathway I) partially turn off the center responses by depolarizing the cones, as the membrane resistance changes associated with surround responses of all BCs are opposite to the resistance changes associated with center responses (**Figure 2(e)**).

Although all BCs share a common surround response pathway (the HC–cone–BC feedback pathway), various types of BCs use different HC and AC synaptic inputs to mediate their surround responses. It is unlikely, for example, that HBC surround responses are directly mediated by chemical synaptic inputs from hyperpolarizing lateral neurons, such as HCs and AC_{OFF}s, because of resistance change mismatch, and thus HBCs may only receive surround inputs from HC–cone–HBC and AC_{ON}–HBC synapses. On the other hand, resistance analysis suggests that DBC surround responses can be mediated by HC–cone–DBC, HC–DBC and AC_{OFF}–DBC chemical synapses, but not the AC_{ON}–DBC synapses. Moreover, dye coupling (**Figure 2(a)**) results indicate that DBC_Cs receive additional surround inputs from wide-field HCs through electrical synapses. Despite the heterogeneity, it is interesting to point out that an ON/OFF crossover inhibition rule applies here: cells with OFF (hyperpolarizing) responses (HCs and AC_{OFF}s) mediate surround inhibitory inputs to ON cells (DBCs); and cells with ON (depolarizing) responses (AC_{ON}s) mediate surround inhibitory inputs to OFF cells (HBCs). ON/OFF crossover inhibition from ACs to GCs have been reported in the salamander and mammalian retinas, and the data shown in **Figures 2** and **3** suggest that it may be a general rule for lateral inhibition in the visual system.

HCs mediate BC surround responses through the feedback synaptic pathway (HC→cone→BC) and/or the feed-forward synapses (HC→BC). Three synaptic mechanisms have been proposed for the HC feedback actions on cones. The first is that HCs release an inhibitory neurotransmitter (gamma aminobutyric acid (GABA) in several

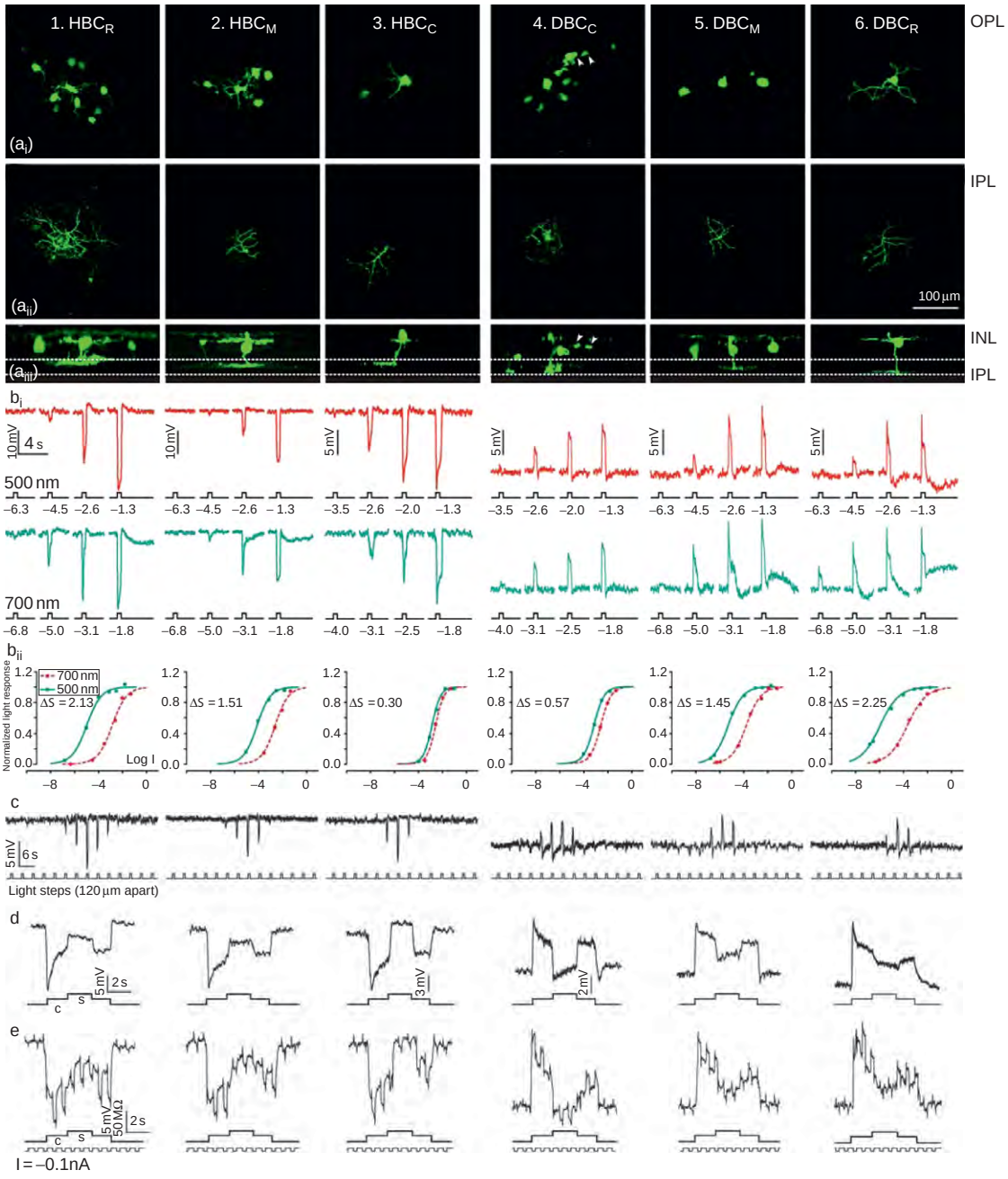

Figure 2 Morphology, light responses, and receptive fields of six types of bipolar cells in the tiger salamander retina. (a) Fluorescent micrographs of a neurobiotin-filled HBC_R (column 1), an HBC_M (column 2), HBC_C (column 3), a DBC_C (column 4), a DBC_M (column 5), and a DBC_R (column 6) viewed with a confocal microscope at the outer INL/OPL level (a_i), the IPL level (a_{ii}), and with *z*-axis rotation (a_{iii}). Scale bar = 100 µm. (b_i) BC voltage responses to 500 nm and 700 nm light steps of various intensities. (b_{ii}) Response-intensity (V-Log I) curves of the responses to 500-nm and 700-nm lights. ΔS (spectral difference, defined as $S_{700} - S_{500}$, where S_{700} and S_{500} are intensities of 700-nm and 500-nm light-eliciting responses of the same amplitude) of the six BCs are: 2.13, 1.51, 0.30, 0.57, 1.45, and 2.25. Since ΔS for the rods is about 3.4 and that for the cones is about 0.1 in the salamander retina, BCs with $\Delta S > 2.0$ are rod-dominated BCs, BCs with $\Delta S < 1.0$ are cone-dominated BCs, and BCs with $1.0 < \Delta S < 2.0$ are mixed rod/cone BCs. (c) Measurements of BC receptive field center diameters (RFCDs) by recording voltage responses to a 100-µm-wide light bar moving stepwise (with 120-µm step increments) across the receptive field. (d) Voltage responses of the six types of BCs elicited by a center light spot (300 µm) and a surround light annulus (700 µm, inner diameter; 2000 µm, outer diameter). The surround light annulus was of the same intensity (700 nm, –2) for all six cells, whereas the intensity of the center light spot was adjusted so that it allowed the annulus to produce the maximum response. (e) Voltage responses of the six types of BCs elicited by a center light spot and a surround light annulus (same as in (d)), and by a train of –0.1-nA/200-ms current pulses passed into the cell by the recording microelectrode through a bridge circuit. From Zhang, A. J. and Wu, S. M. (2009). Receptive fields of retinal bipolar cells are mediated by heterogeneous synaptic circuitry. *Journal of Neuroscience* 29(3): 789–797, with permission from Society for Neuroscience.

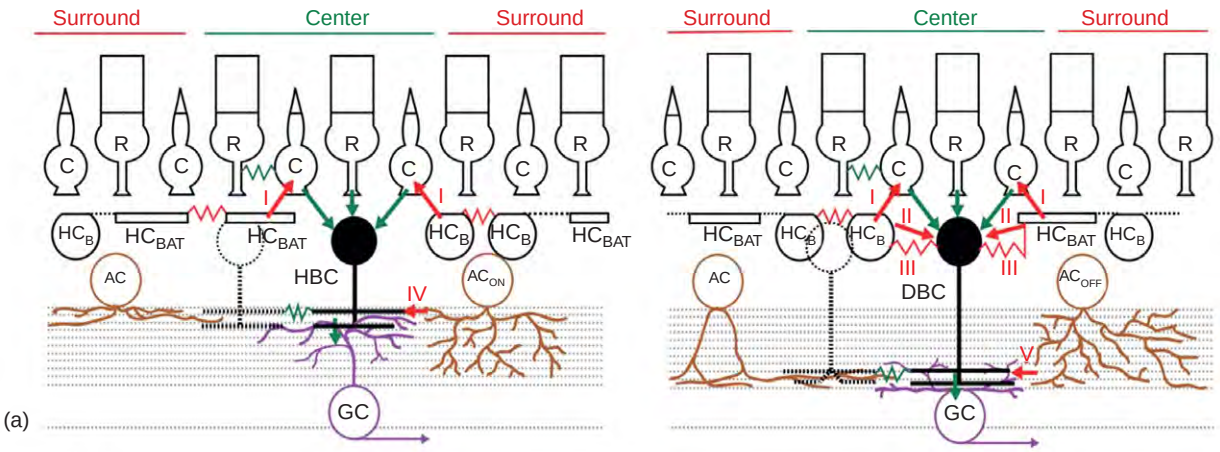

(a)

	Center synaptic organization		Surround synaptic pathways		
	Rod/cone inputs	BC–BC coupling	HC feedback (I) HC → cone → BC	HC feedforward HC → BC (II) chemical	(III) electrical	AC feedback (chemical) (IV) AC_{ON} → BC	(V) AC_{OFF} → BC
HBC_R	Rod: +++ Cone: +	+++	+ hyp (–) dep (+) dep	No	No	Yes (+) dep → dep	No
HBC_M	Rod: ++ Cone: ++	++	++ hyp (–) dep (+) dep	No	No	Yes (+) dep → dep	No
HBC_C	Rod: + Cone: +++	++	+++ hyp (–) dep (+) dep	No	No	Yes (+) dep → dep	No
DBC_C	Rod: + Cone: +++	+ +HC_S	+++ hyp (–) dep (–) dep	Yes hyp (+) hyp	Yes hyp (+) hyp	No	Yes hyp (+) hyp
DBC_M	Rod: ++ Cone: ++	+	++ hyp (–) dep (–) dep	Yes hyp (+) hyp	No	No	Yes hyp (+) hyp
DBC_R	Rod: +++ Cone: +	0	+ hyp (–) dep (–) dep	Yes hyp (+) hyp	No	No	Yes hyp (+) hyp

(b)

Figure 3 Center-surround antagonistic receptive field organization of bipolar cells. (a) Schematic diagrams of center (green) and surround (red) synaptic pathways of HBCs (left) and DBCs (right). R, rod; C, cone; HC_B, B-type HC somas; HC_{BAT}, B-type HC axon terminals; HBC, hyperpolarizing bipolar cell. DBC, depolarizing bipolar cell; AC, amacrine cell; AC_{ON}, ON amacrine cell; AC_{OFF}, OFF amacrine cell; GC, ganglion cell. Arrows: chemical synapses; zigzags: electrical synapses; I–V: five surround synaptic pathways list in (b). (b) Variations in synaptic pathways mediating center (green) and surround (red) responses of the HBC_R, HBC_M, HBC_C, DBC_C, DBC_M, and DBC_Rs. +++: strong; ++: intermediate; +: moderate; yes: possible; no: unlikely. For the possible pathways, response polarities (hyp, hyperpolarization; dep, depolarization) in each neuron and the synaptic sign ((+): sign preserving or (–): sign inverting) in each synapse in the pathways are indicated (e.g., in the HBC_R HC–cone–BC pathway: (hyperpolarization in HC) through a sign-inverting synapse (–) (depolarization in cone) through a sign-preserving synapse (–) (depolarization in BC)). From Zhang, A. J. and Wu, S. M. (2009). Receptive fields of retinal bipolar cells are mediated by heterogeneous synaptic circuitry. *Journal of Neuroscience* 29(3): 789–797, with permission from Society for Neuroscience.

species) in darkness that opens chloride channels in cones, and surround light hyperpolarizes the HCs, suppresses feedback transmitter release, depolarizes the cones, depolarizes the HBCs, and hyperpolarizes the DBCs. The second mechanism is that surround light hyperpolarizes HCs, resulting in an outward current through hemichannels in their dendrites near the cones, charging the cone membrane and modulating calcium currents in cones, increasing their calcium-dependent glutamate release which depolarizes the HBCs and hyperpolarizes the DBCs. The third mechanism is that surround-induced HC hyperpolarization elevates the pH in the HC–cone synaptic cleft, leading to an increase of calcium current in cones and a higher rate of glutamate release which depolarizes the HBCs and hyperpolarizes the DBCs. It is possible that different species under different conditions favor different feedback synaptic mechanisms, and/or different types of HC–cone synapses in the same animal may use one or more of

these three HC–cone feedback mechanisms. This idea is supported by a recent study demonstrating that the responses of salamander GCs to dim surround stimuli are sensitive to GABA blockers and those to bright surround stimuli are sensitive to carbenoxolone, a gap-junction/hemichannel blocker.

The HC–BC feed-forward pathway requires a sign-preserving HC–DBC synapse and a sign-inverting HC–HBC synapse. Studies from salamander retina suggest that HC→DBC feed-forward synapses may be functional. However, application of GABA on BC dendrites in Co^{2+} Ringer's does not elicit any response, indicating that if feed-forward synapses are chemical, the neurotransmitter is not GABA. Histochemical evidence suggests that only about 50–60% of the HCs in the salamander retina are GABAergic, and the identity of neurotransmitter(s) in the rest of the HCs is unknown (but unlikely to be glycine). As illustrated in the salamander (**Figure 2(a)**) and the rabbit retinas, subpopulations of BCs are dye coupled with HCs, raising the possibility that HC–BC electrical coupling may be involved in mediating the HC–BC feed-forward synapses for DBC surround responses.

The AC–BC contribution to BC surround responses are mediated by GABAergic or glycinergic synapses. GABA receptors on ACs and GCs are largely $GABA_A$, and those on BC axon terminals are largely $GABA_C$. Glycine receptors have been localized in ACs, GCs, BC dendrites, and BC axon terminals. These receptors localized in the IPL are postsynaptic to glycinergic ACs, while those in the OPL are postsynaptic to glycinergic interplexiform cells. In the *Xenopus* retina, GABA suppresses the surround responses of the DBCs, but only slightly reduces the surround of the HBCs, and glycine suppresses the surround responses of both DBCs and HBCs. In the tiger salamander, one study shows that GABA reduces the surround responses of a subpopulation of HBCs, but another report reveals that application of picrotoxin and strychnine does not affect the surround responses of either DBCs or HBCs. Recent studies in the primate retina indicate that the HC feedback signal to cones as well as to the surround responses of GCs are not sensitive to GABAergic or glycinergic agents, but sensitive to carbenoxolone, suggesting that the surround responses in GCs are mainly mediated by HC actions on BCs in the outer retina, not by GABAergic or glycinergic AC actions in the inner retina. The reasons for these different GABA/glycine actions on surround responses are unclear. As illustrated in **Figures 2** and **3**, surround responses of different functional types of BCs in the salamander retina are mediated by different combinations of synaptic circuitries: HC→cone (GABA/hemichannel/proton) →BC, HC→BC (chemical/gap junction) and AC→BC (GABA/glycine). It is conceivable that the surround responses of different BCs/GCs from different animals under different conditions are mediated by different combinations of surround synaptic pathways, and thus they are sensitive to different synaptic blockers. The wide variation of synaptic circuitries underlying surround responses of various functional types of BCs allows for flexibility in function-specific modulation of BC/GC receptive fields. Hence different features of spatial and contrast information, such as rod/cone and ON/OFF signals, can be differentially modulated by different lighting and adaptation conditions.

Acknowledgments

This work was supported by grants from NIH (EY 04446), NIH Vision Core (EY 02520), the Retina Research Foundation (Houston), and the Research to Prevent Blindness, Inc.

See also: Dry Eye: An Immune-Based Inflammation; Immunopathogenesis of HSV Keratitis.

Further Reading

Boycott, B. and Wassle, H. (1999). Parallel processing in the mammalian retina: The Proctor lecture. *Investigative Ophthalmology and Visual Science* 40: 1313–1327.

Dowling, J. E. (1987). *The Retina, an Approachable Part of the Brain*. Cambridge, MA: Harvard University Press.

Ghosh, K. K., Bujan, S., Haverkamp, S., Feigenspan, A., and Wassle, H. (2004). Types of bipolar cells in the mouse retina. *Journal of Comparative Neurology* 469: 70–82.

Kamermans, M. and Fahrenfort, I. (2004). Ephaptic interactions within a chemical synapse: Hemichannel-mediated ephaptic inhibition in the retina. *Current Opinion in Neurobiology* 14: 531–541.

Kolb, H., Ripps, H., and Wu, S. M. (2001). Concepts and challenges in retinal biology: A tribute to John E. Dowling. *Progress in Brain Research* 131: 23–29.

Pang, J. J., Gao, F., and Wu, S. M. (2004). Stratum-by-stratum projection of light response attributes by retinal bipolar cells of Ambystoma. *Journal of Physiology* 558: 249–262.

Sterling, P. and Demb, J. B. (2004). Retina. In: Sherpherd, G. M. (ed.) *The Synaptic Organization of the Brain,* 5th edn., pp. 217–269. Oxford: Oxford University Press.

Wu, S. M. (1992). Feedback connections and operation of outer plexiform layer of the retina. *Current Opinion in Neurobiology* 2(4): 462–468.

Wu, S. M. (1994). Synaptic transmission in the outer retina. *Annual Review of Physiology* 56: 141–168.

Wu, S. M. (2003). Intracellular light responses and synaptic organization of the vertebrate retina. In: Kaufman, P. L. and Mosby, A. A. (eds.) *Adler's Physiology of the Eye*, ch. 15, pp. 422–438. St. Louis, MO: Elsevier.

Wu, S. M. (2009). Bipolar cells. In: Squire, L., Albright, T., Bloom, F., Gage, F., and Spitzer, N. (eds.) *Encyclopedia of Neuroscience*, vol. 8, pp. 181–186.

Zhang, A. J. and Wu, S. M. (2009). Receptive fields of retinal bipolar cells are mediated by heterogeneous synaptic circuitry. *Journal of Neuroscience* 29(3): 789–797.

Information Processing: Contrast Sensitivity

M B Manookin and J B Demb, University of Michigan, Ann Arbor, MI, USA

Glossary

Adaptation – The change in response properties of a neuron, which enhance the ability to encode the immediate environment.
Contrast – The percent deviation in light intensity from the mean intensity (as defined over some period of time and region of visual angle).
Filter – The concept of a neuron's receptive field as a tuning function that is matched to certain spatial or temporal frequencies.
Receptive field – The area of space and period of recent time over which changes in light input can modulate the response of a neuron.
Threshold – The lowest contrast level of a spatiotemporal pattern where a neuron can respond to the stimulus reliably (physiology) or where an observer can perceive the stimulus reliably (psychophysics).

Contrast Processing and Adaptation

Humans can see and behave across a wide range of lighting conditions. For example, one can navigate through the woods on a starry night, where each rod photoreceptor absorbs a photon only about once per minute; and yet one can also navigate across the beach on a cloudless day, where cone photoreceptors absorb thousands of photons per second. The mean luminance between these extreme examples can differ by ~100-million-fold. This wide range of intensities poses a computational problem for the retina, because a ganglion cell can fire only about 20 action potentials (spikes) in the ~100 ms integration time of a postsynaptic neuron. Thus, the ganglion cell must continually adjust its sensitivity so that the wide range of light levels (~8 log units) can be encoded with the narrow range of output signals (~1–2 log units).

To deal with the mismatch between input and output, the retina adjusts its sensitivity depending on the mean intensity, through mechanisms of light adaptation. These mechanisms are varied, and they include: the switch between rod photoreceptors (for night vision) and cone photoreceptors (for day vision); intrinsic properties of each receptor type that alter sensitivity depending on mean intensity; and postreceptoral mechanisms within the retinal circuitry. The apparent purpose of light adaptation is to adjust the ganglion cell's response to report, not the absolute intensity, but rather the contrast, or the percentage deviations from the mean intensity.

The contrast of a visual stimulus is a more robust property than the absolute intensity. To illustrate this point, consider a simple example, where an observer gazes at a bird on a background of leaves. Assume that the bird reflects 50% more light toward the observer's eye compared to the leaves (and ignore color in this example). Now imagine that the light reflected to the eye is reduced either by the observer's action (i.e., putting on a pair of sun glasses) or by a change in the light source reflecting off the objects (i.e., a cloud passes overhead, obscuring the sunlight). In either case, the light reflected into the eye is reduced 10-fold or more. However the relative reflectance is unchanged: the bird still reflects 50% more light than the leaves. Hence, it follows that the retina (and most of the visual system) is designed to encode contrast or the relative reflectance of objects within the same scene: the relative reflectance of objects represents a stable property of natural scenes, whereas absolute reflectance does not. Physiological measurements of retinal ganglion cells confirm this idea, showing that responses to a given contrast level are relatively constant over several orders of mean light level.

The Spatial Receptive Field

A ganglion cell calculates contrast over a specific retinal region known as its spatial receptive field. There are approximately 20 different types of ganglion cells whose axons form the optic nerve. These types encode different aspects of visual information, and some are highly selective for features such as wavelength of light or the direction of moving objects. Here, the focus is on the several types of ganglion cell that have a relatively conventional receptive field that can be described with an excitatory center region and an inhibitory surround region.

A ganglion cell's excitatory center corresponds to the retinal region aligned with its dendritic tree. Thus, the photoreceptors within the span of the ganglion cell's dendritic tree would all contribute to driving the excitatory center region. These photoreceptors synapse onto both ON- and OFF-types of bipolar cell, which express distinct glutamate receptors at their dendrites (metabotropic or

ionotropic, respectively) and therefore have opposite responses to light: ON-type cells are excited by light increments, whereas OFF-type cells are excited by light decrements. Most ganglion cell types collect synapses from either ON-type bipolar cells or OFF-type bipolar cells and then inherit the ON- or OFF-center property from these presynaptic bipolar cells.

A ganglion cell's inhibitory surround corresponds to the retinal region that extends beyond the dendritic tree. Thus, an OFF-center cell that is excited by light decrements over the tree is inhibited by light decrements over the surround region, beyond the tree. The center and surround combine to report the relative contrast over space. The center is commonly stronger than the surround, so that a large object covering both the center and surround will drive a center response (e.g., a large bright object will provide some excitation to an ON-center cell). For some cell types (e.g., the X/beta-type ganglion cell of the cat or the midget/parvocellular-projecting ganglion cell of the monkey), the center and surround combine in an approximately linear fashion. Thus, the response to center plus surround stimulation can be predicted reasonably well by summing the separate responses to center and surround measured individually. For other cell types (e.g., the Y/alpha-type of the cat) there is a nonlinear combination of center and surround regions. For these nonlinear receptive fields, the presynaptic bipolar cells may be described by relatively linear receptive fields; the major nonlinearity of the ganglion cell receptive field may arise at the level of the synaptic output of the bipolar cells as they converge onto the ganglion cell. In general, a ganglion cell's excitatory center is driven by the presynaptic bipolar cells, whereas the surround arises at two levels: the horizontal cells in the outer retina and the amacrine cells in the inner retina.

The Temporal Receptive Field

In addition to the two-dimensional spatial component, a ganglion cell's receptive field also has a temporal component. In many cases, ganglion cell responses can be described with a temporal filter that represents the best stimulus for driving a response. Thus, if the time course of the stimulus contrast over the past ~250 ms matches the filter, the response will be maximal. Ganglion cell firing rates can increase above the baseline rate much more than they can decrease below the baseline rate. In extreme cases, some ganglion cell types have essentially no background rate. Thus, a substantial nonlinearity in the ganglion cell's response is the threshold for firing action potentials (also known as rectification). The temporal filter concept must thus be combined with the concept of an output nonlinearity to predict a cell's response to a contrast modulation presented over time (**Figure 1**). A common method for modeling such responses is the linear–nonlinear model. The temporal filter can be measured by presenting a randomly flickering stimulus (commonly called white noise). For example, a spot over the receptive field center could have its intensity modulated over time. The response in the ganglion cell's firing rate could then be correlated with the stimulus to generate the filter. A separate step is used to relate the filtered output (a linear prediction of the temporal response) to

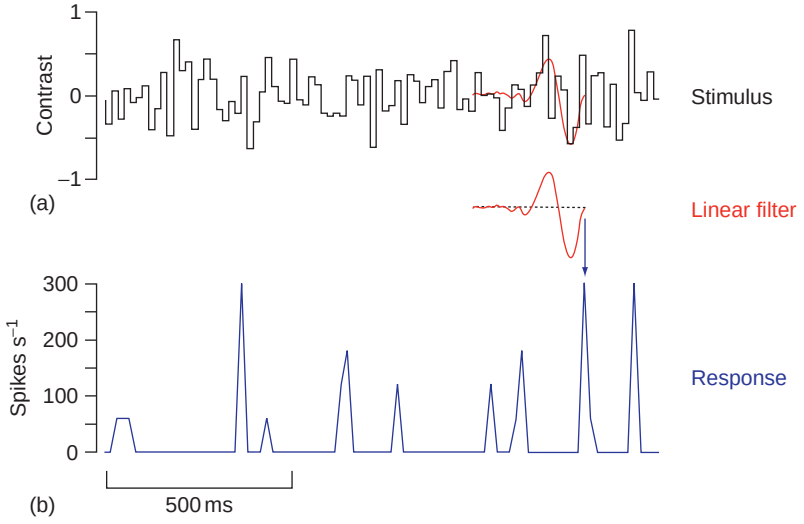

Figure 1 The retina temporally filters visual input. A temporal white-noise stimulus and firing rate response can be correlated to generate the linear filter. The filter represents a model of the temporal receptive field of the ganglion cell. The initial downward deflection (going backwards in time) indicates that the cell is an OFF-center type. The filter (red) is superimposed on the stimulus at a time when the stimulus closely matches the filter and the response output is large.

the actual firing rate; this step represents the nonlinearity associated with firing action potentials and typically includes a threshold for firing and also a point at which the firing rate saturates.

Receptive Field Properties Explain Contrast Sensitivity Functions

For cell types with linear receptive fields, the contrast sensitivity function can be explained by the receptive field properties described over space or time. For example, Figure 2(a) shows a temporal filter and its relationship to sinusoidal modulation of luminance of different temporal frequencies. The biphasic filter is best matched to the 6-Hz frequency and would thus predict a strong response to this frequency. At the lower frequency (1 Hz), the two phases of the filter are stimulated simultaneously and would therefore cancel to some extent; at the high frequency (12 Hz), the two phases of the filter are not stimulated strongly by the modulations and would thus, likewise, yield suboptimal responses. The response as a function of temporal frequency is plotted as the solid line in Figure 2(b). This line represents the cell's temporal tuning function (or temporal contrast sensitivity function).

The same concept of filtering can be applied to the spatial domain (Figure 2(c2) shows a one-dimensional cut through a circular center–surround receptive field). In this case, sinusoidal modulation of light (over space; described in cycles per degree of visual angle) is presented to a center–surround receptive field. The center–surround filter best matches the 8 cycles deg^{-1} stimulus, whereas lower or higher frequencies are suboptimal. The tuning function (solid line in Figure 2(c3)) describes the spatial contrast sensitivity function.

Temporal and spatial contrast sensitivity functions can also be used to describe threshold measurements in human psychophysical experiments. In this case, the spatial or temporal filter is that of the entire visual system. A human is presented with brief stimuli of various spatial or temporal frequency contrast modulation and a threshold is determined (i.e., the lowest contrast at which the pattern can be reliably discriminated from the mean luminance). The perceptual contrast sensitivity function resembles the sensitivity functions of individual ganglion cells, at least superficially. It is difficult to determine how perceptual and neural sensitivity functions are related to one another, because perception depends on the output of many different types of ganglion cell as well as further processing at later stages in the brain.

Disrupting Specific Retinal Pathways Alters Perceptual Contrast Sensitivity in Selective Ways

The retinal ganglion cell axons exit the eye and travel to several different nuclei in the brain, including targets in the brainstem, midbrain, and thalamus. The pathway for

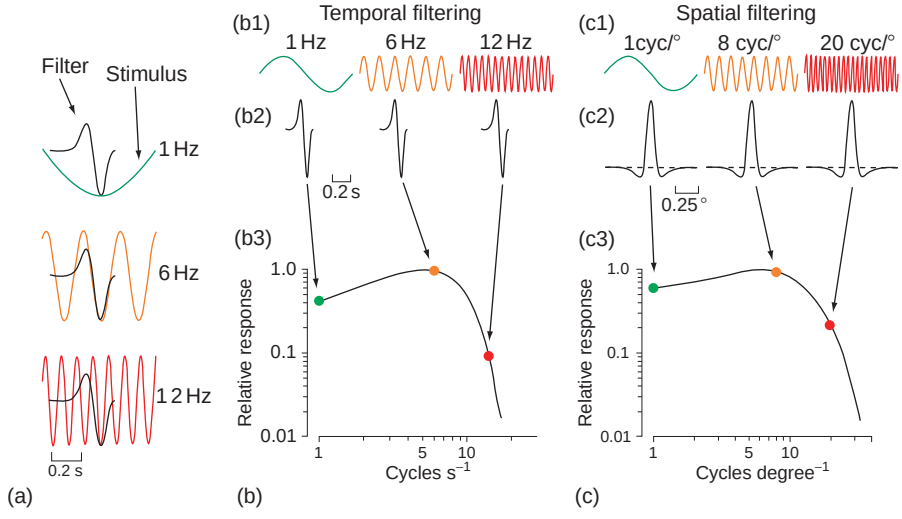

Figure 2 Spatial and temporal filtering explains the contrast sensitivity function.
(a) A temporal filter is shown with stimuli of three frequencies. The 6-Hz stimulus provides the best match to the filter.
(b) Temporal contrast sensitivity function. (b1) Three temporal frequencies (sine waves).
(b2) The filter is best matched to the 6-Hz sine wave. (b3) The sensitivity function represents the filter's normalized response to each frequency.
(c) Spatial contrast sensitivity function. (c1–c3) Same as for part (B) but for spatial frequency stimuli and the spatial filter. The filter shown is a one-dimensional cut through a circular center–surround receptive field.

conscious vision is believed to arise from the retinal projection to the thalamus, where relay cells then project retinal signals to the visual cortex. About a dozen or more different types of ganglion cell project to the lateral geniculate nucleus of the thalamus (LGN); and LGN relay cells provide a major input to primary visual cortex.

In primates, the LGN is organized into six prominent layers. The top four parvocellular (P) layers contain small cell bodies (ON and OFF midget/P cells), whereas the bottom two magnocellular (M) layers contain large cell bodies (ON and OFF parasol/M cells). Both P and M layers are separated by the eye where the ganglion cells originate; thus there are two P layers and one M layer that each receives input from the contralateral eye, whereas the other layers each receives input from the ipsilateral eye. The ON and OFF M and P cells thus account for four of the ~13 types that project to the LGN. The other nine ganglion cell types apparently project to relay cells that either reside in the layers between the M and P layers (the intercalated layers) or intermingle with the M and P cell bodies. These pathways are referred to collectively as koniocellular (K) cells.

To understand the role of the different ganglion cell types in perceptual contrast sensitivity, the M or P layers of the LGN were lesioned. We now understand that these lesion experiments were not entirely selective; the lesions to the P layers, for example, must have also affected some of the other (less numerous) K pathway ganglion cell types that project to the dorsal region of the LGN. Nevertheless, the M and P cells are the most numerous cell types that project to the LGN, and lesions to either the M or P layers yielded distinct deficits on contrast sensitivity measurements. Thus, these deficits are probably explained in large part by the lesions of either M or P cell types.

Lesions to the M layers reduced the monkey's sensitivity for high temporal frequency and low spatial frequency stimuli, whereas lesions to the P layers reduced sensitivity for low-temporal-frequency and high-spatial-frequency stimuli. Thus, the different ends of the monkey's contrast sensitivity function depended most heavily on distinct ganglion cell classes in the retina. There are two clear conclusions from these studies: there was no single cell type that could explain perceptual sensitivity for all possible patterns; and specific spatial or temporal domains of perceptual sensitivity depended most heavily on particular cell types.

Physical Limits to Contrast Sensitivity

Under optimal conditions, humans can detect small spots with contrasts of 1–3%. The most sensitive ganglion cell types can also detect small spots with contrasts of 1–3%. Thus, there may be certain conditions where perceptual thresholds are driven by a small number of ganglion cells and there may be relatively little information lost between the retina and the brain. However, there is a loss between the contrast threshold that could (theoretically) be computed at the level of photon absorptions by the photoreceptors and the threshold measured in the ganglion cell. Recent computational analysis suggests that, under certain conditions, this loss may be a factor of ~10–20.

The ability to detect contrast depends on the statistics of photon arrival and the statistical properties of various cellular processes. Photon arrival follows Poisson statistics, where the mean and the variance are equal. For example, consider a case where a ganglion cell integrates signals over 20 photoreceptors across the retina and over a 100-ms integration time and where the mean rate of photoisomerizations (i.e., absorbed photons) is 50 isomerizations (R^*) per photoreceptor per second (i.e., 5 R^*/photoreceptor/integration time). In this case, the mean R^* rate over the spatial/temporal integration ($20 \times 100 \times 5$) is 10 000 and the variance (across multiple trials) would be the same. Thus, the SD (or noise level) would be the square root or 100 R^*. The signal-to-noise ratio (mean/SD per integration time) would then be $10\,000/100 = 100$. Therefore, the cell in question would have difficulty detecting a difference of less than 1/100 (i.e., SD/mean) or 1% deviation from the mean level (i.e., 1% contrast). The contrast threshold would be worse (i.e., higher) when the mean luminance is lower, the number of integrated photoreceptors is fewer or the temporal integration time decreases.

Similar limitations on contrast sensitivity must arise within the neural circuit of the retina. For example, the release of neurotransmitter at retinal synapses probably obeys Poisson statistics similar to the case of photon arrival. Thus, the ability of the synapses to transfer information at low contrast depends on the release rates at these synapses and the number of synapses that are integrated by a given neuron. For example, the threshold of a cell would be best (i.e., lowest) in the presence of high release rates and a large number of integrated synapses (i.e., high degree of synaptic convergence within the circuitry). Thus, several physiological factors will place neural limits on the contrast threshold of retinal ganglion cells.

See also: Information Processing: Ganglion Cells; Morphology of Interneurons: Amacrine Cells; Morphology of Interneurons: Horizontal Cells; Phototransduction: Adaptation in Cones; Phototransduction: Adaptation in Rods; Phototransduction: Phototransduction in Cones; Phototransduction: Phototransduction in Rods; Retinal Pigment Epithelium: Cytokine Modulation of Epithelial Physiology.

Further Reading

Borghuis, B. G., Sterling, P., and Smith, R. G. (2009). Loss of sensitivity in an analog neural circuit. *Journal of Neuroscience* 29: 3045–3058.

Carandini, M., Demb, J. B., Mante, V., et al. (2005). Do we know what the early visual system does? *Journal of Neuroscience* 25: 10577–10597.

Chichilnisky, E. J. (2001). A simple white noise analysis of neuronal light responses. *Network* 12: 199–213.

Dacey, D. M., Peterson, B. B., Robinson, F. R., and Gamlin, P. D. (2003). Fireworks in the primate retina: *In vitro* photodynamics reveals diverse LGN-projecting ganglion cell types. *Neuron* 37: 15–27.

Dhingra, N. K., Kao, Y. H., Sterling, P., and Smith, R. G. (2003). Contrast threshold of a brisk-transient ganglion cell *in vitro*. *Journal of Neurophysiology* 89: 2360–2369.

Enroth-Cugell, C. and Robson, J. G. (1966). The contrast sensitivity of retinal ganglion cells of the cat. *Journal of Physiology* 187: 517–552.

Field, G. D. and Chichilnisky, E. J. (2007). Information processing in the primate retina: Circuitry and coding. *Annual Review of Neuroscience* 30: 1–30.

Geisler, W. S. (1989). Sequential ideal-observer analysis of visual discriminations. *Psychological Review* 96: 267–314.

Merigan, W. H. and Maunsell, J. H. R. (1993). How parallel are the primate visual pathways? *Annual Review of Neuroscience* 16: 369–402.

Rose, A. (1973). *Vision: Human and Electronic*. New York: Plenum Press.

Sterling, P. and Demb, J. B. (2004). Retina. In: Shephard, G. (ed.) *Synaptic Organization of the Brain,* 5th edn., pp. 217–269. New York: Oxford University Press.

Troy, J. B. and Enroth-Cugell, C. (1993). X and Y ganglion cells inform the cat's brain about contrast in the retinal image. *Experimental Brain Research* 93: 383–390.

Wandell, B. A. (1995). *Foundations of Vision*. Sunderland: MA: Sinauer.

Walraven, J., Enroth-Cugell, C., Hood, D. C., MacLeod, D. I. A., and Schnapf, J. L. (1990). The control of visual sensitivity: Receptoral and postreceptoral processes. In: Spillman, L. and Werner, J. (eds.) *The Neurophysiological Foundations of Visual Perception*, pp. 53–101. New York: Academic Press.

Wässle, H. (2004). Parallel processing in the mammalian retina. *Nature Reviews. Neuroscience* 5: 747–757.

Watson, A. B., Barlow, H. B., and Robson, J. G. (1983). What does the eye see best? *Nature* 302: 419–422.

Information Processing: Direction Sensitivity

Z J Zhou and S Lee, Yale University School of Medicine, New Haven, CT, USA

Glossary

Accessory optic nuclei – A series of small nuclei in the rostral midbrain, near where the optic tract enters the lateral geniculate nucleus. They receive inputs from motion-sensitive ganglion cells and project to the vestibular nuclei, triggering optokinetic movements in response to movement of the visual world across the retina. This system is very important for animals without foveae, but is poorly developed in humans.

Optokinetic nystagmus – The repeated reflexive responses of the eyes to ongoing large-scale movements of the visual scene.

Patch-clamp recording – A sensitive electrophysiological recording technique that permits the measurement of ionic currents flowing through individual ion channels. It uses a glass micropipette that has an open-tip diameter of about 1 μm. The micropipette tip is sealed onto the cell surface, enclosing a membrane surface area or patch that often contains only a few ion channels. Several variations of this technique are commonly applied.

Spatially offset inhibition – An inhibitory synaptic input from the receptive field surround that is asymmetrically offset to one direction.

Two-flash apparent motion stimulation – A visual stimulation paradigm, in which two nearby spots of light are flashed in rapid succession to simulate the motion of a light spot.

Detecting the direction of image movement is an essential task of the visual system. Neurons in many parts of the visual system show directional sensitivity to image motion. The initial computation of movement direction is accomplished in the retina. In the early 1960s, Barlow and co-workers discovered that a subset of output neurons in the rabbit retina responds vigorously to an image moving across its receptive fields in a particular (preferred) direction, but gives little or no response to the same image moving in the opposite (null) direction (Figure 1). These retinal neurons, termed direction-selective ganglion cells (DSGCs), display a directional preference that is independent of the nature of the image, such as contrast, size, and complexity. They are specialized in processing visual information regarding motion and motion direction.

Physiological Functions of DSGCs

In rabbit, a species for which retinal direction selectivity is best characterized, two types of DSGCs have been found: the ON type, which responds to the onset of a small spot of light flashed in the center of the cell's receptive field, and the ON–OFF type, which responds to both the onset and the offset of such a flash. ON DSGCs project their axons to the accessory optic system. They are believed to be involved in the feedback mechanism that stabilizes a moving image on the retina, for example, during the smooth tracking movements of the eyes. These cells respond best to slow image movements ($\sim 0.3^\circ\ s^{-1}$) and contribute significantly to the control of optokinetic nystagmus over the range of stimulus velocities that produce the most complete minimization of image motion on the retina. ON DSGCs are divided into three subtypes, distinguished by their preferred directions pointed roughly toward the anterior, superior, and inferior retina, respectively. Each of these three preferred directions is thought to correspond to a component of the head rotation that activates one of the three pairs of semicircular canals in the inner ears, suggesting that these cells may also detect the slippage of a visual image on the retina during head rotation and provide an error signal that tells the visual servo-system to compensate the difference between head rotation and eye rotation.

ON–OFF DSGCs, on the other hand, project to the superior colliculus and the lateral geniculate nucleus. They are further categorized into four subtypes, characterized by their preferred directions which, respectively, point roughly toward the four cardinal directions in the retina: superior, inferior, anterior, and posterior. It has been suggested that these four directions may correspond to the directions in which the eye is rotated by the four extraocular rectus muscles, indicating that ON–OFF DSGCs are also involved in the feedback mechanism that controls eye movement. However, unlike the ON type, ON–OFF DSGCs give largest responses to fast movements ($\sim 10^\circ\ s^{-1}$ or faster) and respond poorly to slow movements. Their contribution to image stabilization during the slow phase of optokinetic nystagmus may be significant only at stimulus velocities exceeding $\sim 3^\circ\ s^{-1}$. The fact that ON–OFF DSGCs project to the lateral geniculate nucleus in addition to the superior colliculus suggests that these cells may also process directional information of object movement for visual perception. However, the exact physiological functions of ON–OFF DSGCs remain to be understood.

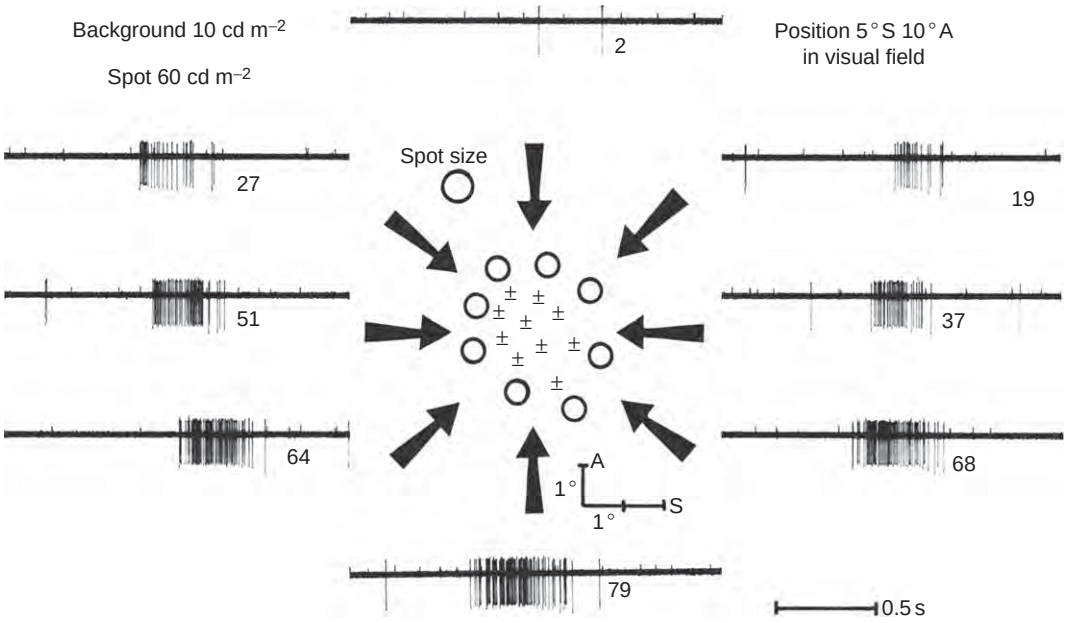

Figure 1 Responses of a directionally selective ganglion cell (recorded from its axon) to stimulus motion in different directions. Map of receptive field in center. Traces show responses (spikes) elicited by the movement of a spot of light across the receptive field in the direction of adjacent arrow. This cell shows a preferred direction pointing upward. Anterior (A) and superior (S) meridians in the visual field are shown together with 1° calibration marks. The number of spikes is shown immediately after each response. Conventions are as follows: ±, response to stationary spot at both ON and OFF; O, no response; there are no responses outside the ring of Os. Adapted from Barlow, H. B., Hill, R. M., and Levick, W. R. (1964). Retinal ganglion cells responding selectively to direction and speed of image motion in the rabbit. *Journal of Physiology* 173: 377–407.

Synaptic Circuitry of DSGCs

As direction selectivity in the retina represents a fundamental form of information processing, it has been regarded as a model system for understanding neuronal computation in the brain. In their 1965 work, Barlow and Levick first suggested that the direction selectivity of ganglion cells is built from sequence-discriminating subunits. The primary mechanism for this discrimination was thought to result from a spatially offset lateral inhibition, which vetoes responses to sequences corresponding to stimulus movement in the null direction. Pharmacological experiments by Daw and colleagues subsequently found that gamma aminobutyric acid (GABA) receptor antagonists block direction selectivity by bringing out strong responses of DSGCs to stimulus movement in the null direction, suggesting that the spatially offset inhibition is mediated by GABA. Direct measurement of the inhibitory inputs to ON–OFF DSGCs became possible in the early 2000s, when whole-cell patch-clamp recordings were made successfully from these cells in the whole-mount rabbit retina by several labs. Fried and co-workers showed that the inhibitory input to ON–OFF DSGCs is larger during stimulus movement in the null direction than that in the preferred direction, and that the inhibitory input arrives ahead of the excitatory input when the stimulus moves in the null, but not in the preferred direction. The spatial extent of the inhibitory input measured by whole-cell patch clamp is offset from the ON–OFF DSGC dendritic field toward the null direction. The excitatory current input to an ON–OFF DSGC is also directionally asymmetric: larger for preferred direction movement than for null direction movement. Similar results were also obtained from ON DSGCs in the mouse retina. These findings establish that the synaptic inputs to a DSGC are already directionally asymmetric.

An important clue to the origin of major synaptic inputs to DSGCs comes from the anatomical structure of these cells. DSGCs have a distinctive morphology, characterized by the looping dendritic branches (**Figure 2**). The dendritic stratification pattern of DSGCs follows the general rule of segregation between the ON and OFF channels in the inner plexiform layer (IPL) of the retina. Thus, ON DSGCs arborize only in the proximal half (ON sublamina) of the IPL, whereas ON–OFF DSGCs arborize in both the proximal and the distal half (OFF sublamina). Both the ON and OFF arborizations stratify narrowly in the IPL, juxtaposing the two narrow cholinergic strata, suggesting that DSGCs receive synaptic inputs from the relatively small number of bipolar and amacrine cell subtypes that terminate specifically in these strata. In particular, cholinergic amacrine cells, which are the only cholinergic cells in the mammalian retina, are expected to provide a significant amount of lateral input

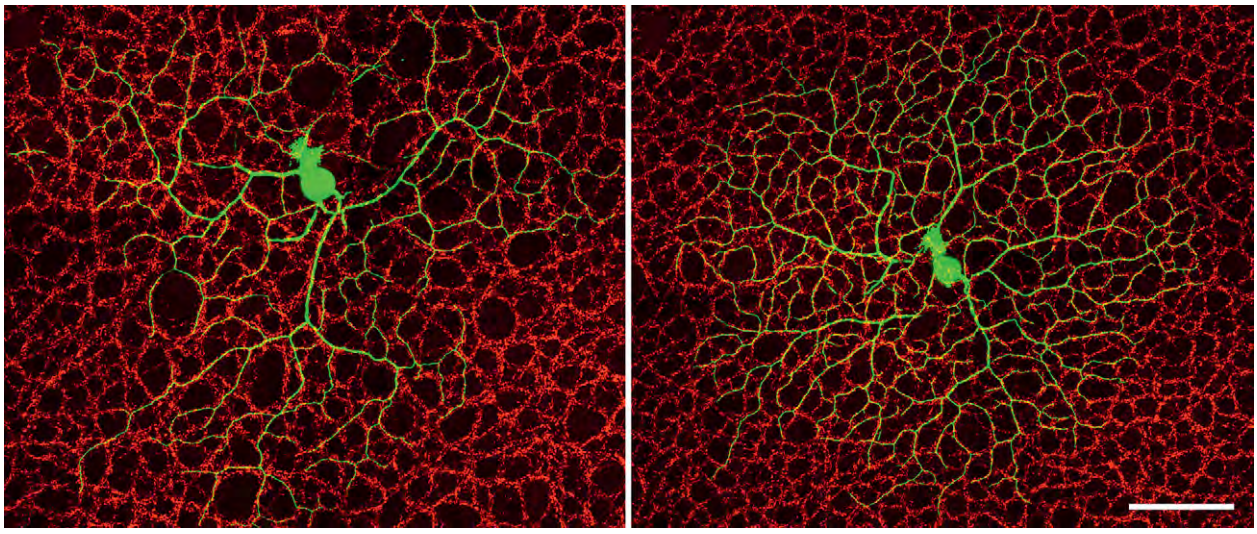

Figure 2 Dendritic morphology of ON–OFF direction-selective ganglion cell. Confocal micrographs of an intracellularly injected ON–OFF DSGC in the whole-mount rabbit retina, showing bistratified dendritic arbors in the ON (left panel) and OFF (right panel) sublamina of the inner plexiform layer. The characteristic looping dendrites co-stratify extensively with the cholinergic plexus (labeled with choline acetyltransferase in red). Scale bar = 100 μm. Adapted from Dong, W., Sun, W., Zhang, Y., Chen, X., and He, S. (2004). *Journal of Physiology* 556: 11–17.

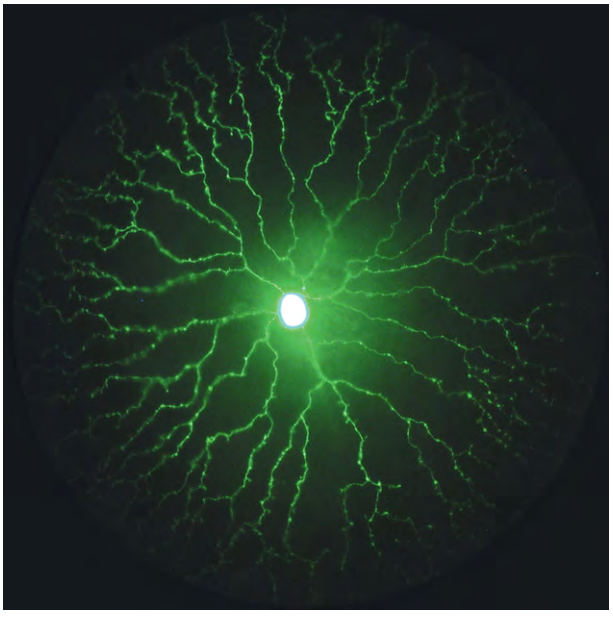

Figure 3 Dendritic morphology of starburst amacrine cell. Fluorescence micrograph of a SAC, with its soma located in the ganglion cell layer in a postnatal day 18 retina of a rabbit. The cell has a radially symmetric dendritic tree and a polar asymmetric synaptic structure. The input synapses from bipolar cell are distributed over the whole dendritic tree, but the output synapses are localized in the distal varicose zone, where synaptic vesicles are concentrated. Unpublished micrograph provided by Lee S and Zhou ZJ.

to DSGCs. Cholinergic amacrine cells are also known as starburst amacrine cells (SACs; Figure 3). They exist as two mirror-symmetric populations across the IPL. They have four to five primary dendrites, each branching out regularly into secondary and tertiary processes, with numerous varicosities imbedded in the distal dendritic zone. The dendritic tree of a SAC emanates from the soma with a nearly perfect radial symmetry, rendering the cell a starburst appearance and hence its popular name. The processes of neighboring SACs overlap significantly and form honeycomb-shaped plexuses which co-fasciculate extensively with the looping dendrites of DSGCs, suggesting intimate synaptic interactions between the two cell types. Indeed, direct synapses from SACs to ON–OFF DSGCs have been observed at the electron microscopic level.

The neurochemical significance of the synapses between SACs and DSGCs became apparent when SACs were found to synthesize and release both acetylcholine (ACh) and GABA, a property that also rendered SACs the first known exception to Dale's principle of one neuron releases one fast neurotransmitter. The GABAergic nature of cholinergic amacrine cells suggests that these cells may provide the crucial, spatially offset GABAergic inhibition to DSGCs, an idea that has been tested and debated extensively in the literature. The co-release of ACh and GABA by SACs also raises the possibility that these two neurotransmitters may be used by SACs in a complimentary manner to enhance the sensitivity of DGSCs to motion and motion direction.

The first functional evidence for a key role of SACs in direction selectivity came from the finding that ablation of SACs by immunotoxins and neurotoxins results in an apparent elimination of the directional discrimination of DSGCs in the mouse retina, as well as a loss of optokinetic nystagmus. This finding demonstrates a critical

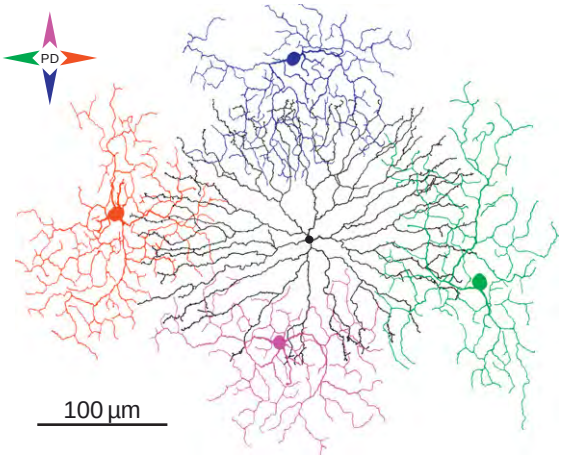

Figure 4 Synaptic circuit of ON–OFF direction selective ganglion cells. ON–OFF DSGCs receive GABAergic inhibitory inputs only from starburst amacrine cell dendrites that point in the null direction, but not in the preferred direction. A single SAC (shown in black) can provide null-direction inhibition to all four subtypes of ON–OFF DSGCs with preferred directions along four orthogonal directions (shown in different colors). For simplicity, only the circuitry in the ON sublamina is shown. Adapted from Taylor, W. R. and Vaney, D. I. (2003). New directions in retinal research. *Trends in Neurosciences* 26(7): 379–385.

link not only between SACs and direction selectivity, but also between direction selectivity and optokinetic nystagmus. Dual patch-clamp recordings from SAC–DSGC pairs in the rabbit retina subsequently demonstrated that DSGCs receive direct GABAergic synaptic inputs from SACs, and that such inputs come only from SACs located on the null side, but not the preferred side of the DSGC. This result establishes that SACs exert a spatially offset GABAergic inhibition on DSGCs through directionally asymmetric hardwiring between SACs and DSGCs, a landmark finding that forms the basis of the current model of the synaptic circuitry of DSGCs (**Figure 4**).

Direction-Selective Responses in SAC Processes

For the asymmetric wiring model of direction selectivity shown in **Figure 4** to work, the release of GABA from each branch of a SAC must also be directionally selective: larger during a null-direction movement and smaller during a preferred-direction movement. Otherwise, the SAC dendrites that synapse on a DSGC from the null direction would still inhibit the DSGC when an image moves to the DSGC receptive center along the preferred direction, even though such an inhibitory input may not precede the glutamatergic excitatory input from bipolar cells. Experiments using apparent motion stimulation also show that the GABAergic input to a DSGC (from SACs on the null side) is strongly suppressed by two-spot flashes that simulate a preferred-direction movement, indicating that GABA release from SAC dendrites is directionally selective. This result suggests that a critical component of the direction-selective mechanism must reside upstream from DSGCs and in SACs.

How does a morphologically symmetric cell like the starburst produce the functional asymmetry required for direction-selective GABA release? A close anatomical examination of the SAC tells us that, despite the striking radial symmetry in the dendritic tree, the synaptic structure of the cell has a profound polar asymmetry. Input synapses on starburst dendrites distribute more or less uniformly along the entire dendritic length, whereas output synapses are localized in the distal varicose zones, where synaptic vesicles are concentrated (**Figure 3**). The distal varicose zones are believed to be electrotonically semi-isolated, due to the thin diameter of the dendrites and a heavy expression of K_{V3} voltage-gated potassium channels on the proximal dendrites. This polar asymmetry in input–output relation, combined with the short electrotonic length of the dendrites, would enable the distal dendrites of a SAC to process directional signals independently, with a preference to centrifugal stimulus movement, as predicted by computational models. In an elegant two-photon Ca^{2+}-imaging experiment, Euler and co-workers showed that distal starburst dendrites respond to spot illumination with intracellular Ca^{2+} transients that are restricted to distal dendrites. Importantly, these local Ca^{2+} responses tended to be directionally selective: stronger for centrifugal than for centripetal stimulus movement.

Two-flash apparent motion experiments further show that the direction selectivity in distal starburst dendrites involves both centrifugal excitation and centripetal inhibition. The underlying mechanism may involve both cell-autonomous properties and synaptic interactions at SAC dendrites. Cell-autonomous properties, such as nonlinear interactions between the activation of voltage-gated calcium channels and a gradient in membrane potential along the SAC dendrites, may contribute to an enhanced response of the distal dendrites to centrifugal image movement. On the other hand, synaptic interactions, particularly GABAergic inhibition from the receptive field surround, play a key role in centripetal inhibition. Dual patch-clamp recording experiments found that neighboring SACs inhibit each other through reciprocal GABAergic synapses. Zhou and Lee proposed that the synaptic mechanism for direction-selective release of GABA in distal starburst dendrites is built primarily from a classic center-surround receptive field structure. Synaptic inputs to the receptive field center are dominated by the glutamatergic input from bipolar cells, whereas synaptic inputs from the receptive field surround are dominated by the direct GABAergic input from neighboring SACs. Such a concentric receptive field structure would normally be directionally symmetric for a neuron that makes an integrative

output decision at the soma or axon hillock. However, since the output decisions of a SAC are made independently in individual distal dendrites, such a concentric center-surround receptive field structure would produce a profound directional asymmetry at distal dendrites, where synaptic inputs received during centrifugal stimulus movement are dominated by excitation, but synaptic inputs received during centripetal stimulus movement are dominated by inhibition. This synaptic mechanism, together with an intrinsic mechanism that promotes centrifugal facilitation, would produce robust direction-selective GABA release from SACs.

Integration of Multiple Cooperative Mechanisms for Direction Selectivity

The direction-selective circuit so far identified consists primarily of DSGCs, SACs, and subsets of bipolar cells, although other amacrine cell types may also participate in the regulation of DSGC receptive fields. Distinct mechanisms of direction selectivity work in concert at three different levels. First, at the DSGC level, direction selectivity is shaped largely by a spatially offset inhibition from SACs, whose distal dendrites release GABA in a direction-selective manner and make GABAergic synapses onto DSGCs asymmetrically from the null direction only. Direction selectivity of DSGCs is also enhanced by the directionally asymmetric excitatory inputs, which may contain both glutamatergic and cholinergic components. In addition, a postsynaptic mechanism, involving local signal computation and spike generation in DSGC dendrites, may further sharpen direction selectivity. Second, at the SAC level, direction selectivity is formed in the distal starburst dendrites by a profound polar asymmetry between centrifugal excitation and centripetal inhibition. GABAergic inhibition, mediated largely by reciprocal inhibition between SACs, plays a key role in suppressing SAC responses to centripetal stimulus motion. However, the nature of lateral synaptic interaction during centrifugal motion is currently unclear. A model based on differential expression of two different chloride transporters proposes that the excitability of GABAergic input changes as the image moves centrifugally or centripetally along a SAC dendrite. Further experiments are required to test directly the predictions of this model. In addition to synaptic interactions, intrinsic cellular properties also play an important role in shaping direction selectivity in SAC dendrites, predominantly by contributing to centrifugal facilitation. Third, at the bipolar cell level, a direction-selective release of glutamate is strongly implicated by the finding of asymmetric excitatory inputs to DSGCs, but the underlying mechanism remains a major missing piece of the puzzle. A key issue is whether local terminals of a bipolar cell axon can function independently and make selective synapses with the dendrites of specific subtypes of DSGCs. An intriguing possibility in this regard is that SACs asymmetrically inhibit specific bipolar cell output synapses, which in turn synapse selectively on DSGCs in a spatially asymmetric manner.

While the critical GABAergic contribution of SACs to direction selectivity is well accepted, the cholinergic role of SACs remains elusive. Various models of cholinergic contributions to direction selectivity and motion sensitivity have been proposed over the years. However, the basic mode of nicotinic cholinergic action in the retina still remains obscure: Does ACh mediate fast neurotransmission at precise synaptic sites between SACs and DSGCs, or does it play a diffuse, paracrine role in modulating the activity of many ganglion cell types? More detailed experimental results are needed before it can be concluded as to how the release of ACh from SACs may enhance the sensitivity of DSGCs to image movement, whether cholinergic interactions enhance direction selectivity, how cholinergic synapses form a neural circuit, and how the cholinergic and GABAergic circuits of SACs interact with each other. Investigations into some of these questions are currently underway and may uncover additional levels of cooperation among synaptic mechanisms of motion and direction selectivity in the near future.

Concluding Remarks

Direction selectivity is a basic form of information processing produced by a relatively simple neuronal circuit in the inner retina. In order for this circuit to accomplish the robust computation required for detecting motion direction, multiple levels of cooperative mechanisms are integrated at each synapse. Such synaptic integration may represent an important feature of network computation in the central nervous system. From an anatomical point of view, the direction-selective circuit in the retina reveals a level of selectivity and precision in network organization that was previously unappreciated in most other parts of the central nervous system. Understanding the developmental mechanisms that control the establishment of the direction-selective circuit in the retina remains a challenging task of future investigation and will shed important light on the development of neuronal circuits in general.

Acknowledgments

This work is supported in part by grants from the National Eye Institute and Research to Prevent Blindness, Inc.

See also: GABA Receptors in the Retina; Information Processing: Amacrine Cells; Information Processing: Bipolar Cells; Information Processing: Ganglion Cells; Information Processing in the Retina; Morphology of

Interneurons: Amacrine Cells; The Role of Acetylcholine and its Receptors in Retinal Processing.

Further Reading

Barlow, H. B. and Levick, W. R. (1965). The mechanism of directionally selective units in rabbit's retina. *Journal of Physiology* 178(3): 477–504.

Barlow, H. B., Hill, R. M., and Levick, W. R. (1964). Retinal ganglion cells responding selectively to direction and speed of image motion in the rabbit. *Journal of Physiology* 173: 377–407.

Dacheux, R. F., Chimento, M. F., and Amthor, F. R. (2003). Synaptic input to the on–off directionally selective ganglion cell in the rabbit retina. *Journal of Comparative Neurology* 456(3): 267–278.

Demb, J. B. (2007). Cellular mechanisms for direction selectivity in the retina. *Neuron* 55(2): 179–186.

Euler, T., Detwiler, P. B., and Denk, W. (2002). Directionally selective calcium signals in dendrites of starburst amacrine cells. *Nature* 418 (6900): 845–852.

Famiglietti, E. V. (1991). Synaptic organization of starburst amacrine cells in rabbit retina: Analysis of serial thin sections by electron microscopy and graphic reconstruction. *Journal of Comparative Neurology* 309(1): 40–70.

Fried, S. I., Munch, T. A., and Werblin, F. S. (2002). Mechanisms and circuitry underlying directional selectivity in the retina. *Nature* 420(6914): 411–414.

Lee, S. and Zhou, Z. J. (2006). The synaptic mechanism of direction selectivity in distal processes of starburst amacrine cells. *Neuron* 51(6): 787–799.

Oyster, C. W., Takahashi, E., and Collewijn, H. (1972). Direction-selective retinal ganglion cells and control of optokinetic nystagmus in the rabbit. *Vision Research* 12(2): 183–193.

Rodieck, R. W. (1998). *The First Steps in Seeing.* Sunderland, MA: Sinauer.

Tauchi, M. and Masland, R. H. (1984). The shape and arrangement of the cholinergic neurons in the rabbit retina. *Proceedings of the Royal Society of London. Series B. Biological Sciences* 223(1230): 101–119.

Taylor, W. R. and Vaney, D. I. (2003). New directions in retinal research. *Trends in Neurosciences* 26(7): 379–385.

Vaney, D. I. (1990). The mosaic of amacrine cells in the mammalian retina. *Progress in Retinal Research* 9: 49–100.

Wyatt, H. J. and Day, N. W. (1976). Specific effects of neurotransmitter antagonists on ganglion cells in rabbit retina. *Science* 191(4223): 204–205.

Yoshida, K., Watanabe, D., Ishikane, H., et al. (2001). A key role of starburst amacrine cells in originating retinal directional selectivity and optokinetic eye movement. *Neuron* 30(3): 771–780.

Information Processing: Ganglion Cells

T A Münch, University of Tübingen, Tübingen, Germany

Glossary

Excitation – The synaptic input to a cell that serves to depolarize and activate it.
Inhibition – The synaptic input to a cell that serves to hyperpolarize and suppress it.
Receptive field – For retinal cells, this refers to a region in the visual environment in which the presence of a visual stimulus will influence the activity of the neuron.

The eye is often compared to a camera, in which the retina plays the role of the film. However, this analogy does not do justice to the remarkable image- and information-processing capabilities of the retina. The roles that horizontal cells, bipolar cells, and amacrine cells play in the information processing in the retina have been discussed elsewhere in the encyclopedia. All their activity merges into the output cells of the retina, the ganglion cells. These cells form a sort of bottleneck through which all the information has to pass, which is destined to reach higher visual centers in the brain.

Ganglion Cell Types

The signals leaving the retina are transmitted by several channels, each channel carrying information about different features of the visual world. Each channel is embodied by a certain type of ganglion cell. It is still controversial how many different types of ganglion cells exist, but 20 should be a reasonable upper limit. Two ganglion cells are considered to belong to the same type if they share a defined set of properties, including morphological, physiological, and genetic properties. However, it is not trivial to define what such characterizing properties should be. Too fine a distinction would artificially separate ganglion cells into different types, even though they might belong to the same type, while a course classification will not do justice to the rich diversity of image-processing capabilities of the retina. For the purpose of this article, the term ganglion cell type will be loosely and pragmatically defined as the population of ganglion cells extracting the same features from the visual world and therefore performing the same function. Later in this article, we describe some specific examples of ganglion cell types and the visual features that activate them. First, however, we discuss some general principles of ganglion cell processing.

Principles of Ganglion Cell Processing

Neural activity in the retina is unusual in the central nervous system as most retinal neurons are analog: they do not fire action potentials; instead, transmitter release is a continuous function of membrane voltage. Ganglion cells are different; they use action potentials to transmit their signals along their axons which form the optic nerve. These cells integrate excitatory input from bipolar cells and inhibitory input from amacrine cells. It is the precise temporal and spatial integration of these inputs that leads to the final spiking output of the ganglion cells. It will become clear from the examples below that it is the inhibitory activity of the amacrine cells that creates most of the specificity in ganglion cell responses. Bipolar cells serve to set up a range of permissive stimuli, that is, the set of stimuli that a ganglion cell could, in principle, respond to. This stimulus space is then strongly restricted by the activity of the inhibitory amacrine cells, resulting in the specific responses of ganglion cell types.

Temporal Processing

Ganglion cells show diverse responses to step changes of light (**Figure 1(a)**). Generally, responses can be divided into ON (activated by increases of light intensity), OFF (activated by decreases of light intensity), and ON–OFF (activated by both increases and decreases of light intensity). The ganglion cells expressing these responses are accordingly termed ON cells, OFF cells, and ON–OFF cells. Within each of these classes, one can find cell types with transient or sustained responses. In addition, different cells have different latencies from stimulus onset until the time of the first spike. For some cell types, Gollisch and Meister demonstrated that the relative spike latency can code for the stimulus intensity (**Figure 1(b)**).

The different temporal response characteristics of ganglion cells are correlated with the level of stratification of ganglion cell dendrites. The dendrites of ON ganglion cells stratify in the inner half of the inner plexiform layer (sublamina b, close to the cell bodies of the ganglion cells), while the dendrites of the OFF ganglion cells stratify in outer half (sublamina a, toward the bipolar cells). The transient cells tend to stratify toward the center of the inner plexiform layer (IPL), while the sustained cells send their dendrites to the two borders of the IPL.

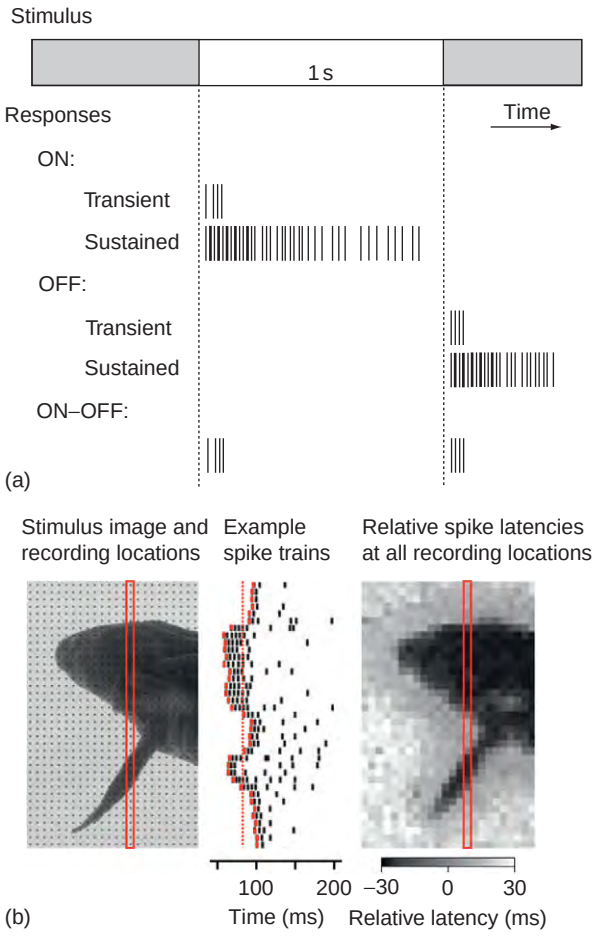

Figure 1 Temporal response characteristics of ganglion cells. (a) Different types of ganglion cells respond differently to the onset of a bright stimulus in the receptive field. ON cells respond at the onset of the stimulus; OFF cells respond at the offset; and ON–OFF cells respond at the both the on- and offset. Within these cell classes, one can find transient and sustained types of responses. (b) The latency of responses of some cell types indicates the intensity of the stimulus. Left: The stimulus image was presented to the retina multiple times at different locations, so that the recorded ganglion cell was located at the positions indicated by the dots. Middle: Spiking responses for the column of recording locations indicated by the red rectangle in the left panel. The first spike after stimulus onset is marked in red. The average time-to-first-spike is indicated by the dotted red line, and serves as time point 0 in the right panel. Right: Relative spike latency for each recording location coded as a grayscale value. Adapted from Gollisch and Meister (2007).

Spatial Processing

Center-Surround Receptive Fields

Many ganglion cell types express antagonistic center-surround receptive fields, first described by Kuffler in 1953. The terms ON and OFF cells defined in the previous paragraph are a shorthand for ON center cell and OFF center cell, describing the response characteristics of the cells when they are stimulated in their receptive field center. When a stimulus spot falls in the surround region, an ON center cell might respond when a bright spot is removed, that is, with an OFF-type response (point 2 below). In his 2001 work, Ralph Nelson summarized the effects that the surround can have on ganglion cell responses. Point 4 of the list given below is equivalent to a size tuning of the response, that is, responses to larger spots can be weaker than responses to smaller spots.

1. Change from sustained to transient center response as stimuli are displaced from center.
2. Responses evoked to opposite stimulus phase with surround stimulation.
3. Active inhibition of the center response with surround stimulation.
4. A maximal response can be evoked only with an optimally sized spot.

Center-surround receptive fields can be successfully modeled as difference of Gaussians, describing two overlaying concentric receptive fields with opposite effects on the cell (**Figure 2**). For small stimuli, the effect of the strong center receptive field prevails. For larger stimuli, the weaker surround begins to show its effect due to its larger radius. Physically, center responses originate from the excitatory input of bipolar cells to the ganglion cell dendrites. Usually, the size of the receptive field center of a ganglion matches the size of its dendritic field quite well. Surround properties originate from the activity of laterally oriented inhibitory interneurons in the retina, namely horizontal cells and amacrine cells. The activity of these cells contributes to the surround at three levels. They suppress the activities of bipolar cells either in the outer retina (horizontal cells) or inner retina (amacrine cells). Amacrine cells also give direct input to ganglion cells, contributing to the inhibitory surround at a third level of interaction.

Tiling

One of the properties characterizing a ganglion cell type is that its members tile the retina. This means that, as a population, the ganglion cells of any type carry information about the whole scene; a single ganglion cell is contributing one pixel. Ganglion cells with small receptive fields (e.g., midget ganglion cells) can convey spatial details of the visual scene (**Figure 3(a)**, left column), while a ganglion cell with a large receptive field (e.g., parasol ganglion cells) will not be able to convey much detailed spatial information (**Figure 1(a)**, right column) – the cell's activity will signal that it was triggered from somewhere within its receptive field, but it is not possible to pinpoint the exact spatial location just from the activity of a single cell, or from the activity of the cell population. The situation is better when the ganglion cells of a type overlap (**Figure 3(b)**), a situation which is frequently

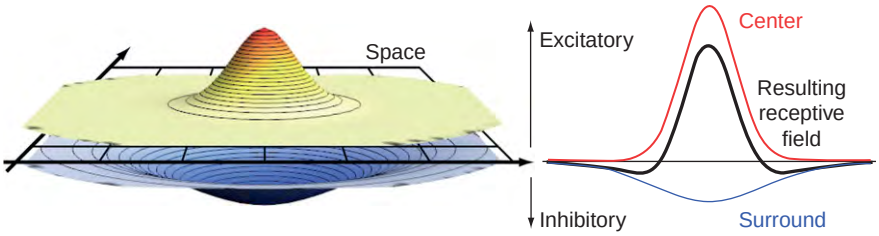

Figure 2 Difference of Gaussian model of center-surround receptive fields. According to this model, the receptive field of a ganglion cell consists of two bell-shaped components, a smaller excitatory component (center), and a larger inhibitory component (surround). The resulting overall receptive field has the shape of a Mexican hat (black curve, right).

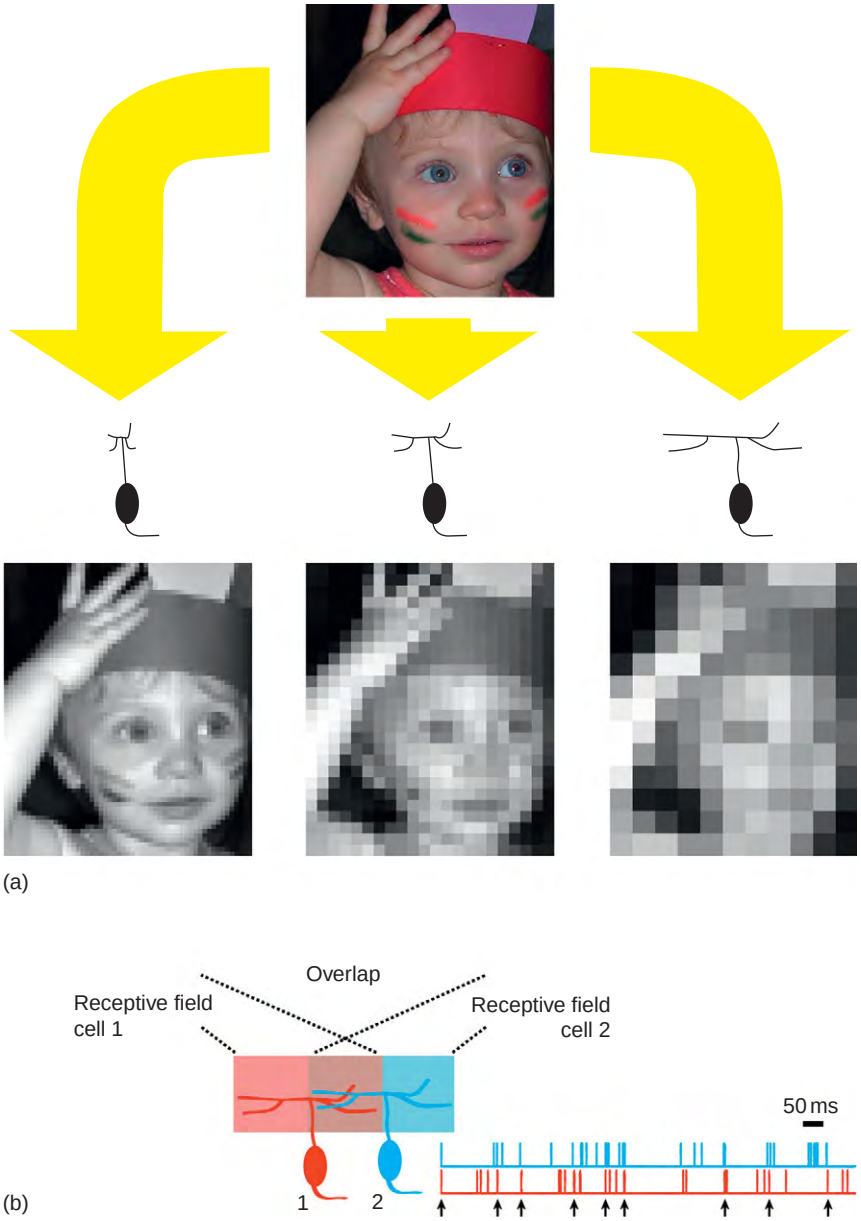

Figure 3 Spatial processing by ganglion cells. (b) Ganglion cells of the same type usually tile the retina so that each region in the visual environment is seen by at least one member of each type. One cell contributes one pixel of the image transmitted to the brain. Ganglion cells with small receptive and dendritic fields convey more detailed spatial information than larger cells. (b) Neighboring ganglion cells often fire action potentials synchronously. One possible mechanism is shared synaptic input. Then, the presence of synchronous spikes is an indication of the presence of an image feature in the region of overlap between two cells, which can increase the spatial resolution of a ganglion cell type. Spike trains adapted from Shlens, J., Rieke, F., and Chichilnisky, E. (2008). Synchronized firing in the retina. *Current Opinion in Neurobiology* 18: 396–402.

encountered (e.g., alpha ganglion cells). When a stimulus feature occurs in the region of overlap between neighboring cells, one can often observe a strongly increased probability of synchronous action potentials of the two cells. In many cells, the main reason for the synchronization is shared synaptic input. Consequently, if the two cells are triggered simultaneously by two separate stimuli occurring in the two nonoverlapping regions of their receptive fields, the firing is not synchronized. The precise relative timing of action potentials can therefore contribute to the spatial information conveyed by the ganglion cell population. More details on modes and mechanisms of synchronous firing in the retina can be found in the 2008 review by Shlens and co-workers.

Stimulus Features that Trigger Ganglion Cell Activity

As mentioned above, any ganglion cell type can be considered as a channel that conveys information about a certain image feature to higher visual centers of the brain. The activity of such a ganglion cell means that (one of) the trigger feature(s) has been present in the visual stimulus in the receptive field of the cell. What are the features that trigger ganglion cell activity?

Ganglion Cells as Spatiotemporal Filters

One way of looking at the processing of visual stimuli by ganglion cells is to interpret them as a bank of spatiotemporal filters (**Figure 4**). Each ganglion cell has certain frequency response characteristics in both space and time. For example, the size of the receptive field together with the surround properties may determine the spatial frequency to which a cell is tuned (small receptive field = high spatial-frequency response). The temporal frequency response is determined not only by cell-autonomous properties of the ganglion cells, but also by the properties of the presynaptic neurons. For example, if the presynaptic neurons are not able to follow a fast-flickering stimulus, neither will be the ganglion cell that is activated by those neurons. Interestingly, ganglion cells with a high spatial-frequency response tend to have a low temporal-frequency response and vice versa. In other words, ganglion cells tend to carry detailed information about space or time, but not both. In general, however, ganglion cells fill up the frequency range in space and time which is occupied by natural stimuli.

Ganglion Cells as Specific Feature Detectors

The following discussion is limited to one important category of visual events in the environment, namely

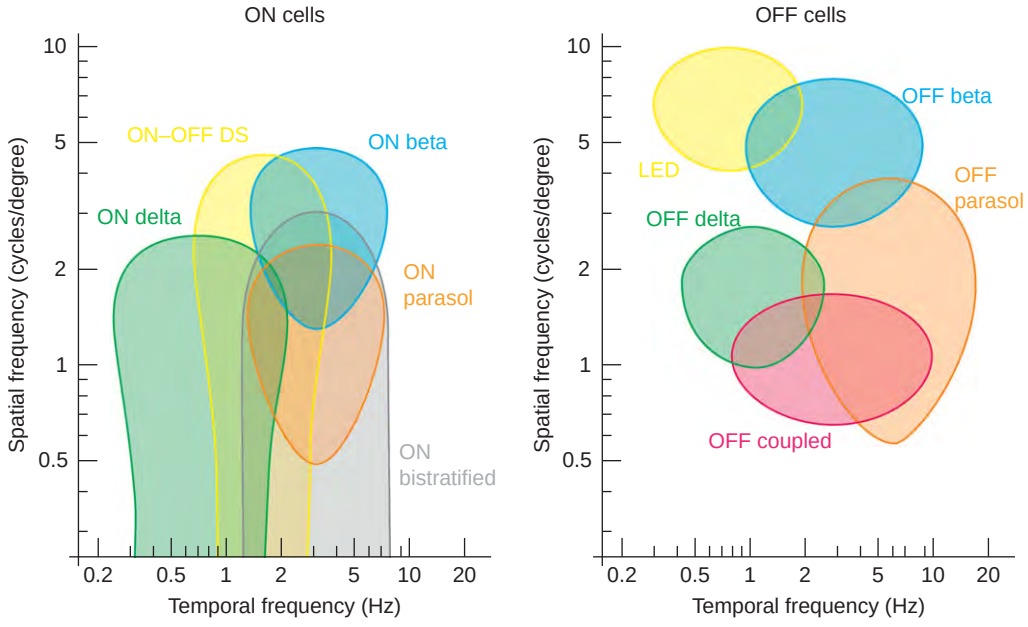

Figure 4 Ganglion cells as spatiotemporal filters. Range of frequencies in space and time over which each ganglion cell type in the rabbit retina responds. The colored blobs represent the full range of responses for each ganglion cell type when measured with a flashed square of light, 600 um on a side. Data have been generated by analyzing the response characteristics in space and time by Al Molnar and Frank Werblin based on data from Roska, B., Molnar, A., and Werblin, F. S. (2006). Parallel processing in retinal ganglion cells: How integration of space–time patterns of excitation and inhibition form the spiking output. *Journal of Neurophysiology* 95: 3810–3822; and Roska, B. and Werblin, F. (2003). Rapid global shifts in natural scenes block spiking in specific ganglion cell types. *Nature Neuroscience* 6: 600–608. Figure courtesy of Frank Werblin.

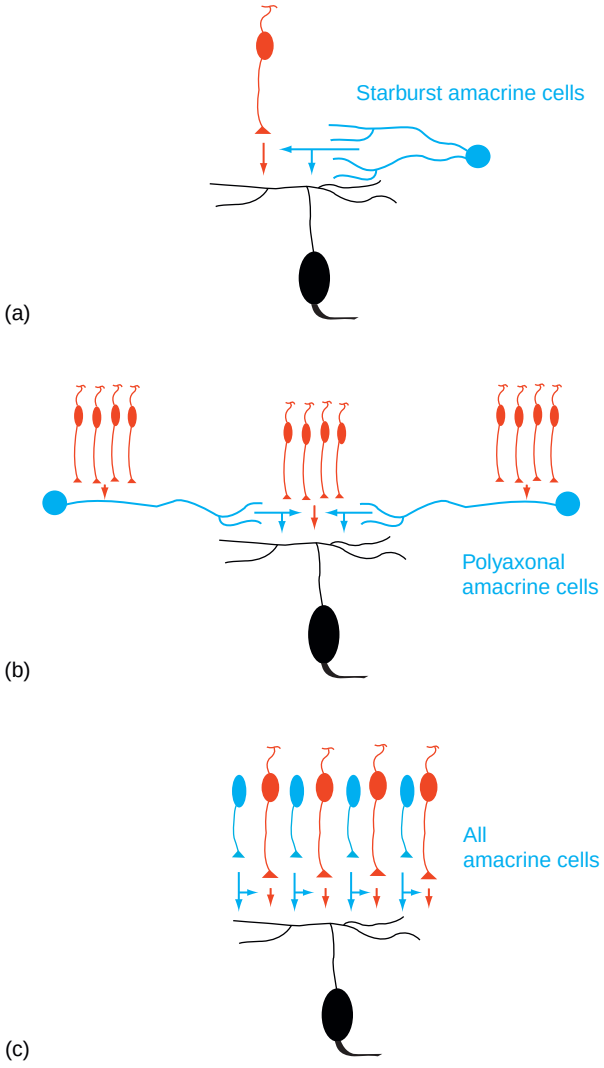

Figure 5 Circuits of movement-encoding ganglion cells. These cells employ common computational principles. The inhibitory circuitry is wired such that unwanted responses are canceled. The targets of the inhibitory input are the dendrites of the ganglion cells and the terminals of the excitatory bipolar cells. The specific wiring diagram is different for each cell type to achieve the desired computation. (a) The inhibitory circuit of direction-selective (DS) ganglion cells is spatially directed and asymmetric. Inhibition is supplied by starburst amacrine cell processes that point in the null direction of the targeted DS cell. The spatial asymmetry creates a temporal difference in the synaptic inputs; inhibition arrives before a suppressed excitatory input for movement in the null direction. (b) Object-motion-sensitive (OMS) cells get long-range inhibitory input from polyaxonal amacrine cells. The OMS cell and the polyaxonal cells get activated by strongly rectifying bipolar cells with similar properties, reporting about the presence of movement. Different trajectories of movement create different temporal sequences of activity, and same trajectories create similar sequences. When an OMS cell sees the same trajectory as a majority of polyaxonal cells, its responses are canceled by the correlated inhibitory activity. When the OMS cell sees a different trajectory, for example, because an object moves within its receptive field relative to the background, it is allowed to respond. Polyaxonal cells have active properties so that the inhibition arrives sufficiently fast at the OMS cell. (c) Approach-sensitive cells receive inhibitory input from AII amacrine cells, which are ON cells. They receive excitatory input from OFF bipolar cells. When dark and bright borders move concurrently within the receptive field, the inhibitory activity elicited by the bright borders cancels the excitatory activity elicited by the dark borders. This situation is encountered by laterally moving small objects or by image drift of a sufficiently detailed scene over the retina. An approaching dark object is expanding in size and has no bright moving image borders, allowing the cell to respond. AII cells get activated through electrical synapses with ON bipolar cells, so that the inhibition arrives sufficiently fast at the approach-sensitive ganglion cell.

that of object motion. Evolution appears to have dedicated a significant amount of retinal hardware to the detection and decoding of moving stimuli. There are at least eight types of direction-selective (DS) ganglion cells (four ON–OFF DS cells, three ON DS cells, and one OFF DS cell) that encode information about the direction of object motion or image drift over the retina. In addition, several ganglion cell types seem to be specialized to recognize the movement of an object relative to global background motion (object-motion-sensitive (OMS) ganglion cells). Recently, a ganglion cell type has been described, which is sensitive to yet another important aspect of object motion, namely when an object is approaching the animal. In the remainder of this article, these different types of motion-sensitive ganglion cells are discussed in greater detail, with emphasis on the underlying mechanism of their response specificity. The basic principle is always the same: responses to unwanted visual stimuli are suppressed by specific inhibitory circuitry (Figure 5).

Direction-selective (DS) ganglion cells

The defining property of DS ganglion cells is that they respond well to a moving object when it moves in a so-called preferred direction. However, when the same object moves in the opposite so-called null direction, they remain silent. The best characterized are the ON–OFF DS cells. Their dendrites are bi-stratified in the ON and OFF sublaminae of the IPL, and the cells respond to both bright and dark objects. The neural circuitry computing the DS responses are present in both the ON and OFF systems, and seem to compute direction selectivity independently from each other. The importance of the inhibitory system can be appreciated by applying blockers of the inhibitory neurotransmitter gamma aminobutyric acid (GABA) to the retina. This results in equal responses to movement in all directions: responses to null-direction movement are uncovered, while responses to preferred-direction movement are hardly changed at all. The directionality of DS ganglion cell behavior is therefore obtained by actively suppressing responses to null-direction movement.

The interneuron responsible for this suppression of null responses is the starburst amacrine cell. Starburst cells have peculiar properties that make them particularly suited for this task. For example, they have an asymmetric spatial distribution of incoming and outgoing synapses along their dendritic processes, which enables them to act at a distance: activation anywhere within the dendritic field can lead to release at the distal tips. In addition, their responses express DS properties themselves. Details of these are discussed elsewhere in the encyclopedia. The most important property responsible for the directional behavior of DS cells, however, is the geometrically specific connectivity between starburst cells and DS ganglion cells, and therefore a circuit property of the retina rather than a cell-autonomous property of either the DS cells or the starburst cells themselves. The geometry of the connectivity is such that only starburst cells located on the null side of the DS cell dendritic field inhibit the DS cell. As a consequence, a stimulus moving in the null direction will first encounter and activate this field of inhibitory starburst cells, which can then perform their action at a distance and inhibit the DS cell before the stimulus also enters the excitatory receptive field of the DS cell. This geometrically asymmetric connectivity can also be observed with static receptive field measurements: The inhibitory receptive field of DS cells is offset to the null side with respect to the excitatory receptive field, which matches the dendritic field quite well. DS cells are, therefore, an example of a cell type that does not have a classical center-surround receptive field.

Inhibitory activity acts at three levels in the DS circuitry to make the DS responses more robust. One level, already mentioned in the previous paragraph, is the geometrically asymmetric inhibition of DS ganglion cells by starburst amacrine cells. Geometric asymmetry is translated by a moving stimulus into a timing difference: during null movement, inhibition will reach the DS cell before excitation; however, during preferred movement, this will not be the case. A second level of inhibition targets the terminals of bipolar cells, and shows the same geometric properties as the inhibition of the DS cell dendrites. The properties of this presynaptic inhibition are consistent with the hypothesis that the same starburst cells that inhibit the DS cell also inhibit the presynaptic bipolar cells that make input to that DS cell. As a consequence, the excitatory input delivered by these bipolar cells is direction-selective because excitation during null-direction movement is strongly reduced. A third level of inhibition relates to the inhibitory input itself. During preferred-direction movement, the inhibitory input to DS cells is suppressed, as a consequence of the above-mentioned directional properties of starburst cell dendritic properties. These directional properties may be brought about, at least partly, by mutually inhibitory interactions between starburst cells.

In summary, because of inhibitory activity at many levels, DS ganglion cells receive directionally asymmetric synaptic inputs: during null-direction movement, they receive early-and-strong inhibitory input together with late-and-weak excitatory input; and during preferred-direction movement, they receive early-and-strong excitatory input with late-and-weak inhibitory input. Internal nonlinear properties of the DS cell itself emphasize the directional differences of the synaptic inputs: it appears that the DS cell contains local dendritic nonlinear properties. Calcium-driven spikes are generated locally in the dendrites when some threshold is crossed. These spikelets travel to the soma where they trigger standard sodium spikes.

Object motion sensitive (OMS) ganglion cells

The visual system constantly has to deal with global image jitter caused by eye, head, and observer movements. It poses a considerable challenge to neglect this global image movement and extract the more relevant movement of objects embedded in this scene. In other words, a ganglion cell with such properties would be active if an object moves within its receptive field (relative to the background), but it would be silent if there is only background movement within the receptive field, even if the local image trajectory is identical in both cases. Markus Meister and colleagues termed such ganglion cells as Object Motion Sensitive (OMS). The responsiveness of such a cell does not depend solely on the local image properties, but on a comparison of local and global properties. The next few paragraphs describe the computational principle of object motion detection.

The excitatory receptive field of OMS ganglion cells consists of small subunits, namely bipolar cells. Each of these subunits is strongly rectifying. This means that each subunit only gives input to the OMS cell if it is strongly activated. This results in relatively sparse excitatory input to the OMS cell.

Inhibitory input is provided by a class of amacrine cells called polyaxonal. Polyaxonal amacrine cells have a relatively small receptive field comparable in size to the OMS ganglion cell, but they have several axonal processes with active properties spreading across a considerable fraction of the whole retina. As a result, an OMS cell can receive inhibitory input from a polyaxonal amacrine cell that looks at a completely different area of the visual scene. Importantly, polyaxonal amacrine cells are electrically coupled with each other, so that they function as a coherent network through which activity can spread. Even though the axonal processes of a single polyaxonal cell are quite sparse, the network of these cells creates a dense mesh of axons. Polyaxonal cells receive similar excitatory input as OMS cells, namely temporally sparse input provided by strongly rectifying bipolar cells. These cells

have a relatively high threshold, so that the polyaxonal network gets activated only if it receives near-simultaneous excitatory input from a large fraction of the visual scene. This condition is met during global image motion, because many of the subunits providing excitatory input to polyaxonal amacrine cells are activated simultaneously. Because of the coupling, all polyaxonal amacrine cells, as a network, fire a burst of action potentials. In time, this results in a relatively sparse sequence of activity in polyaxonal amacrine cells, and consequently in a sparse sequence of inhibitory events in OMS ganglion cells.

An OMS cell therefore receives sequences of excitatory and inhibitory inputs that are temporarily sparse. If there is an object in the receptive field of an OMS cell that moves uncorrelated relative to the global (background) movement, the temporal sequence of the sparse excitatory (local) and sparse inhibitory (global) events will also be uncorrelated. Therefore, the inhibitory events cannot cancel the excitatory events, and the OMS cell will be active. On the other hand, an OMS cell sitting in the background region of the image will receive correlated excitatory and inhibitory inputs, the inhibitory events suppress the excitatory events, and the cell remains silent. In fact, inhibitory input arrives at the OMS cell about 25 ms before the excitatory input, at least in salamander retina, presumably because of the fast active properties of polyaxonal amacrine cells. An OMS cell can, therefore, effectively report the existence of an object moving relative to background.

Recently, in 2008, Baccus and co-workers expanded on their original findings and reported that the main target of the inhibitory input by polyaxonal amacrine cells is not the OMS ganglion cell itself, but the bipolar cell terminals which provide input to the OMS cell.

Saccadic suppression

Roska and Werblin showed that in rabbit retina some ganglion cells are suppressed during saccades, sudden eye movements that serve to shift gaze direction. They suggest that this is due to the inhibitory activity of polyaxonal amacrine cells. This resets the activity of ganglion cells for each visual episode in-between saccades. It is possible that saccadic suppression is a consequence of the same circuitry and mechanism described for OMS ganglion cells in the paragraph above. Roska and Werblin provided a detailed list of ganglion cell types which receive saccadic suppression in rabbit retina, while Meister and colleagues have remained vague about the cell types in rabbit retina, which have the OMS property.

Approach-sensitive ganglion cells

The detection of approaching or looming optical stimuli is important for survival. Such stimuli trigger robust behavioral avoidance responses in basically all animals tested, from insects to humans. Babies as young as 2 weeks react with widening of the eyes, turning of the head, lifting of the arms, and crying when they view a symmetrically expanding shadow on a screen directly in front of them. This suggests that hard-wired neural circuitry exists to detect such looming stimuli and to trigger these protective motor responses. Recently, we described a ganglion cell in the retina that is sensitive to dark approaching visual stimuli, such as widening shadows. Similar to the other cells described earlier, the function of these cells can only be appreciated when one considers the space of null stimuli, that is, the range of stimuli to which the cell does not respond because of active suppression by inhibitory circuitry. In the case of the approach-sensitive ganglion cells, these null stimuli comprise lateral movement of a small object within the receptive field, or lateral drift of the visual scene. In the case of a small, dark, moving object, for example, a hawk flying in sky, the cell will respond when the object is approaching the observer, but it will be suppressed when the object is moving on a lateral trajectory. Lateral drift of a visual scene is encountered during observer head or eye movements, similar to the OMS cells described in the above paragraph, but the mechanism for response suppression is substantially different.

The receptive field of approach-sensitive cells is comprised of small subunits for both the excitatory and inhibitory inputs. The excitatory input is mediated by transient OFF bipolar cells. Whenever a dark stimulus border is moving into a new subunit (i.e., into the receptive field of another bipolar cell), the approach-sensitive ganglion cell receives another episode of excitatory input, resulting in spiking output. This is true for any moving dark border within the receptive field of the ganglion cell, unless these events are canceled by simultaneously moving bright stimulus borders within the receptive field, as it would be encountered by the trailing edge of a laterally moving small dark object, but not by an approaching dark object, which does not create any trailing edges. The reason for the suppression by moving bright image borders is the structure of the inhibitory receptive field: it also consists of small subunits, but of the opposite polarity; the inhibitory input is mediated by ON amacrine cells with a small receptive field. The suppression of null responses is therefore computed on a local scale within the receptive field of ganglion cell.

The most interesting aspect of the approach-sensitive circuitry is the identity of the inhibitory amacrine cell and the specific synaptic connectivity employed. The amacrine cell responsible for the inhibition of the approach-sensitive ganglion cell is the well known AII (pronounced A-two) amacrine cell. AII amacrine cells are a main conduit for visual signals during nighttime vision. They are activated by rod bipolar cells through a glutamatergic chemical synapse, and then pass the signals on to both ON and OFF cone pathways. OFF pathways are activated through a glycinergic chemical synapse. The targets of

these synaptic connections are both the terminals of OFF cone bipolar cells, and the dendrites of OFF ganglion cells. ON pathways are activated through electrical synapses (gap junctions) between the AII cells and the terminals of ON cone bipolar cells. During daytime vision, rods are saturated, and rod bipolar cells are not active. Under these conditions, AII cells are activated mostly by ON cone bipolar cells by virtue of the electrical synapse between these cells. Once activated, AII cells can release glycine and inhibit their targets in the OFF pathway. One such target is the approach-sensitive ganglion cell, and the bipolar cells that activate it.

This pathway for the inhibitory input of the approach-sensitive ganglion cell has properties ideally suited for the approach-sensitive computation. AII cells are small, with a receptive field not larger than that of bipolar cells. Therefore, the excitatory and inhibitory subunits are of compatible size. Another important aspect is the dynamics of the inhibition. As explained above, null stimuli for the approach-sensitive cell are those that have concurrently moving dark and bright borders. The inhibitory input, activated by the bright borders, suppresses responses that would be elicited by the dark borders. This requires the inhibition to arrive at its target fast enough, so that no excitatory signal slips through, similar to the fast inhibitory input arriving at DS cells and at OMS cells. In the case of the AII cells, the speed of inhibition seems to be ensured by the electrical synapse in the pathway. The electrical synapse effectively reduces the number of chemical synapses in the inhibitory pathway to the same number as those in the excitatory pathway.

See also: Information Processing: Direction Sensitivity.

Further Reading

Baccus, S. A., Olveczky, B. P., Manu, M., and Meister, M. (2008). A retinal circuit that computes object motion. *Journal of Neuroscience* 28: 6807–6817.

Demb, J. B. (2007). Cellular mechanisms for direction selectivity in the retina. *Neuron* 55: 179–186.

Fried, S. I., Münch, T. A., and Werblin, F. S. (2002). Mechanisms and circuitry underlying directional selectivity in the retina. *Nature* 420: 411–414.

Gollisch, T. and Meister, M. (2008). Rapid neural coding in the retina with relative spike latencies. *Science* 319: 1108–1111.

Kuffler, S. W. (1953). Discharge patterns and functional organization of mammalian retina. *Journal of Neurophysiology* 16: 37–68.

Nelson, R. (2001). Visual responses of ganglion cells. *From: Webvision – The Organization of the Retina and Visual System* . http://webvision.med.utah.edu/GCPHYS1.HTM (accessed May 2009).

Olveczky, B. P., Baccus, S. A., and Meister, M. (2003). Segregation of object and background motion in the retina. *Nature* 423: 401–408.

Rodiek, R. W. (1998). *The First Steps in Seeing.* Sunderland, MA: Sinauer.

Roska, B., Molnar, A., and Werblin, F. S. (2006). Parallel processing in retinal ganglion cells: How integration of space–time patterns of excitation and inhibition form the spiking output. *Journal of Neurophysiology* 95: 3810–3822.

Roska, B. and Werblin, F. (2003). Rapid global shifts in natural scenes block spiking in specific ganglion cell types. *Nature Neuroscience* 6: 600–608.

Shlens, J., Rieke, F., and Chichilnisky, E. (2008). Synchronized firing in the retina. *Current Opinion in Neurobiology* 18: 396–402.

Wässle, H. (2004). Parallel processing in the mammalian retina. *Nature Reviews* 5: 747–757.

Werblin, F. and Roska, B. (2007). The movies in our eyes. *Scientific American* 296: 72–79.

Information Processing: Horizontal Cells

A A Hirano, UCLA School of Medicine, Los Angeles, CA, USA
S Barnes, Dalhousie University, Halifax, NS, Canada
S L Stella, Jr., UCLA School of Medicine, Los Angeles, CA, USA
N C Brecha, UCLA School of Medicine, Los Angeles, CA, USA; VAGLAHS, Los Angeles, CA, USA

Glossary

Ephaptic transmission – A nonsynaptic electrical interaction mediating cellular communication. Closely apposed neural elements may share signals through an extracellular voltage change caused by the flow of current in a confined, resistive interstitial space between neurons. Changes of extracellular ion concentrations, such as high potassium levels caused by potassium extrusion from an active, depolarized neuron, also affect close-neighboring neurons.

Gain control – The gain or amplification of a graded potential synapse, such as that between photoreceptors and second-order neurons in the retina, is defined as the postsynaptic amplitude divided by presynaptic amplitude. To optimize signal-to-noise ratios, synaptic strength may be controlled by reciprocal signals that increase synaptic gain when signals are small, and reduce the gain when signals are large and saturating.

Gap junctions – The specialized electrical junctions between cells consisting of two connexons, each termed a hemichannel and made up of connexin proteins, which together form an intercellular pore. These mediate rapid electrical events between cells, allow diffusion of ions and small proteins, and are regulated by neuromodulators, including dopamine, nitric oxide, and retinoic acid, in the retina.

Photoreceptor synaptic triad – The synaptic arrangement consisting of two lateral horizontal cell endings or terminals and an ON bipolar cell dendrite that invaginate into a photoreceptor terminal.

Protons – The free hydrogen ions, as H^+ or hydronium ions (H_3O^+), in solution, usually bound (buffered) by other molecular constituents.

Receptive fields – The receptive fields of neurons in the visual system are the regions of retinal surface, receiving an optical projection of visual space, for which light stimulation causes a response in the cell. The classic center-surround antagonistic receptive field typically has a circular center and, forming a ring around the center, an annular surround. The sign of the cell's response to light in the center is the opposite of that in the surround. This receptive-field organization underlies edge detection by enhancing contrast between regions of varying brightness and/or color.

Roll back – A modest, slowly depolarizing trajectory seen in the horizontal cell voltage waveform, counteracting the rapid hyperpolarization of 30–50 mV during the response to a light stimulus. The roll back, whose amplitude is dependent on the intensity and diameter of the stimulus, is considered to be due to inhibitory feedback from horizontal cells to photoreceptors.

Introduction

Visual information is conveyed through the retina from photoreceptors via bipolar cells to ganglion cells, and the signal is modulated by inhibitory lateral interactions provided by horizontal cells in the outer plexiform layer and amacrine cells in the inner plexiform layer. Retinal neurons are characterized by having an antagonistic, concentric center-surround receptive-field organization.

Horizontal cells play a critical role in generating the inhibitory receptive-field surround of cone photoreceptors and bipolar cells in both mammalian and nonmammalian retinas. These cells are characterized by a broad, lateral spread of their processes as well as homologous coupling through gap junctions to other horizontal cells. In mammalian retinas, both A-type and B-type horizontal cells receive input from cone photoreceptors at their dendritic tips, and rod photoreceptors at their axon terminals. Horizontal cells transmit spatially broad visual signals back to photoreceptors and bipolar cells, to generate receptive-field surrounds (**Figure 1**). The antagonistic, center-surround receptive-field spatial organization contributes to visual processing that highlights changes in luminance and contrast to improve visual acuity. Horizontal cells also participate in setting the gain of the photoreceptor synapse through inhibitory feedback of information about local illumination levels, and in lower vertebrates, color-opponent receptive fields are generated through color-specific, antagonistic receptive-field surrounds.

Synaptic Interactions and Gap-Junction Coupling of Horizontal Cell Subclasses

There are two physiological classes of horizontal cells, which code for luminosity and chromaticity, in the vertebrate retina. The luminosity (L-type, or H1) horizontal cell responds to the whole range of visible light with a graded hyperpolarization, due to receiving inputs from all types of cone photoreceptors. The chromaticity (C-type, or H2, H3) horizontal cells respond to certain wavelengths of light with a hyperpolarization and a depolarization to others, in a biphasic or triphasic manner, due to selective connectivity with and feedback onto different spectral subtypes of cone photoreceptors. In this manner, the C-type horizontal cells begin the process of encoding color opponency. In addition, there are also horizontal cells that synapse selectively with rod photoreceptors in some species, including teleosts; however, most lower vertebrates exhibit mixed rod and cone inputs into horizontal cells. Mammals appear to have only the L-type horizontal cells, and these do not exhibit color-opponent properties.

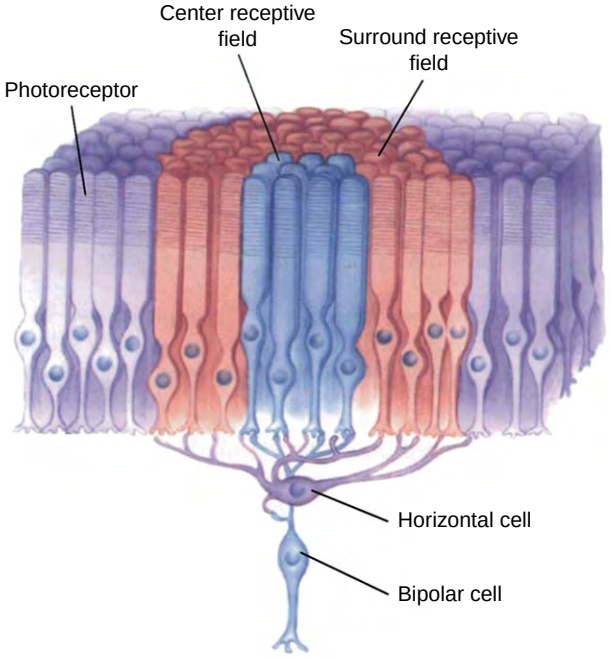

Figure 1 Formation of bipolar cell center-surround antagonistic receptive fields by integration of direct photoreceptor inputs at center of receptive field (shown in blue) and surround photoreceptor inputs (shown in red) carried through a large receptive-field horizontal cell. Horizontal cells are normally homologously coupled, except under the condition of extreme light adaptation. The horizontal cell signal is conducted to the bipolar cell through inhibitory feedback at the photoreceptor terminals and through direct feed-forward signaling to the bipolar cell. Reproduced from figure 9.22 of Bear, M. F., Connors, B. W., and Paradiso, M. A. (eds.) (2007). *Neuroscience: Exploring the Brain*, 3rd edn. Philadelphia, PA: Lippincott Williams & Wilkins.

In general, in mammals, A- and B-type horizontal cell dendrites form synapses with cone photoreceptors, whereas the axon terminal system of the B-type forms synapses with rod photoreceptors. Due to the high electrical resistance in the long axon connecting the axon terminals to the somatodendritic region, the two compartments of the B-type horizontal cell are thought to act as functionally independent units. Horizontal cells receive excitatory glutamatergic input from the photoreceptors and feedback onto the cone and rod terminals, presumably at the horizontal cell endings within the photoreceptor terminals. In darkness, photoreceptors release transmitter; thus, the membrane potential of horizontal cells is relatively depolarized. In response to light, all horizontal cells studied exhibit slow, graded hyperpolarizing potential changes due to the reduction in transmitter release from photoreceptors. These slow potentials were originally called S-potentials (in honor of Gunnar Svaetichin, who initially described them in 1953). With the advent of intracellular dyes, it was shown that S-potentials arose from horizontal cells in the outer retina.

A slow-adapting depolarization is seen in the horizontal cell voltage waveform, immediately following the hyperpolarization seen during the response to a light stimulus (**Figure 2**). This so-called roll back, whose amplitude is dependent on the diameter of the stimulus, as well as on the intensity and duration of the stimulus, is considered to be due to inhibitory feedback from horizontal cells to photoreceptors.

A key feature of horizontal cells is that they form a syncytium through gap-junction coupling between homologous horizontal cell subtypes, such that the networks of A-type horizontal cells are distinct from those formed by the B-type horizontal cells. As a result, the receptive fields of horizontal cells are considerably larger than the spread

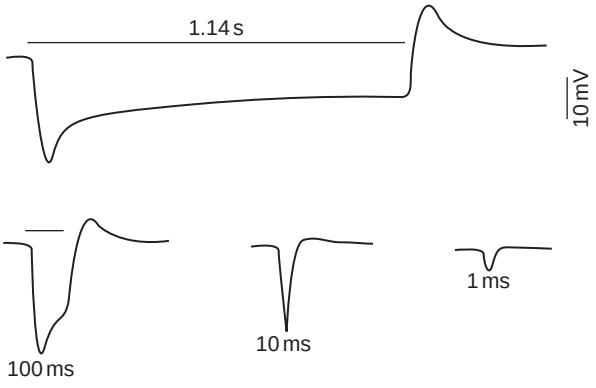

Figure 2 The S-potential in early recordings from the retina of cat, showing horizontal cell responses to bright light stimuli of various durations (1.14 sec, 100, 10, and 1 ms). Vertical bar on right corresponds to 10 mV. Reproduced from figure 8 of Brown, K. T. and Wiesel, T. N. (1959). Intraretinal recording with micropipette electrodes in the intact cat eye. *Journal of Physiology (London)* 159: 537–562, with permission from Wiley-Blackwell.

of their dendritic arborization. Furthermore, the number of coupled cells varies depending on the state of light adaptation of the retina. It is now known that several neuromodulators, including dopamine, nitric oxide, and retinoic acid, act through various signaling systems and distinct retinal circuitry to regulate properties of gap junctions within the coupled network of horizontal cells.

Ionic Conductances of Horizontal Cells and the Response to Light

The ionic conductances that shape the graded potentials of horizontal cells are attributable to the postsynaptic α-amino-3-hydroxyl-5-methyl-4-isoxazole-propionate (AMPA; GluR1, GluR2/3, and GluR4) and kainate (KA2, GluR6) ionotropic glutamate receptors that mediate photoreceptor input and an ensemble of voltage-gated ion channels, ion transport mechanisms, and voltage-insensitive ion channels. **Figure 3** shows a voltage-clamp recording from an isolated goldfish horizontal cell that illustrates several of the voltage-sensitive ion channel currents. In total, there are at least three types of voltage-gated K^+ channels (inward rectifier, delayed rectifier, and transient A-type), two types of voltage-gated Ca^{2+} channels (L- and N-type) and tetrodotoxin (TTX)-sensitive Na^+ channels. Horizontal cells also express hemichannels (formed from a variety of connexins in a species-dependent manner), amiloride-sensitive Na^+/H^+ channels (ENaCs), acid-sensitive Na^+/proton channels (ASICs), as well as a range of electrogenic exchangers for Na^+, Ca^{2+}, Cl^-, K^+, and HCO_3^- (Na^+/Ca^{2+}, $Na^+/Ca^{2+}/K^+$, $Na^+/K^+/2Cl^-$, and AE3) and pumps (Na^+/K^+- and Ca^{2+}-adenosine triphosphate (ATP)ases, H^+-pumping plasma membrane V-ATPases) for maintaining ionic gradients. Finally, inositol 1,4,5-trisphosphate-sensitive and caffeine-sensitive intracellular Ca^{2+} stores contribute to calcium signaling and may influence synaptic transmission.

In the dark, horizontal cell membrane potential is driven by input from photoreceptors releasing L-glutamate acting at AMPA and kainate receptors to depolarize cells to a level near −20 mV (**Figure 4**). The balance of excitatory synaptic input and activation of delayed rectifier K^+ channels set this membrane potential. Reduction of glutamatergic input from photoreceptors by light terminates the depolarizing influence, and the membrane hyperpolarizes toward the potassium equilibrium potential (E_K) where inward rectifier K^+ channels (K_{IR}) activate and dominate the membrane potential. In fact, horizontal cell K_{IR} channels strongly clamp these cells at a potential near −70 mV in the absence of glutamate. The dihydropyridine-sensitive, L-type ($Ca_V1.2$ and 1.3, α1C and D) and N-type Ca^{2+} channels, which normally activate above −50 mV, may mediate vesicular fusion, and produce Ca^{2+} fluxes that activate Ca^{2+}-dependent enzymes, and trigger release of Ca^{2+} from internal stores. Na^+ channels are thought to have roles in accelerating the depolarizing phase of the horizontal cell response at the termination of a light step, and, in coordination with the A-type K^+ channels, participate in oscillatory potential production. Some of these channels are also modulated by neurotransmitters: inward

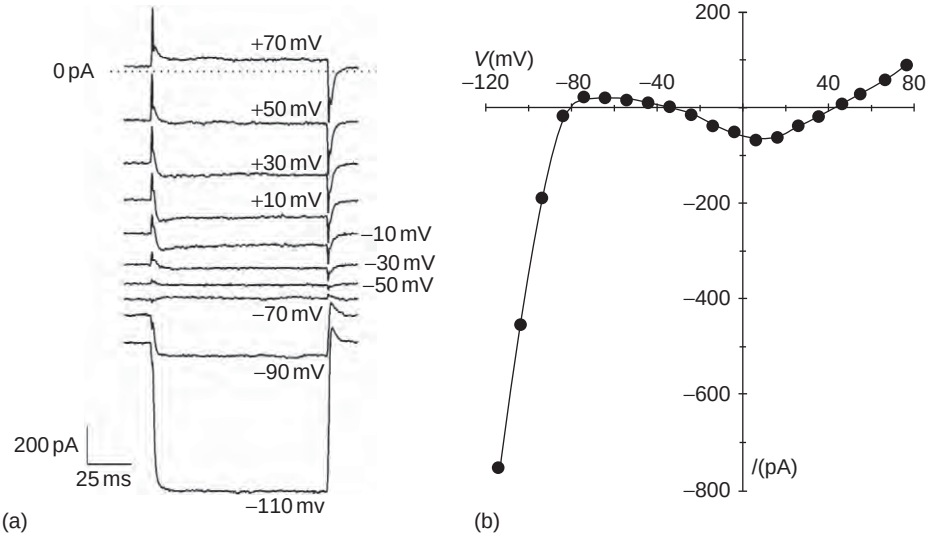

Figure 3 Current–voltage relation of isolated goldfish horizontal cell, recorded from a holding potential of –40 mV with steps in (a) to show temporal characteristics of the response and in (b) a depolarizing ramp voltage clamp protocol. The characteristic N-shape of the *I–V* relation illustrates the prominent inwardly rectifying current carried by K^+ at potentials more negative than –80 mV, an extended negative slope region due to L-type Ca^{2+} channels positive to –40 mV, and modest outward rectification positive to +40 attributable to delayed rectifier K^+ channels and hemichannels. Reproduced from figure 1 of Jonz, M. G. and Barnes, S. (2007). Proton modulation of ion channels in isolated horizontal cells of the goldfish retina. *Journal of Physiology (London)* 581(Pt 2): 529–541, with permission from Wiley-Blackwell.

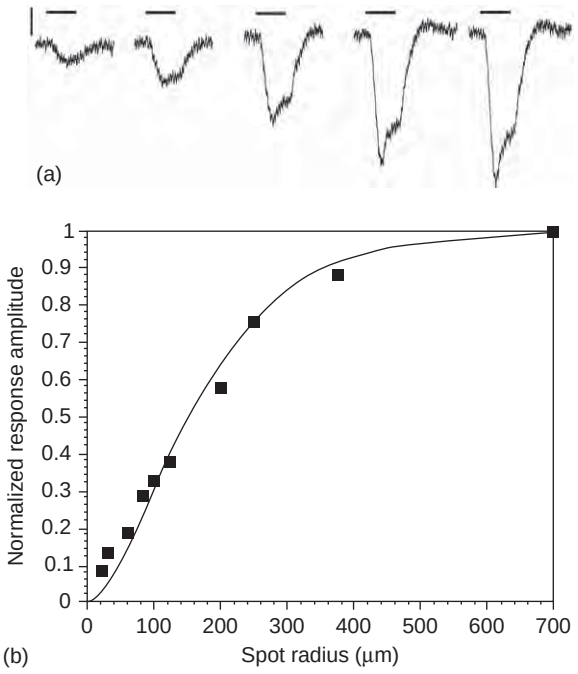

Figure 4 Responses of a mouse horizontal cell to (a) light spots of increasing radius (40, 90, 200, 375, and 700 μm) and constant intensity (log $I/I_0 = -2.1$) lasting 250 ms (horizontal bars). Note the prominent roll back of the hyperpolarization response with the largest spot stimulations, reflecting the engagement of the surround response. Vertical scale bar is 2 mV. (b) Plot of normalized response amplitudes against spot radius. Reproduced from figure 4 of Shelley, J., Dedek, K., Schubert, T., et al. (2006). Horizontal cell receptive fields are reduced in connexin57-deficient mice. *European Journal of Neuroscience* 23(12): 3176–3186, with permission from Wiley-Blackwell.

rectifier K^+ channels and L-type Ca^{2+} channels are suppressed by L-glutamate, and the L-type Ca^{2+} channels are modulated by dopamine in cone-driven horizontal cells.

Cellular Mechanisms of Horizontal Cell Neurotransmission

Lateral inhibition in the outer retina generates receptive-field surrounds of retinal neurons at photoreceptor terminals and at bipolar cell dendrites. In other words, the photoreceptor response can be modulated by light falling on neighboring photoreceptors through horizontal cell feedback. As the diameter of a spot of light increases and the horizontal cell feedback network is engaged, the hyperpolarizing membrane potential response of photoreceptors and horizontal cells exhibit a slow depolarizing sag or roll back in the membrane potential, which is attributed partly to this feedback (**Figure 4**). Although it is generally accepted that horizontal cells provide inhibitory feedback onto photoreceptor terminals, the synaptic and cellular mechanisms underlying this process are poorly understood. There are several proposed mechanisms of synaptic transmission, involving gamma aminobutyric acid (GABA), protons, and an ephaptic mechanism through hemichannels, at the tips of horizontal cells. Discrepancy between findings from different groups may reflect technical issues and different biological strategies used by mammalian versus nonmammalian species, and perhaps even different synaptic mechanisms used by the different horizontal cell subtypes. Furthermore, it is also possible that different cellular mechanisms encode different aspects of visual information or may be used under different light conditions. However, it seems clear that the principal effect of horizontal cell feedback onto cone and rod photoreceptor terminals involves the modulation of their voltage-gated L-type Ca^{2+} channels.

Horizontal Cell Feedback and Feed-Forward

The inhibitory transmitter GABA has been proposed as the horizontal cell neurotransmitter, and the release of GABA is thought to occur through the voltage-modulated action of a plasma membrane GABA transporter (GAT) in nonmammalian retinas and by regulated vesicular release in mammalian retinas, as mammalian horizontal cells do not express GATs. An ephaptic model of feedback onto cone terminals was originally conceived by Byzov and colleagues, and later elaborated to involve hemichannels as current sinks. More recently, evidence has accumulated for protons as a key messenger. In any case, since the ON and OFF bipolar cells depolarize or hyperpolarize, respectively, in response to light-mediated reductions in glutamate release from photoreceptors, it seems simplest that for surround antagonism to affect the two types of bipolar cell responses in a coherent manner, the modulatory effect would be integrated at the presynaptic photoreceptor terminal by a feedback mechanism. To invoke feed-forward surround inhibition requires the horizontal cell transmitter to affect the postsynaptic ON and OFF bipolar cells through mechanisms of opposite polarity.

Several convergent findings indicate that GABA is a mammalian horizontal cell transmitter. One or both of the L-glutamate decarboxylase (GAD) isoforms are found in horizontal cells at the messenger RNA (mRNA) and protein levels. Many, but not all, studies have shown GABA immunoreactivity in horizontal cells of guinea pig, cat, rabbit, and primate retina. In contrast, there are studies reporting low or nondetectable levels of GAD_{67} or GABA immunoreactivity in horizontal cells of the adult mouse and rat retina, whereas GAD immunostaining is present at high levels in horizontal cells of the developing and juvenile mouse retina. The detection of GAD or GABA in the adult retina is influenced by several factors, including differential expression of GAD isoforms and levels of GAD and GABA in horizontal cells, as well as technical issues related to fixation protocols and antibody

specificity. The presence of vesicular GABA transporter (VGAT) immunoreactivity in horizontal cells is consistent with a transmitter role for GABA in mammals, as VGAT mediates the accumulation of GABA into synaptic vesicles. The highest level of VGAT immunostaining is in horizontal cell processes underneath the photoreceptor terminals, and in the dendritic and axonal endings within the synaptic triad.

Feed-Forward onto Bipolar Cell Dendrites

Bipolar cells possess antagonistic receptive-field surrounds, which may be to some extent mediated by horizontal-cell feed-forward transmission onto bipolar cells. At the ultrastructural level, synapses between horizontal cell processes and bipolar cell dendrites have been reported. $GABA_A$ and $GABA_C$ receptor immunoreactivity is localized to bipolar cell dendrites adjacent to horizontal cell processes. In perforated-patch recordings, GABA elicits depolarizing inward currents when applied to dendrites of mouse rod bipolar cells and hyperpolarizing currents when applied to OFF-type cone bipolar cells, consistent with a GABAergic feed-forward input from horizontal cells in the creation of receptive-field surrounds. The inhibitory and excitatory actions of GABA at ON- and OFF-bipolar cell dendrites may be accounted for by the different Cl^- concentrations in bipolar cell dendrites maintained by chloride co-transporters. NKCC (Na-K-2Cl transporter), which accumulates Cl^- intracellularly, has been immunolocalized to dendrites of ON bipolar cells, whereas, KCC2, which extrudes Cl^-, has been localized to those of OFF bipolar cells. The localization of these chloride transporters would predict that chloride equilibrium potential (E_{Cl}) would be positive to the membrane potential (V_m) in the former situation, and E_{Cl} would be negative to V_m in the latter.

While horizontal cell inputs to bipolar cells could be demonstrated by direct current injection into or light stimulation of horizontal cells, it has been more difficult to sort out the contributions of the indirect pathway of horizontal cell to cone photoreceptor to ON bipolar cell from the direct horizontal cell to bipolar cell dendrite pathway. In experiments where L-2-amino-4-phosphonobytyric acid (L-AP4) was used to block photoreceptor input to ON bipolar cells, and by extension the indirect pathway, light stimulation produced a hyperpolarization response in these bipolar cells. From the relative magnitudes of the surround responses with and without L-AP4, about a quarter to a third of the surround response came through the feed-forward horizontal cell to bipolar cell synapse; the majority arose through the feedback to the cone photoreceptor terminals. Low cobalt concentrations (<500 μM) selectively block surround-evoked depolarization of cones (and receptive fields of downstream neurons), without affecting transmission from cones to horizontal cells. It has been proposed that low concentrations of cobalt may act by blocking GABA-induced current in turtle cones, but hemichannels and proton-permeable ENaCs have also been reported to be sensitive to low concentrations of cobalt. Finally, there is anatomical evidence from rabbit retina as well as electrophysiological and tracer evidence from salamander that indicate gap-junction coupling between horizontal cells and cone ON-type bipolar cells.

Feedback onto Photoreceptor Terminals

In turtle and salamander retina, there are extensive data supporting the GABA-mediated inhibitory feedback from horizontal cells to cones. A clear, nonzero reversal potential of this feedback synapse onto cones suggests that the underlying synaptic mechanism is likely chemical, rather than electrical. Moreover, bathing the retina in GABA blocks the feedback response of cone photoreceptors, as would be expected if a decrease in GABA release signals the horizontal cell feedback. In turtle cones, the effect of GABA was hyperpolarizing upon break-in in ruptured patch recordings, suggesting that the reversal potential for chloride in cones was negative to the resting membrane potential. The surround response would reflect a diminution of this hyperpolarizing current. However, the currents evoked by GABA in turtle cones in whole retina preparations were too small to account for feedback, unless enhanced by modulators of $GABA_A$ receptors (e.g., pentobarbital), suggesting that the contribution of the GABA-induced current to surround formation was minor. In salamander cones, the reversal potential for chloride in cones is close to the dark resting potential, suggesting GABAergic disinhibition near the dark potential should produce little membrane-potential change. This result is inconsistent with the postulated role for GABA in generating the feedback depolarization and supports other studies using GABA receptor antagonists, suggesting that GABA does not have a role in horizontal cell to cone photoreceptor feedback.

In contrast, the localization of GABA receptors to photoreceptor terminals is consistent with a feedback role for GABA. Morphological and molecular support for a feedback role includes the expression of $GABA_A$ receptor subunit messenger RNA (mRNA) by photoreceptors detected by *in situ* hybridization immunohistochemistry and single-cell RT-PCR. In addition, cone terminals of pig, mouse, and rat show $GABA_C$ receptor (ρ subunit) immunoreactivity. Similar to the GABA-induced currents in turtle cone pedicles, recordings from mouse and pig cones show the presence of functional $GABA_A$ and $GABA_C$ receptors, whereas rods in porcine and turtle retina exhibit little sensitivity to GABA. In addition to ionotropic GABA receptors, metabotropic $GABA_B$ receptors are expressed on horizontal cell processes, suggesting that GABA may also act presynaptically on horizontal cells. Finally, it is also likely that GABA

acts on autoreceptors on horizontal cells as well as on neighboring horizontal cells, where it would likely be depolarizing as E_{Cl} is above V_m; this would provide positive feedback. Overall, these studies indicate multiple targets for GABA in the outer plexiform layer, which could mediate complex actions of GABA in the outer retina.

There are also findings that argue against the role of GABA in mediating horizontal cell feedback onto cones. Principally, GABA agonists and antagonists do not always appear to affect surround-evoked depolarization of cones. However, the presence of GABA receptors on horizontal cells, bipolar cells, as well as on cone photoreceptors complicates the interpretation of experiments using GABA antagonists. Furthermore, it is clear that small changes in the Ca^{2+} currents produced by feedback are not reflected in large changes in the membrane potential of the photoreceptor.

Ephaptic Transmission between Horizontal Cells and Photoreceptor Terminals

An ephaptic effect has also been hypothesized to underlie the feedback signal from horizontal cells to rod and cone photoreceptors. Originally, this electrical feedback mechanism was proposed to involve only glutamate-gated channels in the tips of horizontal cell processes that invaginate cone synaptic terminals. More recently, evidence for hemichannels at the tips of horizontal cell processes added this conductance mechanism as an additional current sink in the horizontal cell dendrites. Current flowing through the bulk resistance of the interstitial space and into hemichannels and glutamate receptor ion channels is proposed to produce a voltage drop in the synaptic cleft. This extracellular negative potential, in effect, shifts the activation of presynaptic Ca^{2+} channels in the positive direction, reducing the amount of glutamate released by the photoreceptor synapse.

The amplitude of the extracellular voltage drop is a critical function of the current density and the interstitial resistivity, and there is no consensus yet that the amplitude is sufficient to carry the 5–10-mV feedback signals that presynaptic Ca^{2+} channels apparently sense. Furthermore, the time course of an ephaptic response should be nearly instantaneous since it is electrical in nature, but it is well known that there is a slow time course of the roll back of the horizontal cell light response (**Figure 2**). The more rapid depolarization of the photoreceptor (or OFF bipolar cell) in response to strong surround inhibition seems better suited kinetically to the ephaptic effect. Carbenoxolone-induced block of hemichannels has been cited as evidence for ephaptic transmission. However this drug also blocks Ca^{2+} currents in photoreceptors at concentrations used to block ephaptic transmission.

Proton Mediation of Horizontal Cell Feedback

Recent work in turtle, salamander, ground squirrel, primate, zebra fish, and goldfish retina indicates that modulation of the extracellular pH in the synaptic cleft between horizontal cells and photoreceptors may be used to signal feedback to photoreceptors. Evidence that protons modulate voltage-gated Ca^{2+} channels at photoreceptor terminals, carrying the feedback signal, is substantial. The principal evidence is that 1–20-mM HEPES and other pH buffers reversibly block feedback onto photoreceptors by eliminating the shift in activation of the photoreceptor Ca^{2+} channel current. The exact cellular mechanism that controls the pH of the synaptic cleft between photoreceptors and horizontal cells remains undefined, but horizontal cell plasma membrane V-ATPases, ENaCs, ASICs, and hemichannels are possible membrane mechanisms by which horizontal membrane potential could alter cleft pH. Depolarized horizontal cells would produce or contribute to cleft acidification by extruding protons and/or by not taking them up, while hyperpolarized horizontal cells would facilitate cleft alkalinization by not releasing protons and/or by taking them up. The sensitivity of presynaptic Ca^{2+} channels to alterations in extracellular pH suggest that cleft pH is modulated between ~pH 7.0, during the peak of inhibitory feedback signaling, and ~pH 7.8, during maximal horizontal cell hyperpolarization and the absence of presynaptic inhibition. Physiological measurements and estimates of cleft pH changes support the possibility that pH changes of this magnitude occur.

Functional Roles of Horizontal Cells

The proposed functional roles of mammalian horizontal cells are derived from the notion that these cells provide inhibitory feedback onto photoreceptors. This idea is based largely on investigations of nonmammalian model systems that show: (1) a global contribution to retinal adaptation to different mean levels of illumination; (2) a local contribution to spatial processing and contrast enhancement by a spectrally broadband, but spatially restricted feedback to create the antagonistic receptive-field surrounds of photoreceptors, bipolar cells, and ganglion cells; and (3) a local contribution to chromatic processing by a chromatically selective feedback to create color-opponent receptive fields of cones, bipolar cells, and ganglion cells.

Retinal Adaptation

The syncytium of horizontal cells formed through electrical coupling of homologous cells shows characteristic changes with different states of light adaptation. Dark adaptation reduces coupling (from space constant determinations, tracer coupling), smaller receptive-field sizes

(surround-to-center ratio), and decreased sensitivity of horizontal cells. The decreased electrical coupling would also increase input resistance of the cell, resulting in larger voltage changes to a given light stimulus. Several modulators of horizontal-cell gap-junctional coupling have been identified, including dopamine, nitric oxide, and retinoic acid, which appear to mediate the effects of adaptation.

The dopaminergic modulation of horizontal-cell gap-junction conductivity has been reported for both nonmammalian and mammalian retinas. During light stimulation, the levels of dopamine rise in the retina and, through activation of D1 dopamine receptors on horizontal cells in a cyclic adenosine monophosphate (cAMP)-dependent manner, the duration and frequency of gap-junction openings are reduced. This results in the uncoupling of horizontal cells, such that responses of a smaller pool of photoreceptors and, thus, input from a smaller visual area, influence the horizontal cell response, reflected in the reduced surround-to-center (annulus-to-spot) ratios. Findings in rabbit retina indicate that the network of coupled horizontal cells is greatest in dim, scotopic conditions (dim ambient light) and less extensive in darkness and in photopic conditions, that is, the degree of coupling reflects the adaptational state of the retina (**Figure 5**). The retinal circuit underlying the modulation of dopamine release appears to involve a pathway from photoreceptors to ON bipolar cells to dopaminergic amacrine cells to horizontal cells. In addition to differing adaptational states, retinal levels of dopamine vary with a circadian rhythm.

Similar to dopamine, nitric oxide appears to uncouple horizontal cells, modulating the electrical coupling through activation of soluble guanylate cyclase and a cyclic guanosine monophosphate (cGMP)-dependent cascade in horizontal cells. Interestingly, in rabbit retina, nitric oxide also appeared to increase the sensitivity of horizontal cells to light through possibly an indirect action on photoreceptor transduction or at the photoreceptor-horizontal cell synapse, in addition to the increased input resistance resulting from the reduced cellular coupling. This may occur to some extent through the modulation of the ionotropic glutamate receptors found on horizontal cells. It has been speculated that increased nitric oxide production by horizontal cells under dark-adapted conditions and by amacrine cells under light-adapted conditions may account for the biphasic modulation of horizontal cell coupling with adaptational state.

Illumination increases the levels of all *trans*-retinoic acid (at-RA), which is a byproduct of the phototransduction cycle, and thereby correlates with the amount of light illumination. at-RA can uncouple horizontal cells in mouse, rabbit, and carp in a stereospecific manner and can do so in the presence of D1 dopamine receptor antagonist, indicating that it is not acting through modulation of the dopaminergic pathway. In the presence of at-RA, the receptive-field sizes of horizontal cells, as measured by annulus-to-spot ratios, were reduced. In addition to its effects on spatial response characteristics of horizontal cells, at-RA application in dark-adapted retinas could induce effects resembling light adaptation, such as reduced light responsiveness, changes in chromatic properties of H2 horizontal cells in teleosts, decreased gap-junctional permeability, as well as spinule formation in fish horizontal cells.

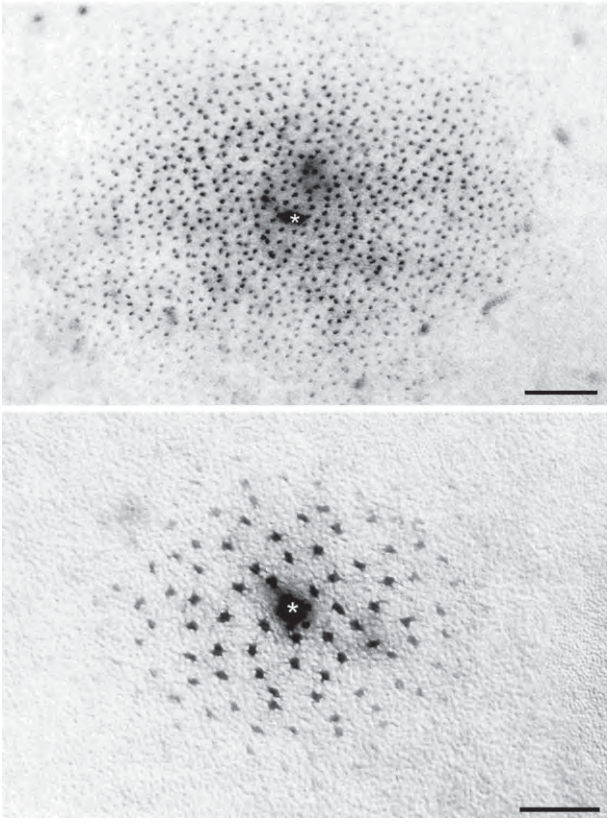

Figure 5 Regulation of horizontal cell tracer coupling by exposure of rabbit retina to different light intensities. (Top) Exposure to dim light intensity (log –6.0) produced coupling of over 1200 cells. (Bottom) Exposure to bright light intensity (log –1.0) produced coupling of 124 cells. Scale = 100 μm in top panel, 50 μm in bottom panel. Adapted from figures 7 and 8 of Xin, D. and Bloomfield, S. A. (1999). Dark- and light-induced changes in coupling between horizontal cells in mammalian retina. *Journal of Comparative Neurology* 405: 75–87.

Gain Control of Synapses in the Outer Retina

The gain of the graded potential synapses between photoreceptors and horizontal cells is defined as the postsynaptic amplitude divided by presynaptic amplitude. High-gain synapses in an open-loop system (e.g., no inhibitory feedback) are inherently unstable, tending to saturate their

postsynaptic targets. To maintain stability and to optimize signal-to-noise ratios, synaptic gain is controlled by reciprocal feedback signals so that gain is high and stable when signals are small, and gain is reduced when signals are large and potentially saturating. Having each photoreceptor synapse under closed-loop inhibitory feedback control imparts gain control to the system.

The ability of the horizontal cell network to adjust to different states of light adaptation permits in part the retina to operate optimally over 10 orders of magnitude of light intensities. The input-output relations of photoreceptor to second-order neurons are modulated by light and dark adaptation. For example, dim background illumination can increase the voltage gain of the rod output synapse by increasing the conductance of horizontal cell kainate receptors through a dopaminergic signaling pathway and enhancing rod Ca^{2+} channel activation. Tonic activation of the feedback synapse by the steady illumination of receptive-field surrounds shifts (or resets) the operating range of bipolar cells to the right along the intensity axis, such that a brighter light is now necessary to elicit a given response.

Spatial and Temporal Processing

The antagonistic center-surround receptive-field organization underlies our ability to detect edges, enhancing contrast between regions of varying brightness and color, and it is ultimately responsible for visual acuity. Baylor and colleagues demonstrated that the turtle cone photoreceptor light response was modulated by light intensity as well as by the pattern of light stimulation, where cone response to center illumination was modified by the stimulation of the surround. Moreover, hyperpolarization of horizontal cells could produce a depolarization in nearby cones. These data indicated that horizontal cells participate in generating antagonistic receptive-field surrounds of cone photoreceptors. The two morphological types of horizontal cells exhibit different spatial summation properties, owing to differing dendritic field sizes and degree of electrical coupling. The reduction of horizontal cell receptive-field sizes in darkness due to uncoupling would further improve spatial contrast ability. Because of their large dendritic fields and electrical coupling, in general, horizontal cells integrate light stimuli over a large area and thus respond well to large light stimuli (i.e., low spatial frequency), whereas small spot stimuli (i.e., high spatial frequency) evoke small responses. The knockout of connexin 57 (Cx57), a gap-junction protein specific to horizontal cells, in mice reduced the receptive-field sizes of horizontal cells, but did not eliminate the rollback in the horizontal cell light response, reflective of negative feedback to cones (**Figure 4**). The knockout diminished the tracer coupling of horizontal cells by 99%, which indicates that Cx57 is the principal connexin in horizontal cells. Furthermore, the regulation of coupling by dopamine was lost, suggesting that gap junctions formed by Cx57 are the targets of this modulation.

In fish, D1 antagonists blocked the uncoupling of horizontal cells produced by flickering light, but not the uncoupling resulting from steady ambient light, suggesting that the temporal characteristics of the light stimulation may affect the pathway activated.

Chromatic Processing

The Stell model emerged from anatomical analysis of the connectivity of color-sensitive cones and three types of cone-driven horizontal cells in fish retina (**Figure 6**). The model accounted for findings that monophasic horizontal cells (H1) hyperpolarize irrespective of wavelength, but peak in the red or long wavelengths, biphasic horizontal cells (H2) hyperpolarize at short and medium wavelengths and depolarize at long wavelengths, and triphasic horizontal cells (H3) hyperpolarize at short and long wavelengths, while depolarizing at medium wavelengths. Hence, monophasic H1 cells signal luminance, whereas the other two types provide color-opponent signals. In the

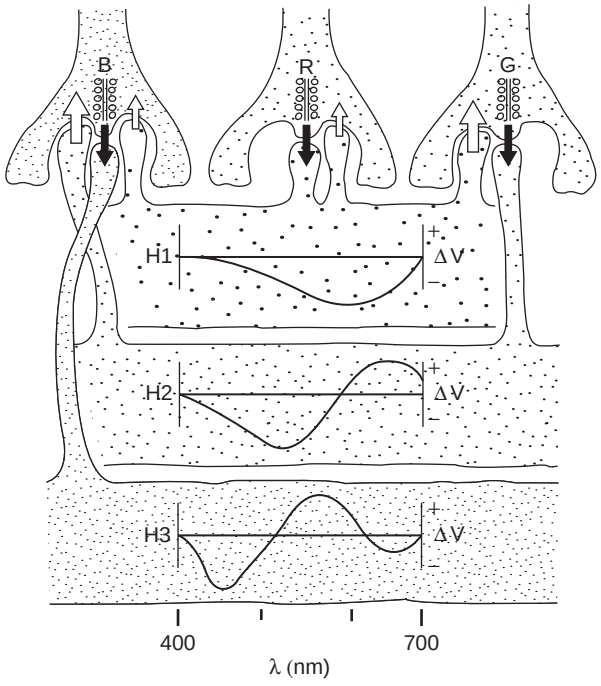

Figure 6 The Stell model of chromatic interactions in the goldfish retina. Cone types are labeled R, G, and B. The H1, H2, and H3 horizontal cells generate monophasic, biphasic, and triphasic spectral response functions by the pathways shown. Synaptic pathways from cones to horizontal cells are shown with filled arrows while feedback pathways are shown in open arrows. Reproduced from figure 2 of Stell, W. K., Lightfoot, D. O., Wheeler, T. G., and Leeper, H. F. (1975). Goldfish retina: Functional polarization of cone horizontal cell dendrites and synapses. *Science* 190(4218): 989–990. Reprinted with permission from AAAS.

case of the H2 red/green biphasic C-type cells, the depolarizing responses to long wavelengths appear to arise from feedback from red-sensitive L-type horizontal cells to green cones, which then synapse onto H2 cells, and, similarly, the depolarizations in the H3 come about through H2 feedback to short wavelength or blue cones, which then drive the H3 cells. Mammalian retinas do not appear to have color-opponent horizontal cells.

Conclusions

The visual system operates over a large range of stimulus intensities. That animals can see in the dark of a moonless night and in near-blinding sun-drenched scenes is a remarkable feat achieved by exploiting the dynamic range of numerous cascaded stages. Several adaptation stages have been described in rods and cones, beginning in the light-transducing outer segments. Modulation of the rod and cone output synapses is another critically important stage, and here adaptation results in large part from horizontal cell feedback and feed-forward, and may alter the form of some receptive fields. Many of the anatomical and biophysical features of the photoreceptor triad synapse are known in great detail, and regulation of the synapse by integrative feedback from horizontal cells is one area of critical importance in retinal neurobiology. Future studies will aid us in understanding the complex analysis of information in the visual system, and, in particular, how the visual system has evolved algorithms that optimize acuity under changing levels of ambient illumination.

Acknowledgment

This work was supported by NEI EY 15573 and a Veterans Administration Senior Career Scientist Award to NB, and CIHR grant MOP10968 to SB.

See also: The Circadian Clock in the Retina Regulates Rod and Cone Pathways; Cone Photoreceptor Cells: Soma and Synapse; GABA Receptors in the Retina; Glutamate Receptors in Retina; Information Processing in the Retina; Morphology of Interneurons: Bipolar Cells; Morphology of Interneurons: Horizontal Cells; Morphology of Interneurons: Interplexiform Cells; Neurotransmitters and Receptors: Dopamine; Physiology of Photoreceptor Synapses and Other Ribbon Synapses; Rod Photoreceptor Cells: Soma and Synapse.

Further Reading

Baylor, D. A., Fuortes, M. G. F., and O'Bryan, P. M. (1971). Receptive fields of cones in the retina of the turtle. *Journal of Physiology (London)* 214: 265–294.

Bear, M. F., Connors, B. W., and Paradiso, M. A. (eds.) (2007). *Neuroscience: Exploring the Brain,* 3rd edn. Philadelphia, PA: Lippincott Williams & Wilkins.

Brown, K. T. and Wiesel, T. N. (1959). Intraretinal recording with micropipette electrodes in the intact cat eye. *Journal of Physiology (London)* 159: 537–562.

Burkhardt, D. A. (1993). Synaptic feedback, depolarization, and color opponency in cone photoreceptors. *Visual Neuroscience* 10: 981–989.

Davenport, C. M., Detwiler, P. B., and Dacey, D. M. (2008). Effects of pH buffering on horizontal and ganglion cell light responses in primate retina: Evidence for the proton hypothesis of surround formation. *Journal of Neuroscience* 28: 456–464.

Hirano, A. A., Brandstätter, J. H., and Brecha, N. C. (2005). Cellular distribution and subcellular localization of molecular components of vesicular transmitter release in horizontal cells of rabbit retina. *Journal of Comparative Neurology* 488: 70–81.

Hirasawa, H. and Kaneko, A. (2003). pH changes in the invaginating synaptic cleft mediate feedback from horizontal cells to cone photoreceptors by modulating Ca^{2+} channels. *Journal of General Physiology* 122: 657–671.

Jonz, M. G. and Barnes, S. (2007). Proton modulation of ion channels in isolated horizontal cells of the goldfish retina. *Journal of Physiology (London)* 581: 529–541.

Kamermans, M. and Fahrenfort, I. (2004). Ephaptic interactions within a chemical synapse: Hemichannel-mediated ephaptic inhibition in the retina. *Current Opinion in Neurobiology* 14: 531–541.

McMahon, D. G., Zhang, D. Q., Ponomareva, L., and Wagner, T. (2001). Synaptic mechanisms of network adaptation in horizontal cells. *Progress in Brain Research* 131: 419–436.

Perlman, I., Kolb, H., and Nelson, R. (2003). Anatomy, circuitry, and physiology of vertebrate horizontal cells. In: Chalupa, L. M. and Werner, J. S. (eds.) *The Visual Neurosciences* vol. 1, pp. 369–394. Cambridge, MA: MIT Press.

Shelley, J., Dedek, K., Schubert, T., et al. (2006). Horizontal cell receptive fields are reduced in connexin57-deficient mice. *European Journal of Neuroscience* 23: 3176–3186.

Stell, W. K., Lightfoot, D. O., Wheeler, T. G., and Leeper, H. F. (1975). Goldfish retina: Functional polarization of cone horizontal cell dendrites and synapses. *Science* 190: 989–990.

Thoreson, W. B., Babai, N., and Bartoletti, T. M. (2008). Feedback from horizontal cells to rod photoreceptors in vertebrate retina. *Journal of Neuroscience* 28: 5691–5695.

Verweij, J., Hornstein, E. P., and Schnapf, J. L. (2003). Surround antagonism in macaque cone photoreceptors. *Journal of Neuroscience* 23: 10249–10257.

Verweij, J., Kamermans, M., and Spekreijse, H. (1996). Horizontal cells feed back to cones by shifting the cone calcium-current activation range. *Vision Research* 36: 3943–3953.

Weiler, R., Pottek, M., He, S., and Vaney, D. I. (2000). Modulation of coupling between retinal horizontal cells by retinoic acid and endogenous dopamine. *Brain Research. Brain Research Reviews* 32: 121–129.

Wu, S. M. (1994). Synaptic transmission in the outer retina. *Annual Review of Physiology* 56: 141–168.

Xin, D. and Bloomfield, S. A. (1999). Dark- and light-induced changes in coupling between horizontal cells in mammalian retina. *Journal of Comparative Neurology* 405: 75–87.

Information Processing: Retinal Adaptation

K R Alexander, University of Illinois at Chicago, Chicago, IL, USA

Glossary

Contrast – Magnitude of luminance variation with respect to mean luminance, defined as Weber contrast (C_w) for discrete stimuli: $C_W = (I_T - I_B)/I_B$, where I_T and I_B refer to the retinal illuminance of a test probe and background, respectively; or as Michelson contrast (C_M) for periodic stimuli: $C_M = (I_{max} - I_{min})/(I_{max} + I_{min})$, where I_{max} is the maximum retinal illuminance and I_{min} is the minimum retinal illuminance.

Gain – Change in the neural response produced by either a change in luminance or a change in contrast over the range for which the stimulus–response function is reasonably linear, specified in units such as impulses per quantum or impulses per percent contrast.

Luminance – Amount of light given off by an extended source, either emitted or reflected, and usually specified in candelas per square meter (cd m^{-2}), although many alternative units exist, including apostilbs (asb), foot-lamberts (ftL), millilamberts (mL), and nits.

Retinal illuminance – Luminance in cd m^{-2} multiplied by pupil area in square millimeters (mm^2) and specified in trolands (td).

Threshold – In psychophysics, the light level that marks the transition from invisibility to visibility, defined as either the absolute threshold ("yes, I see it") or the difference threshold ("yes, it is different"); in electrophysiology, the light level that elicits a criterion neural response amplitude or a criterion change in response amplitude.

The eye can potentially be exposed to an enormous range of light intensities, ranging from a few photons per second under extremely dim lighting conditions to light levels that can be more than 10-billion-fold higher (i.e., a factor of 10^{10} or 10 log units). Furthermore, there may be rapid temporal fluctuations in the light level due to eye movements. In addition, there can be marked changes in the chromatic properties of the visual environment, such as when viewing objects in incandescent room illumination versus outdoors at noon on a sunny day. Remarkably, the visual system is able to cope with the large range of illumination conditions through complex neural mechanisms that are collectively termed adaptation.

It should be noted, however, that there are actually a number of different uses of the term adaptation, ranging from an adjustment to the overall light level to more complex forms, such as spatial frequency adaptation, motion adaptation, and adaptation to artificially induced retinal image distortion or rotation. The emphasis of this article is on adaptation that is presumed to occur within the retina. How do we know which processes are retinal and which involve higher levels of the visual system? One method is to identify neurons within the retina that exhibit the physiological characteristics of the type of adaptation under investigation. This can be determined by recording from single neurons within the retina, by recording simultaneously from groups of neurons using a multi-electrode array, or by recording the electroretinogram (ERG), which is the massed electrical response of the retina. Further insight into the sites and mechanisms of adaptation can be gained through the study of transgenic animals that have a mutation in, or knockout of, putative components of the adaptation process, or of humans who have spontaneously occurring mutations in these components.

A complementary, behavioral method for investigating the site of adaptation is to employ dichoptic stimulation. In this technique, an adapting stimulus is presented to one eye and a test stimulus is presented to the other eye. The goal is to determine whether adaptation of the contralateral eye affects performance for targets presented to the tested eye. The first site at which there is a combination of information from the two eyes occurs at a cortical level. Therefore, if there is interocular transfer of the adaptation, then it is presumed that the primary site of the adaptation is cortical. On the other hand, if there is no evidence of interocular transfer, then the adaptation is presumed to occur at the retinal level.

Based on such considerations, the forms of adaptation that are thought to be predominantly or exclusively retinal in origin are: (1) light adaptation, which refers to the adjustment of the visual system to changes in the overall or mean illumination level; (2) contrast adaptation, which refers to the ability of the visual system to adjust to the variance of the illumination rather than to its mean; (3) chromatic adaptation, which refers to an adjustment to the spectral composition of light; and (4) dark adaptation, which refers to the time-dependent recovery of visual sensitivity in the dark following exposure to light. These forms of adaptation are the subject of this article, although the emphasis is on light adaptation.

In addition to adaptation, though, there are additional strategies that are employed by the visual system to cope with the broad range of illumination levels encountered by the visual system. One strategy is a change in pupil size, which is a mechanical way in which the visual system can partially adjust to varying light levels. As the overall light level increases, the pupil area decreases, which in turn decreases the retinal illuminance. However, the maximum change in pupil area is essentially 16-fold (i.e., a change in diameter from 2 to 8 mm); therefore a change in pupil size can compensate for only a small portion of the potential illumination range. Furthermore, owing to the directional sensitivity of the cone photoreceptors (the Stiles–Crawford effect), light entering the edge of the pupil is a less efficient stimulus for the cone system than light entering the pupil center. Therefore, the effective increase in retinal illuminance with increasing pupil size is actually less than would be predicted based on pupil area.

Another strategy used by the visual system to cope with the large range of environmental light levels is to split the load between the rod and cone systems. The rod system, which is extremely sensitive, covers the lower 3 log units of stimulation, termed the scotopic range. The cone system handles the highest 6 log units, termed the photopic range. Between these two ranges is the mesopic range, within which visual sensitivity can be rod-mediated or cone-mediated, depending on such factors as target wavelength, duration, size, and retinal eccentricity. Thus, the duplex nature of the retina provides a partial solution to the problem of dealing with the wide range of light levels impinging on the retina. However, adaptive processes within the rod and cone systems are also necessary in order to provide useful vision under all illumination conditions.

Light Adaptation

Light adaptation typically refers to the adjustment of the visual system to the overall illumination level. This adjustment allows for an amplification of neural signals relative to noise at low light levels, and prevents or minimizes saturation of the neural response at high light levels. Light adaptation also changes the way in which spatial and temporal information is processed. For example, spatial resolution is typically better at high illumination levels.

Characteristics of Light Adaptation

The typical light adaptation paradigm consists of the presentation of a brief test probe of retinal illuminance I_T against an adapting field of retinal illuminance I_B. The dependent variable is the increment threshold ΔI, defined as:

$$\Delta I = (I_T - I_B) \quad [1]$$

which is usually measured at different values of I_B. The typical threshold versus retinal illuminance or tvi function is illustrated in **Figure 1**. The data points in this figure represent psychophysical increment thresholds for a small achromatic test probe presented foveally against a large achromatic adapting field. The curve represents the log form of the equation:

$$\Delta I = K(I_B + I_0)^n \quad [2]$$

where K and I_0 are fit parameters that represent the absolute threshold and the inflection point of the function, respectively, on log–log coordinates and n determines the slope of the function at high retinal illuminances.

At low adapting levels, the increment threshold is relatively independent of the retinal illuminance of the adapting field. Under these conditions, it is generally assumed that the threshold is governed by the internal noise within the visual system, also termed dark light or eigengrau. As the retinal illuminance of the adapting field increases, the increment threshold begins to rise as the internal noise becomes overwhelmed by the neural response to the adapting field. At high retinal illuminances, the increment threshold is proportional to the adapting field retinal illuminance, such that:

$$\Delta I / I_B = K \quad [3]$$

This relationship is referred to as the Weber–Fechner relationship or Weber's law. On a log–log plot, Weber's law has a slope of 1. An important implication of Weber's

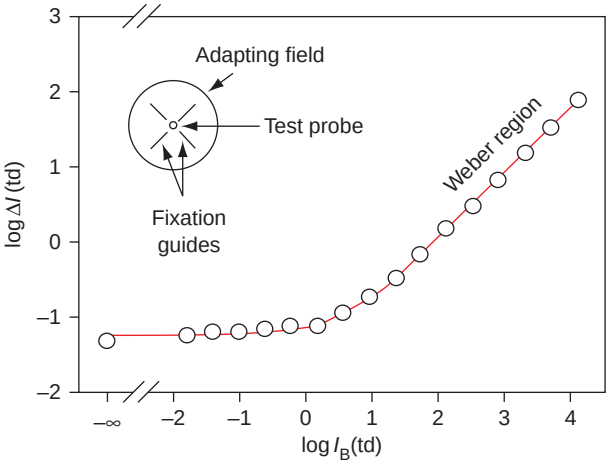

Figure 1 Increment threshold (circles) as a function of adapting field retinal illuminance for a foveally presented brief achromatic test probe in the center of an achromatic adapting field, as depicted in the inset. The curve represents the least-squares best fit of eqn [1].

law is that the visual system is organized to signal contrast rather than absolute luminance. In other words, because $\Delta I/I_B$ is constant within the Weber region, Weber contrast is also constant, regardless of the adapting level.

The data of Figure 1 represent a tvi function for the foveal cone system, but an increment threshold function can also be obtained for the rod system if a short-wavelength test probe, to which the rods are sensitive, is presented in the visual field periphery against a long-wavelength adapting field that desensitizes the cone system. A schematic of a rod increment threshold function is shown in Figure 2. As is the case for the cone system, there is a range of low retinal illuminances over which the rod threshold remains constant. This is followed by a region over which the rod threshold is proportional to the square root of the retinal illuminance (the Rose–deVries region), and then there is a transition to Weber-law behavior. However, a primary difference between the rod and cone increment threshold functions is that the rod function shows saturation, or an upward turn at high retinal illuminances that is steeper than Weber's law. For adapting field retinal illuminances above rod saturation, the cone system mediates detection of the test probe.

Saturation can be observed in individual rod photoreceptors, in the sense that there can be a complete shutdown of the rod circulating current resulting from light exposure. However, there is considerable evidence that psychophysical rod saturation does not represent saturation at the level of the rod photoreceptors, but rather is a property of the pathway through which the rod signals travel. For example, the value of I_B at which the onset of psychophysical rod saturation occurs depends on whether the adapting field is steady or flashed, on the size of the test probe and the wavelength of the adapting field, and on the level of cone stimulation, all of which indicate that postreceptoral factors are involved.

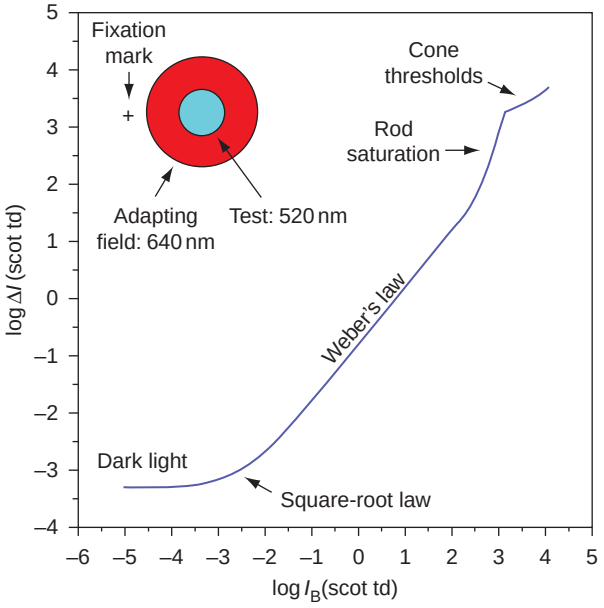

Figure 2 Schematic increment threshold function obtained under rod-isolating conditions. The inset depicts the stimulus configuration, which consists of a large short-wavelength (blue) test probe presented in the visual field periphery against a larger long-wavelength (red) adapting field.

The tvi function of the cone system typically does not show saturation, owing to photopigment bleaching. When cone photopigment molecules become bleached as a result of light exposure, there is less total photopigment within a cone photoreceptor that is available to capture photons. As a result, a proportionally greater level of stimulation is needed to produce the same neural response. At equilibrium, the relationship between p, the fraction of unbleached cone photopigment, and retinal illuminance I in td is:

$$1 - p = I/(I + I_0) \quad [4]$$

where I_0 is the half-bleaching constant of 4.3 log td. The effect of cone photopigment bleaching on vision has been likened to wearing sunglasses, which reduce the retinal illumination by a scaling factor. Photopigment bleaching is a way of avoiding saturation within the cone system but it is not a factor within the rod system, because the rod photoreceptors are saturated by illumination levels that bleach only a few percent of the rhodopsin molecules within an outer segment.

However, saturation within the cone system can be demonstrated if a probe-flash paradigm is used. In this paradigm, the test probe is presented simultaneously with a briefly flashed adapting field. A typical finding is that the threshold rises rapidly with increasing retinal illuminance of the flashed adapting field, such that at high retinal illuminances, the test probe itself is invisible and its presence can only be detected by virtue of an afterimage.

The probe-flash paradigm is a variant of Crawford masking or early light adaptation, in which the increment threshold for a test probe is measured with respect to the time of onset of a transient rather than a steady-state adapting field. Typically, the threshold begins to rise when the test probe is presented slightly before the masking flash. This curious result has been attributed to the differential latencies of the neural responses to the weak test probe and the stronger masking flash. The threshold is highest when the test probe and masking flash have simultaneous onsets. If the test probe is presented during the middle of a long-duration masking flash, then the threshold corresponds approximately to the steady-state level.

Traditionally, studies of light adaptation have used aperiodic test stimuli, such as the light pulses described above. However, there has been another experimental approach to light adaptation that has used periodic test stimuli, such as one whose retinal illuminance varies sinusoidally over time. In this approach, the dependent variable is contrast sensitivity, defined as the reciprocal of

the threshold contrast in Michelson units. A typical finding is that, at low temporal frequencies, contrast sensitivity is invariant with respect to mean retinal illuminance, which corresponds to Weber-law behavior. At high temporal frequencies, however, contrast sensitivity changes with mean retinal illuminance, such that the amplitude of the flicker rather than its contrast determines sensitivity. This finding indicates that there is a high-frequency linearity that discounts the mean retinal illuminance. In addition, the shape of the temporal contrast sensitivity function changes with adaptation level, becoming more band-pass at high retinal illuminances, so that sensitivity to intermediate frequencies becomes enhanced. This shape change has been attributed to a contrast gain-control mechanism.

The explanation for the high-frequency linearity, which is seen both psychophysically and in electrophysiological recordings, remains unclear, although several quantitative models have been proposed to account for it. In fact, a major theoretical challenge has been to develop a computational model that can encompass the adaptational features of data obtained with both periodic and aperiodic stimuli. To date, this attempt has not been entirely successful.

Mechanisms and Sites of Light Adaptation

As illustrated in **Figures 1** and **2**, the rod and cone systems can respond over a considerable range of retinal illuminances. However, individual neurons within the retina can only respond over an approximately 400-fold range of illumination levels. The typical response R of a retinal neuron as a function of retinal illuminance I is illustrated as the solid curve in **Figure 3**. This curve represents a plot of the Naka-Rushton equation:

$$R/R_{\max} = I^n/(I^n + I_s^n) \qquad [5]$$

where $R_{\max}$ is the maximum neural response, I_s is the retinal illuminance that produces $R_{\max}/2$, and n governs the steepness of the function, although n is usually set to 1. This response function is S-shaped when plotted on semi-log coordinates, as in **Figure 3**. A major characteristic of the neural response function is that it shows saturation at high illuminance levels. The response function is considered to represent a static nonlinearity, or one which acts instantaneously with no change over time.

If a retinal neuron only operated according to the solid curve in **Figure 3**, then the presence of an adapting field would lead to response compression. For example, the adapting field indicated by the vertical line in **Figure 3** would produce a neural response that is toward the top of the response range, as indicated by the solid horizontal line. This would then leave little room for an additional response to an increment of light. In fact, if the retinal illuminance of the adapting field were high enough, additional increments of light would be invisible due to response saturation.

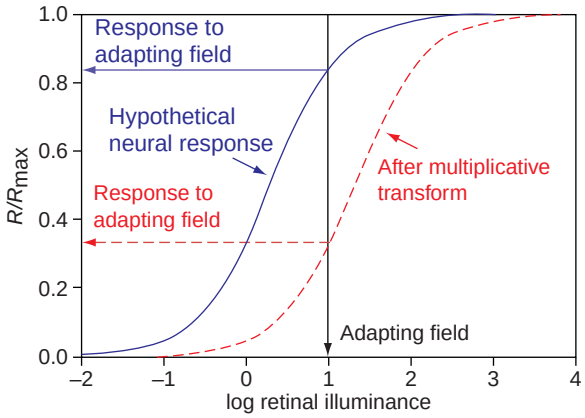

Figure 3 Normalized response amplitude vs. log retinal illuminance for a hypothetical retinal neuron before (solid curve) and after (dashed curve) a multiplicative transform. The vertical line with arrowhead indicates an arbitrary adapting field retinal illuminance, and the horizontal lines represent the hypothetical neural responses to the adapting field, based on the respective illuminance-response functions.

One way in which a neuron can avoid saturation is by shifting its operating range in proportion to the mean level of illumination. This shift of the response function is termed multiplicative adaptation and is illustrated in **Figure 3** as the dashed curve. Multiplicative adaptation is also known as von Kries adaptation, dark glasses adaptation, and automatic gain control. After a multiplicative transform, the same adapting field retinal illuminance produces a smaller neural response, as indicated by the horizontal dashed line in **Figure 3**. This allows for the detection of light increments that would otherwise be invisible without the multiplicative response scaling. Multiplicative adaptation tends to be relatively fast acting, with a time constant on the order of a few tens of milliseconds, and is thought to be the result of a neural feedback circuit.

A second way in which a neuron can avoid saturation is through subtractive adaptation. This form of adaptation subtracts out the neural response to an adapting field, thus bringing the response down out of the saturating range, without affecting the response to a brief test probe. There are both fast and slow forms of subtractive adaptation, although both are typically much slower than multiplicative adaptation, with time constants on the order of seconds to tens of seconds. Fast subtractive adaptation is presumed to represent center-surround antagonism within neuronal receptive fields. Slow subtractive adaptation may be due to a change in the membrane hyperpolarization of retinal neurons.

The rod system is desensitized by dim backgrounds that produce a quantal absorption in only a very few rod photoreceptors. This observation has led to the concept of a rod adaptation pool, according to which signals from

multiple rod photoreceptors are combined in controlling light adaptation. Pooling allows a retinal ganglion cell to respond to light when only a tiny fraction of the rods absorb photons, but it also increases the likelihood of neuronal saturation. Neural pooling can also be a factor with respect to light adaptation within the cone system. Signals from cone photoreceptors are processed by two major parallel pathways: magnocellular (M) and parvocellular (P), which are first organized at the retinal level and extend to the visual cortex. M retinal ganglion cells have a high contrast gain and saturate at relatively low levels of contrast. P ganglion cells have a low contrast gain and a more linear contrast-response function. There is generally a greater degree of spatial integration or pooling within M cells, due to their relatively larger receptive fields. Therefore, M cells are typically more light adapted by a given adapting field than are P cells.

The retinal site or sites of the various neural processes underlying light adaptation remain to be fully explicated. However, the following general conclusions can be drawn. With respect to the cone system, the site of adaptation appears to shift depending on the illumination level. At lower retinal illuminances, adaptation is dominated by postreceptoral processes, sometimes referred to as network adaptation. There is recent evidence that postreceptoral adaptation within the cone system occurs at the synapse between bipolar cells and ganglion cells. At higher retinal illuminances, adaptation occurs primarily within the cone photoreceptors themselves. Rod photoreceptors in the mammalian retina can show adaptation, in that there are changes in sensitivity and response kinetics as a function of illumination level. However, much of the light adaptation within the rod system appears to be postreceptoral in origin, occurring at the synapse between rod bipolar cells and AII amacrine cells.

A potentially powerful way to investigate the relationship between the phenomenology of light adaptation and retinal physiology is to study humans who have genetic mutations that can affect putative components of the adaptational process. An example is a visual condition termed bradyopsia (slow vision) that has been identified recently. Individuals with bradyopsia have mutations in the guanosine triphosphatase-activating protein RGS9 or its anchor protein R9AP, which impedes deactivation of the phototransduction cascade. Bradyopsia is characterized by a slow recovery of sensitivity following a sudden change in illumination and also a loss of motion sensitivity, particularly at low contrasts.

Contrast Adaptation

Contrast adaptation refers to an adjustment to the variance or contrast of the illumination, rather than to its mean level. There are two types of contrast adaptation: spatial and temporal. Spatial contrast adaptation is selective for stimulus spatial frequency and orientation and is therefore predominantly cortical in origin. Temporal contrast adaptation, on the other hand, is observed in recordings from retinal ganglion cells in response to spatially uniform fields of light. Examples of stimuli used to study contrast adaptation are illustrated in **Figure 4**. Both involve the temporal modulation of a uniform field of light. One type of stimulus (**Figure 4**, top) is contrast-modulated sinusoidal flicker, whose mean luminance and temporal frequency remain constant but whose contrast is changed abruptly. The second (**Figure 4**, bottom) is contrast-modulated white noise.

Following a transition from a low-contrast to a high-contrast stimulus, there is an essentially instantaneous change in the gain and temporal response of retinal ganglion cells. This is followed by a slow change in the firing rate that may take several seconds to complete. There are similar fast and slow changes following a transition from a high-contrast to a low-contrast stimulus, including a temporary decrease in the maintained discharge rate, but these changes are typically more sluggish than for a transition to high contrast. Fast contrast adaptation represents the action of a gain-control mechanism, whereas slow contrast adaptation appears to involve membrane hyperpolarization. Temporal contrast adaptation may form the neural substrate for psychophysical flicker adaptation, in which exposure to high-contrast flicker reduces sensitivity for a subsequently viewed low-contrast flickering test stimulus.

Temporal contrast adaptation has been shown to occur at multiple sites within the retina, beginning in bipolar cells and including processes intrinsic to ganglion cells.

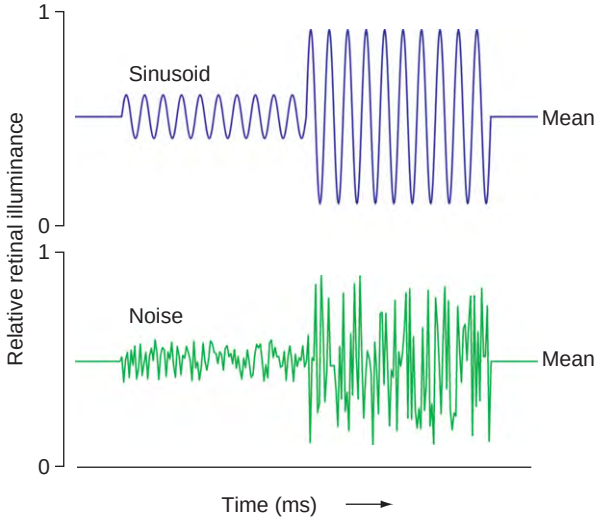

Figure 4 Examples of contrast-modulated stimuli used to study contrast adaptation. The top waveform is a contrast-modulated sinusoid; the bottom waveform represents contrast-modulated noise.

Temporal contrast adaptation is observed in M but not in P ganglion cells, owing in part to the faster temporal response and greater spatial pooling of M cells. Contrast adaptation and mean-luminance adaptation share certain similarities, but whether these forms of adaptation represent a common mechanism or distinct mechanisms remains to be determined.

Chromatic Adaptation

Chromatic adaptation refers to the effect of spectrally selective adapting fields on the detection and appearance of test stimuli of various wavelengths. When chromatic test probes and adapting fields are used to study light adaptation, the increment threshold function of the foveal cone system typically consists of more than one component, as illustrated in **Figure 5**. With the combination of test and adapting field wavelengths shown in **Figure 5**, the test probe is initially detected by a middle-wavelength-sensitive mechanism that becomes progressively more desensitized by the middle-wavelength adapting field. At high retinal illuminances, a short-wavelength-sensitive cone mechanism governs detection.

A change in test wavelength displaces a given tvi function vertically, and a change in adapting field wavelength displaces the tvi function horizontally. Initially, it was thought that the spectral sensitivities of the short-wavelength (S), middle-wavelength (M), and long-wavelength (L) cone photopigments could be derived by evaluating the relative displacements of the tvi functions as the test wavelength and adapting field wavelength were varied. This approach was used by W. S. Stiles to define what are known as π mechanisms. However, instead of identifying three π mechanisms corresponding to the three cone types, seven π mechanisms were derived from this method. The field sensitivities of three of the seven (π_1, π_4, and π_5) correspond approximately to the spectral sensitivities of the S, M, and L cones, respectively. Nevertheless, the shapes of the π_4 and π_5 mechanisms are broader than would be expected from the known spectra of the cone photopigments, and there are other failures of the π mechanisms to correspond to properties predicted by adaptation of the cone photoreceptors.

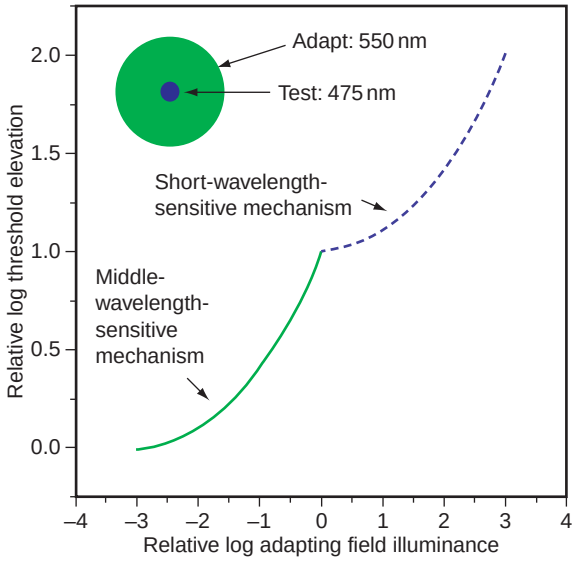

Figure 5 Schematic tvi functions for a 475-nm test probe (blue) presented foveally against a 550-nm adapting field (green), plotted in relative units. The curves represent plots of the tvi template of Stiles, and the lower (green) and upper (blue) branches represent detection by middle-wavelength-sensitive and short-wavelength-sensitive cone mechanisms, respectively.

Partly to account for the mismatch between the properties of the π mechanisms and the cone spectral sensitivities, two-stage models of chromatic adaptation have been developed. The first stage consists of receptor adaptation, and the second stage combines signals from the S, M, and L cones in an opponent manner. The site of the opponent interactions among signals from different cone types has not yet been identified definitively. Candidates include horizontal cells (although these are not typically spectrally opponent), amacrine cells, and possibly gap-junctional connections between photoreceptors.

Chromatic adaptation also refers to a change in the color appearance of a test light as a result of a change in adapting field chromaticity. For example, a monochromatic light that appears yellow in isolation will appear greenish when superimposed on a long-wavelength adapting field. This change in color appearance has been attributed to a relative desensitization of the L-cone photoreceptors through von Kries or multiplicative adaptation. However, there are instances in which photoreceptor desensitization alone cannot account for the changes in color appearance, such as when the level of retinal illuminance is changed, or when a monochromatic light becomes desaturated during extended viewing. These changes in color appearance are presumably due to second-site adaptation in addition to cone photoreceptor adaptation. Two-stage models are also presumed to account for color constancy, in which colored surfaces maintain their appearance despite substantial changes in the spectral content of the illumination, such as the change from sunlight to incandescent lighting.

Dark Adaptation

Following the exposure of the eye to an adapting field that bleaches a significant fraction of photopigment, there is a systematic recovery of visual sensitivity that is referred to as dark adaptation. Whereas light adaptation occurs relatively quickly, dark adaptation can require a substantial period of time, on the order of tens of minutes. Strictly speaking, the term dark adaptation refers to the recovery of sensitivity to a briefly flashed test probe presented in complete darkness following the offset of a bleaching

light. However, there are also variants of bleaching recovery in which the eye is not kept in darkness. These include the photostress recovery test, which measures the recovery of visual acuity following exposure to light from an ophthalmic instrument.

Characteristics of Dark Adaptation

The typical time course of dark adaptation following a bleach is illustrated in Figure 6. The data points in this figure represent thresholds for a test probe of 500 nm, a wavelength to which rod and cone systems are both sensitive. The test probe was presented at a retinal eccentricity of 20°, a retinal locus that contains both rod and cone photoreceptors. Thresholds are plotted relative to a baseline threshold that was measured in the fully dark-adapted state prior to a bleach. The recovery of sensitivity follows a two-branched course, each part of which is reasonably well fit by an exponential function. Immediately following the offset of the bleaching light, the recovery of sensitivity occurs relatively rapidly, and then sensitivity reaches a plateau region. This initial portion represents the recovery of cone system sensitivity. There is then a second region of rapid recovery followed by a slower phase, such that full recovery from a substantial bleach can take 45–50 min. This second region represents the return of rod system sensitivity. The transition point from cone-mediated to rod-mediated thresholds is termed the rod–cone break.

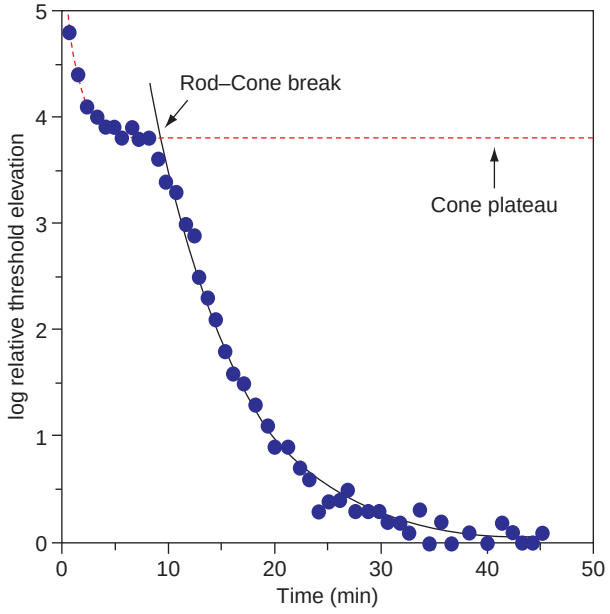

Figure 6 Recovery of visual sensitivity following exposure to a bleaching light, measured with a test probe of 500 nm presented to the peripheral retina in the dark. Thresholds are plotted with respect to the prebleach dark-adapted threshold. The dashed and solid curves are exponential functions fit to the cone-mediated (upper) and rod-mediated (lower) portions of the dark adaptation data, respectively.

Although the rod portion of the dark adaptation function in Figure 6 has been fit with an exponential function, it is more accurately represented by several regions with linear slopes on log-linear coordinates, with each region representing a different physiological process.

The relative vertical placements of the rod and cone dark adaptation curves and the time course of the recovery of sensitivity depend on a number of factors, including the retinal location of testing, the wavelength of the test probe, and the retinal illuminance of the bleaching light. For example, dark adaptation testing at the rod-free fovea reflects only the cone portion of the curve. Long-wavelength test probes, to which the rod system is relatively insensitive, typically produce a less-pronounced and delayed rod–cone break. Weak bleaching lights produce a faster time course of recovery than strong bleaches.

The psychophysical threshold not only is elevated following the offset of a bleaching light, but it is also elevated by the presence of an adapting field. This correspondence has led to the concept of the equivalent background, which holds that the aftereffect of a bleach is equivalent to the presence of a background of real light. This equivalent background, which is sometimes termed dark light, is generally not visible because it is stabilized on the retina. However, it can sometimes be observed in the form of an afterimage. Real light and dark light may have similar properties under some test conditions, but they are not always identical.

Although dark adaptation typically follows the time course illustrated in Figure 6, it is not always the case that sensitivity improves following the offset of a bleaching light. Under certain conditions, sensitivity actually decreases as dark adaptation progresses. One example occurs when the task is to determine the hue threshold or Lie specific threshold, which refers to the retinal illuminance of a test probe at which it appears to have a color. The hue threshold begins to rise at the time of the rod–cone break, rather than remaining constant once the cones have recovered. This rise in the threshold for hue has been attributed to an influence of the recovering rod system on color appearance.

A second example occurs when the task is to determine whether a rapidly flickering test stimulus, presented at a frequency above the rod temporal resolution limit, appears to flicker. The threshold for flicker detection does not remain constant once the cone system has recovered, but instead rises as the rods recover their sensitivity. The rise in the flicker threshold has been attributed to a suppressive effect of the dark-adapting rod system that surrounds the test stimulus on the temporal sensitivity of the cone system.

A threshold elevation during dark adaptation also occurs when the task is to detect a short-wavelength test probe following the offset of a long-wavelength adapting field. In this case, there is a substantial threshold elevation immediately following the adapting field offset, which is

followed by a gradual decrease in threshold. The brief threshold increase, termed transient tritanopia, is thought to represent a change in sensitivity within a postreceptoral opponent color mechanism. Transient tritanopia can also be observed in the ERG, indicating that it is retinal in origin.

Mechanisms of Dark Adaptation

The recovery of sensitivity in the dark, following light exposure, depends ultimately on the regeneration of bleached photopigment. For example, individuals with vitamin A deficiency, which limits the regeneration of rod photopigment, typically have a prolonged time course of rod dark adaptation, and rod thresholds may never reach a normal level. Yet, the recovery of rod sensitivity depends on more than the regeneration of a light absorber. This is demonstrated by the fact that rod thresholds remain elevated by 2 to 4 log units at a time when 90% of rhodopsin has been regenerated following a bleach. It is likely that the presence of various bleaching intermediates, such as metarhodopsin products and free opsin, contribute to the rod threshold elevation during dark adaptation.

In addition to physiological processes occurring within photoreceptors, it is apparent that postreceptoral factors are involved in the recovery of sensitivity during dark adaptation. For example, a change in the size of the test probe can influence the shape of the dark-adaptation curve, although test probe size should have no influence on the rate of photopigment regeneration. Furthermore, dim lights that bleach a trivial amount of photopigment and that have no effect on the receptor potential or on horizontal cell responses in the skate retina, nevertheless, result in an elevation of ERG b-wave and ganglion cell thresholds that requires several minutes to recover. Thus, dark adaptation appears to involve mechanisms at multiple levels within the retina.

Human gene mutations are continuing to provide important insights into the physiological processes underlying dark adaptation. For example, mutations in either the rhodopsin kinase gene or the arrestin gene produce Oguchi disease, in which there is a prolonged recovery of rod sensitivity following light exposure that is thought to be due to impaired deactivation of rhodopsin. Mutations in the RDH5 gene, which encodes the enzyme 11-*cis* retinol dehydrogenase, result in fundus albipunctatus, which is characterized by extremely prolonged rod dark adaptation, presumably due to an impairment in the conversion of 11-*cis* retinol to 11-*cis* retinal.

Conclusion

Retinal adaptation refers to diverse visual phenomena and neural processes, all of which represent the adjustment of the visual system to the prevailing conditions of light stimulation. Through the use of psychophysical and electrophysiological techniques, great progress has been made in understanding the fundamental mechanisms underlying retinal adaptation, but many of the details have yet to be clarified. Studies of transgenic animal models and of naturally occurring human mutations, in which there are alterations in the putative components of adaptation, show great promise in furthering our knowledge of this fundamental visual process.

See also: Anatomically Separate Rod and Cone Signaling Pathways; Information Processing: Contrast Sensitivity; Perimetry; Photopic, Mesopic and Scotopic Vision and Changes in Visual Performance; Phototransduction: Adaptation in Cones; Phototransduction: Adaptation in Rods; Unique Specializations – Functional: Dynamic Range of Vision Systems.

Further Reading

Demb, J. B. (2008). Functional circuitry of visual adaptation in the retina. *Journal of Physiology* 586: 4377–4384.
Dowling, J. E. (1987). *The Retina: An Approachable Part of the Brain.* Cambridge: Belknap Press.
Dunn, F. A., Doan, T., Sampath, A. P., and Rieke, F. (2006). Controlling the gain of rod-mediated signals in the mammalian retina. *The Journal of Neuroscience* 26: 3959–3970.
Dunn, F. A., Lankheet, M. J., and Rieke, F. (2007). Light adaptation in cone vision involves switching between receptor and post-receptor sites. *Nature* 449: 603–606.
Graham, N. and Hood, D. C. (1992). Modeling the dynamics of light adaptation: The merging of two traditions. *Vision Research* 32: 1373–1393.
Hess, R. F., Sharpe, L. T., and Nordby, K. (eds.) (1990). *Night Vision: Basic, Clinical and Applied Aspects.* New York: Cambridge University Press.
Hood, D. C. (1998). Lower-level visual processing and models of light adaptation. *Annual Review of Psychology* 49: 503–535.
Kaplan, E., Lee, B. B., and Shapley, R. M. (1990). New views of primate retinal function. In Osborne, N. N. and Chader, G. T. (eds.) *Progress in Retinal Research,* vol. 9, pp. 273–336. Oxford: Pergamon Press.
Lamb, T. D. and Pugh, E. N., Jr. (2006). Phototransduction, dark adaptation, and rhodopsin regeneration: The Proctor lecture. *Investigative Ophthalmology and Visual Sciences* 47: 5138–5152.
Nishiguchi, K. M., Sandberg, M. A., Kooijman, A. C., et al. (2004). Defects in RGS9 or its anchor protein R9AP in patients with slow photoreceptor deactivation. *Nature* 427: 75–78.
Reeves, A. (2003). Visual adaptation. In Chalupa, L. M. and Werner, J. S. (eds.) *The Visual Neurosciences*, pp. 851–862. Cambridge: MIT Press.
Shapley, R. and Enroth-Cugell, C. (1984). Visual adaptation and retinal gain controls. In Osborne, N. N. and Chader, G. T. (eds.) *Progress in Retinal Research,* vol. 3, pp. 263–346. London: Pergamon.
Shevell, S. K. (ed.) (2003). *The Science of Color,* 2nd edn. Oxford: Elsevier.
Stockman, A. and Sharpe, L. T. (2006). Into the twilight zone: The complexities of mesopic vision and luminous efficiency. *Ophthalmic and Physiological Optics* 26: 225–239.

Relevant Websites

http://webvision.med.utah.edu – Webvision: Light and Dark Adaptation.
http://cvision.ucsd.edu – CVRL Color and Vision database.

Inherited Optic Neuropathies

A A Sadun and C F Chicani, University of Southern California-Keck School of Medicine, Los Angeles, CA, USA

Glossary

Cecocentral scotoma – Visual field defect involving the optic disk area (blind spot) and papillomacular bundle (PMB) fibers.
Cybrid cells – These are a eukaryotic cell line produced by the fusion of a whole cell with a cytoplasmic mitochondria.
Donder's curve – An expected reduction of lenticular accommodation as a function of age.
Dyschromatopsia – A partial or complete loss of color vision.
Genetic penetrance – The degree to which individuals express a genetically determined condition.
Papillomacular fibers – Axons from the smaller retinal ganglion cells that carry the information from the macula.
Searching nystagmus – A condition where both eyes occasionally make a wide, comparatively slow, sweeping movement caused by poor vision.
Tapetoretinal – The region of the photoreceptors and retinal pigment epithelium in the retina.

Inherited optic neuropathies fall under the rubric of metabolic optic neuropathies. Metabolic optic neuropathies share many pathophysiologic and clinical characteristics. Most metabolic optic neuropathies involve derangements that affect mitochondria and oxidative phosphorylation. Acquired metabolic optic neuropathies are further divided into those of toxic and those of nutritional deficiency states. For example, both ethambutol toxicity and vitamin B12 deficiency produce bilateral symmetrical optic neuropathies that are very similar to inherited optic neuropathies.

This article discusses hereditary optic nerve diseases that affect the optic nerve in isolation. Common hereditary optic neuropathies include Leber's hereditary optic neuropathy (LHON), dominant optic atrophy (DOA), and congenital recessive optic atrophy (ROA). Like most acquired optic neuropathies, inherited optic neuropathies involve mitochondrial function. In all cases, mitochondria are impaired either by mutations of their own DNA (mtDNA), or mutations of nuclear DNA involved in the transcription of mitochondrial proteins or substrates for mitochondrial biochemistry. All three have a similar presentation inherited mitochondria optic neuropathy. This makes the diagnosis both challenging and, at the same time, the clinical evaluation similar. The presentation is usually that of bilateral symmetric visual loss with dyschromatopsia, and central or cecocentral visual field defects, which involves the optic disk and papillomacular fibers. This archetypical set of clinical signs reflects the fact that in metabolic optic neuropathies there is a strong predilection for the papillomacular bundle (PMB). The distinctions between acquired and inherited optic neuropathies usually come down to issues of personal history, such as toxic exposure, decreased vitamin intake or malabsorption, and, especially for inherited optic neuropathies, family history. However, because of variable penetrance, the family history in inherited optic neuropathies may not be always positive. Prompt recognition of the characteristic elements from history and physical examinations often precludes unnecessary patient laboratory evaluation.

Leber's Hereditary Optic Neuropathy

LHON was first described in 1871 by Theodore Leber. Later von Hippel, Gowers, and Collins refined our understanding and introduced the term hereditary optic atrophy. As recently as the 1980s, LHON was considered to be a non-Mendelian inherited genetic disorder, since there was no male-to-male transmission. In 1988, Douglas Wallace demonstrated LHON as the first maternally inherited disease to be associated with point mutations in mitochondrial DNA, and it is now considered the most prevalent mitochondrial disorder.

LHON typically manifests as a subacute central loss of vision that predominantly affects young adult males. Age of onset is usually between 15 and 35 years; however, it has been reported to occur as young as 2 and as old as 80 years of age. Almost invariably the second eye is affected, within weeks to months. LHON is usually due to one of three pathogenic mitochondrial DNA (mtDNA) point mutations. These mutations affect nucleotide positions 11778, 3460, and 14484, respectively, in the ND4, ND1, and ND6 subunit genes of complex I which is integral for oxidative phosphorylation in mitochondria. These three primary mutations are responsible for about 95% of LHON cases; other rarer mutations continue to be described. In some pedigrees of LHON, associated systemic features have been reported; these include cardiac abnormalities such as pre-excitation syndromes and

hypertrophic cardiomyopathy, reflex and sensory changes, Charcot-Marie-Tooth disease, and skeletal disorders. It is hypothesized that the respiratory chain dysfunction leads to energy depletion and reactive oxygen species (ROS) accumulation which in turn produce axoplasmic stasis and swelling, thereby blocking ganglion cell function and causing loss of vision. In some patients, this loss of function is reversible in a substantial number of ganglion cells, but in others, a cell-death pathway, probably apoptotic, is activated with subsequent extensive degeneration of the retinal ganglion cell layer and optic nerve. The retinal ganglion cell degeneration and axonal loss occur predominantly in the PMB of the optic nerve.

Biochemical and cellular studies in LHON point to a partial defect of respiratory chain function that may generate either an ATP synthesis defect and/or a chronic increase of oxidative stress through the accumulation of ROS. Histological evidence of myelin pathology in LHON also suggests a role for oxidative stress, possibly affecting oligodendrocytes of the optic nerves. In cell culture studies, LHON cybrid cells, constructed from the merging of heteroplasmic cytoplasm of a cell which had its nucleus removed and the cytoplasm from a second normal cell that had all its mitochondria removed, are forced by the reduced rate of glycolytic flux to utilize oxidative metabolism by a shift from glucose to galactose in the media. This causes these cells to be sensitized to a mitochondrial-mediated apoptosis. It has also been proposed that in cells carrying LHON mutations, there is a decrease in antioxidant defenses. Recent evidence shows that mitochondrial distribution reflects the different energy requirements of the unmyelinated prelaminar axons in comparison to the myelinated retrolaminar axons.

In LHON, the pathologic mutation may be either homoplasmic (involving all the mitochondria) or heteroplasmic (involving only a fraction of the mitochondria). Most heteroplasmic pedigrees have much lower penetrance but surprisingly, the disease is not milder in form. Even with homoplasmic families, penetrance is highly variable. The rate of penetrance varies with the mutation and pedigree, although it is always greater in males. Hence, in a typical family with 11778 mtDNA, 8–10% of the women and 40–50% of the men may suffer devastating and sudden visual loss in young adulthood. This marked incomplete penetrance and gender bias imply that additional mitochondrial and/or nuclear genetic or epigenetic factors must be modulating the phenotypic expression of LHON. It is also likely that environmental factors contribute to the onset of visual failure. For example, there is increasing evidence that tobacco and alcohol consumption plays a role. There is an active search for nuclear genes that might modify the penetrance.

In LHON, fundus changes, such as microangiopathy and nerve fiber layer swelling, have been described to immediately precede or accompany the onset of visual loss (**Figure 1**). This process, although usually bilateral, occurs asynchronously over the course of several weeks to months and eventually evolves to severe optic atrophy and irreversible impairment of vision. The smaller caliber fibers of the PMB are selectively lost at a very early stage of the pathological process, which eventually extends to most of the rest of the nerve leading to optic atrophy.

The acute stage of LHON usually lasts a few weeks. The affected eye characteristically demonstrates an early dropout of the PMB; an edematous appearance of the rest of the nerve fiber layer, especially in the arcuate bundles; and enlarged or telangiectatic and tortuous peripapillary vessels (microangiopathy). There is absence of leakage from the optic disk or peripapillary region on fluorescein angiography These main features are seen on fundus examination, just before or subsequent to the onset of visual loss. In optical coherence tomography (OCT), LHON-affected patients showed extensive thinning of the retinal nerve fiber layer (RNFL), as would be expected in cases of optic atrophy. LHON carriers sometimes show significant RNFL thickening of the arcuate

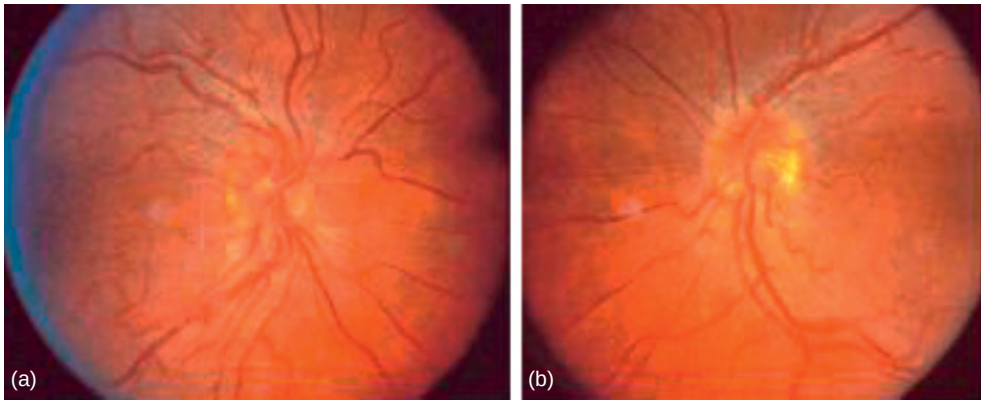

Figure 1 Right (a) and left (b) eyes of a patient with acute phase Leber's hereditary optic neuropathy (LHON). Fundus photographs of both eyes demonstrate hyperemic optic nerve heads, with dilated tortuous vessels, indistinct optic disk margins and swollen retinal nerve fiber layers (pseudoedema of the optic disk). Note also the telangectatic vessels.

bundles, in correlation with similar changes noted by funduscopy or the GDx nerve fiber analyzer, usually in the temporal sector, suggesting that the inferior temporal portion is affected first; this could be a subclinical sign. Several authors have described subclinical changes in the examination of asymptomatic carriers such as subtle optic disk findings, mild dyschromatopsia, OCT, and alterations in electrophysiology suggesting that LHON has some subtle chronic aspects.

In LHON-affected patients, the clinical examination reveals decreased visual acuity, dyschromatopsia, and cecocentral scotoma on visual field examination. There are a few reports of spontaneous recovery, especially with the 14484/ND6 mutation (up to 60% of cases) and in younger patients. Visual recovery may occur in one or both eyes and may happen as late as 10 years after the onset of visual loss. However, most often in LHON-affected individuals, the visual loss progresses and stabilizes within a year, with temporal optic atrophy.

There is currently no clinical evidence for an efficacious treatment to reverse vision loss in LHON. Theoretical considerations have led to the use of several agents involved with mitochondrial energy production and with anti-oxidant capabilities such as coenzyme Q10, succinate, L-carnitine, and vitamins K1, K3, C, B12, folate, and thiamine. Coenzyme Q10 is less likely to offer benefit since it is not transported to the mitochondria in sufficient concentration. A similar agent, Idebenone, has better drug delivery characteristics, and there have been a few encouraging reports and a prospective clinical trial with Idebenone in LHON. Case reports of successful recovery in LHON have to be considered in the light of spontaneous recovery. It remains unlikely that any of these agents alone or in combination will prove consistently useful in the treatment of acute visual loss in LHON or in the prophylactic therapy in asymptomatic family members at risk.

However, it is prudent to recommend the avoidance of agents that might induce oxidative stress or impair mitochondrial energy production. Most specifically, it is imperative to avoid exposure to smoke and alcohol as these environmental factors can trigger the loss of vision in susceptible individuals.

Dominant Optic Atrophy (DOA)

DOA, or Kjer's optic neuropathy, is one of the most common forms of hereditary optic atrophies, with estimated disease prevalence in the range of 1:10 000–1:50 000. Presentation usually occurs at latency age (7–10 years old). It often presents with imperceptible onset, a slowly progressive course, and leads to mild to moderate visual impairment (20/40–20/400). Insofar as onset is insidious and progression is slow, the young patient is often unaware of the visual loss. This usually comes to the parent's attention after a school-based visual screening.

The inheritance of DOA is autosomal dominant. Despite the variability in expression, the penetrance is actually very high. However, the vision impairment is often very mild; hence, the apparent absence of family history may not be accurate. We recommend the direct examination of the parents. DOA presents as mild, bilateral, sometimes asymmetric loss of visual acuity. On examination, there is a central, paracentral, or cecocentral visual field deficit; temporal optic disk pallor, often with a wedge shaped area of temporal excavation (**Figure 2**). There is mild generalized dyschromatopsia. In general, visual prognosis is good. However, patients with DOA often re-present around the age of 35 complaining of further visual loss. In fact, this represents premature presbyopia brought about by their lifelong habit of holding reading material much closer to their faces. Therefore, Donder's curve should not be applied to DOA patients. Instead, they should be offered plus lenses at about age 35 and graduated up to about plus 3.50 by age 50 to compensate for their closer near point.

In the year 2000 came the remarkable news that the genetic cause of dominant optic neuropathy had been identified. The gene OPA1 was, of course, nuclear and located on chromosome 3. However, the OPA1 protein encoded is imported to the mitochondria and serves structural roles in mitochondrial fission, fusion, and transport. Hence, though the genetics are somatic, the problem, like LHON, is in the mitochondria. Subsequently, other DOA genes have been found, as variations on the same theme. In addition to OPA1, there are OPA4 and other OPAs, which have been mapped to the 3q and 18q regions, respectively. All these genes are responsible for mitochondrial structural proteins.

Histological examination exhibited diffuse atrophy of the retinal ganglion cell layer, which is associated with atrophy and loss of myelin within the optic nerves. As in LHON, the retinal ganglion cells and axons lost are predominantly those of the PMB. However, the extent of axonal loss is significantly less in DOA.

In DOA, there is also an increased occurrence of associated sensorineural hearing loss so these patients should be advised to undergo audiology investigation. As in LHON, many agents have been tried as possible treatment options, and none were found to be effective. It remains unclear as to the role of environmental factors. These patients should be offered genetic counseling.

Recessive Optic Atrophy

This autosomal recessive somatic condition is the most uncommon form of inherited optic nerve disease.

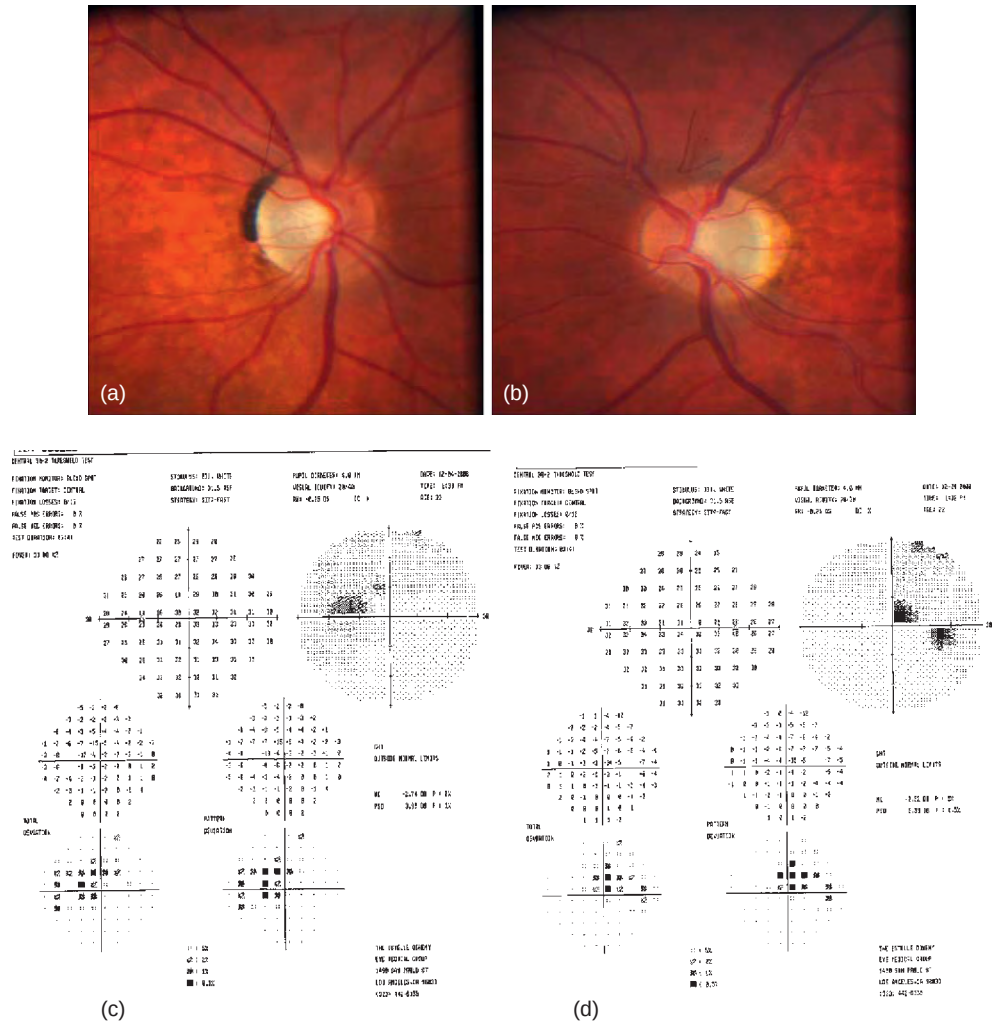

Figure 2 Right (a) and left (b) eyes in a patient with dominant optic atrophy (DOA): Fundus photographs show the characteristic wedge-shaped optic atrophy seen on the temporal side of both optic disks. 2(c) (Left) and 2(d) (Right): DOA. Humphrey Visual Fields demonstrate bilateral cecocentral visual field defects. Patient photographs are through the courtesies of Peter Quiros, MD.

Unlike LHON and DOA, ROA is usually discovered in the first 3–4 years of life. It often presents as severe visual impairment, frequently associated with searching nystagmus. Visual acuity ranges between no light perception (NLP) to 20/400. There is diffuse optic disk atrophy, sometimes with attenuation of the retinal arterioles, similar to that seen in tapetoretinal degenerations. Hence, the differential diagnosis of ROA is not so much a comparison to the other hereditary optic neuropathies as it is a comparison to retinal dystrophies. Electrophysiology using eletroretinography plays an important role in differentiating ROA from tapetoretinal degeneration, retinitis pigmentosa, or Leber's congenital amaurosis, this is normal in ROA and severely impaired in the retinal degenerations.

The gene/chromosome for ROA remains to be identified. Not surprising for an autosomal recessive condition, there are several reports of consanguinity related to ROA.

Other Inherited Conditions with Optic Atrophy

There are several well-characterized syndromes that also include optic atrophy. Wolfram's syndrome which is characterized by diabetes insipidus, diabetes mellitus, optic atrophy, and deafness is linked to the WFS1 gene located on chromosome 4p. Patients with Behr's syndrome, which consists of progressive encephalopathy, mental retardation, ataxia, nystagmus, and pes cavus, may also have optic atrophy. It is linked to the OPA3 gene located on chromosome 19q. Friederich's ataxia often includes vision loss and optic atrophy.

Conclusion

All of the inherited optic neuropathies serve to remind us that the optic nerve is highly dependent on mitochondrial

function. Indeed, acquired optic neuropathies that affect mitochondrial metabolism are often in the differential diagnosis of genetic optic neuropathies. The genetics of LHON involve a mutation of mitochondrial DNA resulting in impairments of complex I, which in turn leads to decreased ATP production and increased ROS. This is in contradistinction to DOA in which the genetics involve nuclear DNA. However, despite the fact that these mutations are somatic, the OPA genes control structural mitochondrial proteins that also limit mitochondrial functions such that the final consequences are similar: decreased ATP production and increased ROS. Hence, inherited optic neuropathies and metabolic optic neuropathies, whether toxic or nutritional, all share the common pathophysiology of producing mitochondrial dysfunction and subsequent retinal ganglion cell loss. Not surprisingly, all mitochondrial optic neuropathies share a similar clinical presentation. If a treatment proves to be effective in one, it is likely to be of benefit in the other mitochondrial optic neuropathies.

Exciting new treatment options with agents that modulate mitochondrial function that have anti-apoptotic effects or are helpful for neuronal survival, are currently being studied. Inherited optic neuropathies may serve as the ideal model with which to test these purportive neuroprotective agents.

See also: Imaging of the Orbit; Orbital Bony Anatomy and Orbital Fractures.

Further Reading

Barboni, P., Savini, G., Valentino, M. L., et al. (2005). Retinal nerve fiber layer evaluation by optical coherence tomography in Leber's hereditary optic neuropathy. *Ophthalmology* 112(1): 120–126.

Carelli, V., Ross-Cisneros, F. N., and Sadun, A. A. (2002). Optic nerve degeneration and mitochondrial dysfunction: Genetic and acquired optic neuropathies. *Neurochemistry International* 40(6): 573–584.

Carelli, V., Ross-Cisneros, F., and Sadun, A. (2004). Mitochondrial dysfunction as a cause of optic neuropathies. *Progress in Retinal and Eye Research* 23: 53–89.

Chalmers, R. M. and Schapira, A. H. V. (1999). Clinical, biochemical and molecular genetic features of Leber's hereditary optic neuropathy. *Biochimica et Biophysica Acta* 1410: 147–158.

Newman, N. J. (1998). Hereditary optic neuropathies. In Miller, N. R. and Newman, N. J. (eds.) *Walsh and Hoyt's Clinical Neuro-Ophthalmology*, pp 742–756. Baltimore: Williams and Wilkins.

Riordan-Eva, P., Sanders, M. D., Govan, G. G., et al. (1995). The clinical features of Leber's hereditary optic neuropathy defined by the presence of a pathogenic mitochondrial DNA mutation. *Brain* 118(2): 319–337.

Sadun, A. A. (2002). Metabolic optic neuropathies. *Seminars in Ophthalmology* 17(1): 29–32.

Sadun, A. A., Carelli, V., Salomao, S. R., et al. (2003). Extensive investigation of large Brazilian pedigree of Italian ancestry (SOA-BR) with 117788/Haplogroup J Leber's hereditary optic neuropathy (LHON). *American Journal of Ophthalmology* 136: 231–238.

Sadun, A., Salomao, S. R., Berezovsky, A., et al. (2006). Subclinical carriers and conversions in Leber's hereditary optic neuropathy: A prospective psychophysical study. *Transactions of the American Ophthalmological Society* 104: 51–61.

Sanchez, R. N., Smith, A. J., Carelli, V., et al. (2006). Leber's hereditary optic neuropathy possibly triggered by exposure to tire fire. *Journal of Neuroophthalmology* 26(4): 268–272.

Smith, J. L., Hoyt, W. F., and Susac, J. O. (1973). Ocular fundus in acute Leber optic neuropathy. *Archives of Ophthalmology* 90(5): 349–354.

Nikoskelainen, E. K. (1994). Clinical picture of LHON. *Clinical Neuroscience* 2: 115–120.

Wallace, D. C., Singh, G., Lott, M. T., et al. (1988). Mitochondrial DNA mutation associated with Leber's hereditary optic neuropathy. *Science* 242: 1427–1430.

Injury and Repair Responses: Retinal Detachment

S K Fisher and G P Lewis, University of California, Santa Barbara, Santa Barbara, CA, USA

Glossary

Glial scar – The proliferation and growth of glial cells (astrocytes and oligodendrocytes in the brain and spinal cord) in response to a physical wound to the central nervous system.
Immunocytochemistry – A laboratory technique that uses antibodies (the primary antibody) targeted to specific peptides or proteins (antigens) in the cell. The primary antibody is made to recognize its specific protein by the immune system of a specific species (i.e., it may be a rabbit immunoglobulin G (IgG) antibody). In addition, it can be bound to an antibody made in a second species (i.e., goat anti-IgG) that is bound with some detectable marker, often a fluorescent dye. Using appropriate imaging techniques, the localization can be subcellular.
Laser scanning confocal microscope – An optical imaging technique used to increase contrast and/or resolution by eliminating out-of-focus planes within a tissue section by using a spatial pinhole. Optical image plane thickness can be selected (usually 0.5–1.0 μm) and images from several optical sections collapsed together, played as a movie loop, or used to reconstruct objects in three dimensions. In biological research, this technique is most commonly used with immunocytochemistry with fluorescent dyes.
Pneumatic retinopexy – A method for repairing a retinal detachment by the injection of expanding gasses (usually sulfur hexafluoride (SF_6) or perfluoropropane (C_3F_8)) into the vitreous cavity.
Retinal detachment – A site-threatening condition that results from the physical separation of two cellular layers of the retina, the retinal pigmented epithelium and the neural retina.
Rhegmatogenous retinal detachment – A specific type of retinal detachment in which the neural retina is torn, allowing fluid from the vitreous to separate the two layers. This type is the most common form of retinal detachment.
Scleral buckle – A surgical method for repairing a retinal detachment by placing a band or bands of material (now usually silicone rubber and/or silicone sponges in a variety of configurations) to encircle the globe and to indent the wall of the eye in the region of the detachment. A scleral buckle is used in conjunction with cyrotherapy or laser treatment to seal the retinal break.
Serous retinal detachment – A retinal detachment that occurs when fluid accumulates between the neural retina and retinal pigmented epithelium, but without a tear in the retina.

Injury to the Retina

Introduction

Retinal glial cells

Damage to the retina, whether a result of physical injury, disease, or a genetic condition, produces similar cellular responses on the part of glial cells. Glial cells are non-neuronal, supportive cells found in all parts of the central nervous system (CNS). In the brain and spinal cord, where they also play an important role in injury, there are two types of true glia: oligodendrocytes and astrocytes. Oligodendrocytes are found in the optic nerve, but not in the retina itself. Astrocytes, similar to those in the brain and spinal cord, are star-shaped cells limited to the bundles of axons that run across the surface of the retina and exit the eye as the optic nerve. The glial cell with the most prominent role in the retina's response to injury is a highly modified, structurally complex radial astrocyte referred to as the Müller cell (first described in the mid-nineteenth century by the German anatomist Heinrich Müller). This cell spans the entire width of the neural retina (**Figure 1**), and, in many ways, its reaction to injury mirrors that of astrocytes. Microglia comprise another cell type important in the retina's response to injury. However, these are not true glia since they are derived from blood-borne marcrophages and have a different developmental lineage than that of astrocytes and Müller cells.

Retinal injury and retinal detachment: A close relationship

Physical injury to the retina can occur in many ways, from a penetrating wound to a spontaneous tearing of the retina in highly myopic individuals. Anytime the retina is physically damaged, there is great risk that the neural retina will separate from the underlying retinal pigmented epithelium (RPE in **Figure 1**) in a condition known as a rhegmatogenous retinal detachment (RD; **Figure 2**; the prefix rhegma is derived from the Greek word meaning a

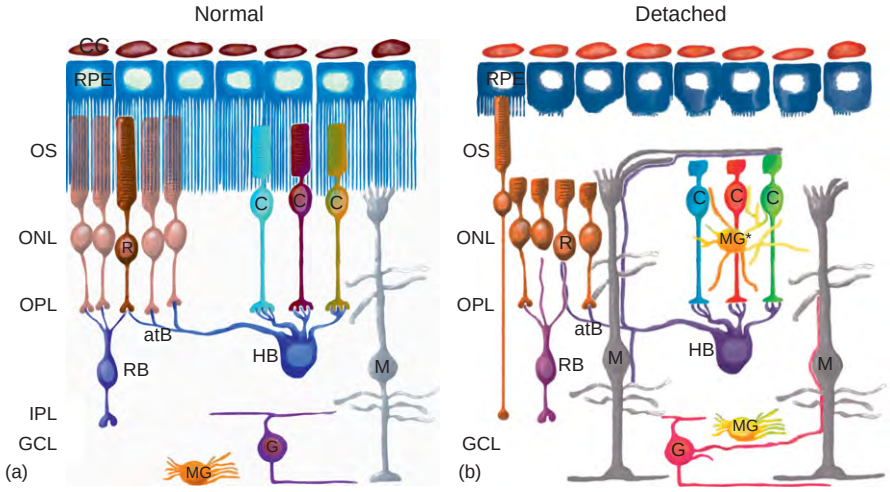

Figure 1 Diagrammatic representation of major cell types in which important reactions to injury of the retina by retinal detachment have been identified. (a) Normal retina and (b) representative changes after detachment. The rod photoreceptor on the left in (b) (gold cell) represents a characteristic response that occurs in some rods after reattachment; that is, they regenerate an axon that grows beyond its normal target, the OPL. CC, choriocapillaris, the main vasculature supply for the RPE and photoreceptor cells; RPE, retinal pigmented epithelium; R and C, rod and cone photoreceptors; OS, outer segments; ONL, outer nuclear layer (cell bodies of rods and cones); OPL, outer plexiform layer (region where photoreceptors synapse with second-order neurons); HB, a subclass of horizontal cells; atB, the axon of the B type horizontal cell; RB, rod bipolar cell; M, Müller's cell (the radial glial cell of the retina); IPL, inner plexiform layer (region where second-order neurons synapse with third-order neurons); GCL, ganglion cell layer, the third-order and output neurons of the retina; MG, microglia; MG*, activated microglia.

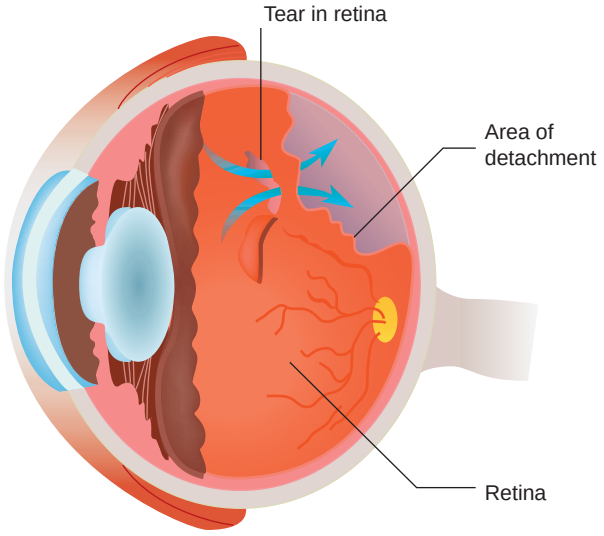

Figure 2 A rhegmatogenous retinal detachment forms when a hole or tear occurs across the neural retina, allowing fluid to flow from the vitreous and separate the neural retina from the retinal pigmented epithelium.

break in continuity). This condition occurs with a prevalence estimated at 1:10 000 in the United States and is usually treated by a retinal surgeon who repairs the retinal tear and reapposes the two layers of tissue. Thus, studying RD is, in essence, a study of retinal injury, and used to demonstrate the variety of cellular responses that can occur in many different insults or injuries to the retina.

What is an RD?

An RD refers to a separation between the neural retina and the RPE. As discussed above, rhegmatogenous detachment (hereafter, simply detachment or RD) involves a specific injury to the retinal tissue. An important physiologicalra mification of such a detachment is an increase in the physical distance between the photoreceptor cells and their blood supply, a highly branched capillary network (the choroicapillaris, which lies behind the RPE; see Figure 1). The choriocapillaris provides nearly all of the oxygen and nutrients to photoreceptors and also carries away metabolic waste products from these extraordinarily active cells. A decrease in oxygen availability across the expanded extracellular space may be a critical step in the rapid degeneration of photoreceptor outer segments that occurs after detachment (Figure 1). A certain number of these photoreceptors are destined to die by apoptosis, in most species reaching a peak about 3 days after detachment and declining thereafter to a low, but steady level. Indeed, some studies in animal models have demonstrated that placing animals in an environment of 70% oxygen has the capacity to stop many of the degenerative effects of detachment including photoreceptor cell death. Detachment also creates a foreign environment for the photoreceptor outer segments as components from the vitreous wash through the tear and into that space. Indeed, it is this movement of fluid through the tear and under the retina that is generally assumed to create and maintain a detachment. Another type of RD is known as a serous

detachment and involves the accumulation of fluid within the same space, but without a retinal tear. Its symptoms and treatment are very different.

Symptoms and signs of RD in people

All detachments are accompanied by some loss of visual function, but this will vary depending upon the size and retinal location, making it difficult to ascribe one set of symptoms to the condition. Diagnosing RD is complex, with many qualifications. Abnormal vision is the only reliable symptom of RD; however, the types of abnormal vision are large and varied: light flashes, floaters, changes in the peripheral visual field, decreased acuity, defective color vision, distorted vision (metamorphopsia), or even unilateral double vision (diplopia). The detachment of the fovea always involves a loss of central visual acuity.

Brief history

Greg Joseph Beer provided the earliest systematic description of RD in the early eighteenth century. After Hermann von Helmholtz recognized the clinical significance of the ophthalmoscope in *c.* 1850, detailed descriptions of detachments and accompanying retinal breaks or tears proliferated rapidly. The first treatment of rhegmatogenous detachment by sealing the retinal break with a red-hot probe occurred in 1889, and was revived as a standard treatment by Jules Gonin in the early 1920s. Gonin devoted much of his research career to studying the relationship between retinal tears and detachment and also was the first to suggest a relationship between detachment duration and successful visual recovery. His technique is credited with moving an inevitably blinding retinal injury into a treatable one. The next major advance occurred 70 years later when Ernst Custodis described the scleral buckle, a band or bands of material (now usually silicone rubber and/or silicone sponges) surgically placed to encircle and indent the wall of the eye in the region of the detachment, thus reapposing the RPE and neural retina. A scleral buckle is used in conjunction with cyrotherapy or laser treatment to seal the retinal break, probably by creating a localized glial scar. In the early 1970s, pneumatic retinopexy, or injection of an expanding gas bubble (sulfur hexafluoride or perfluoropropane), into the vitreous cavity to reappose the retina and RPE became widely used. There is still much ongoing discussion on the use of scleral buckling, primary vitrectomy, and pneumatic retinopexy to treat RD.

Cellular Responses of the Retina to Injury

General Events

Overall, the retina may be described as including two major cellular layers, the RPE and the intimately apposed neural retina. The neural retina is highly organized, consisting of three cellular layers and two synaptic layers (**Figure 1**). Since it is so highly structured, changes in its normal architecture are readily noted by conventional histology and light microscopy as shown in **Figure 3**.

In the 1960s through the 1980s, investigators used combinations of light and electron microscopy to reveal cellular and subcellular structural changes induced by detachment in photoreceptors including outer segment degeneration, loss of mitochondria, and the general disorganization of organelles involved in protein synthesis. It was also recognized in these early structural studies that Müller's cells underwent vast changes in structure (hypertrophy) with growth out of the retina and into the subretinal space (**Figure 3(b)**). In recent years, it has been recognized that cellular effects of detachment occur well beyond the site of separation of the RPE and neural retina. Almost all of the cellular changes have been validated in tissue samples taken from human detachments including the capacity of photoreceptors to regenerate outer segments after surgical reattachment. When immunocytochemistry became a routine laboratory procedure in the late 1980s, and laser scanning confocal imaging allowed the efficient collection of high-resolution immunofluorescence images by light microscopy, it became apparent that cellular responses to detachment were far more complex than the degeneration of photoreceptor outer segments and the hypertrophy of Müller's cells. It first became clear in these animal studies that a number of photoreceptors actually die (see **Figure 3**).

As Müller's cells are the primary players in the retina's gliotic response to injury, they are discussed first and in most detail. In animal models, these range from molecular changes that occur within minutes to hours (e.g., phosphorylation of the fibroblast growth factor receptor 1, and the extracellular signal-regulated kinase, with later synthesis of the AP1 family transcriptional activators cFos and cJun in Müller's cells), cellular changes recognizable within hours (photoreceptor outer segment degeneration) to cellular events that begin in days and can extend for weeks or months (e.g., Müller cell reactivity, rod cell death, glial scar formation, and neuronal remodeling). The cellular level events are summarized in **Figure 4**.

Müller's cells

Except for the death of photoreceptors, the reactivity of Müller's cells may be one of the most important consequences of injury to the retina. The cell body of the Müller cell lies among the interneurons of the inner nuclear layer and extends main stalks in both directions (M in **Figure 1**). The inner stalk expands along the vitreal border of the retina to form a so-called endfoot. Müller's cells are arrayed across the retina to assure that adjacent endfeet form a continuous layer on the vitreal surface (the green cells in **Figure 5(c)** are good examples). They are not, however, linked by tight junctions and, hence,

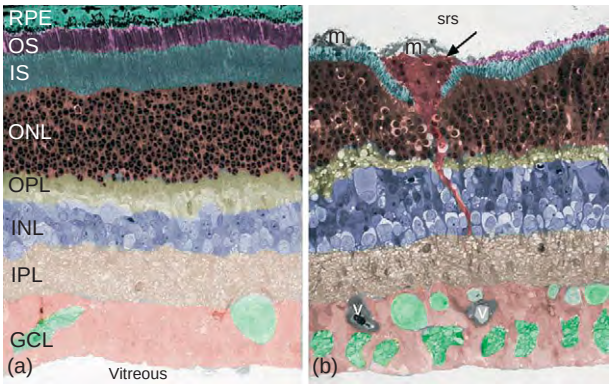

Figure 3 (a) Light micrographs of a normal mammalian retina and (b) micrograph showing the overall disorganization of the retina with a characteristic glial scar in the subretinal space (arrow in (b), dark red) after a retinal detachment. The retinal layers were colored to allow for easier comparison between the two images. The retinal pigmented epithelium (RPE, light green in A) that is anatomically tightly apposed to the photoreceptor outer segments (OS, light purple) in normal retina becomes several hundred micrometers removed from the neural retina after detachment and does not appear in (b). There is a dramatic degeneration of light-sensitive rod and cone outer segments (OS, light purple) and inner segments (IS, light gray) in the detached retina. The latter are responsible for most of the energy production and protein synthesis in normal photoreceptors. The outer nuclear layer (ONL, dark brown) which contains the cell bodies and nuclei of the photoreceptors is greatly thinned in the detached retina as a result of the loss of cells by apoptotic cell death. Notice that many of the photoreceptor cell bodies in (b) appear swollen with clear cytoplasm surrounding highly condensed nuclei, indicative the fact that they are in the process of undergoing apoptosis. The outer plexiform layer (OPL, light green) is greatly thinned in the detached retina by the loss of rod photoreceptor terminals and probably dendrites of second-order neurons whose cell bodies reside in the inner nuclear layer (INL, blue). The INL appears thickened in the detached retina due to the significant swelling of the cells and also due to the hypertrophy and migration of Müller's cells within the layer (see text). Although we know there are subtle changes in the inner plexiform layer (IPL, light brown) after detachment, these are difficult to discern by light microscopy. The endfeet of Müller's cells (pink) form a continuous layer along the vitreous cavity of the retina (vitreous) and assume a somewhat thickened and contorted appearance as they expand after detachment (this effect is more obvious when the Müller cells are specifically stained by immunolabeling as in **Figures 5** and **6**). The cells of the ganglion cell layer (GCL, green) and their axons (green) appear little affected in this thin histological section, but immunolabeling studies show that they undergo significant remodeling through the sprouting of neurites (see **Figure 8(b)**). Müller's cells expanding beyond the boundaries of the retina form a layer of scar tissue on the photoreceptor surface (arrow, dark red), in the subretinal space (srs). The dark round structures embedded in the subretinal scar represent nuclei of Müller's cells that migrate through their processes into the scar as well as some photoreceptor cell bodies that migrate from the ONL to appear among the scar tissue. These subretinal scars can block the regeneration of outer segments after surgical reattachment, and they can also contract, wrinkling and redetaching the retina after reattachment. Two macrophage cells (m) appear in the subretinal space in (b). These cells engulf debris from degenerating outer segments. Two retinal blood vessels (v) appear among the Müller cell endfeet in (b).

extracellular molecules can flow freely between them. Some branching of the main stalk occurs in all retinal layers, but reaches its greatest complexity as the individual cells interweave between all photoreceptor cell bodies so that each is separated from the next by a thin layer of Müller cell cytoplasm. The Müller cell ends as a tuft of microvilli at the level of the photoreceptor inner segments. Thus, this cell is ideally situated to sample the internal environment of the retina, the vitreous, and the space between photoreceptors and RPE. Adhering junctions between adjacent Müller's cells and photoreceptors form a continuous, recognizable layer known as the outer limiting membrane.

Functionally, Müller's cells are responsible for much of the homeostasis of the neural retina. They are known to actively recycle glutamate released as a neurotransmitter by retinal neurons through uptake and conversion to glutamine. Potassium balance, water regulation, and pH balance are all thought to depend strongly on Müller's cells. There is even some evidence that they may act as light pipes – optically funneling light through the retinal layers to the outer segments. While much of the focus of this article is on the formation of glial scars by Müller's cells as part of the injury response, there is also significant experimental evidence that activated Müller's cells can play a neuroprotective role in retinal injuries resulting from excitotoxicity generated by the excess release of the neurotransmitter glutamate.

Müller's cells and RD: Glial scarring

Following RD, there are rapid changes in molecular events in Müller's cells as discussed above. This fairly quickly translates into two major events: proliferation of the cells and hypertrophy or excessive growth. Both are poorly understood, but the latter is known to have important ramifications. If a retina is labeled with markers for DNA synthesis (tritiated-thymidine, bromodeoxyuridine, or antibodies to cell-cycle-specific proteins such as Ki-67), many cell types can be shown to divide, with Müller's cells and microglia being among the most prominent (**Figure 5**).

This newly activated cell division appears to peak 3–4 days after detachment in the feline and rabbit retina, but continues at low levels thereafter as long as the retina is detached. The fate of the daughter cells produced by dividing Müller's cells is still controversial, although, in species such a chick or teleost fish, they appear to regress to an earlier pluripotent stage where they can regenerate retinal neurons. There is scant evidence that this occurs in mammals. Details of how these morphologically complex cells divide or exactly what cell types they produce in the mammalian retina are unknown. One intriguing scenario is that after nuclear division, a daughter nucleus migrates into the outer retina and then buds off a daughter cell. If this is true, the proliferating Müller's cells may indeed

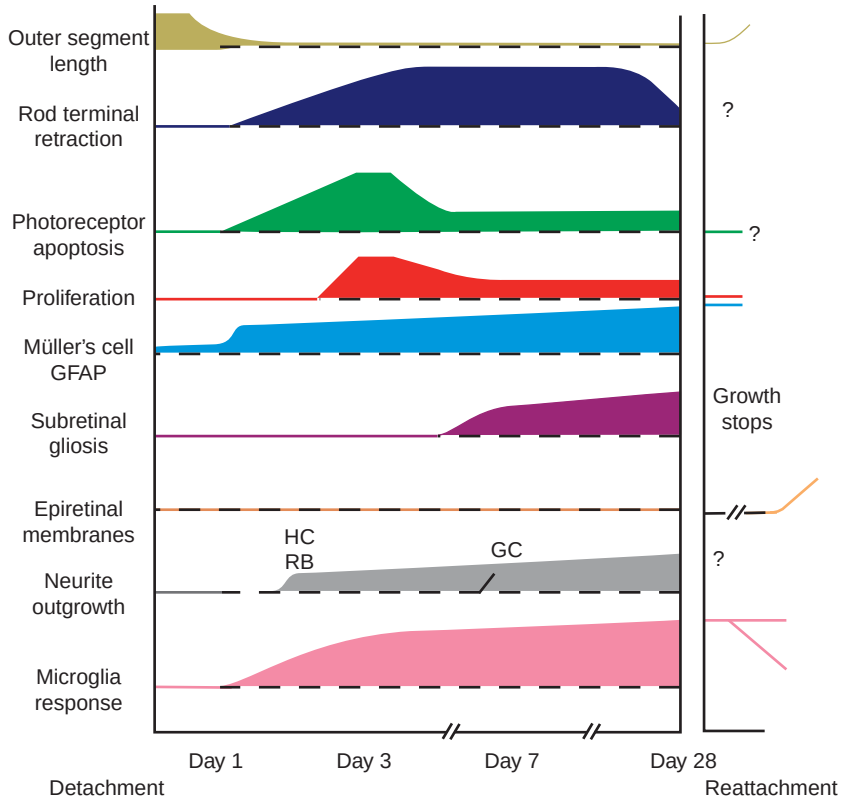

Figure 4 A diagram representing cellular events that occur after retinal detachment. The purpose is to show how the various events are temporally related. For example, outer segments degenerate very quickly with rod terminal retraction and photoreceptor apoptosis starting around the end of the first day of detachment. Epiretinal membranes do not form in the detached retina, but begin forming when the retina is reattached. Their time of formation is highly variable, but can range from weeks to months. Rod terminal retraction and apoptosis are stopped by reattachment, but the timing is unknown. Indeed, following reattachment, rod axons regrow into the outer plexiform layer. Müller cell proliferation is stopped by reattachment, but glial fibrillary acidic protein (GFAP) expression can remain elevated for an unknown period of time. Neurite sprouting occurs from horizontal and rod bipolar cells (HC, RB) before it does from ganglion cells (GC). The microglial response is variable after reattachment, remaining high in areas of poor regeneration, but returning to normal in areas of good regeneration.

be producing a small population of pluripotent cells that have remained unidentified in mammals. The proliferation of glial cells is common to virtually all types of CNS injuries.

Structural remodeling of Müller's cells can be observed as early as 1 day after detachment by the hypertrophy of their main trunk and lateral branches within the retina. At this time, they also decrease their expression of the proteins glutamine synthetase, carbonic anhydrase II, and cellular retinaldehyde-binding protein, and dramatically increase their expression of two intermediate filament proteins, glial fibrillary acidic protein (GFAP) and vimentin (**Figures 6(a)–6(d)**). The increased expression of these two proteins is especially useful as hallmarks of the retina's reaction to injury. Indeed, their tissue expression profile varies by species, but an increased expression of GFAP is widely used as an indicator of retinal stress or injury. In the normal feline retina, both of these proteins are mainly restricted to the endfoot of the Müller cell (**Figures 6(a)** and **6(b)**). There are interesting species differences in the expression of these molecules. In rabbit, ground squirrel, rat, and mouse retinas, vimentin is expressed from the endfoot into the layer of photoreceptors, whereas GFAP is limited to the endfoot or virtually undetectable by immunocytochemistry. GFAP does, in all of these species, occur abundantly in astrocytes while vimentin does not. Following detachment or injury, the proteins rapidly increase their expression so that within a few days, they fill the entire cytoplasm of the cell (**Figures 6(c)** and **6(d)**; see also **Figure 5**). The interesting exception occurs in the cone-dominant ground squirrel retina which increases its expression of vimentin, but not GFAP, and does not show the Müller cell hypertrophy characteristic of the all other species studied. In feline retina, the balance of expression of GFAP and vimentin within individual Müller's cells shifts fairly rapidly over the first few days of detachment. Within a day or so, there is a shift so that GFAP expression in the endfoot increases rapidly as it acquires a more elongated and branched appearance. This is one of the earliest recognizable stages of the hypertrophic growth of these cells after

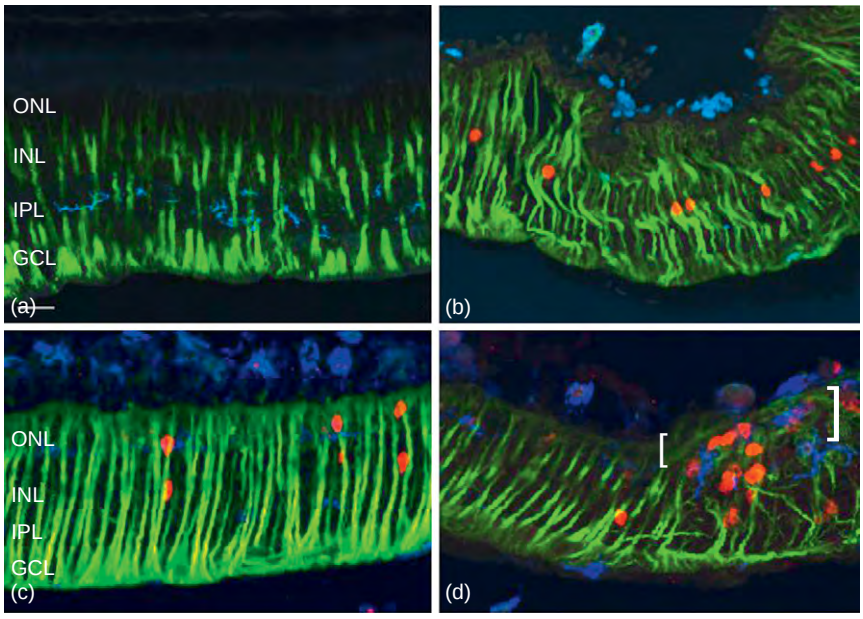

Figure 5 A series of immunofluoresence images acquired by laser scanning confocal microscopy, illustrating the proliferative response of Müller's cells in reaction to retinal detachment and their participation in glial scar formation. The red-colored portions indicate the signal from immunolabeled bromodeoxyuridine, a nucleotide that can become incorporated into DNA as cells undergo DNA synthesis in preparation for division. Green labeling is a marker for Müller's cells and blue a marker for microglia and macrophages. Panel (a) is an image from normal retina. Notice that there are no red cells because neurons and Müller's cells of the adult mammalian retina are postmitotic. In (b)–(d), the bromodexoyuridine-labeled nuclei are associated with Müller's cells. In (b), these occur at the normal location of Müller cell nuclei in the inner nuclear layer (INL), while 24 h later (c), many of them have migrated into the outer nuclear layer (ONL). At a later time point, Müller's cells begin to to form a characteristic glial scar (brackets in (d)) on the photoreceptor layer and many of the bromodeoxyuridine-labeled Müller's cells reside within the glial scar, suggesting a link between Müller cell proliferation and glial scar formation. Notice that many of the microglial cells (blue) occur within the glial scar as well. IPL, inner plexiform layer; GCL, ganglion cell layer. Scale bar = 20 μm.

injury of the retina (**Figures 6(c)** and **6(d)**). By 3 days, GFAP expression increases throughout the cell and the cell shows expansive growth of its processes within the retina, in later stages forming large columns of cytoplasm across the retina and filling space left by dying photoreceptors. An important subpopulation of Müller's cells will eventually grow into the space between the retina and RPE to form glial scars over the photoreceptor surface (**Figures 6(e)** and **6(f)**). Interestingly, these cells will quickly begin heavy expression of vimentin in their outer half. The extension of Müller's cells into the subretinal space is part of a reaction comparable to glial scarring in the brain and spinal cord where the scars block axon growth. Here, they effectively block outer segment regeneration after reattachment. The growth of Müller's cells into this space does not appear to be random, but, in feline retina, spatially associated with the presence of cone photoreceptors (inset to **Figure 6(d)**), suggesting some attraction between cones and the vimentin-rich Müller's cells. There is no molecular mechanism known to underlie this process. Once growth into the subretinal space is initiated, it continues at a rapid pace so that a Müller cell scar can rapidly expand broadly over the photoreceptor surface of the retina (**Figures 6(e)** and **6(f)**). Besides inhibiting outer segment regeneration, these scars also appear permissive for the growth of neurites out of the retina (see below).

Retinal reattachment appears to greatly slow much of the intraretinal hypertrophy of the Müller cells as well as their growth into the subretinal space. It does not, however, completely halt their reactivity since cell division can still occur at low levels. In addition, reattachment appears to stimulate a redirection in the growth of Müller's cells from the subretinal space toward the vitreal surface of the retina where they break through the vitreoretinal interface to form glial scars on this surface of the retina. Curiously, the Müller cell processes that expand into the vitreous predominately express GFAP instead of vimentin. Their growth into the vitreous may mark the beginning for a devastating disease called proliferative vitreoretinopathy (PVR). The Müller cells can form long fibers on the retinal surface and become populated with a variety of other cell types, including RPE and immune cells. There are no pharmacological treatments to date that will inhibit this disease from occurring or reverse its progression. It continues to occur in a small percentage of successful reattachment surgeries. The cellular strands can become contractile, causing a secondary tractional detachment (essentially a rhegmatogenous

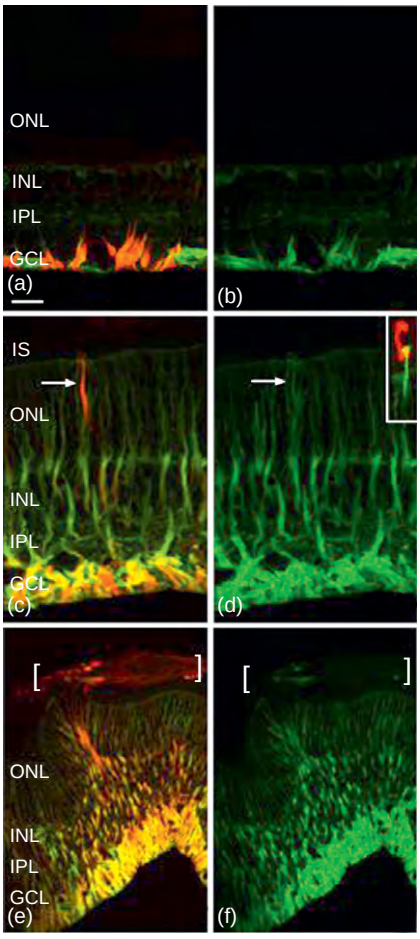

Figure 6 A series of immunofluoresence images acquired by laser scanning confocal microscopy, illustrating the upregulation of the intermediate filament proteins vimentin (red) and GFAP (green) that occurs as Müller's cells react to injury. Panels (a), (c), and (e) show the fluorescent signals from both (when the signals overlap, yellow results). Panels (b)–(e) show only the signal from GFAP. Panels (a) and (b) are images from a normal retina. The retinal astrocytes reside among the ganglion cells with their axons containing GFAP, while the endfeet of the Müller's cells (where these cells terminate on the vitreal border of the retina as shown in **Figure 1**) have a mixture of the two proteins (with vimentin being at a higher level of expression than GFAP). Panels (c)–(f) show the very large uprergulation of both of these molecules as the Müller's cells react to injury. Panels (c) and (d) show that although both increase their expression in Müller's cells after 3 days of detachment, the largest overall increase is associated with GFAP. However, one Müller's cell predominately shows vimentin expressed at its apex (arrow), and this cell is just beginning to grow out of the retina to form a glial scar in the subretinal space (the space created between the neural retina and RPE by the detachment). Panels (e) and (f) show further upregulation of both at 7 days of detachment and also a large subretinal glial scar (brackets) in which the Müller's cell processes predominately express vimentin. The inset to panel (d) shows a characteristic phenomenon where Müller's cell processes (yellow/green) grow out of the retina at the location of cone photoreceptors (red). ONL, outer nuclear layer; IS, photoreceptor inner segment layer; INL, inner nuclear layer; IPL, inner plexiform layer; GCL, ganglion cell layer. Scale bar = 20 μm.

detachment caused by the contractional force generated by this strand of fibrous-like scar tissue). Similar to their counterparts in the subretinal space, these epiretinal membranes can act as substrates for the growth of ganglion cell neurites (discussed below) out of the retina. From these examples, it is clear that Müller's cells are highly involved in the reaction of the retina to detachment. There is evidence in mice which are genetically modified so that they do not express vimentin and GFAP that subretinal scars do not form. There is also some experimental evidence that certain inhibitors of cellular proliferation may help prevent the formation of glial scars. There are currently no drugs that target the former, although inhibiting proliferation of cells with antiproliferative drugs after retinal injury is an area of active investigation.

Injury and Other Cell Types

Photoreceptors

Besides undergoing degeneration of their light-sensitive outer segment, photoreceptors undergo a number of other changes when the retina is detached, or when they lie in the immediate vicinity of retinal injury. Within a day after detachment, they undergo changes in the way they express proteins; the light-sensitive protein, opsin, normally localized in the membranes of the outer segment soon becomes distributed throughout the plasma membrane of the cell (red staining, right side of **Figure 7(a)**), essentially outlining the whole cell. This may occur because the cell cannot construct an outer segment as part of its ongoing membrane renewal process; however, since the cell does continue to synthesize opsin, the protein is then aberrantly inserted into the plasma membrane. Some proteins (e.g., peripherin/rds) remain inside transport vesicles that accumulate within the cytoplasm. Rods and cones appear to differ in this respect inasmuch as cones may actually downregulate much of their protein synthetic machinery, perhaps giving these critical cells a better chance of survival in a stressful environment.

Rod photoreceptors have short axons that retract after detachment, pulling their synaptic terminal back toward the cell body. This can be seen as a loss of synaptic terminals in the outer plexiform layer and the appearance of these terminals among the cell bodies of photoreceptors (**Figures 7(c)** and **7(d)**). Cone photoreceptor axons do not appear to retract, but there are numerous structural modifications in their synapses (**Figures 7(e)** and **7(f)**). Given the complexity of photoreceptor synapses, it seems reasonable to expect that these structural changes effect communication to second-order neurons. Importantly, rod axons appear to regrow back toward their normal location after reattachment; some even overshoot their target and grow into the inner retina (**Figure 7(b)**),

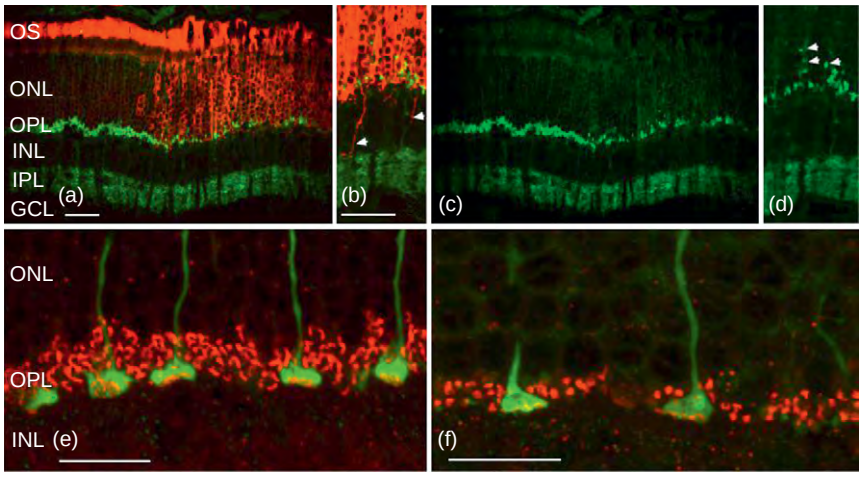

Figure 7 A series of immunofluoresence images acquired by laser scanning confocal microscopy, illustrating various responses of photoreceptor cells caused by detachment. In panels (a)–(d), the retina has actually been surgically reattached, but shows characteristics of both normal morphology and that after detachment. In panels (a) and (b), the retinal sections were labeled with antibodies to the rod photopigment, rhodopsin (red), and a synaptic vesicle protein, synaptophysin (green). Panels (c) and (d) show labeling with synaptophysin alone. In panel (a), the layer of rod outer segments (OS) is uniform in the nondegenerate area to the left, but highly disrupted in the degenerate area to the right. Characteristically, as the OS structure is disrupted by injury, the rhodopsin molecules become distributed throughout the plasma membrane of the rod photoreceptors instead of being restricted to the outer segment, hence the heavy red labeling in the ONL in panels (a) and (b). Also shown in panel (b) is the characteristic overgrowth of some axons (arrowheads) that occur in some rods after reattachment (also see **Figure 1**). The fate of these overgrown axons is unknown. The green labeling compares the organization of the photoreceptor synaptic terminals in areas that are normal (to the left in (a) and (c)) to the organization in areas of photoreceptor degeneration (to the right in (a) and (c)). Notice the sparseness of terminals in areas of degeneration. This is caused largely by the withdrawal of rod axons and the retraction of the terminals into the layer of photoreceptor nuclei (ONL, arrowheads in (d)). Axonal retraction appears to be a common response of rod photoreceptors to retinal injury but the same is not true of cones. Figures (e) and (f)show the responses of cone photoreceptors (green) as well as an organelle characteristic of all photoreceptor synapses, the synaptic ribbon (red). In the normal retina, the cone synaptic terminals are very large by comparison to those of rods and contain many of the synaptic ribbons (red/yellow areas within the green terminals). Rod terminals, on the other hand (unstained in these images), contain only one or two of the crescent-shaped synaptic ribbons. As rod and cone photoreceptors degenerate, cone axons (green) do not withdraw as do those of rods, but the cone synaptic terminals assume a flattened appearance and lose the characteristic synaptic morphology of normal terminals. Notice that the rod synaptic ribbons are transformed from a crescent shape in (e) to a small clumped appearance in (f). There are also many fewer of the rod terminal ribbons in (f) due to the loss of rod synaptic terminals from their normal location in the OPL. OS, layer of photoreceptor outer segments; ONL, outer nuclear layer; OPL, outer plexiform layer; INL, inner nuclear layer; IPL, inner plexiform layer; GCL, ganglion cell layer. Scale bar = 20 μm.

a phenomenon that also occurs in retinal development. There is almost nothing known about the recovery of connections to second-order neurons, but the repopulation of the outer plexiform layer with rod terminals appears imperfect after a month of reattachment. It may be the reformation of synaptic connections that partially accounts for the prolonged period of visual recovery that can occur after reattachment, rather than simply a defect in the recovery of outer segments, since the latter are known to have a remarkable capacity to regenerate and recovery quickly, usually within a few weeks of reattachment.

Second- and Third-Order Neurons

The interneurons of the inner retina and the ganglion cells undergo remarkable structural remodeling as the photoreceptors undergo degenerative changes. Rod bipolar cells and horizontal cells show rapid neurite sprouting with fine thread-like processes extending deep into the outer nuclear layer, usually terminating near withdrawn rod terminals (**Figure 8(a)**). However, many neurites from horizontal cells grow across the retina, following intermediate filament-filled Müller cell processes into the subretinal space (**Figure 8(b)**). Postsynaptic processes are probably pruned from both of these cell types as well. A subpopulation of ganglion cells, those with the largest cell bodies, undergoes changes that mirror the responses of horizontal cells. They upregulate the expression of at least two proteins, GAP 43 and neurofilament protein, both of which are expressed at low levels in adult ganglion cell bodies and dendrites (**Figure 8(b)**). The same cells also sprout neurites that can become extensive and grow into the vitreous or across the retina and into the subretinal space, always following gliotic Müller cell scars.

Thus, the detachment of the neural retina from the RPE initiates a series of events in neurons not just among photoreceptors, but also throughout the retina. Ensuing

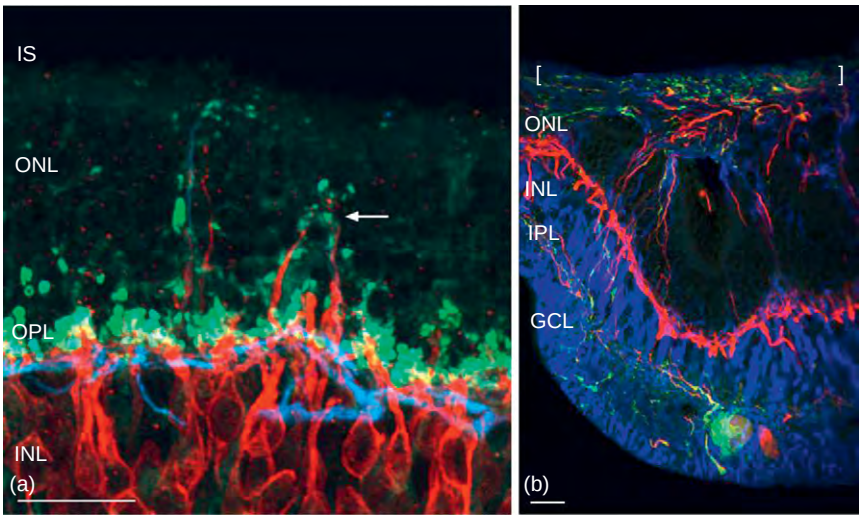

Figure 8 A series of immunofluoresence images acquired by laser scanning confocal microscopy, illustrating the remodeling response of second- and third-order neurons to retinal injury and the relationship of that reaction to glial scars formed by Müller's cells in the subretinal space. (a) All rod bipolar cells (red) label with an antibody to protein kinase C. Synaptic terminals of the photoreceptors (green) are labeled by an antibody to the synaptic vesicle protein synaptophysin. Notice that many of the synaptic terminals have withdrawn into the outer nuclear layer (ONL) as part of the injury response (white arrow). The dendrites of rod bipolar cells normally terminate only among the layer of rod terminals in the outer plexiform layer (OPL), but, in the detached retina, these cells extend neurites deep into the ONL with many of them terminating close to the withdrawn rod terminals. Electron microscopic studies show that these usually do not terminate close enough to the rod terminal to participate in the normal transmission of signals from the rod cells. (b) Horizontal cells and ganglion cells can show extreme remodeling in response to many retinal degenerations including retinal detachment. This image shows processes from horizontal cells (red) and ganglion cells (green) extending across the retina and into a glial scar formed by Müller cell processes in the subretinal space (white brackets). In a normal retina, the horizontal cell postsynaptic processes would terminate among the layer of photoreceptor synaptic terminal in the OPL, and ganglion cell processes would terminate in the IPL where they are postsynaptic to bipolar and amacrine cells. Müller's cells and their processes forming the subretinal scar are labeled with an antibody to GFAP (blue). Scale bar = 20 μm.

changes in synaptic circuitry could have a profound effect on retinal function and there is evidence that the activity of ganglion cells is abnormal in the detached feline retina. The reorganization of synaptic circuitry after reattachment may underlie the long-term changes in vision that are known to occur in many reattachment patients.

Microglia and the Immune Response

Microglial cells are immune cells that normally reside in the inner retina. Almost any injury to the retina will activate these cells, meaning that they begin to proliferate and migrate from their normal location in the inner retina into the photoreceptor layer where they scavenge dead or dying cells (**Figure 9**).

Microglia may cause or prevent photoreceptor cell death by modulating the release of trophic factors from Müller's cells. Macrophages from the circulation enter the subretinal space where they also scavenge debris from degenerated outer segments. Microarray analysis of messenger ribonucleic acid (mRNA) in a number of species has now identified significant changes in the expression levels of many genes involved in the immune and inflammatory responses, with most of these genes being up regulated. In the reattached retina, the presence of microglia correlates strongly with the degree of photoreceptor recovery; areas showing less outer segment recovery have a greater population of microglia distributed among the photoreceptor cells (**Figure 9(c)**). The role of the immune system and the inflammatory response following detachment and retinal injury is only beginning to be appreciated. It is quite clear from cellular localization studies that both macrophages and microglia can populate glial scars formed on either surface of the retina. What role they play there is unknown.

Retinal Pigmented Epithelial cells

Retinal pigmented epithelial cells react to detachment by retracting their highly specialized apical microvillii – actin-filled processes that normally drape the outer segments (**Figure 1**). The cells do, however, retain a fringe of conventional microvilli much like those that appear on cultured RPE cells and these microvilli then have the capability of regenerating after reattachment. RPE cells can also proliferate after injury to the retina and then migrate from their monolayer to form complex assemblies of cells in the expanded subretinal space. This is an important response to injury because these cells are structurally and physiologically polarized so that their apical

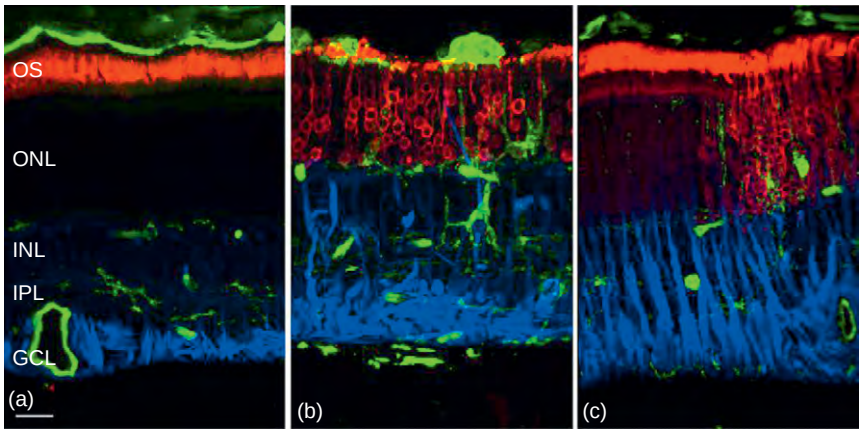

Figure 9 A series of immunofluoresence images acquired by laser scanning confocal microscopy, illustrating the microglial and macrophage component of the response to retinal detachment. Microglia and macrophages (green) are labeled by a lectin molecule that binds to sugar groups on protein molecules. Notice that this lectin also binds to blood vessels that are represented by the large choroidal vessels above the OS and a large inner retinal vessel bridging the GCL/IPL layers in panel (a). Rod photoreceptors (red) are labeled with an antibody to the protein rod opsin, and Müller's cells by an antibody to GFAP (blue). Rod opsin is restricted to the layer of outer segments (OS) and GFAP to the Müller cell endfeet and astrocytes, both in the ganglion cell layer (GCL). The microglia are the green spindly cells within the INL. (b) In a detached retina, the OS are highly degenerated; rod opsin labeling now extends throughout the rod cell plasma membrane and the Müller cells have upregulated the expression of GFAP. Lectin-labeled microglia are now found in the outer retina, and macrophages are present on top of the degenerated outer segments. (c) An example of a retina that has been reattached but shows patchy areas of good and poor outer segment regeneration. In the area of good outer segment regeneration (to the right), opsin is once again restricted to the layer of outer segments and microglia are no longer found in the outer retina. In the area of poor outer segment regeneration, opsin is found distributed throughout the plasma membrane of the rod cells and microglia still reside in the outer retina. Notice that even though this retina was reattached for 28 days after a 3-day period of detachment, there is still a large amount of GFAP in the Müller cells. Scale bar = 20 μm.

and basal surfaces physiologically differ. If a new layer of RPE cells is generated in response to detachment and their basal surface faces the retina, no outer segment regeneration will occur. These cells also have the remarkable ability to migrate across the neural retina and integrate into epiretinal membranes (referred to above as glial scars) that contribute to the disease PVR. Indeed, because of the presence of melanin pigment granules, RPE cells within these membranes are highly visible and, for many years, PVR was thought to be a disease of RPE cell origin. This is still a point of controversy, but it seems clear that RPE cells can be involved along with glia and immune response cells.

Summary

Rhegmatogenous RD is a form of retinal injury that produces cellular responses common to many other injuries. Detachment as well as other physical injuries to the retina can result in long-lasting visual deficits. New information at the cellular and molecular level may lead to an understanding of why successful anatomical reattachment can still leave a patient with imperfect vision or the mechanisms by which some repairs fail. Müller's cells of the retina respond similarly to astrocytes in the brain and spinal cord and there is still much to learn about the role of these enigmatic cells in the retina's responses to injury and its ability to recover.

See also: Rhegmatogenous Retinal Detachment.

Further Reading

Anderson, D. H., Guérin, C. J., Erickson, P. A., Stern, W. H., and Fisher, S. K. (1986). Morphological recovery in the reattached retina. *Investigative Ophthalmology and Visual Science* 27: 168–183.

Bringmann, A., Pannicke, T., Rosche, J., et al. (2006). Müller cells in the healthy and diseased retina. *Progress in Retinal and Eye Research* 25: 397–424.

Cook, B., Lewis, G. P., Fisher, S. K., and Adler, R. (1995). Apoptotic photoreceptor degeneration in experimental retinal detachment. *Investigative Ophthalmology and Visual Science* 36: 990–996.

Fisher, S. K., Lewis, G. P., Linberg, K. A., and Verardo, M. R. (2005). Cellular remodeling in mammalian retina: Results from studies of experimental retinal detachment. *Progress in Retinal and Eye Research* 24: 395–431.

Harada, T., Harada, C., Kohsaka, S., et al. (2002). Microglia–Müller glia cell interactions control neurotrophic factor production during light-induced retinal degeneration. *Journal of Neuroscience* 22: 9228–9236.

Jacobs, G. H., Calderone, J. B., Sakai, T., Lewis, G. P., and Fisher, S. K. (2003). Effects of retinal detachment on S and M cone function in an animal model. In: Mollon, J. D., Pokorny, J., and Knoblauch, K. (eds.) *Normal and Defective Colour Vision*, pp. 381–388. Oxford: Oxford University Press.

Lewis, G. P. and Fisher, S. K. (2003). Upregulation of GFAP in response to retinal injury: Its potential role in glial remodeling and a comparison to vimentin expression. In: Jeon, K. W. (ed.) *International Review of*

Cytology. A Survey of Cell Biology, vol. 230, pp. 263–290. San Diego, CA: Academic Press.
Lewis, G. P. and Fisher, S. K. (2005). Retinal plasticity and interactive cellular remodeling in retinal detachment and reattachment. In: Pinaud, R., Tremere, L., and De Weerd, P. (eds.) *Plasticity in the Visual System: From Genes to Circuits*, pp. 55–78. Dordrecht: Springer.
Lewis, G. P., Sethi, C. S., Charteris, D. G., et al. (2002). The ability of rapid retinal reattachment to stop or reverse the cellular and molecular events initiated by detachment. *Investigative Ophthalmology and Visual Science* 43: 2412–2420.
Lewis, G. P., Sethi, C. S., Carter, K. M., Charteris, D. G., and Fisher, S. K. (2005). Microglial cell activation following retinal detachment: A comparison between species. *Molecular Vision* 11: 491–500.
Ryan, S. (ed.) (2006). *Retina,* 4th edn., vol. I–III. Philadelphia, PA: Mosby.
Sarthy, V. and Ripps, H. (2001). *The Retinal Müller Cell. Structure and Function.* New York: Kluwer/Plenum.
Zacks, D. N., Hanninen, V., Pantcheva, M., et al. (2003). Caspase activation in an experimental model of retinal detachment. *Investigative Ophthalmology and Visual Science* 44: 1262–1267.

Relevant Websites

http://biology.about.com – About.com: Biology. The starting place for exploring biology.
http://www.sciencedirect.com – Current Opinion in Neurobiology.
http://webvision.med.utah.edu – Introduction.
http://www.nei.nih.gov – National Eye Institute, Retinal Detachment.
http://www.sfn.org – SfN Brain Briefings.

Injury and Repair: Light Damage

N A Mandal, R E Anderson, and J D Ash, University of Oklahoma Health Sciences Center, Oklahoma City, OK, USA

Glossary

Acute light damage – Single exposure of intense light (1000–13 000 lux) for a brief period (20 min–24 h), which causes photoreceptor cell death, mainly in the central retina.

Apoptosis – A form of programmed cell death in multicellular organisms, which involves a series of biochemical events leading to a characteristic cell morphology and death. Death and the disposal of cellular debris do not damage the neighboring cells. Light-induced photoreceptor cell death occurs by apoptosis.

Chronic light damage – Exposure to sublethal doses of light (200–800 lux) in a cyclic manner (day–night) for a longer period of time (7–12 weeks). This causes overall thinning of the photoreceptor layer in the entire retina.

Inflammation – The complex biological response of vascular tissues to harmful stimuli such as pathogens, damaged cells, or irritants. It is a protective response by the organism to remove the injurious stimuli as well as initiate the healing process for the tissue.

Photoisomerization – The event in which a light-sensitive molecule absorbs a photon of light energy and undergoes a chemical change. In the current context, the 11-*cis*-retinal chromophore of rhodopsin is isomerized to all-*trans*-retinal, leading to activation of rhodopsin (R*) and initiation of the visual process.

Photostasis – Retinal adaptive response to different levels of cyclic illuminances. In bright cyclic light, rod outer segment (ROS) length is shortened, concentration of rhodopsin per unit of ROS is decreased, and ROS membranes become disorganized, compared to animals raised in dim cyclic light. This remarkable plasticity allows the retina of animals raised in dim and bright cyclic light to catch an equivalent number of photons each day.

Introduction

In 1966, Werner Noell discovered that the exposure of albino rats to bright visible light led to a rapid, specific, and irreversible loss of rod photoreceptor cells. Over the next four decades, this light-damage model has been used extensively to study mechanisms of retinal cell death and to test the efficacy of a variety of putative neuroprotective compounds. In his pioneering work, Noell discovered that photo-bleaching of rhodopsin was absolutely essential for light damage; rats raised on vitamin-A-deficient diets were not sensitive to light damage and the susceptibility to light damage followed the absorption spectrum of the visual pigment rhodopsin. Although the mechanism for initiation of the cell death signal in light damage is not known, recent studies have shown that while activation of rhodopsin is required, the visual transduction pathway downstream is not. Several outstanding reviews have been written on various aspects of light damage and therapeutic interventions. This article focuses on recent advances in identifying potential molecular mechanisms of cell injury and death, as well as the discovery of two independent mechanisms of endogenous self protection which are activated by light and stress in retinal photoreceptors.

There are several major advantages in using light damage to study retinal degeneration. Most inherited retinal degenerations occur over a long period of time with only a few photoreceptors dying each day. This makes it extremely difficult to biochemically study mechanisms of cell death or to study the effectiveness of therapeutic interventions. Light damage, on the other hand, has the advantage to more or less induce cell death in whole populations of photoreceptors at once. In addition, light damage can be tuned in terms of severity by varying the intensity of the light and duration of exposure. Hence, the intensity and duration required to cause a certain level of damage are correlated and a longer exposure can substitute for a higher intensity.

Over the years, two models of light damage have emerged: acute (short bright exposure) and chronic (less bright cyclic exposure). Both lead to retinal degeneration, but have quite different phenotypes. In the acute model, animals placed in light intensities ranging from 1000 to 13 000 lux in a time frame of 20 min to 24 h undergo a rapid and specific loss of rod photoreceptors. An example of acute light damage in a Sprague Dawley (SD) rat is shown in **Figure 1**. There is a clear demarcation of photoreceptor cell death, with normal-appearing retina (yellow arrow) adjacent to an area of moderate-to-massive cell death (white arrows). It is interesting that the subretinal space underlying the normal retina (yellow arrow) has been infiltrated with immune cells, suggesting that an inflammatory process is occurring prior to photoreceptor cell death. The role of inflammation in light damage is

discussed subsequently in this article. A so-called spider graph of the thickness of the outer nuclear layer (ONL, rod nuclei) measured at defined distances from the optic nerve head to the inferior and superior ora serrata along the vertical meridian clearly demonstrates the specific loss of photoreceptor cells in the central superior region of the retina (Figure 2). The chronic light damage model involves raising albino rodents in sublethal levels of cyclic light (200–800 lux, depending upon the strain). Retinas of SD rats raised from birth to 7 weeks of age in 700-lux cyclic light show remarkably normal retinal morphology except for a thinning of the ONL (Figure 3). The loss of photoreceptor cells is quite different from that which occurs in acute light damage, showing no regional differences (Figure 4). An interesting feature of the chronic light damage model is that, although the retina slowly loses photoreceptors, it is protected against the massive loss that occurs when these animals are placed in acute bright light. This point is discussed in detail later on in this article. These two models thus provide a means of testing putative neuroprotective compounds in two experimental paradigms. They are also useful to identify the molecular mechanisms that are responsible for light-induced damage, although the initial sequence of events leading to apoptosis may differ significantly from one protocol to another.

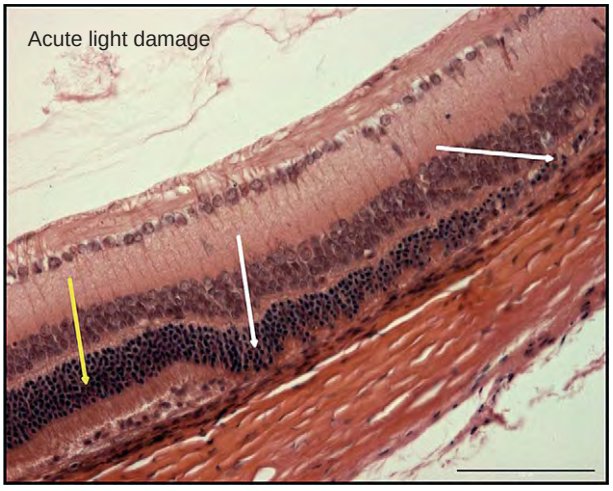

Figure 1 Sprague-Dawley rats were born and raised in 5 lux cyclic light. At 6–7 weeks of age, they were exposed to 2700-lux light for 6 h, after which they were returned to their cyclic light environment for 7 days. The white arrows point to areas of moderate to severe degeneration adjacent to an area of normal retina (yellow arrow).

Role of Rhodopsin Activation in Light Damage

While the precise mechanisms for cell damage are not fully understood, several genes have been identified that regulate photoreceptor sensitivity to light damage. When first identified, the action spectrum of light damage overlapped with the absorption spectrum of rhodopsin, suggesting a role for photoisomerization and phototransduction in cell injury. Indeed, a single, strong rhodopsin bleaching event is sufficient to induce light damage. The role of photoisomerization of 11-*cis*-retinal and rhodopsin activation as a requirement for light damage has been demonstrated pharmacologically and genetically. Pharmacological inhibition of rhodopsin regeneration with either the anesthetic halothane or by retinoic acid analogs, isotretinoin or 13-*cis*-retinoic acid, renders retinal photoreceptors less susceptible to light damage. Therefore, the severity of damage depends on the regeneration of rhodopsin during light exposure.

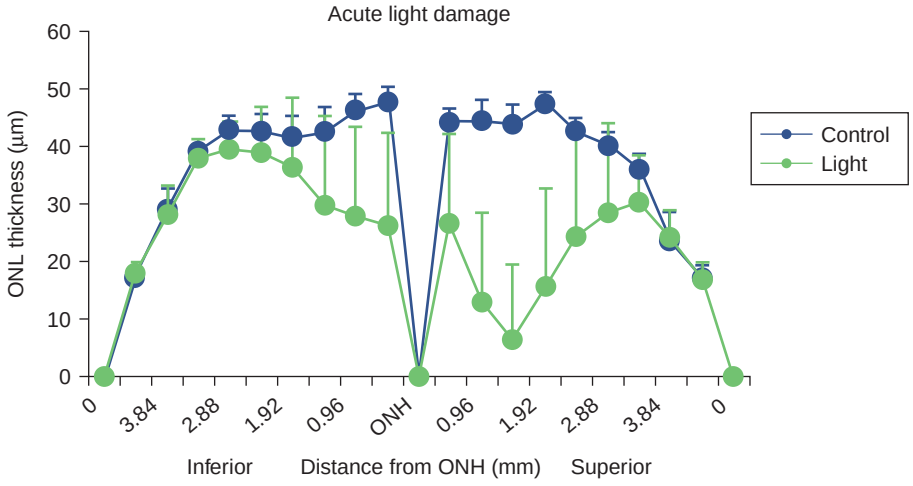

Figure 2 Sprague-Dawley rats were born and raised in 5-lux cyclic light. At 7 weeks of age, they were exposed to 2700-lux light for 6 h, after which they were returned to their cyclic light environment for 7 days. Plotted is the thickness of the outer nuclear layer (ONL) against distance from the optic nerve head (ONH) along the vertical meridian.

This sensitivity may be affected by polymorphisms or disease-causing mutations in opsin. The P23H opsin mutation is known to cause retinitis pigmentosa (RP) in humans. Work by Muna Naash and Daniel Organisciak, using transgenic mice or rats expressing human rod opsin with the P23H mutation, has shown that photoreceptors from these animals degenerate faster in bright cyclic light. Several recent studies have shown that mice with mutations in opsin, and phototransduction termination proteins arrestin and rhodopsin kinase are more sensitive to light damage. These results suggest that a prolonged R* or activated rhodopsin state is responsible for sensitivity to light damage. In more recent years, the Zurich group of Charlotte Reme, Andreas Wenzel, and Christian Grimm confirmed the necessity for rhodopsin photobleaching by demonstrating that mice lacking the RPE65 gene, which encodes a protein necessary for photoisomerization of all-*trans*-retinyl esters, were protected from light-induced cell death. The same group has also shown that a slow rate of rhodopsin regeneration due to an L450M variation in the RPE65 protein also renders mice less susceptible to light damage. However, while activation of rhodopsin is required for acute light damage, activation of phototransduction through guanine nucleotide-binding protein α_t ($G\alpha_t$ or transducin) is not. This was demonstrated in an elegant study by Wenshan Hao using combinations of rhodopsin kinase, arrestin, and transducin knockout mice. The study clearly suggests that a transducin-independent but, rhodopsin-dependent, signaling is required for acute light damage.

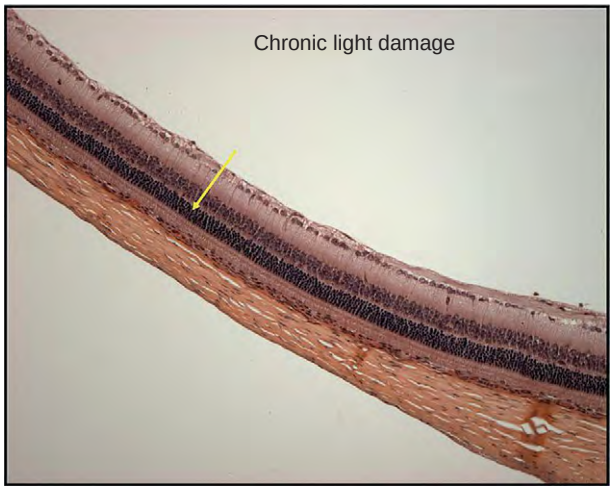

Figure 3 Sprague-Dawley rats were born and raised under 700-lux cyclic light until they were 7 weeks old. The retinas appear normal except for the thinning of the outer nuclear layer (ONL; yellow arrow). ONH, optic nerve head.

Mechanisms of Photic Injury: From Gene Expression to the Molecular Pathway

Gene expression analyses by DNA microarray studies have uncovered several possible molecular mechanisms of cell death in light damage. Our primary focus has been acute light damage (2700–3000 lux for 6 h) in albino mice or rats. This exposure paradigm induces oxidative stress that is sufficient to cause loss (>80%) of the photoreceptor cells in the central retina with no recoverable electroretinogram (ERG). However, cell death does not occur immediately following light exposure. It should be noted that by isolating RNA immediately after light exposure one can assess the stress response of photoreceptors before the onset of cell loss and detectable apoptotic cells in the retina. Therefore, by determining this early response one can decipher the molecular pathways that might regulate light-induced cell death. Retinas harvested

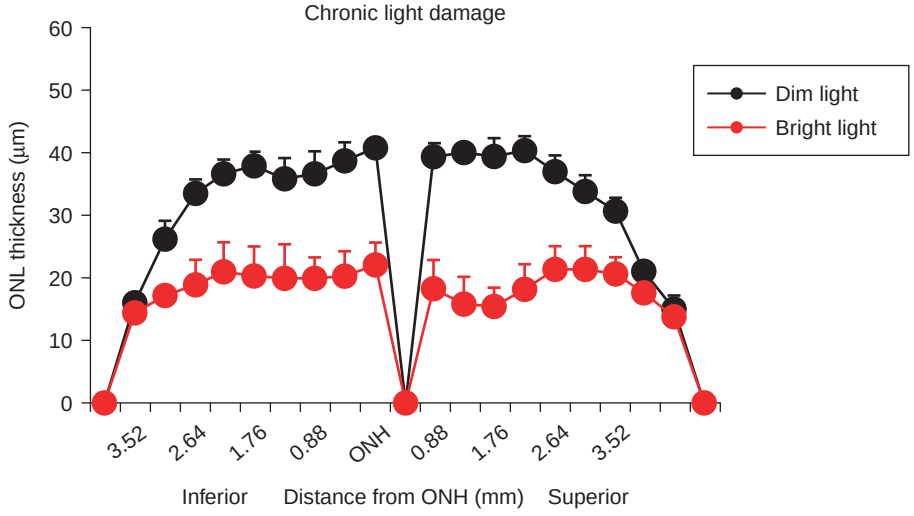

Figure 4 Sprague-Dawley rats were born and raised under 5 lux or 700 lux cyclic light until they were 7 weeks old. Plotted is the thickness of the outer nuclear layer (ONL) against distance from the optic nerve head along the vertical meridian.

immediately after the light exposure were used to generate complementary DNA (cDNA) to expressed messenger RNA (mRNA). The expression of the genes is studied by high-throughput DNA microarray analysis followed by quantitative (real-time) RT-PCR methods (RT-PCR, reverse transcriptase-polymerase chain reaction).

Apoptosis Genes

It has been well documented that apoptosis is the mechanism of photoreceptor cell death in light damage. Light damage induces expression of members of the activator protein 1 (AP-1) transcription factor family: *c-fos*, *FosL1* (*fra-1*), *junB*, and *c-Jun*. The dimeric AP-1 transcription factor is formed by either *c-fos* or *fra-1* binding to Jun proteins. The bright-light-induced apoptosis in retina is dependent upon activation of *c-fos*, and this *c-fos* upregulation plays a critical proapoptotic role, as evidenced from *c-fos* knockout mice, which showed marked resistance to light damage. Further, activation of the glucocorticoid receptor, which inhibits AP-1, also protects against light damage.

There are indications of involvement of other apoptosis genes in light damage. We have observed marked upregulation in the expression of tumor necrosis factor (TNF) receptor superfamily, member 1A (*Tnfrsf1a*), growth arrest and DNA-damage-inducible, beta (*Gadd45b*), and pleckstrin homology-like domain, family A, member 1 (*Phlda1*) genes. The protein encoded by *Tnfrsf1a* is one of the major receptors for the TNF-alpha (TNFα). This receptor can activate nuclear factor kappa-light-chain-enhancer of activated B cells (NFκB), mediate apoptosis, and function as a regulator of inflammation. In addition, the anti-apoptotic protein BCL2-associated athanogene 4 (BAG4/SODD) and adaptor proteins TRADD and TRAF2 have been shown to interact with this receptor. GADD45b can respond to environmental stresses by mediating activation of the p38/JNK pathway, which is involved in the regulation of growth and apoptosis. *Phlda1* encodes an evolutionarily conserved proline–histidine-rich nuclear protein, which may play an important role in the anti-apoptotic effects of insulin-like growth factor-1. In summary, we observed a significant upregulation of many proapoptotic genes, which are mainly involved in the AP-1-mediated apoptotic pathway and did not detect any changes in the caspase-related genes in the initial phase of degeneration.

Role of Oxidant Stress in Light Damage

Oxidant stress has long been implicated in the pathogenesis of light damage. Intense light involves the generation of oxidants in the photoreceptors and the accumulation of oxidatively modified lipids, nucleic acids, and proteins. Oxidant stress is further supported by several reports describing protection from light damage induced by a variety of antioxidants, including ascorbate, dimethylthiourea, thioredoxin, and NG-nitro-L-arginine-methyl ester (L-NAME). We observed that pretreatment with the free radical trap phenyl-*N*-*tert*-butylnitrone (PBN) completely abrogates light-induced degeneration of the retina. The PBN protection not only involves the stabilization of the free radicals, but also suppresses the expression of many proinflammatory and apoptotic genes. Gene expression analysis has shown that light damage upregulates the expression of antioxidant genes heme oxygenase 1 (*Ho-1*), superoxide dismutase (*Sod*), thioredoxin, glutathione peroxidase, ceruloplasmin (*Cp*), and metallothioneins (*Mt*)-1 and-2. Mice expressing mutant SOD1 are highly susceptible to light damage and have accelerated age-dependent degeneration of the retina. CP is a ferroxidase that functions as an antioxidant by oxidizing iron from its ferrous to ferric form. Iron-derived hydroxyl radicals produced by the Fenton reaction may be important mediators of retinal photic injury as systemic administration of the iron chelating reagent desferrioxamine attenuates light-induced damage in rat retinas. Metallothioneins (MTs), another group of antioxidants, are copper- and zinc-binding proteins which can quench superoxide and hydroxyl radicals. Expression of oxidant defense genes further supports the hypothesis that light-induced retinal degeneration involves oxidative stress.

Role of Inflammation in Light Damage

We have noticed recurrent appearance of a host of inflammatory genes in the group of upregulated genes in many light-damage studies. In fact, invading immune cells are often observed in the retina near dying photoreceptors. These can be seen under the relatively normal photoreceptors (yellow arrow, **Figure 1**) adjacent to the injured photoreceptors (white arrows, **Figure 1**). While the connection between inflammation and light damage is not well known, two recent studies have suggested there is a strong link. Work from Barbel Rohrer has shown that genes related to complement activation are upregulated in response to light stress and that elimination of complement factor D reduces susceptibility to light damage. Work from Ying-qin Ni has shown that light stress leads to the upregulation of interlukin 1β (IL-β) and activation of resident microglia. Significantly, the study found that inhibiting microglia activation with naloxone protected photoreceptors from subsequent light damage. These studies suggest that an inflammatory response plays an active role in promoting photoreceptor death in light damage. Inflammation is also becoming recognized as a key factor in many retinopathies, including the epidemic forms of diabetic retinopathies and age-related macular degeneration (AMD). Therefore, a thorough investigation into the inflammatory process in the retina is essential for an understanding of the mechanism of light damage as well as other forms of retinal degeneration.

Light damage rodent models are slowly being recognized as models for retinal inflammation and are suitable models for human AMD. Here we summarize our observation of inflammatory gene expression changes. Photic injury upregulates the expression of many chemokine genes, Ccls (*Ccl2*, *Ccl3*, *Ccl4*, and *Ccl7*) and Cxcls (*Cxcl1*, *Cxcl11*, *Cxcl10*, and *Cxcl9*). Chemokines are a group of small (8–14 kDa), mostly basic, structurally related molecules that regulate cell trafficking of various types of leukocytes through interactions with a subset of guanine nucleotide-binding protein (G-protein-coupled) receptors. These molecules are divided into two major subfamilies, CXC and CC, based on the arrangement of the first two of four conserved cysteine residues; the two cysteines are separated by a single amino acid in CXC chemokines and are adjacent in CC chemokines. Chemokines also play fundamental roles in the development, homeostasis, and function of the immune system, and they have effects on cells of the central nervous system as well as on endothelial cells involved in angiogenesis or angiostasis. *Ccl2* or monocyte chemoattractant protein-1 (*Mcp-1*) upregulation is very robust and very early in the process of acute light damage. They may signal injury and recruit choroidal macrophages to scavenge retinal debris. Homozygous deletion of Ccl2 resulted in a mouse phenotype reported to be similar to human AMD. CCL3, also known as macrophage inflammatory protein-1, or monokine, is involved in the acute inflammatory state in the recruitment and activation of polymorphonuclear leukocytes. CCL4, a cytokine that is upregulated during the inflammatory response, is involved in the recruitment of neutrophils. CCL7 or monocyte chemotactic protein 3, a secreted chemokine, attracts macrophages during inflammation and metastasis. In addition, CXCL10 binds to its receptor CXCR3 and results in pleiotropic effects, including stimulation of monocytes, migration of natural killer and T-cells, and modulation of adhesion molecule expression. Upregulation of CXCL11 indicates probable activation of interferon gamma, which is a potent inducer of CXCL11 transcription.

Besides chemokines, we found significant upregulation of genes, which are either members of classic inflammatory proteins or involved in regulation of cellular inflammation. Expression of intercellular adhesion molecule 1 (*Icam1*), CCAAT/enhancer-binding protein (*Cebpb*/C/EBP, beta), cytokine-cardiotrophin-like cytokine factor 1 (*Clcf1*), lipopolysaccharide-induced TNF factor (*Litaf*), cyclooxygenase 2 (*Cox2*), ring finger protein 125 (*Rnf125*), and *Cd44* genes were significantly upregulated in acute light stress. The protein encoded by the *Cebpb* gene is a basic-leucine zipper (bZIP) transcription factor, which can bind as a homodimer to certain DNA regulatory regions of genes involved in immune and inflammatory responses and has been shown to bind to the IL-1 response element in the IL-6 gene, as well as to regulatory regions of several acute-phase and cytokine genes. The CLCF1 protein belongs to the IL-6 family of cytokines, which are involved in cell signaling through phosphorylation of gp130. Lipopolysaccharide is a potent stimulator of monocytes and macrophages, causing secretion of TNFα and other inflammatory mediators. COX2 is the key enzyme in prostaglandin biosynthesis and acts both as a dioxygenase and as a peroxidase and is involved in inflammation and mitogenesis. The *Rfn125* gene encodes a novel E3 ubiquitin ligase that contains an N-terminal RING finger domain, which may function as a positive regulator in the T-cell receptor signaling pathway. This is a small list of the inflammatory genes (~30% of all the upregulated genes) that are induced in acute light damage and clearly indicates a role in the pathogenesis of light damage.

Tissue Remodeling

Inflammatory signaling events are usually followed by tissue remodeling for the invasion of the macrophages and other cells, which then leads to the process of advanced cell death and removal of debris. We observed significant upregulation of matrix metallopeptidase 3 (*Mmp3*), tissue inhibitor of metallopeptidase 1 (*Timp1*), growth differentiation factor 15 (*Gdf15*), and plasminogen activator, tissue (*Plat*) genes. MMP3 is an endopeptidase that degrades extracellular matrix proteins and TIMP1 acts as an inhibitor of metalloprotease activity; PLAT is an enzyme that also plays a role in cell migration and tissue remodeling.

Transcription Factors

Many of the genes described under apoptosis, oxidative stress, and inflammation are transcription factors. However, there are other transcription factors upregulated in retinal light damage, which are involved in neuronal injury and various processes in cell death and survival. These include early growth response 1 (*Egr1*), zinc finger protein 36 (*Zif36*), activating transcription factor 3 (*Atf3*), and stress-signal transducer and activator of transcription 3 (*Stat3*).

Identification of Two Nonredundant Mechanisms of Endogenous Protection of Photoreceptors

Several recent studies have been designed to reveal pathways that protect photoreceptors from light damage. These studies have identified two independent protective pathways. One pathway is rapidly activated by phosphorylation

following light stimulation, while the second pathway requires induction of new gene expression in response to chronic light stress.

Rhodopsin-Activated Endogenous Protection

Work from Raju Rajala has demonstrated that rhodopsin activation by light results in ligand-independent activation of the insulin receptor, which leads to activation of downstream signaling including increased PI3K and Akt kinase activity in photoreceptors. This activation was subsequently shown to be transducin independent. Genetic inactivation of the insulin receptor, insulin receptor substrate 2 (IRS2), AKT2, or BCL-XL have all led to increased photoreceptor susceptibility to acute light damage. These studies suggest that rhodopsin signaling, independent of transducin, is responsible for the activation of a defense mechanism through the insulin receptor and AKT2. Insulin receptor regulation of AKT2 is an ideal protective pathway for acute changes in light intensity since the entire pathway can be activated quickly through a series of phosphorylation events and does not require new gene expression. However, the AKT2 defense mechanism is overwhelmed as the duration of light exposure or intensity of light begins to induce cell death. It seems that the retina requires a secondary system of protection from chronic stresses such as prolonged bright light exposure and inherited genetic mutations.

Identification of Mechanisms for Chronic Light Stress-Induced Endogenous Protection

Noell's observation that animals raised in bright cyclic light were less susceptible to a subsequent light challenge than those raised in dim cyclic light or darkness inspired the discovery by John Penn and Ted Williams in the 1980s that albino rats born and raised in bright (but sublethal) cyclic light were protected from acute light damage. They discovered an enormous plasticity of the retina. Animals raised in dim cyclic light enhanced their chances of photon capture by lengthening their outer segments and increasing the packing density of rhodopsin in rod outer segment disk membranes. On the other hand, animals raised in relatively bright cyclic light reduced the length of outer segments, which also became somewhat disorganized, and decreased the packing density of rhodopsin in the disk membrane. The net result was to reduce the efficiency of photon capture by rhodopsin. Penn and Williams coined the term photostasis to describe the phenomenon of biochemical and morphological adaptation of the retina to modify efficiency of photon capture in animals exposed to different levels of cyclic light. It was suggested that these changes allowed photoreceptors to capture an equivalent number of photons each day regardless of their light environment. The morphological changes associated with bright cyclic rearing were also accompanied by biochemical changes described by Penn and Anderson that included increased activity of glutathione enzymes (peroxidase, S-transferase, and reductase), elevation of retinal vitamins E and C, and decreased levels of polyunsaturated fatty acids (substrates for lipid peroxidation). These studies suggest that in response to chronic light stress, photoreceptors undergo photostasis to reduce activation of rhodopsin and induce an antioxidant defense. Similar findings have been shown in both mice and rats. Importantly, these stress-induced molecular and morphological adaptations were shown to protect photoreceptors almost completely from acute light damage.

The mechanism by which retinas of rodents raised in bright cyclic light are protected from acute light damage is an important area of research and significant progress has been made toward identifying the factors and receptors that are required, as well as identifying their relevant signal transduction pathways. Since the insulin receptor/PI3K/Akt2 pathway is involved in providing protection from acute light damage, this pathway was considered a likely candidate for chronic light stress-induced protection. However, recent findings suggest that chronic light stress-induced protection is independent of this pathway. Unlike the insulin receptor and AKT2-dependent protection, induced protection requires several days of preconditioning, suggesting that new gene expression is required. This indirectly suggests a different mechanism. In support of this, we have shown that induced protection is independent of AKT phosphorylation, and we have shown that *Akt2* knock-out mice have induced protection that is identical to wild-type mice. The insulin receptor and AKT2 appear to function as a rapid response to an acute injury, but is not necessary or perhaps is unable to protect from chronic injury. These studies demonstrate that there are two mechanisms of endogenous protection, one for acute injury that utilizes the insulin receptor and AKT2, and one for induced protection from chronic injury.

Role of Leukemia Inhibitory Factor

Several groups, including Steinberg, LaVail, Wen, and Stone, have shown that light preconditioning in rats induces the expression of several factors including basic fibroblast growth factor (FGF) (FGF2) and ciliary neurotrophic factor (CNTF). More recently in mice, the Grimm and Ash laboratories have shown that preconditioning induces the expression of leukemia inhibitory factor (LIF), cardiotrophin-like ligand (CLC), onchostatin M (OSM), FGF2, endothelin 2 (End2), and brain-derived neurotrophic factor (BDNF). While many factors are upregulated, it was not known which were responsible for induced protection. Early work from Steinberg and LaVail demonstrated that the intravitreal injection of FGF2, CNTF, LIF, or BDNF resulted in substantial

protection of rat photoreceptors from a subsequent acute light damage independent of preconditioning. Additional work from Wen and Ash has similarly found that injection of LIF, CNTF, or BDNF protects mouse photoreceptors from a subsequent acute light damage. Of these, LIF and CNTF have tremendous therapeutic potential, given their ability to protect photoreceptors not only from acute light damage but also from inherited retinal degenerations.

Studies using intravitreal injections have demonstrated that multiple factors can induce protection, but did not demonstrate which factors were required for chronic light stress-induced protection. We have recently shown that LIF, CNTF, or CLC are the most likely candidates. This was demonstrated using an antagonist (LIF05) to the LIF receptor (LIFR), which blocks the activity of LIF, CNTF, and CLC. Intravitreal injection of LIF05 during light stress preconditioning greatly diminishes stress-induced protection from acute light damage. We also used conditional knock-out mice for the gp130 receptor and found that mice lacking gp130 expression in retinal photoreceptors also lose chronic light stress-induced protection. These recent studies demonstrate that the LIFR and gp130 expression in photoreceptors is essential for stress-induced protection and that the likely ligands are LIF, CLC, or CNTF, since these upregulated cytokines all utilize the LIFR and gp130. Our studies suggest that LIF may be the more important ligand since its expression is induced more than 100-fold following chronic light stress-induced preconditioning.

As described above, stress-induced protection was accompanied by upregulation of oxidant defense enzymes as well as photostasis. More recently, we have injected different doses of LIF into the vitreous of mice to determine whether LIF could induce both events. We found that at lower doses, LIF could induce protection from light damage without reducing photoreceptor sensitivity to light flashes. At higher concentrations, LIF not only induced protection, but also induced photostasis through decreased mRNA and protein expression of opsin, transducin (α and β subunits), and cyclic guanosine monophosphate (GMP) phosphodiesterase (PDE6A and PDE6B). Because of decreased expression of genes required for phototransduction, photoreceptors exhibited reduced efficiency in photon capture. These results demonstrate that LIF is upregulated by chronic bright-light stress and its induced expression is necessary for protection. LIF also has the ability to upregulate both photostasis and oxidant defense mechanisms. These studies clearly establish that in mice, LIF receptor, gp130, and perhaps LIF are essential players in chronic light stress-induced endogenous protection from acute light damage.

Many questions remain to be answered. In particular: Is LIF the essential factor? Which cells induce expression of LIF? Which signal transduction pathways are required for protection? What changes in gene expression are required for protection? In a series of studies, we have shown that intravitreal injection of LIF results in activation of ERK1/2 and STAT3. The pattern of activation changes over time. Within the first 30 min of injection, both phosphorylated ERK1/2 and STAT3 were detected only in Müller's cells and some ganglion cells. Within 4 h, however, all retinal cells were positive for STAT3, while ERK1/2 activation returned to basal levels. Detectable phosphorylated STAT3 remained up to 6 days following a single injection of LIF. Since phosphorylated STAT3 is a transcription factor, these results suggested that LIF could induce gene expression changes in all retinal cells including Müller's cells and photoreceptors.

Concluding Remarks

Light-damage models have led to major advances in our molecular understanding of retinal degeneration through oxidative injury mechanisms and, in the future, light-damage studies will be used to advance our understanding of injury induced by inflammation. Light-damage models have also led to the discovery of two independent mechanisms of endogenous neuroprotection, as well as to the discovery of promising new therapies to prevent or delay inherited retinal degenerations. Indeed, phase I clinical trials using encapsulated cells expressing CNTF have been completed with promising early results, and the study has since progressed into phase II trials. The protective effect of CNTF was initially described in the retina using the light-damage model. This alone should clearly establish the relevance for using light damage to identify potential therapeutic agents. By further defining the mechanisms of cell injury or protection, light-damage studies will likely lead to the development of new and more specific therapies.

See also: Injury and Repair: Retinal Remodeling; Injury and Repair Responses: Retinal Detachment; Phototransduction: Phototransduction in Rods; Phototransduction: Rhodopsin; Phototransduction: The Visual Cycle; Primary Photoreceptor Degenerations: Retinitis Pigmentosa; Primary Photoreceptor Degenerations: Terminology; Retinal Pigment Epithelium: Cytokine Modulation of Epithelial Physiology; Secondary Photoreceptor Degenerations: Age-Related Macular Degeneration.

Further Reading

Boulton, M., Rozanowska, M., and Rozanowski, B. (2001). Retinal photodamage. *Journal of Photochemistry and Photobiology* 64: 144–161.

Chen, L., Wu, W., Dentchev, T., et al. (2004). Light damage induced changes in mouse retinal gene expression. *Experimental Eye Research* 79: 239–247.

Marc, R. E., Jones, B. W., Watt, C. B., et al. (2008). Extreme retinal remodeling triggered by light damage: Implications for age related macular degeneration. *Molecular Vision* 14: 782–806.

Noell, W. K., Organisciak, D. T., Ando, H., Braniecki, M. A., and Durlin, C. (1987). Ascorbate and dietary protective mechanisms in retinal light damage of rats: Electrophysiological, histological and DNA measurements. *Progress in Clinical and Biological Research* 247: 469–483.

Penn, J. S. and Anderson, R. E. (1992). Effects of light history on the rat retina. In: Osborne, N. and Chader, G. (eds.) *Progress in Retinal Research,* vol. 11, pp. 75–98. New York: Pergamon Press.

Penn, J. S. and Thum, L. A. (1987). A comparison of the retinal effects of light damage and high illuminance light history. *Progress in Clinical and Biological Research* 247: 425–438.

Ranchon, I., Chen, S., Alvarez, K., and Anderson, R. E. (2001). Systemic administration of phenyl-*N*-tert-butylnitrone protects the retina from light damage. *Investigative Ophthalmology and Visual Science* 42: 1375–1379.

Reme, C. E., Grimm, C., Hafezi, F., Marti, A., and Wenzel, A. (1998). Apoptotic cell death in retinal degenerations. *Progress in Retinal and Eye Research* 17: 443–464.

Tanito, M., Agbaga, M. P., and Anderson, R. E. (2007). Upregulation of thioredoxin system via Nrf2-antioxidant responsive element pathway in adaptive-retinal neuroprotection *in vivo* and *in vitro*. *Free Radical Biology and Medicine* 42: 1838–1850.

Tanito, M., Kaidzu, S., Ohira, A., and Anderson, R. E. (2008). Topography of retinal damage in light-exposed albino rats. *Experimental Eye Research* 87: 292–295.

Wenzel, A., Grimm, C., Marti, A., et al. (2000). C-fos controls the ''private pathway'' of light-induced apoptosis of retinal photoreceptors. *Journal of Neuroscience* 20: 81–88.

Wenzel, A., Grimm, C., Samardzija, M., and Reme, C. E. (2005). Molecular mechanisms of light-induced photoreceptor apoptosis and neuroprotection for retinal degeneration. *Progress in Retinal and Eye Research* 24: 275–306.

Wu, J., Seregard, S., and Algvere, P. V. (2006). Photochemical damage of the retina. *Survey of Ophthalmology* 51: 461–481.

Injury and Repair: Neovascularization

M E Kleinman and J Ambati, University of Kentucky, Lexington, KY, USA

Glossary

Complement – A complex molecular cascade that directly removes pathogens and activates the host immune system.
Cytokines – The secreted proteins that mediate cellular communication through a specific set of cell-surface receptors.
Extracellular matrix – The extracellular material that supports cell structure and intercellular communication.
Laser-induced injury – A reproducible model of tissue injury with the application of a high-energy laser photocoagulation to the fundus.
Neovascularization – The formation of new blood vessels.
Vascular endothelial growth factor – A potent cytokine that is critical for the process of neovascularization.

Introduction

The retina is a highly organized multicellular system designed to efficiently convert light into electrical signals which can then be transmitted to the brain for cortical integration and, ultimately, visual perception. In an acute setting of retinal injury, the cellular components of the neural retina, retinal pigment epithelium (RPE), and choroid get activated in order to contain the wound, destroy any invading pathogens, and initiate the repair process. As a result of the subsequent proinflammatory surge, blood vessels invade the wound bed to revascularize injured and hypoxic tissue and provide a new source of nutrients to the remodeling tissues. Typically, as in several other peripheral tissues in the human body, such as skin, this vascular growth allows for tissue healing and scar remodeling; however, in the delicate architecture of the retina, these abnormal vessels grow in an unregulated fashion and are susceptible to leakage and rupture. These traits are hardly suitable for the retina's highly specialized function of vision and often lead to neovascularization (NV) as a cause of blindness in the context of retinal disease and injury. NV also contributes to other cellular responses in the injured retina, including gliosis and fibrosis. Through clinical observations and scientific investigation, critical insights into the biology of NV in injury and repair in the retina, RPE, and choroid have modernized our current understanding of the cellular and molecular pathways that drive this pathological process.

Mechanisms of Injury

Retinal, RPE, and choroidal injury may be caused by a plethora of mechanical, cellular, physiologic, photochemical, and iatrogenic processes that are addressed in detail in other sections. Each of these instigating factors, either individually or in concert with one another, is capable of setting off the intricate cascade of factors leading to subretinal NV. A list of some of the common causes of injury-induced NV is provided next.

1. *Mechanical trauma.* Blunt trauma to the eye disorganizes the retinal architecture to varying degrees with displacement of reactive glial cells and RPE to the vitreo-retinal interface. These cells can form a fibrotic scar at the surface of the internal-limiting membrane (ILM), in the case of epiretinal membrane, and even grow into the vitreous as in the case of proliferative vitreo-retinopathy. More ominous is the presence of a choroidal rupture, a finding that is very likely to induce neovascular invasion of the retina through fractures in Bruch's membrane. Over time, these lesions eventually involute but do leave behind a residual fibrotic scar that significantly decreases visual acuity in the area.
2. *Age-related macular degeneration.* One of the most common forms of retinal injury is due to a combination of inflammation, oxidative stress, and photochemical damage secondary to age-related macular degeneration (AMD), a disease which accounts for the epidemic loss of vision in people over 60 years of age in the developed world. Between 10% and 20% of people with AMD will progress to the neovascular or wet form, which is responsible for about 90% of vision loss in patients with AMD. Recent evidence suggests that the gradual accumulation of inflammatory debris in drusen beneath the RPE and within the choroid ultimately leads to the production of proangiogenic cytokines and retinal invasion by abnormal and leaky vasculature. Some of these inflammatory components are comprised of photochemically altered proteins that are linked to intermediate or terminal products of the vitamin-A cycle or lipid-breakdown products released

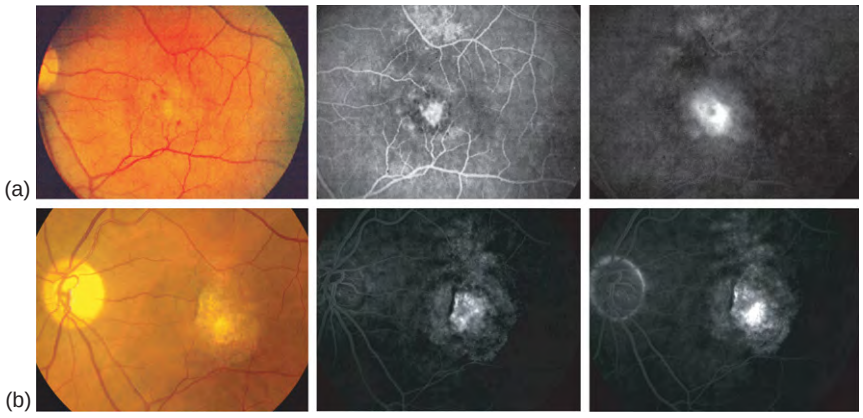

Figure 1 Retinal injury progression through inflammation, neovascularization, and fibrosis. (a) Left to right sequence of images representing CNV (far left, color fundus photography) after an inciting inflammatory event leading to leaky vasculature in the macula as evident on fluorescein angiography (middle, 45-s time point, far right, 10-min time point); (b) The same patient several years later showing subretinal fibrosis (far left) with fluorescein staining scar and RPE dropout (same sequence as above).

by dying photoreceptors and RPE. Neovascular AMD occurs either below the RPE in its occult form or invades the neural retinal in its classic form. Choroidal NV (CNV) can wreak havoc through leakage into the intraretinal or vitreous spaces which acutely decreases visual acuity (Figure 1). Overtime, these NV membranes remodel into fibrotic scars that may still harbor abnormal vasculature and become sites of active NV recurrence.

3. *Diabetic retinopathy.* Diabetic retinopathy (DR) remains the primary cause of vision loss in patients aged less than 65 years. Hyperglycemia induces multiple microvascular abnormalities in the retina, eventually leading to retinal NV.
4. *Vaso-occlusive disease.* The retina receives dual blood supply with the central retinal artery feeding the inner layers and the choroidal vasculature feeding the outer layers, including the highly metabolic photoreceptor segments. Numerous pathologic processes can choke the retinal circulation, including atherosclerosis, vasculitis, thrombosis, and emboli. Retinal venous outflow is through the central retinal vein which is also at risk for collapse, stasis, or thrombosis. Choroidal venous flow exits through the vortex veins where thrombus may also form, albeit in a less-dramatic presentation than the central retinal vein occlusion. Another vascular disease that can trigger massive retinal ischemic injury is giant-cell arteritis, an inflammatory disorder that can occlude the central retinal artery. Ischemic damage to the retina is irreversible approximately 90–100 min after initial insult and can result in a widespread neovascular response in the retina, iris, and angle. These sequelae are the leading causes of enucleation after such catastrophic vascular events in the eye.
5. *Choroidal disease.* Histoplasma capsulatum is a fungal organism endemic to the Ohio and Mississippi river valleys that infects the choroidal tissue and causes localized areas of subretinal NV, which eventually scar over with RPE and glial cells. The organism is rarely isolated; however, patients often show a positive skin-allergy test thus earning this condition the title of presumed ocular histoplasmosis (POHS). Choroidopathies are a group of rare disorders that affect the tissues around the RPE due to either immune dysregulation or infectious disease, most often associated with nematode invasion. Although it is difficult to discern among the different forms of choroidopathy, several of them may lead to the formation of CNV. Multifocal choroiditis (MFC), multiple evanescent white-dot syndrome (MEWDS), bird-shot choroidopathy, serpiginous choroidopathy, and diffuse unilateral subacute neuroretinitis (DUSN) have all been associated with NV, hypothesized to be secondary to inflammation or immune dysregulation.
6. *Cryogenic injury.* Cryotherapy is a widely used treatment modality in vitreoretinal surgery to seal peripheral retinal tears in order to prevent rhegmatogenous retinal detachments. It is also used in combination with scleral buckling to destroy large areas of ischemic retina in order to prevent further NV. In some instances, cryotherapy itself can lead to subretinal NV.
7. *Laser-induced injury.* The use of laser photocoagulation for targeted retinal injury in the treatment of extrafoveal NV and proliferative DR has been widely used with success for several decades. In the treatment of CNV, focal laser injury is able to inhibit growth and decrease leakage from abnormal microvasculature. With panretinal photocoagulation, laser is used to ablate large swaths of the peripheral retina in DR that would otherwise be ischemic, producing proangiogenic factors. It is through the destruction of this pathologic tissue, that NV is spared in the precious visual real estate in the macula. Laser-injured tissues will commonly

remodel into small areas of RPE hyperpigmentation with fibrosis and only go on to develop CNV when high-energy laser photocoagulation is able to break through Bruch's membrane. It is critical to note that laser-induced injury which fractures Bruch's membrane serves as a very well-described animal model of CNV in many different laboratory animals, which is addressed in the following section.

Animal Models of NV after Laser-Induced Injury

In order to study the natural history of injury-induced NV *in vivo,* several experimental models have been developed to mimic the disease process which occurs in humans. Over 25 years ago, Stephen Ryan described a laser-induced injury model of subretinal NV in rhesus monkeys. The same technology has since been used to develop similar models in a variety of research animals, including the mouse. In this model, laser photocoagulation is used to fracture Bruch's membrane, which results in the formation of CNV (**Figure 2**). The laser-induced model captures many of the important features of the human condition including: migration of choroidal endothelial cells into the subretinal space via defects in Bruch's membrane (**Figure 3**), accumulation of subretinal fluid, congregation of leukocytes adjacent to neovascular tufts, gliosis (**Figure 4**), leakage of fluorescein from immature new vessels into the subretinal space, and increased expression of angiogenic growth factors and their receptors in cells and ocular tissues. The cellular and molecular details of retinal injury and repair are discussed below.

Acute Responses to Retinal Injury

Blood–Retina Barrier Breakdown

In a normal uninjured retina, the blood–retina barrier (BRB), comprised of RPE and retinal endothelial cell tight junctions, serves to prevent the influx of circulating proinflammatory cells and proteins where their presence and actions would compromise vision; however, in animal models of high-energy laser injury, there is an immediate disruption in the neural retinal, RPE tight junctions, and Bruch's membrane, leading to BRB breakdown.

Acute Release of Cytokines

With laser injury, thousands of retinal and RPE cells suffer instantaneous thermal damage or death and disperse their intracellular contents into the interstitium. Many pro- and antiangiogenic cytokines which are harbored in cytoplasmic granules are immediately released

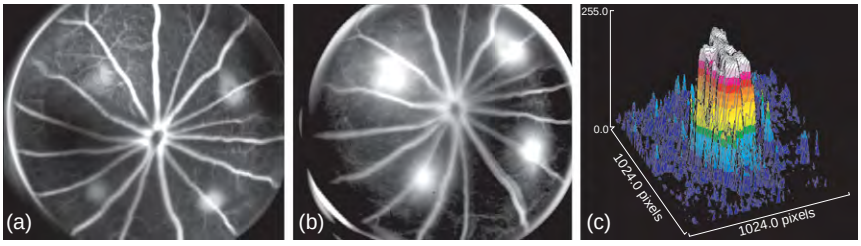

Figure 2 The mouse model of retina injury with laser photocoagulation. (a) An early time-point fundus fluorescein angiogram 7 days after laser injury of the retina, RPE, and Bruch's membrane showing hyperfluorescent hot spots. (b) Later time-point fluorescein angiogram of the same mouse eye exhibiting significant vascular leakage similar to the human form of CNV. (c) Vascular volumetrics and surface mapping reveal the size and shape of the CNV lesion in an important animal model that allows for scientific exploration into the molecular mediators of this process.

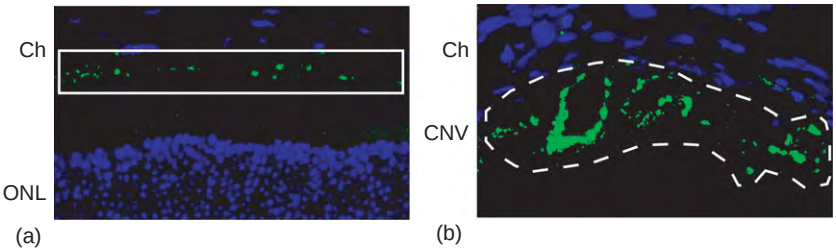

Figure 3 Choroidal vasculature before and after laser injury. (a) In the normal eye, the choroidal vasculature is organized into an extensive capillary network, the choriocapillaris, which exists in a single tissue plane below Bruch's membrane (white box encloses normal mouse choriocapillaris with vasculature appearing green). (b) After laser injury, the vasculature invades the retina where it grows into leaky neovascular membranes (dashed-line marks area of CNV formation 7 days after laser injury of the fundus).

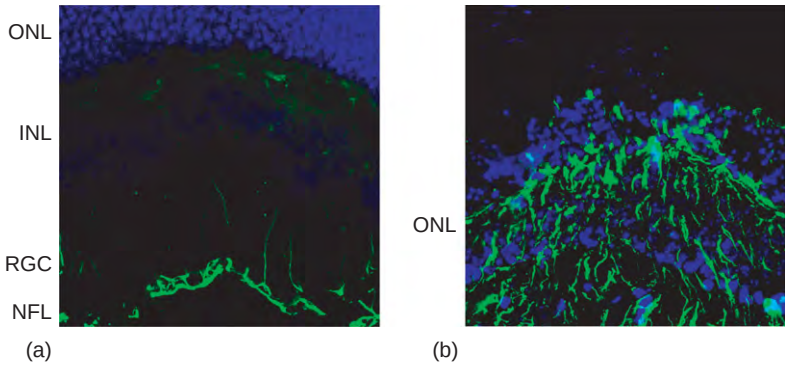

Figure 4 The participation of neural-retina derived cells to CNV pathogenesis. (a) Glial cells (retinal astrocytes shown here with glial-fibrillary acid protein (GFAP)) in green are located in well-demarcated areas of the un-injured neural retina. (b) Upon injury, glial cells migrate to areas of wound healing and proliferate along with endothelial cells while providing both structural and growth-factor support.

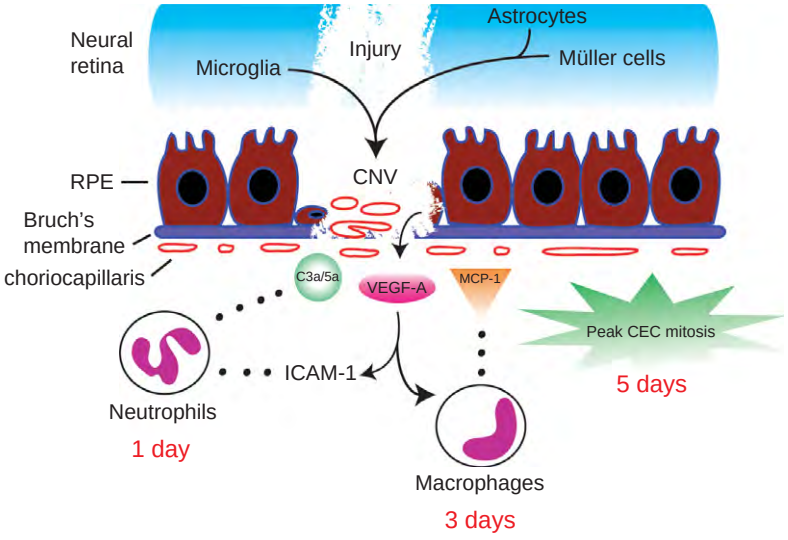

Figure 5 Critical mediators in CNV formation after acute and chronic injury. The initiating step of CNV is often an injury or disease process that induces local inflammation in the retina, RPE, and choroid. Locally produced leukocyte chemoattractants and provascular growth factors are secreted in the wound bed resulting in peak neutrophil infiltration at 1 day, maximal macrophage influx at 3 days, and a spike in choroidal endothelial cell proliferation at 5 days.

inducing the influx of circulating leukocytes into the retinal tissues (Figure 5). There is a paucity of evidence on which resident cells are the sources of these cytokines. RPE cells constitutively produce a wide array of cytokines that are usually secreted in a polarized fashion either toward choriocapillaris or the photoreceptor layer to maintain their relative functions. For example, pigment-epithelium-derived factor (PEDF), a potent antiangiogenic mediator, is secreted from the apical RPE surface toward the photoreceptor layer, while vascular endothelial growth factor-A (VEGF-A), a predominant proangiogenic cytokine, is secreted from the basal RPE toward the choriocapillaris. With injury, this directionality is lost allowing for the disinhibition of angiogenesis in normally avascular tissue planes.

VEGF-A belongs to the highly conserved platelet-derived growth factor (PDGF) family along with several other related proteins that constitute the VEGF subfamily, including placental growth factor (PlGF), VEGF-B, VEGF-C, and VEGF-D. For nomenclature purposes, the original VEGF protein was designated VEGF-A. Multiple isoforms of VEGF-A exist due to alternative splicing of the *Vegfa* gene; however, the 165-amino-acid variant in humans ($VEGF\text{-}A_{165}$) is the most potent and prevalent among the major isoforms expressed during pathologic NV. Many other important components within the VEGF family contribute to injury-related NV. Several genes important in VEGF regulation and activation, such as the coreceptors neuropilin-1 and-2 as well as PlGF, are

acutely upregulated in the setting of laser injury and in some forms of human subretinal NV.

An acute elevation of VEGF-A released from various resident cells types, including RPE, microglia, Müller cells, and retinal astrocytes, transiently induces vascular permeability and upregulates endothelial cell expression of intercellular adhesion molecule (ICAM)-1. In response, there is a marked leukocytosis of injured tissues within 24 h. Resident cells also spew monocyte-chemoattractant protein (MCP)-1 into the wound matrix which acts as a homing device for circulating monocytes expressing its cognate receptor (CCR2). Interleukin-1β (IL-1β), tumor necrosis factor-α (TNF-α), and interleukin-6 (IL-6), all potent cytokines that sequester a wide range of inflammatory cells and induce their proliferation, are increased within 24 h of injury. IL-6 is instrumental in promoting continued expression of VEGF-A, ICAM-1, and MCP-1, which regulate the specific sequence of leukocyte chemotaxis that occurs over the initial 72 h after injury.

Injury-Induced Complement Activation

Complement factors are also a major participant in the robust and rapid retinal tissue response to injury. The complement pathways are comprised of multiple, complex, domino-like cascades engineered to generate massive pro-inflammatory induction through cytokine expression and leukocyte invasion in addition to promoting the self-assembly of molecular components that are capable of directly lysing bacteria and virus-infected cells. The two main active byproducts of complement activation, C3a and C5a, are predominantly responsible for the anaphylactic response. After laser injury, C3a and C5a levels are selectively and swiftly increased in the RPE and choroid within 4 h after photocoagulation with peak concentrations at 12 h. With blockade of C3a and C5a, as in mice that are deficient in C3a or C5a receptors, VEGF-A production is downregulated which may also inhibit leukocyte trafficking. Functional blockade of complement activation may be a valuable preventative therapy to arrest NV progression in patients with retinal disease and injury.

Other Angiogenic Mediators in the Retinal Response to Injury

Several other molecular factors have been implicated in the development of injury-induced NV through descriptive expression analyses in human specimens, including transforming growth factor-beta 1(TGF-β1), PDGF, fibroblast growth factor-2 (FGF-2), insulin-like growth factor-1 (IGF-1), and estrogen. Hepatocyte growth factor (HGF) is produced by RPE, upregulated as early as 6 h after laser injury, and hypothesized to mediate RPE proliferation during tissue repair.

Endogenous antiangiogenic molecules have also been identified such as PEDF and thrombospondin-1 that are decreased in CNV lesions and are capable of regulating NV responses in animal studies. These factors provide yet another level of control in this increasingly complex system of vascular regulation.

Modulation of the Extracellular Matrix

The biologic activities of VEGF-A and other cytokines, which acutely increased after injury, are influenced by the myriad of interactions between cells and the extracellular matrix (ECM). ECM proteins transmit cell–ECM communication and modulate tissue-remodeling events including NV. CNV membranes contain an abundance of ECM proteins similar to those found in granulation tissue during epithelial wound healing. Fibrin, fibronectin, and integrin receptors, all of which are important in ECM-guided angiogenesis, are present in surgically excised CNV membranes. The pathogenesis of injury-induced NV requires invasion of pre-existing ECM and the formation of new vascular conduits (**Figure 6**). Matrix metalloproteinases (MMP-2 and 9), which are capable of ECM dissolution, are upregulated in the acute-phase response. Tissue inhibitors of MMPs (TIMPs), which prevent excessive degradation of ECM by MMPs, are also expressed in CNV membranes thus offering a novel therapeutic target. Another proteinase mechanism, known to be involved in CNV progression, is the urokinase plasminogen activator pathway which is also being evaluated as an alternative treatment modality for pathologic NV.

More recently characterized ECM proteins may also be involved in VEGF-A signaling and NV response after injury. The matricellular protein SPARC (secreted protein, acidic, and rich in cysteine) is involved in tissue remodeling, cellular migration, and angiogenesis through its interaction with VEGF-A. After injury, SPARC expression is acutely decreased thus allowing VEGF-A to activate VEGFR-2 inducing endothelial cell proliferation and migration. In a paradoxical molecular mechanism, intravitreous administration of VEGF-A is able to suppress CNV when delivered after laser injury, whereas VEGF-A treatment prior to laser injury expectedly augments pro-angiogenic tissue response. These data may help improve our understanding of VEGF-A duality in NV induction and enhance the timing of administration of our targeted therapeutics to suppress this unwanted growth.

Cellular Response in Injury-Induced NV

Similar to epithelial wound healing, retinal injury is succeeded by an orchestrated arrival of various inflammatory cell types, a process that is determined by the acute response to injury discussed above. From other

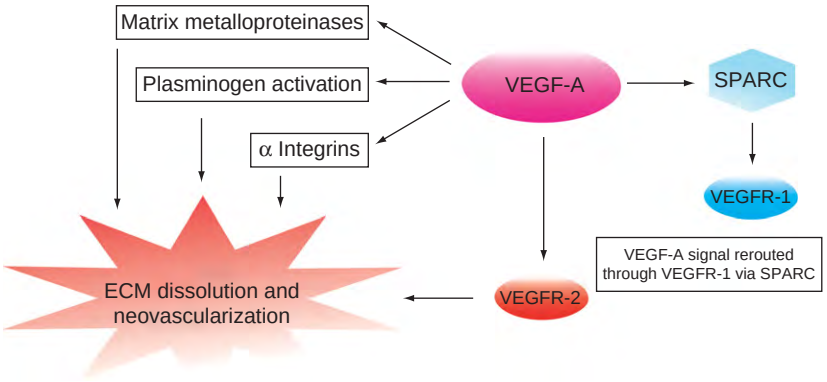

Figure 6 Modulation of the ECM with injury and VEGF-A upregulation. VEGF-A is a major factor in the pathogenesis of CNV through its direct effects on endothelial cell proliferation and modulation of the extracellular matrix. Integrins, plasminogen factors, and MMPs are all upregulated in response to VEGF-A contributing to ECM degradation that promotes neovascular invasion. VEGF-A is also able to curb the endothelial cell responses through its interaction with SPARC which reroutes signal transduction away from the proangiogenic pathways of VEGFR-2 to the nonproliferative cellular pathways of VEGFR-1.

wound-healing studies, it is known that inflammatory cell recruitment is directed by the expression of cytokines such as MCP-1, GROα (also known as CXCL1), and macrophage inflammatory protein-1α and-2 (MIP-1α, MIP-2). Many of these counterparts have been shown to be involved in NV progression in retinal injury.

Neutrophils

With breakdown of the BRB and acute VEGF-A-driven expression of ICAM-1 on the retinal and choroidal endothelia, there is an immediate and rampant neutrophil extravasation into the injured tissues which is maximal at 24 h. In addition to C5a, acute elevations in IL-1β and TNF-α may upregulate interleukin-8 (IL-8) which also acts as a potent neutrophil chemoattractant. These cells serve as a potent proinflammatory stimulus by secreting more VEGF-A along with numerous proangiogenic cytokines into the wound. Moreover, neutrophils are capable of engulfing invading pathogens and destroying them through the release of hypochlorous acid. Without neutrophil participation in wound healing, there is only a partial abrogation of the NV response to laser injury.

Macrophages

The next major influx of circulating proinflammatory leukocytes is the macrophage, which is driven by the enhanced expression of MCP-1 that peaks at 2 days after injury. These professional inflammatory cells home to sites of increased MCP-1 gradients through the expression of its cognate receptor, CCR2. This signaling axis is responsible for maximal macrophage infiltration into the choroid at 3 days post injury. Macrophages are able to respond to the proinflammatory milieu of vascular growth factors and secrete even more VEGF-A in order to aid revascularization and tissue repair. After the arrival of macrophages, endothelial cells continue to increase their mitotic activity with peak proliferation at 5 days post injury. Approximately 1 week after injury, organized subretinal NV membranes are formed, which can be visualized *in vivo* with fluorescein angiography. Without macrophage influx, the ability of laser-injured areas to fully develop CNV is completely eliminated signifying the critical importance of this infiltrating cell in injury-induced NV.

Progenitor/Stem Cells

Pluripotent stem/progenitor cells are also recruited to sites of NV during injury and repair and incorporate into pathologic vasculature. Animal studies have now demonstrated that interfering with stem/progenitor cell homing to the sites of CNV through the modulation of the hypoxia responsive cytokine stromal-derived factor (SDF)-1α and its receptor, CXCR4, inhibits neovascular growth, a finding that offers another potential treatment for the human condition.

Other Infiltrating Cell Types

Although mast cells and eosinophils are able to generate significant proinflammatory stimuli, their contribution to injury-induced NV in the retina is believed to be negligible. B- and T-lymphocytes as well as natural killer cells are also able to infiltrate retina injuries, yet their particular effects and contribution to NV are still unclear but likely to be negligible.

Resident Tissue Cells

Among the resident cells of the retinal, RPE, and choroidal tissues that are involved in injury-induced NV, the

effects of RPE cells, microglia, retinal astrocytes, and Müller cells are the most evident.

Microglia

Microglial cells are tissue macrophages dispersed throughout the normal retina, choroid, and central nervous system. Their primary functions are to respond to the local invasion of pathogens through activation of the innate immune system, promotion of inflammation, and phagocytosis of bacteria and virus-laden cells. Microglia express a unique set of surface markers, as well as the chemokine receptor CX3CR1 which binds to fractalkine (or CX3CL1), a cytokine that is secreted preferentially by inflamed retinal and endothelial cells. CX3CR1 is present on a number of differentiated cell types derived from myeloid progenitor cells, such as dendritic cells, infiltrating macrophages, neutrophils, and some endothelial cells, thus providing another signaling axis for the infiltration of professional inflammatory cells after laser injury.

As part of their immune-surveillance capabilities, microglia express a series of innate immune receptors, called toll-like receptors (TLRs), that recognize pathogen-associated molecular patterns and respond by alarming other immune system components, mediating cellular infiltration, and selectively inducing apoptosis to prevent infectious spread. Several TLRs, including TLR 2–9, all of which are expressed on microglia, are likely to be involved in modulating angiogenesis in the setting of injury, thus creating a significant link between the innate immune response and NV. This immunovascular phenomenon is an area of great interest at this time given the strong evidence that several neovascular-related diseases, including AMD, may be driven by immune-system activation.

VEGF-A, once thought to be a pure vascular mediator, has been discovered to impart significant cellular effects on neural cells including microglia. Similar to blood-derived macrophages, microglia express VEGF receptor-1 (VEGFR-1) enabling their migration toward areas of VEGF-A production. With injury, microglia switch from their quiescent state to become activated, demonstrated by increased cytokine secretion, immune receptor expression, and proliferation.

Retinal astrocytes

Activated microglia may also initiate the reparative process by inducing the chemotaxis and proliferation of retinal astrocytes through TGF-β1, IL-1β, and TNF-α. Unlike microglia, astrocytes may be far more robust in the promotion of immune-mediated inflammation and contribution to glial scarification after retinal injury.

Müller cells

Müller cells are specialized glia that provide structural and trophic support, among numerous other functions, in the retina. In the setting of injury, Müller cells are able to proliferate and dedifferentiate into progenitor-like cells thus providing a potential source for retinal regeneration. Whereas some vertebrates (avian, amphibian, and fish) have been found to demonstrate such reparative potential, there is still controversial evidence on whether Müller cells of the mammalian retina are capable of this phenomenon.

Cellular Responses to VEGF-A Receptor Binding

VEGF-A is a multifaceted cytokine that influences multiple endothelial cell pathways promoting growth, survival, and vascular permeability. Its signal transduction is mediated primarily through two receptor tyrosine kinases, VEGFR-1 and VEGFR-2; however, the latter is implicated as the principal proangiogenic transducer. Both VEGFR-1 and R-2 are expressed in normal human eyes and surgically excised CNV membranes. There is a continuing controversy on the role of VEGFR-1 as a decoy receptor designed to sequester free VEGF-A and prevent excessive VEGFR-2 activation. In multiple models of injury-induced NV, VEGFR-1 has been shown to function bilaterally as both a pro- and antivascular mediator. Importantly, it does not appear that VEGFR-1 does this by simply serving as a decoy, as VEGFR-1 can repress VEGFR-2 mediated endothelial cell proliferation through active signaling after retinal injury. Thus, VEGF-A may possess the ability to function dichotomously in both pro- and anti-angiogenic capacities.

Conclusion

NV in the context of injury and repair is designed to aid the healing process, but, in the fragile and transparent cellular layers of the retina, it wreaks havoc on neural function and visual acuity. Several decades of dedicated molecular science and centuries of clinical observations have yielded an exhaustive foundation of knowledge that has significantly improved our understanding of injury-induced blood vessel growth. These mechanisms are currently being elucidated with such resolution and speed that a detailed molecular map of this disease process may be within our reach in the near future. More importantly, the work has been a tremendous benefit to society, as several targeted therapeutics are now available to the millions of people around the world suffering from neovascular diseases. It is our hope that scientific investigation of the unique biologic responses to retinal injury will continue to reveal critical facets in vasomolecular medicine both in the eye and elsewhere that will aid in the design of advanced therapeutics.

See also: Avascularity of the Cornea; Breakdown of the Blood–Retinal Barrier; Breakdown of the Retinal Pigmented

Epithelium Blood–Retinal Barrier; Central Retinal Vein Occlusion; Immunobiology of Age-Related Macular Degeneration; Injury and Repair: Neovascularization; Injury and Repair: Retinal Remodeling; Injury and Repair Responses: Retinal Detachment; Molecular Mechanisms of Angiostasis; Pathological Retinal Angiogenesis; Primary Photoreceptor Degenerations: Terminology; Retinal Pigment Epithelium: Cytokine Modulation of Epithelial Physiology; Retinal Vasculopathies: Diabetic Retinopathy; Role of Complement in Ocular Immune Response; Secondary Photoreceptor Degenerations: Age-Related Macular Degeneration; Secondary Photoreceptor Degenerations.

Further Reading

Ambati, J., Ambati, B. K., Yoo, S. H., et al. (2003). Age-related macular degeneration: Etiology, pathogenesis, and therapeutic strategies. *Survey Ophthalmology* 48(3): 257–293.

Carmeliet, P. (2005). Angiogenesis in life, disease and medicine. *Nature* 438(7070): 932–936.

Eter, N., Engel, D. R., Meyer, L., et al. (2008). *In vivo* visualization of dendritic cells, macrophages, and microglial cells responding to laser-induced damage in the fundus of the eye. *Investigative Ophthalmology and Visual Science* 49(8): 3649–4358.

Fisher, S. K., Lewis, G. P., Linberg, K. A., et al. (2005). Cellular remodeling in mammalian retina: Results from studies of experimental retinal detachment. *Progress in Retinal and Eye Research* 24(3): 395–431.

Friedlander, M. (2007). Fibrosis and diseases of the eye. *Journal of Clinical Investigation* 117(3): 576–586.

Holtkamp, G. M., Kijlstra, A., Peek, R., et al. (2001). Retinal pigment epithelium–immune system interactions: Cytokine production and cytokine-induced changes. *Progress in Retinal and Eye Research* 20(1): 29–48.

Nozaki, M., Raisler, B. J., Sakurai, E., et al. (2006). Drusen complement components C3a and C5a promote choroidal neovascularization. *Proceedings of the National Academy of Sciences of the United States of America* 103(7): 2328–2333.

Nozaki, M., Sakurai, E., Raisler, B. J., et al. (2006). Loss of sparc-mediated Vegfr-1 suppression after injury reveals a novel antiangiogenic activity of Vegf-A. *Journal of Clinical Investigation* 116(2): 422–429.

Osborne, N. N., Casson, R. J., Wood, J. P., et al. (2004). Retinal ischemia: Mechanisms of damage and potential therapeutic strategies. *Progress in Retinal and Eye Research* 23(1): 91–147.

Pournaras, C. J., Rungger-Brandle, E., Riva, C. E., et al. (2008). Regulation of retinal blood flow in health and disease. *Progress in Retinal and Eye Research* 27(3): 284–330.

Rattner, A. and Nathans, J. (2005). The genomic response to retinal disease and injury: Evidence for endothelin signaling from photoreceptors to glia. *Journal of Neuroscience* 25(18): 4540–4549.

Ryan, S. J. (1982). Subretinal neovascularization. Natural history of an experimental model. *Archives of Ophthalmology* 100(11): 1804–1809.

Ryan, S. J. (2006). *Retina*. Philadelphia, PA: Elsevier.

Vazquez-Chona, F. R., Khan, A. N., Chan, C. K., et al. (2005). Genetic networks controlling retinal injury. *Molecular Visision* 11: 958–970.

Wu, J., Seregard, S., and Algvere, P. V. (2006). Photochemical damage of the retina. *Survey Ophthalmology* 51(5): 461–481.

Injury and Repair: Prostheses

G J Chader, A Horsager, J Weiland, and M S Humayun*, USC School of Medicine, Los Angeles, CA, USA

Glossary

Age-related macular degeneration (AMD) – Retinal degeneration, primarily in the macula that is prevalent in the aging population.
Bare light perception (BLP) – A high level of visual loss but retaining light perception.
Lateral geniculate nucleus (LGN) – One of the central visual areas within the central nervous system.
No light perception (NLP) – A complete lack of visual sensation.
Phosphene – A phenomenon characterized by the experience of seeing light without light entering the eye.
Retinal degenerative diseases (RDDs) – A general term referring to many different types of diseases in which photoreception is lost mainly due to photoreceptor degeneration.
Retinotopy – The spatial organization of the neuronal responses to visual stimuli.
Retinitis pigmentosa (RP) – Retinal degeneration, primarily affecting rod photoreceptor cells starting in the retinal periphery.

Rationale for a Prosthetic Device

The idea of stimulating a portion of the central nervous system (CNS) to elicit formed vision is not new. The need to do this is particularly evident in the case of retinal degenerative diseases (RDDs) in which the retinal photoreceptor cells degenerate and die. The RDD family of diseases has two main branches: retinitis pigmentosa (RP) and macular degeneration (MD). RP primarily affects rod photoreceptor cells, leading initially to loss of dim-light and peripheral vision. It usually is early onset, leaving otherwise normal subjects blind or with severely affected vision for life. RP is thought of as a rare disease with a prevalence of approximately 1:3400 around the world. The MD branch primarily affects cone photoreceptors, degrading central and sharp vision. The most common form of MD, age-related macular degeneration (AMD), strikes later in life (usually >60 years of age), but affects millions around the world. In these diseases, although photoreceptors cells degenerate and ultimately can be lost, other layers of the retina are not as severely affected and remain relatively intact for some time thereafter. Thus, there is a window of opportunity for replacing photoreceptor function with a prosthetic device that will capture visual images, electronically transfer these to remaining secondary neurons of the retina, with subsequent passage to the brain. However, much of the visual processing takes place in the brain so it may be possible to bypass the eye completely with a visual image transmitted directly to vision-processing areas of the brain such as the visual cortex. Both of these approaches have been studied for decades now with the ultimate goal of sight restoration not only in cases of RDD but even when the entire eye has been lost. In fact, each separate anatomical portion of the visual system, such as the retina, the optic nerve, the lateral geniculate nucleus (LGN) of the thalamus, and the primary visual cortex (V1), has been used as a target in attempts at producing visual images.

*Dr. Humayun has a financial interest in Second Sight Medical Products.

Brain Prosthetic Devices

In 1962, Brindley found that application of stimulating pulse trains to his own eye with a corneal electrode interfered with visual light stimulation. This established at least the possibility of direct electrical stimulation of the retina. In 1968, Brindley and Lewin first reported on the use of platinum disk electrodes to stimulate the occipital pole of a subject and elicit independent visual percepts. Dr. William Dobelle followed, starting in about 1974, implanting blind subjects with electrodes mainly over the surface of the visual cortex and evaluating phosphene maps, which represent vision without light actually entering the eye. Although neither the pioneering studies of Brindley nor Dobelle were able to yield a useful, commercial visual prosthetic device, they did establish that phosphenes could be evoked by current pulses from an electrode array and that smaller stimulating electrodes would probably be needed to allow for more focal stimulation of cortex neurons. This led to the fabrication of novel, small, high-density arrays made of biocompatible silicon capable of penetrating the cortex (e.g., the work by Wise et al.). About this time, the National Institutes of Health actively developed a group dedicated to stimulating the primary visual cortex (area VI) using fine-wire electrodes in the hope of sight restoration in blind subjects. Since then, a number of groups (Normann et al. Hambrecht et al., Troyk et al., etc.) have continued to develop a cortical prosthesis. In most of this work, a video

camera is used to capture a visual image, which, through a processor, delivers electrical signals to intracortical electrodes that finally deliver the image to the appropriate brain area(s). To date, this body of work has established that electrical stimulation of the visual cortex can produce phosphenes and that penetrating electrodes allow for the use of low, relatively safe levels of stimulation. The LGN can also be electrically stimulated to produce visual percepts. For example, Pezaris and Reed in 2007 demonstrated that either electrical or visual stimulation of specific receptive fields of the LGN results in highly localized and repeatable eye movements in a nonhuman primate.

Unfortunately, the field of electrical stimulation of brain areas to produce formed vision has only slowly advanced in the last few years. There are currently only a few investigators doing basic research in the area, perhaps because of difficulties in continuing human testing and moving to *bona fide* clinical trials. In contrast, work on retinal prosthetic devices has proceeded briskly, with many groups around the world applying unique concepts and designs in human testing.

Retinal Prosthetic Devices

As the optic nerve is a bundle of ganglion cell axons, it rightfully can be considered as an extension of the neural retina. Optic nerve stimulation became feasible after the development of cuff electrodes for nerve fiber recordings by Hoffer and collaborators in the 1980s. Since then, several groups have demonstrated that such electrodes are effective in generating visual percepts in the blind. A problem with this approach though is that the optic nerve does not maintain spatial organization (retinotopy), making spatial mapping of the stimulus difficult. In the 1950s, a US patent was issued describing the insertion of a light-sensitive selenium cell behind the retina and the subsequent transient restoration of light perception. It was not until the 1990s though that the investigators demonstrated that there were enough inner neurons remaining in the retina of RP patients to warrant prosthesis implantation. Work by Milam, Humayun, and co-workers, for example, reported that about 30% of the ganglion cells remained in advanced RP retinas and an even larger proportion of cells in the inner nuclear layer. Similar studies on eyes procured from AMD patients revealed that both the ganglion cell layer and the inner nuclear layer were relatively well preserved. Thus, in both diseases, enough cells remain such that they can act as a platform for the array and could perhaps adequately transmit an electronic stimulus to the brain. In 1993, the first report was presented by Humayun and colleagues that direct electrical stimulation of the retinal surface could produce visual percepts in a blind human subject. In this case, a man with advanced RP, essentially no light perception (NLP), was able to perceive a spot of light with the temporary electrical stimulation. At that time, many other groups were working in parallel to develop other versions of the retinal prosthetic device – some intraocular, some extraocular.

All these approaches have different pros and cons, both with respect to efficacy and safety. For example, in the extraocular approach, one major hurdle is the relatively large distance between the electrodes and the retina. Chowdhury and co-workers though have presented evidence in an animal model that electrodes placed on the exterior surface of the eye can, in fact, stimulate the retina, evoking responses from the visual cortex. Tano and co-workers have shown that suprachoroidal–transretinal stimulation (with the anode in the fenestrated sclera and the cathode in the vitreous) is able to elicit excitatory electrical potentials (EEPs) from the visual cortex. Within the eye, electronic arrays have been implanted either in the subretinal or epiretinal positions. Subretinal positioning, as used by Zrenner et al., Rizzo and Wyatt, Chow et al., etc., is logical since the array is in the natural position of the lost photoreceptors. This juxtapositioning of the array to the bipolar cells could theoretically maximize the computational processing of the retinal circuitry but could be made difficult or impossible by lack of fidelity of the bipolar–ganglion cell synapse. There is also growing evidence for a substantial gliotic wall in the RDD subretinal space that could effectively limit the signaling from the subretinal implant to the overlying neurons. As shown by Marc in cases of severe RDD, the outer retina (bipolar, horizontal, and, to some extent, amacrine cells) undergoes marked reorganization, altering the synapses, and hence making the approach of stimulating bipolar cells more challenging. In addition, surgical placement of the array in the subretinal space is technically more difficult than placement on the vitreal surface. In epiretinal placement, that is, on the vitreal side, surgery is easier as well as access of the array to other components of the device. In patients, it is not known in either the epiretinal or subretinal situations which cell type or types are stimulated and react to the electrical signal. The epiretinal approach, because it is closer to the ganglion cells, has the theoretical advantage of stimulating this layer with lower currents. This is a distinct advantage since this layer does not undergo as significant a reorganization process in end-stage RDD.

Along with position on the retina, power output is an important consideration. Too little and the device might not be effective; too much could induce pathological changes in addition to an already compromised retina. A possible example of the dangers of too small of a power output is the case of the artificial silicon retina (ASR). In this case, Chow and co-workers used passive photosensitive diode arrays powered by only ambient light within the eye. Specifically, the 2-mm diameter ASR contained 5000 microelectrode-tipped microphotodiodes for light-energy processing with no external power supply. In spite of initial positive reports

from a clinical trial that the ASR could improve vision in a number of implanted RP patients, it was subsequently found by Chow, Pardue, and co-workers that the device itself was ineffective and that the improvement in vision probably resulted from a more generalized neurotrophic effect (i.e., release of neuron-survival factors) due to implantation of the device – active or nonactive. Failure of the ASR led others, such as Zrenner et al. and Palanker et al., to use microelectronics to power subretinal devices. In comparison, the epiretinal devices include radio-frequency (RF) power transmission for wireless operation of the implants.

Clinical Trials

The main clinical indication and usefulness of retinal prosthetic devices as discussed above will be to patients with inherited photoreceptor degenerations such as RP and, ultimately, AMD. Although other forms of therapy are now being considered for these diseases, the electronic prosthetic device should be useful in situations where other proposed therapies are not applicable. Current studies on gene therapy, for example, in specific types of RP such as Leber's congenital amaurosis, seem to be successful, but gene replacement therapy will only be useful if the specific gene mutation is known, and if a sufficient number of viable photoreceptor cells are present to allow for a visual response after therapy. Similarly, pharmaceutical therapy, that is, the use of neurotrophic agents and nutritional therapy, for example, the use of antioxidants, will only be possible if photoreceptors are yet present. In the case where few or no photoreceptors remain, photoreceptor cell transplantation or stem cell transplantation could certainly replenish the photoreceptor layer. However, studies on direct photoreceptor transplantation have yet to show significant functional efficacy and studies on stem cell development into mature photoreceptor neurons have yet to demonstrate safety and efficacy. Thus, to many RDD patients, particularly those with severe or advanced photoreceptor degeneration, the retinal electronic prosthesis could be the best hope for sight restoration.

Many groups around the world are working on prosthetic devices – including Japan, Belgium, Korea, Australia, China, Germany, and the USA – too many to cover in any detail in the current article. Only a few groups of the many excellent approaches have progressed to the stage of intensive human testing. To do this, most of the basic science groups have become associated with companies who provide critical functions such as manufacturing and quality control as well as regulatory expertise. The Zrenner group, for example, works with Retina Implant AG, a second group with Intelligent Medical Implants GmbH (IMI), and a third with Epi-Ret GmbH. In the USA, the Humayun consortium has worked with the company, Second Sight Medical Products Inc. (SSMP), to establish a Food and Drug Administration (FDA)-approved clinical trial with retinal arrays chronically implanted in RP patients.

In the subretinal approach taken by Zrenner and Retina Implant AG, an external energy source is used along with a microphotodiode array (about 3 mm in diameter containing 1600 microphotodiodes) that is implanted in the subretinal space. Experiments on animal models of inherited retinal degeneration have shown that ganglion cells are indeed stimulated by this device. Cortical evoked potentials could also be recorded in some of the animal experiments. Based on these positive preclinical findings, Retinal Implants AG has proceeded to human testing, first studying the short-term effects of the implant in RP patients. More recently, a prospective, open pilot clinical trial has been initiated with the subretinal implant and functional placebo controls. Eligible participants must have inherited retinal degeneration, be blind in at least one eye, or have visual function not compatible with navigation and orientation. The primary outcome is a measure of activities of daily living and orientation as well as safety. Latest information indicates that Retina Implants AG has implanted eight subjects for 4 weeks to date in their trial (clinicaltrials.gov identifier: NCT00515814). IMI GmbH has reported on four subjects with an epiretinal array of 49 electrodes designed to be functional for 18 months (clinicaltrials.gov identifier: NCT00427180). A 25-electrode array, EPI RET3, was implanted for 4 weeks in six subjects (clinical trial identifier: DE/CA21/A07). Finally, SSMP has conducted a long-term trial with a 16-electrode array (clinicaltrials.gov identifier: NCT00279500) and a more recent study with a 60-electrode array (clinicaltrials.gov identifier: NCT000407602).

Due to space limitations, this article will mainly focus on the SSMP effort and its clinical trial as an example of progress with retinal prosthetic devices. In addition, many of the early results from the SSMP trial have been reported and are clearly documented in the scientific literature. Finally, testing of the SSMP device has been continuous since 2002 in specific patients who have not only had regular laboratory testing but also have been able to use the device at home for direct assessment of quality-of-life (QOL) improvements. The approach taken by Humayun and co-workers has been epiretinal with the electrode array tacked on to the vitreal surface of the retina. Work initially started with studies on animal models of inherited retinal degeneration. These studies demonstrated no major problems in terms of inflammation, neovascularization, or encapsulation of the device. These positive safety studies allowed for short-term human testing where electrodes were temporarily juxtaposed to the retina of subjects with advanced RP and activated to ascertain if phosphenes were elicited. Results were positive in that appropriate phosphene signals were reported by the subjects. Since safety was also apparent in these acute studies, more

chronic implantation in the formal setting of a feasibility clinical trial was allowed by the FDA in 2002. The first-generation device used in the trial was called the Argus I; it had 16 electrodes affixed to the retina. Patients who had outer retinal degenerative diseases with a preoperative vision of bare light perception or worse and a nonrecordable electroretinogram (ERG) were chosen. The entire device is complex, with many interacting components that are the result of new technology modified from the cochlear implant. Functionally, the device has an external system that includes a tiny, lightweight video camera housed in the subject's glasses. This allows for image capture and initial processing. Image and power data are sent to the array using RF wireless transfer through a transmitter coil. The microelectronic implant is under the skin on the temporal bone behind the ear. A cable is threaded under the skin toward the orbit and around the eye under the rectus muscles. Once entering the eye through a sclerotomy, it is connected to the array, which is tacked to the retinal surface. The Argus 1 array has 16 platinum electrodes in a 4×4 arrangement within a silicone platform. The array is implanted in the macular region and is approximately 2.0×2.9 mm. It subtends an approximate 10° of visual angle with 14° on the diagonal.

Starting in 2002, six subjects were implanted with the Argus 1 device in the SSMP-sponsored feasibility clinical trial. The results were promising, in that safety was observed both for the subject and the device. No device failures were encountered, and no significant sequelae of the implantation were observed in the subjects. Because the device can be independently monitored and controlled (i.e., through the head-worn video camera or by custom software on a laptop computer), testing continues to date. Valuable longitudinal data have been obtained from this initial study. For example, although not surprising, it was found that the impedance and threshold values were inversely proportional to the distance of the electrode array from the retinal surface and that most of the electrodes had stimulatory thresholds below the safe charge injection limit. Importantly, subjects could spatially resolve the individual electrodes within the array with good resolution of the perceived locations of the elicited phosphenes, good two-point resolution, and good perception of motion direction. There was also a good correlation between percept brightness and stimulation level, demonstrating the ability of the implanted subjects to differentiate between different levels of illumination. Cortical responses were also evoked by the device. The electrically evoked responses (EERs) from the visual cortex are a primary measure of the possibility of functional vision. Most encouragingly, testing for object recognition showed that subjects with the use of the implant could differentiate between a cup, knife, and saucer. In mobility testing, patients could follow a line on the floor and identify and walk toward test doors. In the object recognition test, repeated testing gave scores significantly above chance, statistically at $P < 0.001$. Investigators at SSMP have also just concluded the first detailed study of spatial vision in an Argus I-implant patient definitively showing patterned visual perception with logMAR = 2.21, which is well matched to the sampling limit determined by the spacing of the electrodes. This provides strong evidence that it is possible for the brain to use the special information provided by individual electrodes. However, further testing is ongoing to understand the level of visual acuity obtainable with arrays that have more numerous or more closely spaced electrodes.

Testing of these subjects remains ongoing to determine if their QOL is enhanced, especially since they are able to use the devices at home while not under direct supervision. As might be expected though, differences between the performances of different subjects were observed. This could be based on differences in disease type and on the stage, that is, severity, of the degeneration in the individuals. Factors such as the site of implantation of the array and its proximity to the retinal surface must also be considered. All in all though, it is perhaps surprising that any functional efficacy is observed using the 16-pixel array. Theoretically, with such a simple array, only areas of light/dark should be discerned by the subjects, perhaps modified by shades of gray. That simple objects and letters can be identified though and mobility enhanced perhaps indicates that the brain can indeed make sense out of primitive signals and that, through a patient learning process, useful vision can indeed be restored.

Based on the positive results from both safety and efficacy in the feasibility portion of the trial, SSMP has initiated an international feasibility trial using a second-generation device, the Argus II. This new device has several improved designs, notably, an increased electrode count with up to 60+ electrodes on the retinal array. It also is much smaller than the first-generation device, allowing for an easier and shorter surgery procedure. Finally, as with the Argus I, the Argus II is designed to last the lifetime of the patient. Only severely affected RP patients are chosen to participate, with visual acuity and safety as the primary outcome measures. Secondary outcomes are improvements in orientation and mobility, activities of daily living, and general QOL. Early indications are that the Argus II device is safe (both to subject and device), although this certainly can only be properly assessed over a longer time period. Similarly, early data indicate that there is enhanced efficacy (i.e., improved vision). As alluded to above for the Argus I though, this does not come immediately and is a learning process over a period of months.

Challenges

Although the data presented above are encouraging, significant challenges yet remain in perfecting a prosthetic

device that will restore a high level of functional vision, be it epiretinal, subretinal, or one of the other approaches. For example, it will be important to determine the actual mechanism of action of the array, in particular, which populations of neurons are stimulated. In this way, the efficacy and efficiency of the device might be enhanced, irrespective of future design improvements. Another important area of future investigation must be directed at gaining a better understanding of the different pathologies and how the usefulness of the device is affected by the state of each individual retina. Although significant numbers on inner retinal neurons remain alive in cases of advanced retinal degeneration, neural remodeling takes place such that morphology is altered and synaptic contacts rearranged. Investigators such as Milam, Marc, and Strattoi have presented compelling evidence that inappropriate neurite sprouting takes place in remaining rod, horizontal, and amacrine cells, with abnormal contacts with both neuronal and glial (Müeller) cells. These changes, along with the appearance of a dense fibrotic layer in the subretinal space, could severely affect proper inner retinal cell processing and signal transmission down the optic nerve. The effects of electrical stimulation on the normal retina have been well studied, but the effects on retinas affected with an inherited retinal degeneration are just beginning to be examined. These effects will have to be better defined in different genetic forms of RD and at different stages of disease such that the electrical properties of the device can be tuned and adjusted to individual situations. Similarly, the state of central connections could be a problem, particularly in patients with long-term degeneration (i.e., no or bare light perception) and with patients with very-early-onset degeneration such as Leber's congenital amaurosis in which central connections may not even have been initially formed. All of these factors will vary considerably from subject to subject and will have to be individually assessed in each case. That a level of functional vision has been restored though in a number of older human subjects with severe retinal degeneration indicates that, at least in many cases, enough functional inner retinal neurons and their synaptic connections do remain, and the visual cortex remains functional enough to process the electrically derived information into discernable forms.

Issues of safety also remain, particularly with regard to long-term implants. There is yet the possibility of low-level but cumulative damage from both electrical and mechanical effects of array implantation. Too high an electrical input could not only grossly burn the retina but, more subtly, also induce an altered state of conductivity and responsiveness within the remaining retinal cells. In addition, as preclinical and clinical studies continue, the properties of the implant itself may need to be modified as to materials, size, and shape. On the positive side, implantation of the Argus I began in 2002 with testing continuing to date, giving several years of evidence for not only patient and device safety but also continuation of efficacy.

Future Prospects

From an engineering standpoint, one of the greatest challenges but most exciting prospects for the future is in the enhancement of vision through improved and more sophisticated electronics, for example, an increased number of electrodes impinging on the retina. Theoretically, an electrode count of 1000+ should allow for face recognition and reading ability, leading to a marked improvement in QOL and mainstreaming of patients back into society. With this type of improved function, retinal electronic prosthetic devices should thus be helpful not only to the relatively limited number of patients with RP but also to the millions with AMD.

There are several other obvious but diverse factors that can be studied that should lead to improved action of a retinal prosthesis. One of these would be to assure close and uniform proximity of the array to the retinal surface in the specific cases of epiretinal and subretinal implantation. A bioadhesive glue that is biocompatible and reversible would be useful in this regard, particularly in an epiretinal device. Another area of improvement could be the use of an intraocular rather than extraocular camera. This would allow for more natural object tracking, as the eye rather than the head moves. A third area of interest would be to increase the relatively narrow visual field of the implants currently under study such that peripheral vision is restored. Finally, could it be possible to restore color vision? The implant subjects to date do describe different colors, including blue, yellow, orange, and green. Although not important to most of the visual tasks we perform, colors do abundantly increase our appreciation of our environment and certainly increase QOL.

See also: Injury and Repair: Neovascularization; Injury and Repair: Retinal Remodeling; Injury and Repair: Stem Cells and Transplantation; Injury and Repair Responses: Retinal Detachment; Primary Photoreceptor Degenerations: Retinitis Pigmentosa; Primary Photoreceptor Degenerations: Terminology; Retinal Vasculopathies: Diabetic Retinopathy; Secondary Photoreceptor Degenerations: Age-Related Macular Degeneration; Secondary Photoreceptor Degenerations.

Further Reading

Brindley, G. and Lewin, W. (1968). Short- and long-term stability of cortical electrical phosphenes. *Journal of Physiology (London)* 196: 479–493.

Caspi, A., Dorn, J., McClure, K., et al. (2009). Feasibility study of a retinal prosthesis. Spatial vision with a 16-electrode implant. *Archives of Ophthalmology* 127: 398–401.

Chader, G. (2007). Retina prosthetic devices: The needs, and future potential. In: Tombran-Tink, J., Barnstable, C., and Rizzo, J., III (eds.) *Visual Prosthetics and Ophthalmic Devices*, pp. 1–4. New York: Springer.

Dagniele, G. (2008). Psychophysical evaluation for visual prosthesis. *Annual Review of Biomedical Engineering* 10: 15.1–15.30.

Horsager, A., Greenwald, S., Weiland, J., et al. (2009). Predicting visual sensitivity in retinal prosthesis patients. *Investigative Ophthalmology and Visual Science* 50: 1483–1491.

Humayun, M., Weiland, J., Chader, G., and Greenbaum, E. (eds.) (2007). *Artificial Sight: Basic Research, Biomedical Engineering and Clinical Advances.* New York: Springer.

Javaheri, M., Hahn, D., Lakhanapal, R., Weiland, J., and Humayun, M. (2006). Retinal prostheses for the blind. *Annals of the Academy of Medicine, Singapore* 35: 137–144.

Lowenstein, J., Montezuma, S., and Rizzo, J., III. (2005). Outer retinal degeneration. An electronic retinal prosthesis as a treatment strategy. *Archives of Ophthalmology* 122: 587–596.

Normann, R., Maynard, E., Rousche, P., and Warren, D. (1999). A neural interface for a cortical vision prosthesis. *Vision Research* 39: 2577–2587.

Palanker, D., Vankov, A., Huie, P., and Baccus, S. (2005). Design of a high resolution optoelectronic retinal prosthesis. *Journal of Neural Engineering* 2: S105–S120.

Pezaris, J. and Reid, R. (2007). Demonstration of artificial percepts generated through thalamic microstimulation. *Proceedings of the National Academy of Sciences of the United States America* 104: 7670–7675.

Tombran-Tink, J., Barnstable, C., and Rizzo, J., III (eds.) (2007). *Visual Prosthesis and Ophthalmic Devices: New Hope in Sight.* New York: Springer.

Weiland, J. and Humayun, M. (2005). Retinal prosthesis. *Annual Review of Biomedical Engineering* 15: 361–401.

Yani, D., Weiland, J., Mahadevappa, M., et al. (2007). Visual performance using a retinal prosthesis in three subjects with retinitis pigmentosa. *Americal Journal of Ophthalmology* 143: 820–827.

Zrenner, E. (2002). Will retinal implants restore vision? Science 295: 1022–1025.

Injury and Repair: Retinal Remodeling

R E Marc, University of Utah, Salt Lake City, UT, USA

Glossary

Glial seal – A compaction of the distal microvillar processes of mature Müller cells and their stabilization by intermediate junction to form a barrier to diffusion and cellular movement.
Microneuromas – New, anomalous complexes of synapses by mature neurons.
Migration – The ability of a cell to relocate to a new position in a tissue. It is often thought that mature neurons cannot migrate without de-differentiating, but mature retinal neurons can migrate both intra- and extraretinally without losing their characteristic molecular profiles.
Neuritogenesis – The activation of new dendrites and axons from neurons; typically associated with developing cells, it is vigorously demonstrated by mature neurons in remodeling retinas.
Reprogramming – A major change in the gene expression profile of a cell, typically the expression of genes not characteristic of homeostasis.
Self-signaling – The ability of retinal networks to generate their own excitatory activity in the absence of a photoreceptor drive.

Overview

Retinal remodeling is a collection of molecular and cellular revisions triggered by primary inherited degenerative diseases such as retinitis pigmentosa (RP), Usher syndrome; secondary degenerative diseases with mixed environmental/genetic risks, such as age-related macular degeneration (AMD); and acquired retinal defects such as prolonged retinal detachment and light-induced retinal damage. These revisions include anomalous neuronal rewiring (targeting canonically inappropriate cells) and reprogramming (expressing canonically inappropriate genes or repressing characteristic genes); *de novo* neuritogenesis and synaptogenesis; spontaneous and corruptive self-signaling; bipolar cell (BC) dendrite truncation; supernumerary axon generation; neuronal migration along hypertrophic Müller cell (MC) columns; neuronal death; altered glial molecular profiles; vascular remodeling; and retinal pigmented epithelium (RPE) invasion, vascular occlusion, and hyperpigmentation. Some revisions (e.g., reprogramming) begin as soon as photoreceptor stress is initiated, while others (e.g., synaptogenesis) are manifest only after complete local photoreceptor loss. Importantly, the local survival of even heavily altered cones can prevent much late-stage remodeling, apparently by stabilizing the dendritic compartment of BCs. Remodeling impacts the timing and potential outcomes of gene therapy, survival factor treatments, stem or progenitor cell implantation, retinal transplantation, and bionic implants.

It was not until the detailed imaging studies of Ann Milam (University of Pennsylvania) in the mid-1990s that the nature and scope of remodeling in human RP became evident. More recently, Enrica Strettoi (Centre National de la Recherche Scientifique, Pisa, Italy) and Bryan W. Jones (University of Utah) independently demonstrated that remodeling was also characteristic of animal models of human inherited retinal degenerations. Though remodeling was not initially given much credence despite strong homology to central nervous system (CNS) degenerative disorders, it is now gaining understanding as a serious denouement of retinal disease.

Progression

Remodeling kinetics are largely independent of the source of photoreceptor deafferentation and occur in distinct phases (**Figure 1**). In phase 1, neuronal and glial cells react to photoreceptor stress signals prior to photoreceptor death. In phase 2, neurons, glia, and microglia interact in the processes of photoreceptor death, outer nuclear layer (ONL) decimation, and formation of the glial seal, encapsulating the remnant retina. In phase 3, neural cells respond to deafferentation and non-neural cells form new cytoarchitectures in the remnant retina. The speed of these phases depends on the nature of the degeneration (**Figure 2**). Aggressive primary rod, cone–rod, or cone dystrophies, as well as RPE phagocytosis defects can rapidly transit phases 1 and 2 to extensive phase 3 remodeling. Slower photoreceptor degenerations (e.g., autosomal-dominant RP (adRP) models of rhodopsin mutations) can lead to extended periods of cone survival, delaying the onset of phase 3. In rodent models, the faster overall kinetics are partly due to the small eye and the likely constancy of cell–cell interaction areas. Greater loss of peripheral retina is tolerated in humans as long as the macula is spared.

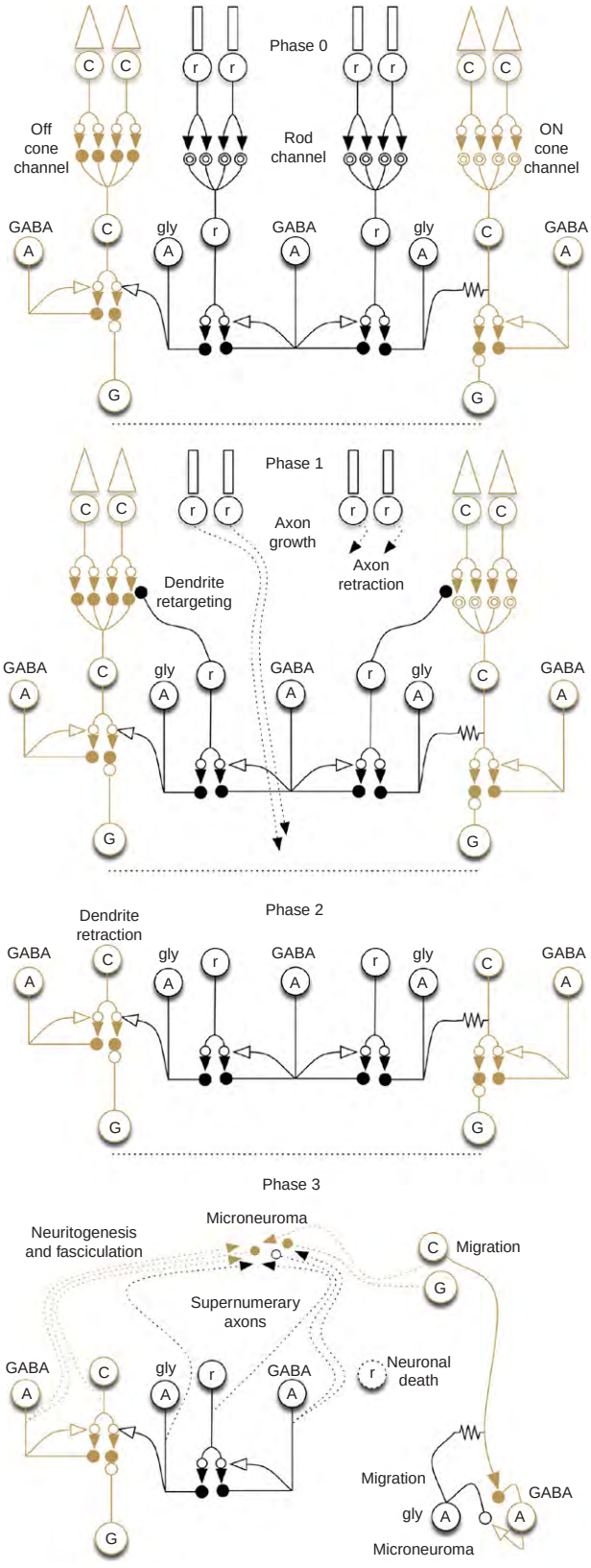

Figure 1 Remodeling phases in the mammalian retina. Phase 0 is the normal retina prior to the onset of acquired or inherited defect stress. The mammalian retina uses separate cone (C) and rod (r) channels prior to converging on retinal GCs (G).

Phase 1

The first evidence that remodeling precedes photoreceptor death was the demonstration that human rods harboring a rhodopsin defect were able to form new fascicles of axons, bypass their normal BC targets, and project into the ganglion cell (GC) layer prior to apoptotic stress and death. Some rodent model degenerations show the same ability. Furthermore, rodents with autosomal-recessive RP, such as the phosphodiesterase B 6 (*Pdeb6*^{rd1}) mouse (the rd1 mouse), show truncated BC dendritic arbors and horizontal cell (HC) axonal fields long before photoreceptor death. MC stress signals and protective alterations in neuronal glutamate receptor expression in light-induced retinal degeneration (LIRD) albino rodents are activated within hours of light-stress onset and long before photoreceptor death.

Phase 2

The degenerations transition to extensive cell-autonomous and/or bystander photoreceptor death. The ONL is dismantled with the involvement of activated microglia and hypertrophic MCs. The details are poorly understood and may vary according to gene defect. For example, dominant mutations that impair rhodopsin trafficking may activate endoplasmic reticulum (ER) stress in several ways such as anomalous protein multimerization, inhibition of proteasome cycling, and activation of the unfolded protein response. This results in a slow dismantling of the ONL by sporadic apoptosis. Conversely, mutations of transduction pathways that trigger calcium-dependent apoptosis are faster and more coherent. In either case, photoreceptor apoptosis and migroglial-initiated bystander cytolysis may create debris zones that must be cleared. The mechanisms of such clearance are unknown. Phase 2 ends with the entombment of the remnant neural retina by a thick seal of distal MC processes similar to the normal outer limiting membrane, with extensive intermediate junctions between the processes. Though often termed a glial scar, there is no evidence that the seal involves astrocyte proliferation as in

Cone BCs receive cone input with either ionotropic sign-conserving glutamate receptors (solid circle) or metabotropic sign-inverting glutamate receptors (double circle), and drive ACs (A) and GCs which decode signals with sign-conserving glutamate receptors. Rod BCs receive rod input with metabotropic sign-inverting glutamate receptors and then drive glycinergic rod ACs, which fan their signals out to ON cone channels through gap junctions (resistor symbol) and OFF cone channels through glycine release decoded by inhibitory receptors (open circles). In phase 1, rod photoreceptors reprogram to either bypass rod BCs with new axons or retract their synapses. Rod BCs both retract dendrites and retarget some to adjacent cone pedicles. In phase 2, photoreceptors are lost and all BCs lose their dendrites. In phase 3, extensive rewiring, neuritogenesis, microneuroma formation, cell migration, and neuronal death occur.

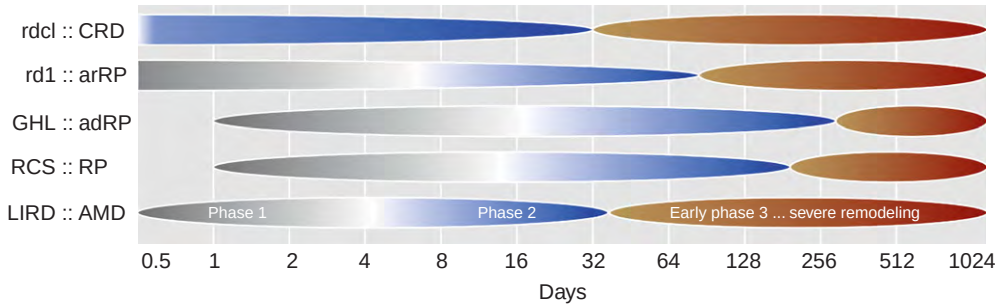

Figure 2 Different forms of retinal degeneration express different kinetics. The abscissa is exponential in time in either postnatal or postlight exposure days. Light-induced retinal degeneration (LIRD) is fast with phase 1 stress appearing almost immediately and phase 2 photoreceptor death extending for a couple of weeks before patches of phase 3 remodeling begin. In the the Royal College of Surgeons (RCS) rat, photoreceptor debris build up in the subretinal space causes stress, but photoreceptor death is not complete for 3 months or more, after which extensive remodeling occurs. The triple mutation valine 20 → glycine, proline 23 → histidine, proline 27 → leucine GHL mouse model of autosomal-dominant RP (adRP) does not begin to show photoreceptor stress until opsin synthesis begins and slowly traverses phase 2 for nearly a year before phase 3 remodeling begins. In contrast, the rd1 model of autosomal-recessive RP (arRP) is already stressed at birth with phase 2 photoreceptor death reaching completion close to 90 days. Similarly the rodless–coneless (rdcl) mouse is a model of cone–rod dystrophy (CRD) and cell death actually begins prenatally. This model spends most of its life in phase 3.

CNS glial scars. There are occasional breaks in the seal that are associated with phase 3 RPE and choroidal vascular invasion of the neural retina and neuronal escape into the choroid.

Phase 2+

In some degenerations, the death of rods is slow and seems to trigger variable bystander killing, leaving clusters of deconstructed cones with apparently functional synaptic contacts. This results in patches of retina suspended in late phase 2 (phase 2+) in a sea of phase 3 retina. The extent to which these preserve vision is unknown, but they definitely provide evidence that even marginal rescue of cones is a critical step if late-phase therapies are to be viable.

Phase 3

After loss of all photoreceptors, the stability of neuronal connectivity in the retina becomes progressively compromised through at least nine distinct processes (see below) including molecular reprogramming, individual cell rewiring, large-scale neuritogenesis, synaptogenesis and microneuroma formation, spontaneous self-signaling, neuronal migration to ectopic foci, progressive neuronal death, MC remodeling and altered gene expression, as well as RPE and vascular remodeling and migration. In severe degenerations, including human late-stage RP and geographic atrophy, the revision of the retina can be so severe that no visual function could ever be restored. In other cases, the neural retina survives but is likely to be so altered that upstream strategies such as subretinal implants, stem/progenitor cell transplants, or even fetal retinal transplants will likely not successfully deliver form vision. Further, there is increasing evidence that bionic implants and transplants do not stabilize phase 3 remodeling and may accelerate it.

Remodeling Events

Reprogramming

Reprogramming is a shift, possibly reversible, in the gene expression of cells to anomalous molecular and anatomic states. This is best known for MCs in retinal stress where intermediate filament expression is elevated and is also becoming evident for retinal neurons, especially in terms of glutamate receptor expression. Receptor reprogramming can begin in phase 1–2 when rods lose the ability to directly signal rod BCs. In the *Pde6b*^{rd1} mouse, the expression, localization, and function of the metabotropic glutamate receptor 6 (mGluR6) essential for proper ON pathway encoding decrease. In both mouse and human RP models, rod ON BCs appear to transiently upregulate expression of ionotropic glutamate receptors (iGluRs). In the LIRD mouse model, rapid upregulation of protective GluR2 subunits occurs within 24 h after initiation of photoreceptor stress. There is also evidence of gamma-aminobutyric acid (GABA) receptor redistribution in ON BCs of the *Pdeb6*^{rd1} mouse. Further, the expression of dendrites in all BCs appears to be completely suppressed after rod and cone loss, and supernumerary axons are formed. While the mechanisms initiating these changes are not yet known, they demonstrate that mature retinal neurons can change their architectures and receptor expressions, while glia can change their architectures and metabolic profiles. More reprogramming events are certain to be found.

Rewiring

Rewiring is the switching of dendritic or axonal targeting. The first known instance of this was the escape of rod synaptic terminals from BC dendrites to form long axonal fascicles (Figure 1), but with no established targets; cones behave similarly in some cases. In other forms of retinal degeneration, photoreceptors retract their synaptic terminals, which may be associated with alterations in the balance of cAMP/cGMP production (Camp, cyclic adenosine and guanosine monophosphate; cGMP, guanosine monophosphate). The numerous reports of BC sprouting in many model degenerations as well as aging mice likely reflect the simple extension of the dendrites still attached to retracting rod synaptic terminals and not true plasticity. More concretely, BCs bereft of rod input transiently retarget dendrites to cone terminals and, though they do not make structurally appropriate ribbon-associated synapses, they do express anomalous iGluRs. This is consistent with the disappearance of the electroretinogram b-wave, despite the fact that no rod BCs die early in phase 2, and with observations that ON center GC responses disappear long before those of OFF center GCs.

Neuritogenesis

Neuritogenesis is the large-scale evolution of new processes by amacrine cells (ACs), BCs, and GCs in phase 3. The mechanism of activation is unknown, but it encompasses all cell classes, suggesting a global signaling process and a pan-neural response. Many new fascicles course just distal to the glial seal and contain mixed neurites in patterns never observed in the normal retina. In other regions, especially near invading RPE processes, large tracts of tiny new neurites with only one or two microtubules form homogeneous fascicles. The tracts can traverse several hundred microns, suggesting significant alteration in the spatial patterning of circuits.

Synaptogenesis and Microneuromas

A logical extension of neuritogenesis is synaptogenesis. The extent to which new synapses are made in the inner plexiform layer (IPL) of phase 3 remodeling retina is not clear, but in regions of the MC's hypertrophy, surrounding migration columns (see below), in the GC layer, and especially in the remnant distal retina, numerous new AC, BC, and GC connections are made. The most distinctive zones are microneuromas, which range from 10 to 100 ìm in width and contain abundant conventional and ribbon synapses. The mechanisms that stimulate new synapse formation are also unknown but seem closely associated with RPE processes. As RPE cells are known to release several growth factors, it is plausible that they are the activators of synaptogenesis. The wiring within microneuromas seems chaotic and, by serial section reconstruction and modeling, such networks appear to be resonant, which is incompatible with visual processing.

Self-Signaling

A number of observations suggest that retinal degenerations lead to spontaneous self-signaling in phase 3 retina. Photopsias (scintillating illusions common in RP) are initiated in the retina and the generator mechanisms can remain quiescent for decades in the absence of vision, only to be reactivated by experimental transocular currents. Spontaneous, erratic retinal waves of depolarization occur in rodent models of RP after light-driven responses are lost. Physiological measures show that rodent ACs and GCs are glutamate-activated in phase 3. GC activation in the phase 3 *Pdeb6*^{rd1} mouse is clearly glutamatergic and not intrinsic. This means that BCs must be voltage modulated in some way. However, most remodeled BCs lack functional glutamate receptors and they must be depolarized by another mechanism. One plausible mechanism is periodic AC membrane potential fluctuations, leading to the modulation of BC anion currents and modulation in BC glutamate release. Some isolated ACs have shown endogenous oscillations in K^+ channel conductance, alternately hyperpolarizing and depolarizing them, presumably modulating GABA (or glycine) release. The isolation of ACs from the normal visual drive in retinal degenerations may unmask this intrinsic capacity. Once self-signaling is initiated, resonant networks created by rewiring or microneuroma formation can rapidly generate periodic activity. Such networks may be inimical to restoration.

Migration

Neuronal migration is a large-scale remodeling event. In most instances, migration is closely associated with both hypertrophy of MCs and anomalous vascular tangles (see below). All forms of cell mixing occur: collections of ACs and BCs can become displaced to the GC layer. Conversely, ACs and even GCs can migrate to the distal margin of the remnant retina. One fundamental question is whether these cells remain functional. Ultrastructurally, cells in migration columns such as GCs seem to have processes extending both distally and proximally much like neuroepithelial cells in development. However, after migration, the original orthotopic processes seem to be retracted. Migrated cells seem heavily connected to microneuromas. A more serious form of migration (emigration) occurs when RPE cells and the basement membrane are focally ablated and the distal seal can surge into the choroid. Large tracts of MCs and neurons can emigrate, decimating the remaining neural structures. This is especially evident in LIRD and suggests that it may play a role in loss of vision in severe nonvascular forms of AMD such as geographic atrophy.

Cell Death

There is little evidence of glial death in remodeling, but the proportions and numbers of survivor neurons change significantly. BCs form the largest cohort of neurons (other than photoreceptors) in normal retina; however, ACs always predominate in phase 3, suggesting that BC death is far more common than AC or GC death. This may be due to the fact that BCs are the only retinal cells that lose all of their glutamatergic input. Neurons require a basal level of Ca influx to maintain homeostatic gene expression and, through self-signaling, ACs and GCs clearly possess the critical glutamatergic input required to provide both transmitter-gated Ca flux and voltage-gated Ca-channel activation; BCs clearly lack that input. As subjects age, ACs and GCs also decrease in number. In any event, the loss of neurons has strong implications for all therapeutic interventions, including epiretinal implants.

MC Remodeling

MCs make up nearly 50% of the mass of the peripheral primate retina and are one of the major drivers of remodeling. While there has been little analysis of phase 1 MC function in inherited retinal degenerations, there is abundant evidence that they respond to rapid, coherent photoreceptor stress initiated by LIRD within hours by increasing intermediate filament expression, displaying distal process hypertrophy in the ONL, and increasing arginine expression (a marker of increased protein synthesis). In phase 2, MCs play a lead role in forming a seal between the remnant RPE and/or choroid. The transport characteristics of that seal are unknown, but its formation is paralleled by a massive increase in MC glutamine levels. MCs normally export glutamine from MCs to surrounding neurons. This transport is voltage sensitive and, similar to many Na-coupled transporters, allows increasing export with depolarization. Depolarization of MCs is closely coupled to light-activated events, and the loss of photoreceptors may play some role in progressive hyperpolarization of MCs and retention of gluamine. However, as the increase in MC glutamine is temporally linked to the formation of the distal seal, the mechanism of glutamine retention appears more complex than just constraining the MC voltage.

RPE Remodeling

In classical RP, invading RPE cells are one of the hallmarks of advanced disease. After formation of the MC seal, certain RPE cells and, sometimes, choriocapillaris endothelia are able to penetrate into the neural retina, forming large complexes of hypertrophic MCs, RPE with altered melanosomes encapsulating invading and remnant retinal capillaries, clusters of new neurites, and columns of migrating neurons. RPE cells seem to be the foci of large-scale morphologic derangements in the survivor retina, but whether they are initiators or responders is not clear. The RPE remains partially intact for long periods in many retinal degenerations, including the Royal College of Surgeons (RCS) rat defect; however, the RPE layer can become broken by patches of invading RPE cells and apical processes. In the RCS rat, apical RPE processes can extend to the GC layer.

Vascular Remodeling

New capillaries invade the neural retina in phase 3, emanating from both vitreal and choroidal sources. Little is known of the fundamental transport properties of these new vessels (e.g., whether they are fenestrated or not), but both molecular and genetic profiling show that neural retina in RP is metabolically deprived. New imaging data as well as electron microscopy suggest that the new vessels are too attenuated and too heavily invested by hypertrophic MCs and RPE to allow proper perfusion of the retina. These anomalous foci may trigger neuronal migration. The stimuli for vascular remodeling remain unknown, but VEGF secretion by invading RPE cells is one plausible source.

Impact of Remodeling on Therapeutics

The potential reversibility of remodeling events varies. For example, phase 1 and 2 changes in reprogramming of gene expression and neurite switching are reminiscent of normal plastic behavior and might respond to the appropriate therapeutic signals. However, phase 3 changes such as rewiring, neuritogenesis, and microneuroma formation, migration, and neuronal cell death are not reversible by any known means. Intermediate phenomena such as MC, RPE, and vascular remodeling are similarly challenging. Human RP patients show the full spectrum of remodeling defects; therefore, most therapies are impacted by a narrowing therapeutic window.

Primary Gene Therapy

All prospective primary gene therapies (those targeting known gene defects) depend on photoreceptor survival. However, it is clear that photoreceptor deconstruction starts long before photoreceptor death. The recent successes with gene therapy for replacing the deficient isomerase (RPE65) in that variant of Leber's congenital amaurosis (LCA) is not likely relevant to primary rod or cone gene defects, nor to defects associated with the accumulation of genotoxic and cytotoxic debris in the

subretinal space such as those due to defects in RPE mer tyrosine kinase (MERTK). In human rod dystrophies, it is clear that mutations impacting rhodopsin trafficking also lead to changes in the inner segment function and photoreceptor architecture. Rod photoreceptor rewiring in human RP is unlikely to be reversible regardless of the success in replacing defective phototransduction genes. So far, gene therapy successes in animal models are largely restricted to prenatal or early postnatal genetic interventions. With the exception of soft diseases such as LCA and stationary night blindness that do not trigger photoreceptor deconstruction, most retinal degenerations clearly have only a tiny window for gene therapy. Primary gene therapies are currently restricted to phase 1.

Survival Factor Therapy

One strategy to retard retinal degeneration involves the use of survival factors such as neurotrophins (e.g., ciliary neurotrophic factor, CNTF) that slow photoreceptor apoptosis. These strategies were validated for slower models of adRP (the rat P23H and S344ter rhodopsin transgenic models). Some argue that the structural preservation afforded by CNTF in these models does not reflect a parallel functional rescue. There is evidence that early postnatal CNTF infusion in other rodent models of RP negatively alters photoreceptor gene expression profiles, activates MC stress signaling, and alters inner retinal organization. Simple survival factor therapy without a known cellular and molecular target is not likely to generalize well across human RP types. At present, survival factors offer little prospect of reversing or retarding remodeling. Survival factor therapies are restricted to phase 1 and early phase 2.

Stem/Neuroprogenitor Cell Therapy

Several groups have shown that isolated stem/ progenitor cells, particularly murine postnatal day 5 rod neuroprogenitor cells, have the potential to intercalate in the ONL and, possibly, repopulate the retina. The efficiency of such intercalation is low and it is not likely that these cells will survive in phase 3 retinas. Penetration of the MC seal is unlikely and several groups have failed to obtain significant numbers of exogenous photoreceptors to extend synapses through it. Direct injection into the retina is likely to activate microglial killing and, in any event, isolates any surviving photoreceptors from the remnant RPE. For photoreceptor progenitor cells to be successful in rescuing vision, they must also lead to cone survival and reconnect with existing neurons before morphologic remodeling begins. This excludes most current RP patients. Stem/neuroprogenitor cell therapies are currently restricted to phase 1 and early phase 2.

Retinal Transplantation

The team of Seiler and Aramant pioneered the effort to insert sheets of fetal retina into the subretinal space of degenerating retina. They have successfully demonstrated long-term photoreceptor survival and some visual driving in rats. Remodeling remains a major barrier in several ways. The extent of transplant-to-host neurite intermingling is small, and the glial seal predominates. Further, the transplanted retina begins to remodel and appears even more susceptible to alteration than the host. This suggests that remodeling signals emanate from the survivor retina. Certainly, after phase 3 BC dendrite truncation in the host retina, a semi-intact fetal retina cannot recapitulate normal circuitry by tandem connections. It is likely that most transplant-to-host connectivity is AC → AC driven and probably functionally random. Even so, such networks can generate light-driven behavior. Though lacking the spatiotemporal precision normal GCs, transplants have the potential for much higher sensitivity, range, and resolution than bionic mechanisms. Retinal transplantation therapies are largely restricted to phases 1–2, but may function if the connection can traverse the glial seal in phase 3 retinas.

Secondary Gene Therapies: Photosensitive Proteins

A recent development of import is the ability to induce expression of photosensitive proteins in survivor neurons by viral or molecular transfection, generating light responses directly in neurons. Several groups have shown that it is possible to express channelrhodopsin 2 (ChR2) in retinal BCs, and elicit ChR2-BC-driven photoresponses in GCs and light–dark preferences in behavioral search. This is an important advance and represents the potential to convert blind retinas into navigational systems without surgical intervention and ancillary equipment. The challenge is to demonstrate that this is possible in phase 3 profoundly blind patients, as they are the most obvious candidates for therapy. This technique has, once again, only been established in phase 2 or earlier models. Further, as with transplantation, there is no evidence that such secondary therapies will be resistant to remodeling, prevent cell death, or overcome signal corruption. A significant amount of basic research remains to be done but, despite promise, secondary gene therapies still seem limited to phases 1–2, although they may function in phase 3, even if randomly targeted.

Bionic Implants

The most successful schemes to restore vision to the profoundly blind from aggressive phase 3 retinal degenerations are epiretinal bionic implants. Surgically placed near the

GC layer, epiretinal implants provide direct current stimulation of retinal GCs or nearby circuitry to activate patches of visual sensation. The argument that such stimulation conflates ON and OFF responses seems irrelevant as several implanted patients can now successfully navigate with such devices. It is clear that the severe remodeling, especially neuronal death, limits candidacy. All implants, whether they are epiretinal, intraretinal, or subretinal, seem to induce further glial and neuronal remodeling. Severe remodeling, BC death, and microneuroma formation will more severely impact subretinal models.

The Importance of Cone Rescue

In every model, the survival of cones seems to delay the onset of phase 3, holding the retina in a phase 2+ state indefinitely. The effect is local and small patches of cones preserve connected BC dendrite structure even when surrounding BCs have lost all dendrites and glutamate receptors. The preservation persists even when cones are severely deconstructed, lacking outer segments and visual pigment expression, and significantly reduced in size. This suggests that cone contact alone, perhaps through synaptic integrins, may be sufficient to preserve BC function. Expression array studies suggest that cone deconstruction may be accelerated by metabolic deprivation. While preserving cones will not rescue vision, it will permit holding the survivor retina in suspended animation, making an array of interventions such as stem/progenitor cell transplantation, fetal retinal sheet transplantation, and secondary gene therapy viable for adults suffering from advanced retinal degenerations. Revisiting survival factor research with a focus on cones may be the critical advance needed for all intervention methods.

See also: Anatomically Separate Rod and Cone Signaling Pathways; Injury and Repair: Light Damage; Injury and Repair: Prostheses; Injury and Repair: Stem Cells and Transplantation; Injury and Repair Responses: Retinal Detachment; Primary Photoreceptor Degenerations: Retinitis Pigmentosa; Secondary Photoreceptor Degenerations: Age-Related Macular Degeneration; Secondary Photoreceptor Degenerations.

Further Reading

Gargini, C., Terzibasi, E., Mazzoni, F., and Strettoi, E. (2007). Retinal organization in the retinal degeneration 10 (rd10) mutant mouse: A morphological and ERG study. *Journal of Comparative Neurology* 500: 222–238.

Gupta, N., Brown, K. E., and Milam, A. H. (2003). Activated microglia in human retinitis pigmentosa, late-onset retinal degeneration, and age-related macular degeneration. *Experimental Eye Research* 76: 463–471.

Jones, B. W., Watt, C. B., Frederick, J. M., et al. (2003). Retinal remodeling triggered by photoreceptor degenerations. *Journal of Comparative Neurology* 464: 1–16.

Li, Z. Y., Kljavin, I. J., and Milam, A. H. (1995). Rod photoreceptor neurite sprouting in retinitis pigmentosa. *Journal of Neuroscience* 15: 5429–5438.

MacLaren, R. E., Pearson, R. A., MacNeil, A., et al. (2006). Retinal repair by transplantation of photoreceptor precursors. *Nature* 444: 203–207.

Marc, R. E., Jones, B. W., Anderson, J. R., et al. (2007). Neural reprogramming in retinal degenerations. *Investigative Ophthalmology and Visual Science* 48: 3364–3371.

Marc, R. E., Jones, B. W., Watt, C. B., et al. (2008). Extreme retinal remodeling triggered by light damage: Implications for AMD. *Molecular Vision* 14: 782–806.

Marc, R. E., Jones, B. W., Watt, C. B., and Strettoi, E. (2003). Neural remodeling in retinal regeneration. *Progress in Retinal and Eye Research* 22: 607–655.

Margolis, D. J., Newkirk, G., Euler, T., and Detwiler, P. B. (2008). Functional stability of retinal ganglion cells after degeneration-induced changes in synaptic input. *Journal of Neuroscience* 28: 6526–6536.

Peng, Y-W., Hao, Y., Petters, R. M., and Wong, F. (2000). Ectopic synaptogenesis in the mammalian retina caused by rod photoreceptor-specific mutations. *Nature Neuroscience* 3: 1121–1127.

Seiler, M. J., Thomas, B. B., Chen, Z., et al. (2008). Retinal transplants restore visual responses: Trans-synaptic tracing from visually responsive sites labels transplant neurons. *European Journal of Neuroscience* 28: 208–220.

Stasheff, S. F. (2008). Emergence of sustained spontaneous hyperactivity and temporary preservation of OFF responses in ganglion cells of the retinal degeneration (rd1) mouse. *Journal of Neurophysiology* 99: 1408–1421.

Strettoi, E., Pignatelli, V., Rossi, C., Porciatti, V., and Falsini, B. (2003). Remodeling of second-order neurons in the retina of rd/rd mutant mice. *Vision Research* 43: 867–877.

Sullivan, R., Penfold, P., and Pow, D. V. (2003). Neuronal migration and glial remodeling in degenerating retinas of aged rats and in nonneovascular AMD. *Investigative Ophthalmology and Visual Science* 44: 856–865.

Varela, C., Igartua, I., De la Rosa, E. J., and De la Villa, P. (2003). Functional modifications in rod bipolar cells in a mouse model of retinitis pigmentosa. *Vision Research* 43: 879–885.

Injury and Repair: Stem Cells and Transplantation

B A Tucker and M J Young, Schepens Eye Research Institute, Harvard Medical School, Boston, MA, USA
H J Klassen, University of California, Irvine, Orange, CA, USA

Glossary

Choriocapillaris – Vascular layer of the eye, located between the sclera and Bruch's membrane.
Ganglioside – A component of the cell membrane involved in signal transduction.
Neuroprotection – Halting apoptotic cell death of neurons through delivery of diffusible growth factors.
Proteoglycans – A unique class of heavily glycosylated glycoproteins.
Tetraspanins – A family of membrane proteins with four transmembrane domains.

Introduction

The use of surgical procedures for the treatment of blinding conditions has a long history, most notably for cataract. In the modern era, refinements in ophthalmologic techniques and pharmacology have greatly expanded the range of available interventions for a host of ocular conditions. Nevertheless, conditions involving the loss of nonregenerating cell types remain a persistent therapeutic challenge. In the case of diseases involving the loss of corneal endothelial cells, tissue transplantation has proven successful, even though the limited availability of donor corneas restricts the use of this approach.

More problematic are diseases involving the loss of retinal neurons and retinal pigment epithelial (RPE) cells where few, if any, options are currently available to the treating clinician. As a group, diseases of this type are common and examples include age-related macular degeneration, retinal detachment, retinitis pigmentosa, as well as various forms of optic neuropathy, including glaucoma. In addition, common retinal vascular diseases such as diabetic retinopathy and vascular occlusive disease frequently involve retinal cell loss. Given the prevalence of visual disability resulting from these conditions, novel methods of both preserving and replacing retinal neurons are sorely needed.

Early Transplant Work

Over the last several decades, experimental work in rodents has made considerable progress in neuroprotection as well as cell and tissue transplantation in the setting of retinal cell loss. Seminal work by LaVail and Steinberg demonstrated the power of growth factor-mediated neuroprotection for retinal degeneration, both hereditary and acquired. Work by Lund's group showed that transplanted retinal tissue can, to a certain extent, engraft and integrate with the recipient visual system. Work by the Turner and Gouras laboratories showed that RPE transplantation can confer survival benefits to host photoreceptors following placement in the subretinal space. This last observation was made in dystrophic Royal College of Surgeons (RCS) rats and was subsequently extended to a variety of manipulations in this model. Taken together, these early studies provided compelling evidence of efficacy in mammals.

Despite the above advances, however, significant limitations remained, thereby encumbering further development of these otherwise promising strategies. In the case of neuroprotection, a major challenge has been to find a method of sustained intraocular delivery that is not neutralized due to the rapid degradation of peptide growth factors by endogenous proteases. For neural transplantation, a perplexing challenge has been to find a method of promoting regeneration across injury-induced gliotic barriers. Furthermore, RPE cell transplantation was challenged by the apparent reluctance of grafted cells to reconstitute an orthotopic epithelial monolayer on Bruch's membrane. In all these cases, a compounding impediment to translation of these strategies was posed by the limited ability of the rodent eye to model an approach with tangible clinical relevance.

Within the past 10 years, new breakthroughs pertaining to the above challenges have emerged from the nascent field of stem cell transplantation, as will be discussed presently.

Neural Progenitor Cells

The first report of successful transplantation of stem-like cells to the retina was from Masayo Takahashi, then working in the laboratory of Fred Gage. The cells used were adult hippocampal progenitor cells (AHPCs), a clonally selected line of highly mitotic cells cultured from the brain of mature rats and genetically altered to express green fluorescent protein (GFP) as a reporter gene. This study showed a remarkable degree of apparently seamless integration of donor AHPCs into the immature retina of normal recipients. Although the cells fell short in terms of marker expression, their morphology, placement, and orientation were strikingly similar to resident retinal cell types.

In addition to working with Gage, we showed that AHPCs can also integrate into the diseased or injured retina of mature rats and that at least a degree of phenotypic marker expression was achievable, thereby underscoring the potential of using stem cells for cell replacement in the setting of common retinal disorders.

Together, these two studies with AHPCs stimulated considerable interest in stem cell research within the scientific community, particularly with respect to retinal applications. Initial work on cultured cells continued to focus on AHPCs as the first cell type with a demonstrated ability to integrate into the cytoarchitecture of the neural retina. These cells were shown to exhibit a number of nonimmunogenic properties and to express a number of important cytokines, as did similar brain-derived cells of human origin. Neural progenitor cells from the brains of human and GFP-mouse brain were compared in terms of surface marker expression. It was found that cultured neural progenitor populations consistently express 3-fucosyl-*N*-acetyl-lactosamine (CD15), GD(2) ganglioside, and the tetraspanin proteins CD9 and CD81 across species, whereas major histocompatibility complex (MHC) expression is more variable, specifically for class I antigens. Transplantation of the mouse cells showed that they exhibited characteristics of an immune-privileged cell type. Similar cells were later derived from the brain of the pig and cat.

Retinal Progenitor Cells

A significant limitation that emerged from the work with brain-derived progenitors was the difficulty in obtaining photoreceptor marker expression from these cells following engraftment in the retina. While it has been shown that recoverin expression can be induced under exceptional circumstances, it remained to be seen whether a stem-like cell could generate cells with outer segments that co-express multiple appropriate markers such as recoverin and rhodopsin. It was this challenge that led us to explore the possibility of deriving transplantable progenitor cell cultures from the mammalian neural retina.

Starting with newborn GFP-transgenic mice, we were able to grow cells from dissociated retinal tissue in the presence of mitogenic stimulation from epidermal growth factor (EGF). These cells were capable of expressing rhodopsin, either in culture under differentiation conditions or following engraftment in the host retina. We have obtained similar findings in work with porcine and human donor tissue of fetal origin. Following differentiation, either *in vitro* or *in vivo*, these cells have been shown to be capable of co-expressing rhodopsin and recoverin, consistent with rod photoreceptor phenotype. Retinal progenitor cells (RPCs) therefore represent a stem-like cell type that provides a potential source of new photoreceptors for retinal repair in the setting of various forms of diseases and injuries.

As mentioned above, transplantation of mature RPE cells for cell replacement has been hampered by the apparent inability of these cells to recreate an epithelial sheet and adhere to Bruch's membrane. In contrast, retinal and various types of neural progenitor cells have also shown an ability to integrate into the RPE monolayer, although it is not yet known if such cells can replace native RPE cells at the functional level. Recent work with pluripotent stem cells suggests that these represent a source for new retinal cells with functional properties.

Induced Pluripotent Stem Cells

A new development in stem cell biology that has changed the way we think about commitment and differentiation is a process known as direct reprogramming (**Figure 1**). Yamanaka and colleagues were the first to demonstrate this technique, in which somatic cells are reprogrammed to become pluripotent stem cells through the addition of several stemness transcription factors. They began with a type of skin cell known as a fibroblast, and inserted four transcription factors (Oct3/4, Klf4, Sox2, and c-Myc) using retroviruses. A subpopulation of the fibroblasts began expressing other markers of embryonic stem (ES) cells, such as nanog, and formed teratomas when transplanted into immunocompromised mice. Careful evaluation of the resulting cells revealed that they indeed had all the properties of ES cells, and have been termed induced pluripotent stem (iPS) cells.

There are several important ramifications of this work. First, this technology offers the promise of creating patient-specific stem cells. One could harvest skin cells from a donor, turn these cells into iPS cells, and subsequently differentiate this population into the cells of interest, which would then be transplanted back into the donor. Importantly, this would obviate the need for chronic immunosuppression and eliminate the risk of immunorejection of the grafted cells. Many of the ethical issues associated with ES cells would also be circumvented by using this technique, although as with most such developments, new and unexpected ethical questions arise. Thus far, no one has created a viable embryo through this technology, and indeed there are many biological hurdles standing in the way of this. However, as the theoretical possibility of using iPS cells for reproductive cloning exists, this work raises novel moral issues.

A number of technical barriers must be overcome before iPS cells can be useful for the treatment of disease. Foremost among these is the use of oncogenes (cancer-associated transcription factors) to reprogram fibroblasts. These genes often lead to tumorogenesis, and indeed scientists have seen cancerous growths from the

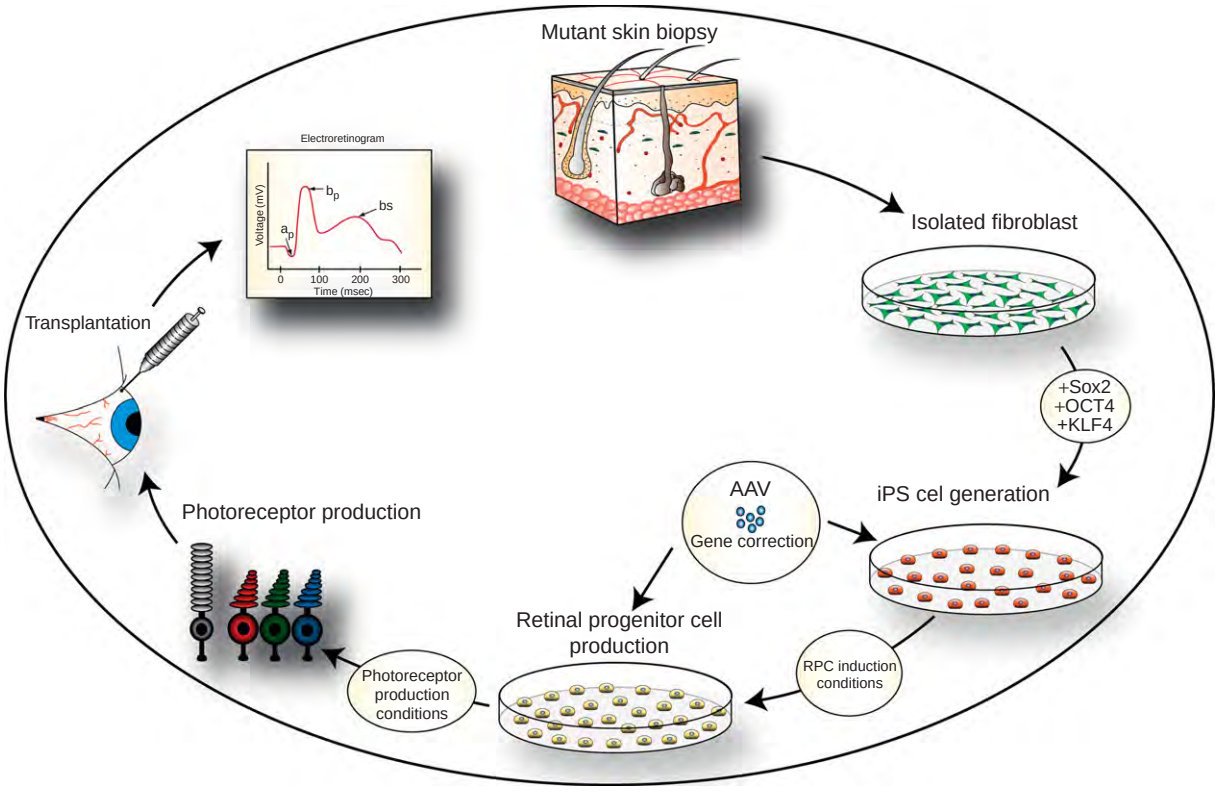

Figure 1 Schematic diagram illustrating the steps toward differentiation of reprogrammed fibroblasts into retinal neurons.

transplanted progeny of iPS cells. In addition, the use of retroviruses to deliver the four factors to the nuclei of the fibroblasts must be replaced by other means before using these cells in the clinic. It is worth noting, however, that in the months that followed the first publication of this technique, a flurry of scientific papers were published in which only two or three of the reprogramming factors were needed, and vectors other than retroviruses were used for gene insertion. This field is developing extremely rapidly, and it is likely only a matter of time until these methodological obstacles are overcome.

Stem Cells for Neuroprotection

In addition to cell replacement, stem-like cells have potential use in retinal neuroprotective strategies. We reported evidence that murine RPCs confer survival benefits to dysfunctional rods following transplantation to the retina of rhodopsin double knock-out mice. This result indicated that RPCs, or their more differentiated progeny, possess an inherent neuroprotective influence that is revealed in this setting. Interestingly, a similar finding was obtained in retinal dystrophic mice in work with a very different type of stem cell derived from the bone marrow.

Elucidating the mechanisms underlying such effects remains a subject of active interest; however, an alternative method for inducing neuroprotection via stem cells is to modify them genetically so as to over-express the therapeutic gene of interest. Gamm and colleagues have shown that brain-derived progenitor cells modified to ever express a GDNF transgene were capable of rescuing photoreceptor cells in the RCS rat following transplantation.

Retinal Transplantation

As suggested above, to achieve functional repair in patients afflicted with retinal degenerative disorders, there is an urgent need to reconstruct, via cellular replacement, the damaged or lost layers of the retina. During the past 30 years attempts have been made in order to achieve retinal regeneration via transplantation of developing donor material. Although significant progress and invaluable information have been acquired, visual restoration using this technique has not been achieved. For instance, although embryonic rat retina was shown to survive without immune rejection, develop normally, and continue to respond to light for up to 3 months post-transplantation, extensive host–donor integration was not identified. Similarly, comparable experiments performed in pig models of retinal dystrophy showed that although healthy retinal tissue from fetal donors survived and maintained proper laminar structure and cellular

organization for up 6 months post-transplantation, this tissue did not integrate with the host retina, and as such, did not aid in visual restoration. These findings collectively suggest that the eye is an amenable site for transplantation; however, the proper donor material or extracellular conditions have yet to be met.

Transplantation Strategies

Stem/progenitor cell transplantation as a means of inducing tissue reconstruction and functional regeneration has garnered extensive interest in the field of regenerative medicine. Unlike the solid tissue transplants mentioned above, stem cells have the ability to integrate within host tissue and develop into retinal specific cell types. For instance, in 2004, we were able to show that a subset of grafted RPCs gave rise to mature retinal ganglion and photoreceptor cells following transplantation. Since then, numerous studies reporting varying degrees of success have utilized an assortment of different cell types, including the fate-restricted photoreceptor precursor and the pluripotent ES cell. Regardless of the cell type used, efficient delivery methods are required. Traditionally, the two transplantation techniques most extensively utilized for cell delivery were vitreal cavity and subretinal space injections. Regardless of species, vitreal cavity injections generally involve insertion of a needle through the pars plana into the vitreal space, where in the case of mice, approximately 1 µl of cell suspension as a bolus is injected (**Figure 2(a)**). The subretinal space, unlike the vitreous, is actually a pseudo-space that is created upon detachment of the retina from the underlying RPE layer. Cellular injections into this space are performed by one of the two techniques. The first, which is very similar to that carried out during vitreal injections, involves entering the eye through the pars plana and inserting a needle beneath the retina via a precut hole, or retinotomy. Through this hole, fluid, most often saline, is injected, creating a retinal detachment and bleb into which the cell of choice can be delivered (**Figure 2(b)**). This approach generally requires a larger vitreal space in which to work and is often performed in larger models of retinal disease, such as the pig and human. The second technique, which is more often employed in smaller organisms such as rodents, is performed by making an incision through the sclera (sclerotomy), choriocapillaris, Bruch's membrane, and overlying RPE, through which a needle is inserted and saline is injected. This again creates a retinal detachment/bleb into which cells can be delivered (**Figure 2(c)**). The reasons for choosing one approach over the other are vast and may range from personal preference to surgical competence. However, more practical reasons for choosing vitreal or subretinal approaches for stem cell transplantation exist, including the type of injury and cell/retinal layer being targeted. For instance, subretinal transplantation would be more beneficial for targeting the retinal photoreceptor layer in retinal degenerative diseases such as retinitis pigmentosa (RP) and age-related macular degeneration (AMD), while vitreal transplantation would be more beneficial for targeting the inner nerve fiber layer in diseases such as glaucoma and various other optic neuropathies. Tailoring the transplantation approach to the specific disease at hand allows for larger numbers of cells to be provided to the area required. For instance, performing vitreous cavity injections of retinal stem cells as a treatment regime for photoreceptor cell replacement requires that the cells migrate through the entire thickness of the remaining retina before arriving at the desired location. With an increased distance for cellular migration, there is a greater chance that cells will take up residence in unwanted retinal layers, thus decreasing the chance that they will actually reach the appropriate target.

Polymer Substrates

Despite choosing the correct transplantation technique, the use of bolus cell injection as a delivery method is actually quite inefficient and typically results in massive cellular efflux, low cellular survival, and poor integration. For example, it has previously been suggested that as little as 0.1% of transplanted retinal stem cells actually survive for an extended period of time following traditional bolus injection. Issues such as these, which hinder functional regeneration, are largely accounted for by the lack of cellular support and trauma associated with the injection processes. For instance, in a recent publication we were able to show that the shearing forces placed on retinal stem cells by passing them through the typical glass injection needle resulted in nearly 60% cell death at 3 days post-passage. When the glass injection needle was replaced with a large bore pipette, cell death was reduced to less than 2%. However, even if a large bore pipette could be used during the transplantation process, the fact remains that a large portion of the cells injected would still be lost to efflux via the implantation port. This is especially true when attempting to place cells into the subretinal space through an opening in either the retina or sclera. One approach that we have developed in an attempt to circumvent these issues is to apply tissue-engineering techniques focused on the use of biodegradable polymer scaffolds as cell delivery vehicles. In one study we were able to show that the transplantation of retinal stem cells on a biocompatible poly(lactic-*co*-glycolic acid) (PLGA) polymer resulted in greatly reduced cell death and prevented leakage and migration of retinal stem cells away from the transplantation site. This resulted in significantly improved cellular integration when compared to bolus cell injections.

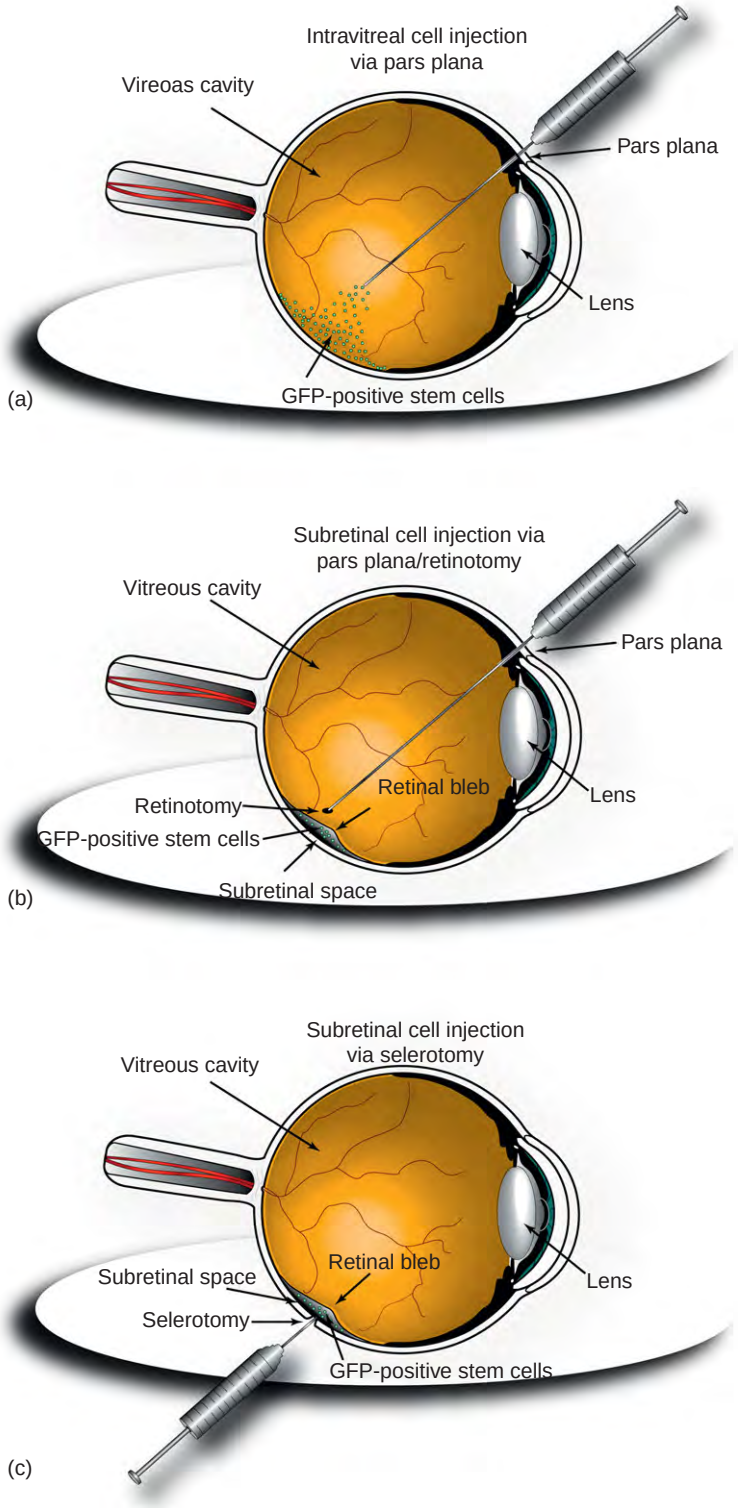

Figure 2 Schematic diagram illustrating three transplantation techniques.

Inhibitory Barriers

Although we have developed an efficient means of cell delivery, in order to achieve functional regeneration via retinal reconstruction/repopulation, a further increase in cellular integration and axonal extension/synapse formation is required. As suggested above, a major contributor to the lack of functional regeneration in the face of efficient

cell delivery is the presence of an inhibitory extracellular environment. Unlike the peripheral nervous system (PNS), the central nervous system (CNS) is stricken with an abundance of myelin-associated extracellular matrix (ECM) proteins, namely MAG, Nogo, and Omgp, which are well known for their ability to inhibit process extension and functional regeneration. The optic nerve, like other CNS locations, is laden with these inhibitory proteins, and as such, their chemical and/or enzymatic neutralization has been shown to significantly enhance retinal ganglion cell axon extension and optic nerve regeneration. Thus, in order for stem cell therapies to be used as an effective treatment for diseases such as glaucoma, which affect the retinal ganglion cell layer and optic nerve, inhibition of these proteins will ultimately be required.

Unlike the optic nerve, the retina is void of myelin, oligodendrocytes, and their associated inhibitory ECM molecules. Thus, these factors are not a concern when attempting to stimulate regeneration in retinal degenerative diseases such as RP and AMD, both of which predominantly affect the retinal outer nuclear layer. Why then are attempts at stimulating retinal regeneration via stem cell transplantation still largely unsuccessful? The lack of functional integration following transplantation is in large part due to the presence of an inhibitory injury induced glial scar that forms during reactive gliosis. In the retina, reactive gliosis is predominantly characterized by Müller glial activation, as indicated by upregulation of intermediate filament proteins such as glial fibrillary acidic protein (GFAP) (**Figure 3(a)**, red) and the projection of processes from their original location (forming the outer limiting membrane) into the subretinal space. Here, these processes proceed to form a dense fibrotic barrier that contains a variety of growth inhibitory ECM/adhesion molecules, which include the chondritin sulfate proteoglycan (CSPG) Neurocan (**Figure 3(a)**, blue) and the hyaluronan-binding glycoprotein CD44 (**Figure 3(b)**, red). Both Neurocan and CD44 have previously been shown to function as chemical inhibitors to axon growth and cellular migration, thus preventing regeneration and functional synapse formation. A variety of approaches have been taken in an attempt to remove these inhibitory ECM molecules, including enzymatic degradation of the proteins themselves. One such enzyme that we have utilized for this purpose is the matrix metalloproteinase 2 (MMP2). MMPs are well known for their ability to degrade a variety of ECM and cell adhesion molecules, including CD44, the CSPGs, and the aforementioned myelin-associated inhibitors. MMP2, in particular, has been shown to cleave both CD44 and Neurocan, thus releasing their negative hold on axonal extension and cellular migration. In a recent study, we discovered that endogenous MMP2 induction resulted in glial barrier-associated CD44 and Neurocan degradation at the outer limits of heavily scarred degenerating retinas, subsequently stimulating integration and synapse formation between the host and healthy transplanted tissue grafts. Conversely, chemical and/or genetic inhibition/removal of MMP2 was shown to completely abolish stem cell migration and retinal repopulation. In light of these findings, we have developed a biodegradable PLGA polymer scaffold that, as in previous permutations, is capable of efficient cell delivery and also possesses the ability to provide a sustained controlled release of active MMP2 following degradation (MMP2-PLGA). Subretinal transplantation of this polymer in conjunction with retinal stem cells as a composite graft has resulted in efficient glial barrier degradation and enhanced stem cell integration. This new polymer scaffold will undoubtedly act as an invaluable transplantation tool

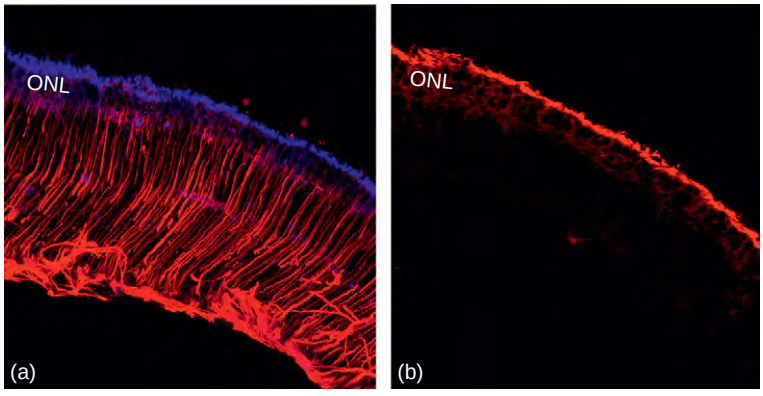

Figure 3 Injury-induced Müller cell activation stimulates inhibitory ECM molecule deposition and glial barrier formation. Eyes from adult retinal degenerative mice (Rho–/–) were enucleated, fixed, cryoprotected, sectioned, and immunostained for GFAP, CD44, and Neurocan. (a) Representative micrograph illustrating CD44 (blue) and GFAP (red) expression in the adult degenerative Rho–/– mouse retina. Activated Müller cells extend processes through the degenerating photoreceptor layer (ONL) into the subretinal space and deposit CD44 at the outer limits of the retina. (b) Representative micrograph illustrating neurocan (red) expression in the adult Rho–/– mouse retina. Inhibitory glial barrier-associated proteins, CD44 and Neurocan, deposited at the outer limits of the degenerating retina. Inhibitory CD44 and Neurocan molecules are intertwined within the degenerating photoreceptor layer, preventing cellular/axonal integration following subretinal transplantation.

for targeted repopulation of the retinal and restoration of vision.

Conclusions

Regardless of the source of the transplanted material, retinal transplants aim to rescue or replace injured photoreceptors. It is likely that each of these objectives will require different cell types as donor tissue. For example, rescue of diseased rods may be accomplished by delivering nonengrafting mesenchymal stem cells, or perhaps with engrafting neural stem cells. In these cases, rescue would be achieved by the delivery of growth factors such as glial cell-derived neurotrophic factor (GDNF) or brain-derived neurotrophic factor (BDNF) in a nonspecific fashion, possibly to cells other than photoreceptors (e.g., Müller glia). Engraftment and long-termed survival is a requirement if rescue of the diseased photoreceptors is to be prolonged. In contrast, repair through reconstruction involves a more complicated and indeed more difficult set of concerns. Cell replacement not only requires engraftment and long-termed survival, but also necessitates differentiation.

A cell type that can differentiate into fully mature, functional photoreceptors narrows the field of players somewhat. While a hematopoetic or stromal stem cell may by somewhat ill-suited to such a task, retinal stem cells or ES cells may be ideal candidates.

See also: Coordinating Division and Differentiation in Retinal Development; Injury and Repair: Retinal Remodeling; Injury and Repair Responses: Retinal Detachment; Primary Photoreceptor Degenerations: Retinitis Pigmentosa; Primary Photoreceptor Degenerations: Terminology; Retinal Ganglion Cell Apoptosis and Neuroprotection; Retinal Histogenesis; The Vascular Stem Cell; Zebrafish: Retinal Development and Regeneration.

Further Reading

Caroni, P. and Schwab, M. E. (1988). Two membrane protein fractions from rat central myelin with inhibitory properties for neurite growth and fibroblast spreading. *Journal of Cell Biology* 106: 1281–1288.

Kajita, M., Itoh, Y., Chiba, T., et al. (2001). Membrane-type 1 matrix metalloproteinase cleaves CD44 and promotes cell migration. *Journal of Cell Biology* 153: 893–904.

Klassen, H. and Lund, R. D. (1987). Retinal transplants can drive a pupillary reflex in host rat brains. *Proceedings of the National Academy of Sciences of the United States of America* 84: 6958–6960.

Klassen, H. J., Ng, T. F., Kurimoto, Y., et al. (2004). Multipotent retinal progenitors express developmental markers, differentiate into retinal neurons, and preserve light-mediated behavior. *Investigative Ophthalmology and Visual Science* 45: 4167–4173.

Lamba, D. A., Karl, M. O., Ware, C. B., and Reh, T. A. (2006). Efficient generation of retinal progenitor cells from human embryonic stem cells. *Proceedings of the National Academy of Sciences of the United States of America* 103: 12769–12774.

LaVail, M. M., Unoki, K., Yasumura, D., et al. (1992). Multiple growth factors, cytokines, and neurotrophins rescue photoreceptors from the damaging effects of constant light. *Proceedings of the National Academy of Sciences of the United States of America* 89: 11249–11253.

MacLaren, R. E., Pearson, R. A., MacNeil, A., et al. (2006). Retinal repair by transplantation of photoreceptor precursors. *Nature* 444: 203–207.

Nakagawa, M., Koyanagi, M., Tanabe, K., et al. (2008). Generation of induced pluripotent stem cells without Myc from mouse and human fibroblasts. *Nature Biotechnology* 26: 101–106.

Osakada, F., Ikeda, H., Mandai, M., et al. (2008). Toward the generation of rod and cone photoreceptors from mouse, monkey and human embryonic stem cells. *Nature Biotechnology* 26: 215–224.

Park, I. H., Zhao, R., West, J. A., et al. (2008). Reprogramming of human somatic cells to pluripotency with defined factors. *Nature* 451: 141–146.

Sheedlo, H. J., Li, L., and Turner, J. E. (1989). Photoreceptor cell rescue in the RCS rat by RPE transplantation: A therapeutic approach in a model of inherited retinal dystrophy. *Progress in Clinical and Biological Research* 314: 645–658.

Takahashi, M., Palmer, T. D., Takahashi, J., and Gage, F. H. (1998). Widespread integration and survival of adult-derived neural progenitor cells in the developing optic retina. *Molecular and Cellular Neuroscience* 12: 340–348.

Tomita, M., Lavik, E., Klassen, H., et al. (2005). Biodegradable polymer composite grafts promote the survival and differentiation of retinal progenitor cells. *Stem Cells* 23: 1579–1588.

Zhang, Y., Klassen, H. J., Tucker, B. A., Perez, M. T., and Young, M. J. (2007). CNS progenitor cells promote a permissive environment for neurite outgrowth via a matrix metalloproteinase-2-dependent mechanism. *Journal of Neuroscience* 27: 4499–4506.

Relevant Websites

http://www.blindness.org – Foundation Fighting Blindness.
http://www.hsci.harvard.edu – Harvard Stem Cell Institute.
http://webvision.med.utah.edu – John Moran Eye Center, University of Utah, Webvision.
http://www.schepens.harvard.edu – Schepens Eye Research Institute, Michael Young.

Innate Immune System and the Eye

M S Gregory, Schepens Eye Research Institute, Harvard Medical School, Boston, MA, USA

Glossary

Endocytosis – The process by which cells absorb molecules, such as proteins, from outside the cell by engulfing them with their cell membrane to form an endosome.
Endophthalmitis – An infection of the posterior of the eye.
Opsinization – The process by which a pathogen or infected cell is marked for destruction by a phagocyte.
Phagocytosis – The engulfment of solid particles, such as bacteria, by the cell membrane to form an internal phagosome.

Introduction

Innate immunity comprises a large number of molecules and cells that recognize and respond rapidly to pathogens, providing immediate defense against infection. However, innate immunity also carries with it the potential of highly destructive inflammation that presents an important dilemma for the eye. Inflammation is necessary for successfully eradicating pathogens. An ideal response would eliminate the microorganisms before they are able to directly damage any ocular tissues. The innate immunity would be limited and produce little or no damage to the surrounding normal tissues. However, some types of ocular infections trigger inflammation that is either (1) insufficient to clear the microorganisms, resulting in direct destruction of ocular tissue by the pathogen, or (2) excessive inflammation that clears the microorganisms, but destroys a significant amount of normal tissue. Either of these two scenarios is undesirable and can lead to significant loss of vision. Therefore, a delicate balance must be achieved between the amount of inflammation required for pathogen clearance and the amount of nonspecific tissue damage.

The innate immune system of the eye is similar to other mucosal surfaces. The first tier is passive consisting of several anatomic, physical, and chemical barriers that work together to prevent infection without inducing inflammation. The second tier is active consisting of cellular and secretory components that together cause acute inflammation aimed at eradicating the pathogen. The delicate tissues of the eye that make up the visual axis (cornea, lens, and retina) have a very low tolerance for inflammation, as a very small amount of damage can produce a significant loss of vision. The two-tiered system helps to prevent unnecessary inflammation and the active mechanisms of innate immunity are only turned on once the passive barriers have been breached. Both the passive and active arms of ocular innate immunity are the focus of this article.

Passive Innate Defense System

Anatomic and Physical Barriers

Several anatomic and physical barriers protect the anterior and posterior of the eye from invading pathogens (Figure 1). The active arm of innate immunity is only triggered when pathogens breach these barriers. The cornea is exposed to the external environment, making the anterior segment highly vulnerable to potential pathogen invasion. Therefore, the anterior segment possesses a multilayer barrier system that includes: eyelids and eyelashes, tear film, and the corneal epithelium. By contrast, the posterior segment is not exposed to the external environment, and is therefore less vulnerable to infection. The critical barriers of the posterior segment include (1) the retinal pigment epithelium (RPE), which lies between the blood-rich choroid and the neural retina, and (2) the posterior lens capsule that forms the barrier between the anterior and posterior segments. Each component of the passive innate defense system is described briefly below.

Eyelids and eyelashes

The outermost barrier of the ocular surface consists of the eyelids and eyelashes. The eyelashes protect the ocular surface from dust and foreign debris. The regular blinking action of the eyelids moves the tears across the ocular surface, washing away potentially colonizing or infecting organisms.

Tear film

Tears form the second barrier, lubricating and protecting the ocular surface. Tears also posses a potent defense system that limits the growth, colonization, and survival of microorganisms. The tear film consists of three layers: the outermost lipid layer, an aqueous layer, and the inner mucus layer (Figure 2). The lipid layer lubricates the eyelid and slows evaporation of the aqueous tear film layer. The aqueous layer forms the major component of the tear film and contains numerous antimicrobial

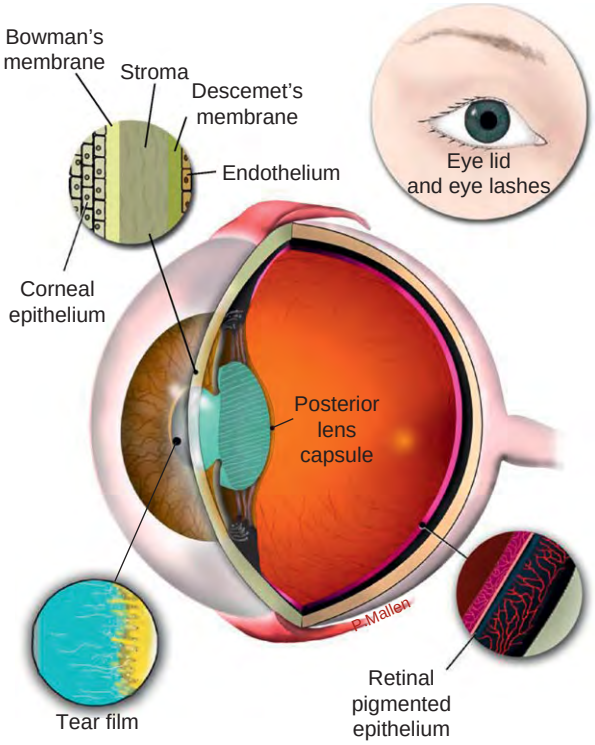

Figure 1 Anatomic and physical barriers of the eye. The eyelid, eye lashes, tear film, and corneal epithelium serve as barriers of the anterior segment of the eye. The posterior lens capsule and RPE serve as barriers of the posterior segment of the eye.

proteins including: lysozyme, lactoferrin, defensins, secretory IgA (sIgA), and complement. Many of these antimicrobial proteins are constitutively expressed and provide early, broad-spectrum protection against invading pathogens and also prevent the overgrowth of commensal bacteria. The innermost mucus layer of the tear film is made up of secreted and membrane-bound mucins that protect the epithelium from debris, pathogens, and desiccation. Mucins are high-molecular weight glycoproteins characterized by extensive *O*-glycosylation. Membrane-bound mucins expressed by the ocular surface epithelia include MUC1, MUC4, and MUC16. Secreted mucins are also found in the mucus layer and include MUC2, MUC5AC, and MUC19. The membrane-bound mucins anchor the ocular tear film to the corneal epithelium and are thought to act as a physical barrier against pathogen penetrance. Secreted mucins bind to pathogens in the tear film, facilitating their clearance from the ocular surface. Under normal conditions, mucin production and secretion by goblet cells and corneal epithelial cells are constitutive. However, mucin production can also be induced via Toll-like receptors (TLRs) expressed on the surface of corneal epithelial cells. Moreover, inflammatory cytokines, such as IL-1β, IL-6, and TNFα, have also been shown to induce mucin production and secretion. Together, these data reveal that constitutively expressed mucins make up a critical component of the passive defense system, while at the same time, upregulation of mucin production and secretion can also be a product of the active arm of innate immunity in the eye.

Corneal epithelium

The final barrier of the ocular surface consists of nonkeratinized stratified epithelial cells bound together by tight junctions. The corneal epithelium acts as a physical barrier to invasion of microorganisms due to the presence of epithelial intercellular tight junctions and the rapid renewal of epithelial cells with frequent shedding of the superficial layers of potentially infected epithelium. As mentioned in the previous section, the epithelium also expresses membrane-bound mucins that inhibit bacterial binding to the epithelial surface and produce several of the antimicrobial factors that are present in the ocular tear film.

Posterior lens capsule

The posterior lens capsule forms a physical barrier between the anterior and posterior segments of the eye after extracapsular cataract surgery and prevents the spread of microorganisms from the anterior chamber into the posterior chamber in the postsurgical eye. The best example of this is the fact that an intact posterior lens capsule is critical in preventing endophthalmitis following cataract surgery. Contamination of the aqueous humor can occur during cataract surgery. However, the pathogens are quickly cleared and endophthalmitis does not develop. By contrast, when the posterior capsule is breached, the rate of endophthalmitis increases significantly. This supports the finding that the anterior segment is much more efficient at clearing bacteria as compared to the posterior segment. Studies suggest the difference in ability to clear pathogens in the anterior versus posterior of the eye may be linked to expression of antimicrobial peptides. One major difference is that the AH is continuously secreted and drained, whereas the vitreous humor is not. The vitreous also offers greater opportunity for microbes to bind its fibrils. However, the exact molecular mechanisms involved remain unclear.

Retinal pigment epithelium

The RPE consists of a single layer of cells joined by tight junctions that lie between the photoreceptors of the neural retina and the blood-rich choroid. The RPE serves multiple functions aimed at protecting and maintaining the health of the neural retina. RPE cells (1) phagocytose shed disks from the photoreceptor outer segments and recycle their components; (2) transport nutrients from the choroid to the retina; (3) absorb light; (4) provide adhesive properties for the retina; and (5) serve as a rich source of cytokines, chemokines, and growth factors. More recently, RPE have also been linked to immunity and have been

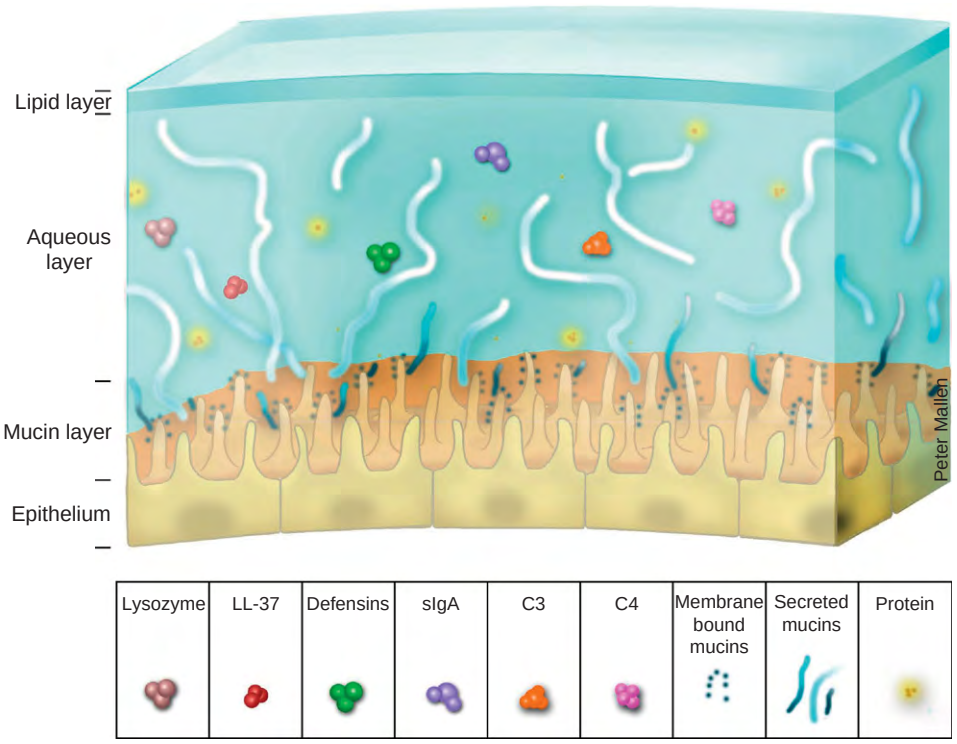

Figure 2 Ocular tear film. The ocular tear film is composed of three layers: the outermost lipid layer, the aqueous layer, and the innermost mucus or mucin layer. The lipid layer lubricates the eyelid and slows evaporation of the aqueous tear film layer. The aqueous layer forms the major component of the tear film and contains numerous antimicrobial proteins including: lysozyme, cathelicidin (LL-37), defensins, secretary IgA (sIgA), and complement components (C3 and C4). The mucin layer acts as a physical barrier against pathogen invasion and consists of both membrane bound and secreted mucins.

shown to behave as antigen-presenting cells that phagocytose pathogens, produce cytokines, and present pathogen-derived peptides to sensitized T cells. Therefore, while RPE acts as a physical barrier to the posterior segment, it is also important in shaping and regulating the adaptive immune response once this barrier has been breached.

Chemical Barriers

In addition to the anatomic and physical barriers designed to block invasive pathogens, there are also a number of soluble factors that inhibit bacterial growth, adherence, and survival. Several of these factors are constitutively expressed at low levels, providing a baseline of protection from foreign pathogens. However, many of these factors can also be upregulated in response to pathogens and inflammation; thus, these become an important product of the active arm of innate immunity. Some of the more important factors are discussed in more detail below.

Lysozyme

Lysozyme is bacteriacidal and makes up 20–40% of the total tear protein. Lysozyme kills bacteria by (1) binding to and creating pores in the bacterial cell wall, or (2) dissolving bacterial membranes by enzymatic digestion.

Secretory phospholipase A_2

Secretory phospholipase A_2 exhibits potent antibacterial activity against Gram-positive bacteria. Similar to lysozyme, secretory phospholipase A_2 dissolves bacterial membranes by hydrolyzing the principal phospholipid, phosphatidylglycerol.

Cathelicidin (LL-37)

LL-37 is a small cationic peptide with potent antimicrobial activity against Gram-positive and Gram-negative bacteria as well some viruses. The precise mechanism of action is incompletely understood, but it is widely believed that the antimicrobial activity is due to disruption of the microbial membrane or viral envelope.

Defensins

Beta defensins are expressed in epithelial cells that line mucosal surfaces such as the cornea. Similar to LL-37, defensins have a broad spectrum of antimicrobial activity and are effective against: Gram-positive and Gram-negative bacteria, fungi, and enveloped viruses. In addition to their antimicrobial activities, defensins modulate a variety of cellular activities including immune cell chemotaxis, epithelial proliferation, cytokine secretion, and stimulation of histamine release from mast cells. Human

corneal epithelial cells constitutively express human beta defensin-1 (hBD-1) and hBD-3. By contrast, hBD-2 is induced in response to corneal injury, infection, or inflammation, and is approximately 10-fold more potent than hBD-1 with an even wider antibacterial spectrum. Therefore, while hBD1 and hBD-3 provide a baseline defense to protect the cornea from infection, upon injury or microbial invasion, hBD-2 is upregulated and displays increased antimicrobial activity.

Lactoferrin

Lactoferrin is bacteriostatic and binds to and depletes iron from the tear film, which is required for microbial metabolism and growth. Lactoferrin is also bactericidal and permeabilizes membranes of Gram-positive and Gram-negative bacteria. Additional functions of lactoferrin have also been described: (1) inhibits biofilm development, (2) inhibits bacterial adhesion to host cells, (3) inhibits intracellular invasion, (4) amplifies apoptotic signals in infected cells, and (5) enhances bactericidal activity of neutrophils.

Lipocalin-A

Lipocalin A prevents bacteria from obtaining iron, an essential nutrient for microorganism survival. However, unlike lactoferrin, lipocalin-A does not bind iron directly. Lipocalin-A inhibits the iron acquisition system of microbes by binding to and blocking microbial sidephores used to transport iron into bacteria.

Secretory IgA

sIgA protects the ocular surface against colonization and possible invasion by pathogenic microorganisms by binding to bacteria and facilitating clearance. In addition, sIgA can opsonize bacteria for phagocytosis.

Complement

Complement components (such as C3 and C4) are constitutively expressed in the tear film and are involved in phagocytic chemotaxis, opsonization, and lysis of bacteria. The eye is unusual in that there is a constitutive low level of activated complement that is present even in uninfected normal eyes. It is believed that this low level of activated complement provides innate immune surveillance of microbes and allows for a rapid activation of the full complement cascade upon pathogen invasion.

Active Innate Defense System

Pattern Recognition Receptors

Innate immunity develops rapidly and is described historically as nonspecific, while adaptive immunity develops slowly and is antigen-specific. However, the discovery of pattern recognition receptors (PRRs) that detect unique pathogen-associated molecular patterns revealed a level of specificity in innate immunity that not only allows discrimination between self and non-self, but also allows the development of innate immunity tailored to specific pathogens, such as bacteria, viruses, and fungi.

There are two classes of PRRs: (1) TLRs and (2) nucleotide-binding oligomerization domain (NOD)-like receptors (NLRs) (**Table 1**). TLRs are expressed on the cell surface and detect pathogens at the cell membrane. TLRs are also expressed within endosomes and detect pathogens that have been endocytosed. By contrast, NLRs are expressed within in the cytoplasm and detect the presence of microbial molecules inside the host cell. These two classes of PRRs are discussed in detail below.

Toll-like receptors

TLRs are type 1 transmembrane proteins with an extracellular domain for ligand binding composed of leucine rich repeats and a cytoplasmic domain for intracellular signaling which is known as the Toll/IL-1 receptor (TIR) domain. TLRs recognize bacteria, viruses, fungi, protozoa, and endogenous ligands, such as heat shock proteins and fibrinogen. Triggering of the TLR leads to activation of the transcription factor, nuclear factor-kappa B (NF-κB), and the expression of pro-inflammatory molecules, such as TNF-α, IL-1, and IL-2. To date, 10 human TLRs have been identified and each TLR has a unique ligand specificity (**Table 1**). TLRs were first identified on innate immune cells: neutrophils, macrophages, monocytes, and dendritic cells. More recently, TLRs were also identified on epithelial cells that lie at the host/environment interface: skin, gastrointestinal tract, respiratory tract, and urogenital tract. Furthermore, several TLRs have been identified on ocular tissue in both the anterior and posterior segment of the eye, including cornea, iris, ciliary body, choroid, and RPE.

Similar to other barrier epithelium, several TLRs have been identified on the RPE and corneal epithelial cells and are vital for sensing microbes and triggering a rapid response to eliminate the pathogen. The study of TLRs in ocular immunity is still relatively new and debate remains over which TLRs are expressed in the eye and whether TLRs are expressed on the cell surface or within endosomes. However, it is clear that TLRs are required for initiation of innate immunity in the eye. This is supported by studies using TLR knockout mice that demonstrate a significant decrease in inflammation characterized by decreased neutrophil infiltration and increased susceptibility to infection in the absence of TLRs.

NOD-like receptors

The NLRs comprise a large family of cytoplasmic PRRs that recognize bacteria and endogenous danger signals such as uric acid (**Table 1**). All members of the NLR family share a conserved NOD. However, the NLR family

Table 1 TLR and NLR expression within the eye

	Ligand	*Location in the eye*
TLR1	Triacyl lipopeptides	Cornea, conjunctiva, RPE[a]
TLR2	Glycolipds, lipopeptides, lipoproteins, PGN, LTA, HSP70, zymosan	Cornea, onjunctiva, RPE
TLR3	dsRNA (viruses)	Cornea, conjunctiva, RPE
TLR4	Lipid A (Gram-negative bateria), LPS, bacterial HSP60, RSV coat protein	Cornea, conjunctiva, iris, ciliary body, choroid, whole retina, RPE
TLR5	Flagellin	Cornea, RPE
TLR6	Diacyl lipopeptides	Conjunctiva, RPE
TLR7	ssRNA (viruses)	Cornea, conjunctiva, RPE
TLR8	ssRNA (virsues)	None detected
TLR9	Unmethylated CpG motifs of bacterial DNA, dsDNA (viruses and bacteria)	Cornea, conjunctiva, RPE
TLR10	N/d	Cornea, conjunctiva, RPE
TLR11	profillin	N/d
NOD1	iE-DAP	Anterior and posterior portions of the eye,[b] HCE-T and HCE[c]
NOD2	MDP	Anterior portion, HCE-T and HCE
NALP1	Cell rupture	HCE-T and HCE
NALP2	N/d	HCE-T and HCE
NALP3	Bacterial RNA, toxins and ATP, uric acid	HCE-T and HCE
NALP10	N/d	HCE-T

[a]RPE: primary cultures of human retinal pigment epithelial cells.
[b]Anterior portion contains corneal tissues; posterior portion contains all other ocular tissues.
[c]HCE-T, SV-40 immortalized human corneal epithelial cell line; HCE, human primary corneal epithelial cells.
TLR, Toll-like receptor; NLR, NOD-like receptors (caspase recruitment domain-containing NODs and pyrin domain-containing NALPs); PGN, peptidoglycan; LTA, lipoteichoic acid; iE-DAP, γ-D-glutamyl-meso-diaminopimelic acid; RSV, respiratory syncytial virus; MDP, muramyl-dipeptide; N/d, not determined.

can be subdivided into three groups based upon their N-terminal domains: caspase recruitment domain (NODs), pyrin domain (NALPs), or baculovirus inhibitor repeat (neuronal apoptosis inhibitor proteins, NAIPs). At present, the human NLR family comprises of 23 proteins, while at least 34 NLR genes have been identified in mice. NALPs are unique in that upon binding to their ligand, NALPs form a complex termed the inflammasome resulting in caspase-1 activation and the release of active IL-1β. Recently, NALP1, 3, and 10 were identified in corneal epithelial cells, but their potential function in regulating ocular innate immunity has not been determined. NAIPs inhibit caspase effectors and are mainly expressed in neurons where their primary role is to protect against apoptosis. NAIPs have not yet been found in ocular tissues. NODs are the most extensively studied members of the NLR family and are expressed in ocular tissue.

Both NOD1 and NOD2 are constitutively expressed within the eye; NOD1 in the anterior and posterior segments of the eye and NOD2 only in the anterior segment. However, which specific tissues express NODs is unknown. NOD1 and NOD2 recognize specific subcomponents of bacterial peptidoglycan. NOD1 recognizes D-γ-glutamyl-meso-diaminopimelic acid, while NOD2 recognizes muramyl dipeptide. Recently, a mutation in NOD2 was linked to the development of uveitis in patients with Blau syndrome, suggesting that cytoplasmic NODs may be important in ocular inflammation. While the importance of NOD receptors in innate immunity and the pathogenesis of inflammatory disease are recognized outside the eye, the study of NODs within the eye is at an early stage. A complete understanding of ocular host defense will require a better understanding of where NODs and other NLRs are expressed and how they regulate innate immunity within the eye.

Complement

Similar to PRRs, the complement system acts as an innate immune surveillance system, detecting the first signs of pathogen invasion. The complement system was first identified as a biochemical cascade of serum proteins that help or complement antibodies to clear pathogens and mark them for opsinization by phagocytes. It is now known, however, that the complement system can also be activated directly by microbial products via the alternative pathway. Several studies demonstrate that complement is constitutively active at low levels in the eye. This is thought to be a primary defense mechanism of the eye against pathogenic infection. Upon pathogen invasion the complement system is further activated to clear the infection through (1) generation of inflammatory factors (C3 and C5a), (2) chemotaxis of phagocytes (C3 and C5a), (3) opsonization of Ab-coated cells (C3b), and (4) lysis of bacteria and virus-infected cells (C8 and C9).

Cytokines, Chemokines, and Effector Cells

Once pathogens breach the passive barriers of the eye and trigger the PRRs or the complement system, the primary function of innate immunity is to eliminate the invading pathogen as quickly as possible. To achieve this innate immunity must: (1) trigger an immediate immune response, (2) amplify the response, (3) clear the pathogens, and (4) activate the adaptive system if the pathogen cannot be cleared quickly. Cytokines, chemokines, and adhesion molecules play critical roles in regulating each of these stages.

Initiation and amplification

PRRs (TLRs and NLRs) recognize microbial products in the earliest phase of host defense and activate many immune and inflammatory genes, the products of which are important in initiating and amplifying antimicrobial immunity. Triggering TLRs on either the corneal epithelium or the RPE leads to activation of NF-κB via the (1) MyD88-dependent or (2) MyD88-independent pathway. The MyD88-dependent pathway is utilized via most TLRs (TLR1, 2, 4, 5, 6, 7, 8, and 9) and leads to the production of proinflammatory cytokines and chemokines (IL-6, IL-8, IL-18, MIP-1, and TNF-α). By contrast, only TLR3 and TLR4 utilize the MyD88-independent pathway and leads to the production of IFN-α and IFN-β. Recruitment of neutrophils into inflamed tissues is controlled predominantly by two chemokines (MIP-2 (= IL-8 in humans) and KC). In *Pseudomonas aeruginosa*-induced corneal keratitis, elevated MIP-2 and KC correspond with increased infiltration of neutrophils. In the posterior segment, elevated TNF-α, IL-1β, and CINC (rat homolog of IL-8) contribute to the breakdown of the blood–retinal barrier and the recruitment of neutrophils in response to *Staphylococcus aureus*. The adhesion molecules ICAM-1 and E-selectin are also upregulated early in iris, ciliary body, and retinal vessels, serving to enhance the infiltration of neutrophils to the site of infection.

Clearing the pathogen

In response to inflammatory cytokines and chemokines, neutrophils and macrophages are recruited to the site of infection. Bacterial clearance by neutrophils is accomplished by (1) phagocytosis, (2) generation of reactive oxygen species, and (3) the release of granule-associated enzymes: cathepsin G, myeloperoxidase, lactoferrin, and elastase. While the recruitment of neutrophils to the site of infection is essential for clearance of the pathogen, the persistence of neutrophils and the prolonged release of inflammatory mediators is also associated with nonspecific host tissue damage. Similar to neutrophils, macrophages also phagocytose and directly kill microbes as part of innate immunity. However, macrophages are also antigen-presenting cells, and as such participate in the development of the adaptive immune response. The natural killer (NK) cell is another important innate effector cell in host defense against viral infections of the cornea such as herpes simplex virus type-1. NK cells respond in an antigen-independent manner and kill virus-infected host cells through the release of perforin and granzymes or through binding of the death receptors Fas and TRAIL-R on the target cell. If innate effector cells fail to clear the infection, adaptive immunity will take over and finish eradicating the pathogen. However, if the infection is successfully cleared, the final and most important step of innate immunity is preventing nonspecific host tissue damage. This is accomplished in the eye through several mechanisms that together make up innate immune privilege.

Innate Immune Privilege

The primary role of innate immunity is to rapidly eradicate invading pathogens through the induction of inflammation. As a general rule, the level of inflammation is proportional to the size and virulence of the infection. Small, nonvirulent infections are cleared by mild inflammation, while larger, more virulent infections induce intense inflammation. The potential danger of inflammation occurs when intense and/or prolonged inflammation threatens the surrounding normal tissue, resulting in nonspecific tissue damage and scarring. The potential danger of inflammation in the eye is magnified by the presence of irreplaceable and highly sensitive ocular tissues. Therefore, it is not surprising that immune privilege in the eye has multiple mechanisms to control innate immunity and limit nonspecific tissue damage. The aqueous humor contains multiple factors that directly inhibit innate immunity including: (1) TGF-β, soluble Fas ligand, and alpha-melanocyte stimulating hormone (inhibit neutrophil activation); (2) macrophage migration inhibitory factor (inhibits NK cell-dependent lysis of target cells); (3) calcitonin gene-related peptide (inhibits nitric oxide release from activated macrophages); and (4) complement regulatory factors: CD46, CD55, CD59, and Crry (inhibit complement activation). These factors work together to limit the damaging consequences of inflammation and to preserve the visual axis. Unfortunately, while these mechanisms evolved to limit local tissue destruction and preserve the visual axis, they may leave the eye more vulnerable to organisms whose virulence often requires a robust inflammatory response for eradication. Therefore, a delicate balance must be made between the amount of inflammation needed for eradicating the pathogen and the amount of nonspecific tissue damage.

Link between Innate and Adaptive Immunity

Innate and adaptive immunity have long been discussed as separate arms of the immune system. However, it is

increasingly clear that they are indeed not separate but highly integrated. Several studies, both outside and inside the eye, identified the dendritic cell as a central link between innate and adaptive immunity. Immature dendritic cells reside in peripheral tissues and through triggering of TLRs, participate in the primary immune response against microbial infections. Immature dendritic cells encounter invading pathogens, capture bacterial antigens, and migrate to the draining lymph node. Once in the lymph node, only mature dendritic cells can efficiently prime naïve T cells and initiate adaptive immunity. Studies using TLR and MYD88 deficient mice, reveal that TLR signaling is required for bacteria-induced maturation of dendritic cells and induction of adaptive immunity. Therefore, TLRs on dendritic cells are essential for (1) sensing the microbe and initiating the immediate innate immune response, as well as (2) inducing the development of an adaptive immune response. While dendritic cells have been identified in the cornea and retina, additional studies are needed to completely understand their function in linking innate and adaptive immunity within the eye.

Conclusion

Innate immunity is a critical first line of defense against ocular infections. However, the regulation of innate immunity within the eye is just beginning to be unraveled. The identification of TLRs and NLRs has provided new insights into the mechanisms of host defense and the pathogenesis of inflammatory diseases. A better understanding of how microbial agents and endogenous host factors interact with TLRs and NLRs in the eye will be critical in advancing our knowledge of the pathogenesis of infectious and noninfectious eye diseases. Moreover, a better understanding of these mechanisms will lead to the identification of new therapeutic targets for treating and preventing sight-threatening infections.

See also: Corneal Epithelium: Wound Healing Junctions, Attachment to Stroma Receptors, Matrix Metalloproteinases, Intracellular Communications; Defense Mechanisms of Tears and Ocular Surface; Immunosuppressive and Anti-Inflammatory Molecules that Maintain Immune Privilege of the Eye; Ocular Mucins; Retinal Pigmented Epithelium Barrier; Role of Complement in Ocular Immune Response; Tear Film Overview.

Further Reading

Banchereau, J. and Steinman, R. M. (1998). Dendritic cells and the control of immunity. *Nature* 392: 245–252.

Creagh, E. M. and O'Neill, A. J. (2006). TLRs, NLRs and RLRs: A trinity of pathogen sensors that co-operate in innate immunity. *Trends in Immunology* 27: 352–357.

Gregory, M., Callegan, M. C., and Gilmore, M. S. (2007). Role of bacterial and host factors in infectious endophthalmitis. *Chemical Immunology and Allergy* 92: 266–275.

Haynes, R. J., McElveen, J. E., Dua, H. S., Tighe, P. J., and Liversidge, J. (2000). Expression of human beta-defensins in intraocular tissues. *Journal of Investigative Ophthalmology and Visual Science* 41: 3026–3031.

Holtkamp, G. M., Kijlstra, A., Peek, R., and de Vos, A. F. (2001). Retinal pigment epithelium–immune system interactions: Cytokine production and cytokine-induced changes. *Progress in Retinal and Eye Research* 20: 29–48.

Kaplan, H. J. and Niederkorn, J. Y. (2007). Regional immunity and immune privilege. *Chemical Immunology and Allergy* 92: 11–26.

Kawai, T. and Akira, S. (2007). TLR signaling. *Seminars in Immunology* 19: 24–32.

Kolls, J. K., McCray, P. B., and Chan, Y. R. (2008). Cytokine-mediated regulation of antimicrobial proteins. *Nature Reviews Immunology* 8: 829–835.

Pearlman, E., Johnson, A., Adhikary, G., et al. (2008). Toll-like receptors at the ocular surface. *Ocular Surface* 6: 108–116.

Rodriguez-Martinez, S., Cancion-Diaz, M. E., Jimenez-Zamudio, L., et al. (2005). TLRs and NODs mRNA expression pattern in healthy mouse eye. *British Journal of Ophthalmology* 89: 904–910.

Sack, R. A., Nunes, I., Beaton, A., and Morris, C. (2001). Host-defense mechanism of the ocular surfaces. *Bioscience Reports* 21: 463–480.

Sohn, J. H., Bora, P. S., Jha, P., et al. (2007). Complement, innate immunity and ocular disease. *Chemical Immunology and Allergy* 92: 105–114.

Streilein, W. J. and Stein-Streilein, J. (2000). Does innate immune privilege exist? *Journal of Leukocyte Biology* 67: 479–487.

Tosi, M. F. (2005). Innate immune responses to infection. *Journal Allergy and Clinical Immunology* 116: 241–249.

Van Vilet, S. J., den Dunnen, J., Gringhuis, S. I., Geijtenbeek, T. B., and Van Kooyk, Y. (2007). Innate signaling and regulation of dendritic cell immunity. *Current Opinion in Immunology* 19: 435–440.

Innate Immunity and Angiogenesis

S Frantz, Medizinische Universitaetsklinik, Wuerzburg, Germany
K A Vincent and R A Kelly, Genzyme Corporation, Framingham, MA, USA

Glossary

Angiogenesis – The definition of angiogenesis – also termed neovascularization – in the context of this article refers to new blood vessel formation and growth following development. The process of angiogenesis is highly sensitive to hypoxia (i.e., a low cellular oxygen content within cells), which is sensed by a family of transcription factors or master switch proteins present in all nucleated cells, termed hypoxia inducible factors (HIFs). These in turn trigger the transcription, synthesis, and release of cascades of pro-angiogenic cytokines, including, among others, vascular endothelial growth factors (VEGFs), hepatocyte growth factor (HGF), and inflammation-related cytokines such as tumor necrosis factor alpha TNF-α.

Hemostasis – Limitation of blood loss following injury due to localized vasoconstriction, pressure applied to the bleeding site, or by mechanical means (e.g., sutures).

HGF – Hepatocyte growth factor (HGF), in addition to its role in hepatic (liver) development, also plays a key role in the growth and remodeling of blood vessels in response to tissue hypoxia as well as triggering release of inflammatory signals that can accelerate and stabilize nascent (i.e., new) arterioles.

Innate immunity – Innate immunity, also termed nonadaptive or natural immunity, is the evolutionarily ancient, germ-line encoded, hardwired components of the immune system, which trigger rapid, albeit relatively nonselective, recognition and subsequent destruction and removal of possible pathogens.
A large and growing number of pathogen-associated molecular patterns (PAMPs) have been identified to date, that are characterized by specific molecular motifs on a wide variety of potentially infectious organisms. These highly conserved molecular motifs are, in turn, recognized or sensed by specific molecular motifs termed pattern recognition receptors (PRRs), which can trigger an initial, rapid innate immune response. Importantly, long-term suppression of specific pathogens in vertebrates requires recognition by, and subsequent activation of, an appropriate innate immune response. Thus, the initial innate, and subsequently acquired, pathogen-specific immune responses are typically both necessary for long-term pathogen suppression.

iNOS (inducible nitric oxide synthase (iNOS)) – It is an enzyme associated with innate immunity as activation of this enzyme can trigger release of relatively large amounts of oxygen radicals that limited pathogen growth. iNOS activation also causes vasodilation which facilitates increased blood flow to regions of injury or infection, as well as producing oxygen radicals that suppress pathogen growth.

PAMPs (pathogen-related molecular pattern ligands) and PRRs (pattern recognition receptors) – These refer to specific, phenotypically stable, molecular motifs, or patterns that are characteristic of infectious organisms but not normal host tissue or cells.

Selection pressure – During evolution, changes in the environment over time, which may affect access to supplies of energy, water, and other essentials, generate a selection pressure in which those organisms whose genetic make-up provides an survival advantage in the current environment may thrive, while those whose genetic background is not as favorable for survival will be at a disadvantage. This concept applies to vertebrates as much as to viral or bacterial evolution.

siRNAs (small interfering RNAs) – siRNA disruptions occur naturally and play an important role in the regulation of the expression and/or degradation of RNA transcripts, which affects the synthesis and/or degradation of multiple proteins. Artificial siRNA constructs are now being widely used as highly specific reagents to selectively increase or suppress transcription of selected gene. Mutiple clinical trials using these novel reagents are now in progress.

Toll-like receptors (TLRs) – TLRs, originally identified in the fruit fly *Drosophila*, are families of trans-membrane proteins that were among the first innate immunity signaling proteins to be identified that provided a contextual, danger signal in the presence of potential pathogens. Different classes of TLRs recognize distinct molecular motifs termed pathogen-associated molecular patterns (PAMPs) on pathogenic organisms. The innate immune system is germ-line encoded in the fly as well as

vertebrates, although the fly has no capacity for a specific adaptive immune response, that is, a more rapid, extensive, and importantly specific immune response following on a repeat challenge to the same pathogen.

Transcription – Transcription refers to the generation of messenger RNA (mRNA) sequence from a DNA sequence template. This is followed by translation of the mRNA sequence into an appropriate sequence of amino acids (i.e., a protein sequence).Vascular endothelial growth factors (VEGFs) – They are families of intercellular signaling proteins or cytokines that are principally involved in regulating blood vessel formation (angiogenesis) and the subsequent growth and remodeling of smaller vessels into larger vessels termed or arterioles, which is termed arteriogenesis.

Inflammation is a coordinated response triggered by either infection or tissue injury, the primary goals of which are the containment and, eventually, removal of pathogens followed by cellular repair and restoration of tissue homeostasis. In general, immunity to infection in vertebrates is mediated by two distinct, but complementary forms of immune response pathways: germ-line encoded innate immunity and acquired immune responses. Acquired (i.e., specific, targeted, and adaptive) immunity recognizes molecular motifs on pathogens by a trial and error process based on successive random gene rearrangement, followed by identification and rapid amplification of antigen receptors on B and T lymphocytes that are highly specific for epitopes on pathogens.

In contrast, the components of innate immunity (i.e., nonadaptive, or natural immunity) are expressed constitutively, act immediately, and are not dependent upon prior exposure to a specific pathogen. The innate immune system recognizes invariant molecular patterns shared by groups of potentially pathogenic microorganisms but not by host tissues, such as bacterial lipopolysaccharides (LPSs, also termed endotoxin), viral double-stranded RNA, or yeast cell wall mannans among others. These pathogen-associated molecular patterns or PAMPs are typically highly conserved since they are essential for the structural integrity and survival of their respective families of microbes. The innate immunity receptors for these largely invariant motifs on potential pathogens are germ-line-encoded, either soluble or cell-associated proteins, that exhibit a broad range of specificities to highly conserved structural motifs on specific families of pathogens (note that the nomenclature for some specific components of innate immunity has not yet been standardized; in this article, we will utilize principally the definitions as originally coined by Medzhitov and Janeway). Unlike the acquired or adaptive arm of the immune system, which gained the ability to evolve highly specific approaches to target pathogens, as noted above, the innate immune response is not a single entity, but rather a collection of relatively independent subsystems or modules. Importantly, selected components of innate immunity signaling also provide a contextual signal, that is, the recognition of highly conserved molecular motifs on potential pathogens.

The innate immune response is obviously imperfect and/or insufficient, however, in that serious infections sometimes do occur, while inappropriate activation or delayed downregulation of an immune response may sometimes injure the host, as in the case of autoimmunity, for example. Only metazoans (vertebrates) have evolved alternative strategies for dealing with repeated pathogen recognition and elimination, including the capacity to mount a more rapid, robust, and, importantly, specific response upon repeat exposure to a pathogenic organism.

Recent work suggests that specific protein sequences or epitopes related to certain products of tissue injury can be detected by innate immunity pattern recognition receptors or PRR's. Coined the Danger hypothesis, this postulate suggests that the appearance of epitopes characteristic of damaged or necrotic tissue, even in the absence of any evidence of an infection, will be recognized by components of the innate immune system. In support of this hypothesis, resting dendritic cells can be activated by damaged cells or necrotic debris, but not by healthy cells, or cells undergoing programmed cell death (i.e., apoptosis).

A review of recent data details a number of aspects of the evolutionary selection pressure that have resulted in strategies that vertebrates have evolved for the control of infection and wound repair. Despite the obvious differences between tissue destruction due to trauma compared to an infectious origin, for example, there are a number of responses to both forms of injury that have many common features. First, there is a high likelihood that some degree of infection will eventually accompany significant amount of tissue injury. Second, mechanisms that are important for pathogen recognition and removal are also necessary for wound repair and healing. For example, macrophages are necessary to both clear cellular debris and initiate tissue remodeling after injury, besides assisting in the suppression of pathogen growth.

Innate Immunity and Wound Healing

Following hemostasis, angiogenesis in injured tissue – an essential component in the process of wound healing – is dependent on the activation of different parts of the innate immune system, including inflammatory cytokines, toll-like receptors (TLRs), the receptor for advanced glycosylation end products (RAGEs), as well as transcription factors such as hypoxia inducible factor 1 alpha

(HIF-1α). The involvement of these essential elements links innate immunity and angiogenesis in the process of wound healing. Innate immunity cytokines – a generic term denoting relatively short, soluble extacellularc signaling proteins, such as angiopoietins, transforming growth factor beta (TGFβ), or members of the several VEGF families and their respective sub-isoforms – are essential for both angiogenesis (i.e., the process of endothelial cell division and sprouting) and arteriogenesis (i.e., the recruitment of pericytes and vascular smooth muscle cells), with subsequent circumferential growth of smaller vessels into arterioles. Inflammatory cytokines, such as tumor necrosis factor alpha (TNFα) and interleukins among others, released by neighboring cells (e.g., macrophages) also contribute to accelerated arteriolar growth, suppression of infection, and preservation of local tissue architecture. However, rapid pathogen growth and/or unrestrained release of inflammatory pro-angiogenic cytokines may also result in excessive tissue fibrosis (scarring), particularly if the initial inflammatory stimulus is not appropriately suppressed as infectious organisms are cleared. Ideally, damaged or infected cells would be phagocytosed (i.e., internalized by neighboring tissue macrophages), triggering only an appropriate degree of inflammation, which would subsequently suppressed as the infection is cleared.

The process of removal of cells with minimal inflammatory reaction is termed programmed cell death or apoptosis. Apoptosis is characterized in part by active suppression of inflammatory cytokine production by specialized scavenger cells (i.e., macrophage-derived, so-called professional phagocytes). In contrast, cells undergoing necrotic cell death induced by, among other causes, tissue trauma, infection, or profound hypoxia and acidosis contribute to a decline in both plasma and mitochondrial membrane potentials, ionic gradients that are essential to maintain cellular homeostasis. Typically, this results in rapid death of numerous cell types and the release of intracellular contents, which in turn triggers the synthesis and release of pro-inflammatory cytokines.

TLRs and Angiogenesis

Cells dying via necrosis also typically induce activation of innate immunity PRRs such as toll-like receptor-2 (TLR-2), which, when activated, initiate transcriptional responses that are qualitatively different from that induced by, for example, LPS binding to its innate immunity receptor, TLR-4. Activation of either signaling pathway leads to a series of distinct but complimentary pro-inflammatory downstream signaling cascades, many of which require activation of nuclear factor kappa B (NFκB)-dependent signaling pathways, which also facilitate both angiogenesis and arteriogenesis (see **Figure 1**).

Commonly encountered bacterial TLR ligands, such as LPS (also termed endotoxin) and flagellin among others can activate endothelial sprouting directly by signaling through TLRs, even in the absence of additional cytokines. The molecular pharmacology contributing to enhanced angiogenesis includes, for example, increased local tissue concentrations of adenosine and adenine nucleotides, autacoids (i.e., nonpeptidic, intercellular small molecule signals) that increase rapidly following cellular injury or ischemia. Animals with targeted disruption – also termed a gene knock-out – of adenosine A2A receptors, for example, exhibit not only less inflammation but also less wound-related angiogenesis following injury, suggesting that release of locally acting autacoids such as adenosine does contribute to accelerated wound healing. Indeed, several mammalian TLRs (specifically TLR2, -4, -7, and -9), in the presence of activating ligands such as LPS or unmethylated CpG motifs, synergistically induce the synthesis and release of multiple families of vascular endothelial growth factor (VEGF) isoforms, in the presence of adenosine acting at A2A receptors. As a consequence, the induction and extent of inflammation-induced angiogenesis is accelerated, while any further release of inflammatory cytokines (e.g., TNF-α, and IL-1β among others) may be moderated or even suppressed. In contrast, in the absence of adenosine release, although TLR activation continues to increase inflammatory cytokine expression, VEGF-A is suppressed (at least in murine macrophages *in vivo*).

This adenosine-mediated angiogenic switch triggers downstream intracellular signal transduction cascades involving intermediate adapter proteins such as MyD88, IRAK4, and TRAF6, among others (see **Figure 1**). Indeed, macrophages from mice with targeted disruption of MyD88 (i.e., MyD88 knock-outs), an essential component of intracellular TLR signaling cascades, as expected did not express any VEGF-A isoforms in response to either TLRs or to adenosine A2AR agonists. These results provide additional insight into the molecular pathways that contribute to wound healing. Skin wounds in $MyD88^{-/-}$ mice, for example, healed at a markedly slower rate than wounds in wild-type animals. Wound contraction and stabilization also decreased, which in turn delayed granulation tissue formation, in part, due to reduced microvascular blood vessel density, each of which was due in large part to a reduction in the expression of several VEGF isoforms, when compared to wild-type (i.e., $MyD88^{+/+}$) animals.

Another signaling pathway involved in innate immunity and the response to tissue injury is high mobility group box-1 (HMGB1), a protein which is released from cells in response to infection or injury. Activated HMGB1 triggers a cascade of innate immunity signaling pathways, including TLR4, as well as activation of several families of pro-angiogenic proteins. This cascade of signaling proteins is manifested, in large part, by the

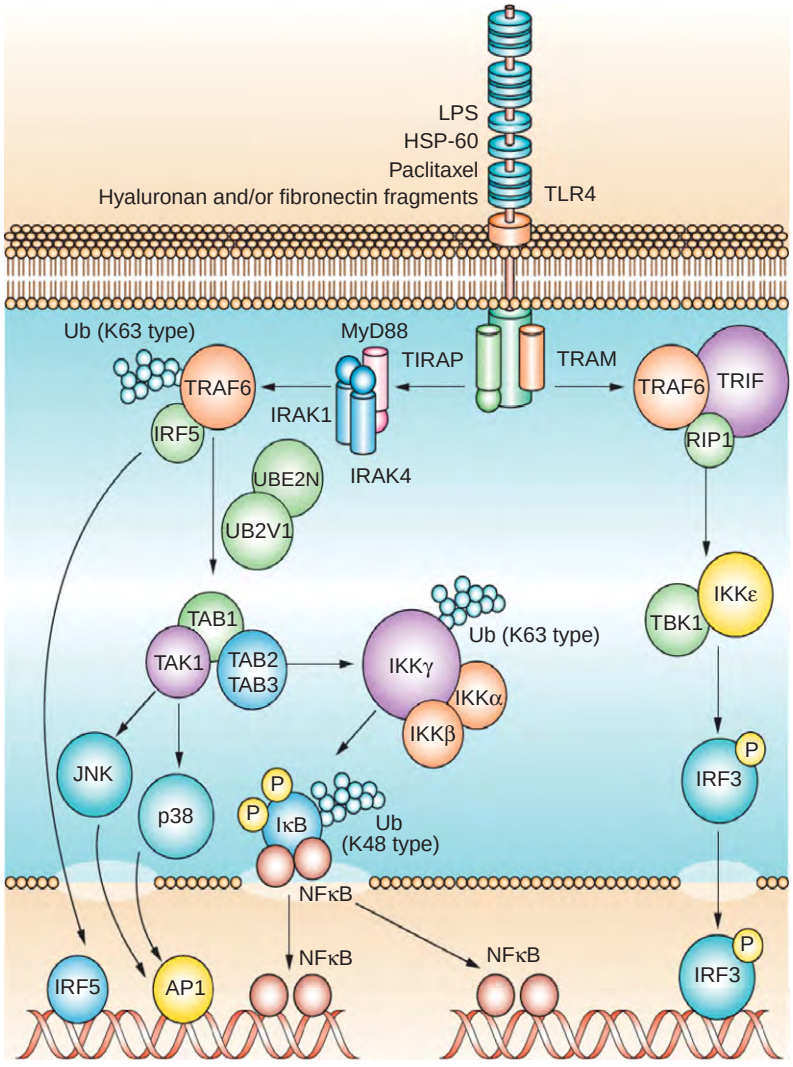

Figure 1 The toll-like receptor signaling pathway. Abbreviations: AP1, activator protein 1; HSP-60, heat shock protein 60; IκB, inhibitor of nuclear factor κ B; IKKα, inhibitor of nuclear factor κ B kinase α; IKKβ, inhibitor of nuclear factor κ B kinase β; IKKε, inhibitor of nuclear factor κ B kinase ε; IKKγ, inhibitor of nuclear factor κ B kinase γ; IRAK1, interleukin 1 receptor-associated kinase 1; IRAK4, interleukin 1 receptor-associated kinase 4; IRF3, interferon regulatory factor 3; IRF5, interferon regulatory factor 5; JNK, c-jun N-terminal kinase; LPS, lipopolysaccharide; MyD88, myeloid differentiation primary response protein; NFκB, nuclear factor κ B; RIP1, receptor-interacting protein 1; TAB1, TAK1-binding protein 1; TAB2–TAB3, TAK1-binding proteins 2 and 3; TAK1 (M3K7), transforming growth factor-β-activated kinase 1; TBK1, serine–threonine-protein kinase; TIRAP, TIR domain-containing adaptor protein; TLR4, toll-like receptor 4; TRAF6, tumor necrosis factor receptor-associated factor 6; TRAM, TRIF-related adaptor molecule; TRIF, TIR-domain-containing adaptor inducing interferon β; Ub, ubiquitin; UB2V1, ubiquitin-conjugating enzyme E2 variant 1; UBE2N, ubiquitin-conjugating enzyme E2N.

RAGEs. Animals with targeted disruption of RAGE, for example, have significantly less heart muscle damage in ischemia-reperfusion assays when compared to normal, wild-type, control animals.

HIF-1α: At the Intersection of Angiogenesis and Innate Immunity

The transcription factor HIF-1α and its related isoforms play a relatively unique role following development, in that they regulate, either directly or indirectly, a series of physiologic regulatory pathways that include both oxidative phosphorylation as well as glycolytic pathways for the generation of ATP. All three HIF isoforms require binding (i.e., dimerization) to a protein termed the arylhydrocarbon receptor nuclear translocator or ARNT for short (also termed HIF-1β), in order to initiate gene transcription. Hypoxia-dependent activity of all of the HIF-1 isoforms is regulated via hydroxylation of highly conserved proline residues, a reaction catalyzed by oxygen-sensing prolylhydroxlyases (PHDs). Induction of

HIF-1α signaling is well known to orchestrate the expression of genes that regulate multiple families of proteins that are involved in angiogenesis and tissue repair. These include most VEGF family members and their related subisoforms, as well as other angiogenic cytokines, including, but not limited to, platelet-derived growth factor (PDGF), PlGF, and the several known angiopoeitin isoforms, among others.

Importantly, the appropriate physiologic suppression of HIF-dependent signaling is equally important with regard to this family of pro-angiogenic transcription factors, depending on the cellular and physiologic context. For example, excessive and/or continuous activation of HIF signaling may lead to vascular malformations, or facilitate the development of a blood supply to a nascent, hypoxic subclinical tumor. There are, therefore, a number of autoregulatory mechanisms that limit HIF isoform activity as tissue hypoxia improves, including upregulation of PHD gene expression, which acts as a feedback mechanism to suppress HIF activity in the short term. During sustained or chronic hypoxia, however, continuous overactivation of PHD signaling appears to induce a new set point or equilibrium for intracellular O_2 homeostasis. This is characterized by sustained low levels of HIF isoform expression despite continuously low intracellular levels of tissue oxygen content, thereby prolonging cell survival.

HIF-1 activation in many cell types also regulates the expression of a number of proteins involved in apoptosis. In endothelial cells studied *in vitro* for example, HIF-1α decreased apoptosis in response to hypoxic stress followed by rapid re-oxygenation (often termed reperfusion injury). This models the common clinical scenario observed in patients who develop a rapidly occlusive clot in, for example, a large coronary artery, resulting in myocardial ischemia or infarction. These are then treated by a clot-dissolving, thrombolytic drug or by coronary artery catheterization and physical removal of the clot. Rapid restoration of oxygenated blood flow into an area of ischemic tissue is essential – particularly in tissues such as the brain, kidney, and the heart – that have a continuously high metabolic demand for oxygen. However, the extent of tissue injury following ischemia is also impacted by the generation of reactive oxygen species (ROSs) which, somewhat counter intuitively perhaps, may result in additional damage to cells despite adequate tissue oxygen levels.

Genomic analyses of selected cell types transfected with constitutively active HIF-1α transgenes have also identified unconventional pro-angiogenic peptides that are regulated by HIF-1α, such as the natriuretic peptides atrial and brain natriuretic factor (ANP and BNP), for example, as well as growth factors such as insulin-like growth factor 1 (IGF-1), IGF-2, insulin-like growth factor binding protein 3 (IGFBP3), fibroblast growth factor 2 (FGF-2), TGFβ1 and epidermal growth factor (EGF), as well as neuregulins and inflammatory cytokines, including TNF-α and interleukin (IL)-1β, among other innate immunity agonists. LPS (i.e., endotoxin) alone, for example, even in the absence of inflammatory cytokines, has been shown to directly activate HIF-1α signaling to a greater extent than hypoxia. Indeed, a central role for HIF-1α in sustaining, if not initiating, inflammation was first revealed by selectively deleting HIF-1α only in leukocytes, using the enzyme *cre*-recombinase. The phenotype of the resulting leukocytes was surprisingly normal, but the affected cells did have reductions in many pro-angiogenic cytokines – all VEGF-A isoforms for example – as well as in genes involved in gluconeogenesis, a reflection of the essential role that the HIF isoforms play in maintaining and regulating energy homeostasis within most cell types. Genetically engineered, myeloid tissue-specific, VHL-deficient (VHL-LysM-CRE) mice lack the ability to suppress HIF-1α activation when oxygen is not limiting. These animals exhibited an exaggerated response to a number of pro-inflammatory signals in several tissues, such as arthritic changes in synovial joint tissue, even in the absence of any documented infectious etiology. Indeed, biopsies from patients with active arthritis exhibited increased levels of HIF-1α and HIF-2α expression in tissue sections, as well as increased bioactivity (i.e., increases in angiogenic cytokines such as VEGF-A isoforms, in synovial biopsies). Also, HIF-1α is known to regulate the expression of the inflammation-inducible isoform of nitric oxide synthase (i.e., iNOS), an effector arm of innate immunity. Levels of NO generated by iNOS are sufficient to induce bacteriostasis, as well as facilitating local vasodilation, both of which would tend to suppress infection and permit more rapid recruitment of inflammatory cells.

Another recently recognized link between HIF signaling and innate immunity was the discovery that induction of HIF-1α is dependent upon, among other pathways discussed above, the activation of NFκB signaling, and in particular IKK-β. More efficient utilization of glycolytic pathways may be one other potential benefit of the physiologic link between HIF-1 and IKK β-mediated regulation of inflammation, both of which are evolutionarily ancient signaling pathways. Consistent with this model are recent data that document increases in expression and transcriptional activity of both HIF-1α *and* HIF-1β (i.e., ARNT) in monocytes during differentiation into tissue macrophages. Indeed, activation of HIF-1α appears to be essential for the functional maturation of macrophage activity. Furthermore, several forms of ROSs – generated by H_2O_2 or by a nicotinamide adenine dinucleotide phosphate (NADPH) oxidase for example – are known to trigger stabilization and nuclear translocation of HIF-1α/ARNT heterodimers, a process that requires initiation of activation of NFκB.

Wound repair also requires sources of energy in the relatively hypoxic, inflammatory milieu of the healing tissue, a process termed metabolic reprogramming, that

is, switching from the use of oxygen as the primary electron donor to anaerobic metabolism. This metabolic switch depends in large part on the activation of the transcription factor peroxisome proliferator activated receptor (PPARα). This adaptation, perhaps somewhat counter-intuitively, results in the restriction of glycolytic intermediates entering into the tri-carboxylic acid cycle (TCA) cycle, while concurrently decreasing oxidative phosphorylation. This adaptation should diminish the risk of severe tissue ischemia, while concurrently minimizing oxygen radical damage to, in this case, skeletal muscle fibers.

Other, related transcriptional regulators that have recently been shown to mitigate tissue hypoxia, by inducing activation of several angiogenenic signaling cascades, include the peroxisome–proliferator-activated receptor coactivator-1α (PCG-1) which, following dimerization with the orphan receptor ERR-α, regulates oxidative phosphorylation, induces gluconeogenesis, and upregulates all VEGF-A isoforms, although by a mechanism that is distinct from HIF-1α/ARNT heterodimer signaling. For example, iron chelators such as desferoxamine, which reliably induce HIFα expression and activation, do not enhance PCG-1α-dependent VEGF isoform secretion).

There is also epigenetic regulatory control of numerous inflammatory and pro-angiogenenic pathways in the context the pathophysiology of cardiovascular diseases. Histone deacetylase (HDAC) inhibitors suppress, for example, TNF-α signaling in monocytes *in vitro*, but not necessarily *in vivo*, depending on the intracellular context. There are also important inter-species differences among mammals, such as the modest activation of human iNOS *in vitro* in response to inflammatory cytokines when compared to the much more robust responses observed in rodents, for example. As these authors note, our understanding of the epigenetic regulation of promoter specificity for many genes targeting innate immunity pathways remain poorly understood. Investigation of these regulatory signaling pathways will obviously continue to inform our knowledge of the roles of epigenetic factors at the interface of inflammation and angiogenesis.

Another area of increasingly focused investigation is the role of RNA silencing in the regulation of host defense, including the function of microRNAs (miRNA) and small interfering RNAs (siRNAs) in controlling gene expression in general. A recent study documented the phenotype of animals with an endothelial cell restricted, targeted deletion of mi-126, a miRNA expressed predominantly in areas of high vascular density, such as the heart and lungs. Deletion of mi-126 results in a number of vascular abnormalities, including, among others, severe ischemic injury in several vascular beds – including the heart – compared to control animals. Similar results with mi-126 were reported by Fish and collaborators in a zebra-fish model.

One of the more remarkable results noted recently are data from Kleinman and colleagues in the context of choroidal neovascularization (CNV). While testing a variety of siRNA constructs targeted to suppress neovascularization (i.e., VEGF-A isoform secretion) in the retina, these investigators noted that even non-targeted 21 nucleotide duplex siRNAs were able to suppress intraocular vascular proliferation as well as targeted constructs. For example, firefly luciferase siRNA, among several other siRNA's tested, was as effective in suppressing VEGF production in the retina as isoform-targeted, VEGF-A siRNA constructs. Given that naked siRNAs are not known to be internalized by mammalian cells, the most tractable hypothesis based on these data suggests that the innate immunity PRRs , and, in particular, TLR-3, recognize 21-mer or longer double-stranded RNA (dsRNAs) and suppress transcription. This additional activity of TLR3 was unanticipated, given that the majority of the work to date on the inflammatory effects downstream of the toll isoforms results in increased, not decreased, inflammation.

Summary

Activation of an innate immune response is among the first lines of defense following tissue injury. Restoration of blood flow to the site of injured tissue (i.e., angiogenesis) is a necessary prerequisite for successful tissue remodeling and wound repair. The HIF families of transcription factors play a pivotal role in both the induction of an innate immune response as well as the triggering of multiple pro-angiogenic signaling cascades that participate in wound repair and regeneration. The coordinated activation of these, among other innate immunity signaling cascades, are essential for initial suppression of pathogen growth, and are required for the release of multiple pro-angiogenic and innate immunity signaling pathways that facilitate tissue repair process which, when successful, results in a gradual return to normal tissue homeostasis.

See also: Adaptive Immune System and the Eye: Mucosal Immunity; Adaptive Immune System and the Eye: T Cell-Mediated Immunity; Angiogenesis in the Eye; Angiogenesis in Wound Healing; Innate Immune System and the Eye; Role of Complement in Ocular Immune Response.

Further Reading

Aragones, J., Schneider, M., Van Geyte, K., et al. (2008). Deficiency or inhibition of oxygen sensor Phd1 induces hypoxia tolerance by reprogramming basal metabolism. *Nature Genetics* 40(2): 170–180.

Arany, Z., Foo, S. Y., Ma, Y., et al. (2008). HIF-independent regulation of VEGF and angiogenesis by the transcriptional coactivator PGC-1alpha. *Nature* 451(7181): 1008–1012.

Barton, G. M. (2008). A calculated response: Control of inflammation by the innate immune system. *Journal of Clinical Investigation* 118(2): 413–420.

Cramer, T., Yamanishi, Y., Clausen, B. E., et al. (2003). HIF-1alpha is essential for myeloid cell-mediated inflammation. *Cell* 112(5): 645–657.

Goda, N., Dozier, S. J., and Johnson, R. S. (2003). HIF-1 in cell cycle regulation, apoptosis, and tumor progression. *Antioxid Redox Signal* 5(4): 467–473.

Gurtner, G. C., Werner, S., Barrandon, Y., and Longaker, M. T. (2008). Wound repair and regeneration. *Nature* 453(7193): 314–321.

Hayden, M. S. and Ghosh, S. (2008). Shared principles in NF-kappaB signaling. *Cell* 132(3): 344–362.

Kawai, T. and Akira, S. (2007). Signaling to NF-kappaB by toll-like receptors. *Trends in Molecular Medicine* 13(11): 460–469.

Kleinman, M. E., Yamada, K., Takeda, A., et al. (2008). Sequence- and target-independent angiogenesis suppression by siRNA via TLR3. *Nature* 452(7187): 591–597.

Matouk, C. C. and Marsden, P. A. (2008). Epigenetic regulation of vascular endothelial gene expression. *Circulation Research* 102(8): 873–887.

Matzinger, P. (2002). The danger model: A renewed sense of self. *Science* 296(5566): 301–305.

Medzhitov, R. (2007). Recognition of microorganisms and activation of the immune response. *Nature* 449(7164): 819–826.

Medzhitov, R. and Janeway, C. A., Jr (1997). Innate immunity: The virtues of a nonclonal system of recognition. *Cell* 91(3): 295–298.

O'Neill, L. A. (2008). 'Fine tuning' TLR signaling. *Nature Immunology* 9(5): 459–461.

Stiehl, D. P., Wirthner, R., Koditz, J., et al. (2006). Increased prolyl 4-hydroxylase domain proteins compensate for decreased oxygen levels. Evidence for an autoregulatory oxygen-sensing system. *Journal of Biological Chemistry* 281(33): 23482–23491.

Intraocular Pressure and Damage of Optic Nerve Axons

R W Nickells, University of Wisconsin, Madison, WI, USA

Glossary

Apoptosis – The molecular and biochemical process by which a cell soma (cell body) is able to disassemble all of its organelles and break apart to be engulfed by neighboring cells. As the process is intrinsic, and tightly regulated by the cell itself, it has often been called a cell suicide program. Apoptosis is the mechanism of cell elimination during development (programmed cell death) and is often the end-stage result of cell loss in a variety of diseases, particularly chronic neurodegenerative disorders. Retinal ganglion cell soma apoptosis is the mechanism of cell loss in glaucoma.

Axons – The single extensions of neurons that act as the conduit for an electrical impulse or signal originating from the soma of the same neuron. They typically terminate in a synapse that contacts one of many dendrites of other neurons. In reference to glaucoma, axons of the retinal ganglion cells pass out of the eye into the optic nerve.

Glia – The abundant non-neuronal cell types in the nervous system. There are many different classifications of glia, but principally they are made up of astrocytes, Müller cells (in the retina), oligodendrocytes or Schwann cells (which synthesize myelin in the central and peripheral nervous systems, respectively), and microglia. Astrocytes and Müller cells are thought to function as neuronal support cells under normal conditions. Microglia are thought to play an important role in the innate immune response of neural tissue.

Lamina cribrosa – In higher primates, it is the connective tissue and neuronal structure comprising the scleral canal at the site where the optic nerve exits the eye. The connective tissue is formed as plates of collagen and basement membrane and the surface of these plates are occupied by astrocytes and a secondary cell type called lamina cribrosa cells. Pore structures exist between the plates through which retinal ganglion cell axons are bundled as they exit the eye. Rodents do not have a lamina cribrosa, but instead have columns of astrocytes that surround the bundles of exiting axons. Because of the lack of connective tissue, this structure has been termed the cellular lamina in these animals.

Optic nerve – It is anatomically described as the second of the 12 paired cranial nerves and is an extension of the central nervous system. The nerve begins at the lamina cribrosa and extends to the lateral geniculate nucleus in higher primates and the superior colliculus in rodents. Shortly after it exits the eye, the fibers of the nerve, which are axons of retinal ganglion cells, become myelinated.

Retinal ganglion cells – The projection neurons that reside in the innermost layer of the retina, and extend axons out of the eye and into the optic nerve. They receive electrical stimulation from photoreceptors by way of bipolar neurons and then convey that stimulus to optical centers in the brain.

Soma – Also known as the cell body, it is anatomically and functionally distinct from the dendrites, axon, and synapse, even though these compartments are all part of the same cell. The soma contains the basic cellular organelles including the nucleus and the majority of endoplasmic reticulum and Golgi bodies. Retinal ganglion cell somas reside in the ganglion cell layer of the retina.

Introduction – Intraocular Pressure as a Risk Factor for Glaucoma

Glaucoma is one of the world's leading causes of blindness, estimated to affect over 60 million people worldwide by the year 2010. It is typically a disease of the elderly and often goes undetected until later stages because progression is usually not associated with pain, or the devastating loss of central vision. Instead, glaucoma progresses slowly, creating a series of small peripheral defects in vision (called scotomas) that are compensated for by processing in the visual centers of an affected individual. The development of these pathological blind spots is principally the result of the regional degeneration of the retinal ganglion cells, involving the loss of both the axon in the optic nerve, and the cell body (soma) in the retina. Once a critical number of cells are lost in the retina, light information from that specific region is unable to be transmitted to the brain.

Because of the slow progressive nature of the disease, early detection is paramount to establish treatments that can attenuate further damage to the retina and optic nerve. A critical part of the early detection arsenal is the association between elevated intraocular pressure (IOP) and glaucoma. Nearly every person with glaucoma has

either elevated IOP, or benefits from having existing levels of IOP lowered. In addition, experimentally induced ocular hypertension is a staple of virtually all animal models of the disease, while lowering elevated IOP in these models is associated with slowing the progression of glaucoma, thus providing experimental evidence for the causal relationship between eye pressure and optic nerve disease.

Currently, there is no clear mechanism that associates elevated IOP with the activation of optic nerve and retinal damage; however, studies over the last several decades have pointed to a viable model linking the two. At present, this model serves as a framework for both current and future hypothesis-driven studies that may help resolve this important question. Understanding the model requires a brief tutorial on the relevant anatomical structures of the eye. In essence, the mammalian eye is a closed hydrostatic system. The optics, which are designed to focus incoming light from the anterior segment of the eye onto the sensory retina lining the posterior segment of the eye, require that the globe be properly inflated. To do this, aqueous humor is secreted by cells of the ciliary body posterior to the iris and drained through the trabecular meshwork and Schlemm's canal, anterior to the iris. As light passes into the eye, and is focused onto the sensory retina, photons are captured by photoreceptors, where they are converted into chemical signals that are then processed by the neural network of the retina until finally reaching the retinal ganglion cells. Ganglion cells transmit these signals through axons that exit the globe, enter the optic nerve, and connect to neurons in visual centers in the brain. Anatomically, the axons from the ganglion cells typically form bundles and exit the globe through a posterior hole in the sclera called the lamina. In small mammals, such as rodents, the axon bundles in the laminar region are supported by columns of glial cells, principally astrocytes. This structure has been called the cellular lamina by some researchers to distinguish it from the lamina cribrosa (LC) found in the eyes of larger mammals such as primates. The LC accommodates larger numbers of ganglion cell axons (in the range of 1 million in higher primates versus 50 000–100 000 in rodents), which necessitates the presence of collagenous beams and plates that support the spaces through which the axon bundles pass (**Figure 1**). Similar to rodents, this region of the optic nerve is also populated with cells, including astrocytes, specialized cells referred to as LC cells, and microglia.

Biomechanical Engineering Studies

In a consideration of how elevated IOP causes the death of retinal ganglion cells, the lamina plays a central role. Several seminal studies on the pathophysiology of glaucoma have pointed to the laminar region of the optic nerve head as the first site of damage in glaucoma. The evidence for this comes from a variety of observations, notably classical studies showing the disruption of both retrograde and anterograde axoplasmic transport in response to elevated IOP (**Figure 2**), and more recent electron microscopic studies showing very early axonal disruption in the nerve head of a mouse model of glaucoma.

Intuitively, the lamina causes something of a dilemma when considering that the eye must be under some kind of pressure in order to maintain normal function, since it is essentially a hole in an otherwise closed, spherical, hydrostatic system. Thus, one might expect that forces generated by hydrostatic pressure within this system would be focused onto the weakest point, such as this small hole. Given the requirement for some level of pressure in the eye, it is likely that the evolutionary development of the lamina would be sufficiently strong enough to support the axons passing through it, so that they are not adversely affected by the forces concentrated on this area. However, in the face of above-normal levels of IOP, which would increase the forces directed at the laminar structure, axons could be damaged if the forces focused on this region exceeded the structural capacity it was designed to withstand.

This rather speculative model has been tested by biomechanical engineers using finite element modeling. In this complicated field of applied engineering, real-life measurements of the tensile strength of biological tissues are taken and used to design small elements that are pieced together to create a three-dimensional model of the biological system in question. Early finite element models of the eye were created based on mathematics of a simple sphere under pressure, and these models helped confirm the basic intuitive idea that forces created by pressure inside the globe create stress and strain on the structural integrity of the lamina (**Figure 1**). Important advances in the field finite element modeling in the study of glaucoma have come from detailed element modeling of both the sclera of the eye and the different components of the primate LC.

Modulation of Glia Behavior at the Optic Nerve Head and Dysfunction of Ganglion Cell Axons

When IOP becomes elevated, resulting in an increase in the stress placed in the laminar region, the cells in this region respond. The precise nature of this response is not fully understood, but detailed gene expression profiles of the optic nerve head region of rats with experimental glaucoma clearly indicate that the glial cells in this region upregulate the expression of genes involved in proliferation and remodeling of the extracellular matrix (ECM). Similar changes in gene expression have been noted in optic nerve astroctytes and LC cells in higher primates

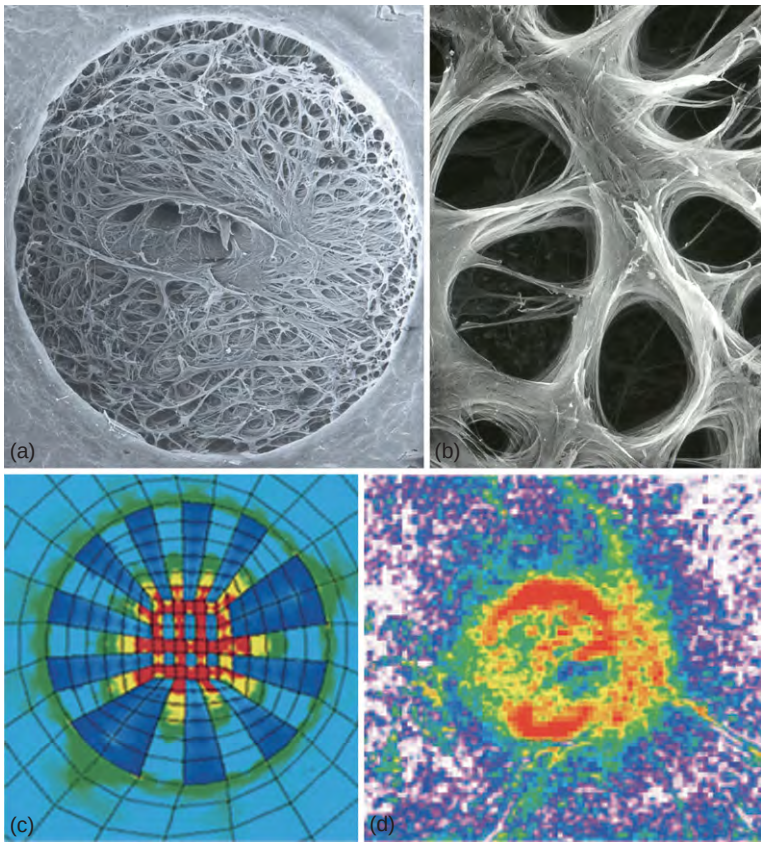

Figure 1 Increased strain associated with elevated IOP is directed onto the lamina cribrosa. (a) Scanning electron micrograph of a human lamina cribrosa after alkali treatment to remove soft tissue. The collagen-based laminar beams create an interacting network of plates and pores (higher magnification in (b)), through which bundles of retinal ganglion cell axons pass as they exit the eye and extend through the optic nerve. The diameter of the human scleral canal is approximately 1.7 mm, and the image shown is from the perspective of the vitreoretinal surface. (c) A contour stress plot of a finite element model of a human lamina. Models such as these predict that stresses generated by elevated IOP are concentrated on the laminar beams, with the highest stress (warm colors) occurring within the central beams. In addition to stress being applied to the beams, detailed histological studies also show an enlargement of the scleral canal. (d) A contour plot of tissue deformation of the lamina of a human donor eye. In this experiment, deformation was calculated as the topographical difference between the vitreoretinal interface when exposed to 15 and 50 mmHg. Experimentally, maximal deformation does not take place at the center of the lamina. (a and b) Courtesy of Dr. Harry A. Quigley, Wilmer Eye Institute, Johns Hopkins School of Medicine. (c) Reproduced from Bellezza, A. J., Hart, R. T., and Burgoyne, C. F. (2000). The optic nerve head as a biomechanical structure: initial finite element modeling. *Investigative Ophthalmology and Visual Science* 41: 2991–3000, with permission from the Association for Research in Vision and Ophthalmology. (d) Reproduced from Sigal, I. A, Flanagan, J. G., Tertinegg, I., and Ethier, C. R. (2004). Finite element modeling of optic nerve head biomechanics. *Investigative Ophthalmology and Visual Science* 45: 4378–4387, with permission from the Association for Research in Vision and Ophthalmology.

with experimental glaucoma and in the human disease. Early interpretations of these changes in gene expression generally assumed that cells in this region were responding to the loss of ganglion cell nerve fibers by laying down a glial scar. This notion has recently been challenged by biomechanical studies of the connective tissue composition of the laminas isolated from monkeys at the very early stages of experimental glaucomatous damage. In detailed three-dimensional reconstructions of serially sectioned nerve heads, in which each section was individually stained for ECM components, this group showed that connective tissue content increased in the laminar region well in advance of the loss of neuronal tissue. Surprisingly, the ratio of connective tissue to neural tissue remained relatively constant, indicative of an increase in the thickness of the laminar region caused by the addition of new ECM material in the posterior region of the lamina and an actual widening of the scleral canal. Progressively, the connective tissue lamina begins to deform posteriorly partly as a function of the loss of ECM material in the anterior portion of the lamina, and, at later stages of glaucomatous progression, partly as a function of the loss of ganglion cell axons entering the optic nerve head. Eventually, the posterior deformation becomes permanent, resulting in the classic cupping of the optic nerve head observed clinically.

The interpretation of these changes in the optic nerve head in early glaucoma is that the glial cells in this region are responding to the tremendous increase in stress and strain induced by the elevation in IOP, by laying down

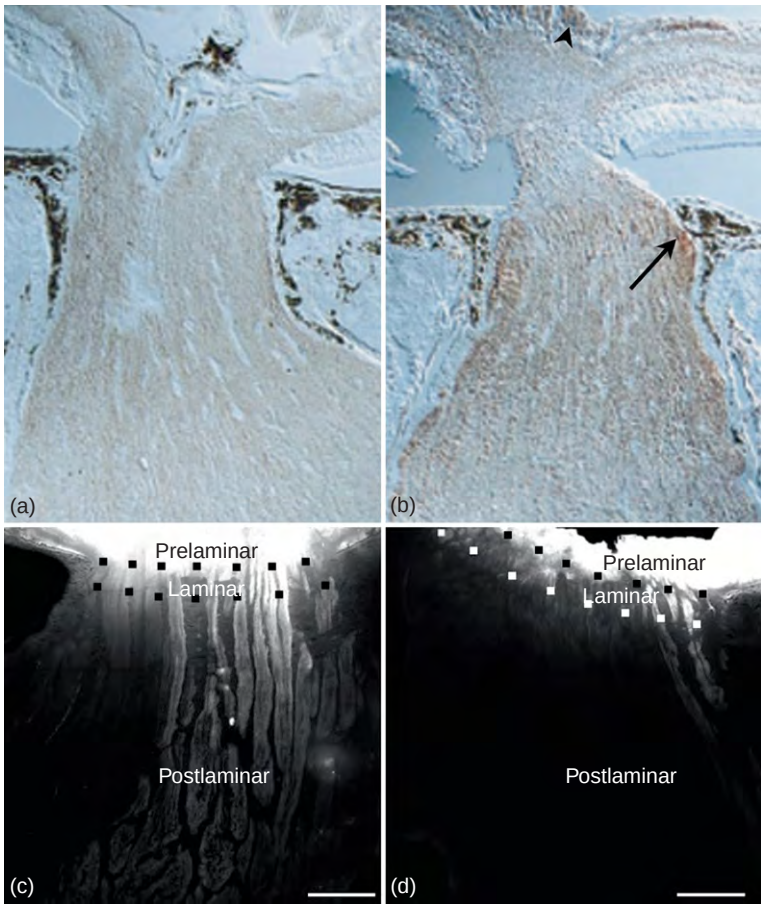

Figure 2 Ocular hypertension and glaucoma are associated with a blockage of axonal transport. (a and b) Immunohistochemical staining for the TrkB neurotrophin receptor in the optic nerve of rat eyes under normal IOP (a) or experimentally induced ocular hypertension (b). The TrkB receptor typically binds neurotrophic factors, such as brain-derived neurotrophic factor (BDNF), at ganglion cell synaptic connections in the brain. Once bound, TrkB is internalized and transported retrogradely to the ganglion cell somas. During periods of ocular hypertension, TrkB receptor accumulates at the level of the cellular lamina in the rat eye (arrow), while focal accumulations of this receptor can also be detected in the nerve fiber layer of the retina (arrowhead). These findings are consistent with a blockade of retrograde axonal transport during ocular hypertension. (c and d) Blockade of anterograde axonal transport in a porcine model of ocular hypertension. In this experiment, rhodamine β-isothiocyanate (RITC) was injected into the vitreous of pig eyes, which were then subjected to elevations in IOP for 6 h (d). Eyes under normal IOP (c) show uptake and transport of the RITC along the axons of the optic nerve. Ocular hypertensive eyes exhibit little to no transport of this dye past the laminar region. (a and b) Reproduced from Pease, M. E., McKinnon, S. J., Quigley, H. A., Kerrigan-Baumrind, L. A., and Zack, D. J. (2000) Obstructed axonal transport of BDNF and its receptor TrkB in experimental glaucoma. *Investigative Ophthalmology and Visual Science* 41: 764–774, with permission from the Association for Research in Vision and Ophthalmology. (c and d) Reproduced from Balaratnasingam, C., Morgan, W. H., Bass, L., et al. (2007) Axonal transport and cytoskeletal changes in the laminar regions after elevated intraocular pressure. *Investigative Ophthalmology and Visual Science* 48: 3632–3644, with permission from the Association for Research in Vision and Ophthalmology. Scale (in (c) and (d)) = 400 μm.

new connective tissue in an effort to increase the mechanical strength of the lamina. Addition of material to the posterior surface of the lamina ensures, at least in the short term, that axons will be minimally damaged in the process. Ultimately, this process appears to be a losing battle, as axons become progressively more damaged and begin to degenerate, the optic nerve head becomes a series of collapsed connective tissue plates. A critical question in the pathophysiology of glaucoma is what ultimately causes the damage to the axons in this region.

Several theories have been postulated for the source of the axonal damage. The earliest of these were contradictory models that postulated either (1) a decrease in blood flow to the optic nerve head, creating an ischemic environment for the ganglion cell axons, or (2) direct mechanical damage to the axons as they passed through the connective tissue plates of the lamina such that they were being crimped as the plates underwent the process of posterior deformation. More recent models have predicted that the altered function of the astrocytes and microglia in this region leads to the release of toxic molecules. Several studies have suggested that these toxins could range from highly reactive nitric oxide radicals mediated by the activity of nitric oxide synthase-(NOS)-2 to tumor necrosis factor α (TNFα), which is produced by astrocytes under stress conditions and can activate retinal ganglion

cell death. Regarding this hypothesis, although many questions remain unanswered, experimental evidence is clear that astrocytes, microglia, and possibly LC cells become reactive in the glaucomatous optic nerve head (Figure 3), leading to molecular and behavioral changes that have been associated with pathology in several other neurodegenerative disorders.

Others, however, have reasoned that the initial responses of glia in the nerve head are just as likely trying to protect the axons as they compensate for the increased mechanical strain. Protective effects of astrocytes can include becoming a source of trophic factors for damaged neurons. In addition, they also act as the principal source of glycogen stores in the central nervous system (CNS), and are typically involved in monitoring and balancing extracellular pH and ionic conditions, which both support neurons and prevent damaging effects. Thus, central questions in our understanding of glaucoma pathology are whether the optic nerve glia simply become unable to continue their role in supporting the ganglion cell axons, or do they instead change to a molecular behavior that contributes to axonal pathology?

Another important consideration in our understanding of the effects of elevated IOP on the optic nerve head is the differential between IOP and arteriolar blood pressure. From a biomechanical standpoint, perfusion pressure to the small capillaries in the nerve head could meet much higher resistance in the face of elevated IOP. Thus, it is reasonable to predict that reduced blood flow would lead to micro-ischemic environments in this region. A similar consideration could also be made for the process of axoplasmic transport, particularly retrograde transport. Taken together, the pressure differential encountered at the lamina of a glaucomatous eye may consummate in a catastrophic stress where neurons are consuming greater amounts of adenosine triphosphate (ATP) to maintain

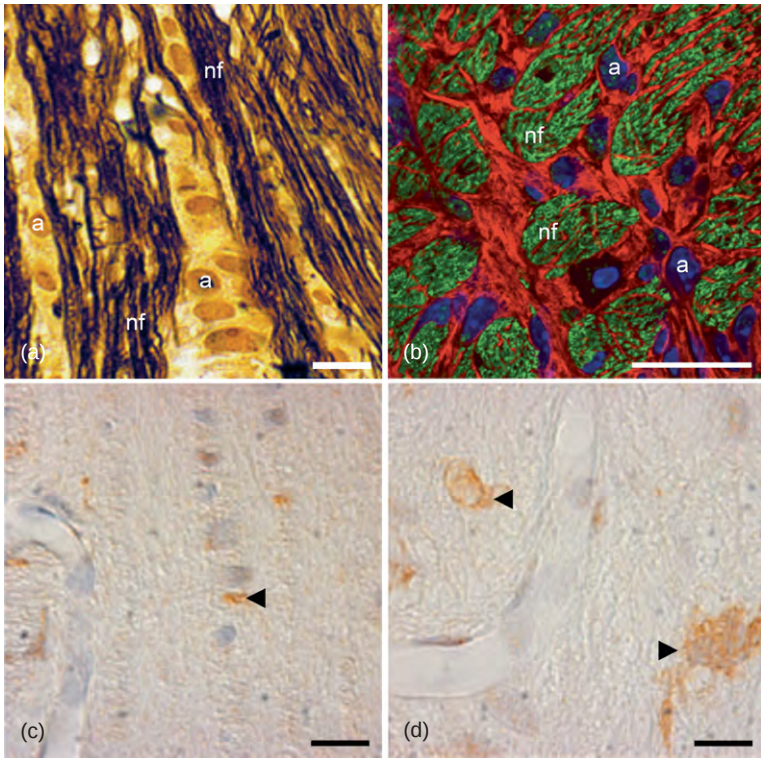

Figure 3 Ocular hypertension is associated with reactive astrocytes and microglia in the optic nerve head. (A) Columns of astrocytes (a) separate bundles of nerve fibers (nf) of ganglion cell axons in the cellular lamina of a young DBA/2J mouse without glaucoma. Longitudinal section, stained with silver impregnation. Scale = 10 μm. (B) In a mouse eye with glaucoma, astrocytes (a) become reactive and express the glial fibrillary acidic protein intermediate filament (stained red). This expression occurs early in disease, as evidenced by nerve fiber bundles (nf: stained green) still mostly intact. Transverse section through the lamina. Scale = 20 μm. (C, D) Images showing microglia expressing the marker gene IBA1 (brown reaction product) in a normal control rat lamina (C), or in the lamina of an eye with experimental glaucoma (D). Arrowheads point to immunopositive cells. Reactive microglia upregulate IBA1 expression. Scale (in (C) and (D)) = 3 μm. (A) Reproduced from Schlamp, C. L., Li, Y., Dietz, J. A., Janssen, K. T., and Nickells, R. W. (2006). Progressive ganglion cell loss and optic nerve degeneration in DBA/2J mice is variable and asymmetric. *BMC Neuroscience* 7: 66. (B) Reproduced from Howell, G. R., Libby, R. T., Jakobs, T. C., et al. (2007). Axons of retinal ganglion cells are insulted in the optic nerve early in DBA/2J glaucoma. *Journal of Cell Biology* 179: 1523–1537, with permission from the Rockefeller University Press. (C, D) Reproduced from Johnson, E. C., Jia, L., Cepurna, W. A., Doser, T. A., and Morrison, J. C. (2007). Global changes in optic nerve head gene expression after exposure to elevated intraocular pressure in a rat glaucoma model. *Investigative Ophthalmology and Visual Science* 48: 3161–3177, with permission from the Association for Research in Vision and Ophthalmology.

axoplasmic transport in the face of reduced access to nutrients and oxygen from both compromised astrocytes and reduced arteriolar blood flow. Ultimately, a scenario may develop where energy supplies are no longer sufficient to sustain transport against the pressure gradient and the axon is forced to execute a self-destruct pathway.

Compartmentalized Self-Destruct Pathways and the Pathology of Glaucoma

A major factor in understanding how elevated IOP leads to ganglion cell death is understanding how ganglion cells die in the first place. Ganglion cells are projection neurons of the CNS. The cell body, or soma, is located in the inner retina, where they take input from neurons in the outer retina through a complex network of dendrites located in the inner plexiform layer. The soma then projects an axon through the nerve fiber layer, which is adjacent to the vitreous, exiting the eye through the lamina into the optic nerve. In simple terms, a ganglion cell has four distinct compartments: the soma, the axon, a synapse at the end of the axon, and the dendritic tree.

Recently, the death of retinal ganglion cells has been evaluated in the context of effects on their individual compartments. Several studies, using genetically engineered mice, in which mutations in specific genes selectively affect the degenerative process of individual compartments, have shown that ganglion cell death can occur in an autonomous, compartment-specific, fashion. Two mutations, in particular, have contributed to the understanding of the process of ganglion cell death in glaucoma. The first of these is a knock-out mutation created in a gene called *Bax*, which is a member of a larger gene family that regulates the intrinsic apoptotic pathway by affecting permeability changes and dysfunction in mitochondria. Although apoptosis is generally considered in the same context as cell death, the term actually describes the self-destruct pathway executed by cell somas. In a defined, naturally occurring form of glaucoma in the DBA/2J inbred line of mouse, *Bax* deficiency was found to completely abrogate ganglion cell soma loss, but not the degeneration of the ganglion cell axons. A second mutant gene, which occurs naturally in mice, is called Wallerian degeneration slow (Wld^S). This mutant gene dramatically reduces the degenerative process called Wallerian degeneration, which is the self-destruct pathway executed by dying axons. In DBA/2J mice carrying the Wld^S mutation, ganglion cell axons are dramatically preserved in the face of ocular hypertension that causes glaucoma in wild-type mice. Importantly, in these mice, ganglion cell somas are also spared compared to wild-type animals. These data provide insight on the timing of events associated with ganglion cell loss. They indicate that axon loss is not prevented by blocking soma loss, while soma loss can be attenuated if axon loss is prevented. Together, this strongly implicates glaucoma as an axogenic disease, distinct from other neurodegenerative disorders where the soma is the fist site of injury. Supporting this model, all studies examining the timing and progression of both optic nerve degeneration and retinal disease in the DBA/2J mouse (**Figure 4**), point to axonal damage preceding the loss of ganglion cell somas.

In a scheme that links elevated IOP to ganglion cell damage and death, the activation of an autonomous self-destruct pathway in the ganglion cell axon will, in turn, lead to the activation of the autonomous apoptotic pathway in the ganglion cell soma. The mechanism by which this occurs is also unknown, but several studies suggest that the loss of axonal transport will reduce the flow of neurotrophic growth factors to ganglion cell somas. This model for the activation of soma death in glaucoma has been coined the neurotrophin hypothesis. During development, the normal pruning of retinal ganglion cells, in which approximately 50% of the cells are eliminated, coincides with an increased dependence on neurotrophic factors for survival. Similarly, application of exogenous neurotrophins, after acute or chronic damage to the optic nerve, is able to prolong ganglion cell survival.

Although these studies are consistent with the neurotrophin hypothesis, there are several caveats that require further explanation and reveal the need for continued study. First, the level of protective effect of exogenous neurotrophins is transient, even if efforts are made to introduce a continuous supply of any given factor over a long period. Second, injury to the optic nerve is known to stimulate the expression of endogenous trophic factors by other cells, particularly macroglia, in the retina, leading to the question of why this increase is not an expression sufficient to sustain ganglion cell somas in the absence of retrograde transport? Part of the reason for this effect may lie within molecular changes occurring in the ganglion cell somas once they have become injured. An early component of the injury process is the silencing of normal gene expression and some of the genes that are downregulated appear to be for the receptors that neurotrophic factors bind to. An alternative explanation is that many of the studies showing the transient effects of exongenous trophic factors are usually examining the effects of only a single factor at a time. Compelling available data suggest that treatments that elicit the infiltration of cells, such as macrophages, provide a much greater and longer-term effect on the survival of ganglion cell somas. In this case, infiltrating cells are likely producing and secreting much more complex mixtures of trophic factors than could be applied by experimental manipulation. Lastly, the signaling pathways activated by neurotrophic factors are variable and highly regulated. One such level of regulation is by the localization of target receptors on neurons, such that receptors bound at the synapse are likely to activate distinct mitogen-activated protein kinase

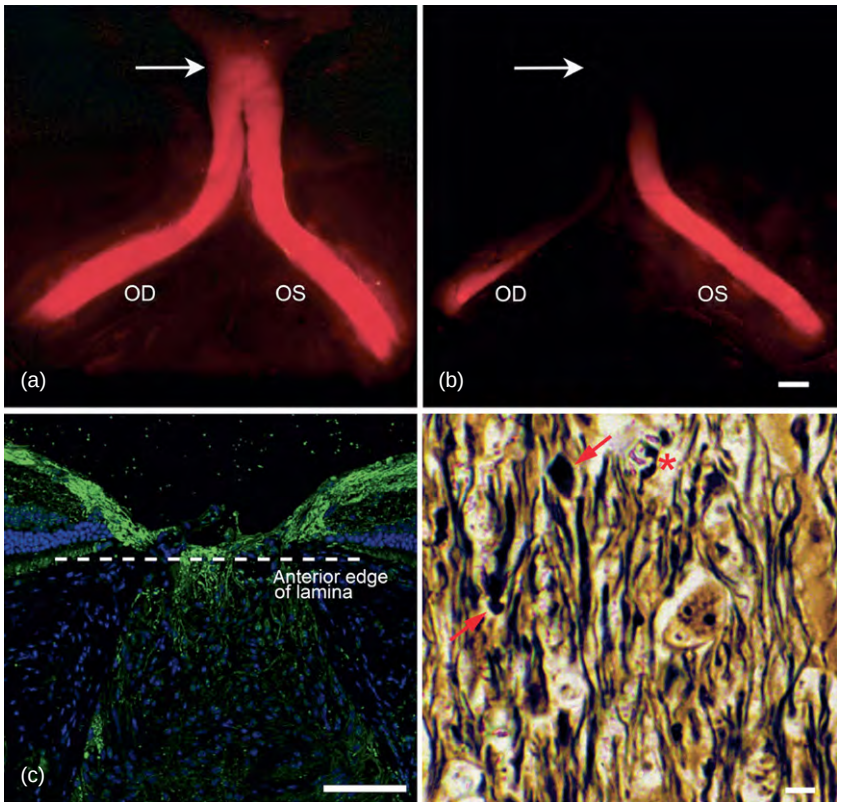

Figure 4 Axon degeneration in the optic nerves of DBA/2J mice with glaucoma. (a and b) Optic nerve tracts of a young mouse without disease (a) or an older mouse with bilateral disease (b). Axons are labeled using a postmortem technique in which DiI is allowed to diffuse along intact axonal tracts from the globe to the optic chiasm (denoted by arrow in both). Both nerves of young mice can be labeled all the way to the chiasm, while mice with glaucoma show partial or incomplete labeling that is typically asymmetric. Scale = 0.5 mm. (c) Axon loss in a DBA/2J mouse mutant for the proapoptotic *Bax* gene (*Bax*$^{-/-}$). Axons of retinal ganglion cells are labeled green. Mice lacking a functional *Bax* gene exhibit complete resistance of ganglion cell somas to glaucoma, but still undergo optic nerve degeneration. In this severe case, axons originating in the nerve fiber layer extend only to the laminar region. Past this point, axons have mostly degenerated, indicating that the point of axonal lesion is at the level of the lamina. Scale = 75 μm. (d) Silver-stained longitudinal section of the post-laminar region of a DBA/2J mouse with glaucoma. Axons, which are stained dark brown to black, are tortuous (asterisk) and often end in bulbous swellings (arrows) indicative of degeneration. Scale = 5 μm. (c) Reproduced from Howell, G. R., Libby, R. T., Jakobs, T.C., et al. (2007) Axons of retinal ganglion cells are insulted in the optic nerve early in DBA/2J glaucoma. *Journal of Cell Biology* 179: 1523–1537, with permission from the Rockefeller University Press.

(MAPK) pathways than the same receptors if they interact with a neurotrophin ligand at the plasma membrane of the cell soma. The activation of distinct MAPK pathways could certainly yield different effects on ganglion cell survival. This was demonstrated by recent studies showing increased survival and gain of function of ganglion cells in cat eyes after a partial optic nerve crush, when the neurotrophic factor, brain-derived neurotrophic factor (BDNF), was applied both as an intravitreal injection and simultaneously infused into the visual cortex.

Acknowledgments

The author would like to thank Dr. Harry A. Quigley for contributing scanning electron microscope images of the human lamina cribrosa and Dr. Cassandra L. Schlamp for preparing the figures. Some of this work was funded by NIH grant R01EY12223 to the author.

See also: Animal Models of Glaucoma; Biomechanics of the Optic Nerve Head; Primary Open-Angle Glaucoma; Retinal Ganglion Cell Apoptosis and Neuroprotection.

Further Reading

Hernandez, M. R. (2000). The optic nerve head in glaucoma: Role of astrocytes in tissue remodeling. *Progress in Retinal and Eye Research* 19: 297–321.

Hernandez, M. R., Andrzejewska, W., and Neufeld, A. (1990). Changes in the extracellular matrix of the human optic nerve head in primary open-angle glaucoma. *American Journal of Ophthalmology* 102: 180–188.

Howell, G. R., Libby, R. T., Jakobs, T. C., et al. (2007). Axons of retinal ganglion cells are insulted in the optic nerve early in DBA/2J glaucoma. *Journal of Cell Biology* 179: 1523–1537.

Johnson, E. C., Guo, Y., Cepurna, W. O., and Morrison, J. C. (2009). Neurotrophin roles in retinal ganglion cell survival: Lessons from rat glaucoma models. *Experimental Eye Research* 88: 808–815.

Johnson, E. C., Morrison, J. C., Farrell, S., et al. (1996). The effect of chronically elevated intraocular pressure on the rat optic nerve head extracellular matrix. *Experimental Eye Research* 62: 663–674.

Libby, R. T., Li, Y., Savinova, O. V., et al. (2005). Susceptibility to neurodegeneration in glaucoma is modified by Bax gene dosage. *PLoS Genetics* 1: 17–26.

Nickells, R. W., Semaan, S. J., and Schlamp, C. L. (2008). Involvement of the *Bcl2* gene family in the signaling and control of retinal ganglion cell death. *Progress in Brain Research* 173: 423–435.

Quigley, H. A., Addicks, E. M., Green, W. R., and Maumenee, A. E. (1981). Optic nerve damage in human glaucoma: II. The site of injury and susceptibility to damage. *Archives of Ophthalmology* 99: 635–649.

Roberts, M. D., Grau, V., Grimm, J., et al. (2009). Remodeling of the connective tissue microarchitecture of the lamina cribrosa in early experimental glaucoma. *Investigative Ophthalmology and Visual Science* 50: 681–690.

Schlamp, C. L., Li, Y., Dietz, J. A., Janssen, K. T., and Nickells, R. W. (2006). Progressive ganglion cell loss and optic nerve degeneration in DBA/2J mice is variable and asymmetric. *BMC Neuroscience* 7: 66.

Schwartz, M., Yoles, E., and Levin, L. A. (1999). 'Axogenic' and 'somagenic' neurodegenerative diseases: Definitions and therapeutic implications. *Molecular Medicine Today* 5: 470–473.

Soto, I., Oglesby, E., Buckingham, B. P., et al. (2008). Retinal ganglion cells downregulate gene expression and lose their axons within the optic nerve head in a mouse glaucoma model. *Journal of Neuroscience* 28: 548–561.

Tezel, G., Hernandez, M. R., and Wax, M. B. (2001). *In vitro* evaluation of reactive astrocyte migration, a component of tissue remodeling in glaucomatous optic nerve head. *Glia* 34: 178–189.

Whitmore, A. V., Libby, R. T., and John, S. W. M. (2005). Glaucoma: Thinking in new ways – a role for autonomous axonal self-destruction and compartmentalised processes? *Progress in Retinal and Eye Research* 24: 639–662.

Yang, Z., Quigley, H. A., Pease, M. E., et al. (2007). Changes in gene expression in experimental glaucoma and optic nerve transection: The equilibrium between protective and detrimental mechanisms. *Investigative Ophthalmology and Visual Science* 48: 5539–5548.

Intraretinal Circuit Formation

J L Morgan, P R Williams, and R O L Wong, University of Washington, Seattle, WA, USA

Introduction

The vertebrate retina is a laminated tissue in which the various component cell types and their synaptic connections are arranged in distinct layers or laminae. This laminar organization, together with a high correspondence between structure and function, makes the vertebrate retina an excellent model system for studying the development of neuronal circuits. The development of retinal circuits generally follows the same sequence of major events for all vertebrates studied thus far. In this article, we provide an overview of the assembly of circuits in the vertebrate retina, primarily focusing on the mouse and zebrafish that have in recent years become key model systems because of the availability of transgenic animals. Circuit assembly involving retinal neurons requires that each cell type forms connections with their appropriate synaptic partners and establishes the correct density of synaptic connections with these synaptic partners. We first briefly review the overall organization of the mature retinal circuitry and then provide the current views on how these circuits are assembled during the development.

Organization of Retinal Circuits of Vertebrates

Figure 1 shows the general morphological organization of the mature vertebrate retina. Cone photoreceptors transmit light-evoked signals to bipolar cells that relay these signals to the output neurons of the retina, the retinal ganglion cells. There are two major functional subclasses of bipolar cells: ON bipolar cells are depolarized by increased illumination, whereas OFF bipolar cells are hyperpolarized. Cone photoreceptors contact cone bipolar cells whereas in general, rod photoreceptors contact a single class of rod bipolar cells, which form a circuit dedicated to low light vision (the rod pathway). Unlike cone bipolar cells, rod bipolar cells do not contact retinal ganglion cells directly, and instead contact AII amacrine cells. Neurotransmission along the vertical pathway comprising photoreceptors–bipolar cells–retinal ganglion cells is mediated by glutamate. Signals transmitted along the vertical pathway are modulated by amacrine interneurons that provide feedforward inhibition directly onto retinal ganglion cells and feedback inhibition onto bipolar cells. In the inner plexiform layer (IPL), lateral inhibition is mediated by either gamma aminobutyric acid (GABA)-ergic or glycinergic transmission from the amacrine cells. In the outer plexiform layer (OPL), photoreceptor transmission is modulated by horizontal cells, although the exact mechanism(s) by which this modulation occurs remains highly debated.

Formation of Retinal Synaptic Laminae

The exquisite lamination of cell bodies and synaptic connections of the vertebrate retina have long attracted investigations into the mechanisms that organize this orderly arrangement. Lamination first emerges in the inner retina where retinal ganglion cells, the first-born neurons, migrate to the basal surface of the retina after cell division at the apical surface. As a ganglion cell layer forms, amacrine interneurons are generated and migrate to the inner retina where the majority of these cells accumulate and form a cell layer next to the ganglion cell layer. As amacrine cells and ganglion cells elaborate their processes, an IPL takes shape. An OPL becomes apparent later as the axons and dendrites of the photoreceptors, bipolar cells and horizontal cells differentiate and become confined to a narrow lamina. Interestingly, horizontal cells differentiate early, at around the time of amacrine and ganglion cell genesis, but they do not reach their laminar position until after the IPL emerges. This sequence of lamination, from inner to outer, thus does not depend strictly on the time course of cell generation and the subsequent migration of the various cell types (summarized in Figure 2). The lamination of the axons and dendrites of each cell type of the retina is described in detail in the following sections in the context of circuit assembly.

Assembly of the Vertical Pathway

The vertical pathway of the retina is the major excitatory pathway, conveying light information from the outer to inner retina through glutamatergic transmission. This pathway from photoreceptors to bipolar cells to retinal ganglion cells develops later than circuits involving lateral connections from amacrine cells and horizontal cells.

In order to understand how vertical circuits in the retina are assembled, many studies have focused on the mechanisms that organize the presynaptic axons and postsynaptic dendrites of cellular components of the vertical pathway into their appropriate laminae. How the axonal

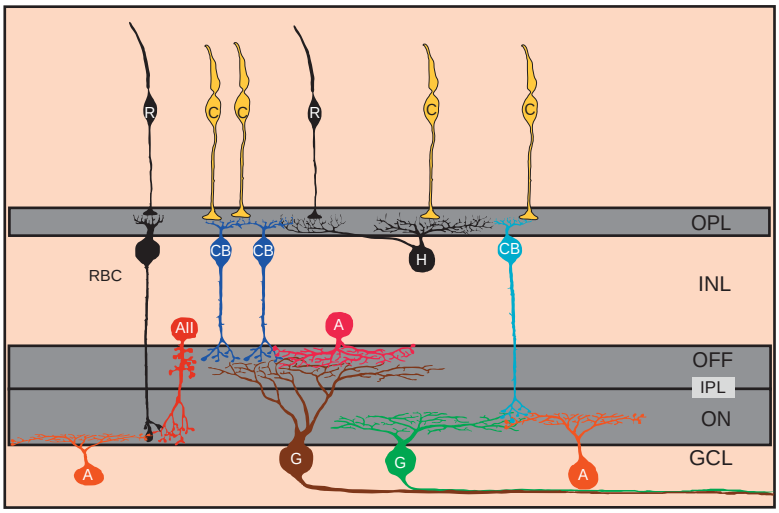

Figure 1 Organization of mature retinal circuits. Schematic of the laminar organization of the various cell types and their intraretinal axonal and dendritic projections is provided on the right. R, rods; C, cones, RBC, rod bipolar cell, CB, cone bipolar cell, H, horizontal cell, A, amacrine cell, AII, AII amacrine cell, G, ganglion cell, IPL, inner plexiform layer, OPL, outer plexiform layer. The IPL is approximately divided into OFF (outer two-fifths) and ON (inner three-fifths) sublaminae.

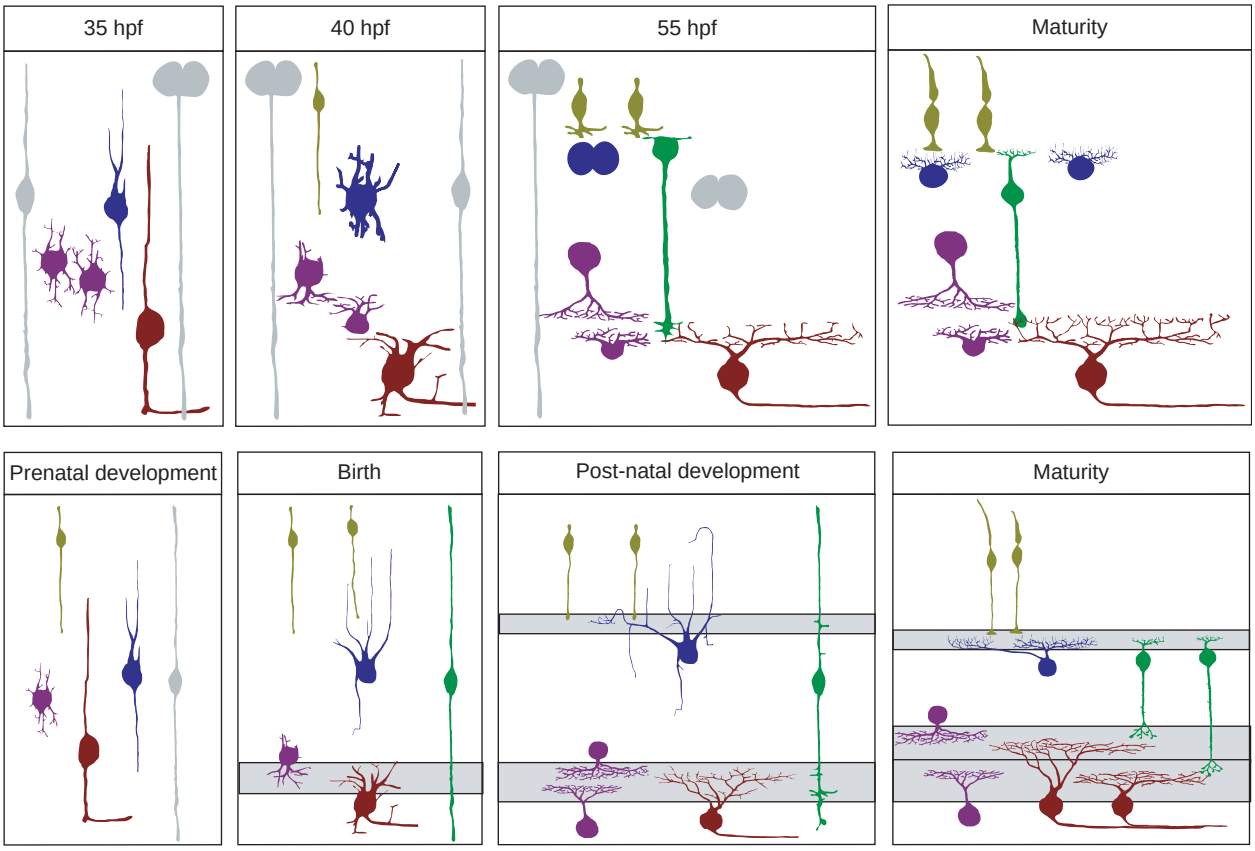

Figure 2 Developmental time-line in retinal circuit assembly. Schematic diagrams illustrating the developmental time-line in the structural assembly of the verteberate retina of mice (below) and zebrafish (above). Development in both species shares some common features, for example, the inner retinal circuits emerge before outer retinal circuits. However, there are some species differences in the developmental organization of the neuronal processes of some cells, especially the developmental remodeling of horizontal cell and ganglion cell dendrites. hpf: hours postfertilization; IPL: inner plexiform layer; OPL: outer plexiform layer.

and dendritic arbors of retinal ganglion cells, bipolar cells, and photoreceptors develop has largely been investigated by imaging labeled cells by light microscopy and by reconstructions from serial electron microscopy. Despite the static nature of the observations, these studies have collectively provided insightful views of how retinal ganglion cells, bipolar cells, and photoreceptors acquire the mature forms of their neuronal processes. More recently, live imaging approaches have captured the dynamic changes in axonal and dendritic architecture of developing retinal neurons, including the retinal ganglion cells and bipolar cells. These time-lapse studies confirmed previous observations and also revealed surprising cellular behaviors resulting in the stratified processes of some types of ganglion cells and bipolar cells.

Retinal Ganglion Cells

Dendritic stratification of retinal ganglion cells has been studied extensively in a variety of species. The stratification level of retinal ganglion cell dendrites is correlated with the type of functional input these neurons receive from cone bipolar cells. As indicated in **Figure 1**, retinal ganglion cells that depolarize to increased illumination have dendritic arbors stratifying in the inner three-fifths of the IPL, whereas ganglion cells stratifying in the outer two-fifths of the IPL hyperpolarize to illumination. In mammalian retinas including cat, rabbit, ferret, mouse, rat, and quokka, immature retinal ganglion cells have dendrites that course through the entire depth of the forming IPL (**Figure 3(a)**). This initially diffuse arrangement is altered with maturation, giving rise to laminated arbors that stratify at depths unique to each subtype of retinal ganglion cell. Such studies have largely focused on ganglion cells that later possess a single monostratified arbor. Retinal ganglion cells that have two stratified arbors in mammalian retina (the bistratified ganglion cells) have not been followed throughout their early differentiation, mainly because of a lack of cell-specific markers for ganglion cell subtypes prior to when their dendrites stratify.

In zebrafish, a large proportion of retinal ganglion cells possess more than one stratified dendritic arbor. Because *in vivo* time-lapse imaging of individual retinal ganglion cells is possible in the transparent zebrafish, the sequence of events leading to the stratification of ganglion cell dendrites can be monitored. Such imaging studies demonstrated that ganglion cells with multiple stratified arbors appear to form each arbor, one stratum at a time (**Figure 3(b)**). These observations in zebrafish raise the possibility that dendrites in mammals and fish may adopt distinct mechanisms to achieve their stratification patterns. Alternatively, retinal ganglion cells that have multiple stratified arbors may develop differently from cells that become monostratified. Thus, future experiments in which bistratified ganglion cells in mammalian retinas can be identified early in their development are needed to distinguish between these possibilities.

What regulates retinal ganglion cell dendritic stratification? Studies in cat and ferret suggested that blockade of neurotransmission affects the emergence of stratified dendritic arbors of the retinal ganglion cells. Chronic application of the amino-phosphonobutyric acid (APB) agonist of the metabotropic glutamate receptor 6 (mGluR6) receptor found on the dendrites of mature ON bipolar cells led to a failure of ganglion cell dendrites to become stratified. However, APB has been shown to suppress the activity of all retinal ganglion cells in the immature ferret retina and thus its site of action is unclear. Examination of mice in which transmission along the vertical pathway is expected to be perturbed led to different observations. In mice lacking

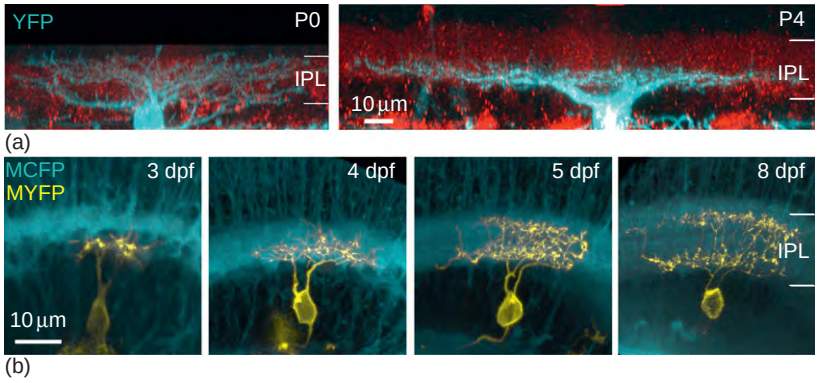

Figure 3 Dendritic stratification of retinal ganglion cells. (a) The dendritic arbors of neonatal retinal ganglion cells (blue) in the mouse retina become stratified with maturation; Red signal is reflected light. P: postnatal day; YFP: yellow fluorescent protein. (b) Dendritic stratification in many zebrafish retinal ganglion cells (yellow) emerges by progressive addition of new strata, one at a time. MYFP: membrane targeted yellow fluorescent protein. MCFP: membrane targeted cyan fluorescent protein (blue) in other retinal neurons. Reproduced with permission from **Figure 5** in Mumm, J. S., Williams, P. R., Godinho, L., et al. (2006). *In vivo* imaging reveals dendritic targeting of laminated afferents by zebrafish retinal ganglion cells. *Neuron* 52: 609–621, with permission from Elsevier.

the mGluR6 receptor, ganglion cell dendritic stratification is normal – in this case, however, one might expect that spontaneous release of neurotransmitter from the bipolar cells is unaffected even though visual stimulation along the ON pathway is abolished. Numerous studies have since been carried out to assess the role of visual experience in regulating dendritic stratification of retinal ganglion cells. Dark-rearing appears to decrease the developmental reduction in the proportion of ON–OFF retinal ganglion cells in mice. This developmental reduction is also less prevalent in mice lacking glycine receptors. In contrast, factors independent of activity have been found to guide dendritic lamination of ganglion cells. In particular, recent studies of the chick retina showed that members of the superfamily of immunoglobulin family of adhesion molecules (sidekicks and DsCam) influence the lamination patterns of retinal ganglion cells and amacrine cells. Although not yet completely worked out, it appears that molecular guidance cues involving adhesion molecules initially guide stratification of ganglion cell dendrites but later visually evoked activity may continue to shape the final lamination patterns of the ganglion cell dendrites.

Bipolar Cells

The development of the axonal terminals of bipolar cells has mostly been studied in a variety of species by single cell labeling methods using Golgi techniques and immunolabeling. Golgi-labeled cells that were presumed to be bipolar cells based on their radial morphology and terminal ending in the IPL appear to confine their axon terminals to specific depths within the IPL even before these cells form dendrites. Immunostaining for recoverin also suggested that ON and OFF bipolar cells stratify early in their differentiation. In transgenic mice, the mGluR6 promoter drives expression of green fluorescent protein in a subset of bipolar cells (ON bipolar cells). Expression is observed when these cells still possess apical and basal processes that are attached to the outer and inner limiting membranes, respectively. Time-lapse imaging of the retinas from these transgenic mice unequivocally demonstrated that axons and dendrites extend from the neuroepithelial-like processes as the bipolar cells differentiate (**Figure 4(a)**). Whether axons and dendrites in other species including zebrafish also develop in a similar manner is yet to be determined. Both axons and dendrites of the mouse ON bipolar cells explore retinal

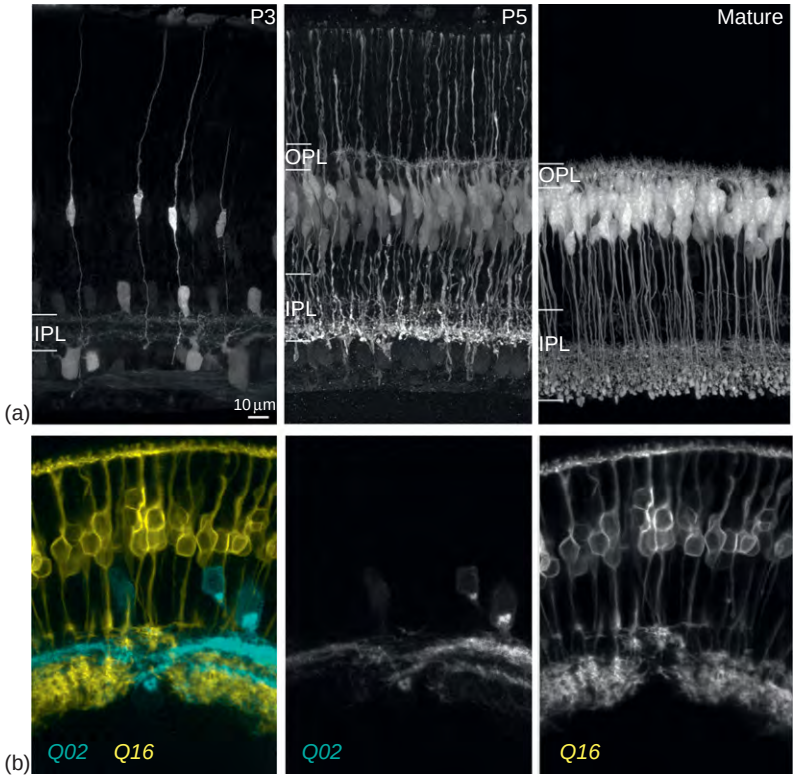

Figure 4 Lamination of bipolar cell axons and dendrites. (a) Green fluorescent protein driven by the mGluR6 promoter in bipolar cells at P3, P5 and mature retina. GFP expressing bipolar cells elaborate dendrites from apical and basal processes oriented vertically and neuroepithelial-like. IPL, inner plexiform layer. Note that upon maturation, dendrites are confined to the OPL (outer plexiform layer) and axons to the IPL. (b) Local perturbation in amacrine cell (blue) and bipolar cell (yellow) lamination visualized in a transgenic zebrafish in which a subset of amacrine cells express cyan fluorescent protein (Q02) and ON bipolar cells express yellow fluorescent protein (Q16) in the background of the *lakritz* mutant, which lacks ganglion cells.

depths outside their final lamination locations, but processes within the appropriate lamina are selectively stabilized with maturation. Process stabilization cues may be provided by other retinal neurons that have already grown stratified arbors in the forming plexiform layers. For example, the axonal terminals of the ON bipolar cells are largely distributed within the inner half of the IPL where they later contact ON ganglion cells. At this stage of axonal elaboration, as discussed later, amacrine cells that stratify in the ON sublamina have already contacted their target ganglion cells. Because amacrine cells can stratify independently of the presence of retinal ganglion cells, it is possible that these interneurons provide laminar cues for the bipolar axons. This hypothesis receives some support from observations in the zebrafish *lakritz* mutant that lacks retinal ganglion cells, in which there are local patches with lamination defects in the amacrine cell neurites although lamination largely occurs across the retina. In these locally perturbed regions, bipolar axon terminals are also abnormally placed (**Figure 4(b)**).

Photoreceptors

Photoreceptors connect to the bipolar cell dendrites once horizontal cells have already entered into synaptic partnerships with the photoreceptors (**Figure 2**). Apart from early Golgi studies, relatively little is known about how individual photoreceptors terminate their axons to form a single lamina in the outer retina during development although several studies have described the maturation of their outer segments. Observations in the ferret retina showed that some photoreceptors even transiently project into the IPL during development, although the functional significance of these projections is not yet known.

Synaptogenesis in the Vertical Pathway

Synaptic connections in the vertical pathway have only recently been studied in detail by light microscopy. Early ultrastructural studies of the IPL and OPL of mammals and zebrafish suggest that ribbon synapses are formed between bipolar cells and retinal ganglion cells after conventional synapses are present (**Figures 5** and **6**). In rodents and zebrafish, contact between photoreceptors and bipolar cells occur about the same time as bipolar cells contact the retinal ganglion cells. However, ribbons appear late at bipolar synapses in the IPL. Detailed serial reconstruction of immature bipolar cell axon terminals in primate retina suggest that ribbons appear after clusters of vesicles are found at appositions between bipolar cell axonal processes and a neighboring process. Interestingly,

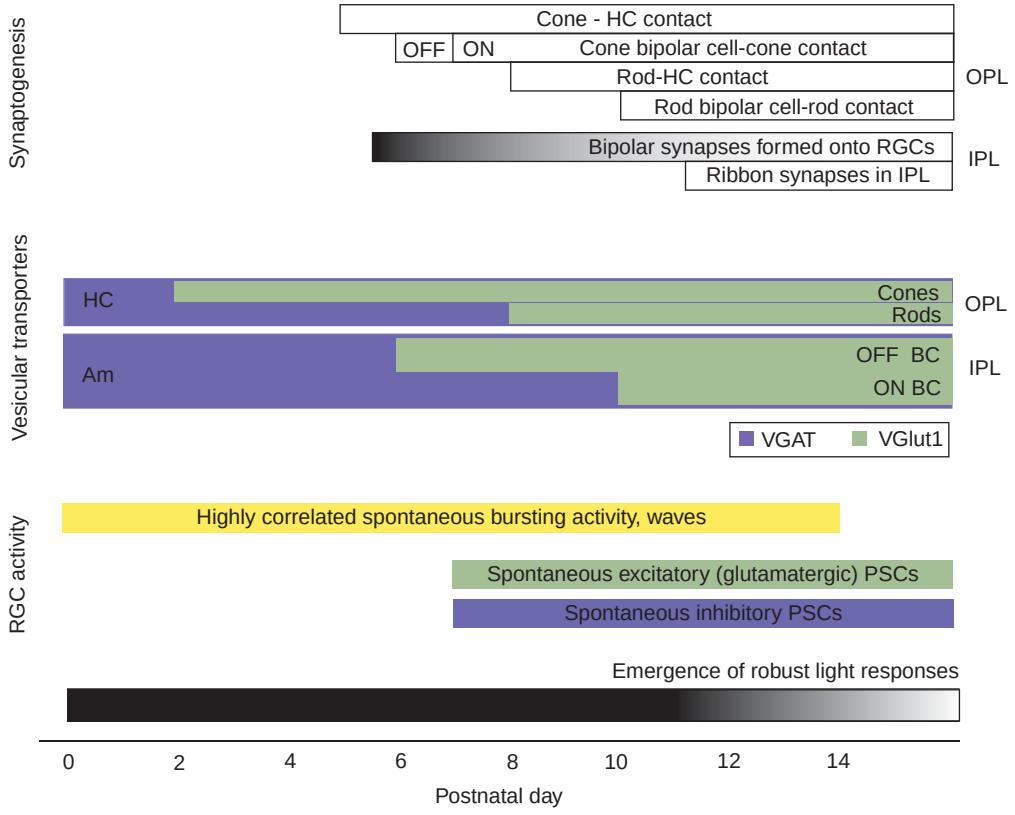

Figure 5 Summary of major developmental events associated with structural and functional assembly of mouse retinal circuits. VGAT, vesicular GABA/glycine transporter; VGlut1, vesicular glutamate transporter; HC, horizontal cells; BC, bipolar cells; PSCs, postsynaptic currents.

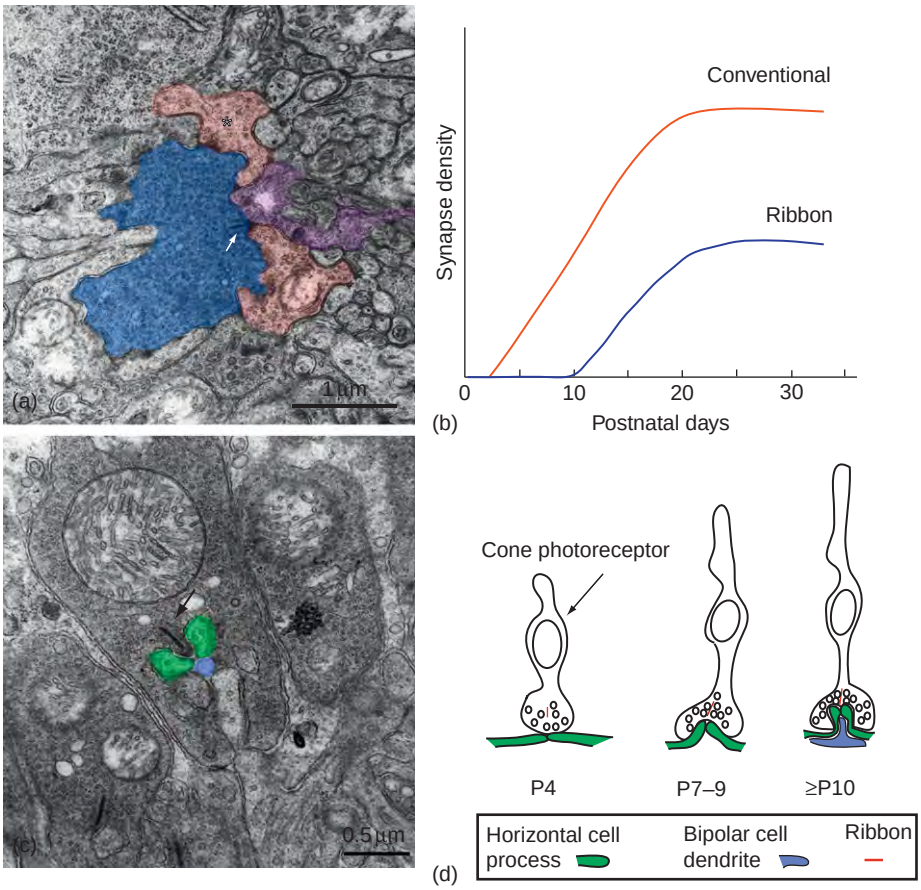

Figure 6 Synaptogenesis in the IPL and OPL. (a) Ultrastructure of ribbon (bipolar cell, blue shading) and conventional (amacrine, pink with asterisk and purple) synapses in a 2-week-old mouse retina. Shown here is a reciprocal synapse between a rod bipolar cell and amacrine cells. Arrow indicates ribbon. (b) Time-line of synaptogenesis in the IPL. (c) Example of a cone photoreceptor triad synapse in the OPL. Arrow indicates a ribbon. Green are horizontal cell processes and blue is bipolar cell process. Micrograph taken by Ed Parker, University of Washington. (d) Schematic illustrating time-line of triad formation in the mouse OPL. (b) Fisher, L. J. (1979). Development of synaptic arrays in the inner plexiform layer of neonatal mouse retina. *Journal of Comparative Neurology* 187: 359–372.

the earliest bipolar synapses appear to be monads, that is, there is only one postsynaptic process, whereas with maturation, bipolar cells synapses occur at junctions with two processes, forming a dyad synapse. The postsynaptic processes may comprise processes from two amacrine cells, an amacrine and a ganglion cell, or two ganglion cells. That bipolar synapses are already present on ganglion cell dendrites prior to the appearance of ribbons is supported by electrophysiological recordings from immature retinal ganglion cells. As discussed in more depth later, spontaneous excitatory postsynaptic currents (sEPSCs) can be recorded from ganglion cells in mammals prior to when ribbons appear. Electron microscope observations of developing mouse retina also suggest that bipolar synapses are present in the outer half (OFF) of the inner plexiform layer prior to their appearance in the inner half (ON) of the inner plexiform layer. There is support for the relatively earlier differentiation of synaptic connections, or at least their structures, in the OFF sublamina of the inner plelxiform layer. For example, in mice, VGluT1 (vesicular glutamate transporter) immunolableing is first observed in the OFF sublamina prior to its appearance in the ON sublamina (**Figure 5**). The significance of this sequence in maturation of the ON and OFF vertical pathways is unclear because light-evoked activity does not emerge until several days later.

Reconstructions of bipolar cell synapses at the ultrastructural level, however, cannot provide a view of the spatial distribution of such inputs on individual ganglion cell dendritic arbors unless extensive serial reconstructions are performed on immature ganglion cells. Using transient transfection methods, recent studies have successfully explored the spatial distribution of bipolar cell inputs on the dendritic arbors of retinal ganglion cells using light microscopy. Expression of fluorescently tagged postsynaptic density protein 95 (PSD95), a scaffolding protein found at glutamatergic postsynaptic sites, revealed the distribution of bipolar cell contacts across the dendritic arbors of ganglion cells in the mouse retina. Quantification of the spatial maps of these synaptic puncta

indicated that in mice, there is a rapid acquisition of glutamatergic postsynaptic sites from postnatal day 5 until eye-opening (Figure 7). Synaptogenesis between bipolar cells and retinal ganglion cells thus appears to proceed mostly prior to eye-opening (around 2 weeks after birth). Interestingly, the density of connections across the dendritic territory of the ganglion cells appears to be fairly invariant with age, even though there is significant structural remodeling (largely reduced dendritic branching density) of the dendritic arbors with maturation. This may reflect the developmental increase in the number of contact sites along the dendrites as dendritic density decreases with age.

Electron microscopy studies clearly indicate that cones form synaptic connections prior to rods. However, to date, there is little information concerning how bipolar cells and photoreceptors establish the specificity in their connectivity patterns during synaptogenesis. Retinas in which rod or cone populations are perturbed provide important insight into the specificity of wiring between rod and cone photoreceptors and their target bipolar cell types. In *nrl*-knockout mice in which rods fail to form and all photoreceptors become cones, rod bipolar cells are contacted by cones. Conversely, in in cyclic nucleotide gated channel A3 (CNGA3) knock-out mice in which cones are present but nonfunctional, cone bipolar cells form synaptic connections with rods. Thus, rod and cone bipolar cells can be targeted nonspecifically by cones and rods in the absence of proper interactions between these pre- and postsynaptic cell types. However, it is not yet clear whether specificity in the wiring between rods and cones and their target bipolar cells is obtained during development after a period of rewiring, or whether there is target selectivity during synaptogenesis. One way to address this question is to follow the development of photoreceptor-bipolar synaptogenesis over time *in vivo*. This can be readily achieved in zebrafish but is more difficult to perform for mammalian retinas. Furthermore, experiments that will determine how the different color cones wire up to the appropriate bipolar cells during development will be important in determining how color circuits are established in cone-dominated retinas.

Assembly of Lateral Circuits

Compared to the vertical pathway, the assembly of circuits that modulate transmission in the inner and outer retina are not as well understood. However, recent studies in which amacrine cells and horizontal cells can be identified early in development have shed new insight into the cellular behaviors of these cells as they form circuits.

Inner Retina – Amacrine Cells

Amacrine cells migrate freely toward the inner retina and appear to stratify shortly upon reaching the border with the forming ganglion cell layer (Figure 2). Serial electron microscopy suggested this pattern of amacrine cell migration and neurite development, which has

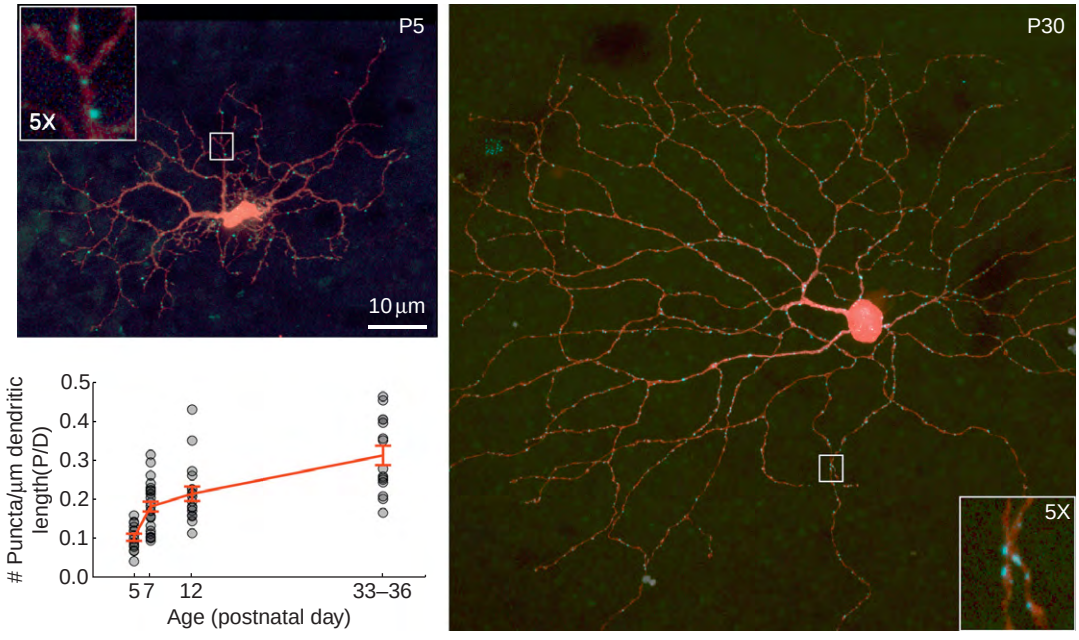

Figure 7 Spatial distribution of glutamatergic postsynaptic sites on developing ganglion cells. Examples of ganglion cells from an immature (postnatal day, P5) and a juvenile (postnatal day, P30) retina for which glutamatergic postsynaptic sites are labeled (blue). Dendrites are labeled by expression of the red fluorescent protein, td-Tomato, and gluamatergic postysnaptic sites by fluorescently tagged postsynaptic density 95 PSD95. Insets in upper left and lower right are 5× magnifications of the areas indicated by the boxes. Lower left: The density of PSD95-YFP (blue) puncta along the dendrites is plotted across ages studied.

subsequently been visualized in real time by *in vivo* imaging of these neurons in the zebrafish retina. Zebrafish amacrine cells very quickly stratify their neurites within the inner or outer half of the IPL as soon as their cell bodies reach their final locations. Thus, amacrine cell neurites do not appear to undergo a period of indiscriminate occupation of the IPL. Whether this pattern of neurite growth also occurs for mammalian amacrine cells, however, is not known although in rodents, cholinergic amacrine cells appear to form their mirror-symmetric laminations at two distinct depths in the IPL early in IPL formation.

The cues that influence the neuritic stratification of amacrine cells are not completely known, but it is evident that ganglion cells are not necessary for this process to occur. In mouse atonal 5 (*Math5*) knock-out mice and in the zebrafish mutant, *lakritz*, both lacking retinal ganglion cells, amacrine cells form stratified arbors. Because bipolar cells differentiate later than amacrine cells, these interneurons are unlikely to provide lamination cues for amacrine cells. The influence of adhesion molecules in the stratification of amacrine cell neurites has, however, been shown in the chick retina. The immunoglobulin superfamily of adhesion molecules, Down syndrome cell adhesion molecule (DsCam), DsCam-like, Sidekick-1 and Sidekick-2 are expressed in nonoverlapping strata in the chick inner plexiform layer. Manipulating the expression of these adhesion molecules in ovo suggests that they are involved in specifying the laminae within which amacrine cells and their target retinal ganglion cells stratify.

As yet, it is unknown what factors regulate synapse density between the amacrine cells and their target retinal ganglion cells. This issue can potentially be investigated by serial reconstructions of the IPL but because there are at least two dozen types of amacrine cells in the mammalian retina, and perhaps an even greater variety in the fish retina, mapping the inputs of specific subtypes of amacrine cells on the dendrites of their postsynaptic ganglion cells is extremely challenging. No doubt, future studies using transgenic approaches to visualize specific amacrine subtypes will be invaluable. Amacrine cells also provide feedback inhibition onto bipolar axon terminals. These feedback synapses have largely been studied in the rod bipolar cell pathway where A17 amacrine cells are known to contact the large axon terminals of rod bipolar cells (see **Figure 6 (a)**). The development of this highly localized reciprocal synapse has yet to be examined in detail but its well-characterized function makes this synapse a good model for studying the development of feedback circuits in general.

Outer Retina – Horizontal Cells

In the outer retina, modulation of transmission along the vertical pathway is provided by horizontal cells. In rodents, horizontal cell dendrites attain a laminated arbor after a period of reorganization (**Figure 2**). Cajal described immature horizontal cells as having a radial rather than lateral arbor. Since then, horizontal cells in rodents have been identified by immunolabeling for the GABA synthesizing enzyme, glutamic acid decarboxylase 67 (GAD67), and by calbindin immunoreactivity. Such labeling confirmed Cajal's early observations and also showed that horizontal cell dendritic stratification occurs as photoreceptors form synaptic connections onto the horizontal cells. Dendritic stratification of horizontal cells does not appear to rely on neurotransmission from photoreceptors because this process occurs even when cone photoreceptors are ablated during development. However, long-term loss of photoreceptor transmission does lead to elaboration of horizontal cell dendrites into the outer nuclear layer where they can receive ectopic contact.

Horizontal cells form contacts with cone photoreceptor terminals prior to the elaboration of bipolar cell dendrites that later invaginate into the cone terminal to form a synaptic triad (**Figure 6(c)** and **6(d)**). The triad comprises a single bipolar cell dendritic tip flanked by two horizontal cell processes at a location opposite to the ribbon in the cone terminal. The assembly of this triad structure has been described by elegant ultrastructural studies in the past but the cues that coordinate the assembly of each component of this synapse are still unknown. **Figure 5** summarizes the time-line of synaptogenesis between the various cell elements contributing to the OPL.

Emergence of Function – Spontaneous and Light-Evoked Activity

Visually evoked signals in the mammalian retina emerge shortly before eye-opening when photoreceptors have formed synaptic connections with the bipolar cells. However, the retina generates its own pattern of activity prior to photoreceptor transmission. In many mammalian species studied thus far, retinal ganglion cells have been found to exhibit bursts of action potentials that occur rhythmically and are synchronized among neighboring cells (**Figure 8**). This synchronized activity takes on the form of propagating waves that spread across the retina in different directions. The wave-like activity pattern has been linked to the refinement of the axonal projection patterns of the retinal ganglion cells to their subcortical targets, but as yet waves have not been found to influence the development of intraretinal circuits in mammals.

Changes in the properties of retinal waves, however, have been informative with regard to the organization and development of retinal circuits. For example, studies of retinal activity in chick, mice, ferret, and rabbit all suggest that early synchronized activity is mediated by gap junctions, then by cholinergic drive and later by glutamatergic transmission. Moreover, ON and OFF retinal

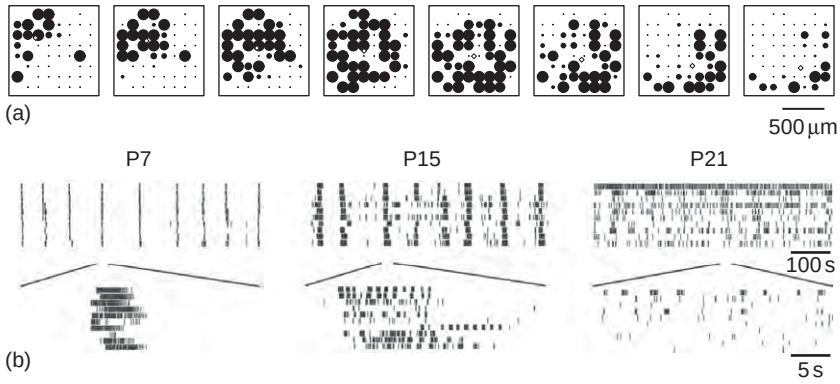

Figure 8 Immature retinal circuits spontaneously generate waves of activity. (a) Multielectrode array recordings (squares) for neonatal mouse retinas showing propagation of a retinal wave over time (left to right). Time between frames is 0.5 s. Each dot represents an electrode site and the size of the dot corresponds to spike rate. (b) Spike rasters from 10 representative cells recorded simultaneously on the array for three postnatal ages; P7, P15, and P21.

ganglion cells are synchronized in their bursting activity during the period when cholinergic drive is necessary for the wave activity. However, as glutamatergic drive takes over, the spontaneous bursting activity of ON and OFF mouse ganglion cells becomes desynchronized: ON ganglion cells burst before OFF ganglion cells. This asynchrony is generated by cross-over inhibition between these parallel pathways. Thus, prior to eye-opening, retinal circuits undergo changes in spontaneous activity patterns of the ganglion cells largely due to alterations in the type of excitatory drive (cholinergic then glutamatergic) and the maturation of inhibitory circuits. At the level of synapses, measurements of synaptic currents from individual retinal ganglion cells show that the amplitudes and frequency of sEPSCs increase with age, even after eye-opening.

Few studies have directly measured the early visual response properties of retinal ganglion cells. Such studies have been difficult to carry out *in vivo* because of the poor optics of the immature eye. As soon as it is possible to record light responses from the retina *ex vivo*, generally a few days before eye-opening, the characteristic center-surround organization of ganglion cell receptive fields can be identified in cat and rabbit. Although the antagonistic surround, mediated by inner and/or outer retinal inhibition, is present when the receptive field centers are first detected, the response properties of the early surrounds appear to be species dependent. The early light responses are weak and adapt rapidly but become robust several days later. However, ON and OFF responses are evident and there is no significant developmental change in the percentage of cells with ON- and OFF-center receptive fields in the cat. In contrast, in ferret and mice, there is a higher proportion of ganglion cells that receives converging ON and OFF input during development. The reduction in the incidence of ON–OFF cells in the ferret has been attributed to dendritic pruning, whereas in mice this reduction is considered to be the result of a decrease in the number of cells with dendritic arbors located at the border of the ON and OFF sublaminae of the IPL. However, in mice, direct correlation between structure and function of individual ganglion cells that have converging ON and OFF input has yet to be obtained. Direction-selective ganglion cells can be found in rabbit retina before eye-opening and the development of the circuitry underlying this visual response property in mouse retinal ganglion cells does not depend on spontaneous retinal wave activity or visual experience. In contrast, the spatial receptive fields of turtle retinal ganglion cells appear to reorganize with maturation. Direction selectivity, orientation preference, and receptive field sizes of turtle ganglion cells are shaped by spontaneous and light-driven activity. Thus, the influence of neurotransmission, especially visual experience, in establishing the precision in wiring of intraretinal circuits appears to vary across species, perhaps due to different developmental constraints that are species specific. Alternatively, such differences may be due to how neurotransmission is altered *in vivo* and the consequence of each manipulation in the transmission of signals between specific cell types.

Conclusions

Much remains to be done in order to elucidate the molecular and cellular mechanisms that are responsible for establishing the many circuits within the vertebrate retina dedicated to the processing of light information. In recent years there have been significant technological advances that allow probing the structural and functional development of retinal circuits. However, cell-type specific markers that will enable tracking the same cell type throughout development are necessary for many future studies. With the increasing availability of transgenic models, it should be possible to directly address the mechanisms that are essential to circuit assembly *in vivo*. Investigating the development of intraretinal circuits is certainly well aided by the immense knowledge of the structure and function of the

adult vertebrate retina, and the comparative anatomy and physiology of its circuits across many species.

See also: GABA Receptors in the Retina; Ganglion Cell Development: Early Steps/Fate; Glutamate Receptors in Retina; Histogenesis, Cell Fate, and Signaling Factors; Information Processing: Amacrine Cells; Information Processing: Bipolar Cells; Information Processing: Ganglion Cells; Information Processing: Horizontal Cells; Information Processing in the Retina; Photoreceptor Development: Early Steps/Fate; Retinal Histogenesis; The Role of Acetylcholine and its Receptors in Retinal Processing.

Further Reading

Cajal, R. Y. (1960). *Studies on Vertebrate Neurogenesis*. Springfield, IL: Thomas.

Eglen, S. J., Sernagor, E., and Wong, R. O. (eds.) (2006). *Mechanisms of Retinal Development.* Cambridge: Cambridge University Press.

Elstrott, J., Anishchenko, A., Greschner, M., et al. (2008). Direction selectivity in the retina is established independent of visual experience and cholinergic retinal waves. *Neuron* 58: 499–506.

Fisher, L. J. (1979). Development of synaptic arrays in the inner plexiform layer of neonatal mouse retina. *Journal of Comparative Neurology* 187: 359–372.

Fuerst, P. G., Koizumi, A., Masland, R. H., and Burgess, R. W. (2008). Neurite arborization and mosaic spacing in the mouse retina require DSCAM. *Nature* 451: 470–474.

Galli-Resta, L., Leone, P., Bottari, D., et al. (2008). The genesis of retinal architecture: An emerging role for mechanical interactions? *Progress in Retinal and Eye Research* 27: 260–283.

Godinho, L., Mumm, J. S., Williams, P. R., et al. (2005). Targeting of amacrine cell neurites to appropriate synaptic laminae in the developing zebrafish retina. *Development* 132: 5069–5079.

Haverkamp, S., Michalakis, S., Claes, E., et al. (2006). Synaptic plasticity in CNGA3(−/−) mice: Cone bipolar cells react on the missing cone input and form ectopic synapses with rods. *Journal of Neuroscience* 26: 5248–5255.

Kay, J. N., Roeser, T., Mumm, J. S., et al. (2004). Transient requirement for ganglion cells during assembly of retinal synaptic layers. *Development* 131: 1331–1342.

Morest, D. K. (1970). The pattern of neurogenesis in the retina of the rat. *Zeitschrift für Anatomie und Entwicklungsgeschichte* 131: 45–67.

Morgan, J. L., Schubert, T., and Wong, R. O. (2008). Developmental patterning of glutamatergic synapses onto retinal ganglion cells. *Neural Development* 3: 8.

Mumm, J. S., Williams, P. R., Godinho, L., et al. (2006). *In vivo* imaging reveals dendritic targeting of laminated afferents by zebrafish retinal ganglion cells. *Neuron* 52: 609–621.

Nishimura, Y. and Rakic, P. (1987). Development of the rhesus monkey retina: II. A three-dimensional analysis of the sequences of synaptic combinations in the inner plexiform layer. *Journal of Comparative Neurology* 262: 290–313.

Schmitt, E. A. and Dowling, J. E. (1999). Early retinal development in the zebrafish, *Danio rerio*: Light and electron microscopic analyses. *Journal of Comparative Neurology* 404: 515–536.

Sernagor, E., Eglen, S. J., Harrris, W., and Wong, R. O. L. (eds.) (2006). *Retinal Development.* Cambridge: Cambridge University Press.

Sernagor, E., Eglen, S. J., and Wong, R. O. (2001). Development of retinal ganglion cell structure and function. *Progress in Retinal and Eye Research* 20: 139–174.

Strettoi, E., Mears, A. J., and Swaroop, A. (2004). Recruitment of the rod pathway by cones in the absence of rods. *Journal of Neuroscience* 24: 7576–7582.

Yamagata, M. and Sanes, J. R. (2008). Dscam and Sidekick proteins direct lamina-specific synaptic connections in vertebrate retina. *Nature* 451: 465–469.

Ion Transport in the Ciliary Epithelium

O Strauß, Klinikum der Universität Regensburg, Regensburg, Germany

Glossary

Functional syncytium – In cells that are coupled to each other by gap junctions, small molecules can freely diffuse between the cells, an effect that synchronizes the cells to a functional unit. A true syncytium is a cell-like body filled with cytoplasm and multiple nuclei.
Primary active transport – A transport of molecules against a concentration gradient which directly uses energy from hydrolysis of adenosine triphosphate.
Secondary active transport – A transport of a molecule against a concentration gradient in which the transport is coupled to the active transport of another molecule. Since the concentration difference of the downhill-transported molecule stems from primary active transport, the transport is then termed secondary active transport.
Transepithelial potential – The voltage difference across an epithelium.
Transepithelial resistance – The electrical resistance across an epithelium.

Introduction

A stably and finely regulated intraocular pressure is of fundamental importance for the maintenance of visual function. The balance between aqueous humor production and outflow defines intraocular pressure. The understanding of the regulation of aqueous humor production represents an important base to lower intraocular pressure in glaucoma. Aqueous humor is produced by active ion transport across the ciliary epithelium. In the course of this active ion transport, anions are transferred from the stromal to the chamber side. The transport of solutes drives a transcellular transport of water through aquaporin water channels. In this article, the basic transport mechanism across the ciliary epithelium is described. When possible, the article focuses on the mechanisms known in primate species, because there are great variations among different species.

Aqueous Humor Production: Active Transport

The ciliary stroma contains fenestrated capillaries which provide the substrate for aqueous humor production. The formation of aqueous humor occurs in an estimated rate of 2–4 $\mu l\,min^{-1}$. Aqueous humor has a defined composition. For example, in aqueous humor there is a much higher ascorbate concentration compared to that in the plasma. Furthermore, it contains only very minor amounts of proteins when compared to plasma, but a variety of signaling molecules. This indicates that a selective active secretion process is responsible for the production of aqueous humor. The secretion process across the ciliary epithelium (**Figure 1**) results in a transepithelial potential of −2.5 mV at the aqueous side (measured in monkey). This transepithelial potential results from the fact that the transport mainly involves movement of anions, in humans mainly Cl^-, across the ciliary epithelium. The net transport of Cl^- is coupled to a net transport of Na^+, K^+, and ascorbate. The transport of solutes across the ciliary epithelium drives osmotically the flow of water across the epithelium through water channels in the nonpigmented epithelium. It should be mentioned that it might be possible that not all of the aqueous humor is produced by the ciliary epithelium only. Concentration differences of, for example, ascorbate between the posterior and the anterior chamber might be explained by a passive volume influx from other epithelia.

The Ciliary Epithelium: A Double-Layered Epithelium Forms a Functional Syncytium

The ciliary epithelium separates the stroma of the ciliary body from the posterior chamber. It is a double-layered epithelium consisting of a pigmented epithelium facing the ciliary body stroma and a nonpigmented epithelium facing the posterior chamber. The two epithelia are in contact with each other through their apical cell membranes. The basolateral membrane of the pigmented epithelium is orientated toward the stromal side, whereas the basolateral membrane of the nonpigmented epithelium faces the side of the aqueous humor. In region of the borders of the ciliary body, posteriorly at the flat pars plana zone close to the ora serrata, and anteriorly at the transition zone between iris and ciliary body, the human ciliary epithelium shows regional structural variations. In the pars plicata, the ciliary epithelium shows deep infoldings and large numbers of mitochondria, indicating the zone of active transepithelial ion transport. Furthermore, the analysis of the intracellular ion composition in the ciliary epithelium using X-ray microprobe analysis also revealed functional variations in the transport activity

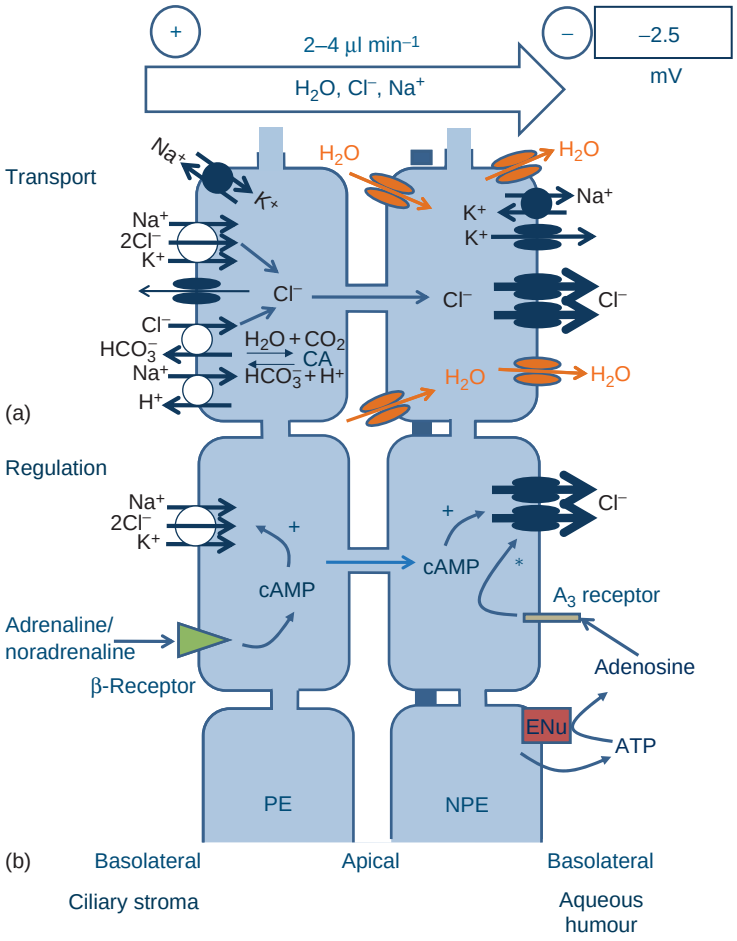

Figure 1 Summary of ion and water transport mechanisms of the ciliary epithelium. (a) Transport of ions. The ciliary epithelium is a functional syncytium: gap junctions (open connections) connect the cells of the pigmented and the nonpigmented epithelium and tight junctions (dark blue bars) between the cells of the nonpigmented epithelium form a barrier. Mainly Cl^- and Na^+ are taken up by the pigmented epithelium by transport mechanisms located in its basolateral membrane. The Na^+/K^+-ATPase establishes a gradient for Na^+ by transporting Na^+ out of the cell. The gradient for sodium is used by the $Na^+/K^+/2Cl^-$ co-transporter to take up Na^+, K^+, and Cl^- into the cell. A second transport mechanism further accumulates Cl^- in the cell: intracellular carbonic anhydrase accelerates the reaction of CO_2 and water into HCO_3^- and H^+; using the gradient for Na^+, H^+ is extracted from the cytosol by the activity of the Na^+/H^+ exchanger which further accelerates the reaction by carbonic anhydrase, leading to accumulation of HCO_3^-; HCO_3^- is transported out of the cell in exchange with Cl^- which increases the amount of Cl^- in the cytosol. Cl^- diffuses through gap junctions into the nonpigmented epithelium and leaves the cell through basolateral Cl channels. Na^+ is eliminated from the cytosol of the nonpigmented epithelium by the activity of the Na^+/K^+-ATPase. K^+ recycles across the basolateral membrane through K^+ channels. This transport of osmolytes drives the transport of water which follows the osmotic gradient though aquaporin water channels across the nonpigmented epithelium. (b) Major regulatory pathways. Activation of β-adrenergic receptors in the pigmented epithelium leads to an increases in intracellular cAMP which activates both the $Na^+/K^+/2Cl^-$ transporter in the basolateral membrane of the pigmented epithelium and the Cl^- channels in the basolateral membrane of the nonpigmented epithelium. ATP, which is released from the ciliary epithelium or adjacent tissues, is degraded into adenosine by ecto-nucleotidases. Adenosine stimulates A_3-receptors which activates an intracellular signaling cascade, resulting in stimulation of the Cl channels in the basolateral membranes of the nonpigmented epithelium. CA, carbonic anhydrase; ENu, ecto-nucleotidase; NPE, nonpigmented epithelium; PE, pigmented epithelium.

of the different regions. The turnover of Na^+, K^+, and Cl^- appeared to be considerably higher in the anterior than in the posterior ciliary epithelium.

The barrier function of the epithelium is provided by the formation of tight junctions between cells of the non-pigmented epithelium at their apical borders. The tight junctions form a major part of the blood–aqueous barrier of the ciliary body. The cells of the pigmented and of the nonpigmented epithelium are functionally connected to each other by gap junctions to form a functional syncytium. Thus, the transport across the ciliary epithelium requires the following steps (**Figure 1(a)**): (1) the pigmented epithelium takes up ions from the stroma of the ciliary body; (2) the ions pass through the gap junctions to the nonpigmented epithelium; and (3) the ions are released into the aqueous humor across the basolateral membranes of the nonpigmented epithelium. Functionally, the ciliary epithelium could be characterized as a tight epithelium,

which means that the major part of the ion transport has to pass through the cells of the epithelium. Due to the low conductance of the tight junctions, only few molecules can pass the paracellular pathway. In fact, flux studies in the bovine ciliary epithelium using L-glucose showed paracellular flux rates comparable to those known in tight epithelia. However, fresh iris–ciliary body preparations from many species showed rather low transepithelial resistances of values lower than 100 Ω cm^2. The explanation for such a small value likely stems from an underestimation of the surface area of the deeply folded ciliary epithelium in these preparations. When the measurements were corrected for the true surface of the unfolded tissue, the resistances reaches values of more than 1000 Ω cm^2, which is comparable to that of other tight epithelia, such as the retinal pigment epithelium. Using transport inhibitors the rate of aqueous humor production can be reduced by 80 %, which indicates the amount of water and solutes transported through the transcellular route.

The Energy for Active Transport

As in all transporting epithelia, the basic drive for active ion transport is provided by the activity of the Na^+/K^+-adenosine triphosphate (ATP)ase. Inhibition of Na^+/K^+-ATPase decreases intraocular pressure and transport of Na^+ in experimental animals. The Na^+/K^+-ATPase uses the energy of ATP hydrolysis to transport Na^+ and K^+ across the cell membrane against a concentration gradient. In this transport, the Na^+/K^+-ATPase removes Na^+ from the intracellular space and transports K^+ into the cell. This primary active transport of Na^+ establishes a gradient for Na^+ across the membrane which is used by secondary active transporters for many substances by coupling their transport to a movement of Na^+ along the established gradient. In the ciliary epithelium, both the pigmented and the nonpigmented epithelium express Na^+/K^+-ATPase. The Na^+/K^+-ATPase is localized in the basolateral membranes and the interdigitations of both the nonpigmented and the pigmented epithelium. Due to a higher expression rate in the nonpigmented epithelium and because of regional variations in the expression of different isoforms, the Na^+/K^+-ATPase activity of the nonpigmented epithelium overcomes the one of the pigmented epithelium. Thus, the transport across the double-layered epithelium is mainly driven by the activity of the Na^+/K^+-ATPase in the nonpigmented epithelium. The activity of the Na^+/K^+-ATPase in the pigmented epithelium may serve housekeeping functions. The activity of the Na^+/K^+-ATPase in the nonpigmented epithelium is further supported by the close neighborhood to basolateral K^+ channels. K^+, which is transported by the Na^+/K^+-ATPase into the cell, recycles across the basolateral membrane into the extracellular space through these K^+ channels. This keeps the gradient for K^+ across the basolateral membrane small and facilitates the Na^+ transport by Na^+/K^+-ATPase. The transport direction, in general, is then defined by the asymmetrically distributed Na^+-dependent co-transporter molecules in the ciliary epithelium.

The Transport Mechanisms

The Uptake of Ions at the Basolateral Membrane of the Pigmented Epithelium

Cl^- is taken up from the stromal side across the basolateral membrane of the pigmented epithelium and accumulates in the cytosol basically by two transport mechanisms which use the Na^+ gradient established by Na^+/K^+-ATPase. The bumetanide-sensitive electroneutral $Na^+/K^+/2Cl^-$ co-transporter takes up Na^+, K^+, and Cl^- from the stromal fluid. Since K^+ can flow back from the cytosol into the stromal extracellular space through K^+ channels, it is mainly Cl^- that accumulates in the cytosol of the pigmented epithelium. The second transport mechanism is provided by the coupled activity of both a Na^+/H^+ exchanger and a Cl^-/HCO_3^- exchanger. The Na^+/H^+ exchanger again uses the gradient for Na^+ to remove protons from the cytosol of the pigmented epithelium. This increases the amount of HCO_3^- in the cytosol from the reaction of H_2O and CO_2. HCO_3^- is then transported out of the cell across the basolateral membrane by the Cl^-/HCO_3^- exchanger by whom an additional influx of Cl^- ions from the stromal side into the cell is generated. The proportion of the two transport mechanisms in the entire transport of the ciliary epithelium is not clear and may vary between different species. However, the combined transport activity of these two transport mechanisms is counterbalanced by basolaterally localized Cl^- channels. Cl^-, which has accumulated in the cytosol of the pigmented epithelium, can recycle back into the stroma through these channels. This decreases the amount of transported Cl^- into the cytosol of the pigmented epithelium and across the ciliary epithelium. As described later, the control of the ratio of transported and recycled Cl^- ions is important for the modulation of the ion and water transport by the ciliary epithelium.

The Transport from the Pigmented Epithelium to the Nonpigmented Epithelium

As described above, the two epithelia are coupled through intercellular gap junctions to form a functional syncytium. The gap junctions are localized between the pigmented and the nonpigmented epithelium, and between the cells of the nonpigmented epithelium. The two combined transport mechanisms, $Na^+/K^+/2Cl^-$ exchanger and Na^+/H^+ exchanger plus Cl^-/HCO_3^- exchanger, lead to a transport of Na^+ and Cl^- into the pigmented epithelium. The ions

flow from the cytosol of the pigmented epithelium into the cytosol of the nonpigmented epithelium through the gap-junction channels which are formed by connexins. So far, different subtypes of connexins were found to be expressed by either the pigmented or the nonpigmented epithelium. Analysis of the gap junctions in the rat showed that Cx40 and Cx43 form gap junctions between the pigmented and the nonpigmented epithelium, whereas Cx26 and Cx31 form the gap junctions between the cells of the nonpigmented epithelium. The identity of the connexins forming gap junctions between the cells of the pigmented epithelium is unclear. Unspecific inhibition of the conductance of gap junction channels by inhibitors, such as oactanol of heptanol, revealed the importance of the gap junctional complexes for the epithelial transport of ions across the ciliary epithelium. Using these blockers, the active ion transport across the ciliary epithelium is reduced by 80%.

The Efflux of Ions across the Basolateral Membrane of the Nonpigmented Epithelium

Under physiological conditions, the efflux of ions across the basolateral membrane of the nonpigmented epithelium into the eye chamber represents the rate-limiting step of the transport of ions by the ciliary epithelium. This is mainly concluded by the difference of driving forces for Cl^- between the cytosol of pigmented and the nonpigmented epithelium and by the fact that the transport activity of the Na^+/K^+-ATPase of the nonpigmented epithelium is dominating over that of the pigmented epithelium. This conclusion means that the uptake of Cl^- by the pigmented epithelium is always larger than the efflux of Cl^- from the cytosol of the nonpigmented epithelium into the eye chamber. Na^+, which reaches the nonpigmented epithelium, is transported out of the cell by the activity of the Na^+/K^+-ATPase. Additionally, it is possible that a part of Na^+ leaves the cell through epithelial Na^+ channels (ENaCs), which were found to be expressed by the nonpigmented epithelium. Cl^- ions leave the cells of the nonpigmented epithelium through basolateral Cl channels. Since the Cl^- efflux out of the nonpigmented epithelium represents the rate-limiting step in the transepithelial transport, the regulation of the Cl channel activity represents a major mechanism in the regulation of aqueous humor formation. So far, it seems to be that the basolateral Cl^- conductance of the nonpigmented epithelium is primarily provided by ClC-3 Cl channels. These Cl channels are regulated by a multitude of different stimuli such as cell swelling or reduced protein kinase C activity. However, data from other stimulatory pathways, such as elevation of intracellular cyclic adenosine monophosphate (cAMP), imply the functional presence of other Cl channels which are so far not identified. Data from the isolated nonpigmented ciliary epithelium imply also the presence of a recycling pathway for Na^+ and Cl^- back from the aqueous side into the cytosol of the nonpigmented epithelium. This recycling pathway could be again provided by the coupled activity of both Na^+/H^+ exchanger and Cl^-/HCO_3^- exchanger in the basolateral membrane of the nonpigmented epithelium.

Aquaporins of the Ciliary Epithelium

The active transport of osmolytes drives the transport of water by osmosis. As mentioned above, the ciliary epithelium has a low paracellular permeability so that every transport has to pass the transcellular route. This transport route is provided by aquaporins, the so-called water channels, which are transmembrane proteins that form a pore to pass water across the cell membrane. In the ciliary epithelium, only the nonpigmented epithelium was found to express aquaporins: aquaporin-1 (AQP1) and aquaporin-4 (AQP4). These aquaporins are likely located in the membranes on both sides, apically and basolaterally, of the tight-junction belt of the nonpigmented epithelium. Thus, the transport route for water consists of the following steps: Since the pigmented epithelium does not express tight junctions, water can freely reach the tight-junction belt of the nonpigmented epithelium. Na^+ and Cl^-, which reach the nonpigmented epithelium through gap junctions from the pigmented epithelium, increase intracellular osmolarity. This drives an osmotic uptake of water through aquaporins. The ATP-driven transport of osmolytes across the basolateral membrane of the nonpigmented epithelium drives the transport of water through aquaporins across the basolateral membrane. Analysis of aquaporin-deficient mice revealed a decreased intraocular pressure due to reduced water transport by the ciliary epithelium.

Regulation of Aqueous Humor Formation

A large variety of signaling molecules was detected which regulate aqueous humor formation. Extracellular stimuli are catecholamines, antinatriuretic peptide, cannabinoids, endothelin, muscarinic agonists, glucocorticoids, prostanoids, and tumor necrosis factor-alpha. These extracellular signaling molecules activate intracellular signaling pathways, which involve cAMP, cyclic guanosine monophosphate (cGMP), NO, Ca^{2+}, pH, protein kinases A and C, tyrosine kinase, or mitogen-activated protein (MAP) kinase.

Regulation of Na^+ and Cl^- Uptake by the Pigmented Epithelium

As mentioned above, the efficiency by which the pigmented epithelium takes up Na^+ and Cl^- is reduced by a recycling pathway for these ions. This pathway is

represented by the combined activity of the Na^+/K^+-ATPase of the pigmented epithelium and the presence of basolateral Cl channels in the pigmented epithelium. These two transporting transmembrane proteins move Na^+ and Cl^- back to the extracellular space of the stromal side. As a pathway which counterbalances the uptake of ions from the stromal side, the recycling pathway can increase or decrease the net uptake of Na^+ and Cl^- and is, thus, important for the regulation of aqueous humor production. Although the Cl^- efflux at the nonpigmented epithelium represents the rate-limiting step in the aqueous humor production, the recycling pathway of the pigmented epithelium is of importance by the fact that the pigmented epithelium is accessible to many signaling molecules from the blood stream or from sympathetic nerve endings. ATP was found to increase the activity of the Cl channels and is therefore a regulator which decreases aqueous humor formation. Stimulation of the ATP receptors, P_2Y_2, triggers the formation of prostaglandin E2, and increases intracellular free Ca^{2+} as well as cytosolic cAMP. The latter second messenger directly activates the so-called maxiCl channels, which have a large Cl conductance and would transport the major proportion of recycled Cl^-.

Modulation of Cl^- Efflux out of the Nonpigmented Epithelium

The Cl^- is the rate-limiting step for the aqueous humor formation by the ciliary epithelium. Thus, the regulation of the Cl channel activity in the nonpigmented epithelium represents an important side for the regulation of aqueous humor production. Since the nonpigmented epithelium is not reachable to mediators from outside of the eye, the regulation of Cl channel activity can only involve intrinsic factors such as cell swelling or autocrine regulatory pathways; indeed, cell swelling appeared as a strong regulator to increase aqueous humor secretion. Furthermore, the stimulation of the A_3 adenosine receptors, inhibition of protein kinase C, or an increase of cytosolic cAMP increases the Cl channel activity and subsequently the formation of aqueous humor.

The Regulation of the Aqueous Humor Formation at the Double-Layered Epithelium

As mentioned above, a multitude of different factors modulate the formation of aqueous humor. Since a clear picture which integrates these pathways into one scenario is lacking, the two most important pathways are described in more detail subsequently (**Figure 1(b)**).

In the isolated epithelia, cAMP appeared as an important regulator. On the one hand, cAMP might reduce the aqueous humor production by activation of Cl channels in the pigmented epithelium and, on the other hand, it might increase the formation of aqueous humor by activation of the basolateral Cl conductance of the nonpigmented epithelium. Indeed, an increase by different cAMP-stimulating mediators had adverse effects on the Cl^- transport of the double-layered epithelium. β-Adrenergic stimulation, which leads to formation of cAMP, increases the aqueous humor production by stimulation of the $Na^+/K^+/2Cl^-$ co-transporter and the Cl channels in the pigmented and the nonpigmented epithelia, respectively. This mechanism is in accordance with the effects of clinically administered β-adrenergic antagonists, which lower the aqueous humor inflow. However, a more general increase in intracellular cAMP production by forskolin activates the cAMP-producing enzyme, adenylyl cyclase, leading to a reduction in the aqueous humor inflow. These effects of cAMP might result from the inhibition of the Na^+/K^+-ATPase in the nonpigmented epithelium, uncoupling of the gap junctional connection between the pigmented and the nonpigmented epithelium and the above-mentioned activation of Cl channels in the pigmented epithelium. It is likely the final response of the double-layered epithelium to cAMP stimulation results from a spatial distribution of local increases in the cAMP concentration, especially for the effects of β-adrenergic stimulation.

A second important pathway that regulates the formation of aqueous humor is that of the stimulation of A_3 adenosine receptors. Knock-out mice, lacking the expression of the adenosine A_3 receptor, were found to show decreased intraocular pressure probably resulting from a decreased transport through the ciliary epithelium. In addition, A_3-receptor-selective agonists increase intraocular pressure, while A_3-receptor-selective antagonists block the effects of adenosine to increase intraocular pressure. Furthermore, a disease-dependent overexpression of A_3 receptors seems to play a role in the development of glaucoma in pseudoexfoliation syndrome. The agonist of the adenosine receptors is either secreted from the adjacent tissue or generated by the presence of ecto-enzymes on the surface of both the pigmented and the nonpigmented epithelium. These enzymes hydrolyze ATP which is released from both the pigmented and the nonpigmented epithelium. Thus, the adenosine-dependent regulation of aqueous humor production represents an intrinsic autocrine pathway, which is of critical importance for the regulation of the transport activity by the nonpigmented epithelium. Indeed, the most profound effect of A_3 receptor stimulation is the increase in the Cl^- conductance of the nonpigmented epithelium.

The Transport of HCO_3^-

As shown above, an HCO_3^--dependent transport pathway seems to increase uptake rates for Na^+ and Cl^- by the

pigmented epithelium and to counterbalance the Cl^- efflux across the basolateral membrane of the nonpigmented epithelium. The role of the HCO_3^- transport in epithelial ion transport across the ciliary epithelium is not fully understood. In humans, the transport by the ciliary epithelium does accumulate Cl^- in the aqueous humor, but not HCO_3^-. However, there are implications for a role of HCO_3^- in the regulation of aqueous humor formation in humans. These implications come from the treatment of glaucoma by lowering intraocular pressure using inhibitors of carbonic anhydrase, which were found to reduce inflow of aqueous humor in monkey. Carbonic anhydrase strongly accelerates the reaction of CO_2 and H_2O to HCO_3^- and H^+ and the reaction vice versa. Indeed, the presence of cytosolic and of membrane-bound carbonic anhydrase has been demonstrated in the ciliary epithelium. In humans, the administration of inhibitors for carbonic anhydrase leads to an increase in the aqueous-to-plasma ratio for HCO_3^- and a decrease in the aqueous-to-plasma ratio for Cl^-. This means that inhibition of carbonic anhydrase seems to decrease the Cl^- transport by the ciliary epithelium and to increase the HCO_3^- transport. Since the Cl^- transport by the human ciliary epithelium seems to be the dominating transport, the reduced inflow of aqueous humor in response to inhibition of carbonic anhydrase results from a decreased transport of Cl^- and water. Thus, in humans the effects of carbonic anhydrase seem to work at the side of the pigmented epithelium. The activity of the membrane-bound carbonic anhydrase would deliver CO_2 and water. CO_2 diffuses into the cell where the cytosolic carbonic anhydrase accelerates the reaction of CO_2 and H_2O to H^+ and HCO_3^-, which enhances the transport by the combined activity of the Na^+/H^+ exchanger and the Cl^-/HCO_3^- exchanger. These two transporter systems accumulate Na^+ and Cl^- in addition to the transport activity of the $Na^+/K^+/2Cl^-$ co-transporter and would increase the net transport of Na^+ and Cl^-. Thus, although the transport across the ciliary epithelium does not accumulate HCO_3^- in the aqueous humor, the modulation of HCO_3^- transport across the basolateral membrane of the pigmented epithelium is of clinical importance, being a target for drugs to lower intraocular pressure.

See also: Ciliary Blood Flow and its Role for Aqueous Humor Formation; Control of Aqueous Humor Flow; Neuroendocrine Properties of the Ciliary Epithelium; Pharmacology of Aqueous Humor Formation; The Role of the Ciliary Body in Aqueous Humor Dynamics. Structural Aspects.

Further Reading

Candia, C. A. and Alvarez, L. J. (2008). Fluid transport in ocular epithelia. *Progress in Retinal and Eye Research* 27: 197–212.

Civan, M. M. (2003). The fall and rise of active chloride transport: Implications for regulation of intraocular pressure. *Journal of Experimental Zoology A Comparative Experimental Biology* 300: 5–13.

Civan, M. M. and Macknight, A. D. (2004). The ins and outs of aqueous humor secretion. *Experimental Eye Research* 78: 625–631.

Coca-Prados, M. and Escribano, J. (2007). New perspectives in aqueous humor secretion and in glaucoma: the ciliary body as a multifunctional neuroendocrine gland. *Progress in Retinal Eye Research* 26: 239–262.

Do, C. W. and Civan, M. M. (2004). Basis of chloride transport in ciliary epithelium. *Journal Membrane Biology* 200: 1–13.

Do, C. W. and Civan, M. M. (2009). Species variation in biology and physiology of the ciliary epithelium: Similarities and differences. *Experimental Eye Research* 88(4): 631–640.

Jacob, T. J. and Civan, M. M. (1996). Role of ion channels in aqueous humor formation. *American Journal of Physiology* 271: C703–C720.

Hamann, S. (2002). Molecular mechanisms of water transport in the eye. *International Reviews in Cytology* 215: 395–431.

Verkman, A. S., Ruiz-Ederra, J., and Levin, M. H. (2008). Functions of aquaporins in the eye. *Progress in Retinal Eye Research* 27: 420–433.

Ionic Permeability and Currents in the Lens

P J Donaldson, University of Auckland, Auckland, New Zealand
K F Webb, University of Nottingham, Nottingham, UK

Glossary

Advection – The transport of a substance by a moving fluid. In the lens the circulating ionic currents create a fluid flow that causes the advection of neutral solutes such as glucose and amino acids into the lens faster than would be predicted by passive diffusion alone.
Conductance – A measure of current (in Amperes (A)) divided by voltage (in Volts (V)) and refers to the rate of ion travel through an ion channel and is often measured in Siemens (S). Most ion channels have a conductance of between 1 and 150 pS (10^{-12} S).
Impedance analysis – An electrophysiological technique which utilizes broadband voltage stimuli delivered and recorded by spatially separated microelectrodes to provide location-specific measurements of resistive pathways within a tissue. This technique has been used to monitor the propagation of these stimuli through the ocular lens, providing information on the resistive coupling of electrical compartments between and around radial columns of lens cells. This analysis is dependent upon the fitting and refinement of a detailed three-dimensional equivalent circuit model, incorporating the relative contributions of membranes and conductive spaces within different lens locations.
Isotonic fluid transport – The theoretical limiting velocity of water flow that is approached as the membrane water permeability approaches infinity and the transmembrane osmotic gradient approaches zero.
Patch clamping – An electrophysiological technique whose discovery made it possible to record currents flowing through individual ion channels. Patch clamp recording utilises a glass micropipette, with a tip diameter of $\sim$ 1mm, to enclose a patch of membrane that often contains just one or a few ion channels. The micropipette is pressed against a cell membrane and suction is applied to assist in the formation of a high resistance ($>10^9$ ohm, GΩ) seal between the glass and the cell membrane. The high resistance of this seal makes it possible to electrically isolate the ion channel currents measured across the membrane patch with little competing noise. Erwin Neher and Bert Sakmann received the Nobel prize in physiology or medicine in 1991 for their contributions to the development of this technique.
Permeability – A description of how fast ions are able to move through an ion channel (the rate of movement). The depth of the energy well for a particular ion generally determines its permeability, or conductance. However, if an energy well is too deep, it can slow down the ion's rate of travel.
Ussing chamber – A physiological recording apparatus consisting of two halves that are clamped together to isolate the apical and basolateral surfaces of an epithelial tissue. The two half chambers are filled with physiological media in order to remove any chemical, mechanical, and electrical driving forces. The vectorial transport of ions across an epithelial tissue produces a potential (voltage) difference across the tissue that is measured using a pair of voltage electrodes placed on either side of the epithelial tissue. Current is injected to balance the potential difference measured across the voltage electrodes via a second pair of current passing electrodes. This so-called short-circuit current (I_{sc}) is a precise measure of net ion transport taking place across the tissue.
Vibrating current probe – An electrophysiological technique used to measure ionic current flowing in the extracellular compartment surrounding tissues. The vibrating probe consists of a voltage-sensitive electrode which is rapidly vibrated between spatially separated locations adjacent to the tissue surface. Calibrating for the resistivity of the bathing fluid allows measurements of current density and direction to be made at locations across an epithelial surface or around a tissue.

The Physiology of Lens Transparency: A Unique Structure and Function

The transparency of the lens is closely linked to the unique structure and function of its component cells. The highly differentiated lens fiber cells which compose the bulk of the lens are derived from an overlying anterior layer of epithelial cells, which exit the cell cycle at the equator to embark upon a differentiation process involving extensive cellular elongation, loss of cellular organelles and nuclei, and the expression of fiber-cell-specific proteins. Fiber cells elongate until they meet other fibers extending

from their opposite hemisphere, meeting and interdigitating at the anterior and posterior poles to form the sutures. Since this process continues throughout life, a gradient of fiber cells at different stages of differentiation is established around an internalized core (the lens nucleus) of mature, anucleate fiber cells. While the transparent properties of the lens are a direct result of its highly ordered tissue architecture, the lens may not be a purely passive optical element. Maintenance of its architecture could require special mechanisms to supply the deeper lying fiber cells with nutrients and remove metabolic waste and to control the volume of these cells.

Because of its size, it has been proposed that the avascular lens cannot rely on passive diffusion alone to transport nutrients to deeper lying cells, or to transport waste products back to the surface. Calculated diffusion rates for substrate entry to the lens center preclude simple diffusional delivery of glucose and other nutrients, whereas passive redistribution of metabolic waste products and ionic entry could lead to excessive accumulation of toxic metabolites in the lens interior. Outer cell layers, lying near the surface and closer to supply of oxygen and nutrients, derive energy from aerobic glycolysis conducted by mitochondria in the anterior epithelium and differentiating fiber cells. In contrast, internalized mature fiber cells are reliant on anaerobic glycolysis for energy production, which produces lactate whose accumulation in the deep lens lowers tissue pH. Thus, opposing gradients of metabolic substrates and waste products are found across the lens radius. In the absence of a blood supply some other transport system must exist by which glucose and other nutrients supply the metabolic needs of mature fiber cells and by which waste products can be removed from the lens interior.

It has been proposed that the lens operates an internal microcirculatory system that preserves tissue architecture and transparency by supplying fiber cells with nutrients, removing wastes, and controlling the volume of fiber cells. Our understanding of this system is not yet complete and is still somewhat controversial. To put the current model of lens transport into perspective it is pertinent to review the historical developments that have led to its formulation.

Early Views of Lens Physiology

Early investigations in lens physiology treated the organ as a kind of giant cell, due to its apparently amorphous interior, high global internal K^+, and low Na^+ concentrations (**Figure 1(a)**). The physiological characterization of the lens began with techniques designed to estimate its global functional properties – such as ion concentrations, intrinsic potential, specific resistances, and current–voltage relationships. Such experiments did not attempt to localize or apportion functional measurements to intralenticular structures, due to the prevalent view that the lens was a homogeneous bag of proteinaceous gel, and was not cellular in nature. As histological and electrophysiological techniques improved, there was a slow paradigm shift driven largely by the growing study of fluid transport and homeostatic mechanisms in other epithelial tissues. Since the anterior surface of the lens is covered by an epithelial cell layer while the posterior surface is not, early studies of lens physiology focused on hypothetical anterior–posterior differences in ion transport (**Figure 1(b)**). By mounting the lens in an Ussing chamber an anteriorly directed positive electrical potential was detected, which appeared to result from Na^+/K^+ exchange mechanisms located at the lens anterior. Thus, the anterior epithelial layer was thought to maintain the welfare of the fiber cell mass by setting and maintaining the lens intrinsic potential and ion balance, creating a functional syncytium driven by a pump-leak mechanism (**Figure 1(b)**). The lens epithelium was thought to contain all active transport and selective ion permeation pathways, while the fiber cells were thought to exist as a distributed leak, against which epithelial transport worked to maintain lens homeostasis. Two-electrode voltage clamp methods, in which separate voltage-sensing and current-passing electrodes were inserted into different locations within a single lens, found that wherever the electrodes were placed a similar potential could be recorded. This was interpreted as evidence of membrane degeneracy in the lens core, where cells were seen as electrochemically passive, or even dead. By contrast, the anterior epithelium was amenable to direct functional study – being capable of maintaining its integrity and structural composition even when stripped from the lens. The fiber mass left behind depolarized and rapidly degenerated on removal of the epithelium, and was thus viewed as functionally inert.

The role of fiber cells in lens physiology remained uncertain, although data hinted at a more defined contribution of inner lens membranes than a simple homogeneous leak. Some of the first data on the internal structure and resistive contribution of cell membranes within the internalized lens came from the application of impedance analysis to the lens which allowed the relative contributions of peripheral and deep fiber cell membranes, connected by a tortuous, resistive extracellular space to be estimated. It was found that internalized fiber cells possessed very high resistance membranes, and the majority of the ion conducting pathways lay within the outer cell layers. In combination with ion replacement experiments, it was found that surface cells contained a large permeability pathway to K^+ ions, while inner fiber membranes were dominated by Na^+ and Cl^- conductances of much lower density. The large amount of fiber cell membrane in the internalized lens ($\sim$100 cm^2 in a small frog lens, vs. $\sim$0.5 cm^2 of epithelial membrane) translates into a significant leakage pathway for Na^+ and Cl^-, which is offset by

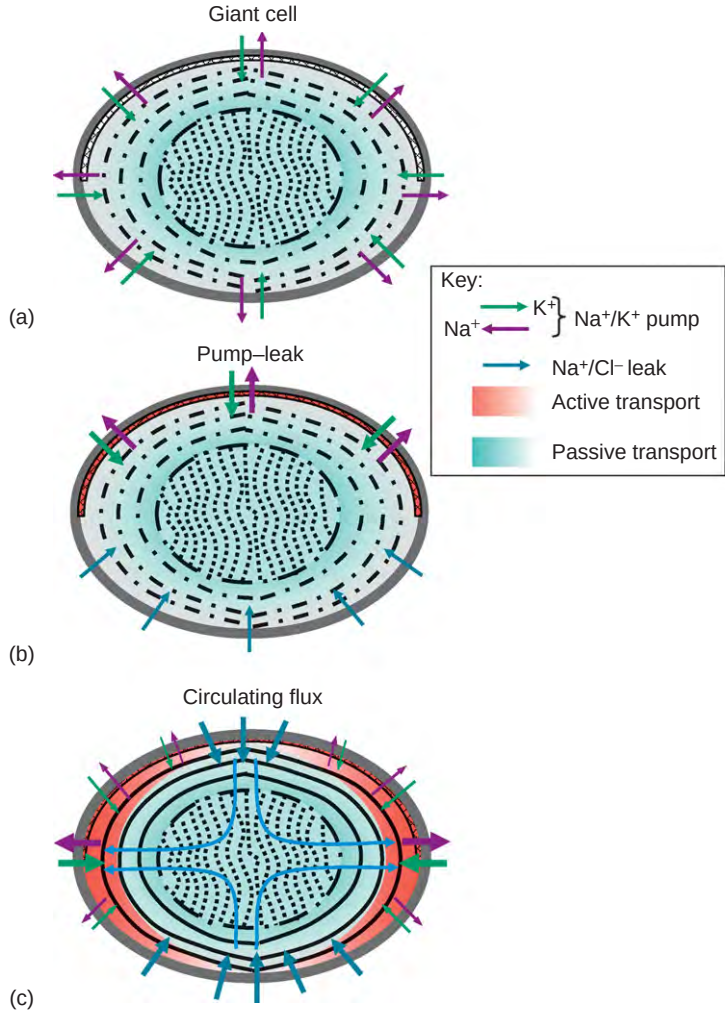

Figure 1 Historical views of lens physiology. (a) The lens was originally thought of as a homogeneous, acellular ''giant cell'' due to the degeneration of fiber cell membranes. Transport across the lens capsule was thought to create an outwardly-directed K^+ and an inwardly-directed Na^+ gradients. (b) In the pump-leak model active transport by the anterior epithelium was believed to drive a posterior–anterior ion flux that compensated for a distributed Na^+/Cl^- leak in the fiber cell mass. (c) The circulating flux model was proposed to account for impedance and vibrating probe data that collectively showed that current flows are directed into the lens at the poles and out of the lens at the equator.

pumping activity at the lens surface. In this revised model transport activity was no longer restricted solely to the anterior epithelium, but to surface cells which includes differentiating fiber cells that retain contact with the capsule.

The next advance in understanding of lens physiology came from the application of a novel electrophysiological approach, the so-called vibrating probe, which measured the magnitude and direction of ionic current flowing in the extracellular compartment around the lens circumference. This technique revealed an outwardly-directed current exited the lens at the equator, whereas inward current was detected at both the anterior and posterior poles (**Figure 1(c)**). In intermediate positions, the current direction appeared to undergo a gradual shift from strongly inwardly-directed over the polar sutures, to strongly outwardly directed at the lens equator (**Figure 2(b)**). The equatorial outward current was found to respond to manipulations in bathing $[K^+]$, and could be reversed in direction by voltage clamping the lens to potentials more negative than E_K. Blockade of Na^+/K^+ ATPase activity by exposure to ouabain lead to a small initial current reduction, that was followed by a slow decline to zero. Decreasing bathing $[Ca^{2+}]$, which lead to large depolarizations in lens potential, caused a sharp rise in equatorially measured current. Radiolabeled Na^+ in the bath solution entered the lens at the poles and eventually exited at the lens equator. Since the equatorial current was outwardly directed, and Na^+/K^+ ATPase activity extrudes Na^+, it was proposed that the measured pattern of lenticular current flow represented a re-entrant cycle of Na^+ movement through the lens structure, entering via the extracellular space and leaving via Na^+/K^+ ATPase activity at the lens equator.

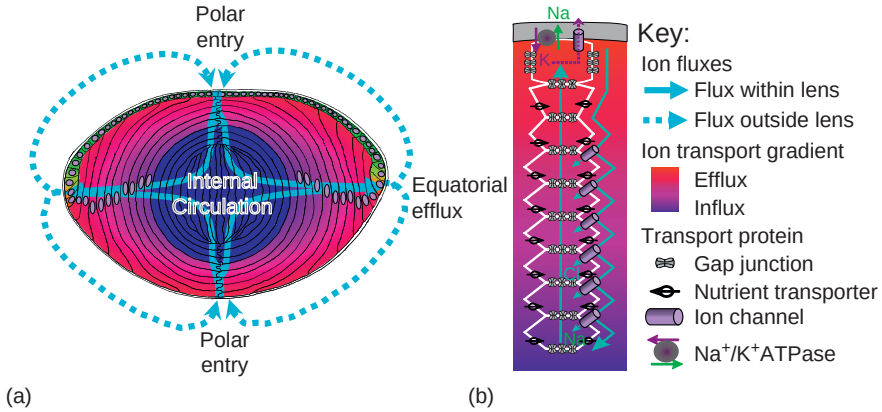

Figure 2 The lens internal micro-circulation system. (a) Current flow pathways around and through the lens carried by circulating ionic fluxes. (b) Schematic diagram showing a column of fiber cells cut in cross section at the lens equator. Current and solutes are proposed to flow into the lens via the extracellular space, to cross fiber cell membranes and to flow outward via an intracellular pathway mediated by gap junction channels. The surface local of Na^+/K^+ ATPase and K^+ channels which is connected to the Na^+ and Cl^- leak pathways in deeper fiber cells via gap junctions generates a circulating flux of ions that drives the circulation system.

K^+ accumulated by pumping activity was allowed to leave equatorial cells by K^+ selective channels, setting a negative membrane potential which was transmitted to the entire lens via gap junctions.

The results obtained by the vibrating probe were eventually verified using a modified Ussing chamber that measured ion fluxes in specific regions of the lens surface. These studies showed patterns of current flow that were spatially similar to those recorded via the vibrating probe. Efflux currents were dominant at the lens equator and an area immediately anterior. Application of the K^+ channel blocker Ba^{2+} eliminated measured currents only if applied to regions including the most equatorial zone, while ouabain produced measurable inhibition of Na^+/K^+ ATPase currents in the equatorial and immediately anterior segment, but not at the lens anterior pole. This location-specific effect of pharmacological agents strongly supports the notion that the physiologically relevant transport processes are concentrated in the equatorial lens.

The Lens Internal Circulation System

Having described from a historical perspective the techniques underpinning the formulation of the lens internal circulation hypothesis, this article now describes the current understanding of the model. Spatial segregation of transport functions within the lens creates a continuous flux of ions through the tissue structure (**Figure 2(a)**). Na^+ and Cl^- enter the lens at both poles via the extracellular space, enter internalized fiber cells via a distributed low level entry pathway, and leave the lens via an intercellular route mediated by gap junctions (**Figure 2(b)**). Mathias and co-workers have shown by biophysical modeling that this vectorial flux of ions produces a continuous flux of fluid and solute through the lens tissue, which appears to act as a lens internal microcirculation. The circulating flux of ions creates an extracellular fluid flow by solvent drag, whose rate has been estimated in the frog lens at approximately 1 μm s^{-1}. This flowing fluid carries with it other solutes, including antioxidants, glucose, and other nutrients; causing them to reach the lens core at a rate exceeding that results from simple diffusion alone. The operation of this lens internal circulation system appears essential to lens transparency since it controls ionic and volume homeostasis in all lens cells, and nutrient delivery and waste removal from the lens core. The constantly moving fluid flux prevents excessive accumulation of lactate and other metabolic products, prevents depletion of Na^+ and other ions from the extracellular space, and prevents the slow leakage of Na^+ and Ca^{2+} into fiber cells from triggering pathological change in the lens core.

Key Membrane Transport Components of the Lens Circulation System

The lens internal circulation system is hypothesized to achieve a constitutive flux of ions and fluid through the lens structure by the concerted action of spatially separated membrane transport pathways. Key components are listed below:

Localization of Active Transport Mechanisms to the Lens Surface

In the lens the active transport of Na^+ ions is achieved by concentrating the expression of functionally active Na^+/K^+ ATPase in the membranes of the surface cells, including the anterior epithelium and equatorial fiber cells. However, ouabain-sensitive pump currents at the equator have been shown to be at least 20-fold higher than those

measured at the poles. Na^+/K^+ ATPase pump proteins are detected throughout the fiber cell mass, but these proteins detected in cortical and nuclear fiber membranes appear to be nonfunctional due to tyrosine phosphorylation. The restriction of functional Na^+/K^+ ATPase pumps to the lens surface makes sense anatomically, since the pumping of ions requires energy, which is in short supply in deeper fiber cells that rely on anaerobic metabolism. Hence, it is the Na^+/K^+ ATPase activity that sets up the ion gradients which become the driving force for passive ion movement within the lens. The intracellular potential and cation gradient thus created are transmitted to the fiber cell mass by extensive gap junctional coupling, allowing secondary active uptake of nutrients and electroneutral ion exchange in internalized cells, which do not themselves maintain a functional pool of Na^+ pumps.

Spatially Differences in Membrane Permeability

Electrical measurement conducted on whole lenses exposed to changes in extracellular ion concentrations have shown that the K^+ permeability is restricted to the surface of the lens, while deeper fiber cells contain Na^+ and Cl^- permeability pathways. Using the patch clamp technique, the lens epithelium was subsequently found to contain K^+ channels which are thought to play a key role in setting lens membrane potential by providing a permeation pathway for K^+ accumulated by Na^+/K^+ ATPase activity in the lens periphery. A variety of inwardly and outwardly rectifying K^+ channels that were differentially sensitive to blockade by agents such as Ba^{2+} and tetraethylammonium (TEA) have been reported to be expressed in the lens epithelium. Not all of these identified channels are found in every species, or even in any one cell. However, despite this diversity of lens epithelial K^+ channel expression, in all species of lens these K^+ channels are important in setting the membrane potential for the underlying fiber cells, which are electrically connected to the epithelial surface via gap junctions. This dependency of the fiber cells on the surface epithelium is graphically illustrated by the inability of fibre cells once isolated to maintain their structural integrity. Fiber cells dissociated from the epithelium depolarize and activate a nonselective leak conductance that allows Ca^{2+} influx, which in turn activates Ca^{2+}-dependent proteases that compromise the structural integrity of these isolated cells.

Equatorial epithelial cells differentiate into fiber cells, and as part of this process there needs to be a switch in cation permeability from a predominantly outwardly directed K^+ conductance at the lens surface, to an inwardly directed Na^+ conductance in deeper fiber cells. Consistent with this switch in cation permeability the Cl^- conductance is expected to change from a peripheral efflux to a deeper influx to preserve electroneutrality. To determine how these changes occur as a function of fiber cell differentiation, fiber cells were isolated from the outer lens cortex in the presence of Gd^{3+}, a general inhibitor of nonselective cation channels, that prevented the membrane depolarization and Ca^{2+} influx that usually occurs when fiber cells are dissociated from the overlying epithelium. In the presence of Gd^{3+} it is possible to measure the membrane properties of isolated fiber cells using the whole cell patch clamp technique and to compare their membrane properties to those of the epithelium. Since fiber cell length *in vitro* has been shown to be predictive of *in vivo* location, length-dependent trends in the electrical properties of isolated fiber cells are able to be related to differentiation-dependent changes in membrane permeability.

Using this approach it was shown that the membrane properties of isolated fiber cells resemble a continuum (**Figure 3**). Short newly differentiated fiber cells tend to have membrane properties that resemble those of their progenitor epithelial cells, being hyperpolarized, electrically tight and dominated by K^+ conductances that are sensitive to Ba^{2+} and TEA (**Figure 3(a)**). As fiber cells elongate, these epithelioid K^+ conductances appear to become buried beneath an outwardly rectifying lyotropic anion channel, which increasingly dominates membrane behavior in longer cells. In short fiber cells this anion conductance was found to be not normally active, but it could be activated by cell swelling. In longer cells the anion conductance appeared to be constitutively active. The lyotropic selectivity sequence of these anion conductances observed in isolated cells appears similar to that measured in intact lenses under isotonic conditions, suggesting that these conductances may have a physiological role within the lens under resting conditions. Two classes of nonselective cation (NSC) channels could be distinguished by their sensitivity to trivalent cations, and were present in parallel to the anion conductance. The presence of these NSC conductances introduced a variable Na^+-permeable leak pathway that depolarized current reversal potentials and contributed a linear component to whole-cell current recordings. If this conductance was allowed to remain active, cell degradation rapidly ensued, triggered by catastrophic membrane influx of Ca^{2+} ions. While one NSC conductance was effectively minimized by the addition of Gd^{3+} to the bathing media, an additional NSC conductance, which proved to be sensitive to La^{3+}, was shown to activate upon isotonic cell shrinkage. Thus, it appears that while epithelial and short fiber cells are dominated by K^+ conductances, longer fiber cells become increasingly dominated by an anion conductance with a low level of cationic leak, which appear differentially sensitive to cell volume in longer cells. These spatially localized differences in ionic permeability, because they are electrically coupled by gap junctions, are believed to drive the internal ionic circulation system.

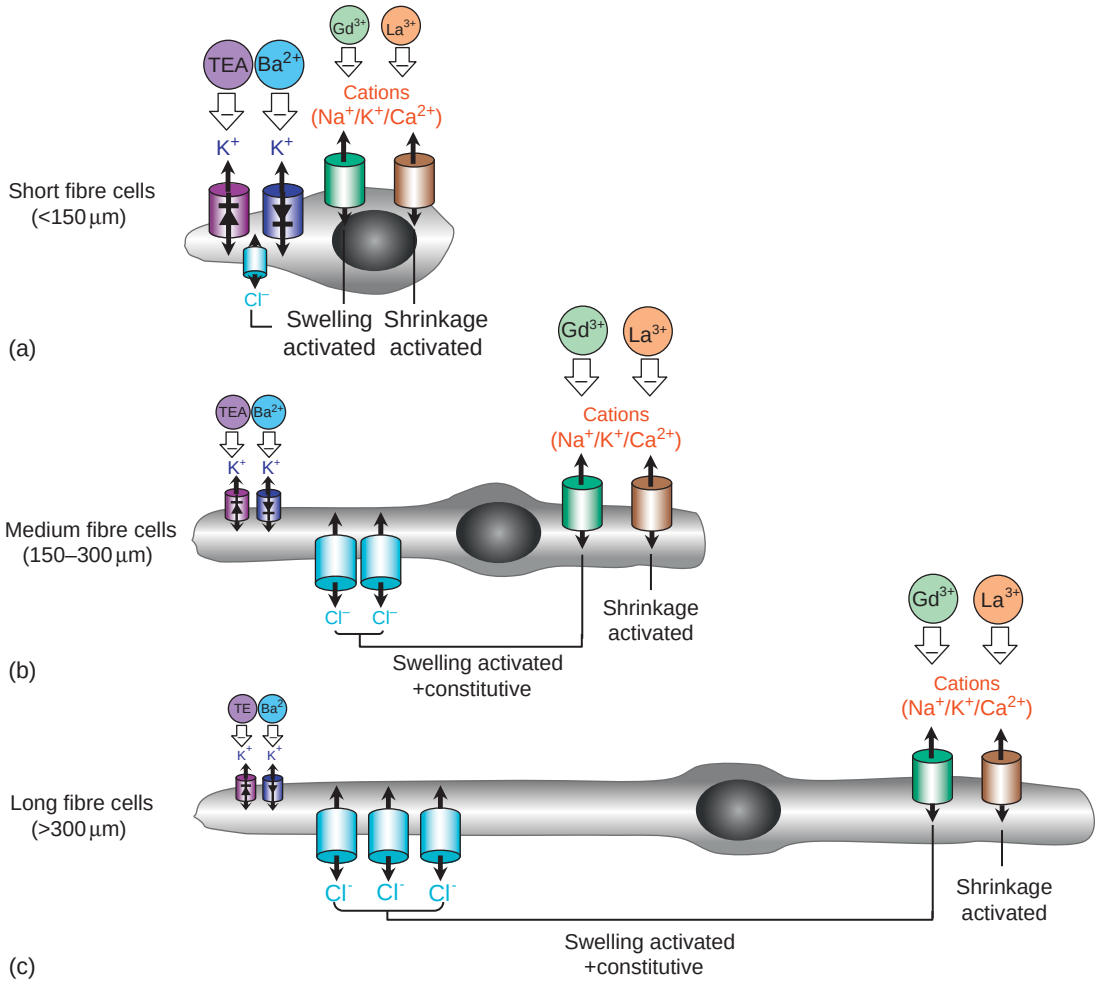

Figure 3 Spatial differences in membrane permeability develop as fiber cell differentiate. (a) The membrane properties of short fiber cells that have just undergone elongation from their progenitor epithelial cells tend to be dominated by Ba^{2+}- and TEA-sensitive K^+ channels, although they contain at least two distinct classes of nonselective cation (NSC) channels and a lyotropic Cl^- channel. The activity of NSC and Cl^- channels is usually low in these short cells but can be activated by changes in cell volume. Medium (b) and longer (c) fiber cells begin to accumulate more Cl^- channels, which, while retaining their volume sensitivity, become constitutively active under isotonic conditions. This increase in Cl^- conductance in longer cells overwhelms the K^+ conductances originally present in the shorter epithelial-like fiber cells.

Directing Gap Junctional Coupling to the Equator

Due to the abundance of gap junction channels, the lens can be considered a syncytium in which all cells have a similar membrane potential. However, regional differences in the distribution and regulation of the gap junction channels exist. In the outer fiber cells, gap junctions are particularly concentrated on the broad sides of the equatorial region of fiber cells, thus providing communication pathways preferentially in a radial direction toward the equator. In the inner fiber cells, the gap junctions are more evenly distributed throughout the cell membrane and provide a more isotropic coupling. This differential distribution of gap junctions helps to direct the outward component of the circulating current to the lens equator where the Na^+ pumps are preferentially localized (**Figure 2(b)**).

Fiber cells throughout the lens are connected to each other via gap junction channels composed of two related connexins, α_3 (Cx46) and α_8 (Cx50). Despite the fact that both of these connexins have the ability to form functional channels when expressed in *Xenopus* oocytes, inherited mutations and null mutants have shown that the presence of both is essential for the maintenance of tissue transparency. Briefly, α_8 appears to be involved in modulating the growth of the lens, while α_3 is important for maintaining cell-to-cell coupling in the lens core. In a wild-type lens the gap junctional coupling in differentiating fiber cells of the outer cortex is about 1.0 S cm^{-2} and falls to around 0.4 S cm^{-2} in the mature fiber cells of the lens core. In the lenses from the α_3 knock-out mice, the conductance is reduced by about 50% in the outer differentiating fibers and can be accounted for by the presence of α_8. However,

in central mature fibers of the α_3 knock-out mouse the coupling conductance drops to zero. This indicates that α_3 is solely responsible for mediating intercellular coupling in the lens core.

Water Permeability and Fluid Flow

The lens circulation model proposes that water follows the circulating Na^+. This requires that the lens fiber and epithelial cell membranes have significant water permeability. The most abundant membrane protein in lens fiber cells, Major Intrinsic Protein 26 (MIP26), was subsequently shown to be a member of the aquaporin (AQP) family of water channels and was renamed AQP0. When exogenously expressed in oocytes, AQP0 forms a water channel, but unlike many other members of the AQP family, it is not sensitive to Hg^{2+} and exhibits a relatively low water permeability. Using vesicles prepared from the rat lens, it was subsequently shown that the water permeability of AQP0 containing vesicles was some 45 μm s^{-1}, was Hg^{2+}-insensitive, and was dramatically reduced by the extraction of AQP0 from the vesicles. AQP0 water permeability has been shown to be sensitive to alterations in intracellular pH and $[Ca^{2+}]_i$, reflecting a potential mechanism to enhance water transport and rectify osmotic imbalances. In contrast, lens epithelial cells that express AQP1 had a membrane water permeability of some 135 μm s^{-1}, which was blocked by Hg^{2+}. Based on the lens circulation model, the water flowing out of each epithelial cell is due to the cumulative entry into many fiber cells. Hence, the water permeability of the epithelial cell membrane needs to be greater than that of fiber cell membrane, as indeed is the case.

Since water fluxes in the lens have been proposed to be isotonic in nature and the Na^+ influx across fiber cell membrane has been measured as 0.3×10^{-11} mol cm^{-2} s^{-1}, then the water flow generated by this solute flux needs to be some 10^{-8} cm s^{-1} to maintain lens osmolarity. Given the water permeability above 45 μm s^{-1}, the fiber cell transmembrane osmotic gradient necessary to generate this flow velocity is only about 0.1 mOsm. Thus, one does indeed expect the circulation to generate a near maximal water flow that approaches isotonic.

Secondary Active Transport of Nutrients

The internal circulation system is hypothesized to generate a bulk flow of fluid and solute which enhances the delivery of substrates to internalized lens cells by accelerating the movement of solute via the extracellular space. Consistent with this view, molecular studies (Table 1) have shown that fiber cells express a full repertoire of transporters that mediate the uptake of glucose and the amino acids involved in the synthesis of the glutathione (GSH), the key antioxidant in the lens.

Furthermore, immunocytochemical localization of these transporters has shown that differences exist in the complement of transporters expressed in the cortex and nucleus of the lens, suggesting that regional differences in nutrient uptake may exist. For example while lens epithelial cells express the facilitative glucose transporter GLUT1, fiber cells express the higher-affinity GLUT3

Table 1 Molecular inventory of nutrient transporter protein expression in different regions of the lens

		Localization					
Transporters	*Species*	*CE*	*NE*	*OC*	*IC*	*C*	*Mode of action*
Glucose transporters							
GLUT1	Rat		√				Facilitative diffusion
GLUT3	Rat			√	√		
SGLUT2	Rat			√	√	√	Secondary active transport
Cystine/glutamate exchanger (Xc-)							
xCT	Rat			√	√	√	Sodium independent antiporter
Glutamate transporters							
EAAT1	Rat			√	√		Secondary active transport
EAAT2	Rat		√	√			
EAAT3	Rat		√	√	√		
EAAT4	Rat			√	√		
EAAT5	Rat			√			
ASCT2	Rat		√	√	√	√	
Glycine transporters							
GLYT1	Rat		√	√	√		Secondary active transport
GLYT2	Rat		√	√	√	√	
Vitamin C transporters							
SVCT2	Human	√					Secondary active transport

CE, cultured epithelial cells; NE, native epithelial cells; OC, outer cortex; IC, inner cortex; C, core; A, anterior surface; E, equatorial surface.

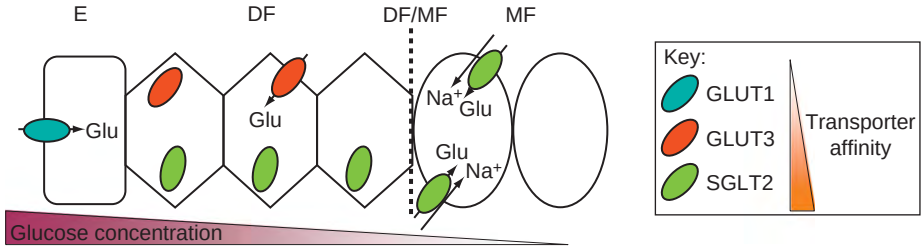

Figure 4 Regional differences in nutrient uptake in the lens. (a) Glucose uptake in the lens is mediated by at least three different transporters. In the epithelium GLUT1 is expressed, while in fiber cells GLUT3 and SGLT2 are expressed. During the course of fiber cell differentiation GLUT3 first becomes inserted into the narrow sides of differentiating fiber cells (DF) in the outer cortex. By contrast, SGLT2 is inserted into membranes of mature fiber cells (MF) from a cytoplasmic pool at the DF/MF transition. It is proposed that this differential expression of glucose transporters establishes an affinity gradient, which increases the ability of deeper fiber cells to extract a diminishing supply of glucose from the extracellular space.

isoform and the sodium-dependent glucose transporter SGLT2 (Figure 4). Both GLUT3 and SGLT2 transporters appear to be present predominantly in the cytoplasm of peripheral fibre cells and become inserted into the plasma membrane at different stages of fiber cell differentiation. GLUT3 is initially inserted into the narrow sides of the differentiating fiber cells, while SGLT2 is abruptly inserted into the membranes of mature fiber cells at the transition zone between differentiating and mature fiber cells that coincides with the loss of cell nuclei. Thus, the differential expression of glucose transporters establishes an affinity gradient which increases the ability of deeper fiber cells to extract a diminishing supply of glucose from the extracellular space. A similar change in the complement of transporters that mediate amino acid uptake in the cortex and nucleus has also been observed.

The expression of sodium-dependent transporters such as SGLT2 in the lens nucleus means that mature fiber cells are able to utilize the energy stored in the sodium gradient to accumulate metabolites such as glucose above their concentration gradients. Reference to the circulation model shows that the Na^+ gradient is ultimately maintained by the active removal of Na^+ at the lens surface. Thus in addition to generating the circulating ion fluxes that underpin the convective delivery of the nutrients to deeper fiber cells, Na^+ efflux at the lens surface also serves to maintain the Na^+ gradient utilized by secondary active transporters to accumulate nutrients in the lens nucleus.

Steady-State Volume Regulation: Balancing Ion Influx and Efflux

Lens transparency is a direct result of its unique cellular structure and any disruption of this structure by either cellular swelling or dilation of the normally tight spaces between the cells increases intralenticular light scattering, and can eventually lead to cataract. Thus, volume regulation at both the cellular and tissue levels is of critical importance for the maintenance of lens transparency. The regulation of lens volume in turn depends on maintaining an appropriate balance between ion influx and efflux so as to prevent the intracellular or extracellular fluid accumulations that induce light scattering. This balance has been experimentally manipulated by utilizing pharmacological reagents to modulate the activity of Cl^- transport proteins implicated in mediating ion influx and efflux in the lens.

The histological analysis of lenses treated with a variety of inhibitors revealed that blocking Cl^- transport induced either one of two spatially distinct tissue damage phenotypes, or on occasions a combination of the two phenotypes (Figure 5). In contrast to the regular cellular architecture observed in control lenses, lenses cultured in the presence of either the Cl^- channel inhibitor 5-nitro-2-(phenylpropylamino)-benzoate (NPPB), or the sodium potassium dependent chloride cotransporter (NKCC) blocker bumetanide, exhibited a localized band of tissue damage (Figure 5(a)). This damage manifests itself as extracellular fluid accumulations between fiber cells located some 150 μm from the lens capsule. In contrast, the predominant effect of culturing lenses in the $K^+/2Cl^-$ co-transporter (KCC) inhibitor [(dihydroninindenyl)oxy] alkanoic acid (DIOA) was a swelling of fiber cells located at the lens periphery, although some deeper extracellular space dilations were evident (Figure 5(b)).

The two distinct damage phenotypes generated by the different inhibitors can be explained with reference to previous experimental measurements of lens membrane potential (Figure 5(c)). By measuring radial differences in the transmembrane potential and the concentration of Cl^- in the whole lens, the electrochemical gradient for Cl^- ion movement (E_{Cl}) can be calculated at different depths into the lens. This analysis predicts that Cl^- will move from the extracellular space into fiber cells in the inner lens, but will be driven from the cytoplasm of fiber cells to the extracellular space in the lens periphery (Figure 5(c)). Therefore, one would expect that an inhibition of Cl^- fluxes would block the uptake of Cl^- from the extracellular space by fiber cells in the inner lens. This would cause an accumulation of Cl^- ions and water in the

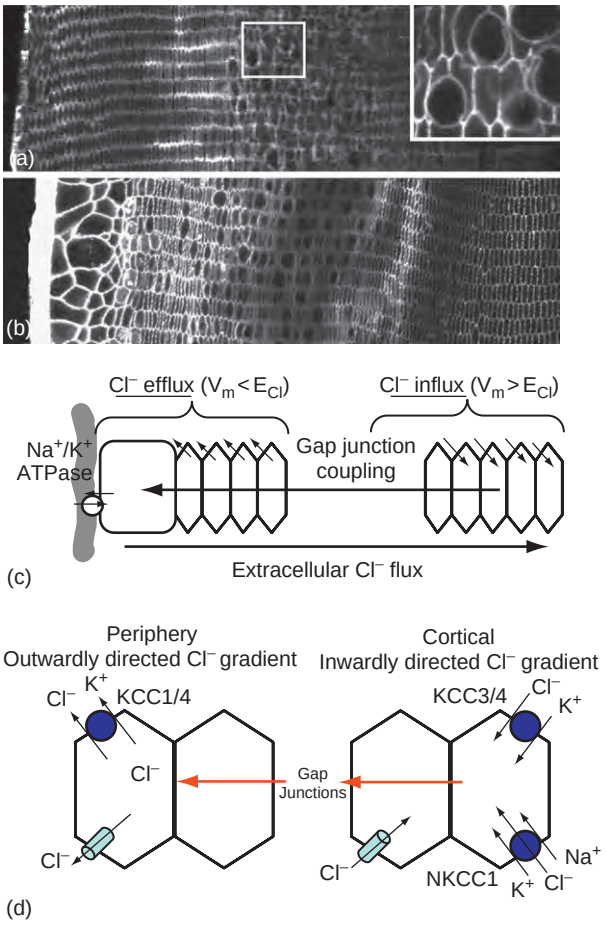

Figure 5 A circulating flux of Cl^- ions contributes to steady-state volume regulation in the rat lens. Confocal images of equatorial sections taken from lenses organ cultured under isotonic conditions showing the distinct morphological effects of blocking either (a) Cl^- channels with 10 μM NPPB or (b) KCC with 10 μM DIOA. (a) Blocking Cl^- influx mediated by Cl^- channels resulted in the accumulation of Cl^- ions and water between deeper fibre cells and the formation of extracellular space dilations in a distinct zone of the lens (insert). (b) Blocking Cl^- channel efflux mediated by KCC produced the intracellular accumulation of osmolytes and the swelling of peripheral fiber cells. Some deeper extracellular space dilations were also evident. (c) Measurements of membrane potential and E_{Cl} predict that in deeper fiber cells the electrochemical gradient favors Cl^- influx while in the periphery it promotes Cl^- efflux. (d) Emerging molecular model of transporters and channels that contribute to volume regulation by mediating ion influx and efflux in different regions of the lens. Since the zones of ion influx and efflux are connected by gap junction channels a circulating flux is established which helps to maintain cell volume. Patch clamp studies indicate that in peripheral fibre cells a volume-sensitive Cl^- channel becomes activated following cell swelling induced by either blockage of KCC (isosmotic cell swelling) or exposure to hyposmotic solutions.

tortuous extracellular space and lead to the formation of extracellular space dilations (Figure 5(a), insert). In the lens periphery, the passive efflux of Cl^- ions from fiber cells would be blocked, thereby causing an intracellular accumulation of osmolytes and resultant fiber cell swelling. These two spatially segregated zones of cell swelling and extracellular space dilations were deemed to be due to the inhibition of Cl^- influx and efflux in deeper and peripheral fiber cells, respectively. Since these pathways are coupled together by gap junctions, they generate a circulating flux of Cl^- ions, which contributes to the maintenance of steady-state lens volume. The two spatially distinct phenotypes observed from pharmacological experiments with anion transport inhibitors indicate that NKCC, KCC, and Cl^- channels all mediate ion uptake in the deeper cells, while KCC mediates ion efflux in peripheral fiber cells.

This relative simple view of circulating Cl^- fluxes derived from these morphological experiments has been confirmed and extended by a series of molecular localization, electrophysiological, and additional morphological studies. Molecular experiments designed to identify the specific proteins responsible for Cl^- influx and efflux have shown that NKCC1 and three of the four known KCC isoforms are expressed in a differentiation-dependent manner in the rat lens, supporting their initial pharmacological detection (Figure 5(d)). KCC1 was restricted to peripheral cells in the efflux zone, NKCC1 and KCC3 were found in both zones in the outer cortex, while KCC4 was expressed throughout the entire lens including the lens core. Although the molecular identity of the Cl^- channels that mediate the circulating Cl^- fluxes remains unclear, patch clamp experiments on longer fiber cells (>120 μm) isolated from the zone of ion influx exhibited a lyotropic anion selectivity sequence ($I^- > Cl^-$), reminiscent of volume-sensitive Cl^- conductances seen in many cell types. In contrast, the membrane properties of shorter fiber cells (<120 μm) isolated from the efflux zone were dominated by a K^+ conductance, and under isotonic conditions appeared to lack a constitutively active Cl^- conductance. Additional morphological experiments performed on organ cultured lenses using the KCC activator *N*-ethylmaleimide (NEM) support a role for KCC isoforms in both Cl^- influx and efflux pathways. NEM-induced stimulation of KCC-mediated Cl^- fluxes caused cell shrinkage in peripheral cells within the efflux zone, but cell swelling in deeper fiber cells of the influx zone. Taken together these data suggest that under isotonic conditions, NKCC1, KCC3/4, and a constitutively active lyotropic Cl^- channel all appear capable of contributing to Cl^- influx in deeper cells. This Cl^- influx in the deeper cells is then conveyed to the more peripheral cells by an intracellular pathway mediated by gap junction channels, where the Cl^- is removed from the lens by KCC transporters (Figure 5(d)). In these peripheral cells if the KCC-mediated efflux is blocked, these cells swell and a normally quiescent Cl^- channel is activated by the cellular swelling that allows Cl^- to efflux the lens.

From this model it is apparent that, under steady-state conditions, if fiber cell volume, and therefore lens transparency, is to be maintained, ion influx and efflux in the

two zones needs to be balanced. Furthermore, since the fluid flows associated with these two zones are dependent on the circulation model, any pathological insult to the circulation system will result in a loss of lens homeostasis that will initiate a cascade of events that ultimately leads to lens cataract.

See also: Accommodation; Cortical Cataract; Lens Fiber Cell Differentiation; Lens Gap Junctions; Lens Structure; Normal Age-Related Changes: Crystallin Modifications, Lens Hardening; Nuclear Cataract; Presbyopia.

Further Reading

Candia, O. A. and Zamudio, A. C. (2002). Regional distribution of the Na^+ and K^+ currents around the crystalline lens of rabbit. *American Journal of Physiology Cell Physiology* 282: C252–C262.

DeRosa, A. M., Martinez-Wittinghan, M. J., Mathias, R. T., and White, T. W. (2005). Intracellular communication in lens development and disease. In: Winterhager, E. (ed.) *Gap Junctions in Development and Disease*, ch. 8, pp. 173–195. Berlin: Springer.

Donaldson, P., Kistler, J., and Mathias, R. T. (2001). Molecular solutions to mammalian lens transparency. *News in Physiological Sciences*, ch.8, 16: 118–123.

Donaldson, P. J., Chee, K. S., Lim, J. C., and Webb, K. F. (2009). Regulation of lens volume: Implications for lens transparency. *Experimental Eye Research* 88(2): 144–150.

Donaldson, P. J. and Lim, J. (2008). Membrane transporters: New roles in lens cataract. In: Rizzo, J. F., Tombran-Tink, J., and Barnstable, C. J. (eds.) *Ocular Transporters in Ophthalmic Diseases and Drug Delivery*, pp. 83–104. Totowa, NJ: Humana Press.

Mathias, R. T., Kistler, J., and Donaldson, P. J. (2007). The lens circulation. *Journal of Membrane Biology* 216: 1–16.

Mathias, R. T., Rae, J. L., and Baldo, G. J. (1997). Physiological properties of the normal lens. *Physiological Reviews* 77: 21–50.

Rae, J. L. (1985). The application of patch clamp methods to ocular epithelia. *Current Eye Research* 4: 409–420.

Rae, J. L., Levis, R. A., and Eisenberg, R. S. (1988). Ionic channels in ocular epithelia. In: Narahashi, T. (ed.) *Ion Channels*, pp. 283–327. New York: Plenum Press.

Robinson, K. R. and Patterson, J. W. (1983). Localization of steady-state currents in the lens. *Current Eye Research* 2: 843–847.

Varadaraj, K., Kumari, S., Shiels, A., and Mathias, R. T. (2005). Regulation of aquaporin water permeability in the lens. *Investigative Ophthalmology and Visual Science* 46: 1393–1402.

Webb, K. F. and Donaldson, P. J. (2008). Differentiation-dependent changes in the membrane properties of fiber cells isolated from the rat lens. *American Journal of Physiology: Cell Physiology* 294: C1133–C1145.

Ischemic Optic Neuropathy

S S Hayreh, University of Iowa, Iowa City, IA, USA

Glossary

Afferent pupillary defect – Reduction in the response of the pupil to direct light.
Giant cell arteritis – An inflammation of the arterial wall, affecting medium and large size arteries.

Ischemic optic neuropathy constitutes one of the major causes of blindness or seriously impaired vision among the middle-aged and elderly population, although no age is immune. Its pathogenesis, clinical features, and management are discussed in this article.

Classification

Ischemic optic neuropathy is an acute ischemic disorder of the optic nerve. Based on the blood-supply pattern, the optic nerve can be divided into two very distinct parts: (1) the anterior part (called the optic nerve head) and (2) the rest of the optic nerve (Figure 1). Ischemic optic neuropathy is of two distinct types.

1. *Anterior ischemic optic neuropathy (AION).* This is due to ischemia of the anterior part of the optic nerve, which is supplied by the posterior ciliary artery (PCA) circulation. Etiologically and pathogenetically, AION is of the following two types: (a) arteritic AION (A-AION), which is due to giant cell arteritis (GCA), and (b) nonarteritic AION (NA-AION), which is due to all other causes and not GCA.
2. *Posterior ischemic optic neuropathy (PION).* This is due to ischemia of a segment of the rest of the optic nerve, which is supplied by multiple sources but not the PCA (Figure 1).

Nonarteritic Anterior Ischemic Optic Neuropathy

This is the most common type of ischemic optic neuropathy and has attracted the most controversy about its pathogenesis and management.

Pathogenesis

Nonarteritic anterior ischemic optic neuropathy (NA-AION) is caused by acute ischemia of the optic nerve head, whose main source of blood supply is from the PCA circulation (Figure 1). Marked interindividual variations in the blood supply of the optic nerve head and its blood-flow patterns profoundly influence the pathogenesis and clinical features of NA-AION.

Etiologically and pathogenetically, NA-AION is of two types:

1. *Transient nonperfusion or hypoperfusion of the optic nerve head circulation.* This is by far the most common cause of NA-AION. All the available evidence indicates that NA-AION is not a thromboembolic disorder. The mechanism causing transient nonperfusion or hypoperfusion of the optic nerve head circulation in NA-AION is multifactorial in nature. In the vast majority of cases, it is a transient fall of blood pressure, most commonly during sleep (nocturnal arterial hypotension – Figure 2) or a nap during the day. Any kind of shock also can cause a transient marked fall of blood pressure. A sharp rise in the intraocular pressure to high levels, as in neovascular glaucoma associated with ocular ischemia, or angle closure glaucoma, can also cause a transient fall in perfusion pressure in the optic nerve head, where perfusion pressure is equal to mean blood pressure minus the intraocular pressure.

   A transient fall of perfusion pressure in the optic nerve head vessels below the critical autoregulatory range level in susceptible persons results in ischemia of the optic nerve head and development of NA-AION. The severity of the ischemia may vary from mild to marked, depending upon the severity and duration of the transient ischemia, and upon other factors influencing the blood flow in the optic nerve head.
2. *Embolic lesions of the arteries/arterioles feeding the optic nerve head.* This is a rare cause of NA-AION. Compared to the hypotensive type of NA-AION, the extent of optic nerve head damage in this type is usually massive, severe, and permanent.

Risk Factors for Development of NA-AION

All available evidence indicates that NA-AION is multifactorial in nature. The risk factors fall into two main categories:

1. Predisposing risk factors:
   (a) *Systemic.* These include arterial hypertension, nocturnal arterial hypotension, diabetes mellitus, ischemic heart disease, hyperlipidemia, atherosclerosis

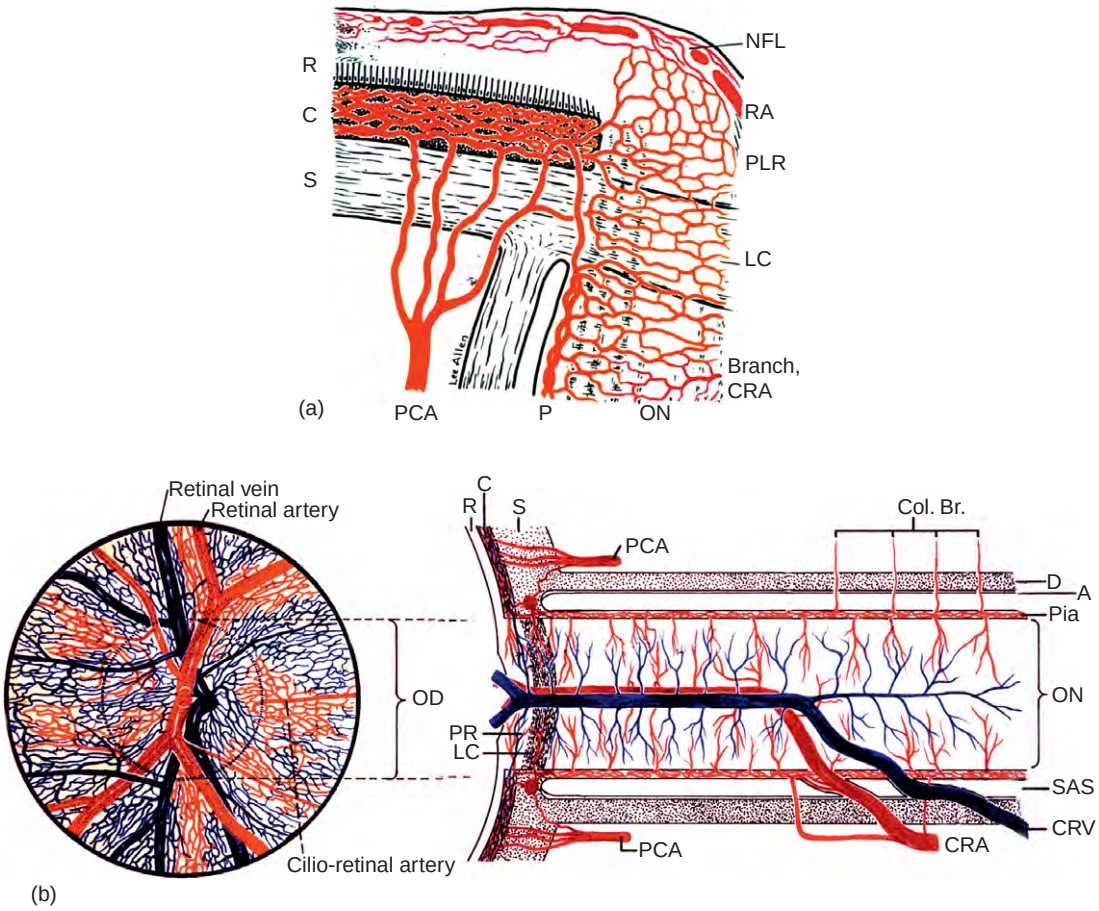

Figure 1 Schematic representation of blood supply of: (a) the optic nerve head and (b) the optic nerve. A, arachnoid; C, choroid; CRA, central retinal artery; Col. Br., collateral branches; CRV, central retinal vein; D, dura; LC, lamina cribrosa; NFL, surface nerve fiber layer of the disk; OD, optic disk; ON, optic nerve; P, pia; PCA, posterior ciliary artery; PR and PLR, prelaminar region; R, retina; RA, retinal arteriole; S, sclera; SAS, subarachnoid space. (a) Reproduced from Hayreh, S. S. (1978). In: Heilmann, K. and Richardson, K. T. (eds.) *Glaucoma: Conceptions of s Disease*, pp. 78–96. Stuttgart: Thieme. (b) Modified from Hayreh, S. S. (1974) *Transactions American Academy of Ophthalmology and Otolaryngology* 78: OP240–OP254.

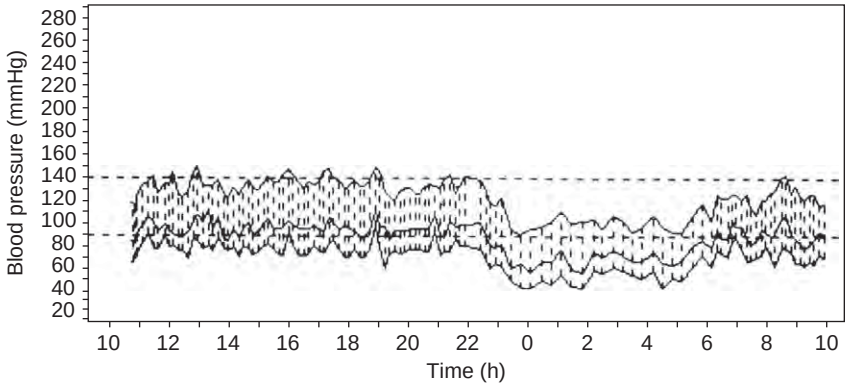

Figure 2 Ambulatory blood pressure monitoring records (based on individual readings) over a 24-h period, starting from about 11 a.m., in a 58-year-old woman with bilateral NA-AION, and on no medication. The blood pressure is perfectly normal during the waking hours but there is marked nocturnal arterial hypotension during sleep. Reproduced from Hayreh et al. (1999) *Ophthalmologica* 213: 76–96.

and arteriosclerosis, sleep apnea, arterial hypotension due to any cause, and migraine.

(b) *Risk factors in the eye and/or the optic nerve head.* These include absent or small cup in the optic disk, marked optic disk edema, raised intraocular pressure, and optic disk drusen. There is a misconception in the ophthalmic community that a small or absent cup is actually the primary factor in the development of the disease; this has resulted in catchy terms like "disk at risk". However, in the multifactorial scenario of the pathogenesis of NA-AION, an absent or small cup is simply a secondary contributing factor once the process of NA-AION has started.

2. Precipitating risk factor(s): in a person with predisposing risk factors present, a precipitating risk factor acts as the final insult (last straw), resulting in ischemia of the optic nerve head and NA-AION. Nocturnal arterial hypotension (**Figure 2**) is the most important factor in this category. Studies have shown that patients with NA-AION typically discover visual loss on waking in the morning, indicating that NA-AION developed during sleep when there is invariably a fall of blood pressure.

Conclusion

A host of systemic and local factors, acting in different combinations and to different extents, may derange the optic nerve head circulation, with some increasing optic nerve head susceptibility to ischemia and others acting as the final insult. Nocturnal arterial hypotension seems to be an important precipitating factor in the susceptible patient. Thus, the pathogenesis of NA-AION is complex but, not, as often stated, unknown.

There is a common perception among ophthalmologists and neurologists that NA-AION and cerebral stroke are similar in nature pathogenetically and in management. It is well established that stroke is a thromboembolic disorder. However, available evidence indicates that NA-AION is pathogenetically a hypotensive disorder, not a thromboembolic disorder. In NA-AION, unlike stroke, (1) there is no association between smoking and NA-AION; (2) aspirin has no beneficial effects in NA-AION; (3) no significant association has been found between NA-AION and thrombophilic risk factors; (4) fluorescein fundus angiography during the early stages of onset of visual loss invariably shows no evidence of complete occlusion of the vessels supplying the optic nerve head (**Figures 3(a) and 3(b)**); and (5) 41% of NA-AION eyes show spontaneous visual improvement, which is rare in a thromboembolic disorder.

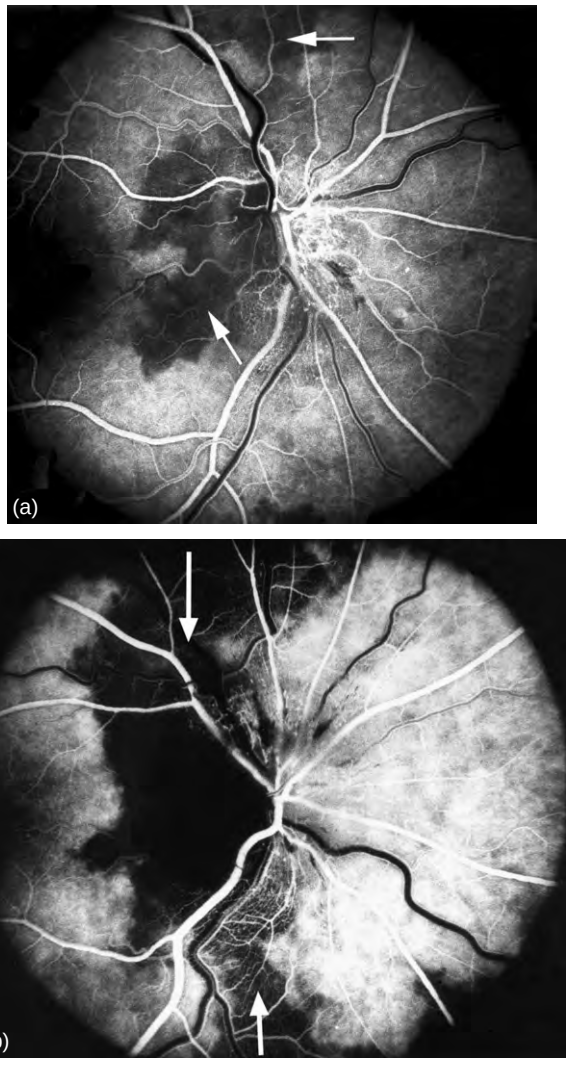

Figure 3 Fluorescein fundus angiograms of eyes with NA-AION. (a) Shows non-filling of temporal part of the peripapillary choroid (oblique arrow) and adjacent optic disk and the choroidal watershed zone (horizontal arrow). (b) Shows non-filling of the choroidal watershed zone (vertical dark band: arrows) between the lateral and medial PCAs and of the temporal part of optic disk. Reproduced from Hayreh, S. S. (1985). Inter-individual variation in blood supply of the optic nerve head. Its importance in various ischemic disorders of the optic nerve head, and glaucoma, low-tension glaucoma and allied disorders. *Documenta Ophthalmologica* 59: 217–246.

Clinical Features of NA-AION

NA-AION is the most common type of ischemic optic neuropathy. It usually has classical symptoms and signs. NA-AION is mostly a disease of the middle-aged and elderly population, although no age is immune. It has been reported in twenty-three percent of patients with NA-AION are under the age of 50 years. It is far more common among the white population than in other racial groups.

1. *Symptoms.* In the vast majority of patients, there is a sudden and painless deterioration of vision, usually discovered on waking in the morning. NA-AION patients often complain of loss of vision toward the nose and less often in the lower part. Later on,

photophobia is a common complaint. Simultaneous bilateral onset of NA-AION is extremely rare.

2. *Signs.* Initial visual acuity may vary from 20/20 (better than 20/40 in 33%) to marked loss. Therefore, a normal visual acuity does not rule out NA-AION. An inferior nasal visual field defect is the most common, followed by an inferior altitudinal defect; a combination of a relative inferior altitudinal defect with absolute inferior nasal defect is the most common pattern in NA-AION (**Figures 4(a) and 4(b)**). The eye shows the presence of a relative afferent pupillary defect in unilateral NA-AION cases, and in some there may be raised intraocular pressure.

At the onset of visual loss, there is always optic disk edema (**Figures 5 and 6(a)**). There are several misconceptions about optic disk edema in NA-AION. The most common one is that in NA-AION the optic disk edema is always pale, which is not at all true initially because the color of optic disk edema in NA-ION initially does not differ from that due to other causes; in some cases there may even be hyperemia of the optic disk (**Figures 5 and 6(a)**). A splinter hemorrhage at the disk margin is common (**Figure 7**). The optic disk edema resolves spontaneously in about 8 weeks, and the disk develops segmental or generalized pallor (**Figure 6(b)**). In the normal fellow eye, the optic disk usually shows either no cup or a small cup, which can be a helpful clue in the diagnosis of NA-AION in doubtful cases.

In diabetics, optic disk changes in NA-AION may have some characteristic diagnostic features. During the initial stages, the optic disk edema is usually, but not always, associated with characteristic prominent, dilated, and frequently telangiectatic vessels over the disk and many more peripapillary retinal hemorrhages than in nondiabetics (**Figures 8(a) and 8(c)**). Because of these disk changes, NA-AION in diabetics has been mistakenly diagnosed as diabetic papillopathy. With the resolution of optic disk edema, vascular changes and hemorrhages also resolve spontaneously (**Figures 8(b) and 8(d)**).

Fluorescein fundus angiography, at the onset of NA-AION, during the very early phase of dye filling in the fundus almost invariably shows delayed filling of the prelaminar region and the peripapillary choroid (**Figure 3(a)**) and/or choroidal watershed zone (**Figure 3(b)**).

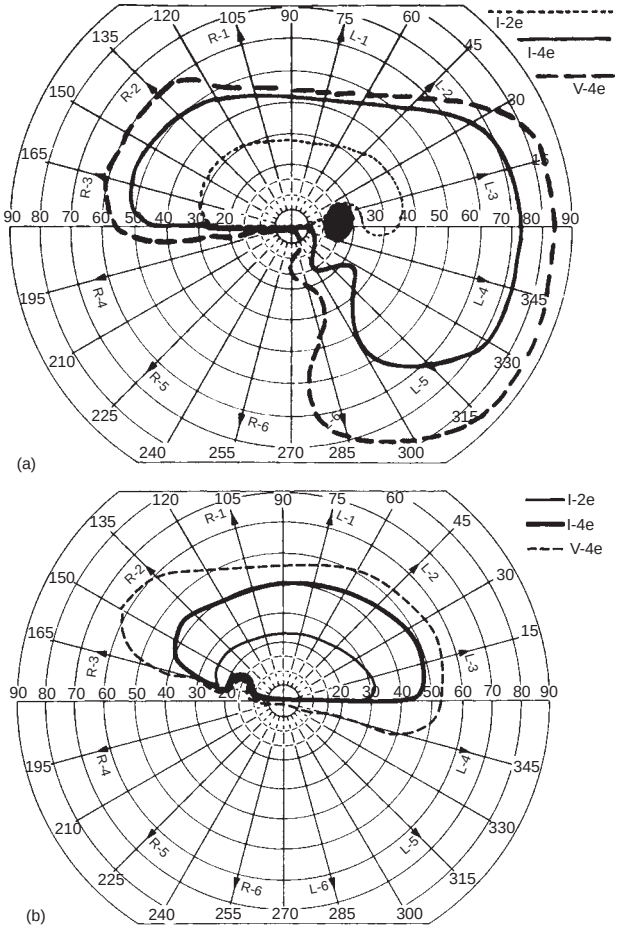

Figure 4 Visual-field defects in NA-AION, plotted with Goldmann perimeter using I-2e, I-4e, and V-4e targets, where the Roman numeral indicates target size, the Arabic numeral indicates relative intensity, and the lowercase letter indicates minor filter adjustment of the light intensity. (a) Shows an inferior altitudinal defect with I-2e and an inferior nasal defect with I-4e and V-4e. (b) Shows an absolute inferior altitudinal defect with I-2e, I-4e, and V-4e. The visual acuity in both eyes was 20/20. Reproduced from Hayreh et al. (2005) *Archives of Ophthalmology* 123:1554–1562.

Bilateral NA-AION

The cumulative probability of the fellow eye developing NA-AION has varied among different studies: 25%

Figure 5 Left fundus photograph showing optic disk edema and hyperemia during the acute phase of NA-AION.

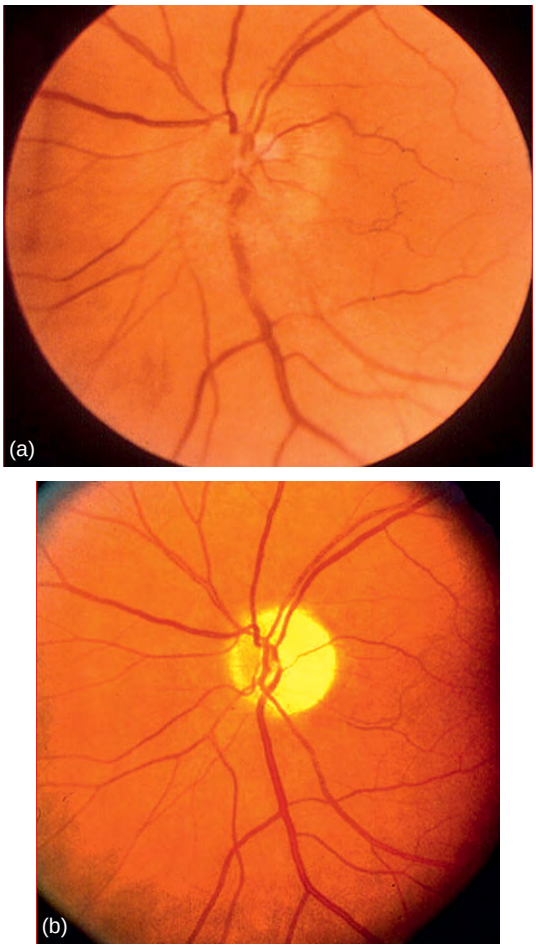

Figure 6 Fundus photographs of left eye of a 53-year-old man. (a) With optic disk edema during the active phase of NA-AION. (b) After resolution of optic disk edema and development of optic disk pallor – more marked in the temporal part than in the nasal part.

within 3 years, 17% in 5 years, and 15% over 5 years. Diabetics have a significantly ($p = 0.003$) greater risk than non-diabetics of NA-AION in the second eye as well as earlier involvement. Simultaneous bilateral onset of NA-AION is extremely rare, except in patients who develop sudden, severe arterial hypotension, for example during hemodialysis or surgical shock.

Recurrence of NA-AION in the same eye

In a study of 829 NA-AION eyes, the overall cumulative percentage of recurrence of NA-AION in the same eye at 2 years was 5.8%. The only significant association for recurrence of NA-AION was with nocturnal arterial hypotension.

NA-AION and phosphodiesterase-5 inhibitors

These agents are currently popular for erectile dysfunction. A critical review of all the reported cases usually shows a good temporal relationship between the ingestion of Viagra and other phosphodiesterase-5 inhibitors and the development of NA-AION, in persons who already have predisposing risk factors.

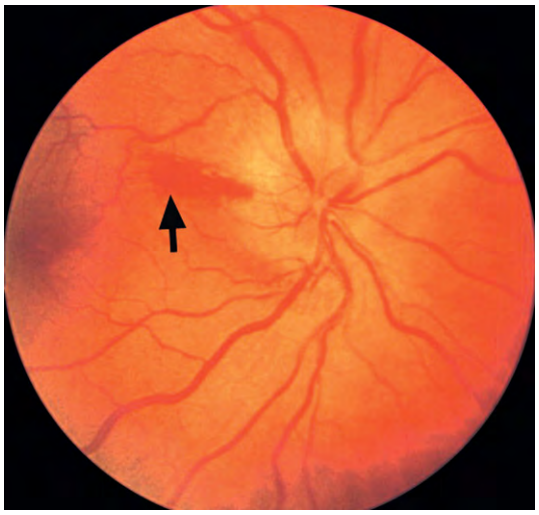

Figure 7 Right fundus photograph showing optic disk edema and hyperemia, with a splinter hemorrhage (arrow) during the acute phase of NA-AION.

Amiodarone and NA-AION

There is a universal belief that amiodarone causes optic neuropathy, called "amiodarone-induced optic neuropathy". However, it is NA-AION produced in the multifactorial scenario by the systemic cardiovascular risk factors for which the drug is given rather than amiodarone *per se* causing it.

Familial NA-AION

There are five reports in the literature representing 10 unrelated families in which more than one member developed NA-AION. It is clinically similar to the classical non-familial NA-AION, with the exception that familial NA-AION occurs in younger patients and has much higher involvement of both eyes than the classical NA-AION. The role of genetic factors in familial NA-AION is not known.

Management of NA-AION

The outcome of all advocated treatments has to be compared with the natural history of a disease, so that natural recovery is not attributed to the beneficial effect of a mode of treatment. Therefore, it is essential to first consider the natural history of visual outcome in NA-AION. This has been investigated by two prospective studies in patients seen within 2 weeks of onset of visual loss and initial visual acuity of 20/70 or worse. Both showed spontaneous visual acuity improvement in 41–43% of the patients and worsening in 15–19% at 6 months. Evaluation of visual fields

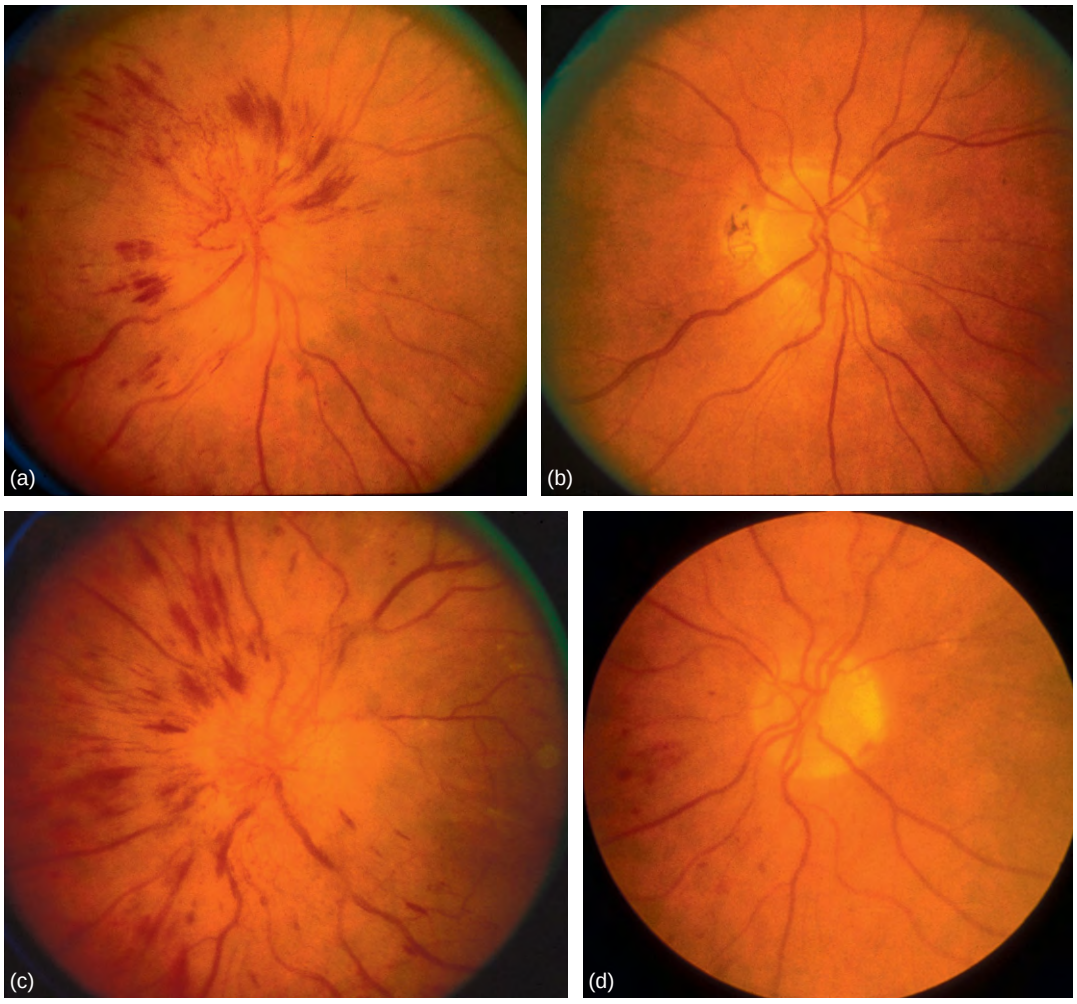

Figure 8 Fundus photographs of both eyes of a 51-year-old woman with adult-onset diabetes mellitus. She developed bilateral NA-AION, first in the right eye ((a) and (b)) and 8 months later in the left eye (c, d). (a, c) On first visit: Fundus photographs show massive optic disk edema with marked telangiectatic vessels on the optic disk, and many retinal hemorrhages. Visual acuity was 20/20 in the left and 20/15 in the right eye. Both eyes had an inferior nasal visual-field defect. (b, d) On resolution of optic disk edema: Fundus photographs show no optic disk edema but mild temporal pallor, no abnormal vessels on optic disk, and no retinal hemorrhages in the right eye (b), and a few resolving hemorrhages in the left eye (d). Reproduced from Hayreh et al. (1981) *Ophthalmologica* 182: 13–28.

with kinetic perimetry showed that of those with moderate-to-severe visual field defect, 26% showed improvement at 6 months. Visual acuity and visual fields showed improvement or further deterioration mainly up to 6 months, with no significant change thereafter.

Management of NA-AION has been a highly controversial subject. A number of treatments have been advocated. Following are the principal ones.

Optic nerve sheath decompression. A study in 1989 claimed that optic nerve sheath decompression improved visual function in "progressive" NA-AION. However, a recent multicenter clinical trial showed that this procedure is not effective and may be harmful, and thus is an inappropriate treatment for NA-AION, because 24% of the eyes with the optic nerve sheath decompression suffered further visual loss as compared to only 12% of eyes simply left alone.

Aspirin. Studies have shown that aspirin in NA-AION provides no long-term benefit in reducing the risk of NA-AION in the fellow eye.

Systemic corticosteroid therapy. A recent large, prospective study evaluated the role of steroid therapy in 696 NA-AION eyes, comparing the visual outcome in treated (364 eyes) versus untreated control (332 eyes) groups. In eyes with initial visual acuity of 20/70 or worse and seen within 2 weeks of onset, there was visual acuity improvement in 70% the treated group compared to 41% the untreated group (odds ratio of improvement: 3.39; 95% CI:1.62, 7.11; $p = 0.001$). Similarly, among those seen within 2 weeks of NA-AION onset and moderate to severe initial visual-field defect, there was improvement in 40% of the treated group and 25% of the untreated group (odds ratio: 2.06, 95% CI: 1.24, 3.40; $p = 0.005$). In

both treated and untreated groups, the visual acuity and visual fields kept improving for up to about 6 months after the onset of NA-AION, but very little thereafter.

Reduction of risk factors. As NA-AION is a multifactorial disease and many risk factors contribute to it, the correct strategy is to try reducing as many risk factors as possible to reduce the risk of developing NA-AION in the second eye or any further episode in the same eye. Nocturnal arterial hypotension is a precipitating risk factor in NA-AION patients with predisposing risk factors. In view of this, management of nocturnal arterial hypotension is an important step in both the management of NA-AION and the prevention of its development in the second eye. It seems NA-AION is emerging in some cases as an iatrogenic disease due to the use of currently available highly potent arterial hypotensive drugs.

Incipient NA-ION

This clinical entity initially presents with asymptomatic optic disk edema and no visual loss attributable to NA-AION. Available evidence indicates that it represents the earliest, asymptomatic clinical stage in the evolution of the NA-AION disease process; therefore, it shares most clinical features with classical NA-AION except for the visual loss initially.

Arteritic AION

The primary cause of A-AION is GCA, although other types of vasculitis can also cause it.

Pathogenesis

The primary cause is GCA, which has a special predilection to involve the PCA, resulting in its thrombotic occlusion. Since the PCA is the main source of blood supply to the optic nerve head (**Figure 1**), occlusion of the PCA results in infarction of a segment or the entire optic nerve head, depending upon the area of the optic nerve head supplied by the occluded PCA. This, in turn, results in development of A-AION.

Clinical Features of GCA and A-AION

GCA is a disease of late middle-aged and elderly persons and is almost 3 times more common in women than in men. There is evidence that GCA is far more common among Caucasians than other races.

Symptoms

GCA patients usually present with systemic symptoms, including anorexia, weight loss, jaw claudication, headache, scalp tenderness, abnormal temporal artery, neck pain, myalgia, malaise, and anemia. However, a study showed that 21% of patients with visual loss due to GCA have no systemic symptoms whatsoever (i.e., occult GCA).

One visual symptom of GCA is episodic transient visual loss, which is an important and an ominous sign of impending visual loss. In one series, it occurred in about one-third of the patients. Most patients with GCA develop visual loss due to A-AION suddenly without any warning. Occasionally there may be diplopia or ocular pain. A rare patient with GCA can suffer from euphoria and even deny any visual loss.

Signs

Visual acuity in eyes with A-AION varies between 20/20 and no light perception, but overall it is much worse than in NA-AION. The extent and severity of visual field defects depends upon the extent of optic nerve head damage caused by ischemia, usually much more extensive and severe than in NA-AION. When there is diplopia, there is extraocular motility abnormality. In uniocular A-AION, there is a relative afferent pupillary defect.

The optic disk always shows edema initially, which usually has a chalky white color (**Figure 9**) – a diagnostic characteristic of A-AION. When disk edema resolves, the optic disk in the vast majority shows cupping which is indistinguishable from that seen in glaucomatous optic neuropathy. In addition to optic disk edema, the fundus may show retinal cotton wool spots, central retinal artery occlusion, cilioretinal artery occlusion (**Figure 10(a)**), and/or choroidal ischemic lesions. Fluorescein fundus angiography done during the early acute stage of the disease shows evidence of occlusion of the PCAs (**Figures 10(b)** and **11**).

Laboratory investigations

Evaluation of erythrocyte sedimentation rate (ESR) and C-reactive protein (CRP) are the most important immediate diagnostic tests in the diagnosis of A-AION and its

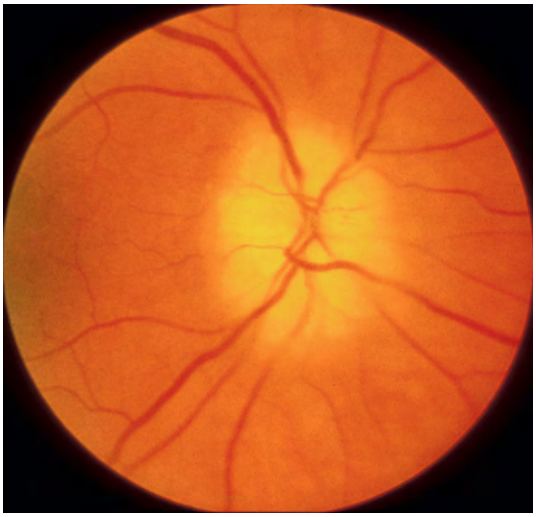

Figure 9 Fundus photograph of right eye with A-AION showing chalky white optic disk edema during the initial stages.

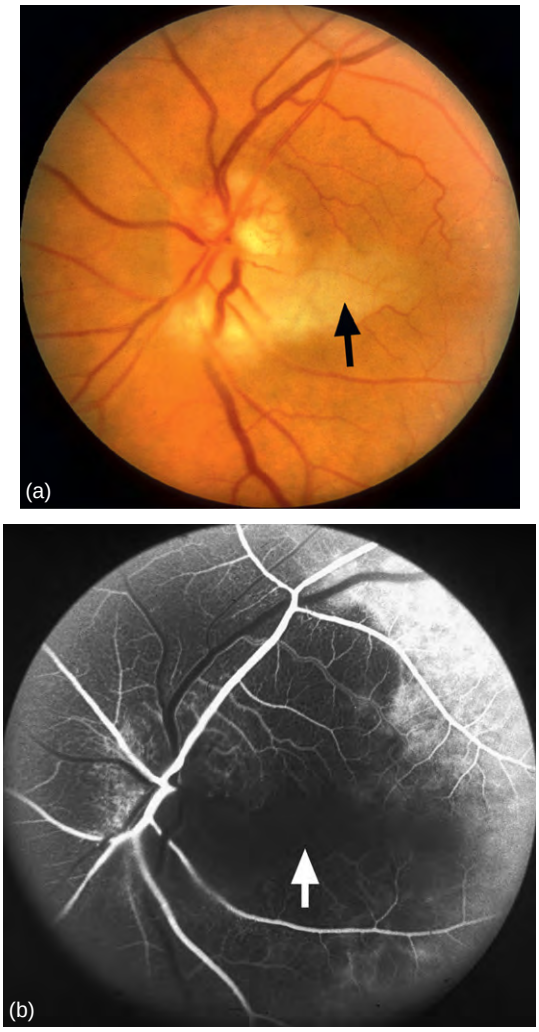

Figure 10 Fundus photograph (a) and fluorescein angiogram (b) of left eye with A-AION associated with cilioretinal artery occlusion. (a) Fundus photograph shows optic disk edema and retinal infarct (arrow) in the distribution of cilioretinal artery. (b) Fluorescein angiogram shows no filling of the choroid and entire optic disk supplied by the medial PCA and of the cilioretinal artery (arrow), but normal filling of the area supplied by the lateral PCA. (a) Reproduced from Hayreh, S. S. (1990). Anterior ischaemic optic neuropathy. Differentiation of arteritic from non-arteritic type and its management. *Eye* 4: 25–41; (b) reproduced from Hayreh S. S. (1978) *International Ophthalmology* 1: 9–l8.

differentiation from NA-AION. Although high ESR is traditionally emphasized as a *sine qua non* for diagnosis of GCA, there are numerous reports of "normal" or "low" ESR in patients with positive temporal artery biopsy for GCA. Normal ESR does not rule out GCA. CRP, on the other hand, is a much more reliable test to diagnose GCA. Thus, both tests should be used for diagnosis of GCA and monitoring of steroid therapy in all patients. Other hematological tests which can help in the diagnosis of GCA include the presence of thrombocytosis, anemia, elevated white blood cell count, and low hemoglobin and hematocrit levels.

Figure 11 Fluorescein fundus angiogram of a right eye with A-AION, showing normal filling of the area supplied by the lateral PCA (including the temporal one-fourth of the optic disk) but no filling of the area supplied by the medial PCA (including the nasal three-fourth of the disk). Reproduced from Hayreh S. S. (1978) *International Ophthalmology* 1: 9–l8.

Management of A-AION

Management of A-AION is actually the management of GCA. Visual loss is preventable with (1) early diagnosis of GCA and (2) immediate and adequate steroid therapy. To establish a definite diagnosis of GCA without delay is the most critical step in the management of GCA. Classically the gold standard for diagnosis of GCA is the five criteria advocated by the American College of Rheumatologists: (1) age $\geq$ 50 years at onset, (2) new onset of localized headache, (3) temporal artery tenderness or decreased temporal artery pulse, (4) elevated ESR (Westergren) $\geq$ 50 mm/hour, and (5) positive temporal artery biopsy. The American College of Rheumatologists states: "A patient shall be classified as having GCA if at least 3 of these 5 criteria are met." However, studies indicate that these criteria are inadequate to prevent blindness in all GCA patients, particularly patients with occult GCA (21%) who never develop any systemic symptoms of GCA. Use of a positive temporal artery biopsy as the definite diagnostic criterion for GCA showed that the odds of a positive temporal artery biopsy were 9 times greater with jaw claudication ($p < 0.0001$), 3.4 times with neck pain ($p = 0.0085$), 2.0 times with ESR (Westergren) 47–107 mm/hour relative to those with ESR <47 mm/hour ($p = 0.0454$), and 3.2 times with CRP >2.45 mg dl compared to CRP <2.45 mg dl ($p = 0.0208$), and 2.0 times when the patients were aged $\geq$75 years as compared to those $\leq$75 years ($p = 0.0105$). Among the other systemic signs and symptoms, the only significant one was anorexia/weight loss ($p = 0.0005$); the rest showed no significant difference from those with negative temporal artery biopsy.

Differentiation of A-AION from NA-AION

When a patient is diagnosed as having AION, the first crucial step in patients aged 50 and over is to identify immediately whether it is arteritic or nonarteritic – missing A-AION can result in disastrous visual loss which is entirely preventable. Collective information provided by the following criteria helps to differentiate the two types of AION reliably.

1. *Systemic symptoms of GCA.* These are discussed above. However, 21% with occult GCA have no systemic symptoms of any kind at all. Patients with NA-AION have no systemic symptoms of GCA.
2. *Visual symptoms.* Amaurosis fugax is highly suggestive of A-AION and is extremely rare in NA-AION.
3. *Hematologic abnormalities.* Immediate evaluation of ESR and CRP is vital in all patients aged 50 and over. As discussed above, elevated ESR and CRP, particularly CRP, is helpful in the diagnosis of GCA. Patients with NA-AION do not show any of these abnormalities, except when a patient has some other concurrent systemic disease.
4. *Early massive visual loss.* There is a much more massive visual loss in A-AION than in NA-AION; however, the presence of perfectly normal visual acuity does not rule out A-AION.
5. *Chalky white optic disk edema* (**Figure 9**). This is almost always diagnostic of arteritic AION and is seen in the majority, but not all, of A-AION eyes.
6. *A-AION associated with cilioretinal artery occlusion* (**Figure 10**). This is almost always diagnostic of A-AION.
7. *Evidence of PCA occlusion on fluorescein fundus angiography* (**Figures 10(b) and 11**). If angiography is performed during the first few days after the onset of A-AION, and the choroid supplied by one or more of the PCAs does not fill, this once again is almost diagnostic of A-AION.
8. *Temporal artery biopsy.* This finally establishes the diagnosis; however, the possibility of an occasional false negative biopsy has to be kept in mind.

Steroid Therapy to Prevent Blindness in GCA

This is a highly controversial subject because practically all the available information is from the rheumatologic literature. Rheumatologists and ophthalmologists have different perspectives which influence their recommendations on steroid therapy for GCA – the regimen advocated by the former primarily concerns managing benign rheumatologic symptoms and signs, whereas the latter confront the probability of blindness. In our 27-year prospective study on steroid therapy in GCA, marked differences were seen between the rheumatologic and ophthalmic steroid therapy regimens. In the light of information from that study, the following guidelines to prevent visual loss are suggested.

1. If there is a reasonable suspicion of GCA, as judged from systemic symptoms, high ESR and CRP (particularly high CRP) and sudden visual loss from A-AION or central retinal artery occlusion, high doses of systemic corticosteroid therapy must be started immediately as an emergency measure.
2. The physician should not wait for the result of the temporal artery biopsy because by the time it is available, the patient may have irreversibly lost further vision.
3. A high-dose steroid therapy (80–120 mg) must be maintained until both the ESR and CRP settle down to stable levels, which usually takes 2–3 weeks, with CRP reducing much earlier than ESR levels (**Figure 12**), followed by gradual tapering of steroid therapy.
4. A titration of the steroid dosage with the levels of ESR and CRP is the only safe and reliable method for tapering down and follow-up of steroid therapy; using clinical symptoms and signs of GCA as a guide, as often recommended by rheumatologists, is a dangerous practice for the prevention of blindness.
5. Patients with GCA show marked interindividual variation in the dosage of corticosteroids they require, their response to steroid therapy, and their therapeutic and tapering regimens of steroid therapy; therefore therapy must always be individualized. No generalization is possible; *NO* one size fits all.
6. The vast majority of GCA patients require a lifelong small dose of steroids to prevent blindness. As our study found no evidence that intravenous mega-dose steroid therapy was more effective than large-dose oral therapy in improving vision or preventing visual deterioration due to GCA, it is recommended that patients initially receive one intravenous mega dose (equivalent to 1 g of prednisone) followed by a high-dose (80–120 mg) of oral prednisone if that patient presents with: (a) a history of amaurosis fugax, (b) complete or marked loss of vision in one eye, or (c) early signs of involvement of the second eye.

Conclusion

If GCA patients are treated promptly and aggressively with an adequate dose of corticosteroids, and reduction of steroid therapy is regulated by using ESR and CRP as the only criteria, not a single patient will suffer any further visual loss 5 days after starting adequate steroid therapy. However, in our study, in spite of early high-dose steroid therapy, only 4% of GCA patients with visual loss showed any visual improvement, and during the first 5 days after the start of the therapy 4% developed further visual loss; but there was no further visual loss after that.

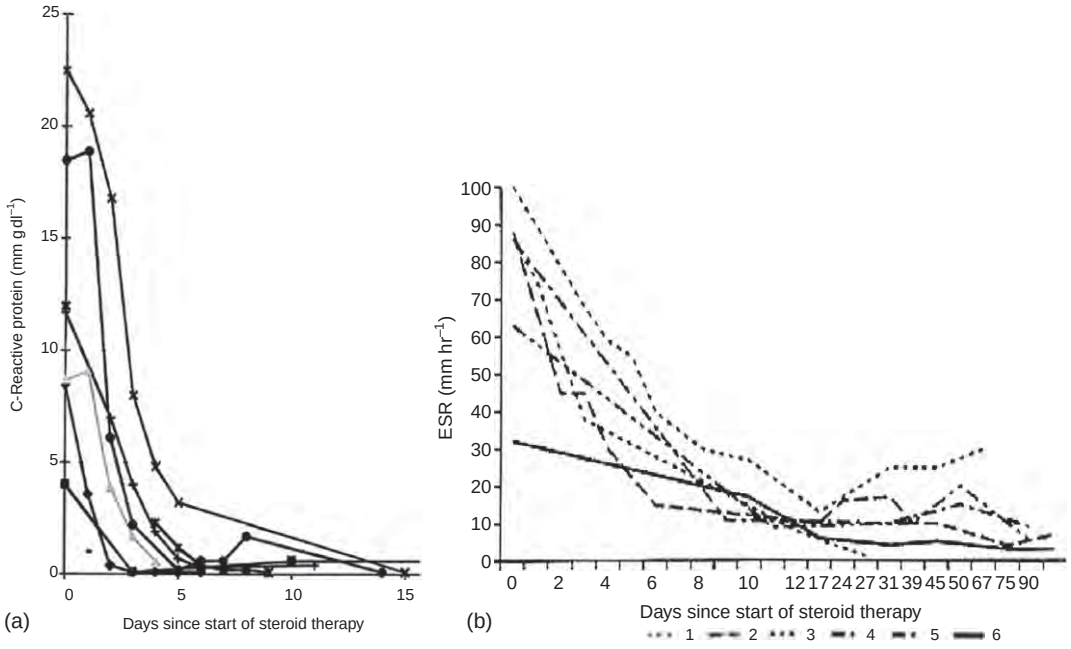

Figure 12 Graphs of (a) C-reactive protein levels and (b) erythrocyte sedimentation rates (ESRs) of six patients with giant cell arteritis, showing their initial responses to high-dose steroid therapy. Reproduced from Hayreh, S. S. and Zimmerman, B. (2003). Management of giant cell arteritis. Our 27-year clinical study: New light on old controversies. *Ophthalmologica* 217: 239–259.

Posterior Ischemic Optic Neuropathy

PION is much less common than AION and is due to ischemia of the optic nerve posterior to the optic nerve head, which is supplied by multiple sources but not the PCA (**Figure 1(b)**). It is a diagnosis of exclusion, and it should be made only after all other possibilities have been carefully ruled out, for example, macular and retinal lesions, NA-AION, retrobulbar optic neuritis, compressive optic neuropathy, other optic disk and optic nerve lesions, neurological lesions, hysteria, even malingering, and a host of other lesions.

Classification

Etiologically, PION can be classified into three types: (1) arteritic PION (A-PION), (2) nonarteritic PION (NA-PION), and (3) surgical PION.

Pathogenesis

Arteritic PION

This is due to GCA when arteritis involves the orbital arteries, which supply the posterior part of the optic nerve (**Figure 1(b)**). A-PION occurs much less commonly than A-AION.

Nonarteritic PION

An association between NA-PION and a variety of systemic diseases has been reported in the literature. In one series, comparison of NA-PION cases with a control population showed a significantly higher prevalence of arterial hypertension, diabetes mellitus, ischemic heart disease, cerebrovascular disease, carotid artery and peripheral vascular disease, and migraine than in NA-PION patients. Thus, the pathogenesis of NA-PION, similar to NA-AION, is multifactorial in nature, with a variety of systemic diseases, other vascular risk factors, and/or local risk factors predisposing an optic nerve to develop PION; defective autoregulation of the optic nerve may also play a role. Finally, some precipitating risk factor acts as the "last straw" to produce PION.

Surgical PION

This type of PION usually tends to cause bilateral, massive visual loss or even complete blindness, which is usually permanent; therefore, it has great medicolegal importance. It is almost invariably associated with prolonged systemic surgical procedures for a variety of conditions, including spinal and other orthopedic surgical procedures, radical neck dissection, coronary artery bypass, hip surgery, nasal surgery, and so on. The pathogenesis of surgical PION is multifactorial in nature. The main factors include severe and prolonged arterial hypotension, hemodilution from administration of a large amount of intravenous fluids to compensate for the blood loss, orbital and periorbital edema, chemosis and anemia, and even direct orbital compression due to the prone position.

Clinical Features of PION

NA-PION, similar to NA-AION, is seen mostly in the middle-aged and elderly population, but no age is immune.

Symptoms

Clinically, patients with A-PION and NA-PION typically present with acute, painless visual loss in one or both eyes, sometimes discovered upon waking up in the morning. In some eyes, it may initially be progressive. Patients with surgical PION discover visual loss as soon as they are alert postoperatively, which may be several days after surgery. Surgical PION usually tends to cause bilateral massive visual loss or even complete blindness, which is usually permanent.

Signs

Visual acuity may vary from 20/20 to no light perception. The most common visual-field defect is central scotoma, alone or in combination with other types of visual-field defects (**Figure 13**). A small number of PION eyes show the reverse pattern, that is, a normal central field with marked loss of peripheral fields (**Figure 14**).

Initially, apart from relative afferent pupillary defect in unilateral PION, the anterior segment, intraocular pressure, and optic disk and fundus are normal on ophthalmoscopy and fluorescein fundus angiography. The disk generally develops pallor within 6–8 weeks, usually more marked in the temporal part. The criteria to differentiate arteritic from nonarteritic PION are basically the same as those for arteritic and nonarteritic AION,

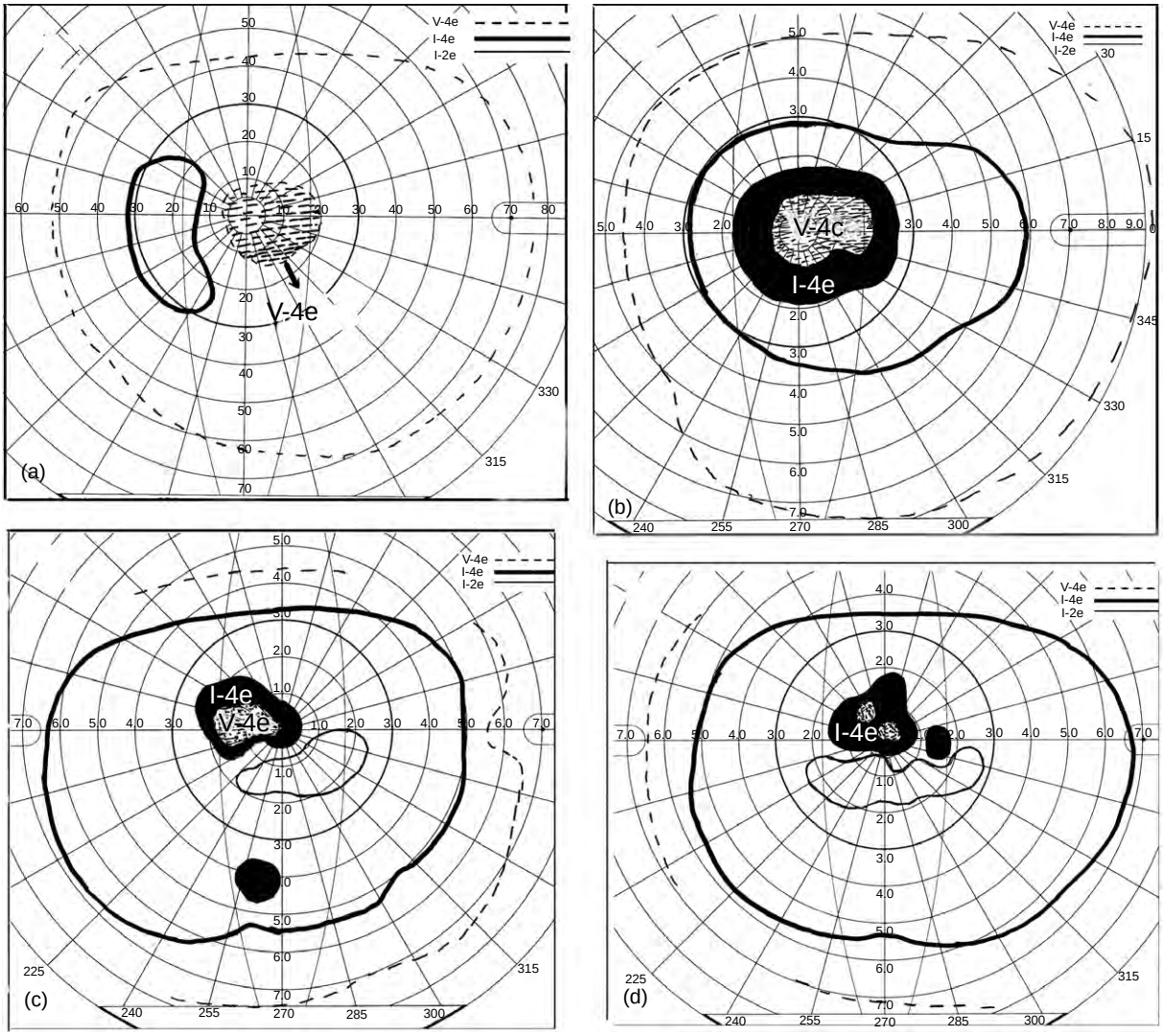

Figure 13 Four visual fields in nonarteritic PION showing varying sizes and densities of central scotoma and other field defects, with normal peripheral visual fields, where the Roman numeral indicates target size, the Arabic numeral indicates relative intensity, and the lowercase letter indicates minor filter adjustment of the light intensity. Reproduced from Hayreh, S. S. (2004). Posterior ischemic optic neuropathy: Clinical features, pathogenesis, and management. *Eye* 18: 1188–1206.

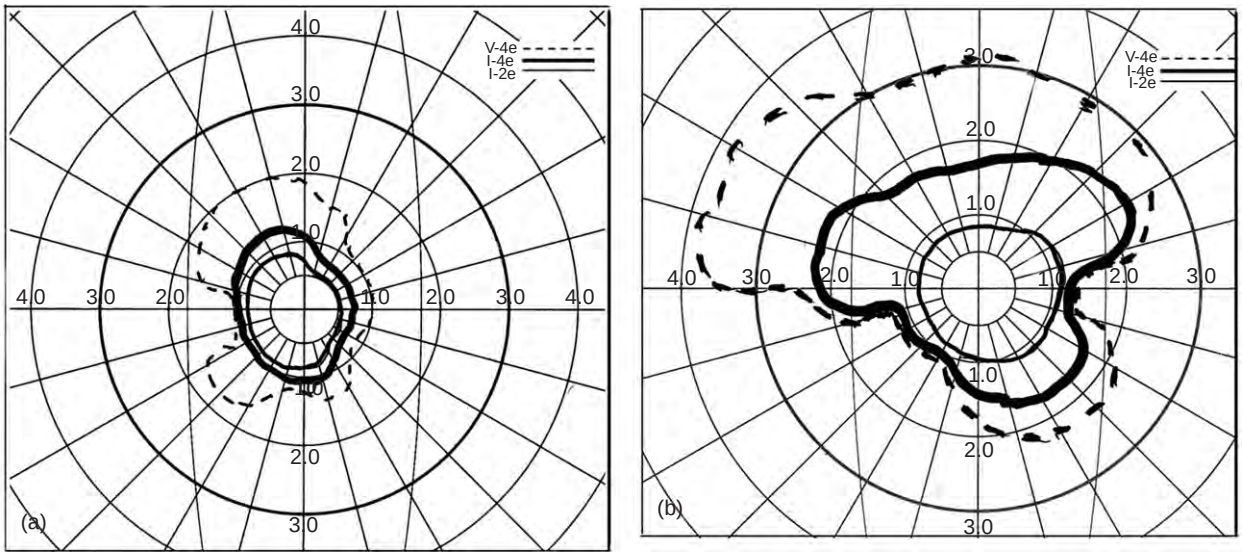

Figure 14 Visual fields of (a) right and (b) left eyes with arteritic PION, showing markedly constricted central visual fields, with complete loss of peripheral fields in both eyes. From Hayreh, S. S. (2004). Posterior ischaemic optic neuropathy: Clinical features, pathogenesis, and management. *Eye* 18: 1188–1206.

discussed above, except that the optic disk and fundus are initially normal in both types of PION.

Management of PION

The management of PION depends upon the type of PION. In all cases other than surgical PION, as in AION, the most important first step in persons aged 50 years or older is always to rule out GCA.

Arteritic PION

Management is similar to that of A-AION discussed above. However, there is usually no visual improvement with systemic steroid therapy.

Nonarteritic PION

The eyes of patients treated with high-dose systemic steroid therapy during the very early stages of the disease show significant improvement in visual acuity and visual field, compared to untreated eyes. However, spontaneous improvement in visual acuity and visual field may also occur to some extent in some eyes without steroid therapy. Since systemic risk factors may play a part in the development of NA-PION, in the management of these patients one should try to reduce as many risk factors as possible so as to reduce the risk of second eye involvement.

Surgical PION

Management amounts to prophylactic measures to prevent development, because once the visual loss occurs, it is usually bilateral, severe, and irreversible. No treatment has been found to be effective to recover or improve the lost vision. Prophylactic measures during surgery include shortening the duration of surgery to a minimum and avoiding: arterial hypotension, excessive fluid replacement and hemodilution, pressure on the eyeball and orbit, and dependent position of the head. Since systemic cardiovascular risk factors may predispose a patient to a higher risk of developing surgical PION, it may be advisable to consider those factors in the decision to perform surgery.

Conclusions

Ischemic optic neuropathy is not a singular disease but a spectrum of several different types, each with its own etiology, pathogenesis, and management. Each must be considered a separate clinical entity. Overall, they constitute one of the major causes of blindness or seriously impaired vision, yet there is marked controversy on their pathogeneses, clinical features, and management. As the signs and symptoms can overlap, correct diagnosis is the key to producing the best visual outcome.

See also: Cranial Nerves and Autonomic Innervation in the Orbit; Imaging of the Orbit; Orbital Bony Anatomy and Orbital Fractures; Orbital Vascular Anatomy.

Further Reading

Hayreh, S. S. (1969). Blood supply of the optic nerve head and its role in optic atrophy, glaucoma, and oedema of the optic disc. *British Journal of Ophthalmology* 53: 721–748.

Hayreh, S. S. (1974). Anterior ischaemic optic neuropathy. I. Terminology and pathogenesis. *British Journal of Ophthalmology* 58: 955–963.

Hayreh, S. S. (1974). Anterior ischaemic optic neuropathy. II. Fundus on ophthalmoscopy and fluorescein angiography. *British Journal of Ophthalmology* 58: 964–980.

Hayreh, S. S. (1985). Inter-individual variation in blood supply of the optic nerve head. Its importance in various ischemic disorders of the optic nerve head, and glaucoma, low-tension glaucoma and allied disorders. *Documenta Ophthalmologica* 59: 217–246.

Hayreh, S. S. (1990). Anterior ischaemic optic neuropathy. Differentiation of arteritic from non-arteritic type and its management. *Eye* 4: 25–41.

Hayreh, S. S. (1996). Acute ischemic disorders of the optic nerve: Pathogenesis, clinical manifestations and management. *Ophthalmology Clinics of North America* 9: 407–442.

Hayreh, S. S. (2001). The blood supply of the optic nerve head and the evaluation of it – myth and reality. *Progress in Retinal and Eye Research* 20: 563–593.

Hayreh, S. S. (2004). Posterior ischaemic optic neuropathy: Clinical features, pathogenesis, and management. *Eye* 18: 1188–1206.

Hayreh, S. S. (2008). Non-arteritic arterior ischaemic optic neuropathy and phosphodiesterase-5 inhibitors. *British Journal of Ophthalmology* 92: 1577–1580.

Hayreh, S. S. (2009). Non-arteritic anterior ischemic optic neuropathy and thrombophila. *Graefe's Archive for Clinical and Experimental Ophthalmology* 247: 577–581.

Hayreh, S. S., Fingert, J. H., Stone, E., and Jacobson, D. M. (2008). Familial non-arteritic anterior ischemic optic neuropathy. *Graefe's Archive for Clinical and Experimental Ophthalmology* 246: 1295–1305.

Hayreh, S. S., Jonas, J. B., and Zimmerman, M. B. (2007). Non-arteritic anterior ischemic optic neuropathy and tobacco smoking. *Ophthalmology* 114: 804–809.

Hayreh, S. S., Podhajsky, P. A., Raman, R., and Zimmerman, B. (1997). Giant cell arteritis: validity and reliability of various diagnostic criteria. *American Journal of Ophthalmology* 123: 285–296.

Hayreh, S. S., Podhajsky, P. A., and Zimmerman, B. (1997). Nonarteritic anterior ischemic optic neuropathy: Time of onset of visual loss. *American Journal of Ophthalmology* 124: 641–647.

Hayreh, S. S., Podhajsky, P. A., and Zimmerman, B. (1998). Occult giant cell arteritis: Ocular manifestations. *American Journal of Ophthalmology* 125: 521–526, 893.

Hayreh, S. S., Podhajsky, P. A., and Zimmerman, B. (1998). Ocular manifestations of giant cell arteritis. *American Journal of Ophthalmology* 125: 509–520.

Hayreh, S. S. and Zimmerman, B. (2003). Management of giant cell arteritis. Our 27-year clinical study: New light on old controversies. *Ophthalmologica* 217: 239–259.

Hayreh, S. S. and Zimmerman, M. B. (2007). Incipient nonarteritic anterior ischemic optic neuropathy. *Ophthalmology* 114: 1763–1772.

Hayreh, S. S. and Zimmerman, M. B. (2007). Optic disc edema in non-arteritic anterior ischemic optic neuropathy. *Graefe's Archive for Clinical and Experimental Ophthalmology* 245: 1107–1121.

Hayreh, S. S. and Zimmerman, M. B. (2008). Nonarteritic anterior ischemic optic neuropathy: Clinical characteristics in diabetic patients versus nondiabetic patients. *Ophthalmology* 115: 1818–1825.

Hayreh, S. S. and Zimmerman, M. B. (2008). Nonarteritic anterior ischemic optic neuropathy: Natural history of visual outcome. *Ophthalmology* 115: 298–305.

Hayreh, S. S. and Zimmerman, M. B. (2008). Non-arteritic anterior ischemic optic neuropathy: Role of systemic corticosteroid therapy. *Graefe's Archive for Clinical and Experimental Ophthalmology* 246: 1029–1046.

Hayreh, S. S., Zimmerman, M. B., Podhajsky, P., and Alward, W. L. M. (1994). Nocturnal arterial hypotension and its role in optic nerve head and ocular ischemic disorders. *American Journal of Ophthalmology* 117: 603–624.

Hunder, G. G., Bloch, D. A., Michel, B. A., et al. (1990). The American College of Rheumatology 1990 criteria for the classification of giant cell arteritis. *Arthritis and Rheumatology* 33: 1122–1128.

Ischemic Optic Neuropathy Decompression Trial Research Group (1995). Optic nerve decompression surgery for nonarteritic anterior ischemic optic neuropathy (NAION) is not effective and may be harmful. *Journal of the American Medical Association* 273: 625–632.

Sadda, S. R., Nee, M., Miller, N. R., et al. (2001). Clinical spectrum of posterior ischemic optic neuropathy. *American Journal of Ophthalmology* 132: 743–750.

K

Knock-Out Mice Models: Cornea, Conjunctiva, Eyelids and Lacrimal Gland

W W-Y Kao, C-Y Liu, and H Liu, University of Cincinnati, Cincinnati, OH, USA

Glossary

Cre – The phage recombinase that catalyzes cyclization recombination of LoxP elements.
EGF – The epidermal growth factor which binds to its receptor, EGFR.
FGF – The family of growth factors involved in angiogenesis, wound healing, and development.
Keratins – The family of structural proteins that are tough and insoluble. Keratin 12 is specific to the cornea.
Keratocan – A member of keratan sulfate proteoglycans that is important for transparency of the cornea.
LoxP – The locus of crossover within P1 phage.
Reverse tetracycline transcriptional activator (rtTA) – Binds to Tet operator sequence 7 and activates transcription of the target gene in the presence of tetracycline (Tet-on system).
Tetracycline operator element – The tetracycline-regulated promoter that contains tetracycline operator sequences, which regulate expression of a downstream gene.

Introduction

Transgenesis, that is, the insertion of an exogenesis gene into an organism such that the gene is transmitted to the offspring, and gene targeting are among the most important biological techniques developed in the twentieth century. The studies of genetically modified mutant mice by transgenesis and gene targeting are of great value to elucidate the pathophysiology of altered gene functions and have greatly increased our knowledge of normal physiology and diseases in humans. They not only provide the means for the generation of animal models that are used to examine the pathogenesis of human diseases caused by altered genetic functions, but also allow the development of gene and cell therapy strategies to treat diseases. For example, the application of transgenesis and gene-targeting techniques opens the door of targeted introduction of genes to cells of diseased tissues, that is, gene therapy. Thus, lost cellular and tissue functions can be restored and diseases are cured.

Transgenesis

Transgenesis through microinjection of cloned DNA into fertilized mouse eggs was first accomplished in the laboratories of Brinster, Costantini, Ruddle, Mintz, and Wagner. The availability of a cell-type-specific promoter is a prerequisite for the success of creating transgenic mouse lines that exhibit altered phenotypes caused by the presence of such reporter gene product in tissues of interest. Since then, the technology of transgenesis has advanced to create inducible transgenic mouse lines in which a reporter gene has a unique spatial and temporal expression pattern by administering antibiotics, hormones, and pheromones to experimental animals. The system usually consists of two transgenic mouse lines, one of which employs a tissue-specific promoter for the expression of a transgene that encodes a fusion protein of a transcription factor and hormone receptor and antibiotic suppressor. The other is a transgenic mouse carrying a reporter gene following the responsive elements of a transcription factors and suppressor. In the bitransgenic offspring from the mating of the two transgenic mice, the reporter genes can be turned on and off when ligands bind to the fusion proteins of transcription factor/receptor and transcription factor/suppressor fusion proteins. For example, tet-ON and tet-OFF system in overexpression of *tet-O-FGF7* by epidermal epithelium under the control of reverse tetracycline transcription activator (rtTA) driven by keratin 5 (K5) and K14 promoters of bitransgenic *K5-rtTA/tet-O-FGF7* and/or *K14-tTA/tet-O-FGF7* mice.

Gene Targeting

In late 1980, Doetschman et al. and Thomas et al. demonstrated that the mouse genome could be modified *in vitro* in embryonic stem cells by homologous recombination. It was subsequently demonstrated that the modified mouse genome could be transmitted to offspring through injection of such genetically modified embryonic stem cells into blastocysts. Since then, many gene-targeting strategies have been developed not only to ablate functional genes (i.e., knock-out), but also to replace target genes with another functional gene and/or a mutant gene of interest (knock-in). These strategies allow us to examine gene function in experimental mouse lines that mimic pathogenesis of human diseases and yield useful information, leading to a better understanding of normal physiology and pathophysiology in humans.

However, many of the altered genes often lead to embryonic lethality and detrimental effects on animal development, limiting their use in studying biology of the ocular surface tissues. To circumvent the pitfalls, one of the strategies is conditional gene knock-out that employs Cre–LoxP system to ablate gene in a cell-type-specific manner.

Tissue-specific gene ablation using Cre–LoxP system

The Cre–LoxP system was developed to avoid embryonic lethality as well as to confine the inactivation of the target gene in a cell- or tissue-specific manner. Cre is a phage recombinase that specifically deletes any DNA sequence flanked by two LoxP elements. The Cre–LoxP system consists of two mouse lines, one of which uses a tissue-/cell-type-specific promoter for the expression of Cre. The other mouse line contains a modified genome in which two LoxP elements are inserted in two introns flanking functionally important exon(s) of the targeted gene by gene-targeting techniques. The LoxP-modified (floxed) gene remains fully functional, except in cells expressing Cre that is under the control of a tissue-specific promoter. Thus, the offspring are characterized by the ablation of the gene in a tissue-/cell-type-specific manner. The system allows the inactivation of the target gene in a single cell type and/or a limited number of cell types, depending on the specificity of the promoter, and reduces the probability of embryonic lethality of the experimental mice. Thus, it permits the analysis of physiological and pathophysiological consequences of the genetic alteration in mature animals.

Pitfalls of Cre–LoxP system: Cryptic Cre expression by germ cells during gametogenesis

We have recently discovered that recombination of floxed genes happens during gametogenesis in several Cre/LoxP bitransgenic mouse lines that express tissue-specific Cre outside the gonads, for example, *Kera-Cre*, *Krt12-Cre*, and *BF1-Cre* mice. The frequency of the promiscuous LoxP/Cre recombination varied in different lines of Cre driver mice and sex of the same driver mice with higher penetrance in male than in female double transgenic mice as well (**Table 1**). Polymerase chain reaction (PCR) and recombination analysis demonstrate recombination of floxed allele occurs during transition from spermatogonia (diploid) to primary spermatocyte (tetraploid) in testis. Thus, target floxed allele(s) are ubiquitously ablated in Cre/LoxP mice intended for tissue-specific gene

Table 1 Excision of floxed alleles during gametogenesis of double transgenic Cre/floxed mice

Father	Mother	Number of Cre^{tg}/floxed mice Total	Δ	Number of Cre^{0}/floxed mice Total	Δ	Percentage of penetrance[c]
KC4.3/ZEG	*C57BL/6*	10	10	10	10	100
KC4.1/ROSAR	*C57BL/6*	4	4	6	6	100
KC1/ZEG	*C57BL/6*	15	15	16	16	100
C57BL/6	*KC4.3/ROSAR*	4	2	1	1	60
$K12^{Cre/w}$/*ZEG*	C57BL/6	NA[a]	NA[a]	13	6	46
C57BL/6	$K12^{Cre/w}$/*ZEG*	NA[a]	NA[a]	27	2	7
$BF1^{Cre}$/*R26R*	*CD-1*	7	5	9	6	69
C57BL/6	*Wnt1-Cre/R26R*	1	0	5	0	0
WntlCre/R26R	*C57BL/6*	1	0	7	0	0
$Tbr2^{f/f}$	$KC4/Tbr2^{f/w}$	18[b]	5	26[b]	5	23
$Smad4^{f/f}$	$KC4.3/Smad4^{f/w}$	6[b]	2	7[b]	3	38

[a]ZEG transgene is on chromosome 11 same as *Krt12*. Thus, the ZEG allele is always co-segregated with the $Krt12^{Cre}$ allele
[b]Homozygous floxed *Tbr2* and *Smad4* alleles
[c]Percentage of penetrance is calculated by number of mice with excised floxed allele divided by the total number of mice carrying floxed allele in each experimental group.
Double transgenic mice were crossbred with wild-type mice, and homozygous $Tbr2^{f/f}$ and $Smad4^{f/f}$ mice. The excision event was determined by the expression of respective reporter gene activities or by PCR of the excised floxed alleles as described in Methods. Cre^{Tg}: hemizygous Cre transgenic mice; Cre^{0}: non-Cre transgenic mice. Reproduced from Weng, D. Y., Zhang, Y., Hayashi, Y. et al., (2008). Promiscuous recombination of *LoxP* alleles during gametogenesis in cornea *Cre* driver mice. *Molecular Vision* 14: 562–571.

deletion. Increasing evidence indicates that many cell-type-specific genes in adults are promiscuously expressed in gonad during gametogenesis. Therefore, the promiscuous expression of Cre recombinase driven by cell-type-specific promoters should always be examined to avoid misinterpretation resulting from haploid deficiency.

Inducible Cre–LoxP system

To overcome the pitfalls of promiscuous Cre expression during gametogenesis, we have developed a doxycycline-inducible tet-ON system to spatially and temporally ablate gene of interest in ocular surface tissues. This tet-ON system employs triple transgenic mice consisting of an ocular-surface tissue-specific promoter rtTA (*Kera-rtTA (KR)*), *Krt12-rtTA* (K12R), and *Pax6$_{OS}$-rtTA* (P6R) (**Table 2**), and tet-O-Cre (TC) transgenes, as well as an $X^{f/f}$ (a LoxP-modified gene). Administration of doxycycline will activate rtTA that subsequently turns on the tet-O-Cre transgenes for the synthesis of Cre recombinase, which then excises the $X^{f/f}$ gene in an ocular-surface tissue-specific manner (as described below).

Strategies of Cornea-Specific Genetic Modification: Transgenic and Knock-Out/Knock-In Mice

Identification of Ocular-Surface Tissue-Specific Promoter

The availability of ocular-surface tissue-specific promoter is a prerequisite for the preparation of experimental animal models in which genetic modifications are made to study the consequence of the loss and/or gain of functions of genes in ocular surface tissues, that is, cornea, conjunctiva, lacrimal glands, and eyelids. To date, our laboratory has identified and characterized two cornea-specific genes: keratin 12 (*Krt12*) and keratocan (*Kera*) genes of corneal epithelium and stroma, respectively, and used transgenesis and gene-targeting techniques to create mouse lines in which the gene functions are altered in a cornea-specific manner. However, it should be noted that many systemic genetically modified mouse lines that were created by conventional systemic gene-targeting techniques and/or transgenesis with non-ocular-surface tissue-specific promoters also manifested pathogenesis in ocular surface tissues. Naturally, these mouse lines often exhibited pathogenesis in other tissues than ocular surface tissues as well. To date, only a few promoters that exhibit ocular surface tissue specificity have been identified, for example, keratocan (*Kera*), keratin 12 (*Krt12*), and modified *Pax6* promoters. It should be noted that there is no tissue-specific promoter available that can be used to create mouse lines in which genetic modifications are limited to conjunctiva, cornea endothelium, and lacrimal gland.

Stromal keratocyte-specific promoter

Keratan sulfate proteoglycans (KSPGs) play a pivotal role in the development and maintenance of corneal transparency. Keratocan, lumican, and mimecan (osteoglycin) are the major KSPGs in vertebrate corneas. We have cloned both the mouse keratocan gene and its complementary DNA (cDNA). The mouse keratocan gene spans approximately 6.5 kb of the mouse genome and contains three exons and two introns. Northern blotting and *in situ* hybridization were employed to examine keratocan gene expression during mouse development. Unlike lumican gene, which is expressed by many tissues other than cornea, keratocan messenger RNA (mRNA) is more selectively expressed in the corneal tissue of the adult mouse. During embryonic development, keratocan mRNA was first detected in periocular mesenchymal cells migrating toward developing corneas on embryonic day 13.5 (E13.5). Its expression was then gradually restricted to corneal stromal cells in between E14.5 and E18.5. Interestingly, keratocan mRNA can be detected in scleral cells of E15.5 embryos, but not in

Table 2 Mouse lines for cornea-specific genetic modification

Mouse lines	*Tissue/cell specificity*	*Induction*	*Function*
Kera-rtTA/tet-*O*-reporter	Stromal keratocytes in adult and neural crest cells in embryo	Doxycycline	Overexpression
Kera-Cre	Stromal keratocytes in adult and neural crest cells in embryo	Not inducible	Gene ablation
Kera-rtTA/tet-*O*-Cre/$X^{f/f}$	Stromal keratocytes in adult and neural crest cells in embryo	Doxycycline	Spatial and temporal gene ablation
Krt12-rtTA/tet-*O*-reporter	Corneal epithelium	Doxycycline	Overexpression
Krt12-Cre	Corneal epithelium	Not inducible	Gene ablation
Krt12-rtTA/tet-*O*-Cre/$X^{f/f}$	Corneal epithelium	Doxycycline	Spatial and temporal gene ablation
$Pax6_{OS}$-rtTA/tet-*O*-reporter	Ocular surface epithelium and lacrimal gland (?)	Doxycycline	Overexpression
$Pax6_{OS}$-rtTA/tet-*O*-Cre/$X^{f/f}$	Ocular surface epithelium and lacrimal gland (?)	Doxycycline	Spatial and temporal gene ablation

E18.5 embryos. In adult eyes, keratocan mRNA can be detected in corneal keratocytes, but not in scleral cells.

To identify and characterize a keratocyte-specific promoter, we have cloned a 3.2-kb genomic DNA fragment 5′of the mouse *Kera* gene, which has promoter activities in driving the expression of reporter genes, for example, β-galactosidase *(β-Gal)*, reverse tetracycline transcription activator (*rtTA*), Cre recombinase (*Cre*), by migrating periocular mesenchymal cells of neural crest origin during embryonic development and by cornea stromal keratocytes in adults. For example, in adult *Kera-βGal* transgenic mice, *β*-galactosidase activity was detected only in cornea, not in other tissues (e.g., lens, retina, sclera, lung, heart, liver, diaphragm, kidney, and brain). In contrast, during ocular development, the spatial–temporal expression patterns of *βGal* reporter gene recapitulated that of endogenous *Kera* expression in mice. Using X-Gal staining, strong *β*-galactosidase activity was first detected in periocular tissues of E13.5 embryos, and restricted to corneal keratocytes at E14.5 and thereafter. Interestingly, in addition to cornea, *β*-galactosidase activity was transiently found in some nonocular tissues, that is, ears, snout, and limbs of embryos of E13.5 and E14.5, but was no longer detected in those tissues of E16.5 embryos. The transient expression of endogenous keratocan in nonocular tissues during embryonic development was confirmed by *in situ* hybridization. Taken together, the observations suggest that the 3.2-kb *Kera* promoter contains sufficient *cis*-regulatory elements to drive heterologous minigene expression in cells expressing keratocan.

Corneal-epithelium-specific promoter

Keratins are a group of water-insoluble proteins that form 10-nm intermediate filaments in all epithelial cells. Approximately 30 different keratin molecules have been identified, which can be divided into acidic and basic neutral subfamilies. *In vivo*, a basic keratin is usually coexpressed and paired with a particular acidic keratin. The expression of keratin pairs is tissue specific, differentiation dependent, and developmentally regulated. Expression of keratin 3/keratin 12 pair has been found in human, bovine, guinea pig, rabbit, and chicken corneas and is regarded as a marker for corneal-type epithelial differentiation. The expression of keratin 12 is restricted to the corneal epithelium. We have identified and cloned the corneal-epithelium-specific K12 keratin (*Krt12*) gene. Using gene gun to deliver *Krt12-LacZ* reporter gene constructs to rabbit corneal epithelium, we have identified the *cis*-regulatory element that is sufficient and necessary for corneal-epithelium-specific expression of the reporter genes. However, the use of conventional transgenesis techniques failed to identify a functional *Krt12* promoter that was capable of driving the expression of reporter genes, for example, *β-Gal*, chloramphenicol acetyl transferase (*CAT*), and green fluorescent proteins (*GFP*s) in corneal epithelium. Transgenesis using lentiviral *Krt12-lacZ* vectors had successfully generated mouse lines that expressed the reporter *LacZ* gene by corneal epithelium, but multiple insertions by the use of lentivirus vector compromised the efficiency of obtaining stable transgenic mice. To overcome the pitfalls, a gene-targeting construct containing an internal ribosomal entry site–reverse tetracycline transcription activator (IRES-rtTA) cassette was inserted into the *Krt12* allele to produce knock-in *Krt12-rtTA* and Krt12-Cre driver mouse lines through gene-targeting techniques (see below).

Ocular-surface epithelium-specific Pax6 promoter ($Pax6_{OS}$)

Pax6 is a regulatory gene with restricted expression and essential functions in the developing eye and pancreas and distinct domains of the central nervous system (CNS). Three conserved transcription start sites (P0, P1, and a) have been identified in the murine *Pax6* locus. Furthermore, the use of transgenic mouse technology has identified the *cis*-regulatory elements controlling the tissue-specific expression of *Pax6*. Specifically, a 107-bp enhancer and a 1.1-kb sequence within the 4.6-kb untranslated region upstream of exon 0 are required to mediate *Pax6* expression in the lens, cornea, lacrimal gland, conjunctiva, or pancreas. Another 530-bp enhancer fragment located downstream of the *Pax6* translational start site is required for expression in the neural retina, the pigment layer of the retina, and the iris. Finally, a 5-kb fragment located between the promoters P0 and P1 can mediate expression into the dorsal telencephalon, the hindbrain, and the spinal cord. The identified *Pax6/cis*-essential elements are highly conserved in pufferfish, mouse, and human DNA and contain binding sites for several transcription factors indicative of the cascade of control events. Corresponding regulatory elements from pufferfish are able to mimic the reporter expression in transgenic mice. Thus, the results indicate a structural and functional conservation of the *Pax6* regulatory elements in the vertebrate genome. This segment of the mouse Pax-6 gene 5′ flanking region is necessary and sufficient for reporter construct expression in components of the eye derived from non-neural ectoderm, for example, lens epithelium and ocular surface epithelium. This transcriptional control element has been used to prepare $Pax6_{OS}$-rtTA (P6R) driver mouse lines for transgene expression.

Ocular Surface Tissue-Specific Driver Mouse Lines

Corneal stroma-specific mouse lines

The mouse keratocan gene (*Kera*) expression tracks the corneal morphogenesis during eye development and becomes restricted to keratocytes of the adult, implicating a cornea-specific gene regulation of the mouse *Kera*. We

have identified and cloned a 3.2-kb genomic DNA fragment 5′ of the mouse *Kera* gene, which is capable of driving the expression of *LacZ* reporter gene that recapitulates the expression patterns of *Kera*. The keratocan promoter has been used to create transgenic mice, for example, *Kera-biglycan*, and *Kera-Cre* and *Kera-rtTA* driver mouse lines. The *Kera-rtTA* (KR) mice can be used to create bitransgenic Kera-rtTA/tet-O-reporter construct and tritransgenic *KR/TC (tet-O-Cre)/X$^{f/f}$* (X, gene of interest) mice for keratocyte-specific doxycycline-inducible transgene expression and gene ablation (**Table 2**).

Corneal-epithelium-specific mouse lines

A similar strategy employing Cre–LoxP and tet-ON systems with keratin 12 promoter (*Krt12*) would allow us to prepare experimental mouse lines that express transgenes and ablate genes in a corneal-epithelium-specific manner. Thus, for many years we tried to identify and isolate a functional keratin 12 promoter for the preparation of corneal-epithelium-specific transgenic and Cre–LoxP mouse lines without success. To circumvent these difficulties, we have prepared mouse lines carrying IRES-Cre and IRES-rtTA reporter genes into the *Krt12* locus through a targeted knock-in strategy.

Unlike prokaryotes, most mammalian mRNAs are monocistronic (i.e., one message encodes one protein). However, some viral mRNAs and/or translationally regulated mRNAs (e.g., fibroblast growth factor 2 (FGF-2) and c-myc) are bicistronic in that they have IRESs in the mRNA that allows a second initiation of translation after the stop codon of the first reading frame for the synthesis of a second protein from the mRNA. Inclusion of such IRES elements in the reporter gene constructs has allowed the generation of transgenic mouse lines that express two proteins encoded by a single transgene.

To create corneal-epithelium-specific gene ablation in mice, a targeting construct containing intron 2 to exon 8 of *Krt12* gene was prepared in which an IRES-Cre and the phosphoglycerate kinase-neomyocin resistance gene (PGK-Neo) reporter genes were inserted right after the stop codon within exon 8 as shown in **Figure 1**. Germ line chimera mice were obtained through conventional gene-targeting techniques using embryonic stem cells. The K12-Cre mice were crossed with reporter Tg(CAG-Bgeo/ALPP)1Lbe (*ZAP*) mice that harbor a transgene containing a chicken β-actin promoter, a floxed *LacZ* gene (two LoxP elements flanked at 5′ and 3′ ends of *LacZ*), and followed by alkaline phosphatase (*AP*) gene in tandem. The Cre activity was assessed by the detection of *LacZ* and expression of *AP* in corneas of the offspring as shown in **Figure 2**. Thus, the K12-Cre knock-in mice can be used to create mouse lines in which any floxed genes are ablated in corneal epithelium. Thus, it will allow us to investigate the role of a gene in corneal morphogenesis and homeostasis through the loss of function without threatening the life of the experimental animals. Using a similar strategy, a gene-targeting construct containing an IRES-rtTA cassette was inserted into the *Krt12* allele to produce a knock-in *Krt12$^{rtTA/w}$* mouse line through gene-targeting techniques (**Figure 1**). The *Krt12$^{rtTA/w}$* knock-in mice were bred with *tet-O-LacZ* reporter mice to obtain *Krt12$^{rtTA/w}$/tet-O-LacZ* bitransgenic mice. The corneal-epithelium-specific expression of the *LacZ* gene was induced in bitransgenic mice by administration of doxycycline in the drinking water and chow as shown in **Figure 3**. To further expand the usefulness of Krt12-rtTA knock-in mice, a tritransgenic *Krt12$^{rtTA/w}$/tet-O-Cre/ZEG* mouse line was prepared in which the expression of enhanced green fluorescence protein (EGFP) was activated by feeding mice doxycycline that subsequently excised the *LacZ* gene from the *ZEG* allele and allowed the expression of EGFP. **Figure 4** shows the doxycycline-induced expression of EGFP by corneal epithelial cells of *Krt12$^{rtTA/w}$/TC/ZEG* mice. ZEG is a transgenic mouse line that has dual reporter genes of a *LacZ* flanked by LoxP, followed by *EGFP* driven by a chicken actin promoter. Chicken actin promoter drives the expression of *LacZ* in all cells except those of which express Cre and show green fluorescence due to the excision of *LacZ* and expression of *EGFP*. Using the strategies, we have prepared several mouse lines that can be used to overexpress transgenes and ablate genes of interest in a cornea-specific manner as summarized in **Table 2**.

Ocular surface tissue-specific Pax6$_{OS}$-rtTA mouse line

We have recently prepared an ocular surface epithelium-rtTA (Pax6$_{OS}$-rtTA) driver mouse line with *cis*-regulatory elements of the 4.6-kb un-translated region upstream of exon 0 of *Pax6*, which mediate *Pax6* expression in the lens, cornea, lacrimal gland, conjunctiva, or pancreas. The bitransgenic *Pax6$_{OS}$-rtTA/Tet-O-EGFP* mice express EGFP upon doxycycline induction (data not shown). This *Pax6$_{OS}$-rtTA* mouse line is useful for generating experimental mice of overexpression of tet-O-transgene and ablation of floxed gene of tritransgenic (*Pax6$_{OS}$-rtTA/tet-O-Cre/X$^{f/f}$*) mice.

Roles of Growth Factors on Ocular Surface Tissue Morphogenesis during Development and Wound Healing Elucidated from Transgenic Mice

Corneal morphogenesis during eye development of vertebrates involves the differentiation of cells from surface ectoderm and the migration of periocular mesenchymal cells of neural crest origin. The differentiation of surface ectoderm gives rise to corneal and conjunctival epithelia of the ocular surface as well as to glandular epithelium, for example, lacrimal and meibomian glands. The

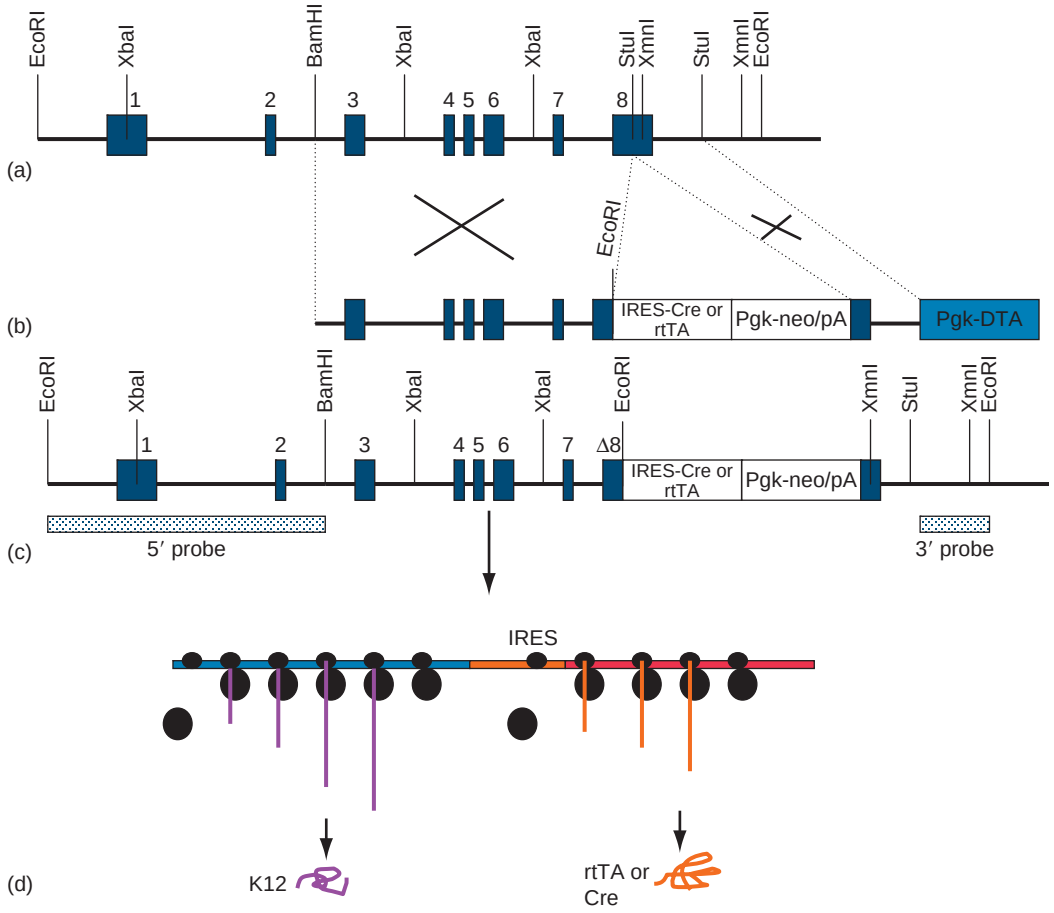

Figure 1 Generation of *Krt12*$^{rtTA/+}$ and *Krt12*$^{Cre/+}$ knock-in mice through gene targeting. (a) Krt12 allele. (b) Targeting vector: the IRES-rtTA (and IRES-Cre) cassette, containing IRES, rtTA (Cre), and SV40-polyA, was cloned in-frame into the corresponding EcoRI/EcoRV site of pKrt12-4.8 3′ to the stop codon in exon 8 of *Krt12*, creating a modified exon 8 that contains the entire 3′ coding region of *Krt12*, IRES-rtTA, and SV4-polyA signals. This was followed by pgk-Neo minigene, untranslated exon 8, and polyadenylation (pA) of *Krt12.* Finally, a negative selection marker gene, diphtheria toxin A fragment (pgkpr-DTA) cassette, was placed on the 5′ end of the targeting vector. Knock-in' shows the predicted structure of a targeted knock-in allele after homologous recombination. (c) Knock-in Krt12 allele through homologous recombination. (d) Bi-cistronic mRNA derived from the Knock-in Krt12 allele. Panels (a), (b), and (c) of this figure are reprinted from Chikama, T. -L., Hayashi, Y., Liu, C. -Y. et al. (2005). Characterization of tetracycline inducible *Krt12*$^{rtTA/+}$/*tet-O-LacZ* mice. *Investigative Ophthalmology and Visual Science* 46: 1966–1972.

mesenchymal cells of neural crest origin become corneal endothelial cells and keratocytes, and the stromal cells of other ocular surface tissues, that is, eyelids, iris, ciliary body, and trabecular meshworks.

The corneal epithelium synthesizes components of extracellular matrix (ECM) for the formation of primary stroma when the lens detaches from the ectoderm during development. In vertebrate corneal development, the first wave of mesenchymal cells that migrate underneath the primary stroma forms the endothelium. The mesenchymal cells of the second wave invade the primary stroma and become keratocytes, which are responsible for the formation of secondary stroma of adult vertebrates. The third waves of mesenchymal cells contribute to the stromas of eyelids, iris, ciliary body, and trabecular meshworks. This orderly cellular migration and differentiation are controlled by cues from various cytokines and the components of ECM, which are under constant remodeling during embryonic development. For example, members of the transforming growth factor beta (TGFβ) superfamily play pivotal roles in embryonic development. However, the precise cytokines and their functions that modulate corneal morphogenesis remain unknown. It is very likely that cytokine signaling may modulate the expression of specific transcription factors that contribute to this orderly corneal morphogenesis during development or vice versa.

TGFβ Receptor Signaling Pathways during Development and Corneal Wound Healing

Role of TGFβ2 on development

TGFβ has a pivotal role in embryonic development. In mammals, three isoforms of TGFβ (β1, -2, and -3) are

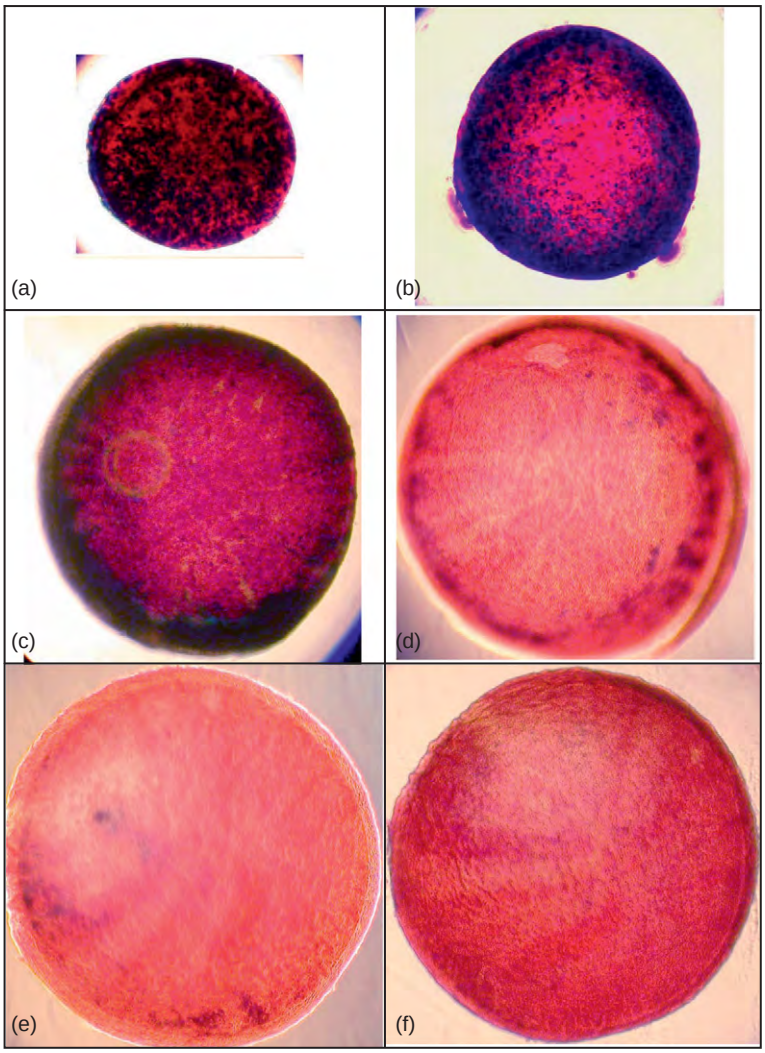

Figure 2 Histograms of X-gal and AP staining of *Krt12*$^{Cre/Cre}$/*ZAP* bitransgenic mice. Corneas from bitransgenic mice at different ages were subjected to histochemistry staining for X-gal and alkaline phosphatase activities. (a) P15 (postnatal day 15); (b) P30; (c) P60; (d) P90; (e), P180; (f) P300. Cells express K12 and AP (alkaline phosphatase) positive were stained red, whereas the K12 negative cells were *LacZ* positive and stained blue. At P15, the expression of *LacZ* (blue) and *AP* (red) shows a mosaic pattern. At P90, almost all central cornea epithelia express K12 and stained red with sporadic blue cells. At P180 and P300, central corneas were stained red with blue cells located at limbus. Reproduced from Tanifuji-Terai, N., Terai, K., Hayashi, Y., et al. (2006). Expression of keratin 12 and maturation of corneal epithelium during development and postnatal growth. *Investigative Ophthalmology and Visual Science* 47: 545–551.

known. Members of TGFβ family are multifunctional cytokines involved in development, tissue repair, and other physiological or pathologic processes. Among the knock-out mice of the three *Tgfb* isoforms, only *Tgfb2*$^{-/-}$ mice exhibit ocular pathology of thin corneal stroma, absence of corneal endothelium, fusion of cornea to lens, a phenotype resembling Peter's and Axenfeld anomaly in humans, and accumulation of hyaline cells in vitreous. Delayed appearance of macrophages in ocular tissues was observed in *Tgfb2*$^{-/-}$mice. Malfunctioning macrophages may account for accumulation of cell mass in vitreous of *Tgfb2*-null mice. In *Tgfb2*$^{-/-}$mice, fewer keratocytes were found in stroma that have a decreased accumulation of ECM; for example, lumican, keratocan, and collagen I were greatly diminished. The thinner stroma resulting from decreased ECM synthesis may account for the decreased cell number in the stroma of *Tgfb2*-null mice. The absence of TGFβ2 did not compromise corneal epithelial cell proliferation, nor enhance apoptosis. Keratin 12 expression was not altered in *Tgfb2*$^{-/-}$mice, implicating that TGFβ signaling is not essential for cornea-type epithelium differentiation. This suggestion is further supported by the observation that ablation of TGFβ type II receptor in *Krt12*$^{Cre/Cre}$/*Tbr2*$^{f/f}$ mice does not cause corneal epithelium anomaly (our unpublished observation).

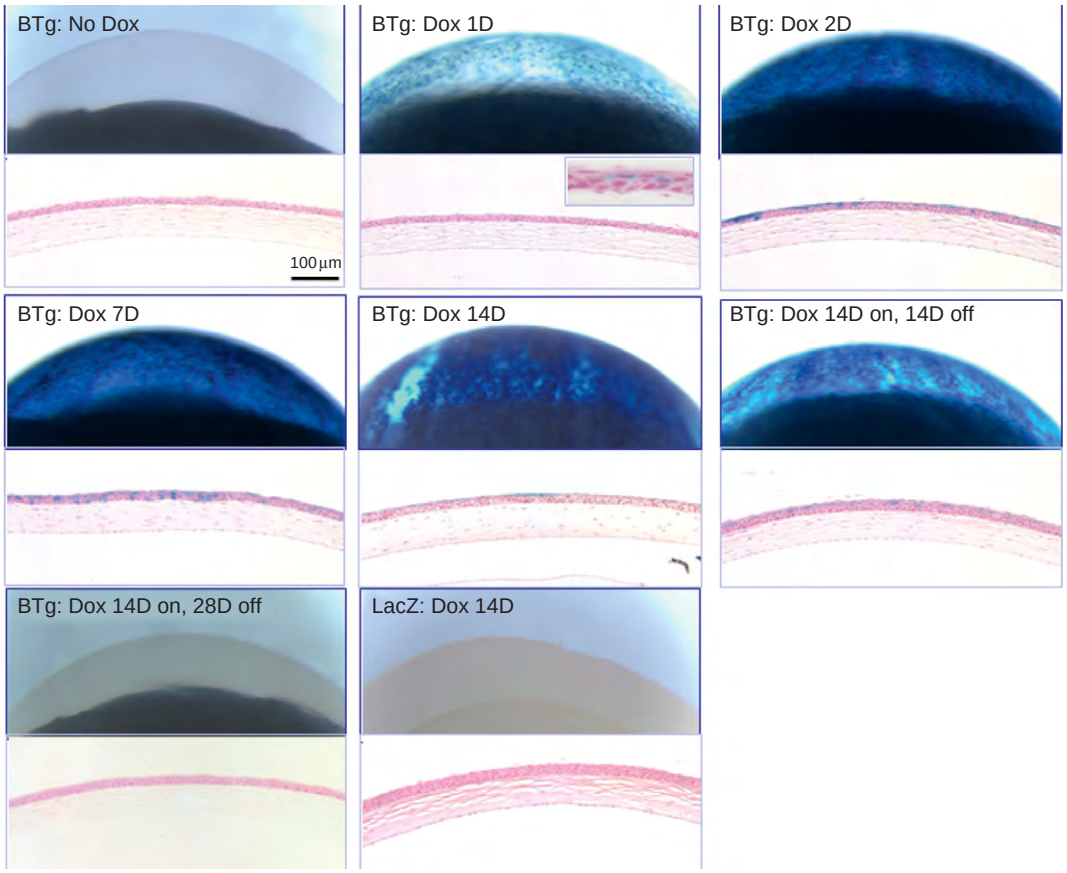

Figure 3 *In situ* analysis of β-galactosidase enzyme activity induction by doxycycline in corneas of *Krt12*$^{rtTA/+}$*/tet-O-LacZ* bitransgenic mice. Stereomicroscopy showed a side view of each eye after whole-mount β-galactosidase staining. Histological examination (lower image of each panel) of the same samples revealed that the β-galactosidase expression was restricted to corneal epithelium. Corneal epithelial cells began to express β-galactosidase in 24 h after doxycycline administration. The number of β-galactosidase expressing cells in BTg mouse with doxycycline increased in the course of time. Not all corneal epithelial cells expressed β-galactosidase was observed even in the maximum level. BTg, bitransgenic; *LacZ*, *tet-O-LacZ* single transgenic. Reproduced from Chikama, T. -I., Hayashi, Y., Liu, C. -Y. et al. (2005). Characterization of tetracycline Inducible *Krt12*$^{rtTA/+}$*/tet-O-LacZ* mice. *Investigative Ophthalmology and Visual Science* 46: 1966–1972.

Role of TGF-β signaling in wound healing of corneal epithelium

Corneal epithelial defects must be rapidly resurfaced to avoid microbial infection and further damage to the underlying stroma. Epithelial healing is achieved by migration of the epithelial sheet to cover the denuded surface and enhanced cell proliferation to reestablish the epithelial stratification quickly after resurfacing. It is of interest to note that in the early phase of healing only one of the two cellular responses, cell migration, takes place, whereas cell proliferation is suppressed. Although cell migration promotes rapid re-epithelialization, the cessation of cell proliferation may impede healing if such cessation is prolonged.

Various growth factors, including TGFβ, orchestrate the behavior of healing corneal epithelium: for example, cell migration and/or proliferation, cell death, and protein synthesis. It has been demonstrated that the TGFβ isoforms and their receptors are present in corneal and limbal epithelia and other supporting tissues (e.g., conjunctiva and tear fluid). Therefore, it has long been speculated that the TGFβ isoforms play pivotal roles in maintaining corneal homeostasis in a paracrine and autocrine fashion as TGFβ inhibits cell proliferation of cultured keratinocytes and corneal epithelial cells *in vitro*, thus it may suppress corneal epithelial cell proliferation *in vivo*. This notion is further supported by the observation in which the administration of anti-TGFβ-neutralizing antibodies reduces scar tissue formation in injured corneas. Recently, it was shown that epithelial debridement causes an upregulation of TGFβ receptor expression on migrating corneal epithelial cells, suggesting that this ligand may have a pivotal role in modulation of functions of migrating corneal epithelial cells during wound healing.

We recently examined the roles of TGF-β signaling pathways in regulating cell migration and proliferation of the healing of corneal epithelium debridement. TGF-β type II receptor (*Tbr2*) floxed mice were bred

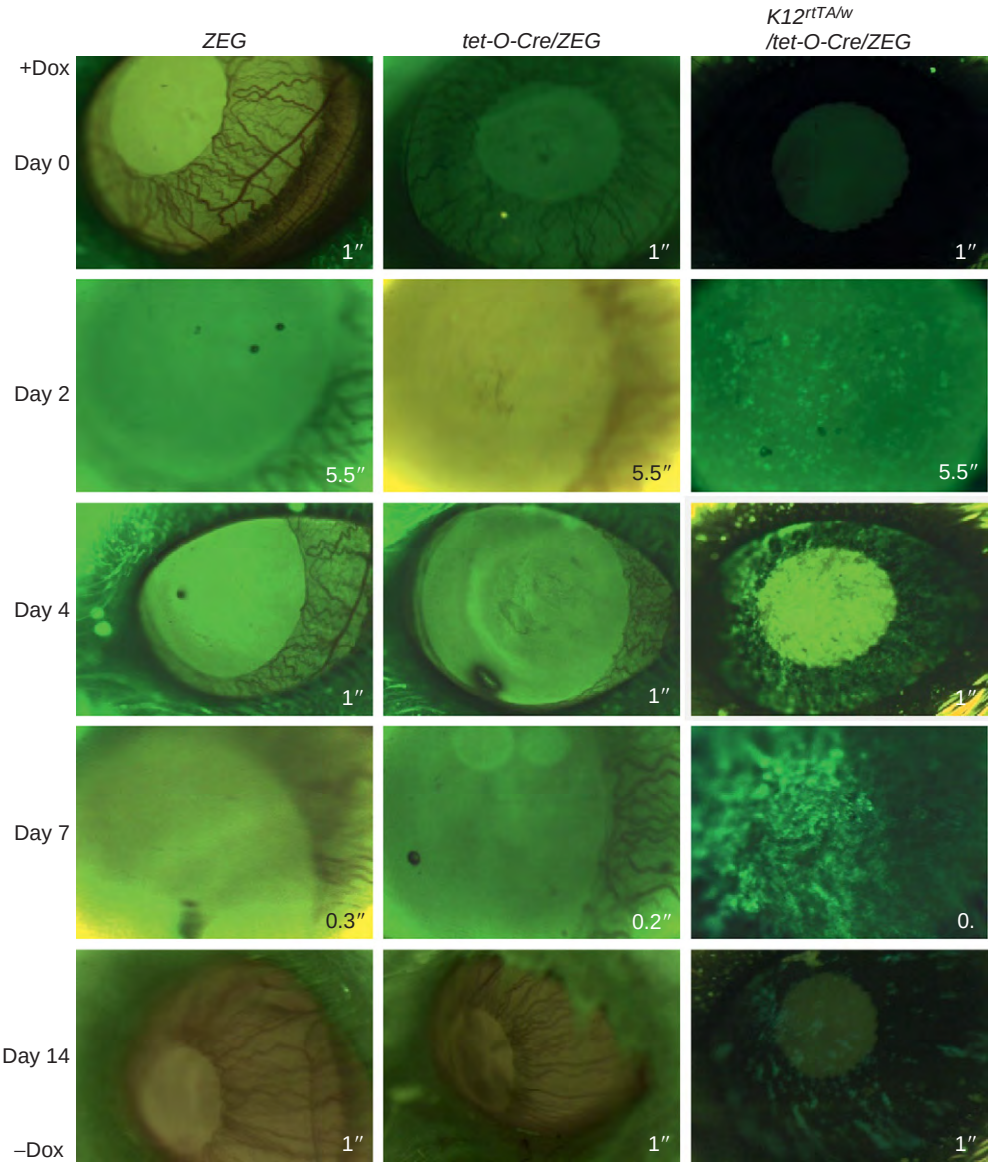

Figure 4 Expression of floxed reporter gene by doxycycline induction Tritransgenic *Krt12/tet-O-Cre/ZEG* mice were fed doxycycline chow for various periods of time. The experimental animals were examined under a ZEISS stereomicrscope with epi-fluorescence attachment. Strong green fluorescence was observed in tritransgenic *Krt12/tet-O-Cre/ZEG* mice after 2 days induction and then declined in 14 days after removal of doxycycline in the diet.

with *Krt12-Cre* mice to generate bitransgenic mice in which the *Tbr2* gene was disrupted selectively in the corneal epithelial cells. Corneal epithelial debridement (2 mm in diameter) was created in 2-month-old bitransgenic $Krt12^{Cre/Cre}/Tbr2^{f/f}$ mice and their littermates as controls $Krt12^{Cre/Cre}/Tbr2^{f/w}$ and $Krt12^{Cre/Cre}/Tbr2^{w/w}$. Our results indicated that corneal epithelium of $Krt12^{Cre/Cre}/Tbr2^{f/f}$ mice exhibited delayed healing of debridement in comparison to that of control littermates that were heterozygous floxed and wild-type *Tbr2*. The naive uninjured corneal epithelium of $Krt12^{Cre/Cre}/Tbr2^{f/f}$ mice exhibited higher cell proliferative activities than controls as determined by BrdU incorporation. It is of interest to note that corneal epithelium debridement caused cessation of epithelial cell proliferation of all experimental mice in 6–12 h, irrespective of whether the *Tbr2* was ablated or not.

Immunohistochemistry using anti-phospho-p38 mitogen-activated protein kinase (MAPK) revealed, following epithelium debridement, that the activation of p38MAPK was seen in 6 h of injury in control mice. In contrast, phosphorylation and nuclear translocation of p38MAPK were markedly delayed in mice lacking Tbr2 in corneal epithelium compared to control mice. The observation is consistent with results of our previous studies, in which we demonstrated that addition of p38MAPK inhibitors blocked cell migration more markedly than

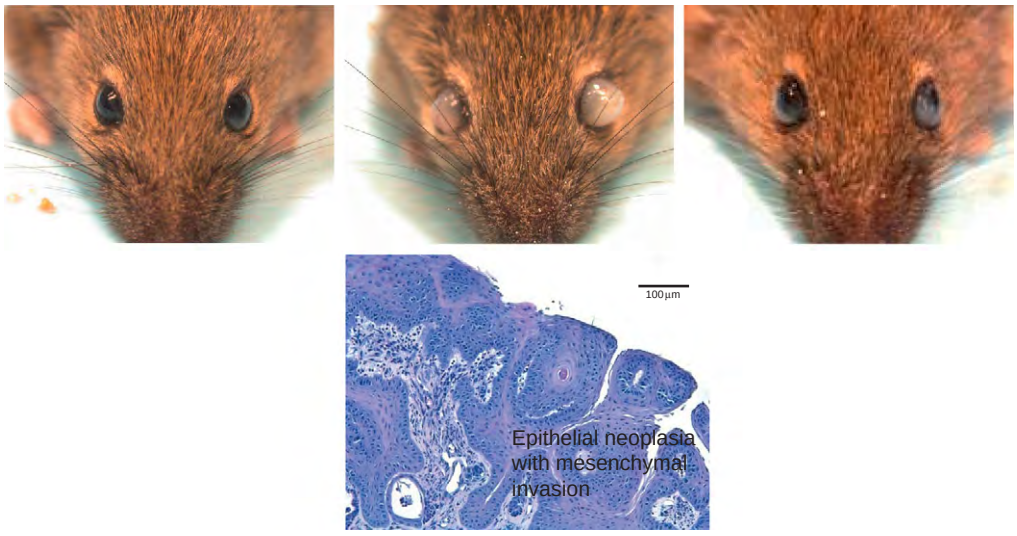

Figure 5 Excess expression of FGF7 by corneal epithelium causing ocular surface squamous neoplasia (OSSN). Krt12-rtTA/tet-*O*-FGF7 bitransgenic mice were obtained by crossbreeding single Krt12-rtTA and tet-*O*-FGF7 mice. The progeny were induced by feeding mothers doxycycline chow at the beginning of mating (E0.5) and until weaning of the pups at postnatal day 18 (P18). The pups were continuously fed doxycycline chow after weaning until sacrifice at P21. Enucleated eyes were subjected to histological examination. The bitransgenic Krt12-rtTA/tet-*O*-FGF7 mice showed bilateral OSSN.

neutralizing anti-TGFβ antibody and enhanced cell proliferation in the injured corneal epithelium. The observation suggested that p38MAPK, but not the mothers against decapentaplegic (Smad, another signaling cascade active by TGFβ) cascade, plays a major role in promoting cell migration and in suppressing cell proliferation in migrating epithelium.

Role of FGF7 in Maintenance of Corneal Homeostasis

During mammalian embryogenesis, epithelial–mesenchymal interactions play a determining role in normal tissue patterning and development. FGF7 (also known as keratinocyte growth factor, KGF), a member of the FGF family, is a mesenchymally derived mitogen for epithelial cells in regulating epithelial cell behavior, as the FGF7 receptor is expressed by epithelial cells. Overexpression of human FGF7 by a crystalline promoter in the eye caused hyperproliferation of embryonic corneal epithelial cells and their subsequent differentiation into functional lacrimal gland-like tissues. This indicates that stimulation of the FGF7 receptor early in development, in surface ectoderm normally destined to form corneal epithelium, is sufficient to alter the fate of these cells. This further suggests that the correct spatial and temporal expression of FGFs plays a critical role in normal lacrimal gland induction. It is of interest to note that overexpression of FGF7 in $Krt12^{rtTA/wt}/tetO\text{-}FGF7$ bitransgenic mice by doxycycline induction during embryonic development resulted in the formation of vascularized cornea with epithelium hyperplasia, resembling human ocular surface squamous neoplasia (OSSN) as shown in Figure 5. The phenotype variations of the two mouse models can be explained by the fact that α-crystalline expression by lens commences at E10–E11.5, whereas the expression of keratin by corneal epithelium begins at E14.5.

EGFR/EGF, TGFα Signaling Pathways on Eyelids Morphogenesis

Transgenic *Kera-Bgn* mice overexpressing biglycan, driven by keratocan promoter under the keratocan promoter, exhibit exposure keratitis and premature eye opening from noninfectious eyelid ulceration due to perturbation of eyelid muscle formation and the failure of meibomian-gland formation. In addition, *in vitro* analysis revealed that biglycan binds to TGFα, thus interrupting epidermal growth factor receptor (EGFR) signaling pathways essential for mesenchymal cell migration induced by eyelid epithelium. The defects of TGFα signaling by excess biglycan were further augmented by the interruption of the autocrine or paracrine loop of the EGFR signaling pathway of heparin-binding (HB)-EGF expression elicited by TGFα.[10] These results are consistent with the notion that under physiological conditions, biglycan secreted by mesenchymal cells serves as a regulatory molecule for the formation of a TGFα gradient serving as a morphogen of eyelid morphogenesis (Figure 6).

MEK kinase 1 (MEKK1) is an MAPK originally identified as an upstream activator for several MAPK pathways. During mouse embryogenesis, MEKK1 controls cell

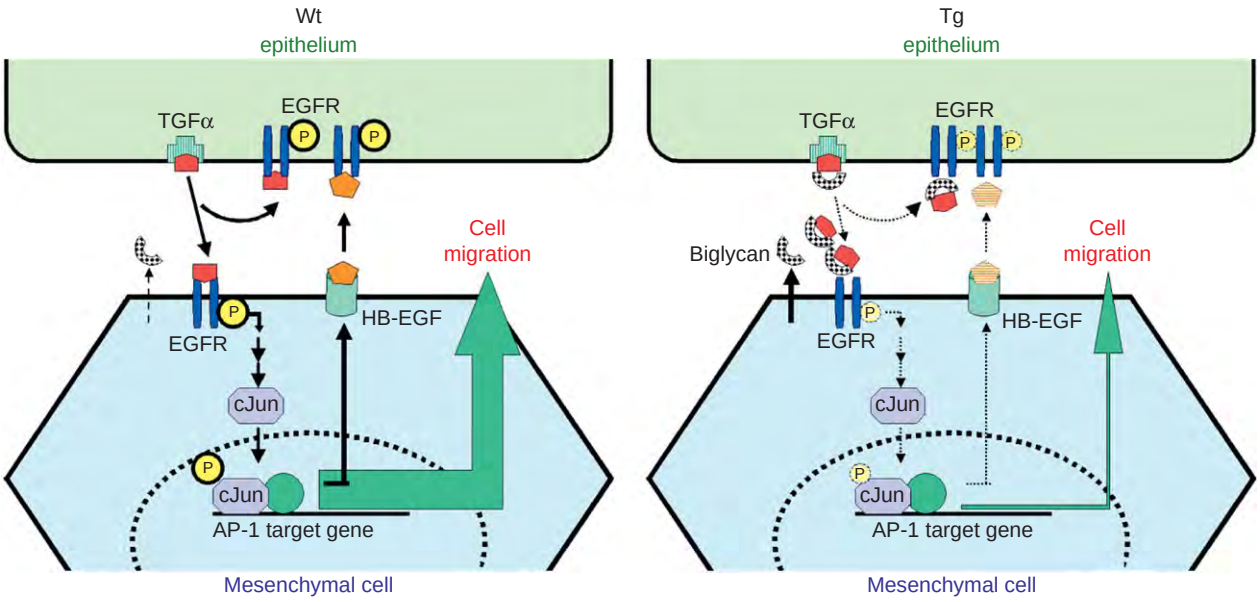

Figure 6 The EGFR signaling mediated by TGF-α during eyelid morphogenesis. The presence of excess biglycan in the *Kera-Bgn* transgenic mice sequesters TGF-α and consequently perturbs the autocrine and/or paracrine loop of EGFR signaling pathways through HB-EGF and impairs mesenchymal cell migration. Reproduced from Hayashi, Y., Liu, C. -Y., Jester, J. V. et al. (2005). Excess biglycan interferes TGF-α signaling required for eyelid morphogenesis. *Developmental Biology* 277: 222–234.

shape changes and formation of actin stress fibers that are required for sealing epidermis in the embryos in a process known as eyelid closure. MEKK1-null mice display eye-open at birth (EOB), a phenotype found also in mice impaired in activin, a subgroup of the TGFβ family, or in EGFR or its ligand TGFα, or in transcription factor c-Jun. Molecular analyses have revealed at least two signaling mechanisms in the control of eyelid closure. One is originated from the activins and is transduced through MEKK1, leading to transcription-independent actin stress fiber formation and transcription-dependent keratinocyte migration. Another is the TGFα/EGFR signal that is transduced through an MEKK1-independent pathway to the activation of the extracellular signal-regulated kinase (ERK) MAPK, which also leads to keratinocyte migration. c-Jun might serve as a connection between the two pathways. As embryonic eyelid closure is a specific morphogenetic process that is easily detectable, genetic mutant mice with EOB will be ideal models to understand the signaling mechanisms in the control of epithelial cell migration and the morphogenetic process of epithelial sheet movement.

Thus, the observation supports the hypothesis that tissue morphogenesis during development is regulated by growth factors and cytokines, and is characterized by constant remodeling of ECM in response to signaling molecules, for example, growth factors, cytokines, and so forth. Proteoglycans that bind growth factors are potential regulators of tissue morphogenesis during embryonic development.

Conclusion: The Clinical Relevance of Tet-ON Mouse Models in Elucidating Pathophysiology of Ocular Surfaces Diseases

Many transgenic and knock-out mice exhibit pathogenesis resembling human ocular surface diseases. Thus, the clinical manifestations of mouse lines can be used as clues for identifying inherited human disease of unknown etiology. However, embryonic lethality and congenital defects of the mouse lines do not allow further examination of the effects of altered genetic functions on pathophysiology of acquired diseases in adults. The difficulties can be overcome by preparing mouse lines of inducible transgene expression, tissue-specific gene ablation, and inducible tissue-specific gene ablation. The conditional transgenic mouse lines will live normally until the administration of doxycycline, which induces expression of the transgene and/or ablation of gene of interest. Use of these genetically modified mouse lines can simulate the pathophysiology of ocular surface diseases, for example, wound healing, tumorigenesis, and irregular hormone and cytokine signaling that offsets homeostasis in adults.

Acknowledgments

This work was supported by NIH grants EY 10556, EY 11845, and EY 13755, Challenge Grant for Research to

Prevent Blindness, Inc., and Unrestricted grant from Ohio Lion Eye Research Foundation.

See also: Conjunctival Goblet Cells; Corneal Epithelium: Cell Biology and Basic Science; Corneal Epithelium: Wound Healing Junctions, Attachment to Stroma Receptors, Matrix Metalloproteinases, Intracellular Communications; Cornea Overview; Gene Therapy for the Cornea, Conjunctiva, and Lacrimal Gland; Lacrimal Gland Hormone Regulation; Lacrimal Gland Overview; Lacrimal Gland Signaling: Neural; Lids: Anatomy, Pathophysiology, Mucocutaneous Junction; Overview of Electrolyte and Fluid Transport Across the Conjunctiva; The Surgical Treatment for Corneal Epithelial Stem Cell Deficiency, Corneal Epithelial Defect, and Peripheral Corneal Ulcer.

Further Reading

Camper, S. A., Saunders, T. L., Kendall, S. K., et al. (1995). Implementing transgenic and embryonic stem cell technology to study gene expression, cell–cell interactions and gene function. *Biology of Reproduction* 52: 246–257.

Chikama, T., Hayashi, Y., Liu, C. Y., et al. (2005). Characterization of tetracycline-inducible bitransgenic Krt12rtTA/+/tet-O-LacZ Mice. *Investigative Ophthalmology and Visual Science* 46: 1966–1972.

Funderburgh, J. L., Corpuz, L. M., Roth, M. R., et al. (1997). Mimecan, the 25-kDa corneal keratan sulfate proteoglycan, is a product of the gene producing osteoglycin. *Journal of Biological Chemistry* 272: 28089–28095.

Hanks, M., Wurst, W., Anson-Cartwright, L., Auerbach, A. B., and Joyner, A. L. (1995). Rescue of the En-1 mutant phenotype by replacement of En-1 with En-2. *Science* 269: 679–682.

Hayashi, Y., Liu, C. Y., Jester, J. J., et al. (2005). Excess biglycan causes eyelid malformation by perturbing muscle development and TGF-alpha signaling. *Developmental Biology* 277: 222–234.

Kao, W. W. (2006). Ocular surface tissue morphogenesis in normal and disease states revealed by genetically modified mice. *Cornea* 25 (supplement 1): S7–S19.

Kao, W. W. and Liu, C.-Y. (2003). The use of transgenic and knock-out mice in the investigation of ocular surface cell biology. *The Ocular Surface* 1: 5–19.

Kao, W. W., Xia, Y., Liu, C. Y., and Saika, S. (2008). Signaling pathways in morphogenesis of cornea and eyelid. *The Ocular Surface* 6: 9–23.

Liu, C. Y., Shiraishi, A., Kao, C. W., et al. (1998). The cloning of mouse keratocan cDNA and genomic DNA and the characterization of its expression during eye development. *Journal of Biological Chemistry* 273: 22584–22588.

Muller, U. (1999). Ten years of gene targeting: Targeted mouse mutants, from vector design to phenotype analysis. *Mechanisms of Development* 82: 3–21.

Saika, S., Okada, Y., Miyamoto, T., et al. (2004). Role of p38 MAP kinase in regulation of cell migration and proliferation in healing corneal epithelium. *Investigative Ophthalmology and Visual Science* 45: 100–109.

Weng, D. Y., Zhang, Y., Hayashi, Y., et al. (2008). Promiscuous recombination of LoxP alleles during gametogenesis in cornea Cre driver mice. *Molecular Vision* 14: 562–571.

Xia, Y. and Kao, W. W. (2004). The signaling pathways in tissue morphogenesis: A lesson from mice with eye-open at birth phenotype. *Biochemical Pharmacology* 68: 997–1001.

Zhang, L., Wang, W., Hayashi, Y., et al. (2003). A role for MEK kinase 1 in TGF-beta/activin-induced epithelium movement and embryonic eyelid closure. *EMBO Journal* 22: 4443–4454.

L

Lacrimal Gland Hormone Regulation

A K Mircheff, D W Warren, and J E Schechter, University of Southern California, Los Angeles, CA, USA

Glossary

CD86 – A co-receptor expressed on the surfaces of antigen-presenting cells. When engaging either of its cognate receptors – CD28 and CTLA-4 – on the surface of T cells, it generates signals essential for T-cell activation and activates signaling cascades within the antigen-presenting cells.
Chemokines – The proteins that promote recruitment of lymphocytes and leukocytes to inflamed tissues and to lymphoid tissues.
Hypophysectomy – The surgical removal of the pituitary gland.
Interferon gamma (IFN-γ) – A cytokine released primarily by T cells and natural killer cells that induces T cells to express the T_H1 phenotype, activates macrophage to express microbicidal functions, and induces B cells to switch from immunoglobulin M (IgM) to complement-fixing IgG isotypes.
Interleukin 1 alpha and 1 beta (IL-1α, IL-1β) – The related cytokines released primarily from macrophages, endothelial cells, and epithelial cells that induce inflammatory responses.
Interleukin 6 (IL-6) – A cytokine that promotes inflammatory responses and supports survival of T and B cells.
Interleukin 12a (IL-12a) – A cytokine released in innate immune responses that induces expression of IFN-γ and, thereby, promotes the evolution of adaptive responses mediated by T_H1 cells.
Lactation – The production and secretion of milk.
Lactogenesis – The secretory differentiation of the mammary epithelium.
Orchiectomy – The surgical removal of the testes.
Sex hormone-binding globulin (SHBG) – A protein which binds estrogens and androgens. It is produced by the liver and secreted into the blood. Estrogens stimulate its production and androgens suppress its production.
Sodium-potassium-dependent ATPase (Na,K-ATPase) – The sodium–potassium pump enzyme; it generates the chemiosmotic energy essential for lacrimal fluid production by pumping Na^+ out of, and K^+ into, the cytosol.
Transforming growth factor-beta (TGF-β) – A cytokine released by T cells and macrophages, as well as by some epithelial cells and mesenchymal cells. Its actions on immune cells include: inhibiting T-cell proliferation and expression of effector functions; inhibiting B cells from proliferating and inducing them to undergo IgM-to-IgA isotype class-switch recombination; and suppressing macrophage activation. It often exerts antiproliferative or pro-apoptotic influences on epithelial cells.

Gender-Related Dimorphisms

The lacrimal glands produce most of the aqueous fluid that comprises the *milieu extérieur* sustaining the live, metabolically active cells of the superficial layers of the cornea and conjunctiva, and insufficient production of this fluid and alterations of its composition are associated with dry eye disease. Because dry eye disease is considerably more prevalent among women, it has seemed intriguing that morphological differences can be readily discerned between the acini – that is, the primary secretory structures of the lacrimal glands – of male and female rats. The structural dimorphisms were, some years ago, found to be accompanied by equally striking biochemical and functional dimorphisms. Classic work by Sullivan and colleagues showed that many of the evident dimorphisms are supported by the higher levels of androgens characteristic of males. However, it is taking much longer to learn how, in mechanistic terms, the gender-related dimorphisms might relate to females' greater predilection

for lacrimal dysfunction. Indeed, one of the first functional dimorphisms to be documented appeared paradoxical: basal precorneal tear volume is smaller in intact male rats than in females, and it increases in males after they are castrated – a surgical maneuver that causes the size of the acini to decrease, that is, to become more female like.

One of the products that the lacrimal glands contribute to the ocular surface fluid is secretory immunoglobulin A (sIgA), which is the effector of the adaptive mucosal immune defense against microbial infection. The lacrimal glands of rats exhibit several readily quantified dimorphisms relating to the production and secretion of dimeric IgA (dIgA). The stromal spaces of the lacrimal glands of male rats are populated by larger numbers of dimeric IgA-secreting plasmacytes. Whole gland extracts contain greater masses of dIgA. Glandular epithelial cells express higher levels of the polymeric Ig receptor (pIgR), which mediates uptake of dimeric dIgA at the stromal-facing surface of the lacrimal epithelium, chaperones it through the cells' transcytotic apparatus, and provides the secretory component (SC) portion of secretory IgA (sIgA). Lacrimal gland fluid from sexually mature male rats contains both more sIgA and SC.

Sex Steroids

Androgens

As noted above, it was established early on that the androgens support the gender-related dimorphisms of acinar size and of precorneal tear volume, which is presumably related to basal rates of lacrimal fluid production. It was also found that the androgens also support epithelial cell expression of pIgR and secretion of SC. However, androgen effects on the numbers of IgA^+-plasmacytes populating the glands' stromal spaces varied considerably among individual animals.

Although different laboratories have reported discrepant findings, there is some evidence for the theoretical paradigm that the androgens exert general trophic influences on the glandular epithelium. Hypophysectomizing rats decreases circulating levels of gonadal and adrenal steroids, as well as pituitary hormones (see **Box 1**). This maneuver reduces the lacrimal glands' gross weight and their weight as a fraction of total body weight. In some studies, administration of dihydrotestosterone (DHT) did not change lacrimal gland weight appreciably. In other studies, administration of DHT partially reversed hypophysectomy-induced decreases in the total amounts of protein and Na,K-ATPase catalytic activity measured in lacrimal gland lysates. Ovariectomizing female rabbits decreases serum sex steroid levels. This maneuver decreased the total protein and DNA contents of lacrimal gland lysates. Administration of DHT prevented the ovariectomy-induced decreases, and it increased the Na,K-ATPase catalytic activity measured in lacrimal gland lysates. Surprisingly, in view of the role Na,K-ATPase plays in lacrimal fluid production, DHT did not increase the basal rate of lacrimal fluid production. However, it significantly increased the volume of fluid intact glands produced when they were stimulated with cholinergic agonists. These findings make it clear that several independent layers of regulation determine lacrimal fluid production: long-term regulation of the mass of cells comprising the glandular epithelium and of the levels at which the epithelial cells transcribe the genes specifying Na,K-ATPase and other ion-transport proteins, and acute regulation – presumably neurally mediated – of the transport proteins' functional states. A more complex paradigm, however, is needed to account for why the magnitude of the lacrimal gland regression caused by ovariectomy is small compared to the extent of atrophy that nuclear magnetic resonance (NMR) imaging studies have documented in the lacrimal glands of aging females. One possible paradigm is that in mature, but not aged, female rabbits the lacrimal glands compensate for ovariectomy-induced loss of testosterone by converting the weak androgen, dihydroepiandrosterone (DHEA) – which is produced by the adrenal cortex (see **Box 1**) – to testosterone and DHT. A second is that the loss of a small trophic influence must be compounded over time before its consequences become evident. A third is that androgens influence other parameters in addition to the cellular mass of the epithelium, and that it is the consequences of loss of those influences that are compounded over time.

In *ex vivo* studies, DHT increased proliferation in models of acinar cells from rabbit lacrimal glands. Compared to the action of epidermal growth factor (EGF), however, the influence of DHT was relatively modest. When Azzarolo and colleagues tested the hypothesis that androgens support the number of cells in the epithelium by preventing apoptosis, as well as by promoting cell proliferation, they found that epithelial cell apoptosis is relatively rare, but plasmacytes in the glands' stromal space began apoptosing within an hour following ovariectomy. Moreover, administration of DHT prevented ovariectomy-induced plasmacyte apoptosis.

The finding that androgen withdrawal leads to a wave of apoptosis in the lacrimal gland plasmacyte population is one of several that accord with the paradigm that their higher levels of androgens protect men both from Sjögren's autoimmune dacryoadenitis and from the histopathophysiological syndrome commonly found in aging women by influencing immunophysiological processes within the gland. Indeed, it has been found that administration of DHT suppresses lacrimal gland disease in certain mouse models for Sjögren's syndrome, and preliminary clinical experiences suggest that androgen supplementation of hormone replacement therapy may improve symptoms and clinical signs in menopausal women with inflammatory autoimmune lacrimal diseases. In the models in which androgen administration is therapeutic, the responses are

Box 1. Regulation of reproductive hormone bioavailability

Figure 1 summarizes factors and feedback interactions that determine the bioavailabilities and local actions of the steroid reproductive hormones.

Hypothalamic neurons release gonadotropin-releasing hormone (GNRH), which stimulates release of LH and FSH by the anterior pituitary. LH and FSH, in turn, stimulate synthesis of estradiol and progesterone in the ovaries, and synthesis of testosterone in the testes. Notably, testosterone is an obligatory precursor in the syntheses of estradiol and progesterone, and total serum testosterone levels increase as estradiol and progesterone levels increase. Progesterone can be converted to testosterone, but estradiol cannot.

The anterior pituitary also produces adrenal corticotropic hormone (ACTH), which is induced by corticotrophin releasing hormone from hypothalamic neurons. ACTH, in turn, increases adrenal synthesis of the glucocorticoids and dihydroepiandrosterone (DHEA). DHEA can be converted to testosterone in peripheral tissues. Androgen target tissues frequently convert testosterone to dihydrotestosterone, a higher affinity ligand for androgen receptors.

The liver plays an indirect but critical role in determining testosterone bioavailability, producing sex hormone binding globulin (SHBG) in response to increasing levels of estradiol and testosterone in the serum. In some cases SHBG sequesters the hormones, reducing their bioavailability. In other cases SHBG-sex steroid hormone complexes exert biological activities by interacting with nonclassical receptors at the surfaces of target cells, rather than with the classical receptors that traffic from the cytosol to the nucleus.

After menopause, the ovarian stroma continues to produce some testosterone and androstenedione. During hormone replacement therapy, however, the exogenous estrogens suppress GnRH release, thus reducing ovarian testosterone production. Exogenous estrogens further decrease testosterone bioavailability by stimulating increased hepatic production of SHGB.

Production of testosterone declines gradually as men age. Production of DHEA declines similarly in women and men. In women, reproductive steroid hormone and prolactin levels vary systematically during the menstrual cycle. They fluctuate, with more individual variation, during the perimenopause. They then remain consistently low postmenopausally, while prolactin levels are decreased only modestly. Estradiol, progesterone, and prolactin levels increase markedly over the course of a pregnancy. The steroid levels decrease abruptly at parturition; prolactin declines more gradually during a nonlactating puerperium, and it remains elevated during lactation.

In contrast to positive regulation of LH, FSH, and ACTH by hypothalamic factors, the release of prolactin by the anterior pituitary is negatively regulated, that is, suppressed, by dopamine produced by hypothalamic neurons. Estradiol increases production of prolactin in the anterior pituitary, while prolactin suppresses estradiol production by acting upstream to suppress release of GNRH. As noted in the text, a number of peripheral tissues in addition to the pituitary produce prolactin.

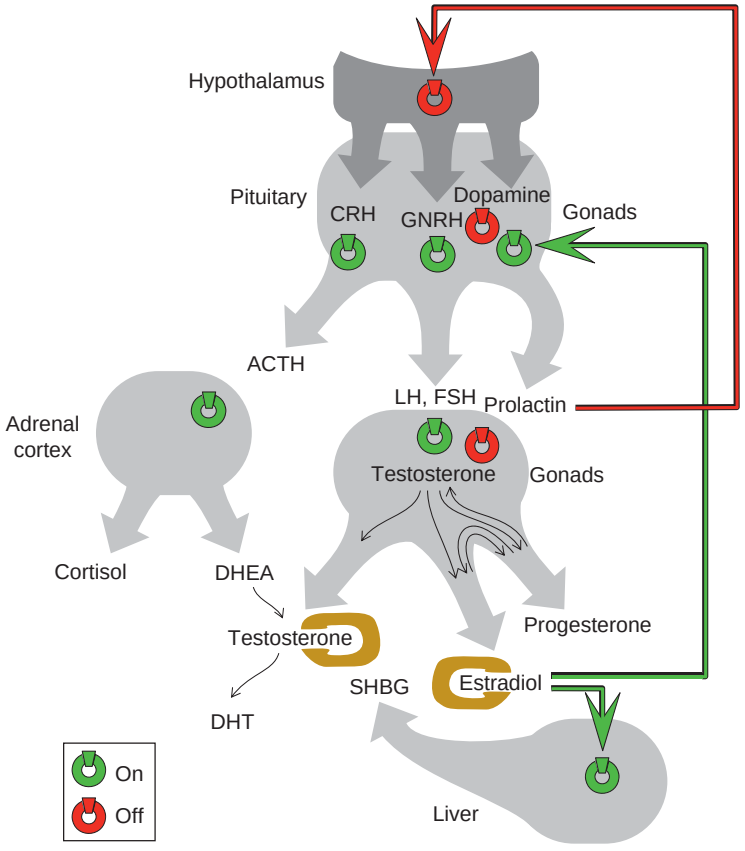

Figure 1 Production, regulation, and interactions of reproductive hormones. The pituitary produces the protein hormones, LH (luteinizing hormone), FSH (follicle stimulating hormone), ACTH (adrenalcorticotropic hormone), and prolactin. LH and FSH stimulate gonadal production of estradiol, progesterone, and testosterone. ACTH stimulates production of cortisol, as well as dihydroepiandrosterone (DHEA). Estradiol stimulates hepatic production of sex hormone binding globulins, which may either sequester steroids, particularly testosterone, reducing their bioavailability, or potentiate their actions by allowing them to bind to unconventional receptors at the surfaces of target cells. Estradiol also increases pituitary production of prolactin. Both prolactin and estrogen mediate negative feedback signals that decrease LH and FSH production.

more pronounced in the lacrimal glands than in other affected organs. This finding led Sullivan and coworkers to propose that the androgens control the expression of critical immunoregulatory paracrine mediators by lacrimal gland epithelial cells. Recent microarray analyses indicate that androgens influence the expression of large numbers of gene transcripts in the lacrimal glands and corneas of mice. Some of the androgen actions might be expected to diminish inflammatory processes. For example, testosterone decreases expression of certain chemokines; interferon (IFN) response factors 4 and 7; caspase-1, which converts the inactive interleukin (IL)-1β precursor to active IL-1β; and the prolactin receptor, which – as discussed below – mediates mitogenic responses both in B and T cells and induces T cells to express IFN-γ. However, other testosterone actions might be expected to enhance inflammatory processes. For example, testosterone increases expression of IL-6; IL-12a; the chemokines CCL1, CCL8, CCL28, CCL5, and CXCL4; CD86; and interferon response factor 5.

Before considering tentative theoretical paradigms that might explain how the androgens might confer protection against dry eye disease, it is necessary to first review the influences other reproductive hormones exert on the lacrimal glands.

Estradiol and Progesterone

Whereas estradiol and testosterone often have opposing actions, Azzarolo and coworkers found that estradiol – like DHT – prevents ovariectomy-induced apoptosis of lacrimal gland plasmacytes. Estradiol does not appear to influence pIgR expression in rat lacrimal epithelial cells. However, tear lactoperoxidase levels vary during the estrus cycle in rats and the menstrual cycle in humans – correlating with the changes in estradiol and progesterone levels. Microarray analyses of mouse lacrimal gland extracts indicate that estradiol and progesterone influence the expression of numerous gene transcripts. They increase expression of the chemokines CCL2 and CXCL15 and decrease expression of FoxP3 – a central transcription factor in regulatory lymphocyte function; these influences might seem consistent with the greater risk for inflammatory lacrimal gland disease in females. However, estradiol and progesterone also decrease expression of CD86, IL-12, and the chemokines CCL6, CCL12, and CCL28 – influences which might be expected to diminish inflammatory responses.

Prolactin

Prolactin is produced by the pituitary gland; as its name implies, its first discovered function was support of lactogenesis and lactation. However, prolactin has also been found to function as an autocrine/intracrine and paracrine mediator in a number of physiological systems. In the immune system, it acts as a mitogenic cytokine for T cells and B cells, and as a differentiation factor for T cells – inducing them to express the prototypical T_H1 cytokine, IFN-γ. Administration of prolactin to hypophysectomized male rats increased Na, K-ATPase catalytic activity in lacrimal gland. However, a number of reports indicate that serum prolactin levels are elevated in women with Sjögren's syndrome and other autoimmune diseases. A study of reproductive hormone influences on lacrimal function revealed that increasing serum prolactin levels within the normal range of values for nonpregnant, nonlactating women were strongly correlated with decreasing lacrimal function – independently of menopausal status and use of estrogen replacement therapy.

Exocrine Products and Autocrine/Intracrine and Paracrine Mediators

While they respond to prolactin as a classic hormone, lacrimal gland epithelial cells also express prolactin, and they secrete it both as an exocrine secretory product and as a paracrine mediator. In the lacrimal glands of normal, nonpregnant female rabbits, immunopositivities for prolactin, as well as for transforming growth factor-beta (TGF-β), EGF, fibroblast growth factor (FGF)-2, are localized preferentially – but not exclusively – in ductal epithelial cells. In both acinar and ductal cells, the cytokine and growth factor immunopositivities are concentrated in the apical cytoplasm. Prolactin is localized in the regulated exocrine secretory vesicles; the mechanisms by which epithelial cells of the rabbit lacrimal gland secrete the other cytokines and growth factors have not been elucidated. Like prolactin and other secretory vesicle-content proteins, TGF-β is released to the fluid forming within the lumen of the acinus-duct system in response to stimulation with cholinergic agonists.

As illustrated in **Figure 1**, lacrimal epithelial cells use their apical recycling endosome and early basolateral endosome as a transcytotic secretory apparatus. It is this apparatus which secretes sIgA and some free SC into the lumena of the acinus-duct system. They also use the early and recycling endosomes as a paracrine secretory apparatus that delivers products to the underlying stromal space. Both transcytotic secretion and paracrine secretion occur constitutively; although they can be accelerated by stimulation with cholinergic agonists, the steady-state pools of secreted products in the endosomes are quite small compared to the pools of products stored in regulated exocrine secretory vesicles. Experiments with *ex vivo* acinar cell models showed that increasing the concentration of prolactin in the ambient medium induces increased transcription of prolactin messenger RNA (mRNA). Increasing epithelial cell prolactin expression or increasing the prolactin concentration in the ambient medium decreased the amount of secretory proteins stored in apical secretory vesicles, and it

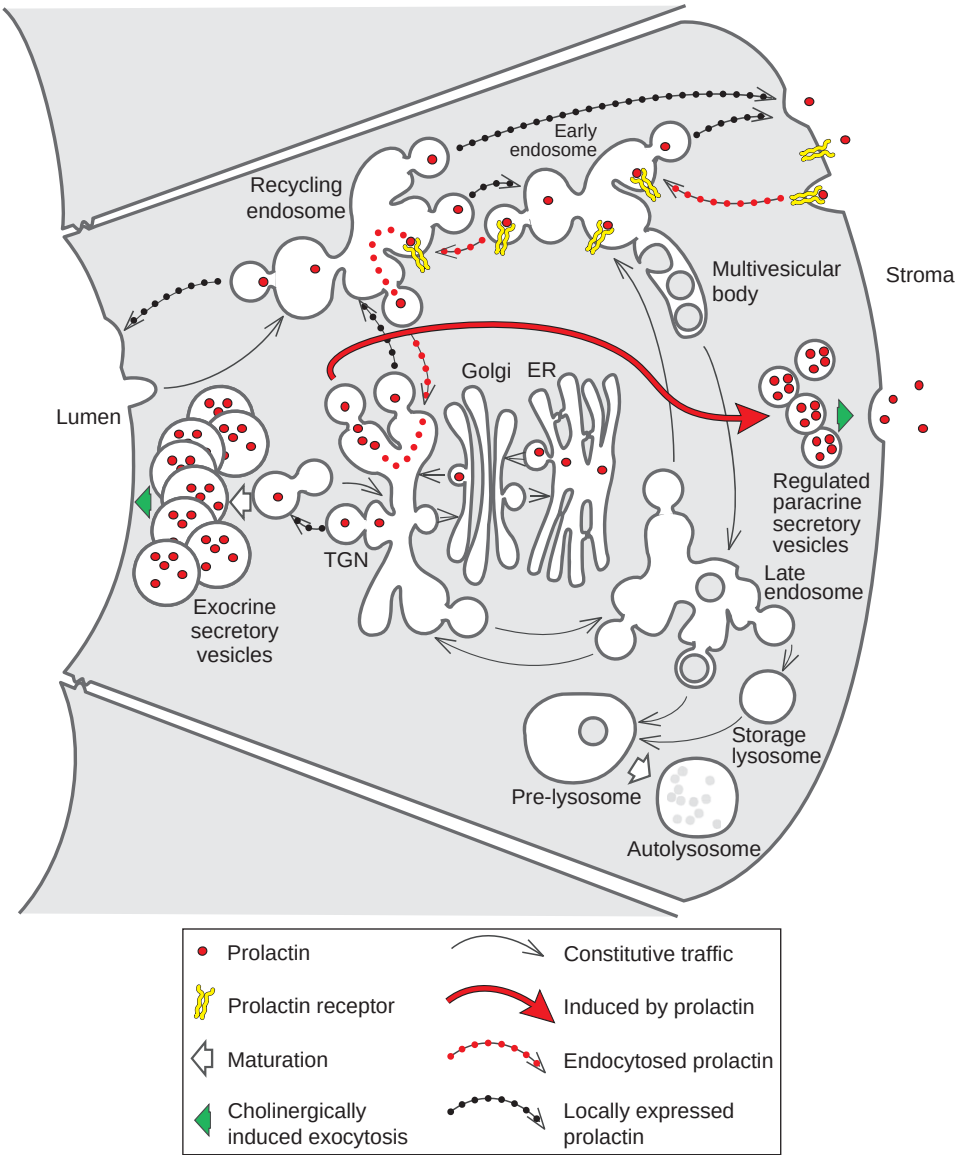

Figure 1 As in other exocrine glands, lacrimal gland epithelial cells use secretory vesicles to secrete proteins into the fluid being produced in the lumena of the acinus-duct system. They also use their early basolateral endosomes and apical recycling endosomes as a transcytotic apparatus to secrete SC and sIgA. Furthermore, the constitutive traffic of transport vesicles from the endosomes to the basolateral plasma membranes secreted paracrine mediators to underlying stromal space. Elevated levels of prolactin induce the cells to express a novel population of regulated paracrine secretory vesicles and decrease their population of exocrine secretory vesicles. The induced paracrine secretory vesicles allow ductal epithelial cells to secrete more prolactin and TGF-β to the stroma, and they allow acinar cells that have endocytosed prolactin from the stroma to recycle it as a paracrine secretory product.

induced the cells to express a novel population of regulated secretory vesicles that accumulated in the basal cytoplasm and released their contents at the basolateral plasma membrane in response to acute cholinergic stimulation.

Immunogold localization studies demonstrated that when acinar cells endocytose prolactin from their ambient medium, they traffic it dually to the endosomes that comprise their constitutive transcytotic-paracrine apparatus and to the secretory vesicles of the novel, induced paracrine apparatus. Thus, when acinar epithelial cells internalize prolactin secreted from the pituitary or from ductal epithelial cells, they may recycle it as a paracrine mediator.

Serum prolactin levels do not differ greatly between normal men and normal, nonpregnant women. However, serum prolactin levels increase markedly during pregnancy, and, by the time a pregnancy reaches term, mean serum prolactin levels are 10- to 20-fold greater than the levels in nonpregnant, nonlactating females. Thus, the physiological hyperprolactinemia of pregnancy has seemed to offer a natural model in which to study prolactin's influences on the lacrimal glands.

Influences of Prolactin, Estradiol, and Progesterone during Pregnancy

The lacrimal glands of nonpregnant, sexually mature female rabbits normally contain small aggregates of lymphocytes and plasmacytes, localized in the stromal spaces surrounding and spanning between venules and interlobular ducts. It might be noted that these are the same sites where the ectopic lymphoid tissues characteristic of Sjögren's dacryoadenitis develop. The immunoarchitecture undergoes a remarkable change during pregnancy, and it remains in the altered state throughout lactation and for some weeks following weaning. By the time a pregnancy reaches term, the aggregates have largely dissipated, and lymphocytes and plasmacytes are primarily located in the thin stromal spaces surrounding acini.

The immunoarchitectural change is associated with several notable cytophysiological changes and functional changes. The basal rate of lacrimal gland fluid production decreases, while the rate of fluid production under cholinergic stimulation increases. Immunopositivities for TGF-β and prolactin increase substantially, and their localizations shift from the apical cytoplasm to the basal cytoplasm. It now appears that these redistributions occur because the novel paracrine secretory apparatus induced by the increased serum prolactin level captures prolactin and TGF-β away from the regulated exocrine secretory pathway. Accordingly, the level of prolactin excreted in lacrimal gland fluid decreases, and TGF-β becomes scarcely detectable.

Experiments that have not yet been published indicate that when ovariectomized rabbits are implanted with sustained-release pellets establishing pregnancy-like serum levels of estradiol and progesterone, the patterns of lymphocyte organization and of TGF-β and prolactin expression and localization change to resemble the patterns characteristic of pregnancy. Thus, estradiol, progesterone, or the two steroid hormones in concert act on ductal epithelial cells to increase their expression TGF-β. They may increase ductal epithelial cell prolactin expression either directly, or indirectly, that is, by increasing pituitary prolactin secretion (see **Box 1**). The increased level of prolactin then directs both mediators away from the regulated exocrine protein-secretion apparatus and directs prolactin into the novel paracrine apparatus.

As discussed below, the changes that occur in the lacrimal glands during pregnancy are analogous to those which occur over roughly the same time in the mammary glands. While the lacrimal glands are accessory organ of the visual system, the mammary glands are accessory organs of the reproductive system. Both glands also are effector organs of the mucosal immune system. Other organs of the male and female reproductive systems also play parallel roles as adaptive mucosal immune system effector organs, and their immunophysiological functions are, likewise, influenced by the reproductive hormones.

Reproductive Hormone Influences on Other Mucosal Immune System Tissues

Neither the testes nor the ovaries are normally populated by IgA^+-plasmacytes. However, in males, IgA^+ cells are abundant in the urethral glands and prostate; they are also present in the seminal vesicles in some species, but not others. Orchiectomizing male rats has little effect on the amount of IgA in the prostate and seminal vesicles; subsequent administration of DHT causes a slight increase of the IgA content of the prostate, but not the seminal vesicle. There is little pIgR expression in the testes, vas deferens, or epididymis, but a significant level of expression in the seminal vesicles and a 20-fold greater level in the prostate. Orchiectomy decreases pIgR expression, and subsequent administration of DHT increases it threefold in the seminal vesicles and fourfold in the prostate. Interestingly, estradiol has no effect on pIgR expression in the seminal vesicles but doubles it in the prostate.

In females, IgA^+ immune cells are abundant in the lamina propria of the fallopian tubes. They are sparse in the endometrium. Since endometrial gland epithelial cells contain IgM^+ and IgA^+, as well as J chain, it may be that the uterine lining secretes Igs derived primarily from the serum, rather than from local plasmacytes. In contrast, IgA^+ cells are abundant within the epithelia and lamina propria of the endocervix, although somewhat less abundant in the ectocervix and vagina. Epithelial expression of pIgR roughly parallels the abundance of IgA^+ cells. The level is significant in the fallopian tubes and endocervix. While there seems to be no clear evidence that pIgR is expressed in the ectocervix and vagina, the level of sIgA in cervical mucus increases just prior to ovulation and remains elevated throughout the luteal phase, and the uterine fluid contains a high level of sIgA throughout pregnancy.

As the alveolar epithelium of the mammary glands develops during pregnancy, ductal epithelial cells are induced to express pIgR, and the glands' stromal spaces become populated by $dIgA^+$-plasmacytes. During lactation, the mammary epithelium secretes sIgA as well as lactoperoxidase and other innate mucosal immune effector molecules. Like the other changes occurring during lactogenesis, the induction of mucosal immune effector functions is controlled by interacting influences of estradiol, progesterone, and prolactin. Most studies of hormonal influences on the mammary glands have been motivated by interest in normal lactogenesis, lactation, and postweaning involution, and in mammary carcinoma – rather than focused on the mammary glands' mucosal immune functions. This work has shown that the systemic hormones orchestrate lactogenesis and lactation, in part, by regulating the expression of autocrine/intracrine and paracrine mediators. The ductal network of the mammary gland develops

during puberty, largely under the influence of estradiol. Prior to pregnancy, TGF-β – which is expressed both by ductal epithelial cells and periductal mesenchymal cells – exerts pro-apoptotic and antiproliferative influences that prevent development of the alveoli – and, during pregnancy, alveolar development depends on the concerted influences of prolactin and progesterone. Increasing progesterone levels increase the abundance of TGF-β, but they also increase expression of EGF, FGF-2, and TGF-alpha (TGF-α) – which abrogate TGF-β's anti proliferative and pro-apoptotic influences. Notably, the expression of prolactin by mammary epithelial cells also increases at this time. Despite its evident synergy with prolactin in promoting lactogenesis, the elevated level of progesterone inhibits lactation. Recent evidence suggests it does so by increasing expression of Wnt-5b, which is thought to maintain the undifferentiated state by promoting nuclear translocation of β-catenin, and by increasing expression of insulin-like growth factor-binding protein (IGFBP-5) – which suppresses insulin-like growth factor signaling. These inhibitory influences are removed and lactation becomes possible at parturition, when production of progesterone is abruptly suppressed.

Certain of the estradiol-, progesterone-, and prolactin-induced mediators that determine development of the mammary epithelium also determine expression of the mammary glands' mucosal immune functions. As reviewed elsewhere in the encyclopedia, TGF-β typically acts as a differentiation factor for immature $dIgA^+$-expressing plasmablasts, inducing them to mature into dIgA-secreting plasmacytes as they arrive at mucosal immune effector sites. Normal plasmacytes – like other bone-marrow-derived cells – express an intrinsic apoptotic program, and their ongoing survival requires that this program be abrogated by survival signals from the local milieu. As noted above, prolactin plays a role in inducing ductal epithelial cells to express pIgR. Its known mitogenic influences on T cells and B cells suggest that it may also act as one of the factors which support the mature plasmacytes' survival. Thus, prolactin may contribute to a counterpoise against plasmacyte's apoptotic program as well as against the pro-apoptotic and antiproliferative influences TGF-β would otherwise exert on both the plasmacytes and the alveolar epithelium. Evidently, this counterpoise is maintained as the levels of TGF-β, prolactin, and other estrogen- and progesterone-dependent factors increase during pregnancy, and it supports expansion of the population of plasmacytes that will produce dIgA for secretion in the milk.

Similar interactions between the sex steroids and prolactin may account for the reproductive hormones' influences on the other mucosal effector organs of the female and male reproductive systems, and the data available so far indicate that they do so for the lacrimal glands, as well.

Counterpoises between Contradictory Signals

Figure 2 summarizes the spatial and temporal actions of the differentiation and survival factors, as they are organized in the lacrimal glands. The notions that plasmacytes express an intrinsic apoptotic program which must constantly be abrogated and that the steady-state pools of paracrine secretory products in lacrimal epithelial cells are small may help explain why they begin undergoing apoptosis so abruptly after ovariectomy. The pools of paracrine secretory products would deplete rapidly after the signals that support their ongoing expression are removed. Unpublished findings that prolactin immunoreactivity is present in the nuclei of plasmacytes seem to confirm that prolactin is one of the lacrimal epithelial paracrine mediators the influence plasmacytes. This may only be part of the explanation; however, and it is possible that testosterone, estradiol, and, perhaps, progesterone as well also might interact with prolactin and other survival factors to generate synergistic signals that maintain plasmacyte survival.

While prolactin may be one of several factors that provide mitogenic signals abrogating TGF-β's pro-apoptotic and antiproliferative influences, it appears that TGF-β may provide a counterpoise to prolactin's lymphoproliferative and proinflammatory influences. As reviewed elsewhere in the encyclopedia, there is evidence that the transcytotic apparatus mucosal epithelial cells use to internalize dIgA and release sIgA into the fluid they produce inevitably secretes a significant burden of autoantigens to the underlying stromal spaces. Thus, newly matured dendritic cells that emigrate from the lacrimal glands to the draining lymph nodes carry with them lacrimal epithelial autoantigens. They process the autoantigens to generate epitopes that their surface MHC class-II molecules will present to $CD4^+$ T cells, and they also release the autoantigens for sampling by IgM^+-B-cell antigen receptors. There is now evidence that TGF-β induces immature dendritic cells to mature into immunosuppressive antigen-presenting cells that prevent proliferation of autoreactive lymphocytes within the lacrimal glands and draining lymph node. Moreover, it is possible that dendritic cells that have matured within the lacrimal glands might also function as tolerogenic antigen-presenting cells – inducing the generation of T_H3 or T_R1 regulatory cells.

Microarray studies have clarified that the reproductive hormones influence the expression of other cytokines and growth factors apart from TGF-β and prolactin in the lacrimal glands. Further work will be needed to determine the extents to which the various mediators are expressed by infiltrating immune cells, acinar and ductal epithelial cells, and mesenchymal cells. Other factors in addition to the reproductive hormones are likely to influence epithelial expression of TGF-β and of prolactin and the plasmacyte

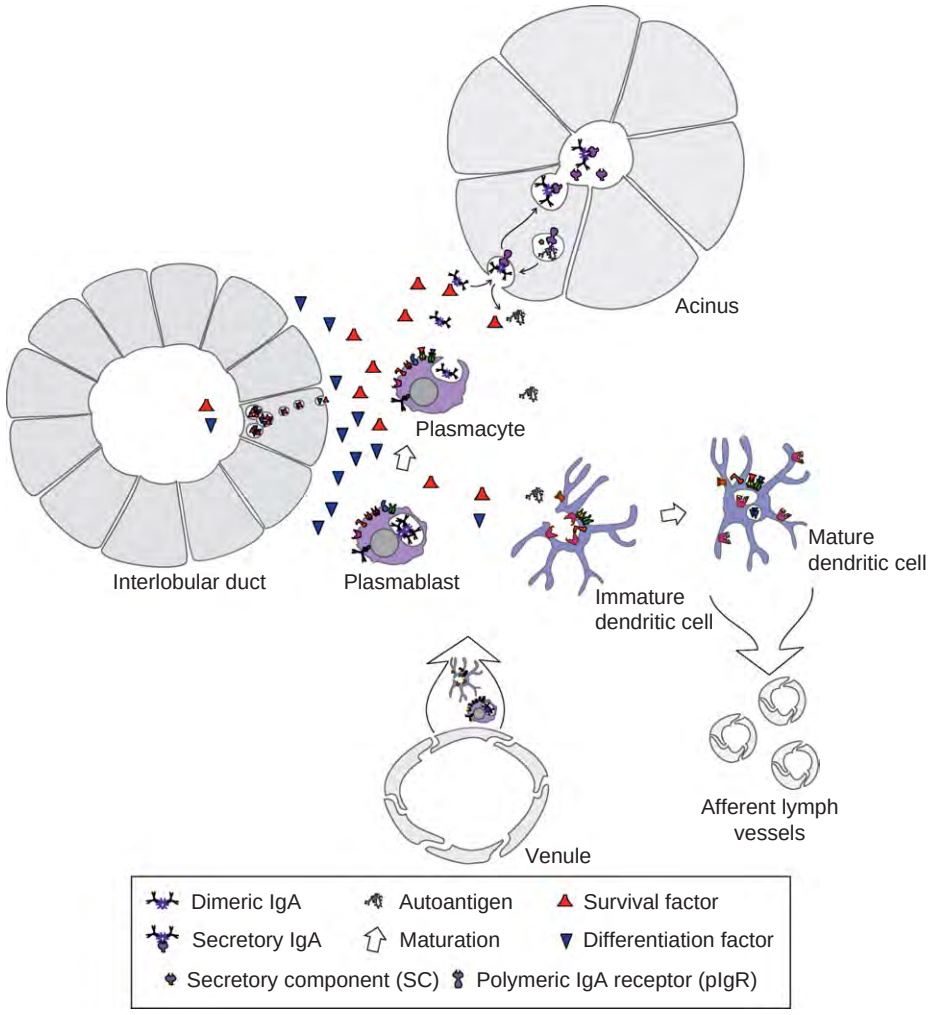

Figure 2 Interlobular duct epithelial cells produce both differentiation factors, such as TGF-β and IL-10, which may also exert pro-apoptotic and immunoregulatory influences. They also produce survival factors, such as EGF, FGF, and prolactin, some of which also may exert mitogenic and proinflammatory influences. The counterpoises of contradictory influences maintain for the lacrimal glands' exocrine functions as well as their mucosal immune functions. For example, TGF-β may support expression of the ductal epithelial phenotype, while FGF, EGF, and prolactin may support both survival of the ductal epithelium and development and survival of the acini. TGF-β induces plasmablasts to undergo terminal differentiation to dIgA-secreting plasmacytes, while prolactin may be one of several mediators that support the plasmacytes' ongoing survival. TGF-β also induces immature dendritic cells that have taken up lacrimal autoantigens to differentiate as regulatory antigen presenting cells.

survival factors. Nevertheless, the concept that the reproductive hormones orchestrate counterpoises between contradictory signals, summarized in **Figure 3**, may lead to detailed paradigms that explain why Sjögren's dacryoadenitis and the common histopathological syndrome are both so much more prevalent among women, and why the onset of clinical dry eye disease is associated with events of the reproductive cycle and life cycle. There are several physiological states during which prolactin-mediated influences might become excessive with respect to the available counterpoises (see **Box 1**). Given the burden of epithelial autoantigens constitutively present in the stromal space of the lacrimal glands, one might predict that such states favor the accumulation of autoreactive T cells and B cells. In a direct experimental test of the hypothesis, an adenovirus vector was used to transiently increase prolactin expression in lacrimal glands of mature female rabbits. As has been reported in preliminary form, increased abundance of prolactin transcripts was accompanied by increased abundances of mRNAs for IFN-γ and TGF-α, as well as accumulation of large lymphocytic infiltrates and apparent formation of germinal centers. Moreover, the lymphocytic foci persisted for weeks after the prolactin mRNA levels returned to normal. Of interest also is a recent report that, after having a primary relative with an autoimmune disease, carrying a pregnancy to term is the second greatest risk factor for Sjögren's syndrome appears to accord with this prediction. Both findings suggest that autoimmune activation can be suppressed after systemic hormone levels have returned to normal, but that autoreactive memory cells

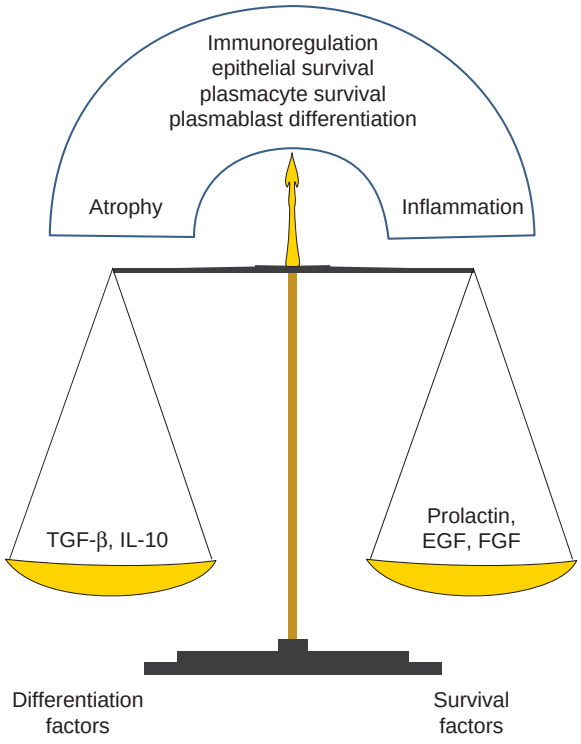

Figure 3 The capacity of the lacrimal gland to perform its exocrine functions – that is, secretion of electrolytes, water, and proteins – and its mucosal immune functions – that is, maintenance of a population of mature, dIgA-secreting plasmablasts and transcytotic delivery of sIgA into the fluid being produced, while avoiding autoimmune inflammatory processes – depends on a system of counterpoises between contradictory influences. The reproductive hormones influence expression of many of the paracrine mediators that exert those influences.

may persist and become activated as the age-related loss of reproductive steroids changes the immunoregulatory signaling milieu within the lacrimal glands.

See also: Adaptive Immune System and the Eye: Mucosal Immunity.

Further Reading

Ariga, H., Edwards, J., and Sullivan, D. A. (1989). Androgen control of autoimmune expression in lacrimal glands of MRL/Mp-lpr/lpr mice. *Clinical Immunology and Immunopathology* 53: 499–508.

Azzarolo, A. M., Eihausen, H., and Schechter, J. (2003). Estrogen prevention of lacrimal gland cell death and lymphocytic infiltration. *Experimental Eye Research* 77: 347–354.

Azzarolo, A. M., Mircheff, A. K., Kaswan, R. L., et al. (1997). Androgen support of lacrimal gland function. *Endocrine* 6: 39–45.

Azzarolo, A. M., Wood, R. L., Mircheff, A. K., et al. (1999). Androgen influence on lacrimal gland apoptosis, necrosis and lymphocytic infiltration. *Investigative Ophthalmology and Visual Science* 40: 523–526.

Bailey, J. P., Nieport, K. M., Herbst, M. P., et al. (2004). Prolactin and transforming growth factor-β signaling exert opposing effects on mammary gland morphogenesis, involution, and the Aky-forkhead pathway. *Molecular Endocrinology* 19: 1171–1184.

Ding, C., Chang, N., Fong, Y. C., et al. (2006). Interacting influences of pregnancy and corneal injury on rabbit lacrimal gland immunoarchitecture and function. *Investigative Ophthalmology and Visual Science* 47: 1368–1375.

Frey, W. H., Nelson, J. D., Frick, M. L., and Elde, R. P. (1986). Prolactin immunoreactivity in human tears and lacrimal gland: Possible implications for tear production. In: Holly, F. J. (ed.) *The Preocular Tear Film in Health, Disease, and Contact Lens Wear*, pp. 798–807. Lubbock, TX: Dry Eye Institute.

Kolek, O., Gajowska, B., Godlewski, M. M., and Motyl, T. (2003). Antiproliferative and apoptotic effect of TGF-β1 in bovine mammary epithelial BME-UV1 cells. *Comparative Biochemistry and Physiology C* 134: 417–430.

Mathers, W. D., Stovall, D., Lane, J. A., Zimmerman, M. B., and Johnson, S. (1998). Menopause and tear function: The influence of prolactin and sex hormones on human tear production. *Cornea* 17: 353–358.

Mircheff, A. K., Wang, Y., de Saint Jean, M., et al. (2005). Mucosal immunity and self-tolerance in the ocular surface system. *Ocular Surface* 4: 182–193.

Priori, R., Medda, E., Conti, F., et al. (2007). Risk factors for Sjögren's syndrome. *Clinical and Experimental Rheumatology* 25: 378–384.

Richards, S. M., Liu, M., Jensen, R. V., et al. (2005). Androgen regulation of gene expression in the mouse lacrimal gland. *Journal of Steroid Biochemistry and Molecular Biology* 96: 401–413.

Rosfjord, E. C. and Dickson, R. B. (1999). Growth factors, apoptosis, and survival of mammary epithelial cells. *Journal of Mammary Gland Biology and Neoplasia* 4: 229–237.

Rudolph, M. C., McManaman, J. L., Hunter, L., Phang, T., and Neville, M. C. (2003). Functional development of the mammary gland: Use of expression profiling and trajectory clustering to reveal changes in gene expression during pregnancy, lactation, and involution. *Journal of Mammary Gland Biology and Neoplasia* 8: 287–307.

Schechter, J., Carey, J., Wallace, M., and Wood, R. (2000). Distributions of growth factors and immune cells are altered in the lacrimal gland during pregnancy and lactation. *Experimental Eye Research* 71: 129–142.

Sullivan, D. A., Kelleher, R. S., Vaerman, J. -P., and Hann, L. E. (1990). Androgen regulation of secretory component synthesis by lacrimal gland acinar cells *in vitro*. *Journal of Immunology* 145: 4238–4244.

Suzuki, T., Schirra, F., Richards, S. M., et al. (2006). Estrogen's and progesterone's impact on gene expression in the mouse lacrimal gland. *Investigative Ophthalmology and Visual Science* 47: 158–168.

Wang, Y., Chiu, C. T., Nakamura, T., et al. (2007). Traffic of endogenous, over-expressed, and endocytosed prolactin in rabbit lacrimal acinar cells. *Experimental Eye Research* 85: 749–761.

Lacrimal Gland Overview

M C Edman, R R Marchelletta, and S F Hamm-Alvarez, University of Southern California School of Pharmacy, Los Angeles, CA, USA

Glossary

Acinus – Originating from the Latin word grape, it refers to the sac-like ending of a secretory exocrine gland.
Endocytosis – The process of internalization of plasma membrane as well as membrane-bound constituents and extracellular fluid by invagination of the plasma membrane, budding of the membrane vesicle, and its movement to the interior. Different types of endocytosis are known, including clathrin-mediated and caveolar endocytosis.
Exocytosis – The process by which a cell releases the contents of secretory vesicles to the extracellular environment by fusion of secretory vesicles with a plasma membrane domain.
Motor proteins – Mechanochemical proteins that utilize the energy of ATP hydrolysis to generate motive force along a polar surface, typically an actin filament or a microtubule.
Rab proteins – Small GTP-binding proteins that utilize the GTP binding and hydrolysis cycle to trigger protein on and off states, and which serve as molecular zip codes to specify the accurate sorting and targeting of membranes.
SNARE proteins – Proteins associated with donor and acceptor membranes which associate to form a fusion pore, allowing the contents of opposing membrane vesicles to intermingle, or allowing the extrusion of membrane-encapsulated contents to the cell exterior.
Transcytosis – The process by which macromolecules are transported through a polarized cell.
***trans*-Golgi network** – A post-Golgi processing compartment responsible for the accurate segregation of contents into membrane vesicles destined for regulated exocytosis, constitutive exocytosis, or for targeting to intracellular membrane compartments.

Anatomy of the Main Lacrimal Gland

The human main lacrimal gland, located laterally above the eye, measures approximately $20 \times 12 \times 5$ mm and has an almond-like shape. The major part of the gland, designated as the orbital portion, or the intraorbital gland, is located in the shallow lacrimal fossa of the frontal bone, while the smaller palpebral, or extraorbital portion, which is separated from the orbital portion by the lateral horn of the levator palpebrae muscle, is located above the temporal segment of the superior conjunctival fornix. In contrast, the mouse and rat have two pairs of lacrimal glands including a small orbital gland which is located laterally beneath the upper lid and a larger extraorbital gland which is located ventral and anterior to the eye. The rabbit lacrimal gland is unusually large and is comprised of a larger portion (4 cm) located below the eye and a smaller portion (0.5 cm) located above the eye. The lacrimal gland is constituted largely (80%) of acinar epithelial cells organized within the tubuloacinar units that are arranged into multiple globuli surrounded by fibrovascular septa. The remaining 20% of the mass of the lacrimal gland is composed of ducts, nerves, myoepithelial cells, leukocytes, and connective tissue. A schematic diagram showing the positioning of the gland relative to the ocular surface and the organization of several of the cell types within the gland is shown in **Figure 1**.

Cell Types within the Lacrimal Gland

Acinar Cells

The acinar epithelial cells within the lacrimal gland are triangular-shaped cuboidal cells organized in single cell layers in clusters with a narrow microvillus-covered apical domain oriented toward a central lumen and a more extensive basolateral domain which faces the tissue interstitium. Tight junctions near the apices segregate these two domains and result in polarization of the cells, which also are cytoplasmically coupled through gap junctions, thus making the acinus a single functional unit. The apical side of the cell is enriched in numerous large (1–2 μm) secretory granules or vesicles, containing proteins released upon cell stimulation, while the Golgi apparatus and endoplasmatic reticulum compartments are located more toward the basolateral side adjacent to the basolateral nucleus. **Figure 2** shows the characteristic distribution of secretory vesicles and other organelles within an acinar cell from mouse lacrimal gland.

Ductal Cells

The lumena of several acini come together to form a duct; each duct merges with others into gradually larger ducts

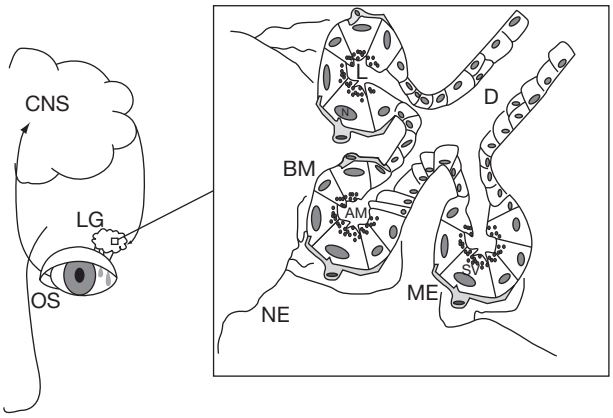

Figure 1 Schematic diagram showing the positioning of the human main lacrimal gland relative to the ocular surface and the organization of several of the cell types within the gland. AM, apical membrane; BM, basolateral membrane; CNS, central nervous system; D, duct; L, lumen; LG, lacrimal gland; ME, myoepithelial cell; N, nucleus; NE, nerve ending; OS, ocular surface; SV, secretory vesicle.

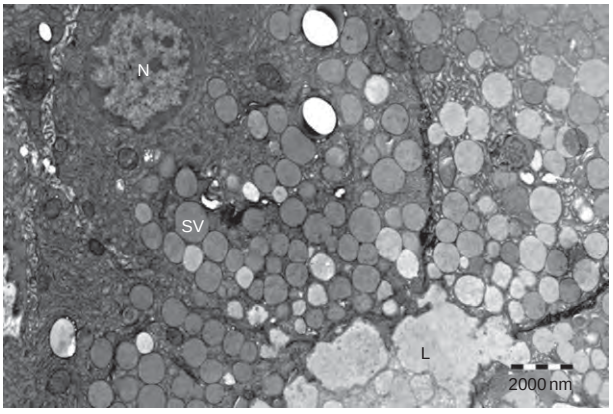

Figure 2 Transmission electron micrograph of mouse lacrimal gland. N, nucleus; L, lumen; SV, secretory vesicle.

that finally, in humans, drain into 6–12 major ducts with openings in the upper lateral fornix. In rat and mice, the ducts from the extraorbital gland join to a single major duct that then joins the duct from the intraorbital gland before it empties onto the conjunctiva in the lateral canthus of the eye. In rabbit, a single duct each forms from the upper and lower portions of the gland, which empty onto the conjunctiva of the upper and lower lids, respectively, near the temporal angle. The ducts are formed by one to two layers of cuboidal epithelial cells. Similar to the acinar cell, the ductal epithelial cells of small ducts are polarized by tight junctions in the apical area. However, in these cells, the Golgi and endoplasmic reticulum are located more apically, and secretory vesicle content is lower. Interlobular ducts are embedded with and supported by perivasculoductal connective tissue containing associated structures such as nerve fibers, capillaries, and mast cells and a dense population of fibroblast-associated collagen fibrils.

Myoepithelial Cells

The acini are surrounded by stellate-shaped myoepithelial cells with long slender processes. The myoepithelial cells not only exhibit characteristics of other epithelial cells, such as expression of cytokeratin, but also exhibit properties of smooth muscle cells such as expression of α-smooth muscle actin. The exact role of the myoepithelial cells in the regulation and maintenance of the lacrimal gland remains unclear, but it has been shown that they express receptors for neurotransmitters, suggesting that they play a role in facilitating the secretion from the lacrimal gland. It is also likely that an important role is to support and maintain the structure of the lacrimal gland.

Bone-marrow-derived Cell Population

The lacrimal gland is a part of the mucosal-associated lymphoid tissue (MALT). The bone-marrow-derived cells in the lacrimal gland are mainly immunoglobulin A (IgA)-producing plasma cells and T and B lymphocytes, but macrophages and mast cells are also present. The bone-marrow-derived cells are clustered into lymphoid follicles scattered in the stroma surrounding the acini.

Innervation of the Lacrimal Gland

The lacrimal gland is innervated by parasympathetic, sympathetic, and sensory nerves. Parasympathetic nerves originate in the lacrimal nucleus of the pons and travel along the nervus intermedius, the deep and superficial petrosal nerves, and the vividian nerve before they synapse in the pterygopalatine ganglion. The postganglionic parasympathetic fibers can take different routes to the lacrimal gland. They leave the ganglion through the pterygopalatine nerves but can also reach the lacrimal gland via the maxillary portion of the trigeminal, the zygomatic, or the lacrimal nerves. Parasympathetic fibers can also travel along a branch of the middle meningeal artery to join the ophthalmic or lacrimal artery *en route* to the lacrimal gland. Sympathetic nerves originate from the superior cervical ganglion and travel along with the parasympathetic nerves through the pterygopalatine ganglion, reaching the lacrimal gland through the lacrimal branch of the zygomatic branch of the maxillary trigeminal nerve that joins the ophthalmic branch of the trigeminal nerve. The sensory nerves innervating the lacrimal gland carry sensory information from the gland through the ophthalmic branch of the trigeminal nerve to the trigeminal ganglion.

The parasympathetic nerves, being the most abundant, regulate the lacrimal gland mainly through the release of neurotransmitters, acetylcholine and vasoactive intestinal

peptide (VIP), with a possible co-secretion of nitric oxide (NO). Acetylcholine activates M_3 muscarinic receptors located in the basolateral membrane of the lacrimal cells, while VIP binds to VIP receptors that are similarly located. The sympathetic nerves exert their effects on the lacrimal gland through release of norepinephrine that binds to α- and β-adrenergic receptors, and possibly through neuropeptide Y receptors also located at the acinar cell basolateral membranes. The sensory nerves release substance P and calcitonin gene-related peptide. Not every individual acinar cell is independently innervated; rather cells that are not directly innervated can respond to stimulation of neighboring cells due to the intercellular gap junctions that connect the cells. The density of synapses within each acinus varies according to the species: in the rat, orbital glands fewer than 15% of acinar cells have an adjoining nerve fiber in contrast to the mouse orbital glands where close to 100% of the cells have an adjoining nerve fiber.

Blood Supply

The main blood supply to the lacrimal gland is not only through the lacrimal artery, a branch of the ophthalmic artery, but it also receives minor contributions from the infraorbital and the meningeal arteries. The veins mainly follow the same pathways as the arteries inside the orbit and drain into the superior ophthalmic vein.

Contents of Lacrimal Fluid

The tear film consists of three layers: a mucus layer located directly above the ocular surface epithelium, an aqueous layer, and a thin external lipid layer. The lacrimal fluid produced by the main lacrimal gland constitutes the major part of the aqueous layer of the tear film, to which the accessory glands of Krause and Wolfring and the ocular surface epithelium also contribute, in a minor fashion. Although the major part of the aqueous layer is water, it also contains electrolytes and a high concentration of proteins. Human tear fluid, for instance, has a protein concentration of about $8\,\mu g\,\mu l^{-1}$. Although the three layers of the tear film largely originate from different sources, these sources can contribute in part to each layer; therefore, it is hard to determine the origin of a specific protein. Recently, researchers identified 419 different proteins in human tear fluid; however, many of these may not have an active function in the tear fluid but are simply debris shed from epithelial cells. Three proteins constitute 80% of the total protein within the aqueous tear film, that is, lipocalin, lysozyme C, and lactoferrin. The functions of the different proteins in the tear fluid are varied. For instance, many proteins contribute to the antimicrobial properties of the tear fluid. Secretory IgA and cytokines are involved in immune responses, while others such as lysozyme C and lactoferrin provide a more direct defense against bacteria. The novel protein, lacritin, acts as a mitogen in corneal regeneration. Other proteins in the lacrimal fluid are involved in diverse activities in wound healing, blood coagulation, and oxidative stress reduction – all functions essential to maintain a healthy ocular surface. The protein pattern of both active and inactive proteins in the tear fluid can reflect disease states, including diabetes, dry eye, and cystic fibrosis.

Mechanisms of Protein Secretion in the Lacrimal Gland

The acinar cells of the lacrimal gland are professional excretory cells that engage in several types of secretion that collectively contribute to the lacrimal fluid. Protein secretion at the apical membrane into lacrimal fluid can be subdivided into several types: regulated exocytosis, constitutive exocytosis, and transcytosis. Regulated exocytosis is a process in which proteins destined for a particular plasma membrane domain are sorted into secretory vesicles after their biosynthesis within a post-Golgi sorting compartment called the *trans*-Golgi network. These secretory vesicles mature and migrate toward the site of release, where they are stored until the appropriate signal triggers their movement and fusion with the acceptor membrane domain. Examples of content proteins thought to be released from the lacrimal acini in animal model systems through regulated exocytosis at the apical plasma membrane include peroxidase and β-hexosaminidase. Constitutive exocytosis occurs, similarly, as components for release to the exterior of the cell are sequestered into vesicles at the *trans*-Golgi network that are immediately targeted to the acceptor membrane. Unlike regulated exocytosis, constitutive exocytosis is not reliant on extracellular activation of receptors by a ligand (such as a hormone or a neurotransmitter) to elicit the event. Although both forms of exocytosis have been observed in lacrimal acini, most studies have focused on the role of regulated exocytosis in the release of proteins at the apical plasma membrane of the acinar cell into lacrimal fluid. The secretory vesicles in the lacrimal gland acinar cells are generally larger (1–2 μm) and considerably more heterogeneous in both size and content compared to vesicles in other exocrine glands such as exocrine pancreas and the salivary gland. The spectrum of proteins secreted from the lacrimal acinar secretory vesicles appear to span a greater functional range than the spectrum release from other exocrine tissues as well, including nutrient and protective factors as well as factors that protect the mucosal surface from pathogens. This is an area of very active research since there are an unusually large number of

proteins of unknown function in the lacrimal gland secretory proteome.

Transcytosis is a process in which material internalized at the basolateral membrane is recruited into vesicles by endocytosis, followed by the movement of these vesicles to apically located compartments, and ultimately their targeting to the apical plasma membrane for release. Major cargo known to be carried through this pathway includes dimeric IgA, through association with the polymeric IgA receptor. Although not specifically characterized in lacrimal acini, other abundant tear proteins, including albumin and transferrin, are known to be transported through transcytotic pathways in other epithelial cells, suggesting that these proteins may be comparably transcytosed into lacrimal fluid by lacrimal acini.

Regulated exocytosis and transcytosis utilize a number of different processes, globally referred to as membrane trafficking, to achieve the unidirectional transport of cargo-laden vesicles over short and long distances followed by their targeted release. Several of these processes have been studied in acinar cells, including cytoskeleton and motor proteins, rab proteins, and soluble *N*-ethylmaleimide-sensitive factor attachment protein receptors or SNARE proteins. All mammalian cells contain filamentous structures collectively referred to as the 'cytoskeleton', which includes actin filaments, intermediate filaments, and microtubules. Each of these structures is formed from individual subunit proteins that exist in equilibrium with polymeric assemblies. Cytoskeletal filaments are critical in maintaining the integrity of cell shape as well as conferring cellular polarity or asymmetry, a function critical in aiding the movement of materials to different membrane domains in a polarized cell. Filamentous actin and microtubules, in particular, participate in several capacities in the movement of membrane vesicles to the apical plasma membrane, where the release of proteins into lacrimal fluid takes place. Microtubule- and actin-dependent membrane transport events can be facilitated either by the use of compressive force associated with cytoskeletal assembly to physically compress or direct membrane traffic, and/or by the use of these polymers as tracks which support the movement of motor proteins which carry membrane vesicles to specific destinations.

In lacrimal acini, actin filaments are localized in a dense network below the apical membrane called the subapical actin network, and this network is also present to a lesser extent below the basolateral membrane. Beneath the subapical actin, the ends of microtubules are anchored. Microtubules extend from the subapical region to the basolateral membrane. Both actin filaments and microtubules sustain aspects of protein secretion in lacrimal acinar cells. When microtubules are disrupted in acinar cells using the agent, nocodazole, stimulated protein secretion is reduced because the microtubule scaffolding required for vesicle motility has been disrupted. Other studies have suggested that a particular motor protein, cytoplasmic dynein, is required for the movement of membrane vesicles involved in secretory vesicle maturation and, possibly, transcytotic vesicle transport, to the subapical cytoplasm.

The subapical actin cytoskeleton plays complex roles in lacrimal acinar secretion. With its location immediately beneath the apical plasma membrane in a dense network, it poses an intracellular barrier for vesicle fusion to the apical membrane. For fusion to occur, this actin barrier must be disassembled to allow access of large secretory vesicle to the apical plasma membrane. Recent work has shown in fact that regions of the actin cytoskeleton located immediately beneath the regions of apical plasma membrane do disassemble, but that actin filaments also reassemble and contract around the base of multiple fusing secretory vesicles. The force generated through compression and retraction of actin filaments toward the apical membrane aids in compound fusion and content extrusion from the fusing vesicles. Regulated exocytosis can therefore be further characterized in lacrimal acini into a type known as multivesicular exocytosis. Two specific actin-dependent motors have been implicated so far in this actin remodeling and compound fusion of activated secretory vesicles, a conventional myosin motor known as nonmuscle myosin 2 and an unconventional myosin motor known as myosin 5c, with the possibility that other members of the myosin motor superfamily may also participate in this complex process.

Other major membrane trafficking effectors that have been implicated in acinar cell protein secretion include rab proteins. Rabs are major effectors of all intracellular steps of membrane trafficking and fusion in the eukaryotic cell, serving as the molecular address code on donor membrane vesicles which specify the acceptor compartment destination. GTP binding and hydrolysis serves as the on/off switch that activates these proteins. Specific rabs are localized to distinct compartments, conferring identity to these compartments. For instance, rab3D is enriched in secretory vesicles in lacrimal acinar cells and appears to regulate compound fusion of these vesicles. Other data suggest that rab27 isoforms also participate in the maturation and fusion of secretory vesicles during regulated exocytosis in lacrimal acini. By analogy with other systems, rab4 and rab5 isoforms are likely to participate in early events in acinar transcytosis, specifically basolateral endocytosis and sorting, while rab 11 isoforms are enriched in apical endosomes and may facilitate terminal transcytotic traffic of materials destined for the lacrimal fluid.

Specific types of SNARE proteins are located on donor and acceptor membranes and interact to form fusion pores which allow membrane contents to mingle or secretory vesicle contents to be extruded to the cell exterior. Several types of SNARE proteins have been demonstrated in lacrimal acini. Regulated exocytosis of secretory vesicles in acini is thought to use both vesicle-associated

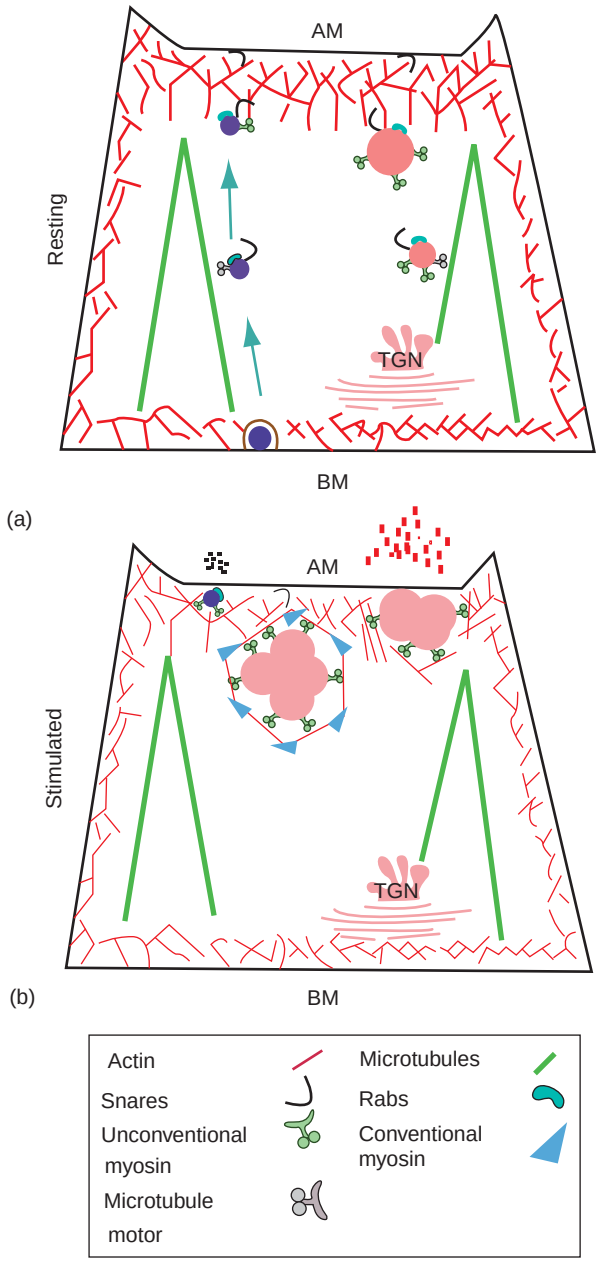

Figure 3 Protein secretion in lacrimal acinar cells at the apical membrane. (a) Depicts vesicles participating in the transcytotic pathway from the basolateral membrane (BM) to the apical membrane (AM) as shown in blue vesicles. Depicted as well is the maturation and movement to the AM of secretory vesicles after budding from the *trans*-Golgi network (TGN) as shown in red vesicles. Initially both transcytosis from the BM and movement from the TGN are reliant on microtubule-based motor proteins. As the vesicles move to the actin-rich subapical region, unconventional myosin motors become important in actin-based movement through the subapical actin network. (b) Depicts multivesicular exocytosis after stimulation with secretogogs such as carbachol. Unconventional myosins such as myosin 5c have been shown to have an important role in the reorganization of actin filaments around clusters of secretory vesicles primed for fusion. Actin and conventional myosins then work together to compress the fusing secretory vesicles and to promote content extrusion. Rab and SNARE proteins participate in the targeting and fusion events in each pathway. It should be noted that the rabs and the SNAREs participating in transcytosis and exocytosis are different for each pathway.

membrane protein 2 (VAMP 2) and VAMP 8 on donor membranes, and syntaxin 2 and SNAP23 on acceptor membranes. Figure 3 shows the organization of the two major protein secretory pathways that contribute proteins to lacrimal fluid: regulated exocytosis and transcytosis, as well as some of the effectors within each pathway.

Morphological analysis of ductal epithelial cells has revealed the presence of large secretory vesicles, presumably containing additional constituents destined for release into the lacrimal fluid. However, due to limitations in the ability to isolate these individual cells and conduct cellular investigations into the membrane trafficking mechanisms, little is known about the precise mechanisms involved in ductal cell exocytosis and transcytosis.

Mechanisms and Regulation of Electrolyte and Water Secretion by the Lacrimal Gland

Acinar Cells

The lacrimal fluid is hypertonic due to a high Cl^- and K^+ content, whereas the levels of Na^+, HCO_3^-, and Ca^{2+} are similar to the plasma levels. The electrolyte concentration of the lacrimal fluid is however not static, but varies with the flow rate to become more isotonic with an accelerated flow rate. Fluid secretion is an osmotic process driven by ion movement through the membrane of the acinar cells. Parasympathetic stimulation of the acinar cells triggers an acute increase of cytosolic Ca^{2+} and adenosine 3′,5′-cyclic monophosphate (cAMP) which opens Cl^- channels in the apical membrane, resulting in a movement of Cl^- into the lumen. The increase in cytosolic Ca^{2+} also activates K^+ channels in the apical as well as the basolateral membrane, causing K^+ to move out of the cell. Na^+ follows the flux of Cl^- and K^+, moving from the basolateral side toward the lumen traveling through paracellular channels between the cells. To maintain an isotonic secretion, water exits the cell through water-channel proteins called aquaporins. The movement of Cl^- and K^+ out of the cell is dependent on their electrochemical gradient, that is, the intracellular concentration of these ions must be higher than in the extracellular fluid. This is made possible by ion pumps and co-transporters located in the basolateral membrane. Na^+/K^+-ATPase transports K^+ into the cell and Na^+ out of the cell; the $Na^+/K^+/2Cl^-$ co-transporter (NKCC1) moves all three ion types into the cell; and Cl^-/HCO_3^- and Na^+/H^+ anti-porters transport Cl^- and Na^+ into the cell and H^+ and HCO_3^- out of the cell. Figure 4 illustrates the ion channels and transporters present in the lacrimal acinar cell.

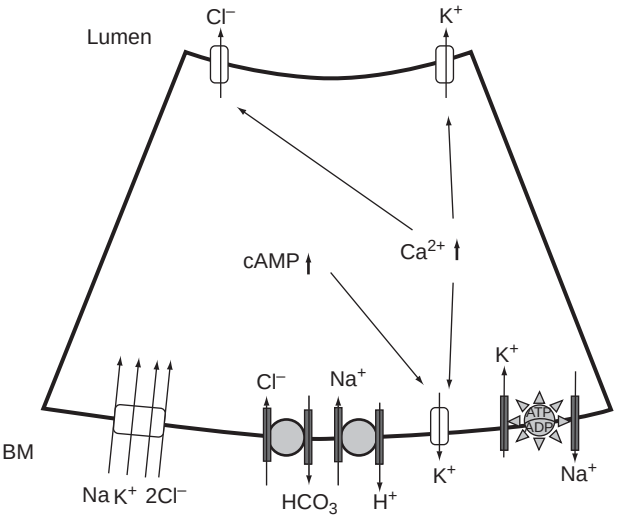

Figure 4 Schematic diagram showing the major ion transporters active in the electrolyte and water release from the lacrimal gland acinar cell. Increases in cytosolic Ca^{2+} and cAMP following neural stimulation opens K^+ and C^- channels, resulting in an outward flux of these ions. Na^+/K^+-ATPase transports K^+ into the cell and Na^+ out of the cell, the $Na^+/K^+/2Cl^-$ co-transporter moves all three ion types into the cell, and Cl^-/HCO_3^- and Na^+/H^+ anti-porters transport Cl^- and Na^+ into the cell and H^+ and HCO_3^- out of the cell.

Ductal Cells

Due to difficulties in specifically isolating the ductal cells, the ion transport mechanisms have not been extensively studied. However, it has been hypothesized that the water and ion transport events continue as the lacrimal fluid travels through the ductal system in a pattern comparable to that in the acinar cells. Recently, several approaches to study the ductal cells have been developed, including microdissection and culturing of individual ducts and laser capture microdissection of individual ductal cells. In these studies, some of the most common acid/base transporters were characterized in the ductal cells. The same work also showed that the ion transport in the ductal cells can be regulated by parasympathetic neurotransmitters. Furthermore, studies showed that the lacrimal fluid released from the acinar cells is isotonic, leading to the hypothesis that the ductal cells are responsible for the high K^+ levels in tears. The finding that Na^+K^+-ATPase and NKCC1 are expressed at higher levels in the ductal cells than in the acinar cells supports this hypothesis.

Conclusion

Previous and ongoing studies have established many of the functions of the principal cells of the lacrimal gland. The major cell type, the acinar cell, is responsible for the regulated release of proteins, fluid, and electrolytes into the lacrimal fluid, while ductal cells appear to further modify the electrolyte composition and likely also contribute additional proteins to the aqueous tear film. Some of the signaling pathways have been elucidated that stimulate the production of lacrimal fluid, while some of the molecular mechanisms involved in the fundamental exocytotic and transcytotic events have likewise been elucidated. However, the complexity of the signaling and membrane trafficking events even in lacrimal acinar cells, the best-studied cell type in this complex organ, means that considerable work remains to be done. Although some insights regarding changes in signaling and membrane trafficking pathways that result in altered production of lacrimal fluid have been obtained in dry eye disorders, considerable additional work is required in order to truly understand the etiology of these disorders. In some studies, changes in tear protein composition have been associated with dry eye disorders, so future challenges also include the identification of tear biomarkers that can be used to diagnose different types of dry eye disorders to aid in determination of the appropriate course of treatment.

See also: Dry Eye: An Immune-Based Inflammation; Innate Immune System and the Eye; Lacrimal Gland Hormone Regulation; Lacrimal Gland Signaling: Neural; Meibomian Glands and Lipid Layer; Tear Film Overview.

Further Reading

Cohen, A. J., Mercandetti, M., and Brazzo, B. G. (eds.) (2006). *The Lacrimal System, Diagnosis, Management and Surgery.* New York: Springer.

Hodges, R. R. and Dartt, D. A. (2003). Regulatory pathways in lacrimal gland epithelium. *International Review of Cytology* 231: 129–196.

Jerdeva, G., Wu, K., Yarber, F. A., et al. (2005). Actin and non-muscle myosin II facilitate apical exocytosis of tear proteins in rabbit lacrimal acinar epithelial cells. *Journal of Cell Science* 118: 4797–4812.

Marchelletta, R. R., Jacobs, D., Schechter, J. E., Cheney, R., and Hamm-Alvarez, S. F. (2008). Myosin Vc facilitates actin filament remodeling and compound fusion of mature secretory vesicles during exocytosis in lacrimal acini. *American Journal of Physiology (Cell Physiology)* 295: C13–C28.

Pflugfelder, S. C., Beuerman, R. W., and Stern, M. E. (eds.) (2004). *Dry Eye and Ocular Surface Disorders.* New York: Marcel Dekker, Inc.

Ubels, J. L., Hoffman, H. M., Srikanth, S., Resau, J. S., and Webb, C. P. (2006). Gene expression in rat lacrimal gland duct cells collected using laser capture microdissection: Evidence for K^+ secretion by duct cells. *Investigative Ophthalmology and Visiual Science* 47: 1876–1885.

Walcott, B., Moore, L., Birzgalis, A., Claros, N., and Brink, P. R. (2002). A model of fluid secretion by the acinar cells of the mouse lacrimal gland. *Advances in Experimental Medicine and Biology* 506(Pt. A): 191–197.

Wu, K., da Costa, S. R., Jerdeva, G., et al. (2006). Mechanisms of exocytosis in lacrimal gland. *Experimental Eye Research* 83: 84–96.

Zierhut, M., Stern, M. E., and Sullivan, D. A. (eds.) (2005). *Immunology of the Lacrimal Gland, Tear Film and Ocular Surface.* New York: Taylor and Francis.

Lacrimal Gland Signaling: Neural

D Zoukhri, Tufts University, Boston, MA, USA

Glossary

Acinar cells – Highly polarized epithelial cells that form an acinus and whose primary function is to secrete proteins, electrolytes, and water.
Exocytosis – The process in which molecules (such as secretory proteins) in a membrane-enclosed vesicle (secretory vesicle or granule) fuse with the plasma membrane and are then released outside the cell.
Muscarinic receptors – A subtype of receptors for the neurotransmitter acetylcholine that is more responsive to muscarine than nicotine.
Neurotransmitters – Chemicals released by neurons to modulate the function of a target cell.
Preocular tear film – A complex and highly structured moist film which covers the bulbar and palpebral conjunctiva, and the cornea. It is composed of water, electrolytes, proteins, mucins, and lipids.
Signal transduction – The biochemical events that conduct the signal of an external stimulus from the cell exterior, through the cell membrane, and into the cytoplasm.

Anatomy of the Lacrimal Gland

The lacrimal gland is a compound tubuloalveolar serous gland composed primarily of acinar, ductal, and myoepithelial cells (Figure 1). Acinar cells account for over 80% of the cell type present in the lacrimal gland and form the site for synthesis, storage, and secretion of proteins. Several of these proteins have antibacterial or growth factor properties and are crucial to the health of the ocular surface. Acinar cells are highly polarized cells with tight junctions surrounding each acinar cell on the luminal side and thus separating the plasma membrane into apical (luminal) and basolateral (serosal) components. The basal portion of the cell contains a large nucleus, rough endoplasmic reticulum, mitochondria, and Golgi apparatus, while the apical portion is filled with secretory granules.

Like the acinar cells, the duct cells are also polarized with the nuclei located basolaterally, whereas the rough endoplasmic reticulum and mitochondria are more apical. The primary function of the ductal cells is to modify the primary fluid secreted by the acinar cells by absorbing or secreting water and electrolytes. The duct cells secrete a KCl-rich solution so that the final secreted lacrimal gland fluid is rich in K^+. It has been estimated that as much as 30% of the volume of the final lacrimal gland fluid is secreted by the duct cells.

The myoepithelial cells lie scattered between the acinar and ducts cells and the basement membrane and are interconnected by gap junctions and desmosomes. These cells are highly branched and contain multiple processes which surround the basal area of the acinar cells (Figure 1). The myoepithelial cells are thought to contract because they contain muscle contractile proteins (α-smooth muscle actin, myosin, and tropomyosin). The contraction of these cells would help expel the fluid out of the acini and the ducts onto the ocular surface. In support of a functional role of lacrimal gland myoepithelial cells, receptors and intracellular signaling molecules for parasympathetic neurotransmitters have been described.

The lacrimal gland contains other cells: plasma cells, B and T cells, dendritic cells, macrophages, and mast cells. Immunoglobulin A (IgA)-positive plasma cells account for the majority of the mononuclear cells in the lacrimal gland. These cells synthesize and secrete IgA, which then is transported into acinar and ductal cells and secreted by these epithelial cells as secretory IgA.

Neural Control of Lacrimal Gland Secretion

To ensure adequate production of the aqueous component of the preocular tear film, lacrimal gland secretion is under tight neural control. To this end, the lacrimal gland is densely innervated by the parasympathetic and sympathetic nervous system (Figure 2). Although scarce, sensory nerves are also present in the lacrimal gland (Figure 2). Nerves are located in close proximity to acinar, ductal, and myoepithelial cells, as well as blood vessels, and hence can control a wide variety of lacrimal gland functions. While each individual cell may not be innervated, gap junctions electrically and chemically connect cells within an acinus so that even noninnervated cells can respond to the neural stimulus.

In the lacrimal gland, parasympathetic nerves contain the neurotransmitters acetylcholine and vasoactive intestinal peptide (VIP). Sympathetic nerves contain the neurotransmitters norepinephrine and neuropeptide Y (NPY).

Sensory nerves contain the neurotransmitters substance P and calcitonin gene-related peptide (CGRP). Acetylcholine and VIP are potent stimuli of lacrimal gland protein and electrolyte/water secretion. Norepinephrine is also a potent stimulus of protein secretion, but a weak stimulus of electrolyte/water secretion. In contrast, NPY and CGRP are weak stimuli of protein secretion, while substance P does not appear to stimulate either protein or electrolyte/water secretion.

The stimulation of lacrimal gland secretion occurs through a neural reflex arc originating from the ocular surface (Figure 3). Neural reflexes are initiated by stimulation of the afferent sensory nerves of the cornea and conjunctiva or by activation of the optic nerve in response to intense light. Efferent parasympathetic and sympathetic nerves of the lacrimal gland are then activated to release their neurotransmitters (Figure 3). The neurotransmitters interact with and activate specific receptors located on the basolateral membranes of acinar and duct cells, which then initiates a cascade of intracellular events known as signal transduction. Activation of these signal transduction pathways induces fusion of the preformed secretory granules with the apical membrane to release secretory proteins into the lumen (Figure 3). To trigger electrolyte and water secretion, ion channels and pumps, located in the apical and basolateral membranes, are also activated.

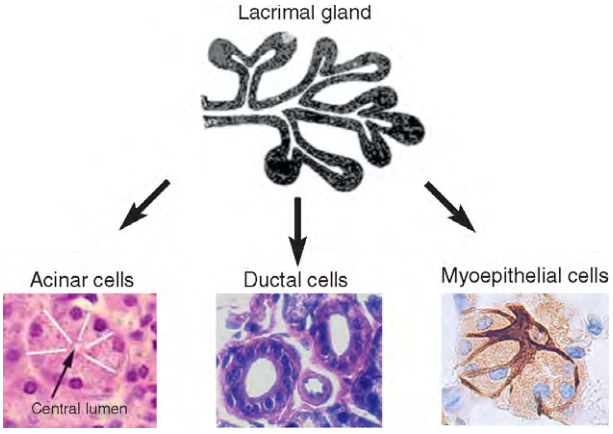

Figure 1 Schematic of the lacrimal gland and photomicrographs showing the three major cell types that it is composed of. The acinar cells, which account for 80% of the cell type present in the lacrimal gland, and ductal cells were stained with hematoxylin and eosin. The myoepithelial cells were identified immunohistochemically (brown stain) using an antibody against α-smooth muscle actin.

Signal Transduction Pathways Activated in the Lacrimal Gland

Signal transduction proceeds in three steps: (1) initiation of the signal by interaction of the ligand (neurotransmitter, neuropeptide, or hormone) with its receptor; (2) amplification of the signal through the interaction of the receptor/G protein/effector enzyme leading to the generation of second-messenger molecules; and (3) termination of the signal through the action of protein phosphatases and membrane pumps to bring the amount of phosphorylated proteins and ions, respectively, back to resting levels (Figure 4).

Cholinergic Agonist-Activated Signal Transduction Pathways

Acetylcholine, released from parasympathetic nerves, activates muscarinic receptors on the basolateral membrane of lacrimal gland cells. Of the five receptor subtypes (M_{1-5}) identified, only the M_3 or glandular subtype is present in the lacrimal gland. These receptors are coupled to the activation of phospholipases C and D (PLC and PLD, respectively) and the activation of the p42/p44 mitogen-activated protein kinase (p42/p44 MAPK, also known as extracellular signal-regulated kinase (ERK)) pathway (Figure 5).

PLC-coupled signaling pathway

Lacrimal gland M_3 receptors are coupled, via the G-protein Gαq, to the effector enzyme PLC. Activated PLC hydrolyzes the plasma membrane lipid, phosphatidylinositol 4,5-bisphosphate (PIP_2), to generate two

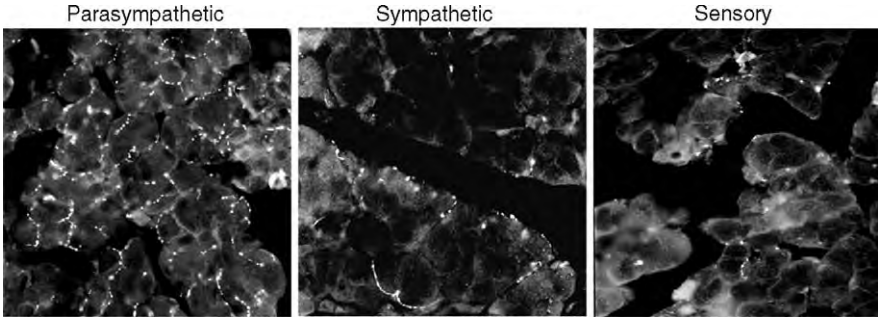

Figure 2 Photomicrographs depicting the innervation of murine lacrimal gland. Nerves were visualized using antibodies against the following neurotransmitters or enzymes: VIP for the parasympathetic nerves, dopamine β-hydroxylase for the sympathetic nerves, and CGRP for the sensory nerves.

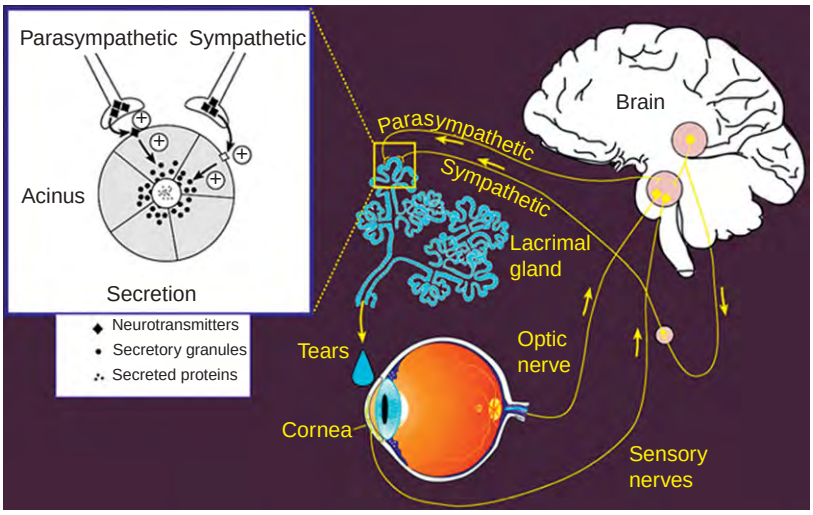

Figure 3 Schematic of the neural reflex arc that controls lacrimal gland secretion. Neural reflexes are initiated by the stimulation of the afferent sensory nerves of the cornea and conjunctiva or by activation of the optic nerve. Efferent parasympathetic and sympathetic nerves of the lacrimal gland are then activated to release their neurotransmitters. The neurotransmitters activate specific receptors located on the basolateral membranes of acinar cells to stimulate secretion.

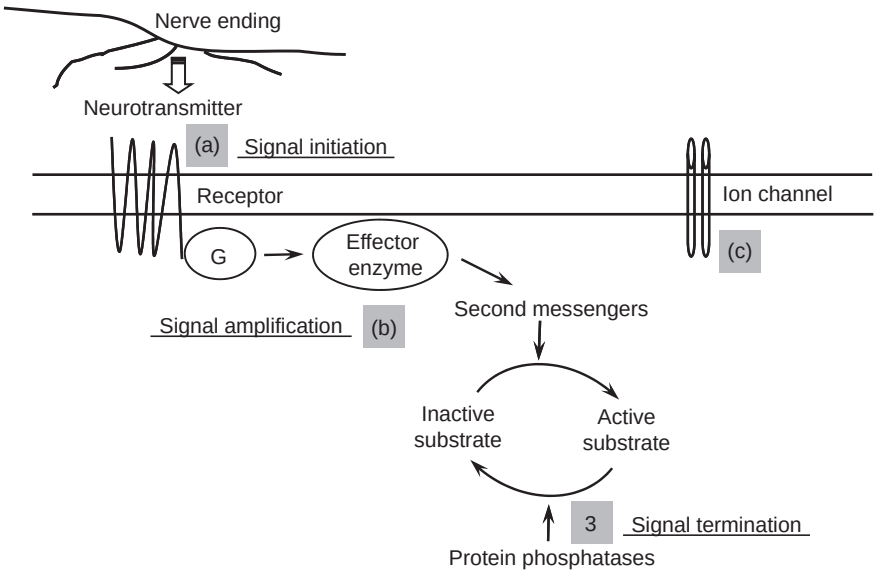

Figure 4 Schematic depicting the three steps involved in signal transduction in response to a neural stimulus: (a) signal initiation by interaction of the neurotransmitter with its receptor; (b) signal amplification through the interaction of the receptor with the G protein and effector enzyme to generate second-messenger molecules; and (c) signal termination through activation of protein phosphatases and membrane pumps.

second-messenger molecules, inositol 1,4,5-trisphosphate (IP_3) and diacylglycerol (DAG; **Figure 5**).

IP_3, a water-soluble molecule, diffuses to the endoplasmic reticulum where Ca^{2+} is stored in an inactive, bound form. It also interacts with specific receptors located on the endoplasmic reticulum to release Ca^{2+} into the cytosol. Depletion of these Ca^{2+} stores leads to an increase in the influx of extracellular Ca^{2+} across the plasma membrane. The IP_3 receptor is a homotetramer of ≈310 kDa each and constitutes one of the largest of all known ion channels. Binding sites for IP_3 are located within the N-terminal domain, whereas the C-terminal regions form the intrinsic Ca^{2+} channel. Multiple isoforms of IP_3 receptor have been cloned. They share significant similarity to each other and are encoded by at least four genes.

The activation of lacrimal gland cholinergic M_3 receptors triggers a biphasic Ca^{2+} response: a rapid (usually referred to as peak) increase in $[Ca^{2+}]_i$ due to IP_3-induced release of Ca^{2+} from intracellular stores, followed by a slow and sustained (usually referred to as plateau) increase in $[Ca^{2+}]_i$ due to influx of Ca^{2+} from the extracellular milieu. Both Ca^{2+} responses are necessary for cholinergic

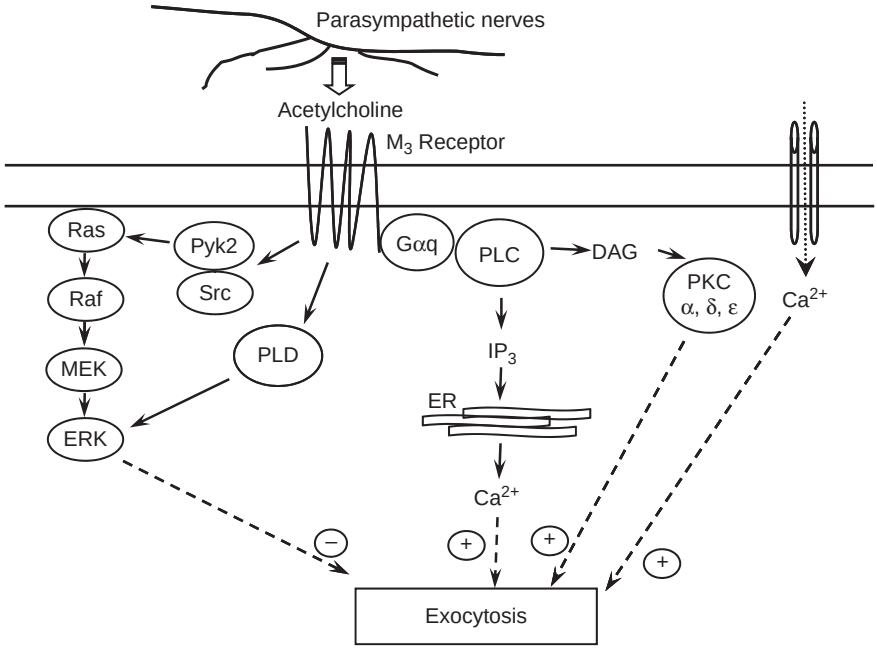

Figure 5 Schematic depicting the main signal transduction pathways activated by acetylcholine to stimulate protein secretion. The activation of lacrimal gland cholinergic receptors activates three main signaling pathways that either enhance (PKC, Ca^{2+}) or attenuate (ERK) protein secretion. The net protein secretory output in response to acetylcholine stimulation will likely depend on the relative contribution of the stimulatory versus the inhibitory signal transduction pathways.

agonist-stimulated protein secretion since chelation of either the intracellular or the extracellular Ca^{2+} leads to complete inhibition of secretion. Ca^{2+} can stimulate secretion alone or do so by activating Ca^{2+} and calmodulin-dependent protein kinases to phosphorylate-specific substrates to cause secretion.

The DAG formed from the hydrolysis of PIP_2 activates protein kinase C (PKC, Figure 5). PKC is a family of closely related isozymes that has been divided into three categories based on structural and functional criteria. A first group, termed conventional PKCs (cPKCs), includes PKCα, -βI, -βII, and -γ isoforms, which have a Ca^{2+}- and DAG-dependent kinase activity. A second group, termed novel PKCs (nPKCs), includes PKCϵ, -δ, -θ, and -η isoforms, which are Ca^{2+}-independent and DAG-stimulated kinases. A third group, termed atypical PKCs (aPKCs), includes PKCζ and -ι/λ isoforms, which are Ca^{2+}- and DAG-independent kinases.

Four isoforms of PKC are expressed in the rat lacrimal gland: one classical, PKCα; two novel, PKCδ, and -ϵ; and one atypical, PKCι/λ. In an attempt to define the role that individual PKC isoforms might play in regulating lacrimal gland functions in response to cholinergic stimulation, isoform-specific peptide inhibitors of PKC were synthesized. These peptides were derived from the unique pseudosubstrate sequences of PKCα, -δ, and -ϵ, and were myristoylated at their N-terminus to make them cell permeant. Indeed, all PKC isoforms have a pseudosubstrate sequence in their N-terminal part, which interacts with the catalytic domain to keep the enzyme inactive in resting cells. Using these peptides, it was shown that cholinergic agonists activate PKCα and -ϵ to a larger extent and PKCδ to a lesser extent, to induce protein secretion. It was also shown that PKCδ and -ϵ, but not -α, negatively modulate cholinergic-induced Ca^{2+} elevation in the lacrimal gland.

PLD-coupled signaling pathway

PLD catalyzes the hydrolysis of membrane phospholipids (preferably phosphatidylcholine), producing phosphatidic acid and the free polar head group. Phosphatidic acid, by itself or after its conversion to DAG by a phosphohydrolase, is an important second-messenger molecule. Besides its hydrolytic activity, PLD possesses the unique ability to catalyze a transphosphatidylation reaction, in the presence of a primary alcohol, in which the phosphatidyl moiety of the phospholipid substrate is transferred to the primary alcohol producing the corresponding phosphatidylalcohol. Accumulation of such unique transphosphatidylation products has been used to detect PLD activity unambiguously in diverse cell types.

Depending on the cell's type, the receptor activation of PLD was shown to occur through mechanisms involving PKC activity, Ca^{2+}, G proteins, or receptor-linked tyrosine kinases. Since PKC activation and Ca^{2+} mobilization are downstream to PLC stimulation, it has been suggested that PLD activation may be secondary to receptor activation of PLC.

Taking advantage of the transphosphatidyl reaction catalyzed by PLD, it was shown that the lacrimal gland contains a PLD activity. Cholinergic agonists, through the muscarinic receptor, stimulate both the hydrolytic activity of PLD to produce phopshatidic acid, as well as the transphosphatidyl reaction. However, if either Ca^{2+} is mobilized or PKC is activated, only the transphosphatidyl reaction is stimulated. This finding implied that cholinergic agonist activation of PLD in the lacrimal gland is not secondary to the activation of PLC by these agonists.

MAPK-coupled signaling pathway

MAPK, also known as ERK, is a dual serine/threonine and tyrosine protein kinase. It is activated through phosphorylation by an MAPK kinase (known as MEK). MEK is also activated through phosphorylation by its upstream MAPK kinase kinase (known as Raf). Raf is activated when the small GTP-binding protein, Ras, is in its GTP-bound form. Depending on the cell's type, Ras can be activated by several mechanisms, including the nonreceptor tyrosine kinases Pyk2 and Src, growth factors receptors, and PKC.

In the lacrimal gland, the activation of MAPK attenuates protein secretion. The activation of MAPK by the M_3 receptor was shown to involve the nonreceptor tyrosine kinases Pyk2 and Src, which in turn activate Ras and, ultimately, MAPK (**Figure 5**). Recent evidence showed that the activation of MAPK by cholinergic agonists is downstream of PLD activation. The mechanisms involved in PLD-mediated activation of MAPK in the lacrimal gland remain to be elucidated.

The termination of the cholinergic signaling pathway involves receptor desensitization, activation of protein phosphatases to dephosphorylate ERK and other phosphorylated substrates, and the activation of ion channels/pumps to return the concentration of cytosolic Ca^{2+} to its resting levels.

In summary, the activation of lacrimal gland cholinergic receptors in response to the parasympathetic neurotransmitter acetylcholine activates three main signaling pathways that either enhance (PKC, Ca^{2+}) or attenuate (ERK) protein secretion (**Figure 5**). The net protein secretory output in response to acetylcholine stimulation will likely depend on the relative contribution of the stimulatory versus the inhibitory signal transduction pathways.

VIP-Activated Signal Transduction Pathways

VIP interacts with specific VIP receptors located on the basolateral membranes of lacrimal gland cells. Two types of VIP receptors have been identified, VIPRI and VIPRII, which are also known as VIPACR1 and VIPACR2, and both of them are expressed in the lacrimal gland, with VIPRI being the predominant type.

Adenylate cyclase-coupled signaling pathway

The VIP receptor uses the G protein $G_{\alpha s}$ to activate the effector enzyme adenylyl cyclase (AC), which produces the second-messenger molecule, cyclic adenosine monophosphate (cAMP) (**Figure 6**). Molecular cloning has identified several isoforms of mammalian AC forming a family of at least 10 enzymes (ACI-X). There are at least three isoforms of AC (ACII, ACIII, and ACIV) present in the lacrimal gland, each having a unique localization.

Although the regulation of AC enzymatic activity is complex and isoform specific, all AC isoforms are activated

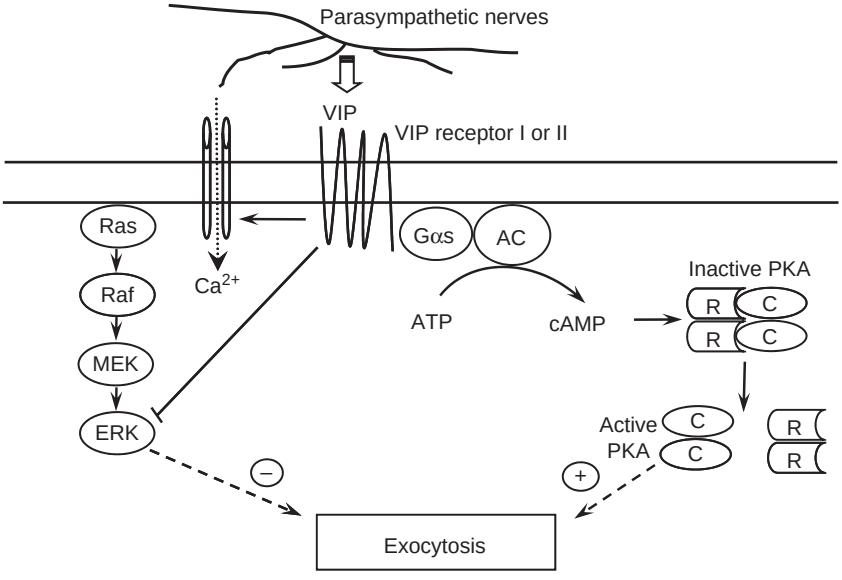

Figure 6 Schematic depicting the main signal transduction pathways activated by the VIP to stimulate protein secretion. The activation of lacrimal gland VIP receptors activates two main signaling pathways that enhance protein secretion.

by Gαs. Increases in the intracellular levels of cAMP lead to activation of protein kinase A (PKA), a ubiquitous serine and threonine protein kinase. In its inactive state, PKA consists of a complex of two catalytic (C) subunits and two regulatory (R) subunits (Figure 6). Binding of cAMP to the R subunit alleviates an autoinhibitory contact that releases the active C subunit (Figure 6). The active kinase is then free to phosphorylate specific protein substrates to stimulate lacrimal gland protein and fluid secretion.

MAPK-coupled signaling pathway

Recently, it has been shown that addition of VIP, exogenous cAMP, or analogs that increase cAMP levels inhibited both basal as well as cholinergic induced activation of MAPK in the lacrimal gland. One implication of these findings is that it could help explain the well-documented synergistic effect that addition of a cAMP along with a Ca^{2+}-/PKC-dependent agonist have on lacrimal gland protein secretion. Indeed, cholinergic agonists activate MAPK, which attenuates protein secretion. When the cAMP pathway is activated, MAPK activity is inhibited; this should alleviate the inhibitory effect that MAPK has on secretion and as a result, protein secretion will be potentiated if both the Ca^{2+}/PKC and the cAMP pathways are activated simultaneously.

The termination of VIP-activated signaling pathways likely includes activation of the cAMP-phosphodiesterase, which converts cAMP to the inactive 5'-AMP. Other signal-terminating mechanisms include desensitization of the VIPR and AC, sequestration of the PKA C subunits by the naturally occurring protein kinase inhibitor (PKI), and activation of protein phosphatases.

α_1-Adrenergic Agonist-Activated Signal Transduction Pathways

Norepinephrine, released from the sympathetic nerves, binds to α_1- and β-adrenergic receptors on lacrimal gland cells. β-Adrenergic receptors are coupled to activation of AC to activate a cAMP-dependent signal transduction pathway, as discussed for VIP. Of the three α_1-adrenergic receptor subtypes (α_{1A}, α_{1C}, and α_{1D}) identified, only the α_{1D} subtype is expressed in the lacrimal gland.

Ca^{2+}- and PKC-coupled signaling pathways

In most exocrine tissues, α_1-adrenergic agonists activate the same pathway as cholinergic agonists (i.e., activation of PLC and PLD). Surprisingly, in the lacrimal gland, α_1-adrenergic agonists do not activate PLC or PLD, although their activation leads to a slight increase in cytosolic Ca^{2+} and to activation of PKC isoforms (Figure 7). To date, the effector enzyme(s) activated by lacrimal gland α_{1D}-adrenergic receptors to mobilize Ca^{2+} and activate PKC is still unknown.

Although Ca^{2+} mobilization in the lacrimal gland in response to adrenergic agonist stimulation is well

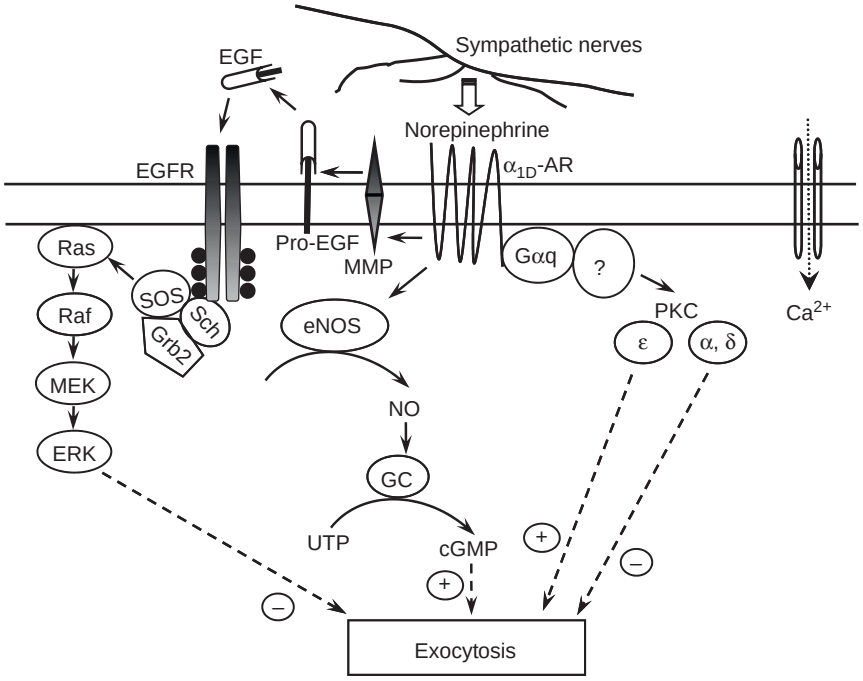

Figure 7 Schematic depicting the main signal transduction pathways activated by the norepinephrine to stimulate protein secretion. The activation of lacrimal gland α_{1D}-adrenergic receptors activates stimulatory pathways, including PKCε and cGMP, and inhibitory pathways, including PKCα, PKCδ, and ERK. It is likely that the net lacrimal gland protein secretion in response to sympathetic stimulation is a balance between these stimulatory and inhibitory signal transduction pathways.

documented, the mechanisms involved are poorly understood. A role for IP_3 has been ruled out since adrenergic agonists do not increase its production as they fail to activate PLC. It has been proposed that cyclic ADP ribose, which activates ryanodine receptors to release Ca^{2+} into the cytosol, might be involved. Other investigators proposed that nitric oxide (NO)-induced generation of cyclic guanosine monophosphate (cGMP) is involved in α_1-adrenergic agonist-induced mobilization of Ca^{2+}.

The role of PKC in α_1-adrenergic agonist-induced lacrimal gland protein secretion has been studied using the myristoylated pseudosubstrate-derived peptides. It was shown that α_1-adrenergic agonists activate three PKC isoforms – PKCα, -δ, and -ϵ. Activation of PKCϵ enhances protein secretion, whereas activation of PKCα and -δ attenuates protein secretion. This is in contrast to the stimulatory effect that PKCα and -δ isoforms have on protein secretion when activated by cholinergic agonists. These findings imply that the effect (inhibitory or stimulatory) of a given isoform of PKC in the lacrimal gland is stimulus dependent and might be dictated by the cellular location of PKC isoforms.

MAPK-coupled signaling pathway

Similar to cholinergic agonists, α_1-adrenergic agonists activate MAPK to attenuate lacrimal gland protein secretion. However, in contrast to the cholinergic pathway, activation of MAPK by the α_{1D}-adrenergic receptor does not involve the nonreceptor tyrosine kinases Pyk2 and Src, but involves activation of the epidermal growth factor receptor (EGFR; **Figure 7**). The EGFR, also known as Erb1, is the prototypical member of the ErbB/EGFR family of receptors which consists of three additional members (ErbB2–4). EGFR is a type 1 transmembrane tyrosine kinase receptor consisting of an extracellular domain (ligand-binding site), a transmembrane domain, and the carboxy-terminal, an intracellular domain containing the tyrosine kinase motif. In addition, the carboxy-terminal domain contains tyrosine residues that become phosphorylated following ligand binding and receptor dimerization. Following receptor activation, several exogenous substrates that contain either Src homology 2 (SH2) or protein tyrosine binding (PTB) motifs are recruited to specific phosphorylated tyrosine residue.

In the lacrimal gland, the activation of the EGFR by α_1-adrenergic agonists occurs through a process termed as transactivation and involves the activation of a metalloproteinase and shedding of EGF (**Figure 7**). Following activation, Shc (an SH2 motif-containing protein) is recruited to the EGFR, followed by recruitment of Grb2 and the guanine nucleotide exchange factor protein, SOS (**Figure 7**). SOS stimulates the exchange of GDP for GTP on Ras and hence leads to its activation. Activated Ras triggers the activation of the MAPK cascade, leading to activation of ERK (**Figure 7**). Similar to the cholinergic pathway, α_1-adrenergic-activated ERK has been shown to attenuate lacrimal gland protein secretion.

NO-coupled signaling pathway

NO, along with L-citruline, is produced from L-arginine in the presence of O_2- and NADPH-derived electrons. This reaction is catalyzed by the enzyme NO synthase (NOS). There are three well-characterized isoforms of NOS expressed by mammalian cells: neuronal NOS (nNOS also known as NOS1), inducible NOS (iNOS or NOS2), and endothelial NOS (eNOS or NOS3). Activation of nNOS and eNOS, but not iNOS, requires calmodulin and an increase in $[Ca^{2+}]$.

It has been shown recently that lacrimal gland α_1-adrenergic receptors are coupled to the NO/cGMP pathway (**Figure 7**). Indeed, it was found that both nNOS and eNOS are expressed in the lacrimal gland. The addition of α_1-adrenergic agonists led to generation of NO, presumably through activation of eNOS and not nNOS. NO, in turn, activates soluble guanylate cyclase to generate cGMP which enhances lacrimal gland protein secretion.

The termination of the α_1-adrenergic signaling pathway is likely to involve receptor desensitization, activation of protein phosphatases to dephosphorylate ERK and other phosphorylated substrates, and the activation cGMP-phosphodiesterase, which converts cGMP to the inactive 5'-GMP.

In summary, the activation of lacrimal gland α_{1D}-adrenergic receptors, in response to the sympathetic neurotransmitter norepinephrine, activates stimulatory pathways (including PKCϵ and cGMP) and inhibitory pathways (including PKCα, PKCδ, and ERK; **Figure 7**). It is likely that the net lacrimal gland protein secretion in response to sympathetic stimulation is a balance between these stimulatory and inhibitory signal transduction pathways.

See also: Adaptive Immune System and the Eye: Mucosal Immunity; Lacrimal Gland Hormone Regulation; Lacrimal Gland Overview; Tear Film; Tear Film Overview.

Further Reading

Botelho, S. Y., Hisada, M., and Fuenmayo, N. (1966). Functional innervation of the lacrimal gland in the cat. *Archives of Ophthalmology* 76: 581–588.

Broad, L., Braun, F., Lievremont, J., et al. (2001). Role of the phospholipase C-inositol 1,4,5-trisphosphate pathway in calcium release-activated calcium current and capacitative calcium entry. *Journal of Biological Chemistry* 276: 15945–15952.

Chen, L., Hodges, R. R., Funaki, C., et al. (2006). The effects of α_{1D}-adrenergic receptors on shedding of biologically active EGF in freshly isolated lacrimal gland epithelial cells. *American Journal of Physiology. Cell Physiology* 291: C946–C956.

Funaki, C., Hodges, R. R., and Dartt, D. A. (2007). Role of cAMP inhibition of p44/p42 mitogen-activated protein kinase in potentiation of protein secretion in rat lacrimal gland. *American Journal of Physiology. Cell Physiology* 293: C1551–C1560.

Hodges, R. R. and Dartt, D. A. (2003). Regulatory pathways in lacrimal gland epithelium. *International Review of Cytology* 231: 129–196.

Hodges, R., Rios, J., Vrouvlianis, J., et al. (2006). Role of protein kinase C, Ca^{2+}, Pyk2 and c-Src in agonist activation of rat lacrimal gland p42/p44 MAPK. *Investigative Ophthalmology and Visual Sciences* 47: 3352–3359.

Ota, I., Zoukhri, D., Hodges, R., et al. (2003). α_1-Adrenergic and cholinergic agonists activate MAPK by separate mechanisms to inhibit secretion in lacrimal gland. *American Journal of Physiology. Cell Physiology* 284: C168–C178.

Wu, K., Jerdeva, G., da Costa, S., et al. (2006). Molecular mechanisms of lacrimal acinar secretory vesicle exocytosis. *Experimental Eye Research* 83: 84–96.

Lens Determination and Induction

T J Plageman, B Chauhan, and R A Lang, Cincinnati Children's Hospital Medical Center, Cincinnati, OH, USA and University of Cincinnati, Cincinnati, OH, USA

Glossary

Induction – A process that occurs during embryonic development in which one tissue signals to an adjacent tissue, altering the differentiation of the responding cells.

Lens fiber cells – Terminally differentiated cells that first form at the posterior of the lens vesicle, the side closest to the developing retina. Fiber cells become highly specialized for light refraction and transparency by the accumulation of large amounts of proteins, called crystallins.

Optic cup – A bilayered structure derived from the optic vesicle, an outpocketing of the forebrain. Invagination of the optic cup occurs at the same time that the lens is invaginating from the lens placode. Cells of the inner layer of the optic cup produce the retina.

Placode – A region of thickened epithelium caused by the crowding and elongation of the epithelial cells. Placodes are the source of several structures in the embryo, including the neural tube, inner ear, and lens.

Introduction

The Lens Is One Type of Light-Focusing Structure

Animals have developed many different types of eyes. These range from the multifaceted ommatidial eyes of insects to the camera eyes of vertebrates. There are some remarkable variations on these basic themes. For example, flies have evolved with their eyes positioned on long stalks as a mechanism of improved peripheral vision and of attracting a mate. There also exists a species of fish with bifocal corneas for simultaneous air and water viewing. These unusual examples indicate the remarkable plasticity, over evolutionary timescales, of the visual system.

In most types of eyes, there is a mechanism for focusing light on photoreceptors. In the familiar vertebrates, both cornea and lens are transparent and refractile and serve together to focus light on the retina. However, other solutions are possible and include variations like the Spookfish where a downward-looking eye uses a mirror-like surface to direct light onto photoreceptors or the solution that evolved in a species of turtle where a thickened cornea serves as the sole means for focusing light. The compound eyes of insects have lenses that are a complex of proteins secreted from the so-called cone cells. In the Duke-Elder volumes, one drawing suggests that a unicellular organism has a subcellular organelle with a lens-like component. These examples suggest that most species have some form of refracting lens and recommend these structures as an interesting subject for analysis. In this article, we review our understanding of development of the vertebrate lens. Most of the analysis has been performed in the popular experimental organisms such as the African clawed frog *Xenopus laevis*, the chick, *Gallus gallus*, the zebrafish *Danio rerio*, and the mouse, *Mus musculus*.

Lens Induction: An Auspicious Beginning

In 1901, Hans Spemann performed optic cup ablation experiments in amphibian embryos that resulted in the failure of a lens to form on the operated side. These experiments led directly to the concept of embryonic induction – the ability of one tissue to direct the fate of another – and began the study of lens induction. The interpretation of these experiments was initially controversial when Mencl identified a mutant salmon with lenses but no other eye components. Since then, many investigators performed similar optic cup ablation experiments, which have shown varying results that probably reflect the delivery of critical lens induction signals at different developmental stages in the different species used. In the mouse, it has become very clear that the retinal primordium and optic cup do provide signals that direct lens development, although over several stages of development and not exclusively. Understanding the nature of these signals is a major goal of the lens induction research field.

The Developmental Biology of Lens Formation

The Lens Undergoes Complex Morphogenesis

Studies in many different vertebrate species have shown that the lens of the eye is derived from the embryonic surface ectoderm (**Figure 1**). Morphologically, lens structures first become apparent when the surface ectoderm overlying the optic cup forms the thickened domain of

epithelium known as a placode, which develops when epithelial cells elongate through mechanisms that are currently not understood.

After placode formation, the presumptive lens begins invagination. This epithelial movement occurs in close coordination with the invagination of the presumptive retina. When the presumptive retina invaginates into the optic vesicle, the bilayered optic cup is formed. During coordinated invagination of the lens placode and presumptive retina, the two epithelia are joined by fine cytoplasmic processes (**Figure 2**). These were originally described in 1902 by Lenhossek and Magitot, then by Mann in 1950, and most recently, in 1980, by McAvoy. These cytoplasmic processes are transient in that they form in the mouse at about E9.0 just before invagination begins, increase in numbers to about one per cell by E10.5, and then disappear by E11.5. It may be that these structures are physical tethers that have a structural function in

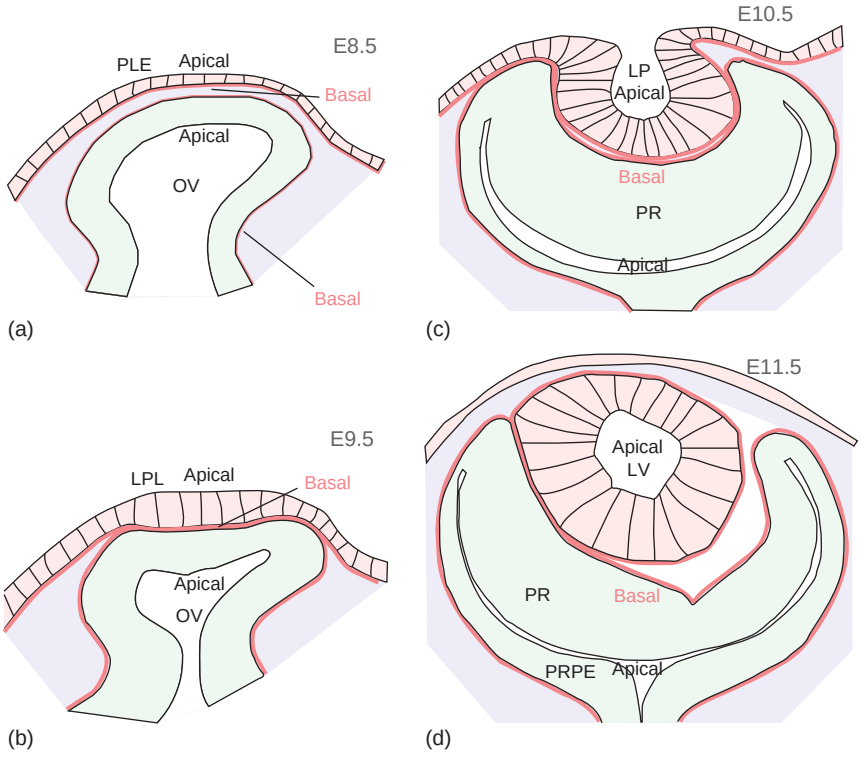

Figure 1 Early morphogenesis of the mouse eye. (a–d) Mouse eye development stages from E8.5 to E11.5 in daily intervals. The three tissue layers involved in eye development include the surface ectoderm (red) the mesenchyme (mauve), and the neuroepithelium of the optic vesicle (green). The apical and basal faces of the epithelia are indicated. PLE, presumptive lens ectoderm; OV, optic vesicle; LPL, lens placode; PR, presumptive retina; LV, lens vesicle; PRPE, presumptive retinal pigmented epithelium.

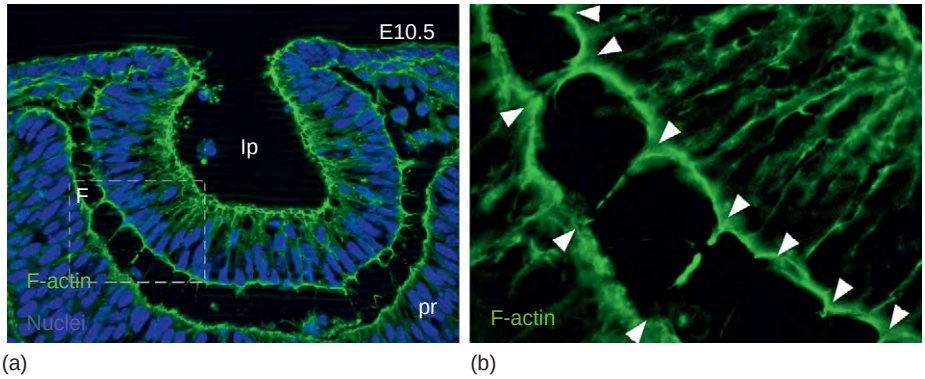

Figure 2 Cytoplasmic processes connect presumptive lens and retina during invagination. (a) An E10.5 mouse eye in section, labeled for F-actin with phalloidin (green) and nuclei (blue). A subregion of (a), indicated by the white dashed line, is shown at higher magnification in (b). The white arrowheads point to the cytoplasmic extension that connects presumptive lens and retinal epithelia. lp, lens pit; pr, presumptive retina.

coordinating epithelial morphogenesis or that they have an active signaling role.

The presumptive lens and retina are epithelia with apposed basal surfaces (**Figure 1**). Transmission electron microscopy studies have shown that fine basal laminae can be detected on both sides of the presumptive lens–presumptive retina interface. This arrangement of epithelial polarity means that during invagination of presumptive lens and retina, presumptive lens is invaginating basally and presumptive retina in the apical direction. Although the mechanisms of invagination are not understood, this opposite epithelial polarity may mean that the mechanisms of invagination in each epithelium are fundamentally distinct.

Johaan Zwaan and Richard Hendrix performed mathematical modeling of cell shape during invagination of the lens placode. Their major goal was to understand the forces required for invagination, but as part of this analysis, they carefully measured changes in epithelial cell shape. They concluded that lens placode invagination is accompanied by a change from cylindrically shaped to conically shaped epithelial cells. Since apical constriction can be an active process imposed, for example, by the Shroom3 molecule, it is tempting to speculate that apical constriction and the formation of conically shaped lens epithelial cells is the driving force behind invagination.

At E10.5 in the mouse, the lens pit is fully invaginated (**Figure 1**). After this, the major morphogenetic movement is the anterior extension of the lens pit epithelium to form a closure pore at the embryo surface. Fusion of the junction epithelium, that is, surface ectoderm distally and lens pit ectoderm proximally, forms the lens stalk, a structure that persists in a variety of mutants with mild lens development defects. Involution of the lens stalk by mechanisms that are not understood results in the formation of separated lens vesicle and the surface ectoderm that will become the corneal epithelium.

Within the lens vesicle, the lens fiber cells, which are the differentiated cell type, begin to form from the posterior wall of the lens vesicle at approximately E12.5. These are the primary lens fiber cells that go on to form the nucleus of the lens. Secondary lens fiber cells differentiate starting at approximately E14.5 from cells at the lens equator. These have migrated to the lens equator and originated in lens epithelial cells that proliferate to provide lens fiber progenitors. The formation of lens fiber cells and the nature of their differentiation program are addressed elsewhere in this encyclopedia.

Is There a Common Placodal Precursor Domain?

It has been suggested that in vertebrates, placode-derived structures such as the olfactory epithelium, lens, ear, and pituitary might all begin their existence at a common placodal region with uniform characteristics that later becomes further regionalized. The idea of a common placodal precursor derives partly from the morphology of some vertebrates – such as frogs – where the U-shaped region at the edge of the neural plate has uniform morphology and also gives rise to all the placodes. In addition, more recent analysis has suggested that there are common molecular characteristics across the placodal progenitor domain. These include expression of certain genes such as Pitx3 (in the zebrafish) and Six1, 2, and Eya2 (in the chick). Indeed, investigations using the chick have suggested that the common placodal precursor first has the characteristics of lens and, then later, under the influence of additional genes, becomes modified regionally to other structures. This whole idea has given further credibility to experiments showing that lenses can arise in unusual places when gene function is modified. These examples include the *you too* mutant zebrafish, where a *Gli2* gene mutation results in an ectopic lens forming from the adenohypophyseal (pituitary) placode, and misexpression of the *Six3* gene in Medaka, which results in an ectopic lens forming from the olfactory placode. Furthermore, in chicks with neural crest elimination, ectopic lenses arise close to the eye and in mice with fibroblast growth factor 4 (Fgf4) overexpression in the head ectoderm, ectopic lenses form in corresponding regions.

Genetic Regulation of Lens Development

Transcription Factors

After more than a decade of analysis, a reasonably sophisticated model has been generated that describes the genetic regulation of lens development in the mouse (**Figure 3** is a simplified version). Central to these pathways is paired box 6 (Pax6), the paired domain and homeodomain-containing transcription factor that has been implicated generally in metazoan eye development. Various experiments show that Pax6 is essential for lens development and that there are two distinct phases of expression. These include the so-called pre-placodal phase in the head surface ectoderm and the placodal phase that can be detected when the placodal morphology is obvious. According to an assessment of Pax6 gene transcription in a Pax6 point mutant, the placodal phase of Pax6 expression is dependent on functional gene product from the earlier, pre-placodal phase. For this reason, the Pax6 gene is often described as autoregulated (**Figure 3**).

The Pax6 gene is large and complex with multiple transcripts that are the consequence of multiple promoters and alternative exon splicing. Long-range sequence alignments of Pax6 gene sequences from a variety of species reveal that there are more than 30 highly conserved regions that presumably have a regulatory function. A few of these have been characterized. The so-called ectoderm enhancer

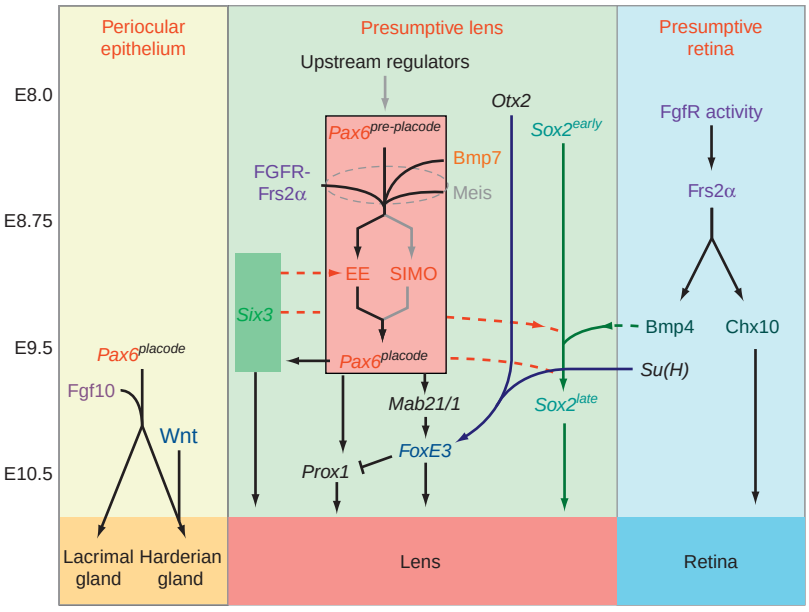

Figure 3 A model for genetic regulation of lens induction in the mouse. In this model, solid arrows represent expression dependency and dashed arrows a direct action. For example, evidence suggests that Six3 can directly bind the ectoderm enhancer (EE) of Pax6. A detailed description of this model is provided in the text.

of Pax6 not only is active in the lens placode but is also active in the surrounding ectoderm that includes the epithelia of the presumptive Harderian gland, lacrimal gland, and conjunctiva. This enhancer is just over 300 bp in length and is more than 90% conserved when comparing mouse and human. Thus far, it has been suggested that the myeloid ecotropic viral insertion site (Meis) transcription factors bind to this enhancer and activate Pax6. Furthermore, it has also been suggested that Six3 regulates Pax6 by binding to the ectoderm enhancer (**Figure 3**).

The so-called single input multiple output (SIMO) element of Pax6 is an enhancer that resides 240 kb downstream of Pax6 in the final intron of the adjacent gene. Heterozygous deletion of the SIMO element in humans or in mice results in an aniridia (without a lens) phenotype like Pax6 heterozygosity. This implies that SIMO is required for Pax6 expression. Since the SIMO element is sufficient to drive gene expression in the presumptive lens, it likely functions in concert with the ectoderm enhancer. This may explain why targeted deletion of the ectoderm enhancer still allows lens formation, albeit a small one.

In a Pax6 somatic mutant where Pax6 is rendered nonfunctional in the lens placode, no lens forms. Furthermore, Pax6 misexpression can lead to the formation of ectopic lenses in many locations. These data have indicated that Pax6 is necessary and sufficient for lens development.

Downstream of Pax6, there are other transcription factors that include Prox1, Six3, and FoxE3 (**Figure 3**). Analysis of Six3 somatic mutants has suggested that Pax6 and Six3 function in a positive-feedback loop that may serve to raise expression levels of both in the early lens. These same Six3 somatic mutants also show that Six3 is required for lens development from the placode stage onward. FoxE3 is a *forkhead* family transcription factor that is mutated in the *dysgenetic lens* mouse. In this mutant, the lens does not separate from the surface ectoderm and remains small. Prox1 is a homeodomain transcription factor that is critical for the development of lens fiber cells in the later lens. FoxE3 suppresses Prox1 expression and regulates the balance of proliferating and differentiating cells in the lens.

The Grainger group has also provided evidence to suggest that inducibility of the FoxE3 in the lens placode is dependent on an Otx2-binding site in a FoxE3 gene enhancer. Otx2 is not sufficient for FoxE3 expression but appears to be a necessary prerequisite. A critical activating signal for FoxE3 is believed to be the suppressor of Hairless (Su(H)) transcription factor that is a transducer of Notch signaling. The finding that the Notch ligand Delta2 is expressed in the optic vesicle explains the source of the Notch signal and is consistent with many years of developmental biology implicating the optic vesicle in lens induction. These findings are also very interesting because they suggest that Otx2, which is expressed broadly in head ectoderm, may be, in part, the basis of lens competence.

FoxE3 expression is also dependent on Pax6, as mentioned above, but analysis of Mab21l1 mutants suggests that this transcription factor acts as an intermediate between Pax6 and FoxE3. It is not yet understood whether Mab21l1 is a direct regulator of FoxE3. We can conclude that FoxE3 expression is dependent on at least three inputs – Otx2, Mab21l1, and Su(H) (**Figure 3**). It is likely

that this type of combinatorial regulation will be commonplace as we dissect lens induction and development mechanisms further.

The sex-determining region (Sry) family transcription factors, Sox1, 2, and 3, have all been implicated in lens development. For example, according to embryological manipulations in the chick, expression of Sox2 in the lens placode is dependent on the underlying optic vesicle. Furthermore, when Sox2 is mutated in the presumptive lens, with a few exceptions, lens development is arrested at the lens pit stage. Since Sox2 expression is unchanged in pre-placodal ectoderm of Pax6 mutant mice (and vice versa), Sox2 and Pax6 are believed to function in parallel at this stage (**Figure 3**). Recent data indicate that after the lens placode has formed, expression of Sox2 is dependent on Pax6. Investigation from the Kondoh group has shown that Pax6 and Sox2 can form a physical complex and, in one important element of lens development, regulate the expression of crystallin genes.

Signaling Pathways Involved in Lens Induction and Development

Bone Morphogenetic Protein

The bone morphogenetic proteins (BMPs) have important roles in the development of many structures in vertebrates. Although a germ-line mouse mutant is difficult to analyze because of early lethality, BMP4 has been implicated in lens induction. The BMP4 mutant does not increase the expression of the transcription factor Sox2 in the early lens, although the expression of Pax6 is unchanged. Since Sox2 has an important role in lens development, the regulation of Sox2 by BMP4 is further confirmation that BMP4 is also an important regulator. These data place BMP4 signaling upstream of Sox2 expression in the current model of the genetic regulation of mouse lens induction (**Figure 3**).

The eye phenotype apparent in the Bmp7 germ-line null mouse is highly variable, but does implicate this signaling molecule in lens induction. In Bmp7-null embryos that show a severe phenotype, there is a failure of the lens placode to form and arrest of eye development that includes the absence of lens fate acquisition and morphogenesis. Consistent with the absence of lens formation, Pax6 is not upregulated in the lens placode and remains at the low level normally observed earlier in the head surface ectoderm. Since Sox2 expression is unaffected in the Bmp7 mutant, it appears to have a function that is distinct from Bmp4. Indeed, the regulation of Pax6 by Bmp7 and Sox2 by BMP4 suggests that these two signaling molecules may function in parallel (**Figure 3**). In some Bmp7-null mutants, the phenotype is very much less severe and results only in a small eye. It is unclear why the Bmp7 phenotype is so variable but phenotypic variability is a characteristic of several of eye development mutants.

Fibroblast Growth Factor

Early work on the role of Fgf signaling in lens fiber cell differentiation prompted investigators to determine whether Fgf signaling might also be required for lens induction. This turned out to be the case with multiple methods of Fgf signaling suppression, indicating that this pathway was involved in lens induction. In particular, mutation of the fibroblast growth factor receptor substrate 2-alpha (Frs2α) adapter protein resulted in reduced Pax6 expression in the lens placode. Since lens placode-specific somatic mutation of Fgf receptors also results in a failure of lens development, it is clear that placodal cells respond to Fgf signaling during induction (other experiments have shown that the presumptive retina is also Fgf pathway responsive) (**Figure 3**).

In Frs2$\alpha^{2F/2F}$ mutants, the FGF signaling pathway is compromised in both presumptive lens and retina. One interesting feature of these mutants is the loss of Bmp4 expression within the optic vesicle and of Six3 expression in optic vesicle and presumptive lens. First, this places Six3 downstream of Fgf signaling. Since Pax6 in the presumptive lens is also dependent on Fgf signaling and Six3 is downstream of Pax6, these findings are consistent with a model in which FGF signaling–Pax6–Six3 is a linear pathway (**Figure 3**).

The dependence of BMP4 expression on FGF signaling is particularly interesting because it might explain how the two pathways are integrated during lens induction. Since BMP4 signaling increases the expression of Sox2, we can argue that BMP4 produced by the presumptive retina stimulates Sox2 expression in the surface ectoderm. Since Pax6 expression in presumptive lens is FGF pathway dependent, this would mean that FGF activates both Pax6 and Sox2 in presumptive lens (**Figure 3**). Recent investigations show that Pax6 and Sox2 cooperate functionally in early lens development.

Wnt

Wnt pathway signaling responses are generally referred to as canonical (involving β-catenin) and noncanonical. There are now many varieties of noncanonical Wnt signaling and although noncanonical Wnt signaling has been implicated in lens development, it is currently unclear which of these varieties. The canonical Wnt signaling system is well characterized but complex (**Figure 4**). Wnt ligands are lipid modified and are thus poorly soluble. Consistent with this, range-of-action experiments suggest that in many settings, Wnt signaling may occur through cell–cell contact. Canonical Wnt signaling requires two membrane components, the *frizzled* receptors and the Drosophila *arrow*-related co-receptors Lrp5 or Lrp6. In the mouse, there are nine Frizzled receptors. Lrp5 and Lrp6 are members of the larger class of low-density

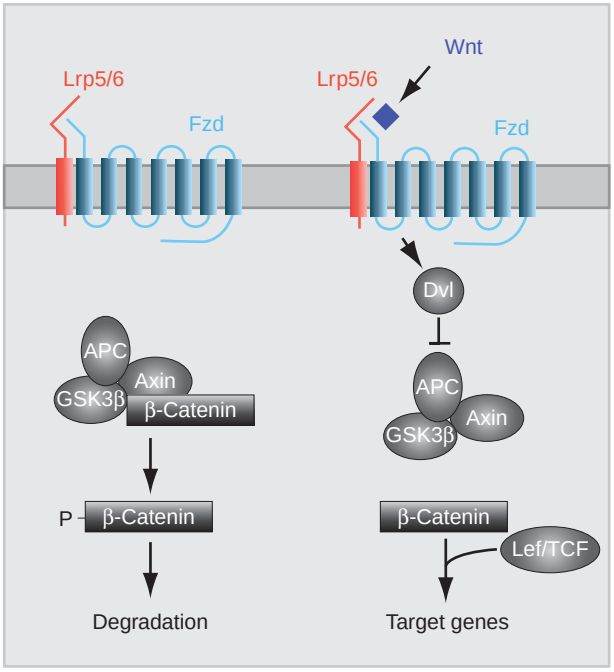

Figure 4 The canonical Wnt signaling system. In the absence of a Wnt ligand, a complex consisting of APC, axin, and GSK3β causes the phosphorylation-mediated degradation of β-catenin. In the presence of a Wnt ligand, Disheveled (Dvl) is activated by the receptor complex and suppresses the APC–axin–GSK3β complex allowing β-catenin to stabilize. In turn, β-catenin associates with transcription factors of the Lef/TCF family and regulates target gene transcription.

lipoprotein receptors, but Lrp5 and Lrp6 are the only ones closely related to arrow, the co-receptor for *Drosophila* Wnt signaling. Wnt ligand engagement by Frizzled/Lrp5/6 complex results activates Dishevelled (Dvl) and suppresses the glycogen synthase kinase-3β (GSK3β), axin, adenomatosis polyposis coli (APC) degradation complex. In the absence of ligands, GSK3β phosphorylates β-catenin and results in its degradation through APC and the proteasome. When Dvl suppresses GSK3β, β-catenin is stabilized, binds TCF/Lef transcription factors and regulates target genes.

Canonical Wnt signaling pathways have been implicated in the regulation of lens development. The McAvoy group has provided evidence that canonical Wnt signaling reporters are expressed in the lens epithelium and that there is a lens epithelial defect in the few *Lrp6* mutant embryos that survive to later stages of lens development. The canonical Wnt signaling pathway has also been implicated in restricting the domain of surface ectoderm that can form lens. This activity is demonstrated when β-catenin function – an essential Wnt pathway component – is functionally deleted from the surface ectoderm. This results in the formation of not only small ectopic lentoid bodies throughout the head ectoderm, but also a large ectopic lentoid structure immediately nasal to the eye. Since there is normally a small region of Wnt-responsive ectoderm that forms the Harderian gland nasal to the eye, this leads to the suggestion that canonical Wnt pathway activity normally redirects ectoderm from a lens fate to a Harderian gland fate (**Figure 3**). This is quite consistent with general conclusion that the canonical Wnt pathway often functions to suppress differentiation. There is a set of genes known to be directly regulated level by the canonical Wnt signaling pathway and presumably some of these participate in lens development.

There are a number of mutant mice in which the optic vesicle fails to develop and, as a consequence, no lens is formed. This is the modern-day equivalent of Spemann's optic cup ablation experiments. The Lhx2 and Rx mutant mice both have this characteristic. In an interesting extension of our understanding of β-catenin function, the Jamrich group has shown that the lens development failure of the Rx mutant mice can be largely rescued by deletion of β-catenin in the presumptive lens. This might mean that the optic vesicle normally suppresses Wnt signaling to permit lens development or that the adhesion function of β-catenin is an important regulator. However, further work is required to understand this in detail.

Notch

The Notch pathway is a well-characterized means to regulate cell fate decision. In many cases, Notch signaling is employed in binary cell fate decisions where two distinct cell types are produced. As touched on above, the Notch signaling pathway has been implicated in lens induction with evidence suggesting that Delta2 in the optic vesicle signals to the overlying presumptive lens ectoderm to initiate expression of FoxE3. It has also been shown that the Notch pathway has a role in later lens development in regulating the balance between lens epithelial and lens fiber cells. This is an appealing setting for the Notch pathway because, again, it represents a binary cell fate decision.

Concluding Comments

The lens has proven an excellent model system for developmental biologists because of its relative simplicity. With the increasing sophistication of genetic tools in the vertebrate models, we can anticipate that our understanding of lens development will become increasingly sophisticated. In particular, the lens is likely to serve as an excellent model system in which to understand the processes of morphogenesis that are such a prominent component of its development.

See also: Lens Fiber Cell Differentiation; Lens Regeneration; Lens Structure.

Further Reading

Chow, R. L., Altmann, C. R., Lang, R. A., and Hemmati-Brivanlou, A. (1999). Pax6 induces ectopic eyes in a vertebrate. *Development* 126: 4213–4222.

Furuta, Y. and Hogan, B. L. M. (1998). BMP4 is essential for lens induction in the mouse embryo. *Genes and Development* 12: 3764–3775.

Lang, R. A. (2004). Pathways regulating lens induction in the mouse. *International Journal of Developmental Biology* 48: 783–791.

Medina-Martinez, O. and Jamrich, M. (2007). Foxe view of lens development and disease. *Development* 134: 1455–1463.

Ogino, H., Fisher, M., and Grainger, R. M. (2008). Convergence of a head-field selector Otx2 and notch signaling: A mechanism for lens specification. *Development* 135: 249–258.

Robinson, M. L. (2006). An essential role for FGF receptor signaling in lens development. *Seminars in Cell and Developmental Biology* 17: 726–740.

Wawersik, S., Purcell, P., Rauchman, M., et al. (1999). BMP7 acts in murine lens placode development. *Developmental Biology* 207: 176–188.

Relevant Website

http://www.stanford.edu/~rnusse/wntwindow.html – The Wnt homepage; 1997–2009 Roel Nusse.

Lens Fiber Cell Differentiation

M L Robinson, Miami University, Oxford, OH, USA

Glossary

Connexins – The membrane proteins which form gap-junction channels that connect the cytoplasm of adjacent cells. Lens fiber cells have abundant fiber-specific connexins (Cx46 or Gja3 and Cx50 or Gja8) that are found in few other tissues.

Lens capsule – An extracellular matrix, secreted by the epithelial and superficial fiber cells, which surrounds the lens. The capsule can be thought of as a multilayered basal lamina, composed of the proteins laminin, type 4 collagen, entactin, and other typical components of basal laminae.

Lens vesicle – The hollow sphere of epithelial cells that results from the invagination of the lens placode early in eye development. Lens epithelial cells are derived from half of the vesicle closest to the surface ectoderm, while primary fiber cells are derived from the half nearest the future retina. These cells elongate and fill the lumen of the vesicle.

Secondary fiber cells – The fiber cells derived from the equatorial region of the lens epithelium. These cells are formed in successive waves throughout life, burying primary fiber cells and older secondary fiber cells deeper in the lens fiber mass.

Primary Fiber Cell Differentiation

In terrestrial vertebrates, the first morphological sign of lens development is the thickening of the surface ectoderm overlying the optic vesicle to form a lens placode (**Figure 1(a)**). The placode subsequently invaginates, forming the lens pit (**Figure 1(b)**). The lens pit deepens and eventually the connection of the pit to the surface, known as the lens stalk, narrows, closes off, and disintegrates, forming the initially hollow lens vesicle (**Figure 1(c)**). All of the cells of the lens vesicle are polarized, with basal surfaces facing outward and apical surfaces facing the lumen of the vesicle.

The lens vesicle contains the precursors of all the cells in the lens. Initially, all cells of the lens vesicle are capable of proliferation, with the fate of each cell determined by its position within the vesicle. The most posterior cells of the vesicle (closest to the developing neural retina) begin elongating as they become the primary lens fiber cells, while the cells lining the anterior hemisphere of the lens will differentiate into the lens epithelium (**Figure 1(d)**). The elongation of the primary fiber cells will continue until the apical ends of the fiber cells have reached the apical surface of the lens epithelial cells lining the anterior of the vesicle. As the lens grows, elongating secondary fiber cells will displace the attachment of the primary fiber cells to their basement membrane (the lens capsule), at the posterior, and to the lens epithelial cells, at the anterior. This process forms the embryonic lens nucleus, which remains in the center of the lens throughout life. During differentiation, all lens fiber cells, whether primary or secondary, withdraw from the cell cycle, elongate, express several fiber-cell-specific proteins (including differentiation-specific crystallins), and will ultimately degrade all intracellular organelles.

The Lens is a Stratified Epithelium

Pax6 is a transcription factor essential for the development of all surface-ectoderm-derived eye structures, including the lens. The Pax6-expressing surface ectoderm, overlying the lens vesicle, will differentiate into the corneal epithelium, conjuctiva, and eyelid epithelium, and the surrounding surface ectoderm that does not express Pax6 will differentiate into epidermis. All of these tissues are stratified epithelia, defined as having multiple layers of cells with only the basal cells remaining in contact with the basement membrane. The lens can also be thought of as a stratified epithelial tissue. Although all of the cells of the lens vesicle and the lens epithelial cells remain attached to the basement membrane (lens capsule), fiber cells eventually lose their attachment to the lens capsule and eventually form layers of fiber cells with the oldest (primary) fiber cells in the center with progressively younger layers of secondary fiber cells, derived from the lens epithelium, at the periphery.

Secondary Fiber Cell Differentiation

Primary fiber cells are only those fiber cells derived from the posterior cells of the lens vesicle. The majority of fiber cells present in the mature lens are derived from the continuous differentiation of lens epithelial cells, which takes place at the lens equator.

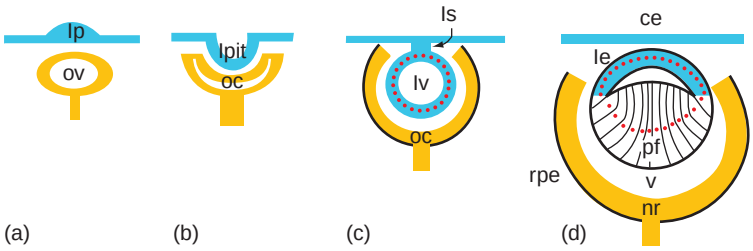

Figure 1 Early stages of terrestrial vertebrate lens development. (a) The first morphological sign of lens development is a thickening of surface ectoderm overlying the optic vesicle (ov) into a lens placode (lp). (b) The lens placode subsequently invaginates to form a lens pit (lpit) as the optic vesicle invaginates to form the optic cup (oc). (c) The lens pit eventually forms a hollow, closed lens vesicle (lv) consisting of a single layer of cells initially joined to the overlying surface ectoderm through a transient lens stalk (ls). At this time, the outer layer of the optic cup starts differentiating into the retina pigment epithelium (rpe). (d) The cells making up the posterior half of the lens vesicle begin the process of elongation signaling the initial differentiation of the primary lens fiber cells (pf). The anterior cells of the lens vesicle will differentiate into the lens epithelium (le) and the overlying surface ectoderm is fated to become the corneal epithelium (ce). The inner layer of the optic cup will subsequently differentiate into the neural retina (nr). The space between the lens and neural retina is where the vitreous (v) will eventually form.

Cell-Cycle Withdrawal

As the lens epithelium differentiates from the anterior lens vesicle cells, lens cell proliferation becomes restricted to a narrow band of cells slightly anterior to the lens equator known as the germinative zone. As cell proliferation in the germinative zone continues, some epithelial cells are displaced toward the equator into a region of postmitotic cells called the transitional zone (in most mammals) or the annular pad (in birds and most reptiles). In mice, the transitional zone is only six to seven cells wide. It is while the cells are in the transitional zone that the very first molecular signs of secondary fiber cell differentiation become apparent. These cells increase their synthesis of the transcription factor Prox1 and the cyclin-dependent kinase inhibitor p57Kip2. The *p57Kip2* gene is paternally imprinted in mammals and is essential for proper cell-cycle withdrawal during fiber differentiation. As cells move through the transitional zone toward the equator, their nuclei go from being randomly arranged to lining up in radial columns called meridional rows (**Figure 2(a)**). This establishment of regular packing order is the first morphological evidence of secondary fiber cell formation and is the genesis of the hexagonal shape (easily seen in lens cross sections along the equatorial plane) maintained by secondary fiber cells throughout their subsequent differentiation stages (**Figure 2(b)**). In contrast, primary fiber cells in the embryonic lens nucleus do not exhibit a regular hexagonal packing shape in cross section (**Figure 2(c)**).

Fiber Cell Elongation

As meridional rows are forming, these differentiating cells begin the process of elongation. There is evidence from chick lens epithelial explants that primary fiber cell elongation is driven by increased cytoplasmic volume resulting both from increased intracellular potassium and by increased protein synthesis. In contrast, morphometric confocal microscopy studies on living mouse lenses demonstrated that initial elongation of secondary fiber cells is not coupled with a directly proportional increase in cell volume. Although fiber cells are much longer than epithelial cells, they are also much thinner, and exhibit a ribbon-like morphology. The driving force for the initial elongation of lens epithelial cells appears to be changes in cell shape mediated by cytoskeletal remodeling. The precise mechanism of this remodeling is not known, but fiber cell elongation is insensitive to nocodazole, suggesting that microtubules are not essential for the process. These young differentiating secondary fiber cells are found at the lens equator and the arrangement of the nuclei of differentiating cells in this region (seen in transverse lens sections) resembles the arc of a bow from which the bow region of the lens received its name (**Figure 2**).

Crystallin Synthesis

Upon differentiation, fiber cells begin synthesizing large quantities of fiber-cell-specific (or fiber-cell-preferred) crystallins, most notably the β-crystallins (in all vertebrate lenses) and γ-crystallins (which are largely missing from birds) and several other taxon-specific crystallins. Crystallins are typically very stable proteins, and collectively crystallins accumulate to extremely high concentrations in the lens fiber cells. The extremely high protein content of lens crystallins is thought to be necessary for short-range order required for the transparency and refractive power of the lens.

Fiber Cell Membranes

As lens fiber cells mature, several membrane specializations occur. There are a number of membrane proteins that are only found in lens fiber cells. The most abundant of these is aquaporin 0 (AQP0); also known as major

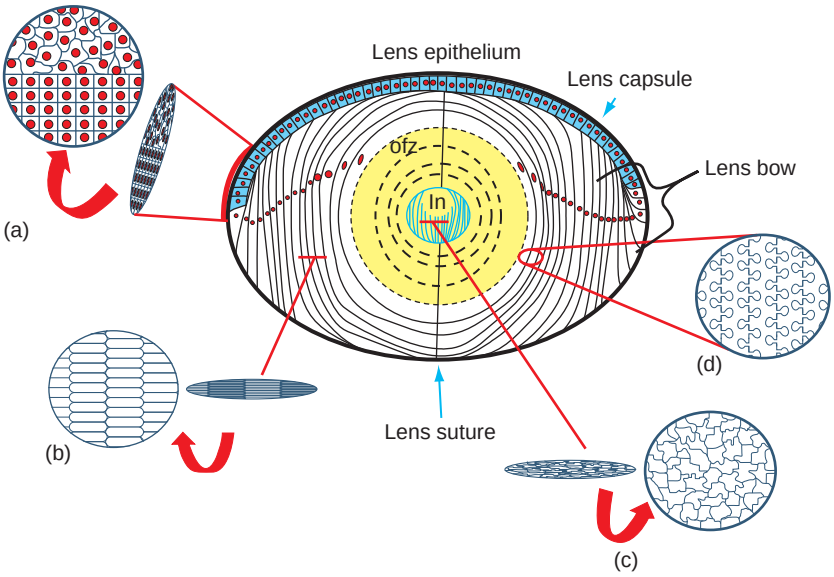

Figure 2 A transverse view of a section of mature lens. The lens epithelium occupies a single layer of cuboidal cells lining the anterior hemisphere of the lens (shaded cells). The entire lens surface is covered with a lens capsule. (a) The first morphological sign of secondary fiber differentiation is the formation of meridional rows of lens cells as previously randomly arranged transitional zone lens epithelial cells approach the equator. These meridional rows of cells begin elongating with basal fiber ends remaining in contact with the lens capsule and apical ends contacting the lens epithelium. The arrangement of nuclei (red circles) when viewed in transverse section form the characteristic lens bow representing the differentiation zone of cortical secondary fiber cells. (b) Cross sections through the lens cortex demonstrate the hexagonal arrangement typical of secondary lens fiber cells. (c) Cross sections through the embryonic lens nucleus (ln) containing the primary lens fiber cells do not resemble the hexagonal arrangement of secondary fiber cell membranes. Eventually, the cortical fiber cells detach from the lens capsule and the lens epithelium and join oppositely oriented lens fiber cells to form anterior and posterior lens sutures, the pattern of which is characteristic for a given species. (d) Fiber cell membranes become progressively more intertwined by ball-and-socket joints as they mature. Just before the destruction of nuclei and other cytoplasmic organelles mature, fiber cell membranes fuse and open large cytoplasmic pores that allow for the movement of proteins and other materials throughout the syncytium of the lens organelle free zone (ofz).

intrinsic protein (MIP) or MIP26, it is the founding member of the aquaporin water channel family of proteins, but its water permeability is much less than that of AQP1 (present in epithelial cells including lens epithelium). AQP0 is also pH dependent, being more active at low pH. It contributes as much as 60% of total fiber cell membrane protein and is responsible for the bulk of water transport between fiber cells. The relatively low water permeability and high abundance of AQP0 suggest that it serves a dual role of both a cell–cell channel and adhesion molecule in the lens. MP20 (also known as lens intrinsic membrane protein 2 (LIM2)) is also an abundant fiber-cell-specific membrane protein. It is a tetraspanin protein thought to act as a transmembrane scaffolding protein aiding in the assembly of membrane signaling complexes. In contrast to AQP0, which is always membrane associated, MP20 is cytoplasmic in young fiber cells and is exclusively localized to the membrane corresponding to the stage when lens nuclei are degraded. Mutations in either AQP0 or MP20 cause cataracts in mice.

The membranes of both lens epithelial cells and lens fiber cells are connected through gap junctions formed by connexin proteins. Although the nomenclature and molecular size of gap-junction orthologs differ among vertebrate species, the lens contains three gap-junction proteins that demonstrate differential expression patterns. The lens epithelium expresses two of these, known as connexin 43 (also known as gap-junction protein, alpha 1 (Gja1)) and connexin 50 (also known as Gja8), in mice and humans. Upon fiber differentiation, connexin 43 expression ceases, connexin 50 expression continues and connexin 46 (also known as Gja3) expression initiates. Connexin 43 is expressed in many tissues, but connexins 46 and 50 are found only in the lens. Subunits of connexins 46 and 50 may mix in fiber cells to form heteromeric gap-junction channels. Mice lacking either connexin 46 or 50 develop cataracts. Connexin 50 also plays a specific role in lens growth as lenses lacking this connexin are significantly smaller than wild-type lenses. While connexins are generally thought to function specifically through the formation of gap junctions, there is some evidence that expression of connexin 45.6 (the chick ortholog of connexin 50) is capable of stimulating fiber cell differentiation, independent of its ability to form a functional gap-junction channel.

As fiber cells mature, several structural membrane modifications develop. Among these is the formation of interdigitations between the lateral surfaces of neighboring fiber cells known as ball-and-socket junctions (**Figure 2(d)**).

These junctions interlock the fiber cells together and help keep adjacent fibers from sliding past each other when the lens stretches during accommodation. In the deeper (older) secondary fiber cells, this interlocking nature is exaggerated by the formation of paddle-like extensions that are formed after organelles are eliminated, suggesting that their formation does not require *de novo* protein synthesis. Finally, in the oldest nuclear fiber cells, a further level of compression is achieved by the formation of accordion-like folds of fiber cells in the plane of the visual axis.

Fiber cells also have both basal and apical membranes. The basal membrane is initially in contact with the lens capsule through an extensive basal membrane complex consisting of a lattice-like network of neural cadherin (N-cadherin), fibrous actin (F-actin), and myosin. The basal ends of the fiber cells adhere to the capsule through α6β1 integrin interaction with capsular laminin-1. The contractile proteins present in the basal membrane complex allow fiber cells to migrate in a posterior direction along the capsule as they mature. The apical membrane of young fiber cells is apposed to the apical membrane of lens epithelial cells. Although there are some gap junctions connecting the apical–apical fiber–epithelial interface, these are relatively rare and it is thought that little molecular transport occurs across this interface. The apical membrane does contain an actin network, but the organization is not as regular as seen in the basal membrane complex. Nevertheless, the apical fiber cell membrane also migrates in an anterior direction as fiber cells mature. As secondary fiber cells elongate in mammals, they assume an opposite-end curvature giving them a three-dimensional S-shape. The basal membrane complex breaks down as the posterior end of the fiber cell reaches the lens suture branch. Likewise, the apical membrane loses its attachment to the epithelium near the anterior suture branch. The basal and apical ends of oppositely oriented fiber cells flare outward relative to their mid-portions and join to form posterior and anterior lens sutures, the pattern of which is characteristic for any given species. In the final phases of lens fiber differentiation, lens cell membranes partially fuse and large pores form creating cytoplasmic connections between fiber cells. This process takes place shortly before intracellular organelles are destroyed and results in what is known as the lens syncytium. Large molecules, including proteins, can diffuse from cell to cell within this most central region of the lens.

Fiber Cell Cytoskeleton

Fiber cells also develop an extensive cytoskeletal network. Although the cell adhesion molecule, N-cadherin, is found in both epithelial cells and fiber cells, it specifically localizes to fiber cell membranes upon differentiation. N-cadherin also co-localizes with F-actin and β-catenin on the lateral membranes of the hexagonally packed fiber cells. In contrast, N-cadherin associates with γ-catenin at the vertices of the fiber cell hexagons. γ-Catenin also associates with desmoplakin and vimentin intermediate filaments in this N-cadherin-based junctional complex. Lens fiber cells also uniquely express components of intermediate beaded filaments, filensin (CP115) and phakinin (CP49). Proteomic studies have demonstrated an interaction of both filensin and phakinin with AQP0 at the cell membrane. Phakinin and vimentin also associate with lengsin at fiber cell membranes. Lengsin is a lens-specific protein related to glutamine synthase which appears to have been evolutionarily recruited to serve as a lens cytoskeletal protein in vertebrates. In mice, lengsin expression initiates in fiber cells just prior to organelle loss. Interestingly, this is precisely the time when beaded filaments undergo a redistribution from being primarily associated with the plasma membrane to being distributed throughout the cytoplasm. Cytoskeletal remodeling is an essential component of both fiber cell elongation and migration. Networks of F-actin and myosin IIB, predominantly localized at the basal membrane complex, are likely regulated by myosin light-chain kinase and small guanosine triphosphate (GTP)-binding proteins such as Rho. Protrusive lamellipodia-like processes have also been observed on both basal and apical fiber cell tips, suggesting that these cellular extensions may play a direct role in the migration of the ends of the fiber cells.

Organelle Elimination

The lack of organelles is one of the most striking features of a fully mature fiber cell. Failure to eliminate organelles from mature fiber cells results in light scattering and cataract formation. Fiber cells are transcriptionally and translationally active until shortly before the loss of nuclei. Evidence for this comes from the expression of at least two proteins (lengsin and hop) in mouse fiber cells between the time of capsule detachment and nuclear loss. The process of nuclear breakdown takes place over some period of time and the morphological events associated with nuclear destruction vary among species. In contrast, the loss of mitochondria and other organelles takes place very rapidly, over the course of a few hours. The end of the nuclear breakdown and loss of other cytoplasmic organelles are coordinated such that there is a sharp boundary between organelle-containing fiber cells and the organelle-free zone (**Figure 2**). The destruction of the nucleus and other cytoplasmic organelles has been compared to the process of apoptosis, but in contrast to apoptosis, fiber cells must remain in place to ensure transparency of the lens as a whole. Recent evidence has also demonstrated that the proteases that initiate the destructive processes in apoptosis (caspase-3, caspase-6, and caspase-7) are not required for organelle breakdown in lens fiber cells. In contrast, DNase IIβ, which is not essential for apoptosis, is required fiber cell denucleation.

Mice lacking this enzyme develop nuclear cataracts and retain DNA-containing nuclear remnants in mature fiber cells. However, mature fiber cells deficient in DNase IIβ do not contain mitochondria and other organelles, suggesting that DNase IIβ is not required to initiate organelle loss. Lactacystin (an inhibitor of the ubiquitin–proteosome pathway) is able to inhibit mitochondrial breakdown in lens fiber cells *in vivo*, suggesting that the ubiquitin–proteosome pathway is required for the creation of the organelle-free zone. The regulatory mechanism that triggers organelle breakdown in the lens is not known. A number of different mutations and perturbations of the lens appear to inhibit nuclear breakdown, but these may be secondary to their disruption of fiber cell homeostasis, as organelle loss is a late event in fiber cell maturation. It has been hypothesized that organelle loss may be triggered by a combination of decreasing oxygen concentration and increasing calcium concentration as fiber cells move further from the superficial layers of the lens cortex, but the resolution of the precise trigger for organelle breakdown remains a matter of debate.

The entire lens is surrounded by a lens capsule which is secreted by the lens cells. This capsule starts out as the basement membrane of the lens vesicle cells and thickens as the lens matures. The capsule ensures that no cells enter or leave the intact lens. Occasional apoptotic cells appear within the lens epithelium during normal development. However, most lens cells remain in the lens for the life of the organism. Analogous to the way the history of a tree is retained within its rings, the developmental history of a lens is also retained within the tissue. The primary fiber cells remain at the center of the lens, forming the embryonic lens nucleus. Therefore, the cells within the embryonic lens nucleus are among the oldest cells in the body. The embryonic lens nucleus is enveloped by layer upon layer of secondary fiber cells with progressively younger cells being found in a central to peripheral gradient. The lens epithelium remains as a single layer of cells lining the anterior lens hemisphere.

Experimental Approaches to Study Lens Fiber Cell Differentiation

Classical experiments by Coulombre and Coulombre in the 1960s provided the first direct evidence that the polarity of the lens (with the epithelium on the anterior lens surface and the differentiated fiber cells posterior to the epithelium) was dictated by extrinsic factors. In these experiments, embryonic chick lenses were surgically reversed such that the lens epithelium faced the retina and the posterior surface of the lens faced the cornea. Within a few days, the epithelial cells on the reversed lens surface formed a new fiber cell mass and the equatorial epithelium migrated anteriorly to form a new epithelium on what had been the posterior face of the lens. This suggested that factors in the vitreous (the gel-like material between the retina and lens) promoted lens fiber differentiation and that factors in the aqueous (fluid between the cornea and lens) promoted lens epithelial maintenance. Similar experiments conducted with mouse eyes by Yamamoto in 1976 reached similar conclusions.

Most of the current molecular understanding of the regulation of fiber differentiation comes from three basic types of experiments. The first of these is the study of primary dissociated lens epithelial cells in culture; the second experimental system is the lens explant; and the third is direct studies in living embryos or genetically manipulated animals.

Dissociated lens epithelial experiments are often done with isolated chick lens epithelial cells grown on different substrates that differentially promote migration or differentiation of these epithelial cells to fiber-like cells present in aggregations of cells called lentoid bodies. These lentoid bodies express fiber-preferred crystallins and exhibit many of the features of normal lens fiber cells. The advantages of these experiments include the relative ease by which these cells can be transfected and grown in culture. The most common criticism of this experimental approach lies in the fact that epithelial cells often behave abnormally when separated from their normal basement membrane.

Lens explants are prepared by removing the fiber cells from the lens while leaving epithelial cells attached to the lens capsule. As the attachment of the lens epithelial cells to the capsule is quite strong, this can be accomplished simply by peeling off the capsule and removing the fiber cell mass. The capsule can then be pinned to a culture dish with the epithelium either above or below the capsule. Epithelial cells cultured in this way can go through all of the stages of fiber differentiation including organelle loss. Another similar approach is the lens capsular bag, where the lens fiber cell mass is removed through a hole in the capsule much the way cataracts are surgically removed in the clinic. Epithelial cells will remain attached to the capsule and the whole capsule with epithelial cells attached can be grown in culture. These approaches have the advantage of being amenable to defined culture conditions without disrupting lens epithelial cell polarity, cell–cell interaction, or cell–basement-membrane interaction.

It is always most powerful to be able to elucidate developmental pathways in the context of normal development. Unfortunately embryonic development *in vivo* is complicated and achieving defined experimental conditions is difficult. Modern genetic techniques that specifically add or subtract genetic information during development have contributed a great deal to our present understanding about regulatory networks involved in lens fiber differentiation. RNA interference (RNAi), morpholinos, and gene targeting in embryonic stem cells can be used to knock down or knock out specific gene expression, while transgenic, *in vivo* electroporation and viral vector strategies can easily add genetic

information to the developing embryo. Although many modern genetic strategies are amenable to manipulating development in a wide variety of species, unless otherwise noted, the references about the role of specific genes during *in vivo* fiber differentiation for the remainder of this article are derived from studies in using transgenic or gene-targeted mice.

Regulation of Fiber Cell Differentiation

Although the precise molecular events initiating primary lens fiber cell differentiation *in vivo* are not known, gene deletion studies in mice have revealed several genes essential for this process. Obviously, transcription factors essential for lens induction (e.g., Pax6) will secondarily be essential for lens fiber cell differentiation. Cells of the lens vesicle initially express a set of characteristic transcription factors, including Foxe3, c-Maf (or L-Maf in the case of chickens and Xenopus), Pax6, Pitx3, Prox1, Six3, and at least one member of the group B1 Sox genes (Sox1, Sox2, and/or Sox3, depending on the species). Genetic studies in several organisms demonstrate that each of these transcription factors is required for lens formation and/or development. While it is sometimes difficult to discern where to draw the line between those genes necessary for lens induction and those required for later stages of lens development, there are genes that appear to be specifically important for fiber cell differentiation. Defects in many of these disrupt normal primary lens fiber differentiation, often resulting in a lens where the fiber cells fail to fill the lumen of the lens vesicle.

Transcription Factors

Primary fiber cells in mice deficient for the transcription factors, c-Maf, Prox1, and Sox1, fail to completely elongate, inefficiently withdraw from the cell cycle, and are missing specific subsets of crystallin proteins. In particular, c-Maf-deficient mice have very low-to-undetectable levels of β- and γ-crystallin expression. The discovery of functional c-Maf-binding sites in the promoters of many crystallin genes suggests that these crystallins are directly regulated by c-Maf. c-Maf-binding sites have not been identified in the promoters of filensin, phakinin, and AQ0, but the expression of all of these genes is greatly reduced in *c-Maf* knock-out mice, suggesting that these genes are indirectly regulated by c-Maf. Likewise, Sox-binding sites are present in the promoters of all of the genes in the mouse gamma crystallin cluster (γA, γB, γC, γD, γE, and γF) and none of these genes is expressed in *Sox1* knock-out mice despite persistence of β-crystallin gene expression. Sox2 and/or Sox3 are important in lens induction of several species as well, but it appears that the role of Sox1 is most important during the fiber differentiation stage of development, at least in mice. Prox1-deficient mice do not express γB or γD crystallins and fail to increase the levels of the cyclin-dependent kinase inhibitor, p57Kip2, which likely explains the failure of lens cells from this mutant to withdraw from the cell cycle. Another transcription factor, Pitx3, is expressed in the lens placode and vesicle and Pitx3 expression within the lens is highest in the bow region. Lenses in mice homozygous for the spontaneous *Pitx3* mutation, *aphakia*, degenerate shortly after the initiation of primary fiber cell differentiation. The phenotype of the Pitx3 mutant mice differs from that of the c-Maf, Sox1, and Prox1 mutants in that there is no persistence of a hollow lens vesicle. It is likely that defective lens development of Pitx3 mutants is more a problem of lens specification/induction than specifically with fiber cell differentiation. Experiments in zebrafish suggesting that Pitx3 is in a genetic pathway upstream of Foxe3, which is required for the normal development of lens epithelial cells, support this notion.

Several other transcription factors need to be down-regulated during fiber cell differentiation. Notably, Pax6, and Foxe3 expression falls during lens fiber cell differentiation and transgene-mediated overexpression of either of these transcription factors in maturing fiber cells results in abnormal differentiation.

Growth Factors

The search for the fiber cell differentiation factor has been going on at least since the experiments of Coulombre and Coulombre demonstrated that factors supplied by the ocular environment control lens fiber differentiation. Vitreous fluid is a rich source of factors that can induce lens fiber differentiation in lens epithelial explants. Multiple lines of evidence suggest that both bone morphogenetic proteins (Bmps) and fibroblast growth factors (Fgfs) are present in the vitreous fluid and play a role in lens fiber differentiation. Experiments performed with dissociated chick lens epithelial cell monolayers have demonstrated that both Fgfs and Bmps are capable of stimulating lens epithelial cell elongation as well as the expression of several fiber-cell-specific genes.

The importance of both Fgf- and Bmp-mediated signal transduction cascades in fiber cell differentiation is also supported by genetic studies in mice. Clearly, Bmp4 and Bmp7 are important for lens induction, as lens formation is inhibited in mice lacking either of these growth factors. The role of Bmps, specifically in fiber cell differentiation, has been more difficult to discern. Mice lacking the type I Bmp receptor, *Acvr1* (*Alk2*), develop elongated fiber cells that express many characteristic fiber cell proteins. These Acvr1-deficient cells did display a defect in cell-cycle withdrawal that normally accompanies fiber cell differentiation, likely due, at least in part, to decreased expression of p57Kip2 (**Figure 3**). Similarly, mouse lenses lacking

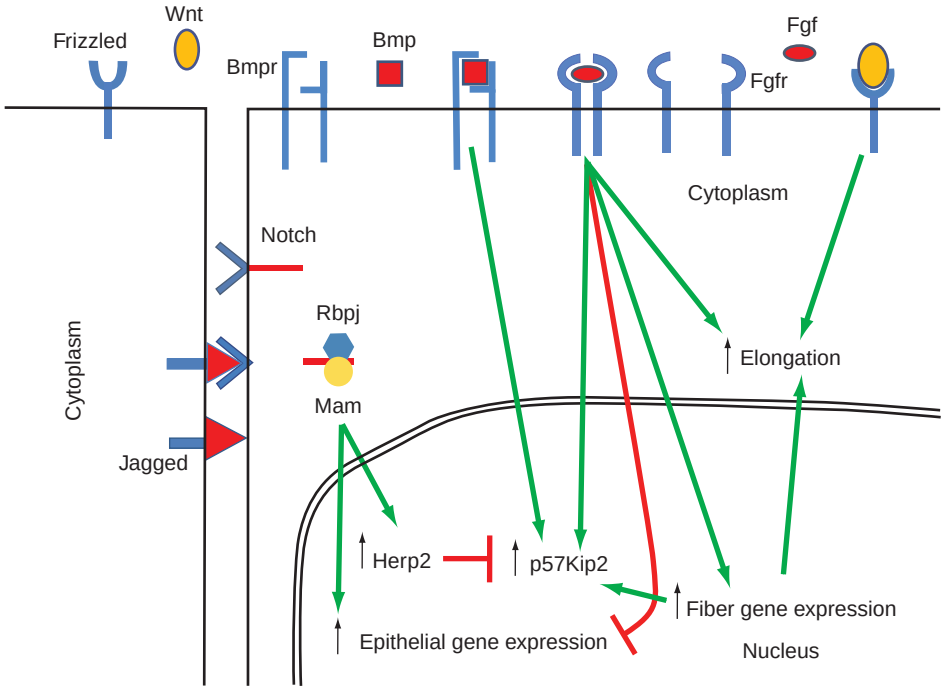

Figure 3 Ligand–receptor signaling controlling fiber differentiation in lens epithelial cells. Adjacent lens epithelial cells are shown with Bmp receptors (Bmprs), Fgf receptors (Fgfrs), Frizzled receptors and Notch receptors embedded in the plasma membrane and soluble Bmp, Fgf, and Wnt ligands as well as cell-associated Jagged ligands. Upon Jagged activation of Notch receptors present on the plasma membrane, the intracellular domain of Notch disassociates with the membrane and associates with Rbpj and Mam proteins to form a transcriptional signaling complex that directly activates expression of Herp2 and directly or indirectly promotes lens epithelial gene expression. Herp2 directly inhibits the promoter for p57Kip2, thus keeping lens epithelial cells in the cell cycle. Bmp and Fgf signaling increase p57Kip2 expression and cell-cycle withdrawal. Fgf signaling also promotes the expression of several lens fiber-cell-specific genes and aids in the repression of gene expression associated with lens epithelial cells. Fgf signaling also promotes lens fiber elongation as does Wnt signaling, most likely acting through the Wnt/planar cell polarity pathway.

intracellular mothers against decapentaplegic (Smad) proteins necessary for canonical Bmp signaling (Smad1, Smad4, or Smad5) exhibit elongating fiber cells that fail to completely exit the cell cycle. Transgenic mice expressing the Bmp inhibitor, noggin, in the lens undergo morphologically normal primary fiber cell differentiation, but display inhibition of secondary fiber cell differentiation. These noggin transgenic mice eventually display a lens epithelial layer that covers most of the lens surface with a loss of the characteristic lens bow. Similar defects in secondary lens fiber differentiation were seen in transgenic mice expressing a soluble Fgf receptor (Fgfr), designed to interfere with endogenous lens Fgfr activity. Fgfs have been shown to promote lens fiber differentiation in dissociated lens epithelial cell monolayers, lens epithelial explants, and in transgenic mice. Lens fiber cells lacking *Fgfr2* elongate and express many genes consistent with fiber cell differentiation but exhibit defects in cell-cycle withdrawal associated with incomplete induction of p57Kip2. Combined deletion of *Fgfr1, Fgfr2*, and *Fgfr3* in the lens vesicle inhibits multiple aspects of both primary and secondary fiber cell differentiation (**Figure 3**). Presumptive fiber cells from these triple *Fgfr* knock-out mice fail to induce p57Kip2 and thus remain in the cell cycle. These cells also do not properly elongate or initiate fiber-cell-specific gene expression; instead, they express genes characteristic of lens epithelial cells, including E-cadherin, Pax6, and Foxe3.

There is also evidence that Wnt signaling plays a role in lens fiber cell differentiation. Although canonical Wnt signaling, through stabilization of β-catenin, has been shown to suppress lens fate in the ectoderm surrounding the lens placode, the lens later expresses a number of Wnt ligands, Wnt (frizzled) receptors and modulators of Wnt signaling. The role of canonical Wnt signaling in fiber cell differentiation is controversial. Reporter mice indicate only a brief period of canonical Wnt signaling in the anterior cells of the lens vesicle and in the early embryonic lens epithelium. Despite this, Wnt3a-conditioned media or overexpression of β-catenin has been shown to activate β-crystallin expression in lens cell cultures. Recent evidence with transgenic mice overexpressing a secreted frizzled-related protein (Sfrp2), a protein that interferes with Wnt signaling, suggests that Wnts play a role in lens development through the noncanonical Wnt/planar cell polarity pathway (**Figure 3**). Fiber cells in Sfrp2 transgenic mice do not elongate completely, leaving a lumen between the primary fiber cells and the lens epithelium. Secondary

fiber cells from the Sfrp2 transgenic mice also exhibited nuclear retention and cytoskeletal disruption. Both the anterior and posterior tips of the fiber cells lacked filopodia-like protrusive processes and failed to appropriately migrate, detach from the capsule, and form sutures, leading to an abnormally shaped lens with fiber cells exhibiting abnormal curvatures.

Notch Signaling

Notch is a cell surface receptor that interacts with membrane-associated ligands, such as Jagged, on neighboring cells. Activation of Notch receptors leads to the release of the intracellular domain which forms a DNA-binding complex in association with Rbpj and Mam proteins to activate transcription. Notch signaling during development typically acts to prevent differentiation, while Notch signaling in the lens epithelium activates the expression of Herp2, which binds to and represses the promoter of p57Kip2, thus maintaining lens epithelial cells in a proliferative state (**Figure 3**). Lens epithelial cells with conditional deletion of Rbpj lose expression of Herp2 and prematurely express p57Kip2, leading to cell-cycle withdrawal and fiber differentiation. These findings are consistent with Notch signaling playing a critical role in the regulation of the choice between proliferation and differentiation in the lens.

Conclusion

Lens fiber differentiation is a complex process that is undoubtedly supported by a number of growth factors, receptors, and transcription factors, only a few of which have been highlighted here. Likewise, these ligand–receptor complexes initiate many intracellular signal transduction cascades that ultimately turn on genes required for fiber cell formation and turn off genes required for lens epithelial maintenance. The elucidation of the complete molecular mechanics of these processes remains an active area of research that is far from complete.

See also: Lens Determination and Induction; Lens Gap Junctions; Lens Structure.

Further Reading

Banks, E. A., Yu, X. S., Shi, Q., and Jiang, J. X. (2007). Promotion of lens epithelial-fiber differentiation by the C-terminus of connexin 45.6 a role independent of gap junction communication. *Journal of Cell Science* 120: 3602–3612.

Bassnett, S. (2005). Three-dimensional reconstruction of cells in the living lens: The relationship between cell length and volume. *Experimental Eye Research* 81: 716–723.

Bassnett, S. (2008). On the mechanism of organelle degradation in the vertebrate lens. *Experimental Eye Research* 88(2): 133–139.

Bassnett, S. and Beebe, D. C. (2004). Lens fiber differentiation. In: Lovicu, F. J. and Robinson, M. L. (eds.) *Development of the Ocular Lens*, pp. 214–244. New York, NY: Cambridge University Press.

Beebe, D., Garcia, C., Wang, X., et al. (2004). Contributions by members of the TGFbeta superfamily to lens development. *International Journal of Developmental Biology* 48: 845–856.

Blankenship, T., Bradshaw, L., Shibata, B., and Fitzgerald, P. (2007). Structural specializations emerging late in mouse lens fiber cell differentiation. *Investigative Ophthalmology and Visual Science* 48: 3269–3276.

Boswell, B. A., Overbeek, P. A., and Musil, L. S. (2008). Essential role of BMPs in FGF-induced secondary lens fiber differentiation. *Developmental Biology* 324: 202–212.

Chen, Y., Stump, R. J., Lovicu, F. J., Shimono, A., and Mcavoy, J. W. (2008). Wnt signaling is required for organization of the lens fiber cell cytoskeleton and development of lens three-dimensional architecture. *Developmental Biology* 324: 161–176.

Gong, X., Cheng, C., and Xia, C. H. (2007). Connexins in lens development and cataractogenesis. *Journal of Membrane Biology* 218: 9–12.

Goudreau, G., Baumer, N., and Gruss, P. (2004). Transcription factors in early lens development. In: Lovicu, F. J. and Robinson, M. L. (eds.) *Development of the Ocular Lens*, pp. 48–68. New York, NY: Cambridge University Press.

Jia, J., Lin, M., Zhang, L., et al. (2007). The Notch signaling pathway controls the size of the ocular lens by directly suppressing p57Kip2 expression. *Molecular and Cellular Biology* 27: 7236–7247.

Kistler, J., Eckert, R., and Donaldson, P. (2004). Lens cell membranes. In: Lovicu, F. J. and Robinson, M. L. (eds.) *Development of the Ocular Lens*, pp. 151–172. New York, NY: Cambridge University Press.

Kuszak, J. R. and Costello, M. J. (2004). The structure of the vertebrate lens. In: Lovicu, F. J. and Robinson, M. L. (eds.) *Development of the Ocular Lens*, pp. 71–118. New York, NY: Cambridge University Press.

Landgren, H., Blixt, A., and Carlsson, P. (2008). Persistent FoxE3 expression blocks cytoskeletal remodeling and organelle degradation during lens fiber differentiation. *Investigative Ophthalmology and Visual Science* 49: 4269–4277.

Lang, R. A. and McAvoy, J. W. (2004). Growth factors in lens development. In: Lovicu, F. J. and Robinson, M. L. (eds.) *Development of the Ocular Lens*, pp. 261–289. New York, NY: Cambridge University Press.

Leonard, M., Chan, Y., and Menko, A. S. (2008). Identification of a novel intermediate filament-linked N-cadherin/gamma-catenin complex involved in the establishment of the cytoarchitecture of differentiated lens fiber cells. *Developmental Biology* 319: 298–308.

Menko, A. S. and Walker, J. L. (2004). Role of matrix and cell adhesion molecules in lens differentiation. In: Lovicu, F. J. and Robinson, M. L. (eds.) *Development of the Ocular Lens*, pp. 245–260. New York, NY: Cambridge University Press.

Quinlan, R. and Prescott, A. (2004). Lens cell cytoskeleton. In: Lovicu, F. J. and Robinson, M. L. (eds.) *Development of the Ocular Lens*, pp. 173–187. New York, NY: Cambridge University Press.

Rajagopal, R., Dattilo, L. K., Kaartinen, V., et al. (2008). Functions of the type 1 BMP receptor Acvr1 (Alk2) in lens development: Cell proliferation, terminal differentiation, and survival. *Investigative Ophthalmology and Visual Science* 49: 4953–4960.

Robinson, M. L. (2006). An essential role for FGF receptor signaling in lens development. *Seminars in Cell and Developmental Biology* 17: 726–740.

Rowan, S., Conley, K. W., Le, T. T., et al. (2008). Notch signaling regulates growth and differentiation in the mammalian lens. *Developmental Biology* 321: 111–122.

Lens Gap Junctions

E C Beyer and V M Berthoud, University of Chicago, Chicago, IL, USA

Glossary

Connexin – A subunit protein component of gap junction channels.
Gap junction – The plasma membrane specialization characterized by the close apposition of the plasma membranes of adjacent cells leaving a gap of 2–3 nm that contains clusters of intercellular channels made of connexins.
Gap junction-mediated intercellular communication – The direct transfer of ions and molecules between the cytoplasm of adjacent cells through gap junction channels.
Lentoid cultures – Lens cells that, in culture, begin to differentiate into fiber cells. In this process, the cells aggregate to form clusters that express increased levels of markers of fiber cell differentiation. Lentoid cultures can be used to study the assembly and regulation of gap junctions in lens fiber-like cells.

Lens Structure and Importance of Intercellular Communication for Lens Function

The lens is a transparent organ suspended between the aqueous humor and the vitreous whose main function is to transmit light and focus it onto the retina. The lens is comprised of two cell types: epithelial cells that form a single layer along the anterior surface and fiber cells that form the bulk of the organ (Figure 1). At the lens equator, epithelial cells differentiate into fiber cells, a process that involves cell elongation and loss of nuclei and organelles. Most of the synthetic and active transport machinery of the lens is present only in the nucleated surface cells. Mature fiber cells have limited metabolic activities, are nondividing, and must survive for the life span of the organism.

As there is no direct blood supply to the organ, specialized mechanisms are required to allow survival of the cells in the interior of the lens. Nutrients for the entire organ derive from the aqueous humor through uptake by the epithelial cells. The lens may have an internal circulation in which flow of ions drives the movement of solutes throughout the organ. A model of this circulation has been developed based on surface currents recorded from lenses. In this model, current (i.e., flow of ions and associated water and solutes) enters the lens along the extracellular spaces at the anterior and posterior poles, it crosses fiber cell membranes in the lens interior, and it flows back to the surface at the equator (through a cell-to-cell pathway). The lens circulatory system provides a pathway for internal fiber cells to obtain essential nutrients, remove potentially toxic metabolites, and maintain resting potentials. Thus, fiber cell survival and the maintenance of transparency depend on the function of epithelial cells and on communication between cells.

Structure and Components of Gap Junctions

Intercellular communication among lens cells is facilitated by an extensive network of gap junction channels. Gap junctions are plasma membrane specializations that contain clusters of intercellular channels that allow direct exchange of cytoplasmic ions and small molecules (<1 kDa) between coupled cells without encountering the extracellular space (Figure 2(a)). A gap junction channel is formed by docking of two hexameric hemichannels or connexons (Figure 2(b)) located in the plasma membranes of apposing cells. The subunit gap junction proteins are members of a family of related polytopic membrane proteins called connexins (CX). The proteins that form vertebrate gap junctions are called connexins. The official names of the human genes encoding these proteins are *GJA1* for CX43, *GJA3* for CX46, and *GJA8* for CX50. This article utilizes only the connexin nomenclature in which different connexins are identified based on their predicted molecular masses in kDa (e.g., CX43 is a 43-kDa protein). To avoid the confusion that arises due to different masses of the orthologous connexins in other species, this article identifies each connexin using the name for its human isoform. There is a second family of vertebrate proteins called pannexins that are related to the innexins which form gap junctions in invertebrates. Although there is pannexin expression in the lens, the pannexins may not form intercellular channels; therefore, they are not included in this article. Connexins contain four transmembrane domains and have both their amino and carboxyl termini located in the cytoplasm (Figure 2(c)). Among connexin family members, the extracellular and transmembrane domains are the most conserved, while the cytoplasmic domains are the most divergent.

Distribution of Connexins within the Lens

Three connexins have been identified in the lens with different, but overlapping, expression patterns (Figure 1). CX43 is produced in lens epithelial cells, but its expression is turned off as epithelial cells in the equatorial region differentiate into fiber cells. CX50 is also expressed in epithelial cells. CX46 and CX50 are abundantly expressed in the differentiating cells and are the only connexins found in lens fiber cells. CX46 and CX50 co-localize at gap junctional plaques and form mixed (hetero-oligomeric) connexons. Despite their similar expression patterns, CX46 and CX50 must have some differences in function, since substitution of CX46 for CX50 in genetically engineered mice does not result in entirely normal lenses.

Transcripts encoding a fourth connexin, CX23, have been detected in lenses of zebrafish embryos and mice. CX23 may be expressed in lens cells of other mammalian species, since it has been identified as an expressed sequence in messenger RNA (mRNA) from whole eyes or lenses. However, no transcripts have been detected in human lenses. This connexin may be involved in fiber cell differentiation, since elongation of fiber cells is abnormal in mice expressing a missense mutant of CX23. However, several issues regarding CX23 have not yet been resolved, including detection of CX23 protein in lens cells, determination of its abundance and, more importantly, its contribution to lens intercellular communication, relative to other connexins. Therefore, CX23 is not included in Figure 1.

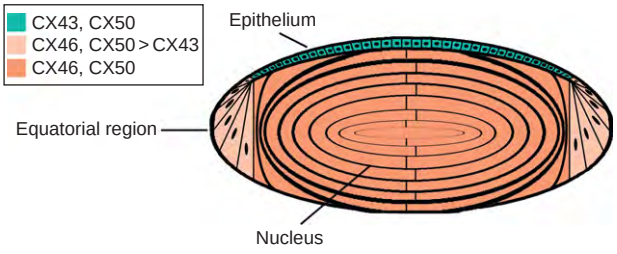

Figure 1 Diagram of the lens showing the distribution of three connexin isoforms. Different colors indicate regions with different connexin expression patterns. Cells from the anterior epithelial layer express CX43 and CX50; cells from the equatorial region express CX43, CX46, and CX50; and fiber cells (including those of the nucleus) contain CX46 and CX50.

Physiology and Pharmacology of Gap Junction-Mediated Intercellular Communication

The behavior of intercellular channels formed of connexins has been studied in expression systems, including paired *Xenopus* oocytes and transfected mammalian cells, using electrophysiological techniques such as voltage clamp and patch clamp. The gap junction conductance between a pair of cells depends on the number of channels, their open probabilities, and their single-channel conductances.

Each connexin forms channels with distinct properties, including unitary conductance, permeability, charge selectivity, gating, and regulation by different protein kinase-dependent pathways. CX43 gap junction channels are permeable to larger molecules than channels formed of CX46 or CX50. Thus, the permeability of gap junction channels in different regions of the lens is determined, in part, by the repertoire of connexins expressed.

Although there are connexin-specific differences in sensitivity to these agents, all gap junction channels are regulated by voltage (transjunctional and sometimes transmembrane), calcium, and pH. High transjunctional voltage, high concentrations of intracellular calcium, and low cytoplasmic pH close gap junction channels. Regulation by transjunctional voltage is not significant in the lens where cells have similar resting potentials. Both calcium- and pH-dependent regulation of gap junctions may be important in the lens, because calcium concentration is higher in the lens perinuclear region and pH decreases toward the lens interior. As in other tissues/organs, closure of gap junctions by voltage, calcium, and pH may contribute to the cellular response to injury in the lens,

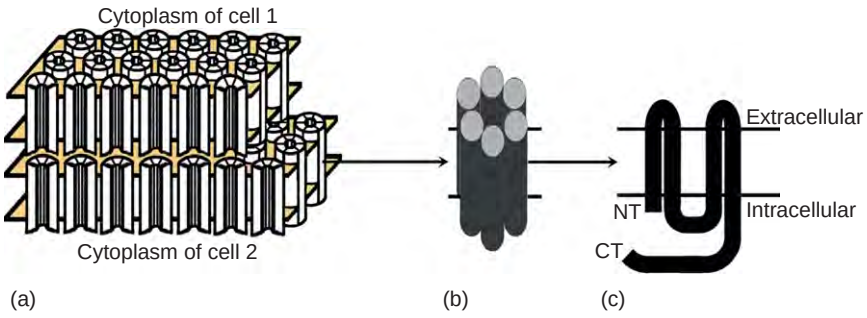

Figure 2 Diagram of a gap junction (a), a hemichannel or connexon (b), and the subunit gap junction protein, connexin (c). NT, amino terminus; CT, carboxyl terminus.

since the resulting disruption of intercellular communication would isolate intact cells from damaged ones.

Gap junction channels can also be closed by several pharmacologic agents, including long-chain alkanols (e.g., heptanol and octanol), anesthetics (e.g., halothane), glycyrrhetinic acid derivatives, oleamide, arachidonic acid or its metabolites, and the antimalarial compounds quinine and mefloquine. All of these are rather nonselective agents that also affect other channels or cellular functions; therefore, they are unlikely to be of therapeutic utility as selective lens gap junction blockers. However, mefloquine inhibits CX50 channels at much lower concentrations than it blocks other connexins; therefore, it has been used to determine the physiological role of CX50 in the lens.

Connexin Functions beyond Intercellular Communication

In addition to forming intercellular channels, connexins can also form hemichannels that introduce large, relatively nonselective conductances in single plasma membranes. (These conductances appear to represent permeation through undocked single connexons.) This phenomenon has been best demonstrated in primary cultures of various cells and in expression systems. One of the most dramatic examples is the large permeability induced by expression of CX46 in single *Xenopus* oocytes that can be gated by modulation of extracellular concentrations of divalent cations, including calcium. As CX46 hemichannels are mechanosensitive, it has been proposed that their opening plays a physiological role during lens accommodation. Opening of such hemichannels has not yet been demonstrated in intact tissues.

Connexins may also be involved in functions not directly associated with their channel-forming ability. Expression of the chicken CX50 ortholog (including nonfunctional mutants) or a chicken CX46 chimera containing the CX50 carboxyl terminus promotes differentiation of chicken lens cells in culture. The mechanism for these nonchannel-induced effects of CX50 has not been clarified, but it has been suggested that it involves interactions of its carboxyl terminus with other cellular proteins to modulate intracellular signaling critical for lens cell differentiation.

CX50 is also required for normal growth of the lens. Mice that are null for CX50 (but not those null for CX46) have small lenses. The decreased lens size appears to result from reduced proliferation of lens epithelial cells, especially during the first few days of postnatal life. It has been speculated that this proliferative deficiency is due to some connexin function other than intercellular exchange of ions, since introduction of CX46 into the CX50 locus does not restore normal lens growth to CX50-null mice. Overexpression of CX50 also leads to a decrease in lens size; thus, the proper level of CX50 expression is required for normal lens development and growth.

Regulation of Connexin Functions by Protein Modification

Similar to many other proteins, connexins are subject to post-translational modifications. A variety of modifications has been detected in the connexins found in different cells and tissues, including phosphorylation, acetylation, ubiquitinylation, S-nitrosylation, fatty acylation, hydroxylation, γ-carboxyglutamylation, and cleavage/partial proteolysis. The functional consequences of many of these protein modifications remain to be determined. Phosphorylation and proteolytic cleavage are the most extensively studied modifications of lens connexins and may be associated with physiological effects on connexin function.

Phosphorylation

Many of the connexins, including CX43, CX46, and CX50, are phosphoproteins. A number of phosphorylated residues and the responsible kinases have been identified. These phosphorylation events are involved in the regulation of channel function or of various steps during formation and degradation of gap junction channels.

CX43 phosphorylation has been extensively studied. In many cell types, the immunoblot pattern of CX43 contains at least three major immunoreactive bands designated NP, P1, and P2. The NP band has the fastest electrophoretic mobility and, in some cases, corresponds to CX43 that is not phosphorylated. P1 and P2 correspond to different phosphorylated forms. The P2 form shows a slower electrophoretic mobility than P1, and its presence has been correlated with localization of the protein to gap junctional plaques and insolubility in Triton X-100. A P3 form with an electrophoretic mobility slower than P2 is observed in some cell lines during mitosis. At least 12 serines and two tyrosines in the carboxyl terminus of CX43 can be phosphorylated by different protein kinases.

In many cell types that express CX43 (including lens epithelial cells), treatment with activators of protein kinase C, PKC, (e.g., 12-*O*-tetradecanoyl phorbol ester, TPA) decreases intercellular communication. In most cases, this treatment is associated with a relative increase in the P1 and P2 forms of CX43 and a decrease in NP. Studies have suggested several different mechanisms for the reduction of gap junction function, including changes in single-channel conductance, channel permeability, connexin trafficking/assembly, and turnover/redistribution of gap junctions.

Several immunoreactive bands corresponding to different phosphorylated forms of CX46 and CX50 are

detectable in lens homogenates. Phosphorylation of the lens fiber cell connexins has been implicated in regulation of intercellular communication, protein stability, and proteolytic cleavage. The sheep CX50 is phosphorylated by casein kinase I, and inhibition of casein kinase I increases intercellular communication between cultured lens cells. Casein-kinase II-mediated phosphorylation of Ser363 in the chicken CX50 regulates its cleavage by a caspase-3-like protease. Phosphorylation may regulate the stability of chicken CX46, since its slowest migrating phosphorylated forms have longer half-lives.

The effects of phorbol esters and PKC activation on fiber cell connexins have been studied in lentoid-containing cultures and lens organ cultures. TPA treatment of cultures from chicken lenses decreases dye coupling between lentoid cells. The TPA-induced decrease in dye coupling is associated with activation of PKCγ and an increase in phosphorylation of chicken CX46 at Ser118, suggesting that phosphorylation leads to channel closure. Rat CX46 hemichannels are also modulated by PKC phosphorylation. A PKC activator reduces the amplitude of hemichannel currents and leads to their inactivation after prolonged incubation, an effect that can be inhibited by PKC inhibitors. Treatment of whole rat lenses with TPA results in increased PKCγ activity, decreased intercellular coupling in the lens cortex, decreased anti-CX50 immunoreactivity in gap junctions, and increased anti-CX50 immunoreactivity in the nonjunctional plasma membrane, suggesting that PKC activation leads to undocking and dispersion of CX50 hemichannels. However, in sheep lentoids, PKC activators have no effects on intercellular communication. These divergent findings may be explained by species differences, because the ovine CX50 ortholog is not a PKC substrate.

Cleavage/Proteolysis

In lens sections, immunofluorescent staining (performed using antibodies directed against epitopes in the carboxyl terminus of fiber cell connexins) shows a substantial decrease of staining intensity in the nuclear region. This reduction has been interpreted as due to proteolysis of this part of the connexin. In agreement with this interpretation, preparations of isolated lens gap junctions contain immunoreactive bands with electrophoretic mobilities corresponding to connexin polypeptides that are full length and to proteolytically cleaved products. While such connexin proteolysis is not seen in all systems, several investigators have suggested that cleavage of lens fiber connexins occurs *in vivo*. Calpains and a caspase-3-like protease have been implicated in connexin cleavage in different species.

The carboxyl terminus of connexins may play an important role in regulating channel activity. Intercellular coupling between lens fibers (but not between epithelial cells) is insensitive to acidification. It has been speculated that the lack of sensitivity results from cleavage of lens fiber connexins. When expressed in exogenous systems, truncated forms of CX50 are unresponsive to pH gating, whereas truncated forms of CX46 show a slight change in acid dissociation constant (K_a), but are still sensitive to pH. These results imply that the pH sensitivity of gap junctions in lens fiber cells is dominated by CX50. Therefore, it has been proposed that the cleavage of fiber cell connexins in the lens interior would allow gap junction channels to stay open in this rather acidic environment, facilitating the exchange of small molecules between fiber cells.

Connexins and Lens Pathologies

Cataracts in Mice with Genetically Manipulated Connexin Levels

The importance of gap junction-mediated lens intercellular communication for the maintenance of lens transparency has been substantiated by a number of genetic studies in mice. Targeted deletion of CX46 or CX50 results in the development of cataracts in homozygous but not heterozygous mice. The CX50-null mice have a more severe cataract than the CX46-null mice. The onset of the cataract phenotype in CX50 knock-out mice occurs within the first postnatal week, and results in a mild nuclear cataract that is characterized by a relative decrease in the solubility of crystallins. The cataracts in CX46-null mice are visible by the third week of age; they are associated with decreased solubility of several crystallins and proteolysis of γ-crystallins. In mice deficient in either of the lens fiber connexins, cataract severity varies with genetic background, suggesting the influence of additional genes. Double knock-out mice lacking both the CX46 and CX50 genes show dense opacities that are far more extensive than those observed in either the CX46- or CX50-single null mice. The increased severity of the opacities in these mice likely reflects the total absence of gap junction-mediated intercellular communication between lens fiber cells. Transgenic mice overexpressing CX50 in differentiating and lens fiber cells also develop severe cataracts, suggesting that any significant alteration of connexin levels in these cells (either absence or a major increase) may lead to cataract formation. The role of CX43 for normal lens function is uncertain. The lenses of prenatal or newborn CX43-null mice appear normal and transparent; however, the long-term effects of the loss of CX43 in the lens have not been determined in these mice, because global deletion of CX43 results in neonatal lethality. (Lens-specific deletion of CX43 has not been studied.)

Cataracts due to Connexin Mutations

The cataract trait in several mutant mouse strains has been mapped to the lens connexin gene loci. The *No2*

mouse, which develops congenital cataracts (especially in homozygotes), carries a missense mutation within the coding region of CX50, resulting in a change of amino acid residue 47 from aspartate to alanine (CX50D47A). Another mouse with cataracts, *lop10*, carries a missense mutation at amino acid residue 22 of CX50 (CX50G22R). Mice carrying a CX50 mutation at amino acid residue 64 (changing it from valine to alanine, CX50V64A) exhibit dominantly inherited cataracts.

More importantly, mutations in lens connexins have been associated with human disease. Missense and frameshift mutations of the CX46 and CX50 genes have been identified in members of families with inherited (usually dominant) cataracts of various different phenotypes. The identified mutations and their positions within the connexin proteins are summarized in **Figure 3**. Mutations in CX43 have been associated with oculodentodigital dysplasia, a disease which is rarely accompanied by cataracts.

Studies of connexin mutants identified in association with a variety of diseases have revealed that the molecular mechanism responsible for cellular pathology may differ among mutants. Mutant connexins could form nonfunctional channels or channels with altered properties (such as gating, conductance, or permeability).

Several cataract-associated mutant connexins have been examined in expression systems to elucidate cell biological and/or functional abnormalities that may lead to cataract formation. The CX46 and CX50 mutants that have been analyzed exhibit loss of function; no gap junction conductance is detected when they are expressed in paired *Xenopus* oocytes or in transfected cells. When co-expressed with wild-type connexins, some mutants exert a dominant-negative effect abolishing gap junction conductance. This behavior may explain the autosomal dominant inheritance of the cataract trait associated with these mutants, since this inhibition would render these individuals effectively null for function of that connexin despite the presence of a wild-type allele. However, co-expression of some other mutants with their wild-type counterparts has no inhibitory effect. Thus, there is an apparent difference in the phenotypic consequences of partial loss of fiber cell connexin function between mice and men; heterozygous connexin-null mice are unaffected, whereas people that are heterozygous for a loss-of-function mutant develop cataracts. Another explanation is that the presence of mutant connexin protein (at about 50% levels due to heterozygosity) is worse for lens transparency than a 50% reduction in expression of that connexin.

In some cases, the loss of function may reflect defects in connexin trafficking, since several mutants do not form gap junction plaques when expressed in transfected cells; rather, the proteins are found in the cytoplasm. In one mutant, CX46fs380, a unique sequence in the mutant CX46 protein (generated by a frame shift) impairs protein trafficking to the plasma membrane.

While cataract formation due to connexin mutations may occur due to impaired intercellular communication, cytoplasmic accumulation of the mutant protein or formation of mutant protein aggregates may also contribute to the phenotype. The CX50 mutant, CX50P88S, forms cytoplasmic multilamellar accumulations. These accumulations may be detrimental to lens function by scattering light and interfering with its transmission and focusing onto the retina. Cytoplasmic accumulations of mutant connexins may also contribute to the loss of lens transparency by acting as nucleation particles for accumulation/aggregation of other proteins or by directly causing cellular damage.

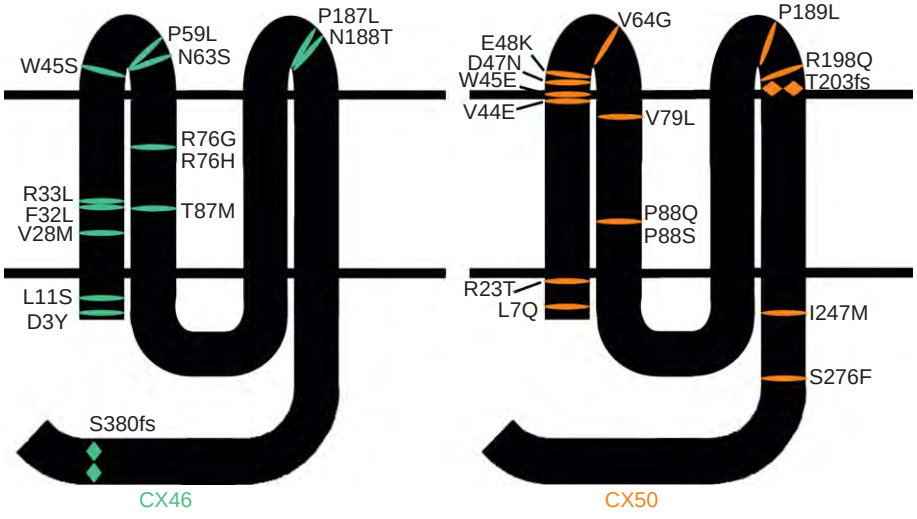

Figure 3 Diagram illustrating the topology of the human lens connexins, CX46 and CX50, is illustrated. The locations of missense (⬭) or frame shift (♦♦) mutations identified in members of families with inherited cataracts are indicated.

Cataract-Causing Insults and Damage to Lens Connexins

Lens proteins, including connexins, can accumulate a variety of post-translational modifications with aging or in association with cataract formation. Oxidation of methionine has been detected in the bovine orthologs of CX46 and CX50. Deamidation of asparagine121 has been detected in the CX50 ortholog. However, it is not certain that these modifications actually occur *in vivo*, since both methionine oxidation and deamidation may occur during sample preparation. The effects of most of these modifications on gap junction-mediated intercellular communication are unknown.

One of the most-studied etiologies of cataract formation is oxidative stress, which may be linked to changes in connexins and gap junctions. Several studies have used H_2O_2 treatment of cultured lens cells or isolated lenses to examine the consequences of oxidative stress. Treatment of chicken lentoid-containing cultures with H_2O_2 leads to dose- and time-dependent changes in the immunoblot pattern of chicken CX46, suggesting that H_2O_2 leads to its differential phosphorylation. A cleaved form of this connexin has been observed following treatment with high concentrations of H_2O_2; this is also associated with cell death. Treatment of a CX43-expressing lens cell line with H_2O_2 leads to an increase in PKCγ activity, an increase in phosphorylation of CX43 in Ser368 as detected by immunoblotting, a decrease in the number of gap junction plaques, and a decrease in dye coupling. Similar effects have also been observed when rat lenses are treated with H_2O_2. Thus, several pieces of data suggest that oxidative stress leads to alterations in lens intercellular communication through activation of protein kinases and alterations in connexin phosphorylation, which may contribute to cataract formation.

See also: Ionic Permeability and Currents in the Lens.

Further Reading

Berthoud, V. M. and Beyer, E. C. (2009). Oxidative stress, lens gap junctions, and cataracts. *Antioxidants and Redox Signalling* 11: 339–353.

Donaldson, P., Kistler, J., and Mathias, R. T. (2001). Molecular solutions to mammalian lens transparency. *News in Physiological Sciences* 16: 118–123.

Gong, X., Cheng, C., and Xia, C. H. (2007). Connexins in lens development and cataractogenesis. *Journal of Membrane Biology* 218: 9–12.

Goodenough, D. A. (1992). The crystalline lens. A system networked by gap junctional intercellular communication. *Seminars in Cell Biology* 3: 49–58.

Harris, A. L. (2001). Emerging issues of connexin channels: Biophysics fills the gap. *Quarterly Reviews of Biophysics* 34: 325–472.

Harris, A. L. and Locke, D. (eds.) (2008). *Connexins: A Guide.* New York: Humana Press.

Jiang, J. X. and Gu, S. (2005). Gap junction- and hemichannel-independent actions of connexins. *Biochimica et Biophysica Acta* 1711: 208–214.

Mathias, R. T., Rae, J. L., and Baldo, G. J. (1997). Physiological properties of the normal lens. *Physiological Reviews* 77: 21–50.

Sáez, J. C., Berthoud, V. M., Brañes, M. C., Martínez, A. D., and Beyer, E. C. (2003). Plasma membrane channels formed by connexins: Their regulation and functions. *Physiological Reviews* 83: 1359–1400.

Solan, J. L. and Lampe, P. D. (2005). Connexin phosphorylation as a regulatory event linked to gap junction channel assembly. *Biochimica et Biophysica Acta* 1711: 154–163.

Sosinsky, G. E. and Nicholson, B. J. (2005). Structural organization of gap junction channels. *Biochimica et Biophysica Acta* 1711: 99–125.

Stout, C., Goodenough, D. A., and Paul, D. L. (2004). Connexins: Functions without junctions. *Current Opinion in Cell Biology* 16: 507–512.

Yeager, M. and Harris, A. L. (2007). Gap junction channel structure in the early 21st century: Facts and fantasies. *Current Opinion in Cell Biology* 19: 521–528.

Relevant Website

http://www.ncbi.nlm.nih.gov – Online Mendelian Inheritance in Man; Gap Junction Protein Alpha-8; Gap Junction Protein Alpha-3.

Lens Regeneration

P A Tsonis, University of Dayton, Dayton, OH, USA

Glossary

Axolotls – Species of aquatic salamanders, *Ambystoma mexicanum,* that do not undergo metamorphosis, retaining gills into adulthood.
Dedifferentiation – Loss of differentiated cellular characteristics, including cell shape and characteristic gene-expression profiles; it may be followed by reacquisition of differentiated characteristics or transdifferentiation to another cell type. In lens regeneration in urodeles, iris cells dedifferentiate, then transdifferentiate to lens.
Dorsalize – Malformed quality in which the gross morphology contains only what are normally dorsal structures.
Epistasis – The effects of one gene are modified by one or several other genes.
Lentectomy – Removal of the lens. This is usually a requirement to initiate the process of lens regeneration.
Urodeles – Living members of the amphibian order *Caudata*, many of which can regenerate multiple body parts.
Ventralizer – Relating to or situated on or close to the anterior aspect of the human body or the lower surface of the body of an animal.

A General Background of Lens Regeneration

Some urodele amphibians are the only animals that, throughout their life, are capable of regenerating their lens following removal of the lens (lentectomy). Regeneration of the lens in adult newts was observed first by Collucci, in 1891, and independently by Wolff, in 1895, after whom the process is often called Wolffian regeneration. A few species of fish and premetamorphic frogs can also regenerate the lens. In the fish and newts, the regenerating lens is derived from the pigment epithelial cells (PECs) of the dorsal iris, whereas in the frog it is derived from the larval cornea. Mammals possess an ability to regenerate the lens, but only when the capsule and associated lens epithelial cells are left behind. This has been studied extensively in rabbits, and recently such studies have been extended to mice and rats. The source of the regenerated lens is the adherent lens epithelial cells that cannot be completely removed. This article concentrates only on the mechanism underlying lens regeneration in newts.

Over the past several decades, many reports have provided important insights about the process and its restriction to only some adult salamanders. First, not all salamanders are capable of lens regeneration. The axolotl, which can regenerate its limbs and tail very well, is unable to regenerate the lens. This mystery might unveil crucial mechanisms (see below). Second, for regeneration to occur, the iris PECs must re-enter the cell cycle and dedifferentiate. These dedifferentiated cells can then differentiate to lens cells. This process has been called lens transdifferentiation. That the regenerate was derived from dedifferentiated cells and not from a contaminating undifferentiated progenitor cell, was convincingly demonstrated by Professor Goro Eguchi and colleagues in studies using clonal cell culture. The ability of the dorsal and not the ventral PECs to transdifferentiate *in vivo* provides another valuable comparison. This is especially true, since ventral PECs are able to transdifferentiate to lens following prolonged culturing. Indeed, newt PECs from the ventral iris as well as retinal pigmented epithelium (RPE) cells from many different vertebrates are capable of transdifferentiation to lentoids after being cultured under certain condition. This is true for even aged human PECs. Much work, especially using chick RPE, has led to the identification of factors that seem to mediate this ability of PECs to transdifferentiate following culture. The most notable of these factors are fibroblast growth factors (FGFs), hyaluronidase, phenylthiourea, and vitamin C. Thus, it appears that the ability for transdifferentiation is present in all PECs, but, *in vivo*, this ability is only expressed by the dorsal iris PECs of the adult newt. This calls for extensive search for factors restricted to the dorsal or ventral iris and for comparative studies with the axolotl. These features have made lens regeneration a primary paradigm in the study of cell plasticity, cell determination, aging, and reprogramming.

The Process of Transdifferentiation and Lens Regeneration

PECs must proliferate to create the lens vesicle and the subsequent lens. Previous studies clearly showed that both the dorsal and ventral iris PECs re-enter the cell cycle, although the ventral PECs do so at a lower rate. These showed that proliferation begins at about 4 days post-lentectomy and that, at that time, both dorsal and ventral

PECs show comparable levels of cell proliferation. Later, proliferation rates are higher in dorsal PECs, but obviously this must correlate with the process of lens regeneration, which has been initiated from the dorsal iris. In relation to this, expression of a hyperphosphorylated form of retinoblastoma (Rb) has been found in the PECs of both the dorsal and ventral iris. Rb is a paramount player in cell-cycle regulation. When it is hyperphosphorylated, it is inactivated and dissociates from E2F transcription factors. Activation of E2Fs allows cells to re-enter the cell cycle. However, treatment with a cyclin-dependent kinase (CDK) inhibitor (which reduces Rb phosphorylation and inhibits proliferation) does not completely inhibit transdifferentiation. In addition, when ventral cells are cultured for about 2 weeks and then implanted as aggregates in the eye cavity, they can never transdifferentiate to lens – even though they undergo considerable proliferation. In different studies, it has been demonstrated that activation of the protease – thrombin – is predominant in the dorsal iris and that inhibition of thrombin activity results in loss of proliferating cells. Nevertheless, PECs from both dorsal and ventral iris are responsive to thrombin when stimulated *in vitro*. This might imply that, while proliferation is necessary to prepare cells for the process of regeneration, it might not be sufficient for their subsequent transdifferentiation. Thus, events other than those involved in cell-cycle re-entry are decisive for transdifferentiation and lens regeneration.

The histological events leading to de-differentiation have been well studied at the microscopic level. Soon after lentectomy, the PECs shed their pigment. Macrophages recruited to the site mediate such a process. Four days postlentectomy (a time frame that coincides with the onset of cell proliferation), the iris is decondensing and the PECs begin to elongate. At about 8–10 days postlentectomy, these cells become columnar and depigmented. The first depigmented cells are obvious at the tip of the dorsal iris. At about 10 days, a lens vesicle has been formed, but no crystallin expression is yet apparent. Many of the genes that are known to be expressed and involved in lens development, such as pax-6, FGFs, FGF receptors, and prox-1 are expressed in the early lens vesicle. After the vesicle is formed, the events of lens differentiation are initiated. At the posterior edge of the vesicle, elongation of the cells ensues with concomitant induction of crystallin synthesis. The elongated cells differentiate to lens fibers and the anterior part of the vesicle becomes the lens epithelium, which continues to contribute by proliferation and differentiation to the growing of the lens (**Figure 1**). Once lens differentiation has started, the process is remarkably similar to embryonic lens development (as far as the sequential appearance of the different crystallins is concerned). Indeed, studies using antibodies to crystallins or cDNA probes have conclusively shown that there is a parallel of their synthesis in the developing and regenerating lens. The crystallins examined were αA, βB1, and γ. All these crystallins appeared, at the same time, at the ventral portion of the lens vesicle (Sato stage IV; nearly 10 days postlentectomy), with γ-crystallin (in contrast with the other two) being specific for the lens fibers and not the lens epithelial cells. The lens epithelium proliferates extensively throughout. As in normal lens development, when lens epithelial cells differentiate to lens fibers, they stop dividing. At the same time events of apoptosis are also observed, but at a minimal rate. It is interesting to note that, even at stages prior to completion of regeneration of the lens, cell death is part of the normal routine.

Gene Expression and Induction of Lens Regeneration

Because lens regeneration normally occurs only from the dorsal iris (and never the ventral) by transdifferentiation of the iris PECs, research focused on finding key differences between the positive cells (dorsal) and the negative ones (ventral). It was hoped that understanding these differences could help induce the ventral iris (as a first step) to regenerate a lens. Studies concentrated on genes that were important for eye development and axis formation. It was first shown that *pax-6*, a known eye master gene, is expressed during dedifferentiation of the PECs and lens regeneration. These initial expression studies indicated that lens regeneration could recapitulate lens development and that, in the adult newt, developmental genes are not irreversibly turned off. FGFs and FGF receptors were also expressed in lens regeneration, with

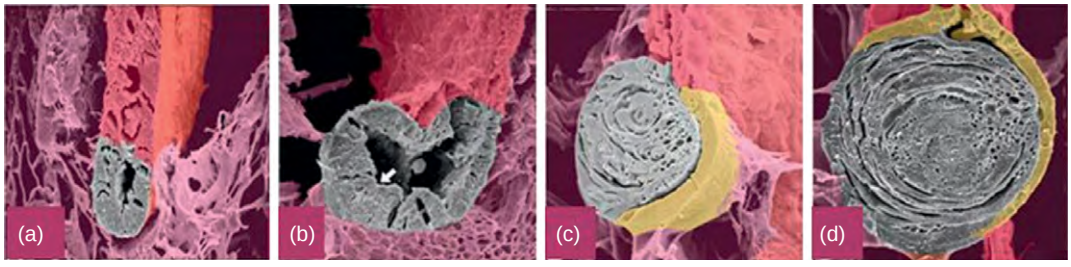

Figure 1 Lens formation from the dorsal iris during regeneration shown through SEM. (a) Day 10 postlentectomy, a lens vesicle forms at the dorsal margin. (b) Day 14, elongation and further lens development as differentiation of lens fibers occur at the posterior part (arrow) of the vesicle. (c) Day 20 of lens reformation. The anterior part becomes the lens epithelium (colored yellow). (d) Day 30, regeneration has concluded.

a preference for expression in the dorsal iris. When exogenous FGF was given to the eye, a second lens could be elicited from the dorsal, but not from the ventral iris. When FGF-receptor signaling was specifically inhibited, lens regeneration was abolished. These data clearly showed that FGF signaling is imperative for normal regeneration.

Other important factors were studied for specific expression and function during lens regeneration. These included key regulators, such as *Hox* genes, *Prox-1*, retinoic acid receptors, cyclin-dependent kinases, complement components, and components of the hedgehog pathway, which played a novel role in lens regeneration. The goal of all these studies was to identify factor(s) that might be good candidates for the induction of lens regeneration and to apply them to the ventral iris to induce regeneration from that site. This was initially accomplished by forced expression in the ventral iris of the transcription factor, six-3, and treatment with retinoic acid. As mentioned above, six-3 is a major eye-development regulator that collaborates with pax-6. Inhibition of the bone morphogenetic protein (BMP) pathway – which lies upstream of the pax-6/six-3 loop – could do exactly the same (**Figure 2**). BMPs are known to influence tissues to become more ventral fates during development. It seems likely that their function controls the identity of dorsal and ventral iris. The basic events and possible pathways that regulate this process are depicted in **Figure 3**.

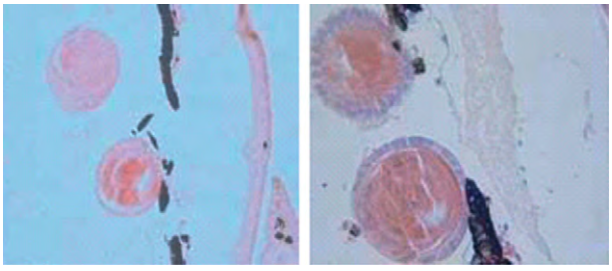

Figure 2 Induction of lens transdifferentiation from a ventral iris implant. On the left panel, the lens was induced by transfecting the ventral iris PECs with six-3 and treated with retinoic acid. On the right panel, the lens was induced by inhibiting the BMPR-1A. Top lens is the host regenerating lens.

Gene Regulation in the Induction of Lens Regeneration

Induction of lens regeneration from the ventral iris was a major accomplishment, which opened new avenues of experimentation. To understand more about the mechanism of induction, a detailed analysis of the expression of six-3, pax-6, and BMP receptors was undertaken. RNA was isolated from the intact dorsal and ventral irises, as well as at days 2, 4, and 8 postlentectomy. This time range was chosen to observe the regulation of these genes throughout the process of dedifferentiation. The results were quite surprising. All of these genes were expressed in the intact dorsal and ventral iris. In fact, levels in the intact ventral iris were higher than in the intact dorsal. However, as dedifferentiation progressed, these genes (especially six-3; **Figure 4(c)** and **(d)**) were selectively upregulated in the dorsal iris. The levels were elevated in the induced ventral irises as well (**Figure 4(f)**). These patterns suggested a mechanism whereby regeneration might be achieved: levels of gene expression must be elevated above a certain threshold. The genes involved are not just absent in the intact irises and specifically appear in the dorsal iris during regeneration.

Epistasis experiments showed that the BMP pathway was upstream the six-3/pax-6 loop. Treatment with the BMP antagonist chordin elevated both pax-6 and six-3 in the ventral iris postlentectomy (**Figure 4(g)**). As during normal eye development, an inhibitor of the BMP pathway (in that case, the BMP antagonist noggin) seems to be the upstream regulator of the eye-forming genetic network.

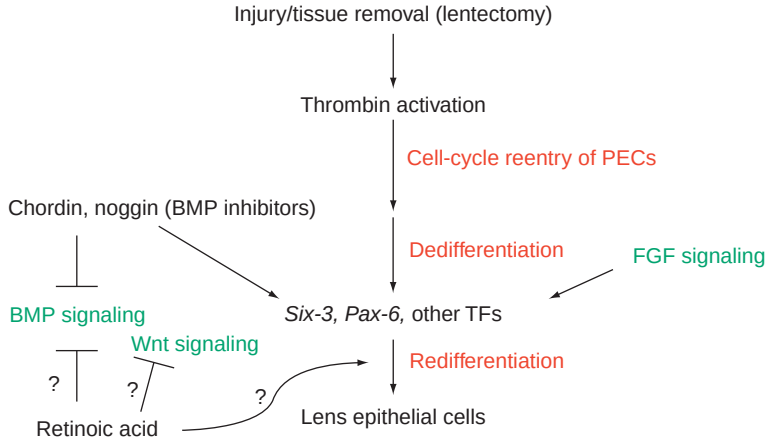

Figure 3 A diagram indicating the basic events and factors whose function has been associated with lens regeneration.

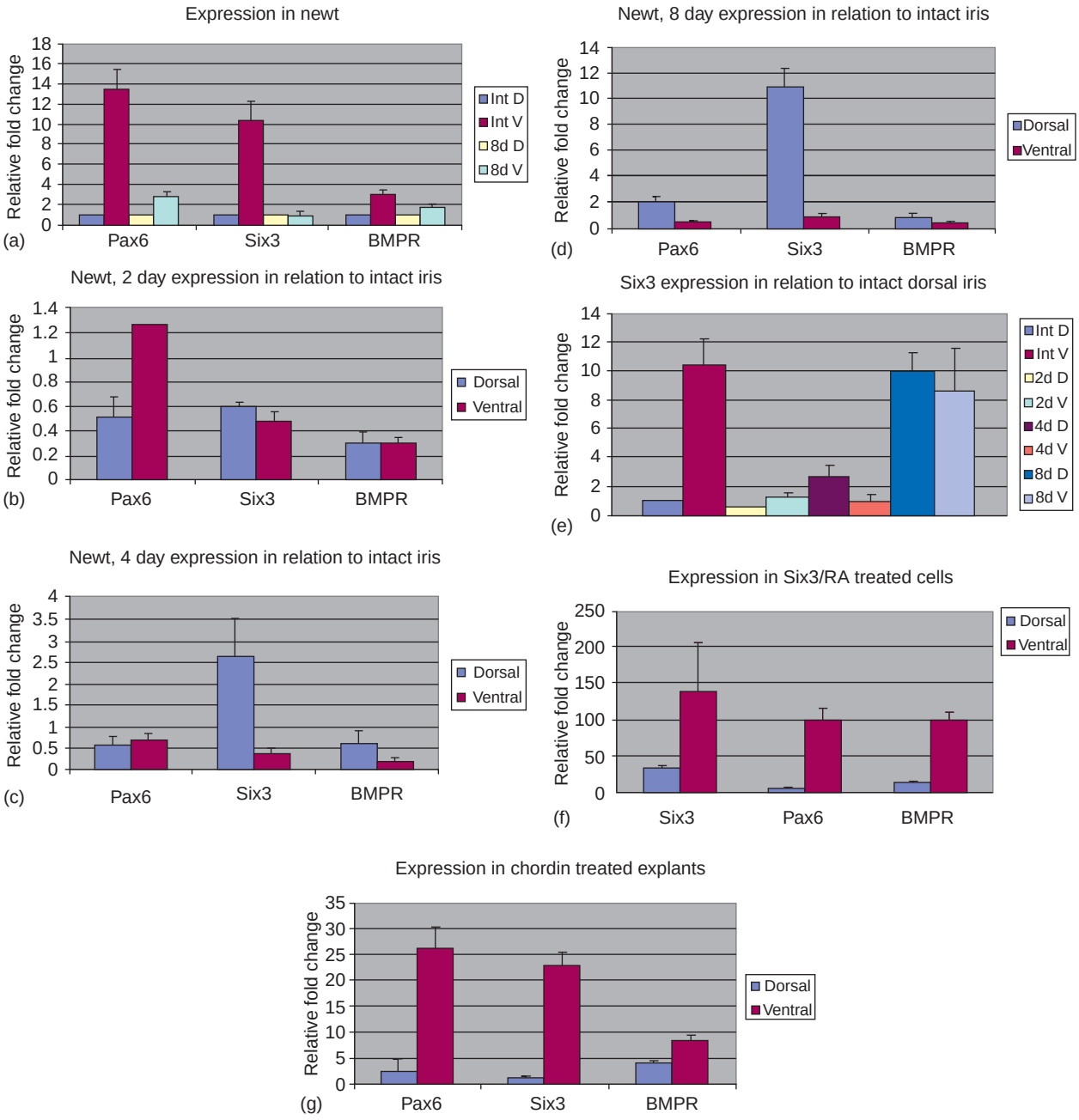

Figure 4 (a–d) Expression of pax-6, six-3, and BMPR-IA during the initial stages of regeneration – 2, 4, and 8 days following lentectomy. Expression in both dorsal and ventral iris is compared with the levels of the intact iris. Gradual increase in the dorsal iris can be seen, especially for six-3. (e) A summary of six-3 expression in relation to the one in intact iris. (f) Expression in six-3/RA treated cells. (g) Expression following chordin treatment. Note upregulation of pax-6 and six-3. Right panels: Comparison of expression levels in the dorsal and ventral iris for newt BMP-1, BMP2/4, and snail. Comparisons are between intact dorsal iris (ND), intact ventral iris (NV), dorsal iris at day 8 following lentectomy (RD) and ventral iris at day 8 following lentectomy (RV). Note a pattern of upregulation in the ventral iris during regeneration (RV vs. NV).

Several interesting points can be stated from the above induction and expression experiments (apart for the already mentioned activity in the ventral iris). First, six-3 was the first of these genes to be upregulated in the dorsal iris at day 4, while pax-6 levels increased at day 8. It was somewhat surprising that pax-6 did not induce regeneration. Second, because BMPs are ventralizers during embryogenesis and their inhibition dorsalizes the embryo, similar events might regulate lens regeneration. In fact, treatment of the dorsal iris with BMPs inhibited its ability for transdifferentiation. Because of this and the obvious involvement of the BMP pathway in lens regeneration, the expression of some BMP-signaling factors was examined to ascertain whether any of these genes would

recapitulate their expression pattern during embryogenesis. This network in *Drosophila* has nearly 90 genes involved in elaborate interactions. To obtain some insight into this idea, expression of the newt orthologs of decapentaplegic (dpp) – BMP2/4 and tolloid-related metalloproteinase (BMP-1) – were examined. BMP2/4 is an activator of ventral-specific genes during embryogenesis. The expression of snail was also evaluated. BMP-1 is ventral specific; it inhibits chordin and thus allows release of BMPs. This action is blocked by its antagonist, sizzled. Snail is activated by dorsal and is a repressor of ventral, neurogenic territory during development. For BMP2/4, BMP1, and snail, a very similar pattern emerged when their expression was examined with quantitative polymerase chain reaction (PCR) during regeneration (**Figure 4**, right panel). While their levels are higher in the intact dorsal iris when compared to the ventral (ND vs. NV in **Figure 4**), during regeneration, this difference became smaller. This might indicate downregulation in the regenerating dorsal iris, which would be consistent with dorsalization. Notably, levels in the ventral iris were increased during regeneration, consistent with ventralization.

Large-Scale Expression Studies

Microarray Analysis

The surprising results of genetic activity in the ventral iris provided new insights with regard to the mechanisms of lens regeneration. Was this a more general pattern, or was it restricted to only a few genes? The expression of nearly 370 cDNAs cloned from the newt was examined via microarray. The results showed that most were expressed in the dorsal and ventral iris. It was interesting to see that genes for tissue remodeling, for example, those for metalloproteinases (**Figure 5**), were expressed in both the dorsal and ventral iris! Clearly, the regeneration-incompetent ventral iris is remodeling in the same way as the dorsal iris.

MicroRNA Regulation During Lens Regeneration

The information available so far indicates that the ventral iris is not really dormant in genetic activity and that, in general, genes that are expressed in the regeneration-competent dorsal iris are also expressed in the regeneration-incompetent ventral iris. In addition, the gene expression data show that the levels of expression are upregulated in the dorsal iris in response to the process of regeneration. To delineate the underlying mechanism of such global regulation, attention turned to microRNAs (miRNAs). miRNAs are short RNAs of about 20–22 neucleotides in length that have sequences complementary to sequences in the 3′-untranslated regions (UTRs) of many different mRNAs. Thus, one miRNA can target hundreds of mRNAs. When a miRNA forms a duplex with its target sequence, protein synthesis is inhibited. Since one miRNA can regulate many mRNAs, it can exert massive effects on gene expression.

The first step was to clone miRNAs from the newt eye. Several miRNAs were identified, among them miRNAs known to be expressed in the eyes of other animals. The newt miRNAs were almost identical to their mouse or to human counterparts. This astonishing sequence conservation among many species is another characteristic of miRNAs and implies conservation of regulation as well. Following this initial step, detailed expression study was performed, using microarrays containing all the mouse and human miRNAs. RNA was isolated from intact and day-8 postlentectomy dorsal and ventral irises. Indeed, it was found that several miRNAs are regulated in the intact irises as well as during regeneration (**Figure 6**).

Table 1 summarizes some of the results of the microarray analysis. Several miRNAs – such as miR124, miR181, and miR184 – are known to be expressed in the eye. In addition, a particular pattern was seen for members of the let7 family. While these miRNAs were expressed at higher levels in the intact dorsal iris, they were all decreased during dedifferentiation. Interestingly, same patterns were seen during regeneration of another tissue, that of hair cells.

These results were the first to associate miRNA expression with regenerative processes and provide great promise for understanding gene regulation. For example, miR148 seems to be ventral-specific (this was verified by quantitative polymerase chain reaction (QPCR); **Figure 7**). Its inhibition might dorsalize the ventral iris and induce regeneration. Likewise, opposite experiments should inhibit regeneration.

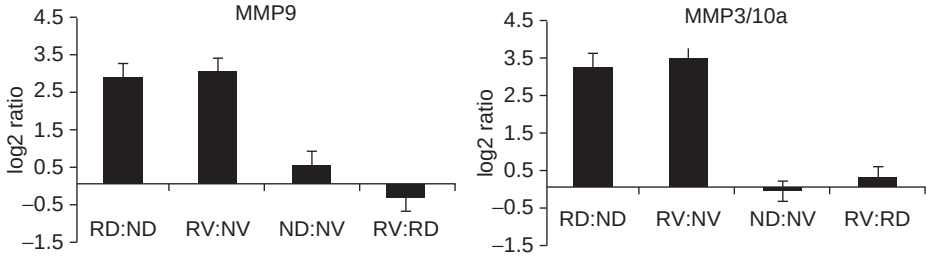

Figure 5 Quantitative PCR results on the expression of MMP9 and MMP3/10a in normal and regeneration-undergoing dorsal and ventral iris. RV:NV means comparison between regenerating ventral iris and normal ventral iris. Note that both in ventral and dorsal irises these genes are upregulated in relation to the values of their normal (intact counterparts), without much differences between each other.

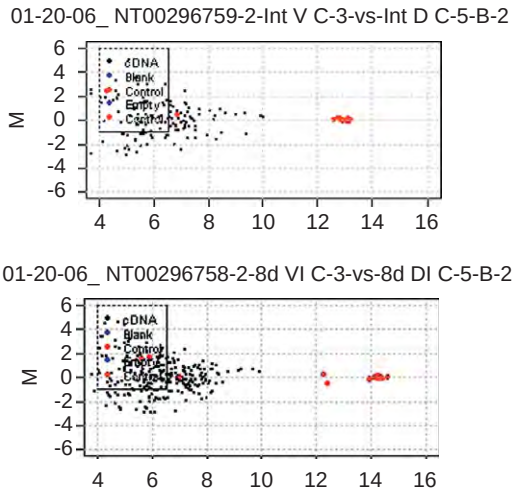

Figure 6 miRNA expression as revealed by microarray analysis. Comparison between intact dorsal and ventral iris (left) and between day 8 dorsal iris (DI) and ventral iris (VI) (right). Each black dot indicates a particular miRNA and, if it is above 0, is upregulated and, below 0, is downregulated. The red dots correspond to controls and as the reader can see they are mostly around value 0.

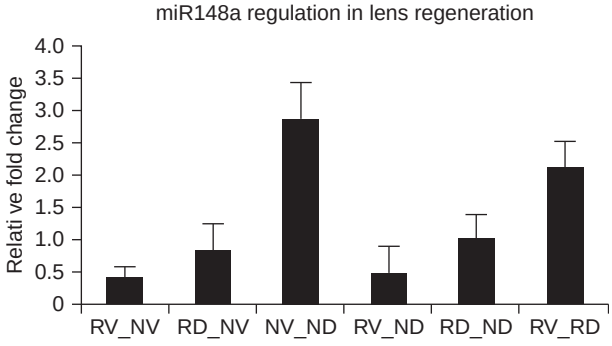

Figure 7 Quantitative PCR analysis of miR148 during lens regeneration. Note that this miRNA is expressed higher in the normal ventral iris as compared with the normal dorsal (NV_ND) and during regeneration (RV_RD).

Table 1 Regulation of selected miRNAs in newt irises

Upregulated in intact dorsal iris	*Upregulated in regeneration dorsal iris*	*Upregulated in intact ventral iris*	*Upregulated in regeneration ventral iris*
mir200	mir200	mir148	mir148
mir125	mir125	mir181	mir181
mir184	mir124	mir299	mir184
let7d		mir370	mir370
mir29			let7a-g
mir204			
let7a-g			

Comparison with the Axolotl

Gene expression was also investigated in the axolotl – another urodele – but one that cannot regenerate the lens. We were, in particular, interested to check gene

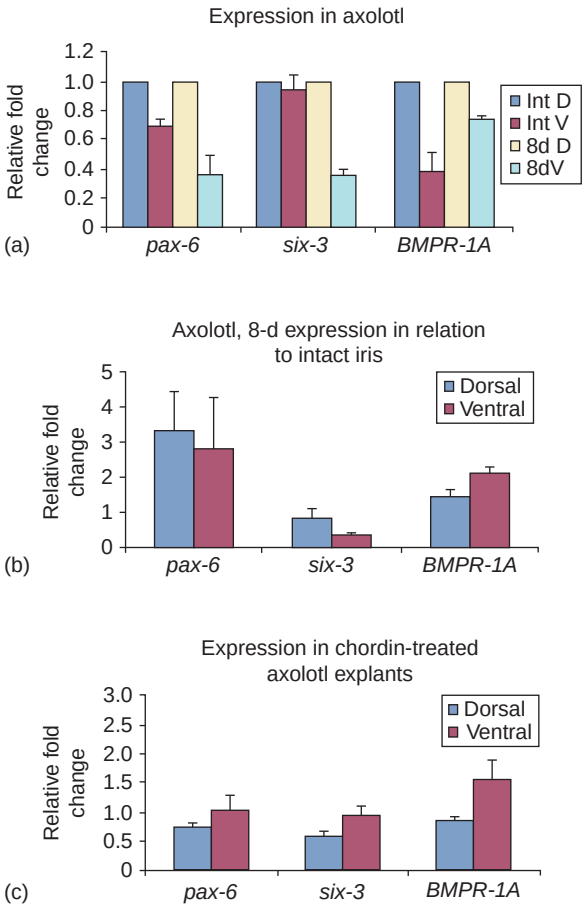

Figure 8 Expression in axolotl. (a) Comparison of pax-6, six-3, and BMPR-IA expression between the axolotl dorsal and ventral iris. Expression is shown in intact irises and 8 days following lentectomy. Values in the dorsal iris have been set to 1 and those in the ventral iris are shown as relative fold changes.
(b) Comparison of expression in 8th-day irises with intact irises.
(c) Expression in chordin-treated iris explants relative to untreated explants.

expression as it pertains to the induction we achieved in the newt ventral iris. QPCR for six-3, pax-6, and BMPR-1A was performed. The results were quite instructive. Unlike the newt, there was no differential expression detected between the intact dorsal or ventral iris (**Figure 8(a)**) and no upregulation of these genes following lentectomy (**Figure 8(b)**). Even though these genes are expressed, they do not follow a pattern similar to the one seen in the newts. Similarly, treatment with chordin did not increase the levels of pax-6 or six-3, as was shown previously in newts (**Figure 8(c)**; compare with **Figure 4(g)**).

This suggests that the axolotl irises cannot really be equated with the newt ventral iris. To corroborate this observation, the expression of several proteins involved in signaling was examined using antibodies that cross-react with both newt and axolotl tissues (verified by Western blot analysis). Some proteins showed increased expression in the newt ventral iris when compared with the newt

Table 2 Expression of proteins and their association with regenerative capabilities in newt and axolotl

Protein	*Abbreviation*	*Newt dorsal vs ventral iris (higher)*	*Newt dorsal vs Axolotl (higher)*	*Consistent with regeneration potential*
Calcium/calmodulin-dependent protein serine kinase 2α	CaMK2a	D	axolotl	NO
Catenin beta 1	Catenin b	V	equal	NO
Epidermal growth factor receptor	EGFR	D	newt	YES
Integrin-linked protein-serine kinase 1	ILK1	equal	newt	NO
Interleukin 1 receptor-associated kinase 4	IRAK4	V	equal	NO
Jun proto-oncogene	jun	V	axolotl	YES
Macrophage-stimulating protein receptor α chain	RONa	D	axolotl	NO
MAP kinase phosphatase 1	MKP1	D	newt	YES
Mitogen-activated protein serine kinase p38 α	P38aMAPK	equal	equal	NO
p21 activated serine kinase 3	PAK3	D	newt	YES
Protein-serine kinase C α	PKCa	D	newt	YES
Suppressor of cytokine signaling 4	SOCS4	V	axolotl	YES
TNF-related apoptosis-inducing ligand	Trail	equal	newt	NO

dorsal iris. These were similarly regulated in the axolotl irises, indicating a similarity of axolotl irises to newt ventral iris. However, many other proteins did not follow this pattern, indicating that the axolotl irises show patterns of protein expression that are different from that seen in the ventral iris of the newt (see **Table 2**).

These observations may have important implications for the potential of the axolotl (or another animal) iris to be induced with the same treatment that induced the newt ventral iris to form a lens. It is, of course, a major goal to induce lens regeneration in other species, but one must be cautious of how to apply the knowledge gained from the newt. Attempts to induce the axolotl irises to transdifferentiate to lens have not yet been successful. With the knowledge described above, this is hardly surprising. It seems most likely that global suppression of regeneration must occur in the newt ventral iris. Induction of lens regeneration in other animals, such as the axolotl, will depend on manipulating this exact molecular signature. The induction of the newt ventral iris is a good starting point, but achieving a similar result in the axolotl may require additional manipulation. Similar issues apply in mice. Even though the jump from amphibian to mammals is a big one, the ultimate goal of this research is to apply it in higher animals. In truth, not much is known about the expression of regulatory genes in adult mouse eye tissues. Most of what is known is derived from studies during development. As an initial step, pax-6 and six-3 mRNA levels were examined in mouse irises by PCR. Several genes that are important in pigment synthesis and in pigment stem cells – among them pax-3, beta-catenin, Sox10, and endothelin – were also studied. Interestingly, pax-6, six-3, and the other genes examined were expressed in the adult mouse dorsal and ventral iris (**Figure 9**) and, as in the axolotl, without apparent regulation following lentectomy. Thus, similar deductions can be drawn for the induction of lens regeneration in mice.

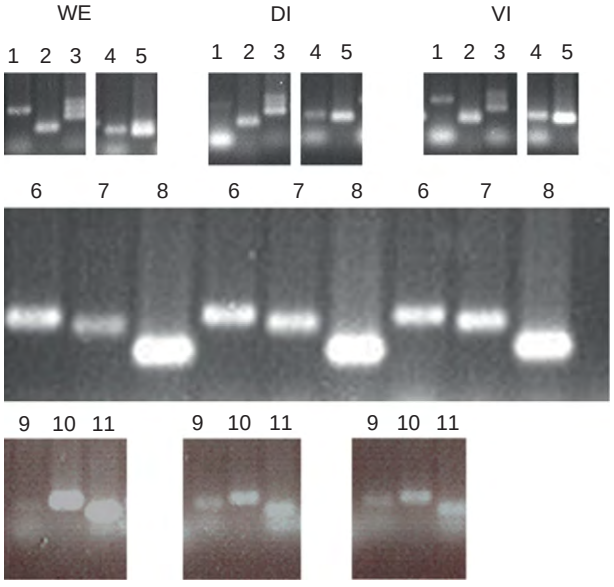

Figure 9 Expression of several genes in mouse whole eye (WE), dorsal iris (DI), and ventral iris (VI). 1: endothelin 3; 2: Endothelin B receptor; 3: pax-6; 4: mitf; 5 and 8: ATP5e (housekeeping); 6: six-3; 7: Sox10; 9: pax-3; 10: beta-catenin; 11: beta-integrin.

Regeneration of the lens in newts has provided a paradigm for regenerative research, in general. The inability of the ventral iris to form a lens is most likely due to a general repression mechanism that prevents it from transdifferentiating to lens. Since many of the mechanisms that are involved in gene repression are quite conserved to be extended and compared in other species than the newt.

See also: Lens Determination and Induction; Lens Fiber Cell Differentiation; Lens Structure; Zebrafish: Retinal Development and Regeneration.

Further Reading

Alvarado, A. S. and Tsonis, P. A. (2006). Bridging the regeneration gap: Genetic insights from diverse animal models. *Nature Reviews Genetics* 7(11): 873–884.

Ambros, V. (2004). The functions of animal microRNAs. *Nature* 431: 350–355.

Call, M. K., Grogg, M. W., Del Rio-Tsonis, K., and Tsonis, P. A. (2004). Lens regeneration in mice: Implications in cataracts. *Experimental Eye Research* 78(2): 297–299.

Davidson, E. H. (2006). *The Regulatory Genome.* San Diego, CA: Academic Press.

Del Rio-Tsonis, K., Jung, J. C., Chiu, I. M., and Tsonis, P. A. (1997). Conservation of fibroblast growth factor function in lens regeneration. *Proceedings of the National Academy of Sciences of the United States of America* 94(25): 13701–13706.

Del Rio-Tsonis, K., Tomarev, S. I., and Tsonis, P. A. (1999). Regulation of Prox 1 during lens regeneration. *Investigative Ophthalmology and Visual Science* 40(9): 2039–2045.

Del Rio-Tsonis, K., Trombley, M. T., McMahon, G., and Tsonis, P. A. (1998). Regulation of lens regeneration by fibroblast growth factor receptor 1. *Developmental Dynamics* 213(1): 140–146.

Del Rio-Tsonis, K. and Tsonis, P. A. (2003). Eye regeneration at the molecular age. *Developmental Dynamics* 226(2): 211–224.

Del Rio-Tsonis, K., Washabaugh, C. H., and Tsonis, P. A. (1995). Expression of pax-6 during urodele eye development and lens regeneration. *Proceedings of the National Academy of Sciences of the United States of America* 92(11): 5092–5096.

DeRobertis, E. M. (2006). Spemanns organizer and self-regulation in amphibian embryos. *Nature Reviews Molecular Cell Biology* 7: 296–302.

Eguchi, G. (1988). Cellular and molecular background of Wolffian lens regeneration. In: Eguchi, G., Okata, T., and Saxen, L. (eds.) *Regulatory Mechanisms in Developmental Processes*, pp. 147–158. Amsterdam: Elsevier.

Grogg, M. W., Call, M. K., Okamoto, M., et al. (2005). BMP inhibition-driven regulation of six-3 underlies induction of newt lens regeneration. *Nature* 438: 858–862.

Gwon, A., Gruber, L. J., Mantras, C., and Cunanan, C. (1993). Lens regeneration in New Zealand albino rabbits after endocapsular cataract extraction. *Investigative Ophthalmology and Visual Science* 34: 2124–2129.

Kimura, Y., Madhavan, M., Mantras, C., and Cunanan, C. (2003). Expression of complement 3 and complement 5 in newt limb and lens regeneration. *Journal of Immunology* 170(5): 2331–2339.

Makarev, E. O., Call, M. K., Grogg, M. W., et al. (2007). Gene expression signatures in the newt irises during lens regeneration. *FEBS Letters* 581: 1865–1870.

Makarev, E. O., Spence, J. R., Del Rio-Tsonis, K., and Tsonis, P. A. (2006). Identification of miRNAs and other small RNAs from the adult newt eye. *Molecular Vision* 7: 1386–1391.

McDevitt, D. S. and Brahma, S. K. (1981). Ontogeny and localization of the alpha-, beta, and gamma-crystallins in newt eye lens development. *Developmental Biology* 84: 449–454.

Stone, L. S. (1967). An investigation recording all salamanders which can and cannot regenerate a lens from the dorsal iris. *Journal of Experimental Zoology* 164: 87–104.

Tsonis, P. A. (2000). Regeneration in vertebrates. *Developmental Biology* 221(2): 273–284.

Tsonis, P. A., Call, M. K., Grogg, M., et al. (2007). MicroRNAs and regeneration: Let-7 members as potential regulators of dedifferentiation in lens and inner ear hair cell regeneration of the adult newt. *Biochemical and Biophysical Research Communications* 362: 940–945.

Tsonis, P. A. and Del Rio-Tsonis, K. (2004). Lens and retina regeneration: Transdifferentiation, stem cells and clinical applications. *Experimental Eye Research* 78(2): 161–172.

Tsonis, P. A. and Makarev, E. (2008). On dorsal/ventral-specific genes in the iris during lens regeneration. *Cellular and Molecular Life Sciences* 65: 41–44.

Tsonis, P. A., Tancous, E., Madhavan, M., and Del Rio-Tsonis, K. (2004). A newt's eye view of lens regeneration. *International Journal of Developmental Biology* 48: 975–980.

Yamada, T. (1977). Control mechanisms in cell type conversion in newt lens regeneration. In: Wolsky, A. (ed.) *Monographs in Developmental Biology* vol. 13, pp. 1–119. Basel: Karger.

Lens Structure

D C Beebe, Washington University, Saint Louis, MO, USA

Glossary

Lens capsule – The thick extracellular matrix that surrounds the lens.
Lens fibers – Elongated cells that make up the bulk of the lens. During their terminal differentiation fiber cells lose all membrane-bound organelles. The absence of organelles and their high protein concentration accounts for the transparency and high refractive index of the lens.
Sutures – Elongated fiber cells cannot taper to infinite thinness as they approach the anterior and posterior poles of the lens. Sutures are structural modifications that adjust for this physical dilemma. Elongating fiber cells may meet cells from the opposite side of the lens at planes (suture planes), or most cells may extend only part way to the pole, forming an umbilical suture.
Zonules – Thin fibrils that anchor the lens capsule to the ciliary epithelium, thereby suspending the lens in the anterior of the eye.

The function of the lens depends on its transparency, its refractive index, the curvature of its refractive surfaces, and its ability to change shape during accommodation. Accommodation is the process by which the power of the lens is increased for near vision. Transparency depends on minimizing light scattering and absorption. Some aspects of lens transparency are addressed below and in the sections on lens fiber cell differentiation and lens protein aging. The lens refractive index depends on the concentration of proteins in the fiber cells, a topic that is discussed below. Lenses may be nearly round or oblate and their anterior and posterior surfaces may have different radii of curvature. Surprisingly, the factors that determine lens shape are poorly understood, although it is clear that, during development and growth, signals from outside the lens influence its shape.

The mature lens is an unusual structure, compared to most in the body, being constructed only from epithelial cells. These cells exist in two states of differentiation, lens epithelial cells and fiber cells (**Figure 1**). The lens is surrounded by a tough, flexible layer of extracellular matrix, the lens capsule, which is secreted by the lens cells at the lens surface. Thin fibrils, the zonules, connect the capsule to the ciliary epithelium to suspend the lens in the anterior of the eye.

The anterior surface of the lens, the surface that faces the cornea, is covered by a monolayer of cuboidal epithelial cells, lying beneath the anterior capsule. The bulk of the lens is formed from a mass of elongated fiber cells. In the adult lens, cells in the central region of the epithelium rarely divide. However, epithelial cells in a narrow band near the lens equator – the germinative zone – proliferate slowly. The daughter cells of these mitotic divisions move toward the lens equator, where, in response to signals from the posterior of the eye, they permanently withdraw from the cell cycle in a region called the transition zone. Cells at the posterior edge of the transition zone elongate to form fiber cells. The elongation of successive waves of fiber cells buries earlier-born fiber cells deeper in the lens. Since new fiber cells are formed all around the lens equator, fiber cell formation generates concentric shells of fiber cells that are formed at the same time. Because no cells are removed from the fiber mass, the lens grows in cell number and size throughout life. Thus, the rate of cell proliferation in the germinative zone determines the rate of fiber cell formation and the size of the lens.

During fiber cell elongation, the basal ends of the fiber cells, which contact the posterior capsule, extend toward the posterior pole of the lens, whereas the apical ends extend anteriorly beneath the lens epithelium. The posterior ends of the fiber cells extend more rapidly than the anterior ends and reach the posterior pole of the lens before the apical ends reach the anterior pole. Fiber cell nuclei tend to remain in the center of the cells. The more rapid elongation of fiber cells toward the posterior pole causes the nuclei to become located more posteriorly in the lens. When the posterior ends reach the posterior pole of the lens, they stop migrating; however, the anterior ends of the fiber cells are still elongating. Therefore, the nuclei gradually shift back in a more anterior direction. The movement of the nuclei during fiber cell elongation, first in a posterior direction and then anteriorly, traces the shape of a bow, which gives this region of elongating fiber cells its name, the lens bow.

When the ends of the fiber cells extend, they encounter a geometric problem. The basal and apical ends of all of the fiber cells in a shell are elongating toward two points, one at the posterior pole and one at the anterior pole. In a practical sense, the ends of the cells can never be narrow enough for all cells to reach the poles.

The lenses of different species deal with this topological problem in one of two ways. In most mammals, amphibians, and some fish, elongating fiber cells meet cells from the opposite side of the lens along planes,

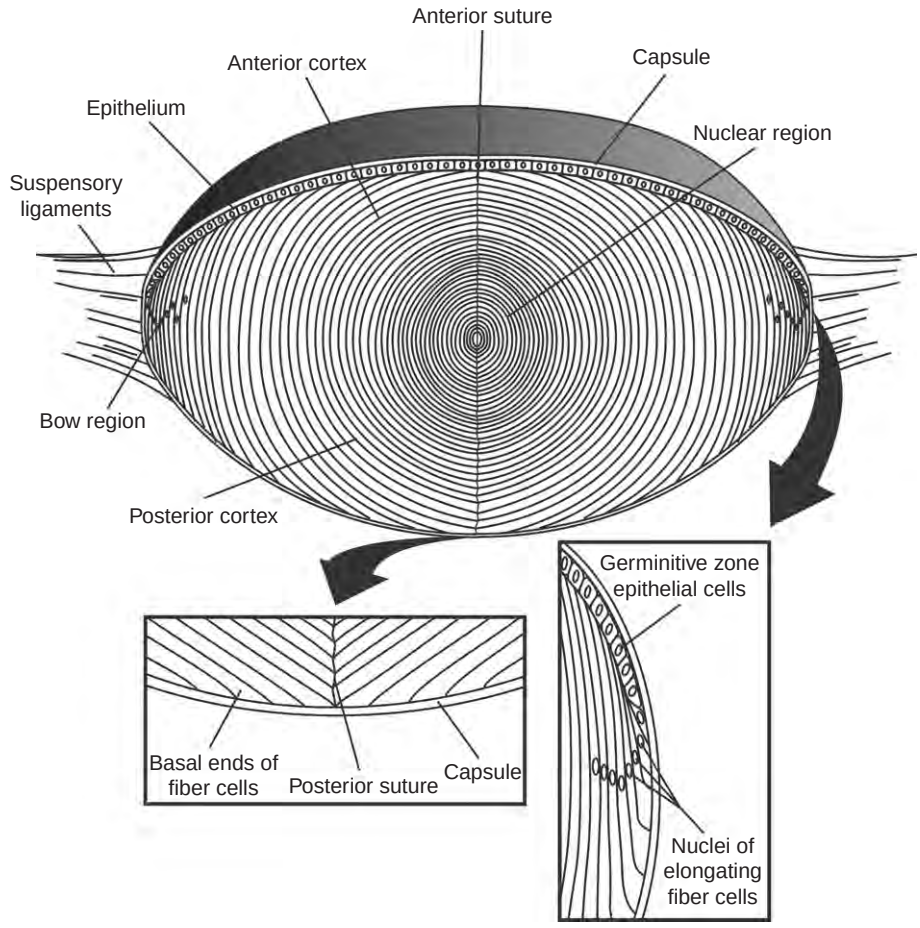

Figure 1 A schematic diagram of the structure of the lens. The inset on the left shows fiber cells meeting at the posterior of the lens, where the sutures are forming. The inset on the right shows detail of the lens equator, where epithelial cells divide, move posteriorly, elongate to form fiber cells, and eventually lose all membrane-bound organelles, including their nuclei. From Beebe, D. (2003). Lens. In: Kaufman, P. L. and Alm, A. (eds.) *Adler's Physiology of the Eye*, 10th edn, pp. 117–158. St. Louis, MO: Mosby.

called sutures. The simplest suture pattern is a line suture, in which the ends of fiber cells meet along a single plane at each pole of the lens. In a more complex variation, the ends of fiber cells meet along three planes, which take the shape of the letter Y (**Figure 2**). In humans and other primates, Y sutures initially form, but become more complex as the lens grows. In humans, the ends of the suture branches bifurcate soon after birth, generating six suture planes from the original three. This process occurs again later in life, resulting in 12 suture branches. In birds and some fish, suture planes do not form; instead, elongating fiber cells gradually taper as they elongate, with most fiber cells stopping before they reach the poles. The few cells that reach the poles contact the ends of cells from the opposite side of the lens, forming an umbilical or point suture.

Line and Y sutures are oriented precisely with respect to the axes of the eye. Y sutures form an upright Y in the anterior of the lens, the side toward the cornea, and an inverted Y at the posterior of the lens. Line sutures have a vertical orientation at the anterior of the lens and are horizontal at its posterior.

The suture patterns may have optical and structural consequences for the lens. Comparison of the optical properties of lenses with Y sutures with the more complex pattern found in primates showed that the more complex suture pattern results in lenses with fewer optical aberrations. The optical properties of lenses with umbilical and Y sutures have not been directly compared. Bird lenses undergo rapid and extensive change of shape during accommodation, suggesting that umbilical sutures may contribute to the ability of the lens to withstand the forces generated in this process. However, fish do not accommodate by changing the shape of the lens, but some have umbilical sutures. Thus, the extent to which the lens changes shape during accommodation is not the only factor that determines the suture pattern.

Sutures are not present early in lens formation. They only form later, as the lens grows and lays down shells of secondary fiber cells. The mechanisms that determine the

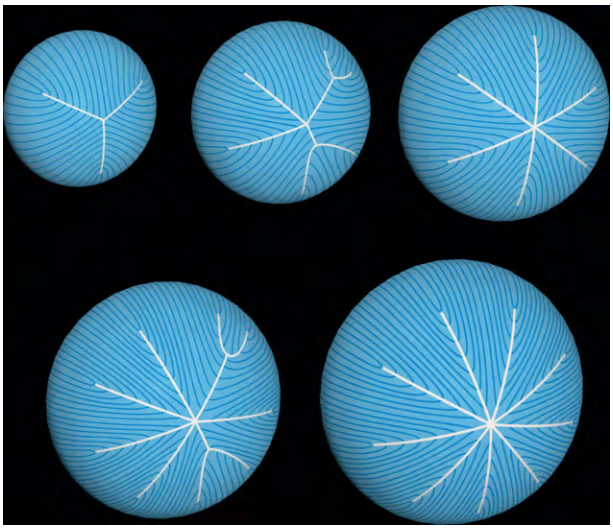

Figure 2 A diagram showing the development of the suture pattern in the human lens. The lens begins with a Y suture pattern. As it grows, newly formed sutures branch near the tips of the existing suture planes. These branch points migrate toward the pole, eventually doubling the number of suture planes. This process continues as the lens grows throughout life with the deposition of successive layers of fiber cells. This figure was kindly provided by Dr. Jer Kuszak. From Beebe, D. (2003). Lens. In: Kaufman, P. L. and Alm, A. (eds.) *Adler's Physiology of the Eye*, 10th edn, pp. 117–158. St. Louis, MO: Mosby.

type of suture pattern and that assure the stereotypical orientation of the sutures in the eye are not known. Similarly, we do not know why different species have acquired different suture patterns during evolution.

After the anterior and posterior ends of the fiber cells reach the sutures, they stop elongating. The lateral membranes of the fiber cells interdigitate, forming interlocking junctions between adjacent cells. These specializations appear to stabilize lens structure. At this stage in their development, fiber cells also partially fuse along their lateral membranes with their neighbors in the same shell. This may assure that the cytoplasm of cells at similar depth in the lens is of uniform refractive index. Soon after fusing, the fiber cells degrade all intracellular, membrane-bound organelles, including the nucleus, mitochondria, and endoplasmic reticulum. Mouse mutants in which nuclear degradation is inhibited have diffuse nuclear cataracts, supporting the idea that organelle degradation increases transparency by reducing light scattering.

Refractive Index

To focus light, any lens must have a refractive index that is different from the medium in which it is suspended. The refractive index of the eye lens is higher than the aqueous and vitreous humors that surround it because it has a higher protein concentration than these fluids. The higher protein content of the lens results largely from the synthesis and stability of the proteins of the lens fiber cells, the lens crystallins. Information about the structure, complexity, and stability of the crystallins is covered elsewhere in this encyclopedia.

Numerous studies have documented the extreme specialization in protein content that occurs during fiber cell differentiation. During lens development, a single crystallin can account for as much as 70% of the total protein content of the lens. There are about 12 crystallin polypeptides in the adult lens, but these account for about 95% of the soluble protein. The abundance of any protein depends on the level to which its mRNA accumulates, the efficiency with which the mRNA is translated, and the relative stability of the resulting protein. The abundance of the crystallins results, in part, from the high level of expression of crystallin mRNAs. This aspect of lens molecular biology is the one most studied. The relative contribution of selective translational efficiency to crystallin accumulation is not known. Although crystallins persist for the life of the lens, experimental studies have not revealed whether they are intrinsically more stable than other cytoplasmic proteins, whether the cytoplasmic environment within the lens fiber cells generally protects against protein degradation, or a combination of these factors.

The protein concentration of the lens cytoplasm increases two- to threefold from the lens surface to its center. This protein gradient creates a gradient of refractive index that largely compensates for the spherical aberration of the lens. Although the existence and importance of this gradient has been appreciated for many years, its origin is not clear. Cells at the surface of a young lens are buried deeper in the lens as it ages. Thus, the protein concentration in their cytoplasm must increase as lens cells age. However, protein synthesis is confined to cells near the lens surface. Therefore, for the most part, the increase in protein concentration in the deeper cells does not result from continued synthesis.

The solubility or osmotic activity of the lens proteins must change as they become more concentrated. If the crystallins were free in solution, the increase in their concentration would result in a decrease in water concentration, creating an osmotic gradient that would draw water into the lens nucleus. Since this does not occur, proteins deeper in the lens must exist in a state that reduces their osmotic activity. This might be accomplished by partial association or gel formation. The mechanisms responsible for the decrease in osmotic activity of the crystallins are not well understood.

Transparency

The high protein concentration in the lens cytoplasm may seem inconsistent with transparency, since light scattering

tends to increase with an increase in protein concentration. Classical studies by Delaye and Tardieu resolved this apparent contradiction by showing that, at the high concentrations present in the lens, short-range interactions between the proteins minimize light scattering. Whether these interactions also account for the reduced osmotic activity of the cytoplasm deep within the lens remains an unanswered question.

The Zonules

Thin fibrils connect the lens capsule to a ring of ciliary epithelial cells on the inner surface of the eye near its anterior margin. These fibrils form the suspensory ligament or zonular apparatus. They are composed largely of the protein fibrillin, a component of the elastic fibrils found throughout connective tissues. However, the zonular fibers are not extensible. In addition to positioning the lens in the visual axis, they transmit force from the ciliary muscles, altering lens shape during accommodation.

See also: Accommodation; Lens Fiber Cell Differentiation; Normal Age-Related Changes: Crystallin Modifications, Lens Hardening.

Further Reading

Bassnett, S. (2002). Lens organelle degradation. *Experimental Eye Research* 74(1): 1–6.

Bassnett, S. and Winzenburger, P. A. (2003). Morphometric analysis of fibre cell growth in the developing chicken lens. *Experimental Eye Research* 76(3): 291–302.

Beebe, D. (2003). Lens. In: Kaufman, P. L. and Alm, A. (eds.) *Adler's Physiology of the Eye*, pp. 117–158. St. Louis, MO: Mosby.

Coulombre, J. L. and Coulombre, A. J. (1969). Lens development. IV. Size, shape, and orientation. *Investigative Ophthalmology* 8(3): 251–257.

Cvekl, A. and Duncan, M. K. (2007). Genetic and epigenetic mechanisms of gene regulation during lens development. *Progress in Retinal and Eye Research* 26(6): 555–597.

Danysh, B. P. and Duncan, M. K. (2009). The lens capsule. *Experimental Eye Research* 88(2): 151–164.

Delaye, M. and Tardieu, A. (1983). Short-range order of crystalline proteins accounts for eye lens transparency. *Nature* 302: 415–417.

Fagerholm, P. P., Philipson, B. T., and Lindstrom, B. (1981). Normal human lens – the distribution of protein. *Experimental Eye Research* 33(6): 615–620.

Kuszak, J. R., Zoltoski, R. K., and Tiedemann, C. E. (2004). Development of lens sutures. *International Journal of Developmental Biology* 48(8–9): 889–902.

Shi, Y., Barton, K., De Maria, A., et al. (2009). The stratified syncytium of the vertebrate lens. *Journal of Cell Science* 122(Pt 10): 1607–1615.

Sivak, J. G. (2004). Through the lens clearly: Phylogeny and development: The proctor lecture. *Investigative Ophthalmology and Visual Science* 45(3): 740–747; 739.

Lids: Anatomy, Pathophysiology, Mucocutaneous Junction

T Wojno, The Emory Clinic, Atlanta, GA, USA

Glossary

Actinic lesion – Dry, scaly, rough-textured patches that form after years of exposure to ultraviolet light, such as sunlight.
Amblyopia – Disorder of the visual system that is characterized by poor or indistinct vision in an eye that is otherwise physically normal.
Anisometropia – Condition in which the two eyes have unequal refractive power.
Blepharitis – Chronic inflammation of the eyelids.
Blepharoplasty – Surgical procedure intended to reshape the upper eyelid or lower eyelid by the removal or repositioning of excess tissue as well as by reinforcement of surrounding muscles and tendons.
Dermatochalasis – Redundant, baggy eyelids.
Ectopion – Outward malposition of the eyelid.
Entropion – Inward malposition of the eyelid.
Lagophthalmos – Inability to close the eye.
Ptosis – Downward malposition of the upper eyelid.
Strabismus – A condition in which the eyes are not properly aligned with each other.
Trichiasis – Misdirected eyelashes.

Anatomy

From a functional perspective, the upper lid can be divided into anterior, middle, and posterior lamellae (Figure 1). In the upper lid, the anterior lamella consists of the skin and orbicularis muscle while the posterior lamella consists of the conjunctiva, tarsus, levator, and Müller's muscle. The middle lamella is the orbital septum and orbital fat. The thin eyelid skin covers the orbicularis muscle, which is functionally divided into the pretarsal, preseptal, and orbital parts. There is no discreet anatomic border to these components of the orbicularis. The levator muscle originates just superior to the annulus of Zinn at the orbital apex and changes from striated muscle to fibrous apponeurosis 15 mm above the superior border of tarsus. The levator inserts into the superior border and anterior surface of the tarsal plate. It is innervated by the third cranial nerve. Müller's muscle is only 10–14 mm long and arises from the underbelly of the levator and inserts into the superior border of tarsus. It is composed of smooth muscle fibers and is adrenergically innervated. The levator and Müller's muscles function to open the upper lid while the orbicularis muscle closes it. The orbital septum is a thin, multilayered sheet of fibrous tissue separating the lid from the orbit. It arises from the superior orbital rim and inserts onto the levator aponeurosis 2–10 mm above the superior border of tarsus in Caucasians, 15 mm or more in blacks and at or below the superior border of tarsus in Asians. Small, fine, fibrous attachments extend from the levator to the subcutaneous tissue. These attachments and the insertion of the septum form the lid crease while the skin above the crease forms the lid fold. There are two fat pockets in the upper lid found nasally and centrally. The upper tarsus is a firm connective tissue usually 10–12 mm in height and 1 mm in thickness.

The lower lid is likewise divided into three functional lamellae: an anterior layer of skin and orbicularis, a posterior layer of conjunctiva and lower lid retractors, and a middle layer of septum and orbital fat (Figure 2). The lower lid retractors are composed of the capsulopalpebral fascia (the equivalent of the levator in the upper lid) and the inferior tarsal muscle (the equivalent of the Müller's muscle in the upper lid). The capsulopalpebral fascia is a fibrous band originating from the underbelly of the inferior rectus muscle that courses anteriorly, enveloping the inferior oblique, and inserts onto the inferior border of tarsus. It is functionally controlled by its origin from the inferior rectus muscle to retract the lower lid inferiorly when the eye looks downward, preserving unobstructed vision. The inferior tarsal muscle is often just scattered smooth muscle fibers intermixed with the capsulopalpebral fascia. As in the upper lid, the septum arises from the orbital rim and inserts on the inferior border of tarsus, often blending with the lower lid retractors. A lower lid crease occasionally exists but is usually less obvious. There are three fat pockets in the lower lid: nasal, central, and temporal (or lateral). The lower tarsus is usually 4–5 mm in height.

The lid margin is the border between the anterior skin–muscle layer and the posterior tarsoconjunctival layer. There are two to three irregular rows of lashes, whose bulbs are embedded just below the skin surface within the orbicularis muscle. Posterior to the lash line are the meibomian gland orifices. These sebaceous glands are embedded within the tarsal plates and run the entire vertical length of the tarsus. There are about 25 of these glands in the upper lid and 20 in the lower lid. The mucocutaneous junction is just posterior to the meibomian

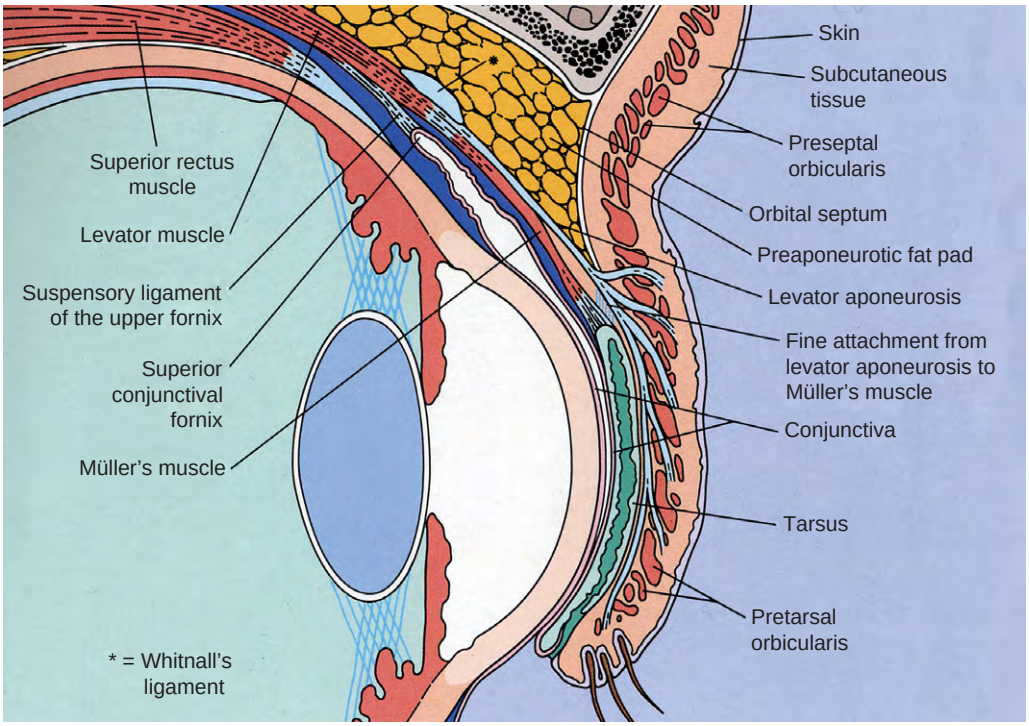

Figure 1 Cross-section of the upper eyelid.

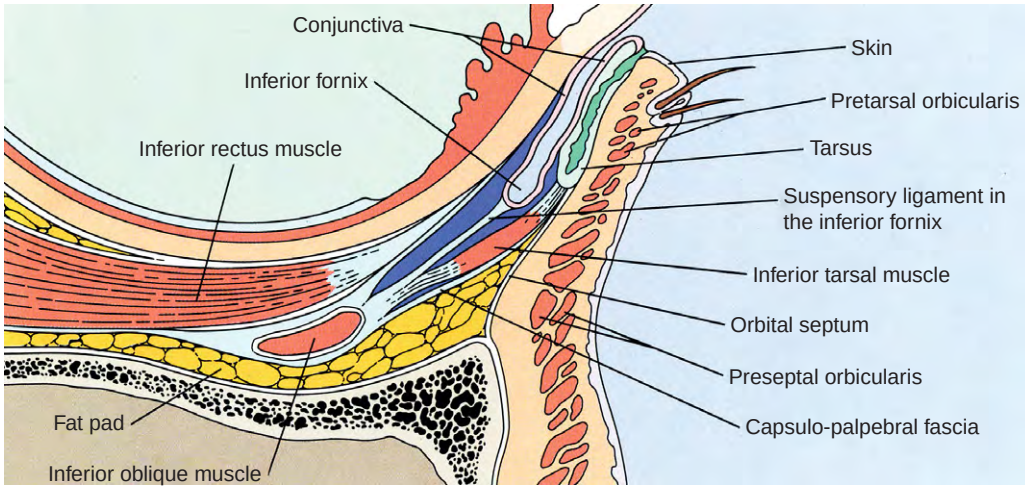

Figure 2 Cross-section of the lower eyelid.

gland orifices. The gray line is a variably visible section of pretarsal muscle (muscle of Riolan) just anterior to the tarsus. Embedded within the lid margin are the apocrine glands of Moll and the sebaceous glands of Zeiss associated with the lash follicles.

The upper and lower lids join laterally where the pretarsal heads of the orbicularis muscle form the lateral canthal tendon, which inserts into the orbital tubercle just posterior to the lateral orbital rim. Medially, the preseptal and pretarsal muscle form the medial canthal tendon, whose anterior and posterior heads surround the lacrimal sac. The lacrimal puncta open on the lid margin 6 mm from the medial commissure of the lids.

Pathophysiology

Dermatochalasis

Dermatochalasis is the normal aging change in the upper and lower lids characterized by loose, redundant skin and

orbicularis muscle often with bulging of the orbital fat pockets (Figure 3). It may be associated with ptosis of the eyebrows and forehead relaxation. When severe in the upper lids, it can limit peripheral vision and obstruct the central visual axis. Lower lid dermatochalasis rarely affects the vision, but in rare cases, fat bulging can be so extreme so as to contact the patient's glasses. Surgical treatment is aimed at removal of the excess skin, orbicularis, and fat.

Ptosis

Lid ptosis is a lower-than-normal position of the upper lid margin (Figure 4). When the lid margin is 2 mm or less from the center of the pupil, the superior visual field is usually significantly obstructed. Ptosis is either congenital or acquired. Congenital ptosis is usually the result of a malformed levator muscle often with a family history. It is unilateral in 75% of cases and bilateral (although often asymmetric) in 25% of cases. It is associated with anisometropia, amblyopia, or strabismus in 30% of cases. In general, the more severe the ptosis, the more dystrophic appears the muscle histologically. In cases of severe congenital ptosis, striated muscle fibers are usually completely absent, totally replaced by fibro-fatty connective tissue.

Figure 3 Dermatochalasis of all four eyelids.

Figure 4 Ptosis of the right upper lid.

Treatment for mild-to-moderate congenital ptosis is to perform levator resection surgery, wherein 12–18 mm of the distal levator and the underlying Müller's muscle is resected and the cut end resewn to the superior border of tarsus. This effectively shortens the muscle, resulting in a higher resting level of the lid on the globe but does not improve the overall movement of the lid. The most common problems post-operatively are undercorrection, overcorrection, or asymmetry of the lids often necessitating reoperation. Surgery induces lagophthalmos that increases with the amount of levator resected. Surprisingly, if done during childhood, lagophthalmos is usually well tolerated throughout the patient's lifetime.

In severe congenital ptosis, the levator is usually so dystrophic that resection is ineffective. In such cases a sling must be performed. In this surgery, autogenous or banked fascia or some alloplastic material is sewn into the tarsus and then threaded under the skin to the frontalis muscle in the forehead. The patient then elevates the lid by contracting the frontalis muscle, which pulls up the lid margin. Most patients do so automatically, resulting in effective lid opening.

Acquired ptosis, usually seen with aging, results from thinning or dehiscence of the levator aponeurosis from the tarsal plate. Any condition, however, that causes lid swelling or stretching (cataract surgery, trauma, contact lens wear, etc.) can result in acquired ptosis. Much less frequently, acquired ptosis is due to actual deterioration of the levator muscle or true muscular dystrophy. The usual treatment of acquired ptosis is to shorten the levator aponeurosis but to a much smaller degree than done with congenital ptosis (usually 4–10 mm). In adults, ptosis repair, when performed bilaterally, is often combined with blepharoplasty surgery for optimal cosmesis. Like in congenital ptosis, undercorrection, overcorrection, and asymmetry are common problems. In adults, however, adjustments can often be accomplished in the office under local anesthesia. Lagophthalmos is generally to be avoided in adult surgery, since the cornea is usually very intolerant of any chronic exposure and can rapidly result in discomfort and even ulceration.

Retraction

The opposite of ptosis, retraction is abnormal elevation of the upper lid or downward positioning of the lower lid (Figure 5). Most cases of upper lid retraction are due to thyroid eye disease resulting from contracture of the upper and lower lid retractors secondary to inflammation.

Figure 5 Retraction of all four lids secondary to thyroid eye disease.

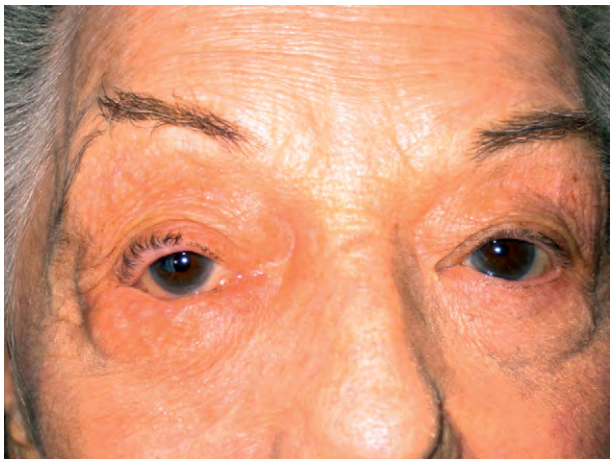

Figure 6 Involutional entropion of the right lower lid.

The lower lids may also retract due to age, associated with poor support from the cheekbones. Retraction due to thyroid eye disease is often associated with exopthalmos or an abnormal anterior displacement of the globe, which further increases the stare – so characteristic of this disease. Patients with retraction often have lagophthalmos, resulting in corneal exposure and irritation. Lower lid retraction is often seen as a normal physiologic variant in people with shallow orbits, especially common in black patients. Retraction is occasionally seen with overexcessive skin excision in blepharoplasty surgery.

Treatment of upper lid retraction in thyroid eye disease consists of graded recession of the levator–Müller's muscle complex superiorly so as to drop the upper lid margin down. Some surgeons insert spacers (autologous or banked tissues) between the recessed, cut edge of the levator–Mueller's muscle complex and the superior border of the tarsus when performing this surgery. In the lower lid, retraction is treated with recession of the lower lid retractors very frequently combined with spacer grafts for additional support of the lower lid. In the upper lid, gravity works in favor of the correction while it works against it in the lower lid. If the retraction is due to skin shortage after blepharoplasty, then skin grafting may be necessary.

Entropion

Entropion is an inward turning of the upper or lower lid margin (**Figure 6**). This results in the lashes rubbing on the globe, causing irritation and even corneal ulceration. Senile or involutional lower lid entropion is common with age and is due to excess horizontal (canthal tendons) and vertical laxity (the lower lid retractors).

This may be intermittent at first but usually progresses to a chronic condition. The lid margin appears to have a distinctive rolled-in appearance and can be reduced by pulling the lid against the lateral orbital rim, effectively tightening the lid. Surgical correction is aimed at correcting the horizontal laxity by resection of the redundant lid margin with resuspension at the lateral canthus. The vertical lid laxity may be corrected by plication of the lower lid retractors to the inferior border of tarsus. An effective repair is one which combines both of these procedures often performed through a lower lid blepharoplasty incision.

Involutional entropion usually does not occur in the upper lid. Such aging changes usually result in ptosis, as discussed above, or in lash ptosis – a downward angulation of the lashes due to relaxation of the anterior lamella of the eyelid in which the lash follicles are embedded. Lash ptosis is often corrected as part of an upper lid blepharoplasty procedure.

Cicatricial entropion may occur in both the upper and lower lids. It is due to vertical shortening of the posterior lamella of the eyelid, the tarsoconjunctival layer. It may be due to autoimmune disorders of the mucous membranes, inflammation, infection, surgery, trauma, or long-term use of glaucoma drops. Often, however, the cause is unclear. All surgeries for cicatricial entropion can be conceptualized as falling into three categories. The first are those that act by outward rotation of the lid margin (prototypical Weis procedure) usually involving a full-thickness, horizontal blepharotomy 4 mm from the lid margin. The second category involves expanding the shortened posterior lamella of the eyelid with grafts (usually buccal mucosa, amniotic membrane, or banked sclera). The third category involves procedures that split the lid margin at the gray line often with insertion of a spacer material, such as mucous membrane, to thicken the lid margin to the point that the lashes no longer rub against the globe. In some cases, the lash-bearing segment of the lid margin may simply be resected after splitting the lid margin.

Trichiasis

Often confused with entropion, trichiasis is inward misdirection of lashes against the globe in the presence of normal lid margin position. Trichiasis may, however, coexist with cicatricial entropion. Trichiasis is caused by the same factors that cause cicatricial entropion but is often idiopathic. Focal trichiasis is often treated by simple epilation of the offending lashes. If recurrent, electrolysis, cryotherapy, or laser may be used. Repeat treatment is often necessary since these modalities will kill the visible offending lashes but not the lashes that are about to bud. For large areas of the lid margin, surgery as outlined above for ciciatricial entropion may be needed. Alternatively, if focal, a segmental resection of the involved lid margin can be performed.

Distichiasis

Distichiasis is an additional row of lashes that grow from the meibomian orifices on the posterior lid margin. Such lashes will rub against the globe causing corneal irritation. Distichiasis may be congenital, often with a family history or acquired due to lid inflammation causing metaplasia of the cells in the posterior layer of the lid margin. It is treated with electrolysis or cryotherapy often after splitting the lid margin to prevent damage to the normal lashes. It may also be treated by direct surgical excision of the offending lashes.

Ectropion

Ectropion is outward rotation of the lower lid margin away from the globe (**Figure 7**). The exposure of the globe and the palpebral conjunctiva results in irritation, corneal damage, and keratinization of the conjunctiva. Epiphora, increased tear production, often results when the lower punctum stands off the globe and cannot adequately drain tears from the eye. Involutional ectropion occurs as an aging change secondary to horizontal lid laxity, mainly in the medial and lateral canthal tendons. Repair is accomplished by horizontal shortening of the redundant lid margin, usually at the lateral canthus, sometimes combined with vertical shortening of the lower lid retractors. When the problem is mainly medial, punctual ectropion, a spindle of conjunctiva and lower lid retractors is resected immediately below the lower punctum. Lower lid ectropion may coexist with retraction, as was discussed above. Involutional ectropion usually does not occur in the upper lid.

Figure 7 Involutional ectropion of the lower lids, worse on the right.

Cicatricial ectropion is due to vertical shortening of the anterior, skin–muscle lamella of the upper or lower lid. It is usually secondary to trauma or skin disorders. In the upper lid, release of the scarred tissue is followed by skin grafting from the opposite upper lid, the retroauricular area, supraclavicular area, or forearm. In the lower lid, horizontal lid shortening is also often required since the chronically ectropic lid often has or develops a component of excess horizontal laxity. In the lower lid, a skin graft may be replaced by advancement of a skin–muscle flap from the surrounding area.

Paralytic ectropion is due to paralysis of the seventh nerve. There is also lagophthalmos due to inability of the upper and lower lids to close. Exposure can be severe and can lead to corneal ulceration. Conservative treatment consists of ocular lubrication, moist chamber devices and lid taping. Tarsorrhaphy may be needed if the cornea dries out in spite of conservative measures. For those cases in which seventh nerve function will not return a gold weight or spring may be placed in the upper lid to counter the lagophthalmos. The lower lid usually needs to be tightened horizontally and often lifted vertically with a posterior lamellar graft or suspension sling of fascia or silicone. Although such treatments are helpful, patients never have a normal blink with any of these procedures.

Floppy Lid Syndrome

This uncommon syndrome is most frequently seen in obese, middle-aged males (**Figure 8**). The upper lid is extremely lax and spontaneously everts often while the patient sleeps and rubs against the pillow. Those affected have a severe papillary conjunctivitis, ropey mucoid discharge, and irritation. Floppy lid syndrome is accompanied by sleep apnea and hypertension. Symptoms can sometimes be controlled by having the patient wear a Fox shield over the eye while sleeping to reduce nocturnal eversion of the lid. Most often, horizontal upper lid shortening is needed along with tightening of the lower lid for control of symptoms.

Common Malignant Eyelid Tumors

Basal cell carcinoma (BCC) is the most common eyelid malignancy accounting for 85–90% of such lesions.

Figure 8 Demonstration of the floppy eyelid syndrome on the left.

Figure 9 Nodular basal cell carcinoma of the left lower lid.

BCC is an actinic lesion and is more common in fair-skinned individuals on sun-exposed parts of the body. It is most common on the lower lid, followed by the medial canthus, upper lid, and lateral canthus. The tumor is classically a firm, nodular lesion with a central ulcer and pearly, vascular border (**Figure 9**). It may also present as an irritating, erythematous patch or rarely be entirely subcutaneous. Lesions of the medial canthus have a propensity for deep invasion into the eye socket. BCC only rarely metastasizes and generally grows very slowly. The preferred treatment is complete excision with frozen section control or by Mohs micrographic surgery usually performed by a specially trained dermatologist. It provides the best cure rate (98–99%) while saving as much normal tissue as possible. Excision is followed by reconstruction of the eyelid defect or occasionally by spontaneous healing if the defect is small or does not involve the lid margin. Radiation therapy is an alternative to surgery but not as effective due to the relatively high recurrence rate (5–20%). Recurrence is also difficult to detect after radiation due to tissue alteration from the treatment. Cryotherapy is sometimes used for small lesions but has similar problems with a relatively high recurrence rate (20–30%) and depigmentation and atrophy of treated tissue.

Squamous cell carcinoma (SCC) accounts for about 5% of periocular malignancies. It too is an actinic lesion, being more common on sun-exposed areas of fair-skinned individuals. Again, the lower lid is the most common location. It most frequently presents as an erythematous, thickened patch with erosion of the involved tissue (**Figure 10**). A nodular subtype is occasionally observed. It may arise from preexisting actinic keratoses, which undergoes malignant transformation 20% of the time. SCC can metastasize through the regional lymphatics or spread along involved sensory nerves. Mohs removal and reconstruction are the preferred therapy. Radiation

Figure 10 Squamous cell carcinoma of the left medial canthus.

therapy is much less effective in SCC and thus is used only for palliation of surgically unresectable tumors. Topical therapy with 5-fluorouracil or imiquimod is a frequent treatment of the premalignant actinic keratosis.

Sebaceous cell carcinoma accounts for about 5% of periocular malignancies but is increasing in frequency, which may be due in part to better pathological diagnosis. It arises from the meibomian glands, the glands of Zeiss, and sebaceous glands of the caruncle. It presents as a nodular lesion, which is often mistaken for a chalazion or a diffuse intraepithelial pattern that looks like a chronic conjunctivitis (pagetoid spread) (**Figure 11**). Because of this, the diagnosis is often delayed until biopsied. It is capable of both regional lymphatic and vascular spread. It is considered deadlier than SCC. Mohs microsurgery may be effective in tumor removal if the tumor is nodular, but pagetoid spread and skip lesions often necessitate wide sampling of the bulbar and palpebral conjunctiva (map biopsy). If diffusely spread, orbital exenteration is

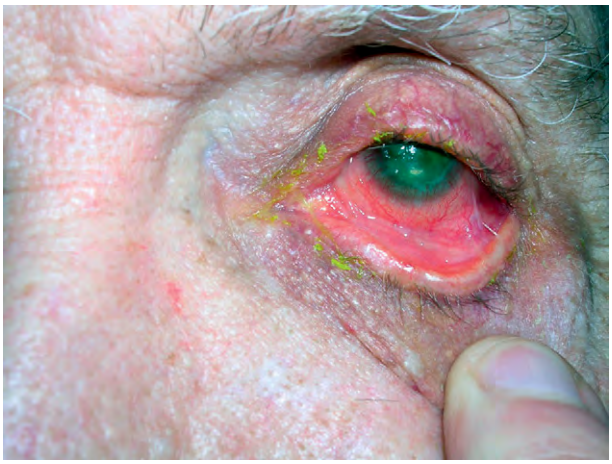

Figure 11 Pagetoid spread of sebaceous cell carcinoma of the conjunctiva of the left lower lid.

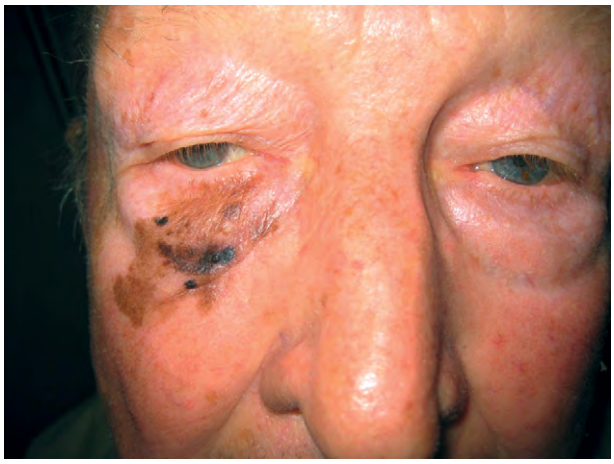

Figure 12 Malignant melanoma of the right lower lid.

usually required. Sebaceous cell carcinoma is relatively radio resistant and responds poorly to chemotherapy.

Malignant melanoma accounts for less than 5% of periocular malignancies, but it too is increasing in frequency (**Figure 12**). It too is an actinic lesion but other less well-defined causes play a role. It arises spontaneously usually as a nodule or in an existing nevus or area of lentigo maligna (intraepithelial tumor). It too is capable of spread through the regional lymphatics and the blood stream. Surgical excision is the treatment of choice, but requires permanent section histology to adequately assess tumor margins. Because of this, the resection of the tumor is often spread over several days (Slow Mohs) followed by reconstruction when margins are clear.

Benign Eyelid Tumors

A variety of benign lesions are found on the lids and periocular skin. The vast majority are of minimal functional significance, but patients frequently request removal for cosmetic reasons. The most common are nevi, inclusion and glandular cysts, seborrheic keratoses, verruca, skin tags, and benign glandular tumors. Simple excision can usually be carried out in the office under local anesthesia.

Inflammatory and Infectious Disorders of the Lids

Chalazion is a lipogranuloma of one of the meibomian glands of the tarsal plate. They arise relatively rapidly over a period of a few days, often with inflammation and discomfort. They can progress to form a chronic pea-sized, firm nodule in the lid (**Figure 13**). The initial treatment is to hot compress the involved lid frequently in the first few days in hopes of opening the obstructed gland. If not effective many will resolve spontaneously over the next several weeks to few months. Patients often request removal for cosmetic reasons. This can usually be done in the office with local anesthesia. An alternative is to inject the chalazion with steroid, which is effective about 50% of the time.

Figure 13 Chalazion of the right upper lid.

Hordeolum is a staphylococcal infection of one of the sebaceous glands of the lid. It presents as an acutely swollen, erythematous, painful nodule on the lid margin (external hordeolum) or on the palpebral conjunctiva (internal hordeolum). Hot compress, topical antibiotics, and surgical drainage are effective. Oral antibiotics may be needed if cellulitis occurs.

Blepharitis is the most common inflammatory disorder of the eyelids characterized by redness, swelling, and irritation with visible crusting. It is a chronic condition characterized by intermittent exacerbations. There are three subtypes, but many patients show combinations of all three. In staphylococcal blepharitis, chronic colonization of the lid margin leads to inflammation from the bacterial toxins and antigens. Slit-lamp examination

reveals characteristic white collarettes around the base of the lashes. In seborrheic blepharitis, there are greasy scales (scurf) found on the lashes and often associated seborrheic dermatitis of the face and scalp. The third form, posterior blepharits (posterior lid margin disease, meibomian gland dysfunction, and meibomianits) is characterized by a change in the normal clear meibomian gland secretion to a thick, cloudy to yellow, oily discharge. Posterior blepharitis is often associated with acne rosacea and chalazia. All forms of blepharitis lead to chronic redness of the conjunctiva, sometimes with papillary hypertrophy. The tear film is often unstable as manifested by a rapid tear break-up time. Dry eye is a frequent association. In addition to the above findings, slit-lamp examination may reveal punctate epithelial erosions (PEEs) of the cornea and marginal corneal erosions due to staphylococcal hypersensitivity. There may be small, rounded domes on the meibomian orifices, manifestations of the thick, inspissated secretions. Digital pressure on the lid may cause the meibomian glands to express material that can, in severe cases, have a cheesy consistency.

Treatment consists of warm compresses to thin the meibomian secretions and eyelid scrubs with baby shampoo or commercially available products to clean the lid margin and express the meibomian glands. Topical antibiotic drops or ointment reduces the bacterial colonization of the lid margin and topical steroids help to control the inflammation. Oral, low-dose tetracycline (50 mg doxycycline per day) is helpful in reducing the meibomian gland discharge and normalizing the pH of the tear film. Oral erythromycin can be used if the patient is intolerant to tetracyclines, pregnant, nursing, or under the age of 12.

See also: Eyelid Anatomy and the Pathophysiology of Blinking; Imaging of the Orbit; Lacrimal Gland Overview; Orbital Bony Anatomy and Orbital Fractures; Orbital Masses and Tumors; Tear Drainage; Thyroid Eye Disease.

Further Reading

Jordan, D. R. and Anderson, R. A. (2000). *Surgical Anatomy of the Ocular Adnexa: A Clinical Approach.* San Francisco, CA: American Academy of Ophthalmology.

Stewart, W. B. (2000). *Surgery of the Eyelid, Orbit, and Lacrimal System.* San Francisco, CA: American Academy of Ophthalmology.

Light-Driven Translocation of Signaling Proteins in Vertebrate Photoreceptors

P D Calvert, SUNY Upstate Medical University, Syracuse, NY, USA
V Y Arshavsky, Duke University, Durham, NC, USA

Glossary

Arrestin – A protein which binds to and inactivates photoactivated rhodopsin. Arrestin binding results in termination of transducin activation.
Light adaptation – The ability of photoreceptors (and the visual system as a whole) to adapt the speed and sensitivity of light responses to ever-changing conditions of ambient illumination.
Phosducin – A protein which interacts with the $\beta\gamma$-subunit of transducin and reduces its membrane affinity.
Recoverin – A regulatory protein which is thought to regulate the speed at which arrestin can bind to photoactivated rhodopsin.
RGS9 – A protein responsible for returning activated transducin in its inactive form.
Transducin – A G protein that mediates the visual signal between the photoactivated visual pigment, rhodopsin, and the downstream effector enzyme, cGMP phosphodiesterase. Transducin consists of two functional subunits, α and $\beta\gamma$.

Introduction

Rod and cone photoreceptors are highly polarized cells which transduce information encoded by photons into electrical activity that can be processed by higher-order neurons. At the one end, photoreceptors have specialized ciliary organelles, outer segments, which are enriched in proteins directly involved in light detection and signal transduction. At the opposite end, synapses convey the information gathered by outer segments to downstream neurons. Vision begins when a molecule of rhodopsin in the outer segment becomes excited by light and activates a G protein, transducin. The transducin α-subunit stimulates its effector, cyclic guanosine monophosphate (cGMP) phosphodiesterase (PDE), which leads to the reduction in intracellular cGMP and to the electrical response mediated by the closure of the cGMP-gated cationic channels in the plasma membrane. The recovery of the photoresponse requires complete inactivation of all these molecular components. Photoexcited rhodopsin is inactivated through its phosphorylation by rhodopsin kinase and arrestin binding, which blocks transducin activation. The rate of rhodopsin phosphorylation, and thus its active lifetime, is regulated by the Ca^{2+}-binding protein, recoverin. Transducin (and accordingly PDE) activation is terminated upon the hydrolysis of GTP tightly bound to transducin α-subunit, a process markedly accelerated by the GTPase activating protein RGS9.

Importantly, three of the above-mentioned proteins (transducin, arrestin, and recoverin) undergo massive light-driven translocation between the major subcellular compartments of photoreceptors (**Figure 1**). In rods, transducin moves out of the outer segment and accumulates primarily in the inner segment, arrestin moves in the opposite direction, and recoverin shifts from the outer segment toward the synapse. In cones, in light arrestin moves in the same direction, whereas transducin moves very little, if at all. Recoverin translocation has not yet been analyzed in cones. A similar phenomenon involving the G protein (G_q), arrestin, and the transient receptor potential-like (TRPL) channel takes place in rhabdomeric invertebrate photoreceptors.

Light Dependency of Protein Translocation

Quantitative experiments revealed that the translocations of arrestin and transducin in rods take place in bright light. The outer segments of the rod contain very little arrestin (estimated under 7% of its total cellular content) in the dark and under moderate illumination. In mouse rods, arrestin begins to move to outer segments when the light intensity reaches a critical threshold, exciting over ~1000 rhodopsins per rod per second, which is within the upper limit at which mammalian rods can signal variations in light. Transducin translocation is also triggered at a threshold light intensity, although brighter, exciting ~5000 rhodopsins per rod per second, an intensity that completely saturates rods. The time required for the completion of protein translocation in saturating light in rods is on the order of tens of minutes. Although no such quantitative measurements are available for cones, available data indicate that cone arrestin translocation also requires fairly bright light. The existence of cone transducin translocation in intact cells remains somewhat

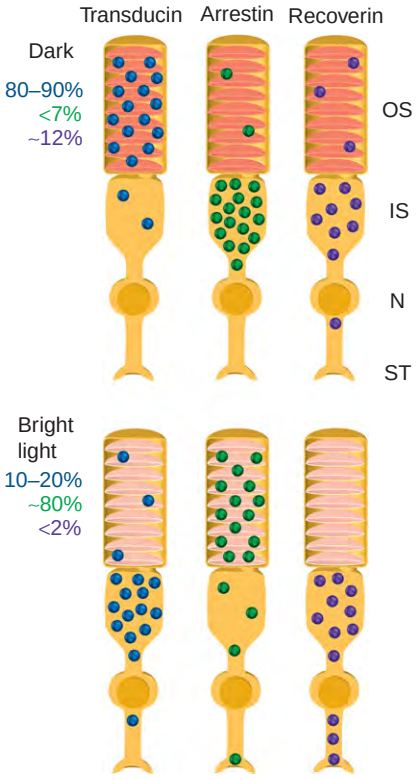

Figure 1 Schematic illustration of transducin, arrestin, and recoverin distribution in dark- and light-adapted rods. The numbers on the left, color-coded to the corresponding translocating proteins, represent the percentage of the proteins found in the outer segments in the dark or following bright light illumination. The subcellular rod compartments are abbreviated on the right: OS – outer segment; IS – inner segment; N – nucleus; ST – synaptic terminal. Reproduced from Calvert, P. D., Strissel, K. J., Schiesser, W. E., Pugh, E. N., Jr., and Arshavsky, V. Y. (2006). Light-driven translocation of signaling proteins in vertebrate photoreceptors. *Trends in Cell Biology* 16: 560–568.

controversial. Most investigators do not see it at any light intensity, whereas one group reports small degree of translocation observed in extremely bright light. The most recent report argues that the inability of cone transducin to efficiently translocate in light reflects specific physicochemical properties of its individual subunits.

Hypotheses on the Functional Roles of Protein Translocation

Photoreceptors adjust their sensitivity over a broad range of ambient light intensities, and protein translocation has been proposed to contribute to this process at the high end of adaptive light intensities. The reduction of transducin content in outer segments of rod in bright light correlates with a reduction in signal amplification in the rhodopsin–transducin–phosphodiesterase cascade, likely due to the reduction in transducin activation rate. This is likely to move the dynamic range over which rods operate to higher light intensities. Although transducin translocation takes place in light that is saturating for rods, this range adjustment may be adaptive after the light is dimmed or extinguished. For example, such a mechanism could be useful as dusk approaches when vision is switching from being cone-dominant to rod-dominant. The fact that transducin translocation is triggered by light intensities that completely saturate rods makes it plausible to suggest that both phenomena, transducin translocation and response saturation, occur for essentially the same reason, the inability of rods to inactivate vast amounts of transducin beyond a certain light intensity. In this context, transducin translocation can be viewed as an elegant self-regulating mechanism triggered at the point where the rod exhausts other means of avoiding response saturation.

Although not yet tested experimentally, arrestin translocation is thought to be adaptive as well. Its increased concentration in the outer segment could reduce the response amplitude and/or accelerate recovery. It could also allow rods and cones to prepare for inactivation of large amounts of photoexcited rhodopsin and its bleach products produced in bright light. Similarly, recoverin translocation from outer segments may increase the amount of rhodopsin kinase available to phosphorylate rhodopsin, thus further reducing light sensitivity.

Light-driven protein translocation, particularly in rods, may also play a neuroprotective role. Rod saturation marks the transition from mesopic (mixed rod/cone) to cone-dominated photopic vision. Under these conditions, rods contribute little to vision and transducin translocation may prevent excessive energy consumption by rods by reducing the number of transducin molecules undergoing the cycle of activation/inactivation. This may, in turn, reduce the metabolic stress in the retina commonly believed to contribute to pathological processes. A reduced level of cellular signaling caused by transducin translocation may also reduce the chance of apoptotic death of the rod. At least in rodents, some forms of apoptosis are suggested to be caused by excessive signaling through the phototransduction cascade. The same argument may be applied to arrestin translocation, whose accumulation in the outer segment in bright light is likely to preamplify rhodopsin shutoff on a sunny day.

Finally, when vision is dominated by cones, rods may perform more of their housekeeping functions, such as checking the integrity of proteins by the ubiquitin proteasome system located in the inner segments.

What Is the Mode of Protein Translocation: Active Transport or Diffusion?

A major currently explored area in this field is whether phototransduction proteins translocate by diffusion or by

active transport via molecular motors. In principle, the mode of translocation of each protein could be different between the light- and dark-induced directions. Most investigators argue against the involvement of molecular motors. One major argument is that all of these proteins (or at least individual subunits in the case of transducin) are fairly soluble and any of their relocation by molecular motors may be negated by the subsequent diffusion throughout the entire cellular volume. Another argument is that, although protein translocation by motors is rapid, it could be easily saturated by the very large number of translocation protein molecules. On the other hand, intracellular diffusion of soluble proteins in rods is also sufficiently rapid to explain the observed protein translocation rates and, unlike molecular motors, could not be saturated by the amount of protein molecules undergoing light-induced translocation. Yet, it should be noted that, based on the impediment of translocation by the cytoskeleton disrupting drugs, some believe that motor systems are involved, particularly in protein translocations in the dark-induced directions.

However, diffusion alone cannot account for the phenomenon because it does not explain any disequilibrium of protein distributions with the free cytoplasmic volume of the rod or cone. Thus, while diffusion serves as the mode of protein movement, the observed patterns of light-dependent protein redistribution may be explained by light-dependent appearance or disappearance of specific protein-binding sites in individual subcellular compartments. The next two sections illustrate these ideas in regard to transducin and arrestin.

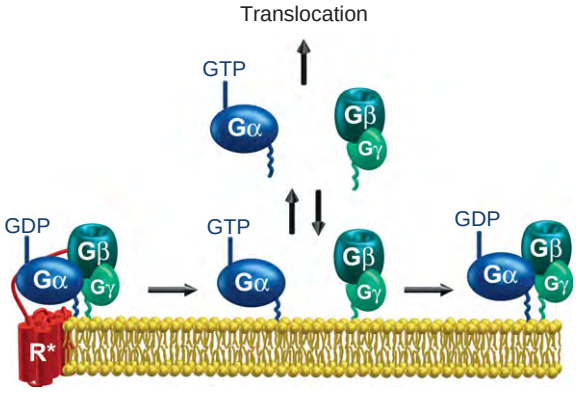

Figure 2 The putative role of transducin subunit dissociation in its translocation. When transducin is activated by photoexcited rhodopsin (R*), its α- and βγ-subunits become separated from one another and the membrane affinity of each is less than that of the heterotrimer. In this state, subunits may dissociate from photoreceptor disk membranes and translocate from the outer segment. The efficiency of translocation is dependent on the time during which transducin subunits stay apart before re-formation of the trimer. This time is determined by the rate of the GTP hydrolysis on the α-subunit and is dependent on the absolute amount of activated transducin. Reproduced from Calvert, P. D., Strissel, K. J., Schiesser, W. E., Pugh, E. N., Jr., and Arshavsky, V. Y. (2006). Light-driven translocation of signaling proteins in vertebrate photoreceptors. *Trends in Cell Biology* 16: 560–568.

Specific Mechanisms of Protein Translocation

Transducin

Recent reports suggest that transducin translocation could be explained by the differences in the membrane affinities of its αβγ heterotrimer compared to the individual α- and βγ-subunits. The heterotrimer is strongly membrane-associated due to the combined action of two lipid modifications: a farnesyl group on the γ-subunit and an acyl group on the α-subunit. Thus, in the dark-adapted rod, transducin heterotrimer is predicted to be concentrated on the disk membranes of the outer segment. When transducin is activated in light, α-subunits bind GTP and dissociate from the βγ-subunits (**Figure 2**). Both subunits become more soluble since each has only one lipid modification, allowing them to diffuse throughout the cytoplasm. Inevitably, GTP hydrolysis by the α-subunit would result in the restoration of the poorly soluble trimer. When this happens in the outer segment, transducin becomes re-attached to the disk membranes; but when it happens in the inner segment, the trimer may adhere to the membranous structures there, causing its transient accumulation. The central assumption of this hypothesis, that transducin subunits move apart from one another, is supported by the difference in their translocation rates and by transducin translocation being facilitated by transgenic or pharmacological manipulations promoting transducin subunits to remain in the dissociated state. The translocation of transducin βγ-subunit is further enhanced by the protein called phosducin. Phosducin reduces membrane association of the βγ-subunit, which presumably allows it to more easily diffuse throughout the cytoplasm.

Another important mechanistic feature of transducin translocation is its light-intensity threshold. This threshold reflects the fact that the cellular content of transducin significantly exceeds that of RGS9, a protein responsible for rapid inactivation of transducin. Light of the threshold intensity produces activated transducin in the amount exceeding the capacity of RGS9 to inactivate it. Consequently, a fraction of activated transducin stays in the active, GTP-bound form (with α- and βγ-subunits dissociated) for a longer time, sufficient for dissociation from the disk membranes and diffusion through the photoreceptor cytoplasm. Accordingly, the knockout of RGS9 allows transducin translocation at a lower light intensity, whereas RGS9 overexpression shifts the threshold to brighter light.

Arrestin

It was first suggested that arrestin is equilibrated throughout the rod cytoplasm in the dark and is trapped in the outer segment in light upon binding to photoexcited rhodopsin. However, recent observations argue that the dark-adapted distribution of arrestin does not match the distribution of the free cytoplasm volume, indicating that most arrestin is bound to sites located in the inner segment. One hypothesis is that these sites are formed by microtubules. It was further proposed that arrestin translocation is explained by a simple competition between constitutive, low-affinity microtubule sites in the inner segment and transient, high-affinity sites in the outer segment formed upon rhodopsin photoexcitation. However, quantitative measurements indicated that, at the minimal light intensity sufficient to trigger arrestin translocation, the number of translocated arrestin molecules exceeds the number of photoactivated rhodopsin molecules by ~30-fold. Even less rhodopsin activation is required to trigger arrestin translocation in knockout mice lacking RGS9 where transducin activation persists longer than normally. Therefore, triggering arrestin translocation is not dependent on the absolute amount of rhodopsin excited by light, but is rather dependent on arrestin release from the inner segment sites by a yet-to-be-identified signaling mechanism downstream from phototransduction.

Proteins' Return in the Dark

The rates of transducin and arrestin return to their dark-adapted locations upon switching from light to dark are much slower than their movement in the light-induced direction, with most measurements indicating that it takes at least an hour. This may be slow enough to be within the capacity of molecular motors, and indeed transducin and arrestin return can be blocked by cytoskeleton disrupting drugs. The specificity of these treatments remains unknown and artifacts such as clogging the connecting cilium could not be ruled out. On the other hand, arrestin and transducin return could also be explained by a combination of diffusion, removal of the light-induced binding sites, and restoration of the dark-adapted sites. Current evidence is insufficient to discriminate between the potential roles of molecular motors and diffusion in transducin and arrestin return to their dark-adapted cellular distributions.

See also: Phototransduction: Adaptation in Cones; Phototransduction: Adaptation in Rods; Phototransduction: Inactivation in Cones; Phototransduction: Inactivation in Rods; Phototransduction: Phototransduction in Cones; Phototransduction: Phototransduction in Rods.

Further Reading

Artemyev, N. O. (2008). Light-dependent compartmentalization of transducin in rod photoreceptors. *Molecular Neurobiology* 37: 44–51.

Brann, M. R. and Cohen, L. V. (1987). Diurnal expression of transducin mRNA and translocation of transducin in rods of rat retina. *Science* 235: 585–587.

Broekhuyse, R. M., Tolhuizen, E. F., Janssen, A. P., and Winkens, H. J. (1985). Light induced shift and binding of S-antigen in retinal rods. *Current Eye Research* 4: 613–618.

Calvert, P. D., Strissel, K. J., Schiesser, W. E., Pugh, E. N. Jr., and Arshavsky, V. Y. (2006). Light-driven translocation of signaling proteins in vertebrate photoreceptors. *Trends in Cell Biology* 16: 560–568.

Fain, G. L. (2006). Why photoreceptors die (and why they don't). *BioEssays* 28: 344–354.

Hanson, S. M., Francis, D. J., Vishnivetskiy, S. A., Klug, C. S., and Gurevich, V. V. (2006). Visual arrestin binding to microtubules involves a distinct conformational change. *Journal of Biological Chemistry* 281: 9765–9772.

Kerov, V., Chen, D. S., Moussaif, M., et al. (2005). Transducin activation state controls its light-dependent translocation in rod photoreceptors. *Journal of Biological Chemistry* 280: 41069–41076.

Nair, K. S., Hanson, S. M., Mendez, A., et al. (2005). Light-dependent redistribution of arrestin in vertebrate rods is an energy-independent process governed by protein–protein interactions. *Neuron* 46: 555–567.

Philp, N. J., Chang, W., and Long, K. (1987). Light-stimulated protein movement in rod photoreceptor cells of the rat retina. *FEBS Letters* 225: 127–132.

Reidel, B., Goldmann, T., Giessl, A., and Wolfrum, U. (2008). The translocation of signaling molecules in dark adapting mammalian rod photoreceptor cells is dependent on the cytoskeleton. *Cell Motility and the Cytoskeleton* 65: 785–800.

Slepak, V. Z. and Hurley, J. B. (2008). Mechanism of light-induced translocation of arrestin and transducin in photoreceptors: Interaction-restricted diffusion. *IUBMB Life* 60: 2–9.

Sokolov, M., Lyubarsky, A. L., Strissel, K. J., et al. (2002). Massive light-driven translocation of transducin between the two major compartments of rod cells: A novel mechanism of light adaptation. *Neuron* 34: 95–106.

Strissel, K. J., Lishko, P. V., Trieu, L. H., et al. (2005). Recoverin undergoes light-dependent intracellular translocation in rod photoreceptors. *Journal of Biological Chemistry* 280: 29250–29255.

Strissel, K. J., Sokolov, M., Trieu, L. H., and Arshavsky, V. Y. (2006). Arrestin translocation is induced at a critical threshold of visual signaling and is superstoichiometric to bleached rhodopsin. *Journal of Neuroscience* 26: 1146–1153.

Whelan, J. P. and McGinnis, J. F. (1988). Light-dependent subcellular movement of photoreceptor proteins. *Journal of Neuroscience Research* 20: 263–270.

Limulus Eyes and Their Circadian Regulation

B-A Battelle, University of Florida, St. Augustine, FL, USA

Glossary

Arhabdomeric cell – The secondary visual cell in *Limulus* median eyes that is not photoreceptive but is electrically coupled to photoreceptors and generates action potentials in response to photoreceptor depolarization.
Chelicerate – A type of arthropod belonging to the group Chelicerata that includes horseshoe crabs, scorpions, spiders, ticks, and mites.
Circadian clock – A biological clock that oscillates with a period of about 24 h even under constant conditions.
Compound eye – An eye that contains a few to many separate photoreceptive units.
Eccentric cell – A secondary visual cell in *Limulus* lateral eye that is not photoreceptive but is electrically coupled to photoreceptors and generates action potentials in response to photoreceptor depolarization.
Lateral inhibition – A mechanism of information processing in nervous systems that increases contrast and resolving power.
Ocellus – A type of eye with a single lens.
Octopamine – A major amine neurotransmitter in invertebrates that is the phenol analog of norepinephrine.
Ommatidium – The photoreceptive unit of compound eyes.
Quantum bump – The response of photoreceptors to a single photon of light.
Rhabdom – A photoreceptive membrane typically elaborated by arthropod photoreceptors that is composed of tightly packed microvilli.

The retinas of animals that live in cyclic light environments typically undergo rhythmic, daily changes in structure and function. These changes underlie the ability of animals to detect images over the large daily fluctuations in ambient illumination, and therefore they are critical for normal vision. Some of these changes, such as light and dark adaptation, are driven solely by fluctuations in illumination, while others are driven solely by signals from internal circadian clocks. Still other changes require interactions between light- and clock-driven biochemical cascades.

In the American horseshoe crab *Limulus polyphemus*, a chelicerate arthropod, circadian changes in vision are dramatic, and as a result, *Limulus* can see at night nearly as well as it can during the day. Since the circadian organization of the *Limulus* visual system is also advantageous for experimental manipulation, *Limulus* has been used to examine in detail the separate and combined effects of diurnal light and the clock on the retina.

The first part of this article describes the organization of the *Limulus* visual system and the circadian input to the eyes. The second part describes the impact of the circadian clock on *Limulus* retinal structure, the photoresponse, photosensitive membrane shedding, and gene expression. The synaptic mechanisms through which the clock influences the eyes are described as well as a clock-driven biochemical cascade in photoreceptors that may underlie some of the observed circadian changes in visual function.

Organization of the *Limulus* Visual System

Limulus has three major types of eyes: lateral, median, and rudimentary (**Figure 1**). The eyes that are obvious by examining the dorsal side of an adult animal are the lateral compound eyes (LE) on the dorsolataral carapace, and a pair of median eyes located on either side of the median dorsal spine near the front of the animal. Rudimentary eyes are found at three different locations, and in an adult animal they are largely hidden from view. Lateral rudimentary eyes are located below the cornea at the posterior edge of each LE, and a pair of fused median rudimentary eyes is located below the carapace between the two median ocelli. Ventral rudimentary eyes consist of a pair of optic nerves that extend anteriorly from the brain just below the cuticle on the ventral side of the animal. They terminate in an end organ located below a wart-like structure visible on the ventral cuticle in front of the mouth.

Lateral Compound Eyes

In an adult animal, each LE contains over 1000 conical lenses, and below each lens there is a single ommatidium, or mini-retina, that is aligned with the long axis of the overlying lens (**Figure 2(a)**) Each ommatidium is composed of 8–12 photoreceptors clustered like the sections of an orange around the dendrite of usually one secondary visual cell called the eccentric cell (**Figures 2(b)** and **2(c)**). The photoreceptors are electrically coupled to the dendrite of the eccentric cell. Two major non-neuronal cells types

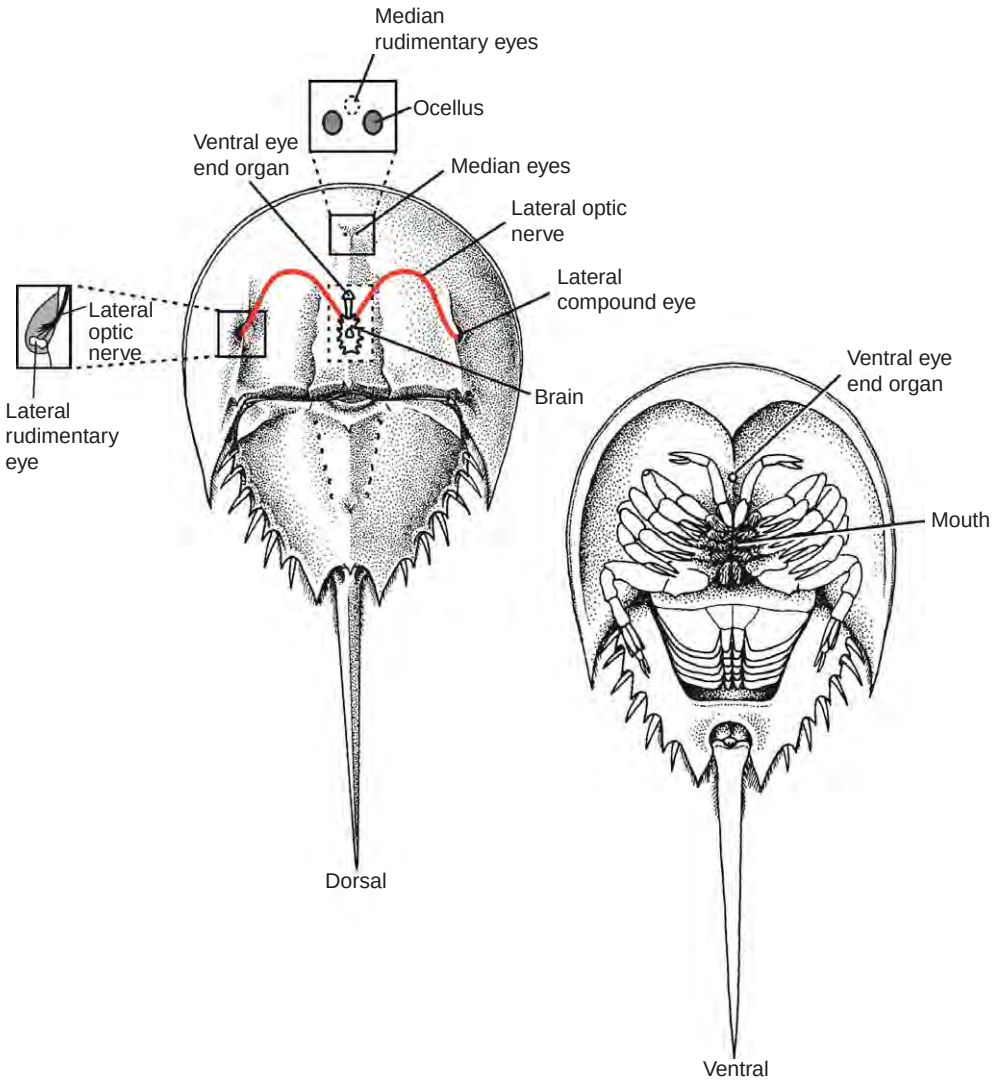

Figure 1 Schematics of dorsal and ventral views of an adult *Limulus* showing the locations of the eyes. The lateral compound eyes and median ocelli are visible on the dorsal carapace. The box at the left shows the location of a lateral rudimentary eye below the cornea at the posterior edge of the lateral compound eye. The box at the top shows the location of the fused median rudimentary eyes below the carapace between the median ocelli. The cutaway in the center shows the position of the brain and ventral rudimentary eyes. Ventral optic nerves extend anteriorly from the brain and terminate in an end organ located just beneath a wart-like structure that is visible on the ventral cuticle in front of the mouth. The long lateral optic nerves are shown in red. Modified from Calman, B. G. et al. (1991). *Journal of Comparative Neurology* 313: 553–562.

are present in ommatidia: cone cells and pigment cells. Cone cell processes occupy the aperture at the base of the lens and separate the lens from photoreceptors. Pigment cells surround each ommatidium and form partitions between photoreceptors.

LE photoreceptors respond with graded depolarizations to visible light, and the eccentric cells to which they are electrically coupled, encode these graded depolarizations as action potentials. Both photoreceptors and eccentric cells have axons that project to optic ganglia in the brain (lamina and medulla) through the lateral optic nerve (**Figure 3(a)**). However, because the lateral optic nerve in an adult animal is long, often over 10 cm, it is unlikely that the graded photoreceptor potentials reach the brain. Therefore, information from LEs is thought to reach the brain only through the activity of the eccentric cells.

In addition to projecting to the brain, eccentric cells extend axon collaterals laterally within the eye to form a neural plexus just below the ommatidia (**Figure 2(a)**). Within this plexus, eccentric cell collaterals from neighboring and even distant ommatidia make reciprocal inhibitory synapses which are the basis for lateral inhibition in the eye. Lateral inhibition, a fundamental mechanism of information processing in nervous systems that increases contrast

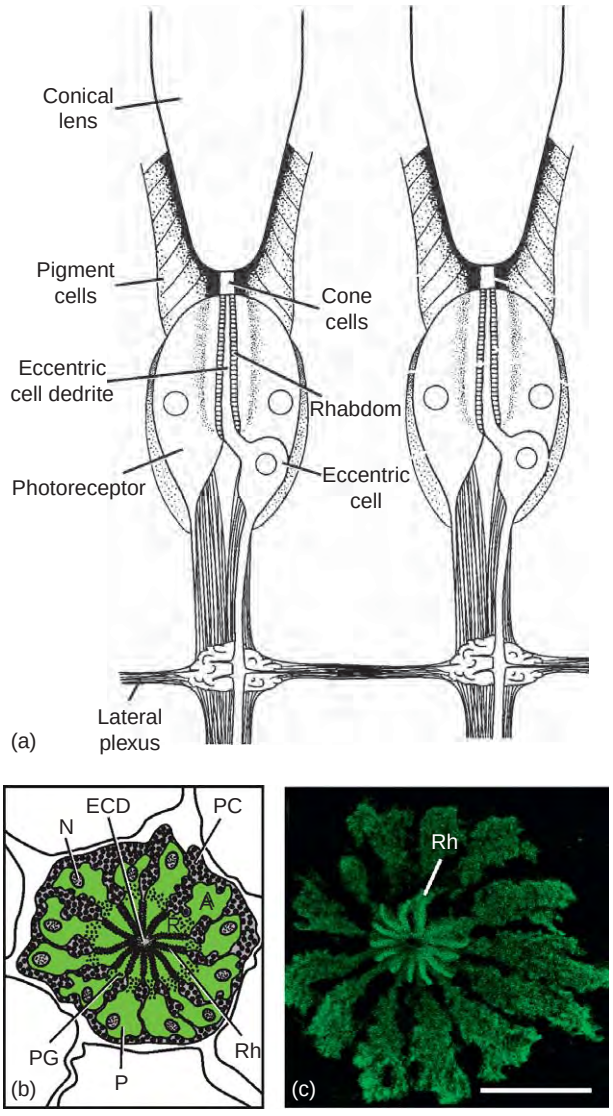

Figure 2 (a) Schematic of a longitudinal section through two ommatidia of the lateral eye, illustrating major cell types. The photoreceptors and eccentric cells project axons into the lateral optic nerve. Eccentric cell axons also project collaterals into a lateral plexus within the eye where they form the reciprocal inhibitory synapses that underlie lateral inhibition. (b) Schematic of a cross section through one ommatidium showing the arrangement of photoreceptors (P), shown in green, around a central eccentric cell dendrite (ECD). The nuclei (N) located in the arhabdomeral lobes (A) of photoreceptors is shown. Screening pigment granules within the photoreceptors (PG) define the junction between the arhabdomeral and rhabdomeral (R) lobes. The asterisk-like structure at the center of the ommatidium is the rhabdom (Rh) formed from the fused photosensitive membranes of neighboring photoreceptors. Pigment cells (PC) surround the ommatidium and form partitions between photoreceptors. (c) Confocal image of one ommatidium from a light-adapted daytime animal immunostained for LpMyo3. LpMyo3 distributes through photoreceptor cell bodies and concentrates at the rhabdom (Rh). Scale bar = 50 μm. (a) and (c) from Battelle, B-A. (2006) *Arthropod Structure and Development* 35: 261–274, with permission from Elsevier.

and resolving power, was first detected experimentally in *Limulus* LE. In vertebrate retinas, this same mechanism is known as center-surround inhibition.

Median Eyes

Median eyes are called ocelli because they have a single spherical lens (**Figure 4**). In median eye retinas, groups of 5–11 photoreceptors are typically associated with at least one secondary visual cell or arhabdomeric cell, but unlike LE ommatidia, these groups are not highly organized and difficult to discern anatomically. The photoreceptors and arhabdomeric cells are embedded in guanophores, cells that contain reflective guanine crystals, and the retina is surrounded by pigment cells.

An interesting feature of median eyes is that they contain two different types of photoreceptors: one that responds to visible light and another that is sensitive to ultraviolet (UV) light. These two photoreceptor types have not yet been distinguished anatomically. Median eye arhabdomeric cells are thought equivalent to LE eccentric cells because, similar to eccentric cells, they are electrically coupled to photoreceptors and generate action potentials in response to graded photoreceptor depolarizations. Median eye photoreceptors and arhabdomeric cells both project axons to ocellar ganglia in the brain through the median optic nerve (**Figure 3(a)**), but only the action potentials of the arhabdomeric cell are thought to reach the brain. Interestingly, arhabdomeric cell action potentials have been detected only in response to UV illumination.

Rudimentary Eyes

The lateral, median, and ventral rudimentary eyes differentiate in the embryo before the more complex LEs and median ocelli, and they presumably provide photic information to the developing embryo. Each rudimentary eye consists of a cluster of large photoreceptors (100 × 160 μm) that are sensitive to visible light. Ventral eye photoreceptors are typically scattered along the length of the ventral optic nerves as well as clustered near the brain and in the end organ (**Figure 3(a)**).

Similar to the photoreceptors in lateral and median eyes, rudimentary eye photoreceptors produce graded depolarizations in response to illuminations, but they have no associated secondary visual cells. Rudimentary photoreceptors project axons to the brain through the lateral, median, or ventral optic nerves, and although their axon diameters are considerably larger than those of lateral and median eye photoreceptors, it still seems unlikely that their graded depolarizations reach the brain in an adult animal. An exception may be the graded

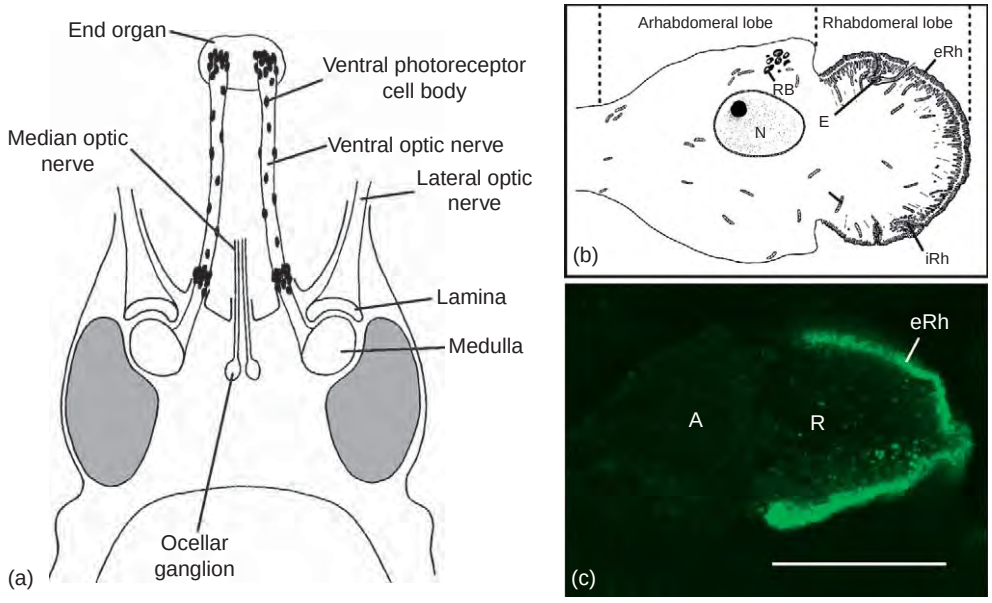

Figure 3 (a) Schematic of a dorsal view of the brain and ventral optic nerves. Ventral photoreceptor cell bodies (dark ovals) are scattered along the ventral optic nerves and clustered at their ends. Also shown are the median and lateral optic nerves and the optic ganglia. (b) Schematic of a ventral photoreceptor showing the rhabdomeral (R) and arhabdomeral (A) lobes, external rhabdom (eRh), internal rhabdom (iRh), efferent terminals near the rhabdom (E), mitochondria (M), ribosomes (RB), and nucleus (N). (c) Confocal image of a 1 μM optical section through a light-adapted ventral photoreceptor immunostained for visual arrestin. Visual arrestin concentrates at the rhabdom in the R lobe. Scale = 50 μm. (a) Modified from Calman, B. G. et al. (1991). *Journal of Comparative Neurology* 313: 553–562. (b) Modified from Calman, B. G. and Chamberlain, S. C. (1982). Distinct lobes of *Limulus* ventral photoreceptors. II. Structure and ultrastructure. *Journal of General Physiology* 80: 839–862, with permission form Rockefeller University Press. (c) from Battelle, B-A. (2006). *Arthropod Structure and Development* 35: 261–274, with permission from Elsevier.

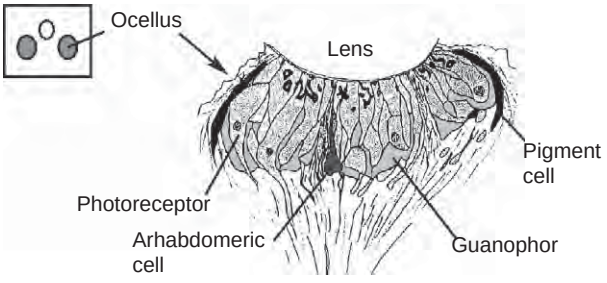

Figure 4 Schematic of a median ocellus cut perpendicular to the carapace. Most of the area proximal to the lens is filled with photoreceptor cells. The dark areas below the lens represent the rhabdoms, which are not highly organized in this eye. Arhabdomeric cells are interspersed among the photoreceptors. Pigment cells surround the structure and reflective guanophores lie nearer the base of the retina. Modified from Jones, J. N. and Brown, J. E. (1971). *Z. Zellforsch* 118: 297–309, with permission from Springer Verlag.

depolarizations produced by ventral photoreceptors located close to the brain.

The Photoreceptors

The photoreceptors are fundamentally similar in the three types of *Limulus* eyes. All are composed of two major compartments: a rhabdomeral lobe and an arhabdomeral lobe (**Figures 2(b), 3(b),** and **3(c)**). The rhabdomeral lobe contains the photosensitive membrane or rhabdom, which in *Limulus*, as in other arthropods, is composed of tightly packed actin-rich microvilli. The arhabdomeral lobe is not photosensitive and contains the nucleus and metabolic machinery of the cell. As described above, all *Limulus* photoreceptors produce graded depolarizations in response to illumination, and with the exception of the median eye UV-sensitive photoreceptors, all respond to visible light with an absorption maximum of about 525 nm. Finally, all *Limulus* photoreceptors, as well as the eccentric cells of the LE and arhabdomeric cells of the median eye, release the inhibitory neurotransmitter histamine. Histamine is also the neurotransmitter used by the photoreceptors of insects and crustaceans.

The rhabdoms in the three types of eyes are organized differently, however, and they are highly organized only in LE ommatidia. In LEs, the rhabdoms of neighboring photoreceptors are fused so that in a cross section of an ommatidium, they appear like an asterisk with the eccentric cell dendrite at the center (**Figures 2(c)** and **2(c)**). The highly complex rhabdoms in median ocelli may project proximally into neighboring photoreceptors or infoldings of photoreceptor membranes may form internal rhabdoms (**Figure 4**). Rudimentary photoreceptors typically have both external and internal rhabdoms (**Figures 3(b)** and

3(c)) and often have more than one rhabdomeral lobe. In addition, rhabdoms of adjacent rudimentary photoreceptors frequently fuse forming a double layer of microvilli.

Among *Limulus* photoreceptors, those of the ventral eyes are the best studied, and their physiology is probably the most thoroughly characterized of any rhabdomeral photoreceptor. Ventral photoreceptors are also significant in the history of vision research. The first intracellular recordings of a photoresponse were made from ventral eye photoreceptors, and physiological studies of these photoreceptors provided the first evidence for the importance of Ca^{++} in light adaptation and a role for phospholipids in the photoresponse.

Circadian Organization of the *Limulus* Visual System

The circadian organization of the *Limulus* visual system is significantly different from that of vertebrates. In vertebrates, one or more circadian oscillators are present within the retina, and in some species, circadian oscillators are present in photoreceptors. In *Limulus*, the circadian oscillators that influence the eyes are located in the brain, not in the eyes. The *Limulus* brain contains bilateral circadian oscillators that remain synchronous through neuronal coupling, and they drive the activity of efferent neurons that project from the brain to all of the eyes.

The cell bodies of clock-driven efferent neurons that project to the eyes are clustered in the cheliceral ganglia located on either side of the base of the brain, and there are about 20 efferent neurons in each ganglion. The axon of each efferent neuron is thought to branch several times in the brain and its branches to project bilaterally out all of the optic nerves and innervate all of the eyes (**Figure 5(a)**). In the eyes, the efferent axons have neurosecretory-like terminals containing both clear vesicles and large, dense, crystalline granules. In LE ommatidia, efferent terminals innervate all cell types (**Figure 5(b)**). In median eyes, efferent terminals contact photoreceptors near the rhabdom, and in rudimentary eyes, efferent axons project to the rhabdomeral lobes of photoreceptors where they terminate directly adjacent to rhabdoms (**Figures 3(b)** and **5(c)**). Circadian efferent neurons, similar to those described in the *Limulus* visual system, also innervate the eyes of scorpions and spiders; therefore, the type of circadian regulation described for *Limulus* eyes appears to be a feature common to chelicerate arthropods, but not to crustaceans and insects.

In *Limulus*, efferent neurons innervating the eyes are active at night and silent during the day. They begin firing bursts of action potentials about 45 min before sunset. These bursts, which are synchronous in all optic nerves, reach a maximum frequency of about 2 Hz during the early evening. The burst rate slows after midnight, and then stops after dawn. This pattern of efferent nerve activity persists in constant darkness, and its phase (the time of day it starts and stops) can be shifted by changing the time of light onset. Thus, efferent nerve activity is clearly circadian.

Effects of the Clock on *Limulus* Eyes

Clock input increases the sensitivity of *Limulus* eyes to light at night, and this effect is most dramatic in LEs. In animals maintained in cyclic light, LEs become about 1 million times more sensitive to light at night compared to the day from the combined effects of dark adaptation and clock input. The effect of the clock is to roughly double the sensitivity obtained with dark adaptation alone.

In animals maintained in constant darkness, the onset of efferent nerve activity near dusk correlates with the increase in LE sensitivity. If the lateral optic nerve is cut during the day, severing the efferent axons and thus preventing clock signals from reaching the LE during the night, there is no nighttime increase in sensitivity. If the lateral optic nerve is cut during the night, interrupting clock input to the eyes, LE sensitivity falls rapidly toward the daytime level. However, if the distal end of a cut lateral optic nerve is stimulated electrically to activate the efferent axons, LE sensitivity increases even during the subjective day. Thus, increased LE sensitivity directly correlates with the activity of the efferent neurons.

In LEs, where the effects of the clock have been studied most thoroughly, the clock influences almost every aspect of retinal function, and studies with these eyes have revealed that the full range of some of the diurnal changes observed involves complex interactions between effects of clock and light (**Table 1**).

Structure

Much of the nighttime increase in LE sensitivity can be attributed to the changes in the structure of ommatidia (**Figure 5(b)**). As the LE transitions into the nighttime state, the aperture at the base of the lens, which is constricted during the day, widens and shortens permitting more photons to reach the underlying photoreceptors. The rhabdom also becomes shorter and wider, adjusting to the larger aperture. These structural changes, which increase photon catch during the night, persist with reduced amplitude in constant darkness in response to clock input alone. However, if clock input is eliminated, all of these rhythmic structural changes are abolished, even in cyclic light. Without clock input, ommatidia assume a structure that is never seen in an intact animal. Thus, these structural changes require clock input, and the effects of the clock are enhanced by cyclic light.

Another diurnal structural change observed in LE photoreceptors that probably contributes to increased nighttime sensitivity is the migration of photoreceptor screening pigment granules. However, unlike the

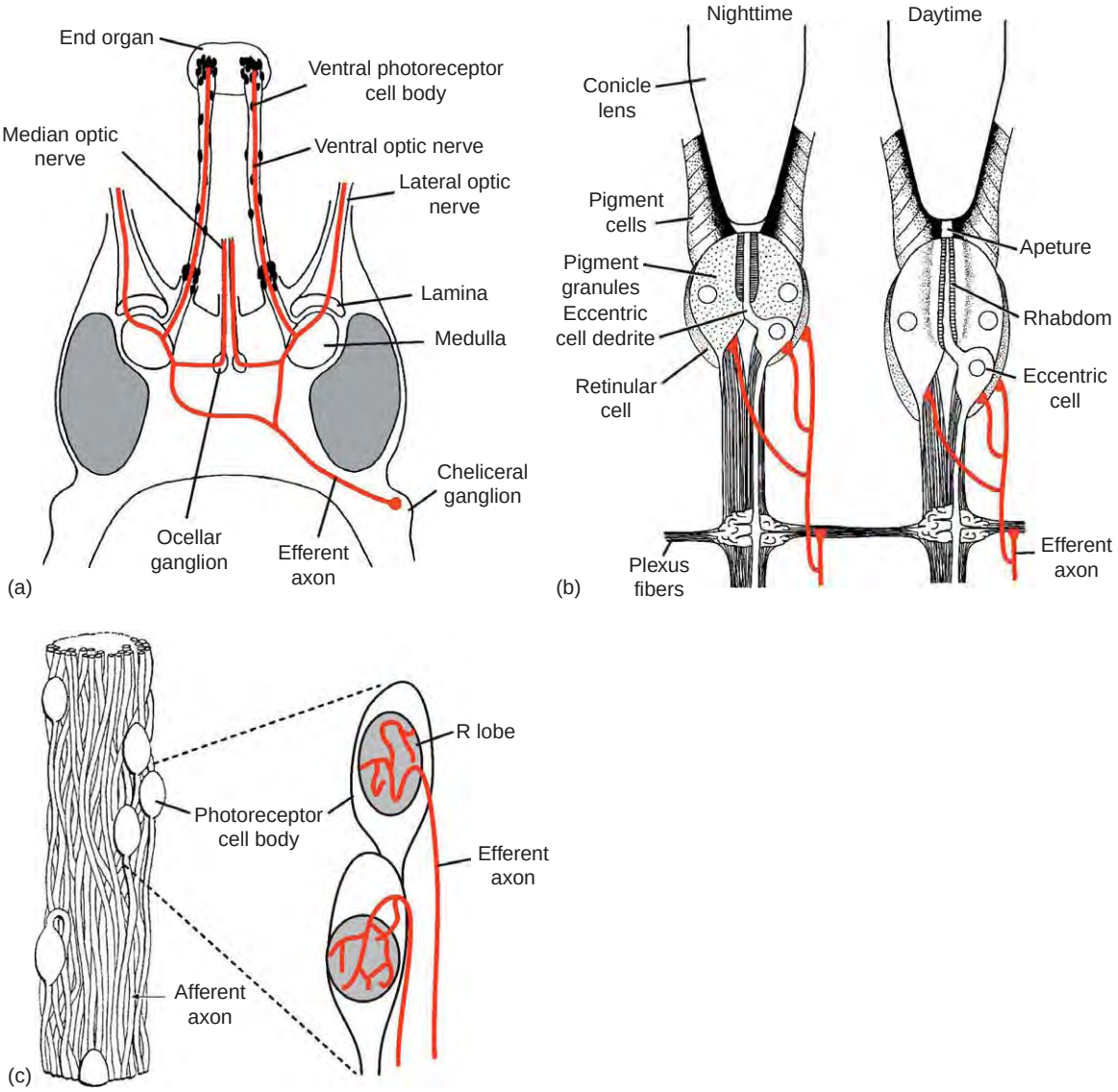

Figure 5 Schematics of circadian efferent neuron projections (shown in red). (a) The cell bodies of the circadian efferent neurons are located in the cheliceral ganglia at the base of the brain. A single idealized efferent neuron branches several times in the brain to project out all of the optic nerves. Modified from Calman, B. G. and Battelle, B-A. (1991). *Visual Neuroscience* 6: 481–495, with permission from Cambridge University Press. (b) Schematic of a longitudinal section through an ommatidium of the lateral eye illustrating projections and terminations of clock-driven efferent neurons, and the nighttime and daytime structure of ommatidia observed when the lateral eye is exposed to cyclic light and clock input. Modified from Barlow and Chamberlain (1979). *Science* 210: 1037–1039. (c) Schematic of efferent projections to ventral photoreceptors. On the left is an enlarged view of a portion of a ventral optic nerve showing ventral photoreceptor cell bodies and axons. On the right, a schematic of the two ventral photoreceptor cell bodies illustrates that the axons of the circadian efferent neurons project specifically to photoreceptor R lobes (shaded areas) and then ramify extensively. Modified from Evans et al. (1983). *Journal of Comparative Neurology* 219: 369–383.

structural changes in the aperture described above, pigment granule migration appears to be regulated entirely by the clock and is not significantly influenced by light. Photoreceptor pigment granules cluster near the junction of the rhabdomeral and arhabdomeral lobes during the day and disperse toward the periphery of the cell during the night (**Figure 5(b)**). This rhythm continues undiminished in eyes maintained in constant darkness and is eliminated in eyes deprived of clock input even when the eyes are exposed to cyclic light.

Physiology

Clock-driven physiological changes in photoreceptors also contribute to increased LE sensitivity. Clock input at night increases the amplitude (gain) and duration of the

Table 1 Lateral eye responses to clock input are influenced by light and mimicked by octopamine and elevated cAMP.

Retinal response to clock input	*Effect of light*	*Mimicked by octopamine and cAMP*
Sensitivity increases	Enhances	Yes
Aperture widens and shortens	Enhances	Inferred[a]
Rhabdom widens and shortens	Enhances	Inferred[a]
Screening pigments disperse		Not tested
Quantum bump gain increases		Yes
Quantum bump duration increases		Yes
Noise decreases		Yes
Transient shedding primed	Triggers	Yes
Arrestin mRNA levels decrease		Yes

[a]Infusions of OA into the LE *in situ* increase LE sensitivity. Since increased sensitivity is largely due to a wider aperture and repositioned rhabdom, the effects of OA on these two parameters are inferred.

response to a single photon (the quantum bump) and decreases the frequency of spontaneous membrane depolarizations recorded in the dark (noise). Thus, the clock increases the signal-to-noise ratio of photoreceptors at night. The onset of these physiological changes correlates directly with the onset of efferent nerve activity and occurs well before the structural changes described above are detected.

Rhabdom Shedding

Similar to the photoreceptors of vertebrates, invertebrate photoreceptors shed some of their photosensitive membrane every day. *Limulus* photoreceptors exhibit two distinct mechanisms for rhabdom shedding: light-triggered transient membrane shedding and light-driven shedding (Figure 6). Both result in the internalization of photosensitive membrane into photoreceptors. Light-driven shedding is similar to the clathrin-mediated endocytosis of activated G-protein coupled receptors described in many other systems, including insect photoreceptors. It continues throughout the day in the light and is mediated by clathrin and arrestin. The clock does not influence this process. On the other hand, light-triggered transient shedding is a unique, synchronous process that rapidly removes membrane from the rhabdom at dawn. During light-triggered transient shedding, large whorls of rhabdomeral membrane are internalized from the base of rhabdomeral microvilli and trafficked into multivesicular bodies. The process is triggered by the dim light of dawn and is complete within an hour after first light. The mechanism for membrane internalization during transient shedding is not yet known. However, importantly from the perspective of this discussion,

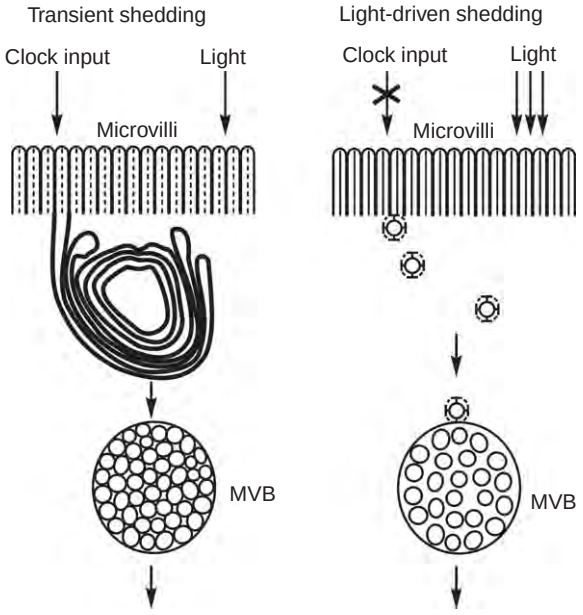

Figure 6 Schematic of transient rhabdom shedding and light-driven shedding. Transient rhabdom shedding must be primed by clock input during the night. It is triggered by the first light of dawn and characterized by the formation of large whorls of rhabdomeral membrane, which subsequently are processed in densely packed multivesicular bodies (MVBs). Light-driven shedding does not require clock input. This progressive process, which continues throughout the day, requires brighter light and involves the clathrin-mediated endocytosis of microvillar membrane from the base of the microvilli. The membranes endocytosed by this process aggregate and form loosely packed MVB. From Sacunas et al. (2002). *Journal of Comparative Neurology* 449: 26–42, with permission from John Wiley & Sons, Inc.

although transient shedding is triggered by light and probably involves the activation of protein kinase (PK) C, it occurs only after photoreceptors have received at least 3 h of clock input and the activation of cyclic adenosine monophosphate (cAMP)-dependent PK.

Gene Expression

In addition to driving structural and physiological changes in photoreceptors and priming transient rhabdom shedding, clock input influences the expression of at least one gene important for the photoresponse. Specifically, clock input to the LE controls an early step in the expression of the gene for visual arrestin (varr). Varr is the protein in photoreceptors responsible for quenching the phototransduction cascade, and as described above, it is also involved in the internalization of rhabdomeral membrane during light-driven shedding. In LEs maintained in constant darkness, clock input during the subjective night causes varr messenger RNA (mRNA) levels in photoreceptors to fall. Circadian fluctuations in varr mRNA levels may lead to a circadian fluctuation in varr

protein levels and thus contribute to some of the circadian changes in the photoresponse described above.

The expression of other photoreceptor proteins probably is also under circadian control, but the clock does not regulate the expression of all proteins important for the photoresponse. For example, *Limulus* opsin mRNA levels are regulated by light, not by the clock. In LEs that receive normal clock input and are exposed to cyclic light, opsin mRNA levels rise during the late afternoon and fall during the night. This rhythm continues in LEs deprived of clock input if they are exposed to cyclic light, and it is eliminated in LEs maintained in the dark even when they receive normal clock input.

Biochemical Processes Mediating Clock Effects on *Limulus* Eyes

Octopamine and the Activation of a cAMP Cascade

When circadian efferent neurons are active during the night, they release the biogenic amine octopamine (OA) from their terminals, and OA, the phenol analog of norepinephrine, is probably most responsible for initiating the circadian changes observed in the eyes. The application of OA to *Limulus* eyes mimics many effects of the clock (Table 1). Other molecules are also released from efferent terminals. Specifically, γ-glutamyl conjugates of OA and tyramine, the precursor of OA, are released, but their physiological relevance is not yet clear. The presence of crystalline granules in efferent terminals suggests that one or more neuropeptides may be released. Crystalline granules are often associated with peptidergic synaptic terminals in invertebrates, but presumptive neuropeptides in the circadian efferent terminals in *Limulus* eyes have not been identified.

In *Limulus* eyes, OA activates membrane receptors that are coupled to adenylyl cyclase stimulating a rise in cAMP in photoreceptors, and any effects of the clock are mediated through the activation of this cAMP cascade (Table 1). There is no evidence for a direct effect of cAMP on *Limulus* photoreceptor physiology; however, there is good evidence that some of the clock-driven changes in the eye require the activation of cAMP-dependent PKA. Therefore, investigations of mechanisms underlying the circadian regulation of photoreceptor function have focused on identifying and characterizing clock-regulated photoreceptor phosphoproteins.

Clock-Driven Protein Phosphorylation

To date, one clock-regulated phosphoprotein in *Limulus* photoreceptors has been identified and partially characterized. It is an unconventional myosin III (LpMyo3), a homolog of the *Drosophila ninaC* gene product that is required in *Drosophila* for normal photoreceptor function and survival. Since their discovery in *Drosophila* and *Limulus* photoreceptors, class III myosins also have been detected in photoreceptors of a variety of invertebrates and vertebrates, including octopus, fish, mice, and humans; thus, these proteins may be important for photoreceptor function in both vertebrates and invertebrates.

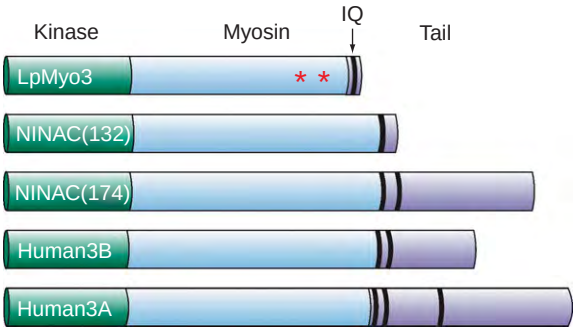

Figure 7 Schematic comparing the domain structure of LpMyo3 with that of the class III myosins expressed in *Drosophila* and humans. One isoform of myo3 has been found in *Limulus*. The two isoforms of myo3 expressed in *Drosophila* are splice variants of the same *ninaC* gene. Human class III myosins are products of two separate genes, *myo3A* and *myo3B*. Each protein contains an N-terminal kinase domain, a myosin domain, and one or more IQ calmodulin-binding motifs (black bars). The tail domains are most variable in length and sequence. LpMyo3 is a target of clock-stimulated phosphorylation within an actin-binding region near the C-terminus of its myosin-like domain (red asterisks).

Class III unconventional myosins are characterized by having an N-terminal kinase domain, a myosin-motor-like domain, one or more IQ calmodulin-binding motifs, and a C-terminal tail of varying lengths (Figure 7). Thus, they are potential signaling molecules as well as potential molecular motors. LpMyo3 is photoreceptor specific, quantitatively a major protein in photoreceptors and distributed throughout the photoreceptor from its cell body to its terminals. During the day in the light, LpMyo3 concentrates over the rays of the photosensitive rhabdom (Figure 2(c)).

LpMyo3 becomes more highly phosphorylated in LEs *in vivo* in response to activation of the circadian efferent input. Its phosphorylation also becomes elevated when intact photoreceptors are incubated *in vitro* with OA, drugs that elevate intracellular cAMP levels and that activate PKA, respectively. Since LpMyo3 is also phosphorylated in response to light, this protein may be particularly important as a substrate upon which light- and clock-driven cascades converge.

Some biochemical properties of LpMyo3 are known. It is a kinase that phosphorylates its own myosin domain as well as other substrates, and its substrate specificity is similar, but not identical, to PKA. LpMyo3 also binds actin, but since its actin binding is insensitive to adenosine triphosphate (ATP) and the protein lacks ATPase activity,

it probably does not function as a molecular motor. Clock-regulated phosphorylation sites in LpMyo3 have also been identified. This information provides clues to how the clock might regulate LpMyo3 and leads to speculations regarding how the phosphorylation of LpMyo3 might influence photoreceptor function.

Clock input to LEs increases the phosphorylation of two sites within the motor-like domain of LpMyo3 within and near an actin-binding interface called loop2 (**Figure 7**). Interestingly, LpMyo3 autophosphorylates these same sites through an intermolecular mechanism. The presence of phosphorylation sites within the actin-binding interface of a myosin is surprising. None of the other 22 classes of myosins that have been described to date becomes phosphorylated in this region. However, mutagenesis studies using other unconventional myosins indicate that changing the net charge in loop2 alters the affinity of myosin for actin. Phosphorylation of LpMyo3 within its actin-binding interface is predicted to reduce its actin affinity.

Actin is concentrated in the rhabdomeral microvilli. Functional consequences of a possible nighttime decrease in the affinity of LpMyo3 for microvillar actin are not yet known, but could be diverse. The Myo3 in *Drosophila* photoreceptors (neither inactivation nor afterpotential C (NINAC)) is thought to bind to and stabilize actin in rhabdomeral microvilli, and in *Drosophila* lacking NINAC, microvillar actin is fragmented or absent. These observations lead to speculations that LpMyo3 phosphorylation participates in circadian processes involving changes in the stability of rhabdomeral actin. One such process is light-triggered transient rhabdom shedding, which involves a transient breakdown of rhabdomeral actin. As described above, although this process is triggered by light, it must be primed by clock input and the activation of PKA. The clock-driven phosphorylation of LpMyo3 by PKA may contribute to the priming event.

LpMyo3 is also a kinase that may phosphorylate one or more proteins involved in the photoresponse. This idea is consistent with observations from *Drosophila*, which show that the photoresponse is abnormal in flies expressing NINAC without its kinase domain. If a change in the affinity of LpMyo3 for actin produces a nighttime decrease in the concentration of LpMyo3 at the rhabdom, the level of phosphorylation of LpMyo3 substrates may also fall and modify the photoresponse. Thus, multiple effects of the clock could be mediated through the modulation of LpMyo3.

Conclusion

The eyes of *Limulus*, with their diverse structures, large photoreceptors, and relatively simple organization, have long served as useful preparations for studying basic mechanisms of vision. Fundamental and broadly relevant aspects of photoreceptor function and sensory information processing were discovered through studies of the *Limulus* visual system. Moreover, studies using *Limulus* have revealed the fundamental importance of circadian rhythms for vision and the complex ways in which clock- and light-driven processes can interact to produce the full range of diurnal changes in retinas. The effects of circadian rhythms observed in *Limulus* LE have many parallels in vertebrate retinas, including those on photoreceptor structure, the photoresponse, and membrane shedding. In addition, circadian clocks in both *Limulus* and vertebrates exert their influence in retinas by regulating the release of biogenic amines and the activity of cyclic-nucleotide-signaling pathways. Mechanisms through which clock-driven signaling pathways influence specific retinal functions are just beginning to be identified, and their discovery remains an important challenge.

See also: Chick Metabolism in the Chick Retina; The Circadian Clock in the Retina Regulates Rod and Cone Pathways; Circadian Regulation of Ion Channels in Photoreceptors; Fish Retinomotor Movements; Genetic Dissection of Invertebrate Phototransduction; Phototransduction in *Limulus* Photoreceptors; Rod and Cone Photoreceptor Cells: Outer-Segment Membrane Renewal.

Further Reading

Barlow, R. B., Jr. (1983). Circadian rhythms in the *Limulus* visual system. *Journal of Neuroscience* 3: 856–870.

Barlow, R. B., Jr., Bolanowski, S. J., Jr., and Brachman, M. L. (1977). Efferent optic nerve fibers mediate circadian rhythms in the *Limulus* eye. *Science* 197: 86–89.

Barlow, R. B., Jr., Chamberlain, S. C., and Lehman, H. K. (1989). Circadian rhythms in the invertebrate retina. In: Stavenga, D. G. and Hardie, R. C. (eds.) *Facets of Vision*, pp. 257–280. Berlin: Springer.

Barlow, R. B., Jr., Chamberlain, S. C., and Levinson, J. Z. (1980). *Limulus* brain modulates the structure and function of the lateral eyes. *Science* 210: 1037–1039.

Battelle, B.-A. (2006). The eyes of *Limulus polyphemus* (Xiphosura, Chelicerata) and their afferent and efferent projections. *Arthropod Structure and Development* 35: 1–14.

Battelle, B.-A. (2008). Circadian rhythms in visual function in *Limulus*. In: Fanjul-Moles, M.-L. and Aguilar-Roblero, R. (eds.) *Comparative Aspects of Circadian Rhythms*, pp. 19–40. Kerala: Transworld Research Network.

Battelle, B.-A., Evans, J. A., and Chamberlain, S. C. (1982). Efferent fibers to *Limulus* eyes synthesize and release octopamine. *Science* 216: 1250–1252.

Calman, B. G. and Chamberlain, S. C. (1982). Distinct lobes of *Limulus* ventral photoreceptors. II. Structure and ultrastructure. *Journal of General Physiology* 80: 839–862.

Cardasis, H. L., Stevens, S. M., McClung, S., et al. (2007). The actin-binding interface of a myosin III is phosphorylated *in vivo* in response to signals from a circadian clock. *Biochemistry* 46: 13907–13919.

Chamberlain, S. C. and Barlow, R. B., Jr. (1984). Transient membrane shedding in *Limulus* photoreceptors: Control mechanisms under natural lighting. *Journal of Neuroscience* 4: 2792–2810.

Chamberlain, S. C. and Barlow, R. B., Jr. (1987). Control of structural rhythms in the lateral eye of *Limulus*: Interactions of natural lighting

and circadian efferent activity. *Journal of Neuroscience* 4: 2794–2810.

Fahrenbach, W. H. (1975). The visual system of the horseshoe crab *Limulus polyphemus*. *International Review of Cytology* 41: 285–349.

Fein, A. and Payne, R. (1989). Phototransduction in *Limulus* ventral photoreceptors: Roles of calcium and inositol trisphosphate. In: Stavenga, D. G. and Hardie, R. C. (eds.) *Facets of Vision*, pp. 173–185. Berlin: Springer.

Hartline, H. K., Wagner, H. G., and Ratliff, F. (1956). Inhibition in the eye of *Limulus*. *Journal of General Physiology* 39: 651–673.

Yeandle, S. (1958). Evidence of quantized slow potentials in the eyes of *Limulus*. *American Journal of Ophthalmology* 46: 82–87.

M

Macular Edema

R N Frank and I Glybina, Kresge Eye Institute, Wayne State University School of Medicine, Detroit, MI, USA

Glossary

Circinate lipid exudates – A round or oval assemblage of intraretinal lipid deposits that is often seen in macular edema, especially in diabetic macular edema. This presumably occurs because plasma exudes from a small retinal blood vessel, or a cluster of retina vessels, in a circular pattern around the abnormal vessel. The portion of this circle, farthest from the leaking vessels, is the thinnest, and as reabsorption of the fluid occurs at that location, the lipoproteins precipitate into the tissues, forming the visible exudates.

Cystoid macular edema – A form of macular edema in which much of the extracellular fluid collects in loculated spaces between the photoreceptor axons of Henle's fiber layer, forming round or oval, fluid-filled spaces. These are called cystoid because they are not lined with a layer of epithelial cells, which would make them true cysts; hence, these spaces are cystoid and not cystic.

Fovea – The central portion of the macula that contains only specialized cone photoreceptors, whose outer segments are narrow and elongated, rather than cone shaped as are extrafoveal cones.

Foveal avascular zone (FAZ) – A specialization of the capillary network in the foveal region of the retinal vasculature in humans and higher primates. There are no blood vessels in the FAZ, presumably as an evolutionary development to permit unimpeded access of light rays to the foveal cone photoreceptors. The FAZ can be readily seen as an approximately circular avascular zone about 1 mm in diameter in retinal vascular digest preparations from enucleated eyes or in good-quality fluorescein angiograms in living eyes.

Foveola – The central portion of the fovea, in which the axons of the cone photoreceptors are swept to the side, leaving only their inner and outer segments exposed to the incoming rays of light.

Henle's fiber layer – The obliquely directed axons of the foveal cone photoreceptors.

Irvine–Gass syndrome (aphakia, or pseudophakia, cystoid macular edema) – This entity was first described during the 1960s by the individuals whose eponymous names it bears. Presumably because of postoperative inflammation after cataract surgery, perifoveal capillaries begin to leak and edema fluid collects in a cystoid pattern in the central macula. The condition is often self-limited but may lead to considerably reduced vision. As demonstrated by fluorescein angiography, it may be accompanied by breakdown of the blood–retinal barrier in the capillary circulation of the optic nerve head.

Macula – The central region of the retina that is specialized for high-resolution vision. It is found in humans and higher primates and is notable histologically for the fact that it contains multiple layers of ganglion cells, while the extramacular retina contains only a single layer.

Macular edema – The thickening of the macular retina by extravasation of fluid, often containing lipid components (which may precipitate into the tissues) from breakdown of the normal blood–tissue barrier at the level of the endothelial cells of the retinal blood vessels in the macula. Fluid can also extravasate from the choroidal capillaries through the retinal pigment epithelium barrier, but this usually produces collections of subretinal fluid, which is distinguishable from the intraretinal fluid of macular edema.

Randomized controlled clinical trial (RCT) – A method of evaluating the efficacy of a new therapeutic procedure in which subjects with a disease under investigation volunteer to be allocated by random selection to a treatment group, or groups,

which will receive the new therapy or therapies under investigation, or to a control group that receives either no treatment or treatment with a placebo or treatment by the method that has been accepted as the current standard of care. Evaluation of the results for each subject is done by observers who are masked, that is, who do not know to which of the treatment, or control, groups the various subjects belong. This method is considered the definitive way to determine the efficacy, or lack of efficacy, of a putative new therapy.

Macular edema, a swelling of the central portion of the human retina, or macula, is a common feature in many diseases. It is a widely recognized complication of diabetic retinopathy, where its prevalence (in the United States) may be of the order of 10% of all individuals with diabetes, varying somewhat by ethnic group but not by type of diabetes (i.e., type 1 or type 2). Macular edema also occurs commonly in retinal vein occlusions, in uveitis, following cataract surgery, as an accompanying feature of some ocular tumors, in hereditary retinal degenerations, such as the retinitis pigmentosa syndromes and, rarely, as an isolated genetic entity apparently in and of itself.

Diagnosis of Macular Edema

Recognition of macular edema as an important clinical entity has been increasing in recent years, and, in particular, since the 1960s with the advent of a variety of new diagnostic techniques. These have included high-magnification, stereoscopic ophthalmoscopy using the slit lamp and several types of contact and noncontact lenses that allow the observer to visualize the edematous macula in a better manner; stereoscopic retinal photography; fluorescein angiography to enable visualization of circulatory dynamics and the physiology/pathology of the macular circulation, even at the capillary level; and, most recently, optical coherence tomography (OCT), a rapid, noninvasive technique that permits accurate measurement of the thickness of the macula, and yields high-resolution tissue sections of the maculae of living subjects with almost histologic clarity.

Anatomy of the Macula

The macula is an anatomic specialization of the neural retina that is unique to humans and to higher primates (**Figure 1(a)–(d)**). It is defined histologically by the presence of multiple layers of retinal ganglion cells (there is only a single layer of ganglion cells in the extramacular retina), and ophthalmoscopically as the region extending from the temporal margin of the optic nerve head to the center of the macula (the foveola, the central depression that is evident clinically in the normal retina), and then for an equal distance temporal to the foveola. In the superior–inferior direction, the macula extends between the two major temporal retinal vascular arcades. It is not clear why, of the entire extent of the human retina, the macula is particularly susceptible to such a large number of disorders, for example, the macular degenerations, or to edema in a large variety of diseases. Speculations entail the likelihood that the macular retina, including both its neural elements and also the macular retinal pigment epithelium, has a higher level of metabolic activity because of its enhanced visual function, including a greater density of cone photoreceptors, a thicker ganglion cell layer, and a greater thickness of retinal pigment epithelial (RPE) cells; or that this enhanced activity necessitates greater blood flow with a greater likelihood of circulatory breakdown, especially in view of the very rich retinal capillary network within the macula and, particularly, in the perifoveal region. Finally, the anatomic specialization of the foveola, in which the foveolar cone axonal and synaptic processes are swept obliquely to all sides, permitting direct access of photic stimuli to the photoreceptor outer segments, may lead pathologically to the accumulation of extracellular edema fluid into ballooning spaces in this axonal region in the entity known as cystoid macular edema.

In studying macular edema in an experimental setting, investigators are hampered by the fact that the macula is an anatomic specialization of the retina that is limited to humans and some higher primates. While certain birds, for example, hawks and eagles, have a fovea, there is no macula in the sense that it is present in the human eye, and the blood circulation of the posterior avian globe is entirely different from that of humans.

Clinical Findings in Macular Edema

The thickening of the central retina is best appreciated by stereoscopic viewing methods, for example, slit-lamp ophthalmoscopy with a contact lens or a handheld high dioptric indirect ophthalmoscope lens. Until recently, multicenter clinical research studies, for example, the Early Treatment Diabetic Retinopathy Study (ETDRS) used stereoscopic retinal photography to evaluate macular thickening. However, relatively minimal central retinal thickening may not be apparent even to the experienced examiner and photographic methods are subject to variability. Therefore, the introduction of OCT, which is discussed in more detail below, has held recent very great interest, but it has also raised some unexpected questions.

In the absence of stereoscopic viewing methods, one can suspect the presence of macular edema by the

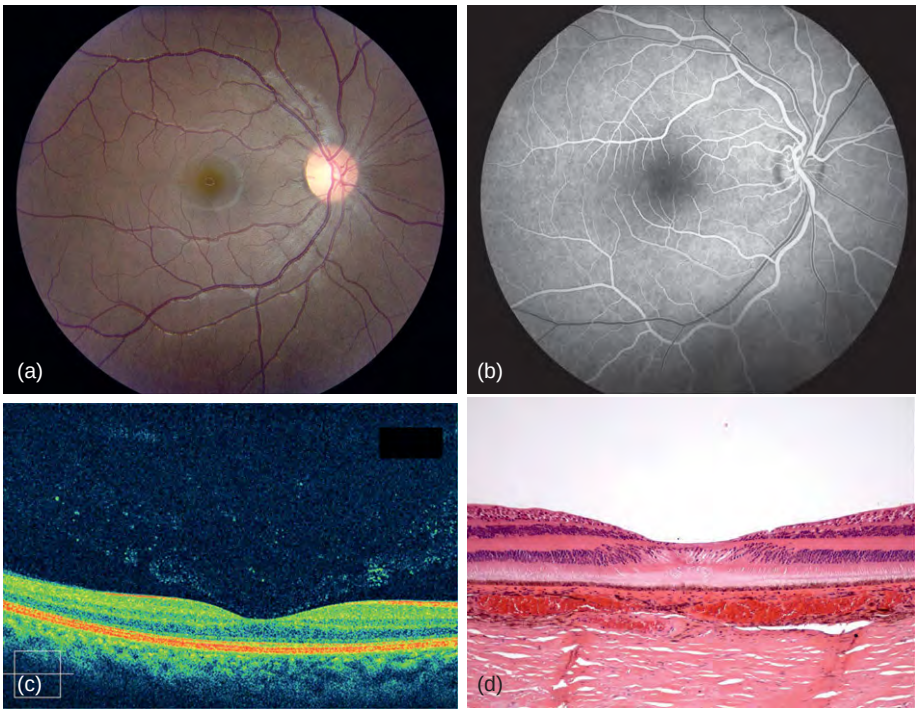

Figure 1 The normal human macula. (a) Color photograph of a normal macula. (b) Fluorescein angiogram of a normal macula. Note the striped pattern of blood flow in the retinal venule. This laminar flow, with the nonfluorescent column of blood cells in the center of the vessel, is typical of early flow in retinal venules. In later phases of the angiogram, the entire vessel will fill in. Note also the sharp margins of the vessels in this normal angiogram, in the normal retinal vasculature, the endothelial lining of the vessels is tight, even to the small (M.W. 327) fluorescein molecule, which is only about 65% bound to plasma proteins. (c) A spectral domain optical coherence tomogram (OCT) of a normal macula. In this high-resolution OCT scan, one can clearly see the cellular layers of the retina. (d) A histologic section of a normal human macula, stained with hematoxylin–eosin. This photomicrograph is courtesy of Ralph Eagle, M.D., Wills Eye Institute, Philadelphia, PA.

presence of certain characteristic retinal lesions. Extensive intraretinal hemorrhages or microaneurysms (dilations of capillary-sized blood vessels, which appear ophthalmoscopically as tiny red dots) in the macular region are indicators of extravascular blood or plasma leakage with resultant macular edema (**Figure 2(a)** and **(b)**). An especially characteristic abnormality, particularly in individuals with diabetes, is the presence of intraretinal lipid deposits. These often have a circular (circinate) configuration (**Figure 2(a)**), which presumably is the result of leakage of plasma from a central vascular lesion, or cluster of lesions (**Figure 2(b)**), with resorption of the edema fluid but not its lipid components around the periphery of the 360° circumference of the zone of leakage, where the thickness of the fluid layer is least and the less-soluble lipid therefore precipitates out of solution. Macular lipid, and edema, have characteristic appearances by OCT, and histologically, as demonstrated in **Figure 2(c)** and **(d)**. It has been known for a number of years that lower blood-lipid values are associated with lesser degrees of macular edema in diabetic subjects, although it is not clear that normalizing blood lipids can entirely prevent the development of macular edema in diabetic subjects.

There have been reports, at least one of which preceded by a number of years the development of OCT for objective measurements of macular thickness, that macular edema can vary over the course of a day. Some patients have noted that their vision, on arising in the morning, was much poorer than later in the day. Several investigators, using OCT, have found that macular thickness in at least some patients with diabetic macular edema is greater immediately after arising from a night's sleep than it is later. Although there are a number of possible causes, the most plausible is a simple gravitational effect, with edema fluid remaining in the upper body during recumbent posture and draining to the lower body when the individual is sitting or standing. However, although this diurnal effect does occur in some individuals, the Diabetic Retinopathy Clinical Research Network, in a study involving many institutions, found it to be infrequent.

Clinically Significant Diabetic Macular Edema

The ETDRS also introduced the term "clinically significant macular edema" to describe those cases in which the

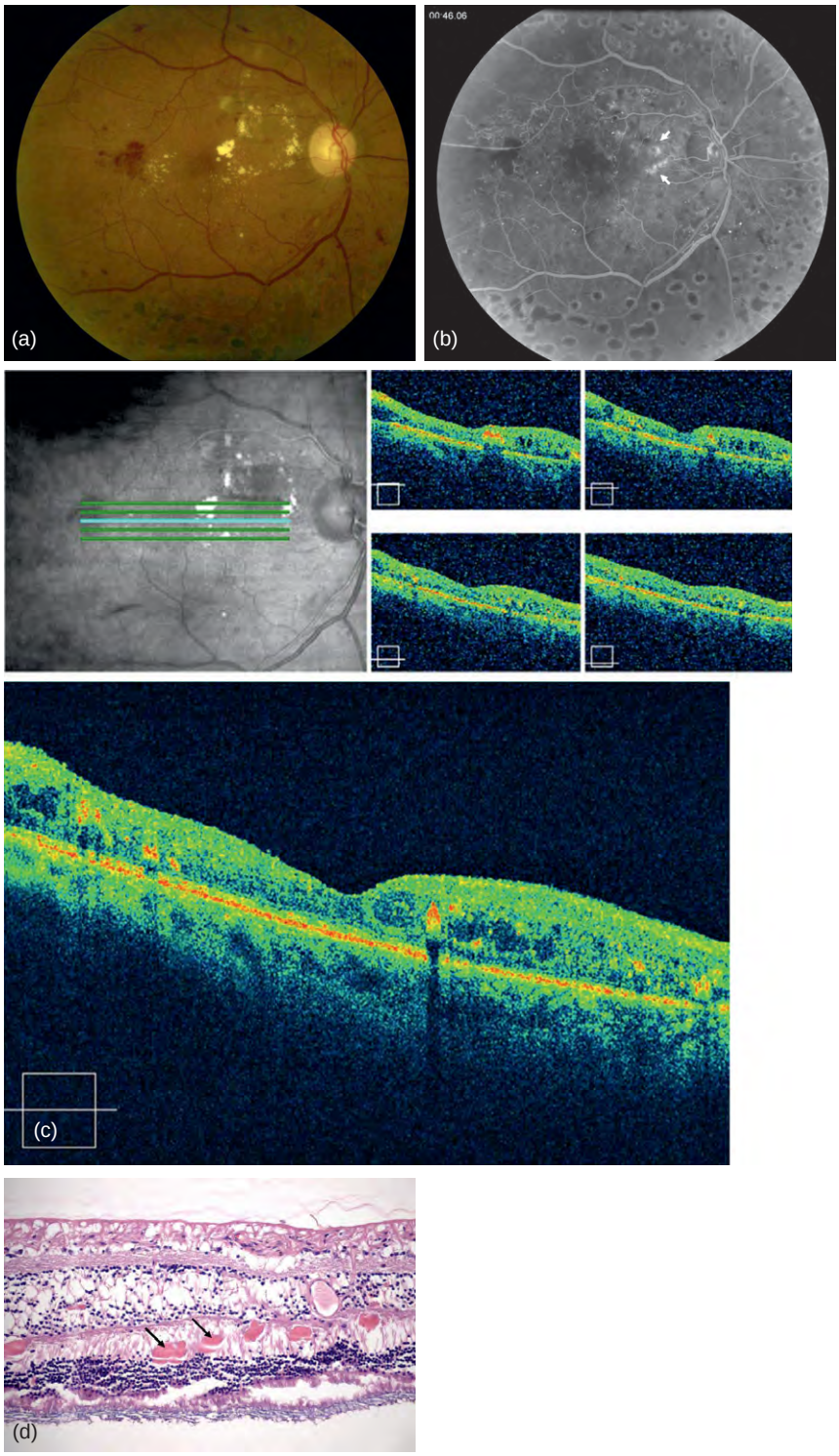

Figure 2 (a) Circinate lipid deposits form a ring in a case of diabetic macular edema. Multiple dot and blot hemorrhages and microaneurysms are also present. (b) A frame from a fluorescein angiogram from this patient, showing a cluster of leaking microaneurysms (arrows) at the center of the lipid ring. (c) Spectral domain OCT scans of this patient, showing intraretinal edema fluid, which appears as round, hollow spaces, and lipid plaques (red-orange densities). The vertical, empty spaces beneath the plaques occur because the plaques absorb the scanning laser beams, producing optical shadows. (d) Histologic section of the neurosensory retina, lacking retinal pigment epithelium and choroid, from an eye with diabetic macular edema (round or/and intraretinal lipid plaques, some of which are shown by arrows). The edema fluid appears as round or oval spaces with smooth borders, while the irregular spaces with ragged edges at the bottom of the micrograph are artifacts created by histologic sectioning. Hematoxylin–eosin stain. Photomicrograph courtesy of Ralph Eagle, M.D., Wills Eye Institute, Philadelphia, PA.

retinal thickening either involved the center of the macula (the fovea and foveola), or was sufficiently close to the center as to constitute a potential threat to the center with likely loss of central vision. The definition of clinically significant diabetic macular edema, as established by the ETDRS, is presented in **Table 1**.

Table 1 Clinically Significant Diabetic Macular Edema

1. Thickening of the retina at or within 500 μm (approximately one-half optic disk diameter) of the center of the macula.
2. Hard exudates at or within 500 μm of the center of the macula, if associated with thickening of adjacent retina (not residual hard exudates remaining after disappearance of retinal thickening).
3. A zone or zones of retinal thickening 1 optic disk area or larger, any part of which is within one disk diameter of the center of the macula.

From Early Treatment Diabetic Retinopathy Study Research Group (1985). Photocoagulation for diabetic macular edema. Early Treatment Diabetic Retinopathy Study Report No. 1. *Archives of Ophthalmology* 103: 1795–1805.

Findings by Fluorescein Angiography

By intravenous fluorescein angiography, in which a solution of sodium fluorescein is injected intravenously through an antecubital vein and rapid sequence photographs are taken using fluorescence optics, it is possible to visualize some of the vascular dynamics of macular edema. Fluorescein is a small molecule (M.W. 327) that is only loosely bound to plasma proteins, for example, only about 65% to albumin, and this small size enables it to leak readily through patent interendothelial cell junctions. Hence, in successive frames of a fluorescein angiogram in patients with diabetic retinopathy or other edema-producing retinal vascular diseases, one can see an increasing fluorescent haze surrounding the microvascular lesions (**Figure 3**). These leaking lesions are often (though surprisingly, not always) associated with macular thickening by OCT examination.

Fluorescein angiography has also demonstrated a specific type of macular edema, so-called cystoid macular edema. The axons of foveal cone photoreceptors are displaced laterally in human and higher primate retinas, thereby permitting light to strike the foveal cone outer

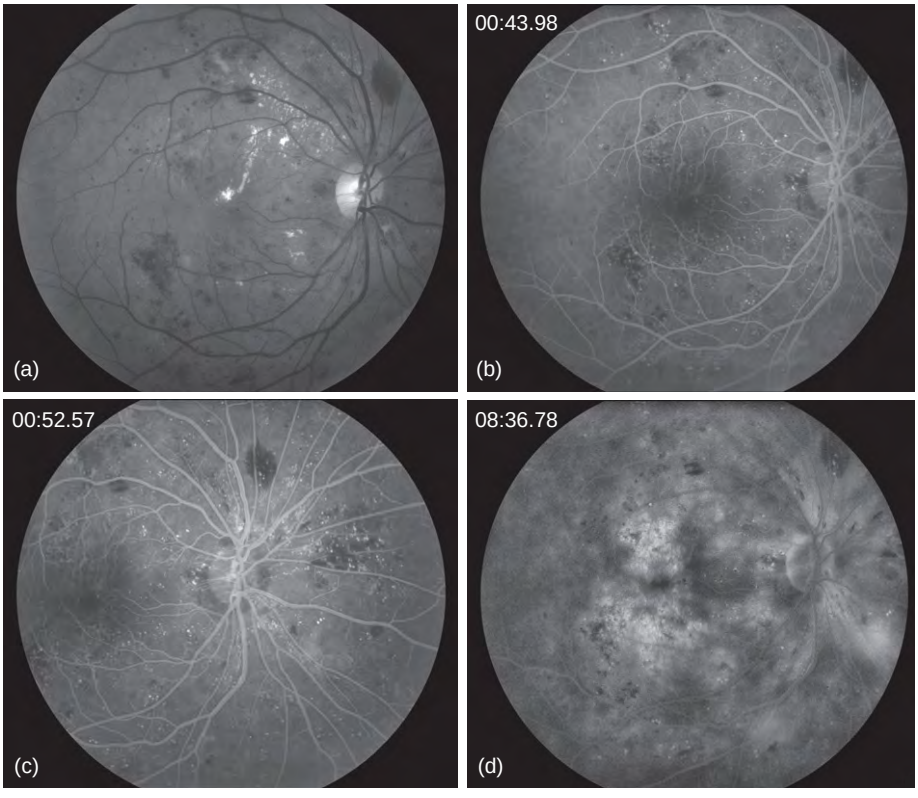

Figure 3 Sequence of angiographic frames showing increasing dye leakage in diabetic macular edema. (a) Red-free initial photograph of the right eye, taken before injection of the dye to show features of the posterior retina. (b) Frame from the fluorescein angiogram taken approximately 44 s from the time of dye injection (timing is indicated by numbers at the top left of the photograph). Arteries and veins have filled, and multiple microaneurysms, which appear as tiny white dots, are apparent. (c) Frame from the fluorescein angiogram taken at approximately 53 s after injection. Dye in the microaneurysms has intensified and has begun to leak from the vessel walls, creating a somewhat blurred appearance. (d) Frame from the angiogram taken approximately 8 min and 37 s from the time of injection. Dye and plasma have leaked profusely from the abnormal vessels into retinal tissue, contributing to the tissue edema.

segments directly, without traversing the inner retinal layers. This lateral displacement produces a unique anatomic arrangement that is known as Henle's fiber layer. The center of the fovea itself is avascular; however, cyst-like extracellular fluid spaces collect within Henle's fiber layer. These can, although often with some difficulty, be visualized by white light ophthalmoscopy using a slit lamp and handheld or contact lens, or sometimes by ophthalmoscopy using a green filter to increase contrast. The characteristic appearance, using fluorescein angiography, is one or more oval, uniformly fluorescent spaces oriented radially around the foveal center similar to petals on a flower, giving rise to the term "petaloid appearance." A single such large cystoid cavity is shown in the fluorescein angiographic frame of **Figure 4(a)**. The cyst-like nature of this cavity is evident on OCT scans (**Figure 4(b)**). Although macular edema may produce severe loss of central visual acuity, vision is often surprisingly preserved in many instances. **Figure 4(c)** shows OCT scans of a patient with bilateral cystoid macular edema, with corresponding microperimetric data printed underneath. This very sensitive visual sensitivity mapping device demonstrates only modest sensitivity loss in each eye, located almost directly corresponding to the position of the cystoid cavities. Visual acuity in each eye, also printed on the figure, is quite good. These cystoid cavities are, of course, not true cysts, since when histologic sections are available, they demonstrate that these fluid-filled spaces are not lined by layers of epithelium (**Figure 4(d)**). Cystoid edema may occur with any of the disorders that produce macular edema. One notable entity was first described during the 1960s, after fluorescein angiography had become widely used, when cystoid macular edema was observed angiographically in many patients who had just undergone seemingly uneventful intracapsular cataract surgery. Often, the postoperative visual acuity in these patients did not recover as fully as might have been expected, and fluorescein angiography revealed a pattern of cystoid macular edema, frequently accompanied by leaking of fluorescent dye from the optic nerve head. This pattern has been called the Irvine–Gass syndrome, after the individuals who initially reported it. With the advent of advanced extracapsular cataract surgical techniques, in which the posterior lens capsule is left in place and a posterior chamber intraocular lens is inserted, the incidence of postcataract surgical cystoid macular edema has been considerably reduced, but it still occurs. While this entity has been associated with various complications of the surgery, it often appears in cases where the surgical procedure was entirely uneventful.

Causes of Macular Edema

All investigators agree that the proximate cause of macular edema, associated with any systemic or ocular disease or drug, is a breakdown of the inner blood–retinal barrier, which is composed of junctional complexes of the endothelial cells of the retinal blood vessels, as opposed to the outer blood–retinal barrier, consisting of the retinal pigment epithelium, which serves as a boundary layer between the neural retina and the choroidal vasculature. Although contents of the vascular lumina can reach the extravascular space by transcellular mechanisms, directly through endothelial cell cytoplasm, most investigators believe that the most frequent pathologic mechanism is the breakdown of intercellular junctional complexes, which normally form a tight boundary between the vascular lumen and the extravascular milieu. This may be caused by specific molecular mechanisms, such as increased levels of vascular endothelial growth factor (VEGF, originally called vascular permeability factor because it was through that function that this molecular family was first discovered), or various inflammatory molecules or cytokines, or through the use of certain topical drugs in the treatment of glaucoma, such as epinephrine or, more recently, prostanoid compounds. Another molecular mechanism that has been of interest is the family of carbonic anhydrase enzymes. A recent paper, which describes proteomic analysis of the vitreous fluid in a series of patients with proliferative diabetic retinopathy and vitreous hemorrhage, who underwent vitrectomy surgery, has reported that these vitreous samples demonstrated a substantial upregulation of the CA-1 isoform of carbonic anhydrase. Injection of this molecule into the vitreous cavity of rats produced generalized retinal edema. Another recent paper cast some doubt on the role of VEGF in diabetic macular edema. These investigators examined the relationship between various single nucleotide polymorphisms (SNPs) in the VEGF gene and its promoter in individuals with various levels of diabetic retinopathy severity in the very large and well-characterized Diabetes Control and Complications Trial/Epidemiology of Diabetes Interventions and Complications (DCCT/EDIC) cohort. They found that there were 18 SNPs in the VEGF gene and its promoter that were significantly associated with severe preproliferative and proliferative retinopathy, but no detectable significant associations of VEGF gene or promoter polymorphisms with diabetic macular edema.

Treatment of Macular Edema

Results from the ETDRS

The ETDRS, a randomized, controlled clinical trial (RCT) of laser treatment and aspirin therapy that involved over 3000 patients with moderate to severe nonproliferative and early proliferative diabetic retinopathy, and/or with macular edema, reported in 1985 that treatment with focal applications of small-diameter

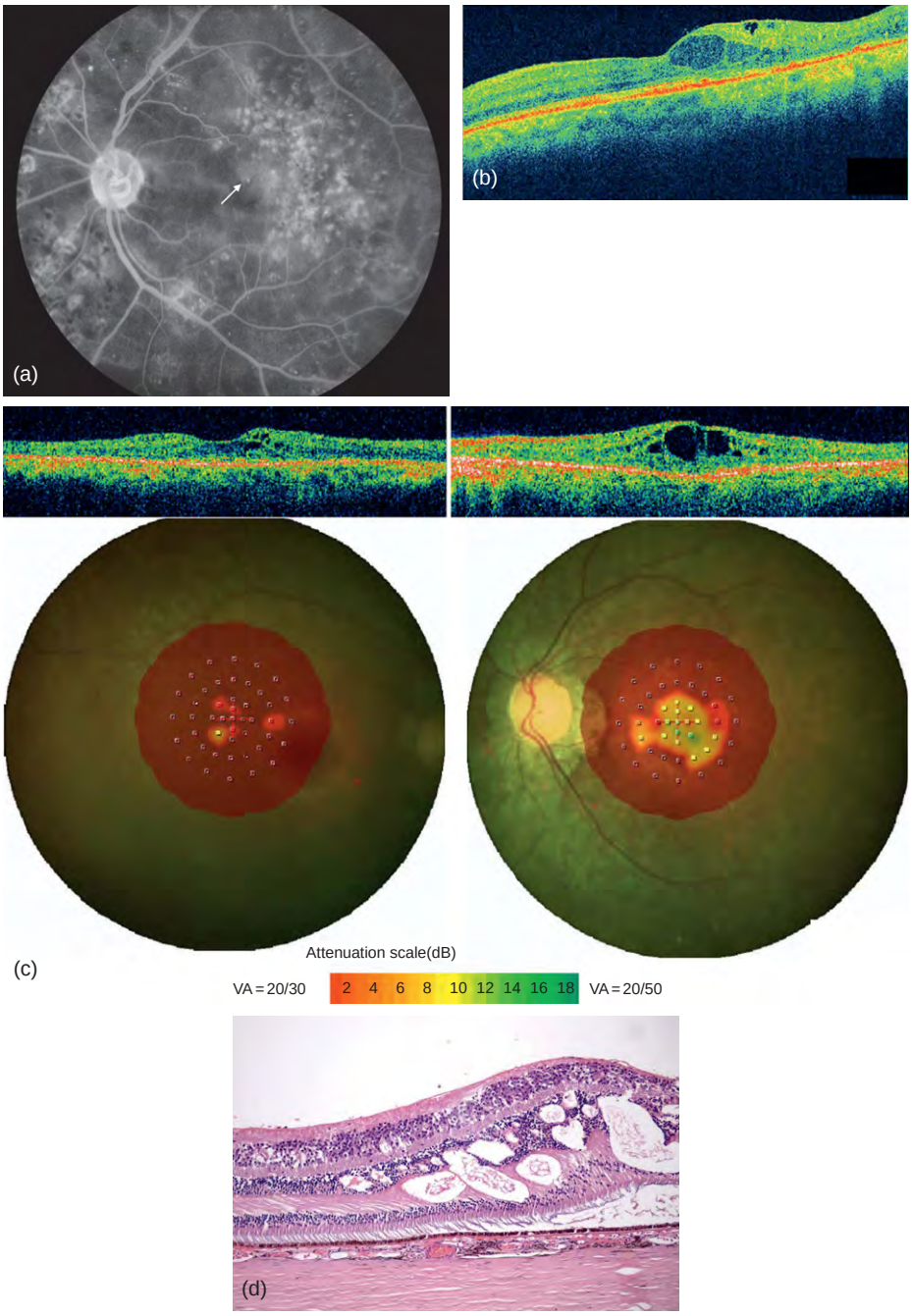

Figure 4 (a) Frame from a fluorescein angiogram of a patient with cystoid macular edema. Edema fluid containing the dye may fill many balloon-like spaces surrounding the center of the macula, producing an appearance similar to multiple radial petals on of flower, a so-called petaloid appearance. Only one such large space, indicated by the arrow, is seen in this photograph. The multiple small, round spots are previous laser treatment burns, which have been placed in a grid pattern. (b) Spectral domain OCT scan of this patient, showing the large cystoid spaces that appear in the angiographic frame in **Figure 4(a)**. (c) Microperimetric study of a patient of Dr. Tamer Mahmoud, who presented with bilateral cystoid macular edema. The microperimetry scans are here placed beneath OCT scans of the corresponding eyes. The color scale at the bottom of the illustration shows increasing loss of retinal sensitivity as one moves from left to right on the scale. (d) H-and-E-stained histopathological section of a retina with macular edema. Note the large fluid-filled vacuoles in the macula. This photomicrograph is courtesy of Ralph Eagle, M.D., Wills Eye Institute, Philadelphia, PA.

(50–100 μm) argon laser burns directly to macular microaneurysms (**Figure 5(a)–(c)**), or with grid laser applications could slow down or arrest the progress of diabetic macular edema with substantial preservation of vision by as much as 50% more in eyes that received treatment than in eyes that were randomly allocated to the no laser treatment group. The ETDRS results are frequently cited as showing that such laser treatment preserves

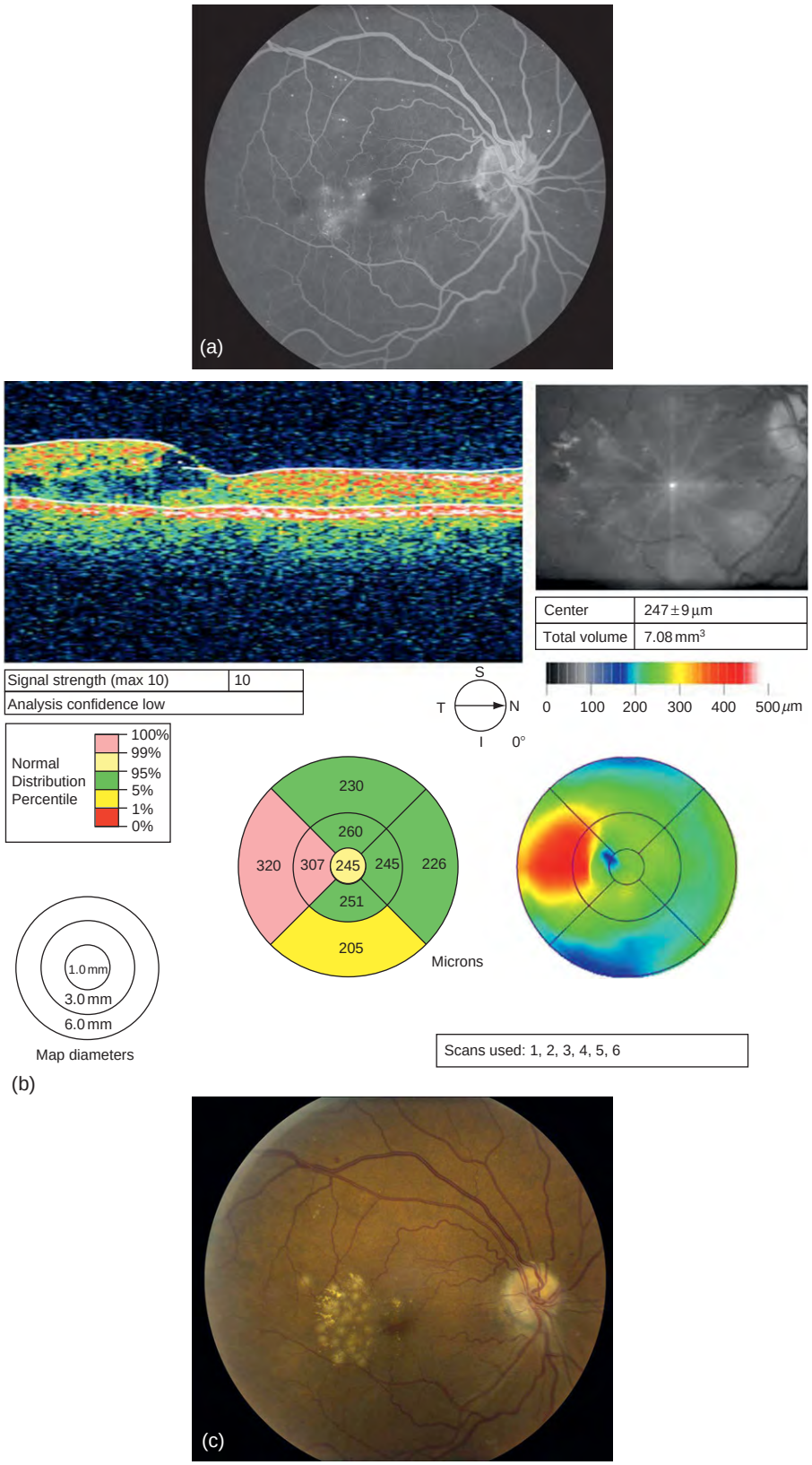

Figure 5 (a) Frame from a fluorescein angiogram showing intense leakage in the right eye of a patient with relatively focal macular edema; (b) Time domain OCT scan showing the region of edema (red-filled zone in the macular map). Color scales indicate retinal thickness. (c) Photograph taken immediately after application of focal argon laser burns, showing localization of the laser treatment to the edematous area.

vision, but does not improve it. However, in this study, a substantial number of the patients initially had good (i.e., better than 20/40) vision and hence were not likely to improve substantially. When one examines the results of the ETDRS patients whose initial vision was less than 20/40, it becomes apparent that laser treatment produced an actual improvement of visual acuity by more than one line on the ETDRS visual acuity chart in more than 40% of these subjects, compared to approximately 25% in the control group. In a more recent RCT, which compared two different techniques for applying focal argon laser treatment for diabetic macular edema, the Diabetic Retinopathy Clinical Research Network found that approximately 30% of patients with initial visual acuity less than 20/40 who received the modified ETDRS laser technique improved their visual acuity by more than three lines on the ETDRS vision chart, a halving of the visual angle, over a 1-year follow-up. At that time (fall, 2008), therefore, laser treatment, involving focal application of small, relatively light-intensity argon laser burns to areas of vascular leakage in the maculae of eyes with diabetic macular edema, and in particular clinically significant macular edema, was considered the treatment of choice. Application of this treatment, however, requires a degree of caution. Because eyes with clinically significant macular edema may not have suffered a loss of central vision (and most eyes with macular edema in the ETDRS had visual acuity at, or better than, 20/40), and because the laser treatment technique employed in this study involves the placement of moderately intense, small-diameter laser burns directly to microaneurysms identified ophthalmoscopically or by fluorescein angiography, placement of such burns to lesions very close to the center of the macula may result in damage to central vision. The use of focal laser photocoagulation for lesions very close to the macular center therefore does require an element of clinical judgment. Hence, the ETDRS recommended that laser treatment for clinically significant macular edema should be considered, but did not establish such treatment as an absolute standard of care.

Results of Other Clinical Trials

Another multicenter RCT, the Branch Vein Occlusion Study, found a significant beneficial effect of focal argon laser photocoagulation for macular edema, and for retinal neovascularization, in this disorder. However, eyes with central retinal vein occlusion, a much more severe condition, received no benefit from focal laser photocoagulation in the Central Vein Occlusion Study.

Focal laser treatment was also shown to be of clear benefit for the treatment of macular edema resulting from branch retinal vein occlusion in another RCT, the Branch Vein Occlusion Study. However, it was ineffective for central retinal vein occlusion in the Central Vein Occlusion Study, yet another RCT. There is no evidence for a beneficial effect of laser treatment for macular edema from any other cause.

As the pathogenesis of macular edema appears to have an inflammatory component, anti-inflammatory therapies have been widely used as treatment for some forms of this disorder. The ETDRS evaluated aspirin at a dose of 650 mg day^{-1}, compared to placebo for severe nonproliferative diabetic retinopathy and for diabetic macular edema and found no beneficial effect. In aphakia or pseudophakia cystoid macular edema, one RCT has demonstrated the efficacy of treatment with a topical nonsteroidal anti-inflammatory eyedrop, although some clinicians combine this with a topical steroid. More recently, a number of investigators have used intravitreal injections of triamcinolone, a steroid molecule, for several forms of macular edema. Although several papers have reported good results of this procedure for diabetic macular edema, a very recent paper detailing the results of a large, multi-institutional RCT in the Diabetic Retinopathy Clinical Research Network found that, over a 2-year follow-up, intravitreal triamcinolone, at 1 and 4 mg doses, was significantly less effective in this disorder than focal laser treatment. These doses of intravitreal triamcinolone have been evaluated for their efficacy in treating macular edema resulting from branch or central retinal vein occlusion in the Standard Care versus COrticosteroid for REtinal vein occlusion (SCORE) study, two multi-institutional randomized, controlled clinical trials sponsored by the U.S. National Eye Institute. For central retinal vein occlusion, these studies found that triamcinolone injected intravitreally in either a 1 or a 4 mg dose produced a significantly higher number of eyes that gained three or more lines of vision over a 1-year follow-up interval than observation alone. One milligram was concluded to be the preferred dose for this indication because of its smaller number of adverse effects. This result is the first time that any treatment has been reported as significantly effective in improving vision in macular edema from a central retinal vein occlusion. However, the concurrent SCORE clinical trial showed that neither of these two steroid doses injected intravitreally produced gains in vision for eyes with macular edema secondary to branch retinal vein occlusion that were superior to those obtained by focal argon laser photocoagulation, the previously accepted standard of care for that entity. Reasons for the different efficacies of steroids and laser for macular edema in diabetic retinopathy and in central and branch retinal vein occlusions remain to be explained.

Another intravitreal steroid, fluocinolone, has been used successfully as a long-term, slow-release implant inserted surgically in the treatment of macular edema resulting from chronic uveitis. Like other steroids, but to a somewhat greater degree, the fluocinolone implant can result in substantial elevations of intraocular pressure, and

in cataract formation. A full evaluation by RCT of the fluocinolone implant for macular edema in diabetes is underway, but clinical trials using this steroid implant involving other disorders in which macular edema is present have not yet been carried out.

Anti-VEGF Therapies and Macular Edema

Because the VEGFs were first recognized as a family of molecules that enhanced vascular permeability and the breakdown of blood–tissue barriers, before their recognition as angiogenic agents, the development of anti-VEGF agents with efficacy against neovascular retinal and choroidal diseases has been followed by clinical studies of these agents as potential treatments for macular edema. RCTs involving ranibizumab (Lucentis, Genentech), a humanized anti-VEGF monoclonal antibody injected intravitreally for diabetic macular edema and for macular edema in retinal vein occlusions are currently underway. A very similar monoclonal antibody, bevacizumab (Avastin, Genentech), developed initially as a cancer therapy, has also been employed in some preliminary clinical trials. One possible objection to the putative role of VEGF in diabetic macular edema, relating to the absence of significant VEGF gene polymorphisms in diabetic macular edema cases, compared to the presence of such changes in cases of severe preproliferative and proliferative diabetic retinopathy, has been discussed above. Another is the clinical observation that diabetic macular edema often occurs in the absence of retinal neovascularization and, conversely, neovascularization may occur without macular edema. If excessive VEGF secretion is essential to the cause of both types of diabetic retinal lesion, then both should occur together much more often than not. However, the issue may be much more complex, and its resolution will require, among other things, the completion of the ongoing clinical trials. There have been a number of reports describing encouraging results from much smaller trials. A report of a small, phase 2 trial of bevacizumab for diabetic macular edema from the Diabetic Retinopathy Clinical Research Network described suggestive evidence of a beneficial effect on macular thickness by OCT and visual acuity in patients injected with this agent, compared to focal argon laser photocoagulation. This trial, however, was quite small and complex in organization (a total of 100 patients, randomized into five treatment groups of 20 each, receiving various combinations of different doses of bevacizumab with or without laser therapy). A final determination of the efficacy of this mode of therapy must therefore await the completion of larger, longer controlled clinical trials.

Other agents that are currently being investigated for the treatment of diabetic macular edema include VEGF-TNF receptor-associated protein (TRAP; aflibercept, Regeneron), a VEGF receptor that is solubilized by being complexed to an immunoglobulin and that, upon intravitreal injection, acts by sponging VEGF molecules from the vitreous, and sirolimus (rapamycin), an antibiotic with immunomodulatory and anti-inflammatory properties, that is also capable of interfering with neovascularization.

A Puzzling Question

The use of OCT evaluations to measure macular thickness and to determine pathologic changes in macular anatomy has led to an unexpected finding. It has been generally assumed, that macular thickness beyond the normal range, and visual acuity, were inversely, and fairly closely, correlated, and central macular thickness determined by OCT has been used as an endpoint (usually a secondary endpoint) of several clinical trials of new therapies for diabetic retinopathy and some other diseases. Although a rough correlation does exist, the Diabetic Retinopathy Clinical Research Network and others who have investigated this question have found that, for diabetic macular edema, the correlation is surprisingly poor (**Figure 6**). We, and others, have found that this poor correlation extends to macular edema in other disorders as well, and our own preliminary results suggest that the slope of the correlation curve of central macular thickness

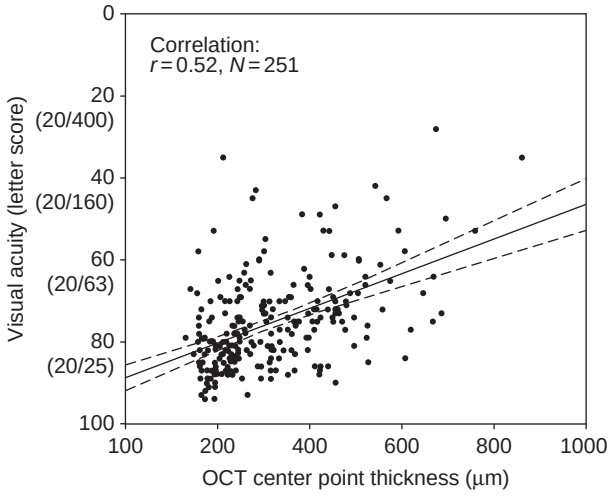

Figure 6 Best-corrected visual acuity, measured on the Early Treatment Diabetic Retinopathy Study (ETDRS) chart, of a large series of patients from the multicenter Diabetic Retinopathy Clinical Research Network, and correlated with macular central point thickness (measured by time domain OCT). The solid line indicates the best-fitting linear correlation curve, while the dashed lines indicate the 95% confidence interval. Although a correlation exists, it is surprisingly poor. Reprinted from DRCR.net Study Group (2007). Relationship between optical coherence tomography-measured central retinal thickness and visual acuity in diabetic macular edema. *Ophthalmology* 114: 525–536, with permission from Elsevier.

versus visual acuity differs for diabetic macular edema and for pseudophakia macular edema (Irvine–Gass syndrome).

The reasons for this unexpected observation are yet to be established. What is the effect of intracellular fluid accumulation versus large amounts of intercellular edema fluid, as in cystoid macular edema? Does edema of much longer duration have an adverse effect on visual acuity, by contrast with more acute occurrences? What kinds of anatomic alterations have an adverse effect on the visual acuity outcome? As a rule, patients whose fluorescein angiograms show extensive nonperfusion of the perifoveal capillary network, or who have a large lipid plaque in the center of the macula, will have poor visual acuity regardless of macular thickness. Are there more subtle

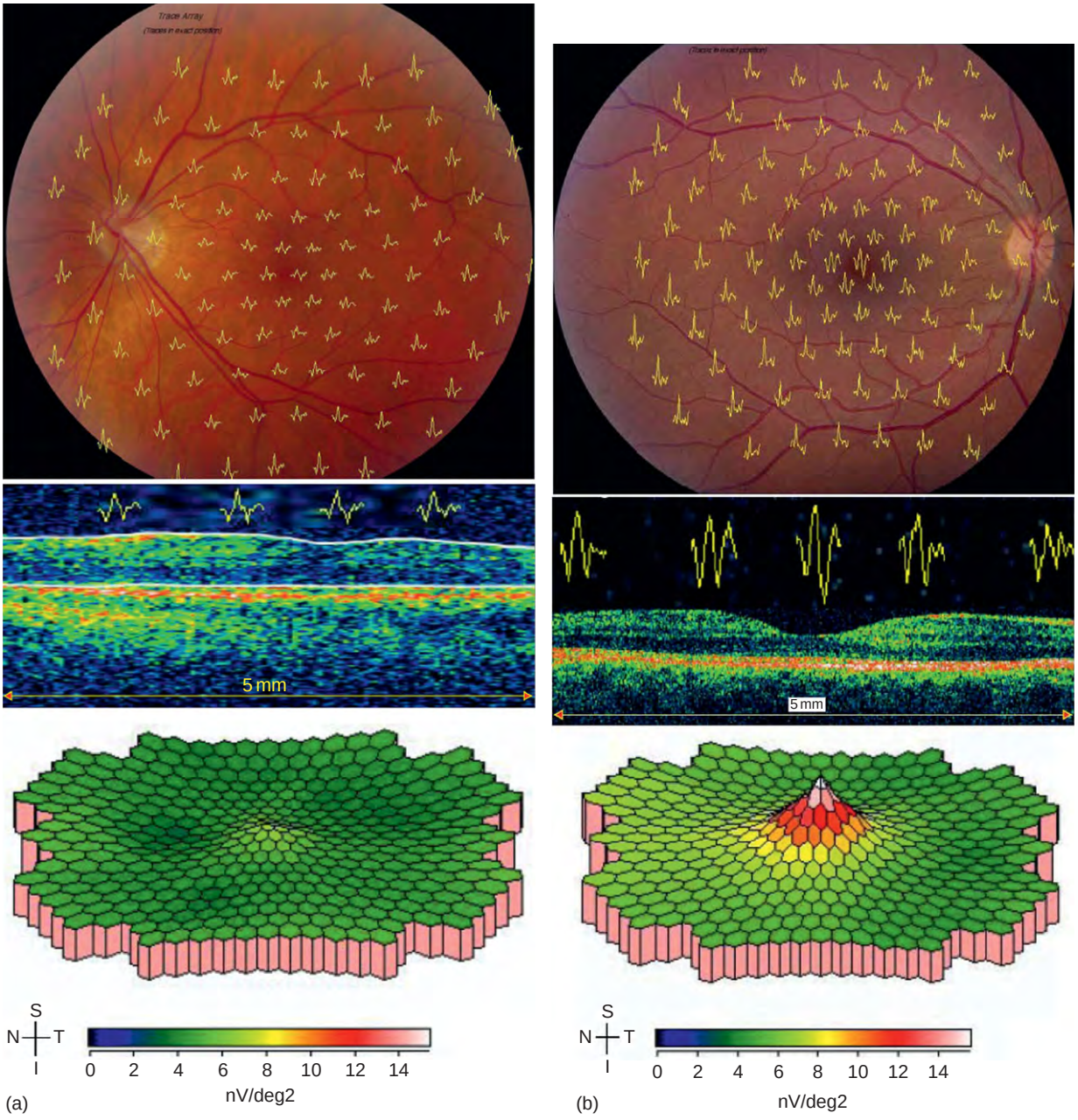

Figure 7 Multifocal electroretinogram (mfERG) traces of (a) A patient with diffuse macular edema and (b) a normal subject. In both figures, the mfERG traces are placed overlying a digital photograph of the individual's posterior retina, such that the site of the mfERG trace corresponds to its anatomic location. Note the diminution of the amplitudes and widening of the traces, indicating a prolongation of the latencies (implicit times) of the electrophysiologic responses to the light stimulus, in the retina with macular edema compared to the normal. Underneath the fundus images are placed time domain OCT scans of the normal and edematous retinas taken in the 180° meridian with overlying, corresponding mfERG responses. At the bottom of each figure is a three-dimensional pseudocolor map of mfERG P1 amplitudes (corresponding to the positive b-wave of a full-field ERG).

anatomic changes that can be detected by newer, high-resolution OCT methods (**Figures 1(c), 2(c)**, and **5(b) and (c)**; compare with **Figure 4(b)**)? Are there aberrations in photoreceptor structure or orientation that can be detected by high-resolution OCT, or by adaptive optics techniques? What prognostic information can be obtained by electrophysiologic methods such as the multifocal electroretinogram (**Figure 7**), that can detect functional alterations in very small regions of the macula? These and other questions remain subjects for investigation in the study of macular edema.

See also: Adaptive Optics; Blood–Retinal Barrier; Breakdown of the Blood–Retinal Barrier; Optical Coherence Tomography.

Further Reading

Aiello, L. P., Avery, R. L., Arrigg, P. G., et al. (1994). Vascular endothelial growth factor in ocular fluid of patients with diabetic retinopathy and other retinal disorders. *New England Journal of Medicine* 331: 1480–1487.

Al-Kateb, H., Mirea, L., Xie, X., et al. (2007). Multiple variants in vascular endothelial growth factor (VEGFA) are risk factors for time to severe retinopathy in type 1 diabetes: The DCCT/EDIC genetics study. *Diabetes* 56: 2161–2168.

Bearse, M. A., Jr., Adams, A. J., Han, Y., et al. (2006). A multifocal electroretinogram model predicting the development of diabetic retinopathy. *Progress in Retinal and Eye Research* 25: 425–448.

Diabetic Retinopathy Clinical Research Network (2008). A randomized trial comparing intravitreal triamcinolone acetonide and focal/grid photocoagulation for diabetic macular edema. *Ophthalmology* 115: 1447–1449.

Diabetic Retinopathy Clinical Research Network, Scott, I. U., Edwards, A. R., et al. (2007). A phase II randomized clinical trial of intravitreal bevacizumab for diabetic macular edema. *Ophthalmology* 114: 1860–1867.

Drexler, W. and Fujimoto, J. G. (2008). State-of-the-art retinal optical coherence tomography. *Progress in Retinal and Eye Research* 27(1): 45–88.

Early Treatment Diabetic Retinopathy Study Research Group (1985). Photocoagulation for diabetic macular edema, Early Treatment Diabetic Retinopathy Study Report No. 1. *Archives of Ophthalmology* 103: 1796–1806.

Frank, R. N. (2004). Medical progress: Diabetic retinopathy. *New England Journal of Medicine* 350: 48–58.

Frank, R. N. (2006). Etiologic mechanisms in diabetic retinopathy. In: Ryan, S. J., Schachat, A. P., Wilkinson, C. P., and Hinton, D. (eds.) *Retina,* 4th edn., ch. 66, pp. 1240–1270. London: Elsevier.

Gao, B. B., Clermont, A., Rook, S., et al. (2007). Extracellular carbonic anhydrase mediates hemorrhagic retinal and cerebral vascular permeability through prekallikrein activation. *Nature Medicine* 13: 181–188.

Gass, J. D. and Norton, E. W. (1966). Cystoid macular edema and papilledema following cataract extraction. A fluorescein fundoscopic and angiographic study. *Archives of Ophthalmology* 76: 646–661.

Huang, D., Swanson, E. A., Lin, C. P., et al. (1991). Optical coherence tomography. *Science* 254: 1178–1181.

Jampol, L. M., Sanders, D. R., and Kraff, M. C. (1984). Prophylaxis and therapy of aphakic cystoid macular edema. *Survey of Ophthalmology* 28(supplement): 535–539.

Schuman, J. S., Puliafito, C. A., and Fujimoto, J. G. (2004). *Optical Coherence Tomography of Ocular Diseases*, 2nd edn. Thorofare, NJ: Slack.

Tezel, T. H., Del Priore, L. V., Flowers, B. E., et al. (1996). Correlation between scanning laser ophthalmoscope microperimetry and anatomic abnormalities in patients with subfoveal neovascularization. *Ophthalmology* 103: 1829–1836.

The SCORE Study Research Group (2009). A randomized trial comparing the efficacy and safety of intravitreal triamcinolone with observation to treat vision loss associated with macular edema secondary to central retinal vein occlusion. The Standard Care vs Corticosteroid for Retinal Vein Occlusion (SCORE) Study Report 5. *Archives of Ophthalmology* 127: 1101–1114.

The SCORE Study Research Group (2009). A randomized trial comparing the efficacy and safety of intravitreal triamcinolone with standard care to treat vision loss associated with macular edema secondary to branch retinal vein occlusion. The Standard Care vs Corticosteroid for Retinal Vein Occlusion (SCORE) Study Report 6. *Archives of Ophthalmology* 127: 1115–1128.

Wojtkowski, M., Srinivasan, V., Fujimoto, J. G., et al. (2005). Three-dimensional retinal imaging with high-speed ultrahigh-resolution optical coherence tomography. *Ophthalmology* 112: 1734–1746.

Meibomian Glands and Lipid Layer

T J Millar, P Mudgil, and S Khanal, University of Western Sydney, NSW, Australia

Glossary

Acinus – A gland that is shaped like a hollow sphere with the gland cells lining the sphere and secreting into the center of the sphere. The secretions are removed from the center of the sphere by a duct.
HMG-CoA – The 3-hydroxy-3-methyl-glutaryl-coenzyme A is a precursor molecule for lipid synthesis with the small precursor molecule attached to a carrier molecule, coenzyme A.
Holocrine – A mechanism of secretion by a gland wherein the whole gland cell is secreted.
Hydrophilic – A substance that dissolves readily in water (water loving).
Hydrophobic – A substance that does not like water. Fats, lipids, and oils are common hydrophobic substances.
mN m^{-1}(millinewtons per meter) – A unit used for measuring surface pressure relative to that of water which is regarded as 0 mN m^{-1}.
Osmolarity – A measure of the number of individual molecules dissolved in water. It is important to cells because water can pass readily through a cell membrane, but the dissolved chemicals in the cytoplasm cannot. Hence, a cell will either take on water or release water depending upon whether its osmolarity is more (hyperosmolar) or less (hypoosmolar) than its environment, respectively.
Refractive index – When light travels from one medium to another, for example, from air into water, it is bent. The refractive index is a measure of the extent to which the light is bent and is a constant for a particular substance.
Tarsal plate – A sheet of fibrous cartilage in the eyelids of mammals that gives the eyelids their stiffness and shape.

Overview

Meibomian glands are a series of fat (lipid)-producing glands found in the upper and lower eyelids of mammals, named after a German anatomist, Heinrich Meibom (1638–1700), who recorded their presence in *De Vasis Palpebrarum Novis Epistola* (1666). In humans, there are 30–40 evenly spread glands in the upper lid and 20–30 in the lower lid (**Figure 1**). Each gland is aligned vertically in the eyelid and located within the tarsal plate (a sheet of fibrous cartilage that gives the eyelids their stiffness and shape) which lies closer to the ocular surface than the dermal surface. Structurally, meibomian glands have a central tubular duct surrounded by grape-like acini (glands). The duct is blind at one end and the other end opens onto the eyelid margin. By everting the lower eyelid, the openings can be readily seen as a row of small dots behind the eyelashes (**Figure 2**).

Phylogenetically, meibomian glands are present in marsupials, but are absent in the two monotremes (echidna, *Tachyglossus aculeatus*; platypus, *Ornithorhynchus anatinus*) that we have studied. They are not present in reptiles or birds. It is believed that many of these animals use a different gland, the harderian gland, to secrete lipids onto the ocular surface. While the distribution and appearance of meibomian glands in other mammals are generally similar to those of humans, this is not always the case. Some species of voles and musk rats have few glands, for example, *Microtus pinetorum*, which has only two large glands in the upper eyelid – one at the medial canthus and the other at the lateral canthus. Whales have neither meibomian glands nor a tarsal plate in the eyelid. Dolphins and sea lions have a very oily secretion in their tears, but this is thought to originate from the harderian gland. Currently, the literature is not clear about the presence or absence of meibomian glands in sea-dwelling mammals. However, it is of interest to note that dolphins, sea lions, and sea otters have no eyelashes (or eyebrows), which means that they also lack the other major sebaceous glands in the eyelid, for example, the glands of Zeis which are the sebaceous glands of the eyelashes.

The major function of the meibomian gland is to supply the main components of the outer layer of the tear film. The tear film is a thin (7–10 μm thick), watery fluid that covers the exposed surface of our eyes (**Figure 3**). Lipids from the meibomian glands are secreted onto the inner margin of the eyelids where they contact and then spread over the aqueous part of the tear film to form a covering layer (~90 nm thick) in contact with the air. This layer is referred to as the lipid layer of the tear film. It is believed to decrease evaporation from the tear film and hence prevent dry eyes. However, this role for the meibomian lipids is by no means certain, and it is likely that it has other roles such as preventing tears from flowing onto the skin and skin lipids from flowing onto the ocular surface, assisting the spread of the tear film over the eye by lowering the surface tension, and forming a watertight seal when the lids are closed. The Meibomian lipids provide a smooth and

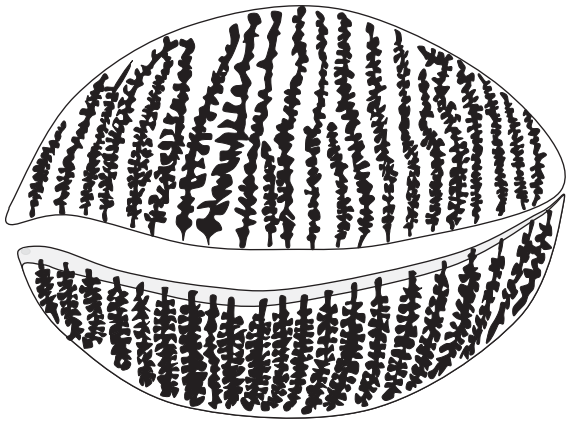

Figure 1 Arrangement of the meibomian glands in the upper and lower eyelids.

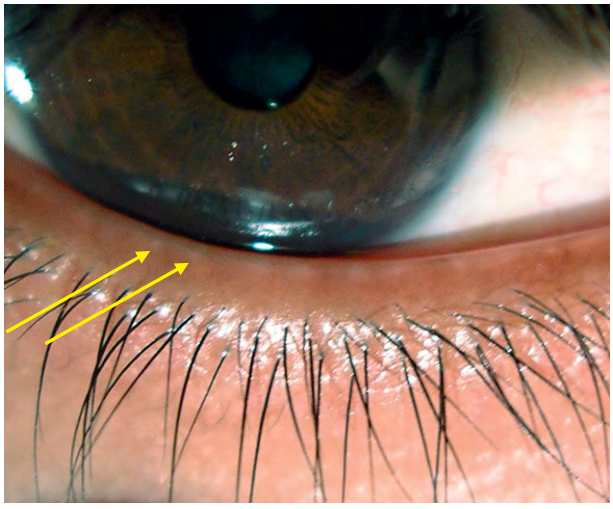

Figure 2 Meibomian gland orifices (arrows) in the lower lid margin.

highly refractive (1.4766 at 589 nm and 35°C) surface. Clinically, a mechanism for measuring tear breakup time (TBUT) is to observe changes to interference colors of the surface layer of the tear film. This can be used as one measure of the tear film performance.

The Lipid Layer of the Tear Film

The lipid layer of the tear film provides an optically smooth surface at the interface between the air and the aqueous part of the tear film. Although the structure of this layer has not been determined, the meibomian lipids form a major component (**Figure 3**). A useful model of the lipid layer, based on the idea that only lipids are present, was developed by McCulley and Shine. The model is presented as a crystalline array, and, while very useful for developing understanding, the lipid layer is unlikely to be crystalline in practice. This model proposed that the wax esters, steryl esters, triglycerides, and hydrocarbons (hydrophobic lipids) from the meibomian glands reside in the outermost layers and are linked to the aqueous subphase by polar lipids (phospholipids, free cholesterol, and free fatty acids). Some of these polar lipids may arise from the aqueous layer of the tear film and others from meibomian lipids and hydrolysis (cleavage) of the wax esters, steryl esters, and triglycerides. These polar lipids have a hydrophobic part which interacts with the hydrophobic lipids and a hydrophilic part that is able to interact with water (the aqueous layer). Assuming that the outer layer of the tear film is entirely made from lipids implies that the interfacial molecules (surfactants) must be polar lipids.

An alternate model proposing that proteins and mucins also contribute to this layer is more realistic. Strong evidence comes from surface tension measurements. It has been found that the surface tension of tears is 42–46 mN m^{-1} and this can only be achieved by a mixture of lipids and proteins and not with meibomian lipids alone. The interaction of meibomian lipids with tear proteins is often cautiously presented as lipids occupying the outer surface of the lipid layer, and the inner surface interacting with proteins from the aqueous layer. A more recent model includes proteins and mucins as integrated parts of this layer (**Figure 3**). Although there has been a focus on lipocalin, an abundant lipid-binding protein in tears, being the main tear protein interacting with the meibomian lipids, lysozyme and lactoferrin may be more involved. Lipocalin is thought to scavenge lipids that have adhered to the epithelial cells of the ocular surface and lipids that are in the aqueous layer. Although it has been claimed that these are then transported to the outer lipid layer, this may not be the case. Once a lipid is bound into the central pocket of lipocalin, lipocalin is in a low-energy state and unlikely to interact with the meibomian lipids at the outer surface of the tear film.

The presence of proteins in the lipid layer has important conceptual implications because they are large molecules with complex mixtures of hydrophobic, hydrophilic, and distinctly charged components. These properties mean that they can unfold and form a range of shapes according to their local molecular environment. Due to this unfolding, it is possible for them to extend across the lipid layer and interact with the hydrophobic lipids and other proteins. As the model suggests, this means that the layer comprises a complex mixture of islands of proteins, islands of lipids, islands of mucins, and various mixtures of these (**Figure 3**). This model is more akin to models for cell membranes and for lung surfactant. Some advantages of this model are that: the outer layer would be a noncollapsible viscoelastic gel; it would allow for the lowest free energy states of the proteins in contact with lipids; and the changes in salt concentrations in the tears

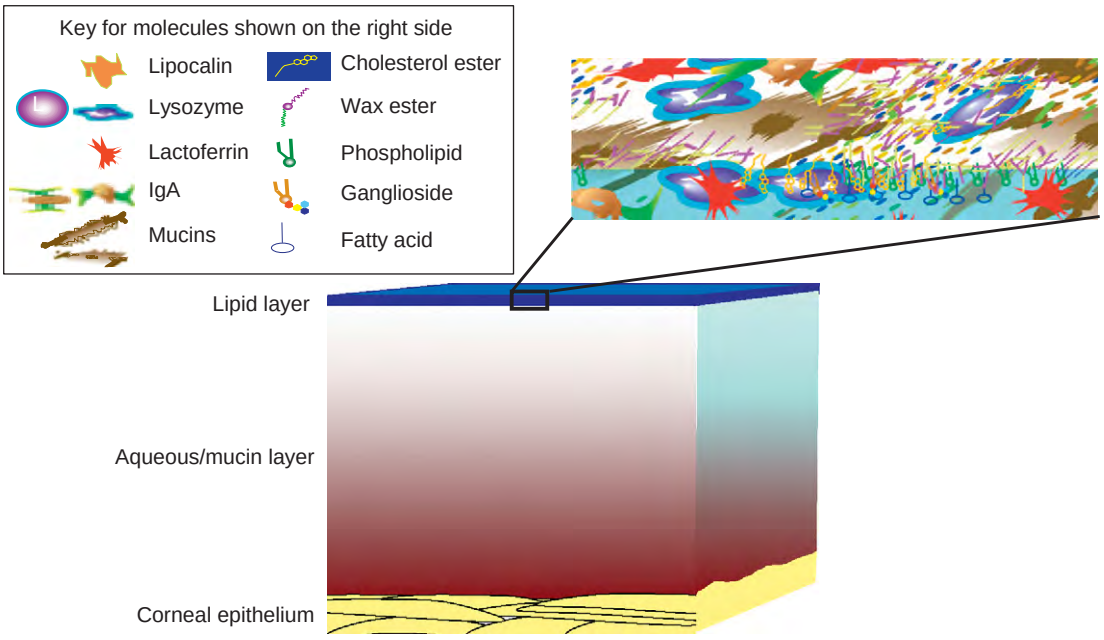

Figure 3 Tear film comprising an outer lipid layer covering an aqueous/mucin layer. The exploded view of the lipid layer shows a mixture of different lipids and denatured proteins (see key).

(e.g., hyperosmolarity) would affect the ability of the proteins to unfold and interact with lipids in the outer layer. Taking these one at a time, the lipid-only model needs some mechanism to spread the lipids over the aqueous surface after a blink. Both phospholipids and mucins have been proposed as enabling this by spreading slightly ahead of the hydrophobic lipids, and this concept also means that a new lipid layer is formed at each blink. Lack of change over a number of blinks to the interference patterns formed by the outer layer of the tear film does not support this concept. However, a noncollapsible viscoelastic gel that would be formed with proteins and mucins in the layer obviates the need for spreading and would account for the consistent interference pattern over a number of blinks. Furthermore, in other fields of study, mixtures of molecules in a liquid environment autoassemble into states of lowest free energy, which means that when lipids and proteins are placed together, they will mix at the molecular level rather than remain separate as the lipid-only model suggests. Some of the proteins can act as the surfactants, meaning that while phospholipids may co-jointly serve as surfactants, they are not absolutely necessary. It has also been found that while lipids alone are not capable of lowering the surface tension to the levels found in tears, mixtures of tear proteins and tear lipids possess that ability. Hyperosmolarity of the tears has the strongest correlation with a dry eye. Salt concentrations have strong effects on how proteins fold; therefore, it is possible that high salt concentrations would affect the folding of proteins and hence their ability to interact with the lipid layer to form a stable outer layer. In turn, this could affect the surface tension and spreading of the outer layer and, consequently, its protective function.

Meibomian Glands

Anatomy and Histology

There are no anatomical differences in the meibomian glands of human males and females. The ducts in humans are approximately 1.6 mm long with the central ducts being slightly longer than the nasal and temporal ducts, and are surrounded by a dense banding of elastic fibers. The ducts are lined by keratinized epithelium and lie nearly 780 µm from the dermal surface of the eyelid. A horny cell layer overlies one or two layers of intermediate cells that rest on cuboidal basal cells connected to a basement membrane, and there is no difference in this appearance between the proximal and distal portions of the duct (**Figure 4**). Acini are arranged circularly around the central duct and are connected to it by short ductules. The acinar cells are distinct from the ductal cells with no keratohyaline granules or lamellar bodies in the acinar cells, and no lipid vesicles in the ductal cells. The acinar cells continually differentiate into holocrine-secreting cells from basal acinar cells. They contain an abundance of smooth endoplasmic reticulum that surrounds the lipid vesicles. These cells also develop from the division of basal cells and move toward the center of the acinus (migration rate of 0.62 µm d^{-1} in rats), and slowly increase in neutral lipid content and in the size of the lipid-containing vesicles. The acinar cells die and gradually breakdown, leaving a

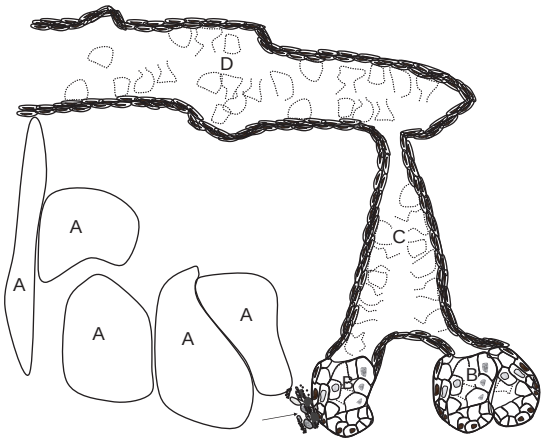

Figure 4 An illustration of meibomian glands and duct. A: Ghosts of acini not filled in with detail. B: Acini showing nucleated basal cells around the periphery which gradually lose their nuclei as they mature and move to the center of the acinus. C: Secondary duct surrounded by ductal cells (stratified epithelium) containing meibomian secretion and cell remnants. D: Main duct surrounded by ductal cells containing meibomian secretion and cell remnants. The arrow shows a bundle of nerve endings close to the acinus but separated by collagen fibers.

lipid mass that is secreted via the duct. In rats, it takes close to 9 days for a cell to migrate to the center of the acinus, and it probably divides twice during this time.

Surrounding the glands is a distinct extracellular matrix comprising collagen types I, II, and IV, aggrecan, dermatan sulfate, and chondroitin-6-sulfate. Close to the acini are numerous unmyelinated varicose nerve fibers with boutons in contact with collagen fibers within the basal lamina of the basal acinar cells. These are mainly parasympathetic fibers which contain the neurotransmitter, acetylcholine, and the neuropeptide vasoactive intestinal polypeptide. The cell bodies for these fibers lie in the pterygopalatine ganglion and their fibers reach the eyelid by the greater petrosal nerve. Preganglionic neurons are ipsilateral and cholinergic, and lie in the superior salivary nucleus located lateral, dorsal, and caudal to the superior olive and lateral, dorsal, and rostral to the facial nucleus. Sympathetic innervation is sparse and mainly associated with blood vessels. Sensory nerve fibers are also sparsely distributed close to the basal region of acini, and these are immunoreactive for the neuropeptides substance P and calcitonin gene-related peptide.

Development

Meibomian glands in humans develop as small, solid epithelial invaginations from the ocular face of the eyelid margin at approximately 9 weeks of development (crown-rump length of 40 mm). By 12 weeks (60 mm), the epithelial growth has extended the depth of the tarsal plate and has a central tube that was formed from apoptosis of the central epithelial cells. At 15 weeks (100 mm), cuboidal secretory cells line the ducts. The upper and lower eyelids are fused during this whole process. At 7.5 months (250 mm), after the eyelids have separated, acini are present, epithelial cells plugging the meibomian gland orifices disintegrate, and secretion begins just prior to birth. A similar process takes place in the mouse; however, in this case, the eyelids are still fused at birth, which is also the time when the first signs of meibomian gland development show, again from the eyelid margin. In contrast to meibomian gland development, eyelashes in humans begin development earlier at 8 weeks (35 mm) as solid epithelial invaginations from the external face of the eyelid margin.

Composition of Meibomian Lipids

The meibomian gland is often referred to as a modified sebaceous gland. In this case, the term sebaceous means lipid producing rather than sebum producing because the composition of the lipids differs from those produced by the sebaceous glands of hair follicles. The main lipid types produced by meibomian glands are wax and steryl esters (60–70%) which are very hydrophobic (dislike water). Wax esters are formed by linking a long-chain carboxylic acid (fatty acid) to a long-chain alcohol (fatty alcohol). Since different fatty acids and fatty alcohols are linked together, the wax esters are a complex family of lipids and their detailed structure varies between species. In humans, oleic acid is the most prevalent fatty acid found in these waxes. Similarly, the steryl esters are mainly cholesterol esters which are formed by linking cholesterol to a long-chain fatty acid. These fatty acids are generally longer than those found in the wax esters. Small amounts of other lipids (mainly polar) – such as mono-, di-, and triglycerides; fatty acids; fatty alcohols; free cholesterol; and phospholipids – make up the remainder. While phospholipids are readily detected in meibomian lipids of rabbits, there is contention as to whether they are a component of human meibomian lipids. This is important because in models of the lipid layer of the tear film, phospholipids are crucial as a link between the hydrophobic molecules (wax and cholesterol esters) and the aqueous layer. If they are not present in the meibomian lipids, then they must be derived from elsewhere, such as the aqueous layer of the tear film, or alternative surfactants need to be present in the model. The nature and mixture of the lipids give them a melting range of 19–33 °C, which means that they are fluid on the ocular surface.

Meibomian Lipid Turnover and Synthesis

Since the meibomian gland is a holocrine gland, lipid turnover is related to the cell turnover rate and the lipids are synthesized by the glands rather than being adsorbed from the bloodstream. For instance, the levels of

cholesterol found in meibomian lipids are independent of cholesterol levels in the blood. Synthesis of the straight-chain fatty acids is typical of elsewhere in the body, occurring in the cytoplasm using acetyl-coenzyme A (CoA) and malonyl-CoA as the starting molecules and fatty acid synthase as the major enzyme. Some of the fatty acids have branching and, at least in rabbits, the branched carbon chains are derived mainly from the amino acids valine and isoleucine. The acyltransferases seem to be nonselective and will connect any fatty acid to a fatty alcohol. Similarly, cholesterol synthesis is typical of other tissues converting β-hydroxy-β-methylglutaryl-CoA to mevalonate, isoprene, squalene, and cholesterol. The acylcholesterol transferase, involved with cholesterol ester synthesis, appears to be selective for longer-chain fatty acids based on the predominance of long-chain fatty acids in cholesterol esters.

The meibomian acinar cells have nuclear androgen receptors and the level of androgens or, more likely, the ratio between androgens and estrogens is critical for controlling lipid synthesis in the meibomian glands. Stimulating androgen receptors increases gene transcription in enzymes associated with fatty acid and cholesterol synthetic pathways (adenosine triphosphate (ATP)-citrate lyase, acetyl-CoA synthase, acetoacetyl-CoA synthase, 3-hydroxy-3-methyl-glutary (HMG)-CoA synthase 1, HMG-CoA reductase, acetyl-CoA carboxylase, glyceraldehyde-3-phosphate dehydrogenase, and sterol regulatory element-binding protein 1 and 2) and hence stimulates lipid production. Androgen deficiency has been associated with meibomian gland dysfunction (MGD) and dry eye. $P2Y_2$ receptor gene expression has also been detected in meibomian gland acini. This suggests that extracellular ATP or UTP might influence lipid synthesis or composition through activation of G proteins. Specific changes to lipid composition through this pathway have not been investigated.

The total amount of meibomian lipids on the lid margins has been estimated and children under 14 years of age showed the lowest levels ($1.5\,\mu g\,mm^{-2}$ lid margin). After puberty, there is a steady increment with age until the late 60s ($3.26\,\mu g\,mm^{-2}$) and throughout this period, males have nearly 10% greater levels than females. Given that one of the reasons for dry eye is insufficient meibomian lipid secretion and that there is an increase in the incidence of dry eye with age, it is surprising that the lowest levels of meibomian lipids have been found in children. Morning and afternoon basal levels are the same and there is no correlation between lid temperature (30–34 °C) and basal levels of meibomian lipids. However, deliberately increasing the eyelid temperature from 33 to 37 °C increases the lipid values on the lid margin by close to 25%. Despite the presence of parasympathetic nerves around the acini, lipid secretion is most likely due to the mechanical force of blinking which causes compression of the territorial fibrocartilaginous matrix that surrounds the meibomian glands. This has been shown by measuring the reappearance of lipids on the eyelid margin after cleaning with an organic solvent. No lipids appear until a blink occurs (3 min was the longest). After approximately 10 blinks, the levels return to nearly a third of their basal levels. It is estimated that close to 10 μg of lipids are delivered per blink and that there is approximately 20–40 times excess basal amount of lipids available on the eyelid margin than what is required for forming a complete lipid layer on the tear film.

How the lipids are removed from the eye is uncertain. It is believed that most of them flow over the eyelid margin onto the skin and eyelashes. This constant flow prevents the skin lipids from contaminating the tear film. It has been shown that skin lipids disrupt the tear film. Some lipids are likely to bind to proteins of the aqueous layer, particularly lipocalin, and are removed with the aqueous layer through the lacrimal ducts. The crusty buildup that collects in the corner of the eye during sleep is primarily a mixture of lipids and mucins and thus another mechanism for removing lipids from the ocular surface.

Pathology of the Meibomian Gland

Disorders of the meibomian glands are manifest by the obstruction of the gland orifices, inflammation, or loss of the glands. This is often associated with one or more of the following: thickening of the lid margin, exaggerated vascularization around the gland orifices, and hyperkeratinization. Meibomian gland diseases are usually more uncomfortable rather than painful and, when chronic, are associated with dry eye which can be very painful. Absence or deficiency of meibomian glands is often congenital.

Clinically, the state of meibomian glands is determined by examining their morphology and function. In eye clinics, the orifices of the glands lining both the upper and lower eyelids are observed through a slit lamp biomicroscope. If a gland is blocked, the orifice appears swollen on the lid margin. Some practitioners also squeeze the lower eyelid gently to expel meibomian lipids. A clear fluid is considered to be normal, whereas a thick, yellowy secretion is an indication of meibomian gland disorder. If excessive pressure is applied, a thick pasty expression can be obtained from people with normal meibomian gland function (**Figure 5**). This technique is used for obtaining meibomian lipids for experimental purposes or for analysis. In research settings, more specific tests are performed to assess meibomian gland function. Transillumination of the lower eyelids is widely used to evaluate the morphology of the glands. In particular, shorter-than-normal meibomian glands and meibomian gland dropout are strong indications of MGD (**Figure 6**). Changes to the shape and form of the glands do not occur with aging,

although expression of secretion is commonly more difficult. A clear, noninvasive view of meibomian glands can be achieved by using infrared light, but the need for specialized equipment means that this technique is only used in a few research laboratories.

Rather than examine the meibomian glands themselves, observation of the lipid layer of the tear film is regarded as an indirect measure of both the quantity and the quality of meibomian gland secretions. Using specialized interferometry, the lipid layer stability, distribution, dynamics, and thickness can be assessed. Generally, a thick amorphous layer is an indication of high-quality meibomian oil secretions and, hence, excellent meibomian gland function. Such a layer is also commonly associated with longer TBUTs, presumably because of the lowered surface tension. The results obtained from tear breakup tests have been shown to be comparable to interferometry findings, although a cause–effect relationship between the two is yet to be established.

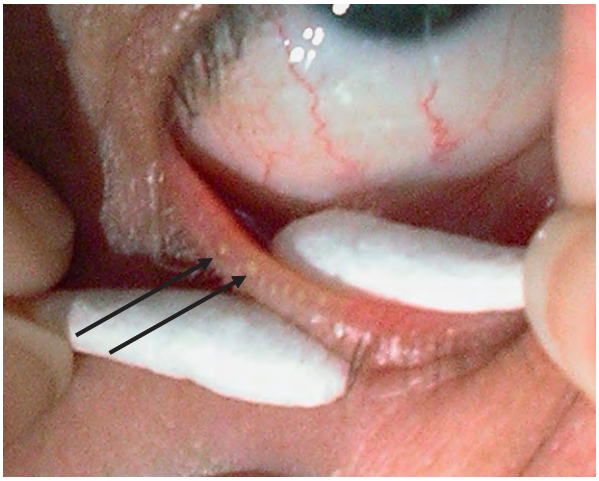

Figure 5 Hard squeezing of meibomian glands. The secretions are indicated by arrows.

Another method for evaluating meibomian gland function indirectly is to measure evaporation from the ocular surface. This is a difficult technique and is normally confined to research settings. Evaporimetry is based on the theory that evaporation from the ocular surface is normally minimal due to the well-spread lipid layer acting as a blanket, and that an inadequate lipid layer or disruption to this lipid layer causes tear evaporation to increase. It is thought to be the cause of evaporative dry eye. However, this idea has been difficult to substantiate and a wide variability in tear evaporation rates has been reported irrespective of the presence or absence of dry eye and, more importantly, the appearance of the lipid layer. Further, a large quantity of lipid on the tear surface does not necessarily correlate with an adequate barrier to evaporation. Evaporative dry eye can occur with an excessively thick lipid layer. Current areas of research center on whether the biochemical composition of the meibomian lipids can influence their surface activity and ability to diminish evaporation, but clear outcomes are still in the future.

Chronic Blepharitis

The term blepharitis has different meanings depending upon the user. Acute blepharitis (normally just called blepharitis) is an infection of the anterior eyelid and *Staphylococcus epidermidis* or *Staphylococcus aureus* are the most likely cause. Chronic blepharitis is caused by dysfunction of the meibomian glands and is synonymous with

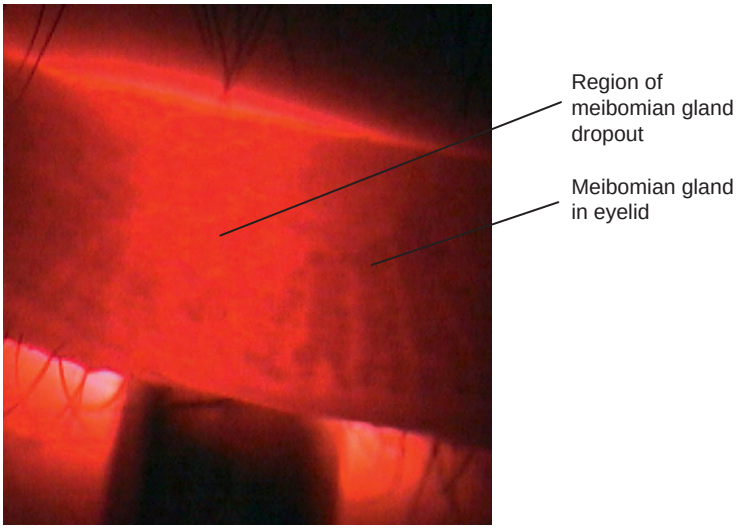

Figure 6 The transillumination of eyelid showing the dark meibomian gland acini. There is meibomian gland dropout in the middle region of the lid. Courtesy of Jerry Paugh, Southern California College of Optometry.

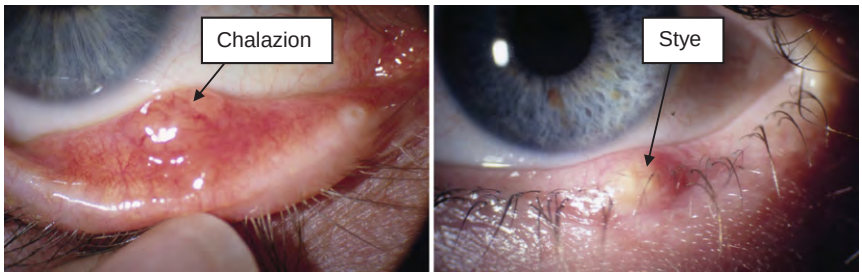

Figure 7 A chalazion appears as a swelling deep within the eyelid. A stye is associated with the eyelashes (infection of the eyelash follicle). Courtesy of Rob Terry, Institute of Eye Research, University of New South Wales.

MGD and posterior blepharitis. Many studies have looked at the association between blepharitis or chronic blepharitis and dry eye. However, the conclusions drawn about the association depend on the definitions being used in the study. Although MGD occurs in nearly three-quarters of patients with chronic blepharitis, it also occurs in approximately 20% of people with normal tear function. In MGD, the orifices of the meibomian glands are blocked, reducing the secretion of meibomian lipids onto the ocular surface. Regular warm compresses help to open the orifices and allow normal lipid secretion. Some patients with chronic blepharitis have similar symptoms to those of dry eye and are prescribed tear lubricants for palliative purposes, that is, they do not resolve the blepharitis.

Chalazion

The blockage of the meibomian glands can lead to formation of a chalazion (**Figure 7**). This is a cyst on the eyelid that is normally sterile and composed of a lipid granuloma. It looks similar to a stye, which is caused by an infected sebaceous gland of the eyelash, but can be easily distinguished clinically because a chalazion is painless and develops gradually, whereas a stye is always painful and forms over a few days. For both conditions, warm compresses are recommended. In extreme cases of chalazion, it is surgically incised and the granulomatous material is removed by curettage. Antibiotics are often prescribed to treat a stye.

Surgical Damage

Treatment of trachoma is a common cause for surgical damage to the meibomian gland. Trachoma, a leading cause of blindness, is an infectious disease of the palpebral conjunctiva that leads to the eyelids folding inward (entropion), causing the lashes to rub against the cornea. The lids, and hence the meibomian glands and ducts, are cut to relieve this condition. It is yet to be determined whether this compromises the functionality of the outer lipid layer of the tear film. Other surgical procedures such as correction of lid malpositioning, particularly ptosis (drooping of the upper eyelid) and genetic entropion, can also sometimes require the cutting of the meibomian glands.

Contact Lenses and the Lipid Layer

Anomalies of the lipid layer, in themselves, are not a deterrent for contact lens wear. Lipids or proteins or both are deposited on contact lenses during wear. These deposits can block the small pores of the contact lenses, which are essential for the passage of air to the cornea for its metabolism. It is impossible to ascertain beforehand how long a contact lens needs to be worn for it to be unsuitable for an individual as the amount and pattern of lipid deposition depends on the composition of the ocular lipids, which can vary between people, and the specific material the lens is made from. Contact lens cleaning agents are designed for the specific type of contact lens and normally contain a surface active agent that removes lipid deposits.

See also: Dry Eye: An Immune-Based Inflammation; Ocular Mucins; Tear Film; Tear Film Overview.

Further Reading

Bron, A. J., Benjamin, L., and Snibson, G. R. (1991). Meibomian gland disease, classification and grading of lid changes. *Eye* 5: 395–411.

Bron, A. J., Tiffany, J. M., Gouveia, S. M., Yokoi, N., and Voon, L. W. (2004). Functional aspects of the tear film lipid layer. *Experimental Eye Research* 78: 347–360.

Butovich, I. A., Millar, T. J., and Ham, B. M. (2008). Understanding and analysing Meibomian lipids – a review. *Current Eye Research* 33: 405–420.

Glasgow, B. J., Marshall, G., Gasymov, O. K., et al. (1999). Tear lipocalins: Potential scavengers for the corneal surface. *Investigative Ophthalmology and Visual Science* 40: 3100–3107.

Goto, E. and Tseng, S. C. G. (2005). Kinetic analysis of tear interference images in aqueous tear deficiency dry eye before and after punctual occlusion. *Investigative Ophthalmology and Visual Science* 44: 1897–1905.

Gouveia, S. M. and Tiffany, J. M. (2005). Human tear viscosity: An interactive role for proteins and lipids. *Biochimica et Biophysica Acta* 1753: 155–163.

Holly, F. J. (1973). Formation and rupture of the tear film. *Experimental Eye Research* 15: 515–525.

Hykin, P. G. and Bron, A. J. (1992). Age related morphological changes in lid margin and Meibomian gland anatomy. *Cornea* 11: 334–342.

Jester, J. V., Nicolaides, N., and Smith, R. E. (1981). Meibomian gland studies: Histologic and ultrastructural investigations. *Investigative Ophthalmology and Visual Science* 20: 537–547.

Mathers, W. (2004). Evaporation from the ocular surface. *Experimental Eye Research* 78: 389–394.

McCulley, J. P. and Shine, W. (1997). A compositional based model for the tear film lipid layer. *Transactions of the American Ophthalmological Society* 55: 79–93.

Millar, T. J., Tragoulias, S. T., Anderton, P. J., et al. (2006). The surface activity of purified ocular mucin at the air–liquid interface and interactions with meibomian lipids. *Cornea* 25: 91–100.

Nagyova, B. and Tiffany, J. M. (1999). Components responsible for the surface tension of human tears. *Current Eye Research* 19: 4–11.

Sullivan, D. A., Sullivan, B. D., Evans, J. E., et al. (2002). Androgen deficiency, Meibomian gland dysfunction, and evaporative dry eye. *Annals of the New York Academy of Science* 966: 211–222.

Tiffany, J. M. (1995). Physiological functions of the Meibomian glands. *Progress in Retinal and Eye Research* 14: 47–74.

Microvillar and Ciliary Photoreceptors in Molluskan Eyes

E Nasi and M del Pilar Gomez, Universidad Nacional de Colombia, Bogotá, Colombia

Glossary

Ciliary photoreceptors – Visual receptor cells in which the photosensitive region is derived from a cilium, a structure protruding from the cell body and characterized by the internal presence of nine longitudinal microtubules arranged in a circular fashion (and sometimes two additional microtubules in the center). Folding of the membrane of the cilium enhances its surface area to accommodate a great number of photopigment molecules.

Circumpallial nerve – Nerve that loops around the mantle of mollusks. It collects the axons from the eyes and projects to central neural ganglia of the animal.

Cyclic nucleotide-gated channels (CNG channels) – Family of ion channels that are ancestrally related to certain voltage-activated channels, but have evolved a different gating mechanism that responds to the binding of cGMP and cAMP to a site located in the intracellular side. They are responsible for generating the receptor potential in a variety of sensory cells, like olfactory neurons and many photoreceptors.

Diacylglycerol (DAG) – Product of the breakdown of phosphatidylinositol bisphosphate (PIP_2) by phospholipase C (PLC). This is the lipid moiety of the molecule and remains membrane bound. It is a prime activator of protein kinase C (PKC).

Guanylate cyclase (GC) – Enzyme responsible for generating the intracellular messenger cyclic guanosine monophosphate (cGMP), using guanosine trisphosphate (GTP) as substrate.

Inositol trisphosphate (IP_3) – Soluble, bioactive product of the breakdown of PIP_2, resulting from the cleavage of the polar head of this phospholipid. It can diffuse from the membrane to the endoplasmic reticulum (ER), where it binds to IP_3 receptors, causing them to expose a calcium-permeable pore and to release calcium contained within the endoplasmic reticulum (ER).

Microvillar photoreceptors – These are also called rhabdomeric photoreceptors. Photoreceptor cells in which the light-sensitive region presents evaginations of the cell membrane in the form of thin cylindrical protrusions, called microvilli. These are internally packed with longitudinal bundles of actin filaments that confer structural stability. The resulting increase in the surface area of the membrane makes it possible to accumulate a large population of photopigment molecules.

Phosphatidylinositol bisphosphate (PIP_2) – Minor phospholipid present in the inner leaflet of the cell membrane. Its enzymatic breakdown by phospholipase C (PLC) yields two bioactive products, namely inositol trisphosphate (IP_3) and diacylglycerol (DAG).

Phosphodiesterase (PDE) – Enzyme that cleaves a phosphodiester bond. In vertebrate photoreceptors, PDE breaks down cGMP, forming the inert compound 5′-GMP, thus leading to the closure of ion channels gated by cGMP.

Phospholipase C (PLC) – Enzyme that hydrolyzes inositol phospholipids in the membrane. A subclass, known as PLC-β, is activated by a guanine-binding protein (G-protein) of the G_q type.

Protein kinase C (PKC) – A class of enzymes capable of transferring a phosphate from an ATP molecule to a serine or threonine residue in a protein. Members of a subclass of these enzymes, known as conventional PKCs, are activated by calcium and/or diacylglycerol, two messenger molecules whose intracellular concentration increases in microvillar photoreceptors after stimulation with light.

pS, Pico-siemens (10^{-12} S) – A measurement unit of conductance. The conductance of a body is 1 S, such that upon applying 1 V across it, an electrical current of 1 A would flow.

Transient receptor potential (TRP), transient receptor potential like (TRPL) – Proteins first identified in the eyes of *Drosophila* as the ion channels subserving the late and the early phase, respectively, of the receptor potential. Genetic mutations leading to the failure to express TRP cause the receptor potential to consist of only the initial, transient phase, hence the name transient receptor potential (TRP).

Visual cells in the animal kingdom are usually partitioned into two distinct categories on the basis of the structure of the light-sensing organelle: in some photoreceptors, all the machinery necessary to absorb photons and generate a receptor potential is contained in a modified cilium; this is the case of the rods and cones in the vertebrate retina. In other cells, that function is subserved by microvilli, as it

occurs, for example, in the photoreceptors of the compound eye of insects. In both designs, the folding of the membrane greatly increases its surface area to accommodate a large number of photopigment molecules – which are integral membrane proteins – thus conferring a high optical density to the cell, making it an efficient and compact light collector.

It is generally accepted that this dichotomy also marks a sharp boundary between the design of vertebrate versus invertebrate retinae. However, the eyes of several marine mollusks, such as those of *Pecten irradians* (Figure 1) and *Lima scabra* challenge such dogma, because they possess a double retina, comprised of microvillar cells in the proximal layer, and ciliary cells in the distal layer. Because each retinal layer gives rise to a separate branch of the optic nerve, which in turn produces either ON or OFF neuronal discharges in response to light, both cell types were thought to be visual receptors. This conjecture was corroborated by intracellular recordings of light-evoked responses in the intact retina. Surprisingly, these light responses have opposite polarities: proximal cells depolarize – as all other invertebrate photoreceptors were known to do – while distal cells hyperpolarize. Because those measurements were conducted under conditions designed to hamper synaptic transmission, it was unlikely that some of the light responses may have been evoked indirectly. Lingering doubts about the coexistence of functionally and structurally different primary visual receptors were dispelled by recordings of light-dependent changes in membrane voltage and membrane current in enzymatically isolated microvillar and ciliary cells.

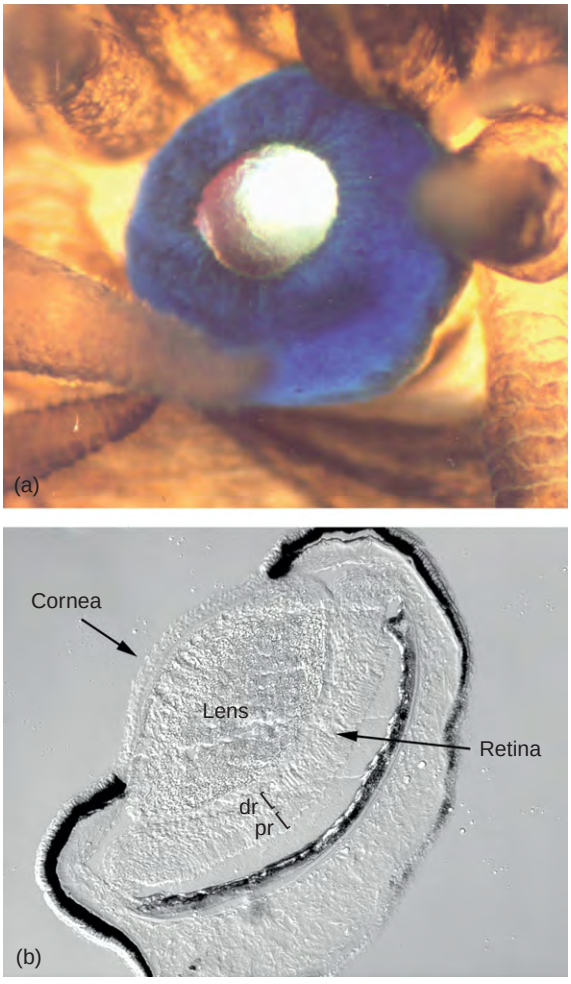

Figure 1 (a) The eye of the scallop, *Pecten irradian,* is of the simple type, possessing a single cornea and lens. The shiny appearance of the pupil is due to the presence of a reflector at the back of the eye, which helps focus light onto the retina. (b) Cryosection of a fixed eye. The retina is comprised of two separate layers, proximal (pr) and distal (dr), each giving rise to a separate branch of the optic nerve.

Microvillar (Rhabdomeric) Photoreceptors

Excitation

The basic properties of the light response in microvillar visual receptors of mollusks are generally similar to those found in other invertebrate eyes. Light produces a depolarizing receptor potential, which is due to an increase in membrane conductance. Because there are no local second-order neurons, light information must be directly encoded by action potentials (Figure 2) propagating along the axons

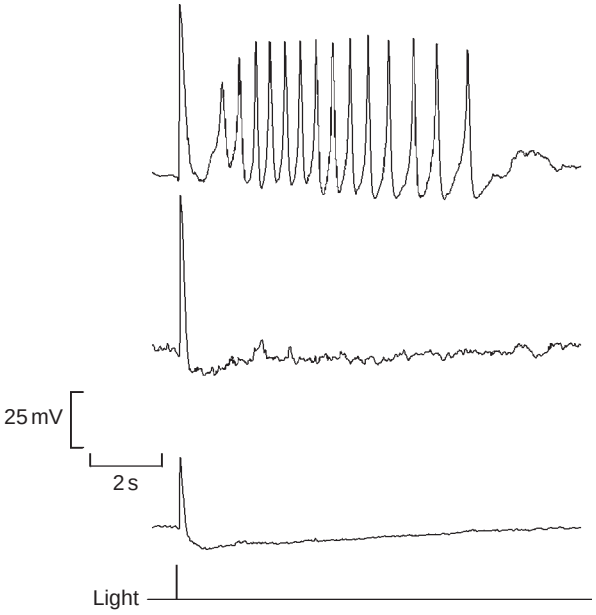

Figure 2 Current-clamp recording of the light response in an isolated microvillar photoreceptor of *Lima*. The membrane voltage was measured through a patch electrode in the whole-cell configuration. Flashes of 100-ms duration were presented, as indicated at the bottom, increasing their intensity at 0.6 log units (from bottom trace to top). A graded depolarization is evoked by light, eventually triggering one or more action potentials. The resting potential was ~–54 mV. Traces were offset vertically for clarity.

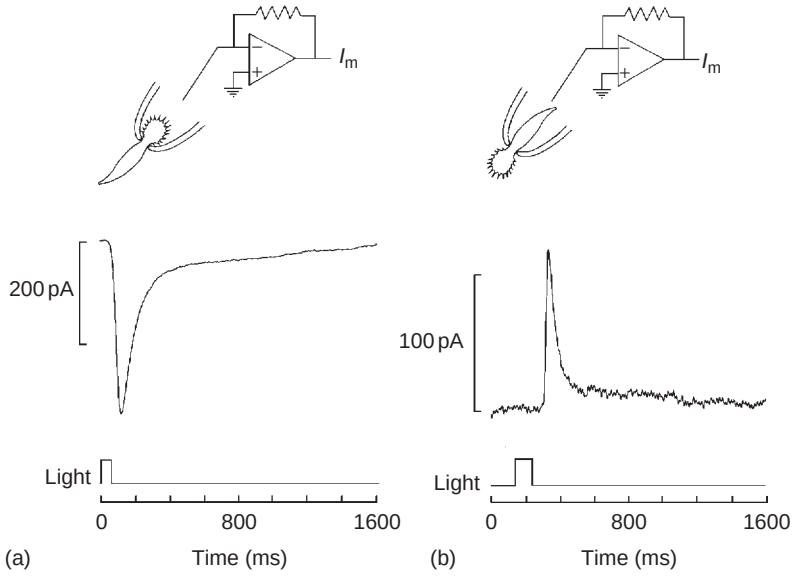

Figure 3 (a) Suction-electrode recording of light-evoked currents in isolated rhabdomeric photoreceptors of *Pecten* with the microvillar lobe inside the electrode. (b) Inverting the orientation of the cell in the pipette reverses the polarity of the recorded current. The active (inward) current is confined to the microvillar lobe of the cell.

that directly emanate from the photoreceptor cells and form the circumpallial nerve. The circumpallial nerve loops around the mantle of mollusks, collects the axons from the eyes, and projects to central neural ganglia of the animal. Voltage-dependent calcium currents contribute to the initiation of regenerative spikes, and, together with voltage- and calcium-dependent potassium currents, help shape the light response. The photocurrent is segregated to the photosensitive microvillar lobe, as clearly demonstrated by suction-electrode measurements (**Figure 3**). The light-sensitive conductance is cationic, permeable to sodium ions, and, to a lesser extent, to K (permeability ratio, p_{Na}:p_K, $\sim$ 1.8:1). Additionally, there is a small contribution of calcium ions, which, however, is quantitatively minute (<3% of the light-evoked inward current). In this respect, these cells differ from *Drosophila*, where the Ca:Na selectivity ratio of light-dependent channels may be as high as 40:1. Such discrepancy may point to the evolution of different strategies for light-triggered calcium mobilization (a phenomenon universally observed in all microvillar receptors tested to date): in *Pecten* and *Lima*, like in some other species (e.g., *Limulus*), photo-induced Ca transients are impervious to the removal of extracellular calcium and reflect release from IP_3-sensitive intracellular stores; such a scheme would have little use for a Ca influx pathway. By contrast, other photoreceptors display minimal – if any – internal release and must therefore depend essentially on Ca-permeable channels at the plasma membrane.

The photo-induced calcium transients of *Pecten* and *Lima* are very large, best monitored with low-affinity fluorescent indicators like Fluo 5F and Calcium Green 5N (K_D $\sim$ 2.3 and 14 μM, respectively; **Figure 4**); they are initiated

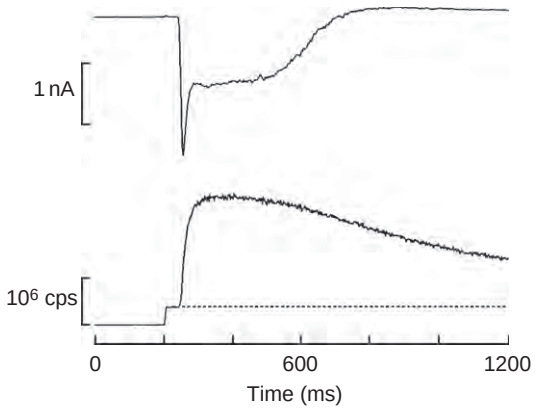

Figure 4 Simultaneous recording of membrane current under voltage clamp (top trace) and fluorescence of the indicator Calcium Green 5N, which was dialyzed through the patch pipette at a concentration of 75 μM (bottom trace). Emitted light was measured with a photomultiplier tube in photon-counting mode; the calibration bar at the bottom refers to counts per second (cps). A large increase in fluorescence above the initial level (indicated by the dashed line) occurred shortly after activating the epifluorescence beam, coincident with the beginning of the photocurrent.

in the light-transducing microvillar lobe, and precede the activation of the electrical response by $\sim$1 ms. Blunting the light-triggered Ca changes with Ca buffers (internal 1,2-bis(o-aminophenoxy)ethane-N,N,N′,N′-tetraacetic acid (BAPTA) or high concentration of ethylene glycol-bis-(β-amino-ethyl ether) N,N,N′,N′-tetraacetic acid (EGTA)) interferes with the light response, dramatically reducing its amplitude and slowing down its kinetics. However, although cytosolic Ca levels are controlled by light and

in turn exert a pivotal regulatory function, Ca does not, in all likelihood, directly activate light-dependent channels. Other events that follow phospholipase C (PLC) activation play a fundamental role; light-activated single-channel currents remain temporally viable in excised, perfused inside-out patches, pointing to membrane-bound signaling elements, rather than soluble messengers like inositol 1,4,5 triphosphate (IP_3) or Ca^{2+}. Diacylglycerol (DAG), the other, membrane-confined product of the breakdown of phosphatidylinositol-bisphosphate (PIP_2), is a plausible candidate. In *Lima*, a variety of DAG analogs, such as 2-dioctanoyl-sn-glycerol (DOG), phorbol 12-myristate 13-acetate (PMA), and (–)-indolactam, increase membrane conductance and evoke an inward current (**Figure 5**) with a similar ionic selectivity as the photoconductance; moreover, DAG analogs and light interact occlusively, suggesting that their effects converge onto a common target. Calcium elevation greatly potentiates and accelerates the effects of DAG analogs, an observation in line with the aforementioned effects of Ca manipulations. The generality of the role of DAG – or some metabolite thereof – in phototransduction remains to be systematically assessed in different species; moreover, even in *Lima*, the robust effects of DAG analogs fall quantitatively short of the speed and magnitude of the electrical response elicited by light. While the discrepancy could be ascribed to technical limitations in the application of chemicals to the cell, the participation of additional messenger molecules should not be ruled out. In other systems, phosphatidylinositol 4,5 bisphosphate (PIP_2), long viewed simply as the substrate of phosholipase C-β (PLC-β) and the precursor of IP_3 and DAG, has emerged as a signaling molecule in its own right. Because PIP_2 levels in the rhabdomeric membrane are bound to drop with light-triggered activation of PLC, a direct participation of this phospholipid in light signaling would call for a negative messenger role, one that helps maintain some element(s) of the transduction cascade in the inactive state. In *Lima*, intracellular administration of PIP_2 specifically antagonizes the light-evoked current while sparing voltage-dependent currents. Moreover, in excised patches of *Pecten* rhabdomeric membrane screened for the exclusive presence of light-activated channels, functional depletion of PIP_2 by antibodies (to avoid confounding by the concomitant generation of its bioactive hydrolysis products) induces the appearance of single-channel currents, which can be silenced by exogenous replenishment of PIP_2. Thus, the visual excitation process may be complex, and involve the interplay of several signaling and modulator molecules, rather than constituting a linear cascade.

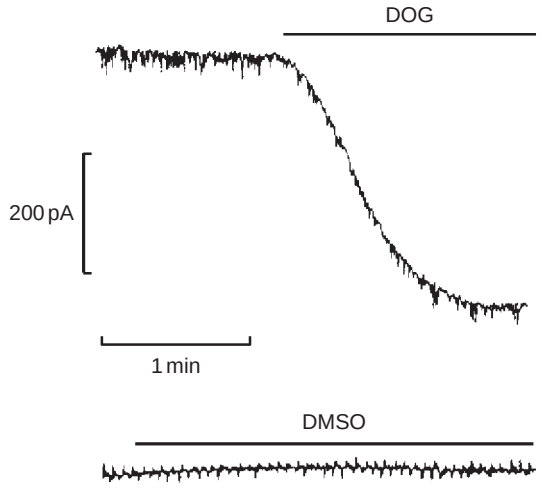

Figure 5 Diacylglycerol (DAG) analogs stimulate the light-sensitive conductance in *Lima* microvillar photoreceptors. Puffer-pipette application of the 2-dioctanoyl-sn-glycerol (DOG, 100 μM) activates an inward current, several hundreds of pA in amplitude, in a cell held under voltage clamp. Control application of dimethyl sulfoxide (DMSO) at the same concentration as that used to dissolve DOG is inert (bottom trace). The current activated by DOG and other diacylglycerol DAG analogs has the same ionic selectivity as the photocurrent; moreover, the analogs interact occlusively with light.

An additional complexity in the visual excitation scheme of molluskan microvillar receptors is the presence of separate populations of ion channels underlying the photocurrent, as subsequently corroborated in *Drosophila* where transient-receptor potential (TRP) and transient-receptor potential-like (TRPL) channels were molecularly identified. Two components of the macroscopic photocurrent of *Lima* can be distinguished by their time course and ion-conduction properties. In *Pecten*, cell-attached patch-clamp recordings in the exposed light-sensitive membrane reveal single-channel currents specifically activated by photostimulation (**Figure 6**) with a unitary conductance of ~48 pS and an additional population of smaller-amplitude currents ~18 pS. The identity of these single-channel currents as the constitutive elements of the macroscopic photoresponse was confirmed by the similarity of kinetics and light sensitivity, extending down to stimulation intensities that only evoke single-photon responses.

Light Adaptation

Modulation of sensitivity is a fundamental process in photoreceptor function, and enables the cell to maintain responsiveness over widely varying levels of ambient illumination. Once again, calcium had been singled out as a critical player as early as in the 1970s in *Limulus*, but its downstream effector(s) remained unclear. Protein kinase C (PKC) is a likely mediator, because some PKC subtypes are activated by calcium (and DAG), and also because in *Drosophila* it is associated with the macromolecular 'light-transduction complex'. Ca-dependent PKCα is selectively expressed in *Lima* eyes, as established by Western blot analysis using isoform-specific antibodies, and localizes in the light-sensing lobe of microvillar photoreceptors. Moreover, upon illumination it translocates from the cytosol to the membrane

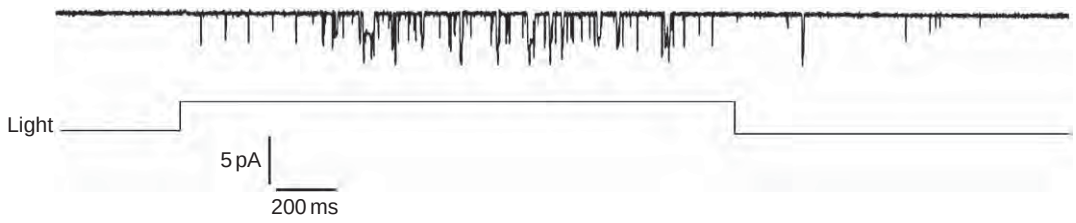

Figure 6 Cell-attached patch-electrode recording on the microvillar lobe of a *Pecten* rhabdomeric photoreceptor. Upon presenting a sustained, dim-light stimulus, single-channel inward currents are elicited. Two populations of light-activated currents are observed, one with a unitary conductance of ~≈48 pS and an additional population of smaller-amplitude currents ~18 pS. No responses are produced by voltage stimulation in the dark (not shown).

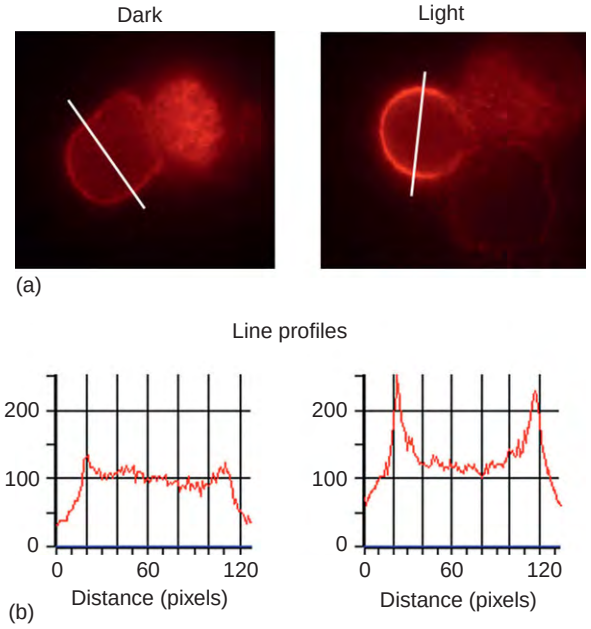

Figure 7 Light-induced translocation of PKCα. (a) Photoreceptor dark adapted for 1 h and directly fixed in paraformaldehyde (left), or illuminated for 3 s just before fixation (right). Anti-PKCα antibodies revealed a different spatial pattern of immunofluorescence in the two conditions, whereas in control cells PKCα is largely distributed diffusely in the cytosol of the microvillar lobe, after light the fluorescence forms a much more pronounced ring around the edges and is nearly absent from the central portion. (b) Intensity profiles of the immunofluorescence, measured along a line cutting across the rhabdomeric lobe.

(a functional assay of its activation), on a similar timescale as the onset of light adaptation (Figure 7). Chemical stimulation of PKC specifically depresses the light response, consistent with its role in desensitization, while pharmacological antagonists of PKC reduced light adaptation. These observations strongly support the involvement of PKC in the calcium-dependent regulation of response sensitivity.

Ciliary Photoreceptors

Photoreceptors of the distal retina function in a profoundly different way. Their resting potential is relatively depolarized (~−35 mV) owing to a high resting g_{Na}/g_K

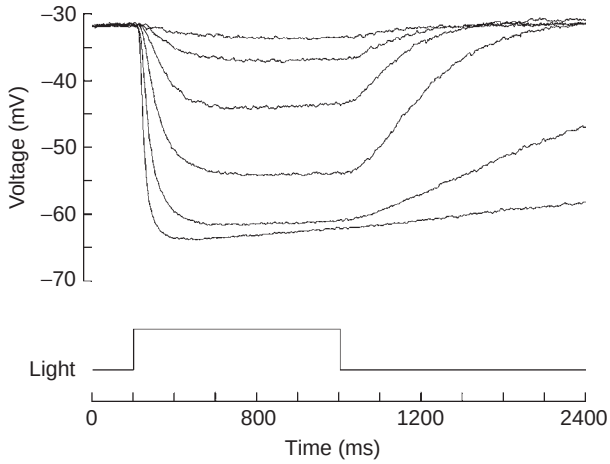

Figure 8 Hyperpolarizing receptor potentials elicited by a 1-s light of increasing intensity (top to bottom trace) in a dissociated ciliary photoreceptor of *Pecten*, measured with a patch electrode in whole-cell current-clamp mode.

ratio, and illumination produces a hyperpolarizing receptor potential graded with light intensity (Figure 8). The light sensitivity is significantly lower than in proximal photoreceptors, but the purpose here is not range fractionation (unlike rods and cones of the vertebrate retinas). Instead, ciliary photoreceptors play a fundamentally different role from that of their microvillar counterparts: the information output ultimately entails action potentials, which, of course, could not be caused by light-induced hyperpolarization. It is a reduction of illumination that causes firing in these axons: the effect of light is to remove, in a time- and intensity-dependent way, the steady-state inactivation of voltage-dependent calcium channels, such that when illumination is decreased (e.g., when an approaching predator casts a shadow on the animal's visual field), the return to a depolarized membrane potential triggers a Ca spike. As such, these cells function as dark detectors and activation of the phototransduction cascade serves the function of priming them to respond to light dimming.

Excitation

The hyperpolarizing receptor potential of ciliary visual receptors also arises from an increase in membrane

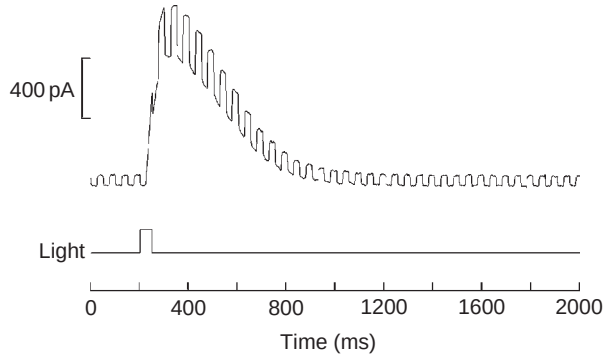

Figure 9 Light-induced increase in membrane conductance in a ciliary photoreceptor, assessed by superimposing a repetitive voltage step on the steady holding potential (10 mV, 100 Hz, and 0.5 duty cycle). When a light response was elicited, the size of membrane current perturbations grew several fold, indicating the opening of ion channels.

conductance (**Figure 9**). The reversal potential is ~–80 mV, close to the calculated value for E_K, the equilibrium potential for potassium, and exhibits a near-perfect Nernstian dependency on the concentration of extracellular potassium. Photostimulation, therefore, opens K-selective channels. Cell-attached patch recording on the ciliary appendages of the cell, presumably the light-sensitive organelles, reveals outwardly directed single-channel currents activated by light but not by voltage, with a unitary conductance ~26 pS.

Light-signaling in distal photoreceptors diverges sharply from that of their microvillar counterparts: the photoresponse is insensitive to both IP_3 and antagonists of the IP_3 receptor, and is also impervious to Ca elevation and to Ca buffering. Moreover, the guanine nucleotide-binding alpha Q protein ($G\alpha_q$) is not expressed in the distal photoreceptors of another member of the *Pectinidae*. These data strongly argue against the involvement of PLC – the canonical transduction cascade of invertebrate vision.

By contrast, substantial data have accumulated in support of a role for cGMP: intracellular application of cGMP or slowly hydrolyzing analogs (but not cAMP) elicits an outward current (**Figure 10(a)**) with similar ion-conduction properties as the light-evoked current: the reversal potential and its dependency on $[K]_o$ are the same (**Figure 10(a)**), and so is the characteristic outward rectification. Both the photocurrent and the current elicited by cGMP are inhibited by the same antagonists, such as l-*cis*-diltiazem. Furthermore, illumination and exogenous cGMP analogs interact occlusively. Activation of cGMP-dependent currents can be obtained in excised membrane patches, suggesting that cGMP operates directly on the channels. It can be concluded that cGMP is the internal final messenger for visual excitation, as it occurs in vertebrate photoreceptors.

Despite the structural and functional similarities of *Pecten* distal photoreceptors with rods and cones, a key difference places these receptors in a novel, distinct subcategory because the photoresponse is due to the opening, rather than the closing, of cGMP-gated channels. This implies that light must elevate cGMP levels, and this calls for an enzymatic machinery different from that of rods and cones. Several clues on the nature of this light-signaling pathway have emerged.

Photopigment, G Protein, and Arrestin

The molecular identity of the photopigment of ciliary receptors was elucidated in the Japanese scallop *Patinopecten yessoensis*, where a novel form of rhodopsin, dubbed SCOP2, was cloned and localized to the distal retinal layer by *in situ* hybridization. As in other invertebrates, the photopigment of scallop ciliary receptors is thermally stable upon illumination. The action spectrum, measured by both the late or the early receptor potential, peaks at 500 nm, and rhodopsin photoisomerization red-shifts its absorption curve by 75 nm; as a consequence, the fractional state of the pigment (rhodopsin (R)/metarhodopsin (M)) is a photoequilibrium that can be manipulated by varying the wavelength of illumination. A massive R to M conversion by blue-light illumination gives rise to prolonged hyperpolarizing after-potentials (or outward after-currents under voltage clamp) that can be reset by illumination with red light. Little is known about the detailed mechanisms that terminate the light response, but antibodies against bovine arrestin label a single band in Western blots of *Pecten* retinal homogenates and decorate ciliary photoreceptors both in cryosections of the eye and in dissociated retinas. Moreover, intracellular dialysis with the same antibodies slow down the falling phase of the photocurrent and allow prolonged after-currents to be elicited by spectrally neutral flashes, indicating that an arrestin-like molecule is implicated in visual excitation turn-off.

Seven transmembrane domain receptors (like rhodopsin), signal through a heterotrimeric G protein, and ciliary photoreceptors are no exception: GTP-γ-S, which interferes with G-protein deactivation, because it is resistant to the GTPase activity of Gα and associated GTPase activating proteins (GAPs), causes the flash response to become sustained. Conversely, GDP-β-S inhibits phototransduction. However, the identity of the G-protein is unusual for visual cells: the only detectable Gα form expressed in the distal retina was molecularly identified as a $G\alpha_o$, by Shichida and colleagues in *P. yessoensis*. A similar $G\alpha_o$, differing in a stretch of 22 amino acids but otherwise identical at the nucleotide level, has been cloned in *P. irradians*; this was also demonstrated to be confined to the layer of ciliary photoreceptors by *in situ* hybridization. Physiological and pharmacological data corroborate the participation of $G\alpha_o$ in light transduction: (1) mastoparan peptide activators of $G\alpha_o$ induce an outward current, which is suppressible by blockers of the light-sensitive conductance; (2) the light response is

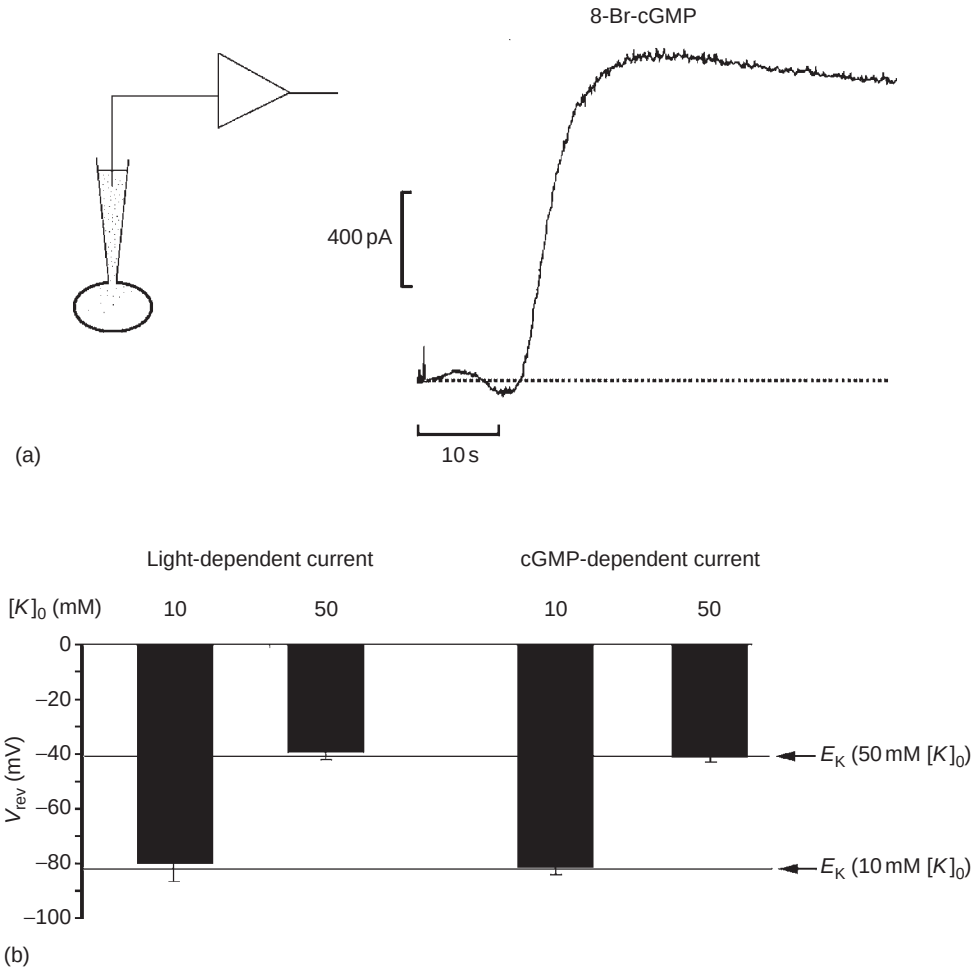

Figure 10 (a) Intracellular dialysis of an isolated ciliary photoreceptor cell with 20 μM of the cGMP analog, 8 bromo-cGMP (8Br-cGMP). Several seconds after rupturing the membrane patch to access the cell interior, a large outward current was evoked. (b) Similarity of the ion selectivity of the current elicited by light and by cGMP analogs. The reversal potential (V_{rev}) of the photocurrent was determined along with that of the current elicited by intracellular application of 8Br-cGMP. The measurements were conducted either in normal extracellular potassium (10 mM), or after elevating its concentration to 50 mM. In all cases, reversal potential V_{rev}, tracked exactly the predicted value of the *K* equilibrium potential, E_K.

inhibited by application of the A-protomer of pertussis toxin (the holotoxin moiety where the ribosyl-transferase activity resides), as predicted from the presence of a cysteine in the fourth position from the carboxy terminus of the $G\alpha_o$ sequence. This is the hallmark for susceptibility to ADP-ribosylation.

Guanylate Cyclase

The downstream mechanisms of visual excitation call for a light-induced elevation of cGMP, which could conceivably arise by either of two schemes: (1) inhibition of a phosphodiesterase (PDE) over a background of constitutive guanylate cyclase (GC) activity (i.e., the mirror image of the cGMP cascade of rods and cones) and (2) light-dependent stimulation of a cyclase (i.e., parallel to the cAMP cascade of olfactory neurons). Pharmacological antagonists of PDE fail to mimic the effects of light (i.e., they do not directly activate the photoconductance, although some of them augment the amplitude of the light response). By contrast, GC antagonists reversibly inhibit the photoresponse, suggesting that light may control cGMP production, rather than degradation (i.e., scheme (2)). Such a notion, unprecedented for visual cells, parallels the well-established role of adenylate cyclase in ciliary neurons of the olfactory epithelium, where cAMP is the internal messenger. The putative light-regulated GC, however, must not be one of the canonical soluble (sGC) or membrane (mGC) forms. First, the light response is impervious to manipulations of the nitric oxide (NO) pathway, which suggests exclusion of a soluble GC. Second, changes in intracellular Ca concentration do not alter the photocurrent, which indicates an essential divergence with respect to the regulatory mechanisms that operate in vertebrate membrane GCs. Most importantly, like in

all G-protein-coupled receptors, rhodopsin signals through a G-protein, and such a regulatory mechanism has not been reported by either class of GC. However, a new family of GCs has been uncovered in lower organisms (e.g., *Plasmodium*, *Paramecium*, and *Dictyostelium*), with the same topology as the G-protein-regulated adenylyl cyclase (class III) of olfactory neurons. In *Dictyostelium*, it has been reported that its activity is regulated by a heterotrimeric G-protein of the G_o subtype. G protein dependency for GC activity has recently been documented in Leydig tumor cells and may thus not be confined to protozoa. In *Pecten* retinal lysates, polyclonal antibodies against the multitransmembrane domain GC of *Paramecium* label a distinct band, with an apparent molecular mass of ~240 kDa, similar to that of the multitransmembrane domain GCs, and greatly exceeding that of either soluble (70–82 kDa) or other membrane-bound GCs (up to 140 kDa).

Light-Dependent Ion Channels

The molecular identity of the ion channels underlying the receptor potential of ciliary photoreceptors has yet to be established. Interestingly, in Western blots of *Pecten* retinal lysates, antibodies raised against CNG-2 (the α-subunit of the transduction channel of olfactory neurons) label a single band of the appropriate apparent molecular mass, 73 kDa; by contrast anti-CNG-1, the vertebrate retina form, and anti-CNG-3 (which is expressed in mammalian heart, kidney, and sperm) produce no signals. In whole-eye cryosections, the same antibodies selectively decorate the distal layer of the retina, where ciliary photoreceptors are found. By confocal fluorescence microscopy in dissociated cells, the target was localized in the ciliary appendages, presumed to be the light-transducing organelles. The results suggest the presence of an olfactory-like CNG channel in distal photoreceptors, with a subcellular distribution compatible with a role in visual excitation.

The light-dependent channels of distal photoreceptors are uniquely interesting because of their gating and ion-selectivity properties. It has long been known that CNG channels are homologous to some voltage-gated K channels, and a common evolutionary origin has been proposed. Nonetheless, the two classes differ sharply in terms of ion permeation, which in CNG channels is characteristically cationic nonselective. The light-dependent channels of hyperpolarizing invertebrate photoreceptors are remarkably similar to both voltage-gated K channels and CNG channels: on the one hand, they are strongly selective for potassium and highly susceptible to blockage by certain K-channel antagonists like 4-aminopyridine. On the other hand, they are gated by cGMP and blocked by various antagonists of the light-sensitive conductance of rods, such as l-*cis*-diltiazem. As such, they seemingly constitute a missing link, bridging the gap between these two superfamilies of ion channels. This raises a question about the origin of their gating mechanism. In *Pecten*, the light-dependent K conductance exhibits a pronounced outward rectification due to voltage-dependent occlusion of the permeation pathway by Ca^{2+} and Mg^{2+} ions, which bind at a site located about half-way through the membrane (electrical distance $\delta \sim 0.6$ from the external surface). Blockage by Ca^{2+} and Mg^{2+} requires an open pore, and the channels can close with a divalent ion trapped inside. These observations suggest that the cGMP-controlled gate must reside near the extracellular side of the channel protein, in sharp contrast with the intracellularly located gate of its voltage-dependent K channel relatives.

Light Adaptation

Because the primary function of ciliary cells is to produce an OFF discharge upon the dimming of a continuous light, the photoresponse is bound to have a prominent sustained component. Nonetheless, during prolonged light stimulation the photocurrent decays to a plateau, and background illumination or conditioning flashes produce all the classical manifestations of light adaptation: shift in the sensitivity curve, compression of the response amplitude range, and acceleration of response kinetics. However, the underlying modulatory mechanisms operate in an unusual way: the lack of a detectable Ca permeability of the light-activated channels and of a functional IP_3 signaling pathway implies that light stimulation is not coupled to either influx or internal release of calcium. In fact, unlike all other known photoreceptors, fluorescent Ca indicators report no discernible light-induced changes in cytosolic calcium. As a consequence, this ion would not be in a position to play a significant role in light adaptation. Not surprisingly, direct manipulations of intracellular Ca, either buffering it with the rapid Ca chelator BAPTA, or, conversely, elevating it to μM levels fails to significantly change basal light sensitivity or to alter adaptation. The Ca-independent signaling pathway responsible for light adaptation appears to implicate cGMP, the same messenger that governs visual excitation: application of cGMP analogs not only activates the photoconductance, but, on a slower timescale, also depresses the light response to an extent that far exceeds what one would expect from the decreased pool of available channels (i.e., a simple competition for a common effector mechanism). This excess reduction of the photoresponse amplitude is accompanied by a shift in the sensitivity curve and acceleration of response kinetics, the hallmark signs of light adaptation (**Figure 11**). Tests with pharmacological antagonists indicate that the changes in sensitivity during light adaptation mediated by cGMP may be in part controlled by a cGMP-dependent protein kinase.

In summary, ciliary photoreceptors found in the retina of several bivalve mollusks diverge sharply from classical (microvillar) invertebrate photoreceptors, and partake instead of several morphological and structural features of vertebrate rods and cones; nonetheless, they utilize a

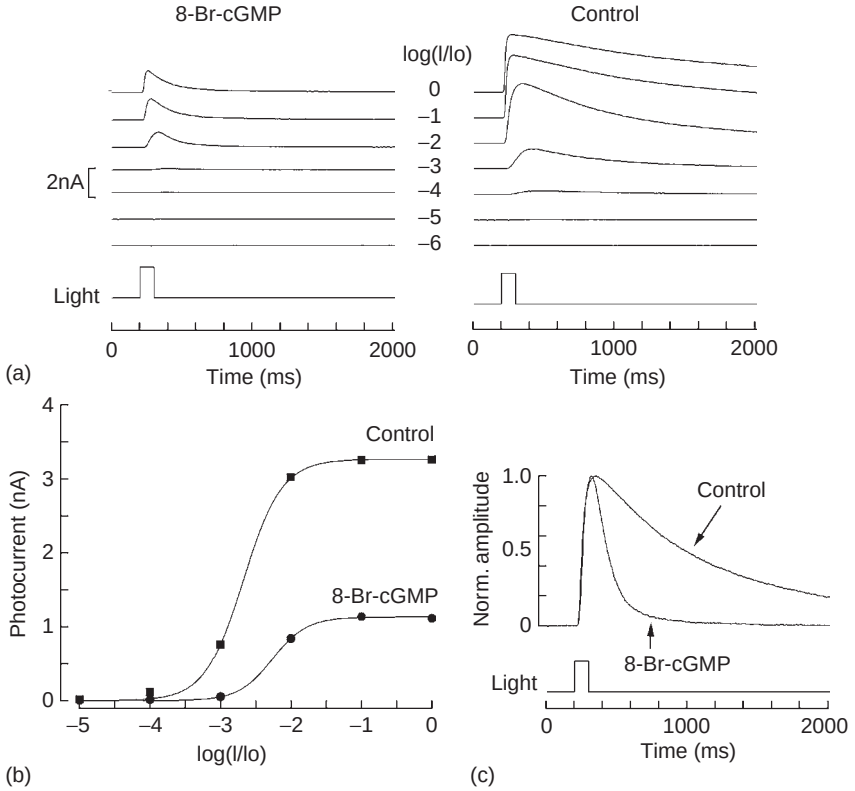

Figure 11 Photoresponse desensitization by cGMP analogs. (a) Current evoked by flashes of increasing intensity (bottom to top trace) delivered to ciliary photoreceptors internally dialyzed with 20 μM 8-Br-cGMP (left) vs. control solution (right). Log intensity for each trace indicated between two sets. (b) Intensity-response relation in the two cases in (a). In addition to the compression of response amplitude, 8-Br-cGMP shifts the curve to the right. (c) Normalized photocurrents (at –2 log) in control conditions vs. 8-Br-cGMP, highlighting the acceleration of the response decay.

fundamentally different cascade both for light transduction and for light adaptation, warranting their inclusion in a novel separate class of light-transducing cells. The parallelism with the odor-transduction cascade of olfactory neurons suggests a common lineage with an ancestral chemoreceptor cell.

See also: Genetic Dissection of Invertebrate Phototransduction; Phototransduction: Inactivation in Rods; Phototransduction in *Limulus* Photoreceptors; Phototransduction: Phototransduction in Cones; Phototransduction: Phototransduction in Rods.

Further Reading

Barber, V. C., Evans, E. M., and Land, M. F. (1967). The fine structure of the eye of the mollusk *Pecten maximus*. *Zeitschrift für Zellforschung und Mikroskopische Anatomie* 76: 295–312.

Cornwall, M. C. and Gorman, A. L. F. (1979). Contribution of calcium and potassium permeability changes to the off response of scallop hyperpolarizing photoreceptors. *Journal of Physiology* 291: 207–232.

Gorman, A. L. F. and McReynolds, J. S. (1969). Hyperpolarizing and depolarizing receptor potentials in the scallop eye. *Science* 165: 309–310.

Gomez, M. and Nasi, E. (1994). The light-sensitive conductance of hyperpolarizing invertebrate photoreceptors: A patch-clamp study. *Journal of General Physiology* 103: 939–956.

Gomez, M. and Nasi, E. (1995). Activation of light-dependent potassium channels in ciliary invertebrate photoreceptors involves cGMP but not the IP_3/Ca cascade. *Neuron* 15: 607–618.

Gomez, M. and Nasi, E. (1998). Membrane current induced by protein kinase C activators in rhabdomeric photoreceptors: implications for visual excitation. *Journal of Neuroscience* 18: 5253–5263.

Gomez, M. and Nasi, E. (2000). Light transduction in invertebrate hyperpolarizing photoreceptors: Involvement of a G_o-regulated guanylate cyclase. *Journal of Neuroscience* 20: 5254–5263.

Gomez, M. and Nasi, E. (2005). A direct signalling role for PIP_2 in the visual excitation process of microvillar receptors. *Journal of Biological Chemistry* 280: 16784–16789.

Gomez, M. and Nasi, E. (2005). Calcium-independent, cGMP-mediated light adaptation in ciliary photoreceptors. *Journal of Neuroscience* 25: 2042–2049.

Kojima, D., Terakita, A., Ishikawa, T., et al. (1997). A novel G_o-mediated phototransduction cascade in scallop visual cells. *Journal of Biological Chemistry* 272: 22979–22982.

Nasi, E. (1991). Two light-dependent conductances in the membrane of *Lima* photoreceptor cells. *Journal of General Physiology* 97: 55–72.

Nasi, E. and Gomez, M. (1992). Light-activated ion channels in solitary photoreceptors from the eye of the scallop *Pecten irradians*. *Journal of General Physiology* 99: 747–769.

Nasi, E. and Gomez, M. (1999). Divalent cation interactions with light-dependent K channels: Kinetics of voltage-dependent block and requirement for an open pore. *Journal of General Physiology* 114: 653–671.

Piccoli, G., Gomez, M., and Nasi, E. (2002). Role of protein kinase C in light adaptation of microvillar photoreceptors. *Journal of Physiology* 543: 481–494.

Molecular and Cellular Mechanisms in Allergic Conjunctivitis

V L Calder, UCL Institute of Ophthalmology, London, UK

Glossary

Allergen – A protein to which the immune system responds.
Amblyopia – Vision disorder characterized by poor or indistinct vision in an eye that is otherwise physically normal.
Atopy – Allergic response in an area not in contact with allergen.
Conjunctiva – Tissue lining of the ocular surface comprised of epithelium and stromal layers. Bulbar conjunctiva covers the outer surface of the eye; tarsal (palpebral) conjunctiva lines the eyelids.
HLA-DR – A transmembrane human major histocompatibility complex 2 family member.
Hyperemia – Increase of blood flow to a portion of the body.
Photophobia – An abnormal sensitivity to light.
Rhinitis – Inflammation of some internal areas of the nose. The primary symptom of rhinitis is nasal dripping.

The term ocular allergy describes a spectrum of clinical conditions, ranging from the common, milder conditions of seasonal and perennial allergic conjunctivitis (SAC, PAC), to the rare but more severe diseases, vernal keratoconjunctivitis (VKC) and atopic keratoconjunctivitis (AKC). This article describes the clinically different subtypes of ocular allergy (classification summarized in Table 1) and our current understanding of the cellular and molecular pathways involved in the different forms of ocular allergy.

Ocular Allergies

Seasonal Allergic Conjunctivitis

SAC, or hay fever, is the most common form of ocular allergy and, in fact, the most common of all ocular disorders. SAC occurs only during the pollen season, the timing being dependent on which pollen is allergenic for that individual (e.g., tree, grass, weed). In countries where pollen seasons are extended, SAC can affect individuals for up to 10 months per year. It can occur at any age but is more frequently seen in children and young adults and the severity tends to lessen with age.

The symptoms of SAC include itching, watering, redness, and swelling of the eyes and lids, and there may be increased discharge. There is often an associated rhinitis and a history of atopy. During the pollen season, the ocular signs can be dramatic, usually affecting both eyes to a similar degree. Edema of the lids and conjunctiva can be mild and often outweighs the degree of hyperemia, giving a milky or pink appearance to the eye. In severe cases the swelling can be gross, with the inability to open the lids and a ballooning out of the conjunctiva termed chemosis, particularly after exposure to high aeroallergen concentrations or after rubbing of the eye. Eversion of the lids to reveal the tarsal conjunctiva demonstrates some hyperemia and mild infiltration of the conjunctiva, leading to a loss of transparency and thickening, with diffuse small inflammatory excrescences known as papillae. Since there is no serious limbal disease or conjunctival scarring, and the cornea is not involved, the visual acuity remains normal. Outside the pollen season the eye examination is normal.

Perennial Allergic Conjunctivitis

PAC is another common ocular allergy with many similarities to SAC but with a very different time course. Since the allergens in PAC are present for most or all of the year, PAC is not seasonal. The disorder is again most frequently and severely seen in children and young adults. House dust mite (*Dermatophagoides pteronyssinus*) is the most common sensitizing allergen but animal hair and dander, molds and other allergens can also induce PAC.

The symptoms are perennial and include ocular itch, discomfort, watering, redness, and some discharge. Patients may be able to correlate symptoms with exposure to an allergen. House dust mite allergy sufferers have a history of symptoms worse in the morning. Approximately one-third have an associated rhinitis, and a family and/or personal atopic history is very common. The clinical appearance is of a mild conjunctival inflammation and clinical signs may be very slight. The bulbar conjunctiva may be slightly red and edematous and the tarsal conjunctiva shows mild to moderate hyperemia, infiltration, and fine papillae. Lid edema is usually mild. Similar to SAC, in PAC there is no conjunctival scarring, or corneal involvement, such that vision is not affected. Due to the continuing presence of the allergens, the resultant inflammation in PAC is more chronic and hence the immunopathology of PAC differs from that of SAC.

Table 1 Classification of ocular allergic diseases

Disease	*Timing*	*Age group*	*Prevalance*	*Keratopathy*	*Sight threatening*	*Course*
SAC	Seasonal	Majority children and young adults	Very common	No	No	Mild, nonprogressive, often resolves
PAC	Perennial	Adult	Common	Common	No	Not serious, nonprogressive
VKC	Seasonal – Perennial if severe	Children	Uncommon	Yes	Yes	Serious, but usually resolves in 2–10 years with good outcome if well managed. Can change into AKC
AKC	Perennial	Adult	Rare	Yes	Yes	Serious and progressive, vision often reduced

SAC, seasonal allergic conjunctivitis; PAC, perennial allergic conjunctivitis; VKC, vernal keratoconjunctivitis; AKC, atopic keratoconjunctivitis.

Vernal Keratoconjunctivitis

VKC is a more serious ocular allergy of childhood. It makes up 0.1–0.5% of ocular disease in the developed world but is more common and much more severe in hot dry countries, especially the Middle East, West Africa, and the Mediterranean. It is a chronic form of conjunctivitis, usually with seasonal exacerbations. In the United Kingdom, VKC is a rare, self-limiting, often seasonal ocular allergy that affects children and young adults, most of which are male (85%) and many have a history of atopy.

The symptoms are worse in the spring and summer but, in severe disease, will last all year. Patients complain of severe itching, discomfort or pain, photophobia, stringy discharge, blurred vision, and difficulty opening the eyes in the morning. The ocular signs can be very asymmetrical. Conjunctival signs are maximal in the superior tarsal conjunctiva and limbus and the heavily inflamed lid may droop (ptosis). The conjunctival surfaces are hyperemic, edematous, and infiltrated, and a stringy mucoid discharge is present. The tarsal conjunctival tissues are densely infiltrated, with papillae that are often giant (>1 mm in diameter, known as cobblestone papillae). The limbus can have discrete swellings or, less often, diffuse hyperemia and inflammation, and the presence of small white chalky deposits (Trantas' dots) is typical of vernal limbitis. In the later stages, fine reticular white scarring may be seen, but this does not lead to significant shrinkage and distortion of the ocular surface as in some cicatrising conjunctival diseases such as AKC (see below).

Visual acuity can be affected by involvement of the cornea (keratopathy), which is most marked in the upper third of the cornea as a result of greater exposure to toxic inflammatory mediators, not mechanical rubbing by the papillae. At its mildest, there is a punctate disturbance of the epithelium, which may coalesce to form a discrete epithelial defect (macroerosion). Deposition of mucus, fibrin, and inflammatory debris can then result in the formation of a shallow oval plaque (or shield) ulcer, which repels the hydrophilic tears and the epithelial-healing response. Herpetic and bacterial corneal infection may occur. In the later stages, scarring of the cornea may lead to permanent visual reduction. Steroid treatment-related complications, and (because of the young age group) sensory-deprivation amblyopia also contribute to the potential for long-term visual loss.

Atopic Keratoconjunctivitis

AKC is the least common but most serious of the ocular allergies. It is a life-long condition that affects adults who have systemic atopic disease, either atopic dermatitis or chronic asthma. The usual onset is in the late teens but, unlike VKC, the disease is persistent and may be relentlessly progressive; occasionally the disease can begin in childhood. AKC is a highly symptomatic disorder with severe itching, pain, watering, stickiness, and redness.

There is usually facial atopic dermatitis involving the eyelids. The lid margins show severe blepharitis (chronic inflammation of the lash follicles and meibomian glands) and are thickened and hyperemic, posteriorly rounded, sometimes keratinized and the lid anatomy may be distorted with ectropion (outwardly turning eyelid), entropion (inwardly turning eyelid), trichiasis (inturning lashes), loss of lashes, and notching. The whole conjunctiva is affected and shows intense infiltration, papillae (which may be giant) and sometimes scarring with linear and reticular white scar tissue, lid to conjunctiva adhesions and shrinkage or loss of the conjunctival sac and secondary lid distortions. Marked limbal inflammation can develop and Trantas' dots may occur. The disease may never affect the cornea, in which case it is sometimes referred to as atopic blepharo-conjunctivitis (ABC); in this situation, the overall inflammation is generally less severe.

The cornea can be affected as a direct effect of the inflammatory process or may be damaged secondarily following extensive changes to the usually protective ocular surface by processes such as continual mechanical trauma, reduced lid protection, or severe loss of conjunctival tear

production. Significant visual acuity reduction due to corneal involvement occurs in 40–70% of the cases. Keratopathy may consist of punctate and macroscopic epithelial defects, filamentary keratitis, plaque ulcer, progressive scarring, neovascularization (with or without lipid deposition), thinning, and secondary corneal infections (herpetic, bacterial, and fungal). Associations between AKC and eye rubbing, keratoconus, atopic cataract, and retinal detachment have been reported.

Cellular Mechanisms in Ocular Allergy

The predominating immune mechanism occurring in SAC is an immediate (type 1) hypersensitivity response whereby conjunctival mast cells (MCs) (**Table 2**) and their secreted products primarily orchestrate the inflammatory response. In contrast, the cellular responses in PAC involve MC to a certain extent, although neutrophils and some T cells have also been detected in the conjunctival tissues, probably recruited as a result of the release of chemokines which attract these cells to the site of inflammation during the persistent allergen-driven inflammatory response. During VKC, studies have identified cells of both innate and adaptive immune responses becoming activated with T lymphocytes and eosinophils predominating, as well as MCs, neutrophils, and other cells infiltrating the conjunctival epithelium and stroma. In AKC, the predominant cell types infiltrating the conjunctival tissues are T cells, eosinophils, and neutrophils. In both VKC and AKC there are alterations to the epithelium and evidence of tissue remodeling and collagen deposition.

Conjunctival MCs

MCs are important effector cells at all mucosal sites including the conjunctiva, where rapid responses are necessary. During SAC, conjunctival MC become activated as a direct result of allergen cross-linking of surface IgE receptors (FcεR1), resulting in degranulation and release of histamine, leukotrienes, proteases, prostaglandins, cytokines, and chemokines (**Figure 1**). This rapid MC histamine response causes the itching characteristic of SAC. Upon binding to its receptors (H1 and H2), histamine induces vascular leakage, resulting in further cellular infiltration of eosinophils and neutrophils from the blood, leading to chemosis. Relative increases in mucosal MC (MC_T) were identified in tarsal conjunctival tissue specimens in SAC whereas increased numbers of both MC_T and connective tissue type (MC_{CT}) MC phenotypes have been detected in both tarsal conjunctival epithelial and substantia propria layers in PAC. The different pattern of MC subset activation occurring in PAC probably reflects the more persistent response to allergen.

Therapeutic intervention in SAC initially focused on the use of topical antihistamines in the form of eye drops, to neutralize the localized effects of the histamine secreted by the degranulating MC. Another therapeutic approach has used MC stabilizing drugs (e.g., sodium chromoglycate) to inhibit release of histamine and other secretagogues from the cells. Combinations of antihistamines with chromolyns have been used to treat the signs and symptoms of SAC for many years. However, more recent topical antiallergic drugs for treating SAC (e.g., azelastine, epinastine, ketotifen, olopatadine) combine antihistamine action with MC stabilization. The additional benefits of these drugs are in their ability to selectively prevent MC secretion of various inflammatory mediators including histamine, as well as cytokines and chemokines. Due to the presence of other cell types in the more chronic forms of ocular allergy, these antiallergic drugs are most effective in SAC and are not effective for the more severe forms of ocular allergy when used alone, but can be of some benefit when given in combination with other anti-inflammatory drugs such as steroids or cyclosporine A (see below). While specific allergen immunotherapy has been successfully used for treating other forms of allergy where the specific allergens are known, it has not been widely used for treating SAC since there is a wide variation among individuals affected with SAC in terms of their allergen responsiveness, with many

Table 2 Summary of cell types in conjunctival tissues in ocular allergy

Disease	*Predominant inflammatory cells*	*Involvement of tissue-resident cells*
SAC	MC_{CT}	None
PAC	MC_{CT} and MC_{CT}, neutrophils, T cells	None
VKC	Eosinophils, $CD4^+$T cells, neutrophils, MC	Fibroblasts, epithelium
AKC	$CD4^+$T cells, eosinophils, neutrophils, MC	Epithelium, fibroblasts

SAC, seasonal allergic conjunctivitis; PAC, perennial allergic conjunctivitis; VKC, vernal keratoconjunctivitis; AKC, atopic keratoconjunctivitis; MC, mast cells; MC_{CT}, mucosal mast cells; MC_{CT}, connective tissue mast cells.

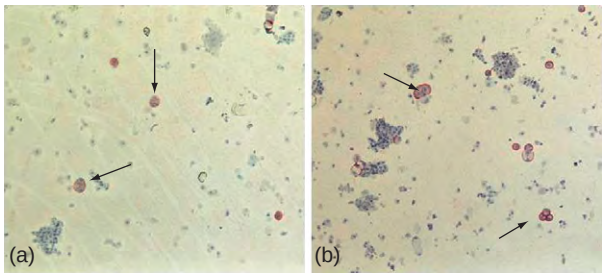

Figure 1 Conjunctival mast cells *in vitro* : (a) Unstimulated mast cells (small arrows); (b) mast cells stimulated via FecR cross-linking (large arrows). Stimulated mast cells form clusters prior to degranulating.

responding to more than one allergen. In the chronic forms of allergic eye disease (VKC, AKC), the conjunctivitis is due less to a direct allergen-specific response, but more an immune-mediated response involving local tissue resident cells, and other nonallergen-specific inflammatory cells. In those severe forms of ocular allergy, specific allergen immunotherapy would not be appropriate.

Conjunctival Eosinophils and Neutrophils

MCs are predominately responsible for SAC, but in more chronic forms of conjunctivitis other cell types have been identified as playing an important role. Some neutrophils and eosinophils have been found in less than half of symptomatic patients with SAC but little or no T cell infiltration was observed. In SAC and PAC, neutrophils and eosinophils have been observed at the site of inflammation, and both of these cell types are able to secrete a wide range of proinflammatory cytokines (interleukin (IL)-3, IL-4, IL-5, IL-6, transforming growth factor alpha (TGF-α), tumor necrosis factor alpha (TNF-α)), chemokines (IL-8, RANTES), and multiple mediators (granule proteins: eosinophil cationic protein, major basic protein, and eosinophil-derived cationic protein) to amplify the inflammatory response. In PAC, due to the presence of eosinophils, neutrophils, and some T cells, several cell-mediated processes are likely to be involved. MC-targeted therapy alone is not an effective treatment for PAC, supporting the hypothesis that there is a complex network of cells contributing to the chronic inflammation in this condition. Recently, intranasal corticosteroids have demonstrated a promising therapeutic effect in relieving the ocular symptoms associated with perennial allergic rhinitis.

In the more severe forms of ocular allergy (VKC and AKC), increased numbers of eosinophils have been detected in the conjunctival tissues, although it has also been found that it is the extent of eosinophil activation expressing intracellular adhesion molecule (ICAM)-1 or a transmembrane human major histocompatibility complex 2 family member (HLA-DR) that correlates more with disease severity than the overall numbers of eosinophils. There are differences between VKC and AKC in the patterns of cytokines which colocalize to conjunctival eosinophils, with those from VKC mainly expressing IL-3, IL-5, IL-6, and granulocyte/macrophage colony stimulating factor (GM-CSF) whereas, in AKC, eosinophils express mainly IL-4, IL-8, and GM-CSF. Although the specific cellular interactions are as yet unclear, these different cytokine profiles point to different eosinophil-mediated pathways being involved in each severe form of ocular allergy.

Conjunctival Lymphocytes

There are very few T cells detected in normal and in SAC conjunctival tissue specimens, which are mainly situated in the epithelial layer. There are a few T cells detectable in PAC but their phenotypes remain unknown. In contrast, immunostaining of tarsal conjunctival tissue specimens from VKC patients have found significantly increased numbers of lymphocytes which are mainly activated $CD4^+$ T cells, localized to the subepithelial layers of the affected tissue. There is also an increased HLA-DR expression within the epithelium and stromal layers of the conjunctival tissues as compared with normal subjects and increased numbers of Langerhans' cells and activated macrophages ($CD68^+$) were also observed. T cell clones, derived from VKC conjunctival tissues, were functionally characterized as Th2-type, since *in situ* hybridization staining demonstrated an increased Th2 cytokine (IL-3, IL-4, and IL-5) mRNA expression in VKC in areas of maximum T cell infiltration (**Figure 2**). In support of these studies, VKC tear samples were found to have increased intracellular T cell expression of IL-4 in more than 60% of the specimens. Further analysis of tear specimens using multiplex bead cytokine arrays, found that IL-4, interferon-gamma (IFN-γ), and IL-10 were all elevated in SAC and VKC in comparison with nonatopic controls. Although such studies do not identify the cellular source of the cytokines, nevertheless they illustrate the differentially activated cytokine pathways in each form of ocular allergy, perhaps due to the different cell types involved in each form of ocular allergy.

Similar to VKC, conjunctival biopsy specimens in AKC were found to have increased numbers of activated $CD4^+$T cells, HLA-DR expression, and cells of the monocyte/macrophage lineage as well as mRNA expression of the Th2 cytokines (IL-3, IL-4, and IL-5) in the stromal tissues. However, in contrast to VKC, there was also a significant increase in the expression of IL-2 mRNA, and in numbers of IFN-γ expressing T cells, suggesting a more Th1-type T cell response in the most severe of the ocular allergic diseases. In support of this, conjunctival biopsy specimen-derived T cell lines from AKC were found to secrete significantly increased levels of IFN-γ, indicative of Th1-T cells. It has thus been proposed that AKC is an

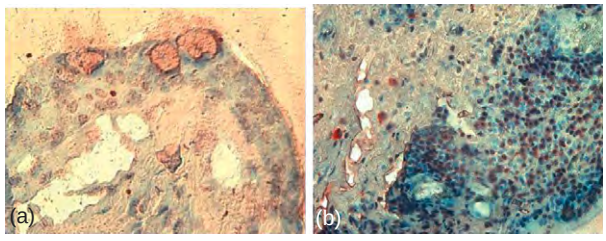

Figure 2 Light microscopy immunostaining of conjunctival biopsy tissue sections for IL-13 expression (brown): (a) weak staining for IL-13 localizing to goblet cells within the epithelial layer in SAC biopsy specimen; (b) intense staining for IL-13 (brown) localizing to mononuclear cells within the subepithelial and epithelial layers in VKC biopsy specimen (magnification ×200).

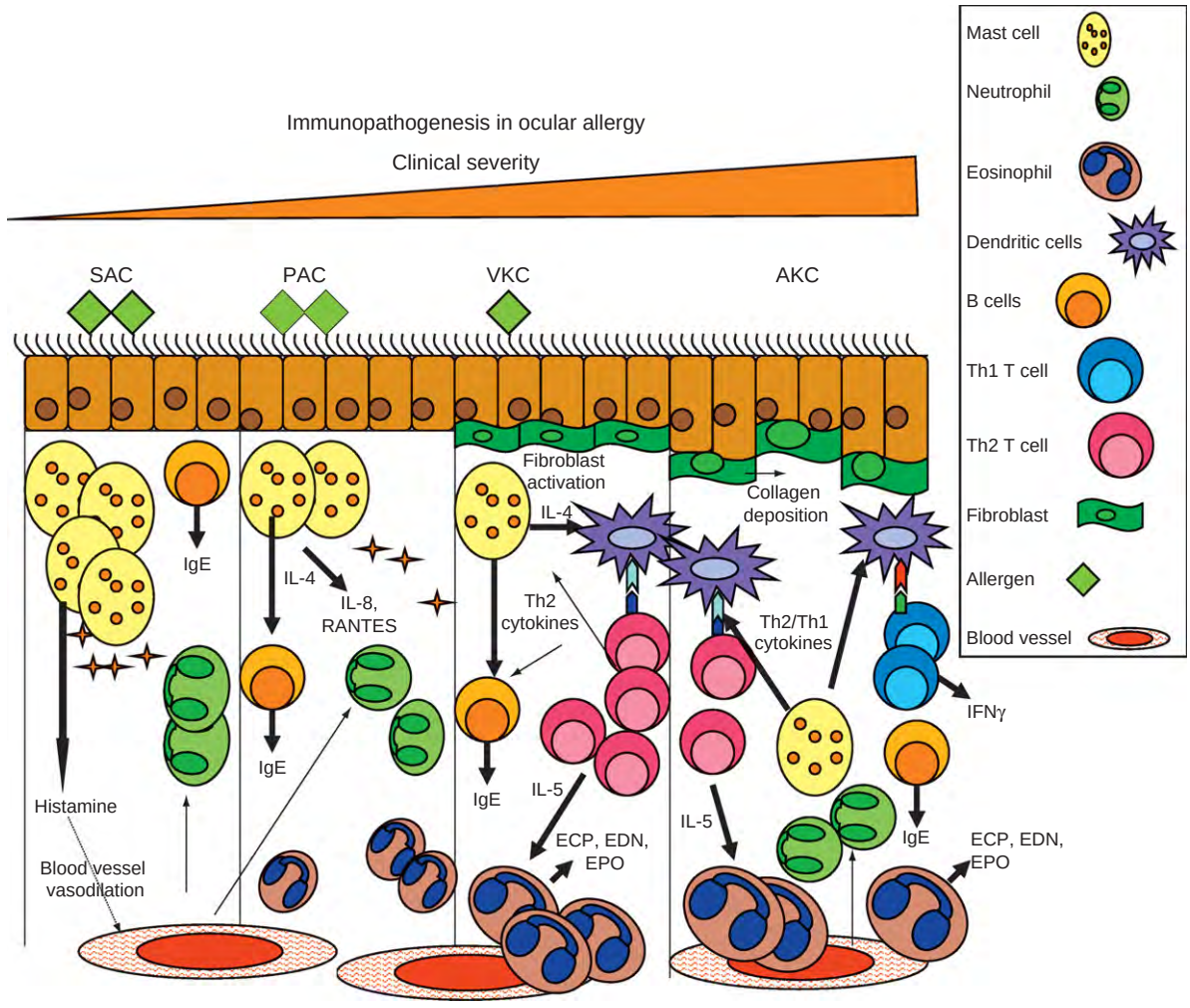

Figure 3 Schematic comparing the different types of immunopathogenis in ocular allergy. SAC, seasonal allergic conjunctivitis; PAC, perennial allergic conjunctivitis; VKC, vernal keratoconjunctivitis; AKC, atopic keratoconjunctivitis.

immune-mediated response involving Th1 T cells, whereas VKC involves a predominant Th2-type T cell response (Figure 3).

Due to the severity of the inflammation in VKC and AKC, immunosuppressive drugs (steroids) are used to dampen the immune response. However, long-term steroid treatment can have serious side effects in the eye, causing raised intraocular pressure which can lead to glaucoma, and cataract formation. Following the identification of T cells and their cytokines within the conjunctival tissues in VKC and AKC, cyclosporine A (CsA; 2% in maize oil) was tested and found to be an effective steroid-sparing treatment for VKC and AKC if administered locally as eye drops.

Conjunctival Epithelial Cells

As a consequence of chronic inflammation at the ocular surface, in particular in AKC, the epithelium can become thickened. Immunostaining of conjunctival epithelial cells from conjunctival biopsies have demonstrated an increased expression of ICAM-1 and HLA-DR, but only in the most severe forms of allergic eye disease (VKC and AKC) and almost no expression of these costimulatory molecules in noninflamed control conjunctival tissues. The ability of conjunctival epithelial cells to express ICAM-1 might allow greater adhesion and recruitment of leukocytes, while the expression of HLA-DR molecules could simply reflect the activation status of the cells, although the possibility of conjunctival epithelial cells presenting antigen to T cells is still to be confirmed. Several *in vitro* studies have used conjunctival epithelial cells, either as primary cultures of cells isolated from biopsy specimens, or as immortalized epithelial cell lines. Upon activation of conjunctival epithelial cells *in vitro*, there is an upregulation of costimulatory molecules, including ICAM-1 and HLA-DR and secretion of various cytokines such as IL-6, CCL8 (IL-8), a potent

Table 3 Summary of cytokines and molecules present in conjunctival tissues

	IL-2	*IL-4*	*IL-5*	*MMP-1, -3, -9*	*IFN γ*	*HLA-DR + epithelium*	*ICAM-1 + eosinophils*
Control	+	+	−/+	+	+	−	−
VKC	−/+	+++	+++	++	++	++	++
AKC	+++	++	+++	nd	+++	++	++

VKC, Vernal keratoconjunctivitis; AKC, atopic keratoconjunctivitis; IL, interleukin; MMP, matrix metalloproteinases; IFN, interferon; HLA-DR, a transmembrane human major histocompatibility complex 2 family member; ICAM, intracellular adhesion molecule.

chemokine for neutrophils. The ability of conjunctival epithelial cells to secrete proinflammatory cytokines and chemokines suggests an important proinflammatory role for these cells (Table 3).

Conjunctival Fibroblasts

In the severe forms of chronic ocular allergy, there is significant tissue remodeling involving collagen deposition and subepithelial fibrosis. Conjunctival biopsy-derived fibroblasts *in vitro* have been found to secrete cytokines (e.g., IL-6), chemokines (e.g., MCP-1), as well as matrix metalloproteinase (MMP)-1 and -9 and tissue inhibitor of matrix metalloproteinase (TIMP)-1. These cells were also found to respond to the Th2 cytokines IL-4 and IL-13, by secreting increased levels of eotaxin-1, IL-6, and RANTES, whereas there was a significant reduction of MMPs. Immunostaining of conjunctival biopsies from noninflamed controls and VKC identified a significant increase in MMP-1, -3, -9, and -13 expression in VKC tissues. Tear levels of MMP-1 and MMP-9 have also been found to be increased in VKC in comparison with controls, which is probably a reflection of the ongoing fibrotic tissue response.

Molecular Mechanisms

The ocular surface of the eye is a mucosal site and plays an important role in protecting the eye from infection through a mucosal barrier as well as supporting both innate and adaptive immune responses as described elsewhere in this encyclopedia. The ocular surface is protected by the presence and continuous production of tears and mucins to prevent binding of antigens, and within the tear fluid, antibodies can be found which will bind to, and activate opsonization of antigens by phagocytes. In addition, the expression of toll-like receptors (TLRs) provides another mechanism at the ocular surface, whereby binding of evolutionarily conserved microbial proteins (pathogen-associated molecular patterns, PAMPs) to these receptors induces innate and adaptive immune responses to break down and remove the invading pathogen. Immunostaining has been used to demonstrate expression of TLR-2, -4, and -9 in healthy conjunctival tissues, with expression mainly in the stromal layers. In comparison, in VKC, there is an increased expression of TLR-4 on both epithelium and stroma, together with a decrease in TLR-9. In AKC, TLR-2 expression has been found to be increased on human primary cultures of conjunctival epithelial cells following exposure to *Staphylococcus aureus*, as well as increases in ICAM-1 and HLA-DR expression and secretion of TNF-α and IL-8. This has been proposed as a mechanism whereby *S. aureus* infection at the ocular surface in AKC could activate a host epithelial cell response. In AKC, *S. aureus* colonization can occur at the ocular surface, probably due to a compromised mucosal barrier during this severe form of ocular allergy.

Costimulatory Molecules in Ocular Allergy

Immunohistochemical studies of tarsal and bulbar conjunctival biopsy specimens demonstrated expression of adhesion molecules, ICAM-1 and e-selectin, to be increased in SAC in comparison with controls. However, this increased expression was only detected during the pollen season and outside the pollen season, the levels returned to those of controls. This pattern of expression correlated with the degree of neutrophil or eosinophil infiltration in the bulbar tissue, suggesting an MC-mediated cell recruitment process.

Expression of HLA-DR and ICAM-1 molecules has been used as markers of cell activation. In AKC, there is an upregulation of HLA-DR expression and ICAM-1, localized to the epithelial cells, suggesting epithelial cell activation, probably as a result of exposure to proinflammatory cytokines as well as TLR activation. In both VKC and AKC there is an upregulation of HLA-DR expression and ICAM-1, localized to the eosinophils which correlated with an enhanced activation of these cells.

IgE in ocular allergy

Total serum IgE levels are significantly increased in VKC than in controls. However, IgE levels are variable among those with ocular allergy and cannot be used as a reliable indicator of disease activity or severity. Studies investigating allergen-specific serum IgE levels have detected a range of allergen specificities. A greater percentage of

VKC patients have specific serum IgE against *D. pteronyssinus* and *Dermatophagoides farinae*, whereas in SAC the specific serum IgE is against grass pollens. Allergen-specific IgE is also increased in tear specimens and there is a highly significant correlation with ocular allergy symptoms, supporting a diagnostic value for specific tear IgE, although limited tear volume restricts its use in routine immunoassays.

Cytokines and Chemokines in Ocular Allergy

Throughout this article, cytokines and chemokines have been discussed in relation to particular cell types. However, cell-free tear specimens have also been studied for the presence of cytokines and chemokines in the various forms of ocular allergy. Studies of VKC tear specimens have detected increased levels of IL-4, IL-10, IFN-γ, eotaxin, and TNF-α in comparison with noninflamed control tears. This correlates well with the enhanced expression of Th2-cytokines detected in isolated T cell clones from conjunctival biopsy specimens from VKC patients, as well as the increased percentages of intracellular IL-4-expressing T cells from tear specimens in VKC. In severe forms of AKC, increased tear levels of eotaxin-1 were found to correlate with increased numbers of eosinophils in tears, although the cellular source of the eotaxin was not identified.

The production of proinflammatory cytokines and chemokines by infiltrating conjunctival T cells could provide a mechanism whereby local tissue resident cells such as conjunctival fibroblasts become involved, since collagen deposition and conjunctival tissue remodeling is considerable in chronic allergic eye disease. Comparing conjunctival biopsy specimens from VKC patients with controls, increased expression of RANTES, eotaxin, monocyte chemotactic protein (MCP)-1, and MCP-3 was detected, reflecting the range of inflammatory cells present. VKC conjunctival tissue expression of the chemokine receptor CXCR3 was found to be specifically localized to T cells, and the CXC chemokine Mig was highly expressed, suggesting an important role for this ligand in recruitment of activated T cells.

In conclusion, tissue-based studies, combined with *in vitro* and *in vivo* models (not discussed in this article), have identified discrete cellular and molecular pathways in each form of ocular allergy, and this knowledge has allowed a more selective therapeutic approach. Nevertheless, currently available therapies for the more chronic forms of ocular allergic disease are limited by their side effects and there is an urgent need for improved treatments which can be given topically to reduce the impact of potential side effects.

See also: Adaptive Immune System and the Eye: Mucosal Immunity; Adaptive Immune System and the Eye: T Cell-Mediated Immunity; Conjunctiva Immune Surveillance; Defense Mechanisms of Tears and Ocular Surface; Innate Immune System and the Eye; Overview of Electrolyte and Fluid Transport Across the Conjunctiva.

Further Reading

Abelson, M. B. and Granet, D. (2006). Ocular allergy in pediatric practice. *Current Allergy and Asthma Reports* 6(4): 306–311.

Blaiss, M. S. (2008). Evolving paradigm in the management of allergic rhinitis-associated ocular symptoms: Role of intranasal corticosteroids. *Current Medical Research and Opinion* 24(3): 821–836.

Bonini, S., Gramiccioni, C., Bonini, M., and Bresciani, M. (2007). Practical approach to diagnosis and treatment of ocular allergy: A 1-year systematic review. *Current Opinion in Allergy and Clinical Immunology* 7(5): 446–449.

Bonini, S., Sacchetti, M., Mantelli, F., and Lambiase, A. (2007). Clinical grading of vernal keratoconjunctivitis. *Current Opinion in Allergy and Clinical Immunology* 7(5): 436–441.

Calonge, M. and Enríquez-de-Salamanca, A. (2005). The role of the conjunctival epithelium in ocular allergy. *Current Opinion in Allergy and Clinical Immunology* 5(5): 441–445.

Calonge, M. and Herreras, J. M. (2007). Clinical grading of atopic keratoconjunctivitis. *Current Opinion in Allergy and Clinical Immunology* 7(5): 442–445.

Dogru, M., Okada, N., Asano-Kato, N., et al. (2005). Atopic ocular surface disease: Implications on tear function and ocular surface mucins. *Cornea* 24(8 supplement): S18–S23.

Fukuda, K., Kumagai, N., Fujitsu, Y., and Nishida, T. (2006). Fibroblasts as local immune modulators in ocular allergic disease. *Allergology International* 55(2): 121–129.

Kumagai, N., Fukuda, K., Fujitsu, Y., Yamamoto, K., and Nishida, T. (2006). Role of structural cells of the cornea and conjunctiva in the pathogenesis of vernal keratoconjunctivitis. *Progress in Retinal and Eye Research* 25(2): 165–187.

Leonardi, A., De Dominicis, C., and Motterle, L. (2007). Immunopathogenesis of ocular allergy: A schematic approach to different clinical entities. *Current Opinion in Allergy and Clinical Immunology* 7(5): 429–435.

Leonardi, A., Motterle, L., and Bortolotti, M. (2008). Allergy and the eye. *Clinical and Experimental Immunology* 153(supplement 1): 17–21.

Mantelli, F. and Argüeso, P. (2008). Functions of ocular surface mucins in health and disease. *Current Opinion in Allergy and Clinical Immunology* 8(5): 477–483.

Micera, A., Stampachiacchiere, B., Aronni, S., dos Santos, M. S., and Lambiase, A. (2005). Toll-like receptors and the eye. *Current Opinion in Allergy and Clinical Immunology* 5(5): 451–458.

Schultz, B. L. (2006). Pharmacology of ocular allergy. *Current Opinion in Allergy and Clinical Immunology* 6(5): 383–389.

Stern, M. E., Siemasko, K. F., and Niederkorn, J. Y. (2005). The Th1/Th2 paradigm in ocular allergy. *Current Opinion in Allergy and Clinical Immunology* 5(5): 446–450.

Molecular Composition of the Vitreous and Aging Changes

P N Bishop, University of Manchester, Manchester, UK

Glossary

Collagen – This is the most abundant protein in the body and characteristically provides tissues with shape and tensile strength. Collagen molecules are composed of three polypeptide chains (called α-chains) that assemble into a triple helix. Collagen molecules form supramolecular structures such as fibrils and sheets.

Extracellular matrix – This is the material on the outside of cells that is composed of proteins, such as collagens, and carbohydrates, such as glycosaminoglycans. It provides mechanical support for cells. In addition, there is a two-way communication between cells and the extracellular matrix that regulates cellular functions, including fate, morphology, proliferation, and migration.

Glycosaminoglycans – These are long chains of carbohydrate consisting of repeating disaccharide units that are found in the extracellular matrix. Because they are highly charged, they attract ions and water, and this allows them to occupy large volumes and create a swelling pressure within tissues. All glycosaminoglycans are attached to a protein core, thereby forming proteoglycans, with the exception of hyaluronan.

Hyaluronan – Also called hyaluronic acid, hyaluronan is a unique glycosaminoglycan because it is not synthesized as attached to a protein core and is not sulfated. It exists as long unmodified chains of the repeating disaccharide units [β1-4 glucuronic acid-β1-3 *N*-acetylglucosamine]$_n$.

Posterior vitreous detachment – A collapse of the residual vitreous gel away from the inner surface of the retina as far anteriorly as the posterior border of the vitreous base. It results from a combination of vitreous liquefaction and weakening of postoral vitreoretinal adhesion. The main plane of cleavage is between the inner limiting lamina of the retina and the cortical vitreous gel, although vitreoschisis can also occur.

Introduction

The vitreous humor is a highly hydrated tissue with a water content of between 98% and 99.7%. It is surrounded by, and attached to, the retina, pars plana, and lens (Figure 1). At the vitreous base, which straddles the ora serrata, there is an unbreakable adhesion between the vitreous and peripheral retina/pars plana, but further posteriorly the adhesion is less strong and weakens with aging. When the vitreous (secondary vitreous in embryological terms) is formed, it is a gel. However, with aging, the vitreous gel gradually and inevitably liquefies. A combination of age-related gel liquefaction and weakening of postbasal vitreoretinal adhesion eventually results in posterior vitreous detachment (PVD) in 25–30% of the population during their lifetime (Figure 2). PVD is the separation of the cortical vitreous from the inner surface of the retina, which consists of a basement membrane called the inner limiting lamina (ILL), up to the posterior border of the vitreous base. PVD plays a central role in disease processes, including rhegmatogenous retinal detachment, macular hole formation, vitreomacular traction syndrome, and proliferative diabetic retinopathy. This article will discuss the macromolecular structure of the vitreous gel and the aging changes that can eventually result in PVD.

Molecular Composition of the Vitreous

Extracellular Matrix

The vitreous is in essence a dilute extracellular matrix. It contains a low number of macrophage-like cells called hyalocytes. These reside in the cortical vitreous and peripheral basal vitreous (Figure 1).

Extracellular matrices are composite structures containing network-forming macromolecules that possess complementary properties. There are fibrillar proteins that endow the tissue with shape, strength, flexibility, and resistance to tractional forces. Then there are charged carbohydrates, particularly glycosaminoglycans (GAGs), that attract counter-ions and water thereby providing a swelling pressure that spaces apart the fibrillar proteins, inflates the tissue and resists compressive forces. In vitreous the main fibrillar proteins are collagens and in mammalian vitreous the predominant GAG is hyaluronan (Figure 3).

Vitreous Collagens

The vitreous gel contains a low concentration of collagen, estimated to be approximately 300 μg ml^{-1} in the adult human eye. Vitreous collagen is mainly synthesized during

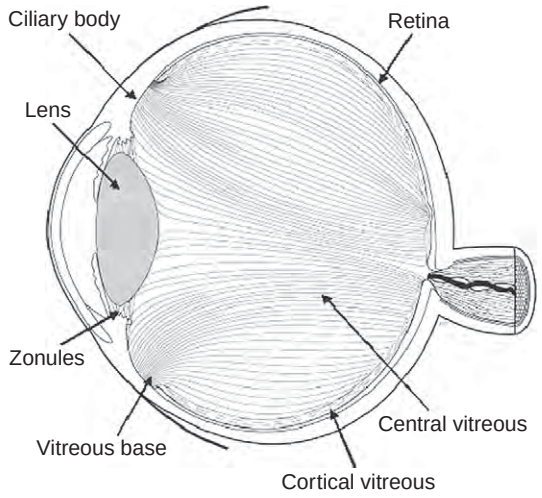

Figure 1 Anatomy of the vitreous. The vitreous is surrounded by and attached to the retina, ciliary body, and lens. The central vitreous forms the bulk of the vitreous body; in this region, the collagen fibrils are at their lowest concentration and tend to be orientated in an anterior–posterior direction. The collagen fibrils of the basal vitreous are at a higher concentration and are orientated perpendicular to the vitreous base, here they insert into the pars plana and the peripheral retina and form an unbreakable adhesion. The vitreous cortex is a thin layer (100–300 μm) that surrounds the central vitreous that has a higher concentration of collagen fibrils than the central vitreous. The anterior cortex courses from the anterior vitreous base across to the posterior surface of the lens. The posterior vitreous cortex lines the surface of the retina behind the vitreous base where it is adherent to the ILL. There is no vitreous cortex over the optic disk and it is thinned over the macula. The cortical collagen fibrils are orientated parallel with the inner retinal surface and they do not generally insert directly into the ILL. Reproduced from Le Goff, M. M., and Bishop, P. N. (2008). Adult vitreous structure and postnatal changes. *Eye* 22: 1214–1222, with permission of the Nature Publishing Group.

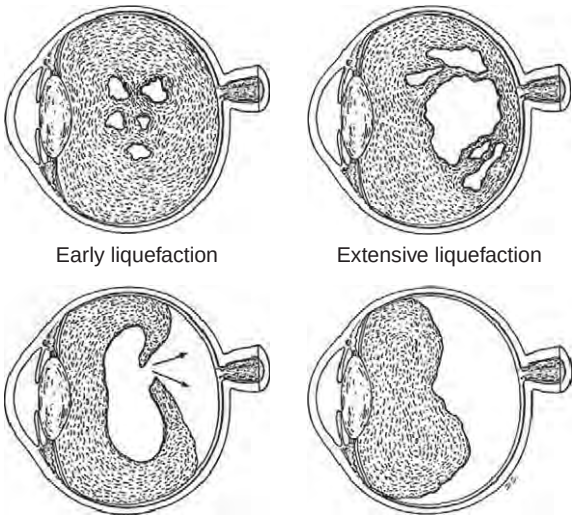

Figure 2 Age-related vitreous liquefaction and PVD. Pockets of liquefaction appear within the central vitreous and these gradually coalesce with aging. There is a concurrent weakening of postoral vitreoretinal adhesion. Eventually, these combined processes can result in PVD where the liquid vitreous dissects the residual cortical gel away from the ILL as far anteriorly as the posterior border of the vitreous base. Reproduced from Le Goff, M. M., and Bishop, P. N. (2008). Adult vitreous structure and postnatal changes. *Eye* 22: 1214–1222, with permission of the Nature Publishing Group.

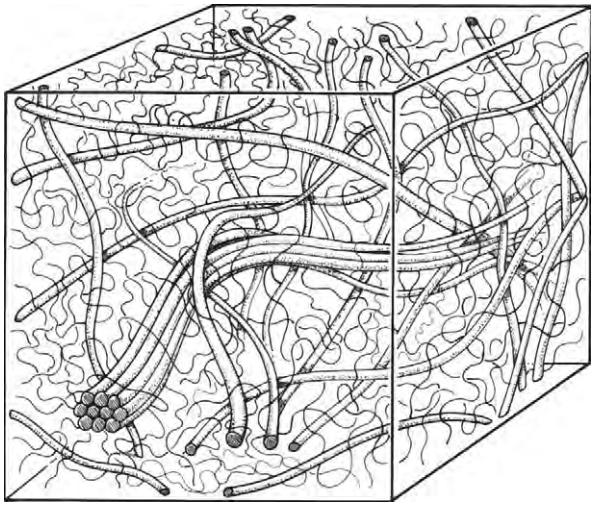

Figure 3 Schematic representation of the cooperation between two networks responsible for the gel structure of the vitreous. A network of collagen fibrils maintains the gel state and provides the vitreous with tensile strength. A network of hyaluronan (thin black lines) fills the spaces between these collagen fibrils and provides a swelling pressure to inflate the gel and help space apart the collagen fibrils. Reproduced from Le Goff, M. M., and Bishop, P. N. (2008). Adult vitreous structure and postnatal changes. *Eye* 22: 1214–1222, with permission of the Nature Publishing Group.

embryonic development and thereafter the rate of synthesis is low. It remains unclear how much degradation of vitreous collagen occurs, but it is likely that the rate of turnover is low and indeed it is possible that collagen fibrils that are formed during embryonic development last throughout life.

Collagen molecules are composed of three polypeptide chains (α-chains) that fold into a characteristic triple-helical configuration. They also contain nontriple helical regions of varying size that are present at each end of the molecule, and in some collagens interrupt the main triple-helical region. The triple-helical fold results from the α-chains having a glycine at every third amino acid, that is, a $(Gly–X–Y)_n$ sequence where X and Y can be any amino acids, but are frequently the imino acids proline and hydroxyproline. Hydroxyproline is important in stabilizing the structure of the collagen triple helix by forming extra hydrogen bonds, while lysine and hydroxylysine residues are necessary for the formation of cross-links which stabilize the collagen fibril.

There are at least 28 different types of collagen molecules (i.e., collagen types I – XXVIII). The commonest collagens are fibril-forming collagens, including types I, II, III and V/XI, but others such as type IV collagen form

sheets (in basement membranes). When fibril-forming collagens are secreted into the extracellular environment they are in a soluble precursor form, the procollagen, and have terminal extensions called N- and C-propeptides. Cleavage of these propeptides by specific enzymes produces a mature collagen with just short noncollagenous (NC) telopeptides at the ends of the triple-helical molecule; this removal (or processing) of the propeptides allows the mature collagen molecules to assemble into fibrils. In some instances the N-propeptides are not removed from fibrillar collagens, but these collagens can still participate in fibril formation and the N-propeptides are then retained on the fibril surfaces.

In vitreous humor nearly all of the collagen is in thin, uniform fibrils that are about 15 nm in diameter. These fibrils are heterotypic (of mixed composition) and contain the fibril-forming collagen types II and V/XI, along with type IX collagen (**Figure 4**). The molecules within the fibrils are cross-linked together to make the fibrils strong and resilient. The collagen fibrils of cartilage have a similar, but not identical, composition and contain collagen types II, XI, and IX. This explains why hereditary collagenopathies such as Stickler syndrome affect both vitreous and cartilage.

Type II collagen

Collagen type II is a fibril-forming collagen that forms the bulk of the vitreous collagen fibrils, accounting for 60–75% of the collagen within the fibrils. It is composed of three identical α-chains, that is, its α-chain composition is $\alpha1(II)_3$. The N-propeptide contains an additional domain that is present in some, but not all of the vitreous type II procollagen, but is absent from cartilage type II procollagen. The presence or absence of this von Willebrand type C domain is dependent on alternative splicing of exon 2 of the type II procollagen gene. Its function remains uncertain, but interestingly it binds transforming growth factor-β and bone morphogenic protein-2, so it may play a role in regulating eye development. This tissue-specific differential splicing of exon 2 explains why patients have been identified with mutations in exon 2 that have a predominantly ocular or ocular only form of Stickler syndrome.

Type V/XI collagen

Type V/XI collagen is a minor component (10–25%) of the heterotypic vitreous collagen fibrils. Its chain composition is probably $\alpha1(XI)_2\alpha2(V)$. The N-terminal domain of type V/XI collagen is not removed by processing and is retained on fibril surfaces where it may play a role in regulating fibril diameter by sterically hindering the lateral growth of the fibrils. There is evidence that a closely related collagen called type V collagen has an essential role in the initiation of collagen fibril formation in tissues where it forms heterotypic fibrils with type I collagen, so type V/XI collagen may have a similar role in initiating collagen fibril formation in the vitreous.

Type IX collagen

Type IX collagen represents up to 25% of the collagen in the heterotypic vitreous fibrils and it is made up of three distinct α-chains, that is, α1(IX)α2(IX)α3(IX). It is not a

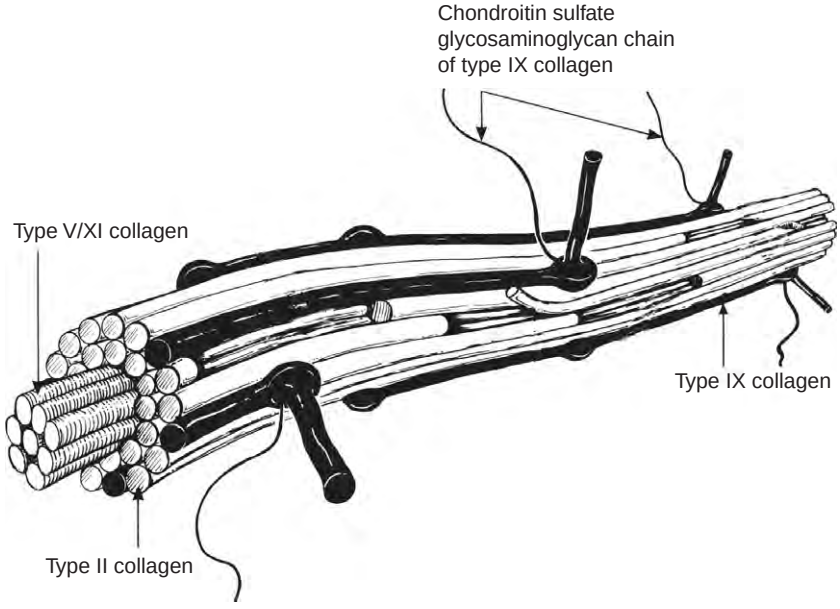

Figure 4 Cartoon representation of the heterotypic collagen fibrils of the vitreous. The fibrils contain collagen types II, V/XI, and IX. Collagen types II and V/XI are fibril-forming collagens that align in staggered arrays to form a central core to the fibrils. Type IX collagen is a chondroitin sulfate proteoglycan that is regularly distributed along the surface of the fibrils. The N-propeptides of type V/XI collagen are retained and located on the surface of the fibrils and some of the N-propeptides of type II collagen may be retained on the fibril surfaces. Reproduced from Bishop, P. (1996). The biochemical structure of mammalian vitreous. *Eye* 10: 664–670, with permission of Macmillan Publishers Ltd.

fibril-forming collagen. Instead it is regularly cross-linked to the surface of the collagen fibrils, which have a core formed by the type II and V/XI collagens. It is a member of the family of fibril-associated collagens with interrupted triple helices (FACIT), which also includes collagen types XII, XIV, and XVI. These collagens have (NC) domains interspersed between collagenous (COL) regions. In the case of type IX collagen there are three COL domains (COL1, COL2, and COL3) interspersed between four NC domains (NC1, NC2, NC3, and NC4). Further complexity is added by the α1(IX) collagen gene (COL9A1) using tissue-specific alternatively spliced transcription start sites, resulting in a form in cartilage that has a globular NC4 domain, but this domain is almost absent in vitreous. The functional significance of these differences remains unclear.

Type IX collagen can exist in proteoglycan and non-proteoglycan forms with the proteoglycan form having a single chondroitin sulfate chain attached to the α2(IX) chain in the NC3 domain. In vitreous, the type IX collagen is synthesized in a proteoglycan form, but the length and sulfation pattern of the chondroitin sulfate chain is species dependent. In mammalian vitreous it has a relatively short chondroitin sulfate chain (15–60 kDa), but in chick vitreous it is very long (approximately 350 kDa).

Synthesis of vitreous collagen

Evidence from a variety of studies suggests that during embryonic development vitreous collagens are mainly synthesized by the ciliary body. The posterior nonpigmented ciliary epithelium secretes the collagen molecules that assemble into fibrils in or around these cells. The fibrils are then extruded into the vitreous cavity. This provides an explanation for the perpendicular orientation of the collagen fibrils in the basal vitreous relative to the nonpigmented ciliary epithelium, and the unbreakable adhesion at the vitreous base.

While the levels are low, there is good evidence that some postnatal vitreous collagen synthesis occurs. Interestingly, this appears to carry on into adulthood and to take place in the peripheral retina. The cells responsible for collagen synthesis in the adult eye are yet to be conclusively identified. This new vitreous collagen synthesis in the adult eye results in the formation of a mat of collagen fibrils on the cellular side of the peripheral ILL. Some of these collagen fibrils break through the ILL and become intertwined with the preexisting cortical vitreous collagen. This process then results in the formation of new unbreakable vitreoretinal adhesions and thereby extends posteriorly at the posterior border of the vitreous base (**Figure 5**). At birth, the vitreous base is at the ora serrata, but it extends posteriorly with aging and has been shown to have migrated over 3.5 mm behind the ora serrata as a result of this process. Irregularities of the posterior border of the vitreous base resulting from uneven posterior extension will predispose to rhegmatogenous retinal detachment during PVD.

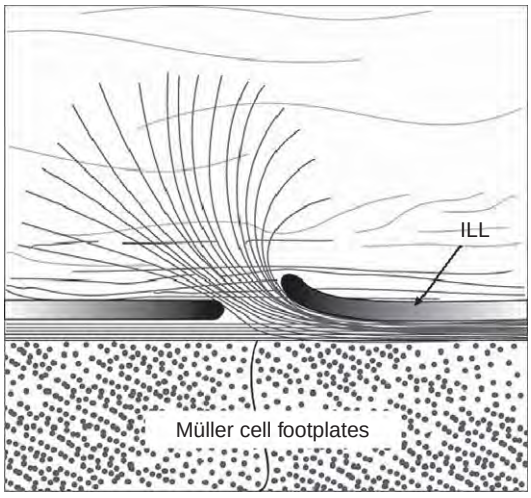

Figure 5 Extension of the posterior border of the vitreous base. There is a very strong adhesion at the vitreoretinal interface within the vitreous base because vitreous collagen fibrils insert directly into the posterior ciliary body and peripheral retina. The vitreous base extends posteriorly into the peripheral retina with aging as a result of the adult peripheral retina synthesizing new collagen. This new collagen forms a mat-like layer on the cellular side of the ILL, and some of this collagen breaks through defects in the ILL and intertwines with preexisting cortical vitreous collagen thereby creating new adhesions and extending the vitreous base posteriorly. Reproduced from Le Goff, M. M., and Bishop, P. N. (2008). Adult vitreous structure and postnatal changes. *Eye* 22: 1214–1222, with permission of the Nature Publishing Group.

NC Proteins and Glycoproteins

Opticin

The heterotypic collagen fibrils of the vitreous are coated with a molecule called opticin. It is a glycoprotein member of the extracellular matrix small leucine-rich repeat protein/proteoglycan (SLRP) family. This family comprises of approximately 11 members and are characterized by a domain containing a number of tandem leucine-rich repeats (LRRs) flanked by disulfide-bonded capping motifs. LRRs are 20–30 amino acid repeats that contain the consensus sequence LXXLXLXXNXL, where L can be a leucine, isoleucine, or valine residue, N is an asparagine, cysteine, or threonine residue and X can be any amino acid. Opticin possesses eight tandem LRRs and an N-terminal extension containing a cluster of sialylated O-linked oligosaccharides. Opticin exists as a dimer in solution as a result of interactions between the LRR domains. Other members of the SLRP family have been shown to play a role in regulating collagen fibril diameter, but this does not appear to be the case for opticin. Instead, opticin appears to modify the vitreous collagen fibril surfaces that are presented to invading cells during pathological processes, such as preretinal neovascularization, and thereby it can attenuate disease processes.

Other proteins and glycoproteins

Vitreous contains many other proteins. Some are derived from the serum and others are produced locally. As well as the molecules described above there are other extracellular matrix components in the vitreous, but their functions remain uncertain. Fibrillin-containing microfibrils have been demonstrated in vitreous. The zonules are composed of bundles of these fibrils and it is unclear whether the vitreous fibrillin-containing microfibrils have a structural role or whether they are a byproduct of zonular synthesis or breakdown. A small amount of type VI collagen is present, this forms its own distinctive microfibrils, but again it is unclear if these have a significant structural role. Fibronectin has been identified in vitreous and it has been postulated that it is involved in vitreoretinal adhesion. A number of other extracellular matrix components have been identified using proteomics in embryonic chick vitreous.

GAGs and Proteoglycans

GAGs are long chains of repeating disaccharide units that undergo varying degrees of modifications during their synthesis, including sulfation, epimerization, and acetylation/deacetylation. These modifications alter the charge of the GAGs and can create specific binding sites for other molecules. All GAGs are attached to a core protein, thereby forming proteoglycans, except hyaluronan which is uniquely synthesized at cell surfaces and is not linked to a core protein.

Hyaluronan

Hyaluronan is the predominant GAG in mammalian vitreous. It is composed of very long carbohydrate chains consisting of the repeating disaccharide [β1-4 glucuronic acid-β1-3 *N*-acetylglucosamine]$_n$. These chains are not modified by sulfation or epimerization. In adult human vitreous, the hyaluronan concentration has been estimated to be between 65 and 400 μg ml^{-1} and the average molecular weight to be 2–4 million.

Chondroitin sulfate proteoglycans

The repeating disaccharide unit of chondroitin sulfate is [β1-4 glucuronic acid-β1-3 *N*-acetylgalactosamine]$_n$. The C-4 and C-6 of the *N*-acetylgalactosamine residues are variably sulfated, and less frequently the C-2 of glucuronic acid. Vitreous is known to contain two chondroitin sulfate proteoglycans, type IX collagen (see section on collagens) and versican. Versican is a large proteoglycan with a central domain that carries multiple chondroitin sulfate chains. At its N-terminus it has a hyaluronan-binding domain that presumably binds vitreous hyaluronan and this binding is stabilized by a link protein. However, as the hyaluronan is in a 150:1 molar excess to the versican and link protein, the structural role of versican in vitreous remains uncertain. Nonetheless, it is of note that the hereditary vitreoretinopathy Wagner syndrome is caused by splice site mutations in versican.

Heparan sulfate proteoglycans

Heparan sulfate and heparin share the same repeating disaccharide unit [β1-4 glucuronic acid-α1-4 *N*-acetylglucosamine]$_n$. The GAG chain is variably modified by sulfation, deacetylation, and epimerization. The degree of modification determines whether the GAG is heparan sulfate or heparin. Heparan sulfate proteoglycans are major components of basement membranes, including the ILL. Heparan sulfate proteoglycans are present in the embryonic vitreous, possibly in transit to form the ILL, but the levels are very low in postnatal eyes.

Supramolecular Organization of the Vitreous

The vitreous collagen fibrils and hyaluronan form two interwoven networks (**Figure 3**). The network of (heterotypic) collagen fibrils is essential for the gel state of the vitreous, as removal of these collagen fibrils converts the vitreous into a viscous liquid. Furthermore, it is through this network of collagen fibrils that tractional forces are transmitted in vitreoretinal diseases. The hyaluronan network inflates the vitreous, increases its mechanical stability and contributes to the spacing of the collagen network, but surprisingly the hyaluronan network can be removed without destroying the vitreous gel, at least in the short term. The long hyaluronan chains form a network primarily through entanglement and this network probably interacts weakly with the collagen fibrillar network.

The vitreous collagen fibrils are long and unbranched. Analysis by freeze-etch rotary shadowing electron microscopy showed that the collagen fibrils are arranged in bundles within the vitreous and form an extended interconnected network by branching between these bundles (**Figure 6(a)**). In the young eye the vitreous collagen fibrils within the bundles appear to run closely together and in parallel, but are not fused. Morphological analyses suggest that the chondroitin sulfate chains of type IX collagen play a role in both connecting together and spacing apart the collagen fibrils within these bundles (**Figure 7**).

Aging Changes that Predispose to PVD

Age-Related Vitreous Liquefaction

The human vitreous humor undergoes an inevitable process of liquefaction (or syneresis) with aging. Initially

small pockets of liquefaction form, but these coalesce with aging to produce more extensive areas; so by the age of 80–90 years typically more than half of the vitreous cavity is filled with liquid. Ultrastructural studies have shown that vitreous collagen fibrils aggregate with aging into macroscopic strands. Age-related vitreous liquefaction is probably caused by this gradual and progressive aggregation of the collagen fibrils resulting in a redistribution of the collagen fibrils, with the aggregated collagen fibrils being concentrated in the residual gel and other areas therefore becoming devoid of collagen fibrils and consequently converted into liquid.

The spacing between the collagen fibrils appears to be maintained by the chondroitin sulfate chains of type IX collagen (**Figures 6** and 7). However, we have shown that there is a progressive loss of type IX collagen from the surface of the human vitreous collagen fibrils with aging, and that the half-life of type IX collagen on the fibril surfaces is just 11 years of age. This loss of type IX collagen (along with its chondroitin sulfate chains) will result in a loss of spacing between the collagen fibrils. Furthermore, the loss of type IX collagen results in the increased exposure of sticky type II collagen on the fibril surfaces, so when the collagen fibrils come into contact (as a result of eye movement) they will have a propensity to fuse irreversibly.

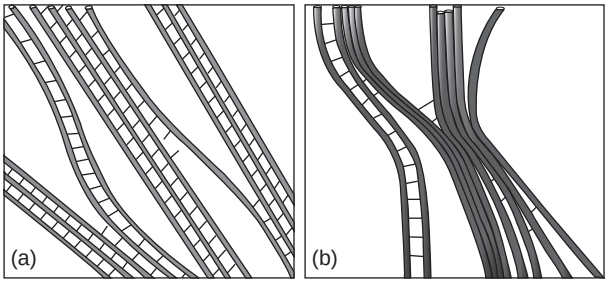

Figure 6 The collagen fibrillar network of the vitreous and aging changes. (a) The collagen fibrils (thick gray lines) form an extended network by being organized into small bundles that are interconnected by collagen fibrils running from one bundle to another. Within each bundle the collagen fibrils are both connected together and spaced apart by the chondroitin sulfate chains of type IX collagen (thin black lines). (b) With aging there is a loss of type IX collagen from the fibril surfaces. The loss of the type IX collagen from the fibril surfaces combined with an increased surface exposure of type II collagen results in aggregation of the collagen fibrils. Reproduced from Le Goff, M. M., and Bishop, P. N. (2008). Adult vitreous structure and postnatal changes. *Eye* 22: 1214–1222, with permission of the Nature Publishing Group.

Figure 7 The role of the chondroitin sulfate chains of type IX collagen in maintaining the spacing between vitreous collagen fibrils. Electron micrographs of vitreous collagen fibrils stained with uranyl acetate (to visualize the collagen fibrils) and the cationic dye Alcian blue (to visualize the chondroitin sulfate chains of type IX collagen). The Alcian blue-stained chondroitin sulfate chains appear to bridge between adjacent collagen fibrils and thereby both space the collagen fibrils apart and link them together. (Scale bar 300 nm).

Weakening of the Vitreoretinal Adhesion

In young eyes there is a relatively strong adhesion between the cortical vitreous and the ILL of the postoral retina, but this weakens with age. The cortical vitreous collagen fibrils do not generally insert directly into the postoral ILL, so it is assumed that the molecular basis of the vitreoretinal adhesion is interactions between components on the surface of cortical vitreous collagen fibrils and macromolecules on the inner surface of the ILL. There is evidence that type XVIII collagen is involved in vitreoretinal adhesion from studies of knockout mice and early PVD in patients with Knobloch syndrome, a rare autosomal recessive condition that results in a lack of type XVIII collagen. Type XVIII collagen is a heparan sulfate proteoglycan. It has been shown that opticin can bind heparan sulfates including those of type XVIII collagen and opticin and type XVIII collagen colocalize at the vitreoretinal interface. Therefore, the opticin on the surface of cortical vitreous collagen fibrils could bind heparan sulfate proteoglycans of the ILL including type XVIII collagen, thereby contributing to vitreoretinal adhesion. However, opticin knockout mice do not appear to develop spontaneous vitreoretinal disinsertion, suggesting that other molecular interactions also contribute to vitreoretinal adhesion, at least in the mouse eye.

Conclusions

Although the vitreous only contains a dilute dispersion of collagen fibrils, it is these fibrils that are central to the gel structure of the vitreous. Molecules on the surface of these collagen fibrils are essential for maintaining the gel state (such as type IX collagen) and play a key role in vitreoretinal adhesion. Alterations in the molecular interactions of the collagen fibrils lead to vitreous liquefaction, weakening of vitreoretinal adhesion, and a consequent predisposition to PVD.

See also: Cellular Origin, Formation and Turnover of the Vitreous; Hereditary Vitreoretinopathies; Hyalocytes.

Further Reading

Bishop, P. N. (2000). Structural macromolecules and supramolecular organisation of the vitreous gel. *Progress in Retinal and Eye Research* 19: 323–344.

Bishop, P. N., Holmes, D. F., Kadler, K. E., McLeod, D., and Bos, K. J. (2004). Age-related changes on the surface of vitreous collagen fibrils. *Investigative Ophthalmology and Visual Science* 45: 1041–1046.

Bos, K. J., Holmes, D. F., Meadows, R. S., et al. (2001). Collagen fibril organisation in mammalian vitreous by freeze etch/rotary shadowing electron microscopy. *Micron* 32: 301–306.

Fukai, N., Eklund, L., Marneros, A. G., et al. (2002). Lack of collagen XVIII/endostatin results in eye abnormalities. *EMBO Journal* 21: 1535–1544.

Wang, J., McLeod, D., Henson, D. B., and Bishop, P. N. (2003). Age-dependent changes in the basal retinovitreal adhesion. *Investigative Ophthalmology and Visual Science* 44: 1793–1800.

Molecular Genetics of Congenital and Juvenile Glaucoma

M Acharya and M A Walter, University of Alberta, Edmonton, AB, Canada

Glossary

Congenital glaucoma – A rare genetic disorder that usually manifests itself at birth or within the first year of life, but may emerge up to the age of 3.
Glaucoma – A multifactorial optic disk neuropathy with a complex genetic basis, in which there is a characteristic acquired loss of retinal ganglion cells and atrophy of the optic nerve.
Juvenile glaucoma – Another subtype of glaucoma based on time of onset. Individuals presenting with open-angle glaucoma before the age of 35 are classified as having juvenile glaucoma.
Mutation – Mutations are changes in nucleotide sequences of an organism's genetic material. Mutations in a gene often have deleterious effects and are often associated with disease.
Open-angle glaucoma – The most common subtype of glaucoma based on anatomy of the anterior chamber of the eye. In open-angle glaucoma, the angle between iris and cornea, often referred to as the iridocorneal angle, remains open.
Trabecular meshwork – A mesh-like structure composed of endothelial cells located between the iris and cornea in the anterior chamber of the eye covering the Schlem's canal. The trabecular meshwork regulates aqueous outflow from the eye thereby maintaining the physical shape of the eye.

Definition of Glaucoma

Glaucoma is the second-largest blinding disorder after cataract. According to the latest estimates, glaucoma affects about 60 million people worldwide. Globally, 12.3% of all blind people suffer from glaucoma. Glaucoma refers to a heterogeneous group of optic neuropathies, with a complex genetic basis. It is a multifactorial optic disk neuropathy, in which there is a characteristic acquired loss of retinal ganglion cells and atrophy of the optic nerve. These neuropathies gradually reduce vision without warning and often without symptoms. At least half of patients with glaucoma do not know they have glaucoma due to lack of symptoms. Untreated glaucoma is a leading cause of irreversible blindness.

Major Subtypes of Glaucoma

Glaucoma is classified according to etiology (primary vs. secondary), anatomy of the anterior chamber (open angle vs. closed angle), and time of onset (infantile vs. juvenile vs. adult). In general, primary glaucoma is broadly classified into three major groups: (1) open-angle glaucoma (OAG), (2) angle-closure glaucoma, and (3) congenital glaucoma (CG) (**Figure 1**). OAG is further subdivided according to age of onset as (1) juvenile OAG (JOAG) and (2) adult-onset glaucoma. In addition, a number of ocular conditions, such as Axenfeld–Rieger syndrome (ARS), Peters anomaly, and nail–patella syndrome (NPS), which result from an abnormal differentiation of neural crest cells, are also reported to be associated with glaucoma (**Table 1**).

Secondary glaucoma can develop due to multiple reasons. The most common types are inflammatory or drug-induced glaucoma. In addition, exfoliation syndrome and pigment dispersion syndrome are two common disorders that can result in secondary glaucoma through blockage of the trabecular meshwork (TM).

Prevalence and Clinical Features of JOAG and CG

OAG is the most common type of glaucoma affecting about 33 million people worldwide. Individuals presenting with OAG before the age of 35 are classified as having JOAG. However, approximately 1% of JOAG patients present clinical symptom before 5 years of age. Almost 39% of JOAG patients present the symptoms between the age range of 15 and 20 and 21% between ages 20 and 25. The glaucoma symptoms of JOAG, which are usually associated with variable severity and phenotypic expression, are severe and respond poorly to treatment.

CG is a rare genetic disorder that usually manifests itself at birth or within the first year of life, but may emerge up to the age of 3. Characteristic clinical features of CG include tearing, photophobia, megalocornea, corneal opacity with characteristic Haab's striae, and enlargement of the eyeball (buphthalmos meaning ox eye) resulting from elevated intraocular pressure (IOP). Unless managed properly, the disease may eventually lead to optic-nerve damage and permanent loss of vision (**Figure 2**). The incidence of CG varies geographically, for example, 1 in 10 000 in Caucasians, 1 in 2500 in Middle East, 1 in 1250 in Romany population of Slovakia, and 1 in 3300 in the Indian state of Andhra Pradesh.

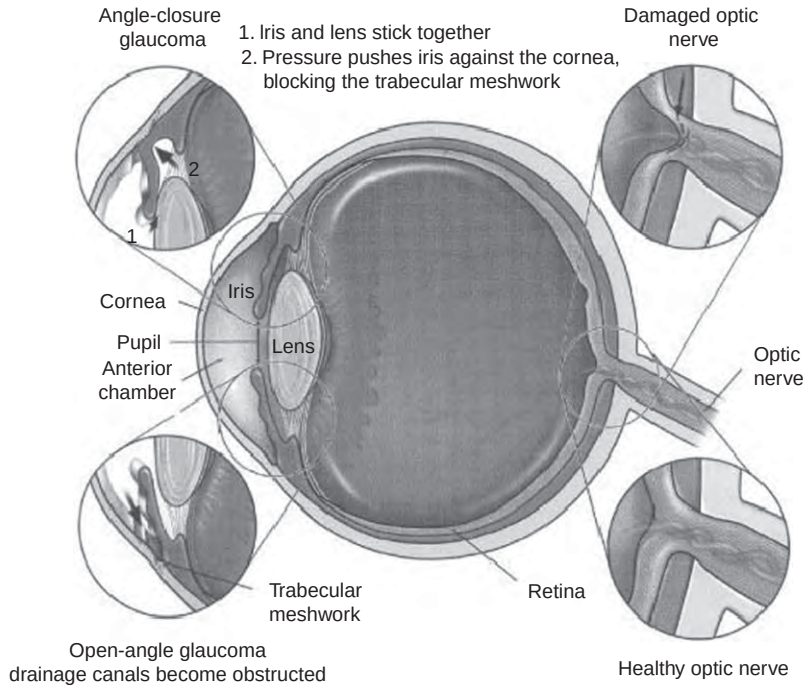

Figure 1 Regions of the eye affected by glaucoma. Cross-sectional diagram of the eye is shown with the areas that are affected under glaucomatous condition. Courtesy of Annual Report of Research to Prevent Blindness, New York, 2001.

Molecular Genetics of JOAG: Mapped Loci and Identified Candidates

OAG (OMIM # 137760) is transmitted both as a monogenic as well as a complex disease. In juvenile- and adult-onset OAG, genetic linkage analysis in affected families clearly suggests autosomal-dominant inheritance with incomplete penetrance. Luntz, in 1979, already suggested that adult-onset OAG is inherited as a non-Mendelian trait, whereas juvenile-onset OAG exhibit autosomal-dominant inheritance. The genetic relationship of adult-onset OAG and JOAG is not yet clear since, while a given OAG family may show a predominant diagnosis of either OAG or JOAG, some family members may have either of the diagnoses. Three JOAG genetic loci have been identified so far (GLC1A or JOAG1, GLC1J or JOAG2, and GLC1K or JOAG3). Details with references have been cited in **Table 1**.

Myocilin (*MYOC*) as a Primary Candidate for JOAG

Overview

In 1993, the first genetic locus for OAG (GLC1A) was identified and, in 1997, the causal gene, myocilin (*MYOC*), (OMIM # 601652) was discovered. In 1997, Polansky and coworkers identified the protein now known as myocilin while studying the effects of steroids on the TM cells in culture. In the eye, the TM cells help regulate eye pressure by controlling the drainage of aqueous humor from the eye. The cultured cells when treated with steroids secreted the same protein, which was called TM-inducible glucocorticoid response protein (TIGR). The gene (*MYOC/TIGR*), located in chromosome 1q24.3, spans about 17 kb region in the genomic DNA and contains three exons. Fingert and coworkers showed by northern blot analysis that *MYOC* is expressed as a 2.3 kb transcript and the translated product is predicted to contain 504 amino acids (57 kDa). Myocilin is a glycoprotein that exists in glycosylated and nonglycosylated forms, with molecular weights of 66 and 55 kDa, respectively, in both intracellular and extracellular locations. Myocilin has two major domains: a myosin-like domain at the N-terminus encoded by exon 1 and an olfactomedin-like domain at the C-terminal region encoded by exon 3.

Analysis of Mutations and Polymorphisms Associated with JOAG in *MYOC*

Known mutations in *MYOC* causing OAG are listed in the Human Genome Mutation Database (HGMD). It is estimated that *MYOC* mutations occur in 2–4% of OAG patients from a variety of ethnic background. Among the three exons of *MYOC*, mutations are mostly clustered in exon 3 (56 mutations), located rarely in exon 1 (eight mutations) and none has been detected so far in exon 2. In 2001 null mice for *MYOC* were created. Interestingly, these null mice had normal morphology of the eye and no

Table 1 Genetic loci associated with glaucoma

Glaucoma type	*Locus*	*Location*	*OMIM #*	*References*	*Gene*	*GenBank accession #*	*References*
Primary open angle glaucoma	GLC1A (JOAG1)	1q21–31	137750	Sheffield et al. (1993)	TIGR/MYOC	*NM_000261*	Stone et al. (1997)
	GLC1B	2cen-q13	606689	Stoilova et al. (1996)			
	GLC1C	3q21–24	601682	Wirtz et al. (1997)			
	GLC1D	8p23	602429	Trifan et al. (1998)			
	GLC1E	10p15–14	602432	Sarfarazi et al. (1998)	OPTN	*NM_021980*	Rezaie et al. (2002)
	GLC1F	7q35–36	603383	Wirtz et al. (1999)			
	GLC1G	5q22.1	609887	Monemi et al. (2005)	WDR36	*NM_139281*	Monemi et al. (2005)
	GLC1H	14q11–13	-	Wiggs et al. (2000)			
	GLC1I	15q11–13	609745	Allingham et al. (2005)			
	GLC1J (JOAG2)	9q22	608695	Wiggs et al. (2004)			
	GLC1K (JOAG3)	20p12	608696	Wiggs et al. (2004)			
	GLC1L	3p21–22	-	Baird et al. (2005)			
	GLC1M	5q22	610535	Pang et al. (2006)			
Primary congenital glaucoma	GLC3A	2p21	231300	Sarfarazi et al. (1995)	CYP1B1	*NM_000104*	Stoilov et al. (1997)
	GLC3B	1p36	600975	Akrasu et al. (1996)			
Other anomalies associated with glaucoma							
Axenfeld–Reiger syndrome	RIEG1	4q25	180500	Semina et al. (1996)	RIEG/PITX2	*NM_000325*	Semina et al. (1996)
	RIEG2	13q14	601499	Philips et al. (1996)			
Iridogonio-dysgenesis	IRID1	6p25	601631	Mears et al. (1996)	FKHL7/FOXC1	*NM_144769*	Mears et al. (1998)
	IRID2	4q25–26	137600	Heon et al. (1995)	PITX2	*NM_000325*	Walter et al. (1996)
Pigment dispersion syndrome	GPDS1	7q35–q36	274600	Anderson et al. (1997)			
Exfoliation syndrome Thorleifsson et al. (2007)	XFG	15q22	177650	Thorleifsson et al. 2007	LOXL1	NM_005576	
Nail–Patella syndrome	NPS	9q34.1	161200	Dreyer et al. 1998	LMX1B	*NM_002316*	Dreyer et al. (1998)

Akarsu, A. N., et al. (1996). A second locus (GLC3B) for primary congenital glaucoma (Buphthalmos) maps to the 1p36 region. *Human Molecular Genetics* 5(8): 1199–1203.
Allingham, R. R., et al. (2005). Early adult-onset POAG linked to 15q11-13 using ordered subset analysis. *Investigative Ophthalmology and Visual Science* 46(6): 2002–2005.
Andersen, J. S., et al. (1997). A gene responsible for the pigment dispersion syndrome maps to chromosome 7q35-q36. *Archives of Ophthalmology* 115(3): 384–388.
Baird, P. N., et al. (2005). Evidence for a novel glaucoma locus at chromosome 3p21-22. *Human Genetics* 117(2–3): 249–257.
Dreyer, S. D., et al. (1998). Mutations in LMX1B cause abnormal skeletal patterning and renal dysplasia in Nail–Patella syndrome. *Nature Genetics* 19(1): 47–50.
Heon, E., et al. (1995). Linkage of autosomal dominant iris hypoplasia to the region of the Rieger syndrome locus (4q25). *Human Molecular Genetics* 4(8): 1435–1439.
Mears, A. J., et al. (1996). Autosomal dominant iridogoniodysgenesis anomaly maps to 6p25. *American Journal of Human Genetics* 59(6): 1321–1327.
Mears, A. J., et al. (1998). Mutations of the forkhead/winged-helix gene, FKHL7, in patients with Axenfeld-Rieger anomaly. *American Journal of Human Genetics* 63(5): 1316–1328.
Monemi, S., et al. (2005). Identification of a novel adult-onset primary open-angle glaucoma (POAG) gene on 5q22.1. *Human Molecular Genetics* 14(6): 725–733.
Pang, C. P., et al. (2006). A genome-wide scan maps a novel juvenile-onset primary open angle glaucoma locus to chromosome 5q. *Molecular Vision* 12: 85–92.
Phillips, J. C., et al. (1996). A second locus for Rieger syndrome maps to chromosome 13q14. *American Journal of Human Genetics* 59(3): 613–619.
Rezaie, T., et al. (2002). Adult-onset primary open-angle glaucoma caused by mutations in optineurin. *Science* 295(5557): 1077–1079.
Sarfarazi, M., et al. (1995). Assignment of a locus (GLC3A) for primary congenital glaucoma (Buphthalmos) to 2p21 and evidence for genetic heterogeneity. *Genomics* 30(2): 171–177.
Sarfarazi, M., et al. (1998). Localization of the fourth locus (GLC1E) for adult-onset primary open-angle glaucoma to the 10p15-p14 region. *American Journal of Human Genetics* 62(3): 641–652.
Semina, E. V., et al. (1996). Cloning and characterization of a novel bicoid-related homeobox transcription factor gene, RIEG, involved in Rieger syndrome. *Nature Genetics* 14(4): 392–399.
Sheffield, V. C., et al. (1993). Genetic linkage of familial open angle glaucoma to chromosome 1q21-q31. *Nature Genetics* 4(1): 47–50.
Stoilov, I., Akarsu, A. N., and Sarfarazi, M. (1997). Identification of three different truncating mutations in cytochrome P4501B1 (CYP1B1) as the principal cause of primary congenital glaucoma (Buphthalmos) in families linked to the GLC3A locus on chromosome 2p21. *Human Molecular Genetics* 6(4): 641–647.
Stoilova, D., et al. (1996). Localization of a locus (GLC1B) for adult-onset primary open angle glaucoma to the 2cen-q13 region. *Genomics* 36(1): 142–150.
Stone, E. M., et al. (1997). Identification of a gene that causes primary open angle glaucoma. *Science* 275(5300): 668–670.
Thorleifsson, G., et al. (2007). Common sequence variants in the LOXL1 gene confer susceptibility to exfoliation glaucoma. *Science* 317(5843): 1397–1400.
Trifan, O. C., et al. (1998). A third locus (GLC1D) for adult-onset primary open-angle glaucoma maps to the 8q23 region. *American Journal of Ophthalmology* 126(1): 17–28.
Walter, M. A., et al. (1996). Autosomal-dominant iridogoniodysgenesis and Axenfeld-Rieger syndrome are genetically distinct. *Ophthalmology* 103(11): 1907–1915.
Wiggs, J. L., et al. (2000). Genome-wide scan for adult onset primary open angle glaucoma. *Human Molecular Genetics* 9(7): 1109–1117.
Wiggs, J. L., et al. (2004). A genomewide scan identifies novel early-onset primary open-angle glaucoma loci on 9q22 and 20p12. *American Journal of Human Genetics* 74(6): 1314–1320.
Wirtz, M. K., et al. (1997). Mapping a gene for adult-onset primary open-angle glaucoma to chromosome 3q. *American Journal of Human Genetics* 60(2): 296–304.
Wirtz, M. K., et al. (1999). GLC1F, a new primary open-angle glaucoma locus, maps to 7q35-q36. *Archives of Ophthalmology* 117(2): 237–241.

Figure 2 Diminishing vision in glaucoma.

glaucomatous features, suggesting that *MYOC* mutation does not cause glaucoma through haplo-insufficiency but through a dominant negative effect.

An interesting *MYOC* mutation (Lys423Glu) was described in a French–Canadian family, which resulted in a dominant negative effect when present in single dosage but had no phenotypic effect when present in both copies of the gene. The findings represent the first example of autosomal dominant metabolic interference. In metabolic interference, homozygosity for the normal allele *XX*, or for the mutant allele *xx*, both result in a normal phenotype. Only the heterozygous condition *Xx* produces an abnormal phenotype because the two alleles, when present together, interact to produce a harmful effect. These mutant proteins, resulting from Lys423Glu and Gln368Stop, in *MYOC* remain sequestered within cells. Furthermore, irrespective of mutant proteins produced from two alleles (homo-oligomer) or formed between wild type and mutant (hetero-oligomer), both remain sequestered within the cell. These researchers suggested a hypothesis that altered biochemical properties of mutant *MYOC* interfere with its secretion, dimerization, or interaction with other extracellular matrix components of the TM. Consistent with this idea, Fan and coworkers reported, in 2006, a Cys245Tyr mutation in *MYOC* in a Chinese glaucoma family, where the Cys245Tyr mutant protein formed homo-multimeric complexes that migrated at molecular weights larger than their wild-type counterparts and remained sequestered intracellularly in COS-7 cells. These data led to the hypothesis that myocilin-associated glaucoma is an endoplasmic reticulum (ER) storage disease, whereby chronic expression of misfolded, nonsecreted myocilin leads to TM cell death, TM dysfunction and, ultimately, a dominant glaucoma phenotype. The potential beneficial effects of facilitating folding and secretion of mutant myocilin suggested a new type of treatment for this form of glaucoma. Recently, it has been shown that mutations in human *MYOC* induce exposure of a cryptic peroxisomal targeting sequence whose interaction with the peroxisomal targeting signal type 1 receptor is necessary for elevation of IOP in a mouse model for human OAG. IOP is considered to be one of the major characteristic features in glaucoma.

Autosomal recessive inheritance was reported to be caused by a nonsense mutation in *MYOC* exon 1 in Koreans. However, a subsequent study from China identified a normal individual who was homozygous for the same mutation, suggesting that this *MYOC* alteration might be a nondisease-causing polymorphism. Among 64 mutations in the *MYOC* identified so far, four (Arg46Stop, Arg82Cys, Pro370Leu, and Thr377Met) mutations occur in mutable DNA motifs (CpG). These mutable motifs in DNA are considered to be the hotspots for mutation. Cooper and Youssofian suggested that deamination of 5-methylcytosine in a CpG dinucleotide followed by DNA replication results in mutation of the CpG to TpG. As described earlier, only eight mutations (Gln19His, Cys25Arg, Arg46Stop, Gln48His, Arg82Cys, Arg91Stop, Arg126Trp, and Arg158Gln) of a total 64 reported in *MYOC* are located in exon 1 of the MYOC gene. With the exceptions of Arg126Trp and Arg158Gln all of these mutations have been detected only in sporadic cases. Since sporadic mutations lack familial segregation data, they have weaker potential to be considered as disease-causing mutations. These findings suggest that the N-terminal region of *MYOC* encoded by exon 1 might harbor functionally less important domain than that contained within exon 3 (the olfactomedin domain).

A number of upstream/promoter region polymorphisms in *MYOC*, for example, −1000 G > C in *MYOC* and −153 T > C in *MYOC* have been suggested to have significant association with POAG including the normal-tension glaucoma. So far, about 50 *MYOC* polymorphisms have been reported, among which two (−83 G > A and Arg76Lys) have been detected in most of the populations examined. In addition, polymorphisms of additional genes have been suggested to have a role in OAG. Lin and coworkers showed a significant association of the p53 polymorphism (Arg72Pro) with Chinese POAG patients. However, additional studies did not find any association of Arg72Pro polymorphism in POAG patients of Indian origin.

While *MYOC* remains the most commonly mutated gene for POAG, several additional genes may also play a role in the disease. It has been recently reported that the polymorphism in *OPA1* is a significant risk factor for normal-tension glaucoma. Besides *MYOC* there were two

more genes reported to be linked with OAG. Mutations in *OPTN* were found to be responsible for 17% normal-tension glaucoma patients while *WDR36* is a potential candidate for OAG.

Molecular Genetics of CG: Mapped Loci and Identified Candidates

Genetic linkage studies revealed that CG mapped to two different loci, GLC3A (OMIM # 231300) located at chromosome 2p21 and GLC3B (OMIM no. 600975, Genbank accession no. NM_000104) located at chromosome 1p36 (**Table 1**). The causal gene at GLC3A locus has been found to be *CYP1B1*, which encodes for the cytochrome P450 enzyme. The causative gene for GLC3B has yet to be identified despite mutational analyses of a large number of genes identified in the chromosomal region (1p36) that contains the GLC3B locus. Following the discovery of association between the *CYP1B1* gene (OMIM # 601771) and GLC3A locus, 55 mutations and 32 polymorphisms have been identified in CYP1B1 in different populations. It is interesting to note that substantial portions of the mutations reported (19 out of 55) are deletion/insertions, implying an inherent instability of the CYP1B1 gene.

Cytochrome P450 1B1 (*CYP1B1*) as a Primary Candidate for CG

Overview

The *CYP1B1* genomic region spans >12 kb and contains three exons. Exon 1 encodes an untranslated portion of the CYP1B1 gene, while exons 2 and 3 encode for a protein containing 543 amino acids. CYP1B1 protein is a membrane-bound cytochrome that contains a transmembrane domain located at the amino-terminal region, and a proline-rich hinge region, which permits flexibility between the membrane-spanning domain and cytoplasmic portion of the molecule. Induced mutations in the hinge region interfere with the proper folding and heme-binding properties of other cytochrome P450 molecules. The C-terminal ends of members of the cytochrome P450 superfamily is highly conserved and contains a set of conserved core structures (CCSs) responsible for the heme-binding ability of these molecules. Between the hinge and the CCS lies a less conserved substrate-binding region.

Analysis of Mutations Associated with CG in *CYP1B1*

The identification of *CYP1B1* mutations in CG is the first example in which mutations in a member of the cytochrome P450 superfamily result in a primary developmental defect. It is thought that *CYP1B1* participates in the metabolism of an as-yet-unknown biologically active molecule that is a participant in eye development. They demonstrated that a stable protein product is produced in the affected subjects of these families, and that the three mutations they described would be expected to result in a product lacking amino acids between 189 and 254 from the C-terminus. This segment harbors the invariant cysteine of all known cytochrome P450 amino sequences; in *CYP1B1* it is *Cys470*. A cytochrome-P450-dependent arachidonate metabolite has been implicated that inhibits Na^+-K^+-ATPase in the cornea in regulating corneal transparency and aqueous humor secretion. This finding is consistent with the clouding of the cornea and increased IOP, two major diagnostic criteria for primary CG.

The involvement of *CYP1B1* in CG populations varies from 20% in Indonesians and Japanese populations to 50% among the Brazilians and about 100% among the Saudi Arabians and Slovakian Gypsies. The Slovakian Gypsies and Saudi Arabian populations exhibited allelic homogeneity largely attributed to consanguinity. Consanguinity is also prevalent in different ethnic groups of India and thus provides an excellent motivation to explore the role of *CYP1B1* in CG in these populations. Interestingly, the involvement of *CYP1B1* in CG was found to be lower (37.50%) in Indian population. This could be due to a lower rate of consanguinity and allelic homogeneity in the Indian populations. Relatively lower frequencies of *CYP1B1* mutations have also been observed in Southeast Asian populations such as Japanese (20%) and Indonesians (about 34%). Interestingly, none of the *CYP1B1* mutations in Japanese and Indonesian populations were found in Indian CG patients. Since Japanese and Indonesian populations reportedly has similar allelic distribution for numerous SNPs in different genes, the overlap in the *CYP1B1* mutation spectrum could be the result of shared ancestry between these two populations.

Genetic Overlap between CG and Juvenile Glaucoma (JOAG)

Involvement of *CYP1B1* in JOAG

The first report of *CYP1B1* involvement in JOAG came in 2002, where Vincent and coworkers showed an Arg368His mutation in *CYP1B1* expedited disease progression in combination with a Gly399Val mutation in *MYOC*. Later, *CYP1B1* was screened in 236 unrelated French–Caucasian OAG patients. They found mutations in 4.6% ($n = 11$) of the patients with no mutation in *MYOC*. In two families, occurrence of CG and OAG in members of a single sibship was found, all of which were compound heterozygous for mutations in the *CYP1B1* gene. Mutations in *CYP1B1* were typically associated with juvenile- and middle-age-onset OAG. Except one, all mutations detected in OAG patients were previously associated with PCG.

It has also been reported that another *CYP1B1* mutation was present in 200 unrelated Indian OAG patients. A R523T mutation in *CYP1B1* is primarily responsible for JOAG. Altogether six *CYP1B1* mutations were found in nine OAG patients (4.5%), consistent with previous reports. Subsequently, heterozygous *CYP1B1* mutations in Spanish OAG patients are present with similar frequency. Thus, it appears that *CYP1B1* has a larger role to play in glaucoma pathogenesis that includes causation of CG, modifying the pathogenesis of OAG, and, on rare occasion, being the primary cause of JOAG.

Recently, it has been reported that an Leu432Val polymorphism in *CYP1B1* is a susceptible factor for OAG. They designated Val432 as susceptible allele and CGGTA as the risk haplotype for OAG. They have shown higher amount of reactive superoxide (ROS) generation in Val432 in *CYP1B1* leading to apoptotic condition that might progress toward OAG. These data suggest that other than *CYP1B1* mutations, cSNPs found in normal individuals could also be functionally associated with OAG.

Involvement of *MYOC* in CG

Involvement of *MYOC* in CG was first described when 200 CG cases were screened for the *MYOC* Gln48His mutation and identified five cases harboring the mutant allele, which also included one homozygote. Interestingly, four of the five PCG cases harboring *MYOC* mutations, including the individual with the homozygous Gln48His mutation lacked any *CYP1B1* defect. These data and other more recent reports are consistent with a direct role of *MYOC* mutations in CG.

Digenic Inheritance in Glaucoma

The concept of defects in two genes gave rise to glaucoma (digenic inheritance) where primarily *MYOC*-linked OAG segregated in a large Guyanese family with *CYP1B1* as potential modifier. In that pedigree, a heterozygous *CYP1B1* mutation (Arg368His) was associated with earlier onset of the disease in patients carrying the *MYOC* mutation (Gly399Val), indicating that a *CYP1B1* mutation might behave as a modifier of the *MYOC* gene. In this family the mean age of onset of carriers of the *MYOC* mutation alone was 51 years, whereas carriers of both the *MYOC* and *CYP1B1* mutations had an average age of onset of 27 years. Similar results were reported, where a combination of *MYOC* and P1B1 variations appeared to be necessary to cause JOAG in an Indian population. These observations suggested that *MYOC* and *CYP1B1* may interact through a common pathway and *MYOC* function may be influenced by changes in *CYP1B1* and mutations of *CYP1B1* might be a cause of POAG or at least a risk factor for this disease. A potential digenic inheritance of *MYOC* and *CYP1B1* mutations leading to CG has been reported. Such digenic interaction is also observed in retinitis pigmentosa (RP) individuals who harbor specific mutations in both the peripherin/RDS and ROM1 genes wherein neither of these mutations in single gene alone causes RP.

Developmental Anomalies and Glaucoma

Since some forms of glaucoma are congenital, it is expected that glaucoma could be associated with ocular conditions that are the result of an abnormal differentiation of the eye. This is born out as the abnormal differential of ocular neural crest cells results in diseases that include glaucoma – for example, ARS, Peters' anomaly, and NPS/hereditary onycho-osteodysplasia (HOOD). These diseases share the features of variable expression of ocular features with high degree of penetrance among affected family members.

ARS is an autosomal-dominant developmental defect of the anterior segment of the eye that often results in glaucomatous blindness. The systemic ARS phenotype variously includes any of small, missing or absent teeth, redundant periumbilical skin, sensory hearing loss, congenital heart defects, and skeletal limb anomalies. The gross changes in eye morphogenesis in ARS are highly penetrant and ARS is associated with an approximately 50% risk of glaucomatous optic nerve damage and visual field loss. ARS is associated with mutations in two transcription factor genes (*PITX2* and *FOXC1*) expressed throughout eye development. However, more than 50% of ARS patients are without any genetic variation in defined loci and genes for ARS, suggesting that ARS has considerable genetic heterogeneity.

The Peters' anomaly is another congenital abnormality associated with glaucoma, which shows a number of ocular phenotypes that include central corneal leukoma (opacity), absence of the posterior corneal stroma and Descemet membrane, and a variable degree of iris and lenticular attachments to the central aspect of the posterior cornea. A number of genes including *PITX2*, *FOXC1*, and *PAX6* have been reported to be associated with Peters' anomaly. A mutation in *CYP1B1* is also causal for Peters' anomaly, and mutations in *CYP1B1* could contribute to 20% of cases of Peters' anomaly. However, the genetic basis for this anomaly is still not clear and, to date, there are no major loci found to be linked with the anomaly.

In addition to these anomalies, several other developmental defects are associated with glaucoma. NPS or HOOD has been shown to be associated with glaucoma by Dryer and coworkers in 1998. NPS is an autosomal-dominant, pleiotropic disorder with features suggestive of a primary defect of connective tissue, and is caused by mutations in LMX1B gene. The encoded protein specifies the development of dorsal structures from mesoderm during limb development. In all of these developmental

abnormalities, the genes mutated in these conditions cause the developmental defects of the eye structure. However, the fact that these genes continue to be expressed in the adult eye suggests that a combination of structural defects that predispose to glaucoma pathogenesis and disruption of functions of these genes in the adult eye together result in glaucoma. It appears that the ARS gene *FOXC1* is involved in stress-response pathways in the adult eye, which is consistent with this hypothesis.

Future Directions

Taken together, these data suggest overlapping genetic mechanisms for causation of both JOAG and CG. Although JOAG and CG are different in terms of age of onset, they share many common anatomical (e.g., angle between iris and cornea remains open) as well as physiological (e.g., elevated IOP) features related to glaucoma. However, there are several distinct morphological features observed in the eye of a CG patient that are not present in patients affected with JOAG. In addition, digenic inheritance in JOAG suggested a genetic connection between *MYOC* and *CYP1B1* that requires thorough investigation at functional level. In 2001, Vincent and coworkers suggested that *MYOC* and *CYP1B1* might interact through a common pathway and proposed that *MYOC* function might be influenced by changes in *CYP1B1*. To date, however, there are no reports of a direct physical interaction between *MYOC* and *CYP1B1*. In all likelihood, there might be one or more unknown substrates of *CYP1B1* acting as missing link in the common pathway through which both *MYOC* and *CYP1B1* interact. Exploration of this area could be particularly fruitful.

From multiple genetic evidences it appears that JOAG and CG are parts of a larger disease spectrum where mutation in a single gene can cause either form of glaucoma. At the same time, some of these forms of glaucoma only result from simultaneous mutations of several genes. Current evidence indicates that *CYP1B1* has a larger role to play in glaucoma pathogenesis, which includes causation of CG, modification of the pathogenesis of OAG, and, on rare occasion, it might be the primary cause for JOAG. Therefore, from the viewpoint of glaucoma molecular diagnostics, both *MYOC* and *CYP1B1* should be routinely screened for disease-causing variants in both JOAG and CG patients.

See also: Animal Models of Glaucoma; Biomechanics of Aqueous Humor Outflow Resistance; Functional Morphology of the Trabecular Meshwork; The Genetics of Primary Open-Angle Glaucoma: A Review; Myocilin; Primary Open-Angle Glaucoma.

Further Reading

Johnson, W. G. (1980). Metabolic interference and the + – heterozygote. A hypothetical form of simple inheritance which is neither dominant nor recessive. *American Journal of Human Genetics* 32: 374–386.

Luntz, M. H. (1979). Congenital, infantile, and juvenile glaucoma. *Ophthalmology* 86(5): 793–802.

Quigley, H. A. (1996). Number of people with glaucoma worldwide. *British Journal of Ophthalmology* 80: 389–393.

Ray, K., Mukhopadhyay, A., and Acharya, M. (2003). Recent advances in molecular genetics of glaucoma. *Molecular and Cellular Biochemistry* 253(1–2): 223–231.

Sarfarazi, M., Akarsu, A. N., Hossain, A., et al. (1995). Assignment of a locus (GLC3A) for primary congenital glaucoma (Buphthalmos) to 2p21 and evidence for genetic heterogeneity. *Genomics* 30(2): 171–177.

Sarfarazi, M., Stoilov, I., and Schenkman, J. B. (2003). Genetics and biochemistry of primary congenital glaucoma. *Ophthalmology Clinics of North America* 16(4): 543–554 vi.

Sheffield, V. C., Stone, E. M., Alward, W. L., et al. (1993). Genetic linkage of familial open angle glaucoma to chromosome 1q21–q31. *Nature Genetics* 4(1): 47–50.

Stoilov, I., Akarsu, A. N., Alozieet, I., et al. (1998). Sequence analysis and homology modeling suggest that primary congenital glaucoma on 2p21 results from mutations disrupting either the hinge region or the conserved core structures of cytochrome P4501B1. *American Journal of Human Genetics* 62(3): 573–584.

Stone, E. M., Fingert, J. H., Alward, W. L., et al. (1997). Identification of a gene that causes primary open angle glaucoma. *Science* 275(5300): 668–670.

Tamm, E. R. (2002). Myocilin and glaucoma: Facts and ideas. *Progress in Retinal and Eye Research* 21(4): 395–428.

Vasiliou, V. and Gonzalez, F. J. (2008). Role of CYP1B1 in glaucoma. *Annual Review of Pharmacology and Toxicology* 48: 333–358.

Zhou, Z. and Vollrath, D. (1999). A cellular assay distinguishes normal and mutant TIGR/myocilin protein. *Human Molecular Genetics* 8(12): 2221–2228.

Relevant Website

http://archive.uwcm.ac.uk – The Human Gene Mutation Database at the Institute of Medical Genetics in Cardiff.

Molecular Mechanisms of Angiostasis

A Sudhakar, Boys Town National Research Hospital, Omaha, NE, USA
R Kalluri, Department of Medicine, Beth Israel Deaconess Medical Center and Harvard Medical School, Boston, MA, USA

Glossary

Basement membranes – Thin sheets of extracellular matrix at the interface between epithelial and mesenchymal tissues that contain type IV collagen, adhesive glycoproteins, and proteoglycans.
Caspase – A type of protein that is involved in apoptosis (a normal process in a cell that leads to its death).
Endothelial cell – Cell type responsible for blood vessel formation, forms inner lumen of blood vessels.
Extracellular matrix – Three-dimensional macromolecular network that forms a structural scaffold and an instructional cellular and tissue environment.
Focal adhesion kinase – An important intracellular mediator of integrin signaling. FAK is phosphorylated and activated on endothelial cell integrin engagement with various ligands.
Integrin – A large family of noncovalently linked, heterodimeric trans-membrane cell-adhesion receptors that also transduce signals from the outside to the inside of the cell and vice versa.
Matrix metalloproteinases – A large family of proteolytic enzymes that preferentially degrade collagens, basement membranes, and other extracellular matrices. They are extremely active during tissue remodeling, cancer and angiogenesis.
Mitogen-activated protein kinases – Important intracellular mediators of integrin signaling. They belong to two major classes, ERK1 and ERK2, and p38 MAPK (MAPKs function downstream of FAK).
Noncollagenous domain 1 – The C-terminal domain of type IV collagen. In type IV collagen, proteolytic cleavage from the parent molecule can release NC1 fragments that can become anti-angiogenic.
Phosphatidylinositol-3 kinase – Important intracellular mediators of integrin signaling (PI3K function downstream of FAK).
RGD – Proteins that contain the Arg–Gly–Asp (RGD) attachment site.

Introduction

Vascular basement membrane (VBM)-derived molecules are regulators of certain biological activities, such as cell growth, differentiation, and angiogenesis. Angiogenesis, the process by which neovasculature is created from native blood vessels, is essential in both normal development and several pathological conditions, such as cancer, rheumatoid arthritis, choroidal neovascularization (CNV) in age-related macular degeneration (AMD), and diabetes. Angiogenesis is regulated by a systematic controlled balance between VBM-derived angiostatic factors and proangiogenic growth factors. In the normal physiological state, equilibrium is maintained between the angiostatic and proangiogenic factors. In cancer, tumor cells require new blood vessels to sustain local growth and escape to distant sites through hematogenous spreading and metastasis. Without angiogenesis, tumor cells cannot survive for long, for this reason, endogenous angiostatic factors which do not engender the same sort of resistance and intolerance as exogenous compounds might be important candidates for anticancer or anti-CNV in AMD therapy, either by themselves or in combination with other agents that are used more routinely in the clinic.

Endogenous angiogenesis inhibitors from extracellular matrix (ECM) include large multifunctional ECM glycoproteins, such as thrombospondin, Endorepellin (a C-terminal end of perlecan), anastellin (a fibronectin fragment), fibulins (C-terminal fragments corresponding to fibulin 1D and the domain 111 of fibulin 5), and endostatin. The discovery of endostatin hastened the investigation to find other matrix components, such as collagen IV, that have the potential to modulate angiogenesis. The proteolytic cleavage of type IV collagen generates noncollagenous (NC1) domains which include: arresten (α1(IV)NC1), canstatin (α2(IV)NC1), tumstatin (α3(IV)NC1), and α6(IV)NC1 domains identified as angiostatic molecules discussed in this article. In this terminology, α indicates the chain in collagen IV (**Figure 1**). Thus, the molecules that are needed to assemble a basement membrane (BM) to maintain the integrity of blood vessels and to prevent the leakage of fluids and loss of proteins can do the opposite under the right circumstances; that is, they have both angiogenic and angiostatic activities. Interestingly, endogenous angiostatic proteins that are derived from type IV collagen

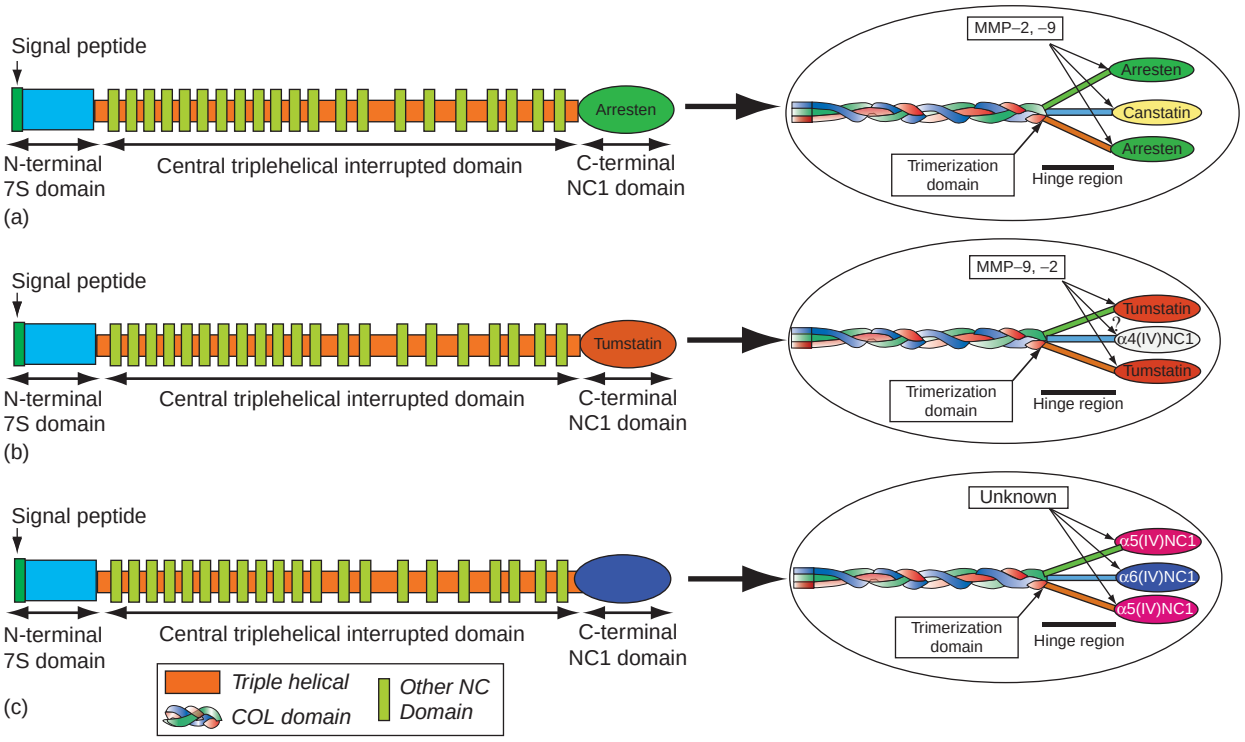

Figure 1 Structural domains of mammalian type IV collagen. (a) Type IV collagen (a single α1(IV) chain is depicted for simplicity) contains an N-terminal cysteine-rich 7S domain, a central triple-helical interrupted domain by noncollagenous (NC) domains, and a C-terminal NC1 domain. The NC1 domain is enlarged as a trimer of $[\alpha1(IV)]_2\alpha2(IV)$. α1(IV) and α2(IV) chains contain the antiangiogenic domains arresten (or α1(IV)NC1) and canstatin (or α2(IV)NC1) (labeled green and yellow oval). (b) α3(IV) chain contains an N-terminal cysteine-rich 7S domain, a triple-helical interrupted domain by NC domains, and a C-terminal NC1 domain shown. The NC1 domain is enlarged as a trimer of $[\alpha3(IV)]_2\alpha4(IV)$. α3(IV) contains the antiangiogenic domain tumstatin (or α3(IV)NC1) (labeled red oval). No antiangiogenic activity has been identified from α4(IV)NC1 domain (labeled white oval). (c) α5(IV) chain contains an N-terminal cysteine-rich 7S domain, a triple-helical domain interrupted by NC domains, and a C-terminal NC1 domain shown. The NC1 domain is enlarged as a trimer of $[\alpha5(IV)]_2\alpha6(IV)$. α6(IV) contains the antiangiogenic NC1 domain (α6(IV)NC1) (labeled blue oval). No antiangiogenic domain has been identified from α5(IV) (labeled pink oval).

possess similar structures that have striking differences in their angiostatic actions.

Type IV collagen NC1 domains exert their effects by interacting with cell-surface integrin receptors that help modulate how cells interact with and are affected by matrix components. The functional receptor for each angiostatic agent derived from type IV collagen is different and specific; α1β1, αVβ5/αVβ3, αVβ3/α3β1, and αVβ3 integrins for arresten, canstatin, tumstatin, and α6(IV)NC1, respectively. This indicates that the mechanism of receptor engagement and downstream signaling events might also be different and specific, although some common intracellular signaling components are modulated. Canstatin and tumstatin function by inhibiting endothelial protein synthesis and promoting apoptosis. Arresten and α6(IV)NC1 seem to interact differently with integrins compared with the typical native ligands from which they are derived. The four fragments are structurally related but differ functionally, which explains why they interact with different integrins and have different effects on angiogenesis. By restricting our focus to these four angiostatic molecules, we hope to emphasize similarities that might also apply to other (perhaps undiscovered) angiostatic matrix molecules and further our understanding of angiostatic activity with potential therapeutic benefit against diseases in which angiogenesis play role.

Physiological and Biological Functions of Type IV Collagen

Type IV collagen is the most abundant constituent of the BM that forms a network-like structure in the ECM. Type IV collagen provides a scaffold in the BM with other macromolecules, such as laminins, heparan sulfate proteoglycans, fibronectin, entactin, and regulates the interaction with adhering cells discussed separately in this article. Type IV collagen is ubiquitously present in VBM and is highly conserved among vertebrates and invertebrates, regulating cell adhesion and migration. Type IV collagen has six α-chains and can exist in atleast three hetero-trimeric triple helical forms $[\alpha1(IV)]_2\alpha2(IV)$, $[\alpha3(IV)]_2\alpha4(IV)$, and $[\alpha5(IV)]_2\alpha6(IV)$ and their genomic localization shows a pair-wise head-to-head arrangement with a

bi-directional promoter that were mapped onto three different chromosomes. Each α(IV) chain in type IV collagen is composed of three distinct domains: a cysteine-rich N-terminal 7S-domain, a central long triple helical collagenous domain with Gly–X–Y repeats (where X and Y represent any amino acids other than glycine, but are often proline and hydroxyproline) interrupted by short NC domain, and a globular C-terminal NC1 domain of ~ 230 amino acids (**Figure 1**). The NC1 domains are involved in the assembly of α-chains to form heterotrimers and the 7S-domains are involved in the covalent assembly of heterotrimers in a complex mesh-like network that serves as a scaffold for BM. Several human genetic diseases provided insights into the physiological role of type IV collagen discussed in this article. Mutations or deletions in Col4α5, Col4α3, and Col4α4 chains are involved in Alport syndrome (defective glomerular BM) and diffused leiomyomatosis (a benign smooth muscle tumor). The C-terminal region of α3 chain of type IV collagen has been identified as an autoantigen involved in Goodpasture syndrome (an immune disease characterized by glomerulonephritis and pulmonary hemorrhage). The α1(IV) and α2(IV) chains are ubiquitous and $[\alpha1(IV)]_2\alpha2(IV)$ heterotrimers are predominant. In humans, no disease is yet linked to mutations in the major α1(IV) and α2(IV) chains.

The $[\alpha1(IV)]_2\alpha2(IV)$ trimers contain a triple helical domain with binding sites for α1β1 and α2β1 integrins. Cells bind to type IV collagen and this binding inhibited by type IV collagen derived peptides was demonstrated in several cell types. A peptide that was derived from NC1 of the α1(IV) chain could promote adhesion of bovine aortic endothelial cells. The functional α1 and α2 type IV collagen chains isolated from the Engelbreth Holm Swarm Sarcoma tumors inhibited capillary endothelial cell proliferation. In primitive invertebrate Hydra vulgaris, addition of NC1 type IV collagen alters morphogenesis, blocking cell aggregate and development. These results confirm that the biological functions of NC1 domains are conformation dependent.

Generation of Angiostatic Domains from Type IV Collagen and Their Signaling Mechanisms

Proteolytic degradation of type IV collagen induces exposure of cryptic sites which is involved in binding of integrins and sends new signals between cells and BM. Several NC1 domains from type IV collagen were detected in the serum of patients suggesting that these domains exist due to physiological cleavage of ECM by proteases. Earlier we reported that arresten, canstatin and tumstatin are proteolytic NC1 peptides generated from α1, α2, and α3 chains of type IV collagen by matrix metalloproteinase (MMP)-9, -2, and -13. Although we gained some preliminary clues for *in vitro* processing of type IV collagen NC1 domains, the exact mechanisms of generation still need to be extensively investigated. In early 2000, several groups focused their attention on potential angiostatic properties of type IV collagen NC1 domains and identified their angiostatic effects.

Different Integrins Mediated Angiostatic Signaling by Tumstatin

Tumstatin, a 28 kDa protein from the C-terminal NC1 fragment of α3(IV) (**Figure 1**), was identified originally as an inhibitor of angiogenesis in early 2000. Inhibition of cell migration using peptide 185–205 amino acids from tumstatin was reported in melanoma and fibrosarcoma cells with a decrease in expression of membrane-bound metalloproteinase (MT1-MMP) and activated MMP-2. Tumstatin inhibits formation of tubular structures in mouse aortic endothelial cells embedded in Matrigel plugs and inhibits growth of different tumors in mouse models (renal cell carcinoma (786-O), CT26 (colon adenocarcinoma), prostate carcinoma (PC3), Lewis lung carcinoma (LLC), human lung cancer (H1299), human prostate cancer (DU145), human fibrosarcoma (HT1080), and teratocarcinoma (SCC-PSA1)). But what are the cell surface integrin receptor(s) involved in these angiostatic actions of tumstatin? It is clear that different integrins are key targets of tumstatin. Tumstatin interacts with endothelial cell via αVβ3 integrin in a vitronectin and RGD-independent fashion. Integrin αVβ3 interacts with tumstatin through two distinct regions, comprising residues 54–132 and 185–203 amino acids. The first site is involved in the angiostatic activity (is sufficient to inhibit *in vitro* and *in vivo* angiogenesis by increasing apoptosis in endothelial cells), whereas the second site is involved in antiproliferative activity on cancer cell lines. These results confirm specific regulatory subdomains in tumstatin control adhesion, proliferation, or apoptosis in various cell types. The functional specificity of these subdomains from tumstatin in endothelial or cancer cells is very interesting. Indeed, the recently published 3D crystal structure of type IV collagen NC1 domain reveals N- and C-homologous subdomains. The major difference between these subdomains for each chain is in the region from residues 86–95 in the N-subdomain and 196–209 in the C-subdomain. These regions overlap two sequences that were previously identified to be having angiostatic and antiproliferative effects in cancer cells. Tumstatin or its peptides interaction with integrins seems to be involved in the disruption of contacts between endothelial or tumor cells and the BM, leading to apoptosis in these cells. Tumstatin also binds to endothelial cells through α6β1 and αVβ5 integrins, but the significance of these integrins interaction is not yet clear.

Tumstatin induces endothelial cell apoptosis by interacting with αVβ3 integrin and inhibits adhesion to VEGF in the matrix, and this effect was potentiated by anti-αVβ3 blocking antibody. The angiostatic activity of tumstatin was conferred by its N-terminal end comprising amino acid residues 54–132 region interaction with integrin αVβ3 and inhibiting activation of focal adhesion kinase (FAK), phosphatidylinositol 3-kinase (PI3K), serine/threonine kinase (Akt/protein kinase B), mammalian target of rapamycin (mTOR), and prevents dissociation of eukaryotic translation initiation factor 4E (eIF4E) from 4E-binding protein 1 (4E-BP1) leading to the inhibition of Cap-dependent translation in proliferating endothelial cells (Figure 2). Furthermore, these findings indicate a specific role for integrins in mediating cell specific inhibition of protein translation suggesting a potential specific mechanism of tumstatin on endothelial cells. α3β1 integrin binds to C-terminal region 185–203 residues associated with

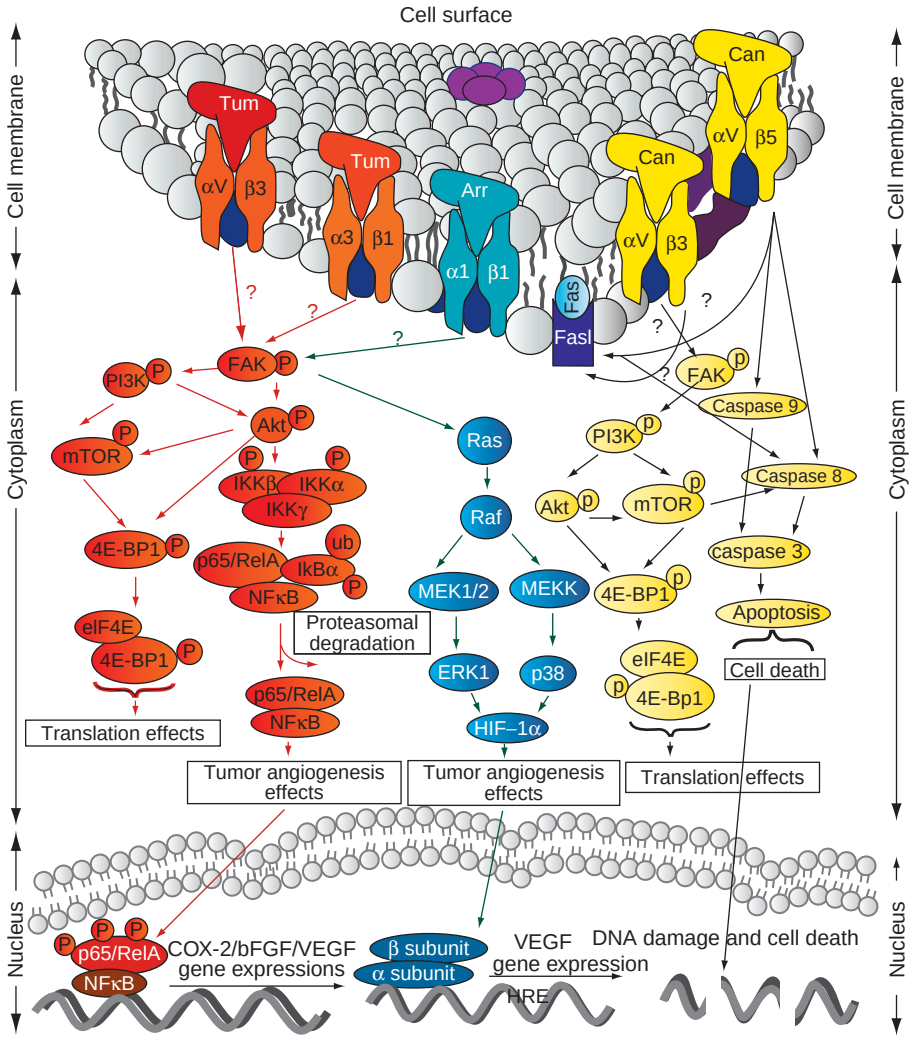

Figure 2 Schematic illustrations of the different integrins mediated signaling pathways evoked by tumstatin (Tum), arresten (Arr), and canstatin (Can) in endothelial cells. Tumstatin (signaling components shown as red ovals), arresten (signaling components depicted as blue ovals), and canstatin (signaling components depicted as yellow ovals) interact with αVβ3/α3β1, α1β1, and αVβ3/αVβ5 integrins, respectively, to inhibit the phosphorylation of FAK. Tumstatin: It binds to αVβ3 and α3β1 integrins and inhibits the pathway that includes phosphorylation of FAK, PI3K, serine/threonine kinase (Akt), mammalian target of rapamycin (mTOR), eIF4E-4E-BP1, and eIF4E to decrease endothelial cell protein synthesis and proliferation. In addition, tumstatin also inhibits NFκB-mediated signaling in hypoxic conditions and leads to inhibition of cyclo-oxygenase (COX-2), VEGF, bFGF expressions, resulting in inhibition of hypoxic tumor angiogenesis. Antagonism of the α3β1 integrin by tumstatin might also cause transdominant inhibition of αVβ3 integrin. Arresten: It binds to α1β1 integrin and inhibit phosphorylation FAK, causes inhibition of Ras (a small GTPase), Raf (a serine/threonine kinase), extracellular signal-related kinase 1 (ERK1), and p38 MAPK pathways that leads to inhibition of HIF-1α and VEGF expression resulting in inhibition of endothelial cell migration, proliferation, tube formation, and apoptosis in proliferating endothelial cells. Canstatin: It binds to αVβ3/αVβ5 integrins and inhibits two apoptotic pathways, involving activation of caspase-8 and casoase-9, leading to activation of caspase-3 on endothelial cells. Canstatin activates procaspase-9 not only through inhibition of the FAK/PI3K/AKT pathways, but also by cross talking mitochondrial pathway through Fas-dependent caspase-8 activation leads to endothelial cell apoptosis.

antitumor activity. These data correlate with earlier findings that tumstatin binds to α3β1 integrin and transdominantly inhibits expression of αVβ3 integrin. Interestingly, recent studies clearly show that in addition to tumor suppressive action of tumstatin or its peptide (T3; C-terminal end comprising amino acid residues 133–244 region of the tumstatin) directly inhibits growth of glioma cells. In addition, a cyclopeptide derived from tumstatin (YSNSG) was also shown to inhibit human melanoma cell proliferation.

Recently, Boosani and coworkers identified that tumstatin inhibits hypoxia-induced cyclo-oxygenase-2 (COX-2) expression in endothelial cells via FAK/Akt/NFκB (nuclear transcription factor-kappa B) pathways, leading to decreased tumor angiogenesis and tumor growth in an α3β1 integrin dependent manner. In addition to COX-2 inhibition, the down stream VEGF and basic fibroblast growth factor (bFGF) protein expression was also inhibited upon tumstatin treatment to endothelial cells. Moreover, several investigators have demonstrated that blockade of COX-2-mediated pathway serves as a therapeutic benefit in different cancer models and potential target for tumor angiogenesis. These findings indicate that there may be several targets for the inhibitory effects of tumstatin in tumor angiogenesis. The above studies support the angiostatic and antitumorogenic activity of tumstatin mediated through αVβ3 and α3β1 integrins (**Figure 2**). Surprisingly, abnormal tumorogenesis is observed in mice lacking tumstatin, indicating that it is playing a role in pathological angiogenesis to decrease tumor progression. However, in a controlled angiogenic process such as wound healing, tumstatin does not affect the overall neovascularization. Although tumstatin is efficient in reducing tumor neovascularization, its exact role needs to be deciphered.

Different Integrins Mediated Angiostatic Signaling by Canstatin

Proteolytic degradation of type IV collagen liberates a 24 kDa peptide from C-terminal NC1 domain of α2 chain, called canstatin [α2(IV)NC1], and this peptide was reported to inhibit tumor-associated angiogenesis. Canstatin binds to the endothelial and tumor cell surface in an αVβ3 and αVβ5 integrin-dependent manner. Canstatin competes with type IV collagen of ECM for cell surface integrin binding and reverses the proliferative and migratory effects induced by cell–ECM interactions. Thus, αVβ3 and αVβ5 integrins appear to mediate the angiostatic and antitumorgenic properties of canstatin. In addition, researchers also determined that canstatin binds to αVβ3 and αVβ5 integrins and induce apoptosis in endothelial and certain tumor cells. Canstatin inhibits the growth of many tumors in human xenograft mouse models, histological studies revealed decreased CD31 positive vasculature. Canstatin strongly inhibits the migration and proliferation of endothelial cells. Moreover, these events are mediated by an upstream event involving canstatin binding to αVβ3 and αVβ5 integrins. Recent findings have shown that canstatin inhibits the phosphorylation of FAK, Akt, mammalian target of rapamycin (mTOR), eukaryotic initiation factor 4E-BP1, and ribosomal S6 kinase in cells. Canstatin binds to αVβ3 and αVβ5 integrins and initiates two apoptotic pathways that include activation of caspase-8 and-9 (both initiators of the downstream apoptotic process), and leads to activation of caspase-3. Canstatin activates caspase-8 by downregulation of Flip levels. Upregulation of Fas/Fas ligand triggers not only cell death directly through caspase-3 activation, but also indirectly through mitochondrial damage via activation of caspase-9 within the apoptosome. On the other hand, phosphorylated FAK/PI3K is known to inactivate the mitochondrial apoptotic pathway by inhibition of caspase-9 (**Figure 2**). Canstatin directly activates procaspase-9 through inhibition of the FAK/PI3K pathway and amplifies the Fas-dependent pathway in mitochondria. Caspase activation in endothelial cells by canstatin might be exploited for treatment of CNV in AMD or therapy in the treatment of cancer.

Recently, the Campochiaro group reported that intravitreous or periocular injections of canstatin caused selective apoptosis of endothelial cells participating in neovascularization resulting in suppression of neovascularization when it was given prior to onset of new vessel sprouting. Importantly, when the canstatin was given after neovascularization had already developed, it caused the new vessels to regress. These results demonstrates that canstatin, which has previously been shown to suppress tumor angiogenesis in xenograft models, is also a strong angiostatic agent in the choroid and is a therapeutic candidate for treatment of choroidal nonvascular in AMD.

Canstatin inhibits FAK/Akt signaling by binding to αVβ3 and αVβ5 integrins and induces distinct signaling pathways to activate caspase-3 in endothelial or in tumor cells. Canstatin initiates two apoptotic pathways, involving activation of caspase-8 and -9, leading to activation of caspase-3. Canstatin activates (1) procaspase-9 directly through inhibition of the FAK/PI3K/Akt pathway and (2) caspase-3 by amplifying indirectly the mitochondrial pathway through Fas-dependent caspase-8 activation; whereas in tumor cells canstatin activates caspase-3 only the mitochondrial pathway (**Figure 2**). Collectively, the available research information suggests that, canstatin binds to αVβ3 and αVβ5 integrins and inactivates FAK downstream signaling, leading to suppression of cell proliferation and migration and thus leading to apoptosis.

Distinct Integrin-Mediated Angiostatic Signaling by Arresten

Arresten is a 26 kDa molecule derived from the NC1 domain of the α1 chain of type IV collagen by proteases. Not much is known yet about arresten, its angiostatic actions are presumably mediating through α1β1. Integrin

α1β1 is a collagen-binding receptor that also binds to other BM components, such as laminin. Blocking of α1β1 integrin interactions with ECM inhibits angiogenesis, which indicates that the integrin α1β1 acts as pro-angiogenic receptor. Among the integrin receptors for collagen, α1β1 integrin activates the Ras/Shc mitogen-activated protein kinase (MAPK) pathway promoting cell proliferation. Arresten binds to α1β1 integrin in a collagen type IV dependent manner and mediates its angiostatic and proapoptotic functions and inhibits angiogenesis by inhibiting endothelial cell proliferation, migration, and tube formation. Significant halt in pathological angiogenesis and tumor growth was reported in α1 integrin knockout mice. Whereas arresten had no effect in α1 integrin null endothelial cells, on the contrary, it significantly inhibited proliferation of wild-type mouse endothelial cells. This confirms the significance of integrin α1β1-mediated signaling of arresten. Arresten inhibits phosphorylation of FAK/Ras/Raf/MEK1/2 and p38 MAPK when mouse lung endothelial cells (MLECs) are plated on collagen type IV matrix. Similar inhibition of FAK/Ras/Raf/MEK1/2 and p38 MAPK phosphorylation was not observed with arresten treatment in α1 integrin null MLECs. Downstream to FAK, Akt/PKB plays an important role in endothelial cell survival signaling. Arresten does not inhibit Akt or phosphatidyl-3-kinase (PI3K) phosphorylation suggesting that arresten regulates migration of endothelial cells in an Akt-independent manner.

In addition, recently, Nyberg and coworkers identified arresten and its active peptides induce endothelial cell apoptosis via downregulation of Bcl-2 (antiapoptotic) and Bcl-xL (antiapoptotic) with no effect on Bax (proapoptotic) expression. These Bcl-family members are significantly involved in the balance of proapoptotic and antiapoptotic signals at the mitochondrial level. The balance of their expression determines whether cells undergo apoptosis. These studies demonstrate that activation of apoptotic signaling in proliferating endothelial cells is sufficient to inhibit or regulate new blood vessel formation. These results are consistent with earlier reports that angiostatic and antitumorogenic activity of arresten is partly mediated via integrin cross talk with a cell-intrinsic apoptotic pathway.

Interestingly hypoxia-induced factor alpha (HIF-1α) and VEGF expression was inhibited by treatment of arresten in hypoxic (lack of oxygen) endothelial cells in an α1β1 and FAK/Ras/Raf/MEK1/2 and p38 MAPK manner (**Figure 2**). HIF-1α is an oxygen-dependent transcriptional activator, which plays crucial roles in the tumor angiogenesis. HIF-1α regulates cellular responses to physiological and pathological hypoxia, and studies demonstrate that HIF-1α is a potential target for tumor angiogenesis. HIF-1α transcriptionally regulates VEGF expression in hypoxic cells and promotes angiogenesis in solid tumors. These findings suggest that HIF-1α is a prime target for anticancer therapies. This hypoxic inhibitory activity might be exploited for antiangiogenic therapy in the treatment of cancer, but more preclinical laboratory studies are needed.

Distinct Integrin-Mediated Angiostatic Signaling by α6(IV)NC1

Recombinant α6(IV)NC1 binds to αVβ3 integrin and inhibits human endothelial cell proliferation and neovascularization of Matrigel plugs in mice. The α6(IV)NC1 suppresses the growth of subcutaneously transplanted Lewis lung carcinoma and also spontaneous pancreatic insulomas that develop in the Rip1Tag2 mice. Inhibition of tumor growth is associated with significantly diminished microvascular density. Collectively, present scientific evidence suggested that α6(IV)NC1 is an another angiostatic molecule that are generated from type IV collagen showing antitumorogenic activity. How α6(IV)NC1 regulates angiostatic activities is not yet clear and further extensive studies are needed to address this molecule as an inhibitor of angiogenesis and to be considered for the future clinical trials

Conclusions and Perspectives

In the last decade, several different endogenous angiostatic molecules have been discovered and their pharmacological studies showed promising angiostatic activity, but their mechanism of action and physiological role are not yet understood. Type IV collagen derived angiostatic molecules binds to different integrins and exert their effects through multiple mechanisms including induction of endothelial cell apoptosis, inhibition of endothelial cell proliferation, migration and tube formation, and inhibition or alteration the functions of proangiogenic growth factors. Three possible conclusions drawn from the signaling mechanisms of type IV collagen derived angiostatic molecules that are shown in **Table 1**. (1) All these collagen type IV derived inhibitors appears to exert their angiostatic effects by binding to specific cell surface integrins. (2) These inhibitors also block the binding of natural ligand/binding partners for proangiogenic receptors/molecules. (3) In addition, possibly by binding to its receptors, these inhibitors cross talk with other cell surface receptors and activate specific caspase-mediated signaling to regulate cell functions.

In addition several angiogenic inhibitors including αV integrin antagonist EMD 121974, 2-methoxyestradiol (panzam) and MMP-2,-9 inhibitor COL-3 etc. are currently in half phases in human clinical trails. Recent study suggests that upregulation of specific proangiogenic factors is a common mechanism for colorectal and renal carcinoma cells to evade inhibition by several of extracellular derived

Table 1 Signaling Mechanisms Mediated by Type IV Collagen Derived Angiogenesis Inhibitors

Angiogenesis inhibitor name	**Arresten (α1(IV)NC1)**	**Canstatin (α2(IV)NC1)**	**Tumstatin (α3(IV)NC1)**	**α6(IV)NC1**
Inhibitor origin	Type IV collagen α1 chain NC1 domain	Type IV collagen α2 chain NC1 domain	Type IV collagen α3 chain NC1 domain	Type IV collagen α6 chain NC1 domain
Generated by	By MMP-2 and -9	By MMP-9 and -2	By MMP-9, -2, -3 and -13	Not known
Integrin binding	α1β1 ?	αVβ5, αVβ3, ?	αVβ3, α3β1, αVβ5, α6β1?	αVβ3, ?
Endothelial proliferation	Effect	Effect	Effect	Effect
Endothelial migration	Effect	Effect	No effect	Not known
Endothelial tube formation	Effect	Effect	Effect	Not known
Anti-angiogenic effects	Inhibits endothelial proliferation and migration	Inhibits endothelial proliferation by activating apoptosis	Inhibits endothelial proliferation and protein synthesis	Inhibits endothelial proliferation
Anti-angiogenic signaling mechanism	FAK/Ras/cRaf/MEK1/2/p38/ERK1/2/HIF1α mediated signaling and Bcl-2 mediated apoptosis.	FAK/Akt/PI3/mTOR/eIF-4E/4E-BP1 signaling and FasL mediated apoptosis	FAK/Akt/PI3K/mTOR/ eIF-4E/4E-BP1 and NFkB/COX-2 mediated signaling	Not known

endogenous angiogenesis inhibitors. Earlier lessons from preclinical trials of angiostatin, endostatin, 2-ME, etc. suggest that more basic research is required for better understanding of the mechanisms of action associated with these inhibitor molecules. Presently, some of the angiostatic agents, such as Bevacizumab, and several other VEGFR tyrosine kinase inhibitors, Vatalanib (PTK787/ZK 222584), Semaxanib (SU5416), Sunitinib (SU11248), Sorafenib (BAY 43-9006), etc., are in clinical trials. Further extensive evaluation of arresten, canstatin, tumstatin, and α6(IV)NC1 through pharmacokinetic studies is needed to address these molecules as an inhibitors of angiogenesis and to be considered for the clinical trials.

Acknowledgments

The original research was supported by NIH grants DK62987, DK61688, CA12550, Champalimaud Foundation Metastatis Research Program and, funds from the Division of Matrix Biology at Beth Israel Deaconness Medical Center to RK; and also supported by Flight Attendant Medical Research Institute Young Clinical Scientist Award Grant FAMRI# 062558, Dobleman Head and Neck Cancer Institute Grant #61905, startup funds of Cell Signaling and Tumor Angiogenesis Laboratory at Boys Town National Research Hospital to AS.

See also: Angiogenesis in Inflammation; Angiogenesis in Response to Hypoxia; Angiogenesis in Wound Healing; Pericytes and Microvascular Remodeling: Regulation of Retinal Angiogenesis; Stability and Functional Integrity of New Blood Vessels; Vessel Regression.

Further Reading

Boosani, C. S., Mannam, A. P., Cosgrove, D., et al. (2007). Regulation of COX-2 mediated signaling by α3 type IV noncollagenous domain in tumor angiogenesis. *Blood Journal* 110: 1168–1177.

Folkman, J. and Kalluri, R. (2002). *Tumor Angiogenesis. Part II Scientific Foundation, Section 1: Cancer Biology. Cancer Medicine,* 6th edn. London: BC Decker.

Hamano, Y., Zeisberg, M., Sugimoto, H., et al. (2003). Physiological levels of tumstatin, a fragment of collagen IV alpha3 chain, are generated by MMP-9 proteolysis and suppress angiogenesis via alphaV beta3 integrin. *Cancer Cell* 3: 589–601.

Kalluri, R. (2002). Discovery of type IV collagen non-collagenous domains as novel integrin ligands and endogenous inhibitors of angiogenesis. *Cold Spring Harbor Symposia on Quantitative Biology* 67: 255–266.

Kalluri, R. (2003). Basement membranes: Structure, assembly and role in tumour angiogenesis. *Nature Reviews Cancer* 3: 422–433.

Maeshima, Y., Colorado, P. C., Torre, A., et al. (2000). Distinct anti-tumor properties of a type IV collagen domain derived from basement membrane. *Journal of Biological Chemistry* 275: 21340–21348.

Maeshima, Y., Sudhakar, A., Lively, J. C., et al. (2002). Tumstatin, an endothelial cell-specific inhibitor of protein synthesis. *Science* 295: 140–143.

Magnon, C., Galaup, A., Mullan, B., et al. (2005). Canstatin acts on endothelial and tumor cells via mitochondrial damage initiated through interaction with αVβ3 and αVβ5 integrins. *Cancer Research* 65: 4353–4361.

Mundel, T. M., Yliniemi, A. M., Maeshima, Y., et al. (2008). Type IV collagen alpha6 chain-derived noncollagenous domain 1 (α6(IV)NC1) inhibits angiogenesis and tumor growth. *International Journal of Cancer* 122: 1738–1744.

Nyberg, P., Xie, L., and Kalluri, R. (2005). Endogenous inhibitors of angiogenesis. *Cancer Research* 65: 3967–3979.

Nyberg, P., Xie, L., Sugimoto, H., et al. (2008). Characterization of the anti-angiogenic properties of arresten, an alpha1beta1 integrin-dependent collagen-derived tumor suppressor. *Experimental Cell Research* 314(18): 3292–3305.

Petitclerc, E., Boutaud, A., Prestayko, A., et al. (2000). New functions for non-collagenous domains of human collagen type IV. Novel integrin ligands inhibiting angiogenesis and tumor growth *in vivo*. *Journal of Biological Chemistry* 275: 8051–8061.

Silva, R. L. E., Kachi, S., Akiyama, H., et al. (2006). Recombinant non-collagenous domain of α2(IV) collagen causes involution of choroidal neovascularization by inducing apoptosis. *Journal of Cellular Physiology* 208: 161–166.

Sudhakar, A. and Boosani, C. S. (2007). Signaling mechanisms of endogenous angiogenesis inhibitors derived from type IV collagen. *Gene Regulation and System Biology* 1: 217–226.

Sudhakar, A. and Boosani, C. S. (2008). Inhibition of tumor angiogenesis by tumstatin: Insights into signaling mechanisms and implications in cancer regression. *Pharmaceutical Research* 12: 2731–2739.

Sudhakar, A., Nyberg, P., Keshamouni, V. G., et al. (2005). Human alpha1 type IV collagen NC1 domain exhibits distinct antiangiogenic activity mediated by alpha1beta1 integrin. *Journal of Clinical Investigation* 115: 2801–2810.

Zhang, X., Hudson, B. G., and Sarras, M. P., Jr (1994). Hydra cell aggregate development is blocked by selective fragment of fibronectin and type IV collagen. *Developmental Biology* 164: 10–23.

Morphology of Interneurons: Amacrine Cells

E Strettoi, Istituto di Neuroscienze CNR, Pisa, Italy

Glossary

Coverage factor – The product of mean dendritic field size and cell density. It gives a measure of the number of neurons of a particular type whose receptive fields overlap a particular point on the retina. Because of their great varieties in shapes and frequencies, amacrine cells of different types can have coverage factors anywhere between 1 and 500.
Retinal mosaic – The ordinate spatial pattern formed over the retinal surface by cells of a certain type, arranged regularly. Each retinal cell type has a unique mosaic that can be described formally in mathematical terms. Starburst amacrine cells tile the retinal surface very regularly, while dopaminergic amacrines have highly irregular mosaics.

Near the end of the nineteenth century, Santiago Ramon y Cajal named amacrine cells those retinal neurons whose cell bodies occupy the innermost tier of the inner nuclear layer (INL) and that ramify at various depths in the inner plexiform layer (IPL). Literally, their name means cells without an axon. From Cajal's initial observations and following early studies based on Golgi-impregnated neurons, the notion emerged that amacrine cells come in all shapes, sizes, and stratification patterns (**Figure 1**). In time, many morphological types were described thanks to the development of various techniques. These included intracellular recordings followed by dye injections, immunocytochemical staining, assorted anatomical tracing methods and, more recently, transgenic expression of fluorescent molecules. At present, it is accepted that the retina of mammals contains more than 26 varieties of amacrine cells; their catalog can be considered substantially complete. Classification schemes with a tendency to emphasize subtle differences among presumptive categories separate amacrine cells in as many as 40 different types. Surely enough, amacrine cells represent the most diverse cell types in the retina, as they comprise more varieties than bipolar and ganglion cells.

In the IPL, amacrine cells receive their excitatory input from bipolar cells and provide inhibitory output onto the dendrites of both other amacrine and ganglion cells. They also establish inhibitory synapses onto the axonal arborizations of bipolar cells. Functionally, amacrine cells are capable of modulating the activity of ganglion cells by direct inhibition, or by inhibiting the activity of bipolar cells that carry excitatory inputs to the inner retina. Many amacrine cells are also coupled by means of gap junctions.

Coupling can be with amacrine cells of the same (homologous) or different (heterologous) type. In addition, amacrine cell processes can be coupled to ganglion cell dendrites. Although many amacrine cells, such as the AIIs, generate graded signals in response to light, it has been shown that certain amacrine cells are capable of producing true action potentials that initiate locally and then propagate into every dendrite, exciting the entire cell. Thus, each amacrine cell can mediate both local as well as long-range lateral inhibition, regulating the spatial and temporal pattern of synaptic outputs from its dendrites.

Despite their name, certain wide-field amacrine cells have long, axon-like processes which probably function as true axons as they represent output fibers of the cell. These particular amacrines have been described as polyaxonal and their soma are often found in an interstitial position, that is, within the IPL. However, their long processes remain confined within the retina and do not contribute to the optic nerve as do the axons of ganglion cells.

Traditionally, amacrine cells have been divided into the broad categories of narrow-field (30–150 μm), small-field (150–300 μm), medium-field (300–500 μm), and wide-field (>500 μm) cells, based on the size of their dendritic field diameters. It is worth pointing out that the dendritic spread of the cells is correlated quite strongly with their degree of stratification. Hence, wide-field cells are highly stratified, medium-field cells are less so, and almost all narrow-field cells span radially across two or more levels of the IPL (**Figure 2**).

The mere size of their dendritic field, however, cannot account for the great variability in the morphology of these interneurons. Multiple classification schemes coexist: some amacrine cells have traditionally maintained numbers from old, partial nomenclatures (i.e., AII amacrines and A17 amacrines), while others are indicated with names reminiscent of their shapes, such as starburst cell, fountain amacrine, flag amacrine, or spider cell. As for bipolar and ganglion cells, a more functional, and therefore relevant criterion of identification involves knowing the stratification level of the cells. It is well known that the IPL can be subdivided into five equally thick strata or sublayers to which amacrine, bipolar, and ganglion cell processes can be assigned. The level of stratification of a given neuron in the IPL is predictive of the polarity of the cell response to light stimuli, so that neurons confined in the outermost two

layers of the IPL, the so-called sublamina a, are excited when the light goes off, while neurons ramified in the innermost three tiers of the IPL, the sublamina b, are excited at the light onset. This strong correlation between anatomy and function makes it convenient to classify neuronal types primarily according to the strata of the IPL in which their processes are confined. Altogether, the combination of dendritic field size, pattern, and depth of stratification within the IPL are sufficient criteria to separate cells into unique types. Supplementary information includes dendritic caliber, size and distribution of varicosities, and the course of dendrites.

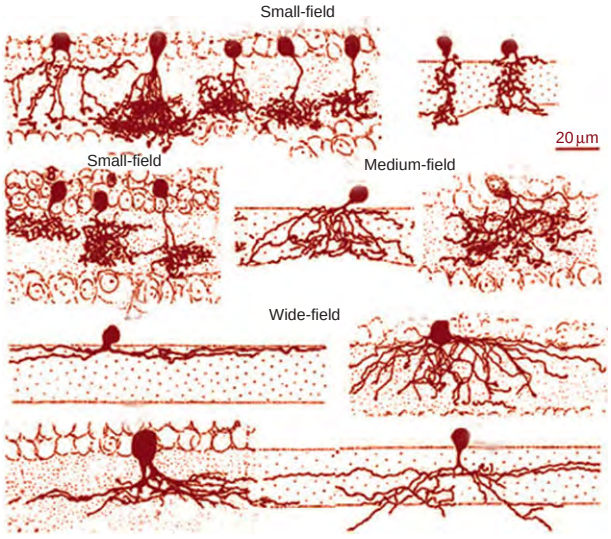

Figure 1 Small-, medium-, and wide-field amacrine cells from the human retina. Golgi silver impregnation. Modified from Poljak, S. (1941). The Retina.

The fact that branching of individual amacrine cells takes place at various levels in the IPL implicates that different amacrine cells contact different types of bipolar and ganglion cells and end up having different functional properties. Indeed, amacrine cells are major players in the retina's processing of visual information. They constitute at least 40% of all neurons in the INL of mammalian retinas and contribute to 64–87% of all synapses in the IPL according to the species. While it was once generally believed that primate retinas were more bipolar dominated as opposed to lower-mammal (i.e., rabbits) retinas, considered more amacrine dominated, quantitative morphology demonstrated that these cells represent some 40% of the INL cells in rabbits, mice, and primates.

Neurotransmitter immunocytochemistry (based on the localization of amino acids or rate-limiting enzymes) has shown that amacrine cells either contain gamma-aminobutyric acid (GABA) or glycine, two inhibitory amino acids used as neurotransmitters ubiquitously in the central nervous system. Remarkably, GABAergic amacrine cells are morphologically wide-field cells, while glycinergic amacrines are small- and medium-field neurons. Glycinergic amacrines are slightly more numerous, at least in the rabbit retina, in which they account for some 56% of all the amacrines. This fits well with the percentage of small-field amacrines (55%) revealed by the technique

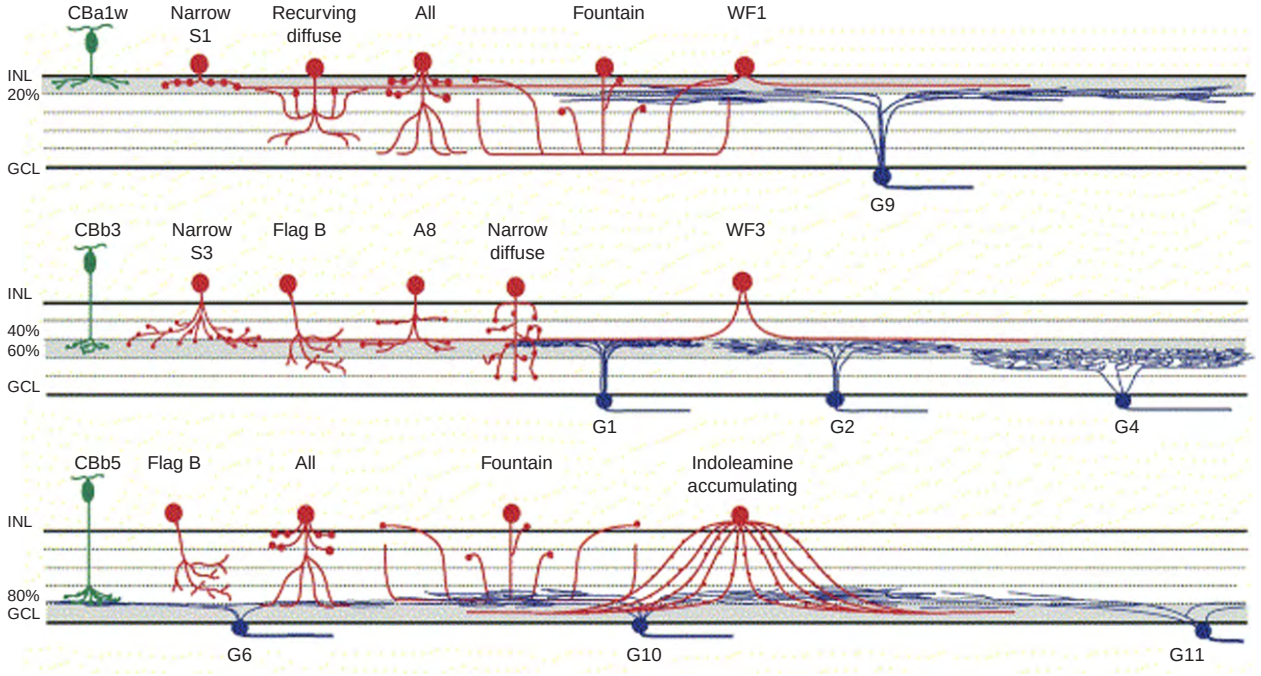

Figure 2 A schematic drawing of some amacrine cells (shown in red), and their spatial relations to known bipolar (green) and ganglion (blue) cell types. From Masland, R. H. (2004). Neuronal cell types. *Current Biology* 14, R497–R500.

of random photofilling. Glycinergic amacrines, with their narrow fields and little overlapping dendrites, mediate radial inhibition in the retina. These cells are meant for vertical transmission rather then for modulation of light signals.

GABAergic amacrines, instead, are more designated for later inhibition, a function traditionally ascribed to amacrine cells in general. In GABAergic amacrines, the fast neurotransmitter GABA usually coexists with another neurotransmitter or neuromodulator; this is typically a peptide, such as somatostatin, substance P, vasoactive intestinal peptide (VIP), and so on. Because they contain high levels of one amino acid, amacrine cells can be identified through their typical amino acidic signature in appropriately stained histological sections of the retina. Noticeably, cholinergic (starburst) amacrine cells are stained with methods revealing both GABA and acetylcholine and are known to corelease both transmitters.

Each particular point of the retina is covered by the dendritic trees of cells of the same type, overlapping to different extents. The parameter indicating the degree of overlapping is known as the coverage factor. This is obtained essentially by histological measurements and is defined as the product of cell density and area of the dendritic tree. A coverage factor of 10 means that a retinal point is covered by the dendritic trees of 10 cells of a given type. Amacrine cells have highly variable coverage factors. In general, small-field amacrine cells have lower coverage factors than wide-field amacrine cells. The well-known indoleamine-accumulating cells (IACs), which comprise two varieties of wide-field amacrines, narrowly stratified in the deepest stratum of the IPL, have coverage factors of 500–900. This means that in each point of the retina, a stack of processes from overlapping IAC cells are regularly piled in sublamina 5 of the IPL. Low-power electron microscopy shows bundles of IAC cells fasciculating in sublamina 5, running parallel to each other and interrupted by the large varicosities of rod bipolar axonal endings, also located at the border with ganglion cell bodies.

Individual types of retinal neuron exhibit regular spacing, such that cells of a certain type maintain a minimum distance from other neurons of the same type. Each cell is surrounded by an exclusion zone from which other cells of the same type are barred. On the contrary, spacing of neurons of different types is completely casual. Amacrine cells adhere to this rule. Because of the availability of cell-specific markers, the mosaics of certain amacrine cells have been described in detail. Starburst amacrine cells can be stained by antibodies against choline acetyl trasferase (ChAT), the rate-limiting enzyme in acetylcholine synthesis; their mosaic is highly characteristic. Similarly, AII amacrine cells can be labeled with antibodies against the protein disabled 1, or, in certain mammals including humans, by parvalbumin antibodies. Dopaminergic amacrines (historically, the first to be described, using enzyme histochemistry) can be revealed by antibodies against tyrosine hydroxylase. Each of these amacrine cells forms over the retinal surface a peculiar, well-recognizable mosaic that can be described formally in rigorous, mathematical terms. Whatever the mechanism leading to mosaic formation during retinal development might be, the regularity of a mosaic is a powerful means to assess that a given cell has been properly identified and correctly assigned to a type. Mutations in various genes controlling retinal development can alter mosaic formation and lead to retinal structural abnormalities.

Multidisciplinary studies on the currently well-known amacrine cell types have led to the notion that, as for other retinal neurons, diversity of shape means diversity of function. This concept is supported by a number of considerations: first, cells whose morphological features are very different have different membrane properties associated with the size of the dendritic tree, the caliber of individual dendrites, and the number and position of input and output synapses with respect to the cell soma. In addition, amacrine processes that occupy different sublayers of the IPL communicate with different sets of bipolar and ganglion cells. Since connectivity shapes function, the functional properties of amacrine cells with different patterns of connections must be different. Also, the area of the dendritic field (which varies greatly among various cells types) is strictly related to the retinal sampling capability (or area of visual space) of a given cell. A different coverage factor also reflects different sampling rates of cells.

The following sections describe two types of amacrine cells whose morphological and functional properties have been studied in detail and appear extremely different. They can be considered as paradigmatic of amacrine-cell-variegated structural and functional aspects.

AII Amacrine Cells

These small-field amacrines were first described in the cat retina by Kolb and co-workers in 1978 and can be considered as hallmark components of the retina of mammals. They bear a distinctive morphology as their dendrites are organized in two different layers: an ovoidal cell body gives rise to a thick, primary dendrite producing two orders of branches – a series of long, thin processes mostly restricted in sublamina 5 of the IPL, near the cell bodies of ganglion cells; and a second set of globose varicosities, called lobular appendages, clustered in a bushy and narrow ramification, spanning vertically through sublaminae 1–2 of the IPL (**Figure 3**). Electron microscopy has demonstrated that AII amacrine cells are placed in a pivotal position along the rod pathway. Scotopic signals transmitted from rods to rod bipolar cells (which belong to the category of ON-center, depolarizing neurons) are conveyed through sign-conserving, glutamatergic synapses to the vitreal dendrites of AII amacrine cells in sublamina 5 of the IPL. At this point, a dichotomy is generated in the rod pathway,

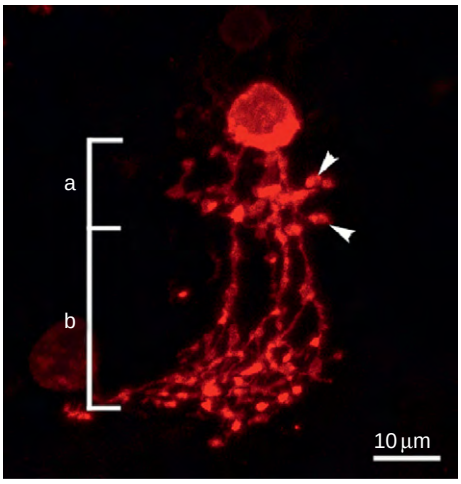

Figure 3 An individual AII amacrine cell from the mouse retina labeled after delivering the fluorescent probe DiI with a gene gun. Note the typical bistratified morphology, with lobular appendages (arrowheads) confined in the outermost part of the inner plexiform layer (IPL), the sublamina a. Long and thin processes of the same amacrine reach the innermost portion of the IPL, the sublamina b.

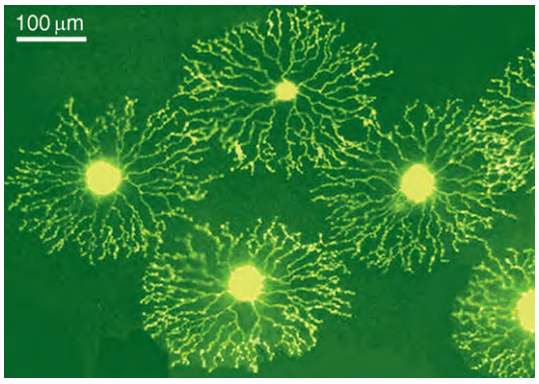

Figure 4 Example of three adjacent starburst amacrines stained by intracellular injection with Lucifer yellow. Reproduced from Vaney, D.I. (1999). Neuronal coupling in the central nervous system: Lessons from the retina. *Novartis Foundation Symposium* 219: 113–125.

as the signal is literally split into two channels by means of the connections of AII amacrines. These cells establish sign-conserving gap junctions with the axonal arbors of cone bipolar cells located in sublamina ON of the IPL, and glycinergic, sign-inverting synapses with axonal endings of cone bipolar cells terminating in sublamina OFF of the IPL. Finally, rod-initiated signals are transferred to the ganglion cell through sign-conserving chemical synapses established by axonal endings of cone bipolar cells in the ON and OFF halves of the IPL. Therefore, the rod pathway ultimately makes use of the axonal endings of cone bipolar cells to gain access to ganglion cells. The five-neuron chain in which the main rod pathway is organized is usually called piggyback arrangement, to indicate the fact that rod-generated signals use a common route, represented by cone bipolars, to exit the retina. AII amacrines are key elements of the piggyback pathway: because of their peculiar morphology and connectivity, they occupy a strategic position when illumination conditions switch from the scotopic range, in which rod photoreceptors are active, to the photopic range, in which cones become functional. AII amacrines, therefore, have to be informed about adaptation in the inner retina. This information is provided, among others, by dopaminergic amacrine cells, which play a relevant role in adaptation processes in the neural retina, and which provide a rich innervation of the primary dendrites of AII amacrine cells in sublamina 1 of the IPL.

Because of their synaptic circuitry, cells such as the AII do not conform to the general concept of amacrine cells as laterally placed, modulatory elements of the retinal connectivity, deputed to lateral transmission of electric signals. Within the rod pathway, AII amacrines occupy a vertical position and rod-generated signals cannot enter ganglion cells without this strategically placed neuronal type. Hence, in very dim light, the AII amacrine is an obligatory connection in the retina's through-pathway. Generally speaking, small-field amacrine cells introduce little more lateral conduction than bipolar cells do; besides the AII, the function of other small-field amacrines is yet to be clarified.

As rod photoreceptors are numerous, AII amacrine cells are also abundant in the retina. Indeed, they are the largest population of amacrine cells accounted for, reaching 11–13% of all the amacrines in the retina of rabbits and mice. The remaining amacrine cell types come at a lower frequency, each reaching 3% maximum of the total population.

Starburst Amacrines

Starburst amacrine cells, so defined thanks to the shape of their circular and rich dendritic tree, are the second, most numerous amacrine cells in mammals, accounting for about 3% of the whole amacrine population. They are a recurrent finding of vertebrate retinas, from dogfish to primates. These neurons have a characteristic, radially symmetric morphology, with higher-order dendritic branches emerging from dichotomous ramification of thicker fibers. In the rabbit retina, their dendritic field size is approximately 400 µm and therefore they belong to the category of wide-field cells (**Figure 4**). It has been shown that starburst amacrines overlap extensively and their dendrites occupy a large percentage of the volume of the IPL. In the rabbit, calculations show that each millimeter of IPL is covered by 6 m of dendrites from starburst amacrine cells, so that the whole retina contains some 2 km of processes from this neuronal type.

Starburst amacrines occur in two, mirror-symmetric populations, composed of almost equal numbers of cells.

In the first group, cell bodies reside in the innermost tier of the INL and dendrites form a narrow plexus in sublamina 2 of the IPL.

These are OFF-starburst cells. In the second population, cell bodies are located in the ganglion cell layer instead and therefore contribute to the heterogeneous group of displaced amacrine cells. Displaced starbursts can be easily identified in the ganglion cell layer even with simple nuclear staining because of the smaller nuclear size and visible regularity of their mosaic. Their dendrites form a second plexus in sublamina 4 of the IPL and are therefore ON-starbursts. Because of their early formation during retinal development and precise positions in the ON and OFF halves of the IPL, the two tiers of starburst dendrites (also known as cholinergic bands) are landmarks often used as references to define the stratification levels of other neurons in the IPL.

In the first days of postnatal development, when retinal neurons are being generated and assembled in regular tiers, waves of light-independent electrical activity traverse the inner retinal surface intermittently. Retinal waves can be recorded from the ganglion cell layer in the form of correlated activity of these neurons. Waves are thought to play an instructive role in the formation of topographic maps of projection neurons in the centralmost visual areas. Pharmacological experiments indicate that developmental waves require the presence of starburst amacrines, releasing both GABA and acetylcholine, the latter acting on nicotinic receptors. The action of both neurotransmitters is excitatory, since GABA has an excitatory role during development. During retinal maturation, starburst cells communicate directly with each other, so that electrical activity generated at one retinal location can propagate to distant areas. However, during the subsequent developmental stages, excitation between starbursts becomes almost undetectable while GABAergic synapses among starburst cells switch from being excitatory to inhibitory.

Starburst cells participate in transretinal waves during early development but their role is totally different in the adult retina. The exact cofasciculation of starburst processes and the dendrites of a highly distinctive ganglion cell type, the ON-OFF directional selective (DS) ganglion cell, which senses stimuli moving in one direction, led to the hypothesis that, in the adult retina, starburst amacrines could provide a major source of synaptic input to this category of neurons. A wealth of data generated the notion that acetylcholine and starburst amacrines in particular, do contribute to the functional properties of directional selectivity. A current view of this complex problem that has fascinated physiologists for decades is that starburst amacrines are capable of releasing the neurotransmitter in a directional fashion, contributing to the tuning of DS ganglion cells for the preferred direction of motion.

Only for a few other types of amacrine cells has a clear role been elucidated. Among them, dopaminergic amacrines, also known as interplexiform cells, have a crucial function in neural adaptation and circadian rhythms; A17 amacrine cells, a long-time known type of wide-field amacrine, are typical local interneurons, providing feedback inhibition to the axonal ending of rod bipolar cells. For most of the amacrine cell types, however, the role is simply inferred on the basis of their costratification with other retinal neurons. Obviously, the fact that our inventory of amacrine cells is presumably complete represents only the first stage in the comprehension of the role of these interneurons. The next step toward a true understanding of retinal architecture will be to learn synaptic and functional interactions of the amacrine cell with individual types of bipolar and ganglion cells, constituting parallel pathways across the retina – a challenge for future years.

See also: Information Processing: Amacrine Cells; Morphology of Interneurons: Interplexiform Cells.

Further Reading

Baccus, S. A. (2007). Timing and computation in inner retinal circuitry. *Annual Review of Physiology* 69: 271–290.

Demb, J. B. (2007). Cellular mechanisms for direction selectivity in the retina. *Neuron* 55: 179–186.

Galli-Resta, L. (2002). Putting neurons in the right places: Local interactions in the genesis of retinal architecture. *Trends in Neuroscience* 25: 638–643.

Jeon, C. J., Strettoi, E., and Masland, R. H. (1998). The major cell populations of the mouse retina. *Journal of Neuroscience* 18: 8936–8946.

MacNeil, M. A., Heussy, J. K., Dacheux, R. F., Raviola, E., and Masland, R. H. (1999). The shapes and numbers of amacrine cells: Matching of photofilled with Golgi-stained cells in the rabbit retina and comparison with other mammalian species. *Journal of Comparative Neurology* 413: 305–326.

MacNeil, M. A. and Masland, R. H. (1998). Extreme diversity among amacrine cells: Implications for function. *Neuron* 20: 971–982.

Marc, R. E., Murry, R. F., Fisher, S. K., et al. (1998). Amino acid signatures in the normal cat retina. *Investigative Ophthalmology and Visual Science* 39: 1685–1693.

Masland, R. H. (2004). Neuronal cell types. *Current Biology* 14: R497–R500.

Masland, R. H. (2005). The many roles of starburst amacrine cells. *Trends in Neuroscience* 28: 395–396.

Masland, R. H. and Raviola, E. (2000). Confronting complexity: Strategies for understanding the microcircuitry of the retina. *Annual Review of Neurosciences* 23: 249–284.

O'Malley, D. M., Sandell, J. H., and Masland, R. H. (1992). Co-release of acetylcholine and GABA by the starburst amacrine cells. *Journal of Neuroscience* 12: 1394–1408.

Sharpe, L. T. and Stockman, A. (1999). Rod pathways: The importance of seeing nothing. *Trends in Neuroscience* 22: 497–504.

Strettoi, E. and Masland, R. H. (1995). The organization of the inner nuclear layer of the rabbit retina. *Journal of Neuroscience* 15: 875–888.

Taylor, W. R. and Vaney, D. I. (2003). New directions in retinal research. *Trends in Neuroscience* 26: 379–385.

Torborg, C. L. and Feller, M. B. (2005). Spontaneous patterned retinal activity and the refinement of retinal projections. *Progress in Neurobiology* 76: 213–235.

Vaney, D. I. (1999). Neuronal coupling in the central nervous system: Lessons from the retina. *Novartis Foundation Symposium* 219: 113–125.

Morphology of Interneurons: Bipolar Cells

S Haverkamp, Max-Planck-Institute for Brain Research, Frankfurt/Main, Germany

Glossary

Clomeleon – A ratiometric genetically encoded indicator comprising a fusion of cyan and yellow fluorescent protein that allows noninvasive chloride measurements in living tissue.
Dyad – Synaptic arrangement of the bipolar cell output synapses within the inner plexiform layer of the retina; the presynaptic ribbon of a dyad is surrounded by vesicles and two postsynaptic elements.
Genuine S-cones – In ventral mouse retina, the great majority of cones express both medium-wavelength (M) and short-wavelength (S) opsin. Blue cone bipolar cells contact only those cones, which express S-opsin only. These are the genuine S-cones.
Landolt club – Process that extends distally from many bipolar cells in cold-blooded vertebrates from the outer plexiform layer to the outer limiting membrane. The function of the Landolt club is not known in any retina.
Midget bipolar cell – The term midget refers to the small spread of their dendritic and axonal arbors. The one-to-one relationship between midget bipolar cells and cones on the dendritic end, and between midget bipolar cells and ganglion cells on the axonal end, is a distinctive property of midget bipolar cells around the fovea.
Type – Members of each cell type show very similar properties, that is, release the same transmitter, make the same connections to other cell types, and generally have the same morphology.

Introduction

The retina contains a large diversity of individual cell types, each carrying out a specific set of functions. They are mainly defined by their morphological appearance. Bipolar cells differ in their dendritic branching pattern, the number of photoreceptors contacted, and the shape and stratification level of their axons in the inner plexiform layer. The cells transfer the light signals from the photoreceptors to amacrine and ganglion cells. They can be subdivided, according to their light responses, into ON and OFF bipolar cells. This functional dichotomy is the result of the expression of different glutamate receptors at the synapses between photoreceptors and bipolar cell dendrites. OFF bipolar cells make flat or basal contacts with cone pedicles, ON bipolar cells make invaginating contacts. The axon terminals of OFF cone bipolar cells terminate in the outer half of the IPL and synapse with the dendrites of OFF ganglion cells, whereas those of ON bipolar cells terminate in the inner half of the IPL and contact the dendrites of ON ganglion cells.

Bipolar Cell Types of the Mammalian Retina

Bipolar cells of the mammalian retina can be subdivided into many different morphological types (**Figure 1**). There are at least nine types of cone bipolar cells and one type of rod bipolar cell. Most mammalian retinas are rod dominated. Therefore, rod bipolar cells form the numerically superior part of the bipolar cell population. Their dendrites make invaginating contacts with rod spherules (**Figure 3(b)**) and their axons terminate in the innermost part of the IPL (**Figure 1**: rod bipolar cell, RB). The number of rods converging on a single rod bipolar cell varies greatly between the species, and, within a species, with retinal eccentricity. In the peripheral human retina, each rod bipolar cell contacts 40–50 rods. Near to the fovea, the dendritic trees become smaller and 15–20 rods are connected. Regardless to retinal eccentricity, convergence in the rod pathway is usually higher than in the cone pathway.

Several types of cone bipolar cells have been recognized in different mammalian species (rabbit: 13, human: 10, cat: 8–10, rat: 9–11, ground squirrel: 6–8). The diagram in (**Figure 1**) compares the bipolar cells of the mouse retina with those of the peripheral macaque monkey retina. The nine putative cone bipolar cell types (labeled 1–9) and the rod bipolar cell of the mouse retina are arranged according to the stratification level of their axon terminals in the IPL. The cells were drawn from vertical sections following intracellular injections. Selective markers, which stain the whole population, are now available for most of the bipolar cell types of the mouse retina (see below). Types 1–4 are OFF cone bipolar cells; types 5–9 are ON cone bipolar cells. The cells contact on average between five and eight neighboring cone pedicles with one exception: type 9 has a wide dendritic tree that appears to be cone selective and it will be shown later that it contacts S-cones.

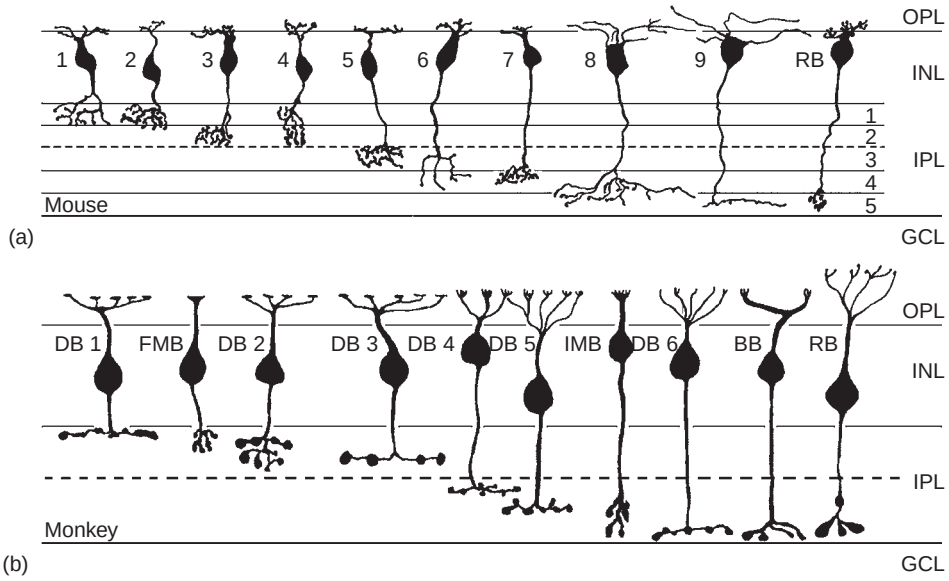

Figure 1 Schematic diagrams of bipolar cells of mouse (a) and primate retina (b). The retinal layers are indicated in (a) for the mouse retina. The inner plexiform layer (IPL) can be subdivided into five sublayers of equal width. The bipolar cell types of the mouse retina were named according to the level of stratification of their axon terminals in the IPL. The dashed horizontal lines dividing the IPL in (a) and (b) represent the border between the OFF-(upper) and the ON-(lower) sublayers. Bipolar cells with axons terminating above this line represent OFF bipolar cells, those with axons terminating below this line represent ON bipolar cells. DB, diffuse bipolar cells; FMB, flat midget bipolar cells; IMB, invaginating midget bipolar cells; BB, blue cone bipolar cells; RB, rod bipolar cells; OPL, outer plexiform layer; INL, inner nuclear layer; GCL, ganglion cell layer. Adapted from Ghosh, K. K., et al. (2004). See Erratum in *Journal of Comparative Neurology* 476: 202–203.

The mouse retina is considered to be rod dominated because only 3% of their photoreceptors are cones. However, the perspective changes if one examines the absolute number of cones; the cone density is about 13 000 cones/mm^2, similar to peripheral cat, rabbit, and macaque monkey retinas. Consequently, the types and retinal distributions of cone bipolar cells are closely similar between mammalian species. The bipolar cell types of the monkey retina (**Figure 1(b)**) were determined initially from Golgi-stained whole mounts. There is a striking similarity between mouse and monkey bipolar cells with respect to the shapes and stratification levels of their axons. However, there is also a clear difference; midget bipolar cells (flat midget bipolar cell (FMB); invaginating midget bipolar cell (IMB)) are only found in the monkey retina. FMB and IMB cells have dendritic trees, which contact a single cone. Bipolar cells contacting several neighboring cone pedicles were named diffuse bipolar cells (DB1–DB6).

Midget Bipolar Cells of the Primate Retina

Primates have trichromatic color vision based on three spectral types of cones: long-wavelength (red or L-), middle-wavelength (green or M-), and short-wavelength (blue or S-) sensitive cones. Midget bipolar cells receive inputs either from red or green cones. Thus, in terms of their input and the polarity of their response, there are four types of midget bipolar cells: red ON, red OFF, green ON, and green OFF. The term midget refers to the small spread of their dendritic and axonal arbors (**Figure 1b**: FMB, IMB). In the central retina, a midget bipolar cell receives direct input from just one cone (**Figure 2(a)**). The bipolar cell axon terminal, which contacts just one ganglion cell, is correspondingly small. This one-to-one relationship between midget bipolar cells and cones on the dendritic end, and between midget bipolar cells and ganglion cells on the axonal end, is a distinctive property of midget bipolar cells around the fovea. Four to five millimeters beyond the fovea, in the near periphery, the midget bipolar cells become two and three headed connecting to two and three cones, respectively (**Figure 2(b)**).

Reconstructions of Golgi-impregnated midget bipolar cells of the primate retina by serial electron microscopy (EM) revealed a clear dichotomy of their dendritic contacts at the cone pedicle base: IMB cells made exclusively invaginating contacts, whereas FMB cells made only flat contacts (**Figure 3(a)**). In central retina, they are all in the vicinity of the ribbons (triad associated, TA), and at eccentricities beyond 3–4 mm, approximately 20% are nontriad associated (NTA). Individual IMB bipolar cells make up to 25 contacts with a cone pedicle, and an FMB cell makes approximately 2–3.5 times that number of basal synapses.

Blue Cone Bipolar Cells

Placental mammals other than primates have only two types of cones: M-cones, in which the visual pigment has an absorption maximum of >500 nm and S-cones with an absorption maximum at <500 nm. They are, therefore, dichromats. In an evolutionary comparison of color

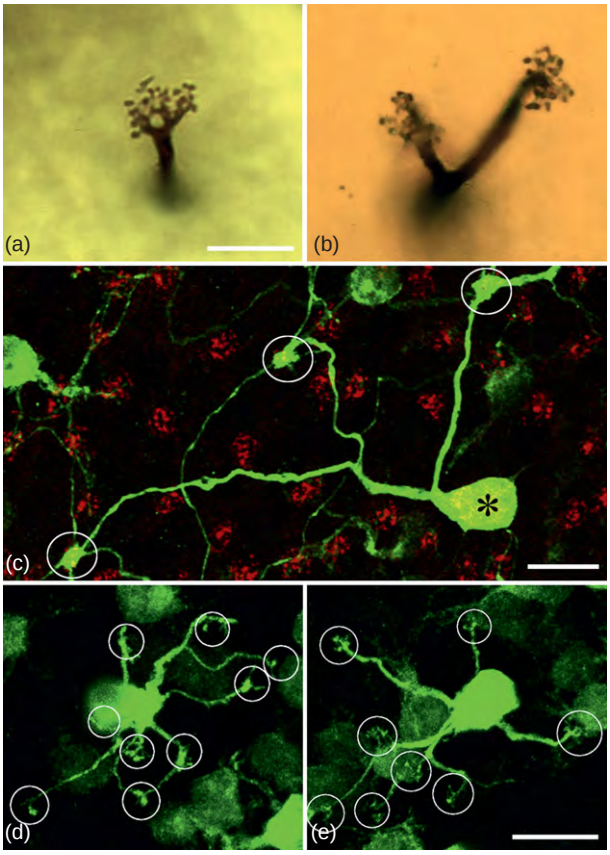

Figure 2 Bipolar cells and their cone contacts in the primate and mouse retina. (a, b) Horizontal view of Golgi-impregnated midget bipolar cells, with the plane of focus at their dendritic tips in the OPL. The micrographs show examples of a single-cone contacting (a) and a two-cone-contacting (b) midget bipolar cell. (c) Horizontal view of a Clomeleon mouse retina (Clm1 line) double labeled for GFP (green) and for GluR5 (red). The clusters of GluR5 puncta represent individual cone pedicles. The dendrites of the blue cone bipolar cell (asterisk) contact three-cone pedicles (circles) and avoid all other pedicles. The BB cell is cone-selective for S-opsin expressing cones. (d, e) Dendritic trees of two type 7 bipolar cells in the Gus-GFP mouse and their cone contacts (circles). Type 7 cells contact on average 8.4 cones. Scale bars = 10 μm. (a, b) Images: courtesy of H. Wässle. From Puller, C., Haverkamp, S., and Grünert, U. (2007). OFF midget bipolar cells in the retina of the marmoset, *Callithrix jacchus*, express AMPA receptors. *Journal of Comparative Neurology* 502: 442–454.

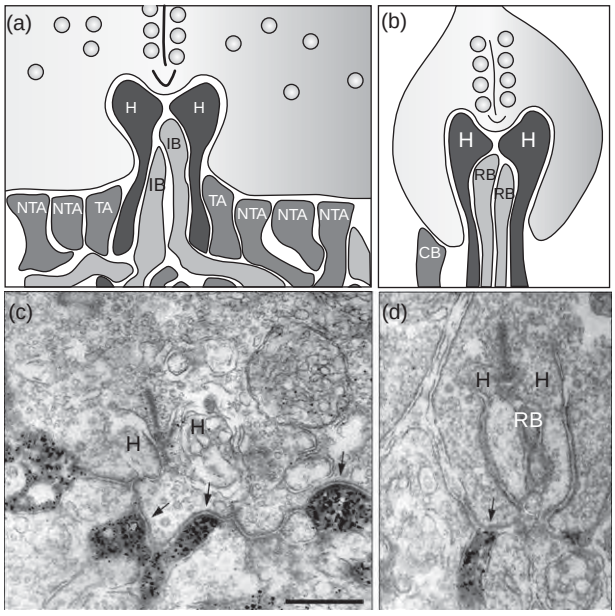

Figure 3 Bipolar cell contacts at photoreceptor terminals. (a, b) Schematic drawings showing the arrangement of contacts at a cone pedicle (a) and rod spherule (b). Horizontal cell processes (H) always end laterally and deeper in the invaginations of both rod and cone terminals. In cone pedicles, the central processes derive from invaginating ON bipolar cells (IB), whereas in rod spherules, the central elements derive from rod bipolar cells (RB). Flat contacts at the base of the cone pedicle are subdivided into triad associated (TA) or nontriad associated (NTA) contacts, depending on their relative distance from the triad. Some cone bipolar cells receive direct input from rods (CB in (b)). (c, d) Type 4 cone bipolar cells of the mouse retina express calsenilin and contact cones as well as rods. Preembedding electron micrographs showing several flat contacts of a calsenilin-positive dendrite at a cone pedicle base (arrows in (c)) and a calsenilin-positive dendrite making a flat contact on a rod spherule (arrow in (d)). Scale bar = 0.5 μm. (a, b) Schematic drawings: courtesy of C. Puller.

pigments, it has been estimated that the L/M separation in the old world primate lineage occurred ~35 million years ago. The separation of the M- and S-cone pigments occurred >500 million years ago and thus represents the phylogenetically ancient, primordial color system. The morphological substrate for the dichromatic color vision common to most placental mammals is the S-cone pathway. Bipolar cells selective for S-cones in the macaque monkey retina have long, smoothly curved dendrites and contact between one and three cone pedicles. Their axons terminate in rather large varicosities in the innermost part of the IPL, close to the ganglion cell layer (BB cells in Figure 1(b)) and innervate the inner tier of the dendritic tree of the small bistratified ganglion cells: These cells are color-opponent and respond to increasing blue light (blue – ON) and decreasing yellow light (yellow – OFF).

Immunostaining with antisera specific for S-opsin has shown that S-cones constitute approximately 10% of the cones in most mammalian retinas. However, in some species S-cones have a very uneven topographical distribution across the retina and many cones express both M- and S-opsin. Recently, a transgenic mouse line could be studied, where Clomeleon, a genetically encoded fluorescence indicator, was expressed under the thy1 promoter. Clomeleon was expressed in ganglion cells, amacrine cells, and bipolar cells.

Clomeleon-labeled ganglion cells, amacrine cells and bipolar cells

Among the bipolar cells the S-cone-selective (blue cone) type could be identified, and the cone-selective contacts

and the retinal distribution could be studied (**Figure 2(c)**). The morphological details of the blue cone bipolar cells match type 9 cells of mice (**Figure 1(a)**) and they are closely similar to the blue cone bipolar cell of the primate retina. It is interesting that in the ventral mouse retina, where most cones express both M- and S-opsin, blue cone bipolar cells contact only those cones, which express S-opsin only. They are the genuine S-cones of the mouse retina. Meanwhile, S-cone-selective bipolar cells have also been verified in ground squirrel and rabbit retina.

Diffuse Bipolar Cells

Most bipolar cell types of the mammalian retina contact between 5 and 10 neighboring cones (**Figure 2(d)** and **2(e)**). In mouse, the number of cone pedicles contacted by individual bipolar cells varied from an average of 5.6 for type 2 cells to an average of 8.4 for type 7 cells. Each and all cones are contacted by at least one member of any given type of bipolar cell (leaving aside the blue cone pathway). Consequently, each cone pedicle is connected to a minimum of eight different bipolar cells. They represent eight separate channels that transfer the light signal into the IPL. Parallel processing, therefore, starts at the first synapse of the retina, the cone pedicle.

Diffuse bipolar cells of the primate retina contact L- and M-cones in their dendritic field non-selectively. Whether all diffuse bipolar cell types also contact S-cones is still a matter of discussion, and it has been proposed that one type of diffuse bipolar cell avoids S-cones in the primate retina. This type would be a good candidate to transfer a yellow (L-plus M-cone) signal into the IPL, where it could contact the outer tier of the dendritic tree of the small bistratified ganglion cells. For the dichromatic ground squirrel retina, it has been shown that diffuse bipolar cells sample cone signals differently: some types receive mixed S/M-cone input and other types receive an almost pure M-cone signal. Bipolar cells that sum signals from S- to M-cones are therefore involved with the transfer of luminosity signals, whereas bipolar cells that carry M-cone signals can have, together with S-cone bipolar cells, a role in color discrimination. Alternatively, these bipolar cells may mediate – due to their relatively small dendritic fields – high acuity vision. This idea would correspond to the fact that the center of the human fovea, which mediates the highest acuity vision, also excludes S-cones.

Like the midget bipolar cells, diffuse bipolar cells also differ in their synaptic contacts with cone pedicles, making either flat or invaginating contacts. EM reconstructions of Golgi-impregnated diffuse bipolar cells of the macaque monkey retina revealed that DB1, DB2, and DB3, which have their axon terminals in the outer IPL and are putative OFF bipolar cells (**Figure 1(b)**), make exclusively basal junctions with the cone pedicle. They always have triad associated (TA) and nontriad associated (NTA) contacts (**Figure 3(a)**). The proportion of TA and NTA contacts varies according to the cell type, as does the average number of contacts per cone, which is between 10 and 20. Bipolar cells DB4, DB5, and DB6 have their axon terminals in the inner part of the IPL and are putative ON bipolar cells. They have an average of between four and eight invaginating synapses per cone pedicle. In addition, they also form basal junctions, in a predominantly TA position. Thus, while the dichotomy 'invaginating = ON, flat = OFF' holds for midget bipolar cells, it does not conform so clearly for diffuse bipolar cells. Therefore, the type of synapse made by a bipolar cell at a cone pedicle, flat versus invaginating, is not the decisive feature; it is rather the glutamate receptor expressed there.

Cone Bipolar Cells with Rod Input

Recent results from rodent and rabbit retina have shown that some OFF cone bipolar cells make also basal contacts with rod spherules and thus receive a direct input from rods. This represents a third route for the rod signal, in addition to the rod bipolar cell circuit, and the gap junctions between rods and cones. In mouse, true-cone-selective OFF bipolar cells (types 1 and 2, **Figure 1(a)**) can be distinguished from types with mixed rod-cone input (types 3 and 4, **Figure 1(a)**). Type 4 bipolar cells make several basal contacts at the cone pedicle base (**Figure 3(c)**) and an individual cell contacts five to eight cones. In addition, some dendrites extend further out into the OPL and contact rod spherules as flat contacts (**Figure 3(d)**). On average, we counted 10 rod spherule contacts per type 4 bipolar cell, and approximately 10% of rods contacted by type 4 bipolar cells.

Immunocytochemical Markers and Transgenic Mouse Lines

The morphological classification of bipolar cells has been made more objective and more quantitative by immunocytochemical markers that selectively label specific cell types. Some of the markers label the same cell types across different species. For instance, rod bipolar cells of all mammals are immunoreactive for protein kinase C α (PKCα). However, other markers, such as calcium-binding proteins, label different cell types in different mammals. Calbindin antibodies label the DB3 OFF cone bipolar cell in the primate retina. However, in the rabbit retina, the calbindin-immunoreactive cell is an ON cone bipolar cell, and in the rat and mouse retina, no bipolar cell expresses calbindin immunoreactivity. Recoverin is another example of a marker that selects different types of bipolar cells in different species. While

in rat and rabbit retinas two types of bipolar cell, an OFF and an ON cone bipolar cell, appear to be labeled, only the OFF midget bipolar cell is labeled in the macaque monkey retina. Even in closely related species, different bipolar cell types can be selected by the same marker. The antibody against the carbohydrate epitope CD15 labels a single population of ON bipolar cells (DB6) in macaque monkey, whereas DB6 cells and OFF midget bipolar cells are labeled in marmoset monkeys. In rabbit, CD15 antibodies label an ON cone bipolar cell, whereas in mouse CD15 is expressed in OFF cone bipolar cells. In contrast, antibodies against the calcium-binding protein CaB5 immunolabel at least three types of bipolar cells in a variety of mammalian species. In all species, rod bipolar cells, one ON cone bipolar cell and at least one OFF cone bipolar cell were labeled (**Figure 4**).

The IPL can be subdivided into five strata of equal thickness (**Figures 1** and **5**). In mouse, these strata can be easily defined by immunolabeling the retina for the calcium-binding protein calretinin (**Figure 5(b)**), which reveals three densely labeled horizontal bands of processes. The outer band (between stratum 1 and 2) contains the processes of the OFF cholinergic amacrine cells and the outer dendritic branches of direction-selective ganglion cells. The band in the inner IPL (between stratum 3 and 4) contains the processes of the ON cholinergic amacrine cells and the inner dendritic branches of direction-selective ganglion cells. The band in the middle of the IPL (between stratum 2 and 3) represents the level of stratification of a nitric oxide synthase (NOS) immunoreactive amacrine cell type and separates the OFF sublamina (outer) from the ON sublamina (inner). The calcium-binding protein 5 (CaB5)-immunoreactive bipolar cells stratify in three strata; in stratum 2 where the type 3 bipolar cells stratify, in stratum

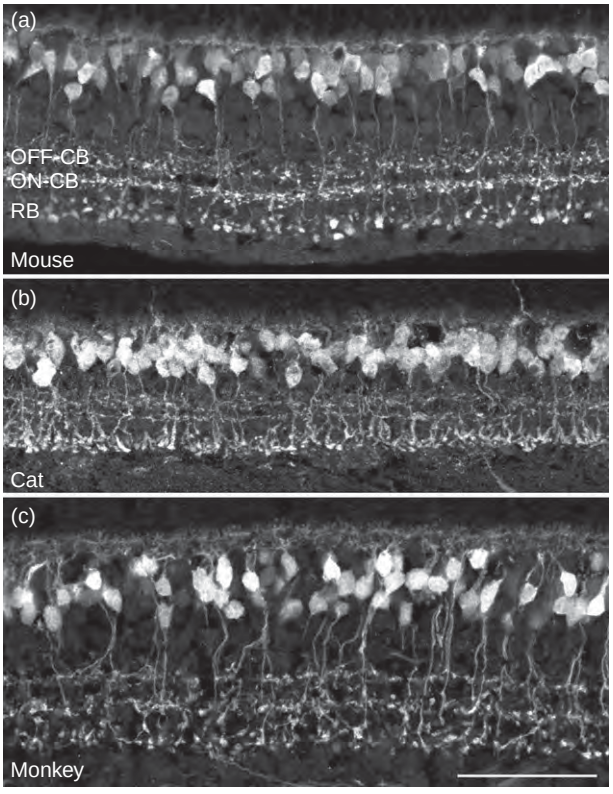

Figure 4 Comparison of CaB5 immunoreactivity in mouse (a), cat (b), and monkey (c) retina. In all three species, rod bipolar cells (RB) and at least one ON cone bipolar (ON-CB) and one OFF cone bipolar cell (OFF-CB) are labeled. Scale bar = 50 μm.

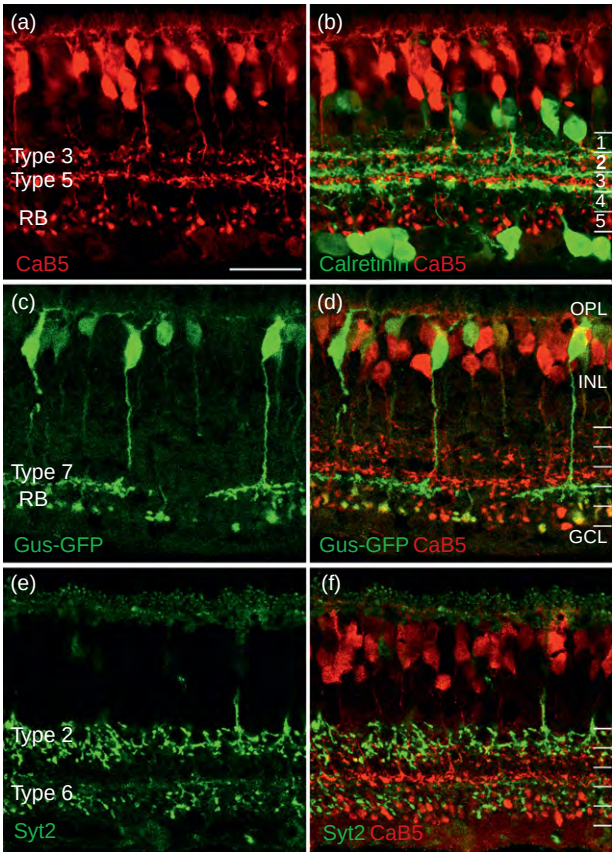

Figure 5 Immunocytochemical staining of mouse bipolar cells. (a, b) Vertical section through a mouse retina that was double immunostained for CaB5 (red) and calretinin (green). Three dendritic strata within the IPL express calretinin and subdivide the IPL into four sublaminae. Three bipolar cell types (type 3, type 5, and RB) express CaB5. Their axons terminate in the IPL in sublamina 2, sublamina 3, and sublamina 5, respectively. (c, d) Vertical section through the Gus–GFP mouse retina immunostained for GFP (green) and CaB5 (red). The retinal layers are indicated (OPL, INL, IPL, subdivided into five sublayers of equal thickness; GCL). Type 7 bipolar cells express high levels of GFP and their axons terminate at the border of sublaminae 3/4. Rod bipolar cells also express GFP, but weakly (double labeled with Cab5 in (d)). (e, f) Vertical section through the mouse retina immunostained for synaptotagmin 2 (Syt2 , green) and CaB5 (red). Type 2 and type 6 bipolar cells express Syt2. Type 2 axons terminate in sublamina 1/2, above the CaB5-labeled type 3 axons; type 6 axons terminate mainly in sublamina 4/5 and intermingle with CaB5-labeled RB axon terminals. Scale bar = 25 μm.

3 where type 5 cells stratify, and in stratum 4/5 where the rod bipolar cells terminate (**Figure 5(a)** and **5(b)**).

We have used several selective markers, either antibodies or the specific expression of fluorescent proteins in transgenic mouse lines, for analyzing the different types of bipolar cells in the mouse retina. Five putative OFF cone bipolar cells were analyzed by selective markers. Type 1 bipolar cells were found to be immunoreactive for the neurokinin 3 receptor (NK3R) and they could also be identified in Clm1 transgenic mice. Type 2 bipolar cells expressed NK3R and synaptotagmin II (Syt2) immunoreactivity (**Figure 5(e)** and **5(f)**). Type 3a and type 3b cells were immunostained for the hyperpolarization-activated cyclic nucleotide-gated potassium channel 4 (HCN4) and the protein kinase A regulatory subunit II β ($PKA_{RII\beta}$), respectively, and type 4 cells expressed the calcium-binding protein, calsenilin. In the case of ON cone bipolar cells, markers for four types were described. Type 5 bipolar cells were labeled in the 5-hydroxytryptamine 3 receptor-EGFP (5HT3R-EGFP) transgenic mouse; however, they represent two types (named 5a and 5b). Type 6 bipolar cells were partially identified because their axons express Syt2 (**Figure 5(e)** and **5(f)**). Type 7 bipolar cells were labeled in the Gus-GFP mouse, a transgenic mouse line where GFP is expressed under the control of the gustducin promoter (**Figures 2(d), 2(e), 5(c)** and **5(d)**) Type 9, the blue cone bipolar cell, has been identified in Clm1 mice. Rod bipolar cells have been immunostained for PKCα. This list suggests that, with the exception of type 8 bipolar cells, selective markers, which stain the whole population, are available for all bipolar cell types of the mouse retina.

Synaptic Contacts of Bipolar Cells in the Inner Plexiform Layer

The axons of bipolar cells terminate in the IPL in lobular swellings (**Figure 6(a)**). Some bipolar cell types, such as DB3 and DB6 of the primate retina and type 7 of the mouse retina, keep their axon terminals within a narrow stratum (**Figure 5(c)** and **5(d)**). Hence, their output will be restricted to the amacrine and ganglion cell dendrites they meet within that stratum. Other bipolar cells such as type 4 and type 6 of the mouse retina occupy with their axon terminals the complete OFF or ON sublamina respectively (**Figure 5(e)** and **5(f)**). They are possibly engaged in contacts with a wider variety of postsynaptic

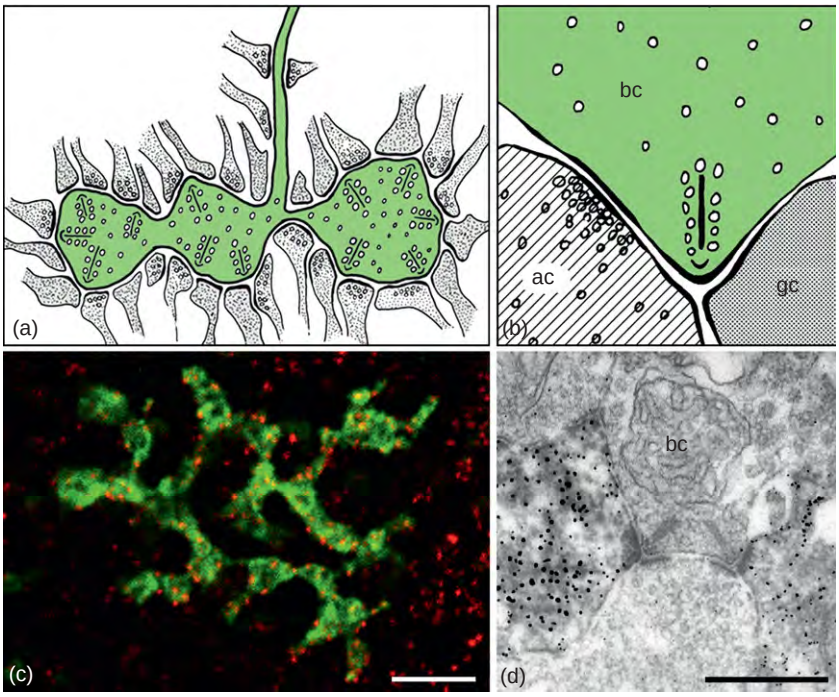

Figure 6 Synaptic output of bipolar cells in the IPL. (a) Schematic diagram of the axon terminal of a cone bipolar cell. It contains many presynaptic ribbons that are flanked by synaptic vesicles. (b) Magnified view of a cone bipolar cell ribbon synapse (dyad). The presynaptic bipolar cell (bc) releases glutamate and the two postsynaptic partners express different sets of glutamate receptors. The amacrine cell, in turn, makes a synapse back onto the bipolar cell terminal (reciprocal synapse). (c) Horizontal view of a GFP-labeled type 7 axon terminal (green) in a Gus-GFP retina. The output synapses are marked (red) by their expression of the ribbon associated C-terminal binding protein 2 (CtBP2/RIBEYE). Altogether, 128 output synapses have been counted at this axon terminal. (d) Electron micrograph of a bipolar cell axon terminal (bc) with two output synapses. Two of the postsynaptic elements are immunolabeled amacrine cell profiles (pre-embedding with glycogen phosphorylase in primate retina). Scale bar = 5 μm in (c), 0.5 μm in (d). ac, amacrine cell; gc, ganglion cell.

neurons. Midget bipolar cells of the primate retina represent a special case, because their axon terminals precisely match in width and depth the dendritic tops of midget ganglion cells, and they together form a densely interconnected glomerulus. The axon terminals of neighboring bipolar cells of a given type usually tile the retina without overlap in the horizontal direction. An interesting question is how the precisely layered and territorial arrangement of axon terminals is formed during embryonic development. Type-specific interactions have to be postulated because terminals of different types can overlap within the same sublamina. Proteins such as the Down's syndrome cell adhesion molecule (Dscam) and an immunoglobulin superfamily protein (Sidekick) are involved in lamina-specific segregations of neuronal processes within the IPL during embryonic development.

Bipolar cell axon terminals provide synaptic output through multiple ribbon synapses (**Figure 6(c)**). We have counted the number of output synapses of the type 7 bipolar cells in the Gus–GFP mouse. The numbers varied between 74 and 128 ($n = 8$) depending on the size of the axon terminals. The number of ribbon synapses made by rod bipolar cells of the rabbit retina was up to 30, compared to only 15 in the rat retina, which reflects the smaller size of rod bipolar axon terminals in rats. The fine structure of the bipolar cell output synapses is shown in **Figure 6(b)**. The presynaptic ribbon is surrounded by vesicles and two postsynaptic elements. This synaptic arrangement is named a dyad. One of the postsynaptic partners at cone bipolar cell dyads is usually a ganglion cell dendrite, while the other one is an amacrine cell process. The amacrine cell process often makes within about 0.5–1.0 μm of the dyad a conventional synapse back onto the bipolar cell axon terminal. This arrangement appears to be a reciprocal synapse and because most amacrine cells are inhibitory, it is the structural correlate of negative feedback at the dyad. Bipolar cell axons receive, in addition to reciprocal synapses, input from amacrine cells not related to the dyads. In the case of rod bipolar cell dyads, both postsynaptic partners are amacrine cells (AI and AII); and AI cells provide the reciprocal synapses.

Costratification of Pre- and Postsynaptic Partners in the Inner Plexiform Layer

Bipolar axons terminate at distinct levels within the IPL, and different types of amacrine and ganglion cells also keep their processes at specific levels within the IPL, which leads to the prediction that they are also engaged in mutual synaptic contacts (**Figure 7**). However, this simple rule has only been verified in a few instances. Midget bipolar cells of the primate retina – both ON and OFF midget – contact midget ganglion cells. Parasol

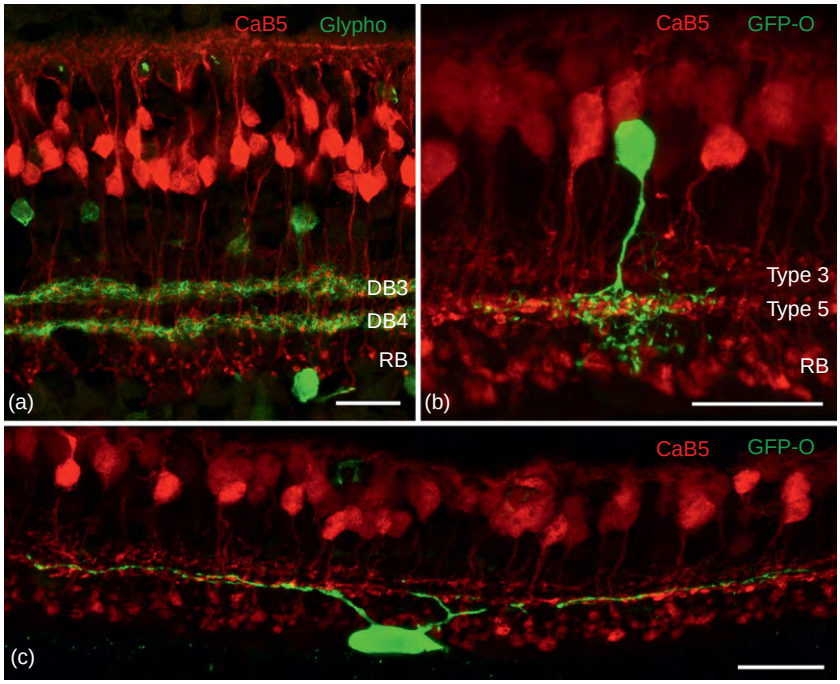

Figure 7 Costratification of pre- and postsynaptic partners in the inner plexiform layer. (a) Vertical section through a primate retina that was double immunostained for CaB5 (red) and glycogen phosphorylase (glypho, green). Axon terminals of CaB5-labeled DB3 and DB4 bipolar cells costratify with the glypho-immunoreactive amacrine cell processes. (b, c) Vertical sections through a transgenic mouse retina where a small set of small-field amacrine cells and ganglion cells express GFP under the control of the thy1 promotor (GFP-O line). Both the small-field amacrine cell with dendrites in the ON-sublamina (b) and the monostratified putative ON ganglion cell (c) costratify with the axon terminals of the type 5 ON bipolar cell. Scale bar = 20 μm.

ganglion cells of the primate retina also occur as OFF and ON pairs and their dendrites stratify in sublamina 2 and sublamina 4, respectively. The OFF parasol cells receive their major, excitatory input from DB3 bipolar cells, and ON-parasol cells most likely from DB5 bipolar cells. In rabbit, ON α ganglion cells stratify just below the ON cholinergic amacrine cells and cofasciculate (distribute together) with the axon terminals of the calbindin-immunoreactive bipolar cells.

The bistratified ON/OFF direction-selective (DS) ganglion cell coincides with the level of stratification of ON and OFF cholinergic amacrine cells. In the rabbit retina, DS ganglion cells receive the majority of their synaptic input from amacrine cells. The axon terminals of the CD15-immunoreactive bipolar cells stratify slightly more distally of the ON cholinergic band. In addition, they follow the pattern of the ON cholinergic dendrites, and are, therefore, good candidates for providing synaptic input to the DS circuitry.

Figure 7(a) shows a double labeling of glycogen phosphorylase (glypho) and CaB5 in the macaque monkey retina. The glypho-immunoreactive cells occur – like the cholinergic amacrine cells – as mirror-symmetrical populations of regular and displaced wide-field amacrine cells. The regular amacrine cells branch in sublamina 2 and co-stratify with DB3 cells; the displaced amacrine cells branch in sublamina 3 and co-stratify with DB4 cells.

Transgenic mouse lines are extremely helpful to study potential contacts between bipolar cells and their postsynaptic partners in the mouse retina. For instance, in the GFP-O line, each mouse expresses GFP in a small and variable set of ganglion cells and small-field amacrine cells. See **Figure 7(b)** for a small-field amacrine cell and **Figure 7(c)** for a monostratified ON ganglion cell, both of which coincide with the type 5 bipolar cell.

Bipolar Cells of Nonmammalian Vertebrates

It has been shown that bipolar cells of a particular cell are usually found in one-half of the IPL or the other, but not in both. In several nonmammalian vertebrates, however, the axon terminals of the bipolar cells are highly stratified, ending on one or several levels in the inner plexiform layer. Most cold-blooded vertebrate retinas contain large bipolar cells, long thought to be rod-related bipolar cells, and small bipolar cells, believed to be cone-related bipolar cells. In fish, it has been shown that many bipolar cells, particularly the larger ones, contact both rods and cones.

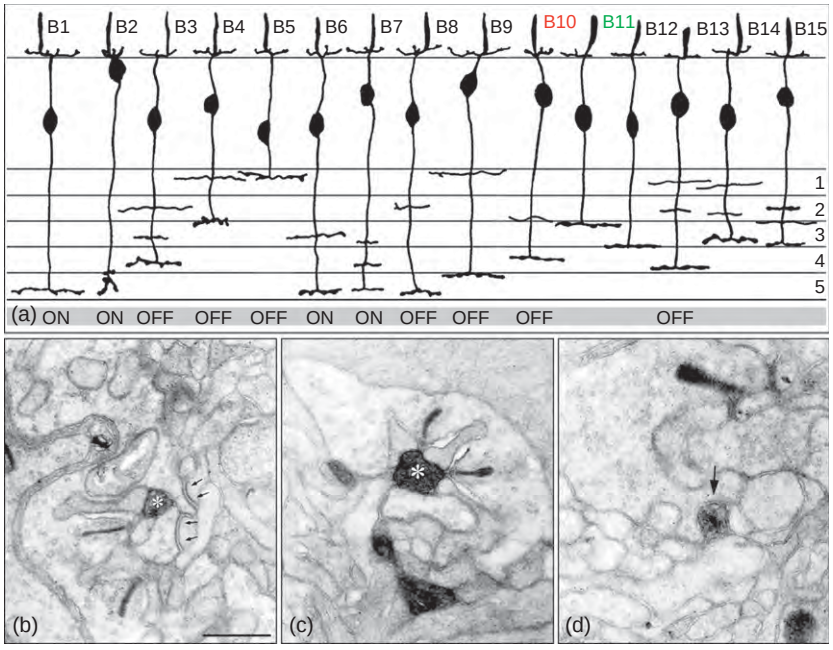

Figure 8 Bipolar cells of the turtle retina. (a) Bipolar cell types B1–B15 in the turtle retina. B1–B9 are from Golgi-impregnated retinae, B10, B11, and B13 from intracellular recordings with subsequent dye injection, and B12, B14, and B15 from Lucifer Yellow injections. The cells are drawn in vertical views with cell bodies, dendrites, and Landolt clubs in the outer retina and the stratification of their axons in the five strata (S1–S5). Several cells are bi- or tristratified. B1, B2, B6, and B7 are ON-center cells; B3, B4, B5, B8, B9, B10, and B13 are OFF-center cells. B10 and B11 are color-opponent cells (B10: red-ON, green/blue-OFF; B11: red-OFF, green/blue-ON). (b)–(d) Electron micrographs showing invaginating, ribbon-associated synapses of an HRP-stained B10 bipolar cell with L-cone pedicles (asterisks in (b) and (c)) and a noninvaginating, basal junction with an M-cone pedicle (arrow in (d)). Two unstained wide-scleft basal junctions in (b) are marked by small arrows. Scale bar = 0.5 μm.

It has also been shown that certain of these bipolar cells are likely to be color-coded, because they contact specific sets of cones. In turtle retina, at least 15 different morphological types of bipolar cells were found (**Figure 8(a)**). Some are monostratified with only a single axon terminal (B1, B2, B5, B11, and B12), several are bistratified (B4, B6, B8, B9, and B10), and some are tristratified (B3, B7, B13, B14, and B15). All seem to have Landolt clubs arising from their dendrites in the outer plexiform layer (OPL) to extend into the outer nuclear layer. A functional organization of the turtle IPL into OFF sublaminae (strata 1 and 2) and ON sublaminae (strata 3, 4, and 5), as has been described for other vertebrate retinas, is quite clear for two types of OFF bipolar cells, which stratify in the two distal strata (B4, B5) and for all four types of ON bipolar cells (B1, B2, B6, and B7). However, some OFF bipolar cells (B3, B9, B10, and B13) have axon terminals in strata 3–5 in addition to their terminations in stratum 1 or 2 (**Figure 8(a)**).

Color-Coded Bipolar Cells in the Turtle Retina

The turtle has excellent color vision, and is at least tetrachromatic. Three cones are sensitive to long wavelengths, one to medium wavelengths, one to short wavelengths, and a further cone to ultraviolet light. The chromatic types of cones can be morphologically identified by the presence and colors of their oil droplets and the shape of their pedicles. Two of the bipolar cell types in turtle are color-opponent: B10 is a red-ON, green/blue-OFF bipolar cell with axons in S2 and S4 and B11 is a red-OFF, green/blue-ON bipolar cell with an axon terminal in S3 (**Figure 8(a)**).

We have analyzed the cone contacts of a horse-radish peroxidase labeled B10 cell by serial EM reconstruction: 45 ribbon-associated synapses were found in single and double L-cones; basal junctions were found in M-cones (**Figure 8(b)–8(d)**). No contacts were found with rods, S-cones, and UV-cones. The results showed that invaginating synapses with L-cones and noninvaginating synapses with M-cones formed the basis of color opponency in an identified bipolar cell for red versus green light stimulation. We suggested sign-inverting transmission from L-cones at invaginating synapses mediated by G-protein-coupled metabotropic glutamate receptors, and sign-conserving transmission from M-cones at wide-cleft basal junctions mediated by ionotrophic (ion-gated) glutamate receptors. For B11 bipolar cells, we would predict that the dendrites express ionotropic glutamate receptors at their contacts with L-cones (red-OFF) and metabotropic glutamate receptors at their contacts with M-cones (green-ON).

See also: Cone Photoreceptor Cells: Soma and Synapse; Information Processing: Bipolar Cells; Morphology of Interneurons: Amacrine Cells; Morphology of Interneurons: Interplexiform Cells; Rod and Cone Photoreceptor Cells: Inner and Outer Segments; Rod Photoreceptor Cells: Soma and Synapse.

Further Reading

Ammermüller, J. and Kolb, H. (1996). Functional architecture of the turtle retina. *Progress in Retinal Research* 15: 393–433.

Boycott, B. B. and Wässle, H. (1991). Morphological classification of bipolar cells in the macaque monkey retina. *European Journal of Neuroscience* 3: 1069–1088.

Boycott, B. B. and Wässle, H. (1999). Parallel processing in the mammalian retina. The Proctor Lecture. *Investigative Ophthalmology and Visual Science* 40: 1313–1327.

Chan, T. L., Martin, P. R., Clunas, N., and Grünert, U. (2001). Bipolar cell diversity in the primate retina: Morphologic and immunocytochemical analysis of a new world monkey, the marmoset *Callithrix jacchus*. *Journal of Comparative Neurology* 437: 219–239.

Euler, T., Schneider, H., and Wässle, H. (1996). Glutamate responses of bipolar cells in a slice preparation of the rat retina. *Journal of Neuroscience* 16: 2934–2944.

Famiglietti, E. V. (1981). Functional architecture of cone bipolar cells in mammalian retina. *Vision Research* 21: 1559–1563.

Ghosh, K. K., Bujan, S., Haverkamp, S., Feigenspan, A., and Wässle, H. (2004). Types of bipolar cells in the mouse retina. *Journal of Comparative Neurology* 469: 70–82.

Haverkamp, S., Möckel, W., and Ammermüller, J. (1999). Different types of synapses with different spectral types of cones underlie color opponency in a bipolar cell of the turtle retina. *Visual Neuroscience* 16: 801–809.

Haverkamp, S., Wässle, H., Dübel, J., et al. (2005). The primordial, blue cone color system of the mouse retina. *Journal of Neuroscience* 25: 5438–5445.

Haverkamp, S., Specht, D., Majumdar, S., et al. (2008). Type 4 OFF cone bipolar cells of the mouse retina express calsenilin and contact cones as well as rods. *Journal of Comparative Neurology* 507: 1087–1101.

Kolb, H. (1970). Organization of the outer plexiform layer of the primate retina: Electron microscopy of Golgi-impregnated cells. *Philosophical Transactions of the Royal Society, London, B* 258: 261–283.

Li, W. and DeVries, S. H. (2006). Bipolar cell pathways for color and luminance vision in a dichromatic mammalian retina. *Nature Neuroscience* 9: 669–675.

MacNeil, M. A., Heussy, J. K., Dacheux, R. F., Raviola, E., and Masland, R. H. (2004). The population of bipolar cells in the rabbit retina. *Journal of Comparative Neurology* 472: 73–86.

Sherry, D. M. and Yazulla, S. (1993). Goldfish bipolar cells and axon terminal patterns: A Golgi study. *Journal of Comparative Neurology* 329: 188–200.

Wässle, H., Puller, C., Müller, F., and Haverkamp, S. (2009). Cone contacts, mosaics and territories of bipolar cells in the mouse retina. *Journal of Neuroscience* 29: 106–117.

Morphology of Interneurons: Horizontal Cells

L Peichl, Max Planck Institute for Brain Research, Frankfurt am Main, Germany

Glossary

Cone pedicle – The axonal synaptic ending of the cone photoreceptor in the outer plexiform layer of the retina; it is commonly a relatively large conical structure that contains about 30 synaptic sites (triads), each having a presynaptic ribbon and three postsynaptic processes.

Connexin – A transmembrane protein; six connexins form a connexon or hemichannel and two connexons form a gap junction. Connexins are a diverse family and can combine into homomeric or heteromeric connexons and gap junctions.

Ephaptic – An action mediated by an electrical contact between nerve cells, without the mediation of a neurotransmitter. In the case of horizontal cells it is mediated by a hemichannel.

Gap junction – A specialized connection between neighboring cells, forming an electrical synapse in the neurons. A gap junction consists of two connexons (hemichannels) that form an intercellular pore across the touching cell membranes. The connexons are connexin hexamers. The pore allows various ions and molecules (e.g., neurobiotin) to pass between the cells. Gap junctions can be regulated (opened and closed) by neuromodulators and thus implement a flexible functional syncytium.

Rod spherule – The axonal synaptic ending of the rod photoreceptor in the outer plexiform layer of the retina; it is a small globular structure that contains two synaptic sites with a presynaptic ribbon and four postsynaptic processes.

Triad – A synaptic arrangement at the synaptic ending of a photoreceptor, located at an invagination of the cone pedicle or rod spherule. The presynaptic side of the triad contains an electron-dense synaptic ribbon for the docking of transmitter vesicles. The postsynaptic side has three invaginating processes, a central bipolar cell dendritic terminal and two lateral horizontal cell terminals. Rod triads receive two biploar cell terminals and two horizontal cell terminals.

General Morphology and Connectivity

Basic Morphology

Horizontal cells are interneurons of the outer retina and the largest neurons present in that region. Their somata are located in the outer part of the inner nuclear layer. Their processes ramify in the outer plexiform layer and form synaptic contacts with the photoreceptors. The horizontal cells of mammals – to which this article is limited – comprise two types, commonly termed A-type and B-type; the terms A-HC or HA and B-HC or HB are also in use. The B-type has a smaller, densely branched dendritic tree with relatively fine dendrites and also has an axon ending in a profusely branched axon terminal system. The A-type has a larger, more sparsely branched dendritic tree with fewer and stouter primary dendrites, and has no axon (**Figure 1(a)**). The dendrites of both types carry clusters of terminals (terminal aggregates) that synapse exclusively with cones. The axon terminal system of the B-type has unclustered terminals that exclusively contact rods (**Figures 1(b)–1(g)**).

The horizontal cell terminals, together with the dendrites of invaginating bipolar cells (ON bipolar cells, depolarizing to the onset of light), insert into invaginations at the base of the photoreceptor terminal (cone pedicle or rod spherule). The synaptic complexes thus formed are referred to as triads. Each cone pedicle possesses a substantial number of invaginations with triads (20–50 in primates), whereas a rod spherule commonly only has one invagination with two triads (**Figures 1(e)–1(g)**). Presynaptically, the triad is marked by a synaptic ribbon that is thought to play a crucial role in the continuous vesicular release of the photoreceptor transmitter glutamate. Postsynaptically, each mammalian triad has a bipolar cell dendritic terminal (two at rod spherules) as a central element, flanked by two horizontal cell terminals as lateral elements. The bipolar cells, via their axonal contacts, pass their signals on to the inner retina. The horizontal cells have no spatially segregated output synapses. The only synaptic contacts they form are with the photoreceptors. These are their input and output sites, representing a local feedback mechanism for the cones (by A-type and B-type dendrites) and the rods (by B-type axon terminals).

Horizontal cells modulate signal transmission from the photoreceptor to the invaginating bipolar cell processes.

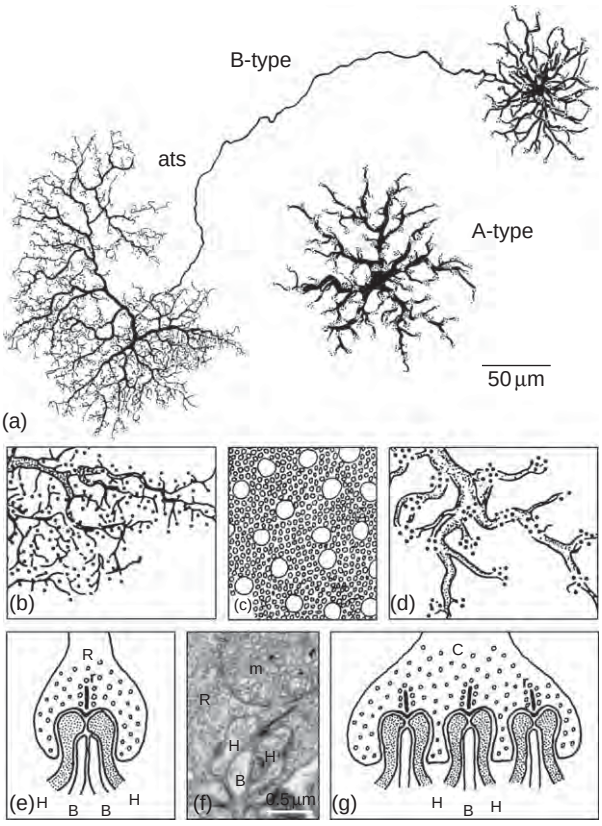

Figure 1 Basic mammalian horizontal cell morphologies. (a) Flat views of a Golgi-stained B-type horizontal cell with axon terminal system (ats) and axonless A-type horizontal cell of cat. Middle row: (b) enlarged part of the B-type ats with single terminals that are the contacts with rods; (c) a schematic photoreceptor pattern with the rather regularly spaced cones surrounded by the more numerous and smaller rods; and (d) part of an A-type dendrite with clustered terminals that are the contacts with cones. Bottom row: (e) schematic triad arrangements at a rod spherule; (f) electron micrograph of a triad in a mouse rod spherule; and (g) schematic triad arrangements at a cone pedicle. R, rod spherule; C, cone pedicle; H, horizontal cell process; B, bipolar cell process; r, presynaptic ribbon; and m, mitochondrion. For details, see text. (a) Adapted from Boycott, B.B., Peichl, L., and Wässle, H. (1978). Morphological types of horizontal cell in the retina of the domestic cat. *Proceedings of the Royal Society* (*London*) *B* 203: 229–245. (f) Image kindly provided by Silke Haverkamp. Adapted from Figure 1 in Peichl, L., Sandmann, D., and Boycott, B. B. (1998). Comparative anatomy and function of mammalian horizontal cells. In: Chalupa, L. M. and Finlay, B. L. (eds.) *Development and Organization of the Retina*: *From Molecules to Function*, pp. 147–172. New York: Plenum Press. With kind permission of Springer Science and Business Media.

The horizontal cell feedback is inhibitory and supposedly creates the antagonistic receptive field surrounds of bipolar cells, thus contributing to the receptive field properties of the ganglion cells. However, the exact nature of the feedback synapse is unknown. There is some evidence that mammalian horizontal cells use the inhibitory transmitter gamma aminobutyric acid (GABA); however, a feedback mediated by electrical conduction (ephaptic, via hemichannels) and pH modulation (proton hypothesis) is also considered. In addition, the horizontal cells probably have feed-forward connections to ON bipolar cells. OFF bipolar cells, which make flat (noninvaginating) contacts at the photoreceptor base, are not in direct apposition to the horizontal cells. It is assumed that the horizontal cell modulation affects them indirectly via the changed photoreceptor output.

The dendritic spread of a horizontal cell is much larger than that of a cone bipolar cell, and activation by cones anywhere in its dendritic field results in an output across the entire dendritic field. Thus, information about the illumination state of cones outside a bipolar cell's input region is picked up by the overlying horizontal cells and negatively fed back to the few cones providing the direct bipolar cell input – the classical lateral inhibition that sharpens contrast sensitivity and acuity. Most likely, the same function is provided for the rod pathway by the B-type axon terminal system.

Photoreceptor Contacts

In the mammalian retina, the rod and cone signals are separately carried by cone and rod bipolar cells, respectively. These major rod and cone pathways only converge in the inner retina. In addition, there is gap-junctional coupling between rods and cones, and a few cone bipolar cells also synapse with rods. Mammalian horizontal cells separately serve the rod and cone pathways.

Contacts with cones

The dendritic fields of horizontal cells are commonly shaped round to oval. Depending on the retinal location, A-type dendritic trees in cat are 80–220 µm in diameter and contact 120–170 cones, whereas B-type dendritic trees are 70–120 µm in diameter and contact 60–90 cones. A- and B-type cells in rabbit are slightly larger but contact similar numbers of cones. In their cone connections, the two horizontal cell types share a common input. Most mammals are cone dichromats with an approximately 90% majority of medium-to-long-wavelength-sensitive (L) cones and a 10% minority of short-wavelength-sensitive (S) cones. In most studied species, both A- and B-type cells contact the vast majority of cones within their dendritic fields; this was considered as evidence that each spectral cone type contacted each horizontal cell type. Soma recordings from cat and rabbit horizontal cells with spectral stimuli confirmed that both types hyperpolarize to all wavelengths. Direct anatomical evidence for the nonselective contacts of both horizontal cell types with both spectral cone types has been obtained in rabbit and tree shrew (**Figures 2** and **3**). In cone triads, the two lateral elements are either two A-type terminals, two B-type terminals, or one A-type and one B-type terminal; in rabbit, these three combinations are found in equal numbers. The current

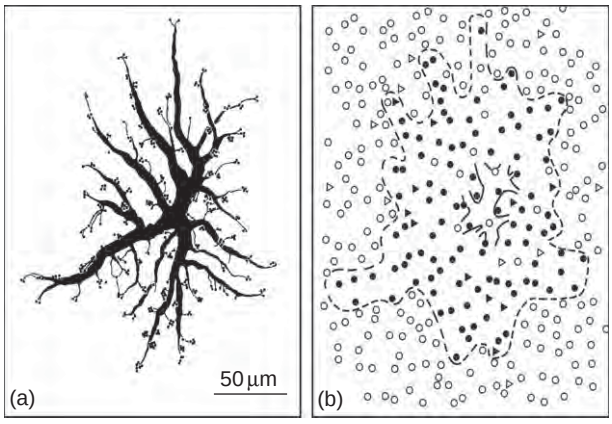

Figure 2 Cone contacts of an A-type horizontal cell in rabbit. (a) Drawing of the Lucifer yellow-injected cell. (b) Cone mosaic overlying the cell, revealed by labeling all cones with the marker peanut agglutinin and identifying the S-cones by an S-opsin antiserum. S-cones are shown as triangles and L-cones as circles. Cones contacted by the A-type cell (dendritic field outline given by broken line) are shown as filled symbols and noncontacted cones as open symbols. The cell contacts most of both spectral cone types in its reach. Reproduced from Figure 4 in Hack, I. and Peichl, L. (1999). Horizontal cells of the rabbit retina are non-selectively connected to the cones. *European Journal of Neuroscience* 11: 2261–2274. With kind permission of Wiley-Blackwell.

view is that mammalian horizontal cells do not participate in color opponency (i.e., the antagonistic interpretation of color opponent channels).

Contacts with rods

Mammalian rods have horizontal cell contacts only with B-type axonal terminals; conversely, B-type axonal terminals connect only to rods. The only reported exception is the cone-dominated gray squirrel retina, where the axon of an H1 cell (B-type equivalent) was described to contact cones and, perhaps, rods. Unlike some other vertebrates, mammals have no type of horizontal cell that is exclusively connected to rods. This role is taken over by the B-type axon terminal system. The B-type axon is not an axon in the functional sense; it does not conduct information from the dendrites and soma to the axon terminal system. The latter is electrically uncoupled from the dendritic part; apparently, the axon is too thin and long (several hundred microns) to conduct the graded potentials that horizontal cells use for signaling. The axonal synaptic connections with the rods resemble those of the dendrites with the cones (**Figures 1(e)–1(g)**). It is thought that the B-type axon terminal system is the independent rod horizontal cell of mammals. Thus, while being one metabolic entity, the B-type cell represents two functional units. Actually, a small rod input is found in soma recordings of both B- and A-type cells; however, this is attributed to direct rod/cone coupling and not to signal transfer through the B-type axon.

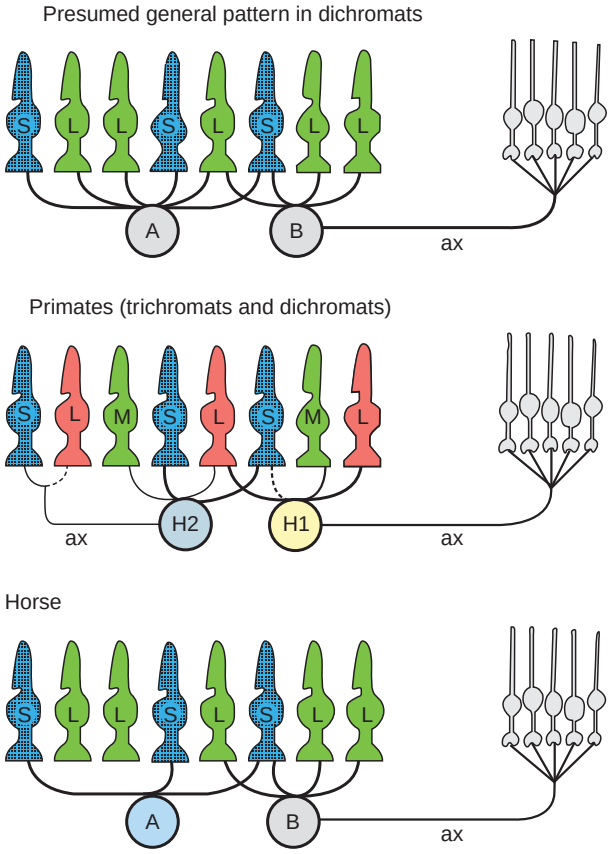

Figure 3 Scheme of the cone and rod contacts of horizontal cells in different mammals. (Top) The presumed general connectivity pattern in dichromats, confirmed in rabbit and tree shrew. A- and B-type cells indiscriminately contact S-cones and L-cones; the B-type axon terminal system contacts rods. (Middle) The connectivity pattern in primates. H1 cells contact M- and L-cones, but largely avoid S-cones (broken contact line); their axon contacts the rods. H2 cells contact S-cones strongly (thick contact line) and M/L-cones less strongly; their axon contacts S-cones, but may also contact M/L-cones. In dichromatic primates, M- and L-cones are only one spectral L type. (Bottom) The connectivity pattern in horse (and probably other equids). The A-type contacts S-cones exclusively, whereas the B-type makes indiscriminate contacts with S-cones and L-cones. The coloring of horizontal cell somata indicates their spectral tuning. Adapted from Figure 9 in Peichl, L., Sandmann, D., and Boycott, B. B. (1998). Comparative anatomy and function of mammalian horizontal cells. In: Chalupa, L. M. and Finlay, B. L. (eds.) *Development and Organization of the Retina*: *From Molecules to Function*, pp. 147–172. New York: Plenum Press. With kind permission of Springer Science and Business Media.

Why are the rods contacted by only one type of process (the B-type axonal terminals) and the cones by two types (A- and B-type dendrites) and what detailed functional difference does that make? An answer is currently not available. The receptive field surround of the ganglion cells becomes broader and shallower with decreasing light levels, and this is interpreted as a useful image-processing strategy. Nevertheless, it is unknown whether and how the rod/horizontal cell connections may be involved.

Population Properties and Gap-Junctional Coupling

The A- and B-type cells form populations that completely cover the retinal surface and thus provide their signals at all points of the retina. Within each population, the cells form a rather regular mosaic, that is, an even tiling of the retinal surface. The horizontal cells, similar to many other neurons, decrease their population density from the central to peripheral retina and conversely increase the size of the individual cells such that the dendritic overlap, or coverage factor, remains approximately constant across the retina. In cat, the density of A-type cells decreases from 800 mm^{-2} to 100 mm^{-2}, and that of B-type cells from 2300 mm^{-2} to 300 mm^{-2}. The coverage factor is approximately four for each type; therefore, each cone can, on average, contact eight horizontal cells. In rabbit, the central–peripheral density gradient is shallower (550 mm^{-2} to 250 mm^{-2} for the A-type and 1375 mm^{-2} to 400 mm^{-2} for the B-type); the coverage factor is approximately six for the A-type and 8–10 for the B-type, somewhat larger than in cat. Several staining methods can be used to stain entire horizontal cell populations. In many mammals, neurofibrillar stains and immunocytochemical staining of the neurofilament proteins specifically reveal the A-type population (**Figure 4(a)**), but in horse, the B-type population is specifically stained. Antibodies against the calcium-binding protein calbindin (CaBP 28 kDa) stain both horizontal cell populations in various mammals (**Figure 4(b)**).

Mammalian horizontal cells are electrically coupled by gap junctions. The coupling is homotypical; there are no gap junctions between A- and B-type cells (**Figure 5**). The gap junctions of A-type cells in rabbit are composed from connexin 50 (Cx50) subunits, and are larger than those of the B-type cells where the connexin is Cx57. The gap junctions of B-type cells in mouse are also formed by Cx57; therefore, the cell-type-specific connexins may be conserved across species. The rod connectivity is similar through the coupling of B-type axon terminals; notably, this coupling is segregated from that of the B-type dendrites (**Figure 5**). Thus, with respect to electrical coupling, the horizontal cells form three separate networks, even though A-type and B-type dendrites largely share their synaptic input and output partners, the cones. The gap junctions are regulated by the ambient light level in a triphasic manner. At intermediate light levels, the horizontal cells are strongly coupled and their signals spread over large distances; in bright and in very low light, the gap junctions are closed and the horizontal cells act as smaller inhibitory units. Dopamine and other neuromodulators are involved in this regulation. Horizontal cell coupling is thought to play an important role in photoreceptor adaptation to different ambient light levels as it serves to collect light information over large areas of the retina.

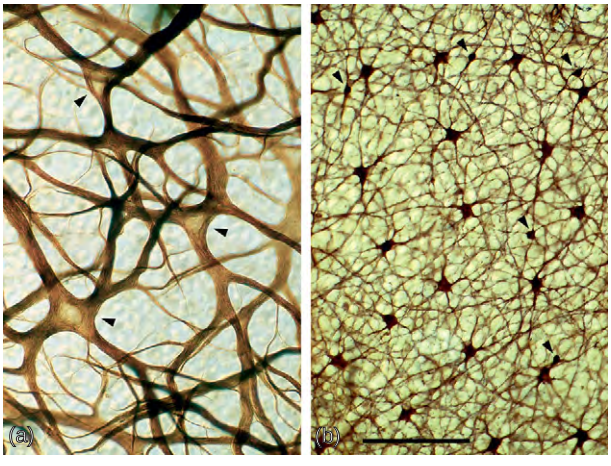

Figure 4 Flat views of population stains of horizontal cells. (a) Neurofibrillar staining of the A-type population in rabbit and (b) calbindin immunostaining of the A- and B-type populations in horse. In both images, the arrowheads indicate A-type somata. The scale bar = 50 μm for (a) and 100 μm for (b).

Diversity of Morphology and Connectivity across Species

None of the basic features listed so far has provided compelling arguments to explain why there should be two horizontal cell types in mammals. Are there really

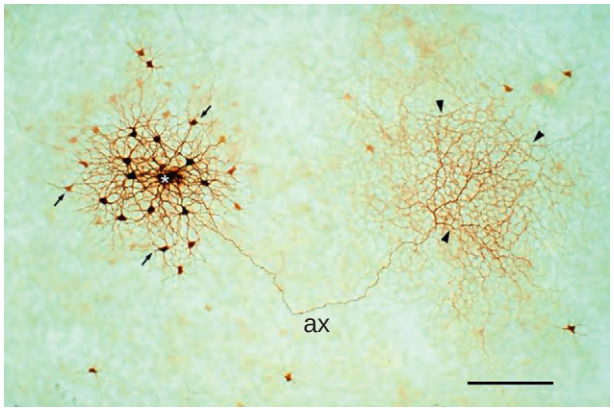

Figure 5 Gap-junctional coupling of rabbit B-type cells. After injection of neurobiotin into a B-type soma (asterisk), the dye spreads to neighboring B-type somata and dendritic trees (some arrowed) via gap junctions between dendrites, but not to neighboring B-type axon terminals or A-type cells. The dye that has diffused intracellularly through the axon (ax) to the axon terminal system of the injected cell then spreads to neighboring axon terminals via gap junctions (right side, arrowheads), and thereon diffuses to some B-type somata through their axons. This shows that gap-junctional coupling is type-specific (homotypic), and that coupling is segregated between B-type dendrites and axons. The scale bar = 100 μm. Image kindly provided by David I. Vaney.

two types in every mammal? Which morphological differences are of functional significance? Are there differences in their specific connection with the cones and, thus, in chromatic processing? A- and B-type horizontal cells have been identified in a range of orders including primates, carnivores, lagomorphs, rodents, and ungulates; both types are present in rod-dominated and cone-dominated retinas. On this basic pattern, an unexpected diversity in morphology and connectivity is superimposed, which has led to modifications in the general definition of mammalian A- and B-type cells.

Variations of Shape

Old World primates including humans were perceived early on as deviating from the general mammalian pattern. Both the H1 cell (B-type equivalent) and the H2 cell have an axon (**Figures 6(a) and 7**). Hence, H2 was regarded as unique to the primate retina. The axon of the H1 cell connects to rods, while that of the H2 cell connects to cones; the dendrites of both types only synapse with cones. As the H2 axon has no rod contacts, this cell can be equated to the A-type of other mammals. However, H2 cells have finer dendrites than H1 cells, the reverse of the presumed characteristic distinction between the A-type and B-type. Cells with the same morphologies also exist in New World monkeys. Moreover, the cone contacts of H1 and H2 cells in both Old World and New World primates differ from those of the B- and A-type cells of other mammals (see below).

In line with the overall more fine-grained processing in primate retina, particularly near the fovea, H1 and H2 cells have higher densities and smaller dendritic fields than the horizontal cells of other mammals. In macaque, H1 and H2 densities near the fovea are 18 400 mm^{-2} and 4,600 mm^{-2}, respectively, dropping to 1000 mm^{-2} and 500 mm^{-2}, respectively, in the peripheral retina. A central H1 cell only contacts 6–7 cones and a peripheral one, 40–50 cones. H2 cells have larger dendritic fields than H1 cells at corresponding locations, conforming to the A-type/B-type differences in other mammals.

In artiodactyls (ox, sheep, pig, and deer), the B-type cells have a robust dendritic tree, while the A-type dendritic tree is delicate (**Figures 8(c) and 7**); with regard to this, they resemble primates. The B-type has a single axon ending in an axon terminal system. The A-type has no axon; however, sometimes, one or a few dendritic processes extend beyond the perimeter of the dendritic field. Our evidence indicates that they are conventional dendrites connected to cones. The suggestion is that the artiodactyl A-type represents an intermediate shape between the roughly symmetric A-type dendritic fields of many mammals and the singular asymmetry of the primate H2 cell's axon, thus placing primate H2 cells at one end of a spectrum of A-type morphologies.

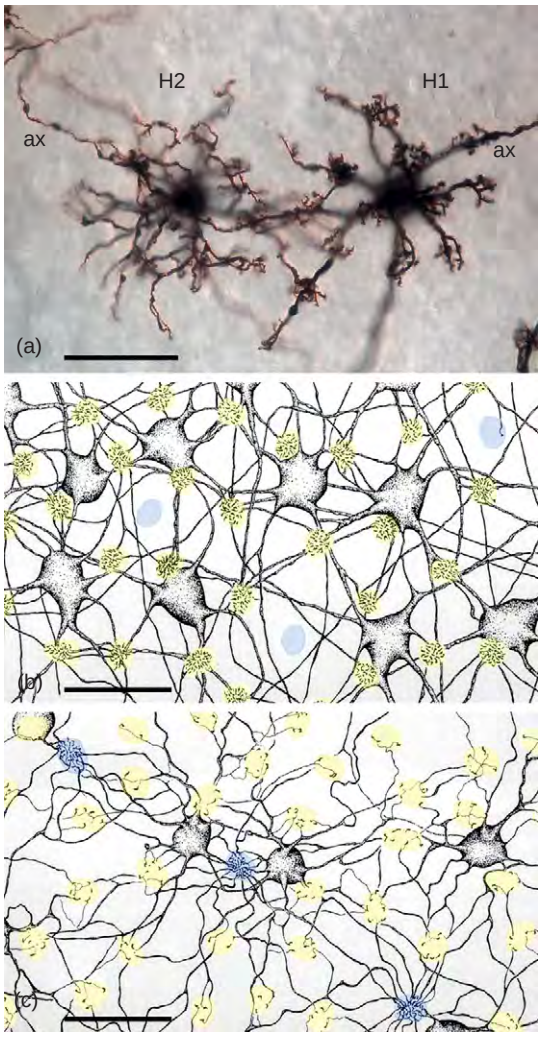

Figure 6 Primate horizontal cells and their cone contacts. (a) Golgi-stained macaque H1 and H2 cells in flat view, focused on the dendritic trees and terminal aggregates (ax, axon). (b) Plexus of macaque H1 cells, stained by a neurobiotin injection in one of the cells; tracer spread to the neighboring H1 cells occurred through the gap junctions. The H1 cells form dense terminal clusters at most cone pedicles (yellow, presumed M- and L-cones), but nearly completely miss the three presumed S-cones (blue). (c) Similarly neurobiotin-labeled macaque H2 cells. They not only strongly innervate the three presumed S-cones (blue), but also contact the other (M and L) cones. The scale bar = 25 μm. Images kindly provided by Dennis Dacey.

In perissodactyls (horse, ass, mule, and zebra), the B-type also has a robust dendritic tree. The single axon is very long, straight, and unusually thick (**Figures 8(d) and 7**). The dendrites of the A-type are very fine and sparsely branched, and there is no indication of an axon (**Figure 7**). The most interesting feature of this A-type cell, however, is its selective connection to the S-cones (see below).

The cone-dominated retina of the tree shrew (*Tupaia belangeri*, Scandentia) has particularly unusual A-type cells (**Figure 9**). They are large and have stout radial

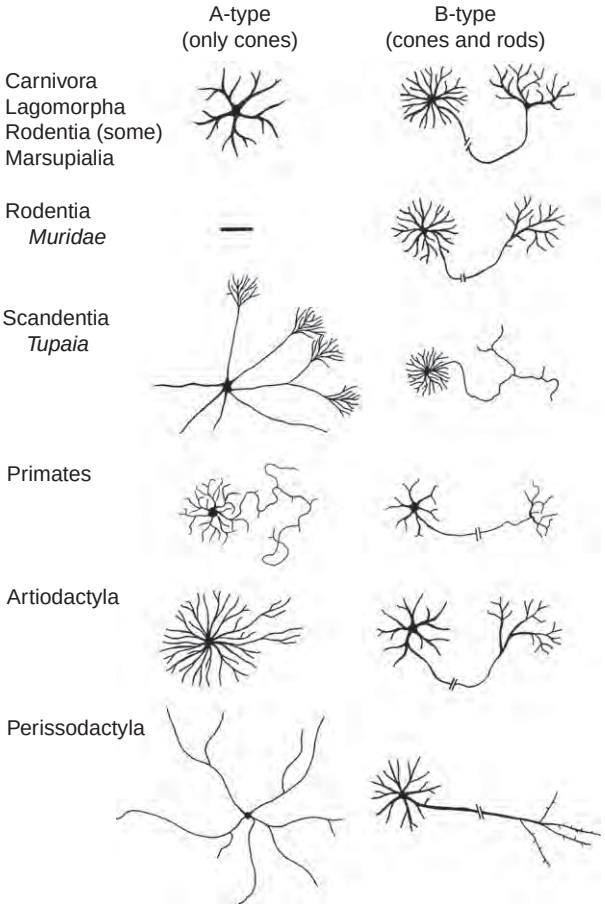

Figure 7 Schematic drawings to show interordinal variations in mammalian A- and B-type horizontal cell morphology. The diagram shows the basic branching patterns but not the synaptic terminals. Interruptions on B-type cells' axons indicate that the axons are longer than drawn. Adapted from Figure 5 in Peichl, L., Sandmann, D., and Boycott, B. B. (1998). Comparative anatomy and function of mammalian horizontal cells. In: Chalupa, L. M. and Finlay, B. L. (eds.) *Development and Organization of the Retina*: *From Molecules to Function*, pp. 147–172. New York: Plenum Press. With kind permission of Springer Science and Business Media.

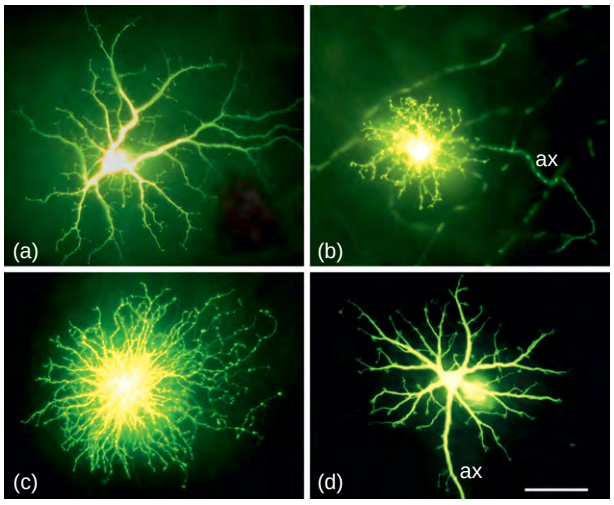

Figure 8 Species variations in horizontal cell morphology; Lucifer yellow-injected cells in flat view. (a) Guinea pig A-type; (b) gerbil B-type; (c) pig A-type; and (d) horse B-type. ax, axon. All cells shown at the same magnification and scale bar = 50 μm.

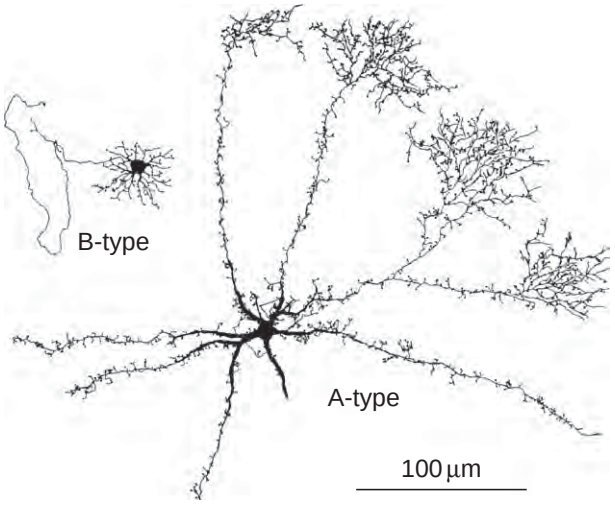

Figure 9 Drawings of Lucifer yellow-injected A- and B-type cells from the cone-dominated retina of the tree shrew. The B-type cell has a conventional dendritic tree and a sparsely branched axon terminal system, whereas the A-type cell has a unique branching pattern. Adapted from Figure 4 in Peichl, L., Sandmann, D., and Boycott, B. B. (1998). Comparative anatomy and function of mammalian horizontal cells. In: Chalupa, L. M. and Finlay, B. L. (eds.) *Development and Organization of the Retina*: *From Molecules to Function*, pp. 147–172. New York: Plenum Press. With kind permission of Springer Science and Business Media.

primary dendrites that rarely branch until the periphery of the dendritic field, where some ramify into unique bushy arborizations. The first description of these cells termed them multiaxonal because the arborizations were reminiscent of B-type axon terminal systems. We then showed that all connections of these cells, including those at the peripheral arborizations, are with cones. The cells thus conform to the basic mammalian A-type connectivity and can be interpreted as a further variety of A-type shape. This shape is not overtly associated with the high cone density in the tree shrew retina because the H2 cell (A-type equivalent) of the equally cone-dominated ground squirrel retina has a rather conventional shape. The B-type cells of the tree shrew are small and have a conventional dendritic tree; however, the axon is very sparsely branched and has only a few terminals (**Figure 9**). This is to be expected because less than 10% of the tree shrew's photoreceptors are rods.

The rodents are the most diverse of the mammalian orders, and their horizontal cells have provided the biggest surprise. The muroid species rat, mouse, gerbil, and Syrian

hamster possess only one type, the axon-bearing B-type (**Figures 8(b)** and **7**); intracellular injections and population analysis gave no evidence for a further type of horizontal cell. So far, the muroid rodents are the only known instance where the basic mammalian pattern of two horizontal cell types has not been found. In some other rodent groups, for example, sciurids and caviomorphs, both types are present (**Figure 8(a)**). The absence of A-type cells does not appear to be associated with nocturnality since the gerbil has active phases at both day and night and possesses a rather high cone proportion of 10–20%. Rat and mouse have a lower cone proportion (1% and 3%, respectively), which is, however, comparable to the cone proportions found in cat and rabbit (2–4%). Apparently, there is no correlation between a low cone/rod ratio and the absence of the A-type.

The morphology of the B-type axon terminal system also varies significantly across mammalian species. Most species have a thin B-type axon of a few hundred microns length that meanders randomly; in horse, the axon is thick, straight, and a few millimeters long. In cat, rabbit, and rat, the axon terminal system is rather densely branched and appears to innervate most of the rods in its field (as many as 3000 in cat). In other species such as primates or horse, the branching is less dense or even sparse. Here, only a minority of the rods present are innervated by any one terminal system. However, as a population, the overlapping axons of several cells ensure full coverage of the rods.

The existence of a third type of horizontal cell has been claimed for primates, the rabbit, and the South American opossum on the basis of individual cells that markedly differed from the other two types in morphology and presumed connectivity. However, other studies have concluded that such cells are encompassed in the normal variation of the standard two types; the most parsimonious interpretation is that these cells are extreme individuals. If horizontal cells with new or unusual morphological features are to be classified as a new type, it should also be demonstrated that this type exists as a population and adequately covers the retina.

The species variations in horizontal cell morphology add to the recognition that the basic blueprint of the mammalian retina is more flexible than is commonly assumed (**Figure 7**). Currently, there is little clarity regarding the meaning of these variations. The absence of the A-type in murids is of practical significance since genetically modified mouse strains are heavily used to elucidate the general principles of mammalian retinal wiring and function. Researchers have to be aware that mouse data on the contribution of horizontal cells to retinal processing may not be readily transferable to other species. On the other hand, mice may provide key insights into the effects that one versus two horizontal cell types have on the properties of ganglion cell receptive fields.

Species with Selective Cone Contacts

Most mammals are cone dichromats with a majority of L-cones and a minority of S-cones. In Old World primates and man, the mammalian L opsin gene has diverged into separate genes for the M (green) and L (red) cone opsins, making these species cone trichromats with refined color vision. Most New World monkeys are cone dichromats by genotype; however, some species were shown to have an L opsin polymorphism that results in a trichromatic phenotype in many females, while the males are dichromats. Hence, the retina of primates was an interesting place to investigate whether the horizontal cells are chromatically selective and might contribute to color processing.

Observations on Golgi-stained human and monkey horizontal cells had indicated that H1 dendrites specifically avoid or undersample the S-cones, whereas H2 dendrites contact all cones and H2 axons exclusively contact S-cones. In a seminal study, Dennis Dacey and his colleagues recorded the responses of H1 and H2 cells to chromatic stimuli in the isolated living macaque retina and demonstrated that H2 cells show the same hyperpolarization at all wavelengths, whereas H1 cells hyperpolarize to M- and L-cone stimuli but do not respond to S-cone stimuli. The recorded cells were injected with the tracer neurobiotin, labeling all members of patches of H1 or H2 cells around an injected cell through the homotypic gap junctions. The population of H1 cells innervates the majority of the cones, but hardly contacts the small fraction of presumed S-cones (**Figure 6(b)**). The H2 population, on the other hand, connects to all cones, but makes particularly numerous contacts with the small fraction of presumed S-cones (**Figure 6(c)**). Studies combining dye-labeling of individual horizontal cells and cone opsin labeling confirmed this connectivity pattern for macaque, orangutan, and chimpanzee. They showed that only close to 15% of the H1 cells contact S-cones, but then only sparsely; the H2 cells contact all cones within reach and have more synapses with each S-cone than with each of the M- and L-cones contacted. The axon of the H2 cell definitely contacts S-cones, but whether it does so exclusively has yet to be determined. Despite the differences in cone connectivity, the physiological recordings indicate that neither the H1 nor the H2 cell is involved in creating spectrally opponent receptive fields of bipolar and ganglion cells.

New World monkeys (where there are dichromatic and trichromatic individuals) have the same cone connectivity pattern of H1 and H2 cell dendrites as macaque and man. This suggests that the special horizontal cell connectivity with S-cones is not correlated with the evolution of trichromacy in the Old World primates. Notably, both horizontal cell types of trichromatic primates are nonselective in their M-cone and L-cone contacts. Apparently, when the red/green processing pathway evolved from a

presumably dichromatic early primate retina, this did not involve alterations in horizontal cell connectivity.

A differential cone connectivity of horizontal cells was also found in the dichromatic horse (**Figure 3**). Its A-type cells have particularly large and sparsely branched dendritic fields with few and widely spaced terminal aggregates. In one Lucifer yellow-filled A-type cell, counterstained with an S-cone marker, all but one of its 45 contacts were with S-cones. Further cells need to be studied to confirm this finding. However, the A-type, similar to the B-type, is a consistently occurring cell population that covers the horse retina (**Figure 4(b)**). Therefore, the horse (and other equids) may possess an A-HC that is selectively connected to S-cones, while the B-type connects to both types of cone.

A similarly S–cone-selective horizontal cell may be present in the cone-dominated retinas of the dichromatic sciurids. The red squirrel and ground squirrel possess an axon-bearing H1 cell (B-type) and an axonless H2 cell (A-type). The density of dendritic terminal aggregates on the H1 cell is high enough to contact all cones present. In contrast, the terminal aggregates on H2 dendrites are spaced so far apart that they can only contact a small fraction of the cones, which presumably are S-cones. It would be worthwhile and now feasible to determine, experimentally, if an S-cone selective horizontal cell is present.

Conclusions and Open Questions

The principal horizontal cell dichotomy of an axon-bearing B-type, which serves rods and cones, and a commonly axonless A-type that only serves cones, holds for most mammals. Thus, the A-type and B-type cells represent basic components of the mammalian retinal blueprint, suggesting an indispensable function. The B-types are necessary in all mammals as they all have cones and rods. However, why is there an additional A-type in the cone pathway? What functional differences are there between the A-type and the B-type? Modeling suggests that the two types with their different dendritic field sizes and spatial summation properties can explain the assumed receptive field characteristics of the cones, and, hence, the receptive field organization of bipolar cells and ganglion cells. The requirements for temporal processing may be another reason for having more than one horizontal cell type. Indeed, horizontal cells in cat differ in their flicker-response properties. However, despite the absence of the A-type, rat and mouse have ganglion cells with center/surround receptive field organizations very similar to rabbit and cat.

Mammalian horizontal cells are rather diverse across species. This diversity encompasses morphological features as well as details of cone connectivity (**Figures 7** and **3**). Thus, some amendments to the textbook characterizations are necessary:

1. Dendritic thickness and dendritic branching pattern are not defining characteristics of either type, unless the order of mammal is specified. Within a given species, the two types differ in their dendritic morphology, which suggests some physiological difference. Does it matter whether the finer dendrites are on the B-type (as in cat and rabbit) or on the A-type (as in primates and artiodactyls)?
2. Across species and orders, the A-type is more variable than the B-type. A-type variability includes axon-like processes in primates, an S-cone preference in primates and horse, and a complete lack of the A-type in some rodents. B-type variability includes dendritic and axonal branching patterns and the near avoidance of S-cones by primate H1 cells.

There is no obvious correlation between these horizontal cell variations and the phylogenetic distance of the corresponding mammalian orders. For example, Carnivora and Lagomorpha are phylogenetically less close than Primates and Scandentia, but the former have very similar horizontal cell morphologies, while those of the latter differ significantly. The peculiarity of a B-type/H1 cell with fine dendrites and an A-type/H2 cell with stout dendrites is shared by artiodactyls, perissodactyls, and primates. Within any one taxon, horizontal cell features are commonly more conserved across species.

There is no obvious correlation between these horizontal cell variations and specific adaptations to different visual requirements and other retinal specializations. Different cone/rod ratios, indicative of a nocturnal or diurnal lifestyle, do not predict the presence of one or two horizontal cell types. Primates with highly developed trichromatic color vision have cone-selective horizontal cells, but so does the dichromatic horse. In addition, the cone selectivity of H1 and H2 cells is the same in New World and Old World primates, which have different levels of color vision.

See also: Cone Photoreceptor Cells: Soma and Synapse; Information Processing: Bipolar Cells; Information Processing: Horizontal Cells; Morphology of Interneurons: Bipolar Cells; Physiology of Photoreceptor Synapses and Other Ribbon Synapses; Rod Photoreceptor Cells: Soma and Synapse.

Further Reading

Ahnelt, P. and Kolb, H. (1994). Horizontal cells and cone photoreceptors in human retina: A Golgi-electron microscopic study of spectral connectivity. *Journal of Comparative Neurology* 343: 406–427.

Boycott, B. B., Peichl, L., and Wässle, H. (1978). Morphological types of horizontal cell in the retina of the domestic cat. *Proceedings of the Royal Society (London) B* 203: 229–245.

Chan, T. L. and Grünert, U. (1998). Horizontal cell connections with short wavelength-sensitive cones in the retina: A comparison

between New World and Old World primates. *Journal of Comparative Neurology* 393: 196–209.
Dacey, D. M., Lee, B. B., Stafford, D. K., Pokorny, J., and Smith, V. C. (1996). Horizontal cells of the primate retina: Cone specificity without spectral opponency. *Science* 271: 656–659.
Hack, I. and Peichl, L. (1999). Horizontal cells of the rabbit retina are non-selectively connected to the cones. *European Journal of Neuroscience* 11: 2261–2274.
Mills, S. L. and Massey, S. C. (1994). Distribution and coverage of A- and B-type horizontal cells stained with neurobiotin in the rabbit retina. *Visual Neuroscience* 11: 549–560.
Peichl, L. and González-Soriano, J. (1994). Morphological types of horizontal cell in rodent retinae: A comparison of rat, mouse, gerbil and guinea pig. *Visual Neuroscience* 11: 501–517.
Peichl, L., Sandmann, D., and Boycott, B. B. (1998). Comparative anatomy and function of mammalian horizontal cells. In Chalupa, L. M. and Finlay, B. L. (eds.) *Development and Organization of the Retina: From Molecules to Function*, pp. 147–172. New York: Plenum Press.
Perlman, I., Kolb, H., and Nelson, R. (2003). Anatomy, circuitry, and physiology of vertebrate horizontal cells. In Chalupa, L. M and Werner, J. S. (eds.) *The Visual Neurosciences* vol. I, pp. 369–394. Cambridge, MA: The MIT Press.
Smith, R. G. (2008). Contributions of horizontal cells. In Masland, R. H. and Albright, T. (eds.) *The Senses: A comprehensive reference* vol. 1, pp. 341–349. Amsterdam: Elsevier.
Wässle, H., Peichl, L., and Boycott, B. B. (1978). Topography of horizontal cells in the retina of the domestic cat. *Proceedings of the Royal Society* (*London*) *B* 203: 269–291.
Wässle, H., Dacey, D. M., Haun, T., et al. (2000). The mosaic of horizontal cells in the macaque monkey retina: With a comment on biplexiform ganglion cells. *Visual Neuroscience* 17: 591–608.

Relevant Website

http://webvision.med.utah.edu – Webvision: The Organization of the Retina and Visual System.

Morphology of Interneurons: Interplexiform Cells

D G McMahon and D-Q Zhang, Vanderbilt University, Nashville, TN, USA

Glossary

Retinitis pigmentosa – A group of inherited disorders characterized by progressive loss of photoreceptors.
Sublamina of inner plexiform layer – Inner plexiform layer is divided into sublamina a (the distal sublamina) and sublamina b (the proximal sublamina). Sublamina a is further divided into two strata, 1 and 2, whereas sublamina b is divided into three strata, 3–5.

Introduction

The canonical flow of visual information in the retina is for light stimuli to be transduced into neurochemical signals by the rod and cone photoreceptors in the outer retina and then passed through the synaptic layers (outer plexiform layer, OPL; inner plexiform layer, IPL) to ganglion cells which then transmit them to the rest of the brain via the optic nerve. Interplexiform neurons are a unique class of retinal amacrine cells that form an intraretinal feedback pathway transmitting adaptational visual signals in the opposite direction, from the inner retina back to the outer retina (**Figure 1**). They receive their synaptic input in the IPL and make their output via interplexiform processes terminating in the OPL. These intraretinal feedback neurons are present in most vertebrate retinas, and in the majority of species these neurons secrete the neurotransmitter dopamine.

Dopaminergic interplexiform cells (IPCs) exert widespread influence on the physiology and function of the retina, reconfiguring retinal circuits and altering the processing of visual signals in the retina, by initiating slow and sustained changes in the physiology of retinal neurons and synapses. In particular, retinal dopamine has been found to act on electrical synapses, or gap junctions, to restrict the flow of visual signals in retinal neural networks at the level of photoreceptors, horizontal cells, and amacrine cells. In addition to the direct synaptic contacts from interplexiform processes in the outer plexiform layer, dopaminergic retinal neurons exert influence throughout the retina by volume transmission, via perfusion of dopamine beyond synaptic zones. Dopamine has been found to affect all major classes of retinal neurons, from photoreceptors to ganglion cells. An overall effect on retinal function of these feedback signals from dopaminergic IPCs is to enhance signaling in cone pathways and to decrease the signaling on rod pathways, optimizing retinal circuitry for photopic visual processing during periods of relatively high light levels. However, roles for dopamine in dark-adapted retinal responses have also been shown. Thus, dopamine and IPCs play key roles in optimizing retinal function over the wide dynamic range of light intensities encountered in the visual environment.

Secretion of dopamine by IPCs is controlled by two factors: background illumination and an intrinsic daily clock in the retina, enhancing cone signals in conditions of bright light and during the day, and rod signals in conditions of dim light and during the night. In addition to this adaptational effect on retinal neural networks, dopamine secreted from IPCs has trophic effects on photoreceptor survival and eye growth that are associated with eye diseases. In the following, we discuss the anatomy, physiology, and significance for human visual health of dopaminergic IPCs.

Morphology of Dopaminergic Interplexiform Neurons

Dopaminergic amacrine (DA) cells are a subpopulation of amacrine cells whose cell bodies lie in the innermost cell row of the inner nuclear layer (INL). DA cell processes ramify extensively in the outermost layer of the IPL where they are both presynaptic to and postsynaptic to other neurons. The total number of DA cells averages 500 per retina, although it varies slightly in different species. IPCs are a class of DA cells in which additional fine processes arising either from the cell body or from one of the dendrites ascend through the INL to the OPL where they form an output plexus for the secretion of dopamine in the outer retina. The IPC was first described in the retina of cat by Gallego in 1971, and was extensively studied by Dowling and co-authors. The percentage of DA-IPCs among DA cells is species dependent. In goldfish, Cebus monkey, and mouse retinas, almost all DA cells are likely to be DA-IPCs, whereas in rabbit, turtle, salamander, and human retinas, interplexiform processes are rarely observed on DA neurons. Approximately 50% of DA cells are DA-IPCs in the rat, *Xenopus* and *Rhesus* monkey retinas.

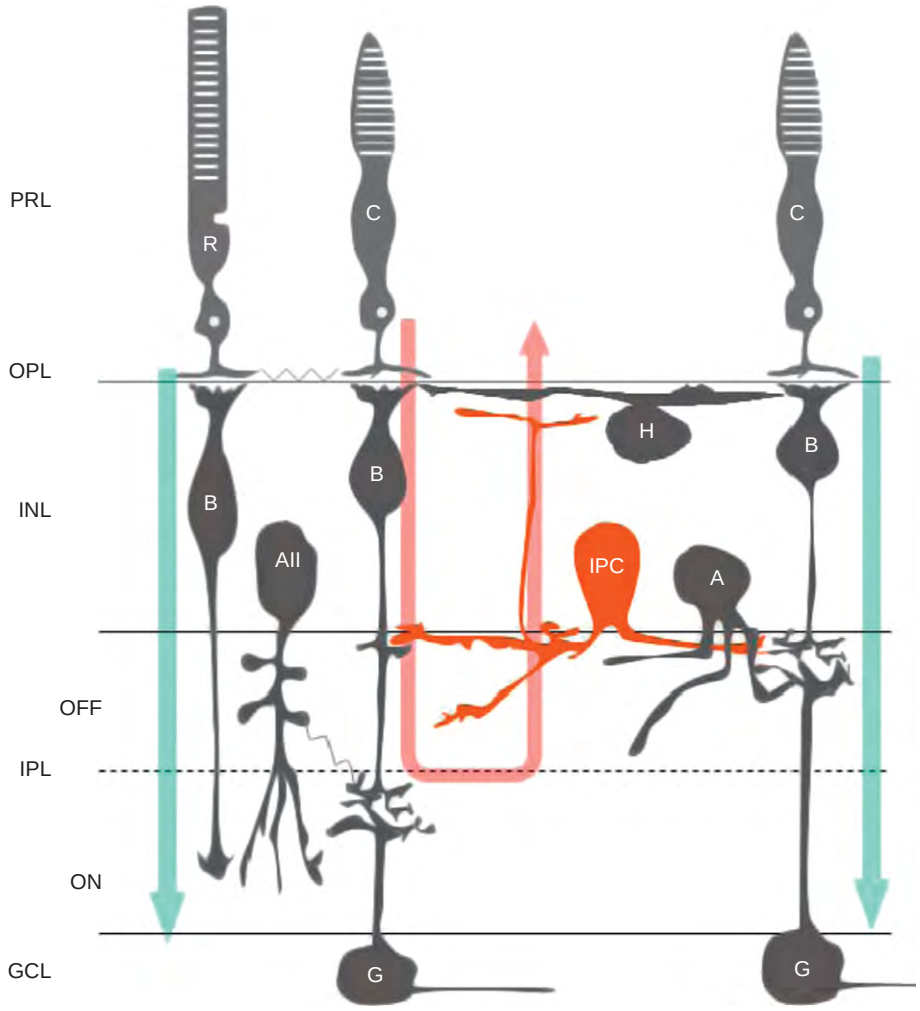

Figure 1 Interplexiform neurons mediate intraretinal feedback. An interplexiform cell (red) is located in the middle of the retina. Straight arrows indicate the canonical flow of visual signals from the outer retina to the inner retina. The U-shape arrow indicates an intraretinal feedback from the inner retina to the outer retina. R, rod; C, cone; H, horizontal cell; B, bipolar cell; AII, AII amacrine cell; IPC, interplexiform cell; A, inhibitory amacrine cell; G, ganglion cell, PRL, photoreceptor layer; OPL, outer plexiform layer; IPL, inner plexiform layer; GCL, ganglion cell layer; OFF, OFF sublamina of the IPL; ON, ON sublamina of the IPL.

Morphology and Distribution

Antibodies against tyrosine hydroxylase, the rate-limiting enzyme of catecholamine synthesis, are commonly used to detect DA cells for characterization of their localization, shape, size, dendritic arborization, and distribution (**Figure 2**). In order to enable targeting of living DA cells for morphological, functional, and molecular analysis, transgenic mouse lines have been created in which the DA cells are labeled with chemical or fluorescent protein reporters, driven by the tyrosine hydroxylase gene promoter. DA cells have three descriptive components to their morphology: soma, dendrites, and axon-like process. The morphology of dopaminergic IPCs is similar to that of other DA cells except for the presence of an additional axon-like process ascending to the OPL.

Soma

Somata of DA cells are either round or ovoid with diameters of 12–15 μm and areas of 100–150 μm^2 (**Figure 2**). In most species, DA cell somata are regularly and sparsely distributed in the innermost aspect of the INL across the entire extent of the retina. The distribution of the DA cells varies across the retina in the rat, with the peak density in the superior temporal quadrant and the lowest density in the inferior nasal quadrant. Occasionally, DA cells are displaced into the ganglion cell layer and, in this case, there is no evidence that these displaced amacrine cells have interplexiform processes.

Dendrites

Two to six primary dendrites arise from the cell body, and branch 4–6 times in the outermost aspect of the OFF

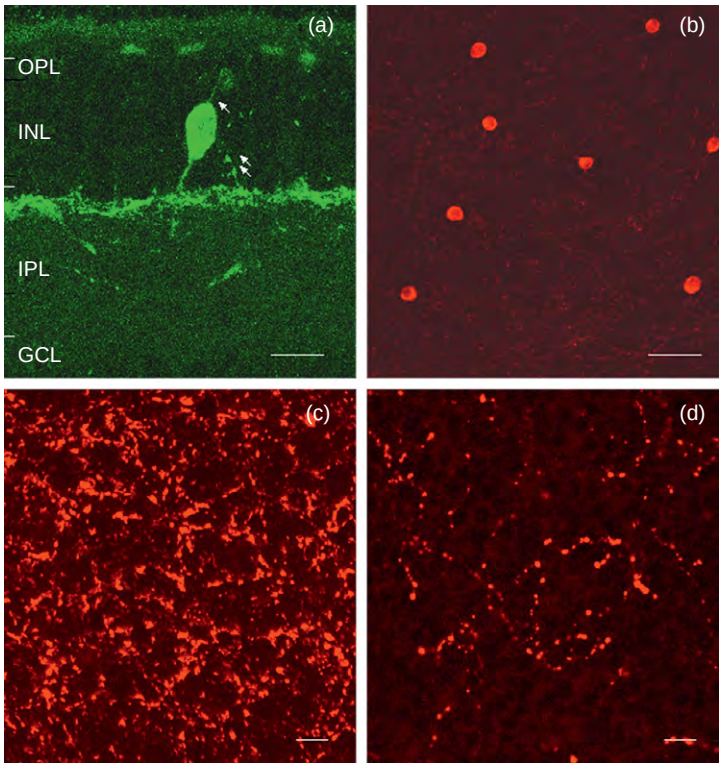

Figure 2 Immunohistochemical localization of TH in the mouse retina. (a) TH-positive soma situated in the INL stratifies at the border between the INL and the IPL in a vertical section. Single arrow and double arrows indicate ascending axon-like processes emerging from the DA cell body and from the plexus in the IPL, respectively. The axon-like processes traverse the INL toward the OPL. Scale bar: 20 μm. (b) Flat-mount view focused on the INL demonstrates the regular distribution of DA cells. Scale bar: 50 μm. (c) Flat-mount view focused on the border between the INL and the IPL shows a dense plexus of dopaminergic processes. Scale bar: 10 μm. (d) Flat-mount view focused on the OPL illustrates a loose plexus of fine dopaminergic processes. Scale bar: 10 μm.

sublamina (stratum 1) of the IPL. These branches radiate symmetrically from the soma and follow a straight somatofugal direction. The thickness of the primary dendrites is up to 4.5 μm and decreases at each bifurcation. The primary dendrites are usually smooth, whereas terminal branches exhibit varicosities (up to 0.5 μm in diameter). The long axis of the dendritic field of individual DA cells is approximately 800 μm. The dendritic fields of adjacent DA cells overlap extensively with a coverage factor of 2–4, forming a dense plexus in stratum 1 of the inner plexifom layer (**Figure 2**). Dendrites from teleost DA cells spread proximally throughout the IPL. In contrast, in mammalian retinas, only occasional processes from the plexus in stratum 1 run deeper into other stratums.

Axon-like fine process

Axon-like processes are quite distinct from the dendrites of DA cells. They are thin, straight, long, and sparsely branched at close to right angles. Teleost DA-IPC axon-like processes form a pronounced plexus in the OPL. DA-IPCs in Cebus monkey have dense plexuses of fine processes in both the outer and inner plexifom layer. In other species, DA cell processess form an extensive dense network in the IPL, whereas the ascending axon-like processes either do not branch or branch within clusters in the OPL. For instance, in the mouse retina, two to three axon-like processes arise either from the soma or from the primary dendrites. Each axon-like process, with multiple successive bifurcations, covers the extensive area of the retina: total length up to 10–25 mm. Thus, axon-like processes can overrun each other and, together with overlapping dendrite networks, form a particularly dense plexus of dopaminergic processes in stratum 1 of the IPL. This process network forms small rings around the origin of the primary dendrites of AII amacrine cells at the INL–IPL margin. Axon-like processes bear varicosities that are thought to be sites of dopamine release. Compared to the dense plexus in the IPL, the OPL plexus of fine dopaminergic processes is more loosely arranged. Axon-like processes also traverse the INL to the OPL, sometimes forming clusters of fine processes (**Figure 2**).

Synaptic Input to DA Neurons

Dopaminergic IPC processes extend widely into the outer and the IPLs. There is anatomical evidence that DA neurons receive synaptic input in the IPL from bipolar

and amacrines cells, as well as centrifugal fibers arising from brain nuclei, and there is functional evidence for retrograde input to DA neurons from ganglion cells.

Input from bipolar cells and amacrine cells

DA cell interplexiform processes are presynaptic to horizontal and bipolar cells in the OPL, and there is no evidence that interplexiform processes are postsynaptic to any cells in the OPL. Electron microscopy of tyrosine hydroxylase immunoreactivity in rhesus monkey, cat, and rabbit has shown that DA cells receive synaptic input from both bipolar cells and inhibitory amacrine cells in mammalian retinas. The size, structure, and position of the bipolar to DA neuron synapses in the IPL suggest that they are from bistratified bipolar cells. Bistratified bipolar cells have also been found in the mouse, fish, turtle, and salamander retinas. In addition, close apposition of bipolar and DA neuron processes has also been observed in deeper layers of the IPL. Therefore, light information generated by photoreceptors may reach DA cells directly from bipolar cells or indirectly from bipolar cells through inhibitory amacrine cells (**Figure 3**).

Input from intrinsically photoreceptive ganglion cells

Intrinsically photoreceptive ganglion cells (ipRGCs) are endogenously photosensitive because they express melanopsin, a photopigment first described in photosensitive dermal melanophores of the frog. They comprise 1–2% of retinal ganglion cells forming a photosensitive network in the inner retina. The ipRGC dendritic processes ramify in the OFF layer of the IPL where they have close contact with DA neuron processes (**Figure 3**). Physiological experiments have suggested that DA cells receive synaptic input from ipRGCs (below). Whether DA cells are postsynaptic to the dendrites of ipRGCs is under investigation.

Input from centrifugal fibers

Many vertebrate retinas receive input from other parts of the brain via retinopetal axons. The efferent input to the retina originates from the ventral thalamus in reptiles, the olfactory bulb in fish, the isthmo-optic nucleus in birds, and the tuberomammillary nucleus of the posterior hypothalamus in mammals. In fish centrifugal fibers make synapses directly onto DA-IPCs. Histamine has been localized to retinopetal axons in the guinea pig, monkey, and rat, and evidence suggests that DA cells receive input from histaminergic centrifugal fibers in mammalian retinas. Thus, IPCs likely form a conduit for feedback to the retina from the rest of the brain as well as for intraretinal feedback signals.

Physiology of Dopaminergic Interplexiform Neurons

Dopamine Reconfigures Retinal Circuits

DA neurons comprise the central neuromodulatory system of the retina, forming an intraretinal feedback

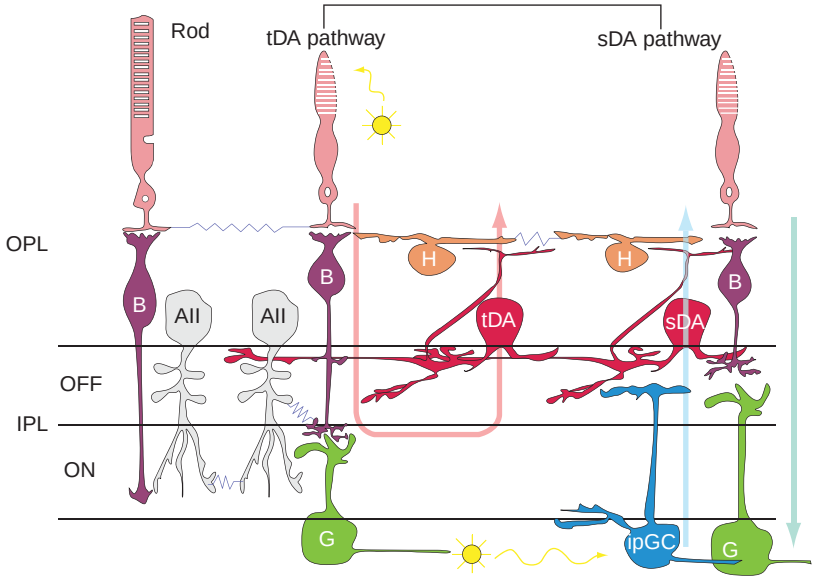

Figure 3 Dopamine neuron light response pathways. DA cells exhibit two classes of light responses: ON-transient and ON-sustained. ON-transient DA cells (tDA) are driven by rod or cone photoreceptors through ON-bipolar cells (tDA pathway), whereas ON-sustained DA neurons (sDA) are driven by melanopsin-expressing intrinsically photoreceptive ganglion cells (sDA pathway). Green straight arrow indicates the canonical flow of rod/cone visual signals from the outer retina to the inner retina. The U-shape red arrow indicates an intraretinal feedback of rod/cone initiated signals from the inner retina to the outer retina. The blue arrow indicates an intraretinal retrograde flow of ganglion cell photoreceptor signals from the inner retina to the outer retina. tDA, transient dopaminergic interplexiform cell; sDA, sustained dopaminergic interplexiform cell; ipGC, intrinsically photoreceptive ganglion cell.

pathway that reconfigures retinal circuits according to prevailing illumination conditions and signals from the retinal circadian clock. Through dopaminergic signaling, they restructure retinal function by modulation of chemical and electrical synapses, as well as by modification of the functional properties of retinal neurons. Both through direct synaptic contacts from interplexiform processes and through volume transmission, DA neurons influence all levels of retinal circuitry and all major classes of retinal neurons. In particular, dopamine regulates multiple neural circuits in the retina by modulating electrical synaptic transmission through gap junctions. This type of circuit modulation was first described in relation to dopaminergic uncoupling of gap junctions mediating electrical synaptic transmission between horizontal cells in teleost fish retinas, an action thought to reduce the size of retinal receptive fields. Subsequently, the regulatory action of dopamine on retinal gap junctions has been found to be a more general phenomenon, with coupling between rods and cones, AII amacrine cells and ganglion cells also being modulated by dopamine. Dopaminergic regulation of both rod–cone coupling and AII amacrine cell coupling serves to restrict the flow of visual signals from rods to retinal ganglion cells during light-adapted conditions in the day, while allowing flow of rod signals in the dark and at night.

In addition to regulating electrical synaptic transmission, retinal dopamine influences retinal circuit function by modifying chemical synaptic transmission, via modulation of glutamate and gamma aminobutyric acid (GABA) receptors. It also alters intrinsic functional properties of retinal neurons via modulation of membrane ion channels, such as voltage-gated sodium currents in bipolar and ganglion cells. Many of the synaptic and cellular changes induced by dopamine are consistent with a role for this transmitter in mediating light-adaptive changes in retinal function. For example, uncoupling of horizontal cells is consistent with a reduction in receptive field size and increased spatial resolution in light-adapted conditions. Restriction of rod signals from the cone pathways in the light and during the day is consistent with this notion as well. Modulation of sodium currents in bipolar cells and ganglion cells is consistent with accelerating light responses in cone pathways and shifting ganglion cell function from photon detection to contrast signaling, respectively. Finally, although IPCs do not directly synapse on photoreceptors, the outermost cells of the neural retina, they significantly influence their function, presumably through volume transmission of dopamine. In addition to regulating circadian rhythms in rod–cone coupling, dopamine influences regulation of the intracellular second messenger cyclic adenosine monophosphate and the timing of circadian secretion of melatonin by photoreceptors.

Light Drives Interplexiform Neurons via Both Conventional and Novel Pathways

One of the persistent puzzles regarding IPCs has been to understand the precise mechanisms by which they are affected by light and thus provide feedback signals within retinal circuits for background illumination. Studies of retinal dopamine release revealed a surprising heterogeneity in the lighting conditions that evoked dopamine release, including flickering light, steady light, and even prolonged darkness. Although studied intensively for more than three decades, the neural mechanisms by which light influences the activity of dopaminergic interplexiform neurons have remained incompletely understood, in part, because the sparse nature of retinal dopaminergic neurons had prevented analysis within intact retinal circuits with electrophysiological approaches that directly measure neuronal activity. Previous studies with anatomical approaches had suggested that retinal DA neurons are a homogeneous population of cells, that their primary input was from inhibitory GABA/glycine amacrine cells in the OFF sublamina of the IPL, and thus that their light responses could be due to disinhibition of OFF responses. Recently, the limitation on *in situ* electrophysiological recording of DA neurons was overcome by creating a transgenic mouse in which DA neurons were genetically marked with a fluorescent protein. Electrophysiological studies of dopaminergic interplexiform neuron light responses yielded the surprising finding that despite being considered a morphologically homogenous class, these neurons are functionally heterogeneous, with distinct neuronal subpopulations exhibiting transient and sustained light responses (**Figure 3**). This cellular heterogeneity is likely the substrate for the observed functional heterogeneity in dopamine regulation by light.

Light-responsive DA neurons fall into two distinct subpopulations (ON-transient and ON-sustained), which are driven by separate synaptic circuits. ON-transient cells are driven by rod or cone photoreceptors through ON-bipolar cells, in a conventional retinal ON-pathway circuit. ON-sustained DA neurons, however, are driven by melanopsin-expressing ipRGCs in a novel intraretinal retrograde light pathway in which ganglion cell photic signals are used for network adaptation within the retina. This novel intraretinal feedback pathway completely reverses the canonical direction of visual signaling, with photoreception being initiated in ganglion cells and dopaminergic signaling potentially modulating rod and cone photoreceptors (**Figure 3**). Thus, the dopaminergic interplexiform system is composed of two functional subpopulations of neurons tuned to distinct aspects of environmental light signals: transient DA neurons (t-DA, **Figure 3**), driven by rod and cone input through ON-bipolar cells that are tuned to rapidly changing background signals and which may mediate the observed dopamine release to flickering light, and sustained DA neurons (s-DA, Figure**3**), driven

by ipRGCs that are tuned to maintained background illumination and which may mediate the observed dopamine release to steady light.

While light stimulates dopamine secretion by dopaminergic retinal neurons, there is also basal release of dopamine in the dark. Studies by Raviola and colleagues showed that isolated DA neurons are spontaneously active, with sodium and calcium currents that support spontaneous spiking and dopamine secretion. Recordings from DA neurons in intact retinas have shown that DA neurons exhibit spontaneous bursts of spikes that are enhanced when input from inhibitory amacrine cells is blocked pharmacologically. In intact retinal circuits, the OFF-channel-driven GABA and glycine input from inhibitory amacrine cells partially suppresses the intrinsic bursting activity of DA neurons. As burst spiking is associated with increased dopamine secretion from midbrain dopaminergic neurons, the input from inhibitory amacrine neurons likely regulates basal secretion of dopamine by retinal DA neurons in the dark.

IPCs Signal Time of Day from the Retinal Clock

The retinal circadian clock shapes retinal function into 'day' and 'night' states timed to the local day–night cycle. This requires intraretinal signaling mechanisms for both the output of clock signals to the downstream retinal processes and the input of the local light cycle to set the phase of the retinal clock. Retinal dopamine, which is under both circadian and light-evoked control, appears to play a critical role in both of these processes. Among its manifold demonstrated effects on retinal neurons and circuits, dopamine regulates circadian rhythms in rod–cone coupling, and the resulting rhythms in spectral sensitivity and rod–cone balance of retinal responses. Several recent results also suggest that dopamine plays a key role in the signaling of light stimuli to the retinal circadian clock. Recent findings that retinal dopamine is a key component of light resetting of the retinal clock and that retinal dopaminergic neurons receive light input from ipRGCs suggest that retinal circadian photoreception is likely mediated by a novel intraretinal retrograde light-transmission circuit in which light signals originate in the ipRGCs and reset the circadian clock through their influence on sustained DA cells.

DA Neurons and Retinal Degenerative Disease

Parkinson's Disease

Parkinson's disease is a neurodegenerative disease caused by degeneration of doapminergic neurons in striatum and substantia nigra. Visual functions such as contrast sensitivity detected by pattern electroretinograms (PERGs) are also impaired in Parkinson's disease since there is concurrent loss of DA neurons in the retina. One possible cause is that dopamine deficiency increases receptive field size of horizontal cells in the outer retina, and of AII amacrine cells in the inner retina, through loss of dopaminergic control of gap junctions, which results in altering receptive field properties of ganglion cells (the primary origin of the PERG response).

Diabetic Retinopathy

Diabetic retinopathy, which is classically defined as a microvasculopathy, is now being viewed as a neurodegenerative disease of the retina. Functional visual deficits detected by electroretinogram (ERG) often occur before the appearance of overt retinal lesions in diabetic retinopathy. The most prominent change of the ERG in early diabetes is a distortion of oscillatory potentials that are thought to derive from the inner retinal neurons including DA cells. Indeed, DA cells initiate programmed cell death in early diabetes, and are lost during the later phases of the disease. Dysfunction of DA cells in diabetic retinas has also been suggested by studies examining retinal dopamine content and tyrosine hydroxylase activity. Together, these studies suggest that DA cells undergo degeneration in diabetes, but the cause remains unclear.

Human Health Implications of the Retinal Clock

Retinal circadian clock signaling modulates human vision, is associated with retinal degenerative diseases, and modifies photoreceptor survival in animal models of human ocular disease. Humans have daily psychophysical rhythms in absolute visual sensitivity, as well as the temporal resolution of vision, with peak scotopic sensitivity occurring at night and peak temporal resolution occurring during the day. These visual rhythms are mediated by corresponding rhythmic changes in retinal function with scotopic ERG b-wave sensitivity, and implicit time decreased during the day. Interestingly, these ERG rhythms are altered in patients with retinitis pigmentosa, indicating a link between circadian regulation of retinal function and this disease, which is a major cause of adult blindness. In addition, macular edema in diabetic retinopathy, intraocular pressure associated with glaucoma, and refractive errors associated with myopia in primates also exhibit circadian regulation. Finally, photoreceptors exhibit circadian-dependent vulnerability to light damage, being more susceptible in the night phase, and that dopamine and melatonin, two neurochemical messengers of the circadian clock, modulate photoreceptor survival in retinal degeneration animal models.

Summary

Retinal interplexiform neurons are a specialized subclass of amacrine cells that mediate intraretinal feedback of photic signals from photoreceptors, ganglion cells, and from brain nuclei to reconfigure retinal circuits according to prevailing illumination and circadian factors. They act primarily through the secretion of the neurotransmitter dopamine, both synaptically and via volume transmission. DA neurons and interplexiform neurons play critical roles in overall retinal function and in visual health by modulating retinal circuits, synchronizing the retinal clock and regulating eye and photoreceptor tropism.

See also: The Circadian Clock in the Retina Regulates Rod and Cone Pathways; Circadian Photoreception; Neurotransmitters and Receptors: Dopamine.

Further Reading

Besharse, J. C. and Luvone, P. M. (1992). Is dopamine a light-adaptive or a dark-adaptive modulator in retina? *Neurochemistry International* 20: 193–199.

Boelen, M. K., Boelen, M. G., and Marshak, D. W. (1998). Light-stimulated release of dopamine from the primate retina is blocked by 1-2-amino-4-phosphonobutyric acid (APB). *Visual Neuroscience* 15: 97–103.

Dacey, D. M. (1990). The dopaminergic amacrine cell. *The Journal of Comparative Neurology* 301: 461–489.

Djamgoz, M. B. A., Hankins, M. W., Hirano, J., and Archer, S. N. (1997). Neurobiology of retinal dopamine in relation to degenerative states of the tissue. *Vision Research* 37: 3509–3529.

Dowling, J. E. and Ehinger, B. (1975). Synaptic organization of the amine-containing interplexiform cells of the goldfish and Cebus monkey retinas. *Science* 188: 270–273.

Gustincich, S., Feigenspan, A., Wu, D. K., Koopman, L. J., and Raviola, E. (1997). Control of dopamine release in the retina: A transgenic approach to neural networks. *Neuron* 18: 723–736.

Hokoc, J. N. and Mariani, A. P. (1987). Tyrosine hydroxylase immunoreactivity in the rhesus monkey retina reveals synapses from bipolar cells to dopaminergic amacrine cells. *Journal of Neuroscience* 7: 2785–2793.

McMahon, D. G., Knapp, A. G., and Dowling, J. E. (1989). Horizontal cell gap junctions: Single-channel conductance and modulation by dopamine. *Proceedings of the National Academy of Sciences USA* 86: 7639–7643.

Mills, S. L. and Massey, S. C. (1995). Differential properties of two gap junctional pathways made by All amacrine cells. *Nature* 377: 734–737.

Ribelayga, C., Cao, Y., and Mangel, S. C. (2008). The circadian clock in the retina controls rod–cone coupling. *Neuron* 59: 790–801.

Ruan, G. X., Allen, G. C., Yamazaki, S., and McMahon, D. G. (2008). An autonomous circadian clock in the inner mouse retina regulated by dopamine and GABA. *PLoS Biology* 6: e249.

Witkovsky, P. and Schütte, M. (1991). The organization of dopaminergic neurons in vertebrate retinas. *Visual Neuroscience* 7: 113–124.

Zhang, D. Q., Stone, J. F., Zhou, T., Ohta, H., and McMahon, D. G. (2004). Characterization of genetically labeled catecholamine neurons in the mouse retina. *Neuroreport* 15: 1761–1765.

Zhang, D. Q., Zhou, T. R., and McMahon, D. G. (2007). Functional heterogeneity of retinal dopaminergic neurons underlying their multiple roles in vision. *Journal of Neuroscience* 27: 692–699.

Zhang, D. Q., Wong, K. Y., Sollars, P. J., Berson, D. M., Pickard, G. E., and McMahon, D. G. (2008). Intraretinal signaling by ganglion cell photoreceptors to dopaminergic amacrine neurons. *Proceedings of the National Academy of Sciences USA* 105: 14181–14186.

Myocilin*

M P Fautsch, Mayo Clinic, Rochester, MN, USA

Glossary

Extracellular matrix – The structural support for cells and tissues in animals or plants. It contains fibrous proteins, polysaccharides, and proteoglycans.
Gene – The portion of DNA that encodes a functional RNA or protein product.
Leucine zipper – The protein motif characterized by a short alpha-helix with a leucine amino acid at every seventh position.
Signal peptide – A short peptide sequence that directs proteins to organelles within a cell.
TATA box – A DNA sequence in the regulatory region of a gene where the transcription factors bind.
Trabecular meshwork – The tissue in the anterior segment of the eye located between the cornea and the ciliary body. It is responsible for filtering and draining aqueous humor from the anterior segment.
Unfolded protein response – A cellular stress response related to an accumulation of misfolded or unfolded proteins in the endoplasmic reticulum.

Discovery of the Glaucoma-Associated Myocilin Gene

The most common form of glaucoma is primary open-angle glaucoma (POAG). This disorder generally occurs between the sixth and eighth decades of life and is accompanied with alterations in visual acuity due to loss of optic nerve function. An early onset or juvenile form of primary open-angle glaucoma (JOAG) occurs between the second and fifth decades of life. In 1997, Edwin Stone and colleagues at the University of Iowa (USA) used genetic linkage studies to identify a glaucoma-associated region to chromosome 1q in a family with an autosomal dominant pedigree for JOAG. Additional studies in other JOAG family pedigrees confirmed chromosome 1q21-1q31 as a glaucoma susceptibility locus.

Concurrent to the genetic studies, Jon Polansky and colleagues studied a protein in human trabecular meshwork cells that was induced following glucocorticoid treatment (originally called trabecular meshwork inducible glucocorticoid response gene (TIGR)). Clinically, the administration of glucocorticoids can result in elevated intraocular pressure (IOP) and if not monitored, may lead to symptoms similar to POAG. Expression of TIGR from cultured human trabecular meshwork cells treated with dexamethasone increased in a time and dose-dependent manner that correlated with the elevated IOP increase observed in patients following steroid treatment. Additionally, studies aimed at identifying candidate genes for inherited retinal disease identified a novel protein with homology to nonmuscle myosin that was expressed in the ciliary rootlet and basal body of the connecting cilium in photoreceptor cells which was termed myocilin (myo- from myosin; -cilin from cilium). Sequence comparisons of both TIGR and myocilin proteins confirmed that these two proteins were identical and that both originated from the same gene *(MYOC/TIGR)*. The *MYOC/TIGR* gene was located within the chromosome 1q21-1q31 glaucoma susceptibility locus. Subsequent studies found that the *TIGR/MYOC* gene contained mutations in up to 36% and 4% of JOAG and POAG patients, respectively. Conventional nomenclature set forth by the Human Genome Organization Committee officially designated the *MYOC/TIGR* gene as *MYOC* and the protein product produced from this gene as myocilin.

MYOC Gene to Myocilin Protein

The gene for human myocilin contains three exons and two introns and spans nearly 17 kb of human genomic sequence at the chromosome 1q24.3-1q25.2 locus (**Figure 1**). The gene produces several transcripts, ranging in size from 1.8 to 2.3 kb, due to differential use of three polyadenylation sites at the 3′ end. The immediate upstream region of the myocilin gene contains several transcriptional regulatory elements, including a TATA-box, nuclear factor kappa-light-chain-enhancer of activated B cells (NF-κB), activating protein (AP)-1 and -2, and an E-box. The E-box is a DNA sequence which lies upstream of a gene in the promoter region. An E-box is bound by an upstream stimulatory factor (USF) and is critical for basal promoter activity. Several glucocorticoid-like response elements have also been identified upstream of the transcription initiation start site. However, none of these appears to function in myocilin's response to steroids. Furthermore, glucocorticoid induction of myocilin is dependent on new protein

*Adapted from Resch, Z. T. and Fautsch, M. P. (2009). Glaucoma-associated myocilin: A better understanding but much more to learn. *Experimental Eye Research* 88: 704–712.

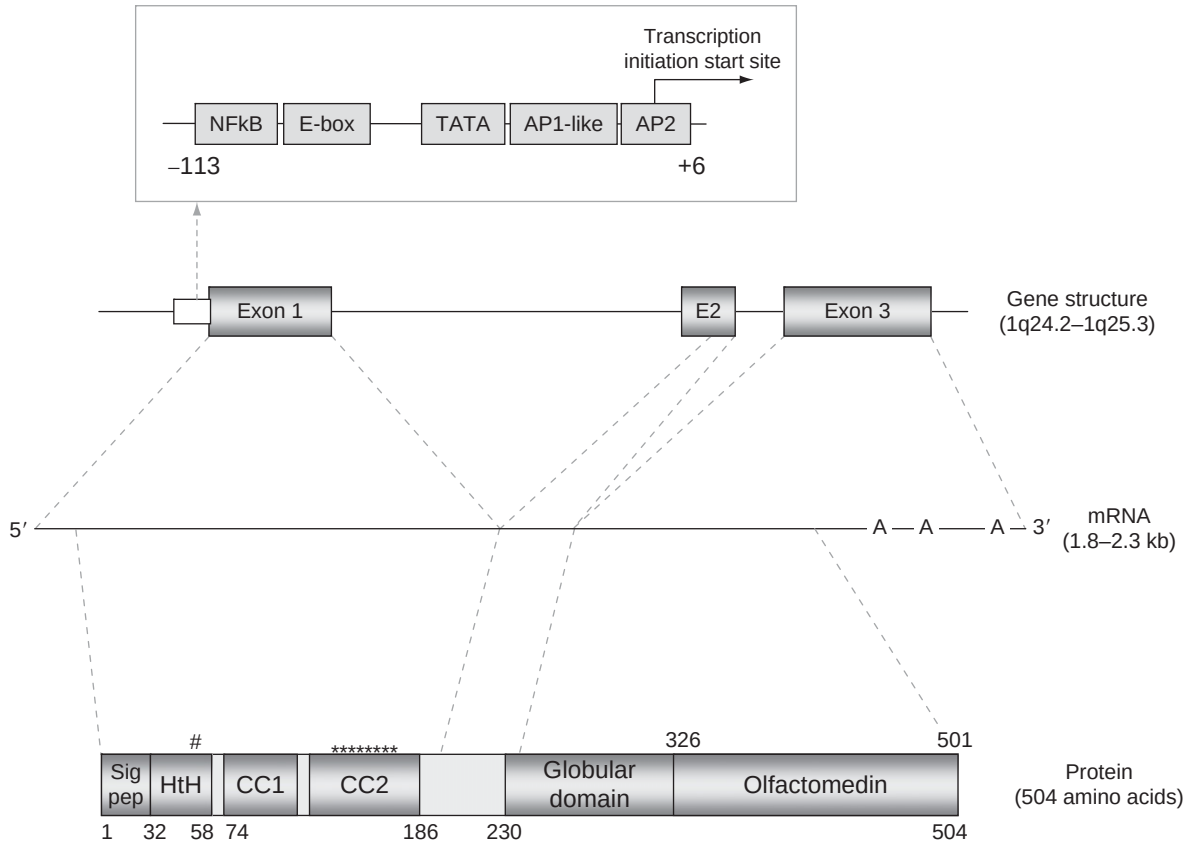

Figure 1 Structure of human *MYOC* gene and myocilin protein. The human *MYOC* gene contains three exons and two introns. The inset shows regions of homology to several promoter and enhancer sequences upstream of Exon 1. The mRNA produced from the *MYOC* gene ranges in size between 1.8 and 2.3 kb. The myocilin protein is 504-amino-acids (aa) long and contains several structural motifs: a signal peptide sequence (aa1–32), a helix–turn–helix (HtH) domain (aa18–58), two coil–coil (CC) domains (aa74–110 and aa118–186), and a C-terminal globular domain (aa230–504) that contains homology to olfactomedins (aa326–501), a protein family involved in many diverse functions. Asterisks represent leucine amino acids involved in the leucine zipper. Number sign denotes N-glycosylation site.

synthesis suggesting that the myocilin steroid response is a secondary effect, not a direct stimulation.

The protein product produced from the myocilin transcript is a 504-amino-acid glycoprotein with a predicted molecular weight of 55.3 kDa. On sodium dodecyl sulfate polyacrylamide gel electrophoresis (SDS-PAGE) gels, myocilin separates as a doublet between 53 and 57 kDa, with the larger of the two proteins migrating slower due to the N-glycosylation at amino acids (aa) 57–59 (Asn-Glu-Ser). A 66-kDa form of myocilin has also been reported. Not all myocilin antibodies recognize this product suggesting that the 66-kDa form of the protein is unique, potentially having several post-translational modifications. Alternatively, the 66-kDa form may not be myocilin, but may represent a myocilin-related protein. Truncated products of myocilin have also been identified. Cleavage of myocilin, possibly by the protease calpain II, can lead to a 23-kDa N-terminal fragment and a 35-kDa C-terminal fragment. The C-terminal form of myocilin has been identified in human aqueous humor and in conditioned media from human trabecular meshwork and embryonic kidney cells (HEK293) engineered to overexpress myocilin.

The N-terminal region of myocilin contains two translation initiation methionine amino acids at aa1 and aa15. A functional signal peptide sequence representing aa1-32 was confirmed for human myocilin by N-terminal sequencing of immunoprecipitated myocilin and *in vitro* using microsomal membranes. Phylogenetic comparison of other myocilin proteins shows that only rat myocilin contains two initiation codons similar to human myocilin. All other myocilin proteins have only one initiation codon that corresponds to the second initiation codon in humans and rat. All species, however, have an N-terminal region characteristic of a signal peptide sequence that suggests an evolutionary conserved function for this region.

In addition to the signal peptide sequence, the N-terminal region of myocilin contains leucine zipper motifs within two coiled-coiled domains (aa74–aa110 and aa118–aa186), the second of which is responsible for exosome-like vesicular binding. Dimerization with itself as well as other

intracellular and extracellular proteins can also occur within this region.

The C-terminal globular region of myocilin (aa230–504) contains homology to a family of proteins called olfactomedins. Over 100 proteins contain an olfactomedin domain. Within these proteins, the olfactomedin domain is highly conserved across species supporting an important role for this domain in the functional aspects of these proteins. Similarly, the olfactomedin domain of myocilin is highly conserved across species (>80%), suggesting this region is important for the structure and functional properties of the protein. The importance of the olfactomedin domain to myocilin function is highlighted by the presence of >90% of the identified glaucoma-associated mutations being found within this domain.

Myocilin Expression and Localization

Myocilin is expressed in a number of tissues within and outside the eye. Within the eye, myocilin expression has been identified in the sclera, ciliary body, choroid, cornea, iris, lamina cribosa, retina, optic nerve, and aqueous and vitreous humor (**Figure 2**). The trabecular meshwork is reported to have the highest level of expression within the eye with similar expression distribution within the uveal, corneoscleral, and juxtacanicular regions. Outside the eye, expression of myocilin is found in highest levels in the skeletal muscle and heart. Other tissues in humans, rats, and mice that express myocilin include the mammary gland, small intestine, thymus, prostate, testis, colon, stomach, thyroid, trachea, bone marrow, and brain. Myocilin has also been detected in Schwann cells and the myelin sheath of peripheral nerves, renal podocytes and mesangial cells, intervertebral disks, and plasma.

Expression of myocilin can be regulated by both its internal and external environment. In addition to mechanical and oxidative stress, transforming growth factor-beta1 (TGF-β1), optineurin, and steroids can stimulate myocilin expression. Conversely, glaucoma medications such as timolol and latanoprost can decrease myocilin expression, while basic fibroblast growth factor (bFGF) and thyroid hormone T_3 can reduce the steroid stimulation of myocilin.

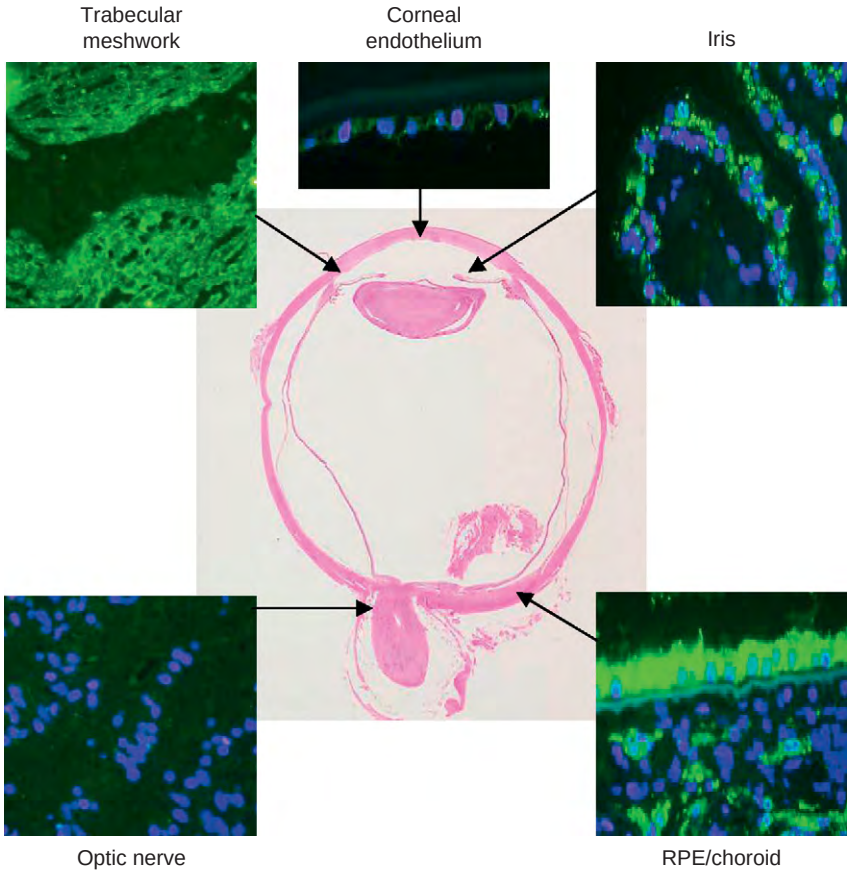

Figure 2 Representative images of myocilin expression within the human eye. Myocilin monoclonal antibodies were used to identify myocilin expression within the trabecular meshwork, corneal endothelium, iris, RPE/choroid, and optic nerve. Magnification: ×400. Blue: nuclei; green: myocilin.

The use of cultured primary human trabecular meshwork cells is an important model system to study the cellular and molecular aspects of these cells. Substrate and growth supplementation can effect the proliferation, morphology, and gene expression of cultured trabecular meshwork cells. Standard culture conditions (use of 10% fetal bovine serum as a growth supplement) can reduce myocilin expression and secretion from cultured trabecular meshwork cells. The use of aqueous humor as a growth supplement, and growth on soft extracellular matrices or on anisotropically ordered nanopatterned substrates can maintain myocilin levels in cultured trabecular meshwork cells similar to that observed *in vivo*. Additionally, topographic cues including shear forces present *in situ* may also play an important role in maintaining normal myocilin production from the trabecular meshwork.

Myocilin has been localized to both intracellular and extracellular compartments. The identification of an N-terminal signal peptide sequence and the presence in aqueous humor indicate that myocilin is secreted from the cell. Proteins with signal peptides are generally synthesized, folded, and processed through the endoplasmic reticulum and Golgi apparatus prior to exposure to the extracellular milieu. Myocilin has been localized within a variety of organelles associated with the secretory pathway, including the endoplasmic reticulum and Golgi apparatus.

In the extracellular matrix, myocilin associates with long-spacing collagens, elastic-like fibers, and sheath-derived plaque material within the trabecular meshwork. Structural components of the extracellular matrix, including fibronectin, laminin, decorin, and collagen types I, III, V, and VI, have all been associated with myocilin binding. Hevin, a member of the BM-40/SPARC/osteonectin family, has also been identified as a myocilin-binding protein.

Inside the cell, myocilin has been reported to associate with several intracellular proteins, including microtubules, myosin regulatory light chain, flotillin, gamma-synuclein, and actin stress fibers. Additionally, myocilin has been found associated with organelles. In the mitochondria, myocilin associates with the inner and outer membranes and in the intramembrane space, but not with mitochondrial matrix. The association between myocilin and mitochondria may be cell specific, having been seen in trabecular meshwork and astrocyte cells, but not in corneal fibroblasts. Furthermore, myocilin appears to associate with exosome-like vesicles. Exosomes are small microvesicles that are transported to the plasma membrane through microvesicular bodies, where they are released into the extracellular compartment. The association with exosomes not only suggests an intracellular localization for myocilin but also indicates that myocilin may be secreted from cells by a nontraditional mechanism.

Function of Myocilin

The normal, physiologic function of myocilin is currently unknown. However, myocilin has some properties consistent with matricellular proteins. Matricellular proteins are extracellular matrix proteins essential for modulating cell–matrix interactions, particularly those involved with cell attachment, cell spreading, inhibiting focal adhesion, and stress-fiber formation. Some matricellular proteins have a de-adhesive effect on cell–matrix attachment. Cells grown on matricellular substrates have altered cell attachments, cytoskeletal reorganization, and changes in cell shape. Most matricellular proteins are tightly regulated at the level of gene expression, especially during development and following cellular injury.

Similar to matricellular proteins, myocilin can be found extracellularly, bound to extracellular matrix, can influence cell–matrix interactions, and is a stress and injury response protein. Culturing of trabecular meshwork cells, skin fibroblasts, and neurons on myocilin substrates reduced cell–matrix adhesion and cell migration (i.e., de-adhesive activity). Furthermore, trabecular meshwork cells that have been wounded by physical disruption in culture exhibit decreased migratory ability and altered morphology, becoming more broad and stellate with the formation of cellular microspikes in the presence of exogenous myocilin treatment.

Intracellularly, myocilin may influence mitochondria function. Overexpression of myocilin in trabecular meshwork cells reduced mitochondrial respiration, potentially sensitizing cells and triggering apoptotic events. This may lead to a loss of trabecular meshwork cells, altering trabecular meshwork function and IOP maintenance.

Myocilin Mutations

Myocilin mutations have been found in up to 36% of JOAG patients and in approximately 4% of individuals with POAG. Over 70 glaucoma-causing mutations have been identified (**Figure 3**). Greater than 90% of these mutations are found in the C-terminal globular domain containing homology to olfactomedins. Myocilin mutations have a strong genotype–phenotype correlation. Individuals with the T377M mutation are generally diagnosed in their fourth decade, later than the P370L mutation (first and second decade) and Y437H (second decade), but earlier than the most common disease-associated mutation in Caucasians, Q368X, which has an average onset in the fifth and sixth decades. IOP differences have also been noted, with individuals carrying the Y437H mutation having mean maximal pressures of 44 mmHg and patients with the Q368X mutation having lower, but still elevated, mean maximal IOP (30 mmHg).

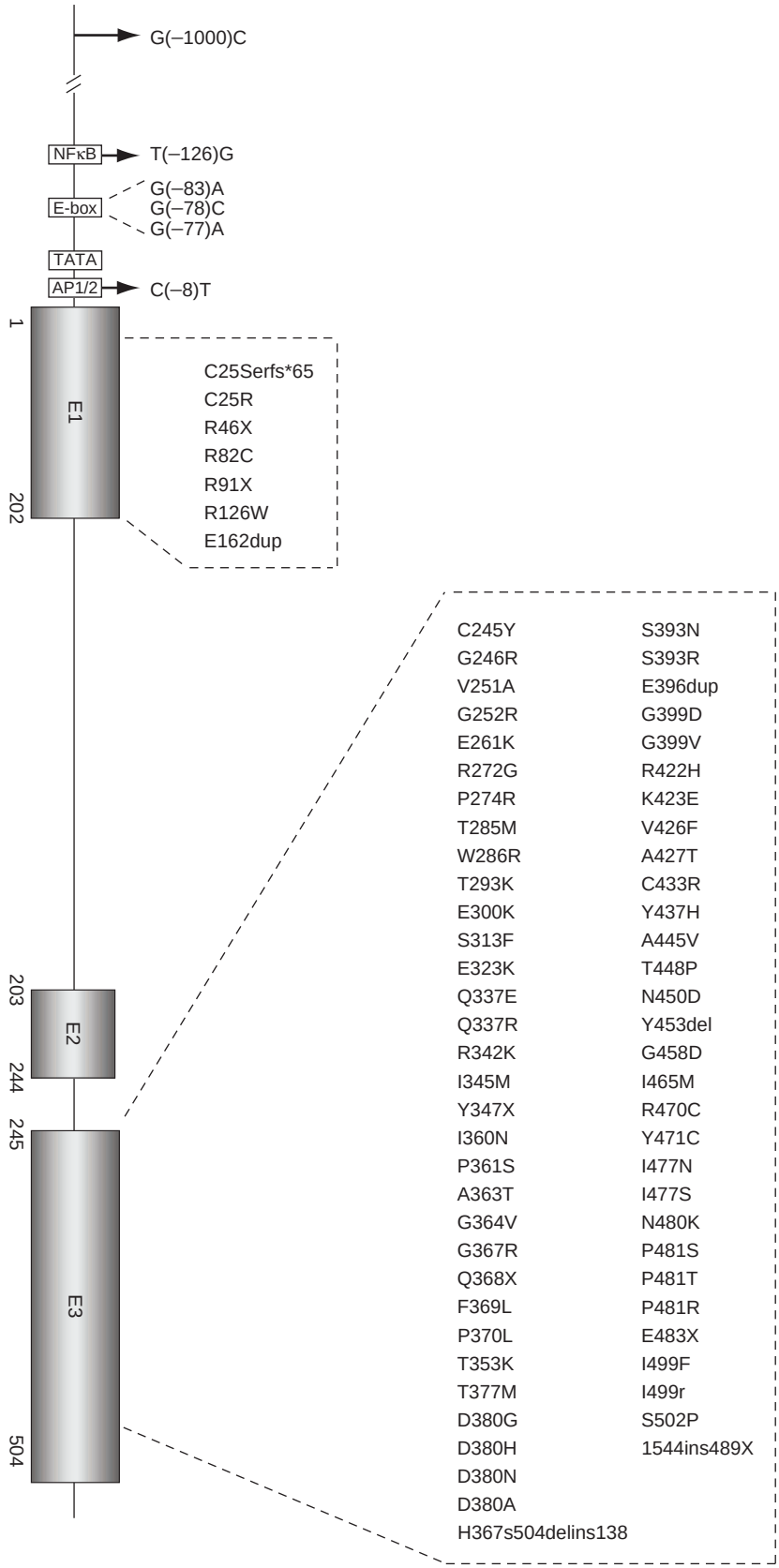

Figure 3 Glaucoma-causing mutations in myocilin. Over 70 glaucoma-causing mutations have been identified in myocilin, with >90% found in exon 3 that contains an olfactomedin-homology domain. Gene structure is shown on right. Numbers under the exons denote codon location in gene sequence. Reproduced from Resch, Z. T. and Fautsch, M. P. (2009). Glaucoma-associated myocilin: A better understanding but much more to learn. *Experimental Eye Research* 88: 704–712, with permission from Elsevier Ltd.

Less than 10% of the glaucoma-causing mutations in myocilin have been identified in the N-terminus. Two involve cysteine amino acids. C25R is in the signal peptide sequence and may interfere with secretion. Mutation of the cysteine amino acid at position 47 may disrupt normal homo- and heteromer disulfide bond formation. Three other mutations involve arginines at aa82, aa91, and aa126. These mutations may disrupt protein–protein interactions within the N-terminal leucine zipper motif.

A unique property of many of the mutant myocilin proteins is their inability to be secreted. Unlike normal myocilin which is secreted, mutant myocilin accumulates within the endoplasmic reticulum as homo- or heterodimers. The protein conformational changes caused by many mutants can be relaxed when cells overexpressing individual myocilin mutants are grown at 30°C. Interestingly, the more virulent glaucoma phenotypes (P370L, I477N, and Y437H) were less sensitive to secretion at 30°C compared to glaucoma phenotypes that are less virulent (T377M, G364V, I499F, and D380A). Additionally, treatment of cells with sodium 4-phenylbutrate increased the secretion of several myocilin mutants (C245Y, P370L, and Y437H), presumably by reducing aggregate formation.

Several sequence variations have been identified in the transcriptional regulatory region. Three of the sequence changes (−77G>C, −78G>C, and −83G>A) were identified in the E-box, a DNA sequence found to be essential for basal transcription regulation of myocilin. The most common sequence variation in the transcriptional control region is a cytosine to guanine base-pair substitution at position −1000 (mt.1(+)). This sequence variation has been reported in up to 20% of POAG patients with a suggestion that individuals with the mt.1(+) variation have a more rapid disease progression. Not all studies have confirmed the association of the mt.1(+) variant with POAG. A genetic test for the mt.1(+) variant (OcuGene) is available for clinical use.

How Does Myocilin Cause Glaucoma?

How myocilin increases IOP and causes glaucoma is unknown. Two theories, supported by clinical and laboratory observations, have been proposed. The first involves overproduction of normal myocilin, while the second focuses on a change of function for the glaucoma-associated mutations.

Normal Myocilin

The first hypothesis regarding myocilin's role in glaucoma revolves around the idea that elevated IOP may be caused by increased levels of normal myocilin, thus resulting in a reduction of outflow facility (increase in outflow resistance) within the trabecular meshwork. Several studies support this hypothesis: (1) the use of myocilin-specific antibodies in immunohistochemical studies indicates that some POAG eyes have elevated levels of myocilin in the trabecular meshwork; (2) dexamethasone treatment of trabecular meshwork monolayer cells or cultures of anterior segments increased myocilin in a time- and dose-dependent manner that correlated with the timing and increase of IOP seen in patients following steroid treatment; (3) primates treated with steroids for 1 year had elevated IOP and a threefold increase in trabecular meshwork myocilin levels; (4) recombinant myocilin overexpressed and isolated from either bacterial lysate or conditioned media from a human transformed trabecular meshwork cell line increased outflow resistance by >90% when perfused into human anterior segments; and (5) myocilin levels are statistically elevated in human aqueous humor by volume and as a percent of total protein in POAG when compared to normal controls (patients undergoing cataract surgery). Some animal models also support a correlation between elevated myocilin levels and IOP: (1) rats that spontaneously develop elevated IOP have a fourfold increase in myocilin transcription; (2) several canine breeds that have primary glaucoma show elevated levels of myocilin in aqueous humor, trabecular meshwork, and nonpigmented ciliary epithelium within regions of the ciliary processes; and (3) beagles genetically susceptible to develop glaucoma have increased levels of myocilin in aqueous humor with a direct relation to the severity of the disease.

Although evidence in human eyes and some animal models seemed to validate the hypothesis that overexpression of myocilin may contribute to elevated IOP, not all studies have confirmed this opinion. Expression of myocilin by an adenovirus in cultured anterior segments decreased IOP rather than increased IOP. Mice bred to overexpress either the mouse or human form of myocilin showed no change in IOP. Steroid-treated rats with elevated IOP contained normal levels of myocilin in the trabecular meshwork and a feline model overexpressing myocilin for >1 year did not show any change in IOP. Furthermore, deletion of one or both copies of myocilin in mice did not have any effect on IOP or ocular morphologies.

As myocilin is a protein induced by several forms of stress, it is reasonable to speculate that increased levels of myocilin may be a secondary effect of elevated IOP, not the primary cause. The overexpression of myocilin has been reported to alter gene expression of several molecules involved in cell adhesion and cell–matrix interactions. Therefore, increased levels of myocilin would not cause the elevated IOP, but may be the result of elevated IOP and potentially influence long-term changes in cellular adhesion.

Glaucoma-Associated Mutant Myocilin

While the mutations within the transcription regulatory region (promoter and enhancer region) may change myocilin messenger RNA (mRNA) and protein expression, the alterations in the protein-coding sequence can alter the three-dimensional structure, effectively masking important charges that regulate cleavage sites and presumably normal function. The sequestration of myocilin mutants in the endoplasmic reticulum may result in a gain of function unrelated to the normal function of myocilin. Clinical evidence supports this notion. Homozygous and heterozygous family members for myocilin mutant R46X, which truncates all but 13 amino acids of the processed protein, do not develop glaucoma. This suggests that normal myocilin may not be a key component in the causality of glaucoma. Furthermore, mice engineered to have zero or one copy of a functional myocilin gene did not have any ocular changes or elevation in IOP. These studies indicate that the lack of normal myocilin expression is not essential for the disease but that myocilin containing mutations may have a different function (gain of function) that may influence the physiologic development of glaucoma.

Mutant myocilin forms heterodimers with normal myocilin, effectively reducing the levels of secreted normal myocilin from trabecular meshwork cells. The sequestration of normal myocilin by mutant myocilin suggests that prolonged expression of mutant myocilin may lead to retention of the mutant (and normal myocilin), causing an endoplasmic reticulum overload response or unfolded protein response. Formation of normal and mutant myocilin heterodimers can form inclusion bodies, decreasing the heteromeric complex from translocating to the cytosol or extracellular milieu. Cells overexpressing myocilin mutants show expression changes in immunoglobulin heavy chain binding protein (BiP), endoplasmic-reticulum-localized eukaryotic initiation factor (eIF-2α) kinase, and activation of caspase 3 and 12. All of these factors are indicative of an endoplasmic reticulum storage disease process that can lead to apoptotic death. Furthermore, if normal myocilin functions as a de-adhesive molecule as postulated, then retention of normal myocilin in the endoplasmic reticulum by mutant myocilin would reduce the level of extracellular myocilin and cause a stiffer, less-pliable trabecular meshwork, possibly resulting in elevated IOP.

Glaucoma is mainly a human disease, with only sporadic cases found in other animals. Therefore, if myocilin is involved in glaucoma, specific characteristics of human myocilin may give us clues as to how mutated myocilin may function. Several lines of evidence support this hypothesis (summarized in **Table 1**). Mice engineered to express the human Y437H mutation have an increase in IOP. Conversely, mice or domestic cats expressing their species equivalent of the human Y437H mutation (Y423H) do not show a change in IOP. Unlike all forms of myocilin from different species, human myocilin contains a unique peroxisomal targeting signal-1 receptor binding site (PTS1R) at the C-terminus. Whether or not the PTS1R-binding site is functional in human cells remains to be determined. However, if the PTS1R site is functional, the shuttling of misfolded mutant myocilin to peroxisomes may lead to cellular stress and death.

Table 1

Myocilin animal models

Species	*Myocilin expressed*	*Effect on IOP*
Mouse	*MYOC* knockout	No effect
Mouse	*MYOC* overexpression[a,b]	No effect
Mouse	Mutant Y437H[a]	Increased
Mouse	Mutant G364V, Y437H[a]	Increased
Mouse	Mutant Q368X, S502P[a]	No effect
Mouse	Mutant Y423H[b]	No effect
Feline[d]	*MYOC* overexpression[c]	No effect
Feline[d]	Mutant Y423H[c]	No effect

Naturally occurring models

Species	*Phenotype*	*Myocilin levels*
Canine	Glaucomatous	Elevated
Beagle	Glaucomatous	Elevated
Rat	Elevated IOP	Elevated

[a]Human myocilin or myocilin mutant.
[b]Murine myocilin or myocilin mutant.
[c]Feline myocilin or myocilin mutant.
[d]Overexpression due to transduction of the anterior chamber with feline-immunodeficiency virus (FIV) containing myocilin. Adapted from Resch, Z. T. and Fautsch, M. P. (2009). Glaucoma-associated myocilin: A better understanding but much more to learn. *Experimental Eye Research* 88: 704–712, with permission from Elsevier Ltd.

Future Directions

Understanding the function of normal myocilin and the glaucoma-associated myocilin mutants is essential to our understanding of myocilin's role in the eye. Myocilin's expression throughout the eye and its secretion into the outflow pathway as part of aqueous humor suggest possible roles for myocilin in maintaining or influencing the aqueous outflow pathway. However, additional studies need to be done to fully elucidate myocilin's normal function and its role in the pathogenesis of JOAG and POAG. Analysis of stress conditions and growth factor/cytokine levels in aqueous humor needs to be assessed to determine whether they have a role in myocilin expression and function in outflow facility. An appreciation of myocilin in concert with other factors, such as the glaucoma-associated proteins cytochrome P450, subfamily 1, polypeptide 1

(CYP1B1), and WD repeat domain 36 (WDR36), is necessary to delineate myocilin's role in normal and disease processes. Future endeavors aimed at myocilin function will be essential to understanding myocilin's role in the eye as well as to other tissues of the body.

See also: Animal Models of Glaucoma; Biological Properties of the Trabecular Meshwork Cells; Biomechanics of Aqueous Humor Outflow Resistance; Control of Aqueous Humor Flow; The Fibrillar Extracellular Matrix of the Trabecular Meshwork; Functional Morphology of the Trabecular Meshwork; The Genetics of Primary Open-Angle Glaucoma: A Review; Molecular Genetics of Congenital and Juvenile Glaucoma; Regulation of Extracellular Matrix Turnover in the Aqueous Humor Outflow Pathways; Steroid-Induced Ocular Hypertension and Effects of Glucocorticoids on the Trabecular Meshwork; Structural Changes in the Trabecular Meshwork with Primary Open Angle Glaucoma.

Further Reading

Alward, W. L. (2000). The genetics of open-angle glaucoma: The story of GLC1A and myocilin. *Eye* 14: 429–436.

Alward, W. L., Kwon, Y. H., Khanna, C. L., et al. (2002). Variations in the myocilin gene in patients with open-angle glaucoma. *Archives of Ophthalmology* 120: 1189–1197.

Fingert, J. H., Heon, E., Liebmann, J. M., et al. (1999). Analysis of myocilin mutations in 1703 glaucoma patients from five different populations. *Human Molecular Genetics* 8: 899–905.

Hewitt, A. W., Mackey, D. A., and Craig, J. E. (2008). Myocilin allele-specific glaucoma phenotype database. *Human Mutation* 29: 207–211.

Kim, B. S., Savinova, O. V., Reedy, M. V., et al. (2001). Targeted disruption of the myocilin gene (MYOC) suggests that human glaucoma-causing mutations are gain of function. *Molecular Cellular Biology* 21: 7707–7713.

Kubota, R., Noda, S., Wang, Y., et al. (1997). A novel myosin-like protein (myocilin) expressed in the connecting cilium of the photoreceptor: Molecular cloning, tissue expression, and chromosomal mapping. *Genomics* 41: 360–369.

Nguyen, T. D., Chen, P., Huang, W. D., et al. (1998). Gene structure and properties of an olfactomedin-related glycoprotein, TIGR, cloned from glucocorticoid-induced trabecular meshwork cells. *Journal of Biological Chemistry* 273: 6341–6350.

Polansky, J. R. (2003). Current perspectives on the TIGR/MYOC gene (myocilin) and glaucoma. *Ophthalmology Clinics of North America* 16: 515–527.

Resch, Z. T. and Fautsch, M. P. (2009). Glaucoma-associated myocilin: A better understanding but much more to learn. *Experimental Eye Research* 88: 704–712.

Stone, E. M., Fingert, J. H., Alward, W. L., et al. (1997). Identification of a gene that causes primary open angle glaucoma. *Science* 275: 668–670.

Tamm, E. R. (2002). Myocilin and glaucoma: Facts and ideas. *Progress in Retinal and Eye Research* 21: 395–428.

Myopia

F A Vera-Diaz, Schepens Eye Research Institute, Harvard Medical School, Boston, MA, USA

Glossary

Accommodation – The changes in optical power by the eye in order to maintain a clear image (focus) as objects are moved closer. This occurs through a process of ciliary muscle contraction and zonular relaxation that causes the elastic-like lens to round up and increase its optical power. Natural loss of accommodation with increasing age is called presbyopia.

Astigmatism – An optical defect in which refractive power is not uniform in all directions (meridians). Light rays entering the eye are bent unequally by different meridians that prevent formation of a sharp image focus on the retina.

Choroidal neovascularization – The creation of new, weak and leaky, blood vessels in the choroid layer of the eye. It is a common symptom of wet age-related macular degeneration and of pathological myopia.

Glaucoma – The neuropathy that affects the optic nerve of the eye and involves loss of retinal ganglion cells in a characteristic pattern causing peripheral visual-field defects.

Retinal detachment – A disorder of the eye in which some layers of the retina peel away from its underlying layers of support tissue. It is a medical emergency and if untreated it may cause partial or total vision loss.

Definition of Myopia: Health and Economic Implications

Myopia, also called near- or shortsightedness, refers to the refractive state of the eye whereby the images of distant objects are focused in front of the retina when the accommodation system is relaxed. It can also be described as the refractive error in which the point conjugate with the retina, the far point of the eye, is located at some finite point in front of the eye. Therefore, light entering the eye has to originate from near objects, within the eye's focal point, or diverged by concave lenses (minus power) in order to be focused on the retina of the myopic eye (**Figure 1**). Distant objects are otherwise perceived as blurred, hence the term nearsightedness. Squinting of the eyes is another symptom of myopia which can, rarely, produce headaches.

Myopia, in particular high myopia, is directly or indirectly associated with a number of ocular health complications that are potentially blinding. Moderate and high levels of myopia – greater than −5.00D – are a predisposing risk factor of reghmatogenous retinal detachment (lifetime risk is greater than 9%). High myopia is also a predisposing factor for open-angle glaucoma, myopic retinopathy, and myopic maculopathy. The increased elongation of the globe may be associated with degenerative changes in the sclera, choroid, Bruch's membrane, retinal pigment epithelium (RPE), and neurosensory retina. There is increased incidence of fundus (posterior part of the eye) lesions (**Figure 2**) such as posterior staphyloma, atrophy of RPE and choroid, lacquer cracks in Bruch's membrane, subretinal hemorrhages, lattice degeneration, pavingstone degeneration, pigmentary degeneration, white with or without pressure, retinal holes or tears, posterior vitreous detachment, macular holes, and choroidal neovascularization (CNV). Of these, CNV is the most common vision-threatening complication. Keratoconus, lens opacities, and increased complications following cataract surgery and pigmentary glaucoma are other associated complications. Although various methods of optical correction of myopia are possible, none changes the abnormally large size and shape of the myopic eye, with consequent thinning of the various layers, and therefore the risk of complications remains. Therefore, frequent complete eye health examinations, with pupillary dilation for comprehensive examination of the fundus, are necessary.

Myopia is a significant public health problem and its rapid increase in prevalence in recent decades is associated with a significant financial burden. In the United States, the annual direct cost of refractive correction with eye glasses alone is estimated to be at least $3.8 billion. Further adding to the cost of myopia are eye examinations, time off work, other optical corrections (e.g., contact lenses), refractive surgery, and other treatments. In the United States, correction of refractive errors, including the cost of glasses, contact lenses and refractive surgery, consumed over 12 billion dollars in 1990.

Although blurred vision resulting from myopia can often be corrected with visual aids, such as glasses, contact lenses, or refractive surgery, uncorrected refractive error is the major cause of visual impairment worldwide, accounting for at least 33% of visual impairments. In the United States, it is estimated that 5.3% of the visual impairments are due to uncorrected refractive errors. In addition, myopia – even if corrected – can be an impediment in certain professions; for example, military pilots and police officers.

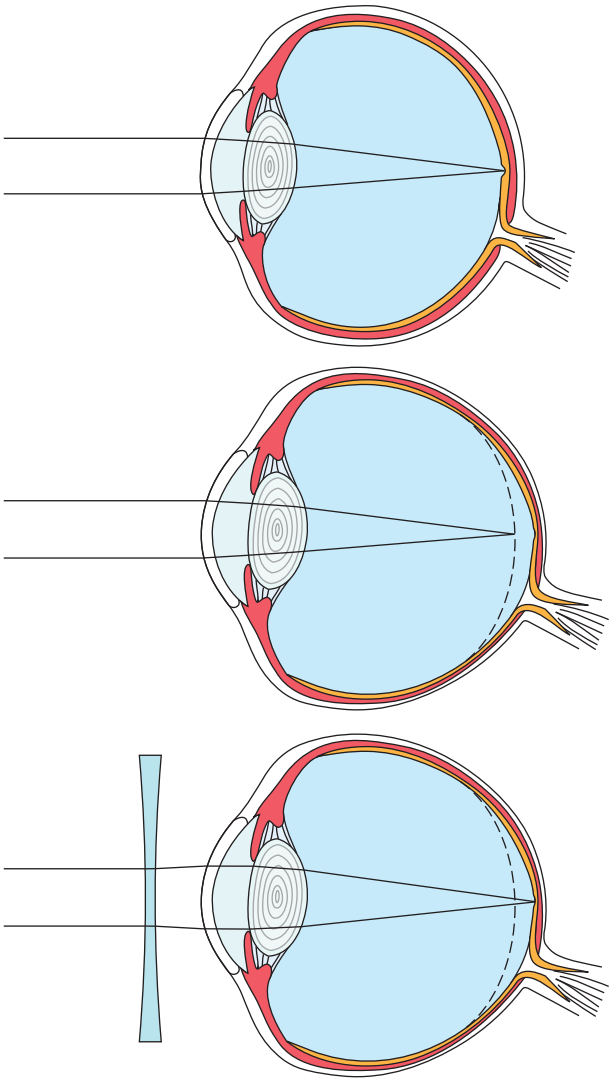

Figure 1 (From top to bottom) Schematic drawing (color) of an emmetropic eye (top) with parallel rays of light focusing at the retina; a longer myopic eye (middle) with parallel rays of light focusing in front of the retina; and a longer myopic eye corrected with a concave lens, the light rays are diverged and now focus at the retina (bottom).

Natural History of Myopia

Emmetropization is the process whereby the refractive components and the axial length of the eye come into balance during postnatal development in order to induce emmetropia (no refractive error). Most infants are hyperopic, and in those born myopic, the myopia typically decreases to reach emmetropia by toddler age. However, in a small population, for instance, premature infants with retinopathy of prematurity, myopia is present at birth and does not regress. By 12 months of age, the frequency distribution of the spherical equivalent becomes leptokurtic (as it is in adults) with the peak at low hyperopia. Results of a large longitudinal study by Gwiazda and colleagues, in 2000, showed that infantile astigmatism is associated with increased astigmatism and myopia during the school years.

Myopia typically develops during the school years, progressing until adulthood, but it may also develop in adults. Progression typically ceases in the teenage years, although it may continue into the 30s. Generally, the annual progression is close to −0.50D in juvenile (8–12-year-old) Caucasians and double that for juvenile Asians. There is a correlation with the age of onset and the final refractive status in adulthood, that is, children who become myopic at an earlier age (6 vs. 11 years) have a higher risk for myopia progression and higher degree of myopia later on.

Refractive error in the adult population follows a leptokurtic distribution with the peak around emmetropia. Later in life, a myopic refractive shift may result due to crystalline lens changes.

Structural Correlates, Molecular and Anatomical Changes in Myopia

In the Aristotelian writings (*c* 330 BC), the condition of shortsightedness was already documented. The optics of myopia, however, were first elucidated by Johannes

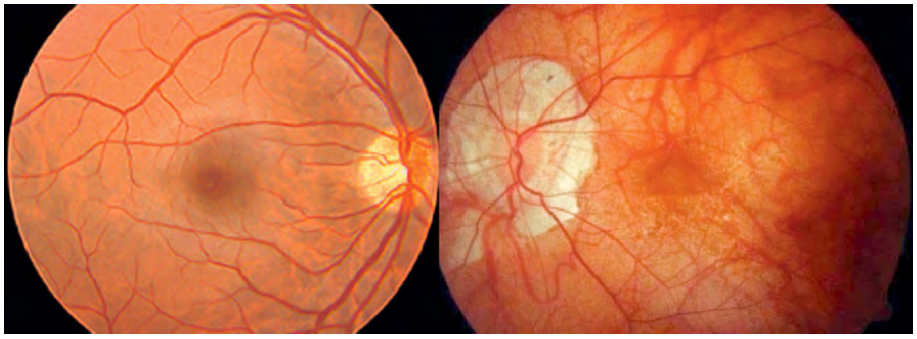

Figure 2 Fundus photograph of a normal emmetropic eye (left) and an eye with pathological myopia (right). Modified photographs from original images from images.google.com

Kepler in his initial *Clarification of Ophthalmic Dioptrics* (1604) when he correctly assumed that the incident light was brought to a focus in front of the retina. The reason for the displacement of the focus in myopic eyes elicited much attention. Some authors believed it was due to abnormal convexity of the lens; others attributed the defect either to an increased convexity of the cornea or to undue length of the globe, while some others described anatomically the unusual distance between the lens and the retina.

Biometric investigations of myopic eyes have confirmed that increased axial length of the eye, particularly vitreous chamber elongation, is the main structural correlate in human myopia. Steeper corneal radius, deeper anterior chambers, and thinner crystalline lenses have also been found; however, these are less consistent findings. The relationship between the eye's axial length and corneal radii (normally 3/1) is generally increased in myopic eyes. Retinal thickness is increased in the fovea, but decreases toward the periphery and it is significantly thinner in myopic eyes beyond the macula. In the 1990s, some studies showed that intraocular pressure (IOP) was related to myopia in children and therefore associated to the pathogenesis of myopia. However, a number of recent studies have refuted this theory with findings of no association between IOP and refractive error prior to or after the onset of myopia in children. Differences in the results may have resulted from ethnic differences.

The protein composition in aqueous humor is different in myopic eyes, suggesting that those proteins could indicate a potential biomarker for myopia development. However, most myopic changes are found in the posterior segment of the eye. The sclera of myopic eyes, even with low or moderate amounts of myopia, exhibits a number of structural changes due to the stretching of the eye, including increased extensibility, narrowing and dissociation of collagen fiber bundles, increased prevalence of stellate fibrils, severe thinning, and reduced collagen content, among others. These differences in scleral structure, and therefore its functionality, translate into a relatively thinned and weakened sclera. As myopic eyes expand during myopia development, the sclera must increase its surface area. Either new tissue must be added or existing tissue remodeled. Results of biochemical and histological studies are generally consistent with the hypothesis of active remodeling of the sclera during myopic growth. Regulatory changes in scleral metabolism could be rapidly evoked by a change in visual conditions which can also regulate the direction of change in eye size (toward hyperopia or myopia). The sclera's role on regulating eye growth and emmetropization and its potential role for preventing myopia warrant further investigation.

Signaling cascades link retinal image processing to scleral growth in myopia. Chemical messengers are released from the retina toward the RPE where secondary messengers are released through Bruch's membrane and transmitted through the choroid to the sclera. The role of substances and transmitters in the retina and choroid, such as glucagons, insulin, early growth response factor-1 (EGR1 or ZENK), dopamine, nitric oxide synthase (NOS) inhibitors, gamma aminobutyric acid (GABA), muscarinic receptor subtypes (M1 and M4), and acetylcholine, is being investigated. Jody Rada and Lisa Palmer have suggested that increased choroidal permeability may represent a mechanism for controlling the rate of delivery of bioactive factors to the sclera to regulate the rate of glycosaminoglycan synthesis in the posterior sclera. Changes in collagen subtype expression and turnover of the normal scleral matrix (matrix metalloproteinase-2) are ultimately responsible for the anatomical changes in collagen fibril morphology and tissue thinning found in myopia. A role of growth factors, such as transforming growth factor beta and specific matrix–cell receptors (integrins), and altered scleral cell phenotype (myofibroblasts), in the scleral regulation of myopia development has been suggested. In addition, several research centers are beginning to map the myopia-associated locus and to identify the gene(s) responsible for myopia (see the section titled 'Etiology of myopia').

Anthropometric measures such as body stature and weight have been associated to myopia. The Genes in Myopia (GEM) Twin Study group from Australia has recently (2008) reported that individuals in the heaviest quartile of weight of their study population had an increased incidence of myopia compared to those in the lightest weight quartile, but the relationship was significant only for females. Previous investigations have also associated myopia with taller and heavier individuals, but not all studies agree.

Classifications of Myopia

The pattern of myopia development is complex and variable; therefore, it makes more sense to refer to "myopias" rather than a single condition of myopia. This complex pattern makes a classification of myopia difficult and has resulted in numerous different classifications being postulated, including:

- *Classification according to the degree of myopia.* (1) Low, (2) moderate, and (3) high. The limits are still arbitrary, a consensus among experts is necessary if studies of prevalence are to be compared. Typically, low myopia refers to amounts between −0.50D and less than −3.00D; moderate refers to amounts between −3.00D and −6.00D; and high would be greater than −6.00D.
- *Ophthalmologic classification based on the fundus changes.* (1) Simple or physiological (no fundus changes) and (2) degenerative or pathological myopia (fundus anomalies).

- *Classification according to progression of myopia.* In 1984, Donders subdivided myopia progression into (1) stationary, (2) temporarily progressive, and (3) chronically progressive (also called malignant or deleterious) myopia. Nowadays, researchers classify myopia based on the progression of the refractive power: (1) stable myopia refers to the refractive error that has not increased more than -0.25D in a period greater than 2years, and (2) progressing myopia refers to greater increases over that period.
- *Classification according to the age of onset.* Typically classified as (1) congenital, (2) infantile, (3) juvenile, and (4) adult myopia. It may also be classified as (1) congenital versus (2) acquired. Research studies classify myopia based on the age of onset: (1) late-onset (15 years or older), and (2) early-onset myopia (14 years or younger).
- *Classification according to the combination of components of the eye.* (1) Refractive, correlation or combination myopia, and (2) component myopia (e.g., due to corneal curvature myopia, lens myopia, and axial myopia).
- *Classification according to presumed etiology.* (1) Environmental versus (2) genetic. Also: (1) physiological myopia, (2) school myopia (due to close work), and (3) excessive myopia (i.e., caused by diseases).
- *Genetic classification.* Dominant type, recessive type, a sex-linked recessive type, etc.
- *Biological classification of myopia.* (1) Physiological or simple myopia as a biological variation of the normal distribution of the eye components, and (2) pathological (progressive or magna) myopia as falling outside the normal distribution.

Clinical forms of myopia include: nocturnal myopia, due to drift in the accommodation state that increases the power of the eye under scotopic conditions, and pseudomyopia, false myopia due to physiological or pathological increased accommodation state.

Epidemiology of Myopia

In the early 1980s, more than 25% of the adult population in the United States and up to 75% in other developed countries, such as Taiwan, was myopic. Twenty years later, approximately 50% of general population in USA and up to 84% of the 16- to 18-year-old group in Taiwan was myopic. Based on a serial cross-sectional study from the Singapore Armed Forces, myopia prevalence has increased in military conscripts from 26% in the late 1970s, to 43% in the 1980s, 66% in the mid-1990s, and to 83% in the late 1990s.

The prevalence of myopia varies with age; it is low in young children, increases in school-age children and young adult cohorts, and decreases in older age groups. Within populations, myopia tends to be initially observed at the ages of 6–8 years with the average annual progression quoted as ranging from −0.10D to −0.60D. Chinese children are predominantly myopic; in 1990, the prevalence was 37% and 50% in the 6–12-year-old group and 13–18-year-old group, respectively. Recent studies in China and Sweden show that the prevalence of myopia is now higher for teenagers. Prevalence is even higher among Taiwanese children: 56% of 12-year-old children and 76% of 15-year-old children are myopes. In the later 1990s in Japan, 43.5% of 12-year-old children and 66% of 17-year-olds were myopes. It can be appreciated that there are racial differences within groups of same-age populations, for example, Chinese and Taiwanese populations show higher prevalence rates than other populations. Myopia prevalence declines to some extent in the population over 45 years of age, which is likely due to an increased prevalence rate in younger populations than an age difference.

The prevalence of myopia varies considerably between races, although it is difficult to ascertain the influence of environmental factors on these differences. In an attempt to account for environmental differences, a number of studies have investigated differences in racial groups living in the same location. In 1999, Lam and Edwards reviewed previous studies on myopia prevalence and concluded that the greatest prevalence of myopia occurs among Japanese, Chinese, and some Native American tribes. These studies take into account that the prevalence of myopia is lower in rural populations and it is affected by educational attainment and socioeconomic status.

Some studies have found a slightly higher prevalence of myopia in females than in males; however, not all agree on this. It seems that the differences in gender are found if the prevalence is measured in younger adults when males and females are not at the same growth level.

Etiology of Myopia

It is currently accepted that the etiology of myopia is complex with genetic and environmental factors playing a role. Understanding the relative contributions of genetic and environmental components is necessary to establish the mechanisms of myopia development and further attempt to arrest its progression. Separating these components is not trivial; for example, educational attainment is strongly influenced by genes, and therefore this risk factor should not solely be considered as an environmental risk factor; twins typically have the same environmental factors and hence should not be considered merely a genetic component.

A century ago, in 1913, Steiger showed that myopia is influenced by genetic factors and is an expression of a range within the normal distribution. A number of early

and recent studies with twins have shown that the concordance of refractive error is greater in monozygotic twins, indicating the existence of a genetic factor in myopia. Further, twin studies have provided evidence of correlation and heritability of a number of traits implicated in myopia. However, there are limitations associated to these studies.

The use of twin studies is also important in the identification of myopia's gene loci. A number of genetic loci have been identified as being linked with myopia. These include loci for high myopia occurring at Xq28 (MYP1), 18p11.31 (MYP 2), 12q23-24 (MYP3), 7q36 (MYP4), 17q21-22 (MYP 5), 4q22-27 (MYP11), and 2q37.1 (MYP12). Other candidate loci have been linked with low and moderate (common) myopia: 22q12 (MYP6), 11p13 (MYP7), 3q26 (MYP8), and 4q12 (MYP9). These linkages provide evidence that myopia is a polygenic disease with multiple and different alleles likely to contribute to different disease subtypes. Multiple familial studies also support a genetic component in myopia, suggesting a definite genetic basis for high myopia, and likely for low myopia. However, to date no candidate genes have been shown to account for even a modest fraction of the familial risk of myopia, and data are conflicting about whether a true association exists. It is likely that there is substantial genetic heterogeneity. In addition, further studies need to assess the relative roles of environmental factors and genetic influences, such as interactions of early-age nearwork and genotype, and the identification of phenotypes for etiologically different subgroups of myopia, for example, age of onset, presence of retinal degenerative changes, or response to treatments. See Schaeffel et al., Young, and the Genes of Myopia (GEM) Twin Group studies in the further reading section for reviews on the molecular basis of myopia.

Environmental factors, particularly nearwork, have been associated to myopia for centuries. Even though associated, nearwork has not yet been proven to be a causative factor. A number of aspects related to nearwork have been associated to myopia development and progression, including reading, cognitive effort during nearwork (with associated educational level and intelligence), lighting, and working distance. Accommodation and inaccuracies of the accommodation response are associated with myopia. Children who are to become myopic show greater inaccuracies of accommodation (greater lags) during near tasks. Accommodation effort, inaccuracies of the accommodation system during distance viewing, and accommodation flexibility have also been associated to myopia (nearwork-induced transient myopia (NITM) – a shift in refractive error due to inability to relax the accommodation).

Evidence for active and visually guided emmetropization (and its failures, such as myopia) is beyond refute. A number of animal models of myopia show that emmetropization can be manipulated and myopia can be induced. Manipulation of the environment can be achieved by imposing a close-work environment, or most commonly by lens-induced myopia (using high-power negative – concave – lenses) or form-deprivation myopia (using diffuser lenses, sutured lids, etc.; **Figure 3**). The most common animal models for myopia are chicks, mice, pigs, and tree shrews. Defocus blur is thought to be the primary cue for emmetropization and myopia. Emmetropization uses blur as visual feedback to regulate eye growth; the system requires detection of blur probably at the level of outer retina (perhaps amacrine and bipolar cells) – via diffusion of signals across RPE and choroid – to then alter scleral matrix (likely through a modulation of proteoglycan synthesis). The amount of defocus blur may increase in those

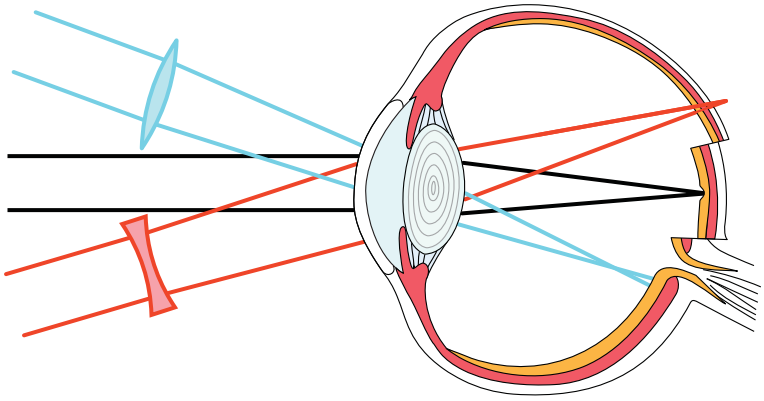

Figure 3 Schematic of an animal model of eye compensation for lens-induced defocus. Blue rays: a positive convex lens placed in front of a normal eye causes the image to form in front of the retina, the eye compensates by slowing down its growth rate and it hence becomes hyperopic (shorter); the eye layers become thickened. Red rays: a negative concave lens placed in front of a normal eye causes the image to form behind the retina, the eye compensates by accelerating its growth rate and it hence becomes myopic (longer); the eye layers become thinner. Black rays: the normal eye. Modified from Wallman, J. and Winawer, J. (2004). Homeostasis of eye growth and the question of myopia. *Neuron* 43, 447–468.

individuals who adapt more to blur, and hence blur adaptation may be a risk factor for myopia. The balance between central and peripheral defocus has been related to myopia, and animal models show that peripheral defocus alone can influence the rate of axial eye growth. Optical aberrations have been suggested to play a role in myopization, as some studies have found higher levels of aberrations in myopic eyes, but their association with myopia is not clear.

Among environmental factors, increasing educational demand seems to be a risk factor for development of myopia. When comparing university student populations with general populations, a much higher rate of myopia progression is found in the university populations. For example, significant differences have been found in the prevalence of myopia among Norwegian university students when compared to the general population of Norway and other Nordic countries. The prevalence of myopia has also been found to be greater in Greek university students and Scandinavian medical students than in the general population of the respective countries. In an interesting study in 1993, Zylbermann and coworkers showed that myopia was more prevalent in Orthodox Jewish boys in Jerusalem compared to Jewish girls, since boys spend up to 16 h day reading religious text, whereas girls receive a similar education to that in Western countries. Educational demands have also been cited as a risk factor in the prevalence of myopia in Young's 1969 work with Eskimo families in Alaska; while only two of the 130 Eskimo parents (all illiterate) were myopic, 60% of the children (required to attend school) became myopic.

Studies show that other environmental factors, such as light levels (related to latitude and the absence of ultraviolet (UV) radiation), contamination, diet, and parental smoking, have been associated to the development of myopia but there is no proven causation.

Children who spend more daytime outdoors are less likely to become myopic. This was a key discussion during the 12th International Myopia Conference in Australia. Following Jones and colleagues' first report in 2002 on the beneficial effects of outdoor exposure, others have found that it is the amount of time spent outdoors, rather than any particular physical activity as it was previously suggested, which may help retard myopia. There is consensus among myopia research groups (Orinda Longitudinal Study of Myopia, Sydney Myopia Study, and Singapore Sharable Content Object Reference Model (SCORM) study) that outdoor time is protective against myopia. The mechanism for this protective effect is unknown.

Mutti and coworkers (in 2002), the Correction of Myopia Evaluation Trial (COMET) group (in 2005), and others have found that parental myopia is a high-risk factor for myopia. Parental myopia may affect myopia with both genetic and environmental components. A theory of genetic predisposition to myopia with environmental triggers, such as nearwork, urban life, and reduced outdoor exposure, is commonly accepted at present. For an update on molecular, structural, and functional studies in humans and animals, including twin studies; prevalence, progression, and risk factors in myopia; the influence of nearwork and outdoor activity in myopia; and therapies for myopia see the 2009 work by McBrien and coworkers.

Correction and Prevention: Clinical Management of Myopia

Myopia may be corrected using visual optical aids such as spectacles, contact lenses, or, increasingly, refractive surgery. Correction of myopia is achieved by placing minor power (concave) lenses in front of the eye (**Figure 1**). The power of the lenses is measured in diopters (D) and corresponds to the inverse of the focal power of the lens. The eye care provider measures the refractive correction using objective (i.e., retinoscopy and autorefractometer) and subjective techniques to determine the lowest-power diverging lens that achieves best visual acuity. A binocular and eye health examination is required to establish the appropriate prescription.

As per the American Optometric Association guidelines, the goals for management of the patient with myopia are clear, comfortable, efficient binocular vision and good ocular health. Low levels of myopia (less than 3.00D) are not corrected in infants and toddlers as it may disappear within 2 years of age and their visual world is close anyway, that is, they can see as far as they need to. Older children or young children with higher amounts of myopia need to be corrected to allow the visual system appropriate development with clear visual input. For adolescents and adults, in general, any degree of myopia should be corrected any time the patient is adversely affected by the lack of clear distance vision; therefore, patients' needs are taken into account when prescribing a myopic correction. Astigmatism may occur in conjunction with myopia. When the degree of myopia is different ($\geq$2.00D) between the two eyes, the condition is called anisometropic myopia (anisomyopia). The material of choice for the eye glasses will also depend on the patient's characteristics (e.g., polycarbonate lenses are given to children) and the degree of the myopia (e.g., high-index, thinner lenses are recommended for higher prescriptions). Contact lenses (soft or gas permeable) are typically well accepted by myopic patients as the size of the retinal image is larger than with glasses, and they avoid visual-field restrictions. Whether spectacles or contact lenses are preferable in a given case depends upon numerous factors, including patient age, motivation, compliance, corneal physiology, and financial considerations. Orthokeratology is a technique of contact lens fitting which flattens the corneal surface over time to transiently reduce myopia.

A number of options to correct myopia with refractive surgery are available. Since the approval of the use of the excimer laser in the 1990s to reshape the cornea, there has been significant development in the correction of myopia. Laser refractive surgery has surpassed other conventional surgical techniques in safety and efficacy. The suitability of refractive surgery needs to be determined on a case-to-case basis and after a thoughtful discussion between the surgeon and the patient. Current refractive surgery options include:

1. *Excimer laser photorefractive keratectomy (PRK).* A procedure in which the corneal power is decreased by laser ablation of the central cornea, the corneal epithelium is scraped away to allow the reshaping of the corneal stroma.
2. *Laser in situ keratomileusis (LASIK).* This was introduced in the mid-1990s and largely replaced PRK. Unlike PRK, a flap is made in the epithelium to permit access to the stroma. LASIK avoids most of the problems of corneal haze, postoperative pain, and slow rehabilitation seen in PRK, but complications are sometimes associated with the flap. Some studies show that LASIK surgery has predictable and stable results in refractive and visual outcomes in correcting moderate to high myopia on long-term follow-up. Refractive stability is maintained over 7 years, with no evidence of progressive late-onset complications. Recently, an alternative mechanical, epi-LASIK technique has shown comparable effective results to LASEK.
3. *Laser epithelial keratomileusis (LASEK).* In this procedure, the epithelium is treated with alcohol and then peeled back to permit reshaping of the underlying layer. It avoids all flap-related complications associated with LASIK and has less postoperative pain and faster recovery than PRK.
4. *Wavefront-guided (WFG)*, or *custom LASIK.* This technique is used to avoid the induced positive spherical aberration typically found after conventional LASIK procedures. It is more advantageous with large pupils (most studies of conventional LASIK have shown a relationship between the diameter of the low-light pupil and complains of visual symptoms after surgery). However, WFG LASIK has all the same risks of conventional surgery.
5. A new procedure of PRK with intraoperative use of topical mitomicym C seems to be more effective than LASIK surgery for moderate myopia.
6. A number of surgical techniques use phakic intraocular lenses implanted in the posterior chamber. These are used for the correction of high myopia.

Despite significant advances, certain limitations and complications exist in these refractive surgery procedures and patient education is essential before a decision is taken. In this rapidly changing field, co-management of patients and consultation of most recent literature are necessary.

None of these correction techniques prevents or treats the condition. A number of approaches and techniques, which are discussed below, have been advocated over the years to prevent, inhibit, and attempt to reverse myopia development.

Positive Additions for Nearwork

The underlying principle of using positive additions is to reduce the accommodative demand at near, as increased accommodative effort is thought to play a role in the development of myopia. Positive additions may be achieved with the undercorrection of spectacles which also leads to a distance undercorrection and therefore defocused images; hence, the use of bifocals and progressive lenses has been suggested. The technique is supported by animal research that has shown that wearing positive lenses induces hyperopia. However, good results on the use of positive additions may not be only dependent on reducing the magnitude of accommodation, but on other oculomotor factors as well. Results of different studies are contradictory, although some reduction in the rate of myopia progression has been found to occur. In particular, the COMET group has found that the progression of myopia slows down in myopic children who have esophoria at near and are treated with positive additions in the form of progressive addition lenses (PALs). Ongoing longitudinal studies are being undertaken in this area.

Contact Lenses

Although some studies have shown that contact lenses (especially hard contact lenses) reduce myopia progression, the mechanism of action is not well understood. However, the success of these techniques is thought to result from corneal curvature changes produced by the contact lenses, which suggests that the changes may be transient.

Vision Therapy and Biofeedback Training

Various forms of accommodative vision therapy have been advocated in the treatment of myopia. The aim of a training program is to reinforce and establish control over the accommodative response. Although there are reports that these techniques can induce a reduction in myopia, there are no masked studies with objective data supporting the usefulness of vision therapy for correcting or preventing the progression of myopia. In most published reports the quantified test was solely unaided visual acuity which improvement may be explained by an improved ability to interpret a blurred retinal image. Myopes of low degree commonly report that their vision seems poorer upon removal of their spectacles compared to that after a period without spectacle wear. This phenomenon is called blur adaptation and accounts for very small to no additive improvement in visual performance.

Rigorous research studies are needed if accommodation biofeedback is to qualify as a method of clinical treatment of myopia.

Pharmacological Treatment

The first drugs to treat the progression of myopia were chosen based on the belief that myopia could be controlled either by the relaxation of accommodation or the reduction of IOP. Hence, cycloplegic agents such as tropicamide and atropine, and adrenergic antagonistic agents have been used in the past with no success. The difficulties resulting from the regular instillation of drugs, such as inconvenience, reading problems, discomfort, pupillary mydriasis, and the possibility of other adverse reactions to the drug, in addition to the lack of clear evidence of the effectiveness of these agents, provoked abandonment of these techniques. Although none of these pharmacological agents used has demonstrated an ability to control myopic progression successfully, for the past few years new approaches to myopia control are considering the importance of muscarinic receptors in myopia development. M1 antagonist pirenzepine and atropine are the newest drugs used in the attempt to slow down the progression of myopia. Atropine is the only pharmacological agent currently studied in clinical trials. Although the site of action of these drugs is unknown, studies in chicks suggest that these drugs act on the cartilaginous sclera to transiently inhibit glycosaminoglycan synthesis and slow down myopia development. Growth factors, such as insulin-like growth factor 1 (IGF-1), basic fibroblast growth factor (bFGF), and retinoic acid have been shown to be effective at controlling ocular growth in animal models and are promising therapeutic agents for high human myopia. Future therapies to slow down the progression of myopia in humans will be directed at altering the retinal–scleral signaling cascade involved in emmetropization.

Correction and Prevention: Clinical Management of Myopia?

In conclusion, the limited success achieved by the various methods of myopia control should not necessarily be interpreted as providing the absence of any relationship between myopia and nearwork. It is possible that once axial elongation has begun, continued visual feedback would produce additional axial elongation irrespective of any external intervention.

See also: Refractive Surgery.

Further Reading

American Optometric Association (1997). Care of the Patient with Myopia, Optometric Clinical Practice Guideline. Association of Optometrists. http://www.aoa.org/myopia.xml (accessed Jun. 2009).

Charman, W. N. (2005). Aberrations and myopia. *Ophthalmic and Physiological Optics* 25: 285–301.

Chen, C. Y.-C. (2007). Heritability and shared environment estimates for myopia and associated ocular biometric traits: The genes in myopia (GEM) family study. *Human Genetics* 121: 511–520.

Curtin, B. J. (1985). *The Myopias: Basic Science and Clinical Management.* Philadelphia, PA: Harper and Row.

Dirani, M., Shekar, S. N., and Baird, P. N. (2008). Adult-onset myopia: The genes in myopia (GEM) twin study. *Investigative Ophthalmology and Vision Science* 49: 3324–3327.

Gilmartin, B. (2004). Myopia: Precedents for research in the twenty-first century. *Clinical and Experimental Ophthalmology* 32(3): 305–324.

Grosvenor, T. P. (1998). *Clinical Management of Myopia.* Boston, MA: Butterworth-Heinemann.

Gwiazda, J., Hyman, L., Dong, L. M., et al. (2007). Factors associated with high myopia after 7 years of follow-up in the Correction of Myopia Evaluation Trial (COMET) cohort. *Ophthalmic Epidemiology* 14(4): 230–237.

Jones, L., Sinnott, L. T., Mutti, D. O., et al. (2007). Parental history of myopia, sports and outdoor activities, and future myopia. *Investigative Ophthalmology and Vision Science* 48: 3524–3532.

Kurzt, D., Hyman, L., Gwiazda, J. E., et al. (2007). Role of parental myopia in the progression of myopia and its interaction with treatment in COMET children. *Investigative Ophthalmology and Vision Science* 48(2): 562–570.

McBrien, N. A., Young, T. L., Pang, C. P., et al. (2009). Myopia: Recent advances in molecular studies; prevalence, progression and risk factors; emmetropization; therapies; optical links; peripheral refraction; sclera and ocular growth; signalling cascades; and animal models. *Optometry and Vision Science* 86(1): 45–66.

Rada, J. A. and Palmer, L. (2007). Choroidal regulation of scleral glycosaminoglycan synthesis during recovery from induced myopia. *Investigative Ophthalmology and Vision Science* 48: 2957–2966.

Rosenfield, M. and Gilmartin, B. (1998). *Myopia and Nearwork.* Oxford: Butterworth-Heinemann.

Saw, S.-M., Gazzard, G., Au Eong, K. G., and Tan, D. T. (2002). Myopia: Attempts to arrest progression. *British Journal of Ophthalmology* 86: 1306–1311.

Saw, S.-M., Tong, L., Chua, W. H., et al. (2005). Incidence and progression of myopia in singaporean school children. *Investigative Ophthalmology and Vision Science* 46: 51–57.

Schaeffel, F., Simon, P., Feldkaemper, M., Ohngemach, S., and Williams, R. W. (2003). Molecular biology of myopia. An invited review. *Clinical and Experimental Optometry* 86(5): 295–307.

Wade, N. J. (1999). *A Natural History Of Vision.* Cambridge, MA: MIT Press.

Wallman, J. and Winawer, J. (2004). Homeostasis of eye growth and the question of myopia. *Neuron* 43: 447–468.

Young, T. L. (2009). Molecular genetics of human myopia: An update. *Optometry and Vision Science* 86(1): E8–E22.

Relevant Website

http://www.revoptom.com – Review of Optometry: Handbook of Ocular Disease Management: Pathological Myopia and Posterior Staphyl.

N

Neuroendocrine Properties of the Ciliary Epithelium

M Coca-Prados, Yale University School of Medicine, New Haven, CT, USA

Glossary

Aqueous humor – The fluid produced by the bilayered ciliary epithelium in the eye.
Endocrine system – An integrated system involving the release of extracellular signaling molecules such as hormones and neuropeptides in chemical communication between cells or tissues.
Intraocular pressure – The balance between the rate of aqueous humor secretion and its resistance to drainage through the trabecular meshwork.
Neuropeptide – A small chain of amino acids (i.e., 3–20 residues) formed from a large precursor (i.e., 200–300 residues) that is progressively cleaved by specific proteolytic enzymes into a biological active peptide.
Prohormone convertases – A group of protease enzymes that clip off the active segments from the larger peptide precursor at single, specific basic residues or pairs of basic residues.

The ciliary epithelium (CE) is a bilayer of polarized neuroepithelial cells, the pigmented epithelium (PE) and the nonpigmented epithelium (NPE), in the anterior segment of the mammalian eye. It forms with the underlying ciliary muscle (CM) and stroma, the ciliary body (CB), a multicellular unit playing multiple and essential functions in the physiology of the eye. The CE is involved in the secretion of aqueous humor and in the accommodation of the lens. It is also believed that the CE in conjunction with the trabecular meshwork (TM) plays a key role in the regulation of outflow of aqueous humor and intraocular pressure (IOP).

The gene expression profile of the CE has revealed the identification of prohormone convertases (PCs; PC1, PC2, PACE4, PC5, and furin) and enzymes (carboxypeptidase E (CPE); peptidylglycine α-amidating monoxygenase), usually restricted to neuroendocrine cells and tissues involved in the processing and maturation of neuroendocrine peptides and regulatory hormones. This finding has been supported by the identification of multiple neuropeptides (i.e., neurotensin (NT), galanin, and somatostatin (SST)) and peptide-hormones (i.e., natriuretic peptides (NPs), endothelin (ET), and angiotensin) in the intact CE, in aqueous humor and in the conditioned medium of cultured CE-derived cells *in vitro*. Some of these peptides are known to exert hypotensive effects in the cardiovascular system by lowering blood pressure, or ocular hypotension when injected in the eye, suggesting the presence of a local endocrine system in the CE that could influence inflow and outflow of aqueous humor and IOP. Although the development and differentiation of endocrine cells along the CE bilayer remain to be studied, peptide-producing cells have been localized in the NPE cell layer, including cells with molecular markers distinctive of neuronal differentiation involved in the biosynthesis of neurotransmitters.

The neuroendocrine peptides released by the CE are believed to act as either classical autocrine factors targeting their cognate receptors on the same peptide-producing cells, or as endocrine/paracrine signals on neighboring cells and tissues. In particular, cells of the conventional and the uveoscleral outflow pathways of aqueous humor are likely main targets of CE-secreted neuropeptides to influence their cellular function. These peptides may also function as neurohormones, neuromodulators, or neurotransmitters by linking inflow and outflow of aqueous by exerting positive and/or negative feedback control on IOP.

The Ciliary Epithelium

The mammalian CE is a bilayer of neuroepithelial cells, the NPE and PE, sharing the same embryological origin with the retina and the retinal pigment epithelium (RPE), respectively. The PE cell layer of the CE is continuous with the RPE and the NPE cell layer is related to the multiple neural and sensory cell layers of the retina.

At least, three anatomical regions have been distinguished along the CE: the pars plicata, the pars plana, and the ora serrata. The first region borders anteriorly with the iris and it is followed by the pars plana, whereas the ora serrata borders posteriorly with the peripheral margin of the retina. The cell polarity of NPE and PE cells along the entire CE is unique in the sense that their respective apical plasma membranes appose each other. Therefore, the basal membrane of NPE and PE cells face distinct microenvironments. The NPE cells face the aqueous humor, whereas the PE cells the stroma (**Figure 1**). Tight junctions, at the apical plasma membrane of NPE cells form a blood–aqueous barrier, preventing paracellular diffusion of plasma proteins from the stroma into the posterior chamber. The multiple gap-junction proteins, known as connexins, coupling NPE and PE cells facilitate the transfer of ions, electrolytes, and the propagation of intracellular signals along the CE as a functional syncytium.

A main function of the CE is the secretion of aqueous humor, a fluid that nourishes the avascular tissues (lens, cornea, and TM) in the anterior segment of the eye. The CE in conjunction with the filtering cells of the TM regulates the IOP, which reflects a balance between the rates of secretion of aqueous humor and its drainage through the outflow pathways. The secretion of aqueous humor and the regulation of IOP are essential for the integrity and normal function of the eye. An abnormal elevation in IOP is, for example, the best-known risk factor in the development of glaucoma, a neuropathy of the optic nerve characterized by the progressive axon degeneration and death of retinal ganglion cells, excavation of the optic nerve head, and loss of visual field, leading often to bilateral blindness. Today, a reduction in the rate of aqueous humor secretion is the most effective pharmacological approach in lowering IOP and in reducing the progression of the disease. Upon secretion, the aqueous humor moves from the posterior toward the anterior chamber through the pupil, leaving the eye through distinct outflow pathways, including the TM and Schlemm's canal, the uveoscleral, and the episcleral vein by mechanisms not totally understood.

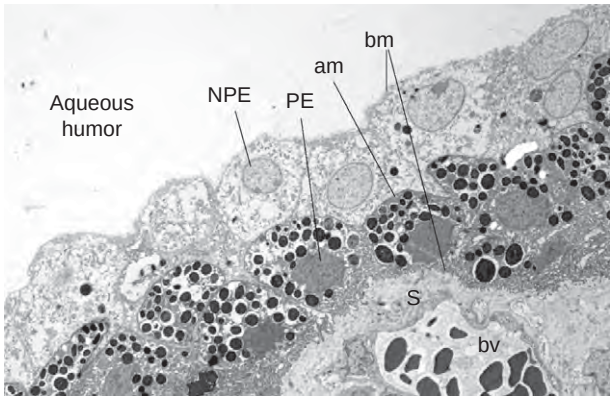

Figure 1 Electron micrograph of a cross section of the ciliary epithelium. The basal membrane (bm) of NPE cells faces the aqueous humor, whereas of the bm of PE cells abuts the stroma (S). The apical membranes (am) of NPE and PE cells appose each other. NPE, nonpigmented; PE, pigmented; bv, blood vessel.

Another function of the CE is accommodation, a mechanism that allows changing the focus of the eye field. Microfibril arrays, known as ciliary zonules, connect the CE and the equator of the lens, and through the contraction–relaxation of the CM, the underlying tissue of the CE, exerts tension in the zonular fibers by modifying the curvature of the lens and its refractive power. The elasticity of the zonular fibers is reduced over age, and in pseudoexfoliation glaucoma they appear to be subject to an increased proteolytic degradation.

In spite of the embryological relationship of the CE with the retina and RPE, little is known about the molecular signals that configure this tissue. Earlier studies have suggested that the lens formation may influence early events in the differentiation of the CE, and that specific signals such as BMP4, BMP7, and transcription factors (CHX10 and PAX6) are important determinants in that process. The PE cell layer of the CE is an extension of the RPE where there is a cellular redistribution of the Na^+/K^+-adenosine triphosphate (ATP)ase from the apical membrane in the RPE toward the basal membrane in PE cells without changing their cellular polarity. On the other hand, the NPE cell layer is related to the multiple cell layers of the retina and it becomes a single polarized cell layer apposing the PE cell layer. Although there is no evidence that the CE harbors photoreceptive cells capable of evoking light-mediated responses, the human CE continues to express (messenger RNA mR and protein) many components associated with the visual phototransduction and the retinoid cycle. The adult CE contains reduced levels of rhodopsin kinase, visual arrestin, cellular retinaldehyde-binding protein (CRALBP), all-*trans*-retinyl esters, and all-*trans*-retinol. Whether these retinal markers are indicative of the presence of presumptive retinal neurons or retinal progenitor cells along the CE is at present unknown.

In recent years, a large body of information has emerged on the cell and molecular biology of the human CE as well, based on the analysis of hundreds of expressed sequence tags (ESTs) isolated by subtractive hybridization from a human CB cDNA library. It has provided a deeper understanding of the multiple biological functions of the human CB (**Table 1**). This article emphasizes the neuroendocrine properties of the CE and the supporting evidences that it is the source of neuropeptides and transmitters in aqueous humor.

Neuroendocrine Genotype of the CE

Earlier studies have shown that the human CE expresses genes for neuropeptides, including NT, galanin, SST, and peptide-hormones and their receptors. These peptides usually are restricted to endocrine cells of the brain,

Table 1 Biological functions assigned to the human ciliary epithelium

1. Aqueous humor transport
2. Accommodation of the lens
3. Synthesis and secretion of plasma proteins, proteases, anti-proteases, and anti-angiogenic and growth factors.
4. Expression of neuropeptides, transmitters, peptide-hormones, and cognate receptors.
5. Expression of immunosuppressive factors: TGFβ2, somatostatin, substance-P.
6. Steroidogenic: steroid-converting enzymes (17β-HSDs and 11βHSDs).
7. Prostaglandins: Cyclooxigenase-2 (COX-2); prostaglandin D2 synthase.
8. Expression of components of rod-phototransduction including: rhodopsin, rhodopsin kinase, and visual arrestin.
9. Expression of components of the visual (retinoid) cycle including: CRALBP, IRBP, CRBP, 11-*cis*-RDH, and LRAT.
10. Expression of glutamate metabolizing enzymes, glutamate receptors (mGluR1b), and glutamate transporters (EAAT1, EAAT5).
11. Expression of GABA receptors (i.e., GABA-C)
12. Circadian clock genes, melatonin rhythm-generating enzymes, and melatonin receptors.
13. Expression of glaucoma genes: myocilin (*MYOC)*, cytochrome P450 *(CYP1B1)*, optineurin *(OPTN)*.

heart, and gastrointestinal tract. The neuronal-like peptides of the human CE (i.e., NT, galanin, and SST) should be considered separately from the peptides that originate from the sympathetic, parasympathetic or sensory ganglions for which nerve endings may be observed in the proximity of PE cells. Transcripts for galanin, NT, or SST, for example, have been detected by RT-PCR or Northern blot analysis on RNA extracted from dissected ciliary processes, a villi-like formation in the *pars plicata*, or from cultured NPE and PE cell lines established from this region. The peptides synthesized and released by the CE have been detected by radioimmunoassay. In many instances, human and bovine CE-derived cells under culture conditions *in vitro* maintain their peptide secretory activity. Therefore, it is unlike that the mRNA detected for each of the above peptides in the CE derives from the ganglia (i.e., ciliary ganglion, pterygopalatine ganglion, superior cervical ganglion, and trigeminal ganglion) innervating the CB.

It has been suggested that peptides released by the CE cells may display multiple functions including their potential influence in the regulation of the rate of aqueous humor secretion and IOP, while also serving as trophic or immunosuppressive factors.

Neuropeptides are synthesized as large precursor polypeptides or pre-propeptides containing the amino acid sequence of the neuropeptide, plus the signal sequence (also known as signal peptide) at its N-terminus that is found in precursor of hormones to be secreted. The precursors are first subjected to endoproteolytic cleavage on the C-terminal of basic residue pairs (Lys-Arg) by PCs, which are members of a family of serine proteinases related to the subtilisin/kexin-type. The C-terminal basic residues are then removed by the CPE, a neuropeptide-processing enzyme resulting in many cases the final step in the biosynthesis of mature peptides. However, some peptides undergo additional post-translational modifications, including amidation, N-terminal acetylation, and serine or threonine phosphorylation. Thus, if the peptide contains a glycine residue preceding the basic cleavage site, it can be further modified by the removal of the glycine residue, generating an amidated carboxyl group by the action of the peptidyl-glycine-α-amidating monooxygenase (PAM).

The capacity of the human CE to process neuropeptide precursors was initially suggested after the isolation and identification of a subtracted cDNA clone (CBS-294) encoding CPE. This finding followed the characterization in the CE of PAM, furin, the PCs PC1, PC2, PACE4, PC5, and the neuroendocrine peptide 7B2. PC1 and PC2 are endoproteolytic enzymes restricted to endocrine cells and neurons, whereas PACE4 and PC5 are found in a wide range of tissues and cells. PC1 and PC2 cleave precursors entering the regulated secretory pathway, while furin process precursors within the constitutive secretory pathway.

There is supporting evidence now that PCs are involved in a number of pathologies, including cancer, neurodegenerative diseases, endocrine disorders, and inflammation. Within the CE, PC1 has been found in the PE cell layer, whereas PC2 in the NPE cell layer. These studies also suggested that the intracellular proteolytic processing of peptide precursors is likely occurring in both cell layers of the CE in a cell-specific fashion. This is consistent with the view that CE cells may be able to process the same precursor into distinct biologically active peptides in PE from NPE cells. For example, the precursor of NT and neuromedin (NN), pre-proNT/NN, is a target of proteolytic processing of both PC1 and PC2 giving rise to distinct cleaved forms. In the brain, NT and NN are detected in equimolar levels, whereas in the intestine NN is detected in larger levels than NT. In the retina, the concentration of NN is higher than NT, whereas in the CB, NT is more abundant than NN. The distinct ratio of NT/NN found in endocrine tissues or cells is dependent on the PC-specific expressed. Precursors of neuropeptides and hormones released from the signal peptide are shuttled to the Golgi apparatus where they are sorted away from other proteins into granules of the regulated secretory pathway. Precursors are also co-packaged with their processing enzymes and they may be subjected to many additional enzymatic modifications (i.e., glycosylation and phosphorylation). The presence of a limited membrane around the secretory granules is characteristic of many secretory granules and their size may range from 20 to 30 nm to as large as 400 nm in diameter. Although neuropeptides and hormones can usually be stored within membrane-bound

Table 2 Expression of endocrine markers, neuropeptides, peptide-hormones, and transmitters in the human CE

Neuropeptide-processing enzymes
Prohormone convertases: PC1, PC2, PACE4, PC5, and furin
Carboxypeptidase E (CPE)
Peptidylglycine α-amidating monooxygenase (PAM)
Neuropeptides and peptide-hormones
7B2
Secretogranin II/secretoneurin
Neurotensin (NT)
Galanin
Somatostatin (SST)
Natriuretic peptides (ANP, BNP, CNP)
Neuropeptide PY
Angiotensinogen (angiotensin II)
Endothelin (ET)
Substance-P

secretory dense-core granules, they can be also stored on translucent secretory vesicles (10–100 nm in diameter).

Protein 7B2 is an acidic protein that resides in the secretory granules of neuroendocrine cells and it functions as a specific chaperone for PC2. The co-expression of PC2/7B2 and additional neuroendocrine-processing enzymes in PE and NPE cells supports the hypothesis that the CE exhibits neuroendocrine properties. Table 2 summarizes a list of neuropeptide markers, peptides, and transmitters expressed in the human CE.

Neuropeptides and Peptide-Hormones of the CE

It is believed that the regulatory peptides released by the CE may exert positive and negative feedback actions on the secretion of aqueous humor and on the secretion of other neuropeptides and hormones. NPs and endothelin ET are among the most extensively studied peptides because of their potent ocular hypotensive effects evidenced by the lowering IOP in experimental animals and in humans. NPs and ET released by the CE exert important regulatory actions on both the site of secretion and the site of drainage of aqueous humor where NPs and ET receptors are present. A more recently identified neuropeptide expressed by the adult human CE is SST, which is also widely distributed in the central nervous system, gastrointestinal tract, and endocrine cells. Within the CE, SST immunoreactivity has been detected sparsely along the NPE cell layer, whereas SST receptors (SSTRs) are widely detected in the retina, iris, and CE. SST is regarded as a neurotransmitter and neuromodulator, exhibiting antisecretory and antiproliferative properties. SST is produced by neuroendocrine, inflammatory, and immune cells in response to a large and diverse number of exogenous and endogenous molecular signals. SST regulates many cellular functions, including the secretion of hormones, neuronal excitability, and vascular

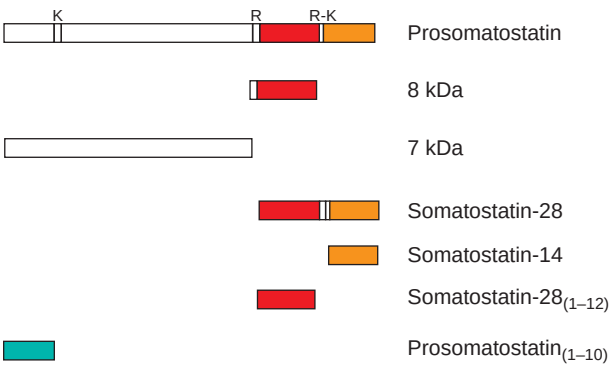

Figure 2 The polypeptide precursor of somatostatin, prosomatostatin, undergoes endoproteolytic cleavage at specific basic residue sites (i.e., arginine (R), lysine (K)), by proprotein convertases PC1 and PC2, to produce distinct biologically active peptides (i.e., somatostatin-28, somatostatin-14).

smooth muscle contractility. SST derives from a 92-amino-acid polypeptide precursor, known as prosomatostatin (pro-SST), which undergoes processing at both the amino and carboxyl-terminal sites of specific pair, basic amino acids into multiple shorter forms, including the biologically active peptides somatostatin-28 (SST-28), and somatostatin-14 (SST-14) (Figure 2).

It has been shown that the PCs, PC1 and PC2, cleave pro-SST into multiple forms, including SST-28 and SST-14, at specific residues with different efficiencies. The inhibitory activity exerted by SST on endocrine, exocrine secretions, and transmitter release, is mediated through at least five distinct SSTRs 1–5. These receptors are coupled to G_i-proteins and upon activation can negatively couple to the adenyl cyclase-cyclic adenosine monophosphate (cAMP) pathway to inhibit stimulated, but not basal, cAMP production, and inhibition of ion exchangers. In the iris, SST has been shown to induce mydriasis by attenuating cholinergic neurotransmitter release and may modulate pupil diameter. In other endocrine systems, activation of SSTRs mediates the inhibition of the growth hormone, glucagons, and insulin secretion.

The NP system has been shown to be present in the CE. It consists of three NPs (ANP, BNP, and CNP), and three distinct receptor subtypes (NPR-A, NPR-B, and NPR-C). Within the ciliary processes, ANP and BNP have been co-localized in the NPE cell layer, and CNP distributed in the vascular endothelium. CNP exhibits the most potent hypotensive effect in the eye when compared to ANP or BNP. The three NPs have been detected in the aqueous humor and in concentrations higher than in plasma, suggesting they are secreted. On the other hand, BNP levels are in higher levels than CNP or ANP. ANP receptors are downregulated in rabbits with experimental glaucoma and ANP levels in aqueous humor are increased as the IOP is increased. The mechanism of

action of the NPR-A and NPR-B receptors is associated with intrinsic guanylyl cyclase (GC) activities producing the second-messenger cyclic guanosine monophosphate (cGMP). In contrast, the NPR-C receptor does not have GC activity and functions as a clearance receptor regulating the level of NPs in aqueous humor.

The potential role of NPs as paracrine modulators of aqueous humor outflow has been suggested. Bremazocine, a relatively selective agonist of κ opioid receptors, lowered IOP by increasing the level of CNP in aqueous humor and increasing outflow. It has been also shown the effect of NPs on the transport systems believed to contribute to fluid secretion across the CE. Inhibitors of the Na^+/H^+-exchanger (NHE), for example, lower IOP when topically applied to the eye. On the other hand, NPs attenuate NHE activity in the CE by inhibiting the Na^+-dependent intracellular pH recovery upon an acid-load, in an order of potency that is similar to their ability to stimulate cGMP in cultured NPE cells. Thus, endogenous NPs could influence aqueous humor secretion by modulating the NHE activity in the CE.

ET is another example of a CE-released peptide in the aqueous humor with ocular hypotensive effects. The effect of lowering IOP has been suggested to occur as a result of the contraction of the CM, which inserts into the TM, resulting in an enhancement of the outflow facility. However, other studies support a potential reduction in aqueous humor secretion due to the inhibition of the Na^+/K^+-ATPase activity by acting on ETB receptors in NPE cells. Such an action could also result in a decrease in aqueous humor formation and contribute to the reduction of IOP.

Potential Neuroendocrine–Immune Circuitry in the Anterior Segment of the Eye

Neuropeptides released by the CE in the aqueous humor may exhibit multiple biological activities, including those associated with a putative neuroendocrine–immune circuit. It has been well recognized that the anterior segment of the mammalian eye is an immune-privileged site, and that antigens injected in the anterior chamber elicit deviant systemic immune responses that are devoid of immunogenic inflammation. This distinctive response, known as anterior chamber-associated immune deviation (ACAID), arises in part by the soluble immunosuppressive and anti-inflammatory factors released by the surrounding tissues in the aqueous humor. The aqueous humor, for example, is able to suppress interferon-γ (INF-γ) production by effector T cells, and neuropeptides present in the aqueous humor, including α-melanocyte stimulating hormone (α-MSH), calcitonin gene-related peptide (CGRP), vasoactive intestinal peptide (VIP), and SST, are capable of suppressing pathogen-induced inflammation in the anterior chamber of the eye. SST, for example, contributes to the immunosuppressive properties of the aqueous humor by promoting the production of the potent immunosuppressive cytokine α-MSH, and by inducing the activation of regulatory T cells. The presence of proinflammatory (i.e., substance-P and CGRP) and anti-inflammatory neuropeptides (i.e., SST) in aqueous humor indicates that there is likely a regulated balance between these factors that influence the ocular immune-privileged microenvironment of the anterior chamber. TGFβ2, a cytokine that promotes immune deviation and immunosuppressive activities, has been detected in high levels in the aqueous humor in approximately 50% of glaucoma patients with primary open-angle glaucoma. High levels of TGFβ2 mRNA are expressed in the human CE, and TM, suggesting that these tissues produce immunosuppressive factors into the aqueous humor. Recent studies have documented that T cells exposed to cultured PE cells of the iris-CB were induced to secrete large amounts of active and latent TGF-β2, a response that was mimicked by exposing T cells to aqueous humor. These observations confirmed that cells from the CE exhibit immunomodulatory functions of their own, since its ability to synthesize and release cytokine factors was independent of the involvement of T cells. The finding that the CE and TM cells expressed cognate receptors for many of the neuropeptides and cytokine released in the aqueous humor may not be coincidental, and it suggests that these factors may act upon autocrine and paracrine based mechanisms to promote immune privilege in the anterior chamber of the eye.

Potential Glutamatergic and Gamma-Aminobutyric Acid (GABA) Systems in the CE

Glutamate (L-Glu) and gamma-aminobutyric acid (GABA) are major excitatory and inhibitory neurotransmitters in the central nervous system (CNS) and retina. However, in recent years it has been shown that components of the glutamatergic are not restricted to the CNS. Glutamatergic systems have been found in peripheral tissues, including bone, pancreas, gastrointestinal tract, testis, and RPE, suggesting that L-Glu functions in these tissues as a chemical transmitter in an autocrine or paracrine fashion. There are observations supporting that NPE cells are pluripotent and capable of proliferating and differentiating into neurons when exposed *in vivo* to growth factors (i.e., insulin and EGF), or into presumptive photoreceptor precursors in response to retinal injury. Further studies have shown evidence supporting neuronal and glial differentiation within the adult CB. In comparison, PE cells from rodents and other adult

mammals in neurosphere-forming assays are capable of generating new neurons with retinal stem/progenitor cell characteristics. These PE-derived cells were shown to harbor stem/progenitor cells with the capacity to give rise to rod photoreceptors, bipolar neurons, and Müller glial cells.

Earlier studies have shown that the CE is capable of synthesizing and breaking down amino acid neurotransmitters. The enzyme glutamine synthetase, involved in the conversion of glutamate into glutamine, was described in NPE cells, and glutamate, GABA, taurine, glutamine, and glycine, and has been measured biochemically in the iris-CB extracts. Post-embedding immunocytochemistry techniques in the zebra fish eye have also revealed that CE cells contain significant basal levels of glutamate, glutamine, and taurine. Overall, these studies indicate that the CE stores neurotransmitter amino acids. Glutamate has been detected in the aqueous humor and in certain forms of retinal diseases and glutamate levels are high suggesting a disruption in glutamate homeostasis. The broad spectrum of peptide-, hormone-, and transmitter-producing cells in the human CE suggests that this tissue harbors a wide range of endocrine cells.

GABA exerts its regulatory actions through ionotropic $GABA_A$ and $GABA_C$, and metabotropic $GABA_B$ receptors. Preliminary studies indicate that $GABA_C$ ρho1- and ρho2-subunits are expressed in the adult human CB (**Table 1**). In the retina, for example, ρho1 transcripts have been identified only in bipolar cells, whereas ρho2 mRNA has shown a more widespread distribution, and ρho3 are in ganglion cells.

What is the putative function of GABAergic systems in non-neuronal tissues? One function that has been widely suggested is that GABA acts in these tissues as an autocrine or paracrine regulator of endocrine functions. Further studies are required to determine whether the $GABA_C$ receptors in the CE are functional and if so what role they play on the neuroendocrine functions of the CE.

Conclusion

The mammalian CE synthesizes and secretes neuropeptides, transmitters, and peptide-hormones into the aqueous humor. The peptides and the neuroendocrine-processing enzymes, so far identified, underscore potential novel neuroendocrine functions of the CE not exclusively restricted to the regulation of aqueous humor secretion and its absorption. The CE-released peptides may also represent functional components of multiple local interactive endocrine loops between the endocrine cells of the CE and the avascular tissues of the anterior segment of the eye. For example, the ocular hypotensive effect of several of CE-released peptides suggested that they may be involved in the local regulation of IOP by linking inflow with outflow of aqueous humor. The CE-peptides may also be involved in the cross talk between the CE and the immune homeostasis of the anterior segment of the eye. Finally, CE-peptides may represent key input/output factors in the circadian rhythm of aqueous humor and/or IOP.

See also: Ciliary Blood Flow and its Role for Aqueous Humor Formation; Control of Aqueous Humor Flow; Functional Morphology of the Trabecular Meshwork; GABA Receptors in the Retina; Glutamate Receptors in Retina; The Immunological Aspects of Aqueous Humor Turnover; Immunosuppressive and Anti-Inflammatory Molecules that Maintain Immune Privilege of the Eye; Ion transport in the Ciliary Epithelium; Neuropeptides: Function; Neuropeptides: Localization; Pharmacology of Aqueous Humor Formation; Pharmacology of the Aqueous Humor Outflow; Phototransduction: The Visual Cycle; The Role of the Ciliary Body in Aqueous Humor Dynamics. Structural Aspects; Uveoscleral Outflow.

Further Reading

Escribano, J. and Coca-Prados, M. (2002). Bioinformatics and reanalysis of subtracted expressed sequence tags from the human ciliary body: Identification of novel biological functions. *Molecular Vision* 8: 315–332.

Escribano, J., Ortego, J., and Coca-Prados, M. (1995). Isolation and characterization of cell-specific cDNA clones from a subtractive library of the ocular ciliary body of a single normal human donor. Transcription and synthesis of plasma proteins. *Journal of Biochemistry (Tokyo)* 118: 921–931.

Fidzinski, P., Salvador-Silva, M., Choritz, L., Geibel, J., and Coca-Prados, M. (2004). Inhibition of NHE-1 Na^+/H^+ exchanger by natriuretic peptides in ocular nonpigmented ciliary epithelium. *American Journal of Physiology. Cell Physiology* 287: C655–C663.

Ghosh, S., Choritz, L., Geibel, J., and Coca-Prados, M. (2006). Somatostatin modulates PI3K-Akt, eNOS and NHE activity in the ciliary epithelium. *Molecular and Cellular Endocrinology* 253: 63–75.

Marc, R. E. and Cameron, D. J. (2001). A molecular phenotype atlas of the zebrafish retina. *Neurocytology* 30: 593–654.

Martínez-Navarrete, G. C., Angulo, A., Martín-Nieto, J., and Cuenca, N. (2008). Gradual morphogenesis of retinal neurons in the peripheral retinal margin of adult monkeys and humans. *Journal of Comparative Neurology* 511: 557–580.

Salvador-Silva, M., Ghosh, S., Bertazolli-Filho, R., et al. (2005). Retinoid processing proteins in the ocular ciliary epithelium. *Molecular Vision* 11: 356–365.

Seidah, N. G. and Chretien, M. (1999). Proprotein and prohormone convertases: A family of subtilases generating diverse bioactive polypeptides. *Brain Research* 848: 45–62.

Troger, J., Doblinger, A., Leierer, J., et al. (2005). Secretoneurin in the peripheral ocular innervation. *Investigative Ophthalmology and Visual Science* 46: 647–654.

Ortego, J. and Coca-Prados, M. (1997). Molecular characterization and differential gene expression of the neuroendocrine-specific genes neurotensin, neurotensin receptor, PC1, PC2, and 7B2 in the human ocular ciliary epithelium. *Journal of Neurochemistry* 69: 1829–1839.

Ortego, J., Escribano, J., Crabb, J., and Coca-Prados, M. (1996). Identification of neuropeptide and neuropeptide-processing enzymes in aqueous humor confers neuroendocrine features to the human ocular ciliary epithelium. *Journal of Neurochemistry* 66: 787–796.

Neuropeptides: Function

N C Brecha, UCLA School of Medicine, Los Angeles, CA, USA; VAGLAHS, Los Angeles, CA, USA
I D Raymond and A A Hirano, UCLA School of Medicine, Los Angeles, CA, USA

Glossary

Calcium imaging physiology – An experimental technique used for detecting and measuring calcium (Ca^{2+}) levels in cells or tissues. Calcium imaging techniques take advantage of calcium indicator dyes, which are molecules that respond to the binding of Ca^{2+} ions by changing their spectral properties.
G-protein-coupled receptor – A large protein family of seven-pass transmembrane receptors that bind molecules and activate intracellular signal transduction pathways to generate cellular responses by coupling to heterotrimeric guanine-triphosphate-binding proteins.
Ion channels – The transmembrane protein complexes that form a water-filled channel across the plasma membrane through which specific inorganic ions can diffuse across their electrochemical gradients.
Paracrine – Acting by volume transmission of transmitters or modulators rather than at chemical synapses in a point-to-point fashion.
Patch-clamp electrophysiology – The study of the electrical properties of biological cells and tissues using electrodes with a high-impedance (gigaohm) seal that permits measurements of small (pA) current and voltage changes.

Introduction

The vertebrate retina contains numerous transmitters and related signaling molecules, including peptides and growth factors, which have multiple roles in the retina, including cellular signaling, growth, and maintenance. The presence, expression, and distribution of peptides, and their receptors in the retina are discussed elsewhere in the encyclopedia. This article mainly focuses on the cellular actions of peptides in the retina. Peptides are characterized by their small size, ranging from 5 to 35 amino acids, and their actions are mediated through guanine-nucleotide-binding protein (G-protein)-coupled receptors (GPCRs) to influence multiple intracellular effectors, including cyclic adenosine monophosphate (cAMP), cyclic guanosine monophosphate (cGMP), Ca^{2+}, protein kinases, and phosphatases. These intracellular effectors modulate ion channels, ligand-gated channels, gap junctions, transporters, and receptors, and affect nuclear transcription factors.

The presence of peptides in the retina was firmly established in the 1970s on the basis of peptide bioactivity and immunoreactivity in retinal extracts, and peptide immunostaining, mainly of amacrine cells. Consistent with the action of peptides in the retina, peptide receptor binding sites have been reported in retinal extracts, and later the expression of their receptors by different retinal cell populations was demonstrated. There is a wide distribution of receptors, with bipolar, amacrine, and ganglion cell populations, expressing different complements of peptide receptors. Interestingly, there is often a difference between the cellular distribution of peptide-containing amacrine cells and their processes compared to the cellular distribution of their receptors, which suggests that peptides can act in a paracrine manner to influence multiple retinal circuits in both the outer and inner retina.

Peptides modulate the cellular activity of retinal neurons and circuits by influencing intracellular signaling pathways. For instance, several different peptides reported in the retina have an effect on cAMP and Ca^{2+} levels, and somatostatin (somatotropin-release-inhibiting factor, SRIF) modulates K^+ and Ca^{2+} currents. SRIF and vasoactive intestinal polypeptide (VIP) also modulate gamma aminobutyric acid-A ($GABA_A$) receptor currents. Through these actions, peptides can change the efficacy of synaptic transmission in the retina by regulating cellular excitability as well as by modulating the release of the fast-acting transmitters, GABA and glutamate, from presynaptic axonal terminals. The overall actions of peptides on retinal neurons are generally characterized as being slow in onset, long lasting and potent at low concentrations, suggestive of a role in adaptive mechanisms. Together, these findings provide support for multiple physiological roles for peptides in the retina.

Peptide Receptor Expression

In general, peptide actions are mediated by GPCRs that influence intracellular signaling pathways, which in turn modulate neuronal excitability and transmitter secretion. Furthermore, there are multiple peptide receptor subtypes for most peptides that are differentially coupled to these intracellular effectors, which markedly increase the diversity of peptide action. For instance, numerous

receptor subtypes mediate the action of neuropeptide Y (NPY), somatostatin (SRIF), and VIP in the nervous system. In retina, there is a similar situation, with peptides expressed by a limited number of rarely occurring amacrine cell populations and multiple peptide receptor subtypes expressed by multiple and distinct retinal cell populations.

Numerous studies report the presence of numerous peptides in the vertebrate retina (**Table 1**). There are also multiple peptide receptors, including those for atrial natriuretic peptide, angiotensin II of the renin-angiotensin system, corticotropin-releasing hormone, NPY, opioid (enkephalin) and opioid-related peptides, SRIF, the tachykinin (TK) peptides (substance P (SP), neurokinin A (NKA), neurokinin B (NKB)), and VIP in some vertebrate retinas. These observations are based on biochemical, molecular biological, and immunohistochemical findings. The best-documented peptides and peptide receptors in the mammalian retina are currently, NPY, SRIF, the TK peptides, and VIP.

Peptide-Binding Sites and Localization

In the late 1980s and early 1990s, the presence of high-affinity peptide-binding sites was reported for several peptides in the vertebrate retina. Biochemical studies showed peptide-binding sites in retinal homogenates, and autoradiographic techniques reported their localization to the plexiform layers. These findings were suggestive of peptide-mediated actions through specific receptors in the retina, although at that time very few peptide receptors had been identified and cloned.

Peptide Receptor messenger RNAs

The identification and cloning of the key peptide receptor genes in the early to mid-1990s provided the tools for determining the expression of specific peptide receptors in the retina. NPY, SRIF, and the TK peptide receptors were reported in the mammalian retina. There are typically multiple subtypes of these receptors, based on both molecular and immunohistochemical findings, and these different subtypes vary in their abundance. These findings confirm that the mammalian retina, as indicated by binding and autoradiographic studies, synthesizes multiple peptide receptors.

Table 1 Peptides and peptide receptors in the retina

Peptides	*Preferred receptors*
Angiotensin II	AT_{1A}, AT_2
Enkephalin (leu_5- and met_5-enkephalin)	delta-, kappa-, mu-opioid receptors
CRH	CRH-binding sites
Neuropeptide Y	Y1, 2, 4, 5
Pituitary adenylate-cyclase-activating polypeptide	PAC1, VAC1, VAC2
Somatostatin	sst_{1-5}
Tachykinin peptides	
• Substance P	NK-1
• Neurokinin A	NK-2
• Neurokinin B	NK-3
Vasoactive intestinal polypeptide	VAC1, VAC2

Peptide Receptor Localization

Peptide receptors, including those that mediate the cellular actions of NPY, SRIF, and the TKs, have been principally studied in the mouse and rat retinas. Several receptor subtypes are expressed in the retina, often by one or more distinct cell types, including photoreceptors, bipolar, amacrine, and ganglion cells. For instance, in rat retina, the neurokinin-1 (NK-1) receptor, which is the preferred receptor for SP, is expressed by GABAergic amacrine cells, while, the NK-3 receptor, which is the preferred receptor for NKB, is expressed by OFF-type bipolar cells.

A frequent observation that has emerged from immunostaining studies is the mismatch between the distribution and number of peptide-containing processes and their receptors. For example, there is a differential distribution of SRIF processes and SRIF subtype (sst) receptors in the inner plexiform layer (IPL). There are examples of several peptides acting at receptors that are located away from the peptide-containing processes, which support the notion of a paracrine mode of action, although this does not rule out direct transmitter actions occurring at or near synaptic specializations where there is a close apposition of peptide- and peptide-receptor-expressing processes.

Intracellular Signaling

The activation of signal transduction cascades by peptides and related analogs in retinal extracts also supports the idea that endogenous peptides are present in the retina and their actions are mediated by specific receptors.

However, there are differences in observations concerning peptide actions on intracellular signaling pathways that may be due to the experimental approaches and sensitivity of the assays, as well as species differences. For instance, both NPY and SRIF inhibit forskolin-induced cAMP accumulation in some, but not all, vertebrate retinas. In contrast, VIP and VIP-related peptides potently stimulate adenylate cyclase activity in many vertebrate retinas. For example, SRIF is reported to stimulate cAMP accumulation in chick and ovine retinas, but SRIF does not affect cAMP accumulation in fish, pigeon, mouse, and rabbit retinas. Furthermore, SRIF inhibits VIP-stimulated adenylate cyclase activity in sheep retina. There is further complexity in evaluating SRIF's action in

retinal homogenates, based on a recent report using both wild-type and sst receptor knock-out mouse lines. This study reported that interactions of sst receptor subtypes as well as levels of sst receptors influenced SRIF potency on adenylate cyclase activity. Finally, the sst_2 receptor is reported to mediate SRIF inhibition of adenylate cyclase activity through a G protein of the $G_{o\alpha}$ type in both mouse and rabbit retina.

In contrast, VIP's potent stimulation of adenylate cyclase activity is well established in many vertebrate retinas. Peptide histidine isoleucine, which is co-expressed with VIP, also stimulates adenylate cyclase activity. In addition, the VIP-related peptides, pituitary adenylate-cyclase-activating polypeptide-27 (PACAP-27) and PACAP-38, are positively coupled to adenylate cyclase activity, and their actions are more potent than VIP, indicating the presence of the PAC1 receptor in retinal homogenates. Furthermore, in rat retinal homogenates, PACAP-27 and PACAP-38, but not VIP, show a dose-dependent stimulation of inositol phosphate levels, suggesting multiple signal transduction pathways for PACAP peptides.

SRIF acting through the sst_2 receptor is also reported to induce nitric oxide production in the retina. Nitric oxide, in turn, would activate soluble guanylate cyclase and increase levels of cGMP. The presence of functional NK receptors has been shown by the dose-dependent stimulation of inositol phosphate accumulation and intracellular Ca^{2+} ($[Ca^{2+}]_i$) mobilization by the TK peptides, SP, NKA, and NKB.

Cellular Signaling

Ca^{2+} Imaging and Ion Channel Physiology

Several peptides, including met_5-enkephalin, NPY, SP, and SRIF, have an action at the cellular level in both nonmammalian and mammalian retinas. For instance, in goldfish retina, met_5-enkephalin, SP, and SRIF partially inhibit voltage-dependent Ca^{2+} currents in isolated mixed bipolar cell axon terminals. In the mammalian retina, low concentrations of NPY, SRIF, or VIP modulate both voltage- and ligand-gated channels in multiple cell types, as discussed below.

Pharmacological studies used isolated rat rod bipolar cells in acute preparations, coupled with Ca^{2+} imaging techniques to characterize the cellular actions of NPY and SRIF. Low concentrations of NPY did not result in detectable changes in $[Ca^{2+}]_i$ levels in rod bipolar cell axon terminals, suggesting that NPY alone does not influence $[Ca^{2+}]_i$ levels. In contrast, there is a dose-dependent inhibition of K^+-evoked increases of $[Ca^{2+}]_i$ with NPY; inhibition is maximal with 1 μM NPY and is also observed with 0.1 nM NPY. Maximal inhibition is also seen with 1 μM C2-NPY and NPY(13–36), selective Y2 receptor agonists. In contrast, no inhibition is observed with Y1, Y4, and Y5 agonists. These findings indicate that NPY acts presynaptically through Y2 receptors to regulate glutamate release from rod bipolar cell axon terminals (**Figure 1**).

There have been several studies of SRIF action at the cellular level. In both isolated rat and rabbit rod bipolar cells, there is no detectable change in $[Ca^{2+}]_i$ levels following direct application of SRIF. However, SRIF strongly inhibits a K^+-stimulated increase of $[Ca^{2+}]_i$ through L-type Ca^{2+} channels in a dose-dependent manner in rat and rabbit rod bipolar cell axon terminals (**Figure 2**). SRIF also enhances GABA-evoked whole-cell currents in amacrine cells likely due to $GABA_A$ receptor phosphorylation, following activation of adenylate cyclase. In rabbit retina, SRIF and octreotide, a SRIF agonist, reduce a K^+-stimulated increase in $[Ca^{2+}]_i$ in rod bipolar cell axon terminals. In addition, SRIF inhibits Ca^+-activated K^+ currents (I_{BK}) in these cells. The octreotide effect is prevented by L-Tyr8Cyanamid 154806, an sst_2 receptor antagonist, indicating that these SRIF effects are likely to be mediated by sst_2 receptor activation.

In salamander photoreceptors, low concentrations of SRIF modulate both voltage-activated K^+ and L-type Ca^{2+} currents. SRIF enhances a delayed outwardly rectifying K^+ current in both rod and cone photoreceptors (**Figure 3**). It differentially modulates L-type Ca^{2+} channels currents: SRIF reduces the Ca^{2+} current in rods and increases the Ca^{2+} current in cones (**Figure 4**). Ca^{2+} imaging experiments of isolated rod and cone photoreceptors produce findings consistent with the electrophysiological findings. Together, these observations suggest that SRIF has a role in the regulation of glutamate release from photoreceptors based on its modulation of both voltage-gated K^+ and Ca^{2+} currents.

Membrane currents are not altered following direct application of VIP to isolated rat rod bipolar and ganglion cells. However, VIP does influence GABAs action at $GABA_A$ receptors. It potentiates GABA-evoked whole-cell currents in bipolar cells by 65% and ganglion cells by 54% (**Figure 5**). The onset of VIP action is slow with a long recovery period. VIP-induced potentiation of whole-cell GABA currents is mediated through phosphorylation of $GABA_A$ receptors, following adenylate cyclase activation. The activation of a cAMP-dependent pathway is consistent with biochemical findings that VIP increases cAMP levels in the mammalian retina. In contrast to these observations in rat, VIP reduces GABA-evoked whole-cell currents of rabbit bipolar cells by about 40%. Finally, in rat amacrine cells, VIP, SRIF, and enkephalin also enhance GABA-evoked whole-cell currents through $GABA_A$ receptor phosphorylation by protein kinase A to increase affinity of $GABA_A$ receptor for GABA. Thus, the peptides appear to fine-tune the inhibition by GABA.

These findings of NPY, SRIF, and VIP action at the cellular level are consistent with biochemical studies

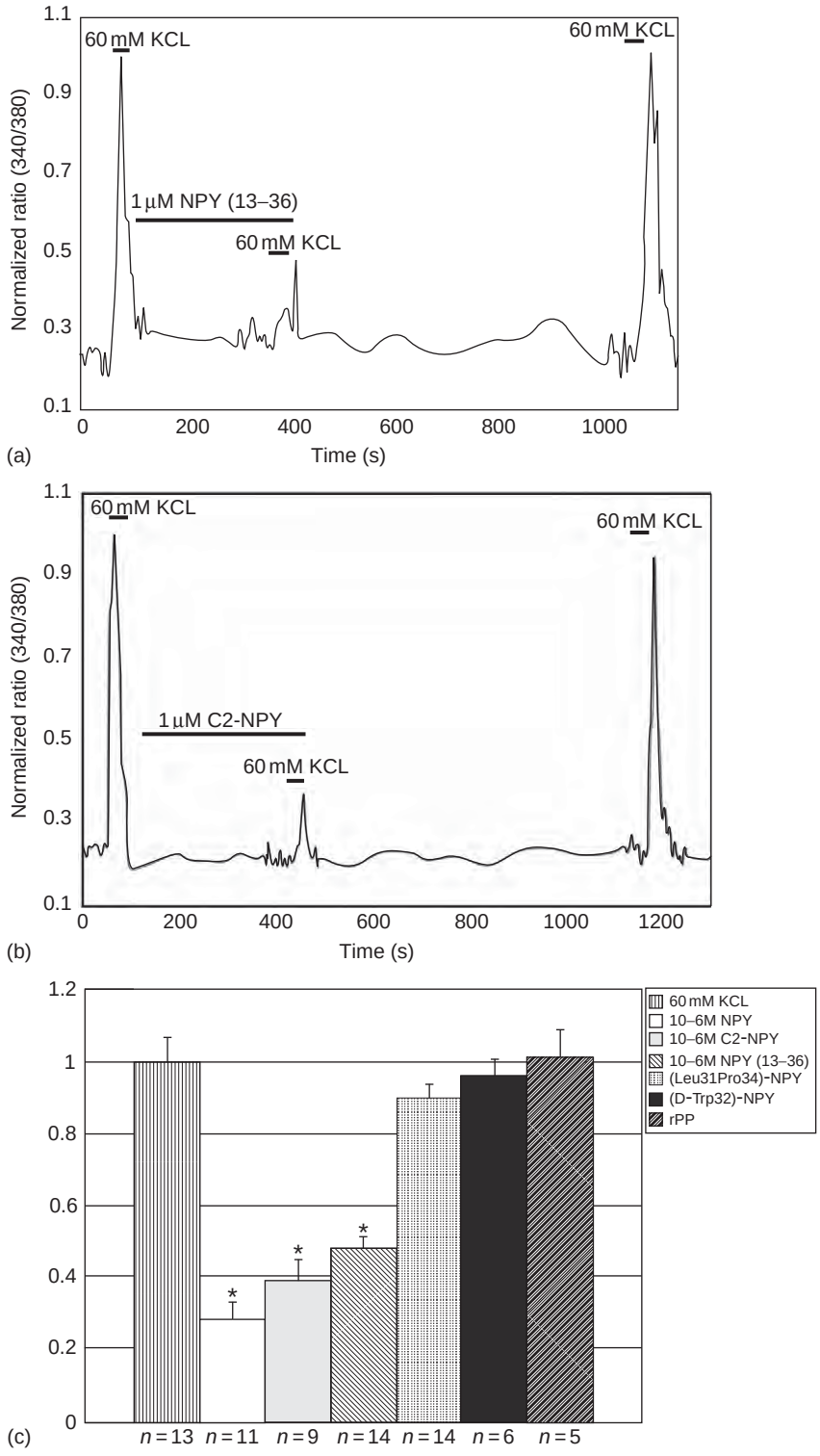

Figure 1 NPY inhibits Ca^{2+} influx into rod bipolar cells through Y2 receptor activation. (a) Micromolar concentrations of Y2 receptor selective agonists NPY (13–36) and (b) C2-NPY inhibits high K^+-induced increases in $[Ca^{2+}]_i$ in rod bipolar cell axonal terminals. The Ca^{2+} responses recover to baseline 10 min after the removal of the peptide. (c) Effect of NPY and selective Y-receptor agonists on depolarization-induced increases in intracellular calcium $[Ca^{2+}]_i$. Summary bar graph comparing the effects of NPY, Y2 receptor selective agonists NPY (13–36) and C2-NPY, Y1 receptor selective agonist $[Leu^{31}Pro^{34}]$-NPY, and Y5 receptor selective agonist $[D\text{-}Trp^{32}]$-NPY. (*) Significant inhibition when compared with high K^+ control ($P < 0.05$). From Figure 4 in D'Angelo, I. and Brecha, N. C. (2004). Y2 receptor expression and inhibition of voltage-dependent Ca^{2+} influx into rod bipolar cell terminals. *Neuroscience* 125: 1039–1049, with kind permission from Elsevier.

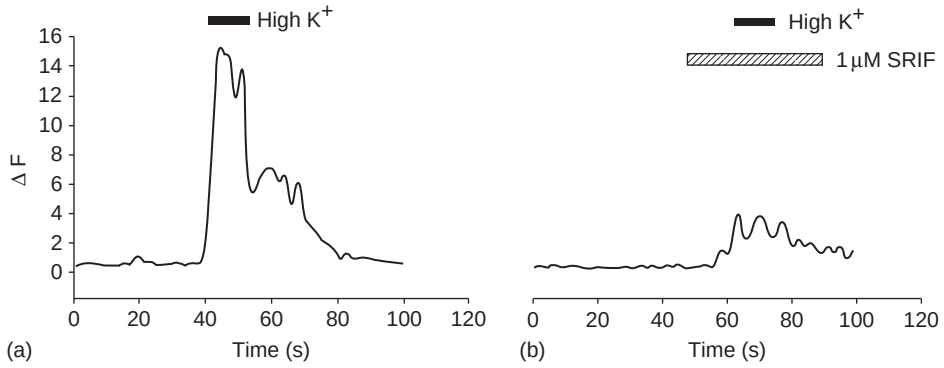

Figure 2 SRIF strongly inhibits a K^+-stimulated increase of intracellular calcium $[Ca^{2+}]_i$ through L-type Ca^{2+} channels in a rod bipolar axon cell terminal. (a) K^+-stimulated increase of $[Ca^{2+}]_i$ in an axonal terminal. (b) Inhibition of K^+-stimulated increase of $[Ca^{2+}]_i$ in an axonal terminal by SRIF treatment (striped bar). From Figure 3 in Johnson, J., Caravelli, M. L., and Brecha, N. C. (2001). Somatostatin inhibits calcium influx into rat rod bipolar cell axonal terminals. *Visual Neuroscience* 18: 101–108.

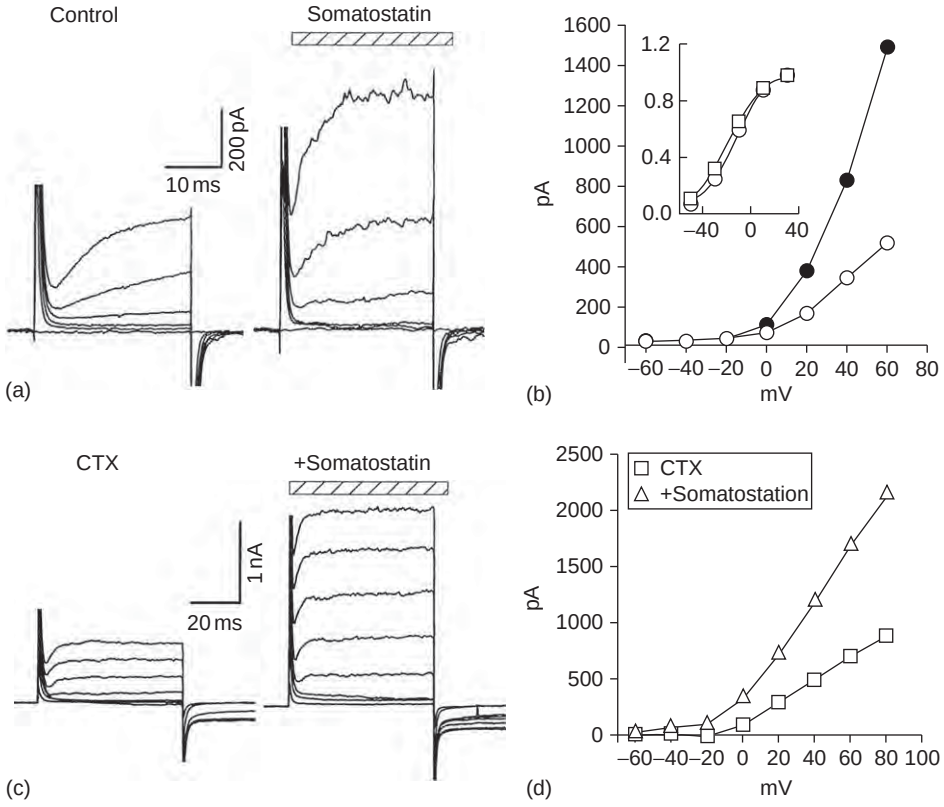

Figure 3 SRIF enhances a delayed outward K^+ current in rods. (a) Somatostatin (SRIF) increased voltage-activated K^+ current. (b) Current–voltage (I–V) relationship of the K^+ current obtained by holding cells at –70 mV and stepping from –60 to +40 mV in 20 mV increments. (c) Charybdotoxin (CTX), which blocks calcium-activated K^+ current, reduced outward current but did not prevent SRIF-induced increases in K^+ currents. (d) I–V relationship of outward current in the presence of CTX. From Figure 2 in Akopian, A., Johnson, J., Gabriel, R., Brecha, N., and Witkovsky, P. (2000). Somatostatin modulates voltage-gated K(+) and Ca(2+) currents in rod and cone photoreceptors of the salamander retina. *Journal of Neuroscience* 20: 929–936.

reporting the presence of peptide receptors and the activation of intracellular effectors in retinal homogenates. They are also consistent with the localization of peptide receptors to different retinal cell types. Together, they show that peptides have multiple cellular actions including modulation of voltage- and ligand-gated ion channels, which would influence intrinsic cellular properties and transmitter release from retinal cells.

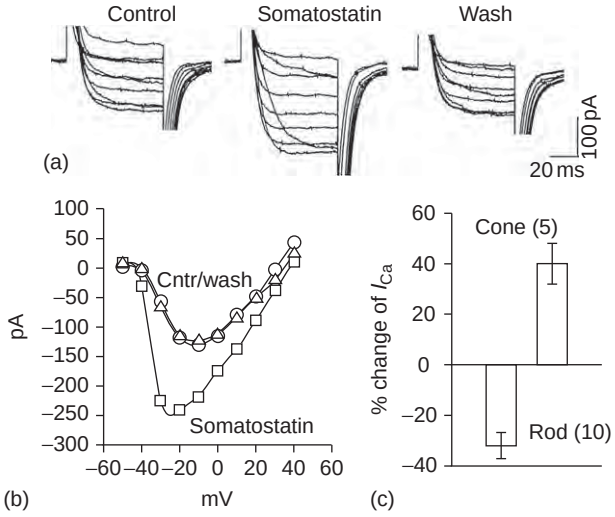

Figure 4 Excitatory effects of somatostatin (SRIF) on the Ca^{2+} current in cones. (a) Cones were held at − 70 mV, and depolarizing pulses were applied from − 40 to +40 mV in 10 mV steps. (b) Current–voltage plot of the data in (a) is shown. (c) A summary of the changes induced in the peak Ca current of rods and cones by SRIF is shown. From Figure 6 in Akopian, A., Johnson, J., Gabriel, R., Brecha, N., and Witkovsky, P. (2000) Somatostatin modulates voltage-gated K(+) and Ca(2+) currents in rod and cone photoreceptors of the salamander retina. *Journal of Neuroscience* 20: 929–936.

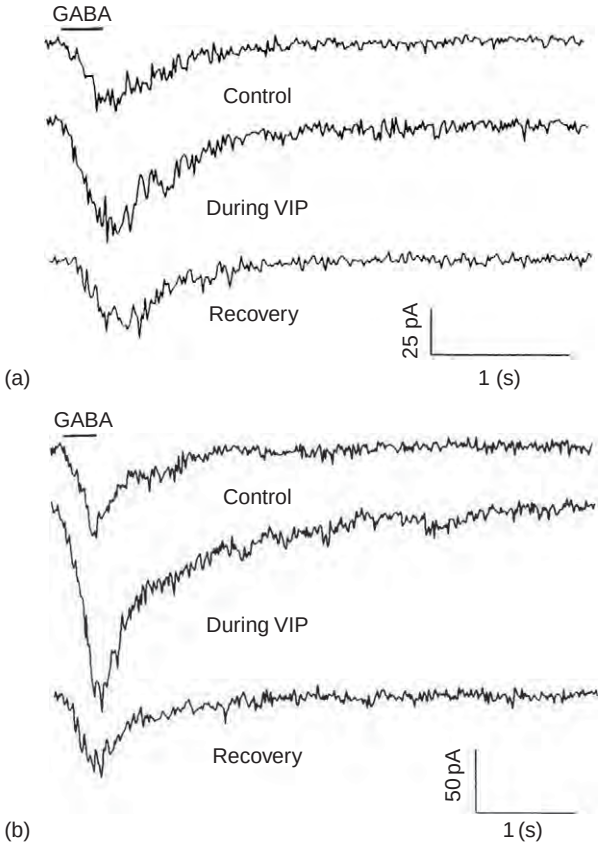

Figure 5 VIP potentiation of GABA-evoked Cl^- current in a bipolar cell (a) and a ganglion cell (b). The whole-cell GABA-evoked currents in both the bipolar and ganglion cells were potentiated after a 11-s application of VIP. From Figure 4 in Veruki, M. L. and Yeh, H. H. (1992). Vasoactive intestinal polypeptide modulates $GABA_A$ receptor function in bipolar cells and ganglion cells of the rat retina. *Journal of Neurophysiology* 67: 791–797.

Functional Studies

Electroretinogram Recording

A limited action of peptides in the retina has been shown using electroretinogram (ERG), which reflects the contribution of electrical activity from the different retinal cell types. The initial a-wave appears to arise from photoreceptors; the b-wave, the activity of primarily second-order bipolar cells and Müller glial cells; the slower c-wave, the activity of the retinal pigment epithelium and Müller cells; and the d-waves, the activity of the OFF pathway. In rabbit retina eyecups, low concentrations of SRIF decreased the amplitude of the b-wave in rabbit eyecup preparations, but several other peptides, including cholecystokinin (CCK) and SP do not appear to affect the ERG.

Extracellular Recordings

In contrast, extracellular recordings have shown that SP, SRIF, and VIP influence multiple retinal cell types in both nonmammalian and mammalian retinal eyecup preparations. Typically, low concentrations of peptides increase the general excitability of cells. In the mudpuppy eyecup preparation, neurotensin and SP increased the firing activity of ganglion cells; however, met_5-enkephalin inhibited them. However, the distribution of μ-opioid receptors is unknown in mudpuppy retina and the action of met_5-enkephalin could be an indirect effect on amacrine cells. These actions are characterized as slow and long lasting. There is also some specificity in peptide action. For example, using a rabbit eyecup preparation as described below, SRIF acts on all ganglion cell types; in contrast, SP acts on most brisk ganglion cells and VIP acts on ON- and OFF-center brisk ganglion cell types, respectively. Overall, peptide actions in this preparation are characterized as being modulatory and too slow to participate in fast, light-evoked responses.

Application of SP at low-to-moderate concentrations excites most brisk ganglion cells, including ON- and OFF-center and ON–OFF directionally selective ganglion cells in the rabbit retina (**Figure 6**). SP exerts these excitatory effects without affecting ganglion cell receptive field properties. The latency of the SP response

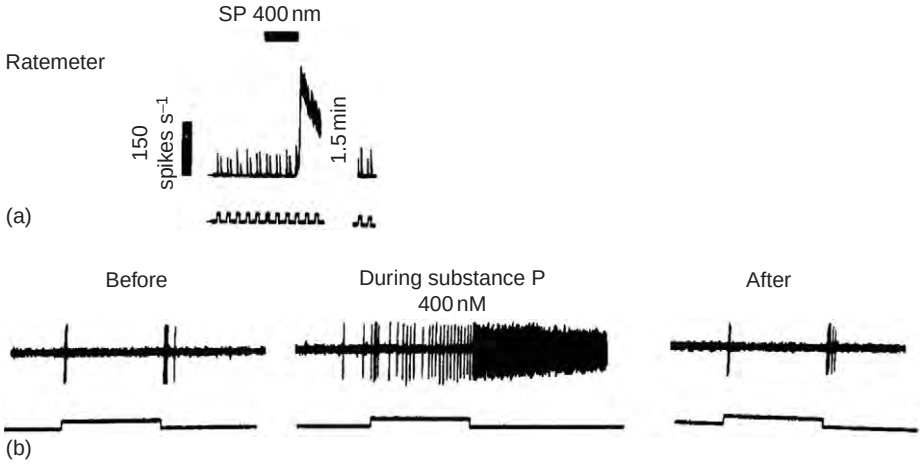

Figure 6 SP excitation of an ON–OFF direction selective ganglion cell responding to a stationary flashing spot. (a) Ratemeter records showing response to flashes (bottom trace) before, during and after application of 400 nM SP (upper bar); calibration bar on right is for 150 spikes s^{-1}. (b) Individual light responses before, during, and after application of SP. Bottom traces show duration of light response and upper traces show spikes. From Figure 1 in Zalutsky, R. A. and Miller, R. F. (1990). The physiology of substance P in the rabbit retina. *Journal of Neuroscience* 10: 394–402.

was shorter than that of SRIF. Furthermore, intracellular recordings show that SP depolarizes some amacrine cells, including GABA-containing amacrine cells. These experiments are consistent with the expression of the SP-specific NK-1 receptor by GABA-containing amacrine cells. SP did not affect horizontal cell activity, consistent with the lack of TK-binding sites and NK-1- or NK-3-receptor immunostaining of horizontal cells. Investigations also report that SP excites most ganglion cells in mudpuppy and fish retina. Together, these findings indicate that TK peptides act in the inner retina and affect the general excitability of ganglion cells and their level of spontaneous activity, rather than altering the characteristics of ganglion cell receptive field properties, as reported for SRIF and VIP in the rabbit retina.

In rabbit retina, low concentrations of SRIF excite all ganglion cell types, change their signal-to-noise ratio discharge activity and shift their center-surround balance toward a more dominant center (**Figure 7**). Similar to other peptides, SRIF actions are characterized as being slow in onset and having a long latency. SRIF is also reported to act on multiple cells in the inner and outer retina; it directly affects bipolar, amacrine, and ganglion cells and influences the horizontal cell network. Moreover, SRIF is reported to increase input resistance of amacrine and bipolar cells, suggesting an action on ion channels or gap junctions. This would be consistent with patch-clamp experiments showing that SRIF affects K^+ and Ca^{2+} currents in retinal neurons. In addition, modulation of gap junctions could be mediated by SRIF-induced dopamine release or nitric oxide production, as suggested by pharmacological studies. Together, these observations indicate that SRIF acts on multiple retinal circuits to produce long-lasting changes in ganglion cell activity and receptive field organization, consistent with the idea that this peptide acts as a modulator to mediate the effects of light adaptation in the retina.

VIP excites ON- and OFF-center brisk ganglion cells in the rabbit retina. Similar to observations using SRIF and SP, VIP is potent at low concentrations and there is a delay in the onset of its action on ganglion cells. The maintained activity of ON- and OFF-center ganglion cells is increased by VIP and their excitatory responses to flashes of light are unaffected or slightly reduced in the presence of VIP. In contrast, VIP has little effect on the maintained activity of ON/OFF directionally selective ganglion cells, and the response of these cells to a moving stimulus. Finally, the action of VIP on ganglion cells in rabbit retina is congruent with other reports of the action of VIP on GABA currents on isolated ganglion cells in the rat retina.

Peptide Influence on Transmitter Release

Several investigators have evaluated the influence of peptides on transmitter release from the retina. The general experimental paradigm is to preload the retina with a radiolabeled transmitter, such as GABA, glycine, or dopamine, and, following a washout period, to add the peptide and measure changes of radiolabeled transmitter levels induced by the peptide. An alternative experimental design is to measure endogenously released transmitter

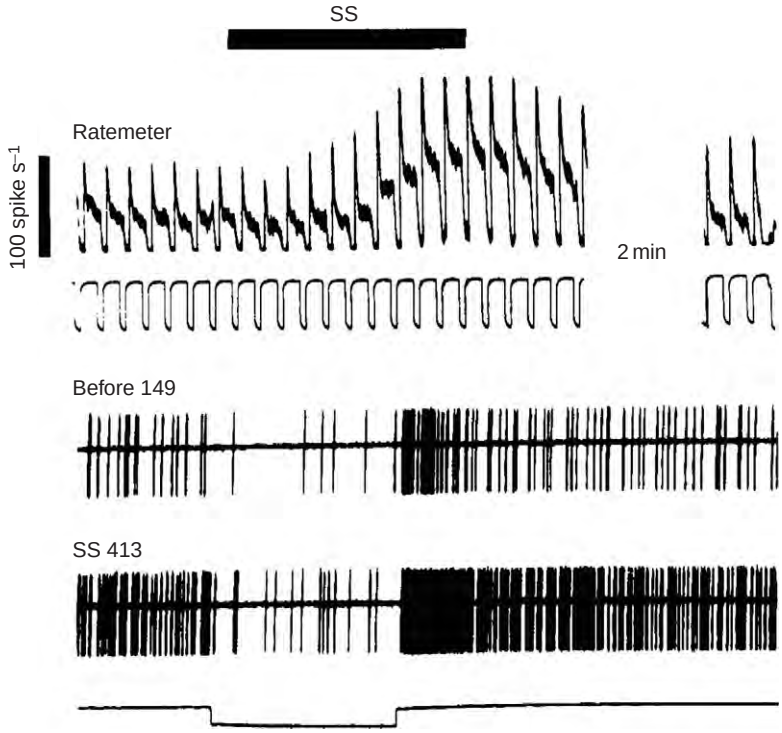

Figure 7 SRIF (somatostatin) excites most ganglion cells. (Top) Ratemeter record before, during, and after application of somatostatin indicated by the bar at top. (Middle and lower) An OFF ganglion cell response before and after 400-nM SRIF application. SS, somatostatin. From Figure 1 in Zalutsky, R. A. and Miller, R. F. (1990). The physiology of somatostatin in the rabbit retina. *Journal of Neuroscience* 10: 383–393.

levels, using radioimmunoassays or by high-pressure liquid chromatography.

Low concentrations of exogenously applied NPY stimulate the release of glycine, dopamine, acetylcholine, and 5-hydroxytryptamine from the vertebrate (frog and rabbit) retina. SRIF stimulates release of dopamine from the rat retina, and pharmacological studies indicate this action is mediated by sst receptors. SP also evoked the release of dopamine from rat retina, and the modulation of Ca^{2+} currents in fish bipolar cells by SP suggests that it may affect transmitter release.

A variant of this experimental approach involves the use of flashing light to stimulate transmitter release to determine if peptides influence light-evoked transmitter release. For example, the μ-opioid receptor agonist, (D-Ala2, MePhe4, Gly-ol5)-enkephalin (DAMGO), increases light-evoked release of acetylcholine from rabbit retina. These latter findings are consistent with-opioid-binding sites distributed homogenously over the IPL and GCL of the rat and monkey retina, and the localization of μ-opioid receptor immunoreactivity by bistratified ganglion cells of the rat retina. Furthermore in rabbit retina, nociceptin, the endogenous ligand for opioid-receptor-like 1, inhibits acetylcholine release evoked by flickering light. In contrast, SP and SRIF do not change the level of light-evoked release of acetylcholine from rabbit retina.

Peptide Function

Experimental findings are consistent with peptides acting as slow transmitters or modulators in the retina. For instance, NPY, PACAP, SP, SRIF, and VIP, acting through GPCRs, influence adenylate cyclase or phospholipase C activity in retinal homogenates and whole retina. Peptides also have potent modulatory effects on both Ca^{2+} and K^+ currents in retinal neurons. Furthermore, SRIF acting through sst_{2A} receptors inhibits the release of the excitatory transmitter glutamate from rod bipolar cells. In addition, the action of GABA at $GABA_A$ receptors is modulated by SRIF and VIP through phosphorylation of $GABA_A$ receptors by protein kinase A in rat rod bipolar, amacrine, and ganglion cells. These examples illustrate the functional role of peptides in regulating both transmitter release and the excitability of retinal neurons.

The concept that peptides act as modulators of retinal circuitry or networks is based on both anatomical and functional findings. Peptide-containing cells in most cases are wide-field amacrine cells that are characterized by a very-low–to-medium cell density. These cells ramify widely and have overlapping processes that cover the entire retinal surface. Therefore, they would have a broad influence on a large number of cells and are unlikely to mediate discrete point-to-point information

processing. Connectivity studies show that most synaptic input onto peptide-containing amacrine cell processes are from amacrine cells, and these cells in turn terminate mainly on amacrine and ganglion cells. Peptides released from these cells could therefore influence multiple cells in a local fashion. In addition, a consistent finding for several peptides is a distinct distribution of peptide-containing and peptide-receptor-bearing processes and cells. These findings suggest that peptides are likely to diffuse from their release sites and act at a distance in a paracrine fashion. Together, these observations support the concept that peptides have a widespread effect on multiple types of retinal neurons.

A feature of many wide-field amacrine cells is the co-expression of GABA and a peptide. For example, in rat, cat, and monkey retina, GABA is co-localized with NPY, SP, and VIP in different amacrine cell types. In addition, glutamate, the predominant ganglion cell transmitter, is co-expressed with PACAP in ganglion cells that innervate the suprachiasmatic nucleus of the hypothalamus. These observations are consistent with findings elsewhere in the nervous system reporting the co-expression and co-release of classical transmitters and peptides from the same cell. Interestingly, a differential release of classic transmitters and peptides depending on the frequency and pattern of cell firing has been shown for several neuronal systems. GABA or glutamate and peptides can act together at the same site, or the peptides can diffuse through the tissue and act at more distant cellular sites. There is evidence for both modes of action in the retina. GABA and peptides released from wide-field amacrine cells may act locally at $GABA_A$ receptors; for instance, both VIP and GABA act on $GABA_A$ receptors expressed by bipolar cell axons and ganglion cells. Peptides can also diffuse from their release site and act in a paracrine manner, as suggested for example, by the different distributions of SRIF immunoreactive processes and sst receptors, which are expressed by multiple retinal cell types.

Functional studies also support the concept that peptides act as modulators of retinal circuitry. In general, the cellular effects of peptides are slow, and they occur at multiple locations in the retina. Both SRIF and VIP produce excitatory changes in the range of seconds to minutes in the spontaneous activity and neuronal discharge patterns of ganglion cells. Moreover, SRIF affects the center-surround balance of all types of ganglion cells. This action of SRIF suggests a role in light/dark adaptation. The role of other peptides in visual function is less well understood. However, as their wide-ranging actions are also likely to be too slow to mediate fast signaling, these peptides will probably also act in modulatory processes that occur on longer timescales and participate in adaptive mechanisms that globally affect the state of retinal circuits and networks.

Conclusion

The vertebrate retina is richly endowed with multiple peptides and peptide receptors; peptides are often localized to a single or at the most a few amacrine cell types, and their receptors are typically expressed by multiple cell types. Peptides act through GPCRs to modulate voltage- and ligand-gated ion channels, and influence neuronal excitability and transmitter release. The pattern of peptide and peptide receptor expression, and the cellular action of peptides being slow in onset, long lasting and potent at low concentrations is congruent with a modulatory role of peptides that would influence multiple cells and cellular networks. This broad modulatory role is consistent with peptides participating in slow signaling events in the retina and influencing adaptive mechanisms.

Acknowledgment

Support for this work was provided by NEI EY 04067 and a Veterans Administration Senior Career Scientist Award.

See also: GABA Receptors in the Retina; Glutamate Receptors in Retina; Neuropeptides: Localization; Neurotransmitters and Receptors: Dopamine; Neurotransmitters and Receptors: Melatonin Receptors; The Role of Acetylcholine and its Receptors in Retinal Processing.

Further Reading

Akopian, A., Johnson, J., Gabriel, R., Brecha, N., and Witkovsky, P. (2000). Somatostatin modulates voltage-gated $K(^{+})$ and $Ca(2^{+})$ currents in rod and cone photoreceptors of the salamander retina. *Journal of Neuroscience* 20: 929–936.

Brecha, N. C. (1983). Retinal neurotransmitters: Histochemical and biochemical studies. In: Emson, P. C. (ed.) *Chemical Neuroanatomy*, pp. 85–129. New York: Raven.

Brecha, N. C. (2003). Peptide and peptide receptor expression and function in the vertebrate retina. In: Chalupa, L. and Werner, J. (eds.) *Visual System*, pp. 334–354. Boston, MA: MIT Press.

Casini, G., Catalani, E., Monte, M. D., and Bagnoli, P. (2005). Functional aspects of the somatostatinergic system in the retina and the potential therapeutic role of somatostatin in retinal disease. *Histology and Histopathology* 20: 615–632.

Cervia, D., Casini, G., and Bagnoli, P. (2008). Physiology and pathology of somatostatin in the mammalian retina: A current view. *Molecular and Cellular Endocrinology* 286: 112–122.

D'Angelo, I. and Brecha, N. C. (2004). Y2 receptor expression and inhibition of voltage-dependent Ca^{2+} influx into rod bipolar cell terminals. *Neuroscience* 125: 1039–1049.

Feigenspan, A. and Bormann, J. (1994). Facilitation of GABAergic signaling in the retina by receptors stimulating adenylate cyclase. *Proceedings of the National Academy of Sciences of the United States of America* 91: 10893–10897.

Hökfelt, T., Broberger, C., Xu, Z. Q., et al. (2000). Neuropeptides – an overview. *Neuropharmacology* 39: 1337–1356.

Jensen, R. J. (1993). Effects of vasoactive intestinal peptide on ganglion cells in the rabbit retina. *Visual Neuroscience* 10: 181–189.

Johnson, J., Caravelli, M. L., and Brecha, N. C. (2001). Somatostatin inhibits calcium influx into rat rod bipolar cell axonal terminals. *Visual Neuroscience* 18: 101–108.

Thermos, K. (2003). Functional mapping of somatostatin receptors in the retina. *A review.Vision Research* 43: 1805–1815.

Veruki, M. L. and Yeh, H. H. (1992). Vasoactive intestinal polypeptide modulates $GABA_A$ receptor function in bipolar cells and ganglion cells of the rat retina. *Journal of Neurophysiology* 67: 791–797.

Zalutsky, R. A. and Miller, R. F. (1990). The physiology of somatostatin in the rabbit retina. *Journal of Neuroscience* 10: 383–393.

Zalutsky, R. A. and Miller, R. F. (1990). The physiology of substance P in the rabbit retina. *Journal of Neuroscience* 10: 394–402.

Neuropeptides: Localization

N C Brecha, UCLA School of Medicine, Los Angeles, CA, USA; VAGLAHS, Los Angeles, CA, USA
A A Hirano and I D Raymond, UCLA School of Medicine, Los Angeles, CA, USA

Glossary

Autoradiography – A histochemical technique used to localize the binding site of a ligand in tissue using radiolabeled ligands (usually ^{131}I, ^{3}H, or ^{35}S) and photographic techniques to detect the isotope.
BAC – A bacterial artificial-chromosome-generated transgenic animals, which are a relatively potent way to generate knock-in transgenic mice that is thought to better recapitulate normal gene expression due to use of a large, chromosomal amount of regulatory genomic DNA surrounding the protein-coding region of the gene.
***In situ* hybridization histochemistry** – A histochemical technique used to localize the cellular localization of messenger RNA.
Isoforms – The different forms of a protein, derived from a single gene that result from alternative splicing or from a family of related genes.
Paracrine – Acting by volume transmission of diffuse messengers rather than at chemical synapses in a point-to-point fashion.

Introduction

The vertebrate retina contains numerous transmitters and related signaling molecules, including peptides and growth factors (Table 1). Peptides and growth factors have multiple roles in the retina, including cellular signaling, growth, and maintenance. This article focuses on the localization of peptides that are primarily involved in cellular signaling, including neurotransmission, and participate in retinal circuitry functions mediating visual information processing. Peptides are characterized by their small size ranging from 5 to 35 amino acids and slow actions that are mediated through multiple guanine-nucleotide-binding protein (G-protein)-coupled receptors (GPCRs), which influence intracellular signaling pathways.

The presence of peptides has been documented in both nonmammalian and mammalian retinas. The most studied peptides in the mammalian retina are neuropeptide Y (NPY), somatostatin (somatotropin-release-inhibiting factor, SRIF), the tachykinins (substance P (SP), neurokinin A (NKA) and neurokinin B (NKB)), and vasoactive intestinal polypeptide (VIP). This article primarily uses these peptides as exemplars of the pattern of peptide expression in the vertebrate retina.

Evidence for abundant peptide expression in the vertebrate retina began with multiple descriptions in the late 1970s of peptide activity in retinal extracts and peptide immunostaining of amacrine cells. These studies established that peptides are usually localized to low-density populations of wide-field amacrine cells; some ganglion cells also express peptides. Consistent with the presence of peptides in the retina is the expression of their receptors, which have a wide distribution, and have been reported in bipolar, amacrine, and ganglion cell populations. Interestingly, there is often a mismatch between the cellular distribution of peptide-containing amacrine cells and their processes compared to the cellular distribution of their receptors. A striking example is the distribution of SRIF and its receptor, SRIF subtype 2A (sst_{2A}, as discussed below), which suggests that peptides mainly act in a paracrine manner, and therefore influence multiple retinal circuits in both the outer and inner retina.

Peptides influence the cellular activity of retinal neurons and circuits by modulating multiple intracellular signaling pathways, which affect transmitter release and intrinsic neuronal properties. Peptide actions are characterized as being slow in onset, long-lasting, and potent at low concentrations, suggestive of a role in adaptive mechanisms. Together, these findings provide strong support for a functional role of peptides in the retina.

Peptide Expression

Bioassays and Radioimmunoassays

In the 1950s, Euler and his colleagues reported the presence of SP bioactivity in dog and bovine retinal extracts. However, it was not until the late 1970s with the development of additional bioassay systems and radioimmunoassays (RIAs) that a rich variety of peptides, including cholecystokinin, the enkephalin peptides, glucagon, SRIF, SP, thyrotropin-releasing hormone, and VIP, was described in vertebrate retinal extracts. At the present time, over 20 peptides have been reported in the vertebrate retina (Table 2) with a greater number of peptides and peptide families in nonmammalian compared to mammalian retinas.

In general, bioassay and RIA studies report low-to-moderate levels of peptides in retinal extracts compared to other tissues and brain regions. In most cases, findings

Table 1 Peptides and peptide receptors in the retina

Peptides	*Preferred receptors*
Neuropeptide Y	Y1, 2, 4, 5, 6
Pituitary adenylate-cyclase-activating polypeptide	PAC1, VAC1, VAC2
Somatostatin	sst_{1-5}
Tachykinin peptides	
• Substance P	NK-1
• Neurokinin A	NK-2
• Neurokinin B	NK-3
Vasoactive intestinal polypeptide	VAC1, VAC2

Table 2 Peptides reported in the vertebrate retina

Angiotensin II
Cholecystokinin
Corticotropin-releasing hormone
Enkephalin
• Leu_5-enkephalin
• Met_5-enkephalin
ß-Endorphin
FMRFamide
Glucagon
Luteinizing–hormone-releasing hormone
Natriuretic peptides
• Atrial natriuretic peptide (α-ANP and γ-ANP)
• Brain natriuretic peptide
• C-type natriuretic peptide
Neurotensin
Neuropeptide Y
Nociceptin
Pituitary adenylate-cyclase-activating polypeptide
Peptide histidine isoleucine
Somatostatin
Tachykinin peptides
• Substance P
• Neurokinin A
• Neurokinin B
Thyrotropin-releasing hormone
Vasoactive intestinal polypeptide

from these investigations are consistent with immunohistochemical studies showing that these peptides are expressed in amacrine and ganglion cells. For instance, SRIF bioactivity and immunoreactivity are in retinal extracts from numerous species, and this peptide is localized to sparsely occurring amacrine and displaced amacrine cells in all species studied to date. Similarly, SP bioactivity and immunoreactivity are reported in the retina of numerous species, and SP immunoreactivity is localized to both amacrine and ganglion cells.

Peptides detected in the retina correspond to those detected in other tissues as to their molecular structure based on gel electrophoresis or high-pressure liquid chromatography and, in more limited cases, on peptide sequencing. These studies revealed that both forms of SRIF, SRIF-14 and SRIF-28, are differentially expressed in the mammalian retina; SRIF-14 is the predominant form in the rat and human retina and SRIF-28, in addition to SRIF-14, is in guinea pig and rabbit retina. Functionally, this finding is likely to be of importance, since SRIF-14 and SRIF-28 preferentially bind to different SRIF receptor subtypes.

Peptide Localization

Peptide Messenger RNA

There have been few investigations documenting peptide messenger RNAs (mRNAs) in the retina. Most studies evaluated mouse, rat, and human retinal extracts using Northern blots and reverse transcription polymerase chain reaction (RT-PCR), and rat retinal sections using *in situ* hybridization histochemistry. A combination of these approaches have been used to show that preprotachykinin (PPT) I mRNA, which generates SP and NKA, and PPT II mRNA, which generates NKB, are expressed in rat retinal extracts. *In situ* hybridization histochemical studies have extended these findings to establish a differential distribution of the tachykinin mRNAs with PPT I mRNA in cells distributed to the inner nuclear layer (INL), inner plexiform layer (IPL), and ganglion cell layer (GCL), and PPT II mRNA in cells distributed to the GCL. *In situ* hybridization histochemical studies have also established the presence of sparsely distributed SRIF mRNA-containing cells in the INL and GCL, while another study showed the co-expression of SRIF mRNA and immunoreactivity in amacrine and displaced amacrine cells. Finally, VIP mRNA and immunoreactivity are in sparsely distributed cell bodies in the inner retina. These findings extend earlier biochemical studies showing that the mammalian retina synthesizes multiple peptides, and it is reasonable to assume that other peptides located in the retina by RIA or immunohistochemistry are also synthesized by retinal neurons.

An alternative approach to evaluating the cellular localization of a peptide is the employment of a transgenic mouse line with the peptide promoter driving the expression of a reporter gene. Although this type of genetic approach has been commonly used in other regions of the nervous system, there have been limited findings reported to date in the retina. The best example is the detection of NPY in amacrine cells in the INL and GCL of a mouse line with ß-galactosidase (ß-gal) expression driven by the NPY promoter. ß-Gal-containing amacrine and displaced amacrine cells are distributed to all retinal regions and they have widely ramifying processes. The pattern of ß-gal expression matched the pattern of NPY immunostaining established using a highly characterized antibody to NPY; there is about 85% co-localization between β-gal expression and NPY immunoreactivity. Thus, independent experimental approaches confirm the pattern of NPY expression in the retina.

Peptide Immunostaining

Beginning in the late 1970s and early 1980s, numerous peptide immunolabelings were described in both non-mammalian and mammalian retinas. Peptide immunostaining was usually localized to distinct populations of amacrine cells, and in some cases, to ganglion cells and their central-nervous-system projections.

Peptide immunoreactivity is commonly localized to wide-field amacrine cell populations distributed to both the proximal INL and the GCL. These cells are characterized by processes that ramify in one or more laminae of the IPL. In addition, these processes arborize widely and overlap to form a network across the retinal surface. Some wide-field amacrine cell types that contain peptide immunoreactivity also have axon-like processes. These amacrine cell types are likely to be polyaxonal amacrine cells characterized by a more restricted dendritic field and multiple axons that extend beyond their field of dendrites. Finally, there are several examples of sparse peptide-containing processes crossing the INL and ramifying in the outer plexiform layer (OPL). These processes are likely to be derived from interplexiform cells, which are characterized by processes that ramify in both the IPL and OPL, and they are often categorized as an amacrine cell variant. These peptide-containing amacrine cell populations are characterized by a very-low-to-moderate cell density. In most cases, their cell bodies are distributed to all retinal regions. In all cases, peptide-containing processes cover the entire retinal surface.

Three examples that illustrate the general features described above are the NPY-, SRIF- and VIP-containing amacrine cells in the mammalian retina.

NPY immunoreactivity is localized to wide-field amacrine cells that are located in both the proximal INL and the GCL. NPY cells have a similar appearance in different mammalian retinas. In the INL, most immunoreactive cells were characterized by small cell bodies and fine processes that ramify primarily in lamina 1 of the IPL. A few cells also ramified in lamina 3 of the IPL. In the GCL, small-to-medium immunoreactive cells ramify primarily in lamina 5 of the IPL. A few immunoreactive processes, originating from somata in the INL and processes in the IPL, ramified in the OPL (**Figure 1**). In rat retina, immunoreactive cells had a regular distribution across the retina and an overall cell density of 280 cells mm^{-2} in INL and 90 cells mm^{-2} in GCL.

SRIF immunoreactivity is localized to sparsely distributed, wide-field amacrine and displaced amacrine cells (**Figure 2**). Immunoreactive somata give rise to thin varicose fibers that form a narrow and continuous plexus in lamina 1 of the IPL. In many species, there is also a narrow plexus of varicose fibers in laminae 3 and 5 of the IPL. Frequently, a smooth, thin-caliber, axon-like process is observed to arise from a cell body or a primary process. A few immunoreactive fibers also cross the INL to ramify in the OPL in both ventral and dorsal retina. These fibers can be traced to the plexus in lamina 1 of the IPL. Finally, in rabbit and cat retinas, there is a dense accumulation of SRIF-immunoreactive fibers along the retinal margin, which form a circumferential band in all retinal regions.

A major feature of the SRIF expression in the mouse, rabbit, cat, and human retina is the predominant distribution of SRIF-containing cell bodies to the ventral retina. These cells form a very low-density cell population. For example, in rabbit retina, cell density ranges from 6 cells mm^{-2} in ventral retina to 11 cells mm^{-2} at the retinal margins. In addition, the total number of SRIF-immunoreactive amacrine cells in these retinas is correspondingly very low.

VIP immunoreactivity is localized to sparsely distributed wide-field amacrine cells, mainly located in the proximal INL. VIP cells have a similar appearance and

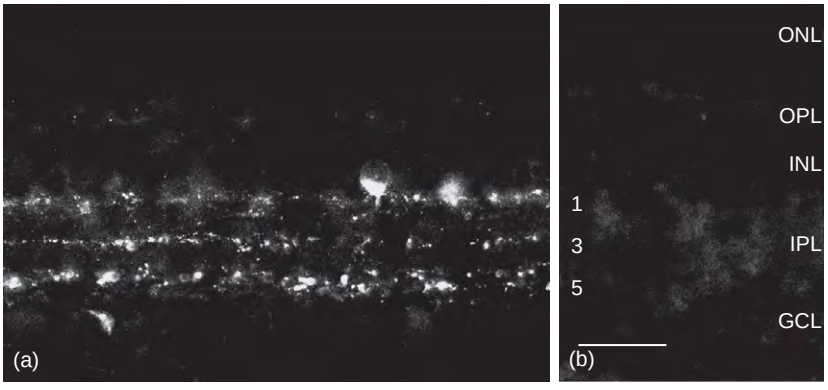

Figure 1 – NPY immunoreactivity in the rat retina. (a) NPY immunostaining of an amacrine cell body in the INL and varicose processes that ramify in laminae 1, 3, and 5 of the IPL. (b) Control experiment; NPY immunostaining was absent from a retinal section incubated with the NPY antibody that was preabsorbed with 10^{-6} M NPY. Vertical sections: scale bar = 30 μm. From Oh, S. J., D'Angelo, I., Lee, E. J., Chun, M. H., and Brecha, N. C. (2002). *Journal of Comparative Neurology* 446(3): 219–234. Copyright 2002, John Wiley & Sons, Inc. Reprinted with permission of John Wiley & Sons, Inc.

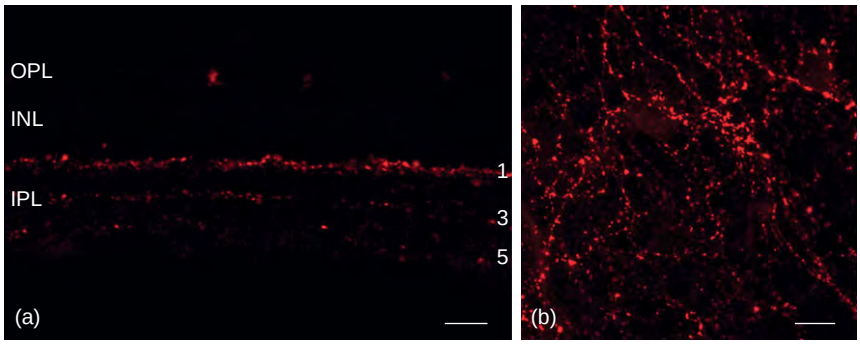

Figure 2 – SRIF immunoreactivity in the mouse retina. (a) SRIF immunoreactive processes are mainly in lamina 1 of the IPL. Sparse occurring processes also ramify in laminae 3 and 5 of the IPL, as well as crossing the INL and ramify in the OPL. (b) Plexus of SRIF immunoreactive processes in lamina 1 of the IPL. (a) Vertical section; scale = 50 μm; (b) Whole-mount preparation; scale = 50 μm.

distribution in different mammalian retinas. VIP immunoreactivity is distributed to multiple varicose processes and collaterals that ramify in laminae 1, 3, and 5 of the IPL in all retinal regions. VIP mRNA-containing and immunoreactive cells also form low-density cell populations in both the INL and GCL. For example, VIP-immunoreactive cells have an overall cell density of 25 cells mm^{-2} in rabbit retina, and there is an overall cell density of 50 cells mm^{-2} in the INL and 12 cells mm^{-2} in the GCL in the monkey retina.

Tachykinin and pituitary adenylate-cyclase-activating polypeptide (PACAP), a peptide in the VIP family, are reported in ganglion cells. These peptide-containing ganglion cells innervate multiple retinorecipient targets.

SP-immunoreactive ganglion cells are present in the frog, rat, hamster, rabbit, monkey, and human retina. These cells have been identified in co-staining experiments following either retrograde labeling of ganglion cells after fluorescent tracers are injected into retinorecipient nuclei or by the loss of ganglion cell immunostaining, following optic nerve section. In hamster, a small number of ganglion cells contain SP immunoreactivity; SP immunoreactivity in the lateral geniculate nucleus (LGN) is eliminated following optic nerve section. In rabbit, about 30% of the ganglion cells contain SP immunoreactivity. These cells have medium-to-large somata and dendrites that ramify extensively in the IPL. Their axons terminate in several retinorecipient nuclei, including the LGN, superior colliculus, and the accessory optic nuclei. In human retina, weakly staining SP-containing ganglion cells have also been identified on the basis of their morphology. Finally, in the *Macaca* monkey retina, the presence of SP-containing ganglion cells is suggested by the partial loss of SP immunostaining in the pregeniculate nucleus and the olivary pretectal nucleus, following bilateral eye enucleation.

There have been a modest number of ultrastructural investigations concerning the connectivity of peptide immunoreactive cells in rat, guinea pig, and primate retina. In general, the main input to peptide immunoreactive processes is from amacrine cells, whereas the major output formed by conventional synapses is onto amacrine and ganglion cells. There is a smaller percentage of input and output connections with bipolar cell axonal terminals. The large number of synaptic connections with amacrine cells indicates that peptide-containing cells are influenced principally by other amacrine cells and to a lesser degree by bipolar cells. There is more limited information about the connectivity of peptide-containing cells in other species, although overall the pattern of connectivity of these cells appears to be quite similar to that observed in monkey retina.

A feature of many wide-field amacrine cells is the co-expression of gamma aminobutyric acid (GABA) and a peptide. For example, in rat, cat, and monkey retina, GABA is co-localized with NPY, SRIF, and VIP. In addition, glutamate, the predominant ganglion cell transmitter, is reported to be co-expressed with PACAP in ganglion cells that innervate the suprachiasmatic nucleus of the hypothalamus. The co-expression of glutamate and SP in ganglion cells is also likely, although not formally demonstrated to date. These observations are consistent with findings elsewhere in the nervous system, reporting the co-expression and co-release of classical transmitters and peptides from the same cell. Interestingly, a differential release of classic transmitters and peptides, depending on the frequency and pattern of cell firing, has been shown in several systems. GABA or glutamate and peptides can act together at the same site, or the peptides can diffuse through the tissue and act at more distant cellular sites. There is evidence for both modes of action in the retina. GABA and peptides released from wide-field amacrine cells may act locally at $GABA_A$ receptors; for instance, both VIP and GABA act on $GABA_A$ receptors expressed by bipolar cell axons and ganglion cells. Peptides can also diffuse from their release site and act in a paracrine manner, as suggested, for example, by the differential distribution of SRIF-containing amacrine cell processes and SRIF receptors, which are expressed by multiple retinal cell types located away from the SRIF-containing processes.

Peptide Receptor Expression

As mentioned above, peptide actions are mediated by multiple GPCRs that influence intracellular signaling pathways, which regulate transmitter secretion and neuronal excitability. For instance, SRIF's cellular actions are mediated by five distinct GPCRs, sst_1–sst_5. There are also two sst_2 isoforms, sst_{2A} and sst_{2B}, from alternative splicing. The cellular actions of the tachykinin peptides are mediated by three receptors, known as NK-1, NK-2, and NK-3, whose preferred ligands are SP, NKA, and NKB, respectively.

Peptide-Binding Sites and Localization

The distribution of peptide receptors was initially evaluated using binding sites with autoradiographic approaches. In the late 1980s and early 1990s, the presence of high-affinity peptide-binding sites for several peptides, including SRIF, tachykinins, and VIP, was reported using radiolabeled peptides. Autoradiographic techniques were also used to define the regional distribution of peptide-binding sites. For example, SRIF-binding sites, identified with radiolabeled SRIF or a radiolabeled SRIF analog, were over the photoreceptor and both plexiform layers of the mouse and rat retina. High-affinity SP- and VIP-binding sites were homogeneously distributed over the IPL and GCL. In addition, NKA- and NKB-binding sites were evenly distributed over the IPL of the guinea pig retina. However, there are major difficulties in defining the cell types associated with these binding sites because of the low resolution of the autoradiographic technique. Furthermore, there are very few selective peptide agonists or antagonists available to distinguish among the different receptor isoforms. For example, octreotide binds to several SRIF receptor subtypes, and there is a high likelihood that multiple receptor subtypes were detected in these autoradiographic studies.

Peptide receptor mRNAs

The identification and cloning of peptide receptor genes in the 1990s have provided the tools for determining the expression of specific peptide receptors in the retina. NPY, SRIF, TK, and VIP receptors have been described most often in the mouse and rat retina. Multiple subtypes of these receptor mRNAs are found in the retina and they vary in their abundance; for example, in rat retina, the sst_2 and sst_4 mRNAs are the most abundant compared to the other sst mRNAs. Similarly, mRNAs of NPY and NK isoforms are present in retinal extracts with different levels of expression. Finally, mRNAs of the selective PACAP receptor, PAC1, and the VIP/PACAP-preferring receptors, VPAC1 and VPAC2, have been reported in retinal extracts. These findings illustrate that multiple peptide receptors are synthesized by the mammalian retina, in agreement with binding, autoradiographic, and immunohistochemical studies.

Pharmacological Studies

The activation of intracellular signaling pathways by peptides and related analogs in retinal extracts also supports the notion that endogenous peptides are present in the retina and they have a functional role that is mediated by specific receptors. For instance, both NPY and SRIF potently inhibit forskolin-induced cyclic adenosine monophosphate (AMP) accumulation, and VIP potently stimulates adenylate cyclase activity in retinal extracts. In addition, PACAP-27 and PACAP-38 are positively coupled to adenylate cyclase activity, and their actions are more potent than VIP, indicating the presence of PAC1. Furthermore, in rat retinal homogenates, PACAP-27 and PACAP-38, but not VIP, show a dose-dependent stimulation of inositol phosphate levels, suggesting multiple signal transduction pathways for PACAP peptides. Finally, the presence of functional NK receptors has been shown by the dose-dependent stimulation of inositol phosphate accumulation and $[Ca^{2+}]_i$ mobilization by the tachykinin peptides, SP, NKA, and NKB.

Pharmacological studies with isolated retinal cells and peptide receptor agonists and, in more limited cases, antagonists have also indicated the presence of pharmacological subtypes of peptide receptors. For instance, Y2, an NPY receptor, and sst_{2A} modulate L-type calcium channels expressed by rod bipolar cells. These investigations along with peptide binding and autoradiographic studies have been valuable in establishing the presence of functional peptide receptors in the retina.

Peptide Receptor Localization

Peptide Receptor mRNAs

In situ hybridization histochemical experiments have documented the cellular expression of NK-1 and NK-3 mRNAs in the rat retina. NK-1 mRNA is located in the INL and GCL, and NK-3 mRNA is mainly distributed to the middle and outer regions of the INL, corresponding to the location of bipolar cell bodies. This pattern of expression matches the NK-1- and NK-3-immunostaining patterns in the mouse and rat retina.

Peptide Receptor Localization

Peptide receptors, including those that mediate the actions of NPY, SRIF, and the TKs, have been mainly studied in the mouse and rat retinas. Several receptor subtypes are expressed in the retina, often by one or

more distinct cell types, including bipolar, amacrine, and ganglion cells.

Sst and NK receptor expressions illustrate the general pattern of cellular localization of peptide receptors, although many details of individual receptor expression remain to be determined in future studies. In some cases, there are marked differences in the pattern of expression of these receptors, when studied using different, well-characterized antibodies. These disparate observations suggest that antibody specificity is a major factor influencing the understanding of peptide receptor expression in the retina. To date, animal models using genetic reporters driven by peptide receptor promoters to localize the cellular expression of peptide receptors have not been reported in the retina. The use of molecular approaches and knock-out lines will be needed to fully characterize the antibodies used for the immunostaining studies, and bacterial artificial chromosome (BAC) transgenics and knock-in mouse lines will be important for establishing the cellular localization of these receptors, independent of immunostaining approaches.

There are major differences in the reported pattern of SRIF receptor expression. For instance, some groups report that numerous amacrine cells in the rat and rabbit retina express sst_1 immunoreactivity. In contrast, other groups using a different antibody report sst_1 immunoreactivity in a distinct population of ganglion cells based on their size, and distribution of dendrites to lamina 3 of the IPL. Several independent studies, using different antibodies, agree that sst_{2A} immunoreactivity is the most abundant SRIF receptor subtype, and it is mainly localized to bipolar cells in mouse, rat, and rabbit retinas (**Figure 3**). Sst_{2A} immunoreactivity is also reported in some wide-field amacrine cells, photoreceptor terminals, and horizontal cells in some species. All investigators agree that ganglion cells express sst_4 immunoreactivity. Sst_4 immunoreactivity is in multiple ganglion cells and numerous multistratified processes in the IPL. Consistent with the immunostaining studies are *in situ* hybridization histochemical experiments describing sst_4 mRNA expression in cells distributed to the INL and GCL. Together, these findings provide strong evidence for the expression of SRIF receptors by ganglion cells. There are no reports of the cellular localization of sst_3 to retinal cells and there is a single report of sst_5 expression in nearly all amacrine cells.

NK-1 immunoreactivity is in numerous amacrine cell bodies in the INL and in some small and large cell bodies in the GCL in the rat retina (**Figure 4**). Immunoreactivity is prominent in all IPL laminae, and in addition there are fine caliber and varicose processes in the OPL, and a few processes in the ganglion cell axon layer. NK-1 immunoreactivity is observed in tyrosine-hydroxylase-containing amacrine cell bodies and their processes. Finally, most NK-1 immunoreactive amacrine cells contain GABA immunoreactivity. The large number of NK-1 immunoreactive cell bodies and the distribution of processes to the IPL suggest that this receptor is expressed by multiple amacrine cell populations. Some ganglion cells, based on cell body size, appearance, and position, are also likely to express NK-1 immunoreactivity.

In contrast, NK-3 immunoreactivity is in bipolar cell bodies distributed to the middle of the INL, and in their dendritic and axonal processes in the OPL and IPL, respectively (**Figure 5**). In the IPL, they ramify in

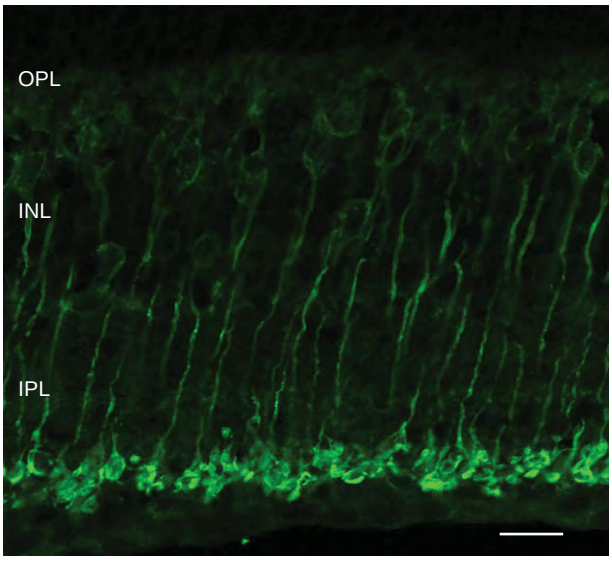

Figure 3 – Sst_{2A} immunoreactive rod bipolar cells in the mouse retina. Sst_{2A} immunostaining of rod bipolar cells, as well as some amacrine cells. Note very high level of expression (bright green) in rod bipolar cell terminals in laminae 5 of the IPL. Vertical section: scale = 15 μm.

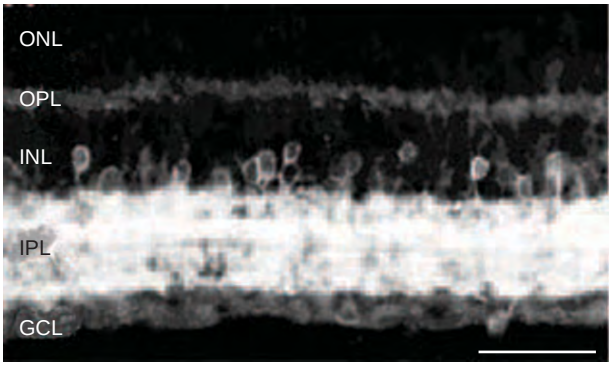

Figure 4 – NK-1 immunoreactivity in amacrine cells of the rat retina. NK-1 immunostaining of multiple amacrine cell bodies in the INL and heavy staining of processes in all laminae of the IPL. The pattern of immunostaining suggests that multiple amacrine cell types express this receptor. Vertical section: scale bar = 50 μm. Adapted from figure 1 in Casini, G., Rickman, D. W., Sternini, C., and Brecha, N. C. (1997) Neurokinin 1 receptor expression in the rat retina. *Journal of Comparative Neurology* 389(3): 496–507. Copyright 1997, John Wiley & Sons, Inc. Reprinted with permission of John Wiley & Sons, Inc.

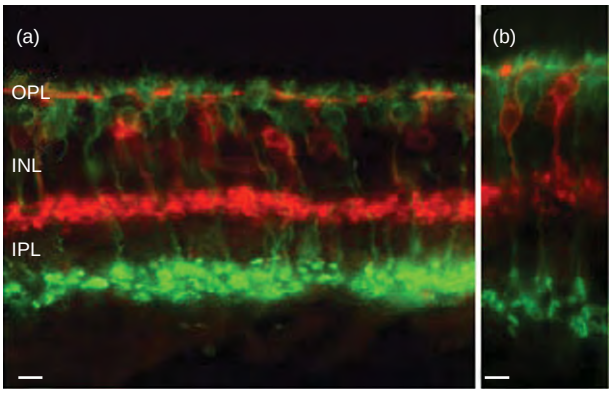

Figure 5 – NK-3 immunoreactivity in bipolar cells of the mouse retina. (a) NK-3 immunoreactive bipolar cells (red) are localized to the INL and labeled processes are in the OPL and laminae 1 and 2 of the IPL. PKC immunoreactivity in rod bipolar cells (green) that ramify in lamina 5 of the IPL. (b) The cell bodies of the NK-3 immunoreactive bipolar cells are clearly distinct from those of the rod bipolar cells. The pattern of NK-3 expression indicates OFF-type cone bipolar cells express this receptor. Vertical section: scale = 10 μm.

laminae 1 and 2, distal to where the type 3 cone bipolar cells stratify, suggesting NK-3 expression in OFF-type bipolar cells. A subset of the NK-3 immunoreactive bipolar cells expresses synaptotagmin 2. This same subgroup of NK-3 immunoreactive bipolar cells contains recoverin, a marker for type 2 bipolar cells. Together, these findings show that NK-3 immunoreactivity is localized to at least two types of OFF-type bipolar cells. In addition, NK-3 immunoreactivity is in tyrosine-hydroxylase-containing amacrine cells. There are no reports of specific NK-2 immunostaining in the retina, although NK-2 mRNA is detected in retinal extracts.

A frequent observation from these studies is the mismatch between the distribution of peptide-containing processes and their receptors. This mismatch supports the notion of a paracrine mode of action for peptides acting at receptors that are located away from the peptide-containing processes, although this does not rule out direct transmitter actions that could occur at synaptic specializations in areas of the IPL where there is apposition of peptide and peptide receptor processes.

Acknowledgment

Support for this work was provided by NEI EY 04067 and a Veterans Administration Senior Career Scientist Award.

See also: Information Processing: Amacrine Cells; Morphology of Interneurons: Amacrine Cells; Neuropeptides: Function.

Further Reading

Brecha, N. C. (1983). Retinal neurotransmitters: Histochemical and biochemical studies. In: Emson, P. C. (ed.) *Chemical Neuroanatomy*, pp. 85–129. New York: Raven.

Brecha, N. C. (2003). Peptide and peptide receptor expression and function in the vertebrate retina. In: Chalupa, L. and Werner, J. (eds.) *Visual System*, pp. 334–354. Boston, MA: MIT Press.

Brecha, N., Johnson, D., Bolz, J., et al. (1987). Substance P-immunoreactive retinal ganglion cells and their central axon terminals in the rabbit. *Nature* 32: 155–158.

Casini, G., Catalani, E., Dal Monte, M., and Bagnoli, P. (2005). Functional aspects of the somatostatinergic system in the retina and the potential therapeutic role of somatostatin in retinal disease. *Histology and Histopathology* 20: 615–632.

Casini, G., Rickman, D. W., Sternini, C., and Brecha, N. C. (1997). Neurokinin 1 receptor expression in the rat retina. *Journal of Comparative Neurology* 389: 496–507.

Cervia, D., Casini, G., and Bagnoli, P. (2008). Physiology and pathology of somatostatin in the mammalian retina: A current view. *Molecular and Cellular Endocrinology* 286: 112–122.

Marshak, D. W. (1989). Peptidergic neurons of the macaque monkey retina. *Neuroscience Research.Supplement* 10: S117–S130.

Thermos, K. (2003). Functional mapping of somatostatin receptors in the retina: A review. *Vision Research* 43: 1805–1815.

Zalutsky, R. A. and Miller, R. F. (1990). The physiology of somatostatin in the rabbit retina. *Journal of Neuroscience* 10: 383–393.

Neurotransmitters and Receptors: Dopamine

P M Iuvone, Emory University School of Medicine, Atlanta, GA, USA

Glossary

Amacrine cells – Neurons with cell bodies located in the proximal part of the inner nuclear layer, and neuronal processes ramifying in the inner plexiform layer.
Circadian rhythms – Changes in biological processes that occur on a daily basis, are driven by autonomous circadian clocks, and provide selective advantage to organisms by allowing them to anticipate temporal changes in their environment.
Interplexiform cells – Neurons with cell bodies in the amacrine cell layer; they are distinguished from amacrine cells by having neuronal processes that project in both the inner and the outer plexiform layers.
Neuromodulators – Chemical transmitters that mediate slow, long-lasting modulatory effects on neurons and neuronal circuits through synaptic or extrasynaptic receptors; they usually have no effect on neuronal membrane potential alone, but modulate the response to other neurotransmitters.
Photopic vision – The vision in bright light that is mediated by cone photoreceptors and cone bipolar cell pathways.

Localization of Dopamine Neurons in the Retina

Dopamine is a member of the catecholamine family of neurotransmitters, which also includes norepinephrine (also known as noradrenaline) and epinephrine (also known as adrenaline). It is the primary catecholamine in the retina; only trace amounts of epinephrine and norepinephrine are found in this tissue. It was first detected in the retina in the 1960s and has been the subject of intensive study ever since.

Dopamine is released from a unique population of neurons with cell bodies in the innermost region of the inner nuclear layer (INL). These neurons have been visualized by formaldehyde-induced histofluorescence and by immunohistochemistry, with antibodies against tyrosine hydroxylase (see **Figure 1**), the rate-limiting enzyme in dopamine biosynthesis. The dopamine neurons have long axons that ramify in sublamina 1 of the inner plexiform layer (IPL), at the border of the INL. The axons contain varicosities (presumptive sites of dopamine release) along their entire length. Although the number of dopamine neurons is small (approximately 500 in mouse retina), the extensive length and branching of the axons result in considerable overlap of processes throughout the retina. Some of the axons form rings around the perikarya of AII amacrine cells, which transmit rod pathway signals in the inner retina. Some processes, likely dendritic, descend further into the IPL. In many species, the processes of the dopamine neurons project toward the outer plexiform layer (OPL; see arrow in **Figure 1(a)**), designating them as interplexiform cells.

Regulation of Dopamine Neuronal Activity

Retinal dopamine neurons spontaneously fire action potentials, stimulating the release of dopamine throughout the cell. Light increases the firing of action potentials and stimulates dopamine synthesis, release, and metabolism. Both transient and sustained light-evoked firing patterns have been observed.

Although the processes of dopamine neurons ramify in the outer portion of the IPL, where OFF bipolar cells make synapses, most evidence suggests that the light responses of dopamine neurons are driven by the ON pathway. Light-evoked dopamine release from monkey and frog retinas is inhibited by L-(+)-2-amino-4-phosphonobutyric acid (L-AP4), which pharmacologically blocks synapses between photoreceptors and ON bipolar cells. Light-evoked firing of most, but not all, dopamine cells in mouse retina is also blocked by L-AP4. In addition, light-evoked dopamine metabolism, commonly observed in the vertebrate retina, is absent in the no b-wave (*nob*) mouse; this mouse has no functional ON pathway due to a mutation in the nyctalopin (*nyx*) gene, but has an intact OFF pathway. Retinal dopamine neurons are excited by glutamate, a bipolar cell transmitter, and inhibited by the amacrine cell transmitters gamma aminobutyric acid (GABA) and glycine. Once released, dopamine diffuses to act on extrasynaptic receptors found on multiple cells types throughout the retina.

Dopamine Neuronal Activity Is Coupled to Dopamine Synthesis and Metabolism

The light-evoked increase in dopamine neuronal activity is not associated with a depletion of the neuromodulator,

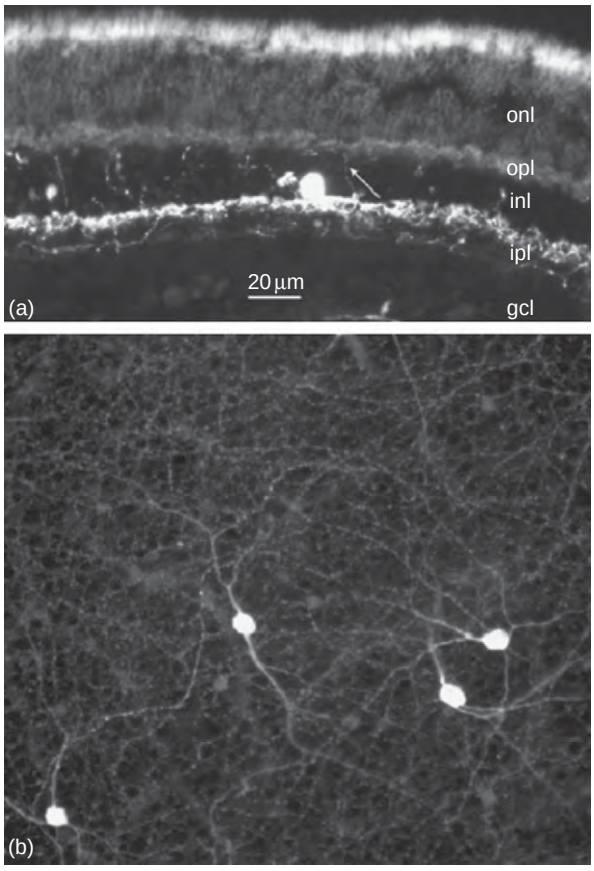

Figure 1 Dopamine amacrine/interplexiform cells of the rat retina. (a) A vertical section through the retina showing a dopamine cell body and processes labeled with an antibody to tyrosine hydroxylase. Note the extensive labeling of processes in sublamina 1 of the ipl and processes ascending to the opl (arrow). onl, outer nuclear layer; opl, outer plexiform layer; inl, inner nuclear layer; ipl, inner plexiform layer; gcl, ganglion cell layer. (b) Whole mount preparation of rat retina showing tyrosine hydroxylase immunoreactive cell bodies and processes from a horizontal view. Note the long, branching processes of the dopamine neurons and the extensive coverage of the ipl with these processes. Reproduced from Figure 1 in Witkovsky, P. (2004). Dopamine and retinal function. *Documenta Ophthalmologica* 108, 17–40. © Kluwer Academic Publishers. With kind permission of Springer Science and Business Media.

and is sometimes correlated with an increase in the steady-state levels of dopamine and it's primary metabolite 3,4-dihydroxyphenylacetic acid (DOPAC). Several mechanisms appear to account for these observations. The dopamine neurons contain plasma membrane dopamine transporters, which recapture a fraction of the dopamine released into the extracellular space. Following reuptake, the dopamine can be repackaged into vesicles for subsequent release or metabolized by monoamine oxidase to form DOPAC. A light-evoked increase of DOPAC levels is a common feature among many vertebrate retinas. More important in maintaining a readily releasable pool of dopamine is a light-evoked increase of dopamine biosynthesis. This occurs through phosphorylation and activation of tyrosine hydroxylase, the rate-limiting enzyme in dopamine synthesis. While tyrosine hydroxylase can be phosphorylated by several protein kinases, the cyclic adenosine monophosphate (cAMP)-dependent kinase (protein kinase A (PKA)) appears to play a prominant role in the light-evoked regulation of tyrosine hydroxylase. The phosphorylation of the enzyme by PKA results in a conformational change that decreases the Km for tetrahydrobiopterin (BH4), the co-factor of tyrosine hydroxylase. This increases the activity of the enzyme at the subsaturating concentrations of BH4 found in retinal dopamine cells.

Circadian Control of Dopamine Release and Metabolism

In addition to being regulated by light, retinal dopamine release and metabolism, in many species, are controlled by circadian clocks that generate daily rhythms that persist in constant ($24\,h\ d^{-1}$) darkness. In these instances, dopamine release and DOPAC levels increase during the subjective day and decrease during the subjective night. In mouse retina, dopamine neurons express circadian clock genes and, therefore, may possess an autonomous circadian clock. However, evidence obtained in several species, including mouse, suggests that the circadian rhythms of dopamine release and metabolism are dependent on another neuromodulator, melatonin, which is synthesized in photoreceptor cells and released in a circadian fashion during the subjective night. Retinal dopamine neurons express melatonin receptors, the activation of which inhibits dopamine release. In turn, dopamine released in the daytime suppresses melatonin formation. Since dopamine receptors are widely distributed in the retina, dopamine plays important roles in the circadian organization of the retina.

Dopamine Receptors

Dopamine receptors are guanine nucleotide-binding protein (G-protein)-coupled receptors. There are five subtypes, organized into two families based on structural and pharmacological similarities: the D1-like and D2-like families (**Table 1**). The individual subtypes are named based on the chronological order in which they were cloned. The D1 family includes the D1 and D5 receptors, while the D2 family consists of D2, D3, and D4 receptors. The D1 and D5 (also known as D1B) receptors are derived from genes without introns; thus, there are no splice variants of the D1-like receptors. They show very similar pharmacologies with respect to selective agonists and antagonists; however, dopamine has a much higher affinity for the D5 receptor than for the D1 subtype. The D2, D3, and

Table 1 Dopamine receptors in the retina

Receptor name	*G protein*	*cAMP response*	*Cellular expression*
D1-like family			
D1	G_s	Δ↑	Horizontal cells, cone bipolar cells, and amacrine cells
D5	G_s	Δ↑	Retinal pigment epithelial cells
D2-like family			
D2	G_i	Δ↓	Dopamine neurons and amacrine cells
D4	G_i	Δ↓	Photoreceptor cells

D4 receptor genes contain introns, and splice variants of the D2 receptor have been characterized. They show similar pharmacologies; however, some selective agonists and antagonists have been identified. A common feature of all dopamine receptors is that they couple to G proteins that regulate cAMP. The D1 family receptors stimulate cAMP formation, while the D2 family members inhibit it. Dopamine receptors have also been reported to affect phospholipase C, Ca^{2+} currents, K^+ currents, and the protein kinases AKT, glycogen synthase kinase-3β (GSK3β), and extracellular signal-regulated kinases (ERK1/2).

Nearly all retinal cell types appear to express dopamine receptors, consistent with dopamine's role as a paracrine neuromodulator that acts on extrasynaptic receptors. Of the D1 family members, dopamine D1 receptor immunoreactivity is found on processes in both the OPL and IPL. The receptors are expressed by horizontal cells, subtypes of cone bipolar cells, and some amacrine cells. There is evidence for the expression of functional D1-like receptors in ganglion cells of goldfish. D5 receptors are expressed by mammalian retinal pigment epithelial (RPE) cells. Of the D2 family members, dopamine D2 receptors are highly expressed by retinal dopamine neurons, and function as autoreceptors that inhibit dopamine release. D2 receptors are also expressed by other unidentified amacrine cells and possibly by some bipolar and ganglion cells. D2 receptors have also been shown to be expressed and functional in guinea pig Müller cells. Dopamine D4 receptors are highly expressed by photoreceptor cells in mammals. The photoreceptors of nonmammalian vertebrates also have D2-like receptors; in addition, these are likely to be D4 receptors based on pharmacological criteria, but no molecular proof of this has been provided yet. D4 messenger ribonucleic acid (mRNA) expression has also been observed in the IPL and ganglion cell layer; however, due to the lack of specific antibodies, the types of cells in these layers have not been identified. Interestingly, neither mRNA nor protein for the dopamine D3 receptor has been found in retina.

Functions of Dopamine in the Retina

The widespread distribution of dopamine receptors coupled with the ability of dopamine to diffuse throughout the retina suggests that this neuromodulator has many functions in regulating retinal physiology, particularly in serving as a chemical signal promoting light adaptive functions. This section describes the effects of dopamine on different cell types within the retina, beginning with the distal retina, and gives examples on how dopamine impacts retinal network adaptation, circadian rhythmicity, and ocular growth.

Retinal Pigment Epithelium

Dopamine D5 receptors stimulate cAMP formation, which inhibits rod outer segment phagocytosis by RPE cells. Cultured bovine RPE cells express D5 receptors and dopamine inhibits phagocytosis by these cells. Thus, dopamine may function as a component of the regulatory mechanism that controls rod outer segment turnover.

Photoreceptor Cells

Dopamine D2/D4 receptors on photoreceptor cells have numerous effects due to their ability to inhibit cAMP formation and decrease intracellular Ca^{2+} concentrations. Dopamine receptor activation inhibits the synthesis of melatonin in photoreceptor cells by inhibiting cAMP formation. It regulates the amplitude of diurnal rhythms of phosphorylation of phosducin by cAMP- and Ca^{2+}-dependent protein kinases. Dopamine has been reported to increase the rate of dephosphorylation of rhodopsin, and probably affects the phosphorylation state of many photoreceptor proteins. Dopamine has been reported to inhibit the hyperpolarization-activated current (I_H) in rods, as well as the activity of Na^+/K^+-adenosine triphosphate (ATP)ase, which balances the dark current. It decreases the intracellular Ca^{2+} concentration of photoreceptor cells and also affects rod–cone coupling, but the effects may vary by species. These effects on currents, Ca^{2+}, and coupling may contribute to a reduction of rod synaptic transfer to bipolar and horizontal cells during the daytime.

Horizontal Cells

Horizontal cells mediate lateral inhibition and synaptic feedback to photoreceptor cells. Different horizontal cell subtypes couple together through gap junctions to form networks. In retinas of both mammalian and nonmammalian vertebrates, the activation of D1-like receptors uncouples the horizontal cells, narrowing their receptive fields. The activation of dopamine D1 receptors in dark-adapted retinas depolarizes horizontal cells and reduces

responses to flickering lights. The depolarization is due to the cAMP-dependent enhancement of glutamate-gated currents through α-amino-3-hydroxyl-5-methyl-4-isoxazole-propionate (AMPA)/kainate glutamate receptors in the horizontal cell membrane; other voltage-gated channels may also be involved.

Bipolar Cells

Although dopamine receptor immunoreactivity has been observed in subtypes of mammalian cone bipolar cells, its function is yet to be investigated. In salamander retina, glutamate responses in OFF cone bipolar cells are enhanced by dopamine, similar to the enhancement observed in horizontal cells. In addition, dopamine has been shown to modulate gamma-aminobutyric acid (GABA)-mediated inhibition of Ca^{2+} influx and neurotransmitter release from bipolar cell terminals. GABAergic amacrine cells synapse onto bipolar cell terminals to provide feedback inhibition of glutamate release via GABA-C receptors. Dopamine, acting on D1 receptors, reverses this inhibition and increases glutamate release.

Amacrine Cells

AII amacrine cells are critical mediators of the rod pathway. They receive excitatory input from rod depolarizing bipolar cells and, thus, depolarize in response to light. They transmit hyperpolarizing light signals to OFF cone bipolar cells through inhibitory glycinergic synapses and depolarizing light signals to ON cone bipolar cells through gap junctions. In addition, AII amacrine cells form homotypic gap junctions with neighboring AII amacrines. The axons of the dopamine neurons surround the perikarya of AII amacrine cells. Dopamine and D1 receptor agonists promote the uncoupling of gap junctions in AII amacrine cells by cAMP-dependent phosphorylation of connexin proteins. The gap junctions between amacrine cells are more sensitive to the uncoupling action of dopamine than those between AII amacrine cells and ON cone bipolar cells. In addition to secreting dopamine, the dopamine amacrine/interplexiform cells also synthesize and release the inhibitory neurotransmitter GABA. The dopamine amacrine/interplexiform cells synapse onto the AII amacrines, where their processes form rings around the perikarya of the AII cells. The active zones of the synapses have GABA-A receptors. Thus, activation of the dopamine amacrine/interplexiform cells is likely to decrease the light response of AII amacrine cells through GABA. Interestingly, D1 dopamine receptors have not been observed in these active zones, suggesting that dopamine diffuses to distal receptors to promote AII–AII cell uncoupling.

Dopamine stimulates acetylcholine release in the retina through D1-like receptors; most acetylcholine in mammalian retina is released from starburst amacrine cells, which function in the circuitry regulating directional selectivity to moving stimuli.

Most of the synapses made by dopamine amacrine/interplexiform cells are onto other amacrine cells. Thus, it is likely that dopamine affects many other functions within the inner retinal circuitry, but the details and functional consequences for visual processing are less clear.

Ganglion Cells

The effects of dopamine on ganglion cells are complex and it is difficult to discern which responses result from direct actions on ganglion cells and which responses reflect effects on retinal circuitry. In the mammalian retina, dopamine appears to decrease the sensitivity to light and strengthen the center surround of ganglion cells. These effects are mediated by dopamine D1-like receptors, and D1 receptor antagonists have opposite effects. A D1 receptor blocker also reduces the response of ON–OFF directionally sensitive ganglion cells to the leading edge of a moving light stimulus. In addition, dopamine strengthens cone pathway input to ganglion cells and reduces rod pathway input.

A small subpopulation of ganglion cells is referred to as intrinsically photosensitive retinal ganglion cells (ipRGCs). These ganglion cells project to the suprachiasmatic nucleus (SCN) of the hypothalamus, the site of the master circadian clock in mammals; to the olivary pretectal nucleus, a relay nucleus in the pupillary light reflex circuit; and to other nuclei involved in nonimage forming vision. These ipRGCs mediate photic entrainment of the circadian clock and are essential for the normal pupillary light reflex. They contain a photopigment, melanopsin, and are directly responsive to light, showing a depolarizing response to illumination. The ipRGCs also receive input from rods and cones through retinal circuitry. In mammals, dopamine amacrine/interplexiform cells are a component of this circuitry and synapse directly onto the ipRGCs. In addition, dopamine drives a circadian rhythm of melanopsin expression in the ipRGCs, at least in rats.

Müller Glial Cells

Müller cells are giant glia that span the width of the neural retina from the outer limiting membrane to the inner limiting membrane. They play important roles in retinal physiology by regulating the extracellular ionic milieu, especially the K^+ concentration. Müller cells are also an important source of trophic factors within the retina. Mammalian Müller cells express dopamine D2 receptor immunoreactivity. The application of dopamine or a D2 receptor agonist decreases K^+ conductance through an inwardly rectifying K^+ channel. These findings indicate that dopamine may influence the extracellular K^+ clearance, thereby affecting neuronal excitability and visual processing in the retinal circuitry.

Role of Dopamine in Photopic Visual Processing

Overall, the effects of dopamine on individual retinal cell types are consistent with an important role for this neuromodulator in visual processing in light-adapted retinas. Dopamine facilitates cone input to the inner retina and diminishes rod input. Extensive rod–cone coupling at night may shunt cone currents to rods, accounting for the apparent lack of cone input at night in the absence of dopamine. The uncoupling of the rod–cone network in the daytime in response to dopamine isolates the cones, strengthening their input signals to the inner retina. The effect of dopamine on horizontal cell coupling narrows receptive fields and makes the center surround organization more compact, enhancing spatial contrast sensitivity. The enhancement of glutamate-gated currents on OFF cone bipolar cells would also be expected to strengthen cone input. In addition, the uncoupling of the AII amacrine cell network by dopamine, together with the inhibitory effect of co-released GABA on AII amacrine cell light responses, should further suppress information flow through the rod pathway. Collectively, activation of the dopamine amacrine/interplexiform cell appears to fine-tune the retinal circuitry for high-resolution, high-contrast, low-sensitivity visual processing under photopic conditions.

Dopamine and Circadian Organization of the Retina

Many cells types in the vertebrate retina express circadian clock genes, including the dopamine amacrine/interplexiform cells. Dopamine can entrain or phase-shift the circadian clock in amphibian photoreceptor cells that regulates melatonin biosynthesis. Dopamine affects the circadian expression of a clock gene reporter (period 2:: luciferase) in the inner retina of mice. In addition, circadian-clock-driven dopamine release drives circadian rhythms of rod–cone coupling in mice and fish, and photoreceptor protein phosphorylation in mouse photoreceptors. With the widespread distribution of dopamine receptors in retina, the ability of dopamine to diffuse throughout the retina, the expression of clock genes in the dopamine amacrine/interplexiform cells, and the large increase in dopaminergic activity at dawn, dopamine may play important, conserved roles in the circadian organization of the retina by entraining and coordinating multiple circadian oscillators.

Dopamine, Retinal Development, Ocular growth, and Myopia

In chick embryo retinal cell cultures, dopamine has been reported to inhibit growth cone motility. In addition, the signaling mechanisms utilized by dopamine receptors appear to change with the developmental stage. Dopamine may play a role in stabilizing synapses during retinal development. However, many of these studies were done with *in vitro* systems, and may not necessarily reflect the development of the retina *in vivo*.

Dopamine may also be involved in ocular development and establishing emmetropia (perfect, focused vision). At birth, most animals are hyperopic, with images focused posterior to the photoreceptors. During the postnatal period, the eye elongates, increasing its own focal length. Under normal conditions, the eye will elongate only to the point that the image is focused on the photoreceptor cells, yielding the condition referred to as emmetropia. However, if the eye grows excessively long, the image will focus in front of the retina, causing myopia (nearsightedness). The growth of the eye in the axial dimension is regulated by the retina through visually guided feedback mechanisms that coordinate the growth of the eye with its optics. If the retinal image is degraded, as in the case of congentital infant cataract, the eye grows excessively long, resulting in myopia. This process is referred to as form-deprivation myopia and has been studied extensively in chicken hatchlings. When a diffuser goggle is placed over the eye of a newly hatched chick, the eye will grow excessively long, resulting in a large myopic refractive error within 1–2 weeks. Interestingly, allowing short periods of vision each day without the diffusers prevents the development of myopia.

Although some controversy exists, dopamine appears to contribute to the retinal circuitry involved in the feedback mechanism controlling emmetropization. Retinal dopamine levels and metabolism are reduced in eyes of chicks exposed to form deprivation. The administration of apomorphine, a dopamine receptor agonist, prevents the development of form-deprivation myopia. Moreover, dopamine receptor antagonists block the ability of short periods of unobstructed vision to prevent the development of myopia.

Summary

Dopamine release is driven by light and regulated by circadian clocks. The neuromodulator regulates multiple functions within the retina primarily by extrasynaptic mechanisms. Dopamine receptors are widely distributed in the retina, and dopamine has the capacity to diffuse from sites of release to distant receptors. A primary function of dopamine is to regulate network adaptation within the retina to optimize vision during the daytime.

Acknowledgements

The research in the author's laboratory is supported by NIH grants EY004864 and EY006360.

See also: Chick Metabolism in the Chick Retina; Circadian Photoreception; Circadian Regulation of Ion

Channels in Photoreceptors; Information Processing: Amacrine Cells; Morphology of Interneurons: Amacrine Cells; Morphology of Interneurons: Interplexiform Cells; Neurotransmitters and Receptors: Melatonin Receptors; The Circadian Clock in the Retina Regulates Rod and Cone Pathways.

Further Reading

Djamgoz, M. B. A., Hankins, M. W., Hirano, J., and Archer, S. N. (1997). Neurobiology of retinal dopamine in relation to degenerative states of the tissue. *Vision Research* 37: 3509–3529.

Green, C. B. and Besharse, J. C. (2004). Retinal circadian clocks and control of retinal physiology. *Journal of Biological Rhythms* 19: 91–102.

Nguyen-Legros, J., Versaux-Botteri, C., and Vernier, P. (1999). Dopamine receptor localization in the mammalian retina. *Molecular Neurobiology* 19: 181–204.

Ruan, G. X., Allen, G. C., Yamazaki, S., and McMahon, D. G. (2008). An autonomous circadian clock in the inner mouse retina regulated by dopamine and GABA. *PLoS Biology* 6: e249.

Tosini, G., Pozdeyev, N., Sakamoto, K., and Iuvone, P. M. (2008). The circadian clock in the mammalian retina. *BioEssays* 30: 624–633.

Witkovsky, P. (2004). Dopamine and retinal function. *Documenta Ophthalmologica* 108: 17–40.

Zhang, D. Q., Zhou, T. R., and McMahon, D. Q. (2007). Functional heterogeneity of retinal dopaminergic neurons underlying their multiple roles in vision. *Journal of Neuroscience* 27: 692–699.

Neurotransmitters and Receptors: Melatonin Receptors

A F Wiechmann, University of Oklahoma College of Medicine, Oklahoma City, OK, USA

Glossary

Circadian rhythm – The term from the Latin *circa* which means around and *diem* which denotes day that is an approximate daily (24-h) periodicity in physiological processes of many organisms.
Diurnal – Activities that are repeated every 24 h, but are not necessarily under the control of a biological clock.
Orthologs – Homologous sequences which are similar to each other because they originated from a common ancestor.
Paracrine – The term from the Latin *para*, which means near, is a form of cell signaling in which the target cell is located within the same tissues as the cell that releases the chemical signal.
Pinealocytes – The main cells of the pineal gland that produce and secrete melatonin into the circulation.
Xenopus – The term from the Latin *strange foot*, which is a genus of frog native to Africa, and commonly used in research as a model organism.

Introduction

Melatonin (*N*-acetyl-5-methoxytryptamine) is an indolamine hormone synthesized by pinealocytes and retinal photoreceptors. The rate of melatonin synthesis, in most species studied, is highest at nighttime, and is considered to be a chemical signal of darkness that entrains circadian rhythms. This hormone synthesized in the pineal gland is secreted immediately into the circulation and acts as an endocrine hormone on distant target sites throughout the body. Melatonin produced in the retina, however, is thought to have a local, or paracrine role. It is thought that melatonin is synthesized and released by the photoreceptors at night, and diffuses throughout the retina to bind to melatonin receptors located on a variety of retinal cells. Since melatonin is a very lipophilic molecule, it diffuses freely through plasma membranes.

The three major subtypes of melatonin receptors are members of the superfamily of guanine nucleotide binding (G-protein)-coupled receptors. Most studies have shown that melatonin receptor activation is coupled to an inhibition of adenylate cyclase activity, although many reports demonstrate that other signaling mechanisms are conveyed by the melatonin signal. Melatonin receptors have been identified in many different retinal cells, including amacrine cells, horizontal cells, ganglion cells, photoreceptors, and the adjacent retinal pigment epithelium (RPE).

Sites of Retinal Melatonin Synthesis

Melatonin Synthesis by Photoreceptors

The photoreceptors appear to be the sites of melatonin synthesis in the retina. They express all of the enzymes involved in melatonin synthesis. Melatonin is synthesized from tryptophan in a series of four enzymatic steps: (1) tryptophan is converted into 5-hydroxytryptophan by tryptophan hydroxylase (TPH); (2) the 5-hydroxytryptophan is then converted into 5-hydroxytryptamine (serotonin) by aromatic amino acid decarboxylase; (3) serotonin is then converted into *N*-acetylserotonin by arylalkylamine N-acetyltransferase (AANAT); and (4) *N*-acetylserotonin is converted into melatonin (*N*-acetyl-5-methoxytryptamine) by hydroxyindole-O-methyltransferase (HIOMT). The enzyme activity and messenger RNA (mRNA) encoding TPH and AANAT exhibit circadian rhythms of expression, with highest levels occurring at night.

There is strong evidence that identifies the photoreceptors as the sites of retinal melatonin synthesis. Melatonin immunoreactivity is localized in the outer nuclear layer (ONL) of the retina which contains the cell soma of the photoreceptors. HIOMT and AANAT protein and mRNA are localized to photoreceptor cytoplasm, and a cyclic rhythm of AANAT activity persists following chemical lesion of the inner retina. The mRNA encoding TPH is localized to photoreceptors, and the photoreceptor layer of the amphibian retina continues to produce melatonin rhythmically in darkness after isolation from the inner retina.

In addition to the photoreceptors, some neurons of the inner retina may have the capacity to produce a small amount of melatonin. Melatonin immunoreactivity is observed in the inner retina, and a low level of AANAT mRNA has been detected in the inner nuclear layer (INL) and ganglion cell layer (GCL). The INL contains the cell soma of amacrine, horizontal, bipolar, and Müller cells. Since some cells in these layers also have melatonin receptors, the synthesis of melatonin by inner retinal neurons may be involved in the circadian activity of cells of the inner retina.

Phylogenetic Relationships between Photoreceptors and Pinealocytes

The ability of photoreceptors and pinealocytes to synthesize melatonin appears to be the consequence of an ancestral relationship between the retina and the pineal gland. Some primitive animals possessed three eyes which may have produced melatonin and were also capable of phototransduction. Pinealocytes of some lower vertebrates are morphologically very similar to retinal photoreceptors, and they synthesize melatonin as well as many proteins that are characteristic of retinal photoreceptors. Furthermore, the photoreceptors of the nonmammalian pineal gland are directly photosensitive, and during the embryologic development of the mammalian pineal gland, the pinealocytes undergo a transient photoreceptor-like differentiation.

It is suggested that the middle, or third eye, eventually evolved into an endocrine organ specialized for the secretion of melatonin into the circulation, in which the melatonin-producing pineal photoreceptors eventually lost their phototransduction capabilities, and the melatonin-producing cells of the lateral eyes evolved into photoreceptors specialized for phototransduction, but maintained their ability to synthesize melatonin. Genes expressing melatonin receptors in peripheral tissues may have also become expressed in ocular tissues, which enabled local paracrine signaling by melatonin in the retina.

Classification of Melatonin Receptors

Melatonin receptor expression has been identified in the retinas of several species. The major types of melatonin receptors that have been cloned are members of the superfamily of G-protein-coupled receptors. Melatonin receptors have been classified as Mel_{1a}, Mel_{1b}, and Mel_{1c} subtypes. These three subtypes are expressed in tissues, including the retinas, of lower vertebrates such as amphibians, fish, and birds. Mammalian melatonin receptors are classified according to their homology to the nonmammalian receptors, and according to their pharmacological properties. In mammals, the Mel_{1a} and Mel_{1b} receptor subtypes are designated as the MT1 and MT2 receptor subtypes, respectively. The mammalian ortholog of the Mel_{1c} subtype has been designated as GPR50, and does not bind melatonin. The G-alpha proteins coupled to melatonin receptors are inhibitory (G_i) to the activation of adenylate cyclase and cyclic adenosine monophosphate (cAMP) production in most tissues studied. However, receptor coupling to other G-alpha proteins ($G_{i\alpha 2}$, $G_{i\alpha 2}$, $G_{i\alpha q}$, $G_{i\alpha s}$, $G_{i\alpha z}$, and $G_{i\alpha 16}$), and hence other signaling pathways, have been reported. Nuclear melatonin receptors, which are members of the RAR-related RZR/ROR orphan nuclear receptor superfamily, have been reported to exist in some tissues, and a melatonin-binding site on the enzyme quinine reductase 2 has been identified and is referred to as the mammalian MT3 melatonin receptor.

Most G-protein-coupled receptors interact with each other to form homodimers or heterodimers. The mammalian MT1 and MT2 melatonin receptors can exist as homodimers and as heterodimers. Dimerization of G-protein-coupled receptors has important functional consequences in regard to receptor affinity, trafficking, and signaling. The relative expression levels of melatonin receptor subtypes in the retina may have a significant impact on the function of melatonin in the target cells.

Sites of Melatonin Receptors in the Retina

Melatonin receptors have been identified not only in several retinal neurons of the inner retina, but also in photoreceptors cells and RPE cells. The identification of melatonin receptors in photoreceptor cells was unanticipated, given that the photoreceptors are the site of retinal melatonin synthesis. The presence of melatonin receptors in photoreceptor cells suggests the possibility of what can be characterized as an intracrine (autocrine) signaling mechanism in response to melatonin, in which a cell synthesizes and releases a signaling molecule, and also has receptors to which the molecule binds and triggers an intracellular response. Another potential role of melatonin receptors in photoreceptor cells is that they may be involved in a negative-feedback mechanism which would enable melatonin to regulate the expression of the receptors to which it binds.

Melatonin Receptors in Photoreceptor Cells

Mel_{1a}, Mel_{1b}, and Mel_{1c} melatonin receptor subtype protein and mRNA have been identified in the photoreceptors of nonmammalian vertebrates, and MT1 receptors in photoreceptors of the mammalian retina. The receptor immunoreactivity has been identified primarily in the photoreceptor membranes of the inner segments, although some cytoplasmic immunoreactivity has been reported for some subtypes, and may represent newly synthesized receptors that have not yet been transported to the plasma membrane, or receptors that have been internalized after activation.

Mel_{1b} and Mel_{1c} melatonin receptor RNA and/or protein are expressed in *Xenopus* photoreceptors, and the MT1 (Mel_{1a}) receptor is localized to photoreceptors of the human retina. In the chicken retina, Mel_{1a} immunoreactivity and melatonin receptor mRNA expression (Mel_{1a}, Mel_{1b}, and Mel_{1c}) are localized to the photoreceptor layer. In the *Xenopus* retina, Mel_{1c} immunoreactivity is observed in the plasma membrane of photoreceptor

inner segments, whereas Mel_{1b} receptor immunoreactivity appears in a punctate pattern in the proximal portion of photoreceptor inner segments. The differential pattern of Mel_{1b} and Mel_{1c} may reflect differential regulation of expression or trafficking of melatonin receptors in photoreceptor cells.

Melatonin Receptors in RPE

The RPE is a monolayer of cuboidal cells located between the vascular choroid layer and the neural retina. It is very closely associated with the retinal photoreceptor cells. This close association reflects the vital function of the RPE to provide physical and metabolic support to the photoreceptors. Circadian signals may play a role in influencing the coordinated interactions between the RPE and its adjacent tissues. The RPE, photoreceptors, retinal neurons, and choroidal cells interact in a coordinated manner for optimal function. Melatonin may play a role in the timing of the circadian phagocytosis of shed photoreceptor outer segments. The distal tips of rod photoreceptor outer segments are shed on a circadian rhythm as part of a renewal process, with peak shedding occurring early in the light period. The shed outer segment tips are phagocytized by the RPE, and melatonin is thought to be involved in this process. Melatonin secreted from photoreceptors at night may activate melatonin receptors on the RPE to regulate some circadian activities of the RPE that are important for optimal photoreceptor activity.

Melatonin inhibits forskolin-stimulated cAMP synthesis in RPE cell cultures, and melatonin affects the RPE membrane potentials and resistances at the apical or basal membrane. The mRNA encoding all three melatonin receptor subtypes is expressed in *Xenopus laevis* RPE but the Mel_{1b} receptor protein is localized only to the apical surface of the *Xenopus* RPE, and is not present on the basal surface. The Mel_{1c} receptor protein has also been localized to the *Xenopus* RPE. The presence of melatonin receptors on the apical microvilli, which directly contact the photoreceptors, but not on the basal membrane of the RPE, suggests that the photoreceptors are more likely to be the source of melatonin that activate melatonin receptors on the RPE rather than melatonin that is produced by the pineal gland and secreted into the general circulation.

Melatonin Receptors in Inner Retinal Neurons

Using autoradiography with ^{125}I-melatonin, it has been demonstrated that melatonin binding occurs in the inner plexiform layer (IPL) of many species. The IPL contains the synaptic terminals between bipolar cells, amacrine cells, horizontal cells, and ganglion cells. Since melatonin inhibits dopamine release from the retina, and high-affinity melatonin binding occurs in the IPL of the retina, the dopaminergic amacrine cell, which forms synaptic contacts in the IPL, has long been considered to be a candidate for the site of action of melatonin in the inner retina. Another candidate cell for melatonin receptor expression is the GABAergic amacrine cell (GABA, gamma aminobutyric acid) of the INL since $GABA_A$ receptor antagonists block melatonin-induced suppression of dopamine release. This suggests that the effect of melatonin on dopamine release may not be mediated only by direct action on dopaminergic cells, but that indirect action on GABAergic amacrine cells may also contribute to the inhibition of dopamine release via melatonin.

The autoradiographic localization of melatonin-binding sites in cells of the inner retina has been confirmed by both *in situ* hybridization and immunocytochemistry. In *Xenopus*, Mel_{1b} and Mel_{1c} RNA expression is localized to the INL, GCL, and photoreceptor inner segments. In the chicken retina, the mRNA encoding the $Mel1_a$, Mel_{1b}, and Mel_{1c} receptor subtypes is present in the INL, GCL, and photoreceptor inner segments. The INL contains the cell soma of bipolar, amacrine, horizontal, and Müller cells. In the human retina, Mel_{1b} receptor mRNA is much more highly expressed than is Mel_{1a} receptor RNA, suggesting that the Mel_{1b} receptor has a more significant role in human retinal physiology.

Using antibodies against specific melatonin receptor subtypes for immunocytochemistry, all three melatonin receptor subtypes (Mel_{1a}, Mel_{1b}, and Mel_{1c}) have been observed in the outer plexiform layer (OPL; the layer that contains the synaptic contacts between photoreceptors, bipolar cells, and horizontal cells) and the IPL. The MT1 (Mel_{1a}) receptor has been localized to horizontal cells in several mammalian species, including human. All three melatonin receptor subtypes appear to be present in horizontal cells of fish and *Xenopus* retina. The MT1 (Mel_{1a}) receptor has also been localized to AII amacrine and GABAergic amacrine cells of the mammalian retina.

Some Mel_{1a} and Mel_{1c} receptor immunoreactivity co-localizes with GABAergic and dopaminergic amacrine cells in the *Xenopus* retina. The presence of Mel_{1a} and Mel_{1c} receptors on dopaminergic and GABAergic amacrine cells is consistent with the observation that melatonin modulates the cyclic release of GABA and dopamine from retinal amacrine cells. In contrast, Mel_{1b} receptor immunoreactivity does not appear to co-localize with markers for dopaminergic and GABAergic neurons in the *Xenopus* retina, suggesting that melatonin does not act directly on GABAergic and dopaminergic amacrine cells through the Mel_{1b} receptor in this species.

In the *Xenopus* retina, the Mel_{1a}, Mel_{1b}, and Mel_{1c} receptor proteins are differentially distributed throughout the retina. In the OPL, for example, presumptive horizontal cell processes are immunoreactive for Mel_{1a} and Mel_{1b} receptor subtypes, but the immunoreactive labels appear to be in different cell processes. Cell somas in the INL are immunoreactive either for Mel_{1b} or Mel_{1a}, or for Mel_{1a} or Mel_{1c}, but not for both. All three melatonin receptor

subtypes appear to be expressed in different populations of ganglion cells in the *Xenopus* retina, and the MT1 subtype is present in ganglion cells of the human and macaque retina.

Melatonin receptor mRNA and protein are rhythmically expressed in *Xenopus* and chicks, with peak levels of Mel_{1c} expression occurring in the day. In chicks, the rhythms of Mel_{1a} and Mel_{1b} receptor protein generally appear to be the opposite to that of Mel_{1c}, with lowest levels occurring in the early morning and higher levels in the evening. The patterns of cyclic rhythms appear to be distinctive for each receptor subtype in the retina. Circadian rhythms in melatonin receptor expression may perhaps be superimposed on the rhythm in retinal melatonin levels to provide an additional level of regulation of the responsiveness of retinal target to melatonin.

Effects of Melatonin on Retinal Function

Modulation of Neurotransmitter Release

Melatonin released from photoreceptors at night diffuses into the extracellular milieu and binds to melatonin receptors on dopaminergic amacrine cells. The activation of the melatonin receptors results in a decrease of dopamine release at nighttime. Thus, retinal dopamine levels are higher during the day and lowest during the night due to the circadian release of melatonin. Resultant lower dopamine levels at night cause a reduction in D_2 dopamine receptor activity on photoreceptors, causing an increase in photoreceptor intracellular cAMP levels that in turn causes an increase in coupling of gap junctions between rod and cone photoreceptors so that rod input dominates the cone horizontal cells. The increased sensitivity of horizontal cells to light at nighttime is therefore mediated at least in part by activation of D_2-like receptors by dopamine released from amacrine cells. A reduction in endogenous retinal dopamine levels causes hyperpolarization of horizontal cells and enhanced dark adaptation.

D_1 dopamine receptors, which are positively coupled to cAMP synthesis, are located on horizontal cells. Melatonin may therefore postsynaptically regulate horizontal cell activity by inhibiting the stimulation of cAMP synthesis in response to D_1 receptor activation. It may bind to receptors on GABAergic amacrine cells, stimulating them to inhibit dopamine release from nearby dopaminergic amacrine cells. In addition, since horizontal cells express melatonin receptors, and melatonin increases horizontal cell sensitivity to light, melatonin may act directly on horizontal cells to increase gap-junctional coupling of horizontal cells. Increased horizontal cell coupling would cause an increase in receptive field size, which would potentially increase the sensitivity of the retina to light during the dark period, since more second-order neurons would respond to a light stimulus.

Melatonin may therefore modulate dopaminergic transmission by a combination of directly reducing dopamine release from amacrine cells, and indirectly by stimulating GABAergic amacrine cells to inhibit dopamine release from dopaminergic amacrine cells, both of which would increase horizontal cell coupling. The resulting increased visual sensitivity at nighttime could be due to increased rod–cone coupling through dopamine binding to D_2 receptors on photoreceptors, or to horizontal cell coupling stimulated by the binding of melatonin to melatonin receptors on horizontal cells. A summary diagram of the known locations of melatonin receptors and the possible interactions with the various target cells is presented in **Figure 1**.

Melatonin increases horizontal cell sensitivity to light in salamander retina, and also potentiates glutamate-induced currents from isolated cone-driven horizontal cells in carp retina by increasing the efficacy and affinity of the glutamate receptor. These observations suggest that melatonin acts directly on melatonin receptors of horizontal cells. Melatonin modulates cyclic guanosine monophosphate (cGMP)-dependent glutaminergic transmission from cones to cone-driven horizontal cells by activation of the Mel_{1a} receptor, causes a depolarization of the H1 horizontal cell membrane potential, and reduces its light responses. These observations suggest that melatonin enhances the circadian sensitivity of rod photoreceptor signaling.

Melatonin has been shown in fish retina to potentiate responses of rod ON bipolar cells to simulated light flashes. This action of melatonin is mediated by the Mel_{1b} receptor, and increases cGMP levels by inhibiting phosphodiesterase activity. Melatonin may bind directly to Mel_{1b} receptors on rod ON bipolar cells to improve the signal/noise ratio for rod signals by enhancing signal transfer from rod photoreceptors to rod bipolar cells. The presence of melatonin receptors by immunocytochemistry has not yet been definitively established in bipolar cells.

Melatonin treatment of isolated rat retinal ganglion cells potentiates glycine-induced currents by increasing the efficacy and channel conductance of a glycine receptor. The inhibitory modulation of glycinergic inputs to ganglion cells may thus be strengthened by stimulation of melatonin receptor activation. This suggests that melatonin may regulate circadian changes in receptive field organization and light sensitivity by binding to melatonin receptors on ganglion cells.

Modulation of Photoreceptor Function

Several reports support the concept of a direct action of melatonin on retinal photoreceptor function. Melatonin induces membrane conductance changes in isolated frog rod photoreceptors, binds with low affinity to structures in the OPL in frog retina, enhances the rate of photoreceptor

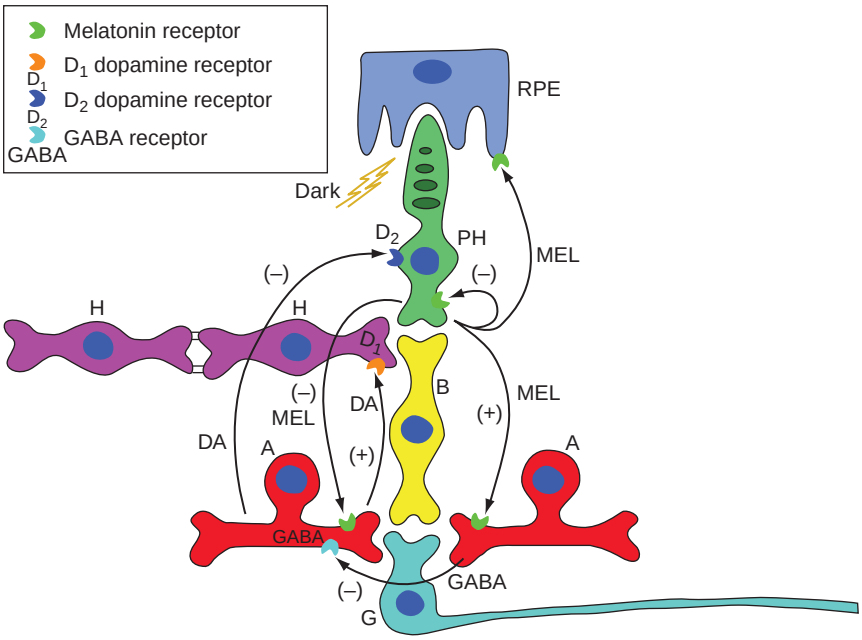

Figure 1 Summary diagram of locations of retinal melatonin receptors and potential interactions among target cells. Melatonin (MEL) is produced by photoreceptors (PH) at nighttime, and diffuses to target cells within the retina. Arrows represent the movement of melatonin to the target cells. The melatonin receptors are represented by a black crescent symbol. Dopamine and GABA receptors are represented by crescent symbols with D_1, D_2, or GABA as identifiers. Melatonin may bind to amacrine cells (A) that release GABA or dopamine (DA) as their neurotransmitter. Melatonin is thought to stimulate (+) GABA release and/or inhibit (–) dopamine release from these cells. GABA inhibits dopamine release from dopaminergic amacrine cells. A lower rate of dopamine release from amacrine cells at nighttime results in lower stimulation of D_1 receptors on horizontal cells (H), which leads to increased coupling of horizontal cells through gap junctions (=), which could cause an increase in receptive field size and increased retinal sensitivity to light. The decreased binding of dopamine at nighttime to D_2 receptors on photoreceptor cells results in an increase in melatonin synthesis, since dopamine inhibits melatonin synthesis in photoreceptors. Melatonin may potentially bind to horizontal cells to directly inhibit the cellular response to D_1 receptor binding. Melatonin may also bind to receptors located on the photoreceptor membrane, which could directly increase rod sensitivity to light, increase rod–cone coupling, and/or regulate synthesis of melatonin. Melatonin may bind to receptors on the apical membrane of retinal pigment epithelial (RPE) cells, to coordinate circadian interactions with photoreceptor outer segments. The possible expression of melatonin receptors on bipolar (B) cells, and the confirmed expression of melatonin receptors on ganglion cells (G) are not indicated by arrows.

outer segment disk shedding, and increases the degree of light-induced photoreceptor cell death. It causes a stimulation of the amplitude of the *a*-wave (rod photoreceptors) and the *b*-wave (inner retinal cells responding to the photoreceptor input) of electroretinogram (ERG) recordings of transgenic frogs that overexpress the Mel_{1c} receptor in rod photoreceptors. This suggests that melatonin acts directly on rod photoreceptors to increase retinal sensitivity to light as part of a dark-adaptation mechanism.

The role of melatonin in dark adaptation suggests a potential mechanism by which melatonin increases the degree of light-induced photoreceptor cell death. Since melatonin appears to increase the sensitivity of the retina to light as part of a dark-adaptation mechanism, an undesirable consequence of this may be an increased sensitivity to the deleterious effects of light. Although signals from the inner retina obviously play a significant role in the circadian activities of retinal photoreceptors, direct action of melatonin on receptors located on photoreceptors may contribute substantially to the functions of melatonin in circadian-regulated activities of the retina.

See also: Chick Metabolism in the Chick Retina; Circadian Photoreception; The Circadian Clock in the Retina Regulates Rod and Cone Pathways; Circadian Regulation of Ion Channels in Photoreceptors; Neurotransmitters and Receptors: Dopamine.

Further Reading

Besharse, J. C. and Dunis, D. A. (1983). Methoxyindoles and photoreceptor metabolism: Activation of rod shedding. *Science* 219: 1341–1342.

Boatright, J. H., Rubim, N. M., and Iuvone, P. M. (1994). Regulation of endogenous dopamine release in amphibian retina by melatonin: The role of GABA. *Visual Neuroscience* 11: 1013–1018.

Dubocovich, M. L. (1983). Melatonin is a potent modulator of dopamine release in the retina. *Nature* 306: 782–784.

Dubocovich, M. L., Cardinali, D. P., Guardiola-Lemaitre, B., et al. (1998). Melatonin receptors. In: Girdlestone, D. (ed.) *The IUPHAR Compendium of Receptor Characterisation and Classification*, vol. I, pp. 188–193. London: UCPHAR Media.

Fujieda, H., Scher, J., Hamadanizadeh, S. A., et al. (2000). Dopaminergic and GABAergic amacrine cells are direct targets of melatonin: Immunocytochemical study of mt_1 melatonin receptor in guinea pig retina. *Visual Neuroscience* 17: 63–70.

Huang, H., Lee, S. C., and Yang, X. L. (2005). Modulation by melatonin of glutamatergic synaptic transmission in the carp retina. *Journal of Physiology* 569: 857–871.

Iuvone, P. M., Tosini, G., Pozdeyev, N., et al. (2005). Circadian clocks, clock networks, arylalkylamine N-acetyltransferase, and melatonin in the retina. *Progress in Retinal and Eye Research* 24: 433–456.

Lundmark, P. O., Pandi-Perumal, S. R., Srinivasan, V., and Cardinali, D. P. (2006). Role of melatonin in the eye and ocular dysfunctions. *Visual Neuroscience* 23: 853–862.

Reppert, S. M., Godson, C., Mahle, C. D., et al. (1995). Molecular characterization of a second melatonin receptor expressed in human retina and brain: The Mel_{1b} melatonin receptor. *Proceedings of the National Academy of Sciences of the United States of America* 92: 8734–8738.

Scher, J., Wankiewicz, E., Brown, G. M., and Fujieda, H. (2002). MT_1 melatonin receptor in the human retina: Expression and localization. *Investigative Ophthalmology and Visual Science* 43: 889–897.

Wiechmann, A. F. and Smith, A. R. (2001). Melatonin receptor RNA is expressed in photoreceptors and displays a cyclic rhythm in *Xenopus* retina. *Molecular Brain Research* 91: 104–111.

Wiechmann, A. F. and Summers, J. A. (2008). Circadian rhythms in the eye: The physiological significance of melatonin receptors in ocular tissues. *Progress in Retinal and Eye Research* 27: 137–160.

Wiechmann, A. F., Vrieze, M. J., Dighe, R. K., and Hu, Y. (2003). Direct modulation of rod photoreceptor responsiveness through a Mel_{1c} melatonin receptor in transgenic *Xenopus laevis* retina. *Investigative Ophthalmology and Visual Science* 44: 4522–4531.

Wiechmann, A. F., Udin, S. B., and Summers Rada, J. A. (2004). Localization of Mel_{1b} melatonin receptor protein expression in ocular tissues of *Xenopus laevis*. *Experimental Eye Research* 79: 585–594.

Young, R. W. and Bok, D. (1969). Participation of the retinal pigment epithelium in the rod outer segment renewal process. *Journal of Cell Biology* 42: 392–403.

Noninvasive Testing Methods: Multifocal Electrophysiology

E E Sutter, The Smith-Kettlewell Eye Research Institute, San Francisco, CA, USA

Glossary

Base interval of stimulation – Stimuli are presented at intervals that are integral multiples of a base interval.
Binary stimulation – The stimulation that switches between two states such as flash/no flash, pattern–contrast-reversing pattern.
First-order kernel – This response component is computed by adding the response signal following base intervals with a stimulus and subtracting the signal following intervals without stimulus. If the response is linear, response contributions from subsequent stimuli must cancel as they are added and subtracted the same number of times. If the response is nonlinear, the following responses depend on the presence of the preceding stimulus. The difference that appears in the first-order kernel is called an induced component.
Inion – The prominent projection of the occipital bone at the lower rear part of the skull.
Lamina cribrosa – A mesh-like structure through which the optic nerve exits the sclera.
m-Sequence stimulation – The binary stimulation controlled by a special class of pseudorandom binary sequences called m-sequences. These sequences have ideal properties for the analysis of nonlinear systems.
Myelination – An electrically insulating material that forms a layer, surrounding the axons of many neurons. Axons of retinal ganglion cells become myelinated at the lamina cribrosa in the optic nerve head. Myelination of axons greatly increases the propagation velocity of action potentials.
Nonlinear response – In the case of binary stimulation, nonlinear means that the contribution of a response to the signal may depend on preceding and immediately following responses or responses in the neighboring areas.
Saltatory nerve conduction – The nerve conduction in myelinated fibers whereby the action potential jumps from gap to gap between the myelinated section.
Second-order, first slice – This response component can roughly be thought of as the difference between the response to two consecutive stimuli and the two stimuli individually presented.

Why Multifocal?

Visual electrophysiology has enjoyed decades of useful applications in the clinic and research. It provides objective measures of function at different stages of visual processing. Until relatively recently, it has been restricted to testing of a single area in the visual field. In the clinic it was generally used as a full field test or a test of a single area or spot in the field. This has greatly limited its sensitivity in diagnosis and in measuring progression and recovery from disease. It was clear from the start that mapping responses across the retina recording focal responses from one small area at a time would have taken very long and would not be practical. Multifocal techniques have overcome this limitation by stimulating a large number of areas concurrently whereby the response of each area is encoded in its temporal stimulation pattern. The special encoding using binary m-sequences permits clean extraction of the focal response contributions from a single signal derived from the cornea or from the scalp over the visual cortex of the brain. The m-sequence encoding has the additional benefit that it provides information on nonlinear response properties such as fast adaptation and recovery from photo stress that can be important clinical indicators.

There are many multifocal protocols available to clinicians. Some of them test the central visual field with lower spatial resolution and short recording times useful for screening. Others offer high resolution for the detection of small scotomata and sensitive assessment of changes in the spatial extent of dysfunction. Yet, other protocols enhance inner retinal and specifically ganglion-cell contributions. These tools permit tailoring the test for a specific clinical purpose. In many laboratories, only one protocol is commonly used and ordered by the clinicians as a multifocal electroretinogram (mfERG). Judicious selection of one of many available tests can lead to faster and more accurate diagnosis and, in some cases, avoid errors. Careful data analysis by a knowledgeable user can tease out local-response abnormalities that might otherwise be missed. A few examples shown below are selected to illustrate this point.

The Basic Principle

The basic principle of mfERG and multifocal visual-evoked potential (mfVEP) recording is schematically illustrated in Figure 1. With both types of recordings, the size of the focal stimuli is scaled with eccentricity to

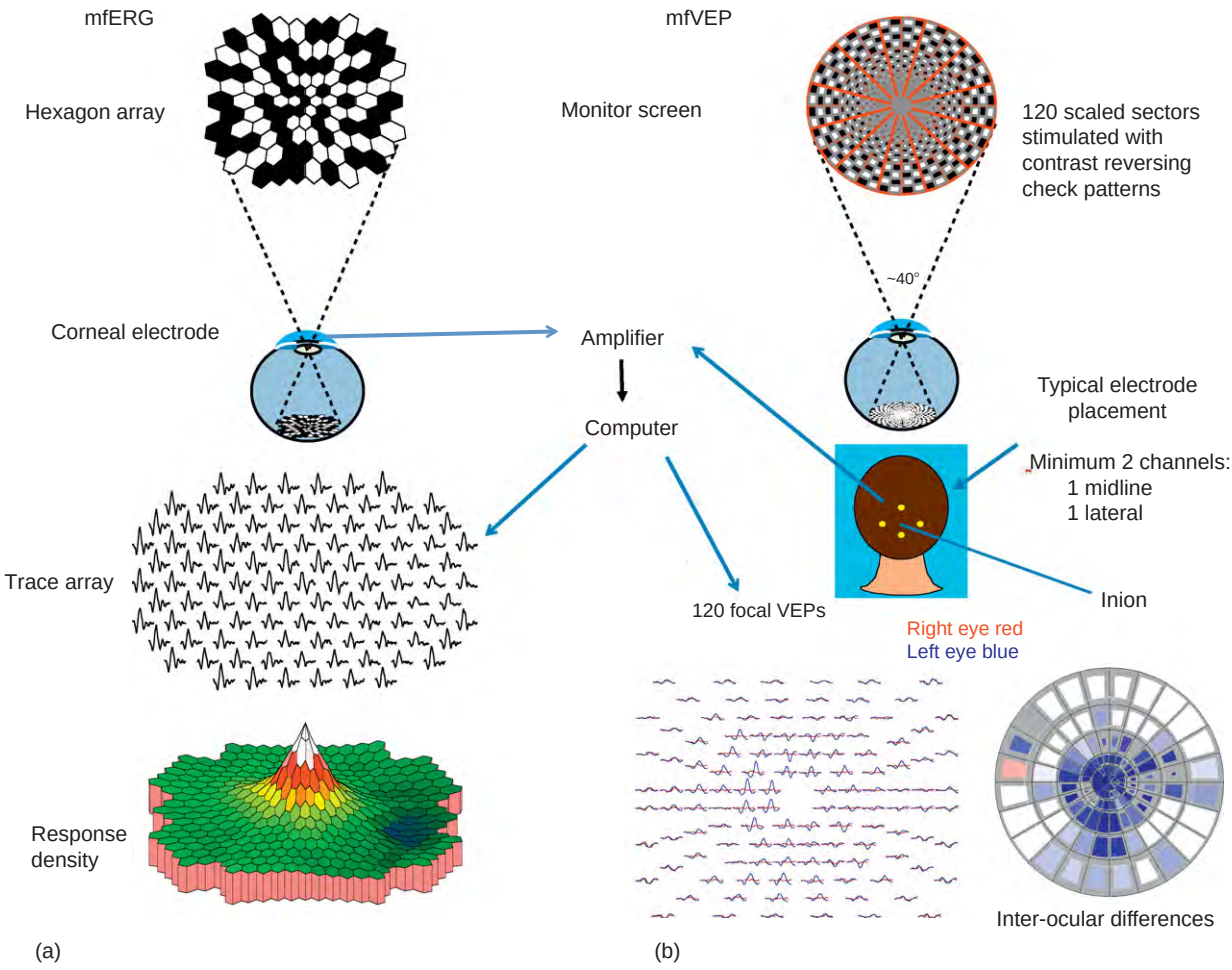

Figure 1 Schematic representation of the derivation of mfERG and mfVEP records. Commonly used stimulus arrays are shown on top. For the mfERG, hexagonal arrays are scaled with eccentricity to achieve similar signal-to-noise ratios across the stimulated field. The focal stimulation is m-sequence modulated flicker. The corneal signal can be derived with any of the available electrode techniques. For mfVEP, recording a dartboard pattern of stimulus elements is used to account for the steep eccentricity scaling of the representation of the visual field on the primary visual cortex. Each sector is stimulated with a contrast-reversing check pattern. Two perpendicular electrode pairs pasted to the scalp over the primary visual cortex cover the different directions of current flow. The data are presented as an expanded array of traces (bottom left) and as a pseudocolor field map (bottom right). The example is from an asymmetric patient. The left eye largely dominates (blue areas) except in the area of the right-eye blind spot (pink patch).

generate approximately the same signal amplitudes across the stimulated field. In the mfERG, we use scaled hexagonal arrays of the kind shown in **Figure 1(a)**. The steeper scaling of the cortical response requires the use of dartboard patterns **Figure 1(b)**. While the mfERG stimulus is usually focal flicker, the cortical responses of the multifocal visual-evoked cortical potential (mfVECP) are best elicited with focal contrast reversal of a check pattern.

Recording of Multifocal Data

All the data presented here have been recorded, analyzed, plotted, and exported with VERIS science 6.0 (Electro-Diagnostic Imaging, Inc, Redwood City, CA, USA). The mfERG data were recorded with a Burian–Allen bipolar contact lens electrode. This electrode and others of similar construction provide the best signal-to-noise ratio. Disposable monopolar electrodes such as the DTL fiber or the HK loop are considered less invasive but provide noisier signals and require longer recording times to achieve the same-quality data. Contact lens electrodes offer the advantage that they correct for corneal astigmatism and prevent drooping eyelids. However, care must be taken that the corneal ring of the electrode is reasonably well centered on the dilated pupil. To be comfortable, the electrode should be selected to fit the size of the eye.

All mfERG records shown here were recorded with a stimulus screen calibrated to produce multifocal flash intensities of 2.7 cd s m^{-2}. In most cases, the patient's fixation stability was monitored with an eye camera. For more recent recordings, fixation was monitored with an

infrared (IR) fundus camera that shows the position of the stimulus array on the fundus of the eye throughout the recording.

Multifocal Stimulators

Originally monochrome cathode ray tubes (CRTs) with a fast white phosphor were commonly used for stimulation. Few color CRTs could reach the required stimulus intensity. While, at this time, some suitable CRT monitors are still available, this technology is rapidly disappearing from the market and is being replaced by flat-panel liquid crystal display (LCD) monitors. The large panels are now bright enough, but achieve high brightness by leaving the pixels on during the entire display frame. This is ideal for pattern-reversal stimulation such as the mfVEPs, but it is not recommended for mfERGs. The switching speed of these panels is also marginal for ERG recording but adequate for mfVEPs. For multifocal flash ERG recording, we would like to have brief focal flash stimuli of no more than 2–3-ms duration at the beginning of each frame. This can be achieved with some of the available microdisplays. DLP projection displays can be used after substantial internal modifications.

Patient Positioning and Data Collection

In many laboratories chin rests are used for stabilization of the patient's head during recording. This is acceptable, but not the best solution. Patients are more comfortable in a reclining chair with a stable adjustable headrest. The reclined position helps to keep contact lens electrodes from dropping out. This arrangement works well in combination with a small stimulator mounted on an articulating arm. It allows adjustment of the angle of the stimulator so that the corneal ring of the contact lens electrode is centered on the patient's pupil.

The stimulus normally consists of a single cycle of a binary m-sequence. Using a longer m-sequence rather than averaging several shorter ones prevents contamination by higher-order kernels and, thus, provides cleaner separation of the local response contributions. For patient comfort, the record is collected in slightly overlapping segments that permit smooth splicing before data processing. Protocols for contact lens electrodes use a segment size of about 30 s. When recording with fiber electrodes, the patient must suppress blinks. To make this easier for the patient, the segment size is reduced to about 15 s.

Data Analysis and Presentation

Focal responses are extracted from the recorded signal using a cross-correlation executed by the fast m-transform. The focal responses may be contaminated with noise from blinks and small eye movements. A special artifact subtraction algorithm helps clean up the data. If the quality is not sufficient for this purpose, the operator can apply spatial filtering whereby each local waveform is averaged with a certain percentage of its nearest neighbors. This greatly improves the waveforms, but leads to some local smearing and is not recommended in cases where dysfunctional areas are suspected to be very small.

Clinically useful parameters of the local response waveforms can be extracted and presented as pseudo-color 2- or 3-dimensional topographic maps. The two most important ones are maps of response density and peak implicit time (time from the stimulus onset to the selected peak). Response densities are derived by dividing each focal-response amplitude by the solid visual angle of the corresponding stimulus patch. Estimating amplitudes of the often noisy focal responses using peak-to-trough measurements is very inaccurate. For this reason, a method of template matching is used. Each focal waveform is multiplied point by point with a normalized template of the underlying response. The template is derived as the average of waveforms in the same retinal region.

Implicit times of specific features of the response waveform, that is, the time from the stimulus onset to the feature are sensitive clinical measures. Of particular importance is the implicit time of the main positive peak *P*1. Estimating *P*1 implicit times using the highest point in the waveform is much too inaccurate when dealing with the noisy local responses. Much more accurate estimates are achieved by means of a template of the underlying waveform. On each focal waveform, the template is shifted into the position of best mean square fit. The location of the peak on the template waveform is then taken as the implicit time estimate. As with the amplitude estimation described above, the template waveform used at each location is the average of waveforms in the same neighborhood.

Dealing with Noisy Data

The main contaminations in mfERG responses are artifacts from blinks and small eye movements. It is possible to detect these artifacts and subtract them from the recorded signal. The process is capable of recovering some of the responses superimposed on the artifact, as long the artifact did not saturate data acquisition. This noise-reduction procedure works very well with mfERG records, but is less effective with mfVEPs where the contamination is usually noise from muscle tone required to maintain head posture rather than discrete artifacts. Here, it is more important to position the head in order to minimize tension.

How Long Does the Test Take?

The kernel extraction is an averaging procedure and, thus, follows the law of averages. Increasing the recording time

by a factor k improves the signal-to-noise ratio by $k^{1/2}$. The duration of a test must be determined by the amount of information to be gained and the signal-to-noise ratio of the derived response.

A multitude of tests can be designed from very short tests to tests lasting perhaps 1 h or more. The longer tests are used when more precise information is required. In the selection of a test, one should consider all the information already known regarding the patient.

Figure 2(a) and 2(b) show the results from two very short recordings derived from the same subject. Sixty-one patches stimulated the central field. Interpolating hexagons were inserted at plotting time to permit a more accurate estimation of the topography. The signal quality was very good in this case and does not reflect what one might get from an average patient in such ultra-short recording times. However, recordings of 2-min duration can be quite adequate for patient screening.

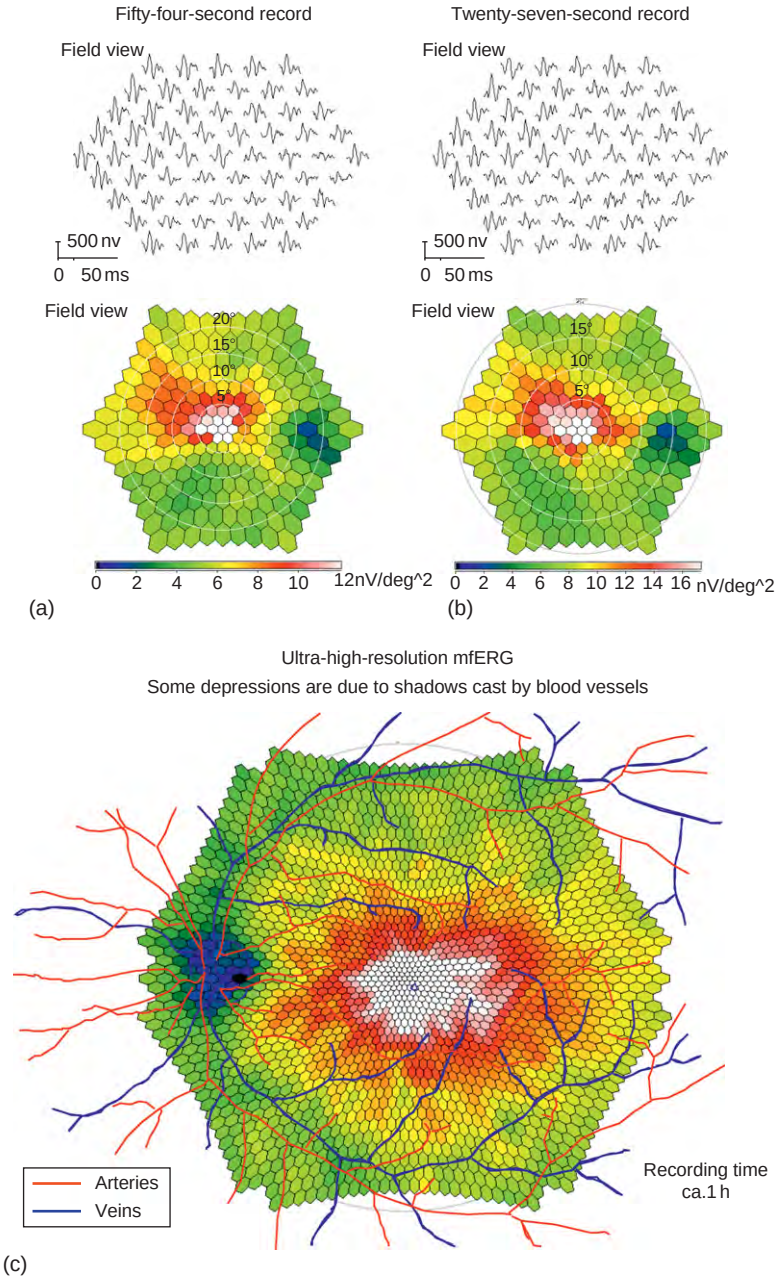

Figure 2 (a) Results from two very short multifocal recordings with 61 stimulus areas. The signals were derived with a bipolar Burian–Allen electrode. (b) High resolution recording using 509 stimulus areas within the central 45° of the visual field. The overlaid vasculature of the subject suggests that the depressed responses in some areas are caused by shadows of major blood vessels and their bifurcations.

Figure 2(c) illustrates a high-resolution recording with a stimulus array of 509 patches. The recording time of about 1 h necessary for this resolution is clearly not feasible in the clinic. The most popular array size uses 103 hexagons and records of 2–7 min length. Some clinics have used 241 hexagons in 7-min tests. Ideally, the spatial resolution of the test should be adjusted to meet the requirements of the clinical problem at hand.

Some Examples from the Retina Clinic

The samples presented below are selected to illustrate uses of different recording and analysis protocols. The clinical significance of the results cannot be discussed here due to space limitations.

Central Serous Retinopathy

The first example is from a male patient with central serous retinopathy (CSR). He was not diagnosed at the time of the recording but complained about a relative central scotoma in his left eye. We selected a 7-min test with 241 hexagonal patches because of the anticipated small spatial extent of the problem. The plots shown represent the average of two records. Individual records are slightly noisier, but would have been quite adequate in this case. Figure 3(a) shows the response density plots of the two eyes. The affected area in the left eye is clearly visible as an excavation in the central peak extending to the area surrounding the optic nerve head. The right eye is normal.

Some pathologies cause local delays in the main positive peak of the first-order waveform called the *P*1 peak indicated by the marks on the traces in Figure 3(c). Such delays are mainly attributed to photoreceptor sensitivity loss. Mapping the peak implicit time can help distinguish between different pathologies. In this CSR case, such delays are found in areas with reduced response density (Figure 3(b)).

Plots of *P*1 implicit time generally show delays in the vicinity of the disk. This feature must be ignored. It is attributed to a contribution to the focal response from scattered light. Some light from the focal stimulation of the highly reflective optic disk is scattered onto the peripheral retina where it elicits a delayed response contribution.

Hydroxychloroquine Retinopathy

A small percentage of patients who take this drug for autoimmune disease develop a bull's eye retinopathy. This dysfunction is, at best, only partially reversible when the patient is taken off the drug. For disease prevention, the mfERG is now proposed as a test for patient screening.

The left column in Figure 4(a) shows a typical example of hydrohychloroquine toxicity. Only the right eye is shown here as the presentation is usually bilaterally symmetric. The array of traces is shown at the top followed by the plots of response density and *P*1 implicit time below. Responses surrounding the center are substantially reduced to about 7–10° eccentricity with some relative sparing of the center.

The bottom plots shows that hydroxychloroquine toxicity does not cause significant changes in peak implicit times. This suggests that the changes are post-receptoral.

Amplitude ratios of ring averages around the fovea are used for diagnosis and assessment of severity of the bull's eye presentation. A plot from an automated screening protocol with statistical evaluation is shown in Figure 5. Ring averages are plotted in Figure 5(a). In Figure 5(b), response densities are plotted against eccentricity in degrees of visual angle and compared to data from a normal cohort. The data are interpolated with a cubic spline. For this analysis, ring averages have been normalized to the outermost ring that is usually minimally affected. The green bands around the normal mean (red line) represent the 2 standard deviation (SD) limit. The heavy black line is the patient's response amplitude. The area where the patient curve falls outside the 2-SD band is colored red. ICS is the index of central sparing used to evaluate the bull's eye configuration. It is computed as the ratio between the red area outside 3° eccentricity and the total red area below the 2-SD band. An ICS number of 1 indicates that all the losses in amplitude relative to the peripheral ring are outside 3° with complete sparing of the center. In a typical maculopathy patient, we find ICS values of around 0.2–0.4.

The importance of considering implicit times as well as response densities in standard clinical testing is illustrated with the example shown in the right-hand column of Figure 4 showing a patient with unknown vision loss.

The patient's visual fields showed a bilateral bull's eye configuration reminiscent of hydroxychloroquine toxicity of Figure 4(a). The perifoaveal relative scotoma seen in the visual field is confirmed by the response density distribution of the mfERG (Figure 4(a)). However, in this case we see substantial delays in the areas with depressed response amplitudes. This finding suggests loss in receptor sensitivity. In this case, topographic mapping of *P*1 implicit times was needed to clearly distinguish this case from hydroxychloroquine toxicity. Latency plots are often necessary to distinguish different pathologies with similar response density topography.

Juvenile X-Linked Retinoschisis

The first-order trace array (Figure 6(a)) and the first-order response density plots (Figure 6(b)) show two areas where amplitudes are still within normal range. However, closer scrutiny reveals that the two areas are very different in their functional properties. Area 1 is normal in the

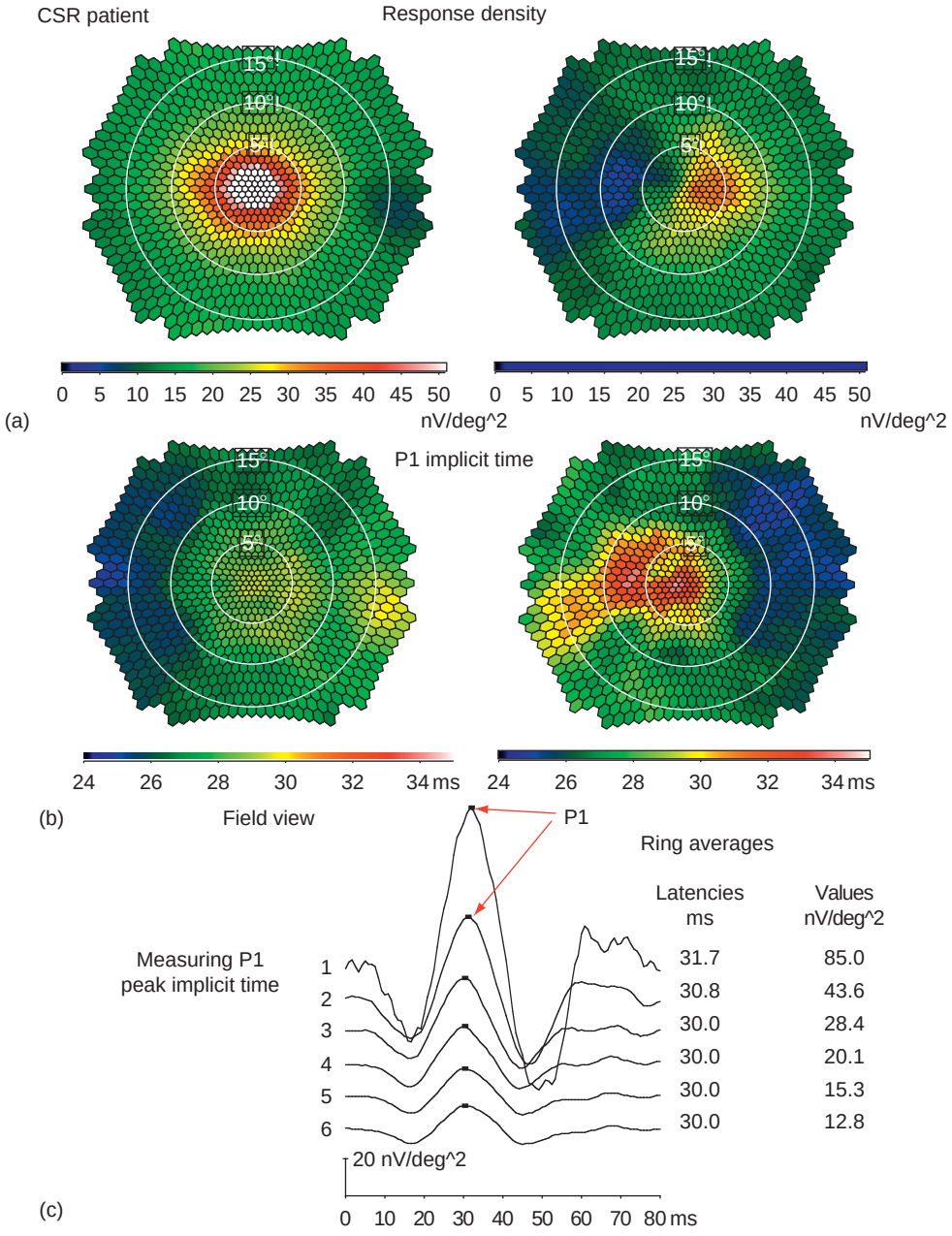

Figure 3 A patient complaining of a relative central scotoma diagnosed as central serous retinopathy with the help of this test. (a) A response density plot derived from two 7-min records. (b) The plot of *P*1 implicit time from the same record. *P*1 implicit times are measured from the time of the focal flash to the first positive peak as shown in (c).

first-order response amplitude as well as the *P*1 implicit time. The dominant higher-order component, the first slice of the second-order kernel, is also within normal range. This component reflects interactions between consecutive flash responses and is thought to originate predominantly in the inner retina. Area 2, on the other hand, has highly abnormal implicit times of close to 40 ms. The second-order component is almost completely absent in this area. This case illustrates the importance of looking not only at response densities but also at peak implicit times and the dominant higher-order kernel.

Detecting Small Central Dysfunction

The patient complained of a very small scotoma. It did not show in the visual field (**Figure 7(b)**) and there was no abnormal ophthalmoscopic finding. The patient drew the scotoma in the Amsler grid at 5° eccentricity (**Figure 7(a)**). Due to the small size of the suspected central dysfunction, we selected a protocol that places all 103 hexagons within the central 12°. The net recording time was 7 min. A distinct depression is seen at the location corresponding to the Amsler grid drawing (**Figure 7(a)**). In such cases, no spatial

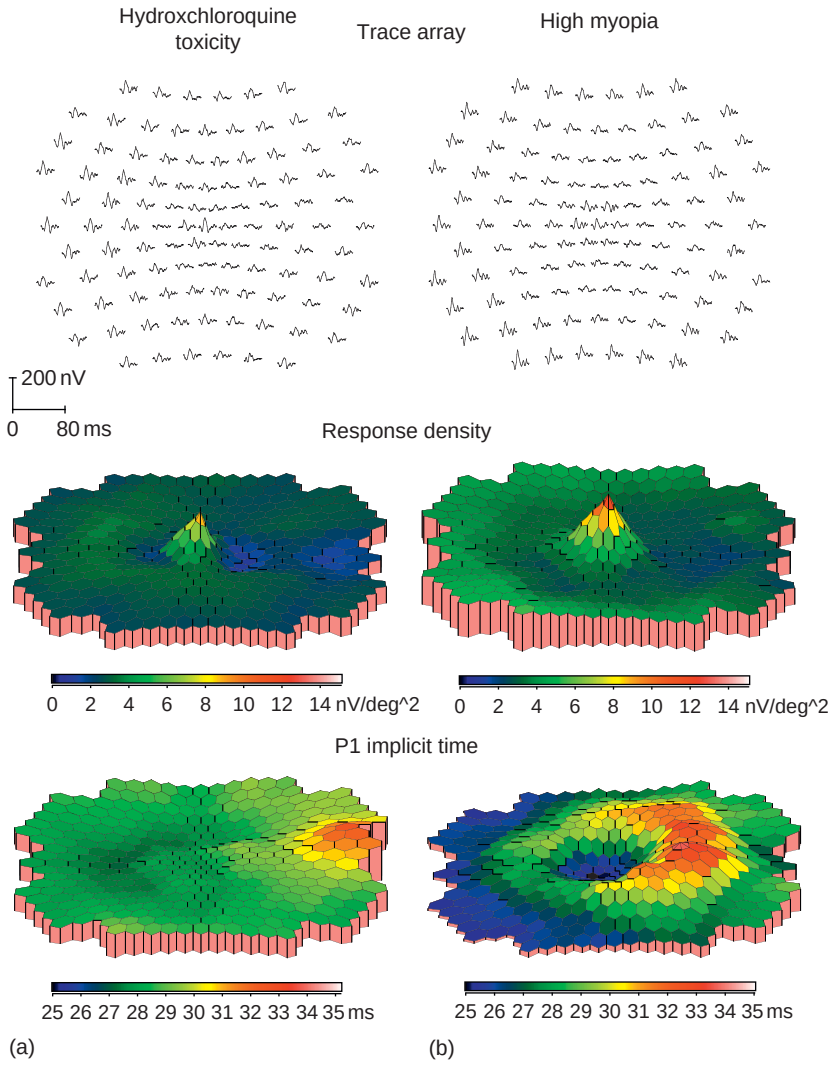

Figure 4 Column (a) shows a typical case of hydroxychloroquine toxicity. The characteristic peri-central amplitude loss is clearly seen in the trace array and the response density plot. The plot of *P*1 implicit time is normal suggesting inner retinal abnormalities. The enhancement in the area of the optic disc is due to scattered light and can be ignored. (b) a patient (high myopia) with a peri-central scotoma resembling hydroxychloroquine retinopathy. The increased implicit times in the depressed areas suggests a different pathogenesis, namely photoreceptor sensitivity loss. Plots of implicit time were needed to distinguish the two pathologies.

filtering could be applied to improve the quality of the focal waveforms as this would greatly reduce the small depression seen in the plot.

Another application of high-resolution central recording of this type is follow-up to macular hole surgery. OCT records document repair of structure, while the mfERG can be used to map recovery of function over time.

Applications to Neuro-Ophthalmology and Glaucoma

Some of the most important future clinical applications of multifocal electrophysiology are expected in the area of neuro-ophthalmology and glaucoma. The integrity of the optic pathway can be tested using the visual-evoked cortical response derived by means of electrodes placed over the visual cortex as schematically illustrated on the right in Figure 1. The response to contrast reversal of a check pattern has been shown to be most sensitive for the detection of conduction losses to the cortex. The introduction of the multifocal pattern visual-evoked response (mfVEP) raised hopes for objective visual field mapping. The main obstacle to this aim is found in the convoluted cortical anatomy onto which the visual field is mapped. Different patches in the visual field generate dipole signal sources of different orientations. Adequate coverage of the visual field requires at least two electrode pairs at perpendicular orientation as well as their sum and difference signals. Uniform coverage is not possible. Comparison

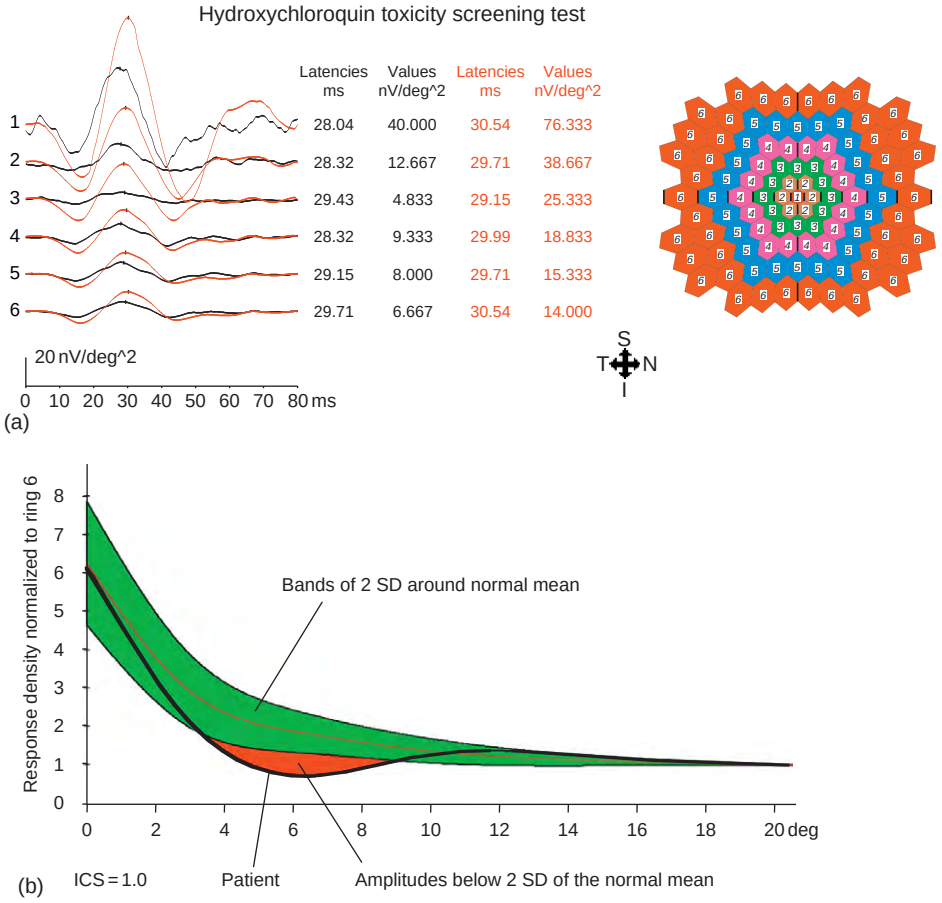

Figure 5 Automated statistical analysis for hydroxychloroquine toxicity screening. (a) responses in six rings for the patient (black) and the mean of 46 normal eyes (red). In (b), the amplitudes are plotted as a function of eccentricity. All data have been normalized to the outermost ring that is relatively unaffected in this condition. The ring averages of 5(a) are plotted as a function of eccentricity in degrees of visual angle with cubic spline interpolation. The green bands indicate 2-SD around the normal mean. The patient plot is in black.

with normative data is problematic due to the intersubject differences in the gross cortical anatomy. However, interocular comparison makes the mfVECP a powerful tool when the pathology is monocular or asymmetric between the eyes. Stimuli at corresponding locations in the visual field of the two eyes project to the same cortical patch and, in normal subjects, elicit virtually identical responses.

The cortical fold at the bottom of the calcarine fissure presents a problem that cannot be addressed with multiple electrodes. Sectors of the stimulus whose projections fall in this cortical area may wrap around the fold such that the same stimulus patch stimulates opposing surfaces of the sulcus generating mutually canceling dipole sources. This leads to characteristic signal dropout in the vicinity of the horizontal meridian. A substantial improvement was achieved by subdividing the sectors further and recording with 120 rather than 60 sectors. To compensate for resulting loss in signal to noise, the signal of each sector is averaged with a given percentage of the surrounding sectors after they have been brought to the same signal polarity. A typical plot of a trace array from a normal subject is shown in **Figure 8(a)**. Traces from the right eye are red, left eye traces blue. In this presentation, the position of the traces is not topographic. They are approximately equally spaced to best utilize the rectangular plot surface. The approximate eccentricities of the waveforms are indicated with black contour lines. The plot was derived from two perpendicular electrode placements, one from electrodes on the midline 4 cm apart and the other from electrodes 4 cm lateral to the inion on both sides. At each stimulus location, the signal-to-noise ratios of the two recorded channels and their sum and difference signals were compared and the best combination was selected. The pseudo-color topographic map of **Figure 8(b)** was derived from the same record. It graphically represents the local differences in response amplitude between the two eyes. The saturation of the color in each stimulus patch indicates the interocular difference while the amount of gray in each patch is a measure of uncertainty. It is derived from the noise level in the record. While some data can also be displayed in numeric form, this graphic representation permits us to capture

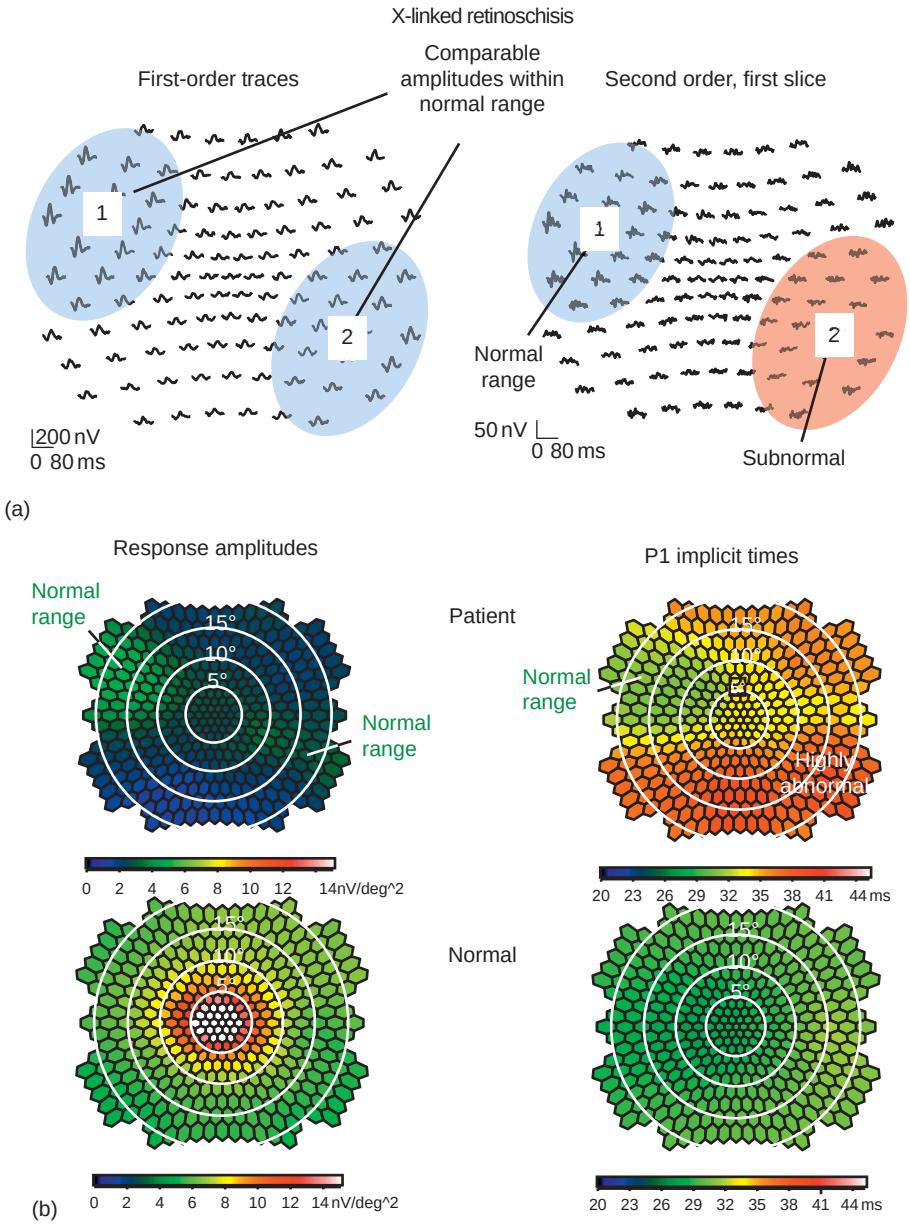

Figure 6 Record from right eye of a patient with x-linked juvenile retinoschisis. (a) The first-order traces show two areas with amplitudes within normal range. However, in area 2, the dominant second-order response contributions are almost completely extinct. (b) The response density plot shows two islands of relatively normal amplitudes. While the *P*1 implicit times are normal in area 1, they are highly abnormal in area 2.

the essence at a glance. Note that even in normal subjects, areas with small interocular differences in the peripheral areas are not unusual.

The mfVECP in Optic Neuritis

An obvious application of the mf VECP is in optic neuritis and multiple sclerosis. It is illustrated here with an example of acute optic neuritis. **Figure 9** shows mf VECP plots recorded in the acute phase and at 2-month intervals during recovery. In the acute phase, the responses within the central 3° of the affected eye are almost extinguished. The first follow-up record shows substantial recovery of amplitudes in this area, while increased implicit times indicate areas of demyelination. In the second follow-up record, the implicit times in the lower part of the fovea are back to normal, while in the upper field the delays persist.

Comparison of the mfVEP and the mf ERG in Optic Neuropathies and Glaucoma

It is well known that the ERG signal contains contributions from retinal ganglion cells and that losses of this cell population can, through a retrograde process, affect other

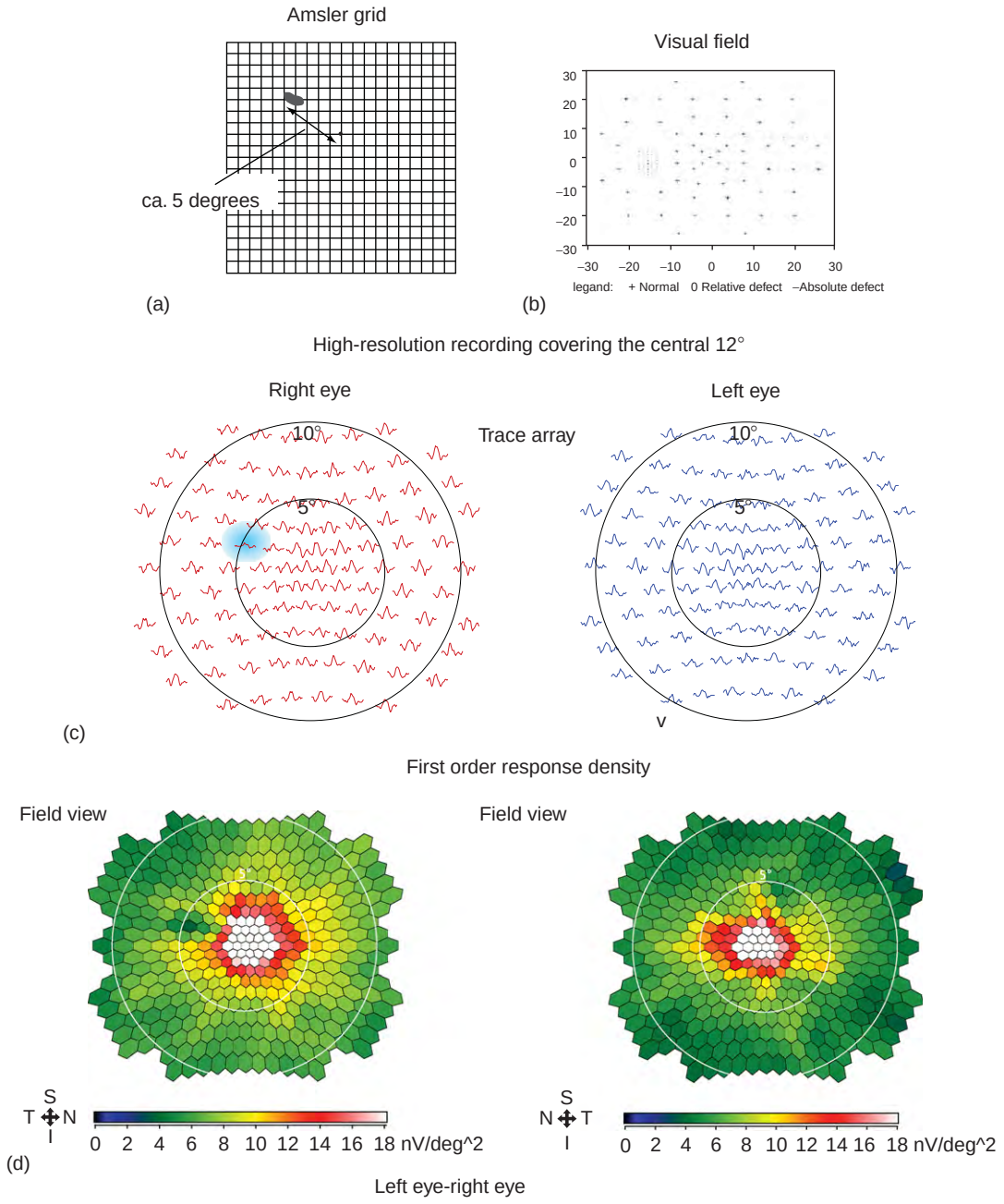

Figure 7 Patient complaining of a small scotoma not ophthalmoscopically visible or in the visual field. Patient draws it in the Amsler grid. A 7-min high resolution mfERG record reveals the dysfunctional patch objectively. (a) Amsler grid, (b) visual field, (c) trace arrays, (d) response density topography.

inner retinal response contributions. However, changes in the ERG signal are rather subtle and have proven difficult to detect in early stages of disease. The ganglion cell contributions to the ERG are small and overlap with signal contributions from other retinal sources, making their isolation and quantitative estimation extremely difficult. The discovery of the optic nerve head component (ONHC) of the ERG raised hope that isolation and mapping of ganglion cell function might become possible. The ONHC is a contribution from optic nerve fibers near the optic nerve head. Its generation is schematically illustrated in Figure 10. The contribution of the ONHC is delayed by the amount of time it takes action potentials to travel from the stimulated retinal patch to the nerve head. It is recognized by its timing, which varies depending on the length of the nerve fibers connecting the stimulus site with the disc. Possible mechanisms for its generation are the sharp bend in the axons where they descend into the cup, the beginning of myelination near the lamina cribrosa and conductive changes in the extracellular

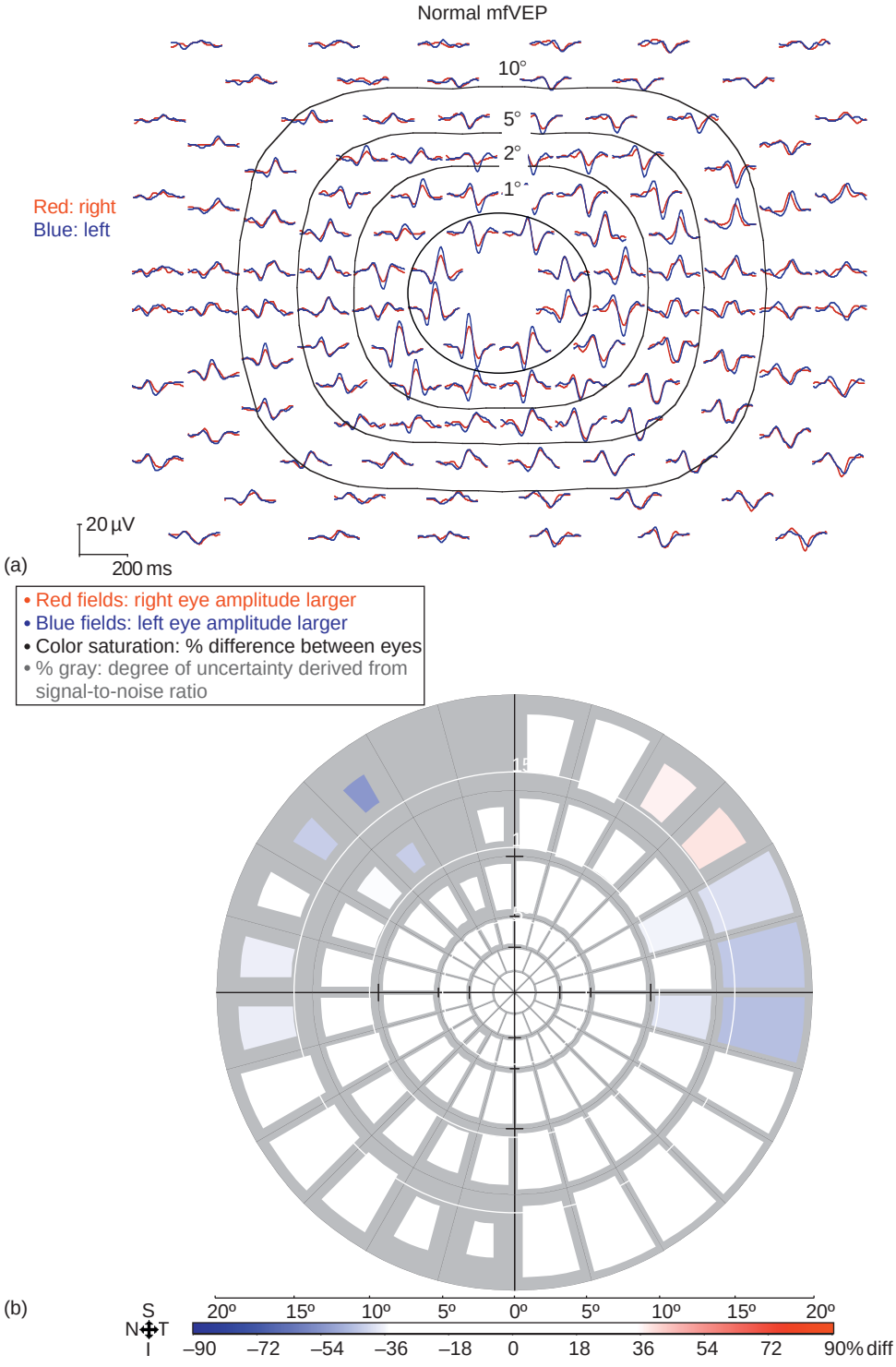

Figure 8 MfVEP of a normal subject. (a) interocular comparison of response traces: right eye red, left eye blue. The distribution of the traces is not topographic but has been arranged for best presentation of the traces in the rectangular plot area. Approximate eccentricities are indicated. (b) Pseudocolor topographic map of interocular differences.

medium. The observation that it can disappear in demyelinating disease while cortical responses are preserved, strongly points toward the transition from membrane conduction to saltatory conduction at the point where myelination begins as the main source of this signal. While mfVEP amplitudes are affected by the cortical anatomy, ONHC amplitudes directly reflect function. Their local evaluation does not require interocular response

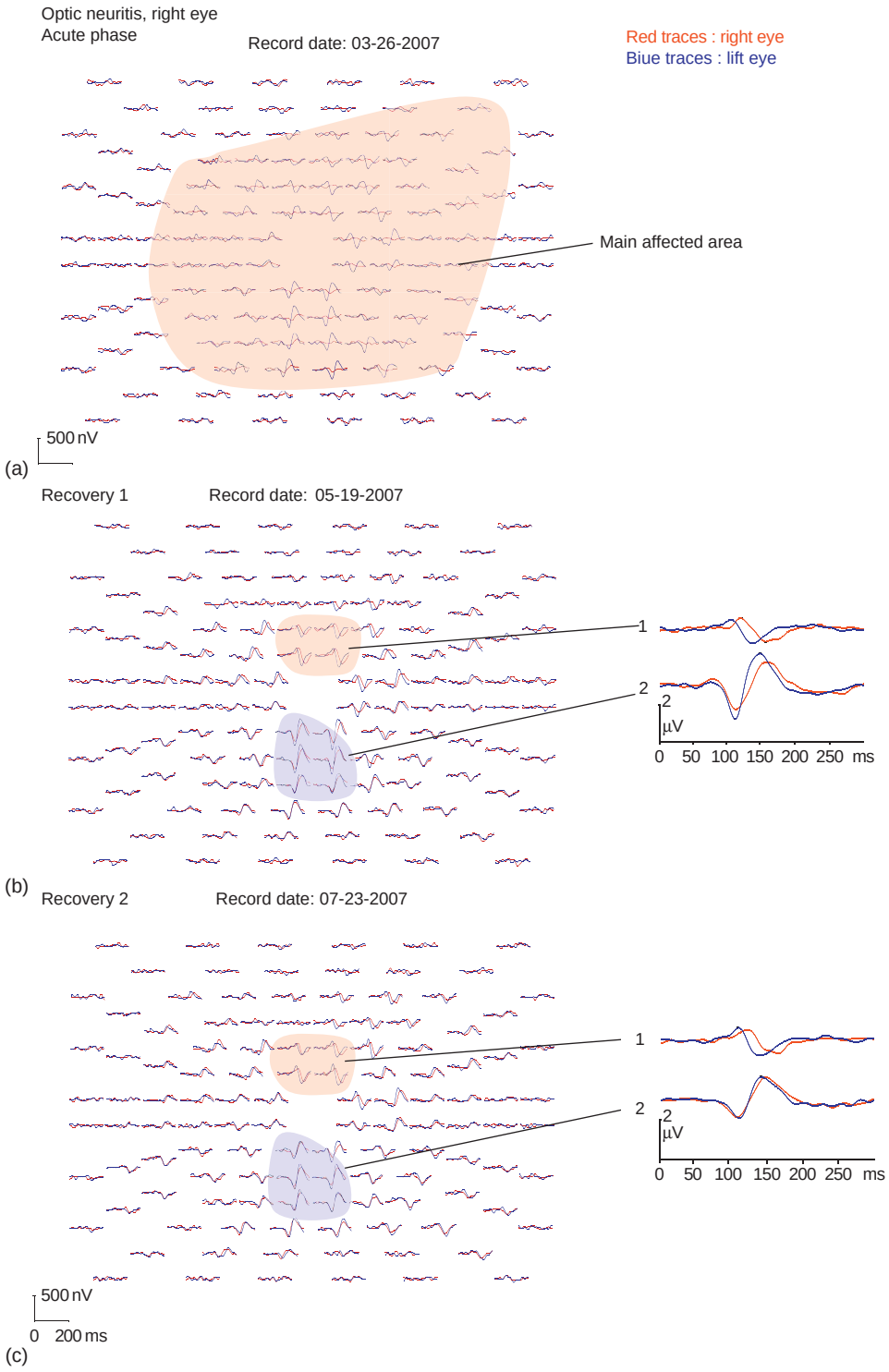

Figure 9 MfVEPs of a patient with optic neuritis. (a) during the acute phase: The red shading indicates the affected area. (b) After 2 months recovery: Amplitudes have largely recovered, but increased implicit times in the central area indicated demyelination. (c) After 4 months recovery: delays in the lower field have largely disappeared while those in the upper field remain.

comparison. In bilateral disease, the ONHC, thus, promises to be more reliable than the mfVECP.

In records collected with the commonly used mfERG protocol, the ONHC is too small to be evaluated (**Figure10(b)** left). The traces are from a ring around the fovea starting from the area near the nerve head, proceeding through the upper field and returning through the lower field (insert on the right). The contributions

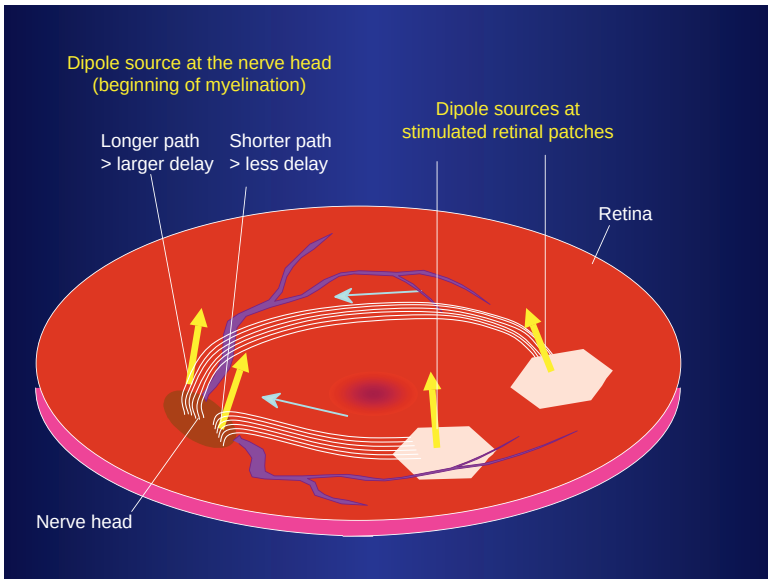

(a)

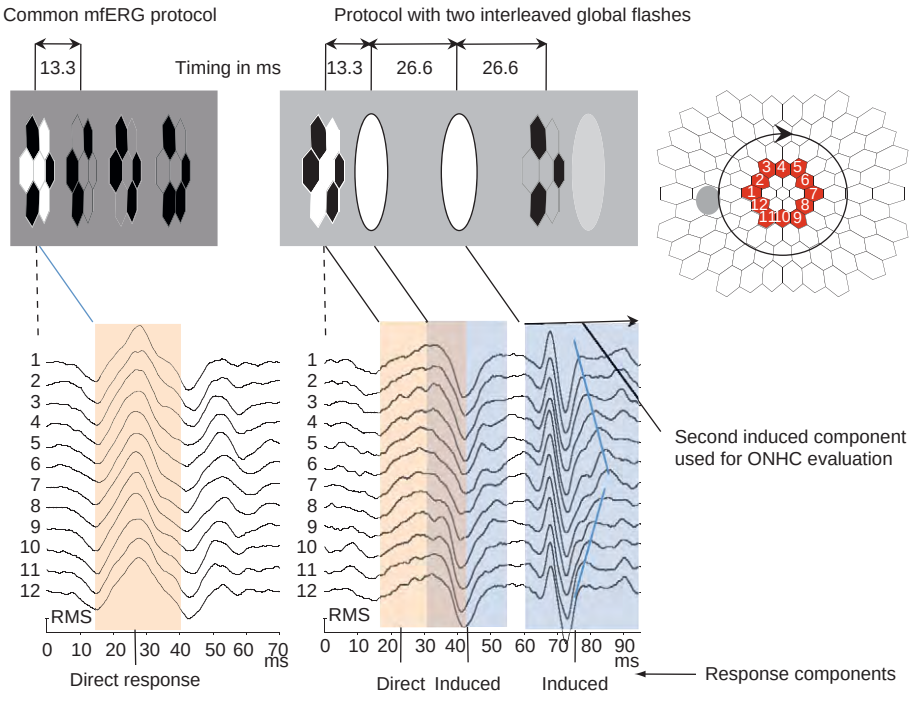

(b)

Figure 10 (a) This is a schematic illustration explaining the generation in the optic nerve head component (ONHC). Two signal sources are thought to contribute to the signal derived from the cornea, one from the stimulated retinal area and the second from the location in the nerve fibers where myelination begins. The latter is delayed relative to the retinal response by travel time of action potential from the stimulation site to the nerve head. It is recognized by this location-dependent delay. (b) Enhancement of the ONHC through the global flash paradigm. (Top) Schematic comparison of the stimulation used in the common m-sequence protocol on the left and the interleaved global flash protocol on the right. (Bottom) First-order traces derived from a normal subject: left, common protocol; and right, global flash protocol. The traces are from a ring around the fovea (insert on right) starting from the vicinity of the nerve head. The thin blue lines indicate the main feature of the ONHC contribution. The second induced component, epoch 60–90 ms, is normally used for visual evaluation.

from the ONHC should thus increase in implicit time to trace 7 and then decrease again. A stimulation protocol is now available that greatly enhances the ONHC as well as inner retinal response contributions. The protocol uses global flashes interleaved at specific intervals between the multifocal stimuli. The principle is illustrated on the right in Figure 10(b). The ONHC is now readily recognized. It consists of those features in the waveforms that shift

to longer implicit times with increasing distance of the stimulus patch from the nerve head. Its main peak is indicated with a thin blue line.

The ONHC can be visually evaluated when traces on rings around the fovea are plotted in vertical columns. A plot of this kind from a normal subject is shown in Figure 11(a). Traces in each ring are plotted starting from the patch nearest the disk, proceeding through the upper field and returning through the lower field.

The delays of the ONHC relative to the retinal contributions to the ERG are known. Propagation velocity of action potentials in the unmyelinated nerve fiber layer is determined by the fiber diameter and varies little between subjects. Aligning the traces to the ONHC before applying some spatial filtering further enhances its visibility and our ability to evaluate it by visual inspection. It is now seen as a vertical ridge in the columns of Figure 11(b).

Until an algorithm for estimation of the ONHC that performs better than a visual evaluation becomes available, the ONHC is mapped and scored as follows: using the computer mouse, traces are marked pink for moderately deficient and red for severely deficient in the ONHC. The corresponding areas automatically appear pink and red in the topographic insert below together with a numeric score (see example of Figure 12).

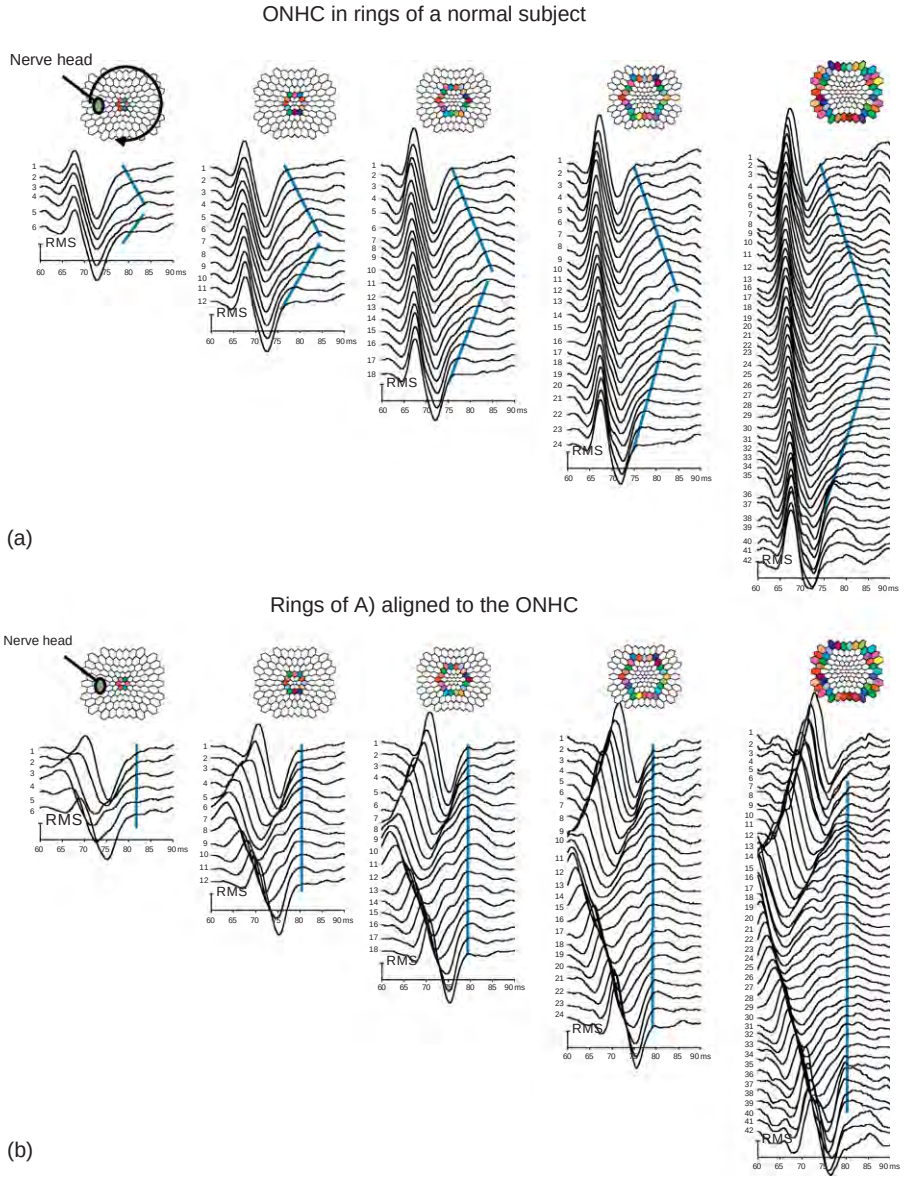

Figure 11 (a) Plots for visual evaluation of the ONHC. Traces on rings around the fovea are plotted in columns. Each ring begins on the side of the optic nerve head, proceeds through the upper field and returns through the lower field. (b) To enhance the appearance of the ONHC, the traces are aligned to ONHC implicit times.

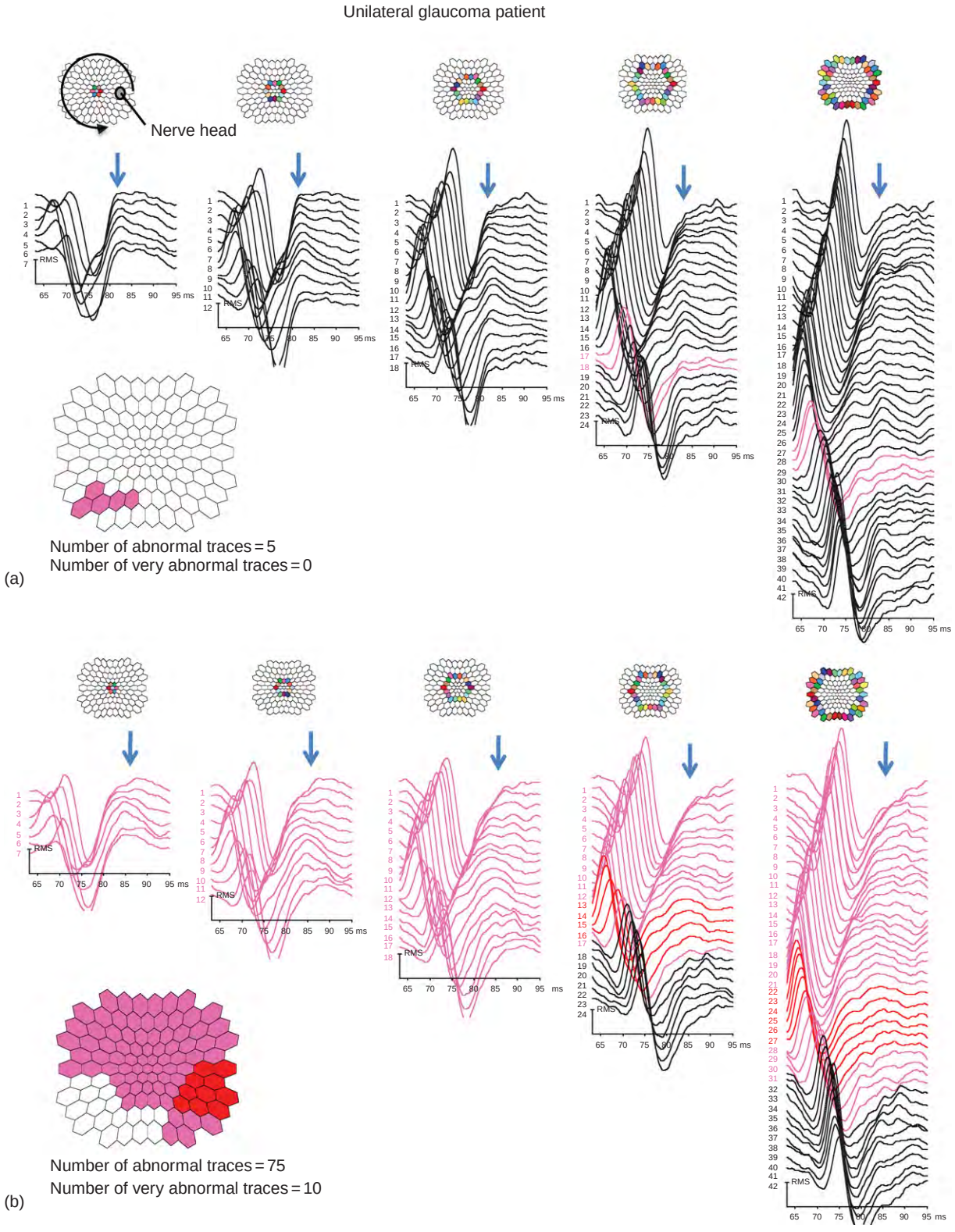

Figure 12 ONHC plots of the patient in **Figure 13**. (a) Unaffected right eye. The ridge from the ONHC contribution indicated with blue arrows is clearly visible and appears normal in most areas; (b) The ONHC ridge has largely disappeared. A residue is visible in the lower field.

Comparison of the mfVEP and the ONHC of the mf ERG in an Asymmetric Glaucoma Patient

To illustrate the performance of currently available electrophysiological function tests, a highly asymmetric glaucoma patient was selected. In Figure 13(a), the mfVEP trace arrays of the two eyes are compared. Figure 13(b) shows an automated topographic analysis of the same data set. The color of the field indicates the eye with the larger response, red for right, and blue for left. The color saturation indicates the percent difference in response amplitude

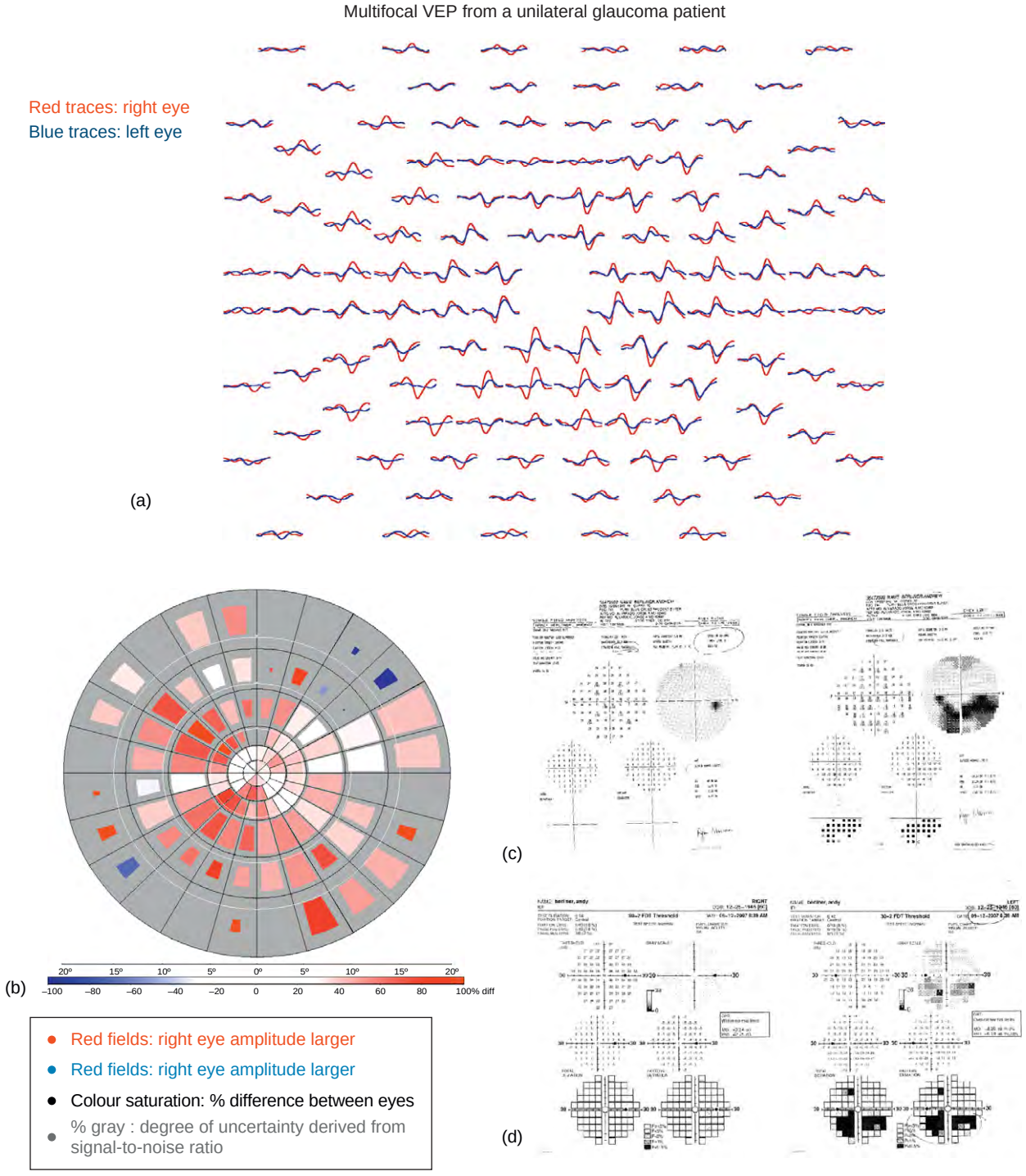

Figure 13 The mfVEP of an asymmetric glaucoma patient: (a) trace arrays of the two eyes; (b) topographic representation of interocular differences shows areas with response deficit in the left eye; (c) visual fields; and (d) perimetry using frequency-doubling technology (FDT) maps for comparison.

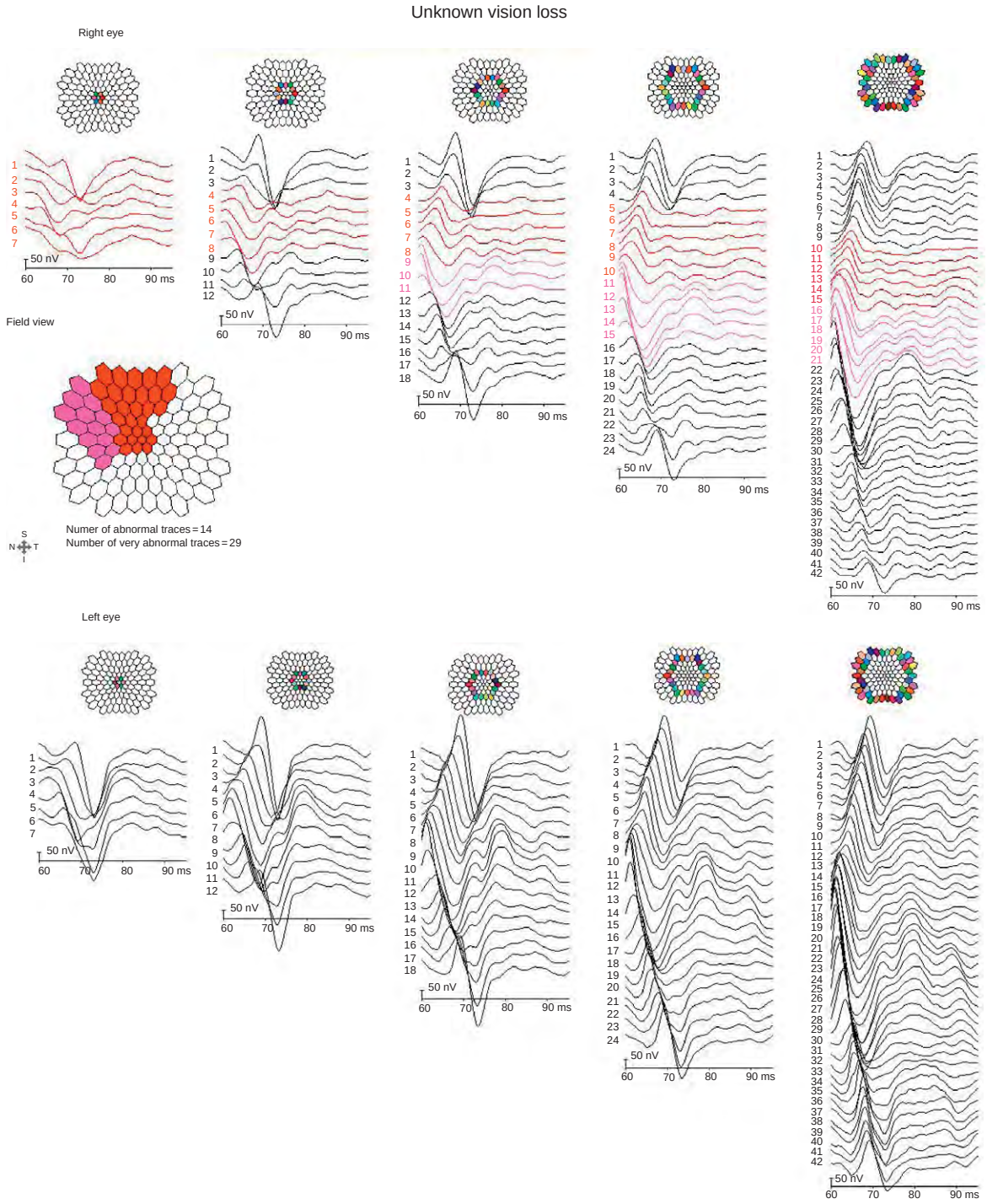

Figure 14 ONHC plots of a person with unknown vision loss. The complete disappearance of the ONHC in areas of the right eye is not consistent with the full visual field (not shown). Conclusion: The disappearance is due to loss of the transition from unmyelinated to myelinated fiber through retrolaminar demyelination rather than conduction loss.

between the eyes. The percentage of gray in each field represents the uncertainty in the estimate based on the signal-to-noise ratio in the record. The numeric version of the plot is not shown here. The inserts (c) and (d) show the visual field and the field mapped with the frequency-doubling technique (FDT) for comparison. **Figure 12(a)** and **12(b)** show the ONHC analysis of the mfERG for the two eyes of the same subject. Traces judged deficient in the ONHC are marked pink or red by the operator depending on the degree of abnormality. The corresponding stimulus areas are marked in the same color in the inset below.

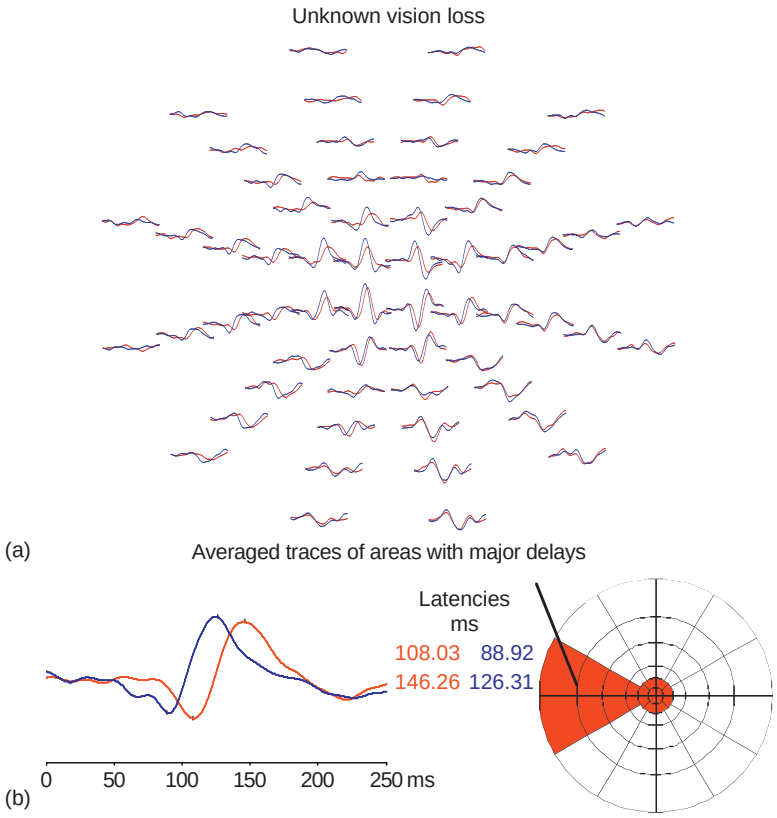

Figure 15 The conclusion from **Figure 14** is confirmed with an mfVEP. In the right eye, we find areas with substantial delays.

Both, the mfVECP and the ONHC data show more extensive losses than the two psychophysical function tests. In such highly asymmetric cases, the mfVECP can be a very sensitive test. It becomes more problematic when both eyes are affected. The ONHC, on the other hand, does not require interocular comparison.

Patient with Unknown Vision Loss

A 53-year-old male patient noticed blurring in his right eye. His visual acuity was V/A 20/30 on the right and 20/20 on the left. Visual fields were normal in both eyes. The common first-order response is somewhat lower in the right eye, but its topographic distribution is within normal range (not shown). The ONHC, on the other hand, is highly abnormal in the right eye, particularly in the center and in some portions of the upper field and completely absent in some areas (**Figure (14)**). The left eye is within normal range. The gross abnormalities in the ONHC are not consistent with the normal visual fields of the patient (not shown). This finding could, therefore, not be attributed to loss of nerve conduction. It could, however be explained by retrolaminar demyelination eliminating the source of the ONHC. This reasoning led to the mfVEP records shown in **Figure 15**. In the right eye, the responses are indeed substantially delayed in the areas with an abnormal ONHC confirming local demyelination. This case is interesting as electrophysiology led to the diagnosis of a patient not suspected of demyelinating disease.

Note that the ONHC is abnormal in some cases of optic neuritis even when substantial cortical delays are observed but not in others. In the above example, there are large cortical delays in areas where the ONHC is preserved. In the case of acute optic neuritis (**Figure 9**), the ONHC was judged within normal range in both eyes. In combination, the three tests (common mfERG, ONHC, and mfVEP protocols) allow us often to localize a dysfunction along the visual pathway.

Summary and Conclusion

Multifocal electrophysiology is not a single tool, but rather a collection of tools. Stimulation and analysis protocols can be optimized for specific clinical applications such as diabetes, AMD, optic neuropathies, etc. Much can still be done to shorten the tests and improve their efficiency. The protocols can be semiautomated to make clinical testing easy. However, the tools have to be paired with the expertise necessary to select the proper tool for each case and interpret the data.

There is a great deal of information contained in multifocal records that is only partially understood and still largely unexploited. Combining tests of function and structure promises to advance the understanding of both types of data and the pathogenesis of diseases. A case in point is the example of x-linked retinoschisis shown in **Figure 6**. The availability of OCT data on the different areas of the retina might have greatly helped our understanding of the connection between function and stricture in this and other similar cases.

Acknowledgment

The studies on which this article is based have been supported in part by NIH grant EY06961.

See also: Adaptive Optics; Optical Coherence Tomography; Primary Photoreceptor Degenerations: Retinitis Pigmentosa; Primary Photoreceptor Degenerations: Terminology; Secondary Photoreceptor Degenerations: Age-Related Macular Degeneration.

Further Reading

Hood, D. C. (2000). Assessing retinal function with the multifocal ERG technique. *Progress in Retinal and Eye Research* 19: 607–646.

Miyake, Y. (2008). *Electrodiagnosis of Retinal Diseases*. Tokyo: Springer.

Sutter, E. E. (2001). Imaging visual function with the multifocal m-sequence technique. *Vision Research* 41: 1241–1255.

Sutter, E. E. (1992). A deterministic approach to nonlinear systems analysis. In: Pinter, R. B. and Nabet, B. (eds.) *Nonlinear Vision*, pp. 171–220. Cleveland, OH: CRC Press.

Normal Age-Related Changes: Crystallin Modifications, Lens Hardening

P Wilmarth, L David, and K Lampi, Oregon Health and Science University, Portland, OR, USA

Glossary

Cataract – A clouding of the eye lens.
Cortex – The outer, soft lens material just inside the capsule.
Crystallins – The major structural proteins in the lens.
Deamidation – Loss of a tertiary amino group on glutamine or asparagines resulting in a carboxyl group and conversion to the corresponding acid.
Disulfide bonds – Oxidation of two cysteine residues resulting in a linkage between them.
Methylation – Addition (+14 Da) of a methyl group to an amino acid residue.
Nucleus – The inner, harder portion of the lens which has several layers.
Oxidation – Addition (+16 Da) of an oxygen atom to an amino acid residue.
Posttranslational modification (PTM) – A chemical or enzymatic alteration to amino acids in proteins that occurs after translation.
Presbyopia – Age-related problem with near vision.
Proteomics – The large-scale identification and quantification of proteins, and the effects of their modifications, interactions, and activities.
Truncation – Proteolytic or spontaneous cleavage of a protein's peptide backbone.

Introduction

The human lens is an avascular, clear tissue with unique protein composition and cellular organization. The bulk of the lens is comprised of terminally differentiated, elongated cells, called lens fiber cells. The most recently synthesized fiber cells are located in the outer (cortical) region of the lens and increasingly older fiber cells are located in the center (nuclear) region. As they mature during normal aging, fiber cells lose their ability to turnover and synthesize new proteins. Consequently, lens proteins persist for the life of the organism. They gradually become modified during aging with the greatest accumulation of modified proteins in the nuclear region. Protein modifications are thought to play major roles in presbyopia, the loss of the ability to focus on nearby objects, and age-related nuclear cataract.

The major proteins in the lens cytosol are called crystallins. Three major groups of crystallins exist in mammalian lenses – α-, β-, and γ-crystallins. α-Crystallins belong to the small heat shock family of proteins, form aggregates of approximately 800 000 Da molecular weight, and are composed of two types of subunits with molecular weights near 20 000 Da. Members of the β/γ-crystallin family contain a highly conserved tertiary structure made up of four Greek key motifs. They have subunit molecular weights ranging from 21 000 to 28 000 Da, due to variations in the length of their N- and C-terminal extensions. While the β-crystallin family forms aggregates containing from 2 to 8 subunits, the γ-crystallins remain as monomers. In young human lenses the major crystallin subunits have been identified as αA, αB, βA1, βA3, βA4, βB1, βB2, βB3, γC, γD, and γS.

Lens crystallins undergo extensive posttranslational modification as the lens ages, with the greatest abundance of modifications in the central nuclear region that contains some of the oldest proteins in the body. Modifications were first detected following protein separations using sodium dodecyl sulfate polyacrylamide gel electrophoresis (SDS-PAGE) and isoelectric focusing. The earliest modifications observed were the truncations of β-crystallin extensions and an increase in acidic species, presumably due to deamidation. Once complete amino acid sequences for the crystallins had been determined, advances in separation and mass spectrometry techniques could be employed to identify specific crystallins and their sites of modifications.

The plasma membranes of fiber cells also have unique compositions. The dominant membrane protein is a water channel, aquaporin 0, expressed only in lens tissue. Aquaporin 0 undergoes a variety of modifications associated with aging and location within the lens. Lens membrane proteins are difficult to work with and little is known about how their functions change with age and whether they have a role in loss of transparency. In middle age, a barrier to diffusion forms that reduces the flow of nutrients and antioxidants to the nuclear region of the lens. This barrier has been suggested to be a precursor to age-related nuclear cataract formation.

Characterization of Lens Posttranslational Modifications

The techniques available to characterize proteins and their posttranslational modifications (PTMs) have changed

dramatically in the past 1–2 decades, as have the design and scale of lens PTM studies. Mass spectrometry has emerged as the method of choice for detecting and localizing PTMs in proteins. Early techniques relied on protein separations and purifications, and reported results were often devoted to a particular crystallin or crystallin family. Mass spectrometry was employed in these early studies to identify types of modifications and localize many of them to specific sites. However, lengthy protein separations may introduce protein modifications and enrich or deplete modified protein forms, possibly biasing the results.

Separations of intact lens protein mixtures by two-dimensional gel electrophoresis (2-DE) have been used frequently in studies of modifications that changed protein isoelectric points (phosphorylation, acetylation, deamidation, etc.) or molecular weight (proteolysis, alternative splicing, cross-linking, etc.). Mass spectrometry in combination with 2-DE allowed definitive protein identifications but frequently failed to localize sites of modifications in less abundant protein forms. The increasing sample complexity of aged lens proteins and their decreasing solubility limit the applicability of 2-DE in advanced age and cataractous lenses. It is not known to what extent 2-DE selects for different soluble protein forms. Proper controls are required to identify artifactual modifications, such as oxidized methionine, that are by-products of 2-DE.

More recently, complex mixture analyses of enzymatic digests of lens tissue have been used to perform large-scale PTM mapping for the first time. This bottom-up technique relies on the separation power and automation of modern liquid chromatography/mass spectrometer systems. Very complicated peptide mixtures can be separated by multidimensional liquid chromatography and the peptides sequenced by tandem mass spectrometry to identify proteins and localize sites of PTMs. This technique has been used in many recent large-scale studies of aged and cataractous lenses and has provided a truly global perspective on lens PTM changes. Recent advances in analysis of PTMs using tandem mass spectrometry have identified a large number of common *in vitro* sample processing artifacts which may have been incorrectly attributed to *in vivo* modifications in early studies. However, by using young lenses as controls, it is possible to discover which modifications are truly associated with lens aging and loss of protein solubility.

The newest application of mass spectrometry to lens research is using high mass accuracy and resolution to characterize intact protein mixtures without enzymatic digestion to peptides. This top-down approach has the potential to identify truncated protein forms, alternatively spliced proteins, and characterize PTMs. It has been used with great success in studies of histone modifications where whole protein purifications were possible. Current technology requires relatively low sample complexity, but water-soluble whole lens proteins, without separation, have been successfully studied using Fourier transform-ion cyclotron resonance mass spectrometry instrumentation. It will be interesting to see if limitations, such as increased protein heterogeneity with age or poor protein solubility in mass spectrometry compatible buffers, can be overcome.

Summary of Early PTM Studies

Modifications of αA and αB that have been reported include truncation of the C-terminal residues, deamidation of asparagine and glutamine residues to aspartic and glutamic acid, respectively, disulfide bond formation, oxidation of methionine and tryptophan residues, and phosphorylation of serine and threonine residues. Extensive racemization and isomerization of aspartate and asparagine residues in αA and αB also occur.

Early studies of human β- and γ-crystallins reported losses of β- and γ-subunits during aging and accumulation of more-acidic protein forms. Human βB1 and βA3/A1 are initially cleaved on their N-terminal extension with more extensive truncations occurring during aging. Forms of these proteins missing portions of their N-terminal extensions have been detected in human lenses of less than 1 year of age and may be associated more with maturation of the lens cells than with aging. The 2-DE patterns of protein from different lenses suggested that the concentration of truncated β-crystallins increased with age and that more truncated forms were localized in the more mature nuclear fibers of the lens. The acidic isoelectric points (pIs) of these truncated β-crystallins also suggested that they had undergone deamidation. The γ-crystallins are also extensively modified by deamidation and the formation of disulfide bonds.

These early studies established that the major modifications that occur in lens with age are N- and C-terminal truncations, deamidation (and associated isomerization/racemization), oxidation, possible disulfide bond formation, and phosphorylation. Available techniques allowed a relatively small number of specific PTM sites to be determined and quantitative information was generally lacking. Recent advances in proteomic techniques have allowed global PTM mapping in the lens and semiquantitative estimates of PTM abundances.

Review of Identified and Localized Lens PTMs

With the advent of biological mass spectrometry, advanced instrumentation, and sophisticated data analysis techniques, unambiguous identification and assignment of PTMs to specific lens protein sites can be performed. This article focuses on human lens modifications that have been localized to specific sites in lens proteins.

We also discuss which modifications are present *in vivo* and which modifications have the strongest correlations with aging. Most of the reported human lens PTM sites have been to the major crystallins. Lens membrane proteins, the beaded filament proteins filensin and phakinin, and many additional minor lens proteins have not received much attention. We limit our review to crystallins, although these other proteins are also likely involved in lens aging changes. Lastly, recent results probing the functional significance of some of these lens modifications will be discussed.

There are over 310 crystallin PTM sites that have been reported so far. A chart of the frequency of reported crystallin modifications is shown in **Figure 1**. Deamidation and oxidation have the largest numbers of reported sites followed by a gradual decrease for the remaining modifications. **Table 1** lists the reported modification sites in human lens crystallins for deamidation, methylation, oxidation, acetylation, and phosphorylation. Sites that have been reported in more than one study are highlighted in bold. We can draw a few conclusions from the patterns in the table. First, specific modifications are often present in multiple crystallins and at multiple sites. This supports the premise that mature fiber cells have few enzymatic processes and the modifications are probably chemically induced. Second, there are many deamidated asparagine and oxidized methionine residues that could have occurred during sample processing. Which modification sites truly occur *in vivo* and are associated with aging?

According to Wilmarth and colleagues, the technique of spectral counting was used to estimate the relative abundance of PTM sites and compare a young control lens to three aged lenses to identify sites that were more abundantly modified in the aged lens. This novel, unrestricted PTM searching strategy also clearly identified a wide variety of artifactual modifications caused by sample processing or electrospray ionization (such as in-source fragmentation, neutral loss of water and ammonia, N-terminal cyclization reactions, N-terminal carbamylation, deamidation, and oxidation). Comparative analysis of the young versus aged lenses identified carbamylation, deamidation, and oxidation sites that were likely to have occurred during sample processing, as these were present at both ages. Lens proteins were separated into water-soluble and water-insoluble fractions to identify which specific *in vivo* modifications could result in loss of crystallin solubility, a likely precursor to loss of lens protein function. Spectral count data taken from **Table 1** in Wilmarth *et al.* is presented in **Figure 2**. It is easy to see from the plot that deamidation is, by far, the most prevalent modification in aged human lens. It is also clear that no other type of modification, except deamidation, significantly increased in abundance with loss of crystallin solubility. The next sections will discuss these types of modifications and their possible roles in lens aging and loss of function.

Deamidation

Excluding the minor crystallins, βA2 and γB, there are 56 asparagines in the crystallins and 39 have been reported as deamidation sites (70%). Similarly, there are 111 glutamines, with 66 reported deamidations (59%). Surface accessibility, neighboring residues, and the three-dimensional structure all influence the rates of deamidation. To identify the sites that are detrimental to lens function, comparative quantitative studies will be required. Deamidation is expected to be faster for asparagine than glutamine and can occur during sample handling. Proper controls, such as comparison of modifications in old lenses with those in young lenses, with crystallin proteins expressed *in vitro*, or with synthetic peptides processed under identical conditions, are needed to ensure that deamidation sites in aged tissues accurately represent those present in the tissue *in vivo*.

As can be seen in **Figures 1** and **2** deamidation was the most prevalent modification in aged human lenses. Over 25 deamidation sites were found at higher frequency in the insoluble proteins than the soluble proteins, suggesting an association between deamidation and insolubilization.

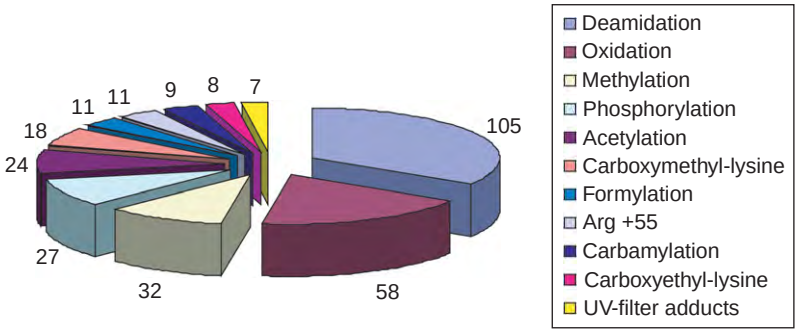

Figure 1 Frequency of reported human lens crystallin PTMs by modification type for 312 reported sites. Kynurenine-based UV filters can form unstable chemical species, react with lens proteins, and may contribute to coloration of aged lenses. The reported modification mass shifts of +28, +58, and +72 Da have been tentatively assigned to formylation, carboxymethyl lysine, and carboxyethyl lysine, respectively.

Table 1 Summary of reported posttranslational modification sites in human lens crystallin proteins for five common modifications

Crystallin	*Deamidation*	*Methylation*	*Oxidation*	*Acetylation*	*Phosphorylation*
Alpha A	**Q6, Q50, Q90, N101, Q104, N123, Q126, Q147**	R21, K88, H154	**M1,** W9, Y18, Y34, **M138**	**N-term, K70, K78,** K88, K145	T13, **S45, S122,** T140
Alpha B	**Q26, N78, Q108, N146**	R22, R50, H83	**M1,** H6, H7, **W9,** Y48, **W60, M68**	**N-term, K92**	**S19, S21,** S43, **S45,** S53, **S59,** S66, **S76**
Beta A2				**N-term**	S30
Beta A3/A1	**Q38, N40, Q42, N54, N62, N103, N120, N133,** Q149, N155, N156, **Q164, Q172,** Q180, **Q203, Q206, Q208**	**C82,** H106, **C117,** R137, **C185**	**M46, W96, W99,** M111, **M126, M151, M161,** W168, **W198,** H201	**N-term, A18 (N-term)**[b], K122, K125, K131	T127, S160
Beta A4	**Q22, Q62, Q64,** Q65, **N82,** N100, **Q111, N113,** Q188	**C165**	**M13,** W16, W79, W148	**N-term**	S34, T43
Beta B1	N15, N57, **N67, Q69,** N81, **Q105, N107, N124,** Q146, **N157, N161, Q166, Q196, Q204, N216, Q222, Q224, Q226, Q235**	C79, R229, R230, K234	**W100, M112, W123, W126, M136, W192, W215, W218, M225**	**N-term,** K5, K159	S9, T11, S31, S76, S80, S106
Beta B2	Q5, Q7, Q12, **N15, N113,** N115, Q137, Q146, Q154, Q162, **Q182, Q184,** Q193, Q196	C37, K41, C66, K67, K120	W58, **M121, W150, M192**	**N-term,** K75, K120	T117
Beta B3	Q78, **N155**	K128	M129	**A2 (N-term)**[c], K128	Y29
Gamma B	***(Q66)***[a], *(Q67)*[a], N161	**C22,** C79	*(W68)*[a], *(M69)*[a], **M102**		*(Y62)*[a], *(Y65)*[a]
Gamma C	N24, **Q26,** N49, Q51, **Q66,** Q67, **Q83, Q112,** N137, Q142, Q148, Q154	**C22,** C79, H116	Y55, W68, **M69, M101, M102,** W130		Y62, Y65
Gamma D	**Q12,** N24, N49, Q67, Q154, **N160**	**C110**	M43, Y45, M69, M146, W156		
Gamma S	**N14, Q16, N53, Q63,** Q70, **N76, Q92,** Q96, **Q106, Q120, N143,** Q148, **Q170**	K6, **C24, C26,** C114	**M58, M73,** M107, M118, **M123, W162**	**N-term**	S166

[a]Gamma B peptide 60–76 is identical to the more-abundant gamma C peptide 60–76.
[b]The N-terminus of beta A1 is residue A18 of beta A3.
[c]Beta B3 sequence incorrectly contains the N-terminal Met residue.
Sites reported in more than one study are highlighted in bold type.

The number of deamidations in the water-soluble proteins increased up to 35 years of age, but then remained constant, while the number of deamidations in the water-insoluble proteins continued to increase with increasing age. This increase in deamidation, particularly between birth and middle age, suggests that deamidation may be a precondition for cataracts and may play a role in hardening of the lens. Hardening of the lens continues throughout life and is especially evident in nuclear sclerotic cataracts discussed elsewhere in this encyclopedia.

Methylation

Methylation is an abundant lens modification that has only recently been discovered. The main sites for crystallin methylation appear to be reactive cysteine residues. In early characterizations of this modification, there were unsuccessful attempts to find the methyltranferase responsible for the methylation. More recent large-scale PTM studies have shown that the number of methylation sites is quite large with methylated cysteine, histidine, and lysine sites all identified in aged lens or nuclear regions of aged lens. This points more and more toward nonenzymatic mechanisms. Currently, it has not been established when methylation is first observed in lens. It is absent in very young lenses and present at moderate levels in older lenses. Methylation was not significantly more abundant in the water-insoluble fractions (Figure 2), so the functional significance of methylation remains unknown. Future studies are needed to see if normally inaccessible cysteine residues become methylated with advance age or during cataract, which could indicate changes in crystallin conformations.

Oxidation

Oxidation is a defining feature of age-related nuclear cataract but the form of oxidation may not be a simple addition of oxygen (a +16 mass increase). Other forms of

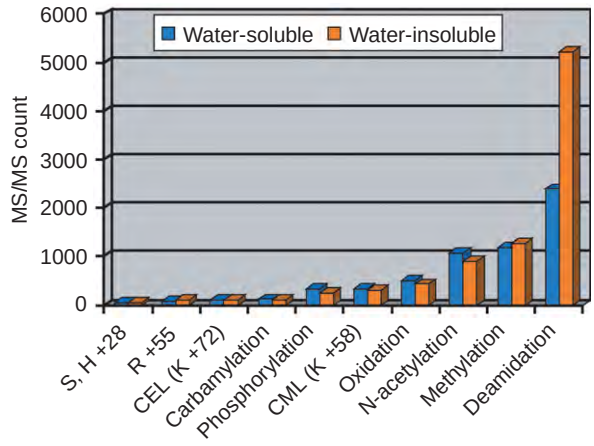

Figure 2 A spectral count comparison of modified peptides of three aged lens samples where water-soluble fractions were compared to water-insoluble fractions. Adapted from Wilmarth, P. A., Tanner, S., Dasari, S., et al. (2006) Age-related changes in human crystallins determined from comparative analysis of post-translational modifications in young and aged lens: Does deamidation contribute to crystallin insolubility? *Journal of Proteome Research* 5(10): 2554–2566.

oxidation, such as disulfides or mixed sulfhydryls, are more difficult to detect in mass spectrometry-based studies. There are 34 methionine residues in the major lens crystallins and 28 have been reported as oxidized (82%). There are 53 tryptophan residues and 42% (22) have been found to be oxidized. Oxidation of methionine can be caused by sample handling, especially in gel-based studies and many of the reported studies failed to demonstrate that methionine oxidation occurred *in vivo*. Tryptophan is much more resistant to artifactual oxidation and it is more likely that these sites, listed in **Table 1**, are true *in vivo* sites of oxidation. Spectral counting data shown in **Figure 2** indicated that the level of oxidation is relatively low in normal aged lenses and was not correlated with loss of solubility. An increase in tryptophan oxidation has been reported in cataractous lenses. The majority of these residues had low solvent accessibility, suggesting that oxidation of tryptophan may serve as a marker of protein unfolding with advanced age or during cataract formation.

Acetylation and Carbamylation

The majority of acetylation in lens occurs cotranslationally at the protein N-terminus for α- and β-crystallins. Data suggest that N-terminal acetylation is essentially quantitative for these proteins and protection of the reactive N-terminus may be advantageous for lens protein longevity. Interestingly, the γ-crystallins are not acetylated although N-terminal carbamylation has been reported. Lysine residues in the α-crystallins are the only other reported sites of acetylation in lens that have been seen in more than one study. It is not known if this modification occurs before, during, or after fiber cell differentiation and its biological significance remains unclear.

Carbamylation of several lysine residues were found to be more abundant in aged than young lens, but were present at similar low levels in water-soluble and water-insoluble fractions (**Figure 2**). Urea is commonly used to denature proteins prior to enzymatic digestion and its by-product (isocyanate) can cause carbamylation during sample processing. Thus, comparisons to control samples or avoiding urea use during sample processing steps are necessary to identify *in vivo* sites.

Phosphorylation

Phosphorylation has been reported at 27 sites in 10 crystallins, and only 7 sites in the α-crystallins have been detected in multiple studies. The reliability of most of these other sites remains unclear. It seems unlikely that phosphorylation would occur in mature fiber cells where enzymatic activities are presumed to be absent, and phosphorylation may be related to fiber cell differentiation or development. The data in **Figure 2** indicated that the levels of phosphorylation were comparable between water-soluble aged lens fractions and water-insoluble fractions. There are few reports that implicate phosphorylation in aging lens changes or cataract formation.

Other Lysine and Arginine Modifications

The unrestricted PTM search strategy used by Wilmarth and colleagues identified several previously unreported types of lens modifications. Lower levels of unusual lysine (+58 Da and +72 Da) and an unknown arginine (+55 Da) modifications were perhaps the most interesting of these modifications. It is speculated that these modification are advanced glycation end products such as carboxymethylation (+58 Da) or carboxyethylation (+72 Da) and may be markers of advanced age or oxidative stress.

Truncation

Extensive proteolysis of lens crystallins has been reported by several laboratories, and the N- and C-terminal extensions of the crystallins are the protein regions the most susceptible to truncation. It has been reported that high-molecular-weight lens protein complexes from aged lenses contain N- and C-terminally truncated fragments of αA and αB. Also, fragments of α-crystallins, β-crystallins, γ-crystallins, filensin, and vimentin have been found in the water-insoluble lens proteins. Increased high-molecular-weight protein complexes and water-insoluble proteins are thought to be detrimental to lens function.

While the bottom-up proteomic approach of digesting proteins by (typically) trypsin is by far the most successful

method to identify and assign PTM sites, it is not very effective in studies of proteolysis and truncation. Truncations, in principle, can be inferred from an atypical semitryptic peptide (either from the N-terminus or the C-terminus of the truncated protein form). However, those peptides may be too small to be detected or produced from other processes (in-source fragmentation, for instance). Gel-based separations have been used most often, but differential N-terminal labeling strategies or top-down methods may provide non-gel alternatives in truncation studies.

Functional Significance of Lens PTMs

The major age-related crystallin modification by far is deamidation. Yet, the functional significance of deamidation in the lens is not known. Deamidation occurs primarily by nonenzymatic reaction mechanisms. In addition to adding a negative charge, which by itself can alter protein structure and function, deamidation can lead to protein backbone cleavage, racemization, and isomerization.

The β-crystallins form complex hetero-oligomers partly due to hydrophobic interactions and hydrogen bonds that stabilize the interacting surfaces between subunits. The α-crystallins also form complex oligomers whose interactions have not been as clearly defined. Nonetheless, α-crystallins have chaperone activity *in vitro* and are likely to have chaperone activity in the lens. It is not surprising that the stabilizing interactions and functional activity of crystallins may be compromised by modifications, such as deamidation and truncation.

In support of the above, numerous studies have shown compromised biophysical properties of deamidated crystallins *in vitro*. Deamidation decreased β-crystallin stability *in vitro*, and similar findings have been reported for α- and γ-crystallins. Soluble aggregates were detected in βA3 when deamidations were introduced on the surface of the protein and surface deamidations in βA3 were more abundant in the insoluble proteins in aged and cataractous lenses. These *in vitro* and *in vivo* studies suggest that the accumulation of extensively modified crystallins and, in particular, deamidated crystallins, may be the reason for the increasing amount of insoluble lens protein that accumulates with age, compromising the transparency of the lens.

Accumulation of extensively modified crystallins during one's life may lead to impaired lens function such as inability to accommodate resulting in presbyopia and eventually to age-related cataracts. Little by little, we are discovering the mechanisms by which these modifications contribute (directly or indirectly) to lens hardening, presbyopia, and age-related nuclear cataract.

A fairly comprehensive tabulation is emerging of the major modifications of lens proteins. However, rigorous quantitative analysis of the differences in the abundance of these modifications in normal and pathologic conditions is still missing. Future experiments must focus on obtaining a large set of graded normal and cataractous human lenses on which a targeted quantitative analysis of the known modifications can be performed. Surprisingly, the biggest hurdle to overcome is not the methods of analysis, but obtaining a significant number of graded control and cataractous lenses to do the study properly.

See also: Nuclear Cataract.

Further Reading

Bloemendal, H., de Jong, W., Jaenicke, R., et al. (2004). Ageing and vision: Structure, stability and function of lens crystallins. *Progress in Biophysics and Molecular Biology* 86(3): 407–485.

David, L. L., Lampi, K. J., Lund, A. L., and Smith, J. B. (1996). The sequence of human betaB1-crystallin cDNA allows mass spectrometric detection of betaB1 protein missing portions of its N-terminal extension. *Journal of Biological Chemistry* 271(8): 4273–4279.

Fujii, N., Ishibashi, Y., Satoh, K., Fujino, M., and Harada, K. (1994). Simultaneous racemization and isomerization at specific aspartic acid residues in alpha B-crystallin from the aged human lens. *Biochimica et Biophysica Acta* 1204(2): 157–163.

Hains, P. G. and Truscott, R. J. (2007). Post-translational modifications in the nuclear region of young, aged, and cataract human lenses. *Journal of Proteome Research* 6(10): 3935–3943.

Hanson, S. R., Hasan, A., Smith, D. L., and Smith, J. B. (2000). The major *in vivo* modifications of the human water-insoluble lens crystallins are disulfide bonds, deamidation, methionine oxidation and backbone cleavage. *Experimental Eye Research* 71(2): 195–207.

Harrington, V., Srivastava, O. P., and Kirk, M. (2007). Proteomic analysis of water insoluble proteins from normal and cataractous human lenses. *Molecular Vision* 13: 1680–1694.

Lampi, K. J., Amyx, K. K., Ahmann, P., and Steel, E. A. (2006). Deamidation in human lens betaB2-crystallin destabilizes the dimer. *Biochemistry* 45(10): 3146–3153.

Lampi, K. J., Ma, Z., Hanson, S. R., et al. (1998). Age-related changes in human lens crystallins identified by two-dimensional electrophoresis and mass spectrometry. *Experimental Eye Research* 67(1): 31–43.

Lapko, V. N., Cerny, R. L., Smith, D. L., and Smith, J. B. (2005). Modifications of human betaA1/betaA3-crystallins include S-methylation, glutathiolation, and truncation. *Protein Science* 14(1): 45–54.

Lapko, V. N., Purkiss, A. G., Smith, D. L., and Smith, J. B. (2002). Deamidation in human gamma S-crystallin from cataractous lenses is influenced by surface exposure. *Biochemistry* 41(27): 8638–8648.

Robinson, N. E. and Robinson, A. B. (2004). Molecular clocks. *Proceedings of the National Academy of Sciences of the United States of America* 98(3): 944–949.

Takata, T., Oxford, J. T., Demeler, B., and Lampi, K. J. (2008). Deamidation destabilizes and triggers aggregation of a lens protein, betaA3-crystallin. *Protein Science* 17(9): 1565–1575.

Takemoto, L. (2001). Deamidation of Asn-143 of gamma S crystallin from protein aggregates of the human lens. *Current Eye Research* 22(2): 148–153.

Truscott, R. J. (2005). Age-related nuclear cataract-oxidation is the key. *Experimental Eye Research* 80(5): 709–725.

Wilmarth, P. A., Tanner, S., Dasari, S., et al. (2006). Age-related changes in human crystallins determined from comparative analysis of post-translational modifications in young and aged lens: Does deamidation contribute to crystallin insolubility? *Journal of Proteome Research* 5(10): 2554–2566.

Nuclear Cataract

R J W Truscott, Sydney University, Sydney, NSW, Australia

Glossary

Nuclear cataract – The opacification of the central region of the lens, usually associated with increased hardening of this region. For this reason, clinicians often refer to this as nuclear sclerotic cataract.
Presbyopia – The increasing loss of ability to focus on near objects with age. Stiffening of the lens cytoplasm is thought to play a major role in presbyopia.
Racemization – The randomization of direction of optical rotation of an optically active molecule. In lens proteins, some amino acids, notably aspartic acid, undergo time-dependent racemization from the L- to the D-form.

Cortical Cataract and Nuclear Cataract

There are two major types of age-related cataract: cortical which affects the outer half of the lens, and nuclear which involves opacification of the lens center. This central region consists of proteins that were synthesized *in utero*.

In contrast to cortical cataract, which is still ill-defined in terms of its molecular etiology, great strides in understanding have recently been made in the area of nuclear cataract. This is certainly not to say that we understand it completely, but there is now a framework.

Classification

It is generally easy to recognize nuclear cataract. The nucleus of the once transparent lens has become opaque and colored. In 1968, Antoinette Pirie used nuclear color as a means of classifying age-related nuclear cataract (ARNC) lenses. This semisubjective classification method has been remarkably successful. Nearly all of the biochemical correlates that are associated with ARNC have been derived using this method. For example, as will be illustrated below, moving from the earliest stage of ARNC (type II) to the most advanced (type IV) has been found to be associated with a progressive increase in urea-insoluble protein, oxidation of methionine, and cysteine and protein cross-linking. Later, other more detailed classification schemes (e.g., various iterations of the Lens Opacity Classification scale (LOCS)) have been introduced.

Cataract is Not the Same as Aging

Too often, even today, lens scientists occasionally lump these two quite distinct phenomena when compiling lists of changes that take place in older lenses. As will become clear later in this review, aging is almost certainly a prerequisite for ARNC, but the changes that take place in aging and ARNC, can and should, be distinguished. A summary outlining the proposed sequential steps in ARNC formation is shown in **Figure 1**.

Features that Distinguish ARNC from Normal Aging

At present, there are four key characteristics that can be used to differentiate ARNC lenses from age-matched normal lenses, and these are discussed below.

Insoluble Protein

Insolubility is a problematic feature since it requires the tissue of interest to be processed in some way, typically by homogenizing it, and the amount of protein that is deemed soluble will depend on the number of extractions, buffer, pH, etc. In normal lenses above the age of 50, approximately half of the total protein in the lens nucleus is no longer soluble in phosphate buffer, pH 7. Since such lenses are still transparent, it is likely that the proteins are not present as a precipitate in the intact lens. We can interpret the laboratory findings in this case to reflect changes in the state of the proteins in the lens.

The onset of ARNC sees the development of a quite separate phenomenon. In these lenses, a new protein fraction can be isolated, which is insoluble even in 8-M urea. This fraction contains most of the color of the ARNC lens and is composed of polypeptides cross-linked by nondisulfide links. The amount of this yellow protein fraction increases progressively in accord with the Pirie classification of ARNC from type II to type III and type IV lenses. In type IV lenses, it comes to represent half of the total nuclear protein. In order to solubilize this yellow protein fraction, a reducing agent such as mercaptoethanol or dithiothreitol must be added to the 8-M urea. In advanced ARNC lenses, a small quantity of protein remains insoluble even after this extraction procedure.

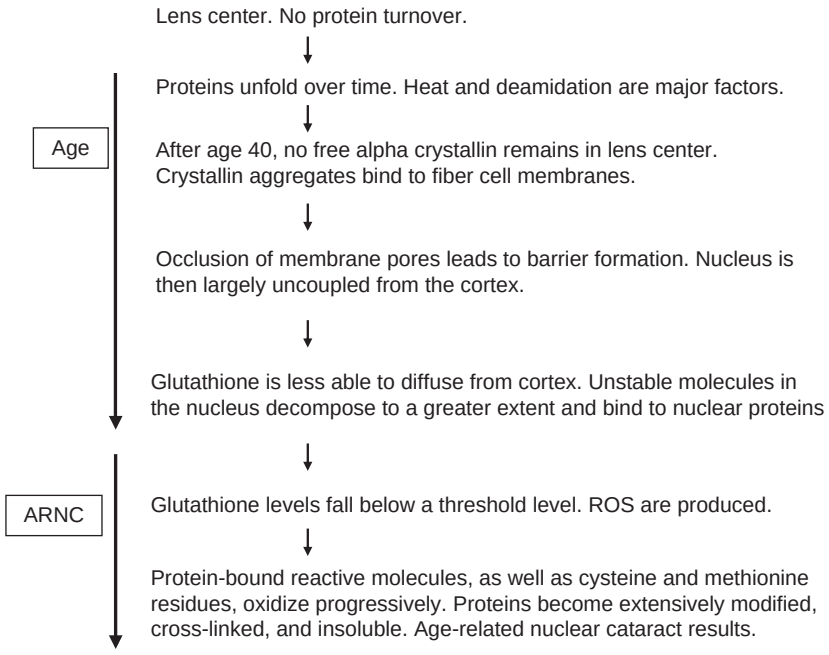

Figure 1 A summary of the sequential steps that take place in the center of the human lens, which may lead to age-related nuclear cataract formation. ROS, reactive oxygen species.

Oxidation

In advanced ARNC lenses, the extent of protein oxidation is unmatched by that of any other biological tissue. In type IV lenses, half of the methionine residues, and more than 90% of cysteines, are oxidized. Oxidation of sulfur-containing amino acids is a hallmark of ARNC. Methionine is oxidized to methionine sulfoxide and the cysteine residues to disulfides.

Oxidation of cysteine, and to a lesser extent methionine, is evident even at the earliest stage (type II) of ARNC and the extent increases as the cataract worsens. This oxidation of proteins can be used to differentiate ARNC lenses from normal lenses, since in aged normal lenses there is almost no methionine sulfoxide and protein thiol levels are typically within the normal range. In some older normal lenses, low amounts of crystallin disulfides can be detected; however, the levels in these lenses are always low, and may reflect the fact that these lenses are soon to become cataractous. All cysteine residues of the crystallins, with the exception of Cys 41 in gamma C and Cys 18 in gamma D crystallin, become oxidized once ARNC develops.

Cross-Linking

In ARNC lenses, two types of cross-links join the crystallins: disulfide and nondisulfide, and both are absent, or in much lower levels, in normal lenses. The extent of protein interchain disulfide bonding in ARNC lenses can be appreciated by the observation that cleavage of such links with reducing agents enables the vast majority of the urea-insoluble protein to become soluble in 8-M urea.

The structure of the nondisulfide bond in ARNC lenses is still unknown and its elucidation would add considerably to our understanding of the processes involved. It is not likely to be the same as that described in a 43-kDa peptide isolated from normal lenses by Spector's group. These authors reported that this novel species may contain a cross-link between crystallins; however, this was not confirmed.

Coloration

Normal human lenses become more colored as they age, and particularly so after age 50. This appears to be primarily due to the binding of breakdown products of reactive molecules, such as ascorbate and kynurenine ultraviolet (UV) filters, to nuclear crystallins. However, in all cases, a yellow hue results.

By contrast, ARNC lenses typically range in color from brown, orange/dark yellow to occasionally black. We still do not know the molecular structures responsible for this pigmentation. Since these colors are found in no other animal cataract, it may well be a human, or at least a primate-specific phenomenon. Since UV filters, such as 3-hydroxykynurenine, are present uniquely in primates, and such molecules readily bind to and tan proteins when exposed to oxygen, it has been postulated that these may be implicated. This hypothesis gained traction when it was discovered that all normal human lenses over the

age of 50 contain measurable levels of 3-hydroxykynurenine bound covalently to proteins in the nucleus. It could be imagined that this binding of reactive molecules to human nuclear crystallins is a potential time bomb waiting to be activated by the arrival of an oxidative environment. Cross-linking and coloration of crystallins would inevitably be the outcome.

Why is ARNC Age-Related?

Epidemiological data suggest that ARNC is inevitable if we are fortunate enough to live for a sufficiently long time. The incidence of ARNC increases substantially as we get older. What aspects of normal aging of the human lens facilitate the later onset of nuclear cataract? To a large extent, this question hinges on the definition of what constitutes normal aging. Substantial progress on the biochemistry of aging of the normal human lens has provided a platform for understanding those aspects that may be the preconditions responsible for subsequent ARNC.

It is now clear that massive changes take place in the normal human lens with age. For example, the stiffness of the center increases approximately 1000-fold in the first few decades of life and this is likely to be the feature that is responsible for presbyopia. Crystallin proteins become deamidated, denatured, and bound to fiber cell membranes. The ratio of free to bound water also changes progressively. After age 50, proteins in the lens center become loaded with covalently bound small molecules. Despite such huge changes, in most cases, the normal aged lens remains transparent. Therefore, which of these substantial alterations is important for the subsequent onset of ARNC?

A Model for ARNC: The Lens Center is an Enzyme-Free Region

In order to understand ARNC, it is first necessary to appreciate that the center of the mature adult lens is an enzyme-free zone. There is no turnover or synthesis of macromolecules in this region. For proteins, it is a life sentence. Although comprehensive data are not available, it would appear that after several decades, all enzymes that were present in the center of the lens, and were therefore synthesized prior to birth, have undergone denaturation and are now inactive. Two studies have demonstrated the presence of enzymes by immunohistochemical methods in the lens core, yet enzyme activity was undetectable. In effect, the center of the middle-aged lens is a chemical incubator where the processes governed in other cells of the body by enzymes, do not apply. The consequences of this are profound.

In order to minimize oxidation and covalent modification of proteins in the lens center, a high concentration of glutathione normally bathes these macromolecules. Glutathione is ideal since it acts not only as an antioxidant, but it can also intercept reactive intermediates and, by reacting with such molecules first, reduce the extent of covalent modification of proteins. Both synthesis of the tripeptide, as well as reduction of oxidized glutathione, takes place in the cortex. It is, therefore, obvious that any impediment to the exchange of glutathione between the cortex and lens nucleus would imperil the stability of nuclear proteins.

Uncoupling the Center from the Lens Cortex

Biophysical studies have demonstrated the onset of a barrier to the diffusion of small molecules within the lens at middle age. This barrier is not absolute, but it impedes the flow of small molecules from the outer parts of the lens into the interior. Interestingly, the existence of the lens barrier has been shown for both glutathione and water. These two molecules may move from cell to cell using quite different pores. In the case of glutathione, movement takes place via gap junctions composed of connexons, whereas water probably diffuses through pores made from the abundant integral membrane protein, aquaporin 0. Since the movement of both molecules are compromised by middle age, it suggests either that both types of channels become less active due possibly to posttranslational modification/cleavage or that a common process within the lens is affecting both types of membrane pores. Recent data suggest that it may be the latter explanation which best fits the data.

Unfolding Crystallins and the Importance of Alpha Crystallin

After age 40, no free alpha crystallin remains in the lens center: all of the chaperone have been used in binding to polypeptides that unfolded over a period of decades. The reasons for the denaturation and unfolding of the crystallins can be traced to the fact that proteins, and particularly some residues within them, are intrinsically unstable over a period of decades. Heat-induced denaturation of polypeptides, combined with deamidation of Gln and Asn residues and the isomerization of Asp/Asn sites, coupled with chemically mediated truncation, combine to destabilize lens proteins.

After age 40, when soluble alpha crystallin has been depleted in the lens center, some marked changes take place in the normal lens. It is at this time when nuclear proteins become increasingly insoluble, and it is noticeable that it is the decade between 40 and 50 in which most changes take place. In recent experiments, we have

demonstrated substantial binding of crystallins to fiber cell membranes during this 10-year period. It seems likely that the interaction of crystallin aggregates with the membranes may well act to clog the pores and, in this way, a barrier may form.

We do not yet understand exactly what processes are necessary to convert a clear middle-aged lens into an ARNC lens. Perhaps the degree of impermeability of the barrier is important in that if diffusion of glutathione from the cortex becomes progressively diminished, a stage may be reached where the environment in the lens core changes from being reducing to oxidative. Maintaining a concentration of glutathione above 1 mM may be crucial, as could be the ability to respond to an increased oxidative insult.

Another Impact of the Lens Barrier

Another feature of the barrier is its role in increasing the residence time of intrinsically unstable molecules in the center of the lens. This latter feature is not generally as well appreciated as the barrier's function in restricting glutathione penetration, but it may be just as important. As noted above, small molecules are able to enter the nucleus after age 50, but their rate of entry is reduced. Similarly, the ability of molecules to move in the reverse direction – from the nucleus to the cortex – will also be hindered. For some molecules that are unstable over a period of hours or days at neutral pH, this factor can be crucial. Two groups of lens constituents that are well known are the kynurenine UV filters and ascorbate. Ascorbate, when it acts as an antioxidant, oxidizes to the unstable triketone, dehydroascorbate. In the absence of sufficient glutathione, which would normally re-reduce the dehydroascorbate, this molecule can bind directly to proteins and it also decomposes to a variety of reactive aldehydes and ketones.

The kynurenine UV filters undergo spontaneous deamination at pH 7. The unsaturated ketones that are produced bind readily to His, Lys, and Cys residues of proteins through their side chains. One of the UV filters, 3-hydroxykynurenine, is an *o*-aminophenol and is therefore highly sensitive to oxidation. It has been proposed that oxidation of 3-hydroxykynurenine that is covalently bound to crystallins, may be responsible for the coloration and cross-linking of polypeptides that characterize ARNC.

Could Sunlight Play a Role in ARNC?

For many years, sunlight was thought to be the prime agent responsible for formation of ARNC. Indeed, it is still mentioned, together with skin cancer, as one of the conditions that will increase as a result of ozone depletion. The premise was that the lens is exposed every day to external light and that over a period of years it was not surprising that the proteins would oxidize. This was especially so since one could readily convert white lens proteins into brown aggregates by exposing them to UV light.

There were, however, some major problems with this hypothesis. First, irradiation destroyed tryptophan (Trp) residues in experimental systems and yet the brown proteins isolated from ARNC lenses did not show any significant reduction in content of Trp. Second, it was unclear why oxidation should be confined to the nuclear lens proteins when light must pass first through the anterior cortex. Third, epidemiology failed to demonstrate any conclusive link between exposure to sunlight and the incidence of ARNC.

The Resurrection of Sunlight?

It is ironic, therefore, that recent experimental data provide an explanation for how UV light could participate in the generation of ARNC. It should be emphasized that this is not evidence for a role of sunlight.

It turns out that protein-bound UV filters behave quite differently from their free kynurenine counterparts. Free UV filters appear to be benign once they absorb UVA light. By contrast, if UV filters are covalently bound, they sensitize the proteins to oxidation. When one considers this fact, in conjunction with the previously mentioned finding that all human lenses after age 50 contain measurable levels of protein-bound UV filters in the nucleus, it is possible to envisage why only the nuclear proteins may oxidize following exposure to ambient UV light. Cortical proteins are modified by UV filter molecules to a much lower degree, as are the nuclear proteins from lenses in people younger than 50. As a consequence, epidemiological evidence may need to be reevaluated. For example, exposure before the age of 50 may have no significant impact, whereas time spent in sunlight after 50 would be expected to be of much greater importance. This is accentuated by the fact that the levels of free UV filters decrease linearly over our life span at approximately 10% per decade. Therefore, older lenses are more susceptible to UV-induced damage.

What is the Primary Oxidant Involved in ARNC?

Oxidative processes are central to the formation of ARNC. It is less certain what the primary oxidant could be. Some oxygen, albeit at low levels, is present in the center of lenses. It has been proposed that increased liquefaction of the vitreous in older people, and in those patients exposed to vitrectomy, may facilitate the diffusion of oxygen from the retina into the lens and therefore

exacerbate ARNC. Such a proposal is supported by separate experimental data where intact lenses and animals, including human infants, have been exposed to hyperbaric oxygen. Experimental studies of UV-filter-modified proteins suggest that singlet oxygen is generated upon irradiation with biologically relevant doses of UVA in the presence of low concentrations of oxygen. Other work using human cataract lenses has revealed that the molecular markers associated with hydroxyl radical damage can be found in ARNC, but not in normal lenses.

Autoxidation of susceptible molecules within the nucleus could generate superoxide locally, which could dismutate into hydrogen peroxide. Peroxide could also potentially diffuse into the interior from mitochondrial electron leakage in the cortex. Certainly, the pattern of oxidation of sulfur-containing amino acids observed in ARNC is what would be expected by exposure of proteins to hydrogen peroxide.

Can ARNC be Prevented?

From the foregoing discussion it is apparent that if nuclear glutathione levels could be maintained in the center of the lens in older people, then it may be possible that ARNC could be delayed, if not prevented. Sadly, this does not seem easy to achieve. Even if one could boost antioxidant levels markedly through dietary or pharmacological means, there would remain the problem of these penetrating the interior of the lens where they are required.

Issues and Questions for the Future

One major impediment to future research on human ARNC is the difficulty in accessing cataract lenses. Phacoemulsification is now almost universal as the technique used to remove cataract lenses and so intact lenses, and even nuclear cores, are becoming increasingly difficult to obtain. This is a huge problem since there appears to be no appropriate nonprimate animal model system that can be employed. Human lenses are unique. As was apparent from the previous parts of this article, it is primarily the changes that take place in the lens over a period of several decades, which appear to be responsible for ARNC. It is, therefore, not an easy condition to model or replicate.

Other Questions

Could Lens Components Other than Crystallins be Involved?

This article has concentrated largely on protein changes as being the dominant factor underlying the etiology of ARNC. Bearing in mind the importance of the barrier and, in particular, membrane interactions of protein aggregates, it is clear that other factors, for example, changes to the lipid composition of the fiber cell membranes, may also play a part in facilitating the formation of the barrier. Preliminary data indicate that substantial changes can be documented in the lipid composition of human lens membranes as a function of age. This remains a topic for future studies, as is the degree to which membrane decomposition and oxidation may be implicated in ARNC.

It is also important to recognize that proteins, other than crystallins, are present in the lens center for all of our lives. The role of cytoskeletal proteins, the intrinsic membrane proteins in particular aquaporin 0, as well as the gap-junctional connexin proteins in ARNC may also be important.

Why Do Some People in India Develop ARNC Much Earlier than Those in Western Nations?

Since it has been reported that ARNC is observed in India more than a decade earlier than in the West, it would seem that a detailed study of people in some Indian regions may shed light on what factors may be responsible for delaying, or accelerating, the onset of ARNC.

Is ARNC Just a Problem that is Lens Specific?

A theme of this article has been that protein denaturation over a period of many decades is at the heart of understanding ARNC. It is becoming increasingly apparent that deducing the impact of changes in protein structure over a period of decades will be important in other human conditions that are associated with aging. The lens is not unique in the body in containing proteins that are present for many decades. Two facets of this longevity, and its relationship to protein unfolding, should be appreciated. First is the intrinsic instability of some amino acid residues. Some were noted briefly in an earlier part of this article, and are well known; others remain to be uncovered. The sites most affected within each protein will depend on the primary, secondary, and tertiary structures, as well as the packing of proteins within each tissue. For example, in the older human lens, deamidation of crystallins is abundant, but is localized to specific regions of each protein.

The second aspect is the role of chemical post-translational modification of proteins over a period of decades. In this sense, the long-lived crystallins of the lens can be viewed simplistically as resembling blotting paper. What are the most important chemical insults over a period of many decades to which proteins are exposed?

It is likely that proteomic investigations may shed light on this aspect.

The relative importance of extralenticular factors, such as the gel state of the vitreous and somatic metabolism, also remain to be established. For example, patients undergoing vitrectomy will, within 12 months, develop ARNC. In addition, patients with ARNC respond differently from age-matched normal subjects in terms of their serum response to an oral dose of Trp and their lenses contain higher-than-normal levels of amino acids. The explanations for these intriguing observations and, in particular, how such findings would relate to the etiology of ARNC, are not yet clear

Conclusion

In summary, there is now a coherent framework for understanding ARNC and why it is that this condition becomes apparent only in our later years. It may well be that the human lens is the ideal system for understanding more general aspects of human aging, particularly those that involve protein modification and denaturation. Lessons derived from the lens may, in the future, be applied more widely to other tissues of the body.

See also: Cortical Cataract; The Epidemiology of Cataract; Genetics of Age-Related Cataract; Genetics of Congenital Cataract; Lens Structure; Normal Age-Related Changes: Crystallin Modifications, Lens Hardening; Posterior Capsule Opacification; Posterior Subcapsular and Anterior Polar Cataract.

Further Reading

Giblin, F. J. (2000). Glutathione: A vital lens antioxidant. *Journal of Ocular Pharmacology and Therapeutics* 16: 121–135.

Harding, J. J. (1991). *Cataract Biochemistry, Epidemiology and Pharmacology*. London: Chapman and Hall.

Heys, K. R., Friedrich, M. K., and Truscott, R. J. W. (2007). Presbyopia and heat. Changes associated with aging of the human lens, suggest a functional role for the small heat shock protein, α-crystallin, in maintaining lens flexibility. *Aging Cell* 6: 1950–1960.

Lampi, K. J., Ma, Z., Hanson, S. R., et al. (1998). Age-related changes in human lens crystallins identified by two-dimensional electrophoresis and mass spectrometry. *Experimental Eye Research* 67: 31–43.

Pirie, A. (1968). Color and solubility of the proteins of human cataracts. *Investigative Ophthalmology* 7: 634–650.

Streete, I. M., Jamie, J. J., and Truscott, R. J. W. (2004). Lenticular levels of free amino acids and UV filters differ significantly between normals and cataract patients. *Investigative Ophthalmology and Visual Science* 45: 4091–4098.

Truscott, R. J. W. (2005). Age-related nuclear cataract – oxidation is the key. *Experimental Eye Research* 80: 709–725.

O

Ocular Media Clarity and Straylight

T J T P van den Berg, L Franssen, and J E Coppens, Netherlands Institute for Neuroscience of the Royal Netherlands Academy of Arts and Sciences, Amsterdam, The Netherlands

Glossary

Angle – In ophthalmology, it is usually measured in degrees (or °) and minutes of arc (or ′). A full circle encompasses 360°, and 1° = 60′. The horizontal human visual field encompasses ± 100°. The scientific standard for angle is the radian, with $2\pi = 360°$.
Commission internationale d'Eclairage **CIE, or International committee on illumination** – International standards committee with representative bodies in virtually all larger countries, acknowledged by ISO.
Disability glare – The effect of straylight on the eye whereby visibility and visual performance are reduced. Disability-glare sensitivity and straylight can be used synonymously according to CIE definition. Discomfort glare is glare that produces discomfort. It does not necessarily interfere with visual performance or visibility.
Glare – The effect produced by a luminance within the visual field that is sufficiently greater than the luminance to which the eyes are adapted to cause annoyance, discomfort (discomfort glare or psychological glare), or loss in visual performance and visibility (disability glare or physiological glare).
Light scatter – The physical effect of irregular material on the transmission of light, whereby part of the light is deflected. Most often scattering by isolated (often optically independent) and small irregularities is considered, resulting in straylight. Sometimes the word scatter is used for small-angle light spreading resulting from large-scale refractile aberrations.
Point-spread function or PSF – The (effective) distribution of light in the eye, deriving from an ideal point source of light, and delivering the unit amount of light to the eye. Properly defined, the PSF integrates to unity. When expressed with the visual angle θ as an independent variable, the functional (as seen) PSF equals $L_{eq}(\theta)/E_{bl}(\text{ster}^{-1})$, with $L_{eq}(\theta)$ the equivalent luminance (as seen), and E_{bl} the illuminance on the eye deriving from the point source.
Steradian – The unit for solid angle, shortened to ster. or sr. A half sphere encompasses 2π steradian.
Straylight – The outer part of the functional PSF of the human eye. As practical limits, values 1–100° are used. It is quantified by means of the straylight parameter $s(\theta)$, defined by $s(\theta) = \theta^2\,\text{PSF}(\theta) = \theta^2\,L_{eq}(\theta)/E_{bl}$. As for most eyes, the dependence on θ is weak, $s(\theta)$ is often shortened to s.
Straylight meter – An instrument for performing a psychophysical test to determine the straylight parameter. The psychophysical tests aim to establish the equivalent luminance L_{eq} deriving from a glare source with calibrated E_{bl} value. Originally, only threshold tests were employed, but more recently, equivalence is established by means of counter-phase flicker, as used in the current, only commercial, instrument (C-Quant by Oculus).

Introduction

Disturbances to the eye media may cause vision loss of several different types. With visual-acuity assessment using a letter chart and other means, the smallest detail that can be resolved is established. With the contrast sensitivity test, testing is extended to include not only the smallest distances, but also differences over somewhat larger distances, typically up to a few tenths of a degree. However, eye-media disturbance can also degrade vision because it may cause light scattering. This results in a veil of straylight over the image, strongly depending on the presence of brightness differences as typical in most visual scenes. The complaints

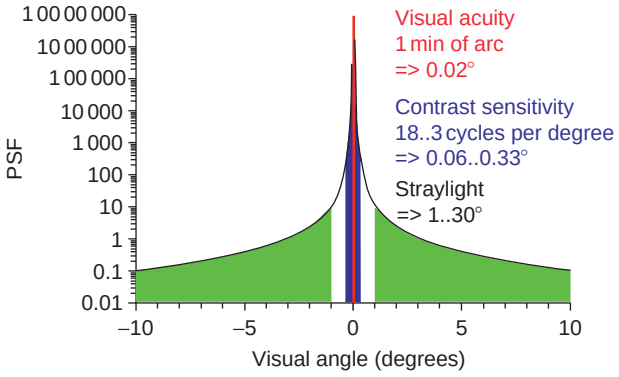

Figure 1 Point-spread function (PSF) of the normal human eye according to the standard formulated for the CIE in 1999. When the eye looks at a point source, the actual light distribution spreads out over the full retina. Different domains of this distribution are indicated, dominating different aspects of visual function. The PSF has steradian^{-1} as unit, and integrates to unity (steradian to be used as variable of integration).

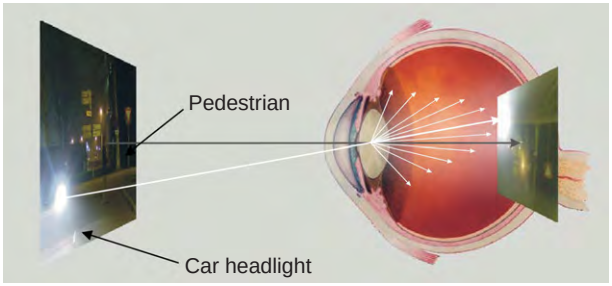

Figure 2 Visualization of retinal straylight. The optical components of the eye form an image of the outside world (left picture) on the retina (right picture). In the case of such a street scene, the picture on the retina is much degraded because part of the light coming from the car headlight is scattered in all forward directions (white arrows in the figure), projecting a veil of light over the retinal image. This veil of light is called straylight. Actually, the left picture simulates what a normal eye would see, and the right picture, what would be seen with an early cataract.

may include hazy vision, increased glare hindrance, loss of contrast and color, etc. These problems are much worsened if visual function is already low from retinal pathology, such as in macular degeneration or glaucoma.

It has long been realized that 20/20 is not enough. Contrast sensitivity was added to better assess full quality of vision. However, contrast sensitivity also was not enough. This can be understood on the basis of the large dynamics of the human eye, as illustrated in Figure 1. Figure 1 shows the point-spread function (PSF) of the normal human eye (for the average Caucasian at 62 years of age), according to the standard observer defined by the *Commission internationale d'Eclairage* (CIE). It gives the light distribution that follows from a point source of light. It shows that a point source does not project on the retina as a point, but strongly spreads out. This spreading of light is caused by several essentially different optical errors of the eye. The PSF dictates the effects of imperfect eye optics on vision. This has been studied over the years in many publications.

Different domains can be identified in the PSF. Ideally, light distribution should only be the central peak up to 1 min of arc, shown in red. The optically ideal PSF is called the Airy pattern, resulting from the fundamental diffractive properties of light, with a central disk extending to 1.22 × wavelength/pupil diameter. With a wavelength of 550 nm, and a pupil diameter of 4 mm, gives 1.2 min of arc for the central disk to become zero (this would be minus infinity in Figure 1 because of the logarithmic scale). However, actual eyes show aberrations causing this central peak to widen. This is the reason why Figure 1 does not show the very steep decline toward minus infinity at 1.2′. The most central area dominates visual acuity. The next area goes on to 10 min of arc (the blue area), which dominates contrast sensitivity (6 cpd corresponds to 5 min of arc band width). However, the light spreading continues over the full retina. The light spreading over 60 min of arc (1°) and more is called straylight. Every area of this PSF is important for quality of vision.

Straylight

Small-angle disturbances to the eye media may cause vision loss of small detail, determined with visual acuity assessment using a letter chart or contrast sensitivity. But how does the light scattered over larger distances affect vision? The light scattered results in a veil of straylight over the retinal image (see Figure 2). The patient's complaints may include hazy vision, increased glare hindrance, loss of contrast and color, etc. If concomitant retinal pathology exists, as macular degeneration, retinal dystrophy, or glaucoma, the problems experienced from straylight are much aggravated, calling for extra attention on straylight in such patients.

It is important to realize that the effect of straylight on vision is totally different from the effect of decreased visual acuity on vision. This is illustrated in the following examples, produced with known realistic means. Daily-life scenes were photographed under three conditions: normal, with a blurring lens, and with a light-scattering filter in front of the camera lens. The blurring lens simulates decreased visual acuity of about 0.4; the scattering filter simulates increased light scattering of around $\log(s) = 1.5$ (see Figure 3). Normal visual acuity would be around 1.5, and a normal straylight value would be around $\log(s) = 0.9$; therefore in both cases, the image is deteriorated by a factor of 4. These pictures illustrate that, in certain daily-life circumstances, increased light scattering has a much stronger effect on the quality of vision than decreased visual acuity.

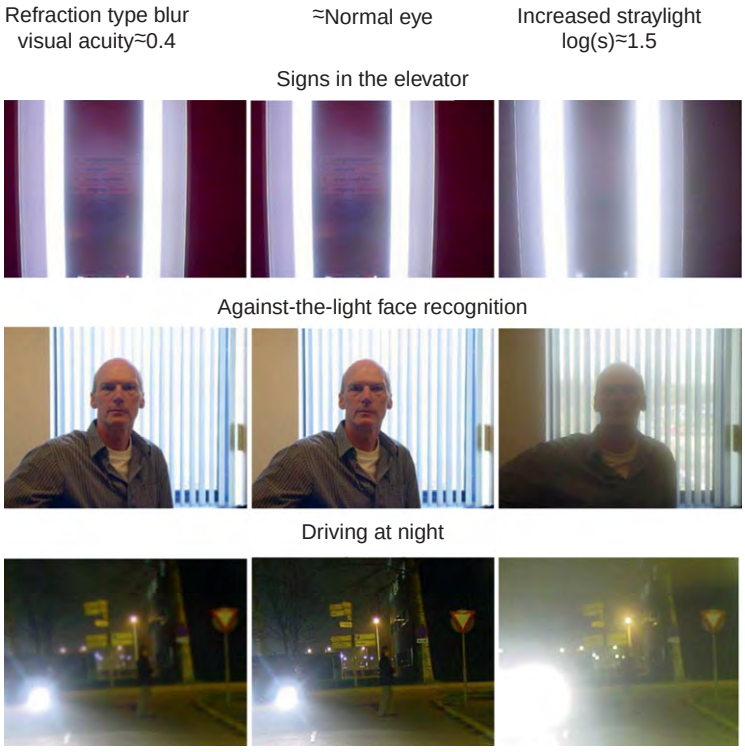

Figure 3 Comparison between refraction type blur (visual acuity around 0.4) and early straylight disturbance (log(s) around 1.5), for different daily-life situations.

History

Since the beginning of the twentieth century, the importance of retinal straylight for visual function has been recognized by several investigators. Cobb introduced the concept of equivalent veiling luminance (L_{eq}) as an apt way to define retinal straylight. Disability glare/retinal straylight, as defined by the CIE, is now quantified by means of this concept of equivalent luminance, that is, the (external) luminance that has the same visual effect as the glare source at some angular distance. Holladay and Stiles applied this concept in their measurements and formulated a disability glare formula, which has been widely used. Nowadays, retinal straylight can also be introduced as the outer skirt of the PSF, outside say, 1°. Since retinal straylight is defined in a functional sense by L_{eq}, the comparison with the PSF only holds if the PSF is also defined in the functional sense. Retinal straylight causes a veiling luminance over the whole retina that adds to the retinal projection of the visual scene, thereby reducing the contrast of the retinal image. Important overview papers were written by Vos. In 1999, a standard was proposed to the CIE (see **Figure 1**) for the normal eye, including age and pigmentation effects.

The first attempts to measure intraocular straylight by means of equivalent luminance involved two types of threshold measurements: thresholds in the presence of a distant glare source and those in the presence of a homogeneous background luminance. From such a series of measurements, the equivalent luminance could be derived, defined as the luminance giving identical thresholds as the glare source (equivalent veil method). This method did not gain practical use, such as in clinical or driver-licensing applications, because it was quite elaborate. As a result, variation was quite large between the older studies. However, the method continued to be used in experimental applications. Some approximate alternatives were designed to circumvent the measurement load. As even more easy-to-use alternatives, the so-called glare testers were introduced, which usually consisted of a visual acuity or contrast sensitivity test, with and without a glare source presented at some angular distance in the visual field. As a result of issues with glare testers, a standard way of glare measurement was never adopted.

To improve on this situation, a dedicated psychophysical method was designed, called the direct compensation (DC) method. In short, this method works as follows: A bright ring-shaped light source around a (dark) test field is presented flickering. Due to intraocular scatter, part of the light from the bright ring-shaped source will be projected on the retina at the location of the test field, inducing a (weak) flicker in the test field. To determine the exact amount of straylight, variable counterphase compensation light is presented in the test field. By adjustment of the amount of compensation light, the flicker perception in the test field

can be extinguished. In this way, the straylight modulation caused by light scattered from the glare source is directly compensated. In 1990, this technique was implemented in a small portable device, called straylight meter. Apart from the group of Van den Berg, this led to studies notably by the groups of Elliott, Kooijman, Schallhorn, and Alexander. However, outside the laboratory it proved to be a difficult technique. In 2003, a better psychophysical approach was defined, called compensation comparison (CC), and implemented in a commercial instrument, by the German firm Oculus, called C-Quant (see Figure 4). The essential difference was that this new approach is suitable for random subjects and for routine clinical use. Moreover, the CC approach enables control over the reliability of the assessment.

Figure 4 The C-Quant instrument from Oculus for measuring the amount of straylight in patient eyes.

Normal Eyes

Figure 5 shows the age dependence of straylight in the normal population. Straylight/disability glare increases with age A by a factor

$$\left[1+\left(\frac{A}{D}\right)^4\right],$$

where D is the age at which the amount of straylight doubles. Values for D were found to be between 62.5 and 70 years. This age dependence was later implemented in a more extensive model including pigmentation as a second parameter. The model was further refined, including age-dependency formulas of different levels of complexity, applicable in different angular-validity domains. This led to a proposal to the CIE for a standard glare observer in 1999, which was accepted as the CIE standard a few years later.

Angular dependence is classically described with the Stiles–Holladay approximation (proportionality to angle^{-2}), holding relatively well between 1° and 30°. As this approximation also holds for aging eyes, including cataracts and other conditions, for most applications, a measurement at one angle suffices. As a consequence, the PSF multiplied with θ^2 (the definition of the straylight parameter s) is more or less constant between 1° and 30°.

Pigmentation of the eye was found to be of importance for quality of vision. Blue-eyed Caucasians were found to have 0.1–0.4 log units higher straylight values compared to pigmented non-Caucasians, depending on angle. This pigmentation dependence is partly caused by variations in transmission of light through the ocular wall. For dark-brown eyes of pigmented individuals, transmission

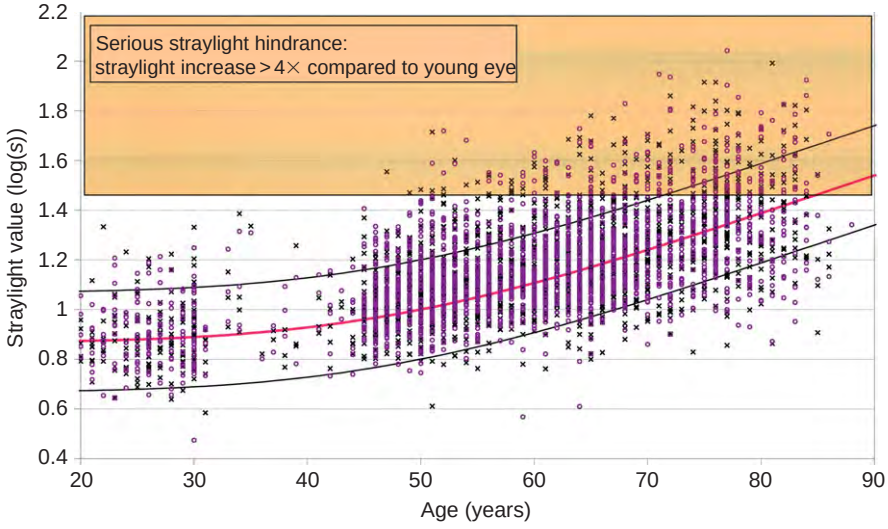

Figure 5 Log(*s*) values at 10° as a function of age for a population of European drivers. Keep in mind that, because of the logarithmic scale, a 0.3 increase in the log(*s*) value means in fact a doubling of the amount of straylight, and a log(*s*) increase of 1 means a tenfold increase in straylight.

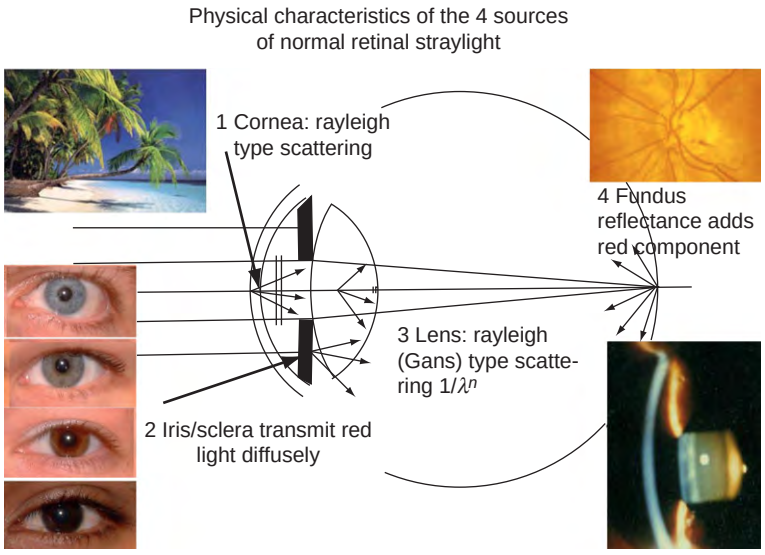

Figure 6 Primary sources of intraocular straylight in the normal eye: corneal scatter, iris, and sclera transparency, lens scatter, and fundus scatter.

was found to be orders of magnitude lower than that for blue-eyed individuals. Furthermore, variations in fundus reflectance are also partly responsible for pigmentation dependence of straylight. In albinism and other defects to pigmentation, the effects can be much stronger. Figure 6 gives an overview of the sources of straylight in the normal eye.

Wavelength dependence of straylight is important as a clue to what processes in the eye might cause straylight. A strong inverse wavelength dependence would signify scatter in the optical media to originate from particles of sizes in the same range as, or smaller than, the wavelength of light. (Like the blue of the sky originates from light scattering by very small irregularities in the air, which is called Rayleigh scatter.) However, depending on pigmentation, eye-wall transmittance and fundal reflections may introduce a straylight component with a wavelength dependence of the opposite sign (red dominant), negating the wavelength dependence from small particle scatter as identified in the lens and cornea.

Sources of straylight in the normal eye at young age are to about equal amounts, the cornea, the lens, and the pigmentation-dependent part. At older age only the lens component changes considerably, so as to dominate the other two, especially if (early) cataract develops. Often, straylight increase is the first complaint, before visual acuity changes.

Cataract

Cataract dependence of straylight was measured in patients with cortical, nuclear, or posterior subcapsular cataract. When compared to visual acuity, on average, the posterior subcapsular type showed the largest straylight increase, but individual results varied considerably. In all cataract types, straylight was often found to be increased considerably while visual acuity was still good; however, in other patients, the reverse was also possible. The important conclusion for ophthalmological practice is that straylight must be taken into account for just assessment of visual problems from cataract, and the decision for cataract surgery.

The angular dependence was found to be about the same for the different cataract types. The behavior was found to be similar to normal (extreme) aging, and it was concluded that, at least with respect to straylight, cataract can be modeled as early aging of the crystalline lens. Light-scattering filters that could be used to simulate the straylight characteristics of cataract were defined (used to create Figure 2). Straylight values after cataract surgery were found to be significantly decreased compared to preoperative values, but still about a factor of 2 above expected (best) levels. The reason is not yet resolved but may partly be due to the intraocular lenses or preclinical forms of posterior capsule opacification (PCO).

Cornea

The cornea proved to be a particularly sensitive organ for straylight increase. In experimentally hydrophilic contact-lens-induced corneal edema on average, a 10% corneal swelling induced a 50% increase in straylight. Variability in this relationship was speculated to be due to changes in the epithelium caused by the contact lens. After contact lens removal, individual straylight values decreased linearly with time, on a similar timescale as the decrease in

corneal swelling. Straylight scores in established contact-lens wearers were found to be significantly greater than in age-matched normals. Rigid gas permeable (RGP) contact lenses were shown to induce more straylight than hydrophilic contact lenses. Subclinical corneal edema seemed to be prevalent in some subjects.

Pathological conditions of the cornea may variably induce increased light scatter, strongly depending on the type of disease. In central crystalline dystrophy, straylight was found to be much increased while visual acuity was relatively well preserved. Alternatively, in posterior polymorphous dystrophy, straylight was not increased, even with impaired visual acuity. In macular and also lattice dystrophy, straylight and visual acuity were affected in a similar way. For deep lamellar endothelial keratoplasty (DLEK) and penetrating keratoplasty (PK), small differences on average between pre- and postoperative straylight values were found. Here the effects of habitual glasses must be mentioned. They were found to induce, as a rule, less straylight than is already present in the eye. The speculative conclusion is that the glass wearer has a tolerance against straylight from his glasses in dependence on his natural level. Higher straylight levels induce him to clean his glasses.

Since the introduction of laser refractive surgery, much concern has been expressed with respect to straylight problems regarding this type of corneal surgery. In radial keratotomy (RK), mean straylight increases by a factor of 1.4 (0.15 log units) in eyes with 4-mm-sized pupils and a factor of 2 (0.3 log units) for 8-mm-sized pupils. These values may be considered as functionally significant increases, but increases of a factor of 6 (0.8 log units) were also found. Studies on photorefractive keratectomy (different varieties are known by acronyms such as PRK, laser-assisted *in situ* keratomileusis (LASIK), and laser-assisted sub-epithelial keratomileusis (LASEK)) provided a less-clear picture. It is well known that a clear haze in the cornea or interface debris as result of the procedure gives subjective complaints, but with the advancement of techniques, these are not often seen. The emerging picture seems that in most cases, straylight does not increase, but that in 5–20% of the cases, depending on the study, significant straylight increase is found, without, in many cases, clear clinical signs.

Forward and Backward Scatter

Straylight reflects the effects of forward light scatter in the eye media. Several methods exist to assess the condition of the eye media using backward light scatter. In fact, the basic ophthalmological tool to evaluate the eye media (the slit lamp) is based on back scatter. Other examples are Scheimpflug slit-image photography, lens opacity meter, and lens opacities classification system (LOCS). One may wonder whether backward light scatter faithfully reflects the functional effect of light scatter in the eye, which is determined by forward light scatter. To address this question, *in vitro* measurements of light scatter in human donor lenses were performed, which showed that backward and forward light scatter are dominated by different light-scattering processes. In correspondence with these *in vitro* studies, patient studies on the comparison between different measures of backward light scatter and forward light scatter showed very variable results. It must be noted here that we consider forward scatter not in a very closely forward direction, but over angles of more than 1°. For more closely forward angles (smaller than 1°) we approach the domain that can be captured with other techniques, such as double-pass and wavefront-sensing approaches.

CIE Standard Observer

As mentioned above, the CIE has adopted standards for the glare of the normal observer. The CIE equations are given here. The total glare function proposed by Vos and Van den Berg (as eqn [8] in the CIE report) does actually give the complete PSF. It reads:

$$\mathrm{PSF} = [L_{\mathrm{eq}}/E_{\mathrm{gl}}]_{\mathrm{total}} = \left[(1-0.08)(A/70)^4\right]\left[\frac{9.2\times10^6}{\left[1+(\theta/0.0046)^2\right]^{1.5}}+\frac{1.5\times10^5}{\left[1+(\theta/0.045)^2\right]^{1.5}}\right] + \left[1+1.6(A/70)^4\right]\left\{\left[\frac{400}{1+(\theta/0.1)^2}+3\times10^{-8}\times\theta^2\right] + p\left[\frac{1300}{\left[1+(\theta/0.1)^2\right]^{1.5}}+\frac{0.8}{\left[1+(\theta/0.1)^2\right]^{0.5}}\right]\right\} + 2.5\times10^{-3}\times p[sr^{-1}],$$

where θ is the glare angle in degrees, A the age in years, and p a pigmentation factor ($p = 0$ for very dark eyes, $p = 0.5$ for brown eyes, and $p = 1.0$ for blue–green-eyed Caucasians).

Figure 1 shows the angular course of this function for $A = 62$ years and $p = 1$. Note that the total dynamics of the PSF span a range of about 10^9, or 1 000 000 000. Due to this enormous range, the differences for the various conditions appear to be very subtle, whereas, in fact, they are functionally very significant. These differences are more clearly represented when the curves are presented in terms of the straylight parameter s by multiplication of the PSF with θ^2. In this way, the approximate $1/\theta^2$ angular dependence is removed, so as to allow a better view of differences, see **Figure 7**.

For practical purposes, the CIE 1999 total glare equation is relatively complicated. Therefore, some simplified equations were formulated. The most simple (given as eqn [9] in the CIE report) version of a disability glare formula seems to be the classic Stiles–Holladay equation, in which the

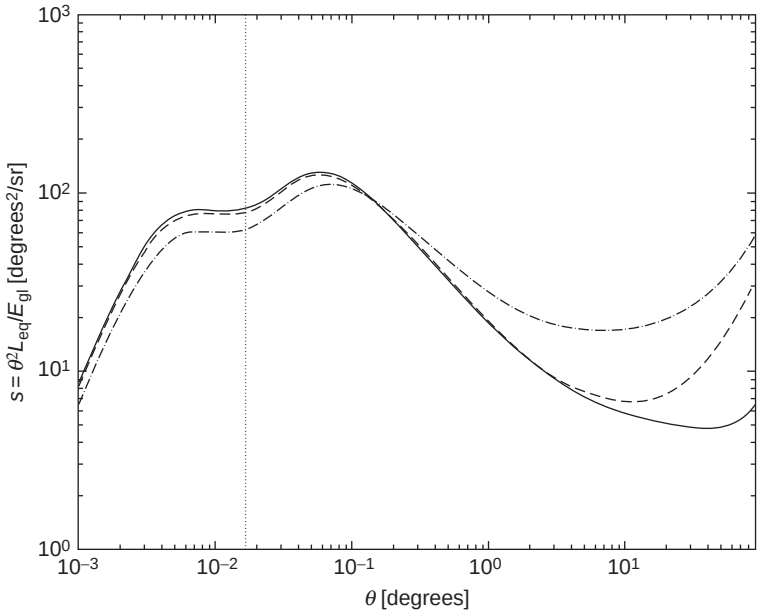

Figure 7 The CIE 1999 total glare function (PSF) multiplied by θ^2 to represent it in terms of the straylight parameter for a 35-year-old negroid (continuous line), a 35-year-old blue–green eyed Caucasian (dashed line), and a 80-year-old blue–green eyed Caucasian (dash–dotted line). The vertical dotted line indicates 1 min of arc. This is customarily assumed to be the smallest detail that can be resolved by an eye having a visual acuity of 1.

constant is multiplied by an age factor. It was called the age-adapted Stiles–Holladay equation:

$$\mathrm{PSF} = \left[L_{eq}/E_{gl}\right]_{S-H,agead} = \left\{1 + [A/70]^4\right\} 10/\theta^2$$

which has a validity domain that runs from 3° to 30°. As it is evident that the Stiles–Holladay equation falls short in particular below 1°, the following equation, the simplified glare equation (eqn [10] in the CIE report[131]), may serve in a more extended angular domain:

$$\mathrm{PSF} = \left[L_{eq}/E_{gl}\right]_{simpl} = 10/\theta^3 + \left\{1 + [A/62.5]^4\right\} 5/\theta^2,$$

which has a validity domain from 0.1° to 30°. To also cover the very large angle domain, more terms of the total glare equation should be taken into account; this is the general glare equation (eqn [11] in the CIE report):

$$\mathrm{PSF} = \left[L_{eq}/E_{gl}\right]_{gen} = 10/\theta^3 + \left[5/\theta^2 + 0.1 \times p/\theta\right] \cdot \left\{1 + [A/62.5]^4\right\} + 2.5 \times 10^{-3} \times p,$$

which has a validity domain that stretches from 0.1° all the way up to the very limit of the field of view, somewhere around 100°.

Relation between Straylight and Other Test Outcomes

Visual Acuity

There is only a weak relation between straylight and visual acuity. This is because straylight is determined by light scattering over larger angles (1–90°), whereas visual acuity is determined by light deflections over small angles (<0.1°, more commonly known as aberrations). Moreover, the physical processes that cause these light deflections are different for the two angular domains. Therefore, changes in one domain do not necessarily mean changes in the other domain. For example, putting a +2 dpt trial lens in front of a subject's eye will definitely change the subject's visual acuity, whereas his/her straylight value will stay precisely the same. On the other hand, putting a fog filter in front of the subject's eye will show a dramatically increased straylight value, whereas visual acuity will hardly decrease. This independence is also illustrated in the practical population by **Figure 8** for a large European-driver study.

Contrast Sensitivity

This is the subject of much misunderstanding. Contrary to what is often believed, straylight affects normal contrast sensitivity only very weakly. It is true that straylight reduces the contrast of the image of the outside world that is projected on the retina. Hence, increased straylight means lower contrast sensitivity. Only the decrease in contrast sensitivity is much smaller than the increase in straylight. This is illustrated in **Figure 9**. Five times increased light scattering lowers the contrast sensitivity function by only 20%; a very small amount, especially when compared to the contrast-lowering effect of blur (decreased visual acuity) or a bifocal implant or contact

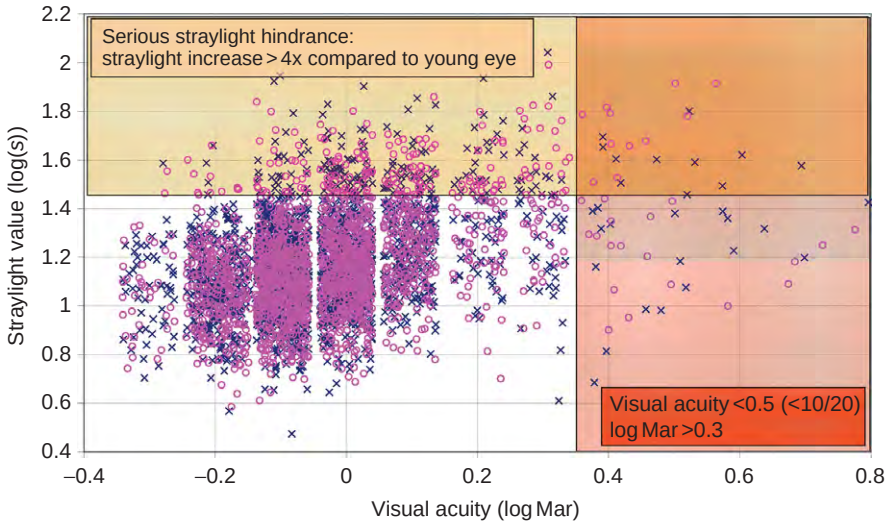

Figure 8 Straylight value as a function of visual acuity for a European driver population. Log(s) values > 1.47 and visual acuities < 0.5 (log MAR > 0.3) are considered serious visual impairments. A lot more individuals in this population are impaired by increased straylight than by decreased visual acuity. Only a very small subgroup suffers from both impairments.

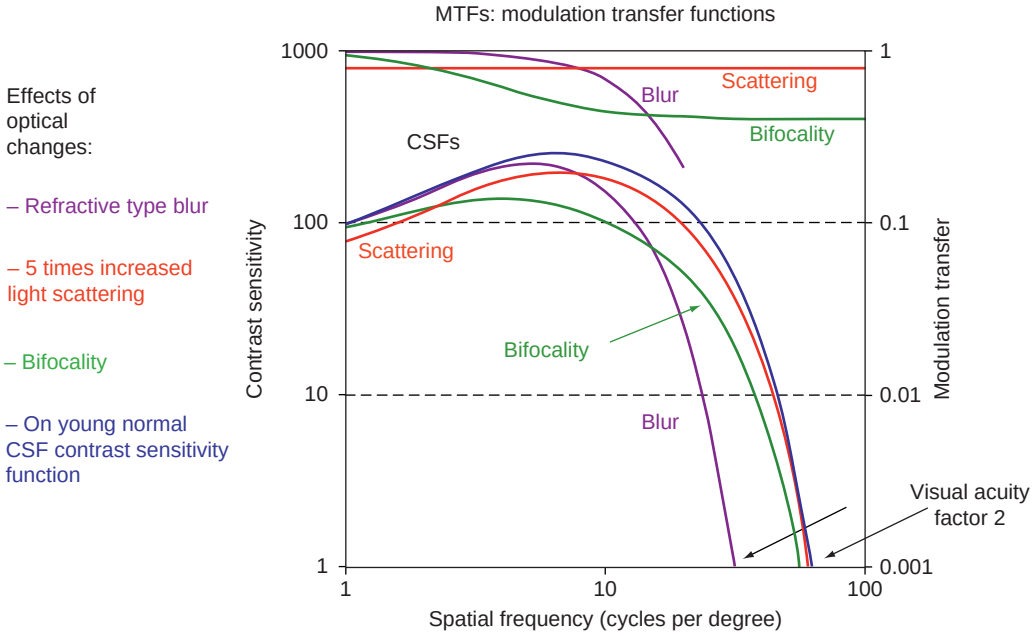

Figure 9 Effects of optical changes on the contrast sensitivity function.

lens. In other words, contrast sensitivity cannot be used as a valid means to assess the amount of straylight.

Glare Sensitivity

Maybe a reason for the misunderstanding is that it is still true that one of the most important effects of straylight is reduction of contrast sensitivity (see the examples in Figure 3). But the point to make here is that in our normal surroundings, huge intensity differences exist. Due to straylight, high-intensity areas influence effective contrasts and, as a consequence, effective contrast sensitivity in low-intensity areas. A better correlation between straylight and contrast sensitivity may be found when contrast sensitivity is measured with a glare source next to the measurement chart. But in that case, differences between subjects will also depend on differences in

contrast sensitivity that already exist without the glare source. Therefore, the parameter that would best relate to the straylight value is the decrease in contrast sensitivity caused by the glare source. There have been attempts to measure glare sensitivity in both ways with so-called glare testers. The Rodenstock Nyktotest, depicted in Figure 10, is an example of the first type (plain contrast sensitivity measurement with a glare source at the side). The second type is in fact a straylight measurement, but in an indirect, and therefore less accurate, way. In theory, it is a valid measurement, which may seem to relate more to all-day real-life circumstances, but in practice, the results appeared to be unreliable and could not be related to the patients' complaints.

Straylight and Slit-Lamp-Based Examination

Using backward light scatter, such as those based on the slit lamp examination principle (e.g., digital slit lamp, Scheimpflug system, lens opacity meter, LOCS), it is possible to assess opacities of the optical media of the eye. Figure 11 gives the LOCS III classification chart developed by Chylack and coworkers. These opacities are partly responsible for the amount of light scattering in the eye, so there may be a relation between the degree of opacity as observed with the slit lamp and the amount of straylight. However, this will not be a one-to-one relation for two reasons. First, as already mentioned, the opacities account for only a part of the total light scattering. For example, the transparency of the iris and sclera, as well as the amount of light reflected from the fundus, are not assessed by the slit lamp examination. Second, with the slit lamp one looks at light that is scattered back from the optical media. This is not the light that reaches the retina, which is the light that is scattered in forward direction. Studies showed that no direct relation exists between the forward and backward scatter. Therefore, it makes more sense to measure the amount of forward scatter, as this is what the patient actually sees and is bothered by.

Figure 10 Rodenstock Nyktotest.

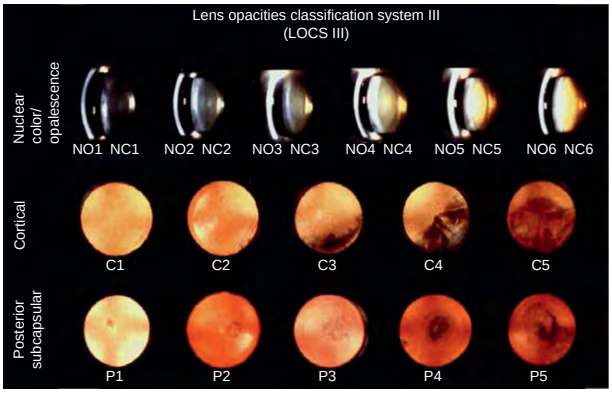

Figure 11 Lens opacities classification system (LOCS) III.

Straylight and Patient Complaints

Patient complaints from increased straylight may be voiced in a variety of ways. It is important to note that straylight defines a functional condition of the eye in a physical way, and the patient complaints will not always correspond with equal precision. As listed above, complaints may include hazy vision, increased glare hindrance, loss of contrast and color, halos around bright lights, and difficulties with against-the-light face recognition. The complaints mentioned or even the words used to describe them may strongly depend on the individual subject. Moreover, it must be mentioned that in the field of glare a particularly subjective type of patient response has been identified, called discomfort glare. As opposed to disability glare, which is the functional effect of glare, discomfort glare is a description of subjective glare. Complaints may be expressed in terms of discomfort, annoyance, fatigue, and even pain. On average, increased disability glare will also lead to more discomfort; however, in some cases, such as with the nowadays-abundant blue-light high-intensity discharge (HID) car headlamps, people might be severely annoyed by light sources that have only a moderate functional glare effect.

Frequently Asked Questions

What Are the Causes of Retinal Straylight?

The amount of retinal straylight is different for each individual, and may even be different for the two eyes of one individual. It depends on age, pigmentation, pathologies, such as cataract, and may change due to human interventions such as refractive surgery.

Normal eye

Within the eye, there are four major sources that contribute to the total amount of straylight: the cornea, the iris and sclera, the eye lens, and the fundus (see **Figure 3**). For a young, healthy, Caucasian eye, the total amount of straylight is, roughly speaking, 1/3 caused by the cornea, 1/3 by the lens, and 1/3 by the iris, sclera, and fundus. These ratios change with age and pigmentation:

- Corneal light scatter is more or less constant with age, but may increase as an unwanted side effect of refractive surgery.
- The iris and sclera are not completely opaque. Depending on the level of pigmentation, some of the light falling on the iris and sclera will be transmitted and contribute to the false light that reaches the retina. This contribution will be low for pigmented non-Caucasians (who have brown eyes), but might be considerable for lightly pigmented blond Caucasians with blue eyes.
- Light scattering by the crystalline lens increases with age, especially when people develop a cataract, which in terms of straylight can be seen as an accelerated aging of the eye lens.
- The fundus does not absorb all the light, so part of the light that reaches the retina will be reflected backward and scatter to different locations on the retina, thus contributing to the total amount of straylight. The amount of this scattered light is pigmentation dependent.

Important causes of increased retinal straylight

Some of the major causes for increase in retinal straylight are:

1. *Early cataract.* If cataract starts to develop, the earliest complaints often are from increased straylight, such as increased glare hindrance when driving at night. In fact, most often the first effect of cataract is that patients stop driving at night. Other complaints may include hazy vision, loss of contrast and color, halos around bright lights, and difficulties with against-the-light face recognition (see examples in **Figure 3**). Why should patients be allowed cataract surgery only on the basis of visual acuity loss?
2. *Corneal disturbances.* Most corneal disturbances as, for example, in corneal dystrophies cause strong increase in straylight. In some cases, visual acuity can be remarkably maintained while straylight deterioration is strong, such as in corneal edema.
3. *Refractive surgery.* In refractive surgery, there is a chance of haze in the cornea. Visual acuity hardly suffers, but complaints from straylight such as glare are of considerable concern.
4. *Contact lenses.* As a rule, contact lenses cause straylight to increase. Deposits or scratches can often be identified as a major cause of increased straylight, but if the cornea reacts to improper (use of) contact lenses, straylight increase can be huge.
5. *Turbidity in the vitreous.* This can cause large increases in straylight, often also without much effect on visual acuity.

What is the Reliability of a Straylight Measurement?

The CC method as implemented in the C-Quant straylight meter measures straylight as the subject actually sees it (and is disturbed by it). However, because it is a psychophysical technique, reliability of individual measurements needs to be checked (as with visual-field measurements). Therefore, a reliability parameter (estimated standard deviation (ESD)) was designed that predicts the accuracy of an individual measurement. In the C-Quant, a limit value of ESD $\leq$ 0.08 is used. In the large European-driver study an overall accuracy of 0.1 log units was found. These accuracies are more than sufficient compared to the effects to be measured (see above).

Does Pupil Size Affect the Straylight Measurement?

This subject is the cause of a lot of misunderstanding. As more glare is experienced at night, one might think that straylight is stronger at night. This may be believed to be caused by a larger pupil size. Indeed, the amount of straylight is higher because of the larger pupil, but also the nonscattered light (which is the light that forms the image on the retina) is increased, and by the same amount. Therefore, the straylight value will not change (the ratio stays the same). However, this is only true in general. On an individual basis, an increase as well as a decrease might happen, depending on the location-dependent scattering properties of the eye. For example, a patient with a centrally located lenticular opacity may get a lower straylight value with larger pupil size. In other words, to assess straylight hindrance at night, it is not needed as a rule to dilate the patient's eye when using the C-Quant.

See also: Acuity; Contrast Sensitivity; Refractive Surgery.

Further Reading

Aslam, T. M., Haider, D., and Murray, I. J. (2007). Principles of disability glare measurement: An ophthalmological perspective. *Acta Ophthalmologica Scandinavica* 85: 354–360.

Cervino, A., Montes-Mico, R., and Hosking, S. L. (2008). Performance of the compensation comparison method for retinal straylight measurement: Effect of patient's age on repeatability. *British Journal of Ophthalmology* 92: 788–791.

Cobb, P. W. (1911). The influence of illumination of the eye on visual acuity. *American Journal of Physiology* 29: 76–99.

de Waard, P. W., IJspeert, J. K., van den Berg, T. J. T. P., and de Jong, P. T. (1992). Intraocular light scattering in age-related cataracts. *Investigative Ophthalmology and Visual Science* 33: 618–625.
de Wit, G. C. and Coppens, J. E. (2003). Straylight of spectacle lenses compared with straylight in the eye. *Optometry and Vision Science* 80: 395–400.
de Wit, G. C., Franssen, L., Coppens, J. E., and van den Berg, T. J. T. P. (2006). Simulating the straylight effects of cataracts. *Journal of Cataract and Refractive Surgery* 32: 294–300.
Elliott, D. B. and Bullimore, M. A. (1993). Assessing the reliability, discriminative ability, and validity of disability glare tests. *Investigative Ophthalmology and Visual Science* 34: 108–119.
Elliott, D. B., Fonn, D., Flanagan, J., and Doughty, M. (1993). Relative sensitivity of clinical tests to hydrophilic lens-induced corneal thickness changes. *Optometry and Vision Science* 70: 1044–1048.
Franssen, L., Coppens, J. E., and van den Berg, T. J. T. P. (2006). Compensation comparison method for assessment of retinal straylight. *Investigative Ophthalmology and Visual Science* 47: 768–776.
Stiles, W. S. and Crawford, B. H. (1937). The effect of a glaring light source on extrafoveal vision. *Proceedings of the Royal Society of London. Series B, Biological Sciences* 122: 255–280.
van den Berg, T. J. T. P. (1995). Analysis of intraocular straylight, especially in relation to age. *Optometry and Vision Science* 72: 52–59.
van den Berg, T. J. T. P., Hagenouw, M. P. J., and Coppens, J. E. (2005). The ciliary corona: Physical model and simulation of the fine needles radiating from point light sources. *Investigative Ophthalmology and Visual Science* 46: 2627–2632.
van den Berg, T. J. T. P., van Rijn, L. J., Michael, R., et al. (2007). Straylight effects with aging and lens extraction. *American Journal of Ophthalmology* 144: 358–363.
Vos, J. J. (1984). Disability glare – a state of the art report. *Commission International de l'Eclairage Journal* 3(2): 39–53.
Vos, J. J. and van den Berg, T. J. T. P. (1999). Report on disability glare. *CIE collection* 135: 1–9.

Relevant Website

http://www.cie.co.at – Commission internationale d'Eclairage CIE, or International committee on illumination.

Ocular Mucins

M Berry, Bristol Eye Hospital, Bristol, UK

Glossary

Alternative splicing – A variation mechanism in which linear combinations of exons are translated, resulting in a variety of mature products encoded by a single gene.
Atomic force microscopy (AFM) – A technique of high-resolution imaging through the measurement of forces between atoms in the sample and those on the instrument tip.
Glycan – The oligosaccharide portion of a glycoconjugate.
Glycocalyx – An outer, carbohydrate-rich coating on the surface of cells.
Glycoforms – Variations in the amount or compositions of oligosaccharides decorating the same peptide core.
Meibomian glands – The special sebaceous glands at the rim of the eyelids that supply the lipid layer of the tear film.
Mucins – A family of large, heavily glycosylated molecules, with most glycan chains O-linked to the peptide core.
Persistence length – A measure of polymer stiffness; it is the length over which correlations in the direction of the tangent are lost.
Reptation – Movement of a long polymer parallel to itself, similar to the movement of a snake.
Tandem repeats – The adjacent repetition of a pattern of two or more nucleotides.
Worm-like model – A model for the behavior of semiflexible polymers, considered continuously flexible.
Young's modulus – A measure of elasticity, defined as the ratio of stress to strain.

Introduction

In addition to the well-defined anatomical blind sac formed by the cornea and conjunctiva, the meibomian and lacrimal glands, the ocular surface comprises a mucosal immune system, rich neural and endocrine loops, as well as the blink reflex. As with other mucosal systems the ocular surface is further integrated into the adaptive immunity of the organism, and into the microbial richness of the outer environment. An additional and specific requirement of the ocular surface is the maintenance of transparency that applies to the cornea as well as to the preocular fluid.

Bathing the exposed part of the outer eye is a complex fluid whose elements are secreted by the wet epithelia, and the lacrimal and meibomian glands. Mucins are the main component of a mucus gel and responsible for its viscoelastic properties. They form a dynamic matrix wetted by a plasma dialysate enriched by secretions from the lacrimal glands and topped by a layer of waxes and lipids originating in the meibomian glands. This fluid is periodically sheared and mixed by the movement of the lids during blinking. Underneath the mucous gel, the epithelial glycocalyx anchors the tear film to the ocular surface: mucins and glycoproteins are the major components of this layer.

Mucin Architecture

A very rich glycosylation, with most sugar chains O-linked through *N*-acetylgalactosamine (GalNAc) to serine or threonine in the peptide core, is diagnostic of mucins. Sugar chains tend to be clustered in discrete regions resulting in concentrations of negative charges. In these high-charge regions the peptide core is rich in serine, threonine, and proline (PTS domains), and repeated sequences of aminoacids (variable number of tandem repeats, hence VNTR domains) are present, specific to the encoding gene. Other regions are less richly glycosylated and contain relatively more N-linked glycan chains, the latter necessary for mucin transit through intracellular microtubules during synthesis. In humans, ocular mucin regions of tens of nanometers seem to be almost naked: the molecular diameter measured in liquid with atomic force microscopy (AFM) is not significantly higher than that of aminoacids in a helix (**Figure 1(a)**), giving mucin polymers the appearance of strings of small beads, small beads of dense bottlebrushes.

Toward the N- and C-termini of mucins, the arrangement of moduli is similar to those found in proteins involved in coagulation (von Willebrand factor, VWF domains), cysteine knots, or SEA (sea urchin sperm protein, enterokinase, and agrin) domains. These are useful in tracing the evolution of mucin genes. Genes encoding for PTS domains and multiple VWF domains (D1–D2–D3 PTS, as in secreted mucins) can be found early in the evolution of metazoa, preceding hemostasis or coagulation

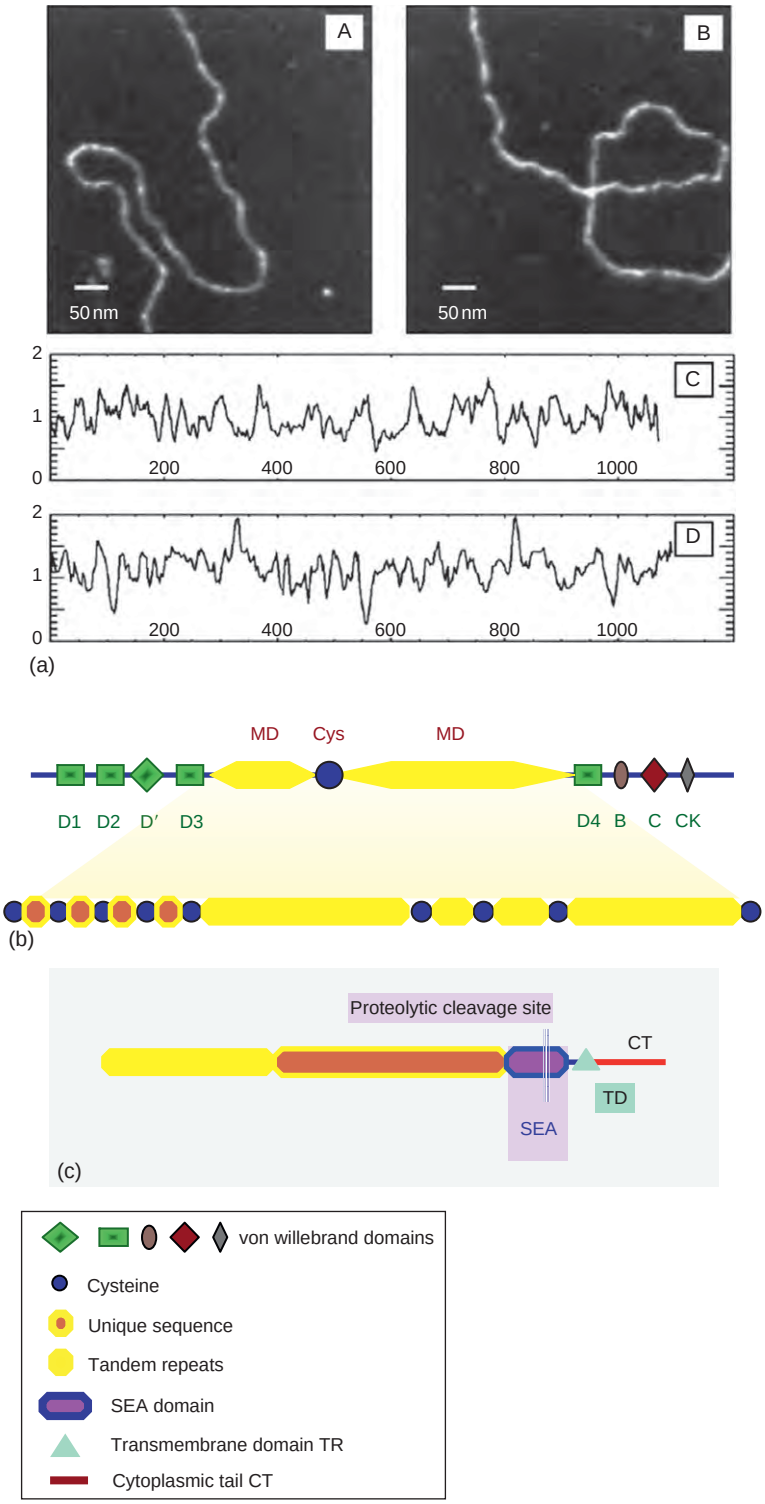

Figure 1 Architecture of ocular mucins deposited on mica (a) Portions of a hydrated human conjunctival mucin molecule imaged with AFM (A, B). The respective height profiles (C, D), highlight the short oligosaccharides of ocular mucins. All axes are in nanometres. Reproduced from McMaster, T. J. (1999). Atomic force microscopy of the submolecular architecture of hydrated ocular mucins. *Biophysical Journal* 77: 533–541. With permission from Biophysical Society. (b) Schematic of a mucin monomer, containing von Willebrand factor domains toward the C- and N-termini (D1, D2, D′, D3, and D4, B, C, and CK, indicated by green labels) and central mucin domains (yellow). A more detailed schematic of PTS domains reveals unique sequences (brown-filled octagons) and tandem repeat regions (yellow octagons) interspersed with cysteins (blue). Most secreted mucins polymerize by disulfide-bonded linear concatenation of such monomers.(c) Schematic of a cell-surface-associated mucin, containing an SEA domain (sea urchin sperm protein, enterokinase, agrin) within which there is a proteolytic cleavage site, a transmembrane domain (TD), and a cytoplasmic tail (CT).

(Figure 1(b)). SEA domain mucins appear in vertebrates, while the auto-catalytically cleaved SEA domain is restricted to mammals (Figure 1(c)).

Regions where the peptide core is extended by the insertion of the first sugar (GalNAc) and repulsion between negatively charged sugar chains alternate with more flexible polypeptide chain stretches, suggesting that mucins behave in solution like stiff random coils. Mucins occupy a large volume which indicates interpenetration of molecular domains at relatively low polymer concentrations. Using the worm-like model, calculations indicate that human ocular mucins are more flexible than DNA molecules of similar length; mucin persistence length is 35 nm and that of DNA is 50 nm. Polymer conformation and stiffness, for example, of human ocular MUC5AC glycoforms, are greatly influenced by the degree and nature of post-translational glycosylation.

Mucin architecture is determinant of mucin role and function at the mucosal surface and in the gel. The organ, developmental state, and physiological status, in turn, affect mucin expression and details of glycosylation. Ocular mucins have short oligosaccharide chains: in humans they are mostly less than six sugars long, negatively charged and terminated in sialic acid, with fucosylation representing less than one-fifth of the sugars (Figures 2 and 3). In dogs and rabbits, glycans are mainly neutral and terminated in fucose and/or GalNAc. The short oligosaccharides might be related to transparency and (relatively fast) turnover of mucins, and terminal sugars to environmental microbiota.

Mucin Families

Mucin genes appeared through a combination of moduli existing in other proteins. The close connection between mucin structure and function gives rise to a classification necessarily reflecting both.

Surface-associated mucins

Some mucins spend part of their life anchored into the apical cell membrane before they are shed into the luminal, that is, tear, fluid. Formerly known as membrane-bound mucins, they are now called cell-surface-associated mucins. These are heterodimers, with a large mucin subunit outside the cell, a (mostly hydrophobic) membrane-spanning region and an intracellular tail. A number of subfamilies are represented at the ocular surface: the mammalian-specific MUC1 with its SEA domain; the MUC16 that contains multiple SEA domains, not all of which are cleaved; and the MUC4 that has VWD but neither cysteine-rich domains nor SEA. Shedding of these mucins is thought to cause changes in the neighboring membrane domains, potentially transferring information to the cell interior. A further possibility is that information is conveyed through the cytoplasmic tail to the cytoskeleton. An important result of surface mucin release in the tear fluid is the renewal of the glycocalyx and the tear fluid itself.

This group of mucins is heterogeneous and most genes also encode splice variants that are secreted: MUC4, a cell-surface mucin in normal cornea and conjunctiva, is a goblet cell mucin in some pterygia (Figure 4). MUC1/SEC, a splice variant of MUC1 that lacks the transmembrane domain and, therefore, results in a soluble, secreted form of MUC1, is present in human cornea and conjunctiva.

Secreted mucins

Milliseconds after the secretion of mucins stored in granules, often in specialized epithelial cells, their volume

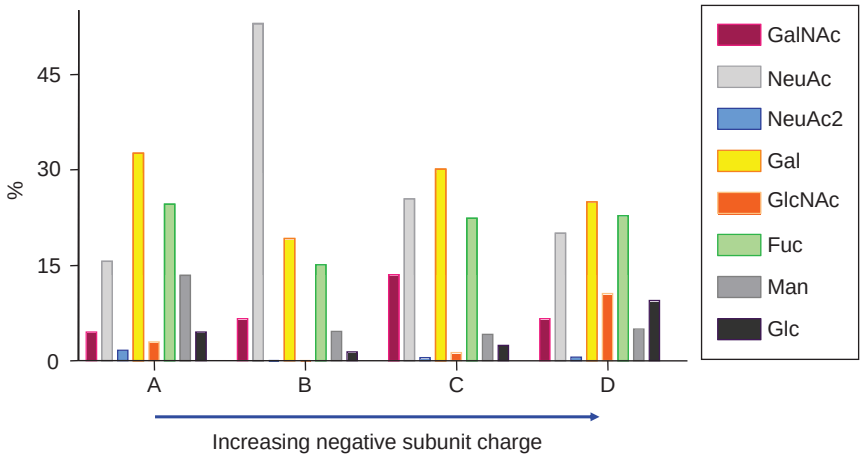

Figure 2 Monosaccharide composition of human ocular mucins. The increase in sialic acids, mono- or di-acetylated (NeuAc, or Neu-Ac2) did not parallel the increase in negative subunit charge (A<B<C<D). High negative charge was conferred by an the appearance and increase of sulfated oligosaccharides (not shown).

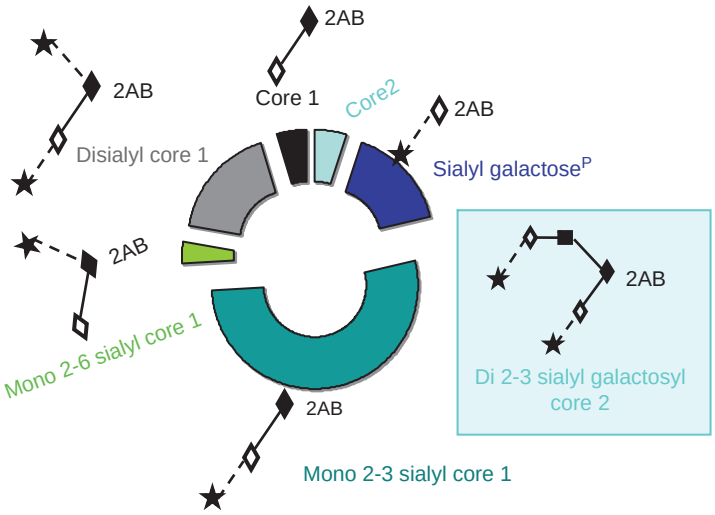

Figure 3 Oligosaccharide composition of human ocular mucins. This pie chart indicates the abundance of the different glycans of purified human ocular mucins obtained by hydrazinolysis. Each sequence is named in the color of its proportion in the total glyco-repertoire, while its structure is indicated in the sugar notation presented below. Notable is the high proportion of sialylated oligosaccharide chains, almost half of which contain α2-3-linked sialic acids. A cautionary note: at present the method used for determining O-linked glycan composition affects the results. Glycochip methods often estimate a higher proportion of core 2 glycans than obtained by hydrazinolysis and HPLC. Notation of sugars in the figure is as follows: ◆ *N*-acetylgalactosamine (GalNAc); ◊ galactose (Gal); ■ *N*-acetylglucosamine (GlcNAc); ★ *N*-acetylneuraminic acid (NeuAc). Solid lines denote β linkages, dashed lines mark α links.

increases 100-fold in the extracellular fluid as a result of hydration. These secreted mucins have a well-defined VWF-D2-D3 PTS architecture, and Cys-rich domains or Cys knots. VWF domains and Cys are involved in the concatenation of mucin subunits (Figure 5). The secreted mucins – MUC2, MUC5AC, MUC5B, MUC7, MUC19, and MUC23 – have been found at the ocular surface, in cells, impressions, and tears. MUC20 messenger RNA (mRNA) has also been identified in the conjunctiva. With the notable exception of MUC7, secreted mucins form linear polymers of subunits linked by disulfide bonds and form gels, and are thus called secreted gel-forming mucins. Polymers extracted from cells (and protected from proteolysis) may be few microns long; in the secretion, submicron lengths dominate. MUC7 oligomers are like spokes of a wheel around a central, yet to be fully described, entity. Though MUC7 is not gel forming, it is found in gels, for example, saliva, from which it has been originally described.

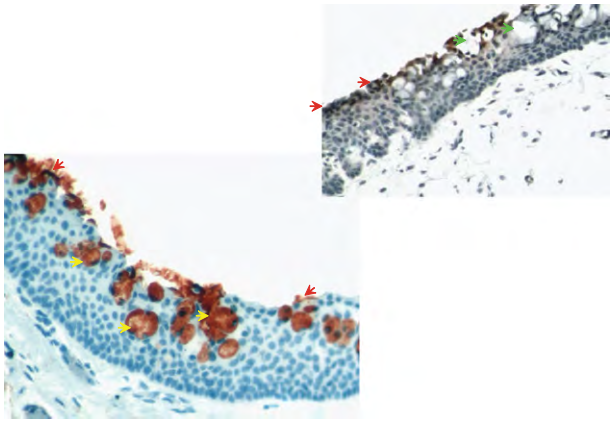

Figure 4 MUC4 alternative splicing in pterygium. In normal conjunctival tissue MUC4 is mainly a surface-associated mucin. In pterygia, triangular growths of the conjunctiva over the cornea, it can be present either as surface associated (red arrows) or secreted (yellow arrows) within prominent goblet cells. Where pterygial MUC4 is surface associated, goblet cells do not light up with anti-MUC4 antibodies (green arrows). MUC4 was visualized with antibody 4F12 (DSHB, Yowa, USA); counterstain: hemalum. Images: courtesy of Friedrich Paulsen, Halle University, Germany.

Biosynthesis and Turnover

Synthetic pathways

Mucin genes account for nearly 4% of genes expressed in the normal conjunctiva, with a further 29% dedicated to glycosyltransferases. During synthesis, molecular species with varying properties are transported to the location corresponding to their stage in this complex process. MUC5AC might take over 2 h from initiation to storage in the secretory granule. The making of secreted mucins starts with the synthesis of the peptide core in the endoplasmic reticulum, where N-linked sugars are also added. Following folding of the C- and N-termini, the peptides dimerize through S–S bonds between cysteine knot

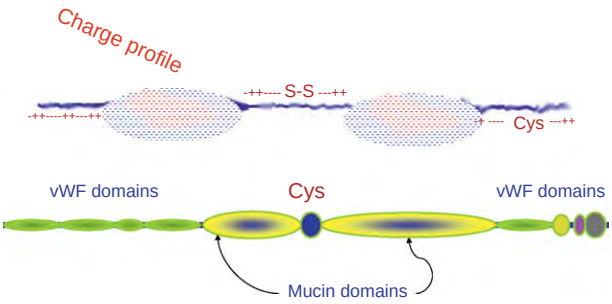

Figure 5 Schematic of secreted mucin structure. Secreted mucins have a well-conserved architecture. Within mucin domains, repeated sequence(s) called tandem repeats are gene specific. The concatenation of mucin subunits gives rise to a polymer with concentrated regions of negative charge, interspersed with less charged, less glycosylated regions. vWF, Von Willebrand factor domains; Cys, cysteine.

domains at the C-termini. O-glycosylation is initiated and elaborated in the *cis*- and medial Golgi. Further polymerization, S–S bonds between VWD3 domains at the N-terminal, occurs in the *trans*-Golgi and the secretory granule. Cell-surface mucins too acquire their N-linked sugars in the endoplasmic reticulum, where the peptide core is cleaved into the two domains, and further glycosylated as these mucins progress through the Golgi. A signal peptide in the N domain localizes cell-surface-associated mucins at the apical membrane; the cytoplasmic domain starts with a signal sequence involved in retention at the plasma membrane and mucin recycling.

Glycosylation

Glycosyltransferases

Mucin glycans are synthesized in the Golgi apparatus. The presence, activity, and localization of glycosyltransferases along the Golgi cisterns are the primary determinants of glycan chain density and sequence. The initial transfer of GalNAc from UDP-GalNAc to the hydroxyl group of Ser/Thr in the peptide backbone is catalyzed by uridine diphosphate GalNAc:polypeptide N-acetylgalactosaminyl transferases (ppGalNAcTs). Subsequent sequential sugar additions are catalyzed by glycosyltransferases (GalNAc-Ts). Nucleotide-sugar synthases and hydrolases, and genes encoding their transport proteins add further dimensions to the function and regulation of mucin molecules.

In other mucosae, for example, respiratory epithelium, epidermal growth factor (EGF), Th2 cytokines, and all-trans retinoic acid alter the expression of GalNAc-Ts, some of which are also downregulated in cancer. Molecular details of transcriptional regulation of glycosylating enzymes are not known for the eye. The final density of glycosylation and chain structure strongly depends on the availability of sugar nucleotides, and competition between enzymes for acceptor intermediates during glycan elongation, incorporating a measure of randomness in the glycan population.

At the human ocular surface, ppGalNAcTs are distributed in an epithelial layer and in a cell-type-specific manner. Isoform –T3 was detected in all the epithelial layers, while –T2 in restricted to basal cells; –T4 is expressed in all apical cells. One member of the family, ppGalNAcT-6, was found in goblet cells only in normal subjects, but in apical cells of conjunctival epithelia in patients with ocular cicatricial pemphigoid, together with the –T2 isoform.

How elongation of oligosaccharide chains is regulated is not yet understood: in humans, rabbit, and dog, ocular mucins have short sugar chains. The same mucin gene product in the respiratory or gastrointestinal mucosa is decorated by chains many tens of sugars long.

The ensemble of human ocular surface enzymes is such that mucin oligosaccharides are negatively charged and mostly terminated in sialylated structures, including the histo-blood Lewis group antigens (sialyl Le^x and sialyl Le^a). The number of different structures is low, barely in double figures, compared with many hundreds in respiratory epithelia from one subject, for example. Histo-blood group antigens are involved in neutrophil adherence and activation. Because of the short chains, sugar epitopes that are cryptic in other mucosae are overt in human ocular mucins, for example, Tn or SialylTn that are richly present in the normal conjunctival epithelium. Which sugars or end groups are exposed in the glycan envelope of the tissue remains to be clarified for the ocular surface. Variation in this envelope is likely to modulate both immune effector cells and bacterial adhesion to the conjunctiva or cornea.

Turnover

Quantities, species, and glycoform composition of mucin populations on the ocular surface are a dynamic result of mucin production, secretion, and degradation. Not all the factors involved in this process are known: immune and infective agents modulate synthesis and secretion, as do neural stimuli; enzymes in the tears contribute to mucin degradation, while tearing and blinking are believed to remove spent mucus from the surface.

There are no data on average half-life of mucins in the preocular fluid. Extraction of large and glycosylated mucin polymers from contact lenses suggests that some escape degradation during waking hours.

Recycling

There is evidence that surface-associated mucins are re-uptaken into the Golgi and re-glycosylated. In the cell lines where these experiments have been done, the final glycosylation of the mucin is different from its original, and, at least for MUC1, the uptake depends on mucin

palmitoylation. It is not known whether this also occurs at the surface of the eye.

Degradation

Bacteria are an essential player in mucin degradation: glycosidases and proteolytic enzymes contribute to mucus gel breakdown and renewal; adherent bacteria are probably wrapped in mucin epitopes (sacrificial epitopes) and removed from the surface. During sleep, neutrophil enzymes degrade the gel and cause or enhance the cleavage of surface-associated mucins, promoting recoating of epithelial surfaces with a mucus gel.

Control of Secretion

Mucins are a defensive secretion, augmented in response to pathogens and stimuli, including mechanical, thermal, and chemical insults (through nocioceptors in cornea and conjunctiva). Though the signaling pathway triggered by the external stimulus might be distinct, the involvement of protein tyrosine kinases, mitogen-activated protein kinases (MAPKs), and transcription factor NF-kappa B are relatively common.

In the conjunctiva, the eicosanoid 15-(*S*)-hydroxy-5,8,11,13-eicosatetraenoic acid (15(*S*)-HETE) stimulates MUC1, but not MUC2, MUC4 release, suggesting mucin-specific control of surface-associated mucin liberation in the tears. Further evidence for gene-product-specific modulation is derived from studies of a human corneal limbal epithelial cell line where matrix metalloproteinase-7 and neutrophil elastase induced the release of MUC16, but not of MUC1 or MUC4.

Nucleotide agonists acting locally through $P2Y_2$ purinoceptors (belonging to the major G-protein-coupled receptor (GPCR) family) on apical membranes of goblet cells provide a major regulatory system for mucin secretion. Cholinergic agonists are potent stimuli of mucin secretion. One of the pathways to secretion is through EGF receptor (EGFR) induction of MAPK. A fast Ca^{2+} sensor for the soluble NSF attachment protein receptor (SNARE) complex (the core machinery of membrane fusion) is essential for regulated secretion.

Individual Variation

It is not known whether the number of goblet cells varies in individuals. Their number, as assayed by impression cytology, represents those that are discharging in response to external stimuli, and depends on external factors, for example, wind, humidity, and spectacle wear. Goblet cell numbers decrease in severe, but not mild, dry eye disease.

Allelic variation, for example, in the number of tandem repeats, is but one source of individual variation. Additionally, variation in glycosyltransferases and in the availability of donor sugars in different physiological states gives rise to potentially large individual variation. However, the size-to-charge ratio of mucin populations is surprisingly well conserved: migration patterns of mucins from conjunctivas of men and women of different ages are similar, suggesting a tight control on the molecular size/charge ratio of intracellular mucins. Conservation of population parameters is also encountered in the largest mucins extracted from tears or contact lenses as shown in **Figures 6 and 7**. Ratios of the different mucin species sampled from the ocular surface showed little variation in asymptomatic contact lens wearers. The variation must therefore be more subtle and is yet to be understood.

Mucin Function

Mucins are essential for the defense of the organ from external factors. Mucins are: (1) lubricants easing the movement of the lids over the surface of the eye; (2) a physical barrier; (3) a trap for microbes; and (4) a matrix where tear constituents among which enzymes, antimicrobial peptides, and other signal molecules fulfill their physiological role. The surface mucins that are richly represented on cornea and conjunctiva are expected to fulfill signaling functions, which are yet to be clearly understood.

Adequate production of mucins is controlled by neural, hormonal, and other signaling networks. In addition,

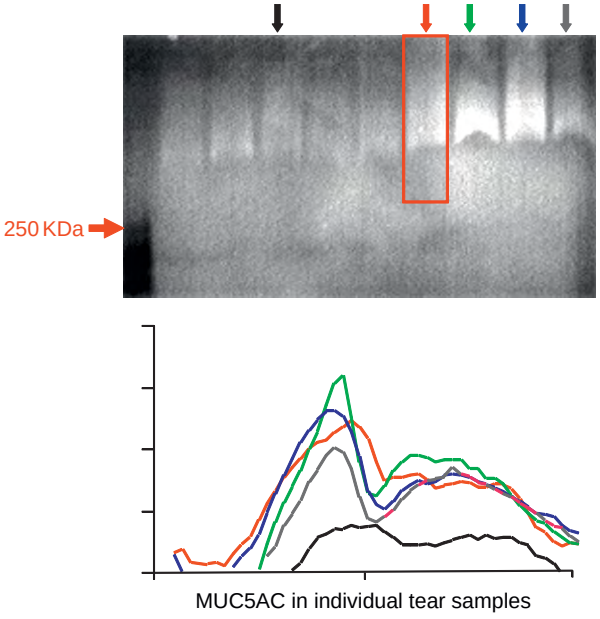

Figure 6 Electrophoresis of MUC5AC from individual tear samples. Very little variation was seen between the mobilities of the largest MUC5AC polymers in tears from nine individuals. Samples (not equalized for protein content) were run on 1% agarose electrophoresis, vacuum blotted, and visualized after incubation with antibody CLH2 to MUC5AC peptide core. The graphic underneath shows details of mobility for the color-coded respective lane.

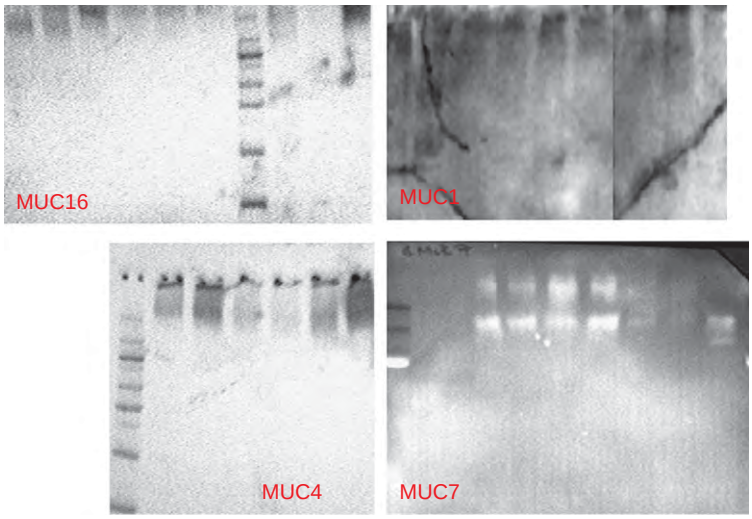

Figure 7 Electrophoretic profile of mucins in individual tear samples. Electrophoresis on NuPage Bis-Tris gels allows analysis of MUC1, MUC4, MUC7, and MUC16 and their fragmentation in individual samples. There are clear similarities in mobility, at least for species sufficiently represented to be detected with these methods.

a massive discharge of mucins occurs as a response to environmental stimuli, from mechanical stimulation to bacterial lipopolysaccharide.

Gel Formation

Mucins adhere to surfaces through either sugars or peptide sequences. In a physiological buffer, sequential adhesions of a mucin lowered onto mica were most often spaced similar to the atoms on this surface, indicating that no region of the molecule is barred from adhering to the substrate. The early events in adhesion are governed by random diffusion. Later (i.e., after the first polymers have adhered), cooperative sequential adsorption occurs, creating regions of high mucin density.

In dilute solutions, mucins reptate, that is, the polymer slides parallel to itself. A long mucin can thus extricate itself from entanglements, like a strand of spaghetti from a tangle.

Mucin polymers associate through long-range hydrogen bonds; they interact with like-charged moieties (e.g., sugars on another polymer) through bridging divalent cations, and form disulfide bonds between unpaired cysteins. Lectin-like site adhesions and hydrophobic domain interactions are also expected to contribute to gel formation, additional to the entanglement of these flexible polymers (**Figure 8**). The ocular surface is covered by a stable and dynamic mucous gel. *In vitro*, the elastic properties of the gel are conserved in time and recover after addition of purified ocular mucin – paralleling the discharge of granules from a goblet cell in the conjunctiva (**Figure 9**). The dynamic nature of the gel can be gleaned in changes in the roughness of its surface, and the temporary oscillations in elastic qualities after intervention. Calcium chelation weakens

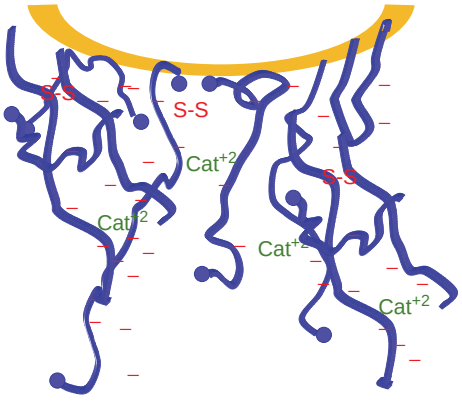

Figure 8 Mucin adsorption and intermolecular bonds. Schematic of mucin adsorption and association (animation). Sugar or peptide-core moieties can adhere to a surface; intermolecular long-range bonds are established between charged epitopes, bridged by divalent cations in solutions, and through unpaired Cys moieties.

human preocular mucus gels: subsequent addition of Ca restores their initial elastic qualities. The gel collapses on mucin depolymerization. Shorter mucins (i.e., $\leq$500 nm long) are more mobile in a model gel than the longest polymers ($\geq$1 µm long). It must be emphasized that the qualities of a gel depend not only on the mucins, but on all its constituents. Intracellular autocatalytic cleavage in the C-termini of MUC5AC is expected to generate reactive termini that form cross-links and enhance gel formation. The pattern of reactivities with antibodies to different parts of MUC5AC suggests that these cleavages occur in normal mucins, but not in those from dry eye patients.

Significant for mucin function is the fact that small entities (compared to pore size) gain more local mobility in a mucin gel than in viscous polymer solution, as

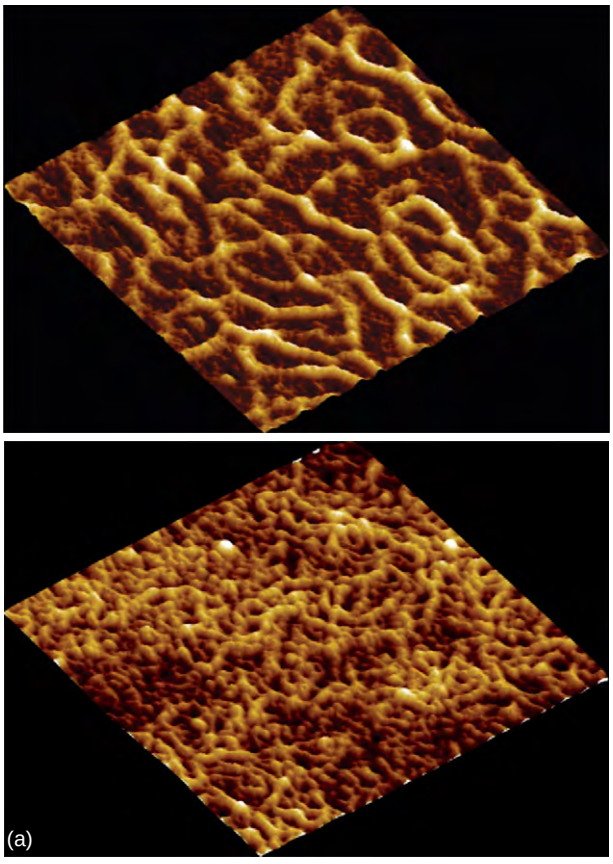

Figure 9 Purified mucin gels *in vitro*. (a) AFM topographical images during formation of mucin gels by repeated deposition of purified mucins on mica, in HEPES buffer (animation). (b) Characteristics of ocular mucin gels *in vitro*. Correlates of Young's modulus (elastic modulus, E*) of the gels were calculated from indenting the gel surface with an AFM tip. These elastic characteristics of the gel were calculated at different depths (of the order of nanometres) within the gel, and differences reflect the effect of the stiff substrate. Elasticity being conserved, as illustrated for three cycles of indentation separated by more than 1 h, indicates that the gel is a stable structure. Throughout this period the gel was kept hydrated in HEPES buffer.

relatively large, typically 200–400-nm, fluid-filled pores open up. Thus, the transport of biologically significant molecules is enhanced in the preocular gel, while micron-sized pathogens are still prevented from penetrating.

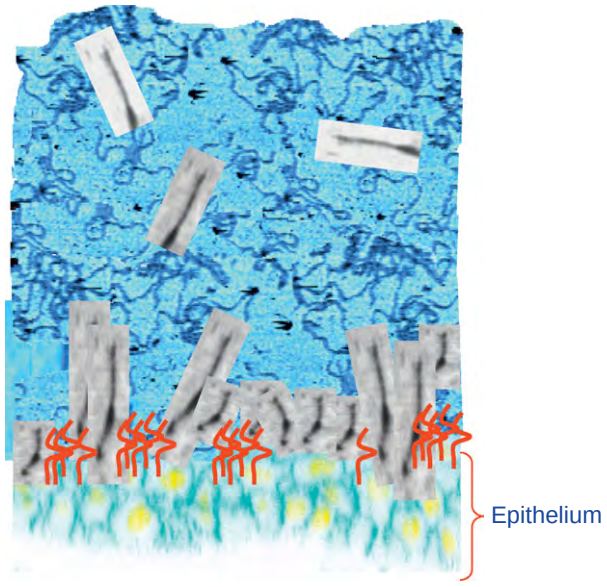

Figure 10 Schematic of the tear film anchoring to the ocular surface. Collage of confocal image of conjunctival epithelium and AFM images of cell surface associated (gray) and secreted mucins (blue). Glycocalyx is schematically shown in red.

Anchoring to the Ocular Surface

Surface tension is responsible for maintaining the tear film onto the ocular surface. Apical epithelial cells of the cornea and conjunctiva express a rich glycocalyx that interfaces with the secreted phase of the fluid. Entanglement, hydrogen bonding, sugar–sugar interactions, and lectin–sugar interactions are all involved in the interpenetration of the sessile and the stirred layer of the preocular fluid (**Figure 10**). Surface-associated mucins are longer than most other glycocalyx components and are expected to penetrate and entangle with elements of the secreted fluid.

Physical and Chemical Barriers

Particles (e.g., from mascara or cigarette smoke) can be seen trapped in the tear film for a period of time, after which they are eliminated from the ocular surface. This mechanism might involve wrapping in mucin or mucin aggregates, and it is also believed to be part of mucin turnover eliminating spent mucins. Sacrificial glycosylated epitopes, to which bacteria or viruses adhere before being eliminated, or which accept reactive molecular species, are also involved in the protective function of mucins.

Mucins are resistant to proteolysis because the peptide core is shielded by sugars. Degradation occurs at specific sites giving rise to small mucin polymers that are very mobile in the mucin gel. The presence of cleavage sites outside the cell membrane to which cell-surface mucins are anchored underlies the turnover of the glycocalyx and tear film itself, for example, through the action of neutrophil enzymes. The same mechanism has a protective

value, when, in response to bacterial enzymes, the cleavage of mucins and portions of gel removes invading organisms from the surface of the eye.

Lubrication

Water lubricates sliding soft surfaces densely covered with bottlebrushes of oligosaccharide chains. Mucin polymers incorporate large quantities of aqueous tears that bridge between negatively charged oligosaccharides. This cushioning layer sustains the pressure of the moving lids, thus decreasing friction. Furthermore, tears lower their viscosity with shear, further easing the blink. *In vitro*, in a physiological buffer, human ocular mucin macromolecular aggregates slide past each other without forming adhesions.

Tear Breakup

Evaporation is the organizing event of tear breakup. The evaporation of water from the liquid trapped in the pores of the gel may cause an increase in salts, and importantly in divalent cations, which causes a local salting-out of mucins and other polyelectrolytes, in turn causing a local collapse of the scaffold, and thus a dry spot on the ocular surface.

Antimicrobial Activity

The ocular surface is not sterile; it hosts commensal bacteria that are part of the normal ocular surface physiology. Mucins are considered to have co-evolved with bacteria. Their mutual relationships result in continued and effective protection of the underlying tissues. Signaling between microflora and host mucosa impacts on local metabolism and immune function in ways which are a current focus of research.

Carbohydrates, including mucin glycans, can be used as an energy source for bacteria. At the ocular surface, mucin oligosaccharides are protected from bacterial degradation by the acetylation of their terminal sugars: most sialic acids are mono-O-acetylated, and a minority di-acetylated. Acetylation prevents or restricts bacterial glycolytic enzymes. A proportion of mucin terminal sugars is sulfated, which also protects from cleavage of the glycan by bacterial enzymes.

For many bacteria, mucins are antiadhesive: denuding a cornea of mucins resulted in a large increase in the number of organisms attached to its surface. This effect can be achieved by mucin glycans interacting with bacterial adhesins and thus blocking them, and because bacteria coated in mucins do not bind to the mucosal surface. Mucins glide over those without any adhesions. In tears, *Pseudomonas aeruginosa* bind to specific oligosaccharide receptors containing sialic acids, and a substantial proportion of glycans are potential receptors. Mucin glycans, however, contain 10 times fewer sialic acids in the α2–6 linkage – the receptor for this bacterial species– than α2–3-linked sialic acids that are not adhesive (**Figure 3**). This example illustrates the two-pronged defensive mechanism of binding and removing in the bulk of the preocular fluid by dissolved moieties, and increasing antiadhesion closer to the epithelial surface.

To degrade complex substrates such as mucins, bacteria need an impressive array of glycosidases and peptidases acting in sequence. These are rarely in the arsenal of a single species, though they can be – and are – expressed by a bacterial community. Commensal bacteria degrade mucins: they cleave sugar chains and peptide backbones, changing the physicochemical characteristic of the mucin molecule. It is thought that in this way the commensal flora contributes to the renewal of the mucus component of the tear film.

Immune Protection

In large epithelial tracts, a link between mucins innate mucosal immunity and mucosal inflammatory responses is provided by modulation of mucin expression by inflammatory cytokines such as interleukins (IL)-1β, IL-4, IL-6, IL-9, IL-13, interferons, tumor necrosis factor-α, or nitric oxide. Neutrophils – the main patrolling cells of the closed eyes – can also stimulate increases in production of both gel-forming and cell-surface mucins through neutrophil elastase. *In vitro*, their degranulation and activation were shown to be different on normal and dry eye mucins.

Clinical Relevance and Pathology

Contact Lens Wear

If all species present in the preocular fluid also adhere to the contact lens without prejudice to its optical properties and gas permeability, a mucin coating should add cushioning, and provide added antimicrobial protection to the ocular surface.

Among mucins adhering to contact lenses there are very large and also (relatively) short mucin polymers, with both secreted and surface-associated mucins well represented. Mucins adherent to contact lenses might act as acceptors for reactive groups produced at the ocular surface. In these mucins, there exist subunits with much higher negative charge than observed in intracellular mucins. Naive wearers deposit more mucins on their lenses than experienced wearers, probably prior to habituation to the stimulus provided by the lens. Contact-lens-induced dry eye does not appear to alter the proportion of mucin species at the ocular surface.

Dry Eye Syndromes

Involvement of mucins in dry eye syndromes is suggested by a number of observations: (1) goblet cell numbers decrease in severe disease; (2) the quality of mucus can be manifestly affected with adherent plaques forming on the ocular surface; (3) ocular surface epithelia are (and feel) dry and even keratinized. The increase in squamous epithelial proliferation and relative (or absolute) decrease in goblet cells in dry eye syndromes highlight the different functions of surface-associated and secreted mucins in the preocular fluid.

Mucin genes are not altered in the conjunctiva of patients with moderate nonimmune (non-Sjögren) dry eye compared to normal conjunctiva. However, the expression of fucosyl- and sialyl-transferases is decreased, consistent with the decrease in sialylation observed in mucins of dry eye patients. Differences between neutrophil adherence and activation (dependent at least in part on fucosylated epitopes) on fields of normal mucins and mucins in Sjögren patients suggest that these differences become more severe with the severity of disease.

See also: Adaptive Immune System and the Eye: Mucosal Immunity; Conjunctival Goblet Cells; Defense Mechanisms of Tears and Ocular Surface; Imaging of the Cornea; Immunopathogenesis of Pseudomonas Keratitis; Innate Immune System and the Eye; Overview of Electrolyte and Fluid Transport Across the Conjunctiva; Tear Film Overview.

Further Reading

Argueso, P. (2003). The cell-layer- and cell-type-specific distribution of GalNAc-transferases in the ocular surface epithelia is altered during keratinization. *Investigative Ophthalmology and Visual Science* 44: 86–92.

Basbaum, C. (1999). Control of mucin transcription by diverse injury-induced signaling pathways. *American Journal of Respiratory and Critical Care Medicine* 160: S44–S48.

Berry, M. (2001). Exploring the molecular adhesion of ocular mucins. *Biomacromolecules* 2: 498–503.

Carlstedt, I. (1985). Mucous glycoproteins: A gel of a problem. *Essays in Biochemistry* 20: 40–75.

Carraway, K. L. (2000). Multiple facets of sialomucin complex/MUC4, a membrane mucin and erbb2 ligand, in tumors and tissues (Y2K update). *Frontiers in Bioscience* 5: D95–D107.

Dartt, D. A. (2000). Regulation of conjunctival goblet cell secretion by Ca2+ and protein kinase C. *Experimental Eye Research* 71: 619–628.

Fleiszig, S. M. J. (1994). Modulation of *Pseudomonas aeruginosa* adherence to the corneal surface by mucus. *Infection and Immunity* 62: 1799–1804.

Gipson, I. K. (1997). Mucin genes expressed by the ocular surface epithelium. *Progress in Retinal Eye and Research* 16: 81–98.

Hattrup, C. L. (2008). Structure and function of the cell surface (tethered) mucins. *Annual Review of Physiology* 70: 431–457.

Imbert, Y. (2006). MUC1 splice variants in human ocular surface tissues: Possible differences between dry eye patients and normal controls. *Experimental Eye Research* 83: 493–501.

Jumblatt, J. E. (1998). Regulation of ocular mucin secretion by P2Y2 nucleotide receptors in rabbit and human conjunctiva. *Experimental Eye Research* 67: 341–346.

McMaster, T. J. (1999). Atomic force microscopy of the submolecular architecture of hydrated ocular mucins. *Biophysical Journal* 77: 533–541.

Perez-Vilar, J. (2007). Mucin granule intraluminal organization. *American Journal of Respiratory Cell and Molecular Biology* 36: 183–190.

Royle, L. (2008). Glycan structures of ocular surface mucins in man, rabbit and dog display species differences. *Glycoconjugate Journal* 25: 763–773.

Sharon, N. (1989). Lectins as cell recognition molecules. *Science* 246: 227–234.

Thornton, D. J. (2008). Structure and function of the polymeric mucins in airways mucus. *Annual Review of Physiology* 70: 459–486.

Relevant Websites

http://www.functionalglycomics.org – Consortium for functional glycomics.

http://www.hugo-international.org – HUGO Gene Nomenclature Committee.

http://www.library.nhs.uk – National Library for Health Specialist Libraries.

http://www.genenames.org/genefamily/muc.php – The HGNC database in 2008: a resource for the human genome.

Optic Nerve: Optic Neuritis

K Hein and M Bähr, University of Göttingen, Göttingen, Germany

Glossary

Apoptosis – A genetically determined process of cell death that is marked by the fragmentation of nuclear DNA, occurs under both pathological and physiological conditions (known as programmed cell death).
Gadolinium – An element of the rare earth family of metals (atomic symbol Gd) used as a paramagnetic contrast agent in magnetic resonance imaging.
Isoelectric focusing – The most sensitive method for protein separation in serum and CSF using agarose gel electrophoresis.
Multiple sclerosis – A chronic autoimmune inflammatory demyelinating disease affecting the central nervous system (CNS) (synonym: encephalomyelitis disseminata).
P100 latency – The time it takes for the signal from the retina to reach the occipital cortex in the brain.
Plasmapheresis (plasma exchange) – A technology for removing pathologic plasma constituents from anticoagulated whole blood by a machine and returning the rest to the donor, usually with saline solution and albumin.
Snellen chart – Chart that contains rows of standardized letters, numbers, or symbols routinely used to assess visual acuity at a distance of 20 feet.
Visual evoked potential – A diagnostic test that measures alterations in the speed of responses to visual events. The patients watch a black-and-white checkerboard and an electroencephalogram (EEG) measures occipital cortex responses.

Definition

Optic neuritis (Latin – *neuritis nervi optici*) is defined as an inflammation of the optic nerve causing a relatively rapid onset of visual failure. Inflammation may occur in the portion of the nerve within the globe (neuropapillitis or anterior optic neuritis) or in the most commonly involved portion behind the globe (retrobulbar neuritis or posterior optic neuritis).

Optic Nerve Anatomy

The optic nerve, ~45 mm in length, can be divided into several segments: intraocular (1 mm), intraorbital (28 mm), canalicular (4–10 mm), and intracranial (3–16 mm). The diameter of the nerve increases from 1 mm at the intraocular point, 3–4 mm in the orbit, to 4–7 mm within the cranial cavity. The orbital section of the optic nerve has a slightly sinuous shape to allow for movements of the eyeball. As part of the brain, the optic nerve is surrounded by meninges. The outer dural sheath and inner arachnoid sheath merge with the sclera. Between the arachnoid sheath and pial sheath lies a cerebrospinal fluid (CSF)-filled space. The optic nerve consists mainly of fibers derived from the ganglion cells of the retina. The fibers emanating from the nasal part of each retina cross over to the other side in the optic chiasm. The nerve fibers originating in the temporal part of the retina do not cross over. From there, the mixed fibers from the two nerves become the optic tract passing through the thalamus and turning into the optic radiation until they reach the visual cortex located in the occipital cortex of the brain.

Immunopathogenesis

An early event in the development of inflammation is considered to be the activation of circulating autoreactive T lymphocytes by factors such as infection, superantigen stimulation, or effects of reactive metabolites or metabolic stress. Activated T lymphocytes interact with the venule endothelium surface to harm and break down the blood–brain barrier. Upregulation of vascular cell adhesion molecules (e.g., intercellular adhesion molecule-1 (ICAM-1)) increases vascular permeability and enables migration of T cells, B cells, and macrophages into the central nervous system (CNS). The activated antigen-specific T cells appear to develop a Th1-dominant profile with production of proinflammatory cytokines (e.g., IL-2, IFNγ, and TNFα). These cytokines exacerbate the inflammation resulting in further recruitment of pathogenic inflammatory cells, which play a direct role in demyelination. Other factors such as demyelinating antibodies, proinflammatory cytokines, and other soluble mediators contribute to myelin and axonal injury. Also the humoral immunity with autoreactive B-lymphocyte expansion with IgG production plays a relevant role in autoimmune inflammation. Despite significant research

progress in this field, the antigen driving the putative cascade of autoimmune inflammation has not been identified, leaving a substantial gap in the understanding of pathogenesis.

Epidemiology

Optic neuritis typically affects young adults with a mean age of 30–35 years. The majority of patients are female. The annual incidence of optic neuritis ranges from 1.4 to 6.4 new cases per 100 000 population. The prevalence is estimated to be 115 per 100 000 population.

Etiology

Various diseases and conditions may cause optic neuritis. The first description of a relationship of optic neuritis to multiple sclerosis (MS) came from Buzzard in 1893. Nowadays, MS is recognized to be the most common etiology for optic neuritis. Up to 50% of MS patients will develop an episode of optic neuritis.

Some other causes of optic neuritis include inflammation of vessels supplying the optic nerve, infectious diseases (e.g., viral encephalitis, sinusitis, meningitis, HIV, tuberculosis, and syphilis) and autoimmune disorders (e.g., lupus erythematosus). Toxic agents can clearly influence optic nerve and retinal function. Among the common offenders are tobacco and alcohol. Drugs (e.g., salicylates, digitalis, amiodaron, and some antibiotics) can also damage the optic nerve. Rarely, tumor metastasis to the optic nerve, diabetes, pernicious anemia, Graves' disease, and trauma lead to optic neuritis.

Some people, especially children, develop optic neuritis following a viral illness such as mumps, measles, or a cold.

Symptoms

Optic neuritis typically presents with a triad of symptoms: loss of vision, dyschromatopsia, and pain during eye movements. The major symptom is vision loss, which occurs over a period of 3–5 days and generally improves within 2–8 weeks. The visual deficit varies from a small central or paracentral scotoma to complete blindness. The initial attack is unilateral in 70% of adult patients and bilateral in 30%. Both eyes are affected with equal regularity. The visual symptoms are usually described as blurring or fogging of vision. Interestingly, some patients become aware of a unilateral visual disturbance by accident when, for some reason, the unaffected eye is covered.

Many patients with optic neuritis may lose some of their color vision in the affected eye, called dyschromatopsia. The colors appear slightly washed out compared to the other eye. In the majority of cases, patients experience tenderness in the eye, which is associated with pain at rest or on eye movement. In some cases, pain on eye movement precedes the visual loss. Positive visual phenomena, such as a sensation of sparks and flashes of light induced by certain eye movements, occur infrequently.

Symptoms of optic neuritis include one or more of the following:

- reduced visual acuity (near or far)
- pain on eye movement
- central scotoma
- dyschromatopsia or impaired color vision
- impaired contrast sensitivity
- afferent pupillary defect, and
- headache

Diagnosis

Optic neuritis can usually be diagnosed from a patient's history, clinical examination, visual-evoked potentials (VEP), CSF investigation and observations from magnetic resonance imaging (MRI).

Clinical Examination

Despite the wide use of MRI and electrophysiological techniques, the diagnosis of optic neuritis depends on accurate clinical assessment. The medical history should also be assessed to determine if exposure to toxins such as lead or methanol may have caused the visual disturbance. Patients with optic neuritis typically contact an ophthalmologist first. A complete visual examination, including a visual acuity test, color vision test, and visualization of the retina and optic disc by indirect ophthalmoscopy, should be performed. However, frequently there is no abnormal appearance of the optic disk during ophthalmoscopy. Occasionally, there may be hyperemia of the optic disk and distension of the large retinal veins. At later stages the margins of the optic disk are blurred and papilledema can be found. Clinical signs such as impaired pupil response may be apparent during an eye examination, but in some cases the eye may appear normal. Central field defects predominate in patients with optic neuritis.

Visual Evoked Potential

VEP is a noninvasive technique to detect pathological changes of the visual system during optic neuritis and is used as a routine clinical test. Commonly used visual stimuli are flashing lights or patterns (e.g., checker boards) on a video screen. The main interest in electrophysiological findings for optic neuritis focus on the so-called P100 latency and VEP amplitude. During the acute phase of the

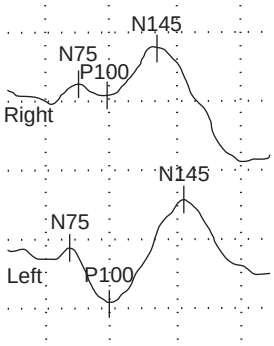

Figure 1 VEP from a 25-year-old woman with a 4-day history of acute right-sided optic neuritis. VEP shows a decrease in amplitude in the affected right eye. VEP amplitude consists of potentials originating in different parts of the brain (N75: area 17; P100: area 18, 19 and partially 17; N145: area 18 and 19).

disease, a decrease in the VEP amplitude, caused by a conduction block of inflamed optic nerve fibers, is a common pathological feature (Figure 1). The depression of the VEP amplitude correlates with the visual acuity and is associated with the degree of atrophy. The prolongation of P100 latency is the main characteristic in the chronic phase and persists over years in up to 70% of patients who suffer from optic neuritis.

Magnetic Resonance Imaging

The principal use of MRI is the evaluation of patients when optic neuritis is the first demyelinating disease event. In a typical case, if accurate clinical assessment has been done, MRI is not required to diagnose and distinguish optic neuritis from other common optic neuropathies. However, the patients with other pathologies such as ischemic or acute compressive optic neuropathy due to a cerebral aneurysm or pituitary tumor may not have the typical features that distinguish these disorders from optic neuritis. In these situations, MRI, when performed with the appropriate examination technique, can make a relevant contribution to the differential diagnosis. The small size and mobility of the optic nerve and artifacts caused by surrounding CSF and orbital fat are technically challenging in optic nerve imaging. Significant progress has been made in developing fat and CSF-suppressed high-resolution imaging. Use of these sequences increases the sensitivity in detecting inflammatory demyelination and optic nerve atrophy. Symptomatic lesions can be detected with sensitivities of 95% in fat-saturated fast spin-echo (FSE) imaging and 94% for the enhancing lesion on fat-saturated T1-weighted imaging following intravenous (IV) gadolinium administration (Figure 2). The abnormal gadolinium enhancement of the affected optic nerve indicates a blood–optic nerve barrier breakdown and is a consistent feature of acute optic neuritis.

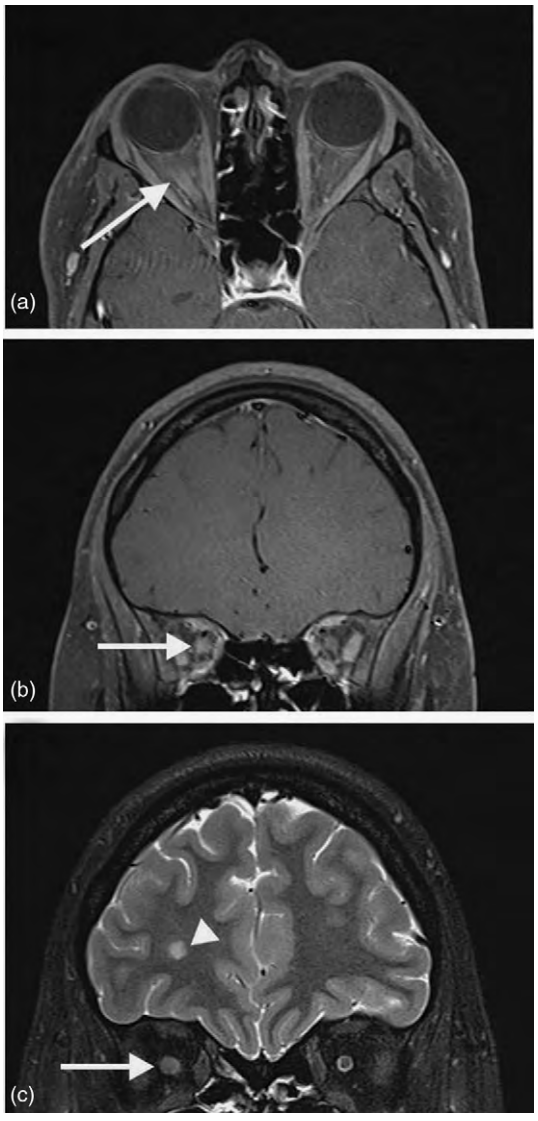

Figure 2 (a) Axial and (b) coronal T1-weighted magnetic resonance images after the IV application of gadolinium. (c) Coronal T2-weighted image from a 25-year-old woman with a 4-day history of acute right-sided optic neuritis demonstrating optic nerve swelling (arrow: diseased optic nerve; arrowhead: demyelinated cerebral lesion).

Cerebrospinal Fluid

CSF analysis is of great relevance to detect an inflammatory process in the brain. The diagnostic sensitivity of single parameters in CSF diagnostics depends on the quality of the applied techniques, especially with isoelectric focusing, and does not have a worldwide standard, such as MRI. In optic neuritis related to MS, typical changes are present in the CSF: slight pleocytosis (max. 50 leucocytes/μl), intrathecal (within the meningeal sheath) IgG production, and additional oligoclonal IgG bands, which are not present in the simultaneously examined serum. The so-called MRZ reaction (intrathecal synthesis of

antibodies against measles, rubella, and varicella-zoster) has a higher diagnostic specificity and is suggested in a European consensus report. Before the use of brain MRI, the detection of CSF pleocytosis and oligoclonal IgG bands provided paraclinical evidence of the dissemination of lesions and met the criteria for the diagnosis of laboratory-supported MS in isolated optic neuritis.

In other autoimmune disorders (e.g., lupus erythematosus and neurosarcoidosis) the cell count is moderately elevated. Verification of oligoclonal IgG bands can be achieved in up to 70% of the cases.

CSF abnormalities in optic neuritis resulting from a viral infection are not specific concerning number of cells, differential cell count, and total protein content and depend particularly on the stage of the disease.

Optical Coherence Tomography

OCT is a relatively new, noninvasive and easy-to-use technology that quantifies the thickness of the peripapillary retinal nerve fiber layer (RNFL), fovea, and macula in real time with highly refined resolution. Originally developed to investigate retinal axonal loss in glaucoma patients, OCT demonstrated a significant reduction of mean RNFL thickness in patients with optic neuritis. Hence, OCT may be useful for observing occult neurodegeneration and monitoring the efficacy of potential neuroprotective therapies in optic neuritis. Serial clinical studies in optic neuritis correlating MRI, clinical, and electrophysiological data are required to establish the use of OCT as an *in vivo* biomarker for axonal loss.

Differential Diagnosis

The differential diagnosis can be divided into several pathophysiological categories: inflammatory/autoimmune diseases, infectious diseases, genetic/hereditary disorders, neoplastic disease, and other demyelinating diseases. Errors in the diagnosis can be minimized if strict clinical criteria are applied and the neurologist is alert to discrepancies in the clinical picture presented (e.g., absence of pain, age of onset, and failure to remit). Also the character of visual symptoms and the type of field defect give additional important information. A slowly progressive unilateral visual failure should always suggest the possibility of compressive etiology. A central field defect can occur with a tumor but, with time, will extend to the periphery. Interestingly, spontaneous improvement in vision may occur in this case. Pain on eye movement is not confined to optic neuritis and can occur in optic nerve glioma, meningioma, and aneurysm. Any of the fundoscopic changes found in optic neuritis may be reproduced by compressive or infiltrative lesions. In such cases, MRI will significantly contribute to the correct diagnosis. The various vascular optic neuropathies generally affect a different age group from optic neuritis and tend to have a poor prognosis.

When both eyes are involved in optic neuritis, simultaneously or sequentially, the disorder must be distinguished from Devic's disease, Leber's hereditary optic neuropathy, nutritional/toxic amblyopia, and functional blindness. Devic's disease, neuromyelitis optica, is characterized by a combination of transverse myelitis and optic neuritis occurring within a finite period of time from each other, typically within weeks. Clinically, the disorder usually has monophasic presentation. The identification of serum anti-aquaphorin-4 antibodies should be helpful for differential diagnosis. Of the hereditary disorders, Leber's optic neuropathy causes optic atrophy with acute or subacute visual loss. This disorder is maternally transmitted and can be diagnosed through genetic testing. In optic neuropathies caused by toxic agents, the overlap of the visual symptoms with those due to optic neuritis is minimal. It often presents as a painless, progressive, bilateral, and symmetrical visual disturbance. Optic nerve pallor is often found in the ophthalmologic examination. Vision loss can be presented as a symptom of Lyme borreliosis optic neuropathy, syphilis, HIV-associated optic neuropathies, and other infectious disorders. In these cases optic nerve involvement tends to be bilateral and MRI and CSF examinations should show a reliable distinction.

Treatment

Treatment of optic neuritis depends on the underlying cause. In a MS-related episode of optic neuritis a course of IV methylprednosolone followed by oral steroids has been found to be helpful. No treatment is also a viable option. The optic neuritis treatment trial (ONTT) has shown that high dose IV steroids (250 mg prednisone every 6 h for 3 days) followed by oral prednisone (1 mg kg^{-1} d^{-1} for 11 days) accelerated visual recovery but did not have any impact on the 6-month and 1-year visual outcome compared with a placebo. An interesting finding of this study was that patients who received IV corticosteroids followed by oral corticosteroids had a temporarily reduced risk of development of a second demyelinating event consistent with MS compared with those who received an oral placebo or treatment with oral corticosteroids only. Oral prednisone has been found to increase the likelihood of recurrent episodes of optic neuritis, and is not recommended for treating the disorder. Patients with severe optic neuritis, who do not respond sufficiently to corticosteroids, can undergo escalating immunotherapy with plasma exchange within 1 month of the first symptoms. In clinical trials up to 60% of patients with optic neuritis had functional improvement after 5 plasmapheresis sessions with an exchange volume of 3000 ml. Long term prophylactic immunomodulatory

therapy with interferon-beta or glatiramer acetate is recommended in patients when optic neuritis is an event of demyelinating disease with a presence of further demyelinated brain lesions shown on the MRI.

Vision loss caused by viral or bacterial infection usually resolves itself once the virus/bacteria are treated. For herpes virus infection the IV treatment with aciclovir ($10\,mg\,kg^{-1}$ every 8 h for 14 days) is recommended. In cases of borrelia infection with neurological symptoms, patients should undergo a treatment session with doxycycline $200\,mg\,d^{-1}$ for 14–21 days. Optic neuritis resulting from toxin damage may improve once the source of the toxin is removed.

Neuroprotective Treatment Strategies

The increasing importance of axonal damage as a major substrate of clinical disability in autoimmune inflammation has led to ongoing research in developing treatment strategies that inhibit degeneration of axons and protect the neuronal cell body from apoptotic cell death. The hypothesis of achieving neuroprotective effects as a secondary phenomenon resulting from the treatment of inflammation and autoimmunity is supported by studies showing close association of axonal damage and inflammation. However, the elimination of the inflammatory component does not necessarily stop the disease progression. MRI studies showed that treatment with methylprednisolone did not limit ongoing lesion lengthening triggered by an episode of optic neuritis nor did it prevent optic nerve atrophy. A detrimental effect of corticosteroids on retinal ganglion cells (RGCs) has even been described in experimental optic neuritis. The effects of cytokines and trophic factors (e.g., erythropoietin, ciliary neurotrophic factor) on neuronal apoptosis appear to be limited; despite preventing neuronal apoptosis, these substances failed to improve visual acuity due to severe and ongoing degeneration of optic nerve fibers in autoimmune optic neuritis. For this reason, anti-inflammatory/immunomodulatory therapies should be combined with primary neuroprotective agents. The potential neuroprotective substances are still in the experimental stage of development, and controlled clinical trials are needed to prove the efficacy and tolerance of these agents.

Prognosis

The vision loss associated with optic neuritis is usually temporary. Spontaneous remission occurs within 2–8 weeks. The majority of patients (65–80%) recover visual acuity of 20/30 (on the Snellen chart) or better. Long-term prognosis depends on the underlying cause of the condition. If a viral infection has triggered the episode, it frequently resolves itself with no aftereffects. If optic neuritis is associated with MS, future episodes are common. Thirty-three percent of optic neuritis cases recur within five years. Each recurrence results in less recovery and worsening vision. There is a strong association between optic neuritis and MS. According to the latest literature, the probability of developing MS within 15 years after onset of optic neuritis is 50% and strongly related to the presence of lesions on a baseline non-contrast-enhanced magnetic resonance image of the brain.

See also: Extraocular Muscles: Extraocular Muscle Anatomy; Extraocular Muscles: Extraocular Muscle Metabolism; Imaging of the Orbit; Intraocular Pressure and Damage of Optic Nerve Axons; Noninvasive Testing Methods: Multifocal Electrophysiology; Optical Coherence Tomography; Orbital Bony Anatomy and Orbital Fractures; Orbital Masses and Tumors; Retinal Ganglion Cell Apoptosis and Neuroprotection.

Further Reading

Andersson, M., Alvarez-Cermeno, J., Bernardi, G., et al. (1994). Cerebrospinal fluid in the diagnosis of multiple sclerosis: A consensus report. *Journal of Neurology, Neurosurgery, and Psychiatry* 57: 897–902.

Beck, R. W. and Gal, R. L. (2008). Treatment of acute optic neuritis: A summary of findings from the optic neuritis treatment trial. *Archives of Ophthalmology* 126: 994–995.

Buzzard, T. (1893). Atrophy of the optic nerve as a symptom of chronic disease of the central nervous system. *British Medical Jornal* 2: 779–784.

Diem, R., Sättler, M. B., and Bähr, M. (2007). Neurodegeneration and protection in autoimmune CNS inflammation. *Journal of Neuroimmunology* 184: 27–36.

Hickman, S. J. (2007). Optic nerve imaging in multiple sclerosis. *Journal of Neuroimaging* 17: 42S–45S.

Hickman, S. J., Brierley, C. M. H., Brex, P. A., et al. (2002). Continuing optic nerve atrophy following optic neuritis: A serial MRI study. *Multiple Sclerosis* 8: 339–342.

Kahle, W., Leonhardt, H., and Platzer, W. (2002). *Color Atlas and Textbook of Human Anatomy,* 4th edn. Stuttgart: Thieme.

Maier, K., Kuhnert, A. V., Taheri, N., et al. (2006). Effects of glatiramer acetate and interferon-beta on neurodegeneration in a model of multiple sclerosis: A comparative study. *American Journal of Pathology* 169: 1353–1364.

Maurer, K. and Eckert, J. (1999). *Praxis der Evozierten Potentiale.* Stuttgart: Enke.

Perkin, G. D. and Rose, F. C. (1979). *Optic Neuritis and Its Differential Diagnosis.* Oxford: Oxford University Press.

Poser, C. M. and Brinar, V. V. (2007). The accuracy of prevalence rates of multiple sclerosis: A critical review. *Neuroepidemiology* 29: 150–155.

Sergott, R. C., Frohman, E., Glanzman, R., and Al-Sabbagh, A: OCT in MS Expert Panel (2007). The role of optical coherence tomography in multiple sclerosis: Expert panel consensus. *Journal of the Neurological Sciences* 263: 3–14.

The Optic Neuritis Study Group (2008). Multiple sclerosis risk after optic neuritis. *Archives of Neurology* 65: 727–732.

Trapp, B. D., Peterson, J., Ransohoff, R. M., et al. (1998). Axonal transection in the lesions of multiple sclerosis. *New England Journal of Medicine* 338(5): 278–285.

Wingerchuk, D. M. and Lucchinetti, C. F. (2007). Comparative immunopathogenesis of acute disseminated encephalomyelitis, neuromyelitis optica, and multiple sclerosis. *Current Opinion in Neurology* 20: 343–350.

Optical Coherence Tomography

W Drexler, Medical University Vienna, Vienna, Austria

Glossary

Adaptive optics (AO) – A technique originally developed for improving imaging performance in astronomy. Applied in vision sciences to correct wave front aberrations introduced by imperfect optics of the human eye to reduce the spot size in the retina and hence transverse resolution of retinal imaging.
Optical coherence tomography (OCT) – Optical analog to ultrasound, for noninvasive three-dimensional micrometer resolution visualization of superficial (up to 2 mm) tissue morphology.
Optophysiology – Optical analog to electrophysiology that enables noninvasive depth resolved optical probing of retinal physiology.

Optical coherence tomography (OCT) is a rapidly emerging noninvasive, optical diagnostic imaging modality enabling *in vivo* cross-sectional tomographic visualization of internal tissue microstructure in biological systems at resolution levels of a few micrometers. Novel high-speed detection techniques as well as development of ultrabroad bandwidth and tunable light sources have recently revolutionized imaging performance and clinical feasibility of OCT. In this view, OCT can now be considered as an optical analog to computed tomography (CT) and magnetic resonance imaging (MRI), not enabling full body imaging, but noninvasive optical biopsy, that is, micrometer/cellular resolution 3D visualization of tissue morphology.

The eye provides easy optical access to the anterior segment and the retina due to its essentially transparent nature. Axial and transverse resolutions are decoupled in OCT. While the axial one is mainly determined by the optical bandwidth of the employed light source, the transverse one is mainly given by the numerical aperture of the optics that is focusing the beam to the tissue. As a consequence, the axial OCT resolution for retinal imaging is not limited by the low-numerical aperture and large depth of focus of the human eye as it does in scanning laser ophthalmosocopy. For this reason, ophthalmic and especially retinal imaging has so far not only been the first, but also the most successful clinical application for OCT. Objectively this is evidenced by the fact that nearly 2500 (49%) of the 5000 OCT publications (including only peer-reviewed articles) have been published in ophthalmic journals. About 1300 (25%) have been published in optical or biomedical journals demonstrating the significant emphasis on OCT technology development since its invention. In addition, more than half a dozen companies offer this technology in its fourth generation for 3D retinal OCT. Considering the fact that OCT has been introduced only about two decades ago, retinal OCT therefore represents the fastest adopted imaging technology in the history of ophthalmology.

Figure 1 depicts an overview of OCT development with respect to axial resolution and data acquisition speed (measurement time) for morphologic (as opposed to functional) retinal imaging. After its first *in vitro* demonstration in 1991 and first *in vivo* imaging studies of the human retina in 1993 (cf. Figure 1(a)–1(d)), OCT has rapidly developed as a noninvasive, optical medical diagnostic imaging modality providing two-dimensional information of retinal structure with resolution about one order of magnitude better than ultrasound. Since its invention, the original idea of OCT was to enable noninvasive optical biopsy, that is, the *in situ* imaging of tissue microstructure with a resolution approaching that of histology, but without the need for tissue excision and postprocessing. As a consequence, two milestone developments that improved key technological OCT parameters – axial resolution and measurement time – significantly contributed to realize the optical biopsy idea of OCT. A first step toward this goal was the introduction of ultrahigh resolution OCT enabling a noticeably superior visualization of tissue microstructure, for example, all major intraretinal layers as well as cellular resolution OCT imaging in nontransparent tissue by improving axial OCT resolution by one order of magnitude from the 10–15 μm to the (sub)micrometer region, accomplishing 2–3 μm in the living human retina (cf. Figure 1(e)–1(g)). Advances in photonics technology including the development of ultrabroad bandwidth and high-speed tunable light sources as well as high-speed detection techniques have enabled a considerable improvement in data acquisition speed from several hundreds of A-scans/s to 30 000 A-scans/s and recently 300 000 A-scans/s (cf. Figure 1(h)–1(j)).

Despite numerous successful and clinically valuable OCT applications in the anterior eye segment (mainly in the cornea and anterior chamber angle), retinal OCT had a significantly higher clinical impact so far. This is mainly due to the lack of competing noninvasive techniques that can provide comparable wealth of information about the living human retina. Hence, the technological improvements that have been accomplished in the last decade not only enabled unprecedented OCT performance that is unique among noninvasive diagnostic

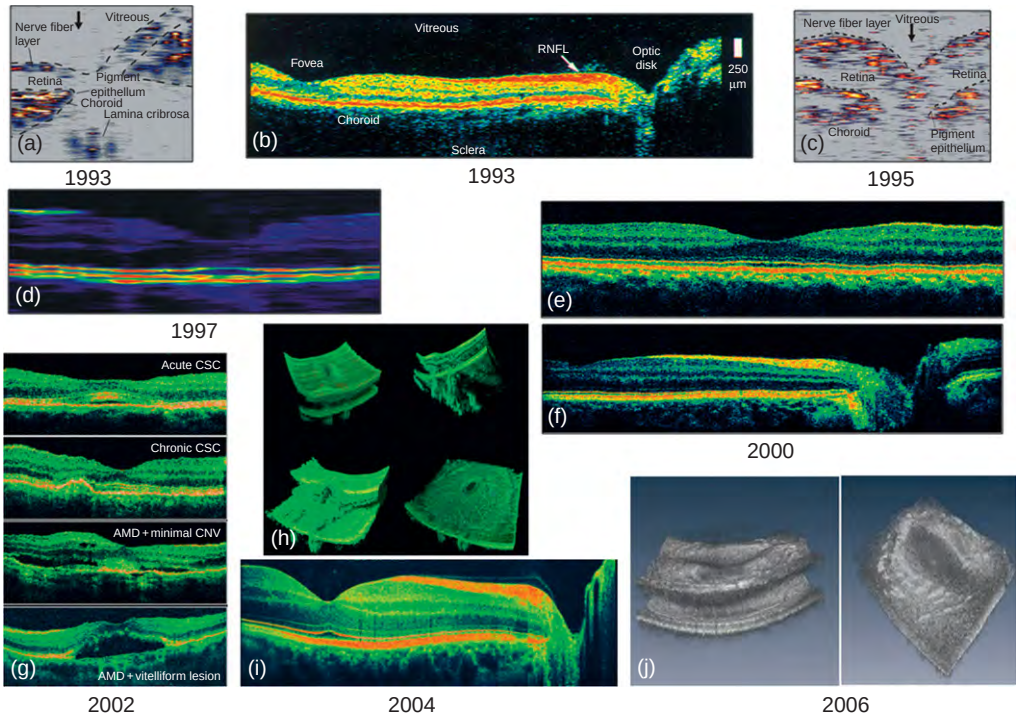

Figure 1 Development of retinal OCT regarding axial resolution and data acquisition. (a, c): First *in vivo* retinal OCT with 10–15 µm axial resolution and 2 A-scans/s; (b) 100 A-scans/s; (d): improved axial resolution (7–9 µm) with 2 A-scans/s; (e, f) first *in vivo* ultrahigh resolution (2–3 µm) with 160 A-scans/s of normal subjects; (g) first ultrahigh resolution OCT in patients; (h) three dimensional; (i) high definition ultrahigh resolution (2–3 µm) with 29 000 A-scans/s; (j) 300 000 A-scans/s and 10 µm axial resolution 3D retinal imaging at 1060 nm with enhanced penetration into the choroid.

techniques, but it also established retinal OCT as a state-of-the art noninvasive, complementary ophthalmic diagnostic methodology. For this reason, this article will mainly focus on retinal OCT.

3D Ultrahigh Resolution Retinal OCT

While third generation commercial retinal OCT systems (Stratus OCT) were based on the so-called time domain OCT, enabling up to 400 A-scans/s (one-dimensional (1D) measurements), fourth generation (spectral or Fourier-domain based) commercial retinal OCT systems, nowadays can perform up to 100 times more measurements enabling either highly sampled (high definition) 2D tomograms or 3D (volumetric) imaging of the retina. This is due to an alternative detection method that uses either a CCD camera-based spectrometer (spectral of Fourier domain), that can be read out quickly or a fast tuneable laser (swept source OCT or frequency domain OCT) as compared to a moving mirror (time domain) to perform a single A-scan. The first version is inherently more efficient and enables to raster scan the retina analog to a scanning laser ophthalmoscope (SLO) but thereby not only acquiring tissue information from a single 2D plane (in focus), but the full morphological depth information from an entire volume with a depth resolution mainly given by the optical bandwidth of the employed light source.

A volumetric data set is acquired for the imaged area that can then be viewed and analyzed in ways similar to those used with CT or MRI scans (cf. **Figure 2(a)** and **2(b)**). Hence, the imaged volume can arbitrarily be cut according to the necessary diagnostic needs, for example, like an ultrahigh resolution SLO in en face (C-mode) tomograms (cf. **Figure 2(c)** and **2(d)**). **Figure 2** demonstrates 3D UHR OCT in the foveal region of a patient with retinal pigment epithelium (RPE) atrophy. Note that the axial dimension is twofold enlarged as compared to the other two dimensions for better visualization. The 3D representation of the macular region is presented at different-angled views (cf. **Figure 2(a)**) depicting the pathological change in the topography of the foveal depression as well as enabling unprecedented views in which the retina can be observed from any direction, including from below (cf. **Figure 2(b)**). **Figure 2(e)–2(h)** present virtual biopsy/surgery using 3D UHR OCT in combination with 3D data rendering which allows the user to excise and remove any given layer or part of the retinal volume to visualize intraretinal morphology.

The clinical benefit of these spectral of Fourier domain-based OCT instruments is demonstrated in highly sampled 3D visualization of the retina during a reasonable short data-acquisition time resulting in more

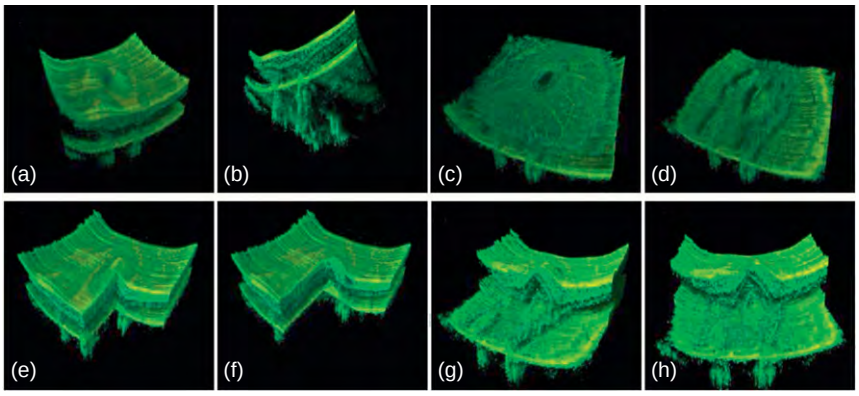

Figure 2 Three-dimensional ultrahigh resolution OCT of the macular region of a patient with retinal pigment epithelium atrophy; (a–d) at different-angled views; (e–h) virtual biopsy allows removal of any given layer or part of the retinal volume to visualize intraretinal morphology.

reliable and reproducible 2D thickness maps of (intra) retinal layers. Furthermore, retinal locations are less likely to be missed that are important for diagnosis since an entire volume is measured instead of deciding the location of B-scans during OCT acquisition. This might result in improved diagnosis of retinal pathologies, better understanding of retinal pathogenesis, as well as enhanced (objective) monitoring of novel therapy approaches.

3D Wide-Field Choroidal OCT

So far, commercially available retinal OCT has mainly been performed in the 800-nm wavelength region. This is mainly due to easy availability of broad bandwidth light sources and detectors (CCD cameras) in this wavelength region. Although OCT systems centered at 800 nm can resolve all major intraretinal layers, they only enable limited penetration beyond the retina, due to multiple scattering and absorption in the melanin-rich RPE. This results in limited visualization of the choriocapillaris and choroid. Moreover, in clinical OCT, turbid ocular media (e.g., cataract or corneal haze) represent a significant challenge when imaging the retina. Since scattering in biological tissues decreases monotonically with increasing wavelength, OCT imaging at 1060 nm can deliver deeper tissue penetration enabling delineation of choroidal structure. Being less sensitive to scattering eye media and enabling enhanced penetration into the choroid up to the choroidal–scleral interface at 1060 nm might therefore significantly improve the clinical feasibility of retinal OCT.

2D time domain-based OCT was initiated about 5 years ago demonstrating improved visualization of superficial choroidal structure. With the introduction of more efficient and hence more sensitive spectral of Fourier domain OCT, 3D OCT at 1060 nm demonstrated wide-field visualization of the entire choroid up to the sclera. In this approach, a cost-effective, easy-to-implement system based on a high-speed InGaAs linear 1024 pixel array (SUI-Goodrich) enabling 47 000 A-scans/s, 5–8 µm axial resolution, and 2.6 mm scanning depth in tissue was developed. **Figure 3** depicts the comparison of 3D OCT at 800 nm (cf. **Figure 3(a)** and **3(b)**) versus 1060 nm (cf. **Figure 3(c)** and **3(d)**) in the same normal eye. Enhanced visualization of the choroid up to the choroidal sclera interface is accomplished using 3D 1060-nm OCT as compared to 3D 800-nm OCT (cf. yellow arrows in **Figure 3(d)**). In the subject with light fundus pigmentation, 3D 1060-nm OCT enables penetration beyond the choroid into the sclera (cf. red arrows in **Figure 3(g)**). High-speed 3D 1060-nm OCT also enables en face visualization of the choroidal vasculature without the use of any contrast agent (cf. **Figure 3(c)**, **3(e)**, and **3(f)**).

High-speed 3D 1060-nm OCT therefore now enables unprecedented visualization of all three choroidal layers giving access to the entire choroidal vasculature. In addition, 2D choroidal thickness maps might have significant impact in the early diagnosis of retinal pathologies such as glaucoma, age-related macular degeneration and might contribute to a better understanding of myopigenesis.

Cellular Resolution Retinal OCT

For retinal OCT imaging, the cornea and the lens act as the imaging objective, thereby determining the numerical aperture and hence the beam diameter in the retina. This diameter specifies the transverse OCT resolution that is of the order of ~20 µm for a beam of ~1-mm diameter (at 800 nm) – approximately one order of magnitude worse than the best axial OCT resolutions accomplished so far. This can be improved by dilating the pupil and increasing the measurement beam diameter. In practice, however, for large pupil diameters, ocular aberrations limit the minimum focused spot size on the retina, even for monochromatic illumination. An alternative and promising

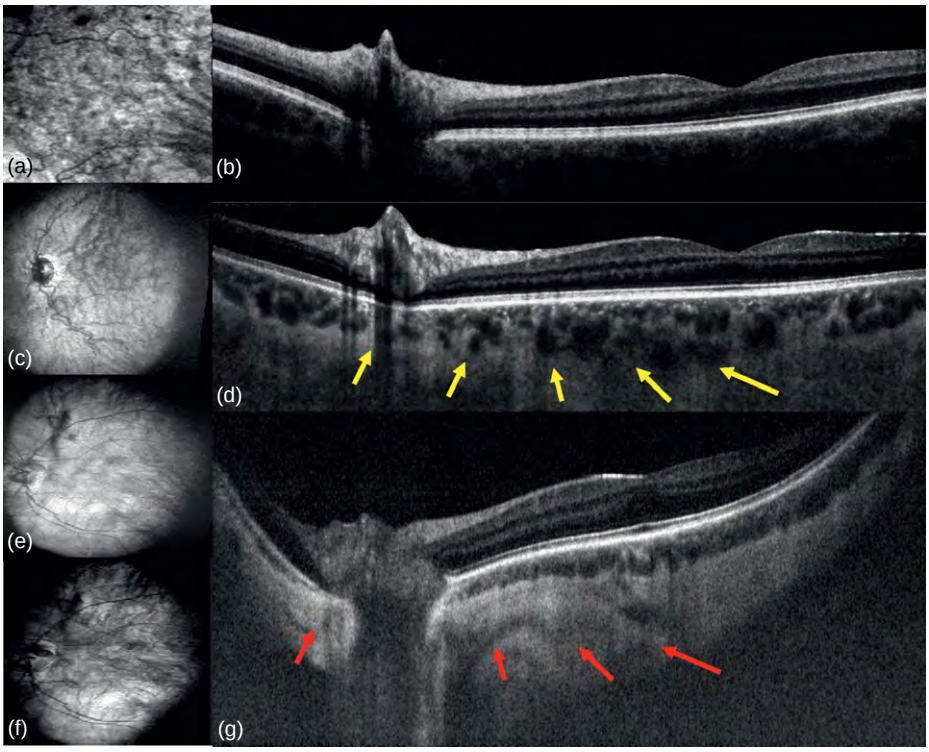

Figure 3 Wide-field three-dimensional choroidal OCT. (a, b) 3D-OCT at 800 nm and (c–g) 1060 nm of a normal retina: (b) high definition (4096 depth scans) 800-nm 3D-OCT scan over 35°; (d, g) high definition (2048 pixel) 1060-nm 3D-OCT scan over 35°; (a) en face view of the choroid using 3D OCT at 800 nm; (c, e, f) en face wide-field (35° × 35°) view using 3D OCT at 1060 nm; yellow arrows indicate enhanced choroidal visualization; red arrows indicate visualization of the sclera.

approach is to use adaptive optics (AO), which was originally developed to improve the resolution of astronomical imaging, to minimize ocular aberrations, reduce retinal spot size, and hence to improve transverse OCT resolution.

In ophthalmic AO a wave front sensor measures the individual ocular aberrations of the investigated eye, calculates an inverse wave front, and sends this information to a correcting device – a deformable mirror – for aberration correction. This procedure is performed in real time in a closed-loop configuration. In a couple of tenths of a second, ocular aberrations are compensated and continuously corrected during the entire measurement procedure. In the present approach, a deformable mirror (Mirao52, Imagine Eyes, France) with a unique performance in terms of amplitude (±50-µm stroke) and linearity was used, allowing for correcting highly aberrated normal or pathologic eyes. Furthermore a 140–160-nm Ti:sapphire laser (Femtolasers Integral, Femtolaser, Vienna, Austria) in combination with a CMOS Basler sprint spL4096-140k camera (Basler AG Germany) enabling 160 000 A-scans/s with 1536 pixels was used, resulting in ultrahigh speed cellular resolution retinal imaging with isotopic resolution of 2–3 µm. Furthermore, the chromatic aberrations of the eye in the 700–900 nm wavelength region of the employed light source have been compensated with a special lens.

The combination of high stroke deformable mirror-based AO, with ultrahigh speed, ultrahigh resolution OCT employing compensation of the eye's chromatic aberrations enabled isotropic OCT resolution of 2–3 µm. It is noteworthy that the extremely high measurement speed in combination with sufficient system sensitivity at this speed is essential to maintain cellular resolution morphology information despite motion artifacts. In analogy to AO, scanning laser ophthalmoscopy measurements, AO OCT raster scans a retinal area, but acquires full morphological information as a function of depth in the region of interest, without the need to scan the depth of focal plane. As a consequence, 3D morphology of single photoreceptor (PR) outer segments in addition to cellular microstructure at the level of the RPE and choriocapillaris can be visualized in the living human retina. **Figure 4** depicts *in vivo* cellular resolution retinal imaging in a normal human retina at about 4° parafoveal. A rendered volume of about 350 × 80 × 100 µm is presented. En face representations at different depths of the volume reveal cellular resolution intraretinal microstructure.

3D information of intraretinal morphology at cellular level might not only revolutionize ophthalmic diagnosis, but also significantly contribute to a more precise interpretation of OCT tomograms. Despite numerous clinical

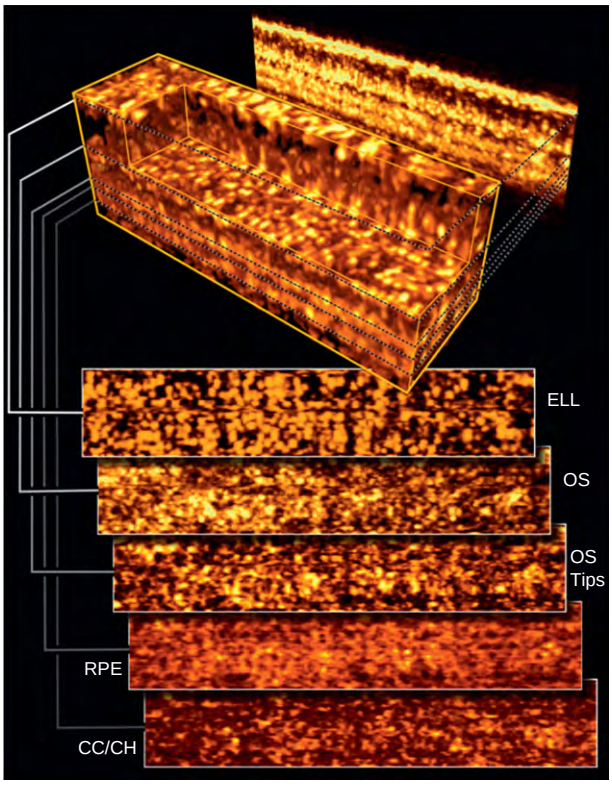

Figure 4 *In vivo* cellular resolution retinal adaptive optics OCT. 3D tomogram and en face cross sections of a normal human retina acquired at 4° parafoveal at 160 000 A-scans/s. Various retinal layers in photoreceptor layer may be distinguished with this technique. From top to bottom slice: ellipsoids (ELL), outer-segment tips (OS), outer segment tips (OS tips), retinal pigment epithelium (RPE), choriocapillaris (CC), and choriocapillaris/choroid (CC/CH). Width of slides corresponds to ~350 × 80 μm.

investigations using UHR OCT and systematic studies comparing histology with UHR OCT in *in vitro* animal models to correctly interpret OCT images, it is noteworthy that a comprehensive, reliable interpretation of all OCT intraretinal layers has not yet been accomplished. Although the state-of-the-art ophthalmic OCT technology enables significantly improved visualization of intraretinal layers, caution is therefore imperative regarding proper interpretation of OCT tomograms, especially of the distal part of the retina. **Figure 5** depicts state-of-the-art OCT interpretation of intraretinal layers in a high definition ultrahigh resolution OCT of the optic disk (a) and foveal (b) region of a normal subject. From the proximal to the distal part of the retina the nerve fiber layer (cf. **Figure 5(a)**, NFL) as well as plexiform layers (cf. **Figure 5(a)**, inner (IPL) and outer plexiform (OPL) layer) appear back-reflecting and therefore as a strong signal in the OCT tomogram. The ganglion cell layer (cf. **Figure 5(a)**, GCL) as well as nuclear layer (cf. **Figure 5(a)**, inner (INL) and outer nuclear (ONL) layer) appear less back-reflecting and therefore as a low signal in the OCT tomogram. The external limiting membrane (cf. **Figure 5(b)**, ELM), the inner and outer PR segments (cf. **Figure 5(b)**, IS PR, OS PR), as well as the choroid (cf. **Figure 5(b)**) are also properly confirmed by literature. Red-labeled layers indicate that caution is imperative and the correct interpretation needs more conclusive studies to confirm correctness. This applies to the internal limiting membrane (cf. **Figure 5(a)**, ILM) and the distal part of the retina involving probably the distal tips of the PRs – sometimes also referred to Verhoeff's membrane (cf. **Figure 5(b)**), the RPE including Bruch's membrane (cf. **Figure 5(b)**, RPE/BM) as well as choriocapillaris (cf. **Figure 5(b)**).

To date, the most distal layer, that is, strongest continuous distal signal in OCT tomograms, has been interpreted as the RPE layer. Although literature describing the light–RPE interaction in the near-infrared region around 800 nm would confirm this interpretation, the relatively thick (up to 30 μm) appearance in OCT tomograms is not supported by histological findings which describe the RPE as a monocellular layer. In addition, the appearance of the RPE and distally adjacent layers as visualized by OCT varies in eyes with different pathologies. **Figure 6** depicts the region indicated with a red rectangle in **Figure 5** but imaged with AO OCT. 3D information at cellular resolution level significantly helps to correlate OCT findings with well-known anatomy from histology and therefore more precisely interpret 2D OCT tomograms. Hence, from the external limiting membrane (cf. ELM in **Figure 6**) toward the distal part of the retina, the first bright (white) signal indicates the junction between inner and outer PR segments. En face cellular resolution representation clearly reveals single ellipsoids. After a thicker, less bright (black) layer indicating a part of the PR outer segment, five signal bands with alternating bright (white) and weak (black) signal appearance is revealed by AO OCT. En face information of the first bright (white) band suggests that this layer corresponds to the outer part/outer tips of the outer PR segments. It is noteworthy that this structure as well as the junction between the inner and outer segment of the PR cannot be resolved within a circular zone of less than 2° parafoveal. Their too-tight spacing and the limited numerical aperture of the human eye in addition to weak contrast has not yet allowed the visualization of PRs in the center (±2° central region) of the fovea. Nevertheless, they are included in this figure for more precise interpretation. The next weak (black) signal band might correspond to the RPE somas, since the adjacent bright (white) signal band is clearly identified to correspond to the RPE layer due to the hexagonal structure of single RPE cells as visualized by AO OCT in the indicated en face view. The next weak (black) signal band might correspond to Bruch's membrane, although literature describes the thickness of this membrane close to the resolution limits of AO OCT. This interpretation is nevertheless supported by the fact that the cellular resolution en face image of the next bright (white) signal band indicates that it might correspond to

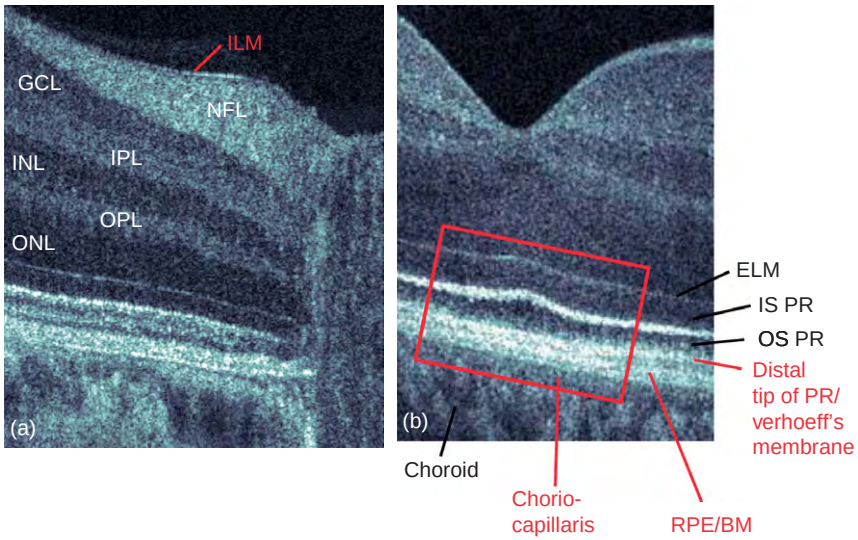

Figure 5 State-of-the-art interpretation of intraretinal layers in OCT. High definition ultrahigh resolution OCT of the optic disk (a) and foveal (b) region of a normal subject. Labeling of intraretinal layers that could properly confirmed by numerous previous studies are labeled white or black. Red-labeled layers indicate that caution is imperative and the correct interpretation needs more conclusive studies to confirm correctness. Nerve fiber layer (NFL), inner (IPL) and outer plexifrom layer (OPL), ganglion cell layer (GCL), inner (INL) and outer nuclear layer (ONL), external limiting membrane (ELM), inner (IS PR) and outer photoreceptor segment (OS PR), choroid, internal limiting membrane (ILM), and distal tips of the photoreceptors – sometimes also referred to Verhoeff's membrane, retinal pigment epithelium including Bruch's membrane (RPE/BM), choriocapillaris. Red square indicates region depicted in **Figure 5**.

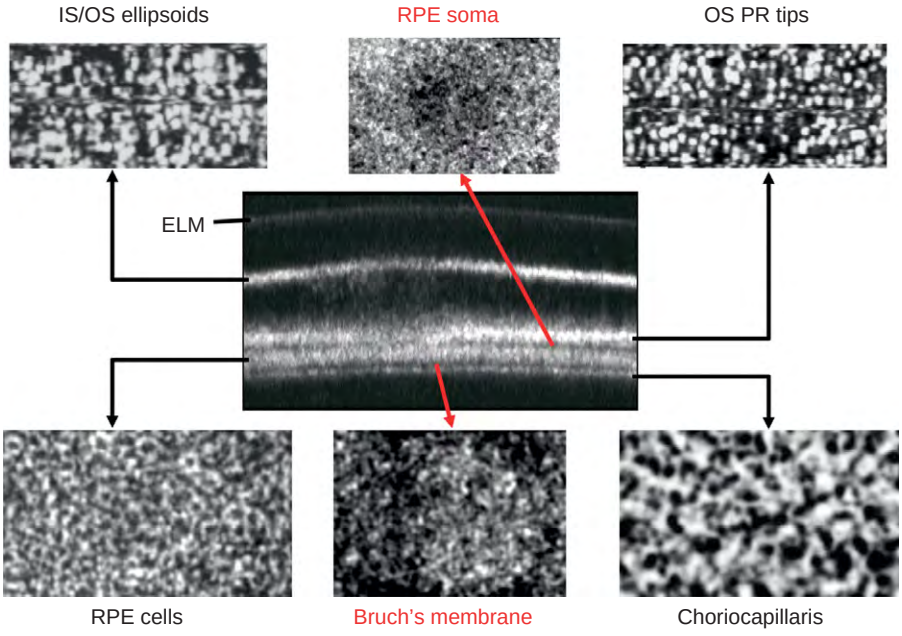

Figure 6 Revised interpretation of the RPE signal band in OCT. Three-dimensional information at cellular resolution level significantly helps to correlate OCT findings with well-known anatomy from histology and therefore more precisely interpret two-dimensional OCT tomograms; external limiting membrane (ELM); photoreceptors can only be resolved within a circular zone of less than 2° parafoveal. Nevertheless, they are included in this figure for more precise interpretation. Two layers are still labeled red indicating that more studies are needed to finally confirm their proper interpretation.

the choriocapillaris. It is noteworthy that despite the superb imaging performance of AO OCT, two layers are still labeled red in **Figure 6** indicating that more studies are needed to finally confirm their proper interpretation.

Figure 7 demonstrates the concept of clinical cellular resolution AO OCT in a patient with type 2 macular telangiectasia. A commercial 3D OCT is used to pre-screen a larger volume to identify suspicious locations.

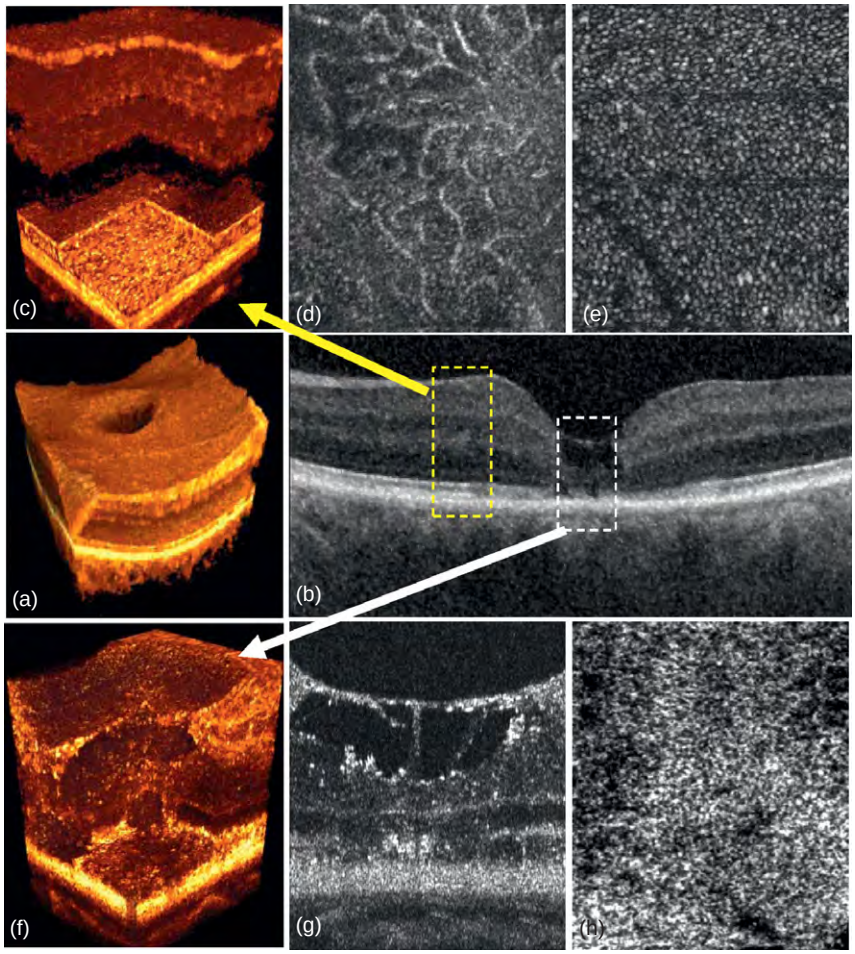

Figure 7 Possible strategy for clinical cellular resolution OCT in a patient with type 2 macular telangiectasia: (a) prescreening over 20°×20° (512 × 128 depth scans) using a commercially available 3D-OCT at 800 nm; (b) detection of impaired intraretinal morphology using a representative cross section from (a); zoom in at a normal (c–e, yellow-dashed square in (b)) and a pathologic ((f–h), white-dashed square in (b)) smaller volumes using cellular resolution OCT; volumetric rendering at 6° parafoveal (c) and 0° (f); en face images at the level of the capillaries in the inner nuclear layer at 6° (d) and at the level of the tips of the outer photoreceptors at 6° (e) extracted from (c); cross sections (g) and en face images at the level of the retinal pigment epithelium (h) extracted from (f).

These areas are then investigated (at the moment still with a separate system) with AO OCT at cellular resolution level revealing quite normal vasculature and PR appearance at 6° parafoveal whereas there is severe impairment at 0°.

Functional Retinal Imaging Using OCT

Numerous functional OCT extensions have been developed in the past of which Doppler OCT, measuring the blood flow velocity and polarization sensitive OCT, imaging depth resolved tissue birefringence have been the most developed and successfully applied in retinal imaging. Noncontact, depth-resolved optical probing of retinal responses to visual stimulation with 10 µm spatial resolution, achieved using functional ultrahigh resolution OCT, has recently been demonstrated. This method relies on the observation that physiological changes in dark-adapted retina caused by light stimulation can result in local variations in tissue reflectivity. This functional extension of OCT can be considered as an optical analog to electrophysiology and has therefore been called optophysiology.

To determine the sensitivity of optophysiology for the detection of changes in retinal reflectivity triggered by light stimulation, a dark-adapted living *in vitro* rabbit retina was exposed to a single flash of white light and optophysiology data were acquired synchronously with electroretinogram (ERG) recordings (cf. **Figure 8**). Throughout the functional experiments the isolated retinas were stimulated with single, 200-ms long white light flashes (cf. yellow rectangle in **Figure 8(c)**, **8(d)**, **8(f)–8(h)**, and **8(j)–8(l)**). A morphological B-scan was first taken from the measurement location (cf. **Figure 8(a)**). Multiple OCT depth reflectivity profiles (A-scans) were then acquired at one transverse location in the retina synchronously with ERG

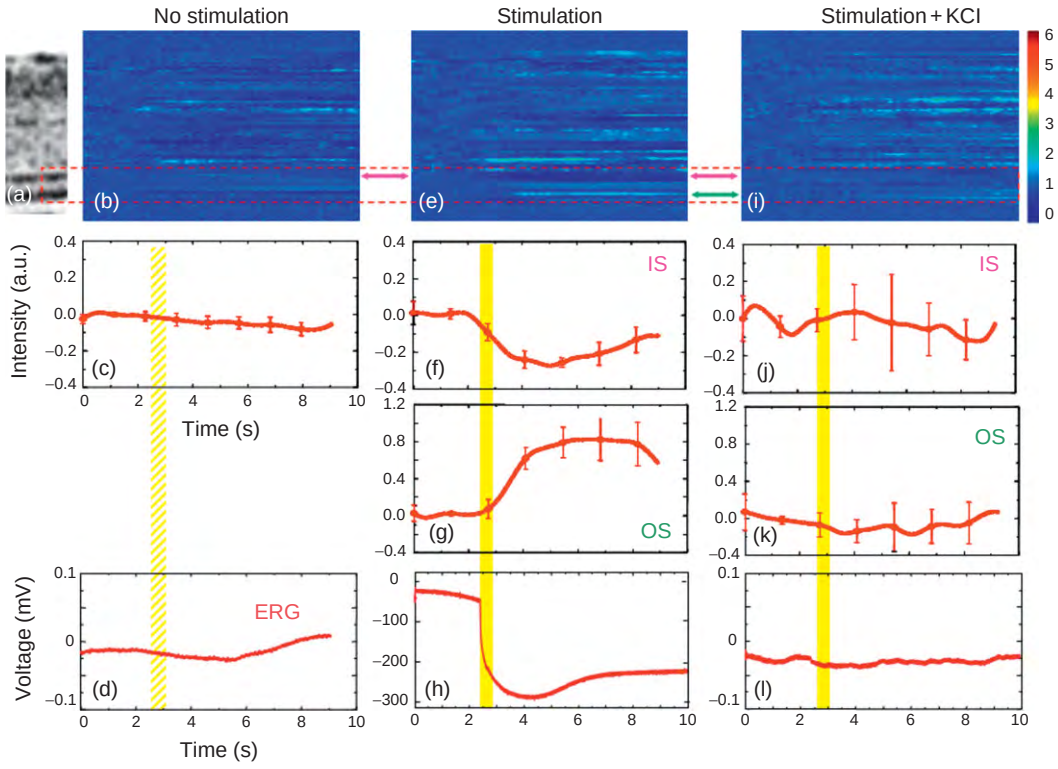

Figure 8 *In vitro* optophysiology in the rabbit retina – optical probing of depth resolved retinal physiology: (a) OCT retinal image of the rabbit retina; (b–d) response during no light stimulus; (e–h) representative single flash stimulus differential M-tomogram and extracted responses from the inner (f) and outer (g) photoreceptor layer; (i–l) case of KCL inhibited photoreceptor function; yellow boxes mark the time duration of the light stimulus; (d, h, l) simultaneous ERG recordings. OS: outer segment; IS: inner segment; ERG: electroretinogram; and KCL: potassium chloride.

recordings. The OCT A-scans were combined to form 2D raw data M-tomograms presenting the retina reflectivity profile as a function of time. The optical data were processed using a cross-correlation algorithm to account for any movement of the retina caused by the solution flow and for calculation of the optical background (average over the pre-stimulation A-scans of each M-tomogram) and generation of differential M-tomograms (cf. **Figure 8(b), 8(e)**, and **8(i)**). Optophysiological signals could be extracted from various retinal layers, so that depth-resolved optical back scattering changes that resulted from physiological processes induced by the optical stimulus could be detected. As expected, in the nonstimulated retina (cf. **Figure 8(b)–8(d)**) the optical reflectivity of the PR layer did not change significantly with time. When the retina is exposed to the light stimulus (marked by the yellow box), changes were seen in optical backscattering at locations corresponding to the inner (cf. **Figure 8(f)**) and outer (cf. **Figure 8(g)**) segment of the PR layer which correlated with changes in the corresponding ERG (cf. **Figure 8(h)**). When potassium chloride (KCL) was applied to the retinal sample to inhibit PR function (cf. **Figure 8(i)–8(l)**), the optical changes observed in the PR inner segment (IS) and outer segment (OS) of the PR layer were close to the optical background level and showed no correlation to the onset of the light stimulus. Depolarization of the cell membranes can occur during conduction of an action potential which could be detected by UHR OCT, but also by detection of spatially resolved change in backscattering over time. The exact origin of the detected optophysiologic signals is unclear but might be related to the dipole reorientation (and therefore refractive index changes) at the PR membrane. Alternatively they could arise from light-induced isomerization of Rhodopsin in the outer PR segment or metabolic changes in the mitochondria of the inner PR segments.

These optophysiological findings in the *in vitro* rabbit model have recently been tried to transfer to the *in vivo* human retina. Due to limitations in coordinating stimulus and data acquisition and the very slow time course of PR recovery after photobleaching stimulus, a protocol that included imaging a normal subject at intervals of about 1 min was used. Dark-adapted human eyes were briefly subjected to localized photobleach. For 20 min prior to, and 30 min after stimulus, volumetric optical coherence tomograms were collected partially overlapping with the bleached region. A location at the peak rod density at 11° temporal was scanned because rod responses are interesting in regards to dark adaptation and rod responses had been successfully observed the rabbit *in vitro* experiments.

The scanned patch was sampled at 512 A-scans in the long axis of the rectangle (fast axis) and 256 samples in the narrow axis (slow axis). Given the 47-kHz A-scan rate of the camera, this volume could be collected in 2.8 s. Twenty double volumes were completed before the subject was exposed to a white, 48 000 cd m^{-2} stimulus, bleaching over 99% of both photopic (duration 6 s) and scoptopic photopigments. As the eye recovered dark accommodation, 35 more double volumes were recorded at 1 min intervals. Tomograms were segmented into retinal layers by a newly described algorithm exploiting information in adjacent B-scans. En face fundus images extracted from major intraretinal layers were laterally registered manually. Time series summarizing the observed backscatter in selected layers for the bleached and unbleached areas are shown with a variety of corrections and normalizations applied: tomograms were corrected for inherent sensitivity roll off; the ratio between other layers and an assumed unchanging layer (RPE) as well as the ratio of stimulated area to unstimulated area were calculated.

Figure 9 depicts results obtained from one normal subject. For each tissue layer in each measured volume, the result of the experiment is summarized by the mean voxel intensity underneath the retinal surface receiving the

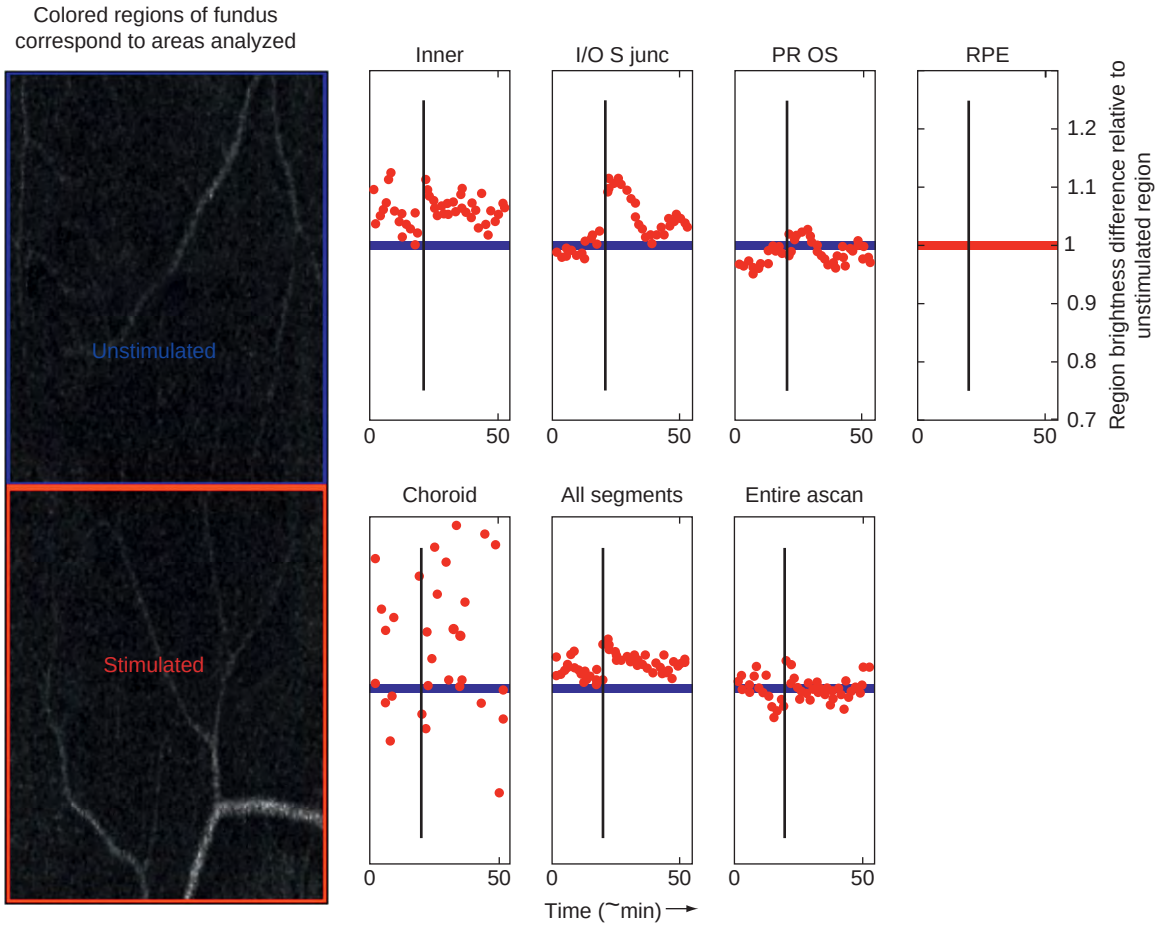

Figure 9 *In vivo* optophysiology in the human retina-A fundus image of the inner–outer segment junction layer is shown at the left to indicate the measured areas defined as unstimulated (blue) and stimulated (red). The volume has been segmented into five anatomical layers using only the most reliably segmented boundaries. The inner retina consists of the NFL, GCL, INL, IPL, and ONL. The choroid is defined from the lower RPE boundary to a thickness 20 pixels deeper (about the thickness of the RPE). All segments is defined from the inner boundary of the NFL to the outer boundary of the RPE. Entire A-scan ignores the segmented boundaries and finds an average pixel intensity over the entire thickness of the recorded A-scan. For each anatomical layer, the average intensity is computed in the stimulated and unstimulated areas and represented as a point in the time series. Twenty volumes acquired before the bleaching stimulus are represented by the points to the left of the vertical black line on each time series plot. Thirty-five volumes recorded after the bleaching stimulus are represented by the point on the right side of the vertical line. Time between acquisitions is about 1 min, so the time axis can be approximately read in units of minutes. Looking at the first four layers, the average pixel intensity appears to track roughly with the IOS distance from the zero delay indicated in the lower right plot. After RPE normalization and a ratio of the stimulated area compared to the unstimulated area, it again appears that there is a relative increase in average pixel intensity in the stimulated area after the stimulus that is most noticeable in the inner–outer segment junction layer that is decaying over a period of about 30 min after the stimulus.

stimulus, and a mean voxel intensity underneath the area without the stimulus. For any particular tissue layer, a time series of this plotted data is expected to show no change in the area without stimulus, and some change in the stimulated area, if there is a change to be observed. The hypothesis is that some layers will show change after stimulus while other layers will not. After the above mentioned normalizations, it appears that an increase larger than the noise level may occur in the inner outer segment region. The decay time for the change (20–30 min) is on the order of the time that the subject observed a persistent after image.

Although the experimental protocol differs from published protocols of studies performed *in vitro* in rabbit and *in vivo* in mouse, the key results are consistent in location and type of change. These, however, could not be convincingly repeated and are therefore presented as an illustration of the techniques used rather than an established observation. Furthermore, the results reported here were only observable in the data after several normalizations. These normalizations are logical, but should be applied with caution. Hence, measuring intrinsic optical signals with OCT in an awake human is challenging. Much needs to be done to deliver both clinically and neurologically significant results. Finally, and probably most importantly, because there is currently a lack of understanding of the physiology that produces intrinsic optical signals, it is difficult to search for the signal using the correct stimulus and measurement protocols. It seems likely that doing more work *in vitro* and with animal models where CCD camera techniques have been highly successful will help identify parameters that are most likely to yield a strong and relevant signal.

Conclusion

Currently, commercial fourth generation 3D ophthalmic OCT systems seem to have a significant diagnostic impact in daily clinical routine as well as novel therapeutic trials. After introducing 3D visualization of the healthy and pathologic human retina, the emphasis now shifts toward filtering out proper biomarkers from this significantly increased amount of information for improved diagnostic decisions. In this respect, it is at the moment not obvious where retinal OCT is heading. Recent developments in OCT technology significantly improved its potential for successful biomedical and clinical applications. These will also be important prerequisites for functional OCT extensions like Doppler OCT, polarization sensitive OCT, and optophysiology.

Despite several proof-of-principle demonstrations of significantly improved state-of-the-art retinal OCT imaging performance sound clinical studies on larger, properly selected patient cohorts are necessary to demonstrate the improved clinical impact and therefore verify the increased technological effort of these novel improvements in retinal OCT modalities.

Acknowledgments

The author wants to acknowledge all members of the biomedical imaging group at the School of Optometry and Vision Sciences, Cardiff University, Alan C. Bird and Catherine A. Egan, Medical Retina Service, Moorfields, London, United Kingdom. Financial and equipment support by the following institutions is also acknowledged: Cardiff University, FP6-IST-NMP-2 STREPT (017128), Action Medical Research (AP1110), DTI (1544C), European Union project FUN OCT (FP7 HEALTH, contract no. 201880); FEMTOLASERS GmbH, Carl Zeiss Meditec Inc., Maxon Computer GmbH, Multiwave Photonics.

See also: Adaptive Optics; Primary Photoreceptor Degenerations: Retinitis Pigmentosa; Primary Photoreceptor Degenerations: Terminology; Rod and Cone Photoreceptor Cells: Inner and Outer Segments; Secondary Photoreceptor Degenerations: Age-Related Macular Degeneration; Secondary Photoreceptor Degenerations.

Further Reading

Bizheva, K., Pflug, R., Hermann, B., et al. (2006). Optophysiology: Depth-resolved probing of retinal physiology with functional ultrahigh-resolution optical coherence tomography. *Proceedings of the National Academy of Sciences of the United States of America* 103: 5066–5071.

Choma, M. A., Sarunic, M. V., Yang, C. H., and Izatt, J. A. (2003). Sensitivity advantage of swept source and Fourier domain optical coherence tomography. *Optics Express* 11: 2183–2189.

de Boer, J. F., Cense, B., Park, B. H., et al. (2003). Improved signal-to-noise ratio in spectral-domain compared with time-domain optical coherence tomography. *Optics Letters* 28: 2067–2069.

Drexler, W. and Fujimoto, J. G. (2008). *Optical Coherence Tomography: Technology and Applications*. New York: Springer.

Drexler, W., Morgner, U., Ghanta, R. K., et al. (2001). Ultrahigh-resolution ophthalmic optical coherence tomography. *Nature Medicine* 7: 502–507.

Drexler, W., Morgner, U., Kartner, F. X., et al. (1999). *In vivo* ultrahigh-resolution optical coherence tomography. *Optics Letters* 24: 1221–1223.

Fercher, A. F., Hitzenberger, C. K., Drexler, W., Kamp, G., and Sattmann, H. (1993). *In-vivo* optical coherence tomography. *American Journal of Ophthalmology* 116: 113–115.

Fernandez, E. J., Hermann, B., Povazay, B., et al. (2008). Ultrahigh resolution optical coherence tomography and pancorrection for cellular imaging of the living human retina. *Optics Express* 16: 11083–11094.

Fujimoto, J. G., Brezinski, M. E., Tearney, G. J., et al. (1995). Optical biopsy and imaging using optical coherence tomography. *Nature Medicine* 1: 970–972.

Huang, D., Swanson, E. A., Lin, C. P., et al. (1991). Optical coherence tomography. *Science* 254: 1178–1181.

Huber, R., Wojtkowski, M., and Fujimoto, J. G. (2006). Fourier Domain Mode Locking (FDML): A new laser operating regime and applications for optical coherence tomography. *Optics Express* 14: 3225–3237.

Leitgeb, R., Hitzenberger, C. K., and Fercher, A. F. (2003). Performance of fourier domain vs. time domain optical coherence tomography. *Optics Express* 11: 889–894.

Považay, B., Hofer, B., Torti, C., et al. (2009). Impact of enhanced resolution, speed and penetration on three-dimensional retinal optical coherence tomography. *Optics Express* 17: 4134–4150.

Schuman, J. S., Puliafito, C. A., and Fujimoto, J. G. (2004). *Optical Coherence Tomography of Ocular Disease*. Thorofare, NJ: Slack.

Srinivasan, V. J., Adler, D. C., Chen, Y., et al. (2008). Ultrahigh-speed optical coherence tomography for three-dimensional and en face imaging of the retina and optic nerve head. *Investigative Ophthalmology and Visual Science* 49: 5103–5110.

Swanson, E. A., Izatt, J. A., and Hee, M. R. (1993). *In-vivo* retinal imaging by optical coherence tomography. *Optics Letters* 18: 1864–1866.

Tumlinson, A., Hermann, B., Hofer, B., et al. (2009). Techniques for extraction of depth resolved *in vivo* human retinal intrinsic optical signals with optical coherence tomography. *Japanese Journal of Ophthalmology* 53(4): 315–326.

Unterhuber, A., Považay, B., Hermann, B., et al. (2005). *In vivo* retinal optical coherence tomography at 1040 nm-enhanced penetration into the choroid. *Optics Express* 13: 3252–3258.

Orbital Bony Anatomy and Orbital Fractures

R A Zaldívar, M S Lee, and A R Harrison, University of Minnesota, Minneapolis, MN, USA

Glossary

Cantholysis – A surgical section of a canthus or a canthal ligament.
Canthotomy – An incision of the canthus.
Dehiscence – The opening of a previously closed wound. It is often associated with contents emerging from the open wound.
Enophthalmos – A posterior displacement of the eyeball into the orbit.
Hypertelorism – An increase in the interorbital distance.
Hypoesthesia – Decreased tactile sensitivity.
Lagophthalmos – An incomplete or defective closure of the eyelids.
Meningitis – An inflammation of the protective membranes covering the central nervous system.
Mucocele – A soft mucus-filled enlargement.
Oculocardiac reflex – A decrease in the pulse rate associated with traction applied to the extraocular muscles and/or compression of the eyeball.
Proptosis – A forward displacement of the eye in the orbit.
Trochlea – The fibrous loop in the superiomedial orbit through which the tendon of the superior oblique muscle passes.

The Bony Orbit

Early in embryogenesis, the bony orbit develops from the mesenchyme that encircles the optic vesicle. Initially, the optic axes are positioned approximately 160–180° apart. The optic cups begin to rotate anteriorly at the same time as the orbital bones are formed. At birth, this angle is reduced to approximately 45°. Hypertelorism, or increased interorbital distance, may develop if there is incomplete rotation. Premature ossification of orbital bones may result in reduced orbital volume and proptosis, as seen in Crouzon's disease.

The adult bony orbit is four walled and pyramidal in shape. The average volume of the orbit is 30 cc. The orbital diameter measures approximately 4 cm in width and 3.5 cm in height at the base or anterior entrance, and has a depth of about 4.5 cm (Figure 1). The widest portion of the orbit is 1 cm just inside the bony rim. The lateral orbital walls subtend a 90° angle, and the medial walls are roughly parallel to each other.

The Orbital Rim

The orbital rim is formed superiorly from the frontal bone, laterally from the zygomatic bone, and inferiorly from the zygomatic and maxillary bones (Figure 2). The inferior-medial portion of the rim continues to form the anterior lacrimal crest on the frontal process of the maxilla, whereas the superior-medial rim continues to form the posterior lacrimal crest. Throughout, the rim is mainly rounded and thickened (greatest laterally). This serves to protect the eye from trauma.

A neurovascular bundle traverses through the medial third of the superior rim. Often (75%), it consists of a notch and the remainder of the time it travels through a true foramen, the supraorbital foramen. This is an important landmark both for brow surgery and to facilitate the identification of the inferior oblique. A vertical line from the notch to the inferior rim is the point anterior to where the inferior oblique originates. The infraorbital foramen, conducting the infraorbital artery, vein and nerve, is also located in this vertical plane, usually 4–10 mm below the central portion of the rim. When performing orbital floor surgery, care must be taken in elevating the periosteum below this level so as not to injure this bundle.

The Medial Orbital Wall

The medial walls are nearly parallel to each other and with the mid-sagittal plane. The wall measures approximately 4.5–5.0 cm from the orbital rim to the orbital apex. It is formed by the maxillary, lacrimal, ethmoid, and sphenoid bones (Figure 3). The maxillary and lacrimal bones join to form the anterior and posterior portions of the lacrimal sac fossa, respectively. Posterior to the lacrimal fossa is the lamina papyracea of the ethmoidal labyrinth. This is the thinnest bone of the bony orbit measuring approximately 0.2–0.4 mm in thickness. This is clinically important in that it is easily fractured in trauma and during surgery, and is a minimal barrier to the spread of infection from the adjacent ethmoid sinuses. Dehiscences or erosions of the bony wall secondary to chronic sinusitis may produce mucoceles either from the ethmoidal or frontal sinuses.

Superiorly, at the junction of the lamina papyracea and the orbital plate of the frontal bone is the frontoethmoid

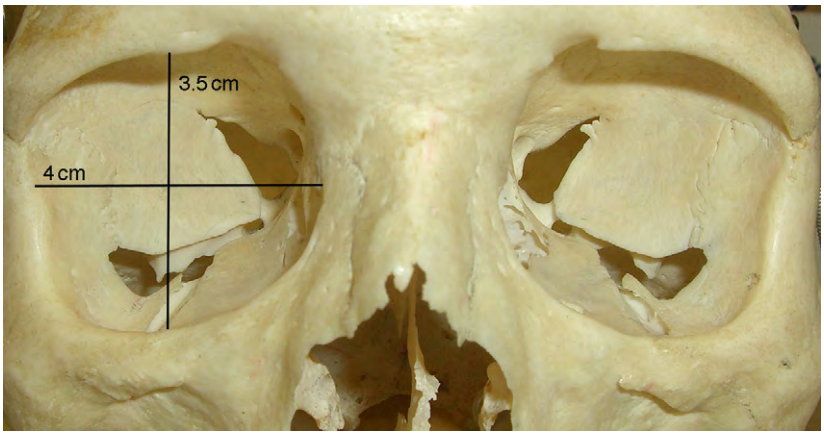

Figure 1 Anterior view of the bony orbit with horizontal and vertical dimensions indicated.

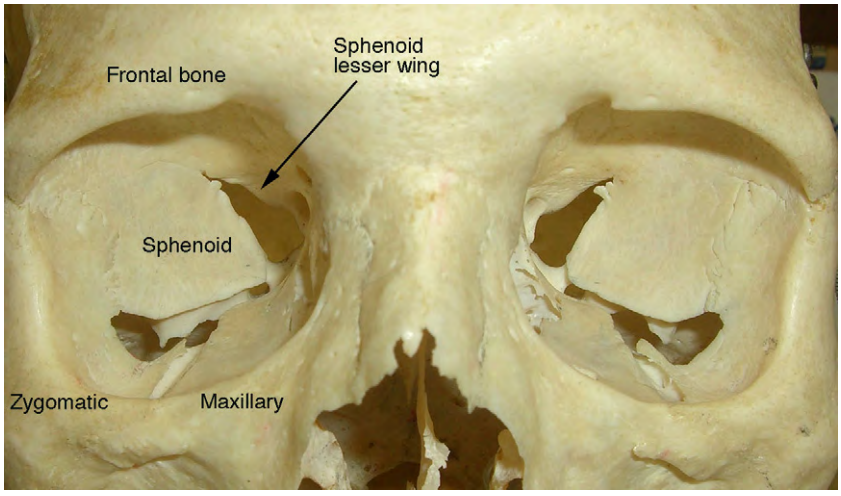

Figure 2 Anterior view of the bony orbit with the bones that form the orbital margin identified.

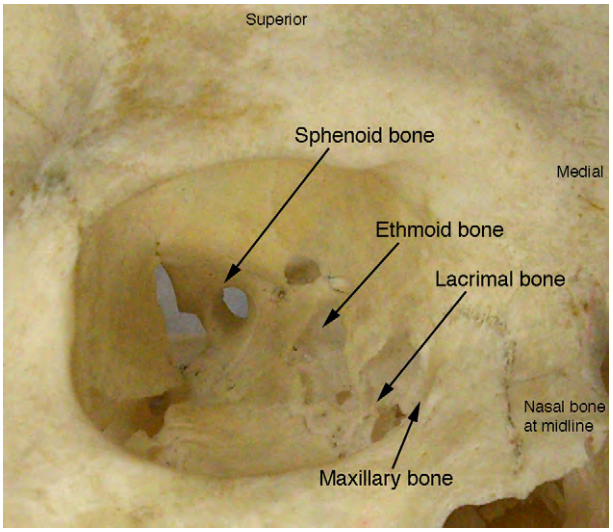

Figure 3 Lateral view of the medial wall of the bony orbit with the main bones identified.

suture line. This is the approximate roof of the ethmoid and floor of the anterior cranial fossa. There are openings at this level for the anterior and posterior ethmoidal vessels and nerves. The anterior foramen is an average of 24 mm behind the anterior lacrimal crest, whereas the posterior foramen is approximately 12 mm posterior to the anterior foramen and 6 mm from the optic canal. These foramina are clinically important as they serve as landmarks for the cribriform plate.

The Orbital Roof

The orbital roof is triangular in shape and formed by the frontal bone and the lesser wing of the sphenoid bone posteriorly (Figure 4). Superolaterally is a concave depression known as the lacrimal gland fossa. Approximately 4 mm posterior to the rim, along the superomedial portion of the roof, is a fibrocartilaginous trochlea for the superior oblique tendon. Careful repositioning of the

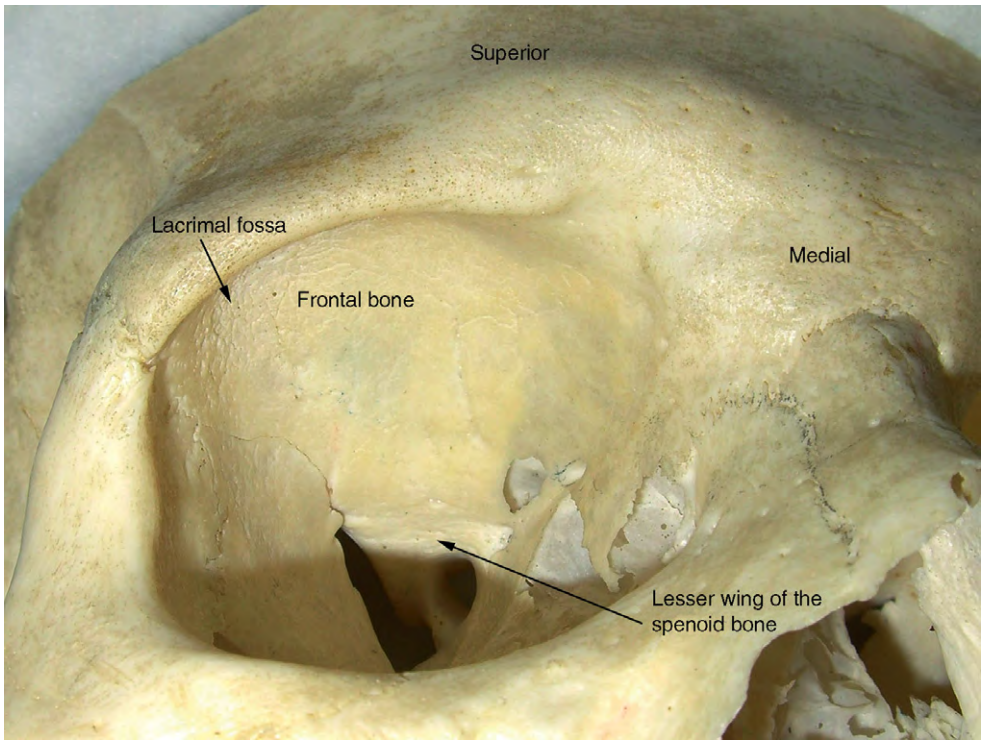

Figure 4 Inferior view of the roof of the bony orbit with the main bones identified.

trochlea on the superomedial surface of the orbit after surgery will help prevent postoperative motility disturbances.

The medial and superior aspects of the orbital roof are adjacent to the ethmoidal and frontal sinuses, respectively. Like the medial wall, the roof is thin and can become secondarily involved with chronic sinus disease. In addition, care must be taken during surgery as damage to the roof can result in a cerebrospinal fluid leak and meningitis. Along the apical, posteromedial portion of the roof lies the optic canal. It is bound by the sphenoid bone medially, the lesser wing of the sphenoid bone superiorly, and the optic strut laterally and inferiorly.

The Lateral Orbital Wall

The lateral orbital wall is the thickest and strongest of the orbital walls. It is composed of the zygomatic bone anteriorly and the greater wing of the sphenoid posteriorly (Figure 5). The medial and lateral walls are approximately the same length (45–50 mm); however, because the lateral wall is at 45° to the medial wall, the lateral orbital rim is approximately 1 cm posterior to the medial rim. The thinnest part of the lateral wall is at the zygomaticosphenoidal suture approximately 1 cm posterior to the orbital rim. This is important when taking off the lateral wall for deep orbital surgery as it allows for outfracture and removal for additional exposure.

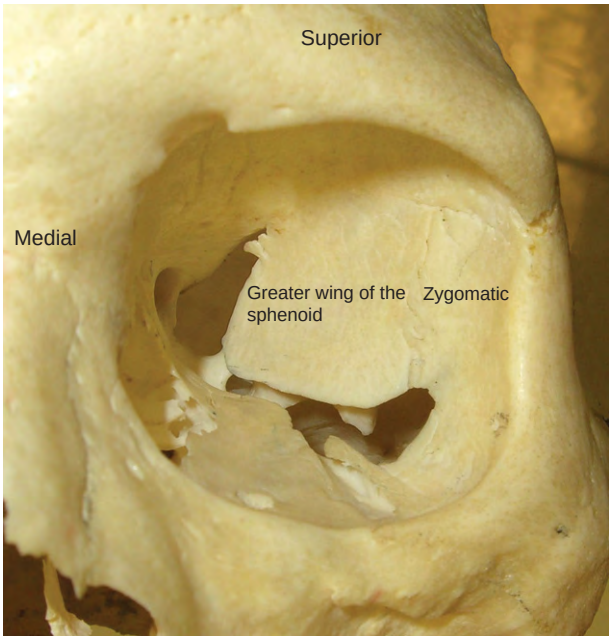

Figure 5 Medial view of the lateral wall of the bony orbit with the main bones identified.

The superior and inferior orbital fissures separate the lateral wall from the roof and floor, respectively. The superior orbital fissure lies between the greater and lesser wings of the sphenoid and transmits the third, fourth, ophthalmic division of the fifth and the sixth cranial

nerves from the middle crania fossa. The ophthalmic veins, a branch of the ophthalmic artery, and the sympathetic root of the ciliary ganglion are also transmitted through this fissure. The inferior orbital fissure transmits the zygomatic branch of the maxillary division of the fifth nerve, the infraorbital nerve and vessel, and the venous communications between the inferior ophthalmic veins and the pterygoid plexus. Along the lateral wall are also several small foramina that perforate the wall just behind the rim laterally and inferiorly. They transmit branches of the lacrimal artery and zygomatic nerve out of the orbit as the zygomaticotemporal and zygomaticofacial neurovascular bundles.

The Orbital Floor

The floor of the orbit is formed by the zygomatic bone, the orbital surface of the maxilla, and the orbital process of the palatine bone (**Figure 6**). It is the shortest of the orbital walls (~40 mm). Similar to the roof, it is triangular in shape. Posteriorly, the floor is separated from the lateral wall by the inferior orbital fissure. It continues anteriorly as the infraorbital groove and canal. The canal runs approximately in the center of the floor from posterior to anterior and carries the maxillary division of the trigeminal nerve and associated infraorbital artery. This bundle exits approximately 4–10 mm inferior to the orbital rim through the infraorbital foramen. The visualization of this groove during orbital floor surgery is important in preventing inadvertent trigeminal hypoesthesia. Medial to the infraorbital canal is the thinnest portion of the orbit where most blowout fractures occur. It is also where the floor is decompressed for surgical treatment of patients with thyroid eye disease.

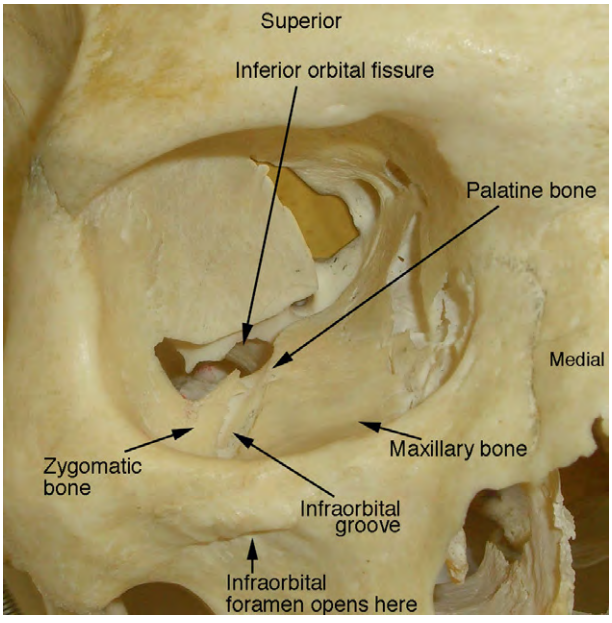

Figure 6 Superior view of the floor of the bony orbit with the main bones and fissures identified.

Orbital Fractures

Blunt trauma to the eye and orbit can cause injury to the thin orbital walls. It is believed that both direct and indirect forces are involved in injury to the orbital bones. The indirect injury occurs as a result of increased hydraulic forces in the confined area of the orbit causing the bone to buckle or blowout into the sinuses. The inferior and medial walls are the most susceptible to this injury. When the fracture is confined to the floor or medial wall, the term pure blowout fracture is used. With more severe injuries, the fractures can extend beyond the orbit, producing rim displacement and maxillary buttress fractures and even separation of the midface from the skull base (Le Fort III; **Figure 7**).

Indications for blowout fracture repair of the orbital floor include rectus muscle entrapment, enophthalmos greater than 2 mm, and large fractures (>50% of the floor or wall). These large floor fractures will often lead to enophthalmos, globe malposition, or both. Similar indications for medial wall repair are used. Repair is often performed within 2–3 weeks after injury. This allows time for the edema to subside, yet is within a window of time that postinflammatory adhesions are not well formed. However, in pediatric cases with clear entrapment, there is evidence that surgery should proceed as soon as possible to limit ischemic damage to the muscle. This group can present with various symptoms when there is a history of trauma. These may include bradycardia, nausea, or syncope secondary to the oculocardiac reflex and warrant early repair.

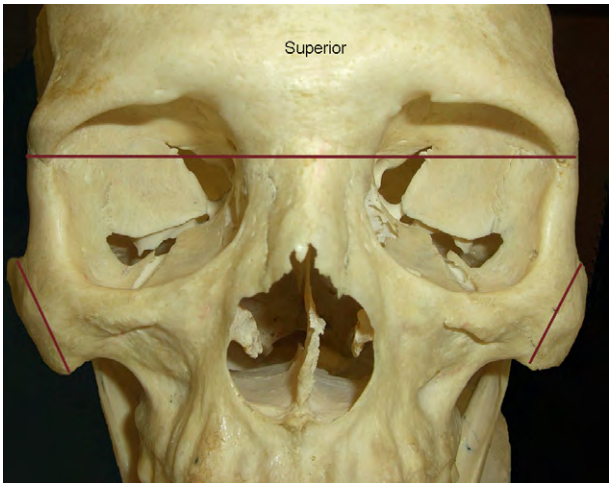

Figure 7 Maroon lines indicate location of a Le Fort III fracture, which is composed of a horizontal fracture that includes the frontozygomatic sutures, the greater wings of the sphenoid, the ethmoid and nasal bones, and a second fracture through the zygomatic arches. This results in a separation from the rest of the cranial bones of the maxillary and zygomatic bones.

Orbital Floor (Blowout) Fracture

Various approaches to the orbital floor have been described, including a subciliary incision or through a laceration of the lower lid sustained during the injury; however, the degree of postoperative sequelae, including lower-eyelid retraction and lagophthalmos, has led to a shift to a tranconjunctival approach. This approach is associated with fewer complications and has gained widespread acceptance.

First, local anesthesia is infiltrated into the lateral canthal and lower eyelid with 1% lidocaine with epinephrine (1:100 000) mixed 50:50 with 0.5% Marcaine (bupivacaine). Forced ductions are performed bilaterally to determine the amount of restriction prior to repair. A 10–15-mm lateral canthotomy is performed in a relaxed skin tension line using a No. 15 Bard-Parker blade (**Figure 8(a)**). Using a curved iris scissors or monopolar cautery, the incision is carried down to the lateral orbital rim periosteum over the zygoma. The inferior crus of the lateral canthal tendon is released (**Figure 8(b)**). The conjunctiva and inferior lid retractors are incised just below the tarsus from the lateral canthus incision to just lateral to the caruncle (**Figure 8(c)**). A Desmarres retractor can be used to retract the tarsal conjunctiva anteriorly. The incision is carried down to the orbital rim periosteum. A malleable retractor is then used to retract the orbital septum and fat. The inferior orbital rim periosteum is incised and gently dissected from the orbital floor with a periosteal elevator (Freer or Coddle elevator; **Figure 8(d)**). The malleable retractor is then repositioned in the subperiorbital plane, and using a hand-over-hand technique, the fracture is exposed (**Figure 8(e)**). Herniated orbital tissue is

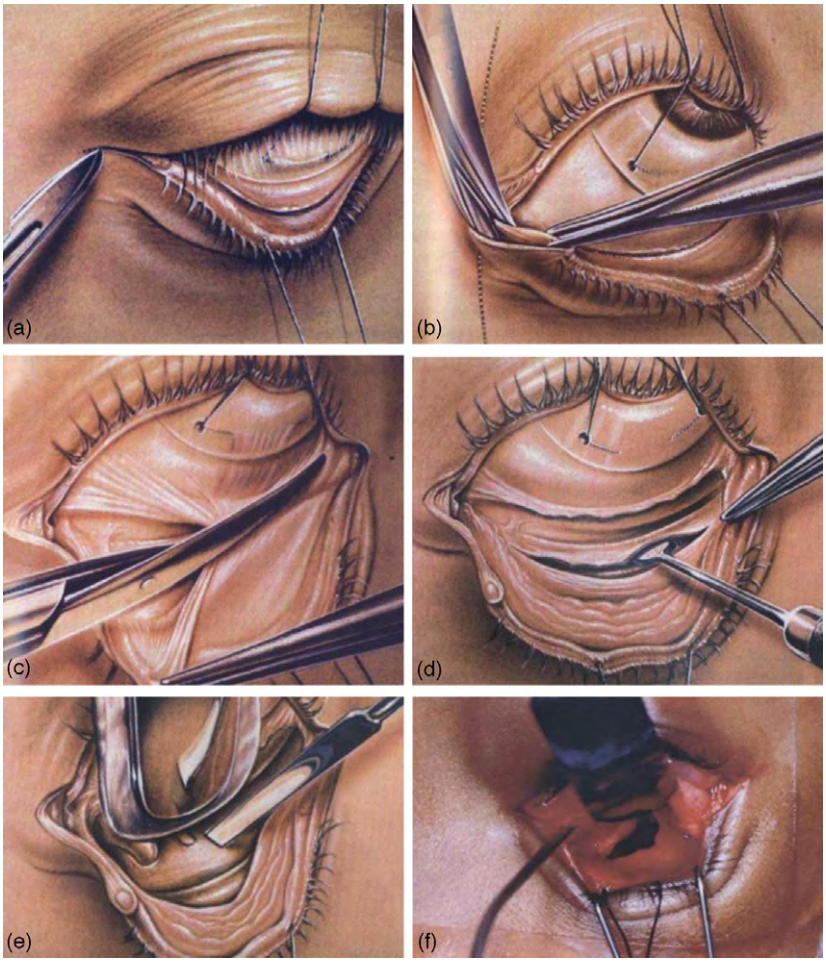

Figure 8 (a) A lateral canthotomy incision is made down to the periosteal level in order to expose the lateral canthal periosteum. This is important in order to be able to reattach the tarsoteninous strap. (b) Next, a lateral cantholysis is performed, which detaches the inferior crus of the lateral canthal tendon from the lateral orbital rim. (c) This incision is made transconjunctivally to extend the horizontal length of the eyelid to the caruncle medially, at a distance of 4 mm below the inferior border of the tarsus. (d) Using a periosteal elevator, the subperiosteal dissection is begun. The periosteum is thicker at the arcus marginalis, and can be grasped to aid dissection. (e) The retraction of the orbital contents superiorly is performed with a malleable retractor, and a subperiosteal pocket is formed. (f) Herniated orbital tissues are elevated in order to visualize the fracture site completely and ensure there is no remaining trapped tissue remaining at the fracture site.

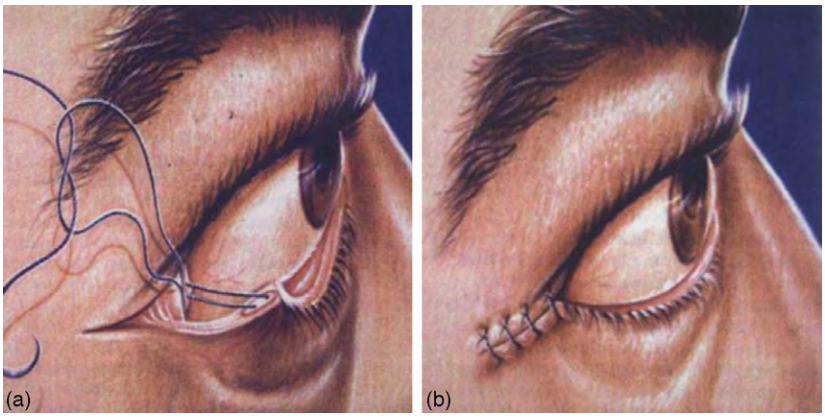

Figure 9 (a) The retractors and periosteum are closed, followed by reattachment of the lateral canthal tendon to the periosteum at the lateral orbital rim. (b) Careful approximation of the eyelid margins during closure is important, which are here closed using a horizontal mattress suture.

gently elevated through the fracture site with blunt dissection until the entire rim of the fracture can be identified (Figure 8(f)). It is important to ensure complete exposure of the fracture to avoid the possibility of leaving entrapped orbital tissue. If the orbital contents are entrapped, the fracture may be enlarged to free the tissue. Bony fragments may be removed with Takahashi forceps. Hemostasis is maintained with bipolar cautery. A paper or foil template is then cut and placed over the fracture site to adequately span the entire bony defect. An alloplastic sheet such as porous polyethylene Medpor (Porex, College Park, GA, USA) or nylon foil sheet SupraFoil (Supramid Alexandria, VA, USA) is then fashioned using the template as a guide. The volume can also be addressed by adding additional sheets. The implant should be positioned posterior to the anterior orbital rim to minimize extrusion. Usually, no fixation is required; however, if the implant tends to ride forward, one can create a small flap into the anterior part of the alloplastic sheet and tuck into the fracture site. Forced ductions are performed to demonstrate the free movement of the globe. The anterior periosteum is closed with a single 5-0 polyglactin suture centrally to prevent anterior migration of the implant. The inferior crus of the lateral canthal tendon is then sutured to the superolateral portion of the orbital rim in a mattress fashion with a double armed 5-0 polyglactin suture (Figure 9(a)). The lateral canthal angle is reformed with a 6-0 polyglactin suture placed through the gray line of the upper, and then lower, eyelid. The lateral canthotomy skin incision is reapproximated with 6-0 Fast Absorbing Plain Gut suture (Ethicon, Inc., Somerville, NJ, USA) in a running or interrupted fashion (Figure 9(b)). The conjunctival incision is not closed. Antibiotic ophthalmic ointment is placed along the lateral canthotomy incision, and antibiotic/steroid combination drops are used for 1 week postoperatively.

In cases where the entire floor is absent and no medial and or lateral edge exists to support the Medpor sheet, a Synthes titanium orbital floor implant (Synthes (USA), Paoli, PA, USA) or a Medpor Titan implant can be positioned over the defect and fixed rigidly to the orbital rim. If, however, the rim fractures are unstable, they should be stabilized first utilizing a screw and plating system, followed by repair of the orbit floor.

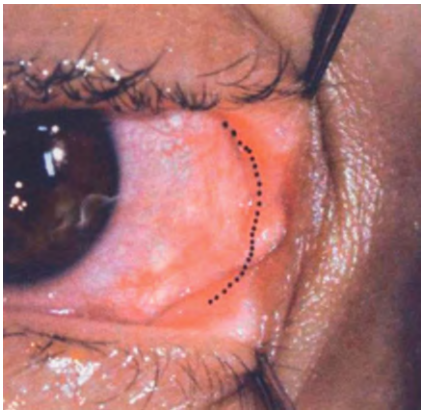

Figure 10 Access to the medial orbit by a transcaruncular incision line.

Medial Wall Fractures

Medial wall fractures often occur in combination with floor or other orbital trauma; however, isolated fractures of the medial wall can occur. If this is the case, they can be observed only if there is no evidence of medial rectus entrapment, the bony defect is nondisplaced or small, and enophthalmos greater than 2 mm is not present. Should it need repair, various approaches can be employed depending on the size.

A small fracture of the medial wall can be approached by a transcaruncular technique (Figure 10). The transcaruncular approach allows moderate access to the orbit without a visible skin incision. An incision is made

through the conjunctiva and Tenon's capsule just medial to the bulk of the caruncle and extends superiorly and inferiorly in the fornices. Dissection is then carried just posterior to the lacrimal sac. A malleable retractor is used to retract the globe and orbital tissues. The periosteum is incised posterior to the lacrimal sac, and periosteal elevators are used to expose the fracture. Once all edges of the fracture have been exposed, a Medpor sheet, or equivalent barrier sheet, can be placed to cover the entire fracture (**Figure 11**). No fixation screws or sutures are needed. Forced ductions are then checked to assure there is no entrapment of muscle.

Lynch incision or a direct approach can be used if the fracture is large or if combined with a large floor defect. The medial canthal area is infiltrated with local anesthetic. The Lynch incision is performed by marking a gull wing approximately 5 mm anterior to the medial canthus (**Figure 12**). Hemostasis is obtained with monopolar cautery and the periosteum is exposed. The periosteum is incised and elevated using a Freer elevator. The lacrimal sac and medial canthal tendon are elevated with the periosteum. A malleable retractor is positioned in the subperiosteal space, and the full extent of the fracture is exposed (**Figure 13**). Then, as with the smaller fractures, the herniated orbital tissue is gently elevated through the fracture site with blunt dissection until the entire rim of the fracture can be identified. The fracture can be enlarged if the orbital contents are entrapped. A template is cut and placed over the fracture site to adequately span the entire bony defect. An alloplastic sheet of Medpor is then cut using the template and placed over the defect. If the defect is greater than 50% of the medial wall or unstable, a combined titanium alloplastic sheet (MED TITAN) can be used to fix the defect. Care must be taken to protect the lacrimal sac by placing a notch in the sheet. Combined floor and medial wall fractures are repaired using the lateral canthotomy approach to the floor combined with the medial Lynch or transcaruncular approach. The anterior periorbita is closed with 5-0 polyglactin suture in an interrupted fashion, the deep tissues are closed with interrupted or running 5-0 polyglactin suture, and the skin is closed with a running 6-0 Fast Absorbing Plain Gut suture. Antibiotic ointment is applied over the wound.

Zygomatic–Maxillary Complex Fractures (Tripod)

Zygomatic–maxillary complex fractures involve the inferior and lateral orbital rim, zygomatic arch, and lateral

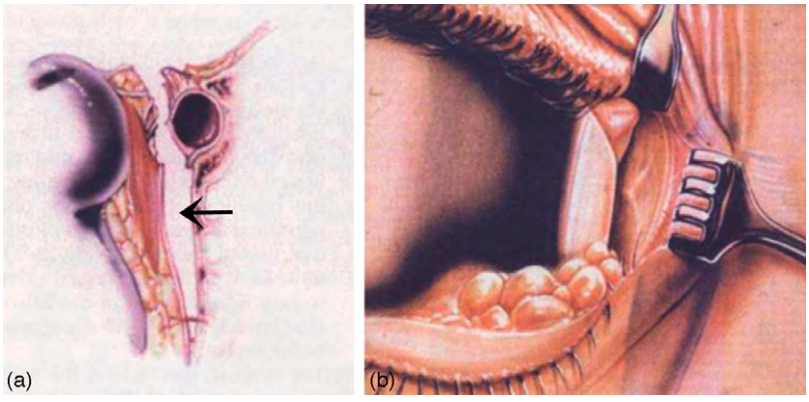

Figure 11 (a) Axial view of the transcaruncular approach to the medial extraperiosteal orbital space, indicated by the black arrow. (b) View of the medial orbital wall. Retractors are used to displace the lacrimal sac medially, while another retractor displaces the orbital contents temporally.

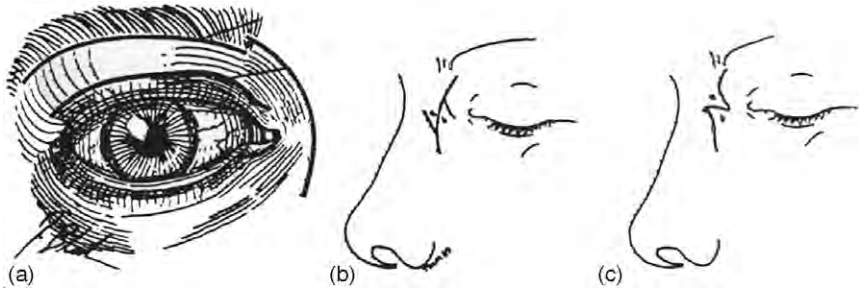

Figure 12 (a) Lynch incision. (b and c) Variations of the standard Lynch incision.

wall of the maxillary sinus. Left uncorrected, these fractures may produce flattening and depression of the cheek in addition to impingement on the coronoid process of the mandible, leading to pain and difficulty in opening the mouth. These fractures should be repaired within the first 2 weeks of injury with open, meticulous anatomic reduction of the fracture and fixation.

The lateral canthal and lower-eyelid areas are infiltrated with local anesthetic. A lateral canthotomy is performed as shown in **Figure 8**. Using the monopolar cautery, the incision is carried down to the lateral orbital rim periosteum over the zygoma. The upper and lower crus of the lateral canthal tendon are released, and the lateral wall periosteum is incised 2 mm lateral to the orbital rim and gently dissected from the zygoma and maxillary bone to define the fracture sites. The periosteum is then dissected from the lateral orbital wall. The conjunctiva and inferior lid retractors are incised below the tarsus from the lateral canthus to just lateral to the caruncle. A Desmarres retractor is used to retract the tarsal conjunctiva inferiorly, and the incision is deepened to the orbital periosteum. The orbital septum and fat are retracted with a malleable retractor and the inferior orbital rim periosteum is incised. A periosteal elevator is used to dissect the periosteum from the orbital floor and malleable retractors are then used to expose the full extent of the fracture using a hand-over-hand technique (**Figure 8**). To ensure the exact realignment and stabilization of the maxillary buttress, a superior buccal sulcus incision is made from the base of the canine to the base of the second bicuspid (**Figure 14**). The subperiosteal plane is created to expose the fracture. The displaced bone is reduced to the correct anatomic position using a towel clip or Kolker clamp. The fragments can be stabilized with miniplates. The periosteum over the lateral and inferior orbital rims is closed with interrupted 5-0 polyglactin sutures. The upper and lower crus of the lateral canthal tendon are reunited with a 5-0 polyglactin suture, and this suture is secured to the lateral orbital periosteum. The lateral canthal angle is reformed with a 6-0 polyglactin suture placed in the gray line of the upper, and then lower, eyelid. The lateral canthotomy skin incision is reapproximated with 6-0 Fast Absorbing Plain Gut suture in a running or interrupted fashion. The conjunctival incision is not closed, whereas the buccal incision is closed with 3-0 chromic sutures. Antibiotic ophthalmic ointment is placed in the inferior fornix and over the lateral canthus.

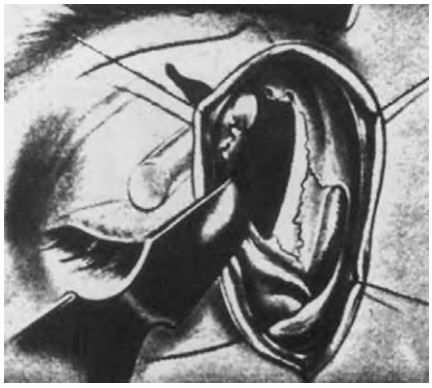

Figure 13 This dissection approach results in an extensive view of the medial orbital wall. The suture lines emerging laterally and medially represent the incision line.

Postoperative Care

In the immediate postoperative period, a delayed retrobulbar hemorrhage is the main concern. The patient and family should be made aware of these symptoms (increased pain and sudden proptosis) and if present, the vision should be checked one eye at a time to establish its presence. The inability of the patient to see or open the

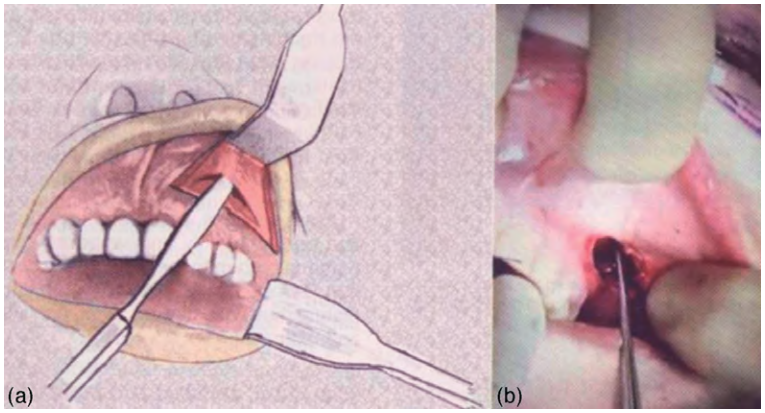

Figure 14 (a) At 10–15 mm superior to the mucogingival junction, a gingivobuccal (sublabial) incision is made at the level of the first molar tooth. (b) As the incision proceeds anteriorly, it is made for inferiorly as it nears the piriform rim. This is 5 mm superior to the mucogingival junction.

eyelid because of tense swelling should be evaluated immediately and may necessitate the release of sutures and a return to the operating room to manage any persistent bleeding. Pupils are often unreliable after surgery due to the effects of epinephrine in the local anesthetic and systemic medications given by the anesthesia staff.

As with care following orbital fractures, patients are warned not to blow their nose as air can enter into the orbit, and, if allowed to develop sufficient pressure, it can lead to vision loss via central retinal artery occlusion. Air in the orbit can be drained with a large bore needle and syringe of sterile water. The presence of bubbles in the water confirms the release of air. Intravenous antibiotics are recommended at the time of surgery if an implant is placed, and generally the patients are given postoperative antibiotics for 5–7 days. Antibiotic ointment is placed in the fornices and on any surgical wounds at the end of the surgery and then used twice a day for 1 week. Sports and significant exertion can be resumed around 6 weeks postoperatively.

Complications associated with orbital implants are infrequent; however, they may include fistula formation, migration, motility restriction, infection, globe elevation, cyst formation, proptosis, and optic nerve trauma. As mentioned earlier, care should be taken to avoid injury to the lacrimal sac by appropriately sizing the implant and cutting a notch as described. A thorough understanding of orbital and facial anatomy combined with appropriate surgical techniques will help limit these complications.

See also: Cranial Nerves and Autonomic Innervation in the Orbit; Orbital Masses and Tumors; Orbital Vascular Anatomy.

Further Reading

Doxanas, M. T. and Anderson, R. L. (1984). *Clinical Orbital Anatomy*. Baltimore, MD: Williams and Wilkins.

Dutton, J. J. (1994). *Atlas of Clinical and Surgical Orbital Anatomy*. Philadelphia, PA: W.B. Saunders Company.

Wobig, J. L. and Dailey, R. A. (2004). *Oculofacial Plastic Surgery.* New York: Thieme.

Zide, B. M. and Jelks, G. W. (2006). *Surgical Anatomy around the Orbit: The System of Zones A Continuation of Surgical Anatomy of the Orbit.* Philadelphia, PA: Lippincott Williams and Wilkins.

Orbital Masses and Tumors

S Morris, Brighton and Sussex University Hospitals, Brighton, UK
V Gauba, Imperial Healthcare Institute, Dubai, UAE
I Mavrikakis, University of Athens, Athens, Greece

Glossary

Choristoma – A benign tumor, which contains normal tissues but is found in abnormal locations.
Ectopia – An abnormal congenital or acquired position of an organ or a part.
Hamartoma – A benign focal malformation that resembles a neoplasm in the tissue of its origin. It is composed of tissue elements normally found at that site, but which grow in a disorganized mass.
Mass effect – Damage to the globe, optic nerve, and/or tissues in the orbit due the bulk of a tumor, the blockage of fluid, or excess accumulation of the fluid within the bony orbit.
Mohs surgery – Created by a general surgeon, Dr. Fredrick E Mohs, it is a microscopically controlled surgery that is highly effective for common types of skin cancer.
Proptosis – Any nonendocrine-mediated protrusion of the globe.

This article discusses tumors and masses that occur in the human orbit. It is divided into sections based on the tissue origin of each tumor type and each disease entity.

Neoplasia

Neurogenic Tumors

Optic nerve gliomas

Juvenile pilocytic astrocytoma is a low-grade, slow-growing pilocytic astrocytoma of the optic nerve derived from glial cells, which usually presents before the second decade of age. Isolated lesions are more typical; however, diffuse tumors are found in conjunction with neurofibromatosis type 1 (NF1). Optic nerve gliomas (**Figure 1**) may involve any part of the optic nerve and can be subdivided according to location into orbital, orbitocranial, chiasmal, and diffuse/multifocal types. Clinical signs depend on the location; the more anterior tumors present with visual loss, increasing proptosis, and optic disk swelling or atrophy, whereas those nearer the chiasm cause a more insidious field of vision loss and hypothalamic symptoms or hydrocephalus. Imaging usually negates the need for biopsy due to the characteristic features of an enlarged fusiform optic nerve with smooth intact dural margins, kinking of the nerve, cystic degeneration of the tumor, and, rarely, sparse calcification seen on a computerized tomography (CT) scan. The management is generally conservative; however, chiasmal or parachiasmal tumors may need chemotherapy, radiotherapy, or shunting procedures, and more localized, accessible tumors of the optic nerve are excised if very large or rapidly progressive.

Malignant optic nerve glioma (glioblastoma) is an aggressive primary tumor of the optic nerve occurring in middle-aged adults. It may occur from a lower-grade astrocytoma but usually occurs *de novo* as glioblastoma multiforme and is not usually associated with neurofibromatosis. It displays rapid growth with local spread extending swiftly into the nervous system. Early visual deterioration progresses quickly into blindness and death. CT imaging demonstrates an enlargement of the optic nerve or chiasm in three-quarters of the patients; the diagnosis is by biopsy. Treatment options include radiotherapy, chemotherapy, or surgical excision, but these only offer a delay in fatality.

Meningioma is the most common primary tumor of the central nervous system in adulthood arising from meningothelial cap cells of the arachnoid villi. The orbital and visual effects are dependent on the location of the tumor – intracranial, within the optic canal, or along the optic nerve. Characteristic retinochoroidal (optociliary) shunts are seen at the optic disk margin with optic nerve sheath tumors. Growth along the optic nerve sheath may be extradural, subdural, or combined. Intracranial sites affecting the visual pathway commonly include the sphenoid ridge, suprasellar area, and the olfactory groove. There is a strong female preponderance, and the tumor typically presents in middle age. However, it can occur more aggressively in younger males. Imaging with CT may reveal hyperostosis of the adjacent bone, calcification of the tumor, railroad tracking (central lucent areas), and diffuse enlargement. Magnetic resonance imaging (MRI) scans show dense uniform enhancement with gadolinium. The management usually consists of regular observation and neuroimaging. If intervention is required, surgical excision or debulking offers a good prognosis. However, blindness frequently occurs due to direct damage of the optic nerve, and irradiation may be preferred.

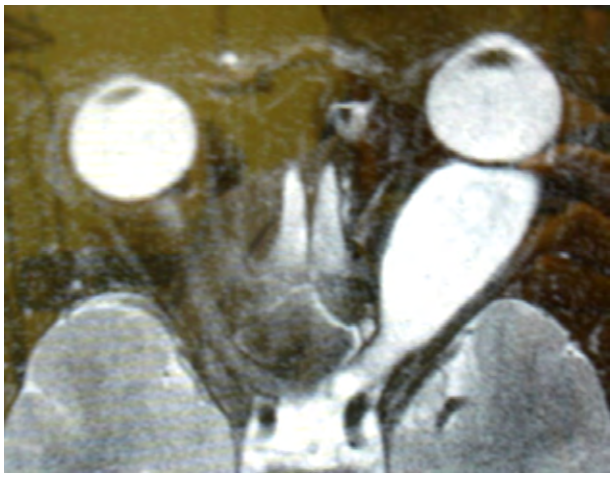

Figure 1 Axial T2-weighted magnetic resonance imaging with gadolinium enhancement of a left optic nerve glioma. Note the hyperintense fusiform mass that extends through the optic canal to the optic chiasm.

Medulloepitheliomas (neuroepitheliomas) of the optic nerve is a benign or malignant tumor of the optic nerve head found in children arising embryologically from the medullary epithelium of the optic vesicle. It needs to be distinguished from optic nerve glioma.

Hemangiopericytoma is an uncommon, noninfiltrative, vascular tumor of the pericytes that may be found in the orbit. It can be benign, intermediate, or malignant depending on the histopathological criteria, and is described as sinusoidal, solid, or mixed type. It causes a symptomatic mass effect within the orbit, but may also occur as an optic nerve lesion. Despite excision, it has a propensity to recur, and benign tumors may metastasize.

Peripheral nerve tumors

Neurofibroma is a benign nerve sheath tumor of the peripheral nervous system. Schwann cells are the neoplastic origin; however, other endoneurial cells and elements are present. The tumor may be plexiform, fusiform, or diffuse in shape. Neurofibromas of the orbit are broadly divided into dermal isolated lesions of a single nerve, diffuse infiltrations, and plexiform lesions of multiple nerve bundles. All types can be found in NF1. Localized isolated lesions can appear similar to schwannoma on imaging. The diffuse and plexiform lesions appear irregular with ill-defined borders and are best seen with fat suppression. No known treatment can stop the progression of neurofibromatosis or cure it. Individual neurofibromas can usually be removed surgically or shrunk with radiation therapy. Surgical removal often requires removing the nerve with the fibrous tumor.

NF1 is an autosomal-dominant disorder with low and variable expressivity affecting the nervous system, due to a mutation of neurofibromin chromosome 17q11.2. Diagnostic criteria require the presence of two or more classic features: at least six café au lait macules, two or more single neurofibromas or one plexiform neurofibroma, optic nerve glioma, axillary or inguinal freckling, Lisch nodules (iris hamartomas), a first degree relative with NF1, or distinct skeletal abnormalities such as sphenoid dysplasia.

NF2 is a rare autosomal-dominant disorder caused by mutation of merlin chromosome 22q12 and characterized by the development of bilateral acoustic neuromas, meningiomas, spinal schwannomas, and posterior subcapsular lens opacities. Combined retinal and pigment epithelial hamartomas, astrocytic hamartomas, and optic nerve gliomas may be visible on fundoscopy.

Plexiform neurofibroma is the most common peripheral nerve sheath tumor of the orbit involving multiple nerve bundles, causing periorbital and orbital soft-tissue hypertrophy, primary or compensatory bony changes, and ocular abnormalities. The management is usually cosmetic, but surgical excision is extremely difficult due to the high vascularity of these tumors and complex integration with surrounding structures. Malignant transformation is extremely rare.

Diffuse neurofibromas are rare, dermal, benign nerve sheath tumors that infiltrate normal surrounding structures. Subcutaneous involvement of the upper eyelid causes the classic S-shaped deformity.

Amputation neuroma is a disorganized overgrowth of regenerating severed peripheral nerves. Mechanical factors may precipitate the formation. Lesions can occur postenucleation causing proptosis and severe pain. Its management involves surgical excision.

Schwannoma (neurilemmoma) is a slowly progressive, noninfiltrative, benign tumor of the peripheral nerves arising from Schwann cells. Typically, the lesions are solitary, presenting in adulthood, and rarely occur within the periorbita. Orbital signs are related to the mass effect, dependent on location, and need to be distinguished from other slow-growing orbital tumors. Imaging shows well-delineated lesions with variable density dependent on intralesional cyst formation. If the patient requires intervention, then a complete surgical excision of the encapsulated tumor is preferential. Exceptionally rarely, schwannomas develop malignant change.

Malignant peripheral nerve sheath tumor (neurofibrosarcoma, neurogenic sarcoma, and malignant schwannoma) is a soft-tissue sarcoma of the nerve sheath, which may or may not arise from Schwann cells. Nearly half of them occur in patients with NF1. Due to the locally aggressive nature, radioresistance, and metastatic spread, the 5-year survival rate from this tumor is extremely low. Rarely, some tumors run a more indolent course. Radical surgical excision/exenteration offers the best prognosis.

Rare tumors of neuroectodermal origin

Alveolar soft part sarcoma is a soft-tissue tumor of uncertain cellular origin occurring in children and young

adults, more commonly female. It usually occurs on extremities but may occur in the orbit as a slow-growing mass. Its treatment is by wide surgical excision with a good prognosis for orbital primary lesions.

Granular cell tumor is a slow-growing, usually benign tumor of spindle cells dense in granular eosinophilic cytoplasm and thought to be of neural origin. Typically, the tumor occurs in the tongue or subcutaneous tissues, but can be orbital, ocular, or periorbital.

Paraganglioma (chemodectoma) is a rare, neuroendocrine tumor arising from glomus cells (chemoreceptors of blood vessels that are part of the paraganglion system) and is described according to their location within the abdomen, thorax, or the head and neck. Within the orbit, they are thought to arise from the ciliary ganglion. Tumors are usually encapsulated, comprising nests of cells (Zellballen), and have a low rate of malignancy or metastases. However, they tend to recur after incomplete orbital resection. Radiotherapy may have a role.

Primary orbital carcinoid tumors are slow-growing tumors of amine precursor uptake and decarboxylation (APUD) cells that are usually benign, but with malignant potential. A small proportion of these lesions are associated with the carcinoid syndrome. The majority arises in the gut, but primary and secondary lesions have been described within the orbit. Similar to other slow-growing tumors of the orbit, complete surgical excision is recommended.

Neuroepithelioma is an extremely rare neoplasm of the peripheral nerve that has an aggressive course and is difficult to treat.

Esthesioneuroblastoma (olfactory neuroblastoma) is a neuroectodermal tumor arising from the olfactory epithelium that commonly extends into the orbit. It differs from neuroblastoma in that it does not arise from the sympathetic nervous system; however, classification remains controversial. Those occurring in the cranium and orbit have a poorer prognosis. The management requires aggressive surgical excision with adjunctive radiotherapy and chemotherapy.

Primary neuroblastoma is a neuroendocrine tumor of varying levels of differentiation arising from the neuroblasts of the sympathetic nervous system. Of the orbit, it is typically metastatic from the adrenal gland and presents in children. However, primary orbital neuroblastoma has been reported, which needs to be distinguished from the less aggressive neuroendocrine tumors, such as carcinoid.

Primary ganglioneuroma is a benign neuroendocrine tumor of the sympathetic nerve fibers. Typically, older children present with a well-delineated mass of the posterior mediastinum or retroperitoneum, although it can rarely occur within the orbit.

Primary orbital melanoma is a rare, malignant tumor of orbital melanocytes that is a distinct clinical entity from secondary or metastatic melanomas that arise from the globe or melanocytes elsewhere. It presents more commonly in association with congenital ocular/oculodermal melanocytosis or hypercellular blue nevus. It starts off as a well-circumscribed lesion with enhancement on MRI; yet, prognosis is poor due to the propensity to metastasize. Its treatment is aggressive – wide excision/exenteration of the mass intact with adjuvant irradiation and chemotherapy.

Retinal anlage tumor (pigmented retinal choristoma/melanotic neuroectodermal tumor (MNET) of infancy/melanotic progonoma/congenital melanocarcinoma/melanotic adamantinoma/pigmented epulis of infancy) is a primary melanocytic tumor of infancy that usually begins in the jaw and occasionally affects the orbital soft tissue. It contains two cell types resembling retinal pigment epithelial cells (hence the name retinal anlage tumor) and neuroblastic cells. Complete wide excision, including bony removal, is usually required.

Ectomesenchymal tumor is a neoplasm derived from neural crest cell origin.

Mesenchymal Tumors

Striated muscle tumors

Rhabdomyosarcoma is the most common soft-tissue sarcoma (tumor of connective tissues) and primary malignancy of childhood arising from mesenchymal skeletal muscle development. Rhabdomyosarcoma commonly arises from within the orbit but can occur as a secondary extension from the sinuses or nasal cavity. Typical presentation is of rapidly advancing, nonaxial globe proptosis with eyelid swelling which may be painless. Histology reveals rhabdomyoblasts, and tumors are classified according to the cell pattern – embryonal, alveolar, undifferentiated, and anaplastic. Imaging assists in diagnosis; CT scans show moderately well-delineated homogenous tumors that usually spare bone and extraocular muscles and enhance with contrast. Prognosis depends on the cell type, the alveolar and undifferentiated sarcomas having the least favorable outcome. The management includes tissue diagnosis and tumor staging. If possible, the whole tumor should be excised intact. Most patients require adjuvant irradiation or chemotherapy.

Rhabdoid tumor is an extremely aggressive, malignant neoplasm of uncertain pathogenesis that appears similar to rhabdomyosarcoma but lacks rhabdomyoblasts. It occurs mainly in children and was initially described as a variant of Wilm's tumor of the kidney. Orbital involvement presents with rapid proptosis and globe displacement. Despite surgical excision, radiotherapy, and chemotherapy, the prognosis is generally very poor.

Rhabdomyoma is a benign tumor of skeletal muscle derivation occurring extremely rarely within the orbit. It is a well-differentiated, circumscribed tumor that can be excised, debulked, or observed. Cardiac rhabdomyomas are associated with tuberous sclerosis.

Endodermal sinus tumor (yolk sac tumor) is a malignant germ cell tumor which can not only occur within gonadal sites of young children as infantile embryonal carcinoma, but can also present as a fulminant neoplasm of the orbit. These malignant endodermal cells secrete α-fetoprotein, which helps to differentiate the tumor. The treatment includes a combination of surgery, and chemotherapy and recent advances of the latter have improved the prognosis.

Smooth muscle tumors

Leiomyoma is a benign, smooth muscle neoplasm that most commonly occurs within the uterus and gastrointestinal tract. It rarely occurs within the orbit as a well-defined, indolent mass, histologically similar in appearance to a nerve sheath tumor or fibrous histiocytoma. After incomplete excision, it may recur.

Leiomyosarcoma is a malignant, smooth muscle neoplasm that typically involves the uterus of women in their sixties. Orbital tumors have been reported and may occur postirradiation for retinoblastoma. It presents like other rapidly enlarging infiltrative orbital tumors with progressive nonaxial globe proptosis. Histology reveals anaplastic spindle cells positive for smooth muscle antigen (SMA). Wide excision/exenteration of orbital lesions combined with chemotherapy or irradiation may be required.

Adipose tumors

Lipoma is an extremely common, benign soft tissue tumor of the adipose tissue. Subtypes are classified according to cell type and location. Lipomas are rare within the orbit; however, if they do occur, they present as a distinct mass within the orbital fat and cause a localized displacement of tissues. The diagnosis is usually made postexcision, and the prognosis is excellent.

Liposarcoma is a malignant, soft tissue tumor arising from adipose cells. It has a widespread distribution, rarely occurring in the orbit where it causes a slowly progressive mass effect. Liposarcomas are classified into well-differentiated, myxoid, round cell, and pleomorphic cell types. Those in the orbit tend to be low-grade, well-differentiated, or myxoid types. The management is by complete surgical excision and may benefit from adjunctive radiotherapy.

Fibrous tissue tumors

Fibroma is a benign tumor of mesenchymal origin composed of fibrous tissue. It occasionally occurs as a non-infiltrative mass of the orbit. After surgical excision, it is found to be composed of a paucicellular population of fibroblasts separated by collagen with the absence of inflammatory cells.

Nodular fasciitis (nodular pseudosarcomatous fasciitis/subcutaneous pseudosarcomatous fibromatosis) is a benign nodular lesion, usually of the extremities, caused by a proliferation of connective tissue, and thought to be a reparative process secondary to trauma. It most commonly involves the superficial fascia and, as it develops rapidly, can be mistaken for sarcoma. Orbital nodular fasciitis is reported, usually occurring more anteriorly rather than deep in the orbit. The management is by complete surgical excision.

Fibromatosis is an infiltrative, nonmetastasizing, fibrous soft tissue tumor that sits in between a fibroma and a fibrosarcoma in the level of progression. Lesions are composed of well-differentiated fibroblasts. If smooth muscle elements are present, the term myofibromatosis is used. Congenital generalized fibromatosis is usually fatal, with multiple tumors occurring throughout the body of newborns. Orbital lesions occur, and treatment is by wide surgical excision followed by periodic monitoring. Myofibromas of the orbit tend to be solitary with a benign course. Regression of fibromatosis can occur.

Fibrosarcoma is a malignant, locally aggressive tumor of fibrous soft tissue comprised of immature spindle-shaped fibroblasts with a propensity to metastasize. Cells are typically aligned in a herringbone pattern. Reclassification of other spindle cell tumors has decreased the true incidence of this condition. Orbital tumors can be primary lesions or may arise secondary to spread from adjacent sinuses or after radiotherapy. Incomplete surgical removal from the orbit is common; thus, this tumor tends to recur. Wide excision/exenteration is needed.

Solitary fibrous tumor is a benign neoplasm of fibrous soft tissue that differs from other spindle cell tumors by the absence of a histopathological pattern. It occurs as a unilateral, well-circumscribed, orbital lesion of any age group and causes a slow mass effect. Malignant transformation is rare. Incomplete surgical excision can cause localized infiltrative recurrence.

Epithelioid sarcoma is a rare, aggressive mesenchymal malignancy with an epithelioid pattern. It commonly occurs in the extremities of young people, particularly the tendon sheaths, but has been reported in the orbit.

Myxoma is a benign tumor of mesenchymal origin, where connective tissue becomes filled with a mucinous matrix. The majority occurs within the heart, in particular the left atrium. Malignant tumors of myxoid appearance need to be excluded prior to diagnosis. True orbital myxomas are extremely rare. A complete surgical excision of this soft tumor is difficult due to the lack of a capsule, thus resulting in its recurrence.

Giant cell angiofibroma is a benign, spindle cell tumor of mesenchymal origin comprising multiple giant cells within the stroma and blood vessels. It very occasionally occurs within the orbit, presenting as an anterior mass.

Dermatofibrosarcoma protuberans is a neoplasm of fibroblasts affecting the dermis of the skin throughout the body. Local invasion, metastases, and recurrences are possible. It can occur in the periorbita and thus invade the orbital tissues. Mohs surgery is effective in excision of the sarcoma.

Histiocytic tumors

Fibrous histiocytoma is a tumor of mesenchymal origin containing fibroblasts and histiocytes that can be benign, locally aggressive, or malignant. It presents either as a superficial lesion, usually on lower extremities, or as a deep tumor – common within the adult orbit. Conventional fibrous histiocytoma tends to be a slow-growing, relatively firm mass, but more aggressive variants occur with infiltrative features and a tendency to recur, and rarely metastasize. Complete surgical resection is best.

Primary Bone Tumors

Benign fibro-osseous and cartilaginous lesions

Osteoma is a benign, slow-growing tumor of the bone, found most commonly in the paranasal and frontal sinuses but the tumor can extend into the orbit. It may take a sessile or pedunculated shape. The symptoms include a mass effect, and pain is common. Three histological subtypes exist – compact, cancellous, and fibrous. The management includes observation and surgical excision, recurrence being rare.

Fibrous dysplasia (Figure 2) is a benign, slowly progressive fibro-osseous malformation causing replacement of the medullary bone with fibrous tissue and osteoid, thought to be due to an arrest in the normal bone development. It may be monostotic (more common and often affecting the craniofacial bones) or polyostotic (involving many bones) as seen in McCune–Albright syndrome. Orbital symptoms reflect the gradual compressive effects. Imaging may reveal a ground-glass appearance to the expanded bone. Surgery tends to be reserved for cases with functional defects, rare malignant transformation, or pain.

Ossifying fibroma (fibro-osseous dysplasia) is a benign, acquired tumor of the bone that is most commonly found in the mandible but, occasionally, does present in the orbit. Typically, it starts as a monostotic lesion that gradually expands and spreads to adjacent bones. It is more aggressive in nature than fibrous dysplasia; thus, surgical excision should be performed early.

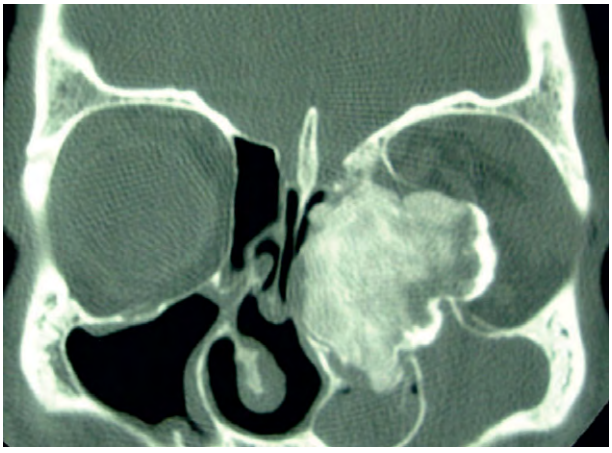

Figure 2 Coronal computed tomography bony view of an ill-defined, hyperdense lesion with a sclerotic margin arising from the ethmoid region and invading the left orbit. The lesion presents a characteristic pagetoid appearance with alternating areas of radiolucency and radiodensity. Histopathological examination revealed this lesion to be fibrous dysplasia.

Osteoblastoma is an uncommon, benign, primary tumor of the bone consisting of osteoblasts that produce the osteoid and primitive woven bone. While it predominantly arises in the spine and long tubular bones of young people, it is unusual for it to be found in the orbit. The mass effect causes compressive symptoms and pain. A rare, aggressive variant of this tumor that metastasizes exists. Complete direct surgical excision is generally curative.

Chondroma is an encapsulated, benign, indolent cartilaginous tumor of chondrocytes that commonly occurs in the bone. Occasionally, it becomes large enough to be symptomatic. It is rare in the orbit owing to the fact that the only normal cartilaginous material in the orbit is the trochlea of the superior oblique. Its management is by observation or excisional biopsy. Malignant change is possible.

Reactive lesions

Cholesterol granuloma is a benign, very slow growing tumor of the bone, formed by a reactive response to crystallized cholesterol and thought to be secondary to trauma or hemorrhage. It typically occurs in the middle ear and temporal bone, but may affect the orbit. Imaging reveals osteolysis, bony expansion, and erosion, and foreign body giant cells are seen microscopically. Curettage is curative.

An aneurysmal bone cyst is a rapidly expansile osteolytic lesion, usually of the long bones and spine and, typically, secondary to neoplasm or trauma. It may be intra- or extraosseus. Orbital cases cause mass and compressive effects. Curettage is generally successful in treatment.

Giant cell (reparative) granuloma is a benign, granulomatous proliferation of the bone, thought to be a reparative response to hemorrhage caused by trauma. It usually involves the maxilla, mandible, or phalanges, but can occur in the orbit. Localized bony destruction and collection of blood cysts are seen. It needs to be distinguished from the more aggressive giant cell tumor and brown tumor of hyperparathyroidism. Its treatment is usually by curettage.

The brown tumor of hyperparathyroidism is a benign, granulomatous proliferation of the bone in association with hyperparathyroidism. Increased osteoclastic activity causes bony destruction and hemorrhage. Treatment of the underlying hyperparathyroidism resolves the tumor.

Neoplasms

Osteosarcoma is the most common primary malignant neoplasm of the bone usually arising *de novo* and occurring in the long bones of children and young adults. It consists

of osteoblastic cell proliferation forming a tumoral bone that shows lysis, sclerosis, and expansion. It can arise secondary to underlying bone pathology, such as Paget's disease, prior irradiation, or a precursor tumor. In addition, it occurs as a secondary tumor in patients with familial retinoblastoma. Orbital lesions usually arise from the maxillary spread. Its management is by surgery with pre- and postoperative chemotherapy and subsequent irradiation. The prognosis depends on the stage, site, size, degree of induced necrosis by chemotherapy, and presence of metastases; however, generally, it is poor.

Chondrosarcoma is a malignant, locally aggressive tumor of the bone composed of anaplastic chondrocytes. It may develop from an underlying benign bony tumor. It most frequently occurs in long bones but can spread to the orbit from the adjacent sinuses. The symptoms are caused by mass effect and infiltration. Depending on the speed of growth and prognosis, the tumors are graded 1–3, with grade 1 being the slowest. If possible, ablative surgery is ideal. Adjunctive chemotherapy or irradiation may have a role.

Mesenchymal chondrosarcoma is a variant of chondrosarcoma that arises from the bone or extraskeletal soft tissue and is typically aggressive with a potential to metastasize.

Ewing's sarcoma is a malignant round-cell tumor found in the bone or soft tissue and thought to be of the same family as neuroectodermal tumors. It most commonly occurs in male teenagers. Orbital tumors arise from metastases or secondary spread, causing a fairly rapid mass effect. Treatment with neoadjuvent chemotherapy, radical surgical resection, and subsequent radiotherapy provides a reasonable prognosis for localized disease.

Myeloma (plasmacytoma) is a hematological malignancy of bone marrow plasma cells. The orbital bone may be affected and tends to present subacutely in older patients.

Langerhans' cell histiocytosis (old term histiocytosis X) is an unusual neoplasm of bone and soft tissues characterized by the clonal proliferation of Langerhans cells, a specialized histiocyte of the epidermal dendritic cell type. On histopathogical examination, these cells sit within an eosinophilic granuloma. The tumor may occur in localized or disseminated forms and can be seen in the orbit. The Hand–Schuller–Christian triad of diabetes insipidus, proptosis, and lytic bone lesions occurs due to multifocal lesions affecting the pituitary. Lettere–Siwe disease is caused by multifocal lesions of many tissues and has a poor prognosis. However, localized disease has a better outlook and is responsive to curettage and systemic or local steroid treatment.

Giant cell tumor (osteoclastoma) is a neoplasm of osteoclast-like giant cells that typically affects long bones in adulthood. Malignant change and metastases may occur. It rarely occurs in the orbit, usually being due to spread from the sphenoid bone.

Intraosseous hemangioma is a benign vascular tumor of the bone, hamartomatous in nature, similar to hemangiomas found elsewhere. It can present in the orbital, particularly frontal, bone as a slowly growing orbital mass associated with pain. Surgical excision is complicated by hemorrhage. Prior embolization may be possible.

Secondary Tumors of the Orbit

Neoplasia of the sinus and nasopharynx

Squamous cell carcinoma is a malignant tumor of anaplastic squamous epithelial cells. The tumor can remain *in situ* (Bowen's disease) or be invasive. Orbital lesions usually occur from direct extension of the eyelid, adnexal, and conjunctival tumors or invasion from the sinuses and nasopharynx. Posterior orbital tumors have a worse prognosis with a greater incidence of metastases at presentation.

Transitional carcinoma of the orbit is a neoplasm of the schneiderian epithelium of the nasal cavity or paranasal sinuses that has invaded the orbit. Tumors are usually multiple, benign, and papillomatous, although malignant transformation occurs in some individuals.

Adenoid cystic carcinoma is a malignant neoplasm of mixed glandular components usually seen in the head and neck region, in particular the salivary glands. Typically, these tumors stay indolent for a period before local invasion and, thus, are detected late. Orbital tumors occur due to spread from the lacrimal gland or paranasal sinuses. Perineural infiltration causes pain and parasthesia. The primary treatment is surgical excision. Adjuvant radiotherapy can be beneficial.

Adenocarcinoma is a malignant epithelial neoplasm of the exocrine glandular tissue. Orbital adenocarcinoma may occur due to the localized spread from the eyelid and adnexa, the sinuses and nasopharynx, or from metastases.

Odontogenic tumors are those arising from the mandible or maxilla that very rarely invade the orbit, for example: ameloblastoma, ameloblastic fibosarcoma, and calcifying epithelial odontogenic tumor.

Orbital extension of eyelid tumors

Basal cell carcinoma of the eyelid is a malignant, slow-growing epithelial tumor of the eyelid skin. Various forms are recognized: nodular, cystic, pigmented, sclerosing, superficial, or baso-squamoid. Orbital invasion is usually a result of advanced disease, recurrence, or the sclerosing (morpheiform) variant.

Sebaceous carcinoma of the ocular adnexa is an aggressive, malignant, epithelial tumor of the sebaceous glands of the eyelids and caruncle. Late diagnosis is typical due to mimicry of other common lid lesions. Orbital involvement is by secondary invasion and has a poor prognosis.

Merkel cell carcinoma is a rare, highly aggressive, and metastasizing malignant neuroendocrine tumor of the skin, usually occurring within the head and neck region.

Eyelid tumors are uncommon. Orbital invasion usually occurs after tumor recurrence.

Mucinous sweat gland adenocarcinoma is a rare, malignant carcinoma of sweat gland origin. An extension from the adnexa into the orbit is possible.

Infiltrating signet-ring carcinoma is an exceptionally rare, malignant carcinoma of eccrine gland origin with a diffuse, histiocytoid appearance microscopically. Orbital spread is possible.

Apocrine gland carcinoma is a rare, malignant carcinoma of apocrine gland origin, for example, an anaplastic cyst of Moll. Secondary orbital extension has been reported.

Secondary tumors arising from the conjunctiva

Conjunctival melanoma is an uncommon malignancy of melanocytes that arises in the conjunctiva. The neoplasms develop within underlying primary acquired melanosis (superficial epithelial pigmentation) or, less frequently, from underlying naevi, or can arise *de novo*. Orbital extension is more typical from other sites.

Orbital extension of ocular malignancies

Uveal melanoma is a malignant neoplasm of melanocytes occurring in the uveal tissue. Orbital involvement is from extrascleral spread and postenucleation orbital recurrence. Its treatment is by partial or complete enucleation/exenteration with plaque or orbital radiotherapy.

Retinoblastoma of the orbit is secondary to spread from a malignant intraocular tumor of the retina. After breach of Bruch's membrane, extension occurs via the choroid, optic nerve, and blood vessels, invading into the orbit and metastasizing. Orbital involvement is treated aggressively with radical excision of the tumor, chemotherapy, and radiotherapy.

Medulloepithelioma of ciliary body is a congenital neuroepithelial tumor of the ciliary body that may be benign or malignant. Medulloepithelioma may also very rarely occur adjacent to and within the optic nerve. Orbital, intracranial extension, and metastases are possible.

Orbital extension of lacrimal sac tumors

Lacrimal sac epithelial tumors occur as exophytic, inverted, or mixed papillomatous lesions, being further subdivided into squamous, transitional, or mixed cell type. They can also arise as *de novo* carcinomas. The histological cell types of those arising *de novo* include squamous cell, transitional cell, adenoid cystic, mucoepidermoid, adenocarcinoma, or poorly differentiated cells. Benign mixed tumors and oncocytomas can also occur from the lacrimal sac.

Lacrimal sac nonepithelial tumors include those of mesenchymal origin (fibrous histiocytoma, hemangiopericytoma, and lipoma), lymphomas, melanoma, granulocytic sarcomas, and neural tumors (neurilemmoma and neurofibroma).

Lacrimal Gland Neoplasia

Tumors of the lacrimal gland are usually classified as epithelial or nonepithelial in embryonic origin and can be benign or malignant. The more common epithelial tumors are the benign pleomorphic adenoma or carcinoma in pleomorphic adenoma and the malignant tumors such as adenoid cystic carcinoma, carcinoma ex pleomorphic adenoma, mucoepidermoid carcinoma, and adenocarcinoma. Nonepithelial tumors typically consist of mesenchymal neoplasms, lymphoproliferations, and metastases.

Pleomorphic adenoma (**Figure 3**) of the lacrimal gland (benign, mixed tumor) is a benign, slowly progressive, epithelial tumor of the lacrimal gland consisting of a mix of epithelial and mesenchymal elements. It usually arises from the orbital lobe and affects young to middle-aged adults. It clinically presents with a unilateral progressive mass in the superotemporal anterior orbit that is relatively pain free. Imaging reveals a round circumscribed mass without bony destruction. Complete extirpation is essential. Over time, this tumor can undergo malignant change.

Carcinoma in pleomorphic adenoma (circumscribed/carcinoma *in situ*) is a circumscribed, noninvasive focus of malignancy within a pleomorphic adenoma that is usually only diagnosed by histopathology. Clinically, there may be a sudden change in the behavior of a previously indolent lacrimal mass. The anaplastic focus is usually adenocarcinoma but may be adenoid cystic, squamous, or sarcomatoid.

Oncocytoma is a rare, benign, slow-growing epithelial tumor composed of oncoctyes – large polygonal granular eosinophilic cells with small, hyperchromatic nuclei. Tumors are found in the kidney, salivary glands, lacrimal sac, conjunctiva, accessory lacrimal glands, and, rarely, the lacrimal gland.

Warthin's tumor (papillary cystadenoma lymphomatosum) is a benign, epithelial tumor of the salivary glands – the second most common parotid gland tumor. It is rare in the lacrimal gland.

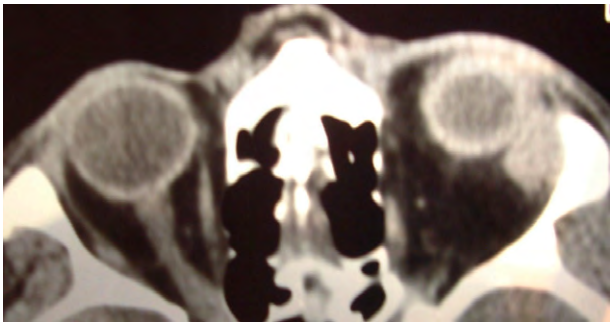

Figure 3 Axial computed tomography soft-tissue view showing an ovoid circumscribed mass in the left lacrimal fossa. Note the characteristic expansion of the lacrimal fossa. The tumor was removed en bloc and proved to be a pleomorphic adenoma.

Myoepithelioma is a benign, epithelial tumor of the lacrimal and salivary glands composed almost entirely of myoepithelial cells.

Adenoid cystic carcinoma of the lacrimal gland is the most common malignant epithelial tumor of the lacrimal gland. It usually presents around the age of 40 but has a bimodal occurrence in the second and fourth decade. Classic histopathological patterns are: cribriform (cystic spaces lined by malignant cells giving a swiss cheese appearance), solid (basaloid), tubular (ductal), sclerosing, and comedocarcinomatous. Tumors may display mixed patterns. In contrast to benign tumors, proptosis is rapid; pain is usually present and associated with ipsilateral parasthesia. Imaging reveals bony destruction. Management is difficult and prognosis is poor. Complete removal may be possible; however, if there is breach of the capsule, then orbital exenteration and bony removal with supplemental radiation and chemotherapy offer the best hope.

Carcinoma ex pleomorphic adenoma (noncircumscribed) is an invasive tumor of any lacrimal gland cell type originating from a pleomorphic adenoma – residual foci of the underlying pleomorphic tumor are evident on histology.

Mucoepidermoid carcinoma of the lacrimal gland is a malignant tumor of the lacrimal gland consisting of varying proportions of luminal epithelial and myoepithelial cell origin and mucin.

Adenocarcinoma of the lacrimal gland is a malignant, aggressively infiltrative epithelial tumor of the lacrimal gland that demonstrates glandular or ductal differentiation. Rapidly growing painful lacrimal masses occur with metastatic spread. Prompt exenteration and radiotherapy increase survival.

Polymorphous low-grade adenocarcinoma is a malignant, epithelial tumor that shows variable histological growth patterns and may be confused with adenoid cystic carcinoma. However, it is well circumscribed and less aggressive in nature. Metastases are less common.

Ductal adenocarcinoma of the lacrimal gland is a malignant epithelial tumor of the lacrimal gland showing proliferation of anaplastic luminal epithelial cells and cystic distension.

Sebaceous adenocarcinoma of the lacrimal gland is a rare, malignant, epithelial tumor of the lacrimal gland usually arising secondary to a preexisting benign mixed tumor or anaplastic carcinoma.

Acinic cell adenocarcinoma of the lacrimal gland is a rare, malignant, epithelial tumor of the lacrimal gland of acinar cell origin. This tumor is seen more typically from the sebaceous gland.

Basal cell adenocarcinoma of the lacrimal gland is a rare, malignant, epithelial tumor of the lacrimal gland of basal epithelioid cells that is slowly infiltrative and has low potential to metastasize.

Epithelial–myoepithelial carcinoma is a low-grade malignant tumor composed of a biphasic cell population of myoepithelial cells and ductal cells. It is more typical of the sebaceous gland but may occur in the lacrimal gland.

Lymphocytic Tumors

Lymphocytic processes in the orbit have received great attention in the last two decades with an increase in our understanding due to more sophisticated molecular and immunodiagnostic techniques. The most frequently encountered lymphocytic orbital tumors are low-grade, slowly-developing lymphoproliferations which tend to develop insidiously and, often, without any pain. They are frequently located anteriorly in the extraconal orbital compartment and tend to be cohesive and mould to adjacent structures on imaging. The underlying disease process is often that of a B-cell lymphoma (small cell), soft-tissue plasmacytoma, having atypical or reactive lymphoproliferations. Other types of orbital lymphocytic processes include: fulminant orbital infiltration by leukemic infiltrates, Hodgkin's lymphoma, or malignant histiocytosis; secondary orbital infiltration from bone or skin lesions; and neuro-ophthalmic lesions in the orbit usually from late disseminated leukemias or lymphomas. These are summarized in **Table 1** in terms of four clinical orbital lymphocytic processes, common mode of presentation, and the common disease processes involved.

If an orbital lesion is the primary presentation of a lymphoproliferative process, then a biopsy must be performed to establish histopathological diagnosis. This can be done by open-incision technique or fine-needle aspiration, the former being the preferred method where one cubic centimeter of tissue is adequate to aid in the diagnosis and allow for immunophenotyping and molecular studies.

A spectrum of lymphocytic processes exists, ranging from reactive lymphoid hyperplasia (RLH) through to frank lymphoma. RLH is a histological diagnosis where biopsy specimens typically show focal lymphoid aggregates. The lesions are usually slightly nodular with a firm to rubbery consistency most frequently in the anterior rather than deep orbit. They are often painless, frequently resemble other lymphoproliferative disorders on imaging, and usually respond well to corticosteroid immunosuppression. Indeterminate lesions are where the morphology is highly atypical but not quite lymphomatous, with lack of molecular or immunophenotypic evidence to suggest lymphoma. They are similar to low-grade lymphoma of the orbit in their presentation and clinical course.

The majority of orbital lymphoproliferations is of B-cell origin, with most lesions being composed of small B-cells that closely resemble normal lymphocytes, making the histological diagnosis particularly difficult.

Table 1 Orbital lymphocytic tumors

Orbital lymphocytic process	*Common mode of presentation*	*Common disease processes*
Orbital masses	Insidious, painless orbital masses, frequently anterior, little functional interference with cohesive appearance on imaging	B-cell lymphomas (small cell) Atypical lymphoproliferations Reactive lymphoid hyperplasia (RLH) Soft-tissue plamacytomas
Fulminant orbital infiltration	More rapid onset of orbital mass and infiltrative effect	Fungal infections Orbital cellulitis Secondary infections (immunocompromised host) Nonspecific orbital inflammatory syndromes
Secondary orbital infiltration	Diverse modes of presentation	B-cell lymphoma (large cell) Plasma cell tumors Burkitt's lymphoma Langerhans' cell histiocytosis T-cell lymphomas Myeloid leukemias
Neuro-ophthalmic lesions	CNS disturbance or invasion of ocular structures	Low-grade intracranial infections or inflammations Intracranial malignancies

The onset is usually in the sixth and seventh decade of life. These lesions are mostly found in the anterior orbit but sometimes have a subconjunctival component. On imaging, they tend to be extraconal and mould or encompass ocular and orbital structures typically without any associated functional deficit. A multidisciplinary approach to managing the patient is most appropriate. Localized disease can be targeted with local radiotherapy, whereas more widespread disease may warrant chemotherapeutic intervention. Emerging monoclonal antibodies against specific lymphocytes may prominently impact the management of lymphoma.

Diffuse large B-cell (DLBC) lymphoma is uncommon in the orbit but is the second most frequent orbital non-Hodgkin's lymphoma. Burkitt's lymphoma is a high-grade and high-risk lymphocytic undifferentiated neoplasm and is linked to Epstein–Barr virus, malaria, or human immunodeficiency virus infection. It is a rapidly disseminating lymphoma but usually presents as a solitary growth with a male preponderance. T-cell lymphomas refer to a broad spectrum of neoplasms in three main categories: precursor T-cell lymphoma, peripheral T-cell lymphomas, and cutaneous T-cell lymphomas. Ocular and orbital involvement usually indicates extracutaneous spread, and their management is based on the extent of involvement. Among childhood malignancies of the orbit, acute leukemia and granulocytic sarcoma are frequent causes of unilateral proptosis, second to rhabdomyosarcoma. Orbital involvement in such cases is a poor prognostic indicator.

Solitary plasma cell tumors are often slow-growing, circumscribed, soft-tissue tumors of the orbit and can be divided histopathologically into polyclonal reactive or monoclonal plasma cell tumors. Histologically, they are not too dissimilar to multiple myeloma, and the distinction comes from careful clinical evaluation and identifying the lack of other associated findings. Unlike non-Hodgkin's lymphoma, orbital involvement of Hodgkin's lymphoma is rare and mostly takes place during the final phases of the disease, reflecting dissemination and aggressive disease.

Langerhans' cell histiocytosis causes rare lesions occurring mostly in children, with a male predilection, and only 10% have any ophthalmic manifestations. It is thought to result from abnormal epidermal accumulations of specialized histiocytes from the dendritic cell family. It typically shows Birbeck granules (cytoplasmic racquet-shaped granules) on electron microscopy. The prognosis is related to the patient's age, extent of the disease, and likely progression, with mortality reducing as the age increases.

Structural Lesions

Cystic Lesions

The multitude of classifications of these lesions indicates their diversity. They can be either with or without epithelial lining. Further divisions can be based on the tissue type, location, and etiology. All cystic lesions share the common feature of a fairly spherical cavity containing material of a different density than the surrounding tissue. Various orbital lesions may have cystic components and may be multilocular. When cystic lesions involve or are adjacent to the bone, they tend to excavate and expand the bone locally if the lesions are encapsulated or cause bony lysis if the cyst margins are more irregular. Identifying cystic lesions from solid ones is part of the diagnostic process in such cases.

Congenital epithelial cysts include dermoid and epidermoid cysts. Orbital and periorbital dermoids are developmental choriostomas and are thought to arise from ectodermal nests pinched off at suture lines. They have a preponderance to be located in the upper outer quadrant of the orbit but may develop virtually anywhere within and adjacent to the orbit. They typically develop slowly and displace other structures by exerting a mass effect. They can be clinically subdivided into superficial

and deep lesions. They tend to have adnexal structures, such as pilosebaceous units, adjacent to the epithelial lining in contrast to epidermoids, which are only lined by the squamous epithelium. Overall, the majority requires complete extirpation, whereas some superficial lesions may be observed.

Acquired cysts include mucoceles and lacrimal cysts. Mucoceles are slowly expanding cystic lesions which originate from the sinuses. They mostly contain a clear to slightly yellow mucoid material, within which they can rarely form a pyocele if the contents become infected. They tend to be expansive and noninfiltrative, and exert a mass effect which can present clinically in a manner typical to the location of origin. For instance, frontal sinus mucoceles tend to displace the globe down and out with minimal proptosis, especially if located anteriorly. Various other ocular effects can result, such as diplopia, vision loss, and swelling, depending on which sinus is involved. The management is surgical and involves removing the cyst lining, re-establishing normal drainage, or obliterating the sinus. Lacrimal ductal cysts (**Figure 4**), otherwise known as dacryops, are uncommon and are classically mobile, tense, fluctuant, slowly growing swellings that become visible in the superior–temporal conjunctival cul-de-sac upon eversion of the upper lid. The management, if symptomatic or bothersome, is complete excision or marsupialization.

Tumors and Ectopias

Dermolipoma (**Figure 5**) is an ectopia of the skin to the conjunctiva and can cause frequent clinical confusion with true orbital dermoids. It often occurs in the area of the lacrimal ducts and, therefore, superficial excision to remove the lesion must ensure that these ducts are not damaged.

Lacrimal ectopia, although not infrequently found in the adnexal area, is rarely noted deep in the orbit. Surgical excision reduces the risk of progressive chronic inflammation of the orbit.

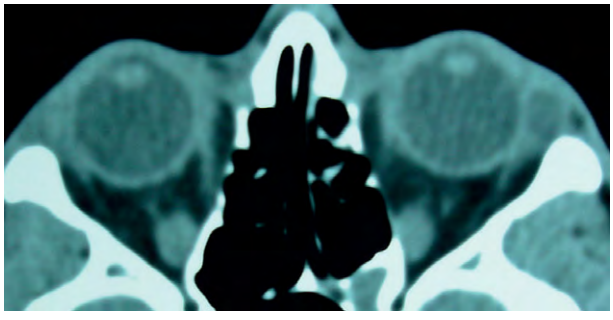

Figure 4 Axial computed tomography soft-tissue view demonstrating a cystic lesion (lacrimal ductal cyst) near the left anterior orbital rim.

Orbital teratoma is an uncommon tumor composed of tissues derived from more than one germ layer and usually from all three and, thus, is thought to arise from the pluripotential embryonic tissue. Aggressive excision or even exenteration may be required. It forms part of the differential diagnosis of a rapidly growing large orbital tumor in infancy along with lesions such as orbital hemangioma and rhabdomyosarcoma.

Inflammatory Diseases

Nonspecific Orbital Inflammations

This heterogeneous group of syndromes all have clinical hallmarks of inflammation, are generally acute or subacute in their onset, and are composed histologically of polymorphous inflammatory cell infiltrations. The location of inflammation often defines the clinical categories of these conditions. On imaging, they typically have an irregular margin adjacent to the primary focus of inflammation in addition to evidence of tissue swelling and enhancement with contrast media. An arbitrary but clinically useful subdivision of these conditions consists of five categories: myositic, lacrimal, anterior, apical, and diffuse. The rapid steroid responsiveness, especially as applied to pain, is almost pathognomonic of this group of conditions.

Myositic inflammation

Orbital myositis (**Figure 6**) is the most frequently encountered nonspecific inflammatory orbital syndrome. Clinically, it tends to have an isolated, recurrent, or atypical presentation. In the more common isolated or recurrent disease, typical presentation includes periorbital inflammation and swelling, retrobulbar pain, along with limitation and pain on eye movement. Visual acuity is often normal and focal conjunctival injection and proptosis may be clinically evident. Imaging reveals fusiform

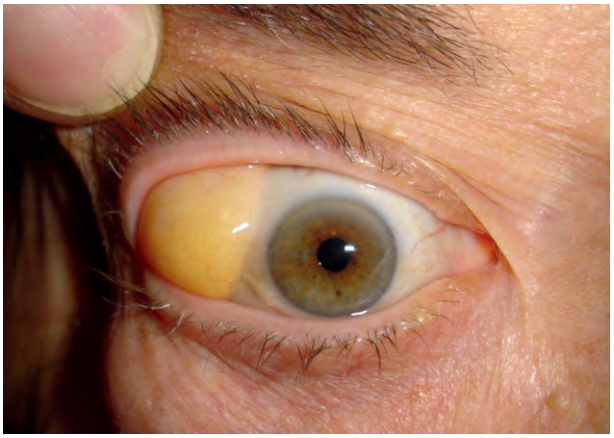

Figure 5 Rounded dermolipoma superotemporally in the right eye of a patient.

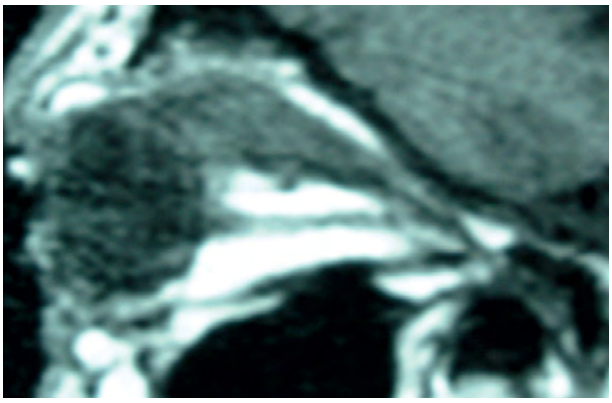

Figure 6 Sagital T2-weighted magnetic resonance imaging with gadolinium enhancement showing orbital myositis. Note the thickened superior rectus muscle and tendon.

enlargement of the whole muscle including the tendon, in contrast to thyroid orbitopathy. Typically, isolated cases tend to involve one muscle, whereas recurrent cases tend to involve multiple muscles and can be bilateral. In the atypical cases, pain may be absent without any limitation of ocular movement; however, abnormal or unusual imaging usually prompts the need for a diagnostic biopsy.

The predominant differential diagnosis for idiopathic myositis is Graves' orbitopathy. In contrast to idiopathic myositis, dysthyroid myopathy tends to be painless at onset, asymmetric, and slowly progressive with lid retraction and potential deterioration of visual function in addition to relative sparing of the tendon insertion of the muscle. The management for idiopathic myositis tends to range from simple nonsteroidal anti-inflammatory drugs in isolated unilateral cases, through to immunosuppressive agents and radiotherapy in bilateral, recurrent, or apex-involving cases.

Lacrimal inflammation

Dacryoadenitis describes inflammation of the lacrimal gland. The typical acute or subacute presentation consists of pain, tenderness, and injection of the temporal portion of the upper lid and conjunctival fornix giving an S-shaped deformity of the lid. The lacrimal gland itself is often palpable and tender, and pouting of the lacrimal ducts may be noted on biomicroscopy. Imaging shows irregular swelling of the lacrimal gland and adjacent tissues. Approximately 50% of nonspecific lacrimal gland inflammations may have an associated systemic disorder such as sarcoid, lymphoma, Wegener's granulomatosis, sclerosing inflammation, or any of a myriad of autoimmune disorders. This is more commonly identified in chronic presentations, and a biopsy is warranted in such situations.

Management for acute dacryoadenitis is to maintain a high index of suspicion for systemic disease and to promptly biopsy if justified. Oral corticosteroids in moderate tapering doses (starting with 40 mg prednisolone) will resolve the inflammatory episode within 1–3 months in the majority of nonspecific acute inflammatory cases.

Anterior and diffuse inflammation

In anterior orbital inflammation, the main focus involves the globe and adjacent orbit. Presenting features include moderate pain, ptosis, proptosis, and, in some cases, reduced vision. There may also be some ocular findings such as uveitis, papillitis, or exudative retinal detachments. This syndrome tends to present in children and young adults. Cases with diffuse disease not only have similar features, but also involve the extraocular muscles and neurosensory structures. On imaging, the infiltration is irregular and produces scleral and choroidal thickening. Ultrasonography may reveal prominence of the Tenon space with doubling of the optic nerve shadow (T sign). Treatment is generally with oral prednisone, usually starting at 60 mg and tapering over 2–3 months. This usually produces a dramatic response with a marked reduction in pain. Resolution can be monitored by repeat imaging. Recalcitrant cases, particularly in adults, should be considered for biopsy.

Apical inflammation

This condition presents with early pain on movement or diplopia in a disproportionate extent to the degree of inflammatory signs. Imaging displays the apical focus of inflammation. Apical disease should rarely be treated nonspecifically without a very careful follow-up, systemic evaluation, and consideration of biopsy, since a wide variety of diagnoses can present the same way.

Specific Inflammations of the Orbit

Infections – orbital cellulitis and sinusitis (microbial)

Clinically, orbital cellulitis is generally associated with axial displacement of the globe, whereas abscess formation within the orbit, particularly in the subperiosteal space, usually causes nonaxial displacement. Posterior subperiosteal tracking may lead to dramatic visual loss and neurosensory compromise due to apical compression. The increase in intraorbital tension may also lead to permanent visual loss. The most devastating complication is the spread to the cavernous sinus, leading to cavernous sinus thrombosis. Alternatively, the infection may spread into the intracranial cavity, leading to a subdural empyema or intracranial abscess. Current imaging technology allows for earlier recognition of orbital and periorbital involvement and is useful for evaluation of severity and guiding management. An abscess can be identified on imaging by a poorly defined mass with contrast enhancement of the rim.

The management and outcomes differ in adults and children. The majority of children do not need sinus or abscess drainage, whereas adults more frequently require this, particularly if there is orbital tension and threat to vision. The main principles of management consist of preventing ocular and nonocular complications, using appropriate antibiotics, surgical drainage when necessary (i.e., significant abscess with globe tenting, increased proptosis, deterioration of vision, or extraocular movements), and careful follow-up.

Fungal infections

Aspergillosis presents in the orbit in a disseminated form that causes microscopic angiitis or by the relatively slow development of a localized infiltrative mass usually originating from the adjacent sinus. It can occur in healthy people but is more common in predisposed individuals with recurrent sinusitis and polyps. Early diagnosis can be aided by the use of aspiration cytology. Once diagnosed, extensive debridement, local irrigation with antifungals, and systemic therapy are the hallmarks of management.

Tuberculosis and syphilis

Orbital tuberculoma is another manifestation of hematological spread and is associated with the development of an infiltrative orbital mass which may cause neurosensory deficits. Diagnosis may be aided by fine needle aspiration biopsy. Primary soft tissue gumma may occur with syphilitic orbital involvement which may also involve the extraocular muscles or lacrimal gland.

Parasitic infections

Hydatid cyst (Echinococcosis) is an infestation of the intestines of dogs, sheep, and other animals which may parasitize humans during its larval stage and spread around the body to form cystic spaces. Orbital cysts are seen infrequently. Onset is usually insidious and dominated by mass effect, but rupture of the cyst may be associated with a more acute fulminant inflammatory course and may be a complication of surgical incision or injury. Diagnosis is made by imaging of a cystic lesion within the orbit which may have evidence of calcification. Biological tests can substantiate these findings. Treatment is excision of an intact cyst either by a direct or lateral orbital route.

Vasculitis

Inflammatory diseases such as Wegner's granulomatosis may present by proptosis associated with a destructive orbital inflammatory mass. This is often bilateral and usually causes irreversible morbidity unless treated. An orbital biopsy can confirm the diagnosis prior to treating with aggressive immunosuppression.

Idiopathic sclerosing inflammation

The clinical features of this condition are dominated by a cicatricial infiltration associated with mass effect and mild inflammation. The characteristic imaging finding is a homogeneously enhancing mass with irregular margins. Prompt early biopsy and diagnosis followed by immunosuppression and immunomodulation are integral to the management of this condition.

Sarcoidosis

The clinical presentation usually consists of a mass effect, rarely associated with evidence of inflammation, with more than half of the patients presenting with lacrimal gland involvement. Other ocular findings may also be evident.

Other lesions

Less frequently encountered orbital inflammatory lesions such as orbital xanthogranulomas, consisting of chronic inflammatory infiltrate with lipid-laden histiocytes, predominantly respond initially to steroids. A reasonable degree of suspicion and suitable threshold for orbital biopsy must remain in the management of most orbital inflammatory lesions.

Vascular Lesions

Arteriovenous Malformations

High-flow arteriovenous malformations are characterized by antigrade arterial flow through the lesion to the venous side. Clinical features include pulsating exophthalmos and occasional episodes of hemorrhage or thrombosis. On imaging, these lesions are characterized by irregular, rapidly enhancing masses. For the most part, arteriovenous malformations are kept under observation; however, recurrent hemorrhaging or pain may require intervention.

Cavernous hemangiomas behave like low-flow arteriovenous malformations, although they are considered to be vascular hamartomas. Clinically, these lesions are benign noninfiltrating tumors that exert a slowly progressive mass effect. CT scans typically show a very well defined oval or rounded mass with distinct margins, which enhances with contrast. Intervention is unnecessary unless there is some functional or cosmetic concern.

Venous Malformations

Distensible venous malformations can be superficial, deep, combined, or complex lesions. The superficial malformations are seen as tortuous, epibulbar, or eyelid lesions, whereas the deeper ones are characterized by intermittent proptosis, evidence of enophthalmos due to fat atrophy, and pain on expansion brought about by physical effort or bending. Imaging features include

enlargement of the lesion on direct coronal CT, and expansion with Valsava maneuver during dynamic CT or MRI. Intervention is unnecessary unless there is pain, progressive expansion, or cosmetic concerns.

Nondistensible venous malformations are characterized by episodes of acute exacerbation and remission, due to hemorrhage or thrombosis within the lesion leading to sudden proptosis, echymosis, and pain. Indications for intervention include extreme orbital pressure and cosmetic disfigurement.

Lymphatic and Combined Venous Lymphatic Malformations (Lymphangioma)

These are no or low-flow vascular hamartomas that derive from the venous system embryologically and have differentiated, in part or whole, to lymphatic vessels. These lesions need to be separated hemodynamically from orbital varices. They can be superficial, deep, a combination of the above or complex if they involve the cheek, neck, face, and so on. The superficial are visible lesions of the conjunctiva or eyelid and consist of multiple clear cysts. If cosmetically unacceptable, they may be removed with relative ease. Deep lesions present with sudden proptosis due to spontaneous hemorrhage. In addition, they may have acute changes related to upper respiratory conditions. Imaging may demonstrate either a cyst with rim enhancement or a solid lesion with cystic components. Indications for intervention include acute orbital hemorrhage, cyst expansion, or significant cosmetic disfigurement.

Adult Lymphangiomas

These lesions are characterized by slowly evolving proptosis and the presence of a relatively homogenous intraconal mass, which is well defined anteriorly but poorly defined posteriorly, and may mimic cavernous hemangiomas clinically.

Capillary Hemangiomas

Capillary hemangiomas represent an abnormal growth of blood vessels with varying degrees of endothelial proliferation. They have a female predominance and usually present within the first months of life, starting as small, flat foci that undergo rapid expansion, followed typically by regression; this may take months to years. These lesions can be superficial, deep, combined, or complex. Superficial ones are the so-called strawberry nevi and are confined to the dermis. Steroid therapy or surgery may be needed if they bleed frequently or lead to obstruction of the visual axis. Deep lesions are characterized by proptosis or globe displacement. When palpable, they have a rubbery, soft consistency and may be collapsed to a degree with modest pressure. On imaging, the margins of these lesions vary from moderately well defined to infiltrating. The majority of these lesions regress spontaneously; however, larger lesions with considerable proptosis or visual axis obstruction may require treatment with systemic or local steroids and surgery.

See also: Cranial Nerves and Autonomic Innervation in the Orbit; Imaging of the Orbit; Orbital Bony Anatomy and Orbital Fractures; Orbital Soft Tissue Biomechanics; Orbital Vascular Anatomy; Thyroid Eye Disease.

Further Reading

Rootman, J. (2003). *Diseases of the Orbit: A Multidisciplinary Approach,* 2nd edn. Philadelphia, PA: Lippincott Williams and Wilkins.

Shields, J. A. and Shields, C. L. (2008). *Eyelid, Conjunctival, and Orbital Tumors: An Atlas and Textbook,* 2nd edn. Philadelphia, PA: Lippincott Williams and Wilkins.

Orbital Soft Tissue Biomechanics

S Schutte, Delft University of Technology, Delft, The Netherlands
G Asmussen, Carl-Ludwig-Institut für Physiologie der Universität Leipzig, Leipzig, Germany
F van Keulen, C P Botha, F-W Goudsmit, and F C T van der Helm, Delft University of Technology, Delft, The Netherlands
H J Simonsz, Erasmus Medical Centre, Rotterdam, The Netherlands

Glossary

Anisotropic materials – These materials do not behave the same way in all directions. Muscle tissue, for example, has a different mechanical behavior in the fiber direction than in the directions perpendicular to the fiber direction.
Coulomb friction model – The frictional forces are determined by a coefficient of friction (either static or dynamic) and the normal forces that are exerted between the surfaces.
Continuum mechanics – It deals with the mechanical behavior of structures that can be modeled as a continuum. The microlevel behavior within a structure, for instance, cross-bridge dynamics within a muscle, is not modeled in detail but only the overall mechanical behavior is considered.
Friction – It is the force resisting the relative motion of two surfaces in contact. When the surfaces are moving, friction converts kinetic energy into thermal energy.
Inhomogeneous materials – These materials do not have the same composition throughout, and the mechanical properties depend on the location within the material. The orbital fat, for instance, is highly inhomogeneous as the connective tissue sheets orientation and density varies throughout the orbit.
Isotropic materials – These materials show the same mechanical behaviour in all directions.
Loss modulus – It is a measure for the energy that is dissipated in the material in deformation; this represents the viscous part of the energy needed for deformation.
Poisson's ratio – When a material is compressed in one direction, it will expand in the other two directions. A measure for this expansion is the Poisson's ratio. Incompressible media, like the orbital fat, have a Poisson's ratio close to the value of 0.5.
Storage modulus – It is a measure for the energy that is stored in the material in deformation; this represents the elastic part of the energy needed for deformation.
Stress – The intensity of the internal forces acting within a body across imaginary internal surfaces, as a reaction to external applied forces and body forces. Stress is a measure for the amount of force exerted per unit area.
Strain – The proportion of deformation to original size.
Viscoelastic behavior – The stress required for a certain deformation depends on the material properties. A viscoelastic material shows both elastic and viscous behavior. Elastic behavior entails that the energy that was used to deform the structure is returned when the structure is unloaded. Viscous behavior causes energy to be dissipated in the loading cycle and depends on the rate of deformation. Response (in terms of strain and stress) of a viscoelastic material to loading depends on the loading timescale and loading history. Hence, there is no direct relation between stress and strain.
A loading–unloading cycle of viscoelastic material will show a hysteresis loop in the stress–strain curve: more energy is required during the loading than returned during the unloading.
Young's modulus – The ratio of the stress to the strain, often also called the modulus of elasticity. Young's modulus is only meaningful in the range in which the stress is proportional to the strain.

Introduction

The human eye is suspended inside the orbit, a bony cavity in the skull. The orbit is filled with fat (adipose tissue) that supports the eye and eye muscles in different directions of gaze. Four rectus muscles control the horizontal and vertical position of the eye and two oblique muscles control the torsional position of the eye (**Figure 1**). The optic nerve, which transmits visual information from the retina to the brain, courses posteriorly from the eye to the apex of the orbit through the orbital fat.

A miraculous interaction between pressure and tensile forces in the soft tissues keeps the eye in place while a large range of rotational motion is enabled. For a correct

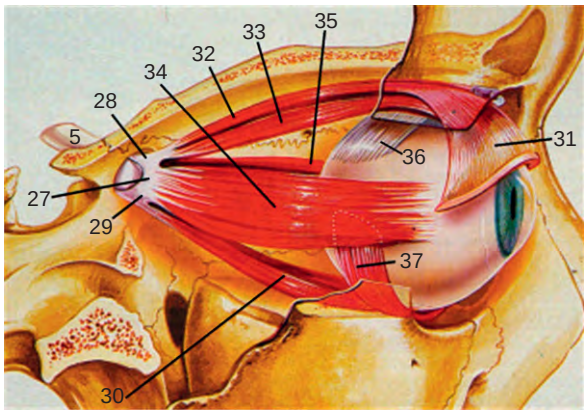

Figure 1 A schematic representation of the eye in the orbit and the six extraocular muscles from the lateral view. 5: optic nerve, 27: origin of lateral rectus muscle from tendinous annulus, 28: combined origin of superior rectus and levator palpebrae superioris muscles from tendinous annulus, 29: origin of inferior rectus from tendinous annulus, 30: inferior rectus muscle, 31: levator aponeurosis, 32: levator palepebrae superioris muscle, 33: superior rectus muscle, 34: lateral rectus muscle, 35: medial rectus muscle, 36: tendinous insertion of the superior oblique muscle, 37: inferior oblique muscle. Reproduced from Rootman, J. (1988). *Diseases the Orbit*, 2nd edn. Lippincott Williams and Wilkins, http://lww.com. With permission from Lippincott Williams and Wilkins.

biomechanical representation of the three-dimensional shapes and volumes of the morphological structures, their material properties, and interactions, we can use continuum mechanics. The mechanical behavior is determined by (1) the geometrical shapes of the tissues, (2) their material properties, (3) their mechanical interactions, and (4) the mechanical load cases. In the following we discuss these four factors.

The first important factor is the geometry of the tissues. The three-dimensional shape of the muscle, for instance, influences the internal mechanics of the muscle fibers and also the resulting direction of pull of the muscles on the eye.

Second, orbital biomechanics depends on the material properties of the tissues. If external forces are applied to a material structure, it will undergo a deformation. The material properties of a structure determine the relation between stress and strain within the structure. Next, equilibrium equations determine the relation between stresses and external loads.

Sclera, for instance, shows less deformation under a certain stress than orbital fat. Most engineering materials, like steel, show a linear (i.e., proportional) relation between stress and strain, provided the deformations remain sufficiently small. The linear elastic material properties of isotropic materials are usually described by the Young's modulus and the Poisson's ratio.

Most biological soft tissues, however, show a more complex relation between stress and strain and usually do not have a linear relation. This is caused by rearrangements within the material that take place on a microscale; for instance, rearrangement of collagen fibers. In order to determine the exact material properties, experimental testing is needed. In addition to the nonlinear elasticity, the orbital tissues show viscoelastic behavior, and are anisotropic and inhomogeneous. The density of connective tissue sheets in the orbital fat, for instance, is much higher adjacent to the eye than directly behind the eye (inhomogeneity) and the sheets have a distinct direction which causes different mechanical behavior in that direction (anisotropy). This plays an important role, and cannot be disregarded when analyzing orbital biomechanics.

The third determinant of orbital biomechanics is mechanical contact interaction between tissues. The extraocular muscles, orbital fat, and the eye mechanically interact and exert forces on each other at every location where they contact. Clearly, contact has a large influence on the resulting strain and stress state, and the corresponding displacements found. The structures might also slide with respect to each other, in which the type and amount of friction becomes important as well. The medial rectus, for example, slides with respect to the medial orbital wall. In case of a trauma with an orbital fracture the muscle can get 'trapped' in the fracture. Sliding is not possible in this case, and eye movements are limited.

The final determinant of orbital biomechanics is the load case that is applied to the orbital structures. The most common load cases are muscle contractions, and blunt impact, tumor growth, or muscle expansion in Graves' disease can constitute application of a load to the orbital tissues as well.

In the following, we discuss the main factors (the geometries of the orbital structures, their material properties, their mechanical interactions, and load cases) that play a role in understanding soft tissue biomechanics and the suspension of the eye in the orbit.

Geometry of the Orbital Structures

The main structures that determine the biomechanical behavior in the orbit are the eye, the six extraocular muscles, the optic nerve, the orbital fat with its containing connective tissue sheets, and the bony orbit. Smaller structures, like blood vessels and nerves, have little influence on the overall mechanical behavior. Anteriorly, the eyelids exert a low pressure on the eye.

There is a large body of anatomical and histological literature that describes the anatomy of the orbit in detail. The currently available imaging techniques, like computed tomography (CT) and magnetic resonance imaging (MRI), enable a detailed view on the *in vivo* three-dimensional shapes of the geometries. In addition, the deformation of the structures can be visualized dynamically in different directions of gaze.

Material Properties

Eye Muscles

The oculomotor system has a diverse repertoire of actions, including steady fixation, slow vergence movements, pursuit movements at various speeds, and high-speed saccades over a wide range of angles. The functional requirements to the motor system are twofold. First, it must be able to keep the eye in a particular position of gaze and second, fast and directed movements must be possible. High eye velocities – velocities of over $600^\circ\,s^{-1}$ have been measured – impose specific requirements on the eye muscles.

The six extraocular muscles (EOMs) are structurally and functionally unique among the cross-striated muscles of vertebrates. For proper function, each muscle needs fatigue resistance, and force and velocity development. As these properties are not found in one fiber simultaneously, these conditions are met by deployment of different kinds of motor units. Most skeletal muscles have a mixed muscle-fiber-type composition, resulting in the functional properties of the muscle. The functional and structural requirements of the EOMs are reflected in complex muscle-fiber types described in mammalian EOMs. Their fibers have been classified into different types on the basis of their color, location, their enzyme- and immunohistochemistry, and their innervation. This system of classification differs markedly from that normally used to classify limb muscle fibers.

At optimum length (LO), that is, the length at which the muscle develops maximum force, the EOMs are the fastest among the cross-striated muscles. In animals, the contraction and the half-relaxation times are about 6 ms (range 4.5–7.0 ms). The maximum shortening velocity of the sarcomeres of EOMs is about $60\,\mu m\,s^{-1}$. This corresponds to an angular rotation velocity of the eye of about $850^\circ\,s^{-1}$ and is in the same order of magnitude as the fastest saccadic eye movements. Furthermore, the maximum shortening velocity appears to be virtually independent of the size of the animal, as has been observed in body and limb skeletal muscles.

The reasons for the uncommon combination of an exceptionally high shortening velocity and a high fatigue resistance are a high oxidative as well as a high glycolytic capacity in one and the same muscle fiber, in comparison with body skeletal muscles. The combination of a high shortening velocity and a high fatigue resistance in EOM is only possible with a relatively low force output. This is not so much of a problem, as inertia and rotational stiffness of the eye are relatively low. In general the EOMs produce a tension of about the half observed in skeletal muscles. These muscles EOMs have less contractile material per cross-sectional area; the fibers are thin and much room is taken by mitochondria, by capillaries needed for oxidative metabolism, and by a well-developed sarcotubular system. An additional reason for the relatively low force development is the presence of slow tonic fibres. EOMs also contain some multiply innervated slow-tonic muscle fibers. These are common in skeletal muscles of lower vertebrates, but rare in those of mammals.

In the classic way of looking at the action of EOMs, the mechanical behavior is regarded in terms of force–length and force–velocity relations. The force developed by a muscle during isometric contraction varies with the muscle's length and its contraction velocity (**Figure 2**). The passive, that is, without neural activation, length–tension relation shows an approximately exponential course. The length–tension relationship of stimulated muscles is approximately linear. The maximum tension development of single twitches is usually found at an extension of the muscle of approximately 1.15 times the rest length (range 1.1–1.2). This length, LO, is normally used as the working point to investigate the contractile properties of the muscles. Also the muscle tension developed in response to tetanic stimulation has maximum values at this extension.

Several lumped models have been developed to describe the mechanical behavior of muscles. Most of these models describe the developed force as a function of time, length, and activation, and the three-dimensional tissue behavior is disregarded. The future of modeling the mechanical eye muscle behavior lies in developing physically nonlinear continuum models. These models are being developed for limb muscles but this modeling approach has not yet been followed for EOMs. Such approaches allow, for instance, implementation of recruitment mechanisms or cross-bridge dynamics based upon Huxley-type models. These types of models have shown that muscles exhibit interesting mechanical behavior that has been neglected in the classic approach. Strain, for instance, is not uniform throughout the muscle: during muscle contraction it is possible that the muscle belly shortens while near the insertion the muscle is extended.

Orbital Fat

Orbital fat is an important entity within the orbital structures. In the human body, most fat is located beneath the skin and around internal organs. Around organs, it provides protective suspension and under the skin its main function is to provide thermal isolation and energy reserve. The main role of the orbital fat is to support the orbital structures but, at the same time, allow for eye rotations. It fills the orbital cavity, surrounding the eye and muscles and mechanically supports the globe and the nerves and vessels within the orbit.

Histological examinations have shown that the orbital fat is a loosely to strongly connected cellular material. The orbital fat consists of specialized connective tissue sheets that form small compartments that are filled with adipocytes, or fat cells (**Figure 3**). These cells contain a large lipid droplet surrounded by a ring of cytoplasm.

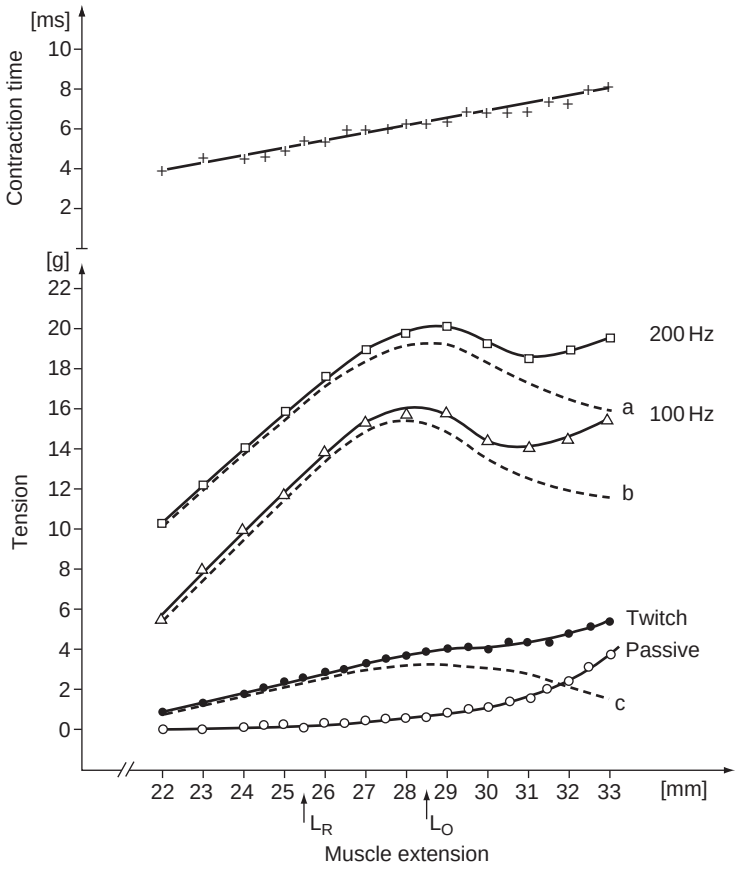

Figure 2 A force length diagram of a rabbit (♀; 4.2 kg body wt.) *in vitro* inferior oblique muscle at 35°C. Passive elongation (○–○) shows an exponential increase. The graph shows tetanic tension (●–●), tetanic tension at stimulation frequencies of 100 Hz (□–□) and 200 Hz (△ – △), and contraction time (+–+). The dashed lines illustrate the net tension of single twitches (c) and tetanic contractions (a, b). L_r – resting length of the muscle *in situ*; L_o optimum length. Reproduced from Asmussen, G. and Gaunitz, U. (1981). Mechanical properties of the isolated inferior oblique muscle of the rabbit. *Pflügers Archiv European Journal of Physiology* 392(2): 183–190. With permission from Springer.

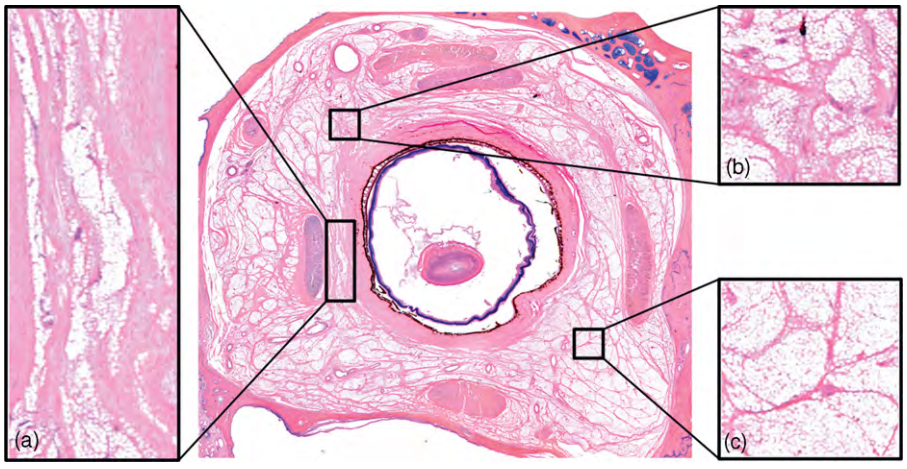

Figure 3 A frontal section of a human orbit (26-year-old person, 80 μm section, hematoxylin–eosin stain) by Koornneef (unpublished). The orbital fat consists of specialized connective tissue sheets that form small compartments that are filled with adipocytes, or fat cells. The orbital fat is a highly inhomogeneous structure, magnifications (b) and (c) show the varying size of the connective tissue compartments containing the fat. In addition, the orbital fat is highly anisotropic. Magnification (a) shows that connective tissue sheets between the medial rectus muscle and the eye, for instance, are oriented parallel to the muscle.

The orbital fat shows a highly anisotropic and inhomogeneous structure: the connective tissue compartments containing the fat vary in size, shape, and orientation. In the retrobulbar area, within the muscle cone, the compartments are large and have less fibrous sheets than anteriorly, in the area between the medial rectus muscle and the orbital wall, for instance. The structure of compartments containing the orbital fat seems to depend on the local mechanical requirements: behind the eye, where pressure is evenly distributed, they are large; adjacent to the eye, where the pressure gradient is steep, they are small. Connective tissue sheets between the medial rectus muscle and the eye, for instance, are oriented parallel to the muscle. This orientation allows the muscle to be quasi-rolled upon the eye when the eye abducts, while the orbital fat is squeezed out superiorly, inferiorly, and posteriorly.

Anterior in the orbit, the density of connective tissue sheets within the adipose tissue is higher and the sheets contain more collagen, elastin, and smooth muscle. The connective tissue sheets do not have a distinct geometry and show an amorphous structure.

The mechanical behavior of a viscoelastic material-like orbital fat can be described by its storage modulus (G') and loss modulus (G''). The storage and loss modulus can be determined in an experiment under oscillatory conditions, for instance, with a rheometer. Such a device applies a strain to the tissue in an oscillatory fashion at various frequencies and records the generated torque. From these recordings the moduli of the tissue can be estimated. In this type of experiment the anisotropy and inhomogenity of the tissues are neglected even though the orbital fat is highly anisotropic and inhomogeneous. The mechanical behavior of calf and monkey orbital fat has been measured (**Figure 4**). The elastic shear modulus (G') and viscous shear modulus (G'') of the orbital fat are low, and G'' is low compared to the G'. G' and G'' were found to be between 250 and 500 Pa for calves, and between 500 and 900 Pa for monkeys. The viscous shear modulus for calf orbital fat was found to be between 80 and 150 Pa, and for monkey orbital fat it was between 300 and 500 Pa.

As the viscous shear modulus is low, little energy is lost during eye movements. In kidney fat, G' and G'' are higher, possibly because this fat primarily has a dampening function. The viscous shear modulus remains approximately the same with increasing angular velocity during sinusoidal deformation. This means that relatively less energy is lost at higher velocities. In polymer mechanics, this phenomenon is called shear thinning.

Sclera

The human sclera performs several important functions for the visual and mechanical performance of the eye. It provides protection to the intraocular contents and its opacity ensures that internal light scattering does not affect the retinal image. The sclera is build up mainly out of collagen fibers with diameters ranging from 20 to 250 nm, entangled in bundles that vary in size.

The thickness of the sclera varies from approx. 1–1.3 mm at the posterior pole to 0.4–0.6 mm behind the insertions of the rectus muscles. From the insertion of extraocular muscles toward the limbus (the edge between the cornea and the sclera), the thickness gradually increases to 0.8 mm, where it blends with the cornea. The conjunctiva, a mucous membrane, attaches to the sclera at the limbus and covers the sclera.

The shape of the eye is maintained by the intraocular pressure that acts against the membrane stiffness of the scleral tissue. The pressure within the eye is approx 18 mmHg or 2.4 kPa. Due to the relatively high stiffness of sclera (2.60 ± 2.13 MPa; measured at 0.6 cm min^{-1}), the mechanical integrity of the eye is damaged after relatively small volume changes, for instance, after a perforation.

Optic Nerve

The optic nerve is contained within the optic nerve sheath that includes cerebrospinal fluid at intracranial pressure. The outermost sheath of the optic nerve resembles the epineurium of peripheral nerves and consists mainly of connective tissue that is the same as the meningeal ensheathments around the brain and spinal cord, dura, and arachnoid. In healthy subjects, the pressure inside the optic nerve sheath is higher than the pressure within the orbital fat. This causes the optic nerve sheath to behave like a protective tube around the optic nerve.

Contact Behavior at the Interface between Structures

An important determinant of the mechanics in the orbit is the contact behavior between the different structures. During eye rotations, the soft tissues in the orbit undergo displacements and deformations. At the interface layers between the tissues, sliding may occur, or the structures may be tautly connected. If tautly connected, the structures are able to transfer forces and moments in every direction. If structures are sliding, the transferred force is primarily in the direction perpendicular to the interface layer. In the direction of the interface layer, the transferred force depends on the type of friction that occurs. The type and amount of friction has to be found empirically. Friction can be described with a friction model. The most commonly used friction model is the model of Coulomb, in which the friction is described by a friction coefficient. However, a large number of friction models exist to describe the behavior of different types of friction

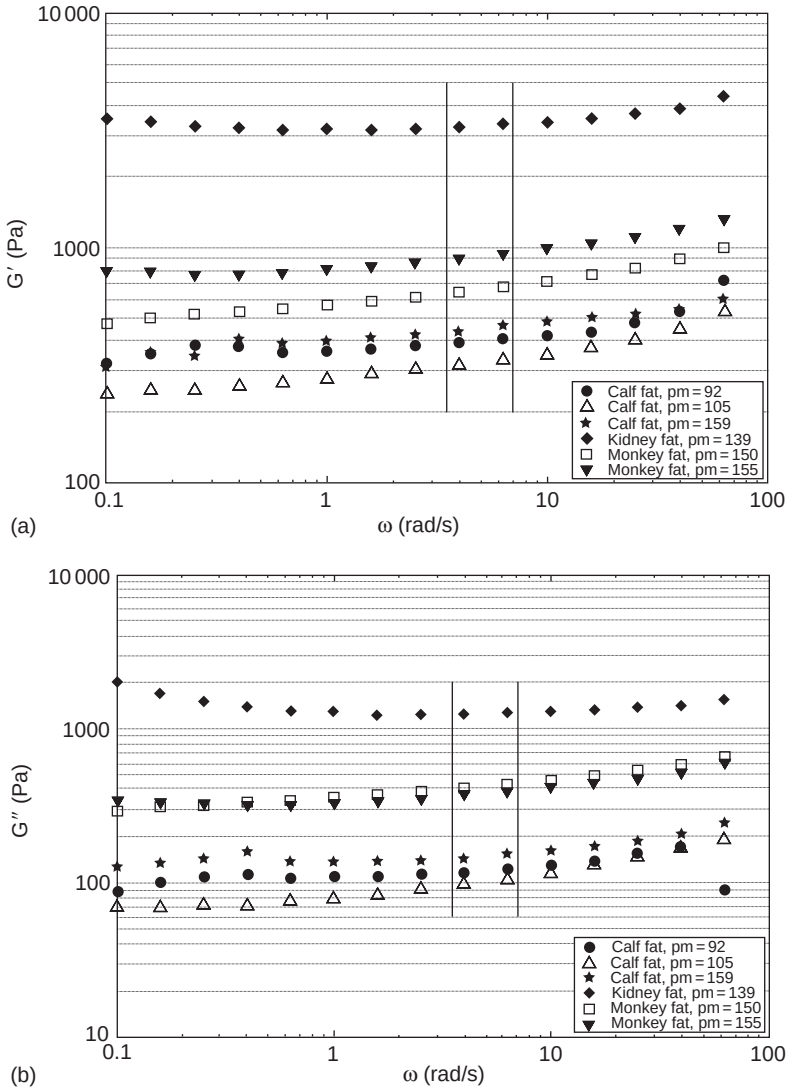

Figure 4 (a) Storage modulus (G′) and (b) loss modulus of the orbital fat of calves and rhesus monkey. Horizontal axis: angular velocity (ω) in rad s^{-1}. Vertical axis: storage modulus (a) and loss modulus (b) expressed in Pa. In order to illustrate the rate of deformation that occurs during eye movements, two vertical bars indicate approximate deformation that occurs during 100 and 200° s^{-1} saccades. Pm, post mortem period in minutes. Reproduced from Schoemaker, I., Hoefnagel, P. P. W., Mastenbroek, T. J., et al. (2006). Elasticity, viscosity, and deformation of orbital fat. *Investigative Ophthalmology and Visual Science* 47(11): 4819–4826. With permission from the Association for Research in Vision and Ophthalmology.

with different parameters. Frictional forces have a large influence on the resulting strain and stress state in the structures and their corresponding displacements. The nature of the lubricating fluid and the types of articular surfaces are important determinants for the friction. Little is known about the types of friction in the orbit. Sliding in synovial joints of the human body is usually facilitated by a synovial-fluid-like substance that is composed mainly of glycosaminoglycans and glycoproteins, which are long unbranched polysaccharides. These molecules are very large and can contain a large amount of water which makes them excellent lubricators.

Connected Structures

At a number of locations in the orbit, the mechanical interactions between the structures are clear. At the insertions of the six EOMs, the tendons are tautly connected to the sclera. Muscular fibers that connect directly to the sclera without a tendon have been described. At their origins, the proximal tendons of the EOMs are tautly connected to the tendinous annulus (of Zinn) in the apex. The origins of the EOMs are attached to the periorbit by interlocking of the tendinous and muscular fibers. The tendon of the superior oblique muscle courses from

its insertion through the trochlea to the apex of the orbit. The trochlea is a fibro-cartilage pulley that is attached to the medial wall of the orbit. A synovial membrane lines the inner surface of the trochlea. Possibly, synovial fluid lubricates the sliding interface between the trochlea and the superior oblique tendon. At the posterior pole of the eye, the optic nerve sheath is merged into the sclera. At its proximal end the optic nerve sheath is encompassed by the EOM origins at the tendinous annulus.

Sliding at the Interface between Structures

The human eye is able to rotate at high angular velocities and has an angular range of 100 degrees horizontally and 90 degrees vertically. It is able to do all of this with almost no translation of its center. It seems evident that the orbital fat plays an important role in keeping the eye in place during eye movements. The fat acts a supportive cushion for the eye and at the same time supports the optic nerve and other nerves, vessels, and the EOMs.

The large range of motion is partly facilitated by sliding at the interface between the sclera and Tenon's capsule, the connective tissue that surrounds the globe and the extraocular muscles. The interface is lubricated, and the eye is able to rotate within Tenon's capsule because of its spherical shape. On the other hand, free rotation of the eye within Tenon's capsule is impeded because the optic nerve leaves the eye posteriorly and crosses the potential subtenon's space. Further, the insertions of the eye muscles rotate with the eye and exert force on the orbital fat. These two effects and others cause the orbital fat to deform and to move, in part, with the eye rotation. The orbital fat directly behind the eye follows approximately half of the eye rotation. The remainder is accounted for by sliding of the eye in Tenon's capsule. Posterior in the orbit, the deformation resulting from eye rotations is less.

Contracting muscles move with respect to their surrounding tissues and sliding occurs between parts of the EOMs and the orbital fat. As the muscles are surrounded by connective tissues, just like the blood vessels and nerves, the mechanism of sliding comes down to sliding between connective tissue fascias. The EOMs slide with respect to the orbital wall. When sliding is hampered, for instance, in case of an orbital fracture when a muscle is trapped in the fracture, eye motility is limited.

MRI studies have demonstrated that the optic nerve slides with respect to the orbital fat. The amount of friction that exists between these structures has not been measured, but is likely to be low.

Connective Tissue Connections

The eye is covered by Tenon's capsule, a thin fibrous membrane that starts at the limbus and covers the eye to the optic nerve. To attach at their insertions, the EOMs course through portals in this capsule.

The inferior tarsal ligament (Lockwood's) is a connective tissue that connects the inferior side of the inferior rectus muscle and the inferior oblique. Posteriorly, this connects to the lacrimal crest. Anteriorly, this attaches to the capsulopalpebral fascia, lower eyelid retractors, and Tenon's capsule. Medially and laterally, it connects into the canthal tendons and orbital walls.

The superior tarsal ligament (Whitnall's) is a condensation of connective tissue sheets overlying the anterior superior part of the levator palpebrae that extends laterally and medially to the orbital walls.

At the level of the posterior pole of the eye, connective tissue bands (often referred to as pulley bands, or pulley slings) are connected to the rectus muscles and course anteriorly to the orbital wall. The function of these bands is heavily disputed. A function in stabilizing the muscle paths is claimed.

Other Interface Layers

The human orbit exhibits more interface layers that influence the overall mechanical behavior, for instance, between the rectus muscles and the orbital walls, between the superior oblique muscle tendon and the superior rectus, between the inferior oblique muscle and the inferior rectus muscle, the muscle tendons and the eye, and between the optic nerve sheath and the orbital fat. The frictional properties of these interactions are largely unknown.

Load Cases: Muscle Contraction, Orbital Disease, Blunt Impact, etc.

The most common load cases in the human orbit are muscle contractions. Neural activation of the EOMs results in force development in the muscles. The muscle forces act against inertia of the structures, stiffness and damping of the antagonistic muscle and of the orbital fat, and against friction in the contact layers. As a result of the muscle contraction, the eye starts to move. If the muscle activation remains constant, a new equilibrium position of the eye will be reached.

In primary gaze, the four rectus muscles have a base tension that causes pressure within the orbital fat. Such a pressure is contained by the connective tissue sheets. Directly behind the eye the pressure is at its highest, gradually diminishing in the anterior direction.

In Graves' disease the EOMs and orbital fat expand. As the bony orbit is stiff with respect to its contents and because the orbital fat is nearly incompressible, pressure in the orbit increases. As a result, the eye is pushed forward and pressure on the optic nerve rises. A similar

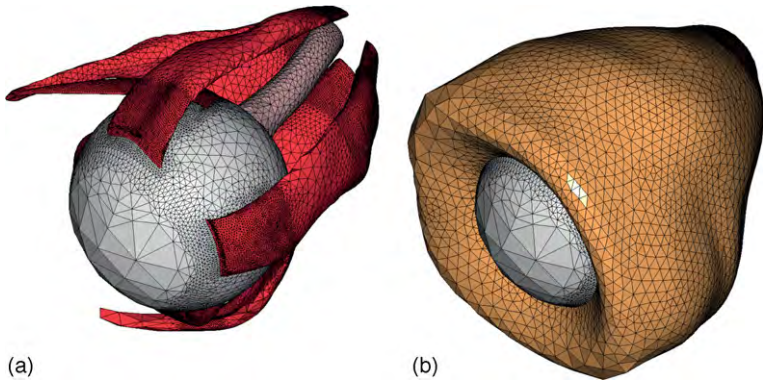

Figure 5 (a) The 3D mesh of the Delft finite-element model of orbital biomechanics. The geometry of the eye, the optic nerve, and the six extraocular muscles have been subdivided into a large number of tetrahedra. The orbital fat (b) encompasses the orbital structures.

process can occur when any other volume-increasing process takes place, like an orbital tumor.

After blunt impact on the orbit, for instance, a tennis ball on the eye, the pressure inside the orbit can rise to the extent that the mechanical load on the bony orbit exceeds its strength. A fracture can occur at the weakest spot, usually the orbital floor. In case of an orbital floor fracture, the inferior rectus muscle can get trapped in the fracture. This limits down gaze as the force developed by the inferior rectus muscle is transferred to the bony orbit. In upgaze, rotation of the eye is limited by the trapped muscle and the force developed by the superior rectus muscle pulls the eye back into the orbit.

Computational Modeling

In order to obtain better insight in orbital biomechanics, mechanical simulations can be employed to evaluate the effect of load cases. A simulation model can provide insight into the internal stress and strain distributions of tissues and contact forces, which cannot be derived from imaging data alone. A computational simulation method that is suited to numerically simulate the complex three-dimensional geometries, and anisotropic and inhomogeneous material properties, tissue interactions and load cases, is the finite-element analysis (FEA) method.

Several open source and commercially available software programs exist to develop FEA models. For an FEA model of orbital biomechanics, firstly the geometries, for example, eye, optic nerve, and EOMs, must be obtained from MRI. Subsequently, the geometries are segmented and mathematically described to be read into the FEA program. The complex geometries should then be subdivided into a number of simple elements, like tetrahedra (**Figure 5**) or hexagons. Each of the elements has to be assigned its material properties in accordance with the material properties of the actual structure, measured *in vivo* or post mortem. At the interface layers, for example, between the EOMs and the orbital fat, the optic nerve and the orbital fat, and the eye and the orbital fat, sliding should be simulated with a contact algorithm. Finally, load cases are applied to the model. After application of a load case, for instance, a base tension in the four rectus muscles, the resulting deformations and stresses in the tissue can be evaluated (**Figure 6**). An FEA model needs extensive validation, for instance, by comparing the deformations of the constituting tissues recorded with MRI (**Figure 7**) to the deformations predicted by the FEA model.

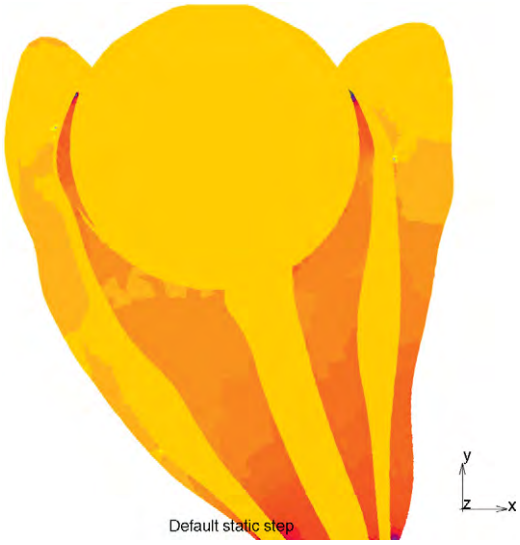

Figure 6 A transverse view on the results of a finite-element simulation at the level of the optic nerve. This simulation shows the pressure gradients in the orbital fat as a result of base tension in the rectus muscles. The yellow represents the globe, optic nerve, and extraocular muscles. The red represents the pressure gradients, with the darkest color representing the highest pressure. The orbital fat was modeled as an incompressible homogenous, isotropic material. The gradient is highest between the horizontal rectus muscles, which partly explains the outward curvature of the muscles. X represents medial and Y anterior.

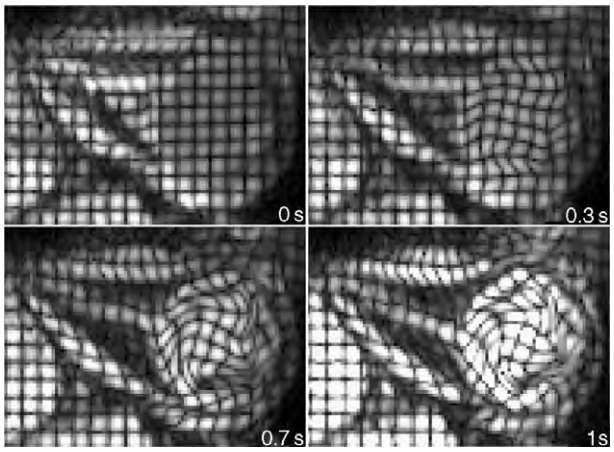

Figure 7 The tissue deformations in the orbit as a result of muscle contractions and relaxations are complex and nonuniform. The MRI sequence CSPAMM (Complementary SPAtial Modulation of Magnetization) can be used to study these deformations. Before the images are acquired, the magnetization of the tissue is periodically modulated in two perpendicular directions, so-called tissue tagging. The figure shows four CSPAMM MR images of the same transverse slice during eye movement. The magnetization is modulated to create a grid bind with the tissue (see time 0 s). The deformation of this grid (during time) depicts the differential movements within homogeneous tissues, such as in the extraocular muscles. Adapted from Piccirelli et al. (2007). Extraocular muscle deformation assessed by motion-encoded MRI during eye movement in healthy subjects. *Journal of Vision.* 7(14): 5.1–10. With permission from ARVO.

The coming years are likely to see improvement of the FEA models of the orbit and, thereby, our understanding of orbital biomechanics. *In vivo* or post mortem measurements of the mechanical behavior at contact layers and measurements of the inhomogeneity and anisotropy of the materials will allow improved modeling of orbital soft tissue biomechanics.

See also: Cranial Nerves and Autonomic Innervation in the Orbit; Extraocular Muscles: Extraocular Muscle Anatomy; Extraocular Muscles: Extraocular Muscle Metabolism; Imaging of the Orbit; Orbital Bony Anatomy and Orbital Fractures; Orbital Vascular Anatomy.

Further Reading

Asmussen, G. and Gaunitz, U. (1981). Mechanical properties of the isolated inferior oblique muscle of the rabbit. *Pflügers Archiv European Journal of Physiology* 392(2): 183–190.

Fung, Y. C. (1993). *Biomechanics: Mechanical Properties of Living Tissues.* New York: Springer.

Koornneef, L. (1976). *Spatial Aspects of Orbital Musculo-Fibrous Tissue in Man.* Amsterdam: Swets and Zeitlinger.

McMahon, T. A. (1984). *Muscles, Reflexes, and Locomotion.* Princeton, NJ: University Presses of California.

Piccirelli, M., Luechinger, R., Rutz, A. K., Boesiger, P., and Bergamin, O. (2007). Extraocular muscle deformation assessed by motion-encoded MRI during eye movement in healthy subjects. *Journal of Vision* 7(14): 5.1–10.

Rootman, J. (1988). *Diseases the Orbit,* 2nd edn. Lippincott Williams and Wilkin.

Schoemaker, I., Hoefnagel, P. P. W., Mastenbroek, T. J., et al. (2006). Elasticity, viscosity, and deformation of orbital fat. *Investigative Ophthalmology and Visual Science* 47(11): 4819–4826.

Schutte, S., van den Bedem, S. P., van Keulen, F., van der Helm, F. C., and Simonsz, H. (2006). A finite element analysis model of orbital biomechanics. *Vision Research* 46(11): 1724–1731.

Scott, A. B. (1979). *Ocular Motility* in *Physiology of the Human Eye and Visual System*, by R. E. Records. Hagerstown, MD: Harper & Row Publishers.

Orbital Vascular Anatomy

A E Semmer, L K McLoon, and M S Lee, University of Minnesota, Minneapolis, MN, USA

Glossary

Anastamosis – The collateral communication between blood vessels. They enlarge to facilitate compensatory blood flow when one of the vessels is obstructed.
Fistula – An abnormal communication between an artery and vein.

A thorough knowledge of the vascular anatomy in the orbit and periorbital tissues is critical for understanding alterations due to disease as well as avoiding these vessels during surgery in and around the orbit. The complexity and interindividual variability of the vessel anatomy is quite significant, and thus understanding the possible differences between orbits is particularly important for ensuring maximum preservation of blood supply and limiting bleeding within the orbit during surgical procedures.

The first major branch of the internal carotid, the ophthalmic artery, is the source of most of the orbital blood supply, with minor contributions from the external carotid circulation. Branching patterns of the ophthalmic artery may vary widely, but common patterns have been identified. Its distal branches form important anastomoses with the external carotid circulation that can sustain orbital blood flow in pathologic conditions involving the internal carotid artery (ICA). The orbital venous system is even more variable than the orbital arteries. Unlike the vasculature in most areas of the human body, the orbital arteries and veins do not run in parallel. Generally, the superior and inferior ophthalmic veins drain orbital blood into the cavernous sinus posteriorly. The orbital veins are valveless, so alternative drainage can occur through veins that connect to the facial veins anteriorly and the pterygoid venous system inferiorly.

Arterial Blood Supply

The ophthalmic artery provides the major blood supply to the orbit. It is the first major branch of the ICA. Branches of the ophthalmic artery anastomose with distal branches of the external carotid artery (ECA), creating important connections between the internal and external carotid circulations (**Figure 1**). The orbital arterial supply will be described first from the internal carotid contributions followed by the external carotid contributions. The most common anatomical configurations will be emphasized with discussions of common variants.

Internal Carotid Artery

At the upper limit of the thyroid cartilage, the common carotid artery bifurcates into the ICA and ECAs. The ICA ascends the neck without branching and enters the skull base through the carotid canal, an opening in the petrous portion of the temporal bone. The ICA runs anteromedially through the carotid canal, continuing through the foramen lacerum to emerge in the posterior cavernous sinus. The ICA winds through the cavernous sinus forming an elongated S shape referred to as the carotid siphon. From its entrance into the posterior cavernous sinus, the ICA travels slightly superiorly and then anteriorly before turning abruptly superiorly and piercing the dural roof of the cavernous sinus, just medial to the anterior clinoid process of the sphenoid bone. The carotid siphon then curves posteriorly, and then anterosuperiorly to reach the inferolateral optic nerve. Within the cavernous sinus, the ICA consistently gives off a meningohypophyseal trunk, which supplies the intracavernous oculomotor, trochlear, and abducens nerves, as well as portions of the pituitary gland. The artery of the inferior cavernous sinus and the capsular arteries are more variable intracavernous ICA branches.

The first major intradural branch of the ICA is the ophthalmic artery, which arises just distal to the carotid siphon. In 10% of cases, the ophthalmic artery actually arises from the ICA within the cavernous sinus external to the dura. Rarely, the external carotid circulation contributes to the ophthalmic artery's origin. The most common variant origin arises from the middle meningeal artery (MMA) either as a single trunk or from two separate ICA and MMA trunks. Isolated descriptions also exist of ophthalmic arteries arising from the middle cerebral artery, the anterior cerebral artery, the posterior communicating artery, and the basilar artery.

Usually, the ophthalmic artery arises from the anterior wall of the ICA inferior to the optic nerve. It then runs anterolaterally inferior to the optic nerve to enter the optic canal, running with the optic nerve. Multiple small arteries arise from the ICA near the origin of the ophthalmic artery. These arteries supply the pituitary infundibulum, the intracranial portion of the optic nerve, and the

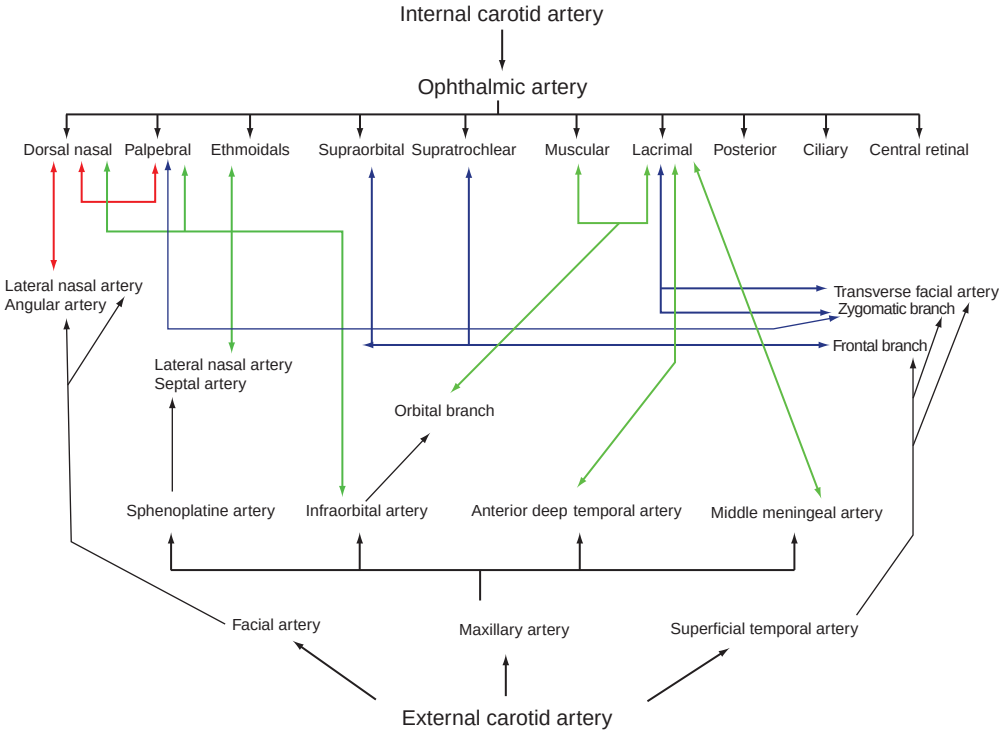

Figure 1 Orbital anastamoses. This diagram depicts the key anastamoses between branches of the ophthalmic and the external carotid arteries. Double arrowheads signify anastamotic connections. Red indicates anastamoses with the facial artery, green indicates anastamoses with the maxillary artery, and blue arrows designate anastamoses with the superficial temporal artery. Based on Hayreh, S. S. (1963). Arteries of the orbit in the human being. *British Journal of Surgery* 50: 938–953.

optic chiasm. Distal to the ophthalmic artery, the ICA gives off the posterior communicating and anterior choroidal arteries to form the anterior circle of Willis. The terminal branches of the ICA are the anterior and middle cerebral arteries that supply blood to the brain parenchyma.

Ophthalmic Artery

The ophthalmic artery provides the major blood supply to the orbit. It is the first major branch of the ICA. Distal branches of the ICA form important anastamotic connections with the external carotid circulation that can provide collateral blood flow to the orbit. Branches of the ophthalmic artery are extremely variable, but common patterns have been identified. The ophthalmic artery will be described in three parts: (1) intracranial, (2) intracanalicular, and (3) intraorbital. The most common branching patterns will be discussed here along with common variants.

Intracranial

The intracranial segment of the ophthalmic artery describes the length of the vessel from its branch point off the internal carotid until it enters the optic canal. This portion of the ophthalmic artery is usually subdural (85%) and intimately associated with the ICA and the inferior aspect of the optic nerve. These structures are often linked by fibrous connective tissue. The average length of the intracranial ophthalmic artery is 2.6 mm, but can be as long as 7 mm. Typically, there are no branches off this arterial segment.

Intracanalicular

The intracanalicular ophthalmic artery runs in the optic canal, inferior to the optic nerve until it emerges in the orbit. The artery gradually pierces the dura surrounding the intraorbital optic nerve to enter the subdural space. Thus, within the optic canal, the artery becomes physically separated from the optic nerve by a dural barrier. The intracanalicular ophthalmic artery sends small branches to the intracanalicular optic nerve through fibrous bands connecting the dura to the optic nerve. Traumatic injury to the optic canal can tear these fibrous bands, interrupting the blood supply to the optic nerve and causes ischemic damage. Rarely, the ophthalmic artery enters the orbit through a separate bony canal.

Intraorbital

The extreme variability of the ophthalmic artery and its branches becomes evident in its intraorbital course. Hayreh has done the most comprehensive anatomical

descriptions of the ophthalmic artery. While their systematic dissections never revealed any identical intraorbital branching patterns of the ophthalmic arteries, they identified common patterns associated with whether the intraorbital ophthalmic artery crosses superior or inferior to the optic nerve.

The intraorbital ophthalmic artery can be divided into three segments (**Figure 2**). The first part begins at the orbital apex and is attached by loose connective tissue and fat to the inferior aspect of the optic nerve as it courses anteriorly along the inferolateral margin. The artery then crosses to the medial orbit. The point at which the artery turns medially to cross superior (83%) or inferior (17%) to the optic nerve is called the angle and marks the division between the first and second intraorbital ophthalmic artery segments. The second segment of the ophthalmic artery is defined as the length of artery that crosses the optic nerve from lateral to medial. It is only loosely connected to the dural nerve sheath. The vertical position of this arterial segment with respect to the optic nerve determines which arterial branching pattern will commonly be seen. The division between the second and third parts of the ophthalmic artery is called "the bend." This is a well-defined point on the superiomedial aspect of the optic nerve, where the ophthalmic artery turns to head anteromedially through the orbit. Distal to "the bend," the ophthalmic artery loses its intimate association with the optic nerve and is anchored to the medial orbital wall by the ethmoidal vessels. This arterial segment is quite tortuous, allowing the ophthalmic artery to withstand ocular movement without compromising blood supply. It heads medially and passes anterosuperiorly between the

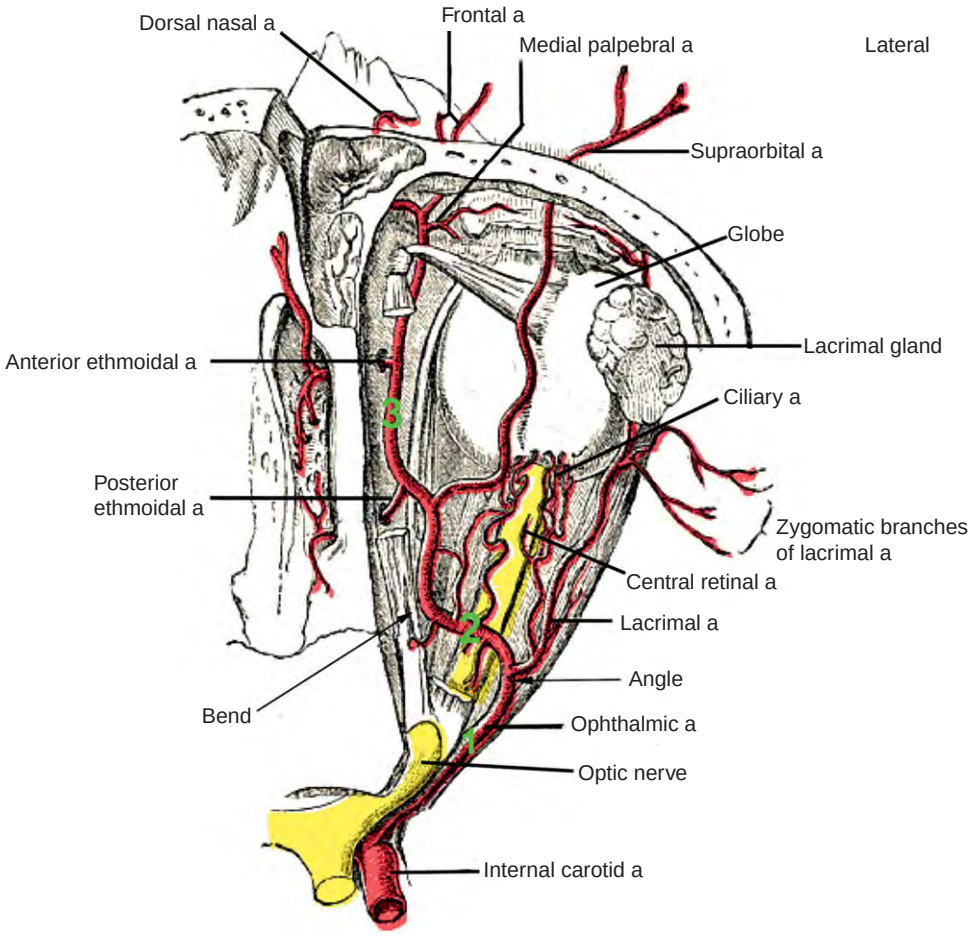

Figure 2 The intraorbital ophthalmic artery and its branches. The branching patterns of the ophthalmic artery are highly variable, but common patterns have been identified. This Figure illustrates the general course of the ophthalmic artery as is crosses over the optic nerve and courses through the medial orbit. The angle and the bend are important landmarks that separate the intraorbital ophthalmic artery into three sections. The first segment (1) runs from the orbital apex to the angle and is intimately associated with the optic nerve. The second segment (2) runs between the angle and the bend. It crosses medially either superior or inferior to the optic nerve. The spatial orientation of the second segment of the intraorbital ophthalmic artery dictates which common branching pattern may be expected in an individual orbit. The third segment runs from the bend along the medial orbital wall until the terminal arterial branches emerge from the orbit. This segment of the ophthalmic artery is the most tortuous. Adapted from Gray's Anatomy, 20th edition, copyright expired.

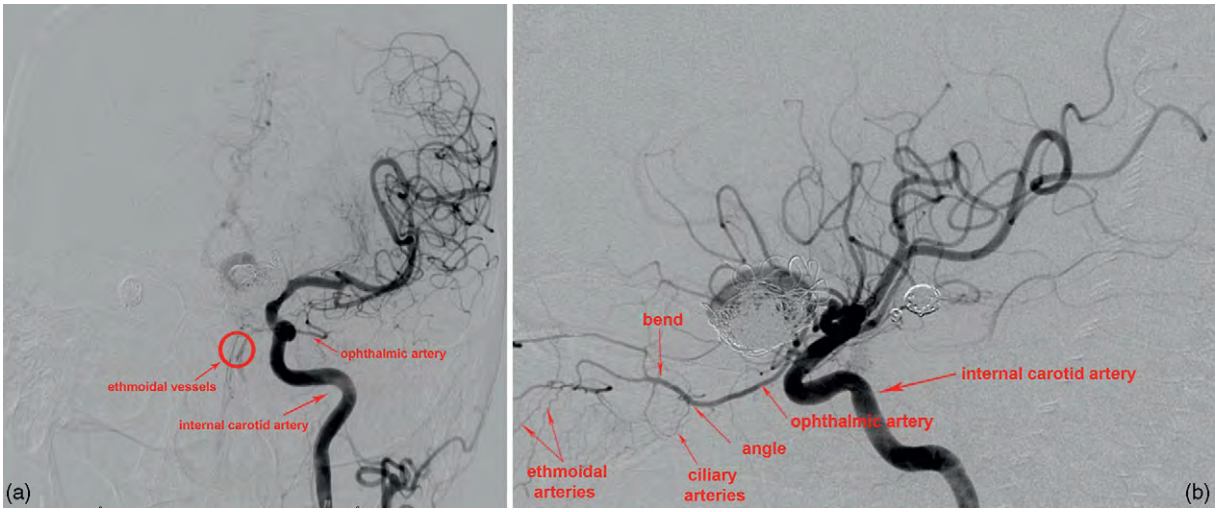

Figure 3 Angiograms depicting the orbital arterial vasculature. (a) Anterior–posterior view of the left internal carotid artery (ICA) shows the left ophthalmic artery coursing anterolaterally after its origin from the supraclinoid segment of the ICA. This ophthalmic artery has prominent ethmoidal branches (circle) coursing along the nasal septum. (b) Lateral projection of left ICA injection, early arterial phase showing most of the intraorbital course of the ophthalmic artery including the proximal, main trunk of the ophthalmic artery, the angle, the bend, and the anterior and posterior ethmoidal vessels. Images courtesy of Dr. Ramachandra Tummala, Department of Neurosurgery, University of Minnesota.

medial rectus and superior oblique muscles. It runs inferior to the trochlea before its terminal branches emerge from the superiomedial orbital angle, midway between the medial palpebral ligament and the superior orbital margin (Figure 3).

Branching patterns of the intraorbital ophthalmic artery are extremely variable. In Hayreh's systematic study of 59 human orbits, no identical ophthalmic artery branching patterns were seen. The main pattern distinction depends on whether the second segment of the ophthalmic artery crosses superior or inferior to the optic nerve and can be traced to varying patterns in fetal arterial development. As the ophthalmic artery develops, a vascular ring forms around the optic nerve. Typically, the larger dorsal portion of the vascular ring persists, while the ventral portion regresses, resulting in the ophthalmic artery crossing superior to the optic nerve 83% of the time. When the dorsal segment of the fetal vascular ring regresses, the ophthalmic artery crosses inferior to the optic nerve.

While the variability of the intraorbital branching pattern of the ophthalmic artery cannot be overemphasized, the most common branching patterns based on order of origin are outlined in Table 1. The following descriptions of the intraorbital ophthalmic arterial branches are organized topographically by the ocular, orbital, and extraorbital blood supplies.

Table 1 Common branching patterns of the ophthalmic artery

	Crossing pattern of ophthalmic artery	
Order of origin	*Superior to the optic nerve (83%)*	*Inferior to the optic nerve (17%)*
1	Central retinal	Lateral posterior ciliary
2	Lateral posterior ciliary	Central retinal
3	Lacrimal	Medial muscular
4	Muscular to superior rectus and/or levator	Medial posterior ciliary
5	Posterior ethmoid	Lacrimal
6	Supraorbital	Muscular to superior rectus and/or levator
7	Medial posterior ciliary	Posterior ethmoid
8	Medial muscular	Supraorbital
9	Muscular to superior oblique and medial rectus	Muscular to superior oblique and medial rectus
10	Anterior ethmoid	Anterior ethmoid
11	Medial palpebral	Medial palpebral
Terminal	Dorsal nasal	Dorsal nasal
Terminal	Supratrochlear	Supratrochlear

Based on Hayreh, S. S. (1962). The ophthalmic artery. III. Branches. *British Journal of Ophthalmology* 46: 212–247.

Ocular Branches

The ocular branches include the central retinal artery, the anterior ciliary arteries, the lateral and medial posterior ciliary arteries, and small collateral branches to the optic nerve. The central retinal artery is typically the first branch of the ophthalmic artery. It runs along the inferior aspect of the optic nerve before piercing the optic nerve sheath 5–15 mm posterior to the globe. Once the artery has entered the neural sheath, it makes its way to the

center of the optic nerve substance, supplying blood to the surrounding nerve as it courses toward the optic nerve head where its terminal branches divide to supply the inner retina. The central retinal artery is the sole blood supply to the inner two-thirds of the retina. The terminal branches of the central retinal artery are end arteries, meaning that a proximal occlusion will completely cut off blood supply to that portion of the retina. More distal occlusions can lead to segmental retinal ischemia.

The number of posterior ciliary arteries is variable. They typically arise as two to three trunks that divide into multiple short ciliary arteries and a medial and lateral long posterior ciliary artery that extend from the ophthalmic artery to the posterior globe. Up to five posterior ciliary artery branches have been described. The short ciliary arteries pierce the sclera near the optic nerve and directly supply the choroidal vessels that nourish the outer one-third of the retina. They form the anastamotic circle of Zinn and Haller, adjacent to the optic nerve that feeds the optic disc. In approximately 15% of the population, the short posterior ciliary arteries give off one or more cilioretinal arteries to supply the inner two-thirds of the macula in addition to the central retinal artery. When present, the cilioretinal artery can provide collateral circulation to the macula in a central retinal artery occlusion. The medial and lateral long posterior ciliary arteries run toward either side of the globe along the horizontal meridian, passing between the choroid and the sclera to anastamose with the anterior ciliary arteries. It supplies the ciliary muscle, iris, and part of the choroid.

Orbital Branches

The orbital branches of the ophthalmic artery include the lacrimal artery, extraocular muscular arteries, and small branches that supply the orbital periosteum and areolar tissue. The lacrimal artery typically branches from the second part of the ophthalmic artery between "the angle" and "the bend." It runs along the lateral orbital wall above the superior border of the lateral rectus muscle with the lacrimal nerve to supply the lacrimal gland. The lacrimal artery gives off the recurrent meningeal, zygomatic, and lateral palpebral arteries. The recurrent meningeal artery exits the orbit through the superior orbital fissure and anastamoses with branches of the MMA, connecting the internal and external carotid circulations. The lateral palpebral arteries supply the lateral eyelids and conjunctiva.

Multiple muscular arteries arise from the ophthalmic artery branches to supply the extraocular muscles. The lateral and medial muscular branches are the most prominent, and provide the major extraocular muscle blood supply. The lateral muscular artery typically arises from the second segment of the ophthalmic artery and supplies the lateral rectus, superior rectus, superior oblique, and levator palpebrae superioris. The medial muscular branch typically arises from the third segment of the ophthalmic artery medial to the optic nerve to supply the medial and inferior rectus, and the inferior oblique. After running the length of the muscle, the muscular branch in each rectus muscle gives off two anterior ciliary arteries, except for the lateral rectus that typically contributes only one, which run in the rectus tendons before piercing the sclera near the limbus to anastamose with the posterior ciliary arteries to supply anterior segment structures and choroid. Interruption of anterior ciliary blood flow can lead to a rare, but well-defined complication of strabismus surgery: anterior segment ischemia. This has typically been reported when three to four rectus muscles are removed during strabismus surgery, but has been reported in cases involving fewer muscles in patients with underlying predispositions to orbital ischemia. Anterior segment ischemia is more common in vertical muscle surgery, most likely because collateral flow from the long posterior ciliary arteries along the equator of the globe can compensate for lateral and medial anterior ciliary blood flow.

Extraorbital Branches

The extraorbital branches include the anterior and posterior ethmoidal arteries, the supraorbital artery, the medial palpebral artery, and the terminal ophthalmic artery branches: the dorsal nasal and supratrochlear arteries. The posterior and anterior ethmoidal arteries typically arise from the third segment of the ophthalmic artery and course through the medial orbit before passing through the posterior and anterior ethmoidal canals, respectively, into the ethmoid air cells. The presence of the posterior ethmoidal artery is variable. Hayreh reported absence of the posterior ethmoidal artery in 15% of specimens where the ophthalmic artery crosses under the optic nerve, and 19% of ophthalmic arteries that cross over the optic nerve. In the majority of cases, however, the posterior ethmoidal artery runs between the superior oblique muscle and the levator muscles. It enters the posterior ethmoidal canal with the posterior ethmoidal nerve to supply blood to the posterior ethmoid air cells, the meninges of the anterior cranial fossa, and the upper nasal mucosa.

The anterior ethmoidal artery is larger and more consistent than its posterior counterpart. It runs between the superior oblique and medial rectus and passes through the anterior ethmoidal canal with the anterior ethmoidal nerve to supply the anterior and middle ethmoidal air cells, the frontal sinus, and the anterior cranial fossa dura. Nasal branches supply skin on the lateral wall of the nose.

The supraorbital artery typically arises off the second portion of the ophthalmic artery. It joins the supraorbital nerve as is courses anterosuperiorly through the medial orbit. The supraorbital artery emerges on the face through the supraorbital notch or foramen to supply the levator

muscle aponeurosis anteriorly, upper eyelid, scalp, and forehead muscles.

Two medial palpebral arteries arise either directly from each ophthalmic artery or from a common trunk to supply the upper and low eyelids. They enter the eyelids superior and inferior to the medial palpebral ligaments and anastamose with the lateral palpebral arteries that branch off the lacrimal artery.

The dorsal nasal and supratrochlear arteries are the terminal branches of the ophthalmic artery. The dorsal nasal artery pierces the orbital septum above the medial canthal tendon to anastomose with the angular and nasal branches of the facial artery, connecting the external and internal carotid circulations. It supplies the scalp and forehead near the midline, and occasionally the lacrimal sac. The supratrochlear artery is typically the larger terminal branch of the ophthalmic artery. It pierces the orbital septum superior to the trochlea with the supratrochlear nerve and ascends the superior orbital margin to supply the skin, muscles, and scalp near the midline.

External Carotid Artery

The ECA provides minor vascular tributaries that form important anastamotic connections between the internal and external carotid circulations (**Figure 1**). In pathologic or anomalous anatomic conditions in which the internal carotid blood flow is slowly compromised, these anastomoses can enlarge to maintain orbital perfusion.

The common carotid artery bifurcates into the ICA and ECA at the upper border of the thyroid cartilage. As the ECA ascends the neck, it first curves slightly anteriorly, and then posteriorly as it courses toward the neck of the mandible, where it divides into its terminal branches: the superficial temporal and maxillary arteries. The major ECA branches are the superior thyroid, ascending pharyngeal, lingual, facial, occipital, posterior auricular, superficial temporal, and maxillary arteries. The facial, superficial temporal, and maxillary arteries supply orbital structures. Only these ECA branches are discussed further.

The facial artery supplies blood to oral, pharyngeal, and mid-lower facial structures. It is a very tortuous vessel, which allows it to withstand movement during speaking and chewing. The facial artery branches off the ECA near the angle of the mandible. It dives deep to the posterior belly of the digastric and stylohyoid muscles and enters a groove on the posterior aspect of the submandibular gland. The facial artery then emerges on the face, crosses superiorly over the body of the mandible to the angle of the mouth, and ascends lateral to the nose to terminate as the angular artery in the medial canthal region. The angular artery has an anastamotic connection with the dorsal nasal artery, a terminal branch of the ophthalmic artery off the ICA to connect the internal and external carotid circulations.

The superficial temporal artery is one of the two terminal ECA branches. It arises from the ECA within the substance of the parotid gland posterior to the neck of the mandible and ascends the scalp, anterior to the ear. Within the parotid gland, the superficial temporal artery gives off the transverse facial artery, which supplies the parotid gland and duct and the masseter muscle. The superficial temporal artery then ascends to cross above the posterior zygomatic process where it gives off two branches: (1) the middle temporal artery that supplies the temporalis muscle and (2) the zygomatic artery that supplies the orbicularis oculi muscle before anastomosing with the lacrimal and palpebral branches of the ophthalmic artery. Within 2–5 cm of crossing the zygomatic process, 90% of superficial temporal arteries split into a frontal and parietal branch. Anomalous patterns exist in approximately 10% of the population, with the most common variant being an additional frontal branch. Other variations include an additional parietal branch, a more proximal branch point off the superficial temporal artery, or no branching at all. The frontal branch supplies the facial muscles, skin, and pericranium of the anterior scalp and anastomoses with the supraorbital artery. The posterior branch anastomoses with the posterior auricular and occipital arteries to supply the posterior scalp.

The maxillary (internal maxillary) artery is the larger terminal ECA branch that supplies the deep structures of the face and sends intracranial branches to the dura and trigeminal ganglion. The artery can be split into three sections: (1) mandibular, (2) pterygoid, and (3) pterygopalatine. The mandibular portion of the maxillary artery runs anteriorly between the mandibular ramus and the sphenomandibular ligament insertion. It gives off the anterior tympanic, deep auricular, and middle meningeal arteries (MMA).

The MMA provides the largest dural blood supply. It ascends between the external pterygoid muscle and the sphenomandibular ligament and passes through the foramen spinosum in the sphenoid bone to enter the cranium. Blunt head trauma can result in MMA rupture leading to an epidural hematoma. Orbital branches of the MMA pass through the superior orbital fissure to anastomose with the lacrimal artery and/or other ophthalmic artery tributaries. Occasionally, the ophthalmic artery originates from one of these orbital MMA branches. Additional anastomoses between the internal and external carotid circulations may exist between small branches off the MMA that anastomose with the meningohypophyseal trunk within the cavernous sinus.

The pterygoid portion of the maxillary artery does not typically contribute blood supply to the orbit. It ascends the external surface of the medial pterygoid muscle medial to the ramus of the mandible, making its way

anteriorly, and entering the pterygoid fossa. It gives off branches to the pterygoid, masseter, and buccinator muscles as well as deep branches to the temporalis muscle and pericranium.

The pterygopalatine portion of the maxillary artery lies in the pterygopalatine fossa. It gives off six major branches: (1) the posterior superior alveolar artery, (2) the infraorbital artery, (3) the descending palatine artery, (4) the artery of the pterygoid canal, (5) a pharyngeal branch, and (6) the sphenopalatine artery. The infraorbital artery runs along the infraorbital groove and canal with the infraorbital nerve, where it gives off branches to the inferior oblique and inferior rectus muscles and anastomoses with the lacrimal and the third segment of the ophthalmic artery. This artery emerges on the face through the infraorbital foramen and ascends toward the medial canthal region to anastomose with the angular branch of the facial artery and the dorsal nasal artery off the internal carotid.

Venous Drainage

The orbital veins are extremely complex and variable. The exact number and configuration of the orbital veins are controversial because of their high variability. Unlike venous systems throughout the rest of the body, the orbital veins do not parallel the orbital arteries. One exception is the superior ophthalmic vein, which has a similar course to the ophthalmic artery. The superior and inferior ophthalmic veins represent the principal drainage systems of the orbit (**Figure 4**). Variably present orbital veins include the middle and medial ophthalmic veins and various collaterals that interconnect the superior and inferior orbital venous systems. Primary drainage is to the cavernous sinus; however, various interconnections also exist with the facial veins and the pterygoid plexus. The orbital veins are valveless, allowing pressure-dependent drainage through these alternative routes.

The superior ophthalmic vein is the largest and most consistently present orbital vein. Its diameter ranges from 2 mm to 1 cm. The superior ophthalmic vein is formed by the confluence of the supraorbital and angular veins near the superomedial orbital rim. The supraorbital vein enters the orbit and runs along the orbital roof superior to the trochlea. The angular vein pierces the orbicularis oculi muscle and enters the orbit through an opening in the orbital septum to join the supraorbital vein, just posterior to the trochlea in the anteromedial orbit. Various superior ophthalmic vein roots have been described, including a singular root formed by the convergence of the supraorbital and angular veins anterior to the trochlea.

The course of the superior ophthalmic vein is relatively constant compared to the rest of the orbital veins. In general, it follows the ophthalmic artery through the orbit. From the superomedial orbital angle, the superior ophthalmic vein enters the orbital cone near the medial border of the superior rectus muscle. It runs within the intraconal adipose tissue, crossing inferior to the superior rectus at the muscle's lateral border. The superior ophthalmic vein then runs posteriorly along the lateral aspect of the superior rectus before exiting the orbit through the superior

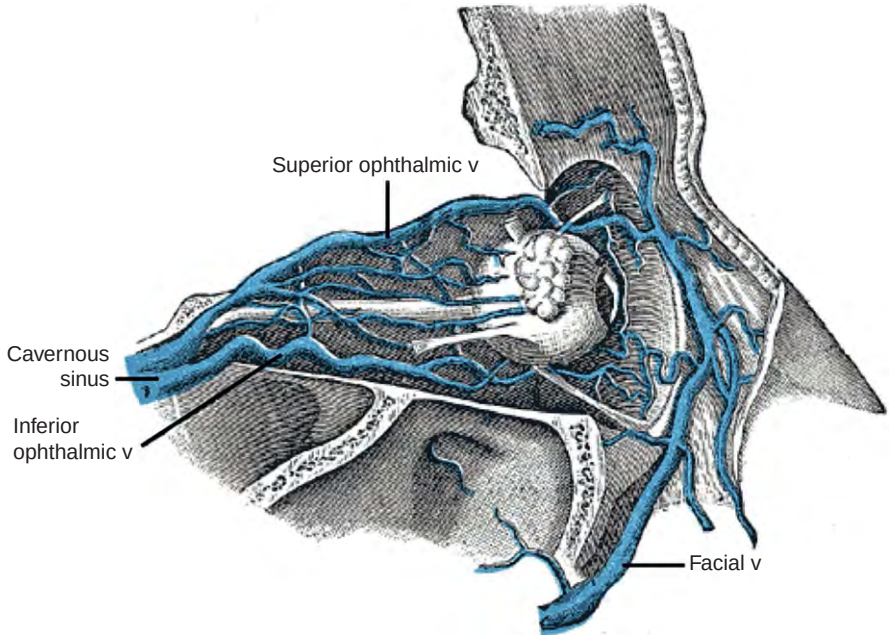

Figure 4 The orbital venous system. The orbital veins are highly variable; however, the superior and inferior ophthalmic veins are relatively constant. The inferior ophthalmic vein frequently empties into the superior ophthalmic vein prior to exiting the orbit through the superior orbital fissure to enter the cavernous sinus. Adapted from Gray's Anatomy, 20th edition, copyright expired.

orbital fissure and emptying into the cavernous sinus. The medial palpebral, superior vortex, anterior ethmoidal, lacrimal, central retinal, muscular, and inferior ophthalmic veins, typically, all drain into the superior ophthalmic. The muscular veins are often the most variable orbital veins; however, the veins from the superior rectus and superior oblique muscles consistently drain into the superior ophthalmic vein (**Figure 5**).

While there is some debate regarding the course and existence of the inferior orbital vein, most investigators agree that the venous drainage of the inferior orbit begins as a diffuse venous plexus on the orbital floor that receives venous blood from the inferior eyelid, lacrimal sac, inferior extraocular muscles, and the inferior vortex veins. When present, the inferior orbital vein typically arises from the posterior inferior venous plexus in the mid-orbit and runs posteriorly between the inferior rectus muscle and the optic nerve. In the posterior orbit, the inferior orbital vein commonly runs along the lateral border of the inferior rectus, before heading superiorly to join the superior ophthalmic vein, prior to its exiting the orbit through the superior orbital fissure into the cavernous sinus. The inferior orbital vein can also enter directly into the cavernous sinus without converging with the superior ophthalmic vein.

Inconstant orbital veins include the middle and medial ophthalmic veins. The middle ophthalmic vein drains the inferior orbit and runs between the superior and inferior ophthalmic veins in the posterior orbit before emptying into the superior ophthalmic vein. The medial ophthalmic vein arises from the angular vein or anterior superior ophthalmic vein. When present, the medial ophthalmic vein runs along the medial orbital wall and empties either into the superior ophthalmic vein or directly into the cavernous sinus. Cheung and McNab found that the medial ophthalmic vein consistently empties into the superior ophthalmic vein. The medial ophthalmic vein has been reported to connect the medial collateral, ethmoidal, and medial muscular veins to the superior ophthalmic vein through a venous loop.

Multiple, variable collateral veins typically connect the superior and inferior venous systems. Cheung and McNab described only medial and lateral collateral veins. Henry described anterior, medial, lateral, and posterior collateral veins that were also found identified by Brismar to be present in 91%, 97%, 72%, and 19% of individuals, respectively, based on orbital phlebography. A collateral branch that drains to the pterygoid plexus is another common variant.

The central retinal vein drains blood from the retina and intraorbital optic nerve. It runs with the central retinal artery within the substance of the optic nerve. It exits the optic nerve sheath 8–15 mm posterior to the globe and typically passes directly through the superior orbital fissure into the cavernous sinus. It can also join the superior or inferior ophthalmic veins within the orbit. Hayreh found that the central retinal vein runs within the surrounding dura after exiting the optic nerve. An optic nerve sheath meningioma involving the dura containing the central retinal vein gradually occludes it, which may cause development of the characteristic retinociliary collateral veins that are indicative of optic nerve sheath meningiomas.

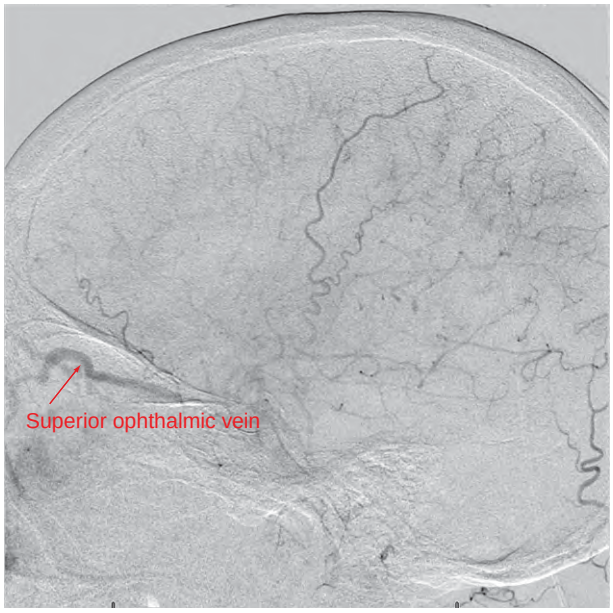

Figure 5 Angiogram depicting the superior ophthalmic vein. Lateral view of the early venous phase of the right internal carotid injection reveals a prominent superior ophthalmic vein providing collateral venous drainage into the cavernous sinus in a patient with a left temporal lob hemorrhage. The superior ophthalmic vein is typically only seen on angiography in pathological conditions. Images courtesy of Dr. Ramachandra Tummala, Department of Neurosurgery, University of Minnesota.

Cavernous Sinus

The cavernous sinuses are paired venous plexuses situated just lateral to the sella turcica on the superior aspect of the sphenoid bone. They receive the majority of orbital venous blood. Each cavernous sinus extends from the superior orbital fissure anteriorly to the apex of the petrous portion of the temporal bone posteriorly. Each cavernous sinus is approximately 3 cm long, 1 cm wide, and 0.5 cm high. Superiorly, the cavernous sinus is bordered by the anterior and posterior clinoid processes. The floor of the cavernous sinus contains the foramen lacerum, foramen ovale, and foramen rotundum.

The cavernous sinus receives venous blood from the orbit and drains posteriorly through the superior and inferior petrosal sinuses. It is the primary drainage reservoir for the orbital veins; however, the absence of valves in

the cavernous sinus and the orbital veins allows for alternative pressure-dependent drainage through the facial veins or pterygoid plexus. This is a potential path for facial infections to spread into the cavernous sinus and throughout the dura. Venous drainage into the cavernous sinus varies depending on the highly variable orbital venous configurations. The superior ophthalmic vein consistently drains through the superior orbital fissure. The inferior ophthalmic vein and the inconstant orbital veins variably drain into the superior ophthalmic vein, or directly into the cavernous sinus.

Contents of the Cavernous Sinus

The ICA runs through the medial cavernous sinus surrounded by a web of sympathetic fibers. The abducens nerve runs through the lateral cavernous sinus. Within the lateral wall of the sinus, from superior to inferior, lies the oculomotor nerve (CN III), trochlear nerve (CN IV), and the ophthalmic (CN V1) and maxillary (CN V2) divisions of the trigeminal nerve (Figure 6).

Clinical Correlate: Orbital Vascular Pathology

Arterial and Venous Occlusions

While the anastomoses between the internal and external carotid circulations can often compensate for a gradual compromise in orbital blood flow, acute interruptions in ocular blood flow can have clinically significant visual consequences.

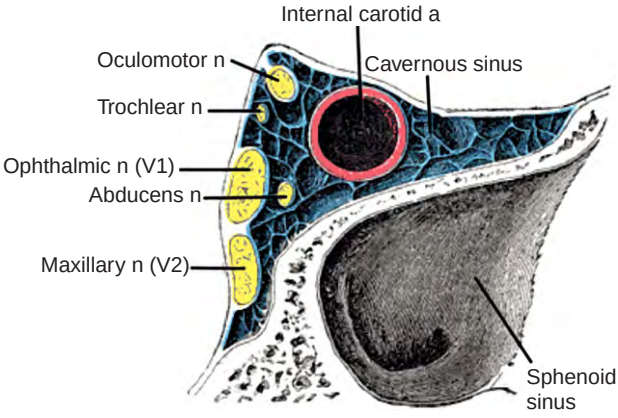

Figure 6 Contents of the cavernous sinus. The cavernous sinus is a venous network that serves as the primary drainage for orbital venous blood. The internal carotid artery, the oculomotor nerve, the trochlear nerve, abducens nerve, and the ophthalmic and maxillary divisions of the trigeminal nerve all run through the cavernous sinus. Adapted from Gray's Anatomy, 20th edition, copyright expired.

Transient monocular vision loss, or amaurosis fugax, results when blood flow in the central retinal artery, ophthalmic artery, or ciliary arteries is compromised. Common etiologies include embolic occlusion, vasospasm, and giant cell arteritis (GCA). Atherosclerotic disease proximal to the affected artery can cause an ocular transient ischemic attack (TIA) when cholesterol emboli released from an atherosclerotic lesion transiently occlude an ophthalmic vessel, or when a severely stenotic proximal vessel results in hypoperfusion. Cardiac emboli from atrial fibrillation, valvular heart disease, or atrial myxoma can cause the same obstructions but typically results in permanent occlusion.

Embolic occlusion of the central retinal artery (CRAO) or one of its branches (BRAO) typically resolves over time, but even transient ischemic retinal injury may result in permanent visual loss in the affected retinal areas. CRAO may result in peripheral field loss with spared central visual acuity if the cilioretinal arteries are spared. Granulomatous inflammation can also cause CRAO and BRAO. Furthermore, vasculitis of the short posterior ciliary arteries can result in arteritic anterior ischemic optic neuropathy (AION).

Occlusion of the central retinal vein (CRVO) or its branches (BRVO) causes loss of vision when venous congestion inhibits retinal capillary blood flow. Patients typically present with acute blurry vision and segmentally distributed intraretinal hemorrhages on examination. CRVO is associated with glaucoma, hypertension, diabetes mellitus, and cardiovascular disease. The strong association with atherosclerotic disease can be explained by the common sheath shared by the central retinal artery and vein, allowing easy compression the central retinal vein.

Cavernous Carotid Artery Aneurysm

ICA aneurysms within the cavernous sinus may present with visual complaints due to compression of the cranial nerves III, IV, and/or VI. Aneurysms can become quite large (>2 cm) before symptoms begin. If the aneurysm extends through the roof of the cavernous sinus into the subarachnoid space, there is a risk of subarachnoid hemorrhage. Aneurysmal involvement of the ophthalmic artery is also possible, putting the orbital circulation at risk. Treatment of these aneurysms involves coiling or ICA ligation to cause thrombosis within the aneurysm.

Carotid–Cavernous Sinus Fistula

A direct connection between the ICAs within the cavernous sinus can lead to the formation of a fistula between the ICA and venous cavernous sinus (Figure 7). Carotid–cavernous

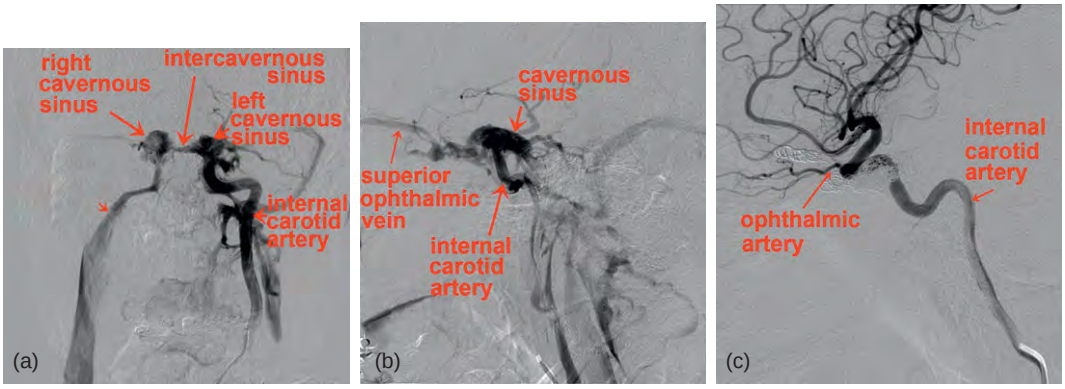

Figure 7 Angiograms depicting a carotid–cavernous sinus fistula (CCF) before and after treatment. (a) Anterior–posterior view of a left internal carotid artery (ICA) injection demonstrating a direct connection, or fistula, between the left cavernous sinus and the left internal carotid artery. The injection also shows filling of the intercavernous and right cavernous sinuses. (b) Lateral view of the CCF after ICA injection demonstrates collateral drainage of the cavernous sinus through the superior ophthalmic vein. (c) Following coil embolization repair of the CCF, ICA injection shows normal arterial filling of the internal carotid arterial vasculature, including the ophthalmic artery. Images courtesy of Dr. Ramachandra Tummala, Department of Neurosurgery, University of Minnesota.

Figure 8 Carotid–cavernous sinus fistula (CCF). These photos depict many of the common clinical features of a CCF, including chemosis, eyelid edema, proptosis, ophthalmoplegia, and arterialization of the conjunctival vessels. (a) The patient is unable to fully depress the left eye. Note that the upper eyelids are manually retracted by the clinician. (b) The patient is staring straight ahead.

Figure 9 Arterialization of the conjunctival veins. This close-up photograph demonstrates how a carotid–cavernous sinus fistula can lead to orbital venous congestion that arterializes the conjunctival veins in the right orbit of this patient. The veins seen here are injected and tortuous, indicating high blood flow and pressure in the orbital venous system.

sinus fistulas (CCFs) can be traumatic or spontaneous, rapid or insidious. The fistula between arterial and venous blood disrupts the orbital pressure gradient and causes a reversal of venous blood flow through the orbital veins. Signs and symptoms of a CCF include chemosis, eyelid edema, central retinal venous congestion, proptosis, arterialization of the conjunctival vessels (Figures 8 and 9), diplopia secondary to oculomotor, trochlear, or abducens nerve palsy, and an audible orbital bruit (the sound of turbulent blood flow heard by the patient or by a clinician with a stethoscope). Approximately 50% of CCFs with low-velocity blood flow will close spontaneously and may not require any intervention. In the presence of a neuro-ophthalmologic deficit or posterior venous drainage, coils can be placed in the cavernous sinus to occlude the fistula (Figure 7).

Cavernous Sinus Thrombosis

Infectious cavernous sinus thrombosis results from the progression of facial infections through the facial vein or pterygoid plexus to the cavernous sinus through the superior ophthalmic vein. Sinus and dental infections can also extend into the cavernous sinus. Signs and symptoms include fever, orbital congestion, lacrimation, conjunctival edema, swelling, proptosis, and ophthalmoparesis from compression of the abducens, oculomotor, or trochlear nerves. Progression of thrombosis to the rest of the cerebral venous sinuses can result in increased intracranial pressure and stroke. Treatment includes antibiotics, anticoagulation,

systemic steroids, and possibly surgery. Noninfectious cavernous sinus thrombosis can result from hypercoagulable states, including polycythemia, sickle cell crisis, and paroxymal nocturnal hemoglobinuria. However, the overwhelming majority of these are infectious.

Orbital Surgical Surface Anatomy

Dacryocystorhinostomy

Abnormal tearing, or epiphora, occurs when the nasolacrimal duct is obstructed and tears cannot drain normally from the lacrimal sac to the inferior meatus inferior to the inferior nasal turbinate. Obstruction can be congenital or acquired through recurrent dacrocystitis or cannaliculitis, dacrolithiasis, trauma, malignancy, or underlying nasal pathology. Surgical repair with dacryocystorhinostomy (DCR) creates a new direct connection between the lacrimal sac and the nasal mucosa for drainage. DCR approach can be external or endoscopic. Both techniques must take care to avoid the angular artery, which lies beneath the obicularis oculi muscle, 6–8 mm medial of the inner canthus and 5 mm anterior of the lacrimal sac.

Temporal Artery Biopsy

Giant cell arteritis (GCA) is a systemic vasculitis that can lead to rapid, irreversible blindness if left untreated. Classic symptoms include headache, scalp tenderness, and jaw claudication. Definitive diagnosis requires temporal artery biopsy. The superficial temporal artery is easily accessible for biopsy as it lies just under the skin while ascending the temporal region and anterior scalp. In cases where the ipsilateral ICA is occluded, collateral flow through the ECA occurs. Resection of the temporal artery in such cases may result in a stroke. Prior to biopsy, the vessel is compressed by hand and the patient is observed for focal neurologic deficits. A positive biopsy reveals lymphocyte, macrophage, and giant cell infiltration of the arterial wall. A negative biopsy does not rule out the possibility of disease.

See also: Cranial Nerves and Autonomic Innervation in the Orbit; Extraocular Muscles: Extraocular Muscle Anatomy; Imaging of the Orbit; Ischemic Optic Neuropathy; Orbital Bony Anatomy and Orbital Fractures.

Further Reading

Cheung, N. and McNab, A. A. (2003). Venous anatomy of the orbit. *Investigative Ophthalmology and Visual Science* 44: 988–995.

Hayreh, S. S. (1962). The ophthalmic artery. III. Branches. *British Journal of Ophthalmology* 46: 212–247.

Hayreh, S. S. (1963). Arteries of the orbit in the human being. *British Journal of Surgery* 50: 938–953.

Hayreh, S. S. (2006). Orbital vascular anatomy. *Eye* 20: 1130–1144.

Miller, N. (1998). Anatomy and physiology of the cerebral vascular system. In: Miller, N. R. and Newman, N. J. (eds.) *Walsh and Hoyt's Clinical Neuro-Ophthalmology,* 5th edn., pp. 2869–2974. Philadelphia, PA: Williams and Wilkins.

Overview of Electrolyte and Fluid Transport Across the Conjunctiva

O A Candia and L J Alvarez, Mount Sinai School of Medicine, New York, NY, USA

Glossary

Short-circuit current – The short-circuit current (I_{sc}) across tissues isolated within an Ussing chamber is defined as the charge flow per time, per the cross-sectional area of the epithelium that is exposed to the bathing solutions, when the tissue is short-circuited by clamping the transepithelial voltage (PD_t) to zero with an external circuit. The I_{sc} is a current that circulates through the tissue and the external circuit thereby completing a closed loop. Because of this, the I_{sc} enters the tissue across one surface and leaves across the other. Monitoring the I_{sc} provides a continuous measure of the net charged flow of current across the transcellular pathways of the tissue. There is no net flow across the paracellular pathways in the short-circuited condition if the tissue is bathed bilaterally with solutions containing identical ionic concentrations. Adding drugs that affect the ionic channels or electrogenic elements within the membranes of the epithelium will affect the magnitude of the I_{sc}.

Transepithelial resistance – An epithelium can be considered to be comprised of an arrangement of resistance elements or resistors. This arrangement is most simply modeled in a multilayered epithelium as two resistors in series, namely R_a (the resistance of the apical membrane) and R_b (the resistance of the basolateral membrane). These resistances are shunted by a parallel resistor, R_{shunt}, which is the cumulative resistance of the paracellular pathways. As such, transepithelial resistance (R_t) is defined as follows:

$$R_t = \frac{(R_a + R_b) \times R_{shunt}}{R_a + R_b + R_{shunt}}$$

In the conjunctiva, R_{shunt} tends to be lower than the transcellular pathway. This leads to small measured changes in R_t when drugs that selectively affect either R_a or R_b are added. For example, potassium channel blockers should selectively increase R_b, but the effect on the measured R_t parameter is relatively smaller in the conjunctiva than in the corneal epithelium, which is a tight epithelium, that is, a tissue with a high R_{shunt}.

Transepithelial voltage – Epithelial cells transport ions and thereby generate a transepithelial voltage (PD_t). The generation of PD_t requires (i) an asymmetric distribution of ion channels and electrogenic transporters on the apical and basolateral sides of the tissue, and (ii) the presence of tight junction proteins between adjacent cells in the superficial epithelium to impede the flow of ions along the paracellular pathways.

Unidirectional fluxes – Across epithelia isolated in Ussing-type chambers, a unidirectional flux of a substance (e.g., a radiolabeled electrolyte or water molecule) is its rate of translocation across the tissue from the bathing solution within one hemichamber to the contralateral bath, disregarding any counterbalancing flux in the opposite direction. In practice, unidirectional fluxes are measured in the apical-to-basolateral direction, and again in the basolateral-to-apical direction. A difference in the magnitude of these two unidirectional fluxes provides a measure of the net flux, for example, there is a net chloride flux across the conjunctiva in the basolateral-to-apical direction.

Ussing chamber – A device designed by Hans Ussing in 1951 to originally study vectorial ion transport across the frog skin. It has since been modified (i.e., an Ussing-type arrangement) by many investigators to characterize electrolyte transport across various epithelial tissues including epithelia of the eye. This approach has significantly contributed to our understanding of how electrolytes are transported. The Ussing-type methodology entails two aspects. One is the chamber itself, which is constructed to hold the dimensions of a particular tissue, and enable it to be bathed bilaterally. The second aspect is the external electrical circuitry, which can be designed to measure transepithelial voltage, resistance, and current. The effects of pharmacological agents on the electrical parameters generated by the epithelium can be studied by applying test compounds unilaterally to either the apical-side or basolateral-side baths.

Introduction

The conjunctiva and the corneal epithelium together form the ocular surface. The conjunctiva (from late Latin, feminine of conjunctivus, or conjoining) is in essence a connection (conjunction) between the eyelids, the sclera of the eyeball, and the cornea. It lines the posterior surface of the

eyelids (the palpebral conjunctiva) and the exposed, anterior aspect of the globe (the bulbar conjunctiva). The latter is loosely attached to the sclera of the eyeball, and translucent, thereby exposing the so-called 'white of the eye'; it merges with the corneal epithelium at the limbus, which constitutes the edge of the cornea. The palpebral conjunctiva is tightly adherent to the eyelid.

The space, lined by the conjunctiva, between the lids and the globe is known as the conjunctival sac. The bottom of the sac, which is unattached to the eyelids or to the eyeball, is known as the fornix, forniceal region, or conjunctival fold. The untethered nature of the fornix allows the eyeball to move freely. The conjunctival sac varies in size depending upon the degree to which the lids are open. The depths of the unextended sac in humans are about 14–16 mm superiorly and 9–11 mm inferiorly. The total surface area of the conjunctiva is about 9 and 17 times larger than that of the cornea in rabbits and humans, respectively. The lacrimal glands, which secrete tears, open into the superior fornix.

The palpebral conjunctiva contains the openings of the lacrimal canaliculi, which allow tears within the conjunctival sac to drain into the nasal cavity. The vasculature of the palpebral conjunctiva is clearly visible within the tissue upon examining the posterior surface of the eyelid. In contrast, the bulbar conjunctiva is normally colorless, unless its vessels are dilated as a result of inflammation (conjunctivitis). The conjunctival vessels arise from a peripheral palpebral arcade and from the anterior ciliary arteries. Blood comes mostly from the orbit, but anastomoses with the facial system.

Conjunctival innervation is mediated by the ophthalmic division of the trigeminal nerve. The conjunctiva is extensively innervated with adrenergic, cholinergic, and peptidergic fibers identified in various species. In general, the largest numbers of nerves present are sympathetic, with fewer parasympathetic and sensory nerves. The parasympathetic nerves contain the neurotransmitters acetylcholine and vasoactive intestinal peptide; the sympathetic nerves, norepinephrine and neuropeptide Y; and the sensory nerves, substance P and calcitonin-gene-related peptide.

The major roles of the conjunctiva are:

(1) to contribute to tear production by secreting electrolytes and fluid;
(2) to modify the composition of the tear film by secreting mucins and lipids, and absorbing various organic compounds found in tears; and
(3) to contribute to the resistance of the eye to infection by providing protection against microorganisms.

The conjunctiva is comprised of an epithelium and an underlying stroma. The epithelium is embryologically related to, and anatomically continuous with, the epithelium of the upper airway. Within the conjunctival epithelium are goblet cells, which are specialized epithelial cells that function as unicellular mucus glands. The goblet cells secrete the mucin component of the tear film, which consists of three layers, each of which is secreted by different cells. Secreted mucins constitute the inner layer of the tear film and serve as wetting agents that keep the apical, hydrophobic aspects of the corneal and conjunctival epithelia hydrated. The middle, aqueous layer of the tear film contains water, electrolytes, immunoglobulin A (IgA), glucose, and proteins (including antibacterial enzymes). This layer is primarily secreted by the main and accessory lacrimal glands; the latter glands of Krause and Wolfring flank the main lacrimal duct near the superior fornix. It is possible that the conjunctiva also contributes to this layer under basal conditions when the lacrimal glands are not stimulated. The outer, lipid layer of the tear film contains a fat mixture that is secreted by the meibomian glands that line the eyelids. This layer functions to reduce evaporation of the aqueous layer.

Underlying the conjunctival epithelium, the connective tissue contains blood vessels, nerves, conjunctival glands, mast cells, and leukocytes including macrophages. The latter, defensive cells can be recruited in large numbers to an injury site on the ocular surface due to disruption of the barrier properties of the epithelium. They may also release paracrine-signaling agents that affect the transport properties of the epithelium, and certain leukocyte populations can also serve as antigen-presenting cells.

Recent work has characterized the active transport properties of the conjunctival epithelium. The epithelium is capable of transporting fluid as a consequence of a sufficiently high water permeability bestowed by endogenous water channels (aquaporins) and transepithelial solute movement due to active transport mechanisms. This article includes a synopsis of the current understanding of the electrolyte and fluid transport across the conjunctiva.

Conjunctival Epithelium

A primary role of all epithelial tissues, including those in the conjunctiva, is the absorption and/or secretion of fluid. In brief, two main elements are necessary for fluid movement across a membrane or a set of membranes: (1) the driving force represented by an osmotic gradient (or hydrostatic pressure), and (2) a water pathway represented by water channels (aquaporins) and the lipid bilayer. Thus, all fluid secretion or reabsorption is a consequence of the osmotic gradient created by active electrolyte transport, with the direction of fluid movement identical to that of the net transepithelial solute transport. To date, extensive, functional characterizations of the electrolyte transport properties of the conjunctival epithelium have been done only on the isolated rabbit conjunctiva. The epithelium of this species exhibits mechanisms that simultaneously mediate Na^+ absorption and Cl^- secretion. The relative proportions of these oppositely directed functions varies considerably from one individual rabbit conjunctival

specimen to another, for reasons that are unknown, but in general Cl^- transport is predominant. On average, the ratio of Cl^- secretion to Na^+ absorption is about 1.5 to 1, suggesting that the rabbit epithelium can function primarily as a chloride-secreting epithelium potentially capable of moving fluid into the conjunctival sac. However, it must also be noted that a small proportion of conjunctival specimens exhibited a Na^+ absorptive rate larger than the rate of Cl^- secretion.

Morphologically, the epithelia of the rabbit bulbar, forniceal, and palpebral regions have distinct appearances (**Figure 1**). The bulbar epithelium appears columnar and thinner than the other sections with goblet cells present. It is as thick as two to three cell layers and packed irregularly. In the forniceal area, the number of cell layers increases to three or four with a greater abundance of goblet cells. From this region to the lid margin, a transition within the palpebral epithelium is evident with the number of goblet cells diminishing, and the epithelial cells becoming more stratified. Species differences in morphology among mammalian conjunctivae have been described.

Excluding variations in the number of goblet cells, the epithelial cells within each conjunctival region appear homogeneous, which suggests that both absorptive and secretory activities coexist within an individual epithelial cell. If so, the conjunctival epithelium exhibits a rare property among epithelia in that the transport functions for Na^+ absorption and Cl^- secretion are not segregated in distinct cell types, and the transport rates for these oppositely directed functions are nearly equivalent in isolated conjunctivae under *in vitro* conditions.

Regardless of the normal, physiologic direction of fluid movement across the human conjunctiva, it is clear that inhibiting reabsorption and/or stimulating secretion may have a beneficial effect by increasing the aqueous layer of the tear film in individuals with a tear-fluid deficit due to various lacrimal gland deficiencies.

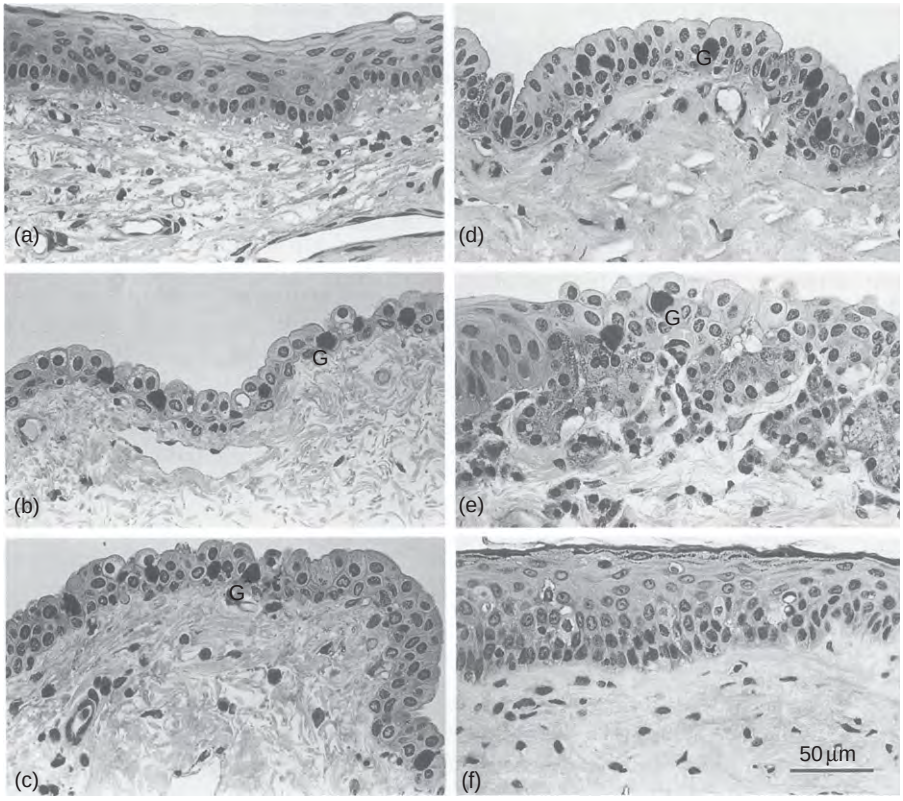

Figure 1 Histological sections of the rabbit limbal and conjunctival regions. (a) The limbal epithelium upon a highly vascularized stroma. (b) The bulbar conjunctival epithelium. There are goblet cells (G) present among the epithelial cells. (c) The forniceal epithelium nearest the bulbar region. (d) Another section of the forniceal epithelium, within which the goblet cells become more numerous relative to the bulbar region. The forniceal epithelium is thicker than the bulbar epithelium. (e) The palpebral epithelium near the forniceal region that is characterized by a decrease in the number of goblet cells and abundant lymphoid tissue. (f) The palpebral epithelium closer to the eyelid margin. It is more stratified than the other conjunctival regions and devoid of goblet cells. Adapted from Wei, Z. G., Sun, T. T., and Lavker, R. M. (1996). Rabbit conjunctival and corneal epithelial cells belong to two separate lineages. *Investigative Ophthalmology and Visual Science* 37: 523–533.

Bioelectric Studies on the Isolated Rabbit Conjunctiva

The ionic transport systems potentially mediating the absorptive and/or secretory functions of an epithelium can be efficiently characterized by isolating the epithelium under an Ussing-type arrangement. With this method, a flat piece of an epithelium is dissected with some of its underlying connective tissue or stroma maintained in place to provide structural support. The thickness of the entire dissected preparation is usually about 1 mm, of which about 0.05 mm represents the epithelial cellular compartment. The isolated tissue is then positioned between two hemichambers, which when closed together result in the tissue serving as a partition separating the cavities of the two hemichambers. In this situation, the apical surface of the epithelium interfaces with the cavity of one hemichamber, while the basal surface attached to the underlying stroma interfaces with the contralateral chamber. Each hemichamber is then filled with a physiological solution to simultaneously bathe the two surfaces of the *in vitro* preparation.

The rabbit conjunctiva serves as a fairly good specimen for this approach given its relatively large surface area, as well as the fact that the conjunctival sac can be removed nearly intact as a cylinder and then cut longitudinally to convert it to a flat epithelium that is easily mounted between Ussing-type hemichambers. Typically, about 0.5 cm^2 of cross-sectional area of tissue is bilaterally exposed to the bathing solutions within the chambers. A negative aspect of this approach with the conjunctiva is that the epithelium seems to be relatively frail (when compared to the corneal epithelium) as its integrity deteriorates following several hours of isolation within the chambers. Nevertheless, useful electrophysiological experiments can be designed and informative data are obtainable.

Upon isolation of an epithelial preparation, such as the conjunctiva, within the divided chambers, a potential difference (PD) develops across the tissue. The PD is a consequence of the active transport of electrolytes by the epithelium, which spends metabolic energy to maintain ionic gradients between the cellular compartment and the extracellular bath. An epithelium will exhibit a negative intracellular voltage with respect to both the apical-side bathing solution and the stromal-side (basolateral) solution. Typically, the positive voltage of the stromal-side bath (PD_s) with respect to the cellular compartment occurs because of the electrogenic Na^+–K^+ ATPase, which extrudes three Na^+ ions for two imported K^+ ions, and the fact that the cellular K^+ ion concentration is above equilibrium, so that K^+ will constantly efflux through K^+ channels toward the stromal (basolateral) bath (**Figure 2** shows an overview of the major transport elements found in the conjunctival epithelium). The Na^+–K^+ ATPase functions incessantly to maintain cellular K^+ above equilibrium. The positive voltage of the apical-side bath (PD_a) with respect to the cellular compartment is less positive than PD_s. As such, a transepithelial PD (PD_t) exists, which equals the difference between the PDs across the respective contralateral surfaces of the epithelium ($PD_t = PD_a - PD_s$; and has a negative sign with PD_s taken as reference). PD_a is less positive with respect to the cellular compartment than is PD_s because of the efflux of Cl^- via channels in the apical domain toward the apical-side bath, and in the case of the conjunctiva, an influx of Na^+ also occurs via electrogenic transporters that are in the apical membrane (**Figure 2**).

PD_t can only exist if tight junctions are present in the epithelium, which is the case in the conjunctiva. These elements are located between the lateral membranes of the most superficial epithelial cells and form a resistance barrier that impedes the diffusion of ions from the contralateral bathing solutions through the paracellular pathways between the epithelial cells. Without the presence of tight junctions, ionic flows in the paracellular pathway would

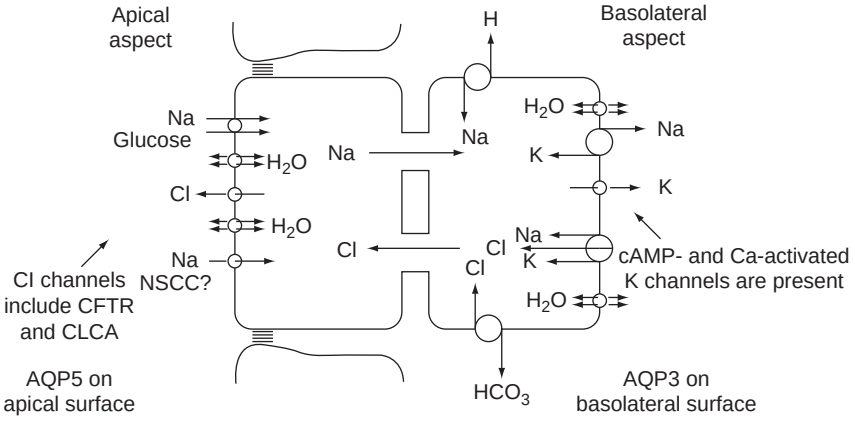

Figure 2 Summary cartoon of the major transport elements found in the rabbit conjunctiva with water fluxes indicated with double arrows. NSCC, nonselective cation channels; CFTR, cystic fibrosis transmembrane conductance regulator (which has chloride channel activity); CLCA, calcium-activated chloride channel; AQP5, aquaporins homolog type 5; AQP3, aquaporins homolog type 3.

short-circuit PD_t, because PD_a and PD_s would still exist and result in a net movement of anions from the apical-side bath to the stromal-side bath through the paracellular pathways, and a net movement of cations in the opposite direction through the paracellular pathways.

The Ussing-type chambers used to isolate the conjunctiva have ports for inserting electrodes into the bathing solutions to directly measure PD_t. In addition, there are ports for current-sending electrodes. These are used to short-circuit PD_t with an external circuit connected to an automatic voltage clamp that constantly maintains $PD_t = 0$ mV. The amount of current needed for this is continuously recorded and known as the short-circuit current (I_{sc}). The I_{sc} represents a real-time measure of the net transepithelial movement of electrolytes across the transcellular pathways of the tissue due to metabolically dependent active transport. As PD_t is maintained at 0 mV, there is no net movement of electrolytes through the paracellular pathways, even if tight junctions were, in principle, not present.

Transepithelial electrical resistance (R_t) can be determined by applying Ohm's law to the measured PD_t (under open-circuit conditions) and the measured I_{sc} (under short-circuited conditions), or by measuring the amount of current necessary to offset the short-circuited condition by a few mV for a few seconds. Either approach gives identical measures of R_t with the conjunctiva.

As alluded to above, the integrity of the conjunctival epithelium appears to degenerate following a prolonged period in the chamber. This is observed as a spontaneous, gradual decline in R_t. It appears that there is a loss in paracellular resistance (i.e., tight-junction structure may change with time *in vitro*) since the R_t decline occurs in the presence of a steady I_{sc}. As noted, under the short-circuited conditions, increases in paracellular ion movement do not result in a net flow across this pathway given the absence of a PD across the epithelium and identical electrolyte concentrations on each side of the preparation. As such, the I_{sc} continues to measure net transcellular flow of electrolytes in experiments with symmetrical solutions. However, changes in conjunctival R_t in response to the additions of various drugs frequently underestimate changes in membrane resistance. This is because transcellular resistance is proportionally larger than paracellular resistance, which means that large changes in transcellular resistance are recorded as smaller changes when measuring conjunctival R_t.

Nonetheless, the initial measurements of conjunctival R_t upon the isolation of fresh preparations within the divided chambers provide a good indication of the barrier properties of the epithelium. This is because the electrical resistances of both the cell membranes as well as the paracellular pathways contribute to the R_t measurement. The paracellular pathways of the *in situ* conjunctiva at the ocular surface allow for the passive diffusion of hydrophilic solutes across the conjunctiva. Passive paracellular transport of electrolytes across the conjunctiva *in vivo*, which is analogous to the open-circuit situation *in vitro*, occurs because of gradients created by the transcellular mechanisms. In addition, cell-impermeable, hydrophilic solutes applied to the conjunctival sac may diffuse across the epithelium through the paracellular route. The transepithelial permeability of such solutes decreases with increased solute size. Tight junctions located at the apical-most aspect of an epithelium create the major barrier for the movement of solutes across all epithelia including the conjunctiva. However, the paracellular route varies considerably among epithelia in terms of permeability to solutes and electrical resistance. R_t measurements can range at least 1000-fold between highly resistant and so-called leaky epithelia. In some tissues, electron microscopy studies have correlated the ultrastructure of the tight junctions with the measured R_t values obtained *in vitro*. In general, the number of tight-junction strands along the apical-basal axis is proportional to the junctional resistance. R_t values from freshly isolated rabbit conjunctival epithelia are in the range of 1–2 $k\Omega\ cm^2$, with many studies reporting an average value of $\approx$1 $k\Omega\ cm^2$. This suggests that the conjunctival epithelium is a moderately tight epithelium. For comparison, R_t measurements of the rabbit corneal epithelium and rabbit corneal endothelium are $\approx$7–9 $k\Omega\ cm^2$ and 0.01–0.07 $k\Omega\ cm^2$, respectively. As such, the electrical resistances of the corneal epithelium and endothelium vary over a range of about 100-fold, and the conjunctiva exhibits an intermediary value. The fact that the measured R_t of the freshly isolated conjunctiva is so high also indicates that tight junctions must exist between the surface goblet cells and the most superficial stratified epithelial cells. An explanation as to why R_t declines with prolonged time *in vitro* remains to be evinced, but barrier resistance is physiologically regulated in other systems. The stable I_{sc} recorded during the spontaneous R_t decline indicates that the epithelial cells have remained metabolically viable.

Electrolyte Transport Systems of the Rabbit Conjunctiva

The bioelectrical approach discussed above has been used to determine the major electrolyte transport systems present in the rabbit conjunctival epithelium. In work done to date, the short-circuiting methodology was used to characterize transcellular transport. Such transport is energy dependent, and controlled by the tissue-specific profile of transporters and channels along the apical and basolateral membranes of the epithelium. The conjunctival apical membranes interface with the tears and the basolateral membranes interface with the paracellular pathways from the tight junctions to the basement membranes at the

stroma. Transport mechanisms in the tissue are generally uncovered by electrolyte substitution experiments, and the application of relatively specific drugs (i.e., channel blockers, channel openers, transporter inhibitors, etc.) to the bathing solutions of conjunctiva isolated in the divided chambers. In some cases, the identity of channels and transporters that were identified in electrophysiological experiments were corroborated with immunoblotting and immunohistochemcial observations.

Identical to other Cl^--secreting epithelia, the rabbit conjunctival epithelium has a basolateral bumetanide-sensitive Cl^- uptake process (mediated by the Na^+–K^+–$2Cl^-$cotransporter, NKCC1) positioned in series with apical Cl^- channels, including cystic fibrosis transmembrane conductance regulator (CFTR). In addition, Na^+/H^+ and Cl^-/HCO_3^- exchangers exist in parallel in the basolateral membrane and can also mediate Cl^- uptake (**Figure 2**).

Oppositely directed, electrogenic Na^+ reabsorption is amiloride-insensitive, indicating the absence of the major epithelial Na^+ channel (ENaC) at the apical surface, and occurs through a Na^+-dependent cotransporter for glucose. Nonselective cation channels (NSCCs) were identified in whole-cell patch clamping of freshly isolated conjunctival epithelial cells and such channels may also reside at the apical surface. A transcellular Na^+ movement occurs because the apical uptake mechanisms for Na^+ exist in series with the basolaterally located Na^+–K^+ pump (**Figure 2**).

Other electrogenic Na^+-dependent uptake mechanisms at the apical surface were demonstrated by adding the transported substrates to the apical bath. Transport systems for amino acids, nucleosides, L-lactate, and di- and tri-peptides were evidenced in this manner because such compounds are normally not included in the physiological solutions used to bathe the *in vitro* preparations. The addition of such compounds to the apical bath results in a short-circuit current stimulation. In the cases of the amino acids and nucleosides, the largest I_{sc} stimulations occurred with L-arginine and uridine, respectively. The roles of these carriers are not firmly established. It is thought that these transport systems may clear the tear fluid of these compounds in either nonphysiologic or pathophysiological states of the ocular surface when excess amounts of such solutes might have leaked into tears.

Results from protocols for immunoblotting and the immunofluorescent labeling of frozen sections from separately isolated bulbar and palpebral regions of the conjunctival epithelium indicated that the proteins for the Na^+–glucose cotransporter, Na^+–K^+ ATPase, and Na^+–K^+–$2Cl^-$ cotransporter are uniformly distributed throughout the conjunctiva. These observations suggest that despite stark differences in the regional morphology of the bulbar and palpebral regions, the entire conjunctival epithelium exhibits the elements for transepithelial Na^+ and Cl^- transport.

Regulation of Epithelial Ion Transport in Rabbit Conjunctiva

Currently, information on the regulation of electrolyte transport by the conjunctival epithelium is somewhat limited. This is because the characterization of the macroscopic electrolyte transport properties of this tissue, as measured in bicameral Ussing-type chambers, was begun relatively recently. Hence, many fundamental aspects of the tissue have not been elucidated. One underlying rationale for studying conjunctival transport is to define the secretory functions of the epithelium. This effort could prove to have utility in ameliorating complications from dry-eye diseases, and some progress has been made in this regard. Because of the large surface area of the conjunctival epithelium, active transport by conjunctiva with accompanying fluid secretion could, hypothetically, contribute a significant fraction of tear production, which is normally provided in healthy individuals by the lacrimal gland. Upon stimulation, the transepithelial conjunctival contribution could be greater.

As commonly found in Cl^--secreting epithelia, the exposure of the conjunctiva to secretogogues that increase either cell calcium or cyclic adenosine monophosphate (cAMP) stimulates transepithelial Cl^- fluxes and the I_{sc}. The latter intracellular messenger can be increased in the conjunctival epithelium with forskolin (a direct stimulator of adenylyl cyclase), dibutyryl-cAMP (a cell permeable form of cAMP), 3-isobutyl-1-methyl-xanthine (IBMX, a nonselective phosphodiesterase inhibitor), rolipram (an inhibitor specific for cAMP-phosphodiesterase type IV), or epinephrine (a nonselective adrenergic agonist). In addition, these agents also increase the transconjunctival I_{sc} under Cl^--free conditions indicating that the increased cAMP levels also stimulate the Na^+ absorptive activity of the epithelium. The increase in Na^+ absorption has been attributed to a protein kinase A (PKA)-regulated, barium-inhibitable, basolateral K^+ conductance in the rabbit conjunctival epithelial cells. One or more different types of K^+ channels that have not yet been identified may mediate this K^+ conductance. The stimulation of the PKA-gated K^+ channels hyperpolarizes the negative cell potential relative to the bathing solutions and favors both the uptake of Na^+ across the apical face and the efflux of Cl^- into the tears. There is evidence that apical Cl^- channels are also gated by PKA, particularly in the case of CFTR. In the short-circuited conjunctiva, cAMP has a central role in coordinating simultaneous changes in apical Cl^- and basolateral K^+ conductances to enable stimulations in the transcellular transport of Cl^- in the stromal-to-apical direction and of Na^+ in the opposite direction.

Should both absorptive and secretory mechanisms coexist within the same cell, such cAMP-evoked stimulations of the *in vivo* conjunctiva would, in principle, deplete the epithelium of KCl and reduce cellular volume, while Na^+ and Cl^- move in opposite directions both trans- and

paracellularly. Experimental measurements of net water fluxes across the isolated conjunctiva (under open-circuit conditions) indicate an increased fluid movement in the stromal (basolateral)-to-apical direction in response to cAMP, likely due to the higher rate of Cl^- secretion relative to Na^+ absorption. Fluid flow occurs under open-circuit conditions, which is the situation *in vivo*. The dominant transport system, apparently Cl^-, will be transported mainly transcellularly, while Na^+ will reverse from its net tear-to-stroma direction found under short-circuit conditions to move paracellularly as a companion ion to neutralize the Cl^- charge and create a possible isotonic fluid at the apical surface. In open circuit, there would still be a transcellular movement of Na^+ toward the stroma, and a paracellular movement of Cl^- toward the stroma, but the magnitude of these flows will be less than the net of Na^+ and Cl^- secreted into tears (**Figure 3**). cAMP stimulates all flows and increases the net.

Other effective secretogogues in the rabbit conjunctiva are: (1) 1-ethyl-2-benzimidazolinone (EBIO), a Cl^- and K^+ channel opener that elicits electrophysiological effects similar to those of cAMP, although different subtypes of channels are likely involved; and (2) the nucleotide uridine 5′-triphosphate (UTP), which stimulates Cl^- secretion through $P2Y_2$ receptors upon exogenous application to the apical-side bath. Of these, only the latter has been tested on net fluid movement across isolated conjunctivae and found to be a useful stimulant. Recently, synthetic $P2Y_2$ agonists (e.g., diquafosol tetrasodium, which is also known as INS365) have been studied in clinical trials. Such agents are administered 4–5 times daily, and there is a time-dependent loss of efficacy that is observable in the data produced by such trials. This may be because $P2Y_2$-receptor activation is often transitory due to the nature of the Ca^{2+} signal itself (through the phospholipase C-sensitive calcium signaling pathways) and the fact that purinergic agonists produce receptor desensitization from which recovery is slow. Yet currently, the use of purinergic agonists appears a suitable approach to palliate dry eye because of not only the stimulatory effects on conjunctival Cl^- secretion and fluid transport, but also the fact that purinergics serve as mucin secretogogues from conjunctival goblet cells. As such, purinergics appear to have utility in conserving the composition of the tear film.

The established receptors that stimulate electrolyte and fluid secretion in the stromal-to-tear direction under open-circuit conditions are schematically presented in **Figure 4**. The specific channel subtypes activated by calcium and cAMP remain to be conclusively identified.

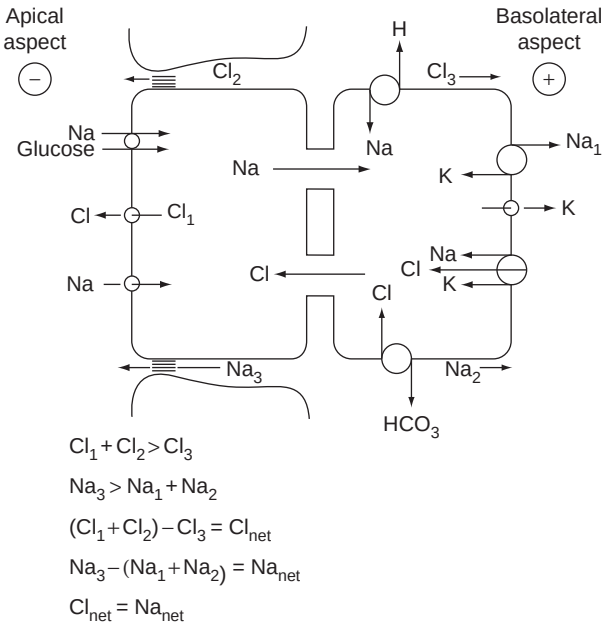

Figure 3 A simplified model of the sodium and chloride flows across the rabbit conjunctiva under open-circuit conditions, which are analogous to the *in vivo* situation. Some transporters present in the epithelium have been omitted for clarity. Cl_1 is the transcellular efflux of chloride via chloride channels in the apical domain. Cl_2 is the paracellular movement of chloride in the stromal-to-tear direction. Cl_3 is the paracellular movement of chloride in the tear-to-stromal direction. Na_1 is the sodium efflux mediated by the sodium-potassium ATPase pump. Na_2 is the paracellular movement of sodium in the tear-to-stromal direction, while Na_3 is the paracellular movement of sodium in the opposite direction. In open-circuit, the tear-side (apical) bath will have a negative potential relative to that of the basolateral-side bath. Cations will thus flow in the paracellular pathways toward the tear side, while anions will flow in the opposite direction. There is also the possibility that some potassium will move along the paracellular pathways toward the tears. The sodium–potassium–chloride cotransporter in the basolateral membranes drives the transcellular movement of chloride. The net flux of sodium and chloride into the tears results in a net fluid transport across the conjunctiva. Flux relationships are indicated at the bottom of the figure by equations.

Fluid Transport Studies across Isolated Rabbit Conjunctiva

Two commonly used methods to measure water fluxes across various epithelia have been applied to the excised, isolated rabbit conjunctiva: (1) unidirectional/diffusional flow with tritiated water (^3H_2O); and (2) net water flow by volumetric procedures.

With method 1, the diffusion permeability coefficient, P_{dw}, is expressed in cm s^{-1} and given by:

$$P_{dw} = \mathcal{J}_{dw}/A \cdot V_w \cdot C_w$$

where, A is the area of the membrane (cm^2), V_w is the partial volume of water (cm^3 mol^{-1}), C_w is the concentration of water (mol cm^{-3}), and $\mathcal{J}_{dw}$ is the measured unidirectional H_2O flux in cm^3 s^{-1}.

In this case, a two-compartment chamber is used. The tissue is mounted between compartments; ^3H_2O is added to one side and samples are taken periodically from both

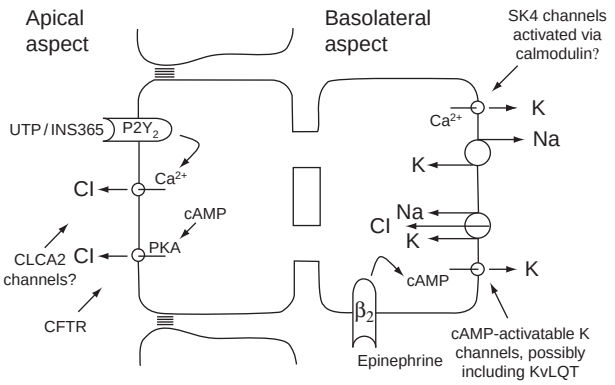

Figure 4 Cartoon of the established receptors that stimulate electrolyte and fluid secretion in the stromal-to-tear direction under open-circuit conditions, which are analogous to the *in vivo* situation. Some transporters present in the epithelium have been omitted for clarity. The specific channel subtypes activated by calcium and cAMP remain unverified. Abbreviations: UTP (uridine 5′-triphosphate); INS365 (a synthetic activator of the $P2Y_2$ receptor); $P2Y_2$ (a receptor subtype for the pyrimidine, UTP, that triggers calcium signaling via the phosphoinositide pathway); CLCA2 (a calcium-activated chloride channel subtype thought to be present in the conjunctiva); CFTR (cystic fibrosis transmembrane conductance regulator, which mediates a cAMP-gated chloride conductance via PKA); SK4 (a potassium channel subtype thought to be present in the conjunctiva that is activated by calcium, possibly via calmodulin, a calcium-regulatory protein); KvLQT (a potassium channel protein subunit linked to cAMP-activated potassium conductances). The presence of the above channel subtypes has been suggested from the expression levels of message in gene microarray assays of human conjunctiva, but the operational existence of the putative channel proteins has not yet been confirmed in functional experiments.

sides to determine the diffusion of ^3H_2O, which is proportional to $\mathcal{J}_{dw}$.

With method 2, the osmotic permeability coefficient, P_f, is expressed in cm s^{-1} and can be calculated from the following expression:

$$P_f = \mathcal{J}_v / A \cdot V_w \cdot \Delta C_s$$

where $\mathcal{J}_v$ (the measured net H_2O flux) is expressed in $cm^3\ s^{-1}$ and ΔC_s is the difference in solute concentration (mol cm^{-3}). For this approach, a two-compartment arrangement could also be used, along with a graduated capillary tube, or appropriate detection system, in order to directly measure $\mathcal{J}_v$ as a function of time.

Unidirectional fluxes of water determined with ^3H_2O (method 1) are usually large and similar in both directions. Thus, a small difference (the net volumetric flow, or $\mathcal{J}_v$, which is detected directly with method 2) is difficult to detect by method 1 and is usually not calculated as a difference between two unidirectional fluxes. For example, in the case of the conjunctival epithelium, unidirectional water fluxes ($\mathcal{J}_{dw}$) across the tissue are statistically identical in either direction, and have a magnitude ≈60-fold larger than the reported values for the net flux ($\mathcal{J}_v$) of fluid secreted to the tear side by the isolated conjunctiva (≈4–6 µl h^{-1} cm^{-2}, using method 2 (a volumetric approach). Because of this discrepancy in magnitude, it is unfeasible (if not impossible) to calculate $\mathcal{J}_v$ as the difference between the two, relatively large, unidirectional fluxes in the opposite directions. However, method 1 (a diffusional approach) is useful for determining the effects of agents or various experimental conditions on water permeability (P_{dw}); because although labeled water will cross cell membranes via all available pathways – lipid bilayer, aquaporins, and other channels, the measurements of $\mathcal{J}_{dw}$, which reflect P_{dw}, change equally in both directions when an experimental maneuver changes the water permeability of the epithelium.

From diffusional water fluxes ($\mathcal{J}_{dw}$) and mannitol fluxes it was determined that the conjunctival apical surface is highly permeable to water, and that the transepithelial water permeability (10^{-4} cm s^{-1}) exceeded the paracellular permeability (10^{-6} cm s^{-1}). A recently described element contributing to the water permeability of the apical surface is the water channel homolog known as aquaporin type 5 (AQP5). Generally, epithelia exhibit distinct AQPs in the apical and basolateral domains, and in the case of the conjunctiva, AQP3 is expressed in the lateral membranes. Together, AQP5 and AQP3 may be necessary in the conjunctiva for transepithelial fluid transport. AQP5 could serve as a potential target for pharmacological upregulation to enhance fluid secretion given that cAMP via PKA activity has been reported to increase the expression levels of this water channel at both transcriptional and posttranscriptional levels in other cell systems.

From measurements of $\mathcal{J}_v$, a spontaneous fluid transport across the isolated conjunctival epithelium in the basolateral-to-apical direction has been described, a property consistent with the more dominant Cl^- secretory activity of the tissue. As noted, the reported fluid secretion rates were ≈4–6 µl h^{-1} cm^{-2}. This flow was dependent upon transepithelial electrolyte transport given its abolition by ouabain, sensitivity to K^+ channel blockade, and Cl^- dependency. In addition, in experiments that increased the Na^+ absorptive activity by raising the glucose concentration (to 25 mM) of the apical bath, fluid transport was inhibited by 77%; an inhibition that did not occur with a similar concentration of mannitol. Studies found that the fluid transport rate was increased (≈50–100 %) by Cl^- secretogogues that included purinergic agonists acting via $P2Y_2$ receptors. As purinergic agonists stimulate mucin secretion by conjunctival goblet cells, it seems plausible that the roles of epithelial Cl^- transport include the hydration of mucins upon release.

Overall, the conjunctival epithelium has sufficient water permeability and the transporters necessary to contribute significant fluid to the tear film (≈50 µl h^{-1} based upon its total surface area). This level of fluid flow is sufficiently large that it may represent a baseline tear

secretion beyond that contributed by the lacrimal gland, which mediates reflex tearing under neuronal control. It is not yet clear if the innervation of the conjunctiva directly regulates the rate of fluid transported across the conjunctiva *in vivo*. However, the transport systems of the conjunctiva can potentially be manipulated pharmacologically.

See also: Antigen-Presenting Cells in the Eye and Ocular Surface; Cornea Overview; Corneal Angiogenesis; Imaging of the Cornea; Stem Cells of the Ocular Surface.

Further Reading

Anderson, J. M. (2001). Molecular structure of tight junctions and their role in epithelial transport. *News in Physiological Sciences* 16: 126–130.

Bron, A., Tripathi, R., and Tripathi, B. (eds.) (1997). *Wolff's Anatomy of the Eye and Orbit,* 8th edn. London: Chapman and Hall.

Candia, O. A. (2004). Electrolyte and fluid transport across corneal, conjunctival and lens epithelia. *Experimental Eye Research* 78: 527–535.

Dartt, D. A. (2004). Control of mucin production by ocular surface epithelial cells. *Experimental Eye Research* 78: 173–185.

Gipson, I. K. and Argüeso, P. (2003). Role of mucins in the function of the corneal and conjunctival epithelia. *International Review of Cytology* 231: 1–49.

Hosoya, K., Lee, V. H., and Kim, K. J. (2005). Roles of the conjunctiva in ocular drug delivery: A review of conjunctival transport mechanisms and their regulation. *European Journal of Pharmaceutics and Biopharmaceutics* 60: 227–240.

Kaufman, P. L. and Alm, A. (eds.) (2003). *Adler's Physiology of the Eye, Clinical Application,* 10th edn. St. Louis, MS: Mosby.

Li, H., Sheppard, D. N., and Hug, M. J. (2004). Transepithelial electrical measurements with the Ussing chamber. *Journal of Cystic Fibrosis* 3(supplement 2): 123–126.

Nichols, K. K., Yerxa, B., and Kellerman, D. J. (2004). Diquafosol tetrasodium: A novel dry eye therapy. *Expert Opinion on Investigational Drugs* 13: 47–54.

Oen, H., Cheng, P., Turner, H. C., Alvarez, L. J., and Candia, O. A. (2006). Identification and localization of aquaporin 5 in the mammalian conjunctival epithelium. *Experimental Eye Research* 83: 995–998.

Tiffany, J. M. (2008). The normal tear film. *Developments in Ophthalmology* 41: 1–20.

Ussing, H. H. (1949). Transport of ions across cellular membranes. *Physiological Reviews* 29: 127–155.

Wei, Z. G., Sun, T. T., and Lavker, R. M. (1996). Rabbit conjunctival and corneal epithelial cells belong to two separate lineages. *Investigative Ophthalmology and Visual Science* 37: 523–533.

P

Pathogenesis and Immunology of Bacterial Endophthalmitis

T Suzuki and M S Gilmore, Schepens Eye Research Institute, Boston, MA, USA

Glossary

Biofilm – A structured community of microorganisms encapsulated within a self-developed polymeric matrix.
Complement – A biochemical cascade that helps clear pathogens from contaminated tissue.
Quorum sensing – The regulation of gene expression in response to fluctuations in cell-population density.
Toll-like receptors – A family of pattern recognition receptors that initiate a rapid host innate immune response to microbial components.

Bacterial endophthalmitis is one of the most severe and sight-threatening ocular infectious diseases. It is characterized by massive inflammation and tissue damage caused by both bacteria and the subsequent immune response. Bacterial endophthalmitis is not common, and usually occurs in the context of ocular surgery, trauma, or hematogenous spread of organism to the eye. As an invariably sight-threatening infection, however, it is important to understand its pathogenesis and the host response.

Classification

Bacterial endophthalmitis is classified into two categories: exogenous, in which case bacteria enter into eye as a result of ocular surgery or trauma, or endogenous, caused by circulating organisms that migrate from other parts of body to the eye. The range of infectious pathogens depends on the causative trigger (Table 1).

Exogenous Endophthalmitis

Postoperative Endophthalmitis

Postoperative endophthalmitis is a severe complication of ocular surgeries, such as cataract surgery, glaucoma surgery, or vitrectomy. Endophthalmitis after cataract surgery usually occurs in the postoperative period, and the prevalence in most studies varies between 0.05% and 0.2%. Although the technical procedures used in cataract surgery are improving, the incidence of endophthalmitis has not changed and may be increasing. The leading causes of postoperative endophthalmitis include staphylococci, streptococci, *Enterococcus faecalis*, and *Propionibacterium acnes*. The visual prognosis depends on the kind of pathogen, and *Staphylococcus aureus*, streptococci, and *Enterococcus faecalis* infections often lead to significant vision loss. External bacterial flora is often the cause of acute postoperative endophthalmitis. External bacterial flora probably enters the anterior chamber through the surgical wound; in fact, contamination of the anterior chamber at the end of surgery has been noted to be as high as 5.7–21.1%.

Although intraoperative or postoperative contamination of the anterior chamber seems to be the initial step of endophthalmitis, the mechanisms by which a bacterium goes on to cause endophthalmitis relates to the pathogenicity of the organism and the host response. Endophthalmitis after cataract surgery usually follows one of two courses – early or late onset. The former occurs within days of surgery, presents with acute inflammation, and is often caused by *S. aureus*, streptococci, or enterococci. Late-onset endophthalmitis is characterized by chronic inflammation and is mainly caused by low-virulence microorganisms such as coagulase-negative staphylococci or *Propionibacterium acnes*.

Bleb-Related Endophthalmitis

The formation of a filtration bleb is often the next step for medically refractory glaucoma. The filtration bleb is formed between the conjunctiva and the sclera, and aqueous humor filters into the bleb. If the bleb is damaged, there can be direct communication between the anterior chamber and the external eye. Organisms infecting a bleb can easily spread into not only the anterior chamber, but also the posterior chamber, leading to endophthalmitis. The leading

Table 1 Classification of bacterial endophthalmitis and causative agents

Classification	*Causative agents*
Exogenous endophthalmitis	
Postoperative endophthalmitis	*Staphylococci, Streptococci, Enterococci, P. acnes*
Bleb-related endophthalmitis	*Staphylococci, Streptococci*
Post-traumatic endophthalmitis	*Staphylococci, Streptococci Bacillus* sp., *P. aeruginosa*
Endogenous endophthalmitis	*Staphylococci, Streptococci K. pneumoniae, E. coli*

causes of bleb-related endophthalmitis are toxigenic organisms *Streptococcus pneumoniae* and *Staphylococcus aureus*, and it is tempting to speculate that cytolysins expressed by these microbes may facilitate translocation through the bleb.

Post-Traumatic Endophthalmitis

Endophthalmitis is a complication of traumatic injury, and often progresses rapidly and leads to severe destruction of ocular tissue. Common etiologic agents of post-traumatic endophthalmitis include *Bacillus cereus, Pseudomonas aeruginosa,* fungi, and other organisms from the environment, along with staphylococci and streptococci from the ocular surface. In contrast to the causative agents of postoperative endophthalmitis, the number of bacterial cells which contaminates the eye during trauma may be large. The pathogenesis of endophthalmitis is often fulminant, which appears to stem from both microbial toxins and a robust host response. It may be that environmental organisms, such as *B. cereus* with little shared evolutionary history with humans, have not evolved mechanisms or properties that result in the type of tolerance that is seen to commensal organisms, and, as a result, they are quickly and robustly recognized as foreign.

Endophthalmitis Associated with Microbial Keratitis

Similar to post-traumatic endophthalmitis, endophthalmitis stemming from progression of microbial keratitis can cause severe damage to ocular tissue. Where healthcare is readily available, antimicrobial therapy against keratitis is usually effective in preventing the advance of the infection, and as a result bacterial endophthalmitis after keratitis is a rare complication. However, treatment failure in an era of advancing antibiotic resistance represents an important threat.

Endogenous Endophthalmitis

Little is known about the pathogenic mechanisms of endogenous endophthalmitis. It is mainly associated with immunocompromised patients, and those with liver abscess, pneumonia, or other serious underlying conditions. Precisely how these conditions contribute to the blood-borne spread of bacteria to eye in endogenous endophthalmitis is not well understood. The kinds of pathogens involved with this infection depend mainly on the predisposing condition. For example, *Klebsiella pneumoniae* is the predominant pathogen in patients with liver abscess. *E. coli,* staphylococci, and streptococci are also the major causative agents of endogenous bacterial endophthalmitis.

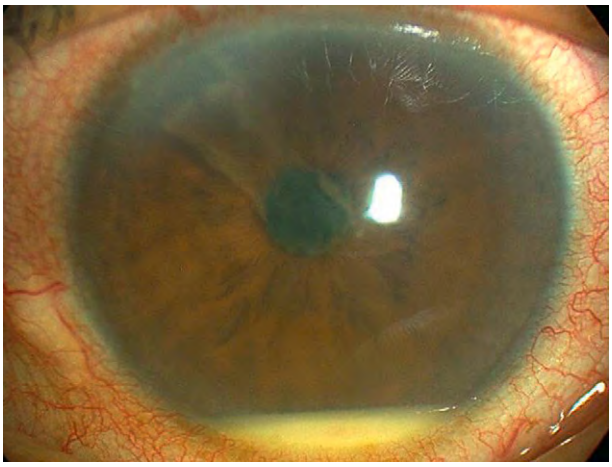

Figure 1 *E. faecalis* endophthalmitis following cataract surgery. Note the hypopyon and fibrin formation in the anterior chamber.

Clinical Findings

Patients who are suffering from acute endophthalmitis usually complain of blurred vision and/or pain. Slit lamp microscopy is used to detect characteristic hyperemia of conjunctiva vessels, ciliary injection, corneal opacity, hypopyon, and cell infiltration in the anterior chamber (**Figure 1**). A late clinical sign is the observation of vitreous opacity. Although it might be difficult to observe the fundus because of haziness in the visual path, retinal hemorrhage can also occur.

As for acute endophthalmitis, delayed-onset endophthalmitis may occur after cataract surgery with intraocular lens (IOL) implantation. This type of endophthalmitis is characterized by an indolent, subclinical inflammation that may evolve over weeks before keratoprecipitates, and a small number of inflammatory cells in anterior chamber raise the index of suspicion (**Figure 2**).

Virulence Factors of Bacteria Causing Endophthalmitis

Several microbial virulence factors that contribute to vision loss in endophthalmitis now have been identified and studied in molecular detail. Rabbit, rat, and mouse

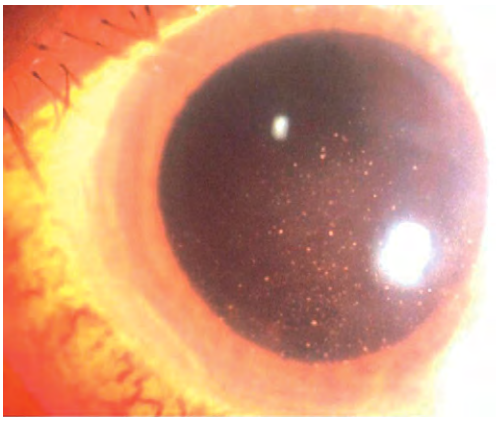

Figure 2 Low-grade endophthalmitis. Note the numerous keratic precipitates on the corneal endothelium. Reproduced from figure 1 in Suzuki, T. (2005). *Journal of Cataract and Refractive Surgery*, 31(10): 2019–2020, with permission from Elsevier.

Table 2 Virulence factor of pathogen in endophthalmitis

Pathogen	*Virulence factor*
S. aureus	Alpha-toxin, beta-toxin, *agr/sar* quorum sensing
E. faecalis	Cytolysin, gelatinase, serine protease, *fsr* quorum sensing
S. pneumoniae	Pneumolysin, autolysin
B. cereus	Motility, swarming, *plcR* quorum sensing
K. pneumoniae	Hypermucoviscosity

models of endophthalmitis have all been used to dissect the disease process. Studies using isogenic strains of bacteria differing only in the production of a toxin or virulence factor have been especially informative in unambiguously demonstrating the role of a particular toxin in contributing to the outcome of infection (Table 2).

Pathogenic Mechanisms

Quorum Sensing

A number of bacterial virulence factors involved in endophthalmitis are controlled by bacterial quorum-sensing systems. Quorum-regulated genes are induced or repressed, depending upon the local density of the bacterial population and accumulation of an extracellular signal. The extracellular signal, or autoinducer, may be a homoserine lactone, peptide, quinolone, or other metabolite. The low turnover of vitreous in the closed posterior segment may contribute to rapid accumulation of quorum molecules.

Biofilm Formation

A biofilm is a structured community of microorganisms encapsulated within a self-developed polymeric matrix, and adherent to a living or inert surface. Although little is known about a precise role of biofilms in bacterial endophthalmitis, biofilm-producing bacteria can attach firmly to the IOL lens. The role of biofilm formation as an impediment to clearance, or contributing to inflammation, is a subject of current study.

Toxin Production

As discussed below, toxin production is central to the pathogenesis of endophthalmitis. Toxins making important contributions to the pathogenesis of infection vary by organism, making it difficult to generalize. However, most of those for which a role has been demonstrated are membrane active.

Virulence Factors of Main Pathogen

Staphylococci

Staphylococci are major causes of postoperative and post-traumatic endophthalmitis. Coagulase-negative staphylococci express relatively few toxins, but are the most common causes of postoperative endophthalmitis. Those infections tend to be mild and usually resolve with limited visual loss. In contrast, infection caused by highly toxigenic *S. aureus*, which is only slightly less common, tends to be more severe, often resulting in visual loss, providing *prima facie* evidence for the role of toxins in endophthalmitis.

Although bacterial contamination of the anterior chamber during surgery is common, cases of endophthalmitis are rare. It has been speculated that biofilm formation, possibly on the implanted lens, may impede the clearance of these microorganisms. Biofilm formation may contribute to circumvention of an immune response and to limitation of the effectiveness of antibiotics. Coagulase-negative as well as *S. aureus* produce biofilms on biomaterials including the IOL lens (Figure 3). Case reports have correlated contaminated IOL lenses with endophthalmitis.

Staphylococcus epidermidis appears to attach to the IOL lens through a polysaccharide intercellular adhesin. The prevalence of potentially biofilm-forming *S. epidermidis* isolates is high in the conjunctival sac, which may be the source for biofilm-forming organisms on the IOL lens. Thus, development of materials that resist bacterial colonization is of high priority.

Once organisms are established, the next step in the pathogenesis of infection is damage to ocular tissue. Rabbit eyes infected with *S. aureus* strains deficient in alpha-toxin, beta-toxin, or both toxins were less inflamed and retained greater retinal function than eyes infected with wild-type toxigenic *S. aureus*. Furthermore, eyes infected with *S. aureus* strains deficient in quorum-sensing systems *agr* and *sar*, which control *S. aureus* toxins and adhesins,

exhibited reduced damage of ocular tissues. Staphylococci are increasingly resistant to a number of antimicrobials complicating rapid resolution of endophthalmitis potentially increasing exposure to toxin-mediated damage.

Enterococci

Enterococcus faecalis, a common cause of endophthalmitis after cataract surgery, is also associated with substantial loss of vision. The endophthalmitis vitrectomy study revealed that endophthalmitis caused by enterococci and streptococci was associated with the worst visual outcome. Several studies have examined the contribution of enterococcal virulence factors to the pathogenesis of *E. faecalis* endophthalmitis. The cytolysin expressed by some strains of *E. faecalis* was shown to be a key determinant of the severity and treatability of enterococcal endophthalmitis. If enterococci were nontoxigenic, the infection responded well to treatment with effective antimicrobials in combination with dexamethasone. However, if the infection was caused by an identical organism additionally expressing the cytolysin, this therapeutic regimen was rendered completely ineffective.

Gelatinase and serine protease are secreted proteases that are regulated by a quorum-sensing system termed *fsr*; in addition, they have been reported to be associated with the retinal destruction. These proteases further have been shown to play a role in endophthalmitis of aphakic eye after cataract surgery. *E. faecalis* proteases may promote organism spread by penetrating the posterior lens capsule. Bacterial migration from the anterior chamber to the posterior chamber is a key event in the progression of endophthalmitis; in the posterior segment, severe retinal damage may result (**Figure 4**). A surface adhesin of *E. faecalis*, aggregation substance, contributes to altered localization of the organism but otherwise appears to play a minor role.

In addition to these virulence traits, *E. faecalis* is intrinsically resistant to many antibiotics and is also capable of producing biofilm on IOL lens material. Both of these factors make infections with this organism very difficult to treat.

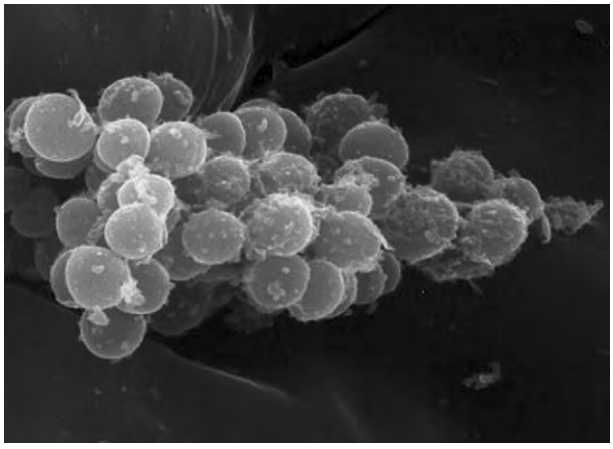

Figure 3 Biofilm-producing *Staphylococci.*

Streptococci

As noted above, streptococci can cause traumatic or postoperative endophthalmitis and are leading agents of bleb-related endophthalmitis. This infection results in severe visual loss. *S. pneumoniae* expresses pneumolysin and autolysin. These virulence factors contribute to the visual outcome of endophthalmitis.

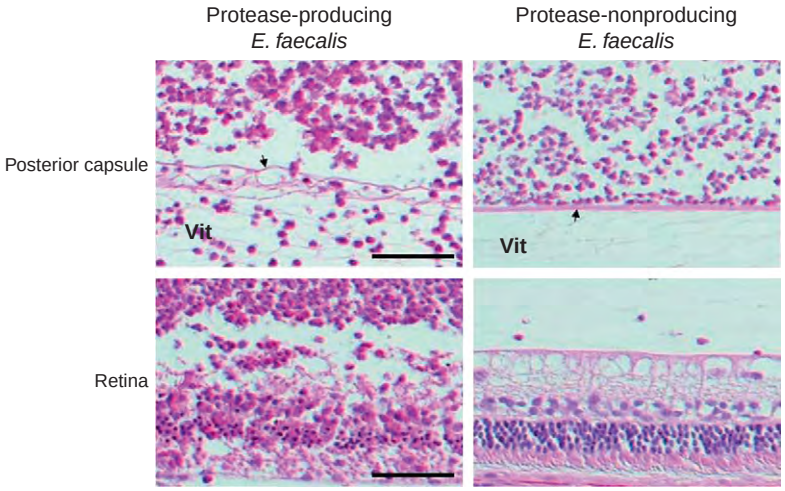

Figure 4 Histological analysis of experimental *E. faecalis* endophthalmitis. Degradation of posterior lens capsule (arrowhead) and destruction of photoreceptor segments were observed in eyes inoculated with protease-producing *E. faecalis*. Scale bar = 50 μm. Vit, vitreous cavity. Adapted from **figure 5** in Suzuki, T. (2008). *Journal of Cataract and Refractive Surgery*, 34(10): 1776–1784, with permission from Elsevier.

Bacillus

Bacillus spp. are leading agents of post-traumatic endophthalmitis, which is uniquely explosive in its evolution, leading rapidly to visual loss. Although speculated early to be an important contributor to the fulminance of *B. cereus* infection, one hemolysin termed hemolysin BL or HBL, was shown to make a relatively minor contribution to the course and severity of disease. *B. cereus* cytolytic factors are regulated by a quorum-sensing system termed *plcR*. Isogenic *plcR*-deficient mutants of *B. thuringiensis* (a derivative of *B. cereus* used as a surrogate in these tests) are significantly attenuated in severity in a rabbit model of endophthalmitis, but the infection nevertheless remains explosive, showing that these toxins collectively made a surprisingly minor contribution to the pathogenesis of infection. As *Bacillus* spp. are aerophilic and motile, it was hypothesized that chemotaxis along an oxygen gradient led to the margination of *B. cereus* to the blood–retina barrier, leading to its compromise and ensuing inflammation. This hypothesis was tested directly in a rabbit model, where motile and nonmotile *B. cereus* strains were compared. It was observed that deficiencies in swarming prevented *Bacillus* from migrating to the anterior segment, leading to less severe anterior segment disease.

Propionibacterium acnes

Propionibacterium acnes is the leading cause of late-onset postoperative endophthalmitis, which is characterized by a chronic indolent course, and is frequently associated with recurrence after standard endophthalmitis treatment. The precise role of *P. acnes* virulence traits, however, is unclear. *Propionibacterium acnes* produces a variety of chemotactic factors and proinflammatory molecules that are responsible for inflammatory and immunomodulatory properties. These factors may be associated with pathogenesis of endophthalmitis, but have not been tested directly.

Gram-Negative Rods

Gram-negative rods, such as *Pseudomonas aeruginosa*, *Klebsiella pneumoniae, Serratia marscescens*, and *Escherichia coli*, are rarer causes of postoperative endophthalmitis, but cause post-traumatic or endogenous endophthalmitis and are usually associated with poor visual outcome. Although there are few experimental studies regarding the pathogenesis of Gram-negative rods in endophthalmitis, hypermucoviscosity is an important phenotype in the pathogenesis of experimental *K. pneumoniae* endophthalmitis.

The Host Response in Endophthalmitis

As noted earlier, breach of the globe following surgery or trauma is a major predisposing factor for endophthalmitis. The low rates of endophthalmitis, compared to the rate of contaminated traumatic injury or contamination during surgery, suggest that the host response plays an important role in eliminating organisms, preventing many more endophthalmitis. The other side of an effective host defense, however, is that an overly exuberant inflammatory response can induce irreversible damage of ocular tissues, including the retina. The balance between defense and destructive inflammation is only beginning to be understood in the context of endophthalmitis.

Defense against Bacteria

Toll-Like Receptors

Toll-like receptors (TLRs) are a family of pattern recognition receptors that initiate a rapid host innate immune response to microbial components, known as pathogen-associated molecular patterns (PAMPs). Ligand binding to TLRs results in activation of cellular signaling pathways that regulate expression of genes involved in inflammation and immunity. In humans, 10 types of TLR family receptors (TLR1–10) have been identified. PAMPs recognized by TLR 2 and 4 are the lipoteicoic acid of Gram-positive bacteria and the lipopolysaccharide of Gram-negative bacteria, respectively. The precise action of TLR in endophthalmitis is still unclear; however, recent *in vitro* and *in vivo* studies have demonstrated the expression and function of TLRs in the eye. In these studies, it was noted that TLR-2, TLR-4, and TLR-9 are expressed in the retina and retinal pigment epithelial cells and could play a role in protecting against or responding to bacterial pathogens in posterior segment.

Complement

The complement system is a biochemical cascade that helps clear pathogens from contaminated tissue. It is part of the innate immune system, although it can be recruited and activated by the adaptive immune response. It is known that several aqueous humor factors possess complement-inhibitory activity. The level of complement components in the eye is lower than in the serum, even in inflamed eyes. Studies using guinea pigs, rendered deficient in complement by treatment with cobra venom factor, suggested a role for complement in defense against *S. aureus* IOL infection. However, when mice that were genetically deficient in the central complement component, C3, were used, complement was comparatively inconsequential in the outcome of endophthalmitis.

Cellular infiltration

Clinical findings, such as hypopyon and dense infiltration of cells in the anterior or posterior segments, are characteristic features of endophthalmitis. The cells present are

mainly polymorphonuclear cells and are found in highest numbers in the vitreous cavity, trabecular meshwork, anterior and posterior lens capsule, ciliary body, retina, and the choroid. Neutrophils are recruited into eye through several cytokine signals. However, the rate and magnitude of cellular infiltration depend on the pathogen. For example, endophthalmitis caused by *S. epidermidis* is often associated with delayed onset of infiltration. Little is known about what determines the onset of infiltration in the context of endophthalmitis. Although neutrophils play a large role in the killing of pathogens, they produce retinotoxic products, such as metalloprotease or oxyradicals, which result in severe damage of retina. Therefore, for successful treatment, it is important to control cellular infiltration in endophthalmitis.

Proinflammatory Cytokines

Tumor necrosis factor alpha (TNF-α) is a cytokine involved in systemic inflammation and is a member of a group of cytokines that stimulate the acute phase reaction. In the eye, TNF-α is produced by astrocytes and by histiocyte-like cells in the iris ciliary body. It induces apoptotic cell death, cellular proliferation, differentiation, and inflammation. The primary role of TNF-α is in the regulation of immune cells. TNF-α is a strong activator of nuclear factor kappa B (NF-κB), a universally present transcriptional regulator that regulates the expression of chemokines, growth factors, and cell adhesion molecules. This cytokine is important for IOL pathogen containment by PMNs during experimental *B. cereus* endophthalmitis. In the absence of TNF-α, fewer PMNs migrate into the eye, facilitating faster bacterial replication and loss of retinal function. Thus, TNF-α might play a critical role in endophthalmitis.

Similar to TNF-α, Fas ligand (FasL) belongs to the TNF family and is a type II transmembrane protein. The binding of FasL with its receptor induces apoptosis. The FasL–receptor interactions play an important role in limiting the response of the immune system. Although it was hypothesized that limiting FasL–receptor interactions would enhance the host response in the eye (by limiting a key factor that limits the host response), when directly tested in C57B6 mice it was found to have the opposite effect. FasL knockout mice were not more resistant to infection, but were more sensitive, suggesting that FasL has an important role in activating infiltrating polymorphonuclear neutrophils (PMNs).

Interleukin-1 (IL-1) is a pro-inflammatory cytokine that is produced by macrophages, monocytes, and dendritic cells and is involved in immune defense against infection. Inside of the eye, IL-1 is produced in the Müller cells and ciliary body cells in response to different uveitogenic stimuli, and induces other inflammatory mediators such as prostaglandins, phospholipase A_2, collagenases, and other proinflammatory cytokines (IL-6 and TNF).

IL-6 is produced by numerous cell types and acts as both a proinflammatory and anti-inflammatory cytokine. IL-6 is induced by other cytokines such as (IL-1, gamma-interferon, and TNF-α). In the eye, IL-6 is produced primarily by retinal pigment epithelial cells. The role of IL-6 as an anti-inflammatory cytokine is mediated through its inhibitory effects on TNF-α and IL-1, and these effects may influence bacterial endophthalmitis.

Immunosuppressive Microenvironment of the Eye

Anticomplement Factors

The ocular microenvironment maintains immune privilege by manipulating regional innate and adaptive immunity away from inflammatory responses. Aqueous humor contains a rich supply of constitutively produced immunosuppressive molecules that prevent pathogen-induced inflammation. The aqueous humor contains neuropeptides, such as α-melanocyte-stimulating hormone and calcitonin gene-related peptide, which along with transforming growth factor-β, suppress the activation and inflammatory activity of macrophages. Although these factors have important roles in minimizing ocular damage by inflammation in endophthalmitis, they might help bacteria avoid clearance.

Anterior-Chamber-Associated Immune Deviation

The anterior chamber is a unique immune-privileged site, governed by anterior-chamber-associated immune deviation (ACAID), as characterized by Streilein and associates. Generally, delayed-type hypersensitivity (DTH) induces a high degree of immunogenic inflammation in which interferon-γ is a principal effector; however, in ACAID, DTH is profoundly suppressed, whereas the humoral immune response is intact or even enhanced. The role of ACAID in limiting damage in IOL infection, either in the anterior or posterior segment, is not well characterized. As noted earlier, bacteria in most cases enter the eye through the anterior chamber, where they may be initially recognized. The extent to which ACAID delays or limits this or limits the host response in the posterior segment is only now being studied.

Conclusion

Severe cases of bacterial endophthalmitis are characterized by massive inflammation in the eye. Although the disease is not common, when it does occur, it can lead to significant damage in the ocular tissue. The visual prognosis of this disease depends on virulence factors of the pathogen and the resulting host response, but the details

of this are only beginning to be understood. It is clear that bacterial toxins and proteases are important in the pathogenesis of enterococcal and staphylococcal infection, but it appears that other cellular traits, such as motility, play more important roles in infections caused by *B. cereus*. Biofilms undoubtedly contribute to the challenge of eliminating an infection, either by antimicrobials or the host response, once it sets in. On the one hand, the multiplicity of factors makes it difficult to generalize and design a single therapeutic approach to improve visual outcome. On the other hand, having multiple targets increases the likelihood that at least some of them may prove to be points for successful intervention in mitigating the destruction that occurs in this infection.

See also: Immunosuppressive and Anti-Inflammatory Molecules that Maintain Immune Privilege of the Eye; Innate Immune System and the Eye; Pharmacology of Aqueous Humor Formation; Role of Complement in Ocular Immune Response.

Further Reading

Behlau, I. and Gilmore, M. S. (2008). Microbial biofilms in ophthalmology and infectious disease. *Archives of Ophthalmology* 126: 1572–1581.

Callegan, M. C., Booth, M. C., Jett, B. D., and Gilmore, M. S. (1999). Pathogenesis of gram-positive bacterial endophthalmitis. *Infection and Immunity* 67: 3348–3356.

Callegan, M. C., Engelbert, M., Parke, D. W., 2nd, Jett, B. D., and Gilmore, M. S. (2002). Bacterial endophthalmitis: Epidemiology, therapeutics, and bacterium–host interactions. *Clinical Microbiology Reviews* 15: 111–124.

Callegan, M. C., Gilmore, M. S., Gregory, M., et al. (2007). Bacterial endophthalmitis: Therapeutic challenges and host–pathogen interactions. *Progress in Retinal and Eye Research* 26: 189–203.

Chang, J. H., McCluskey, P. J., and Wakefield, D. (2006). Toll-like receptors in ocular immunity and the immunopathogenesis of inflammatory eye disease. *British Journal of Ophthalmology* 90: 103–108.

Gregory, M., Callegan, M. C., and Gilmore, M. S. (2007). Role of bacterial and host factors in infectious endophthalmitis. *Chemical Immunology and Allergy* 92: 266–275.

Griffith, T. S., Brunner, T., Fletcher, S. M., Green, D. R., and Ferguson, T. A. (1995). Fas ligand-induced apoptosis as a mechanism of immune privilege. *Science* 270: 1189–1192.

Jackson, T. L., Eykyn, S. J., Graham, E. M., and Stanford, M. R. (2003). Endogenous bacterial endophthalmitis: A 17-year prospective series and review of 267 reported cases. *Survey of Ophthalmology* 48: 403–423.

Lieb, D. F., Scott, I. U., Flynn, H. W., Jr., Miller, D., and Feuer, W. J. (2003). Open globe injuries with positive intraocular cultures: Factors influencing final visual acuity outcomes. *Ophthalmology* 110: 1560–1566.

Streilein, J. W. (1996). Ocular immune privilege and the Faustian dilemma. The Proctor lecture. *Investigative Ophthalmology and Visual Science* 37: 1940–1950.

Taban, M., Behrens, A., Newcomb, R. L., et al. (2005). Acute endophthalmitis following cataract surgery: A systematic review of the literature. *Archives of Ophthalmology* 123: 613–620.

Taylor, A. W. (2003). A review of the influence of aqueous humor on immunity. *Ocular Immunology and Inflammation* 11: 231–241.

The Endophthalmitis Vitrectomy Study Group (1986). Microbiologic factors and visual outcome in the endophthalmitis vitrectomy study. *American Journal of Ophthalmology* 122: 830–846.

Tosi, M. F. (2005). Innate immune responses to infection. *Journal of Allergy and Clinical Immunology* 116: 241–249.

West, E. S., Behrens, A., McDonnell, P. J., Tielsch, J. M., and Schein, O. D. (2005). The incidence of endophthalmitis after cataract surgery among the U.S. Medicare population increased between 1994 and 2001. *Ophthalmology* 112: 1388–1394.

Pathogenesis of Fungal Keratitis

E Pearlman, S Leal, A Tarabishy, Y Sun, L Szczotka-Flynn, Y Imamura, P Mukherjee, and J Chandra, Case Western Reserve University, Cleveland, OH, USA
M Momany and S Hastings-Cowden, University of Athens, Athens, GA, USA
M Ghannoum, Case Western Reserve University, Cleveland, OH, USA

Glossary

Biofilm – The microbial secretion of an extracellular matrix surrounding the organisms.
Conidia – These are fungal spores.
Matrix metalloproteinases (MMPs) – The proteases that participate in tissue remodeling, wound healing, and inflammation.
Multipurpose solution (MPS) – The contact lens care products that are used to disinfect daily-wear contact lenses.
Toll-like receptor (TLR) – A family of surface and endosomal receptors that recognize microbial products. TLR signaling induces production of proinflammatory and chemotactic cytokines and antimicrobial peptides.

Contact-Lens-Associated Fungal Keratitis

In June 2006, the Centers for Disease Control and Prevention (CDC) *Fusarium* investigation team (Chang and colleagues) reported 318 cases of *Fusarium* keratitis, with 164 confirmed cases in 33 states and one US territory, although smaller outbreaks were reported in Singapore, Hong Kong, and France. The age group was between 12 and 83, with a median age of 41; 94% wore soft contact lenses; and keratoplasty was needed for 34%. (Examples of contact-lens-associated *Fusarium* keratitis are shown by Alfonso and colleagues.) The CDC study demonstrated a clear relation to the use of Bausch and Lomb Renu with MoistureLock multipurpose solution (MPS), and the number of cases of *Fusarium* keratitis dropped shortly after withdrawal of this product. As unopened bottles were sterile, and *Fusarium* can be readily isolated from sink and shower drains, the CDC report concluded that the source of infection was in the patients' homes. However, although the report implies that poor lens care habits were involved, it became clear that *Fusarium* clinical isolates were more resistant to disinfectants in the lens care solution than CDC strains that were used for comparison. Moreover, resistance was related to the ability of the microorganism's capacity to form biofilm (see below). Reports from several regions of the USA, including Florida and San Francisco, described cases of contact-lens-associated *Fusarium* keratitis demonstrating severe corneal opacification and descemetocele formation (hernia of Descemet's membrane), most of which required keratoplasty. The CDC also reported that the number of cases of *Fusarium* keratitis dropped after Renu with Moisture Lock was voluntarily withdrawn from the market. However, several cases have been reported subsequently that were not due to this lens care product and were most likely due to increased awareness of *Fusarium*, although the causes were not always apparent.

Biofilm Formation in Contact-Lens-Associated Keratitis

Biofilm is defined as microbial secretion of an extracellular matrix surrounding the organisms. Biofilm formation allows the organisms to resist antibiotics (20–1000 times more resistant than planktonic forms), and to host immune responses. The CDC report on the contact-lens-associated outbreak of *Fusarium* keratitis also suggested that biofilm formation contributes to the resistance phenotype, as bacterial biofilm can form on contact lenses and lens cases. Bacterial biofilms can be generated rapidly on contact lenses and may therefore contribute to the pathogenesis of keratitis and endophthalmitis. Imamura and co-workers showed that *Fusarium* forms a biofilm on silicone hydrogel contact lenses; furthermore, the architecture, thickness, and composition of the biofilm differ according to the contact lens type. It is likely that the conidia germinate on the contact lens surface, and favorable conditions allow biofilm development. Once the biofilm is formed, the organisms are more resistant to antifungal agents, including those in multipurpose lens care solutions. Consistent with this notion, the *Fusarium* strain used to test lens care solutions did not form a biofilm and was more sensitive to lens care solutions (**Figure 1**).

Keratitis Caused by *Candida*

Candida species are the most common pathogenic yeast associated with keratitis. *Candida albicans* is part of the normal commensal flora; however, these organisms can cause opportunistic corneal infections in immunosuppressed

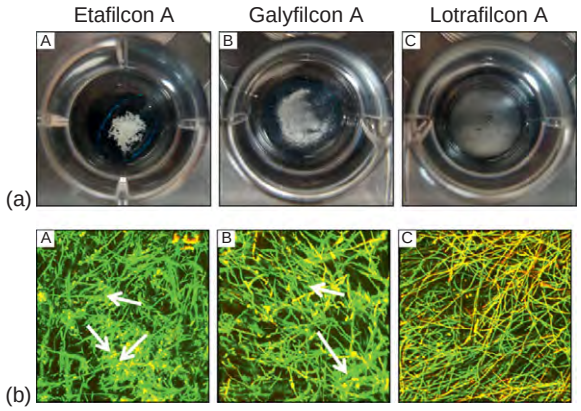

Figure 1 *Fusarium* biofilm formed on different soft contact lenses. (a) *Fusarium* conidia were incubated with each contact lens for 2 h, after which time the lenses were removed and incubated a further 48 h. Biofilms were formed by FSSC 1-b isolate MRL8609 on soft contact lenses, and their gross morphologies were imaged using a digital camera. All lenses tested supported biofilm formation by strain MRL8609. (b) The *Fusarium* FSSC 1-b strain MRL8609 was allowed to form mature biofilms on Etafilcon A silicon hydrogel contact lenses and then was stained with ConA and FUN1 dyes to show extracellular matrix (red) and live organisms (green). Stained lens-containing biofilms were analyzed by confocal scanning laser microscopy. Etafilcon A (A), galyfilcon A (B), lotrafilcon A (C), balafilcon A. Arrows indicate extracellular matrix in the biofilms. Similar results were found for *C. albicans* (not shown). Reprinted from Imamura, Y., Chandra, J., Mukherjee, P. K., et al. (2008). *Fusarium* and *Candida albicans* biofilms on soft contact lenses: Model development, influence of lens type, and susceptibility to lens care solutions. *Antimicrobial Agents and Chemotherapy* 52: 171–182.

individuals or following trauma or surgery. In contrast to filamentous fungi in which trauma is the major predisposing condition, *Candida* is primarily associated with therapeutic contact lenses, steroid use or immunosuppressive disease, and corneal surgery. In these dimorphic organisms, the yeast stage initially infects the cornea, and then germinates to form pseudohyphae in the corneal stroma. *Candida* produces a number of proteases and **phospholipases** (**particularly phospholipase B**) that facilitate their penetration through the cornea and contribute to tissue destruction. Using *C. albicans* mutants in a murine model of keratitis, Jackson and colleagues showed that *C. albicans* virulence depends on expression of genes encoding or regulating hyphal formation, but not genes regulating adherence.

Fungal Keratitis Associated with Trauma

Although relatively rare in North America and Europe, filamentous fungi are among the most common causes of microbial keratitis and corneal ulcers in India, China, and Ghana. In the southern USA, *Fusarium solani* and *Fusarium oxysporum* are the most common causes of mycotic keratitis, with *Aspergillus* species being the second most common cause, including *A. fumigatus*, *A. niger*, and *A. nidulans*.

Corneal trauma is the main predisposing factor, and the incidence of fungal keratitis increases during harvest season, which is consistent with the majority of cases associated with agricultural work, where it affects more males than females of working age. Trauma can be caused by numerous factors, such as airborne soil and plant material. Filamentous fungi are ubiquitous in the environment, especially on plants, and the fungal spores (conidia) can penetrate the corneal epithelium, germinate in the stroma, and if unchecked by the host response or effective antifungal therapy, fungal hyphae will grow in the corneal stroma, penetrate Descemet's membrane, and invade the anterior chamber.

Role of Matrix Metalloproteinases in Fungal Keratitis

Matrix metalloproteinases (MMPs) have an important role in tissue remodeling, wound healing, and inflammation. Rohini and co-workers examined human tears from fungal keratitis patients and corneal sections after keratoplasty and detected elevated collagenases MMP-2 and MMP-8, and the MMP-9 gelatinase, which is consistent with the activation and degranulation of infiltrating neutrophils. In addition to microbial killing, which is primarily mediated by oxygen radicals, neutrophils also prevent microbial dissemination by releasing MMPs and causing local tissue damage. Dong and co-workers as well as Mitchell and co-workers showed that MMP-2 and MMP-9 were also elevated in rabbit and mouse models of *Fusarium* and *Candida* keratitis, and Lin and colleagues demonstrated a role for MMP-8 in corneal inflammation by mediating breakdown of collagen and release of chemotactic Pro–Gly–Pro peptides, which then facilitate neutrophil migration through the cornea. Although differences between *Aspergillus* and *Fusarium* growth in the stroma have been reported by Xie and colleagues, it is not clear at present how this relates to MMP activity, or if there is a difference in protease production by these organisms.

Role of Innate Immunity in Fungal Keratitis

Since the 1960s, it has been apparent that the host immune response regulates fungal growth and the outcome of the infection. In rabbit and murine models of *Fusarium* and *Candida* keratitis in which either conidia or yeast is applied topically to the abraded epithelium, or is injected intrastromally, a neutrophil-rich cellular infiltrate into the corneal stroma ultimately clears the infection. However, subverting the host response by systemic

treatment with cyclophosphamide leads to increased hyphal penetration of the corneal stroma, decreased cellular infiltration, (especially neutrophils), and the unchecked growth of hyphae, causing corneal perforation. These results indicate that the host response plays a critical role in restricting fungal growth in the cornea. To characterize the host response to fungal challenge, *Candida*-infected corneas were processed for microarray analysis, which demonstrated that the proinflammatory cytokines, interleukin-1 (IL-1) and tumor necrosis factor-alpha (TNF-α), were upregulated. To characterize the innate immune response, Tarabishy and colleagues injected *Fusarium* conidia into the corneal stroma of immunocompetent C57BL/6 and mice on the same genetic background in which genes related to the Toll-Like Receptor (TLR) family of pathogen recognition molecules were knocked out. **Figure 2** shows that 6 h after intrastromal injection of 10 000 conidia, hyphae were detected in the corneal stroma of C57BL/6 mice and in mice in which the gene for the MyD88 adaptor molecule common to most TLRs and IL-1R1 is mutated. Although a cellular infiltrate was detected in the peripheral cornea of C57BL/6 mice, this infiltrate was absent in MyD88$^{-/-}$ mice. **Figure 3** shows that whereas C57BL/6 mice rapidly develop corneal opacification associated with a pronounced infiltrate and clear the organisms, MyD88$^{-/-}$ mice had delayed cellular infiltration, and even though neutrophils were recruited to the corneal stroma, they were unable to clear the organisms (**Figures 4** and **5**). *Fusarium* hyphae are detected throughout the cornea (**Figure 5**), which perforated within 4 days. Subsequent experiments showed that IL-1R1 is required for neutrophil recruitment to the cornea, whereas TLR4 is important for fungal killing.

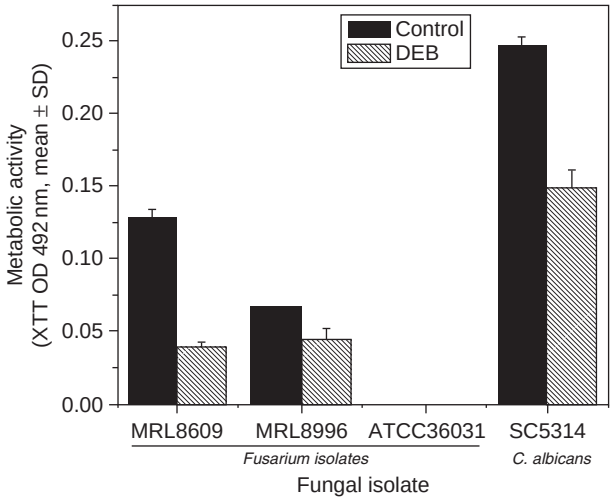

Figure 2 *Fusarium* strain differences in biofilm formation on lotrafilcon A lenses. Biofilms were formed in the absence or presence of DEB (which inhibits biofilm formation) on a lotrafilcon A lens using the FSSC 2-c ATCC 36031 reference isolate or clinical isolate FSSC 1-b (MRL8609), FOSC 3-a (MRL8996). Biofilms were quantified using the XTT metabolic activity assay. Data represent means (+/– SDs) calculated from three separate experiments. Reprinted from Imamura, Y., Chandra, J., Mukherjee, P. K., et al. (2008). *Fusarium* and *Candida albicans* biofilms on soft contact lenses: Model development, influence of lens type, and susceptibility to lens care solutions. *Antimicrobial Agents and Chemotherapy* 52: 171–182.

Murine Model of *Aspergillus* Keratitis

Aspergillus species, the second most common cause of fungal keratitis after *Fusarium*, are also ubiquitous in the environment, and most people inhale hundreds of conidia daily. Although pulmonary aspergillosis occurs primarily in immunosuppressed individuals, this is not the case in keratitis, where the risk factors are similar to those of *Fusarium*, that is, the highest incidence is associated with agriculture and trauma. In addition, *Aspergillus* conidia are smaller than *Fusarium* conidia, can therefore penetrate deeper into the lungs, and likely also penetrate deeper into the corneal stroma. We generated a strain of *Aspergillus fumigatus* expressing a red fluorescent protein, and injected conidia into the corneal stroma of C57BL/6 mice. **Figure 6** shows that after 24 h, the cornea is opaque. However, **Figure 6(b)** also shows that the presence of corneal opacities coincides with the presence of *Aspergillus*. **Figure 6(c)** shows higher magnification of hyphae in the corneal stroma. Ongoing studies are examining the role of the host response and *Aspergillus* virulence factors in the pathogenesis of this disease.

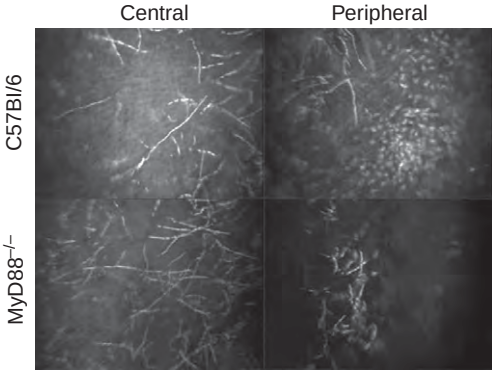

Figure 3 *In vivo* confocal microscopy of *Fusarium* keratitis in C57BL/6 and MyD88$^{-/-}$ corneas. C57BL/6 and MyD88$^{-/-}$ mice were injected intrastromally with 1 × 104 conidia from a clinical isolate of *F. oxysporum*. After 6 h, mice were examined by *in vivo* confocal microscopy (Confoscan). Representative images from the central and peripheral corneal stroma are shown. Note the presence of hyphae in the central corneal stroma of C57BL/6 and MyD88$^{-/-}$ mice (a, c); however, a cellular infiltrate is present in the peripheral cornea of C57BL/6, but not MyD88$^{-/-}$ mice (b, d). Reprinted from Tarabishy, A. B., Aldabagh, B., Sun, Y., et al. (2008). MyD88 regulation of *Fusarium* keratitis is dependent on TLR4 and IL-1R1 but not TLR2. *Journal of Immunology* 181: 593–600.

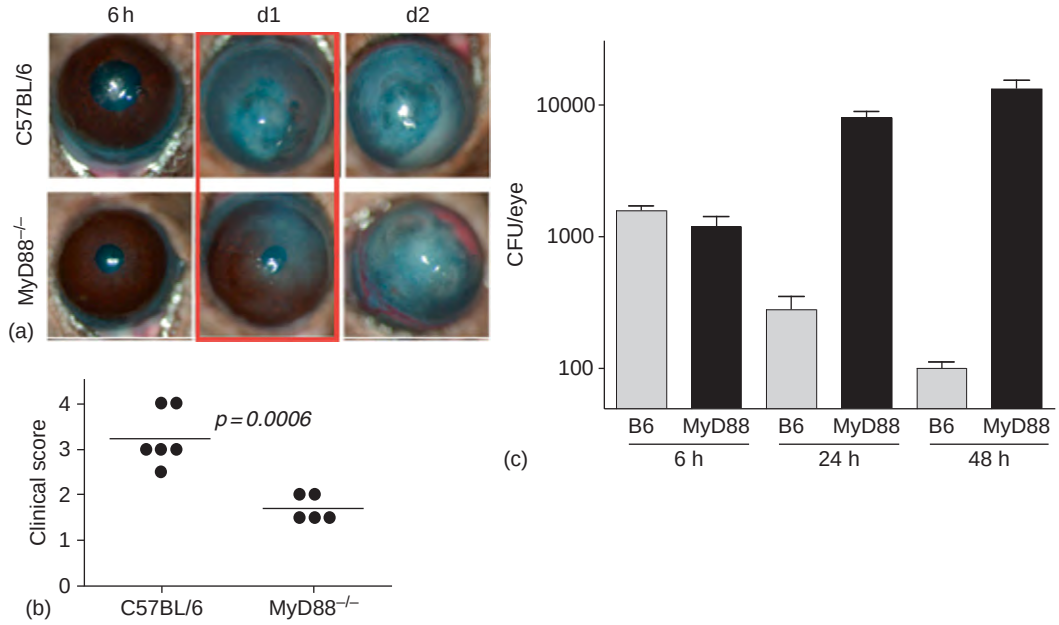

Figure 4 Fungal keratitis in C57BL/6 and MyD88$^{-/-}$ mice. Mice were injected intrastromally with 1 × 104 conidia from a clinical isolate of *F. oxysporum* as described above. Corneal opacification, CFU, and histology were examined by standard methods. (a, b) Corneal opacification in MyD88$^{-/-}$ mice was impaired at 24 h, but increased until 72 h after which time MyD88$^{-/-}$ corneas perforated, whereas C57BL/6 corneas eventually resolved. **(c)** CFU decreased in C57BL/6 mice over time, whereas *Fusarium* replicated in the corneas of MyD88$^{-/-}$ mice. Reprinted from Tarabishy, A. B., Aldabagh, B., Sun, Y., et al. (2008). MyD88 regulation of *Fusarium* keratitis is dependent on TLR4 and IL-1R1 but not TLR2. *Journal of Immunology* 181: 593–600.

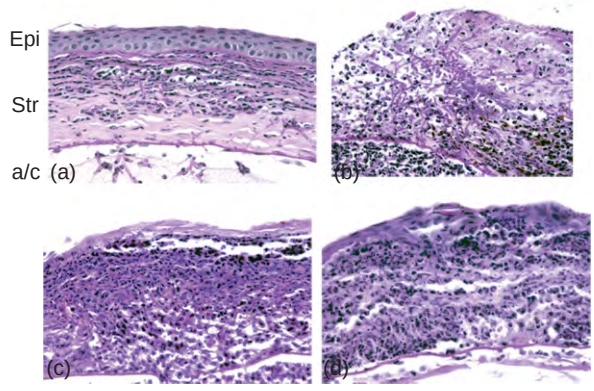

Figure 5 Impaired cellular infiltration in MyD88$^{-/-}$ mice (a, b) Histological analysis in MyD88$^{-/-}$ corneas after PAS staining shows *Fusarium* hyphae penetrating Descemet's membrane after 24 h, and growing in the stroma and anterior chamber after 48 h despite the presence of a cellular infiltrate. In contrast, there was an early and pronounced cellular infiltrate in C57BL/6 mice (c, d) comprised mostly of neutrophils. Reprinted from Tarabishy, A. B., Aldabagh, B., Sun, Y., et al. (2008). MyD88 regulation of *Fusarium* keratitis is dependent on TLR4 and IL-1R1 but not TLR2. *Journal of Immunology* 181: 593–600.

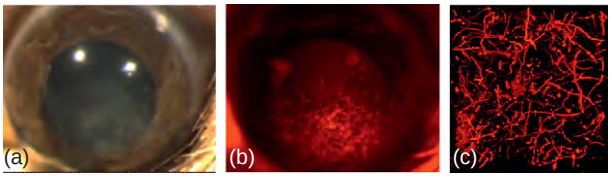

Figure 6 *Aspergillus fumigatus* in murine cornea. *Aspergillus fumigatus* was transfected with a plasmid expressing m-cherry. Conidia were injected into the corneal stroma of C57BL/6 mice, and after 24 h, corneas were examined by light (a) and fluorescence (b) microscopy. (c) Whole mount cornea examined by confocal microscopy.

Conclusions

The pathogenesis of fungal keratitis depends on the balance between the host response and expression of fungal virulence factors. Although some mediators of innate immunity and fungal virulence factors have been identified, it will require a combination of human and animal studies to determine the course of events leading to fungal killing and resolution of infection. Human disease correlates are particularly difficult to study; however, Bochud and co-workers showed that polymorphisms in TLR4 are associated with susceptibility to systemic aspergillosis; therefore, it is possible that TLR4 also mediates susceptibility to *Aspergillus* keratitis.

Acknowledgments

Studies presented in this article were supported by NIH grant EY18362 (EP) and EY11373 (EP), by DE017486-01A1 (MAG) and R01DE 13932 (MAG), and by the Research to Prevent Blindness Foundation and the Ohio Lions Eye Research Foundation.

See also: Contact Lenses; Corneal Epithelium: Response to Infection; Innate Immune System and the Eye.

Further Reading

Alfonso, E. C., Cantu-Dibildox, J., Munir, W. M., et al. (2006). Insurgence of *Fusarium* keratitis associated with contact lens wear. *Archives of Ophthalmology* 124: 941–947.

Bharathi, M. J., Ramakrishnan, R., Meenakshi, R., et al. (2007). Microbial keratitis in South India: Influence of risk factors, climate, and geographical variation. *Ophthalmic Epidemiology* 14: 61–69.

Bochud, P. Y., Chien, J. W., Marr, K. A., et al. (2008). Toll-like receptor 4 polymorphisms and aspergillosis in stem-cell transplantation. *New England Journal of Medicine* 359: 1766–1777.

Chang, D. C., Grant, G. B., O'Donnell, K., et al. (2006). Multistate outbreak of *Fusarium* keratitis associated with use of a contact lens solution. *Journal of the American Medical Association* 296: 953–963.

Dong, X., Shi, W., Zeng, Q., and Xie, L. (2005). Roles of adherence and matrix metalloproteinases in growth patterns of fungal pathogens in cornea. *Current Eye Research* 30: 613–620.

Grant, G. B., Fridkin, S., Chang, D. C., and Park, B. J. (2007). Postrecall surveillance following a multistate *Fusarium* keratitis outbreak, 2004 through 2006. *Journal of the American Medical Association* 298: 2867–2868.

Imamura, Y., Chandra, J., Mukherjee, P. K., et al. (2008). *Fusarium* and *Candida* albicans biofilms on soft contact lenses: Model development, influence of lens type, and susceptibility to lens care solutions. *Antimicrobial Agents and Chemotherapy* 52: 171–182.

Jackson, B. E., Wilhelmus, K. R., and Mitchell, B. M. (2007). Genetically regulated filamentation contributes to *Candida* albicans virulence during corneal infection. *Microbial Pathogenesis* 42: 88–93.

Mitchell, B. M., Wu, T. G., Chong, E. M., Pate, J. C., and Wilhelmus, K. R. (2007). Expression of matrix metalloproteinases 2 and 9 in experimental corneal injury and fungal keratitis. *Cornea* 26: 589–593.

Pearlman, E., Johnson, A., Adhikary, G., et al. (2008). Toll-like receptors at the ocular surface. *Ocular Surface* 6: 108–116.

Rohini, G., Murugeswari, P., Prajna, N. V., Lalitha, P., and Muthukkaruppan, V. (2007). Matrix metalloproteinases (MMP-8, MMP-9) and the tissue inhibitors of metalloproteinases (TIMP-1, TIMP-2) in patients with fungal keratitis. *Cornea* 26: 207–211.

Tarabishy, A. B., Aldabagh, B., Sun, Y., et al. (2008). MyD88 regulation of *Fusarium* keratitis is dependent on TLR4 and IL-1R1 but not TLR2. *Journal of Immunology* 181: 593–600.

Wu, T. G., Keasler, V. V., Mitchell, B. M., and Wilhelmus, K. R. (2004). Immunosuppression affects the severity of experimental *Fusarium* solani keratitis. *Journal of Infectious Diseases* 190: 192–198.

Xie, L., Zhai, H., Shi, W., et al. (2008). Hyphal growth patterns and recurrence of fungal keratitis after lamellar keratoplasty. *Ophthalmology* 115: 983–987.

Yuan, X., Mitchell, B. M., and Wilhelmus, K. R. (2008). Gene profiling and signaling pathways of *Candida* albicans keratitis. *Molecular Vision* 14: 1792–1798.

Pathogenesis of Uveitis in Humans

J V Forrester, University of Aberdeen, Aberdeen, UK

Glossary

Alarmins – The molecules that register danger and, thus, activate the adaptive immune system. These occur in the absence of infection but are capable of inducing inflammation.

Dendritic cells (DCs) – The professional antigen-presenting cells that process and present antigens to T cells.

Experimental autoimmune uveitis (EAU) – An animal model of posterior segment uveitis is elicited when rodents are immunized with interphotoreceptor binding peptide (IRBP) or retinal S-antigen (S-Ag) emulsified in complete Freund's adjuvant (CFA). The inflammation is usually progressive and destroys the retina.

Immune privilege – A condition in which immune responses are either blunted or deviated such that inflammation is reduced and sometimes completely silenced. This is present in the eye and brain and is believed to be an adaptation for controlling inflammation in organs with limited regenerative capabilities.

Pathogen-associated molecular patterns (PAMPs) – The molecular arrays that are present on various microorganisms and are recognized by elements of the innate and adaptive immune systems. These are believed to be important red flags for alerting the immune system, especially cells of the innate immune system, which act as first responders.

T regulatory cells (T regs) – The lymphocytes that maintain self-tolerance and suppress adaptive immune responses. They are believed to be important in preventing or dampening autoimmune responses.

Introduction

Uveitis is a misnomer. The anatomical term for the middle coat of the eye, the uvea, derives from the Latin word meaning grape and was applied to this layer of the eye wall by eighteenth-century anatomists due to the similarity of the intact globe to a large black grape when the outer scleral layer has been removed. The uvea is the lymphovascular layer of the eye and was originally considered to be the target site or locus of inflammation in uveitis. However, although many cases of inflammation could be directly attributed to an infectious agent, numerous studies over many years failed to identify any specific cause in a majority of cases. This led experimental pathologists to the idea of uveitis as an autoimmune condition, and indeed sympathetic ophthalmia, a condition in which the uninjured eye becomes inflamed after penetrating injury to the first eye, probably ranks as the first-described autoimmune disease. Sympathetic ophthalmia had been known from the time of Hippocrates, and was given its name by William McKenzie in 1854, but it was not until the young science of immunology had emerged that this condition was considered autoimmune, that is, a breakdown in tolerance to self-antigens, leading to a specific inflammatory disease.

Since sympathetic ophthalmia was clearly organ specific, and the uvea seemed to be the site of inflammation, it was inevitable that the uveal tract was considered to be the site where the specific self-antigen (autoantigen) was located. Experimental studies were embarked upon to prove this point. These were similar to experiments in other presumed autoimmune animal models of disease, such as encephalomyelitis, where antigenic extracts of brain and spinal cord material were shown to induce inflammation of the central nervous system (CNS) after intradermal inoculation into guinea pigs in an oily emulsion with adiuvant, usually extracts of mycobacteria (complete Freund's adiuvant (CFA)). However, repeated attempts to induce experimental uveitis using intradermal extracts of uveal tissue were not very effective or reproducible. In contrast, a single extract of retinal tissue produced a massive, aggressive, organ-specific ocular inflammation (panuveitis) and further experiments identified the retinal photoreceptor as the source of specific antigens which could cause uveitis/uveoretinitis. This produced a significant conceptual shift in the nature of uveitis as a disease, and has since broadened into considering inflammation of the uveal tract *per se* (uveitis) as one aspect of intraocular inflammation which is distinguishable from extraocular inflammation involving the conjunctiva, the eye lids, or the ocular adnexae. The importance of these experimental studies in shaping our ideas about human uveitis cannot be underestimated.

Currently, it is recognized that there are several retinal and other ocular autoantigens which can induce eye-specific inflammation and that the many clinical forms of human uveitis represent a spectrum of disease which can be

reproduced in different animal models using one or several retinal antigens, that is, there is a common pathway for the pathogenesis of many forms of intraocular inflammation and this includes infectious causes (**Figures 1(a) and 1(b)**). It is important, however, to note that certain pathogens and autoantigens commonly present with characteristic and recognizable clinical signs, which may allow a specific clinical diagnosis, for example, infective cytomegalovirus (CMV) retinitis and autoimmune Vogt–Koyanagi–Harada (VKH) disease, in which one of the autoantigens is a tyrosinase-related protein. Nevertheless, the underlying tissue-damaging processes in most forms of uveitis have many similarities. Interestingly, there is recent evidence that there may be immunological cross-reactivity between tyrosinase peptides and CMV envelope protein peptides.

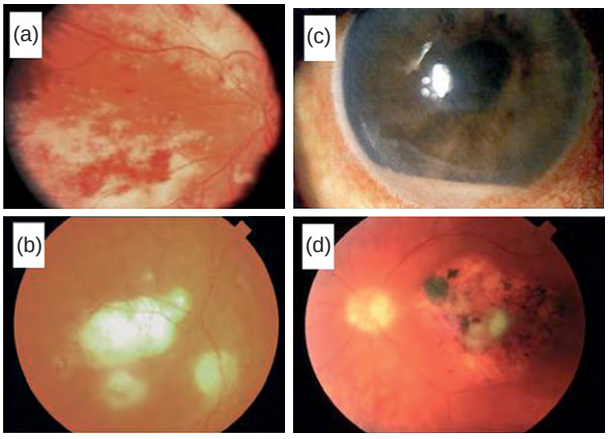

Figure 1 Photographs (a), (b), and (d), show posterior segment of the eye, and (c) shows the anterior segment of the eye of infective and noninfective human uveitis. (a) cytomegalovirus uveoretinitis; (b) toxoplasma chorioretintis; (c) and (d) Behcet's disease.

Causes of Human Uveitis

For centuries, ocular inflammation associated with infective and contagious diseases such as syphilis, rubella, and tuberculosis (TB) has been recognized. All known classes of microorganisms can cause uveitiic disease (**Figure 2**). Whether the ocular damage is caused directly by the infective agent or is the result of the host response to the infectious agent is often not clear, and is only resolved by recourse to a trial of specific therapy, for example, with an antiviral agent.

Infectious Uveitis

Viral disease

Many viruses can cause intraocular inflammation but most of these are of the herpes group, such as herpes simplex, herpes zoster, or CMV. Herpetic infections are contracted during early childhood and in most cases are subclinical. However, the virus remains latent in the ganglia of the nerves and may be reactivated during stress. Recent studies in herpes simplex have revealed that viral latency is achieved in part through virus-specific regulatory $CD8^+$ T cells residing in contact with the latently infected neural cell bodies. This may explain why viral reactivation with severe retinitis and encephalitis occurs in immunocompromised patients. In addition to herpetic disease, other viral diseases affecting the eye which can cause uveoretinitis and retinal vasculitis include

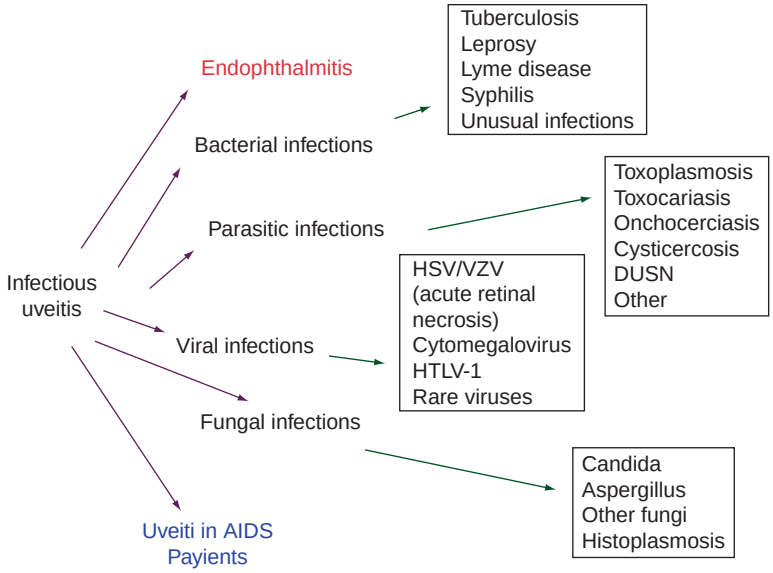

Figure 2 Infective causes of uveitis. HSV, herpes simplex virus; VZV; varicella zoster virus, HTLV-1, human T lymphotrophic virus-1; DUSN, diffuse unilateral subacute neuroretinitis (caused by parasitic worms).

ricekttsial disease and dengue virus, as well as West Nile fever, both of which are vector-borne diseases. The clinical manifestations are indistinguishable from idiopathic retinal vasculitis and frequently there is involvement of the macula in dengue fever while West Nile fever presents as a self-limiting multifocal choroiditis.

In the pathogenesis of viral disease, there is little doubt that replicating virus kills infected cells and in the case of herpes virus, this usually applies to epithelial or neuronal cells. In the eye, direct infection of the retinal nerves and/or the retinal pigment epithelium may explain the progressive clinical brush-fire signs typical of CMV retinitis and HSV-induced acute retinal necrosis, and progression in untreated acquired immune deficiency syndrome (AIDS) patients probably reflects this unchecked disease. However, in immunocompetent individuals with, for instance, HSV-associated recurrent anterior uveitis, or in treated AIDS patients with immune-recovery uveitis, the intraocular inflammation is probably not directly due to the virus but to the host-antiviral immune response.

Parasitic disease

The recognition that toxoplasmosis was a common cause of posterior uveitis, more common than TB, was due to the observations on excised eyes by Wilder Foerster, who demonstrated characteristic trophozoites in 41 adult eyes enucleated for pain and blindness. Despite this, congenital toxoplasmosis contracted *in utero* from maternal infection was considered the main type of ocular toxoplasmosis. It was not till the advent of AIDS that the extremely widespread subclinical infection with toxoplasmosis acquired in adulthood, mostly through ingestion of infected meat and detectable by rising frequency of antitoxoplasma antibodies in the general population, was widely appreciated although authors such as Rieger had suggested this. Pathogenetically, therefore, parasitic infection with toxoplasma organisms is the norm for many adults worldwide and a level of unconscious symbiosis is reached probably because this parasite is intracellular and has disabled macrophage-killing mechanisms while utilizing release of interferon gamma (IFNγ) to suppress CNS inflammation. Only in a few individuals does the organism die *in vivo* and this sets up an inflammatory reaction which is severe if it involves a critical tissue such as the macular area of the retina, or a vital CNS or liver component. As always, in patients who are immunocompromised, as in AIDS patients, the likelihood of this occurring is greatly increased since, although the immune system is evaded, it is not completely disabled and this delicate balance between infection and parasitization is disturbed in AIDS patients.

Other parasitic diseases, such as toxocara, loa loa, cysticercosis, and similar nematodes, can also damage the eye and may do so directly as extracellualr pathogens, as they track through the tissues leaving a pigmentary retinochoroiditis, or a vitreous abscess.

Fungal infections

Most fungal infections are quasi-commensal since they tend to colonize mucosal and skin surfaces. However, they can on occasion invade the tissues, and produce severe systemic infections. Certain fungal infections can directly damage ocular tissues such as the retina and vitreous if they gain access through the bloodstream to the eye, as in intravenous drug users who use infected needles and inject infected substances. In these cases, damage is usually due to the innate immune response induced in the tissues by the organism. For instance, *Candida albicans* generates a massive polymorphonuclear response with abscess formation and tissue damage due to the release of proteolytic enzymes. The pathogenesis of ocular disease in these cases is relatively clear.

More recently, subtle low-grade uveitic disease has been attributed to fungal infection. In the USA, certain forms of subretinal neovascularization with membrane formation have been attributed to low-grade inflammation caused by histoplasma. However, the evidence for histoplasma infection is minimal in these cases, since a similar if not identical clinical condition occurs in Europe and in nonendemic regions of the USA where histoplasma, a soil-residing organism, does not occur. More recently, evidence of antifungal immune reactivity to Candida antigens has been found in patients with certain forms of chronic, progressive posterior uveitis such as serpiginous choroiditis and the ill-defined condition, acute zonal occult outer retinopathy (AZOOR), and thus the possibility that low-grade chronic uveitis may represent damage due to a host-antifungal response from a persistent systemic source of infection requires further investigation.

Pathogenetically, chronic low-grade experimental autoimmune uveoretinitis can be associated with subretinal/intraretinal neovascularization in the late stages, and so a general pathological mechanism may explain this type of uveitic disease, which can produce devastating blindness.

Bacterial infections

Direct suppurative bacterial intraocular infection is not generally regarded as uveitis, but is considered a specific condition, that is, endophthalmitis. It is usually a consequence of direct intraocular inoculation of bacteria as a result of penetrating injury or surgery. However, some forms of postoperative infection can produce a grumbling low-grade inflammation, which is indistinguishable from chronic non-infectious uveitis and only resolve when the intraocular lens implant and the lens capsular bag containing the organism (e.g., propionbacterium) are removed.

Endogenous metastatic bacterial endophthalmitis can also occur usually as part of septicemia from a source of infection elsewhere such as in the kidney or gall bladder.

Bacterial infections may also underlie the pathogenesis of nonendophthalmitic uveitic disease. In patients with

various forms of posterior uveitis including multifocal choroiditis, retinal vasculitis, or panuveitis, infectious agents such as TB, syphilis, *Borrelia burgdorferi* (Lyme disease), and other micro-organisms are considered causative, particularly in endemic areas.

The relationship between active infection and tissue-destructive disease is complex: is loss of function and/or death due to the direct effects of the organism or due to the host defense response as it attempts to get rid of the organism? In this respect, TB presents a model example. Active TB is a global problem and it is estimated that one-third of the world's population is infected. However, the vast majority of patients (>90%) do not have symptoms, that is, the infection is latent. In some recent studies using a sensitive IFNγ-releasing assay, said to be specific for TB, some common and even obscure uveitic conditions have been attributed to tuberculosis. However, there is some concern over the high level of false positives using this assay.

The organism *Mycobacterium tuberculosis* (MTb) infects and resides in macrophages. Nonpathogenic forms of the bacterium kill the macrophage by apoptosis, a process which permits the apoptotic cell membrane to envelop the MTb and prevent its replication. The dead macrophage and its contents are phagocytosed, degraded, and removed by other macrophages. Pathogenic MTb evades this immune response by preventing the apoptotic process and induce a level of necrosis (central caseation) which permits MTb proliferation in the center of the immune granuloma, a structure now recognized to have a degree of immune privilege. A progressively stronger immunological reaction then develops with mounting tissue damage, while the surviving and proliferating MTb act as a sustained source of antigen. In patients with TB-associated disease, especially uveitic disease, it is unclear whether the uveitis is a direct result of infection of ocular tissues or whether it is, as for other infectious diseases, a host response to mycobacterial antigens, released from dead or dying bacteria. The adiuvant effect of mycobacteria is well known to immunologists and a chronic source of extraocular infection could provide a similar *in vivo* adiuvant effect in the presence of cross-reactive antigen. Alternatively, the protective effect of vaccination for MTb could actually generate IFNγ-producing $CD4^+$ Th1 cells which, while limiting bacterial growth, may have a deleterious effect on tissues. Evidence exists that the differential ability of pathogens to induce cytokine in antigen-presenting cells determines the outcome of the infection.

Noninfectious Uveitis

Associated with systemic disease

Several noninfectious conditions are associated with uveitis including sarcoidosis, tubulointerstitial nephritis, and HLA-B27-associated diseases such as ankylosing spondylitis, juvenile idiopathic arthritis, and inflammatory bowel disease. In some of these diseases, the condition is restricted to the anterior segment, while in others there is selective posterior-segment involvement. The etiology and pathogenesis of many of these conditions are obscure but they are commonly believed to be due to autoimmunity to one of more antigens, some of which are widely distributed such as collagen type II or connective tissue proteoglycans, while others are tissue restricted. Sarcoidosis is unusual in this respect in that it has many of the pathological features of TB without the central caseation in the granulomatous lesions. Accordingly, many believe that it has an atypical mycobacterial infectious origin.

As part of a characteristic syndrome

Behcet's disease

This condition also has many characteristics of an infectious disease without clear evidence of an infectious cause. Although described as an entity by Behcet and Adamatiades in the early part of the twentieth century, the condition has an ancient history, being first described by Hippocrates in his book Epidemion. Behcet's disease is common in the Middle East and Asia and has devastating effects on the eye and the CNS, leading to blindness in many cases, mostly due to an occlusive vasculitis. The ocular lesions are very similar to idiopathic retinal vasculitis. Immunologically, it has been difficult to identify any single autoantigen which may be involved and attention has been more recently directed toward a role for the innate immune system in this disease, as a form of auto-inflammatory disease. In particular, polymorphisms in the pathogen-recognition receptor, CARD15 have been described as well as involvement of the natural killer (NK) cell/dendritic cell (DC) cytokine interleukin 15 (IL15).

VKH disease

VKH disease, also known for many years, is a common cause of uveoretinitis in the Far East. Although thought to have a possible infectious etiology, autoimmunity to melanocytic antigens has been demonstrated, and experimentally, antigens to tyrosinase and to tyrosinase-related proteins can produce a similar disease in animals. Interestingly, IL23 and IL17 have been implicated in the pathogenesis of disease in humans.

Idiopathic

This last group of conditions probably comprises the most frequent set of conditions and includes idiopathic retinal vasculitis, multifocal choroiditis, intermediate uveitis, and its variants such as pars planitis, and several vague conditions known as the white-dot syndromes which have considerable clinical overlap. Included in this is sympathetic ophthalmia, probably the first uveitic condition as well

as the first autoimmune disease recognized. Considerable effort has been expended attempting to demonstrate autoimmunity to retinal antigens in many of these conditions and some good evidence has been generated. Despite the fact that several retinal antigens are now recognized as autoantigens, interphotoreceptor retinal-binding protein and its epitopes appear to be a dominant antigen in human disease. However, it is unlikely that a single antigen is the sole culprit particularly for chronic prolonged disease in which inter- and intramolecular epitope spreading are likely to generate reactivities to several potential uveitogenic peptides. The best evidence that idiopathic uveitis is immune mediated, if not directly autoantigenic, is the beneficial response to immunosuppressive agents, an observation that also applies to infectious uveitis, such as toxoplasmosis and tuberculosis, in which there is likely to be a significant and potentially tissue-damaging host immune response.

Classification of Human Uveitis in the Context of Pathological Signs

The bewildering variety of infectious and noninfectious conditions that can present as uveitis or intraocular inflammation has hindered the classification and delayed understanding of the pathological processes at play. Recently, a clinical classification of uveitis has been introduced by the standardization of uveitis nomenclature (SUN) group which has assisted in simplifying the clinical description of uveitis and this should be of considerable value in conducting studies of therapies which will be comparable between centers.

Thus, uveitis is categorized as anterior, intermediate, or posterior on an anatomical basis.

In addition, it is helpful when describing sight-threatening disease to restrict the description to a minimum number of signs which represent activity. Thus, anterior uveitis can be graded for severity on the level of cells and flare (protein) in the anterior chamber, while posterior uveitis can be graded on four basic signs: the level of haze in the vitreous cavity (due to vitreous cellular infiltrates), the number and size of chorioretinal infiltrates (microgranulomata), the degree of retinal vessel inflammation (retinal vasculitis), and the presence of edema (usually macular edema, and also optic nerve swelling and in severe cases, exudative retinal detachment). These signs roughly approximate to the classical signs of inflammation in any tissue and are helpful in correlating pathogenetic mechanisms in experimental and clinical disease.

Pathogenetic Mechanisms in Uveitic Disease

Inflammation is the response of the tissues, or the whole organism, to attack. Attack usually takes the form of invasion by foreign (nonself) microorganisms mediated by pathogen-associated molecular patterns (PAMPs), or can be due to various forms of trauma (danger-associated molecular patterns, DAMPs or alarmins). The organism can also respond to self-antigens if these are altered in any way or presented in a different format or context. Some believe that autoimmune disease is merely an extension of the organism's response to a danger signal represented by pathogenic microorganisms or altered self. Nonpathogenic (commensal) microorganisms and normal self-antigens do not constitute danger and no response occurs to them. This concept can be taken further into the organism by suggesting that some tissues, such as the skin and the lung, respond strongly to danger, and to a wider range of signals, than other tissues such as the brain and the eye. Thus, this provides a novel perspective on immune privilege of certain tissues, of which the eye is the paramount example.

From the above information on the many causes of uveitis in humans, uveitis can be considered the response of the intraocular compartment to a danger signal. This might be an infectious agent (*vide supra* toxoplasma) or it might be an immune-privileged photoreceptor antigen released from the eye after injury (*vide supra* sympathetic ophthalmia). In both cases, the antigen resides in the healthy tissues without causing inflammation, but when the circumstances or conditions change, inflammation ensues.

Thus, the antigen resides in the eye but the cells which induce the inflammation occur outside the eye. In addition, in the case of antigens, a specific (T-cell) response is required. How does this occur?

Tolerance and Its Dysregulation

The initial response to danger signals occurs through the innate immune system in which certain PAMPs are recognized by cells such as DCs and macrophages, NK cells, and gamma–delta T cells. PAMPs activate signal-transduction cascades and induce gene transcription in innate immune cells to generate proinflammatory cytokines. In addition, these cells process foreign antigens, which are then presented to T cells, activating them to enter clonal expansion, release cytokines, and express homing molecules for migration to the site of foreign antigen where they recruit further inflammatory cells, thus removing the antigen, downregulating the inflammation, and repairing the tissue. Self-antigens may also activate PAMPs through generation of DAMPs (alarmins) molecules, which register danger in the absence of infection and induce a similar inflammatory response in the appropriate conditions.

A potentially tissue-damaging response such as the above must be tightly regulated. Regulation of responses to self is mediated through tolerance. Tolerance is generated centrally by essentially deleting all potential self-reactive T-cell clones that might be generated by random

T-cell receptor recombinatorial mechanisms (a similar process occurs in B cells for immunoglobulin molecules), and in the periphery by anergy, deletion, and by generation of a special set of cells known as T regulatory cells (Tregs). Tolerance to nonpathogenic organisms, and even to some potentially pathogenic organisms, is also generated via peripheral mechanisms such as Tregs and by evolutionarily robust evasive tactics utilized by each type of microorganism. Thus, latency, for instance, in herpes viruses and in TB (it is estimated that less than 10% of individuals infected by TB have active disease), represents one form of immune evasion adopted by the microorganism. In a similar manner, the toxoplasma organism resides intact inside macrophages whose killing mechanisms have been disabled.

Self-Antigens versus Foreign Antigens

In inflammatory disease, this homeostatic balance is disturbed. In infectious disease, the organism responds by generating a powerful inflammatory response to get rid of the foreign antigen. In tissues such as the skin, repair of the tissue ensues but an adaptive T- and B-cell response is generated. In tissues such as the eye, the organism may not be able to invoke an immune response because of privilege but memory T cells are now present in the organism available for recall responses, should there be re-infection or even a nonspecific injury (DAMP) response which leads to a cross-reactive immune response. T-cell responses in particular are somewhat degenerate in that a single T cell can respond to a range of antigenic peptides at different levels. Thus, this supposedly tightly regulated adaptive immune response is leaky and cells activated by foreign antigens may have the potential to cross-react with self or other foreign antigens. Clinically, this bystander response is recognized by the increased risk of a recurrent attack of uveitis in patients who have an intercurrent unrelated infection.

Are Antigen-Specific Cells Required to Cause Damage?

As can be deduced from the above discussion, antigen specificity may not be exclusive and, indeed, since there are not only many self-antigens but also many antigens on a single microorganism, it is likely that immune-mediated damage will reflect responses to sets of antigens rather than a single antigen. Despite this, it is recognized that one or a restricted set of antigens in any condition is dominant. In contrast, cells recruited to the tissue to promote damage are relatively nonspecific, although they may be programmed for different activities. These include inflammatory macrophages and T/B cells brought in as part of the overall inflammatory response. For this reason, therapeutic approaches which target the cells causing the damage, such as macrophages and cytokine-producing cells, have proven to be effective in human uveitis, even where the specific causes are unknown.

Cells Regulating Disease

These concepts allow for new approaches to the control of human uveitis. As indicated above, cells regulating inflammation include Tregs which are probably important in downregulating or limiting inflammation. The most well-studied Treg population are the $CD4^+CD25^+$ T cells which occur naturally in the bloodstream at a level of around 3–8%. Two types of Tregs occur, natural Tregs and antigen-specific Tregs. Antigen-specific Tregs are the more suppressive cell type but they can be suppressive to a broad range of T-cell specificities.

Clinical studies of patients with autoimmune diseases, including VKH disease, have suggested that Treg populations are reduced and it has been hypothesized that this permits autoaggressive Tregs to act unhindered. Recent studies on patients with noninfectious uveitis have shown that Treg populations in the bloodstream are reduced, supporting this mechanism of pathogenesis. Experimental studies of autoimmune diabetes, as well as uveoretinitis, have also shown that vaccination with peptide-pulsed DCs suppresses inflammation by expanding Tregs. This approach could be considered for customized control of human uveitis.

Conclusion

In recent years, it has become clear that the classical division between infectious and noninfectious causes of immune-mediated diseases has become blurred at least in pathogenetic terms. On the one hand, there are many obviously infectious causes of sight-threatening uveitis, which respond well to specific antibiotic treatment, but many others in which the immune component (host response) may itself lead to severe tissue damage; this can be ameliorated by immunosuppressive treatments. On the other hand, well-defined autoimmune, noninfectious uveitis has been difficult to demonstrate in humans despite the well-described experimental models of autoimmune disease. Perhaps, there is a collaboration between the microbe and the host, the resultant of which can lead to many outcomes, including the most beneficial one to the host (i.e., clearance of the microbe), parasitism and latency, which are beneficial to the microbes (the most common outcome), or chronic disease in which active infection may be suspected but difficult to detect (e.g., sarcoidosis), but a dysregulated immune response sustains

a chronic, persistent response to sequestered (foreign or self) antigen. This unifying view of disease pathogenesis may help us to develop alternative approaches to their management.

See also: Adaptive Immune System and the Eye: T Cell-Mediated Immunity; Immunobiology of *Acanthamoeba* Keratitis; Immunopathogenesis of Onchocerciasis (River Blindness); Immunopathogenesis of Pseudomonas Keratitis; Innate Immune System and the Eye; Microvillar and Ciliary Photoreceptors in Molluskan Eyes; Pathogenesis and Immunology of Bacterial Endophthalmitis; Pathogenesis of Fungal Keratitis; Pathogenesis of Uveitis in Humans; Photoresponse in Squid; Primary Open-Angle Glaucoma.

Further Reading

Al-Otaibi, L. M., Porter, S. R., and Poate, T. W. (2005). Behcet's disease: A review. *Journal of Dental Research* 84: 209–222.

Ben Ezra, D. and Forrester, J. V. (1995). Fundal white dots: The spectrum of a similar pathological process. *British Journal of Ophthalmology* 79: 856–860.

Caspi, R. (2008). Autoimmunity in the immune privileged eye: Pathogenic and regulatory T cells. *Immunologic Research* 42(1–3): 41–50.

de Smet, M. D. and Chan, C. C. (2001). Regulation of ocular inflammation – what experimental and human studies have taught us. *Progress in Retinal and Eye Research* 20: 761–797.

Drake, W. P. and Newman, L. S. (2006). Mycobacterial antigens may be important in sarcoidosis pathogenesis. *Current Opinion in Pulmonary Medicine* 12: 359–363.

Dye, C., Scheele, S., Dolin, P., Pathania, V., and Raviglione, M. C. (1999). Consensus statement. Global burden of tuberculosis: Estimated incidence, prevalence, and mortality by country. WHO Global Surveillance and Monitoring Project. *Journal of the American Medical Association* 282: 677–686.

Faure, J. P. (1980). Autoimmunity and the retina. *Current Topics in Eye Research* 2: 215–302.

Forrester, J. V. (1991). Uveitis: Pathogenesis. *Lancet* 338: 1498–1501.

Forrester, J. V., Okada, A., BenEzra, D., and Ohno, S. (1998). *Posterior Segment Intraocular Inflammation: Guidelines*. The Hague: Kugler.

Forrester, J. V., Xu, H., Lambe, T., and Cornall, R. (2008). Immune privilege or privileged immunity? *Mucosal Immunology* 1: 372–381.

Imrie, F. R. and Dick, A. D. (2007). Biologics in the treatment of uveitis. *Current Opinion in Ophthalmology* 18: 481–486.

Jabs, D. A., Nussenblatt, R. B., and Rosenbaum, J. T. (2005). Standardization of uveitis nomenclature for reporting clinical data. Results of the First International Workshop. *American Journal of Ophthalmology* 140: 509–516.

Kerr, E. C., Copland, D. A., Dick, A. D., and Nicholson, L. B. (2008). The dynamics of leukocyte infiltration in experimental autoimmune uveoretinitis. *Progress in Retinal and Eye Research* 27: 527–535.

Lang, C., Gross, U., and Luder, C. G. (2007). Subversion of innate and adaptive immune responses by *Toxoplasma gondii*. *Parasitology Research* 100: 191–203.

Lau, A. W., Biester, S., Cornall, R. J., and Forrester, J. V. (2008). Lipopolysaccharide-activated IL-10-secreting dendritic cells suppress experimental autoimmune uveoretinitis by MHCII-dependent activation of CD62L-expressing regulatory T cells. *Journal of Immunology* 180: 3889–3899.

Mellor, A. L. and Munn, D. H. (2008). Creating immune privilege: Active local suppression that benefits friends, but protects foes. *Nature Reviews* 8: 74–80.

Oppenheim, J. J., Tewary, P., de la Rosa, G., and Yang, D. (2007). Alarmins initiate host defense. *Advances in Experimental Medicine and Biology* 601: 185–194.

Wacker, W. B. (1991). Proctor lecture. Experimental allergic uveitis. Investigations of retinal autoimmunity and the immunopathologic responses evoked. *Investigative Ophthalmology and Visual Science* 32: 3119–3128.

Wekerle, H. (1991). Immunopathogenesis of multiple sclerosis. *Acta Neurologica* 13: 197–204.

Wilder, H. C. (1952). Toxoplasma chorioretinitis in adults: A preliminary study of forty-one cases diagnosed by microscopic examination [letter]. *Archives of Ophthalmology* 47: 425.

Pathological Retinal Angiogenesis

A P Adamis, University of Illinois, Chicago, IL, USA

Glossary

Angiogenesis – The formation of new vessels from differentiated vasculature.
Chemoattractant – A chemical agent that induces cell migration (chemotaxis) toward the agent.
Embryogenesis – The phase of prenatal development involved in the establishment of the basic body form.
Hypoxia – A decrease below normal in the oxygen levels of a tissue.
Ischemia – Local loss of blood supply, with concomitant hypoxia, due to mechanical obstruction or degeneration of blood vessels.
Neovascularization – Proliferation of blood vessels in tissues not normally containing them or proliferation of blood vessels of a different kind than usual.
Uveitis – Inflammation of the uveal tract, which includes the iris, ciliary body, and choroid.
Vasculogenesis – Blood vessel formation occurring *de novo* from embryonic endothelial precursor cells (angioblasts).

Introduction

Research into the physiological development of the retinal vasculature and various ocular neovascular diseases has led to a deeper understanding of the molecular and cellular mechanisms underlying normal and pathological retinal vascularization. During embryogenesis, the developing retina is initially supplied by the hyaloid vasculature, which is then supplanted by a vascular plexus that originates at the optic nerve head and spreads peripherally. Subsequent remodeling and pruning leads to the formation of two additional parallel networks in the nerve fiber and inner plexiform layers, together with a circular avascular zone at the fovea.

Two basic mechanisms, vasculogenesis and angiogenesis, underlie the formation of new blood vessels; their relative contribution to the formation of the superficial retinal vasculature is a focus of some disagreement. Vasculogenesis, the differentiation of blood vessels from angioblasts, has been proposed as the mechanism for the formation of primary retinal vascular plexus, with deeper layers developing by angiogenesis; in contrast, it has been argued that all three vascular layers develop through angiogenesis, the formation of new vessels from differentiated vasculature. This process involves both sprouting from differentiated tip cells as well as intussusception, the splitting of existing vessels. The question as to the importance of vasculogenesis ultimately depends on the cellular identity of retinal precursors, and it is possible that some of the discrepancies may reflect species differences among mammals.

With respect to pathological retinal neovascularization, there is general agreement that angiogenesis is the driving mechanism. Many retinal neovascular conditions are associated with ischemia, with the resultant hypoxia leading to the upregulation of proangiogenic molecules. Depending on the particular disease, different pathophysiological mechanisms lead to a common endpoint of local ischemia and neovascularization. In central retinal vein occlusion, ischemia is a direct result of venous blockage. In proliferative diabetic retinopathy (PDR), the mechanism is more complex; the accumulation of polyols, reactive oxygen intermediates, and advanced glycation end products results in inflammation accompanied by retinal leukostasis leading to vascular injury, capillary blockage, and dropout. A third mechanism for ischemia-mediated neovascularization is seen in retinopathy of prematurity (ROP) in which premature birth interrupts the normal retinal vascular development; not only is postnatal tissue oxygen significantly higher than *in utero* but the effects are compounded by the use of oxygen therapy as well. Ultimately, these high oxygen levels lead to an increased rate of vascular pruning with ischemia-mediated increases in vascular endothelial growth factor (VEGF) levels and the resultant rebound aberrant neovascularization, which can be accompanied by retinal detachment. Finally, it should be noted that not all pathological retinal neovascularization is related to hypoxia since it is also observed in inflammatory conditions such as severe uveitis.

Promoters and Inhibitors of Angiogenesis

Over the past two decades, the identification and study of modes of action of proangiogenic and antiangiogenic factors have yielded an extensive list in both categories (see Table 1). While much of this work has been directed to developing treatments for cancer, considerable progress has also been made in elucidating the importance of these factors in ocular neovascular diseases. This article

Table 1 Proangiogenic and antiangiogenic factors

Proangiogenic and antiangiogenic factors	
Proangiogenic factors	*Antiangiogenic factors*
Angiogenin	Angioarrestin
Angiopoietin-1	Angiostatin (plasminogen fragment)
Complement factors C3 and C5	Antiangiogenic antithrombin III
Cryptic collagen IV fragment	Cartilage-derived inhibitor (CDI)
Developmentally regulated endothelial locus 1 (Del-1)	CD59 complement fragment
Ephrins/Ephs	Endostatin (collagen XVIII fragment)
Erythropoietin	Fibronectin fragment
Fibroblast growth factors; acidic (aFGF) and basic (bFGF)	Growth-related oncogene (Gro-β)
Follistatin	Heparinases
Granulocyte colony-stimulating factor (G-CSF)	Heparin hexasaccharide fragment
Hepatocyte growth factor (HGF)/ scatter factor (SF)	Human chorionic gonadotropin (hCG)
Interleukin-8 (IL-8)	Interferon α/β/γ
α5 integrins	Interferon-inducible protein (IP-10)
Leptin	Interleukin-12
Matrix metalloproteinases	Kringle 5 (plasminogen fragment)
Midkine	Metalloproteinase inhibitors (TIMPs)
Notch/D114	2-Methoxyestradiol
Pigment epithelium-derived growth factor	Pigment epithelium-derived growth factor
Placental growth factor	Placental ribonuclease inhibitor
Platelet-derived endothelial cell growth factor (PDECGF)	Plasminogen activator inhibitor
Platelet-derived growth factor-B (PDGF-B)	Platelet factor-4 (PF4)
Pleiotrophin (PTN)	Prolactin 16-kD fragment
Progranulin	Proliferin-related protein (PRP)
Proliferin	Retinoids
Transforming growth factor-α (TGF-α)	Slit/Robo4
Transforming growth factor-β (TGF-β)	Soluble VEGFR1
Tumor necrosis factor-α (TNF-α)	Tryptophanyl-tRNA synthase fragment
Vascular endothelial growth factor (VEGF)	VEGFxxxb
	Tetrahydrocortisol-S
	Thrombospondin-1 (TSP-1)
	Transforming growth factor-β (TGF-β)
	Vasculostatin
	Vasostatin (calreticulin fragment)

Reproduced from: Angiogenesis Foundation. Understanding angiogenesis. List of known angiogenic growth factors. Available at: http://www.angio.org/understanding/content_understanding.html.

Table 2 Actions of VEGF in promoting angiogenesis

- Endothelial cell mitogen
- Endothelial cell survival factor
- Chemoattractant for bone marrow-derived endothelial cells
- Chemoattractant for monocyte lineage cells
- Inducer of synthesis of endothelial nitric oxide synthase and consequent elevation of nitric oxide, itself a promoter of angiogenesis
- Inducer of synthesis of enzymes promoting blood vessel extravasation
  - Matrix metalloproteinases
  - Plasminogen activator

examines the evidence for those molecules whose roles are best understood in the context of pathological retinal angiogenesis.

Promoters of Angiogenesis

Vascular endothelial growth factor

VEGF (also known as VEGF-A) is a 45-kDa homodimeric glycoprotein that is the most potent known promoter of angiogenesis. It exists in a variety of isoforms and acts as a ligand for two receptor tyrosine kinases: VEGF receptor-1 (VEGFR1) and VEGF receptor-2 (VEGFR2). As a key regulator of angiogenesis, VEGF has a variety of proangiogenic actions (**Table 2**). Given the importance of ischemia in many retinal neovascular diseases, it is of particular relevance that retinal expression of VEGF is upregulated by hypoxia. In addition, it is an extremely potent known promoter of vascular permeability, 50 000 times stronger than histamine, thereby contributing to the edema that is often a central factor in vision loss.

The importance of VEGF in pathological retinal neovascularization has been established from both clinical and preclinical studies. The clinical work is correlative, demonstrating that ocular VEGF levels are increased in diseases such as diabetic retinopathy (DR), diabetic macular edema (DME), ROP, neovascular glaucoma, and retinal vein occlusion and in choroidal neovascular membranes from eyes of patients with age-related macular degeneration (AMD). With respect to the preclinical work, elevations of VEGF, whether by laser-induced retinal vein occlusion, direct injection, or transgenic approaches, all have proved capable of inducing ocular neovascularization.

Moreover, VEGF elevation has also been shown to be necessary for the neovascular response since blocking VEGF signaling prevents blood vessel growth. The approaches employed in these experiments have included the use of anti-VEGF antibodies or fragments thereof, an anti-VEGF aptamer, VEGFR fusion proteins, a nonangiogenic isoform of VEGF, antisense oligonucleotides, and small interfering RNAs. This work already has resulted in the clinical approval of two agents for the treatment of

AMD, pegaptanib and ranibizumab. Additionally, bevacizumab, a monoclonal antibody related to ranibizumab, increasingly is being used off-label for the treatment of AMD and other ocular neovascular diseases while VEGF-Trap, a fusion protein combining components of both VEGFR1 and VEGFR2, currently is being examined in a phase 3 trial as a treatment for AMD.

Studies have further demonstrated that ocular neovascular diseases such as AMD and DR bear many hallmarks of an inflammatory process, with VEGF acting as a pro-inflammatory cytokine. Genetic studies have revealed that the risk of AMD is strongly correlated with polymorphisms of several components of the complement cascade. In addition, retinal leukostasis is believed to be important in the capillary dropout characteristic of DR, leading to the development of ischemia. Furthermore, while the molecular mechanisms involved in ischemia-mediated ocular neovascularization remain to be fully elucidated, the influx of inflammatory cells, including monocytes/macrophages (**Figure 1**) and neutrophils, is important for its development. Both of these cell types release VEGF. Since VEGF acts as a chemoattractant for macrophages while upregulating the expression of intercellular adhesion molecule-1 (ICAM-1), a molecule that promotes leukocyte adhesion, on influx of these inflammatory cells provides an inherent positive-feedback mechanism promoting neovascularization.

In detailed studies of VEGF action, the VEGF165 isoform proved to be especially active as an inflammatory cytokine, since it was highly expressed during ischemia-mediated neovascularization. VEGF165 was also more potent than VEGF121, another common isoform, both

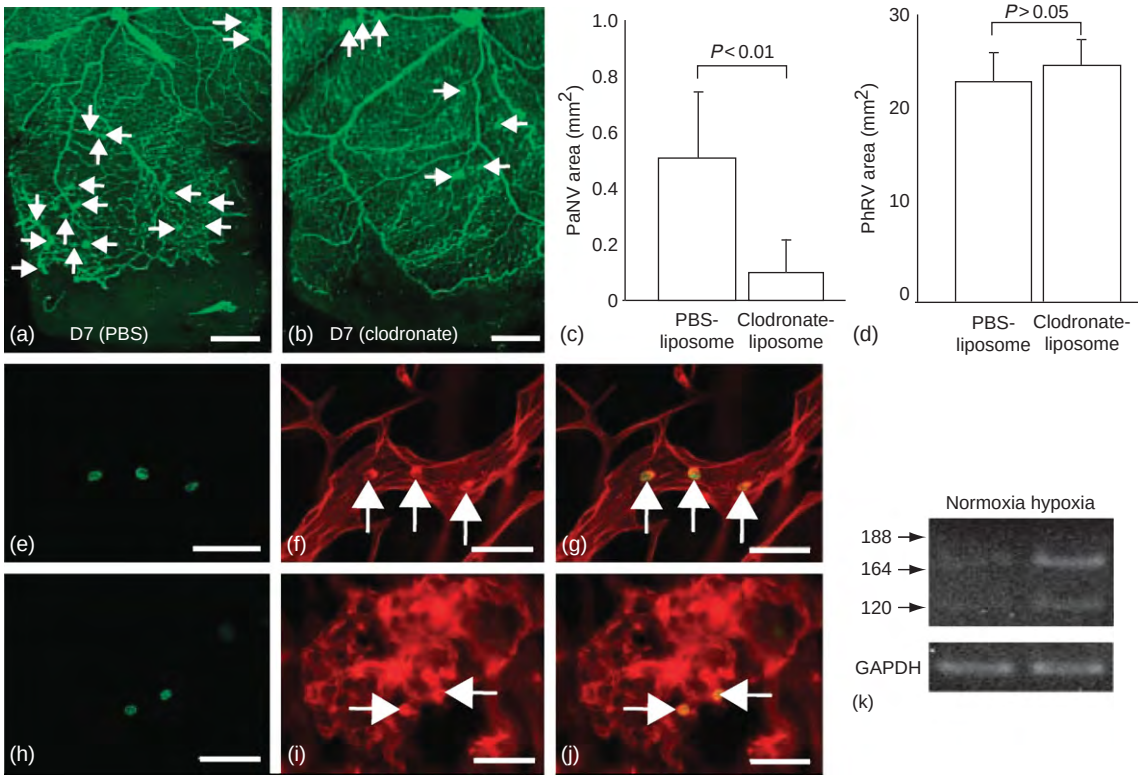

Figure 1 Monocytes contribute to pathological retinal neovascularization. In a ROP model, postnatal day zero (P0) rats were maintained for 10 days in 80% oxygen, interrupted daily by 30 min in room air followed by a progressive return to 80% oxygen. This treatment led to an avascular retina. On P10, corresponding to study day 0 (D0), retinal revascularization was induced by maintaining the rats in room air for an additional seven days (D7). (a–c) At D7, pathological neovascularization (PaNV; arrows in (a) and (b)) was significantly inhibited by treatment with clodronate liposomes compared to phosphate buffered saline (PBS) control liposomes ($n = 8$ for both treatments; mean ± standard deviation). (d) Physiological retinal vascular area (PhRV) was not significantly affected by treatment with clodronate liposomes ($P > 0.05$). (e–j) Influx of monocytes was observed just before and during pathological neovascularization (h–j). Monocytes were labeled with a fluorescein conjugated antibody to CD13 (e and h) while rhodamine-conjugated Concanavalin A was used to label the retinal vasculature and adherent leukocytes (f and i). As shown by superposition of these figures (panels (g) and (j)), the Concanavalin A and CD13 staining co-localized, indicating that the adherent leukocytes were monocytes. (k) In cultured peripheral blood monocytes obtained from retinopathologic rats at D7, exposure to hypoxia (1% oxygen) led to a marked increase in the expression of vascular endothelial growth factor mRNA compared to exposure to normoxia (21% oxygen). GAPDH; glyceraldehyde 3-phosphate dehydrogenase (used as a loading control). Scale bars: (a and b) 0.5 mm and (e–j) 50 μm. Originally published in *The Journal of Experimental Medicine.* doi:10.1084/jem.20022027.

as a macrophage chemoattractant and as a promoter of ICAM-1 upregulation.

Placental growth factor

Placental growth factor (PlGF) is a structurally related member of the same superfamily as VEGF, with all four PlGF isoforms acting as ligands for VEGFR1. PlGF has been implicated in a variety of physiological processes, including serving as a chemoattractant for monocytes and endothelial progenitor cells. Although ablation of the PlGF gene did not prevent embryonic angiogenesis, loss of PlGF led to impaired angiogenesis during conditions of ischemia and inflammation. In murine models, PlGF was found to be essential for the full expression of pathological neovascularization in laser-induced choroidal neovascularization (CNV) as well as for angiogenesis in tumors that were resistant to VEGFR inhibitors. Moreover, intravitreal injection of PlGF was shown to induce retinal edema in a rodent model, reflecting a disruptive effect on the retinal pigment epithelium. PlGF accordingly has attracted interest as a possible therapeutic target, and inhibition of its function is believed to contribute to the efficacy of VEGF-Trap, which, as discussed above, has been engineered to include the binding sites of both VEGFR1 and VEGFR2.

Platelet-derived growth factor

The platelet-derived growth factor (PDGF) family includes four members (PDGF-A through PDGF-D), with active forms being dimers and usually occurring in the homodimeric form. They serve as ligands for two receptor kinases, PDGFR-α and PDGFR-β. PDGF-B, acting through PDGFR-β, mediates most of the actions of PDGF in vascular development. Gene knock-out of either PDGF-B or PDGFR-β resulted in perinatal death owing to vascular deformities. In addition to promoting endothelial cell proliferation and capillary tube formation, PDGF-B signaling is especially important for the proliferation and recruitment of mural cells (pericytes and vascular smooth muscle cells) to the embryonic vasculature and for the maintenance of pericyte coverage (**Figure 2**). These actions are also essential for proper retinal vascular development. Endothelial cell-restricted ablation of PDGF-B produced defective pericyte coverage of retinal vessels and associated proliferative retinopathy; a similar phenotype resulted from the administration of an inhibitor to PDGFR signaling.

Investigations have demonstrated a complex interaction between PDGF and VEGF. During embryonic development, pericyte coverage was found to lag behind growth of retinal capillaries for several days, giving rise

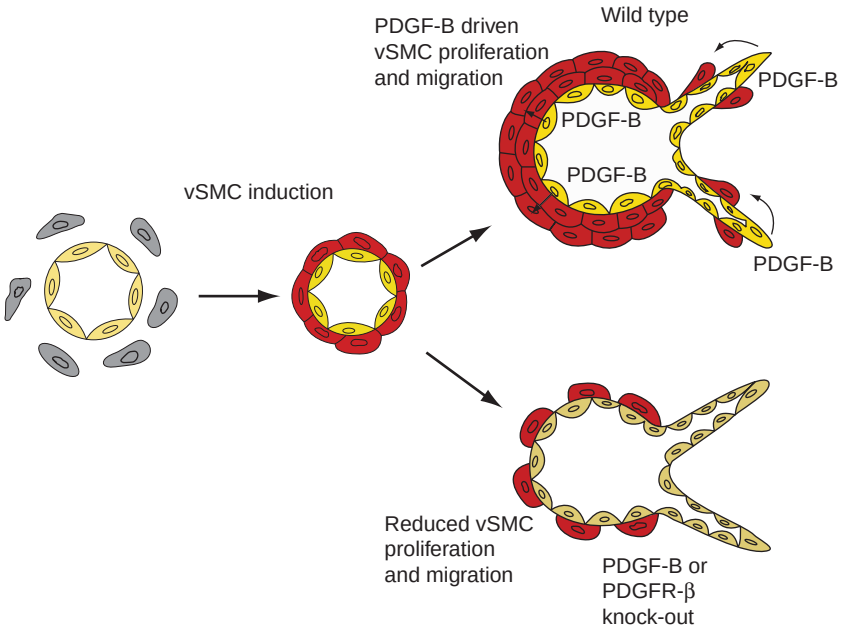

Figure 2 Platelet-Derived Growth Factor (PDGF)-B regulates the development of blood vessel walls. During blood vessel development, the nascent endothelial tube (yellow) is surrounded by undifferentiated mesenchymal cells (gray) that are induced to differentiate into vascular smooth muscle cells (vSMC) and to form a surrounding sheath (red). During further development of the vascular network, with concomitant growth and sprouting of blood vessels, PDGF-B derived from the endothelium further promotes vSMC proliferation and migration. These proliferative and migratory responses are reduced in mice in which PDGF-B or the corresponding receptor, PDGFR-β, have been genetically ablated, leading to defective coating of capillaries by pericytes as well as to vSMC hypoplasia in larger vessels. Reproduced with permission from Hellstrom, M., Kalen, M., Lindahl, P., Abramsson, A., and Betsholtz, C. (1999). Role of PDGF-B and PDGFR-beta in recruitment of vascular smooth muscle cells and pericytes during embryonic blood vessel formation in the mouse. *Development* 126: 3047–3055.

to an optimum window in which nascent blood vessels were especially vulnerable to VEGF depletion. Further investigations have revealed that the inhibition of both PDGF and VEGF signaling is quite effective in inhibiting ocular neovascularization. In experiments with three different murine models, VEGF inhibition was more effective for immature vessels while mature vessels were sensitive to PDGF-B. In every case, however, the most effective inhibition was achieved by interference with both signaling pathways (**Figure 3**).

Notch

The Notch family of cell surface proteins, consisting in mammals of four members, Notch1 through Notch4, is activated by ligands of the Jagged and Delta families and regulates pattern formation of numerous tissues, including those of the kidney, nervous system, and cardiovascular system. In its actions in the vascular system, the principal ligand for Notch is Dll4. Several recent studies have identified a key role for this signaling pathway as a negative regulator of retinal vessel patterning. Even heterozygous ablation of the dll4 gene led to dramatic increases in branching while other approaches to inhibiting the Notch pathway also caused excessive tip-cell (specialized endothelial cells which form the leading edge of vascular sprouts to initiate vessel branching) formation and endothelial cell proliferation. In a tumor model, blockade of the Notch pathway increased tumor vascularity but the vessels were nonproductive, resulting in decreased tumor growth. These findings are believed to reflect the importance of Dll4/Notch signaling in the negative regulation of VEGF-mediated angiogenic sprouting (**Figure 4**). Finally, the loss of Notch3 signaling mechanism has been found to interfere with mural cell differentiation, an action that may reflect Notch-mediated upregulation of PDGFR-β in vascular smooth muscle cells.

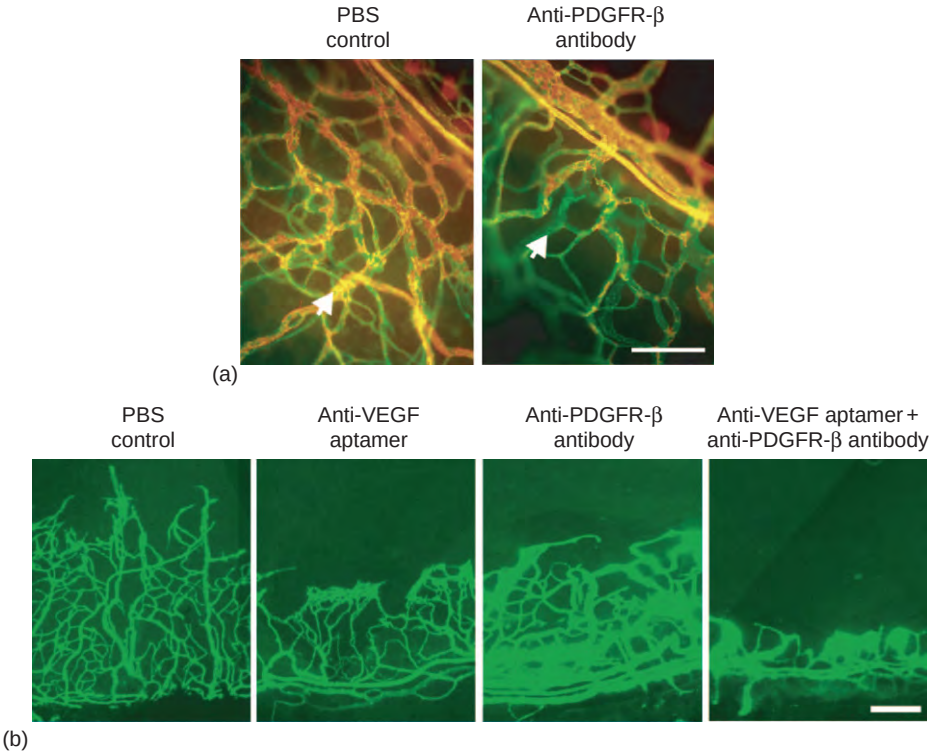

Figure 3 The role of platelet-derived growth factor (PDGF)-B in blood vessel growth and mural cell coverage in a corneal neovascularization model. (a) Endothelial cells were labeled by staining with lectin (green) and mural cells were stained with an antibody against smooth muscle actin (red). Starting at 10 days following corneal injury, mice received daily intraperitoneal injections of an anti-PDGFR-β antibody or phosphate-buffered saline (PBS) and were sacrificed at 20 days postinjury. Treatment with the anti-PDGFR-β antibody led to reduced mural cell coverage compared to controls (arrows). Scale bar = 20 μm. (b) Following induction of corneal injury, mice received daily intraperitoneal injections of one of the following: PBS; a polyethylene-glycolated antivascular endothelial growth factor (VEGF) aptamer; an anti-PDGFR-β antibody, or both the antiVEGF aptamer and the anti-PDGFR-β antibody. Neovasculature (green) was stained by fluorescein isothiocyanate–Concanavalin A. Neovascularization was significantly reduced by the antiVEGF aptamer compared with either PBS or the anti-PDGFR-β antibody ($P < 0.01$); inhibition of both VEGF and PDGF-B signaling led to a further significant reduction ($P < 0.05$), compared to inhibition of VEGF signaling alone. Scale bar = 100 μm. Adapted from Jo, N., Mailhos, C., Ju, M., et al. (2006). Inhibition of platelet-derived growth factor B signaling enhances the efficacy of anti-vascular endothelial growth factor therapy in multiple models of ocular neovascularization. *American Journal of Pathology* 168: 2036–2053. Copyright – The American Society for Investigative Pathology.

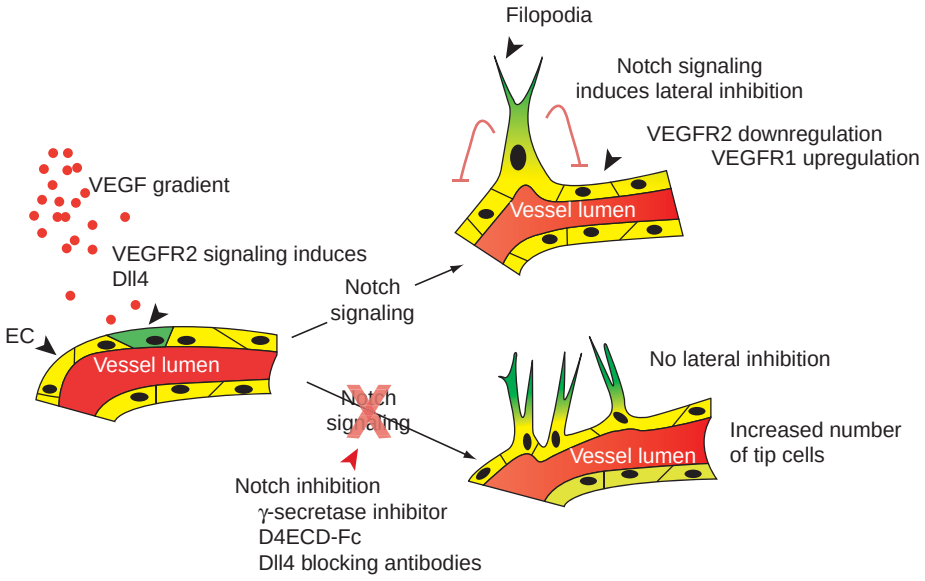

Figure 4 Role of Dll4/Notch in preventing tip-cell formation and branching. Schematic representation showing how Dll4/Notch signaling prevents excessive branching by inhibiting tip-cell phenotype. In response to a local gradient of vascular endothelial growth factor (VEGF), endothelial cells become tip cells and induce local Dll4 expression. This in turn activates Notch signaling in the neighboring cells and prevents these cells from becoming tip cells (lateral inhibition) through the induction of VEGFR1 and the downregulation of VEGFR2. Subsequently, these cells will become trunk/stalk cells and adopt the proliferative behavior necessary for vessel elongation. In the absence of Notch signaling, lateral inhibition is not induced and multiple branching occurs. Adapted from Sainson, R. C. and Harris, A. L. (2008). Regulation of angiogenesis by homotypic and heterotypic notch signalling in endothelial cells and pericytes: From basic research to potential therapies. *Angiogenesis* 11: 41–51, with permission from Springer.

Tumor necrosis factor-α

Tumor necrosis factor-α (TNF-α), a member of a large superfamily of cytokines and their receptors that are involved in regulating numerous physiological processes, is an important mediator of inflammation. Clinical studies have detected TNF-α in the fibrovascular membranes of patients with PDR and CNV. In two small case series, intravenous administration of infliximab, a monoclonal antibody directed against TNF-α, led to the regression of CNV in patients with AMD and to the alleviation of macular edema in patients with DME. In addition, a case report has described a similar regression of uveitis-induced neovascularization with this approach.

The mechanisms underlying the actions of TNF-α in ocular neovascularization have yet to be elucidated. TNF-α has been found to upregulate the synthesis of a number of genes that are important for angiogenesis, including VEGF, VEGFR2, angiopoietins 1 and 2 (Ang1 and Ang2), matrix metalloproteinases (MMPs) 2 and 9, PDGF-B, and the Notch ligand Jagged-1. The increase in Jagged-1 may account for the recent finding that TNF-α can induce the formation of tip cells.

Gene ablation studies in mice have been inconsistent, with some studies finding inhibition of retinal neovascularization in response to interference with TNF-α signaling, while others did not. Inhibition of laser-induced CNV by agents targeting TNF-α has been observed, though, both with intravitreal injection of infliximab and intraperitoneal administration of etanercept, a fusion protein containing the TNF-α receptor. Also, TNF-α signaling was determined to be important for ischemia-mediated neovascularization in the hind limbs of mice. Taken together, these data suggest that TNF-α may serve as a potential molecular target for controlling ocular neovascularization.

Ephrins and Ephs

Ephrins are a family of ligands that bind to the Eph receptor tyrosine kinases. The ephrins fall into two broad classes, the ephrinAs, which are attached to the cell membrane by a glycosylphosphatidyl anchor, and the ephrinBs, which span the cellular membrane and possess a cytoplasmic signaling domain (**Figure 5**). There is a corresponding division among the Eph kinases, which fall into A and B subclasses, with ephrinAs binding primarily to EphAs and ephrinBs to EphBs. Because of the tethered nature of the ephrins, ephrin–Eph signaling requires cell–cell contact and can proceed in either the forward or reverse direction. In addition to angiogenesis, ephrin–Eph interactions are required for the proper development of the nervous and cardiovascular systems as well as such processes as insulin secretion and trafficking of immune cells.

Evidence has been adduced supporting the roles of both major Eph/ephrin classes in angiogenesis, including retinal neovascularization. A soluble EphA-containing fusion protein significantly inhibited VEGF- or ephrinA1-induced

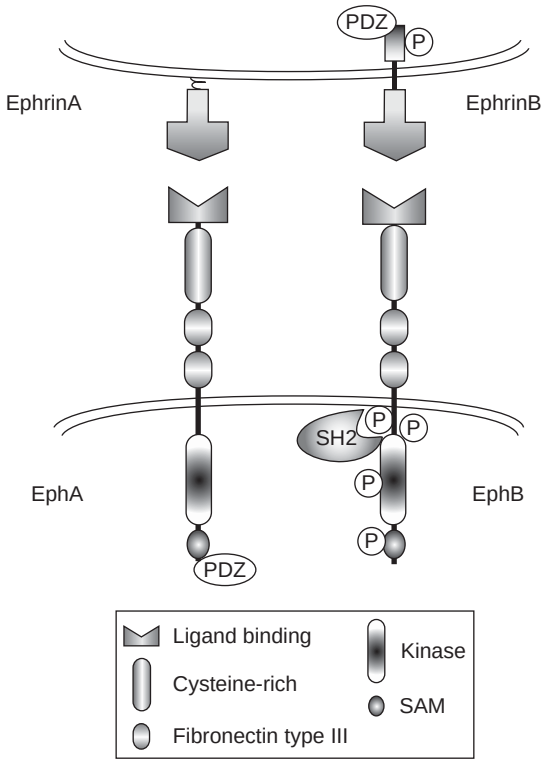

Figure 5 Ephrins and their Eph receptors. While both ephrins and Eph receptors are membrane-tethered proteins, ephrinBs traverse the membrane and possess a cytoplasmic signaling domain while ephrinAs do not. Ephrin–Eph binding results in receptor clustering followed by autophosphorylation of multiple tyrosine residues and docking of downstream effectors through *src*-homology domains. The presence of a sterile alpha motif (SAM) and a PDZ domain (shown here for the carboxy terminus of EphA but also present in EphB) promotes ligand-induced receptor clustering. Adapted from Dodelet, V. C. and Pasquale, E. B. (2000). Eph receptors and ephrin ligands: Embryogenesis to tumorigenesis. *Oncogene* 19: 5614–5619, with permission from Nature Publishing Group.

endothelial cell migration and assembly into capillary tubes *in vitro*, and when injected intravitreally the fusion protein also suppressed retinal neovascularization in a murine ROP model.

More extensive data are available implicating ephrinB/Eph signaling. In clinical studies, both EphB2 and EphB3 were found to be expressed in fibroproliferative membranes of patients with ischemic ocular neovascularization. Genetic ablation of either ephrinB2 or EphB4 led to homozygous embryonic lethality owing to aberrant development of the vasculature. Analysis of expression patterns suggested that ephrinB2 is expressed mainly on arteries and EphB4 on veins, and that these molecules act in defining arterial or venous identity.

Preclinical studies of the role of ephrinB/EphB in ocular neovascularization have not been consistent, however. In corneal models, neovascularization was promoted by ephrinB2, or fusion proteins containing it, and by an EphB1 fusion construct. In contrast, administration of soluble forms of EphB4 inhibited laser-induced CNV in rats as well as ischemia-induced retinal neovascularization in mice; the inhibition of retinal neovascularization also was seen when using soluble ephrinB2. Further work clearly is required if the ephrin/Eph systems can be considered as potential therapeutic targets.

Angiopoietins

Ang1 and Ang2 are members of a family of secreted ligands for Tie2, a receptor tyrosine kinase whose function is essential for vascular development and remodeling. Although Ang1 and Ang2 both activate Tie2, they usually act antagonistically. Similar lethal phenotypes involving gross vascular defects resulted from genetic ablation of Tie2 or Ang1 as well as from the overexpression of Ang2. While the effects of both Ang1 and Ang2 are complex, the overall action of Ang1 is to stabilize the quiescent vasculature while Ang2 is a destabilizing agent for the vascular endothelium (**Figure 6**).

Ang1, which is secreted by vascular smooth muscle cells, acts as a survival factor for endothelial cells *in vitro* and also can promote endothelial cell sprouting and tissue invasion of new blood vessels. In transgenic mice, co-expression of VEGF and Ang1 led to an additive effect on angiogenesis, but co-expression of Ang1 was found to suppress the leakiness of vessels induced by VEGF alone. Recently, this stabilizing effect has been shown to involve Ang1-mediated inhibition of the VEGF-induced internalization of vascular endothelial cadherin, a key component of adherent junctions. In addition, Ang1 inhibited other VEGF-mediated pro-inflammatory actions, including the upregulation of tissue factor, ICAM-1, and vascular cell adhesion molecule-1. Intravitreal injection of Ang1 also prevented many of the inflammatory changes characteristic of DR. In transgenic models, overexpression of Ang1 inhibited the development of laser-induced CNV and retinal neovascularization.

In contrast to the stabilizing effects of Ang1, Ang2 is primarily a destabilizing agent. In clinical studies, elevated levels of Ang2 and VEGF were detected in the vitreous of patients with DR as well as in choroidal neovascular membranes. Ang2 is synthesized by arterial smooth muscle cells and by endothelial cells where it is stored in Weibel-Palade bodies upon activation in response to stimuli such as thrombin or histamine, and sensitizes the endothelium to pro-inflammatory cytokines such as TNF-α. In addition to being upregulated by hypoxia and VEGF, Ang2 appears to act in concert with VEGF in many contexts, including enhancement of endothelial cell permeability. In several different rodent models, Ang2 was found to co-operate with VEGF in promoting neovascularization, but if VEGF levels were low, overexpression of Ang2 led to its regression.

Taken together, these findings suggest that Ang1 could have therapeutic potential as an antiangiogenic agent on

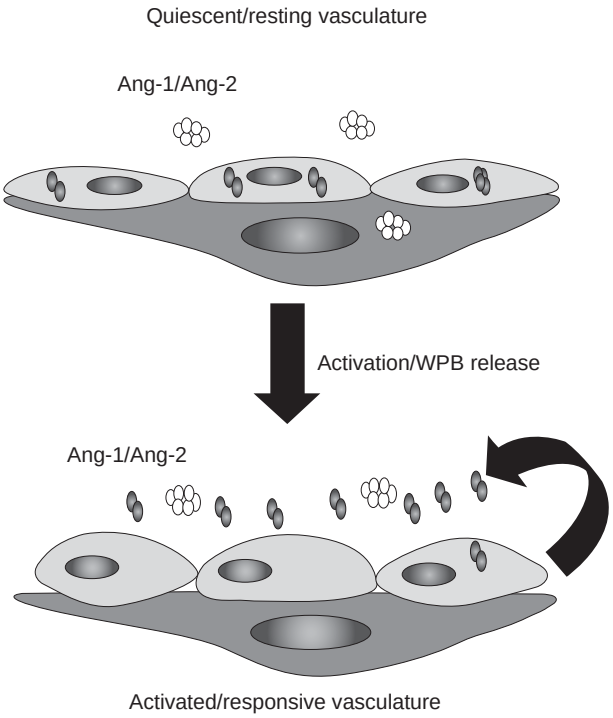

Figure 6 Regulation of vascular responsiveness by Ang1 and Ang2. Angiopoietin 1 (Ang1) (multimeric, white) is secreted constitutively at a low level by mural (periendothelial) cells, and acts on the quiescent endothelium to sustain a low-level activation of Tie2, thereby helping to maintain the luminal cell surface in an antithrombotic and antiadhesive state. Ang2 (dimeric, gray) is stored in Weibel-Palade bodies (WPB) in the endothelium and during endothelial cell activation is released from them, along with other stored factors, leading to the Ang1/Ang2 ratio being altered more in favor of Ang2. As a result, the endothelial cell layer becomes destabilized and more responsive to pro-inflammatory stimuli. Reproduced with permission from Pfaff, D., Fiedler, U., and Augustin, H. G. (2006). Emerging roles of the Angiopoietin–Tie and the ephrin–Eph systems as regulators of cell trafficking. *Journal of Leukocyte Biology* 80: 719–726.

its own. For Ang2, the situation is more complex, although it may have promise if administered together with a VEGF-suppressive agent.

Erythropoietin

While primarily identified as a promoter of erythropoiesis, erythropoietin also acts as a neuroprotective agent and as a promoter of angiogenesis. It plays an essential role in establishing the vascular network following vasculogenesis in that homozygous deletion of erythropoietin or its receptor leads to embryonic lethality with extensive vascular anomalies. In ischemic conditions, erythropoietin (which is itself upregulated by hypoxia) upregulates VEGF and VEGFR2 and promotes the recruitment of bone marrow-derived endothelial progenitor cells.

Correlative clinical findings implicate erythropoietin in ocular neovascular disease. Elevated ocular levels of erythropoietin were detected in patients with DME and PDR; in addition, treatment of premature infants with erythropoietin has been correlated with an increased risk of ROP. Preclinical studies are limited to one report in which intravitreal administration of a soluble erythropoietin receptor inhibited ischemia-induced neovascularization in a murine model. While not extensive, the available data suggest that further studies are warranted.

Integrins

Integrins comprise a large family of transmembrane cell surface receptors that transduce signals from ligands in the extracellular matrix to the cytoplasm. Each integrin is composed of one α and one β subunit; each subunit class contains many representatives, and more than 24 α–β combinations have been observed. The principal focus of integrin research has been their relevance to cancer, and in this context they play important roles in angiogenesis.

Studies with small molecule antagonists have identified a role for the $\alpha_5\beta_1$ integrin in murine models of ocular neovascularization. These inhibitors include JSM5562, which inhibited corneal neovascularization, and a related molecule, JSM6427, which inhibited laser-induced CNV and ischemia-induced retinal neovascularization. Studies indicated that $\alpha_5\beta_1$ contributed to an angiogenic pathway that was distinct from VEGF-mediated angiogenesis, suggesting that combinatorial approaches may offer the promise of even greater efficacy.

Matrix metalloproteinases

The MMPs comprise a large family of enzymes that degrade the extracellular matrix, facilitating the tissue penetration of nascent blood vessels. While the primary focus of their physiological impact has been in the context of cancer, they also have been shown to be involved in ocular neovascularization. MMP action has been implicated in the exposure of a cryptic epitope of collagen IV that promoted laser-induced CNV in a murine model. MMPs also generated soluble fragments of VEGF from matrix-bound forms; as MMP expression by cultured retinal pigment epithelium cells is upregulated by VEGF, this may provide for a positive feedback amplification of the angiogenic response.

Components of the complement cascade

In addition to the genetic studies implicating specific mutations in the complement system as risk factors for AMD (see above), both clinical and preclinical studies have directly implicated factors C3a and C5a in promoting ocular neovascularization. Both of these factors have been found in the drusen of patients with AMD as well as in the eyes of mice with laser-induced CNV; genetic ablation of their corresponding receptors reduced VEGF expression, leukocyte recruitment, and induction of CNV. Moreover, these

factors induced upregulation of VEGF expression when injected intravitreally in mice. Similar effects on CNV and VEGF expression were found in mice in which factor C3 was ablated. Finally, depletion of complement by administration of cobra venom factor has been shown to inhibit the development of the inflammation, which is often accompanied by neovascularization, in an animal model of uveitis. Taken together, these findings suggest that targeting certain components of the complement cascade could provide a therapeutic option for treating ocular neovascularization.

Inhibitors of Angiogenesis

Pigment epithelium-derived factor

Pigment epithelium-derived factor (PEDF) is a 50-kDa glycoprotein, originally found to be expressed in the retinal pigment epithelium that exhibits properties directly opposing VEGF: inhibition of VEGF signaling through VEGFR1, downregulation of VEGF expression in the context of ischemia, and inhibition of VEGF-induced increases in endothelial cell permeability. PEDF induces macrophage apoptosis, suggesting that it serves also as a modulator of inflammation. Systemic or intravitreal administration of PEDF, as well as its expression from a transgene, was found to inhibit ischemia-induced retinal neovascularization in mice. PEDF also induced apoptosis of cultured endothelial cells and suppression of VEGF-induced endothelial cell proliferation and migration. However, one study reported that the effects of PEDF were dose dependent, with both laser-induced CNV and endothelial cell differentiation *in vitro* being inhibited at low doses and promoted at high doses. Clinical data have been similarly inconsistent. While the expression of PEDF in Bruch's membrane was reduced in patients with AMD relative to controls, vitreous levels of PEDF were elevated in patients with PDR. The potential of PEDF as an antiangiogenic agent for ocular neovascularization thus remains to be established.

VEGFxxxb isoforms

VEGFxxxb denotes a parallel family of alternately spliced VEGF isoforms that are identical in length to the canonical VEGF family but differing in the last six amino acids. VEGFxxxb isoforms can bind VEGFR2 but have little or no ability to initiate downstream pathways. They therefore act as competitive inhibitors of VEGF. In clinical studies, VEGFxxxb was found to predominate in the vitreous of control eyes but to constitute only 12% in patients with PDR; similar downregulation of VEGFxxxb has been observed in several cancers. In preclinical studies, VEGFxxxb inhibited both corneal and retinal neovascularization. These findings suggest that downregulation of VEGFxxxb levels may contribute to pathological neovascularization and that members of this family may have potential as antiangiogenic therapies.

Soluble VEGF receptor 1

Soluble VEGFR1, also generated by alternative splicing, is a natural inhibitor that can bind VEGF but lacks the exons required for signaling. It is essential for maintaining the avascularity of the cornea. As an integral component of the engineered therapeutic agent VEGF-Trap (see above), the ligand-binding site currently is being evaluated in clinical trials as a VEGF-targeting agent.

Complementary regulatory protein CD59

In addition to containing components that promote pathological neovascularization, the complement cascade also includes regulatory components that are potential antiangiogenic agents. One such candidate protein is CD59, whose ablation facilitated the development of CNV in mice; in the converse experiment, laser-induced CNV was inhibited by intravitreal or intraperitoneal administration of a soluble fusion protein containing CD59.

Tryptophanyl-tRNA synthase fragment

Tryptophanyl-tRNA synthase fragment (T2-TrpRS), another naturally occurring molecule, was found to inhibit physiological retinal angiogenesis in mice as well as ischemia-induced preretinal neovascularization. Recently, it was shown that intravitreal injection of T2-TrpRS, together with an anti-VEGF aptamer, led to potent inhibition of ischemia-induced retinal neovascularization, suggesting yet another avenue for combinatorial therapy.

Slit/Roundabout4

Slit/Roundabout4 (Robo4) is a member of a family of transmembrane receptors for the Slit family of secreted ligands. While Slit/Robo signaling was initially shown to be important in neuronal patterning, it also has been implicated in angiogenesis. Recently, intravitreal injection of Slit2 was found to inhibit both ischemia-induced neovascularization and VEGF-retinal permeability; none of these effects were seen if Robo4 was genetically ablated. Slit2-mediated inhibition of VEGF-induced endothelial cell migration and tube formation also was dependent on the presence of Robo4. Taken together, these data suggest that Slit/Robo4 axis acts as a negative regulator of VEGF-induced proangiogenic signaling.

Other inhibitors

In addition to the inhibitors discussed herein, numerous other molecules have been identified that also possess antiangiogenic activity but whose involvement in ocular neovascularization is not as well characterized (**Table 1**).

New Directions in Antiangiogenic Therapy

While most research into pathological angiogenesis has been directed toward ablating the unwanted vasculature, recent studies into the control of malignant tumors suggest

that antiangiogenic therapy may act to normalize, rather than to destroy, the tumor vasculature. This normalization facilitated tumor penetration of chemotherapeutic agents and increased their efficiency. Similar concepts have emerged from studies of Dll4/Notch signaling where inhibition led to more profuse tumor vasculature but slower tumor growth. The molecular mechanisms underlying vascular normalization are yet to be determined. Inhibition of the regulator of G protein signaling 5 (RGS5), a protein found in pericytes, has been shown to promote vascular normalization in a mouse tumor model; this allowed the influx of immune cells into the tumor parenchyma and led to increased survival. Upregulation of RGS5 resulted in a significant reduction in the susceptibility of nascent vessels to regression by VEGF inhibition, suggesting that RGS5 contributes to pericyte-endothelial cell interactions and vascular maturation.

Normalization of the vasculature also has been proposed as a contributor to the utility of antiangiogenic therapy in pathological ocular neovascular diseases. Retinal neovascularization may reflect an adaptive response to hypoxia that has gone awry. It remains to be seen whether inducing regression or normalization of aberrant retinal vasculature will be the most effective in providing favorable visual outcomes.

Conclusions

The systematic study of the mechanisms underlying physiological and pathological angiogenesis has yielded a wealth of knowledge as to underlying molecular and cellular mechanisms involved in retinal neovascular diseases, including the actions of proangiogenic and antiangiogenic factors that modulate these processes. Drugs targeting VEGF have already proved their clinical utility. It is clear, moreover, that a variety of other agents offer promise, either alone or as adjunctive therapy with agents targeting VEGF, and that there is reason for optimism that the range of treatments for retinal neovascular diseases soon will be expanded.

See also: Angiogenesis in Inflammation; Angiogenesis in Response to Hypoxia; Breakdown of the Retinal Pigmented Epithelium Blood–Retinal Barrier; Development of the Retinal Vasculature; Normal Age-Related Changes: Crystallin Modifications, Lens Hardening; Retinal Vasculopathies: Diabetic Retinopathy; Retinopathy of Prematurity; Vessel Regression.

Further Reading

Adamis, A. P. (2002). Is diabetic retinopathy an inflammatory disease? *British Journal of Ophthalmology* 86: 363–365.

Andrae, J., Gallini, R., and Betsholtz, C. (2008). Role of platelet-derived growth factors in physiology and medicine. *Genes and Development* 22: 1276–1312.

Arcasoy, M. O. (2008). The non-haematopoietic biological effects of erythropoietin. *British Journal of Haematology* 141: 14–31.

Avraamides, C. J., Garmy-Susini, B., and Varner, J. A. (2008). Integrins in angiogenesis and lymphangiogenesis. *Nature Reviews Cancer* 8: 604–617.

Bora, N. S., Jha, P., and Bora, P. S. (2008). The role of complement in ocular pathology. *Seminars in Immunopathology* 30: 85–95.

Dodelet, V. C. and Pasquale, E. B. (2000). Eph receptors and ephrin ligands: Embryogenesis to tumorigenesis. *Oncogene* 19: 5614–5619.

Ferrara, N., Damico, L., Shams, N., Lowman, H., and Kim, R. (2006). Development of ranibizumab, an anti-vascular endothelial growth factor antigen binding fragment, as therapy for neovascular age-related macular degeneration. *Retina* 26: 859–870.

Fiedler, U. and Augustin, H. G. (2006). Angiopoietins: A link between angiogenesis and inflammation. *Trends in Immunology* 27: 552–558.

Gragoudas, E. S., Adamis, A. P., Cunningham, E. T., Jr., et al. (2004). Pegaptanib for neovascular age-related macular degeneration. *New England Journal of Medicine* 351: 2805–2816.

Hellstrom, M., Kalen, M., Lindahl, P., Abramsson, A., and Betsholtz, C. (1999). Role of PDGF-B and PDGFR-beta in recruitment of vascular smooth muscle cells and pericytes during embryonic blood vessel formation in the mouse. *Development* 126: 3047–3055.

Ishida, S., Usui, T., Yamashiro, K., et al. (2003). VEGF164-mediated inflammation is required for pathological, but not physiological, ischemia-induced retinal neovascularization. *Journal of Experimental Medicine* 198: 483–489.

Jo, N., Mailhos, C., Ju, M., et al. (2006). Inhibition of platelet-derived growth factor B signaling enhances the efficacy of anti-vascular endothelial growth factor therapy in multiple models of ocular neovascularization. *American Journal of Pathology* 168: 2036–2053.

Pfaff, D., Fiedler, U., and Augustin, H. G. (2006). Emerging roles of the Angiopoietin-Tie and the ephrin-Eph systems as regulators of cell trafficking. *Journal of Leukocyte Biology* 80: 719–726.

Ribatti, D. (2008). The discovery of the placental growth factor and its role in angiogenesis: A historical review. *Angiogenesis* 11: 215–221.

Rosenfeld, P. J., Brown, D. M., Heier, J. S., et al. (2006). Ranibizumab for neovascular age-related macular degeneration. *New England Journal of Medicine* 355: 1419–1431.

Sainson, R. C. and Harris, A. L. (2008). Regulation of angiogenesis by homotypic and heterotypic notch signalling in endothelial cells and pericytes: From basic research to potential therapies. *Angiogenesis* 11: 41–51.

Penetrating Keratoplasty

T H Flynn and D F P Larkin, Moorfields Eye Hospital, London, UK

Glossary

Afferent and efferent components of allogeneic response – Afferent arm of the immune response is the inductive stage in which antigens are presented to T lymphocytes in lymph nodes. Efferent arm of the allogeneic response is the stage in which T cells and antibodies are generated and are available to mediate graft rejection or protection from infectious agents.
Alloantigen – An antigen present in some, but not all, individuals of the same species.
Alloreactive – The reaction of lymphocytes or antibodies with alloantigens.
Anterior chamber-associated immune deviation – Systemic downregulation of antigen-specific cell-mediated immunity that is induced when antigens are introduced into the anterior chamber of the eye.
Delayed-type hypersensitivity – Immune response consisting mostly of T cells that develops 24–72 h after exposure to antigen.
Immune privilege – Condition in which immune responses are suppressed or downregulated.
Indirect and direct allorecognition – Two pathways whereby immune responses to histocompatibility antigens on a corneal allograft elicit an immune response and ultimately allograft rejection. Indirect pathway occurs when host-derived antigen presenting cells reprocess antigens from the allograft. Direct pathway involves direct stimulation of the host's T lymphocytes by major histocompatibility antigens expressed on the corneal allograft.

Penetrating Keratoplasty: Indications and Survival

Penetrating keratoplasty, or full thickness corneal transplantation, is the surgical procedure most commonly used in management of blinding corneal disease. Overall graft survival rates in corneal transplantation are similar to those in cadaveric renal transplantation: this indicates that the impact of corneal graft failure, due in most patients to allogeneic rejection, is significant, even if very few of the cornea patients receive oral immunosuppression as prophylaxis. In this way, corneal transplantation is one clinical circumstance in which immune homeostasis of the eye might seem undermined. However, in those patients in whom irreversible transplant rejection occurs, the selective targeting of immune-mediated injury to donor cells is a striking example of protection of host ocular tissue from bystander injury – afferent and efferent components of the allogeneic response in tandem maintaining immune homeostasis of the eye.

Large cohort outcome studies have identified a number of factors on multivariate analysis which, if present, have a statistically significant detrimental effect on corneal graft survival. These are a previous ipsilateral failed graft, ipsilateral ocular inflammation, vascularization of the recipient cornea, and the primary corneal diagnosis. In most patients, these factors increase risk of graft failure by immune rejection.

Corneal Immune Privilege

Apart from the specific diagnoses of keratoconus and Fuchs endothelial disease, few of the common indications for corneal transplantation can truly be considered low rejection risk. Nevertheless, it is clear that corneal transplants do enjoy comparative immune privilege. Early investigators attributed the immune privilege of the cornea entirely to its lack of vascularity, that is, sequestration of alloantigen from the immune response. There is no doubt that this is an important factor. Animal models and large human cohort studies have identified recipient corneal vascularization as the most significant factor conferring high rejection risk in multivariate analyses. In fact, the cornea is an immune-privileged tissue situated in and transplanted to an immune-privileged site.

Immune-Privileged Tissue

A number of factors are known to contribute to the relative immune privilege of the cornea as a tissue.

- On a gross level, the normal cornea is isolated from circulating immune cells due to (1) its avascular nature and (2) the blood–aqueous barrier.
- Until relatively recently, the cornea was thought to contain no passenger antigen-presenting cells (APCs). Recent work has established that it does, in fact, contain APCs but that they are immature and do not express major histocompatibility complex (MHC) class II in the normal setting. Subsequently, the normal cornea is

devoid of lymphatics to transport APCs. Experimental studies which increase the numbers of passenger APCs in the donor cornea have been shown to erode immune privilege and increase the direct component of allorecognition. Because in clinical transplantation normal avascular donor cornea is grafted, high rejection risk status is conferred by vascularization or inflammation of the residual host cornea.

- The stroma and endothelium have low immunogenicity.
- The endothelium, which is the most important target in rejection, expresses (i) low levels of MHC class I and II and (ii) high levels of Fas ligand which induces apoptosis in alloreactive T-lymphocyte cells and protects the graft.

Immune-Privileged Site

The cornea, or specifically its endothelium, constitutes the anterior boundary of the anterior chamber which has been shown to be an immune-privileged site by Medawar in one of the earliest studies of this concept. The aqueous humor in contact with the endothelial cells contains high levels of immunoregulatory proteins such as transforming growth factor beta (TGF-β). In addition, antigen placed in the anterior chamber of the eye alters the immune response (anterior chamber-associated immune deviation or ACAID) to subsequent exposure to the antigen even at a different site. Antigen from the anterior chamber leaves the eye via several pathways but at least some leaves via the conventional aqueous outflow pathway and travels to the spleen. There the interaction of antigen, natural killer (NK), T cells, B cells, and γδ T cells induces a type of operational tolerance.

Clinical Features of Corneal Graft Rejection

Selective rejection signs can be observed in the epithelium, stroma, and endothelium of donor cornea in the human. The corneal endothelial cell monolayer controls stromal hydration, which has an essential role in transparency and transmission of light (Figure 1). As (1) these cells do not have mitotic capability and (2) following uncomplicated corneal transplantation the endothelial cell monolayer density declines at an even faster rate than in health, rejection of the endothelial layer is a terminal threat to graft transparency unless reversed sufficiently early. Even if reversed by treatment, a proportion of endothelial cells is lost.

Patients with isolated epithelial rejection are often asymptomatic. In epithelial rejection, an elevated curvilinear opaque line is seen on the epithelium. However, epithelial rejection is direct evidence that the recipient has been sensitized to the graft and may progress to rejection of the deeper corneal layers. The clinical symptoms and signs of stromal rejection have two patterns. It more frequently manifests as subepithelial opacities. These infiltrates have a similar appearance to those seen in adenovirus viral keratitis but are seen only in the donor cornea. This type of stromal rejection is often asymptomatic, but like epithelial rejection it may precede the onset of a more severe and visually significant process. Rejection of the deeper stroma results in spreading graft opacification and decreased visual acuity.

Endothelial rejection usually presents with discomfort and decreased visual acuity. A line of leukocytes may, over a period of days, be seen migrating across the donor endothelium leaving edematous stroma in its wake (Figure 2). This line often spreads out like a wave from an area of deep vascularization to the graft host junction. Alternatively, a

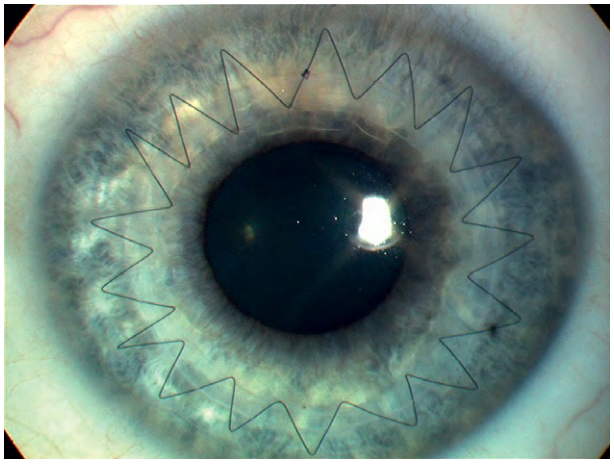

Figure 1 Transparent corneal transplant 8 months following surgery. The donor cornea is fully transparent, indicating normal endothelial function. Both recipient and donor cornea are avascular.

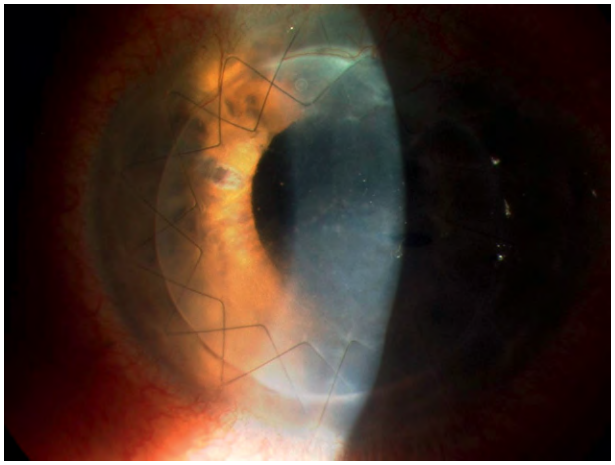

Figure 2 Endothelial rejection is indicated by the demarcated region of donor corneal opacification bordered by a horizontal linear opacity. Vascularization to the superior graft periphery can also be seen.

Table 1 Summary of cellular steps to corneal transplant destruction

	Direct pathway of antigen presentation	*Indirect pathway of antigen presentation*	*Low risk*	*High risk*
1	Egress of donor APCs	Host APCs infiltrate graft	Few recipient cornea APCs	More recipient cornea APCs
		Egress of host APCs bearing antigen	↓MHC II expression	↑MHC II expression
		Egress of host APC from anterior uvea bearing antigen shed from endothelium	Few lymphatics	Lymphatics *in situ*
			Indirect antigen presentation	Direct antigen presentation
			''Quiet'' eye	Inflamed eye
2	Direct priming of T lymphocytes (afferent allorecognition)	''Indirect'' priming of T lymphocytes (afferent allorecognition)	↓MHC II	↑MHC II
			↓Costimulatory molecules	↑Costimulatory molecules
			ACAID	Erosion of ACAID
3	Exposure of circulating primed lymphocytes and other leukocytes to graft	Exposure of circulating primed lymphocytes and other leukocytes to graft	Avascular cornea	Vascular cornea
			''Quiet'' eye	Inflamed eye
4	Recognition of alloantigen (efferent allorecognition)	Recognition of alloantigen (efferent allorecognition)	↓MHC expression	↑MHC expression
5	Recruitment of other effector cells	Recruitment of other effector cells		

APC – antigen presenting cell; MHC – major histocompatibility complex; ACAID – anterior chamber-associated immune deviation.

more diffuse corneal edema may be seen with diffuse keratitic precipitates of variable density. In all cases, there are visible cells in the anterior chamber and the signs of inflammation and of endothelial dysfunction are limited to the donor tissue, demonstrating specificity of the allogeneic response.

Pathogenesis of Rejection

Current understanding of the pathway to rejection of donor cornea following penetrating keratoplasty will be described in terms of the afferent component or sensitization, in which donor transplant antigens are recognized and processed, and the effector component. Components of the allogeneic response in low and high rejection risk corneal transplantation are summarized in Table 1.

Afferent Mechanisms and Components

Histocompatibility antigens

Otherwise known as transplantation antigens, these are proteins and peptides derived from donor cells; in most forms of transplantation, the most potent are class I and class II molecules of the MHC. Additional transplantation antigens termed minor histocompatibility antigens also induce allogeneic tissue rejection. The designation of major or minor refers to the relative importance of these antigens in vascularized organ transplants and may be quite inaccurate in corneal transplantation, in which, for example, minor H antigen appears to be relatively more important than MHC antigens.

Published evidence from several laboratories indicates that following transplantation recipient APCs enter the graft and endocytose exogenous alloantigen. APCs then migrate to the local lymph node where the alloantigen is presented on MHC class II molecules to naive CD4 cells and on MHC class I to naive CD8 cells. APC-associated antigen may be detected in the draining lymph node within hours of corneal transplantation. The exogenous antigen in question could be either a donor minor histocompatibility antigen or part of a donor major histocompatibility antigen. One self APC activates both CD4 and CD8 cells in what is known as the three-cell model of alloantigen presentation.

Direct and indirect alloantigen recognition

The type of antigen presentation by recipient APCs outlined above is termed indirect antigen presentation. Another form of antigen presentation, unique to the transplantation, is direct antigen presentation mediated by donor APCs transplanted within the graft (passenger leukocytes). According to the concept of self-restriction, alloantigen presented by these cells should not be recognized

by host T cells if the major histocompatibility antigens are not matched. In reality, the alloantigens are recognized by a significant number of host T cells. Some of these lymphocytes may recognize, and be primed, by the alloantigenic MHC molecule itself regardless of the peptide it bears. This method of antigen presentation is consistent with the three-cell model and in vascularized organ grafts directly primed T cells constitute ~90% of the alloreactive cells during acute graft rejection.

With its lack of mature resident APCs and lymphatics, the cornea would appear to be poorly equipped to facilitate antigen presentation via the direct route. This is confirmed by studies which show that the indirect route of antigen presentation plays a more prominent role in low-risk corneal transplantation. This lack of influence of the direct route may explain the following findings which are on first consideration counterintuitive:

- In human studies, MHC class I and particularly class II matching of corneal grafts has shown no convincing survival benefit.
- In animal studies, mismatches in minor rather than major histocompatiblity antigens have been shown to be equally or more important in influencing graft survival.

Further experimental evidence suggests that some of the factors which confer immune privilege do so by minimizing or preventing direct antigen presentation and that in erosion of immune privilege (i.e., in high-risk grafts) the direct route of antigen presentation becomes relatively more prominent. Nevertheless, the indirect route of antigen presentation is sufficient to induce sensitization.

T-lymphocyte activation

In the lymph node the MHC–peptide complex interacts with the T cell receptor (TCR), a complex cell surface receptor. The vigor of the T cell response following presentation of antigen is variable and dependent on the nature of the dendritic cell itself, the affinity of the clonotypic TCR for the MHC–peptide complex in question, the state of the T cell (naive, memory), soluble factors in the immediate microenvironment (cytokines and chemokines), and the interactions between accessory (adhesion and costimulatory) molecules.

Once a T cell is activated in the lymph node, there is rapid clonal expansion of alloantigen-specific T cells which enter the circulation. The lifespan of these cells is limited and it follows that there is a limited window of opportunity for these cells to bring about graft destruction in the absence of continuous antigenic stimulation. The rapid expansion of T cells is followed by contraction as many effector T cells undergo apoptosis. Memory (central and effector) cells make up part of the T cell repertoire thereafter.

Effector Mechanisms

Once primed in the regional lymph nodes, activated lymphocytes enter the peripheral circulation. The avascular nature of the cornea and the blood–aqueous barrier provide barriers to immune cell infiltration and endothelial cell destruction. In the case of vascularized corneas, immune cells have easier access to graft antigens/cells.

The nature of graft-infiltrating cells in corneal allograft rejection has been studied in human and animal pathological specimens. The cell types which appear in the highest numbers and with the greatest consistency are CD4+ and CD8+ lymphocytes of the adaptive immune system, and innate immunity component macrophages and NK cells. The presence of a cell in a tissue during rejection does not prove that the cell has an effector functional role: the important questions as to which cells cause endothelial cell destruction and by what mechanism(s) remain poorly understood. For instance, the mechanisms of allorecognition in the effector stage of graft rejection are unclear. A particular conundrum has been the question of how indirectly primed T cells (host MHC(+mH) molecules) can recognize antigen on donor cells (donor MHC(+mH) molecules). The discovery of a semidirect pathway of antigen presentation, whereby recipient APCs present whole donor MHC molecules as well as their own MHC molecules, provides a possible explanation for this but has not been demonstrated experimentally in corneal transplantation.

T lymphocytes

Because both CD4 and CD8 have been found in pathological specimens of rejected corneal grafts, much interest has fallen on the roles of these cells in corneal graft rejection. Several studies have demonstrated the presence of two distinct lymphocyte populations in response to a corneal allograft. One group appear to be CD4+ and are activated by indirect presentation of alloantigen. The other group are CD8+ cells with direct specificity for alloantigen. CD8+ cells act directly on target cells and are cytotoxic but it appears that CD8+ cells are less important in corneal graft rejection than in other organs. While CD4+ cells have the capacity using FasL to be directly cytotoxic, their primary modus operandi in corneal graft rejection appears to be via delayed-type hypersensitivity (DTH), by secreting cytokines and recruiting other cells such as macrophages. The evidence for role of CD4+ cells is supported by the finding that DTH responses rather than cytotoxic responses are found in rejectors of corneal grafts. We may conclude from findings in several laboratories that CD4+ cells play a more important role than CD8+ cells in graft rejection under most conditions but that either cell type may mediate rejection and that neither is essential for the process. However, there is considerable redundancy within the allogeneic response, with several lines of investigation supporting alternative cellular pathways for graft destruction.

Macrophages

The heavy mononuclear cell infiltrate in rejected grafts is in keeping with a DTH reaction. Depletion of corneal macrophages with clodronate liposomes prolongs corneal graft survival in rats, and macrophages have been shown to be necessary as APCs rather than as effector cells. However, cells of monocyte/macrophage lineage have been shown to be the dominant cell type in human aqueous humor during acute endothelial rejection. The function(s) of these cells in the effector arm of the rejection process remains unknown.

NK cells

NK cells of the innate immune system have been found in rejected corneal grafts and in the aqueous humor of experimental animals with corneal allograft rejection. These cells usually function in the elimination of virally infected cells. The default function of an NK cell is to kill any cell with which it comes in contact. Only the presence of self MHC class I on the cell inhibits this process. *In vitro* studies have demonstrated the capacity of NK cells to kill allogeneic corneal endothelial cells, so these cells are likely to be functionally active in the efferent arm of rejection.

Breakdown of immune privilege?

In a high rejection risk transplant there is a preexisting erosion of immune privilege at one or more of these steps mentioned in section "Immune-privileged Tissue". Low rejection risk grafts that reject later may be thought of as grafts that have acquired high rejection risk characteristics due to breakdown of immune privilege. In nonvascularized corneas, immune rejection occurring months or years after transplantation is often seen to be preceded by a local episode of alloantigen-independent inflammation (e.g., loosened transplant suture, bacterial suture-associated infection, and recurrent herpetic infection) which may lead to recruitment of immune-competent cells, angiogenesis, lymphangiogenesis, and upregulation of MHC molecules on the graft cells. Each step and the factors within it contributing to immune privilege are reasonably well understood but the extent to which one step inevitably follows the preceding one is less clear. We may ask of grafts which are not rejected, whether the recipient has not been sensitized due to the immune system not seeing the antigen (ignorance of the alloantigen), whether the immune system has seen the antigen but does not or cannot mount a response (tolerance of the antigen), or whether the immune system has seen the antigen and been sensitized but its effector cells cannot see the target antigen due to sequestration of the graft in its avascular bed.

While it is tempting to speculate that a single step exists, manipulation of which would induce tolerance or absolute immune privilege in all cases, it is far more likely that the relative contributions to immune privilege at each step is different for each person and for each graft and there is no factor contributing to immune privilege that cannot be overcome by one of the many redundant cellular pathways and mechanisms known to bring about rejection.

Treatment of Rejection

The mainstay of treatment for established rejection is intensive topical corticosteroid treatment. The most commonly used regimen is prednisolone acetate 1% or dexamethasone 0.1% hourly. This treatment effectively suppresses graft inflammation but once inflammation has been suppressed, the question of whether graft clarity will return depends on the extent to which the endothelium has been damaged. Topical corticosteroids influence effector cells such as T cells and macrophages in the cornea chiefly by inducing the expression of anti-inflammatory genes (Annexin-1, SLPI) and repressing the expression of proinflammatory genes (cytokines, chemokines, adhesion molecules, and MHC molecules). Inhibition of IL-2 receptor production inhibits T cell proliferation but this may not be an important effect of topical treatment as T cell proliferation occurs quite distal to the site of application in the regional lymph nodes. Corticosteroids also affect dendritic cell (DC) function and have been shown to alter cytokine production, to induce apoptosis in DCs and to delay DC maturation with resultant impairment of antigen presentation. Corticosteroids inhibit angiogenesis but this is unlikely to be relevant in setting of acute rejection. While some clinicians treat endothelial rejection with systemic as well as topical corticosteroid, a trial of intravenous methylprednisolone in addition to intensive topical treatment did not show an improvement in outcome compared with topical treatment alone.

Prevention of Rejection

The key to minimizing immune-mediated graft failure in patients is a dual strategy of (1) identifying pre- and post-transplant those at high risk of rejection, tailoring their management appropriately and (2) educating graft recipients as to the signs and symptoms of rejection. Preoperative risk factors for rejection include unmodifiable factors such as a previously rejected ipsilateral graft or previous herpetic keratitis and factors which are modifiable to a greater or lesser degree such as corneal vascularization or active external eye inflammation. All ocular inflammation should be brought under control where possible before elective corneal transplantation. A degree of regression of corneal vessels may be induced by topical steroid treatment particularly in an inflamed cornea. More established vessels may be difficult to treat. Of most concern are deep vessels and vessels close to the (projected) graft–host interface. Inhibition of formation

of lymphatic vessels from preexisting lymphatic vessels (lymphangiogenesis) in the host cornea has been shown to prevent or delay graft rejection by inhibiting APC egress and sensitization to alloantigen. Antivascular endothelial growth factor (anti-VEGF) treatment is a promising area for future investigation as it may help to mitigate both the afferent (lymphangiogensis) and efferent (angiogenesis) arms of the immune response to allogeneic cornea.

One rational approach to management of transplants at high rejection risk is the use of systemic immunosuppression with calcineurin inhibitors to prevent alloreactive T cell clonal expansion. Unfortunately, there is no robust evidence favoring any such regimes and complete absence of randomized trials. In grafts not at high risk of rejection, very long-term local immunosuppression with topical corticosteroid may be useful in preventing rejection but the benefit must be weighed against such risks as glaucoma, susceptibility to infection, and impaired corneal wound healing. In the postoperative period, patients presenting with alloantigen-independent ocular surface inflammation, such as suture loosening, should be treated promptly and aggressively.

See also: Adaptive Immune System and the Eye: T Cell-Mediated Immunity; Antigen-Presenting Cells in the Eye and Ocular Surface; Dynamic Immunoregulatory Processes that Sustain Immune Privilege in the Eye; Immunosuppressive and Anti-Inflammatory Molecules that Maintain Immune Privilege of the Eye; Role of Complement in Ocular Immune Response.

Further Reading

Barnes, P. J. (2006). How corticosteroids control inflammation: Quintiles Prize Lecture 2005. *British Journal of Pharmacology* 148: 245–254.

Ferguson, T. A. and Griffith, T. S. (2006). A vision of cell death: Fas ligand and immune privilege 10 years later. *Immunological Reviews* 213: 228–238.

Fu, H., Larkin, D. F. P., and George, A. J. T. (2008). Immune modulation in corneal transplantation. *Transplantation Reviews* 22: 105–115.

Hamrah, P., Liu, Y., Zhang, Q., and Dana, M. R. (2003). The corneal stroma is endowed with a significant number of resident dendritic cells. *Investigative Ophthalmology and Visual Science* 44: 581–589.

Herrera, O. B., Golshayan, D., Tibbott, R., et al. (2004). A novel pathway of alloantigen presentation by dendritic cells. *Journal of Immunology* 173: 4828–4837.

Katami, M. (1991). Corneal transplantation – immunologically privileged status. *Eye* 5: 528–548.

Niederkorn, J. Y. (2006). See no evil, hear no evil, do no evil: The lessons of immune privilege. *Nature Immunology* 7: 354–359.

Rogers, N. J. and Lechler, R. I. (2001). Allorecognition. *American Journal of Transplantation* 1: 97–102.

Streilein, J. W., Wilbanks, G. A., Taylor, A., and Cousins, S. (1992). Eye-derived cytokines and the immunosuppressive intraocular microenvironment: A review. *Current Eye Research* 11(supplement): 41–47.

Williams, K. A. and Coster, D. J. (2007). The immunobiology of corneal transplantation. *Transplantation* 84: 806–813.

Williams, K. A., Esterman, A. J., Bartlett, C., et al. (2006). How effective is penetrating corneal transplantation? Factors influencing long-term outcome in multivariate analysis. *Transplantation* 81: 896–901.

Pericytes and Microvascular Remodeling: Regulation of Retinal Angiogenesis

I M Herman, Tufts University School of Medicine, Boston, MA, USA

Glossary

Cytoskeleton – The cellular organelle that constitutes the mechanically deformable, dynamic, and structurally rigid components that enable cell shape changes, cell cycle progression, and migration. Major components include the actin- and myosin-based system, the microtubule-based system, and the intermediate filament system.
Diabetic retinopathy – Pathologic disorder accompanying diabetes wherein unwanted cellular dystrophy and proliferation can give rise to vision loss. Components involved include, but are not restricted to, the retinal microvascular cells, including their associating extracellular matrix elements as well as neural retinal components. Proliferative diabetic retinopathy is heralded by ischemic insult, loss of vascular perfusion, fibrovascular lesion formation, microaneurysm formation, retinal detachment, and vision loss.
Pericyte – Discovered in the late 1800s by the French naturalist, Charles Rouget. Initially bearing the discoverer's namesake, Rouget cells were renamed during the early twentieth century by Nobel laureate, August Krogh, who confirmed and extended Rouget's original observations regarding the perivascular placement of these contractile cells. More recent work has revealed and significantly extended the regulatory roles that pericytes play in controlling capillary growth and contractile phenotype during development and disease.
Rho GEF – Rho guanine exchange factor(s) (GEF) are a class of small molecular weight protein components that specifically associate/bind to Rho GTPases enhancing the duty cycle of GTP hydrolysis, fostering the conversion of GTP to GDP, thus influencing the efficiency or activity of RhoGTPase function.
Rho GTPase – A member of the ras-related superfamily of guanine nucleotide-binding proteins that hydrolyzes guanosine triphosphate (GTP), converting it to the guanosine diphosphate (GDP)-bound form. Rho GTPase acts as a molecular switch within living cells. Upon GTP hydrolysis, Rho GTP is known to activate (phosphorylate) a number of key downstream effectors responsible for reversibly regulating cytoskeletal remodeling, mechanical tension, and cellular dynamics.
SMAD – A transforming growth factor (TGF)-β signal transducer that moves from cytoplasm to nucleus and regulates transcription.

Overview

Development of the adult retinal microcirculation is complex. As is the case in every human tissue bed or organ system, retinal microvascular morphogenesis is both tightly regulated and highly dependent upon the diverse signaling cascades that drive vascular cell proliferation and differentiation. Without question, retinal development is sustainable by the intimate relationship that exists between the neural and vascular retina where metabolites and available survival or growth factors help to shape microvascular remodeling during ocular angiogenesis, regardless of whether these adaptations are observed during development or in association with aging-related or chronic disease states such as diabetes. Indeed, as recent research findings and clinical studies suggest, nascent vessels are born, pruned, stabilized, and destabilized because of the regulatory roles that pericytes play in modulating retinal endothelial cell dynamics.

Retinal Microvascular Dynamics: Cell–Cell Interactions

During retinal microvascular development, there is considerable partnering between pericytes and nonvascular cells. For example, astrocytes transiently express vascular endothelial growth factor (VEGF) as they migrate across the retinal ganglion cell layer. Importantly, this transretinal migration precedes the formation of the superficial retinal microvessels and contributes to the formation of the deeper retinal microcirculation. As the glial cells migrate, VEGF gradients modify endothelial growth, cell–cell contacts, and subsequent structural alterations in basement membrane architecture. Just as these complex cell- and matrix-dependent remodeling events help to initiate and maintain the physiologic vasculature, neuronal and

vascular cell pathology contribute to a physiologic hypoxia. Thus, perictyes, astrocytes, and Müller cells are also contributory or are causally linked to the severe complications observed during diabetic retinopathy, age-related macular degeneration, or neovascular glaucoma, which contribute to the inception and etiology of pathologic angiogenesis. However, there are significant gaps in our understanding the angiogenic switch mechanisms responsible for inducing the recurrent rounds of pathologic angiogenesis observed during these chronic retinal diseased states. It seems likely that common molecular and cellular mechanisms deployed during developmental angiogenesis are recapitulated during the pathologic remodeling observed during diabetes, but we are uncertain whether hypoxic insult, microthrombus formation, or altered microvascular reactivity and permeability are responsible. What are the initiating signals that reactivate the previously quiescent adult retinal microvasculature? Are the initiating events plasma derived, linked with endothelial activation downstream of platelet derangements? Could platelet-driven or endothelial-initiated events signal through the associating pericytes to initiate incipient angiogenesis? Or, are there pericyte-driven, but endothelial-dependent signaling events responsible for initiating the loss or dedifferentiation presumed to take place during diabetes? Without question, early work indicated that pericyte loss and acellular capillaries might reflect an advanced state of microvascular remodeling marking the vascular proliferative disorders observed during diabetes; but, our unraveling the molecular and cellular mechanisms that govern the initiating events responsible for the switch from a growth-arrested endothelium to one that is actively proliferating and engaged in pathologic angiogenesis remains a topic of considerable scientific interest and clinical investigation. Dissection of these endothelial- and pericyte-associated signaling pathways, which govern the onset of vascular proliferative disorders, will help to enable new opportunities aimed at abrogating retinal pathology and the pathologic angiogenesis observed during diabetes or age-related macular degeneration.

Retinal Pericytes and Diabetes-Induced Vascular Proliferative Disorders

It has been long recognized that endothelial cells share and coproduce a common basement membrane through which direct contact with pericytes can be achieved. Ultrastructural evidence supports the notion that when pericytes emerge and associate with the developing capillary, there is a marked cessation of vessel growth. Interestingly, pericyte growth and recruitment is positively regulated by platelet-derived growth factor (PDGF)-B; endothelium-restricted ablation of PDGF-B generates viable mice with extensive inter- and intra-individual variations, including the density of pericytes throughout the central nervous system (CNS) and the retina. This strong inverse relationship between pericyte density and the range of retinal microvascular abnormalities observed in retinopathies suggests that aberrations in pericyte signal transduction or pericyte depletion serve as initiating events that lead to retinopathy. There is evidence using murine models and transgenesis approaches in support of this notion; and, *in vivo*, pericyte dropout has been observed during diabetes. But importantly, pericyte dedifferentiation and the phenotypic modulation that ensue are endothelial dependent, that is, controlled by endothelial-synthesized basement membrane components that are likely to regulate capillary growth state and tonus. Thus, the absence of pericytes and the retinal neovascularization observed during diabetic retinopathy has led investigators to postulate that pericytes suppress retinal capillary endothelial cell growth. Indeed, there seems to be a robust pericyte dependence on microvascular remodeling, either via matrix-initiated signals or via cell-dependent contacts. Yet, the upstream regulators that control the role pericyte stabilization of capillary quiescence or endothelial growth arrest are currently unknown and the subject of intensive investigation.

As mentioned, the molecular and cellular mechanisms by which pericytes suppress endothelial cell proliferation and stabilize the microvasculature have not been completely elucidated; but, *in vitro* experimentation using cocultures of pericytes with endothelial cells have recently revealed both transforming growth factor (TGF)-β1-dependent and, now, TGF-β1-independent processes. In turn, we suspect that these *in vitro* observations reflect local *in vivo* microenvironmental cues emanating downstream of platelet and endothelial activation. Indeed, during diabetes endothelial expression of vascular cell adhesion molecule (VCAM) is induced, neutrophil–endothelial interactions are fostered, and microthrombus formation ensues. However, the initiating events that specifically control microvascular remodeling and which are downstream of platelet activation during pathologic angiogenesis have not been fully characterized. In fact, recent work reveals that perturbation of Rho GTP signaling in retinal pericytes is sufficient to alter retinal capillary endothelial growth state, that is elevating pericyte Rho GTP levels reverses the TGF-b1-dominated, endothelial growth-arrested phenotype, even in spite of sustained cell–cell contacts. Quantitative analyses of the latent or activated TGF-β1 present within media conditioned by endothelial cells, alone, or in co-culture with wild-type or Rho GTP-overexpressing pericytes indicate that other pericyte-dependent signaling mechanisms, which are outside of the TGFβ family, might be causing the reversal of endothelial cell growth arrest observed.

Pericyte Rho GTP Signaling: A Role in Pathologic Angiogenesis?

Our recent work has revealed a pivotal role for Rho GTP signaling in controlling pericyte contractile phenoptype. Signaling through an isoactin-specific signaling cascade, these findings have simultaneously uncovered what may be a mechanically linked series of initiating events that function to activate capillary endothelial growth and angiogenesis during ocular vascular proliferative disorders. Indeed, altering pericyte Rho GTP status uncouples the TGFb- and cell-contact-mediated growth arrested state, which keeps endothelial cells restrained within Go, the resting phase of the growth cell cycle. These data also point to upstream signals and downstream effectors that are likely to be outside the signaling analogues of mothers against decapentaplegic (SMAD)- and vascular smooth muscle actin (VSMA)-regulated events that control pericyte cytoskeletal remodeling or endothelial growth. There are several likely candidates, which could foster these observable aberrations in pericyte-dependent, endothelial growth arrest. Soluble mediators originating in the blood, produced locally by the microvascular cells or elaborated by neighboring supporting cells, could play key roles in modulating pericyte–endothelial interactions during diabetes. For example, there are a multitude of platelet-derived bioactivities that might be locally released downstream of platelet–endothelial interactions, especially during diabetes when the endothelial cell surface is notably altered. In turn, endothelial-synthesized or pericyte-generated activities could also be strategic in the signal transduction cascades leading to this angiogenic switch (Figure 1). Indeed, just this past year, bioactive lipids, which are produced by blood platelets, for example, sphingosine-1 phosphate (S1P), have been reported to modulate angiogenesis. Genetic ablation of a key G-coupled receptor that mediates S1P signaling, S1PR-2, which is predominantly found on vascular smooth muscle cells, was also demonstrated to reduce ischemia-driven angiogenesis in the mouse retina. Perhaps, the convergence of the sphingosine and Rho GTP-dependent signaling pathways offers inroads into understanding the molecular signaling events responsible for regulating pathologic angiogenesis. Indeed, pharmacologic inhibitors of sphingosine kinase, which is required for S1P synthesis, have now been reported to reduce vascular leakage in diabetic retinopathy. In addition, Igarashi and colleagues have demonstrated that aortic endothelial cell S1P receptor expression is induced following VEGF stimulation. The latter occurs concomitantly with activation of endothelial nitric oxide synthase, suggesting that each of these independent events indicates a crosstalk between sphingolipid and endothelial growth factor receptor signaling. Despite these reports, the mechanisms regulating S1P function within the retinal microvasculature, physiologically and pathologically, have not been established. These findings, together with work ongoing in our laboratory, will likely prove pivotal in unveiling upstream signaling events determining the pericyte-dependent control of endothelial proliferation during pathologic angiogenesis. Anticipated outcomes of these experiments may help to lay the experimental infrastructure for innovative anti-angiogenic therapeutic approaches aimed at abrogating the unwanted angiogenesis accompanying diabetic retinopathy or age-related macular degeneration. Platelet–endothelial interactions during diabetes or subsequent platelet S1P release may contribute to elicit local endothelial activation and, possibly, microthrombus formation. This, in turn, could stimulate VCAM expression and downstream

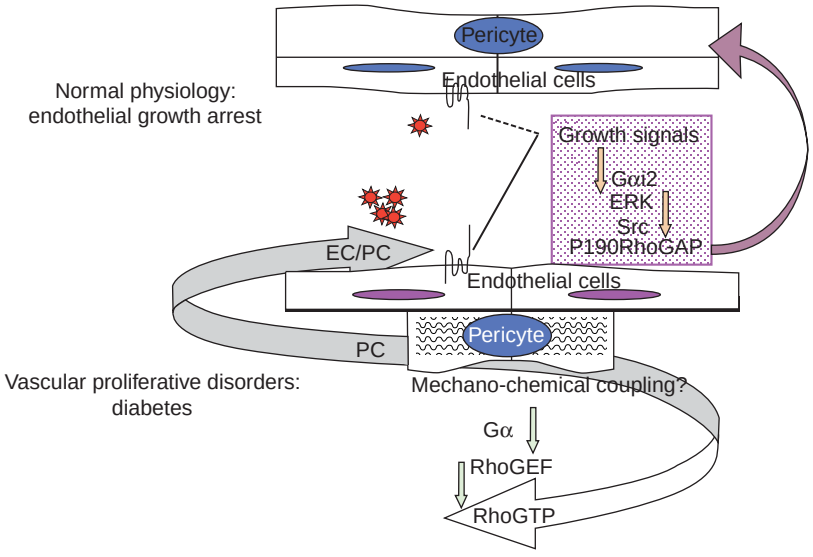

Figure 1 Mechanistic model depicting the putative up- and downstream regulatory roles for Rho GTP-dependent signaling in retinal pericytes and endothelial cells during proliferative diabetic retinopathy.

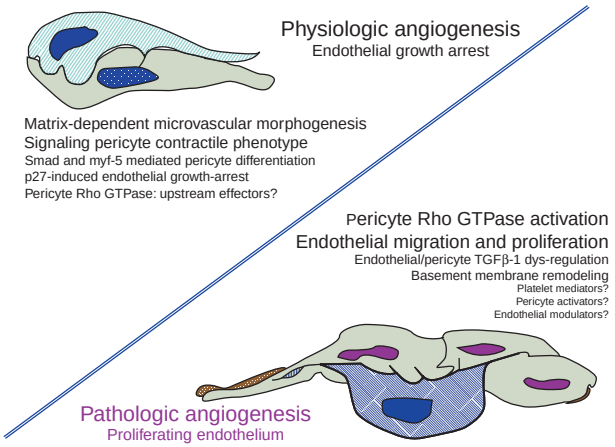

Figure 2 Model depicting the molecular and cellular events controlling the dynamic and reciprocal signaling pathways governing physiological and pathological angiogenesis.

Gq-S1PR signaling (**Figure 1**). While reasonably well worked out in smooth muscle cells, there is little information to suggest that such a signaling mechanism exists within the retinal microvasculature. Surely, diabetes-dependent perturbations in pericyte–endothelial interactions might arise downstream of platelet-dependent S1P release. As recently published findings suggest, more work will be required before we understand the mechanical and biochemical events that are up- or downstream of microvascular endothelial and pericyte Rho GTP-dependent signaling, which controls what we predict will be the angiogenic switch that is linked to the onset and severity of proliferative diabetic retinopathy (**Figure 2**).

Acknowledgments

The author acknowledges the longstanding support from NIH that has helped to advance our understanding of physiologic and pathologic mechanisms of ocular angiogenesis during development and disease (NIH R01-EY 09033, R01-EY15125, R21 EY 19533).

See also: Angiogenesis in the Eye; Angiogenesis in Wound Healing; Development of the Retinal Vasculature; Hemangiogenesis versus Lymphangiogenesis; Molecular Mechanisms of Angiostasis; Pathological Retinal Angiogenesis; Retinal Vasculopathies: Diabetic Retinopathy; Stability and Functional Integrity of New Blood Vessels; Vessel Regression.

Further Reading

Antonelli-Orlidge, A., Saunders, K. B., Smith, S. R., and D'Amore, P. A. (1989). An activated form of transforming growth factor beta is produced by cocultures of endothelial cells and pericytes. *Proceedings of the National Academy of Sciences of the United States of America* 86: 4544–4548.

Benjamin, L. E., Hemo, I., and Keshet, E. (1998). A plasticity window for blood vessel remodelling is defined by pericyte coverage of the preformed endothelial network and is regulated by PDGF-B and VEGF. *Development* 125: 1591–1598.

D'Amore, P. A., Orlidge, A., and Herman, I. M. (1987). Growth control in the retinal vasculature. In: Osborne, N. and Chader, G. (eds.) *Progress in Retinal Research*, vol. 7, pp. 233–259. Oxford: Permagon Press.

Darland, D. C., Massingham, L. J., Smith, S. R., et al. (2003). Pericyte production of cell-associated VEGF is differentiation-dependent and is associated with endothelial survival. *Developmental Biology* 264: 275–288.

Gerhardt, H., Wolburg, H., and Redies, C. (2000). N-cadherin mediates pericytic–endothelial interaction during brain angiogenesis in the chicken. *Developmental Dynamics* 218: 472–479.

Hirschi, K., Rohovsky, S. A., and D'Amore, P. A. (1998). PDGF, TGF-ß and heterotypic cell–cell interactions mediate the recruitment and differentiation of 10T1/2 cells to a smooth muscle cell fate. *Journal of Cell Biology* 141: 805–814.

Igarashi, J., Erwin, P. A., Dantas, A. P., Chen, H., and Michel, T. (2003). VEGF induces S1P1 receptors in endothelial cells: Implications for cross-talk between sphingolipid and growth factor receptors. *Proceedings of the National Academy of Sciences of the United States of America* 100: 10664–10669.

Kolyada, A. Y., Riley, K. N., and Herman, I. M. (2003). Rho GTPase signaling modulates cell shape and contractile phenotype in an isoactin-specific manner. *American Journal of Physiology – Cell Physiology* 285: 1116–1121.

Kutcher, M. E. and Herman, I. M. (2009). The pericyte: Cellular regulator of microvascular blood flow. *Microvascular Research* 77(3): 235–246.

Kutcher, M. E., Kolyada, A. Y., Surks, H. K., and Herman, I. M. (2007). Pericyte Rho GTPase mediates both pericyte contractile phenotype and capillary endothelial growth state. *American Journal of Pathology* 171: 693–701.

Lindahl, P., Johansson, B. R., Leveen, P., and Betsholtz, C. (1997). Pericyte loss and microaneurysm formation in PDGF-B-deficient mice. *Science* 277: 242–245.

Lindblom, P., Gerhardt, H., Liebner, S., et al. (2003). Endothelial PDGF-B retention is required for proper investment of pericytes in the microvessel wall. *Genes and Development* 17: 1835–1840.

Maines, L. W., French, K. J., Wolpert, E. B., Antonetti, D. A., and Smith, C. D. (2006). Pharmacologic manipulation of sphingosine kinase in retinal endothelial cells: Implications for angiogenic ocular diseases. *Investigative Ophthalmology and Visual Science* 47: 5022–5031.

Newcomb, P. M. and Herman, I. M. (1993). Pericyte growth and contractile phenotype: Modulation by endothelial-synthesized matrix and comparison with aortic smooth muscle. *Journal of Cell Physiology* 155: 385–393.

Orlidge, A. and D'Amore, P. A. (1987). Inhibition of capillary endothelial cell growth by pericytes and smooth muscle cells. *Journal of Cell Biology* 105: 1455–1462.

Regan, J. N. and Majesky, M. W. (2009). Building a vessel wall with notch signaling. *Circulation Research* 104: 419–421.

Saint-Geniez, M., Maharaj, A. S., Walshe, T. E., et al. (2008). Endogenous VEGF is required for visual function: Evidence for a survival role on Müller cells and photoreceptors. *PLoS ONE* 3: e3554.

Sato, Y. and Rifkin, D. B. (1989). Inhibition of endothelial cell movement by pericytes and smooth muscle cells: Activation of a latent transforming growth factor-beta 1-like molecule by plasmin during co-culture. *Journal of Cell Biology* 109: 309–315.

Saunders, W. B., Bohnsack, B. L., Faske, J. B., et al. (2006). Co-regulation of vascular tube stabilization by endothelial cell TIMP-2 and pericyte TIMP-3. *Journal of Cell Biology* 175: 179–191.

Skoura, A., Sanchez, T., Claffey, K., et al. (2007). Essential role sphingosine 1-phospahate receptor 2 in pathological angiogenesis of the mouse retina. *Journal of Clinical Investigation* 117: 2506–2516.

von Tell, D., Armulik, A., and Betsholtz, C. (2005). Pericytes and vascular stability. *Experimental Cell Research* 312: 623–629.

Perimetry

D B Henson, University of Manchester, Manchester, UK

Glossary

Change probability – Change probability compares each test location with that of a baseline measure and establishes whether or not there has been any significant change. Results are presented in the form of a visual field plot where each location is classified according to a series of cut-off probability levels, for example, $p < 0.05$.

Kinetic perimetry – With the kinetic examination strategies, the perimetrist selects a stimulus of a given size and intensity and moves it from outside the visual field toward its center noting the position at which it first becomes visible.

Perimetry – Perimetry, or campimetry, is the technique used to measure the extent of the visual field or to assess the sensitivity of the visual system to stimuli presented within the visual field (IPS standards).

Standard achromatic perimetry (SAP) – SAP is the most widely used form of perimetry where a white stimulus is projected onto a white background, often called white-on-white perimetry.

Static threshold perimetry – In static threshold perimetry, an estimate of the patient's sensitivity is derived at a series of predetermined test locations.

Visual field – Tate and Lynn defined the visual field as "all the space that one eye can see at any given instant," it normally extends from the fixation axis: 60° up, 75° down, 100° temporally, and 60° nasally. The superior and nasal fields are limited by facial contours.

Perimetric Techniques

Kinetic Perimetry

With the kinetic examination strategies, the perimetrist selects a stimulus of a given size and intensity and moves it from outside the visual field toward its center noting the position at which it first becomes visible. This is repeated along a series of different meridians and the points at which the stimulus first became visible are then joined together by a line which is called an isopter. Scotomas within the area of an isopter are detected by continuing to move the stimulus toward the center of the visual field after it has first been detected. The patient is asked to report, if at any time, it disappears.

The perimetrist can repeat the whole process with stimuli of different sizes and/or intensities, in order to build up a map of the patient's visual field, such as that given in Figure 1. Kinetic examination strategies were very popular in the early days of perimetry. They have, however, been largely replaced by static techniques although they are still retained for specific cases such as small residual islands of vision and where patients have difficulty in performing automated perimetry.

Static Threshold Perimetry

In static threshold perimetry, an estimate of the patient's sensitivity is derived at a series of predetermined test locations. There are many different algorithms that can be used to establish the threshold and a great deal of effort has gone into deriving ones that minimize test time and error (difference between the true and the measured threshold).

The first widely used threshold algorithm (Full Threshold) was developed by Spahr and Bebie and their colleagues. It is a two-reversal staircase strategy in which the step size reduced from 4 to 2 dB after the first reversal.

This algorithm suffers from four major drawbacks:

1. long test time,
2. demanding and exhausting for the patient,
3. poor repeatability, and
4. a significant learning effect.

In an attempt to shorten test times, the fast threshold staircase algorithm was introduced, in which there was a single step size of 3 dB with only one reversal. While being faster, this algorithm is more variable than the Full Threshold algorithm and thus has not been widely adopted in clinical practice.

Tendency-orientated perimetry was similarly developed in order to reduce test times. The algorithm combines data from several neighboring locations and reduces test times by effectively reducing spatial resolution.

The Swedish interactive threshold algorithm (SITA) is currently one of the most widely used algorithms. It is considerably faster than the full threshold algorithm (approximately 5 min per eye for a normal field) with similar repeatability. This has been achieved by:

1. using maximum-likelihood procedures in combination with a 4–2 dB staircase algorithm;
2. removing the need for false-positive catch trials; and

3. speeding up the rate of stimulus presentation in patients who respond quickly. The SITA algorithm monitors the patient's response rate and adjusts the presentation rate accordingly.

The SITA algorithm is currently available in two forms, standard and fast. SITA Fast has more liberal terminating criteria to further reduce overall test times.

Static Suprathreshold Perimetry

In a suprathreshold examination, the stimuli are initially presented at an intensity that is calculated to be above the patient's threshold. If the stimuli are seen then it is assumed that no significant defect exists. This strategy has largely been developed as a screening procedure for conditions such as glaucoma.

There are many different types of suprathreshold tests and Table 1 highlights some of the major differences.

Selection of the test intensity is an important part of a suprathreshold test. If the intensity is set too high then the test will become insensitive to shallow defects. If the intensity is set too low then the test looses specificity. Most suprathreshold tests set the intensity at 5–6 dB above the threshold estimate.

Multiple stimulus tests are faster (approximately twice as fast in a person without a defect). The need to verbally respond to each presentation helps maintain patient attention, improves threshold estimates and reduces variability.

Test Targets

Most modern perimeters use stimuli whose sizes were defined by Goldmann (see Table 2).

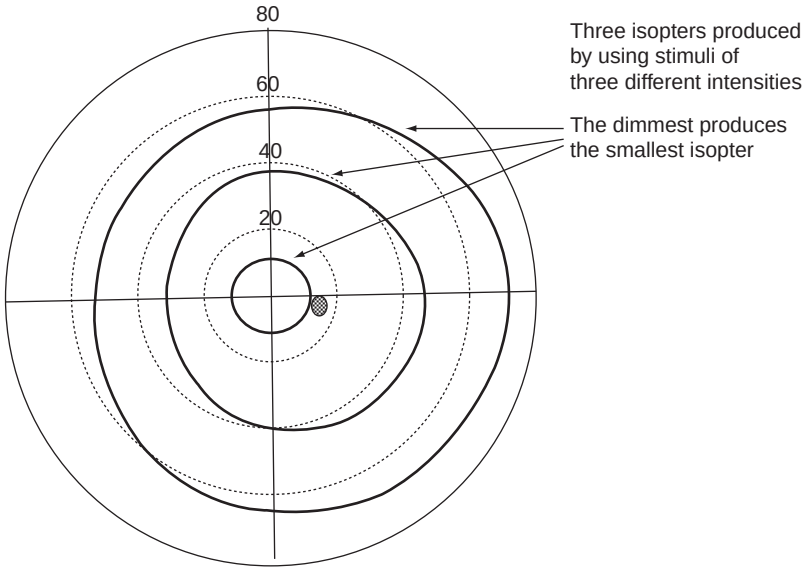

Figure 1 A map of a patient's visual field produced through kinetic perimetry using test stimuli of three different intensities. The dimmest test produces the smallest isopter.

Table 1 The different types of suprathreshold visual field test strategies

Test intensity	Fixed across the whole field	Used to test the visual field of drivers where the intensity is well above the estimated threshold
	Increases with eccentricity	Most common, with the increase matched to a database of threshold measures and age
Threshold setting	Age related	The test intensity is based upon the age of the patient.
	From measurement	The test intensity is based upon a series of threshold estimates at a few test locations, usually 4
Presentation	Single stimulus	Test locations are presented one at a time and the patient indicates when they see the stimulus by pressing a response button
	Multiple stimulus	Test locations are presented in patterns of 2–4 stimuli and the patient verbally reports the number seen
Algorithm	Standard	If stimulus is missed, it is presented a second time and only if missed twice is it marked as a miss. Pass criterion is one seen out of up to two presentations
	Multisampling	Pass criterion is raised, a typical one being three seen out of up to five presentations

Table 2 Goldmann stimulus sizes

Goldmann size	*Nominal size (mm^2)*	*Angular subtence (min of arc)*
0	0.0625	3.78
I	0.25	7.68
II	1.0	15.36
III	4.0	30.71
IV	16	61.3
V	64	122.56

Standard Achromatic Perimetry

Standard achromatic perimetry (SAP) is the most widely used form of perimetry where a white stimulus is projected onto a white background, often called white-on-white perimetry. It normally uses a size III or V Goldmann stimulus on a background luminance of 31.5 apostilbs (10 cd m^{-2}). The intensity of the stimuli is given in decibels of attenuation from a fixed value of 10 000 apostilbs (this can vary from instrument to instrument). Thus, 0 dB corresponds to 10 000 abs, 10 dB to 1000 abs, and 20 dB to 100 abs.

Short-Wavelength Automated Perimetry

Patients with glaucoma often have an associated color vision defect in which their sensitivity to blue light is reduced. This observation led researchers to question whether or not the blue sensitive mechanism was more susceptible to glaucomatous damage and whether or not a perimeter that specifically targeted the blue mechanism might not be more sensitive than those that use the conventional SAP stimuli.

A problem encountered when trying to test the blue mechanism is the relatively low sensitivity of blue cones. Even at short wavelengths (440 nm) the blue sensitive cones are only marginally more sensitive than the red and green cones. Selective damage to the blue cones would have relatively little effect upon sensitivity as the red and green cones would simply step in once the blue cone sensitivity dropped below that of the other receptors. To overcome this problem, the red and green cones are desensitized by adapting the eye to a yellow light. **Figure 2** shows the sensitivity of the three receptors after adaptation. The blue cones are exposed at 440 nm wavelength. The extent of exposure is important. If we consider that any damage to the blue cones mechanism is likely to lower its sensitivity we can see from **Figure 2** just how much loss can be tolerated before the red and green receptors again become the most sensitive (approximately 1.5 log units).

There have been a number of studies that have demonstrated that blue-yellow defects precede those for SAP, however, the test has not been widely adopted because:

1. blue-yellow perimetry is particularly sensitive to lens opacities;
2. short-wavelength automated perimetry is more variable than SAP;
3. patients find the test difficult; and
4. most patients seen in a glaucoma clinic either have no visual field loss or have defects that can be detected with SAP.

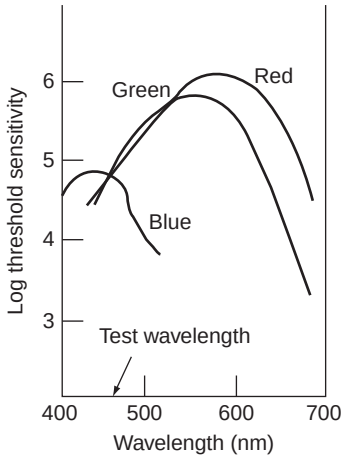

Figure 2 The log threshold sensitivity of the blue, green, and red cone systems after adaptation with a yellow light that desensitizes the red and green cones. Under these conditions the blue cones can be tested using 440 nm wavelength test light. Note that even after adaption, blue cones are approximately 1.5 log units less sensitive than green and red cones.

High-Pass Resolution Perimetry (Ring Perimetry)

High-pass resolution perimetry uses ring-shaped targets of varying size (see **Figure 3**). The luminance inside each ring target is the same as the background while the core of the ring is brighter and its inner and outer edges darker. The overall intensity profile of the ring is such that when it cannot be resolved it cannot be detected. Patients press a response key when they see the stimulus (presentation time 165 ms) and a repetitive bracketing strategy is used to establish the minimum resolvable ring size.

High-pass resolution perimetry has good sensitivity and specificity when compared to SAP. It has also been shown to have threshold variability that is independent of sensitivity and can detect progressive loss earlier than conventional perimetry. High-pass resolution perimetry is also fairly fast taking on average only 5.5 min to test 50 locations.

On the negative side, the technique is sensitive to blur, either refractive or due to media changes, unable to measure defect depth within small circumscribed lesions, and is unable to detect scotomata whose size is less than the local liminal test target. With the current monitor technology, there is also a relatively small dynamic range of stimuli which limits the test ability to monitor loss in patients with significant loss.

Figure 3 High-pass resolution perimetry uses ring-shaped targets of varying size. The luminance inside each ring target is the same as the background while the core of the ring is brighter and its inner and outer edges darker. The overall intensity profile of the ring is such that when it cannot be resolved it cannot be detected. Patients press a response key when they see the stimulus (presentation time 165 ms) and a repetitive bracketing strategy is used to establish the minimum resolvable ring size.

Frequency-Doubling Technology Perimeter

The frequency-doubling technology (FDT) perimeter is based upon an illusion known as frequency doubling, in which an alternating sinusoidal grating of low spatial frequency (<4 cpd) appears, at certain temporal frequencies (>15 Hz), to have twice as many lines. This illusion is believed to be mediated by the magnocellular (M-cell) pathway and in particular by the large fiber diameter *My* ganglion cells which constitute 1.5–2.5% of all retinal ganglion cells.

Recent investigations of ganglion cell fiber loss in glaucoma have led to the development of a number of theories. One theory is that there is selective loss of M-cell fibers during the early stages of this condition. Another is that there is selective loss of large diameter axons and a third is that mechanisms with little redundancy (sparse representation) are likely to show losses earlier than those with greater redundancy. As FDT is believed to be based upon large-diameter M-cell fibers, which are sparsely represented, a screening test based upon this illusion should, according to all these theories, be particularly sensitive to early glaucomatous loss. However, while FDT perimeter uses the appropriate spatial and temporal frequencies for the illusion, the task presented to the patient is one of contrast sensitivity, that is, the patient is being asked when he/she can detect the appearance of a target in the peripheral field not when he/she sees the frequency-doubling illusion.

The FDT perimeter uses 0.25 cpd stimulus that subtend 10° at a temporal frequency of 25 Hz. A modified binary search strategy is used to test 17 locations. Threshold and suprathreshold test strategies have good sensitivities and specificities and the instrument has many attractive characteristics for glaucoma screening. It is a small, self-contained, portable instrument that is not sensitive to background illumination levels. It does not require a corrective lens for refractive errors (results are reported to be independent of refractive error up to ±7.00 D) and it is relatively fast.

A second-generation FDT perimeter, Humphrey Matrix, was produced in 2005. This instrument uses a range of stimulus sizes (10°, 5°, and 2°), two spatial frequencies (0.25 and 0.5 cpd) and three temporal frequencies (25, 18, and 12 Hz) to give a wider range of test programs including those that mimic those widely used in SAP (24-2, 10-2). These modifications overcome the major drawback of poor spatial resolution in the earlier instrument.

Reliability Estimates

Most modern perimeters incorporate methods for estimating the reliability of the patient's responses. Widely used measures are fixation accuracy, false-positive response rate, and false-negative response rate. The relationship between these reliability measures and test–retest variability is, however, poor.

Fixation Accuracy

The simplest technique for monitoring fixation is observation by the perimetrist either with the aid of a telescope or camera. Such techniques are totally dependent upon the perimetrist's judgment and continued vigilance.

Some perimeters incorporate a fixation monitor that indicates when fixation has been lost. Most fixation monitors cannot differentiate between rotations of the eye, which occur when the patient looks away from the fixation target, and translations of the eye. A translation of the eye, such as a slight sideways movement of the head, does not necessarily mean that fixation has been lost or that the angular subtence of the perimetric stimuli has been changed by a significant amount. Automatic fixation monitors are also generally insensitive to small, but significant, fixation errors (e.g., 1°).

Most modern perimeters incorporate the Heijl–Krakau technique for sampling fixation. With this technique stimuli are occasionally presented in the region of the patient's blind spot. If fixation is maintained during these presentations the stimulus will not be seen. If, on the other hand, fixation is lost then the stimulus is likely to fall outside of the blind spot and elicit a response from the patient. A frequently quoted cut off for reliable fixation errors is less than 33% of presentations. There is no evidence on which to base this cut-off value and the relatively small number of trials (on average there are only 10–12 fixation trials in a perimetric test) mean that the precision of the estimated rate is very low. As the position of the blind spot varies from one individual to another it is necessary, at the onset of the examination, to have a little routine which establishes the blind spot's location. The accuracy of this routine is important as errors may later manifest themselves

as numerous fixation errors in a patient who has maintained good fixation.

The major advantages of the Heijl–Krakau technique are its simplicity and ease of implementation. Its disadvantages are:

1. It only samples fixation.
2. It increases the examination time.
3. It is unlikely to detect small fixation errors as the standard target subtends ≈0.5° and the blind spot an area of 5° × 7°.

At present, the best method is direct observation by the perimetrist. This technique is not only sensitive but also, via verbal feedback, can result in an improvement in the fixation accuracy for subsequent presentations.

False-Positive Responses

Single stimulus static test programs derive an estimate of the false-positive response rate with a number of catch trials (when the instrument goes through the motions of presenting a stimulus but does not actually present one). If the patient responds to one of these catch trials then this is classified as a false-positive response. In the SITA test algorithms this catch trial method has been replaced by one based upon response times (interval between the presentation of a stimulus and the patient pressing the response button). Olsson and colleagues were able to show a good relationship between the number of response times that fell outside a patient's normal response window and the false-positive response rate. They also demonstrated that estimates based upon response times were more repeatable than those based upon catch trials. An added advantage of using response times is that it reduces, slightly, the overall test time. Many patients do not give a single false-positive response during a visual field test and it is important to remember the false-positive response rate is a poor predictor of test–retest variability. A less than 33% false-positive rate is often used to differentiate reliable from unreliable results, again there is no evidence on which to base this cut-off value and the relatively small number trials means that the precision of the estimate is poor. More stringent cut-offs are often used in research studies.

False-Negative Responses

An estimate of the false-negative response rate is obtained by retesting a location with a stimulus whose intensity is above the already established threshold. If the patient fails to respond positively to this presentation then this is classified as a false-negative. False-negative responses are often found to increase with the extent of visual field damage and this is believed to be due to the relationship between variability and sensitivity. Most patients have a low false-positive rate and those with a rate above 33% are often classified as unreliable although more stringent cut-offs are often used in research trials. Again there is no evidence to support this cut-off value and the number of trials means that the precision of the estimate is poor.

Clearly, if the patient makes a high proportion of errors then his/her results must be viewed with a certain amount of suspicion. The judgment of an attending perimetrist is, however, often of greater value than these reliability estimates.

Analytical Techniques

Total Deviation and Pattern Deviation Plots

Total deviation and pattern deviation maps take the threshold data from a visual field examination and calculate, for each test location, whether or not the threshold values are significantly different from those of a normal eye of the same age. They rely upon the perimeter having a database of threshold values from normal eyes in order to perform these calculations. Pattern deviation values differ from total deviation values in that they have been adjusted for overall shifts in sensitivity. For example, we might get a patient whose overall sensitivity is below that of a normal patient of the same age. In this case, some locations may be highlighted as being abnormal on the total deviation map but not on the pattern deviation map. This adjustment is based upon the findings from some of the most sensitive test locations, that is, if these are above or below normal then all values are shifted down or up.

Total and pattern deviation probability maps use the distribution of total and pattern deviation values within a normal population, to calculate the probability of each threshold estimate coming from a normal eye. The results are expressed in the standard statistical way, that is, as being beyond the 5%, 2%, 1%, or 0.5% probability level.

Global Indices

Flammer and colleagues proposed that the visual field defects associated with glaucoma could be divided into three different categories: (1) those that cause an overall depression in the sensitivity of the eye, (2) those that cause local defects, and (3) those that cause an increase in the variability of results; and that each category could be represented by an index. They called these three indices mean defect, loss variation, and short-term fluctuation.

The concept of using three separate indices to represent a glaucomatous visual field has found very wide acceptance within the ophthalmological professions and most visual field instruments now incorporate a set of algorithms which compute these or very similar indices. The name given to these indices varies from one instrument to another, as does the form of calculation. In the

Humphrey instrument they are called mean deviation, pattern standard deviation, and short-term fluctuation and the values are weighted according to the normal variance seen at each location.

Mean defect (deviation) (MD) gives the average difference between the threshold values and those from an age-matched control. Loss variance is a measure of the spread of defect values which increases when there is a local defect. An alternative measure of spread is the standard deviation (SD). This statistic has the advantage of giving a measure of spread in decibels and is now used in preference to variance measures. In the Humphrey perimeter this is called pattern standard deviation (PSD) while in the Octopus it is called sLV, which stands for the square root of the loss variance, that is, the SD. Short-term fluctuation is a measure of variability in threshold estimates derived from repeat testing a subset of locations. However, a global estimate of variability is of limited value as it is now recognized that variability is dependent upon sensitivity and varies across the visual field.

MD and sLV or PSD can be plotted over time to aid the detection of progressive loss. They can also be plotted against each other to give a measure of the extent of loss, Brusini staging system. The sensitivity of MD to media opacities, such as cataract, has led to the development of a new global index for the Humphrey perimeter called the visual field index (VFI). This index gives a percentage measure of the residual field and uses pattern deviation values and a weighting system based upon cortical magnification to give a more representative measure of a patient's visual function.

The Glaucoma Hemifield Test (GHT) (Humphrey) and cluster analysis (Octopus) are additional indices designed to help detect rather than quantify glaucomatous visual field loss. They are designed to detect vertical asymmetry between the superior and inferior hemifields. The GHT looks at the asymmetry in pattern deviation probability values between five areas in the superior field and their mirror images in the inferior field, while the Octopus cluster analysis uses the defect values within each of five slightly different clusters within the superior and inferior visual field. Both use a database of normal values to establish whether or not a response is outside normal limits.

Linear Regression

Linear regression can be applied to a longitudinal series of:

1. global indices (MD, PSD, VFI),
2. clusters of test locations (Octopus cluster analysis), or
3. individual test locations (point-wise analysis).

The significance of any change over time and the gradient of the regression line can be used for predicting long-term outcomes.

The Progressor software package presents the findings from a point-wise regression analysis in a particularly novel way that retains the information on both the depth of the defect and the significance of any change while the Peridata software package (Peridata) color codes each test location according to the significance of any change. From these charts the clinician can ascertain whether or not any progressive changes are close to fixation or at the edge of the visual field, where they may have been influenced by artifacts such as a droopy upper lid.

The accuracy of a regression analysis and any predictions is dependent upon the number of examinations. Several research groups have concluded that we really need about five visual field results before we can reliably calculate the gradient of the regression line.

Change Probability

Change probability compares each test location with that of a baseline measure and establishes whether or not there has been any significant change. Results are presented in the form of a visual field plot where each location is classified according to a series of cut-off probability levels, for example, $p < 0.05$. The baseline value is often the average of two visual field results (to give a better estimate) that need not be the first ones recorded, that is, we can establish whether there has been any significant change from intermediate results.

Change probability analysis takes into account the relationship between variability and sensitivity. One of the criticisms of change probability is that it does not use the information obtained in intermediate examinations, that is, it only compares the current finding with the baseline value. The recently introduced Progression Analysis Probability plot for the Humphrey Visual Field Analyzer uses different symbols to code whether or not the change has occurred in just the current, last two, or last three examinations.

See also: Intraocular Pressure and Damage of Optic Nerve Axons; Primary Open-Angle Glaucoma; Retinal Ganglion Cell Apoptosis and Neuroprotection; Structural Changes in the Trabecular Meshwork with Primary Open Angle Glaucoma; The Genetics of Primary Open-Angle Glaucoma: A Review.

Further Reading

Anderson, A. J., Johnson, C. A., Fingeret, M., et al. (2005). Characteristics of the normal database for the Humphrey Matrix perimeter. *Investigative Ophthalmology and Visual Science* 46: 1540–1548.

Artes, P. H., Henson, D. B., Harper, R., and McLeod, D. (2003). Detection and quantification of visual field loss: A comparison of perimetric strategies by computer simulation. *Investigative Ophthalmology and Visual Science* 44: 2582–2587.

Bengtsson, B. (2000). Reliability of computerised perimetric threshold tests as assessed by reliability indices and threshold reproducibility in patients with suspect and manifest glaucoma. *Acta Ophthalmologica* 78: 519–522.

Bengtsson, B. and Heijl, A. (2008). A visual field index for calculation of glaucoma rate of progression. *American Journal of Ophthalmology* 49: 66–76.

Bengtsson, B., Olsson, J., Heijl, A., and Rootzen, H. (1997). A new generation of algorithms for computerised perimetry, SITA. *Acta Ophthalmologica* 75: 368–375.

Brusini, P. and Filacorda, S. (2006). Enhanced glaucoma staging system (GSS2) for classifying functional damage in glaucoma. *Journal of Glaucoma* 15: 40–46.

Cello, K. E., Nelson-Quigg, J. M., and Johnson, C. A. (2000). Frequency doubling technology perimetry for detection of glaucomatous visual field loss. *American Journal of Ophthalmology* 129: 314–322.

Chauhan, B. C., House, P. H., McCormick, T. A., and LeBlanc, R. P. (1999). Comparison of conventional and high-pass resolution perimetry in a prospective study of patients with glaucoma and healthy controls. *Archives of Ophthalmology* 117: 24–33.

Flammer, J., Drance, S. M., Augustiny, L., and Funkhouser, A. (1985). Quantification of glaucomatous visual field defects with automated perimetry. *Investigative Ophthalmology and Visual Science* 26: 176–181.

Frisen, L. (1987). A computer-graphics visual field screener using high-pass spatial frequency resolution and multiple feedback devices. *Documenta*. *Ophthalmologica Proceedings Series* 49: 441–446.

Henson, D. B. and Artes, P. H. (2002). New developments in supra-threshold perimetry. *Opthalmic and Physiological Optics* 22: 463–468.

Henson, D. B., Chaudry, S., Artes, P. H., Faragher, E. B., and Ansons, A. (2000). Response variability in the visual field: Comparison of optic neuritis, glaucoma, ocular hypertension and normal eyes. *Investigative Ophthalmology and Visual Science* 41: 417–421.

Johnson, C. A., Adams, A. J., Casson, E. J., and Brandt, J. D. (1993). Blue-on-yellow perimetry can predict the progression of glaucomatous damage. *Archives of Ophthalmology* 111: 645–650.

King, A. J. W., Taguri, A., Wadood, A. C., and Azuara-Blanco, A. (2003). Comparison of two fast strategies, SITA fast and TOP, for the assessment of visual fields in glaucoma patients. *Archives of Ophthalmology* 240: 481–487.

Miranda, M. and Henson, D. B. (2008). Perimetric sensitivity and response variability in glaucoma with single stimulus automated perimetry and multiple stimulus perimetry with verbal feedback. *Acta Ophthalmologica* 86: 202–206.

Morales, J., Weitzman, M. L., and Gonzalez de la Rosa, M. (2000). Comparison between Tendency-Oriented Perimetry (TOP) and octopus threshold perimetry. *Ophthalmology* 107: 134–142.

Olsson, J., Bengtsson, B., Heijl, A., and Rootzen, H. (1997). An improved method to estimate frequency of false-positive answers in computerized perimetry. *Acta Ophthalmologica* 75: 18–183.

Viswanathan, A. C., Fitzke, F., and Hitchins, R. A. (1997). Early detection of visual field progression in glaucoma: A comparison of PROGRESSOR and STATPAC 2. *British Journal of Ophthalmology* 81: 1037–1042.

Relevant Websites

http://webeye.ophth.uiowa.edu – University of Iowa Health Care; IPS Standards: Imaging and Perimetric Society.

http://www.peridata.org – Peridata; Peridata Software GmbH.

Pharmacological Vitreolysis

A Gandorfer, Augenklinik der Ludwig-Maximilians-Universität, München, Germany

Glossary

Internal limiting membrane (ILM) – The inner border of the retina composed of the basement membrane of retinal glial cells (Müller cells).
Microplasmin – The recombinant form of human plasminogen containing the catalytic domain of the enzyme.
Plasmin – A serine protease mediating fibrinolysis.
Posterior vitreous detachment (PVD) – Separation of the vitreous cortex from the retina either spontaneously or surgically/pharmacologically.
Synchisis – Liquefaction of the vitreous gel.
Syneresis – Separation of the vitreous from the retina.
Vitreoretinal interface – The functional complex between the retina and the vitreous, that is, between the internal limiting membrane of the retina and collagen fibers forming the vitreous cortex.
Vitreoschisis – Splitting of the vitreous cortex, leaving a layer of cortical vitreous behind at the retina, thereby resulting in an incomplete posterior vitreous detachment.
Vitreous liquefaction – Converting the gel-like status of the vitreous into a liquid status.

Introduction

Pharmacological vitreolysis is among the top five wish list of medical and surgical retina specialists. Separating the vitreous cortex completely from the retina by pharmacological means would be a major achievement compared to today's mechanical techniques of vitrectomy. As incomplete vitreoretinal separation and vitreoschisis play a central role in the progression of commonly and potentially blinding diseases such as diabetic retinopathy and maculopathy, proliferative vitreoretinopathy (PVR), and vitreomacular traction syndromes, induction of complete posterior vitreous detachment (PVD) by pharmacological means has a major impact on both surgical techniques and public health aspects.

Enzyme-assisted induction of PVD enables the surgeon to create a clean retinal surface which cannot be achieved by mechanical means currently. Moreover, complete vitreoretinal separation without directly approaching the retina and macula by bent needles or forceps would make surgery easier and safer. In children and young adults and in patients with firm vitreoretinal adhesion, complete separation of the vitreous from the retina would be possible. This would help to improve both the anatomical and functional outcome by eliminating remnants of vitreous which act as a scaffold and promoter of persistent and recurrent cellular proliferation. In progressively blinding diseases such as diabetic retinopathy, separating the vitreous from the retina before neovascular and fibrocellular proliferation grow into the vitreous cortex would prevent advanced stages of the disease. Finally, pharmacological vitrectomy holds the potential of improving retinal oxygen levels in hypoxic retinal diseases in a more applicable way compared with mechanical vitrectomy. This is of particular importance, given the increasing incidence of diabetic retinopathy in the world. The goal of enzymatic vitreous disruption is to manipulate the vitreous collagen pharmacologically, both centrally, achieving liquefaction, as well as along the vitreoretinal interface to induce PVD, and to create a cleavage plane more safely and cleaner than can be achieved by mechanical means.

The Role of the Vitreous in Disease

The vitreous, and in particular the vitreoretinal interface, plays an important role in the pathogenesis of many retinal disorders. An abnormal interface has been implicated in vitreomacular traction syndrome, macular holes, diabetic macular edema, proliferative diabetic retinopathy, retinal detachment, and PVR. A common finding in these entities is a vitreous which is firmly attached to the retina, thereby preventing complete PVD. Even in cases of vitreous liquefaction, the vitreous cortex remains attached to the retina, forming the so-called vitreoschisis, which acts as a scaffold for fibrocellular and fibrovascular proliferations. This may increase traction on the retina, leading to significant patient morbidity and surgical failure.

The Objectives of Pharmacological Vitreolysis

Vitrectomy is the treatment modality of choice in these patients, and complete removal of the cortical hyaloid is critical for success of the operation. However, mechanical separation of the vitreous from the retina is incomplete as cortical vitreous fibrils are left behind on the internal

limiting membrane (ILM) of the retina. Removal of the ILM creates a new vitreomacular interface by eliminating the vitreous cortex and proliferative tissue. ILM removal, however, requires direct manipulation of the macula which can potentially result in retinal damage, leading to functional defects, such as central or paracentral scotomata (an area of diminished vision within the visual field). Ultrastructural analysis of peeled ILM specimens has shown damage to Müller cells and avulsion of macular ganglion cells. Although ILM peeling appears safe in clinical terms, it may not be the best option in terms of safety and visual benefit.

Cleaving the vitreoretinal interface at the vitreal side of the ILM would be a logical approach to relieve traction as the ILM itself cannot exert traction. Traction is generated by contractile cells at the vitreoretinal interface. In most instances, these cells proliferate on a layer of vitreous cortex which remains attached at the ILM after incomplete PVD. From an ultrastructural point of view, separation of the cortical vitreous completely from the ILM would eliminate the cellular proliferations, thereby relieving the traction they generate.

Complete separation of the vitreous from the retina by enzymatic means would remove the pathologic tissue from the retina, and eliminate the scaffold for cellular reproliferation. Diabetic eyes, especially, are characterized by a firm vitreoretinal attachment and a thickened and taut vitreous cortex which frequently contains cellular proliferations. Given that some cells have been shown to produce vasoactive and vasoproliferative substances, such as vascular endothelial growth factor and others, complete removal of the vitreous cortex with embedded cells could lead back to a more physiological state of the vitreomacular interface in patients with diabetic macular edema.

Moreover, a clean ILM, without remnants of the cortical vitreous, would hypothetically prevent the growth of fibrovascular membranes out of the retina as these newly formed vessels commonly proliferate within and along the cortical hyaloid. Given that a complete PVD was achieved by a relatively atraumatic intravitreal injection and not by an operation such as vitrectomy, pharmacologic vitreolysis could be discussed in select cases as a prophylactic treatment regime to prevent proliferative diabetic retinopathy.

Another mechanism of action of enzymatically induced PVD and vitreous liquefaction is an alteration of molecular flux into the vitreous cavity, out of the vitreous cavity, and across the vitreoretinal interface. It has been known since the 1980s that oxygen levels within the vitreous cavity are higher in vitrectomized eyes compared to nonvitrectomized eyes. Recently, it has been demonstrated that the oxygen supply of the retina can be modified by a microplasmin-induced PVD and vitreous liquefaction. It is noteworthy that liquefaction alone did not have this effect. Obviously, the vitreous cortex acts as a barrier for molecules when crossing the vitreoretinal border, and this may not only be the case for oxygen, but also when other molecules are produced within the eye or even when they are injected intravitreally. A better oxygen supply of the retina addresses diseases with hypoxia such as diabetic retinopathy and retinal vein occlusion, both complicated by macular edema and neovascularization, and those in which anti-vascular endothelial growth factor (VEGF) treatment is performed in order to decrease intravitreal VEGF levels, such as age-related macular degeneration (AMD). Interestingly, eyes with wet AMD also show a significantly higher percentage of attached vitreous at the macula compared to dry AMD eyes as well as eyes without AMD. Separation of the posterior hyaloid from the retina and liquefaction alters the molecular flux across the vitreoretinal interface, and it might be expected that larger molecules are even more affected by the barrier function of the cortical vitreous than small molecules such as oxygen are.

The summary of potential objectives of pharmacologic vitreolysis (**Figure 1**) includes complete vitreoretinal separation, resulting in a clean ILM, less manipulation at the vitreoretinal interface compared to current vitrectomy techniques, a well-defined cleavage plane at the vitreal side of the ILM to remove fibrocellular traction, better oxygen supply of the retina due to an alteration of the molecular flux, and a less traumatic and potentially prophylactic treatment regime in select cases in the future.

Enzyme Candidates for Vitreous Disruption

Chondroitinase

A 240-kDa chondroitin sulfate proteoglycan is associated with the vitreoretinal interface (**Table 1**). The greatest immunoreactivity of this proteoglycan has been observed in regions of firm vitreoretinal adhesion, such as the vitreous base and the papillary margin, suggesting a major role in vitreoretinal adhesion. The enzyme chondroitinase cleaves this proteoglycan and has been studied as an adjunct in vitrectomy in two human donor eyes and in 57 cynomolgus monkeys. Intravitreal injection of the enzyme separated the vitreous from the retina without damaging the ILM. Three monkeys have been followed for 14–16 months after surgery without any adverse effects. Chondroitinase has also been utilized to detach epiretinal membranes in four monkeys, providing evidence that chondroitin sulfate proteoglycan participates in the adhesion of epiretinal membranes to the ILM. Unfortunately, no further preclinical or clinical results have been reported yet.

Hyaluronidase

Hyaluronan represents one of the two major macromolecules of the vitreous, and is supposed to maintain the three-dimensional structure of the vitreous gel by coating

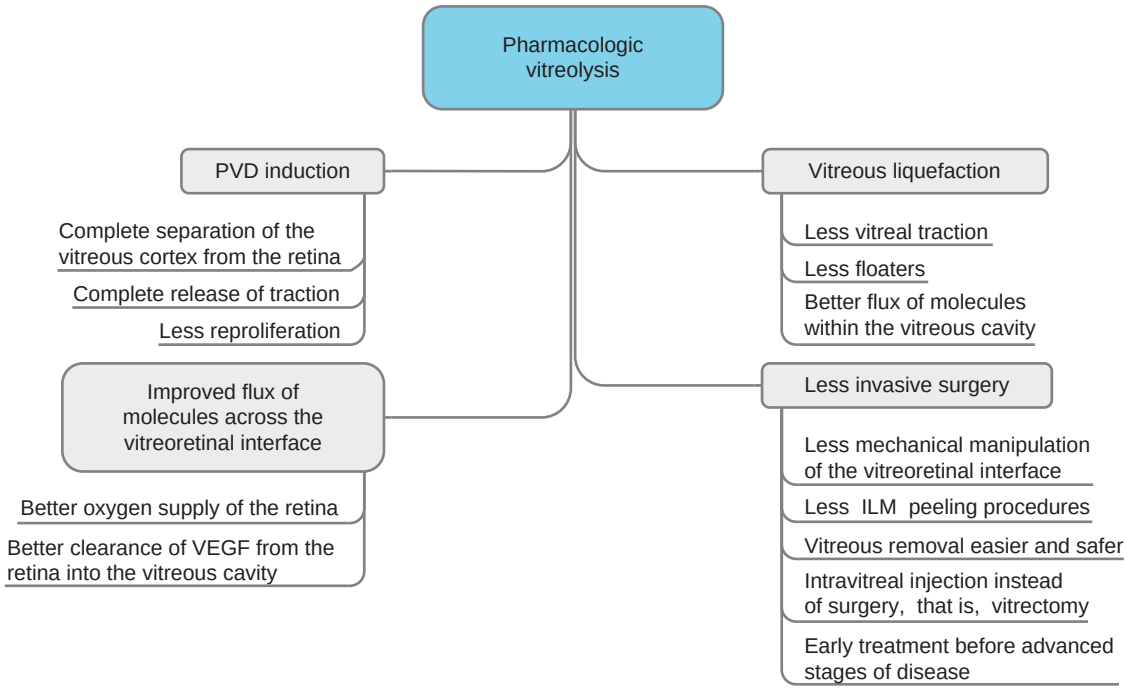

Figure 1 The objectives of pharmacologic vitreolysis.

Table 1 Enzyme candidates for enzymatic vitreous disruption

Enzyme	*Target*	*Effect*
Chondoitinase	Chondroitinsulfate at the vitreoretinal interface	PVD in animal models
Hyaluronidase	Hyaluronan	Liquefaction
Dispase	Type IV collagen	PVD, inner retinal damage
Plasmin/Microplasmin	Laminin and fibronectin at the vitreoretinal interface MMP-2 activation	PVD and liquefaction

PVD, posterior vitreous detachment; MMP, matrix metalloproteinase.

the collagen fibrils and by bridging them with interconnecting filaments. Hyaluronidase (Vitrase®) cleaves hyaluronan and has been suggested to liquify the vitreous.

A phase-III clinical trial has shown that 55 IU of highly purified ovine hyaluronidase (Vitrase®) helps to clear eyes with vitreous hemorrhage 1 month after intravitreal application. In a companion article on the safety results, no serious safety issues were reported. In particular, the incidence of retinal detachment was not statistically different between treated eyes and control groups. No assessment, however, was performed in terms of PVD induction, and previous experimental trials of hyaluronidase in rabbits failed to achieve PVD.

Dispase

Dispase, a neutral 41-kDa protease isolated from *Bacillus polymyxa*, selectively cleaves type IV collagen and fibronectin. The enzyme facilitated PVD in enucleated porcine and human eyes, and in pig eyes *in vivo*. However, partial digestion of the ILM was observed in postmortem eyes, exposing the mosaic pattern of Müller cell endfeet. In rabbit eyes *in vivo* and in human eyes 15 min before enucleation, intravitreal injection of dispase caused intraretinal hemorrhages and ILM disruption at bleeding sites. In this series, there was no effect of dispase on PVD induction.

As dispase acts on type IV collagen, forming the main structural protein of basement membranes including the ILM, changes of the inner retina following application of the enzyme are not surprising. The enzyme has been shown to effectively induce PVR in rabbits in a dose-dependent fashion, known as the dispase model of PVR; in addition, in case future studies are planned, there is a definite need to investigate the safety issues of the enzyme.

Plasmin and Microplasmin

Plasmin is a nonspecific serine protease mediating the fibrinolytic process. It also acts on a variety of glycoproteins including laminin and fibronectin, both of which are

present at the vitreoretinal interface. In 1993, PVD could be achieved in rabbit eyes by intravitreal injection of the enzyme followed by vitrectomy. In 1999, Hikichi and co-workers confirmed complete PVD after injection of 1 U plasmin and 0.5 ml SF_6 gas in the rabbit model, without evidence of retinal toxicity.

We investigated the effect of plasmin in porcine postmortem eyes and in human donor eyes. In porcine eyes, we observed a dose-dependent separation of the vitreous cortex from the ILM after intravitreal injection, without additional vitrectomy or gas injection. In scanning electron microscopy, a bare ILM was achieved by 1 U of porcine plasmin 60 min after injection, and with 2 U of plasmin 30 and 60 min after injection, respectively. In control fellow eyes which were injected with balanced salt solution (BSS), the cortical vitreous remained attached to the retina. In human donor eyes, 2 U of human plasmin from pooled plasma achieved complete PVD 30 min after injection, whereas the vitreoretinal surface of the fellow eyes was covered by collagen fibrils. In both studies, transmission electron microscopy revealed a clean and perfectly preserved ILM in plasmin-treated eyes, and no evidence of inner retinal damage. Li and colleagues confirmed these results, and reported a reduced immunoreactivity of the vitreoretinal interface for laminin and fibronectin following application of plasmin.

In an experimental setting simulating the application of plasmin as an adjunct to vitrectomy, we injected human donor eyes with 1 U of plasmin, followed by vitrectomy 30 min thereafter. All plasmin-treated eyes showed complete PVD, whereas the control eyes which were vitrectomized conventionally had various amounts of the cortical vitreous still present at the vitreoretinal interface.

Plasmin is not available for clinical application, and alternative strategies have been pursued to administer the enzyme in vitreoretinal surgery. Tissue plasminogen activator was injected into the vitreous in an attempt to generate plasmin by intravitreal activation of endogenous plasminogen. In an animal model in rabbit eyes, complete PVD was observed in all eyes treated with 25-μg tissue plasminogen activator. Breakdown of the blood–retinal barrier was necessary to allow plasminogen to enter the vitreous, and this was induced by cryocoagulation. In two clinical pilot studies, 25-μg tissue plasminogen activator was injected into the vitreous of patients with proliferative diabetic retinopathy 15 min before vitrectomy. The results of both studies, however, were contradictory in terms of PVD induction and clinical benefit. More recently, Peyman's group demonstrated PVD induction in rabbit eyes by an intravitreal administration of recombinant lysine-plasminogen and recombinant urokinase.

Autologous Plasmin

Autologous plasminogen purified from the patient's own plasma by affinity chromatography was converted to plasmin by streptokinase *in vitro*. A measure of 0.4 U of autologous plasmin enzyme (APE) was injected into the vitreous in patients with pediatric macular holes, diabetic retinopathy, and stage 3 idiopathic macular holes, followed by vitrectomy after 15 min. All APE-treated eyes achieved spontaneous or easy removal of the posterior hyaloids, including one eye that had vitreoschisis over areas of detached retina.

Microplasmin

Recombinant microplasmin (ThromboGenics Ltd., Leuven, Dublin, New York), a truncated molecule containing the catalytic domain of human plasmin, has been administered successfully into the vitreous of human and porcine postmortem eyes, and in rabbit and cat eyes *in vivo*. In all experimental settings, complete PVD was achieved in a dose-dependent fashion. No alteration of the inner retina was seen, and there was no change in antigenity of neurons and glial cells. Microplasmin was further tested in different animal models sponsored by the manufacturer, and a first clinical trial (the microplasmin in vitrectomy I (MIVI-I) trial) was designed then.

The MIVI-I trial investigated the effect of microplasmin given 1 h, 1 day, and 1 week before vitrectomy in patients with vitreomacular traction. The results of this trial have been published recently, and it can be said that the pharmacologic effect of microplasmin was promising and further trials are now underway to show the efficacy and safety of this recombinant enzyme in different clinical settings, such as vitreomacular traction syndromes, including macular holes, diabetic macular edema, and AMD.

Summary

There are at least four reasons to pursue enzymatic vitreous disruption. First, some retinal diseases that are currently treated by mechanical manipulation of the vitreoretinal interface could be managed more safely by pharmacologic technique. Second, enzymatic vitreous disruption may achieve better anatomic and, thus, potentially functional results by creating a cleaner cleavage plane between the vitreous and the retina than can currently be achieved by vitrectomy techniques. This is of particular importance in eyes with incomplete removal of the cortical vitreous from the retina, and those with vitreoschisis, such as diabetic eyes. Third, as incomplete PVD has been shown to be associated with the development of aggressive fibrovascular proliferation and macular edema, pharmacologic induction of complete PVD could prevent progression of diabetic retinopathy if given before advanced stages of diabetic eye disease. Fourth, cleaving the cortical hyaloid completely from the retina changes

the molecular flux across the vitreoretinal interface and improves the oxygen supply to the retina.

Plasmin holds the promise of inducing complete PVD without morphologic alteration of the retina. Several independent studies confirmed a dose-dependent and complete vitreoretinal separation, associated with perfect preservation of the ultrastructure of the ILM and the retina. In addition, a dose-dependent liquefaction of the vitreous induced by microplasmin has been demonstrated by dynamic light scattering in dissected porcine vitreous and in intact pig eyes. The combination of PVD induction and liquefaction in one molecule is one major advantage of plasmin and microplasmin compared with other enzymes tested, as liquefaction alone carries the risk of tractional retinal breaks. So far, the safety profile and the effects of microplasmin and plasmin are promising. Clinical trials will demonstrate whether practice can hold what theory has promised.

See also: Proliferative Vitreoretinopathy; Regulation of Intraocular Oxygen by the Vitreous Gel; Retinal Vasculopathies: Diabetic Retinopathy; Retinopathy of Prematurity; Rhegmatogenous Retinal Detachment; The Role of the Vitreous in Macular Hole Formation; Vitreous Anatomy, Aging, and Anomalous Posterior Vitreous Detachment

Further Reading

Bishop, P. (1996). The biochemical structure of mammalian vitreous. *Eye* 10: 664–670.

Gandorfer, A. (2007). The need for pharmacology in vitreoretinal surgery. *Klinische Monatsblätter für Augenheilkunde* 224: 900–904.

Gandorfer, A. (2008). Enzymatic vitreous disruption. *Eye* 22: 1273–1277.

Gandorfer, A., Putz, E., Welge-Lüßen, U., et al. (2001). Ultrastructure of the vitreoretinal interface following plasmin assisted vitrectomy. *British Journal of Ophthalmology* 85: 6–10.

Gandorfer, A., Rohleder, M., Sethi, C., et al. (2004). Posterior vitreous detachment induced by microplasmin. *Investigative Ophthalmology and Visual Science* 45: 641–617.

Quiram, P. A., Leverenz, V. R., Baker, R. M., et al. (2007). Microplasmin-induced posterior vitreous detachment affects vitreous oxygen levels. *Retina* 27: 1090–1096.

Trese, M. (2002). Enzymatic-assisted vitrectomy. *Eye* 16: 365–368.

Trese, M. T., Williams, G. A., and Hartzer, M. K. (2000). A new approach to stage 3 macular holes. *Ophthalmology* 107: 1607–1611.

Sebag, J. (1992). Anatomy and pathology of the vitreo-retinal interface. *Eye* 6: 541–552.

Sebag, J. (1998). Pharmacologic vitreolysis. *Retina* 18: 1–3.

Sebag, J. (2002). Is pharmacologic vitreolysis brewing? *Retina* 22: 1–3.

Sebag, J., Ansari, R. R., and Suh, K. I. (2007). Pharmacologic vitreolysis with microplasmin increases vitreous diffusion coefficients. *Graefe's Archive of Clinical and Experimental Ophthalmology* 245: 576–580.

Stefansson, E. (2009). Physiology of vitreous surgery. *Graefe's Archive of Clinical and Experimental Ophthalmology* 247: 147–163.

Verstraeten, T. C., Chapman, C., Hartzer, M., et al. (1993). Pharmacologic induction of posterior vitreous detachment in the rabbit. *Archives of Ophthalmology* 111: 849–854.

Pharmacology of Aqueous Humor Formation

C B Toris, Nebraska Medical Center, Omaha, NE, USA

Glossary

Aqueous flow – The flow rate of aqueous humor from the posterior chamber into the anterior chamber. It is measured by fluorophotometry and is considered to estimate aqueous humor production.
Aqueous humor production – The secretion rate of aqueous humor from the ciliary processes into the posterior chamber.
Fluorophotometry – The technique of measuring the amount of fluorescein in the cornea and anterior chamber. The disappearance rate of fluorescein over a period of a couple of hours is used in the calculation of aqueous flow.
Inflow – The flow of aqueous humor from the posterior to anterior chamber.
Outflow – The flow of aqueous humor out of the eye through the anterior chamber angle.

Physiology of Aqueous Humor Production

Aqueous humor performs several important functions in the eye (Figure 1). It is the source of nutrients for the avascular tissues of the anterior chamber, including the cornea and lens, and it removes their waste products. In addition, its controlled circulation around the anterior chamber and out through the anterior chamber angle is necessary for the maintenance of intraocular pressure (IOP).

The secretion of aqueous humor is a process requiring ultrafiltration and active transport. Ciliary processes are exquisitely designed for this purpose (Figure 1). They contain a stromal core with a rich supply of capillaries and two layers of epithelial cells positioned apex to apex. The innermost layer of nonpigmented ciliary epithelial cells is interconnected by tight junctions and the outer layer consists of pigmented ciliary epithelial cells interconnected by gap junctions. Plasma filtrate enters the interstitial spaces of the stromal core through capillary fenestrations (ultrafiltration). Plasma proteins are blocked from entering the posterior chamber by the tight junctions in the apical region of the intercellular spaces of the nonpigmented ciliary epithelium. This design creates a high protein concentration and high oncotic pressure in the tissue fluid and a reduction in the transcapillary difference in the oncotic pressure. Hydrostatic and oncotic pressure differences across the ciliary epithelium favor movement of water into the ciliary processes from the posterior chamber. Therefore, movement of fluid into the posterior chamber requires secretion. This is done by active transport of ions from the nonpigmented ciliary epithelium cells into the clefts between the cells. The major ions involved in this process are Na^+, HCO_3^-, and Cl^-. The osmotic pressure in the intercellular clefts increases as ions are pumped in. Water and its solutes follow and eventually move out of the clefts and into the posterior chamber. Enzymatic inhibitors of these transport processes significantly reduce aqueous flow.

In the healthy eye, the inflow and outflow of aqueous humor have a circadian rhythm which maintains a predictable pattern of IOP throughout a 24-h period. Chronic and extreme variations from this natural rhythm can cause serious sight-threatening conditions. At one extreme is the persistent elevation in IOP, which increases the risk of glaucoma; a well-documented means of treating glaucoma is to reduce IOP by slowing the production rate of aqueous humor. At the other extreme is chronically low IOP (hypotony), which increases the risk of sight-threatening conditions, including corneal changes, accelerated cataract formation, choroidal fluid, maculopathy, cystoid macular edema, or optic disk edema. Stimulating aqueous humor production and increasing IOP in a consistent and predictable manner should provide a means of treating the hypotony and its associated conditions. Dopaminergic drugs have been investigated for this purpose; however, increasing IOP in a safe and controlled manner remains an unmet need.

The circadian rhythm of aqueous humor production is thought to follow circadian changes in autonomic tone and circulating corticosteroids. Supporting this is the strong evidence that the ciliary processes are under autonomic control. Agonists that increase cyclic adenosine monophosphate (cAMP), such as beta-2 (β_2) adrenergic agonists, tend to increase aqueous humor production, while those that reduce cAMP, such as α_2 adrenergic agonists, tend to decrease it. During the day, when background autonomic tone is relatively high and aqueous humor is being produced at a relatively fast rate, α_2 adrenergic agonists and β-blockers effectively reduce aqueous flow and IOP. However, at night when adrenergic tone is relatively low and aqueous humor is being produced at about half its daytime rate, α_1 adrenergic agonists and β-blockers have little effect on aqueous flow and IOP.

Aqueous Flow Suppressants

Some aqueous flow suppressants, also known as inflow drugs, have been available for decades to treat glaucoma. These drugs are categorized as carbonic anhydrase inhibitors (CAIs), β-blockers, and sympathomimetics including α and mixed adrenergic receptor agonists. Clinically available inflow drugs are listed in Table 1.

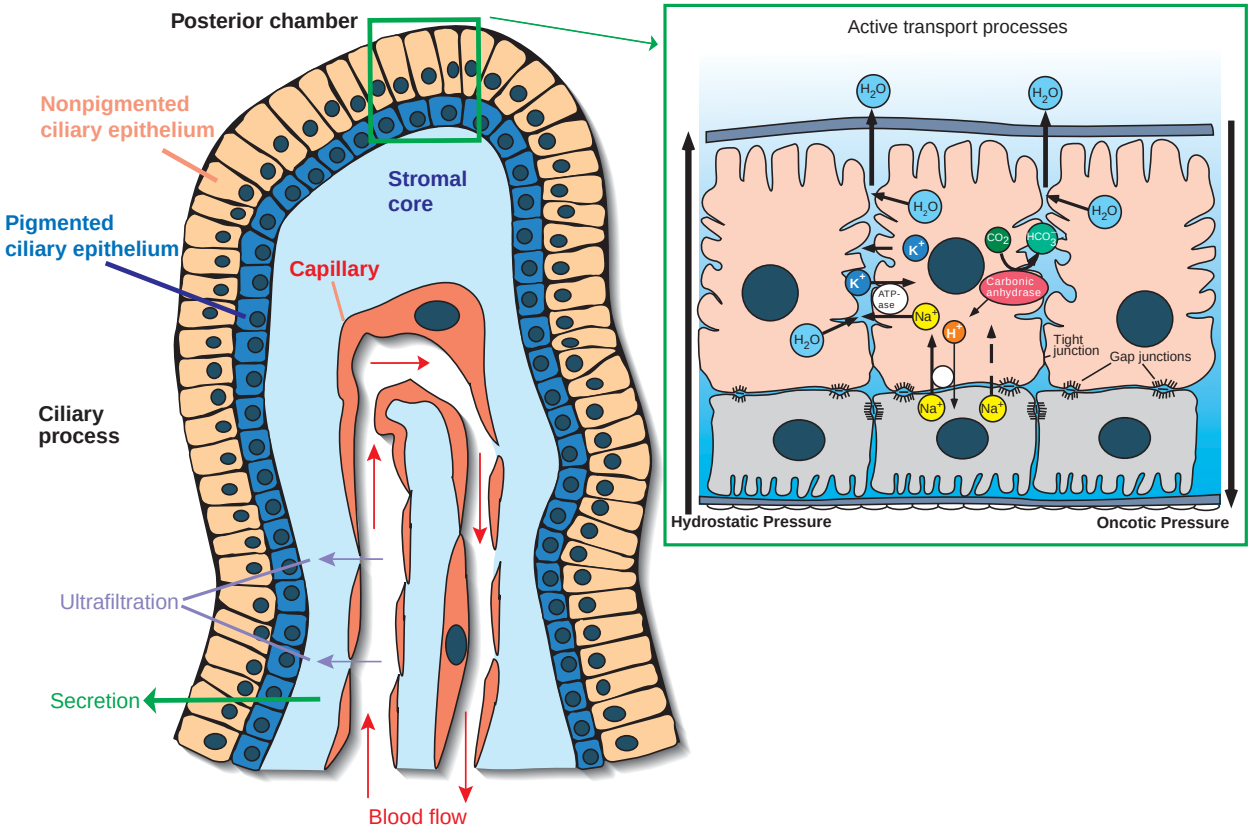

Figure 1 On the left is a ciliary process with a stromal core and capillary network surrounded by two epithelial layers, the nonpigmented and the pigmented ciliary epithelium. Plasma filtrate moves through the capillary fenestrations into the stroma by ultrafiltration and aqueous humor is secreted across the epithelial layers by an active transport process shown at the right.

Table 1 Clinically used drugs that reduce aqueous humor production

	Generic name	*Brand name*
β-blockers	Timolol maleate	Timoptic, Timoptic XE, Istalol
	Timolol hemihydrates	Betimol
	Levobunolol HCl	Betagan
	Carteolol HCl	Ocupress
	Metipranolol HCl	Optipranolol
	Betaxolol HCl	Betoptic
Carbonic anhydrase inhibitors	Dorzolamide HCl	Trusopt
	Brinzolamide HCl	Azopt
	Acetazolamide	Diamox
	Methazolamide	Neptazane
α_2-adrenergic agonists	Apraclonidine HCl	Iopidine
	Brimonidine tartrate	Alphagan
α- and β-adrenergic agonists[a]	Epinephrine HCl	Glaucon, Epifrin, Epinal, Epitrate, Eppy
	Dipivefrin, Dipivelol epinephrine	Propine
Combination drugs	Timolol + dorzolamide	Cosopt
	Timolol + brimonidine	Combigan

[a]Both increases and decreases in aqueous flow have been reported.

Carbonic Anhydrase Inhibitors

Bicarbonate ions are produced in the ciliary body by hydration of carbon dioxide under the control of carbonic anhydrase (**Figure 1**). Under normal conditions, bicarbonate is secreted into the posterior chamber, drawing water with it by osmosis. Inhibition of the carbonic anhydrase enzyme slows the rate of water movement into the posterior chamber, and aqueous production is reduced. If all else remain unchanged, this will decrease IOP.

When administered during the day, oral acetazolamide, a systemic CAI reduces aqueous flow quickly by approximately 30%. However, when administered at night, at a time when aqueous flow is normally low, its effectiveness is inconsistent. One clinical study of acetazolamide reported a decrease in aqueous flow at night, but another study found that it worked no better than placebo.

Systemic CAIs may cause some unpleasant and potentially serious side effects in some patients, which is why significant effort was invested in developing topical CAIs. These drugs, including brinzolamide and dorzolamide, can readily penetrate the cornea and have a very high affinity for ocular carbonic anhydrase. However, for several reasons they are only half as effective as acetazolamide at slowing the production rate of aqueous humor. To lower IOP, topical CAIs must penetrate the cornea and block 99% of the local carbonic anhydrase in ciliary processes. Systemic CAIs reach the ciliary processes through the vasculature, thus avoiding the corneal barriers. Additionally, systemic CAIs may produce extraocular effects that contribute to the IOP reduction. Due to its local delivery, extraocular effects of topical CAIs are expected to be minimal.

β-Adrenergic Antagonists (β-Blockers)

β-Blockers reduce aqueous flow by inhibiting sympathetic nerve activity in the ciliary processes. During the day, timolol suppresses aqueous flow by 28–50%. β-Blockers do not reduce IOP at night when autonomic tone is low because they cannot reduce aqueous flow further than the normally low nocturnal rate. There is additivity of the IOP and aqueous flow effect when β-blockers and CAIs are combined because of the different mechanisms by which these drugs reduce aqueous flow.

Adrenergic Agonists

Adrenergic agonists are drugs that stimulate α_1, α_2, and/or β-adrenergic receptors. Despite 50 years of study, there is no consensus as to the precise mechanism for the IOP reduction of some of these drugs. Although epinephrine, a mixed α_1, α_2, and β-adrenergic receptor agonist, is generally thought to stimulate aqueous production based on many clinical studies, some studies found no effect on or even a decrease in aqueous flow with epinephrine treatment. Epinephrine has complex and dynamic effects on the production and drainage of aqueous humor likely because of its differential activity at multiple receptors. The differing pharmacodynamic effects may depend on which receptor action predominates at the time of the measurement. Recently, more selective agonists at the $\alpha_2$receptor have been developed into efficacious IOP-lowering drugs. Two of these are apraclonidine and brimonidine.

Apraclonidine, an α_2-adrenergic agonist with some α_1-adrenergic activity, was developed initially for the topical treatment of ocular hypertension. Due to the high incidence of allergic reactions to this drug, apraclonidine is no longer routinely used for chronic treatment of ocular hypertension. It reportedly reduces IOP by reducing aqueous flow in addition to some possible effects on outflow.

Brimonidine is a more selective α_2 agonist than apraclonidine but some α_1 activity remains. Within an hour of topical administration, brimonidine reduces IOP by decreasing aqueous flow. In rabbits, one drop of brimonidine causes strong vasoconstriction in blood vessels of the uvea, reduced blood flow to the ciliary body, and insufficient delivery of oxygen and/or other essential energy sources to the ciliary processes. Without a substantial energy source, the production rate of aqueous humor slows. With continued use, the effect of brimonidine on aqueous flow fades and blood flow returns to its normal rate. While this is happening, an effect on outflow, specifically uveoscleral outflow, develops and IOP remains below pretreatment levels.

Although brimonidine and apraclonidine belong to the same class of drugs, their mechanisms of action are not identical. This may be related to the receptor selectivity of each drug. Possible receptors targeted differentially by these drugs include two imidazoline subtypes and four α_2 adrenergic subtypes. Additionally, two of the four known subtypes of α_1 agonists have been found in the anterior segment of the eye. The ocular hypotensive effect of brimonidine in the primate may be mediated through stimulation of an imidazoline receptor rather than an α_2 receptor. The effect of apraclonidine may be through stimulation of a combination of α_1 and α_2 receptors.

When β-blockers and α_2 agonists are combined, the IOP effect is additive despite the fact that both classes of drug reduce aqueous flow. Clearly, the aqueous flow reduction by the different classes of inflow drug is not mediated entirely by the same pathway.

Aqueous Humor Stimulants

At times, stimulation of aqueous flow is desirable, especially in the treatment of chronic hypotony. Currently, ibopamine is the only drug developed to treat hypotony. It is a prodrug of N-methyldopamine with α-adrenergic

properties that is hydrolyzed to epinine in the aqueous humor. It is believed that the D1-dopaminergic activity is responsible for the increase in aqueous humor production and adrenergic stimulation is responsible for its mydriatic effect. Efficacy of ibopamine has been disappointing leaving the need for an effective aqueous flow stimulant unfulfilled.

Prostaglandin $F_{2\alpha}$ analogs produce a small but significant increase in aqueous flow. This increase does not raise IOP because of concomitant increases in outflow facility and uveoscleral outflow. The outflow effects more than compensate for the inflow effect and IOP is substantially reduced. These drugs are used in the treatment of ocular hypertension and glaucoma. The small increase in aqueous flow by prostaglandin analogs is not considered to be clinically relevant.

Conclusions

A clearer understanding of the physiology of aqueous humor production has helped to clarify the mechanisms by which IOP is maintained and inflow drugs work. Several classes of inflow drugs are prescribed for glaucoma therapy, including β-blockers, CAIs, α_2 adrenergic agonists, and other sympathomimetics. Each class reduces aqueous flow by different mechanisms. β-Blockers block cAMP and reduce the autonomic tone needed to produce aqueous humor. CAIs block carbonic anhydrase which prevents the synthesis of bicarbonate, a key step in aqueous secretion. Sympathomimetics have mixed effects on aqueous production, depending on which receptor subtype is stimulated and to what degree.

Suppression of aqueous flow is not the preferred therapy for glaucoma because disturbing the production and flow of this essential fluid could potentially stress the eye in other ways. New classes of drugs under development for the treatment of elevated IOP are designed to target the outflow tissues rather than the inflow tissues because abnormalities in the outflow pathways are usually the source of the IOP elevation.

See also: Control of Aqueous Humor Flow; Ion transport in the Ciliary Epithelium; Pharmacology of the Aqueous Humor Outflow; The Role of the Ciliary Body in Aqueous Humor Dynamics. Structural Aspects.

Further Reading

Bill, A. (1975). Blood circulation and fluid dynamics in the eye. *Physiological Reviews* 55: 383–417.

Brubaker, R. F. (1991). Flow of aqueous humor in humans. *Investigative Ophthalmology and Visual Science* 32: 3145–3166.

Gabelt, B. T., Kiland, J. A., Tian, B., and Kaufman, P. L. (2007). Aqueous humor: Secretion and dynamics. In: Tasman, W. and Jaeger, E. A. (eds.) *Duane's Ophthalmology* vol. 2, ch. 6, pp. 1–72. Philadelphia, PA: Lippincott-Raven.

Kiel, J. W. (1998). Physiology of the intraocular pressure. In: Fehér, J. (ed.) *Glaucoma*, pp. 79–107. Budapest: Akadémiai Kiadó.

Toris, C. B. and Camras, C. B. (2008). Aqueous humor dynamics II, clinical studies. The eye's aqueous humor. In: Civan, M. M. (ed.) *Current Topics in Membranes* vol. 62, ch. 8, pp. 231–272. San Diego, CA: Elsevier.

Pharmacology of the Aqueous Humor Outflow

K P B Cracknell and I Grierson, School of Clinical Sciences, Liverpool, UK

Glossary

Adrenergic agonists – These are compounds that mimic the peripheral effects of epinephrine (adrenaline).
Cholinergic agents – These are compounds that enhance the effects mediated by acetylcholine in the central and/or peripheral nervous system.
Miotics – Compounds that cause constriction of the pupil.
Parasypathomimetic agents – These are compounds that stimulate or mimic the parasympathetic nervous system.
Prostaglandin – Local hormone composed of lipids with 20 carbon atoms including a five-carbon ring.
Prostamide – A fatty acid amide compound similar to a prostaglandin, except that oxygen bonded to carbonyl group is replaced by a nitrogen-bearing substituent. This change significantly alters the electronic and stearic properties of the molecule.

Introduction

Much research has been carried out regarding direct medical means of enhancing ganglion cell survival in primary open angle glaucoma (POAG). However, the only therapeutic approach currently in use is the indirect neuroprotective route of lowering intraocular pressure (IOP). Antiglaucoma medications that lower IOP do so by several mechanisms that include (1) reducing the production rate of aqueous humor, (2) increasing drainage through the nonconventional or uveoscleral route, (3) enhancing drainage of aqueous humor through the conventional route via the trabecular meshwork and canal of Schlemm, and (4) combinations of the aforementioned (1), (2), and (3).

In POAG, there are a range of cellular and extracellular changes in the outflow system that contributes to a poorly understood functional failure of the tissues. However, it is this drainage failure that precipitates an IOP elevation. Of course, by no means do all glaucoma patients have elevated IOP but even the normal tension patients appear to benefit from medical reduction of their IOP. In theory, the physiologically most attractive pressure-lowering option has to be the enhancement of aqueous passage through the conventional drainage route, after all this is where there is pathology. In addition, the trabecular meshwork relies on the aqueous humor for its nutrition, well-being, and survival. There are several classes of antiglaucoma drugs that act on the outflow pathways and they include the miotics (pilocarpine), adrenergic stimulators (epinephrine or adrenalin), and a range of prostaglandins (PGs). A brief description of their mode of action on the various outflow routes is given in this article.

Drugs in Clinical Use That Act upon the Aqueous Humor Outflow Routes

Cholinergic Agents (Miotics)

The cholinergic parasympathomimetic agents that have been in use for the treatment of glaucoma include phospholine iodide, carbachol, and pilocarpine and among these pilocarpine has been by far the most widely used. They act either directly (pilocarpine), indirectly (phospholine iodide), or both (carbachol) on muscarinic receptors to increase the outflow of aqueous humor and effect pupil constriction. Miotics are not in widespread use as they once were, with phospholine iodide and carbachol hardly used in glaucoma treatment at all, and pilocarpine has assumed the status of being a second or even third option drug.

Pilocarpine is a plant alkaloid that is extracted from the leaves of the South American tree *Pilocarpus jaborandi*, and its chemical structure is shown in **Figure 1**. It was introduced in 1876, when it became one of the first commonly used medical treatments for glaucoma, and remarkably, it has remained an important antiglaucoma medication till date. An agent with such a long pedigree is undoubtedly good at what it is supposed to do, and it does lower IOP very effectively. Pilocarpine has systemic side effects, although not too many so it is preferred by the ophthalmologist but frequently loathed by the patient who has to come to terms with needing to take the drops several times a day, stinging on application, narrowed pupils, and blurred vision. Today, the cholinergic agent is applied more often in the form of a fixed combination, delivered by means of an ocusert, or given as a gel rather than as the more traditional stand alone eye drops.

Many years ago Ernst Barany and his team were able to show that pilocarpine induced contraction of the ciliary muscle. Principally, the longitudinal fibers pull the conventional outflow system and stretch the trabeculae, thus opening up the pathways for aqueous humor drainage

(see Figure 2). He surmised that pilocarpine might produce, as a result, a leaky endothelium in the wall of Schlemm's canal. Certainly they were able to infer from rather clever ciliary muscle disinsertion experiments that separating the muscle from the trabecular meshwork abolished the pilocarpine's IOP-lowering effect, as would be predicted if the drainage action of the miotic was primarily brought about by its action on the ciliary muscle. In this context, it is thought likely that all the cholinergic agents have a similar action on the ciliary muscle and presumably the outflow system. There is some morphological evidence to support this contention with at least the long-acting miotic, phospholine iodide.

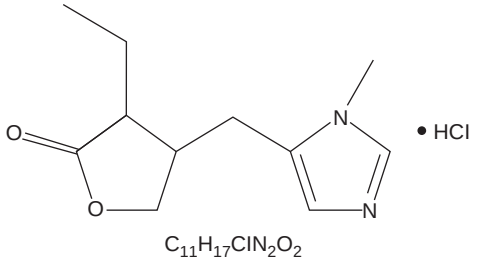

Figure 1 Chemical structure of pilocarpine.

The work on the pilocarpine action in monkeys was repeated by us and also in a number of humans showing essentially the same result. From histological sections, we measured the angle subtended by the cross-section of the sclera sulcus and the sclera spur which was around 15° of arch greater in the pilocarpine-treated group than in our untreated controls. Muscle contraction induced displacement of the spur in a trigger-like action thus pulling on the trabeculae and widening drainage pathways. As it is known that tendon-like structures (made up of extracellular matrix materials) extend from the sclera spur all the way up to Schlemm's canal, it is highly likely that it is altered and that turned out to be the case. We noted a significant distension of the inner wall of Schlemm's canal whose endothelium had an abundance of giant vacuoles and transcellular pores – so we had ultrastructural evidence that Barany's leaky endothelium proposal was essentially correct.

The predominant outflow action of pilocarpine is indirect but is there any evidence of a direct action within the outflow pathways themselves? On first examination, the absence of an IOP-lowering effect of any substance following ciliary muscle disinsertion argues against a direct action although these surgical manipulations tell us more about the relationship between the ciliary muscle and the

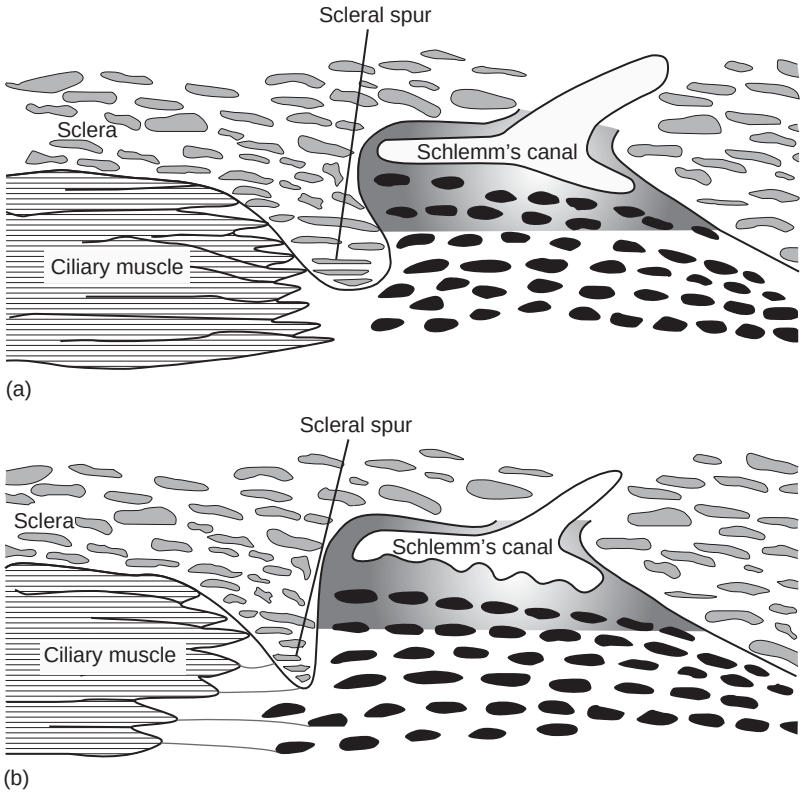

Figure 2 Schematic diagram illustrating the mode of action of pilocarpine: (a) the appearance of the ciliary muscle and trabecular meshwork in the normal meshwork; (b) following the application of pilocarpine the ciliary muscle is contracted, this contraction has pulled the scleral spur and opened up the spaces of the trabecular meshwork.

trabecular meshwork rather than what is going on in the meshwork tissue itself. As we now know, the trabecular meshwork is not a passive filter but has a cell population with characteristics in common with smooth muscle cells. Pharmacological examination of intact trabecular meshwork *in vitro* (which was isolated from the ciliary muscle) showed that pilocarpine contracted the cells in the mesh causing decreased outflow in these preparations. Thus, pilocarpine's overwhelming indirect action via the ciliary muscle opens up drainage through the outflow system despite a minor negative drainage effect caused by a local tightening effect.

Adrenergic Agonists

It is generally considered that the IOP lowering associated with adrenergic agonists such as epinephrine, diprivefrine (a prodrug-releasing epinephrine), and isoproterenol was primarily by a direct action on the conventional outflow system to produce a decrease in resistance. A less marked drainage increase through the uveoscleral outflow pathways is reported particularly in nonprimate animals. Evidence that epinephrine, for example, has more than a minor effect on aqueous production is controversial although that was the prevailing belief when epinephrine was first introduced as a potential antiglaucoma agent over 50 years ago. The outflow effect of adrenergic agonists is poorly understood but it does seem to be negated by the nonselective beta blocker timolol and also the effect is lost *ex vivo* by the eye being subjected to post-mortem delay. Epinephrine (adrenalin) has the chemical structure shown in **Figure 3**.

Cultured human trabecular meshwork cells and trabecular tissue *in vivo* contain $beta_2$-adrenergic receptors and epinephrine causes the intracellular accumulation and extracellular release of cyclic AMP from these cells. Both epinephrine and isoproterenol, using $beta_2$-adrenergic and possibly other (alpha) receptors, cause trabecular meshwork cells to become reduced in size with widening of their intercellular spaces. Such a direct drug action on cell morphology, presumably acting through the cell cytoskeleton, has functional consequences and epinephrine-induced inhibition of mitotic activity and phagocytosis in trabecular meshwork cells in tissue culture has been reported. What immediate benefit, if any, there are on the trabecular meshwork cells, caused by the functional and morphological changes which affect the increased outflow is not fully appreciated. In the longer term, the adrenergic agonist effect on trabecular meshwork cells might compromise tissue function and/or cell survival. The latter would be of particular concern given that excessive trabecular cell loss is part of the meshwork pathology in POAG.

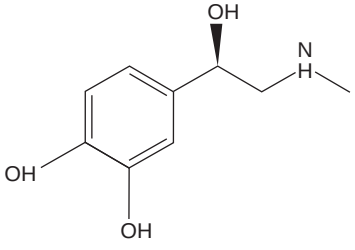

$C_9H_{13}NO_3$

Figure 3 Chemical structure of epinephrine.

It is of some interest that both epinephrine and isoproterenol produce a size-reduction effect on Schlemm's canal endothelial cells in tissue culture similar to that described for trabecular meshwork cells. When the Schlemm's canal cells are established and subsequently organized into monolayers on Millipore filters then exposed to adrenergic agonists, these agents make the endothelial cell layers more permeable and so increase their hydraulic conductivity for at least a few hours. If such canal endothelial cell shrinkage takes place *in situ*, particularly in the inner wall endothelium of Schlemm's canal, then undoubtedly the resistance of the outflow system would decrease because of drug-induced widening of cell-to-cell spaces. Cyclic AMP is likely to have a second messenger role in this process because it has been shown that cyclic AMP analogs increase aqueous humor drainage and so implicate cyclic AMP in the mediation of the adrenergic agonist effect.

Increased permeability and aqueous flow through the canal endothelium is a hypothetical mechanism of action that is worthy of further testing. It is unfortunate that very little fundamental research has taken place to date on adrenergic agonist action within the outflow system and surrounding tissues. However, the role of epinephrine *per se* in glaucoma treatment is small because of patient tolerance to the adrenergic agonist and concern over local (stinging, orbital pain, and allergic blepharoconjunctivitis) or systemic (cardiac arrhythmias and systemic hypertension) side effects. The development of dipivefrin (a lipophilic prodrug formed by the addition of two pivalic acid groups to the epinephrine molecule) provided the much needed benefit of more efficient penetration into the eye at which point esterases removed the pivalic acid to release epinephrine. Unfortunately efficacy was not improved and the side-effect problem was not sufficiently dampened down.

PG Analogs

The relatively new groups of agents, the topical PG analogs, were designed specifically to maximize entry into the eye, exploit their IOP-lowering properties for the treatment of glaucoma and ocular hypertension, and minimize the tendency present in natural PGs to produce

red eye, irritation, and a foreign body sensation. The first two PG analogs that went into clinical use were unoprostone (Rescula) and latanoprost (Xalatan) and of the two, latanoprost was initially the more widely available. Thereafter, travoprost (Travatan) and bimatoprost (Lumigan) were licensed for glaucoma use while Tafluprost, the most recent PG, was in the process of seeking license approval (see **Table 1**).

It is not strictly the case that all the groups are true PGs as such. Bimatoprost is considered to be a prostamide because it is derived from anandamide which has both structural and pharmacological similarities to $PGF_{2\alpha}$ ethanolamide; it is accepted by some to be essentially different although the classification as a prostamide separate from the rest remains controversial. Despite the fact that bimatoprost's chemical structure is similar to the various $PGF_{2\alpha}$ analogs (see **Figure 4**), there are differences such as the fact that bimatoprost is poorly metabolized compared, for example, to latanoprost. As a group the PG analogs and the like, with perhaps the exception of unoprostone (Rescula), have remarkable IOP-lowering capabilities. This has led to their very rapid adoption as a first-line choice for glaucoma therapy.

The PGs have a poor ability to cross biological membranes, and as a consequence they require a carrier-mediated transport (i.e., receptor) to pass into cells. PGs interact with cells by attaching to specific receptor sites on the cell surface. The PGs are comprised of a family of five naturally occurring compounds. Each of the PGs has a particular affinity for a specific receptor site. However, naturally occurring PGs have a low selectivity for their specific PG receptor, and as a consequence they are found to be bound to a whole variety of receptor sites, whereas the synthetic PG analogs are much more selective. The naturally occurring $PGF_{2\alpha}$ has a binding affinity for the FP receptor, along with the EP_1, EP_2, and EP_3 receptor sites. All the $PGF_{2\alpha}$ analogs in use have a particular affinity to the FP receptor site but they are more selective agonists of this receptor with reduced affinity for the other receptors. However, the various analogs do have differing affinities for the other receptor subtypes, for example, latanoprost has a much reduced effect on the EP_2 receptor, and travoprost has a low affinity for all the EP receptors. It is indeed this selectivity which has improved the drug's therapeutic profiles. Certainly, the mechanism of action of the more conventional PG analogs seems to be that they function as FP receptor antagonists; although this may also, to some extent, be the case for bimatoprost, evidence for FP receptor antagonism as a major mechanism of its mode of action remains more controversial.

The mechanisms by which the PG analogs (including prostamides) in current clinical use produce their ocular hypotensive effects are not yet fully understood, but the FP receptor does seem to play an essential role for the majority of them. Studies examining FP receptor-deficient mice have shown that these animals at least do not exhibit any IOP-lowering action when exposed to latanoprost, travoprost, unoprostone, or even bimatoprost. Further research with receptor-deficient mice has shown that the IOP-lowering action of the newest analog, tafluprost, is also mediated through the prostanoid FP receptor. It has been demonstrated with reasonable clarity that the prostaniod IOP-lowering action does not appear to involve any marked alteration to the production rate of aqueous humor. On the contrary, early investigations of the drainage-improving action of latanoprost heavily implicated the uveoscleral drainage pathway as the major site of aqueous outflow increase producing the bulk of the IOP reduction. The conventional outflow pathway, via the trabecular meshwork and Schlemm's canal, is responsible for around 80% of the aqueous drainage in the normal eye, whereas the nonconventional or uveoscleral pathway (whereby aqueous passes through the adventitia of the ciliary muscle and across the sclera to reach the vortex vessels) accounts for most of the remainder. It was shown that latanoprost doubled uveoscleral drainage in human eyes and in some monkeys (where uveoscleral drainage is naturally high); outflow through this pathway increased from 30% to 60% in humans following latanoprost exposure. It has been the general belief that the other PG analogs also enhanced uveoscleral drainage, at least as part of their overall IOP-lowering action. There are three potential mechanisms proposed (relaxation of ciliary muscle, remodeling of the extracellular matrix, and vasodilatation causing tissue expansion), by which PGs could be increasing the uveoscleral outflow.

Vasodilation is strongly stimulated by the natural PGs; however, it has been demonstrated that the synthetic PGs (particularly latanoprost) do not significantly influence vasodilation. Hence, this mode of action seems to have been ruled out.

Table 1 Commercially available prostaglandin drugs and usage regimes

Drug	*Manufacturer*	*Dosage*	*Drug concentration*
Latanoprost Xalatan®	Pfizer	One drop once a day	0.005% solution
Unoprostone Rescula®	Novartis	One drop twice daily	0.15% solution
Travoprost Travatan®	Alcon	One drop once a day	0.004% solution
Bimatoprost Lumigan®	Allergan	One drop once a day	0.03% solution
Tafluprost	Santen	One drop once a day	0.005% solution

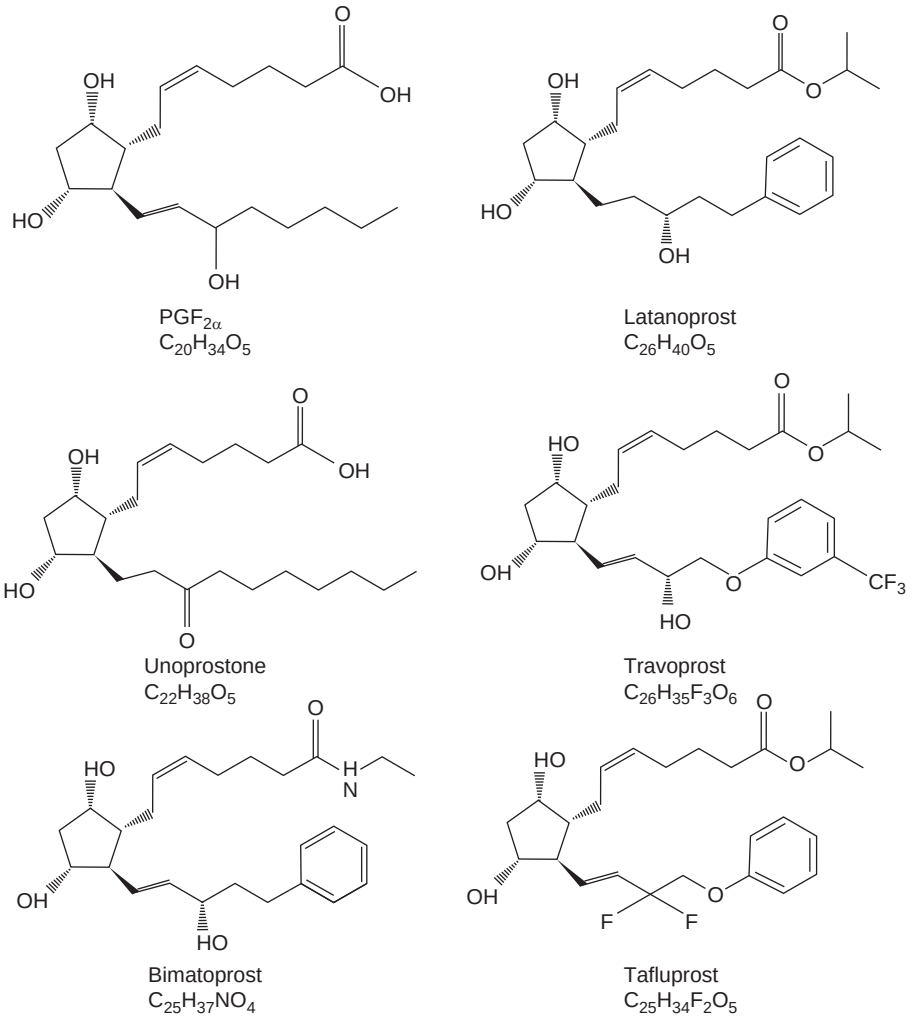

Figure 4 Chemical structures of the PGs in current use for the treatment of glaucoma.

For obvious reasons, attention has focused on PG-induced action on the uveoscleral drainage pathway where remodeling of the extracellular matrix between the muscle bundles of the ciliary body takes place. There appears to be an age-related decrease in the uveoscleral outflow both in humans and monkeys. This accompanies a morphological change seen in the aged ciliary muscle, of a buildup of extracellular material which reduces the spaces around the muscle bundles. In contrast, in aged monkey eyes treated with $PGF_{2\alpha}$ demonstrated a reduction in the extracellular matrix and an increase in interstitial spaces, mimicking the appearance of that seen in young eyes. The effects of PGs at the subcellular level in the ciliary muscle cells have been investigated and it was found that $PGF_{2\alpha}$ disrupted the turnover of some extracellular matrix components which presumably leads to a widening of the uveoscleral pathway. Latanoprost acid, in particular, has been shown to decrease some of the extracellular matrix components (specifically collagens I, III, and IV, laminin, fibronectin, and hyaluronan) in cultured human ciliary muscle cells. However, in monkeys 10 days of topical treatment with 3 μg latanoprost reduced the amount of collagens IV and VI in the ciliary body. In addition, the PG analogs remodel the extracellular matrix components of the intercellular environment of the ciliary tissue by synthesizing a range of matrix metalloproteinases and their inhibitors. Therefore, it is highly likely that all drugs in this class, to a lesser or greater extent, modulate the extracellular matrix materials that reside in the uveoscleral pathway to produce (at least part of) their aqueous outflow enhancing effect.

As far as relaxation of ciliary muscle *in vitro* is concerned, work using $PGF_{2\alpha}$ demonstrated a weak relaxation of monkey ciliary muscle strips. In monkeys, large doses of pilocarpine were found to partially inhibit the IOP-reduction effect produced by $PGF_{2\alpha}$. This IOP reduction is explained by the pilocarpine contraction of the ciliary muscle, from this it can be deduced that it is likely that some of the effect of $PGF_{2\alpha}$ is by causing a relaxation of the ciliary muscle.

Initial studies suggested that PGs had virtually no effect on the trabecular meshwork tissue or, for that matter, on drainage of aqueous humor through the conventional outflow pathway. However, there were some inconsistencies (true for most members of this class of drugs), and they may well relate to the difficulty of accurately measuring relatively small changes in conventional drainage facility, especially when uveoscleral drainage is enhanced. However, more recent work (e.g., that using organ cultured human anterior segments where a much clearer assessment of conventional drainage can be obtained) showed that PGs (specifically latanoprost) do reduce the resistance to aqueous outflow through this pressure-sensitive route. Matrix metalloproteinase analysis surprisingly did not show much change. Indeed, both organ and tissue culture models have been sufficiently robust to show a quite marked increase in outflow facility associated with the prostamide action of bimatoprost. In addition, much work has been done that indicates that unoprostone has an effect on trabecular meshwork cell contractility that may well promote conventional drainage. In general, it remains to be established whether or not extracellular matrix alteration, trabecular meshwork cell contractility, a combination of both, or even some other mechanism is behind the pressure-sensitive increase in outflow that seems to be produced by the PGs.

A combination of clinical, animal, and *in vitro* investigations provides evidence that underlines the fact that the PG analogs and their allies lower IOP by increasing the drainage of aqueous humor out of the eye. For most of these drugs, the important mechanism of action is on the uveoscleral drainage pathway but it is likely that they all produce some enhancement of conventional drainage. At least, for maybe unoprostone, the enhancement of conventional drainage may be of greater significance than for the others in this class of drugs.

The PGs are reported to be essentially free from major systemic side effects but they do have local side effects. The ocular side effects associated with these drugs are:

- conjunctival hyperaemia (5–15% with latanoprost to 35–50% with travoprost);
- ocular irritation (up to 15% of patients);
- burning sensation and dry eye (8% incidence);
- uveitis and cystoid macular edema are rare but severe events that occur in eyes that are susceptible due to other predisposing conditions such as diabetic retinopathy, and complicated cataract surgery;
- increased pigmentation of the iris (incidence highest with latanoprost); and
- increased growth of hair follicles.

The incidence of red eye, irritation, and a foreign body sensation with natural $PGF_{2\alpha}$ were high, and as a consequence much effort has been applied to attempts to subdue these side effects with the analogs. The efforts have significantly reduced the incidence although by no means have these side effects been entirely eliminated. Although it needs to be borne in mind that some drug preparations have a fairly high concentration of preservative which inevitably will contribute to the red eye.

The increased ocular pigmentation is a side effect that is specific to the PGs and as such has been the subject of much scrutiny. Eye-lid color change is uncommon with an incidence of only 1.5–2.9%. Eyelash darkening and thickening incidence has a wide variation in incidence between the different drugs (travoprost 0.7–76%, bimatoprost 3–36%, and latanoprost 0–25%). All of these color-change side effects are reversible upon the cessation of the PG drops.

Darkening of the iris is an irreversible change associated with PG use and has been investigated thoroughly in the case of latanoprost as this was the first drug to exhibit the effect. The findings to date suggest that there is no pathology associated with the darkening and that the color change is brought about by small but significant increase in the size of the individual melanin granules. It is considered at present that this side effect is purely cosmetic change with no significant pathological implications.

See also: Biological Properties of the Trabecular Meshwork Cells; Biomechanics of Aqueous Humor Outflow Resistance; Control of Aqueous Humor Flow; Functional Morphology of the Trabecular Meshwork; Myocilin; Pharmacology of Aqueous Humor Formation; Primary Open-Angle Glaucoma; Regulation of Extracellular Matrix Turnover in the Aqueous Humor Outflow Pathways; Role of Proteoglycans in the Trabecular Meshwork; Structural Changes in the Trabecular Meshwork with Primary Open Angle Glaucoma; The Biology of Schlemm's Canal; Uveoscleral Outflow.

Further Reading

Alvarado, J. A., Murphy, C. G., Franse-Carman, L., Chen, J., and Underwood, J. L. (1998). Effect of beta-adrenergic agonists on paracellular width and fluid flow across outflow pathway cells. *Investigative Ophthalmology and Visual Science* 39: 1813–1822.

Bahler, C. K., Howell, K. G., Hann, C. R., Fautsch, M. P., and Johnson, D. H. (2008). Prostaglandins increase trabecular meshwork outflow facility in cultured human anterior segments. *American Journal of Ophthalmology* 145: 114–119.

Barany, E. H. (1966). The mode of action of miotics on outflow resistance. A study of pilocarpine in the vervet monkey *Cercopithecus ethiops*. *Transactions of the Ophthalmological Societies of the United Kingdom* 86: 539–578.

Cracknell, K. P. B., Grierson, I., and Hogg, P. (2007). Morphometric effects of long-term exposure to latanoprost. *Ophthalmology* 114: 938–948.

Erickson-Lamy, K. A. and Nathanson, J. A. (1992). Epinephrine increases facility of outflow and cyclic-Amp content in the human eye *in vitro*. *Investigative Ophthalmology and Visual Science* 33: 2672–2678.

Grierson, I., Lee, W. R., and Abraham, S. (1978). Effects of pilocarpine on morphology of human outflow apparatus. *British Journal of Ophthalmology* 62: 302–313.

Ota, T., Aihara, M., Narumiya, S., and Araie, M. (2005). The effects of prostaglandin analogues on IOP in prostanoid FP-receptor-deficient mice. *Investigative Ophthalmology and Visual Science* 46: 4159–4163.

Toris, C. B., Camras, C. B., and Yablonski, M. E. (1993). Effects of Phxa41, a new prostaglandin-F(2-alpha) analog, on aqueous-humor dynamics in human eyes. *Ophthalmology* 100: 1297–1304.

Toris, C. B., Gabelt, B. T., and Kaufman, P. L. (2008). Update on the mechanism of action of topical prostaglandins for intraocular pressure reduction. *Survey of Ophthalmology* 53: S107–S120.

Tripathi, B. J. and Tripathi, R. C. (1984). Effect of epinephrine *in vitro* on the morphology, phagocytosis, and mitotic activity of human trabecular endothelium. *Experimental Eye Research* 39: 731–744.

Wan, Z., Woodward, D. F., Cornell, C. L., et al. (2007). Bimatoprost, prostamide activity, and conventional drainage. *Investigative Ophthalmology and Visual Science* 48: 4107–4115.

Wiederholt, M. (1998). Direct involvement of trabecular meshwork in the regulation of aqueous humor outflow. *Current Opinion in Ophthalmology* 9: 46–49.

Photopic, Mesopic and Scotopic Vision and Changes in Visual Performance

J L Barbur, City University, London, UK
A Stockman, UCL Institute of Ophthalmology, London, UK

Glossary

Contrast sensitivity function (CSF) – The reciprocal of contrast threshold measured as a function of spatial frequency in a spatial CSF or as a function of temporal frequency in a temporal CSF.
Higher order aberrations (HOAs) – These aberrations in the eye describe imperfections in the optics that cannot, in general, be corrected for with conventional refraction (i.e., sphere and cylinder components).
Mesopic – The range of intermediate light levels between cone threshold and rod saturation where both rod and cone signals contribute to a visual response.
Photopic – The range of high light levels above rod saturation where vision is mediated by signals from cone photoreceptors.
Scotopic – The range of low light levels below cone threshold where visual responses rely entirely on rod signals.
Spectral luminous efficiency (SLE) – The SLE function represents an appropriate measure of detector spectral responsivity, which in the case of the human eye is used to convert radiant flux to an equivalent photometric flux.
Spectral power distribution (SPD) – This describes the wavelength distribution of radiant flux (power) emitted by a source or surface.
Spectral radiance – A quantity that describes the radiant flux (power) within a narrow wavelength interval emitted by a source or surface in a given direction per unit solid angle, per unit area of the source.
Spectral responsivity (SR) – The SR of a detector of radiation is a measure of the spectral sensitivity of the detector and represents the signal generated per unit incident radiant flux as a function of wavelength.

Introduction

Arguably, the most important feat of human vision is its ability to operate effectively over the enormous 10 000-million-fold range of illumination levels to which it can be exposed, from starlight to bright sunlight (see Figure 1). Moreover, it achieves this despite the limitations imposed by individual neurons in the visual system, many of which have dynamic ranges of no more than about 100-fold. Sensitivity regulation over such a massive range cannot be achieved without compromise. One compromise is to share the range between two different types of photoreceptors: the sensitive rods, functioning at lower scotopic levels of illumination, and the less-sensitive cones, functioning at higher photopic levels, the two working together at intermediate mesopic levels. Another important compromise is the trade-off between increased sensitivity at lower light levels, and improved temporal and spatial acuity at higher light levels. As the light level increases, high sensitivity is no longer needed and is traded for improvements in spatial and temporal acuity. These adjustments occur separately within the rod and the cone systems, but the rod system has a lower acuity and higher sensitivity compatible with its operation at lower light levels.

There are ~100 million rods, but only 5 million cones in the human retina. The 5 million cones are most densely packed in a small region of the retina at the center of our vision, where photopic vision is best. Cones are less sensitive to light but respond more quickly than rods. The cones and their postreceptoral pathways operate well at higher light levels in the upper mesopic and photopic range. Over most of this range, processes of light adaptation within the retina ensure that the operation of the cone photoreceptors adjusts to changes in light level to provide a useful dynamic range of about 100, which remains relatively independent of light level. When the light level is lower, the cone system increases its sensitivity by increasing the spatial and temporal extents over which light is summed, as a result of which spatial and temporal acuity is reduced. Even at very high light levels, bleaching of the light-sensitive pigment in the cone protects its output from saturating and thus failing to signal changes in light. By contrast, rods and their pathways operate well at lower light levels in the scotopic and lower mesopic ranges. The rods and rod pathways are optimized for these levels. The rods are more sensitive and much slower than the cones, so that they integrate light over time, and their postreceptoral pathways integrate light over space. Capable of single-photon detection at the lowest levels, the rod system ceases to operate effectively at the top of the mesopic range.

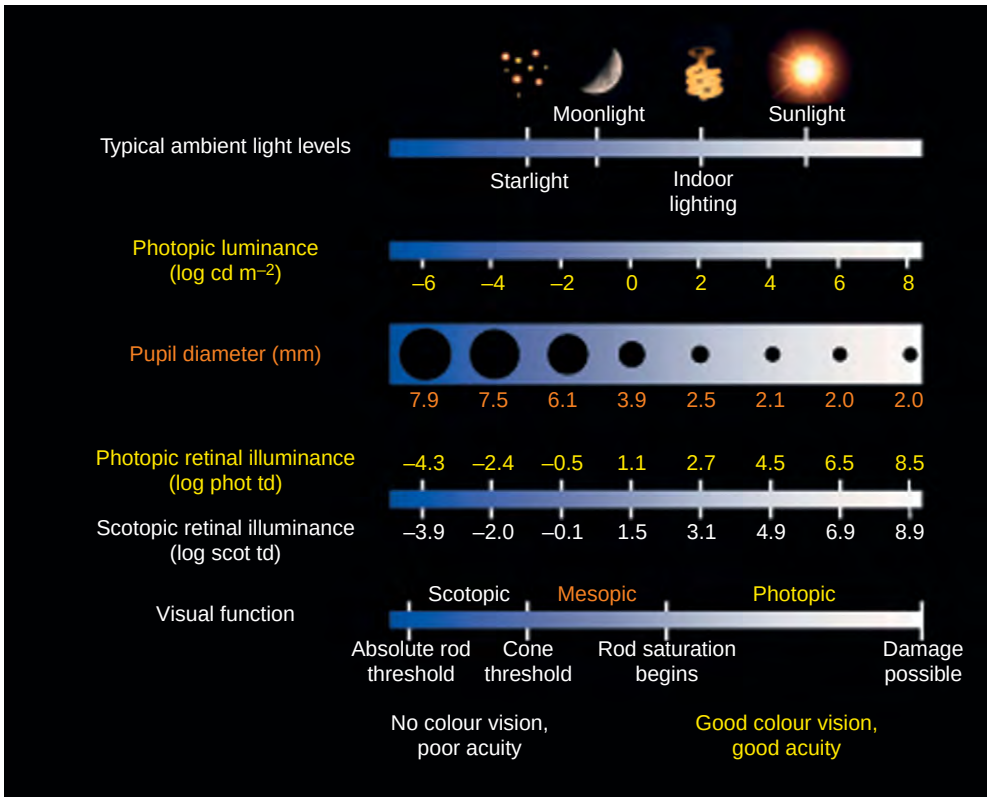

Figure 1 Illumination levels. Typical ambient light levels are compared with photopic luminance (log phot. cd m^{-2}), mean pupil diameter (mm), photopic and scotopic retinal illuminance (log photopic and scotopic trolands, respectively), and visual function. The scotopic, mesopic, and photopic regions are defined according to whether rods alone, rods and cones, or cones alone contribute to a visual response. The conversion from photopic to scotopic values assumes a white standard CIE D_{65} illumination. Based on **Figure 1** of Stockman, A. and Sharpe, L. T. (2006). Into the twilight zone: The complexities of mesopic vision and luminous efficiency. *Ophthalmic and Physiological Optics* 26: 225–239.

Mesopic vision describes the range of light levels over which signals from both rods and cones contribute to the visual response. This range extends just over a 1000-fold from cone threshold to rod saturation, and encompasses light levels that are often found in occupational environments. At mesopic levels, the spectral composition of the illuminant plays an important role in determining the relative strengths of rod and cone signals (see **Figure 2**). Marked changes in visual performance that vary over the visual field are observed as the level of illumination is lowered and/or the spectral composition of the illuminant is modified. The gradual increase in rod signals as the light level decreases causes changes in the overall spectral sensitivity of the eye that has consequences for the visual effectiveness of the illuminant spectral power distribution (SPD) (i.e., the intensity of the light as a function of wavelength). Mesopic luminous efficiency is inherently complex, and therefore difficult to standardize or model, because it depends on the outputs of both the rod and the cone photoreceptors. Not only are there differences in the photoreceptor spectral sensitivities, but there are also differences in the properties of the postreceptoral pathways through which the rod and cone signals are transmitted. The nature and balance of these pathways are constantly changing with changes in light level in the mesopic range.

Much effort has gone into establishing spectral responsivity functions that are appropriate for photopic, mesopic, and scotopic lighting conditions. This approach rests on the assumption that visual performance can be adequately predicted by weighting the intensity of the light reaching the eye (the radiant flux) with functions that reflect the spectral responsivity of the eye at high, intermediate, and low light levels. Some success has been achieved at low light levels in the scotopic range, but this success reflects the fact that the spectral responsivity is determined by a single photoreceptor type, the rods, which have a single type of photosensitive molecule. The approach has been less successful at photopic levels, where responsivity depends on up to three cone photoreceptors, and least successful at mesopic levels where it depends on different types of rod and cone photoreceptor systems with markedly different properties. In this article, we present data on

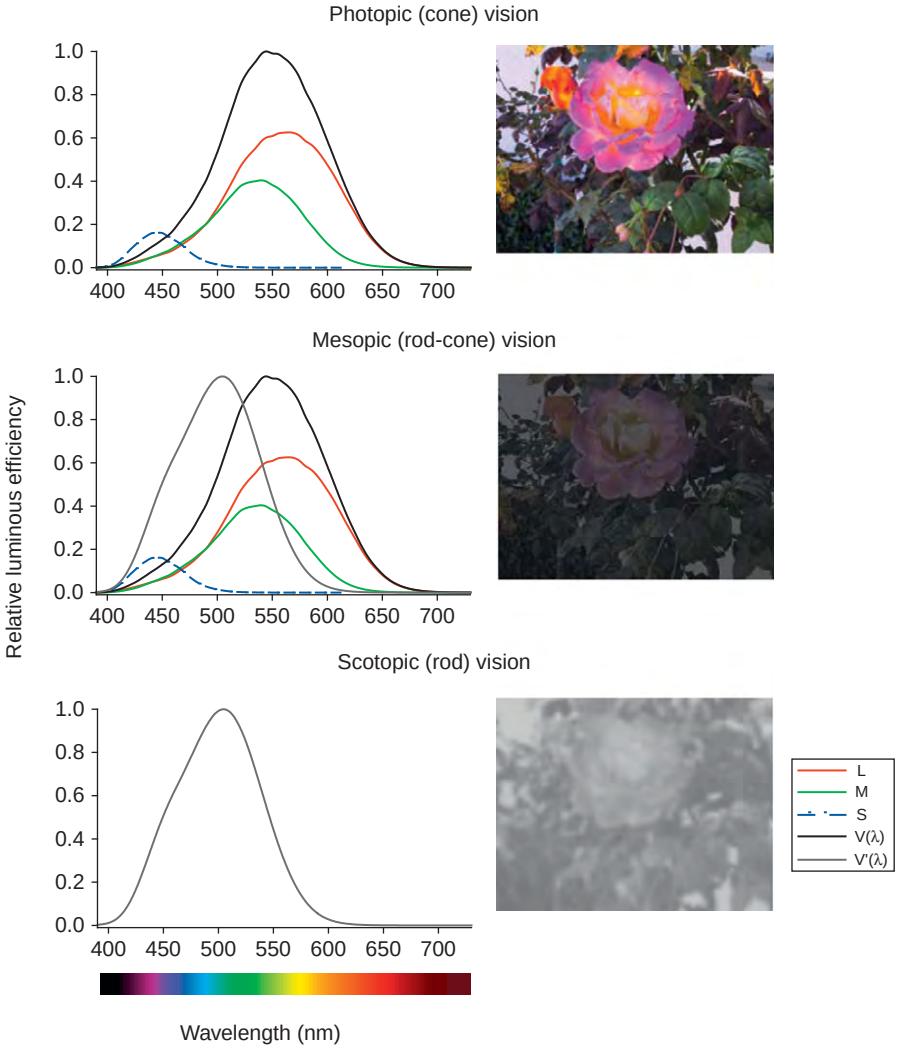

Figure 2 The useful range of light levels can be divided into three regions: the photopic range that yields best temporal and spatial contrast acuity and color discrimination, the mesopic range where color signals become less important, our temporal responses become more sluggish, and the world appears dark, and the scotopic range where the world appears brighter, but we can no longer discriminate color differences and can only see large, high-contrast objects. The spectral sensitivities of the photoreceptors are shown. The relative heights of the M- and L-cone spectral sensitivities reflect their assumed relative contributions to V(λ). The S-cone function is dashed to signify that its contribution to luminous efficiency is minimal. The photographs on the right illustrate how our vision changes as the eye adapts to mesopic and scotopic illumination.

how visual performance changes with light level. We argue that the changes in performance are much more profound than the changes in spectral sensitivity as captured by changes in luminous efficiency functions.

The Concept of Luminous Efficiency Function

The traditional development of photometry has been strongly influenced by radiometry and the properties of an ideal detector of radiation, which is assumed to exhibit response linearity and additivity and has a well-defined spectral responsivity (in the case of the eye at photopic levels, $V(\lambda)$). Let the radiant light fluxes Θ_1 and Θ_2, respectively, produce signals S_1 and S_2 when the detector is exposed to each flux separately. Response linearity means that when the detector is exposed to $\Theta_1 + \Theta_2$ together, the signal generated must equal $S_1 + S_2$, irrespective of the intensity and the spectral composition of Θ_1 and Θ_2. When this is the case, the spectral responsivity curve of the detector becomes a particularly useful quantity since it provides the means of computing the detector signal in response to any broadband, spectral distribution of light flux. This is achieved by simply integrating the radiant flux (weighted at each wavelength by the spectral luminous

efficiency function or $V(\lambda)$) over the spectral range for which $V(\lambda)$ and $\Theta(\lambda)$ are both nonzero to give:

$$\Theta_V \sim \int V(\lambda)\Theta(\lambda)d\lambda, \quad [1]$$

where Θ_V is usually described as the luminous flux. The simplicity of this approach continues to be important and relevant in the more applied areas of vision science, for example, in lighting engineering and photometry. Spectral luminous efficiency functions (i.e., curves that specify the spectral responsivity of the eye, and thus the effectiveness of lights) have been produced using a number of different experimental approaches for both photopic vision (when only cone photoreceptor signals are involved) and for scotopic vision (when vision relies entirely on rod signals). The response linearity of the eye is, however, very limited. Lights that are intense enough to adapt the visual response give rise to nonlinearities that break down the additivity required by eqn [1]. At photopic and mesopic levels, where up to four photoreceptors can contribute to the visual response, additivity is even more limited. As the wavelength or SPD of the illuminant changes, and the photoreceptors selectively adapt, so also do the relative contributions of the different photoreceptors to luminous efficiency. Mesopic and photopic luminous efficiency functions, in general, are not therefore fixed in spectral sensitivity.

Spectral luminous efficiency functions are currently used to provide a means of quantifying the total luminous flux associated with broad-band and narrow-band sources, and for computing the luminance contrast of an illuminated object with respect to that of the surrounding background. When the relative SPD of an object matches that of its surrounding background, the computed contrast is independent of the assumed spectral responsivity curve. However, for objects that differ in SPD from their surrounding background, the computed contrast is strongly dependent on the choice of spectral luminous efficiency function. Moreover, at photopic levels, perceived color differences can also contribute significantly to perceived object contrast, as a result of which any efforts to produce a single spectral luminous efficiency function to account for both the quantity of luminous flux and perceived contrast has severe limitations. In the mesopic range, when rod contrast signals also contribute to object conspicuity, prediction of effective contrast becomes even more challenging. The relative rod and cone contributions to luminous efficiency vary continuously with the illumination level, the spectral composition of the adapting background, the location of the stimulus in the visual field, and the temporal and spatial characteristics of the stimulus. A number of studies have attempted, with limited success, to model these complex interactions. Yet, any model based only on changes in spectral sensitivity is unlikely to capture the effects of the large number of parameters that have been shown experimentally to affect object appearance.

In the remainder of this article, we will be less concerned with the need to produce fixed spectral luminous efficiency functions appropriate for either the photopic or the mesopic range. Instead, we focus on describing how key aspects of visual performance change with ambient light level.

Quality of Vision and Light Level

Spatial Acuity, Spatial Contrast Sensitivity, and Light Level

An important aspect of visual performance is the ability to see fine spatial detail. A simple functional test is to measure the threshold luminance contrast (i.e., $\Delta L/L_b$, where ΔL represents the increment in stimulus luminance with respect to the surrounding background (L_b)) needed to resolve letters or some other visual stimuli when the angular subtense of stimulus elements is larger than the high-contrast resolution limit of the eye. The latter is often taken to be $1'$ of arc and corresponds to a letter size of $\sim 5'$ of arc. In order to avoid eye strain and to minimize the effects of microfluctuations of accommodation, a stimulus size three times the spatial resolution limit of the eye or larger is often employed in various occupational environments. For these reasons, the data shown in **Figure 3** were measured using a Landolt ring stimulus of $3'$ gap size. The orientation of the gap was restricted to four possible locations (i.e., top right, top left, bottom right, and bottom left) and the subject's task was to press one of four buttons to indicate the position of the gap. Two different groups of normal subjects (with high-contrast acuity of $1'$ of arc or better) were involved in this study. The photopic thresholds follow a tight distribution, while the mesopic thresholds are larger and exhibit significantly increased variability. Interestingly, about 50% of the 219 subjects examined under mesopic conditions exhibit thresholds that fall within the normal 2σ (σ: standard deviation) limits of the photopic range.

The results show no significant correlation with either age or the quality of the observer's optics (in terms of the mean-wavefront, higher order aberrations (HOAs)). **Figure 4** shows similar data as a function of retinal illuminance for a single subject measured at the fovea and $\pm 2.5^{\circ}$ away from fixation, along the horizontal meridian. In this experiment, the pupil size was measured every 20 ms and the luminance of the visual display was adjusted appropriately in order to maintain constant retinal illuminance. The results show a large $\sim$2.2-log unit increase in foveal contrast acuity thresholds over the 1000-fold change in retinal illuminance. Contrast acuity at low light levels in the mesopic range is extremely poor and below 0.6 photopic trolands (phot. td, a measure of photopic retinal illuminance) the periphery becomes more sensitive than the foveal region because of the distribution of rods and cones across the retina.

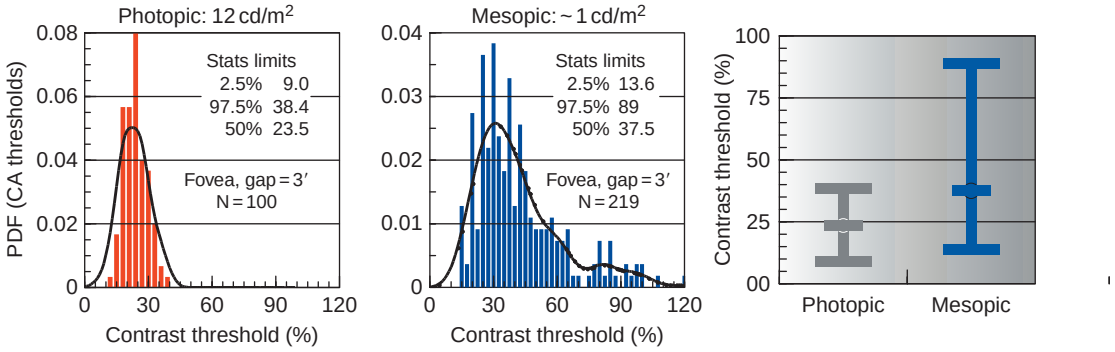

Figure 3 Low photopic and high mesopic measurements of contrast thresholds for gap orientation discrimination using Landolt ring stimuli of 3′ gap size. One hundred subjects participated in the photopic study and 219 subjects carried out the mesopic test. All subjects had normal Snellen acuity and the age distribution was as follows: photopic: mean = 23 years, standard deviation (sd) = ±7, mesopic: mean = 28 years, sd = ±14. The histogram shows the probability distribution function (PDF) of the contrast acuity (CA) thresholds measured as % luminance contrast (i.e., $\Delta L/L_b$, where ΔL represents the increment in stimulus luminance with respect to the surrounding background (L_b)). The statistical limits from each graph are shown as vertical bars to illustrate the overlap in photopic and mesopic thresholds.

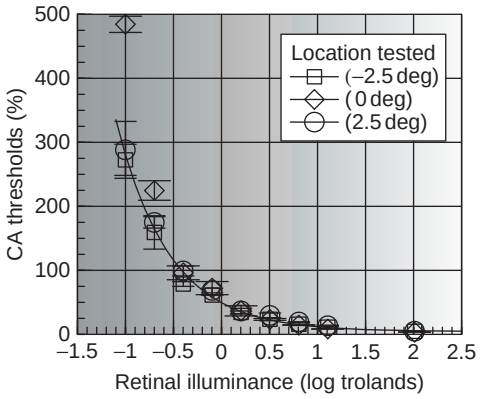

Figure 4 Contrast acuity thresholds ($\Delta L/L_b$) measured at the fovea and ±2.5° in the periphery, as a function of retinal illuminance, for a 3′-gap Landolt ring stimulus. Spectrally calibrated neutral density filters were employed to achieve the full range of retinal illuminance. Pupil size was monitored continuously and this measurement was used to adjust the luminance of the display to maintain constant retinal illuminance. The correlated color temperature of the background field was ~6500K (CIE (*x, y*) – chromaticity coordinates: 0.305, 0.323). The three stimulus locations were interleaved randomly and the subject's task was to report the orientation of the gap (i.e., top right, top left, bottom right, or bottom left) by pressing one of four buttons located at the corners of a square, each button corresponding with one of the gap locations.

Contrast acuity measurements, although functionally important, only partly characterize how the spatial properties of the visual system change with retinal illuminance. A more complete characterization is provided by the spatial contrast sensitivity function or CSF, which defines the sensitivity (i.e., the reciprocal of the contrast threshold) for the detection of sinusoidal gratings (smoothly changing black-and-white stripes) as a function of their spatial frequency (i.e., as they change from coarse to increasingly fine stripes). Loosely speaking, the contrast describes local, spatial differences between the object of interest (the stripes, in this case) and its background (the mean background level), and often correlates with subjective measures such as object conspicuity. In a typical CSF experiment, the observer is presented with sinusoidal gratings of a given spatial frequency, and is asked to vary its contrast to find the contrast at which the grating is just visible. This threshold measurement is then repeated at a series of spatial frequencies to build up a complete CSF. Several spatial CSFs measured by van Nes and Bouman as a function of retinal illuminance are shown in **Figure 5**. As the illumination level increases, the CSFs change in shape from being low-pass (i.e., falling monotonically with increasing spatial frequency) to being much broader, slightly band-pass functions (i.e., peaking in sensitivity at some intermediate frequency and falling off in sensitivity at lower and higher frequencies).

There are two notable features of the data in **Figure 5**. First, at low spatial frequencies, the contrast sensitivity becomes roughly constant above about 0.09 phot. td. Thus, the contrast sensitivity becomes independent of the illumination level at higher photopic levels. Second, at higher spatial frequencies, the highest spatial frequency that can just be seen, which corresponds to the spatial acuity measurements just discussed, improves markedly, increasing from 5 cycles per degree at 0.0009 phot. td to 55 cycles per degree at 5900 phot. td. These two features reflect, in part, the decrease in the spatial extent of visual integration with increasing light level.

In general, the visual system is good at spatial-contrast detection to the extent that, under optimal conditions, the threshold contrast can be as low at 0.2% (see **Figure 5**). By contrast, the visual system is poor at estimating the amount of total luminous flux, a task which is presumably

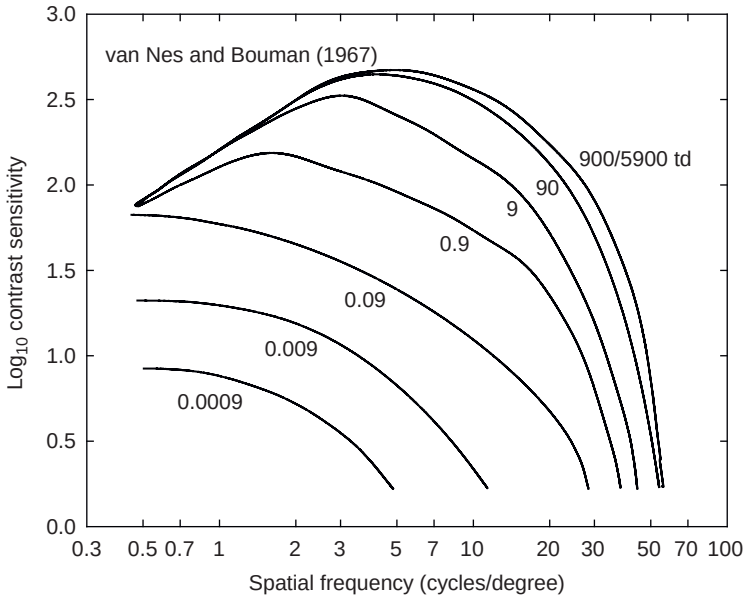

Figure 5 Spatial contrast sensitivity functions from 0.0009 to 5900 td measured by van Nes and Bouman (1967). The CSFs for 5900 td and 900 td are identical. A 2-mm diameter entrance pupil was used, so that these CSFs will be diffraction limited at highest illumination levels. Replotted from van Nes, F. L. and Bouman, M. A. (1967). Spatial modulation transfer in the human eye. *Journal of the Optical Society of America* 57: 401–406.

evolutionarily less important than the detection of faint edges and boundaries that reveal the presence of objects in the visual field.

Pupil Size, Higher order Aberrations, and Light Level

The size of the pupil affects retinal illuminance, depth of field, diffraction, and HOAs. In addition, it can also affect scattered light in the eye, when the light scattering is nonuniform over the pupil. The most important and best-studied afferent visual signal that drives the pupil is generated by changes in the ambient illumination, and this pathway is associated entirely with subcortical projections. Other pathways are also involved, but the corresponding pupil changes are more transient and smaller in amplitude. Aging affects steady-state pupil size, but in general the pupil varies from 2 mm in bright sunlight to over 8 mm in the dark (see **Figure 1**). The HOAs of the eye, mostly spherical aberration, increase rapidly with pupil diameter. Under natural conditions, this corresponds to either mesopic or scotopic vision. **Figure 6(a)** shows how the average wavefront aberration of the eye varies with pupil diameter. At low light levels, the pupil of the eye is large and consequently the quality of the retinal image is affected by increased aberrations and scattered light. When the light level is high, HOAs become very small and diffraction becomes more important and can often limit most the quality of the retinal image that can be achieved.

The potential of improving spatial vision by reducing HOAs using customized, wavefront-guided corneal refractive surgery has been of considerable interest. Since the size of the pupil significantly affects the aberrations in the eye (**Figure 6(a)**), any experimental assessment of the benefit of HOA correction must compare performance with and without correction using the natural pupil size. The visual benefit for contrast acuity that results from HOA correction is shown in **Figure 6(b)** for ambient light levels in the range 140–0.01 cd m^{-2}. Although HOA correction undoubtedly improves retinal image quality for large pupil sizes in mesopic and scotopic vision, the visual benefit for everyday visual performance as measured by contrast acuity is limited, largely as a result of the poor spatial resolution of mesopic and scotopic vision. The results of **Figure 6(b)** suggest that the spatial CSFs shown in **Figure 5** are well matched to the increases in the HOAs with increasing pupil size. As the light level decreases and the pupil size and HOAs increase, the retina is less able to resolve higher spatial frequencies, and thus the most deleterious effects of the increasing aberrations are invisible.

Flicker Perception

Similar to the changes in the spatial properties of the visual system that accompany light adaptation, the changes in its temporal properties can also be characterized by contrast sensitivity measurements. A temporal CSF defines the sensitivity for the detection of flicker as a function of temporal frequency. In a typical experiment, the observer is presented with a uniform disk that flickers sinusoidally

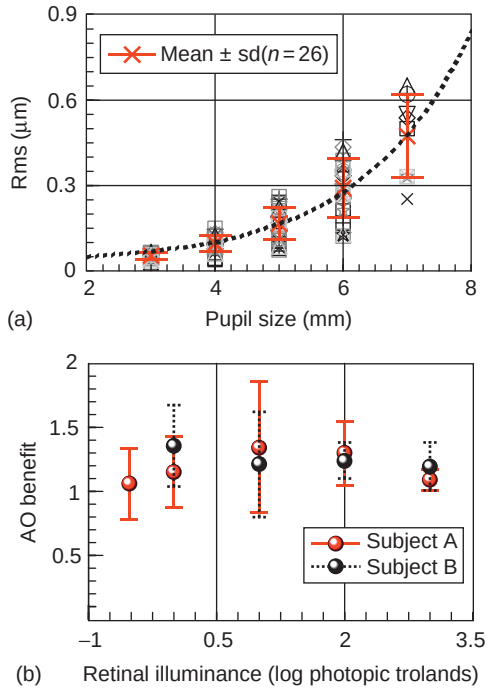

Figure 6 Mean root mean square (rms) wavefront aberration (a parameter that relates to the quality of the retinal image) was measured in 26 subjects and is plotted as a function of pupil diameter. The error bars show ±sd for this subject group. Section B plots the visual benefit (defined as the ratio of contrast sensitivities measured with and without correction of higher order aberrations in the eye), as a function of retinal illuminance. The visual benefit that follows correction of higher order aberrations is small when the retina is adapted to the corresponding ambient illumination. Replotted from Van Kvansakul, J., Rodriguez-Carmona, M., Edgar, D. F., et al. (2006). Supplementation with the carotenoids lutein or zeaxanthin improves human visual performance. *Ophthalmic and Physiological Optics* 26: 362–371; and Dalimier, E., Dainty, J. C., and Barbur, J. L. (2008). Effects of higher-order aberrations on contrast acuity as a function of light level. *Journal of Modern Optics* 55: 791–803.

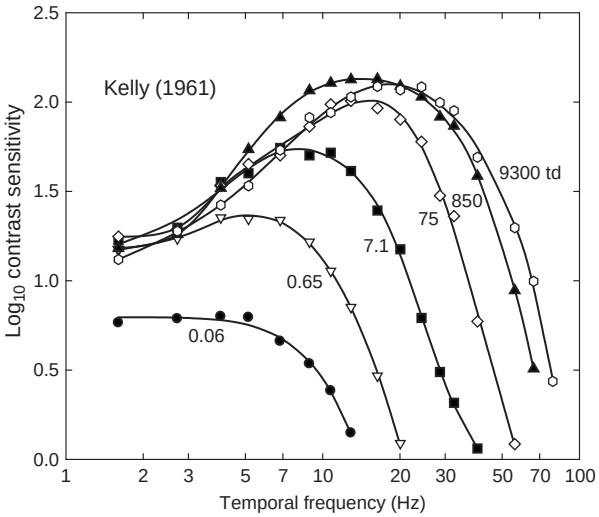

Figure 7 Temporal contrast sensitivity functions from 0.006 to 9300 td measured by Kelly (1962). Replotted from Kelly (1962). Visual responses to time-dependent stimuli I. Amplitude sensitivity measurements. *Journal of the Optical Society of America* 51: 422–429.

at some temporal frequency, and is then asked to adjust its flicker contrast (sometimes called ripple ratio or modulation) until the flicker is just visible. This threshold measurement is subsequently repeated at a series of temporal frequencies to build up a complete CSF. **Figure 7** shows temporal CSFs measured by Kelly as a function of retinal illuminance. These functions have several characteristics in common with the spatial CSFs shown in **Figure 5**. As the illumination level is increased, the temporal CSFs, like the spatial CSFs, change from being low-pass to slightly band-pass.

Other features are also shared between the spatial and temporal CSFs. First, at low temporal frequencies, like low spatial frequencies, the contrast sensitivity becomes roughly constant and therefore independent of light level – in this case, at 0.65 phot. td and above. Second, as the retinal illuminance is increased, the highest temporal frequency that can just be seen (i.e., the temporal acuity limit, which is also known as the critical fusion frequency) increases from about 13 Hz at 0.06 phot. td to 80 Hz at 9300 phot. td.

The changes in the shapes of the temporal CSFs and the reduction in integration time both reflect a speeding up of the visual response with light adaptation. This speeding up can be assessed more directly by measuring the differences in visual delay between the two eyes when they are in different states of adaptation. **Figure 8(a)** shows how the cone response speeds up as the retinal illuminance in one eye is increased (relative to the cone response in the other eye fixed at a retinal illuminance of 4.16 log phot. td). In terms of phase delay (where 360° is one cycle of flicker), the response speeds up, for example, at 10 Hz, by about 150° between 1.05 and 4.16 log phot. td. This is equal to 150/360 or 0.42 of a cycle, which, given that one 10-Hz cycle lasts 100 ms, represents a speeding up of roughly 42 ms. The visual response mediated by rods also speeds up over the scotopic range. **Figure 8(b)** shows the rod response in one eye with varying retinal illumination relative to the rod response in the other eye fixed at a retinal illuminance of 1.3 log scot. td. At 4 Hz, the response speeds up by 135° or 0.38 cycles between −3.3 and −0.8 log scot. td. This translates to a speeding up of roughly 94 ms. These results illustrate that changes in visual delay can be substantial. Visual performance, in terms of the speed of the visual response, improves markedly as the rod or the cone systems light adapt.

At mesopic levels, the situation is more complicated. Although the rod system is relatively light adapted and the cone system relatively unadapted at these levels, the rod system is still more sluggish than the cone system. These differences reflect intrinsic differences between the speeds of the responses of the rod and cone

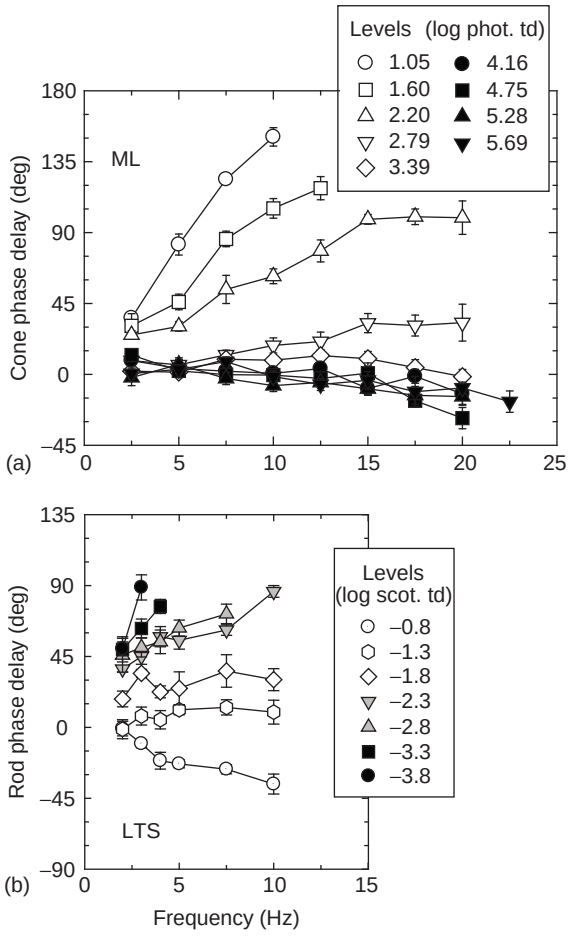

Figure 8 Binocular phase-delay measurements made between the two eyes in different states of adaptation. (a) M-cone phase delays in degrees between signals generated in the left eye and those generated in the right eye for observer ML. The adaptation level in the right eye was fixed at 4.16 log phot. td; that in the left eye was varied according to the key. Data replotted from Figure 5 of Stockman, A., Langendörfer, M., Smithson, H. E., and Sharpe, L. T. (2006). Human cone light adaptation: From behavioral measurements to molecular mechanisms. *Journal of Vision* 6: 1194–1213. (b) Rod phase delays degrees between signals generated in the left eye relative and those generated in the right eye for observer LTS. The adaptation level in the right eye was fixed at −1.30 log scot. td; that in the left eye was varied according to the key. Data replotted from Figure 9 of Stockman and Sharpe (2006). Into the twilight zone: The complexities of mesopic vision and luminous efficiency. *Ophthalmic and Physiological Optics* 26: 225–239.

photoreceptors, as well as differences between the rod and cone postreceptoral pathways. The situation is further complicated by an abrupt transition that occurs within the rod system at mesopic levels from a slow, sensitive postreceptoral pathway to a faster, more insensitive one. Due to the complex differences between the temporal properties of rod- and cone-mediated vision, mesopic measures of luminous efficiency and visual performance will be strongly dependent not only on the relative sensitivities of the rods and cones, but also on the temporal characteristics of the stimuli used to make those measurements. Thus, targets of different duration are likely to produce mesopic results with different rod to cone weightings.

Color Vision and Light Level

Color signals contribute significantly to the detection and appearance of objects, particularly when the photopic luminance contrast of the stimulus is low. In fact, in terms of cone-contrast signals under optimal conditions, the eye sees color better than it sees luminance. Other studies also show that even the pupil of the eye responds more vigorously to chromatic than to luminance signals when small stimuli are involved. Color can be perceived at or near the cone-detection threshold. For instance, the appearance of a spectrally green target is achromatic at scotopic levels, but takes on a clearly green tinge at mesopic levels. Color affects the conspicuity of stimuli. In general, the effective contrast of visual stimuli can be expressed as a complex function of photopic and scotopic luminance contrast with significant contributions from red/green and yellow/blue color signals in the photopic range. Importantly, chromatic signals also contribute to the perception of brightness (but not to luminance). In the mesopic range, cone signals become less effective, but the stronger rod signals do not appear to contribute significantly to color vision, particularly when threshold measurements are involved. When the stimulus is well above threshold, rod signals affect both the color appearance and the overall conspicuity of the stimulus.

Conclusions

The idea that the performance of the visual system can be usefully characterized over a 10 000-million-fold range of light levels by just three spectral luminous efficiency functions, corresponding to the scotopic, mesopic, and photopic ranges, is overly ambitious. Any model based solely on spectral sensitivity is unlikely to capture the effects of the large number of parameters that can influence object appearance. Here, we have focused on the way in which other key aspects of visual performance, such as spatial and temporal contrast sensitivity and acuity, visual delay, and color sensitivity, change with light level. We argue that only by linking such changes with changes in spectral luminous efficiency could we reasonably hope to predict visual performance, particularly at mesopic levels where the characteristics of the rod and cone systems are so different.

See also: Acuity; Chromatic Function of the Cone; Color Blindness: Acquired; Color Blindness: Inherited; Contrast Sensitivity; Information Processing: Contrast Sensitivity;

Information Processing: Retinal Adaptation; Phototransduction: Adaptation in Cones; Phototransduction: Adaptation in Rods; Phototransduction: Inactivation in Cones; Phototransduction: Phototransduction in Cones; Phototransduction: Phototransduction in Rods; Phototransduction: Rhodopsin; Phototransduction: The Visual Cycle; Pupil.

Further Reading

Chisholm, C. M., Evans, A. D., Harlow, J. A., and Barbur, J. L. (2003). New test to assess pilot's vision following refractive surgery. *Aviation, Space, and Environmental Medicine* 74(5): 551–559.

Dalimier, E., Dainty, J. C., and Barbur, J. L. (2008). Effects of higher-order aberrations on contrast acuity as a function of light level. *Journal of Modern Optics* 55: 791–803.

Kelly, D. H. (1961). Visual responses to time-dependent stimuli I. Amplitude sensitivity measurements. *Journal of the Optical Society of America* 51: 422–429.

Kvansakul, J., Rodriguez-Carmona, M., Edgar, D. F., et al. (2006). Supplementation with the carotenoids lutein or zeaxanthin improves human visual performance. *Ophthalmic and Physiological Optics* 26: 362–371.

Sharpe, L. T. and Stockman, A. (1999). Two rod pathways: The importance of seeing nothing. *Trends in Neurosciences* 22: 497–504.

Stockman, A., Jägle, H., Pirzer, M., and Sharpe, L. T. (2008). The dependence of luminous efficiency on chromatic adaptation. *Journal of Vision* 8(16): 1–26.

Stockman, A., Langendörfer, M., Smithson, H. E., and Sharpe, L. T. (2006). Human cone light adaptation: From behavioral measurements to molecular mechanisms. *Journal of Vision* 6: 1194–1213.

Stockman, A. and Sharpe, L. T. (2006). Into the twilight zone: The complexities of mesopic vision and luminous efficiency. *Ophthalmic and Physiological Optics* 26: 225–239.

van Nes, F. L. and Bouman, M. A. (1967). Spatial modulation transfer in the human eye. *Journal of the Optical Society of America* 57: 401–406.

Walkey, H. C. and Barbur, J. L. (guest editorial) (2006). Shedding new light on the twilight zone. *Ophthalmic and Physiological Optics* 26: 223–224.

Walkey, H. C., Barbur, J. L., Harlow, A., and Makous, W. (2001). Measurements of chromatic sensitivity in the mesopic range. *Color Research and Application* 26: 36–42.

Walkey, H. C., Barbur, J. L., Harlow, J. A., et al. (2005). Effective contrast of colored stimuli in the mesopic range: A metric for perceived contrast based on achromatic luminance contrast. *Journal of the Optical Society of America* 22: 17–28.

Photoreceptor Development: Early Steps/Fate

I Nasonkin, T Cogliati, and A Swaroop, National Institutes of Health, Bethesda, MD, USA

Published by Elsevier Ltd.

Glossary

Cell competence – In the context of retinal development, it refers to the characteristic ability of retinal progenitor cells (RPCs) to generate particular retinal cell types. It is determined by a combination of intrinsic and extrinsic factors.

Cell-fate determination – An early step (generally irreversible) in the developmental process leading to the acquisition of a differentiated cellular phenotype.

Cell-fate specification – Developmental process leading to the acquisition of a reversible cell fate, generally preceding determination.

Conditional knockout mouse – A genetically engineered mouse in which targeted deletion of gene(s) of interest can be temporally and/or spatially controlled.

Knockout mouse – A genetically engineered mouse carrying targeted deletion of one or more genes that is transmitted through the germ-line. Knockout mice in which gene function is completely ablated are referred to as *null* for that gene.

Phototaxis – Movement in response to light stimuli.

Precursor – For the purposes of this article, and in agreement with previously published material, the term precursor is used for a postmitotic cell committed to a specific cell fate but not having the differentiated cell function or phenotype. Other authors may use the term precursor interchangeably with the term progenitor.

Progenitor – For the purposes of this article and in agreement with previously presented material, a progenitor is a proliferating, undifferentiated, multipotent, yet developmentally restricted, cell that expresses a combination of genes biasing its fate toward one or multiple differentiated retinal phenotypes.

Rhabdomere – A visual pigment-containing organelle, characterized by numerous microvilli, normally found on the apical surface of photoreceptors, mostly in arthropods. Its counterpart in vertebrates is the outer segment of rods and cones.

Transgenic mouse – A mouse genetically engineered with random integration of one or more exogenous genes (transgenes) in its genome. Expression of the transgene can be cell/tissue specific and controlled over time.

Introduction

Rod and cone photoreceptors are highly specialized sensory neurons responsible for the detection of visual stimuli. They convert quanta of light into signals that are transmitted via interneurons (bipolar cells) to projection neurons (retinal ganglion cells (RGCs)) and then to the brain, where neuronal electrical stimuli are interpreted as visual sensation. In vertebrates, rod and cone photoreceptors are characterized by the expression of rhodopsin and cone opsins, respectively. Opsins belong to a family of membrane-bound guanine nucleotide binding protein-coupled receptors, which are covalently linked to a vitamin A-derived retinaldehyde chromophore and are responsible for initiating the phototransduction cascade.

The capacity to detect and respond to changes in environmental illumination is a fundamental survival skill present, to different degrees, in all living beings. Opsin-like molecules first appeared in prokaryotes (bacteria and archaea) and could function as proton-pumps to transfer energy within a unicellular organism. Activation of opsin-like molecules in response to circadian rhythms and dark–light cycles might sustain a primitive form of flagella and pili phototaxis. The capacity to perceive light stimuli further evolved in protozoa, where opsins allow for rudimental vision to sense the environment and guide adaptive movements. However, only metazoans (animals) display anatomical structures dedicated to detection and processing of light stimuli, with graded complexity from the pit eyes of worms and mollusks to the camera-type eyes of vertebrates, all of which contain light-responsive photoreceptors.

Evolution has resulted in two primary types of photoreceptor cells: rhabdomeric and ciliated. In both, the cell membrane has evolved to accommodate the maximum number of opsin molecules to increase the probability that one is activated by a single photon of light. Photoreceptors in most invertebrates are rhabdomeric with thousands of opsin-containing microvilli, whereas most vertebrates have a ciliated structure containing multiple invaginations of opsin-rich stack of membranous disks, known as the outer segment. Furthermore, as described elsewhere in this encyclopedia, other marine mollusks – such as the Pectin – contain rhabdomeric and ciliary photoreceptors in separate layers in the same retina. While phototransduction leads to membrane depolarization in rhabdomeric photoreceptors, it results in hyperpolarization in ciliated photoreceptors. Developmental

processes also differ between invertebrates and vertebrates, even in those species displaying a camera-type structure. In the former (e.g., the octopus), the eye is of epidermal origin and mature photoreceptors face the vitreous cavity. In the latter, the eye develops from the neural plate (neuroectodermal origin) and mature photoreceptors are oriented away from the vitreous.

This article follows the developmental pathway that results in the generation of rods and cones from pools of retinal progenitor cells (RPCs) in the mammalian retina. We describe the factors involved in photoreceptor cell-fate specification, determination, and maturation. We have focused on human photoreceptors for their relevance in retinal degenerative diseases and on the mouse because of abundant available literature in this model pertaining to photoreceptor development.

Photoreceptor Development

Rod and Cone Pattern in Human and Mouse Retina

Photoreceptors are characterized by distinct morphology and synaptic connections that reflect their unique functions in light detection and visual process. Rod photoreceptors function in dim light, whereas cones are responsible for chromatic vision and visual acuity in bright light. These differences in light sensitivity are made possible by distinct visual pigments (opsins) and other proteins that mediate the phototransduction cascade.

All rod photoreceptors express rhodopsin from the *OPN2/RP4/RHO* gene and display peak sensitivity at a wavelength of approximately 500 nm. Cone photoreceptors can be further distinguished in different subtypes, based on the wavelength sensitivity conferred by their characteristic opsin photopigment. Humans and old world primates have three subtypes of cone photoreceptors. Cones sensitive to blue light express short-wavelength-sensitive (S)-opsin from the *OPN1SW* gene (S cones); cones sensitive to green light express medium-wavelength-sensitive (M)-opsin from the *OPN1MW2* gene (M cones); whereas those sensitive to red light express long wavelength-sensitive (L)-opsin from the *OPN1LW* gene (L cones). On the other hand, only S-opsin and M-opsin from *Opn1sw* and *Opn1mw* genes, respectively, are expressed in mouse cone photoreceptors.

In humans and mice, rods represent over 95% of the photoreceptors. The remaining 5% (human) and 3% (mouse) are cone photoreceptor subtypes. Rods and cones are arranged in a spatial mosaic in the human retina, where cones are concentrated in a region at the center of the macula – the fovea. The innermost 100-μm-wide central fovea – known as the pure cone area – contains a dense population of L and M cones and it is completely devoid of S cones, which are distributed in the peripheral fovea. Rods appear only approximately 300 μm from the center of the fovea and their density peaks outside the fovea at the eccentricity of the optic disc. A smaller proportion of cones are found interspersed within the more numerous rods in the peripheral retina. The ratio of L-to-M cones in the pure cone area and between central and peripheral retina varies considerably among individuals, and no characteristic cone-subtype distribution pattern is evident.

In the mouse retina, rods are relatively homogeneously distributed, and there is no structure resembling the human fovea. However, S- and M-opsins are expressed in cones in a reciprocal dorsal-to-ventral gradient with S-opsin-expressing cones localized predominantly in the ventral portion of the retina and M-opsin cones predominantly in the dorsal region. Differences in photoreceptor subtypes and distribution are reflected in the developmental events that generate photoreceptors in the human and mouse retina.

Development of Cone and Rod Photoreceptors

The retinal neuroepithelium is populated by proliferating, undifferentiated, multipotent RPCs (neuroblasts), from which all neural retinal cell types – including rod and cone photoreceptors – are generated during retinogenesis. Cell birth refers to the time when a cell exits the final mitotic cycle and commits to a specific differentiated fate. Birth-dating studies in the murine retina have shown that RPCs destined to become cone photoreceptors exit the cell cycle between embryonic day (E) 11 and E18 starting from the central retina and proceeding toward the periphery (**Figure 1(a)**). In an overlapping wave, rod progenitors exit the cell cycle between E12 and postnatal day (P) 10. Initiation of opsin protein expression occurs later, with S-opsin protein first detected around E19, followed by rhodopsin around P2 and M-opsin around P7.

Immunohistochemical analysis of the developing human retina, together with data from Macaque monkeys, suggests that cone photoreceptors are generated in the human retina starting from the prospective fovea in a period of time from fetal week (Fw) 8 to Fw34 (**Figure 1(b)**). In humans, rod genesis begins after cone birth around Fw10 but overlaps with cone genesis and continues into the first 8 months of postnatal life. Unlike the mouse, S-opsin expression in humans initiates around Fw12, preceding rhodopsin and L-/M-ospin expression, which are evident by Fw15. In humans, synaptic and neurotransmitter proteins are expressed in association with the initiation of synaptogenesis during the lag period between cone genesis and production of cone opsin. However, synaptogenesis in rods occurs only after the onset of rhodopsin synthesis.

In the mouse, the above-mentioned events occur first in the center of the retina and proceed toward the periphery; this is similar to humans where, generally, new developmental events start in the pure cone area. In the early postnatal human retina, the fovea is still immature with a

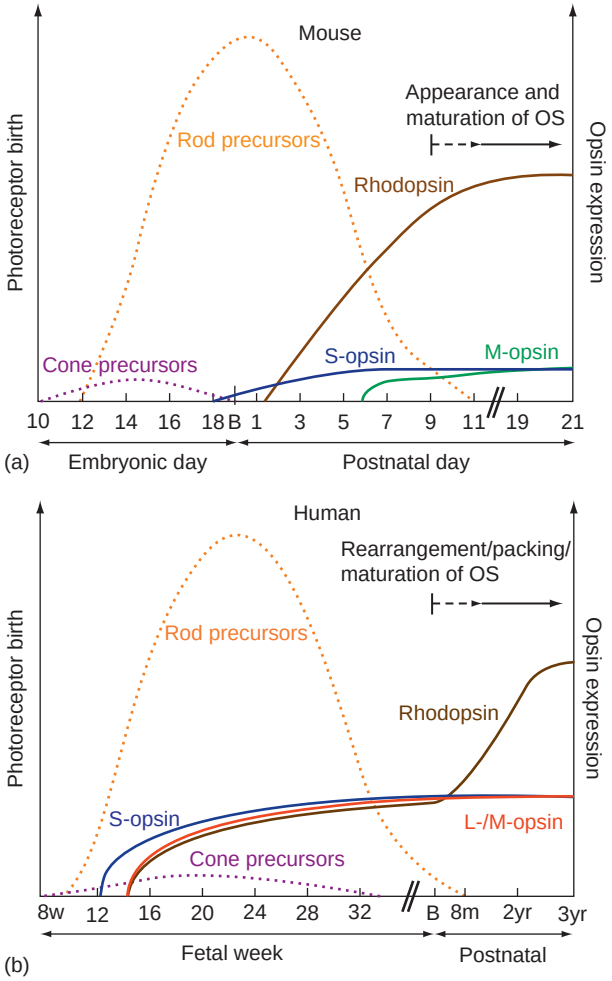

Figure 1 Photoreceptor development in mouse (a) and human (b) retina. In the first stage of photoreceptor development, prospective cone and rod precursors exit the cell cycle in sequential (cone first and rod after), yet overlapping waves (dotted lines). Postmitotic cells lose their apical process while retaining their connection to the outer limiting membrane and have elongated cuboidal morphology (cones) or a round shape (rods). The amplitude of the dotted curves in (a) and (b) represents the proportion of cells becoming postmitotic and fated to differentiate into cones (purple) and rods (orange), and the period of time in which all cells exit the cell cycle. Synthesis of specific opsins initiates the differentiation stage. Solid lines in (a) and (b) illustrate the temporal protein expression pattern of rhodopsin (brown), S-opsin (blue), M-opsin (green), and L-/M-opsin (red). In the mouse (a), S-opsin (blue) is expressed first, followed by rhodopsin (brown) and then M-opsin (green). The relative amount of rhodopsin expressed is considerably higher than S- and M-opsin, consistent with the higher proportion of rods (>95%) in the photoreceptor cell population. Photoreceptor maturation is completed between the second and the third postnatal week (arrow). In the human (b), S-opsin is synthesized first, followed shortly after by overlapping rhodopsin and L-/M-opsins. Rhodopsin production increases dramatically after birth, coincidental with outer segment formation and maturation. Cone and rod photoreceptors are rearranged after birth, with packing of cones in the fovea (dashed arrow). Outer segments continue to expand until they reach their mature size by the third year of age (solid arrow). B, birth; OS, outer segment.

greater proportion of rods than cones at the edge of the pure cone area. The mature fovea becomes evident by 1 year of age with the characteristic packaging of cones in the center. Rod outer segments continue to grow in length well into the first postnatal years until the human retina reaches full maturation by approximately 3–5 years of age.

Factors Affecting Photoreceptor Genesis

In the stereotypical progression of cell differentiation in the retina, cone genesis is initiated from common proliferating RPCs, in a sequential manner after RGCs and before horizontal and amacrine neurons. Rod birth is initiated later compared to cone genesis, but it precedes bipolar and Müller glia cells. However, the time intervals during which full complements of cone and rod photoreceptors are generated largely overlap (see **Figure 1**). Lineage and birth-dating analyses of mouse retina indicate that photoreceptor cell-fate decisions are made at the time of terminal mitosis; however, additional investigations are necessary. Two key elements control the commitment and differentiation of photoreceptors: gene-regulatory networks that confer competence to the RPC and dictate differentiation events (**Figures 2** and **3**), and extrinsic factors that modulate transcriptional cascades in differentiating RPCs and later modulate cell–cell communication (**Figure 2**). In addition, epigenetic mechanisms (such as chromatin modifications) appear to play a significant role in directing photoreceptor specification and differentiation.

Early Stages in Photoreceptor Development

From RPC to Photoreceptor Precursor

At the time of their last mitosis and prior to exiting the cell cycle, RPCs fated to become photoreceptors upregulate the expression of paired-class homeodomain transcription factor orthodenticle protein homolog 2 (OTX2) (**Figure 2**). In the mouse, OTX2 is first detected at E11.5–12.5 in the retinal neuroblastic layer (**Figure 3**). OTX2 expression increases thereafter, concomitantly with early cone and rod development, and persists in the postnatal mouse retina in bipolar and photoreceptor cells. *Otx2* plays an important role as an early factor that specifies photoreceptor cell fate, and probably as a late factor that may promote terminal differentiation by participating in upregulation of photoreceptor-specific genes. When *Otx2* is conditionally knocked out in the developing mouse eye, photoreceptors do not develop and are replaced by amacrine-like cells. Furthermore, when *Otx2* is ubiquitously expressed in RPCs, all cells follow the photoreceptor fate. In humans, *OTX2*

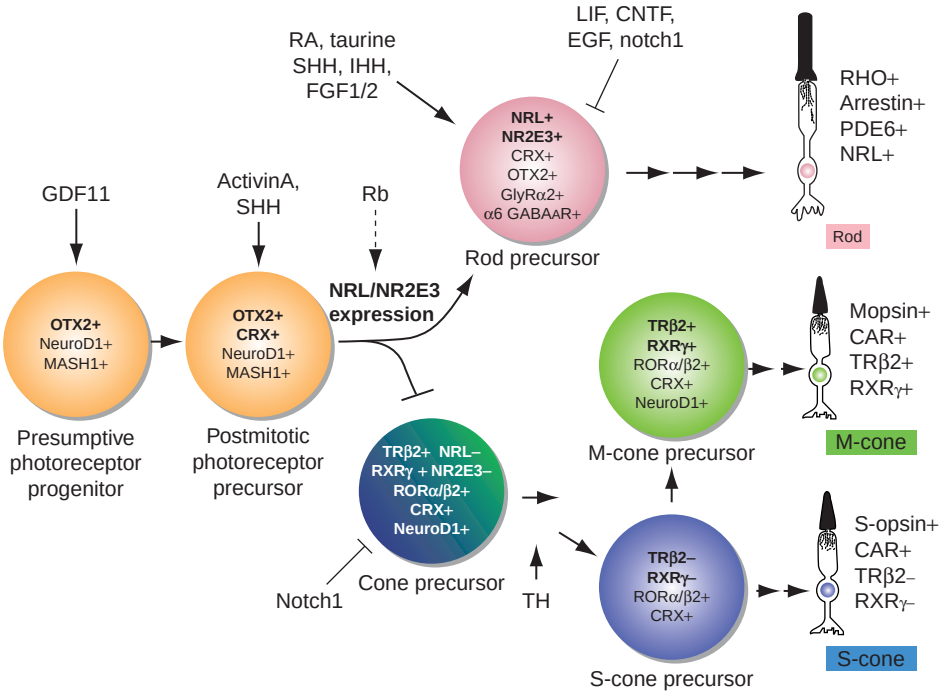

Figure 2 A model of photoreceptor development in the murine retina. Rods, S and M cones are generated from a common pool of retinal progenitor cells (RPCs), which exit the cell cycle at specific times during retinogenesis. A synergistic interaction between intrinsic and extrinsic factors progressively restricts cell fate, biasing individual cells toward differentiation into a unique mature cell type. Some of the known molecules involved are illustrated here. Proteins that appear to be major contributors to specification/determination of cell fate are shown in bold. Expression of OTX2 and CRX defines the postmitotic pool of cells fated to become photoreceptors (photoreceptor precursors). Expression of NRL and its target NR2E3 determines rod photoreceptor cell fate, whereas their absence leads to cone fate. NRL/NR2E3-expressing rod precursors progress through multiple transition stages and become functional rod photoreceptors when rhodopsin and phototransduction protein synthesis occurs and outer segments are mature. Photoreceptor precursors that do not express NRL/NR2E3 progress toward the cone lineage. Upon downregulation of TRβ2 and RXRγ, cone precursors become S cone precursors and synthesize S-opsin. For M cone precursors to develop, S-opsin expression must then be repressed by the heterodimer TRβ2/RXRγ, and M-opsin synthesis initiated by another TRβ2-containing complex. S- and M-opsin expression followed by outer segment maturation complete cone differentiation. The current model supports the existence of a default S-cone pathway that requires active inhibition by NRL/NR2E3 and by TRβ2/RXRγ to allow differentiation of rods and M cones, respectively. The roles of other cell intrinsic and extrinsic factors are further described in the text. Arrows indicate active promotion and truncated lines indicate inhibition of a developmental stage. Dotted lines indicate tentative roles. See the text for explanation of abbreviations.

mutations are associated with retinal diseases, such as anophthalmia, microphthalmia, and coloboma.

At the molecular level, OTX2 is shown to activate the promoter of cone–rod homeobox (CRX) transcription factor, a closely related homeodomain transcription factor. The two transcription factors (OTX2 and CRX) appear to promote completion of photoreceptor differentiation programs (**Figure 2**). CRX does not contribute to photoreceptor cell specification, but is essential for terminal differentiation and maintenance. In *Crx-null* mice, despite normal photoreceptor genesis, morphogenesis is incomplete as outer segments fail to elongate, and photoreceptors do not produce a full complement of phototransduction proteins. These abnormal photoreceptors undergo synaptogenesis, but their synaptic endings appear malformed and eventually degenerate. Mutations in the human *CRX* result in retinopathies, including Leber congenital amaurosis (LCA), cone–rod dystrophy, and retinitis pigmentosa (RP).

Another protein suggested to participate in photoreceptor cell development is the basic helix-loop-helix (bHLH) transcription factor NeuroD1 (**Figure 2**). *NeuroD1* is expressed in developing and differentiated rod and cone photoreceptors. Its targeted deletion in the mouse, however, causes only a modest decrease in photoreceptor number. NeuroD1 acts in combination with another bHLH transcription factor, MASH1, which may contribute to regulating the timing of photoreceptor differentiation as its targeted deletion in mouse leads to delay in photoreceptor development.

Very early, at the time of photoreceptor specification, postmitotic precursor cells become committed toward rod or cone fates. The Maf family basic motif-leucine zipper transcription factor NRL and its target, the

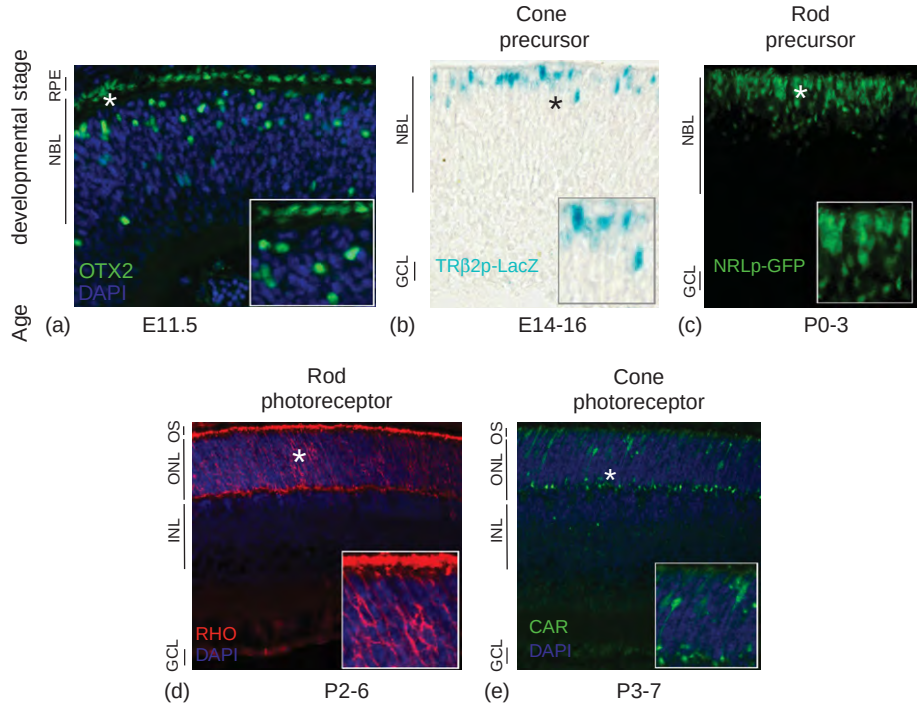

Figure 3 Stages of photoreceptor development in murine retina. Developmental stages are characterized by unique markers. Postmitotic photoreceptor precursors (a) can be detected by immunohistochemistry (IHC) with anti-OTX2 antibodies (green). Intermediate stages leading to cone or rod precursors are less delineated. However, cone precursors are characterized by the expression of TRβ2 and RXRγ, while rod precursors can be distinguished for NRL and NR2E3 expression. When the *lacZ* reporter gene driven by the *Trβ2* promoter is expressed in transgenic mice (b), cone precursors, normally expressing TRβ2, express LacZ (cyan). Similarly, rod precursors in a transgenic mouse expressing green fluorescent protein (GFP) under control of *Nrl* promoter (c) become fluorescent (green). Mature photoreceptors are identified by expression, at the RNA level first and protein level after, of their characteristic opsins and phototransduction proteins. Rod (d) and cone (e) photoreceptors are visualized by IHC with antirhodopsin (red) and anticone arrestin (green) antibodies, respectively. Areas labeled with an asterisk in (a)–(e) are enlarged in the inlets. Images are provided by Dustin Hambright ((a), (d), and (e)), Li Jia and Douglas Forrest (b), and Jerome Roger (c). RPE, retinal pigment epithelium; NBL, neuroblastic layer; GCL, ganglion cell layer; OS, outer segments; ONL, outer nuclear layer; INL, inner nuclear layer; E, embryonic day; P, postnatal day; DAPI, 4'-6-diamidino-2-phenylindole (nuclear staining); CAR, cone arrestin.

photoreceptor-specific orphan nuclear receptor NR2E3, are the primary determinants of rod versus cone cell-fate determination. It appears that S cone cell fate is specified as a default pathway and that inhibition of this pathway by NRL/NR2E3 is permissive to rod specification (**Figure 2**).

From Cone Precursor to Cone Photoreceptor

Cones are the first photoreceptor cell type to exit the cell cycle in all vertebrates (**Figure 1**). However, their differentiation takes a few days (mouse) to weeks (human) and is complete only after a majority of rods have become postmitotic. Cone precursors must go through an additional specification process that determines distinct cone subtypes (L, M, or S in humans, and M or S in mouse).

Studies of cone-photoreceptor-fate determination rely 8w?>on the detection of specific opsins at the mRNA or protein level, thus overlapping with studies on opsin gene regulation. In mouse and human cone precursors, S-opsin expression is detected first, followed by M-opsin expression (**Figure 1**). Variable numbers of photoreceptors go through a transitional state in which both opsins are expressed, before S-opsin is downregulated and M-opsin predominates. In the adult mouse retina, a prevalent population of photoreceptors coexpresses both pigments, whereas cone photoreceptors in the human retina express a single opsin.

In mice, onset of cone opsin expression is regulated by numerous factors; these include CRX, members of the nuclear receptor family, thyroid hormone nuclear receptor beta 2 isoform (TRβ2) and retinoid X nuclear receptor gamma (RXRγ), and of the retinoic acid (RA) receptor-related orphan receptor – RORα and RORβ2. RORα and RORβ2 are expressed in postmitotic cone-photoreceptor precursors and directly regulate S-opsin expression synergistically with CRX. Furthermore, RORα also appears to regulate the expression of M-opsin through direct binding to its promoter, highlighting a potentially more complex role in cone differentiation. Notably, *Rorβ2-null*

mice lack outer segments, suggesting RORβ2 plays an additional role in promoting photoreceptor maturation.

TRβ2 and RXRγ are also expressed in postmitotic cone precursors in the neonatal mouse retina (**Figures 2** and **3**) and act as transcriptional repressors of S-opsin expression. In fact, both receptors are downregulated concomitant with the initial onset of S-opsin expression and upregulated at a later stage in M cones in the dorsal retina to suppress S-opsin. Further evidence comes from studies of *Rxrγ-null* and *Trβ2-null* mice. Both nuclear receptors are necessary to repress S-opsin expression and probably act in concert on the S-opsin promoter. However, only TRβ2 is required for M-opsin expression, making it a key regulator of M cone differentiation. *Trβ2* gene appears to be regulated by a transcriptional complex containing NeuroD1. Although NeuroD1 alone is not sufficient to initiate *Trβ2* expression, it is required for sustained gene activation, thus supporting its role in M cone differentiation.

To date, there is no evidence involving RA in cone development in the mouse or human. On the other hand, TH has been suggested to regulate the ratio and patterning of cone-photoreceptor subtypes through changes in geographical distribution in the developing retina.

From Rod Precursor to Rod Photoreceptor

NRL is the master regulator of rod cell fate and serves as the unique defining signature of newborn rod photoreceptors (see **Figures 2** and **3**). NRL induces the expression of NR2E3. Following this, NRL and NR2E3 – together with CRX – lead to the expression pattern typical of mature rod photoreceptors (**Figure 2**). In mice *null* for the *Nrl* gene, all rods are converted to cones. Targeted deletion of *Nr2e3* in the mouse leads to enhanced S-cones with hybrid photoreceptors. Transgenic expression of *Nr2e3* in *Nrl-null* mice suppresses cone differentiation and leads to the generation of rod-like photoreceptors, yet NR2E3 is not sufficient to produce functional rods. These data support a model in which active induction by NRL and NR2E3 in CRX-expressing photoreceptor precursors is required for rod cell-fate determination with simultaneous inhibition of the cone pathway (**Figure 2**).

Mutations in NRL are associated with retinal degenerative diseases, including autosomal dominant and recessive RP, and retinopathies with varying phenotypes. Loss of NR2E3 in humans leads to enhanced S-cone syndrome, Goldmann–Favre syndrome, and similar retinopathies with increased S-cone function.

The retinoblastoma (*Rb*) gene appears to be an important intrinsic regulator of rod development. In the postnatal mouse retina, *Rb* is expressed in mitotic RPCs, where it regulates timely exit from the cell cycle, and in differentiating rod photoreceptors. When *Rb* is deleted, RPCs continue to proliferate and rod photoreceptors do not develop. Unlike *Nrl*- and *Nr2e3-null* mice, rod photoreceptors in *Rb-null* mice do not change their fate to cones (cone number remains unmodified). Rather, their development is arrested at the progenitor stage. It remains unclear from the current literature whether Rb is instructive or permissive for rod-photoreceptor cell fate.

Several extrinsic factors contribute to signaling for rod development (**Figure 2**). Cell–cell interaction mediated by Notch1 is known to sustain the undifferentiated and proliferating state of RPCs, repressing neuronal fate in general. Recently, Notch1 signaling has been shown to specifically inhibit photoreceptor fate, that is, cone in the embryonic and rod in the postnatal mouse retina. This function of Notch1 may allow differentiation of other neuronal cell types as light detection evolved from uniquely photoreceptor-based, in lower species, to multiple cell-type-mediated, in higher species. Other extrinsic factors inhibiting rod fate are leukocyte inhibitory factor (LIF), ciliary neurotrophic factor (CNTF), and epidermal growth factor (EGF).

Taurine, secreted by RGCs, is suggested to stimulate rod photoreceptor production through glycine (Gly) and gamma aminobutyric acid (GABA(A)) receptors. The hypothesis that taurine and its receptor GlyRα2 have a role in promoting rod cell fate awaits further validation.

Proper maturation and/or migration and integration of young rods into the outer nuclear layer (ONL) may require gradients of Indian Hedgehog (IHH) secreted by the retinal pigment epithelium (RPE), and Sonic Hedgehog (SHH) secreted by RGCs. IHH may also have a role in the specification of photoreceptor fate, possibly inducing *Nrl* in photoreceptor precursors. Similarly, fibroblast growth factor (FGF) family members – acidic FGF (FGF1) and basic FGF (FGF2) – are implicated in rod maturation and may induce NRL expression.

The role of RA in promoting rod photoreceptor differentiation is still unclear, though it can induce *Nrl* expression and RA-responsive sites are present in the *Nrl* promoter. However, retinoic acid receptor (*RAR*)β2/*RARγ*2 double *null* mutant mice contain a normal photoreceptor complement.

Activin A – a transforming growth factor beta (TGFβ)-like protein expressed by extraocular mesenchyme and RPE – promotes photoreceptor development *in vitro* and *in vivo*, and increases the number of photoreceptor cells in rat retinal cultures. *In vitro*, it causes RPCs to exit the cell cycle and biases them to become rods, but not cones. *In vivo*, mice with homozygous deletion of *activinA* show substantial decrease in the number of photoreceptors. Finally, growth differentiation factor 11 (GDF11) and related TGFβ family members control the competence of mitotic progenitors to acquire rod cell fate. *GDF11-null* retinas have more RGCs at the expense of photoreceptors.

Maturation of Photoreceptors

Cones are generated in mice during the prenatal period. Rod photoreceptor birth overlaps with the genesis of all retinal cell types, though most rods are born postnatally (**Figure 1**). Maturation of committed precursors to differentiated functional photoreceptors is a lengthy process and involves expression of cell-type-specific phototransduction genes, biogenesis of outer segments, and formation of synapses with specific interneurons. Expression of most photoreceptor-enriched genes depends on the synergistic or antagonistic actions of NRL, NR2E3, and CRX and their interaction with other regulatory proteins. In most instances, these proteins co-occupy the promoter/enhancer regions of their target genes. Mutations in the target genes of NRL and CRX are associated with retinal dysfunction.

Studies with transgenic and knockout mice, together with microarray and chromatin immunoprecipitation analysis, have yielded valuable information about gene-regulatory networks that guide photoreceptor differentiation and maturation. As NRL and its direct target nuclear receptor NR2E3 determine rod cell fate, these two transcription factors activate the expression of rod-specific genes and repress cone-gene expression. NRL, even in the absence of NR2E3, can activate all rod-specific genes (e.g., rhodopsin, PDE-α, PDE-β) but the repression of cone genes (e.g., S-opsin) is not efficient, leading to hybrid photoreceptors in mice expressing NRL but not NR2E3 (rd7 mice). NR2E3, on the contrary, can repress cone genes but it is unable to efficiently activate rod genes in the absence of NRL. Both NRL and NR2E3 interact with a multitude of regulatory proteins to accomplish transcriptional regulation. NRL is a highly phosphorylated protein and its function is modulated by several kinases. NRL also interacts with TATA-binding protein (TBP) and, presumably, brings the basal transcriptional machinery to target gene promoters. Recent studies have shown a key role for the protein inhibitor of activated STAT3 (PIAS-3) in the sumoylation of NR2E3, adding another level of control in gene expression and consequently rod differentiation. A combined action of NRL and NR2E3 is essential to generate functional rod photoreceptors.

CRX, on the other hand, acts as an enhancer of both rod and cone genes. While photoreceptors are produced even in the absence of CRX, these cells do not elaborate outer segments because of the low expression of most, if not all, phototransduction and structural proteins. CRX is, therefore, necessary to produce functional photoreceptors. CRX also interacts with coactivator proteins that possess histone acetyltransferase (HAT) activity and recruits HATs to promoter/enhancer regions to acetylate histone H3, thereby inducing and maintaining chromatin configurations that facilitate binding of NRL, NR2E3, and RNA polymerase II. These recently described molecular mechanisms underscore the importance of as yet poorly understood epigenetic factors in determining retinal photoreceptor cell fate and maturation.

Current Research in Photoreceptor Development

Cell interactions and intrinsic cellular mechanisms modulate gene expression and regulate photoreceptor differentiation. Among these, chromatin remodeling and small regulatory RNAs have attracted attention in recent years.

Histone methylation/acetylation are key epigenetic modifications that govern chromatin dynamics. The role of chromatin-modifying activities in directing tissue-specific development is an active area of investigation. Histone acetylation is emerging as an important mechanism in regulating photoreceptor development. Acetylation of histone H3 by HATs – recruited by CRX – appears important in maintaining chromatin configurations permissive to NRL/NR2E3 transcriptional activity in developing rods. Furthermore, histone deacetylase 4 (HDAC4) activity is shown to promote the survival of newly differentiated photoreceptors. More recently, the chromatin-remodeling complex Baf60c has been identified in differentiating, but not mature, retinal cells.

A family of three DNA methyltransferases, Dnmt1, Dnmt3a, and Dnmt3b, partially cooperate to establish and maintain genomic DNA methylation patterns. The presence of high levels of Dnmt3a and of Dnmt3b in the mouse rostral neural tube, including the optic grooves and cranial neural folds at E8.5, and in the area of evaginating optic vesicles at E9.5 is suggestive of the role Dnmts play in eye development. Epigenetic chromatin-remodeling mechanisms are also active in retinal neuroblasts undergoing cell-fate commitment, and are likely to contribute to retina-restricted patterns of gene expression. For example, hypomethylation is suggested to modulate interphotoreceptor retinoid-binding protein (IRBP) gene activation during photoreceptor genesis. Little is known about the influence of methylation on retinal cell fate, yet it is plausible that DNA methylation is actively involved in establishing RPC competence.

MicroRNAs (miRs) are short (18–24 nucleotides), noncoding, RNA sequences that modulate gene expression by binding the 3′ (and 5′) untranslated region (UTR) of their target RNAs, thus regulating their stability and translation. They originate as longer RNA transcripts that are processed and cleaved by the subsequent activity of two RNase III endonucleases – the Drosha-DGCR8 complex and Dicer. MiRs could play a gene-regulatory role in development (including retinal) that is comparable to that of transcription factors. For example, in the *Drosophila* eye,

miR-7 is activated by EGF-receptor (EGFR) signaling in cells undergoing the initial steps in photoreceptor differentiation. Furthermore, conditional *Dicer-null* mutation in the developing retina results in apparently normal retinal structure – albeit interspersed with rosettes and fated to progressive degeneration – pointing to the role of miRs in normal photoreceptor genesis and function. Further studies are warranted to fully elucidate the role of miRs in photoreceptors in general and in their development in particular.

Conclusions

When investigating cellular events and molecular mechanisms, the accuracy of models is only as good as the methods used to collect the data and the relevance to human retinal development of the animal model used. Future studies in other vertebrate species (e.g., zebrafish) and in human embryonic stem cells, with more sophisticated tools to dissect cell-fate specification/determination mechanisms, and the analysis of the vast amount of *omic* data available will permit integration of current photoreceptor development models to more closely represent the relevance to human disease. It is the authors' auspice that this article be read as the starting point to stimulate the reader's curiosity to further investigate the field of retinal developmental neurobiology for more in-depth understanding and up-to-date breakthroughs.

See also: Coordinating Division and Differentiation in Retinal Development; Embryology and Early Patterning; Histogenesis, Cell Fate, and Signaling Factors; Microvillar and Ciliary Photoreceptors in Molluskan Eyes; Phototransduction: Phototransduction in Cones; Phototransduction: Phototransduction in Rods; Retinal Histogenesis; Zebrafish: Retinal Development and Regeneration.

Further Reading

Adler, R. and Raymond, P. A. (2008). Have we achieved a unified model of photoreceptor cell fate specification in vertebrates? *Brain Research* 4: 134–150.

Chen, J., Rattner, A., and Nathans, J. (2005). The photoreceptor-specific nulear receptor Nr2e3 represses transcription of multiple cone-specific genes. *Journal of Neuroscience* 25: 118–129.

Cheng, H., Aleman, T. S., Cideciyan, A. V., et al. (2006). *In vivo* function of the orphan nuclear receptor NR2E3 in establishing photoreceptor identity during mammalian retinal development. *Human Molecular Genetics* 15: 2588–2602.

Fishman, R. S. (2008). Evolution and the eye: The Darwin bicentennial and the sesquicentennial of the origin of species. *Archives of Ophthalmology* 126: 1586–1592.

Hatakeyama, J. and Kageyama, R. (2004). Retinal cell fate determination and bHLH factors. *Seminars in Cell and Developmental Biology* 15: 83–89.

Hendrickson, A., Bumsted-O'Brien, K., Natoli, R., et al. (2008). Rod photoreceptor differentiation in fetal and infant human retina. *Experimental Eye Research* 87: 415–426.

Lamba, D., Nelson, G., Kari, M. O., and Reh, T. A. (2008). Specification, histogenesis, and photoreceptor development in the mouse retina. In: Chalupa, L. M. and Williams, R. W. (eds.) *Eye, Retina, and Visual System of the Mouse*, pp. 299–310. Cambridge, MA: MIT Press.

Livesey, F. J. and Cepko, C. L. (2001). Vertebrate neural cell-fate determination: Lessons from the retina. *Nature Reviews Neuroscience* 2: 109–118.

Mears, A. J., Kondo, M., Swain, P. K., et al. (2001). Nrl is required for rod photoreceptor development. *Nature Genetics* 29: 447–452.

Ng, L., Hurley, J. B., Dierks, B., et al. (2001). A thyroid hormone receptor that is required for the development of green cone photoreceptors. *Nature Genetics* 27: 94–98.

Nishida, A., Furukawa, A., Koike, C., et al. (2003). Otx2 homeobox gene controls retinal photoreceptor cell fate and pineal gland development. *Nature Neuroscience* 6: 1255–1263.

Oh, E. C., Khan, N., Novelli, E., et al. (2007). Transformation of cone precursors to functional rod photoreceptors by bZIP transcription factor NRL. *Proceedings of the National Academy of Sciences of the United States of America* 104: 1679–1684.

Onishi, A., Peng, G.-H., Hsu, C., et al. (2009). Pias3-dependent SUMOylation directs rod photoreceptor development. *Neuron* 61: 234–246.

Roberts, M. R., Srinivas, M., Forrest, D., et al. (2006). Making the gradient: Thyroid hormone regulates cone opsin expression in the developing mouse retina. *Proceedings of the National Academy of Sciences of the United States of America* 103: 6218–6223.

Zhang, J., Gray, J., Wu, L., et al. (2004). Rb regulates proliferation and rod photoreceptor development in the mouse retina. *Nature Genetics* 36: 351–360.

Photoresponse in Squid

J Mitchell and W Swardfager, University of Toronto, Toronto, ON, Canada

Glossary

Arhabdomeral lobe – The proximal segment of the photoreceptor cell containing the nucleus and other organelles.
Arrestin – A protein that binds to metarhodopsin and arrests phototransduction by inhibiting metarhodopsin activation of its target gaunine nucleotide-binding protein.
Calpain-like protease – An enzyme isolated from squid photoreceptors that, like calpain, requires millimolar concentrations of calcium for its proteolytic activity.
Metaretinochrome – The conformation of retinochrome when retinal has been photoisomerized to 11-*cis*-retinal.
Metarhodopsin – The light-activated conformation of opsin when bound to all-*trans* retinal.
Retinochrome – A photosensitive protein that binds all-*trans* retinal.
Rhabdomeral lobe – The distal segment of the photoreceptor cell containing the molecular machinery of phototransduction.
Rhabdomere – The collective surfaces of the distal segment composed of densely packed microvilli.
Rhodopsin kinase – An enzyme that adds phosphates onto serine or threonine residues in the carboxyl-terminus of metarhodopsin.

Introduction

Squid, like most invertebrates, have light-sensing organs. The visual systems of squid are composed of camera-type eyes. Incoming light passes through a single lens and an image is formed on the light-sensing cells of the retina in the anterior chamber of the eye. The retina consists of a single layer of photoreceptive neurons that are segmented in structure. The outer segment, also known as the rhabdomeral lobe, contains the protein machinery of phototransduction. The inner segment, or the arhabdomeral lobe, contains the cellular organelles involved in protein synthesis and the soma contains the cell nucleus. Axons arising from the soma of the photoreceptors comprise the optic nerve that projects to the squid brain (Figure 1).

The photoreceptor outer-segment membrane forms densely packed microvilli that greatly increase the surface area of the membrane available to capture incoming photons of light (see enlargement in Figure 1). Embedded in the membrane are the rhodopsin receptors containing light-sensitive chromophores. Light activation of rhodopsin sets off a cascade of molecular interactions that culminate in depolarization of the photoreceptor membrane (Figure 2). In recent years, many of the molecular components of the light-activated signaling system have been identified and a review of our current knowledge of these components is outlined here. Equally important to vision are the molecular mechanisms that inhibit signal transduction after transmission of the light signal (Figure 3). These mechanisms are not well understood; however, many of the components of the inactivation pathway have been revealed and these will also be discussed.

Molecular Components of Squid Visual Signal Transduction

The squid visual signal transduction system is composed of a light-sensitive receptor, rhodopsin, that transduces its activation signal via a heterotrimeric G protein (G_q) to a phospholipase C (PLC) enzyme. Activated phospholipases hydrolyze membrane phospholipids liberating soluble inositiol 1,4,5-trisphosphate (IP_3) and membrane-bound diacylglycerol (DAG). While it is still not clear how these second messengers stimulate membrane depolarization, it probably involves release of calcium from the submicrovillar tubules as a result of IP_3 stimulation of receptors on these organelles and perhaps direct stimulation of transient receptor potential (TRP)-like channels in the membrane by DAG. Together, these mechanisms raise intracellular calcium and increase membrane depolarization.

Squid Rhodopsin

Squid rhodopsin consists of a guanine nucleotide-binding protein-coupled receptor (GPCR) or opsin bound to a light-absorbing retinoid chromophore. Squid opsin genes have been cloned from *Loligo forbesi, Loligo pealei,* and *Todarodes pacificus*, and they share 45% sequence identity with other invertebrate and vertebrate opsins. However,

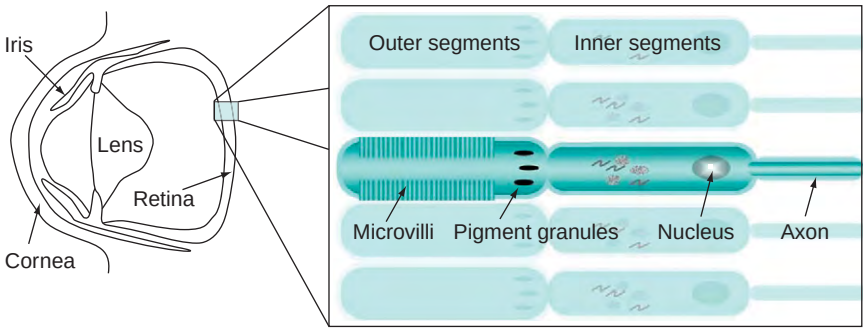

Figure 1 Structure of the squid eye and photoreceptors. Squid have camera-type eyes in which incident light enters the eye and an image is focused through a lens onto the retina in the anterior chamber of the eye. The enlargement on the right shows the orientation of the photoreceptors in the retina. The outer (rhabdomeral) segments contain the microvillar membranes in which rhodopsin and all of the photoreceptor proteins are embedded or associated. The inner (arhabdomeral) segments contain the cell organelles while the photoreceptor cell axons compose the optic nerve that extends to the brain.

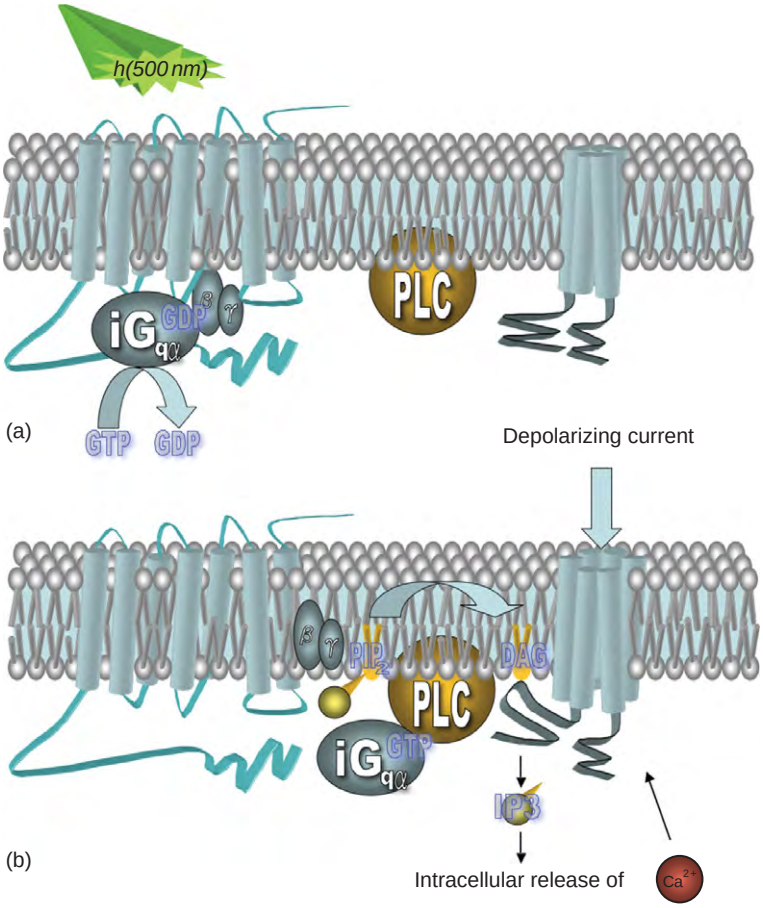

Figure 2 Activation of the squid visual system. (a) In the dark state, rhodopsin is likely coupled to an inactive (GDP-bound) invertebrate G_q (iG_q) protein. On absorption of a photon, 11-*cis*-retinal isomerizes to all-*trans*-retinal changing rhodopsin to metarhodopsin, which stimulates GDP–GTP exchange on the $iG_q\alpha$ subunit. (b) Activated $iG_q\alpha$-GTP changes conformation to interact with PLC stimulating the enzyme to hydrolyze phosphoinositol 4,5-bisphosphate (PIP_2) to inositol 1,4,5-trisphosphate (IP_3) and leaving DAG in the membrane. IP_3 stimulates the release of calcium (Ca^{2+}) from submicrovillar stores and, together with DAG, stimulates opening of an ion channel in the membrane. Membrane depolarization is transmitted to the optic lobe of the squid brain through the photoreceptor cell axons.

squid opsins are about 100 residues larger than those of vertebrates, primarily owing to the addition of a proline-rich carboxyl-terminal tail. Squid rhodopsins bear structural hallmarks of the GPCR superfamily, including amino-terminal sites of N-linked glycosylation, carboxyl-terminal sites of palmitoylation, a disulfide bridge between two extracellular loops, proline residues in the α-helices of the transmembrane domains, and a (D/E)R(Y/W)

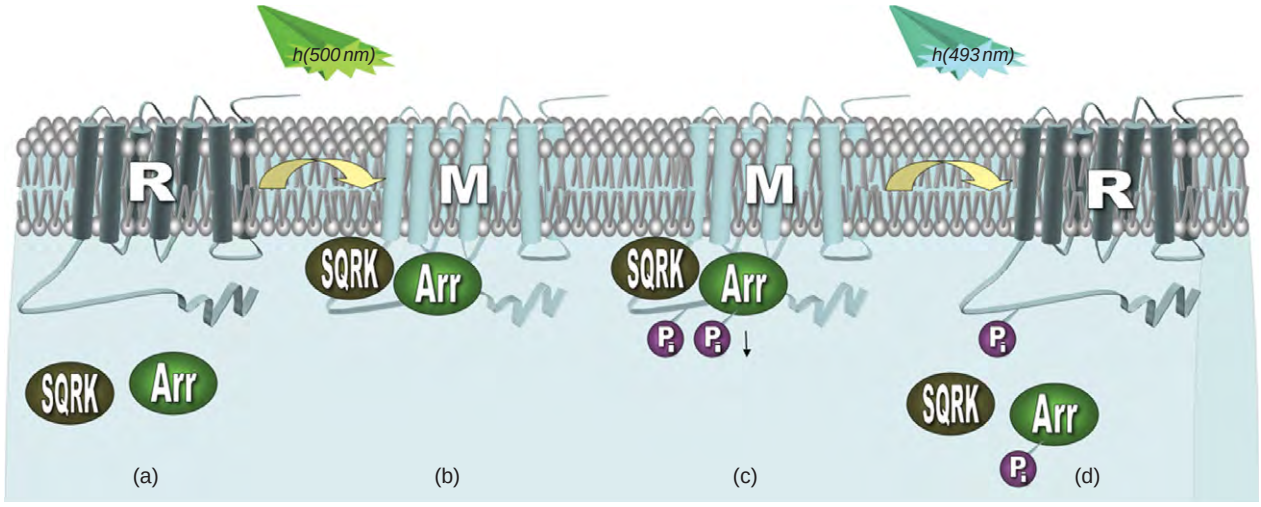

Figure 3 Inactivation of the squid visual system. (a) Rhodopsin (R) stimulation by light (*h* 500 nm) stimulates a conformational change to metarhodopsin (M). (b) SQRK and arrestin (Arr) both bind with high affinity to metarhodopsin. Arrestin binding obstructs further interaction of metarhodopsin with iG_q, uncoupling metarhodopsin from further stimulation of the signal transduction system. (c) SQRK phosphorylates metarhodopsin and following an increase in intracellular Ca^{2+} concentration, SQRK also phosphorylates arrestin. (d) A second light stimulus (*h* 493 nm) isomerizes all-*trans*-retinal back to 11-*cis*-retinal and converts metarhodopsin back to rhodopsin. Phosphorylation of arrestin and rhodopsin by SQRK may facilitate dissociation of the two proteins to return the system back to the dark state, which is primed to receive subsequent stimulation by light.

sequence in the third helix which is involved in G protein interactions.

The presence of a proline-rich carboxyl-terminal tail is unique to cephalopod rhodopsins. This motif consists of 9–10 repeats of the pentapeptide Pro–Pro–Gln–Gly–Tyr that may facilitate receptor trafficking and morphogenesis. Though unique among rhodopsins, tandem repeats of proline-rich sequences are found in other protein families, where they are often associated with protein–protein interactions. Rhodopsin–rhodopsin interactions may be of structural importance in the cephalopod rhabdomere, since rhodopsin networks form in the microvilli of the rhabdomeral lobe. In native membranes, electron microscopy has revealed both poorly ordered rhodopsin clusters of 4–10 molecules and ordered rhodopsin pentameres. Intermolecular interaction is mediated in part by the rhodopsin carboxyl-termini, which aggregate and extend intracellularly from the membrane surface. In contrast, when the carboxyl-terminal is cleaved, crystalline lattice formation is observed both in reconstituted membranes and in crystallized rhodopsin. These more highly ordered crystalline arrays may be favored by interactions between transmembrane domains of adjacent molecules. It has therefore been suggested that the proline-rich region may function, in part, to limit crystalline array formation in native membranes, contributing instead to the formation of less-ordered rhodopsin clusters that confer membrane superstructure. Unfortunately, technical considerations prevent the observation of the squid rhodopsin crystal structure with an intact proline-rich tail, precluding definitive structural analysis.

The majority of opsins are covalently linked to an 11-*cis*-retinal chromophore and squid rhodopsin employs the 4-hydroxy-retinal derivative. In the squid, retinal is attached via a protonated Schiff's base linkage to a lysine residue in transmembrane domain 7 (residue 303 in *Loligo* and 305 in *Todarodes*). In contrast to the mammalian opsins, however, where the Schiff's base is stabilized using a glutamic acid residue of transmembrane domain 3 as a counterion, the crystal structure of *Todarodes* reveals the counterion to be a glutamic acid at residue 180, which is located between transmembrane helices 3 and 4.

On absorption of a photon, 11-*cis*-retinal isomerizes to all-*trans*-retinal in a few hundred femtoseconds, which induces conformational changes in the opsin component. In invertebrates, the product of photoexcitation is an active metarhodopsin that is comparable in stability to inactivated rhodopsin. This contrasts the situation in vertebrates, where rhodopsin undergoes rapid sequential transitions between several unstable intermediate states. In vertebrates, all-*trans*-retinal is released during thermal relaxation of photoexcitation products and rhodopsin must be regenerated through subsequent recombination of opsin with another molecule of 11-*cis*-retinal. In the squid, however, the retinoid chromophore can remain attached to opsin throughout the rhodopsin activation cycle, and in a subsequent deactivating photoconversion event, invertebrate metarhodopsin can be converted to inactive rhodopsin by photon absorption. Thus, photobleaching may not be inevitable in the squid retina. The spectral sensitivities of squid rhodopsin and metarhodopsin differ by only a few nanometers (493 and 500 nm,

respectively) suggesting that the same visual stimulus could be both activating and inactivating. Due to the comparable stabilities and interconverting wavelengths of rhodopsin and metarhodopsin, it has been suggested that substantial populations of each could exist at steady state in the squid eye. However, retinas obtained from freshly caught squid are found to contain almost exclusively rhodopsin, a finding that suggests a highly efficient inactivation pathway.

In addition to rhodopsin, cephalopod photoreceptor cells contain retinochrome, a second photosensitive retinal-binding protein implicated in rhodopsin regeneration. Squid retinochrome from *Todarodes pacificus* has been cloned, revealing a 301-amino-acid protein. The structure of retinochrome resembles that of rhodopsin, but its retinoid occupancy is reversed; whereas rhodopsin binds 11-*cis*-retinal and produces all-*trans*-retinal on photoisomerization to metarhodopsin, retinochrome binds and photoisomerises all-*trans*-retinal to 11-*cis*-retinal in its conversion to metaretinochrome. Metaretinochrome then releases 11-*cis*-retinal, providing it to rhodopsin via a shuttling protein known as retinal-binding protein (RALBP). In the dark, metaretinochrome is localized in the arhabdomeral lobe, where it releases 11-*cis*-retinal and, subsequently, binds all-*trans*-retinal released from metarhodopsin. Soluble RALBP then shuttles 11-*cis*-retinal to the rhabdomeral microvilli, where it binds retinal-free opsin, which may have arisen as a photoproduct or by synthesis *de novo*, in order to generate rhodopsin. Light-dependent translocation of both rhodopsin and retinochrome has been documented. In the dark, rhodopsin and retinochrome colocalize at the base of the microvilli, while in the light rhodopsin redistributes along the entire area of the microvillar membrane, and retinochrome becomes more plentiful in the rhabdomeral lobe. Dynamic control of the availability of rhodopsin (and other light-absorbing pigments and signaling proteins) in signaling compartments may modulate the cascade and rhodopsin regeneration. Thus, the eye can adjust to dim or bright ambient light conditions, accurately perceive objects in each, and regenerate rhodopsin when necessary.

Squid Visual Guanine Nucleotide-Binding Protein, G_q

Squid rhodopsin couples to its effector enzyme, a PLC, via a heterotrimeric G protein belonging to the G_q subfamily. Like all G proteins in this family, squid G_q is composed of three nonidentical subunits, α, β, and γ. These subunits are associated with each other in the inactive state with GDP bound to the α subunit. In this state, the G protein is tightly bound to the rhabdomeric membrane, likely in association with rhodopsin. Upon 11-*cis*-retinal isomerization by light, a conformational change in the receptor causes a conformational change in the G protein subunits, which opens up the gunanine nucleotide-binding site on the α subunit allowing GDP to be exchanged for GTP. In the GTP-bound state, $G_q\alpha$ has a lower affinity for rhodopsin and its $\beta\gamma$ partners, but gains a higher affinity for its effector, PLC. PLC is recruited to the rhabdomeric membrane to interact with activated $G_q\alpha$ and its substrate phosphotidylinositol 4,5-bisphosphate. $G_q\alpha$ binding activates the PLC enzyme and at the same time the PLC stimulates the GTPase activity of $G_q\alpha$ resulting in hydrolysis of the terminal phosphate group on the bound GTP, thus rendering the G protein once again inactive in the GDP-bound state. Reassociation of the G protein subunits completes the cycle of activation and inactivation back to the basal state. The G protein is then ready to receive the next signal from rhodopsin.

G_q protein subunits have been purified and cDNA sequences encoding the proteins have been reported from *L. forbesi* and *L. pealei*. *Loligo* $G_q\alpha$ is similar in amino acid sequence to $G_q\alpha$ proteins of other species with a conserved guanine nucleotide-binding domain and three switch regions that are the major sites of conformational change in the protein when GDP is exchanged for GTP on the protein. The sites of interaction between a G protein α subunit and its receptor are primarily in the two ends of the protein. The carboxyl-terminus of squid $G_q\alpha$ is identical to that found in G_q proteins from other species; however, the amino-terminus of the protein in all invertebrates lacks a six-amino-acid extension found in mammalian $G_q\alpha$. Studies using *L. pealei* $G_q\alpha$ expressed in mammalian cells suggest that the modified amino-terminus found in invertebrate proteins increases the efficacy of G protein activation by receptors.

The amino-terminus is also the site of posttranslational addition of palmitic acid on one or more of the two cysteine residues at position 3 and 4 of the $G_q\alpha$ subunit. This lipid modification helps maintain membrane association of the G_q protein and is particularly important for keeping $G_q\alpha$ attached to the membrane following activation by the receptor when $G_q\alpha$ dissociates from the receptor and $G_q\beta\gamma$ subunits.

The $G_q\beta\gamma$ subunits have not been examined extensively. They appear to have similar functions to other G protein $\beta\gamma$ subunits in that they associate with the $G_q\alpha$ subunit when it is bound to GDP and dissociate when $G_q\alpha$ is bound to GTP. The $\beta\gamma$ subunits are tightly associated with the retinal membranes at all times and lipid modifications of the γ subunit may contribute to this localization. *Loligo* Gβ has a similar sequence to that of all other G protein β subunits, whereas *Loligo* Gγ is quite distinct from Gγ subunits of other species. $G_q\beta\gamma$ subunits do not activate purified PLC from squid eyes. Further studies will be required to determine if squid G protein $\beta\gamma$ subunits have any additional roles in visual signal transduction.

Squid Visual PLC

The protein stimulated by activated G_q in the squid visual system is PLC. The protein has been purified and the amino acid sequence determined from *L. pealei*. Immunoblot analysis of many squid tissues showed that the visual PLC is uniquely expressed in the photoreceptor membranes. Squid visual PLC is a 140 kDa protein that has significant sequence similarity and a domain structure that is common to phospholipase β enzymes; a PH domain that helps the protein bind to membranes, X and Y catalytic domains, and a C2 domain that is likely the site of calcium binding to the enzyme. In the absence of light stimulus to the photoreceptors, intracellular calcium concentrations are low and the PLC has very little catalytic activity. Upon activation of rhodopsin, the catalytic activity of the phospholipase is highly stimulated by the binding of activated $G_q\alpha$ to domains in the carboxyl-terminal end of the protein known as P and G boxes. The enzyme hydrolyzes membrane phospholipids with preference for phosphatidylinositol 4,5-bisphosphate, which is converted into inositol 1,4,5-trisphosphate (IP_3) and DAG. A network of submicrovillar tubules has been observed beneath the microvilli that may express IP_3 receptors and release stored calcium in response to IP_3 activation. A rapid rise in intracellular calcium may help to maintain PLC activity as these enzymes are stimulated in the presence of elevated calcium concentrations.

In addition to the role that calcium plays in visual signal transduction, high (millimolar) calcium concentrations can activate a calpain-like protease found in the squid retina. This protease can cleave several proteins in the visual signaling pathway. Calpain cleaves PLC near the carboxyl-terminus and renders the protein insensitive to $G_q\alpha$ activation. The protease can also cleave rhodopsin near its carboxyl-terminus removing the proline-rich repeat sequence from the rest of the molecule. Calcium activation of this protease may therefore play a role in freeing rhodopsin and G_q to allow for greater membrane turnover following prolonged light exposure.

Light-Activated Ion Channel

The final component in the visual signal transduction system is the channel regulated by PLC hydrolysis of membrane lipids. This component of the squid visual system has been characterized in only one report; an electrophysiological recording made from an isolated *L. pealei* photoreceptor. Light stimulation of the squid photoreceptor evoked an inward current with a peak amplitude greater than 1000 pA and channel activity was most frequently recorded when the patch electrode was placed near the apical tip of the cell where microvilli are present.

A squid photoreceptor channel has been identified and cloned from *L. forbesi* and it was found to be most homologous to that of the visual transient receptor potential (TRP) ion channels identified in *Drosophila*. TRP and an additional TRP-like channel have been shown to constitute the light-activated response in *Drosophila*. Analysis of the amino acid sequence of the squid channel suggests a protein with six or eight membrane spanning segments. The amino-terminus contains an ankyrin-like repeat sequence similar to that found in *Drosophila* TRP channels, and may account for the association of the protein with the cytoskeleton during purification. The carboxyl-terminus of the squid channel is considerably shorter than that found in the *Drosophila* TRP channel and lacks the proline-rich repeat sequence suggested to link TRP to intracellular Ca^{2+} stores. Expression of a peptide composed of the squid channel carboxyl-terminus bound to calcium-calmodulin *in vitro*. These studies suggest that the squid channel may be regulated differently from that of *Drosophila*, however, since the squid channel has not yet been characterized, its properties and the mechanisms by which it is regulated by the PLC signaling cascade remain speculative.

Desensitization of Visual Signal Transduction

Once rhodopsin has been activated, a series of protein–protein interactions occur within the photoreceptor cell to terminate signal transduction and restore the photoreceptor to its inactive state. Like most GPCRs, activated squid rhodopsin is phosphorylated by a G-protein-coupled receptor kinase (GRK) also called rhodopsin kinase. Light-activated rhodopsin also binds arrestin and biochemical studies using purified arrestin have demonstrated that this uncouples rhodopsin from activation of G_q.

Squid Rhodopsin Kinase

The squid visual system expresses a kinase that has sequence and functional similarity with other GRKs. The most extensively studied GRKs are the mammalian rhodopsin kinases (GRK1 and GRK7) and β-adrenergic receptor kinases (GRK2 and GRK3). Interestingly, molecular cloning of squid rhodopsin kinase (SQRK) revealed much higher sequence similarity to the mammalian β-adrenergic receptor kinase GRK2 (66%) than to GRK1 (33%), which terminates signaling in the mammalian visual system. This is a common theme among invertebrate rhodopsin kinases, as eye-specific GRK1 cloned from *Drosophila* and octopus rhodopsin kinase (ORK) also bear higher sequence identity to GRK2 than to GRK1. The structural similarities between SQRK and GRK2 include a central

serine/threonine kinase catalytic domain, a structurally conserved amino-terminal domain bearing an RGS domain, a conserved carboxyl-terminal sequence and a PH domain in the carboxyl-terminal. In GRK2, it has been established that a carboxyl-terminal region partially overlapping the PH domain associates with the G protein βγ subunits hence facilitating membrane localization in a stimulus-dependent manner. These structural similarities suggest that the phosphorylation of squid rhodopsin may more closely resemble the phosphorylation event of the mammalian β-adrenergic receptor than that of mammalian rhodopsin. SQRK structural motifs bearing high homology to the GRK2 Ca^{2+}/CaM-binding domain and the GRK2 clathrin box motif suggest that Ca^{2+} may have a role in regulating SQRK activity and that SQRK may also bind to the clathrin heavy chain and play a role in endocytosis. To date, functional characterization of SQRK has confirmed that purified SQRK is able to phosphorylate squid rhodopsin in rhabdomeric membranes in a light-dependent manner. SQRK phosphorylation of rhodopsin requires GTP and Mg^{2+} ion cofactors that may relate to the need to activate the G_q protein to allow SQRK access to rhodopsin.

Squid Visual Arrestin

Squid visual arrestin (sArr) has been cloned, purified, and characterized with respect to its functional interactions with rhabdomeric membranes. Squid arrestin from *L. pealei* is a 400-amino-acid protein with an estimated mass of 55 kDa that is expressed exclusively in eye tissue. Sequence identity between sArr and those from *Drosophila* and *Limulus* are 42% and 37%, respectively (sequence similarity including conservative substitutions is considerably higher, at 61% and 60%, respectively). Of the mammalian arrestins, visual arrestin from *L. pealei* shares highest identity with β-arrestins (44% identity and 64% similarity to β-arrestin1; 42% identity and 63% similarity to β-arrestin2). Squid visual arrestin is only 32% identical to mammalian visual arrestin, conservatively substituted to 49% similarity. This pattern of similarity parallels that between invertebrate rhodopsin kinase and mammalian β-adrenergic receptor kinases, and suggests that the functional interactions with invertebrate rhodopsin resemble those of the mammalian β-adrenergic receptor more closely than those of mammalian rhodopsin.

For many GPCRs, including mammalian rhodopsin, it has been demonstrated that receptor phosphorylation enhances high-affinity binding of arrestin. Accordingly, the primary structure of squid arrestin contains both conserved residues associated with both high- and low-affinity phosphate interactions. However, purified sArr does not seem to require rhodopsin phosphorylation to bind light-activated rhodopsin. This parallels biochemical studies in *Drosophila*, where purified Arr2 can bind to phosphorylated and unphosphorylated light-activated rhodopsin with comparable affinity. Further, light-dependent binding of Arr2 was equivocal in wild type and mutants where rhodopsin cannot be phosphorylated (both a truncation mutation lacking the phosphorylation site, and a serine to alanine point mutation that retains a similar structure but which cannot be phosphorylated). These findings are consistent with observations that the phosphorylation-deficient rhodopsin mutants display similar deactivation kinetics. Thus for invertebrates, the role of rhodopsin phosphorylation in arrestin binding is unclear, and light activation of rhodopsin may be sufficient.

Squid visual arrestin associates with the rhabdomeric membrane in a light-dependent manner and inhibits light-activated GTPase activity. This is consistent with the notion that recruitment and stoichiometric binding to the intracellular surface can uncouple G_q from the receptor and terminate signaling by a competitive mechanism. In the dark, squid arrestin also has appreciable affinity for the rhabdomeric membrane, an interaction which can be abrogated by inositol 1,2,3,4,5,6-hexakisphosphate (IP_6), a soluble analog of the membrane lipid phosphatidylinositol 3,4,5-triphosphate. This suggests that arrestin can also bind to membrane phospholipids, an interaction that studies in *Drosophila* suggest may mediate arrestin trafficking along an elaborate system of cytoplasmic structural components.

The primary structure of sArr includes five fingerprint motifs that correspond with domains of distinct functional importance conserved among the arrestin family; a region that recognizes receptor activation, a domain rich in hydrophobic interactions, a domain that recognizes receptor phosphorylation, a carboxyl-terminal regulatory domain, and a conserved amino-terminal domain. Overall, the arrestin molecule adopts a concave saddle-like conformation consisting of amino- and carboxyl-terminal domains rich in antiparallel β-sheets that hinge on a central polar core region of buried salt bridges that are disrupted when the molecule encounters the activated receptor. The primary sequence of sArr contains ^{26}Asp, ^{169}Arg, ^{293}Asn, ^{300}Asp, and ^{381}Arg, which are identical to bovine visual arrestin (except ^{293}Asn, which is a conservative substitution). These five essential conserved residues are contained within consensus sequences of five to eight identical or conservatively substituted amino acids that form the salt bridges buried in the polar core. Both the amino- and carboxyl-terminal domains mediate high-affinity binding to rhodopsin intracellular loops and these regions are located exclusively on the concave side of arrestin. Arrestin binding to rhodopsin thus occludes the binding of the G protein, preventing catalysis of GTP exchange, and uncoupling the receptor from its effector.

Interestingly, sArr can be phosphorylated by SQRK, a novel function among the GRK family. This contrasts the phosphorylation of *Drosophila* and *Limulus* visual arrestins, which are phosphorylated by Ca^{2+}/calmodulin-dependent kinase II. Phosphorylation of purified sArr requires SQRK, membranes, light-activated rhodopsin, and the presence of Ca^{2+}. Though the kinase is different, Ca^{2+} dependence is common to *Limulus* and *Drosophila*. Studies in *Drosophila* show that the kinetics of invertebrate visual arrestin phosphorylation are fast (seconds after illumination, 43% of *Drosophila* Arr2 is phosphorylated) and that arrestin phosphorylation can facilitate its release from rhodopsin once arrestin-bound metarhodopsin is photoconverted back to its inactive state. A similar role for squid arrestin phosphorylation has been found, as phosphorylated arrestin dissociates from dark-adapted membranes more readily than unphosphorylated arrestin.

Conclusion

Many of the molecular components of the squid visual system have been identified and characterized. Studies have suggested many similarities between the squid and other invertebrate visual systems. The strength of the squid system has been in the abundance of retinal tissue that makes protein purification and characterization feasible. These biochemical studies have complemented the power of genetic manipulations in the *Drosophila* system and the ease of electrophysiology in *Limulus*. Further studies are still required to determine the roles of rhodopsin and arrestin phosphorylations as well as identification of the many proteins involved in resetting the signaling components in the dark. We still know very little about how the activation of PLC results in membrane depolarization and the characteristics of the ion channels in the microvillar membranes. Future studies may eventually reveal all the molecular machinery of this fascinating visual system.

See also: Circadian Photoreception; Genetic Dissection of Invertebrate Phototransduction; Microvillar and Ciliary Photoreceptors in Molluskan Eyes; Phototransduction in *Limulus* Photoreceptors; Phototransduction: Inactivation in Cones; Phototransduction: Inactivation in Rods; Phototransduction: Phototransduction in Cones; Phototransduction: Phototransduction in Rods; Phototransduction: Rhodopsin; The Evolution of Opsins; The Photoreceptor Outer Segment as a Sensory Cilium.

Further Reading

Go, L. and Mitchell, J. (2007). Receptor coupling properties of the invertebrate visual guanine nucleotide-binding protein iGqα. *Cellular Signalling* 19: 1919–1927.

Mayeenuddin, L. H., Bamsey, C., and Mitchell, J. (2001). Retinal phospholipase C from squid is a regulator of Gq alpha GTPase activity. *Journal of Neurochemistry* 78: 1350–1358.

Mayeenuddin, L. H. and Mitchell, J. (2001). cDNA cloning and characterization of a novel squid rhodopsin kinase encoding multiple modular domains. *Visual Neuroscience* 18: 907–915.

Monk, P. D., Carne, A., Liu, S.-H., et al. (1996). Isolation, cloning and characterization of a trp homologue from squid (*Loligo forbesi*) photoreceptor membranes. *Journal of Neurochemistry* 67: 2227–2235.

Murakami, M. and Kouyama, T. (2008). Crustal structure of squid rhodopsin. *Nature* 453: 363–367.

Nasi, E. and Gomez, M. (1992). Electrophysiological recordings in solitary photoreceptors from the retina of squid, *Loligo pealei*. *Visual Neuroscience* 8: 349–358.

Ryba, N. J., Findlay, J. B., and Reid, J. D. (1993). The molecular cloning of the squid (*Loligo forbesi*) visual Gq-alpha subunit and its expression in *Saccharomyces cerevisiae*. *Biochemical Journal* 292: 333–341.

Swardfager, W. and Mitchell, J. (2007). Purification of visual arrestin from squid photoreceptors and characterization of arrestin interaction with rhodopsin and rhodopsin kinase. *Journal of Neurochemistry* 101: 223–231.

Venien-Bryan, C., Davies, A., Langmack, K., et al. (1995). Effect of C-terminal proline repeats in ordered packing of squid rhodopsin and its mobility in membranes. *FEBS Letters* 359: 45–49.

Walrond, J. P. and Szuts, E. Z. (1992). Submicrovillar tubules in distal segments of squid photoreceptors detected by rapid freezing. *Journal of Neuroscience* 12: 1490–1501.

Phototransduction in *Limulus* Photoreceptors

R Payne and Y Wang, University of Maryland, College Park, MD, USA

Glossary

Confocal fluorescence microscopy – An optical microscopy method that uses a focused laser spot to measure fluorescence within an extremely small volume.
Cytosol – The liquid portion of a cell's contents, or cytoplasm.
Depolarization – A positive-going change in the membrane potential of a cell.
Diacylglycerol (DAG) – A glyceride consisting of two fatty acid chains covalently bound to a glycerol molecule through ester linkages.
d-*myo*-Inositol (1,4,5) trisphosphate (IP_3) – An inositol derivative having three phosphate groups covalently bound to the inositol ring.
Guanine-nucleotide-binding protein (G protein) – A family of signaling proteins that are activated by the exchange of guanine triphosphate for guanine diphosphate bound to the protein.
On-cell patch clamp – An electrophysiological recording technique that uses a polished glass micropipette to measure currents flowing through a small patch of cellular plasma membrane containing ion channels.
Phosphoinositide – A phospholipid containing a polar inositol headgroup.
Smooth endoplasmic reticulum (SER) – A network of membrane sacs found in animal cells that, among other things, functions as a store of calcium ions.
Transient receptor potential (TRP) channels – A widespread family of ion channels. The light-activated channels of *Drosophila* are founding members of the family.

Arrangement of Eyes in *Limulus*

American horseshoe crabs (*Limulus polyphemus*) have 10 eyes. They have two large lateral compound eyes, each containing about 1000 clusters of photoreceptors or ommatidia. A small lens within each ommatidium focuses light from a small patch of visual space onto each photoreceptor cluster, which transmits information about local changes in light intensity to the brain through a nerve fiber. There are five additional eyes on the top side of its first (anterior) major body section, two median eyes, one endoparietal eye, and two rudimentary lateral eyes. Two ventral eyes are located on the underside of the animal above the mouth (Figure 1). Photoreceptors located on the telson (tail) constitute the 10th eye. Of these eyes, the lateral compound, median ocellar and ventral eyes have been extensively studied. All have microvillar photoreceptors, in which the visual pigment, rhodopsin, is embedded in the membrane of finger-like projections of the plasma membrane called microvilli (Figure 2). Each eye has allowed for a study of different aspects of invertebrate vision. The large compound eyes have been favorite preparations for the study of image processing by compound eyes, the biochemistry of visual transduction, and the circadian control of visual sensitivity. The medial eye has been studied for its sensitivity to ultraviolet (UV) light which has allowed the elucidation of the physiological consequences of the reversible photoisomerization of invertebrate rhodopsin. Lastly, the ventral eyes have played a role in the understanding of phototransduction in invertebrate photoreceptors.

The Microvillus is the Cellular Structure Mediating Visual Transduction

Central to the performance of each photoreceptor cell is the rhabdomere – an array of photoreceptive microvilli positioned so as to maximally absorb light entering the eye. Each microvillus is a cylindrical outgrowth of the plasma membrane, 50–80 nm in diameter and 0.5–2 μm in length (Figure 2). Electron micrographs often show an axial filament within each microvillus. The axial filament contains a bundle of actin filaments with their + ends directed toward the tip of the microvillus. The actin filaments appear to extend through the bottom of the microvillus into the cytoplasm, through fenestrations in submicrovillar cisternae (SMC) of smooth endoplasmic reticulum (SER). The actin cytoskeleton is responsible for the presence of an unconventional motor protein, myosin III, in the microvilli of *Limulus* lateral eye photoreceptors. The membrane of a typical microvillus contains 1000 or more particles, which are presumed to be mostly molecules of the visual pigment, rhodopsin, which absorbs light and initiates the physiological response of the photoreceptor. A photoreceptor might possess 10^5 microvilli, resulting in a total rhodopsin content of $\sim 10^8$ molecules, comparable to that of vertebrate retinal photoreceptors.

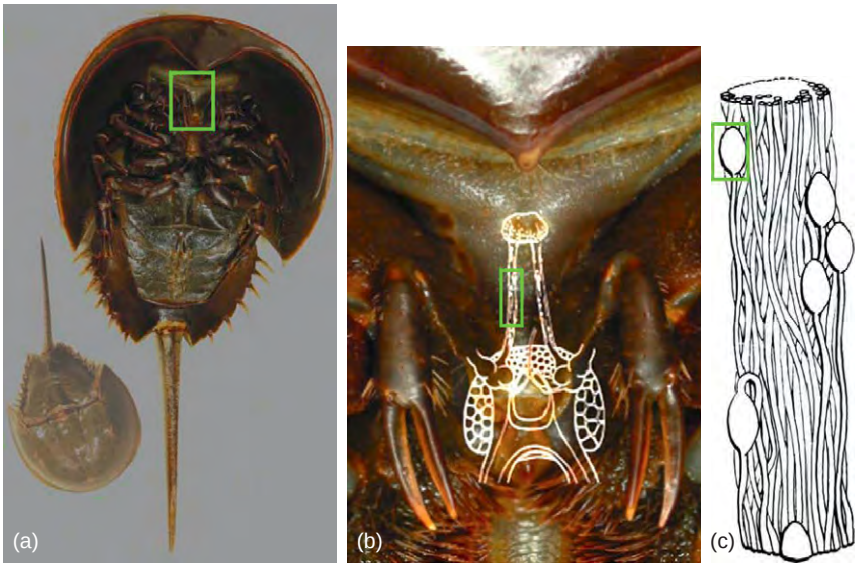

Figure 1 (a) Underside and top side (inset) of the Atlantic horseshoe crab (*Limulus polyphemus*). The green box shows the area enlarged in (b). (b) Enlarged view of the underside, just above the mouthparts. The drawn overlay shows the arrangement of the ventral nerves (green box, enlarged in (c)) and ventral eyes under the skin. The ventral nerves lead from the brain (just above the mouthparts at the bottom of the figure) to the ventral eyes above. (c) Diagram of ventral nerve axons and attached photoreceptor cell bodies (green box). Drawings in (b) and (c) are adapted from Calman, B. G. and Chamberlain, S. C. (1982). *Journal of General Physiology* 80: 839–862.

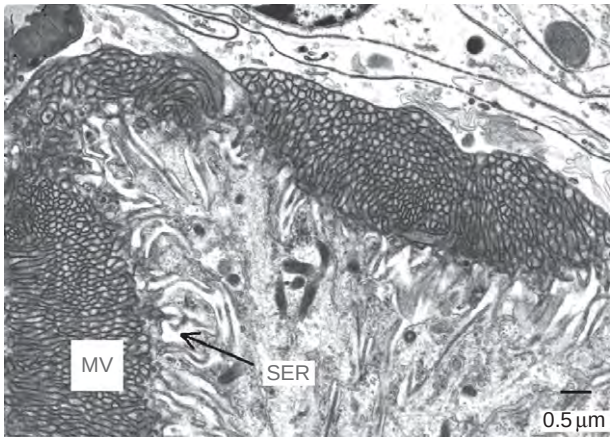

Figure 2 Electron micrograph of a section through the R-lobe of a ventral photoreceptor, showing the microvilli (MV) and submicrovillar cisternae of smooth endoplasmic reticulum (SER; arrow). Adapted from Dabdoub, A., Payne, R., and Jinks, R. N. (2002). *Journal of Comparative Neurology* 442: 217–225. Copyright 2009 Wiley-Liss, Inc.

Studies of Visual Transduction Using *Limulus* Ventral Photoreceptors

The *Limulus* ventral photoreceptor (**Figure 3**) is a highly polarized cell divided into two lobes, analogous to the inner and outer segments of vertebrate retinal photoreceptors. The rhabdomeral (R) lobe bears microvilli on its plasma membrane and is therefore light sensitive. The light-insensitive arhabdomeral (A) lobe contains the cell's nucleus. An axon projects from the A lobe toward the animal's central nervous system. Ventral photoreceptors were originally chosen as a model for invertebrate phototransduction because of their large size (>200 µm). This facilitates insertion of multiple electrodes and makes it possible to clamp the membrane potential of the cells, measure electrical current flow across the plasma membrane, and inject compounds of interest into the cytoplasm (**Figure 4**).

The essential electrical response to illumination is the activation of a very large flow of current into the cell, carried mostly by sodium ions (**Figure 4**). The result is a depolarization (positive-going change) of the cell membrane which is graded with light intensity, of up to 60 mV. The reversal potential of the light-sensitive current is between +10 mV and +20 mV and its dependence on extracellular ion concentrations indicates that this conductance is sodium- and potassium-, but not Ca^{2+}-permeable. This is in contrast to the light-activated transient receptor potential (TRP) channel conductance in the photoreceptors of the fruit fly, *Drosophila*, which is highly Ca^{2+} permeable.

The study of ventral photoreceptors has revealed that they have remarkable performance characteristics, most notably the very large amplification of the transduction process. Amplification refers to the amount of charge that is carried across the plasma membrane as a result of excitation by a single photon. In ventral photoreceptors, this gain can be directly measured because the single-photon response, termed a quantum bump, is easily recorded using glass micropipettes. In response to very dim illumination,

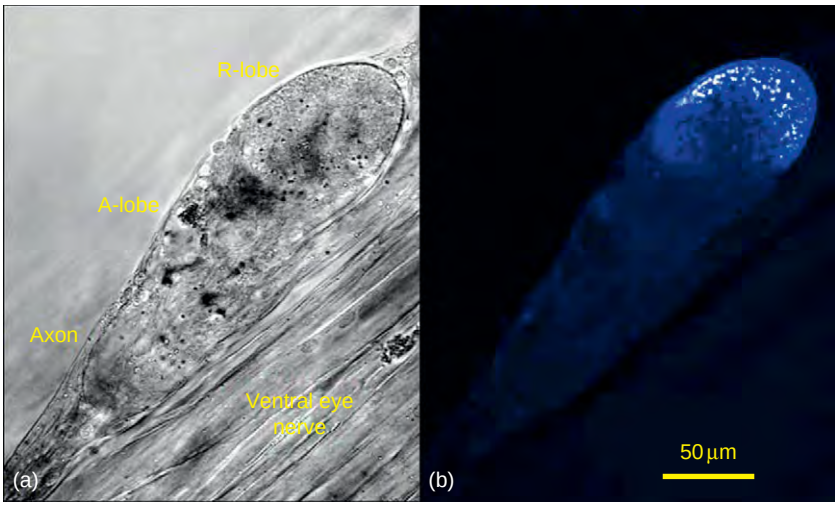

Figure 3 (a) Light micrograph of a ventral photoreceptor. R-lobe, rhabdomeral lobe; A-lobe, arhabdomeral lobe. (b) Immunolocalization (blue) of rhodopsin within the same photoreceptor cell. The ventral photoreceptor has two lobes, a light-sensitive rhabdomeral lobe (R-lobe), which bears rhodopsin-containing microvilli on its plasma membrane and is analogous to the outer segments of vertebrate photoreceptors, and a light-insensitive arhabdomeral lobe (A-lobe), which is analogous to the inner segment of vertebrate photoreceptors. From Battelle, B. A. et al. (2001). *Journal of Comparative Neurology* 435: 211–225. Copyright 2009 Wiley-Liss, Inc.

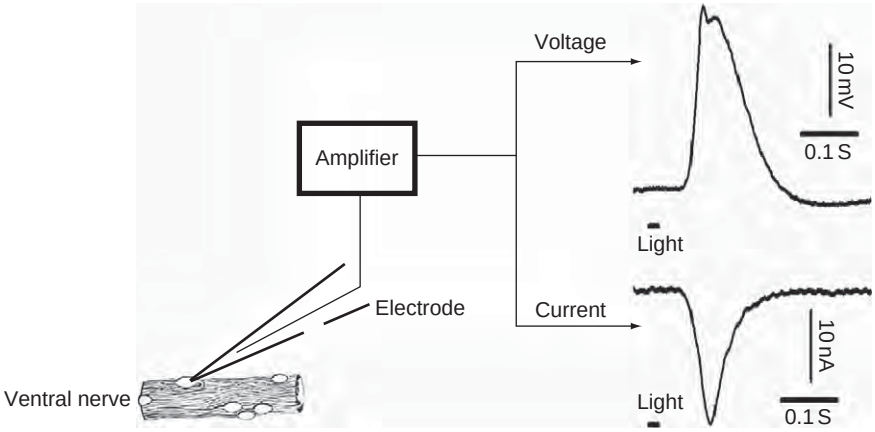

Figure 4 Experimental arrangement for recording electrical activity (membrane potential and voltage clamp currents, right) from ventral photoreceptors impaled with a glass micropipette, left.

quantum bumps over 10 mV in amplitude occur randomly as individual photons are effectively absorbed by rhodopsin molecules. Under voltage clamp, the peak current across the membrane generated by an effectively absorbed photon can exceed 1 nA and appears to be generated over several square microns of membrane surface, containing hundreds of microvilli. The comparatively large currents flowing indicate that quantum bumps are caused by the passage across the plasma membrane of hundreds of millions of cations through ion channels. By contrast, in the smaller *Drosophila* photoreceptors or amphibian rods, a single-photon event involves a maximum current of less than 10 pA. *Limulus* photoreceptors achieve this large amplification in only 100–200 ms, faster than amphibian rods. A further remarkable feature of *Limulus* photoreceptors is their broad dynamic range. Whereas most vertebrate rods work over about a 4-log-unit range of light intensity before saturating, *Limulus* photoreceptors work over 8. They achieve this range through a strong adaptation process that reduces amplification at high light intensity. The large dynamic range of these cells obviates the need for the dual system of photoreceptors (rods and cones) used to achieve a large dynamic range in the vertebrate eye.

The Light-Sensitive Conductance Consists of the Summed Effect of Conventional Ion Channels

The glial cells that surround individual ventral photoreceptors can be removed, exposing the plasma membrane surface. This preparation allows On-cell patch-clamp

recording of single ion channels in the microvillar membrane. As expected, channels whose opening was triggered by light were recorded by this method, with single-channel conductance ranging from 18 to 50 pS. Identification of these channels as the light-activated conductance requires establishing a close correspondence between the properties of individual channel currents and those of photocurrents recorded from the whole cell. Depolarizing potentials applied in the dark did not open the channels; therefore the light-activated opening was not just a secondary consequence of the depolarizing receptor potential. Light-evoked single-channel activity was graded with light intensity, reduced by light adaptation, and the single-channel currents reversed in the same membrane potential range as the macroscopic photocurrent. While these characteristics are consistent with the recorded channels being those that carry the light-activated current, definitive molecular or pharmacological proof is still needed.

The Response of the Ventral Photoreceptor is Mediated by the Phosphoinositide Cascade

A large body of evidence now demonstrates that the phosphoinositide (PI) pathway links the absorption of light to the activation of ion channels in the plasma membrane of invertebrate microvillar photoreceptors (Figure 5). The PI pathway is a mechanism for releasing intracellular messengers upon the activation of a receptor protein, using inositol phospholipids as a substrate. In microvillar photoreceptor cells, the receptor protein is rhodopsin and the cascade is localized to the membrane of the microvilli that cover the plasma membrane of the light-sensitive R-lobe. Activated rhodopsin catalyzes the exchange of guanine triphosphate (GTP) for guanine diphosphate (GDP) bound to the alpha subunit of a heterotrimeric GTP-binding protein of the G_q subfamily ($G_{q\alpha}$), which in turn activates phospholipase C (PLC). PLC cleaves phosphatidylinositol 4,5 bisphosphate (PIP_2), a minor membrane phospholipid, into a lipid messenger, diacylglycerol (DAG), and the water-soluble messenger, d-*myo*-inositol 1,4,5 trisphosphate (IP_3). In support of this biochemical pathway, light-activated PIP_2 hydrolysis and/or IP_3 production has been reported in ventral photoreceptors of *Limulus*. $G_{q\alpha}$ has been amplified and sequenced from *Limulus* ventral eye tissue and immunolocalized to the rhabdomeral microvilli. Pharmacological agents that inhibit PLC, neomycin and U-73122, dramatically desensitize the light response of *Limulus* photoreceptors.

The PI Cascade Generates at Least Two Intracellular Messenger Molecules

The PI cascade generates two messenger molecules with very different properties (Figure 5) DAG is essentially confined to the plasma membrane, while IP_3 can diffuse into the surrounding cytoplasm. In addition, the decline of the precursor, PIP_2 may act as an additional signal within

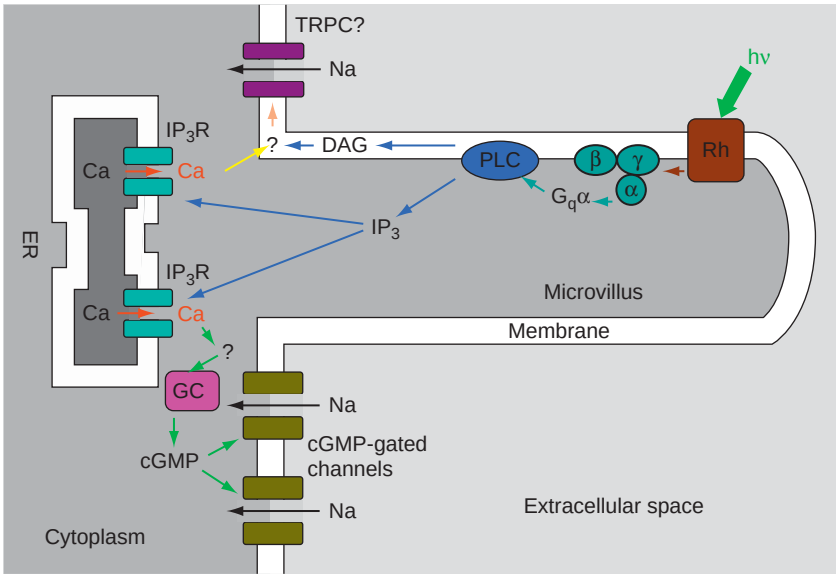

Figure 5 Diagram of mechanisms proposed to mediate phototransduction within a microvillus of the *Limulus* photoreceptor. cGMP, cyclic guanosine monophosphate; DAG, diacylglycerol; ER, endoplasmic reticulum; $G_q\alpha$, alpha subunit of a heterotrimeric GTP-binding protein of the G_q subfamily; β,γ, beta and gamma subunits of a heterotrimeric GTP binding protein of the G_q sub-family; GC, guanylate cyclase; IP_3, d-*myo*-inositol (1,4,5) trisphosphate; IP_3R, d-*myo*-inositol (1,4,5) trisphosphate receptor; PLC, phospholipase C; Rh, rhodopsin; TRPC, transient receptor channel C.

the membrane. The difficult task of assessing the relative roles of these messengers in activating the light-sensitive ion channels has dominated research on the invertebrate phototransduction cascade.

Roles of IP_3 and Intracellular Ca^{2+} Ions in Excitation of *Limulus* Ventral Photoreceptors

There is no evidence that IP_3 can itself activate the light-sensitive channels of ventral photoreceptors. The best-characterized alternative target of IP_3 is a Ca^{2+} channel, the IP_3 receptor protein (IP_3R), located in the membrane of endoplasmic reticulum (ER). IP_3 therefore releases Ca^{2+} from intracellular stores within the ER. In *Limulus* photoreceptors, suitable calcium stores are located close to the base of the rhodopsin-containing microvilli – the subrhabdomeral cisternae (SMC) of SER. Extensions of the SMC are juxtaposed less than 100 nm from the bases of the microvilli. The cytoplasm of both the R lobe containing the SER and, to a lesser extent, the A lobe are immunoreactive when probed with an anti-IP_3R antibody.

In darkness, ventral photoreceptors, like most cells, maintain a low free cytosolic Ca^{2+} concentration ($[Ca^{2+}]_i$) of 200–600 nM. Release of calcium from the SMC results in a very large elevation of $[Ca^{2+}]_i$ during the first few hundred milliseconds of the light response. Confocal fluorescent light microscopy has enabled the measurement of the light-induced elevation of $[Ca^{2+}]_i$ in ventral photoreceptors at spots within 4 μm of the microvillar membrane in the R lobe (**Figures 6** and **7**).

Following a very bright flash, $[Ca^{2+}]_i$ begins to rise after a latent period of approximately 20 ms. Thereafter, $[Ca^{2+}]_i$ rises at an initial rate of 1–2 mM s^{-1} to reach a peak of 100–200 μM within 200 ms. For less-intense flashes, the peak elevation of $[Ca^{2+}]_i$ is graded with flash intensity, increasing from 2 μM to more than 140 μM as light intensity increases from 10 effective photons to 10 000 effective photons. For the dimmest flashes so far investigated, these concentrations represent ~600 free Ca^{2+} ions per effective photon generated within the confocal measurement volume.

Very high levels of $[Ca^{2+}]_i$ are reached only transiently upon illumination. Following a dim or moderate-intensity light flash, $[Ca^{2+}]_i$ falls close to its resting value within 1 s, although a small lingering elevation may persist for up to a minute afterward. Even during sustained intense illumination, $[Ca^{2+}]_i$ falls within 5 s to a sustained plateau elevation of less than 20 μM. As expected, if calcium release from stores occurs, the light-induced rise in $[Ca^{2+}]_i$ is unaltered by removal and chelation of extracellular Ca^{2+}, but is severely reduced by pharmacological agents expected to deplete Ca^{2+} stores.

IP_3 Can Release Ca^{2+} from the SER

Microinjections of IP_3, or photolysis of caged IP_3, rapidly release Ca^{2+} from the R lobe in darkness (**Figure 8**). Photolysis of caged IP_3 by UV light delivered to a spot beneath the microvillar membrane results in local elevations of Ca^{2+} that are comparable in magnitude and rate

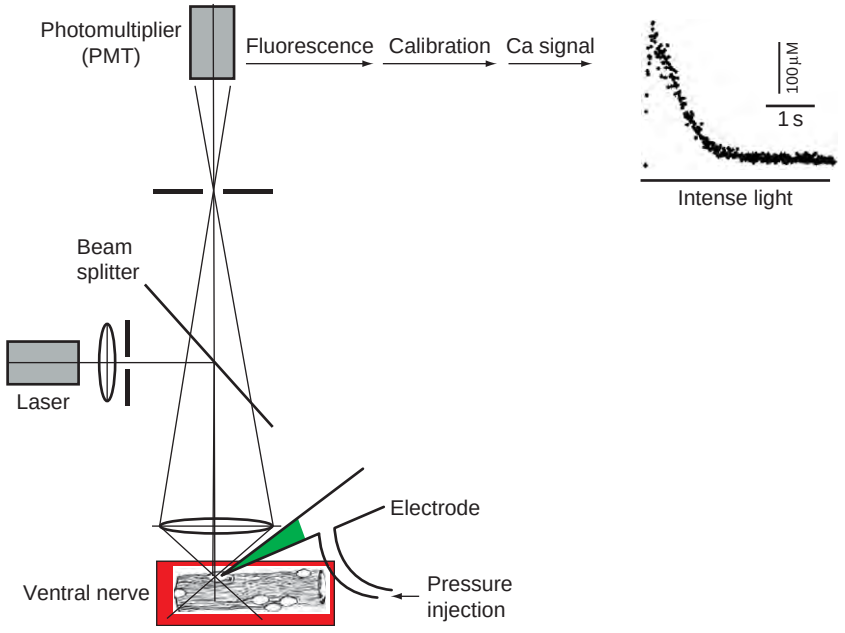

Figure 6 Diagram of confocal microscopy method (left) and recordings of light-activated Ca2+ signals (right) from a Ca^{2+}-sensitive fluorescent indicator dye (indicated in green) injected into the photoreceptor and recorded close to the microvillar membrane of the R-lobe.

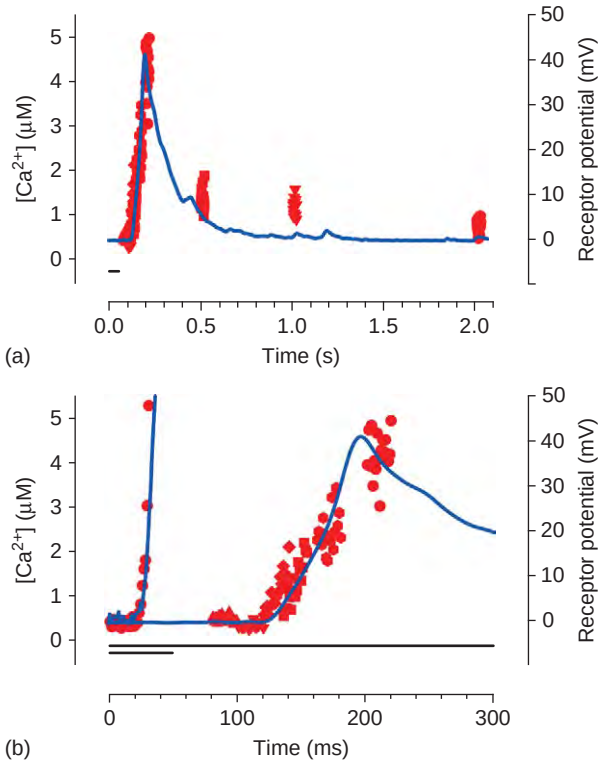

Figure 7 (a) Receptor potential (solid line) and reconstructed elevation of $[Ca^{2+}]_i$ (red symbols) recorded following a flash from an attenuated laser beam that delivered ~50 effective photons to a photoreceptor. The bar beneath the trace indicates the timing of the flash. (b) The responses to the dim flash used in (b) are shown on an expanded timescale on the right. On the left is shown the rising edge of the responses to a much brighter step of light produced by the unattenuated laser beam, delivering $\sim 10^8$ effective photons per second. The bars below the traces indicate the onset and duration of the stimuli. Adapted from Payne, R. and Demas, J. (2000). *Journal of General Physiology* 115: 735–748.

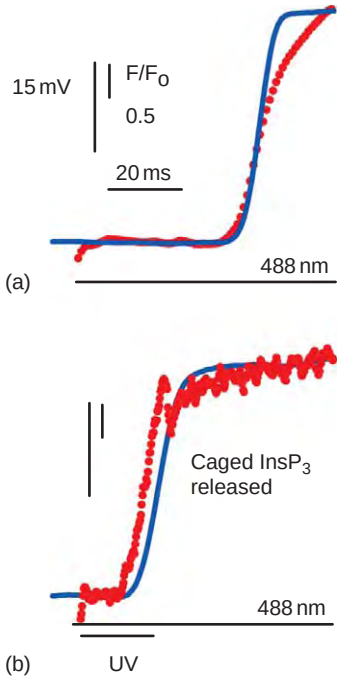

Figure 8 Timing of Ca^{2+} release by caged InsP3. Photoreceptors were loaded with caged IP_3 and the Ca^{2+} indicator dye fluo-3; 488 nm and UV laser beams were focused onto the edge of the R-lobe. As an indicator of $[Ca^{2+}]_i$, uncalibrated dye fluorescence is shown, expressed as a fraction of the background fluorescence during the latent period of the response (F/F_0). (a) Membrane potential (solid line) and fluo-3 fluorescence (red dots) recorded during illumination by the 488-nm laser alone, stimulating $Ca2^+$ release and depolarization through the photoisomerization of rhodopsin, that is, through the natural phototransduction pathway. Laser stimulation began at the beginning of the fluorescence trace. (b) Effect of superimposing a 20-ms duration UV flash and so releasing caged InsP3 into the cytoplasm of the cell, stimulating an earlier release of Ca^{2+} directly from the SER. Adapted from Ukhanov, K. and Payne, R. (1997). *Journal of Neuroscience* 17: 1701–1709.

of rise to those elicited by bright visible light. However, the latency of the Ca^{2+} signal that follows illumination by visible light is ~30 ms longer than that of the response to the release of caged IP_3 (compare **Figures 8(a) with 8(b)**), the difference being presumably the time required for light to activate the PI pathway. There is therefore convincing evidence that the light-induced release of Ca^{2+} from internal stores is mediated by the PI pathway acting on IP_3Rs in SER that are closely juxtaposed to the microvillar membrane.

Released Ca^{2+} Ions can Activate an Inward Current

Pulsed pressure injections of solutions containing 1–2 mM Ca^{2+} into the R lobe of ventral photoreceptors activates a current in the plasma membrane of up to 20 nA, with a similar reversal potential, sodium dependence, and outward rectification to that activated by light. Release of Ca^{2+} ions through IP_3 activates the same conductance, indicating that the $[Ca^{2+}]_i$ generated through the endogenous Ca^{2+} release pathway is sufficient. The current, typically 5–20 nA in amplitude following a pulse of 100 μM IP_3, generates a transient depolarization of the photoreceptor lasting for less than 1 s. The coupling between the elevation of $[Ca^{2+}]_i$ and the depolarization of the photoreceptor is rapid. Depolarization follows caged IP_3-induced Ca^{2+} release after 2.5 ± 3.3 ms (**Figure 8**), while photolysis of caged Ca^{2+} (*O*-nitrophenyl ethylene glycol tetraacetic acid (EGTA)) at the edge of the R lobe activates current within 1.8 ± 0.7 ms.

Light-Induced Ca^{2+} Release can be Detected before the Electrical Response

The above experiments indicate that micromolar $[Ca^{2+}]_i$, released from internal stores by IP_3, can activate an

inward current through the plasma membrane within a few milliseconds. It follows that if light-induced Ca^{2+} release is to act similarly, then a component of the photocurrent must be initiated a few milliseconds after $Ca2^{+}$ is released. Certainly, the onset of the two signals is highly correlated if measured confocally beneath the microvillar membrane. The time for $[Ca^{2+}]_i$ to exceed 2 μM is approximately equal to that for the receptor potential to exceed 8 mV (mean difference: 2.2 ± 6.4 ms). However, the question of which event occurs first is difficult to address, since two signals with different noise levels are compared (**Figure 7**). The detection of the Ca^{2+} signal lead the electrical response by up to 5 ms within about one-third of cells examined. The lag in other cells could indicate the presence of an early Ca^{2+}-independent component of the response present in some cells, but it is difficult to be sure of this because the placement of the confocal measuring spot relative to the microvillar membrane is critical. However, in any case, given the rapidity with which Ca^{2+} can elicit an inward current (1–3 ms; see above) and the fact that it takes the photocurrent 50 ms to rise to peak, this timing appears to be sufficient for released Ca^{2+} ions to contribute to the activation of the photocurrent during the rising edge of the response to light.

How Does IP_3-Induced Ca^{2+} Release Activate Inward Current and is this Current Flowing through the Light-Sensitive Conductance?

Given the detailed evidence above, it seems reasonable to propose that IP_3-induced Ca^{2+} release can activate the light-activated conductance in ventral photoreceptors (**Figure 5**). However, the molecular nature of the channel and the site of calcium's action are not yet known. An ideal preparation for electrophysiology, ventral photoreceptors do not have the advantage of molecular genetic approaches that have allowed the identification of the light-sensitive channels in *Drosophila* as members of the TRP family. Still, two hypotheses have been developed for the nature of the light-activated ion channels based on physiological and molecular evidence.

The first hypothesis is that the channels are not Ca^{2+}-gated, but are cyclic guanosine monophosphate (cGMP) gated. This seems a remote possibility at first, given the evidence that IP_3-induced Ca^{2+} release can rapidly activate a plasma membrane conductance in intact cells. However, the proposal that a further messenger exists downstream from Ca^{2+} is driven by the experimental inability of Ca^{2+} to directly activate ion channels when applied to the inside of patches of plasma membrane excised from the rhabdomeral lobe. Instead, application of cGMP activated channels in a minority of excised patches. The channel events activated during application of cGMP had a similar conductance to light-activated channels, similar reversal potential when bathed in media mimicking intracellular and extracellular ion concentrations and a similar increase in open probability upon membrane depolarization. Since intracellular injections of cGMP or its analogs depolarize the photoreceptor, it was proposed that cGMP might be a terminal messenger in the visual cascade in ventral photoreceptors, as well as in vertebrate rods and cones. A putative cGMP-gated channel has been sequenced from ventral photoreceptors and localized to the microvillar photoreceptors. However, to reconcile this hypothesis with the large body of evidence for the initiation of the light response by the PI pathway, some coupling mechanism must be found to link IP_3-induced Ca^{2+} release to the production of cGMP. There is some pharmacological evidence that a Ca^{2+}-activated guanylate cyclase (GC) might provide this link (**Figure 5**), but no biochemical or molecular evidence has so far been obtained for this hypothesis.

The second hypothesis is that *Limulus* channels are members of the TRP family which, unlike *Drosophila* TRP and TRPL, do not display a high Ca^{2+}- permeability (**Figure 5**). TRP channel homologs have been cloned from ventral photoreceptor messenger RNA (mRNA), and an established activator of some TRP-family channels, the synthetic lipid, 1-oleoyl-2-acetyl-*sn*-glycerol (OAG), activates a conductance with reversal potential similar to that activated by light. Activation of this conductance by OAG apparently requires the presence of free Ca^{2+} ions in the injection pipette, which may explain why extracellularly applied OAG has no effect and why there is a complete dependence of the light response on light-induced Ca^{2+} release from intracellular stores. The hypothesis of a *Limulus* homolog of the TRP channel provides a testable alternative to the proposed role of a cyclic nucleotide channel and may resolve the differences in phototransduction between *Limulus* and *Drosophila* photoreceptors.

Adaptation, a Decrease in the Sensitivity of the Visual Cascade, is Mediated by Small, Lingering Elevations of Ca^{2+}

The onset of prolonged illumination of ventral photoreceptors, or the huge elevations of $[Ca^{2+}]_i$ that occur following flashes of light are not sustained but fall back to the micromolar range within seconds. Concurrently, the photocurrent also falls from tens or hundreds of nA to a few nA. These declines are the result of a decrease in the photoreceptor's sensitivity that prevents saturation of the photoreceptors in bright light and so extends its dynamic range. The initial light-induced elevation of $[Ca^{2+}]_i$ therefore appears to function as a feedback signal that subsequently reduces the sensitivity of the visual cascade.

In support of this concept, slow injection of Ca^{2+} ions into the cytosol of ventral photoreceptors diminishes the sensitivity and latency of the light response, mimicking the effect of an adapting light. Injection of Ca^{2+} chelators, such as EGTA or 1,2-bis(o-aminophenoxy)ethane-N,N,N′,N′-tetraacetic acid (BAPTA), not only slows down and diminishes the initial photocurrent, but also blocks the decline of the light-induced current during prolonged illumination. The site of this feedback inhibition of the light response by Ca^{2+} could be at several points in the phototransduction cascade. For example, IP_3-induced Ca^{2+} release is known to be inhibited by lingering elevations of $[Ca^{2+}]_i$ in ventral photoreceptors. In addition, pharmacological activation of protein kinase C greatly reduces the sensitivity of the light-induced current, apparently acting upstream of IP_3-induced Ca^{2+} release.

Drosophila and *Limulus* Photoreceptors Operate Differently and Illustrate Two General Mechanisms Coupling the PI Cascade to an Electrical Response

The two most extensively studied microvillar photoreceptors, those of *Limulus* and *Drosophila*, have many aspects of their phototransduction mechanism in common. Both are thought to utilize the PI cascade to open non-selective cation channels and both exhibit large elevations of $[Ca^{2+}]_i$, which are necessary for signal amplification and speed, as well as light adaptation. However, there are also clear differences: *Limulus* photoreceptors utilize IP_3-induced Ca^{2+} release to elevate intracellular free Ca^{2+} ion concentrations, while *Drosophila* photoreceptors are thought to utilize DAG or derived products to open Ca^{2+}-permeable TRP channels that allow Ca^{2+} entry from the extracellular space. The photoreceptors of the two species are therefore specific examples of two general mechanisms in cells for coupling the PI pathway to $[Ca^{2+}]_i$ elevation. Why is there this difference? One explanation is the need in *Limulus* for the extra amplification provided by IP_3-induced Ca^{2+} release. One IP_3 molecule can release hundreds of Ca^{2+} ions from the ER through the IP_3R channel. These Ca^{2+} ions can then diffuse along the inner surface of the plasma membrane to activate downstream targets, such as the hundreds of channels required to open in order to produce a significant quantal event in these giant photoreceptors. The trade-off for this amplification is slower speed. The extra amplification step (Ca^{2+} release) required in the visual cascade may explain why *Limulus* photoreceptors are slower than fly photoreceptors to respond to light. This speed difference is entirely reasonable, given the animals' differing demands on their visual systems. Horseshoe crabs do not fly; rather they use their lateral eyes to find mates near moonlit beaches.

Extension of Phototransduction Mechanisms to other Microvillar Photoreceptor Types

Detailed knowledge of the mechanisms of both *Limulus* and *Drosophila* photoreceptors may outline general approaches used by other cell types to the problem of tailoring the outcome of the PI cascade to the need for either speed or amplification. An outstanding question is the extent to which other photoreceptor types utilize these mechanisms. It is apparent that light-induced Ca^{2+} release from intracellular stores occurs in photoreceptors of the file clam, leech, and honeybee. Furthermore, the light-sensitive channels that mediate the immediate electrical response in the file clam are relatively impermeable to Ca^{2+} ions, like those of *Limulus*, but not *Drosophila*. Barnacle photoreceptors, on the other hand, like those of *Drosophila*, display prominent light-induced Ca^{2+} influx. Thus, elements of the two mechanisms for coupling phototransduction to an elevation of Ca^{2+} seem to be scattered across the invertebrate phyla. Whether there is a functional or evolutionary rationale for these differences remains to be seen. Indeed, it is not known yet whether photoreceptors in the other eight eyes of *Limulus* function similarly to the much-studied ventral eye.

See also: Circadian Rhythms in the Fly's Visual System; The Evolution of Opsins; Genetic Dissection of Invertebrate Phototransduction; *Limulus* Eyes and Their Circadian Regulation; Microvillar and Ciliary Photoreceptors in Molluskan Eyes; Photoresponse in Squid.

Further Reading

Bandyopadhyay, B. C. and Payne, R. (2004). Variants of TRP ion channel mRNA present in horseshoe crab ventral eye and brain. *Journal of Neurochemistry* 91: 825–835.

Battelle, B. A. (2006). The eyes of *Limulus polyphemus* (Xiphosura, Chelicerata) and their afferent and efferent projections. *Arthropod Structure and Development* 35: 261–274.

Brown, J. E. and Blinks, J. R. (1974). Changes in intracellular free calcium concentration during illumination of invertebrate photoreceptors. *Journal of General Physiology* 64: 643–665.

Brown, J. E., Rubin, L. J., Ghalayini, A. J., et al. (1984). *myo*-Inositol polyphosphate may be a messenger for visual excitation in *Limulus* photoreceptors. *Nature* 311: 160–162.

Chen, F. H., Baumann, A., Payne, R., and Lisman, J. E. (2001). A cGMP-gated channel subunit in *Limulus* photoreceptors. *Visual Neuroscience* 18: 517–526.

Fein, A., Payne, R., Corson, D. W., Berridge, M. J., and Irvine, R. F. (1984). Photoreceptor excitation and adaptation by inositol 1,4,5 trisphosphate. *Nature* 311: 157–160.

Hardie, R. C. and Minke, B. (1992). The *trp* gene is essential for a light-activated Ca^{2+} channel in *Drosophila* photoreceptors. *Neuron* 8: 643.

Nasi, E., Gomez, M., and Payne, R. (2000). Phototransduction mechanisms in microvillar and ciliary photoreceptors of invertebrates. In: Hoff, A. J., Stavenga, D. G., de Grip, W. J., and Pugh, E. N. (eds.) *Molecular Mechanisms in Visual Transduction – Handbook of Biological Physics,* vol. 3, pp. 389–448. Amsterdam: Elsevier Science.

Phototransduction: Adaptation in Cones

T D Lamb, The Australian National University, Canberra, ACT, Australia

Glossary

Avoidance of saturation – The ability of cones (but not rods) to continue functioning in steady background illumination of arbitrarily high intensity.
Light adaptation – The rapid adjustment of sensitivity and kinetics (of the entire visual system, or of the photoreceptors) that occurs in response to altered ambient light intensity. The adjustment is rapid irrespective of whether the change is an increase or decrease in intensity, provided that the change is not too great.
Saturation – The failure of the photoreceptors (or of the visual system) to respond to incremental illumination in the presence of appropriately bright illumination. The rod photoreceptors saturate at a relatively low background intensity; in contrast, the cone photoreceptors avoid saturation by steady backgrounds, no matter how bright the light is.
Weber's law – The reduction in visual sensitivity that occurs in inverse proportion to the intensity of the ambient background illumination. This corresponds to a rise in visual threshold in direct proportion to the ambient illumination.

Performance of the Photopic (Cone) System

Workhorse of Vision

For human vision, the photopic cone system can be considered the workhorse of vision, because it is operational under almost all of the conditions that we (in a modern world) experience. Thus, it is our photopic system that provides our sense of vision under all lighting conditions, apart from exceptionally low levels such as starlight conditions. Under moonlight conditions, our scotopic and photopic systems are both functional, over an intensity range that is termed mesopic. If you are ever in doubt as to whether you are using your photopic system under twilight or nighttime conditions, there is a simple test: if you are able to detect any color in the scene, then your cones are active; your rods may also be active, but this is one test of whether there is any cone activity at that level of intensities. In addition, the photopic system remains functional at all higher intensities, up to the brightest sunlit conditions than we ever experience.

It is interesting to consider that, despite their enormous importance to our vision, cones make up perhaps only 5% of the population of photoreceptors over most of our peripheral retina. This relatively low proportion of cone photoreceptors in the peripheral retina is entirely adequate for our normal peripheral vision, which requires only relatively low spatial acuity. Even though the great majority of peripheral photoreceptors are rods, they are simply not used under most of the circumstances that we think of as vision – thus, they are only used at exceedingly low ambient lighting levels. The reason for the great numerical preponderance of rods is to be able to capture every available photon at those very low light intensities.

Rapid Response and Moderate Sensitivity

In survival terms, one of the greatest advantages of cones over rods is their much faster speed of response. The responses of our rods, even when they are light adapted, are much too slow to allow us to function visually at the speeds that are required to escape predators and to capture prey. Cones, instead, are specialized so as to permit extremely rapid signaling of visual stimuli to the brain.

Cones are often described as having much lower sensitivity than rods, but this view is misleading, especially when considered in terms of the rapidly changing visual stimuli that the cones are specialized for signaling. Although the peak sensitivity to a brief flash of light may be perhaps 30-fold lower in a cone than in a rod, the sensitivity to rapidly fluctuating stimuli is considerably higher in cones than in rods; thus, the slow response of the rods makes them quite insensitive to rapidly changing stimuli. When expressed in terms of the efficacy of activation within the G-protein cascade of phototransduction, the amplification in cones and rods appears to be essentially indistinguishable – the real difference is in the speed of inactivation.

Avoidance of Saturation

The second crucial feature of cones, in terms of survival advantage, is their amazing ability to avoid saturation no matter how intense the steady background illumination becomes. This property stands in stark contrast to the situation in rods, which are completely incapable of responding once the background exceeds a relatively low level (corresponding roughly to twilight illumination). One of the major challenges in photoreceptor research is

to provide a clear understanding of how it is that cones are able to avoid saturation at arbitrarily high light intensities, whereas rods succumb to saturation at very low light intensities. As will be described below, considerable advances have recently been made toward providing this understanding.

Light Adaptation of the Cones

Cone photoreceptors undergo light adaptation over an enormously wide range of intensities, and it is likely that almost all of the adaptation that is observed in the overall photopic visual system is mediated by these changes occurring at the level of the receptor cells. This section describes the adaptational effects that occur in the cone photoreceptors.

Flashes on Backgrounds: Desensitization and Acceleration

Figure 1 illustrates the responses of a cone photoreceptor to the same set of flashes presented under three different conditions; the flashes *A–F* were of progressively greater intensity from left to right, but were exactly the same in each of the three panels. In (a), the flashes were presented in darkness, and represent a standard dark-adapted flash family; in (b), the same flashes were presented shortly after a dim steady background had been turned on; and in (c), the same flashes were presented after the onset of a brighter background. In the presence of the background illumination, the amplitude of the responses to dim flashes was smaller. For example, for the second flash intensity, *B*, the response amplitude becomes markedly smaller from (a) to (b) to (c). In other words, backgrounds of increasing intensity progressively desensitized the cone's incremental

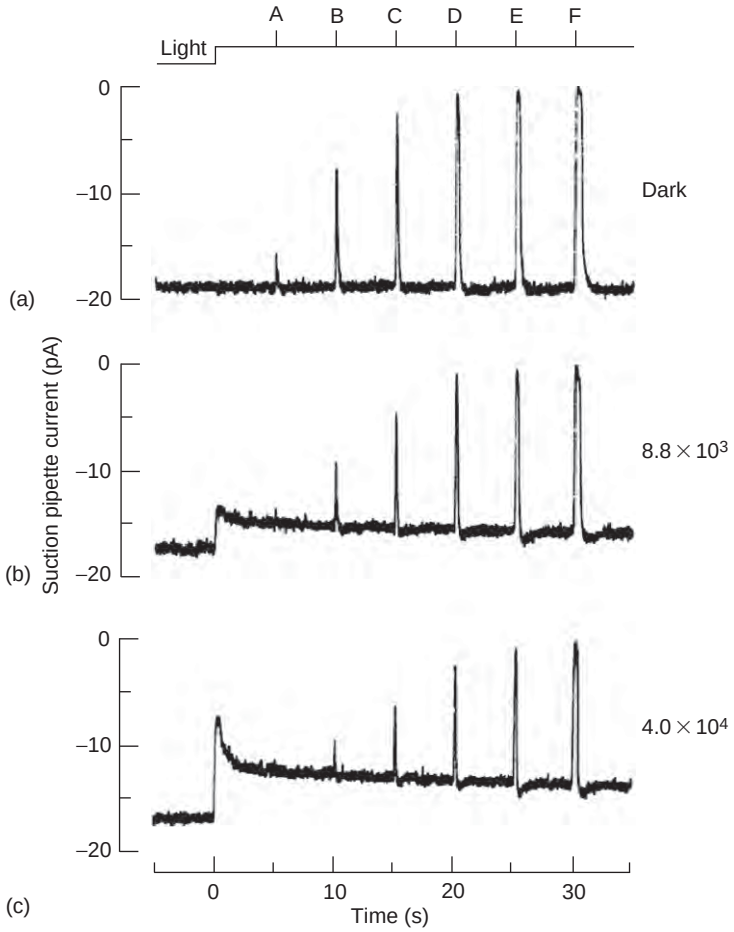

Figure 1 Circulating current of a salamander cone in response to flashes and steps of illumination. Timing of illumination is indicated by the marker trace at the top; flashes *A–F* increased in intensity by factors of ~4, and were the same intensity in each of (a)–(c). In (a), these flashes were presented in darkness; in (b) and (c) the same flashes were presented on steady backgrounds that had been switched on at time zero; the background in (c) was ~4 times brighter than in (b). Reproduced from Matthews, H. R., Fain, G. L., Murphy, R. L. W., and Lamb, T. D. (1990). Light adaptation in cones of the salamander: A role for cytoplasmic calcium concentration. *Journal of Physiology* 420: 447–469.

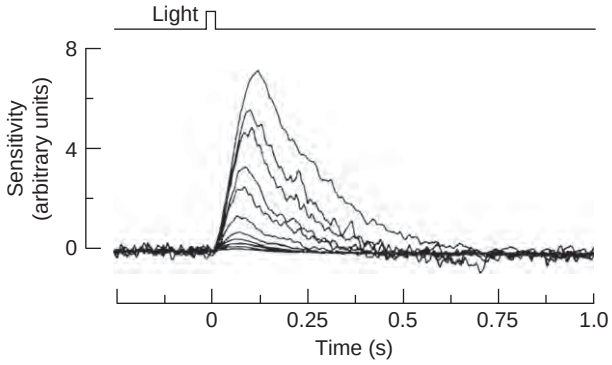

Figure 2 Incremental responses of a salamander cone to test flashes presented on backgrounds of increasing intensity. The largest trace is for a dim flash presented in darkness, while the other traces correspond to the same test flash presented on backgrounds. In fact, in the presence of brighter backgrounds, the test flash intensity was increased in order to obtain measurable responses, and the plotted traces have therefore been scaled as response divided by test flash intensity, so as to provide a direct measure of sensitivity. Reproduced with permission from Matthews, H. R., Fain, G. L., Murphy, R. L. W., and Lamb, T. D. (1990). Light adaptation in cones of the salamander: A role for cytoplasmic calcium concentration. *Journal of Physiology* 420: 447–469.

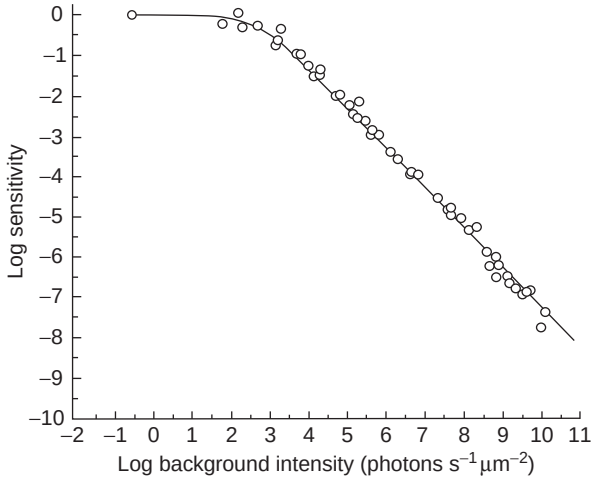

Figure 3 Cone sensitivity as a function of background intensity. Data are plotted in double logarithmic coordinates, and were obtained from intracellular measurements averaged from 15 cones in the turtle eyecup preparation. The experiments used laser illumination to achieve very high background intensities, and monitored step sensitivity rather than the more conventional flash sensitivity. The smooth curve plots Weber's law, given by eqn [1]. Reproduced from Burkhardt, D. A. (1994). Light adaptation and photopigment bleaching in cone photoreceptors *in situ* in the retina of the turtle. *Journal of Neuroscience* 14: 1091–1105.

response. Such behavior is very characteristic of photoreceptors, and these responses from cones are qualitatively similar to those obtained from rods.

The manner in which the response to a dim flash is modified by the presence of backgrounds of different intensity is illustrated in **Figure 2**. The largest trace is the response to a dim flash presented under fully dark-adapted conditions, while the other traces are for the same flash presented on backgrounds of progressively brighter intensity. (In fact, in order to maintain responses of measurable amplitude, the flash intensity was increased in the presence of backgrounds, and the traces actually plot response divided by flash intensity; i.e., the response sensitivity.)

The traces in **Figure 2** demonstrate that the effect of backgrounds of increasing intensity is to both desensitize and accelerate the response to an incremental dim flash. This behavior of cones is very similar to that exhibited by rods.

Dependence of Sensitivity on Background Intensity: Weber's Law

By plotting the peak amplitude of each of the traces in **Figure 2** as a function of the background intensity on which it was measured, one obtains a sensitivity versus background plot of the type illustrated in **Figure 3**.

The results plotted in **Figure 3** were obtained over an extremely wide range of background intensities by Dwight Burkhardt using a laser source of illumination. Importantly, the preparation was the intact eyecup (of the turtle), so that the photoreceptors remained in contact with the retinal pigment epithelium (RPE) and thereby experienced normal regeneration of visual pigment, in order that meaningful results could be obtained even at very high background intensities. (One methodological difference between the results plotted in **Figure 3** and the results that are more usually plotted is that step sensitivities rather than flash sensitivities are plotted; however, this does not, in practice, make much of a difference.)

For background intensities from 10^3 to 10^{11} photons $\mu m^{-2}\ s^{-1}$, the relationship between log sensitivity and log background intensity is a straight line with a slope of -1; in other words, over roughly 8 log units of background, the turtle cone's sensitivity declines inversely with background intensity. The curve plotted near the points in **Figure 3** represents Weber's law, described by:

$$\frac{S}{S_D} = \frac{1}{1 + (I/I_0)} \qquad [1]$$

where S is flash sensitivity, S_D is its dark-adapted value, I is the background intensity, and I_0 is the half-desensitizing intensity, also known as the dark-adapted equivalent background intensity. The good fit of the Weber's law expression shows, very importantly, that cone photoreceptors in the intact eyecup are able to completely avoid saturation, even at enormously high intensities of steady illumination. This feature represents a crucial distinction between the properties of cones and rods. The circulating current of rods is shut off at quite low background intensities, so that

the rods are unresponsive to superimposed stimuli, in the presence of background illumination of moderate intensity.

In the same set of experiments, Burkhardt measured the intensity at which 90% of the pigment was in the bleached state, and found this to be around 10^6 photons $\mu m^{-2}\ s^{-1}$. For all intensities above that level, the observed Weber's law behavior can be accounted for in terms of pigment bleaching. For each additional 10-fold increase in intensity, there will be a 10-fold reduction in the amount of pigment remaining available to absorb light, and hence there will necessarily be a 10-fold reduction in sensitivity in the absence of any other change of parameters of transduction in the outer segment. In other words, if the photoreceptor is able to avoid saturation up to intensities that cause substantial bleaches, then it will be able to exhibit Weber's law desensitization at higher intensities purely by means of pigment bleaching. Cones are able to function up to this critical intensity, whereas rods saturate at much lower intensities.

Extremely Rapid Recovery of Cone Photocurrent

In order to measure the performance of mammalian cones in the presence of extremely bright background illumination, it is necessary to use a preparation in which the cones are in contact with the RPE (as was the case in the experiments above with turtle cones). Accordingly, it is not appropriate to use suction-pipette experiments at very high intensities. On the other hand, experiments measuring the electroretinogram (ERG) in the intact eye are very suitable.

Results from an experiment designed to measure the kinetics of recovery of the circulating current of human cone photoreceptors, upon extinction of steady illumination that bleached 90% of the visual pigment, are illustrated in **Figure 4**. This Figure shows recordings of the a-wave of the human ERG, which monitors primarily the response of photoreceptors; and at these incredibly high intensities, only the cone photoreceptors are responding. The left panel shows the response to a bright flash superimposed on the intense steady background, while the right panel shows the response obtained at extinction of that background. As indicated by the right-hand pair of vertical scales, the bright flash responses established the zero level of circulating current, as well as the level of circulating current during the intense background (i.e., unity on the inner scale). Separate measurements (not shown) established the dark current (i.e., unity on the outer right-hand scale). Even during the presence of the intense steady background, the cone circulating current was roughly 50% of its original level in darkness.

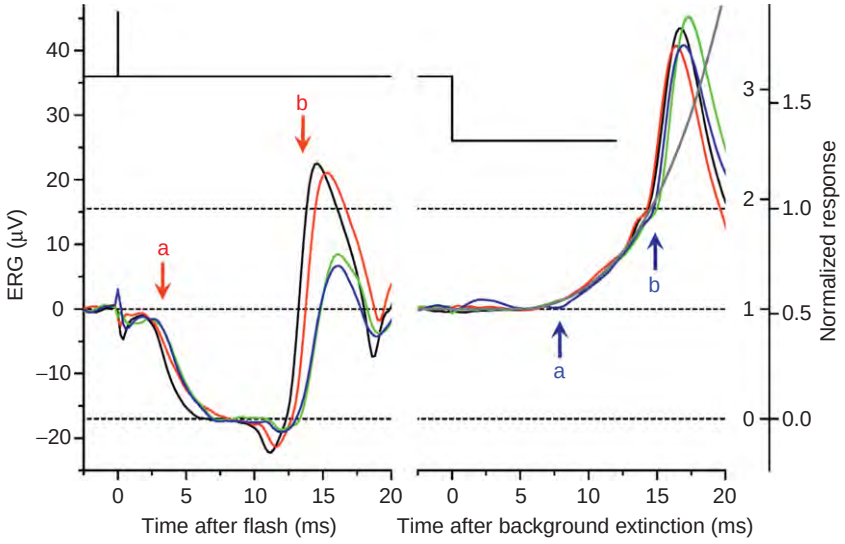

Figure 4 Extremely rapid recovery of human cone photocurrent upon extinction of intense illumination, measured with the ERG. The four colored traces plot ERG responses from two subjects, at two different flash intensities. The light stimulus is monitored by the black traces at the top. Left panel is for an intense flash presented on the intense steady background; right panel is for extinction of that background. The ON a-wave and b-wave elicited by the bright flash are indicated by the red arrows; the OFF a-wave and b-wave elicited by extinction of the background are indicated by the blue arrows. The b-wave is roughly similar in the two cases, and arises from postreceptoral activity. The OFF a-wave represents recovery of the cone circulating current, and begins around 7 ms after the intense background is turned off. Dashed horizontal lines represent the following levels of cone circulating current (from bottom): zero level, steady level during intense background, dark level, as indicated by the two normalized scales on the right. Reproduced from Kenkre, J. S., Moran, N. A., Lamb, T. D., and Mahroo, O. A. R. (2005). Extremely rapid recovery of human cone circulating current at the extinction of bleaching exposures. *Journal of Physiology* 567: 95–112.

The traces on the right show the ERG a-wave upon extinction of the intense background. Little change occurs for the first 7 ms, but thereafter a substantial upward response occurs, the OFF a-wave indicated by the blue arrow, until about 15 ms after extinction of the background; at this point, the a-wave is obscured by spike-like activity of the b-wave. There is compelling evidence that the a-wave traces for these subjects monitor the recovery of the cone circulating current. On this basis, the cone circulating current is essentially fully recovered within about 15 ms after extinction of illumination so intense that it bleaches 90% of the cone pigment. This is extremely rapid recovery, at least when compared with the time course of recovery following intense flashes delivered from darkness. The next section considers the speed that is required for the shut-off reactions of phototransduction, in order to be able to account for recovery of the circulating current as fast as is shown in **Figure 4**. The smooth gray curve near the measured traces in the right-hand panel of **Figure 4** was calculated from the model presented in the next section, using the short time constants listed in **Table 1**.

Extremely rapid recovery of cone circulating current, as inferred from the results of **Figure 4**, is also required in order to account for classical experiments on the flicker-fusion frequency of human subjects. Even at quite low photopic intensities, human subjects are able to detect square-wave flicker at a frequency of around 50 Hz using peripheral vision. However, at higher intensities, the flicker-fusion frequency increases to 100 Hz or more. At a frequency of 100 Hz, the illumination is being switched on and off at intervals of 5 ms each. Thus, in order for the flicker to be detectable, some degree of recovery of cone circulating current must have occurred within 5 ms. Hence, this finding is broadly consistent with the time course inferred from **Figure 4**.

Molecular Basis of Cone Light Adaptation

Reaction Steps Underlying Rapid Recovery of the Cone's Light Response

Figure 5 presents a schematic of the reaction steps underlying phototransduction in cones, where shut-off reactions and the lifetimes (or turnover times) of important intermediates are indicated in red.

For mammalian cones, the speed of the various shut-off reactions shown in the schematic of **Figure 5** has been estimated in a number of recent studies using intact preparations. In the case of monkey cones, the parameters were extracted through theoretical modeling of results obtained from intracellular recordings of horizontal cells in the retina–RPE–choroid preparation. In the case of human cones, the parameters were extracted through theoretical modeling of ERG results, including those of the type illustrated in **Figure 4**. The shut-off reactions have been found to be extremely rapid, and the parameters that have been reported are summarized in **Table 1**.

The collected estimates in **Table 1** are consistent with the notion that all four of the shut-off time constants in human cones are extremely short, with values in the range of 3–18 ms; in fact, it appears that three of the time constants could be around 5 ms or less, and one around

Table 1 Shut-off time constants estimated for mammalian cones and rods

	τ_R ms	τ_E ms	τ_{Ca} ms	$\tau_{cG} = 1/\beta$ (intense) ms	Preparation	Ref.
Cone		18			Human ERG	1
	5	13		4	Human ERG	2
	3	9	3	4	Monkey retina	3
	3	10	3	6	Human ERG	4
Rod	70	200			Mouse suction pipette	5

Estimates for the four shut-off time constants (τ_R, τ_E, τ_{Ca}, and τ_{cG}) obtained from recent experiments are tabulated.
Note that it is not usually possible to determine which is which for the two time constants τ_R and τ_E; however, in the case of the rod results, this identification was made using other experiments.
The time constants for cones are around 20 times faster than for rods.
The studies from which these results were obtained are as follows:
1: Friedburg, C., Allen, C. P., Mason, P. J., and Lamb, T. D. (2004). Contribution of cone photoreceptors and post-receptoral mechanisms to the human photopic electroretinogram. *Journal of Physiology* 556: 819–834.
2: Kenkre, J. S., Moran, N. A., Lamb, T. D., and Mahroo, O. A. R. (2005). Extremely rapid recovery of human cone circulating current at the extinction of bleaching exposures. *Journal of Physiology* 567: 95–112.
3: van Hateren, J. H. (2005). A cellular and molecular model of response kinetics and adaptation in primate cones and horizontal cells. *Journal of Vision* **5**, 331-347.
4: van Hateren, J. H. & Lamb, T. D. (2006). The photocurrent response of human cones is fast and monophasic. *BMC Neuroscience* **7**, 34.
5: Krispel, C. M., Chen, D., Melling, N., Chen, Y.-J., Martemyanov, K. A., Quillinan, N., Arshavsky, V. Y., Wensel, T. G., Chen, C.-K. & Burns, M. E. (2008). RGS expression rate-limits recovery of rod photoresponses. *Neuron* **51**, 409–416.

10–15 ms. (Note that the turnover time for cyclic guanosine monophosphate (cGMP), τ_{cG}, listed in Table 1 represents the value applicable during very intense illumination; under dark-adapted conditions, when the light-induced activity of the phosphodiesterase (PDE) is relatively low, this time constant is likely to be much longer.)

The shut-off time constants for the activated visual pigment (R*) and the activated G-protein/PDE (E*), τ_R and τ_E, are around 20-fold shorter in human cones than in mouse rods, with values of ~80 and ~200 ms having been reported in rods.

Cone Avoidance of Saturation

Work done in collaboration with Edward N. Pugh, Jr. has shown that the ability of the cones to avoid saturation is explicable in terms of the combination of these two 20-fold shorter time constants and the bleaching of cone visual pigment.

In human rod photoreceptors *in vivo*, the circulating current is halved at a steady intensity of ~70 scotopic trolands (600 R* s^{-1}), with complete saturation occurring at ~1000 scotopic trolands (~10^4 R* s^{-1}). If the activation gain of transduction is the same in human cones as in human rods, then the two very short cone time constants would elevate the intensities required for half and full saturation by some ~400×, to levels of ~240 000 and ~4 × 10^6 R* s^{-1} in cones. An additional factor is that the cGMP-gated channels of mammalian cones (in contrast to those of rods) show increased cGMP-binding affinity when Ca^{2+} falls, thereby further increasing the R* rate required for saturation.

How do these estimated rates of isomerization compare with the maximum rate at which the cone visual pigment can be bleached during steady illumination? At steady state, the rate of photoisomerization equals the rate of pigment regeneration, which is set by the delivery of 11-*cis* retinal to opsin. For human L/M cones, the maximal rate of regeneration has been measured as ~45% min^{-1}, or 0.75% s^{-1}. If the outer segment contains ~40 million pigment molecules, then the maximal rate of photoisomerization during intense steady light will be ~300 000 R* s^{-1}. This rate cannot be exceeded in the steady state because a higher rate of isomerization would lead to such a low level of cone pigment available to absorb light that the rate could simply not be maintained.

Hence, from the numbers in the preceding paragraphs, the rate of photoisomerization required to saturate the human cone current exceeds the highest rate of isomerization of cone pigment molecules (~300 000 R* s^{-1}) that can be elicited by a steady light of arbitrarily high intensity. Therefore, the human cone photoreceptor cannot be saturated by steady lights, no matter how bright they are. This is not to say that the cone can never be saturated; if an intense light is presented from dark-adapted conditions (when the cone initially has a full complement of visual pigment), then it will transiently be driven into saturation until bleaching reduces the amount of visual pigment to a suitably low level.

Modeling of Human Cone Light Adaptation

A computational model of human cone light adaptation has been developed by Hans van Hateren and Herman Snippe, which puts factors of the type described in the preceding section into a comprehensive theoretical/numerical model. They take a molecular description of the steps in cone phototransduction closely similar to that illustrated in Figure 5, including pigment bleaching, and

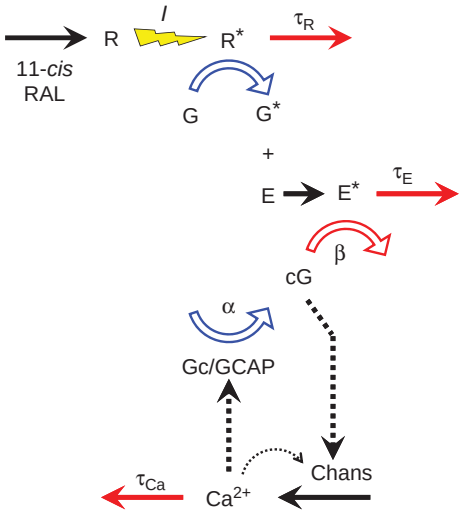

Figure 5 Reaction steps underlying the cone's rapid recovery. Visual pigment (R) is formed by delivery of 11-*cis* retinal (11-*cis* RAL). Light (of intensity *I*) activates the visual pigment, and the activated pigment (R*) is inactivated with a time constant τ_R. R* activates the guanine-nucleotide-binding G protein to G*, which then binds to phosphodiesterase (E) to form active G*–E* (E*). The active G*–E* complex (E*) has a lifetime τ_E. E* hydrolyzes cGMP (cG) with a rate constant β. The increase in β is proportional to steady intensity *I*, and to the product of the R* and E* lifetimes; that is, $\beta = \beta_{Dark} + (A/n_{cG})\,\tau_R\,\tau_E\,I$ (see Nikonov, S., Lamb, T. D., and Pugh, E. N., Jr. (2000). The role of steady phosphodiesterase activity in the kinetics and sensitivity of the light-adapted salamander rod photoresponse. *Journal of General Physiology* 116: 795–824). cGMP is formed by guanylyl cyclase (GC), under regulation by the Ca^{2+}-sensitive guanylyl-cyclase-activating proteins (GCAPs). When present, cG causes opening of ion channels (chans) in the plasma membrane, admitting Ca^{2+}. Ca^{2+} has a powerful negative-feedback action through GCAPs onto the rate α of cGMP synthesis. Ca^{2+} is removed from the cytoplasm with a time constant τ_{Ca}. Reproduced from Lamb, T. D. and Pugh, E. N., Jr. (2006). Avoidance of saturation in human cones is explained by very rapid inactivation reactions and pigment bleaching. *Investigative Ophthalmology and Visual Science* 47, E-Abstract 3714, with permission from the Association for Research in Vision and Ophthalmology.

they express the system in terms of differential equations. Their simulations predict that human cones will indeed conform to Weber's law over a very wide range of background intensities, and that they will not saturate with steady intensities of any level. Thus, there is now a comprehensive description of the process of light adaptation in human cones and, in particular, of the ability of human cones to avoid saturation.

See also: Phototransduction: Adaptation in Rods; Phototransduction: Phototransduction in Cones.

Further Reading

Burkhardt, D. A. (1994). Light adaptation and photopigment bleaching in cone photoreceptors *in situ* in the retina of the turtle. *Journal of Neuroscience* 14: 1091–1105.

Friedburg, C., Allen, C. P., Mason, P. J., and Lamb, T. D. (2004). Contribution of cone photoreceptors and post-receptoral mechanisms to the human photopic electroretinogram. *Journal of Physiology* 556: 819–834.

Kenkre, J. S., Moran, N. A., Lamb, T. D., and Mahroo, O. A. R. (2005). Extremely rapid recovery of human cone circulating current at the extinction of bleaching exposures. *Journal of Physiology* 567: 95–112.

Lamb, T. D. and Pugh, E. N., Jr. (2006). Avoidance of saturation in human cones is explained by very rapid inactivation reactions and pigment bleaching. *Investigative Ophthalmology and Visual Science* 47, E-Abstract 3714.

Matthews, H. R., Fain, G. L., Murphy, R. L. W., and Lamb, T. D. (1990). Light adaptation in cones of the salamander: A role for cytoplasmic calcium concentration. *Journal of Physiology* 420: 447–469.

Nikonov, S., Lamb, T. D., and Pugh, E. N., Jr. (2000). The role of steady phosphodiesterase activity in the kinetics and sensitivity of the light-adapted salamander rod photoresponse. *Journal of General Physiology* 116: 795–824.

Pugh, E. N., Jr., Nikonov, S., and Lamb, T. D. (1999). Molecular mechanisms of vertebrate photoreceptor light adaptation. *Current Opinion in Neurobiology* 9: 410–418.

Pugh, E. N., Jr. and Lamb, T. D. (2000). Phototransduction in vertebrate rods and cones: Molecular mechanisms of amplification, recovery and light adaptation. In: Stavenga, D. G., de Grip, W. J., and Pugh, E. N., Jr. (eds.) *Handbook of Biological Physics. Molecular Mechanisms of Visual Transduction* vol. 3, ch. 5, pp. 183–255. Amsterdam: Elsevier.

van Hateren, J. H. and Lamb, T. D. (2006). The photocurrent response of human cones is fast and monophasic. *BMC Neuroscience* 7: 34.

van Hateren, J. H. and Snippe, H. P. (2007). Simulating human cones from mid-mesopic up to high-photopic luminances. *Journal of Vision* 7(4): 1.

Phototransduction: Adaptation in Rods

T D Lamb, Australian National University, Canberra, ACT, Australia

Glossary

Dark adaptation – The very slow recovery of visual sensitivity that occurs upon the return to darkness following exposure of the eye to extremely intense (and possibly prolonged) illumination. Full recovery of the human visual system takes about 45 min, after a total bleach of all the rhodopsin.

Light adaptation – The rapid adjustment of sensitivity and kinetics (of the entire visual system or of the photoreceptors) that occurs in response to altered ambient light intensity. The adjustment is rapid irrespective of whether the change is an increase or decrease in intensity, provided that the change is not too great.

Saturation – The failure of the photoreceptors (or of the visual system) to respond to incremental illumination in the presence of appropriately bright illumination. The rod photoreceptors saturate at a relatively low background intensity; in contrast, the cone photoreceptors avoid saturation by steady backgrounds, no matter how bright the light is.

Weber's law – The reduction in visual sensitivity that occurs in inverse proportion to the intensity of the ambient background illumination. This corresponds to a rise in visual threshold in direct proportion to the ambient illumination.

Vision over a Billion-Fold Range of Light Intensities

Our visual system operates effectively over an enormously wide range of intensities, of at least a billion-fold, from around 10^{-4} cd m^{-2} under shaded starlight conditions to around 10^{5} cd m^{-2} under intense sunlight. Changes in pupil area account for only about 1 log unit of this >9-log-unit range, since the pupil diameter changes from a maximum of 8 mm to a minimum of 2.5 mm, corresponding to a 10-fold reduction in area. Instead, the great bulk of the operational range is achieved by the combination of, first, a switch between the rod (scotopic) and cone (photopic) pathways in our duplex visual system and, second, the ability of each of these photoreceptor systems to operate over a range of 5 log units (100 000-fold) or more.

This ability of the visual system (or of any of its component parts, such as the photoreceptors) to adjust its performance to the ambient level of illumination is known as light adaptation; the adjustment typically occurs very rapidly (within seconds), whether the light intensity is increasing or decreasing. The term dark adaptation is reserved for the special case of recovery in darkness, following exposure of the eye to extremely bright and/or prolonged illumination that activates (bleaches) a substantial fraction of the visual pigment, rhodopsin. Dark adaptation occurs slowly, and the full recovery of the scotopic visual system after a very large bleach can take as much as an hour.

The changes that accompany light adaptation are beneficial to the possessor of the eye. At very low intensities, the sensitivity is increased to the utmost that is possible so that the rod photoreceptors reliably signal the arrival of individual photons and the scotopic visual system operates in a photon-counting mode. The ability of the scotopic system to operate at incredibly low intensities is enhanced by two deliberate trade-offs – of reduced spatial resolution (increased spatial summation) and reduced temporal resolution (increased temporal integration) – that permit more reliable detection of small signals in the presence of noise. Similar trade-offs are used in the photopic system so that as the ambient illumination decreases from daylight levels toward twilight levels, one's spatial and temporal resolution deteriorate; this is why, in cricket, bad light stops play.

In contrast, the changes that characterize dark adaptation are disadvantageous. To be essentially blind to dim stimuli, for some considerable time following intense light exposure, cannot in any way be useful to an organism. Indeed, for a caveman, entering a cave from bright sunshine, it may have been a serious handicap to have been unable to see well for tens of minutes. Why should such an apparently unsatisfactory situation have persisted? A possible reason could be because it represents an unfortunate downside that has somehow resulted from the enhancements that were needed in order to enable the scotopic system to detect individual photons, and thereby be able to function at incredibly low light levels.

Performance of the Scotopic (Rod) System

For the rod pathway, the dominant mechanisms of scotopic light adaptation result from alterations of signal processing at postsynaptic stages within the retina, and the

rods themselves adapt over only a modest range of intensities before being driven into saturation. This is illustrated in **Figure 1**, which compares the changes in sensitivity of the rod photoreceptors and of the overall visual system during scotopic light adaptation.

The blue symbols and curve plot the relative sensitivity of the overall visual system, measured psychophysically, while the red symbols and curve plot the relative sensitivity of primate rod photoreceptors. Importantly, the overall scotopic visual system begins desensitizing at intensities around 1000 times lower than those required to begin desensitizing the rod photoreceptors. This occurs because the postreceptoral scotopic system is able to integrate photon signals from large numbers of rod photoreceptors, thereby gaining increased sensitivity, while introducing the need to begin desensitizing at much lower background intensities in order to avoid saturation. Hence, the rod photoreceptors maintain their maximal sensitivity over several log units of the lowest intensity regime (up to ~10 isomerizations per second) where the visual system needs to exhibit gradual desensitization.

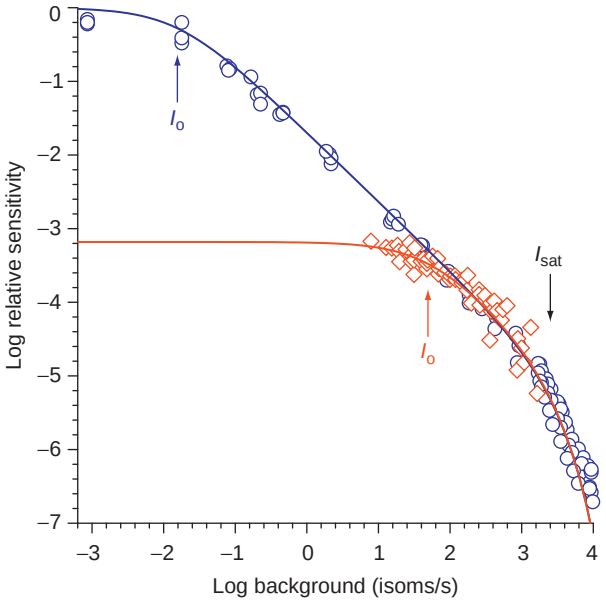

Figure 1 Sensitivity of the human scotopic visual system (blue) and of monkey rod photoreceptors (red) as functions of background intensity in double logarithmic coordinates. The blue symbols are from human psychophysical measurements and the blue curve plots Weber law desensitization in conjunction with saturation, as described by eqn [1], with parameters $I_0 = 0.016$ photoisomerizations per second (blue arrow) and $I_{sat} = 2500$ photoisomerizations per second (black arrow). The red symbols are from suction pipette measurements from isolated rod photoreceptors of monkeys (*Macaca fascicularis*); these symbols have been shifted vertically to align with the blue symbols in the upper intensity range. The red curve also plots eqn [1] with the same value of I_{sat}, but with $I_0 = 50$ photoisomerizations per second (red arrow). Data for the blue symbols are from Figure 3 of Aguilar, M. and Stiles, W. S. (1954). Saturation of the rod mechanism of the retina at high levels of stimulation. *Optica Acta* 1: 59–65. Their troland values were converted using a factor of $K = 8.6$ photoisomerizations per second per troland. Data for the filled symbols are from Figure 9A and Table III of Tamura, T., Nakatani, K., and Yau, K.-W. (1991). Calcium feedback and sensitivity regulation in primate rods. *Journal of General Physiology* 98: 95–130.

When the background intensity is reduced from relatively high scotopic intensities (moving from right to the left along the *x*-axis in **Figure 1**), the sensitivity of rods, and of the scotopic visual system, steadily rises. However, below the intensities indicated by the blue and red arrows, the sensitivity of, first, the rods and, second, the visual system fails to continue increasing, as if the respective mechanism were experiencing a phenomenon equivalent to light. Accordingly, the arrowed intensities for the rods and for the scotopic visual system have been referred to as equivalent background intensities. Clearly, the equivalent background for the scotopic system (around 0.016 photoisomerizations per second) is several log units lower than the equivalent background intensity for the rods (around 50 isomerizations per second).

The curves in **Figure 1** plot desensitization according to the combination of Weber's law with saturation at high intensities, as described by

$$\frac{S}{S_D} = \frac{1}{1 + (I/I_0)} \exp(-I/I_{sat}) \qquad [1]$$

where S is flash sensitivity, S_D is its dark-adapted value, and I is the background intensity. The first term on the right-hand side expresses Weber's law, where I_0 is the equivalent background intensity mentioned above. This first term indicates that, at low background intensities (when $I << I_0$) the sensitivity S approaches a constant level (its dark-adapted value, S_D), while for brighter backgrounds (when $I >> I_0$) the sensitivity declines inversely with background intensity.

At higher scotopic intensities, both the rods and the overall scotopic system exhibit saturation, characterized by a steep decline in sensitivity with increasing background intensity. This behavior is described by the second term on the right-hand side in eqn [1], where I_{sat} is termed the saturation intensity of around 2500 isomerizations per second. It is almost certain that saturation of the overall scotopic system results directly from saturation of the rods.

The span of intensities from I_0 (the equivalent background) to I_{sat} (the saturation intensity) is known as the Weber region and, in this range of background intensities, the sensitivity declines inversely with background intensity; that is, $S \propto 1/I$. Since the contrast in a visual stimulus is, likewise, inversely proportional to background intensity (i.e., contrast = $\Delta I/I$), this Weber region is characterized by a fixed level of contrast sensitivity; that is, a given level of contrast elicits a fixed size of response. Thus, an important feature of Weber's law light adaptation is that it provides automatic extraction of visual contrast.

For mammalian rods, the Weber region encompasses only 1–2 log units of intensity, though for the larger rods of lower vertebrates, it may encompass a slightly wider range of about 3 log units. On the other hand, for the overall scotopic system, the Weber region covers a much wider range of at least 5 log units (i.e., over 100 000-fold). In addition, for cone photoreceptors, it extends over an even wider range.

The Purpose of Light Adaptation: Optimization of Performance

The purpose of light adaptation is to permit the visual system (or any neuron within it) to provide the best performance possible at that particular level of illumination. However, it is not always clear what constitutes best. For example, for the rod photoreceptors, it is clear that at very low ambient levels of illumination, their sensitivity should be as high as possible. However, we cannot readily anticipate the time course of their response that will be optimal.

Avoidance of Saturation: Range Extension

As the ambient light intensity increases, it is important that the rod (or any other cell) should avoid saturating, or else it will be unable to signal. By preventing saturation, light adaptation permits a photoreceptor to extend the range of intensities over which it operates. Although the rods achieve light adaptation over a limited range of intensities, the cones excel, and are able to avoid saturation no matter how bright the steady illumination becomes. Why has evolution permitted the rods to be driven into saturation by relatively low intensities? In part, it is because the photopic (cone) system is functional at these intensities, so that there is no disadvantage if the rods saturate. Not only is there no disadvantage – in fact, there is a distinct advantage when the rods saturate, in conserving energy during daylight conditions. Maintenance of the rod circulating current, in darkness and at low light levels, represents an extremely high metabolic load on the cells, and the elimination of this load when the cones are functional provides a major benefit to retinal metabolism. From this perspective, the limited range of rod light adaptation is beneficial, whereas an extended range (as occurs in cones) would be detrimental.

Extraction of Contrast Information and Optimization of Response Kinetics

In addition to the very important function of extending the operating range of the photoreceptor, there are two other ways in which photoreceptor light adaptation optimizes the cell's response. First, as described above in relation to eqn [1], it permits the extraction of contrast in the visual scene, independent of the absolute level of illumination. Second, it provides real-time adjustment of the time course of the response to an incremental flash of light, in a manner that is presumed to be optimal for the visual system. Thus, at very low background intensities, the response is sluggish, and postreceptoral elements are able to integrate visual signals over relatively long times. At progressively higher background intensities, the response becomes progressively accelerated, thereby improving the time resolution of the system. However, we do not have sufficient information yet to be able to describe exactly how it is that kinetic changes of this kind are actually optimal for the visual system.

Light Adaptation of the Rod Photoreceptors: Range Extension, Desensitization, and Acceleration

In the presence of background illumination, it is not only the overall visual system that adapts, but also the rod photoreceptors themselves display light adaptation, characterized by an extension of their operating range and by desensitization and acceleration of the incremental flash response.

Prevention of Rod Photoreceptor Saturation: Range Extension

The response of a salamander rod to the onset of steady illumination at different intensities is illustrated in **Figure 2**. At the beginning of the step of light, the rod's response begins rising according to what is predicted from the time integral of the flash response, but very soon deviates, falling well below the linear prediction (upper panel). Characteristically, the response to such a step of light typically exhibits an early peak followed by a sag. This deviation from the simplest linear prediction is a crucial aspect of light adaptation – if this deviation did not occur, then the rod would be driven into saturation by lights of very low intensity. Such saturation can be induced by exposing the rod to a solution that clamps the cytoplasmic calcium concentration; in the presence of calcium-clamping solution (lower panel), the responses of the rod follow the predictions of the smooth theoretical curves, and a very low intensity (labeled 2) saturates the rod. This result shows that at least a part of the rod's ability to continue operating in backgrounds of moderate intensity (i.e., the extension of its operating range) is a consequence of changes in cytoplasmic calcium concentration; the molecular mechanisms that contribute to this will be discussed below.

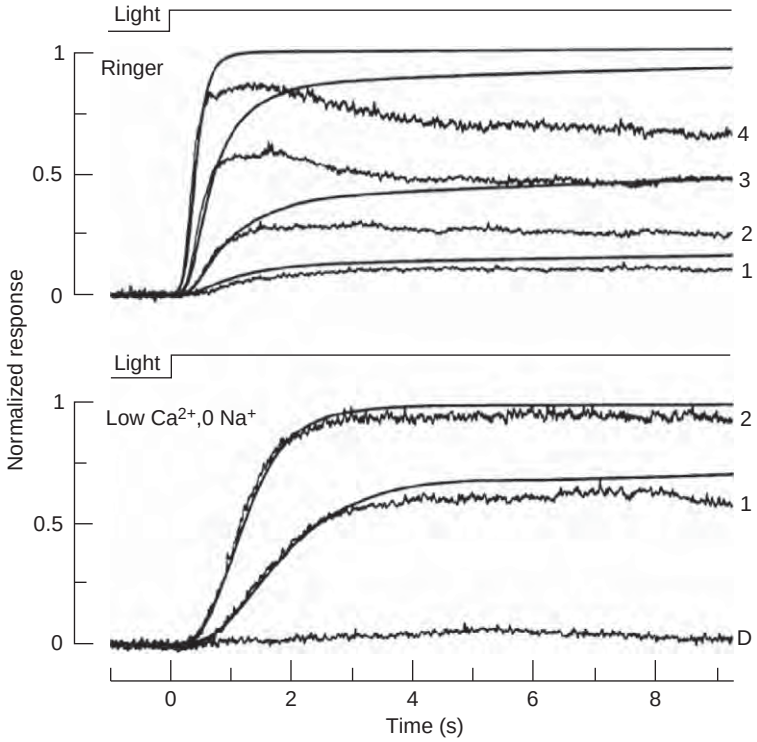

Figure 2 Responses of a salamander rod to onset of steps of light of different intensity. Upper panel: under control conditions (Ringer solution). Lower panel: in the presence of Ca^{2+}-clamping solution. The step intensities increased by factors of ~4 for traces labeled 1–4; D, darkness. The smooth curves are predictions obtained by integrating the measured dim flash response (not shown), and represent the step responses that are predicted in the absence of any adaptation. Reproduced from Fain, G. L., Lamb, T. D., Matthews, H. R., and Murphy, R. L. W. (1989). Cytoplasmic calcium as the messenger for light adaptation in salamander rods. *Journal of Physiology* 416: 215–243.

Desensitization and Acceleration

The manner in which background illumination modifies the rod's response to a dim test flash is illustrated in **Figure 3**. The uppermost trace is for a dim flash presented in darkness, while the remaining traces are for exactly the same flash presented on backgrounds of successively higher intensity. Characteristically, the flash response becomes progressively more desensitized and accelerated with backgrounds of higher intensity. Thus, the peak of the incremental flash response moves downward and leftward as the background intensity increases.

By plotting the peak amplitude of the flash response as a function of the background intensity upon which it was elicited, one obtains a plot of the kind indicated by the red symbols in **Figure 1**, where sensitivity declines according to Weber's law, given above in eqn [1].

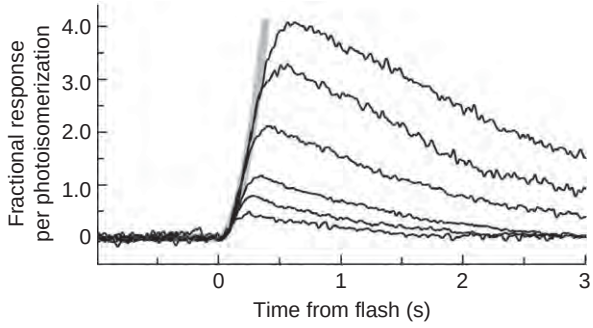

Figure 3 Dim flash responses of a salamander rod obtained in the dark (top trace) or in the presence of backgrounds of progressively higher intensity**.** Each trace was obtained by taking the raw response and dividing by the circulating current, and then dividing by the flash intensity. Reproduced from Pugh, E. N., Jr., Nikonov, S., and Lamb, T. D. (1999). Molecular mechanisms of vertebrate photoreceptor light adaptation. *Current Opinion in Neurobiology* 9: 410–418.

Unaltered Rising Phase, but Accelerated Recovery

For the incremental flash responses in **Figure 3**, the vertical scale has been adjusted to take account of changes in the level of circulating current remaining in the presence of the different background intensities. Thus, rather than plotting raw sensitivity (response per photoisomerization), **Figure 3** instead plots the fractional response

(i.e., the incremental response as a fraction of the circulating current at that background) per photoisomerization. This has been done in order to provide a direct measure of the level of activation of the guanine nucleotide-binding protein (G protein) cascade of phototransduction; thus, it can be shown that the level of cascade activation is best measured by the fractional channel opening, which in turn is measured by the incremental response expressed as a fraction of the existing circulating current. When plotted in this manner, the incremental responses in **Figure 3** demonstrate the remarkable property that the onset phase of the response is invariant; that is, the traces for different background intensities exhibit a common rise at early times, indicated by the smooth gray trace. This behavior indicates that the amplification parameter describing the activation steps in phototransduction is unaltered during light adaptation; in other words, light adaptation causes no change in the efficacy of the activation steps in phototransduction. Instead, it is clear that light adaptation causes a marked speeding up of the shut-off steps in the transduction cascade. The molecular identity of the steps that are accelerated is analyzed below.

Saturation of the Rod Photocurrent at Higher Background Intensities

At higher background intensities, the rod circulating current is completely suppressed. Thus, in the upper panel of **Figure 2**, intensities higher than those labeled 4 cause the response simply to rise to its maximum level (corresponding to the closure of all cyclic guanosine monophosphate (cGMP)-gated channels in the outer segment) and, as a result, incremental stimuli are unable to elicit any incremental response so that the cell's response is saturated. Typically, such saturation sets in exponentially with increasing background intensity, as described by the second term on the right of eqn [1].

Calcium-Dependent Mechanisms of Rapid Light Adaptation in Rod Photoreceptors

The mechanisms that contribute to light adaptation in photoreceptors (i.e., to the alteration in response properties of the photoreceptors upon exposure to background illumination) are closely associated with the mechanisms of response recovery. These mechanisms of adaptation can be classified broadly as (1) those that are calcium dependent and (2) those that do not involve calcium. Both categories are important; yet, the noncalcium-dependent mechanisms have frequently been overlooked.

Role of Calcium: Resensitization through Prevention of Saturation

When cGMP-gated ion channels in the outer segment are closed in response to light, the cytoplasmic concentration of calcium drops. This drop in Ca^{2+} concentration is vitally important to light adaptation, though it is crucial to emphasize that it does not cause the desensitization that characterizes photoreceptor light adaptation. Quite the contrary: the drop in Ca^{2+} concentration actually rescues the rod from the saturation that would otherwise be induced by light, and thereby prevents the onset of massive desensitization at relatively low intensities of background illumination. Thus, the light-induced drop in Ca^{2+} acts to increase the rod's sensitivity above the drastically reduced level that would occur either if the Ca^{2+} concentration did not alter or if the rod's calcium-dependent mechanisms were inoperative.

Powerful Negative-Feedback Loop Mediated by Calcium

Calcium is the cytoplasmic messenger for a very powerful negative-feedback loop that tends to stabilize the rod's circulating current. If ever the Ca^{2+} concentration drops (e.g., in response to light, or as a result of some other perturbation), then, as described below, a number of changes occur very rapidly. These changes are stimulated by the unbinding of Ca^{2+} from at least three classes of calcium-sensitive protein: (1) guanylyl cyclase activator proteins (GCAPs) 1 and 2, which activate guanylyl cyclase; (2) recoverin, which regulates the lifetime of activated rhodopsin; and (3) calmodulin, which modulates the opening of cGMP-gated channels. Calcium's action via each of these pathways leads to the opening of cGMP-gated channels, thereby increasing the circulating current and admitting Ca^{2+} ions from the extracellular medium. This influx of Ca^{2+} ions tends to counteract the initial reduction in Ca^{2+} concentration, thereby completing a negative-feedback loop.

Each of these molecular mechanisms contributing to the calcium negative-feedback loop contributes toward extending the rod's operational range of light intensities by helping prevent saturation of the circulating current. Thus, each of these three molecular mechanisms assists in rescuing the rod from saturation and hence increasing, rather than decreasing, the rod's sensitivity compared with the case that would exist if the mechanism were absent. Each of the three mechanisms is most effective over some range of calcium levels, and a corresponding range of light intensities. Overall, the most powerful of the three (at least in rods) is the GCAPs' activation of guanylyl cyclase.

Since the various components of the calcium negative-feedback loop act quite rapidly, they contribute to determining not only the photoreceptor's sensitivity in the

presence of background illumination, but also the kinetics of its response to an incremental flash presented on the background. The importance of altered Ca^{2+} concentration in setting the incremental flash response kinetics can be demonstrated by incorporating a calcium buffer (such as 1,2-bis(o-aminophenoxy)ethane-N,N,N′,N′-tetraacetic acid (BAPTA)) into the outer segment. Although the flash response begins rising exactly as in control conditions, it does not begin recovering as soon and, instead, rises to a substantially larger and later peak with slower final recovery (see also **Figure 4**).

Three Calcium-Sensitive Molecular Pathways

Guanylyl cyclase activation

In response to a drop in calcium concentration, Ca^{2+} will unbind from the GCAP proteins (GCAP1 and GCAP2), thereby activating guanylyl cyclase and stimulating the production of cGMP at a greatly increased rate, leading to the opening of cGMP-gated channels.

The cyclase activity increases roughly as the fourth power of the drop in Ca^{2+} concentration, and furthermore (as also applies for the other two routes considered below), the number of channels open increases approximately as the cube of the cGMP concentration. Because of the cascading of two such steep dependencies, any small fractional change in Ca^{2+} concentration stimulates a large and opposite fractional change in channel opening; that is, the fractional change in channel opening is opposite in sign to, and up to 12× the magnitude of, the originating fractional change in Ca^{2+} concentration. As a result, this molecular mechanism is the most potent of the three that contribute to the calcium negative-feedback loop and, hence, to setting the adaptational state in rods. It is especially dominant at relatively bright background intensities, corresponding to low Ca^{2+} concentrations, and is therefore the most important in extending the rod's operating range to high intensities.

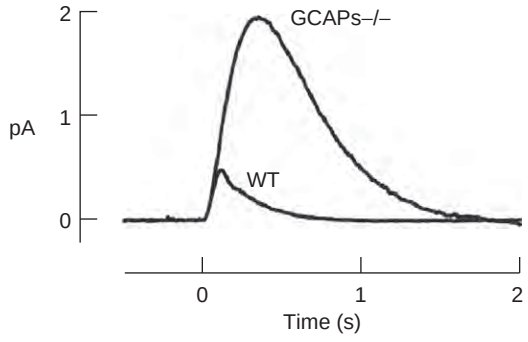

Figure 4 Single-photon responses from rods of wild-type (WT) and GCAPs knock-out (GCAPs−/−) mice. Suction pipette recordings from single rods, analyzed to extract the mean response to a single photoisomerization. Circulating current in rods of both strains averaged 12 pA. Reproduced from Burns, M. E., Mendez, A., Chen, J., and Baylor, D. A. (2002). Dynamics of cyclic GMP synthesis in retinal rods. *Neuron* 36: 81–91.

The role of the GCAPs/guanylyl cyclase component of the Ca^{2+} feedback loop in setting the waveform of the incremental flash response is illustrated in **Figure 4**, where averaged responses are shown for two classes of rod: rods from wild-type (WT) mice and rods from GCAPs knock-out mice. In a manner very similar to that seen in rods containing the calcium buffer BAPTA, the response in the GCAPs knockout case begins rising exactly as for the control (WT) case, but it does not recover as soon; therefore, the response continues rising and reaches a larger and later peak.

Shortened R lifetime*

Activated rhodopsin (R*) is inactivated by multiple phosphorylation steps mediated by rhodopsin kinase (GRK1) followed by binding of arrestin. It is generally assumed that the decline in R* activity follows exponential kinetics, and can therefore be described by a characteristic lifetime, τ_R; however, it is worth bearing in mind that there is no direct evidence for this assumption. It was established by Satoru Kawamura that GRK1's phosphorylation of R* is calcium dependent and that the effect is mediated by the calcium-binding protein recoverin. The molecular mechanism of this dependence is not entirely clear; however, some evidence suggests that the calcium-bound form of recoverin binds to GRK1, thereby preventing it from interacting with R*. In any case, it is proposed that a reduction in Ca^{2+} concentration leads to a shortened R* lifetime, τ_R.

The slowest time constant in the phototransduction cascade (the so-called dominant time constant, τ_{dom}) can be estimated from the steepness of the relationship between the duration that the rod is held in saturation by a bright flash and the flash intensity. Over the years, there has been considerable debate as to whether this dominant time constant is set by the R* lifetime, τ_R, or, instead, by the lifetime τ_E of the transducin–phosphodiesterase (PDE) complex (the effector). The situation may be species dependent; however, in mouse rods, it has now been clearly established by Marie Burns' group that, under dark resting conditions, the dominant time constant is that of transducin–PDE, with $\tau_E \approx 200$ ms, while the R* lifetime is shorter, with $\tau_R \leq 80$ ms. In the scenario where the R* lifetime is shorter than the transducin–PDE lifetime, further light-induced shortening of τ_R is likely to have very little effect on the response kinetics, but will instead cause a reduction in sensitivity because fewer molecules of transducin will be activated during the R* lifetime.

Although it remains difficult to establish the effectiveness of any individual mechanism in an intact rod with a functional calcium feedback loop, it appears that the recoverin-mediated reduction in R* lifetime plays a moderate role, especially at relatively low background intensities.

Channel reactivation

In response to a drop in calcium concentration, Ca^{2+} unbinds from calmodulin (in the case of the rods), leading to a lowered dissociation constant ($K_{½}$) for the binding of cGMP to the channels. The effect of the lowered $K_{½}$ is that any given concentration of cGMP will cause the opening of a larger fraction of the cGMP-gated channels, leading to an increase in circulating current and the influx of more calcium. However, the potency of this effect is low in rods, and the mechanism contributes only weakly to rod adaptation. In contrast, cones possess a much more powerful mechanism, mediated by a different calcium-sensitive protein.

Rod Photoreceptor Light Adaptation Independent of Calcium

There are at least three classes of noncalcium-dependent phenomena that represent mechanisms of light adaptation in rod photoreceptors, insofar as the properties of the response to light are altered in comparison with the dark-adapted state. First, there is response compression, whereby the reduced level of circulating current in the presence of steady background illumination reduces the size of the flash response. This phenomenon will not be discussed here, in part because it is both very well known and very simple and also because (in philosophical terms) it can be viewed as a failure of light adaptation; in comparison, cones cope much better and effectively avoid response compression by feedback mechanisms that maintain the circulating current. Second, there is pigment depletion. However, this is never relevant in rod light adaptation because the rods are driven into saturation even by very low levels of bleached pigment (see section titled 'Dark adaptation of the rods: Very slow recovery from bleaching'). Third, there is a direct effect of PDE activation, which is now considered.

Accelerated Turnover of cGMP

In a rod outer segment in darkness, the activity of the PDE is low; therefore, the turnover rate constant for cGMP (denoted β) is low, with a correspondingly long turnover time constant for cGMP, $\tau_{cGMP} = 1/\beta$, of around 1 s in amphibian rods and around 200 ms in mammalian rods. The magnitude of this parameter has a major effect on both the sensitivity and the kinetics of the rod's response to a flash. Thus, when the PDE activity increases in steady illumination, the shorter turnover time for cGMP contributes to both desensitization and acceleration of the photoresponse (compared with the case that would have applied, had the steady level of PDE activity not increased).

To provide an intuitive understanding of this mechanism, it is helpful to consider what we have referred to previously as the bathtub analogy. Imagine a container of water, such as a tall cylinder, and let the height of water in the cylinder represent the level (concentration) of cGMP in the outer segment. The rate at which water runs out of the cylinder, through a drain hole at the base, is proportional both to the height of water and to the size of the opening, representing the cGMP level and the PDE activity, β, respectively. Likewise, the rate at which water flows in to the cylinder through a tap at the top represents the activity of guanylyl cyclase, α. When a steady state is reached, the height of water will equal the rate of influx divided by the size of the drain hole; that is, $cGMP = \alpha/\beta$. Importantly, whenever the water level is perturbed from this steady-state level (e.g., upon a brief opening of an additional drain hole), the level will re-equilibrate with a time constant $\tau_{cGMP} = 1/\beta$ (provided that the rate of influx through the tap remains constant). Hence, if the drain hole is small (and the inflow via the tap correspondingly small), then any perturbation in water level elicited by a transient additional outflow will be corrected only slowly; if the drain hole is large (and the influx correspondingly large), then any perturbation will be rapidly corrected. Furthermore, though perhaps less intuitively, it can be shown that for a noninstantaneous perturbation, corresponding to the normal flash response, not only will the kinetics of recovery be faster, but the peak also will be smaller.

Hence, the effect of the increased PDE activity during steady illumination is both to accelerate the response kinetics and to reduce the peak amplitude (i.e., reduce the sensitivity) to an incremental flash. Calculations show that in rods the 20-fold increase in β during steady illumination provides the primary mechanism underlying the measured shortening of the time to peak and the decrease in flash sensitivity.

Slow Changes in Rods: Light Adaptation or Dark Adaptation?

In addition to the conventional features of rod photoreceptor light adaptation that occur extremely rapidly (on a subsecond time scale), other changes have been reported to occur over a time frame of minutes of exposure, in response to lights that saturate the cell's response. As the effects of these changes are very slow, and can only be observed in darkness when the adapting exposure is extinguished, there is a semantic issue as to whether these phenomena should be thought of as light adaptation or as dark adaptation.

Light-Induced Change in the Dominant Time Constant

It has recently been shown by Marie Burns' group that exposure of mouse rods to a just-saturating intensity of

around 1000 photoisomerizations per second, for 1 min or more, leads to a persistent speeding of the bright-flash response upon extinction of the background. The change did not involve any reduction in the activation phase of transduction, but instead involved a reduction in the dominant time constant of response recovery; typically, the dominant time constant τ_{dom} dropped from around 200 ms under dark-adapted conditions to around 100 ms immediately after extinction of the saturating light. The adaptational effect developed relatively slowly, building up over 60 s or so, and it required a rhodopsin bleach level of around 2% for full effect. The effect was relatively long lasting, declining with a time constant of around 80 s.

The molecular mechanism giving rise to this adaptational effect is not known, though some evidence suggests that it corresponds to a reduction in lifetime of the activated transducin–PDE complex. If so, it represents a phenomenon distinct from the actions of dimmer adapting lights.

Light-Induced Translocation of Proteins

The light-induced translocation of transducin, recoverin, and arrestin in photoreceptors is dealt with in detail elsewhere in this encyclopedia and, therefore, mentioned only briefly here. Movements of protein are elicited only at quite bright intensities (generally in the saturating range) and occur over a time scale of many minutes. In mouse rods, intensities above 3000 photoisomerizations per second for 30 min (which bleach a substantial fraction of the rhodopsin) trigger the movement of transducin from the outer segment to the inner segment, while slightly lower intensities of 1000 photoisomerizations per second or more trigger the movement of arrestin in the opposite direction; recoverin also leaves the outer segment in bright light.

Protein movements of these kinds may well affect the adaptational state of the rod, though this is yet to be established clearly. Since the movements are triggered only by saturating light intensities, the electrical effects cannot readily be observed during the illumination because the circulating current is completely suppressed. One possibility is that the protein translocation contributes to some form of conservation – for example, lowering the guanosine 5′-triphosphate (GTP) consumption involved in the continual (and maximal) activation of transducin during daylight conditions. Alternatively, it may be that the changes help prepare the rod for its return to lower intensities, as occurs around dusk. Interestingly, in one attempt that was made to detect any change in the amplification constant of human rods (using the electroretinogram (ERG)) following exposures to intensities that elicit transducin translocation in mouse rods, no change in amplification was detectable.

Dark Adaptation of the Rods: Very Slow Recovery from Bleaching

Following exposure of our eye to very intense illumination, our visual threshold is greatly elevated and may take tens of minutes to recover fully. Closely comparable effects can be measured in the overall visual system and at the level of the rod photoreceptors or the rod bipolar cells. The slow recovery of sensitivity is referred to as dark adaptation or bleaching adaptation; however, it should be noted that this use of the term adaptation is something of a misnomer. Adaptation normally refers to beneficial adjustments; yet, the changes that accompany intense illumination are distinctly disadvantageous – thus, there can be no advantage in being almost blind following exposure to intense light.

The recovery of visual threshold for a human subject is plotted in **Figure 5**, following the cessation of nine light exposures that bleached from 0.5% to 98% of the rhodopsin. For a bleach of 20%, the visual threshold was initially elevated by 3.5 log units. This indicates that the elevation of threshold is out of all proportion to the fraction of pigment remaining unbleached; even though 80% of the rhodopsin remained functional, the threshold was raised 3000-fold. Instead, there is overwhelming evidence that the phenomenon arises from the presence within the outer segment of unregenerated opsin (i.e., the presence of the protein part of the visual pigment, prior to its recombination with the regenerated 11-*cis* retinal).

Remarkably, the recovery of scotopic (rod-mediated) threshold exhibits a region of common slope across all the bleach levels, as indicated by the parallel red lines in **Figure 5**. This region is termed the S2 component of recovery, and has a slope $\Psi_{S2} = -0.24$ log unit min^{-1} that is characteristic of dark adaptation recovery in normal (young adult) human eyes; also characteristic is the nature of the rightward shift of the recovery traces as a function of increasing bleach level – the form of this shift is as expected for a rate-limited (zero-order) recovery process, as distinct from an exponential (first-order) recovery process.

From a detailed analysis of results of this kind, in combination with knowledge of the retinoid cycle, Trevor Lamb and Edward Pugh developed a cellular model that can account for human dark adaptation behavior. They postulated that (1) the presence of opsin (without chromophore) gives rise to a phenomenon closely equivalent to light, through activation of the G protein cascade of transduction and (2) the elimination of opsin via its reconversion to rhodopsin follows rate-limited kinetics because of a limitation in the supply of 11-*cis* retinal that results from the movement of this substance from a pool in the retinal pigment epithelium.

Application of this cellular model has provided an accurate account of (1) the regeneration of visual pigment

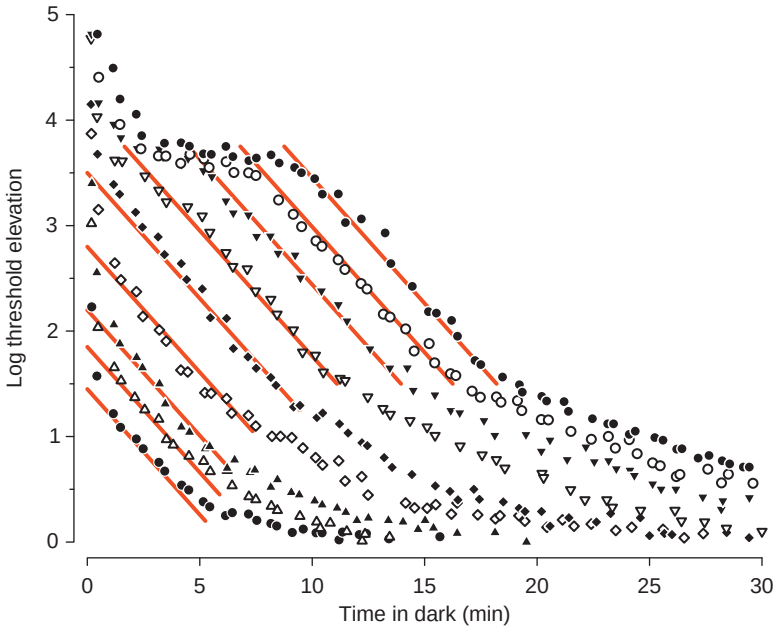

Figure 5 Human psychophysical dark adaptation. Recovery of log threshold elevation in a normal human observer is plotted as a function of time in darkness, after a wide range of bleaching exposures (from 0.5% to 98%). Parallel red lines represent component S2, with a slope of –0.24 decades min^{-1} (see text). The lateral shift between the lines is consistent with the rate-limited delivery of 11-*cis* retinal from the RPE to opsin in the outer segments. Reproduced from Lamb, T. D. and Pugh, E. N., Jr. (2006). Phototransduction, dark adaptation, and rhodopsin regeneration. The Proctor Lecture. *Investigative Ophthalmology and Visual Science* 47: 5138–5152, with permission of the Association for Research in Vision and Ophthalmology.

in humans and other mammals, measured by retinal densitometry; (2) normal human dark adaptation behavior (as in **Figure 5**); and (3) the slowed regeneration of pigment and the slowed dark adaptation that is characteristic of a number of diseases that affect the photoreceptors and/or retinal pigment epithelium.

See also: Light-Driven Translocation of Signaling Proteins in Vertebrate Photoreceptors; Phototransduction: Adaptation in Cones; Phototransduction: Inactivation in Rods; Phototransduction: Phototransduction in Rods; Phototransduction: The Visual Cycle.

Further Reading

Cameron, A. M., Mahroo, O. A. R., and Lamb, T. D. (2006). Dark adaptation of human rod bipolar cells measured from the *b*–wave of the scotopic electroretinogram. *Journal of Physiology* 575: 507–526.

Krispel, C. M., Chen, C-K., Simon, M. I., and Burns, M. E. (2003). Novel form of adaptation in mouse retinal rods speeds recovery of phototransduction. *Journal of General Physiology* 122: 703–712.

Lamb, T. D. and Pugh, E. N., Jr. (2004). Dark adaptation and the retinoid cycle of vision. *Progress in Retinal and Eye Research* 23: 307–380.

Lamb, T. D. and Pugh, E. N., Jr. (2006). Phototransduction, dark adaptation, and rhodopsin regeneration. The Proctor Lecture. *Investigative Ophthalmology and Visual Science* 47: 5138–5152.

Nikonov, S., Lamb, T. D., and Pugh, E. N., Jr. (2000). The role of steady phosphodiesterase activity in the kinetics and sensitivity of the light-adapted salamander rod photoresponse. *Journal of General Physiology* 116: 795–824.

Pugh, E. N., Jr. and Lamb, T. D. (2000). Phototransduction in vertebrate rods and cones: Molecular mechanisms of amplification, recovery and light adaptation. In: Stavenga, D. G., de Grip, W. J., and Pugh, E. N., Jr (eds.) *Handbook of Biological Physics, Vol. 3, Molecular Mechanisms of Visual Transduction, ch. 5*, pp. 183–255. Amsterdam: Elsevier.

Pugh, E. N., Jr., Nikonov, S., and Lamb, T. D. (1999). Molecular mechanisms of vertebrate photoreceptor light adaptation. *Current Opinion in Neurobiology* 9: 410–418.

Tamura, T., Nakatani, K., and Yau, K-W. (1991). Calcium feedback and sensitivity regulation in primate rods. *Journal of General Physiology* 98: 95–130.

Phototransduction: Inactivation in Cones

V V Gurevich and E V Gurevich, Vanderbilt University, Nashville, TN, USA

Glossary

Arrestin – A protein that selectively binds light-activated phosphorylated photopigment and blocks further signal transduction. Cones express two subtypes, arrestin1 and arrestin4 (often termed rod and cone arrestins, respectively).
Cone opsins – Light receptors, consisting of the protein part (opsin) and 11-*cis*-retinal covalently attached via Schiff base to a lysine in the seventh transmembrane domain. All opsins are members of superfamily of G-protein-coupled receptors (GPCRs), the largest family of signaling proteins in animals (mammals have ~1000 different GPCRs).
GCAP – Guanylyl cyclase activating protein is a member of the superfamily of EF-hand-containing calcium-binding proteins. Cones express two homologs, GCAP1 and GCAP2, which in the calcium-liganded form inhibit and in magnesium-liganded form enhance the activity of retinal guanylyl cyclase (retGC).
GRKs – G-protein-coupled receptor kinases that specifically phosphorylate active forms of their cognate receptors. Cones express rhodopsin kinase (systematic name: GRK1) and a cone-specific form GRK7. However, mice do not have GRK7; therefore, photopigments in mouse cones and rods are phosphorylated by a single isoform, GRK1.
Phosphodiesterase (PDE) – The photoreceptor-specific cyclic guanosine monophosphate (cGMP) PDE, PDE6. Cone PDE6 is a heterotetramer, consisting of two identical catalytic α'-subunits and two inhibitory γ-subunits. PDE rapidly hydrolyzes cGMP upon its activation by transducin, when its catalytic activity approaches the theoretical limit set by the rate of cGMP diffusion.
RetGC – Retinal guanylyl cyclase is structurally related to receptor guanylyl cyclases. Cones predominantly express RetGC1, in contrast to rods that express RetGC1 and RetGC2 at comparable levels.
RGS9-1 – Photoreceptor-specific short isoform of the regulator of G-protein signaling 9 expressed in both rods and cones. It interacts with the complex of the guanosine triphosphate (GTP)-liganded active α-subunit of transducin with PDEγ and facilitates its intrinsic GTPase activity, thereby directly inactivating transducin and indirectly PDE. Cones express much more RGS9-1 than rods.
Transducin – Photoreceptor-specific heterotrimeric G protein that couples to light-activated opsins. Its α-subunit belongs to Gi/o family. All types of cones express the same α-subunit that is different from the rod variant.

Rod photoreceptors are often described as a marvel of molecular engineering, which creates an impression that cones are just noisier and less-sensitive rods. In fact, as light sensors, cones are just as amazing: their adaptability gives cones a much wider dynamic range covering more than seven orders of magnitude of light intensity without saturation. Cones begin to function in the light of the full moon reflected from objects in the night and are still adequate for a direct look at the sun. Mostly for technical reasons, the biochemistry of cone photoreceptors, particularly the molecular mechanisms underlying adaptation, is not as well studied as the signaling in rods. The assumption that the signaling and shutoff mechanisms in cones and rods are qualitatively similar is often used to fill the gaps in our knowledge of cone biochemistry. To avoid repetition, here we emphasize known differences between the cone and rod inactivation mechanisms.

Cone Signaling Cascade

Cone opsins are closely related to rhodopsin and belong to the same branch of the G-protein-coupled receptor superfamily. Gene duplication events in early vertebrate evolution produced five groups of light receptors: rhodopsins and four classes of cone opsins. Mammals lost half of cone opsin classes, retaining only two. Light activates cone opsins via induced isomerization of 11-*cis*-retinal covalently attached to a lysine in the seventh transmembrane domain. Cone opsins use the same 11-*cis*-retinal as rhodopsin, but have very different spectral sensitivity, with maxima ranging from 360 nm (ultraviolet) to 575 nm (red). Spectral tuning of covalently linked retinal is achieved by changing its environment in the retinal-binding pocket of opsin. Light-activated cone opsins couple to cone transducin, which, in turn, activates the cone subtype of phosphodiesterase 6 (PDE6). Subsequently,

a decrease of cytoplasmic cyclic guanosine monophosphate (cGMP) reduces the influx of Na^+ and Ca^{2+} through the cone variant of cGMP-gated channels, resulting in cell hyperpolarization. Similar to rods, the decrease in Ca^{2+} concentration and consequent replacement of bound Ca^{2+} with Mg^{2+} converts guanylate cyclase activating proteins (GCAPs) from inhibitors to activators of retinal guanylate cyclase (RetGC). The latter replenishes cGMP lost during the light response, which opens the channels, thereby restoring cytoplasmic Ca^{2+} to the original levels. Thus, the activation and deactivation mechanisms employed by rods and cones are quite similar. However, subtle differences at every step of the pathway, including differences in the subtypes of signaling proteins involved, their expression levels, and the geometry of the cell, result in striking functional specialization of the two types of photoreceptors.

Shutoff of the Light-Activated Cone Opsins

As far as signaling is concerned, the key difference between rhodopsin and cone opsins is lower thermal stability of the latter. Because cone opsins spontaneously activate with much higher probability than rhodopsin and readily release retinal even in the dark, cones generate noise that is orders of magnitude higher than in rods. This rules out the detection of signals below the noise level (e.g., a few photons) and makes even completely dark-adapted cones pre-desensitized and ready to operate at light levels they can detect. Loose attachment of the retinal to opsin also results in a significantly faster spontaneous decay of the light-activated cone opsin. For example, mouse cone S-opsin transgenically expressed in rods lacking arrestin was estimated to decay ~40 times faster than rhodopsin coexpressed in the same cell. However, this spontaneous decay with a time constant of ~1.3 s is still much slower than the rate of recovery in cones.

Evolution equipped cones with a more elaborate (and presumably more efficient) photopigment shutoff machinery than that found in rods. The opsin inactivation is accelerated by pigment phosphorylation followed by arrestin binding. In most species, cones express two G-protein receptor kinase (GRK) subtypes: GRK1 (shared with rods) and cone-specific GRK7. It is likely that the co-expression of GRK7 with higher enzymatic activity accelerates opsin phosphorylation in cones. However, it should be noted that mice and rats are rare exceptions: these nocturnal rodents have only GRK1 in both types of photoreceptors. Cones also express two arrestin subtypes, arrestin1 and cone-specific arrestin4 (formerly known as rod and cone arrestins, respectively). Arrestin1 is present in cones at ~50-fold molar excess over arrestin4. A recent study in knock-out animals shows that both arrestins contribute comparably to the shutoff of the photopigment in cones. It is not entirely clear why cones express two arrestin subtypes, rather than a higher level of one subtype, especially considering that the cone opsin transgenically expressed in mouse rods is rapidly and efficiently deactivated by rod arrestin1.

Two functional differences between these arrestins provide some clues. Arrestin1 has high propensity to self-associate, cooperatively forming dimers and tetramers at physiological concentrations. Even in the dark-adapted rod, where the outer segment contains a small fraction of the total arrestin1, most of arrestin1 is a tetramer. It has been unambiguously shown that only monomeric arrestin1 is an active rhodopsin-binding species; therefore, oligomers appear to be storage forms. In contrast, cone-specific arrestin4 does not self-associate at physiologically relevant concentrations; therefore, the whole complement of arrestin4 present in cones is an active monomer. Recent estimates of their expression and arrestin1 self-association constants suggest that dark-adapted cones have in the outer segment ~60 μM of arrestin4 and ~30 μM (5% of the total) of monomeric arrestin1 ready to bind phosphorylated opsin at any time, in addition to a huge backup supply of arrestin1 oligomers.

The second important difference lies in the stability of the arrestin complex with phosphorylated opsin. Arrestin1 forms very stable complexes that take the bound molecule of phosphopigment out of the game for a long time. This is important in the rod to ensure the fidelity of the shutoff. In order to release completely inactive rhodopsin upon dissociation, arrestin1 must stay bound until metarhodopsin II (Meta II) slowly decays and likely until it is regenerated with 11-*cis*-retinal. In contrast, arrestin4 forms fairly transient complexes with phosphorylated cone opsins, likely to ensure the quick return of the opsin back into the active pool. This is important for cone photoreceptors that function at a high rate of pigment bleaching. Although we do not know with certainty why cones express both arrestin subtypes, one scenario appears to provide a plausible explanation. Given the concentrations of the two arrestins in cones, in moderately bright light arrestin4 likely has an advantage, so that the majority of phosphorylated cone opsin would be rapidly recycled to the signaling-competent pool. Increasing levels of illumination inducing massive pigment bleaching would force the cell to draw increasingly on the virtually inexhaustible supply of arrestin1, which forms long-lived complexes with the opsin. The recent finding that arrestin1 plays a more prominent role in cone recovery after very bright flashes is consistent with this model. The formation of arrestin1-opsin complexes would take larger and larger fraction of the pigment out of action for a relatively long time, possibly serving as one of the mechanisms of light adaptation. Even though a cone-specific visual cycle involving

Müller glia provides 11-*cis*-retinal faster than the canonical retinal pigment epithelium-based visual cycle supplying rods, very bright light bleaches cone pigment faster than it can be regenerated. This loss of functional opsin was proposed to reduce light capture, acting as a mechanism of adaptation. It is entirely possible that in bright light, both incomplete regeneration of opsin and its binding by arrestin1 cooperate to limit the active pool, thereby reducing light sensitivity of cones.

Overall, cones combine less-stable photopigment with more sophisticated machinery of its inactivation (**Figure 1**). These factors apparently contribute to faster shutoff at the opsin level and likely provide cone-specific mechanisms for light adaptation.

Inactivation of Transducin and PDE

It is generally accepted that the activation of cone transducin by cone opsins and that of cone PDE6 by the guanosine triphosphate (GTP)-liganded α-subunit of cone transducin proceeds in similar ways to corresponding processes in rods. All three subunits of cone transducin differ from their rod counterparts, but the significance of this specialization is uncertain. In fact, cone S-opsin transgenically expressed in mouse rods efficiently activates the signaling cascade coupling to rod transducin. Cone PDE6 is an $\alpha'_2\gamma_2$ heterotetramer, in contrast to the $\alpha\beta\gamma_2$ version in rods, but the functional significance of the use of different catalytic subunits remains to be elucidated. There is one biochemical difference that undoubtedly contributes to the much faster inactivation of transducin-PDE6 complex in cones: ~10-fold higher level of the regulator of G-protein signaling 9-1 (RGS9-1) expression. It has been convincingly shown that the deactivation at this step rate limits the recovery kinetics in rods, and that the level of RGS9-1, which accelerates self-inactivating GTPase of transducin α-subunit, sets the speed of transducin-PDE6 inactivation. Thus, the shutoff at the opsin and transducin-PDE6 level in cones is much faster than corresponding processes in rods; however, it is still not clear which step is rate limiting in cone recovery.

Restoration of cGMP and Intracellular Calcium Level

Similar to the situation in rods, cone activation results in a drop in the intracellular Ca^{2+} concentration due to the closure of the cGMP-gated channels mediating the bulk of Ca^{2+} entry. In order to return to the initial state after opsin and PDE6 are fully inactivated, cones need to restore cytoplasmic cGMP hydrolyzed by PDE6. Cones and rods use the same negative-feedback mechanism that translates the drop in Ca^{2+} resulting from the reduction in the cGMP level into a signal to make more cGMP. Ca^{2+} dissociates from GCAPs when its cytoplasmic concentration drops in the light. The replacement of lost Ca^{2+} by Mg^{2+} converts GCAPs from inhibitors to activators of RetGC. The generated cGMP opens the channels, and the consequent increase in cytoplasmic Ca^{2+} stops further cGMP synthesis. Cones apparently express the same combination of GCAP1 and GCAP2 (which differ in their Ca^{2+} sensitivity) as rods. The functional significance of the predominance of the RetGC1 isoform in cones (in contrast to similar levels of RetGC1 and RetGC2 in rods) is not clear.

Several important differences between rods and cones are known to be responsible for much faster cone recovery. First, the rate of recovery depends on the absolute amounts of cGMP and Ca^{2+} that need to be replenished. Here cones hold an obvious advantage due to the much smaller volume of their outer segments: the hydrolysis or synthesis of the same absolute amount of cGMP leads to a more significant change in its concentration. Similarly, the closure of the same fraction of cGMP-gated channels leads to a more profound drop in intracellular Ca^{2+} in cones. However, geometry is only part of the story. The channel expressed in cones has a different subunit composition and ion preference. About 35% of the inward current via the cone cGMP-gated channel is carried by Ca^{2+}, whereas in rods this fraction is only ~20%. Thus, the closure of the same fraction of channels upon PDE6 activation results in a substantially greater change in the absolute number of Ca^{2+} ions entering the cell. Increased Ca^{2+} influx in cones is balanced by its accelerated extrusion via Na^+/K^+–Ca^{2+}-exchanger, so that the turnover of Ca^{2+} in cone outer segments is more rapid. The combination of faster constitutive extrusion, larger fraction of the current carried by Ca^{2+} through cGMP-gated channels, and much smaller outer segment volume greatly increases the rate of Ca^{2+} drop in response to light stimulus, speeding up RetGC activation and cGMP resynthesis. High intracellular Ca^{2+} reduces the sensitivity of the channels to cGMP, so that when the intracellular Ca^{2+} drops, the channels become more sensitive to the cytoplasmic cGMP and therefore reopen faster. This mechanism operates in both types of photoreceptors, but it is more powerful in cones, further contributing to accelerated recovery.

Conclusions

Cone photoreceptors use essentially the same molecular mechanisms of signal shutoff at the opsin level as rods. At this step, cones achieve much higher speed of inactivation by employing, in addition to GRK1 and arrestin1

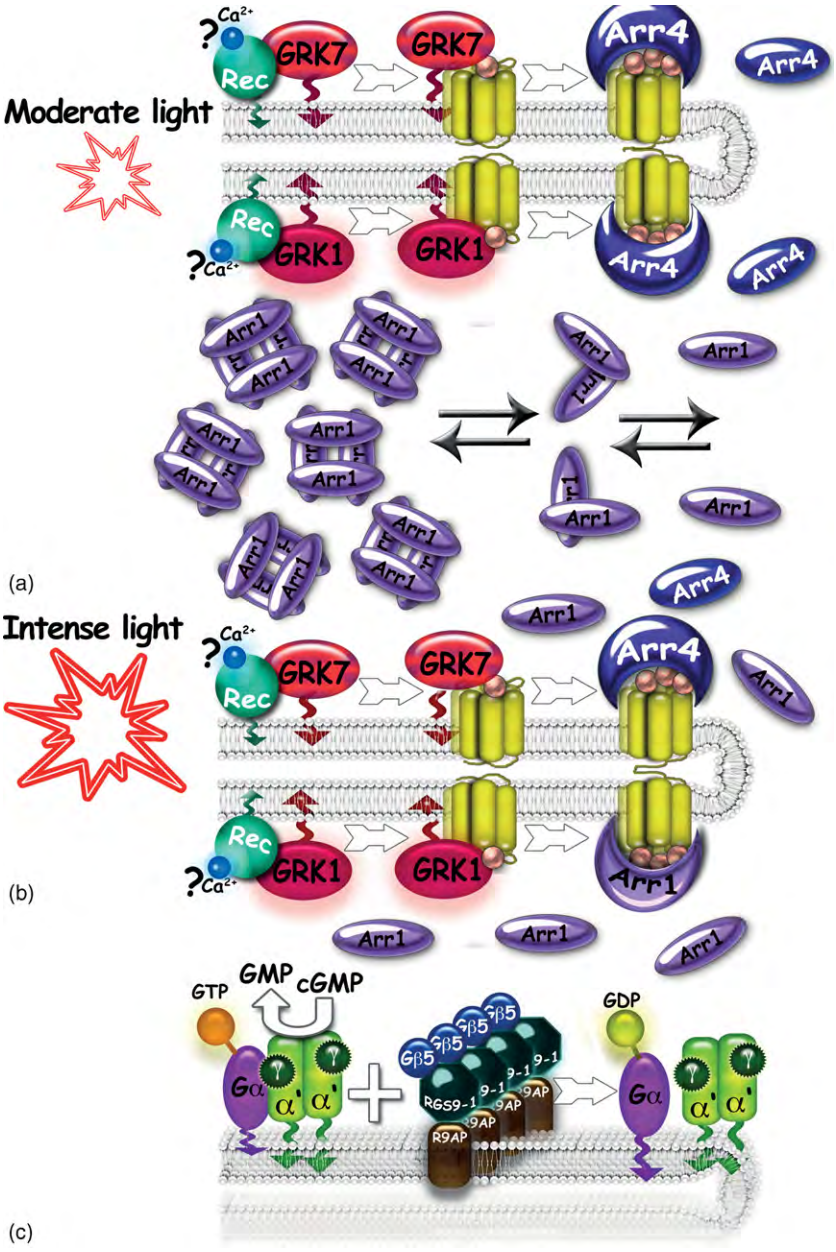

Figure 1 Biochemical mechanisms of rapid inactivation in cones. (a) Cone opsins are phosphorylated by both GRK1 and GRK7 coexpressed in cones of most vertebrates, including humans. At moderate light levels, the signaling by phosphorylated photopigment is largely quenched by constitutively monomeric arrestin4, which forms transient complexes with the receptor. (b) During massive opsin activation in very bright light, the amount of expressed arrestin4 becomes insufficient to quench all active opsins; therefore, cones increasingly use coexpressed arrestin1, which forms longer-lived complexes with phosphorylated cone opsins. The consumption of monomeric arrestin1 by the photopigment shifts its monomer–dimer–tetramer equilibrium toward dissociation of oligomers, which generates virtually inexhaustible supply of binding-competent monomer. (c) RGS9-1 is expressed at ~10-fold-higher level in cones than in rods, ensuring much faster inactivation of transducin and PDE. Cone opsin is shown as a bundle of seven transmembrane domains; opsin-attached phosphates are shown as spheres; lipid modifications anchoring recoverin, GRK1, GRK7, α-subunit of transducin, and catalytic α′-subunits of PDE are shown as membrane-imbedded arrows. Rec: recoverin, Arr1: arrestin1, and arr4: arrestin4.

used by rods, cone-specific GRK7 and arrestin4. The presence of two GRKs speeds up the phosphorylation of light-activated opsin, whereas the expression of two arrestin subtypes with very different functional characteristics likely results in a gradual switch from rapidly reversible arrestin4 interaction with phospho-opsin at moderate light levels to semi-irreversible binding of arrestin1 in very bright light. Inactivation at the transducin/PDE

level is accelerated by a 10-fold higher expression of RGS9-1 in cones. Two key features ensure faster recovery in cones than in rods. Faster Ca^{2+} turnover due to higher influx through cone-specific cGMP-gated channels and efflux via Na^{+}/K^{+}–Ca^{2+}-exchanger generate greater net changes in the number of Ca^{2+} ions in the outer segment when the same fraction of the channels is closed. Due to much smaller outer-segment volume, the same net change in the number of cGMP molecules or Ca^{2+} ions produces greater changes in the concentration of these second messengers. Rapid response and recovery gives cones better temporal resolution than rods. The high speed of activation and inactivation in combination with more powerful adaptation mechanisms (many of which still need to be elucidated at the molecular level) allows cones to function in a broad range of light levels without saturation.

See also: Phototransduction: Adaptation in Cones; Phototransduction: Inactivation in Rods; Phototransduction: Phototransduction in Cones; Phototransduction: Phototransduction in Rods; Phototransduction: Rhodopsin.

Further Reading

Cote, R. H. (2006). Photoreceptor phosphodiesterase (PDE6): A G-protein-activated PDE regulating visual excitation in rod and cone photoreceptor cells. In: Beavo, J. A., Francis, S. H., and Houslay, M. D. (eds.) *Cyclic Nucleotide Phosphodiesterases in Health and Disease*, pp 165–193. Boca Raton, FL: CRC Press.

Dizhoor, A. M., Olshevskaya, E. V., and Peshenko, V I. (2006). Calcium sensitivity of photoreceptor guanylyl cyclase (RetGC) and congenital photoreceptor degeneration: Modeling *in vitro* and *in vivo*. In: Philippov, P. P. and Koch, K.-W. (eds.) *Neuronal Calcium Sensor Proteins*, pp 203–219. New York: Nova Science Publishers, Inc.

Gurevich, V. V., Hanson, S. M., Gurevich, E. V., and Vishnivetskiy, S. A. (2007). How rod arrestin achieved perfection: Regulation of its availability and binding selectivity. In: Kisselev, O. and Fliesler, S. J. (eds.) *Signal Transduction in the Retina. Methods in Signal Transduction Series*, pp 55–88. Boca Raton, FL: CRC Press.

Hanson, S. M., Van Eps, N., Francis, D. J., et al. (2007). Structure and function of the visual arrestin oligomer. *European Molecular Biology Organization Journal* 26: 1726–1736.

Knox, B. E. and Solessio, E. (2006). Shedding light on cones. *The Journal of General Physiology* 127: 355–358.

Korenbrot, J. I. and Rebrik, T. I. (2002). Tuning outer segment Ca^{2+} homeostasis to phototransduction in rods and cones. *Advances in Experimental Medicine and Biology* 514: 179–203.

Nikonov, S. S., Brown, B. M., Davis, J. A., et al. (2008). Mouse cones require an arrestin for normal inactivation of phototransduction. *Neuron* 59: 462–474.

Phototransduction: Inactivation in Rods

V V Gurevich and E V Gurevich, Vanderbilt University, Nashville, TN, USA

Glossary

Arrestin (also known as S-antigen, 48-kDa protein, and rod or visual arrestin; systematic name: arrestin1) – A protein that selectively binds light-activated phosphorylated rhodopsin and blocks further signal transduction.

Guanylyl cyclase activating protein (GCAP) – A member of the superfamily of EF-hand-containing calcium-binding proteins. Rods express two homologs, GCAP1 and GCAP2, which in calcium-liganded form inhibit and in magnesium-liganded form enhance the activity of retinal guanylyl cyclase (retGC).

Phosphodiesterase (PDE) – Photoreceptor-specific cGMP phosphodiesterase, PDE6. Rod PDE6 is a heterotetramer, consisting of two nonidentical catalytic subunits (α- and β-) and two inhibitory γ-subunits. PDE6 rapidly hydrolyzes cyclic guanosine monophosphate (cGMP) upon its activation by transducin. In fully activated state, its catalytic activity approaches the limit set by the rate of cGMP diffusion.

RetGC – It is structurally related to receptor guanylyl cyclases. Rods express comparable levels of two homologs, RetGC1 and RetGC2.

Regulator of G-protein signaling 9 (RGS9-1) – Photoreceptor-specific short isoform of the regulator of G-protein signaling 9 expressed in both rods and cones. It interacts with the complex of the guanosine triphosphate (GTP)-liganded active α-subunit of transducin with PDEγ and facilitates its intrinsic GTPase activity, thereby directly inactivating transducin and indirectly PDE.

Rhodopsin – Light receptor, consisting of the protein part (opsin) and 11-*cis*-retinal covalently attached via Schiff base to a lysine in the seventh transmembrane domain. A member of the superfamily of G-protein-coupled receptors (GPCRs), also known as seven transmembrane domain receptors (7TMRs), the largest family of signaling proteins in animals (mammals have $\sim$1000 different GPCRs).

Rhodopsin kinase (RK) (systematic name: GRK1) – It is a member of the G-protein-coupled receptor kinase (GRK) family expressed in both rods and cones.

Transducin – Photoreceptor-specific heterotrimeric G protein that couples to light-activated rhodopsin. Its α-subunit belongs to Gi/o family.

As light sensors, vertebrate rod photoreceptors are a remarkable evolutionary achievement: rods yield amazingly low noise despite the presence of 10^8–10^9 molecules of the light receptor rhodopsin, and demonstrate single-photon sensitivity and a dynamic range of seven orders of magnitude of light intensity. This level of perfection is achieved through several unique structural and biochemical adaptations. The rod outer segment (OS) is a specialized signaling compartment containing rhodopsin molecules tightly packed in disks. It is separated from the inner segment (IS), which is a mitochondria-rich power station providing huge amounts of energy. Several soluble signaling proteins move between the two compartments depending on the illumination, ensuring their on-demand delivery to the OS. The OS concentrations of transducin (Td) and arrestin, the proteins that transmit and shut down rhodopsin signaling, respectively, change by at least 10-fold. An important functional feature of the rod is that every biochemical step in the pathway between photon capture and the change in synaptic output has its own dedicated shutoff mechanism.

What Needs to Be Inactivated: Overview of the Signaling Cascade

Rhodopsin activation by a photon of light is the first step in visual signaling. Due to extremely high concentration of its cognate G protein, Td, and rapid diffusion of both active rhodopsin (Rh*) and Td in the plane of the disk membrane, Rh* activates a molecule of Td every few milliseconds, generating 50–100 active Td (Td*) during its lifetime. These events occur in the two-dimensional space on the cytoplasmic surface of disk membranes. Each Td* binds the inhibitory γ-subunit of cyclic guanosine monophosphate (cGMP) phosphodiesterase (PDE6), turning the enzyme on. Each molecule of active PDE6 hydrolyzes several cGMP molecules per millisecond, producing a rapid drop in the cGMP concentration in the three-dimensional cytoplasmic space. This results in closure of cGMP-gated Na^+/Ca^{2+} channels on the

plasma membrane. In rods, light activation of a single rhodopsin translates into the hydrolysis of ~100 000 cGMP molecules. The channels are heterotetramers, with each subunit carrying a cGMP-binding site in its C-terminal domain. Highly cooperative cGMP binding to the four sites in the channel greatly increases its response to the change in cGMP concentration. The decrease of the inward current hyperpolarizes the rod, reducing neurotransmitter release in its output synapse.

Several features of the rod signaling machinery bring its light sensitivity within the range of its physical limit: the detection of single photons. First, the concentration of signaling molecules in the rod OS is orders of magnitude higher than in normal cells: ~3 mM rhodopsin (compared to low nanomolar concentrations of related receptors elsewhere), ~0.3 mM Td, ~60 μM PDE, and so on. Second, all three signaling proteins involved have much lower basal activity than their counterparts in other cells. This results in an incredibly low noise level, making signal-to-noise ratio favorable for the detection of even an extremely weak signal. Third, very efficient shutoff mechanisms at every step of the pathway rapidly terminate the signaling, allowing for an exquisite subsecond temporal resolution of mammalian rods.

Shutoff of the Light-Activated Rhodopsin

Rhodopsin is a prototypical G-protein-coupled receptor. In contrast to ~1000 other members of this superfamily, it has virtually no basal activity, because it is effectively suppressed by the covalently attached inverse agonist, 11-*cis*-retinal. Retinal is converted by light into the all-*trans* form, which is a potent agonist of rhodopsin. The fact that it remains covalently attached to the receptor (in contrast to other GPCRs where bound and free agonists are in dynamic equilibrium) ensures a powerful burst of signaling. Through a series of short-lived photoproducts, light-activated rhodopsin reaches the Metarhodopsin II (Meta II) state, which is an active form (Rh*) that couples to Td. Meta II is in equilibrium with the two other states, Meta I and Meta III, which are believed to be inactive, or at least considerably less active than Meta II. Ultimately, all-*trans*-retinal dissociates, yielding empty protein opsin, which has orders of magnitude lower ability to activate Td than Meta II. However, this spontaneous deactivation of rhodopsin is inadequate as a shutoff mechanism for two reasons. At physiological temperatures, rhodopsin decay takes about a minute, which would greatly compromise temporal resolution. Moreover, the activity of opsin, which is much higher than that of dark rhodopsin, would generate considerable noise, compromising rod sensitivity. Therefore, rods use a sophisticated two-step mechanism to achieve rapid and complete rhodopsin deactivation.

First, light-activated rhodopsin is phosphorylated by rhodopsin kinase (RK). Similar to Td, RK is activated by binding to Rh*. Therefore, it selectively phosphorylates the active form of rhodopsin. It should be noted that at low light levels, RK was reported to phosphorylate multiple rhodopsin molecules for each light-activated one, likely by targeting neighboring inactive rhodopsins in the crowded disk membrane. In mammals, RK activity is believed to be held in check by its interaction with Ca^{2+}-loaded recoverin. As a result, RK is fully unleashed only after a brief delay, which allows Td activation to continue until the Ca^{2+} concentration in the rod actually drops. However, low affinity of recoverin for Ca^{2+} ($K_D \sim 5$ μM) is the weak point of this model. Current estimates of the Ca^{2+} concentrations in the dark- and light-adapted mouse OS are ~250 nM and ~25 nM, respectively, so that only a very small fraction of recoverin would be Ca^{2+}-loaded in either. In addition, unlike RK, recoverin predominantly localizes in the inner segment. Still, rods express 50 molecules of recoverin for each RK, so a relatively small change in the Ca^{2+} occupancy of a fraction of recoverin present in the OS could conceivably play a role in RK regulation.

Phosphorylation *per se* reduces, but does not abolish the ability of rhodopsin to activate Td. In the next step, arrestin binds active phosphorylated rhodopsin (P-Rh*), shielding its cytoplasmic tip and precluding further Td interaction. Arrestin apparently remains bound until rhodopsin decays to opsin, and very likely even longer, until opsin is regenerated with 11-*cis*-retinal to the truly inactive dark rhodopsin. Arrestin has several dedicated phosphate-binding residues and other elements that specifically interact with light-activated rhodopsin independently of its phosphorylation state. These partial interactions mediate relatively low-affinity binding to dark P-Rh and unphosphorylated Rh*, respectively. Arrestin elements participating in these interactions also serve as sensors, allowing arrestin to test the functional state of the rhodopsin molecule it encounters and then quickly dissociate from its low-affinity targets, dark Rh, dark P-Rh, or Rh*. In contrast to all other forms, P-Rh* simultaneously engages both sets of elements. This turns the two sensors on at the same time, allowing the arrestin transition into a high-affinity rhodopsin-binding state. This transition involves a global conformational change in arrestin, which mobilizes additional arrestin elements for the interaction. Thus, arrestin works as a molecular coincidence detector, swinging into action only when the rhodopsin molecule it encounters is both active and phosphorylated. The model of sequential multisite interaction readily explains exquisite arrestin selectivity, that is, manifold difference in arrestin binding to Rh* and dark P-Rh on the one hand, and to its preferred target P-Rh* on the other. The salt bridge between positively charged Arg175 and negatively charged Asp296, which is one of the

intramolecular interactions holding arrestin in its basal state, was identified as the main phosphate sensor in arrestin. Rhodopsin-attached phosphates bind Arg175 and neutralize its charge, thereby breaking the salt bridge and facilitating arrestin transition into its active conformation. The reversal of either charge by targeted mutagenesis yields mutants with reduced need for rhodopsin-attached phosphates that bind Rh* with much higher affinity than wild-type protein.

Rhodopsin has multiple phosphorylation sites in its C-terminus. The issue of the number of rhodopsin-attached phosphates necessary for high-affinity arrestin binding was resolved only recently. Studies performed *in vitro* with rhodopsin carrying defined number of phosphates and *in vivo* with mice expressing rhodopsin mutants with different number of sites show that rhodopsin multi-phosphorylation is required. A single rhodopsin-attached phosphate does not appreciably increase arrestin affinity, two somewhat enhance the binding, and three phosphates are necessary for high-affinity interaction *in vitro* and for the rapid shutoff of photoresponse *in vivo*. Whereas arrestin binding does not further increase when Rh* has more than three phosphates, the presence of additional phosphorylation sites on Rh accelerates the shutoff of the photoresponse *in vivo*. This likely reflects the kinetic effect of the abundance of sites that remain available to RK on partially phosphorylated rhodopsin. For example, rhodopsin with three sites would have only one possible RK target left after the incorporation of two phosphates, whereas rhodopsin with six sites would still have four available targets at the same level of phosphorylation. Thus, supernumerary sites would ensure that the magic number of three phosphates per rhodopsin is achieved faster.

Inactivation of Td and PDE

Td is a prototypical heterotrimeric G protein consisting of α-, β-, and γ-subunits. In the inactive state, the αβγ-trimer has guanosine diphosphate (GDP) in the nucleotide-binding site of the α-subunit. In this state, lipid modifications of both α-(N-terminal myristoyl) and γ-(C-terminal farnesyl) subunits provide a fairly strong membrane anchor. This restricts the Td diffusion to the plane of the disk membrane and enforces the orientation favorable for Rh* interaction, thereby maximizing its chances of encountering active rhodopsin and being activated by it. The Td interaction with Rh* opens its nucleotide-binding pocket, whereupon GDP promptly falls out and is immediately replaced by GTP simply because the latter is much more abundant in the cytoplasm. The GTP-liganded α-subunit dissociates from Rh* and βγ-dimer. Tdα-GTP binds the inhibitory γ-subunit of cGMP PDE, greatly increasing PDE activity by relieving the inhibition. Importantly, the separation of the two parts of Td heterotrimer dramatically weakens their membrane anchoring, so that active Tdα-GTP can jump off the disk where it was generated by Rh* and activate PDE on neighboring discs, spreading the signaling in three dimensions. Due to its very high catalytic activity (kcat $\sim 2000\ s^{-1}$ per subunit), active PDE rapidly reduces cGMP concentration in its vicinity, which leads to the closure of cGMP-gated channels and hyperpolarization of the rod within milliseconds of rhodopsin activation by light (**Figure 1**).

Similar to other heterotrimeric G proteins, Tdα has GTPase activity, which serves as a built-in self-inactivation mechanism. However, the intrinsic GTPase of free Tdα is very slow. Interaction of Tdα with PDE γ-subunit increases the activity of its GTPase. The interaction of Tdα–GTP–PDEγ complex with rod-specific GTPase activating protein (GAP) increases the GTPase activity even further. GAP consists of the short isoform of RGS9, Gβ5 (homolog of G-protein β-subunits), and another protein that provides membrane anchor for the complex, RGS9 anchoring protein (R9AP). Low basal GTPase of Tdα gives it time to diffuse around searching for PDE to activate without losing the signal in the transmission. The dramatic acceleration of the GTPase activity of Tdα by the PDE and GAP ensures that the signal is terminated quickly after it is received by PDE, improving the temporal resolution of the photoreceptor cell. The recent finding that the expression of the GAP complex in rods increases the rate of the response shutoff in a dose-dependent manner convincingly demonstrated that the inactivation of Tdα–GTP–PDEγ complex is the rate-limiting step in this process. These elegant experiments also revealed that when this step is maximally accelerated, the recovery kinetics becomes dominated by some other process with the time constant of ~80 ms. This number sets the upper limit for the next slowest step, which could be one of the following: the average lifetime of active Rh*; the release of PDEγ from Tdα-GDP; reassociation of PDEγ with PDE catalytic subunits; or even the time free Tdα-GTP spends searching for PDE and/or docking to it.

Resynthesis of cGMP and Restoration of Calcium Level

Obviously, to return to its initial state and become ready to respond to the next photon with the same vigor, the rod photoreceptor needs to do more than just turn off Rh* and all Td and PDE molecules activated by it. The response leaves, in its wake, substantially reduced cytoplasmic cGMP concentration and very low intracellular calcium due to the closure of the cGMP-gated channels that are responsible for the bulk of Ca^{2+} entry into the OS. Photoreceptors are equipped with an

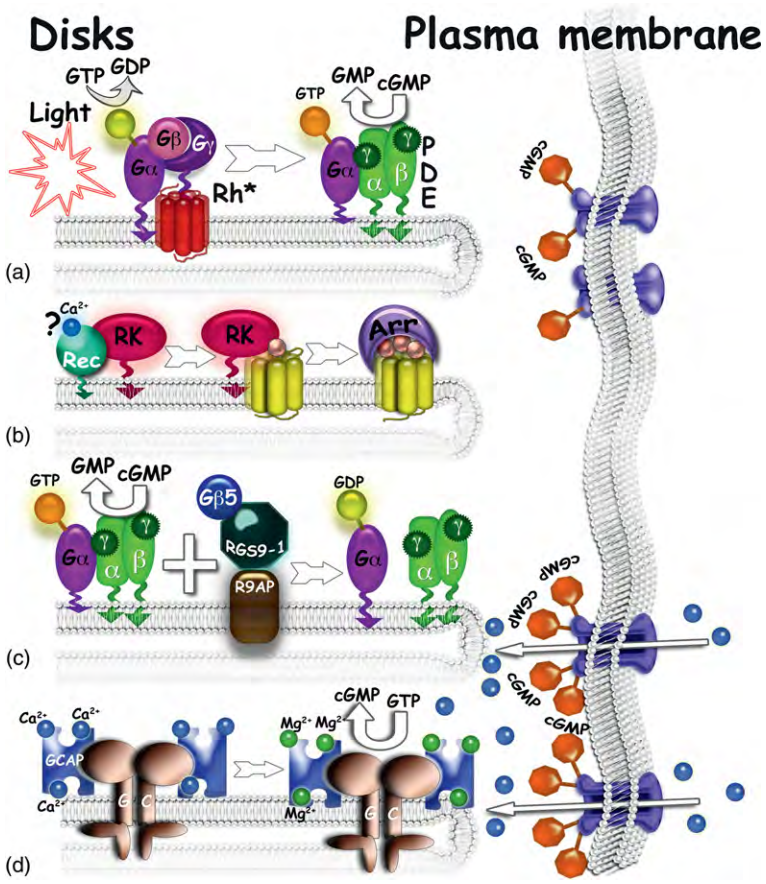

Figure 1 Biochemical mechanisms of signal inactivation in rods. (a) Visual amplification cascade. Light-activated rhodopsin (Rh*) catalyzes GDP/GTP exchange on visual G protein, Td, sequentially activating dozens of Td molecules. Inactive Td is an $\alpha\beta\gamma$-heterotrimer, whereas upon activation the GTP-liganded α-subunit dissociates from the $\beta\gamma$-dimer and binds the inhibitory γ-subunit of rod PDE (which is an $\alpha\beta\gamma_2$ heterotetramer). This activates PDE, which hydrolyzes massive amounts of cGMP (over 100000 molecules per one Rh*). The decrease in cytoplasmic cGMP closes cGMP-gated cation channels on the plasma membrane (right panel). Channel closure reduces the influx of Na^+ and Ca^{2+}, hyperpolarizing the cell up to 1 mV per one Rh*. (b) Rh* is phosphorylated by the rhodopsin kinase (RK, systematic name GRK1), which is expressed in rods and cones of all vertebrates. In the dark, RK may be kept away from rhodopsin via its interaction with Ca^{2+}-liganded recoverin (Rec). Multiphosphorylation prepares Rh* for arrestin (Arr) binding. Arrestin shields the cytoplasmic tip of rhodopsin, sterically blocking its interactions with transducin, thereby completing rhodopsin inactivation. (c) The intrinsic GTPase activity of the Td α-subunit serves as a built-in inactivation mechanism. Its interaction with PDEγ and RGS9-1 (which exists in constitutive complex with Gβ5 and membrane anchoring protein R9AP) greatly facilitates GTP hydrolysis, ensuring rapid inactivation of Td and PDE. (d) In the dark, retinal guanylyl cyclase (GC) is inhibited by Ca^{2+}-liganded GCAPs. Light-induced closure of the cGMP-gated channels results in the drop in cytoplasmic Ca^{2+}. Its replacement with Mg^{2+} on the metal-binding sites of GCAPs converts them into GC activators. GC replenishes the cytoplasmic cGMP and consequent opening of the channels restores cytoplasmic Ca^{2+}, thereby turning off GC. Rhodopsin is shown as a bundle of seven transmembrane domains; Rhodopsin-attached phosphates are shown as spheres; lipid modifications anchoring recoverin, GRK1, α- and γ-subunits of Td, and catalytic α- and β-subunits of rod PDE are shown as membrane-imbedded arrows. Arr, arrestin1; GC, gyanylyl cyclase; Rec, recoverin; Rh*, light-activated rhodopsin; RK, rhodopsin kinase.

ingenious negative-feedback mechanism that translates the drop in Ca^{2+} resulting from the reduction in cGMP level into a signal to replenish it. In photoreceptors, cGMP is synthesized by retinal guanylyl cyclases (retGCs). RetGCs are related to a family of hormone-regulated guanylyl cyclases, such as atrial natriuretic factor receptor, which have extracellular hormone-binding domain connected via a single transmembrane helix to the intracellular guanylyl cyclase domain. Similar to these receptors, retGCs are dimeric, with each monomer equipped with a catalytic domain and an extracellular domain. Interestingly, Mg^{2+} and GTP are bound by two different subunits forming the active catalytic site. As far as we know, the extracellular domain of retGCs neither binds any ligands nor participates in the enzyme regulation. Instead, the activity of retGCs is tightly regulated by their interaction via intracellular elements with GCAPs. GCAPs, as well as recoverin, are members of the neuronal calcium sensor protein branch of the superfamily of calcium-binding proteins containing EF hands (that includes calmodulin).

Similar to other members of this family, GCAPs have four EF hands, three of which actually bind divalent cations. Strictly speaking, GCAPs are Ca^{2+}–Mg^{2+}-binding proteins. The word activating in their name is a bit misleading: Mg^{2+}-liganded GCAPs activate retGCs, whereas Ca^{2+}-liganded forms actually inhibit cGMP synthesis. Thus, in dark-adapted rods with high free-Ca^{2+} concentrations (estimates range from 250 to 600 nM in different species), GCAPs keep the retGC activity at low level. This makes perfect sense, because high Ca^{2+} indicates that there is enough free cGMP ($\sim$2–5 μM) to keep the channels open. Light-induced decrease of intracellular Ca^{2+} (to 5–50 nM, based on different estimates) is the direct result of channel closure, reflecting reduced cGMP in need of replenishing. The loss of bound Ca^{2+} and its replacement by Mg^{2+} (which is always $\sim$1 mM in the cytoplasm) switches GCAPs from the inhibitory to the activating mode exactly when rapid cGMP synthesis is necessary to restore its level. Increasing cGMP opens more channels, thereby gradually restoring Ca^{2+}. Rising Ca^{2+} displaces Mg^{2+} on GCAPs, progressively reducing retGC activity, so that the cell returns to the initial state. After a dim flash, this process often overshoots, leading to a transient increase in the cGMP and Ca^{2+} concentration, likely because PDE is inactivated faster than retGC. The absence of GCAPs slows down cGMP resynthesis, so that light-induced PDE activity results in a more profound decrease of cGMP than in the normal rod. This results in closure of more channels and greatly increases the amplitude of single-photon response. This compromises temporal resolution, prolonging the rising and falling phase of the light response, and limits the working range of rods to lower light levels.

Interestingly, vertebrate photoreceptors express two isoforms of retGC, retGC1 and retGC2, and at least two GCAPs, GCAP1 and GCAP2. The presence of two isoforms of each protein in rods of all vertebrates, including fish, clearly indicates that the different isoforms have nonredundant functions. RetGCs are membrane proteins, suggesting that retGC1 and retGC2 may be localized to different membranes within the OS. RetGC1 was reliably detected in disks, and the possibility that a fraction may also be present in the plasma membrane remains open. The localization of RetGC2 was not studied with sufficient spatial resolution. Since retGC is a dimer, two isoforms of RetGC could give rise to three types of dimers, two homo- and one heterodimer. The fact that each subunit interacts with either GCAP1 or GCAP2 further expands the number of combinatorial possibilities. Definitive experiments, such as knockouts of individual isoforms of either protein, singly and in different combinations, are needed to fully elucidate the biochemistry of the Ca^{2+} feedback mechanism. A recent study of GCAP2 knockout mice revealed that although each GCAP is responsible for about half of the total retGC activation, the functions of the two proteins are quite distinct. Due to lower affinity for Ca^{2+}, GCAP1 switches to the activation mode as soon as the concentration of Ca^{2+} begins to fall, whereas GCAP2 responds later, when Ca^{2+} levels drop further. Thus, together the two GCAPs ensure graded increase in retGC activity in a wider range of Ca^{2+} concentrations than either one could have covered alone.

Another issue in need of clarification is the physiological role of a remarkable buffering capacity of the OS cytoplasm for both second messengers. According to current estimates, total cGMP in the OS is as high as $\sim$50 μM, with only 2–5 μM of it being free and the rest bound to the noncatalytic sites on PDE α- and β-subunits. The polycationic region of PDEγ appears to stabilize the interaction of cGMP with these sites. Reciprocally, the presence of cGMP in noncatalytic sites enhances the interaction of the α- and β-subunits with PDEγ. This mechanism implies that PDE activation by Td would release cGMP from noncatalytic sites. The role of this event in the photoresponse remains unclear. Similarly, free Ca^{2+} represents only a small fraction of the total Ca^{2+} in the OS cytoplasm, the rest being bound to several abundant proteins, such as recoverin, GCAPs, and calmodulin. Ca^{2+} binding by these proteins is a two-way street: on the one hand, it critically regulates their function, on the other hand, by soaking up Ca^{2+}, they significantly change its concentration, modulating the input they respond to. Obviously, Ca^{2+} and cGMP buffering cannot be separated by purely experimental means from other functional modalities of the proteins involved. Therefore, rigorous experimentation must be supplemented with detailed biochemically realistic mathematical modeling to distinguish between the effects of binding on protein activity and on the concentration of free second messenger in the cytoplasm, which is necessary to elucidate the exact biological roles of both.

Light-Dependent Protein Translocation and Rod Signaling

Arrestin localization to the OS in the light and to the IS in the dark was first described in 1985, before the role of this protein in signal termination was established. The subsequent discovery that Td also translocates in a light-dependent fashion, moving in the opposite direction, suggested an idea that translocation may underlie well-known adaptation of rods to different light levels. Preferential localization in the dark-adapted rod of a signal transducer to the rhodopsin-rich OS and a signal terminator to the IS could increase light sensitivity by slowing down shutoff. Conversely, the removal of Td from the OS and accumulation of arrestin in this compartment in the light could significantly reduce it by decreasing the number of Td molecules activated by

Rh* and speeding up rhodopsin inactivation. Subsequent studies showed that the fraction of recoverin, which presumably slows down rhodopsin phosphorylation by keeping RK away from Rh*, in the OS decreases dramatically from 12% in the dark to less than 2% in the light (the bulk of recoverin localizes to the IS in both conditions). The amplification constant in light-adapted rods was found to decrease ~10-fold, in line with the reduction of Td concentration in the OS. While these results support the idea that Td translocation plays a role in rod adaptation, by fully explaining the changes in sensitivity by Td movement alone, they effectively rule out any significant contribution of the translocation of other proteins. The recent finding that phosducin, which interacts with free βγ-dimer released upon Td activation and demonstrates robust translocation from the OS in the light, does not contribute to rod adaptation, supports this notion. The movement of Td, arrestin, phosducin, and recoverin in both directions is a relatively slow process that takes many minutes, which does not seem adequate to explain much faster photoreceptor adaptation. The translocation of arrestin in both directions is energy independent. It is driven in the dark by its low-affinity interactions with microtubules, particularly abundant in IS, and in the light by its binding to light-activated forms of rhodopsin. These findings suggest that the translocation of arrestin and other proteins is more likely to play a role in rod survival during daytime than in relatively fast light/dark adaptation. However, the translocation of different proteins may have distinct functions, which to a large extent remain to be elucidated.

Why Rods Do Not Have an Action Potential

In most neurons, extracellular Ca^{2+} enters presynaptic terminals during an action potential. A brief increase in its local concentration triggers transient exocytosis of neurotrasmitter-containing vesicles. In contrast, vertebrate rod photoreceptors work backward. In the dark, rods are partially depolarized (OS membrane potential is about −35 mV) due to massive influx of Na^+ and Ca^{2+} ions through cGMP-gated channels. This results in continuous release of the neurotransmitter (L-glutamate) from ribbon synapses. By virtue of closing cGMP-gated channels, light of increasing intensity induces progressive hyperpolarization of rods up to –60 mV (a change of ~25 mV). The activation of a single rhodopsin changes the membrane potential by as much as 1 mV. Thus, light intensity is encoded in the extent of hyperpolarization, which determines the magnitude of the decrease of neurotransmitter release. This mechanism makes the signaling graded, in contrast to the all-or-nothing type in neurons with a conventional action potential. It directly couples the change in membrane potential with synaptic activity, so that both the closure of the cGMP-gated channels upon light stimulation and their reopening upon signal termination described above immediately translate into corresponding changes in neurotransmitter release. The absence of thresholds ensures that the information is not lost in transmission, so that the brain can take full advantage of the single-photon sensitivity of the rod photoreceptors. In addition, this mechanism creates a natural ceiling: a full stop of neurotransmitter release is the maximum possible effect of the illumination of any intensity.

Conclusions

In many respects, rod photoreceptors are virtually perfect light sensors that combine single-photon sensitivity with a surprisingly wide dynamic range. Exquisitely timed and extremely efficient inactivation at every step of the signaling cascade between light absorption by rhodopsin and changes in the membrane potential plays an important role in their function. Not surprisingly, molecular errors in this complex multistep inactivation mechanism due to mutations in key proteins underlie a variety of congenital visual disorders in humans, ranging in severity from night blindness to retinal degeneration.

See also: Light-Driven Translocation of Signaling Proteins in Vertebrate Photoreceptors; Phototransduction: Adaptation in Cones; Phototransduction: Adaptation in Rods; Phototransduction: Inactivation in Cones; Phototransduction: Phototransduction in Cones; Phototransduction: Phototransduction in Rods; Phototransduction: Rhodopsin.

Further Reading

Burns, M. E. and Arshavsky, V. Y. (2005). Beyond counting photons: Trials and trends in vertebrate visual transduction. *Neuron* 48: 387–401.

Cote, R. H. (2006). Photoreceptor phosphodiesterase (PDE6): A G-protein-activated PDE regulating visual excitation in rod and cone photoreceptor cells. In: Beavo, J. A., Francis, S. H., and Houslay, M. D. (eds.) *Cyclic Nucleotide Phosphodiesterases in Health and Disease*, pp. 165–193. Boca Raton, FL: CRC Press.

Dizhoor, A. M., Olshevskaya, E. V., and Peshenko, I. V. (2006). Calcium sensitivity of photoreceptor guanylyl cyclase (RetGC) and congenital photoreceptor degeneration: Modeling *in vitro* and *in vivo*. In: Philippov, P. P. and Koch, K.-W. (eds.) *Neuronal Calcium Sensor Proteins*, pp. 203–219. New York: Nova Science Publishers, Inc.

Gurevich, V. V. and Gurevich, E. V. (2004). The molecular acrobatics of arrestin activation. *Trends in Pharmacological Science* 25: 105–111.

Gurevich, V. V., Hanson, S. M., Gurevich, E. V., and Vishnivetskiy, S. A. (2007). How rod arrestin achieved perfection: Regulation of its availability and binding selectivity. In: Kisselev, O. and Fliesler, S. J. (eds.) *Signal Transduction in the Retina, Methods in Signal Transduction Series*, pp. 55–88. Boca Raton, FL: CRC Press.

Phototransduction: Phototransduction in Cones

V J Kefalov, Washington University School of Medicine, Saint Louis, MO, USA

Glossary

Dark adaptation – The mechanism that allows photoreceptors to recover their sensitivity to dark-adapted levels following exposure to bright light.
Light adaptation – The mechanism that allows photoreceptors to reduce their sensitivity in the presence of steady light.
Phototransduction cascade – A series of reactions in the outer segments of photoreceptors through which the energy of a photon is converted into a change in the membrane potential of the cell.
Visual cycle – A series of reactions initiated by the activation of the visual pigment by light and terminating in resetting the pigment to its inactive, ground state. It involves the decay of the photoactivated visual pigment to free opsin and all-*trans* retinal, the recycling of chromophore from all-*trans* to 11-*cis* outside of photoreceptors, and the regeneration of the visual pigment molecule.
Visual pigment – A G-protein-coupled receptor consisting of protein, opsin, covalently linked to a chromophore, 11-*cis* retinal. The absorption of a photon by the visual pigment is the initial step in activating the phototransduction cascade.

Introduction

Cone photoreceptors mediate our vision during the day and provide us with fine spatial and temporal resolution as well as color perception. In most species, cones are located mostly in the central area of the retina where the image directly in front of the eyes is projected. Unlike rods, where the signal from hundreds of photoreceptors is integrated for optimized photon detection in low light conditions, signals from individual cones are relayed to the brain. As a result, the spatial resolution of our central vision, driven primarily by the cones, is excellent, whereas that of our peripheral vision, driven by the rods, is significantly lower. Color discrimination is achieved as each cone typically expresses a single type of visual pigment which conveys different spectral sensitivity to different cone types. While single photoreceptors cannot discriminate colors as the degree of photoactivation depends not only on the wavelength of the stimulus but also on its intensity, the visual system extracts that information by comparing the signals coming from the different cone types. An interesting exception to the one cell–one pigment rule is the mouse retina where green and ultraviolet cone visual pigments are coexpressed in the same cells. The functional significance of that arrangement is not clear.

Functional Properties of Cones

Cones use a phototransduction cascade, similar to the one well characterized in rods, to convert the energy of light into an electrical signal. In addition, cone phototransduction proteins are homologous, or sometimes even identical, to the ones found in rods. Yet, cones have functional properties that are distinct from those of rods and that are suited for their role as bright-light detectors. First, cones are significantly less sensitive than rods. The rod phototransduction cascade is tuned for high amplification which allows rods to achieve the maximal physically possible sensitivity and generate a detectable single photon response. As such enormous gain requires buildup of the reactions of the phototransduction cascade, the trade-off is the slow kinetics of rod responses. Cones, on the other hand, are 30- to 100-fold less sensitive than rods (**Figure 1**) and require the simultaneous activation of tens to hundreds of visual pigment molecules to generate a detectable response. As a result of the low amplification of their phototransduction cascade, cones are not sensitive enough to function under low light conditions, depriving us of color vision in dim light. Instead, the low cone phototransduction gain shifts their dynamic range toward brighter light conditions and enables cones to function during the day. The low signal amplification in cones is made possible by the rapid inactivation of their phototransduction cascade. This results in the second notable difference from rods, namely, that cone responses are typically several fold faster than rod responses. The rapid activation and subsequent inactivation of the cone phototransduction cascade reactions provides the basis for the high temporal resolution of cone-mediated vision (**Figure 1**). The rapid activation of cones results in short latency of detection, whereas their rapid inactivation enables discrimination of stimuli spaced closely in time. In contrast, the slower rod responses limit the temporal resolution of rod-mediated vision. Third, following exposure to bright light, cones fully recover their sensitivity within a few minutes. Rods, in contrast, experience a long

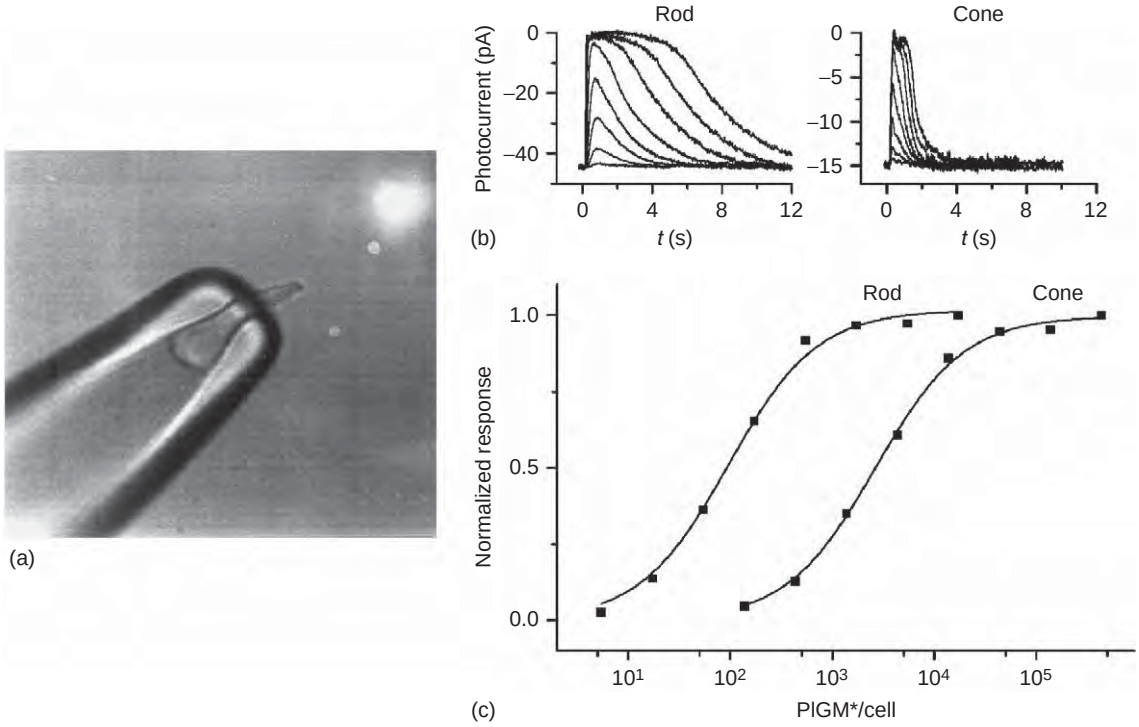

Figure 1 Comparison of rod and cone photoresponses. (a) Salamander red cone drawn in a suction pipet electrode with the outer segment protruding out. (b) Families of photoresponses from a salamander rod (left) and a red cone (right) to brief test flashes of increasing intensity delivered at $t = 0$. Note the significantly faster response kinetics of cone responses compared to rod responses. (c) Normalized intensity–response curves for the same two cells. Note the significantly lower cone sensitivity compared to the rod sensitivity.

refractory period following exposure to bright light and can take up to an hour for a complete recovery of their sensitivity. This process, known as dark adaptation, prevents cones from becoming refractory and allows us to retain visual perception in a quickly changing light environment. Finally, cones have a remarkable ability to adjust their sensitivity over a very wide range and remain photosensitive even in extremely bright light. Rods, in contrast, saturate in even moderately bright light and remain nonfunctional during most of the day. This process, known as light adaptation, prevents cones from saturating in bright light and allows us to see throughout the day. With rods saturated, cones are responsible for most of the visual information reaching our brain during the day. In fact, with the introduction of artificial lighting, humans rely almost exclusively on cones both during the day and at night. This is why cone disorders, such as macular degeneration, the most common cause of blindness in the elderly, have a devastating effect on vision.

Obstacles for Studying Cone Phototransduction

The last several decades have seen a tremendous advance in our understanding of the function of photoreceptors. The development of electrophysiological tools for studying the function of single photoreceptors, together with biochemical and genetic tools have revealed the mechanism of phototransduction and provided quantitative description of the reactions involved in it. Unfortunately, these advances have been almost exclusively limited to rods. The great abundance of rods in most mammalian retinas (95% of all photoreceptors in human and 97% in mouse retinas) has facilitated the purification and biochemical study of rod phototransduction proteins. In contrast, the small fraction of cones and the homology between rod and cone phototransduction proteins have rendered comparable studies from cone proteins technically challenging. A further obstacle has been the fragility of mammalian cone photoreceptors, which has rendered physiological studies from cones also significantly more challenging than comparable rod studies. As a result, while mammalian rod phototransduction has been characterized in quantitative details, most of what we currently know about cone phototransduction is derived from studies of amphibian and fish photoreceptors. Based on the similarities in structure and transduction proteins between rods and cones, it has been assumed that phototransduction in cones follows the same set of reactions as phototransduction in rods. There exist, however, important quantitative phototransduction differences in

rods and cones pertinent to their function in dim and bright light, respectively. The phototransduction cascade in cones will be discussed here in the context of the much better understood rod phototransduction cascade.

In both, rods and cones, phototransduction takes place in specialized compartments, called outer segments, which consist of stacks of membrane disks, similar to a stack of coins. Unlike in rods, where these disks are surrounded by, but not connected to, the plasma membrane, in cones these disks are formed from invaginations of the plasma membrane. As a result, the plasma membrane of cone outer segment has significantly higher area, a factor possibly important for the rapid flow of molecules in and out of the cell. The transduction channels are cGMP-gated nonselective cation channels held open in darkness by the binding of free cGMP in the outer segment. Cone cGMP channels are homologous to those found in rods and in olfactory neurons and consist of two cyclic nucleotide-gated alpha 3 (CNGA3) and two cyclic nucleotide-gated beta 3 (CNGB3) subunits. In darkness, the influx of Na^+ and Ca^{2+} through these channels depolarizes the cells to about −40 mV, which results in the steady release of the neurotransmitter glutamate from the cone synaptic terminal. Photoactivation of the cell results in the hydrolysis of cGMP, closure of the transduction channels, hyperpolarization of the cell, and reduction in the release of neurotransmitter from the cone synaptic terminal.

Cone Visual Pigment and Phototransduction

Phototransduction in cones is initiated by the activation of cone visual pigments by the absorption of a photon. The cone visual pigments, similar to rod pigments, consist of protein, opsin, covalently attached to a chromophore, typically 11-*cis* retinal. Cone opsins have a moderate level (∼50%) of homology to rod opsins. The visual chromophore is a derivative of vitamin A (all-*trans* retinol), which is converted in the pigment epithelium into 11-*cis* retinal and then transported to the photoreceptor's outer segments where it combines with opsin to form the visual pigment. The visual pigment is expressed at very high levels in the disks of the outer segment (3.5 mM), so that a photon traveling along the outer segment has a ∼40% chance of activating a pigment molecule. Interestingly, the concentrations of rod and cone visual pigments in the outer segment as well as their extinction coefficients are similar. In addition, the probability that a pigment molecule will become activated once a photon has been absorbed (quantum efficiency) is also comparable between rod and cone pigments. Thus, with respect to the pigment distribution and optical properties, only the typically smaller size of the cone outer segment compared to that of the rod contributes to the lower sensitivity of cones.

Studies with amphibian photoreceptors indicate that the different stability of rod and cone pigments modulates their respective phototransduction cascades. First, studies of transgenic *Xenopus* rods expressing red cone opsin have allowed the direct observation of physiological responses to the activation of a single cone pigment molecule. This has made possible the determination of the rate of spontaneous thermal activation of red cone pigments, which produces a response identical to the activation by a photon. The molecular rate of thermal activation measured in this way is ∼10 000 times higher for red cone pigment than for rod pigment. As a result, amphibian red cones experience ∼200 pigment activations per second in darkness. This level of dark activity is comparable to the total dark noise measured from salamander red cones, indicating that most of the noise in these cells originates in the thermal activation of the pigment. This spontaneous activity acts as background light to induce adaptation and, therefore, desensitization and acceleration of the flash response. A second mechanism by which the stability of the visual pigment contributes to the differences between rods and cones is based on the covalent bond between opsin and retinal in their respective pigments. Both biochemical and physiological studies indicate that the formation of the covalent bond between opsin and chromophore is reversible in cones but not in rods. As a result, the visual pigment in cones, but not in rods, can spontaneously dissociate into free opsin and 11-*cis* retinal. The very low level of free 11-*cis* retinal in the outer segment (only ∼0.1% of the pigment content) shifts the equilibrium between free and chromophore-bound cone opsin so that even in dark-adapted cones, there is ∼10% free opsin. At this high level, the total catalytic activity of free opsin, though weak per single molecule, is sufficient to induce adaptation and further reduce the sensitivity and accelerate the kinetics of the cone flash responses.

The effects of cone pigment properties on mammalian photoreceptor function have not been well characterized. Interestingly, studies from transgenic mouse rods expressing cone pigments indicate that, though still significantly higher than that of rod pigment, the rate of thermal activation of cone pigment is not high enough to affect cone photosensitivity significantly. A possible explanation for the relatively low thermal activity of cone pigments in mammalian species compared to amphibians might be that they use a slightly different chromophore (11-*cis* retinal or A1) than most amphibian photoreceptors (11-*cis* 3-dehydroretinal or A2). The reversibility of cone pigment formation and its possible effect on cone function have not yet been examined in mammalian cones. Finally, differences in the properties of rod and cone visual

pigment also contribute to the very different rates of dark adaptation in rods and cones.

Activation of Cone Phototransduction

Once activated, the visual pigment binds to and activates a heterotrimeric G protein, called transducin (G_t). This triggers the exchange of GDP for GTP on the α-subunit of transducin ($G_{t\alpha}$) and the dissociation of $G_{t\alpha}$·GTP from $G_{t\beta\gamma}$. This represents the initial amplification step in phototransduction as one visual pigment molecule can activate multiple G_t molecules. Rod and cone transducins are closely related and the primary structures of their α-subunits are ~80% identical, with even higher identity in the region of interaction with the visual pigment. Biochemical studies indicate that rod and cone pigments have comparable binding affinities for rod transducin and that they activate rod transducin with similar kinetics. Furthermore, studies with transgenic animals coexpressing rod and cone visual pigments in the same photoreceptor have shown that rod and cone pigments produce comparable responses. Thus, cone pigments expressed in rods produce a response with rod-like amplification and kinetics and, conversely, rod pigments expressed in cones produce a response with cone-like amplification and kinetics. These results indicate that the activation of the phototransduction cascade by the visual pigment and the inactivation of the visual pigment are not determined by its properties but rather, by the downstream transduction reactions, including the activation of transducin. Indeed, biochemical studies of fish photoreceptors have shown that the activation of transducin is ~25 times less effective in cones compared to rods. This lower activation efficiency would contribute to the lower amplification of the signal and, therefore, to the lower sensitivity of cones. It is not clear yet whether the lower activation of transducin in cones is due to the properties of the cone isoform of transducin or due to the faster inactivation of pigment in cones compared to rods. An interesting recent observation is that exposure to bright light in rods triggers translocation of the subunits of activated transducin from the outer to the inner segment. In contrast, in cones, such translocation does not occur, possibly because transducin subunits are inactivated and re-form a trimer faster than in rods. The mechanism of this light-dependent translocation is still not well understood and is an active area of research.

Once activated by the visual pigment, $G_{t\alpha}$·GTP in turn activates cGMP phosphodiesterase (PDE) by binding to its inhibitory subunit PDEγ and removing its inhibition on the catalytic PDEαβ. The resulting hydrolysis of cGMP by PDE leads to the closure of cGMP-gated channels in the cone outer segment and the hyperpolarization of the photoreceptor to produce the light response. While cone PDE has 60% identity to rod PDE, biochemical studies of fish photoreceptors indicate that the activation of PDE by transducin might also be ~10 times less effective in cones compared to rods, contributing further to the lower cone sensitivity.

Inactivation of Cone Phototransduction

Response termination is achieved as the visual pigment, transducin, and PDE are inactivated and the concentration of cGMP is restored to its dark, preflash level. Though these reactions in cones are not well characterized, it is clear that, similar to their activation, quantitative differences in the inactivation of phototransduction reactions in rods and cones contribute to the lower sensitivity and faster response kinetics of cones. The activity of the visual pigment is initially partially quenched when it is phosphorylated by a G-protein receptor kinase (GRK). Phosphorylation of activated visual pigment is ~50 times faster in cones compared to rods. It appears that this faster phosphorylation is the result of two factors – higher expression of GRK in cones and higher efficiency of cone GRK (GRK7) compared to rod GRK (GRK1). While most species, including human, express GRK1 in rods and GRK7 in cones, the mouse retina is unusual as its rods and cones share the same kinase, GRK1. In this case, the faster pigment inactivation in cones is most likely due to the higher concentration of GRK1 and possibly also to differential modulation of that reaction by the calcium-binding protein recoverin.

Following phosphorylation, complete inactivation of the phosphorylated visual pigment is achieved by the subsequent binding of a protein called arrestin. The cone isoform of arrestin (Arr4) has about 50% identity to rod arrestin (Arr1). The mouse retina again represents an unusual case, as in addition to Arr4, mouse cones also express Arr1. Interestingly, the ratio of arrestin to visual pigment is 7 times higher in cones compared to rods. In dark-adapted rods, most of arrestin is in the inner segment and does not, therefore, contribute to the inactivation of rod visual pigment. As a result, the quantity of arrestin in the outer segments of rods is only a few percent of their visual pigment. Exposure to bright light triggers the translocation of arrestin from the inner to the outer segment for more efficient pigment inactivation. While arrestin also transloactes in cones, the total quantity of arrestin in their outer segments in darkness is comparable to that of their visual pigment. Recent studies from mouse cones lacking both rod and cone arrestins reveal that either arrestin is capable of inactivating cone visual pigment though Arr1 is much more abundant than Arr4 in cones. Studies with transgenic rods expressing cone S-opsin and either rod or

cone arrestin further demonstrate that rod arrestin is more efficient at inactivating cone pigment than cone arrestin. The relatively low expression of Arr4 in cones and its relative inefficiency suggest a possible additional role for this protein. The coexpression of two arrestins and their high concentration in cone outer segments would contribute to the rapid cone pigment inactivation and are consistent with the more rapid pigment inactivation and faster response termination in cones compared to rods.

$G_{t\alpha}$·GTP is inactivated as GTP is hydrolyzed into GDP. This reaction is catalyzed by PDEγ as part of a GTPase-activating protein (GAP) complex that consists, in addition, of regulator of G-protein signaling (RGS9), RGS9 anchoring protein (R9AP), and a G_β subunit ($G_{\beta 5}$). The rod and cone PDEγ have comparable potencies for inhibiting PDE and also for enhancing the hydrolysis of GTP by the GAP complex. In contrast, even though the identical RGS9 protein is present in rods and in cones, its concentration is more than 10 times higher in cones compared to rods. Deletion of RGS9 in the mouse greatly retards cone response inactivation, and mutations in RGS9 have been associated with slow cone deactivation in patients. Thus, while the extent to which the differences in GAP activity in rods and cones contribute to their functional differences is not well understood, RGS9 and the GAP complex clearly play an important role in the inactivation of cone phototransduction.

The final step in photoresponse termination involves the upregulation of synthesis of cGMP by guanylyl cyclase (GC) to restore the concentration of free cGMP in the outer segment and reopen the cGMP-gated channels. While rods express two isoforms of GC, that is, GC1 and GC2, cones appear to express predominantly, if not exclusively, GC1. The role of GC2 in rods is not clear as its deletion produces only a mild change in rod physiology. It is also not understood how modulation of GC by the pair of GC-activating proteins (GCAP1 and GCAP2) contributes to the unique functional properties of cones. Although the distribution of GCAPs between rods and cones in different species is ambiguous, it appears that GCAP2 is prevalent in rods, while GCAP1 is expressed at high levels in cones. The possible role of GCAPs in mediating light adaptation in cones is discussed below in the context of light adaptation.

Dark Adaptation of Cones

Quantitative differences between the phototransduction cascades of rods and cones not only contribute to the difference in sensitivity and kinetics of photoresponses as discussed above, but also play a role for the very different adaptation properties of rods and cones. The ability to recover their sensitivity rapidly following exposure to bright light, or dark-adapt, is critical for the function of cones as daytime photoreceptors. The absorption of a photon by the visual pigment not only triggers its activation, but also results in its eventual decay into free opsin and all-*trans* retinal. Dark adaptation of both, rods and cones, after exposure to bright light requires regeneration of the visual pigment from opsin and 11-*cis* retinal. However, the speed of pigment regeneration, and hence sensitivity recovery, is very different in rods and cones, with full recovery requiring less than 5 min in cones and up to an hour in rods (see **Figure 2**).

Several factors contribute to the rapid pigment regeneration in cones. First, the decay of the photoactivated pigment to free opsin and all-*trans* retinal occurs in seconds for cone pigments compared to minutes for rod pigments. Second, the reduction of all-*trans* retinal into all-*trans* retinol, which takes place in the outer segment and is catalyzed by retinol dehydrogenase (RDH), is also 10–40 times faster in cones compared to rods. The reduction reaction requires the cofactor nicotinamide adenine

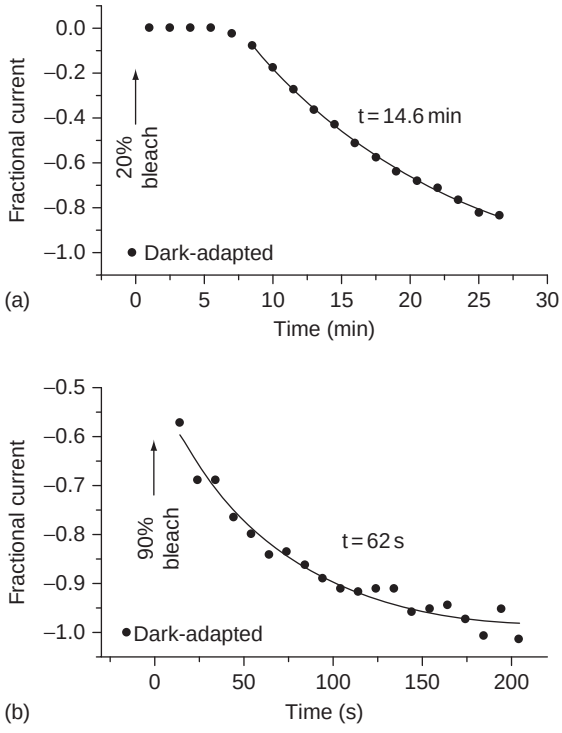

Figure 2 Comparison of rod and cone dark adaptation. Recovery of the circulating (dark) current in salamander rod (a) and red cone (b) measured with a suction electrode. Cells were exposed to bright light that activated (bleached) 20% of the rod pigment and 90% of the cone pigment. The recording was done in the presence of exogenous 11-*cis* retinal to enable pigment regeneration in the isolated cells. Current recovery is fit by a single exponential decay function (solid line). Note the significantly faster recovery of the current in cone compared to the current in the rod.

dinucleotide phosphate oxidase (NADPH). While it is possible that the faster reduction of all-*trans* retinal in cones is due to the different properties of rod and cone RDH enzymes, a more likely hypothesis is that the reduction reaction is limited by the supply of NADPH from the inner segment. Third, single-cell measurements from amphibian photoreceptors indicate that the clearance of all-*trans* retinol from the outer segment is ~25 times faster in cones compared to rods. However, the actual difference in these rates in the intact retina might be affected by factors such as the proximity to the pigment epithelium and the action of extracellular chromophore-binding proteins such as interphotoreceptor retinoid-binding protein (IRBP). Finally, the formation of the covalent bond between opsin and 11-*cis* retinal during pigment regeneration occurs in seconds in cones and minutes in rods. Together, these factors contribute to the faster turnover of cone visual pigment and the faster dark adaptation of cones compared to rods.

In addition to the effects of faster visual pigment decay and regeneration, cone dark adaptation is accelerated by the noncovalent interaction between opsin and 11-*cis* retinal. Pigment regeneration requires the initial binding of 11-*cis* retinal in the chromophore pocket of free opsin. While in rods, the noncovalent binding of retinal activates the opsin molecule and desensitizes the rods, in cones, this reaction has the opposite effect and inactivates cone opsin. As a result, the noncovalent binding of 11-*cis* retinal to opsin delays dark adaptation in rods but accelerates it in cones, as it allows cones to substantially recover their sensitivity even before the regeneration of their visual pigment.

Recent biochemical studies indicate that another mechanism contributing to the faster dark adaptation of cones compared to rods is based on the supply of recycled chromophore for pigment regeneration. The canonical visual cycle involves the pigment epithelium, where all-*trans* retinol is converted into 11-*cis* retinal via a series of enzymatic reactions and then transported back to the photoreceptors for incorporation into opsin. The rapid dark adaptation of cones and their ability to maintain adequate levels of pigment and remain light sensitive even in steady bright light require rapid pigment regeneration, hence rapid recycling of chromophore for cones. However, the slow rate of chromophore turnover in the pigment epithelium and the competition for recycled chromophore between cone opsin and overwhelming levels of rod opsin in most rod-dominant species indicate that the canonical pigment epithelium visual cycle might not be sufficient to meet the chromophore demand of cones. Indeed, recent biochemical studies from cone-dominant species have brought up the idea of a second, cone-specific pathway for recycling of chromophore located within the retina and possibly relying on the Müller cells. The role of this novel cycle in mammalian rod-dominant species is still controversial. However, recent physiological experiments with amphibian photoreceptors demonstrate the function of a retina visual cycle under physiological conditions in a rod-dominant retina. Importantly, the combined action of the pigment epithelium and the retina visual cycles is required for the rapid and complete dark adaptation of cones.

Light Adaptation in Cones

In contrast to rods, which saturate in moderate light and are not responsive during the day, cones have the ability to adapt their sensitivity and remain functional over a very wide range of light intensity. Studies with amphibian and fish photoreceptors indicate that, similar to the case of rods, cone adaptation is mediated by intracellular calcium, modulated by the activation of the phototransduction cascade. In the dark, the continuous current entering the outer segment through the cGMP-gated channels is carried in part by calcium, which is returned to the extracellular space via a $Na^+/(Ca^{2+}, K^+)$ exchanger. Following photoactivation and the closure of cGMP channels, calcium continues to be exported out of the cell through the $Na^+/(Ca^{2+}, K^+)$ exchanger until a new equilibrium is reached. As a result, activation by light causes a decline in the concentration of calcium in the outer segment of the cell. This triggers the calcium-mediated negative feedback on phototransduction, which in rods is required for eventually terminating the signal and for adapting the cell in response to light. Interestingly, calcium constitutes a larger fraction of the total ionic flux in and out of the outer segment of cones compared to rods. Thus, in cones of amphibians and fish, the fraction of photocurrent carried by calcium is about 35% compared to 20% in rods. As would be expected from the need to maintain a steady calcium concentration in darkness, the matching rates of extrusion of calcium via the $Na^+/(Ca^{2+}, K^+)$ exchanger are also higher in cones compared to rods. The combination of faster turnover of calcium in cones and their smaller volume compared to rods allows calcium in cones to decline several times faster upon light stimulation. In addition, their range of calcium concentrations from darkness to bright light is threefold wider than that in rods. These quantitative differences create the potential for more powerful modulation of phototransduction by calcium in cones compared to rods consistent with the ability of cones to adapt better and faster to various light conditions than rods.

The mechanisms by which calcium modulates the cone phototransduction cascade are not well understood. However, comparison between cone and rod phototransduction reveals several interesting points. One mechanism by which calcium modulates phototransduction in rods involves inactivation of the visual pigment via

phosphorylation by rhodopsin kinase. This reaction is modulated by the calcium-binding protein recoverin (also known as S-modulin). Recoverin is a member of the EF-hand superfamily and exerts its effect by inhibiting phosphorylation of rhodopsin by rhodopsin kinase at high calcium levels. In rods, inhibition of rhodopsin kinase by recoverin regulates phototransduction in darkness, in high calcium conditions, but has little effect during light adaptation, in low calcium conditions. The role of recoverin in modulating cone phototransduction in darkness and during light adaptation is not known. However, rods and cones share the same isoforms of recoverin and rhodopsin kinase. In addition, calcium modulates the sites and extent of pigment phosphorylation in cones but not in rods. Finally, unlike in rods, in cones, the calcium-dependent inactivation of cone visual pigment could be the rate-limiting step for the shutoff of the cone photoresponse.

Another mechanism by which calcium modulates phototransduction in rods involves the synthesis of cGMP by GC. As discussed above, this reaction is modulated by GCAP1 and GCAP2. GCAPs modulate GC in rods up to 20-fold as they inhibit it at high intracellular calcium levels and activate it at low calcium levels. While the simultaneous deletion of GCAP1 and GCAP2 delays the recovery of cone light responses, the extent to which GCAPs modulate cone phototransduction in darkness and during light adaptation is not known.

Finally, calcium is also believed to directly modulate the cGMP-gated channels in cones. The Ca^{2+}-dependent modulation of cGMP current is minimal in amphibian and undetectable in mammalian rods. In contrast, cone cGMP channels are directly modulated by Ca^{2+} both in fish and in mammalian retina. The molecular mechanism of cone channel modulation remains to be discovered. While calmodulin binds to and modulates heterologously expressed cGMP-gated channels, its role in the intact cone photoreceptor has been questioned.

Epilog

These are exciting times for studying cone phototransduction. Until recently, technical issues such as the low abundance of cone photoreceptors in rod-dominant retinas and the fragility of mammalian cone photoreceptors have held back the biochemical and physiological studies of cones. As a result, despite the crucial role of cones for our daytime vision, mammalian cone phototransduction has been poorly understood. Recent development of several genetically modified mice has turned the tables. One example is the Nrl knockout mouse. Nrl is a transcription factor required for rod photoreceptor differentiation and its deletion produces a retina populated exclusively by cone-like photoreceptors. This makes possible the purification and biochemical characterization of mammalian cone phototransduction proteins. The Nrl knockout retina has also been used recently for physiological studies of cone photoreceptors. Other examples of useful genetically modified mice include those lacking the rod visual pigment (rhodopsin knockout) and the rod $G_{t\alpha}$ subunit (transducin α knockout). The lack of functional rods in both of these retinas makes possible the physiological identification and study of cone photoreceptors. This approach was most recently used to investigate the role of Arr1 and Arr4 in the inactivation of mouse cone pigments. The combination of new genetic models and improved physiological tools provides promise for studies of mammalian cone photoreceptors using the full range of tools that have been so successful in characterizing the function of mammalian rods. This should allow not only quantitative characterization of the cone phototransduction cascade but also understanding the mechanisms for cone dark and light adaptation which make cones invaluable as our daytime photoreceptors.

See also: Light-Driven Translocation of Signaling Proteins in Vertebrate Photoreceptors; Phototransduction: Adaptation in Cones; Phototransduction: Adaptation in Rods; Phototransduction: Inactivation in Cones; Phototransduction: Inactivation in Rods; Phototransduction: Phototransduction in Rods; Phototransduction: Rhodopsin; Phototransduction: The Visual Cycle.

Further Reading

Donner, K. (1992). Noise and the absolute thresholds of cone and rod vision. *Vision Research* 32: 853–866.

Ebrey, T. and Koutalos, Y. (2001). Vertebrate photoreceptors. *Progress in Retinal and Eye Research* 20: 49–94.

Fu, Y. and Yau, K. W. (2007). Phototransduction in mouse rods and cones. *Pflugers Archive: European Journal of Physiology* 454: 805–819.

Hecht, S., Haig, C., and Chase, A. M. (1937). Rod and cone dark adaptation. *Journal of General Physiology* 20: 831–850.

Holcman, D. and Korenbrot, J. I. (2005). The limit of photoreceptor sensitivity: Molecular mechanisms of dark noise in retinal cones. *Journal of General Physiology* 125: 641–660.

Kawamura, S. and Tachibanaki, S. (2008). Rod and cone photoreceptors: Molecular basis of the difference in their physiology. *Comparative Biochemistry and Physiology Part A: Molecular and Integrative Physiology* 150: 369–377.

Kefalov, V., Fu, Y., Marsh-Armstrong, N., and Yau, K. W. (2003). Role of visual pigment properties in rod and cone phototransduction. *Nature* 425: 526–531.

Kefalov, V. J., Estevez, M. E., Kono, M., et al. (2005). Breaking the covalent bond – A pigment property that contributes to desensitization in cones. *Neuron* 46: 879–890.

Korenbrot, J. I. and Rebrik, T. I. (2002). Tuning outer segment Ca^{2+} homeostasis to phototransduction in rods and cones. *Advances in Experimental Medicine and Biology* 514: 179–203.

Mata, N. L., Radu, R. A., Clemmons, R. C., and Travis, G. H. (2002). Isomerization and oxidation of vitamin A in cone-dominant retinas: A novel pathway for visual-pigment regeneration in daylight. *Neuron* 36: 69–80.

Nikonov, S. S., Brown, B. M., Davis, J. A., et al. (2008). Mouse cones require an arrestin for normal activation of phototransduction. *Neuron* 59: 462–474.

Rebrik, T. I. and Korenbrot, J. I. (2004). In intact mammalian photoreceptors, Ca^{2+}-dependent modulation of cGMP-gated ion channels is detectable in cones but not in rods. *Journal of General Physiology* 123: 63–75.

Rieke, F. and Baylor, D. A. (2000). Origin and functional impact of dark noise in retinal cones. *Neuron* 26: 181–186.

Tachibanaki, S., Arinobu, D., Shimauchi-Matsukawa, Y., Tsushima, S., and Kawamura, S. (2005). Highly effective phosphorylation by G protein-coupled receptor kinase 7 of light-activated visual pigment in cones. *Proceedings of the National Academy of Sciences of the United Sates of America* 102: 9329–9334.

Wald, G., Brown, P. K., and Smith, P. H. (1955). Iodopsin. *Journal of General Physiology* 38: 623–681.

Yau, K. W. (1994). Phototransduction mechanism in retinal rods and cones. The Friedenwald Lecture. *Investigative Ophthalmology and Visual Science* 35: 9–32.

Phototransduction: Phototransduction in Rods

Y Fu, Department of Ophthalmology and Visual Sciences, University of Utah, Salt Lake City, UT, USA

Glossary

Dark current – Also called circulating current. Current generated by constant influx of Na^+/Ca^{2+} into the rod outer segment through cGMP-gated channels, which is balanced by an outward current flowing across the inner segment membrane that mainly carried by potassium channels.
Dark light – Signals produced by thermal activation of rhodopsin in the dark, which adapt the visual system like real background light.
Phototransduction – The conversion of a light signal to an electrical signal in a photoreceptor cell.
Quantum efficiency – The ratio between the number of photoactivated molecules and the number of molecules that absorbed a photon.
Single-photon response – Electrical signal triggered by a single photon in a rod cell.
Suction-electrode recording – The recording of light-sensitive current of a single rod (or cone) by drawing its outer segment (or inner segment) into a suction electrode.

Introduction

Image-forming vision in vertebrates is mediated by two types of photoreceptors: the rods and the cones. Rods are specialized for dim-light (scotopic) vision while cones mediate vision in bright light (photopic). Great progress has been made in understanding rod phototransduction since the introduction of the suction-electrode recording technique in the late 1970s. The light-sensitive current of individual amphibian and mammalian (including primate) photoreceptors can be recorded with this method. Bovine retina, on the other hand, has been a favorite preparation for studying phototransduction by biochemists because of the abundance of tissue available. The mouse, however, has become an increasingly popular animal model for study in the past decade through the advent of gene-targeting techniques. When combined with electrophysiology, mouse genetics provides unmatched power in elucidating the *in vivo* functions of key phototransduction proteins, most of which have been knocked out, overexpressed, or mutated in rods, yielding a rich body of information on the mechanisms underlying the amplification, recovery, and adaptation of rod photoresponses. The details of the activation phase of rod phototransduction are now established. A quantitative description, the Lamb–Pugh model, is achieved that reproduces the activation kinetics of the rod response under physiological conditions. In this article, the focus is on the activation phase of rod phototransduction with particular emphasis on the molecular mechanisms underlying its high signal amplification feature.

Vertebrate Rods Are Highly Efficient Photon Detectors

Psychophysical experiments performed by Hecht, Schlaer, and Pirenne in 1942 suggested that human retinal rods can detect single photons. Thirty-seven years later, suction-electrode recordings from isolated toad rods by Baylor, Lamb, and Yau confirmed this remarkable ability of vertebrate rods (Figure 1). The amazing ability of vertebrate rods to detect single photons can be attributed to at least three factors: high quantum efficiency of photoactivation, low intrinsic noise, and a powerful signal amplification cascade. Two other factors greatly increase the photon capture ability of vertebrate rods, numerical dominance of rods over cones, and a highly specialized outer segment structure. The dense stack of disks of the rod outer segment ensures that virtually every photon traveling axially will be captured. In a sense, vertebrate rods can be viewed as sophisticated three-dimensional photon capture devices.

Phototransduction in Rods: A G-Protein-Signaling Pathway

Rod phototransduction is one of the best-characterized G-protein-signaling pathways. The receptor is rhodopsin (R), the G protein is transducin (G), and the effector is cyclic guanosine monophosphate (cGMP) phosphodiesterase (PDE or PDE6). Upon photon absorption, the rhodopsin molecule becomes enzymatically active (R^*) and catalyzes the activation of the G-protein transducin to G^*. Transducin, in turn, activates the effector PDE to PDE^*. PDE^* hydrolyzes the diffusible messenger cGMP. The resulting decrease in the cytoplasmic-free cGMP concentration leads to the closure of the cGMP-gated channels on the plasma membrane. Channel closure leads to localized reduction on the influx of cations into the outer segment, which results in membrane hyperpolarization, that is, the intracellular voltage becoming more negative (Figure 2).

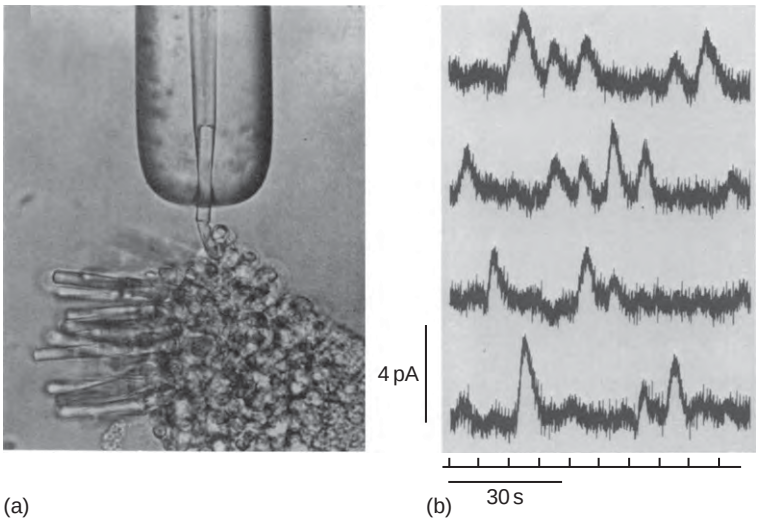

Figure 1 Suction-electrode recording on the membrane current of a single toad rod. (a) The outer segment of a rod projecting from a piece of retina was sucked in position in a suction electrode. Proximal end of cell remains attached to retina. Boundary between inner and outer segments is visible. (b) Response of rod outer segment to a series of 40 consecutive dim flashes, 20 ms flash delivering 0.029 photons μm^{-2} at 500 nm, flash timing monitored below. The rod showed no response to some flashes, or a small response of ~1 pA to others, and occasionally a larger response. This suggests that the flash response is quantized, as might be expected when on average very few photons are absorbed. With further analysis, the authors demonstrated that each quantal electrical event resulted from a single photo-isomerization with mean amplitude of ~1 pA – the single-photon response. Modified from Baylor et al. (1979) *Journal of Physiology*, 288: 589–611 (a) and 288: 613–634 (b), with permission from Blackwell Publishing.

This hyperpolarization decreases or terminates the dark glutamate release at the synaptic terminal. The signal is further processed by other neurons in the retina before being transmitted to higher centers in the brain.

Following light activation, a timely recovery of the photoreceptor is essential so that it can respond to subsequently absorbed photons, and signal rapid changes in illumination. This recovery from light requires the efficient inactivation of each of the activated components: R*, G*, and PDE*, as well as the efficient regeneration of rhodopsin (R) and the rapid restoration of the cGMP concentration. The termination rates of the activation steps set the time course of the photoresponse.

Although rod phototransduction is the best-characterized sensory transduction pathway, rods differ from other sensory cells in that light leads to hyperpolarization rather than depolarization. Rods respond to light with graded hyperpolarization whose amplitude increases monotonically as a function of flash intensity until saturation. One hallmark of rod phototransduction is the reproducibility of its single-photon response in both amplitude and kinetics. This is quite remarkable considering the fact that events generated by single molecules are stochastic in nature. The study on the underlying mechanisms has long been a hot topic in the vision field. Recent research pointed to two possible mechanisms: (1) Rhodopsin inactivation is averaged over multiple shutoff steps so that the integrated R* activity varies less than otherwise controlled by a single step. (2) Averaging over the deactivation of multiple G-protein molecules.

High Quantum Efficiency of Photoactivation

The quantum efficiency of photoactivation measures the probability that the adsorption of a photon initiates photoactivation. This probability is defined as the ratio between the number of photoactivated molecules and the number of molecules that absorbed a photon. Quantum efficiency of visual pigments is wavelength independent at ~0.7 in the spectrum of visible light. This suggests that every absorbed photon in the visible range can activate rhodopsin equally well. The quantum efficiency of 0.7 is very similar across all visual pigments. This high efficiency seems to be a common feature of most vertebrate visual pigments.

The Great Thermal Stability of Rhodopsin

Unlike chemosensory systems, phototransduction is not triggered by the binding of a chemical ligand to the receptor, rhodopsin. Instead, the chemical, 11-*cis*-retinal in birds and land-based animals (or 11-*cis*-3,4-dehydroretinal in aquatic animals), is prebound to rhodopsin. Photon absorption triggers the *cis*- to *trans*-isomerization of the retinoid. This isomerization rapidly converts the ligand from a powerful antagonist to a powerful agonist, leading to the formation of a series of spectrally distinct intermediates of rhodopsin in the order of bathorhodopsin, lumirhodopsin, metarhodopsin I (Meta I), and metarhodopsin II (Meta II) within a few milliseconds. Meta II is

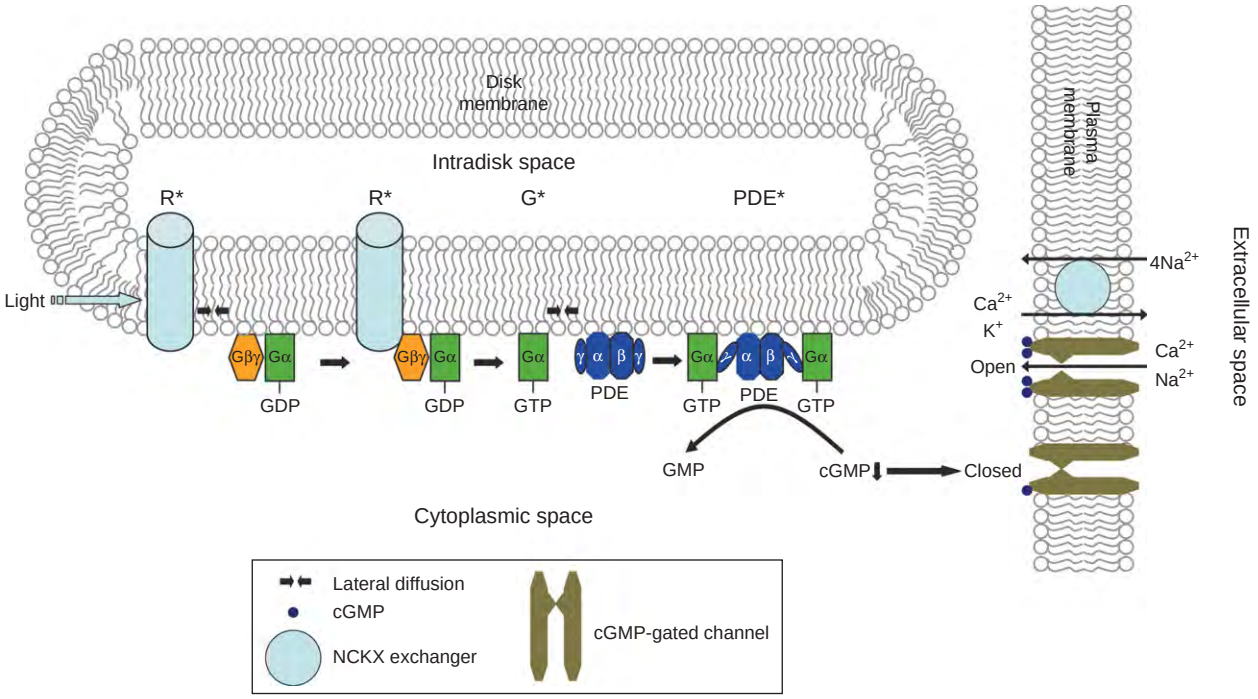

Figure 2 Schematic representation on the activation of vertebrate rod phototransduction. Following photon absorption, the activated rhodopsin (R*) activates the heterotrimeric G protein, catalyzing the exchange of GDP for GTP, producing the active Gα*-GTP. Two Gα*-GTPs bind to the two inhibitory γ-subunits of PDE, thereby releasing the inhibition on the catalytic α- and β-subunits, forming PDE*, which in turn catalyzes the hydrolysis of cGMP. The consequent decrease in the cytoplasmic-free cGMP concentration leads to the closure of the cGMP-gated channels on the plasma membrane and blockage of the influx of cations into the outer segment, which results in the reduction of the circulating dark current.

the active form of rhodopsin (R*), which in turn activates the downstream G protein, transducin. Because free opsin can weakly activate the transduction cascade, the antagonist role of 11-*cis*-retinal in the dark is important to keep the noise low in rods.

Even with 11-*cis*-retinal attached, rhodopsin occasionally undergoes spontaneous (thermal) activation in the dark, producing responses identical to those triggered by photons. This noise is often expressed as dark light because the noise adapts the visual system like real background light. This activity sets the limit on scotopic sensitivity, the visual sensitivity in darkness or dim light. To achieve the single-photon-detection sensitivity, rods not only need to have a high amplification system, but also need to have extremely low noise, or to be very quiet in the dark. This quietness can be partly attributed to the great thermal stability of rhodopsin. In a toad rod, the rate of thermal activation of rhodopsin was measured to be ~0.03 event s^{-1} rod^{-1} at 22 °C, corresponding to an average wait of 2000 years for the spontaneous activation of a given rhodopsin molecule to occur, based on a total of 2×10^9 rhodopsin molecules per cell. This great stability makes it possible for rods to pack many rhodopsin molecules to the rod disks to increase its photon-capture ability while keeping the dark noise low.

It should be mentioned that the question of dark noise in vision has had a long intellectual history from the point of view of psychophysics and system neuroscience. As early as 1940s and 1950s, Hecht and Barlow have estimated the amount of dark light in human rods based on psychophysical experiments. More than 30 years later, Baylor and colleagues used suction-electrode recording technique on primate rods to demonstrate that the very low quantal noise from rhodopsin, corresponding to ~0.01 event s^{-1} rod^{-1} in darkness, indeed matches the human psychophysical scotopic threshold. The quantitative agreement between the quantal noise measured from single rods and that measured in human psychophysics was considered a breakthrough in the vision field and a wonderful convergence between cell physiology and human psychophysics/system neuroscience – the goal of modern neuroscience after all.

The Activation of Transducin Constitutes the First Amplification Step

The second component of the rod phototransduction is the 81-kDa heterotrimeric G-protein, transducin (G_t, or $G\alpha_{t1}\beta_1\gamma_1$), which forms a subfamily of heterotrimeric G proteins. The molecular weight for α-, β-, and γ-subunits of rod transducin is approximately 39, 36, and 6 kDa, respectively. Transducin is present at ~10% the amount of rhodopsin in the disk membrane. Although transducin

subunits are soluble, the holo-transducin is firmly anchored to the disk membranes by a farnesyl lipid group that is post-translationally attached to the carboxy-terminal of the γ-subunit and an acyl group on the amino-terminal of the α-subunit. Therefore, photo-activated rhodopsin (R*) can only interact and activate transducin through lateral diffusion at the membrane surface.

Like many other G proteins, transducin exists in one of the two states: the GDP-bound inactive state and the GTP-bound active state. Binding of R* catalyzes the exchange of GTP for GDP on the α-subunit. The active Gα-GTP (G*) dissociates from R* as well as its native partner, Gβγ, and interacts with PDE to carry the signal forward. In the meantime, R* is able to activate additional molecules of transducin. Transducin activation by R* represents the first amplification step in the phototransduction cascade. The estimated rate of transducin activation by a single R* varied from 10 to over 3000 s^{-1} at room temperature. A rate of ~120 s^{-1} was later reported to be more consistent with biochemical, light-scattering, and electrophysiological measurements. The rate is roughly doubled in mammalian rods due to the higher body temperature. Until recently, it was believed that over a hundred transducins are activated during the lifetime of a single R* in mammalian rods. This number is now revised to be ~20 in mouse rods, based on the shorter life time of R* (80 ms) and activation rate of transducin by R* (240 s^{-1}).

The importance of transducin for conveying the signal from R* to PDE was manifested from animal models deficient in Gα and human patients carrying Gα mutations. It was found that rods of $G\alpha_{t1}$-null mice (*Gnat1*$^{-/-}$) lost all light sensitivity. In human, a mis-sense mutation in *Gnat1* (encoding the rod $G\alpha_{t1}$) is implicated in autosomal-dominant congenital stationary night blindness of Nougaret, caused by constitutive activation of rod phototransduction. The *gnat1*$^{-/-}$ mouse line has proven to be a valuable tool for blocking rod phototransduction to study cone phototransduction and circadian photoreception. It was also used successfully to delineate two apoptotic pathways in light-induced retinal degeneration. Bright light triggers apoptosis of photoreceptors through a mechanism requiring the activation of rhodopsin but not transducin signaling. In contrast, low-intensity light induces apoptosis that is predominantly dependent on transducin signaling.

The High Catalytic Power of PDE Accounts For the Second Amplification Step

PDE is the third component of rod phototransduction. It is a hetero-tetrameric protein consisting of two catalytic subunits, α- and β-, and two identical γ-subunits. PDE is anchored to the disk membrane by a hydrophobic isoprenyl group (compounds that are derived from isoprene, 2-methylbuta-1,3-diene, linearly linked together) post-translationally attached to the C-termini of the two catalytic subunits. As for transducin activation, PDE activation by G is through lateral diffusion on the rod disk membrane. Each catalytic subunit has two high-affinity noncatalytic binding sites and one catalytic binding site for cGMP. The noncatalytic sites were suggested to modulate the binding affinity between PDEγ and PDEαβ. The amount of PDE is ~1–2% of rhodopsin. Thus, the first three components of phototransduction are present in the ratio of 100R:10G:1PDE. In the dark, the two γ-subunits act as inhibitory subunits by binding to the two catalytic subunits and significantly reducing the hydrolysis of cGMP. In the light, Gα-GTP encounters PDEγ and sterically displaces the latter, therefore relieving its inhibitory effect on the catalytic subunits and permitting the hydrolysis of cGMP to proceed (**Figure 2**). Since each G* can only activate one PDEγ, two G*'s are required to fully activate a holo PDE. This is likely the scenario *in vivo* during light activation due to the excess amount of G over PDE and the presence of many molecules of G* activated by rhodopsin.

In contrast to the amplification achieved during transducin activation by R*, the activation of PDE by G* constitutes no gain, that is, with an efficiency approaching 1 (one G*, one activated PDE catalytic subunit) or 0.5 in terms of PDE holoenzyme. It is the catalytic power of PDE* that provides the second amplification step. It was reported that PDE* hydrolyzes cGMP at a rate close to the limit set by aqueous diffusion, with a K_m of ~10 μM and a K_{cat} of 2200 s^{-1}, making it one of the most efficient enzymes *in vivo*.

In addition to the noise produced by spontaneous activation of rhodopsin, spontaneous activation of individual catalytic PDE subunits produces the continuous noise, which accounts ~30–80% (depending on the species) of the total dark noise variance in rods. The basal spontaneous PDE activity balances constitutive guanylate cyclase activity in the dark, therefore maintaining a steady-free cGMP level. It also has the function of increasing the rate of cGMP turnover and consequently speeding up the dim flash response.

One might have expected that the deletion of PDEγ from mouse rods would unleash the full catalytic power of PDEαβ. However, it was found, in the absence of PDEγ that the PDEαβ dimer actually lacked catalytic activity, and the photoreceptors of the mutant mouse rapidly degenerated. Thus, the inhibitory PDEγ subunit appears to be necessary for the integrity of the catalytic PDEαβ subunits. The degeneration might be caused by an abnormally high cGMP concentration due to the lack of hydrolysis. A related example is the *rd* mouse, which is the oldest and one of the best-known models for retinal degeneration. The rod cells in the *rd* mouse begin to degenerate at about postnatal day 8, followed by cones;

by 4 weeks, virtually no rod photoreceptors are left. Degeneration in this mouse model is preceded by the accumulation of cGMP in the retina, correlated with deficient activity of the rod PDE due to a mutation in the PDEβ subunit. It is worth noting that the *rd* mouse was instrumental in suggesting that inner retinal neurons could mediate non-image-forming vision.

cGMP Is the Second Messenger Mediating Rod Phototransduction

By 1970, scientists generally believed that a second messenger was required to mediate the rod photoresponse based on several lines of evidence. First, light absorption occurs on the rod disk membrane, whereas the light-sensitive conductance is in the plasma membrane. Since rod disks are separate from the plasma membrane, a second messenger is required to connect the two. Second, the dim-flash response of rods lasts a few seconds, which is too long to be accounted by the open time of known membrane conductance. However, it took more than a decade before the identity of the second messenger was finally determined to be cGMP. The fierce battle was fought on the validity between two competing candidates, Ca^{2+} and cGMP. According to the Ca^{2+} hypothesis, which was first proposed by Hagins, the concentration of intracellular free Ca^{2+} is low in the dark and rises in the light to block light-sensitive current. The main supporting evidence is that reducing the concentration of external Ca^{2+} dramatically increases the dark current, suggesting that internal Ca^{2+} inhibits the dark current. On the other hand, the cGMP hypothesis proposed that the concentration of cGMP was high in the dark to maintain a cGMP-dependent conductance. Light led to the hydrolysis of cGMP and the subsequent closing of the conductance. The supporting evidence is that intracellular injection of cGMP increases the amplititude and latency of the photoresponse. Adding to the complexity is the finding that the free cGMP concentration varies inversely with the free Ca^{2+} concentration in rods, making it difficult to separate the effect of the two.

This debate was finally settled with the discovery of cGMP-gated channels in rods by Fesenko and colleagues in 1985. By using the patch-clamp technique, they showed that cGMP increased a cation conductance of inside-out patches of outer-segment plasma membrane without the need of ATP. The direct channel gating by cGMP is surprising because cyclic nucleotides were generally believed to act through cyclic-nucleotide-dependent kinases and protein phosphorylation on target proteins at that time. This dogma partially explained scientists' reluctance to embrace the cGMP hypothesis because protein phosphorylation was too slow. Another monumental work by Yau and Nakatani was published at the same year that helped the anointment of cGMP as the right candidate. An identical cGMP-gated cation conductance was found on a truncated rod outer segment with an intact plasma membrane. Most importantly, this conductance could be suppressed by light, suggesting that the long-sought light-sensitive conductance is the cGMP-gated conductance. The publications by Fesenko and Yau marked the end of the Ca^{2+} hypothesis.

The cGMP-Gated Channel Provides the Final Step of Signal Amplification

The cGMP-gated channel belongs to the family of cyclic-nucleotide-gated (CNG) channels, which are nonselective cation channels. The channel is located on the plasma membrane with a density of 400–1000 μm^{-2} and is the last component in the activation phase of phototransduction. Rod CNG channels consist of CNGA1 (or α1) and CNGB1 (or β1) subunits. CNGA1 subunit forms functional homomeric channels by themselves when heterologously expressed. Although CNGB1 does not form functional channels by themselves, it confers several properties typical of native channels when coexpressed with the CNGA1 subunit: flickery opening behavior, increased sensitivity to L-*cis*-diltiazem, (a CNG channel–specific inhibitor) and weaker block by extracellular calcium. For a long time, the rod channel was believed to be a hetero-tetramer consisting of two CNGA1 and two CNGB1 subunits. In 2002, a number of laboratories made the surprising discovery that the rod channel actually has a 3CNGA1:1CNGB1 subunit composition. In humans, mutations in CNGA1 cause retinitis pigmentosa. CNGB1 subunits were found to be crucial for the targeting of the native CNG channel in rods. Thus, only trace amounts of the CNGA1 subunit were found on the rod outer segments in CNGB1-null mice and the majority of rod photoreceptors failed to respond to light.

The gating of the rod channel by cGMP is cooperative with a Hill coefficient of ~3; therefore, the light-triggered suppression of the dark current is 3 times larger than the decrease in the intracellular cGMP concentration. This is the last step of signal amplification in rod phototransduction. The combined amplification provided by rhodopsin, PDE, and CNG channels is very high ($\sim 10^5$–10^6), ensuring the high sensitivity of rods, including the ability of rods to detect single photons.

In the dark, the concentration of free cGMP in the rod outer segment was estimated to be several μM, which is lower than the $K_{1/2}$ (~10–40 μM depending on Ca^{2+} concentration), the concentration of cGMP necessary to half-maximally activate the channel. As a result, only ~1% of the CNG channels are open! In other words, 99% of the channels are already closed in the dark and light can only suppress the remaining 1% channels. This explains

why current induced by cGMP injection is more than 10 times larger than the dark current.

The inward current through the cGMP channel is composed of ~85% Na^+ because Na^+ is the predominant external cation and the channel is nonselective to monovalent cations. The remaining current is mainly carried by Ca^{2+} with a minor contribution from Mg^{2+}. Extracellular Ca^{2+} actually partially blocks the channel to reduce its conductance under physiological conditions. The inward current is balanced by an outward current flowing across the inner-segment membrane, which is mainly carried by potassium channels. This circulating current is also called dark current in both rods and cones. Unlike other ligand-gated channels, the CNG channel does not desensitize to cGMP, which is important for rods to maintain a steady dark current ranging between 20 and 70 pA in vertebrate rods. The rod photoresponse is essentially a transient suppression of the circulating current. It was estimated that the dark current was carried by ~10 000 channels. The participation of large numbers of micro-channels averages out the channels noise, that is, reduces an otherwise substantial stochastic channel noise if the dark current were carried out by a few macro-channels. This feature improves the sensitivity of rods.

Two extrusion mechanisms are critical in maintaining ionic balance in rods. An energy-dependent Na–K ATPase at the inner segment pumped Na^+ out and K^+ into the cells. A Na/Ca,K exchanger (NCKX) in the outer-segment plasma membrane extrudes one Ca^{2+} and one K^+ outward in exchange for four Na^+ inward producing the net entry of one positive charge. The exchanger and the CNG channel were found to form a stable complex on the plasma membrane, likely as a way to control the stoichiometry between the two, which is critical for regulating Ca^{2+} concentration in the rod outer segment. During the light response, the influx of Ca^{2+} is reduced due to the closure of some CNG channels while the efflux of Ca^{2+} through the exchanger is maintained. The resulting Ca^{2+} decline triggers negative feedback to produce light adaptation.

See also: Phototransduction: Adaptation in Cones; Phototransduction: Adaptation in Rods; Phototransduction: Inactivation in Cones; Phototransduction: Inactivation in Rods; Phototransduction: Phototransduction in Cones; Phototransduction: The Visual Cycle; Primary Photoreceptor Degenerations: Retinitis Pigmentosa; Primary Photoreceptor Degenerations: Terminology; Secondary Photoreceptor Degenerations: Age-Related Macular Degeneration; Secondary Photoreceptor Degenerations.

Further Reading

Arshavsky, V. Y., Lamb, T. D., and Pugh, E. N., Jr. (2002). G proteins and phototransduction. *Annual Review of Physiology* 64: 153–187.

Baylor, D. A., Lamb, T. D., and Yau, K. W. (1979a). The membrane current of single rod outer segments. *Journal of Physiology* 288: 589–611.

Baylor, D. A., Lamb, T. D., and Yau, K. W. (1979b). Responses of retinal rods to single photons. *Journal of Physiology* 288: 618–634.

Burns, M. E. and Arshavsky, V. Y. (2005). Beyond counting photons: Trials and trends in vertebrate visual transduction. *Neuron* 48: 387–401.

Burns, M. E. and Baylor, D. A. (2001). Activation, deactivation, and adaptation in vertebrate photoreceptor cells. *Annual Review of Neuroscience* 24: 779–805.

Fu, Y. and Yau, K. W. (2007). Phototransduction in mouse rods and cones. *Pflugers Archiv – European Journal of Physiology* 454: 805–819.

Luo, D. G., Xue, T., and Yau, K. W. (2008). How vision begins: An odyssey. *Proceedings of the National Academy of Sciences of the United States of America* 105: 9855–9862.

Pugh, E. N., Jr. and Lamb, T. D. (2000). Phototransduction in vertebrate rods and cones: Molecular mechanisms of amplification, recovery and light adaptation. In: Stavenga, D. G., de Grip, W. J., and Pugh, E. N., Jr. (eds.) *Handbook of Biological Physics, Vol. 3: Molecular Mechanisms of Visual Transduction*, pp. 183–255. Amsterdam: Elsevier.

Phototransduction: Rhodopsin

L P Pulagam and K Palczewski, Case Western Reserve University, Cleveland, OH, USA

Glossary

GPCRs – G protein-coupled receptors are membrane receptor proteins with a seven-transmembrane helical topology that are capable of activating G proteins.
G proteins – Heterotrimeric intracellular proteins so named because they bind to the guanine nucleotides, guanosine diphosphate in an inactive state and guanosine triphosphate in an active state.
GRK1 – G protein-coupled receptor kinase 1 (rhodopsin kinase) is a highly specific protein kinase that catalyzes phosphorylation of photoactivated rhodopsin thereby triggering its deactivation.
LCA – Leber's congenital amaurosis is an inherited degenerative disease of the retina that results in a severe loss of vision.
Photoisomerization – The structural change between chromophore geometric isomers (*cis* to *trans*) caused by photoexcitation. For rhodopsin, photoisomerization of its chromophore leads to activation of this receptor.
ROSs – Rod outer segments are the cylindrical outer portions of rod cells, each containing hundreds of membranous disks enveloped by the cellular (plasma) membrane.
RP – Retinitis pigmentosa is the name of a heterogeneous group of progressively blinding degenerations of the human retina caused by mutations in genes encoding photoreceptor proteins with an autosomal dominant (adRP), autosomal recessive (arRP), or X-linked pattern of inheritance.
Schiff base – A functional chemical group containing a carbon–nitrogen double bond. The retinylidene moiety is a chemical link between retinal and an amino group, for example, Lys^{296} of opsin.

Vision is an important biological sensing mechanism that involves conversion of light signals received by the eye into electrical nerve impulses transmitted to the brain by a process called phototransduction, consisting of a cascade of biological processes that occur in photoreceptor cells (rod and cone cells) of the retina. In the absence of light, photoreceptors are depolarized to a membrane resting potential of –40 mV. In the presence of light, the plasma membrane of the photoreceptor cells becomes hyperpolarized to –70 mV, resulting in a reduced amount of neurotransmitter released to downstream neurons. This article focuses on rhodopsin structure that relates to its function as a G protein-coupled receptor (GPCR).

Rod Cells and Rhodopsin

The vertebrate rod cell, a highly differentiated postmitotic neuron, is characteristically long, cylindrical, and primarily consists of an outer segment connected to an inner segment via a cilium (**Figures 1(a)** and **1(b)**). The rod outer segment (ROS) contains a stack of disk membranes enclosed by the plasma (cell) membrane, whereas the rod inner segment (RIS) contains the metabolic machinery for this cell. Rhodopsin is processed in the endoplasmic reticulum and transferred to the Golgi membranes of the RIS for additional processing of its carbohydrate moieties. Then rhodopsin-containing Golgi vesicles fuse with the apical plasma membrane of the inner segment and the rhodopsin molecules are transported through the rod cell cilium to the ROS where they form disk membranes. Mutations in the C-terminal region of rhodopsin inhibit transport of rhodopsin to ROS, indicating that this region is essential for recognition by the transport machinery.

A mammalian ROS consists of a stack of 1000–2000 disks enclosed by the plasma membrane. A cryo-electron tomography image of murine ROS (**Figure 1(c)**) also reveals that the thickness of a single disk membrane is 8 nm. Rhodopsin comprises >90% of all proteins in disk membranes and occupies 50% of the disk membrane volume. It is also present at a lower density in the plasma membrane of rod cells, and its expression is essential for ROS formation, which is absent in knock-out $Rho^{-/-}$ mice. In wild-type mice, there are approximately 8×10^4 rhodopsin molecules per disk and 3.96×10^{14} per eye. The power spectra of negatively stained disk membranes from bovine ROS (**Figure 1(d)**) reveals a diffuse diffraction ring at $\sim(45\,\text{Å})^{-1}$, indicating paracrystallinity of rhodopsin. Organization of the seven helices of rhodopsin was first ascertained by using a low-resolution imaging method called electron crystallography. Rhodopsin is unequally distributed in disk membranes. Electron tomographs of the ROS reveal both high- and low-density regions (**Figure 1(e)**). An atomic force microscopic image of native disk membranes showed that the average packing density of rhodopsin monomers is $48\,300 \pm 8000\,\mu m^{-2}$. Recent atomic force microscopic studies disclosing the arrangement of rhodopsin in native mouse disk membranes revealed that rhodopsin and opsin form structural dimers arranged in

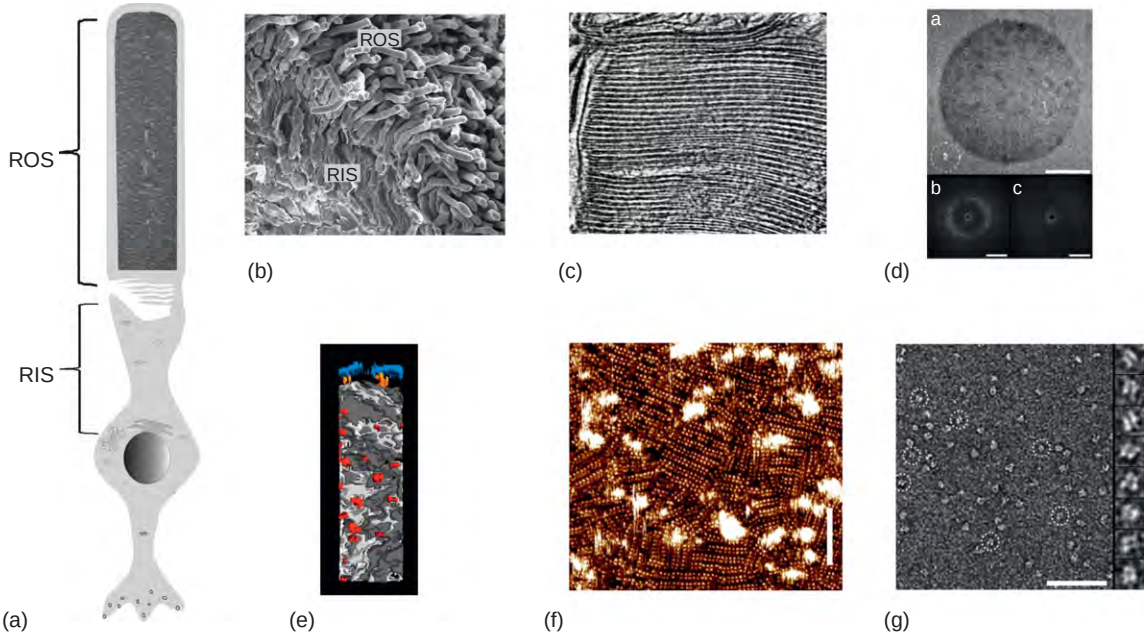

Figure 1 Vertebrate retina and rhodopsin. (A) Diagram of a rod cell. Vertebrate rod cells are postmitotic neurons with highly differentiated rod outer segments (ROSs) connected to rod inner segments (RISs) that generate proteins and energy to sustain phototransduction. ROSs consist of hundreds of stacked disk membranes enveloped by a plasma membrane. The main component of disk membranes is rhodopsin. Biochemical processes involving rhodopsin in the ROS allow rapid transduction of a light signal to graded hyperpolarization of the plasma membrane resulting from a decrease of light-sensitive conductance in ROS cGMP-gated cation channels. (B) Scanning electron micrograph of mouse retina. Rod cells comprise ~70% of all 6.4 million retinal cells, whereas cone cells represent <2%. (C) An *x–y* slice electron tomogram of vitrified mouse ROS. Disk membranes consist of a phospholipid bilayer studded with rhodopsin. (D) Transmission electron microscopy of negatively stained native disk membranes from mouse rod photoreceptors adsorbed on carbon film. (a) Morphology of a native bovine disk membrane. (b) Average of five power spectra calculated from broken circle outlined region shown inside the disk membrane in (a). A diffuse power diffraction signal is evident, indicating paracrystallinity of rhodopsin. (c) Average of five power spectra calculated from broken circle outlined region shown outside the disk membrane in (a). No power diffraction is evident. Scale bars: (a) = 2000 Å; (b and c) = 40 $Å^{-1}$. (E) The density of disk membranes is not uniform, indicating that rhodopsin is unevenly distributed in the mouse membrane. The distribution of high- (dark gray) and low- (light gray) density regions is shown in a top view of a single disk. Areas of low density (gray value < 0.33) represent 29% and areas of high density (gray value > 0.33) represent 71% of the disk volume. Gray values were obtained by computing the gray value for each voxel (three-dimensional pixel) in a disk membrane volume of 10 disks. Spacer proteins connecting two disks are colored red and the plasma membrane is colored blue. (F) Topograph obtained by using atomic-force microscopy shows the paracrystalline arrangement of rhodopsin dimers in the native disk membrane of mouse rod photoreceptors. Vertical brightness ranges: 1.6 nm. Scale bar = 50 nm. (G) Transmission electron microscopy of negatively stained disk membranes solubilized by n-dodecyl-β-D-maltoside. Rhodopsin dimers are clearly discerned on the carbon film. Magnified selected particles marked by broken circles are shown on the right. Scale bar = 500 Å. Frame size of the magnified particles in the gallery is 104 Å. (C and E) From Nickell et al. (2007). Originally published in *The Journal of Cell Biology*. (doi:10.1083/jcb.200612010). (F) Adapted from figure 2a in Fotiadis D. (2003). Atomic-force microscopy: Rhodopsin dimers in native disc membranes. *Nature* 421: 127–128. (D and G) Adapted from figure 3 in Suda K. (2004). The supramolecular structure of the GPCR rhodopsin in solution and native disc membranes. *Molecular Membrane Biology* 21: 435–446: Taylor and Francis.

paracrystalline arrays of rows (Figure 1(f)). Previous studies also support the importance of dimerization/oligomerization as necessary for the function of many, if not all GPCRs. Negative staining of detergent (*n*-dodecyl-β-D-maltoside)-solubilized disk membranes shows bi-lobed, roughly conical structures with lengths of ~65 Å, and these lobes are separated from each other by ~32 Å (Figure 1(g)).

Structure of Rhodopsin

Rhodopsin is a transmembrane protein consisting of an apoprotein, the 348 amino acid residue-long opsin (Figure 2), linked to a chromophore, 11-*cis*-retinal. The chromophore is bound covalently via a protonated Schiff base to the Lys^{296}-containing side chain of the opsin. Bovine rhodopsin also is post-translationally modified. The N-terminal Met is acetylated, and Cys^{322} and Cys^{323} of the C-terminus are palmitoylated, which is very common in GPCRs. In addition, a disulfide bond exists between $Cys^{110\ (H\text{-}III)}$ and $Cys^{187\ (E\text{-}II)}$. Rhodopsin is glycosylated at Asn^{2} and Asn^{15} by the hexasaccharide sequence $(Man)_3Glc(Nac)_3$. The molecular mass of bovine opsin with its post-translational changes (palmitoylation, acetylation of the N terminus and glycosylation) is 42 002.

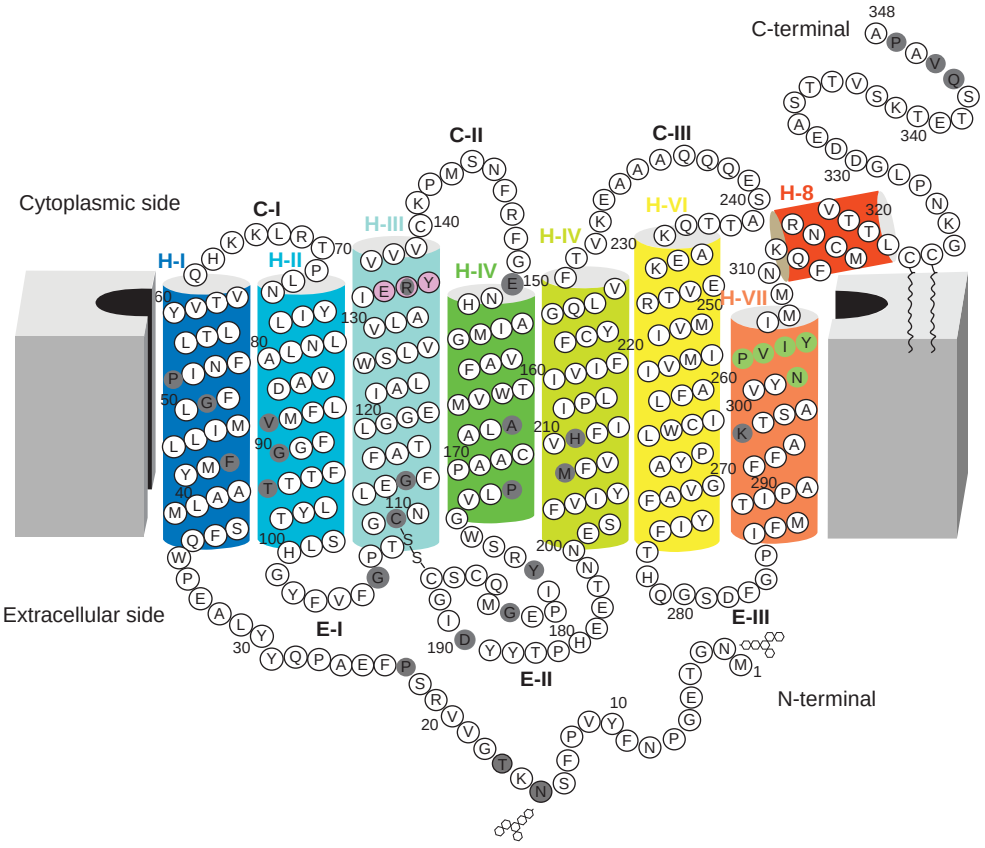

Figure 2 Two-dimensional representation of rhodopsin. Rhodopsin has seven transmembrane α-helices, C-I, C-II, and C-III depict its cytoplasmic loops, and E-I, E-II, and E-III represent the extracellular loops in this diagram. Stability of the helical segment is increased by the disulfide Cys^{110}–Cys^{187} bridge (shown as-S-S-), a highly conserved feature among many GPCRs. The chromophore, 11-*cis*-retinal, not shown here, is attached to Lys^{296} via a protonated Schiff base. Asn^{2} and Asn^{15} are sites of glycosylation by conserved glycans, Met^{1} is acetylated and Cys^{322} and Cys^{323} are palmitoylated. The predominant phosphorylation sites are Ser^{334}, Ser^{338}, and Ser^{343}. The whole C-terminal region is highly mobile but, as shown by using a model peptide, it may become more rigid when bound to arrestin. The highly conserved domains among GPCRs, (D/E)R(Y/W) (colored in pink) in helix 3 and NPXXY in helix VII (colored in green), are important for transforming the receptor from an inactive to a G protein-coupled conformation. Nonsense/missense mutations in rhodopsin leading to retinitis pigmentosa are colored in dark gray.

Rhodopsin was crystallized from detergent solutions. The three-dimensional structure of bovine rhodopsin at 2.8 Å, the first high-resolution structure reported for a GPCR, reveals the internal organization of this receptor molecule (**Figure 3**). Rhodopsin folds into seven transmembrane helices (H-I–H-VII) that vary in length from 20 to 33 amino acid residues, and one cytoplasmic helix (H-8). The transmembrane residues are irregular and tilted at various angles due to their Gly and Pro residues. Further advances in rhodopsin crystallization were recently reviewed.

The N-terminal region of rhodopsin is located intradiscally (extracellular) and the C-terminal region is cytoplasmic (intracellular), each region possessing three interhelical loops. The extracellular region consists of four distorted β-strands, three interhelical loops and the doubly glycosylated N-terminal domain. The extracellular region from residues 173–198 acts as a plug for the chromophore-binding pocket (**Figures 4(a)** and **4(b)**). The cytoplasmic surface contains 14 positively charged residues, whereas the extracellular side contains only three positively charged residues, an arrangement that agrees with the positive inside rule for multispanning eukaryotic membrane proteins. The intracellular/cytoplasmic region of rhodopsin is essential for its vectorial transport from the site of synthesis to the ROS and it also plays important roles in G protein activation and photoactivated rhodopsin desensitization.

A highly conserved (D/E)R(Y/W) motif in the GPCR A family is formed by the tripeptide, Glu^{134}-Arg^{135}-Tyr^{136}, located in the cytoplasmic region of bovine rhodopsin (**Figure 4(a)**). The carboxylate group of Glu^{134} forms a salt bridge with Arg^{135}, a highly conserved residue among GPCRs, and Arg^{135} also interacts with Glu^{247} and Thr^{251} in H-VI. The ionization state of Glu^{134} is sensitive to its environment, such that protonation of this residue causes rhodopsin activation (from meta IIa to meta IIb). This motif plays an important role in conformational changes in the structure of GPCRs that lead to their activation.

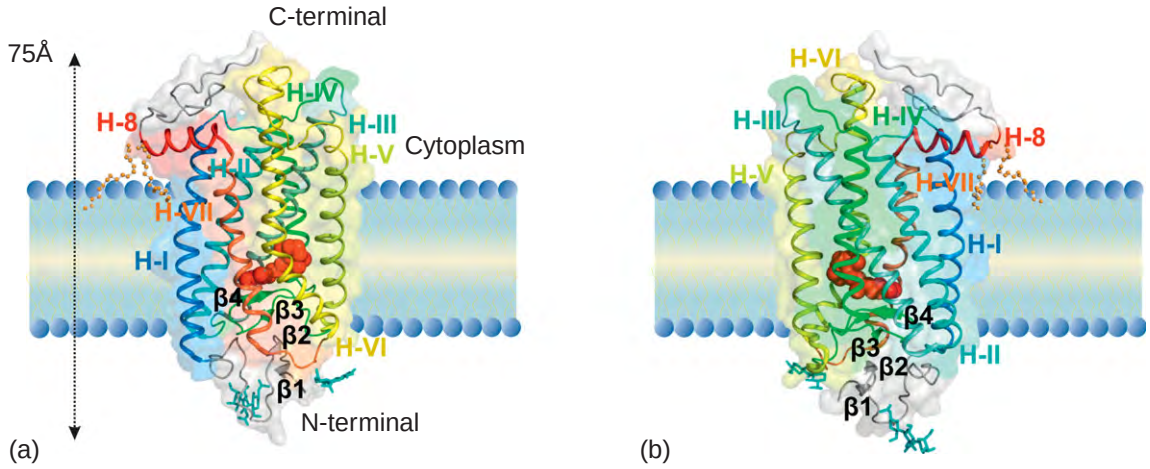

Figure 3 Structure of rhodopsin. (a) Rhodopsin has seven transmembrane helices (H-I to H-VII) and one peripheral helix (H-8). The transmembrane segments are α-helical, but these helices are highly distorted and tilted. Helices are displayed as ribbons and colored from blue (H-I) to red (H-8), as in the visible light spectrum. Helix labels are shown in the same color as their respective helices. N-terminal and C-terminal ends are colored gray. A palmitoyl group (orange-colored ball and stick representation) is attached to each of the two Cys residues at the end of helix H-8. Removal of this group has only a minor effect on phototransduction. β_1–β_4 are distorted β strands. The carbohydrate moieties (cyan-colored stick representation) are at Asn^2 and Asn^{15}. The Gly^3 to Pro^{12} region forms the first β-hairpin that runs parallel to the expected plane of the membrane. Arg^{177} to Asp^{190} leave helix H-4 to form a second twisted β-hairpin on the extracellular side. Rhodopsin is represented in a space-filled background and the plane of the lipid bilayer is shown. (b) Opposite side of rhodopsin shown in **Figure 2(a)**. (pdb code: 1U19.pdb)

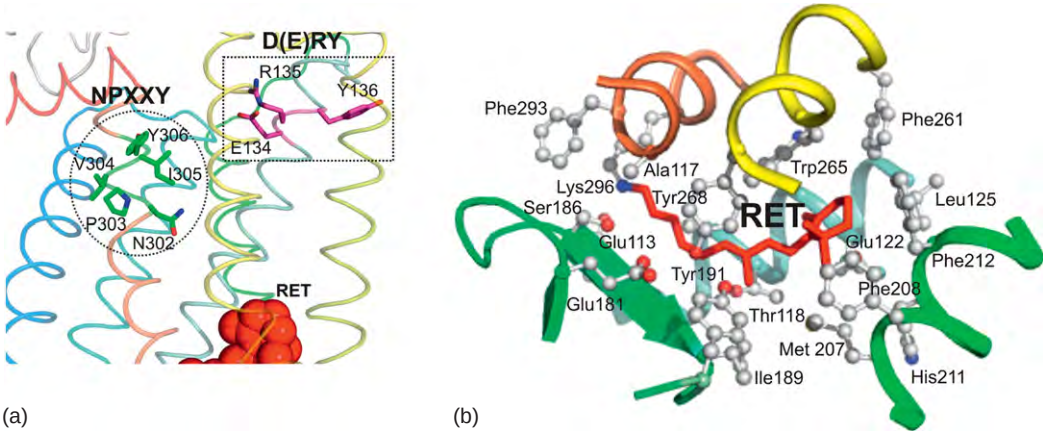

Figure 4 Functional regions of rhodopsin. (a) Conserved NPXXY and (D/E)R(Y/W) motifs in rhodopsin. Amino acid residues of these motifs are rendered as sticks, retinal (RET) is shown in the CPK color scheme as red, and helices are displayed as ribbons. (b) Retinal (RET)-binding site. Amino acid residues within about 5 Å are displayed to show the side chain environment surrounding the 11-*cis*-retinylidene group. Residues are represented as balls and sticks and retinal is shown in stick form (red). See text for explanation/discussion. Helices are colored as in **Figure 3**.

Another highly conserved NPXXY (Asn-Pro-Xaa-Xaa-Tyr) motif located at the end of helix VII and the beginning of H-8, is also close to the cytoplasmic region. Both the D(E)RY and NPXXY regions control the meta II (active) state of rhodopsin, and the NPXXY sequence is likely to be involved in G protein coupling (**Figure 4(a)**). The greatest distortion in H-VI is imposed by Pro^{267} (a highly conserved residue among GPCRs) and H-VII is elongated due the presence of Pro^{291} and Pro^{303} (parts of NPXXY) located in close proximity to Lys^{296}, the retinal-binding residue. Highly conserved Glu^{122} and His^{211} are located at the Zn^{2+}-binding site. The interaction between the β ionone ring and H-III occurs at Glu^{122}, one of the residues that determine the rate of meta II decay (**Figure 4(b)**).

Chromophore-Binding Site

Visual pigments of both rod and cone cells contain the chromophore, 11-*cis*-retinal, bound covalently to a Lys side chain (Lys^{296} in bovine rhodopsin) via a protonated Schiff base. The absorption maximum (λ_{max}) of free

solubilized 11-*cis*-retinal is about 380 nm. When this chromophore binds to opsins, its λ_{max} shifts toward longer wave lengths (a red shift) ranging from 435 nm (frog rods) to 560 nm (human cones). The protonated Schiff base linkage is responsible for about 70 nm of this shift. A further red shift results from the retinal-binding-pocket environment, especially its counter ion, which is Glu113 in vertebrate rhodopsins. In bovine rhodopsin, the λ_{max} of mutant E113Q (Glu to Gln) is dramatically shifted from 498 nm to ~380 nm. The absorption maximum also varies according to the interaction sites of the opsin molecule with the chromophore, especially dipolar interactions near the β ionone ring. Therefore, the λ_{max} absorption of visual pigments varies from species to species that differ with respect to their opsin protein sequences.

The chromophore in rhodopsin is located in the core of the seven transmembrane helices, closer to the extracellular side of the disk membrane. 11-*cis*-Retinal helps maintain rhodopsin in an inactive state (**Figure 4(b)**). The retinal-binding pocket is formed by helices H-III, H-V, H-VI, and H-VII and the antiparallel β sheet of the N-terminal plug, part of extracellular loop II (E-II in **Figure 2**). Although the retinal-binding site is very hydrophobic (**Figure 4(b)**), four charged residues, specifically $Glu^{113\ (H\text{-}III)}$, $Glu^{122\ (H\text{-}III)}$, $Glu^{181\ (\beta\ sheet)}$, and $Lys^{296\ (H\text{-}VII)}$, are located near the chromophore. $Lys^{296\ (H\text{-}VII)}$ donates an amino group to form a protonated Schiff base and $Glu^{113\ (H\text{-}III)}$, which is 3.6 Å away from the Schiff base, acts as a counter ion for this linkage. The positive charge on the protonated Schiff base is energetically unstable in the hydrophobic protein core but the $Glu^{113\ (H\text{-}III)}$ counter ion stabilizes the base by shifting its pK_a from neutral to alkaline. Highly conserved among all known vertebrate visual pigments, $Glu^{113\ (H\text{-}III)}$ plays three important roles: (1) It keeps rhodopsin in its resting state by participating in the salt bridge with the Schiff base. Disruption of this bridge allows the H-VI motion that occurs upon photoactivation. (2) It prevents spontaneous hydrolysis of the Schiff base by stabilizing the protonated Schiff base via increasing its K_a by as much as 10^7. (3) It causes a major bathochromic (longer wavelength) shift in the maximum wavelength absorption of visual pigments. Longer wavelength absorption is essential because the front of the eye in most animals does not allow ultraviolet (UV) light to reach the retina. Steric hindrance, resulting either from mutating $Gly^{121\ (H\text{-}III)}$ or substituting larger R groups at the C9 position, causes transducin (G_t) activation in the dark whereas lack of the C9 methyl group impedes photoactivation.

Opsin reacts within minutes with 11-*cis*-retinal to form rhodopsin. Similarly, 7-*cis* and 9-*cis* retinal also form visual pigments. In contrast, all-*trans*-retinal and 13-*cis*-retinal cannot regenerate opsin. The crystal structure of rhodopsin reveals that the chromophore-binding pocket is well defined, suggesting that the binding pocket has high specificity for the Schiff base and the β ionone ring. The exact location of these two components restricts the length of the chromophore-binding site. Therefore, 7-*cis*, 9-*cis*, and double and triple *cis* retinal analogs that have similar lengths and structures can regenerate the opsin, whereas chromophore analogs that are either shorter or longer than 11-*cis*-retinal cannot.

Rhodopsin Cycle – Retinal Isomerization

Inactive rhodopsin is activated upon light absorption, which induces a *cis–trans* isomerization that converts 11-*cis*-retinal to all-*trans*-retinal. The activation process can be divided into three phases (**Figure 5**).

1. Light-induced *cis–trans* isomerization of the retinylidene.
2. Thermal relaxation of the retinylidene–protein complex.
3. Hydrolysis of the Schiff base linkage, leading to formation of rhodopsin's active meta II state.

Light absorption induces isomerization of 11-*cis*-retinylidene to all-*trans*-retinylidene, resulting in a transient intermediate called photorhodopsin, formed by the fastest chemical reaction (200 fs) in the rhodopsin cycle. Photorhodopsin is converted first into a thermally stable and high-energy intermediate product called bathorhodopsin. About 60% of the incident photon energy is stored in bathorhodopsin and then used to drive further conformational changes. In this state, the chromophore is in an 11-*trans*-15-*anti* conformation, a distorted all-*trans* conformation that results from steric restriction caused by the polyene chain of the retinal and the protein side chains. The β ionone ring and Schiff base are located in a conformation similar to that of rhodopsin in the dark, but Thr^{181} and Glu^{113} are slightly moved. Then the blue-shifted intermediate (BSI) is produced during the thermal relaxation of bathorhodopsin, but BSI can be observed only by time-resolved measurements during subsequent formation of lumirhodopsin. The distorted all-*trans*-retinal in bathorhodopsin relaxes by dislocation of the β ionone ring in lumirhodopsin. Displacement of this ring reflects the movement of helix III aided by interactions between other helices, that result in a slightly disordered structure during the transition from the dark state to lumirhodopsin. In particular, Thr^{181} and Glu^{122} (which are moved slightly in bathorhodopsin) become significantly moved due to the β ionone ring displacement. Lumirhodopsin then relaxes further into meta I. Although the conformation of the chromophore in meta I closely resembles that in lumirhodopsin and the Schiff base proton is still hydrogen bonded, the overall structure is similar to rhodopsin. Meta I is further converted to meta II in two steps that can be separated by 20 ms in detergent-solubilized samples: (1) Conversion of meta I to meta IIa, accompanied by proton transfer from the Schiff base to the counterion Glu^{113}. (2) Subsequent uptake of a proton from the cytoplasm leading to meta IIb formation. The proton acceptor here is $Glu^{134\ (H\text{-}III)}$, thus meta IIa and meta IIb are in a pH-dependent equilibrium regulated by proton uptake

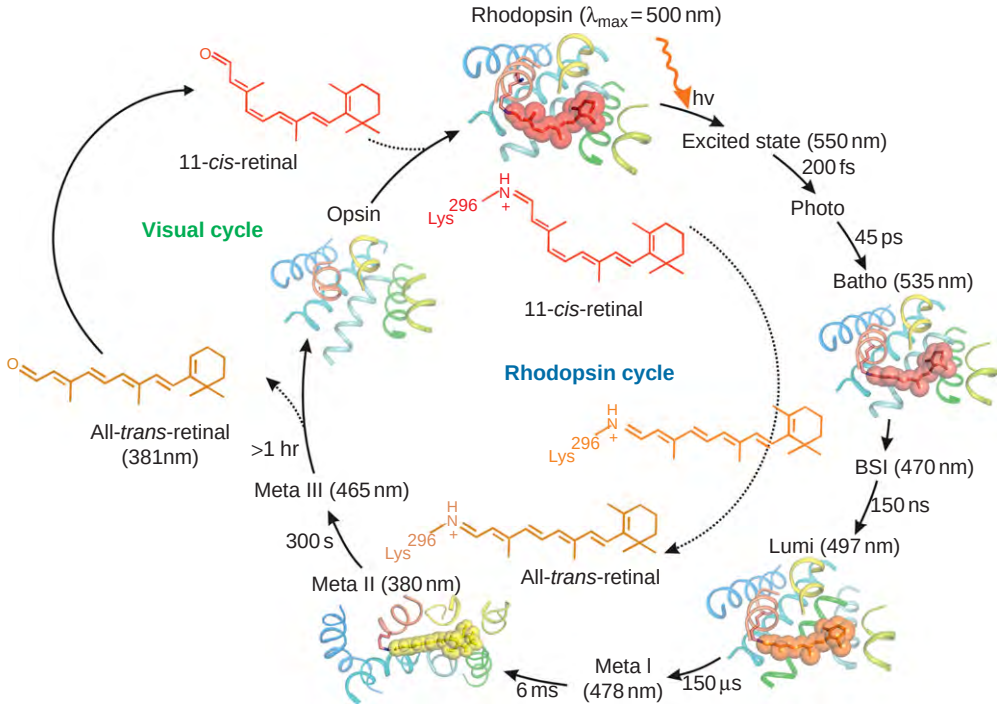

Figure 5 Schematic illustration of the rhodopsin cycle. Rhodopsin consists of an apoprotein called opsin and the bound chromophore, 11-*cis*-retinylidene, a geometric isomer of vitamin A in aldehyde form that imparts a red color to this protein. Upon light activation, rhodopsin transforms into opsin via many intermediate states. In the dark, rhodopsin contains the 11-*cis*-retinal chromophore attached to Lys^{296} (rendered as sticks) of helix H-VII in a protonated Schiff base linkage. Upon absorption of a photon, the chromophore is isomerized with ~65% probability from a *cis* C^{11}–C^{12} double bond to a *trans* conformation. In addition, with light activation, rhodopsin transforms into the photointermediate, bathorhodopsin (Batho), which thermally relaxes to BSI followed by lumirhodopsin (Lumi), which then changes to Meta I. During the transition of meta I to meta II, the all-*trans*-retinylidene Schiff base becomes deprotonated. Meta II, the signaling state capable of G protein activation, ultimately decays to free all-*trans*-retinal and opsin. The released photoisomerized chromophore, all-*trans*-retinal, is reduced to an alcohol by short chain alcohol dehydrogenases, such as prRDH, retSDR, and RDH12. The all-*trans*-retinal then diffuses into the retinal pigmented epithelium. There it undergoes enzymatic transformation back to 11-*cis*-retinal in a metabolic pathway known as the visual cycle. The replenished 11-*cis*-retinal then combines with opsin to form rhodopsin, thereby completing the rhodopsin cycle. The λ_{max} in nm as well as the duration (fs-s) of the various components are shown.

at Glu^{134} (part of E/DRY motif). However, only meta IIb can trigger G_t activation. Deprotonation of the Schiff base is characterized by a large UV shift of the absorption maximum from 478 nm in meta I to 380 nm in meta II. A low-resolution crystal structure of a bovine-deprotonated Schiff base meta II-like rhodopsin has been elucidated. Finally, meta II decays into opsin and all-*trans*-retinal. Free opsin exhibits the largest conformational changes as compared to dark-state rhodopsin (Figure 5).

Visual Cycle – Rhodopsin Regeneration

The visual cycle consists of a series of reactions by which all-*trans*-retinal released from opsin isomerizes back into 11-*cis*-retinal that again binds to the opsin (Figure 5). This cyclic process does not require light. The released all-*trans*-retinal is transformed first to all-*trans*-retinol by a retinal dehydrogenase (RDH) in the ROS. The all-*trans*-retinol is transferred to the retinal pigment epithelium (RPE) where it is esterified by lecithin:retinol acyltransferase (LRAT), and later isomerized to 11-*cis*-retinol by a retinol isomerase. 11-*cis*-RDH then converts 11-*cis*-retinol back to 11-*cis*-retinal, which leaves the RPE to regenerate the opsin in the ROS.

Vertebrate versus Invertebrate Rhodopsins

Enzymatic regeneration of rhodopsin does not occur in invertebrate visual systems where rhodopsin and metarhodopsin are photoconvertible. Upon photon absorption, 11-*cis*-retinal (or its analogs) of rhodopsin is converted into all-*trans*-retinal of metarhodopsin, and then irradiation of metarhodopsin changes the all-*trans*-retinal back to 11-*cis*-retinal by a process called photoregeneration.

Notably, invertebrates differ from vertebrates in the photoactivation of rhodopsin. Absorption of a photon by

invertebrate rhodopsin leads to a stable meta II, but retinal remains in the retinal-binding pocket. This contrasts to vertebrate rhodopsin where retinal leaves the meta II-binding pocket. Invertebrate phototransduction also involves an inositol-1,4,5-triphosphate signaling cascade (cyclic-guanosine monophosphate (GMP) in vertebrates) and a G_q-type G protein (G_t in vertebrates) that is stimulated by photoactivated rhodopsin.

Three-dimensional structures of bovine (vertebrate) rhodopsin and squid (invertebrate) rhodopsin show structural similarities in the arrangement of their transmembrane helices (Figure 6). Squid rhodopsin is a 50-kDa protein composed of 488 amino acid residues. A proline-rich 10-kDa C-terminal extension compared with bovine rhodopsin is important for intracellular trafficking of this rhodopsin, and its deletion does not affect G protein activation. Like other GPCRs, squid rhodopsin forms a disulfide bridge between Cys^{108} and Cys^{186} for proper folding of the E-II loop. The NPXXY and (D/E)R(Y/W) regions of squid rhodopsin are similar to those of bovine rhodopsin. However, Val in the NPXXY motif, and Glu in the (D/E)R(Y/W) motif of bovine rhodopsin are replaced by Met and Asp, respectively, in squid rhodopsin (Figure 6(b)). Their structural similarity implies that the functional difference between vertebrate and invertebrate rhodopsins might be due to specific interactions between

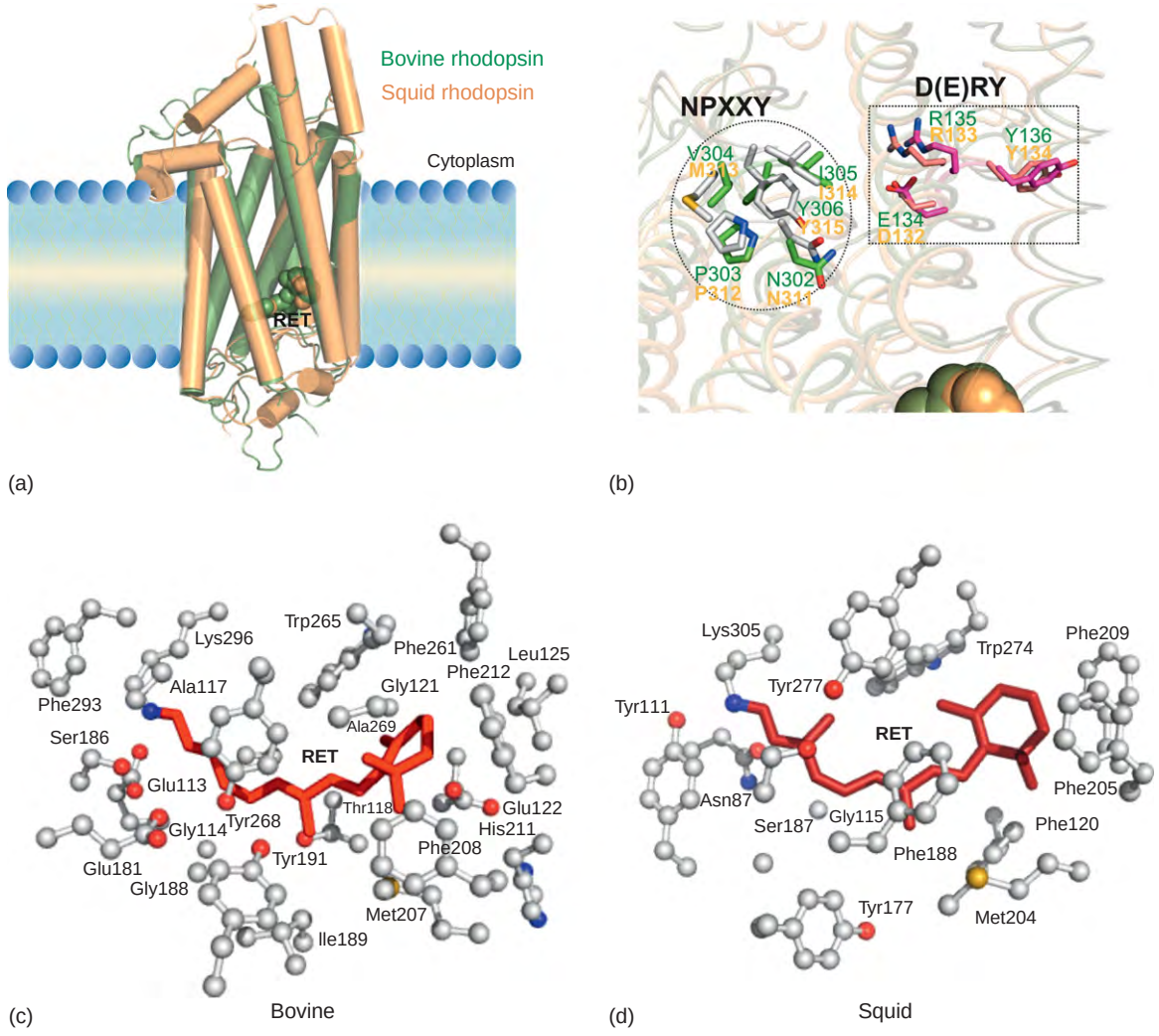

Figure 6 Bovine rhodopsin vs. squid rhodopsin. (a) Superimposition of bovine and squid rhodopsin structures. Helices are displayed in cartoon style, retinal (RET) is rendered as CPK balls, and the planar lipid bilayer is shown. (b) Conserved NPXXY and (D/E)R(Y/W) motifs of both bovine (green) and squid (yellow) rhodopsins are compared. Amino acids of these motifs are rendered as sticks, retinal is rendered as CPK balls, and helices are displayed as ribbons. (c) Retinal-binding site of bovine rhodopsin. Amino acid residues within about 5 Å are displayed to show the side-chain environment surrounding the 11-*cis*-retinylidene group. Residues are rendered as balls and sticks and retinal is shown in stick form (red). (d) Retinal-binding site of squid rhodopsin. Amino acid residues within about 5 Å are displayed to reveal the side-chain environment surrounding the 11-*cis*-retinylidene group. Residues are rendered as balls and sticks and retinal is shown in stick form (red). See text for explanation/discussion.

retinal and the amino acid sequence of the retinal-binding site. These binding sites are compared in Figures 6(c) and 6(d). In squid rhodopsin, the highly conserved Glu^{180} is too far away from the retinal-binding pocket and Asn^{185} is located between Glu^{180} and the Schiff base. Asn^{185} is assumed to move after photoisomerization of retinal, to mediate an indirect interaction between Glu^{180} and the retinal Schiff base. In the dark state, either Asn^{87} or Tyr^{111}, which is highly conserved among all invertebrates, might act as a hydrogen-binding partner (counter ion) for the Schiff base. These residues are replaced by Gly^{89} and Glu^{113} in bovine rhodopsin.

Signaling Cycle

After photoactivation, an active meta II state of rhodopsin triggers the activation of transducin (G_t protein). This form of rhodopsin is capable of activating G_t proteins during the relatively prolonged period of its activation. Accordingly, rhodopsin activity is regulated by its phosphorylation, a common feature among many GPCRs. This regulatory process is also important for rod cells to recover their responsiveness during dark adaptation. Desensitization of rhodopsin involves two steps: (1) phosphorylation of meta II, reducing the rate of transducin activation and (2) binding of arrestin to meta II, completely ending transducin activation by rhodopsin (Figure 7). This phosphorylation is carried out by rhodopsin kinase, a specific kinase also known as GRK1. Rhodopsin kinase phosphorylates specific serines in the rhodopsin C-terminal sequence. However, upon light illumination, GRK1 is released from recoverin and phosphorylates rhodopsin at multiple sites. Ser^{343}, Ser^{338}, and Ser^{334}, located in the C terminal domain on the cytoplasmic side of rhodopsin, are the main sites for this phosphorylation. Some threonine residues in this domain are also phosphorylated. Phosphorylation of this cytoplasmic domain reduces the ability of the G_t protein to bind to meta II, but it does not completely stop G_t activation. By binding to phosphorylated-meta II, arrestin prevents the interaction of G_t with meta II, and thus completely terminates G_t activation. At least three phosphorylated sites are required for high-affinity binding of the rhodopsin–arrestin complex. Arrestin dissociates from rhodopsin as meta II decays and loses all-*trans*-retinal. Then phosphorylated opsin is dephosphorylated by protein phosphatase 2A (PrP2A). The resulting free opsin is readily regenerated by 11-*cis*-retinal and continues recycling through the signaling cascade. A fraction of meta II directly dissociates into all-*trans*-retinal and opsin.

Rhodopsin Interaction with Other Proteins

According to X-ray crystallographic models and atomic force microscopic studies, H-IV–H-V of rhodopsin contact

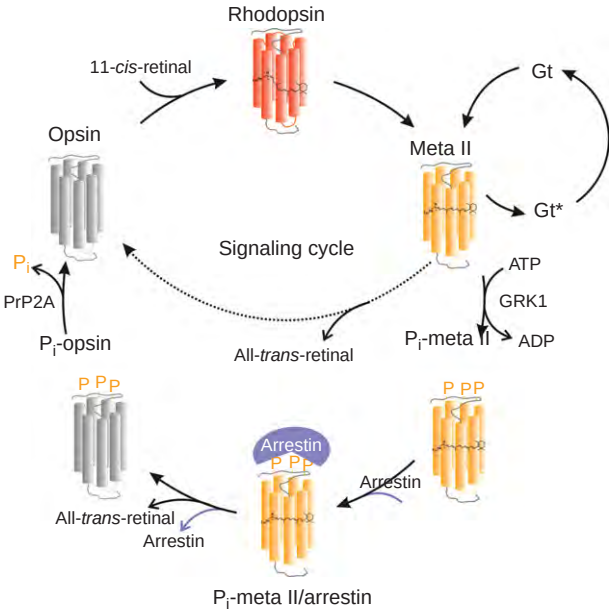

Figure 7 Interaction of rhodopsin with partner proteins. Phototransduction starts with the absorption of light by rhodopsin that causes photoisomerization of 11-*cis*-retinal to all-*trans*-retinal. Photoisomerization of this chromophore induces conformational changes in rhodopsin leading to formation of meta II, the signaling state of rhodopsin. Meta II binds and activates a large number of photoreceptor-specific G protein molecules, transducins (Gt), by catalyzing the exchange of guanosine triphosphate (GTP) for guanosine diphosphate (GDP) on transducin's α-subunit, Gtα. Deactivation of meta II and consequent Gt-mediated signaling starts with binding of the GPCR kinase called GRK1 (or rhodopsin kinase) that catalyzes subsequent phosphorylation of Ser and Thr residues in the C-terminus of rhodopsin. Phosphorylated rhodopsin then is capped by binding to arrestin, which prevents any residual Gt activation by meta II. The complex of phosphorylated rhodopsin–arrestin loses all-*trans*-retinal and then arrestin, after which the phosphorylated opsin is dephosphorylated by the action of protein phosphatase 2A (PrP2A). All-*trans*-retinal is transformed, through a series of steps, to 11-*cis*-retinal, which rebinds to opsin (as shown in Figure 4), thereby continuing rhodopsin signaling. A fraction of meta II loses all-*trans*-retinal (without phosphorylation) and directly transforms to opsin.

each other in a rhodopsin dimer. The sizes of G_t, GRK1, and arrestin proteins also favor the hypothesis of their interaction with the rhodopsin dimers. Previously reported models of rhodopsin with these proteins are discussed below. These complexes have yet to be resolved by crystallography.

Rhodopsin–G_t

In its inactive state, G_t is a membrane-associated protein that consists of α, β, and γ subunits with one guanosine diphosphate (GDP) noncovalently bound to the α-subunit. Post-translational modification of the α-(myristoylation) and γ-(farnesylation) subunits help this protein to associate with the membrane. A model for the rhodopsin–G_t complex has been reported (Figure 8(a)). Spectroscopic,

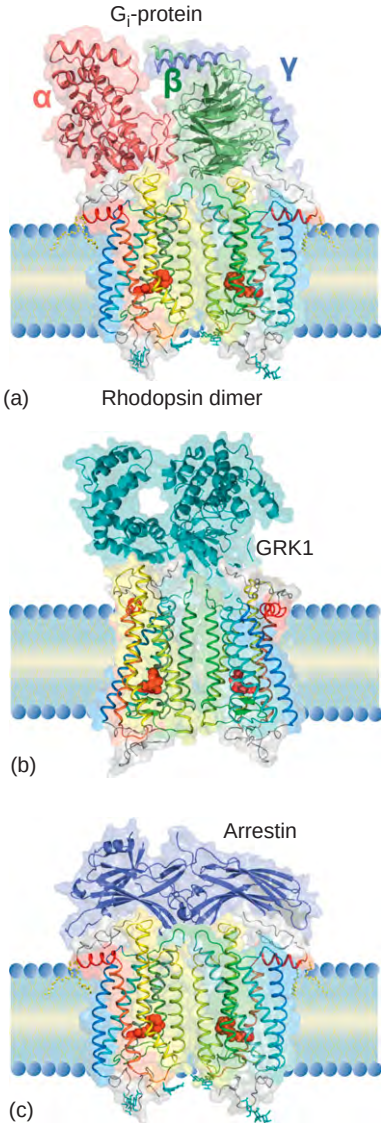

Figure 8 Conceptual models of rhodopsin dimers interacting with Gt, GRK1 and arrestin. (a) Rhodopsin dimer bound to one heterotrimeric Gt. Gtα is colored red, Gtβ is colored green, and Gtγ is colored blue. Gt occupies a single rhodopsin dimer, with only one rhodopsin monomer requiring activation. Helices of rhodopsin are colored as in **Figure 2**. (b) A rhodopsin monomer is modeled such that its third cytoplasmic loop (C-III) lies close to the proposed receptor-docking site for GRK1. This allows the GRK1 active site to have easy access to the C-tail of activated rhodopsin or of a neighboring unactivated rhodopsin in the same membrane plane, thereby allowing high gain phosphorylation of the ROS. (c) This theoretical model reflects the interaction of one arrestin molecule with a rhodopsin dimer. Molecules are represented in a space-filled background and the plane of the lipid bilayer is shown. No structural optimization was performed.

biochemical, and peptide competition experiments reveal that cytoplasmic loops II, III, H-8, and the C-terminal tail of rhodopsin interact with transducin. The interacting sites of transducin are the C-terminal tail, N-terminal helix, the α4–β6–α5 region of the α-subunit, and the farnesylated C-terminal region of the γ-subunit.

Rhodopsin–GRK1

GRK1 phosphorylates multiple sites on the C-terminal tail that is freely accessible in both active and inactive states of rhodopsin (**Figure 8(b)**). A single activated rhodopsin (meta II) molecule can induce the phosphorylation of hundreds of other rhodopsins. Cytoplasmic loops II and III of rhodopsin are the most important sites for binding of GRK1, and the N-terminal 30 residues of GRK1 are important for this interaction. Inactivating mutations in GRK1 are found in human patients with Oguchi disease, a stationary form of night blindness characterized by a substantial delay in recovery of dark vision after photobleaching.

Rhodopsin–Arrestin

Arrestin binds to photoactivated-phosphorylated rhodopsin (**Figure 8(c)**). Biochemical analysis of the arrestin–rhodopsin complex reveals that several domains of arrestin are essential for this interaction. In particular, the region from residues 163 to 189 is essential for binding to activated-phosphorylated rhodopsin, but not to unphosphorylated rhodopsin. Lysine and arginine residues of arrestin are also very important for specific binding, but only to phosphorylated rhodopsin.

Mutations in Rhodopsin and Retinal Diseases

Mutations in the genes encoding many proteins involved in phototransduction and the visual and signaling cycles have been implicated in causing blinding diseases of humans such as Leber's congenital amaurosis (LCA), Stargardt macular degeneration, congenital cone–rod dystrophy, and retinitis pigmentosa (RP). More than 100 rhodopsin mutants resulting in human eye diseases have been identified (**Figure 2**). Some mutations result in degeneration of rod cells, while some affect the function of rhodopsin. Mutations at the C-terminal tail impair rhodopsin trafficking from RISs to the ROSs. Mutations, for example Pro^{23} to His, which lead to rhodopsin misfolding will not allow the protein to reach disk membranes of ROS. Nonetheless, the ROSs degenerate and finally cause blindness. The Lys^{296} mutant is unable to bind chromophore, thereby compromising rhodopsin function. Mutations, for example Ala^{292} to Glu, which lead to human congenital night blindness do not involve ROS degeneration but rather compromise human vision under dim light. Mutations of proteins in the visual cycle also cause eye diseases. For example, inactivating mutations in the *LRAT* gene cause LCA. The $Lrat^{-/-}$ knock-out mouse with *LRAT*-mediated retinal dystrophy evidences only traces of retinoid compounds in ocular tissues, resulting in impaired vision from birth. The ROS are shortened in $Lrat^{-/-}$ mice, and photoreceptors degenerate very slowly. This disease can be treated by

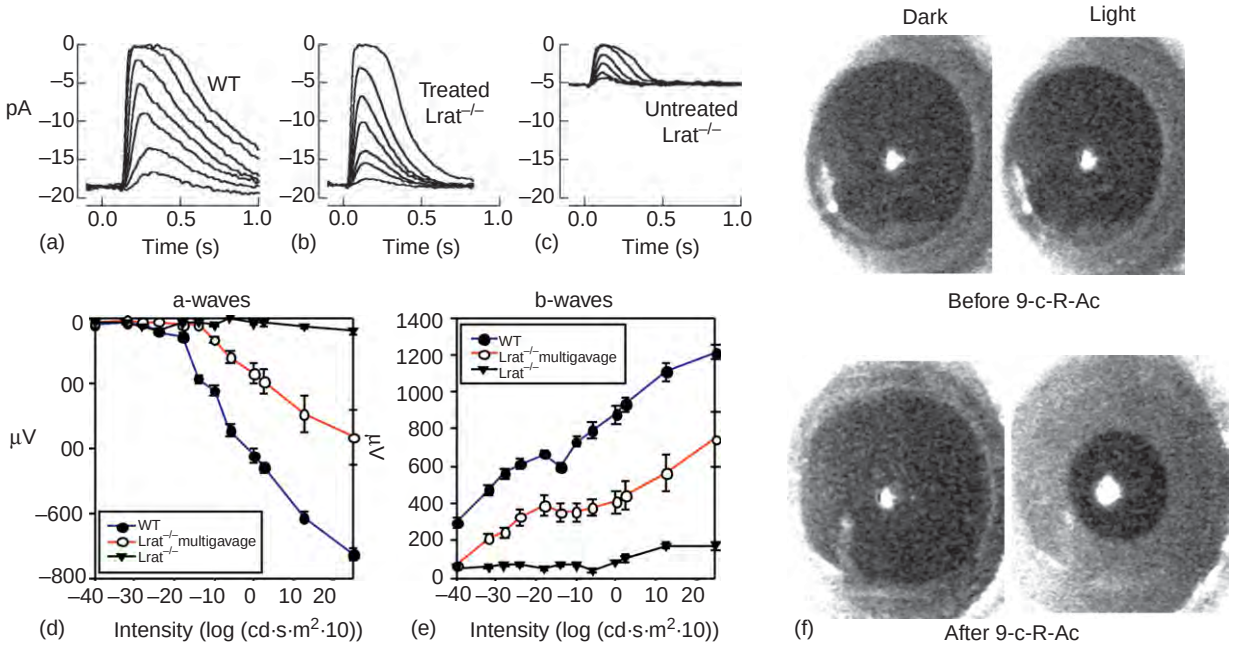

Figure 9 Rescue of visual responses measured by single-cell recording and ERG responses of single *WT* and *Lrat*$^{-/-}$ mouse rod cells. (a) Flash families measured for a *Lrat*$^{+/+}$ mouse (WT) rod, (b) a *Lrat*$^{-/-}$ rod from a mouse that had received a single gavage with 9-*cis*-R-Ac (9-*cis*-retinyl acetate), and (c) a control *Lrat*$^{-/-}$ mouse rod. Rods were obtained from 8-week-old mice. Each panel superimposes averaged responses to 5–20 repeats of a flash; flash strength was increased by a factor of 2 to produce each successively larger response. (d and e) Comparisons of scotopic single-flash ERG recordings from *Lrat*$^{+/+}$ (WT) control mice, 9-*cis*-R-Ac gavaged *Lrat*$^{-/-}$ mice and *Lrat*$^{-/-}$ untreated mice. *Lrat*$^{-/-}$ mice were gavaged 9 times with 5 μmol of 9-*cis*-R-Ac during a 1-month period. (f) Light-induced pupillary constriction of *Lrat*$^{-/-}$ mice before and after treatment with 9-*cis*-R-Ac. All together, these experiments show that 9-*cis*-retinyl acetate restored retinal function in this animal model of LCA. Adapted from figures 4 and 6 in Batten M. L. (2005). Pharmacological and rAAV gene therapy rescue of visual functions in a blind mouse model of Leber congenital amaurosis. *PLOS Medicine* 2(11): e333.

dietary intake of active chromophores or their 9-*cis*-precursors. Oral supplementation of *Lrat*$^{-/-}$ mice with 9-*cis*-retinyl acetate restored retinal function (**Figure 9**).

See also: Phototransduction: Phototransduction in Rods; Phototransduction: The Visual Cycle; Rod and Cone Photoreceptor Cells: Inner and Outer Segments; Rod Photoreceptor Cells: Soma and Synapse.

Further Reading

Arshavsky, V. Y., Lamb, T. D., and Pugh, E. N., Jr. (2002). G proteins and phototransduction. *Annual Review of Physiology* 64: 153–187.

Filipek, S., Stenkamp, R. E., Teller, D. C., and Palczewski, K. (2003). G protein-coupled receptor rhodopsin: A prospectus. *Annual Review of Physiology* 65: 851–879.

Fotiadis, D., Liang, Y., Filipek, S., et al. (2003). Atomic-force microscopy: Rhodopsin dimers in native disc membranes. *Nature* 421: 127–128.

Hargrave, P. A., McDowell, J. H., Curtis, D. R., et al. (1983). The structure of bovine rhodopsin. *Biophysics of Structure and Mechanism* 9: 235–244.

Menon, S. T., Han, M., and Sakmar, T. P. (2001). Rhodopsin: Structural basis of molecular physiology. *Physiological Reviews* 81: 1659–1688.

Muller, D. J., Wu, N., and Palczewski, K. (2008). Vertebrate membrane proteins: Structure, function, and insights from biophysical approaches. *Pharmacological Reviews* 60: 43–78.

Okada, T., Sugihara, M., Bondar, A. N., et al. (2004). The retinal conformation and its environment in rhodopsin in light of a new 2.2 Å crystal structure. *Journal of Molecular Biology* 342: 571–583.

Palczewski, K. (2006). G protein-coupled receptor rhodopsin. *Annual Review of Biochemistry* 75: 743–767.

Palczewski, K., Kumasaka, T., Hori, T., et al. (2000). Crystal structure of rhodopsin: A G protein-coupled receptor. *Science* 289: 739–745.

Park, J. H., Scheerer, P., Hofmann, K. P., Choe, H. W., and Ernst, O. P. (2008). Crystal structure of the ligand-free G-protein-coupled receptor opsin. *Nature* 454: 183–187.

Park, P. S., Lodowski, D. T., and Palczewski, K. (2008). Activation of G-protein-coupled receptors: Beyond two-state models and tertiary conformational changes. *Annual Review of Pharmacology and Toxicology* 48: 107–141.

Rao, V. R. and Oprian, D. D. (1996). Activating mutations of rhodopsin and other G protein-coupled receptors. *Annual Review of Biophysics and Biomolecular Structure* 25: 287–314.

Ridge, K. D. and Palczewski, K. (2007). Visual rhodopsin sees the light: Structure and mechanism of G protein signaling. *Journal of Biological Chemistry* 282: 9297–9301.

Salom, D., Lodowski, D. T., Stenkamp, R. E., et al. (2006). Crystal structure of a photoactivated deprotonated intermediate of rhodopsin. *Proceedings of the National Academy of Sciences of the United States of America* 103: 16123–16128.

Travis, G. H., Golczak, M., Moise, A. R., and Palczewski, K. (2007). Diseases caused by defects in the visual cycle: Retinoids as potential therapeutic agents. *Annual Review of Pharmacology and Toxicology* 47: 469–512.

Phototransduction: The Visual Cycle

G H Travis, UCLA School of Medicine, Los Angeles, CA, USA

Glossary

Lipofuscin – Fluorescent pigment granules found within cells of the RPE. Lipofuscin contains oxidized fatty acids and condensation of products of retinaldehyde with phosphatidylethanolamine, such as A2E. Lipofuscin is thought to arise from the incomplete digestion of phagocytosed outer segments. Components of lipofuscin, including A2E, are cytotoxic and thought to play a role in the etiology of macular degeneration.

Opsin visual pigment – Opsin pigments are light-sensitive complexes containing a protein and an 11-*cis*-retinaldehyde chromophore.

Outer segment – An elongated light-sensitive structure attached to the connecting cilium of rod and cone photoreceptors. The outer segment comprises a stack of approximately 1000 membranous disks. These disks are loaded with rhodopsin or cone opsin visual pigments.

Retinyl ester – A conjugate of vitamin A (retinol) with a fatty acid. Retinyl esters represent stable, nontoxic, and water-insoluble storage forms of retinol. Retinyl esters are also the substrate for Rpe65-isomerase in RPE cells.

Retinaldehyde – An oxidized form of retinol. Retinaldehydes are highly reactive and potentially cytotoxic. The 11-*cis* isomer of retinaldehyde (11-*cis*-RAL) is the light-sensitive chromophore in rhodopsin and cone-opsin visual pigments.

Schiff base – It is also called an imine. Results from the reaction of a primary amine (as in lysine or phosphatidylethanolamine) with a carbonyl group (as in retinaldehyde) to form a carbon–nitrogen double bond with loss of a water molecule. Formation of a Schiff base is reversible.

The vertebrate retina contains two classes of light-sensitive cells, rods and cones. Both cell types contain a membranous structure called the outer segment (OS), which are loaded with rhodopsin or cone-opsin visual pigments. These pigments are members of the G-protein-coupled receptor superfamily. Each rod OS contains approximately 10^8 rhodopsin pigments. The ligand for these pigments is 11-*cis*-retinaldehyde (11-*cis*-RAL), which is covalently coupled to a lysine in the opsin protein through a Schiff-base linkage. Absorption of a photon by an opsin pigment induces photoisomerization of the 11-*cis*-RAL chromophore to all-*trans*-retinaldehyde (all-*trans*-RAL). This isomerization converts the pigment to active metarhodopsin II, which stimulates the visual-transduction cascade. After a brief period, metarhodopsin II is inactivated by rhodopsin kinase-mediated phosphorylation and subsequent capping by arrestin. Next, all-*trans*-RAL dissociates from the inactivated opsin pigment. To restore light sensitivity, the bleached apo-opsin recombines with another 11-*cis*-RAL, forming a new rhodopsin or cone-opsin pigment. To maintain continuous vision in light, the all-*trans*-RAL released by bleached pigments must be converted back to 11-*cis*-RAL. This process is carried out by a multistep enzyme pathway called the visual cycle (**Figure 1**). The first two catalytic steps of this pathway occur in photoreceptors, while the remaining steps take place in cells of the retinal pigment epithelium (RPE). The RPE is an epithelial monolayer adjacent to the photoreceptors. Apical processes of RPE cells interdigitate with the photoreceptor OS. The regeneration of visual chromophore is one of the several collaborations between photoreceptors and RPEs; and cone opsins may have access to an alternative source of 11-*cis*-RAL chromophore. This alternative retinoid pathway is present in Müller glial cells.

Clearance of All-*trans*-RAL from OS Disks

Following photoactivation and subsequent deactivation of the opsin pigment, all-*trans*-RAL probably exits between transmembrane (TM) helices, TM1 and TM7, into the lipid bilayer. The all-*trans*-RAL diffuses within the bilayer until it encounters the amine headgroup of a phosphatidylethanolamine, which may condense with the all-*trans*-RAL to form the Schiff base, *N*-retinylidene-phosphatidylethanolamine (*N*-ret-PE). This condensation reaction is reversible. On the cytoplasmic surface of the OS disk-membrane, all-*trans*-RAL is reduced to all-*trans*-retinol (all-*trans*-ROL), driving dissociation of *N*-ret-PE (see below). However, all-*trans*-RAL can be temporarily trapped as *N*-ret-PE on the intradiscal surface. An adenosine triphosphate (ATP)-binding cassette transporter called ABCA4 (also ABCR or rim-protein) is present in the disks of rod and cone OS. Mice with a knockout mutation in the *abca4* gene show delayed clearance of all-*trans*-RAL and elevated *N*-ret-PE in the retina following exposure to light. *In vitro* studies suggest that ABCA4 is an outwardly directed flippase for

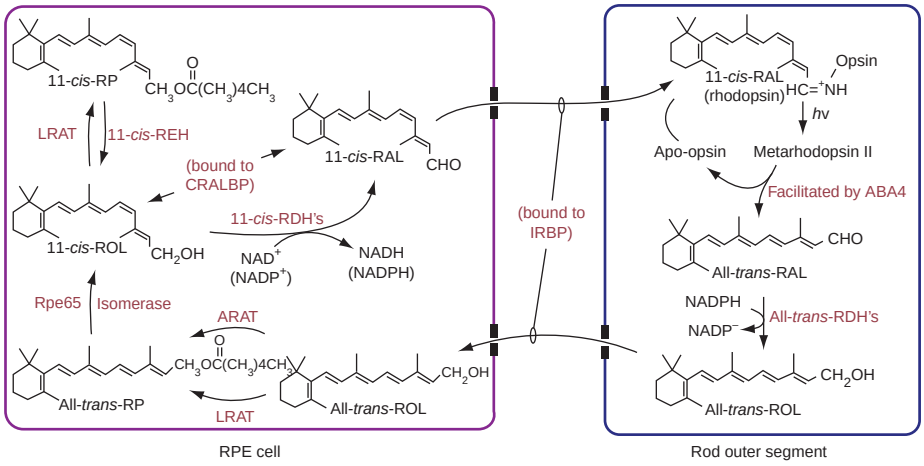

Figure 1 Visual cycle. Following absorption of a photon ($h\nu$), 11-*cis*-RAL Schiff base in rhodopsin is isomerized to all-*trans*-RAL, converting the receptor to active metarhodopsin II. Subsequently, the all-*trans*-RAL dissociates from apo-opsin. ABCA4 transports all-*trans*-RAL (as *N*-ret-PE) across the disk bilayer from the interior to the cytoplasmic leaflet. The all-*trans*-RAL is reduced to all-*trans*-ROL by one or more all-*trans*-RDH's that use NADPH as a cofactor. The all-*trans*-ROL is released by the OS to IRBP in the IPM. The all-*trans*-ROL is carried by IRBP to the apical RPE, where it is taken up and esterified by LRAT or ARAT to yield an all-*trans*-RE such as all-*trans*-RP. The all-*trans*-RP is isomerized and hydrolyzed by Rpe65 to yield 11-*cis*-ROL. The 11-*cis*-ROL may be oxidized by one or more 11-*cis*-RDH to yield 11-*cis*-RAL chromophore. Alternatively, the 11-*cis*-ROL may be secondarily esterified by LRAT or ARAT to yield an 11-*cis*-RE, such as 11-*cis*-RP, representing a preisomerized storage form of chromophore precursor. When needed, the 11-*cis*-RP is hydrolyzed by 11-*cis*-REH to yield 11-*cis*-ROL. 11-*cis*-ROL and 11-*cis*-RAL are bound to CRALBP in RPE cells. The 11-*cis*-RAL is released by the RPE into the IPM where it binds to IRBP. Finally, the 11-*cis*-RAL is delivered to the OS where it recombines with apo-opsin to form a new visual pigment.

N-ret-PE, consistent with the biochemical phenotype in *abca4*$^{-/-}$ mice. Thus, ABCA4 appears to facilitate the removal of all-*trans*-RAL from disk membranes for subsequent reduction to all-*trans*-ROL. Mutations in the human *ABCA4* gene cause Stargardt macular degeneration and a subset of recessive cone–rod dystrophy in humans. Stargardt patients and *abca4*$^{-/-}$ mice accumulate toxic lipofuscin pigments in RPE cells. Buildup of these fluorescent pigments is important in the pathogenesis of photoreceptor degeneration in Stargardt's disease.

Reduction of All-*trans*-RAL to All-*trans*-ROL

This reaction is carried out in photoreceptor OS by a member of the short-chain dehydrogenase/reductase family called photoreceptor retinol dehydrogenase (prRDH) or RDH8. RDH8 uses nicotinamide adenine dinucleotide phosphate oxidase (NADPH) as a co-factor. In *rdh8*$^{-/-}$ knockout mice, reduction of all-*trans*-RAL to all-*trans*-ROL is slowed but not halted, suggesting that RDH8 function is complemented in photoreceptors by at least one other retinol dehydrogenase. Photoreceptors contain a second retinol dehydrogenase called RDH12 that also catalyzes NADPH-dependent reduction of all-*trans*-RAL to all-*trans*-ROL. Mice with a knockout mutation in the *rdh12* gene show mildly slowed reduction of all-*trans*-RAL to all-*trans*-ROL, and protection from light-induced photoreceptor degeneration. Unlike RDH8, which is expressed in photoreceptor OS, RDH12 is expressed in photoreceptor inner segments. This distribution is unexpected given that all-*trans*-RAL is released following light exposure into the OS. RDH12 may play a detoxifying role in the inner segment by reducing all-*trans*-RAL that escaped reduction by RDH8 in the OS. Mutations in *RDH12* cause a severe recessive blinding disease called Leber congenital amaurosis (LCA). No mutations in *RDH8* have been associated with a retinal dystrophy in humans. Mice with a knockout mutation in the *rdh8* gene show normal kinetics of rhodopsin regeneration and delayed recovery of sensitivity following exposure to bright light. An identical pattern is seen in *abca4*$^{-/-}$ mice. ABCR and all-*trans*-ROL dehydrogenase act sequentially in the visual cycle to remove all-*trans*-RAL following a photobleach (**Figure 1**). Delayed dark adaptation in *rdh8*$^{-/-}$ and *abca4*$^{-/-}$ mice is probably due to noncovalent reassociation of all-*trans*-RAL with apo-opsin to form a noisy photoproduct that activates transducin.

Transfer of All-*trans*-ROL from Photoreceptors to the RPE

Interphotoreceptor retinoid-binding protein (IRBP) is secreted by photoreceptors and present at a high concentration in the extracellular space. Besides IRBP, this space is filled with extracellular matrix material and is called the

interphotoreceptor matrix (IPM). IRBP contains binding sites for both 11-*cis*- and all-*trans*-retinoids. IRBP has been shown to accelerate the removal of all-*trans*-ROL from bleached photoreceptors. The uptake of all-*trans*-ROL by IRBP may involve a receptor on the OS plasma membrane. Retinoids bound to IRBP are protected from oxidation and isomerization during transit through the IPM. Mice with a knockout mutation in the *irbp* gene show accumulation of all-*trans*-ROL in the retina, and reduced all-*trans*-REs in the RPE following light exposure. These mice also show accumulation of 11-*cis*-RAL in the RPE and reduced 11-*cis*-RAL in the retina following light exposure. These results suggest that IRBP functions to extract all-*trans*-ROL from bleached photoreceptors, and 11-*cis*-RAL from RPE cells. Mutations in the *RBP3* gene for IRBP cause the inherited blinding disease, recessive retinitis pigmentosa in a small subset of cases.

Another all-*trans*-ROL-binding protein, cellular retinol–binding protein type-1 (CRBP1), is present in RPE cells. CRBP1 is a soluble protein that binds all-*trans*-ROL with 100-fold higher affinity than does IRBP. This difference in affinity drives the uptake of all-*trans*-ROL from the IPM into RPE cells. Compared with wild-type mice, $crbp1^{-/-}$ knockout mice contain reduced all-*trans*-REs in the RPE and higher all-*trans*-ROL in the retina following light exposure. This biochemical phenotype is similar to the phenotype in $irbp^{-/-}$ mice.

Synthesis of Retinyl Esters

The major retinyl-ester synthase in RPE cells is lecithin: retinol acyl transferase (LRAT), which catalyzes the transfer of a fatty-acyl group from the *sn*1 position in phosphatidylcholine to all-*trans*-ROL (see **Figure 1**). The resulting all-*trans*-retinyl esters (all-*trans*-REs) are water-insoluble, and represent a stable and nontoxic storage form of vitamin A. Mice with a knockout mutation in the *lrat* gene contain virtually no all-*trans*-REs or other visual retinoids in their ocular tissues. Accordingly, $lrat^{-/-}$ mice are totally blind. Mutations in the human *LRAT* gene are yet another cause of recessive LCA.

Another retinyl-ester synthase activity, called acyl-CoA: retinol acyltransferase (ARAT), is present in RPE cells. Unlike LRAT, ARAT uses palmitoyl coenzyme A (palm CoA) as an acyl donor. Two enzymes have been shown to posses ARAT activity. Diacylglycerol acyltransferase type-1 (DGAT1), which catalyzes palm CoA-dependent synthesis of triglycerides from diacylglycerol, also catalyzes palm CoA-dependent synthesis of all-*trans*-REs from all-*trans*-ROL. Multifunctional *O*-acyltransferase (MFAT) also possesses ARAT catalytic activity. The very low level of all-*trans*-REs in the RPE of $lrat^{-/-}$ mice despite the presence of ARAT activity is due to the 10-fold higher K_M for all-*trans*-ROL substrate of ARAT versus LRAT. ARAT preferentially uses free all-*trans*-ROL as a substrate in contrast to LRAT, which uses holo-CRBP1.

Retinoid Isomerization

Conversion of a planar all-*trans*-retinoid to the strained 11-*cis* configuration is energetically unfavorable. Rpe65-isomerase uses all-*trans*-REs as substrate and catalyzes two reactions: hydrolysis of the carboxylate ester, and *trans* to *cis* isomerization of the C11–C12 double bond in the retinoid. Accordingly, the energy released by ester hydrolysis (−5.0 kcal $mole^{-1}$) is used to drive isomerization (+4.1 kcal $mole^{-1}$). Rpe65 is homologous to β-carotene oxygenase in mammals and apocarotene oxygenase (ACO) in cyanobacteria. The X-ray diffraction analysis showed that ACO has a seven-bladed β-propeller structure, with a Fe^{2+}-4-His arrangement at its axis. The four His residues that define the Fe^{2+}-binding site are conserved in all members of the ACO family including Rpe65. Rpe65 was shown to bind Fe^{2+}, which is required for its catalytic activity. Rpe65 is strongly associated with membranes but contains no membrane-spanning segments. Mice with a knockout mutation in the *rpe65* gene contain high levels of all-*trans*-REs in the RPE and no detectable 11-*cis*-RAL. Accordingly, $rpe65^{-/-}$ photoreceptors contain only apoopsin, and the mice have no detectable visual function. Despite blocked synthesis of visual chromophore, photoreceptor morphology is nearly normal in $rpe65^{-/-}$ mice. Visual function has been restored in $rpe65^{-/-}$ mice and dogs by administering exogenous visual chromophore. Injection of recombinant adeno-associated virus (AAV) containing a wild-type *rpe65* gene into the subretinal space (between RPE cells and photoreceptors) of $rpe65^{-/-}$ mice partially rescued the blindness phenotype. More recently, patients with *RPE65*-mediated LCA received subretinal injections of a similar *RPE65*-containing AAV. Encouragingly, these blind patients partially recovered visual function with expression of wild-type Rpe65 in their RPE.

The 11-*cis*-ROL synthesized by Rpe65 binds to cellular retinaldehyde-binding protein (CRALBP) in RPE cells. CRALBP also binds 11-*cis*-RAL. Mutations in the gene for CRALBP (*RLBP1*) cause several inherited retinal dystrophies including recessive retinitis pigmentosa. A newly synthesized molecule of 11-*cis*-ROL has two potential fates. As discussed below, it can be oxidized to 11-*cis*-RAL for use as visual chromophore. Alternatively, it can be esterified by LRAT to form an 11-*cis*-RE. 11-*cis*-REs represent a storage form of preisomerized chromophore precursor. Hydrolysis of 11-*cis*-REs is catalyzed by 11-*cis*-retinyl ester hydrolase (11-*cis*-REH) in the plasma membrane of RPE cells. The protein responsible for 11-*cis*-REH activity in RPE cells has not yet been identified.

Synthesis of 11-*cis*-RAL Chromophore

The final step in the visual cycle is oxidation of 11-*cis*-ROL to 11-*cis*-RAL. This reaction is catalyzed by 11-*cis*-ROL-dehydrogenase type-5 (RDH5), which uses NAD^+ as a cofactor. Mice with a knockout mutation in the *rdh5* gene show accumulation of 11-*cis*-ROL and 11-*cis*-REs in the RPE, and delayed recovery of rod sensitivity following light exposure. 11-*cis*-RAL is synthesized in *rdh5* $^{-/-}$ mice, albeit at a reduced rate, suggesting that RPE cells express at least one other 11-*cis*-ROL-dehydrogenase. RDH11 catalyzes $NADP^+$-dependent oxidation of 11-*cis*-ROL to 11-*cis*-RAL in the RPE. Surprisingly, *rdh5* $^{-/-}$, *rdh11* $^{-/-}$ double-knockout mice also synthesize 11-*cis*-RAL, although more slowly than in *rdh5* $^{-/-}$ or *rdh11* $^{-/-}$ single-knockout mice, and much more slowly than in wild-type mice. Thus, extensive functional redundancy exists for the oxidation of 11-*cis*-ROL in RPE cells, similar to the functional redundancy for reduction of all-*trans*-RAL in photoreceptors. 11-*cis*-RAL is strongly bound to CRALBP in RPE cells. CRALBP has been shown to interact with a protein complex on the cytoplasmic surface of the apical plasma membrane. From this position, 11-*cis*-RAL is transferred across the plasma membrane to bind IRBP in the IPM. This process may involve a receptor for IRBP on RPE cells.

Regeneration of Rhodopsin or Cone Opsin

The final step in the visual cycle is regeneration of a visual pigment from an apo-opsin and 11-*cis*-RAL. The mechanism whereby 11-*cis*-RAL is transferred from IRBP in the IPM to apo-opsin in the OS disk is unknown. It may involve an IRBP receptor on the OS plasma membrane, or simple diffusion of the 11-*cis*-RAL. No retinoid-binding protein has been identified in OS. The interaction of 11-*cis*-RAL with an apo-opsin involves a two-step process. First, a weak noncovalent complex is formed with 11-*cis*-RAL binding to a hypothesized entrance site on the opsin. Second, the 11-*cis*-RAL moves into the hydrophobic pocket and forms a Schiff base. This step is virtually irreversible in the case of rhodopsin. Once formed, rhodopsin is extremely quiet, with a spontaneous thermal-activation rate of one isomerization every 2000 years. In contrast to rhodopsin, recombination of 11-*cis*-RAL with the apo-cone-opsins is less favorable thermodynamically. Unlike rhodopsin, 11-*cis*-RAL freely dissociates from cone-opsins. For example, a dark-adapted red cone contains approximately 10% apo-cone-opsin due to spontaneous dissociation of chromophore. This effect contributes to the higher noise and much lower sensitivity of cones versus rods. It is also explains the tendency of rods to steal visual chromophore from cones when the availability of 11-*cis*-RAL is limited.

Regulation of the Visual Cycle

In the dark, photoreceptors stop releasing all-*trans*-ROL. Residual all-*trans*-ROL is esterified by LRAT. The major retinoids present in a dark-adapted eye are all-*trans*-REs in the RPE and 11-*cis*-RALs in photoreceptor visual pigments. How does the visual cycle know to stop converting all-*trans*-REs into 11-*cis*-RAL chromophore in the dark? One mechanism is the strong inhibition of Rpe65 by its product, 11-*cis*-ROL. When rhodopsin is fully regenerated and CRALBP is saturated, further synthesis of 11-*cis*-ROL by Rpe65 is inhibited.

A second mode of visual-cycle regulation involves an opsin protein called RPE-retinal G-protein receptor (RGR) opsin, expressed in RPE cells. Within RPE cells, all-*trans*-REs are stored in two compartments, internal membranes and oil droplets. Rpe65 associates with internal membrane but not lipid droplets. Hence, RPE internal membranes contain a pool of all-*trans*-REs available as substrate for isomerization, while lipid droplets contain a storage pool of all-*trans*-REs. This storage pool is potentially much larger than the isomerase pool in membranes. RGR opsin mediates light-dependent transfer of all-*trans*-REs from the storage compartment to the membrane compartment for isomerization. In light, where the requirement for visual chromophore is high, RGR opsin stimulates synthesis of 11-*cis*-ROL by increasing substrate availability to Rpe65. Consistently, mice with a knockout mutation in the *rgr* gene synthesize less 11-*cis*-RAL in the light and accumulate all-*trans*-REs. Mutations in the human *RGR* gene cause autosomal dominant retinitis pigmentosa.

See also: Phototransduction: Inactivation in Cones; Phototransduction: Inactivation in Rods; Phototransduction: Phototransduction in Cones; Phototransduction: Phototransduction in Rods; Phototransduction: Rhodopsin.

Further Reading

Batten, M. L., Imanishi, Y., Maeda, T., et al. (2004). Lecithin–retinol acyltransferase is essential for accumulation of all-*trans*-retinyl esters in the eye and in the liver. *Journal of Biological Chemistry* 279: 10422–10432.

Beharry, S., Zhong, M., and Molday, R. S. (2004). *N*-retinylidene-phosphatidylethanolamine is the preferred retinoid substrate for the photoreceptor-specific ABC transporter ABCA4 (ABCR). *Journal of Biological Chemistry* 279: 53972–53979.

Cideciyan, A. V., Aleman, T. S., Boye, S. L., et al. (2008). Human gene therapy for rpe65 isomerase deficiency activates the retinoid cycle of vision but with slow rod kinetics. *Proceedings of the National Academy of Sciences of the United States of America* 105: 15112–15117.

Gollapalli, D. R. and Rando, R. R. (2003). All-*trans*-retinyl esters are the substrates for isomerization in the vertebrate visual cycle. *Biochemistry* 42: 5809–5818.

Jin, M., Li, S., Moghrabi, W. N., Sun, H., and Travis, G. H. (2005). Rpe65 is the retinoid isomerase in bovine retinal pigment epithelium. *Cell* 122: 449–459.

Kaschula, C. H., Jin, M. H., Desmond-Smith, N. S., and Travis, G. H. (2006). Acyl coa:retinol acyltransferase (ARAT) activity is present in bovine retinal pigment epithelium. *Experimental Eye Research* 82: 111–121.

Kefalov, V. J., Estevez, M. E., Kono, M., et al. (2005). Breaking the covalent bond – a pigment property that contributes to desensitization in cones. *Neuron* 46: 879–890.

Lamb, T. D. and Pugh, E. N. (2004). Dark adaptation and the retinoid cycle of vision. *Progress in Retinal and Eye Research* 23: 307–380.

Maeda, A., Maeda, T., Imanishi, Y., et al. (2006). Retinol dehydrogenase (RDH12) protects photoreceptors from light-induced degeneration in mice. *Journal of Biological Chemistry* 281: 37697–37704.

Mata, N. L., Weng, J., and Travis, G. H. (2000). Biosynthesis of a major lipofuscin fluorophore in mice and humans with ABCR-mediated retinal and macular degeneration. *Proceedings of the National Academy of Sciences of the United States of America* 97: 7154–7159.

Radu, R. A., Hu, J., Peng, J., et al. (2008). Retinal pigment epithelium-retinal g protein receptor-opsin mediates light-dependent translocation of all-*trans*-retinyl esters for synthesis of visual chromophore in retinal pigment epithelial cells. *Journal of Biological Chemistry* 283: 19730–19738.

Redmond, T. M., Yu, S., Lee, E., et al. (1998). Rpe65 is necessary for production of 11-*cis*-vitamin A in the retinal visual cycle. *Nature Genetics* 20: 344–351.

Travis, G. H., Golczak, M., Moise, A. R., and Palczewski, K. (2007). Diseases caused by defects in the visual cycle: Retinoids as potential therapeutic agents. *Annual Review of Pharmacology and Toxicology* 47: 469–512.

Weng, J., Mata, N. L., Azarian, S. M., et al. (1999). Insights into the function of rim protein in photoreceptors and etiology of Stargardt's disease from the phenotype in ABCR knockout mice. *Cell* 98: 13–23.

Winston, A. and Rando, R. R. (1998). Regulation of isomerohydrolase activity in the visual cycle. *Biochemistry* 37: 2044–2050.

Physiological Anatomy of the Choroidal Vasculature

S S Hayreh, University of Iowa, Iowa City, IA, USA

Glossary

Choriocapillaris – A network of choroidal capillaries with a lumen of 10–50 μm and many fenestrations (openings) in its wall.
Fluorescein fundus angiography – A technique for examining the circulation of the retina using injection of sodium fluorescein into the systemic circulation. The angiogram is obtained by photographing the fluorescence emitted after illumination of the retina.
Ischemia – Restriction of blood supply with resultant damage or dysfunction of tissue.
Watershed zone – The border between the territories of distribution of any two end arteries.

The posterior part of the wall of the eyeball consists of three layers, which are, from the outside inward: the sclera, choroid, and retina. The choroid essentially consists of a thick layer of blood vessels, with some pigment. The blood vessels in the choroid are arranged, from the outside inward, in three ill-differentiated layers: (1) a layer of large vessels, (2) a layer of small vessels, and (3) the choriocapillaris. In the perichoroidal space, there are branches of the ciliary nerves, which form complex plexuses in the vascular layer so that the choroid has a rich nerve supply.

Unlike the neighboring retina, the importance of the choroid has until recently been ill-understood, despite the fact that it has many unique and important features, including the following:

1. Approximately 85% of the total ocular blood flow is in the choroid.
2. Choroidal blood flow is 20 times greater than that of retina.
3. Choroidal blood flow is the highest of any system in the body.
4. The choroidal circulation supplies 80% of the retina (outer 130 μm – up to the outer part of the inner nuclear layer), while the retinal vessels supply only 20%. When an eye has a cilioretinal artery, the choroid supplies the entire thickness of the retina in the area supplied by the cilioretinal artery.
5. Oxygen of the choroidal venous blood is 95% of that in the choroidal arterial blood.
6. Unlike capillaries elsewhere in the eye, the choriocapillaris has a lumen of 10–50 μm.
7. The choriocapillaris has many fenestrations in its wall. Therefore, there is no blood–ocular barrier in the choroid.
8. The peripapillary choroid is the main source of blood supply to the optic nerve head.

Blood Supply of the Choroid

Arterial Supply

The choroid is entirely supplied by the posterior ciliary arteries (PCAs). There is a good deal of confusion as to the nomenclature, number, origin, and distribution of the PCAs in humans. Based on our anatomical study of 59 human ophthalmic arteries and their branches, the following PCA types can be identified.

Posterior ciliary arteries

These arteries arise from the ophthalmic artery (**Figures 1(a)** and **1(b)**). In humans, the ophthalmic artery gives out one (in 3%), two (in 48%), three (in 39%), four (in 8%), or five (in 2%) PCAs. Usually, two or three PCAs supply an eye; when there are more than three PCAs, the additional arteries are usually small in size. The PCAs usually enter the eyeball medial and lateral to the optic nerve and occasionally at other sites. The PCAs are named according to their relationship to the optic nerve at their site of entry into the eyeball:

Medial PCA. This lies medial to the optic nerve and may be one (in nearly 70%) or two (in nearly 30%) in number.

Lateral PCA. This lies lateral to the optic nerve, and there may be one (in nearly 75%), two (in nearly 20%), or none (in nearly 3%).

Superior PCA. This is seen in only 9% and may be one (in 7%) or two (in 2%); and is usually small in size.

Branches of the main PCAs

After their origin from the ophthalmic artery, the various PCAs run forward (**Figure 2(a)**), divide into a large number of small branches, and pierce the sclera near the optic nerve (**Figure 2(b)**). They have the following branches:

1. *Long PCAs.* They are two long PCAs – one on the medial and the other on the lateral side. They run forward horizontally.

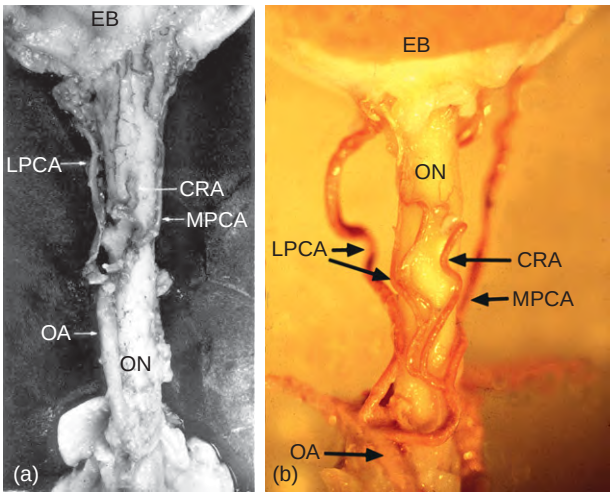

Figure 1 Photographs of inferior surface of the intraorbital part of the optic nerve (ON) and adjacent eyeball (EB) of (a) human and (b) rhesus monkey, showing ophthalmic artery (OA) with its lateral (LPCA) and medial (MPCA) posterior ciliary arteries and central retinal artery (CRA). Note a common trunk of origin of MPCA and CRA from the ophthalmic artery. (a) Reproduced from Hayreh, S. S. (1970). *British Journal of Ophthalmology* 54: 289–311.

2. *Short PCAs (SPCAs)*. There may be up to 20 SPCAs. They are further subdivided into two subgroups:
   (a) Paraoptic SPCAs enter the eyeball closest to the optic nerve (**Figure 2(b)**). Available evidence suggests that the optic nerve head is mostly supplied by the paraoptic SPCAs.
   (b) Distal SPCAs: The majority of the short PCAs are distal; they enter the eyeball midway between the paraoptic SPCAs and long PCAs on either side of the optic nerve (**Figure 2(b)**). They mainly supply the choroid.

From this account it is evident that there may be one to five PCAs and then three sets of branches of the PCAs supplying three different areas. It is inaccurate to use the term PCA loosely and as a generic term, covering all types of PCA and their branches.

Ocular supply by the PCAs

The short PCAs supply the following (**Figure 3**): (1) the choroid as far as the equator, and (2) the overlying retina to a depth of about 130 µm, including the retinal pigment epithelium and up to the outer part of the inner nuclear layer. If a cilioretinal artery is present, then the entire thickness of the retina is supplied in the distribution of the cilioretinal artery. (3) The PCA circulation is the main source of blood supply to the optic nerve head and the adjacent retrolaminar part of the optic nerve.

Each long PCA supplies a sector of the choroid, starting almost immediately from the point where it joins the choroid temporal to the macular region after having pierced the sclera, and extending forward to the ciliary body and iris. It also supplies the corresponding segment of the anterior uvea.

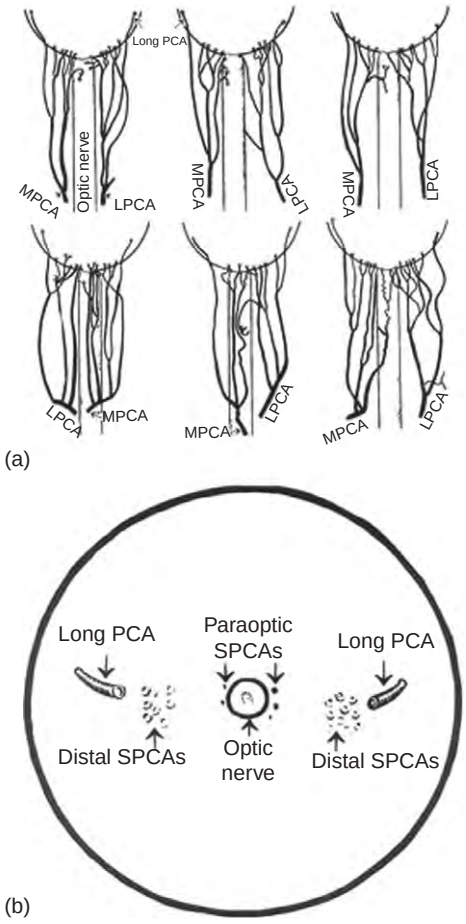

Figure 2 Diagrammatic representation of (a) the actual branching pattern of medial and lateral PCAs in six eyes, and (b) the site of entry of the various long and short PCAs, as seen on the back of the eyeball. Reproduced from Hayreh, S. S. (1999). *Current Concepts on Ocular Blood Flow in Glaucoma*. Pillunat et al. (eds.) pp. 3–31. The Hague: Kugler.

Venous Drainage

Vortex veins

The choroid has a large number of thin-walled veins, which finally drain into the vortex veins. There are usually four vortex veins (**Figure 4**). Each drains the veins not only from the corresponding quadrant of the choroid but also from the same quadrant of the iris and ciliary body.

Choriovaginal vein. In addition to the vortex vein, in some eyes, a vein may be seen which passes from the choroid through the sclera closely adjacent to the optic nerve head (**Figure 5**). It drains into the venous plexus of the pial sheath of the optic nerve. This choriovaginal vein occurs more frequently in highly myopic eyes than others.

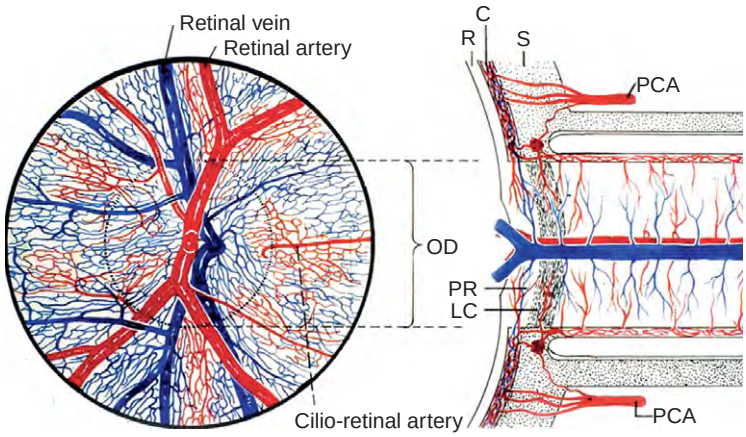

Figure 3 Schematic representation of blood supply of the optic nerve head by the PCA and retinal vasculature with a cilioretinal artery. C, choroid; LC, lamina cribrosa; OD, optic disk; PCA, posterior ciliary artery; PR, prelaminar region; R, retina; S, sclera. Modified from Hayreh, S. S. (1974) *Transactions – American Academy of Ophthalmology* 78: OP240–OP254.

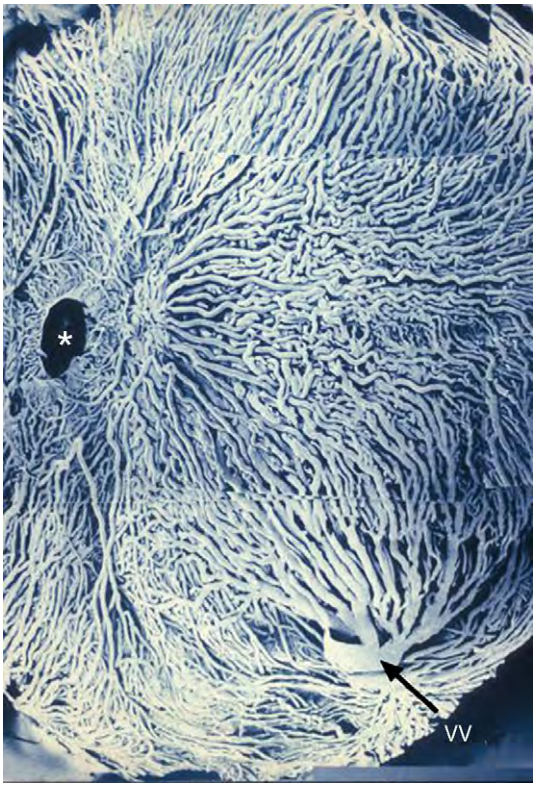

Figure 4 A plastic cast of the choroidal vascular bed of macaque monkey seen from the outside. The star marks the hole corresponding to the optic disk. VV, vortex vein. Reproduced by courtesy of Professor Koichi Shimizu.

Figure 5 Fundus photograph of left human eye showing the choriovaginal vein (arrow).

Since 1755, when Johann Gottfried Zinn, based on his studies, first described the anatomy of the choroidal vascular bed in *Descriptio Anatomica Oculi Humani*, extensive anatomical studies of the choroidal vascular bed have been conducted, mostly by studying casts prepared by the postmortem injection of a variety of materials and lately by studying the casts by scanning electron microscopy. These studies have formed the basis for the classical anatomical textbook description of the choroidal vasculature. According to most of these descriptions:

1. Extensive anastomoses exist between the various branches of all the SPCAs.
2. The SPCAs anastomose with the anterior ciliary arteries at the equator of the eye.
3. The choriocapillaris is arranged in one plane as a single continuous layer of wide lumen capillaries and they form a continuous anastomotic network over the entire choroid (**Figure 6**).
4. The choroidal veins communicate freely and the vortex veins have no segmental distribution (**Figure 4**).

Thus, postmortem cast studies of the choroidal vascular bed have consistently led to the conclusion that (1) there is NO segmental distribution in it, (2) the choroidal vessels anastomose freely with one another (**Figures 4** and **6**),

(3) PCAs anastomose with anterior ciliary arteries, and (4) there are interarterial as well as arteriovenous anastomoses. The casts have also suggested that the choriocapillaris forms a continuous vascular network and choroidal veins anastomose freely (**Figure 6**). However, it is well known that inflammatory, metastatic, ischemic, and degenerative lesions in the choroid are usually localized. Moreover, a number of clinical and experimental observations reported in the literature suggest that the PCAs have a segmental supply to the choroid. To resolve this controversy, the normal *in vivo* circulation and physiological anatomy of the choroidal vascular bed have been investigated experimentally in rhesus monkeys and clinically in humans by means of fluorescein fundus angiography (since 1969). These angiographic studies have virtually revolutionized our concept of the choroidal vascular bed, demonstrating its segmental nature (see above), and helping to explain the pathogeneses of some obscure fundus lesions. The following account represents our current knowledge on the subject.

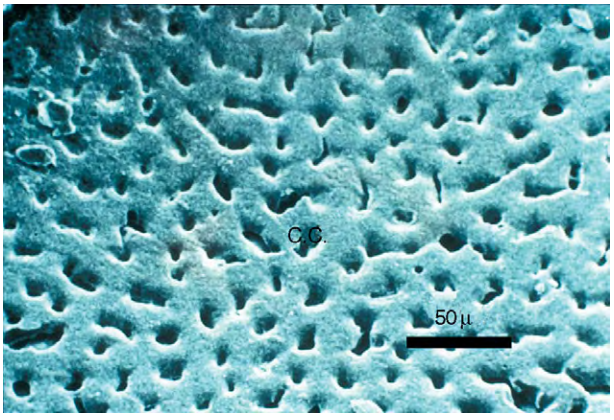

Figure 6 A plastic cast of choriocapillaris vascular bed of macaque monkey. Reproduced by courtesy of Professor Koichi Shimizu.

Normal *In Vivo* Circulation and Physiologic Anatomy of the Choroidal Vascular Bed

Experimental and clinical fluorescein fundus angiographic studies have demonstrated that the choroidal vascular bed is an end-arterial, segmental vascular system, almost similar to that seen in the retinal vasculature.

Posterior ciliary arteries

In the human, each PCA supplies the corresponding segment of the choroid. However, there is marked interindividual variation in the area supplied by each PCA.

The medial PCA

This may supply the entire nasal choroid up to the level of the fovea (**Figure 7(a)**), including the entire optic nerve head, or a part of the optic nerve head (**Figures 7 (b)** and **7(c)**) or its supply may stop short nasal to the nasal peripapillary choroid, so that it may take no part in the blood supply of the optic nerve head; or there may be any variation between these two extremes.

The lateral PCA

This supplies the area of the choroid not supplied by the medial PCA or vice versa. When there are more than one medial or lateral PCAs, the area supplied by each may correspond to only one quadrant or to only a sector.

The superior PCA

When present, this supplies a superior sector (**Figure 8**).

With the interindividual variation in number of PCAs and their distribution (see above), there may be an extremely variable pattern of distribution in the choroid from eye to eye. Clinical and experimental studies have shown that the various PCAs have a segmental supply and

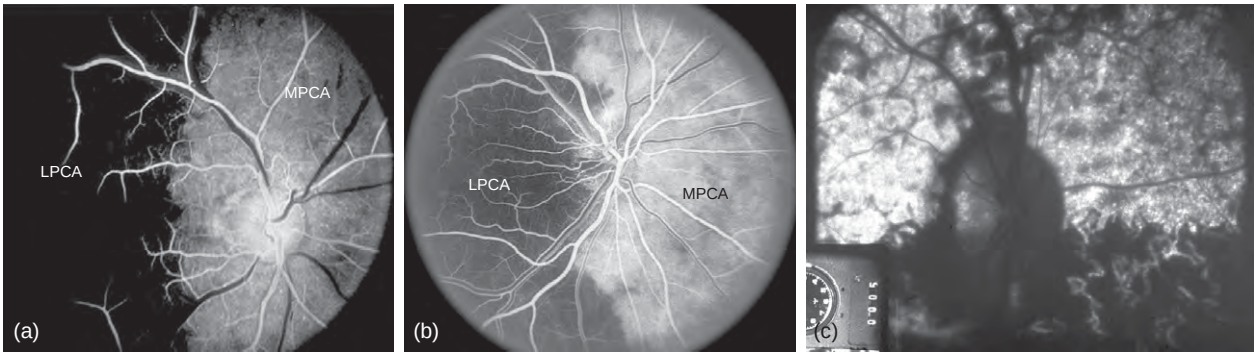

Figure 7 Fluorescein fundus angiograms of two human eyes (a, b) showing two examples of variations in the areas of supply in the choroid and the optic disk by the medial and lateral posterior ciliary artery (MPCA and LPCA, respectively) in different eyes. (c) Fluorescein fundus angiograms of a normal right eye of a healthy monkey showing filling of upper half of the choroid and optic disk with a well-demarcated horizontal border. (a) Reproduced from Hayreh, S. S. (1982). *Archives of Ophthalmology* 100: 1855–1896. (b) Reproduced from Hayreh, S. S. (1985). *Documenta Ophthalmologica* 59: 217–246. (c) Reproduced from Hayreh, S. S. (1970). *British Journal of Ophthalmology* 54: 289–311.

do not anastomose with one another; each behaves like an end artery.

The SPCAs

These supply segments of the choroid extending radially from the posterior pole to the equator; each segment varies greatly in shape, size, and location and has irregular borders (**Figures 9** and **10(a)–10(c)**). Smaller subdivisions of the short PCAs supply still smaller segments of irregular shape and size, having a geographic pattern. Ultimately, each terminal choroidal arteriole supplies a lobule of choriocapillaris. There may be a marked spatial variation in the filling of the various choroidal segments, which explains the well-defined geographical filling defects commonly seen on fluorescein angiography in the normal choroid. These physiological choroidal filling defects have often been mistaken for pathological filling defects. Our criterion to differentiate normal from abnormal filling defects in the choroid is to correlate the filling defects with the normal retinal vascular filling. If the choroidal filling defect disappears when the major retinal veins start to fill, it is normal, but if it is delayed then it is usually abnormal.

Long PCAs

These supply a wedge-shaped sector of the choroid, with its apex posteriorly, extending radially and temporally from the temporal border of the macular region (**Figures 9** and **11**).

Choriocapillaris

Fluorescein angiographic studies have shown that each terminal choroidal arteriole supplies an independent segment (lobule) of choriocapillaris, with the arteriole joining the segment in its center and the draining venules lying around the periphery of this segment (**Figures 12** and **13**). Each lobule of the choriocapillaris is an independent unit (of a polygonal shape in the posterior fundus), with no anastomosis with the adjacent segments *in vivo*. The lobules are arranged like a mosaic, the borders of the mosaic being formed by the venous channels. The size of each lobule of the choriocapillaris varies, and in our studies, it was usually about one-quarter of the disk diameter or less. The choriocapillaris is most densely packed at the posterior pole and progressively become less densely arranged toward the periphery. Unlike the retinal capillaries, the choriocapillaris have no blood barrier in the choriocapillaris because their endothelial fenestrations make them highly permeable.

Vortex veins

Experimental occlusion of the various vortex veins has shown that *in vivo* there is poor communication between the adjacent veins (**Figure 14**).

Choroidal anastomoses

The presence of interarterial and arteriovenous anastomoses in the choroid has been well documented in all the postmortem injection studies. Likewise, interarterial anastomoses between the branches of the PCAs and the anterior ciliary arteries have been documented in those studies. Nonetheless, no *in vivo* experimental or clinical studies, involving acute occlusion of the PCAs or their

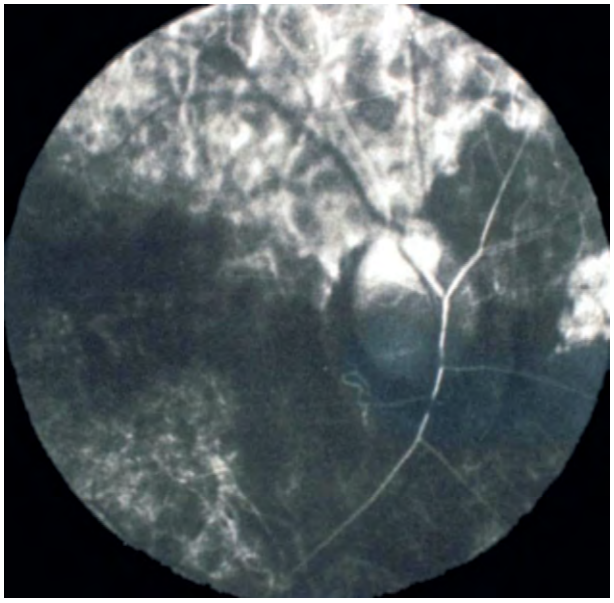

Figure 8 Fluorescein fundus angiogram, of a normal human right eye, shows filling of the superior PCA and corresponding part of the optic disk. Reproduced from Hayreh, S. S. (1974). *British Journal of Ophthalmology* 58: 955–963.

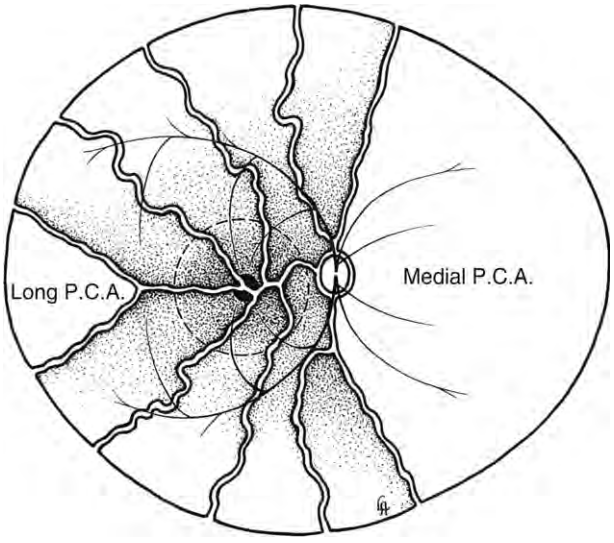

Figure 9 Diagrammatic representation of distribution by various temporal short PCAs and their watershed zones in the posterior part of the fundus. Dotted circle in the region of distribution of the temporal short PCAs represents the macular region. Areas of supply by the medial PCA and the temporal long PCA are also shown. Reproduced from Hayreh, S. S. (1974). *Graefe's Archive for Clinical and Experimental Ophthalmology* 192: 181–196.

smaller divisions, have shown any evidence at all of the presence of such anastomoses.

Segmental Nature of the Choroidal Vascular Bed

Fluorescein angiography clearly shows that blood flow in the choroidal arterial, choriocapillaris, and choroidal venous beds is strictly segmental, with no anastomoses between the adjacent segments at any level. The PCAs and choroidal arteries, right down to the terminal choroidal arterioles, are end arteries. These findings totally contradict the old concept, based on postmortem injection studies, that the entire choroidal vascular bed is one continuous, freely communicating system. Clearly, there is a serious disparity between the postmortem injection and the *in vivo* studies – the former misled us badly for more than two centuries. The reason for this discrepancy is that when the cast material is injected under pressure in the postmortem studies, the vessels fill from all sources, irrespective of the normal blood flow pattern, and, therefore, give information about the morphological conduits only, while the *in vivo* studies with fluorescein angiography reveal the actual pattern of the blood flow in those channels. It is also possible that in the living eye the neural supply to the potential anastomotic channels, seen on postmortem injection studies, may influence the pattern of blood flow; however, as yet, we have no definite explanation for this important disparity. In any case, what matters clinically, in explaining different vascular disorders, is the *in vivo* circulatory pattern.

Watershed Zones in the Choroidal Vascular Bed

When a tissue is supplied by two or more end arteries, the border between the territories of distribution of any two end arteries is called a watershed zone. The occurrence of such watershed zones between the various cerebral arteries is well known, as is also the case in some other organs having end-arterial systems. The significance of the watershed zones is that in the event of a fall in the perfusion pressure in the vascular bed of one or more of the end arteries, the watershed zone, being an area of comparatively poor vascularity, is most vulnerable to ischemia. The development of watershed infarcts in the cerebral cortex is well known.

From the foregoing discussion, it is evident that PCAs and their subdivisions, right down to the terminal choroidal arterioles, are end arteries. The choroidal vascular bed, therefore, has watershed zones. These zones are

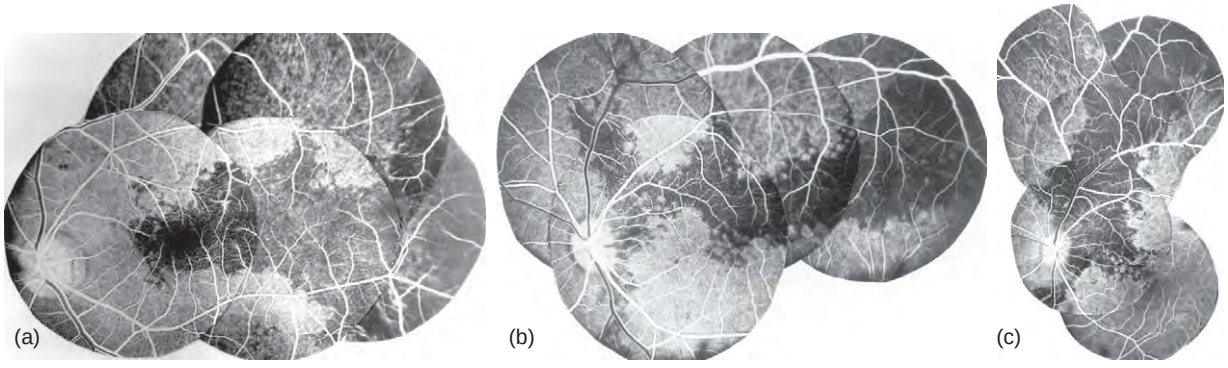

Figure 10 Fluorescein fundus angiograms of 3 (a–c) rhesus monkey eyes after experimental occlusion of different short PCAs, showing the variability in the areas of supply by the 3 different occluded arteries (dark areas). Reproduced from Hayreh, S. S. (1974). *Graefe's Archive for Clinical and Experimental Ophthalmology* 192: 181–196.

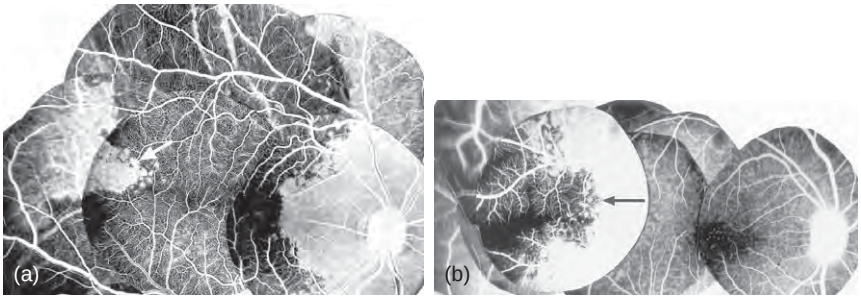

Figure 11 Fluorescein fundus angiograms of two eyes of rhesus monkey showing the area of supply by the long PCA (arrow). (a) After experimental occlusion of all short PCAs but leaving a normal long PCA. (b) After experimental occlusion of long PCA only. Reproduced from Hayreh, S. S. (1974). *Graefe's Archive for Clinical and Experimental Ophthalmology* 192: 197–213.

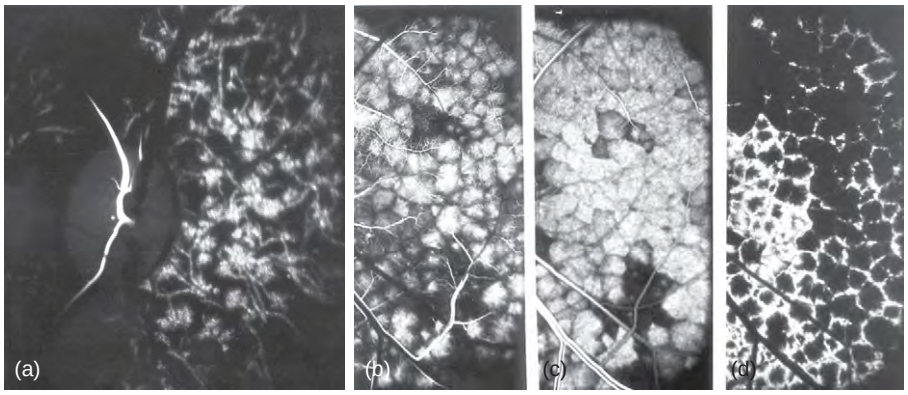

Figure 12 Fluorescein fundus angiograms of a rhesus monkey eye at the posterior pole, showing different phases in choriocapillaris filling. (a) Very early filling phase, where the choriocapillaris is seen as bunches of tiny fluorescent spots at the ends of terminal choroidal arterioles. (b) The early arterial filling phase of the choriocapillaris, showing each lobule of the choriocapillaris (supplied by the terminal choroidal arteriole) forming a big fluorescent spot. Each spot is surrounded by a polygonal unfilled zone, producing a mosaic pattern in the choriocapillaris. (c) Peak arterial filling phase. Note the extraordinarily well-defined mosaic pattern, in which each unit of the mosaic is an independent entity. Some isolated lobules remain unfilled or fill slowly. This suggests that there is no communication between adjacent lobules. (d) Venous phase of the choriocapillaris filling, showing a honeycomb pattern; the fluorescent pattern is the reverse of that seen in figure (b), that is, the fluorescent areas are nonfluorescent and vice versa. Reproduced from Hayreh, S. S. (1974). The choriocapillaris. *Graefe's Archives for Clinical and Experimental Ophthalmology* 192: 165–179.

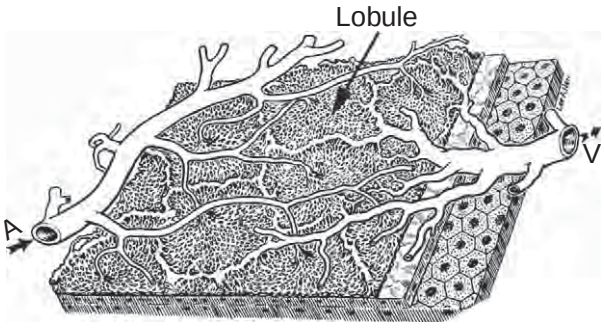

Figure 13 A three-dimensional schematic representation of the choriocapillaris lobular pattern. A, choroidal arteriole; V, choroidal veins. Reproduced with permission from Hayreh, S. S. (1974). The choriocapillaris. *Graefe's Archives for Clinical and Experimental Ophthalmology* 192: 165–179.

located (1) between the PCAs, (2) between the SPCAs, (3) between anterior ciliary arteries and SPCAs, and (4) between adjacent vortex veins.

Between PCAs

Fluorescein fundus angiographic studies have clearly shown the presence of watershed zones between the various PCAs (**Figure 15**).

When there are two (medial and lateral) PCAs

As discussed above, the area of the choroid supplied by the medial and lateral PCAs shows marked interindividual variation, which must result in a wide variation in the location of the watershed zone between the two (**Figure 16**).

Figure 14 Fluorescein fundus angiogram of right eye of a rhesus monkey after occlusion of superior nasal and inferior temporal vortex veins, showing normal filling of superior temporal and inferior nasal quadrants of the choroid but incomplete filling of the quadrants with the occluded veins, and sharp borders between the complete and incomplete filling quadrants. Reproduced from Hayreh, S. S. (1973). *British Journal of Ophthalmology* 57: 217–238.

Figure 17 is a diagrammatic representation of some common locations of the watershed zone between the medial and lateral PCAs. The watershed zone may be situated temporal to the peripapillary choroid, or pass through the temporal

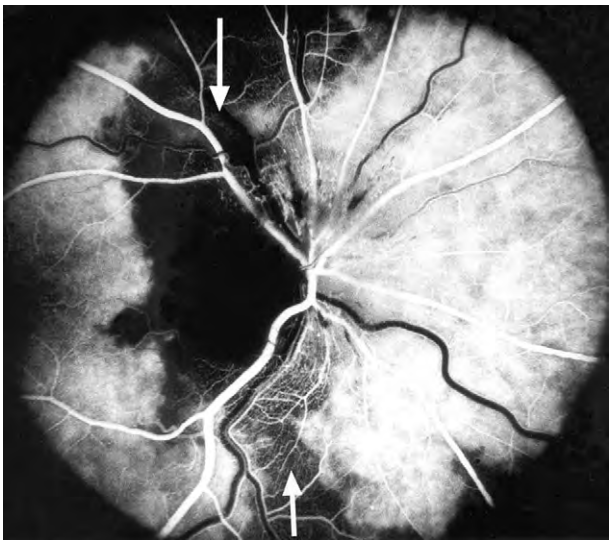

Figure 15 Fluorescein fundus angiogram of right human eye showing nonfilling of the choroidal watershed zone (arrows, vertical dark band) between the lateral and medial PCAs and of the temporal part of optic disk. Reproduced from Hayreh, S. S. (1985). *Documenta Ophthalmologica* 59: 217–246.

peripapillary choroid, one or the other part of the optic disk or medial peripapillary choroid, or the entire optic disk may lie in the watershed zone. There may even be various combinations of the above.

In our fluorescein fundus angiographic studies in eyes with glaucomatous optic neuropathy, where we could outline the watershed zone, we found the incidence of the various locations of the watershed zone as shown in Figure 18; the most common (60%) site was the temporal part of the optic disk and the adjacent peripapillary choroid.

When there are three or more PCAs

The location of the watershed zones varies according to the number of the PCAs and their locations. Figure 19 shows diagrammatically the various combinations of watershed zones, which can occur when an eye has more than two PCAs. The watershed zone filling defect may involve only the upper (Figure 20(a)) or the lower half (Figure 20(b)) of the vertical watershed zone.

Between SPCAs

Figures 9 and 21 are a diagrammatic representation of the watershed zones between the various SPCAs, as revealed by our fluorescein angiographic studies in experimental occlusion of the temporal SPCAs in rhesus monkeys. The area supplied by each SPCA has a well-defined margin, with watershed zones situated between adjacent SPCAs. All the temporal SPCAs enter the eyeball in the macular region and spread out radially to the periphery of the fundus to supply the temporal half of the choroid (Figure 21). It is, therefore, natural that most of the segments of the choroid supplied by the temporal SPCAs and their watershed zones meet in the macular region (Figures 9 and 21). This was a consistent pattern in our studies. It is well established that an area where numerous watershed zones meet is usually an area of comparatively poor vascularity and in the event of circulatory insufficiency, most vulnerable to ischemia.

Between the Anterior Ciliary and SPCAs

This is located in the equatorial region of the choroid (Figure 21). Experimental and clinical studies showed no anastomoses between SPCAs and anterior ciliary arteries. This is because (1) there is no choroidal filling from anterior ciliary arteries when there is PCA occlusion, and (2) when there is anterior ciliary artery occlusion, the normal blood flow in the PCAs does not prevent the development of anterior segment ischemia. Reticular pigmentary degeneration in the location of this watershed zone is not uncommon in elderly patients with severe carotid artery disease, arteriosclerosis, and other conditions associated with vascular insufficiency.

Between the Vortex Veins

Experimental studies on vortex vein occlusion in rhesus monkeys have revealed that the various vortex veins show no free anastomoses (Figure 14), and that the watershed zones between the four vortex veins extend antero–posteriorly through the entire length of the uveal tract – a horizontal watershed zone between the upper and lower vortex veins passes through the optic disk and macular region, while a vertical watershed zone between the temporal and nasal vortex veins passes between the optic disk and macular region (Figure 23).

What then is the clinical significance of all this information about the watershed zones of the PCAs and SPCAs?

Clinical Importance of Watershed Zones Between the PCAs

Role of the watershed zone in relation to the optic disk in the production of anterior ischemic optic neuropathy and other ischemic disorders of the optic nerve head. Since the PCA circulation is the main source of blood supply to the optic nerve head, the location of the watershed zone between the PCAs is crucial in ischemic disorders of the optic nerve head. Our studies indicate that the location of the watershed zone contributes toward the vulnerability of the corresponding part of the optic nerve head to ischemia. If the watershed zone is located away from the optic disk (Figure 16(a)), the optic nerve head is comparatively less

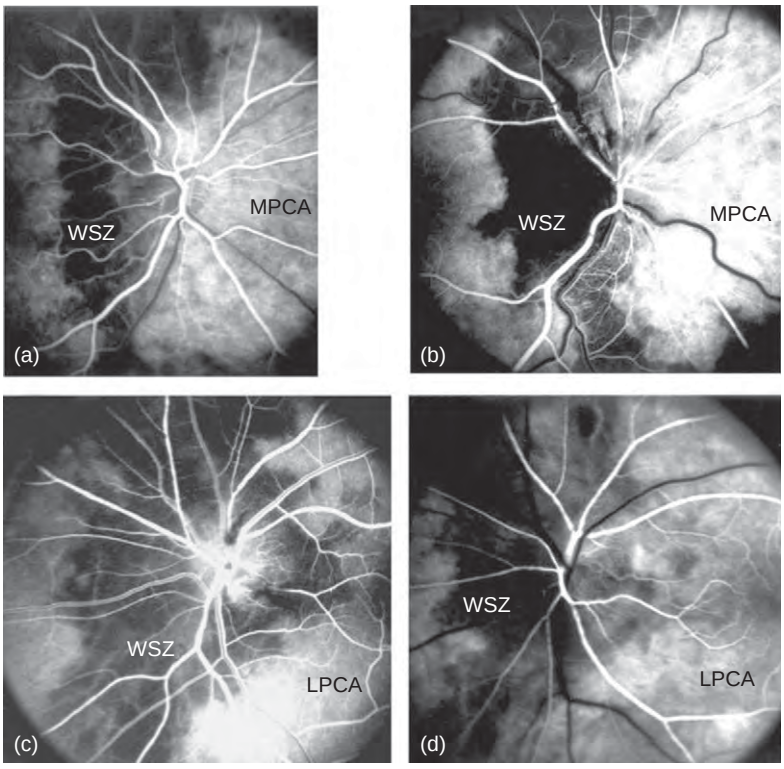

Figure 16 Fluorescein fundus angiograms of four human eyes, showing different locations of the watershed zone (WSZ, vertical dark bands) in relation to the optic disk. Watershed zone lying temporal to the optic disk in (a), passing through the temporal part of the optic disk and adjacent peripapillary choroid in (b), and passing through the nasal part of the disk and adjacent peripapillary choroid in (d), and with the optic disk lying in the center of the watershed zone in (c). Reproduced from Hayreh, S. S. (1985). *Documenta Ophthalmologica* 59: 217–246.

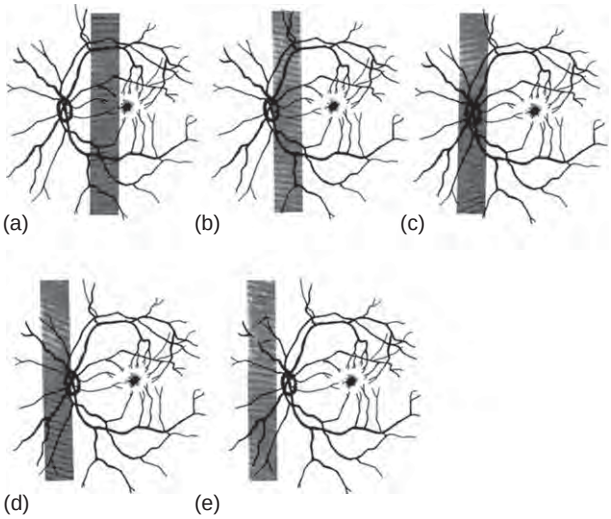

Figure 17 Diagrammatic representation of some of the locations of the watershed zone (shaded area) between the medial and lateral PCAs in human eyes. Reproduced from Hayreh, S. S. (1988). In: Bernstein E. F (ed.) *Amaurosis Fugax*, pp. 1–23. New York: Springer.

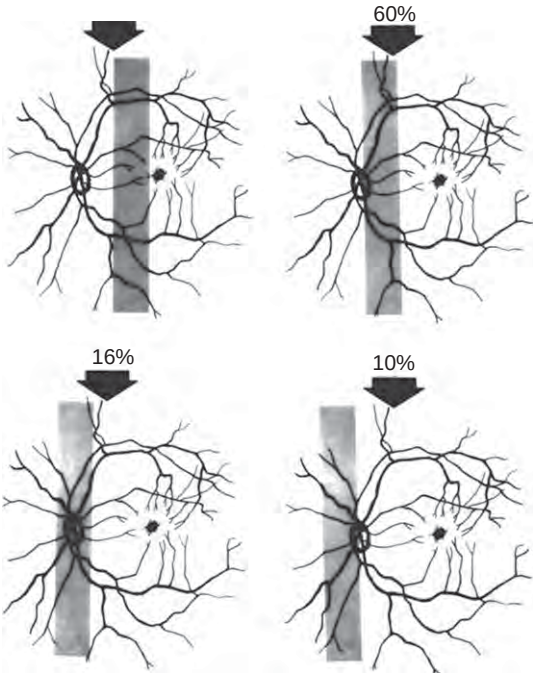

Figure 18 Diagrammatic representation of some of the locations of the watershed zones (shaded area) between the medial and lateral PCAs seen in glaucomatous optic neuropathy in human eyes, and their incidence in three of them. Reproduced from Hayreh, S. S. (1989). In: Lambrou G. N. and Greve E. L. (eds.) *Ocular Blood Flow in Glaucoma*, pp. 3–54. Amsterdam: Kugler and Ghedini.

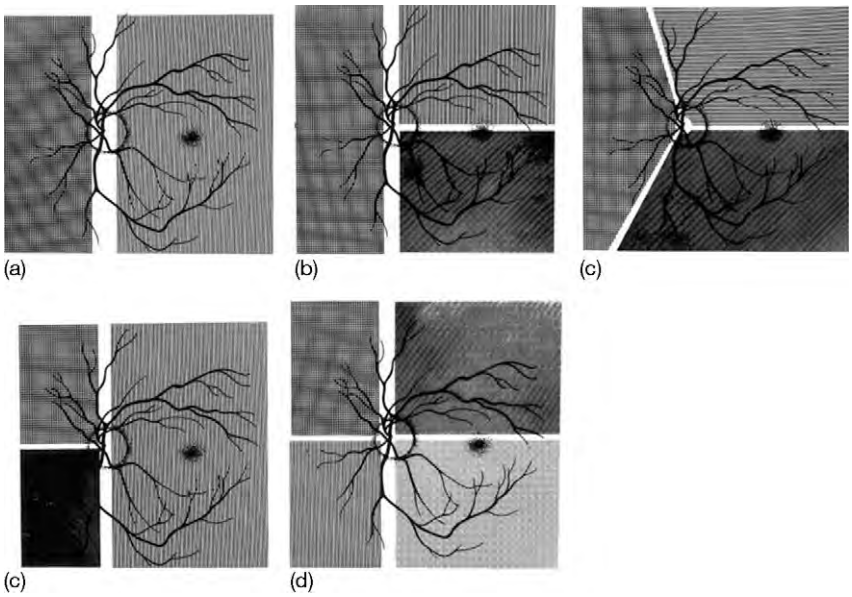

Figure 19 Diagrammatic representations of some examples of the locations of the borders between the territories of eyes with two or more PCAs. (a) With two PCAs: one medial and the other lateral. (b–d) With three PCAs in different combinations. (b, c) With one medial and two lateral PCAs, and (d) one lateral and two medial. (e) With four PCAs: two medial and two lateral. Reproduced from Hayreh, S. S. (1989) In: Lambrou, G. N. and Greve, E. L. (eds.) *Ocular Blood Flow in Glaucoma*, pp. 3–54. Amsterdam: Kugler and Ghedini.

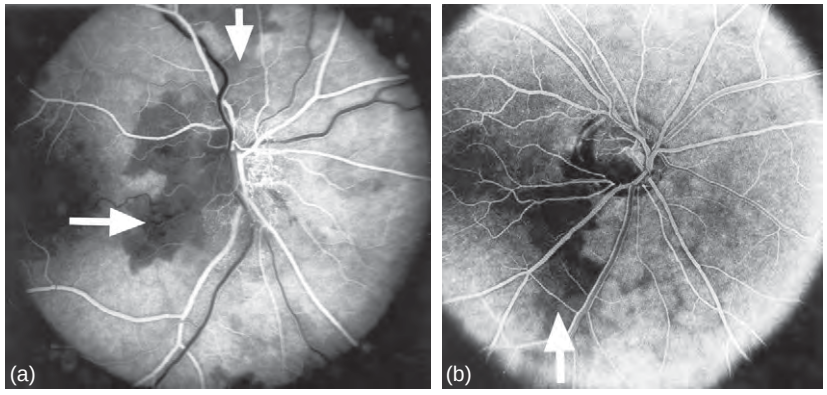

Figure 20 Fluorescein fundus angiograms of two human eyes, showing nonfilling of: (a) temporal part of the peripapillary choroid (lower arrow) and adjacent optic disk and of upper half of the choroidal watershed zone (upper arrow), and (b) inferior watershed zone (arrow). Reproduced from Hayreh, S. S. (1985). *Documenta Ophthalmologica* 59: 217–246.

vulnerable to ischemia than if the watershed zone passes through it (**Figures 16(b)** and **16(d)**). Conversely, the part of the optic disk that lies in the watershed zone is more vulnerable to ischemia than the part that does not. Furthermore, when the entire optic disk lies in the center of a watershed zone (**Figure 16(c)**), that disk is particularly vulnerable to ischemia. The marked variation in the location of the watershed zone in relation to the optic disk produces a marked interindividual variation in the susceptibility to ischemia of optic nerve head.

Importance of the location of multiple watershed zones of the SPCAs in the macular choroid and its possible role in production of various macular ischemic lesions. As discussed above, all the temporal SPCAs pierce the sclera and join the choroid in the macular region, and then run radially toward the equator (**Figures 21** and **22**), so that the apical parts of the various segments supplied by the SPCAs meet each other in the center of the macular region (**Figures 9, 10** and **21**). Therefore, the watershed zones between the several SPCAs meet in the macular region. As already noted, an area

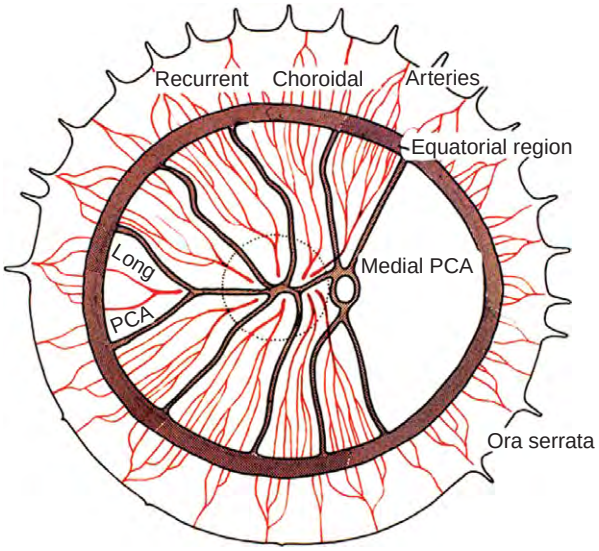

Figure 21 Diagrammatic representation of the distribution by the various ciliary arteries in the choroid and their watershed zones. The choroid posterior to the equator is supplied by the medial and lateral PCAs. In the area supplied by the lateral PCA, the segments supplied by the various short PCAs and the one by the long PCA are shown, with the watershed zones between them (dotted circle in this area indicates the macular region). Recurrent choroidal arteries from the anterior ciliary arteries and supposedly the greater arterial circle of the iris supply in front of the equator. The watershed zone between the anterior and posterior choroidal arteries lies in the equatorial region. Reproduced from Hayreh, S. S. (1981). *Ophthalmologica* 183: 11–19.

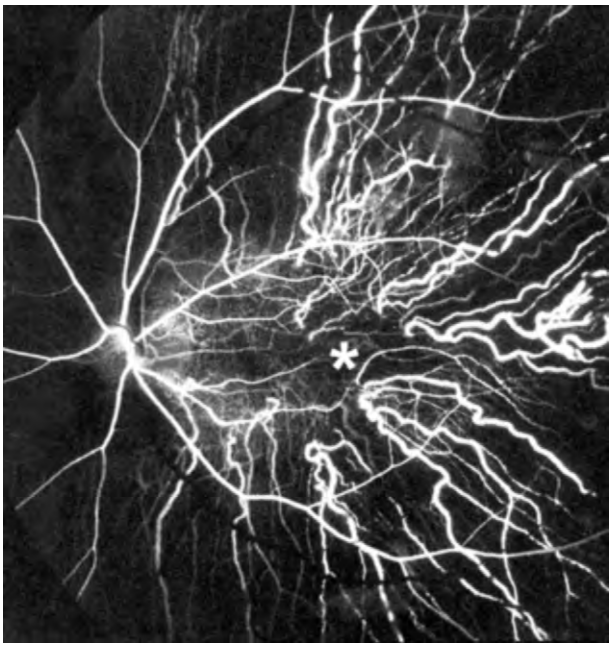

Figure 22 Fluorescein fundus angiogram of a normal human eye, showing the sites of entry of the short PCAs and their radiating course in the choroid. Star marks the center of the macular region. Note that no artery lies in the center of the macular region. Reproduced from Hayreh, S. S. (1983). Physiological anatomy of the choroidal vascular bed. *International Ophthalmology* 6: 85–93.

where multiple watershed zones meet is an area of poor vascularity and most vulnerable to ischemic disorders. There is further evidence suggesting that the macular choroid is more vulnerable to ischemic disorders than other parts of the choroid. For example:

1. In experimental studies on malignant arterial hypertension in rhesus monkeys, choroidal ischemic lesions were most prominent in the macular region and fluorescein fundus angiography revealed a marked, selective delayed filling of the macular choroid, particularly its central part (**Figures 24(a)** and **24(b)**).
2. In experimental studies in rhesus monkeys, when the perfusion pressure in the ocular vessels was reduced, fluorescein angiography revealed delayed filling of the watershed zones in the macular choroid, and of the central choriocapillaris (**Figure 25**).
3. There have been reports of selective localized senile atrophy of the choriocapillaris and in some cases even of large choroidal vessels, in the macular choroid.

In the light of all this information, it is quite logical that in eyes with marked generalized atherosclerosis and arteriosclerosis of the choroidal vessels, the macular choroid would be most vulnerable to ischemic disorders, by virtue of the numerous watershed zones meeting in that location. Similarly, eyes with generalized chronic choroidal ischemia often display a reticular pigmentary degeneration in the equatorial region (the region of the equatorial watershed zone between the anterior and posterior ciliary circulation; **Figure 26**), particularly on the nasal side.

In conclusion, watershed zones may play an important role in making that part of the choroid or the optic nerve head more vulnerable to ischemic lesions. The clinical importance of this is that watershed zone(s) between the PCAs may play a role in ischemic disorders of the optic nerve head, for example, anterior ischemic optic neuropathy and glaucomatous optic neuropathy. Watershed zones between SPCAs may play a role in some macular lesions, for example, macular involvement by hypertensive choroidopathy and probably age-related macular degeneration.

Submacular Choroid

Because of the well-known localized involvement of the macular region in a large number of conditions, a good deal of interest has centered on the submacular choroid. In spite of some claims that there may be a special macular artery, all the available evidence is against the existence of any such artery. All the temporal SPCAs enter the eyeball in the macular region and each artery then radiates toward the periphery, similar to the spokes of a wheel

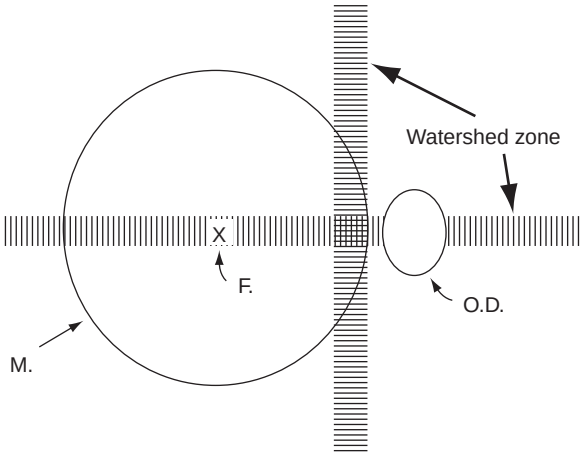

Figure 23 Diagrammatic representation of vertical and horizontal watershed zones between the various vortex veins in rhesus monkeys. F and X, foveola; M, macular region; OD, optic disk. Reproduced from Hayreh, S. S. (1974). Submacular choroidal vascular pattern. *Graefe's Archives for Clinical and Experimental Ophthalmology* 192: 181–196.

(**Figures 21** and **22**); each one of the SPCAs in the macular region gives branches to the submacular choriocapillaris. The sites of entry of the various SPCAs are usually situated some distance away from the center of the macular region (**Figure 22**), and each artery, near its site of entry, gives recurrent centripetal macular branches, which together supply the macular region. Each temporal SPCA supplies a segment of the choroid, with no anastomoses between adjacent segments (**Figures 10(a)–10(c)**). Most of the segments and their watershed zones meet in the macular region (**Figures 9** and **21**). Similarly, the four quadrants of the uveal tract drained by the four vortex veins and their watershed zones meet in the macular region (**Figure 23**). It has been consistently stated that the submacular choroid has a more abundant arterial supply than other parts of the choroid. This impression is based essentially on the fact that the submacular choroid is much thicker than elsewhere. This is because all the temporal SPCAs pierce the sclera in the macular region to join the choroid in the submacular choroidal region (**Figure 22**), and are thus

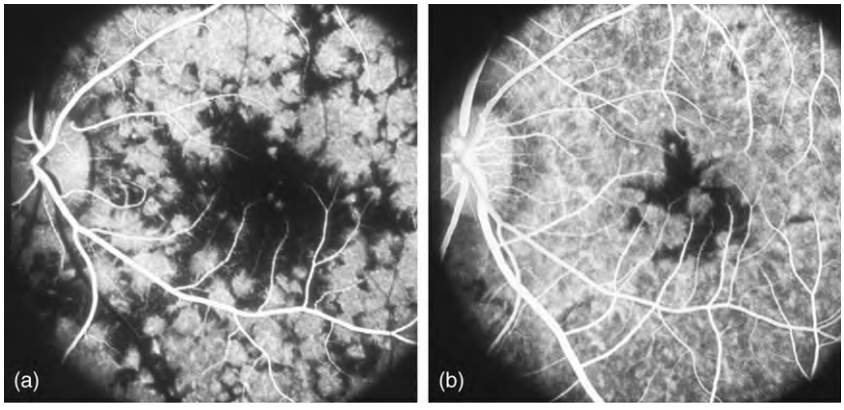

Figure 24 Fluorescein fundus angiograms of left eye of a rhesus monkey with malignant arterial hypertension, during (a) arterial and (b) late venous phases, showing marked delay (dark area) in filling of the submacular choroid. Reproduced from Hayreh, S. S., Servais, G. E., and Virdi, P. S. (1986). Fundus lesions in malignant hypertension – VI. *Ophthalmology* 93: 1383–1400.

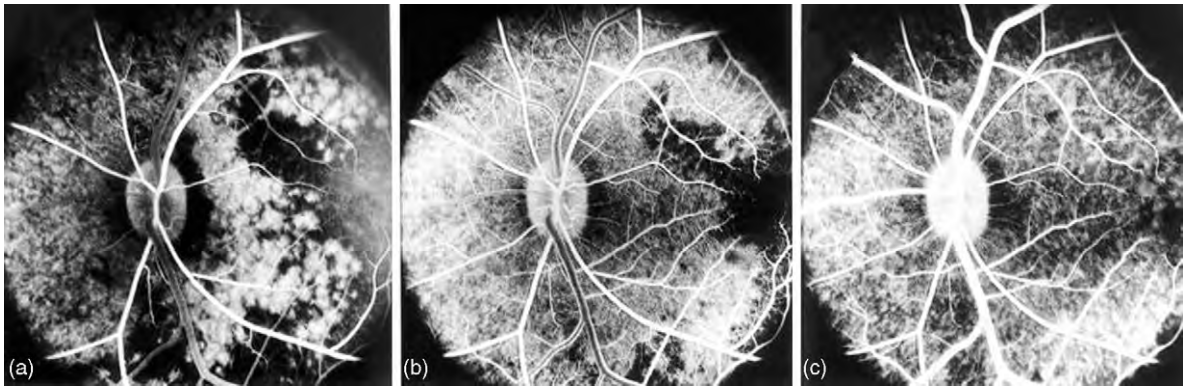

Figure 25 Fluorescein fundus angiograms in left eye of a rhesus monkey, after reduced perfusion pressure in the eye, (a) 9.1, (b) 11.2, and (c) 17.2 s after intravenous injection of fluorescein. Note slow filling of the choroid, particularly marked in the watershed zones between the various temporal short PCAs and in the macular region in (a) and (b). Reproduced from Hayreh, S. S. (1981). *Ophthalmologica* 183: 11–19.

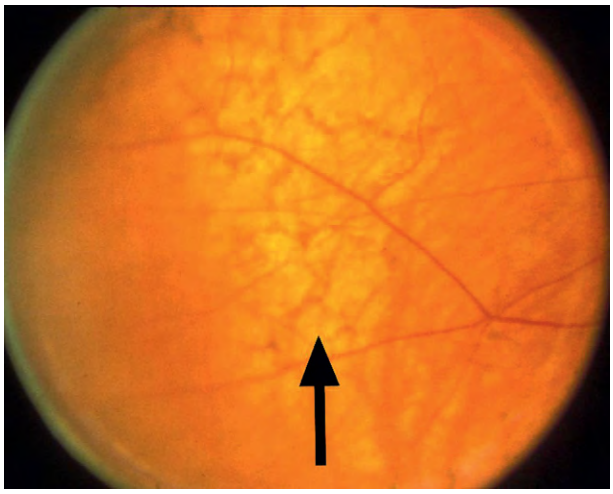

Figure 26 Reticular pigmentary degeneration (arrow) in the equatorial region of a patient with age-related macular degeneration. The pigment accumulates in lines forming irregular polygons. Reproduced from Hayreh, S. S. (1981). *Ophthalmologica* 183: 11–19.

aggregated together in this region. A mere increase in the number of arteries in the submacular choroid does not increase the blood supply and nutrition to that area. Terminal choroidal arterioles supplying the macular choriocapillaris are usually short, vertical, and enter the choriocapillaris perpendicularly and abruptly as compared to those going to the choriocapillaris in the peripheral choroid. This anatomical peculiarity of the submacular terminal choroidal arterioles would make the macular choriocapillaris much more vulnerable to embolism than the peripheral choriocapillaris.

Peripapillary Choroid

The peripapillary choroid is a very important part of the choroidal vascular bed since it is the main source of blood supply to the prelaminar and retrolaminar parts of the optic nerve (**Figure 3**). The branches supplying the optic nerve head arise essentially from the arteries in the peripapillary choroid and not from the choriocapillaris which stop abruptly at the disk margin. The peripapillary choroid is supplied by branches from the SPCAs. Similar to the rest of the choroid, postmortem cast studies have consistently shown free anastomoses in the peripapillary choroidal arteries so as to form a continuous vascular network. Experimental and clinical *in vivo* fluorescein fundus angiographic studies, however, have clearly demonstrated the segmental nature of the peripapillary choroid (**Figures 16(b)–16(d)** and **20(a)** and **20(b)**), which explains the segmental occurrence of anterior ischemic optic neuropathy.

See also: Choroidal Neovascularization; Orbital Vascular Anatomy; Physiological Anatomy of the Retinal Vasculature; Retinal Pigment Epithelial–Choroid Interactions; The Vascular Stem Cell.

Further Reading

Ducournau, D. (1979). *Systematisation vasculaire de la choroide*. Lyon: Association Corporative des Etudiants en Médecine de Lyon.
Hayreh, S. S. (1962). The ophthalmic artery-III. *British Journal of Ophthalmology* 46: 212–247.
Hayreh, S. S. (1974). The choriocapillaris. *Graefe's Archives for Clinical and Experimental Ophthalmology* 192: 165–179.
Hayreh, S. S. (1974). Submacular choroidal vascular pattern. *Graefe's Archives for Clinical and Experimental Ophthalmology* 192: 181–196.
Hayreh, S. S. (1974). The long posterior ciliary arteries. *Graefe's Archives for Clinical and Experimental Ophthalmology* 192: 197–213.
Hayreh, S. S. (1975). Segmental nature of the choroidal vasculature. *British Journal of Ophthalmology* 59: 631–648.
Hayreh, S. S. (1983). Acute occlusive disorders of the choroidal vasculature. *International Ophthalmology* 6: 139–148.
Hayreh, S. S. (1983). Macular lesions secondary to choroidal vascular disorders. *International Ophthalmology* 6: 161–170.
Hayreh, S. S. (1983). Physiological anatomy of the choroidal vascular bed. *International Ophthalmology* 6: 85–93.
Hayreh, S. S. and Baines, J. A. B. (1972). Occlusion of the posterior ciliary artery I. *British Journal of Ophthalmology* 56: 719–735.
Hayreh, S. S. and Baines, J. A. B. (1972). Occlusion of the posterior ciliary artery II. *British Journal of Ophthalmology* 56: 736–753.
Hayreh, S. S. and Baines, J. A. B. (1973). Occlusion of the vortex veins. *British Journal of Ophthalmology* 57: 217–238.
Hayreh, S. S., Servais, G. E., and Virdi, P. S. (1986). Fundus lesions in malignant hypertension – VI. *Ophthalmology* 93: 1383–1400.
Richard, G. (1992). *Choroidal Circulation.* Stuttgart: Thieme.
Ring, H. G. and Fujino, T. (1967). Observations on the anatomy and pathology of the choroidal vasculature. *Archives of Ophthalmology* 78: 431–444.
Shimizu, K. and Ujiie, K. (1978). *Structure of Ocular Vessels.* Tokyo: Igaku-Shoin.
Wybar, K. C. (1954). Vascular anatomy of the choroid in relation to selective localization of ocular disease. *British Journal of Ophthalmology* 38: 513–527.

Physiological Anatomy of the Retinal Vasculature

S S Hayreh, University of Iowa, Iowa City, IA, USA

Glossary

Blood flow autoregulation – The property of a tissue or an organ (i.e., retina) to maintain constant blood flow during changes in perfusion pressure.
Blood–retinal barrier – The system of occluding cellular junctions in the retinal pigmented epithelium and retinal vascular endothelium that prevents free movement of fluid and macromolecules from the blood into the retina.
Cilioretinal artery – A retinal artery which arises from the choriod or the posterior ciliary artery, and is found as a variant in some individuals.
Cotton wool spots – White patches on the retina observed on fundus examination and are caused by local obstruction of the tiny arteries supplying that area.
Fluorescein fundus angiography – Fundus photographs taken in rapid sequence following injection of the fluorescent dye, fluorescein. This provides important information about blood flow as the dye reaches the retinal and choroidal vasculature.

The retina has a dual blood supply; the retinal vasculature supplies only the inner retinal layers up to the inner part of the inner nuclear layer (**Figure 1**), while the choroidal vascular bed supplies the outer 130 μm – up to the outer part of the inner nuclear layer, so that retinal vessels supply only 20% of the retina while the choroid supplies 80%. In this article, the discussion is restricted to the retinal component.

Arterial Supply of the Retina

The main arterial supply of the retina is by the central retinal artery (CRA). In some eyes, another artery, called the cilioretinal artery, may supply a highly variable part of the retina.

Central Retinal Artery

The CRA is usually the first branch of the ophthalmic artery, arising as an independent branch or in common with one of the posterior ciliary arteries (**Figure 2**). Its course can be divided into three distinct parts: (1) intra-orbital (lying below the optic nerve (ON) – (**Figure 2**)), (2) intravaginal (lying in the space between the ON and its sheath), and (3) intraneural (lying in the ON) (**Figure 3**). It enters the ON about 10 mm posterior to the eyeball (**Figures 2** and **3**). A variable number of branches arise from each of its three parts, which anastomose with the surrounding branches from other arteries, mostly in the pial plexus of the ON (**Figure 3**). At the optic disk, the CRA usually first divides into two and then each of them further divides into its various branches (**Figure 4**). The lumen of the intraneural part of the CRA is approximately 200 μm.

Cilioretinal Artery

The cilioretinal artery is either a direct branch of one of the posterior ciliary arteries or arises from the peripapillary choroid and enters the retina by hooking around the Bruch's membrane at the disk margin – usually on the temporal side (**Figures 3** and **5**). Based on ophthalmoscopy, the incidence of the occurrence of the cilioretinal artery reported by different authors varies from 6% to 25%. However, fluorescein fundus angiography provides the most reliable data because the cilioretinal artery fills synchronously with the choroidal filling, which usually starts to fill before the retinal circulation (**Figure 6(a)**). An artery which, on ophthalmoscopy, may look similar to a cilioretinal artery may in fact be an intraneural branch of the CRA emerging at the optic disk – not a true cilioretinal artery. A fluorescein fundus angiographic study of 2000 eyes showed one or more cilioretinal arteries in 32% of the eyes and in both eyes in 15% of persons. There is great variability in size, number, and distribution of the cilioretinal arteries. The area of the retina supplied by the cilioretinal arteries varies markedly, from a tiny region to a large sector of the retina. Eyes where one-fourth to half of the retina is supplied by a cilioretinal artery have been observed (**Figure 6(a)**). Rarely, the CRA is missing and the entire retina is supplied by the cilioretinal artery (**Figure 6(b)**). The outer part of the entire retina is always supplied by the posterior ciliary artery. When a cilioretinal artery is present, in the part of the retina supplied by it, the entire thickness of the retina receives its blood supply from the posterior ciliary artery.

The blood flow in the retinal vascular bed depends upon the perfusion pressure, which is equal to the difference

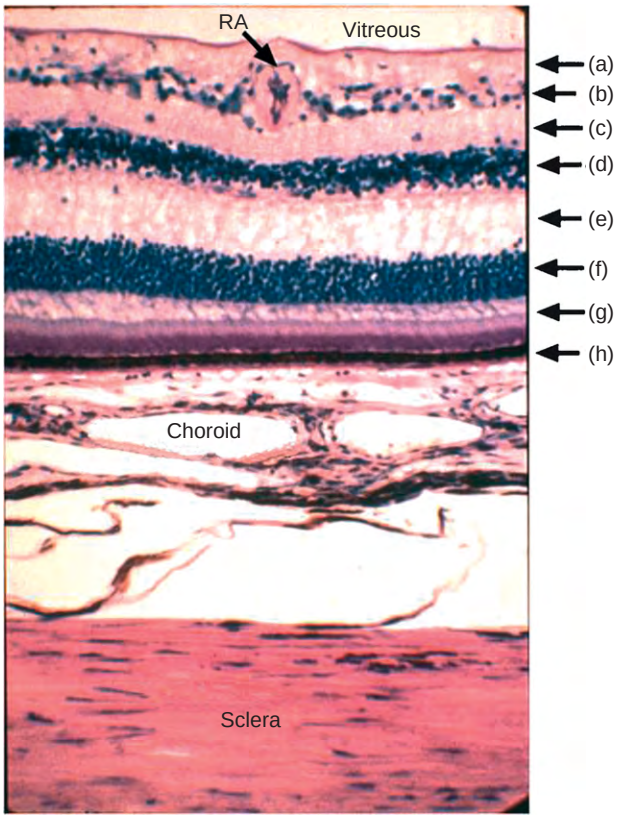

Figure 1 Light micrograph of the retina, choroid, and sclera. The retinal layers are identified as: (a) nerve fiber layer; (b) ganglion cell layer; (c) inner plexiform layer; (d) inner nuclear layer; (e) outer plexiform layer; (f) outer nuclear layer; (g) rod and cone layer; and (h) retinal pigment epithelial layer. RA, retinal arteriole.

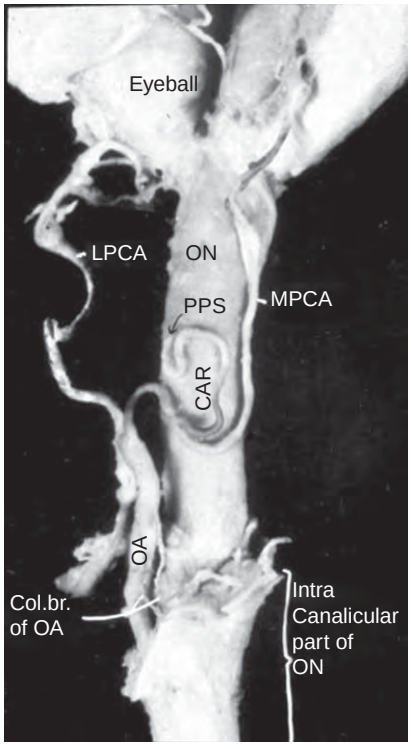

Figure 2 View from under surface of the human eyeball and optic nerve (ON) showing central artery of the retina (CAR) and its site of penetration into the optic nerve sheath (PPS), medial (MPCA) and lateral (LPCA) posterior ciliary arteries, and ophthalmic artery (OA). Reproduced with permission from Singh (Hayreh), S. and Dass, R. (1960). The central artery of the retina I. Origin and course. *British Journal of Ophthalmology* 44: 193–212.

between the retinal arterial and venous pressures. The CRA and cilioretinal artery belong to two arterial systems with different physiological properties. This raises an important physiological issue in eyes with a cilioretinal artery when that eye develops central retinal vein occlusion in which the retinal venous pressure rises suddenly to a high level. The CRA arises directly from the ophthalmic artery and the retinal vascular bed supplied by it has an efficient blood flow autoregulation (see below), so that when there is a fall in perfusion pressure in the retinal arterial bed, caused by a rise in the retinal venous pressure, the autoregulatory mechanism in the central retinal arterial vascular bed kicks in trying to maintain retinal circulation. By contrast, the cilioretinal artery belongs to the choroidal vascular system, which has no autoregulation, so that when the venous pressure rises, there is no corresponding compensatory autoregulatory mechanism. Moreover, the perfusion pressure in the choroidal vascular bed normally is lower than that in the CRA, and there is no corresponding rise of pressure in the choroidal venous bed. In view of all these factors, the following scenario occurs in an eye with cilioretinal artery developing central retinal vein occlusion: sudden occlusion of the central retinal vein results in a marked rise of intraluminal pressure in the entire retinal capillary bed; when that intraluminal pressure rises above the pressure in the cilioretinal artery, the result is a hemodynamic block in the cilioretinal artery, producing cilioretinal artery occlusion (**Figure 7**).

Intraretinal Branches of the CRA

Each of the two main branches (superior and inferior) of the CRA at the optic disk usually divides into temporal and nasal branches, which supply the four quadrants of the retina (**Figure 4**); however, there is marked variation in their vascular pattern. In the retina, the arrangement of the branches and their subdivisions is highly variable, so much so that each eye has a different pattern (**Figures 4** and **7**). It has been suggested that the pattern could be used for personal identification like a finger print. Usually, there is a dichotomous or right-angle branching pattern. The various branches, by multiple divisions, finally end in terminal or precapillary arterioles, which are usually not visible on ophthalmoscopy. Terminal arterioles play an important role in the regulation of retinal blood flow by constriction or dilatation.

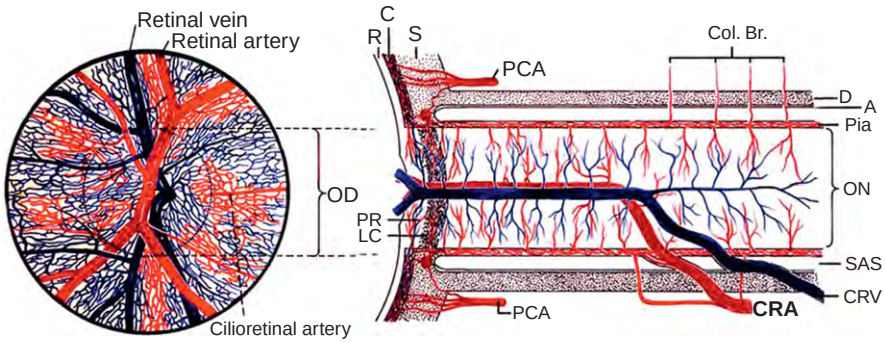

Figure 3 Schematic representation of blood supply of the optic nerve. A, Arachnoid; C, choroid; CRA, central retinal artery; Col. Br., collateral branches; CRV, central retinal vein; D, dura; LC, lamina cribrosa; OD, optic disc; ON, optic nerve; PCA, posterior ciliary artery; PR, prelaminar region; R, retina; S sclera; SAS, subarachnoid space. Modified with permission from Hayreh, S. S. (1974). Anatomy and physiology of the optic nerve head. *Transactions of the American Academy of Ophthalmology and Otolaryngology* 78: OP240–OP254.

There has been a controversy about the true nature of the arteries in the retina. According to some accounts these are small arteries. Others, however, consider them as arterioles after the first branching in the retina because they possess the following anatomic properties, typically seen in arterioles: (1) the widest part of the lumen of the retinal arterioles is near the optic disk and there its diameter is about 100 µm, which is typically the diameter of an arteriole; and (2) unlike arteries, they possess neither an internal elastic lamina nor a continuous muscular coat. This differentiation from the arteries is important in understanding their pathological involvement in some diseases, such as giant cell arteritis. In the retina, there are no interarterial or arteriovenous anastomoses, so that the retinal vascular bed is an end-arterial system.

These intraretinal arterial branches mainly lie in the nerve fiber and ganglion cell layer, usually under the internal limiting membrane (**Figure 1**); however, at the arteriovenous crossing they may extend down to the inner nuclear layer.

Figure 4 Normal human fundus – left eye.

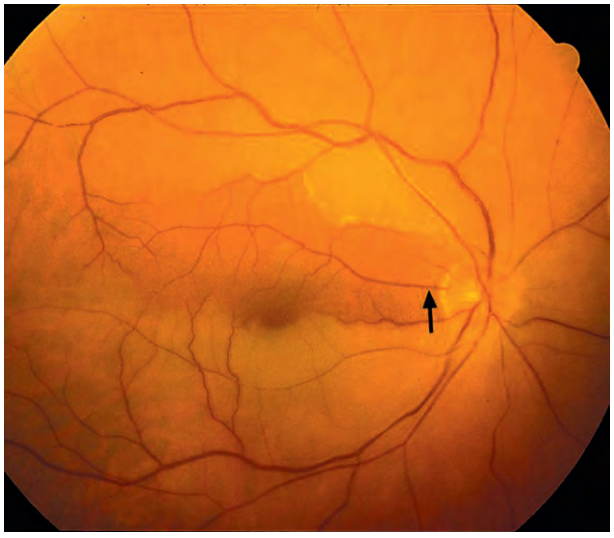

Figure 5 Ophthalmoscopic appearance of right eye with central retinal artery occlusion (pale retina) and a normal cilioretinal artery in the area of normal retina (arrow).

Retinal Capillary Bed

Each terminal arteriole gives out a plexus of 10–20 interconnected capillaries (**Figure 8**). Capillaries lie between the feeding arterioles and venules (**Figure 8**). Around the retinal arteries, there is a capillary-free zone (**Figure 8**). The retinal capillaries are arranged in two layers (**Figure 9**): (1) a superficial layer in the ganglion cell and nerve fiber layers, and (2) a deeper layer in the inner nuclear layer which is denser and more complex than the superficial layer. However, in the posterior retina, there may be three layers in the peripapillary region and there is only one layer in the perifoveal region. Furthermore, in the peripheral retina the deep layer disappears and only the superficial layer is left, with a wider network. At the extreme periphery of the retina, there is an avascular zone about 1.5 mm width.

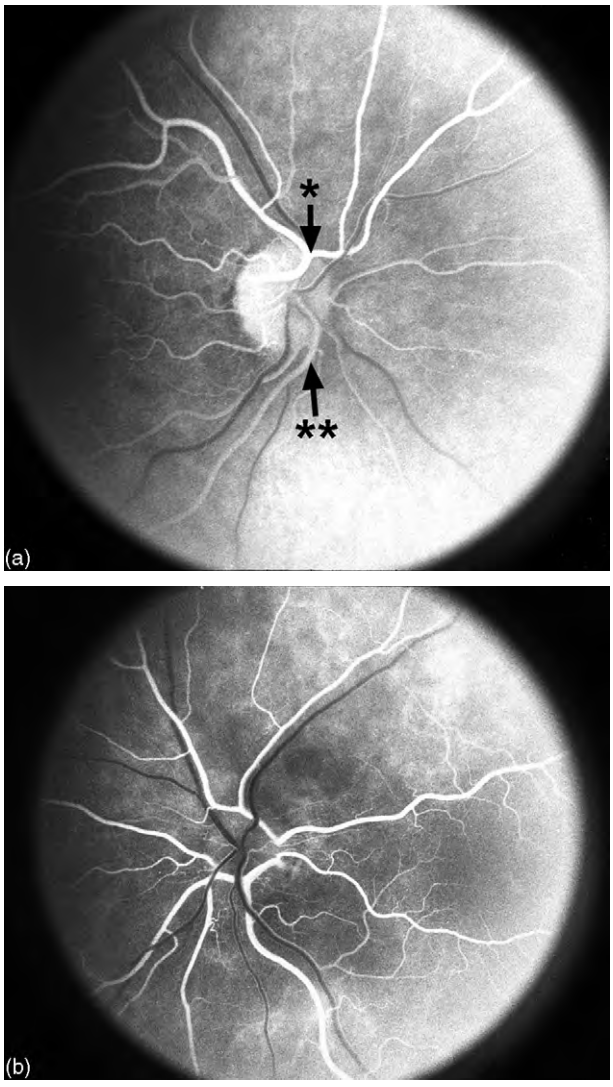

Figure 6 Fluorescein fundus angiograms of (a) right and (b) left eyes of a person. (a) The right eye has one large cilioretinal artery (one asterisk) supplying the superior one-third of the retina that starts to fill before the central retinal artery (two asterisks) which supplies the rest of the retina. (b) The left eye has two large branching cilioretinal arteries (white) – the one above branches in the upper half and the other below branches in the lower half. This eye lacks a central retinal artery.

Figure 7 Fundus photograph of right eye with nonischemic central retinal vein occlusion associated with cilioretinal artery occlusion (arrow).

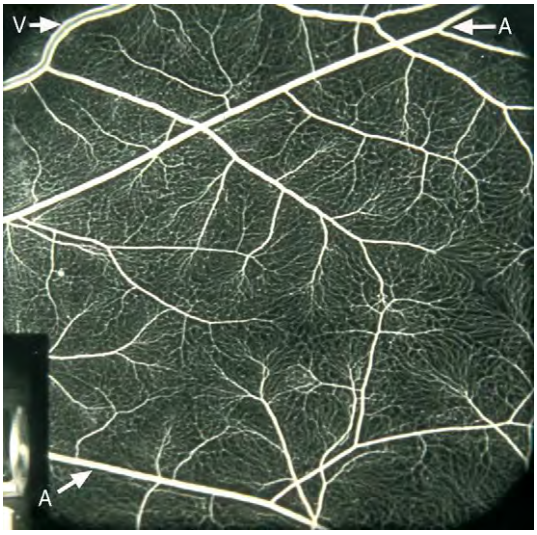

Figure 8 Fluorescein fundus angiogram showing retinal vessels and capillary network. A, retinal arteriole; V, retinal vein.

In addition to the retinal capillary bed described above, there is a distinct retinal capillary bed called the radial peripapillary capillaries, which were first described in 1940 (**Figures 9** and **10**). They have the following special characteristics compared to other retinal capillaries:

1. They are long, straight capillaries, measuring several hundred microns to several millimeters.
2. They form the most superficial layer (**Figure 9**) lying among the superficial nerve fibers, along the superior and inferior temporal arcades of retinal vessels and the peripapillary region (**Figure 10**).
3. They rarely anastomose with one another.
4. They arise from the peripapillary retinal arterioles lying deeper in the retina, and drain into retinal venules or veins on the optic disk (**Figure 3**).

Because of these characteristics, the radial peripapillary capillaries assume importance in the development of several lesions. For example, cotton wool spots are often located in the distribution of the radial peripapillary capillaries, which indicates that the latter may play a role in the pathogenesis of cotton wool spots. In addition, in chronic optic disk edema these capillaries become dilated and develop microaneurysms and hemorrhages.

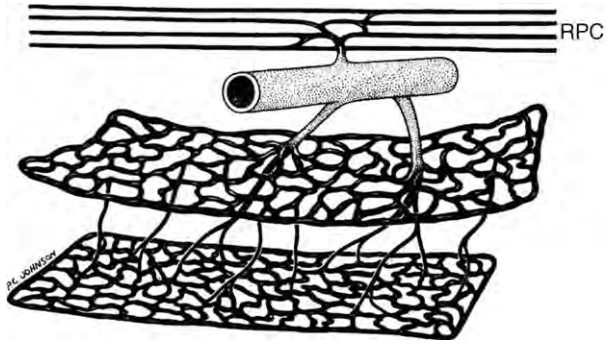

Figure 9 Schematic representation of two layers of the retinal capillaries and radial peripapillary capillaries (RPC). Reproduced with permission from Henkind, P. (1969). Microcirculation of peripapillary retina. *Transactions of the American Academy of Ophthalmology and Otolaryngology* 73: 890–897.

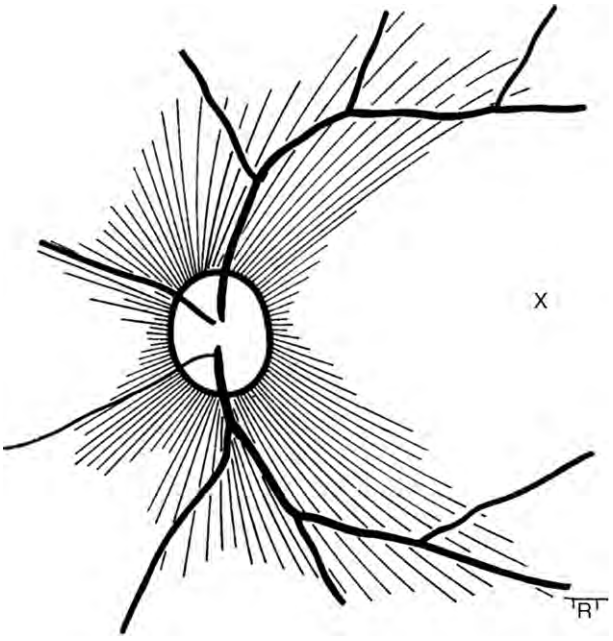

Figure 10 Schematic representation of radial peripapillary capillaries. Site of foveola (X). Reproduced with permission from Henkind, P. (1967). Radial peripapillary capillaries of the retina: I. Anatomy: Human and comparative. *British Journal of Ophthalmology* 51: 115–123.

In the macular region, the capillaries are supplied by arterioles arising from the superior and inferior temporal arteries (**Figure 4**). Their thickness decreases toward the center of the macula where they are arranged in a single layer. The capillaries are absent in the foveal region, with a capillary-free zone of about 400–500 μm in diameter (**Figure 11**).

The wall of the retinal capillaries consists of endothelial cells, pericytes, and basement membrane. Their diameter varies from 3.5 to 6 μm. The endothelial cells have

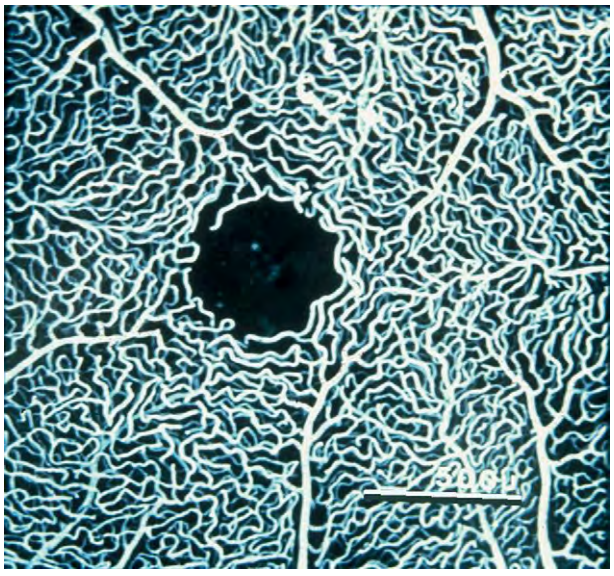

Figure 11 A cast of retinal capillaries in the macular region of a monkey showing the foveal avascular zone in the center. Courtesy of Professor Koichi Shimizu.

tight-cell junctions, which constitute a blood–retinal barrier (see below). In addition to the endothelial cells, there are also pericytes which form a discontinuous layer within the basement membrane of the capillaries. They have a contractile property, by virtue of which they may play a role in regulating blood flow in the capillaries and autoregulation of blood flow (see below). Pericytes are lost preferentially in diabetes so that they may have a role in diabetic retinopathy; it is suggested that diabetic pericyte loss is the result of their migration. Migration of pericytes is also involved in the regulation of angiogenesis.

Retinal Venous Drainage

The postcapillary venules drain the blood from the capillaries but, occasionally, capillaries may join a major vein directly. The terminal arterioles and postcapillary venules are situated in an alternating pattern, with the capillary bed in between the two (**Figure 8**). The postcapillary venules drain into bigger venules and finally into the branch retinal veins. The lumen of the major branch retinal veins, just before they join to form the central retinal vein, is about 200 μm. In the central part of the retina, the branch retinal veins and arteries usually run in close association and at places cross one another (**Figures 4, 5,** and **7**). On the other hand, in the peripheral retina, the veins do not follow the course of the arteries. Various retinal arteries and veins in the retina cross each other at arteriovenous crossings (**Figures 4, 5,** and **7**). In a study of 189 normal eyes, at the sites of arteriovenous crossing, the artery crossed over the vein in 68% and was the reverse

in the remainder. However, in eyes with branch retinal vein occlusion, the artery crossed over the vein at the site of occlusion in 98% of the cases, indicating that pattern of arteriovenous crossing plays a role in the development of branch retinal vein occlusion. At the site of arteriovenous crossing, the artery and vein share a common fibrous coat and are separated by only a thin endothelial lining and basement membrane.

The superior branch veins usually join to form a superior trunk and the inferior branch veins, an inferior trunk. These superior and inferior trunks join on the optic disk to form the central retinal vein (**Figure 3**). However, in 20% of eyes, the superior and inferior trunks do not join together at the disk but enter the optic disk as two separate trunks; this represents a congenital anomaly (**Figure 12**). During the third month of intrauterine life, there are always two trunks of the central retinal vein in the ON, one on either side of the CRA (**Figure 13**), and one of the two trunks usually disappears before birth; however, in 20% of eyes, a dual-trunked central retinal vein persists into adult life. In such eyes, only one of the two trunks may develop occlusion in the ON, resulting in development of the clinical entity called hemi-central retinal vein occlusion (**Figure 12**).

The central retinal vein travels in the ON temporal to the artery, where the central retinal vein and artery lie in the center of the ON, surrounded by a fibrous tissue envelope (**Figure 14**). During its intraneural course, the vein receives many tributaries (**Figure 3**). The central retinal vein exits the ON and its sheath (**Figure 15**), and finally drains into either the superior ophthalmic vein or directly into the cavernous sinus.

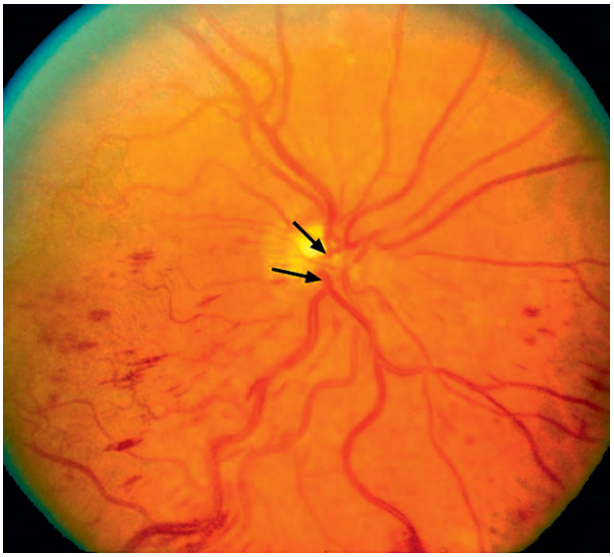

Figure 12 Fundus photograph of an eye with inferior hemicentral retinal vein occlusion, involving the lower trunk of the central retinal vein. Two trunks (arrows) of the central retinal vein enter the optic disk separately above and below.

Nerve Supply

The intraorbital and intraneural portions of the CRA have an adrenergic nerve supply from a sympathetic nerve called the nerve of Tiedemann (**Figure 16**); however, the retinal branches of the CRA have no adrenergic nerve supply. Therefore, there is no autonomic innervation of the retinal vascular bed.

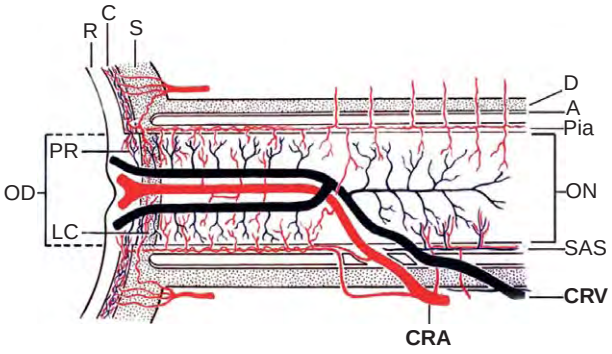

Figure 13 Schematic representation of two trunks of the central retinal vein in the anterior part of the optic nerve. A, Arachnoid; C, choroid; CRA, central retinal artery; Col. Br., collateral branches; CRV, central retinal vein; D, dura; LC, lamina cribrosa; OD, optic disc; ON, optic nerve; PCA, posterior ciliary artery; PR, prelaminar region; R, retina; S, sclera; SAS, subarachnoid space.

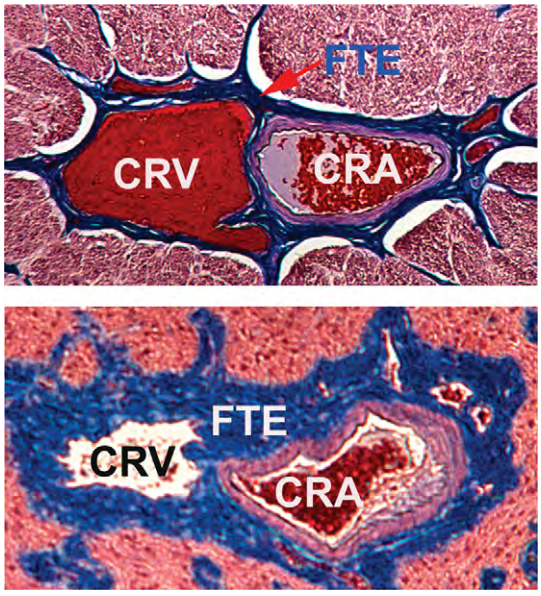

Figure 14 Histological sections (Masson's trichrome staining) showing the central retinal vessels and surrounding fibrous tissue envelope, as seen in a transverse section of the central part of the retrolaminar region of the optic nerve, in a normal rhesus monkey (above) and in a rhesus monkey with experimental arterial hypertension, atherosclerosis and glaucoma (below). CRA =Central retinal artery, CRV = central retinal vein; FTE = fibrous tissue envelope.

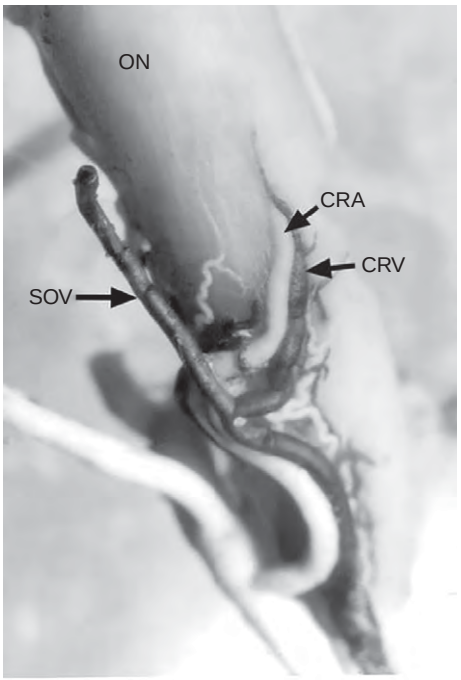

Figure 15 View from under surface of optic nerve in a rhesus monkey showing the intraorbital part of the central retinal vessels and their site of penetration into the sheath of the optic nerve. CRA, central retinal artery; CRV, central retinal vein; ON, optic nerve; SOV, superior ophthalmic vein. Reproduced with permission from Hayreh, S. S. (1965). Occlusion of the central retinal vessels. *British Journal of Ophthalmology* 49: 626–645.

Blood–Retinal Barrier

The retina has two types of blood–retinal barriers.

Inner blood–retinal barrier. This lies in the retinal vessels. It is produced by the tight cell junctions between the endothelial cells of the vessels (due to the presence of extensive zonulae occludentes). The tight interendothelial cell junctions block movement of macromolecules from the lumen toward the interstitial space. Pericytes, Müller cells, and astrocytes also contribute to the proper functioning of this barrier.

Outer blood–retinal barrier. Tight cell junctions between the retinal pigment epithelial cells (**Figure 1**) also produce a blood–retinal barrier, preventing the leakage of fluid from the choroid into the retina. This barrier breaks down when the retinal pigment epithelial cells are destroyed or subjected to ischemia, as in hypertensive choroidopathy.

The blood–retinal barrier plays an important role in the regulation of the microenvironment in the retina. An intact blood–retinal barrier is essential for maintaining retinal structure and function. Breakdown of this barrier results in increased vascular permeability of the capillaries, which causes retinal edema, as seen in a variety of retinopathies. Breakdown of the inner blood–retinal barrier may be caused by acute distension of the vessel walls, ischemia, chemical influences, defects in the endothelial cells, or failure of the active transport system.

The retinal tissue itself has no barrier in its stroma, therefore fluid may diffuse from one part to the adjacent areas.

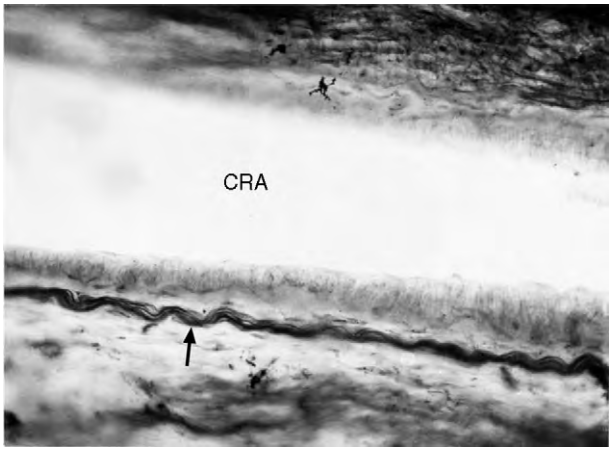

Figure 16 Light micrograph of a longitudinal section of optic nerve of a rhesus monkey, showing central retinal artery (CRA) in the center of the nerve and nerve of Tiedemann (arrow) running parallel with the wall of the central retinal artery. (Gros-Schultze's stain). Reproduced with permission from Hayreh, S. S., Vrabec, Fr. (1966). The structure of the head of the optic nerve in rhesus monkey. *American Journal of Ophthalmology* 62: 136–150.

Autoregulation of Retinal Blood Flow

The object of blood flow autoregulation in a tissue is to maintain relatively constant blood flow during changes in perfusion pressure. This is an important mechanism to regulate blood flow. The retinal circulation has efficient autoregulation. The exact mechanism and site of autoregulation are still unclear except that it most probably operates by altering the vascular resistance. It is generally considered as a feature of the terminal arterioles; so with the rise or fall of perfusion pressure beyond normal levels, the terminal arterioles constrict or dilate, respectively, to regulate the vascular resistance and thereby the blood flow. Recent studies have suggested that pericytes in the retinal capillaries play a role in autoregulation as well because of their contractile property. The metabolic needs of the tissue also regulate the autoregulation. Autoregulation works within a critical range of perfusion pressure, and it breaks down with any rise or fall of the perfusion pressure beyond the critical autoregulatory range.

The vascular endothelium plays an active role in the vasomotor function of both macro- and microvasculatures, including maintenance of vascular tone and regulation of blood flow. Recent studies suggest that vascular-endothelial-derived vasoactive agents (e.g., endothelin-1, thromboxane A_2, and prostaglandin H_2 – vasoconstrictors; and nitric oxide – a vasodilator) profoundly modulate local vascular tone and, thereby, may also play a role in autoregulation. Mechanical stretching and increases in arteriolar transmural pressure induce the endothelial cells to release contracting factors affecting the tone of arteriolar smooth muscle cells and pericytes. Therefore, damage to vascular endothelium (as in arteriosclerosis, atherosclerosis, hypercholesterolemia, aging, diabetes mellitus, ischemia, and possibly from other causes) may be associated with abnormalities in the production of endothelial vasoactive agents, and consequent autoregulation abnormalities.

See also: Blood–Retinal Barrier; Breakdown of the Blood–Retinal Barrier; Breakdown of the Retinal Pigmented Epithelium Blood–Retinal Barrier; Central Retinal Vein Occlusion; Orbital Vascular Anatomy; Pathological Retinal Angiogenesis; Physiological Anatomy of the Choroidal Vasculature.

Further Reading

Anderson, D. R. (1996). Glaucoma, capillaries and pericytes 1. Blood flow regulation. *Ophthalmologica* 210: 257–262.

Cunha-Vaz, J. G. (1976). The blood–retinal barriers. *Documenta Ophthalmologica* 41: 287–327.

Duke-Elder, S. and Wybar, K. C. (1961). Anatomy of the visual system. In: Duke-Elder, S. (ed.) *System of Ophthalmology* vol. 2, pp. 363–382. London: Kimpton.

Haefliger, I. O., Meyer, P., Flammer, J., and Lüscher, T. F. (1994). The vascular endothelium as a regulator of the ocular circulation: A new concept in ophthalmology? *Survey of Ophthalmology* 39: 123–132.

Hayreh, S. S. (1963). The cilio-retinal arteries. *British Journal of Ophthalmology* 47: 71–89.

Hayreh, S. S. and Hayreh, M. S. (1980). Hemi-central retinal vein occlusion. Pathogenesis, clinical features, and natural history. *Archives of Ophthalmology* 98: 1600–1609.

Hayreh, S. S., Fraterrigo, L., and Jonas, J. (2008). Central retinal vein occlusion associated with cilioretinal artery occlusion. *Retina* 28: 581–594.

Henkind, P. (1967). Radial peripapillary capillaries of the retina: I. Anatomy: Human and comparative. *British Journal of Ophthalmology* 51: 115–123.

Henkind, P. (1969). Microcirculation of peripapillary retina. *Transactions of the American Academy of Ophthalmology and Otolaryngology* 73: 890–897.

Justice, J. Jr. and Lehmann, R. P. (1976). Cilioretinal arteries. A study based on review of stereo fundus photographs and fluorescein angiographic findings. *Archives of Ophthalmology* 94: 1355–1358.

Kaur, C., Foulds, W. S., and Ling, E. A. (2008). Blood–retinal barrier in hypoxic ischaemic conditions: Basic concepts, clinical features and management. *Progress in Retinal and Eye Research* 27(6): 622–647.

Pournaras, C. J., Rungger-Brändle, E., Riva, C. E., Hardarso, S. H., and Stefansson, E. (2008). Regulation of retinal blood flow in health and disease. *Progress in Retinal and Eye Research* 27: 284–330.

Singh (Hayreh), S. and Dass, R. (1960). The central artery of the retina I. Origin and course. *British Journal of Ophthalmology* 44: 193–212.

Singh (Hayreh), S. and Dass, R. (1960). The central artery of the retina II. Distribution and anastomoses. *British Journal of Ophthalmology* 44: 280–299.

Weinberg, D., Dodwell, D. G., and Fern, S. A. (1990). Anatomy of arteriovenous crossings in branch retinal vein occlusion. *American Journal of Ophthalmology* 109: 298–302.

Wise, G. N., Dollery, C. T., and Henkind, P. (1971). *The Retinal Circulation*, pp. 20–54. New York: Harper and Row.

Physiology of Photoreceptor Synapses and Other Ribbon Synapses

W B Thoreson, University of Nebraska Medical Center, Omaha, NE, USA

Glossary

Ca^{2+} microdomains – Local submembrane regions of elevated intracellular Ca^{2+} caused by the influx of Ca^{2+} through nearby Ca^{2+} channels.
Calcium-induced calcium release (CICR) – Release into the cytoplasm of Ca^{2+} ions stored in the endoplasmic reticulum that is triggered by the Ca^{2+}-dependent activation of ryanodine receptors.
ERG b-wave – The electroretinogram (ERG) is a massed electrical response of the retina to light that can be recorded by electrodes on the surface of the cornea. ON bipolar cells provide the source of the b-wave of the ERG. A selective reduction in the b-wave indicates a reduction in signaling between photoreceptors and ON bipolar cells.
L-type calcium currents – Currents from high-voltage-activated CaV1.1 (alpha 1S), CaV1.2 (alpha 1C), CaV1.3 (alpha 1D), or CaV1.4 (alpha 1F) calcium channels which show sustained activation and can be selectively blocked by dihydropyridine antagonists.
OFF bipolar cells – Second-order retinal bipolar cells which exhibit a hyperpolarizing response to light mediated by non-NMDA ionotropic glutamate receptors.
ON bipolar cells – Second-order retinal bipolar cell subtypes which exhibit a depolarizing response to light mediated by mGluR6 metabotropic glutamate receptors.
Readily releasable pool – A pool of synaptic vesicles primed for rapid release by elevation of intracellular calcium.
SNARE proteins – SNAP and NSF attachment receptors are a family of proteins participating in vesicle fusion. They can be subdivided into vesicle SNAREs (v-SNAREs), which attach to vesicles, and target SNAREs (t-SNAREs), which associate with the plasma membrane.
Synaptic ribbon – An electron dense presynaptic structure that tethers synaptic vesicles in nerve terminals of sensory neurons including photoreceptors, retinal bipolar cells, hair cells, pinealocytes, and electroreceptors.
Total internal reflectance (TIRF) microscopy – By taking advantage of the subwavelength evanescent field of light created by reflections at the interface between a cell and coverslip, TIRF microscopy can be used to visualize subwavelength structures such as synaptic vesicles.

Anatomy of the Ribbon Synapse

Structures of the electron dense ribbons found at the synapses of retinal photoreceptors and bipolar cells differ depending on cell type. In cross section, photoreceptor ribbons appear as ~35 nm thick bars, but in three dimensions they form flat, ribbon-like structures. Mammalian rods have one to two ribbons that can be up to 2 μm in length and extend up to 1 μm into the cytoplasm. Each wraps around the synaptic ridge to form crescent or horseshoe shapes. The ribbons in mammalian cone are smaller, typically less than 1 μm long and extend only a few hundred nanometers into the cytoplasm. They are shaped like surfboards, and typically a dozen or more ribbons are in each cone terminal. Sitting just below the photoreceptor ribbon is a trough-like arciform density. Ribbons in bipolar cells are planar, like those in rods, but they are smaller than both rod and cone ribbons.

The focus of this review is on ribbon synapses in retina; however, ribbon synapses are not unique to retina. They are present in other sensory neurons, including pinealocytes, electroreceptors in the lateral line organ of fishes, and hair cells of the cochlea and vestibular apparatus. Again, the ribbons in the synapses of these cells have different structures depending on cell type. For example, hair cell ribbons are small spheres.

The ribbon synapses of photoreceptor terminals contain many more synaptic vesicles than conventional synapses. Conventional synapses have 10–100 vesicles near each presynaptic density compared to the synaptic terminal of a lizard cone, which contains ~170 000 vesicles or 7000 vesicles per ribbon. Furthermore, ~85% of the vesicles at ribbon synapses are freely mobile and readily participate in release compared to ~20% of vesicles at conventional synapses. The expanded mobility of vesicles at ribbon synapses may be due to the absence of synapsins which have been proposed to tether synaptic vesicles at conventional synapses. The small subset of vesicles in photoreceptor terminals that are tethered to synaptic ribbons are attached by fine filaments (**Figure 1**).

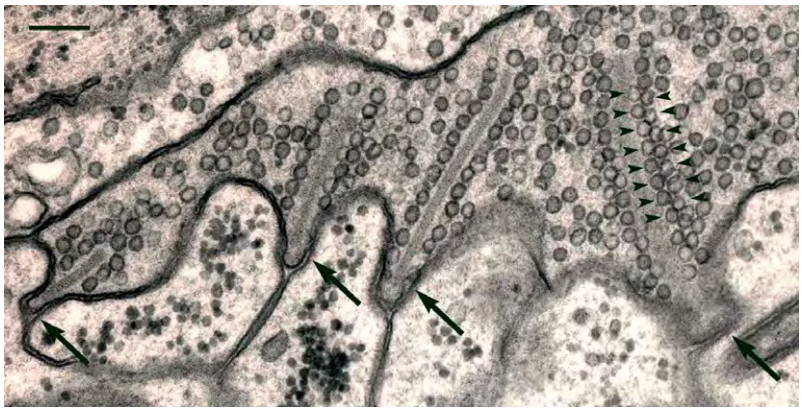

Figure 1 Ribbon-style active zones (arrows) in a salamander rod photoreceptor. A tangential section through the ribbon at right shows the hexagonal packing of vesicles on the ribbon (arrowheads). Scale = 200 nm. Adapted from Thoreson, W. B., Rabl, K., Townes-Anderson, E., and Heidelberger, R. (2004) A highly Ca^{2+}-sensitive pool of vesicles contributes to linearity at the rod photoreceptor ribbon synapse. *Neuron* 42: 595–605, with permission from Elsevier.

Vesicle Pools and Vesicular Release at Synaptic Ribbons

Newly tethered vesicles can be found throughout the ribbon, indicating that vesicles either freely enter the ribbon at any position or redistribute rapidly about the ribbon face after attachment. However, once attached to the ribbon, vesicles exit only from the base. Vesicles tethered on the bottom first to third rows of the ribbon contact the plasma membrane along the synaptic ridge. These vesicles constitute a pool that can be released rapidly in response to increased Ca^{2+} levels. In bipolar cells, the fastest component of vesicular release equals the number of vesicles tethered along the bottom row of the ribbon, and maintained depolarization stimulates release of the total number of vesicles lining the entire ribbon. Similarly, the total releasable pool in rod photoreceptors equals the number of vesicles tethered to the entire ribbon (~700 vesicles in amphibian rods), and there is an ultrafast component similar to the number of vesicles tethered at the ribbon base (~30 vesicles). Because of their smaller size, cone ribbons have a smaller releasable pool than rod ribbons.

In contrast with bipolar and photoreceptor cells, the ultrafast release component in hair cells exceeds the number of vesicles lining the bottom row by nearly 10-fold, and the total releasable pool exceeds the number of vesicles lining the ribbon six- to eightfold. The large ultrafast or rapidly releasable pool could be explained by compound fusion between adjacent vesicles as discussed later. The large size of the total pool suggests that vesicles released from the ribbon are replenished rapidly from the surrounding cytoplasm.

Vesicular transmitter release clearly occurs at the ribbons in ribbon synapses, but the ribbons may not be the only site of transmitter release. Photoreceptors also contact bipolar cell dendrites at flat or basal junctions identified by pre- and postsynaptic membrane densities. In mammalian retina, the basal junctions of cones only contact OFF-type bipolar cells and the dendrites of many OFF-type bipolar cells are not directly apposed to synaptic ribbons. In salamander retinas, the architecture of photoreceptor input to bipolar cells is different, and OFF bipolar cells receive ~80% of their contacts from ribbon synapses and only ~20% from basal junctions. On the other hand, salamander ON-type bipolar cells receive ~ 20% of their contacts from ribbons synapses and ~80% from basal junctions.

Basal junctions lack the vesicle clusters which typify conventional synapses; however, the absence in mammals of direct ribbon contacts onto many OFF bipolar cells led to the suggestion that they necessarily receive synaptic input from basal junctions. This idea was tested in experiments that compared synaptic events recorded simultaneously from two OFF bipolar cells – one that contacted photoreceptors only at basal junctions and a neighbor whose dendrites approach the ribbon. These studies showed that glutamate released at a synaptic ribbon can diffuse rapidly to bipolar cell processes at basal junctions. This finding shows that glutamate released at the ribbon can reach basal junctions, although it does not exclude the possibility of additional nonribbon release events.

The question of whether nonribbon release events occur in ribbon synapses has been addressed further by using total internal reflectance (TIRF) microscopy to visualize single-vesicle fusion events. Studies of release from bipolar cells indicate that up to 1/3 of fusion events occur at ectopic sites away from the ribbon including much of the release during sustained depolarization. Studies on hair cells from mice with disrupted ribbon anchoring also suggest a role for nonribbon sites in sustained release by showing that sustained release is unchanged although fast release is diminished. However,

in photoreceptors, as discussed later, there is evidence suggesting that sustained release occurs predominately at the ribbon.

Role of the Ribbon in Release

The functions of the ribbon in release are not fully understood. It has been widely suggested that the ribbon may operate like a conveyor belt, acting as a molecular motor to accelerate delivery of vesicles to their release sites. Consistent with this possibility is the presence of a kinesin motor protein, KIF3A, at the ribbon. However, release of vesicles attached to the ribbons does not require ATP, although ATP is needed for subsequent replenishment and priming of vesicles. Ribbons are also not necessary for sustaining high-frequency release since it can be observed at conventional central nervous system (CNS) synapses without ribbons. In fact, during sustained release from photoreceptor ribbons, the delivery of vesicles to the base of the ribbon is actually slower than the rate predicted from delivery by simple diffusion. Thus, rather than accelerating release, synaptic ribbons in cones appear to slow the rates of sustained release by constraining the rate of vesicle delivery to the base. By making release more regular, such a mechanism could improve the ability to detect small intensity changes that produce small changes in release rate.

Another hypothesis of ribbon function is that it may operate as a vesicle trap. In this scenario, vesicles moving about the terminal by Brownian motion occasionally collide with the ribbon face where they are captured like flies to fly paper and then delivered to the base for release.

Ribbons may assist in vesicle priming. The match between releasable pool size and the number of vesicles tethered to rod or bipolar cell ribbons indicates that tethered vesicles are primed for release. Furthermore, members of the RIM family of proteins involved in vesicle priming localize to the ribbon. RIM proteins are synaptic proteins required for normal neurotransmitter release.

Another proposed role for the ribbon is to facilitate compound fusion during depolarization by promoting fusion between neighboring vesicles on adjacent rows of the ribbon. Compound fusion could explain the finding in hair cells that many more vesicles fuse rapidly after stimulation than are anchored at the base of the ribbon. The possibility of compound fusion in hair cells is supported by statistical properties of fluctuations in postsynaptic currents and presynaptic exocytotic capacitance changes. There is also ultrastructural and electrophysiological evidence for compound or coordinated fusion of multiple vesicles at bipolar cell synapses.

Ribbons may perform more than one of these functions. They may capture vesicles, prime them for release, regulate their delivery to release sites, and facilitate compound fusion. To sort out the unique functions of ribbons and ribbon synapse, the biochemistry and electrophysiological properties of ribbon synapse are being studied in detail.

Synaptic Proteins

Ribbon synapses contain many of the same proteins as conventional synapses. For example, conventional and ribbon synapses both employ SNARE proteins in vesicle fusion: synaptobrevin (VAMP1 and 2), SNAP-25, and syntaxin. Ribbon synapses also possess Munc 18-1, Munc 13-1, RIM, and rab3A proteins which assist with assembly of the SNARE complex and vesicle priming. RIM1 is distributed across the ribbon, whereas RIM2 localizes to the ribbon base, suggesting that they may have different roles.

In addition to many similarities, there are also differences among the proteins at ribbon and conventional synapses. In place of syntaxin-1 found at many conventional synapses, ribbon synapses utilize syntaxin-3b. In place of complexins 1 and 2 that interact with the SNARE complex at many synapses, ribbon synapses possess complexins 3 and 4. Ribbon synapses lack synapsins. The functional consequences of these differences remain to be explained.

As in conventional synapses, a rise in intracellular free Ca^{2+} is required for neurotransmitter release, but the identity of the calcium sensor(s) at ribbon synapses is unsettled. Synaptotagmin I is the principal calcium sensor at most conventional synapses. Antibodies to synaptotagmin I/II label photoreceptor and bipolar cell ribbon synapses in mouse and bovine retina but do not label these synapses in goldfish and salamander retina, which are instead labeled by antibodies to synaptotagmin III. In hair cells, it has been proposed that otoferlin, not synaptotagmin, is the principal calcium sensor for exocytosis.

The most conspicuous difference between ribbon and conventional synapses is the presence of the ribbon-specific protein, ribeye. Ribbons are constructed from interdomain interactions between adjoining ribeye molecules. Each bipolar cell ribbon is formed from ~4000 ribeye molecules and the 10-fold greater surface area of rod ribbons suggests that they are built from ~40 000 ribeye molecules. Ribeye is an alternative transcript of the gene for transcriptional repressor C-terminal-binding protein 2 (CtBP-2) with a unique ribbon-specific A domain and an enzymatic B domain. Interactions between ribeye molecules are regulated by NAD and NADH levels, suggesting a mechanism by which changes in the metabolic state of the terminal could contribute to observed circadian changes in ribbon structure.

As mentioned above, the kinesin KIF3A is located at the ribbon, but since ATP-driven molecular motors are

not needed for vesicle release from the ribbon, the role of KIF3A at the ribbon is unclear. However, kinesin motor proteins interact with plant homologs of CtBP, indicating that the interaction of kinesins with the major structural protein in ribbon synapses is highly conserved. It has also been proposed that KIF3A may assist with circadian changes in ribbon structure.

Interactions among synaptic proteins help maintain the structure of the ribbon. Interactions between ribeye and the cytomatrix scaffold protein bassoon anchor ribbons to the active zone. Bassoon also tethers ribbons in hair cells and pinealocytes. Bipolar cells lack bassoon but possess a related protein, piccolo. In photoreceptors, piccolo is located further up the ribbon than bassoon.

Interactions between cytoskeletal proteins, membrane-spanning dystroglycan proteins, and extracellular matrix pikachurin proteins are important for maintaining contacts between photoreceptor ribbon synapses and their postsynaptic targets. Disrupting these interactions leads to reductions in the electroretinogram (ERG) b-wave (indicating a reduction in ON bipolar cell responses) in patients with muscular dystrophy.

Interactions between ribeye and Unc119, a protein that is highly expressed in photoreceptors, may help localize Ca^{2+} channels to the base of the ribbon. Unc 119 can bind to both ribeye and the calcium-binding protein CaBP4. CaBP4 binds in turn to Ca^{2+} channels in photoreceptor terminals. Mutations in Unc 119 lead to cone/rod degeneration.

Photoreceptor Calcium Channels

Glutamate release from photoreceptors requires an influx of Ca^{2+} through Ca^{2+} channels. However, unlike conventional synapses that use N- and P-type calcium channels, photoreceptors and other ribbon synapses rely on dihydropyridine-sensitive, L-type calcium channels. L-type calcium channels are classified by their α1 pore forming subunits into CaV1.1-CaV1.4 subtypes. Mutations in CaV1.4 (also known as α1F) cause incomplete congenital stationary night blindness and antibodies to CaV1.4 label mammalian rod terminals, suggesting that CaV1.4 is the principal subtype in rods. Rods and long-wavelength sensitive cones also appear to possess CaV1.3 channels but CaV1.3 antibodies do not label short-wavelength-sensitive cones, suggesting that they possess a different channel subtype.

Calcium channels cluster beneath the ribbon. Freeze fracture electron micrographs from mammalian cones show clusters of ~500 polyhedral transmembrane particles, each with a central dimple, beneath the arciform density of each ribbon. Sites of calcium influx co-localize with ribeye-binding peptides and antibodies to L-type calcium channels co-localize with antibodies to bassoon and ribeye.

Properties of single-calcium channels recorded from amphibian rod photoreceptors are similar to those of L-type calcium channels in other tissues. Single-CaV1.4 channels expressed in HEK293 cells showed a tiny single-channel conductance and extremely low open probability. However, it is unlikely that these properties are retained *in vivo* since they imply an unrealistically large number of channels per ribbon (>15 000).

Photoreceptor calcium currents (I_{Ca}) exhibit a sigmoidal voltage dependence (**Figure 2**). When measured under the same experimental conditions, the voltage dependence of I_{Ca} (calcium current) in rods and cones of different species are remarkably similar. Typically, photoreceptor I_{Ca} activates above −60 mV and is fully activated around −20 mV. I_{Ca} attains about a third of its

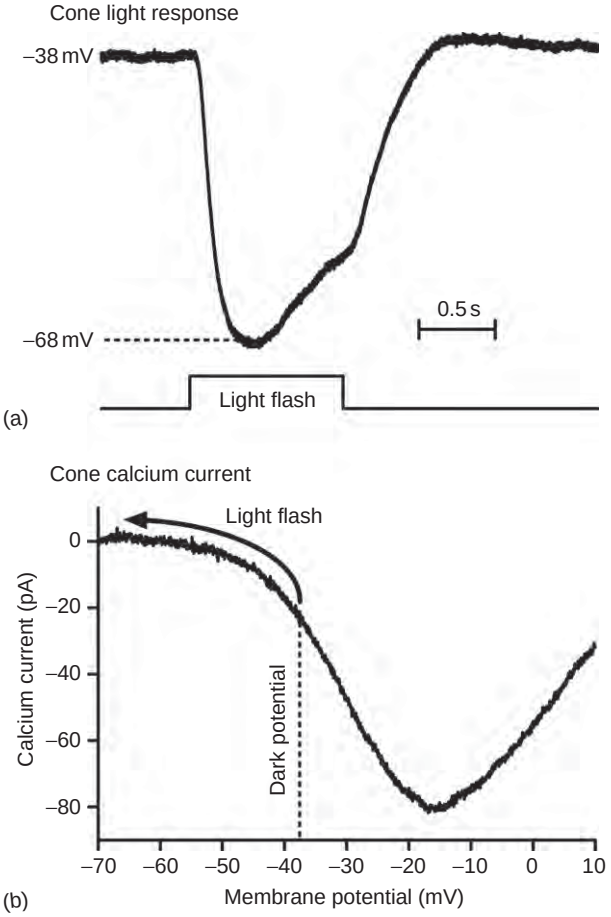

Figure 2 Influence of light-evoked changes in membrane potential on cone calcium currents. (a) Response of a salamander cone to a bright flash of light. (b) Calcium current averaged from eight salamander cones evoked by a ramp voltage protocol (0.5 mV ms^{-1}). By convention, the influx of positively charged Ca^{2+} ions into cones is shown as negative or inward current. The dark potential of the cone in (a) is denoted by the dashed line and the reduction in I_{Ca} caused by the hyperpolarizing light response is shown by the arrow.

peak amplitude at the dark resting potential (ca. –40 mV). The hyperpolarizing light response of a rod or cone photoreceptor diminishes I_{Ca} and thereby diminishes Ca^{2+}-dependent release. The sigmoidal voltage dependence of I_{Ca} contributes to response compression at higher intensities. As illustrated in **Figure 2**, the first 10 mV of membrane hyperpolarization during a cone light response causes a much greater decrease in I_{Ca} than the next 10 mV. This diminished responsiveness at more hyperpolarized potentials is sufficiently pronounced at rod synapses that it has been described as response clipping. There is evidence that Ca^{2+} influx through cGMP-gated cation channels can stimulate synaptic release from cones but the role that these channels play in release under normal physiological conditions is not clear.

Photoreceptor I_{Ca} shows limited and slowly developing inactivation involving both voltage- and calcium-dependent mechanisms. Limited inactivation is important for sustaining synaptic release in darkness when photoreceptors are continuously depolarized. Although the amplitude of I_{Ca} declines slowly in darkness, changes in I_{Ca} produced by brief changes in illumination mirror the sigmoidal voltage dependence of I_{Ca}.

Along with pore-forming α1 subunits, calcium channels possess accessory β and α2/δ subunits. Knockout of β2 subunits almost completely abolishes both the ERG b-wave and staining for CaV1.4 in the outer plexiform layer indicating that β2 subunits are the predominant subtype at photoreceptor synapses. Mutations in α2/δ type 4 subunits lead to disordered ribbons, reduced scotopic b-waves, absent photopic b-waves, and a human cone dystrophy, suggesting that this accessory subunit is associated with calcium channels in photoreceptors, particularly cones.

The calcium-binding protein, CaBP4, is closely associated with photoreceptor calcium channels. When heterologously expressed in the presence of CaBP4, the voltage dependence of CaV1.3 and CaV1.4 I_{Ca} is shifted to more negative potentials, similar to the voltage dependence of I_{Ca} in photoreceptors. By shifting activation to more positive potentials, mutations in CaBP4 reduce the amplitude of I_{Ca} in the normal physiological range and thereby reduce synaptic output from photoreceptors. The reduction in rod output accompanying CaBP4 mutations causes congenital stationary night blindness.

Role of Intracellular Ca^{2+} in Release

Free calcium levels in the photoreceptor synapse are tightly regulated by a variety of mechanisms to maintain synaptic output and prevent calcium overload during the continual influx of Ca^{2+} in darkness.

One way to remove Ca^{2+} from the cytoplasm is to pump it into the endoplasmic reticulum using sarco- and endoplasmic reticulum ATPases (SERCA). SERCA 2A predominates in photoreceptor terminals. The release of calcium from these sequestered stores by calcium-induced calcium release (CICR) can amplify calcium entry through L-type calcium channels. CICR in retina is mediated by a retina-specific variant of the type 2 ryanodine receptor. In rods, CICR amplifies synaptic release and increases the likelihood of the simultaneous fusion of multiple vesicles. CICR also contributes to synaptic release from ribbon synapses in vestibular hair cells. Calcium imaging studies show evidence for CICR in cone cell bodies but it does not appear to contribute to synaptic release. Immunohistochemical studies suggest IP3 receptors, which mediate the release of intracellular Ca^{2+} in many cell types, may be present in cone terminals. However, there is no physiological evidence for IP3-mediated release of calcium in photoreceptors.

Depletion of calcium from intracellular stores triggers the opening of calcium-permeable channels in the plasma membrane to facilitate store refilling. Store-operated calcium entry can influence synaptic release by regulating basal calcium levels in photoreceptor terminals.

Calcium can also be removed from the cytoplasm by pumping it out of the cell. Calcium is removed from outer segments by a Na/Ca exchanger whereas extrusion from inner segments and synaptic terminals rely more on plasma membrane calcium ATPases (PMCA). PMCA2 antibodies label photoreceptor terminals and PMCA2 knockout mice show significant reductions in rod-driven responses, suggesting that this subtype is particularly important in regulating calcium levels in rod terminals.

Calcium buffering by cytoplasmic proteins provides a much more rapid way to reduce free calcium levels than extrusion. The principle calcium buffers are calbindin, calretinin, and parvalbumin although many signaling proteins (e.g., calmodulin, synaptotagmin, and CaBP4) also bind calcium. There is considerable species variability, but cones typically possess the fast, low mobility buffer calbindin whereas the higher mobility buffers calretinin and parvalbumin are less common in photoreceptors.

Supplementing these mechanisms, large calcium increases in rods and cones can be buffered by mitochondrial uptake.

Physiology of Release at Photoreceptor Synapses

Photoreceptors hyperpolarize to light and decreases in light intensity cause photoreceptors to depolarize. Depolarization increases the open probability of Ca^{2+} channels clustered beneath the ribbon. The opening of Ca^{2+}

channels increases $[Ca^{2+}]_i$, stimulating fusion of vesicles at the base of the ribbon. The calcium sensors in bipolar and hair cells have a low affinity for calcium requiring $>10\,\mu M$ calcium to stimulate exocytosis. Release from bipolar cells and most other CNS neurons exhibits high cooperativity consistent with the binding of as many as five Ca^{2+} ions required for release. The release mechanism employed by photoreceptors differs from these synapses by showing a much higher affinity for Ca^{2+} whereby submicromolar calcium levels can stimulate release. This high affinity is consistent with the possible involvement of synaptotagmin III, which has a higher affinity for calcium than synaptotagmin I or II. In addition to higher Ca^{2+} affinity, release from photoreceptors shows lower cooperativity for Ca^{2+} binding ($N \leq 3$).

Ca^{2+} channels are close to the ribbon and thus opening of a channel will expose nearby release sites to high $[Ca^{2+}]$. Opening only a few channels is sufficient to stimulate fusion of a vesicle. Increasing the number of active Ca^{2+} channels increases the number of active Ca^{2+} microdomains and this in turn increases the number of active release sites. Because the number of active release sites increases linearly with I_{Ca} amplitude, there is a linear relationship between I_{Ca} and release at hair cell synapses. This mechanism may also contribute to linearity between I_{Ca} and release at photoreceptor synapses although linearity at this synapse is also promoted by use of a sensor with a low cooperativity for calcium binding ($N \leq 3$).

Synaptic release at ribbon synapses involves two components: a transient burst of release stimulated by abrupt membrane depolarization and the slower, sustained release that accompanies maintained depolarization. In bipolar cells, as with many other neurons, fast release requires very high levels of Ca^{2+} whereas slow sustained release is triggered by low Ca^{2+} levels. The separate control of fast release by low Ca^{2+} affinity sensors and slow release by high Ca^{2+} affinity sensors is consistent with the idea that fast and slow release in bipolar and hair cells may occur at ribbon and nonribbon sites, respectively.

Unlike bipolar cells, fast and slow release from photoreceptors exhibit the same high affinity for Ca^{2+}, suggesting that both components of release occur at the same site. Thus, sustained release from photoreceptors appears to be predominately due to continued release of vesicles from the ribbon, albeit at lower rates than those attained during fast transient release. Because of the high affinity for Ca^{2+} exhibited by the release apparatus in photoreceptors, micromolar levels of Ca^{2+} present at the base of the ribbon in darkness are sufficient to stimulate fusion of vesicles at the base of the ribbon almost immediately after docking. As a consequence, the base of the cone ribbon is largely devoid of vesicles in darkness. This means that in darkness, calcium channel openings often occur beneath empty release sites. The rate of sustained release in darkness is therefore not directly controlled by the stochastic opening of individual Ca^{2+} channels, but by the rate at which vesicles are delivered and readied for release at the base of the ribbon.

Release rates decline when photoreceptors hyperpolarize, allowing vesicles to be replenished at release sites along the base of the ribbon. With a sufficiently long and bright flash of light, the entire readily releasable pool of vesicles can be replenished. When the cone depolarizes at light offset, the rapid release of this replenished pool of vesicles can evoke a large off response in second-order neurons.

Photoreceptors release vesicles continuously at a rate of ~10–20 vesicles per ribbon per second in darkness. Cones can respond to light intensities spanning a 10 000-fold range, but this sustained release rate can encode only 10–20 distinguishable levels of steady light if synaptic release exhibits Poisson release statistics. If sustained release is controlled by the rate of vesicle delivery down the ribbon rather than the stochastic openings of individual calcium channels, this will make the rate of sustained release more regular. Regularization allows discrimination of a greater number of light levels than predicted for a Poisson release process. The high rates of release from cones that can be attained at light offset allow for the encoding of up to 100 distinguishable light decrements. This may account for psychophysical results showing a greater sensitivity to decrements than increments of light.

Rods exhibit slower release kinetics than cones, roughly matched to the slow kinetics of rod light responses. Rod and cone synapses have similar ribbons, I_{Ca} with similar properties, and similarly rapid, high affinity calcium sensors, suggesting that differences in Ca^{2+} handling and buffering may be responsible for rod/cone differences in release kinetics.

The continuous release of vesicles from photoreceptor synapses in darkness is balanced by compensatory endocytosis of vesicles. Photoreceptors rely largely on clathrin-mediated endocytosis whereas bipolar cells and hair cells rely more on bulk retrieval of large endosomes. Visualization of single vesicles at bipolar cell terminals by TIRF microscopy show that the vast majority of vesicles undergo full collapse during fusion indicating that kiss-and-run retrieval of fully formed vesicles is minimal at this synapse.

Disease-Related Mutations in Synaptic Proteins at the Photoreceptor Synapse

Given that all visual information must pass through the photoreceptor synapse, it is not surprising that mutations in synaptic proteins of photoreceptors can produce visual deficits. For example, rod–cone dystrophies can be caused by mutations in Rab3 interacting protein (RIM1),

UNC-119, or Ca^{2+} channel $\alpha 2/\delta$ subunits. Congenital stationary night blindness can be caused by mutations in the rod CaV1.4 Ca^{2+} channel or CaBP4. Misregulation of glutamate release by photoreceptors and bipolar cells may also contribute to excitotoxic damage in neurodegenerative diseases of the retina.

See also: Cone Photoreceptor Cells: Soma and Synapse; Glutamate Receptors in Retina; Rod Photoreceptor Cells: Soma and Synapse.

Further Reading

Choi, S. Y., Borghuis, B. G., Rea, R., et al. (2005). Encoding light intensity by the cone photoreceptor synapse. *Neuron* 48: 555–562.

Daiger, S. P., Sullivan, L. S., and Browne, S. J. (2009). *RetNet – Retinal Information Network*. http://www.sph.uth.tmc.edu/retnet (accessed July 2009).

DeVries, S. H., Li, W., and Saszik, S. (2006). Parallel processing in two transmitter microenvironments at the cone photoreceptor synapse. *Neuron* 50: 735–748.

Dowling, J. E. (1987). *The Retina: An Approachable Part of the Brain*. Cambridge, MA: Harvard University Press.

Heidelberger, R., Thoreson, W. B., and Witkovsky, P. (2005). Synaptic transmission at retinal ribbon synapses. *Progress in Retinal and Eye Research* 24: 682–720.

Jackman, S., Choi, S.-Y., Thoreson, W. B., et al. (2009). Role of the synaptic ribbon in transmitting the cone light response. *Nature Neuroscience* 12: 303–310.

Kolb, H., Fernandez, E., and Nelson, R. (2009). *Webvision: The Organization of the Retina and Visual System*. http://webvision.med.utah.edu (accessed July 2009).

Krizaj, D. and Copenhagen, D. R. (2002). Calcium regulation in photoreceptors. *Frontiers in Bioscience* 7: 2023–2044.

LoGiudice, L. and Matthews, G. (2007). Endocytosis at ribbon synapses. *Traffic* 8: 1123–1128.

Prescott, E. D. and Zenisek, D. (2005). Recent progress towards understanding the synaptic ribbon. *Current Opinions in Neurobiology* 15: 431–436.

Rodieck, R. (1998). *The First Steps in Seeing*. Sunderland, MA: Sinauer.

Sterling, P. and Matthews, G. (2005). Structure and function of ribbon synapses. *Trends in Neuroscience* 28: 20–29.

Thoreson, W. B., Rabl, K., Townes-Anderson, E., and Heidelberger, R. (2004). A highly Ca^{2+}-sensitive pool of vesicles contributes to linearity at the rod photoreceptor ribbon synapse. *Neuron* 42: 595–605.

tom Dieck, S. and Branstatter, J. H. (2006). Ribbon synapses of the retina. *Cell and Tissue Research* 326: 339–346.

Pigment Dispersion Syndrome and Pigmentary Glaucoma

R Ritch, The New York Eye and Ear Infirmary, New York, NY, USA

Glossary

Krukenberg spindle – Typical spindle-shaped pigment deposition on the cornea of patients with pigment dispersion syndrome.
Pigment dispersion syndrome – An autosomal dominant disorder in which iridozonular friction mechanically disrupts the iris pigment epithelium dispersing pigment granules throughout the anterior eye segment.
Pigmentary glaucoma – Form of glaucoma that may develop in patients with pigment dispersion syndrome.
Reverse pupillary block – A condition in which the extend of iridolenticular contact is greater than normal, reducing the ability of aqueous humor to equilibrate between the anterior and posterior chambers, and leading to increased pressure in the anterior chamber that pushes the iris posteriorly.

History

In 1899, Krukenberg described spindle-shaped pigment deposition on the cornea. Two years later, von Hippel suggested that pigment obstructing the aqueous outflow system could lead to elevated intraocular pressure (IOP). Levinsohn first suggested that pigment in the anterior chamber angle of patients with glaucoma originated from the iris pigment epithelium (IPE). A cause and effect relationship between pigment and glaucoma found both support and opposition.

In 1949, Sugar and Barbour described two young, myopic men with Krukenberg spindles, trabecular hyperpigmentation, and open angles, whose IOP increased with mydriasis and decreased with pilocarpine. They identified the disorder as a rare, distinct form of glaucoma, which they termed as pigmentary glaucoma (PG). More patients were subsequently reported, and in 1966 Sugar reviewed 147 cases in the literature, describing several additional features, including bilaterality, frequent association with myopia, greater incidence in men than in women, and a relatively young age of onset. These features were confirmed by Scheie and Cameron.

In the 1950s, the discovery of iris transillumination defects led to the concept that the trabecular pigment originated from the IPE and perhaps the ciliary body. Congenital atrophy or degeneration of the IPE was suggested as a cause of loss of iris pigment. In 1979, Campbell proposed the pathogenesis to involve mechanical damage to the IPE during rubbing of the posterior iris against the anterior zonular bundles during physiologic pupillary movement. Karickhoff presented the concept of reverse pupillary block, in which abnormally extensive iridolenticular contact in eyes with PDS prevents equilibration of aqueous between the anterior and posterior chambers (**Figure 1**). Ritch and colleagues found PDS in 2.45% of the Caucasians in a mass screening, extending the concept of the prevalence of this entity by an order of magnitude. Subsequently, the autosomal dominant inheritance, natural history, reversibility, and more precise therapeutic approaches have become increasingly delineated. Ultrasound biomicroscopic studies have revealed new insights into the pathophysiology of PDS (**Figure 2**).

Pathophysiology

In 1958, Scheie and Fleischauer described iris transillumination defects associated with PDS and noted a pale and waxy appearance of the ciliary body in a few patients, attributing their findings to congenital IPE atrophy. Fine and colleagues examined the eyes of a 55-year-old man who had been found to have PDS without glaucoma at age 43. In the iris mid-periphery, there was an abrupt transition from normal to abnormal IPE, accompanied by hyperplasia of the iris dilator muscle with marked hyperplasia of the muscle spur of Grunert at the iris root. Rodrigues and colleagues, in contrast, reported a focally thickened dilator muscle with thinning in the areas of epithelial atrophy and found an increased number of immature melanosomes, suggesting a developmental defect.

Kupfer and colleagues believed the primary lesion in PDS to be epithelial in origin. The dilator fibers of the inner IPE appeared to be hypertrophic and hyperplastic, resembling the sphincter muscle, and were associated with degenerated neural elements. They hypothesized that the primary defect in the inner IPE could be the result of interruption of sympathetic innervation. The relevance of dilator muscle hyperplasia and nerve fiber degeneration to the disease process remains unknown; however, epinephrine compounds, alone or in combination with other agents, have been suggested to be more effective in patients with PG than in those with primary open-angle glaucoma (POAG).

The theory that posterior bowing of the iris brings it into contact with the anterior zonular bundles was proposed by Campbell. The location and number of the transillumination defects correlated with the position and number of the

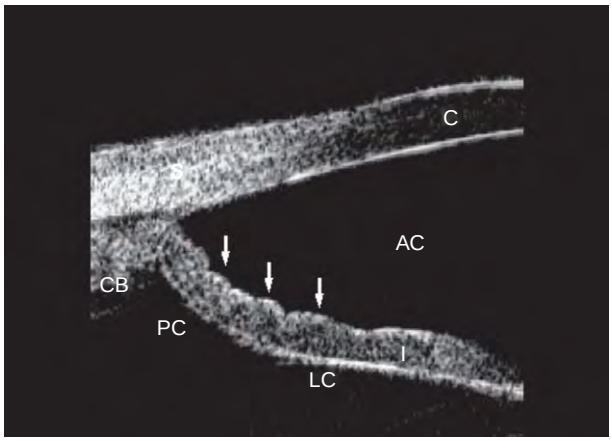

Figure 1 Typical UBM appearance of an eye with pigment dispersion syndrome. The extent of iridolenticular contact is greater than normal, reducing the ability of aqueous to equilibrate between the anterior (AC) and posterior (PC) chambers, leading to increased pressure in the anterior chamber pushing the iris posteriorly (arrows), resulting in reverse pupillary block. Liebmann, J. M. and Ritch, R. (2000). Pigment dispersion syndrome and pigmentary glaucoma. In: Fingeret, M. (ed.) *Primary Care of the Glaucomas*, 2nd edn., pp. 427–442. Philadelphia: McGraw-Hill.

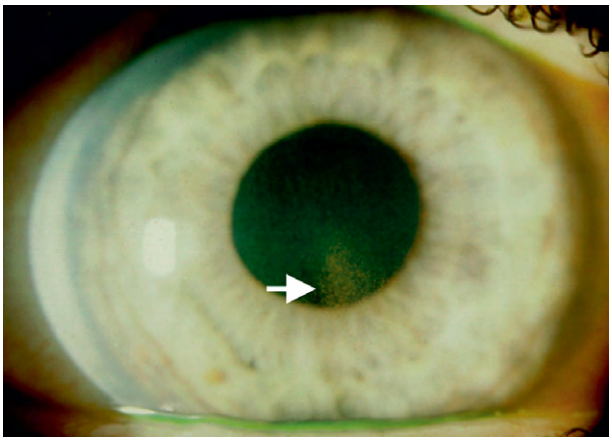

Figure 2 Krukenberg spindle (arrow). Liebmann, J. M. and Ritch, R. (2000). Pigment dispersion syndrome and pigmentary glaucoma. In: Fingeret, M. (ed.) *Primary Care of the Glaucomas*, 2nd edn., pp. 427–442. Philadelphia: McGraw-Hill.

underlying zonular bundles. He hypothesized that iridozonular friction during pupillary movement disrupts the IPE, releasing pigment into the posterior chamber, noting that hyperplasia of the iris dilator muscle was localized to areas of iridozonular contact. Scanning electron microscopic observations supported this hypothesis, which is now accepted as the underlying mechanism of PDS.

There is debate, however, over whether posterior bowing of the iris with iridozonular contact is sufficient in itself to cause PDS. Ultrasound biomicroscopy (UBM) performed during accommodation or exercise reveals accentuation of the iris concavity not only in patients with PDS, but also in normals, particularly myopes. It is possible that a predisposing factor in addition to iridozonular contact, perhaps congenital, is required to allow disruption of the pigment epithelium. Scuderi and colleagues found psychophysical evidence of decreased retinal pigment epithelial function in eyes with PDS by electro-oculography, suggesting primary involvement of the retinal pigment epithelium in PDS. In another study, the mean ratios of the light-peak amplitude to dark-trough amplitude of patients with PDS and PG were found to be significantly lower than the mean ratios of normal controls and patients with POAG, respectively. The pigment epithelium of the iris is continuous with those of the ciliary body and retina. Retinal pigment epithelial dystrophies have rarely been associated with PDS.

Ultrasound Biomicroscopy

UBM has enabled us to elucidate a number of facets of the pathophysiology of PDS. The size of the iris appears overly large relative to that of the anterior segment. This may be the basic anatomic cause of the mid-peripheral iris concavity predisposing to iridozonular contact. Iridolenticular contact is greater in eyes with PDS than in normal eyes and decreases after laser iridotomy is performed to eliminate reverse pupillary block (**Figure 3**). Mathematical modeling, treating the aqueous humor as a Newtonian fluid and the iris as a linear elastic solid, suggests that passive iris deformation can produce the iris contours observed using UBM. Sokol and colleagues compared patients with PDS to age-, sex-, and refraction-matched controls and found a greater mean iris-trabecular meshwork distance in the PDS group (**Figure 4**). Thus, iridozonular contact appears to be facilitated by a congenitally more posterior iris insertion.

The question has again been raised as to whether posterior bowing of the iris and iridozonular contact is sufficient in itself to cause PDS. UBM performed during accommodation reveals accentuation of the iris concavity, not only in patients with PDS but also in normals, particularly myopes. This accentuation also occurs in both normals and PDS patients after exercise. It is possible that many people have iridozonular contact, but that a predisposing factor is required to effect disruption of the IPE.

UBM has shown iridozonular and iridociliary contact in PDS. While iridociliary contact has not been proven to liberate pigment, the occasional extension of transillumination defects into the periphery of the iris, creating an appearance similar to that of an exclamation point, suggests that contact between the two surfaces may damage the pigment epithelium of both and may account retrospectively for the observation of Scheie and Fleischauer regarding the pale and waxy appearance of some ciliary processes.

Electron Microscopy

Trabecular cells are filled with pigment and show various stages of degeneration. Electron microscopic examination

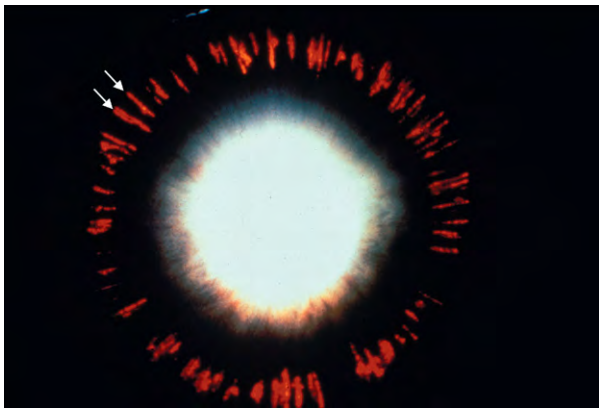

(a)

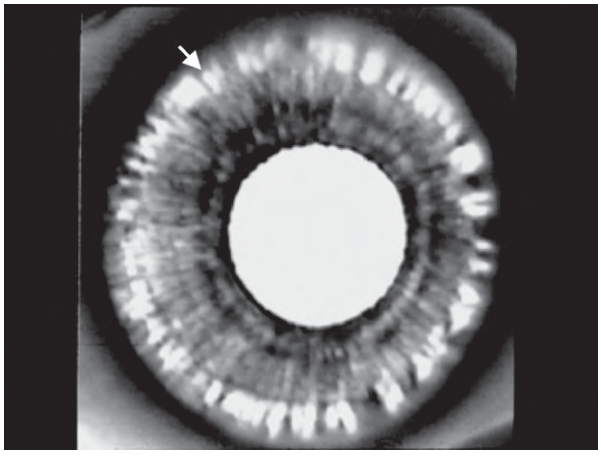

(b)

Figure 3 Mid-peripheral, slit-like, radial iris transillumination defects (arrows). (a). Slit-lamp appearance and (b). Infrared pupillography. Infrared videopupillography is a useful technique to detect and document the number of transillumination defects.

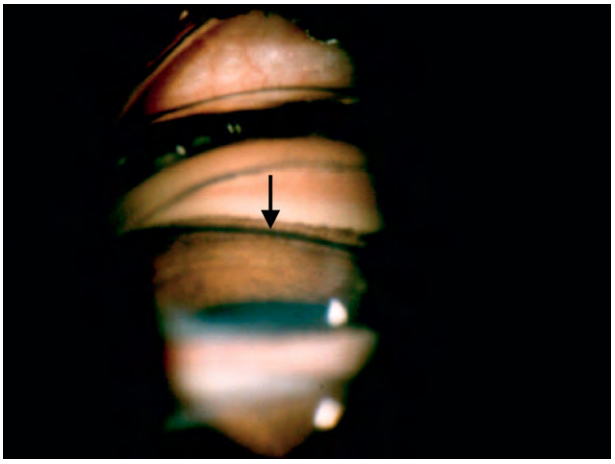

Figure 4 Dense, homogeneous pigmentation (arrow) of the trabecular meshwork in a 35-year-old man with pigment dispersion syndrome. Liebmann, J. M. and Ritch, R. (2000). Pigment dispersion syndrome and pigmentary glaucoma. In: Fingeret, M. (ed.) *Primary Care of the Glaucomas*, 2nd edn., pp. 427–442. Philadelphia: McGraw-Hill.

of the trabecular meshwork shows cells lining the trabecular beams lifting off and disintegrating. There is trabecular cell loss, loss of intertrabecular spaces, fusion of lamellae, and an increase in extracellular material under the inner wall of Schlemm's canal, while the intertrabecular spaces contain cellular debris, but not pigment. These observations suggest that plugging of the trabecular spaces by pigment and cell debris together with fragmentation and collapse of trabecular sheets contribute to the decrease in the facility of outflow that occurs in PG. It is possible that failure or breakdown of endothelial phagocytic function may be involved as well. When eyes with PDS with elevated IOP are compared to normal eyes, the aqueous humor dynamics are similar between the two groups, indicating that a reduction in outflow facility alone is responsible for elevated IOP.

Blinking

When eyelid blinking is prevented in PDS patients, aqueous humor builds up in the posterior chamber and the iris assumes a planar and even a convex configuration. As the volume of the posterior chamber increases relative to that of the anterior chamber, the iris gradually flattens, iridolenticular contact diminishes, and iridozonular and iridociliary process distances increase. In the most pronounced cases, iridolenticular contact disappears, the iris sphincter lifting completely off the surface of the lens without the posterior chamber losing its expanded volume (**Figure 5**). When PDS patients are permitted to blink and are then rescanned, the concave iris configuration is restored.

The mechanism by which blinking affects the anatomy of the anterior segment appears to be a mechanical one. Campbell proposed that a blink initially deforms the cornea, transiently increasing IOP and pushing the iris posteriorly against the lens. Chew and colleagues demonstrated that during blinking of the nictitating membrane in the chick eye, the cornea indents in a wave from the periphery to the center and that anterior chamber depth similarly decreases. Extrapolating this finding to humans, we have hypothesized that blinking acts as a mechanical pump to push a bolus of aqueous humor from the posterior chamber to the anterior chamber. A pressure wave is created, pushing the iris posteriorly toward the zonules. This wave begins at the iris periphery and moves centrally, pushing aqueous before it into the anterior chamber and emptying the posterior chamber.

Abnormally extensive iridolenticular contact in eyes with PDS prevents equilibration of aqueous between the anterior and posterior chambers (reverse pupillary block). The now increased volume of aqueous in the anterior chamber helps to maintain the mid-peripheral iris concavity. As aqueous leaves the eye through the trabecular meshwork and enters through ciliary secretion, the volume of the anterior chamber decreases while the volume

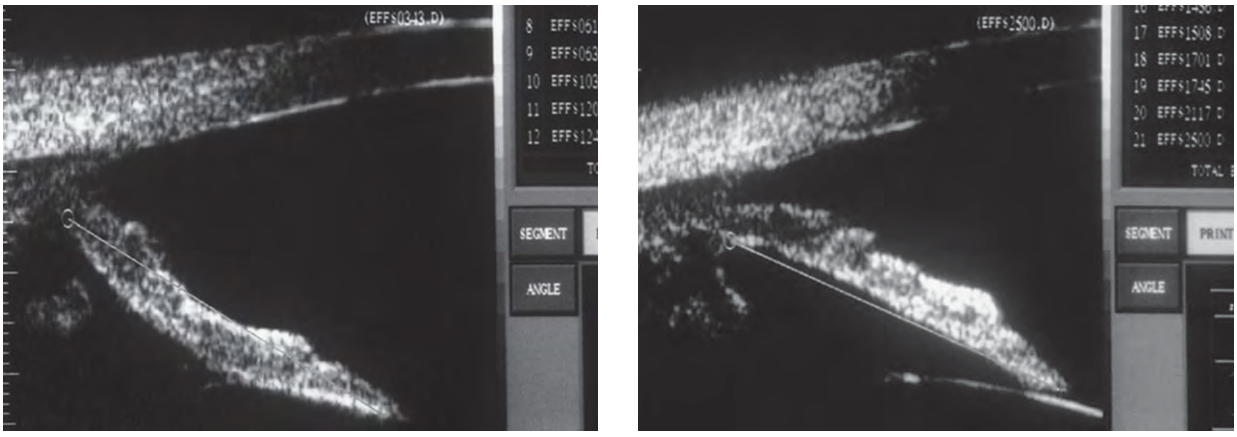

(a) (b)

Figure 5 (a, b) Inhibition of blinking for several minutes causes the iris concavity to disappear as the posterior chamber fills with aqueous, and the iris contour eventually becomes convex.

of the posterior chamber increases, until the next blink starts the cycle once again. Interestingly, increasing myopia is also a predictor of increasing iridolenticular contact, independent of the presence of PDS. This may explain why myopia enhances the phenotypic expression of the genetic abnormality underlying PDS. It also raises the question as to whether decreased trabecular function and reduction of the aqueous outflow coefficient might serve to accentuate the iris concavity.

Accommodation

Accommodation in normal, young individuals and in PDS patients may affect iris contour. Accommodation in normal eyes causes an iris concavity indistinguishable from that in PDS, but recent evidence shows that this effect is lessened with age. Contraction of the ciliary ring allows shallowing of the anterior chamber, anterior lens movement, and increased iridolenticular contact. Aqueous in the anterior chamber is forced into the angle recess and the peripheral iris becomes more concave. As accommodation is relaxed, the iris resumes its initial configuration.

Accommodation might enhance pigment liberation in two ways. In addition to posterior iris bowing during accommodation, the pupil constricts. Relaxation of accommodation accompanied by pupillary dilation might result in additional iridozonular friction. UBM during accommodation in eyes with PDS shows iridozonular contact at the lens margin, consistent with the usual position of iris transillumination defects. The magnitude of the posterior iris bowing is a function of the amount of accommodation exerted.

Scanning following administration of pilocarpine shows resolution of the iris concavity and iridozonular contact in all eyes. Pilocarpine produces a convex rather than a planar configuration. Laser iridotomy relieves reverse pupillary block by allowing aqueous to flow from the anterior to the posterior chamber and produces a planar iris configuration. Iridotomy appears to prevent the accentuation of the iris concavity which accompanies accommodation.

Exercise

Some PDS patients may experience pigment-induced IOP elevation after exercise or with pupillary dilation. This is most commonly associated with activities that include bouncing, such as jogging or playing basketball. However, bicycle exercise increased the iris concavity by UBM both in normals and in eyes with PDS, an effect which was eliminated in the latter by laser iridotomy. Vibration-induced increased trabecular pigmentation has also been reported in rock drillers. The exercise-induced release of pigment and elevation of IOP can be completely blocked by pilocarpine, but iridotomy does so incompletely. A rise in IOP after dilation may be delayed by hours, and patients with PDS should always have IOP measured and the anterior chamber examined for pigment dispersion after dilation. If IOP is elevated or there is extensive pigment liberation, this phenomenon should be kept in mind.

Clinical Findings

Anterior segment

Loss of iris pigment appears clinically as a mid-peripheral, radial, slit-like pattern of transillumination defects seen most commonly inferonasally and most easily in eyes with blue irides. The defects can sometimes be seen by retroillumination, but infrared videography provides the most sensitive method of detection and may be more helpful in black patients. Pigment particles tend to aggregate in the furrows of the iris surface (**Figure 6**). Rarely, dense,

asymmetric pigment on the iris face can cause heterochromia when involvement is asymmetric.

Asymmetric involvement may lead to anisocoria, with the larger pupil found in the eye with greater pigment loss from the iris. Alward and Haynes suggested the presence of an efferent defect in the eye with the larger pupil. The pupil may be distorted in the direction of maximal iris transillumination, possibly as a result of hyperplasia of the iris dilator muscle (see below).

Corneal endothelial pigment generally appears as a central, vertical, brown band of pigment on the corneal endothelium, the shape being attributed to aqueous convection currents. The pigment is phagocytosed by endothelial cells, but endothelial cell density and corneal thickness remain unchanged compared to controls. Coincident PDS and megalocornea has been reported, in one study involving four of eight boys referred for megalocornea and elevated IOP. Anterior megalophthalmos with megalocornea has been reported in two sisters with PG.

In PDS, the anterior chamber is deeper both centrally and peripherally than can be explained by sex, age, or refractive error. Davidson and colleagues compared the central and peripheral anterior chamber depths of patients with PDS to controls and found the anterior chamber to be deeper and the anterior chamber volume greater in the PDS group, more so inferiorly. In patients with unilateral PDS the anterior chamber was deeper and the lens flattens in the involved eyes. Patients with PDS have flatter corneas than myopic age- and refraction-matched controls, but no difference in axial length. Quantification of aqueous melanin granules in the anterior chamber yields a positive correlation with IOP.

The angle is characteristically widely open, with a homogeneous, dense pigmented band on the trabecular meshwork. Pigment may also be deposited on Schwalbe's line and on the corneal shelf anterior to it, distinguishable from a Sampaolesi line by the presence of finer and darker particles. The iris insertion is posterior and the peripheral iris approach is often most concave in the mid-periphery. In younger patients, the scleral spur may be poorly demarcated, blending with the ciliary face due to pigment deposition on these structures. Pigment may be deposited on the zonules (**Figure 7**), on the posterior capsule of the lens, where it is apposed to the anterior hyaloid face at the insertion of the posterior zonular fibers (Zentmayer ring, **Figure 8**), on the posterior lens central to Weigert's ligament (**Figure 9**), and on the anterior vitreous face when that has separated from the lens (**Figure 10**).

Posterior segment

Investigators have found no differences between PG and primary open-angle glaucoma in terms of the size and shape of the optic disk, configuration of the neuroretinal rim, depth of the optic cup, area of the alpha zone of parapapillary atrophy, diameter of retinal vessels at the disc border, and frequency of disc hemorrhages and localized retinal

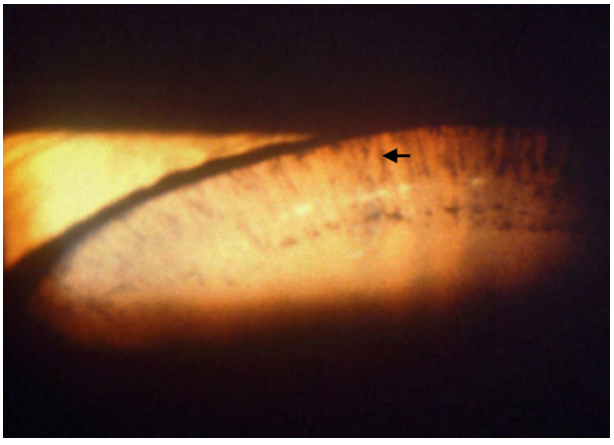

Figure 7 Pigment on the zonules (arrow).

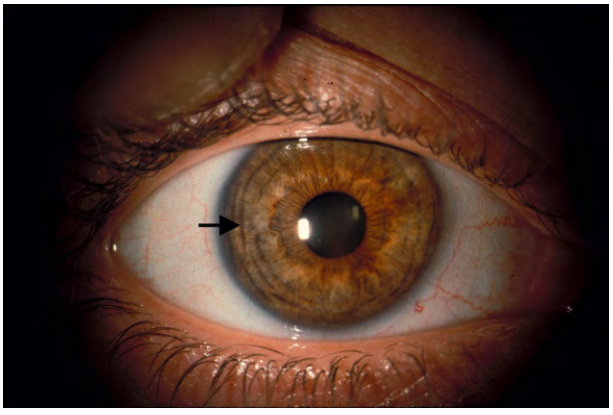

Figure 6 In cases with more pronounced pigment liberation, pigment granules may accumulate in iris furrows, where they are visible as concentric rings (arrow).

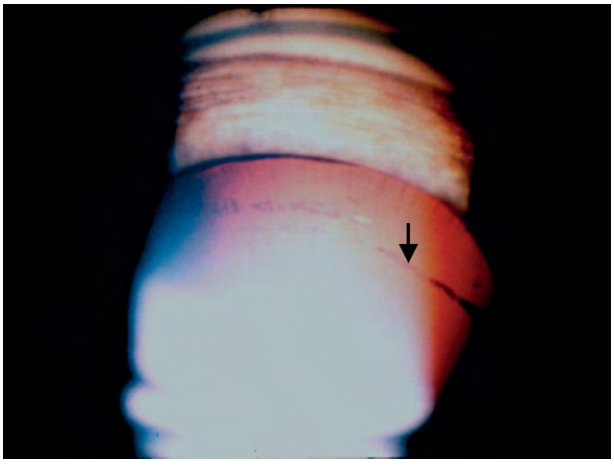

Figure 8 Pigment on the posterior lens capsule at the site of zonular insertion (arrow).

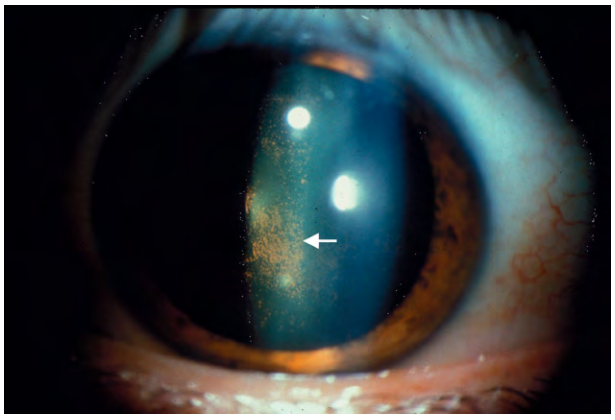

Figure 9 Pigment on the posterior lens capsule (arrow).

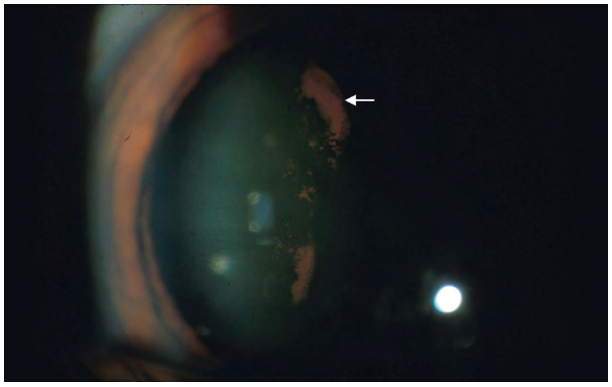

Figure 10 Pigment on the anterior vitreous face (arrow).

nerve fiber-layer defects. A recent study by scanning laser polarimetry in patients with PDS found the retinal nerve fiber layer thickness to be between that of patients with PG and normals.

PDS is associated with a high incidence of retinal detachment. Most detachments occur in phakic men who are not highly myopic. Miotics have been incriminated in precipitating these. It is significant that the incidence of retinal detachment in PDS is 6–8% independent of miotic treatment, and when detachment is associated temporally with miotics, a pre-existing lesion was most likely present. Lattice degeneration is commonly found in myopes and may be hereditary. Its incidence appears to be higher for all degrees of myopia in patients with PDS than in the general population. Despite the fact that comparable prevalences of lattice degeneration in blacks and whites have been demonstrated at autopsy, PDS and retinal detachment are both uncommon in blacks.

Demographics of Pigment Dispersion Syndrome

Heredity

Occasionally families with Krukenberg spindles were reported prior to the 1980s, with subsequent reports describing familial PDS. McDermott and colleagues examined relatives of 21 probands and found involvement in 36% of parents and 50% of siblings, but none in children under the age of 21 years. This suggested a strong pattern of autosomal dominance, with phenotypic onset beginning in the mid-20s. That Caucasians are almost exclusively affected is also consistent with a genetic origin.

Loci for PDS have been reported at chromosome 7q35-36 and 18q, suggesting genetic heterogeneity. The gene for phenylthiocarbamide tasting is located in this region and was once associated with primary open-angle glaucoma. A re-examination of this phenomenon showed no difference between patients with PDS, PG, and juvenile POAG.

Gender

Men and women are equally affected by PDS, but men develop PG about 3 times as often as women and at a younger age. Since the prevalence of myopia in the United States is similar between men and women, refractive error differences cannot explain this observation.

Race

PDS is found almost exclusively in Caucasians. PDS has been reported in African-Americans, but African-American patients with PDS reported a significantly greater percentage of Caucasian ancestry and were more lightly complected than controls. Rare cases have been reported in Asia.

Refractive error

About 60–80% of the patients with PDS and PG are myopes and 20% are emmetropes. Eyes with PG are significantly more myopic than those with PDS and refractive error is correlated with the age of onset of glaucoma.

Asymmetric involvement

Since PDS is a bilateral disorder, asymmetric involvement requires explanation and may be informative of the disease pathogenesis. A second disorder may make one eye worse. The most common cause in older patients appears to be the development of exfoliation syndrome in one eye in patients who had had PDS or PG in earlier life. This combination is an example of an overlap syndrome. Angle recession in one eye has also been reported.

It is also possible for one eye to have a second disorder which reduces the severity of PDS, such as unilateral traumatic cataract extraction in youth prior to the onset of pigment dispersion or development of unilateral cataract during the pigment dispersion phase, which decreases iridozonular contact by causing pupillary block. Trauma resulting in an iridectomy and an iris coloboma leading to protection against PDS has been reported. Horner's syndrome may have a protective effect, while Adie's pupil has been associated with PDS in the same eye.

In other cases, mild to marked asymmetry may exist without any other evident process. Kaiser-Kupfer and colleagues reported four normotensive patients with markedly asymmetric involvement and no obvious cause for asymmetry. Three had anterior chamber depths 0.2 mm greater in the affected eye. UBM has revealed that in all cases of PDS where asymmetric pigment dispersion is present there is either increased relative pupillary block in the less-involved eye (reducing peripheral iridozonular contact) or greater iridozonular contact in the more-involved eye. There is greater iridolenticular contact and a more posterior iris insertion in the more-involved eye.

Clinical Course

Active phase

The mean age of onset of PDS is probably in the mid-20s, when patients enter the pigment liberation phase. Patients in their early teens have been reported. Early in the disease, pigment liberation in the anterior chamber and the characteristic peripheral iris concavity may be the only detectable signs. Neither any pigment has collected on the corneal endothelium nor have iris transillumination defects developed. The youngest patients reported have been aged 12, 14, and 15. McDermott and colleagues found no children of probands with PDS under age 21; however, further studies are warranted.

The phenotypic expression of PDS varies widely, and is difficult to detect early in the disease process. It is not known whether the variability in phenotypic expression is hereditary, environmental, or a combination of both. For instance, the concavity due to iris position and size (genetic) could be affected by the cumulative amount of accommodation (environmental).

Regression phase

Loss of accommodation with the onset of presbyopia and development of relative pupillary block secondary to increased lens thickness with age presumably lead to the cessation of pigment liberation in middle age. Older patients with PDS as well as normals develop little or no accentuation of the iris concavity with accommodation. The severity of involvement of both PDS and PG decreases in middle age when pigment liberation ceases presumably because pigment can pass out of the trabecular meshwork with age. Transillumination defects may disappear and the IOP may return toward normal. Some patients treated with long-term miotic therapy have been able to reduce or discontinue treatment for glaucoma. Older patients presenting with glaucoma may have only very subtle manifestations, if any, of PDS, and may be misdiagnosed as primary open-angle glaucoma or normal-tension glaucoma. That remission of PG occurred in a young patient following lens subluxation provided early confirmation of Campbell's hypothesized mechanism for pigment liberation.

Trabecular pigmentation is initially dense and homogeneous for 360°. During the regression phase, it becomes lighter and more localized to the filtering portion of the meshwork. When the trabecular meshwork begins to recover, the normal pigment pattern reverses and the pigment band becomes darker superiorly than inferiorly. We have termed this the pigment reversal sign and in older patients, it may be the only finding suggestive of previous PDS (**Figure 11**). Although it cannot be regarded as diagnostic, examination of the patient's offspring may be confirmatory. The pigment reversal sign may also be found in patients after long-term miotic therapy in patients with PDS/PG.

Conversion to Glaucoma

The frequency with which PDS converts to PG has probably been greatly overestimated. The three studies which have examined patients longitudinally suggest that up to 50% will eventually develop glaucoma. However, the true rate of PDS in the general population may be an

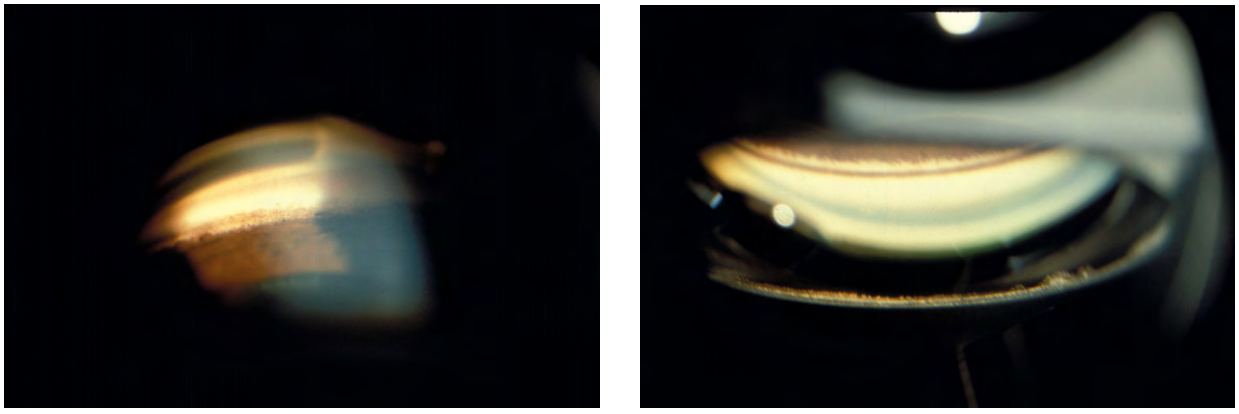

(a) (b)

Figure 11 (a, b) Pigment reversal sign.

order of magnitude greater than had previously been suspected. Wilensky and colleagues found only 2 of 43 patients with Krukenberg spindles developed visual field loss during a mean of 5.8 years of follow-up. In a retrospective community-based study of 113 patients with PDS followed for 24 years, nine developed PG or elevated IOP requiring therapy. The probability of converting to PG was 10% at 5 years and 15% at 15 years.

Differential Diagnosis

Other disorders can produce abnormal pigment dispersion. Exfoliation syndrome may produce dense trabecular pigmentation. A typical Krukenberg spindle does not develop; rather, a more evenly distributed flecking of pigment develops on the posterior surface of the corneal endothelium. The diagnosis is made by discerning the typical pattern of exfoliation material within the eye in association with pigment dispersion. Patients who have had PDS can develop exfoliation syndrome in later life. We are finding this combination increasingly common as patients with known PDS have been followed into middle age. Secondary pigment dispersion has also been reported associated with iris pigment epithelial cysts, iris nevus, and melanocytoma of the ciliary body. Iris, ciliary body, or even posterior segment melanomas (if the anterior hyaloid face is disrupted) can be associated with dispersed pigment. Pigmented tumor cells or pigment-laden macrophages may cause considerable darkening of the anterior and posterior chambers. The typical signs of PDS/PG are absent: there is no Krukenberg spindle; there are no transillumination defects; and the tumor is usually readily apparent. Inflammation involving the posterior surface of the iris can occasionally disperse a moderate amount of pigment often clumped in the inferior angle.

A secondary form of PDS capable of causing glaucoma has been described following implantation of a posterior chamber intraocular lens and after penetrating keratoplasty with a posterior chamber intraocular lens. In this situation, ongoing postoperative contact between the iris and the abnormally positioned lens causes release of pigment. Posterior chamber phakic refractive lenses have also been reported to induce PDS through contact between the lens and the iris, as has piggyback lens implantation.

Pigmented long anterior zonules (PLAZ), originally described as retro-iridial lines of Vogt, is a bilateral disorder in which abnormally long and anteriorly inserted zonules are present on the face of the anterior lens capsule (Figure 12). This creates a type of pigment dispersion as the zonules rub against the posterior surface of the iris, liberating pigment into the anterior chamber. Krukenberg spindles, densely pigmented trabecular meshwork, and pigmented zonules may be seen. Iris transillumination defects are not found. Unlike PDS, PLAZ is common in black patients, and its incidence increases with hyperopia, age, and female gender. In some cases, PLAZ is associated with a CTRP5 mutation and late-onset macular degeneration.

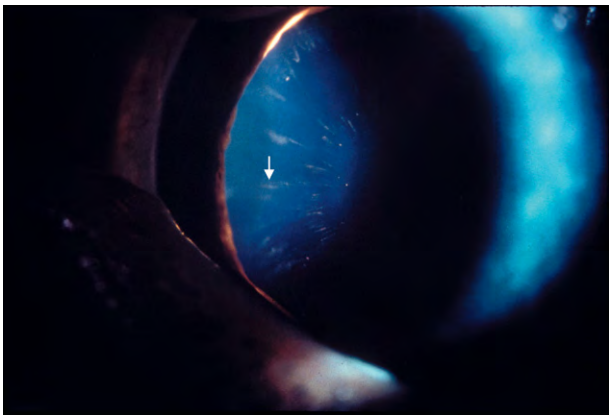

Figure 12 Pigmented long anterior zonule syndrome.

Treatment

While PG is often treated identically with POAG, the unique mechanism of development of elevated IOP in PDS warrants a very different approach to therapy. Miotics both constrict the pupil, eliminating iridozonular contact, and increase aqueous outflow, lowering IOP, thus allowing the pathophysiologic process to begin to reverse, and should be in principle the drug of choice to initiate therapy. Miotics may prevent progression of the disease and the development of glaucoma by both inhibiting iris pigment release and by enhancing clearance of the pigment through the trabecular meshwork. The peripheral retina should be examined carefully and appropriate steps taken if lattice is present. Miotic drops are poorly tolerated because of accommodative spasm and induced myopia in young patients, causing difficulty functioning in work-related situations and activities such as sports and driving, particularly at night. Pilocarpine Ocuserts were the best delivery system for pilocarpine, and we had excellent success with them. Unfortunately, their manufacture was discontinued.

Prostaglandin analogs, which increase uveoscleral outflow, produce an excellent IOP response in patients with PDS and are now our first line choice of drug. In a prospective, randomized, double-masked study, Latanoprost 0.005% qhs was more effective at lowering IOP than timolol bid, which also produced a significant reduction in heart rate. We have found prostaglandin analogs to be effective as monotherapy, and their IOP-lowering effects are also additive in patients already on miotic therapy.

Aqueous suppressants have theoretical disadvantages compared with cholinergic agonists for PG. They decrease IOP by reducing aqueous flow, which could diminish the rate of clearance of the pigment from the trabecular meshwork and conceivably exacerbate the disease process.

Furthermore, reduced aqueous flow into the posterior chamber may exacerbate reverse pupillary block, allowing for more rubbing of the posterior iris surface against the zonules and more pigment release. Furthermore, nonselective beta blockers are likely to suppress younger patients' exercise-induced tachycardia and interfere with exercise tolerance.

Just as argon laser iridotomy is used to eliminate relative pupillary block, it has been advocated for the treatment of PDS as a means of eliminating reverse pupillary block (**Figure 13**). In relative pupillary block, iridotomy results in opening of the angle and increased iridolenticular contact, while in reverse pupillary block, it produces narrowing of the angle and decreased iridolenticular contact. Neodymium-YAG laser iridotomy has been reported to cause a significantly greater postoperative elevation in IOP after iridotomy when performed on eyes with PDS compared to eyes with relative occludable angles. Flattening of the iris contour both clinically and on UBM occurs after iridotomy, although perhaps not in all cases. A reduction of IOP has been reported to correlate with loss of the iris concavity. The number of melanin granules in the anterior chamber is decreased after iridotomy. In one study, 21 patients with PDS underwent unilateral iridotomy and a rise in IOP of more than 5 mmHg was reported in 11/21 untreated other eyes during a 2-year follow-up. No other study of PDS has reported this much high proportion of rise in IOP in normotensive eyes with PDS in such a short time, nor have we observed such rises in our patients. In a review of 23 patients with PDS and elevated IOP with no or mild glaucomatous damage having undergone laser iridotomy, Wang and colleagues found no significant long-term IOP reduction in the lasered eyes compared to the medically treated other eyes. Reistad reported 60 patients collected from American Glaucoma Society members who underwent unilateral laser iridotomy for PG. While the lasered eye had a greater IOP reduction after a minimum of 2 years of follow-up, the magnitude of the effect was explained by a higher baseline IOP in the treated eye, and the study was deemed inconclusive.

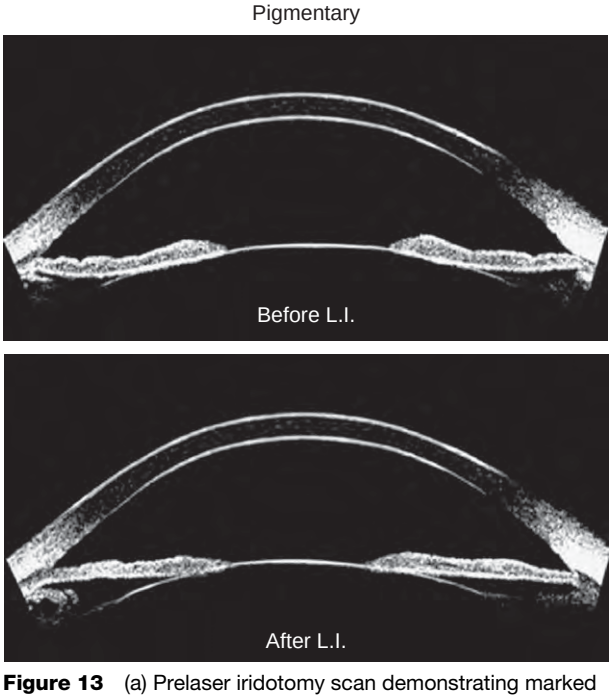

Figure 13 (a) Prelaser iridotomy scan demonstrating marked iris concavity and central iris contact with anterior lens capsule and zonules. (b) Postlaser iridotomy scan shows resolution of iris concavity and decreased length of iris contact with anterior lens capsule.

Patient selection for laser iridotomy is important. By preventing pigment liberation from the iris, the meshwork should theoretically have time to clear itself of pigment already deposited and reduce or eliminate further deposition. Therefore, patients should still be in an early stage of the disease, such as the pigment liberation stage. If pigment is liberated into the anterior chamber with pupillary dilation, it is suggestive that the patient is still in this stage. Patients who have uncontrolled glaucoma and are facing surgery are also poor candidates for laser iridotomy, since perhaps years are required to achieve functional reconstitution of the trabecular meshwork. Generally, we have restricted iridotomy to patients under 45 years of age who have elevated IOP with no damage or early glaucomatous damage. Since not all patients with PDS go on to develop elevated IOP, and since the iridotomy procedure itself results in significant pigment liberation, we do not advocate treating normotensive eyes.

The success rate of argon laser trabeculoplasty (ALT) in PG is greater in younger patients than in older ones and decreases with age. Pigment in younger patients is largely in the uveoscleral and corneoscleral meshworks, whereas in older patients, it is primarily localized to the juxtacanalicular meshwork and the back wall of Schlemm's canal. A larger portion of patients fail within a shorter period of time compared to POAG patients. Initially successful trabeculoplasty may be followed by a sudden, late rise in IOP, similar to that seen in exfoliative glaucoma. Patients in the pigment liberation stage who undergo ALT should be maintained on miotics or undergo laser iridotomy after ALT to prevent further contact between the iris and zonules.

Selective laser trabeculoplasty should be approached with caution at this point. Severe, irreversible IOP rises have been reported after this procedure. We advocate using low-power applications over 180° of trabecular meshwork and repeating the procedure as necessary.

See also: Animal Models of Glaucoma; Biomechanics of Aqueous Humor Outflow Resistance; Blinking Mechanisms; Control of Aqueous Humor Flow; Primary Open-Angle Glaucoma; The Genetics of Primary Open-Angle Glaucoma: A Review; The Immunological Aspects of Aqueous Humor Turnover.

Further Reading

Adam, R. S., Pavlin, C. J., and Ulanski, L. J. (2004). Ultrasound biomicroscopic analysis of iris profile changes with accommodation in pigmentary glaucoma and relationship to age. *American Journal of Ophthalmology* 138: 652–654.

Campbell, D. G. (1979). Pigmentary dispersion and glaucoma: A new theory. *Archives of Ophthalmology* 97: 1667–1672.

Campbell, D. G. (1996). Pigmentary glaucoma. In: Ritch, R., Shields, M. B., and Krupin, T. (eds.) *Pigmentary Glaucoma,* vol. 2, pp. 975–991. St. Louis, MO: CV Mosby.

Gottanka, J., Johnson, D. H., Grehn, F., and Lutjen-Drecoll, E. (2006). Histologic findings in pigment dispersion syndrome and pigmentary glaucoma. *Journal of Glaucoma* 15: 142–151.

Greenstein, V. C., Seiple, W., Liebmann, J., and Ritch, R. (2001). Retinal pigment epithelial dysfunction in pigment dispersion syndrome: Implications for the theory of pathogenesis. *Archives of Ophthalmology* 119: 1291–1298.

Liebmann, J. M., Tello, C., Chew, S.-J., Cohen, H., and Ritch, R. (1995). Prevention of blinking alters iris configuration in pigment dispersion syndrome and in normal eyes. *Ophthalmology* 102: 446–455.

Moroi, S. E., Lark, K. K., Sieving, P. A., et al. (2003). Retro-iridial lines of Vogt and pigment dispersion. *American Journal of Ophthalmology* 136: 1176–1178.

Pavlin, C. J., Macken, P., Trope, G., Harasiewicz, K., and Foster, F. S. (1996). Accommodation and iridotomy in the pigment dispersion syndrome. *Ophthalmic Surgery, Lasers and Imaging* 27: 113–120.

Reistad, E., Shields, M. B., Campbell, D. G., et al. (2005). The influence of peripheral iridotomy on the intraocular pressure course in patients with pigmentary glaucoma. *Journal of Glaucoma* 14: 255–259.

Ritch, R. (1996). A unification hypothesis of pigment dispersion syndrome. *Transactions of the American Ophthalmological Society* 94: 381–409.

Ritch, R. (2004). Pigment dispersion syndrome – update 2003. In: Grehn, F. and Stamper, R. (eds.) *Glaucoma*, pp. 177–192. Berlin: Springer.

Ritch, R., Liebmann, J. M., Robin, A. L., et al. (1993). Argon laser trabeculoplasty in pigmentary glaucoma. *Ophthalmology* 100: 909–913.

Scheie, H. G. and Cameron, J. D. (1981). Pigment dispersion syndrome: A clinical study. *British Journal Ophthalmology* 65: 264–269.

Scuderi, G. L., Ricci, F., Nucci, C., Galasso, M. J., and Cerulli, L. (1998). Electro-oculography in pigment dispersion syndrome. *Ophthalmic Research* 30: 23–29.

Siddiqui, Y., Ten Hulzen, R. D., Cameron, J. D., Hodge, D. O., and Johnson, D. H. (2003). What is the risk of developing pigmentary glaucoma from pigment dispersion syndrome? *American Journal of Ophthalmology* 135: 794–799.

Polarized-Light Vision in Land and Aquatic Animals

T W Cronin, University of Maryland Baltimore County, Baltimore, MD, USA

Glossary

Chromophore – As used here, a small molecule that when bound to a protein causes the complex to absorb light at visible or near-visible wavelengths. The chromophore for visual pigments, in which the protein component is opsin, is either 11-*cis* retinal or a very similar molecule.

Circular polarization – As used here, a type of polarization of light in which the electric vector, or *e*-vector, rotates one full circle for each wavelength traveled by the light, thus describing a circle as seen from the wave front or a helix as seen from the side. Circular polarization can be either right-handed or left-handed, depending on the direction of rotation.

Dichroism – The property of a substance to absorb polarized light of one *e*-vector orientation more strongly than of other orientations, thus transmitting linearly polarized light.

Dielectric – Refers to chemical compounds or substances that do not conduct electricity. Water and most biological molecules are dielectric.

***e*-Vector** – The electrical vector of an electromagnetic wave. For polarized light, the *e*-vector orientation is usually taken to be the plane of polarization.

Linear polarization – Sometimes called plane polarization. Refers to light in which the *e*-vectors of the constituent photons are all oriented on the same axis, or in the same plane.

Microvillus – A membranous protrusion from a cell surface shaped like a tiny tube, typically only a few cell membrane thicknesses in radius.

Polarized light – The light in which the *e*-vector lies in a plane (for linearly polarized light) or rotates through a full circle once for each wavelength (circularly polarized light).

Rayleigh scattering – A type of scattering of electromagnetic energy caused by interactions of the energy with particles much smaller than the wavelength of the energy. Rayleigh scattering produces the blue color of the sky and also produces a celestial polarization pattern by scattering of sunlight.

Specular reflection – Reflection as from a mirror, where the reflected ray leaves the surface at the same angle that the incident ray arrived. Specular reflection is typical of shiny surfaces; examples in nature include shiny leaves, insect cuticle, wet skin, or the surface of smooth water.

Light is made up of streams of photons, the elementary particles that carry electromagnetic energy. Each of these photons can be thought of as a miniature electromagnetic wave, which has a single wavelength related to the energy it carries (the distance the photon travels from one energy maximum to the next, inversely proportional to the photon's frequency) and a single plane within which the electrical energy vibrates – the polarization angle, properly called the *e*-vector (for electrical vector) angle. Note that since the energy is electromagnetic, there are both electrical vectors and magnetic vectors present, normal to each other. For consistency, throughout this article reference is made only to the *e*-vector. Therefore, a beam of light, containing countless photons, is characterized by its intensity (the number of photons delivered per unit time), its spectrum (the distribution of wavelengths of all the photons in the beam), and its polarization (the distribution of the planes of vibration, or *e*-vector angles, of all the photons in the beam).

The most common form of polarization, linear (or plane) polarization, has two descriptors: the overall *e*-vector angle, which is the mean angle of all planes of vibration of the constituent photons, and the degree of polarization, which is the fraction of energy of all photons vibrating within the plane of the *e*-vector angle. Of course, in a typical beam consisting of photons of mixed wavelengths, these polarization parameters generally vary with wavelength, creating a polarization spectrum. In this article, only linearly polarized light is discussed unless otherwise noted.

Like many vertebrates, humans are not generally aware of light's polarization properties, but the visual systems of most animals perceive light's polarization and use this ability to regulate their behavior. To help us understand what visualizing polarization would be like, the polarization properties of light can be analogized to its color properties. The spectrum of light produces the sensation of color, with a perceived hue (the predominant wavelength of constituent photons) and purity or saturation (the overall distribution of wavelengths around that of the hue itself). Hue is therefore analogous to the *e*-vector (the predominant angle of polarization of constituent photons) and saturation to the degree of polarization (the distribution of angles around this). In fact, polarization fields are often portrayed as images using false colors where angle is coded into hue and degree of polarization into saturation. Such a display can also include the coding of overall brightness as the intensity at each point, to provide a complete description of the polarized-light field.

Polarized Light in Nature

There are no natural sources of polarized light of known biological significance. Nevertheless, linearly polarized light is abundant in natural scenery. Light can become polarized in many ways, but the most important processes in nature are through differential absorption, differential reflection, or differential scattering (**Figure 1**).

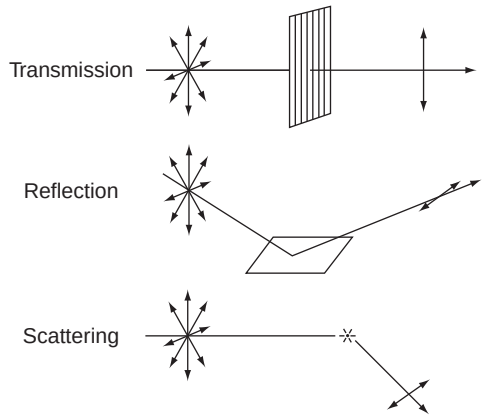

Figure 1 The three most common ways by which linearly polarized light is created either in nature or in the laboratory. At the top part of the figure, the polarization is produced by transmission through some dichroic material, with its preferential plane of transmission symbolized by the vertically parallel lines. Light emerging from a perfect dichroic material becomes fully linearly polarized. Dichroic polarizers are relatively rare in nature, and account for only a minor fraction of the polarized light observed in natural light fields. The middle part of the figure illustrates polarization by reflection from a smooth, dielectric surface. At a particular angle, known as Brewster's angle, the reflected light is fully polarized parallel to the surface. Most biological surfaces are dielectric, as is the surface of water, so much light reflected from shiny natural surfaces is highly polarized. The bottom section of the figure illustrates polarization induced by scattering. When the scattering angle is orthogonal to the axis of the ray being scattered, the scattered light is fully polarized at an *e*-vector angle perpendicular to the plane containing the original ray and the scattered ray.

Some natural or artificial transparent materials preferentially transmit one *e*-vector plane while absorbing others, usually because of aligned molecules within the material. This property, known as dichroism, is not particularly common in biological systems, but there are important exceptions, including the inherent dichroism of visual pigment molecules described later. Reflection of light from dielectric surfaces produces polarization parallel to the surface (**Figure 1**). Therefore, bodies of water and many surfaces in natural scenery reflect horizontally polarized light. Rayleigh scattering from molecules and suspended particles in air produces a well-known pattern of polarization in the sky. Scattering-induced polarization varies with the scattering angle, being greatest (often near 100% polarization) for scattering perpendicular to the axis of the incoming ray (**Figure 1**). As a result, skylight polarization reaches its maximum in a band that stretches across the sky at 90° to the sun. The axis of the *e*-vector of the scattered ray is perpendicular to the plane defined by the incoming ray and the scattered ray, such that the band of maximum sky polarization has its *e*-vectors oriented tangentially to the great circle 90° from the sun's position. At dawn or dusk, this band stretches vertically across the celestial hemisphere (**Figure 2**). Since Rayleigh scattering is most effective at short wavelengths, skylight polarization is strongest in the ultraviolet. Scattering from water molecules and very small particles suspended in natural waters also produces polarization (**Figure 3**), although it rarely reaches the very high degrees of polarization seen in the sky. Light scattering in water is optically different from the processes

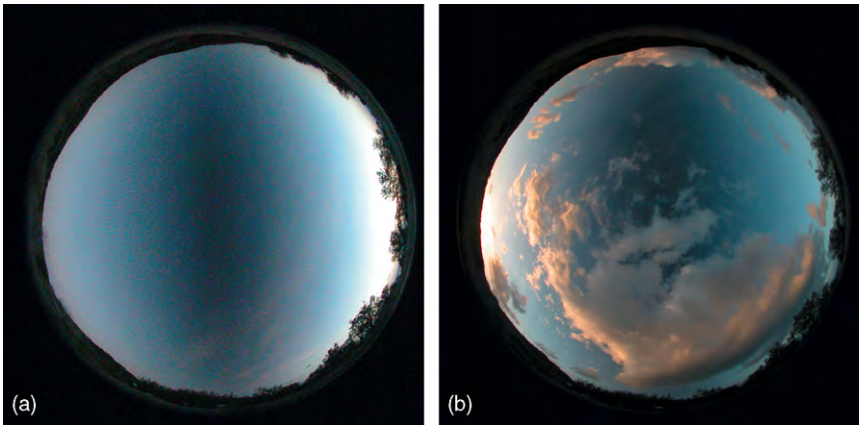

Figure 2 Polarization in the sky at twilight produced by Rayleigh scattering, imaged through a fisheye lens fitted with a linear polarizer with the transmission axis oriented to the right and left. Thus, vertically polarized light is not transmitted to the camera and shows as a dark band in the sky. In these photographs, taken at the same location and not enhanced or retouched in any way, North is to the top and West to the right. (a) Polarization in a clear sky at dusk. Note the clearly visible band of strong polarization passing from North to South through the zenith. (b) Polarization in a partly cloudy sky at dawn. The polarization is still clearly visible, but the presence of clouds depolarizes the skylight.

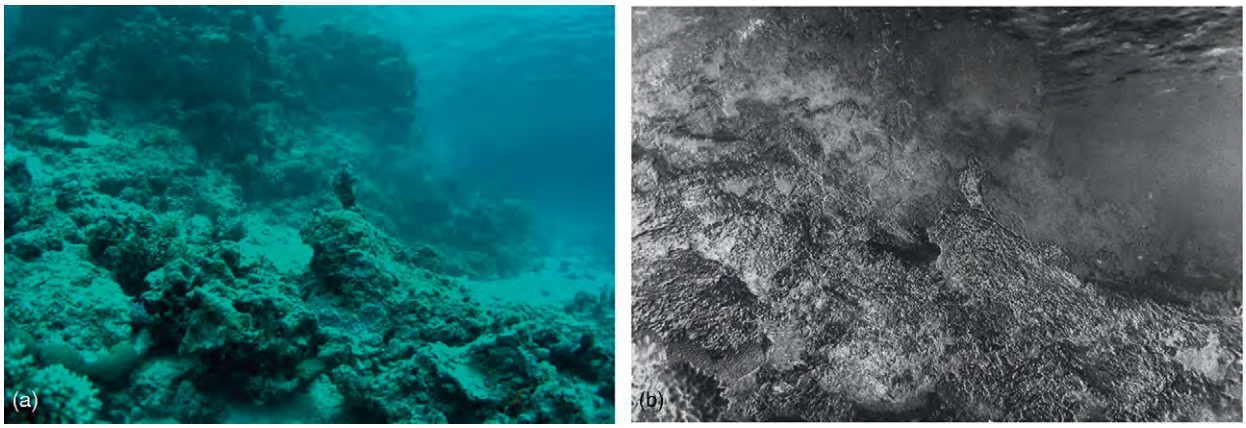

Figure 3 Polarization of light underwater produced by scattering from water molecules and suspended particles. (a) An unaltered image of an underwater scene at a depth of about 7 m, showing coral reef and rubble. (b) The same scene shown as a polarization image, with the degree of polarization encoded by brightness. The maximum degree of polarization in this scene is about 50%. Note that the parts of the scene that are fairly near the camera and that appear darkest in the normal photograph are most polarized. This occurs because the water between these dark regions and the camera scatters mostly horizontally polarized light.

operating in air, and polarization in water typically reaches its maximum value at blue-green wavelengths.

Thus, in the sky and underwater, scattering of incoming light produces partial polarization that varies with solar position and direction of view, and reflection of light from the air–water interface or from shiny surfaces (e.g., leaves, wet surfaces, animal skin, scales, or cuticle) produces strong polarization in geometrically favorable circumstances. If a terrestrial animal has polarized-light vision, the sky presents a reliable pattern useful for navigation, but in contrast, the chaotic and unpredictable pattern of polarized-light reflection produces false, pointillistic images that can mask or taint the true colors and locations of objects. Consequently, as described later, photoreceptors in animals that would normally be sensitive to the polarization of light are sometimes structurally modified to destroy polarization sensitivity.

The situation is almost always simpler in water than in air, particularly at depths greater than a few meters. Due to refraction at the air/water interface, illumination from the sun or moon is confined to within 46° of overhead position. The resulting polarization field, while variable to some extent, has horizontally oriented *e*-vectors much of the time, and the degree of polarization is almost always lower than in air. The pointillistic reflection of polarized light from objects is virtually gone underwater, as the refractive index gradient between water and most natural objects is much lower than in air, such that there is little specular reflection of light (required to produce polarization from dielectric surfaces). The predictable surround, typically low degree of polarization, and minimal polarized-light reflective noise would seem to make polarization vision in water of little utility, yet many aquatic animals have excellent polarization sensitivity. Currently, it is not always clear what biological advantages are provided by such visual abilities.

Polarization Sensitivity and Polarization Vision

Polarization Responses of Photoreceptor Cells

Light is absorbed in visual photoreceptors of all animals by molecules of visual pigment, which consist of a chromophore (derived from vitamin A or a close chemical analog) linked to a protein, termed opsin. Just as each visual pigment molecule has its characteristic absorption spectrum, which ultimately determines the spectral sensitivity of the photoreceptor within which it resides, it also has an inherent polarization sensitivity. This exists because the chromophore itself is dichroic, absorbing preferentially when the *e*-vector of an incident photon is parallel to the long axis of the molecule. Since the chromophores of visual pigment lie nearly parallel to the membranes of photoreceptors, when light arrives perpendicular to these membranes the incident photons are likely to be polarized parallel to the absorption axes of some of the visual pigment chromophores. The way in which these chromophores are aligned within the photoreceptor cell as a whole determine whether or not the receptor responds differentially to polarized light, and thus whether it has inherent polarization sensitivity (**Figure 4**).

In the rod and cone photoreceptors of vertebrate retinas, photoreceptive membranes are arranged in a series of parallel layers, either in flattened disks (rods) or lamellae formed from folded membrane sheets (cones). Since light generally strikes these layers normal to their surfaces, it encounters visual pigments that are arrayed at

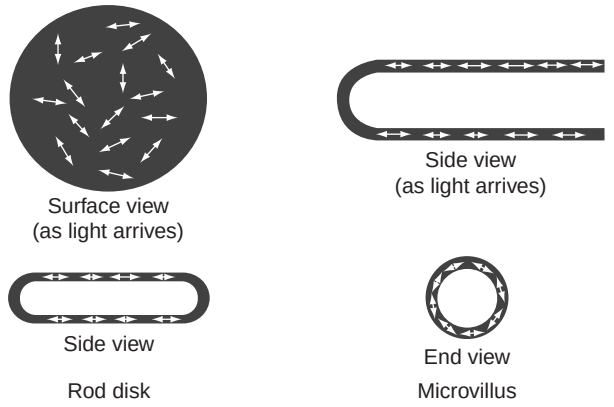

Figure 4 An illustration to show absorption of polarized light by vertebrate rod photoreceptors (left; cone photoreceptors would have similar properties) and by microvillar photoreceptors like those of arthropods or cephalopod mollusks (right). In life, light arrives normal to the flat surfaces of rod disks and encounters randomly oriented chromophores of visual pigment lying within the disk membrane (symbolized by double-headed arrows to indicate the preferred axis of polarization for best absorption). Since the orientation is fully random, there is no preferential absorption of any given *e*-vector angle. If light were to arrive from the side of the disk, it would encounter chromophores that are restrained to angles near that of the membranes themselves, favoring the absorption of horizontally polarized light. In microvillar photoreceptors (right), light arrives orthogonal to the long axis of each microvillus, and encounters visual pigment chromophores that are oriented roughly parallel to the axis of the microvillus. Thus, the microvillus as a whole preferentially absorbs light polarized parallel to its axis. If light were to impinge on the microvillus from the end, it would encounter chromophores arrayed at all possible angles around the circumference of the microvillus, and no preferred absorption orientation would exist.

all possible orientations (Figure 4, top-left). Consequently, rods and cones rarely have an overall polarization response, even though the individual molecules of visual pigment are dichroic. The situation would be very different if light impinged on rods or cones from the side (i.e., normal to the long axes of their outer segments). It would then meet chromophores lying in the planes of the membrane layers, and all chromophores would preferentially absorb light polarized nearly parallel to the membrane. Note that while the individual chromophores have random arrangements in the membrane's plane, and thus absorb light from this direction with varying effectiveness (suggested by the variable lengths of the double-headed arrows), they always absorb light polarized in the membrane's plane most effectively.

The photosensitive membranes of photoreceptor cells of arthropods (crustaceans, insects, etc.) and cephalopods (octopus, squid, and cuttlefish) are constructed from bundles of microvilli. In each microvillus, for reasons that are not yet fully understood, the molecules of visual pigments are arranged such that their chromophores are roughly parallel to the axis of the microvillus. The microvilli typically extend out perpendicular to the axis of the receptor cell as a whole, such that light arrives perpendicular to each microvillus. In this orientation, each microvillus preferentially absorbs light polarized parallel to its axis, such that if microvilli are arranged parallel throughout the receptor as a whole, the cell will be polarization-sensitive. Note that this property requires no other cellular specializations, and as a result, almost all microvillar photoreceptor cells have some level of polarization sensitivity.

Polarization sensitivity

Having receptor cells that respond differentially to polarized light is only the first requirement for polarization sensitivity at higher levels of neural analysis. For the nervous system to be able to analyze light's polarization, sets of photoreceptors with different preferred polarization orientations must be compared, typically through opponent processing. This type of analysis is like that of color vision, where sets of photoreceptors with differential spectral sensitivity are compared for color processing. Recall that polarization of light has three attributes: intensity, degree of polarization, and polarization angle. Thus, for full awareness of light's polarization at a given point in the visual field, independent inputs from three receptor sets must be analyzed. Interestingly, few animals do this; in almost all cases, only two receptor sets with orthogonal microvilli are compared. This is reasonably effective in practice, because natural polarization tends to be predictable, such that if the receptor sets are appropriately oriented, the polarization is well analyzed. Two-channel polarization analysis can be extended to full polarization sensitivity if the receptors are rotated relative to the stimulus, although this has rarely been observed in practice.

The animal groups for which the mechanisms of polarization sensitivity are best understood are the insects, the crustaceans, and the cephalopod mollusks (octopus and squid). All of these have microvillar photoreceptors, and in most species the receptors are arranged orthogonally. Crustaceans and insects have compound eyes that are particularly well designed for analyzing polarized light. Each unit of the eye contains a group of photoreceptor cells, such that each unit of the compound eye can potentially serve as an independent polarization detector. For two-axis polarization sensitivity, subsets of receptors in each group have orthogonal microvilli. In insects, these subsets often extend into a central, fused photoreceptor from four sides, with microvilli entering from opposite sides abutting near the center. Viewed from the tip of the receptor group, the overall arrangement ends up having two cell sets with horizontal microvilli and two with vertical microvilli (Figure 5). Crustaceans have a similar system, but here the orthogonal sets of microvilli exist in successive layers, making the entire composite

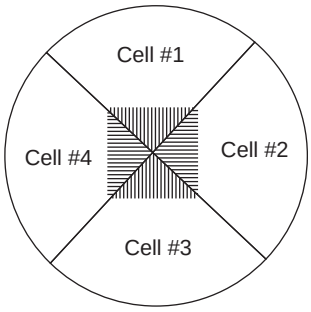

Figure 5 A schematic diagram of the structure of typical polarization-sensitive photoreceptors such as would be found in the compound eyes of insects. The receptor is viewed in a section as seen on the axis of the photoreceptor group. In life, these receptors would form a bundle of cells arranged in a circle and together forming a tall cylinder with the microvilli arranged in a smaller cylinder running down its middle. Each cell forms a section of the overall receptor (a single cell in this diagram can represent either one receptor cell or two cells lying side-by-side with parallel microvilli). Note that cells on opposite sides of the receptor extend parallel microvilli toward the junction in the center, and thus have parallel polarization sensitivity. Since two sets of receptors exist, with either horizontally oriented or vertically oriented microvilli, the receptor group as a whole can provide information for two-axis polarization analysis. Receptors of crustaceans are similar to this, but each layer of the joint photoreceptor contains microvilli from only one subset of cells, with either horizontally arrayed or vertically arrayed orientations. Successive layers of the receptor contain microvilli from the other subset of cells, and thus the receptor cylinder has stacks of mutually orthogonal microvillar layers which can contribute to two-axis polarization analysis. Photoreceptors of cephalopods are somewhat different from these, since they are arrayed continuously side-by-side throughout a retina, but each junction of four cells forms a set of microvilli organized like those in the center of the diagrammatic insect photoreceptor illustrated here. Cephalopod receptor cells also form parallel microvilli on the opposite side of each cell. Consequently, each cell contributes to two junctions of microvilli, one on each side of the cell. Again, with two primary axes of orientation of microvilli, separate cells can contribute to two-axis polarization sensitivity.

photoreceptor like a pile of a large number of circular segments, each having microvilli orthogonal to the segments immediately above and below. Finally, the cephalopods (which do not have compound eyes, but instead have a single lens eye structured much like a vertebrate camera eye) arrange their microvillar receptors such that each cell has microvilli on two opposing sides (like a two-sided toothbrush). The mosaic of cells forms junctions similar to what is pictured in the center of Figure 5, except that each of the four cells in this figure would form another junction on the opposite side with yet other cells. In all these cases, the cells with parallel microvilli viewing one point in space join to form one polarization channel, and those with microvilli orthogonal to these join for the opponent channel.

Vertebrate polarization sensitivity is more difficult to explain, and it is fair to say that we are still not able to account for it satisfactorily. Nevertheless, there is no doubt at all that some vertebrates sense light's polarization. Recall that end-on stimulation of rods and cones is unlikely to produce any differential sensitivity to the plane of polarization, because chromophores are randomly oriented for such light (Figure 4). If vertebrate photoreceptor cell outer segments were slanted relative to the axes of impinging rays of light, this would confer some polarization sensitivity. It appears that in at least some fishes, the outer segments of some classes of cones lie on their sides, tilting their lamellae vertically in the retina. If all cones of a given class lay parallel, or were organized into orthogonal classes, this could permit the retina as a whole to achieve an overall polarization sense. There is recent evidence that some rod or cone classes are measurably dichroic to end-on illumination. The origin of this dichroism is unclear, but it could be caused by parallel tilting of the rod disks or cone lamellae.

Polarization vision

If an animal has polarization sensitivity, it can obviously respond in some way to a polarization stimulus. As described later, these responses are frequently hard-wired and inflexible, and the polarization sense that drives them does not correspond to what is normally conceived of as vision, which implies a perception of space, form, and individual objects. The term polarization vision refers to a polarization sense analogous to color vision, whereby animals visualize polarization attributes of features within the overall field of view and use polarization variations to enhance the visibility, contrast, or features of particular objects. In principle, an animal that is capable of polarization vision perceives the visual world as a pattern varying in polarization features among receptive fields. While polarization sensitivity is most useful for orientation or for organizing simple responses, polarization vision offers the potential to direct complex behavior such as predation, camouflage generation or breaking, and signal detection. There is only weak evidence of this ability in some vertebrates, but many species of both arthropods and cephalopods probably use true polarization vision in ways that are discussed later.

Disentangling polarization and color sensitivity

Many – perhaps most – animals that are sensitive to polarized light also have color vision. This presents both perceptual and sensory-processing challenges, as it is generally not desirable to mix these visual modalities. For example, if a receptor cell that contributes to a perceptual color channel has some residual polarization sensitivity, color appearance will be altered by stimuli that contain polarized light. This is most often a problem for

animals with microvillar photoreceptors due to their inherent polarization bias. The cephalopods have firmly dealt with this issue by discarding color vision entirely – the great majority of octopuses, squids, and cuttlefishes have only a single spectral receptor class in their retinas, restricting vision entirely to the intensity and polarizational domains. Many crustaceans have reached a similar solution, devoting nearly all of their receptors to polarized-light reception. Some crustacean species, however, separate color and polarization processing, using a single spectral class for polarization analysis while reserving a set of other polarization-insensitive classes for color vision. This solution is used, for example, by stomatopod crustaceans, also known as mantis shrimps. Insects also commonly separate color-sensitive from polarization-sensitive receptors, isolating their polarization receptors to just one part of the visual field and often using only ultraviolet receptors for polarization analysis. Some insect species destroy polarization sensitivity in photoreceptors by twisting the entire receptor group around its long axis. In a few cases, surprisingly, insects unify polarization and color perception in the same receptor cells, interpreting some stimuli by combining these two modalities into a single signal. Some butterfly species, for instance, examine potential ovoposition sites in this way. In vertebrates, however, as with other aspects of polarized-light photoreception, it is unknown how (or even if) polarized-light processing is kept separate from color processing. This could be a difficult problem, as it is thought that some vertebrates use different spectral types of cones to sense different polarization planes, a technique that immediately must mix color and polarization information at the first level of light detection.

The Contributions of Polarized-Light Perception to Behavior

Sensing polarized light seems strange to us, but for most animals it is as fundamental to their visual perception as color vision is to humans. Indeed, as will be described shortly, in many animals polarized-light perception plays similar roles to those assumed by color vision, and it can even work together with color vision to improve visual interpretation of stimuli. However, there are many situations where polarized light is used for special purposes unique to this modality. Among these are water surface detection and skylight navigation.

Water surfaces reflect horizontally polarized light, as illustrated in **Figure 1**. This is why sunglasses with polarizing lenses make it easier for fisherman to see fish – the lenses are oriented to block horizontally polarized light, reducing the glare from the water's surface and clarifying the visibility of objects in the water itself. Many flying insects, including adult water beetles and mayflies, use the reflected polarization in the opposite way – their eyes are adapted to respond strongly to large expanses of horizontal polarization below the horizon, which in nature invariably correspond to water surfaces. The insects respond by diving into the water, or by alighting on its surface to ovoposit. This simple response is extremely reliable in nature, but can lead to disastrous consequences for the insects today, when many shiny, horizontal surfaces are man-made. Parking lots, oil ponds, and even the painted surfaces of cars and other manufactured objects induce the same response, which in these cases is frequently lethal.

Scattering of sunlight in the clear sky produces a highly reliable pattern of polarization (**Figure 2**), recognized by the visual systems of many insects (including bees, ants, and crickets) as well as by other arthropods including some spiders and crustaceans. The pattern is used for navigation, as it is a perfect indicator of the current position of the sun, persisting even when the sun is not visible behind an obscuring object or landscape feature, or when the sun is hidden by clouds. Thus, navigation is possible even on quite cloudy (but not wholly overcast) days. Most insects that navigate using skylight polarization devote a small region of the compound eye, called the dorsal rim, to perceiving the pattern, and most require only a small patch of clear sky to orient. Navigation using the location of the sun or skylight polarization patterns is not simple, as the solar position drifts through the sky with changing dynamics throughout the seasons, and insects must be able to compensate for these changes each day as they manage their foraging excursions. Some insects, including dung-foraging scarab beetles, use skylight polarization created by moonlight to navigate during their nocturnal rambles. In an interesting vertebrate example, migrating birds are thought to use skylight patterns of polarization at twilight to calibrate their magnetic compasses.

The tasks described so far are analogous to map senses, simple reflexes, or other perceptual abilities that are not strictly visual in the sense that we humans understand it. In other words, these types of abilities do not examine features or objects in the outside world except in very general ways. However, there are animals that actually see patterns of polarization in a fashion that is quite analogous to the way that we perceive the external world – they use polarization vision to recognize objects, to enhance contrast of prey, or to see signals of conspecific animals. Some animals, in fact, can be trained to discriminate objects that we see as identical but that differ in the patterns of polarization that they reflect or transmit. Octopus and mantis shrimps learn such tasks.

Near the water's surface, the skylight polarization pattern penetrates and is therefore available as an orientation cue. Deeper than this, underwater polarization is only rarely usable for navigation (although it can be used to orient vertical migration) because it is frequently weak,

often oriented near the horizontal plane, and quite variable depending on the background (Figure 3). Nevertheless, the background polarization can be used to enhance the contrast of the visual world and make midwater objects more visible. Squids take advantage of this, making them more effective predators on fishes and transparent planktonic prey against a polarized background than against a depolarized one. Presumably, they use their polarized-light sense to detect differences in polarization between the prey and the background, making objects of similar overall brightness appear distinguishable.

If squids and cuttlefishes can distinguish objects based on polarization, it should not be surprising that they also have body patterns that reflect polarized light, undetectable by many marine animals, and apparently employ these patterns to communicate with each other. The polarization patterns are actively controlled by the animal producing them and can appear and disappear in fractions of seconds. When displayed, the polarization reflections remain highly visible to a conspecific individual even as the signaler changes its posture or moves its arms about.

Two other groups of animals, one marine and one terrestrial, are currently known to recognize and respond to polarization signals. Mantis shrimps produce an abundance of signals based on patterns of polarized light reflected from their carapace (Figure 6), and use these signals during mating and aggressive displays. Like the cephalopods, of course, they are marine invertebrates and conduct their diplays underwater. One group of insects, however, uses polarized-light signals in the open air. Many species of tropical butterflies find mates in the diffuse light under the rainforest canopy. Here, the background polarization is relatively weak, and the strong polarization pattern of the sky is rarely visible. Thus, the polarization produced by reflection from scales on butterfly wings can act as an unusually strong, visible signal.

Sensitivity to Circularly Polarized Light

This discussion of polarized-light sensitivity would not be complete without mention of a recently discovered visual modality, sensitivity to circularly polarized light. Circular polarization differs from linear polarization, the type discussed exclusively until now, in that the *e*-vector does not remain within a single plane, but instead rotates around the axis of the beam of light. Circularly polarized light is not common in nature, and its presence cannot be detected with standard polarization-sensing systems. Despite this, one group of animals, the mantis shrimps, perceives circularly polarized light and produces circularly polarized signals by reflection. This ability is particularly unexpected because there is no known source of circular polarization underwater other than signals from other mantis shrimps, so it is difficult to explain how and why the ability originally arose. It is possible that circular polarization sensitivity in these animals first appeared as an accidental epiphenomenon related to the unusual way in which their linear polarization system is assembled, and that this led to the elaboration of signals based on circularly polarized light. See the suggested reading for a more detailed account of this unusual finding.

Summary

The ability to perceive and respond to linearly polarized light is widespread among animals, occurring in many vertebrates and invertebrates. Some of these species use polarization for general tasks that do not require precise imaging, such as finding water or navigating using patterns of scattered polarized light in the sky. Others truly see polarized objects and use this imaging ability to detect prey and recognize signals from conspecifics. Our poor understanding of the biology of polarized-light sensitivity

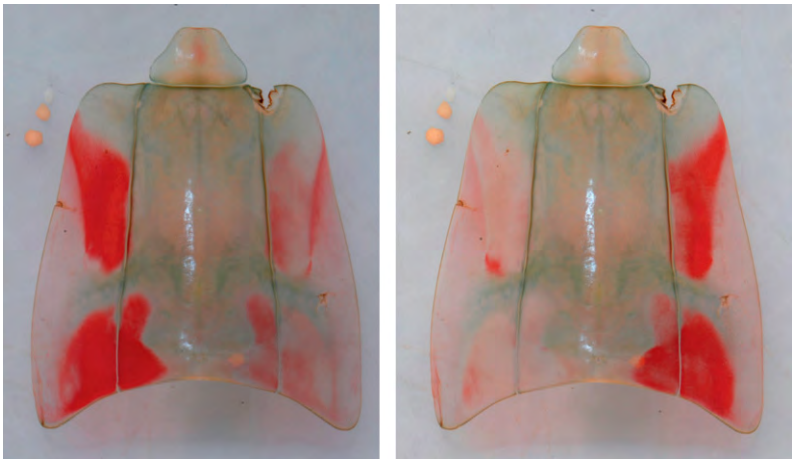

Figure 6 Polarization signals reflected from the shed carapace (or molt) of the stomatopod crustacean, or mantis shrimp, *Odontodactylus cultrifer*. These patterns of polarization are visualized through a linearly polarizing filter rotated to two orientations at 90° to each other. Signals like these are used during aggressive or mating displays of mantis shrimps. Photograph by T. H. Chiou.

in vertebrates, and the recent discovery of circular polarization sensitivity in mantis shrimps, suggest that there are other aspects to polarized-light sensitivity and to polarization vision that still remain to be revealed.

See also: Microvillar and Ciliary Photoreceptors in Molluskan Eyes; Photoresponse in Squid; Phototransduction: Rhodopsin; Rod and Cone Photoreceptor Cells: Inner and Outer Segments; The Colorful Visual World of Butterflies; The Evolution of Opsins.

Further Reading

Chiou, T. -H., Kleinlogel, S., Cronin, T. W., et al. (2008). Circular polarisation vision in a stomatopod crustacean. *Current Biology* 18: 429–434.

Cronin, T. W., Shashar, N., Caldwell, R. L., et al. (2003). Polarization vision and its role in biological signaling. *Integrative and Comparative Biology* 43: 549–558.

Dacke, M., Doan, T. A., and O'Carroll, D. C. (2001). Polarized light detection in spiders. *Journal of Experimental Biology* 204: 2481–2490.

Hawryshyn, C. W. (1992). Polarization vision in fish. *American Scientist* 80: 164–175.

Horváth, G. and Varjú, D. (2004). *Polarized Light in Animal Vision: Polarization Patterns in Nature*. Berlin: Springer.

Muheim, R., Phillips, J. B., and Akesson, S. (2006). Polarized light cues underlie compass calibration in migratory songbirds. *Science* 313: 837–839.

Shashar, N., Rutledge, P., and Cronin, T. W. (1996). Polarization vision in cuttlefish: A concealed communication channel? *Journal of Experimental Biology* 199: 2077–2084.

Sweeney, A., Jiggins, C., and Johnsen, S. (2003). Polarized light as a butterfly mating signal. *Nature* 423: 31–32.

Waterman, T. H. (1981). Polarization sensitivity. In: Autrum, H. (ed.) *Handbook of Sensory Physiology* VII/6B, pp. 281–469. Berlin: Springer.

Wehner, R. (2001). Polarization vision – a uniform sensory capacity? *Journal of Experimental Biology* 204: 2589–2596.

Post-Golgi Trafficking and Ciliary Targeting of Rhodopsin

D Deretic, University of New Mexico, Albuquerque, NM, USA

Glossary

Cell polarity – The asymmetry in cell shape, protein distributions, and cell functions.

Golgi complex – A biosynthetic organelle comprised of a stack of membranous cisternae that are involved in protein modifications, such as processing of N-linked sugars as well as sorting and transport of membrane proteins. Newly synthesized membrane and secretory proteins enter the stack through the *cis*-Golgi, progress through the medial cisternae and exit at the *trans*-Golgi.

Phosphatidylinositol-4,5-bisphosphate ($PI(4,5)P_2$) – An essential second messenger as well as lipid regulator of membrane trafficking. Along with its precursor phosphatidylinositol-4-phosphate (PI(4)P), it regulates Arfs and is regulated by them, providing a positive-feedback loop that regulates membrane trafficking.

Post-Golgi transport carriers (TCs) – The post-Golgi vesicles that carry cargo to the plasma membrane. It is now clear that these carriers are large pleiomorphic structures, rather than small vesicles, as previously believed, thus the term vesicles has been replaced with transport carriers.

Small GTPases – The members of the low-molecular-weight (20–25 kDa) Ras super family of guanosine-triphosphate (GTP)-binding proteins comprised of at least four large families, including the Arfs and the Rabs. Small GTPases function by providing directionality to membrane traffic through the molecular switch whose ON and OFF states are triggered by binding and hydrolysis of GTP. The nucleotide-bound state determines the affinity of interactions with regulatory proteins and the downstream effectors of small GTPases.

SNARE proteins – The soluble N-ethylmaleimide-sensitive factor attachment protein receptor (SNARE) proteins are major components of the intracellular machinery responsible for targeted membrane delivery. SNAREs were identified as membrane receptors for the soluble N-ethylmaleimide-sensitive factor (NSF) attachment protein (SNAP) in the cell-free system that reconstituted intra-Golgi trafficking. SNARE proteins form complexes, which are generally composed of a four helical bundle that bridges opposing membranes and brings them into close proximity to initiate fusion.

The *trans*-Golgi network (TGN) – A tubular network in the close proximity to the *trans*-Golgi cisternae that represents the central sorting station of the cell, where proteins and lipids destined for different subcellular domains are segregated from each other and sorted into post-Golgi TCs.

Introduction

Retinal rod photoreceptors are exquisitely complex polarized cells that carry photon detection and visual transduction that are essential as the first step in vision. Following the final cell division of their precursors, photoreceptors attain a level of polarity that is nearly unmatched in other cells of the body. Maintaining this organization throughout the lifetime of the organism is a prerequisite for vision. Proper targeting and retention of the macromolecular complexes involved in the visual transduction cascade are accomplished by the highly coordinated action of protein and lipid regulators that together constitute the membrane trafficking machinery. Specific components of this machinery involved in the directed delivery of rhodopsin and its associated proteins and lipids are only beginning to emerge.

Photoreceptor Polarity

Rod photoreceptors are modified neurons with specialized light-sensing organelle, the rod outer segment (ROS). The ROS is filled with membranous disks housing the phototransduction machinery that converts photon absorption by rhodopsin into changes in neurotransmitter release, thus transmitting photosensory information to the visual cortex. The light-sensing machinery is comprised of peripheral and integral membrane proteins of the ROS. It is continuously replenished through ROS disk membrane renewal, followed by its removal through daily shedding and phagocytosis by retinal pigment epithelial (RPE) cells.

The ROS disk membrane proteins are embedded in a low-viscosity lipid bilayer milieu comprised of unsaturated long-chain phospholipids highly enriched in omega-3 docosahexaenoic acid (DHA, 22:6(n-3)), which is essential for sensory membrane function and for cell

survival. The exceptionally high content of polyunsaturated DHA phospholipids renders ROS membranes highly susceptible to light and oxidative damage.

ROSs initially form from primary cilia, and a short 9+0 (nonmotile) connecting cilium remains in the adult as the only path of communication between the ROS and the photoreceptor rod inner segment (RIS). The RIS houses mitochondria and biosynthetic membranes involved in oxidative metabolism and membrane protein and lipid biosynthesis, respectively. The photoreceptor-connecting cilium corresponds to the transition zone of primary cilia, which is considered a gateway for the admission of specific proteins to this privileged intracellular compartment.

The primary cilium is the site of assembly of large molecular complexes involved in intraflagellar transport (IFT). IFT protein 20 (IFT20) subunit links mammalian IFT complex with the microtubule motor, kinesin II. The base of the cilium is a region of particularly high lipid ordering, separating the ciliary membrane from the surrounding plasma membrane due to high cholesterol content and glycosphingolipid products of the phosphatidylinositol 4-phosphate (PI(4)P)- and Arf-dependent effector four-phosphate-adaptor protein 2 (FAPP2). Cholesterol rings have also been reported to surround the photoreceptor connecting cilium. Lipid ordering might be important for the docking of the basal body to the plasma membrane or the extension of the ciliary axoneme, both essential processes in ciliogenesis.

The RIS is separated from the nuclear and synaptic domains by adherens junctions (AJs) that comprise a continuous adhesion belt, the outer limiting membrane (OLM). Interestingly, this junctional region lacks tight junctions that normally confine plasma membrane proteins to their respective domains. Nonetheless, rod membrane proteins are strictly confined to their specialized domains and the maintenance of polarity is essential for the cell's function and survival. The photoreceptor synaptic terminal contains specialized ribbon synapses that are responsible for the tonic release of neurotransmitters, which is interrupted by photon capture.

Photoreceptor cytoskeletal networks and molecular motors play a major role in the cell polarity. Microfilaments provide structural support by encircling the RIS beneath the plasma membrane and are anchored at the AJs. Other polar dynamic actin networks and filaments are also dispersed through the cell, most notably in the distal portion of the cilium, at the sites of ROS disk formation where they regulate the growth of nascent disks. Actin-based motility through the cilium is thought to be mediated by myosin VIIa, the product of the Usher syndrome (USH) 1B (Usher1B) gene. An array of microtubules radiates into the RIS from the microtubule-organizing center nucleated by a pair of centrioles located below the cilium. Microtubules generate polar networks that generally determine the position of membrane organelles and allow intracellular motility. Heterotrimeric molecular plus end-directed motor kinesin-II and homodimeric KIF17 mediate microtubule-dependent trafficking into the ROS. The absence of KIF3A subunit of kinesin-II causes membrane accumulation in the RIS and cell death. Cytoplasmic dyneins 1 and 2 mediate retrograde trafficking to the centrosome from the RIS and the ROS, respectively.

Photoreceptor Biosynthetic Membrane Trafficking: Endoplasmic Reticulum, Golgi, and Post-Golgi Transport Carriers

ROS integral membrane proteins are synthesized on the rough endoplasmic reticulum (ER), pass through the Golgi apparatus, and are then incorporated into post-Golgi vesicles or, in current terminology, rhodopsin transport carriers (RTCs) that bud from the *trans*-Golgi network (TGN), the central membrane sorting station of the cell, and are transported to a docking site near the base of the cilium. Along with rhodopsin, DHA phospholipids are co-transported on RTCs, which fuse with the specialized domain separating the ciliary membrane from the surrounding RIS plasma membrane, thereby regulating the replenishment of light-sensitive ROS membranes. Rhodopsin represents 90% of the newly synthesized protein in rod photoreceptors, and its biosynthetic pathway is best understood. In the 1980s, the laboratories of David S. Papermaster and Joseph C. Besharse combined electron microscope (EM) immunocytochemistry, autoradiography, and freeze-fracture analysis and demonstrated that newly synthesized rhodopsin is transported vectorially to the base of the cilium on membranous carriers. Membrane biosynthesis was also studied by pulse–chase experiments that established the kinetics of movement of newly synthesized rhodopsin through membrane compartments separated by subcellular fractionation. This methodology was subsequently refined by Deretic and Papermaster to incorporate high-resolution linear sucrose gradients, which separated the low-density post-Golgi carriers from other subcellular organelles, including the Golgi, TGN, plasma membrane, and synaptic vesicles.

Successful isolation of post-Golgi RTCs provided not only insight into their molecular composition, but was also the basis for the development of the retinal cell-free assay that reconstitutes RTC budding *in vitro*. The development of this assay in our laboratory led to the discovery that rhodopsin contains a sorting signal within its five C-terminal amino acids that regulates its incorporation into RTCs as they bud from the TGN. Abundant evidence points to the role of the amino acid sequence valine-x-proline-x (VxPx motif) in rhodopsin's C-terminal domain as a sorting signal into RTCs and delivery to the cilium and the ROS. In our retinal cell-free system a monoclonal antibody, whose antigenic site is within the five C-terminal

amino acids of rhodopsin, and synthetic peptides corresponding to the C-terminus of rhodopsin inhibit RTC budding from the TGN. Studies in a number of laboratories employing transgenic animals expressing rhodopsin lacking the sorting signal, or rhodopsin–C-terminal fusion proteins carrying autosomal dominant retinitis pigmentosa (adRP) mutations, confirmed that the absence of the correct sorting information results in the targeting to the RIS plasma membrane and the synapse *in vivo*.

Because of the exceptionally high membrane turnover, photoreceptors are vulnerable to mutations that affect membrane trafficking. Among the rhodopsin mutations with the most severe phenotypes are those that alter the rhodopsin C-terminal VxPx targeting motif. Rhodopsin C-terminal mutations cause rapid photoreceptor cell death, retinal degeneration, and blindness in adRP. Within the VxPx targeting motif, V345 and P347 are the primary sites of C-terminal adRP mutations involving single amino acid substitutions.

To dissect the sorting machinery that regulates RTC budding, targeting, and fusion, it was essential to identify the resident proteins of this organelle. These studies indicated a succession of binding on RTCs of members of the small guanosine triphosphate (GTP)-binding protein families (G proteins or small GTPases) that are the known regulators of membrane trafficking.

Small GTPases of the Rab and Arf Families and Their Regulators in Rhodopsin Trafficking

Rabs

Directed delivery of membrane cargo is mediated through vesicular transport regulated by the small GTPases of the Rab and Arf families, which play a central role in organizing intracellular membrane trafficking. All GTPases function by providing a universal molecular switch whose ON and OFF states are triggered by binding and hydrolysis of GTP. Small GTPases are in a dynamic equilibrium between the cytosol and the membranes maintained by the interactions with a number of regulatory proteins, including nucleotide exchange factors (GEFs), GTPase-activating proteins (GAPs), and their downstream effectors, and the affinity of these interactions is determined by the nucleotide-bound state. The Rab family of small GTPases includes over 60 members that are generally designated numerically (i.e., Rab6, Rab8, and Rab11). Upon GTP binding, activated Rabs recruit a multitude of effectors that organize membrane domains involved in the tethering of membranes to other membranes and to cytoskeletal elements, thus conferring directionality to membrane traffic. Macromolecular complexes organized by Rabs provide a unique identity to membrane microdomains within cellular organelles. Consequently, a change in Rabs, termed Rab conversion, changes the membrane identity and accompanies cargo progression through intracellular compartments.

Rab6 regulates retrograde transport between the Golgi and the ER, but in cells with hypertrophied synthesis of simple membranes it also associates with post-Golgi carriers. In photoreceptor cells, Rab6 is associated with the Golgi, TGN, and RTCs. It was demonstrated in *Drosophila* that Rab6 regulates rhodopsin trafficking, and that the expression of the GTPase-deficient mutant of Rab6 leads to retinal degeneration.

Rab11 has been localized to both the Golgi and the recycling endosomes, which are involved in return of plasma membrane receptors to the cell surface through endocytosis. However, the Golgi-associated function of Rab11 is less well understood. The specific functions of Rab11 in apparently divergent cellular processes are probably based on its ability to interact with different effector molecules that belong to the family of Rab11-interacting proteins (FIPs), which are localized in different trafficking pathways. Rab11 is associated with photoreceptor TGN and RTCs where it interacts with FIP3. At the TGN, Rab11 and FIP3 are incorporated into a ciliary targeting complex regulated by the small GTPase Arf4, described below. Sustained presence of Rab11 on RTCs suggests that Rab11 might also interact with the conserved octameric Sec6/8 complex, also known as the exocyst in yeast. The Sec6/8 complex tethers the Rab11/FIP3-positive membranes and is involved in tethering RTCs to the RIS plasma membrane. Exocyst complex localizes to the cilia in polarized epithelial cells, and we also find it at the base of the photoreceptor cilium. In *Drosophila*, interaction of the Sec6/8 complex with Rab11 plays a role in the tethering of membranes carrying rhodopsin. Rab11 may also cooperate with another RTC-associated Rab, Rab8. A handover from Rab11 to Rab8, or Rab conversion, may occur at the base of the cilium to couple the final stages of traffic along the ciliary pathway.

Rab8 regulates polarized trafficking in epithelial cells and neurons through its activity on cytoskeleton remodeling necessary for membrane outgrowth and the formation of cellular protrusions. It has recently emerged as a major player in ciliogenesis. In retinal photoreceptors, Rab8 regulates RTCs fusion and ROS biogenesis. It acts at the base of the cilium in conjunction with another small GTPase (Rac1), phosphatidylinositol-4,5-bisphosphate ($PI(4,5)P_2$), actin and the phosphoinositide- and actin-binding protein moesin. In addition, Sec6/8 complex is also likely to function as one of Rab8 effectors in ciliogenesis. Transgenic *Xenopus* with photoreceptor-specific expression of GFP-Rab8Q67L dominant-active mutants show normal photoreceptor cell morphology, but cause slow retinal degeneration, whereas GFP-Rab8T22N GTPase-deficient dominant-negative mutants show a defect in membrane tethering and accumulate RTCs in

the vicinity of the cilium, leading to rod cell death and rapid retinal degeneration. Emerging evidence points to Rab8 as a central regulator of the biogenesis of primary cilia, suggesting that its regulation of rhodopsin trafficking may be a part of a broad and more general role for Rab8 in the regulation of ciliogenesis.

Mutations that affect regulatory proteins of small GTPases and their interacting proteins have been found to cause X-linked retinitis pigmentosa (RP), autosomal recessive Leber congenital amaurosis (LCA), and choroideremia. Rab escort protein 1 (Rep1), encoded by the choroideremia gene is a subunit of geranylgeranyl transferase, the enzyme that isoprenylates Rab proteins. Rab8-interacting proteins, Optineurin and Huntingtin, are also linked to the neurodegenerative diseases primary open-angle glaucoma (POAG) and Huntington's disease, respectively. Rab8, Optineurin, and Huntingtin are collectively involved in the linkage of membrane organelles to the cytoskeleton, suggesting that the breakdown of this linkage may be a common theme in retinal degeneration and in other neurodegenerative diseases.

Arfs

The Arf family of small GTPases includes three different groups of proteins: the Arfs, Arf-like proteins (Arls), and SARs. Arfs were originally discovered as ADP-ribosylation factors, but in 2006 the new nomenclature for the human Arf family of GTP-binding proteins, formerly known as ARF, ARL, and SAR proteins, has been established. Arfs are no longer called ADP-ribosylation factors (ARFs), since ADP-ribosylation appears unrelated to their physiological function. Arf family members regulate membrane trafficking, lipid metabolism, organelle morphology, and cytoskeleton dynamics. These functions were elucidated for the abundant class I Golgi Arfs, Arf1 and Arf3, and the plasma membrane-associated Arf6. The loss of a single class I or class II Arf has little effect on membrane trafficking, but the deletion of pairs of Arfs causes distinct defects. This suggests a pair-wise engagement of Arfs and a certain redundancy in their function. Arf function depends on GTP hydrolysis mediated by Arf GAPs, which are essential for coupling the proofreading of cargo incorporation to the budding of membrane carriers and are often incorporated into protein coats.

The selection and packaging of sensory receptors and membrane cargo targeted to the primary cilia and cilia-derived sensory organelles are critical to replenish the ciliary membrane, yet it remains poorly understood. Our recent studies have demonstrated that rhodopsin C-terminal VxPx targeting signal binds Arf4 to regulate incorporation of rhodopsin into RTCs at the TGN. The function of the class II Golgi-associated Arfs, Arf4 and Arf5, is least understood, yet the direct and specific binding of the VxPx-targeting motif to Arf4 suggests a distinct role for this particular Arf in the generation of RTCs. The targeting VxPx motif binds Arf4 and recruits it to the TGN, leading to assembly of a ciliary targeting complex. This complex is comprised of two small GTPases, Arf4 and Rab11, the Rab11/Arf effector FIP3, and an Arf-GAP/effector ASAP1. The localization of the ciliary targeting complex in photoreceptors is illustrated in **Figure 1**. ASAP1 catalyzes phosphatidylinositol 4,5-bisphosphate (PIP_2)-dependent GTP hydrolysis on Arf4. Transgenic frogs expressing an Arf4 mutant impaired in ASAP1-mediated GTP hydrolysis, display dysfunctional rhodopsin trafficking and cytoskeletal and morphological defects, resulting in retinal degeneration. FIP3, which binds Arf4, also forms a ternary complex with Rab11 and ASAP1 and stimulates Arf GAP activity of ASAP1. Emerging evidence points to the role of ASAP1 and FIP3 as a functional module that provides temporally and spatially restricted hydrolysis of GTP bound to Arf4 at the TGN. Since ASAP1 and FIP3 act as homodimers, they may oligomerize to form a protein coat that regulates ciliary targeting, a specialized form of the TGN-to-plasma membrane trafficking.

Rhodopsin provides the spatial control for the ciliary targeting module by recruiting Arf4 to the carrier budding sites at the TGN through its VxPx targeting signal. Surprisingly, the VxPx motif is not unique to rhodopsin, but is present in other membrane proteins targeted to primary cilia such as polycystins 1 and 2, and the cyclic nucleotide-gated channel CNGB1b subunit. The VxPx from polycystin-2 also binds Arf4, suggesting that the targeting complex recruited through Arf4 is a part of conserved machinery involved in the selection and packaging of the cargo destined for delivery to the cilium.

SNAREs and their Regulators in Rhodopsin Trafficking

In addition to GTPases and their effectors, the soluble N-ethylmaleimide-sensitive factor attachment protein receptor (SNARE) proteins are major components of the intracellular machinery responsible for targeted membrane delivery. SNAREs are considered to be directly involved in membrane fusion. After the tethering step, SNAREs are activated on the opposing donor and target membranes to form a complex that bridges the two membranes and brings them into close proximity to initiate fusion. Although SNARE pairing alone is not sufficient to determine the specificity of organelle fusion, cognate SNAREs are correctly paired in biological membranes, based on proofreading and polarized distribution leading to their relative enrichment at the appropriate fusion sites. Rabs also function by concentrating and activating SNAREs, accessory proteins and lipids, at the sites of membrane fusion and are thus required for carrier docking and fusion with the target organelle.

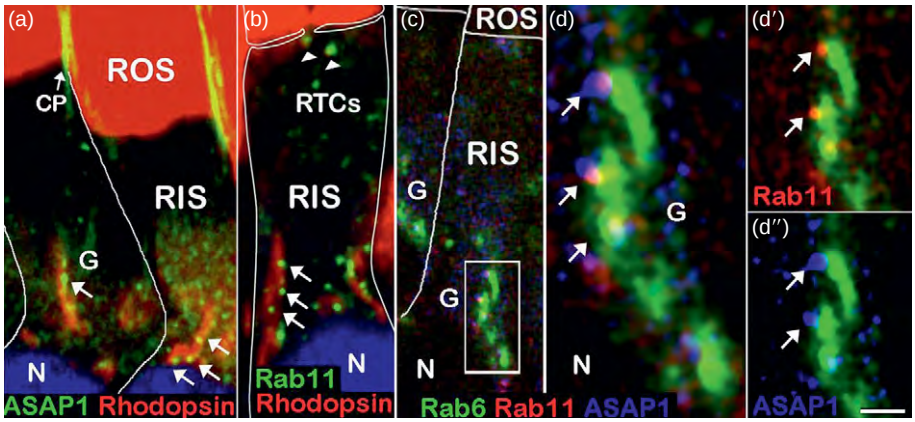

Figure 1 The Arf GAPASAP1 co-localizes with Rab11 on nascent RTCs at the *trans*-Golgi network (TGN). (a) A confocal optical section (0.7 μm) of frog retina labeled with anti-rhodopsin C-terminal mAb 11D5 (red) and anti-ASAP1 (green). Anti-rhodopsin antibody labels the rod outer segment (ROS) and the Golgi (G) in the rod inner segment (RIS), where ASAP1-positive puncta (yellow, arrows) line up with regular periodicity. ASAP1 is also detected in calycal processes (CP) that evaginate from the RIS and surround the base of the ROS. Nuclei (N) are stained with TO-PRO-3 (blue). (b) A confocal optical section labeled with anti-rhodopsin C-terminal mAb 11D5 (red) and anti-Rab11 (green). Rab11-positive puncta (yellow, arrows) aligned with rhodopsin-laden Golgi. Rab11 is also present on RTCs (arrowheads). Nuclei (N) are stained with TO-PRO-3 (blue). (c) ASAP1 (blue) and Rab11 (red) colocalize in the bud-like profiles at the tips of the *trans*-Golgi (Rab6, green) (boxed area magnified in (d). (d) Magnified *trans*-Golgi area from panel C, with ASAP1- and Rab11-positive buds (arrows), which likely represent the TGN. (d′ and d″). Rab11 (red) and ASAP1 (blue) are shown separately. Scale bar = 3 μm in (a)–(c), 0.7 μm in (d), 1 μm in (d′) and (d″). Modified from Mazelova, J., Astuto-Gribble, L., Inoue, H., Tam, B. M., Schonteich, E., Prekeris, R., Moritz, O. L., Randazzo, P. A., and Deretic, D. (2009). Ciliary targeting motif VxPx directs assembly of a trafficking module through Arf4. *EMBO J* 28: 183–192.

SNARE complexes are generally composed of a four-helical bundle bridging opposing membranes and bringing them into close proximity to initiate fusion. Fusion with the plasma membrane requires formation of a complex between syntaxins (Qa SNAREs) and VAMPs (R-SNAREs), each contributing one helix to the four-helix SNARE bundle, and Qbc SNAREs, either neuronal SNAP-25 or non-neuronal SNAP-23, which provide two helices to the central layer of the core complex. SNAREs are targeted to appropriate membrane domains based on specific sequences. The polarized distribution of Qa SNAREs is likely to contribute additional specificity of membrane targeting by promoting fusion with only certain target membranes. Recent evidence suggests that the local lipid environment, particularly phospholipids enriched in omega-3 and omega-6 fatty acids, also contributes to regulate SNARE function.

The membrane fusion event through which RTCs deliver rhodopsin to the cilium is mediated by a SNARE complex. Syntaxin 3 and SNAP-25 are the Q-SNAREs for the fusion of incoming RTCs with the RIS plasma membrane and, therefore, regulators of ROS biogenesis in photoreceptors. The distribution of these SNAREs in photoreceptors is illustrated in Figure 2. Remarkably, omega-3 DHA enhances syntaxin 3 incorporation into SNARE complexes at RTC fusion sites and promotes ciliary membrane expansion and ROS biogenesis. Microtubules direct the restricted distribution of syntaxin 3, consistent with the membrane cytoskeleton playing an essential role in concentrating RTC fusion regulators around the cilium. Syntaxin 3 is the major partner for SNAP-25 in photoreceptor cells; however, SNAP-25 pairing with syntaxin 1A, or 1B, may regulate a distinct trafficking pathway in the RIS. Interestingly, Syntaxin 3 is also found at the base of mouse ROS, suggesting an additional role for this SNARE in rodent rods.

ROS is a Modified Primary Cilium

Almost all cells possess primary cilia that house an array of signal transduction modules. Long underappreciated, the cilium has recently received a great deal of attention due to the ciliary involvement in a wide range of human diseases, including retinal degeneration, polycystic kidney disease (PKD), Bardet–Biedl syndrome (BBS), and neural tube defects. Many cilium disease proteins were detected in the mouse photoreceptor ciliary proteome. Ciliary involvement in a wide range of retinal diseases has come into sharp focus in the past several years, with the molecular mechanism underlying these diseases being rapidly elucidated. Several human syndromes, including Senior–Loken syndrome, Jeune syndrome, and BBS, are also characterized by both cystic kidneys and retinal degeneration, which are often found in combination with skeletal defects or other abnormalities such as obesity, polydactyly, hypogenitalism, and developmental delay that might also be caused by defects in cilia. The organization of the small GTPases,

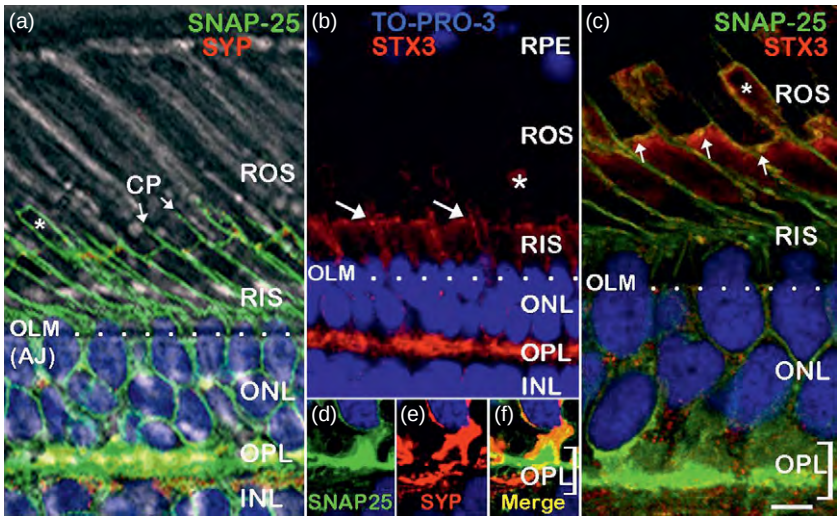

Figure 2 SNAP-25 is a photoreceptor RIS plasma membrane (PM) and synaptic SNARE, whereas syntaxin 3 is concentrated in the RIS PM. (a) A confocal optical section (0.7 μm) of frog retina labeled with anti-SNAP-25 N-terminal mAb (green) and anti-syntaxin 3 (STX3, red). Nuclei are stained with TO-PRO-3 (blue). Anti-SNAP-25 (green) outlines the photoreceptor PM. The calycal processes (CP), which are in continuum with the RIS PM, also contain SNAP-25. The ROS, which are visible by DIC, are completely devoid of this SNARE. AJ, adherens junctions that form the outer limiting membrane (OLM, dotted line). The retinal layers are: ONL-outer nuclear, OPL-outer plexiform, INL-inner nuclear. SNAP-25 co-localizes with synaptophysin (SYP, red) in the OPL, which encompasses the synapses of rods and cones with the rod bipolar, cone bipolar, and horizontal cells. Asterisks indicate the protruding RIS of green rods, a minor subpopulation that accounts for ~5% of total rods. (b) A confocal optical section labeled with anti-syntaxin 3 (STX3, red), which is highly concentrated in the RIS PM (arrows), but is absent from the ROS, and from the RPE. Syntaxin 3 is also abundant in the OPL. Nuclei are stained with TO-PRO-3 (blue). (c) SNAP-25 and syntaxin 3 co-localize (yellow) in the RIS at the RTC fusion sites in the vicinity of cilia (arrows). Syntaxin 3 is also abundant in the inner (lower) half of the OPL (large bracket), where bipolar and horizontal cells are localized, but not in the outer (upper) half where photoreceptor synapses are localized. (d–f). SNAP-25 (green in (d)) co-localizes with synaptophysin (red in (e)) in the photoreceptor synapses (yellow in (f)). However, SNAP-25 is abundant in the bipolar and horizontal cell processes in the OPL (green in (f)), where synaptophysin is not detected. Scale bar = 8 μm in (a), 10 μm in (b), 7 μm in (c)–(f). Modified from Mazelova, J., Ransom, N., Astuto-Gribble, L., Wilson, M. C., and Deretic, D. (2009). Syntaxin 3 and SNAP-25 pairing, regulated by omega-3 docosahexaenoic acid (DHA), controls the delivery of rhodopsin for the biogenesis of cilia-derived sensory organelles, the rod outer segments. *Journal of Cell Science* 122: 2003–2013.

SNAREs and their regulators involved in the ciliary targeting of rhodopsin is schematically illustrated in **Figure 3**.

Twelve BBS genes have been identified. A complex composed of seven BBS proteins, the BBSome, localizes to the base of the cilium and is required for ciliogenesis. BBS3, which is not a part of BBSome encodes the Arf family GTPase Arl6. Strikingly, Rabin8, the GDP/GTP exchange factor that activates Rab8, localizes to the basal body and contacts the BBSome. In cultured epithelial cells, activated Rab8 enters the primary cilium and promotes extension of the ciliary membrane. This explains the accumulation of RTCs below the cilium in photoreceptors expressing mutant Rab8. Strikingly, activated Rab8, in its GTP-bound form interacts with another centrosomal/ciliary protein CEP290/BBS14/NPHP6, which is not a part of the BBSome. Thus, BBS may be caused by defects in Rab8-mediated vesicular transport to the cilium.

An extraordinary array of retinopathy-associated ciliary proteins includes X-linked RP1, which is localized to the proximal cilium and involved in disk morphogenesis, and RP2, which was recently identified as a GAP for the Arf family GTPase Arl3 that is involved in kidney and photoreceptor development. A major player in ciliary morphogenesis is retinitis pigmentosa GTPase regulator (RPGR), which is homologous to RCC1, the nucleotide exchange factor for the small GTPase Ran. Mutations in the retina-specific ORF15 isoform of RPGR (RPGR (ORF15)) were found in X-linked RP3, which is associated with 10–20% of RP. RPGR appears to be a part of a ciliary and basal body protein network that, when disrupted, can result in Leber congenital amaurosis, Senior–Loken syndrome, nephronophthisis, or Joubert syndrome. RPGR (ORF15) co-localizes with RPGRIP1 at centrioles and basal bodies and interacts with nucleophosmin. RPGRIP1, which is affected in patients with LCA, anchors RPGR to the photoreceptor connecting cilium and participates in disk morphogenesis. RPGR also interacts with calmodulin and nephrocystin-5, a ciliary IQ domain protein, which is mutated in Senior–Loken syndrome, and with the centrosomal/ciliary protein CEP290/BBS14/NPHP6, which is truncated in early-onset retinal degeneration in the rd16 mouse. In addition,

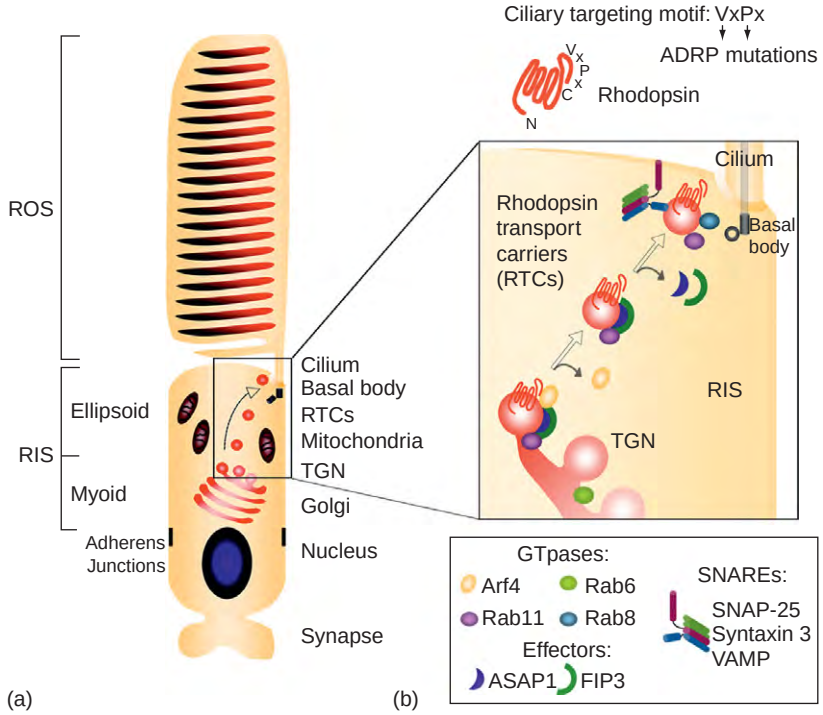

Figure 3 Post-Golgi trafficking and ciliary targeting of rhodopsin (a) Diagram of the rod photoreceptor cell. Cilium protrudes from the cell body (RIS) and elaborates the ROS filled with membranous disks containing photopigment rhodopsin and associated phototransduction machinery. Following synthesis in the RER, newly synthesized rhodopsin traverses the Golgi and the TGN, localized in the myoid region of the RIS, where it is incorporated into transport carriers (RTCs). RTCs travel from the TGN, though the mitochondria-laden ellipsoid region of the RIS, to the base of the cilium where they fuse with the RIS PM. Adherens junctions separate the RIS from the synapse. Little is known about membrane targeting to the RIS PM and the synapse. (b) Polarized trafficking of post-Golgi RTCs is dependent on the rhodopsin C-terminal VxPx ciliary targeting motif. ADRP mutations in the VxPx motif are indicated. Selected proteins involved in the recognition of the VxPx motif, sorting of rhodopsin into the RTCs and their targeting to the cilium are shown in the enlarged area of the RIS. Rhodopsin C-terminal binds to, and recruits Arf4 to the TGN membrane, leading to assembly of a ciliary targeting complex. This complex is comprised of two small GTPases Arf4 and Rab11, the Rab11/Arf effector FIP3, and an Arf-GAP/effector ASAP1. The small GTPases Rab6 regulates trafficking through the Golgi, whereas Rab8 regulates RTC fusion. Syntaxin 3 and SNAP-25 are a part of the SNARE complex that catalyzes RTC fusion at the base of the cilium.

mutations in the gene encoding the basal body protein RPGRIP1L (RPGRIP-like), a nephrocystin-4 interactor, cause Joubert syndrome.

Another ciliary and basal body protein network linked to myosin VIIa is disrupted in human USH, the most frequent cause of combined deafness–blindness. USH is genetically heterogeneous with three clinical types, USH1–3. The scaffold protein harmonin (USH1C) integrates USH1 and USH2 molecules into protein networks. The Usher protein network is organized by the scaffold proteins SANS (USH1G), which provides a linkage to the microtubule transport machinery, and whirlin (USH2D), which anchors USH2Ab and very large G-protein-coupled receptor 1b (VLGR1b). Remarkably, the USH protein network is also a part of the periciliary ridge complex (PRC), a specialized membrane domain for docking and fusion of RTCs in Xenopus photoreceptors. Finally, the Usher protein network is linked to the Crumbs polarity complex in the retina and mutations in Crumbs cause retinitis pigmentosa (RP12).

Conclusions and Summary

Numerous diseases arise from defects in proteins that participate in membrane protein trafficking, vectorial transport, and assembly of outer segment membranes. Thus, maintenance of photoreceptor cell polarity is of utmost importance for their health and survival, and ultimately for vision.

See also: Genetic Dissection of Invertebrate Phototransduction; The Photoreceptor Outer Segment as a Sensory Cilium; Physiology of Photoreceptor Synapses and Other Ribbon Synapses; Primary Photoreceptor Degenerations: Retinitis Pigmentosa; Primary Photoreceptor Degenerations: Terminology; Retinal Degeneration through the Eye of the Fly; Rod and Cone Photoreceptor Cells: Inner and Outer Segments; Rod and Cone Photoreceptor Cells: Outer-Segment Membrane Renewal; Secondary Photoreceptor Degenerations: Age-Related Macular Degeneration; *Xenopus laevis* as a Model for Understanding Retinal Diseases.

Further Reading

Cai, H., Reinisch, K., and Ferro-Novick, S. (2007). Coats, tethers, Rabs, and SNAREs work together to mediate the intracellular destination of a transport vesicle. *Developmental Cell* 12: 671–682.

Deretic, D., Schmerl, S., Hargrave, P. A., Arendt, A., and McDowell, J. H. (1998). Regulation of sorting and post-Golgi trafficking of rhodopsin by its C-terminal sequence QVS(A)PA. *Proceedings of the National Academy of Sciences of the United States of America* 95: 10620–10625.

Deretic, D., Williams, A. H., Ransom, N., et al. (2005). Rhodopsin C-terminus, the site of mutations causing retinal disease, regulates trafficking by binding to ARF4. *Proceedings of the National Academy of Sciences of the United States of America* 102: 3301–3306.

Gillingham, A. K. and Munro, S. (2007). The small G proteins of the Arf family and their regulators. *Annual Review of Cell and Developmental Biology* 23: 579–611.

Green, E. S., Menz, M. D., LaVail, M. M., and Flannery, J. G. (2000). Characterization of rhodopsin mis-sorting and constitutive activation in a transgenic rat model of retinitis pigmentosa. *Investigative Ophthalmology and Visual Science* 41: 1546–1553.

Leroux, M. R. (2007). Taking vesicular transport to the cilium. *Cell* 129: 1041–1043.

Malsam, J., Kreye, S., and Sollner, T. H. (2008). Membrane fusion: SNAREs and regulation. *Cellular and Molecular Life Sciences* 65: 2814–2832.

Mazelova, J., Astuto-Gribble, L., Inoue, H., et al. (2009). Ciliary targeting motif VxPx directs assembly of a trafficking module through Arf4. *EMBO Journal* 28: 183–192.

Mazelova, J., Ransom, N., Astuto-Gribble, L., Wilson, M. C., and Deretic, D. (2009). Syntaxin 3 and SNAP-25 pairing, regulated by omega-3 docosahexaenoic acid (DHA), controls the delivery of rhodopsin for the biogenesis of cilia-derived sensory organelles, the rod outer segments. *Journal of Cell Science* 122: 2003–2013.

Moritz, O. L., Tam, B. M., Hurd, L. L., et al. (2001). Mutant rab8 Impairs docking and fusion of rhodopsin-bearing post-Golgi membranes and causes cell death of transgenic *Xenopus* rods. *Molecular Biology of the Cell* 12: 2341–2351.

Nachury, M. V., Loktev, A. V., Zhang, Q., et al. (2007). A core complex of BBS proteins cooperates with the GTPase Rab8 to promote ciliary membrane biogenesis. *Cell* 129: 1201–1213.

Papermaster, D. S., Schneider, B. G., and Besharse, J. C. (1985). Vesicular transport of newly synthesized opsin from the Golgi apparatus toward the rod outer segment. Ultrastructural immunocytochemical and autoradiographic evidence in *Xenopus* retinas. *Investigative Ophthalmology and Visual Science* 26: 1386–1404.

Shi, G., Concepcion, F. A., and Chen, J. (2004). Targeting od visual pigments to rod outer segment in rhodopsin knockout mice. In: Williams, D. S. (ed.) *Photoreceptor Cell Biology and Inherited Retinal Degenerations*, pp. 93–109. Singapore: World Scientific Publishing.

Tam, B. M., Moritz, O. L., Hurd, L. B., and Papermaster, D. S. (2000). Identification of an outer segment targeting signal in the COOH terminus of rhodopsin using transgenic *Xenopus laevis*. *Journal of Cell Biology* 151: 1369–1380.

Wandinger-Ness, A. and Deretic, D. (2008). Rab8a. *UCSD-Nature Molecule Pages.* Nature Publishing Group. doi:10.1038/mp.a001997.001901.

Relevant Websites

http://www.retina-international.com – Retina International.

http://www.signaling-gateway.org – The UCSD-Nature Signaling Gateway.

http://www.sph.uth.tmc.edu/RetNet/ – Retinal Information Network.

http://webvision.med.utah.edu – WEBVISION: The organization of the retina and visual system.

Posterior Capsule Opacification

I M Wormstone, University of East Anglia, Norwich, UK

Glossary

Capsulotomy or Nd:YAG capsulotomy – An opening made in the posterior capsule, usually with a Nd:YAG (neodymium-doped yttrium aluminum garnet) laser, which is intended to remove opacified tissue from the visual axis.

Epithelial-mesenchymal transition – The transformation of epithelial cells to a cell type that resembles mesenchyme. This process is associated with loss of the tight cell adhesions between epithelial cells, the onset of cell migration, and the synthesis of large amounts of a collagenous extracellular matrix.

Rhexis or capsulorhexis – The opening that is made in the anterior capsule through which the opaque fiber cells are removed during cataract surgery.

General Background

Cataract is a general term, describing any opacity of the lens. It appears in many forms and affects the sight of tens of millions of people throughout the world. At present, there is no cure for cataract; therefore, surgical intervention is required to alleviate this problem. With the development of modern cataract surgery, hopes were high that the problem of cataract had been resolved. This surgical procedure involves creating a circular window in the anterior capsule, which provides access to the fiber mass, the most common site of opacity. The fiber cells can then be removed. Some residual fiber cells remain and these can also be removed using irrigation and aspiration. The product of this operation is known as a capsular bag (Figure 1). The capsular bag serves a number of purposes in that it maintains separation of the anterior and posterior chambers and importantly can house an artificial lens commonly known as an intraocular lens, which provides refractive power. Initially, this procedure is extremely effective, but secondary visual loss can result. Despite the rigors of surgical manipulation, a number of lens epithelial cells remain and a wound-healing response is initiated by these cells. The remaining population of lens epithelial cells re-colonize the denuded regions of the anterior capsule, grow onto the outer surface of the anterior capsule, and migrate onto the intraocular lens surface. Most critically, they begin to colonize the previously cell-free posterior capsule and, consequently, encroach upon the visual axis. These cells can then transform in to several different cell phenotypes, which can lead to altered refractive indices within the bag through increased matrix deposition, fiber cell differentiation, bladder cell formation, and matrix deformation (wrinkling/contraction). This condition is known as secondary cataract, after-cataract, and most commonly posterior capsule opacification (PCO; Figure 1). Ultimately, PCO can cause a significant reduction in visual quality and necessitates a secondary procedure to treat posterior capsule opacification. This typically involves the use of a neodymium-doped yttrium aluminium garnet (Nd:YAG) laser to ablate the cells and central posterior capsule of the patient in order to restore a clear path of light through the visual axis.

The original concept of modern cataract surgery was formed in the 1940s by Sir Harold Ridley, but it was not commonly employed until the 1980s. While this procedure is infinitely superior to its predecessor, which involved the complete removal of the lens, the problem of PCO has continued to affect the long-term outcome of modern cataract surgery. While the importance of PCO is often dismissed by surgeons as resolved or insignificant, this notion is not supported by the available literature. A more balanced view is that, through an evolutionary process, cataract surgery and intraocular lense (IOL) design have improved to such an extent that PCO within 2 years of surgery, determined by Nd:YAG capsulotomy rates, has fallen from ~30% to ~10%. This is a significant achievement, but we must consider that 10% of cataract patients is still >1 million people per annum and that more will develop visually deteriorating PCO at stages later than 2 years. In addition, virtually all patients undergoing cataract surgery will develop PCO to some extent, which may still affect vision. PCO therefore is not a problem that should be dismissed and requires even greater efforts to further reduce the rate of incidence. This idea is given even greater support because of the ambition to introduce accommodating lenses as a routine part of cataract surgery. At present, these lenses have very high rates of PCO. Unless this issue can be addressed, their introduction will be limited.

Regulatory Systems and Management of PCO

In this section, the factors that can influence PCO will be discussed. In order to improve the treatment of PCO, it is important to understand the systems which control its development. Consequently, the biological factors that

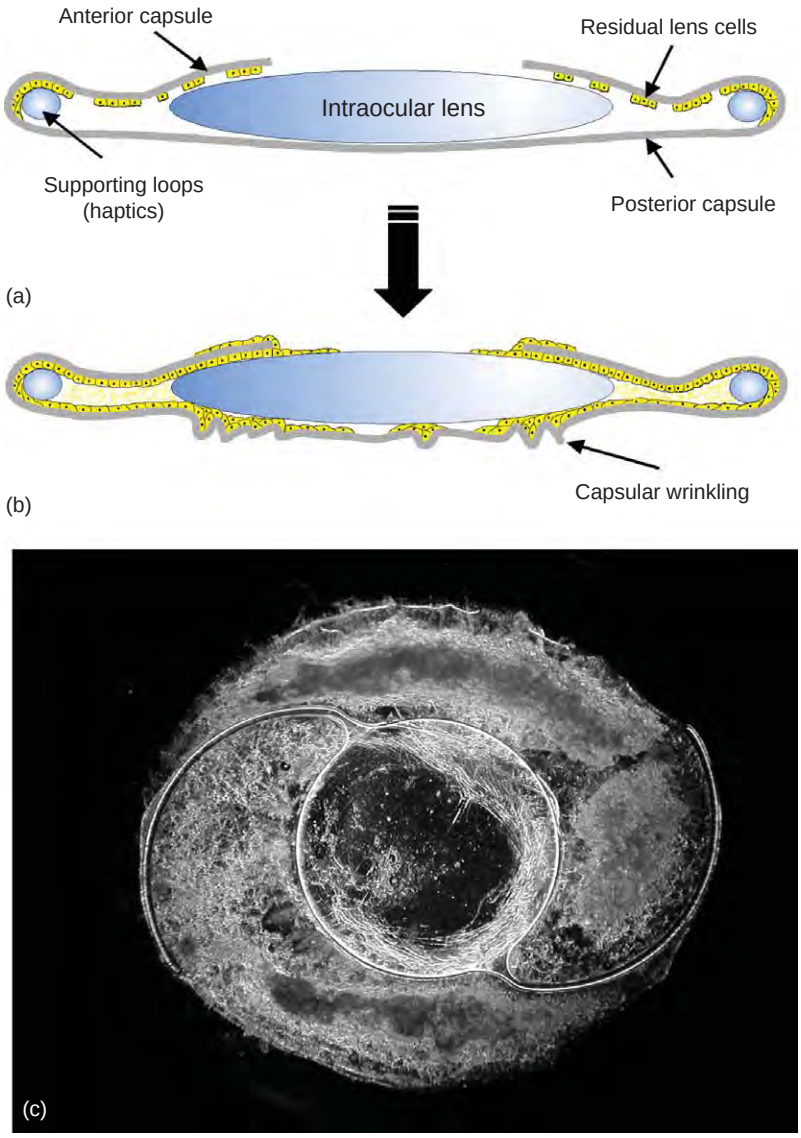

Figure 1 A schematic representation of (a) the postsurgical capsular bag and (b) the extensive growth and modification that gives rise to posterior capsule opacification. (c) A dark-field micrograph of a capsular bag removed from a donor eye that had undergone cataract surgery prior to death that exhibits light scattering regions beneath an intraocular lens. Reproduced from Wormstone, I. M., Wang, L., and Liu, C. S. (2009). Posterior capsule opacification. *Experimental Eye Research* 88: 257–269, with permission from Elsevier.

have been identified will be covered here along with surgical advances, including IOL design, which are, in effect, physical methods designed to overcome or suppress a biological response. It is important to consider the biological processes that contribute to PCO (**Figure 2**). In essence one can consider these to be cell migration, cell division, differentiation into fiber cells, transdifferentiation from an epithelial cell type to a myofibroblast, matrix deposition, and matrix contraction. In order to understand the problem of PCO, one needs to have knowledge of the factors that drive these processes. Through identification of regulatory systems, specific components can be identified and used as therapeutic targets or a physical mechanism can be used to prevent a specific event occurring (e.g., by IOL design). The understanding of the condition and the development of treatment are integrally linked. In due course, putative therapeutic approaches will be discussed, but when considering an approach to prevent PCO there are several options. One method is to kill the entire population of lens epithelial cells within the bag, a second is to prevent proliferation/migration and thus prevent any cell encroachment on the visual axis, while another option is to prevent matrix contraction/fibrosis on the posterior capsule. There are arguments and counter-arguments for each of these strategies. With regard to complete removal of the epithelial cell population, it is possible that a naked capsule will either

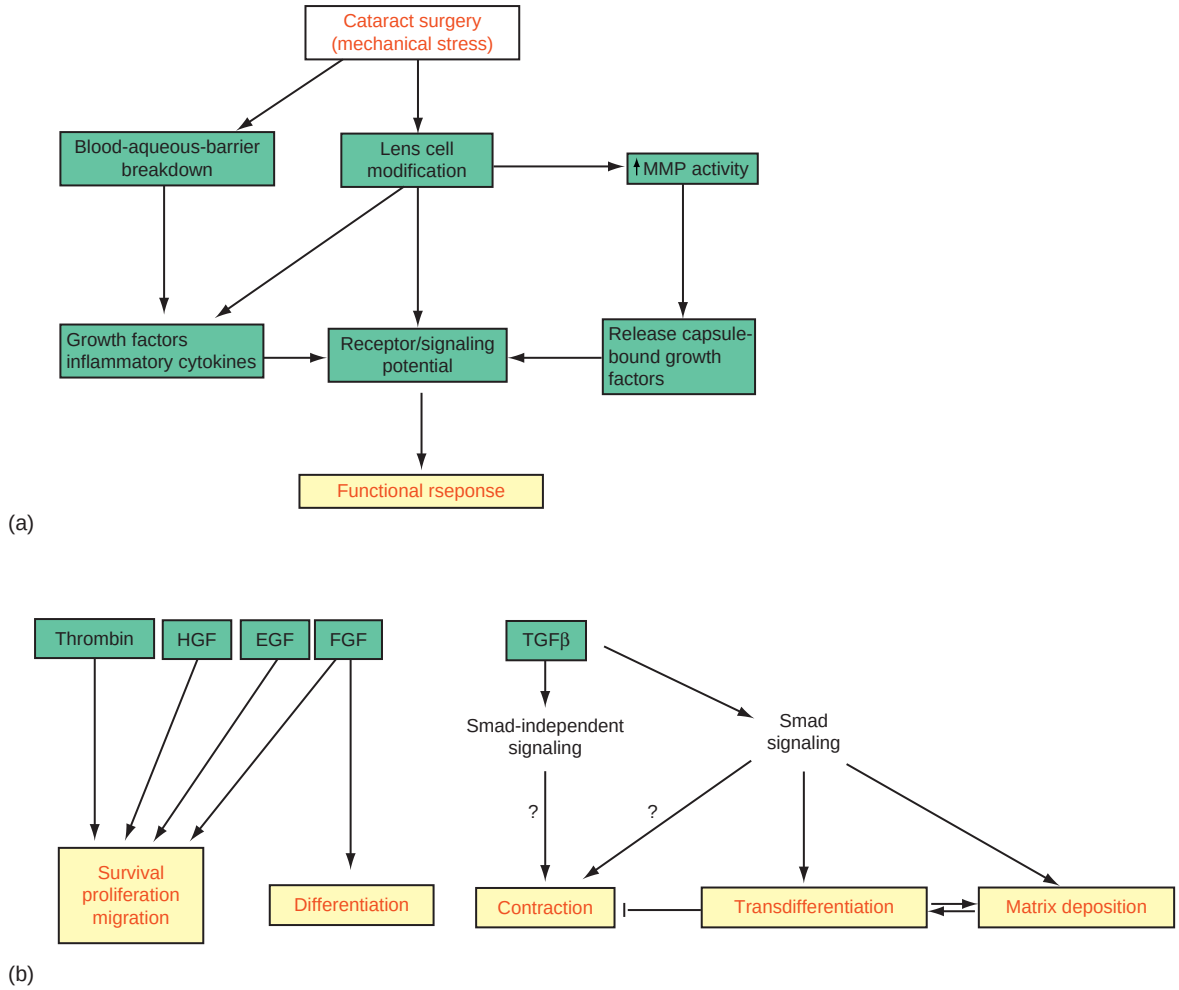

Figure 2 A schematic overview of (a) the wound-healing events following cataract surgery that will ultimately give rise to PCO and (b) the relationship between growth factors and functional events associated with PCO. From Wormstone, I. M., Wang, L., and Liu, C. S. (2009). Posterior capsule opacification. *Experimental Eye Research* 88: 257–269.

degenerate, for example, through the action of matrix degrading enzymes or, with the absence of cellular maintenance, become altered, such that it occludes the visual axis. It may, however, continue to permit light to pass along the visual axis unaffected. In relation to the prevention of proliferation, migration, and fibrosis, it could be argued that maintaining the cell population is attractive, but there are still concerns about the period for which effective therapy can be sustained. In all cases, if an agent is used to achieve an effect, it is important that its actions are exclusive to lens epithelial cells; damage to other tissues would render any treatment unsuitable for clinical use. Consequently, the method of drug delivery is also of great importance when considering a pharmacological solution to PCO.

Surgical Factors

The incidence of PCO can be affected by the quality of surgery, for example, maintaining the entire rhexis edge in contact with the anterior IOL optical surface has been shown to significantly reduce PCO rate. However, significant efforts have been made to change surgical practice. In pediatric cases surgeons have employed for some time a double rhexis approach, such that in addition to the standard capsulorhexis on the anterior capsule, a capsulorhexis is also carried out on the posterior capsule before implanting an IOL. The theory behind this being that without a matrix the cells cannot encroach on the visual axis. This procedure has now been adapted further and is known as the bag-in-the-lens technique and involves placing the rhexis edges in a groove along the IOL perimeter. The clinical results from this method are promising, such that no Nd:YAG laser treatment was performed on a study cohort within 1 year of cataract surgery. This method may be viewed as technically difficult, but it does provide a valid surgical approach to manage PCO.

From a number of clinical trials studying different materials, construction, and design of IOLs, the greatest

benefit appears to result from a square design at the optic edge or from capsular tension rings. This helps prevent PCO through a physical characteristic and is reported to create a barrier that suppresses the movement of cells onto the posterior capsule. This improved design is undoubtedly beneficial. Nevertheless, Nd:YAG capsulotomy is still carried out in approximately 10% of patients who have been implanted with these lenses. A patient implanted with a fixed focus IOL will have refractive power, but glasses or other corrective lenses are still often required because of limited ability to accommodate. The future area of development lies with focusable (accommodating) IOLs. However, with these lenses the barrier provided by the square-edge, fixed focus IOLs is no longer effective. Recently, it has been reported that 50% of patients implanted with a 1CU accommodating lens required Nd:YAG capsulotomy 2 years following surgery. In addition, the changes observed with posterior capsule opacification prevent the focus-shift mechanism of accommodating IOLs to function, thus stopping the IOL from moving forward with accommodative effort. If this next-generation IOL technology is to be introduced, PCO needs to be effectively managed.

Biological Factors

There are two basic levels of regulation of lens cells following cataract surgery. The first can be termed paracrine factors, which are often introduced following a breach of the blood aqueous barrier and an inflammatory response. The second is autocrine factors that are synthesized by the lens. PCO is not an instant problem; it can progress over weeks and years. Therefore, to understand the nature of PCO development it is important to understand the relative contributions of both paracrine and autocrine control. In the days following cataract surgery, protein levels in the aqueous humour are high. This allows many blood proteins to reach the remaining lens epithelial cells and, through activation of receptors, initiate a functional response that could contribute to PCO. However, these elevated protein levels are relatively short-lived and return to baseline within a few weeks or months, whereas PCO often becomes a clinical problem years after surgery. This slow, but persistent progression is most likely explained by the autocrine regulation of lens cells. Previous work has shown that lens cells can survive and synthesize proteins in serum-free medium, provided they remain attached to the lens capsule. Moreover, it has also been shown that the majority of the survival protein, transferrin, within the aqueous humor is synthesized by the lens. This survival response, therefore, exists within lens cells. Thus, PCO can be considered as a two-phase process. In the first phase, the response dominated by the introduction of paracrine factors. It is followed by a second slow, but persistent phase, resulting largely from the independent behavior of lens cells. A number of molecules have been identified that can act as paracrine or autocrine factors or both.

Survival, proliferation, migration, and differentiation

The normal lens requires specific functional tasks to take place in specific places. Proliferation, migration, and differentiation are normal events in the lens and, consequently, a number of the factors regulating these processes have been identified. In relation to PCO, the rate of change is increased, but the regulatory principles still apply. Proliferation, in association with migration, is an important aspect of wound healing and PCO. In one study, it has been shown that creating a small capsulorhexis can increase the rate of proliferation in the lens when compared to the intact lens; removal of fibers increased this rate further. Human capsular bags cultured for 3 days in serum-free medium also exhibited a higher number of positive cells, which were largely situated at the equatorial zone, the natural site of cell division. Addition of serum increased the dividing population, again predominantly at the equator. Fiber differentiation also occurs in the peripheral regions of the capsular bag and is often known as Soemerring's ring. While this does not usually encroach on the visual axis, it can provide peripheral glare and cause the IOL to become displaced.

One protein associated with proliferation, migration, and differentiation is fibroblast growth factor (FGF). Using rat lens epithelial explants as an experimental model, McAvoy and Chamberlain showed that basic FGF could give rise to peak rates of proliferation, migration, and differentiation at 0.15, 3, and 40 ng ml^{-1} respectively. Acidic FGF also induced the same effects in a similar pattern, but the concentrations required were an order of magnitude greater. Similarly, human primary cells also demonstrated 10-fold higher sensitivity to basic FGF over acidic FGF. Basic FGF and FGF receptor 1 (FGFR-1), the elements of a potential autocrine pathway, were identified using reverse ranscriptase polymer chain reaction (RT-PCR) in cultured human lens capsular bags. Basic FGF was also detected using enzyme-linked immunosorbent assay (ELISA). Interestingly, the degree of messenger RNA for the ligand and receptor appeared to be greater in cultured bags compared with native human lens epithelium. Moreover, capsular bags removed from donors who had previously undergone cataract surgery also exhibit RNA encoding FGF and FGFR-1. The levels detected were similar to cultured capsular bags. The functional role of this autocrine system was tested by blocking FGFR-1 using a specific inhibitor, SU5402, which caused a retardation of growth. In addition, the affinity of lens cells for FGF has been exploited as a strategy to prevent PCO by using an FGF–saporin complex bound to a heparin surface-modified IOL. The basis of this approach is that when FGF binds to the appropriate receptors on the epithelial cells, internalization of the complex occurs,

including the saporin, which will then lead to cell death. Unfortunately, this particular system produced some side effects, including transient corneal oedema and iris depigmentation.

Epidermal growth factor (EGF) when applied to lens cell cultures has also been shown to induce proliferation. Using human capsular bag cultures, it has been shown that 10 ng ml^{-1} EGF can increase growth across the posterior capsule; moreover, inhibiting the EGF receptor, using the selective inhibitor AG1478, significantly slowed growth rate. The ability of EGF to induce differentiation of epithelial cells to fibers has also been demonstrated by the capacity to form lentoid bodies that express gamma crystallin.

Hepatocyte growth factor (HGF) has been identified in capsular bags removed from donors who had previously undergone cataract surgery. Cells growing on both the anterior and posterior capsules showed increased c-met (HGF receptor) expression in response to surgical trauma, when compared to native epithelium. In addition, HGF was detected in the medium in the first few days of culture and declined with time. Employing the capsular bag model, application of c-met antibody retarded the rate of growth across the posterior capsule.

Application of thrombin, which is typically associated with the blood coagulation cascade, to the human lens cell line FHL 124 resulted in the activation of the extracellular-regulated kinase (ERK) cascade, a rise in intracellular calcium, and enhanced phosphorylation of Akt. Moreover, in capsular bag experiments, an increased rate of growth across the posterior capsule was observed in response to thrombin. The receptor mediating these events is PAR1, which was determined by the use of specific activating peptides for the four PAR members and detection of message using RT-PCR. Disruption to the blood aqueous barrier, as a consequence of surgery, introduces blood proteins, including thrombin, and is, therefore, likely to affect lens cell behavior.

Many growth factors activate shared signaling pathways. Consequently, signaling components and pathways are a source of great interest to the PCO field. Application of U0126, a mitogen-activated protein kinase kinase (MEK) inhibitor that disables MAP kinase signaling to capsular bag cultures, caused a retardation of growth, but not complete growth arrest suggesting that multiple signaling pathways are involved. Using a chick capsular bag model, the role of Src family kinases (SFKs) has been investigated. Application of PP1 an SFK inhibitor was capable of inhibiting migration on to the posterior capsule. In addition, application of the proteosome inhibitor, MG132, to the human lens epithelial cell line, HLE B-3, caused a reduced rate of proliferation in the presence of different growth stimuli. In addition, cell cycle regulatory proteins p21 and p27 were increased in association with growth inhibition. Intracellular calcium signaling is also a key mechanism in the regulation of lens cells. It has been shown that the application of thapsigargin, a calcium ATPase inhibitor that effectively ablates calcium signaling, results in reduced protein synthesis, proliferation, and increased apoptosis. When directly coated onto an IOL, thapsigargin successfully killed all cells within the capsular bag. However, this coating was too basic and did not account for the physical stress associated with entry through the corneal/scleral tunnel. Recent advances in drug delivery can overcome some of these problems. The Perfect Capsule system is one method that has been investigated in the clinic and laboratory and seems to be a promising approach. This is a means to thoroughly perfuse the capsule with a solution or drug prior to the introduction of an IOL. Human capsular bags prepared *in vitro* were cultured following a 2 min application of 100 μM thapsigargin, which caused complete ablation of the lens epithelial cell population. Interestingly, other agents were also applied to capsular bags in this fashion. Distilled water appeared to cause cell death in the short term, but at the end-point of the study, cell growth was similar to untreated controls. Three molar of NaCl and 250 μg ml^{-1} 5-fluorouracil (5-FU), a drug that interferes with cell growth, had some inhibitory effect, but growth on the posterior capsule was still extensive. Higher doses of 5-FU did cause a significant reduction in coverage of the central posterior capsule, but at day 28 it was evident that viable cells remained on the anterior capsule and on the peripheral posterior capsule. Therefore, it is predicted that 5-FU would retard PCO development, but not prevent it. Interestingly, direct comparison between *in vitro* capsular bag data and the clinic can now be made. Application of distilled water, using the Perfect Capsule system, has been performed in patients. The data from the human capsular bags predicted that distilled water would be ineffective and this proved to be the case clinically. Moreover, the role of the capsular bag model to predict pharmacological responses was strengthened recently. The profile of sensitivity to the agents described earlier differed in human and rabbit *in vitro* capsular bag cultures, such that thapsigargin was ineffective in the rabbit and 5-FU was the most effective at inhibiting growth. Both thapsigargin and 5-FU have also been studied using an *in vivo* rabbit system. The drugs were again delivered using the Perfect Capsule device. As with the *in vitro* results, thapsigargin was ineffective, while 5-FU was successful. This collection of data is important; as it shows that the pharmacological profile in rabbits differs from humans and that the *in vitro* model strongly predicts the pharmacological response *in vivo* for a given species.

Transdifferentiation, matrix contraction, and matrix deposition

A single monolayer of cells would not significantly disturb the light path. Light scatter that we associate with PCO is actually associated with changes in refractive index caused

by matrix contraction, that is, a wrinkling of the posterior capsule along with cell aggregation and matrix deposition. These are, in effect, fibrotic events and are common in pathologies throughout the body. With respect to fibrosis, epithelial–mesenchymal transition or transdifferentiation is often implicated. In the case of lens cells, a transformation from an epithelial cell phenotype to a myofibroblast is often described and is identified by expression of the marker protein, α-smooth muscle actin (α-SMA). Analysis of post-mortem material has shown that, in cases with PCO, there is evidence of contraction, cell aggregation, and matrix deposition in association with α-SMA expressing cells. The most likely candidate to cause this response is the cytokine, transforming growth factor-β (TGFβ). Understanding the role of TGFβ in lens fibrosis has become a major area of investigation. *In vitro* studies using rat explants, cell lines, and the human capsular model have demonstrated that the addition of TGFβ can induce marked transdifferentiation, matrix deposition, and cause matrix contraction.

Levels of active TGFβ are known to increase following injury, which arises from increased production and activation of a latent form of the cytokine, due to proteolytic cleavage of TGFβ binding proteins. The major isoform found in the eye is TGFβ2, but TGFβ1 and TGFβ3 can also be introduced following a breakdown of the blood-aqueous barrier. It has been reported that TGFβ-regulated Smad signaling proteins are present in the nuclei of cells in capsular bags following cataract surgery and wound healing responses can be suppressed by TGFβ antibodies. Therefore, TGFβ is available to lens cells following surgery and is capable of inducing the responses observed *in vivo*.

Post-mortem analysis of a capsular bag received from a donor 1 month following cataract surgery provided evidence of matrix contraction/wrinkling of the posterior capsule and transdifferentiation. Importantly, addition of TGFβ2 to *in vitro* human capsular bags replicated these events over a similar time frame. These effects could be produced after exposure to 10 ng ml^{-1} TGFβ for the first 2 days of culture or after exposure for the complete 28 day culture duration. The fact that significant long-term changes can result from a relatively short exposure to TGFβ is important because the level of active TGFβ in the aqueous humor of patients is likely to be highest within the first week following surgery; the results observed *in vitro* therefore support the idea that this increase is sufficient to provide a long-term contribution to PCO development. There are two possible mechanisms by which this could be achieved: first, through a positive feedback TGFβ level can be increased following TGFβ exposure and second TGFβ can bind to the lens capsule. One substrate with which TGFβ is reported to associate is collagen type IV, which constitutes the bulk of the lens capsule.

A commonly held view is that transdifferentiation of lens epithelial cells into the myofibroblast phenotype is a prerequisite for matrix contraction to occur. This notion is based on the assumption that α-SMA forms an integral part in the formation of contractile apparatus. Much of the evidence to support this theory is circumstantial based on the observation that α-SMA is expressed and matrix contraction occurs in response to TGFβ; on the face of it, this seems plausible. However, it has recently been shown, using the FHL 124 human lens cell line, that transdifferentiation does not appear to drive TGFβ-mediated matrix contraction. This argument is based on a number of results. A comparative study of TGFβ1 and TGFβ2 showed that the latter was a more potent inducer of transdifferentiation, but with respect to matrix contraction TGFβ1 was more potent. Moreover, through the use of siRNA targeted against α-SMA, TGFβ-induced α-SMA expression was suppressed, but matrix contraction was enhanced. In addition, using Arg-Gly-Asp-Ser (RGDS) peptide to block fibronectin/fibronectin receptor (α5β1 integrin) interaction, which is a process also reported to mediate transdifferentiation, leads to an enhanced rate of contraction. Therefore, TGFβ is capable of stimulating cells to undergo both transdifferentiation and matrix contraction, but the signaling pathways driving these events are different.

In terms of putative prevention of PCO, attempts to maintain a lens cell phenotype have been investigated. Application of lithium chloride (LiCl) to rat explant cultures successfully maintained the epithelial cells in a polarized state. In maintaining this phenotype, proliferation and migration were inhibited. Moreover, treatment with LiCl also prevented TGFβ-induced transdifferentiation, such that α-SMA expression was significantly suppressed. TGFβ has also been blocked directly, using a fully human monoclonal anti-TGFβ2 antibody. This antibody neutralizes the effects of TGFβ in a human lens cell line and *in vitro* human capsular bag model. A 2-day period of exposure to an *in vitro* capsular bag was sufficient to suppress TGFβ-induced matrix contraction, α-SMA expression, and Smad signaling for extended periods. The antibody is adsorbed by the lens capsule, which extends the longevity of its actions. However, it is important to note that neutralization of a single TGFβ isoform is probably insufficient to yield a positive therapeutic effect, due to the availability of other TGFβ isoforms following surgery; inhibition of all TGFβ isoforms could be a more productive route.

Summary

While improved IOL design has reduced the incidence of PCO, the problem still remains. Moreover, PCO is

impeding the introduction of accommodating lenses as a routine part of surgery. We are gaining a greater understanding of the biological mechanisms underpinning PCO development. Targeted inhibition of these mechanisms is likely to be of benefit to patients. It is important that both surgical and biological approaches are developed in concert to manage PCO and, as a result, improve the quality of life of millions.

See also: Lens Fiber Cell Differentiation; Lens Regeneration; Lens Structure; Posterior Subcapsular and Anterior Polar Cataract.

Further Reading

Awasthi, N. and Wagner, B. J (2006). Suppression of human lens epithelial cell proliferation by proteasome inhibition, a potential defense against posterior capsular opacification. *Investigative Ophthalmology and Visual Science* 47: 4482–4489.

Choi, J., Park, S. Y., and Joo, C. K. (2004). Hepatocyte growth factor induces proliferation of lens epithelial cells through activation of ERK1/2 and JNK/SAPK. *Investigative Ophthalmology and Visual Science* 45: 2696–2704.

Dawes, L. J., Eldred, J. A., Anderson, I. K., et al. (2008). TGF beta-induced contraction is not promoted by fibronectin-fibronectin receptor interaction, or alpha SMA expression. *Investigative Ophthalmology and Visual Science* 49: 650–661.

De Groot, V., Tassignon, M. J., and Vrensen, G. F. (2005). Effect of bag-in-the-lens implantation on posterior capsule opacification in human donor eyes and rabbit eyes. *Journal of Cataract and Refractive Surgery* 31: 398–405.

Duncan, G., Wang, L., Neilson, G. J., and Wormstone, I. M. (2007). Lens cell survival after exposure to stress in the closed capsular bag. *Investigative Ophthalmology and Visual Science* 48: 2701–2707.

Hancox, J., Spalton, D., Heatley, C., et al. (2007). Fellow-eye comparison of posterior capsule opacification rates after implantation of 1CU accommodating and AcrySof MA30 monofocal intraocular lenses. *Journal of Cataract and Refractive Surgery* 33: 413–417.

James, C., Collison, D. J., and Duncan, G. (2005). Characterization and functional activity of thrombin receptors in the human lens. *Investigative Ophthalmology and Visual Science* 46: 925–932.

Maidment, J. M., Duncan, G., Tamiya, S., et al. (2004). Regional differences in tyrosine kinase receptor signaling components determine differential growth patterns in the human lens. *Investigative Ophthalmology and Visual Science* 45: 1427–1435.

McAvoy, J. W. and Chamberlain, C. G. (1989). Fibroblast growth factor (FGF) induces different responses in lens epithelial cells depending on its concentration. *Development* 107: 221–228.

Saika, S., Miyamoto, T., Ishida, I., et al. (2002). TGFbeta-Smad signalling in postoperative human lens epithelial cells. *British Journal of Ophthalmology* 86: 1428–1433.

Stump, R. J., Lovicu, F. J., Ang, S. L., et al. (2006). Lithium stabilizes the polarized lens epithelial phenotype and inhibits proliferation, migration, and epithelial mesenchymal transition. *Journal of Pathology* 210: 249–257.

Walker, J. L., Wolff, I. M., Zhang, L., and Menko, A. S. (2007). Activation of SRC kinases signals induction of posterior capsule opacification. *Investigative Ophthalmology and Visual Science* 48: 2214–2223.

Wormstone, I. M., Del Rio-Tsonis, K., McMahon, G., et al. (2001). FGF: An autocrine regulator of human lens cell growth independent of added stimuli. *Investigative Ophthalmology and Visual Science* 42: 1305–1311.

Wormstone, I. M., Tamiya, S., Anderson, I., and Duncan, G. (2002). TGF-beta2-induced matrix modification and cell transdifferentiation in the human lens capsular bag. *Investigative Ophthalmology and Visual Science* 43: 2301–2308.

Wormstone, I. M., Wang, L., and Liu, C. S. (2009). Posterior capsule opacification. *Experimental Eye Research* 88: 257–269.

Posterior Subcapsular and Anterior Polar Cataract

C-K Joo, J-C Choi, and H-G Kwan, Catholic University, Seoul, South Korea
H Kim, Baekseok University, Cheonan, South Korea

Glossary

Amblyopia – Visual impairment resulting, in most cases, from an opacity or refractive error early in life, when the visual maps in the brain are undergoing functional refinement.
Curvilinear capsulorhexis – A surgical technique by which the anterior lens capsule and associated lens epithelial cells are removed at the beginning of modern cataract surgery. In the case of lenses with anterior polar cataracts, most or all of the opacity is removed in this process.
Fibrosis – A cellular response to injury involving the accumulation of excessive amounts of extracellular matrix materials. The excessive matrix interferes with the normal function of the tissue. In the case of lens fibrosis, the lens epithelial cell moves out of the epithelial cell layer but scattering light does not occur. The epithelial cells that moved are transformed by fibrosis and then the normal lens structure is broken down in the fibrosis zone.
Transdifferentiation – The conversion of one differentiated cell type to another. In this case, the conversion of lens epithelial cells to a myofibroblast-like cell.

Prevalence

Posterior subcapsular and anterior polar cataracts are often seen in patients younger than those presenting with nuclear, cortical, or mixed cataracts.

The prevalence of posterior subcapsular cataract was 10.2% in an Australian urban population over 40 years of age. In a population-based, cross-sectional study of elderly Chinese, the prevalence of posterior subcapsular cataract was 4.3%. The proportion of these cataracts in subjects in the age range of 40–49 years and 50–59 years was 1.2% and 4.1%, respectively. The proportion of female patients with incident posterior subcapsular cataracts has been reported to be 57.7%, suggesting that, like other age-related cataracts, females may be more susceptible to the condition.

Although the prevalence of anterior polar cataracts has not been reported in population-based studies, the prevalence of anterior polar cataracts as a fraction of total cataract patients is generally agreed to be quite low. However, in Korea, the prevalence of anterior polar cataract in total cataracts was high in comparison to the experience in other countries. In a hospital-based study, of the total percentage of all patients presenting for cataract surgery, 6.02% had anterior polar cataracts; of these, 87.0% were male. The mean age of patients with anterior polar cataract was 52.7 years; 38.9% were younger than 50 years of age, 42.6% were in their 50s, 14.8% in their 60s, and 3.7% in their 70s. The unusual geographic, age, and sex distribution of these opacities has not been explained.

Mechanisms

Cataractogenesis and Lens Epithelial Cells

The lens epithelium is the first site in the lens that is exposed to an insult coming through the cornea or in the aqueous humor that may result in cataract. Although lens epithelial cells have the machinery to combat cataractogenic insults, any damage to these cells may lead to cataract. Aging, stress, ultraviolet radiation, hydrogen peroxide, and cytokines are cataractogenic factors that may activate lens epithelial cell proliferation, migration, extracellular matrix (ECM) accumulation, and epithelial–mesenchymal transition (EMT), leading to cataract formation.

Anterior Polar Cataract

Anterior polar cataract is caused by the transdifferentiation and abnormal proliferation of lens epithelial cells and the accumulation of an abnormal ECM that is secreted by these cells.

Epithelial–Mesenchymal Transition

During the formation of anterior polar cataracts, lens epithelial cells transdifferentiate into large plaques of spindle-shaped, contractile cells, called myofibroblasts, by the process of epithelial–mesenchymal transition (EMT). EMT is a highly conserved, fundamental process that occurs during many phases of embryonic development in multicellular organisms. In mammals, EMT first occurs at the blastula stage, during the formation of the parietal endoderm, which later contributes to the formation of extraembryonic tissues. EMT is, later, involved in gastrulation, the formation of neural crest cells, and many other developmental processes. EMT or EMT-like processes also occur in a variety of disease mechanisms, including renal fibrosis, liver cirrhosis, and cancer metastasis.

Pathological fibrosis in various tissues involves modulation of the interaction between the cells and molecules of the ECM. Transforming growth factor-beta (TGF-β) has been implicated as a strong inducer of fibrotic diseases in many cell types. It is one of the well-characterized cytokines driving the transformation and pathological fibrosis of lens epithelial cells. When the monolayer lens epithelium is treated with TGF-β, the cells lose contacts with their neighbors and acquire a bipolar, elongated shape, bundles of microfilaments, and enriched rough endoplasmic reticulum. These are changes typical of EMT. Therefore, exposure to increased levels of TGF-β is a risk factor in the formation of anterior polar cataracts.

The accumulation and rearrangement of the ECM in anterior polar cataracts suggest that these cataracts involve alterations in the synthesis and/or degradation of matrix proteins. Many researchers have reported that ECM accumulates in anterior polar cataract tissue, including collagen types I and III, and fibronectin. These matrix components are also found in postoperative capsule opacification and are considered to be produced by fibroblast-like lens epithelial cells. Studies have also reported on the role of matrix metalloproteinases (MMPs) in cataract. The secretion of MMP-2 and MMP-9 was stimulated by the TGF-β or hydrogen peroxide in lens epithelial cells and MMP secretion induced transformation of lens epithelial cells. Inhibitors of MMPs have been reported to inhibit the formation of fibrotic plaques in cultured lenses.

It has been suggested that various growth factors may be involved in regulating matrix macromolecule production. TGF-β and fibroblast growth factor-2 (FGF-2) are the most likely candidates. Members of the FGF family are present in a gradient from anterior to posterior in the eye. FGFs regulate epithelial cell proliferation, migration, and differentiation. Both the mitogen-activated protein kinase (MAPK) and phosphoinositide 3-kinase (PI3K) signaling pathways have been implicated as downstream mediators of FGF-induced proliferation and differentiation. Members of the TGF-β and Wnt families of growth factors – which are involved in various stages of lens development – can also regulate the ability of lens epithelial cells to undergo EMT.

Steroid-Induced Cataract

Chronic treatment of patients or animals with steroids may induce a posterior subcapsular opacity in the lens. Steroid-induced posterior subcapsular cataracts occur bilaterally and are easily differentiated from the more common senile nuclear or cortical cataract and some other forms of posterior subcapsular cataract. At the cellular level, steroid-induced cataracts are associated with nucleated epithelial cells that migrate from the equatorial region to the posterior region of the lens.

Glucocorticoid

Glucocorticoids are highly effective anti-inflammatory agents for allergy, asthma, rheumatoid arthritis, and other autoimmune diseases. However, a significant risk exists for the development of complications when glucocorticoids are administered for an extended period at relatively high doses. One of the ocular complications of steroid treatment is the development of cataracts – specifically posterior subcapsular cataracts (PSCs). Despite studies of steroid-induced cataracts, the precise molecular mechanisms involved are unclear, partly because it is difficult to procure human samples.

A few animal models have been developed to examine the effects of glucocorticoids on the lens. After an intravitreal injection of glucocorticoid, opacification appeared in the rabbit lens beneath the posterior capsule. Long-term administration of steroids to rats also induced cataracts, in rats, that were similar to human steroid-induced cataracts. However, it takes more than 8 months to produce phenotypic changes with the *in vivo* model system. One of the mechanisms suggested for posterior subcapsular capsules formation is the inhibition of Na-K-ATPase by corticosteroids. This would increase intracellular sodium concentrations and decreases potassium levels, which leads to the accumulation of water within lens fiber cells.

Lens Epithelial Cell Migration

E-cadherin is a cell-adhesion protein that is normally expressed by lens epithelial cells. Decreased expression of E-cadherin protein followed the administration of steroids. This may account for the abnormal migration of epithelial cells along the capsule. Because the abnormal cells may have been impeded in their differentiation into fiber cells, it is possible that the adhesion of fiber cells to the posterior capsule or the interaction between fiber cells was disrupted. Therefore, the opacity may be caused by the abnormal migration of lens epithelial cells.

Additionally, the posterior capsular opacity by steroid requires signaling mediated by the glucocorticoid receptor. Glucocorticoids may induce new-gene expression including genes involved in signal transduction, transcription factor activity, cytoskeleton, ECM, cell adhesion, membrane transport, and cell cycle in the lens epithelial cells.

Clinical Aspects

Even though anterior polar cataracts and posterior subcapsular cataract involve the same mechanism of visual disturbance and both occur in the visual axis, patients experience more severe visual symptoms with posterior subcapsular opacities. Patients may have relatively little visual impairment with anterior polar cataracts, but may

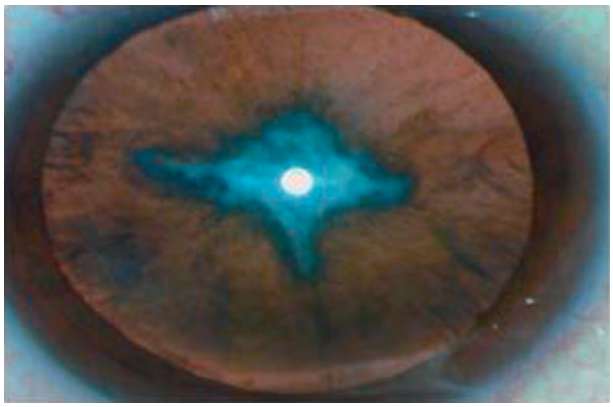

Figure 1 Anterior polar cataract. Courtesy of Choun-Ki Joo MD PhD.

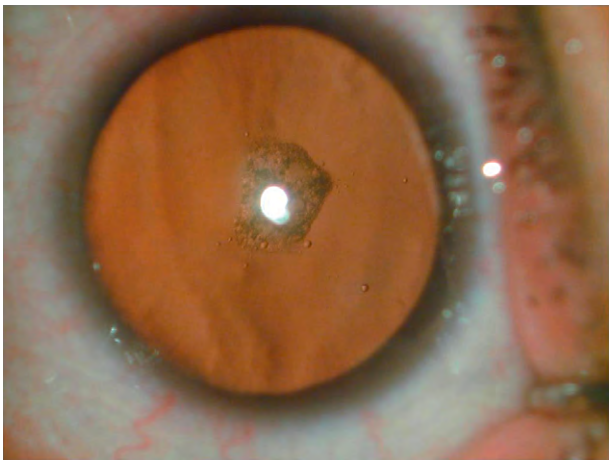

Figure 2 Posterior subcapsular cataract. Courtesy of Choun-Ki Joo MD PhD.

be severely impaired by PSCs. During cataract surgery, the anterior polar-type cataract may be removed easily after continuous curvilinear capsulorhexis, followed by phacoemulsification.

Anterior polar cataracts may present as a congenital (autosomal dominant inherited) or acquired opacities, secondary to uveitis or trauma. In the slit-lamp examination, anterior polar cataract usually has a star shape. It can lie flat on the lens surface or protrude forward from the lens as a small pyramid. However, the cause of most anterior polar cataracts is unknown in the Korean medical literature (**Figure 1**).

Anterior polar cataracts are divided into two groups. Opacities associated with the lens capsule and cataracts also involve the anterior lens fiber cells. Several theories may explain the mechanism of congenital anterior polar cataract. One suggests that the opacity may develop from an intrauterine infection, causing the transformation of epithelial cells. According to another theory, normal nutrition of the lens may be adversely influenced by a persistent vascular tunica that can lead to lens opacity.

Generally, anterior polar cataracts do not affect visual acuity as severely as those at the posterior pole. Traditionally, it has been thought that anterior polar cataracts <2 mm in size are unlikely to interfere with vision sufficiently to induce amblyopia. However, Jaafar and Robb noted a surprisingly high incidence of visual morbidity in 63 patients with anterior polar cataracts. More than one-third of patients were found to have strabismus, anisometropia, or amblyopia. They found that amblyopia did not result from enlargement of anterior polar opacities but occurred secondary to strabismus, anisometropia, and the presence of asymmetrically shaped opacities. Wheeler and colleagues also reported a high incidence of amblyopia. Amblyopia was related to three probable causative factors: (1) size of the opacity, (2) asymmetry of the opacity, and (3) superimposition of cortical changes.

Posterior subcapsular cataracts (**Figure 2**) occur at the posterior pole of the lens and are most often related with the aging process. They are mainly due to posterior migration of lens epithelial cells from the equator. These epithelial cells cluster, form balloon cells, and interdigitate with adjacent lens fibers and the deeper cortical fibers, breaking them down. The result is the lacy, granular, iridescent appearance of PSCs.

Patients with PSCs tend to have relatively good distance-acuity in low-light conditions, but markedly reduced near vision with glare in bright light or with night driving. The reason for this is that the reduced aperture in brighter light prevents the entrance of the more peripheral light rays, resulting in more light passing through the opacity. In PSCs, the opacity is also closer to the nodal point of the eye. It has been suggested that this is the reason that the PSC decreases visual acuity more significantly than does anterior polar cataract, although this remains a controversial explanation.

Posterior subcapsular cataract is the typical cataract type seen with different intraocular diseases (high myopia, retinitis pigmentosa, diabetes mellitus, uveitis, etc.), trauma, or drugs (corticosteroids, antimalarial agents, etc.). However, the cause of the cataract cannot be established from only the ocular appearances. PSCs may develop as isolated entities or may be associated with other types of lens opacities. Often, some granules and vacuoles are found in front of the posterior opacity.

The PSC is one of the most difficult challenges for the cataract surgeon because of the increased tendency for rupture of the posterior capsule during cataract removal. Osher and colleagues reported a 26% incidence of capsule rupture in a series of 31 cases, and Vasavada and Singh reported a 36% incidence in a series of 22 cases. Das and colleagues reported that posterior capsule rupture occurred in 25 (31%) eyes, and was more common in young patients (<40 years). These authors reported that posterior capsule rupture was more common in extracapsular cataract extraction with phacoemulsification. Many

Table 1 Comparison of the main features of anterior polar and posterior subcapsular cataracts

Cataract type	*Anterior polar cataract*	*Posterior subcapsular cataract*
Location	Anterior visual axis	Posterior visual axis
Causes	Congenital, uveitis, trauma	Aging, intraocular disease, drugs (steroids), ionizing radiation
Effect on visual acuity	In congenital cases, little effect or increased risk of amblyopia. In acquired cases, effect mostly in early stages	Impairment, even in early stages; glare and decreased visual acuity, especially in bright sunlight or when driving at night; vision better in dim illumination
Surgical outcome	Easily removed after continuous curvilinear capsulorhexis and standard cataract surgery	High incidence of posterior capsular rupture

techniques have been introduced to protect the posterior capsule during cataract surgery. Howard Fine and colleagues placed emphasis on avoiding pressure on the posterior capsule and stated that careful viscodissection of lens material will help the surgeon successfully meet this challenge. A comparison of anterior polar cataract and PSC is presented in Table 1.

See also: Cortical Cataract; The Epidemiology of Cataract; Genetics of Age-Related Cataract; Genetics of Congenital Cataract; Lens Structure; Normal Age-Related Changes: Crystallin Modifications, Lens Hardening; Nuclear Cataract; Posterior Capsule Opacification.

Further Reading

Das, S., Khanna, R., Mohiuddin, S. M., and Ramamurthy, B. (2008). Surgical and visual outcomes for posterior polar cataract. *British Journal of Ophthalmology* 92: 1476–1478.

De Iongh, R. U., Wederell, E., Lovicu, F. J., and McAvoy, J. W. (2005). Transforming growth factor-beta-induced epithelial-mesenchymal transition in the lens: A model for cataract formation. *Cells Tissues Organs* 179: 43–55.

Eshaghian, J. and Streeten, B. W. (1980). Human posterior subcapsular cataract: An ultrastructural study of the posteriorly migrating cells. *Archives of Ophthalmology* 98: 134–143.

Fine, I. H., Packer, M., and Hoffman, R. S. (2003). Management of posterior polar cataract. *Journal of Cataract and Refractive Surgery* 29: 16–19.

Font, R. L. and Brownstein, S. (1974). A light and electron microscopic study of anterior subcapsular cataracts. *American Journal of Ophthalmology* 78: 972–984.

Hennis, A., Wu, S.-Y., Nemesure, B., and Leske, C. (2004). Risk factors for incident cortical and posterior subcapsular lens opacities in the Barbados eye studies. *Archives of Ophthalmology* 122: 525–530.

Ishida, I., Saika, S., Okada, Y., and Ohnishi, Y. (2005). Growth factor deposition in anterior subcapsular cataract. *Journal of Cataract and Refractive Surgery* 31: 1219–1225.

Jaafar, M. S. and Robb, R. M. (1984). Congenital anterior polar cataract: A review of 63 cases. *Ophthalmology* 91: 249–254.

Joo, C. K., Lee, E. H., Kim, J. C., et al. (1999). Degeneration and transdifferentiation of human lens epithelial cells in nuclear and anterior polar cataracts. *Journal of Cataract and Refractive Surgery* 25: 652–658.

Kim, H. and Joo, C.-K. (2008). The prevalence and demographic characteristics of anterior polar cataract in a hospital-based study in Korea. *Korean Journal of Ophthalmology* 22: 77–80.

Kleiman, N. J. and Worgul, B. V. (1994). The lens. In: Tasman, W. (ed.) *Duane's Foundations of Clinical Ophthalmology*, pp. 1–15. Philadelphia, PA: Lippincott.

Lee, E. H. and Joo, C. K. (2000). Role of transforming growth factor-beta inducible gene betaig-h3 in anterior polar cataracts. *Investigative Ophthalmology and Visual Science* 41: 1840–1845.

Lyu, J., Kim, J. A., Chung, S. K., Kim, K. S., and Joo, C. K. (2003). Alteration of cadherin in dexamethasone-induced cataract organ-cultured rat lens. *Investigative Ophthalmology and Visual Science* 44: 2034–2040.

MacCarty, C. A., Mukesh, B. N., Fu, C. L., and Taylor, H. R. (1999). The epidemiology of cataract in Australia. *American Journal of Ophthalmology* 128: 446–465.

Marcantonio, J. M., Syam, P. P., Liu, C. S., and Duncan, G. (2003). Epithelial transdifferentiation and cataract in the human lens. *Experimental Eye Research* 77: 339–346.

Nagy, L., Módis, K., Kertész, P., Vámosi, E., and Balázs, A. (2004). Anterior polar cataract as a cause of monocular diplopia. *Journal of Cataract and Refractive Surgery* 30(7): 1596–1597.

Osher, R. H., Yu, B. C.-Y., and Koch, D. D. (1990). Posterior polar cataracts: A predisposition to intraoperative posterior capsule rupture. *Journal of Cataract and Refractive Surgery* 16: 157–162.

Seomun, Y., Kim, J., Lee, E. H., and Joo, C. K. (2001). Overexpression of matrix metalloproteinase-2 mediates phenotypic transformation of lens epithelial cells. *Biochemical Journal* 358: 41–48.

Vasavada, A. R. and Singh, R. (1999). Phacoemulsification in posterior polar developmental cataracts. In: Lu, L. W. and Fine, I. H. (eds.) *Phacoemulsification in Difficult and Challenging Cases*, pp. 121–128. New York, NY: Thieme.

Wederell, E. D. and de Iongh, R. U. (2006). Extracellular matrix and integrin signaling in lens development and cataract. *Seminars in Cell and Developmental Biology* 17: 759–776.

Wheeler, D. T., Mullaney, P. B., Awad, A., and Zwaan, J. (1999). Pyramidal anterior polar cataracts. *Ophthalmology* 106: 2362–2367.

Xu, L., Cui, T., Zhang, S., et al. (2006). Prevalence and risk factors of lens opacities in urban and rural Chinese in Beijing. *Ophthalmology* 113: 747–755.

Presbyopia

A Glasser, University of Houston, Houston, TX, USA

Glossary

Accommodation – The dioptric change in optical power of the eye to focus at near. In the young phakic eye, this occurs through an increase in the lens anterior and posterior surface curvatures.
Cataract – An optical opacification of the natural lens that most often occurs through the natural process of aging, but can also result from injury to the lens. A cataract can ultimately reduce the quality of vision if the cataract develops within an area of the lens through which light normally passes to reach the retina.
Depth of field – The range of movement of an object in object space over which there is no perceptible change in focus of the image.
Depth of focus – The range of movement of the image in image space over which there is no perceptible change in focus of the image.
Emmetropia (or an emmetropic eye) – An eye without a refractive error (i.e., without hyperopia or myopia). An unaccommodated emmetropic eye would be normally focused for infinity.
Far point – The point of focus of the eyes when accommodation is relaxed. For an emmetropic eye, this is optical infinity.
Hyperopia (referred to as far-sighted) – A refractive error of the eye in which, technically, the eye is in focus for a virtual object behind the retina, that is, the far point of a hyperopic eye is behind the retina. For a hyperopic eye, there is no distance in front of the eyes at which an object can be positioned so that the image is in focus on the retina when accommodation is relaxed.
Myopia (referred to as near-sighted) – A refractive error in which the eye is focused for an object that is closer to the eye than optical infinity, that is, the far point of the eye is at a closer distance to the eye than optical infinity.
Near point – The closest point of focus of the eyes when the eyes are maximally accommodated.
Phakic eye – An eye that still retains the natural lens.
Presbyopia – The age-related loss of accommodative amplitude which is primarily due to a loss in the ability of the lens to undergo accommodative optical changes. Ultimately, by about 55 years of age the human eye completely loses the ability to accommodate.
Pseudo-accommodation – Some degree of functional near vision that can be attained through nonaccommodative means such as due to ocular aberrations, multifocal optics (such as from a contact lens or an intraocular lens (IOL)), or an increased depth of field of the eye.
Pseudophakic eye – An eye in which a cataract surgical operation has been performed to remove the natural phakic lens to replace it with an artificial IOL.

Accommodation

Accommodation is defined as a dioptric change in power of the eye with an effort to focus at near. In the natural young phakic eye, accommodation is due to an increase in the optical power of the lens. The increase in the optical power of the lens comes about through an increase in the lens anterior and posterior surface curvatures. An effort to focus on a near object results in a contraction of the ciliary muscle, an inward movement of the inner apex of the ciliary body toward the axis of the eye. This results in a relaxation of zonular tension around the lens equator to allow the elastic capsule surrounding the lens to mold the young lens into a more spherical and accommodated form. Accommodation is not simply the ability of a distance-corrected eye to see clearly at near. For example, in a complete presbyope with no accommodation, some degree of functional near vision can be achieved by placing a multifocal contact lens on the cornea. The multifocal contact lens may permit the presbyopic eye some degree of simultaneous focus at both near and distance. This is not an active process but is due to the multifocal optics of the contact lens. The ability of an eye to achieve some degree of functional near visual acuity without active accommodation is called pseudo-accommodation. Many factors can contribute to pseudo-accommodation including an increased depth of field of the eye due to multifocal optics, a small pupil diameter which results in an increase in depth of field, or the presence of ocular optical aberrations such as astigmatism, spherical aberration, or coma. Further, if vision is available to both eyes, some degree of simultaneous near and distance vision can be achieved with one eye corrected for distance and the other corrected for near. This is monovision and as with pseudo-accommodation it can provide some relief to the

symptoms of presbyopia to allow a patient to see at both distance and near, but it is clearly very different from the active optical change in power of the eye that occurs with accommodation.

Presbyopia

Presbyopia is defined as the gradual and progressive age-related loss of accommodative amplitude and is ultimately due to an age-related loss in the ability of the lens to undergo accommodative optical changes (**Figure 1**). Presbyopia is ubiquitous in that every person who lives to beyond 50–55 years of age will ultimately and inevitably, completely lose the ability to accommodate. The impact and symptoms of presbyopia are felt most strongly by emmetropes and uncorrected hyperopes. An emmetropic eye, with a far point at optical infinity, must accommodate to focus clearly on objects at any distance closer to the eyes than optical infinity. The hyperopic eye, with a far point behind the eye, must accommodate to focus clearly on an object at any distance in front of the eye, including for an object at optical infinity. This is only possible if the hyperopic eye has sufficient amplitude of accommodation

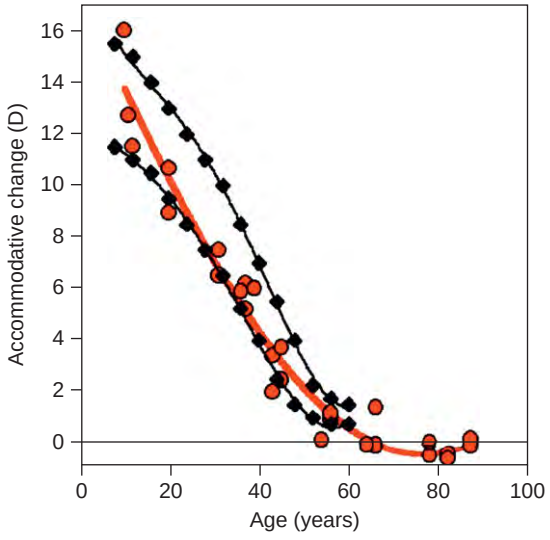

Figure 1 Mechanical stretching studies on human eye bank eyes (red circles) ranging from 10 to 86 years of age show that young human lenses are able to undergo about 12–16 D of accommodative change and that by the age of about 60 years the same amount of mechanical stretching fails to produce any systematic accommodative change in optical power of lenses over 60 years of age. The data from enucleated human eyes are plotted together with the range of subjectively measured accommodative amplitudes from more than 1000 human subjects (black diamonds) taken from Duane (1912). Reproduced from Glasser, A. and Campbell, M. C. W. (1998). Presbyopia and the optical changes in the human crystalline lens with age. *Vision Research* 38: 219, with permission from Elsevier.

to overcome the hyperopic defocus as well as the vergence due to the near object. Myopes suffer the symptoms of presbyopia to a lesser degree than emmetropes and hyperopes. The far point of the uncorrected myopic eye is at a distance in front of the eye closer than optical infinity and therefore myopes can focus on objects at this distance without the need to accommodate by simply removing their distance correction.

Presbyopia represents a complete failure of the normal physiological function of accommodation roughly two-thirds of the way through the normal human life span. The progression of presbyopia actually begins early in life (**Figure 1**) and results in a gradual and progressive decrease in objectively measured accommodative amplitude from about 10 D around 10 years of age ultimately to 0 D by about 55 years of age. The word presbyopia (Greek, *presbys* meaning an aged person and *opsis* meaning vision) possibly derives from Aristotle's use of the term presbytas to describe those who see well at distance, but poorly at near. Historically, the term presbyopia was used to describe the condition where the near point has receded too far from the eye for normal near-vision tasks due to a loss of accommodation. Since the accommodative mechanism was first described by Helmholtz and Gullstrand, it has generally been understood that presbyopia results from an age-related loss of accommodation due to an increase in stiffness of the lens. Normal, emmetropic individuals start to experience the symptoms of presbyopia by about 40–45 years of age. These symptoms include blurred vision at near, visual fatigue or headache after attempting to read at near for prolonged periods, or an inability to sustain clear vision at a normal reading distance. These symptoms usually occur when the amplitude of accommodation decreases to below about 3–4 D. For patients first experiencing the symptoms of presbyopia, it often appears that presbyopia is of sudden onset. However, presbyopia progresses gradually for many years and it is only by about 40–45 years of age that patients for the first time start experiencing the symptoms of not having sufficient accommodation to adjust the focus of their eyes for the habitual reading or working distance.

Our current understanding of the accommodative mechanism and the age-related changes in the eye comes from studying human eyes as well as the eyes of rhesus and cynomolgus monkeys. The anatomy of the accommodative apparatus of the rhesus monkey eye is similar to that of humans. Young rhesus monkeys have high accommodative amplitudes and rhesus monkeys are the only animal species known to experience the same age-related loss of accommodation as humans. Although the life span of rhesus monkeys is shorter than that of humans, they develop presbyopia with a similar relative age-course as humans when adjusted for life span. Presbyopia may be a symptom of outliving the functional life span of the

accommodative system due to increased longevity. Few tissues in the body continue to grow throughout life. Among those that do are nails, hair, and the lens. There are no adverse consequences to continued growth of nails and hair and failure of the primary physiological function of essential organs, such as the heart and liver, would ultimately be incompatible with life; however, in the case of the lens, continued growth ultimately results in a loss of one of its primary functions, that is, accommodation. Loss of accommodation may simply represent the organism outliving one of the physiological functions of the lens. For humans who might once have had a life span less than 40 years, presbyopia would never have become symptomatic. In monkeys in the wild in which life span is shorter than in captivity, reduced life span may be exacerbated by a loss of normal visual function, including accommodation. However, it has also been suggested that from an evolutionary perspective, presbyopia may be adaptive in the hierarchy of monkeys where time spent by the alpha male and other elders on the lookout, scanning the distance for predators rather than performing near-vision tasks requiring accommodation may serve as an important survival strategy for the troop. The modern-day near-obsession with presbyopia may be as much due to suffering the symptoms longer as it is due to the perceived negative connotations or cosmetic insult attributed to reading glasses.

Age-Related Changes in the Eye

There are a myriad of age-related changes in the various anatomical components of the eye involved in the accommodative mechanism that could possibly contribute to the loss of accommodation. For accommodation to occur, there must be a fine balance of forces between the stiffness of the lens nucleus and cortex, the elasticity of the lens capsule and the zonular fibers, and the ciliary muscle and ciliary body. Any disruption to this balance of forces could contribute to a loss of accommodation. Age-related changes have been reported in just about every aspect of the accommodative anatomy and potentially any of these age-related changes could contribute to the loss of accommodation. The most important aspects of the accommodative system are the ciliary muscle which serves as the engine that drives accommodation, the zonular fibers that extend from the ciliary body to insert around the lens equator and in the unaccommodated eye apply an outward-directed tension to maintain the lens in a relatively flattened and unaccommodated state, the lens capsule surrounding the lens that provides the force to change the shape of the lens, and the lens nucleus and cortex that must undergo a change in shape to allow accommodation to occur. Age-related changes have been described in all these tissues. For example, there is a progressive age-related decrease in area and length of the ciliary muscle as well as a change in the configuration of the ciliary muscle (**Figure 2**). There is a decrease in area of the longitudinal and reticular fibers of the ciliary muscle and an increase in area of the circular fibers of the muscle. With increasing age in the unaccommodated eye, the ciliary muscle appears more like an accommodated ciliary muscle with a progressive forward and inward movement of the inner apex of the ciliary muscle and ciliary body. This may occur in part due to the ciliary body being gradually pulled inward by increasing tension on the zonular fibers inserting around the lens equator

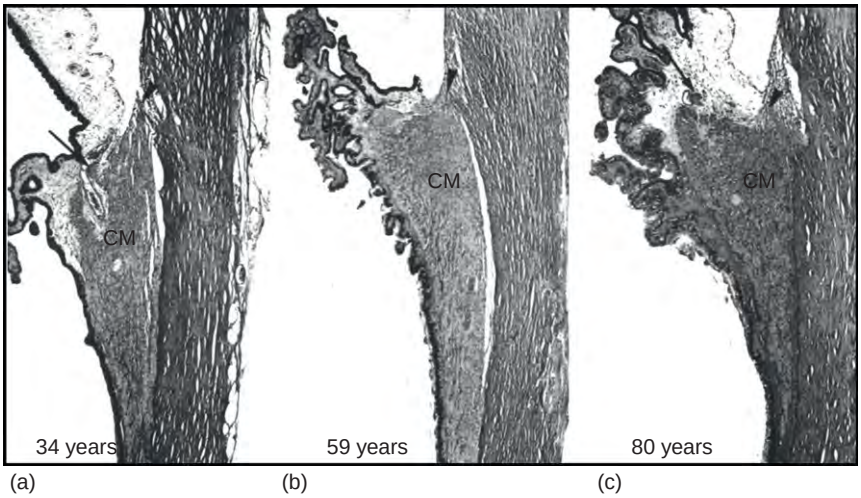

Figure 2 With increasing age the unaccommodated, atropinized human ciliary muscle shows a configurational change such that the older ciliary muscle appears more like an accommodated ciliary muscle with the inner apical region advancing forward of the scleral spur. Reproduced from Tamm, S., Tamm, E., and Rohen, J. W. (1992). Age-related changes of the human ciliary muscle. A quantitative morphometric study. *Mechanisms of Ageing and Development* 62: 217, with permission from Elsevier.

(see below), or simply due to growth-related changes in the ciliary muscle. There are also age-related changes in the relative distribution of ciliary muscle fibers within the ciliary muscle and other morphological changes in the ciliary muscle. The age-related configurational change of the ciliary muscle results in a decrease in the circumlental space with increasing age. In rhesus monkeys, there is an age-related loss of compliance of the posterior attachment of the ciliary which may serve to reduce the ciliary muscle motility; however, there is no age-related loss of contractility of the isolated rhesus monkey ciliary muscle. In spite of the age-related changes in the ciliary muscle, it still remains active with an accommodative effort even in complete presbyopes. The ciliary muscle is, like the iris, an intraocular muscle. The iris is known to continue to contract throughout life in response increased illumination to constrict the pupil. Similarly, the ciliary muscle is unlikely to become quiescent even in complete presbyopes. Convergence, pupil constriction, and accommodation are neurologically coupled in the brain. Every attempt to focus at near or even to converge the two eyes to achieve single, binocular vision on a near object will result in a neuronal stimulus to the ciliary muscle to cause a contraction even in the presbyopic eye. Accommodative contraction of the ciliary muscle occurs with an effort to focus at near in presbyopes even in the absence of any accommodative changes in lens thickness or lens diameter, thereby demonstrating that the ciliary muscle moves even though no accommodative optical change occurs in the lens or eye. Similarly, in rhesus monkeys, irrespective of age, accommodative movements of the ciliary body are always greater than the accommodative movements of the lens. This shows that accommodative movements of the lens limit accommodation through all ages and that at its end point, presbyopia is not due to a loss in contractility of the ciliary muscle.

Age-Related Changes in the Lens

The lens is surrounded by the thin, elastic lens capsule. Lens epithelial cells line the anterior surface of the lens under the capsule. These epithelial cells, like epithelial cells in the rest of the body (such as on the skin and those lining the gut), continue to proliferate throughout life. However, unlike the epithelial cells on the skin and lining the gut which can slough off, because the lens is surrounded by the capsule, lens epithelial cellular proliferation results in a continued age-related increase in mass, size, and volume of the lens. The mass of the isolated human lens increases linearly with age after adolescence (**Figure 3**). Lens axial thickness increases linearly with age, but without a systematic increase in lens diameter (**Figure 4**). The increased volume and axial thickness without a systematic increase in equatorial diameter

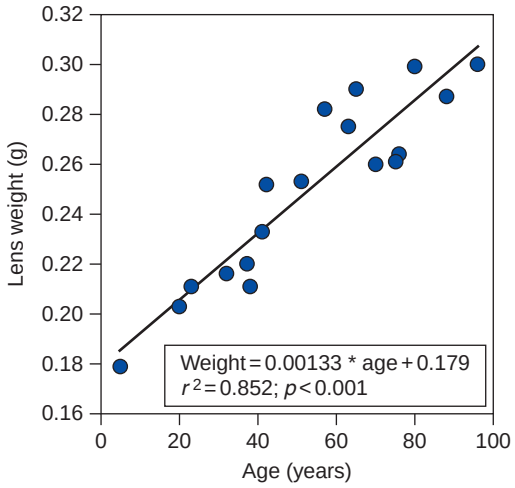

Figure 3 Wet weight of isolated human lenses from donor eyes aged 5–96 years of age increases linearly reflecting the increased growth of the lens. Reproduced from Glasser, A. and Campbell, M. C. W. (1999). Biometric, optical and physical changes in the isolated human crystalline lens with age in relation to presbyopia. *Vision Research* 39: 1998, with permission from Elsevier.

result in an increase in the lens anterior surface curvature. Posterior lens surface curvature does not change systematically with increasing age. The continued growth of the lens results in a decrease in anterior chamber depth of the eye and an increase in anterior segment length (the distance from the cornea to the posterior lens surface). The anterior most zonular fiber insertion into the capsule undergoes an anterior shift with increasing age. This may result in an increased zonular tension around the lens equator and could be partially responsible for the configurational changes observed in the ciliary muscle (described above). In addition, there are internal changes in the lens. Optically evident so-called zones of discontinuity observed with slit-lamp illumination are thought to represent visible boundaries between the nucleus and cortex. These visible zones of discontinuity show that there is a greater increase in axial thickness of the cortex of the lens than of the nucleus with increasing age.

The age-related increases in lens anterior surface curvature and axial thickness may make the older lens appear to be in a more accommodated form and might therefore be expected to result in a progressive age-related increase in optical power of the unaccommodated lens resulting in a myopic progression of the eye. However, presbyopia is characterized by a loss of near vision, rather than a myopic progression with increasing age. This leads to what has been referred to as the lens paradox, that is, how it is that the eye progressively loses near vision despite changes in the lens that might be expected to increase the power of the lens and eye, leading to a more myopic eye. The resolution to this paradox resides in the fact that there is a progressive age-related decrease

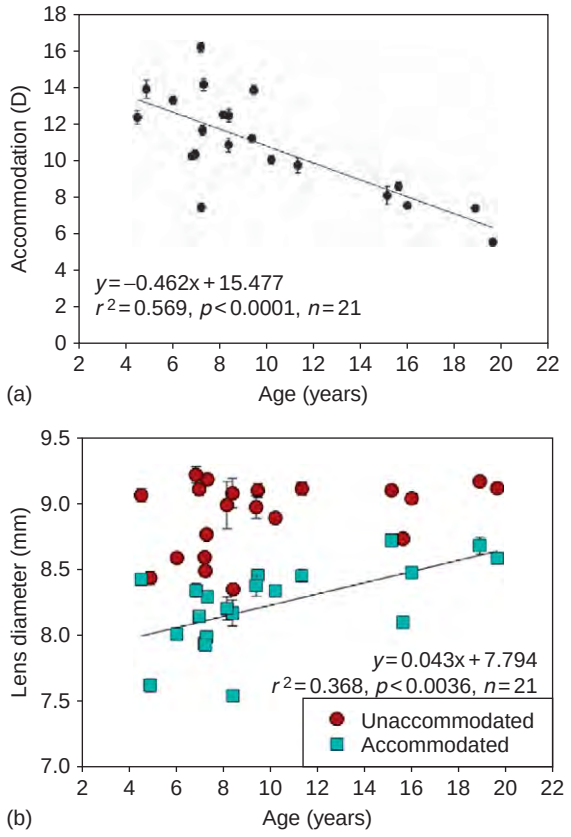

Figure 4 (a) Age-related loss of pilocarpine-stimulated accommodation in 21 rhesus monkeys ranging in age between 5 and 20 years of age. (b) Unaccommodated lens equatorial diameter (circles) as a function of age show no systematic change with increasing age. Pilocarpine-stimulated accommodation causes a decrease in lens diameter (squares) with the accommodative change in lens diameter decreasing with increasing age. Reproduced from Wendt, M., Croft, M. A., McDonald, J., et al. (2008). Lens diameter and thickness as a function of age and pharmacologically stimulated accommodation in rhesus monkeys. *Experimental Eye Research* 86: 751, with permission from Elsevier.

in the overall refractive index of the nucleus. The lens has a gradient refractive index with a greater refractive index at the center of the lens than at the periphery. This gradient refractive index adds additional refractive power to the lens. The refractive index of the surface of the lens does not change systematically with increasing age. The age-related decrease in refractive index of the nucleus can be explained by the observed aggregation, insolubilization, and precipitation of lens proteins (the lens crystallins) and a resulting increase in free water content of the aging lens nucleus. In spite of the age-related increase in anterior lens surface curvatures, which would tend to increase lens power, the increased lens thickness and the reduced nuclear refractive index actually result in a slight overall age-related decrease in lens power in the unaccommodated eye.

Age-Related Changes in the Capsule

The elasticity of the lens capsule produces the accommodative change in shape of the young lens and as such, age-related changes in the properties of the capsule may influence the ability of the capsule to mold the lens. In a young eye, zonular tension around the lens equatorial region holds the lens in a relatively flattened and unaccommodated state. If these zonular fibers are cut, the young lens is molded into a maximally accommodated form by the capsule. If the lens capsule is then carefully cut and removed from the young lens, the isolated, decapsulated lens substance returns to an unaccommodated form. This means that the resting state of the young isolated, decapsulated lens is maximally unaccommodated, whereas with the capsule on, but without zonular tension, the lens is maximally accommodated. The change in shape of the lens substance from the accommodate to the unaccommodated form with decapsulation progressively decreases with increasing age to the point that removing the capsule from a presbyopic lens results in no change in shape of this older lens. The implications of this are that in the older eye, either the capsule has lost the elasticity to mold the presbyopic lens or the presbyopic lens has become too stiff for the capsule to mold it or both changes have occurred with increasing age. Mechanical stretching studies of isolated rings from the anterior surface of human lens capsules show that the elastic modulus increases with increasing age up to about 35 years of age with no significant change thereafter (**Figure 5**). Thus, the capsule may actually become increasingly effective at transmitting accommodative forces to the lens with increasing age during the pre-presbyopic years.

Increased Stiffness of the Lens

The progressive age-related increase in stiffness of the lens is now widely regarded as the primary cause of the age-related loss of accommodation. The lens substance growing in size and mass within the confines of the capsule becomes progressively more compacted and undergoes an exponential increase in stiffness (**Figure 6**). This results in an over fourfold increase in stiffness between approximately 5 and 100 years of age. In the young lens, the nucleus is softer than the cortex. With increasing age, the stiffness of both the nucleus and cortex increases but there is a greater increase in stiffness of the nucleus than the cortex (**Figure 7**). At about 35 years of age, the stiffness of the nucleus and cortex is approximately the same, but after this age the nucleus becomes progressively stiffer than the cortex. This represents a change in the stiffness gradient of the lens with a relatively greater increase in stiffness at the center of the lens and a smaller increase in stiffness

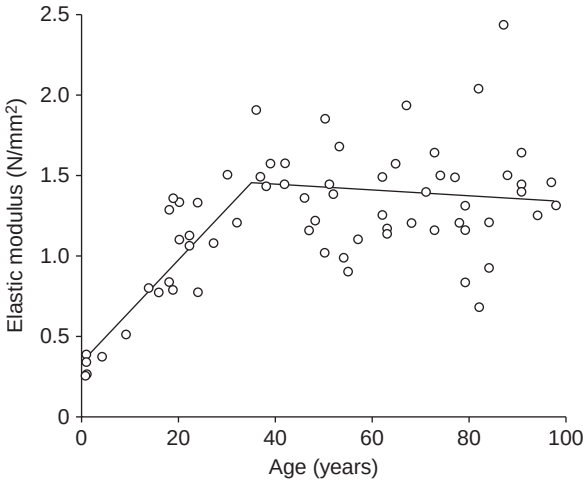

Figure 5 For low strains representing the range that might be expected to occur with accommodation (0–10% of breaking strain) there is an age-related increase, up to age 35, in the elastic modulus of capsular rings cut from the anterior surface of human lens capsules. After the age of 35, there is no systematic change in anterior capsular ring elastic modulus. These data suggest that the human lens capsule actually becomes increasingly effective at transmitting the forces to the lens that are required for accommodation to occur. Reproduced from Krag, S. and Andreassen, T. T. (2003). Mechanical properties of the human lens capsule. *Progress in Retinal and Eye Research* 22: 757, with permission from Elsevier.

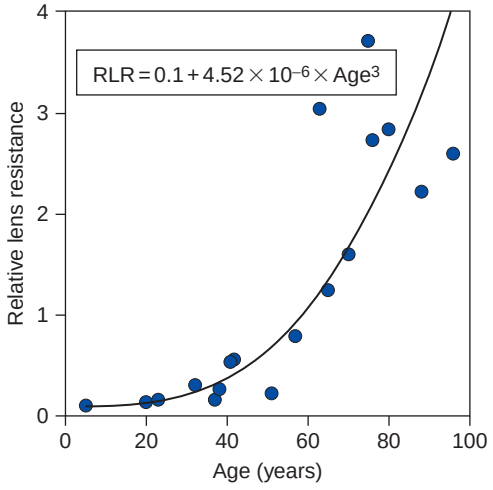

Figure 6 Mechanical squeezing of isolated, intact human lenses shows an exponential increase in resistance of the human lens between 5 and 96 years of age. Reproduced from Glasser, A. and Campbell, M. C. W. (1999). Biometric, optical and physical changes in the isolated human crystalline lens with age in relation to presbyopia. *Vision Research* 39: 2006, with permission from Elsevier.

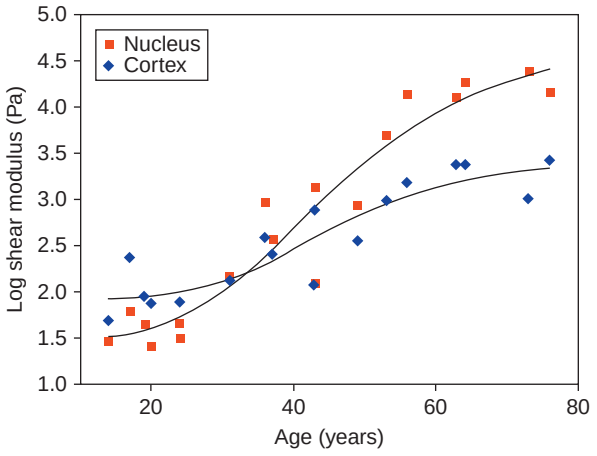

Figure 7 A probe inserted into different regions of equatorially sectioned human lenses shows that in the younger lenses the sheer modulus of the nucleus is less than the cortex, but with increasing age there is a greater increase in the sheer modulus of the nucleus than the cortex. Reproduced from Heys, K. R., Cram, S. L., and Truscott, R. J. (2004). Massive increase in the stiffness of the human lens nucleus with age: The basis for presbyopia? *Molecular Vision* 10: 959, with permission from Molecular Vision.

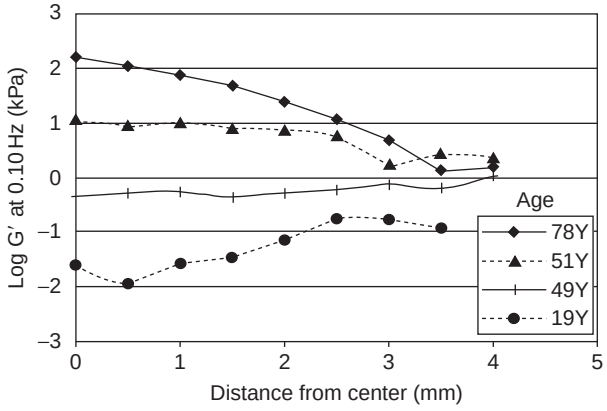

Figure 8 Sheer modulus values determined from inserting a probe into four equatorially sectioned human lenses. In the youngest lens, the sheer modulus is lowest at the center of the lens and increases progressively toward the cortex, whereas in the oldest lens, the sheer modulus is greatest at the cortex and decreases toward the cortex. Both the nucleus and the cortex undergo an increase in sheer modulus with increasing age, with a relatively greater increase toward the center of the lens than toward the periphery. This represents not only an increase in stiffness of the lens, but also a relative increase in the stiffness gradient. Reproduced from Weeber, H. A., Eckert, G., Pechhold, W., and van der Heijde, R. G. L. (2007). Stiffness gradient in the crystalline lens. *Graefe's Archives for Clinical and Experimental Ophthalmology* 245: 1362, with kind permission of Springer Science + Business Media.

progressively further from the center of the lens toward the surface (**Figure 8**). Although accommodation is essentially completely lost by age 55, the increase in stiffness of the lens continues throughout life. This suggests that the age at which accommodation is lost simply represents a time point in the continuum of age-related changes occurring in the lens. It is likely that as the stiffness of the lens nucleus and cortex progresses, there is a progressive change in the fine

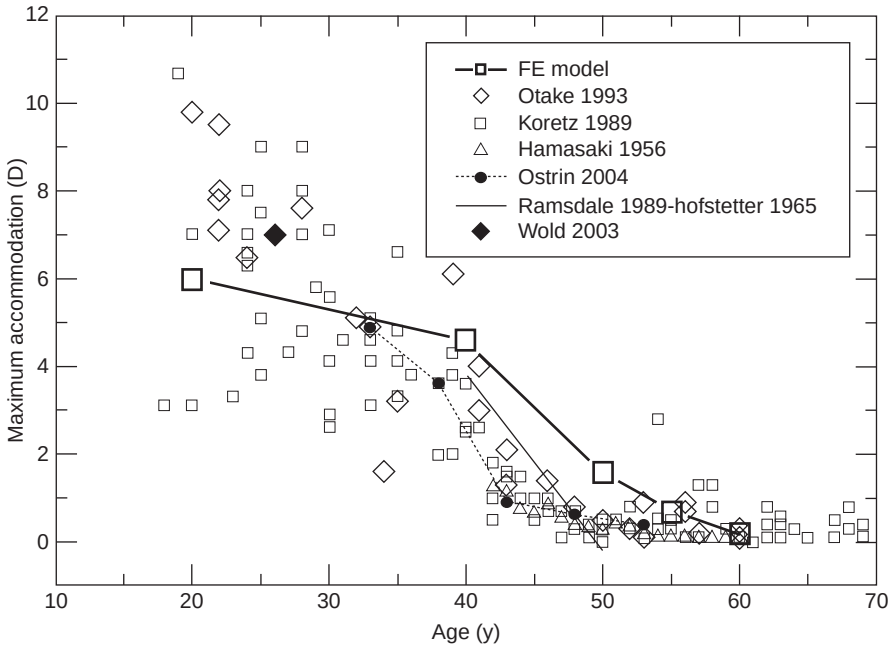

Figure 9 The age-related decrease in the accommodative response in a finite element (FE) model of accommodation (FE model) of a 40-year-old lens in which the only age-dependent parameter modeled was the empirically measured age-related change in stiffness gradient of the lens. The response from the model is compared with objectively measured accommodative response amplitudes from a variety of different human clinical studies. The FE model incorporating an age-dependent stiffness gradient in the lens is able to capture most of the age-related decrease in accommodative amplitude observed in human clinical studies. Reproduced from Weeber, H. A. and van der Heijde, R. G. (2007). On the relationship between lens stiffness and accommodative amplitude. *Experimental Eye Research* 85: 605, with permission from Elsevier.

balance of forces within the lens substance, capsule, and zonules such that ultimately a point is reached when the accommodative forces that can be generated on the lens by the capsule is insufficient to overcome the resistance of the stiffer lens. In the young eye, accommodation results in an increase in thickness of the nucleus but without a change in thickness of the cortex. It is therefore the cortex surrounding the lens that may be molding the lens to allow the lens to undergo the changes in shape required for accommodation to occur. This system may be effective at producing changes in shape of the nucleus when the nucleus is less stiff than the cortex as in the young lens, but this process may become increasingly ineffective as the nucleus becomes stiffer than the cortex. Finite element modeling shows that the age-related loss of accommodation can be relatively accurately predicted by incorporating the age-related change in stiffness gradient of the lens without incorporating age-related changes in other parameters of the model (such as lens size and surface curvatures) (**Figure 9**). Modeling an overall increase in stiffness of the lens as opposed to the stiffness gradient is less predictive of the age-related loss of accommodation. This further suggests that the fine balance of forces between the lens nucleus and cortex is important to allow accommodation to occur and that this fine balance of forces is also ultimately lost by the progressive age-related changes that occur in the lens.

See also: Accommodation.

Further Reading

Dubbelman, M., van der Heijde, G. L., and Weeber, H. A. (2005). Change in shape of the aging human crystalline lens with accommodation. *Vision Research* 45: 117–132.

Glasser, A. and Campbell, M. C. W. (1998). Presbyopia and the optical changes in the human crystalline lens with age. *Vision Research* 38: 209–229.

Glasser, A. and Campbell, M. C. W. (1999). Biometric, optical and physical changes in the isolated human crystalline lens with age in relation to presbyopia. *Vision Research* 39: 1991–2015.

Glasser, A., Croft, M. A., and Kaufman, P. L. (2001). Aging of the human crystalline lens and presbyopia. *International Ophthalmology Clinics* 41: 1–15.

Heys, K. R., Cram, S. L., and Truscott, R. J. (2004). Massive increase in the stiffness of the human lens nucleus with age: The basis for presbyopia? *Molecular Vision* 10: 956–963.

Krag, S. and Andreassen, T. T. (2003). Mechanical properties of the human lens capsule. *Progress in Retinal and Eye Research* 22: 749–767.

Poyer, J. F., Kaufman, P. L., and Flügel, C. (1993). Age does not affect contractile responses of the isolated rhesus monkey ciliary muscle to muscarinic agonists. *Current Eye Research* 12: 413–422.

Stachs, O., Martin, H., Kirchhoff, A., et al. (2002). Monitoring accommodative ciliary muscle function using three-dimensional ultrasound. *Graefe's Archives for Clinical and Experimental Ophthalmology* 240: 906–912.

Strenk, S. A., Semmlow, J. L., Strenk, L. M., et al. (1999). Age-related changes in human ciliary muscle and lens: A magnetic resonance

imaging study. *Investigative Ophthalmology and Visual Science* 40: 1162–1169.

Tamm, E., Croft, M. A., Jungkunz, W., Lütjen-Drecoll, E., and Kaufman, P. L. (1992). Age-related loss of ciliary muscle mobility in the rhesus: Role of the choroid. *Archives of Ophthalmology* 110: 871–876.

Tamm, S., Tamm, E., and Rohen, J. W. (1992). Age-related changes of the human ciliary muscle. A quantitative morphometric study. *Mechanisms of Ageing and Development* 62: 209–221.

Weeber, H. A. and van der Heijde, R. G. (2007). On the relationship between lens stiffness and accommodative amplitude. *Experimental Eye Research* 85: 602–607.

Weeber, H. A., Eckert, G., Pechhold, W., and van der Heijde, R. G. L. (2007). Stiffness gradient in the crystalline lens. *Graefe's Archives for Clinical and Experimental Ophthalmology* 245: 1357–1366.

Wendt, M., Croft, M. A., McDonald, J., Kaufman, P. L., and Glasser, A. (2008). Lens diameter and thickness as a function of age and pharmacologically stimulated accommodation in rhesus monkeys. *Experimental Eye Research* 86: 746–752.

Primary Open-Angle Glaucoma

D Spiegel, University of Regensburg, Regensburg, Germany

Glossary

Bjerrum's area – An arc-shaped area from 5° to 30° in the central visual field, it is the site of typical visual defects in primary open-angle glaucoma.
Chamber angle – The angle between the cornea and the iris.
Gonioscopy – Method to gain a view of the iridocorneal angle by means of a goniolens or gonioscope in conjunction with a slit lamp or operating microscope.
Iridocorneal angle – Angle between the iris and cornea at the periphery of the anterior chamber.
Laser trabeculoplasty – Laser treatment in primary open-angle glaucoma which increases the aqueous humor outflow through the trabecular meshwork.
Myopia – Visual defect where light is focused in front of the retina rather than on it.
Perimetry – A method used to detect visual field defects in glaucoma.

Introduction

Primary open-angle glaucoma (POAG) is characterized by an open anterior chamber angle without any gonioscopic abnormalities. A relatively elevated intraocular pressure (IOP) is considered to cause damage and loss of retinal ganglion cells, which results in typical glaucomatous alterations of the optic nerve head. The loss of ganglion cells corresponds to the loss of visual field in a clinical pattern typical for glaucoma. Consecutively, this will lead to blindness in untreated aggressive cases.

Most of the patients affected with POAG do not recognize any symptoms before a substantial loss of ganglion cells occurs, which causes an advanced irreversible visual field defect. Therefore, POAG is still the second most common cause (12.3%) for blindness in the world (2002 WHO).

The main risk factors for developing and worsening of glaucoma have been identified as age, IOP, family history, myopia, and diabetes mellitus. These factors play an important role in the diagnosis and treatment of the disease.

Definition

Primary open-angle glaucoma is defined as an acquired optic neuropathy, based on a chronic progressive loss of retinal nerve fibers and retinal ganglion cells. These ganglion cell losses are responsible for a typical glaucomatous pattern of visual field defects. In POAG, the iridocorneal angle must be open and there should be no secondary etiology.

Clinically, the signs for glaucoma include: a relatively elevated IOP, glaucomatous optic disk damage, nerve fiber bundle losses seen in the red free retinal image, and visual field defects in a pattern that is typical of glaucoma.

Pathophysiology

To date, the pathogenesis of POAG is still not fully understood. It is believed that the relatively elevated IOP results from increased resistance within the aqueous drainage system. Changes in the trabecular meshwork are considered to be responsible for the outflow restriction. Other reasons for optic neuropathy may include mechanical theories – based on direct pressure-induced damage to the retinal ganglion cell axons at the level of the lamina cribrosa. On the other hand, vascular theories propose microvasculatory changes that result in ischemia in the optic nerve head.

Risk Factors

The term risk factor refers either to risk factors for an increase of prevalence and incidence or for the worsening of POAG.

The prevalence and incidence of POAG increase with higher IOP, older age, Afro-Caribbean race, positive family history, myopia, and diabetes mellitus – the last two are still under debate. Elevated IOP of over 26 mmHg has a 13-fold risk for glaucoma. Age is the second most important risk factor. The prevalence of POAG is 2.1% for individuals over the age of 40. Hereby, the range of prevalence is found to be 0.3% at 40, 3.3% at 70, and over 10% in humans over 80 years of age. The Afro-Caribbean race tends to have a 3.8-fold higher incidence of glaucoma than the white population. Individuals with a family history of glaucoma have a 3.14-fold higher relative risk of developing glaucoma. The highest association is found in siblings of glaucomatous patients. Some of the studies demonstrated that patients with diabetes mellitus have a 1.93-fold, and those with myopia have a 1.88-fold, higher risk of POAG.

The risk factors for worsening of the glaucomatous disease are: IOP above the target pressure, disk hemorrhages, stage of glaucomatous damage, age, perfusion

pressure, history of cardiovascular diseases, and reduced central corneal thickness.

Intraocular Pressure

In the last century, the search for the upper limit of a normal pressure was based on a Gaussian distribution of the IOP in the normal population, in which the readings of the pressure in excess of two standard deviations was 20.5 mmHg, resulting in a fixed pressure value of −21 mmHg. Since elevated IOP has been dropped from the modern definition of glaucoma, this definition (IOP > 21 mmHg) is no longer acceptable. As of now, it is more important to determine the target pressure in each individual patient, considering the increased IOP as a risk factor for developing – and worsening of – glaucoma. Therefore, the target pressure is defined as a level of IOP under which the disease of glaucoma in the individual patient does not progress. To assess the target pressure, several nonevidence-proofed suggestions are made based on the stage of glaucoma and the results of the latest large glaucoma studies with regard to the treatment and natural course of glaucoma (see **Table 1**).

The golden standard for IOP measurement is taken by the Goldmann applanatory tonometer (GAT). Other methods used include noncontact air pulse tonometry, Tono-Pen, or dynamic contour tonometry.

The GAT measurements are influenced by the central corneal thickness. A thicker cornea (above 550 µm) leads to false higher readings and a thinner cornea to false lower IOP measurements. Edema in the cornea causes false lower IOPs. Following refractive corneal surgery, the IOP measured is also substantially lower. Therefore, this needs to be taken into consideration in diagnosis and treatment of glaucoma as well.

The IOP increases with age. From birth to the age of 12 years, the IOP slowly increases from 7 to 12 ±3 mmHg. In healthy adults, the IOP ranges from 10 to 21 mmHg.

Optic Disk Appearance in POAG

The most important objective signs for detecting glaucoma are changes of the optic nerve head (optic disk), which can be detected by direct ophthalmoscopy on slit-lamp examination. The leading clinical signs for glaucoma can be divided into qualitative and quantitative changes at the optic disk. The qualitative signs can again be classified into signs that are found nearly in all eyes with glaucoma only and signs that are also found in up to 50% of healthy eyes.

Definitive qualitative signs for glaucoma at the optic disk are baring of vessels, notches in the optic nerve-head rim, disk hemorrhages, and a peripapillary atrophy zone-β. Less certain signs at the optic disk for glaucoma are bayoneting vessels, nasal cupping of the optic disk, and a bare lamina cribrosa (see **Figure 1(a–c)**).

The baring of vessels develops after the loss of nerve tissue at the optic rim. Once the nerve tissue is reduced, the vessel is left hanging over the lamina cribrosa similarly to a bridge. Afterward, the vessel will slide down to the floor of the bottom of the lamina cribrosa. This entity is only seen in damaged disks. Circumscriptive sectional loss of healthy optic rim results in so-called notches. These notches of the optic nerve-head rim are located most commonly in the upper temporal and lower temporal rim. Peripapillary chorioidal atrophies slowly increase in eyes affected by glaucoma. There are two zones distinguished: zone-β – which is adherent to the disk – and zone-α – which is located temporal to zone-β. While zone-α is frequently seen in healthy eyes, zone-β is found in 62% of glaucomatous eyes and in only 22% of healthy eyes. Bayoneting vessels are retinal vessels which have the form of a bayonet when leaving the optic nerve head. Due to the nerve tissue loss, the excavation of the disk is so extensive that the vessel is hidden under the rim. With the progression of the glaucoma, this sign becomes more pronounced. Nasal cupping is seen when the rim loss of the nerve head can be noticed nasal to the main retinal vessel trunk. In summary, all qualitative signs, except disk hemorrhage, can be directly related to the loss of nerve tissue at the optic disk.

The quantitative signs for glaucoma are the cup-to-disk ratio (CDR) and the nerve-fiber thickness. The CDR is the equation of the optic disk size to the healthy optic rim. In glaucoma-damaged eyes, the vertical CDR is larger than the horizontal CDR. It is believed that the optic nerve head at the lamina cribrosa is more vulnerable

Table 1 Delphi panel recommendations for initial target pressures

Patients with elevated IOP	*Target pressure (mm Hg)*	*Range (mm Hg)*	*Minimum % IOD reduction*
Early glaucoma damage	18	16–21	25%
Moderate glaucoma damage	16	14–18	30%
Advanced glaucoma damage	12	10–14	35% (40%)
Glaucoma suspect	22	18–24	20%
Normal tension glaucoma (early)		30%	
Normal tension glaucoma		35%	Hawai 2002

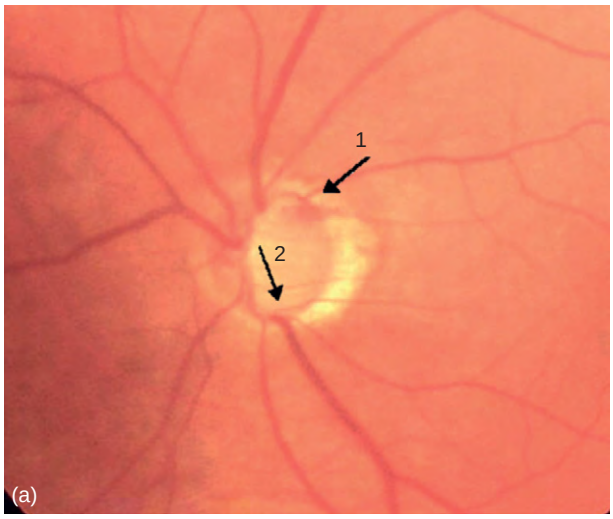

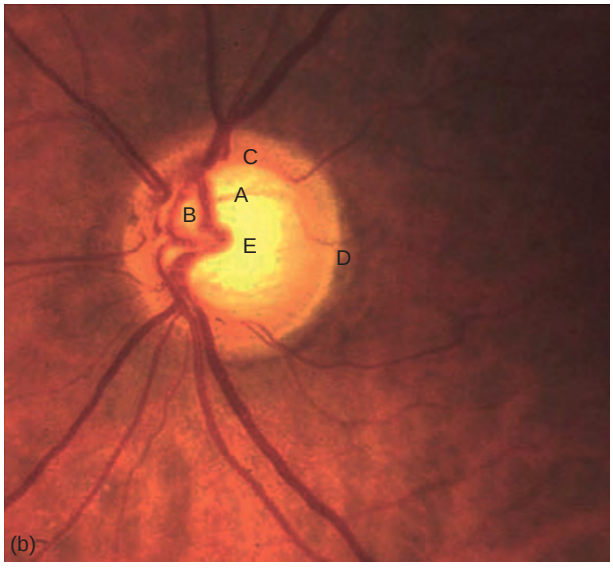

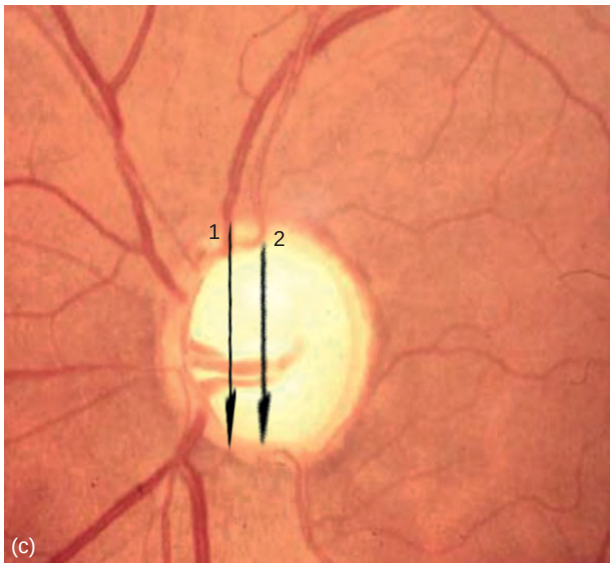

to raised IOP in the inferior and superior cups. In a normal disk, the healthy rim on average is broadest in the inferior temporal sector followed, in a declining fashion, by the superior temporal, nasal, and temporal sector; this is described as the "isn't" rule. The nerve-fiber-bundle loss can be seen at the level of the retina ophthalmoscopically in red-free light.

For a long time, a CDR >0.5 was considered suspicious for glaucoma. However, in larger disks the CDR will be greater than in smaller disk, since the retinal fibers are quite constant in numbers and, thus, a greater CDR would be mistaken for glaucomatous cupping in a larger disk. On the other hand, in a smaller disk the cupping might be underestimated and glaucomatous damage overlooked.

For documentation of the optic nerve head and/or the nerve-fibre layer, methods such as colored fundus photos, scanning images with laser light (Heidelberg Retinal Tomography (HRT)), nerve fiber analyzer (GDx), or optic coherence tomography (OCT) are currently in use. These methods allow a quantification of the nerve tissue or layer and are used for the detection of slow progression of nerve-tissue loss typical in glaucoma.

Visual Field

Visual field defects demonstrate the functional impairment as a result of nerve-fiber loss and localized nerve-fiber-bundle defects. To definitely determine the presence of glaucomatous damage, the detection of visual field defects is necessary; however, this requires the subjective test of perimetry. Since the testing of the visual field needs concentration and good compliance from the patient, a learning curve can be observed in visual field testing. Thus, the first visual field taken from a patient is usually not valid.

The conventional standard method to detect visual field defects attributable to glaucoma is the static computerized perimetry, known as standardized automated perimetry (SAP). Different types of perimeters from different companies are in use, all of which fulfill the standards of testing for glaucoma patients. However, the testing conditions are not the same in each of these instruments (e.g., background illumination) and the numbers representing loss of light sensitivity are not comparable between different instruments. Therefore, the detection of glaucomatous defects and worsening of the functional impairment need the same kind of perimeter with the same testing program.

Figure 1 (a) Optic disk hemorrhage in glaucoma (arrow 1) and notch (arrow 2). (b) Signs for glaucoma on a disk. A: baring vessel, B: nasal cupping, C: bayoneting of vessels, D: parapapillary atrophy (zone-β), and E: bare lamina cribrosa, vertically pronounced CDR. (c) Advanced glaucomatous disk cup (arrow 2)-to-disk (arrow 1) ratio of 0.9.

Nonconventional perimetric methods are developed and utilized in order to detect defects in glaucoma earlier. These methods include short-wavelength automated perimetry (SWAP) or blue/yellow-perimetry, frequency-doubling technology (FDT), high-pass resolution perimetry (HRP), and flicker perimetry. The value of these methods for early detection of glaucomatous defects is still under debate and, in the future, longitudinal studies are warranted. At present, SAP is the standard method for diagnosis and assessment for treatment in glaucoma.

To detect typical visual defects in glaucoma, the central 30° visual field – which requires up to 20 min of testing – is sufficient. To avoid patient fatigue, 24° programs are in use, which reduce the testing time from 8 to 13 min.

Since the beginning of the last century, a typical pattern of visual defects could be found in patients having glaucoma. These patterns help to diagnose glaucoma and to detect the disease at the earliest. The breakthrough in the early detection of defects in glaucoma was the work of Jannik Petersen Bjerrum, at the University of Copenhagen, who found small paracentral defects in the central 30° visual field. Since then, glaucomatous defects have been defined systematically.

The typical visual defects in glaucomatous patients include nasal steps, small localized defects (scotomas) in Bjerrum's area (an arc-shaped area from 5° to 30° in the central visual field but sparing a central island of fixation), enlarged blind spots, and small sector-shaped temporal defects. Most often, the defects occur in the upper central area and in the lower nasal step area. However, glaucomatous visual defects can also occur in any location of the upper or lower Bjerrum's area. The progressing visual field is characterized by scotomas increasing in size and depth – mainly in an episodic manner – by fresh scotomas or sector-shaped defects, or by generalized loss of retinal sensitivity. The progression can occur suddenly but, often, is more gradual. The disease is usually asymmetrically present in both eyes and can lead to a compensation of visual impairment resulting in one normal field for the patient. This might be the main reason for the late subjective recognition of the disease. The late stage of visual impairment is characterized by subtotal loss of the peripheral and paracentral visual field, in which the central island and a temporal peripheral field is spared (see **Figure 2**).

Treatment

At present, the treatment of glaucoma comprises of lowering of the IOP to below a certain target pressure, below which the disease is considered to be nonprogressive. The quality of life of the patient should be taken into consideration when choosing the therapeutic options in terms of side effects of the treatment.

There are two possible physiological ways of lowering the IOP: to reduce the production of aqueous humor and/or to increase the aqueous humor outflow through the trabecular meshwork or into the suprachorioidal space.

These can be achieved by local medications – in the form of eye drops – by laser surgery and/or surgical interventions.

Medical Treatments

There are six different medical treatment groups: β-blockers, α_2-selective adrenergic agonists, prostaglandin derivates, carbonic anhydrase inhibitors, pilocarpine, and dipiverin/epinephrine.

β-blockers, α_2-selective adrenergic agonists, and carbonic anhydrase inhibitors reduce the aqueous humor production, whereas pilocarpine increases the aqueous humor outflow through the trabecular meshwork. Dipiverin and epinephrine are nonselective adrenergic agents, which reduce aqueous humor production and increase the aqueous humor outflow simultaneously. In contrast, prostaglandin derivatives increase the outflow of aqueous humor only through the subchorioidal space. The range of IOP reduction is different for each group and varies on average from 15% to 33% according to different studies, depending on the baseline pressures. Prostaglandins have proven to have the best effect in lowering IOP – up to 33%. The use of combined medications may lead to an additional effect and reaches 50% IOP reduction. Due to the half-life of each different medication, the frequency of application varies from once daily to 4 times a day. The higher frequency of application of eye drops can result in a reduced effectiveness of medical treatment because of the variability subject to patient compliance.

Laser Treatments

Argon laser trabeculoplasty (ALT) and selective laser trabeculoplasty (SLT) are laser treatments used in POAG that increase the outflow at the site of the trabecular meshwork. The production of the aqueous humor can be reduced by laser coagulation of the ciliary body with cyclophotocoagulation (CPC).

Both ALT and SLT are applied gonioscopically at the anterior chamber angle where the trabecular meshwork can be located. Individual spots are circumferentially applied on to the trabecular meshwork. The results of both methods do not appear to be substantially different. A pressure reduction of about 30% can be achieved; however, the effect diminishes across 5 years and repeated application has been demonstrated to have a much lower effect. Both methods are used to achieve a reduction in medications or as a procedure for gaining time to delay surgical intervention in patients with less aggressive glaucomatous disease. On the other hand, CPC can reduce the

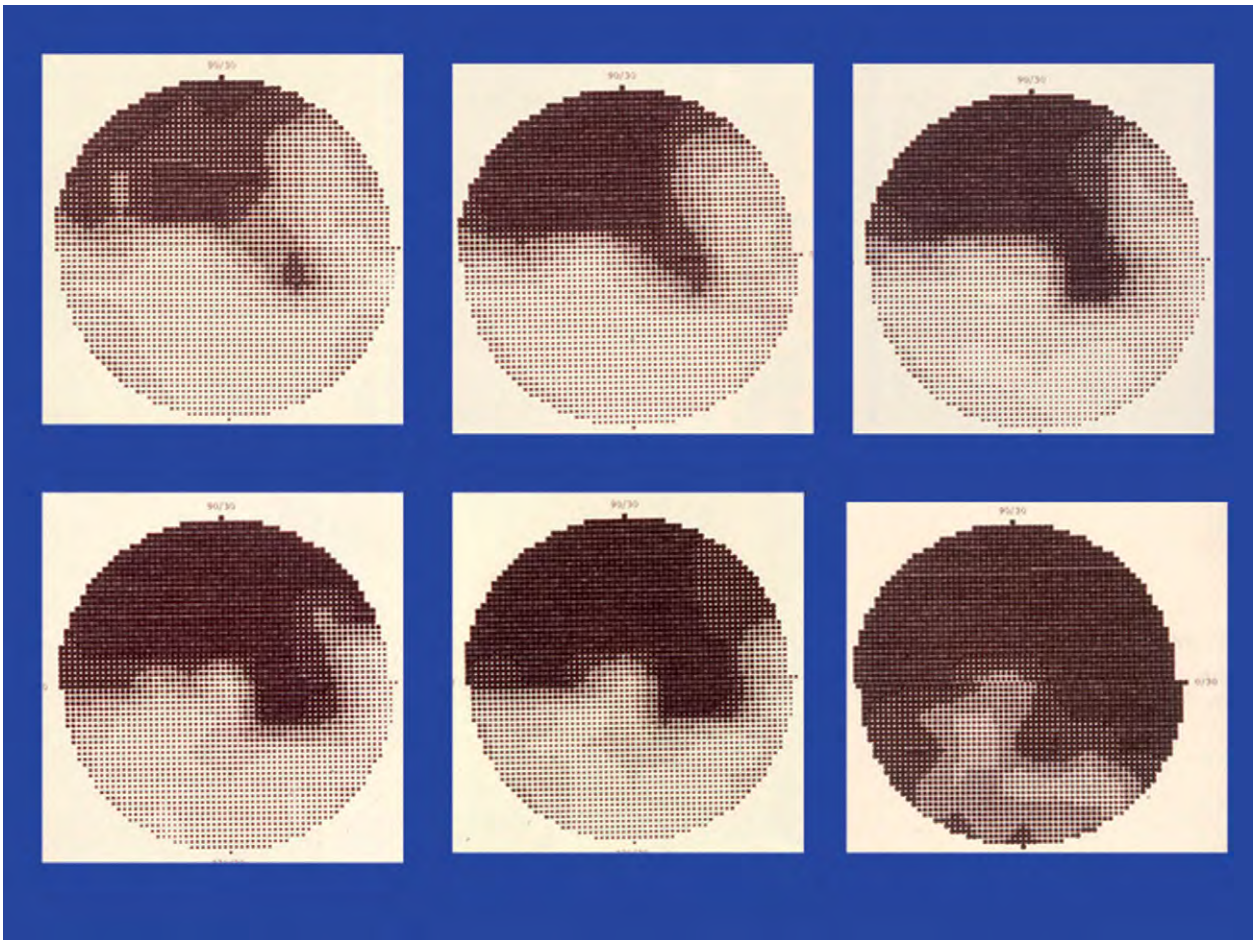

Figure 2 Natural course and field progression observed in a patient who refused treatment.

production of aqueous humor. In CPC, a diode laser is trans-sclerally applied to coagulate the tissue of the ciliary body. Conventionally, the method was applied to eyes in which other surgical methods were less successful. Side effects such as inflammation and hypotony (low IOP) can occur. CPC is safer and has fewer complications in comparison to freezing techniques (cyclocryo) that were commonly used previously.

Surgical Treatment

The most commonly performed surgical procedures are trabeculectomy with or without antimetabolites (mitomycin C or 5-fluorouracil) and implantation of shunts such as the Baerveldt, Molteno, Krupin Implants (without a valve mechanism) and the Ahmed valve (with a valve mechanism). All of these surgical procedures create a fistula that connects the anterior chamber to the subconjunctival space. Thus, they are categorized as fistulating penetrating procedures. These procedures can lower the IOP to 50% or more, independent of the baseline pressure. However, the short- and long-term side effects and complications must be carefully taken into consideration based on the needs and the situation of the individual patient.

Nonpenetrating procedures (canaloplasty, viscocanaloplasty, deep sclerectomy, etc.) and procedures that connect the anterior chamber with Schlemm's canal (trabeculotomy, i-stent) have lesser side effects. However, the long-term pressure reduction is less than what is seen in fistulating penetrating procedures.

The decision of a therapy regimen for POAG includes medical treatment, laser treatment, surgical procedures, and a combination of any/or all of the above-mentioned treatments and is based upon the required target pressure, the side effects of the chosen treatment, the anatomy of the eye, and the individual situation and needs of the patient.

See also: Control of Aqueous Humor Flow; Functional Morphology of the Trabecular Meshwork; Intraocular Pressure and Damage of Optic Nerve Axons; Pharmacology of Aqueous Humor Formation; Pharmacology of the Aqueous Humor Outflow; Structural Changes in the Trabecular Meshwork with Primary Open Angle Glaucoma.

Further Reading

Allingham, R. R., Shields, M. B., Damji, K. F., et al. (2005). *Shield's: Textbook of Glaucoma*, 5th edn. Philadelphia, PA: Lippincott Williams and Wilkins.

European Glaucoma Society (2008). *Terminology and Guidelines for Glaucoma*, 3rd edn. http://www.eugs.org/ebook-new.asp (accessed July 2009).

Kwon, Y. H. and Caprioli, J. (2009). Primary open-angle glaucoma. In: Tasman, W. and Jaeger, E. A. (eds.) *Duane's Ophthalmology,* 15th edn. Philadelphia, PA: Lippincott Williams and Wilkins.

Rivera, J. L., Bell, N. P., and Feldman, R. M. (2008). Risk factors for primary open angle glaucoma progression: What we know and what we need to know. *Current Opinion of Ophthalmology* 19: 102–106.

Primary Photoreceptor Degenerations: Retinitis Pigmentosa

M E Pennesi, P J Francis, and R G Weleber, Oregon Health and Sciences University, Portland, OR, USA

Glossary

Allied disorders – Retinitis pigmentosa (RP) is often grouped with a class of more stable, inherited retinal disorders collectively referred to as RP and allied disorders. Some of these allied disorders cause similar clinic findings as RP, e.g., nyctalopia (night blindness), but usually do not show progression and deterioration with time. An example is congenital stationary night blindness (CSNB), which can present with nyctalopia and decreased rod and cone function on the electroretinogram (ERG). Unlike RP, most patients with CSNB have stable visual function. X-linked CSNB is caused by mutations in nyctalopin (NYX) and L-type voltage dependent calcium channel (CACNA1F). Although the majority of mutations of rhodopsin causes typical RP, rare mutations, such as G90D in rhodopsin, produce night blindness with such mild progression late in life that they have been called stationary night blindness. Another allied disorder is achromatopsia, which is caused by mutations in cyclic nucleotide-gated channel subunits (CNGA2, CNGB3) or guanine nucleotide alpha-binding protein 2 (GNAT2). Achromatopsia is associated with severely decreased central and color vision, photophobia, and nystagmus. These symptoms are similar to those that can be seen with some cone–rod dystrophies. Indeed, later in life some modest foveal atrophy can occur and cases of progressive cone–rod dystrophy have been associated with mutations of some of the achromatopsia genes. However, unlike cone–rod dystrophies, which invariably progress, achromatopsia is, in the vast majority of cases, stationary.

Cone dystrophy – Cone photoreceptors are affected and rod photoreceptors are minimally affected or spared in cone dystrophy. Many cases of early cone dystrophies with time will develop significant rod abnormalities.

Cone–rod dystrophy – Cone-rod dystrophy, as a group, involves both photoreceptors with cones affected more than rods. Certain forms of RP present with greater cone than rod involvement on ERG and these patients have been termed to have cone–rod RP. However, in cone–rod dystrophies as a group the primary defect lies in cones and secondaryrod loss occurs with time. Most investigators consider primary cone–rod dystrophy separate from RP.

Extrinsic factor – An agent external to the organism that contributes to or is causative of a disease state. This can include drugs, foods, normal nutrients (excess or deficiency), toxins, inhaled chemicals, infectious agents, and exposures to radiation such as light, sound, and high-energy particles.

Intrinsic factor – An agent that is inherent to the organism that contributes to or is causative of a disease state.

Mixed intrinsic and extrinsic etiology for a secondary photoreceptor degeneration – This occurs when a person has a genetic variant that creates a toxic metabolite in the presence of an extrinsic molecule that would normally not be encountered.

Mixed model of primary and secondary photoreceptor degeneration – This is considered when a genetic alteration within the photoreceptors is insufficient to cause photoreceptor degeneration by itself, but predisposes to degeneration in the presence of an extrinsic or intrinsic agent. A second mode of combined primary and secondary photoreceptor degeneration is when one group of photoreceptors, such as the rod photoreceptors, undergoes a primary degenerative process that is due to a mutation in a gene that is expressed in those photoreceptors and precipitates apoptosis, which leads to a secondary degenerative process, in this example cones, due to alterations in the cellular environment induced by death of neighboring cells.

Primary retinal degeneration – This occurs when cells in the retina, usually photoreceptors, die secondary to a process that originates within the retina itself. An example of a primary retinal degeneration is RP, which is caused by mutations in genes that encode proteins important for retinal function. A disease can be classified as a primary retinal degeneration if the genetic defect is such that correction of expression of the normal gene product in the photoreceptors is required to correct the abnormality and arrest the degeneration.

Primary retinal degeneration with secondary photoreceptor degeneration – This occurs when photoreceptor degeneration is the result of mutation(s) of a gene that exists in other retinal cells, for example,

retinal pigment epithelial (RPE) cells. Correction of the genetic defect would require modification of the effects of those other retinal cells (e.g, RPE cells).

Retinal atrophy – A broad term encompassing not only processes that occur with retinal degenerations, but also abnormal retinal tissue or cellular loss due to developmental defects and malnutrition.

Retinal degeneration – A process whereby cells in the retina undergo cell death by apoptosis. Most retinal degenerations affect both rod and cone photoreceptors, but some disorders reflect damage that occurs principally in other cell types, e.g., the RPE in Stargardt's disease and other ABCA4-related retinopathies. Secondary degeneration of the RPE is also common. Transsynaptic degeneration of higher-order cells, bipolar and ganglion cells, can also occur. The general term retinal degeneration should be distinguished from the more specific term, photoreceptor degeneration.

Retinal dystrophy – A broad term that not only encompasses retinal degenerations, but also includes abnormal retinal function due to developmental defects and malnutrition.

Retinitis pigmentosa (RP) – A heterogeneous group of diseases that result in degeneration of the rod and cone photoreceptors and secondarily the RPE. This degeneration usually leads to a loss of night vision due to the early degeneration of rods, constricted visual fields, decreased responses on ERG, and ultimately a decrease in visual acuity once macular cones begin to degenerate. Typical fundus findings include midperipheral atrophy of the pigment epithelium, bone spicule pigments, retinal vessel attenuation, and waxy pallor of the optic nerve. The term RP usually refers to only rod-cone dystrophies; however, cone-rod dystrophies and cone dystrophies are sometimes grouped under this term.

Rod–cone dystrophy – A retinal dystrophy in which the rod photoreceptors are affected more than the cones. Most forms of RP manifest as rod–cone dystrophies.

Secondary photoreceptor degeneration of the extrinsic type – A secondary photoreceptor degeneration of the extrinsic type exists if, despite the underlying molecular defect, one could avoid the photoreceptor degeneration by preventing an individual's exposure to an extrinsic agent or condition (e.g., toxin, drug, infectious agent, light, and trauma).

Secondary photoreceptor degeneration of the intrinsic type – If one can prevent photoreceptor degeneration by correcting or reversing a systemic or ocular metabolic or immune process, then it is a secondary photoreceptor degeneration of the intrinsic type.

Background

Retinitis pigmentosa (RP) is caused by a large number of genetic defects that result in a characteristic pattern of degeneration of the rod and cone photoreceptors and the retinal pigment epithelium (RPE). This degeneration usually leads to a loss of night vision due to the early degeneration of rods, constricted visual fields, decreased responses on electroretinogram (ERG), and ultimately a decrease in visual acuity once macular cones begin to degenerate. The typical fundus exam in RP reveals midperipheral atrophy of the pigment epithelium, bone spicule pigmentation, retinal vessel attenuation, and waxy pallor of the optic nerve (Figure 1).

RP was first named by the Dutch ophthalmologist, Frans Cornelius Donders, in the mid-nineteenth century, although earlier clinical descriptions of the disease exist. The term retinitis pigmentosa is somewhat of a misnomer because inflammation is not thought to be the primary pathological mechanism. Rather, mutations in over 100 genes have been shown to cause RP and its allied disorders, and there still remain a significant number of genes yet to be identified. To keep track of the ever-growing list of genes implicated in this disease, a comprehensive online database, Retnet, has been established by Dr. Stephen Daiger.

One of the most fascinating aspects of RP is that mutations in genes that encode functionally distinct

Figure 1 Classic fundus appearance in retinitis pigmentosa demonstrating bone spicule pigmentation, vascular atrophy, retinal pigment epithelium atrophy, and waxy pallor of the optic nerve. From Weleber, R. and Evan, K. G. (2006). Retinitis pigmentosa and allied disorders. In: Ryan, S. J. (ed.) *The Retina*, 4th edn., vol. 1, chap. 17, pp. 395–498. Philadelphia, PA: Elsevier.

proteins result in a common degenerative pathway. Some of the many examples include genes involved in the structural integrity of the photoreceptors and cilia, the retinoid cycle, the phototransduction cascade, the extracellular matrix, cellular metabolism, intracellular trafficking, and RNA processing.

Prevalence

The worldwide prevalence for all forms of RP has been reported to be approximately 1:4000. While most studies have focused on the prevalence in European/Caucasian populations, the occurrence of RP has been reported throughout the world.

Inheritance

All forms of Mendelian inheritance have been reported but autosomal dominant, recessive, and X-linked traits are most frequently seen. Rarely RP is inherited as a digenic disorder or through the maternal line as a mitochondrial disease.

Autosomal Recessive

RP patients with a family history of similarly affected relatives are called multiplex, whereas those with no family history are classified as simplex. Simplex individuals are usually assumed to represent autosomal recessive inheritance, although some of these cases may be *de novo* dominant mutations or unrecognized X-linked inheritance. When simplex cases are included, autosomal recessive cases of RP have been reported to account for approximately 50–60% of all cases, with the exact percentage varying from country to country. Some of the most commonly affected genes are usherin (*USH2A*), a gene that is involved in both Usher syndrome and autosomal recessive RP, and the phosphodiesterase beta subunit (*PDE6B*), a gene involved in phototransduction.

X-Linked RP

X-linked RP results from mutations of genes on the X chromosome and represents approximately 5–15% of patients with RP. To date, six genes that cause retinal degeneration have been linked to the X chromosome. Two genes, retinitis pigmentosa GTPase regulator (*RPGR*) and retinitis pigmentosa 2 (*RP2*), are known, and several genes remain to be identified.

Males with X-linked RP typically have more severe retinal degeneration compared to autosomal recessive and dominant forms of the disease. The actual rate of degeneration is likely similar to the other forms, but the age of onset appears to be earlier.

Female carriers are thought to have a mosaic retina in which some of the cells express the normal allele, while others express the mutant allele. The fundus findings in female carriers of X-linked RP can vary from very subtle changes, such as mottling of the RPE, to more severe disease with some patients showing the classic bone spicule pigmentation. Even in the cases of female carriers with a normal appearing fundus, changes are usually apparent on the ERG.

Autosomal Dominant

Patients with autosomal dominant RP often have a family history of the disease, although there are cases of incomplete penetrance and *de novo* mutations. Autosomal dominant mutations account for approximately 30–40% of patients with RP. In general, patients with autosomal dominant RP tend to be less affected than patients with X-linked or autosomal recessive RP. Some of the most commonly mutated genes include rhodopsin (*RHO*) and retinitis pigmentosa 1 (*RP1*).

Nonsyndromic versus Syndromic Retinal Degeneration

Most cases of RP are nonsyndromic and the pathology is limited to the eye. However, RP can also be associated with dysfunctions in other organ systems, with many of these cases comprising defined syndromes.

The most common syndromic association with RP is Usher syndrome, which is an autosomal recessive disorder and is divided into three subtypes based on clinical findings. Patients with type I Usher syndrome present with severe, but nonprogressive congenital hearing loss, balance problems, and RP. In type II Usher syndrome, patients have less severe hearing loss, RP, and normal balance. Patients with type III Usher syndrome, start with symptoms similar to type II but later progress to type I. The retinal findings in Usher syndrome are indistinguishable from those characteristic of nonsyndromic autosomal recessive RP. Eleven genes have been found to cause Usher syndrome. Considering the presumed shared evolutionary ancestry of photoreceptors and cochlear hair cells, it is likely that some of these genes share similar functions.

Bardet–Biedl syndrome (BBS) is an autosomal recessive disorder in which RP is a universal finding. Other commonly associated features include postaxial polydactyly, truncal obesity, abnormalities of cognition, and renal disease. Mutations in 12 genes have been implicated in BBS. Many of these genes encode proteins that are important for the formation or function of the cilia (**Figure 2**).

Some other syndromes that can present with RP include: abetalipoproteinemia (Bassen–ornzweig disease), Alström

Figure 2 (a) Fundus photos of patient with Bardet–Biedl syndrome (BBS), demonstrating the classical changes of RP that include bone spicule pigmentation, vascular attenuation, and waxy pallor of the optic nerve. (b) Scars on the foot of a patient with BBS from removal of an extra digit. (c) Similar scars on the hand.

syndrome, chronic progressive external ophthalmoplegia (CPEO), Friedreich's ataxia, incontinentia pigmenti (Bloch–Schulzberg syndrome), Joubert syndrome, Kearns–Sayre syndrome, mucopolysaccharide disorders, neuronal ceroid lipofuscinoisis (Batten disease), Refsum disease (infantile and adult), Senior–Loken syndrome, and spinocerebellar ataxia type 7.

Classification of RP

One often confounding feature of RP is the many different ways in which the disease can be classified. RP can be classified by its mode of inheritance, age of onset, fundus appearance, pattern of functional vision loss, or by genetic mutation.

As mentioned previously, RP is often characterized by its pattern of inheritance. With the advent of genetic testing, patients are increasingly being tested and classified according to which genes are mutated (see **Table 1** for the most common mutations and **Table 2** for description of genes). The phenotype and course of the disease can show significant variation with different mutations in the same gene. Likewise, there can also exist significant phenotypic variations between two people who harbor the same mutation. Ultimately, classification by genetic defects will likely prove to be the most useful way to segregate and treat patients with RP. However, many genes remain to be discovered and genetic testing is not yet universally available to test for all mutations in known genes. For these reasons, it is useful to examine the ways in which RP has been categorized in the past.

Table 1 Most common genes causing retinitis pigmentosa by inheritance

	Most common genes causing retinitis pigmentosa
Autosomal recessive RP (including Usher syndrome)	*USH2A, PDE6B, PDE6A, MYO7A, CRB1, RGR, CNGB1, RPE65*
Autosomal dominant RP	*Rho* (rhodopsin), *RP1, PRPF31, PRPF3, RDS/ROM*
X-linked RP	*RPGR, RP2*

Classification by Age of Onset

Severe forms of RP that manifest before the first year of life are referred to as Leber congenital amaurosis (LCA). The forms of RP occurring between 1 and 5 years have been termed juvenile RP or severe early childhood-onset retinal dystrophy (SECORD). LCA is characterized by

Table 2 Genes, protein, diseases, and function

Gene symbol	*Protein*	*Diseases*	*Function*
ALMS1	Alström syndrome protein 1	Alström syndrome	Exact function unknown, may play a role in ciliogenesis
CACNA1F	Calcuim-channel, voltage-dependent, alpha 1F subunit	Incomplete CSNB, AIED, and other X-linked CRD (CORDX3, Maori disease, CSNB with retinal and optic atrophy)	Acts as a subunit in the major voltage-sensitive calcium channel in rod and cone photoreceptor terminals. Required for the calcium flux into photoreceptors (rods and cones) that is needed for sustaining the tonic neuro-transmitter release from presynaptic terminals. Required for formation/ maintenance of ribbon synapses
CEP290	Centrosomal protein CEP290	Joubert syndrome, LCA	Localizes to cilium, may mediate G-protein trafficking
CHM	Rab escort protein 1 (REP-1)	Choroideremia	Participates in post-translational lipid modifications of proteins to enable membrane attachments that are essential in membrane trafficking. Acts as a geranylgeranyl transferase and appears required for specific Rab pathways.
CNGA2	Cyclic nucleotide-gated channel – subunit alpha 2	Achromatopsia	Codes for the alpha subunit of the cyclic nucleotide-gated channels in cones
CNGB1	Cyclic nucleotide-gated channel – subunit B1	arRP	Codes for the beta subunit of the cyclic nucleotide gated channels in rods
CNGB3	Cyclic nucleotide gated channel – subunit beta 1	Achromatopsia	Codes for the beta subunit of the cyclic nucleotide-gated channels in cones
CRB1	Homolog of crumbs	arRP, LCA	Homologous to crumbs in the *Drosophila*, where it plays a role in cell–cell interactions and photoreceptor polarity
GNAT2	Transducin alpha 2	Achromatopsia	Plays a role in the photoreceptor phototransduction cascade. Forms a complex with the beta and gamma subunits and acts to convert cGMP to GMP
MYO7A	Myosin-VIIA	Usher syndrome type IA	May play a role in trafficking of ribbon-synaptic vesicle complexes and renewal of the outer photoreceptors disks
NYX	Nyctalopin	CSNB	Predicted secreted protein important for development of ON bipolar cell signaling pathways
OAT	Ornithine-∂-aminotransferase	Gyrate atrophy	Catalyzes the conversion of L-ornithine and a 2-oxo acid to L-glutamate 5-semialdehyde and an L-amino acid
PDE6A	Phospodiesterase alpha subunit	arRP	Plays a role in the photoreceptor phototransduction cascade. Forms a complex with the beta and gamma subunits and acts to convert cGMP to GMP
PDE6B	Phospodiesterase beta subunit	arRP	Plays a role in the photoreceptor phototransduction cascade. Forms a complex with the alpha and gamma subunits and acts to convert cGMP to GMP
PHYH	phytanoyl-CoA 2-hydroxylase	Refsum disease	Catalyzes the first step in the alpha-oxidation of phytanic acid
PRPF3	PRPF3	adRP	Forms part of a spliceosome complex for mRNA processing
PRPF31	PRPF31	adRP	Forms part of a spliceosome complex for mRNA processing
RDH5	11-*cis* retinol dehydrogenase	Fundus albipunctata	11-*cis* RDH is found in the RPE, where it catalyzes the final step in the biosynthesis of 11-*cis* retinaldehyde, the visual chromophore for both rods and cones
RDS	Peripherin	RP, pattern dystrophy	Interacts with Rom-1 as the major morphogen for disk formation and to stabilize photoreceptor disks
RGR	Retinal g-protein-coupled receptor	arRP, adRP	Expressed in the RPE and Müller cells and plays a role in retinoid recycling
RHO	Rhodopsin	adRP, arRP CSNB	Mediates the detection of photons through light-induced isomerization of 11-*cis* to all-trans retinal, which triggers a conformational change leading to G-protein activation and release of all-trans retinal

Continued

Table 2 Continued

Gene symbol	*Protein*	*Diseases*	*Function*
RLBP1	Cellular retinaldehyde-binding protein 1-like protein 1	arRP, retinitis punctata albescens, Bothnia dystrophy, Newfoundland rod–cone dystrophy	Plays a role in visual pigment regeneration: carrier for endogenous 11-*cis*-retinol and 11-*cis*-retinal, major 11-*cis*-retinol acceptor in the isomerization step of the rod visual cycle, stimulating isomerization of all-*trans*- to 11-*cis*-retinol, facilitates oxidation of 11-*cis*-retinol to 11-*cis*-retinal by 11-*cis*-retinol dehydrogenase (RDH5)
ROM	Rom-1	Digenic RP	Interacts with peripherin to stabilize photoreceptor disks
RP1	RP1	adRP	Localizes to photoreceptor cilium, may play a role in transport of proteins between inner and outer segments
RP2	RP2	xlRP	Exact function unknown. Stimulates GTPase activity of tubulin and may function to link cell membrane with cytoskeleton
RPE65	RPE65	arRP, LCA	Expressed in the RPE and acts in retinoid metabolism to isomerizes all-trans-retinal ester to 11-*cis* retinol
RPGR	Retinitis pigmentosa GTPase regulator	xlRP	Exact function unknown. Localizes to cilium and may act to maintain protein polarization across the cilium
USH2A	Usherin	Usher syndrome type II, arRP	Exact function unknown, Interacts with collagen IV and fibronectin and may be required for stable integration into the basement membrane

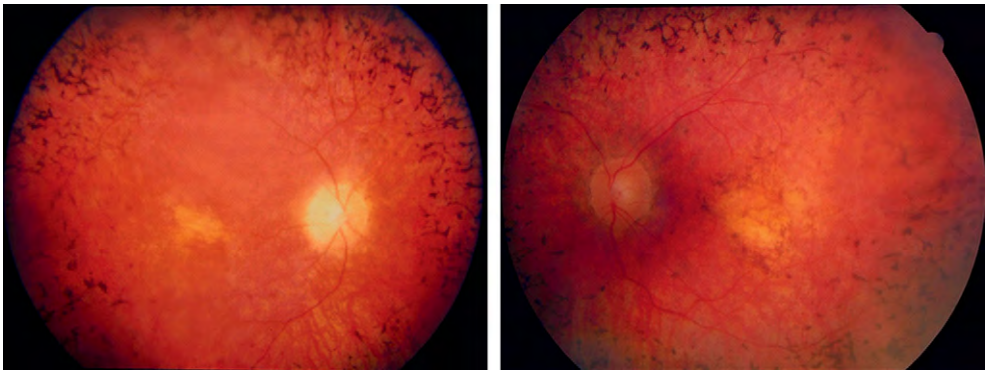

Figure 3 Fundus photographs of a 16-year-old patient with Leber congenital amaurosis. There is waxy pallor of the optic nerve, severe vascular attenuation, RPE atrophy most notable in the macula, and bone spicule pigmentations.

severe vision loss, nystagmus, unrecordable ERGs, and poorly responsive pupils (amaurosis). Mutations in at least 16 genes have been found to cause LCA and most of these are inherited in an autosomal recessive fashion. Juvenile RP/SECORD is thought to be caused by less severe mutations in the same set of genes as LCA, and more mild mutations in some of these genes have been implicated in recessive RP (Figure 3).

Classification by Fundus Appearance

The classic fundus appearance in RP is described below (see the subsection titled 'Fundus findings'). Deviations from this classic fundus appearance have given rise to several alternative terms for pigmentary retinopathies including: inverse RP, concentric RP, sector RP, retinitis punctata albescens, fundus albipunctatus, RP with preserved peri-arteriolar RPE, pigmented perivenous retinochoroidal atrophy, and retinitis sine pigmento. Some of these terms are falling out of usage as genetic characterization of the disease is becoming more common.

There have been many cases of unilateral RP described and it has been proposed that this could be caused by a somatic mutation. However, there is yet to be a histologically confirmed case of RP caused by a somatic mutation. Most of these cases likely represent other diseases that can mimic RP and cause a pigmentary retinopathy.

Classification by Functional Loss

Historically, adult RP was categorized as either type I (rod dysfunction) or type II (rod and cone dysfunction) based on psychophysical testing. These classifications were further refined on the basis of electrophysiological findings to include the categories: rod–cone dystrophy, cone–rod dystrophy, or cone dystrophy. Most forms of RP are rod–cone dystrophies in which rod photoreceptor death occurs first and is later followed by subsequent cone photoreceptor death. This article will use the term RP to describe the most common form, namely rod–cone dystrophy. The forms of RP that cause cone and cone–rod dystrophy will be denoted accordingly.

Mechanism of Disease

RP and its allied disorders are caused by mutations in over 100 genes and likely the same number remains to be elucidated. Ultimately, these mutations lead to photoreceptor death by apoptosis. It is still not fully understood how mutations in genes, which code for an array of functionally different proteins, result in a common pathway to photoreceptor death.

Mutations can result in decreased expression of a given protein, cause loss of function of that protein, or imbue a gain of function. In autosomal recessive forms of RP, there is a loss of expression or function when both copies of a given gene are mutated. In contrast, autosomal dominant forms of RP are thought to be caused by gain-of-function mutations, where the mutated protein becomes toxic or interferes with the function of the remaining normal forms of that protein (dominant negative effect). In autosomal dominant RP, the most common mutations are found in *RHO*. These dominant mutations can lead to forms of *RHO* that do not inactivate properly or are not transported to the outer segment.

An example of one well-studied mutation that causes autosomal dominant RP is the P23H mutation in the *RHO* gene. This mutation results in misfolding of the protein such that it is sequestered in the endoplasmic reticulum and is never transported to the outer segment. The misfolded proteins accumulate creating aggregations that activate an unfolded protein response. Dysregulation of these responses may lead to photoreceptor death although the exact mechanism has yet to be determined.

Clinical Presentation

Symptoms

Most frequently, the earliest symptom of RP is night blindness that precedes visual-field change and, in some, retinal pathology. In children, parents may comment that their child is afraid or becomes distressed in the dark. Older children often comment on poor vision compared with their fully sighted peers. In adults, difficulties with night driving are frequent. The second cardinal symptom of RP is progressive peripheral visual-field loss. Since central vision is spared early in the course of the disease, some patients do not notice this loss of visual field until the degeneration has become quite advanced.

Another common symptom of RP is problems with dark adaptation, such as difficulties adjusting to dim illumination when entering a movie theater. Additionally, as the disease progresses, patients can develop photophobia. Color vision is typically normal early in the disease but with progression, blue–yellow defects become apparent. Flashes of light, or photopsias, are experienced by most patients.

Patients with cone and cone–rod dystrophies can present with early photophobia, decreased central vision, and impaired color vision. These patients will typically have worse visual acuity than patients with rod–cone dystrophies due to earlier involvement of macular cones.

Refraction

Refractive errors in patients with RP have been studied and, on average, these patients are more myopic and have a greater degree of astigmatism than those in the general population. By contrast, patients with early-onset forms of RP, such as LCA or SECORD, tend to have hyperopic refractions.

Anterior Segment and Cataract

The external ocular exam and anterior segment are typically unremarkable in nonsyndromic forms of RP. However, there does appear to be a higher rate of keratoconus and glaucoma in patients with RP. Posterior subcapsular cataracts are common and often can become visually significant. Cataract extraction is beneficial in patients with RP if the cataract is thought to be the vision-limiting factor.

Fundus Findings

The characteristic signs on fundus examination include midperipheral atrophy of the pigment epithelium, intraretinal pigment accumulation (bone spicules; **Figure 1**), retinal vessel attenuation, and waxy pallor of the optic nerve. A yellowish ring of peripapillary atrophy is sometimes seen in patients with RP as well as with optic nerve head drusen. A minor number of vitreous cells are commonly observed in patients with RP. Cystoid macular edema is common in patients with RP and can often result in significantly decreased vision. Rarely, patients can develop a Coats-like retinopathy.

Diagnostic Tests for RP

Dark Adaptation

Dark adaptation can be a useful test in patients with RP. Patients who manifest with a rod–cone dystrophy will usually have a detectable increase in final dark-adapted thresholds and show delayed dark-adaptation curves. Prolonged dark adaptation is especially common among patients with *RHO* mutations. Elevations of the early cone segment of the dark-adaptation curve may be particularly noticed by patients, more so than elevations of the rod segment (Figure 4).

Visual Fields

Visual fields are not only useful for making the diagnosis of RP, but are also one of the most useful objective methods for monitoring progression of the disease. Decreased visual-field sensitivity results from photoreceptor loss (Figure 5).

The earliest change seen as measured by kinetic perimetry is concentric constriction or decreased sensitivity with static perimetry in diffuse disease and relative midperipheral scotomas seen in the in regional disease. As these midperipheral scotomas or regions of decreased sensitivity enlarge and deepen, severe tunnel vision results. Eventually, macular function fails and visual field becomes difficult or impossible to measure by conventional perimetry. Although visual function may be reduced to light perception only, it is rare for patients to become completely blind. With the exception of female carriers in X-linked RP, visual-field loss is usually symmetrical. Marked asymmetry should raise concern for diseases that mimic RP (Figure 6).

The rate of visual-field loss has been shown to be exponential. This rate is thought to be similar for the different forms of inheritance once correction has been made for the critical age of onset. Massof and Finkelstein found that patients lost about 50% of their visual field every 4.5 years. The superior visual field, which corresponds to the inferior retina, is often more affected than inferior visual fields. Based on this finding, it has been suggested that increased levels of light may play a role in accelerating retinal degeneration and this in turn may play a role in the forms of RP with greater damage in the inferior retina.

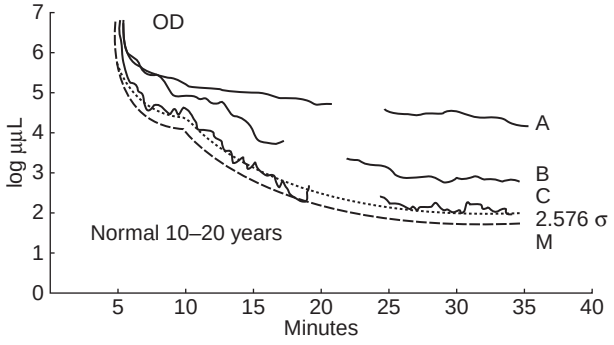

Figure 4 Example of dark-adaptation curves in a normal subject (dashed lines represent the mean normal response, dotted lines represent the upper limit of normal) and patients with retinitis pigmentosa (solid lines). From Weleber, R. and Evan, K. G. (2006). Retinitis pigmentosa and allied disorders. In: Ryan, S. J. (ed.) *The Retina*, 4th edn., vol. 1, chap. 17, pp. 395–498. Philadelphia, PA: Elsevier.

Electroretinograms

ERGs play a crucial role in the diagnosis of RP because these electrophysiological recordings are sensitive enough to detect decreased photoreceptor function early in the disease when fundus findings and visual fields may be minimally altered. In addition, ERGs are particularly

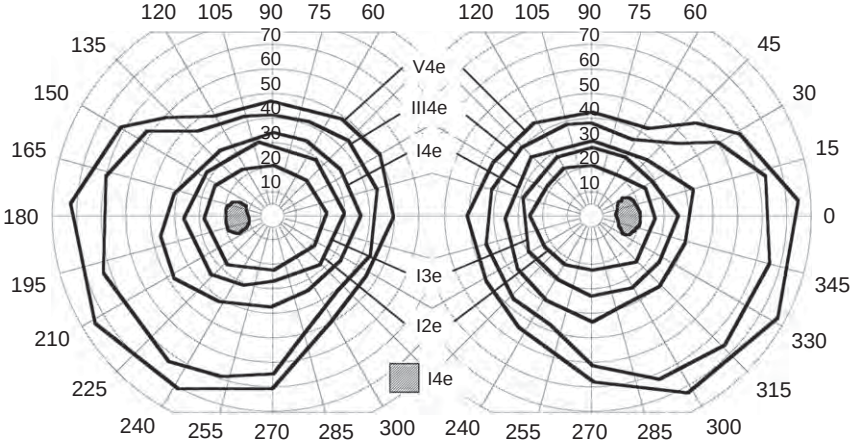

Figure 5 Example of a mildly abnormal kinetic visual field in a patient with early retinitis pigmentosa demonstrating the responses to different-sized targets. The gap between the size III4e and size I4e isopters is greater than normal, indicating loss of sensitivity in this region. The blind spot (region containing the optic nerve head and therefore no photoreceptor cells) is plotted in each eye just temporal to the fovea.

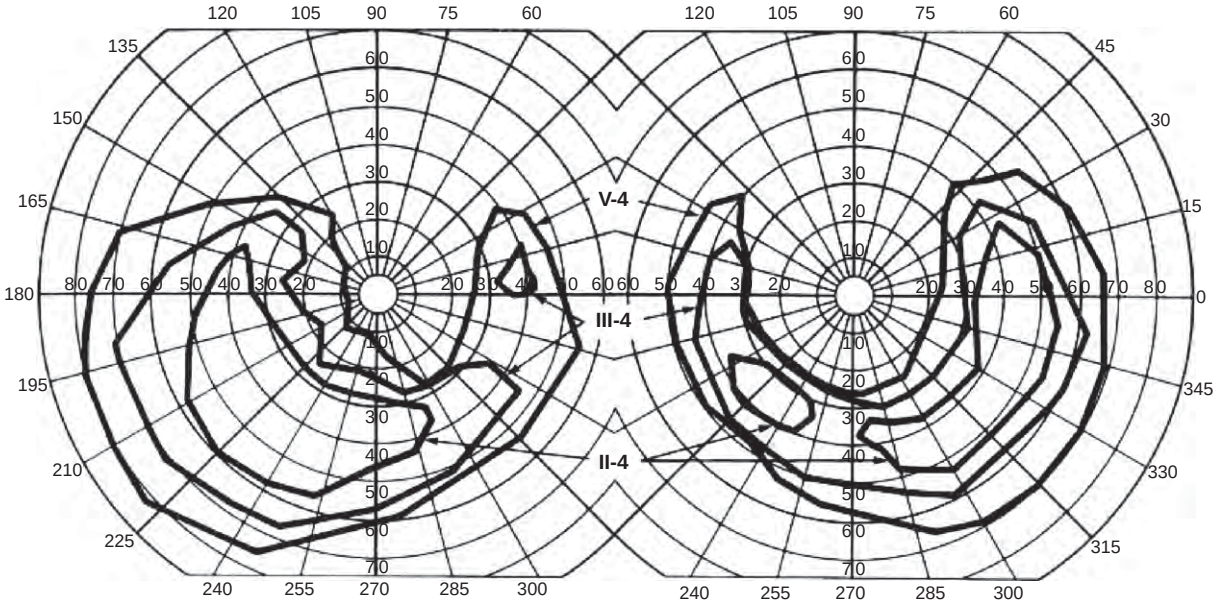

Figure 6 Kinetic visual fields obtained from patient with retinitis pigmentosa. Note the relative preservation of inferior fields, which correlated with preserved superior retina. From Weleber, R. and Evan, K. G. (2006). Retinitis pigmentosa and allied disorders. In: Ryan, S. J. (ed.) *The Retina*, 4th edn., vol. 1, chap. 17, pp. 395–498. Philadelphia, PA: Elsevier.

useful to assess visual function in preverbal infants and children. Almost all patients with symptomatic RP will have detectable changes on the ERG at the time of diagnosis. While the ERG is useful for the diagnosis of RP, visual fields are better for monitoring of the course of the disease. In severe cases of RP, such as LCA, the ERG may be not recordable.

Patients with RP can show decreased amplitude and timing of the major components of the ERG. Caution must be taken when interpreting decreases in the amplitude of an ERG because poor contact of the electrodes, deviations of the eye, and high myopia can affect the amplitude of the signal. When present, delayed timing tends to be a more robust indicator of dysfunction.

By analyzing the different components of the ERG, different forms of RP can be classified. Degeneration of the rod and cone photoreceptors leads to a decrease in the amplitude of different waveforms of the ERG and can also increase the timing or latency of the peaks of these waveforms. The most common forms of RP manifest as a rod–cone dystrophy and the first detectable changes will be apparent on the scotopic ERG. Decreases in the b-wave amplitude and timing of the peak of the b-wave are indicative of early rod photoreceptor death. Further loss of rod cells leads to further decreases in the b-wave amplitude and decreased amplitude of the a-wave responses at higher intensities. Patients with a cone–rod dystrophy have normal, or lesser defect of b-wave responses to dim scotopic stimuli, but typically have more markedly abnormal ERGs to 30-Hz flicker or single-flash stimuli measured under photopic conditions (**Figures 7–9**).

Fundus Photography/Fluorescein Angiography

Documentation by fundus photography can assist in monitoring changes in patients with RP. Fluorescein angiography in patients with RP will demonstrate hyperfluorescence in areas of RPE atrophy and can highlight areas of cystoid macular edema. However, fluorescein angiography has largely been supplanted by optical coherence tomography (OCT) for detecting cystoid maculopathy. In addition, concerns about light exposure accelerating certain forms of RP in animal models have prompted many ophthalmologists to exercise caution in obtaining excessive photographs.

Optical Coherence Tomography

OCT provides a noninvasive cross-sectional image of the retina. It is very useful in patients with RP when there is a question of cystoid macular edema. The ability to detect cystoid macular edema by OCT often obviates the need to get a fluorescein angiogram.

Differential Diagnosis

It is important to realize that RP is not the only cause of a pigmentary retinopathy but many other diseases can mimic RP. Significant asymmetry or the onset of symptoms in an elderly patient should raise suspicion for one of the diseases that mimics RP.

Trauma to the eye can disrupt the retina and result in pigment migration of the RPE into the retina with the formation of bone spicules. By a similar mechanism,

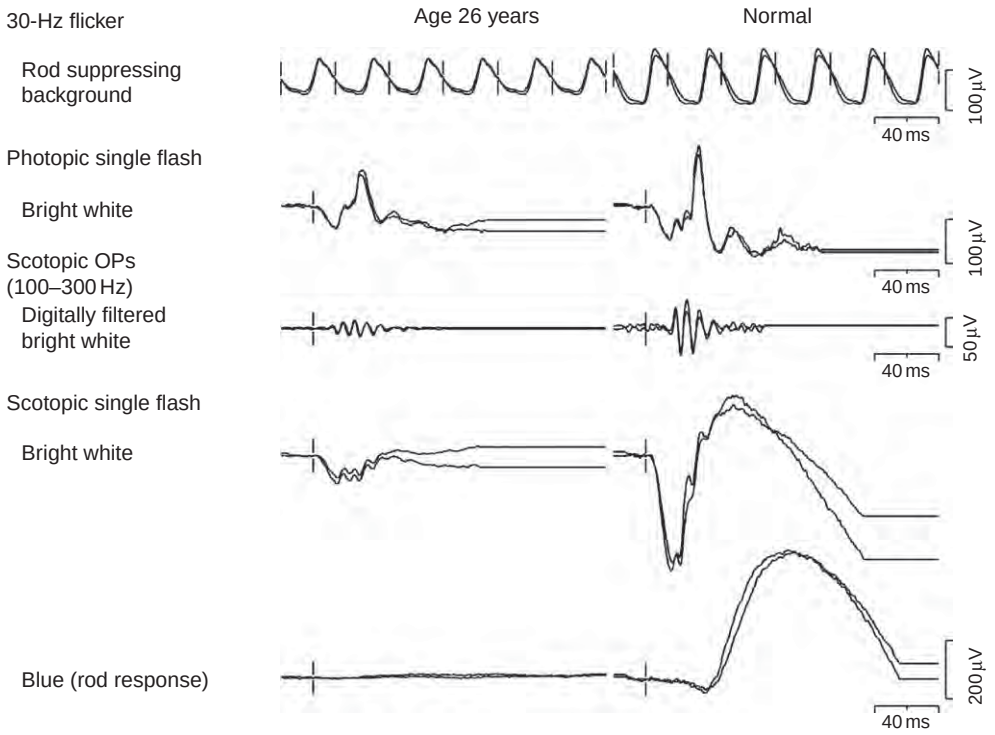

Figure 7 ERGs recorded from a patient with autosomal recessive RP (left column) compared to a control patient (right column). This patient is demonstrative of a rod–cone dystrophy. There is a flat response to the dim blue flash under scotopic conditions, which specifically stimulates rods. The bright flash under scotopic conditions normally elicits mixed responses from both rods and cones. In this case, the response is severely attenuated and the small amount of signal is likely coming from the cone system. Under light-adapted conditions (photopic single flash and 30-Hz flicker), which selectively stimulate the cones, the response is only slightly decreased consistent with the categorization of a rod–cone dystrophy.

ophthalmic artery occlusions and old retinal detachments can present with a pigmentary retinopathy.

Additionally, infections caused by syphilis, toxoplasmosis, and herpes viruses can lead to a pigmentary retinopathy. Congenital rubella infection can often be misdiagnosed as RP or Usher syndrome because these patients present with deafness and a fine, speckled pigmentary retinopathy. The key to differentiating patients with rubella from those with RP is that patients with rubella retinopathy will have normal or near normal responses by ERG (**Figure 10**).

Diffuse unilateral neuroretinitis (DUSN) is caused by a chronic infection with a nematode. In the early stages, this disease can be distinguished due to the appearance of crops of yellowish, deep choroidal infiltrates, neuroretinitis, and sometimes, visualization of the worm itself. However, late in the disease, with the exception of being unilateral, the fundus appearance is identical to RP with the fundus showing bone spicules, vascular attenuation, and optic atrophy (**Figure 11**).

Inflammatory diseases that cause a posterior uveitis can cause chronic changes that mimic the pigmentary changes of RP. Some examples include sarcoidosis, birdshot chorioidoretinopathy, serpiginous retinopathy, Behcet disease, and acute zonal occult outer retinopathy (AZOOR).

Certain drugs can cause pigmentary retinopathies and their usage must be excluded prior to making a diagnosis of RP. One example is thioridazine (Mellaril), an antipsychotic drug, which mimics RP by causing decreased night vision, RPE atrophy, and a pigmentary retinopathy. Hydroxychloroquine (Plaquenil) is used to treat systemic lupus erythematous and rheumatoid arthritis and when taken for extended period of time or at higher doses can lead to central vision loss. Other drugs that have been found to cause pigmentary retinopathies include chlorpromazine, chloroquine, and quinine.

Autoimmune retinopathy is an incompletely understood disease resulting from antibodies to retinal antigens and can present with many of the same features of RP, such as decreased vision, visual-field loss, and decreased ERGs. Unlike the other diseases that mimic RP, autoimmune retinopathy does not present with a pigmentary retinopathy and, in many cases, the fundus appearance can be normal or only show vascular attenuation. A subset of cases of autoimmune retinopathy is associated with carcinomas in other parts of the body. Two examples of this entity are cancer-associated retinopathy (CAR), which often arises from small cell carcinoma of the lung and melanoma-associated retinopathy (MAR). CAR patients may test positive for antibodies directed against retinal

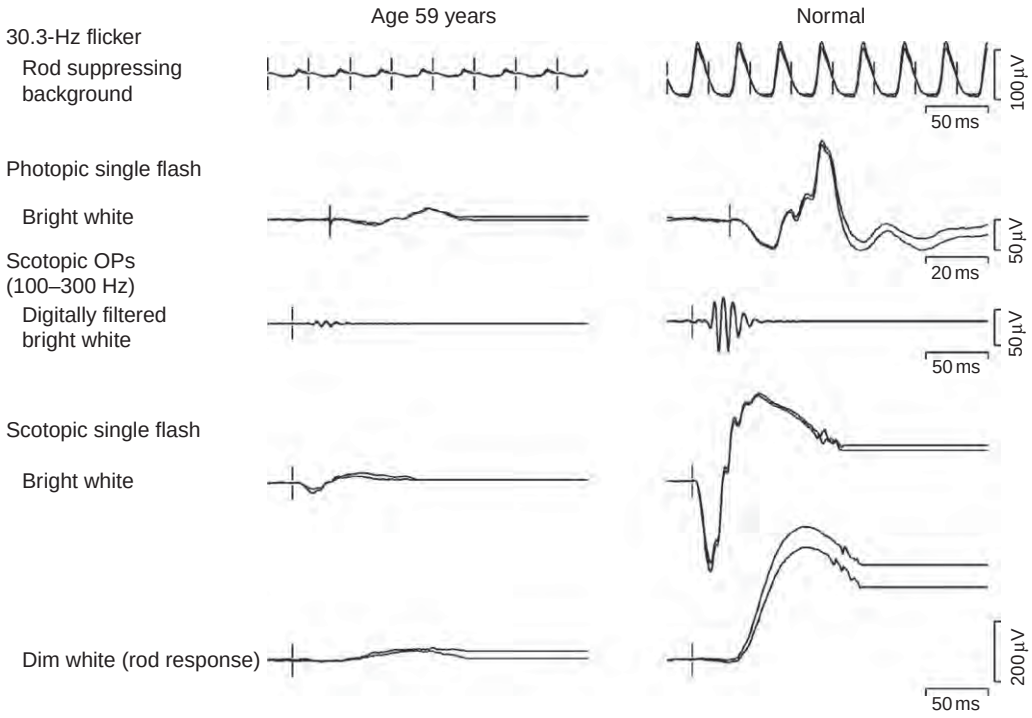

Figure 8 ERGs recorded from a patient with peripherin/*RDS* null mutation (left column) compared to a control patient (right column). This patient is demonstrative of a rod–cone dystrophy where the rods and cones are equally affected. It is of importance that peripherin is expressed in both rods and cones. There is a severely diminished response to the dim white flash under scotopic conditions, which specifically stimulates rods. The bright flash under scotopic conditions normally elicits a mixed response from both rods and cones. In this case, the response is severely attenuated. Under light-adapted conditions (photopic single flash and 30-Hz flicker), which selectively stimulate the cones, the response is also severely decreased consistent with the categorization of an equal rod–cone dystrophy.

antigens, such as anti-recoverin or anti-enolase, while MAR patients may test positive for antibodies directed against bipolar cells.

Prognosis in RP

It is uncommon for a patient with RP to lose all light perception. A study by Grover et al. in 1999 showed that only 0.5% of patients over the age of 45 had no light perception and 50% retained vision better than 20/40. In the typical rod–cone dystrophies, visual loss usually starts in the midperiphery with central visual acuity being spared for many years. Most patients will eventually qualify as being legally blind, often secondary to decreased visual fields prior to being disqualified on the account of decreased central visual acuity. RP is a slowly progressive disease and many patients will eventually experience decreased central acuity, most often from decrease in cone photoreceptor density, macular edema, epiretinal membranes, or retinal pigment defects. However, when there is an unexpected decrease of central acuity, the development of cataracts or cystoid macular edema should be suspected because these sequelae are more amenable to treatment.

Current Treatments

Currently, there is no known cure for most forms of RP, although some treatments have been shown to slow down the progression of the disease and future therapies are promising.

Treatable Forms of RP

A few rare forms of RP are amenable to specific treatments. It is important to rule out these treatable forms of RP because prompt therapy can prevent further damage. The treatable forms of RP include abetalipoproteinemia and adult Refsum disease.

Resources/Support for Patients with RP

The diagnosis of RP can be both frightening and confusing to patients. In addition to having their questions answered by the physician, patients can benefit by meeting with a genetic counselor who can take a detailed family history and answer questions about heritability. Patients should be referred to the many organizations or websites dedicated to providing support for this disease, such as the Foundation Fighting Blindness.

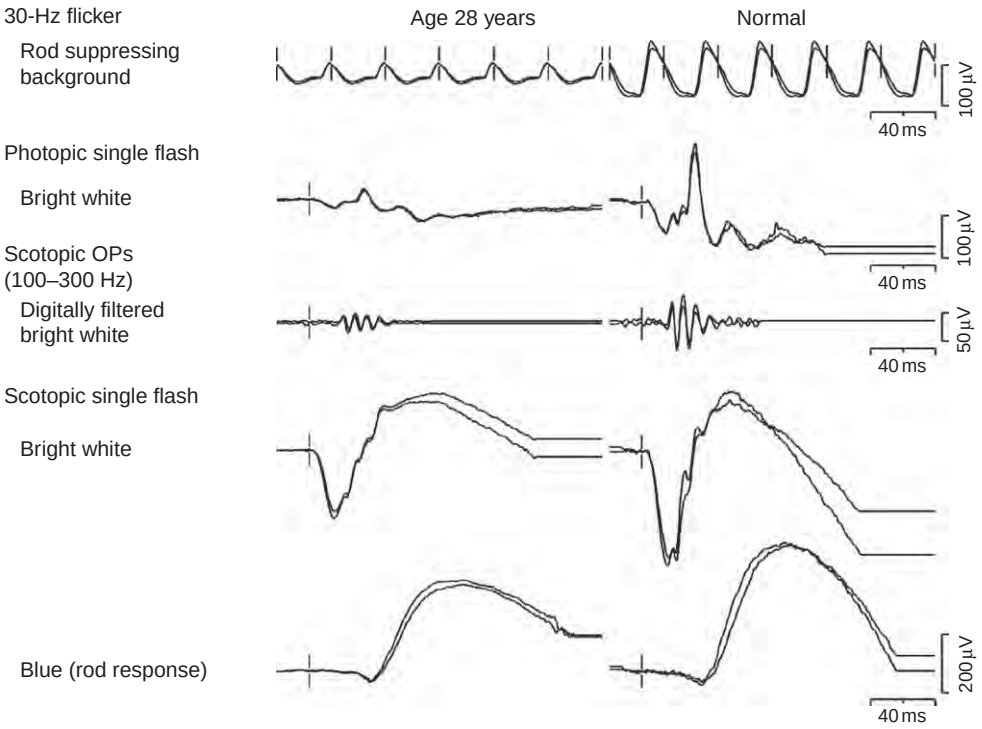

Figure 9 ERGs recorded from a patient with autosomal recessive RP (left column) compared to a control patient (right column). This patient is demonstrative of a cone–rod form of RP. There is a mildly diminished response to the dim blue flash under scotopic conditions, which specifically stimulates rods. The bright flash under scotopic conditions normally elicits a mixed response from both rods and cones. In this case, the response is only moderately attenuated. Under light-adapted conditions (photopic single flash and 30-Hz flicker), which selectively stimulate the cones, the response is severely decreased consistent with the categorization of a cone–rod dystrophy.

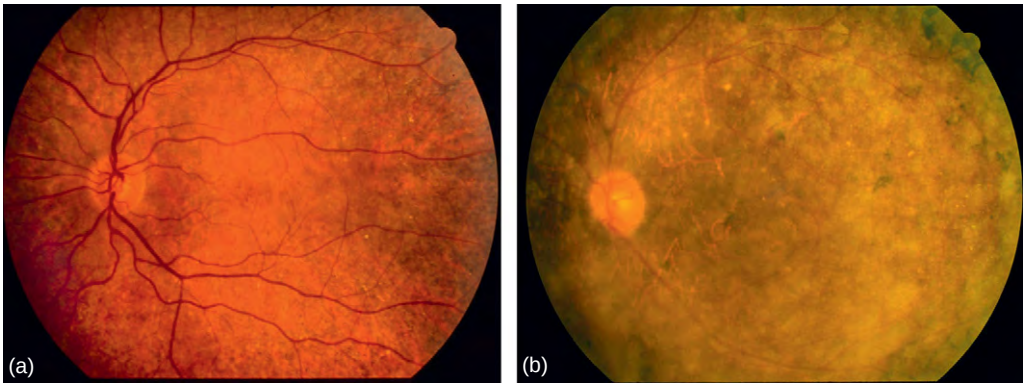

Figure 10 (a) An example of rubella retinopathy. Note the fine, mottled pigmentary changes and normal-appearing nerve and vessels. Unlike RP, ERG testing in this patient would be expected to be normal. (b) Example of a pigmentary retinopathy caused by syphilis.

Optimizing Remaining Vision

It is important that patients with RP have an up-to-date refraction to optimize remaining vision. Patients with significantly decreased visual acuity greatly benefit from a referral to low vision services. A variety of different magnifying devices are available to assist patients with RP. For example, night-vision devices can assist with navigation in dim conditions, although a bright, wide, beam flashlight may be a more cost-effective solution. Various magnifiers and closed-circuit televisions (CCTVs) are available to enhance reading vision.

Cataractogenesis is frequent in patients with RP. Functional visual improvement can be achieved by cataract surgery in carefully selected individuals with suitable remaining retinal function. The risks of surgery are increased in these individuals who should be counseled specifically regarding the risks of postoperative cystoid macular edema.

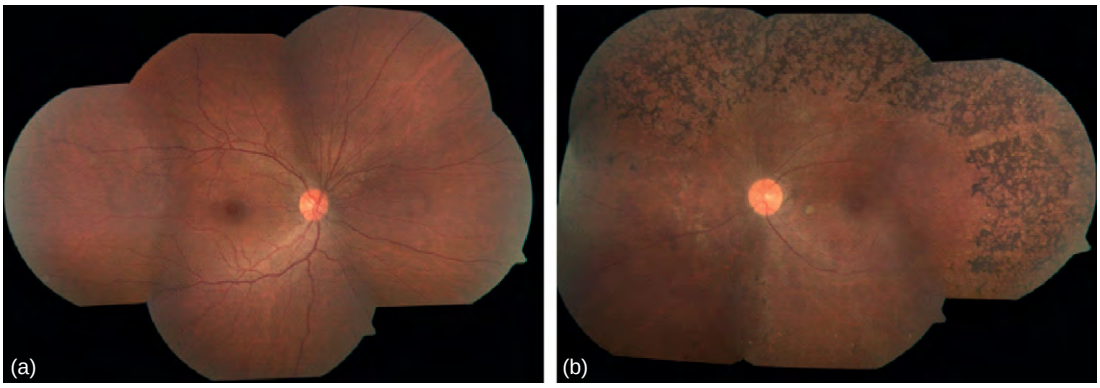

Figure 11 (a) Normal fundus from a patient with diffuse unilateral subacute neuroretinitis (DUSN). (b) The affected eye in the same patient. Note that appearance is identical to RP, demonstrating waxy pallor of the nerve, vascular attenuation, bone-spicule pigmentation, and RPE atrophy.

Cystoid macular edema in RP has been treated with carbonic anhydrase inhibitors such as oral acetazolamide (Diamox) or topical dorzolamide (Trusopt). These medicines can improve vision in some RP patients with cystoid macular edema; however, their efficacy can decrease with time and many patients cannot tolerate the side effects induced by these medicines.

Vitamin A

Observational studies of patients with RP taking vitamin A and vitamin E supplementation demonstrated a slower decline in cone ERGs than expected and led to a randomized, controlled, double-masked trial, to assess if these supplements could slow down retinal degeneration. Additional subgroup analyses in this study suggested that oral supplementation with 15 000 IU of vitamin A modestly slowed down the loss of ERG amplitude over a 5-year period in certain individuals with RP. Currently, vitamin A supplementation is frequently recommended but its use is not universal. High doses of vitamin A supplementation have also been associated with elevated liver enzymes, elevated triglycerides, and an increased risk of osteoporosis. It seems prudent to check annual liver function tests and triglyceride levels for all patients and bone density scans in older patients taking vitamin A supplementation. Vitamin A should be avoided in children, pregnant women, and those with decreased liver function.

Additionally, from a mechanistic disease perspective, vitamin A should be avoided in forms of RP caused by mutations in the gene *ABCA4* due to evidence in animal models of accelerated retinal degeneration. *ABCA4* codes for the ABCR protein, which is important for transport of vitamin A-derived all-trans-retinal from the disk to the photoreceptor cytoplasm. Mutations in this gene are responsible for Stargardt macular dystrophy and rarely can also cause autosomal recessive RP.

Docosahexanoic Acid

Docosahexanoic acid (DHA) is an important omega-3 fatty acid that comprises 30–40% of fatty acids in the retina. The exact role of DHA is not known, but it has been proposed to play a role maintaining membrane fluidity, mediating 11-*cis* retinal transport, and acting as a precursor for neuroprotective factors. Studies in patients with X-linked RP suggested that decreased levels of DHA correlate with decreased ERG responses and have prompted studies to evaluate if supplementation with DHA might slow down retinal degeneration. Two prospective, randomized, double-masked studies (one in patients with X-linked, the other in patients with all forms of RP) failed to show a significant benefit of DHA. However, considering the low risk of adverse effects, many centers do recommend DHA supplementation to patients with RP.

Neuroprotection/CNTF

A relatively new strategy for the treatment of RP is to prevent photoreceptor loss by the delivery of neuroprotective factors. Numerous studies in animal models have documented the successful rescue of photoreceptor degeneration by neurotrophic factors. A delivery system for one of these factors, human ciliary neurotrophic factor (CNTF), has been developed using encapsulated cell technology. These devices use RPE cells that have been transfected to express CNTF and are enclosed by a semipermeable membrane which allows nutrients to diffuse in, but prevents immune attack on the cells. Phase I studies, implanting this device in patients with RP, have been completed without any major adverse events. Phase II studies, which will be able to better assess any visual improvement, are underway.

Gene Therapy

Replacement of defective genes in autosomal recessive forms of RP holds much promise. Currently, three groups

have used an adeno-associated viral vector to deliver normal copies of the all-trans-retinol isomerase (*RPE65*) in patients with LCA. The treatment has thus far been well tolerated and some patients have demonstrated improvement in subjective vision and to some more objective tests such as pupillary reflexes. Gene therapy holds much promise for treating RP, but several challenges remain. RP and its allied disorders are caused by mutations in over 100 genes. Designing a multitude of vectors for each of these genes poses an arduous challenge.

Autologous RPE Transplantation

Replacement of RPE cells has been attempted using suspensions or sheets of cultured RPE cells or autologous grafts. Engraftment of these injected cells has been demonstrated in animal models. Rescue of photoreceptor degeneration has been achieved suggesting that transplanted RPE cells may modulate photoreceptor death. However, in spite of early photoreceptor rescue in these animal models, long-term restoration of vision has been disappointing.

Stem-Cell-Based Therapies

Cell-based therapy using stem cells is currently being intensely explored for rescuing vision. There are two fundamentally different strategies: one is to limit the progress of photoreceptor loss by introducing cells before such loss has progressed too far; the other is to replace lost photoreceptors. Stem cells are multipotent cells capable of self-renewal and have the potential to develop into many specific cell types. Their capacity for proliferative expansion to a large scale and their ability to produce a number of growth factors make them attractive candidates to be used to replace or repair damaged cells in adult organisms.

Microelectrode Implants

One novel concept for treatment of RP is to bypass the loss of the photoreceptors by electronically stimulating the retina, optic nerve, or visual cortex using microelectrode implants.

Expression of Photosensitive Proteins

A very recent approach for treating RP has been the strategy to bypass photoreceptor loss by using viral vectors to express light-sensitive proteins, such as channel rhodopsin, into postreceptor ganglion cells. Early experiments in small animals have demonstrated successful responses from ganglion cells using this strategy. Much work remains to be done, including how to obtain high enough expression to provide adequate sensitivity for useful vision.

Conclusions

RP is a significant cause of vision loss in adults and children. Diagnosis is best made by careful history and clinical examination combined with retinal electrophysiology and psychophysical testing. For some individuals, genetic testing can identify causative mutations. While there is currently no cure for RP, many treatment options are emerging and future therapies are promising.

See also: Adaptive Optics; Injury and Repair: Prostheses; Primary Photoreceptor Degenerations: Terminology.

Further Reading

Berson, E. L., Rosner, B., Sandberg, M. A., et al. (1993). A randomized trial of vitamin A and vitamin E supplementation for retinitis pigmentosa. *Archives of Ophthalmology* 111: 761–772.

Berson, E. L., Rosner, B., Sandberg, M. A., et al. (2004). Clinical trial of docosahexaenoic acid in patients with retinitis pigmentosa receiving vitamin A treatment. *Archives of Ophthalmology* 122: 1297–1305.

Fishman, G. A., Farber, M. D., and Derlacki, D. J. (1988). X-linked retinitis pigmentosa. Profile of clinical findings. *Archives of Ophthalmology* 106: 369–375.

Grant, C. A. and Berson, E. L. (2001). Treatable forms of retinitis pigmentosa associated with systemic neurological disorders. *International Ophthalmology Clinics* 41: 103–110.

Grover, S., Fishman, G. A., Anderson, R. J., et al. (1999). Visual acuity impairment in patients with retinitis pigmentosa at age 45 years or older. *Ophthalmology* 106: 1780–1785.

Hamel, C. P. (2007). Cone rod dystrophies. *Orphanet Journal of Rare Diseases* 2: 7.

Hartong, D. T., Berson, E. L., and Dryja, T. P. (2006). Retinitis pigmentosa. *Lancet* 368: 1795–1809.

Heckenlively, J. R. (1988). *Retinitis Pigmentosa.* Philadelphia, PA: Lippincott.

Hoffman, D. R., Locke, K. G., Wheaton, D. H., et al. (2004). A randomized, placebo-controlled clinical trial of docosahexaenoic acid supplementation for X-linked retinitis pigmentosa. *American Journal of Ophthalmology* 137: 704–718.

Radu, R. A., Yuan, Q., Hu, J., et al. (2008). Accelerated accumulation of lipofuscin pigments in the RPE of a mouse model for ABCA4-mediated retinal dystrophies following vitamin A supplementation. *Investigative Ophthalmology and Visual Science* 49: 3821–3829.

Sieving, P. A., Caruso, R. C., Tao, W., et al. (2006). Ciliary neurotrophic factor (CNTF) for human retinal degeneration: Phase I trial of CNTF delivered by encapsulated cell intraocular implants. *Proceedings of the National Academy of Sciences of the United States of America* 103: 3896–3901.

Weleber, R. G. and Gregory-Evans, K. (2006). Retinitis pigmentosa and allied disorders. In: Ryan, S. J. (ed.) *The Retina* 395–498. Philadelphia, PA: Elsevier.

Relevant Websites

http://www.ncbi.nlm.nih.gov – Online Mendelian Inheritance in Man (OMIM).

http://www.sph.uth.tmc.edu – Retinal Information Network (Retnet).

Primary Photoreceptor Degenerations: Terminology

M E Pennesi, P J Francis, and R G Weleber, Oregon Health and Sciences University, Portland, OR, USA

Glossary

Allied disorders – Retinitis pigmentosa (RP) is often grouped with a class of more stable, inherited retinal disorders collectively referred to as RP and allied disorders. Some of these allied disorders cause similar clinic findings as RP, e.g., nyctalopia (night blindness), but usually do not show progression and deterioration with time. An example is congenital stationary night blindness (CSNB), which can present with nyctalopia and decreased rod and cone function on the electroretinogram (ERG). Unlike RP, most patients with CSNB have stable visual function. X-linked CSNB is caused by mutations in nyctalopin (NYX) and L-type voltage dependent calcium channel (CACNA1F). Although the majority of mutations of rhodopsin causes typical RP, rare mutations, such as G90D in rhodopsin, produce night blindness with such mild progression late in life that they have been called stationary night blindness. Another allied disorder is achromatopsia, which is caused by mutations in cyclic nucleotide-gated channel subunits (CNGA2, CNGB3) or guanine nucleotide alpha-binding protein 2 (GNAT2). Achromatopsia is associated with severely decreased central and color vision, photophobia, and nystagmus. These symptoms are similar to those that can be seen with some cone–rod dystrophies. Indeed, later in life some modest foveal atrophy can occur and cases of progressive cone–rod dystrophy have been associated with mutations of some of the achromatopsia genes. However, unlike cone–rod dystrophies, which invariably progress, achromatopsia is, in the vast majority of cases, stationary.

Cone dystrophy – Cone photoreceptors are affected and rod photoreceptors are minimally affected or spared in cone dystrophy. Many cases of early cone dystrophies with time will develop significant rod abnormalities.

Cone–rod dystrophy – Cone–rod dystrophy, as a group, involves both photoreceptors with cones affected more than rods. Certain forms of RP present with greater cone than rod involvement on ERG and these patients have been termed to have cone–rod RP. However, in cone–rod dystrophies as a group the primary defect lies in cones and secondaryrod loss occurs with time. Most investigators consider primary cone–rod dystrophy separate from RP.

Extrinsic factor – An agent external to the organism that contributes to or is causative of a disease state. This can include drugs, foods, normal nutrients (excess or deficiency), toxins, inhaled chemicals, infectious agents, and exposures to radiation such as light, sound, and high-energy particles.

Intrinsic factor – An agent that is inherent to the organism that contributes to or is causative of a disease state.

Mixed intrinsic and extrinsic etiology for a secondary photoreceptor degeneration – This occurs when a person has a genetic variant that creates a toxic metabolite in the presence of an extrinsic molecule that would normally not be encountered.

Mixed model of primary and secondary photoreceptor degeneration – This is considered when a genetic alteration within the photoreceptors is insufficient to cause photoreceptor degeneration by itself, but predisposes to degeneration in the presence of an extrinsic or intrinsic agent. A second mode of combined primary and secondary photoreceptor degeneration is when one group of photoreceptors, such as the rod photoreceptors, undergoes a primary degenerative process that is due to a mutation in a gene that is expressed in those photoreceptors and precipitates apoptosis, which leads to a secondary degenerative process, in this example cones, due to alterations in the cellular environment induced by death of neighboring cells.

Primary retinal degeneration – This occurs when cells in the retina, usually photoreceptors, die secondary to a process that originates within the retina itself. An example of a primary retinal degeneration is RP, which is caused by mutations in genes that encode proteins important for retinal function. A disease can be classified as a primary retinal degeneration if the genetic defect is such that correction of expression of the normal gene product in the photoreceptors is required to correct the abnormality and arrest the degeneration.

Primary retinal degeneration with secondary photoreceptor degeneration – This occurs when photoreceptor degeneration is the result of mutation(s) of a gene that exists in other retinal cells, for

example, retinal pigment epithelial (RPE) cells. Correction of the genetic defect would require modification of the effects of those other retinal cells (e.g, RPE cells).

Retinal atrophy – A broad term encompassing not only processes that occur with retinal degenerations, but also abnormal retinal tissue or cellular loss due to developmental defects and malnutrition.

Retinal degeneration – A process whereby cells in the retina undergo cell death by apoptosis. Most retinal degenerations affect both rod and cone photoreceptors, but some disorders reflect damage that occurs principally in other cell types, e.g., the RPE in Stargardt's disease and other ABCA4-related retinopathies. Secondary degeneration of the RPE is also common. Transsynaptic degeneration of higher-order cells, bipolar and ganglion cells, can also occur. The general term retinal degeneration should be distinguished from the more specific term, photoreceptor degeneration.

Retinal dystrophy – A broad term that not only encompasses retinal degenerations, but also includes abnormal retinal function due to developmental defects and malnutrition.

Retinitis pigmentosa (RP) – A heterogeneous group of diseases that result in degeneration of the rod and cone photoreceptors and secondarily the RPE. This degeneration usually leads to a loss of night vision due to the early degeneration of rods, constricted visual fields, decreased responses on ERG, and ultimately a decrease in visual acuity once macular cones begin to degenerate. Typical fundus findings include midperipheral atrophy of the pigment epithelium, bone spicule pigments, retinal vessel attenuation, and waxy pallor of the optic nerve. The term RP usually refers to only rod–cone dystrophies; however, cone–rod dystrophies and cone dystrophies are sometimes grouped under this term.

Rod–cone dystrophy – A retinal dystrophy in which the rod photoreceptors are affected more than the cones. Most forms of RP manifest as rod–cone dystrophies.

Secondary photoreceptor degeneration of the extrinsic type – A secondary photoreceptor degeneration of the extrinsic type exists if, despite the underlying molecular defect, one could avoid the photoreceptor degeneration by preventing an individual's exposure to an extrinsic agent or condition (e.g., toxin, drug, infectious agent, light, and trauma).

Secondary photoreceptor degeneration of the intrinsic type – If one can prevent photoreceptor degeneration by correcting or reversing a systemic or ocular metabolic or immune process, then it is a secondary photoreceptor degeneration of the intrinsic type.

Histological and Fundus Features of Retinitis Pigmentosa

The fundus exam in retinitis pigmentosa (RP) reveals mid-peripheral atrophy of the pigment epithelium, bone spicule pigments greater in the periphery than centrally, retinal vessel attenuation, and waxy pallor of the optic nerve.

Bone Spicule Pigmentation

Bone spicules are intraretinal accumulations of melanin pigment that result from the migration of retinal pigmented epithelial (RPE) cells into the retina after photoreceptor death. These spicules are commonly found in a perivascular pattern and may encircle and occlude these vessels, and are a typical feature of RP. However, there are cases of RP that do not present with bone spicules as well as other disease processes, such as trauma and infection, can result in an appearance that mimics RP by presenting with bone spicules (**Figure 1**).

Waxy Pallor of the Optic Nerve

Much as the name implies, waxy pallor of the optic nerve refers to the funduscopic appearance of the optic nerve seen in many patients with RP. When retinal photoreceptors die, Müller cells and astrocytes in the retina undergo gliosis to form scar tissues. It is thought that this process may lead to the waxy pallor of the optic nerve (**Figure 2**).

Peripapillary/Optic Nerve Head Drusen

Peripapillary drusen/optic nerve drusen are found more commonly in patients with RP. Peripapilliary drusen are histologically different from the drusen found in macular degeneration and are found near or within the optic nerve head. They are thought to result from accumulations of materials in the axons of ganglion cells by axoplasmic stasis and can become calcified with time. Such drusen can cause isolated and asymmetrical visual-field defects, which can be slowly progressive (**Figure 3**).

Bull's Eye Maculopathy

A bull's eye maculopathy results from photoreceptor loss and retinal thinning in a parafoveal distribution. It is often apparent on color fundus photos, but can be visualized on

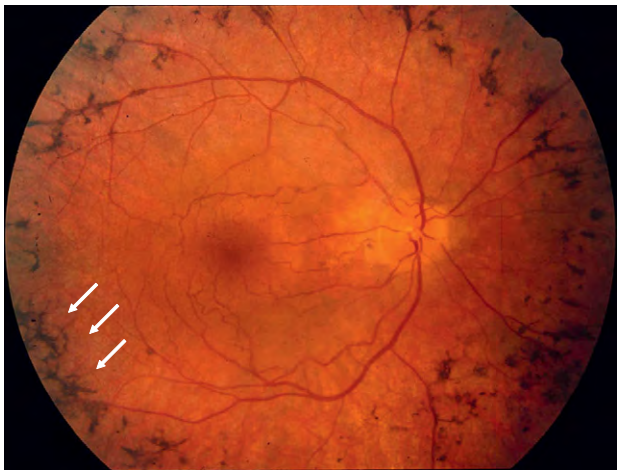

Figure 1 A fundus photo of a patient with retinitis pigmentosa demonstrating intraretinal pigment accumulations (white arrows), also known as bone spicules, which are a common finding in retinitis pigmentosa. They are caused by the migration of retinal pigment epithelial cells into the retina after photoreceptor degeneration. Modified from Weleber, R. and Evan, K. G. (2006). Retinitis pigmentosa and allied disorders. In: Ryan, S. J. (ed.) *The Retina*, 4th edn., vol. 1, chap. 17, pp. 395–498. Philadelphia, PA: Elsevier.

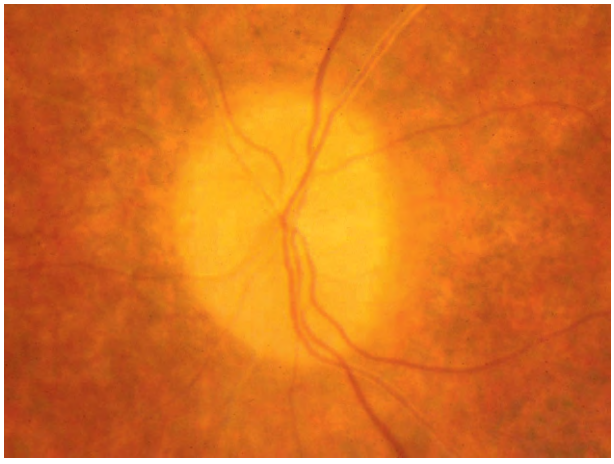

Figure 2 An example of the waxy nerve pallor seen in patients with RP. Also note the vascular attenuation and sheathing.

fluorescein angiography as well. Bull's eye maculopathies are most commonly not only seen in cone–rod dystrophies, but can also be seen in other diseases such as Stargardt's macular dystrophy, Batten's disease, and with hydroxychloroquine (Plaquenil) toxicity (**Figure 4**).

Coats-Like Response

Coats disease is characterized by peripheral retinal telangiectasias, which are dilations of retinal blood vessels, and is usually seen in young males. Rarely, patients with RP can develop localized areas of vascular telangiectasias with exudation similar to those seen in Coats disease. Extravasation of fluid from these vessels can lead to an exudative retinal detachment. This process is termed a Coats-like response (**Figure 5**).

Classification of RP by Fundus Pattern

Classic Pattern for RP

The classic pattern on fundus exam in RP reveals mid-peripheral atrophy of the pigment epithelium, bone spicule pigments in the periphery greater than centrally, retinal vessel attenuation, and waxy pallor of the optic nerve (**Figure 6**).

Inverse RP

The term inverse RP refers to a funduscopic pattern where the central retina exhibits more pigmentary changes and RPE atrophy than the periphery. This term is falling out of favor, as it is now understood that this pattern is often seen with advanced cone and cone–rod dystrophies, as well as some instances of secondary pigmentary retinopathies.

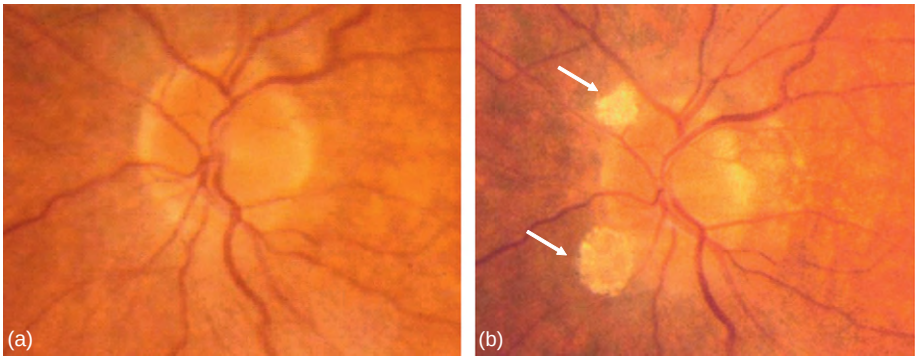

Figure 3 (a) Patient with retinitis pigmentosa – note the lack of a normal physiological cup, which raises the concern for buried drusen. (b) The same patient seen years later who demonstrates peripapillary drusen (arrows).

Concentric RP

Concentric RP is a defined by a subgroup of patients who show a consistent pattern of centripetal vision loss from the far periphery toward the center. This distinguishes it from the classic pattern of RP, which starts in the mid-periphery and progresses both outward and inward. Histological studies have shown an abrupt transition between diseased and normal areas of retina.

Sector RP

Sector RP is a term that refers to the fundus appearance where abnormal pigmentation and atrophy is confined to only one area of the retina, usually an arc inferior to the macula. Debate exists whether this term is specific for certain gene defects or is a stage in evolution of what will become a more generalized process with time. Autosomal recessive or autosomal dominant regional disease can be characterized by such a sectorial pattern at least in early disease. The pattern is usually symmetrical between the two eyes. Mutations in rhodopsin (*RHO*) have been associated with sector RP. These patients are often less symptomatic and their electroretinograms (ERGs) are much less reduced than patients with diffuse or more widespread RP. Early generalized RP can mimic sector RP and, therefore, the diagnosis of sector RP must remain provisional for at least 10 years (**Figure 7**).

Figure 4 A fundus photo demonstrating a Bull's eye maculopathy (dark surrounded by light area).

RP Sine Pigmento

The term RP sine pigmento is applied to the early stages of RP where the classical findings of visual-field loss, decreased ERGs, and vascular attenuation may be present, but there is a lack of bone spicules on the fundus exam. This is thought to represent an early manifestation of the disease and most patients will eventually develop bone spicules, although often not until later stages. Another term in use is pauci-pigmentary retinopathy. In the case of patients who develop symptoms later in life and have a normal, or minimally abnormal, fundus appearance, a work-up for autoimmune retinopathy should be considered.

Tapetal-Like Reflex/Sheen

Tapetal-like sheen is a yellowish-white metallic reflex that can be seen in young males with X-linked RP, women who are carriers of this disease, and patients with cone–rod dystrophy. As the disease advances and RPE atrophy progresses, this reflex can fade. This finding is not pathognomonic of RP because it can be seen in other allied disorders (**Figure 8**).

RP with Preserved Peri-Arteriolar RPE

RP with preserved peri-arteriolar RPE (PPARPE) has been found in families with mutations in the crumbs

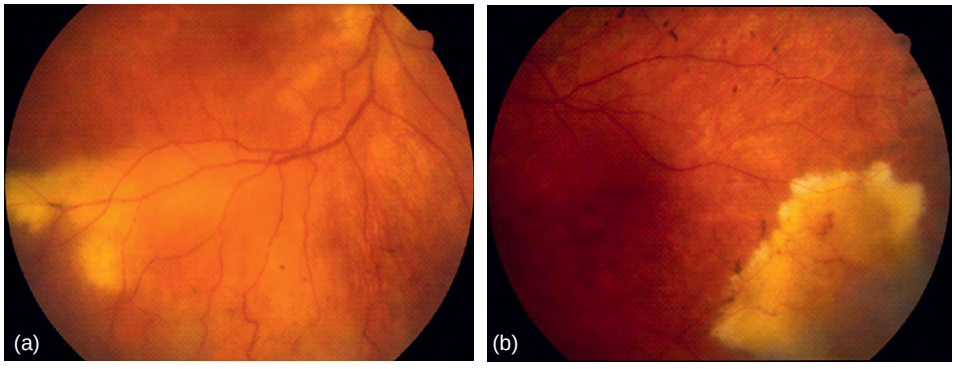

Figure 5 Both (a) and (b) show fundus photos from a patient with RP and a Coat's-like response. Note the yellowish subretinal exudates.

homolog 1 gene (*CRB1*). These patients present with the typical findings of RP, but for reasons not understood, have preservation of the RPE near arterioles.

Pigmented Paravenous Retinochoroidal Atrophy

In pigmented paravenous retinochoroidal atrophy (PPRCA), degeneration and accumulation of bone spicules are limited to the areas around the retinal veins. These patients are often asymptomatic, but with careful testing, scotomas corresponding to the areas of degeneration can be identified. Typically, the ERG is minimally reduced and disease is thought to be, at most, slowly progressive. Although PPRCA has been thought not to be inherited, mutations in the *CRB1* gene have been found in families demonstrating dominant inheritance (**Figure 9**).

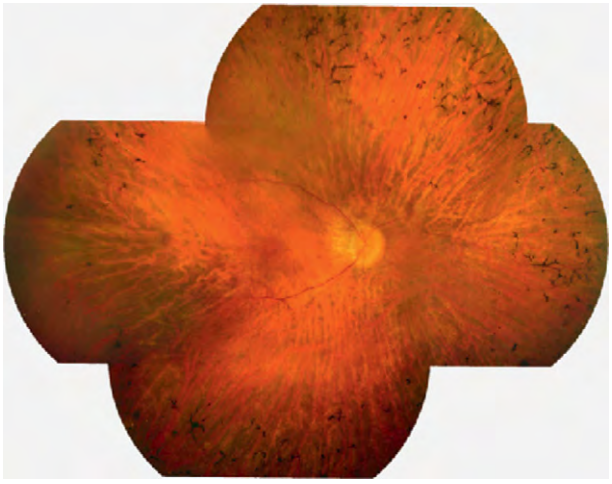

Figure 6 Fundus photo of a typical patient with RP. Note the pallor of the optic nerve, the vascular attenuation, atrophy of the pigment epithelium, and bone-spicules. Reproduced from Weleber, R. G., Butler, N. S., Murphey, W. H., Sheffield, V. C., and Stone, E. M. (1997). X-linked retinitis pigmentosa associated with a two base-pair insertion in codon 99 of the RP3 gene RPGR. *Archives of Ophthalmology* 115: 1429–1435.

Fundus Albipunctata

Fundus albipunctata is an autosomal recessive disease that does not result in a retinal degeneration like RP, but can cause a congenital stationary night blindness. It is more accurately classified as an allied disorder. It is caused by mutations in the retinol dehydrogenase 5 gene (*RDH5*), which results in problems regenerating visual pigment. As a result, these patients have severely decreased rod recovery with prolonged dark adaptation. The fundus exam shows many discrete yellowish-white dots at the level of the RPE. Atrophic lesions in the macula can occur in many patients in later years (**Figure 10**).

Retinitis Punctata Albescens

Retinitis punctata albescens is an autosomal recessive disease caused by mutations in the retinaldehyde-binding protein 1 gene (*RLBP1*). Similar to fundus albipunctata, this disease presents with severe night blindness and small, discrete, yellowish-white lesions in the fundus, but can have a pigmentary retinopathy as well. Later stages of RPA may develop diffuse disease similar to advanced RP.

Gyrate Atrophy

Gyrate atrophy is an autosomal recessive form of diffuse choroidal atrophy caused by mutations of the gene (*OAT*) for ornithine-∂-aminotransferase (OAT). The deficiency of this enzyme results in elevated plasma and tissue levels of ornithine, which exert a cytotoxic effect on the RPE, possibly by endpoint inhibition of a common intermediate for proline synthesis, L-Δ^1-pyrroline-5-carboxylic acid (P5C), which is normally formed from ornithine by OAT and from glutamic acid by P5C synthase. The early stage of gyrate atrophy is associated with sharply demarcated areas of peripheral chorioretinal atrophy. Later stages develop more diffuse and generalized total vascular choroidal atrophy. Dietary restriction of arginine, the precursor for ornithine, can be beneficial. Additionally, a rare subset of patients has been shown to respond with lowered

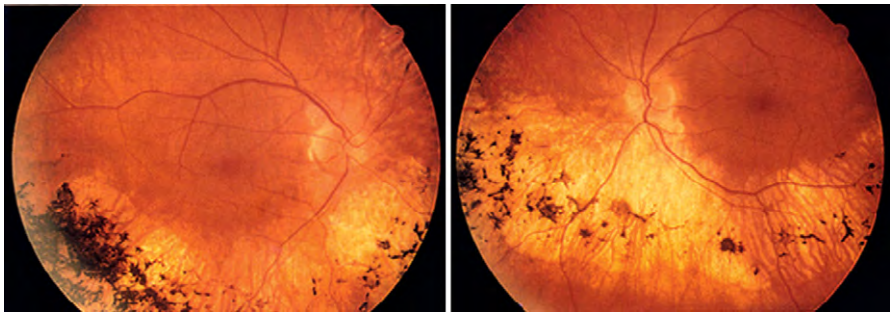

Figure 7 An example of sector RP. From Weleber, R. and Evan, K. G. (2006). Retinitis pigmentosa and allied disorders. In: Ryan, S. J. (ed.) *The Retina*, 4th edn., vol. 1, chap. 17, pp. 395–498. Philadelphia, PA: Elsevier.

Figure 8 An example of tapetal-retinal sheen seen in a carrier of X-linked retinitis pigmentosa.

Figure 9 Example of pigmented paravenous retinal choroidal atrophy.

Figure 10 A fundus photograph of fundus albipunctata. Note the characteristic punctate white dots.

ornithine levels to treatment with vitamin B6 (pyridoxine HCL), which acts as a co-factor for the defective enzyme. Disorders such as gyrate atrophy blur the distinction between primary and secondary retinal degenerations leading to the realization that it is difficult to draw the line between RP and allied diseases (**Figure 11**).

Choroideremia

Choroideremia is an X-linked disease, which is caused by a mutation in the *CHM* gene and leads to progressive degeneration of the retina, RPE, and choroid. The *CHM* gene encodes the homolog of the Rab escort protein 1 (REP1) which is thought to be important in the function of a Rab geranylgeranyl transferase. Choroideremia can often be mistaken for X-linked RP, as the two diseases can share several features including: nyctalopia, retinal RPE atrophy, pigmentary changes, and decreased ERGs and X-linked inheritance. Unlike the waxy nerve pallor seen in RP, patients with choroideremia will often have a normal-appearing nerve and relative preservation of the macula and peripapillary retina (**Figure 12**).

Syndromic Forms of RP

Abetalipoproteinemia

Also known as Bassen–Kornzweig syndrome, abetalipoproteinemia results from a deficiency of beta lipoproteins, which are necessary for normal absorption of fat-soluble vitamins from the gut, leading to poor absorption of vitamins A, D, E, and K. The syndrome is characterized by low levels of fat-soluble vitamins, ataxia, acanthocytosis,

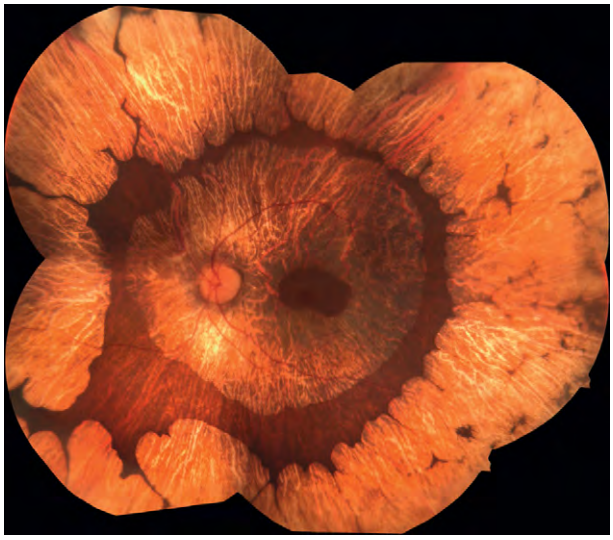

Figure 11 Gyrate atrophy. Note the scalloped peripheral areas of chorioretinal degeneration as well as central atrophy.

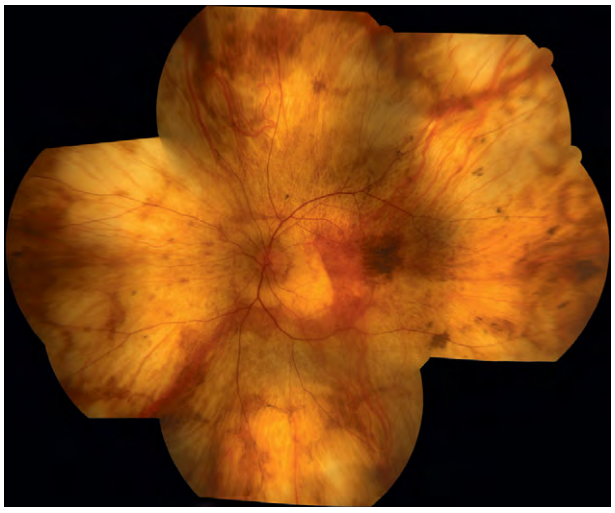

Figure 12 An example of choroideremia demonstrating large areas of chorioretinal atrophy with some macular sparing.

and RP. Treatment with combined vitamin A and vitamin E has been shown to prevent or slow retinal degeneration and, in rare patients, reverse the dark adaptation and ERG defects.

Alström Syndrome

Alström syndrome is an autosomal recessive disease characterized by deafness, obesity, diabetes, cardiomyopathy, and RP. This syndrome shares many overlapping features with Bardet–Biedl syndrome (BBS) and, indeed, much like the genes implicated in BBS, the gene involved in this syndrome, Alström syndrome 1 (*ALMS1*), is thought to play an important role in the structure and function of the cilium.

Bardet–Biedl Syndrome

The details on Bardet–Biedl syndrome are discussed elsewhere in this encyclopedia.

Chronic Progressive External Ophthalmoplegia/ Kearns–Sayre Syndrome

Chronic progressive external ophthalmoplegia (CPEO) and Kearns–Sayre syndrome are mitochondrial myopathies that cause progressive muscle paralysis and pigmentary retinal degeneration. Kearns–Sayre syndrome is associated with sudden cardiac death.

Friedreich's Ataxia

This is an autosomal recessive neurodegenerative disease caused by a trinucleotide repeat expansion in an intron of the frataxin gene (*FXN*), leading to silencing of the gene's protein product, frataxin. The resulting disease causes muscle weakness, ataxia, cardiac hypertrophy, deafness, and retinal degeneration.

Vitamin E Deficiency

Mutations in the alpha-tocopherol transferase protein gene lead to vitamin E deficiency and cause a Friedreich-like ataxia associated with RP. Treatment with oral vitamin E has been shown to halt both the neurological and visual manifestations of this disease.

Incontinentia Pigmenti (Bloch–Schulzberg Syndrome)

Incontinentia pigmenti (Bloch–Schulzberg syndrome) is an X-linked dominant disorder caused by mutations in the nuclear factor kappa-light-chain-enhancer of activated B cells (NFκB) essential modulator gene, *NEMO*, and is usually lethal in males. Affected females demonstrate abnormal teeth and nails, hyperpigmentation of the skin, and central nervous system defects. Retinal findings in these patients include peripheral telangiectasias, hypopigmentation of the fundus, and a pigmentary retinopathy.

Joubert Syndrome

Also known as cerebellooculorenal syndrome, Joubert syndrome is an autosomal recessive disease caused by mutations in 11 different genes. One causative gene, the centrosomal protein 290 (*CEP290*), has also been associated with Senior–Loken syndrome and nonsyndromic Leber congenital amaurosis. Patients with Joubert syndrome have hypoplasia of the cerebellar vermis, and also renal problems and retinal dystrophy. The hypoplasia of the cerebellar peduncles of the midbrain creates a characteristic radiological finding on CT scans termed the molar tooth sign.

Mucopolysaccharide Disorders

Mucopolysaccharide (MPS) disorders can also present with a pigmented retinopathy, some examples of which are Hurler syndrome (MPS type IH), Scheie syndrome (MPS type IS), and Hunter syndrome (MPS type II).

Neuronal Ceroid Lipofuscinosis (Batten Disease)

Neuronal ceroid lipofuscinosis (Batten disease) is a group of autosomal recessive neurodegenerative diseases that result from the accumulation of lipofuscin. This disease is characterized by vision loss, seizures, progressive motor and cognitive dysfunction, and retinal degeneration. Eight genes (*CLN1–CLN8*) have been associated with this disease.

Infantile Refsum Disease

This disease is caused by defective peroxisomes and patients with this disease present with RP, hearing loss, hepatomegaly, and mental retardation. Unlike the adult form of the disease where specific peroxisomal enzymes are defective, the infantile form is characterized by a complete defect in perixosomal biogenesis. Levels of phytanic acid, very long chain fatty acids, and pipecolic acids are elevated. The disease is ultimately fatal.

Adult Refsum Disease

This disease is an autosomal recessive peroxisomal disorder characterized by elevated levels of phytanic acid, which lead to RP, anosmia, deafness, ataxia, cardiac arrhythmias, skeletal anomalies, and polyneuropathy. Mutations in the gene *PAHX*, which encodes phytanoyl-CoA 2-dydroxylases, have been shown to be responsible for some cases of adult Refsum disease. Treatment for adult Refsum disease includes plasmapheresis and dietary restrictions of phytanic acid and its precursors.

Senior–Loken Syndrome

This syndrome is an autosomal recessive disease that also falls under the umbrella of ciliopathies and can share some of the same features as Joubert syndrome (see the section titled 'Syndromic forms of RP'). This disease is characterized by Leber's congenital amaurosis and nephronophthisis (cystic kidneys).

Spinocerebellar Ataxia Type 7

This is an autosomal dominant neurodegenerative disease caused by a trinucleotide expansion in the ataxin 7 gene (*ATXN7*). The disease is characterized by cerebellar ataxias, dysphagia, dysarthria, and a cone–rod dystrophy.

Usher Syndrome

The details of Usher Syndrome are discussed elsewhere in this encyclopedia.

Visual Testing in RP

Terminology of Light Adaptation

The retina can respond to an astonishing 9 log units of light. Rods and cones differ in their sensitivity, temporal characteristics, and response to background lights. Depending on the intensity of a stimulus and background light present, different classes of cells respond. Scotopic refers to conditions under which only rods are functional. Mesopic refers to conditions under which both rods and cones are functional. Photopic refers to conditions under which only cones are functional.

Dark Adaptation

Dark adaption is measured with a Goldmann–Weekers dark adaptometer. Each eye is tested separately by first bleaching the rod and cone photopigments with an intense light and then measuring the brightness of a second light needed to achieve a threshold response. A dark adaptation curve can be drawn by repeating this threshold measurement over time after the bleaching light has been turned off. The normal recovery curve can be separated into two segments. The first segment occurs as cones recover from the bleaching light. The rods are much slower to recover and contribute to the second segment of the curve.

Visual Fields

The details on visual fields are discussed elsewhere in this encyclopedia.

ERG Terminology

The ERG is a fundamentally important test for studying RP and allied disorders. Different forms of RP can be classified based on the ERG response. Just as the electrocardiogram (EKG) measures the electrical activity of the heart through surface electrodes placed on the chest, the ERG measures the electrical activity generated by the retina to flashes of light through electrodes placed on the eye. The standard ERG is most commonly measured using an electrode embedded in a contact lens. Reference electrodes are placed on the forehead and ears. The International Society of Clinical Electrophysiology in Vision (ISCEV) has developed standardized methods for eliciting and recording the ERG.

Full-Field ERG

With the full-field ERG, flashes of light are delivered into a Ganzfeld diffuser, which ensures a uniform distribution of the light to the retina. It is important to realize that the full-field ERG measures a summed response from all of the cells in the retina. Therefore, the visual acuity and the ERG response may not correlate. For example, a patient could have a small scar in the center of the fovea that significantly decreases the vision, but the recordings of the ERG could be normal; the opposite can also be true. A patient could have an extinguished ERG due to peripheral degeneration, but still maintain 20/20 visual acuity due to preservation of the central fovea. For this reason, it is important to correlate visual acuity and ERG recordings along with visual-field results.

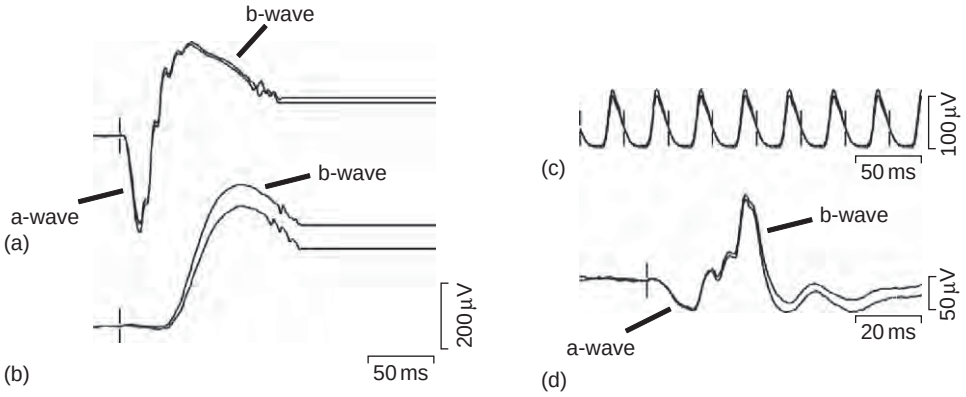

Figure 13 Components of a normal ERG. (a) Scotopic response to bright flash, which stimulates both rods and cones. Note the mixed a-wave, b-wave, and oscillatory potentials (superimposed on b-wave). (b) Scotopic response to a dim white flash, which stimulates only the rods. Note the rod-driven b-wave. (c) Photopic response to a 30-Hz flash, which isolates cones. (d) Response to a single flash under photopic conditions, which also isolates cones. Note the cone a-wave, b-wave, and oscillatory potentials (superimposed on b-wave).

Multifocal ERG

The full-field ERG can demonstrate a large disparity between the ERG signal and the visual acuity. To better detect localized retinal dysfunction in the macula, the multifocal ERG (mfERG) is very useful. The mfERG uses an m-sequence-derived check board pattern to selectively stimulate and isolate electrical activity from the retina. Specifically, the mfERG tests the macula under mesopic or photopic conditions, and therefore is primarily indicative of macular cone function.

Rod-Isolated ERG Response

The ERG can be recorded under dark-adapted (scotopic) conditions or light-adapted (photopic) conditions. When dim flashes are delivered under scotopic conditions, only the rod photoreceptors are stimulated. Such a flash elicits a positive electrical potential termed the b-wave. The scotopic b-wave arises from responses elicited by the rod bipolar cells. As the intensity of the flash increases, the b-wave grows in amplitude and, at higher intensities, a negative potential generated by the rod photoreceptors emerges and is termed the a-wave. Oscillations imposed on the b-wave are generated by higher-order retinal circuitry and are termed the oscillatory potentials.

Mixed Rod–Cone ERG Response

At even higher intensities, both the rod and cone photoreceptors are stimulated to generate a mixed scotopic response. Contributions from the cones contribute to the growing a-wave, while activity of the cone bipolar cells contributes to the b-wave. Once the intensity of the light has become intense enough to saturate the photoreceptors, the a-wave will cease to increase in amplitude. The amplitude from baseline to the peak of the a-wave is termed the saturated a-wave amplitude and the time to the peak of the a-wave is the implicit time. The b-wave amplitude is measured from the trough of the a-wave to the peak of the b-wave.

Cone-Isolated ERG Response

The electrical activity of the cone photoreceptors can be isolated in two ways. The first is to measure the response to 30-Hz flicker flashes for which the cones have sufficient time to recover but the rods do not. The repetitive stimulus elicits a sinusoidal-like response. The peak-to-peak amplitude and the time to peak of this response relative to the stimulus can both be measured. The second method is to turn on a background light, which saturates the rod photoreceptors but minimally affects the cones (photopic conditions). Flashes under these conditions will elicit a cone-driven a-wave and b-wave as well as oscillatory potentials (**Figure 13**).

See also: Anatomically Separate Rod and Cone Signaling Pathways; Noninvasive Testing Methods: Multifocal Electrophysiology; Primary Photoreceptor Degenerations: Retinitis Pigmentosa; Secondary Photoreceptor Degenerations: Age-Related Macular Degeneration.

Further Reading

Berson, E. L., Rosner, B., Sandberg, M. A., et al. (1993). A randomized trial of vitamin A and vitamin E supplementation for retinitis pigmentosa. *Archives of Ophthalmology* 111: 761–772.

Berson, E. L., Rosner, B., Sandberg, M. A., et al. (2004). Clinical trial of docosahexaenoic acid in patients with retinitis pigmentosa receiving vitamin A treatment. *Archives of Ophthalmology* 122: 1297–1305.

Fishman, G. A., Farber, M. D., and Derlacki, D. J. (1988). X-linked retinitis pigmentosa. Profile of clinical findings. *Archives of Ophthalmology* 106: 369–375.
Grant, C. A. and Berson, E. L. (2001). Treatable forms of retinitis pigmentosa associated with systemic neurological disorders. *International Ophthalmology Clinics* 41: 103–110.
Grover, S., Fishman, G. A., Anderson, R. J., et al. (1999). Visual acuity impairment in patients with retinitis pigmentosa at age 45 years or older. *Ophthalmology* 106: 1780–1785.
Hamel, C. P. (2007). Cone rod dystrophies. *Orphanet Journal of Rare Diseases* 2: 7.
Hartong, D. T., Berson, E. L., and Dryja, T. P. (2006). Retinitis pigmentosa. *Lancet* 368: 1795–1809.
Heckenlively, J. R. (1988). *Retinitis Pigmentosa.* Philadelphia, PA: Lippincott.
Hoffman, D. R., Locke, K. G., Wheaton, D. H., et al. (2004). A randomized, placebo-controlled clinical trial of docosahexaenoic acid supplementation for X-linked retinitis pigmentosa. *American Journal of Ophthalmology* 137: 704–718.
Radu, R. A., Yuan, Q., Hu, J., et al. (2008). Accelerated accumulation of lipofuscin pigments in the RPE of a mouse model for ABCA4-mediated retinal dystrophies following vitamin A supplementation. *Investigative Ophthalmology and Visual Science* 49: 3821–3829.
Sieving, P. A., Caruso, R. C., Tao, W., et al. (2006). Ciliary neurotrophic factor (CNTF) for human retinal degeneration: Phase I trial of CNTF delivered by encapsulated cell intraocular implants. *Proceedings of the National Academy of Sciences of the United States of America* 103: 3896–3901.
Weleber, R. G. and Gregory-Evans, K. (2006). Retinitis pigmentosa and allied disorders. In: Ryan, S. J. (ed.) *The Retina*, pp. 395–498. Philadelphia, PA: Elsevier.

Relevant Websites

http://www.ncbi.nlm.nih.gov – National Center for Biotechnology Information, OMIM.
http://www.sph.uth.tmc.edu – The University of Texas School of Public Health, Retinal Information Network (Retnet).

Proliferative Vitreoretinopathy

P Hiscott, University of Liverpool, Liverpool, UK; Royal Liverpool University Hospital, Liverpool, UK
D Wong, University of Hong Kong, Hong Kong, People's Republic of China

Glossary

Cytokeratins – A family of proteins found in the cytoskeleton (intermediate filaments) of epithelial cells.
Glial fibrillary acidic protein – A protein found in the cytoskeleton (intermediate filaments) of glial cells.
Immunohistochemistry – The localization of antigens, especially proteins, in tissue sections by antigen-antibody reactions. The reaction sites are visualized by a label such as a chromogen (typically a brown or red dye).
Myofibroblast – A fibroblast-like cell with some of the features of smooth muscle, including contractile properties.

Introduction

In 1983, the Retina Society Terminology Committee published a landmark paper in which the term proliferative vitreoretinopathy (PVR) was proposed for a condition that had been recognized as the major cause of failure of retinal detachment surgery. Previous names for this disease included preretinal organization, massive vitreous retraction (MVR), massive preretinal retraction (MPR), and massive periretinal proliferation (MPP) – terms that highlighted some of the main clinical features of the disorder.

In this condition, following a retinal detachment, cells leave their normal location in the retina and migrate to the retinal surfaces. Here, the cells proliferate to form membranes. Although many of these membranes consist of only a thin layer of (glial) cells and produce no clinical problems or symptoms, in about 10% of retinal detachment patients the membranes develop into thicker scar-like tissues that are able to contract. It is this ability of the membranes to contract that leads to the clinical picture of PVR.

Definition

PVR is strictly defined as a complication of rhegmatogenous retinal detachment that is characterized by the formation of membranes on both surfaces of the detached retina and on the posterior surface of the detached vitreous gel.

Location of PVR Membranes

The membranes on the vitreous surface of the retina are usually called epiretinal membranes and these are the most common membranes of PVR. Membranes that form beneath the detached retina (i.e., between the neuroretina and the retinal pigment epithelium) are termed sub- or retro-retinal membranes. Membranes on the posterior surface of the vitreous gel are known as posterior hyaloid membranes and typically are continuous with epiretinal membranes in PVR (hence they tend to have a similar composition). The expression periretinal membrane is sometimes used to encompass all membranes around the retina.

In addition, membranes can extend into the vitreous base and anteriorly over the pars plicata to the back of the iris: a condition known as anterior PVR. There is also evidence that PVR can have a distinct component within the neuroretina itself – a situation that may be called intraretinal PVR (iPVR).

It is clear that cellular proliferation can occur at several of the above sites in the same eye. It is also important to recognize that membrane formation can occur in a wide variety of diseases other than retinal detachment. For example, the ischemic retinopathies can also lead to epiretinal and posterior hyaloid membranes although the membranes in these conditions are usually heavily vascularized and thus differ from PVR membranes (see below).

The Significance of Membrane Formation in PVR

In PVR, the membranes may contract so that they exert traction on adjacent tissues. Epiretinal membranes tend to produce tangential traction on the retinal surface. The effect of this retinal traction is to cause retinal folding and/or (re)detachment of the sensory retina (**Figure 1**). Such an effect can be localized, as for example when an epiretinal membrane over the macular (epimacular membrane) causes folding of the macular (macular pucker) or in a peripheral membrane causes a star fold (**Figure 2**). On the other hand, epiretinal membranes may be diffuse, rather than localized, covering much of the retinal surface.

The traction from epiretinal membranes can be mild, causing no more than subtle surface wrinkling of the inner retina. Moderate traction can cause marked folds of the retina. Severe traction can be associated with

displacement of retinal vessels and ectopia of the fovea. The effect of the traction is, however, not just two dimensional (2-D). The newer generation of Optical Coherence Tomography systems provides high-resolution cross-sectional views or reconstructed 3-D images of the retina (Figure 2). These images clearly show that the traction may be superficial but sometimes the whole thickness of the retina is involved. Thus, these signs can indicate the development of PVR.

Clinically, we often see the effect of traction rather than the epiretinal membranes themselves: on the attached retina, epiretinal membranes can be difficult to visualize (Figure 1). Nonetheless, the epiretinal membranes are present and exerting isometric' traction on the retina. The effect of this traction may only become apparent once the retina becomes detached, at which point one may observe star folds or retinal breaks with rolled edges when the traction in the tissue is focal. In addition, when the epiretinal membrane is diffuse, the detached retina will appear to have reduced mobility. Anterior PVR membranes will draw the pre-equatorial retina anteriorly toward the ciliary processes, whereas epiretinal membranes in the post-equatorial retina tend to contract the retina into a cone configuration. The combination of the anterior and posterior traction systems on a totally detached retina will give rise to a so-called closed funnel (Figure 3).

Subretinal membranes, particularly in the form of bands, are apt to elevate the neuroretina like a sheet on a washing line or, in the case of a circular band, like a napkin in a napkin ring. Posterior hyaloid membranes can produce circumferential or, if the vitreous base is involved, anteroposterior traction.

Particularly in eyes that have undergone previous vitrectomy or trauma, proliferative tissue can extend into the vitreous base and anteriorly toward the pars plicata of the ciliary body, the iris and even as far as the pupil margin. Traction in this latter situation may lead to traction on the ciliary body (hypotony can result) and posterior displacement of the iris.

Figure 1 Fundus photograph showing detached, inferior retina with diffuse PVR.

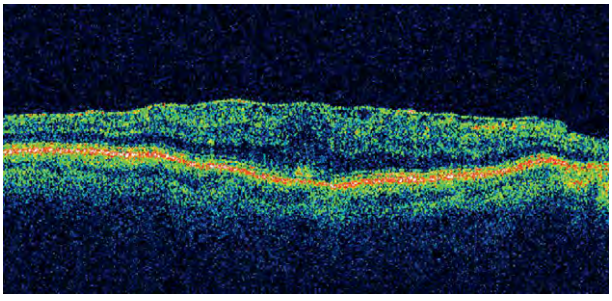

Figure 2 OCT image of retina showing a thin epiretinal membrane and subjacent retinal distortion.

The Cells Involved in PVR

It is now accepted that PVR combines reaction to damage by astrocytes of the central nervous system (gliosis) with fibrosis. In this context, the gliosis involves Müller cells and retinal astrocytes, while the fibrosis includes metaplasia or transdifferentiation of the retinal pigment epithelial (RPE) cells. Although retinal glia and RPE cells are thus major players in PVR, it is also apparent that a variety of other cell types are involved in the disease.

Figure 3 Section through an eye with PVR and a closed-funnel retinal detachment. Retinal folds can be seen. The eye is aphakic and there are anterior PVR membranes that also involve the iris.

Glial Cells

There is compelling evidence from a variety of morphological, immunohistochemical, *in vitro*, and experimental studies that astrocytes and Müller cells are involved in PVR membranes, particularly in epiretinal and, to a lesser extent, subretinal membranes.

Within PVR epiretinal membranes, glial cells often form layers in the tissue (**Figure 4**). These layers are adherent to fibrous components of the membranes and, in both human and experimental PVR, the cells can sometimes be traced through defects in the retinal inner limiting lamina into the retina itself. These observations

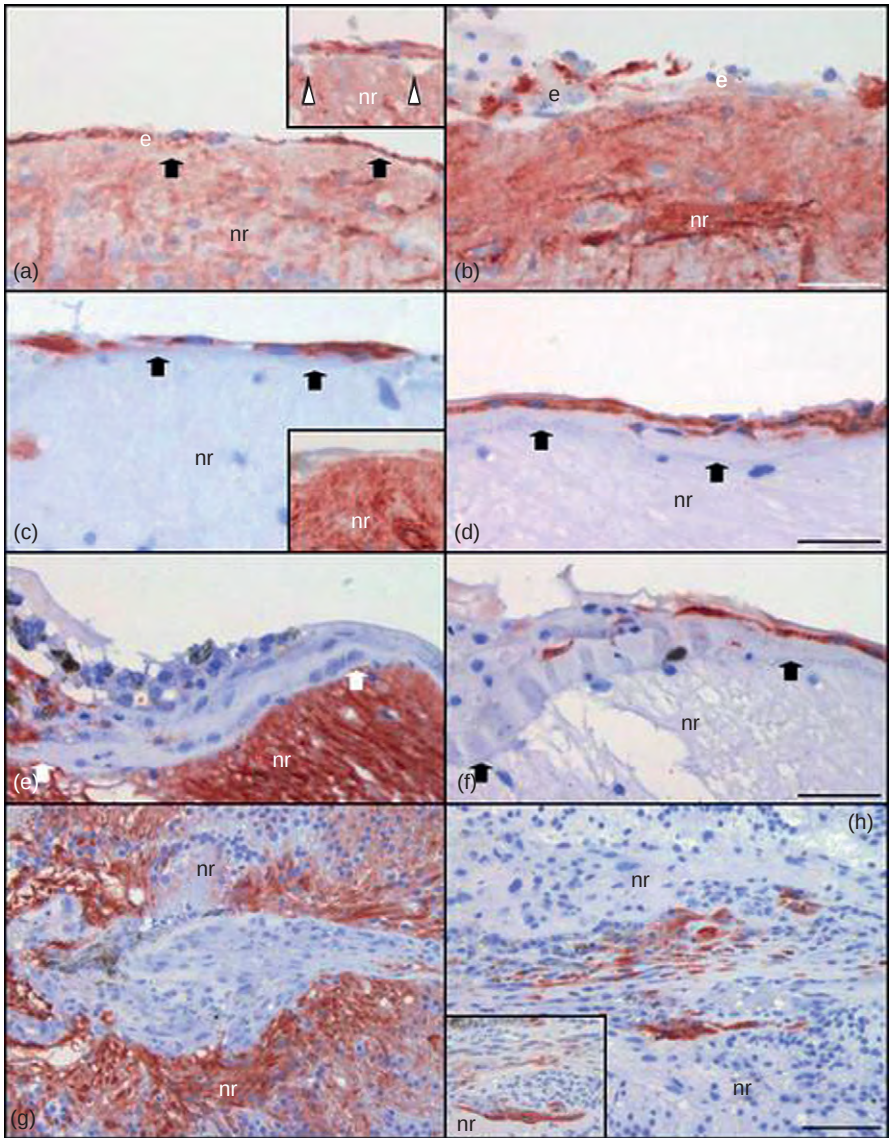

Figure 4 (a–h) Sections through neuroretina (nr) with PVR membranes in enucleated eyes. The sections have been stained with the immunohistochemical method for glial elements with an antibody to glial fibrillary acidic protein (see insets in (a–c) , and also (e) and (g)) or for RPE elements with antibody to cytokeratin 7 ((c), (d), (f), and (h)) or to a range of cytokeratins (inset in (h)): red-brown reaction product, hematoxylin counterstain. (a) The retina is gliotic and there is an epiretinal membrane 'e' composed of a glial monolayer. The internal limiting lamina is marked (arrows). Inset: this epiretinal membrane is composed of a double layer of glia and there is some distortion of the internal limiting membrane (arrowheads). (b) The epiretinal membrane 'e' is composed of glial and nonglial cells. Again, the underlying retina is gliotic. (c and d) Epiretinal RPE cells are seen. The subjacent retina is gliotic (inset in (c)). The internal limiting lamina is marked (arrows). Parts (e) and (f) show the same area of the same specimen: the epiretinal membrane contains both glial (e) and RPE (f) components. The internal limiting lamina is marked (arrows). Parts (g) and (h) show the same area of the same specimen: the retina is folded, disorganized, and gliotic. There is a PVR membrane containing fibroblastic RPE cells and a few glia. Some of the fibroblast-like cells do not label for glial or RPE markers, even with an antibody that reacts with a range of cytokeratins (inset in (h)): their origin is unclear. Scale bars: (a–f) 50 μm; (g and h) 100 μm.

have led to the concept that glial cells traversing the vitreoretinal interface serve to anchor the epiretinal membrane to the retina and that the epiretinal glia may form a substrate or scaffold that other cells might use to produce the rest of the epiretinal tissue. In support of this notion, experimental models have demonstrated that glial cells can break through the retinal inner limiting lamina early in the formation of epiretinal membranes and spread across the retinal surface to form sheets that other cells may adhere to. Failure of glial sheets to become populated by other cells may account for arrest of the disease process at an early stage and the production of asymptomatic or nonproblematic subtle membranes on either surface of the neuroretina.

RPE Cells

The same sorts of methods that were used to detect glia in PVR membranes have been employed to demonstrate RPE cells. Indeed, it is now widely accepted that RPE cells are major components of PVR membranes and the presence of large numbers of RPE cells in epiretinal membranes is one of the distinguishing factors between PVR membranes and epiretinal membranes caused by other diseases. Early in the development of PVR, RPE cells leave their normal location at the chorioretinal interface and either migrate or are swept with subretinal fluid movements to the surfaces of the detached retina. Here, the cells may attach to early membranes (**Figure 4**). In the case of epiretinal membranes, RPE cells may adhere to glia that have already arrived, while in subretinal membranes it has been suggested that the cells may in addition settle on fibrin deposits. Some RPE cells may also migrate into or through the neuroretina.

RPE cells have a remarkable propensity to undergo metaplasia or transdifferentiation. As a result, an RPE cell may change from a polarized, sedentary pigmented cuboidal epithelial cell to a nonpigmented fibroblastic cell, a migratory macrophage-like cell, a cell in a gland-like structure or even a bone-forming cell (**Figure 4**). In PVR membranes, RPE cells most often adopt fibroblastic or macrophagic phenotypes, though they may attempt to (re-)form a polarized monolayer as well.

Fibroblastic Cells

PVR membranes often have a substantial fibrous element that consists of fibroblastic cells in extracellular matrix. Many of these cells are of RPE origin (**Figure 4**). Others may be derived from perivascular sources such as adventitial cells of larger retinal vessels.

There has been much interest in the role of fibroblastic cells in PVR membranes for two reasons. First, they are believed to be responsible for generating most of the tractional forces within the tissue. Second, the cells are thought to be responsible for the production of the bulk of the extracellular matrix in the membranes. There is still debate about how these cells may produce traction: theories include smooth muscle-like contraction of the (myofibroblastic) cells and cell–matrix interactions that cause shortening of matrix elements.

Macrophages

In addition to macrophagic RPE cells, macrophages of hematogenous origin are involved in PVR. Macrophages are especially abundant in membranes arising in the presence of some tamponade agents (see below).

Irrespective of their origin, macrophages are believed to have a number of important roles in PVR. In the early stages of the disease, they produce mitogens, chemotactic agents, and growth factors that probably have a role in cell recruitment to and proliferation in the membranes. Growth factors and enzymes produced by macrophages later in the disease process may be involved in matrix synthesis and remodeling.

Vascular Elements

Blood vessels are found in around 10–20% of PVR membranes but, in contrast to periretinal membranes of conditions such as central retinal vein occlusion and proliferative diabetic retinopathy, blood vessels usually do not form a major component of the tissue. However, vessels are probably more abundant in anterior PVR membranes (**Figure 5**).

Other Cells

T lymphocytes, including CD4 and CD8 positive cells, have been found in PVR membranes. Some of these cells express interleukin-2 receptor, suggesting that they are activated and capable of promoting the cellular events in the tissue. Ciliary body epithelial cells have been reported in the membranes of anterior PVR (**Figure 5**). Hyalocyte-like cells have been described in epiretinal membranes generally and it has been suggested that hyalocytes may give rise to some of the fibroblastic and macrophagic cells in the epiretinal tissues. Recently, ganglion cell neurites have been observed in experimental and human epi- and subretinal membranes. They are co-localized with glia, suggesting active outgrowth into the periretinal tissues.

The Extracellular Matrix in PVR Membranes

PVR membranes contain a matrix that, in terms of composition, is similar to the one seen in a healing skin wound (**Figure 6**). These components include structural proteins

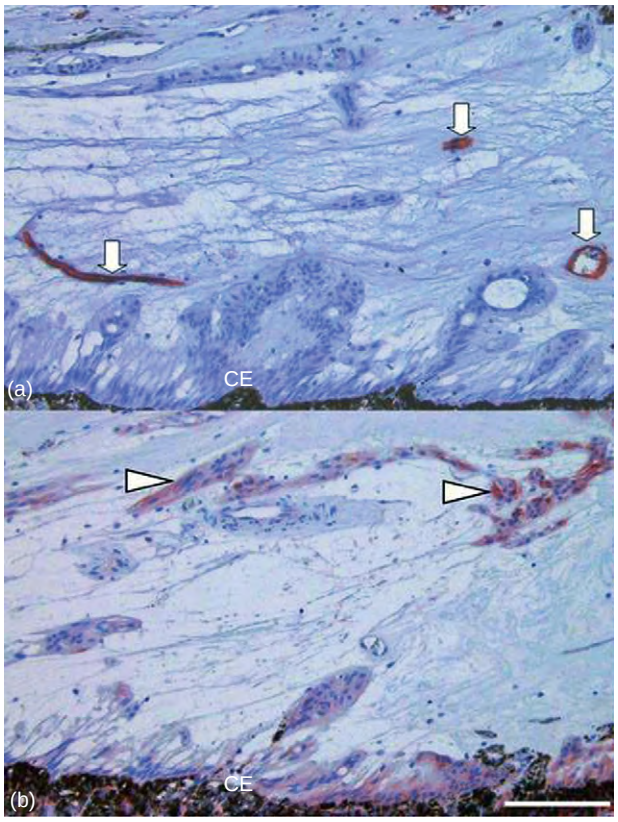

Figure 5 Anterior PVR membrane extending over distorted ciliary epithelium (CE) in an enucleated eye. (a) Stained with the immunohistochemical method for the endothelial marker CD34: note that there are blood vessels in the membranes (arrows). (b) Stained with the immunohistochemical method for cytokeratins: note that in addition to cells in the membranes (arrowheads), the CE normally expresses cytokeratins too. Thus, it is possible that at least some of the epithelial cells in anterior PVR membranes are of CB rather than RPE origin (hematoxylin counterstain, scale bar: 200 μm).

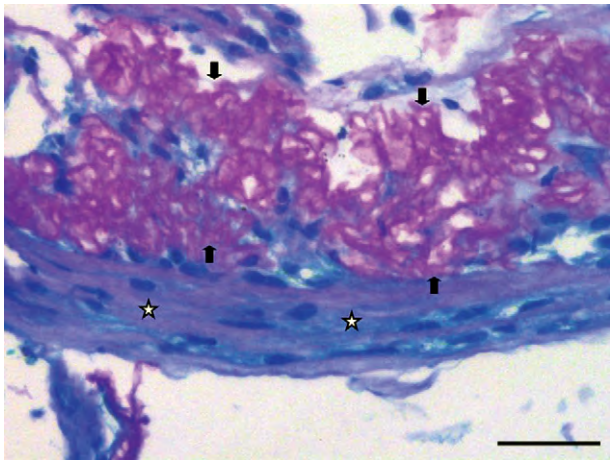

Figure 6 Section through a surgically excised PVR epiretinal membrane. The tissue contains a fibrous element (stars). Convoluted retinal internal limiting membrane is also present (arrows). Periodic acid Schiff reagent, hematoxylin counterstain. Scale bar: 50 μm.

such as collagens and elastic fiber precursors, adhesive glycoproteins like fibronectins and laminins, glycosaminoglycans, matricellular proteins such as tenascins and thrombospondins, and matrix enzymes like matrix metalloproteinases together with their inhibitors.

Much of the matrix in PVR is produced locally by the membrane cells themselves, though there is evidence that some components enter from elsewhere. For example, some blood derivatives like plasma fibronectin are found in PVR membranes. Irrespective of origin, the extracellular matrix in PVR membranes increases with time and there is a corresponding decrease in cellularity of the tissue. Indeed, this change in cellularity together with the contractile nature of the tissue and the presence of fibroblastic cells in matrix gave rise to comparisons between PVR membranes and healing wounds.

As in healing wounds generally, the matrix is more than a passive space filler: there is good evidence that PVR matrix is an important regulator of cell behavior (notably migration and proliferation) in the tissue. For example, there have been a number of reports demonstrating that cells in PVR membranes express a range of cell-surface receptors for the various matrix components around them (e.g., integrins) and experimental studies implicating the importance of such receptors in contraction in PVR models. Moreover, early matrix may have adhesive properties that aid cohesion of the developing tissue. There is also evidence of matrix remodeling in more established membranes. Longstanding PVR membranes are often densely fibrous. It is also worth noting that, when surgically excised, PVR membrane specimens often contain internal limiting membrane from the retina. This material tends to become convoluted in the tissue (**Figure 6**), presumably as a result of tractional forces upon it.

Pathogenesis and Natural History

Although the pathogenesis of PVR is not fully elucidated, our understanding of the disease is at the point where logical therapies can be designed and implemented.

Fundamental to the development of PVR is retinal detachment, itself dependent upon degenerative changes in the vitreous and retina. Vitreous degeneration (syneresis) is a normal aging process that can be accelerated by conditions such as myopia or trauma and results in the formation of fluid and formed components. Attachments between formed vitreous and retina may permit rotational tractional forces, such as dynamic traction from saccadic eye movements, to be transmitted between the two structures. In turn, a retinal tear may form and fluid vitreous pass through the hole in the retina to give rise to a (rhegmatogenous) retinal detachment.

There is experimental evidence that some changes associated with PVR can occur within a day of retinal

detachment. In retinal detachment, together with entry of fluid vitreous to the subretinal space, there is breakdown of the blood–retina barrier with accumulation of plasma proteins in the vicinity of the retina and influx of blood-borne inflammatory cells. Thus, there is aggregation of hematogenous and locally derived proteins and cytokines, including plasma glycoproteins, and growth and differentiation factors. Many of the components of this collection have chemotactic and/or mitogenic properties for RPE and glial cells. In fact, RPE cells can be observed to detach from Bruch's membrane and may be transported to the surfaces of the detached retina while glia may breech the retinal inner limiting lamina (see above) in retinal detachment.

The above reaction to retinal detachment might set the scene for PVR formation, as we have seen only a minority of retinal detachment patients develop the condition. It thus appears that additional factors are required and, indeed, a number of clinical risk factors have been identified (see below). These include factors that would be expected to elevate the concentrations of chemotactic and mitogenic chemical mediators and increase the influx of inflammatory cells to the retinal surfaces, such as hemorrhage, multiple surgical interventions, and large surface area of RPE cells exposed to detachment.

Cells displaced to the surfaces of the detached retina can be seen to adhere to each other as well as the retinal surface. These very early membranes lack matrix but they do possess adhesive glycoproteins like fibronectins. Moreover, a number of matricellular proteins including thrombospondin 1 are also present. It has been hypothesized that fibronectin and thrombospondin 1 can form a provisional matrix in healing wounds. Thus, it is possible that they provide some integrity to developing PVR membranes as well as an adhesion substrate for the cells.

Once in the developing membranes, the cells proliferate. Proliferation is assumed to increase the amount of membrane tissue and it can be detected as long as a year after the onset of the disease. In this respect, PVR differs from skin wounds where proliferation is restricted to a short wave early in the process. It is thought that cells also migrate along the retinal surfaces toward developing membranes, perhaps in response to local chemotactic agent production in the new tissue.

In addition to cell recruitment, cell migration in PVR membranes might also be a mechanism by which tractional forces are generated (motile cells impart a force on their substrate). Thus, it may be that cell migration, myofibroblastic contraction, and cell–matrix interactions (see above) can all be involved in membrane contraction.

The buildup of extracellular matrix with time in PVR membranes is matched by a reduction in cellularity of the tissue (**Figure 6**). Cell loss in PVR membranes probably occurs through apoptosis and nonapoptotic pathways. Ultimately, untreated PVR membranes become paucicellular and fibrous in nature.

Intraretinal PVR

The concept that retina-shortening cellular changes may occur within the neuroretina itself in PVR is relatively recent. Nevertheless, it is now clear that several cell types, including Müller cells and astrocytes, not only become reactive but also do replicate in the retina in PVR and it is thought that this gliosis contributes to retinal shortening. RPE cells are also involved in this process, although their numbers appear to be small compared to the numbers in periretinal membranes. Moreover, gliosis, with or without epiretinal and/or subretinal membranes, can cause marked retinal distortion and localized retinal thickening that can lead to the formation of a focal mass (**Figure 7**). Indeed, similarities in the microscopic appearances of localized PVR masses and vasoproliferative tumors of the retina, including the presence of RPE cells in both lesions (**Figure 8**), have led to speculation that some vasoproliferative tumors may be part of the spectrum of PVR.

Incidence and Risk Factors

It is often stated that PVR afflicts around 10% of all patients with retinal detachment. However, it is clear that some patients are at much greater risk of developing the condition than others. The most important risk factor for postoperative PVR seems to be preoperative PVR. A variety of clinical risk factors have been identified or suggested, including size and number of retinal holes, extent and duration of the detachment, the presence of blood and/or intraocular inflammation, aphakia, preoperative choroidal detachment, early stages of the disease or poor visual acuity prior to initial surgery, and

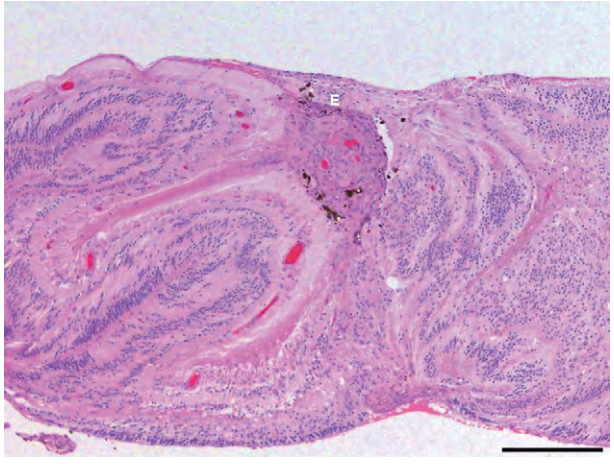

Figure 7 Gliotic, disorganized, thickened retina that has full-thickness folds in association with epiretinal membrane (E), in a section of an eye removed for complications of PVR. The retinal changes give rise to the formation of a localized mass (hematoxylin and eosin; scale bar: 500 μm).

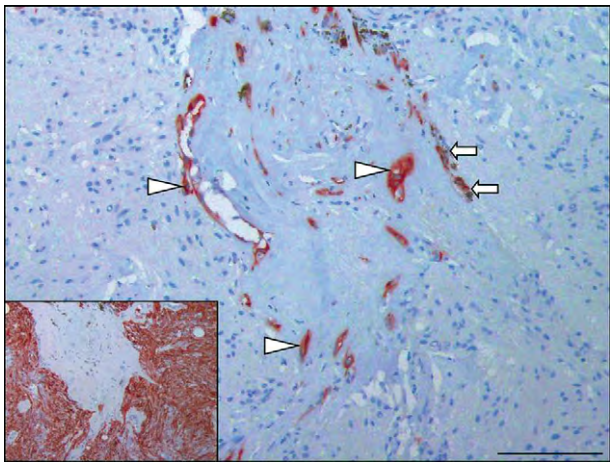

Figure 8 Section showing part of a vasoproliferative tumor (reactive retinal glioangiosis) in an eye removed for complications of retinal detachment. The lesion contains scattered RPE cells (arrowheads), revealed (red) by immunohistochemical staining for cytokeratin 7 (hematoxylin counterstain). A few of these cells contain melanin pigment (*arrows*). Staining of the lesion for glial cells (*inset*: immunohistochemical staining red, hematoxylin counterstain) confirms that the retinal tissue is gliotic and disorganized. Scale bar: 200μm

multiple previous attempts at re-attaching the detached retina. Methods employed during the primary retinal detachment surgery may also increase the risk of PVR. Thus, there is evidence that cryopexy, choice of tamponade agent, and vitrectomy impact on the risk of developing PVR.

Clinical Classification of Proliferative Vitreoretinopathy

There are several attempts to classify PVR according to the clinical features of the retinal detachment. These classifications are descriptive and help surgeons communicate, especially with regard to surgical approaches in the management of the condition. Thus, they are useful for surgical planning and are not based on pathobiology. PVR classifications are also not prognostic. They do not correlate well with visual prognosis or anatomical success with treatment. The classification is also not related to the stages of the disease. It is just the clinical picture at one snapshot in time. Despite their many shortcomings, clinical PVR classifications are widely used in clinical trials and for clinicopathological correlates.

Several classifications have been suggested, based on the clinical manifestations of the disease. For the most part, there is commonality between these systems with regard to the earlier or milder stages of the disease, whereas the schemes tend to diverge in their classification of later or more advanced stages of PVR.

Within these systems, stage A (minimal) is usually regarded as the presence of vitreous haze and pigment clumps, whereas stage B (moderate) is typically recognized as wrinkling of the retinal surface, decreased vitreous mobility, and increased retinal stiffness.

With respect to the more severe or later stages of PVR, some schemes separate the advanced stages by the number of quadrants of the retina involved. Thus, for example, the Retina Society Terminology Committee classification of 1983 associates stage C (marked) disease with fixed retinal folding and adds a number to reflect the number of quadrants involved (e.g., C-3 is fixed folds involving three quadrants of retina). In this system, stage D (massive) reflects the involvement of all four retinal quadrants. In addition, stage D is graded 1–3 depending on how extensive the folding of the retina is (D-1 being an open funnel of totally detached retina, D-3 being a closed funnel so that the optic nerve head cannot be seen: **Figure 3**).

Other schemes classify the more severe stages of PVR into anterior and posterior groups, according to the location of the disease with reference to the retinal equator. In these systems, the number of retinal quadrants involved by the disease is again used so that PVR involving fixed folds in, say, two quadrants of retina posterior to the equator would be classed P2 or CP2 (stage D is generally discarded in these schemes). The schemes employing anterior and posterior also add a contraction type, depending on the extent of epiretinal membrane (focal or diffuse), the presence of subretinal membrane, or posterior hyaloid/vitreous base proliferation.

Management

There is much interest in preventing proliferation of membranes after retinal detachment surgery by treating high-risk patients with combinations of agents. One such combination is the antiproliferative drug 5-fluorouracil and low-molecular-weight heparin (which binds growth factors). This combination has been shown to reduce the incidence of PVR in high-risk retinal detachment patients undergoing vitrectomy.

Once established, PVR membranes are removed by microsurgery so that the retina can be reattached. Again, there is much interest in the use of pharmacological measures to stop membrane recurrence after PVR surgery. For example, there is evidence that daunomycin used preoperatively can reduce the requirement for repeat surgery in these patients.

Tamponade agents to maintain retinal attachment are frequently employed during and after surgery for retinal detachment and PVR. These agents incorporate gases (e.g., air) and liquids (e.g., silicone oil). Liquids have a tendency to emulsify in the eye, particularly if they are

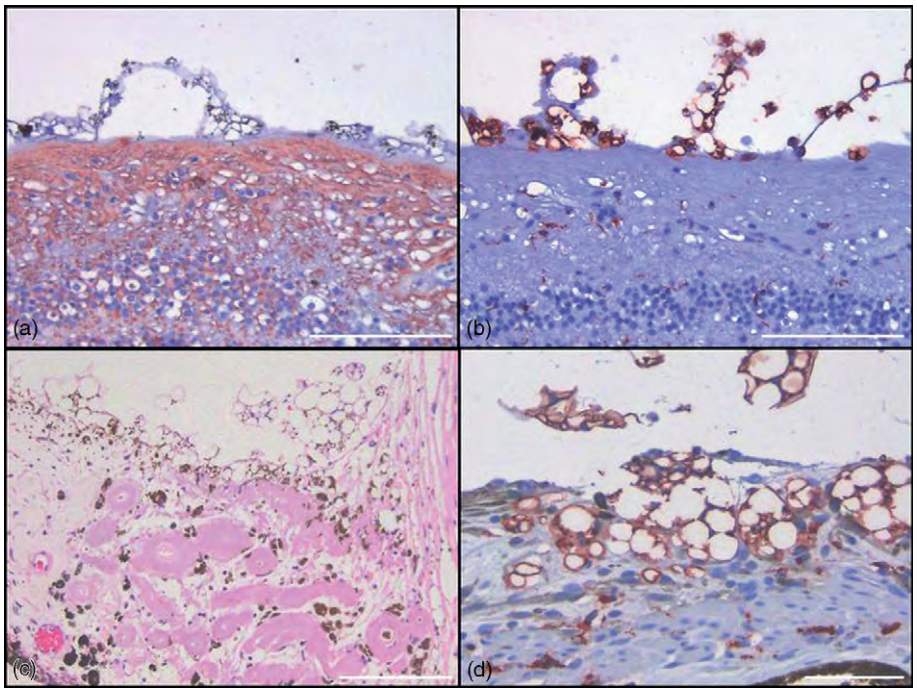

Figure 9 Photomicrographs from sections of an eye removed following liquid tamponade use in the treatment of PVR. Parts (a) and (b) show the vitreoretinal interface with numerous vacuolated cells that label for the macrophage marker CD68 (b), but not the glial marker glial fibrillary acidic protein (a). Similar cells are seen in the drainage angle (c) and in the anterior chamber and iris (d). The features are consistent with macrophage reaction to emulsified liquid tamponade agent (hematoxylin and eosin (c); immunohistochemical staining, red reaction product (a), (b), and (d); scale bars (a), (b), and (d): 100 μm; (c) 200 μm).

of low viscosity. The result is the formation of droplets of various sizes in the vitreous cavity or even elsewhere in the eye (such as in the aqueous if tamponade gains access to the anterior chamber: **Figure 9**). Thus, emulsification of tamponade agent may impact on the pathology of PVR membranes. It appears that the droplets can stimulate a foreign body-type reaction and attract macrophages to the retinal surface (**Figure 9**). New membranes may develop and these tissues characteristically have the microscopic appearances of PVR membranes containing granulomata to emulsified oil.

Outcomes

Successful treatment in PVR has often been measured in terms of final retinal reattachment rates. The assumption is that effective anti-PVR therapy would lead to an increased rate of successful reattachment. This assumption may or may not hold true. It is often missed or untreated holes that lead to retinal redetachment and not necessarily PVR, which may or may not be controlled by the anti-PVR drugs. Indeed, a totally ineffective anti-PVR treatment may be compatible with anatomical success so long as the epiretinal membranes do not act on the retina to produce another retinal break or cause tractional retinal detachment. Hence, anatomical success rate is a poor proxy for PVR control. Another important point is that anatomical success does not guarantee visual recovery. The advancement of surgery in the last few years has greatly increased the final anatomical success rate. Disappointingly, this success rate has not been translated into visual improvement. In retinal detachment patients, the fellow eye is also likely to be involved in sight-threatening pathology so that many PVR patients end up with visual impairment in both eyes.

Conclusions

Despite intense research over the last 25 years that has improved our understanding of the condition, PVR remains the major cause of failure after retinal detachment surgery. Nevertheless, continuing advances in both surgical and pharmacological manipulation of the disease, based on an expanding knowledge of PVR pathobiology, can be expected to reduce the impact of the disease in the future.

See also: Cellular Origin, Formation and Turnover of the Vitreous; Molecular Composition of the Vitreous and Aging Changes; Rhegmatogenous Retinal Detachment; Vitreous Anatomy, Aging, and Anomalous Posterior Vitreous Detachment.

Further Reading

Asaria, R. H., Kon, C. H., Bunce, C., et al. (2001). Adjuvant 5-fluorouracil and heparin prevents proliferative vitreoretinopathy: Results from a randomized, double-blind, controlled clinical trial. *Ophthalmology* 108: 1179–1183.

Charteris, D. G. (1995). Proliferative vitreoretinopathy: Pathobiology, surgical management, and adjunctive treatment. *British Journal of Ophthalmology* 79: 953–960.

Colthurst, M., Williams, R. L., Hiscott, P., and Grierson, I. (2000). Biomaterials used in the posterior segment of the eye. *Biomaterials* 21: 649–665.

Fisher, S. K., Lewis, G. P., Linberg, K. A., and Verardo, M. R. (2005). Cellular remodeling in mammalian retina: Results from studies of experimental retinal detachment. *Progress in Retinal and Eye Research* 24: 395–431.

Heimann, K. and Wiedemann, P. (1989). *Proliferative Vitreoretinopathy.* Heidelberg: Kaden.

Hiscott, P. and Mudhar, H. (2008). Is vasoproliferative tumour (reactive retinal glioangiosis) part of the spectrum of proliferative vitreoretinopathy? *Eye* 23: 1851–1858.

Hiscott, P. and Sheridan, C. (1998). The retinal pigment epithelium, epiretinal membranes and proliferative vitreoretinopathy. In: Marmor, M. F. and Wolfensberger, T. J. (eds.) *Retinal Pigment Epithelium – Function and Disease*, pp. 478–491. New York: Oxford University Press.

Hiscott, P., Morino, I., Alexander, R., Grierson, I., and Gregor, Z. (1989). Cellular components of subretinal membranes in proliferative vitreoretinopathy. *Eye* 3: 606–610.

Hiscott, P., Sheridan, C., Magee, R., and Grierson, I. (1999). Matrix and the retinal pigment epithelium in proliferative retinal disease. *Progress in Retinal and Eye Research* 18: 167–190.

Kampik, A., Kenyon, K. R., Michels, R. G., Green, W. R., and de la Cruz, Z. C. (1981). Epiretinal and vitreous membranes. Comparative study of 56 cases. *Archives of Ophthalmology* 99: 1445–1454.

Kirchhof, B. and Wong, D. (eds.) (2005) *Vitreo-Retinal Surgery. Essentials in Ophthalmology.* Berlin: Springer.

Machemer, R. and Laqua, H. (1975). Pigment epithelium proliferation in retinal detachment (massive periretinal proliferation). *American Journal of Ophthalmology* 80: 1–23.

Pastor, J. C., de la Rúa, E. R., and Martín, F. (2002). Proliferative vitreoretinopathy: Risk factors and pathobiology. *Progress in Retinal and Eye Research* 21: 127–144.

The Retina Society Terminology Committee (1983). The classification of retinal detachment with proliferative vitreoretinopathy. *Ophthalmology* 90: 121–125.

Wiedemann, P., Hilgers, R. D., Bauer, P., and Heimann, K. (1998). Adjunctive daunorubicin in the treatment of proliferative vitreoretinopathy: Results of a multicenter clinical trial. Daunomycin study group. *American Journal of Ophthalmology* 126: 550–559.

Relevant Website

http://www.youtube.com – Number of videos concerning PVR and its management.

Properties and Functions of the Vessels of the Ciliary Body

E L van der Merwe and S H Kidson, University of Cape Town, Cape Town, South Africa

Glossary

Fenestrations – Derived from fenestra, the Latin word for window, 60–80 nm pores in the endothelium spanned by a diaphragm of radially oriented fibrils that regulate the diffusion of small molecules and amounts.
Occludin – A 65-kDa integral plasma-membrane protein that is a major constitutent of tight junctions.
Ora serrata – Junction between the retina and the ciliary body that marks the transition from the simple nonphotosensitive area of the retina to the complex, multilayered photosensitive region.
Pars plana – Part of the ciliary body just beyond the ora serrata is smooth.

Arterial and Venous Supply of the Ciliary Body

The ciliary body (CB) forms part of the anterior segment of the eye and is composed of the ciliary processes and the ciliary muscle. It extends from the iris root anteriorly to the ora serrata posteriorly. The CB is divided into two regions: the pars plana and the pars plicata. The pars plicata consists of ciliary muscles and ciliary processes. The ciliary processes are organized in a radial pattern, with alternating major and minor processes. Each process is composed of two epithelial layers encapsulating a capillary network embedded in a loose connective tissue. The large surface area of the CB enables the secretion of components of the aqueous humour and glycoproteins of the vitreous body. The CB connects to the lens by zonula fibres, thus enabling accommodation.

The CB has the highest density of blood vessels in the eye, and its vascular organization is extremely complex (Figure 1). This complexity, density, and redundancy ensures consistent perfusion of the anterior segment, even following interruption of arteriole supply routes, and thus facilitates homeostatic control of aqueous humor production. The CB has two main blood supplies: the anterior ciliary arteries, and the medial and lateral long posterior arteries which traverse the interior. Superficially, the anterior ciliary arteries arise from the muscular arteries supplying the four recti (superior, lateral, medial, and inferior). These arteries are derived from the ophthalmic artery. The anterior ciliary arteries continue anteriorly and branch at or just before the limbus. One branch supplies the episcleral arterial circle and conjunctiva in the superficial limbus while the other penetrates the limbus and enters the vascular bed of the ciliary muscle. Arterioles that branch off the penetrating anterior ciliary artery undergo further divisions where they interconnect with the capillary bed of the ciliary muscle (Figure 2). These vessels also anastomose with those that arise from the long posterior ciliary arteries to form the intramuscular circle of the CB that lies within the outer portion (exterior regions) of the ciliary muscle. This anastomotic ring artery supplies the superficial (outer) and posterior region of the ciliary muscle.

The other source of blood to the CB is via the major arterial circle (MAC) of the iris (also called the circulus iridis major (Figure 3) which lies between the ciliary muscle and the ciliary process and is located near the root of the iris). According to some reports, in the human eye the MAC is formed mainly from vessels that arise from the medial and lateral long posterior arteries that have bifurcated near the anterior choroid, and, which are orientated in the circumferential plane. Others report that branches of the intramuscular circle form the MAC. In addition, within this region, anastomoses are formed between branches of the anterior ciliary artery and the long posterior ciliary artery. The supply to the anterior and inner regions of the ciliary muscle is derived from arterioles that branch off the MAC.

In the human and primate eye, each ciliary process receives blood from an anterior and posterior arteriole that branch off the MAC. The anterior branches supply the anterior portion of the ciliary process which includes the marginal region and the lateral branching capillaries which supply the anterior portion of the neighboring processes. Thus, intercommunication between ciliary processes occurs through the lateral branching capillaries supplied by the anterior arteriole. The posterior arteriole supplies the inner, basal, and posterior portion of the process and to the minor ciliary processes. In ungulates, rodents, and carnivores, all ciliary processes receive blood solely from the posterior arteriole that arises from the MAC. Venous drainage is via the pars plana into the choroidal veins. Whereas the anterior arterioles have focal constrictions, the posterior arterioles are devoid of these.

The pars plana lies posterior to the ciliary processes and therefore has several sources of vessels. One is from the iris in the form of tributaries, another is from the basal capillaries/venules that lie within the first and third

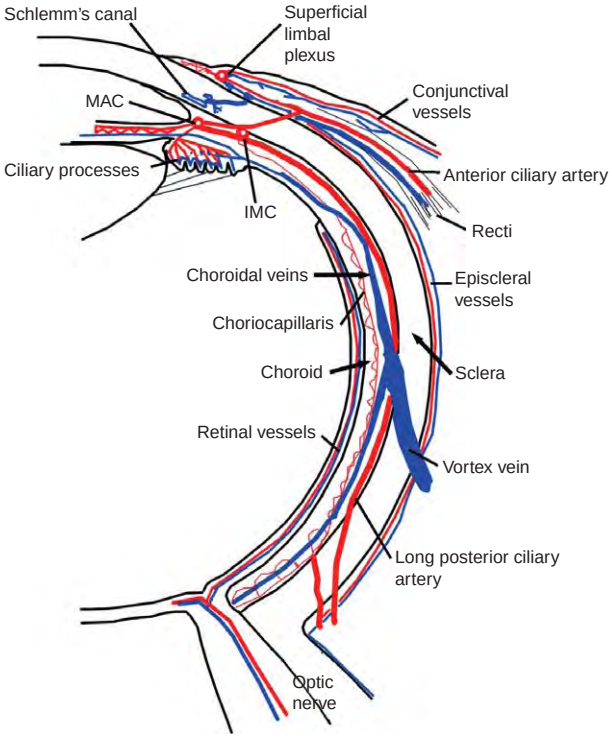

Figure 1 Schematic depicting the arterial supply to and the venous drainage from the anterior segment and ciliary body. The anterior ciliary arteries arise from the vasculature of the external ocular muscle (recti). One branch penetrates the sclera posterior to the limbus. The long posterior ciliary arteries penetrate the sclera near the optic nerve and traverse between the sclera and the choroid. Details of the blood supply to the ciliary body are shown in **Figures 2–4**. Blood drains from the ciliary body into the choroidal veins which converge into the vortex vein to leave the eye. Drawing adapted from Figure 10.25a in Bron, A. J., Ramesh, C., Tripathi, R. C., and Tripathi, B. J. (1997). The posterior chamber and ciliary body. In: *Wolff's Anatomy of the Eye and Orbit*, 8th edn., ch. 10. London: Chapman and Hall Medical. Leber, T. (1872) in Albrecht von Graefe's Archives (for clinical and experimental) Ophthalmology. Berlin: Springer Verlag.

territories (not the marginal capillaries), and the third source is from the venules arising from the marginal capillaries of the processes. These arterioles/capillaries drain into the choroidal veins which pass through the pars plana and drain into the vortex veins. The vortex veins exit the eye through the sclera just posterior to the equator of the globe.

Vascular Organization of the CB

The angioarchiteture of the ciliary process and vasculature is very complex. The vasculature and ciliary processes develop concommittantly, and it would appear that the patterning of the ciliary capillaries dictates the final pattern and organization of the processes. In the human and primate eye, the angioarchitecture is organized into different territories (**Figure 4**). The first territory includes vessels at the anterior end of the major processes at the crests of the processes. This region consists of the short anterior arterioles (precapillary) that branch off the MAC to feed the lateral branches. These lateral branches do not feed into the marginal capillaries but drain into isolated venules that run posteriorly without further connections to the rest of the vasculature in the ciliary processes. The second vascular territory includes the marginal vessels in the anterior end and also the center portion and basal regions of the major processes. The third territory comprises the vasculature of the minor processes. The angioarchitecture of the ciliary muscle is organized into a densely packed network of capillaries that are orientated in parallel to the longitudinal axis of the muscle fibers. Within the anterior portion of the pars plana, the vessels interconnect with the vessels located in the valleys between the ciliary processes, and with those from the anterior portion of the ciliary muscle. Posterior to this, the vessels are arranged in parallel rows orientated in the anterior–posterior plane. The vessels are large and flat with few interconnections with neighboring vessels. In the most posterior portion of the pars plana, the vessels are organized into a connecting meshwork similar to that seen in the choriocapillaris.

Characteristics and Properties of the CB Capillaries

The blood vessels of the ciliary processes have a number of unique properties that relate to the production and regulation of aqueous humor. There are two types of blood capillaries in the CB: those in the stroma of the processes are fenestrated, a property necessary for the production, and regulation of aqueous humor. The short ciliary arterioles that feed into the marginal capillaries (precapillary arterioles) are surrounded by two to three layers of smooth muscle. They characteristically have constrictions at their distal portions before they join to the marginal capillaries. In the rat, the arterioles that branch off MAC, the smooth muscle cells become less dense toward the more distal regions of these arterioles. The smooth muscle cells are replaced by pericytes (more stellate-like cells) in this region and are orientated in the circular plane around the vessel acting as a sphincter. This formation is thought to assist with regulating flow into the marginal capillaries. In the mouse eye, these constrictions are not present, and instead one sees constrictions/strangulations in the posterior portion (distal region) of the marginal capillaries.

The most marked characteristic of the vessels in the ciliary processes is the large irregularly dilated marginal capillaries. They have wide dilated lumens between 15 and 30 μm in diameter. These capillaries are lined by fenestrated endothelium where fenestrations are present throughout the entire capillary, a feature that ensures maximal area for aqueous humor production. In the rat eye, the marginal capillaries are surrounded by an open

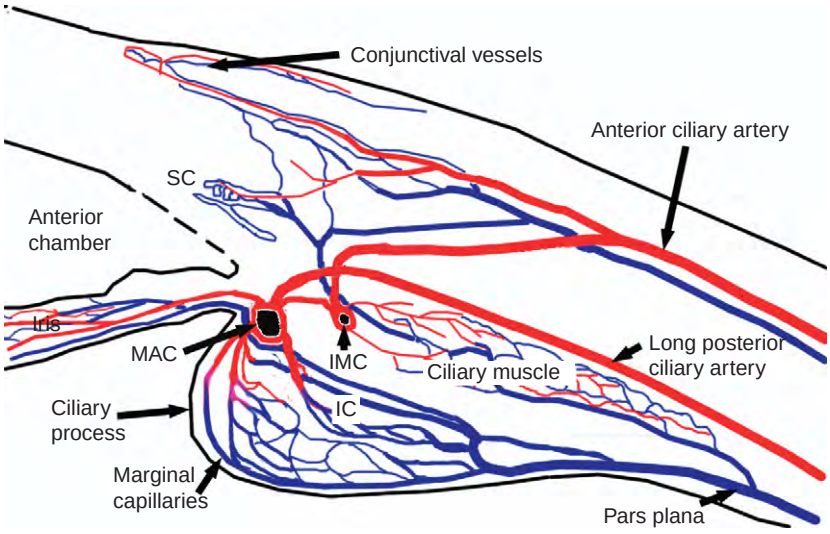

Figure 2 Schematic showing the arterial supply to and venous drainage from the ciliary body. The ciliary body receives its blood supply from the intramuscular arterial circle of the ciliary body (IMC) and the major arterial circle of the iris (MAC). These circular arteries are supplied by seven anterior ciliary arteries and the medial and lateral long posterior ciliary arteries. The anterior ciliary artery sends a branch through the sclera which gives off several branches that feed the ciliary muscle. The MAC is formed from the bifurcations of the medial and lateral long posterior arteries, but is also thought to have its origin in the arterioles that arise from the IMC. The ciliary processes receive their blood supply via the MAC. Blood drains from the ciliary processes and ciliary muscle into the pars plana. SC = Schlemm's canal which drains into aqueous vessels. Adapted from an original drawing from Lauber H., after Maggiore, L. in Bron, A. J., Ramesh, C., Tripathi, R. C., and Tripathi, B. J. (1997). *Wolff's Anatomy of the Eye and Orbit*, 8th edn. London: Chapman and Hall Medical. Lauber, H. (after Maggiore) (1936) in Der Strahlenkörper (Corpus ciliare). D. Die Nerven des Strahlnekörpers, in Handbuch der mikrsopischen Anatomie (ed. W. Von Mollendorf), Berlin: Springer.

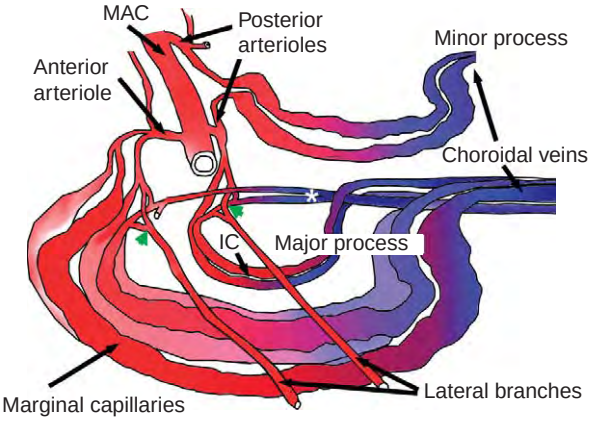

Figure 3 Drawing depicting the general vascular organization and the arterial feeds of the major and minor ciliary processes. The anterior and posterior arterioles that branch off the major arterial circle of the iris (MAC), supply the capillaries of the major and minor processes, respectively. Several smaller vessels that arise from the anterior arteriole feed into the marginal capillaries of the major process. Branches of the posterior arteriole feed the internal capillaries (IC) of the major process. Blood supply to the capillaries of the minor processes is derived from more than one posterior arteriole. Anastomoses (green arrowheads) occur between the lateral branches, some marginal or central capillaries of the major processes and the basally located capillaries that extend posteriorly (white star). Modified from Morrison, J. C. and van Buskirk, E. M. (1984). *American Journal of Ophthalmology* 97: 372–383 in Figure 10.28b in Bron, A. J., Ramesh, C., Tripathi, R. C., and Tripathi, B. J. (1997). The choroid and uveal vessels. In: *Wolff's Anatomy of the Eye and Orbit*, 8th edn, ch. 11. London: Chapman and Hall Medical.

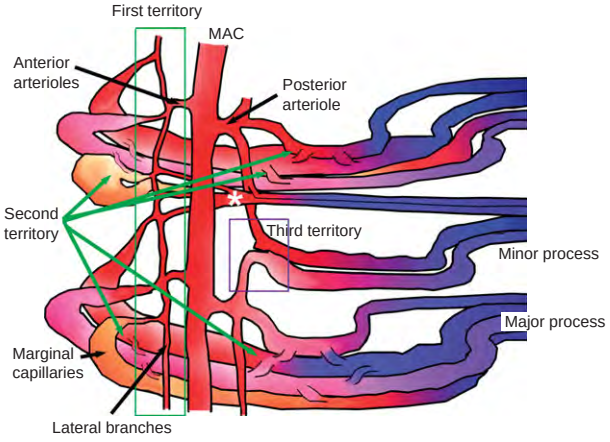

Figure 4 Schematic depicting the vascular territories of the ciliary processes. The first terroritory (outlined in the green box) includes the anterior arterioles, the lateral branches and the vessels arising from the latter that drain into the basally located venules (white star). The second territory (indicated by the green arrows), includes the marginal capillaries and the capillary network (shown as short connections) that connect to these and the internal capillaries (IC) of the major process. The third territory (outlined in the purple box) includes the capillaries that arise from the posterior arterioles, and the vasculature of the minor processes. According to some authors the vessels in the posterior third of the major processes also fall within the third vascular territory. Modified from Morrison, J. C. and van Buskirk, E. M. (1986). *Transactions of Ophthalmological Society of the United Kingdom* 105: 13 in Figure 11.25f in Bron, A. J., Ramesh, C., Tripathi, R. C., and Tripathi, B. J. (1997). The posterior chamber and ciliary body. In: *Wolff's Anatomy of the Eye and Orbit*, 8th edn., ch. 10. London: Chapman and Hall of Medical.

network of pericytes with their processes aligned along the longitudinal and circumferential planes. The processes of these pericytes are irregular and contain spines and are thought to play a role in regulating the permeability of the capillaries. A possible mechanism here may be to cover the fenestrations or constricting their diameters. In the mouse eye, blood vessels in the ciliary processes do not express tight junction proteins ZO-1 or occludin. Thus, movement of plasma constituents can move freely from the intravascular compartment through the paracellular route to the interstitial space. In contrast, blood vessels located near the base of the processes express ZO-1 and occludin, thus indicating different functional territories within the processes. Interestingly, an endothelial barrier protein which is expressed in the capillary endothelium of barrier vessels such as the retinal and iris vessels (also in nonfenestrated vessels in the brain) is highly expressed by the endothelium of the marginal capillaries in those within the CB of the rat. In contrast, these proteins are not expressed in capillaries located in the basal regions. Although the function in the CB is unknown, loss of this antigen is associated with increased vascular permeability in the brain. In particular, its association with an unmistakenly permeable endothelium is not clear.

It appears that the intravascular pressure within the CB is achieved by autoregulatory mechanisms in order to continue perfusion of aqueous humour under variable physiological conditions. Evidence for this is the presence of adrenergic and cholinergic nerve endings that are associated with the vasculature in the ciliary processes seen in several species, including humans. By stimulating the sympathetic and parasympathetic neural systems, studies have shown reduced and increased flow through the ciliary processes, respectively.

The diameter of the vessels of the ciliary muscle is small and the endothelium lining of these vessels is thicker than those of the capillaries in the ciliary processes. Fenestrations are few or absent in capillaries of the ciliary muscle. Capillaries of the pars plana are likely to be similar to that of the choriocapillaris which is fenestrated.

Comparative Angioarchitecture of the Ciliary Processes in Other Species

The vascular organization within the ciliary processes differs widely between rodents, ungulates, carnivores, and primates. The latter is similar to humans. Constrictions in the precapillary arterioles are present in all species but differ in their location along the arteriole. In rabbits, ungulates, rodents, and carnivores, the sole source of blood to the CB is via the MAC, whereas in primates and humans, the ciliary processes receive blood from both anterior and posterior arterioles that branch off the MAC. In rodents each arteriole that branches off the MAC gives rise to further branches which then supply a number of ciliary processes. In carnivores (dogs and cats), each ciliary process is supplied from individual arterioles that branch off the MAC. In ungulates, the branches off the MAC branch extensively over the iris root to form a plexus from which large ciliary process arterioles arise to supply each process. The internal organization of the ciliary processes differs widely between species, with rodents having a similar organization but simpler to that of primates and humans.

See also: Ciliary Blood Flow and its Role for Aqueous Humor Formation; Functional Morphology of the Trabecular Meshwork; Ion transport in the Ciliary Epithelium; The Role of the Ciliary Body in Aqueous Humor Dynamics. Structural Aspects.

Further Reading

Bron, A. J., Ramesh, C., Tripathi, R. C., and Tripathi, B. J. (1997). The posterior chamber and ciliary body: The choroid and uveal vessels. In: *Wolff's Anatomy of the Eye and Orbit,* 8th edn., ch. 10; 11. London: Chapman and Hall Medical.

Fujiwara, T., Tenkova, T. I., and Kondo, M. (1999). Wall cytoarchitecture of the rat ciliary process microvasculature revealed with scanning electron microscopy. *Anatomical Record* 254: 261–268.

Funk, R. and Rohen, J. W. (1990). Scanning electron microscopic study on the vasculature of the human anterior segment, especially with respect to the ciliary processes. *Experimental Eye Research* 45: 651–661.

Hayreh, S. S. (2004). Posterior ciliary artery circulation in health and disease. The Weisenfeld lecture. *Investigative Ophthalmology and Visual Science* 45: 749–757.

Hirsh, M., Renard, G., Faure, J. P., and Pouliquen, Y. (1978). Endothelial cell junctions in the ciliary body microvasculature. *Albrecht v. Graefes Archive for Clinical and Experimental Ophthalmology* 208: 69–76.

Morrison, J. C. and Freddo, T. F. (1996). Anatomy, microcirculation and ultrastructure of the ciliary body. In: Rich, R., Shields, M. B., and Krupin, T. (eds.) *The Glaucomas* 2nd edn., vol. 1, pp. 125–131. St. Louis, MO: Mosby.

Morrison, J. C., Fraunfelder, F. W., Milne, S. T., and Moore, C. G. (1995). Limbal microvasculature of the rat eye. *Investigative Ophthalmology and Visual Science* 36: 751–756.

Morrison, J. C. and van Buskirk, E. M. (1984). Ciliary process microvasculature of the primate eye. *American Journal of Ophthalmology* 97: 372–383.

Morrison, J. C. and van Buskirk, E. M. (1986). Microanatomy and modulation of the ciliary vasculature. *Transactions of Ophthalmological Society of the United Kingdom* 105: 13.

Napier, H. R. L. and Kidson, S. H. (2007). Molecular events in early development of the ciliary body: A question of folding. *Experimental Eye Research* 84: 615–625.

Pseudoexfoliation Syndrome and Glaucoma

U Schlötzer-Schrehardt, University of Erlangen-Nürnberg, Erlangen, Germany

Glossary

Cross-linking – The lateral linking of protein strands to one another via covalent bonds, resulting in a polymer network that becomes stronger and more resistant to degradation.
Elastic fibers – The bundles of stretchable proteins found in the extracellular matrix of connective tissue and produced by fibroblasts and vascular smooth-muscle cells. Elastic fibers are formed by elastic microfibrils and amorphous elastin.
Elastic microfibrils – The macromolecular assemblies of the extracellular matrix, which have unique extensible properties. They are heterogenous in composition and may consist of fibrillins, latent transforming growth factor-β-binding proteins, fibulins, emilins, microfibrillar-associated glycoproteins, and microfibril-associated proteins. They occur as isolated bundles devoid of elastin (e.g., zonules) or act as a template for elastin deposition within elastic fibers.
Elastosis – The degenerative changes in connective tissues resulting from breakdown of elastic fibers and accumulation of increased amounts of abnormal elastotic material.
Extracellular matrix – A complex structural entity surrounding and supporting cells within animal tissues, which includes the interstitial matrix and the basement membrane. It consists of structural proteins (e.g., collagen and elastin), glycoproteins (e.g., fibronectin and laminin), and proteoglycans.
Lysyl oxidase-like 1 (LOXL1) – A member of the lysyl oxidase family of enzymes that catalyzes the covalent cross-linking of collagen and elastin in connective tissues through oxidative deamination of lysine or hydroxylysine side chains.
Pseudoexfoliation (PEX) syndrome – A generalized disorder of the extracellular matrix, often leading to glaucoma. The term pseudoexfoliation syndrome results from dandruff-like deposits on the surface of the lens, as if the lens capsule has exfoliated. It is also called exfoliation syndrome.
Single nucleotide polymorphisms (SNPs) – The DNA sequence variations occurring when a single nucleotide – A, T, C, or G – in the genome differs between members of a species (or between paired chromosomes in an individual).

Pseudoexfoliation Syndrome

Definition

Pseudoexfoliation (PEX) syndrome is a common, age-related systemic disorder of the extracellular matrix characterized by pathologic accumulation of an abnormal fibrillar material in various intra- and extraocular tissues. It is clinically diagnosed by observation of dandruff-like white flakes deposited on ocular structures that line the aqueous-bathed surfaces of the anterior segment, particularly the anterior lens surface and the pupillary border of the iris. The terms pseudoexfoliation or exfoliation syndrome have been widely used for this entity, although the process does not represent a true exfoliation of the lens capsule, like in infrared (glass-blower's) cataract.

Epidemiology

PEX syndrome was first described in Finland by Lindberg in 1917, and at one time was considered to be much more common throughout Scandinavia than elsewhere. It has, however, been realized, that PEX syndrome occurs in all geographic regions worldwide with reported prevalence rates averaging about 10–20% of the general population over the age of 60. In all populations, the frequency rises with increasing age, with its incidence doubling every decade after the age of 50, and females are more frequently affected in most series. Despite its worldwide distribution, there is a clear tendency for the condition to cluster geographically and in certain racial or ethnic subgroups. There is a high prevalence of PEX syndrome in Finland, Lapland, Iceland, Norway, and Northern Russia, where it affects 10–13% of persons aged 50–69 years and 21–35% those over 70 years of age. Similar figures apply to Saudi Arabia, Mediterranean and Baltic countries, and among the Navajo Indians in the United States of America and Australian Aborigines. Recent reports suggest that it is equally common in Ethiopia and South Africa, and The Gambia in West Africa. In contrast, PEX syndrome occurs in only 3–10% of persons over 60 years of age in most European populations and in parts of the United States. Although common in Japan and Mongolia, it is rare in southern China and in the Malay population.

Etiology and Pathogenesis

Genetics

The reasons for true differences in prevalence rates between age-matched geographical and ethnic populations

remain unknown, but appear to be mainly related to genetic variability. Both population-based and pedigree-based studies have shown that genetic factors contribute to the pathogenesis of PEX syndrome, which has been suggested to be inherited as an autosomal dominant trait with late onset and incomplete penetrance. In the past, several chromosomal regions have been tentatively associated with PEX, including the putative gene loci 2p16, 2q35-36, and 3q13-q21. A recent genome-wide scan of 1000 microsatellite markers in a Finnish family suggested a strong linkage to 18q12.1-21.33 and a weaker linkage to chromosomes 2q, 17p, and 19q, which are possible regions of linkage to primary open-angle glaucoma (POAG). Apolipoprotein E gene variants and the ε2 allele were also found to be associated with an increased risk of developing PEX in a Turkish population, whereas the ε3 allele was found to be protective.

In a recent landmark study, the genetic etiology of PEX syndrome and glaucoma has been further specified. Performing a genome-wide association study, Thorleifsson and coworkers detected three common sequence variants or single-nucleotide polymorphisms (SNPs) in the *LOXL1* gene on chromosome 15q24.1 to be strongly associated with both PEX syndrome and PEX glaucoma in Scandinavian populations from Iceland and Sweden. Strikingly, these disease-associated polymorphisms accounted for virtually all PEX cases within the populations studied and appeared to confer risk of glaucoma mainly through PEX. A high-risk haplotype (G–G), that is, a combination of alleles on one chromosome, formed by two nonsynonymous coding SNPs, rs1048661 (R141L), and rs3825942 (G153D), in exon 1 of *LOXL1* increased the risk for PEX by factor 27. Individuals carrying two copies of this high-risk haplotype on both corresponding homologous chromosomes, that is, the high-risk diplotype, would have a 700 times increased risk of developing PEX than those carrying the low-risk haplotype. Compared with the general population, the risk of developing PEX is about 2.5-fold, because approximately 25% of the unaffected controls were also found to carry the high-risk diplotype. Following this discovery, several replication studies in populations from the United States, Australia, Europe, Japan, and India confirmed genetic susceptibility of *LOXL1* polymorphisms to PEX syndrome/glaucoma and verified the *LOXL1* gene as a major genetic risk factor for this condition worldwide. In most study populations, SNP rs3825942 (G153D) has been reported to be the primary risk-associated variant, whereas SNP rs1048661 (R141L) showed a different allele frequency in Japanese patients with PEX or was not significantly associated with PEX in other populations at all. However, because many individuals that carry the *LOXL1* risk alleles do not have PEX, there may be limited usefulness in genetic testing for these variants.

LOXL1 is a pivotal enzyme in extracellular matrix formation. It is a member of the lysyl oxidase family of enzymes that catalyze the covalent cross-linking of collagen and elastin in connective tissues through oxidative deamination of lysine or hydroxylysine side chains. They comprise five characterized members: lysyl oxidase (LOX) and lysyl oxidase-like 1–4 (LOXL1–4). LOXL1 seems to be specifically required for tropoelastin cross-linking and has been shown to be involved in elastic fiber formation, maintenance, and remodeling, particularly during dynamic processes such as tissue injury, fibrosis, cancer, and development. In order to fulfill its cross-linking function, the LOXL1 pro-peptide is selectively targeted to elastic microfibrils at sites of elastogenesis by binding to both tropoelastin and fibulin-5. Following attachment to the scaffolding structure, the pro-peptide is cleaved off by the endo-metalloproteinase procollagen-C-terminal proteinase (bone morphogenetic protein 1) for catalytic activation of the enzyme. Both PEX-associated coding SNPs of *LOXL1* reside in exon 1, which encodes the unique N-terminal domain that is required both for proper enzyme activation and for substrate recognition and binding. The available data suggest that LOXL1 is upregulated in the early phase of PEX fibrogenesis together with elastic fiber components, such as tropoelastin, fibrillin-1, and fibulin-2, and participates in the formation of the aberrant fibrillar aggregates accumulating in tissues of PEX patients.

However, a number of nongenetic factors, including ultraviolet light exposure, dietary factors, autoimmunity, infectious agents, and trauma, have also been hypothesized to be involved in pathogenesis, but have not been proven. Interestingly, the exceptional diagnosis of PEX in younger patients under the age of 40 seems to be generally preceded by prior intraocular surgery or trauma to the anterior segment, particularly to the iris, or to occur after corneal transplantation with grafts from elderly donors. These events may serve as a trigger for the premature development of PEX in a predisposed individual or even point to the possibility of a transmissible etiology. Altogether, it appears that PEX syndrome represents a complex, multifactorial, late-onset disease, involving both genetic and nongenetic factors in its etiopathogenesis.

Pathogenesis

The specific pathogenesis of PEX syndrome and the exact chemical composition of PEX material are still not known. However, the pathologic process is characterized by the chronic accumulation of an abnormal fibrillar matrix product, which is either the result of an excessive production or insufficient breakdown or both, and which is regarded as pathognomonic for the disease, based on its unique light microscopic and ultrastructural criteria.

By light microscopy, PEX material usually appears as periodic acid-Schiff (PAS)-positive, bush-like, nodular, or feathery aggregates on the surfaces of anterior-segment tissues. Transmission electron microscopy shows the

aggregates to be composed of randomly arranged, electron-dense, fuzzy fibrils, 25–50 nm in diameter, frequently with 20–25- or 45–50-nm crossbanding (Figure 1).

These composite fibers are generally associated with microfibrils, 8–10 nm in diameter, which resemble elastic microfibrils and which appear to aggregate laterally into mature PEX fibrils. However, the microfibrillar core of the complex fibers is usually hidden by an apparent coating with electron-dense amorphous material.

Immunohistochemical studies have shown PEX material to represent a complex glycoprotein/proteoglycan structure bearing epitopes of the basement membrane and elastic fiber system. The characteristic fibrils contain predominantly epitopes of elastic fibers, such as elastin, tropoelastin, amyloid P, vitronectin, and components of elastic microfibrils, such as fibrillin-1, microfibril-associated glycoprotein (MAGP-1), and latent transforming growth factor-beta (TGF-β)-binding proteins (LTBP-1 and

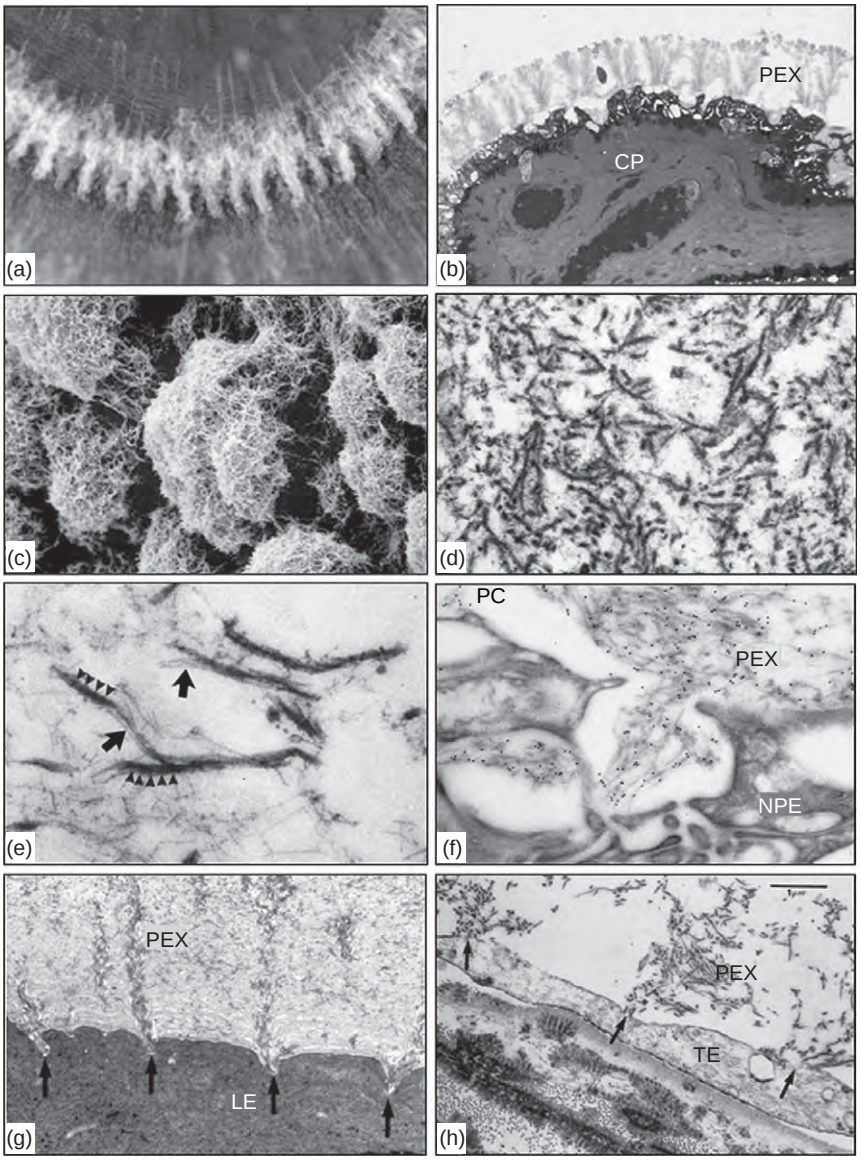

Figure 1 Light and electron micrographs showing structure and origin of PEX material. (a) Macroscopic appearance of PEX deposits on ciliary processes and zonules; (b) bush-like, feathery PEX deposits on ciliary process (CP) by light microscopy (toluidine blue; × 400); (c) scanning electron micrograph of PEX deposits; (d) ultrastructure of PEX fibrils; (e) aggregation of microfibrils (arrows) into mature PEX fibrils showing crossbands at 50 nm (arrowheads); (f) immunogold labeling using antibodies against fibrillin-1 showing clear association of the gold marker with PEX fibrils emerging from a nonpigmented ciliary epithelial cell (NPE); (g) intracapsular PEX fibrils emerging from pits (arrows) in the preequatorial lens epithelium (LE); (h) apparent production of PEX fibrils (arrows) by a trabecular endothelial cell (TE). Adapted from Schlötzer-Schrehardt, U. and Naumann, G. O. H. (2008). Pseudoexfoliation syndrome: Pathological manifestations of relevance to intraocular surgery. In: Naumann, G. O. H., Holbach, L., and Kruse, F. E. (eds.) *Applied Pathology for Ophthalmic Microsurgeons*, 1st edn., p. 356, figure 6.3.1, Berlin: Springer, with permission from Springer.

LTBP-2). Abundantly associated glycosaminoglycans (heparin sulfate, chondroitin sulfate, hyaluronan, etc.) are indicative of excessive glycosylation processes. A direct analytical approach by using liquid chromatography coupled with tandem-mass spectrometry (LC–MS/MS) has confirmed PEX material to consist of the elastic fiber components fibrillin-1, fibulin-2, vitronectin, and amyloid P-component, the basement membrane components laminin and fibronectin, the proteoglycans syndecan-3 and versican, metalloproteases of the a disintegrin and metalloprotease (ADAM) family, the extracellular chaperone clusterin, and complement factor C1q. Together, these findings support the notion that PEX material represents an elastotic material arising from abnormal aggregation of elastic microfibril components interacting with multiple ligands.

A variety of unrelated epithelial and mesenchymal cell types participate in the excessive and disordered synthesis of the fibrillar PEX material at multiple intra- and extraocular sites. In the eye, PEX fibers have been demonstrated in close association with the pre-equatorial lens epithelium, the nonpigmented ciliary epithelium, the iris pigment epithelium, the trabecular endothelium, the corneal endothelium, and virtually all cell types in the iris stroma. Passive distribution of PEX material by the aqueous humor seems to be responsible for abnormal deposits on the central anterior lens capsule, the zonules, the anterior hyaloid surface, and artificial lenses, if present. In extraocular locations, PEX fibers could be identified in close proximity to connective tissue fibroblasts, vascular wall cells, smooth and striated muscle cells, and heart muscle cells. Therefore, the abnormal matrix process virtually affects all anterior segment tissues as well as vessel walls, muscle tissues, and connective tissue portions of skin and visceral organs throughout the body.

Molecular pathophysiology

Gene expression analyses revealed a set of genes differentially expressed in anterior-segment tissues of PEX eyes, which were mainly involved in extracellular-matrix metabolism and in cellular stress. One set of genes consistently upregulated in anterior segment tissues from different PEX patients comprised the elastic microfibril components fibrillin-1, LTBP-1, and LTBP-2, the cross-linking enzyme transglutaminase (TGase)-2, tissue inhibitor of matrix metalloproteinase (TIMP)-2, TGF-β1, several heat-shock proteins (Hsp 27, Hsp 40, and Hsp 60), proinflammatory cytokines, apolipoprotein D, and the adenosine receptor (AdoR)-A3. Genes reproducibly downregulated in PEX tissues included TIMP-1, the extracellular chaperone clusterin, the antioxidant defense enzymes glutathione-S-transferases (mGST-1, GST-T1), components of the ubiquitin–proteasome pathway (ubiquitin-conjugating enzymes E2A and E2B), several DNA repair proteins (ERCC1, hMLH1, and GADD 153), the transcription factor Id-3, and serum amyloide A1.

Apart from increased concentrations of various growth factors (bFGF, HGF, CTGF, and TGF-β1) in the aqueous humor of PEX patients, the growth factor TGF-β1, which is a major modulator of matrix formation in many fibrotic diseases, is considered a key mediator in the fibrotic PEX process. It is significantly increased in the aqueous humor of PEX patients, both in its latent and active form, it is upregulated and actively produced by anterior segment tissues, and it is known to regulate most of the genes found to be differentially expressed in PEX eyes, for example, fibrillin-1, LTBP-1 and-2, TGase-2, and clusterin. Binding of TGF-β1 to PEX material via the TGF-β-binding proteins LTBP-1 and-2 may represent a mechanism of regulation of growth-factor activity in PEX eyes. Whereas the TGF-β3 isoform was also reported to be significantly increased in aqueous humor of PEX patients, levels of TGF-β2 were significantly higher in the aqueous humor of POAG patients but not of PEX patients.

Changes in the local matrix metalloproteinase (MMP)/TIMP balance and reduced MMP activity in aqueous humor and tissues may further promote the abnormal matrix accumulation in PEX syndrome. Significantly increased concentrations of MMP-2, MMP-3, TIMP-1, and TIMP-2 were detected in aqueous humor samples from PEX patients with and without glaucoma compared to control patients with cataract. However, the levels of endogenously active MMP-2, which is the major MMP in human aqueous humor, were significantly decreased as was the ratio of MMP-2 to TIMP-2, resulting in a molar excess of TIMP-2 over MMP-2 in PEX samples. An imbalance of MMPs and TIMPs has been also reported on the tissue level, particularly in trabecular meshwork specimens from PEX glaucoma patients.

Moreover, there is increasing evidence that cellular stress conditions, such as oxidative stress and ischemia/hypoxia, constitute major mechanisms involved in the pathobiology of PEX syndrome. Significantly reduced levels of antioxidative protective factors (e.g., ascorbic acid and glutathione) and increased levels of oxidative stress markers (e.g., 8-isoprostaglandin-F2α and malondialdehyde) in aqueous humor, serum, and tissues are indicative of a faulty antioxidative defense system and increased oxidative stress in the anterior chamber of PEX eyes. PEX is also associated with ocular ischemia, particularly iris hypoperfusion and anterior chamber hypoxia, and with a reduced ocular and retrobulbar micro- and macrovascular blood flow occurring in PEX patients with or without glaucoma. The vasoactive peptide endothelin-1 has been shown to be significantly increased in the aqueous humor of normotensive PEX patients compared with that of age-matched controls, while levels of nitric oxide, a potent physiological vasodilator, were decreased in a small number of PEX patients. This dysbalance may play a role in the

obliterative vasculopathy of the iris causing local ischemia early in the disease process. Elevated homocysteine levels in the aqueous humor of patients with PEX may further contribute to ischemic alterations, such as endothelial dysfunction, oxidative stress, enhancement of platelet aggregation, reduction of nitric oxide bioavailability, and abnormal perivascular matrix metabolism.

Pathogenetic concept

Immunohistochemical, biochemical, and molecular biologic data support the current pathogenetic concept of PEX syndrome as a type of stress-induced elastosis, an elastic microfibrillopathy, associated with the excessive production of elastic microfibril components and their aggregation into typical mature PEX fibrils by a variety of potentially elastogenic cell types. Growth factors, particularly TGF-β1, increased cellular and oxidative stress, a dysfunction of the cellular protection and proteasome system, low-grade inflammatory processes, and genetic variations in the *LOXL1* gene coding for a key enzyme of elastogenesis appear to contribute to the stable accumulation of the elastotic PEX material in the course of this fibrotic matrix process. Due to a proteolytic imbalance between MMPs and TIMPs and extensive cross-linking processes involved in fiber formation, the pathologic material is not properly degraded but progressively accumulates within the tissues over time.

Clinical Findings

Diagnosis

The most important diagnostic criteria of PEX syndrome are the whitish flake-like deposits of PEX material on anterior-segment structures, particularly on the anterior lens surface and the pupillary margin, occasionally also on the posterior surface of the cornea, the anterior surface of intraocular lens implants, and the anterior vitreous face in aphakic eyes. However, the majority of intraocular PEX deposits cannot be observed by direct biomicroscopy, and the accumulations on zonules, ciliary processes, and trabecular meshwork may be only detected by gonioscopy or high-resolution ultrasound biomicroscopy.

The characteristic target-shaped pattern of PEX material accumulation on the lens, consisting of a rather homogenous central disk, an intermediate clear zone, and a peripheral granular zone with nodular vegetations, can be only seen after pupillary dilation. In routine examinations without pupillary dilation, the diagnosis may be easily missed, because the central disk, corresponding to the size of the pupil, may be very subtle or even absent in 20–50% of cases. In addition to PEX material deposits, several other mostly pigment-related clinical signs aid in the diagnosis, including pigment dispersion in the anterior chamber after pupillary dilation, peripupillary atrophy producing a characteristic moth-eaten transillumination pattern, pupillary ruff defects, and pigment deposition on anterior-chamber structures, such as the iris sphincter region, corneal endothelium, and trabecular meshwork. Pigment is also characteristically deposited on or anterior to Schwalbe's line forming one or more undulating lines of pigment in the peripheral cornea (Sampaolesi's line). Pigment dispersion is caused by mechanical friction of the peripupillary iris against the rough anterior lens surface during pupillary movement. Further PEX-associated clinical signs that can alert the clinician to the presence of PEX include phacodonesis, iris stroma atrophy, iris hemorrhages after pupillary dilation, increased aqueous flare values, posterior synechiae, elevated intraocular pressure (IOP), and insufficient pupillary dilation, particularly if asymmetrically present.

However, the classical picture of lens deposits represents a very late stage of the disease, which is preceded by a long, chronic, preclinical course of several years. By thorough biomicroscopic examination, a diffuse-matte grayish film on the entire surface of the anterior lens capsule can be observed prior to the formation of typical PEX deposits. This layer is thought to represent a precursor of PEX material which is initially diffusely deposited on the lens surface from the aqueous humor. As this precapsular layer becomes thicker, focal defects begin to form in the midperipheral zone by abrasive movements of the iris, which further enlarge and become confluent to form the classical picture of manifest PEX syndrome. Ancillary clinical signs, which define patients as PEX suspects, comprise peripupillary atrophy, anterior-chamber pigment dispersion, and deposition on anterior-segment structures, and poor mydriasis. In addition, examination by high-resolution ultrasound biomicroscopy has been shown to be useful for detecting early deposits of PEX material on zonules, particularly in cases with inadequate pupillary dilation or opaque media.

Asymmetry of involvement

PEX patients can present with either unilateral or bilateral involvement, which may be markedly asymmetric. In several large series, PEX syndrome was unilateral at the time of diagnosis in about 50–70% of patients and the conversion rates to bilaterality were found to vary from 15% to 40% within 5 years. Clinically, the involved eye often has a poorer visual acuity, more advanced lens opacity, higher IOP, a smaller pupil, and a more pronounced trabecular pigmentation than the noninvolved fellow eye. However, in the majority of clinically unilateral cases, there are subtle histopathological changes, such as PEX deposits in the conjunctiva and in the iris, particularly in the dilator muscle and blood-vessel walls, of the clinically uninvolved fellow eyes. Therefore, PEX syndrome can be diagnosed prior to the clinically visible appearance of classic PEX material on the lens surface by electron microscopy of conjunctival biopsies. These

early changes support the concept of PEX syndrome as a generalized, basically bilateral disorder with a clinically marked asymmetric presentation. The reasons for this asymmetric involvement remain unknown.

Ocular manifestations and complications

All anterior-segment structures are involved in the PEX process leading to characteristic tissue alterations, which predispose to a broad spectrum of potential intraocular complications:

1. The zonules are affected early in the course of the PEX process and may undergo degeneration and separation from their attachments to the ciliary body and lens. In the pre-equatorial lens capsule, corresponding to the proliferative zone of the lens epithelium and the zone of zonular anchorage, bundles of PEX fibrils appear to originate from the adjacent lens epithelial cells, disrupt the capsule proper, and invade the zonular lamella, resulting in separation of the zonules from their insertion onto the capsule. Similarly, at their origin and anchorage in the nonpigmented ciliary epithelium, the zonular bundles are separated from their connection to the disrupted epithelial basement membrane by intercalating PEX fibers. These alterations are usually not visible on clinical examination, being hidden behind the iris, but give rise to a marked instability of the zonular apparatus producing a characteristic phacodonesis or inferior displacement of the lens. Anterior lens movement can occur, particularly under miotic therapy, resulting in pupillary or even ciliary block-angle-closure glaucoma, which is more common in eyes with PEX.
2. Iris changes are an early and consistent feature of PEX eyes and involve all iris structures and cell types. Clinically, the iris of PEX patients is characteristically rigid with reduced dilating properties, which has been attributed to a combination of PEX fiber deposition in the stroma and muscle tissues along with degenerative changes of the stroma, including sphincter and dilator muscles. The posterior iris pigment epithelium exhibits marked degenerative changes with focal-membrane ruptures and liberation of pigment granules resulting in the diagnostically important moth-eaten pattern of peripupillary atrophy accompanied by a characteristic dispersion of pigment granules following pharmacological dilatation. Involvement of the iris stromal vessels has major functional consequences. Iris blood vessels may become degenerated or obliterated resulting in iris hypoperfusion and reduced partial pressure of oxygen in the anterior chamber. On fluorescein or indocyanine green angiography, changes including iris-vessel dropout and dye leakage may be seen. Spontaneous intrastromal hemorrhages, without rubeosis iridis, after mydriasis indicate significant vascular damage. Another important consequence of the iris vasculopathy is a chronic breakdown of the blood-aqueous barrier in eyes with PEX syndrome, which manifests clinically as a pseudouveitis with elevated aqueous flare values. Blood–aqueous barrier dysfunction is compromised to a greater extent in eyes with PEX compared to eyes without PEX following intraocular surgery, including cataract surgery, trabeculectomy, and laser trabeculoplasty.
3. In eyes with advanced PEX syndrome, focal retrocorneal flakes of PEX material can be clinically observed adhering to the corneal endothelium. Ultrastructural evidence suggests focal *in situ* production of PEX fibers by corneal endothelial cells. Associated with these specific changes, the corneal endothelium shows focal degeneration, phagocytosis of melanin granules, and abnormal extracellular matrix production, resulting in an irregular thickening of Descemet's membrane. Combination of clinical and histopathological observations leads to the concept of a specific PEX-associated keratopathy. The damaged and dysfunctional corneal endothelium in PEX eyes increases the risk of early corneal endothelial decompensation with normal or after moderate rises in IOP, for example, after mydriasis, or after minor intraoperative trauma. It can even result in irreversible corneal endothelial decompensation requiring penetrating keratoplasty.
4. Lens opacification, most commonly of a nuclear type, is long known to be associated with PEX syndrome and is the most common cause for PEX patients to require surgical intervention. Cataract development may be causally linked to the presence of ocular ischemia, aqueous hypoxia, increased growth-factor levels, or reduced protection against ultraviolet radiation by lower levels of ascorbic acid in the aqueous humor of PEX eyes. Traditionally, cataract surgery in eyes with PEX has been considered a challenge because of weakened zonules and reduced pupillary diameter. Intraoperative and postoperative surgical complications, such as zonular ruptures, vitreous loss, blood–aqueous barrier breakdown, anterior capsule fibrosis/contraction, secondary cataract, and decentration or dislocation of the lens implant, have been reported to be more common and more serious than in eyes without PEX. Today, the common use of phacoemulsification with anterior capsulorhexis by experienced surgeons has provided significantly better results with a lower rate of intraoperative complications compared with the conventional extracapsular cataract-extraction technique. However, this has been replaced by a growing number of case reports on late intraocular lens displacement/dislocation after uneventful phacoemulsification due to progressive postoperative zonular weakening.

Systemic manifestations

Aggregates of PEX material were identified by electron microscopy in autopsy specimens of heart, lung, liver, kidney, gall bladder, and cerebral meninges in patients with PEX. In these extraocular locations, PEX material was primarily found in connective tissue portions of visceral organs, often in the periphery of blood vessels. These findings suggested that ocular PEX syndrome is part of a general disorder of the extracellular matrix and that patients with PEX may suffer from increased comorbidity. Subsequently, many studies have examined potential clinical consequences of these deposits and attempted to establish an association between PEX syndrome and systemic diseases. In the meantime, a growing number of small-scale studies are part of an emerging clinical spectrum in which PEX syndrome appears to be associated with cardiovascular and cerebrovascular diseases. These include transient ischemic attacks, a history of angina pectoris, arterial hypertension, myocardial infarction, or stroke, aneurysms of the abdominal aorta, asymptomatic myocardial dysfunction, ischemic white-matter lesions in the brain, Alzheimer's disease, and sensorineural hearing loss. A more recent study retrospectively investigating 1150 patients with either PEX glaucoma or POAG found a significantly higher frequency of chronic cerebral disorders (e.g., senile dementia and cerebral ischemia) and acute cerebrovascular events (e.g., thromboses, embolies, and hemorrhages) in the PEX group. The prevalence of mild-to-moderate hyperhomocysteinemia, which may be related to significantly decreased plasma levels of vitamin B6, B12, and folate, has been suggested as one possible cause for an increased vascular risk in PEX patients. However, the mortality rate appears not to be increased in PEX patients. Therefore, prospective, randomized multicenter studies are indicated to finally resolve these issues.

Pseudoexfoliation Glaucoma

The most serious known complication of PEX syndrome is secondary open-angle glaucoma, affecting 20–60% of patients in different series. PEX-associated open-angle glaucoma accounts for approximately 20–25% of all open-angle glaucomas and currently represents the most common identifiable cause of glaucoma overall. In some populations (e.g., Baltic, Mediterranean, and Arabian), the frequency of PEX-associated secondary glaucoma may reach a higher percentage of the population than the primary form of the disease. The probability of PEX eyes to develop glaucoma has been reported to vary from 5% to 35% within 5 years and from 15% to 40% within 10 years. Patients with PEX are twice as likely to convert from ocular hypertension to glaucoma as those without PEX. Factors associated with conversion to PEX glaucoma were initial IOP, degree of pupil dilation, and difference in IOP between the fellow eyes. Accordingly, the frequency of PEX syndrome is usually high among glaucoma patients and has been reported to range from 10% to 30% in the United States and from 50% to 60% in Northern Europe.

Clinical Characteristics

Compared to POAG, PEX glaucoma has a more serious clinical course and worse prognosis. It is typically associated with higher mean IOP levels, greater diurnal pressure fluctuations, marked pressure spikes, higher frequency and severity of optic nerve damage, more rapid visual-field loss, poorer response to medications, and more frequent necessity for surgical intervention. PEX glaucoma further differs from POAG by a more frequent asymmetry of manifestation, more pronounced chamber-angle pigmentation, and acute pressure rises after mydriasis. In contrast to patients with POAG, patients with PEX glaucoma behave like normal persons after steroid application, that is, only one-third respond with a distinct pressure rise. There is a greater rate of conversion of ocular hypertensive patients to PEX glaucoma than to POAG and damage progresses more rapidly in patients with PEX glaucoma than in patients with POAG. In the Early Manifest Glaucoma Trial, the presence of PEX was the most important independent risk factor for progression. The percentage area of optic-disk pallor was shown to be significantly greater in PEX eyes than in control eyes and the mean disk area has been reported to be significantly smaller in eyes with PEX, with or without glaucoma, than in POAG eyes and normal control eyes. A significant correlation between the IOP level at the time of diagnosis and the mean visual-field defect as well as between diurnal IOP fluctuations and retinal-nerve-fiber-layer thickness could be only established in patients with PEX glaucoma, but not with POAG. These findings suggest that glaucomatous damage in PEX patients may be more directly related to IOP than in POAG patients.

Patients with PEX are also at increased risk for developing significant but transient IOP rises following diagnostic pupillary dilation due to dispersion of pigment granules and PEX material in the anterior chamber. The maximum of pigment liberation and pressure elevation, which can rise up to 30 mmHg above baseline IOP, may peak only 2–3 h post dilation and go back to normal levels after 10–15 h. Such pressure peaks can even mimic an acute glaucoma including pain, a red eye, corneal edema, and pressure rises over 50 mmHg.

Glaucoma in PEX syndrome usually occurs in the presence of an open chamber angle, but an association between PEX and angle-closure glaucoma is not rare either. As eyes with PEX syndrome often have narrowed chamber angles and smaller anterior chamber volumes in the presence of a weak zonular apparatus, a minimal

anterior subluxation of the lens predisposes to the development of angle-closure glaucoma through a pupillary block mechanism. Further features of PEX eyes that may predispose to the development of pupillary-block-angle-closure glaucoma include the formation of posterior synechiae, an increased iris rigidity and decreased iris motility, an impairment of the blood–aqueous barrier, and increased protein concentrations of aqueous humor. Miotics may aggravate both pupillary block and forward movement of the lens–iris diaphragm. In extreme and rather rare cases with marked zonular laxity, anterior displacement of the lens may be so pronounced that a ciliary block-angle-closure glaucoma (malignant glaucoma) is induced by contraction of the ciliary muscle. Secondary-angle-closure glaucoma following central retinal vein occlusion with rubeosis iridis (neovascular glaucoma) may also occur in PEX eyes, because retinal vein occlusion appears to be more common in patients with PEX syndrome/glaucoma.

Pathomechanisms of Glaucoma Development

Progressive accumulation of abnormal PEX deposits in the outflow structures is presumed to account for the increased outflow resistance in the trabecular meshwork and in the uveoscleral outflow pathways. In fact, PEX deposits can be observed throughout both outflow pathways, mainly in the anterior portions of the ciliary muscle, on the inner surface of the trabecular meshwork, beneath the inner and outer wall of Schlemm's canal, in the periphery of intrascleral aqueous collector channels, aqueous veins and episcleral veins, and in the suprachoroidal space. The focus of PEX material accumulation and pathological alterations is the juxtacanalicular tissue beneath the inner wall of Schlemm's canal, the site of greatest resistance to aqueous outflow. This critical area becomes thickened through gradual deposition of PEX material, which appears to be locally produced by the endothelial cells lining Schlemm's canal. The amount of PEX material accumulating in the outflow pathways has been shown to correlate with the IOP level and severity of optic-nerve damage, indicating a direct causative relationship between the matrix alterations in the meshwork and glaucomatous optic-nerve damage. There seems, however, no significant correlation between the clinically visible PEX material on the anterior lens capsule and IOP or glaucoma severity. Accumulation of PEX material in the juxtacanalicular region of the meshwork is also associated with a disruption of the normal elastic fiber network surrounding Schlemm's canal and may result in a progressive destabilization and disorganization of the normal tissue architecture leading to narrowing and focal collapse of the canal lumen in more advanced cases.

Abnormal matrix metabolism in the outflow structures may be associated with cellular dysfunction. Phospholipase A2, a housekeeping enzyme in phospholipid remodeling and removal of oxidized phospholipids from cell membranes, was significantly decreased in the trabecular meshwork of eyes with PEX glaucoma when compared to normal controls or patients with POAG. These observations may indicate abnormal physiological functions, decreased structural stability, and reduced protection against oxidative stress in trabecular meshwork cells of PEX eyes.

Increased trabecular meshwork pigmentation is a prominent and early clinical sign of PEX eyes, the pigment probably deriving from the degenerate iris-pigment epithelium. Although there seems to be a positive correlation with IOP level, the degree of chamber-angle pigmentation did not correlate with the degree of glaucomatous disk damage in most studies, arguing against a decisive role of pigment dispersion in chronic pressure rise. Pigment dispersion and deposition in the trabecular meshwork may, however, lead to acute and transient pressure rises after pupillary dilation. By electron microscopy, pigment granules are invariably present within trabecular endothelial cells, preferably in the innermost uveal portions of the meshwork, and are therefore rapidly cleared from the outflow pathways through phagocytosis by endothelial cells.

Although PEX glaucoma is characteristically a high-pressure disease with a predominant mechanical component of optic-nerve damage, pressure-independent risk factors, such as an impaired ocular and retrobulbar perfusion and structural alterations of the lamina cribrosa, may be present and further increase the individual risk for glaucomatous damage. A prospective study showed that in normotensive PEX patients with clinically unilateral involvement, in whom IOP was equal throughout the follow-up period, disk changes took place only in the involved eye, suggesting that the PEX process itself may be a risk factor for optic-disk changes. In fact, a pronounced elastosis can be observed in the connective tissue sheets of the lamina cribrosa of PEX eyes, which may adversely affect tissue elasticity and increase the susceptibility of optic-nerve fibers toward mechanical and vascular damage. Moreover, accumulations of elastotic and PEX materials are detected in the walls of various retrobulbar vessels, for example, the posterior ciliary arteries and retinal arteries, which may adversely affect vessel elasticity and perfusion parameters.

Therapeutic Aspects

In the management of PEX glaucoma, the stepwise approach from medical to surgical therapy is currently similar to that followed in POAG, but has to be complied with more consistently. In this regard, the importance of early recognition and accurate diagnosis of the pathologic features, rigorous reduction and stabilization of mean and diurnal 24-h IOP, careful examinations at narrow intervals, expectations of a higher complication rate during surgery,

and close attention to postoperative follow-up have to be emphasized. Konstas and coworkers demonstrated the benefit of IOP reduction and suggested a target IOP of <17 mmHg and lower to prevent or slow progressive damage. As peak levels of IOP are usually found in the early morning outside office hours, single IOP measurements are not sufficient for assessing mean IOP levels in PEX patients. PEX has been shown to be an important independent risk factor for glaucoma development in patients with ocular hypertension, implying that patients with PEX and ocular hypertension should receive medical treatment.

Medical therapy

In many PEX glaucoma cases, it is more difficult to reach the target IOP with monotherapy, and combination therapy, along with diurnal pressure monitoring and examinations at shorter intervals, is often required. Any therapy should, however, aim to reduce both mean IOP and 24-h IOP fluctuations.

To date, there are few comparative studies with respect to the efficacy of medications in controlling IOP in PEX glaucoma patients. Prostaglandin derivatives are more effective than beta-blockers in lowering mean and diurnal IOP in eyes with PEX glaucoma, but no significant differences between latanoprost and a fixed combination of timolol and dorzolamide have been reported. Comparing the effect of latanoprost versus bimatoprost on the diurnal IOP in patients with PEX glaucoma in a prospective, three-center, crossover study, mean diurnal IOP was significantly lower with bimatoprost than with latanoprost. In another prospective crossover comparison, latanoprost and travoprost both significantly reduced the 24-h IOP in patients with PEX glaucoma, but travoprost demonstrated a greater hypotensive efficacy in the late afternoon. In another prospective study of patients with hypertensive PEX syndrome receiving latanoprost, travoprost, or bimatoprost therapy, the mean 24-h range of IOP was significantly lower with travoprost. Unoprostone was also reported to provide a clinically significant IOP-lowering effect for patients with PEX glaucoma.

Despite good pressure-lowering effects and several potential benefits of miotic agents, for example, reduction of pupillary movement, there are some hazards of miotic use in PEX patients. Aggravation of blood–aqueous barrier breakdown, reduced pupillary movement promoting the formation of posterior synechiae, aggravation of lens opacities, and induction of pupillary or ciliary block glaucoma in eyes with marked zonular instability, may complicate management. Aqueous suppressants result in decreased aqueous flow through the trabecular meshwork, and this may conceivably lead to worsening of trabecular function and further compromise the degenerative ciliary epithelium.

Laser therapy

Argon laser trabeculoplasty (ALT) often has an immediate pressure-lowering effect, with reported initial success rates up to 80%, perhaps by easier heat absorption due to increased trabecular pigmentation. However, the success rates decrease with time and by 3 years, there is a substantial failure rate averaging 50% in both POAG and PEX eyes. Primary ALT seems to be a good first-line therapy in PEX glaucoma patients, as it can delay the use of medical therapy for up to 8 years in a significant proportion of these patients. Postlaser complications are more common in PEX eyes and comprise inflammatory reactions and IOP spikes, requiring careful follow-up together with anti-inflammatory therapy and pressure control in the early postoperative phase.

Selective laser trabeculoplasty (SLT) may be an effective and safe alternative to ALT in the treatment of PEX glaucoma.

Surgical therapy

As long-term effects of medical therapy and laser treatment are often unsatisfactory in patients with PEX glaucoma, surgical intervention may be earlier and more frequently necessary than in other forms of glaucoma. In cases of extremely high IOP fluctuations, a primary filtration surgery may be considered. Whereas routine trabeculectomy is most often applied, a relatively new surgical approach to improve chamber-angle facility by aspiration of debris and PEX material on the inner surface of the meshwork has been specifically developed for treating PEX glaucoma. Although efficacious in decreasing IOP in the early course, the effect of this trabecular aspiration technique appears to regress by time, being often limited to a few weeks only – possibly due to disregard of the juxtacanalicular region of the trabecular meshwork, where the bulk of PEX material is deposited. Successful results for IOP reduction in PEX glaucoma were also reported for sclerocanalectomy and for nonpenetrating deep sclerectomy. Whatever technique selected, antifibrotic agents may be used in order to limit the risk of postoperative scarring.

Filtration surgery combined with phacoemulsification does not seem to adversely influence the success rate, but has been reported to reduce the frequency and magnitude of postoperative pressure elevation. Cataract extraction alone may also improve IOP control in hypertensive patients with PEX syndrome and appears to be more effective than in POAG and cataract patients.

Peri- and postoperative surgical complications, such as inflammatory responses, fibrin reactions, formation of synechiae, and IOP spikes, are more common and more serious in PEX eyes than in eyes without PEX and can be directly attributed to the exaggerated and prolonged breakdown of the blood–aqueous barrier and anterior-segment hypoxia. The presence of abnormal iris vessels

can lead to intraoperative hemorrhage during iridectomy and postoperative hyphema. Weakened zonular support may allow vitreous loss, intraoperative lens movement, or even subluxation. Preoperative treatment with corticosteroids may therefore be beneficial along with more intensive and prolonged postoperative anti-inflammatory therapy and IOP control.

See also: Biological Properties of the Trabecular Meshwork Cells; Biomechanics of Aqueous Humor Outflow Resistance; Functional Morphology of the Trabecular Meshwork; Pharmacology of Aqueous Humor Formation; Pharmacology of the Aqueous Humor Outflow; Pigment Dispersion Syndrome and Pigmentary Glaucoma; Primary Open-Angle Glaucoma; Regulation of Extracellular Matrix Turnover in the Aqueous Humor Outflow Pathways; Structural Changes in the Trabecular Meshwork with Primary Open Angle Glaucoma; The Biology of Schlemm's Canal; The Fibrillar Extracellular Matrix of the Trabecular Meshwork; The Genetics of Primary Open-Angle Glaucoma: A Review; The Role of Oxidative Stress in the Trabecular Meshwork; The Role of the Ciliary Body in Aqueous Humor Dynamics. Structural Aspects; Uveoscleral Outflow.

Further Reading

Conway, R. M., Schlötzer-Schrehardt, U., Küchle, M., and Naumann, G. O. H. (2004). Pseudoexfoliation syndrome: Pathologic manifestations of relevance to intraocular surgery. *Clinical and Experimental Ophthalmology* 32: 199–210.

Hollo, G. and Konstas, A. G. P. (eds.) (2008). *Exfoliation Syndrome and Exfoliation Glaucoma.* Savona, Italy: Dogma.

Konstas, A. G. P., Tsironi, S., and Ritch, R. (2006). Current concepts in the pathogenesis and management of exfoliation syndrome and exfoliative glaucoma. *Comprehensive Ophthalmology Update* 7: 131–141.

Naumann, G. O. H., Schlötzer-Schrehardt, U., and Küchle, M. (1998). Pseudoexfoliation syndrome for the comprehensive ophthalmologist. Intraocular and systemic manifestations. *Ophthalmology* 105: 951–968.

Ritch, R. and Schlötzer-Schrehardt, U. (2001). Exfoliation syndrome. *Survey of Ophthalmology* 45: 265–315.

Ritch, R., Schlötzer-Schrehardt, U., and Konstas, A. G. P. (2003). Why is glaucoma associated with exfoliation syndrome? *Progress in Retinal and Eye Research* 22: 253–275.

Schlötzer-Schrehardt, U. (2008). Molecular pathology of pseudoexfoliation syndrome/glaucoma – new insights from LOXL1 gene associations. *Experimental Eye Research* 88: 776–785.

Schlötzer-Schrehardt, U. and Naumann, G. O. H. (1997). Pseudoexfoliations-Syndrom: Morphologie und Komplikationen. In: Naumann, G. O. H. (ed.) *Pathologie des Auges,* 2nd edn., pp. 1373–1422. Berlin: Springer.

Schlötzer-Schrehardt, U. and Naumann, G. O. H. (2004). Pseudoexfoliation glaucoma. In: Grehn, F., Stamper, R., Krieglstein, G. K., and Weinreb, R. N. (eds.) *Glaucoma. Essentials in Ophthalmology,* 1st edn., pp. 157–176. Berlin: Springer.

Schlötzer-Schrehardt, U. and Naumann, G. O. H. (2006). Perspective – ocular and systemic pseudoexfoliation syndrome. *American Journal of Ophthalmology* 141: 921–937.

Schlötzer-Schrehardt, U. and Naumann, G. O. H. (2008). Pseudoexfoliation syndrome: Pathological manifestations of relevance to intraocular surgery. In: Naumann, G. O. H., Holbach, L., and Kruse, F. E. (eds.) *Applied Pathology for Ophthalmic Microsurgeons,* 1st edn., pp. 354–377. Berlin: Springer.

Schlötzer-Schrehardt, U. and Naumann, G. O. H. (2008). Trabecular mechanisms of intraocular pressure elevations: Pseudoexfoliation syndrome. In: Tombran-Tink, J., Barnstable, C. J., and Shields, M. B. (eds.) *Mechanisms of the Glaucomas: Disease Processes and Therapeutic Modalities,* 1st edn., pp. 117–138. New York: Humana Press.

Schlötzer-Schrehardt, U. and Streeten, B. W. (2008). Pseudoexfoliation syndrome. In: Klintworth, G. K. and Garner, A. (eds.) *Pathobiology of Ocular Disease,* 3rd edn., pp. 505–536. London: Informa Healthcare.

Schlötzer-Schrehardt, U., Pasutto, F., Sommer, P., et al. (2008). Genotype-correlated expression of lysyl oxidase-like 1 in ocular tissues of patients with pseudoexfoliation syndrome/glaucoma and normal patients. *American Journal of Pathology* 173: 1724–1735.

Thorleifsson, G., Magnusson, K. P., Sulem, P., et al. (2007). Common sequence variants in the LOXL1 gene confer susceptibility to exfoliation glaucoma. *Science* 317: 1397–1400.

Pupil

P D R Gamlin and D H McDougal, University of Alabama at Birmingham, Birmingham, AL, USA

Glossary

Accommodation – A change in the refractive power of the crystalline lens of the eye.
Intrinsically photosensitive retinal ganglion cells (ipRGCs) – The ganglion cells expressing a photopigment, melanopsin, that is intrinsically light sensitive.
Miosis – Pupillary constriction.
Mydriasis – Pupillary dilation.
Pupillary light reflex (PLR) – The constriction of the pupil that is elicited by an increase in illumination of the retina.

Advantages of a Mobile Pupil

The normal human pupil can change diameter from 8 to 1.5 mm, which corresponds to approximately a 30-fold change in area and almost a 1.5-log unit change in retinal irradiance. Although the visual system can operate over a 10-log unit range of lighting levels through the process of adaptation, it can take several minutes for optimum sensitivity to return after an abrupt increase or decrease in retinal illumination. The rapid control of retinal irradiance by the iris allows the visual system to more quickly regain optimal sensitivity by dampening fast changes in ambient lighting levels and by requiring less retinal adaptation for a given change in environmental lighting levels.

However, changes in pupil size affect not only retinal illumination, but also diffraction, optical aberrations, and depth of focus of the eye. These factors differentially affect visual performance and, given changing environmental lighting conditions and visual tasks, the nervous system continuously modulates pupil diameter for optimal visual performance.

The diffraction of light rays by an aperture is a major limiting factor in the resolution of an image in any optical system. The amount of disruption in image quality caused by diffraction at a circular aperture decreases as the size of the opening increases. Therefore, as pupil diameter increases, there is decreased degradation in retinal image quality caused by diffraction. In contrast to diffraction, the image-degrading effects of optical aberrations increase as aperture diameter increases. Therefore, as pupil diameter increases, the degradative effects of optical aberrations also increase, and offset the benefits gained by reduced diffraction at larger pupil diameters. Over the normal range of pupillary diameter, diffraction impacts image quality less than optical aberration, and the optimal pupil diameter is therefore approximately between 2 and 4 mm.

Along with diffraction and optical aberrations, defocus is an important determinate of retinal image quality. Although the pupil does not refract or focus light, it influences the depth of field of the eye. Depth of field is the range of distance in depth in which objects appear to be in focus. For example, when one reads a book, the power of the crystalline lens of the eyes changes in order to bring the text on the page into focus through a process called accommodation. With the eyes accommodated on the book, all objects within a range in front of and behind the book will also appear in focus. This range is called the depth of field and it is primarily dependent both on viewing distance and pupil diameter. When the viewing distance is held constant, the depth of field increases with decreases in pupil diameter, and therefore the pupil diameter can affect the focus of the retinal image.

Clearly, a mobile pupil allows the nervous system to optimize retinal irradiance, diffraction, ocular aberrations, and depth of focus despite differing conditions and visual tasks. For example, across a range of daylight (photopic) luminances, pupil size corresponds to that required for the highest visual acuity, and the maximal information capacity of the retinal image. On the other hand, under low light (scotopic) conditions in which poorer retinal image quality can be tolerated due to the lower resolution of rod photoreceptors, the pupil dilates sufficiently to maximize the retinal illumination. Further evidence for the optimization of pupil diameter for differing visual tasks is evident in the pupillary near response (PNR). When the viewing distance changes from far to near, the pupils constrict to increase the field of view and reduce the retinal image defocus. This compensates for the decrease in the effective field of view that naturally occurs when viewing distance decreases (see the section titled 'Pupillary near response' for more details).

Overview of the Pathways Controlling Pupil Diameter

A summary diagram of the afferent, central, and efferent pathways controlling pupil diameter is shown in **Figure 1**. This figure shows the iris musculature innervated by autonomic efferents from both the parasympathetic and sympathetic components of the autonomic nervous system

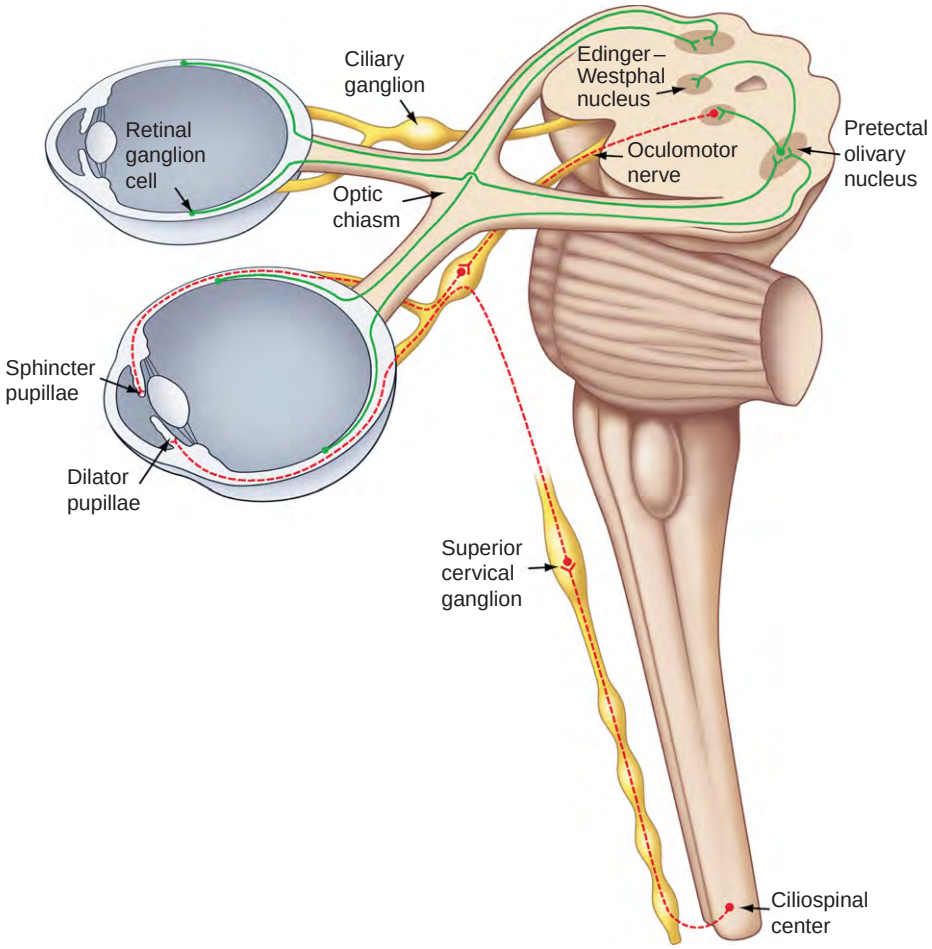

Figure 1 Anatomical drawing showing the direct and consensual pupillary light reflex (PLR) pathways and the parasympathetic and sympathetic innervation of the iris in primates. The bilateral projection from the retina to the pretectum is also shown. The pretectal olivary nucleus receives input from the temporal retina of the ipsilateral eye and the nasal retina of the contralateral eye. The pretectal olivary nucleus projects bilaterally to the Edinger–Westphal (EW) nucleus, which contains parasympathetic, preganglionic, and pupilloconstriction neurons. The axons of these preganglionic neurons travel in the third cranial nerve to synapse upon postganglionic pupilloconstriction neurons in the ciliary ganglion. The axons of these postganglionic neurons leave the ciliary ganglion and enter the eye through the short ciliary nerves, and travel through the choroid to innervate the sphincter muscle of the iris. The sympathetic preganglionic pupillodilation neurons are found at the C8-T1 segmental levels of the spinal cord. The axons of these neurons project from the spinal cord through the dorsal roots and enter the sympathetic trunk, and then project rostrally to the superior cervical ganglion where they synapse with the postganglionic neurons. These postganglionic neurons project from the superior cervical ganglion through the neck and carotid plexus, and into the orbit of the eye. These fibers enter the eye either by passing through the ciliary ganglion and entering the short ciliary nerves, or bypassing the ciliary ganglion and entering via the long ciliary nerves (for clarity, only one of these alternative pathways is shown). Upon entering the eye, these axons travel through the choroid and innervate the dilator muscle of the iris. From McDougal, D. H. and Gamlin, P. D. R. (2008). Pupillary control pathways. In: Basbaum, A. I., Kaneko, A, Shepherd, G. M., et al. (eds) *The Senses: A Comprehensive Reference*, *Vol 1: Vision 1*, pp. 521–536. San Diego, CA: Academic Press.

(ANS). The parasympathetic component of the ANS innervates the sphincter pupillae muscle of the iris. The preganglionic parasympathetic fibers controlling the sphincter pupillae originate from neurons in the Edinger–Westphal (EW) nucleus, the autonomic subdivision of the third cranial nerve nucleus, and travel through the third cranial nerve to the ciliary ganglion, which is located within the orbit of the eye (see **Figure 1**). Within the ciliary ganglion, the preganglionic pupilloconstriction neurons form cholinergic, nicotinic synapses with the postganglionic neurons. The axons of these postganglionic neurons leave the ciliary ganglion to enter the eye through the short ciliary nerves and travel to the iris. Here, they release acetylcholine, which acts on the muscarinic receptors of the sphincter pupillae (see **Figure 2**).

The sympathetic component of the ANS innervates the dilator pupillae muscle. The preganglionic sympathetic neurons, which control pupillary dilation, are located in the C8-T1 segments of the spinal cord, a region termed the ciliospinal center of Budge (and Waller). The

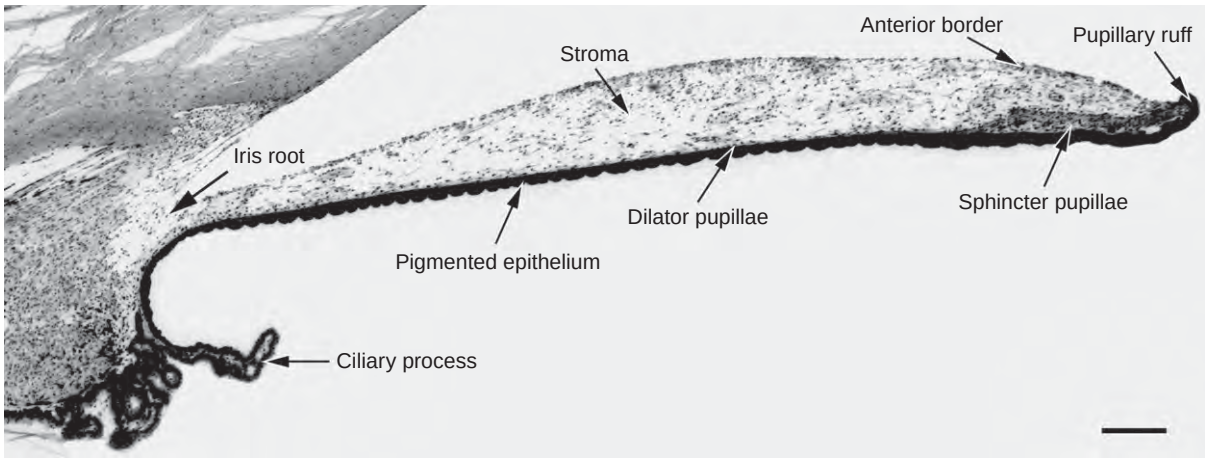

Figure 2 Low-power photomicrograph of a cross section of the macaque iris. Scale = 200 μm. From McDougal, D. H. and Gamlin, P. D. R. (2008). Pupillary control pathways. In: Basbaum, A. I., Kaneko, A, Shepherd, G. M., et al. (eds.) *The Senses: A Comprehensive Reference*, *Vol 1: Vision 1*, pp. 521–536. San Diego, CA: Academic Press.

axons of these preganglionic neurons project to the sympathetic chain and travel in the sympathetic trunk to the superior cervical ganglion. Within the superior cervical ganglion, the preganglionic axons form nicotinic, cholinergic synapses with postganglionic pupillodilation neurons. The axons of these postganglionic neurons project from the superior cervical ganglion to the orbit, where they enter the eye through the short and long ciliary nerves and travel to the iris (see **Figure 1**). Here, they release norepinephrine, which acts on the adrenoreceptors of the dilator muscle (see **Figure 2**).

Iris Musculature

In a cross-section of the iris, the sphincter pupillae can be seen as an annular band of smooth muscle (100–170 μm thick; 0.7–1.0 mm wide) encircling the pupil (**Figure 2**). The sphincter, which is located in the posterior iris immediately anterior to the pigmented epithelium, interdigitates with the surrounding stroma and connects to the dilator muscle fibers. The smooth muscle cells of the sphincter are clustered in small bundles and connected by gap junctions. These gap junctions ensure synchronized contraction of the sphincter muscle. The sphincter receives muscarinic, cholinergic innervation from the short ciliary nerves – parasympathetic, postganglionic fibers arising from the ciliary ganglion.

The dilator pupillae is composed of radially oriented smooth muscle fibers that are myoepithelial in origin. Individual fibers are approximately 50 μm long and 5–7 μm wide. In the pupillary zone, dilator muscle processes fuse with the sphincter pupillae, while peripherally, their processes attach to the ciliary body. Contraction of the dilator muscle pulls the pupillary margin toward the ciliary body.

Pupillary Light Reflex

Description

The pupillary light reflex (PLR) is the constriction of the pupil that is elicited by an increase in illumination of the retina. The direct PLR, present in virtually all vertebrates, is the constriction of the pupil in the same eye as that stimulated with light. The consensual PLR is the constriction of the pupil in the eye opposite to the eye stimulated with light. In mammals with laterally placed eyes, such as the rat and rabbit, the direct PLR is more pronounced than the consensual PLR. However, in those mammalian species with frontally placed eyes, such as humans and monkeys, the direct and consensual PLRs are essentially equal. An example of a human consensual PLR produced by two different wavelengths of light is shown in **Figure 3**. The PLR has traditionally been divided into two separate pathways based on the clinical manifestations of the defects in this reflex. The afferent pathway is composed of both the retinal cells that project to the pretectum as well as their recipient neurons, which project bilaterally to the EW nucleus (**Figure 1**). The efferent pathway is composed of the preganglionic pupilloconstriction fibers of the EW nucleus and their postganglionic recipient neurons in the ciliary ganglion, which project to the sphincter muscle of the iris (**Figure 1**).

Afferent Pathway

The first neurons in the afferent pathway of the PLR are retinal ganglion cells. It has recently been recognized that this reflex in rodents and primates is driven predominantly by a unique subset of intrinsically photosensitive retinal ganglion cells (ipRGCs) which project to the pretectal olivary nucleus (PON), a small nucleus in the

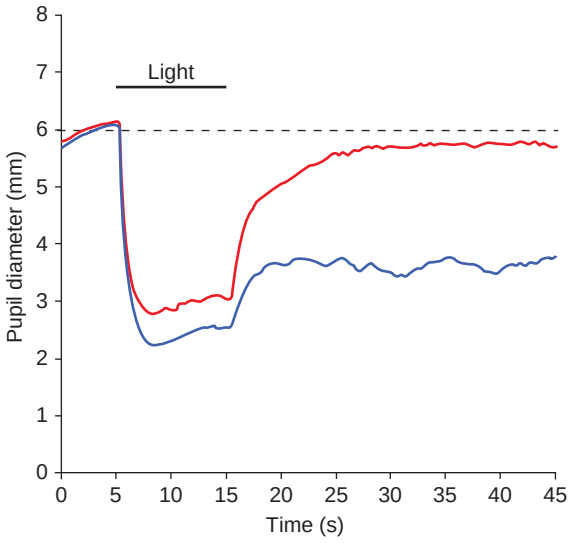

Figure 3 Pupilloconstriction elicited by a 10-s light stimulus of 493-nm wavelength light at 14.0 log quanta cm^{-2} per second irradiance (blue trace), and 613-nm wavelength light at 14.1 log quanta cm^{-2} per second irradiance (red trace). Note that a 473-nm stimulus, which effectively activates the intrinsic photoresponse of intrinsically photosensitive retinal ganglion cells (ipRGCs), drives a larger pupillary response than the 613-nm stimulus (red trace), which does not effectively activate the intrinsic photoresponse of ipRGCs at this irradiance level. Note that the pupilloconstriction induced by the 473-nm light is maintained following stimulus offset. From McDougal, D. H. and Gamlin, P. D. R. (2008). Pupillary control pathways. In: Basbaum, A. I., Kaneko, A, Shepherd, G. M., et al. (eds.) *The Senses: A Comprehensive Reference*, *Vol 1: Vision 1*, pp. 521–536. San Diego, CA: Academic Press.

pretectum; the pretectum is located in the dorsal lateral aspect of the midbrain at the level of the superior colliculus (see **Figure 1**).

Intrinsically photosensitive retinal ganglion cells

Prior to 2000, it was assumed that the PLR was driven by retinal ganglion cells which received light signals exclusively from rod and cone photoreceptors, which up to that time were the only known photoreceptive cells in the retina. However, recent studies have demonstrated that the PLR is driven predominantly by retinal ganglion cells which, unlike any other retinal ganglion cell class, are intrinsically photosensitive. The intrinsic photoresponse of these neurons, which is mediated by the photopigment melanopsin, presumably compensates for the adaptation of rod and cone photoreceptors, and serves to maintain pupilloconstriction during steady-state exposure at all photopic (daylight) illuminance levels. In addition to their intrinsic light-driven signal, it is clear that ipRGCs receive rod and cone inputs. In response to a pulse of light, intracellular recordings from these cells show a characteristic transient burst of neural activity at stimulus onset, which rapidly decays to a plateau of sustained activity that often extends well past stimulus offset. The initial burst of neural activity is mediated by a rapidly adapting cone-mediated photoresponse, while the sustained activity is driven predominantly by the intrinsic response of these cells, although there is growing evidence for a rod contribution to this sustained activity under steady-state lighting conditions.

IpRGCs project to the PON of rodents and primates, and they play a major role in pupillary responses. Monkeys and rodents with nonfunctional rod and cone photoreceptors but functional melanopsin-containing ipRGCs display a PLR; however, the reflex has a higher irradiance threshold than normal. Mice with ipRGCs lacking melanopsin also display PLR, but their pupils fail to constrict maximally in bright lights. Taken together, these results show that both the intrinsic photoresponse of ipRGCs and their classical photoreceptor inputs provide signals of retinal irradiance that drive the PLR. Additional studies further suggest that the influence of rod and cone photoreceptors on the pupillary light reflex is mediated exclusively through their inputs to ipRGCs.

The intrinsic photoresponse of ipRGCs can also affect pupillary behavior in the absence of ongoing light stimulation. As noted above, ipRGCs encode stimulus irradiance through an elevation of firing rate that continues well beyond stimulus offset. Indeed, bright light stimuli can produce a prolonged pupillary constriction in humans that can persist up to 20 min after the light has been extinguished (see **Figure 3**). Experiments in primates, including humans, demonstrate that this prolonged pupillary constriction in darkness is mediated almost entirely by the intrinsic photoresponse of ipRGCs.

Pretectal olivary nucleus

The first relay in the afferent pathway of the PLR consists of luminance neurons within the PON, which receives direct retinal input. PON luminance neurons are characterized by tonic firing rates that increase with increases in retinal illuminance. In primates, these neurons exhibit a transient burst of activity followed by sustained tonic activity in response to increases in retinal illuminance. In addition, the tonic firing rate of these cells is proportional to retinal illuminance over at least a 3 log unit range of stimulus intensities in primates and in rats. Electrical microstimulation of the PON in rats and monkeys elicits pupilloconstriction at short latencies, and lesions of the PON in rats produce deficits in pupillomotor function. These results strongly suggest that luminance neurons within the PON mediate the PLR. In addition to retinal afferents, the PON also receives significant cortical, ventral thalamic, and midbrain inputs which may also have an influence on the PLR or other pupillary movements. Owing to its importance for the PLR, the best-described efferent projection of the PON is to the EW nucleus. However, the PON has been shown to project to a number

of other targets, such as the hypothalamus, pons, and medulla that may also influence pupillary behavior.

Efferent Pathway

The efferent leg of the PLR begins with preganglionic pupilloconstriction neurons of the EW nucleus that project through the third cranial nerve to the ciliary ganglion (see **Figure 1**).

The EW nucleus is a distinct nucleus of the midbrain, lying immediately dorsal to the oculomotor complex. It is located just ventral and lateral to the cerebral aqueduct at the level of the superior colliculus (see **Figure 1**). Evidence for the course of the efferent parasympathetic pupillary pathway and the importance of the EW nucleus in pupilloconstriction comes from electrical stimulation studies in the vicinity of EW nucleus that elicit pupilloconstriction in a variety of animal models. Within the ciliary ganglion, which is approximately 3 mm in size, and located 2–3 mm posterior to the globe and lateral to the optic nerve, the axons of the preganglionic neurons synapse with the postganglionic pupilloconstriction neurons. The axons of these postganglionic neurons leave the ciliary ganglion to enter the eye via the short ciliary nerves to innervate the sphincter muscle of the iris.

Sympathetic Influences on the PLR

It is generally agreed that the parasympathetic pathway discussed above is the primary route of pupillary constriction associated with the PLR. However, there is some evidence that increases in retinal illumination may cause a reduction in the tone of the dilator muscle of the iris through the sympathetic pathway outlined in **Figure 1**, and thus enhance the PLR. Studies in cats have shown a light-induced inhibition of postganglionic pupillodilation fibers at the level of the long ciliary nerves, and preganglionic, pupillodilation fibers at the level of the cervical sympathetic nerve. These studies found that the pupillodilation fibers were inhibited by light in an intensity-dependent manner, that is, a more intense light brought about a greater inhibition in firing rate. However, these findings have not been replicated in primates, in which the evidence suggests that the sympathetic system does not contribute to the dynamics of the PLR and only contributes to tonic modulation of pupil diameter.

The Pupillary Near Response

Description

The PNR is the pupillary constriction associated with a change in viewing distance from far to near that occurs in primates including humans. When the eyes move from viewing a far object to viewing a near object, three oculomotor responses occur. The eyes converge to bring the image of the object onto the fovea of each retina, the refractive power of the crystalline lens is adjusted to bring the image of the object into focus on the retina, and the pupil constricts. These collective processes are classically referred to as the near response or the near triad.

Efferent Pathway of the PNR

The PNR is thought to be driven solely by an increased drive to the sphincter muscle of the iris through the parasympathetic efferent pathway. Therefore, the neural control pathway of the PNR shares a common efferent pathway with the PLR, although the afferent inputs responsible for the PNR are more complex. The neural signals driving these two reflexes most likely converge at the EW nucleus, since the activity of PON luminance neurons is not correlated with pupil constriction during near viewing. Further, certain clinical neurological conditions are characterized by an intact PNR despite the absence of the PLR (light-near dissociation).

It is generally accepted that preganglionic neurons in the EW nucleus drive the PNR as well as the PLR. However, it has not been determined if separate subpopulations of neurons exist in EW nucleus devoted exclusively to either the PLR or the PNR, or whether the same population of neurons drives pupillary constriction in both reflexes, although the latter seems most likely.

Afferent Influences on the PNR

Early investigations attempted to determine whether the PNR was driven primarily by ocular convergence or accommodation, the other two components of the near triad. Some studies found that the PNR was more closely associated with accommodation than with convergence. Other studies found a greater association with convergence, and even reported that the PNR was totally absent during some blur-driven accommodative responses. These conflicting results are likely a product of an incomplete disassociation between the convergence and accommodation systems during these experiments, as these two systems have been shown to be highly interdependent. A more modern view of the afferent influences controlling the PNR has recently emerged. In this view, the PNR is not seen as resulting from either accommodation or convergence alone, but as a separate output of the neural pathways that drive both accommodation and convergence.

A number of brain areas play a role in controlling the near triad. These include cortical areas, such as extrastriate cortex, parietal cortex, frontal eye fields, as well as the cerebellum and the midbrain. Of particular interest to the PNR, is the supraoculomotor area of the midbrain, which lies just dorsal and lateral to the oculomotor nucleus. The supraoculomotor area contains near response cells which

are modulated by both vergence and accommodation. These cells project to medial rectus motoneurons, and thus contribute to vergence eye movements. It seems likely that these cells also project to EW nucleus and are responsible for carrying the signal from the accommodation and convergence controller to the preganglionic, pupilloconstrictor neurons.

Additional Cortical Influences on Pupillary Responses

In addition to cortical afferents mediating the PNR, the pupil is also influenced by both visual and nonvisual cortical regions. These afferents manifest themselves as small changes in pupil diameter during presentation of visual stimuli such as colored stimuli and gratings, as well as nonvisual stimuli such as auditory tones, and even during higher-order cortical functions such as problem solving. These observations provide clear evidence that cortex exerts an influence on pupillary behavior, which therefore cannot be thought of as entirely reflexive in nature.

Visually Mediated Cortical Influences on Pupillary Behavior

Small pupillary constrictions have been shown to occur in both human and monkeys with the presentation of complex visual stimuli, even when the stimuli do not involve a change in viewing distance or retinal illuminance. Changes in stimulus attributes such as color, spatial frequency, or apparent motion produce such cortically mediated pupillary responses. Deficits in these pupillary responses are observed in humans with lesions to cortical areas involved in processing one or more of these stimulus characteristics. In addition, lesions of rostral inferior temporal cortex but not V4 in macaques abolish pupillary responses to chromatically modulated gratings.

Task-Evoked Pupillary Responses

In the early 1960s, Hess and colleagues published a series of papers which reported modulations in human pupillary diameter associated with complex cognitive processes such as subjective attitudes or mental activity. Later studies failed to replicate the findings relating pupillary dynamics to subjective attitudes, although the findings related to mental activity have been replicated and extensively studied. The small pupillary dilations associated with increased mental activity, or task-evoked pupillary responses (TEPRs), have now become a well-established tool of cognitive psychology. These pupillary responses are generally reported to vary in magnitude from 0.2 to 0.7 mm, and have been shown to correlate with cognitive load across diverse functions, such as sensory perception, memory, language, and attention. TEPRs have been repeatedly shown to monotonically vary with the degree of mental activity required by a task as measured by other objective criterion such as reaction time and the extent of cortical activation indicated by positron emission tomography (PET) scan, and this has allowed TEPRs to be utilized successfully to empirically test theories of language processing and intelligence.

Although the behavioral phenomenon of TEPRs has been extensively studied and quantified, little is known of the underlying neurophysiology that drives these responses. It has been suggested that they may be driven by noradrenergic projections from the locus ceruleus since the activity of neurons in this nucleus has been show to correlate with both pupil diameter and task-related events.

Influence of Alertness on Pupillary Behavior

Since the muscles of the iris are controlled by the ANS, environmental or physiological conditions which cause changes in overall autonomic function can have a significant effect on pupillary behavior. Even though the environment or physiological conditions which produce the change in autonomic tone may not have a direct influence on the visual system, they may still manifest themselves through an affect on pupil diameter.

Arousal

Situations or stimuli which produce an emotional or startle response often produce a profound pupillary dilation. This effect is mediated through the hypothalamus, the brain area responsible for the integration of autonomic function. This integration allows for the coordination of the various functions of the ANS and often leads to global changes in the balance between the sympathetic and parasympathetic branches of the ANS. For example, an unexpected loud noise may produce a startle response which is characterized by increases in heart rate, respiratory rate, and pupil diameter; it is caused by a systemic increase in sympathetic tone mediated through the hypothalamus. This global increase in sympathetic tone can affect pupil diameter via activation of the pupillodilation centers of the spinal cord and inhibition of the pupilloconstriction neurons of EW nucleus. Neurons within the hypothalamus project to the sympathetic preganglionic pupillodilation neurons of the thoracic spinal cord. This direct effect of hypothalamic activation on pupil diameter can be shown through microstimulation of the posterior hypothalamus, which often causes rapid pupil dilation. Increase in sympathetic tone can also produce inhibition

of pupilloconstriction neurons of EW nucleus via the influence of ascending neuromodulatory pathways.

The hypothalamus is also the site at which autonomic function is regulated by the central nervous system through connections with the limbic system and cortical structures. The limbic system of the brain, which is responsible for emotions and short-term memory, has a direct connection to the hypothalamus and therefore can have significant effects on autonomic balance. Situations or stimuli which produce an intense emotional response are often accompanied by pupillary dilation, which is certainly mediated through limbic connections to the hypothalamus. In addition, cortical influences on the hypothalamus allow a wide variety of stimuli to effect autonomic tone and thus pupil diameter.

Sleep

Sleep has a pronounced effect on the ANS, specifically a reduction in sympathetic outflow and an increase in parasympathetic outflow. Given this overall trend, it is not surprising that pupillary behavior during sleep is characterized by prolonged constriction of the pupil. It has been shown that sleep-induced pupillary constriction persists in animals with lesions of the preganglionic sympathetic pupillodilation fibers. This suggests that the sleep-induced pupillary changes are mediated by an activation of the preganglionic parasympathetic pupilloconstriction fibers of the EW nucleus.

Ascending Neuromodulatory Systems

The ascending neuromodulatory systems of the midbrain and brainstem can have a variety of effects on pupillary behavior. These nuclei are the origin of neuromodulatory fibers which release dopamine, norepinephrine, histamine, and serotonin at a number of brain areas implicated in pupillary control. These neuromodulatory systems appear to be critical in the regulation of sleep and arousal, as well as autonomic regulation and cortical plasticity. In addition to these global neuromodulatory effects, all or some of which could have a profound influence on pupillary behavior, there is some evidence for a direct inhibition of pupilloconstriction neurons in the EW nucleus by adrenergic neurons originating from the locus ceruleus in a number of animal models. However, other studies in humans and rabbits have failed to find this direct noradrenergic inhibition of EW nucleus pupilloconstriction neurons and it has been suggested that this effect might be mediated by dopaminergic neurons in these species. Drugs which agonize or antagonize these neuromodulatory neurotransmitters have been found to differentially affect pupillary behavior in a wide range of animal models and human studies. These differential effects are most likely due to the both interspecies variability in the projections of these neuromodulatory fibers, as well as the differential activation of multiple brain areas implicated in pupillary behavior due to the extensive projections of these neuromodulators.

Acknowledgments

This work was supported by NIH grant EY09380 and the EyeSight Foundation of Alabama.

See also: Acuity; Binocular Vergence Eye Movements and the Near Response; Chromatic Function of the Cone; Circadian Photoreception; Information Processing: Ganglion Cells; Photopic, Mesopic and Scotopic Vision and Changes in Visual Performance.

Further Reading

Barbur, J. L. (2003). Learning from the pupil – studies of basic mechanisms and clinical applications. In: Chalupa, L. M. and Werner, J. S. (eds.) *The Visual Neurosciences*, pp. 641–656. Cambridge, MA: MIT Press.

Beatty, J. and Lucero-Wagoner, B. (2000). The pupillary system. In: Cacioppo, J. T., Berntson, G., and Tassinary, L. G. (eds.) *Handbook of Psychophysiology*, 2nd edn., pp. 142–162. Cambridge: Cambridge University Press.

Berson, D. M. (2003). Strange vision: Ganglion cells as circadian photoreceptors. *Trends in Neuroscience* 26: 314–320.

Bron, A. J., Tripathi, R. C., Tripathi, B. J., and Wolff, E. (1997). *Wolff's Anatomy of the Eye and Orbit*. London: Chapman and Hall Medical.

Busettini, C., Davison, R. C., and Gamlin, P. D. R. (2009). Vergence eye movements. In: Squire, L. (ed.) *Encyclopedia of Neuroscience*, vol. 10, pp. 75–84. Oxford: Elsevier.

Charman, W. N. (1995). Optics of the eye. In: Bass, M. (ed.) *Handbook of Optics*, pp. 24.3–24.54. New York: McGraw-Hill.

Gamlin, P. D. (2000). Functions of the Edinger–Westphal nucleus. In: Burnstock, G. and Sillito, A. M. (eds.) *Nervous Control of the Eye*, pp. 117–154. Binghamton, NY: Harwood Academic.

Gamlin, P. D. (2005). The pretectum: Connections and oculomotor-related roles. *Progress in Brain Research* 151: 379–405.

Gamlin, P. D., McDougal, D. H., Pokomy, J., et al. (2007). Human and macaque pupil responses driven by melanopsin-containing retinal ganglion cells. *Vision Research* 47(7): 946–954.

Kardon, R. H. (2005). Anatomy and physiology of the autonomic nervous system. In: Miller, N. R., Walsh, F. B., Biousse, V., and Hoyt, W. F. (eds.) *Walsh and Hoyt's Clinical Neuro-Ophthalmology,* vol. 3, pp. 649–714. Baltimore, MD: Lippincott Williams and Wilkins.

Kawasaki, A. (2005). Disorders of pupillary function, accommodation, and lacrimation. In: Miller, N. R., Walsh, F. B., Biousse, V., and Hoyt, W. F. (eds.) *Walsh and Hoyt's Clinical Neuro-Ophthalmology,* vol. 3, pp. 739–804. Baltimore, MD: Lippincott Williams and Wilkins.

Loewenfeld, I. E. and Lowenstein, O. (1993). *The Pupil: Anatomy, Physiology, and Clinical Applications*. Ames, IA: Iowa State University Press.

McDougal, D. H. and Gamlin, P. D. R. (2008). Pupillary control pathways. In: Basbaum, A. I., Kaneko, A., Shepherd, G. M., et al. (eds.) *The Senses: A Comprehensive Reference, Vol 1: Vision 1*, pp. 521–536. San Diego, CA: Academic Press.

Oyster, C. W. (1999). *The Human Eye: Structure and Function*, pp. 411–446. Sunderland, MA: Sinauer Associates.

R

Refractive Surgery

S Marcos, L Llorente, C Dorronsoro, and J Merayo-Lloves, Consejo Superior de Investigaciones Científicas, Madrid, Spain

Glossary

Aberrations – Phase deviations from the ideal wave front measured at the pupil plane. Aberrometers measure local ray deviations, which are fitted to the derivatives of the wave aberration, usually expressed as a Zernike polynomial expansion. A relevant aberration in the human eye (and particularly after standard refractive surgery) is spherical aberration (which results in peripheral rays converging on a different plane than central rays). A common optical quality metric derived from the wave aberration is the root mean square (RMS) wave-front error.

Ablation profile – Corneal tissue that needs to be removed at each location to produce the desired change in corneal power. Generally, the ablation-profile equation is converted into the number of laser pulses to be applied at each location.

Asphericity – Parameter used to describe the deviation of the anterior corneal surface from a sphere. The corneal surface can be fitted to a conic section using the apical radius of curvature and the eccentricity e (variation of this curve with distance from the apex). Asphericity Q is defined as $-e^2$, with the surface represented by the following equation: $(X^2+Y^2)+(1+Q)Z^2-2ZR=0$. For a sphere $Q=0$, a typical cornea shows an asphericity $Q=-0.26$; a surface with zero spherical aberration should have an asphericity $Q=-0.52$; an oblate surface (exhibiting positive spherical aberration) will have $Q>0$; and a prolate surface (exhibiting low positive spherical aberration or negative) will have $Q<0$.

Beer–Lambert law – Law governing the photoablation of the corneal tissue by excimer laser. The depth of ablated material is proportional to the logarithm of the laser fluence (relative to the ablation threshold).

Contrast-sensitivity function (CSF) – The contrast-sensitivity function represents the minimum subjectively discernible contrast as a function of spatial frequency. It typically has an inverted-U shape, peaking at around 4 cycles per degree (c/deg), with sensitivity decreasing on either side of the peak. The shape of the CSF is determined by the properties of the visual neurons and the optical aberrations of the eye. Other factors affecting the CSF are pupil diameter and luminance. CSF is a more sensitive measure of changes in visual quality following a change in the optics (such as that produced by refractive surgery) than visual acuity.

Excimer laser – Laser producing stimulated emission after electrical discharge forming dimers or complexes, emitting typically ultraviolet (UV) light. Lasers applied in refractive surgery use a combination of Argon (as inert compound) and fluorine (reactive gas) and emit at 193 nm. The excimer lasers are well suited to remove exceptionally fine layers of surface material (particularly, biological matter and organic compounds) by disrupting the molecular bonds of the tissue, through ablation rather than burning, leaving the remainder of the material almost intact. Lasers used in refractive surgery have fluences typically ranging between 120 and 400 mJ cm^{-2}.

Laser-assisted *in situ* keratomileusis (LASIK) – Corneal refractive surgery technique which involves the creation of a thin flap on the cornea, folding it to enable remodeling of the tissue underneath with laser and repositioning the flap back after the corneal ablation has been performed.

Modulation-transfer function (MTF) – Optical function representing the contrast degradation by an optical system as a function of spatial frequency. Factors affecting the MTF are diffraction (pupil size),

optical aberrations, scattering, and wavelength. The ocular MTF is a low-pass function, with a cut-off frequency at around 70 c/deg.

Munnerlyn formula – Equation on which standard ablation algorithms for corneal refractive surgery are based. The corneal tissue to be removed is a lenticule with an anterior radius of curvature equal to the preoperative corneal radius and the posterior radius of curvature equal to the postoperative corneal radius (easily related with the attempted correction). A parabolic approximation of the Munnerlyn formula states that the depth of the ablation (in microns) per diopter of refractive change is equal to the square of the optical ablation zone measured in millimeters, divided by 3.

Optical zone – Area of the cornea where the ablation algorithm is applied. For the same attempted correction, smaller optical zones require less ablation depth. However, small optical zones can severely compromise vision if they are smaller than pupil diameter. A transition zone around the optical zone is created to avoid an abrupt step between treated and untreated areas.

Short Historical Background of Corneal Refractive Surgery

Corneal refractive surgery has become, in recent years, a popular surgical approach to correct ametropia. Table 1 depicts highlights of refractive surgery history in chronological order. The first surgical procedure that achieved a change in corneal power by relaxation through corneal incision was radial keratotomy (RK). First attempts of incisional corneal surgery date from 1885 onward. The technique evolved through the 1930s and 1940s to the early 1980s when Fyodorov developed a systematic and more predictable RK procedure that he applied to thousands of patients. In the 1960s, Barraquer invented keratomileusis – the first lamellar surgical technique. This technique consisted of separating a thin layer of the superficial corneal tissue using a microkeratome, removing a small piece of cornea, which was frozen and then reshaped using a lathe, and suturing it back into place. However, it was only in the late 1980s, when excimer lasers were developed at IBM, that their excellent properties for micromachining of biological tissue and organic materials were identified by Srinivasan. In the 1980s, Stephen Trokel applied, for the first time, an argon-fluoride excimer laser to remove tissue in bovine corneas, following previous mechanical removal of the outer layer of the cornea (corneal epithelium) to treat ametropia, thus giving birth to photorefractive keratectomy (PRK).

Table 1 Chronology of corneal refractive surgery

1898	The basic principles of radial keratotomy are laid up by Dr. Lans (the Netherlands)
1930	Pioneering work on corneal incisions is performed by Dr. Tsutomu Sato (Japan)
1948	The first surgical techniques to reshape the cornea (freezing a corneal flap, reshaping it on a lathe and placing it back) are performed by Dr. José Barrarquer (Colombia)
1960s	Radial keratotomy is developed by Dr. Fyodorov (Russia)
1978	Radial keratotomy is introduced in the US by Dr. Leo Bores
1975–79	Excimer Laser Technology is developed. Dr. Srinavasan (IBM Laboratories, USA) foresees the potential of the interactions of laser and biological tissue
1983	The use of excimer laser to remove corneal tissue is described by Dr. Stephen Trokel (USA)
1988	The first excimer treatment on a human eye is performed by Dr. Teo Seiler (Germany)
1989	The benefits of performing PRK after a flap was removed were theorized and experimented by Dr. Pallikaris (Greece) and Lucio Buratto (Italy)
1991	The first LASIK procedure is performed by Dr. Stephen Brint in the United States
1995	FDA approves excimer laser for refractive surgery (PRK) to correct myopia
1999	First excimer lasers approved to perform LASIK surgery
1999	LASEK (a surface ablation procedure in which the epithelium is removed with alcohol) is introduced by Dr. Massimo Camellin (Italy)
2000	FDA approves LASIK surgery for hyperopia
2002	Wavefront-guided LASIK approved for custom correction
2002	Femtosecond laser flap removal approved by FDA
2003	First Epi-LASIK (epithelium mechanically removed) procedures performed by Dr. Pallikaris (Greece)

However, PRK was limited by unpredictability in higher ranges of refractive error and higher risk of corneal haze after surgery. In the 1990s, Pallikaris combined these two techniques (keratomileusis and PRK), creating the laser-assisted *in situ* keratomileusis (LASIK), which has become the most popular refractive surgery technique (see the section titled 'The LASIK procedure'). Today, faster lasers, larger spot areas, bladeless flap creation, intraoperative pachymetry, and wave-front-optimized and wave-front-guided techniques have significantly improved the reliability of the procedure compared to that of 1991. Nonetheless, the fundamental limitations of excimer lasers, the limited corneal thickness (particularly in the presence of the flap), and undesirable destruction of corneal nerves have spawned research into many alternatives to standard LASIK, including laser-assisted subepithelial keratomileusis (LASEK) or Epi-LASIK, which aim at combining the advantages of surface ablations such as PRK with those of LASIK surgery. Although safety and efficacy, and refraction predictability of PRK and LASIK are high, complaints of decreased vision and glare in mesopic and

scotopic light levels, that is, night-vision problems, exist. Haze, halos, and increased optical aberrations are attributed to cause visual degradation, particularly in eyes that had undergone high refraction corrections. Several questions are still open today: proper transfer of the ablation profile to the cornea, wound healing, biological response, corneal biomechanics, microstructural stromal changes, and long-term healing. The implementation of aberrometry in refractive surgery has meant a turning point in the history of laser refractive surgery since – along with other technological advances including improvements in surgical lasers (such as flying spot lasers), ablation algorithms, and eye-tracking – the measurement of ocular wave aberrations has opened the potential for improved refractive surgery, aiming not only at correcting refractive errors but also to minimize optical aberrations of the eye.

The LASIK Procedure

Figure 1 illustrates a LASIK procedure. In this technique, a hinged flap is created by means of a microkeratome, and folded back to leave the stroma exposed. To create the flap, a corneal suction ring is applied to the eye, holding the eye in place. Once the eye is immobilized, the flap is created. This process is achieved with a mechanical microkeratome using a metal blade, or more recently a femtosecond laser microkeratome. A hinge is left at one end of this flap. The flap is folded back, revealing the stroma, the middle section of the cornea. An excimer laser is then used to photoablate the stroma. For treatment of myopia, the central cornea is flattened and experiences a deeper ablation than the periphery. For a hyperopic treatment, the outer area of the optical zone experiences deeper ablation than the central area resulting in a cone-like corneal profile. After the laser has reshaped the stromal layer, the LASIK flap is carefully repositioned over the treatment area by the surgeon and checked for the presence of air bubbles, debris, and proper fit on the eye. The flap remains in position by natural adhesion until healing is completed.

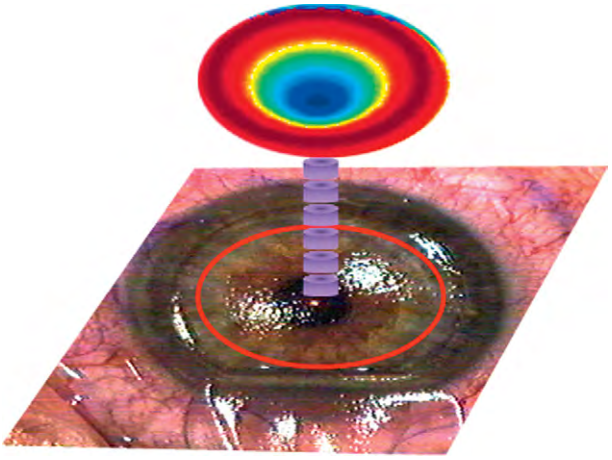

Figure 1 Illustration of a LASIK procedure. A flap is lifted and the exposed stroma ablated with excimer laser pulses according to the programmed ablation profile following which the flap is repositioned.

Corneal Refractive Surgery, Wound Healing, and Haze

The corneal response to laser refractive surgery induces keratocyte apoptosis immediately following the procedure. Proliferation and migration of keratocytes begins within 12–24 h, giving rise to activated keratocytes and myofibroblasts, which are critical components in the wound-healing cascade. Myofibroblasts and newly synthesized extracellular matrix play a major role in haze formation and regression due to stromal remodeling. The timing, intensity, and spatial distribution of wound healing vary significantly between LASIK and PRK. PRK involves injury on a broader area and removal of the epithelium, epithelial basement membrane, Bowman's layer, and a portion of the anterior stroma, while LASIK leaves these structures relatively undisturbed, except at the flap margin. Figure 2 depicts immunohistology microscopic images of excised corneas in an avian model following PRK (5, 15, and 30 days following surgery), showing the distribution of myofibroblasts.

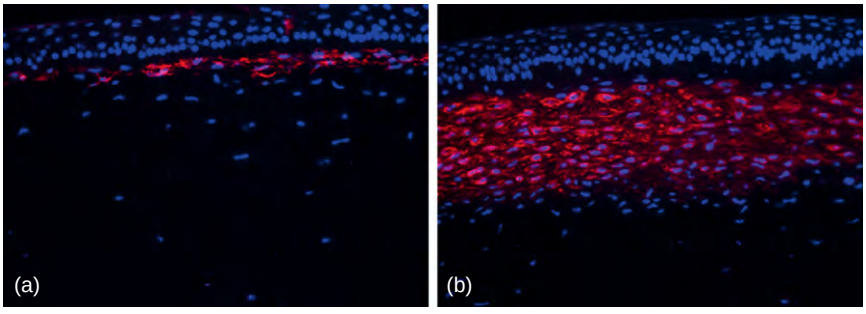

Figure 2 Immunohistology of chicken corneas following PRK, stained for alpha smooth muscle myosin (α-SMA) as a marker for myofibroblasts ((a) 6 days and (b) 30 days). Magnification 200×. From Merayo-Lloves, J., Yañez, B., Mayo, A., Martín, R., and Pastor, J. C. (2001). Experimental model of corneal haze. *Journal of Refractive Surgery* 17: 696–699.

Refractive regression is a major challenge following PRK for myopia, hyperopia, and astigmatism, especially for high levels of correction, and is both more common and more pronounced than the regression following LASIK. The source of regression is attributed to differential changes in the thickness of the cornea due to a combination of stromal remodeling and epithelial hyperplasia. The intensity of the corneal response is related to the magnitude of attempted treatment.

Corneal Refractive Surgery, Optical Aberrations, and Visual Quality

One of the most important side effects of standard refractive surgery is the induction of higher-order aberrations. Early studies based on corneal topography showed that while defocus or astigmatism are generally successfully corrected, refractive surgery (RK, PRK, and LASIK) increased the amount of corneal aberrations. In addition, the distribution of aberrations changed from the third-order dominance found in normal subjects, to fourth-order dominance. This increase in corneal aberrations correlates well with the decrease found in contrast sensitivity. Seiler and colleagues, in standard myopic PRK (15 eyes, mean preoperative spherical error = −4.8 D), and Moreno–Barriuso and colleagues, in standard myopic LASIK (22 eyes, mean preoperative spherical error = −6.5 D), measured, for the first time, the changes in the total aberration pattern induced by either type of surgery. Both studies found a significant increase in third- and higher-order aberrations (by a factor of 4.2 and 1.9 in the root mean square (RMS), respectively). The larger increase occurred for spherical and third-order aberrations. The changes of total spherical aberrations are not fully accounted by changes in the anterior corneal surface. In all eyes, total spherical aberration increased slightly less than corneal aberrations, likely due to significant changes in the posterior corneal shape (shifting toward more negative values of spherical aberration). The increase in the total spherical aberration is highly correlated to the amount of spherical error corrected, and it is associated with an increase in corneal asphericity.

Changes of corneal and total aberrations with LASIK surgery for hyperopia are even higher than those for LASIK surgery for myopia. While spherical aberration becomes more positive following myopic LASIK, it shifts toward negative values following hyperopic LASIK. For the same absolute amount of correction, the absolute increase of corneal spherical aberration is larger with hyperopic LASIK. **Figure 3** shows wave pre- and postoperative high-order aberration patterns in patients that had undergone myopic LASIK and hyperopic LASIK. **Figure 4** compares the induced aberration (total and corneal) following myopic and hyperopic LASIK, respectively.

Modulation-transfer functions (MTFs) can be computed from the measured wave aberrations, and the optical changes can be compared to the visual changes (measured in terms of contrast-sensitivity function (CSF)). Marcos and colleagues found that the decrease in the MTF (between 3 and 18 cycles per degree (c/deg)) was 1.38 – similar to the decrease in the CSF, by a factor of 1.51 (in the same spatial frequency range) – on average in a group of 22 eyes that had undergone LASIK surgery for myopia. This indicates that the increase in optical aberrations plays a major role in the decrease of visual quality following LASIK. **Figure 5** shows pre- and postoperative MTF and CSF, for 3-mm pupils, and the pre/post contrast ratio as a function of spatial frequency.

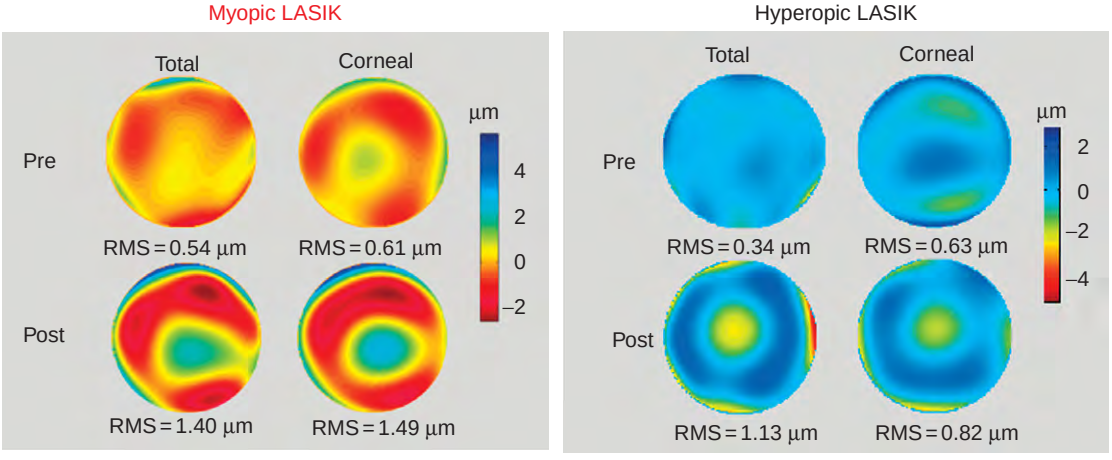

Figure 3 Examples of corneal and total wave aberrations (third- and higher-order aberrations) before and after LASIK surgery for myopia (left panel) and hyperopia (right panel). The increase in aberrations is indicated by the increased RMS. Following surgery, the total aberration map is dominated by the corneal contribution, primarily by positive spherical aberration following myopic LASIK and by negative spherical aberration following hyperopic LASIK. From Marcos, S., Barbero, B., Llorente, L., and Merayo-Lloves, J. (2001). Optical response to LASIK for myopia from total and corneal aberrations. *Investigative Ophthalmology and Visual Science* 42: 3349–3356.

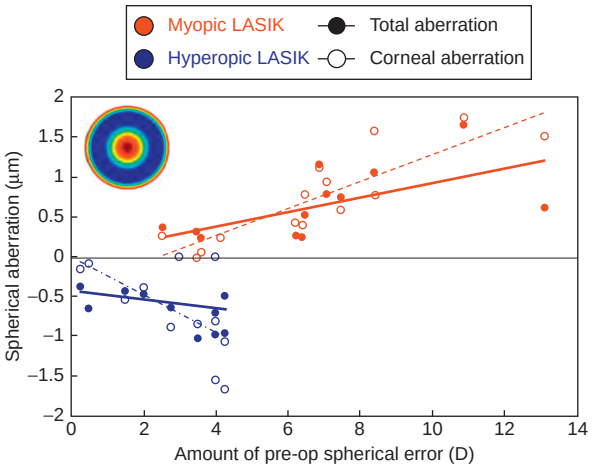

Figure 4 Induced spherical aberration vs. spherical correction (positive for hyperopia and negative for myopia). Corneal spherical aberration increases at a rate of 0.17 μm D^{-1} in myopic LASIK and –0.23 μm D^{-1} in hyperopic LASIK. Total spherical aberration increases at a rate of 0.09 μm D^{-1} in myopic LASIK and –0.06 μm D^{-1} in hyperopic LASIK. The inset depicts the fourth-order spherical-aberration Zernike term. From Llorente, L., Barbero, B., Merayo, J., and Marcos, S. (2004). Changes in corneal and total aberrations induced by LASIK surgery for hyperopia. *Journal of Refractive Surgery* 20: 203–216.

Causes for Spherical Aberration Increase Following Corneal Refractive Surgery

The causes for the increase of spherical aberration (and corneal asphericity) are still not well understood. Computer simulations of the postoperative corneal shape following subtraction of the standard ablation pattern (Munnerlyn equation) performed on real preoperative corneal elevation maps do not show the increased corneal asphericity found clinically. A parabolic approximation of this equation induces a slight increase of corneal asphericity, but much less than is found experimentally. It is likely that much of the discrepancy is due to the fact that the energy is not properly transferred onto the cornea, due to changes in laser efficiency across the corneal surface. Several authors have derived theoretical expressions (based on the Beer–Lambert law and Fresnel equations) to account for the laser-energy losses from the center to the periphery of the cornea. **Figure 6** depicts average results on 13 patients of postoperative corneal asphericities following computer simulation of the Munnerlyn ablation pattern (and its parabolic approximation), directly or considering laser-efficiency changes across the cornea (based on the equations proposed by Jiménez and colleagues), in

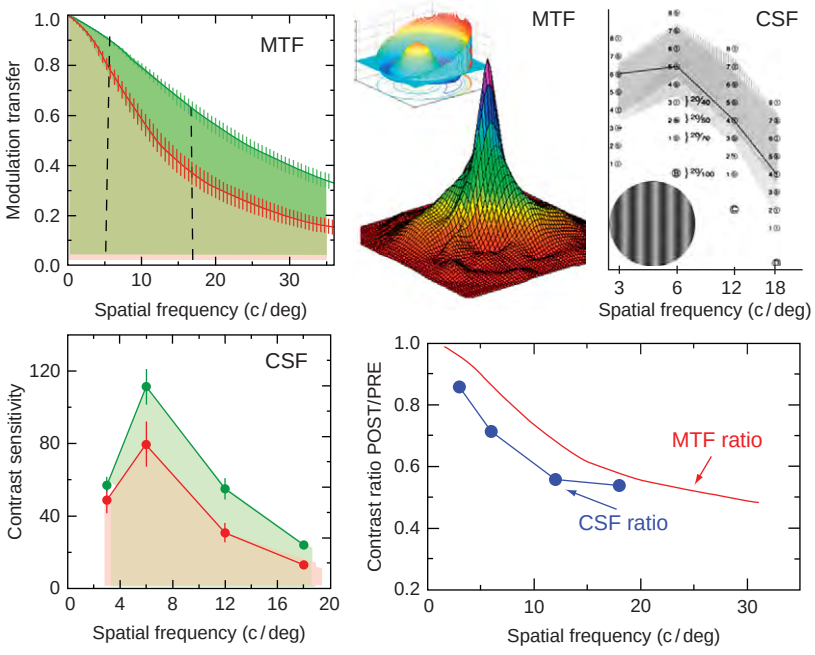

Figure 5 Illustration of the estimation of the MTF from the measured wave aberration, and of the measured CSF, using a clinical gold standard (CVS1000, Vectorvision), in the upper-right panel. Average preoperative MTF (in green) and postoperative MTF (in red), horizontal sections, in the upper-left panel. Average preoperative CSF (in green) and postoperative MTF (in red) for vertical gratings, in the lower-left panel. The area under the curve (shaded in green and red, respectively) between 3 and 18 c/deg was used as a metric for optical quality. The ratio of the area under the MTF decreased by a factor of 1.38, and under the CSF by a factor of 1.51 – indicating that the optical changes have a similar visual impact. The lower-right panel shows the ratio of the MTF and the CSF post/pre as a function of spatial frequency. The drop in contrast follows the same trend for both the MTF and the CSF. Data are average of 22 eyes that had undergone refractive surgery for myopia (between –2.5 and –13 D spherical correction), for undilated pupils. Marcos, S. (2001). Aberrations and visual performance following standard laser vision correction. *Journal of Refractive Surgery* 17: 596–601.

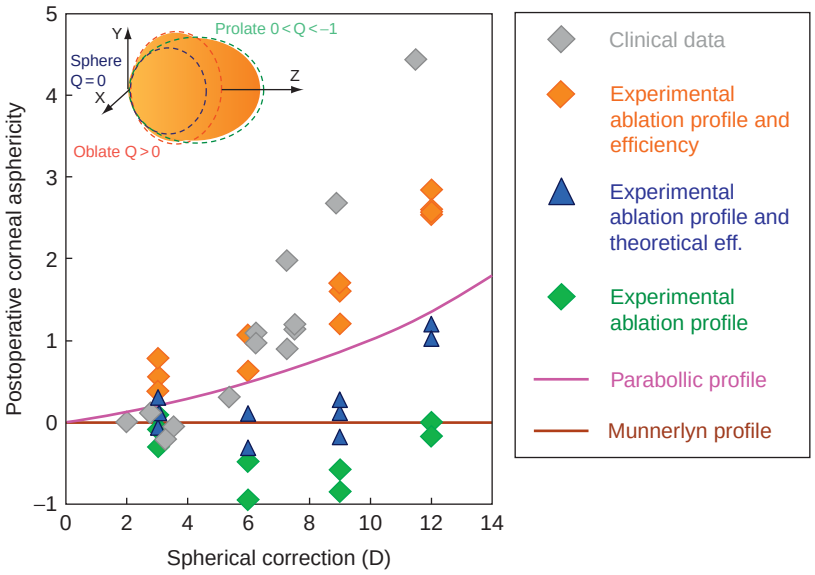

Figure 6 Postoperative corneal asphericity following LASIK surgery for myopia as a function of preoperative spherical error. The graph shows experimental postoperative data from patients – estimations from a virtual surgery using the experimental ablation profile measured on PMMA flat surfaces (and a conversion factor from PMMA to cornea) and an experimentally measured laser-efficiency factor (which takes into account the energy loss from the center to the periphery), estimations from a virtual surgery using the experimental ablation profile and a theoretical laser-efficiency factor, estimations from the experimental ablation profile, the Munnerlyn profile, and its parabolic approximation without considering laser-efficiency losses. From Cano, D., Barbero, B., and Marcos, S. (2004). Comparison of real and computer-simulated outcomes of LASIK refractive surgery. *Journal of the Optical Society of America A* 21: 926–936. and Dorronsoro, C., Cano, D., Merayo, J., and Marcos, S. (2006). Experiments on PMMA models to predict the impact of corneal refractive surgery on corneal shape. *Optics Express* 14: 6142–6156.

comparison with average preoperative asphericities and real postoperative asphericities in the same eyes.

An interesting approach to the understanding of the induction of spherical aberration is the ablation of plastic spherical surfaces, which are subject to geometrical effects but not biomechanical response. Ablation of poly(methyl methacrylate) (PMMA)-model eyes produces an increase in spherical aberration, similar to the increase found in real corneas. In addition, a comparison of the ablation profile of flat and spherical surfaces allows direct estimation of the laser-efficiency losses on PMMA, which can be extrapolated to corneal tissue, without relying on the exact knowledge of the ablation profile programmed into the laser system, and without the approximation of the theoretical approaches. Figure 6 shows estimated postoperative corneal asphericities following direct subtraction of the ablation profile obtained experimentally from profilometry of flat plastic surfaces and also considering the experimental efficiency factor.

Corneal Biomechanical Effects in Refractive Surgery

Although not fully understood, it seems clear that the biomechanical properties of the cornea change following refractive surgery. RK relied fully on the mechanical relaxation of the cornea following incisions. During PRK, LASIK, or any other procedure involving central ablation, corneal lamellae are severed. In a simple elastic shell model, if considered alone, this would result in corneal steepening. However, it has been suggested that a lamellar tension relaxation in the peripheral stroma occurs which produces a compression of the anterior cornea and central flattening. The elastic modulus of the residual stromal bed and the corneal shear strength likely change following surgery, as the cohesive forces among lamellae, stromal swelling pressure, are affected by the procedure. These effects have a potential relevance in the pathogenesis of ectasia, characterized by a progressive thinning and a progressive central and inferior steepening of the cornea, affecting 0.3% of the LASIK patients, although a careful identification of patients with preexisting corneal pathology (keratoconus) and reducing the risk of mechanical instability by leaving a minimal residual stromal thickness (of 300 μm or more) has proved to reduce the occurrence of corneal ectasia greatly. The change in the dynamical response of the cornea, inherent to its biomechanical properties, also affects the measurement of intraocular pressure with standard tonometers, which assume normalized values of corneal elasticity.

Other Side Effects and Complications of PRK and LASIK

Apart from the indicated increased aberrations (resulting in halos and ghost images), haze and loss of best-corrected

contrast sensitivity, other potential complications may occur during or following surgery. The most common side effect from refractive surgery is dry eye (occurring in 36% of patients), diffuse lamellar keratitis (2.3%), flap complications including slipped flap, debris or growth under flap and flap striae (0.244%), infection (0.4%), epithelial ingrowth (0.1%), glare, and light sensitivity.

Safety, Efficacy, and Satisfaction of LASIK

An average of 700 000 patients in the US undergo LASIK annually. To date, more than 28.3 million LASIK procedures have been performed worldwide. Collectively, 7830 patients (representing 16 502 eyes) participated in clinical trials from 1993 to 2005. In April 2008, the Food and Drug Administration (FDA) reaffirmed the safety and efficacy of the LASIK procedure. Although the number of patient complaints has increased in the last few years, the postoperative visual outcomes have improved in the most recent studies. In FDA studies recruiting patients that had undergone surgery prior to 2000, 1.4% of patients lost two lines or more of best spectacle-corrected visual acuity (BSCVA) versus 0.6% in studies after 2000. Prior to 2000, 1.68% of patients with a preoperative BSCVA 20/20 or higher had a postoperative BSCVA 20/25 or higher, compared with 0.16% after 2000. The surveys determining patient satisfaction with LASIK have found most patients satisfied, with satisfaction ranging between 92% and 98%. A meta-analysis – dated March 2008, performed by the American Society of Cataract and Refractive Surgery over 3000 peer-reviewed articles published over the past 10 years in clinical journals from around the world, including 19 studies comprising 2200 patients – that looked directly at satisfaction, revealed a 95.4% patient satisfaction rate among LASIK patients worldwide.

Toward an Optimization of the Corneal Refractive Surgery Procedure

Recent technological advances in refractive surgery include high-frequency eye-tracking, improved laser-delivery systems, and flap creation by femtosecond lasers. The availability of clinical aberrometers, and flying spot technology, led to the development of wave-front-guided ablation profiles – aiming not only at correcting defocus and astigmatism, but also the eye's high-order aberrations. However, major efforts must still focus on preventing the induction of high-order aberrations (particularly spherical aberration) by the procedure, particularly as these are not necessarily

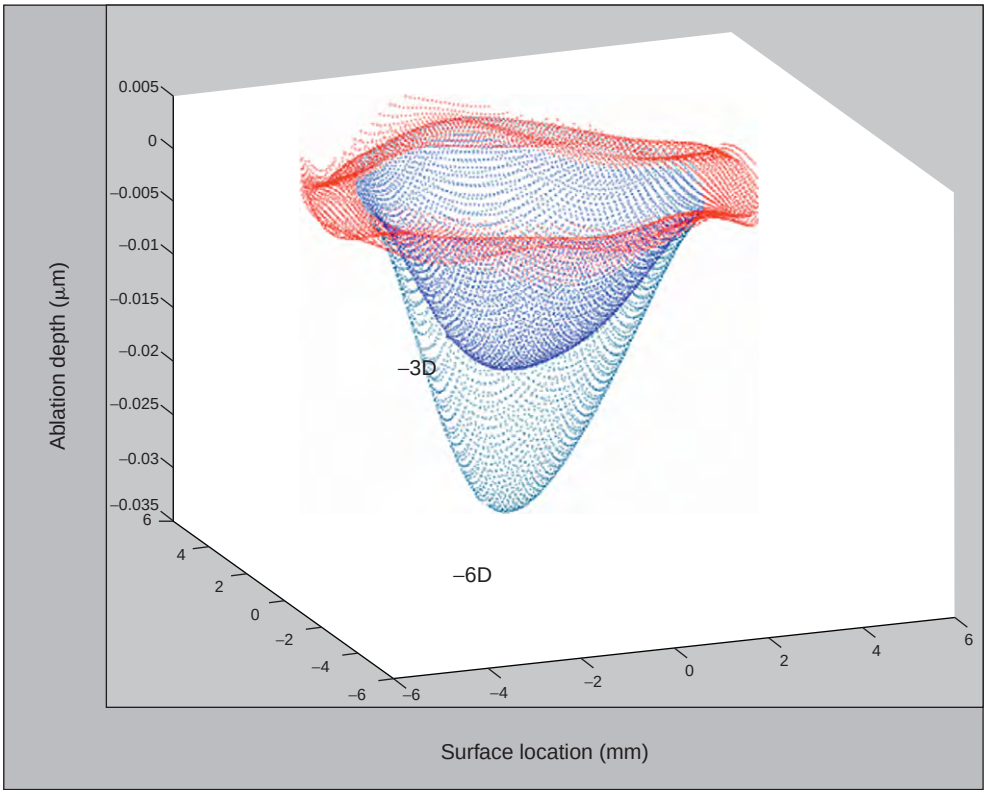

Figure 7 Ablation profiles –6 and –3 D spherical corrections measured experimentally by subtraction of pre- and postablation corneal topographies of PMMA corneal models. From Dorronsoro, C., Cano, D., Merayo, J., and Marcos, S. (2006). Experiments on PMMA models to predict the impact of corneal refractive surgery on corneal shape. *Optics Express* 14: 6142–6156.

inherent to ablation algorithm (despite its simplicity, the standard Munnerlyn algorithm does not induce spherical aberration). Approaches range from theoretical correction of the ablation profile to empirical adjustment of the attempted corneal asphericity. Undoubtedly, a proper characterization of the ablation algorithm, and a calibration of the ablation pattern created by the laser is critical to achieve the desired postoperative corneal shape. Plastic models (in PMMA, and, more recently, a semi-rigid contact lens material – Filofocon A) have been proposed as calibration models for refractive surgery, and their ablation properties have been thoroughly studied. **Figure 7** shows an example of the ablation profile recorded on a plastic material and measured using noncontact profilometry. To date, empirical adjustments of the ablation normogram have – based on population average data – compensated for deviations from ametropia systematically found following surgery. However, customized corrections require a deeper knowledge of ablation, physical effects of the role of corneal hydration, and of the contribution of corneal biomechanical effects and their inter-individual variations on the refractive and high-order aberration outcomes. A fine control of the ablation profile and the biomechanical response will likely expand the range of applications of refractive surgery into presbyopic treatments. As an emerging technology, corneal collagen cross-linking is starting to be applied following refractive surgery as a way to control corneal ectasia by increasing corneal stiffness.

Other technologies further in the track include solide-state ultraviolet (UV) lasers and femtosecond lasers. Diode-pumbed UV laser, using a solide-state laser crystal as the laser medium and nonlinear crystals for frequency conversion instead of the high-voltage gas discharge of excimer lasers, are a safer, more stable, compact, and less expensive alternative to gas-operated excimer lasers. On the other hand, femtosecond lasers use ultrashort pulses (as opposed to pulse durations in the range of nanosecond or picosecond in excimer lasers) which allow laser–tissue interactions characterized by significantly smaller and more deterministic photodisruptive energy thresholds, as well as reduced shock waves and smaller cavitation bubbles, which result in smoother surface quality. Lamellar procedures (keratomileusis) as well as lenticule removal are envisaged with this procedure.

See also: Corneal Nerves: Anatomy; Cornea Overview; Hyperopia; Myopia; Refractive Surgery and Inlays.

Further Reading

Applegate, R. A., Hilmantel, G., and Howland, H. C. (1996). Corneal aberrations increase with the magnitude of radial keratotomy refractive correction. *Optometry and Vision Science* 73(9): 585–589.

Applegate, R. A. and Howland, H. C. (1997). Refractive surgery, optical aberrations, and visual perfomance. *Journal of Refractive Surgery* 13: 295–299.

Buratto, L. and Brint, S. F. (eds.) (2003). *Custom LASIK: Surgical Techniques and Commplications.* Thorofare, NJ: Slack.

Cano, D., Barbero, B., and Marcos, S. (2004). Comparison of real and computer-simulated outcomes of LASIK refractive surgery. *Journal of the Optical Society of America A* 21: 926–936.

Dorronsoro, C., Cano, D., Merayo, J., and Marcos, S. (2006). Experiments on PMMA models to predict the impact of corneal refractive surgery on corneal shape. *Optics Express* 14: 6142–6156.

Dorronsoro, C., Siegel, J., Remon, L., and Marcos, S. (2008). Suitability of Filofocon A and PMMA for experimental models in excimer laser ablation refractive surgery. *Optics Express* 16: 20955–20967.

Dupps, W. and Wilson, S. (2006). Biomechanics and wound healing in the cornea. *Experimental Eye Research* 83: 709–720.

Jiménez, J., Anera, R., Jiménez del Barco, L., and Hita, E. (2002). Effect on laser-ablation algorithms of reflection losses and nonnormal incidence on the anterior cornea. *Applied Physics Letters* 81(8): 1521–1523.

Krueger, R., Applegate, R. A., and MacRae, S. (eds.) (2004). *Wavefront Customized Visual Correction: The Quest for Super Vision II.* Thorofare, NJ: Slack.

Llorente, L., Barbero, B., Merayo, J., and Marcos, S. (2004). Changes in corneal and total aberrations induced by LASIK surgery for hyperopia. *Journal of Refractive Surgery* 20: 203–216.

Marcos, S. (2001). Aberrations and visual performance following standard laser vision correction. *Journal of Refractive Surgery* 17: 596–601.

Marcos, S., Barbero, B., Llorente, L., and Merayo-Lloves, J. (2001). Optical response to LASIK for myopia from total and corneal aberrations. *Investigative Ophthalmology and Visual Science* 42: 3349–3356.

Marcos, S., Cano, D., and Barbero, S. (2003). The increase of corneal asphericity after standard myopic LASIK surgery is not inherent to the Munnerlyn algorithm. *Journal of Refractive Surgery* 19: 592–596.

Merayo-Lloves, J., Yañez, B., Mayo, A., Martín, R., and Pastor, J. C. (2001). Experimental model of corneal haze. *Journal of Refractive Surgery* 17: 696–699.

Moreno-Barriuso, E., Merayo-Lloves, J., Marcos, S., et al. (2001). Ocular aberrations before and after myopic corneal refractive surgery: LASIK-induced changes measured with laser ray tracing. *Investigative Ophthalmology and Visual Science* 42: 1396–1403.

Mrochen, M., Krueger, R., Bueeler, M., and Seiler, T. (2002). Aberration-sensing and wavefront-guided laser *in situ* keratomileusis: Management of decentered ablation. *Journal of Refractive Surgery* 18: 418–429.

Netto, M. V., Mohan, R. R., Ambrósio, R., Jr., et al. (2005). Wound healing in the cornea: A review of refractive surgery complications and new prospects for therapy. *Cornea* 24: 509–522.

Pallikaris, I. G., Agarwal, S., and Agarwal, A. (2003). *Refractive Surgery.* Thorofare, NJ: Slack.

Seiler, T., Kaemmerer, M., Mierdel, P., and Krinke, H.-E. (2000). Ocular optical aberrations after photorefractive keratectomy for myopia and myopic astigmatism. *Archive of Ophthalmology* 118: 17–21.

Relevant Websites

http://www.geteyesmart.org – American Academy of Ophthalmology and Its Partners.

http://www.ascrs.org – American Society of Cataract and Refractive Surgery (ASCRS).

http://www.escrs.org – European Society of Cataract and Refractive Surgery.

http://www.aao.org/isrs – International Society of Refractive Surgery.

http://www.fda.gov – US Food and Drug Administration.

http://www.vision.csic.es – Visual Optics and Biophotonics Lab, Instituto de Optica, CSIC.

Refractive Surgery and Inlays

R M M A Nuijts, M Doors, N G Tahzib, and L P J Cruysberg, University Hospital Maastricht, Maastricht, The Netherlands

Glossary

Astigmatism – A refractive defect in which vision is blurred due to the inability of the optics of the eye to focus a point object into a sharp, focused image on the retina due to an irregular or toric curvature of the cornea or lens.
Cycloplegic refraction – A measurement of the refractive state of the eye without the effects of accommodation. A cycloplegic drop is used to temporarily paralyze the accommodation muscle.
Corneal ectasia – A serious complication involving a cone-like bulging of the cornea following its weakening during laser *in situ* keratomileusis (LASIK).
Diffuse lamellar keratitis – Noninfectious inflammatory complication of LASIK.
Form fruste keratoconus – An abortive form of bulging of the cornea.
Hyperopia – Refractive defect caused by an eye that is too short or a cornea that is too flat, so that images focus at a point behind the retina. It is also called farsightedness.
Intracorneal ring (IRC) – Small ring inserted into the periphery of the cornea to change its shape and correct nearsightedness.
Laser-assisted subepithelial keratectomy (LASEK) – A refractive surgery where only the corneal epithelia is cut to reshape the cornea.
Laser *in situ* keratomileusis (LASIK) – A refractive surgery where the corneal epithelia and stroma is cut to reshape the cornea.
Manifest – Easily seen.
Myopia – Refractive defect of the eye where the light focuses in front of the retina rather than on the retina. It is also called nearsightedness.
Photorefractive keratectomy (PRK) – A refractive surgery where the corneal epithelia is removed to reshape the cornea.
Presbyopia – Reduced ability to see near objects caused by loss if the elasticity of the lens.
Radial keratotomy (RK) – Surgical procedure to correct myopia where radial incisions are made into the cornea at precise depths allowing the sides of the cornea to bulge out and flatten the central cornea.

Introduction

Corneal refractive surgery offers the patient the possibility of becoming independent of spectacles and/or contact lenses. The attainment of this treatment goal is of particular importance to individuals who are restricted in their professional and social life by their contact lens or spectacle intolerance. The developments and outcomes of various refractive surgery techniques have received increasing attention in the medical literature and public media. This phenomenon is mainly related to the numerous success stories and the dramatic changes achieved by correction of the refractive error and the resultant independence of spectacles and contact lenses.

Numerous corneal refractive surgery techniques are available for the correction of refractive errors, with the majority of treatments consisting of myopic and myopic–astigmatic corrections. The field of refractive surgery has greatly evolved since the commencement of excimer laser treatments and surgical implantations of corneal inlays. The techniques have been refined and are continually evolving to be more specifically directed toward the individual optical design. The optical system can differ greatly between individuals and depends on various factors, such as the amount of the refractive error and the degree of optical aberrations. Therefore, laser-ablation techniques have changed from the standard correction of the refractive error to personalized and optimized laser treatments and from broad-beam to scanning-spot or flying-spot devices.

This article presents an overview of the available corneal refractive procedures and their outcomes.

Radial Keratotomy

Prior to the popularity of excimer photoablative refractive surgery, the technique of radial keratotomy (RK) was among the most widely used surgical techniques for the correction of myopia. RK involves making deep radial incisions in the paracentral and peripheral anterior cornea using a diamond blade knife. The technique results in the flattening of the central corneal curvature and steepening of the peripheral area, which reduces the degree of myopia.

The number of RK incisions, diameter of the optic zone, and patient age determine the refractive outcome after RK. Incision direction was shown to be another predictor, with

the centripetal (vs. the centrifugal) incision decreasing myopia to a higher degree.

Although the treatment by RK initially resulted in satisfactory refractive results, it appeared not to be as predictable as current refractive surgery techniques. The Prospective Evaluation of Radial Keratotomy (PERK) study was a nine-center clinical trial which analyzed the long-term (10-year) effects and stability of myopic RK (with a range of −2.00 to −8.75 diopters (D)). They showed that 53% of eyes achieved an uncorrected visual acuity (UCVA) ≥20/20, and 85% of eyes achieved UCVA of ≥20/40. They also showed that 38% of eyes had a refractive error within ±0.50 D and 60% ± 1.0 D of the intended correction.

A common and challenging side effect of RK was the development of secondary and progressive hyperopia. This hyperopic shift occurred in 43% of reported cases, with an additional incidence of 1–2% annually. A less common side effect following RK is the development of irregular astigmatism, which can be induced by the intersection of the incisions with the visual axis or by the eccentricity of the optical zone. Some other side effects are fluctuating vision and glare.

Apart from treating myopia, RK has also been used for the correction of astigmatism (also known as arcuate keratotomy), although the predictability of this technique is known to be slightly less than that for the correction of myopia. The procedure has been shown to be an effective and safe method for correcting moderate to severe naturally occurring astigmatism.

The popularity of RK has declined since the approval of the excimer laser in 1995, due to the superior outcomes of photorefractive keratectomy (PRK) and LASIK. However, keratotomy techniques (arcuate keratotomy and limbal relaxing incisions) are still used for the treatment of astigmatism in cataract surgery and in postsurgical patients.

Photorefractive Keratectomy

In the early 1990s, PRK was the main treatment for low-to-moderate myopia. This technique went through various developments, varying from laser systems, to treatment algorithms, to the choice of transition and ablation zones. The treatment involves the use of a far-ultraviolet (193-nm) argon fluoride excimer laser, which permanently removes the most anterior portion of the corneal stromal tissue in a very precise manner. The ablation occurs with minimal damage to the adjacent corneal tissue. Prior to the performance of the laser-ablation procedure, the corneal epithelium is removed – either manually with a blade or a rotating brush or after alcohol administration. Afterward, a bandage contact lens is applied on the treated corneal surface.

Short-term problems following PRK include discomfort in the first 24 h; a delay in visual recovery lasting 3–5 days during epithelial healing; and a loss of corneal transparency – also called haze – lasting weeks to months following the procedure. PRK ablations often show an immediate postoperative hyperopic shift, due to a thinner epithelium. The hyperopic shift is often compensated by a period of regression that stabilizes between 1 and 6 months. Refractive stability after PRK is generally achieved after 6 months to 1 year and is maintained for up to a period of 5 years.

Long-term studies on the outcome of PRK found no evidence of progressive time-dependent hyperopic shift or late regression, with trace haze in 4% after 12 years with no loss of best-corrected visual acuity (BCVA). In general, corneal haze was transient and decreases rapidly 1 year after treatment.

Laser *in situ* Keratomileusis

The technique of LASIK was first described in 1991. The surgical technique includes the creation of an epithelial-stromal flap using a microkeratome. The flap is attached to the periphery of the cornea by a hinge of uncut tissue and has a diameter of 8–10 mm. When using the mechanical microkeratome, the thickness of the flap ranges between 130 μm (with the newest microkeratomes) and 180 μm (with the older microkeratomes). Subsequently the flap is peeled back and ablation of the corneal stroma is performed using an excimer laser. Following the photoablation, the flap is repositioned on the treated corneal stroma (**Figure 1**). The introduction of this technique meant a major change in the field of refractive surgery. The side effects associated with PRK made LASIK treatment the leading procedure in refractive surgery. The popularity of LASIK is related to the relatively fast visual recovery time, minimal discomfort immediately following treatment, and the minimal incidence of haze.

For low-to-moderate myopia (less than 6 D), LASIK has proven to be very effective, predictable, and safe – achieving an UCVA of 20/40 or more in 86–100% of eyes and an UCVA of 20/20 in 45–94% of eyes. The technique has shown to achieve a very accurate correction, with 71–96% of eyes achieving a refractive error within ±0.50 D of the intended correction and 88–100% of eyes within ±1.00 D of the intended correction. For moderate-to-high myopia (>−6.0 D), the results show more variation.

Since PRK and LASIK candidates typically have healthy eyes, achieving and maintaining high levels of (subjective) satisfaction after surgery are very important. In 2005, a clinical study showed that the overall patient satisfaction

Figure 1 Schematic LASIK-procedure: first the creation of the flap after which the flap is peeled back, then eximer laser ablation of the corneal stroma, and third repositioning of the flap on the treated corneal stroma.

following LASIK treatment was 4.10 ± 0.71 (a score of 5 meaning that the patient was totally satisfied). Patients are generally very satisfied with their uncorrected vision, visual recovery, and quality of life following LASIK treatment, with the majority of patients reporting that they would have the surgery again (92.3%), if required.

Myopic regression is a condition that can occur after LASIK. The risk of myopic regression increases with the degree of preoperative myopia and patient age. Long-term studies on LASIK for treatment of moderate and extreme myopia showed a trend toward myopic regression, changing from 52–96% of eyes within ±1.0 D of the attempted correction after 1 year to 46–91% after 5–6-years follow-up. In contrast, LASIK studies with lower degrees of preoperative myopia (<−6.0 D) show stable visual results during long-term follow-up.

Although the risks associated with LASIK are considered to be low, intraoperative and postoperative flap-related complications are sight threatening and have resulted in a permanent loss of BCVA. The overall incidence of intraoperative LASIK-flap complications – such as incomplete flaps, buttonholes, free caps, and torn flaps – is approximately 4%. Postoperative flap-related complications include diffuse lamellar keratitis, infection, spontaneously or trauma-related flap displacement, and epithelial ingrowth.

Furthermore, LASIK may cause (transient) dry eyes, which may be related to the neurotrophic effects of cutting the nerves during the creation of the flap. It tends to resolve 6–9 months following LASIK treatment, as the nerves grow back into the flap.

Despite the aim of many surgeons to keep the residual corneal thickness of the stromal bed at least 250 μm, postoperative corneal ectasia (dilation) may occur following LASIK treatment. This rare, but important, complication seems to be related to biomechanical changes in the cornea after treatment and occurs at rates much lower than 1%. Risk factors that might contribute to the development of ectasia following LASIK have been suggested to be: high intraocular pressure, irregular topography, thin corneas, thin remaining corneal beds, forme fruste keratoconus, thick corneal flaps, large optical zones, and, possibly, high myopia.

Laser-Assisted Subepithelial Keratectomy

LASEK aims to preserve the original anatomy of the cornea and to avoid potential risks posed by the creation of a LASIK flap. The treatment is, in fact, a blend of PRK and LASIK, aiming to decrease the potential complications of the two treatments. In LASEK treatment, diluted ethanol solution is applied to loosen the corneal epithelium, following which the epithelium is partially removed from Bowman's layer, leaving it connected only at a hinge. Laser treatment is applied directly to Bowman's layer, and afterwards the epithelial sheet is placed back over the treated stroma. The eye is covered by a bandage contact lens to prevent movement of the epithelial flap due to blinking and eye movements.

LASEK does not have the risk of flap-related complications such as with LASIK, because LASEK can easily be converted to the PRK procedure if the epithelial flap tears or breaks. Furthermore, a larger residual bed is created – which retains the cornea's biomechanical strength and reduces the risk of corneal ectasia associated with LASIK. One of the main therapeutic advantages of LASEK is that it can be performed in cases in which LASIK may be contraindicated. These include eyes with thin, steep, and flat corneas; epithelial basement-membrane dystrophy; large pupils (requiring wider and, therefore, deeper ablations); higher myopia; and deep-set eyes or tight orbits.

Reports have shown that LASEK is a safe, effective, and predictable treatment, which can be seen as a good alternative to LASIK and PRK for the surgical correction of myopia. A major review of the literature showed that 95% of eyes achieved an UCVA ≥ 20/40 and 74% ≥20/20. Seventy-four percent of eyes achieved a refraction within ±0.5 D of the desired refraction and 90% of eyes were within ±1.0 D of the desired refraction. Loss of two or more lines of BCVA was demonstrated in 2% of eyes.

Comparing LASEK with PRK and LASIK, it has been indicated that the recovery period following LASEK is shorter than that following PRK, but might be somewhat slower than that following LASIK. Discomfort following LASEK seems to be less than after PRK, which is probably

related to the fact that the epithelial flap acts as a biological therapeutic lens that protects the ablated stroma. However, other studies have demonstrated that the epithelial flap is probably not viable, is replaced by regenerated epithelial cells, and, as such, does not provide advantages in comparison to PRK.

The biological properties of the epithelium might inhibit haze formation following the LASEK treatment. Furthermore, the procedure can be combined with the use of mitomycin-C (MMC) – a cytostatic drug known to inhibit proliferating cells and can be used to prevent postablation corneal haze in high-risk cases, such as in patients requiring retreatment.

Epithelial Laser *in situ* Keratomileusis (epi-LASIK)

Epi-LASIK uses a modified microkeratome (epikeratome) to create a thin corneal epithelial flap before surface ablation is performed. The blade and the angle of cutting of the epikeratome are optimized for a subepithelial dissection, which does not disrupt the corneal stroma such as the LASIK microkeratome. The difference between epi-LASIK and LASEK is that the separation of the epithelium is obtained mechanically without the use of alcohol. Epi-LASIK has been proposed as a safe alternative to LASIK and is especially suitable for patients with low-to-moderate myopia and myopic astigmatism, thin corneas, and in individuals with steeper or flatter corneas, where the cutting of a LASIK flap could potentially impose flap-related complications. The healing period and visual recovery tends to be slower than traditional LASIK. Postoperative discomfort usually occurs within the first 48 h after surgery.

A recent study presented the 1-year results of epi-LASIK and stated that this technique is a safe and efficient method for the correction of low and moderate myopia, demonstrating that all of the eyes treated reached an UCVA of 20/40 or better and 86% an UCVA of 20/20 or better. More than 80% of eyes were within 0.5 D of the attempted correction and 97% were within 1 D of the attempted correction.

In comparison with LASEK, it has been suggested that the incidence of haze following ablation of the cornea is lower with epi-LASIK. Longer-term clinical studies are needed to confirm the reported results on epi-LASIK.

Femtosecond Laser *in situ* Keratomileusis (FS-LASIK)

At the beginning of this century the femtosecond laser, which creates a corneal flap by vaporizing small volumes of tissue using micro-photodisruption at a predetermined depth, was introduced. Furthermore, when using the femtosecond laser, the flap thickness is much more accurate and thinner (between 90 and 110 μm) than with the excimer laser. The corneal flaps can also be customized with a variable flap thickness and diameter based on the requirements of the patient.

The greatest benefit of these thinner femtosecond-created flaps is that they result in a greater stability of the cornea when compared to mechanically created flaps. It has been described that the greatest strength of the cornea lies within the first 150 μm of the cornea. Thus, thinner flaps will help to protect the integrity of the cornea and will lead to thicker residual stromal beds, which results in a decreased risk of corneal ectasia. Studies have shown that flaps created with a femtosecond laser provide better visual results than flaps created with a microkeratome. Furthermore, FS-LASIK demonstrates better visual outcomes than PRK in the first 6 months of follow-up. Following this period, both treatments show similar visual results. As for epi-LASIK, long-term follow-up studies are required to demonstrate the efficacy and safety of FS-LASIK.

Potential limitations of the femtosecond laser include increased costs of the procedure, increased surgical time, and a higher incidence of diffuse lamellar keratitis. The use of topical corticosteroids keeps the last complication at manageable levels. Furthermore, the newer high-frequency femtosecond lasers will probably diminish the incidence of diffuse lamellar keratitis.

Treatment of Hyperopia

Photorefractive keratectomy, LASIK, and LASEK can also be applied for the treatment of low hyperopia (<2 D). In hyperopic treatments, most of the laser ablation is located at the periphery of the treatment zone. Mechanical weakening of the peripheral cornea might lead to a forward-bowing of the central cornea, which increases the intended laser effect. These biomechanical changes and a different wound healing cause increased levels of regression following the hyperopic treatment. Therefore, only low levels of hyperopia can be treated using laser refractive surgery.

The Food and Drug Administration (FDA)-approved studies investigating the treatment of low hyperopia using LASIK showed that 90% of eyes achieved a UCVA $\geq$ 20/40 and only 63% a UCVA $\geq$ 20/20. Sixty-seven percent of eyes achieved a refraction within $\pm$0.5 D of the desired refraction and 90% of eyes were within $\pm$1.0 D of the desired refraction. Loss of two or more lines of BCVA was demonstrated in almost 2% of eyes after more than 3 months of follow-up. Hyperopic PRK and LASEK treatments show similar clinical results when compared to hyperopic LASIK treatments.

General Side Effects of Laser Refractive Surgery

Although many developments in keratorefractive surgical techniques have improved the clinical outcome and have shown great success rates, several quality-of-vision problems have been reported. Qualitative visual disturbances can affect patients' daily activities and include subjective complaints such as glare, halos, and difficulty with night driving. These complaints are more likely to occur with laser corrections of more than 7–8 D of myopia or more than 2–3 D of hyperopia and often diminish after the first six postoperative months. Glare, halos, and night-vision complaints may be attributed to a loss of contrast sensitivity or low-contrast visual acuity. These complaints have been described after all refractive surgery techniques, varying in degrees of incidence.

Reports on patient satisfaction following LASIK treatment showed that predictors for night-vision complaints can include:

- preoperative high levels of myopia (more than 5 D),
- advanced age,
- a flatter preoperative corneal curvature,
- surgical enhancements,
- optical zones <6 mm,
- postoperative residual refractive error >0.5 D from emmetropia (normal refraction), and
- postoperative residual cylinder – a type of higher-order aberration (HOA) of the cornea.

Remarkably, pupil size was not shown to be a significant predictor of night-vision complaints in any of these studies. There is variable evidence in the literature on excluding patients based on large pupil size. It has been suggested in the past that a large pupil, in combination with a small optical zone, is a dominant factor leading to increased night-vision complaints. However, other recent studies demonstrate that the correlation between pupil size and night-vision complaints or between night-vision complaints and the pupil–optical zone disparity is much less critical than previously thought. Pupil size seems to indeed be a significant predictor of glare and halos following LASIK, especially in the first postoperative month, yet it was demonstrated that pupil size is not a significant variable 6 or 12 months following treatment. Postoperative remodeling of the corneal shape by the epithelium may be responsible for these findings.

Other common complications of laser refractive surgery include under- and overcorrection (30%), irregular astigmatism (30%), and dry eyes (4–30%, depending on the type of refractive treatment).

Wave front and Laser Refractive Surgery

When applying conventional laser refractive surgery, the ablations are calculated using the data obtained during manifest and cycloplegic refractions. However, HOAs can cause glare and halos and lead to decreased quality of vision. Wave front technology was developed to categorize and limit the amount of HOA induced by refractive surgery. The wave front sensor measures defocus, astigmatism, and total and individual HOA. Customized wave front-guided corneal ablation combines wave front sensing and wave front correction and, therefore, corrects refractive errors beyond spherical and cylindrical errors.

Over the last decade, several clinical reports have studied HOAs in refractive surgery patients. Some of these studies have shown an increase in patient satisfaction, reduced night-vision complaints, and a lower increase of HOA following wave front-guided treatments, compared to conventional ablation; however, more and larger randomized studies are needed to further analyze and validate the results of these treatments. At the present time, it is not clear whether the excellent results are due to an improved postoperative asphericity profile or the consequence of treating the preexistent HOAs.

Corneal Inlays

The use of corneal inlays as a refractive procedure involves the insertion of a synthetic or biological material into the cornea, which changes the refractive power of the eye by either altering the anterior corneal curvature, or the refractive index of the inlay material, or a combination of these two mechanisms. These inlays can be placed in the stroma or beneath the epithelium of the cornea. The main advantage of this technique over the above-mentioned laser refractive treatments is the reversibility of the procedure.

The inlay material has to meet various physical and biological characteristics in order to minimize complications. Biological materials have shown to be biodegradable and insufficiently permeable to maintain a healthy cornea. Furthermore, hydrogel inlays have been demonstrated to be biocompatible but have insufficient porosity to maintain optimal nutrient flow. Many complications, including corneal haze, epithelial thinning, inlay encapsulation, epithelial opacification, corneal vascularisation, inlay decentration, and fibrosis, have been reported following the implantation of corneal inlays.

At present, a phase 1 trial is being conducted using a synthetic corneal inlay made of a polymer of perfluoropolyether, which is placed into the stroma following the creation of a corneal flap with a microkeratome. The study involves implantation of the inlays in unsighted eyes. Despite the experimental phase of these synthetic inlays, it is believed that they might meet all the required physical and biological characteristics which will help minimize the above-mentioned complications.

Corneal inlays have been developed not only to correct myopia and hyperopia, but also to correct presbyopia.

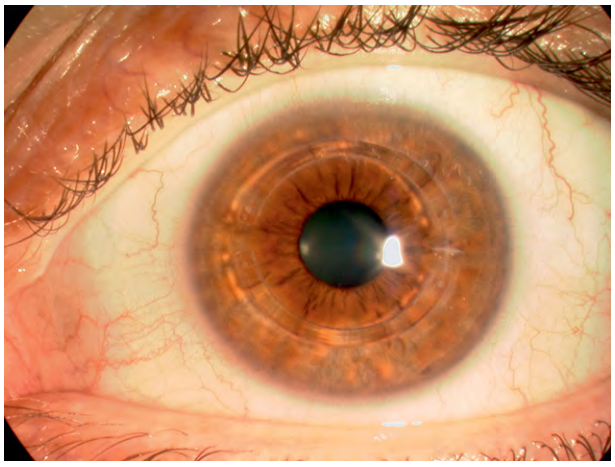

Figure 2 Patient with two intracorneal ring segments (Intacs).

These presbyopic inlays are designed to be implanted in the nondominant eye and have a pinhole optic, which increases the depth of focus. They are currently under investigation in the United States and Europe.

Intracorneal Rings (ICR)

Since 1999 the use of ICR segments, also known as Intacs, has been approved by the United States FDA for the correction of low myopia (less than 4 D) and low astigmatism ($\leq$1 D). These ring segments are curved and made of polymethylmethacrylate. They can be inserted into the peripheral cornea through corneal channels, which are created by a microkeratome or by a femtosecond laser, at about 70% of the corneal depth (**Figure 2**). They aim to expand and flatten the corneal surface.

ICR have some important advantages over laser refractive surgery: there is no abrasion of the cornea, less risk of corneal haze or scarring, the visual axis is spared from treatment, there is no flap creation and, therefore, no flap-related complications, and the procedure is reversible.

Complications following ICR implantation include induced astigmatism – which is the most common complication – extrusion of the ring, dry eye syndrome, and infectious keratitis.

In the treatment of low myopia, the visual results of ICRs seem to be similar to the results following laser refractive surgery. However, ICRs are mainly used to improve visual outcomes in patients with keratoconus, post-LASIK ectasia, or other ectatic disorders.

Conclusion

In conclusion, for the treatment of patients with low-to-moderate myopia, PRK, LASIK, and LASEK have all shown to produce stable and predictable results with an excellent safety profile. Patient selection is crucial to ensure high postoperative patient satisfaction and to diminish the risks of adverse effects. LASIK has the advantage of rapid visual recovery and minimal discomfort and, therefore, has become the most widely performed refractive surgery technique, associated with high patient satisfaction. However, mechanical microkeratome-assisted LASIK displays more complications due to the creation of a flap and might cause more induced HOAs, which is why some surgeons have switched to PRK or LASEK. In the near future, FS-LASIK might become the recommended treatment, but a longer follow-up is needed to ensure long-term stability and safety.

See also: Cornea Overview; Hyperopia; Myopia; Refractive Surgery; The Surgical Treatment for Corneal Epithelial Stem Cell Deficiency, Corneal Epithelial Defect, and Peripheral Corneal Ulcer.

Further Reading

Alio, J. L., Muftuoglu, O., Ortiz, D., et al. (2008). Ten-year follow-up of laser *in situ* keratomileusis for myopia of up to –10 diopters. *American Journal of Ophthalmology* 145: 46–54.

Choi, D. M., Thompson, R. W., and Price, F. W. (2002). Incisional refractive surgery. *Current Opinion in Ophthalmology* 13: 237–241.

Fan-Paul, N. I., Li, J., Miller, J. S., and Florakis, G. J. (2002). Night vision disturbances after corneal refractive surgery. *Survey of Ophthalmology* 47: 533–546.

Guell, J. L. (2005). Are intracorneal rings still useful in refractive surgery? *Current Opinion in Ophthalmology* 16: 260–265.

Katsanevaki, V. J., Kalyvianaki, M. I., Kavroulaki, D. S., and Pallikaris, I. G. (2007). One-year clinical results after epi-lasik for myopia. *Ophthalmology* 114: 1111–1117.

Nuijts, R. M., Nabar, V. A., Hament, W. J., and Eggink, F. A. (2002). Wavefront-guided versus standard laser *in situ* keratomileusis to correct low to moderate myopia. *Journal of Cataract and Refractive Surgery* 28: 1907–1913.

Pop, M. and Payette, Y. (2004). Risk factors for night vision complaints after LASIK for myopia. *Ophthalmology* 111: 3–10.

Rajan, M. S., Jaycock, P., O'Brart, D., Nystrom, H. H., and Marshall, J. (2004). A long-term study of photorefractive keratectomy; 12-year follow-up. *Ophthalmology* 111: 1813–1824.

Sakimoto, T., Rosenblatt, M. I., and Azar, D. T. (2006). Laser eye surgery for refractive errors. *Lancet* 367: 1432–1447.

Slade, S. G. (2008). Thin-flap laser-assisted *in situ* keratomileusis. *Current Opinion in Ophthalmology* 19: 325–329.

Sugar, A., Rapuano, C. J., Culbertson, W. W., et al. (2002). Laser *in situ* keratomileusis for myopia and astigmatism: Safety and efficacy: A report by the American Academy of Ophthalmology. *Ophthalmology* 109: 175–187.

Sweeney, D. F., Vannas, A., Hughes, T. C., et al. (2008). Synthetic corneal inlays. *Clinical and Experimental Optometry* 91: 56–66.

Tahzib, N. G., Bootsma, S. J., Eggink, F. A., Nabar, V. A., and Nuijts, R. M. (2005). Functional outcomes and patient satisfaction after laser *in situ* keratomileusis for correction of myopia. *Journal of Cataract and Refractive Surgery* 31: 1943–1951.

Taneri, S., Zieske, J. D., and Azar, D. T. (2004). Evolution, techniques, clinical outcomes, and pathophysiology of LASEK: Review of the literature. *Survey of Ophthalmology* 49: 576–602.

Waring, G. O., Lynn, M. J., and McDonnell, P. J. (1994). Results of the prospective evaluation of radial keratotomy (PERK) study 10 years after surgery. *Archives of Ophthalmology* 112: 1298–1308.

Relevant Website

http://www.intacsforkeratoconus.com – Intacs Corneal Implants.

Regulation of Corneal Endothelial Cell Proliferation

Q Lu, T A Fuchsluger, and U V Jurkunas, Schepens Eye Research Institute, Boston, MA, USA

Glossary

Cell cycle – Series of events that occur in order for a cell to divide. This cycle is divided into phases where the G0 (gap 0) is resting or quiescent phase; G1 (gap 1) is the synthesis of enzymes necessary for DNA replication; S phase is when DNA synthesis occurs; G2 (gap 2) phase involves the production of microtubules; M phase is the division of the cell into daughter cells.
Corneal dystrophies – Conditions in which the cornea is altered without the presence of any inflammation, infection, or other eye disease.
Cyclins and cyclin-dependent kinases (CDKs) – Cyclins act as the regulatory subunits while CDKs act as the catalytic subunits of an activated heterodimer. Neither cyclins nor CDKs are active in the absence of one another. CDKs are constitutively expressed in cells, whereas cyclins are synthesized at specific stages of the cell cycle, in response to various molecular signals.
Descemet's membrane – A specialized form of extracellular matrix separating corneal endothelial cells from corneal stroma.
E2F – A group of genes that encodes a family of transcription factors.
Epidermal growth factor (EGF) – Compound that promotes cell growth and differentiation.
Mitogen – A chemical substance that induces cell division.
Retinoblastoma gene – A gene whose protein is dysfunctional in many types of cancer.
Tight junction – A junction between two cells composed of the junctional membrane. This acts as a selective barrier to small molecules and as a total barrier to large molecules.
Transforming growth factor (TGF) – Used as a polypeptide growth factors, TGF is produced in many cell types and is involved in cellular development.

Background

Mammalian corneal endothelial cells (CECs) are derived from neural crest cells of mesenchyme and form a monolayer in the inner portion of the cornea (**Figure 1**). The corneal endothelium is attached to the Descemet's membrane (DM) and is in direct contact with the aqueous humor. Its main function is to maintain corneal transparency by regulating corneal hydration. CECs contain numerous Na^+–K^+-adenosine triphosphatases (ATPases) that pump fluid out of the stroma to counteract the corneal tendency to swell. In addition, tight junctions between the CECs provide a barrier that prevents the influx of fluid from aqueous humor into the stroma. CEC number gradually declines with age (**Figure 2**). Since CECs do not proliferate *in vivo* and have a limited ability to regenerate, the loss of endothelial cells is permanent. Certain corneal pathologies, such as dystrophies, infections, and trauma, can lead to an accelerated loss of CECs and a compromise in the endothelial cell layer integrity. As a result, the cornea is unable to maintain its water balance and corneal edema ensues, clinically resulting loss of clarity and a decline in visual acuity.

Cell Cycle Progression, G1/S Transition and its Cell Cycle Regulators

Mammalian cell cycles can be divided into four phases, including G1 phase (gap phase 1), S phase (DNA synthesis), G2 phase (gap phase 2), and M phase (mitosis). The entire process of cell cycle progression is controlled by a variety of regulatory proteins (**Figure 3**). Among them, cyclin-dependent kinases (CDKs) are the engine cores that promote cell cycle progression. CDKs generally remain at a constant level throughout the cell cycle, while their binding partners, cyclins, and post-translational modifiers, kinases and phosphatases, undergo periodic fluctuations throughout the cell cycle. During this process, negative regulatory protein cyclin-dependent kinase inhibitors (CDKIs) also play an important role in cell cycle progression.

During the G1/S transition (**Figure 3**), CDKs 2, 4, 6 and their regulators control the cell transition to the S-phase. Association of CDK4 or CDK6 with D-type cyclins (Cyc D) is critical for G1 phase progression, whereas the association of CDK2 and cyclin E (Cyc E) fosters the initiation of the S phase. Both complexes, Cyc D–CDK4/6 and Cyc E–CDK2, are involved in phosphorylation of retinoblastoma gene (Rb) and a subsequent G1/S transition. During this process, two main families of CDKIs play an important role in regulating G1/S transition: inhibitor of CDK (INK) and CDK-interacting protein/cyclin-dependent kinase inhibitory protein (CIP/KIP). The INK protein, p16, is a

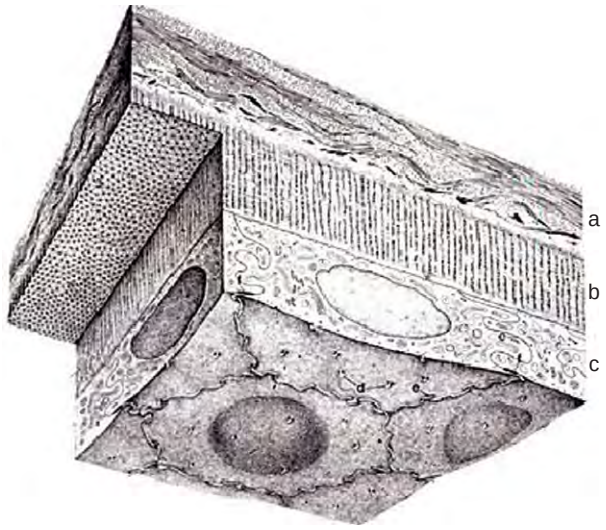

Figure 1 Ultrastructure of a human cornea: (a) epithelium, (b) stroma, and (c) endothelium.

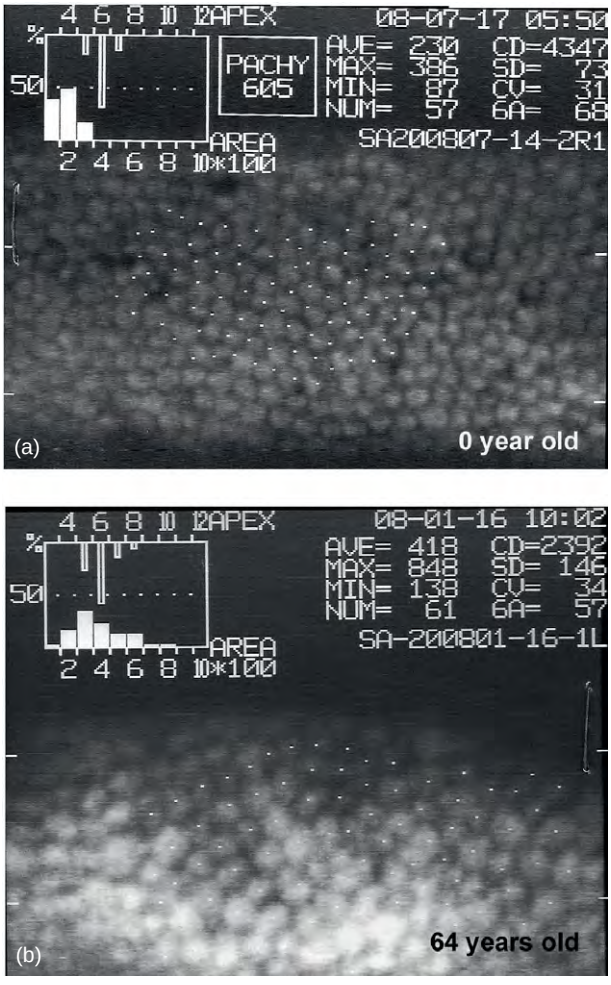

Figure 2 Physiological loss of human corneas endothelial cells: (a) in a newborn (cell density (CD) = 4347 cells mm^{-2}) and (b) in a 60-year-old normal eye (CD = 2392 cells mm^{-2}).

competitive inhibitor of CDK4/6-Cyc D complex, while the CIP/KIP proteins, p21 and p27, serve as competitive inhibitors of CDK2–Cyc E complex. The G1/S phase transition features two consecutive steps: (1) Early G1 progression involves mitogen-dependent accumulation of cyclin D, sequestration of p21, and cyclin D-dependent phosphorylation of retinoblastoma gene (Rb) (2) Late G1 progression depends on phosphorylation and degradation of p27 and additional phosphorylation of Rb by Cyc E/CDK2. Full phosphorylation of Rb leads to its dissociation from E2F and ultimately activation of E2F, which is a main transcription factor involved in the G1/S transition (**Figure 3**).

G1 Phase Cell Cycle Arrest in CECs *in vivo*

Human corneal endothelial cells (HCECs) do not divide *in vivo* sufficiently to replenish lost cells due to aging, trauma, or disease. HCECs exhibit no positive staining with Ki67, a marker of actively cycling cells. However, HCECs exhibit *in situ* staining with the key cycle cell regulators, such as cyclins D, E, and A. Such staining pattern which is similar to the one seen in limbal epithelium known to contain slow-cycling stem cells, points to the fact that CECs are arrested in the G1 phase rather than having permanently exited from the cell cycle. Possible mechanisms accounting for such G1 phase cell cycle arrest are contact inhibition, interaction with the extracellular matrix (ECM), and presence of transforming growth factor (TGF)-β2 in the aqueous humor (**Figure 4**).

Cell–Cell Contact Inhibition

Contact-dependent inhibition of cell proliferation is a well described phenomenon. In corneal endothelium, majority of studies on cell–cell contact inhibition have been performed in neonatal rats, since rats have an immature corneal endothelium at birth, unlike the other species. In neonatal rats, the number of CECs staining positively for bromo-deoxyuridine (BrdU), an S-phase marker, gradually decreased between postnatal days 1 and 13. After postnatal day 13, positive BrdU staining was no longer detectable. Stable cell–cell and cell–substrate contacts gradually formed, and monolayer maturation was complete between postnatal days 14 and 21. These studies showed a correlation between decreased proliferation and increased monolayer formation, underlying the importance of cell–cell contact inhibition in the maturation of endothelial monolayer.

Consistent with these findings, treatment of corneal endothelial monolayer with ethylenediaminetetraacetate (EDTA), a calcium chelator which releases cells from

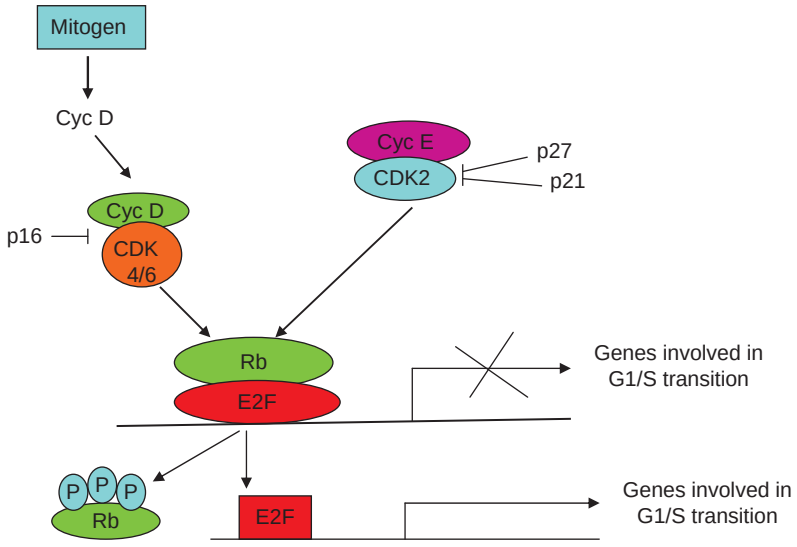

Figure 3 Cell cycle regulators involved in G1/S transition.

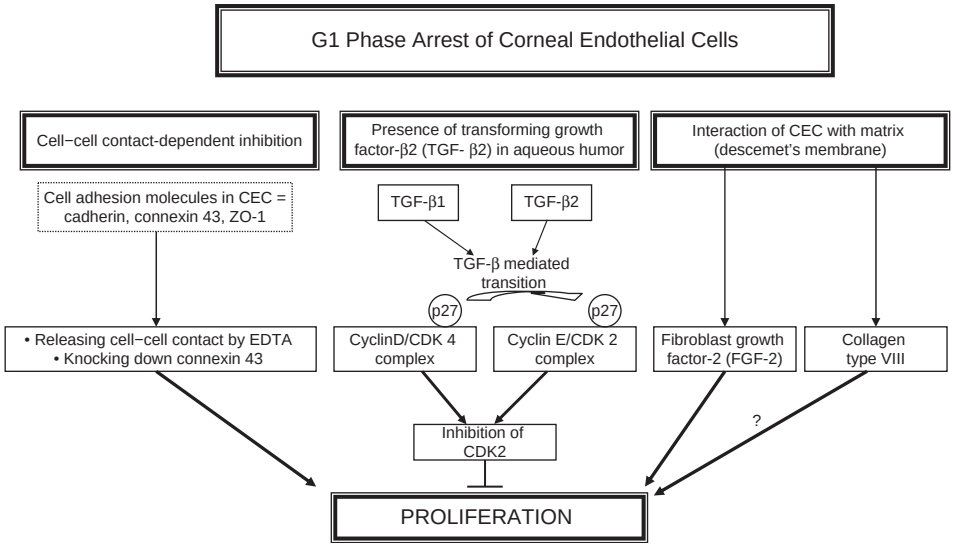

Figure 4 Possible mechanisms involved in G1 phase cell cycle arrest of corneal endothelial cells.

cell–cell contact, has been shown to promote cell proliferation. CEC proliferation can be regulated by calcium levels due to the presence of several cell adhesion proteins that are calcium sensitive and maintain cells in the state of contact inhibition. The main cell adhesion molecules involved in CEC physiology are cadherins, zonula occludens, and connexins (Cx). Exposure of CECs to calcium-free medium resulted in loosening of apical junctions, loss of barrier function, and corneal edema. This effect was reversible by exposing the endothelial cells to calcium. The attempts to break these intercellular interactions have been successful in promoting endothelial cell proliferation, and providing promise to regenerating CEC in traumatic and degenerative situations. These findings indicate that cell–cell contact inhibition may play an important role in the growth arrest status of CECs.

It was demonstrated that knocking down one of the major connexins, Cx43 resulted in a significant increase in the number of actively proliferating CECs. Using the rat model, corneal endothelial scrape injuries were simultaneously applied with Cx43 antisense oligodeoxynucleotide, small interfering RNA, or adenovirus (CMV–Cx43–mRFP1) into the anterior chamber. Changes in Cx43 expression were analyzed by immunolabeling (ZO-1, alpha-smooth muscle actin (SMA), Cx43). While, the endothelial–mesenchymal transition/transformation

after injury was inhibited, Cx43 knock-down induced proliferation of the corneal endothelium.

DNA-binding transcription factors, including the members of the BTB/POZ-zinc finger protein family, might be involved in the signaling pathway of cell–cell contact-induced growth inhibition as well. Among the family members, the promyelocytic leukemia zinc finger protein (PLZF) gene specifically inhibits the transcription of genes involved in G1/S transition, such as cyclin A2 and c-myc. The expression of PLZF is closely related with cell–cell contact. Its expression is high in confluent cells, and treatment with EDTA to disrupt cell–cell contact decreases PLZF messenger RNA (mRNA) levels. Similarly, overexpression of PLZF has been found to inhibit cell proliferation. N-Cadherin is thought to be a potential upstream signaling molecule that regulates PLZF mRNA levels.

Studies showed that p27, a CDKI-type protein, is also involved in the mediation of cell cycle arrest induced by cell–cell contact. Increased expression of p27 in the developing corneal endothelium is well correlated with the cessation of the proliferation in wild-type mice. On the other hand, p27 knock-out mice show prolonged postnatal period of CEC proliferation when compared with their wild-type counterparts. These data indicate that p27 plays an important role in contact-inhibition-mediated growth arrested in CEC.

The Presence of Antiproliferative TGF-β2 in the Aqueous Humor

In many cell types, TGF-β2 inhibits proliferation by inducing G1-phase arrest. CECs are in direct contact with aqueous humor containing TGF-β2. Both exogenous TGF-β2 and active TGF-β2 in rat aqueous humor inhibit S-phase entry in rat CECs. The effect of TGF-β2 may be mediated by CDK4 and p27. In CECs treated with TGF-β2, CDK4 synthesis is inhibited and p27 is mobilized from the cyclin D-CDK 4 complex into the cyclin E-CDK 2 complex to inhibit CDK 2 activity. Furthermore, TGF-β2 prevents phosphorylation of p27 and maintains p27 in an active form.

The Interaction Between CECs and Extracellular Matrix

ECM provides an important microenvironment for cell adhesion, migration, growth, differentiation, and signal transduction. DM is a specialized form of ECM separating CECs from corneal stroma. One difference between infant and adult human corneal DM is that collagen VIII, the major component of DM, shifted from the endothelial face of DM in infant to the stromal side of the DM in the adult. It is not fully understood whether compositional differences of collagen VIII are responsible for the differences in CECs growth potential from young and adult humans. In a mouse model, the complete lack of type VIII collagen leads to dysgenesis (abnormal development) of the anterior ocular segment and enlarged CECs with reduced cell density. Hence, collagen VIII may serve as an important component of matrix that stimulates CEC growth during embryonic development. It is possible that adult DM has structural differences that foster endothelial growth arrest, associated with adult corneas. Proteomic analysis revealed that there is an age-related increase in TGFβ-induced protein content and proteolytic processing of the human corneal endothelium and DM complex.

What Do We Know From Primary and Subcultured CECs

Human and other mammalian CECs can be isolated and subcultured *in vitro*, indicating that endothelium still retains some replicative capacity. Such studies may provide better understanding of the regulatory mechanisms involved in CECs proliferation. Age-related decrease in sensitivity to mitogen or growth factors has been observed in cultured HCECs. It is still controversial whether the corneal periphery has more replicative capacity compared to central region. E2F is a key transcription factor involved in the G1/S transition of CECs, and overexpression of one of its isoforms E2F2 has been shown to promote proliferation. Various upstream signals including protein kinase C (PKC) and fibroblast growth factor (FGF)-2 might also play an important role in the proliferation of cultured CECs.

Age-Related Decrease in Sensitivity to Mitogen or Growth Factors in Cultured HCECs

Donor age negatively affects the proliferative capacity of cultured HCEC. In cultured HCEC a decrease in proliferative capacity is accompanied by changes in morphology and cell density. CECs cultured from older donors show an increase in cell size and a decrease in overall cell density. Different expression levels of cell cycle regulators were studied in cultured HCEC from younger and older donors. Increased expression of CDKIs such as p21 and p16 were seen in HCEC from older donors when compared with those from younger donors. On the other hand, transfection of p27 siRNA was sufficient to promote proliferation in confluent cultures of HCECs from younger (<30 years old), but not from older donors (>60 years old). This suggests that inhibition of proliferation in older donors is regulated by other mechanisms in addition to p27. It is known that an age-dependent increase in expression of negative cell cycle regulators p21 and p16 might be among those mechanisms.

Protein tyrosine phosphatase (PTP) plays a negative role in regulating epidermal growth factor (EGF) signaling pathway. PTP1B is a widely expressed nonreceptor PTP originally identified in placentas. It downregulates the EGF signaling pathway by dephosphorylating epidermal growth factor receptor (EGFR) and inhibition of PTB1B promotes S phase entry. Increased PTP1B activity was detected in HCECs from older donors and reduced proliferative activity in response to EGF in those cells is partly due to increased PTP1B activity.

Comparison of Proliferative Capacity of HCECs from Central and Peripheral Regions

It is still controversial whether the peripheral endothelium has more potential for cell division than the central endothelium. p53 is a negative cell cycle regulator; it inhibits cell division primarily through a p21 pathway. It was found that p53 and its family member TAp63 are highly expressed in central rather than in peripheral endothelium, supporting that there is a greater potential for cell proliferation in the peripheral. However, studies by other group have shown that HCECs cultured from both the central and peripheral areas are capable of cell division in response to serum and their proliferation rates are same.

Overexpression of E2F2 Promotes Proliferation of CEC

E2F family proteins are key transcription factors for genes involved in the cell cycle progression. Three isoforms of this family (E2F1, E2F2, and E2F3) play an important role in G1/S transition. Overexpression of E2F2 promotes cell proliferation in rabbit CECs by increasing the proliferation marker ki67 and cylin B (G2 phase cell cycle regulator).

PKC Signaling Pathways in Regulating Proliferation of CECs

PKC comprises a family of serine/threonine protein kinases, which play an important role in regulating proliferation in many cell types. Several PKC isoforms, including PKC-alpha, -betaII, -delta, -epsilon, -iota, -eta, -gamma, and –theta, were detected in CECs. PKC activity, in particular PKC-alpha and -epsilon activity, is important in promoting CEC proliferation. Inhibition of PKC activity prohibits G1/S-phase progression and reduces cyclin E protein levels in cultured rat CECs.

FGF-2 Signaling Pathway

FGF-2 is a component of DM. As a member of the FGF family, it is a multifunctional regulator of cell development, differentiation, regeneration, senescence, proliferation, and migration. The biological actions of FGF-2 are mediated through transmembrane cell surface receptors that possess tyrosine kinase activity. There are four isoforms of FGF-2. Only the 24-kDa nuclear FGF-2 isoform induced by corneal endothelium modulation factor (CEMF) may be involved in cell proliferation. Phospholipase C gamma (PLC-gamma) or phosphoinositide 3-kinases (PI3 kinase) serve as a downstream signaling pathway in FGF-2-mediated proliferation of rabbit CEC proliferation. Both PLC-gamma and PI3 kinase may utilize Cdk4 and p27 while exerting the mitogenic signal.

Summary

Understanding of the regulatory mechanisms involved in CEC proliferation is important in the context of regenerative medicine. Since corneal endothelium does not divide *in vivo*, manipulation of the factors involved in this cell cycle can be used to expand endothelium for regenerative purposes. Such developments would bring a great promise to the development of the treatment strategies for both exogenous and endogenous corneal endotheliopathies, hopefully bypassing the need for allogeneic corneal transplantation.

See also: Corneal Endothelium: Overview; Regulation of Corneal Endothelial Function.

Further Reading

Bednarz, J., Teifel, M., Friedl, P., and Engelmann, K. (2000). Immortalization of human corneal endothelial cells using electroporation protocol optimized for human corneal endothelial and human retinal pigment epithelial cells. *Acta Ohthalmologica Scandinavica* 78: 130–136.

Coqueret, O. (2002). Linking cyclins to transcriptional control. *Gene* 299: 35–55.

Enomoto, K., Mimura, T., Harris, D. L., and Joyce, N. C. (2006). Age differences in cyclin-dependent kinase inhibitor expression and Rb hyperphosphorylation in human corneal endothelial cells. *Investigative Ophthalmology and Visual Science* 47: 4330–4340.

Harris, D. L. and Joyce, N. C. (2007). Protein tyrosine phosphatase, PTP1B, expression and activity in rat corneal endothelial cells. *Molecular Vision* 13: 785–796.

He, Y., Weng, J., Li, Q., Knauf, H. P., and Wilson, S. E. (1997). Fuchs' corneal endothelial cells transduced with the human papilloma virus E6/E7 oncogenes. *Experimental Eye Research* 65: 135–142.

Hopfer, U., Fukai, N., Hopfer, H., et al. (2005). Targeted disruption of Col8a1 and Col8a2 genes in mice leads to anterior segment abnormalities in the eye. *FASEB Journal* 19: 1232–1244.

Joko, T., Nanba, D., Shiba, F., et al. (2007). Effects of promyelocytic leukemia zinc finger protein on the proliferation of cultured human corneal endothelial cells. *Molecular Vision* 13: 649–658.

Joyce, N. C. (2003). Proliferative capacity of the corneal endothelium. *Progress in Retinal and Eye Research* 22: 359–389.

Joyce, N. C., Harris, D. L., and Zieske, J. D. (1998). Mitotic inhibition of corneal endothelium in neonatal rats. *Investigative Ophthalmology and Visual Science* 39: 2572–2583.

Jurkunas, U. V., Bitar, M. S., and Rawe, I. M. (2009). Co-localization of increased transforming growth factor beta induced protein (TGFBIp) and clusterin expression in guttae of Fuchs endothelial corneal dystrophy patients. *Investigative Ophthalmology and Visual Science* 50(3): 1129–1136.

Kabosova, A., Azar, D. T., Bannikov, G. A., et al. (2006). p27kip1 siRNA induces proliferation in corneal endothelial cells from young but not older donors. *Investigative Ophthalmology and Visual Science* 47: 4803–4809.

Konomi, K., Zhu, C., Harris, D., and Joyce, N. C. (2005). Comparison of the proliferative capacity of human corneal endothelial cells from the central and peripheral areas. *Investigative Ophthalmology and Visual Science* 46: 4086–4091.

McAlister, J. C., Joyce, N. C., Harris, D. L., Ali, R. R., and Larkin, D. F. (2005). Induction of replication in human corneal endothelial cells by E2F2 transcription factor cDNA transfer. *Investigative Ophthalmology and Visual Science* 46: 3597–3603.

Nakano, Y., Oyamada, M., Dai, P., et al. (2008). Connexin43 knockdown accelerates wound healing but inhibits mesenchymal transition after corneal endothelial injury *in vivo*. *Investigative Ophthalmology and Visual Science* 49: 93–104.

Paull, A. C. and Whikehart, D. R. (2005). Expression of the p53 family of proteins in central and peripheral human corneal endothelial cells. *Molecular Vision* 11: 328–334.

Sasaki, T., Sorokin, L. M., Steiner-Champliaud, M. F., et al. (2007). Compositional differences between infant and adult human corneal basement membranes. *Investigative Ophthalmology and Visual Science* 48: 4989–4999.

Yoshida, K., Kase, S., Nakayama, K., et al. (2004). Involvement of p27KIP1 in the proliferation of the developing corneal endothelium. *Investigative Ophthalmology and Visual Science* 45: 2163–2167.

Zhu, C. and Joyce, N. C. (2004). Proliferative response of corneal endothelial cells from young and older donors. *Investigative Ophthalmology and Visual Science* 45: 1743–1751.

Regulation of Corneal Endothelial Function

J A Bonanno and S P Srinivas, Indiana University, Bloomington, IN, USA

Glossary

Aquaporins – The water channels that facilitate water movement across the plasma membrane.
Deturgescence – The removal of water from the cornea stroma to counteract edema.
Guttata – Excresances of Descemet's membrane (basement membrane of the corneal endothelium) produced by abnormal endothelial cells.
Peri-junctional actomyosin ring (PAMR) – A Dense band of actin cytoskeleton found proximal to the apical junction complex.
Pump-leak mechanism – The maintenance of corneal deturgescence in which endothelial active fluid transport (the pump) exactly counters the passive leak directed into the stroma.
Tight junctions – The intercellular junctions at the apical domain of endothelial cells which occlude the paracellular space.
Transendothelial electrical resistance (TER) – Dependent on the integrity of the tight junctions.

Corneal Endothelial Function

Stromal Swelling Pressure and Maintenance of Transparency

The transparency of the cornea stroma is dependent on the tissue hydration. The stroma is composed of 200 or more lamellae, 2-μm thick with widths varying from 10 to 250 μm that span from limbus to limbus and overlap each other at varying orientations. The total thickness of the human stroma varies from 450 to 550 μm. Each lamella is composed of parallel strands of collagen (type I) and associated glycosaminoglycans (GAGs). Between the layers of overlapping lamellae are the keratocytes – a very flat, stellate-shaped cell that is responsible for producing collagen and GAGs and maintaining the stromal structure. The GAGs act as spacers between the collagen fibers. At normal stromal hydration, this space is ~30 nm and is very uniform. Because the refractive index of collagen and the GAGs ground substance are significantly different, a random orientation of collagen fibers and varying fiber diameter (which is characteristic of the sclera) would produce an opaque tissue. However, because there is almost no variation in fiber diameter and the spacing between fibers is uniform, light scattered off-axis through the stroma is <10%. GAGs, however, are very hydrophilic and exert a swelling pressure leading to imbibition of water across the relatively leaky endothelium at the posterior surface. Thus, if a bare piece of stroma is placed in saline, it will swell to many times the normal thickness. This stromal edema produces large variations in collagen-fiber spacing and consequentially increased light scatter, corneal haze, and *in vivo* produces diminished visual acuity. Loss of endothelial cells from surgical trauma or disease, for example, Fuchs' endothelial dystrophy, results in corneal edema. These observations together with *in vitro* physiological studies indicate that the maintenance of stromal hydration is primarily dependent on the corneal endothelium.

The pioneering work of David Maurice first showed that the corneal endothelium actively pumps water from stroma to anterior chamber. This pump exactly counterbalances the leak into the stroma, which is driven by the GAG-dependent swelling pressure. Therefore, the stromal hydration is maintained relatively constant and stromal transparency is preserved. This is often called the Pump–Leak hypothesis for maintenance of corneal hydration and is illustrated in Figure 1.

Endothelial Barrier Function

The tight junctions (TJs) of the corneal endothelium, although leaky (trans-endothelial resistance (TER) ~ 25 Ω cm^{-2}), restrain fluid leak into the stroma. This constitutes the barrier function of the endothelium, and complements fluid-pump function in the regulation of stromal hydration. Despite the leakiness of the endothelium, breakdown of its TJs in the absence of an increase in fluid-pump activity results in corneal edema. In addition to this direct effect, edema could be enhanced further by the fact that TJs also influence the fluid pump function through two indirect mechanisms. First, intact TJs prevent dissipation of local osmotic gradients across the endothelium set up by ion-transport mechanisms by restraining solute back-flux through the paracellular space (i.e., gate function of TJs). Secondly, intact TJs are indispensable for the maintenance of apical-basal polarity of the ion-transport proteins. This is achieved by limiting their lateral diffusion of the membrane proteins (i.e., fence function of TJs). When the polarity of the transport mechanisms is compromised, a vectorial ionic movement and hence fluid transport cannot occur. Thus, the TJs of the endothelium not only restrain fluid leak into the stroma, but also form a principal determinant of the endothelial fluid-pump activity (Figure 2).

Nutrition/Waste Removal

One requirement for corneal transparency is the absence of blood and blood vessels. As such, corneal nutrition must come from the tears, the limbus, and/or the anterior chamber. The stratified squamous epithelium is a very tight barrier, and there are no transporters for nutrients such as glucose. However, the epithelium is permeable to hydrophobic nutrients such as oxygen and wastes, for example, carbon dioxide (CO_2). Because of the long diffusion distances from the limbus, its contribution to overall corneal nutrition is minimal. Therefore, most of the nutrition and removal of wastes – for example, lactic acid – occurs across the endothelium. The corneal endothelium expresses glucose transporters to facilitate uptake into the stroma to nourish keratocytes and the corneal epithelium. Similarly, the endothelium expresses lactic acid transporters to remove this end product of anaerobic glycolysis. Approximately 85% of the glucose consumed by the cornea goes through anaerobic glycolysis because of the relative paucity of mitochondria in the epithelial cells and keratocytes. The relative lack of mitochondria is presumably another strategy to minimize light scatter and enhance transparency.

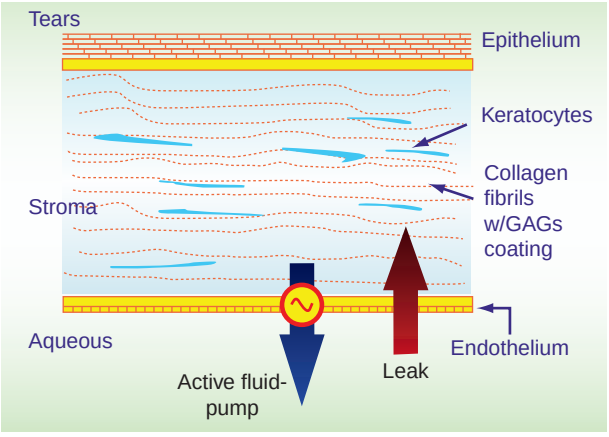

Figure 1 Pump–Leak hypothesis for maintenance of corneal hydration. Stromal glycosaminoglycans (GAGs) are negatively charged hydrophilic molecules that exert a swelling pressure that draws water across the limiting layers (epithelium and endothelium). This is the tissue leak. The endothelial pump must exactly counterbalance the leak so that stromal hydration and transparency are maintained.

Corneal Endothelial Transport

Active Transport

Following discovery that the endothelium was responsible for maintaining stromal hydration, it was shown that the endothelial pump was dependent on active transport. In contrast to corneal epithelial cells and keratocytes, endothelial cells have a very high mitochondrial density. Poisoning the mitochondria reduces the pump activity indicating that it is dependent on the availability of adenosine triphosphate (ATP). Furthermore, exposure of endothelium to the cardiac glycoside ouabain – which blocks the membrane Na^+,K^+-ATPase – also inhibits the pump activity. The Na^+,K^+-ATPase provides the ion gradients across cell membranes that drive secondary transporters, for example, Na^+:K^+:$2Cl^-$ cotransport, Na^+/H^+ exchange, and $Na^+ : 2HCO_3^-$ cotransport, and anion channels that may participate in ion-coupled fluid secretion. A classic fluid-transport mechanism might include basolateral cotransporters and apical anion channels providing a pathway for vectorial ion fluxes that could be osmotically coupled to water transport.

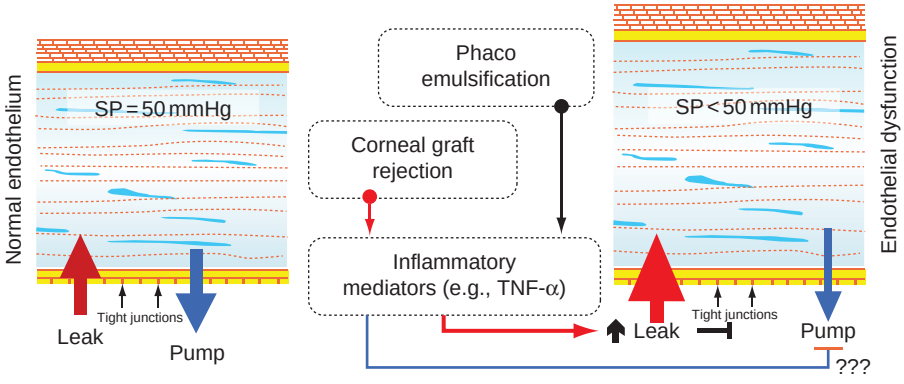

Figure 2 Barrier integrity is essential for stromal hydration control: Fluid leak into the stroma through the paracellular space – determined by the barrier integrity – is driven by a hydraulic gradient equivalent to swelling pressure (SP) of ~ 50 mmHg at normal stromal hydration. Despite the leaky nature of the endothelium (TER < 25 Ω cm^2), stromal thickness is held constant by the fluid-pump mechanism, which counterbalances the fluid leak. When the barrier integrity breaks down, the pump mechanism cannot cope with the leak and hence stromal edema becomes inevitable. Inflammatory stress – which can reduce the barrier integrity – is not known to stimulate the pump function concomitantly. In fact, when the tight junctions are compromised, the fluid-pump mechanism cannot be sustained since the local osmotic gradients generated by ion transport are dissipated by futile solute back-flux.

Bicarbonate/Carbonic Anhydrase

Early studies have shown that the endothelial pump is significantly inhibited in the absence of bicarbonate suggesting that bicarbonate transporters and anion channels may be components of the endothelial pump. A role for bicarbonate was strengthened when it was found that carbonic anhydrase inhibitors (CAIs) – applied directly to the endothelium – also slowed the pump. With the advent of topical carbonic anhydrase inhibitors to lower intraocular pressure (IOP), there was some concern that this could cause corneal edema. However, numerous clinical studies have shown that in humans with normal endothelial cell counts, topical CAIs do not cause corneal edema. Only when cell counts are low and/or in the presence of significant endothelial guttata have topical CAIs been shown to cause corneal edema. This suggests that whatever role bicarbonate/CA activity has in pump activity, there must be a large functional reserve. Interestingly, endothelial pump activity can be maintained in the absence of bicarbonate, but only when bicarbonate is substituted with a high concentration of another buffer. These observations suggest that part of the role of bicarbonate/CA in the endothelial pump may be its buffering capacity, possibly for lactic acid.

Anion Transporters and Channels

Several anion transporters and channels that could participate in a bicarbonate secretory pump mechanism are expressed in corneal endothelium. At the basolateral (stromal side) membrane, the sodium bicarbonate cotransporter (NBCe1) is highly expressed (**Figure 3**). This protein transports one Na^+ with two HCO_3^- ions into the cells from the stroma. Application of the anion transport inhibitor 4,4′-diisothiocyanatostilbene-2,2′-disulphonic acid (DIDS) or genetic knockdown of NBCe1 expression using siRNA significantly reduces bicarbonate uptake and transendothelial bicarbonate flux. DIDS also results in corneal swelling *in vitro*, suggesting that this anion-transport process has an important role in the endothelial pump activity. NBCe1 is responsible for the large Na^+-dependent (Cl^- independent) bicarbonate permeability of the basolateral membrane. The bicarbonate permeability of the apical membrane of the corneal endothelium is about one-third of basolateral membrane and it is independent of Na^+ or Cl^-, suggesting that the smaller apical permeability is conferred by a channel. To date, only two apical anion channels have been described in the corneal endothelium – the cystic fibrosis transmembrane regulator (CFTR) and a calcium-activated chloride channel (CaCC). These channels are permeable to both Cl^- and HCO_3^- in about a 5:1 ratio. Physiological experiments with rabbit corneas have shown, however, that CFTR-channel inhibitors have no effect on the endothelial pump rate. Furthermore, siRNA knockdown of CFTR in cultured cells – while inhibiting cyclic adenosine monophosphate (cAMP)-activated anion flux, did not change the basal bicarbonate flux. This is consistent with clinical studies that indicate normal corneal thickness and function in cystic fibrosis patients. Similarly, siRNA knockdown of CaCC channels had no effect on basal bicarbonate permeability, but reduced calcium-activated flux. To date, the nature of the apical HCO_3^- transport remains unknown.

Recent studies have also shown that removal of Cl^- will also produce significant corneal swelling *in vitro*,

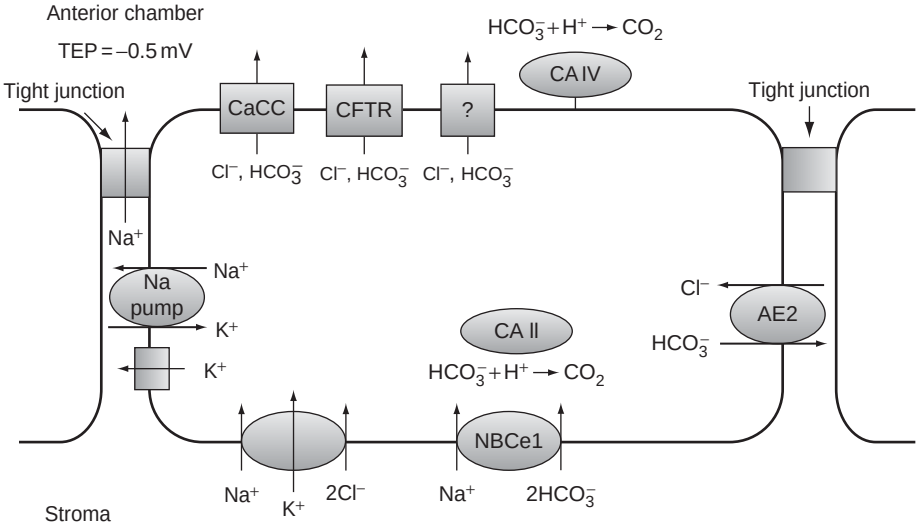

Figure 3 Model for transendothelial bicarbonate transport. NBCe1 uses the inward [Na^+] gradient to transport bicarbonate into the cell at the basolateral surface. This is facilitated by carbonic anhydrase II (CAII). Anion channels at the apical surface that are permeable to bicarbonate can provide an efflux pathway. CAIV is present on the apical surface and may facilitate net HCO_3^- flux. A chloride transport pathway is also in place, which may only be activated during endothelial stress.

suggesting the possibility that both anions – Cl^- and HCO_3^- – participate directly in the pump mechanism. In fact, the basolateral membrane expresses the Na^+:K^+:$2Cl^-$ cotransporter and the cytoplasmic [Cl^-] is 35 mM, which is above electrochemical equilibrium (**Figure 3**). Thus the potential for apical anion channel mediated Cl^- flux is in place. However, the highly specific inhibitor of the Na^+:K^+:$2Cl^-$ cotransporter – bumetanide – has no effect on corneal thickness *in vitro*. In addition, studies examining transendothelial Cl^- fluxes have been equivocal. This indicates that a basal Cl^- flux across the endothelium is unlikely to have a role in the pump mechanism. The presence of Cl^- may have two other roles that could support HCO_3^- fluxes. First, because NBCe1 is electrogenic ($1\ Na^+ : 2HCO_3^-$), membrane potential hyperpolarization (e.g., from −50 to −65 mV) will stop NBCe1 dependent HCO_3^- influx. Cl^- efflux through CFTR or other unidentified anion channels could dissipate the hyperpolarizing effects of NBCe1 activity. Second, the anion exchanger AE2 is expressed on the basolateral membrane as shown in the rabbit corneal endothelium. Thus, the transmembrane Cl^- gradient can help regulate intracellular [HCO_3^-]. Further studies are needed to elucidate the role of Cl^- or Cl^- transporters in the corneal endothelial pump mechanism. **Figure 3** illustrates a possible model for bicarbonate transport.

Aquaporin-1 (AQP1)

Aquaporin-1 (AQP1) water channels are highly expressed on both apical and basolateral membranes of corneal endothelium. No other AQP channel is expressed in the corneal endothelium. AQP1 confers a very high osmotic permeability and allows for rapid cell-volume regulation in response to anisosmotic solutions. In AQP1-knockout mice, corneal endothelial cell osmotic permeability is reduced, as expected. Corneal de-swelling rates are also significantly reduced. This indicates that a significant amount of water flux across the endothelium – at least under non-steady-state conditions – is transcellular. However, steady-state corneal thickness of these mice is slightly thinner than wild-type mice. This result may indicate that the pathway for water fluxes driven by the pump and the leak (GAGs-dependent stromal swelling pressure) is the same, which would result in no net effect. Thus AQP1 (and AQP5 in the corneal epithelium) may be present to increase the rate of water fluxes in response to osmotic changes that can occur, for example, following eye closure or exposure to hypotonicity that occurs during swimming.

Pump Mechanism

The conventional view of epithelial cell secretion and absorption of water is that these cells create local osmotic differences in the lateral spaces between the cells and/or on the apical surfaces of cells within an unstirred layer. These osmotic gradients are the driving forces for water movement across cellular membranes. This standing gradient osmotic theory, first developed by Diamond and Bossert, has come under fire as a general mechanism for fluid transport. For example, in many epithelial cells – including the corneal endothelium – there is no evidence that these gradients exist. This has led to the consideration of other mechanisms, such as electro-osmosis, which has been championed by Jorge Fischbarg for the corneal endothelium. In this theory, cells generate a transepithelial potential (0.5 mV apical-side negative in corneal endothelium) that draws counter-ions – for example, Na^+ – through a paracellular pathway that is ion specific. This produces electro-osmotic coupling across the TJ. Another mechanism for fluid transport across epithelial cells that has been recently developed is the cotransporter model. In this model, water is directly transported or coupled with the movement of the associated ions and metabolites within the cotransporter protein. Since the endothelium expresses several cotransporters – for example, $1Na^+$:$2HCO_3^-$ and Na^+:K^+:$2Cl^-$ cotransporters – and at least two monocarboxylic acid (lactic acid) cotransporters – MCT1 and MCT2 – there is potential for downhill fluid transport by this mechanism.

Barrier Integrity

Barrier integrity – which implies resistance to diffusion of solutes or fluid leak through the paracellular pathway – is dependent on the TJs. TJs are supramolecular assemblies localized at the apical domain of epithelial/endothelial monolayers. The transmembrane molecules (occludins, claudins, and junctional adhesion molecule (JAM)) – which are all expressed in corneal endothelium associated with the TJs – these transmembrane molecules of one cell interact with their homotypic counterparts in the neighboring cells. This interaction – facilitated by intercellular tethering forces through Ca^{2+}-dependent adherence junctions (AJs) – brings about occlusion of the paracellular space. The cytoplasmic domains of the transmembrane molecules of the TJs are structurally linked to a thick band of cortical actin cytoskeleton (called peri-junctional actomyosin ring (PAMR)) via adapter molecules such as zona occludens-1 (ZO-1). For AJs, the association with PAMR is mediated through catenins. The adapter molecules of both AJs and TJs also form a scaffold for a number of signaling molecules which are now implicated in the control of the stability of AJs and TJs and hence in the regulation of barrier integrity. Recent studies have demonstrated that increased contractility of the PAMR induces a breakdown of the barrier integrity through a reduction of the intercellular tethering forces at the TJs and AJs and also possibly through redistribution

of the AJ and TJ molecules at the apical junctional complex. An increase in contractility of the actin cytoskeleton is induced by an increase in the phosphorylation of the regulatory light chain of myosin II (also called myosin light chain or MLC; 20 kDa). Recent studies have shed light on the importance of actomyosin contraction in the regulation of corneal endothelial barrier integrity.

MLC Phosphorylation and Actomyosin Contraction

Phosphorylation of myosin light chain (MLC) – which is bound to the motor protein myosin II – induces actomyosin interaction resulting in increased contractility of the actin cytoskeleton (**Figure 4**). The extent of MLC phosphorylation is regulated by two opposing pathways: myosin light-chain kinase (MLCK)-driven phosphorylation, and myosin light-chain phosphatase (MLCP)-driven dephosphorylation. MLCK is activated after binding to the Ca^{2+}-calmodulin complex and its activity is dedicated to MLC phosphorylation. MLCK activity is also modulated by other protein kinases by direct phosphorylation, especially the large-size isoform of MLCK called vascular endothelial cell MLCK (EC-MLCK; 220 kDa). MLCP is a hetero-trimeric complex consisting of PP1Cδ (the catalytic subunit), the myosin-binding subunit (MYPT1; 130 kDa), and a small subunit of unknown function (M20). Phosphorylation of MYPT1 by Rho kinase (at Thr-696 and Thr-850) – a downstream effector of the small GTPase RhoA – inhibits the phosphatase activity of PP1Cδ. Protein kinase C (PKC) isoforms also inhibit the activity of MLCP through phosphorylation of CPI-17 (PKC-activated 17-kDa inhibitor protein of type 1 phosphatase) and consequent inactivation of PP1Cδ. Thus, activation of Rho kinase and/or PKC results in contraction of the actin cytoskeleton and a breakdown in barrier integrity.

Effect of MLC Phosphorylation on Corneal Endothelium Barrier Integrity

The mechanisms associated with MLC phosphorylation – which are well characterized in smooth muscle cells – are also present in corneal endothelial cells as demonstrated in several recent studies. Thus, it is now known that corneal endothelial cells – similar to vascular endothelial

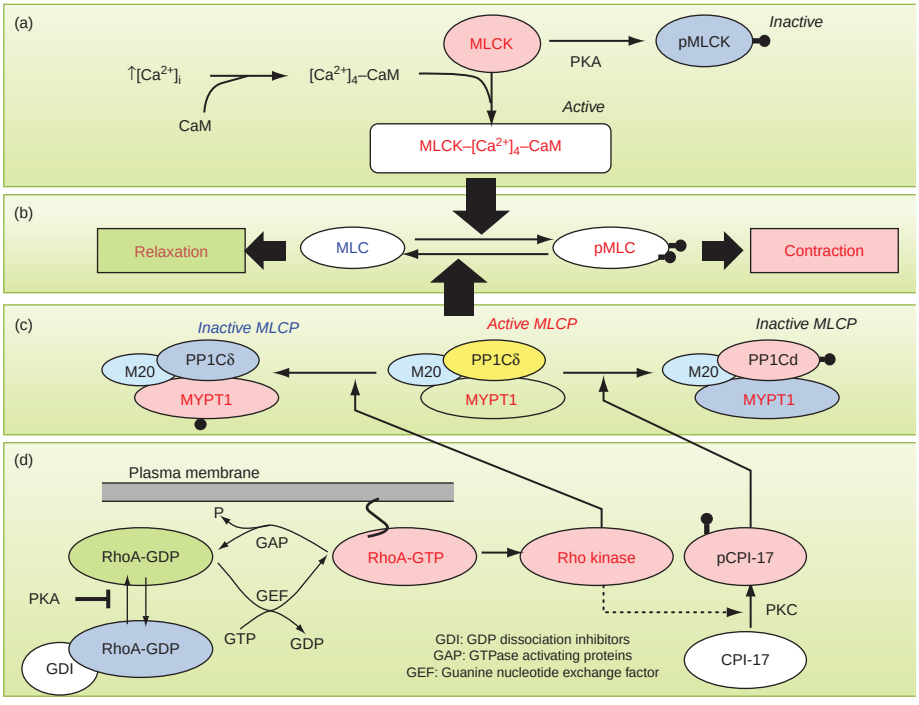

Figure 4 Regulation of myosin light-chain (MLC) phosphorylation in the corneal endothelium. (a) MLC phosphorylation is catalyzed by Ca^{2+}-Calmodulin-dependent myosin light-chain kinase (MLCK). Expression of both endothelial and smooth muscle isoforms is known in corneal endothelium. (b) MLC phosphorylation promotes actomyosin contraction. (c) MLCK activity is opposed by myosin light-chain phosphatase (MLCP), which catalyzes dephosphorylation of pMLC. MLCP is a heterotrimeric complex consisting of MYPT1 (a regulatory subunit), PP1Cδ (the catalytic subunit), and M20 (function unknown). (d) Rho kinase – effector of RhoA – phosphorylates MYPT1. This inhibits PP1Cδ. When RhoA is phosphorylated by protein kinase A (PKA) at its Ser-188, dissociation of RhoA-GDI from RhoA-GDP is opposed. Guanine exchange factors (GEFs) promote the release of GDP and subsequent binding to GTP; G-protein accelerating proteins (GAPs) stimulate the GTPase activity of RhoA; guanine nucleotide-dissociation inhibitor (GDIs) stabilize the inactive state of RhoA. Yet unidentified isoforms of PKC phosphorylate CPI-17 leading to inhibition of PP1Cδ.

cells – possess both EC-MLCK and a smaller smooth muscle isoform of MLCK (SM-MLCK; 120 kDa). In addition, myosin II isoforms (myosin IIA and IIB) are also expressed in the endothelium. To show the importance of MLC phosphorylation and its effects on the corneal endothelial barrier integrity, several G-protein-coupled receptor (GPCR) agonists have been employed. Thus, thrombin – which activates the RhoA–Rho-kinase axis through Gα12/13-coupled PAR-1 receptors in corneal endothelial cells – led to an increase in MLC phosphorylation. This was found to disrupt PAMR with a concomitant breakdown of the barrier integrity. Pretreatment with ML-7 – a selective inhibitor of MLCK – could not significantly block the thrombin-induced MLC phosphorylation. However, the Rho-kinase inhibitor Y-27632 was effective in blocking the thrombin effect. These findings indicate the dominance of the RhoA-mediated Ca^{2+}-independent pathway downstream of PAR-1 activation. The importance of the Ca^{2+}- and PKC-dependent mechanisms in MLC phosphorylation, however, have also been demonstrated independently through activation of histamine H1 receptors, which are coupled to Gαq/11 G-protein and are not known to activate RhoA. Thus, histamine-induced MLC phosphorylation and the resultant loss of endothelial barrier integrity could be suppressed by ML-7 and chelerythrine (a nonspecific PKC inhibitor). Taken together, these data have emphasized a strong role for actin cytoskeleton in the regulation of the endothelial barrier integrity and also suggest that bioactive factors and proinflammatory mediators found in the aqueous humor may influence the barrier function through their respective cell surface receptors.

Transplantation Failure and Tumor Necrosis Factor

Tumor necrosis factor (TNF-α) is a 17-KDa proinflammatory cytokine implicated in corneal endothelial failure during graft rejection (**Figure 2**). TNF-α mRNA has been detected in corneal allografts undergoing rejection, and TNF-α protein levels are significantly elevated in the aqueous humor and the serum of hosts that reject corneal allografts. A study with rabbit corneas has demonstrated that TNF-α breaks down the barrier integrity of the endothelial cells concomitant with disruption of actin cytoskeleton. The cytokine is well known to breakdown barrier integrity in vascular endothelial cells. Some of the important molecular mechanisms involved include activation of RhoA, MLC phosphorylation, significant loss of PAMR, microtubule disassembly secondary to activation of p38 MAP kinase, mobilization of oxidative stress, and formation of stress fibers. In recent studies with bovine corneal endothelium, it is becoming evident that TNF-α also induces disassembly of microtubules concomitant with a gradual loss of barrier integrity and disappearance of PAMR. These effects could be blocked by pretreatment with paclitaxel, SB-203580 (a selective inhibitor of p38 MAP kinase), and inhibitors of matrix metalloproteinases. These results suggest that a number of mechanisms are involved in the breakdown of the barrier integrity in response to TNF-α which converges directly and indirectly on actin and microtubule cytoskeleton.

Regulation of Transport Activity and Barrier Integrity

Adenosine, Soluble Adenylate Cyclase, and cAMP

The corneal endothelial fluid pump is thought to proceed at one rate and when this rate matches the leak rate driven by the stromal GAGs, corneal hydration and thickness reaches a steady state. There are other forces that can influence the leak rate including evaporative loss across the epithelial surface and contact lens-induced hypoxic stimulation of epithelial lactate production, which can produce substantial additions to stromal osmotic pressure. There is no evidence that the pump speeds up when the cornea is edematous or slows down if the cornea thins.

Shortly after it was clear that the endothelium was actively transporting water, it was discovered that the rate of fluid transport could be increased by the addition of adenosine. Later, it was shown that adenosine increases intracellular [cAMP] in endothelial cells through activation of adenosine $A2_b$ receptors. Other approaches that increase cAMP within the cells – for example, stimulating adenylate cyclase (AC) directly or inhibiting phosphodiesterase – also increased corneal endothelial fluid-transport rates. More recently, the expression of a new type of AC, called soluble AC (sAC), was shown in corneal endothelium. Unlike the transmembrane-linked adenylate cyclases, sAC is distributed throughout the cytoplasm and it is activated by HCO_3^- and Ca^{2+}. Because of the robust $1Na^+$:$2HCO_3^-$ cotransporter in endothelial cells, the sAC is active and raises the basal [cAMP] by ~50%, suggesting that it may have a small role in maintaining basal fluid transport rates. Raising cAMP activates protein kinase A (PKA) and this demonstrably phosphorylates the apical CFTR channel, increases apical Cl^- and HCO_3^- permeability, and increases transendothelial HCO_3^- flux. Together, this could contribute to the increased fluid transport observed by increasing cAMP. Corneal endothelial cells can produce adenosine from ATP at the apical surface. When stressed, corneal endothelial cells release more ATP – which, when converted to adenosine, will enhance fluid transport and could help counter the negative effects of the stress.

Role of cAMP–PKA axis in the Regulation of Barrier Integrity

An *in vitro* study with rabbit cornea first showed that adenosine could also promote corneal deturgescence through enhanced barrier integrity. Consistent with this finding, several recent studies have shown that adenosine induces MLC dephosphorylation through mobilization of cAMP–PKA axis via $A2_b$ receptors as noted above. More importantly, consistent with MLC dephosphorylation, exposure to adenosine led to an increase in the barrier integrity as measured by the trans-endothelial electrical resistance. Similar findings were noted with extracellular ATP – which was found to undergo extracellular hydrolysis resulting in formation of adenosine and subsequent activation of $A2_b$ receptors. In addition to these findings, forskolin (direct activator of adenylate cyclase), adenosine, and ATP have been found to overcome thrombin- and histamine-induced MLC phosphorylation as well as loss of barrier integrity. At the molecular level, the locus of action of elevated cAMP is also becoming evident. PKA is known to induce MLC dephosphorylation through modulation of the RhoA–Rho-kinase axis. One potential mechanism involves direct phosphorylation of RhoA by PKA and consequent increase in the affinity of the small guanosine triphosphatase (GTPase) to its guanosine diphosphate (GDP) dissociation inhibitor (GDI). An alternative mechanism involves direct phosphorylation of MYPT1 by PKA. The latter is known to prevent Rho kinase from phosphorylating MYPT1 leading to inactivation of MLCP. cAMP may also influence cell–cell adhesion through activation of a small GTPase, namely Rap1. This involves activation of Epac – a guanine nucleotide-exchange factor (GEF) for Rap1. Activated Rap1 promotes formation of AJs, presumably through enhanced cadherin ligation.

Summary and Perspective

The corneal endothelium is responsible for maintaining corneal hydration and transparency. Active transport processes – through mechanisms that are not fully elucidated – provide a Pump that exactly counterbalances the stromal glycosaminoglycan induced Leak. The Pump is regulated through cAMP-dependent signaling that acts on components of ion transport and the barrier integrity of the endothelial monolayer. Further understanding of the Pump and Leak mechanisms are needed to provide medical therapies that could maintain stromal deturgescence in diseased or traumatized corneal endothelium.

See also: Corneal Endothelium: Overview; The Corneal Stroma; Regulation of Corneal Endothelial Cell Proliferation.

Further Reading

Bonanno, J. A. (2003). Identity and regulation of ion transport mechanisms in the corneal endothelium. *Progress in Retinal and Eye Research* 22(1): 69–94.

Dikstein, S. and Maurice, D. M. (1972). The metabolic basis to the fluid pump in the cornea. *Journal of Physiology* 221(1): 29–41.

Doughty, M. J. and Maurice, D. M. (1988). Bicarbonate sensitivity of rabbit corneal endothelium fluid pump *in vitro*. *Investigative Ophthalmology and Visual Science* 29(2): 216–223.

Fischbarg, J., Diecke, F. P., Iserovich, P., and Rubashkin, A. (2006). The role of the tight junction in paracellular fluid transport across corneal endothelium. Electro-osmosis as a driving force. *Journal of Membrane Biology* 210(2): 117–130.

Fischbarg, J. and Lim, J. (1974). Role of cations, anions, and carbonic anhydrase in fluid transport across rabbit corneal endothelium. *Journal of Physiology* 241: 647–675.

Hodson, S. and Miller, F. (1976). The bicarbonate ion pump in the endothelium which regulates the hydration of rabbit cornea. *Journal of Physiology* 263: 563–577.

Li, J., Sun, X. C., and Bonanno, J. A. (2005). Role of NBC1 in apical and basolateral HCO_3^- permeabilities and transendothelial HCO_3^- fluxes in bovine corneal endothelium. *American Journal of Physiology. Cell Physiology* 288(3): C739–C746.

Maurice, D. (1972). The location of the fluid pump in the cornea. *Journal of Physiology* 221: 43–54.

Riley, M., Winkler, B., Starnes, C. A., and Peters, M. I. (1996). Adenosine promotes gulation of corneal hydration through cyclic adenosine monophosphate. *Investigative Ophthalmology and Visual Science* 37: 1–10.

Satpathy, M., Gallagher, P., Lizotte-Waniewski, M., and Srinivas, S. P. (2004). Thrombin-induced phosphorylation of the regulatory light chain of myosin II in cultured bovine corneal endothelial cells. *Experimental Eye Research* 79: 477–486.

Srinivas, S. P., Satpathy, M., Gallagher, P., Larivière, E., and Van Driessche, W. (2004). Adenosine induces dephosphorylation of myosin II regulatory light chain in cultured bovine corneal endothelial cells. *Experimental Eye Research* 79: 543–551.

Srinivas, S. P., Satpathy, M., Guo, Y., and Anandan, V. (2006). Histamine-induced phosphorylation of the regulatory light chain of myosin II disrupts the barrier integrity of corneal endothelial cells. *Investigative Ophthalmology Visual Science* 47: 4011–4018.

Regulation of Extracellular Matrix Turnover in the Aqueous Humor Outflow Pathways*

R Fuchshofer and E R Tamm, University of Regensburg, Regensburg, Germany

Glossary

Bone morphogenetic proteins (BMPs) – A group of growth factors originally named for its ability to induce the formation of bone and cartilage. BMP2 to BMP7 belong to the transforming growth factor-β superfamily and have important roles during development.

Cytokine – A protein or polypeptide that is used in cellular communication.

Growth factor – A protein capable of stimulating growth, proliferation, and differentiation of cells. The term growth factor is often used interchangeably with the term cytokine.

Pseudoexfoliation glaucoma – A form of open-angle glaucoma characterized by granular material at the pupillary margin of the iris and throughout the inner surface of the anterior chamber.

Smads – A class of proteins that modulate the activity of the TGF-β superfamily of ligands. Smad proteins are homologs to the protein mothers against decapentaplegic (MAD) in *Drosophila melanogaster* and the protein SMA in *Caenorhabditis elegans*. The name is a combination of the two.

Thrombospondin-1 – An adhesive glycoprotein that mediates cell-to-cell and cell-to-matrix interactions.

Transforming growth factor-β (TGF-β) – A secreted protein that exists in three isoforms called TGF-β1, TGF-β2, and TGF-β3. TGF-β's belong to a superfamily of proteins known as the transforming growth factor-β superfamily.

Introduction

In primary open-angle glaucoma (POAG), a major cause of blindness worldwide, the critical risk factor for axonal damage at the optic nerve head is an intraocular pressure (IOP), which is very high for the health of the optic nerve head. IOP is increased in POAG when aqueous humor (AH) outflow resistance in the juxtacanalicular tissue (JCT) region of the human trabecular meshwork (TM) is abnormally high. The mechanisms that are responsible for the increase in TM outflow resistance in POAG are unclear. There is some evidence, however, that changes in the amount and quality of the TM extracellular matrix (ECM) are involved, as eyes with POAG show a significant increase in fibrillar ECM in the JCT outflow pathways. Our knowledge on the molecular factors that govern ECM turnover in the TM has considerably increased in recent years. It has become quite clear that quality and quantity of ECM in the TM are regulated by several signaling molecules that interact with each other to promote synthesis, degradation, or extracellular modification of the ECM. This article reviews the growing list of molecules that act in a complex network to influence ECM homoeostasis in the TM.

Transforming Growth Factor-β

Transforming growth factor-β (TGF-β) is a member of a family of dimeric polypeptide growth factors. There are three isoforms of TGF-β: TGF-β1, TGF-β2, and TGF-β3, which are each encoded by a distinct gene. In the normal anterior eye, TGF-β2 appears to be the predominant isoform as it is found at relatively high concentrations in the AH of normal eyes. This isoform is very likely secreted into the AH from the epithelial cells of ciliary body and lens.

Immunohistochemical studies have shown immunoreactivity for TGF-β1 in the stroma of the ciliary processes, while TGF-β3 was not detected in structures of the anterior eye. The normal TM does not label with antibodies against the various TGF-β isoforms, but cultured TM cells are capable of secreting TGF-β2 and TGF-β1, and expressing receptors for both factors. The physiological role of TGF-β2 in the AH appears to be tightly linked with the immunosuppressive environment of the anterior chamber and the phenomenon of anterior-chamber-associated immune deviation (ACAID).

Among the factors that modulate ECM turnover in the TM, TGF-β2 is the one which is most likely involved in the pathological ECM increase in POAG. Multiple groups have reported significantly higher levels of TGF-β2 in the AH collected from human POAG eyes as compared with AH from patients who underwent cataract operation. The factors which cause or contribute to the increase in TGF-β2 in the AH of patients with POAG are unclear.

*An adaptation and extension of Fuchshofer, R. and Tamm, E. R. (2009). Modulation of extracellular matrix turnover in the trabecular meshwork. *Experimental Eye Research* 88: 683–688. http://www.sciencedirect.com/science/journal/00144835.

In addition, there is no information available on the nature of the ocular tissues which secrete higher-than-normal amounts of TGF-β2 in the AH, but because of the direction of AH flow, ciliary body and lens are more likely candidates than the TM. The increase in TGF-β2 appears to be typical for POAG and not to be directly caused by an increase in IOP, as patients with pseudoexfoliation glaucoma do not show elevated levels of TGF-β2 in their AH. In contrast, AH of patients with pseudoexfoliation syndrome or glaucoma contains elevated amounts of TGF-β1 and TGF-β3.

In multiple disorders throughout the body, TGF-β signaling mediates a pathological increase in ECM secretion and deposition, and is causatively involved in fibrosis. It is reasonable to assume that the passage of higher-than-normal amounts of TGF-β2 through the TM will induce changes in TM gene expression that may result in an increase in TM ECM deposition. Experimental support for this assumption comes from experiments involving anterior eye segment perfusion cultures, in which perfusion with TGF-β2 promoted a focal accumulation of fine fibrillar extracellular material in the TM and an increase in fibronectin synthesis, effects that were correlated with a reduction in outflow facility. Comparable results were obtained in experiments involving monkey anterior eye segment organ cultures, in which perfusion with TGF-β2 caused a decrease in outflow facility by ~40% compared to pretreatment baseline. The decrease in outflow facility correlated with an increase in cochlin, a secreted protein that comprises the major noncollagen component of the ECM of the inner ear, and is present in glaucomatous TM, but absent in the normal TM. In addition, numerous studies provided evidence that treatment of TM cells in monolayer cell culture leads to a substantial increase in the expression and synthesis of a broad variety of ECM proteins (collagens III, IV, and VI, elastin, fibronectin, versican, laminin, and myocilin), all of which contribute to the ECM of the TM *in situ*.

TGF-β2 treatment of cultured TM cells also stimulates the synthesis of proteins that modify turnover and deposition of ECM. Accordingly, TGF-β2 induces in TM cells the expression of tissue transglutaminase and its messenger RNA (mRNA), as well as its action on irreversible and covalent cross-linking of fibronectin. Moreover, TGF-β2 leads to an increased TM synthesis of plasminogen activator inhibitor (PAI-1), which is a potent inhibitor of matrix metalloproteinases (MMPs). In the TM, PAI-1 appears to primarily inhibit MMP2, an enzyme that degrades collagen type IV, the major structural component of basement membranes. The expression of matrix Gla protein (MGP), which is among the most highly expressed genes in fresh human TM, is significantly downregulated following treatment with TGF-β2. In certain soft tissues, MGP is important to prevent ectopic calcification, and mice that are deficient in Mgp ($Mgp^{-/-}$) develop severe vascular atherosclerosis and calcification. While the available data on the morphology and pathology of human TM in POAG very clearly indicate that a major calcification process comparable to that in atherosclerosis is absent in the TM, it is certainly tempting to speculate that a more subtle mineralization of the TM ECM or a comparable process is involved in the structural changes of the TM in POAG, and that TGF-β signaling is causatively involved.

It is of interest to note that TGF-β signaling does not only effect ECM turnover in the TM, but also acts on the TM actin cytoskeleton, as treatment with TGF-β1 induces the expression of α-smooth muscle actin in cultured TM cells. α-Smooth muscle actin is the isoform of actin that is expressed in smooth muscle cells and myofibroblasts, a cell type that predominates in connective tissues of healing wounds and scars. In myofibroblasts, the induction of α-smooth muscle actin by TGF-β1 substantially enhances cell traction force. In the normal TM *in situ*, some cells are immunoreactive for α-smooth muscle actin, while virtually all cells in the scleral spur region, close to the posterior attachment of the TM, express this actin isoform. There is the distinct possibility that an increase in the activity of TGF-β signaling in the eye increases the number of α-smooth muscle actin-positive cells in the TM, thereby increasing TM cell tone, an effect that has been shown to correlate with an increase in outflow resistance.

TGF-β Activation and Thrombospondin-1

TGF-β signaling is not only involved in ECM turnover, but also acts in other extremely important biological processes throughout the body and in the eye, including proliferation, apoptosis, and modulation of the immune system. Accordingly, defects in TGF-β function are associated not only with fibrosis, but also with other pathological states such as tumor cell growth and autoimmune diseases. Because of their multifunctional role, the activity of TGF-β *in vivo* needs to be subject to tight control mechanisms. TGF-β's are secreted as large latent complexes (LLCs), which are unable to interact with cellular receptors, a mechanism that prevents uncontrolled activation of the TGF-β signaling pathway. LLCs consist of the native TGF-β dimer which is noncovalently associated with its propeptide, the latency-associated protein (LAP), and of a second gene product, the latent TGF-β-binding protein (LTBP) which binds covalently to LAP. Mammalian cells express four different LTBP isoforms, of which only three (LTBP-1, -3, and -4) can associate with TGF-β. Following secretion, the LLC may be covalently linked to the ECM through the N-terminus of LTBP. Upon TGF-β activation, TGF-β is liberated from both LAP and LTBP.

Since TGF-β2 in the AH of normal and POAG eyes is mostly found in its latent, inactive form, it seems reasonable to assume that its effects on TM biology will considerably increase, if it is locally activated in the TM. *In vitro*, active

TGF-β is generated by extremes of pH, heat, or chaotropic agents, mechanisms that are not likely to be of physiological relevance for TGF-β activation *in vivo*. The physiological mechanisms of TGF-β activation *in vivo* may involve proteolytic processing as *in vitro* studies have identified a number of proteases, including plasmin, MMP-2, and MMP-9 as activators of latent TGF-β. TM cells would be capable to activate TGF-β by proteolysis, as they express active tissue plasminogen activator (t-PA), and MMP-2.

A very potent activator of latent TGF-β *in vivo* and *in vitro* is thrombospondin-1 (TSP-1), a matricellular protein which belongs to a small family of secreted glycoproteins. Matricellular proteins are secreted proteins that influence cell function by modulating cell–matrix interactions. TSP-1 might be critical for TGF-β activation in the TM, as there is a considerable constitutive TSP-1 expression in the JCT of the human TM (**Figure 1**). In the TM of patients with POAG, an increase of immunoreactivity

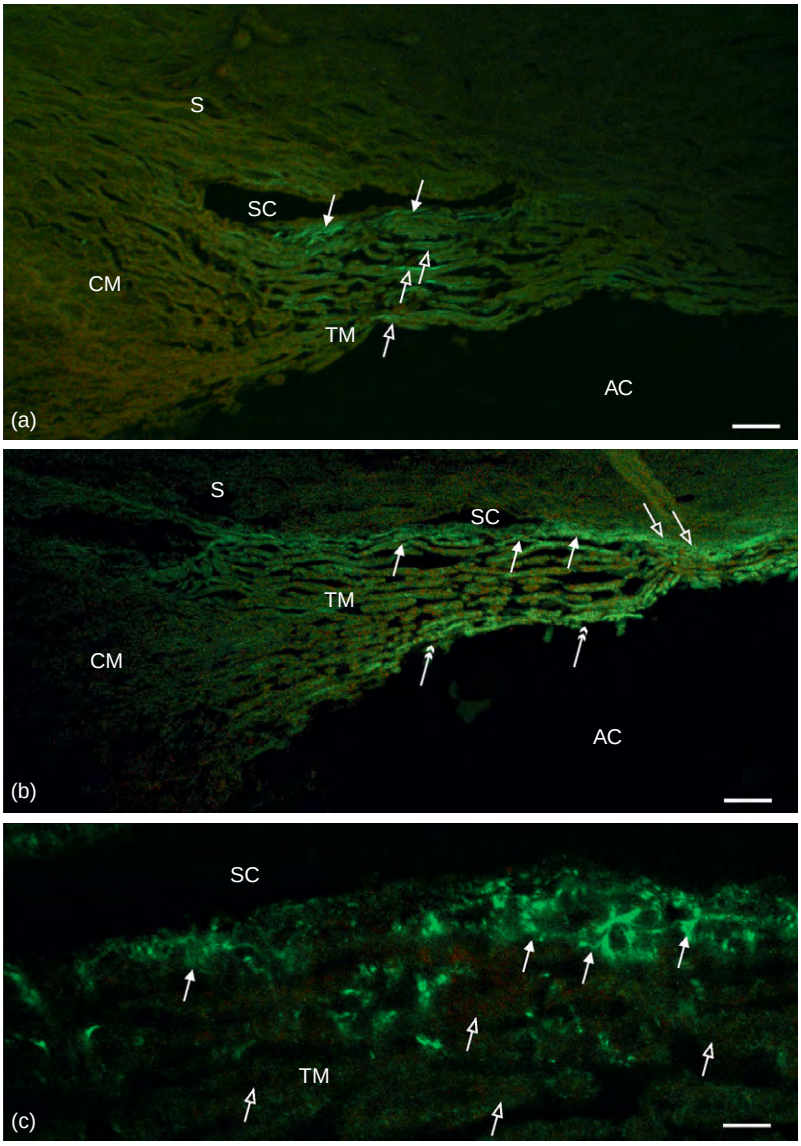

Figure 1 Immunohistochemistry for TSP-1 in the TM of normal human donors. (a) The TM of a 52-year-old donor shows immunoreactivity for TSP-1 in focal areas of the juxtacanalicular region (solid arrows). In addition, focal staining of uveal and corneoscleral TM cells is observed (open arrows). (b) In the TM of a 70-year-old donor, there is continuous labeling for TSP-1 in the juxtacanalicular region (solid arrows), which extends to the area of Schwalbe's line (open arrows). In addition, there is intense labeling of the anterior uveal TM (double arrows). (c) Upon higher magnification, juxtacanalicular immunoreactivity for TSP-1 is predominately localized to extracellular areas surrounding juxtacanalicular TM cells (solid arrows). In contrast, the connective tissue core of the corneoscleral TM lamellae is largely negative for TSP-1 (open arrows). Magnification bar = 47 μm (a, b); 6.6 μm (c). AC, anterior chamber; SC, Schlemm's canal; CM, ciliary muscle; S, sclera. From Flügel-Koch, C., Ohlmann, A., Fuchshofer, R., Welge-Lüssen, U., and Tamm, E. R. (2004). Thrombospondin-1 in the trabecular meshwork: Localization in normal and glaucomatous eyes, and induction by TGF-beta1 and dexamethasone *in vitro*. *Experimental Eye Research* 79: 649–663.

for TSP-1 has been observed in about one-third of patient eyes that were investigated (Figure 2). The expression of TSP-1 in TM cells is induced upon treatment with TGF-β1 and TGF-β2, indicating the presence of self-amplifying mechanisms for TGF-β signaling in the TM outflow pathways.

Another mechanism of activation depends on the direct interaction between integrin αvβ6 and LAP. Integrin-mediated TGF-β activation in the TM would only be relevant for TGF-β1, but not for TGF-β2, as it requires an integrin-binding arginine–glycine–aspartic acid (RGD) sequence in LAP, which is missing in the LAP of TGF-β2. Integrins are dimeric cell surface receptors that connect the cytoskeleton with the ECM. Since latent TGF-β1 binds simultaneously to the ECM through LTBP and to integrin αvβ6 through LAP, it has been hypothesized that mechanical traction is the relevant *in vivo* stimulus for integrin-mediated TGF-β1 activation.

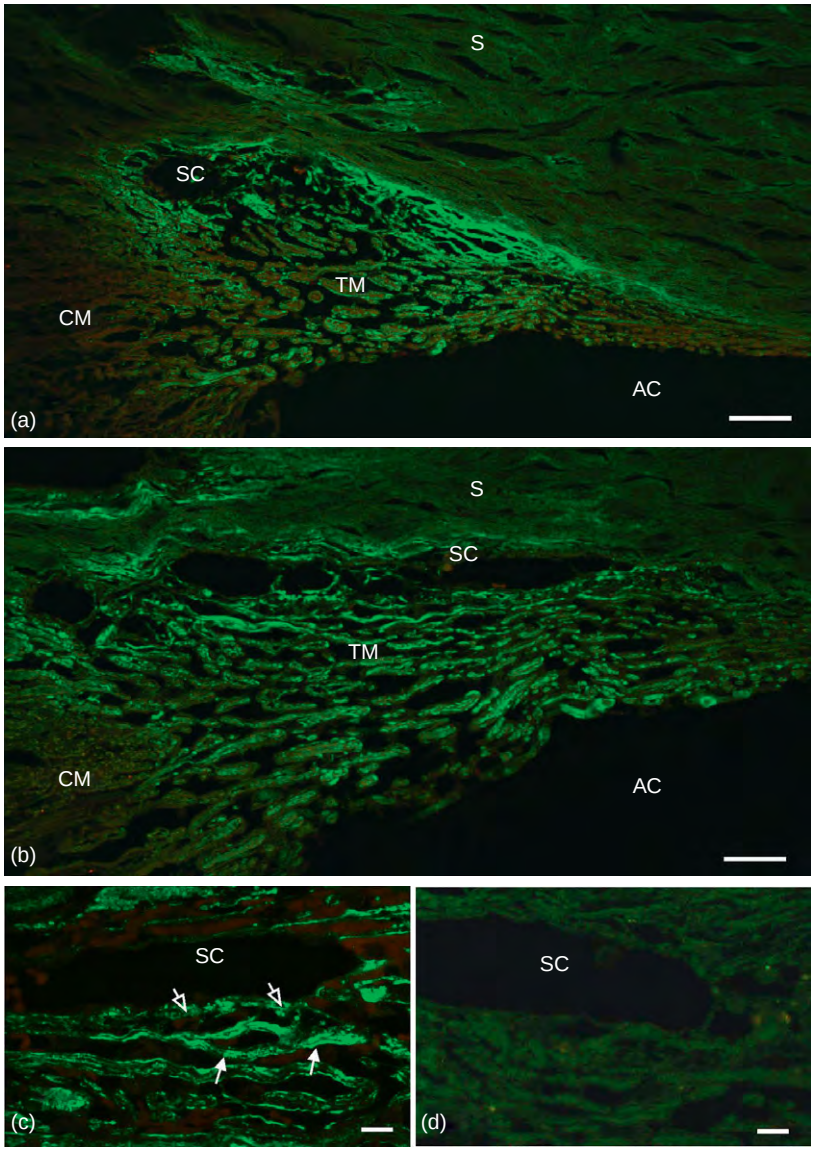

Figure 2 Immunohistochemistry for TSP-1 in the TM of a 67-year-old patient with POAG (a), and a 71-year-old patient with POAG after long-term treatment with topical steroids (b). (a, b) In the TM of both patients, intense immunoreactivity for TSP-1 is observed throughout all regions of the TM. TSP-1 labeling is also observed in the scleral tissue that lines the outer wall of Schlemm's canal and the collector channels, which originate from it. (c) Upon higher magnification, the cells lining the corneoscleral and uveal trabecular lamellae are labeled (solid arrows). In addition, positive staining is observed in the connective tissue core of the lamellae (open arrows). (d) In a control section, no positive immunoreactivity for TSP-1 is observed. Magnification bar = 47 μm (a, b); 6.6 μm (c, d). AC, anterior chamber; SC, Schlemm's canal; CM, ciliary muscle; S, sclera. From Flügel-Koch, C., Ohlmann, A., Fuchshofer, R., Welge-Lüssen, U., and Tamm, E. R. (2004). Thrombospondin-1 in the trabecular meshwork: Localization in normal and glaucomatous eyes, and induction by TGF-beta1 and dexamethasone *in vitro*. *Experimental Eye Research* 79: 649–663.

Clearly, in the living eye, mechanical traction between TM cells and their surrounding ECM would be augmented by an increase in stretch or strain in the TM, for instance, due to an increase in IOP. It is of interest to note that cyclic mechanical stretch of cultured TM cells activates the promoter of TGF-β1 and induces its expression in TM cells. Taken together, the action of TGF-β signaling on TM cells may depend not only on the presence and the amounts TGF-β2 in the AH, but also on that of TGF-β1, which is locally secreted and activated in the TM. Treatment with both TGF-β1 and TGF-β2 induces the expression of TGF-β1 in TM cells, indicating that self-amplifying mechanisms are capable to substantially augment the biological actions of TGF-β signaling on the TM outflow pathways. Upon activation, the biological effects of TGF-β1 and TGF-β2 on TM cells should be rather similar, as they bind to the same cellular receptors, albeit with different affinity, and initiate similar intracellular signaling cascades.

Connective Tissue Growth Factor

Connective tissue growth factor (CTGF) is a member of the CCN (CTGF, cysteine-rich angiogenic protein 61, and nephroblastoma overexpression gene) family of regulatory proteins. In the eye, the expression of CTGF has been found in TM, iris sphincter and ciliary muscle cells, retinal vascular endothelial cells, epi- and subretinal membranes, plaques of human anterior subcapsular cataracts, corneal scars, tear fluid, and pterygia. CTGF has also been detected in the AH and recent studies reported that the concentration of CTGF is increased in the AH of patients with pseudoexfoliation syndrome. CTGF has been identified as a critical downstream mediator of the fibrogenic action of TGF-βs. Similar to TGF-β's, the expression of CTGF is upregulated in a substantial number of disorders that are associated with a pathological increase in ECM, including scleroderma, renal and pulmonary fibrosis, inflammatory bowel disease, and atherosclerosis. The expression of CTGF in the fresh TM is considerably high. As in other tissues, treatment of cultured TM cells with TGF-β2 causes an increase in CTGF expression. CTGF is also found in higher amounts in the TM following mechanical stretch, an effect that is probably induced by the action of TGF-β1, which is also upregulated in TM cells by stretch.

In a recent study, it was shown that recombinant CTGF is as potent as TGF-β2 to induce ECM expression in TM cells. Following treatment with CTGF, an increase was observed in the expression of fibronectin, and of the collagen types I, III, IV, and VI (**Figure 3**). Moreover, transfection with CTGF-specific small interfering (si) RNA inhibited the TGF-β2-induced upregulation of CTGF and fibronectin, providing evidence that CTGF acts also in the TM as downstream mediator of TGF-β2 signaling. CTGF did not affect the expression of MMP-2, MMP 9, or PAI-1, indicating that CTGF mediates the TGF-β2-induced expression of TM ECM components, but is apparently not a downstream mediator of the effects of TGF-β2 on the extracellular proteolytic system in the TM. The effects of CTGF on TM cells were not restricted to the expression of ECM molecules, as TM cells synthesized also higher amounts of the integrin subunits, αv and β1, following treatment with CTGF.

CTGF is among the most highly expressed genes in the human TM, and it is tempting to speculate that the function of CTGF signaling in the TM involves the remodeling of cell–matrix adhesions in response to an increase in stress or strain in the TM, especially as CTGF induces the integrin subunit β1, an important component of fibronectin and collagen type IV binding integrins. While remodeling of JCT, cell–matrix adhesions might be the primary role of CTGF in the normal TM, a pathological increase in CTGF expression, for example, caused by activation of the abnormally high TGF-β2 levels in the AH of patients with POAG, could result in an increase in JCT ECM.

Bone Morphogenic Proteins

The action of TGF-β2 and CTGF on ECM turnover in the TM is strongly antagonized by bone morphogenetic protein-7 (BMP-7), a growth factor of the BMP family. BMP-7 is a 35-kDa homodimeric protein and member of the TGF-β superfamily of cysteine knot cytokines. In embryonic life, BMP-7 plays a critical role during renal and eye development. In the adult organism, the expression of BMP-7 is retained in the eye, in which its expression and that of its receptors have been shown in cornea, TM, and optic nerve. BMP-7 strongly antagonizes *in vitro* the TGF-β2-induced expression of a broad panel of molecules, which would result in an accumulation of ECM in the TM *in situ*. While treatment of human TM cells with TGF-β2 induces the expression of CTGF, TSP-1, fibronectin, collagen types IV and VI, and PAI-1, these effects are inhibited when TGF-β2 is added in combination with BMP-7 (**Figure 4**). BMP-7 by itself has no effects on the expression of all of these molecules. As BMP-7 is expressed in the adult TM *in situ*, it seems more than reasonable to assume that it similarly modulates and antagonizes the effects of TGF-β2 signaling on the TM *in vivo*. This protein has been shown to suppress TGF-β-induced effects on ECM synthesis also in other systems. In the cornea, BMP-7 antagonizes TGF-β-induced effects on corneal scarring. In the kidney, it counteracts an epithelial-to-mesenchymal transition that is induced by TGF-β1 and reverses chronic renal injury. In addition, BMP-7 antagonizes the TGF-β-dependent fibrogenesis in mesangial cells of the kidney-glomerulus. BMP-4 has very similar activities on the

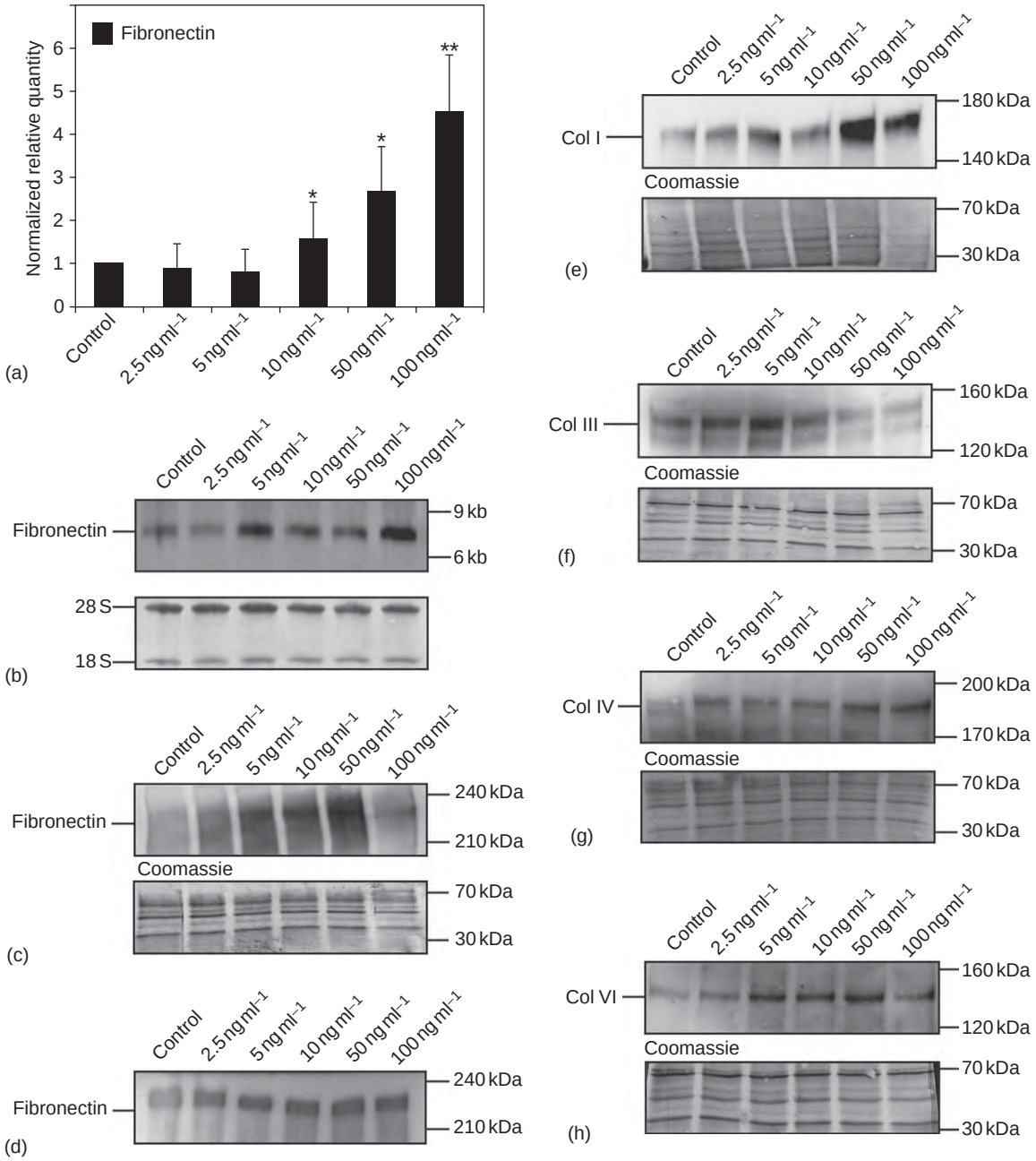

Figure 3 CTGF and its influence on the expression of ECM molecules in HTM cells. (a) Real-time RT-PCR analysis for mRNA of FN in RNA from cultured HTM cells after treatment with 2.5–100 ng ml^{-1} CTGF for 24 h. Means ± SD of four independent experiments run in duplicate are shown. GNB2L was used as reference gene. The mean value obtained with RNA from untreated cells was set at 1. Asterisks mark statistically significant differences between control and CTGF treated cells (*$p < 0.05$; **$p < 0.02$). (b) Northern blot analysis for the mRNA of FN in RNA from cultured HTM cells after treatment with 2.5–100 ng ml^{-1} CTGF for 24 h. Integrity of RNA and equal loading were controlled by staining for ribosomal RNA with methylene blue. (c–h) Western blot analysis of FN ((c) cell lysate; (d) culture medium; 220 kDa), collagen type I ((d); 160 kDa), collagen type III ((e); 140 kDa), collagen 4α2 ((f); 180 kDa), and collagen 6α2 ((g); 140 kDa) in proteins from cultured HTM cells after treatment with 2.5–100 ng ml^{-1} CTGF for 24 h. Membranes were stained with Coomassie blue to confirm equal loading of proteins. From Junglas, B., Yu, A. H. L., Welge-Lüssen, U., Tamm, E. R., and Fuchshofer, R. (2009). Connective tissue growth factor induces extracellular matrix deposition in human trabecular meshwork cells. *Experimental Eye Research* 88: 1065–1075.

biology of TM cells as BMP-7 and also counteracts the action of TGF-β. Cultured TM cells treated with TGF-β 2 significantly increase fibronectin synthesis, while BMP-4 blocks the induction of fibronectin.

There are a number of molecules that regulate the signaling action of BMP family members, including that of BMP-7 and BMP-4, by binding to BMPs and preventing the ligand from interacting with the cellular receptor

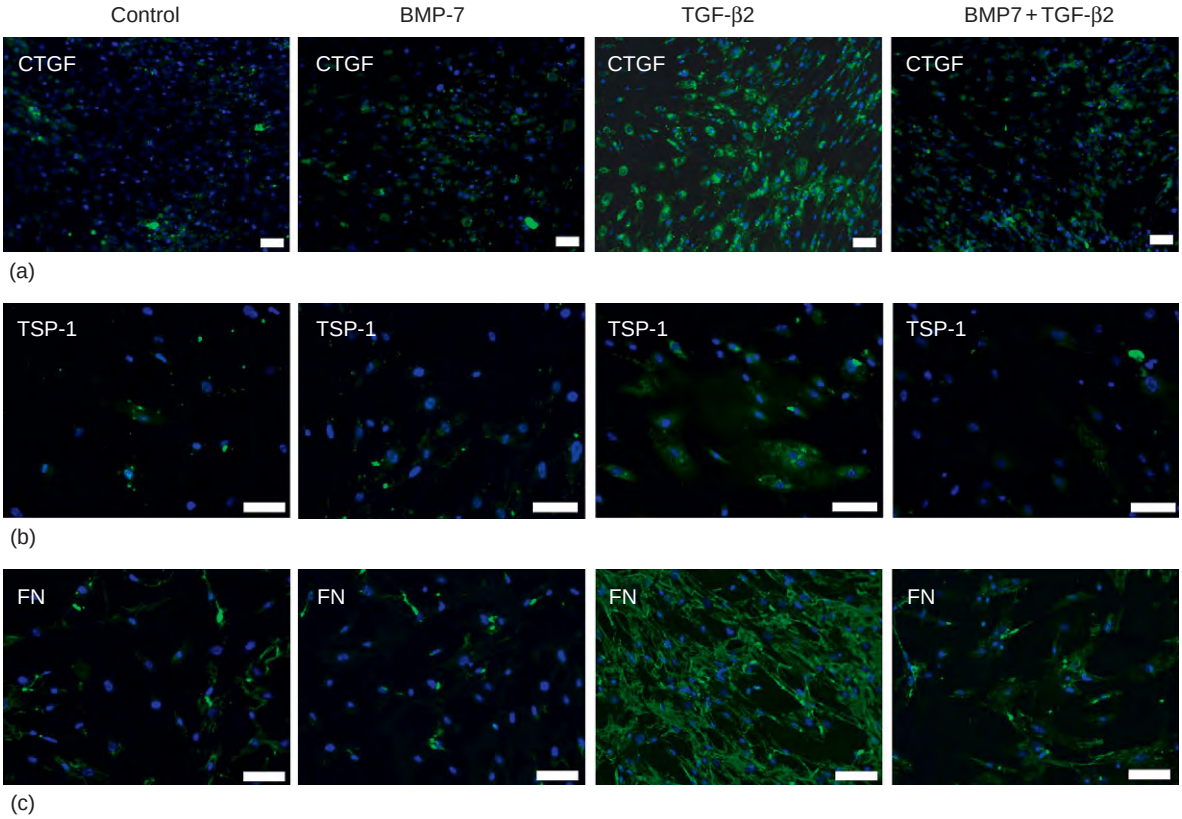

Figure 4 Immunoreactivity for connective tissue growth factor (CTGF, (a)), thrombospondin-1 (TSP-1, (b)), and fibronectin (FN, (c)) in cultured human trabecular meshwork cells following treatment with 300-pM bone morphogenetic protein-7 (BMP-7), 300-pM transforming growth factor-β2 (TGF-β2), or a combination of both. Treatment with 300-pM BMP-7 caused no changes in immunoreactivity. In contrast, after treatment with 300-pM TGF-β2, the intensity of staining for CTGF, TSP-1, and FN was considerably enhanced, an effect that was markedly reduced following treatment with a combination of BMP-7 and TGF-β2. Inset in (a) shows immunoreactivity for CTGF in cellular vesicles (arrowhead). Magnification bar = 100 μm. From Fuchshofer, R., Yu, A. H., Welge-Lüssen, U., and Tamm, E. R. (2007). Bone morphogenetic protein-7 is an antagonist of transforming growth factor-beta2 in human trabecular meshwork cells. *Investigative Ophthalmology and Visual Science* 48: 715–726, with permission from Association for Research in Vision and Ophthalmology.

complex. The expression of some of these BMP-associated molecules that act as BMP antagonists, such as follistatin, gremlin, and chordin, has been observed in TM cells. Applying gene chip analyses, the expression of molecules involved in BMP signaling was profiled and compared between normal TM cells and those from donors with POAG. As a result of this study, an upregulation of gremlin and its mRNA was found in POAG samples. In subsequent experiments, it was shown that gremlin blocks the negative effect of BMP-4 on the TGF-β2 induced upregulation of fibronectin. In anterior segment perfused organ cultures, gremlin added to the medium causes an elevation of outflow resistance strongly indicating that the BMP signaling pathway is involved in the modulation of TM outflow resistance.

Smad7

In order to learn more about the signaling network that is induced in TM cells treated with BMP-7, TGF-β2, or the combination of both factors, a microarray study was performed to identify genes that are differentially regulated following these treatment protocols. While multiple antagonistic and synergistic effects on the expression of a considerable number of genes with different functional properties were observed, it was also noted that both growth factors caused a substantial induction of Smad7. In contrast to receptor-associated Smads, such as Smad2 and Smad3, which mediate TGF-β signaling, Smad7 is an inhibitory Smad that functions as intracellular antagonist that inhibits TGF-β signaling. Since TGF-β1 and BMP-7 induce the expression of Smad7 in several cell types, the concept has been proposed that Smad7 plays an essential role in an autoinhibitory negative-feedback regulation of TGF-β signaling. Several mechanisms have been suggested on how Smad7 exerts its negative effects on TGF-β signaling. Smad7 inhibits signaling through stable binding to activated type I receptors and competition with receptor-associated Smads for receptor activation. In addition, Smad7 can

recruit the E3 ubiquitin ligases, Smurf1 and Smurf2, to the type I receptors, resulting in receptor ubiquitination, degradation, and termination of signaling. Finally, it appears also to act in the nucleus to disrupt the formation of the TGF-β-induced functional Smad–DNA complex. Indeed, by performing experiments with siRNA specific for Smad7, it could be confirmed that the knockdown of Smad7 mRNA expression in TM cells completely inhibits the antagonizing effects of BMP7 on TGF-β2 signaling (**Figure 5**).

The results strongly indicate that Smad7 is a key molecule to prevent TGF-β2-induced gene expression in the TM. The model would imply that TGF-β2 induces Smad7 in TM cells, an effect that shortens the time interval during

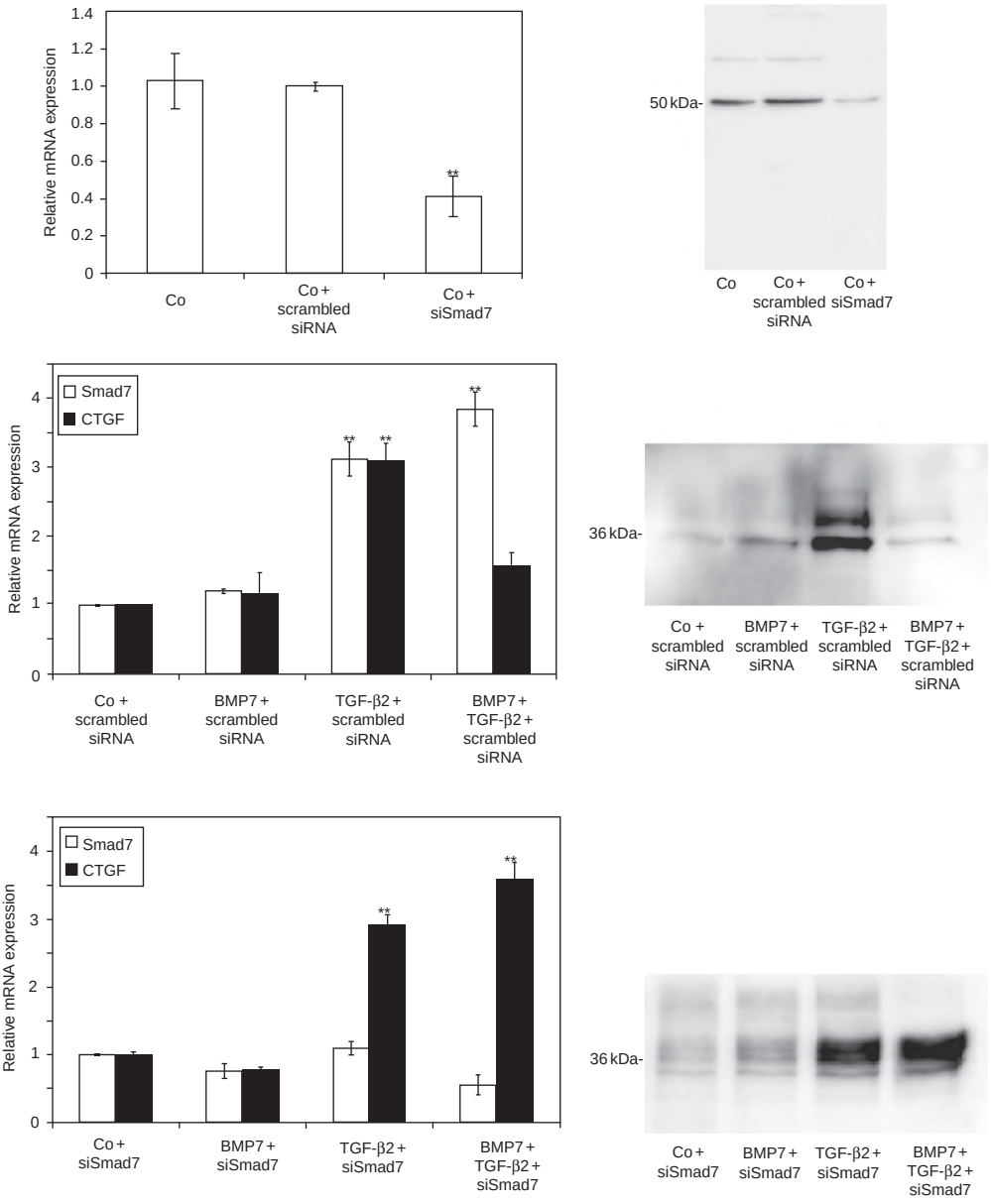

Figure 5 Silencing of Smad7 mRNA following transfection with specific siRNA (siSmad7) or scrambled siRNA, and its effects on Smad7 and CTGF expression in untreated HTM cells (Co), or cells treated with BMP-7, TGF-β2, or combined BMP-7/TGF-β2. (a) Real-time RT-PCR for Smad7 mRNA and Western blot analysis for Smad7. (b) Real-time RT-PCR for Smad7 and CTGF mRNA, and Western blot analysis for CTGF in culture medium of HTM cells transfected with scrambled siRNA. (c) Real-time RT-PCR for Smad7 and CTGF mRNA, and Western blot analysis for CTGF in culture medium of HTM cells transfected with siRNA against Smad7. For real-time RT-PCR experiments, means ± standard deviations of four independent experiments run in duplicate are shown (*$p < 0.05$; **$p < 0.01$). The amounts of Smad7 mRNA were normalized to that of GAPDH. From Fuchshofer, R., Stephan, D. A., Russell, P., and Tamm, E. R. (2009). Gene expression profiling of TGFβ2- and/or BMP7-treated trabecular meshwork cells: Identification of Smad7 as a critical inhibitor of TGF-β2 signaling. *Experimental Eye Research* 88: 1020–1032.

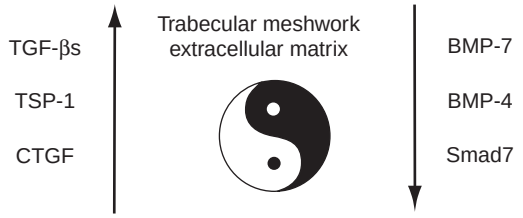

Figure 6 Molecules that modulate extracellular matrix homeostasis in the trabecular meshwork (TM). Transforming growth factor-β's (TGF-β's), thrombospondin-1 (TSP-1), and connective tissue growth factor (CTGF) contribute to induce ECM deposition in the TM. Bone morphogenetic proteins (BMP)-7 and -4 antagonize the effects of TGF-β-signaling on matrix deposition, an effect that requires Smad7. From Fuchshofer, R. and Tamm, E. R. (2009). Modulation of extracellular matrix turnover in the trabecular meshwork. *Experimental Eye Research* 88: 683–688.

which TGF-β2-signaling is promoting the expression of its specific target genes. If BMP7 is added to TGF-β2, the expression of target genes is blunted or completely prevented, as the available amounts of Smad7 are induced to much higher levels than when TGF-β2 would act alone.

Conclusions

In recent years, important parts of the signaling network have been identified, which regulate homeostasis of ECM turnover in the TM (**Figure 6**). TGF-β, which derives from the AH or may be locally expressed, induces the expression of a variety of TM ECM molecules. The action of TGF-β very likely requires activation by TSP-1 and is partly mediated by its downstream mediator CTGF, both of which are constitutively expressed in the TM. BMP-7 and BMP-4 effectively antagonize the effects of TGF-β2 on matrix deposition. The antagonizing effects of BMP-7 are mediated in TM cells through Smad7.

See also: The Fibrillar Extracellular Matrix of the Trabecular Meshwork; Functional Morphology of the Trabecular Meshwork; Pseudoexfoliation Syndrome and Glaucoma; Role of Proteoglycans in the Trabecular Meshwork; Structural Changes in the Trabecular Meshwork with Primary Open Angle Glaucoma.

Further Reading

Adams, J. C. (2001). Thrombospondins: Multifunctional regulators of cell interactions. *Annual Review of Cell and Development Biology* 17: 25–51.

Annes, J. P., Munger, J. S., and Rifkin, D. B. (2003). Making sense of latent TGFβ activation. *Journal of Cell Science* 116: 217–224.

Blobe, G. C., Schiemann, W. P., and Lodish, H. F. (2000). Role of transforming growth factor beta in human disease. *New England Journal of Medicine* 342: 1350–1358.

Fleenor, D. L., Shepard, A. R., Hellberg, P. E., et al. (2006). TGFbeta2-induced changes in human trabecular meshwork: Implications for intraocular pressure. *Investigative Ophthalmology and Visual Science* 47: 226–234.

Flügel-Koch, C., Ohlmann, A., Fuchshofer, R., Welge-Lüssen, U., and Tamm, E. R. (2004). Thrombospondin-1 in the trabecular meshwork: Localization in normal and glaucomatous eyes, and induction by TGF-beta1 and dexamethasone *in vitro*. *Experimental Eye Research* 79: 649–663.

Fuchshofer, R., Stephan, D. A., Russell, P., and Tamm, E. R. (2009). Gene expression profiling of TGFβ2-and/or BMP7-treated trabecular meshwork cells: Identification of Smad7 as a critical inhibitor of TGF-β2 signaling. *Experimental Eye Research* 88: 1020–1032.

Fuchshofer, R. and Tamm, E. R. (2009). Modulation of extracellular matrix turnover in the trabecular meshwork. *Experimental Eye Research* 88: 683–688.

Fuchshofer, R., Yu, A. H., Welge-Lüssen, U., and Tamm, E. R. (2007). Bone morphogenetic protein-7 is an antagonist of transforming growth factor-beta2 in human trabecular meshwork cells. *Investigative Ophthalmology and Visual Science* 48: 715–726.

Gottanka, J., Chan, D., Eichhorn, M., Lütjen-Drecoll, E., and Ethier, C. R. (2004). Effects of TGF-β2 in perfused human eyes. *Investigative Ophthalmology and Visual Science* 45: 153–158.

Itoh, S. and ten Dijke, P. (2007). Negative regulation of TGF-beta receptor/Smad signal transduction. *Current Opinion in Cell Biology* 19: 176–184.

Johnson, M. (2006). What controls aqueous humour outflow resistance? *Experimental Eye Research* 82: 545–557.

Junglas, B., Yu, A. H. L., Welge-Lüssen, U., Tamm, E. R., and Fuchshofer, R. (2009). Connective tissue growth factor induces extracellular matrix deposition in human trabecular meshwork cells. *Experimental Eye Research* 88: 1065–1075.

Leask, A. and Abraham, D. J. (2004). TGF-beta signaling and the fibrotic response. *FASEB Journal* 18: 816–827.

Tamm, E. R. and Fuchshofer, R. (2007). What increases outflow resistance in primary open-angle glaucoma? *Survey of Ophthalmology* 52(supplement 2): S101–S104.

Tripathi, R. C., Li, J., Chan, W. F. A., and Tripathi, B. J. (1994). Aqueous humor in glaucomatous eyes contains an increased level of TGF-β2. *Experimental Eye Research* 58: 723–727.

Wordinger, R. J., Fleenor, D. L., Hellberg, P. E., et al. (2007). Effects of TGF-beta2, BMP-4, and gremlin in the trabecular meshwork: Implications for glaucoma. *Investigative Ophthalmology and Visual Science* 48: 1191–1200.

Regulation of Intraocular Oxygen by the Vitreous Gel

N M Holekamp, Barnes Retina Institute, St. Louis, MO, USA
Y-B Shui and D C Beebe, Washington University, St. Louis, MO, USA

Glossary

Ascorbate – An ion of ascorbic acid; it is an antioxidant and a cofactor in vital enzymatic reactions. Almost all organisms manufacture ascorbate internally, with humans a notable exception. L-ascorbate is the biologically active form of vitamin C.
Intraocular oxygen tension – Oxygen as measured in mmHg by an optical oxygen-sensing probe when the probe is placed inside the eye, usually at various locations within the vitreous or aqueous humor of the eye.
Liquefaction – The process by which the gelatinous nature of the vitreous gel degenerates into liquid, and it usually accompanies aging.
Nuclear sclerotic cataract – A type of cataract characterized by increasing hardness or density at the center of the crystalline lens. Believed to be due to oxidation of nuclear proteins within the lens, and it usually occurs with aging.
Open-angle glaucoma – The most common type of glaucoma caused by gradual increase in resistance to normal outflow of aqueous from eye despite an apparently open anterior chamber angle. If untreated, results in gradual painless irreversible loss of vision.
Oxygen consumption – The process by which oxygen is a substrate in a biochemical reaction leading to the formation of a new product and a reduction in molecular oxygen.
Vitreous gel – The transparent, colorless, gelatinous mass comprised of water, fine collagen fibrils, and hyaluronic acid that fills rear the two-thirds of the eye between the lens and the retina. The water content of the vitreous is 98% yet the vitreous has a viscosity 2–4 times that of pure water, giving it a gelatinous consistency.

Introduction

The anatomy of the eye brings highly vascularized, oxygenated structures such as the retina, the ciliary body, and the iris within close proximity of avascular, relatively low oxygen structures such as the crystalline lens, aqueous, and vitreous. It is critical to the health of the eye that the low oxygen structures remain in a hypoxic environment. Thus, intraocular oxygen must be tightly regulated. There is new evidence that the human vitreous gel has the important biophysical function of oxygen consumption and therefore intraocular oxygen regulation. This function is markedly reduced as the gel undergoes age-related vitreous liquefaction or removal by vitrectomy surgery. Thus, a new understanding of vitreous gel function suggests that vitreous liquefaction may be central to the pathologic process in which excessive intraocular oxygen leads to oxidation-induced conditions such as nuclear sclerotic cataract and open-angle glaucoma.

Mapping of Intraocular Oxygen: Oxygen Gradients

Recent work by researchers at the Washington University School of Medicine in St. Louis has provided a partial map of intraocular oxygen tension in the human eye. Inhaled room air consists of 21% oxygen. Figure 1 shows that the avascular and translucent spaces of the eye are characterized by an oxygen tension below 4%. The definition of hypoxia is 5% oxygen or less. Thus, a large proportion of the human eye, specifically the avascular structures, exists under hypoxic conditions.

Figure 2 shows the actual oxygen measurements as measured by an optical oxygen probe that measures oxygen tension through fluorescence decay. In the anterior chamber there is a concentration gradient of oxygen from 25 mmHg right behind the central cornea to 3 mmHg just in front of the crystalline lens. Oxygen diffuses across the cornea into the anterior chamber. Both the aqueous and the crystalline lens have the ability to act as an oxygen sink to consume or metabolize the oxygen. In the posterior chamber, there is a concentration gradient from 9 mmHg adjacent to the ciliary body to 7 mmHg in the center of the vitreous cavity. Although not shown in Figure 2, oxygen tension at the retina has been measured by other investigators and was found to be quite high as expected, exceeding 30 mmHg. Thus, in the posterior segment most of the molecular oxygen comes from the retina. The vitreous gel acts as the sink to consume or metabolize the oxygen.

Figure 3 compares the oxygen mapping of the human to the oxygen mapping of the rabbit. The most notable difference is that in the posterior segment of the eye, the oxygen concentration gradient in the human is lowest in

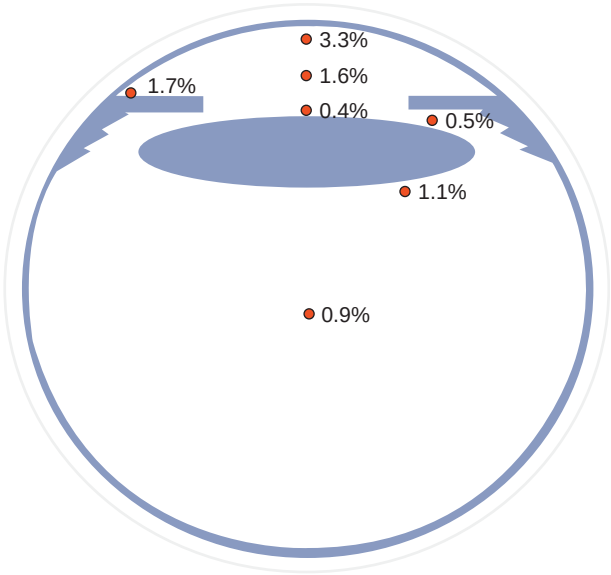

Figure 1 Oxygen distribution in the human eye (%). Reproduced from Holekamp, N. M., Shui, Y. B., and Beebe, D. C. (2005). Vitrectomy surgery increases oxygen exposure to the lens: A possible mechanism for nuclear cataract formation. *American Journal of Ophthalmology* 139(2): 302–310, with permission from American Journal of Ophthalmology.

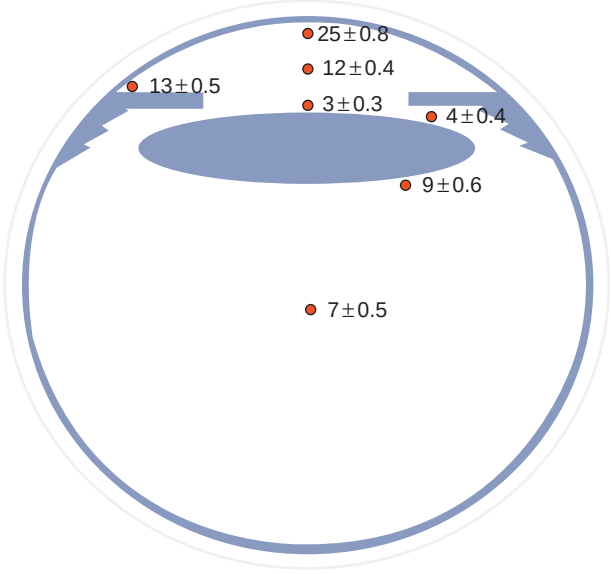

Figure 2 Oxygen distribution in the human eye (mmHg). Reproduced from Holekamp, N. M., Shui, Y. B., and Beebe, D. C. (2005). Vitrectomy surgery increases oxygen exposure to the lens: A possible mechanism for nuclear cataract formation. *American Journal of Ophthalmology* 139(2): 302–310, with permission from American Journal of Ophthalmology.

the center of the vitreous gel, while the oxygen concentration gradient for the rabbit is lowest at the posterior surface of the lens. This elucidates an important difference in intraocular oxygen regulation between the species. In humans, the vitreous has the largest capacity to consume oxygen, while in the rabbit this important biochemical property resides mostly in the lens. Corroborating evidence is provided by the work of colleagues at the Washington University School of Medicine who found that the human eye differs from most other laboratory animals studied: the human vitreous has a much larger capacity to consume oxygen than the human lens. In animals, this relationship appears to be reversed. The animal lens has a much greater capacity to consume oxygen than the animal vitreous. Thus, in most animals, the lens protects itself from oxidative damage. In humans, it is primarily the vitreous gel that protects the lens from oxidative damage. This difference between humans and experimental animals may help explain why there is currently no animal model of nuclear sclerotic cataract.

The Vitreous Gel Consumes Oxygen: Experiments with Cadaver Vitreous

The vitreous gel is the largest component structure in the human eye and is located centrally between the highly oxygenated retina and the hypoxic crystalline lens. Within the vitreous gel is a steep oxygen concentration gradient. In order to maintain this gradient the vitreous gel must consume oxygen. **Figure 4** shows the results of an experiment in which a small sample of cadaver vitreous was placed in an oxygen-impermeable glass tube sealed with an optical oxygen probe. Oxygen tension starts out quite high at 120 mmHg and slowly falls to zero within 2 h. Thus, cadaver vitreous consumes oxygen. This metabolism is unaffected by boiling of the vitreous gel, suggesting an acellular, heat-resistant process.

The postulated biochemical reaction in which vitreous consumes oxygen is shown in **Figure 5**. In the presence of heat-stable, metal ion catalysts and the enzyme catalase, two molecules of oxygen react with one molecule of ascorbate to produce one molecule of oxygen and two molecules of water, with dihydroascorbate and hydrogen peroxide serving as intermediate products. It is important to note that water and ascorbate alone will not consume oxygen. Thus, factors important to this proposed chemical reaction are intrinsic to the vitreous gel.

The heat-stable catalyst in vitreous that promotes the ascorbate–oxygen reaction is not known. The oxidation of ascorbate can be catalyzed by metal ions, like copper or iron, and trace concentrations of metals have been detected in human vitreous. Although ethylenediaminetetraacetic acid (EDTA) completely prevents copper from catalyzing the oxidation of ascorbate by oxygen in a model reaction, treatment of vitreous with 10 mM EDTA slightly enhances the consumption of oxygen by vitreous humor. Compounds that bind iron and inhibit its ability to catalyze oxidation reactions only partially inhibit the ascorbate-dependent consumption of oxygen. This suggests that free iron contributes to this reaction,

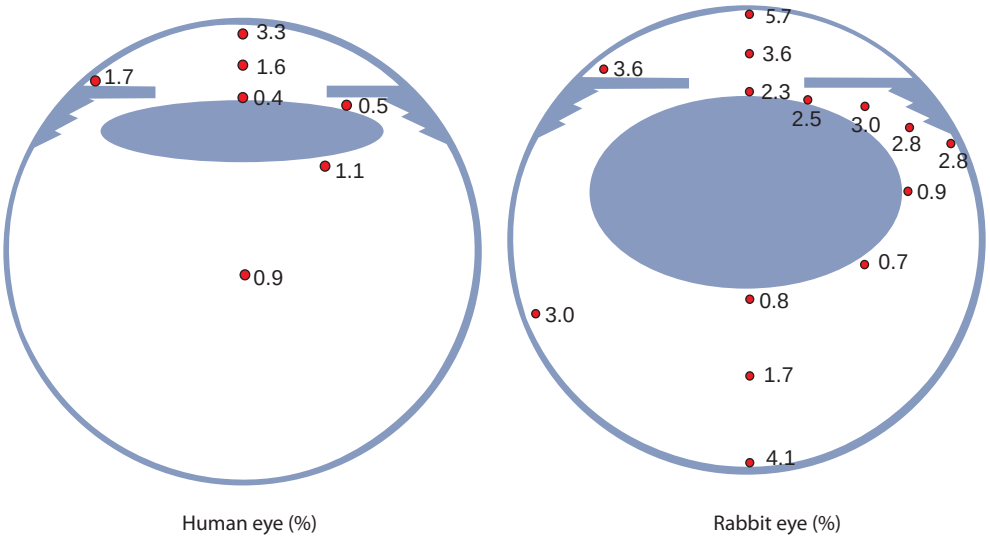

Figure 3 A comparison of oxygen levels in humans and rabbit. Reproduced from Holekamp, N. M., Shui, Y. B., and Beebe, D. C. (2005). Vitrectomy surgery increases oxygen exposure to the lens: A possible mechanism for nuclear cataract formation. *American Journal of Ophthalmology* 139(2): 302–310, with permission from American Journal of Ophthalmology; Shui, Y. B., Fu, J. J., Garcia, C., et al. (2006). Oxygen distribution in the rabbit eye and oxygen consumption by the lens. *Investigative Ophthalmology and Visual Science* 47(4): 1571–1580. Copyright Association for Research in Vision and Ophthalmology.

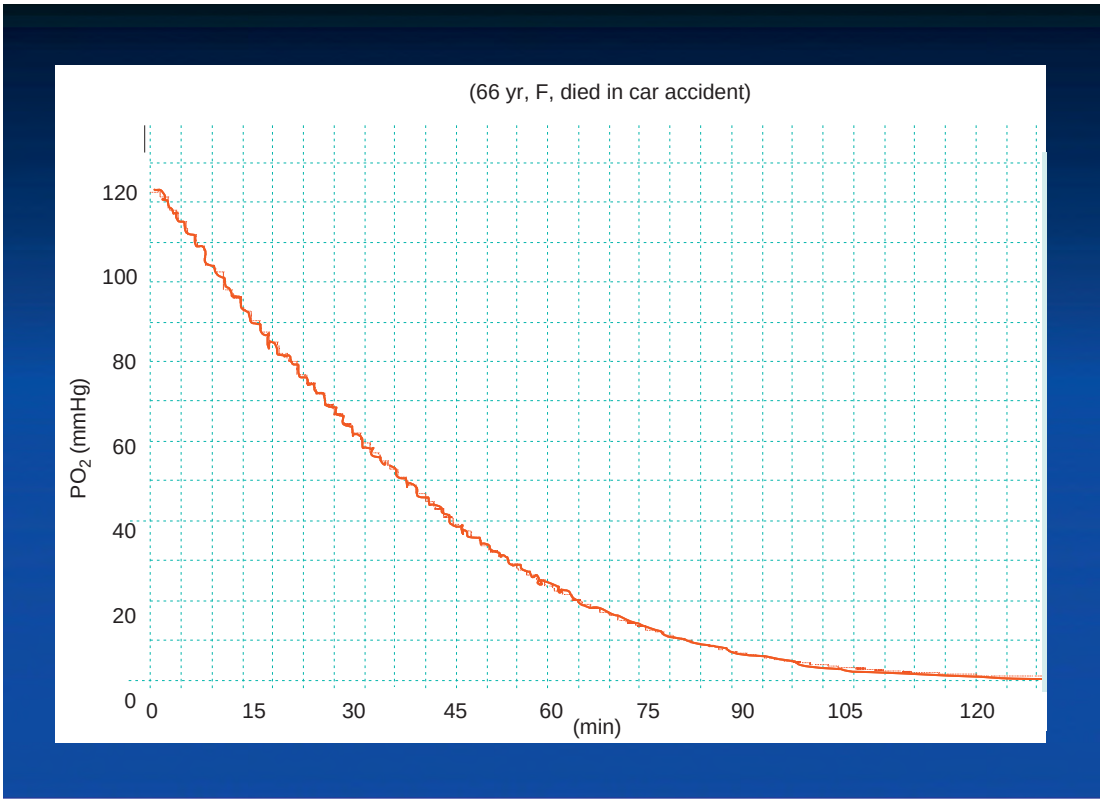

Figure 4 Human cadaver vitreous consumes oxygen *in vitro*. Reproduced from Shui, Y. B., Holekamp, N. M., Kramer, B. C., et al. (2009). The gel state of the vitreous and ascorbate-dependent oxygen consumption: Relationship to the etiology of nuclear cataract. *Archives of Ophthalmology* 127(4): 475–482, with permission from Barnes Retina Institute.

but at least one other catalyst is also involved. These additional factors have not yet been fully elucidated.

Additional experiments with cadaver vitreous indicate that the rate at which the vitreous consumes oxygen varies proportionally to concentration of ascorbate in the vitreous gel, as shown in **Figure 6**.

Ascorbate in the Vitreous Gel

Ascorbate is essentially ascorbic acid or vitamin C. The concentration of ascorbate in human vitreous is remarkably high compared to other animal species. In a recent study, the mean concentration of ascorbate in the human vitreous gel was found to be approximately 2 mM. Blood levels are only 50–60 μM, suggesting a 33- to 40-fold difference. The high concentration of ascorbate in the vitreous is maintained by a sodium-dependent ascorbate transporter (SLC23A2) in the pigmented layer of the ciliary epithelium. The function of such high levels of ascorbate in the vitreous gel was once speculative, but now appears to be critical to the role of the vitreous gel in maintaining a low oxygen environment for the crystalline lens. It is important to note that as the vitreous gel consumes oxygen both the oxygen and the ascorbate are consumed in the reaction. Active transport of ascorbate into the vitreous gel is the only known mechanism by which to maintain a physiologic level. Little is known about the human transport molecule. However, the rat ortholog of this transporter shows half-maximal saturation at ~10 μM ascorbic acid, well below the concentration in human blood. Unless ascorbate transport by human ciliary epithelial cells is markedly different compared to rats, dietary supplementation with vitamin C is unlikely to significantly increase the concentration of ascorbate in the vitreous gel. This observation is consistent with large epidemiologic studies showing that oral vitamin C supplementation has minimal effect on the incidence or progression of nuclear cataract.

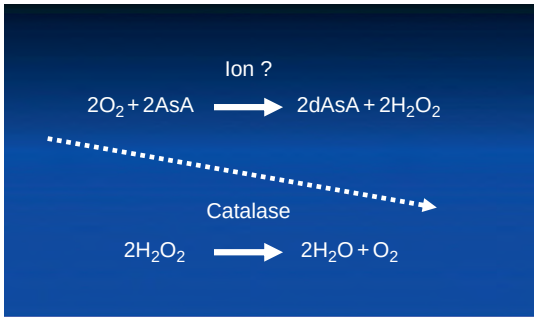

Figure 5 Proposed mechanism of oxygen consumption by ascorbate in vitreous gel. AsA, ascorbic acid; dAsA, dehydroascorbic acid.

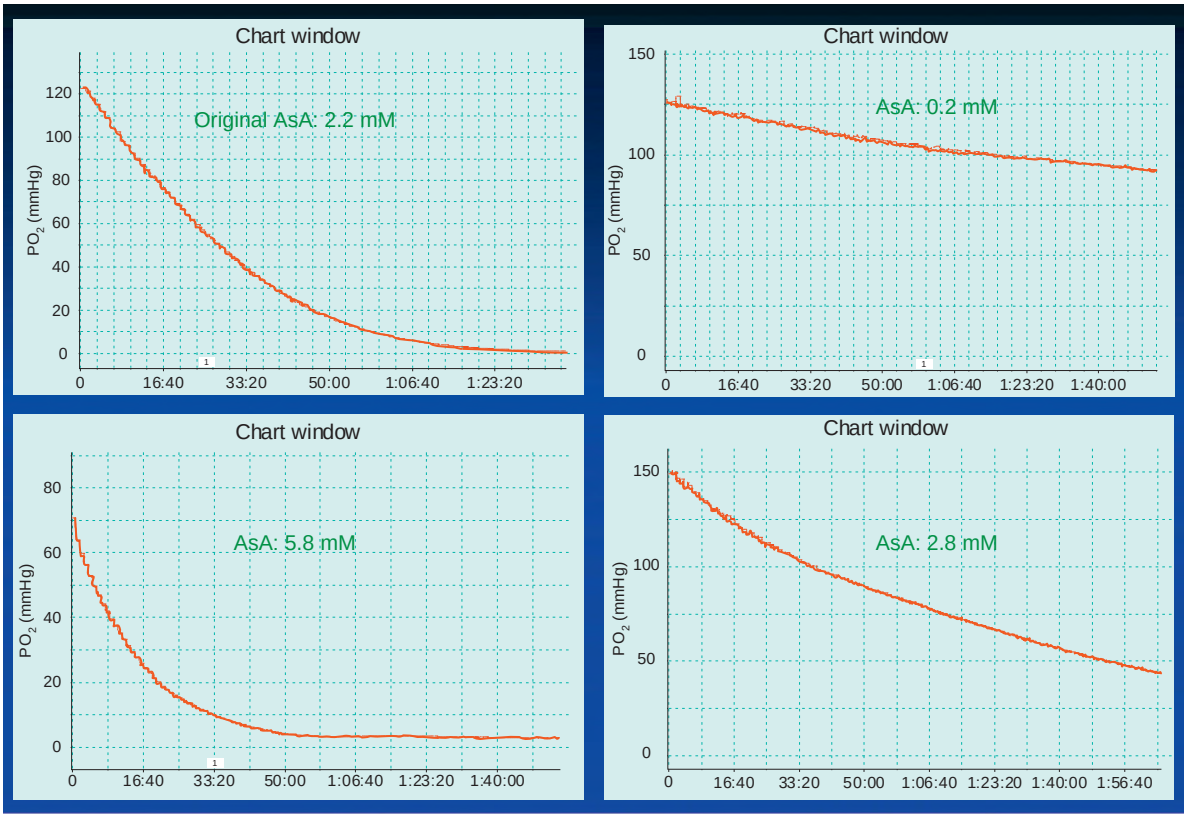

Figure 6 (Top left) O_2 consumption in fresh human cadaver vitreous. (Top right) O_2 consumption in vitreous depleted of AsA by exposure to 21% O_2. (Bottom left) Depleted vitreous with 5.0 mM AsA added. (Bottom right) Depleted vitreous with 2.5 mM AsA added.

Oxygen Consumption in the Human Vitreous Gel

Laboratory experiments on the consumption of oxygen by human cadaver vitreous have been duplicated with samples of fresh human vitreous obtained at the time of vitrectomy surgery. Figure 7 shows a normal rate of oxygen consumption in vitreous gel obtained from a 55-year-old patient undergoing vitrectomy surgery for the first time. In contrast, Figure 8 shows a markedly slower rate of oxygen consumption in vitreous fluid obtained from a 79-year-old patient undergoing vitrectomy surgery for the third time. The fluid obtained from the 79-year-old patient was not gel but rather liquid, most likely the aqueous humor that fills the posterior segment after vitrectomy surgery. A comparison of Figures 7 and 8 suggest that the gel nature of the vitreous is important to its ability to consume oxygen. In fact, this proves to be true when large numbers of eyes are compared. Gel vitreous consumes oxygen at a significantly higher rate that liquid vitreous. Furthermore, gel vitreous has a significantly higher concentration of ascorbic acid than liquid vitreous.

The Importance of the Gel Structure of the Vitreous

Oxygen moving from the retina toward the crystalline lens will diffuse through gel as easily as water. The difference, however, between gel and liquid is flow or currents moving across the retinal surface. When the vitreous is mostly in the gel state, oxygen diffusing into the gel from retinal vessels is taken up and metabolized by nearby retinal tissue, as shown by oxygen microelectrode studies in experimental animals. However, when the vitreous liquefies, oxygen diffusing from the retinal vessels is readily carried away and distributed throughout the eye by fluid currents generated by convection and movement of the eyes or head. Therefore, as suggested above, the critical difference between gel and liquid vitreous may be the extent of mixing that occurs. The more that oxygen is mixed with the vitreous fluid, the more opportunity it will have to react with ascorbate. If the rate of transport of ascorbate into the eye is constant, the net result of increased mixing would be a lower concentration of ascorbate in the vitreous fluid, slowing down the consumption of oxygen. This hypothesis is consistent with previous studies in

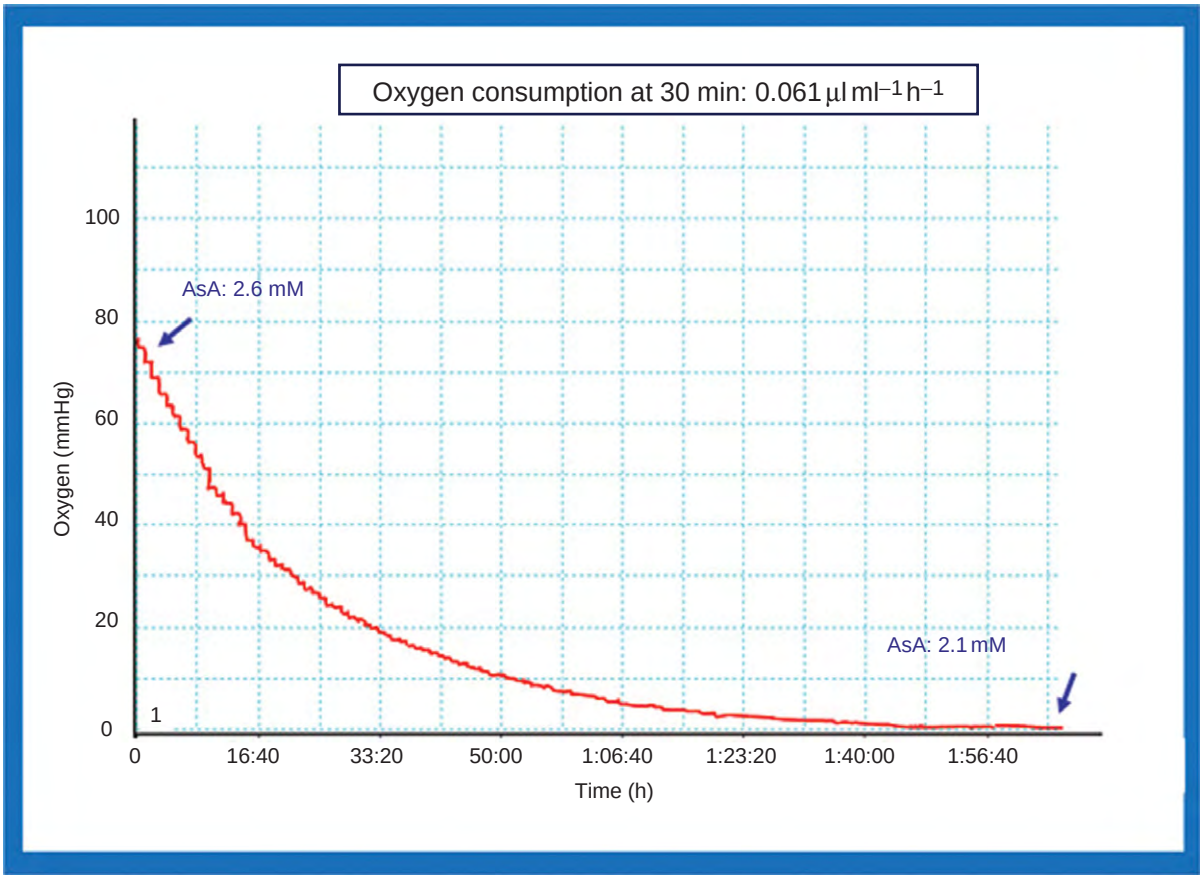

Figure 7 A 55-year-old-patient WF; first vitrectomy.

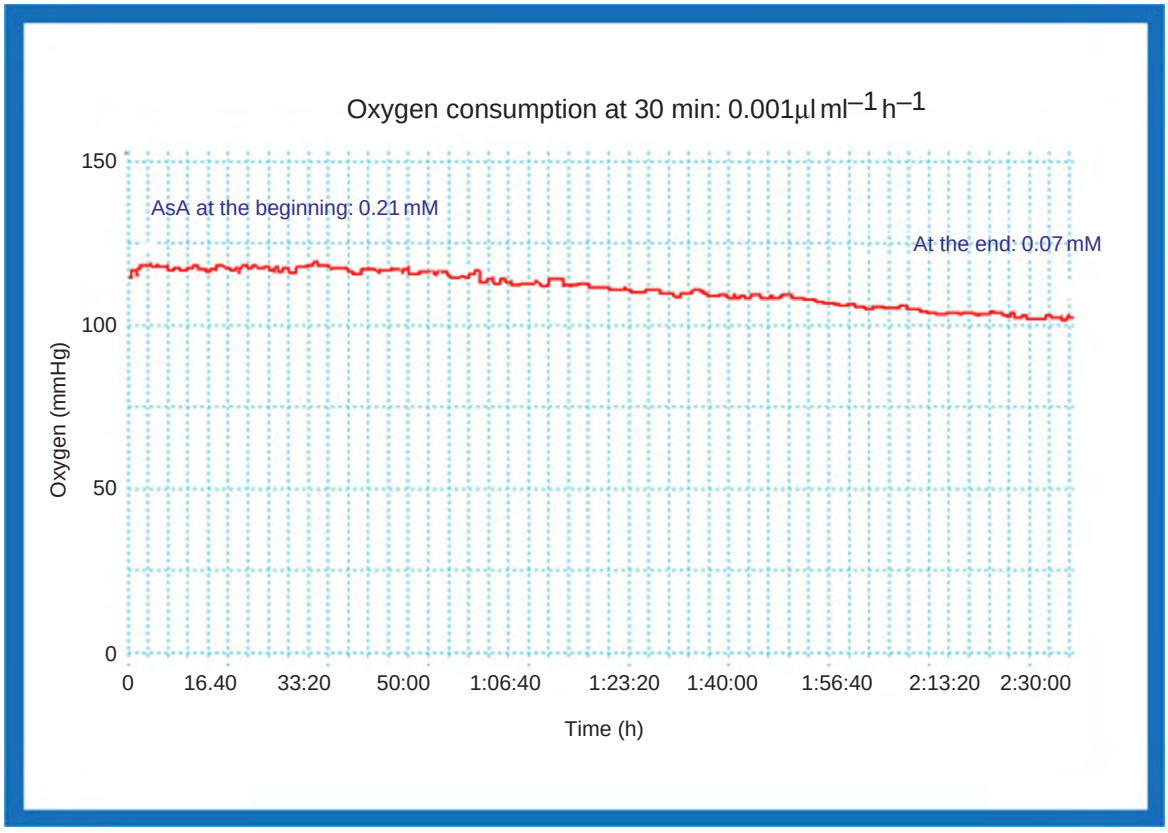

Figure 8 A 78-year-old patient WF; third vitrectomy.

which oxygen tension in the posterior segment of the eye was found to be higher in eyes that had the vitreous gel removed by vitrectomy surgery and physiologically replaced with aqueous.

Vitreous Liquefaction/Surgery Leads to Loss of Vitreous Gel Function

One newly identified function of the vitreous gel is to consume oxygen and protect the crystalline lens from oxidation of the nuclear proteins that ultimately leads to nuclear cataract. As the vitreous gel liquefies, this function diminishes. Harocopos and co-workers have documented the importance of vitreous liquefaction in nuclear cataract formation. **Figure 9** shows the results of a study of almost 100 cadaver eyes in which the degree of vitreous liquefaction correlates with degree of nuclear sclerotic cataract, independent of age.

Vitrectomy surgery is tantamount to instantaneous vitreous liquefaction. Vitrectomy surgery in phakic patients over the age of 50 years leads to significant nuclear cataract progression within 2 years. With few exceptions (as discussed below), such patients will invariably require cataract surgery within 2 years. Patients under the age of 50 likely have a cushion of formed vitreous gel immediately behind

Correlates	Adjusted for:	Partial Spearman coefficient	*P*-value
NS and liq.	Age	0.37	<0.0001
NS and age	Liquefaction	0.57	<0.0001

Figure 9 Liquefaction independent of age contributes to nuclear cataract. Reproduced from Harocopos, G. J., Shui, Y., McKinnon, M., Holekamp, N. M., Gordon, M. O., and Beebe, D. C. (2004). Importance of vitreous liquefaction in age-related cataract. *Investigative Ophthalmology and Visual Science* 45(1): 77–85. Copyright Association for Research in Vision and Ophthalmology.

the lens that is not removed at the time of vitrectomy. This may prove sufficient to consume oxygen and protect the lens from oxidative damage. Alternatively, a younger lens may retain some ability of its own to consume oxygen and protect itself. If these patients who undergo vitrectomy surgery prior to the age of 50 are followed for a period of 10 or more years, a milky-white discoloration of the nucleus of the crystalline lens with a myopic shift can be

noted. Another exception is that diabetic patients develop less-frequent and less-dense post-vitrectomy nuclear cataract than nondiabetic individuals. This may be explained by the fact that diabetic individuals have lower intraocular oxygen tension following vitrectomy. As noted above, the molecular oxygen is coming from the vascularized tissues of the eye. These patients are likely to have relative ischemia due to the microvascular complications of diabetes mellitus.

Corroborating evidence that surgical removal of the vitreous gel leads to loss of vitreous gel function and progressive nuclear sclerotic cataract can be found in a study of nonvitrectomizing vitreous surgery. In 2005, Sawa and co-workers published a series of 30 patients, median age of 70 years, who underwent nonvitrectomizing vitreous surgery in which an epiretinal membrane was delaminated without removal of vitreous gel or infusion of balanced salt solution. Scheimpflug lens photographs were taken at baseline and at a median of 5 years of follow-up. In contrast to what would be expected in this group of older patients, there was no significant progression of nuclear cataract.

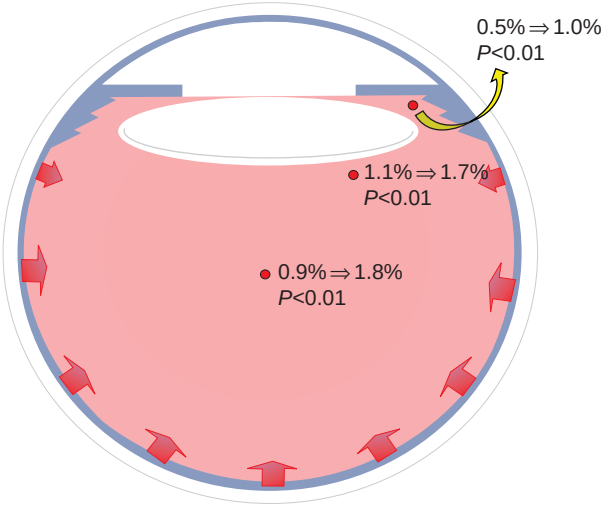

Figure 10 Oxygen levels increase long term after vitrectomy surgery. Reproduced from Holekamp, N. M., Shui, Y. B., and Beebe, D. C. (2005). Vitrectomy surgery increases oxygen exposure to the lens: A possible mechanism for nuclear cataract formation. *American Journal of Ophthalmology* 139(2): 302–310, with permission from American Journal of Ophthalmology.

Intraocular Oxygen Tension after Vitrectomy Surgery

Referring back to **Figures 1** and **2**, intraocular oxygen mapping of the human eye indicates that there are standing intraocular oxygen gradients. The vitreous gel maintains those gradients. Similar measurements taken immediately after removal of the vitreous gel through vitrectomy surgery shows that those gradients are lost. Similar measurements taken many months to years after vitrectomy surgery indicate that the intraocular oxygen tension is chronically higher. This reduction in oxygen consumption by the vitreous and the resultant loss of oxygen gradients and the elevation in intraocular oxygen tension transmit throughout the posterior pole up to the iris plane. **Figure 10** shows that the intraocular oxygen tension is statistically significantly higher long term after vitrectomy surgery. The human crystalline lens also has the ability to consume oxygen, although to a lesser extent than the vitreous gel. The lens may act as a physical and functional barrier to the increased oxygen tension in the posterior segment being transmitted to the anterior chamber. **Figure 11** indicates the changes in anterior chamber oxygen tension that occur when the crystalline lens is removed by cataract surgery. The anterior chamber oxygen tension increases, and this change has statistical significance centrally.

The vitreous gel and, to a lesser extent, the crystalline lens have the ability to consume oxygen and regulate intraocular oxygen tension. The loss of the vitreous gel after vitrectomy surgery raises intraocular oxygen tension and leads to nuclear sclerotic cataract. Once the opacified

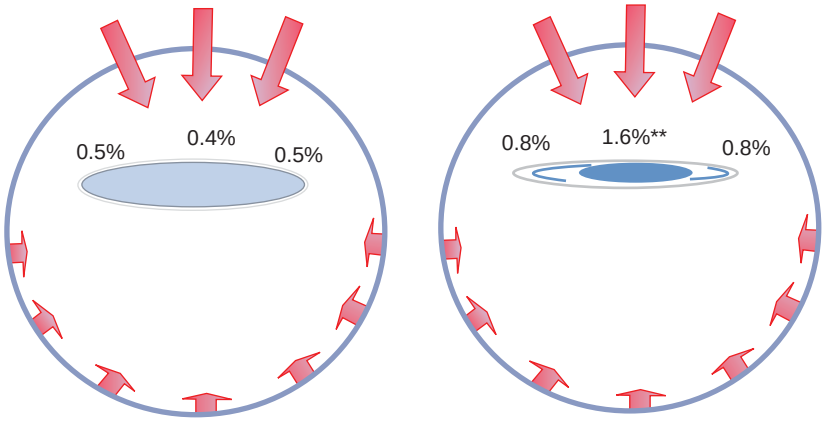

Figure 11 Cataract surgery increases anterior chamber oxygen levels.

lens is removed with cataract surgery the anterior chamber also experiences increased intraocular oxygen tension. In 2006, Stanley Chang hypothesized and supported with a large retrospective clinical study that 15–20% of eyes undergoing vitrectomy surgery followed by cataract surgery will develop open-angle glaucoma if followed long term. This work was duplicated recently by Luk and coworkers. There is growing evidence that oxidative stress may damage the cells of the trabecular meshwork as well as induce apoptotic neuronal cell death, two important mechanisms of open-angle glaucoma. Thus, removing the vitreous gel with vitrectomy surgery and removing the crystalline lens with cataract surgery render the eye devoid of two important tissues with the ability to consume oxygen and regulate intraocular oxygen.

Conclusion

Intraocular oxygen tension is highly regulated. In the human eye, the vitreous gel is the predominant intraocular tissue with the important biophysical property to consume molecular oxygen. It does so in an acellular, ascorbate-dependent chemical reaction. In addition, the gel nature of the vitreous is essential to this function. As the gel vitreous undergoes age-related liquefaction or surgical removal, the ability to consume oxygen is markedly reduced. The result is a significant long-term loss of normal intraocular oxygen concentration gradients and chronic elevation of intraocular oxygen tension. Thus, vitreous liquefaction or surgical removal may be an abnormal or pathologic state contributing to oxidation-mediated disease processes such as nuclear sclerotic cataract or open-angle glaucoma.

In summary, an intact vitreous gel is central to a healthy human eye. Currently, vitreous liquefaction is unavoidable in the human eye. The mechanism underlying this process is poorly understood. Very few mammals experience vitreous liquefaction, making the use of an animal model difficult. Currently, there are no major research efforts to prevent age-related vitreous liquefaction or to identify its causes. Future research on the vitreous gel should focus on the following areas: understanding and ultimately preventing vitreous liquefaction, methods to supplement liquefied vitreous with sufficient ascorbate to reestablish normal oxygen consumption capacity, vitreous substitutes that re-create the gel structure, and finding artificial means to regulate intraocular oxygen tension as the vitreous gel liquefies or is surgically removed.

See also: Anti-Angiogenic Properties of Vitreous; Molecular Composition of the Vitreous and Aging Changes; Nuclear Cataract; Pharmacological Vitreolysis; The Physiological Consequences of Vitreous Composition; The Role of Oxidative Stress in the Trabecular Meshwork.

Further Reading

Barton, K. A., Shui, Y. B., Petrash, J. M., and Beebe, D. C. (2007). Comment on: the Stokes–Einstein equation and the physiological effects of vitreous surgery. *Acta Ophthalmologica Scandinavica* 85: 339–340.

Chang, S. (2006). LXII Edward Jackson lecture: Open angle glaucoma after vitrectomy. *American Journal of Ophthalmology* 141: 1033–1043.

Harocopos, G. J., Shui, Y., McKinnon, M., et al. (2004). Importance of vitreous liquefaction in age-related cataract. *Investigative Ophthalmology and Visual Science* 45: 77–85.

Holekamp, N. H. (2010). The vitreous gel: More than meets the eye. *American Journal of Ophthalmology* 149: 32–36.

Holekamp, N. M., Shui, Y. B., and Beebe, D. C. (2005). Vitrectomy surgery increases oxygen exposure to the lens: A possible mechanism for nuclear cataract formation. *American Journal of Ophthalmology* 139(2): 302–310.

Holekamp, N. H., Shui, Y. B., and Beebe, D. C. (2006). Lower intraocular oxygen tension in diabetics: Possible contribution to decreased incidence of nuclear sclerotic cataract. *American Journal of Ophthalmology* 141(6): 1027–1032.

Izzotti, A., Bagnis, A., and Sacca, S. C. (2006). The role of oxidative stress in glaucoma. *Mutation Research* 612: 105–114.

Luk, F. O., Kwok, A. K., Lai, T. Y. Y., and Lam, D. S. (2009). Presence of crystalline lens as a protective factor for the late development of open angle glaucoma following vitrectomy. *Retina* 29(2): 218–224.

Melberg, N. S. and Thomas, M. A. (1995). Nuclear sclerotic cataract after vitrectomy in patients younger than 50 years of age. *Ophthalmology* 102: 1466–1471.

Quiram, P. A., Leverenz, V. R., Baker, Dang, R. M., et al. (2007). Microplasmin-induced posterior vitreous detachment affects vitreous oxygen levels. *Retina* 27: 1090–1096.

Sawa, M., Ohji, M., Kusaka, S., et al. (2005). Nonvitrectomizing vitreous surgery for epiretinal membrane long-term follow-up. *Ophthalmology* 112: 1402–1408.

Shui, Y. B., Holekamp, N. M., Kramer, B. C., et al. (2009). The gel state of the vitreous and ascorbate-dependent oxygen consumption: Relationship to the etiology of nuclear cataracts. *Archives of Ophthalmology* 127: 475–482.

Stefansson, E., Novack, R. L., and Hatchell, D. L. (1990). Vitrectomy prevents retinal hypoxia in branch retinal vein occlusion. *Investigative Ophthalmology and Visual Science* 31: 284–289.

Truscott, R. J. (2005). Age-related nuclear cataract-oxidation is the key. *Experimental Eye Research* 80: 709–725.

Tsukaguchi, H., Tokui, T., Mackenzie, B., et al. (1999). A family of mammalian Na^+-dependent L-ascorbic acid transporters. *Nature* 399(6731): 70–75.

Retinal Cannabinoids

S Yazulla, Stony Brook University, Stony Brook, NY, USA

Glossary

Age-related macula degeneration (AMD) – It comprises a variety of diseases, mainly of the elderly, that involves loss of vision in the central region of the retina.
Endocannabinoids – Natural chemicals in the body that are mimicked by the active component of marijuana.
Monoamine oxidase (MAO) – An enzyme that degrades dopamine.
Snellen acuity – A test of visual acuity that uses a standard sized "E" in four orientations.
Transient receptor potential type vanilloid 1 receptor (TRPV1) – An ionotropic receptor that increases intracellular calcium either by entry through the plasma membrane or from intracellular stores. It is activated by noxious heat, capsaicin, and the endocannabinoid, anandamide.
Vernier acuity – A test of visual acuity that tests the ability to detect displacement of two lines end-to-end.

Marijuana and the Endocannabinoids

The active component of the marijuana plant *Cannabis sativa*, Δ^9-tetrahydrocannabinol (THC), mimics endogenous chemicals, endocannabinoids (eCBs) that activate membrane receptors. eCBs include a variety of amide, ester, and ether derivatives of arachidonic acid. The most widely studied of these are arachidonoyl ethanolamide (anandamide, AEA) and *sn*-2 arachidonoyl glycerol (2-AG) (Figure 1). Other eCBs have been identified with varying degrees, or no affinity for cannabinoid receptors, and also compete with AEA and 2-AG for metabolizing enzymes. In this way, they modulate activity by competition at the receptors or by affecting substrate availability for metabolism.

Synthesis and Release

Unlike water-soluble transmitters, AEA and 2-AG are lipophilic and not stored in synaptic vesicles. Rather, membrane phospholipids are metabolized on demand to liberate AEA and 2-AG by calcium-dependent phospholipases. The precursor of AEA is *N*-arachidonyolphosphatidyl ethanolamine (NAPE), formed by calcium-dependent transfer of arachidonic acid (AA) from arachidonoylphosphatidylcholine to phosphatidylethanolamine (PE). There are multiple pathways for AEA liberation from the membrane. First, NAPE is hydrolyzed by phospholipase D (PLD) to release AEA and phosphatidic acid. Second, NAPE is hydrolyzed to *N*-acyl-lyso-PE by phospholipase A_1/A_2; then, AEA is released by lysophospholipase D. Third, phospholipase C (PLC) cleaves NAPE to generate phosphoanandamide, which is dephosphorylated to liberate AEA. The PLC pathway may be involved in the on-demand synthesis of AEA rather than in maintaining basal tissue levels of AEA. The primary pathway for 2-AG synthesis involves hydrolysis of diacylglycerols (DAG) by DAG lipase isozymes, DAGLα and DAGLβ. DAGs may be produced by the PLC β-catalyzed hydrolysis of phophotidylinositol or hydrolysis of phosphatidic acid by a phosphohydrolase. AEA and 2-AG freely diffuse within the membrane where they interact with the active sites of degradative enzymes and receptors. AEA binds reversibly to serum albumin, and it is likely that such binding is critical for the movement of AEA and 2-AG in blood, the extracellular matrix, and the cytoplasm. The presence and localization of AEA and 2-AG are inferred from the distribution of receptors, synthesizing and inactivating enzymes as well as physiological effects on identified cells.

Inactivation

AEA and 2-AG are inactivated following intracellular accumulation by fatty acid amide hydrolase (FAAH), monoacylglycerol lipase (MGL), cyclooxygenase-2 (COX-2), and lipoxygenase (LOX). AEA and 2-AG are hydrolyzed by FAAH into AA and ethanolamine or glycerol, respectively. 2-AG, but not AEA, is hydrolyzed by MGL. Following hydrolysis of AEA or 2-AG, AA is incorporated into membrane phospholipids. COX-2 oxidizes arachidonic acid, AEA, and 2-AG to prostamides or prostaglandin glyceryl esters, leading to prostaglandins. In addition, oxidation of AA by LOX produces 12-(S)-hydroperoxyeicosatetraenoic acid (15-(S)-HPETE), 5-(S)-HETE, and leukotriene B_4, all of which are agonists of TRPV1 receptors (Figure 2).The effects of AEA and 2-AG are modulated by the balance of metabolic enzymes that is specific to each cell type.

Receptors

Effects of cannabinoids are mediated by metabotropic (G-protein-coupled receptors (GPCRs)) and ionotropic

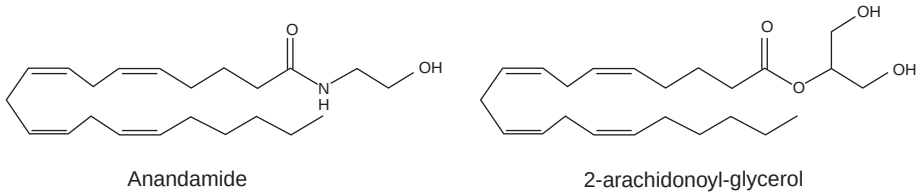

Figure 1 Chemical structures of endocannabinoids: arachidonoyl-ethanolamide (anandamide, AEA) and 2-arachidonoyl-glycerol (2-AG).

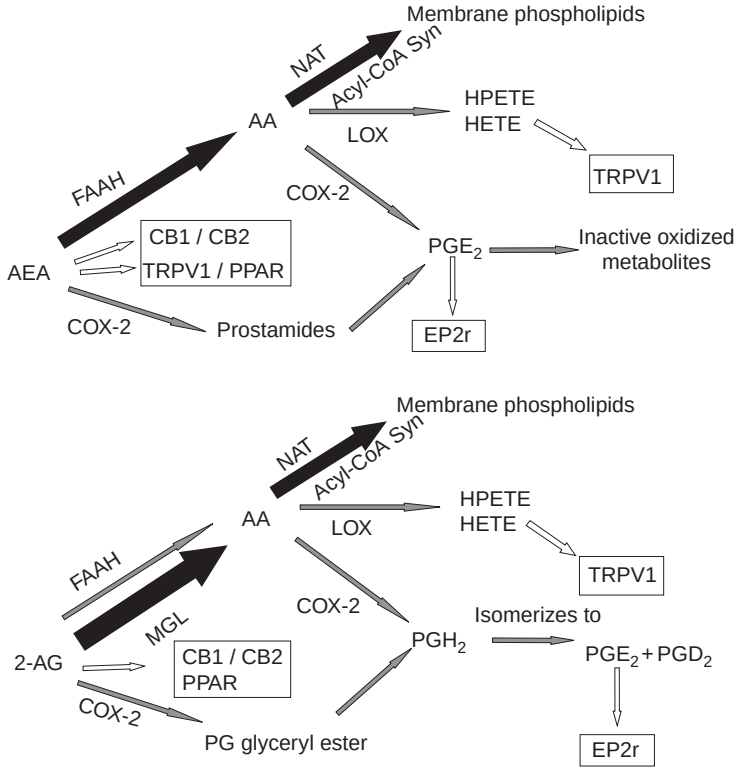

Figure 2 This schematic illustrates some of the metabolic pathways for the degradation of AEA and 2-AG. In the dominant pathways (bold arrows), AEA and 2-AG are hydrolyzed to arachidonic acid (AA), and then rapidly incorporated into membrane phospholipids via *N*-acyltransferase (NAT) and acyl-Coenzyme A synthetase. Lesser pathways (shaded arrows) involve oxidation by cyclooxygenase-2 (COX-2) of AEA, 2-AG, and AA to prostaglandins (PGE_2 and PGD_2). Additionally, AA may be oxidized by lipoxygenase (LOX) to 12-(S)- and 15-(S)-HPETE and 5-(S)-HETE. Hollow arrows show that AEA and 2-AG are endoligands for CB1, CB2, and PPAR receptors, while AEA also activates TRPV1 receptors. Metabolites of COX-2 oxidation activate EP2 receptors, and metabolites of LOX oxidation activate TRPV1 receptors.

(ion channel) receptors (Figure 2). In general, activation of cannabinoid 1 receptors (CB1Rs), via heterotrimeric guanosine-5'-triphosphate (GTP)-binding proteins Gi/o (Gi/o), modulates voltage-gated K^+ and Ca^{2+} conductances, resulting in a reduction of neurotransmitter release, particularly γ-aminobutyric acid (GABA) and glutamate. CB2 receptors, which also signal through Gi/o, are expressed in cells of the immune system and the central nervous system (CNS), particularly in astrocytes. There is evidence for additional cannabinoid receptors, perhaps GPCR 55. AEA, but not 2-AG, activates the ionotropic transient receptor potential type vanilloid 1 receptor (TRPV1) that increases intracellular calcium either by entry through the plasma membrane or from intracellular stores. Prostamides and prostaglandin glycerol esters, produced by eCB oxidation by COX-2, bind to a variety of prostaglandin receptors. eCBs are ligands for peroxisome proliferator-activated receptors (PPARs), members of the nuclear receptor superfamily that are involved in lipid metabolism, insulin sensitivity, regulation of inflammation, and cell proliferation.

Distribution and Function

CB1Rs are the most numerous GPCRs in the brain. eCBs, their receptors, and metabolizing enzymes are enriched in

brain regions associated with the physiological and psychomotor effects of cannabis. AEA and 2-AG have short- and long-term effects on synaptic plasticity and neuroprotection. The effects depend largely on retrograde transmission in which postsynaptic dendrites release an eCB that binds to presynaptic CB1Rs to reduce transmitter release. Retrograde release of eCBs is evoked by two mechanisms. In a voltage-dependent mechanism, depolarization of postsynaptic dendrites by L-glutamate opens voltage-gated calcium channels. The increase in intracellular Ca^{2+} activates Ca-dependent PLD to release an eCB. A second mechanism involves activation of heterotrimeric GTP-binding protein $G_{q/11}$ ($G_{q/11}$) coupled metabotropic receptors, usually group I metabotropic glutamate receptors (mGluRs), mGluR1 and mGluR5, and muscarinic receptors (M1 and M3). By enzymatic cascades that may or may not release calcium from intracellular stores, eCBs are released from the plasma membrane. The eCB-induced reduction of presynaptic glutamate and GABA release contributes to synaptic plasticity, while the reduction of glutamate release inhibits excitotoxicity following ischemia. Evidence implicates 2-AG more so than AEA in plasticity, while both AEA and 2-AG are involved in neuroprotection.

Cannabinoids and Ocular Tissues

Marijuana induces conjunctival vasodilation and reduces intraocular pressure (IOP), but is not a mydriatic. These effects are mediated locally by eCBs as demonstrated in the ciliary body, iris, choroid, and trabecular meshwork in mammalian tissues. THC, as low as 10^{-12} M, increases monoamine oxidase (MAO) activity in the bovine trabecular meshwork, choroid, and ciliary processes but not in the iris. Hydrolysis of anandamide has been measured in the porcine iris, choroid, lacrimal gland, and optic nerve. CB1 mRNA and CB1R-immunoreactivity (IR) have been detected in the ciliary body, trabecular meshwork, and conjunctival epithelium of rat, mouse, bovine, and human. AEA and 2-AG have been measured by gas chromatography in human ocular tissues. The content of eCBs varies in certain disease states, suggesting the importance of eCBs in maintaining ocular homeostasis. For example, 2-AG levels are lower in the ciliary body of patients with glaucoma. However, in diabetic retinopathy there are higher levels of 2-AG only in the iris, and increased levels of AEA in the retina, ciliary body, and cornea. Eyes of patients with age-related macula degeneration (AMD) also show increases of AEA in the retina, choroid, ciliary body, and cornea. Topically applied AEA reduces IOP by activation of CB1R and activation of the prostaglandin E 2 receptor (EP2R) after conversion of AEA to prostamides (see **Figure 2**). Administration of either AEA or THC to human nonpigmented epithelium (NPE) cells induces COX-2 expression, indicating a relationship among prostaglandins, COX-2, and eCBs in lowering IOP. In addition, EP2 receptors have been localized in the NPE of mouse, porcine, and human ciliary body.

Cannabinoids – Retinal Anatomy

Early studies of the effects of cannabis on vision were performed in concert with the effects of alcohol in order to examine the influence on visual motor behaviors as they related to driving. Anecdotal reports also came from studies citing side effects of cannabis when used as an analgesic. Effects on vision are subtle and include blurred and double vision, a reduction in vernier and Snellen acuity, alterations in color discrimination, an increase in photosensitivity and an increase in recovery from foveal glare. It is unlikely that all of these effects of marijuana are due to cortical or preretinal sites because processes of light–dark adaptation take place in the retina. Knockout mice that lack CB1Rs or FAAH are not blind, but the effects on vision have not been studied.

Biochemical Assay

The first evidence for cannabinoids in the retina was the demonstration that THC induced an increase in MAO activity, indicating a role in dopaminergic transmission. Later, FAAH-mediated hydrolysis of ^{3}H-AEA was shown in homogenates of porcine, bovine, and goldfish retinas. AEA and 2-AG were detected in mammalian retina by gas chromatography. Release of AEA from bovine retinal extracts in a physiological buffer demonstrated that the extracts contained the metabolic machinery necessary for eCB release, the precursor NAPE, and PLD.

Localization – Cannabinoid Receptors

CB1Rs have been localized by immunohistochemistry in the retinas of numerous species, including human, monkey, mouse, rat, chick, salamander, and goldfish. Despite differences in detail, there is a common theme. In general, the most prominent label is in cells of the through pathway: photoreceptors, bipolar cells, and ganglion cells. Cone pedicles in all species contain CB1Rs. Rod spherules appear to be labeled in all species except goldfish. Ultrastructural analysis has been performed exclusively on goldfish cones. CB1R-IR is on plasma membrane at the perimeter of the pedicle as well as within the invagination. CB1R-IR is not immediately apposed to the synaptic ribbon, but is at some distance from it. Regarding bipolar cells in mammals, CB1R-IR is restricted to rod bipolar cells as confirmed by double labeling with antisera against PKC. In goldfish, there is a higher proportion (~3:1) of CB1R-IR in ON bipolar cells compared to OFF bipolar

cells. This difference holds for mixed rod–cone bipolar cells as well as for cone bipolar cells. CB1R-IR, on the bipolar cell synaptic terminal membrane, is not adjacent to the synaptic ribbons. Rather, the CB1R-IR is always some distance removed from the ribbon, the same as observed for the cone pedicles.

Regarding rat horizontal cells, CB1R-IR is confined to the cell bodies and is not present on the dendrites, unlike bipolar cells. CB1R-IR is also found on a population of large amacrine cells, identified in rat as a rare type that is immunoreactive for PKC and GABA. In goldfish, CB1R-IR is on presynaptic membrane of amacrine cell boutons. These boutons appear throughout the depth of the inner plexiform layer and are presynaptic to bipolar cell terminals and small processes derived from ganglion cells. It is likely that these CB1R-immunoreactive processes are from a single type of diffuse amacrine cell.

CB1R-IR is on Müller's cells in goldfish but not in any other preparation. There are inconsistent reports of CB1R-IR in mammalian astrocytes, microglia, and oligodendrocytes. Activation of CB1Rs inhibits excitatory amino acid transport and induces glutamate release from astrocytes in the mammalian brain. CB1R and CB2R are involved in gliotic responses to injury. The interaction of eCBs and glia has not been investigated in the retina. CB2 mRNA was described in all cellular layers of the rat retina; this could include glial labeling, particularly Müller's cells.

Localization – Metabolizing Enzymes

There is relatively little information regarding the distribution of eCB metabolizing enzymes in the retina. The distribution of FAAH-IR in the rat and mouse is quite different from that in the fish. FAAH-IR, in rat and mouse, is most prominent in medium size and large ganglion cells, while weaker FAAH-IR is observed in the soma of horizontal cells, large dopaminergic amacrine cells, dendrites of starburst amacrine cells, and Müller's cells. FAAH-immunoreactive bipolar cells in rat and mouse are exclusively cone bipolar cells, in contrast to CB1R-IR that is exclusively in rod bipolar cells. In goldfish, FAAH-IR is present over cone photoreceptors, Müller's cells, and some amacrine cells, not ganglion cells as in mouse and rat. The distribution of FAAH-IR as it relates to FAAH activity was studied in goldfish retina. ^{3}H-AEA is hydrolyzed by FAAH with ^{3}H-AA rapidly incorporated into membrane phospholipids. Silver-grain deposition represents the trapping of ^{3}H-arachidonic acid in the plasma membrane. FAAH-IR and specific ^{3}H-AEA uptake showed the same pattern over cone photoreceptors, Müller's cells, and some amacrine cells. The co-distribution of FAAH-IR and ^{3}H-AEA uptake indicates that the bulk clearance of AEA from the extracellular space in the retina occurs as a consequence of a concentration gradient across the plasma membrane created by FAAH activity.

AEA is a ligand for the TRPV1 receptor whose binding site is on an intracellular domain. As FAAH and TRPV1 are integral membrane proteins of the endoplasmic reticulum and plasma membrane, respectively, FAAH activity may regulate the levels of AEA for TRPV1 activation. Also, following the hydrolysis of AEA by FAAH, LOX metabolites of AA could activate TRPV1. AEA then could act as an intracellular mediator by being produced from and/or degraded by the same neurons that express TRPV1 receptors. Supporting anatomical evidence for this scheme was provided first in goldfish in which co-localization of TRPV1-IR with FAAH-IR occurs in three types of amacrine cells, two of which are GABAergic. These cells ramify in interplexiform layer sublaminae *a* and *b*, indicating a general function in the OFF, ON, and ON/OFF pathways. The role would depend on the downstream cascade following the increase in calcium concentration.

MGL-IR co-localizes with FAAH-IR over medium size and large ganglion cells and with CB1R-IR in all rod bipolar cells in rat and mouse. In rat retina, COX-2-IR is constitutive in horizontal, amacrine, and ganglion cells. Following transient ischemia, COX-2 is upregulated in these cell types and induced in Müller's cells. This pattern in rat differs from mouse in which COX-2 is restricted to bipolar cell bodies and their axons. COX-2 bipolar cells are a mixed group, with 65% rod bipolar cells and 35% cone bipolar cells. Also rod bipolar cells are of two types: 68% contain COX-2-IR and 32% do not.

The cannabinergic system in vertebrate retinas, as indicated by CB1R-IR, FAAH-IR, COX-2-IR, and MGL-IR, is concentrated in the through pathway of photoreceptors, bipolar cells, and ganglion cells (**Table 1**).These cells for the most part use L-glutamate as their neurotransmitter. Cells of the inhibitory lateral pathways, horizontal cells and amacrine cells, do not feature as prominently. Exceptions are some horizontal cells, dopaminergic amacrine cells, and cholinergic starburst amacrine cells that label weakly for FAAH-IR. Bipolar cells tend to be of the on type and differentiated by rod and cone input. CB1R-IR and MGL-IR are restricted to rod bipolar cells, FAAH-IR to cone bipolar cells, and COX-2-IR to subtypes of rod and cone bipolar cells.

Cannabinoids – Retinal Physiology

Effects on Transmitter Release

Stimulation of CB1Rs via $G_{i/o}$ reduces voltage- and Ca^{2+}-evoked release of [^{3}H]-noradrenaline and [^{3}H]-dopamine in guinea pig retina. Agonists of CB1Rs, but not CB2Rs, inhibit K^{+}- and ischemia-evoked [^{3}H]

Table 1 The general distribution of CB1 receptors, FAAH, MGL, and COX-2 immunoreactivities in the retina of a variety of species as determined by immunohistochemistry

Species	*CB1*	*FAAH*	*MGL*	*COX-2*
Fish	Cones	Cones		
	25% OFF BC / 100% ON BC			
	Diffuse AC	TRPV1 AC		
	Müller's cells	Müller's cells		
Rat/Mouse	Rods/cones			
		HC (weak)		
	Rod BC	Cone BC	Rod BC	Rod/cone BC
	PKC AC	DA AC/ACh AC (weak)		
	Ganglion cells	Ganglion cells	Ganglion cells	
Salamander	Rods/cones/ganglion cells			
Chick	Rods/cones/ganglion cells			
Monkey	Rods/cones/ganglion cells			

BC – bipolar cells, AC – amacrine cells, DA – dopamine. Specific details may be found in the citations indicated for each species.

D-aspartate release from isolated bovine retina. Uptake of [^{3}H] D-aspartate identifies high-affinity uptake sites for L-glutamate and L-aspartate in photoreceptors, a small percentage of ganglion cells and Müller's cells. The rank order of potency for the CB1 agonists differs for K^+- and ischemia-evoked release. As photoreceptors are more resistant to ischemia than ganglion cells, the difference in the rank order could reflect the relative potencies of the agonists on CB1Rs on these cell types.

Effects on Ganglion cells

CB1R-mediated activity was demonstrated in rat retinal ganglion cells by [^{35}S]GTPγS autoradiography and reverse transcription polymerase chain reaction (RT-PCR). Voltage-activated Ca^{2+} currents in cultured rat ganglion cells are suppressed by cannabinoid agonist, WIN 55,212-2, an effect that is blocked by CB1 antagonists, SR141716A and AM281. The presence of CB1R function on rat retinal ganglion cells appears unusual in that CB1Rs tend to be at presynaptic boutons. One possibility is that CB1Rs are present on associational ganglion cells, whose axons and axon collaterals do not leave the retina. Rat and mouse ganglion cells also contain FAAH and MGL, putting them in position to regulate AEA and 2-AG as potential retrograde transmitters for suppression of bipolar cell and amacrine cell activity.

Effects on Bipolar Cells

CB1-mediated inhibition of L-type calcium (I_{ca}) and delayed rectifier ($I_{K(V)}$) currents has been reported for ON-bipolar cells of salamander and goldfish. As yet there are no data on OFF-bipolar cells. The voltage-activation range of the currents is not altered, but simply scaled down over the entire activation range. Goldfish mixed rod–cone (Mb) bipolar cells also have D1 dopamine receptors that enhance I_{Ca} and $I_{K(V)}$ via G protein G_s. CB1R agonists and dopamine oppose each other to modulate $I_{K(V)}$ of Mb bipolar cells. Co-application of WIN 55,212-2 (0.1–0.25 μM) reversibly blocks the enhancement induced by 10 μM dopamine even though low concentrations of WIN 55,212-2 have no effect when applied alone. The effects of dopamine and cannabinoid agonists on $I_{K(V)}$ occur within the physiological range of Mb bipolar cell function (∼–25 to 0 mV). $I_{K(V)}$ would be activated during the on portion of the response and, as a counter current, would modulate the peak:plateau ratio of the response. CB1R activation should make the Mb bipolar cell on response more tonic by suppressing the hyperpolarizing effect of $I_{K(V)}$, whereas D1 receptor activation should make the on response more phasic by enhancing $I_{K(V)}$. The effect on ganglion cells should be relatively tonic responses in scotopic (dark-adapted) conditions and relatively phasic responses in photopic (light-adapted) conditions. CB1-induced suppression of calcium currents should reduce transmitter release and reset sensitivity to further increments.

Cannabinoids and Photoreceptors

Voltage-Gated Currents

CB1-mediated modulation of photoreceptor membrane currents has only been reported for tiger salamander and goldfish. The voltage-activation ranges of these currents are not affected. Salamander rods and cones responded differently to WIN 55,212-2. I_K is suppressed in single cones and rods, whereas I_{Ca} is suppressed in cones but enhanced in rods. The differential effect on I_{Ca} and I_K in rods would increase transmitter release, resulting in the reduction of sensitivity, which is an apparent counter-adaptive effect. Goldfish cones show a biphasic response

to WIN 55,212-2: an enhancement of I_K, I_{Cl}, and I_{Ca} via G_s at concentrations $<1\,\mu M$, and suppression via $G_{i/o}$ at concentrations $>1\,\mu M$. The data obtained with retrograde suppression, to be described below, suggest that the enhancement produced by WIN 55,212-2 may be due to agonist-specific trafficking in which binding of agonists to CB1Rs favors coupling to different G proteins. For example, WIN 55,212-2 increases intracellular calcium by $G_{q/11}$ coupling in human trabecular meshwork cells, while other CB1 agonists, including THC, 2-AG, CP55940, and methanandamide couple to $G_{i/o}$ but not to $G_{q/11}$. The caution is that the data obtained with WIN 55,212-2 may or may not apply to other agonists or the eCBs.

An effect of evoked released of eCBs in the retina was demonstrated in goldfish. Retrograde suppression of membrane currents in goldfish cones in a retinal slice was achieved by applying a puff of saline with 70 mM KCl or an mGluR1 agonist, RS-3,5-dihydrophyenylglycine (DHPG), through a pipette at an Mb bipolar cell body while recording $I_{K(V)}$ from cone inner segments under whole-cell voltage clamp (**Figure 3(a)**). Retrograde inhibition of $I_{K(V)}$ was reversible and stable over several hours

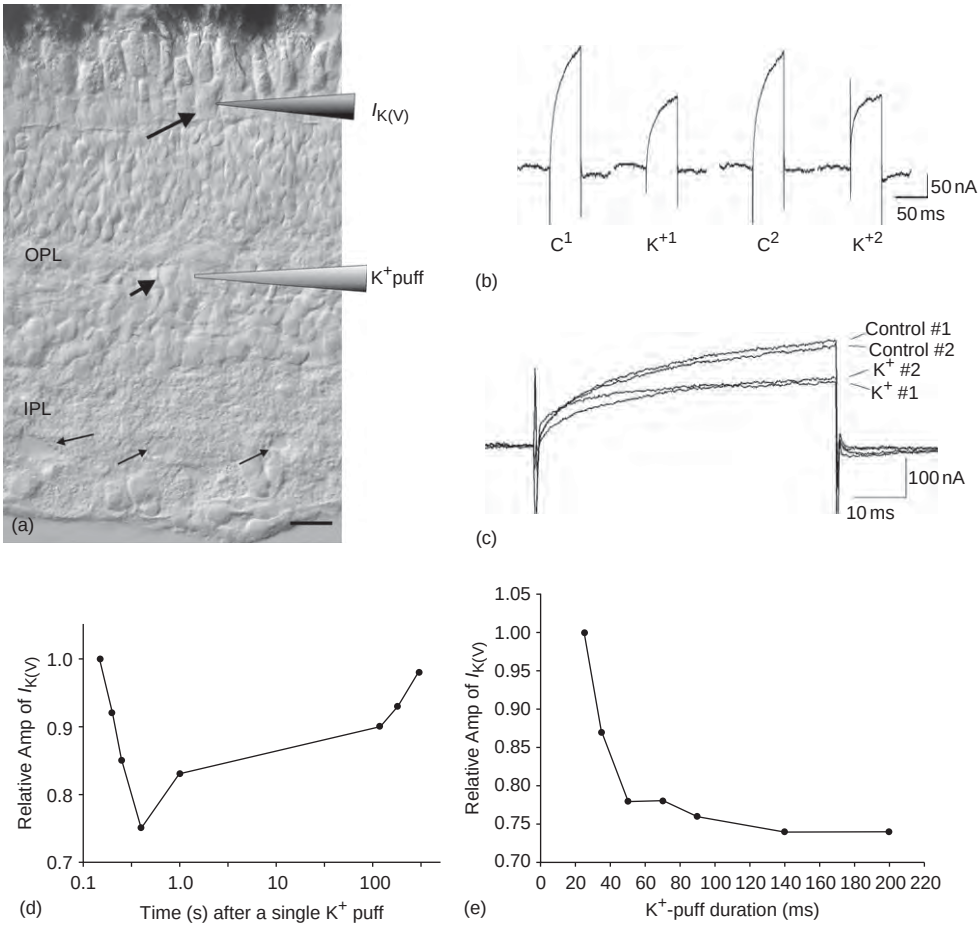

Figure 3 Properties of the retrograde responses of cones. (a) An illustration of the method used to detect retrograde responses in goldfish cones in a retinal slice. Whole cell recordings of $I_{K(V)}$ were obtained from long-single cones (long arrow). A puff pipette, containing 70 mM KCl, was positioned slightly upstream and at the cell body of an Mb bipolar cell (short arrow). Thin arrows indicate the synaptic terminals of Mb bipolar cells. OPL – outer plexiform layer, IPL – inner plexiform layer. Calibration bar = 20 μm. (b), (c) Sequential and overlay of raw records of $I_{K(V)}$ from a single cone evoked by a 50-ms depolarizing pulse to +54 mV from a holding potential of –70 mV. The records have not been normalized. A 50-ms K^+ puff was delivered twice. $I_{K(V)}$ in response to K^+ puff #1 was reduced compared to that evoked for the prepuff control #1. The cone was allowed to recover for 30 min after K^+ puff #1. $I_{K(V)}$ returned to control amplitude (C2, control #2). The K^+ puff #2 produced an equivalent reduction in $I_{K(V)}$. (d) Time course (log scale) of the reduction of $I_{K(V)}$ in response to a single 50-ms puff of K^+ shows a latency of about 200 ms following the puff, a peak response at about 500 ms, and a gradual return to control level by 5 min. (e) Effect of K^+ puff duration on $I_{K(V)}$. These data were obtained from a single cone over 4 h. After a prepuff control value of $I_{K(V)}$ was obtained, a 25-ms K^+ puff was administered and the effect on $I_{K(V)}$ was determined. The cell was allowed to recover for 30 min and another prepuff control and a K^+ puff of a longer duration was administered. This sequence was followed for all puff durations. Thus, the value plotted for each puff duration is relative to its own prepuff control. There was no effect with a puff of ≤25 ms duration. Near maximal suppression of $I_{K(V)}$ at about 25% was achieved with a puff of 50 ms and there was little additional effect with puffs as long as 200 ms. Reproduced from Fan, S. F. and Yazulla, S. (2007). Retrograde endocannabinoid inhibition of goldfish retinal cones in mediated by 2-arachidonoyl glycerol. *Visual Neuroscience* 24: 257–267.

(Figures 3(b) and 3(c)). It had a latency of about 200 ms after a K^+ puff, was reduced on average by 25%, and had a halftime of 3.4 min to recover (Figure 3(d)). Retrograde suppression of $I_{K(V)}$ was unaffected by a combination of the GABA receptor antagonist, picrotoxin, and α-amino-3-hydroxyl-5-methyl-4-isoxazole-propionate (AMPA) glutamate receptor antagonist, 6-cyano-7-nitroquinoxaline-2,3-dione (CNQX), but blocked completely by the CB1 antagonist, SR141716A, indicating mediation by CB1 receptors. Experiments with the FAAH inhibitor (URB597), a COX-2 inhibitor (nimesulide), and a blocker of 2-AG synthesis (Orlistat) indicated that 2-AG, rather than AEA, is the retrograde eCB.

Two conditions evoke 2-AG release from Mb bipolar cells, strong depolarization and activation of mGluR1, corresponding to voltage-dependent and voltage-independent mechanisms. Rods and cones release glutamate at a steady rate under any ambient illumination; this rate is increased by decrements of light intensity and decreased by increments in light intensity. Voltage-dependent release of 2-AG would occur following depolarization of the Mb bipolar cell in response to a light flash. The retrograde suppression of glutamate release from cones would be a positive feedback that would amplify the reduction in cone transmitter release initially caused by increasing light intensity. This may not be physiologically relevant because the halftime to recover from a 50-ms stimulus is several minutes. The long half-life of the suppressive effect should make this mechanism insensitive to rapid changes in intensity.

The voltage-independent mechanism that provides negative feedback on glutamate release may be more functional. Hypothetically, glutamate, released during ambient illumination, stimulates mGluR1α on Mb bipolar cells tonically to maintain a steady release of 2-AG via a $G_{q/11}$ mechanism. The degree of feedback inhibition of glutamate release from cones varies inversely with ambient illumination; the

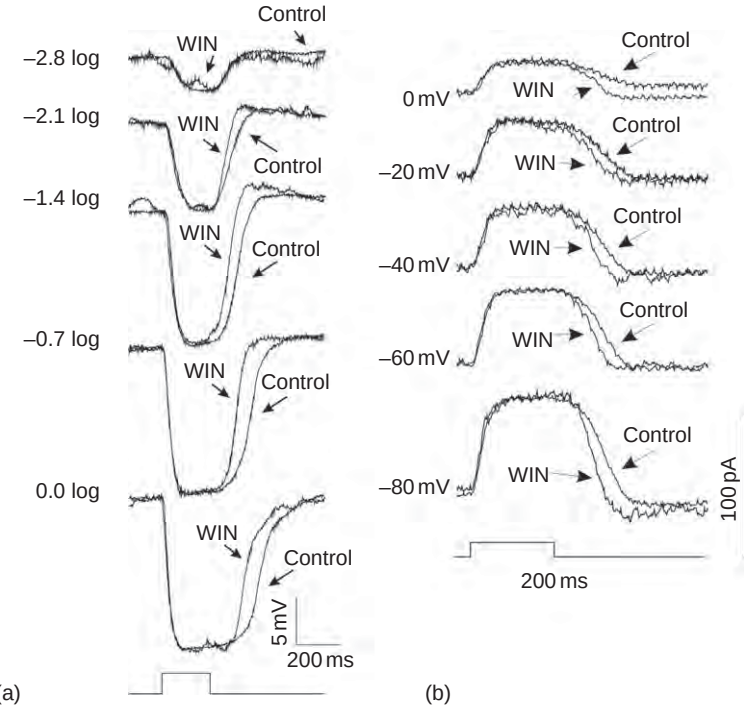

Figure 4 Effect of WIN 55,212-2 on the responses of goldfish cones in an isolated retinal preparation to flashes of light. (a) Voltage-light responses of an L-cone under current clamp to a 200-ms light stimulus of increasing intensities (log unit changes, top to bottom) for Control conditions and after 8 min in 10 μM WIN 55,212-2. Indicated at the left are relative stimulus intensities. The response amplitudes in the control and WIN conditions differed from each other by about 10%. To facilitate comparison, the traces were normalized and superimposed. Except for the dimmest intensity (-2.8 log), there was a speeding up of the response to light offset and an enhancement of the overshoot at two intermediate intensities. There was no effect on the response to light onset or on the plateau phase of the response. The 5 mV calibration refers to the control response. (b) Current-light responses of an L-cone at different holding potentials to a 200-ms light stimulus of approximately half-maximal intensity in control and 10 μM WIN 55,212-2. The timing of the light stimulus is indicated at the bottom of the figure. The amplitude of the light response decreased with decreasing holding potential because the holding potential approached the reversal potential of the photocurrent. The response amplitudes in the control and WIN conditions differed from each other by 5–20%. To facilitate comparison, the traces were normalized and superimposed. Speeding up of the response to light offset in response to WIN 55,212-2 is apparent at all holding potentials. There was no effect of WIN 55,212-2 on the response to light onset or plateau phases of the light response. The holding potential did not change the kinetics of the light responses. The 100 pA calibration refers to the control response. Modified from Struik, M., Yazulla, S., and Kamermans, M. (2006). Cannabinoid agonist WIN 55212-2 speeds up the cone light offset response in goldfish. *Visual Neuroscience* 23: 285–293.

dimmer the background, the stronger the negative feedback. As background is increased, feedback is reduced. Thus, ambient illumination produces an eCB tone that maintains transmitter release from cones within narrow limits. In this way, the ability of the cone to respond to increases and decreases of light intensity is maintained regardless of background. Retrograde transmission occurs even though Mb bipolar cells were hyperpolarized by glutamate acting on either the excitatory amino acid transporter (EAAT) or mGluR6 receptor. The retrograde effect was suppression of currents and not biphasic as expected from data obtained with low concentrations of WIN 55,212-2. It was this finding that led to the idea that the enhancing effect of WIN 55,212-2 on goldfish cones and salamander rods was due to agonist specific trafficking.

WIN 55,212-2 Affects the Cone Light Response

WIN 55,212-2 affects not only cone membrane currents, indicative of presynaptic modulation, but also the response of cones to light. Goldfish cones in an isolated retina preparation were stimulated by light in combination with voltage- and current-clamp protocols (**Figure 4**). WIN 55,212-2 (10 μM) has no effect on the absolute sensitivity of the cones or the kinetics of the onset response. However, the light offset response is faster and the depolarizing overshoot is enhanced. This effect is seen at all but dim intensities (**Figure 4(a)**) and is independent of holding potential (**Figure 4(b)**). This is found under current-clamp as well as under voltage-clamp conditions, indicating modulation of the cyclic guanosine monophosphate (cGMP)-gated channels in the cone outer segment rather than by voltage-dependent currents. The effects of WIN 55,212-2 are not blocked by SR141716A, indicating that CB1Rs are not involved. Given a train of flashes, the photocurrent recovers more quickly with WIN 55,212-2, such that the peak-to-peak response to succeeding flashes is increased. This effect, combined with the shortened recovery time to the offset of bright flashes, could increase contrast detection or critical flicker frequency. A concern is whether the effect of WIN 55,212-2 on the photoresponse would be observed with other CB1 agonists or eCBs because the effect of WIN 55,212-2 is not mediated by CB1 receptors.

In summary, cannabinoids presynaptically suppress the synaptic output of photoreceptors and on-bipolar cells. The effect is subtle as might be expected since smoking marijuana does not produce blindness. Evidence for effects of cannabinoids on amacrine cells is strongest for their suppression of dopamine release. Dopamine, a signal for light adaptation in the retina, antagonizes the action of cannabinoids in on-bipolar cells. eCBs are critically involved in neuronal plasticity. This also appears to include light and dark adaptation, processes of neuronal plasticity that occur in the retina.

Cannabinoids – Development and Neuroprotection

Studies regarding the effects of prenatal-marijuana use on children show deficits on visual habituation, tremors, and startle responses in neonates of 4–30 days old, but no effects on children of 1–6 years old. Problems with behavior, visual perceptual tasks, language comprehension, attention, and memory in 9-year-olds are attributed to effects on the prefrontal cortex, an area enriched in CB1Rs. Although CB1R localization and effects on GABA release have been studied in embryonic rat and chick retinas, no studies have investigated or commented on the effects of manipulating eCBs on retinal development.

The end point of glaucoma is ganglion cell death by apoptosis that may be caused by optic nerve injury following compression or ischemia. CB1 agonists (THC and cannabidiol) as well as inhibition of FAAH protect ganglion cells from glutamate excitotoxicity and ischemia caused by increased IOP. In contrast, COX-2 contributes to neuronal cell death following ischemia or NMDA-toxicity in glial cells, retinal pigment epithelium (RPE), and ganglion cells, while COX-2 blockers prevent ganglion cell apoptosis. Despite progress on the interaction of eCBs, COX-2 metabolites, and EP2 receptors in neuroprotection in the brain, such information is lacking in the retina.

Conclusion

The cannabinergic system is concentrated in the through pathway of the retina. Cannabinoids suppress dopamine release from amacrine cells and presynaptically inhibit potassium currents and glutamate release from cones and on-bipolar cells. How this relates to light and dark adaptation, receptive field formation, temporal properties of ganglion cell responses, and ultimately visual behavior needs to be addressed. eCBs are the most recently described neuromodulators to be studied extensively in neural and non-neural tissues. The existence of multiple eCBs, degradative enzymes, and receptors paints a picture of great complexity. They are important for their role in neuroplasticity and neuroprotection. Further study will verify the importance of eCBs in the retina as well.

See also: Glutamate Receptors in Retina; Information Processing: Amacrine Cells; Information Processing: Bipolar Cells; Information Processing: Ganglion Cells; Information Processing: Horizontal Cells; Neurotransmitters and Receptors: Dopamine; Phototransduction: Adaptation in Cones.

Further Reading

Fan, S. F. and Yazulla, S. (2007). Retrograde endocannabinoid inhibition of goldfish retinal cones is mediated by 2-arachidonoyl glycerol. *Visual Neuroscience* 24: 257–267.

Glaser, S. T., Deutsch, D. D., Studholme, K. M., Zimov, S., and Yazulla, S. (2005). Endocannabinoids in the intact retina: ^{3}H-anandamide uptake, fatty acid amide hydrolase immunoreactivity and hydrolysis of anandamide. *Visual Neuroscience* 22: 693–705.

Iversen, L. L. (2000). *The Science of Marijuana.* New York: Oxford University Press.

Nucci, C., Gasperi, V., Tartaglione, R., et al. (2007). Involvement of the endocannabinoid system in retinal damage after high intracellular pressure-induced ischemia in rats. *Investigative Ophthalmology Visual Science* 48: 2997–3004.

Onaivi, E. S., Sugiura, T., and Di Marzo, V. (eds.) (2006). *Endocannabinoids: The Brain and Body's Marijuana and Beyond.* Boca Raton: CRC Press.

Straiker, A. and Sullivan, J. M. (2003). Cannabinoid receptor activation differentially modulates ion channels in photoreceptors of the tiger salamander. *Journal of Neurophysiology* 89: 2647–2654.

Straiker, A., Stella, N., Piomelli, D., et al. (1999). Cannabinoid CB1 receptors and ligands in vertebrate retina: Localization and function of an endogenous signaling system. *Proceedings of the National Academy of Sciences of the United State of America* 96: 14565–14570.

Struik, M., Yazulla, S., and Kamermans, M. (2006). Cannabinoid agonist WIN 55212-2 speeds up the cone light offset response in goldfish. *Visual Neuroscience* 23: 285–293.

Tomida, I., Pertwee, R. G., and Azuara-Blanco, A. (2004). Cannabinoids and glaucoma. *British Journal of Ophthalmology* 88: 708–713.

Yazulla, S. (2008). Endocannabinoids in the retina: From marijuana to neuroprotection. *Progress in Retinal and Eye Research* 27(5): 501–526.

Yazulla, S., Studholme, K. M., McIntosh, H. H., and Deutsch, D. G. (1999). Immunocytochemical localization of cannabinoid CB1 receptor and fatty acid amide hydrolase in rat retina. *Journal of Comparative Neurology* 415: 80–90.

Yazulla, S., Studholme, K. M., McIntosh, H. H., and Fan, S. F. (2000). Cannabinoid receptors on goldfish retinal bipolar cells: Electron-microscope immunocytochemistry and whole-cell recordings. *Visual Neuroscience* 17: 391–401.

Relevant Websites

http://cannabinoidsociety.org/ – This is the official website of the International Cannabinoid Research Society. It provides updates and background information on all aspect of the endocannabinoid field.

http://webvision.med.utah.edu/ – This website from the University of Utah provides extensive coverage of retinal anatomy and physiology, particularly mammals.

Retinal Degeneration through the Eye of the Fly

N J Colley, University of Wisconsin, Madison, WI, USA

Glossary

ABC-type multidrug transporter – A family of adenosine-triphosphate-binding cassette (ABC) transmembrane proteins that transports various molecules, including proteins, ions, sugars, and lipids, across extracellular and intracellular membranes using energy derived from adenosine triphosphate (ATP).
Allele – One member of a pair of genes occupying a specific location on a chromosome (locus) that controls the same trait, for example, eye color.
cGMP phosphodiesterase (PDE) – This enzyme is found in several tissues, including the rod and cone photoreceptor cells, and it belongs to a large family of cyclic nucleotide PDEs that catalyze the hydrolysis of cyclic adenosine monophosphate (cAMP) and cyclic guanosine monophosphate (cGMP) into AMP and GMP, respectively.
Class B scavenger receptors – A family of proteins, which includes the scavenger receptor class B type I (SR-BI), and CD36, which are cell surface receptors that mediate lipid uptake. They are also thought to play an important role in vitamin A metabolism by mediating the uptake of carotenoids into cells.
Cyclophilin – A protein that binds the immunosuppressant drug, cyclosporin, which is often used to suppress tissue rejection following an organ transplantation. The protein displays peptidyl prolyl *cis–trans* isomerase activity, which catalyzes the *cis/trans* isomerization of peptide bonds on proline residues and is thought to play a role in protein folding.
Flippases – The enzymes located in the membrane that aid in the movement of phospholipid molecules between the two leaflets that comprise a cell's membrane. The process requires energy derived from ATP.
Homeodomain-containing transcription factors – A homeobox is a DNA sequence found within genes that regulates developmental processes in animals, fungi, and plants. A homeobox is about 183-DNA-bp long and it encodes a 61-amino-acid protein domain, called the homeodomain, which binds DNA and plays a key role in the regulation of gene expression.
Paired domain – A conserved domain found in a set of transcription factor proteins which are important in regulating gene expression during development. Paired box (PAX) genes belong to the PAX family of transcription factors.
Rab-GTPase – These are small guanine-nucleotide-binding proteins (G proteins) conserved from yeast to humans and are members of the Ras superfamily of small GTPases. They function in distinct steps in membrane trafficking pathways, including vesicle formation, actin- and tubulin-dependent vesicle movement, and membrane fusion events.
Retinitis pigmentosa (RP) – A heterogeneous group of genetically inherited retinal degeneration disorders leading to progressive loss in vision. Many people with RP retain some sight all their life, others become legally blind in childhood, and some become legally blind in their 40s or 50s. The progression of RP is different in each case.
Rhabdomere – The light-sensing organelle of the *Drosophila* photoreceptor cell. It is the functional equivalent of the outer segment of vertebrate rod and cone cells. A rhabdomere is made up of 60 000 tightly packed microvilli, and each microvillus is 50 nm in diameter and about 1–2 μm in length.
Second-site modifier screens – The genetic screens that are designed to detect a mutation in a second locus (gene) that enhances or suppresses the effect of an existing mutation.

'Prized pest'
You hover over the soft, brown
bananas like a floater, in and out
of my vision, you whose eyes
are so much like my own.

Who am I, dear one,
to swat at you, send you
swirling toward the ceiling
when, really, we share
the same humble beginnings.
And you in your simplicity
hold the key to my complexity.

Let me set out a plate of the sweetest
peaches, invite you to rest
on the arm of my chair,
however late it is.

Marilyn Annucci

Each model organism used to study retinal degenerative diseases has the advantage that others lack. Frogs, fish, rats, and mice have all provided great insights, but it is the tiny fruit fly, *Drosophila melanogaster*, that has played a central role in elucidating the molecular genetics of eye development and the early identification of mutations that cause retinal degeneration. The first mutations in *Drosophila* known to cause retinal degeneration were identified in the 1960s by the pioneering studies of Bill Pak and co-workers. At that time, these findings were only of interest to a few investigators. It was thought that animals as different as flies and humans could not share a similar genetic makeup and, therefore, the amount of transferable knowledge would be limited.

The revolutionary finding that put flies into the spotlight was the one showing that genes controlling pattern formation and development in flies could also do so in humans. In the 1980s, homeodomain-containing transcription factors were found to be essential during development in *Drosophila* for directing the production of appendages, such as the legs and the antennae. Almost identical homeodomain-containing genes were found in the genomes of a wide range of organisms, including humans and mice. This knowledge led to the conclusion that organisms as different as flies and humans contain nearly identical genes. A few years later, working on eye development, Walter Gehring's lab cloned the *eyeless* gene in *Drosophila*. They discovered that *eyeless* is a transcription factor, containing a paired domain and a homeodomain, that directs eye formation. The *eyeless* gene is related to the mouse and human *Pax6* genes (paired box), and the *eyeless*/*Pax6* genes regulate a cascade of genetic processes involved in eye development. Mutations in these genes result in aniridia in humans, a Small eye (*Sey*) phenotype in mice and an *eyeless* phenotype in *Drosophila*. Aniridia is a congenital condition that is characterized by incomplete iris formation. Further, when expressed in flies, both the *Drosophila eyeless* gene and the mouse *Pax6* gene (*Small eye*, or *Sey*) were able to direct the production of ectopic compound eyes. That *Sey* induced the formation of compound eyes and not mouse structures revealed that mice and flies share signaling components that are interchangeable. The proteins encoded by these genes share 94% identity in the paired domain and 90% identity in the homeodomain. It is remarkable that *eyeless* is not only essential for eye formation, but also its ectopic expression can override other developmental processes in a variety of tissues. For example, *eyeless* is capable of directing leg, wing, and antennal tissues to form eyes. As a result of these findings, *eyeless*/*Pax6* was dubbed a master regulatory gene for eye formation during development. These landmark discoveries led to an explosion of exciting work in the 1990s that prompted a reassessment of the evolution of eyes. A complex network of eye determination genes direct eye formation, including another Pax6, *twin of eyeless* (*toy*), *sine oculis (so)*, *eyes absent (eya)*, and *dacshund (dac)*. Counterparts of these genes play a role in mammalian eye development and have been implicated in a variety of human diseases. These studies reveal that even though the compound eye of the fly looks very different from mammalian eyes, both share similar signaling pathways that are able to substitute for each other to form an eye.

Due to these elegant findings, it is now widely accepted that many genes are functionally equivalent between flies and humans. In addition, the same (or similar) mutations cause disease in both species. In fact, nearly three-fourths of all human disease genes have related sequences in *Drosophila*. Examples include gene mutations involved in retinal degeneration, deafness, skeletal malformations, cognitive impairment, cancer, immunity, alcoholism, cocaine and nicotine addiction, heart disease, metabolic and storage diseases, Alzheimer's disease, Parkinson's disease, and Huntington's disease.

At the turn of the twentieth century in the hands of Thomas Hunt Morgan, the founding father of *Drosophila* research, *Drosophila* emerged as a powerful genetic workhorse. In 1910, Morgan identified the first mutation in *Drosophila*, which was a spontaneous *white* eye-pigment mutation that caused a normally red-eyed fly to be white eyed (**Figure 1(a)**). This first allele transformed our understanding of genetics and heredity. The *white* gene encodes a membrane-associated, adenosine triphosphate (ATP)-binding, ATP-binding cassette (ABC)-type multidrug transporter required for the transport of pigment precursors involved in eye pigment biosynthesis. In humans, mutations in the *ABCA4* gene (also *ABCR*) account for approximately 3% of autosomal recessive retinitis pigmentosa (RP) and are linked to both recessive cone–rod dystrophy and recessive Stargardt macular dystrophy. Similar to the *Drosophila white* gene, the *ABCA4* gene encodes a membrane-bound, ATP-binding transporter that in humans localizes to the rims of rod and cone outer segment disks. The ABCA4 transporter serves as a flippase in the retinoid cycle. When the *ABC4* gene is mutated, toxic detergent-like by-products accumulate in the retinal pigment epithelium (RPE) leading to severe pathology. Therefore, the *white* gene, discovered at the turn of the century, was subsequently found to encode an ABC-type transporter required for eye pigment biosynthesis in *Drosophila*, and is related to another ABC-type transporter in the human eye that is involved in the retinoid cycle and several types of retinal diseases.

Not only do we share many genes in common with flies, but we also share a great deal of the same metabolic and signaling pathways. Flies are now being used as genetic models for the National Aeronautics and Space Administration (NASA) astronauts and are providing vital information on how space travel and gravitational changes alter gene expression. Work on flies continues to reveal

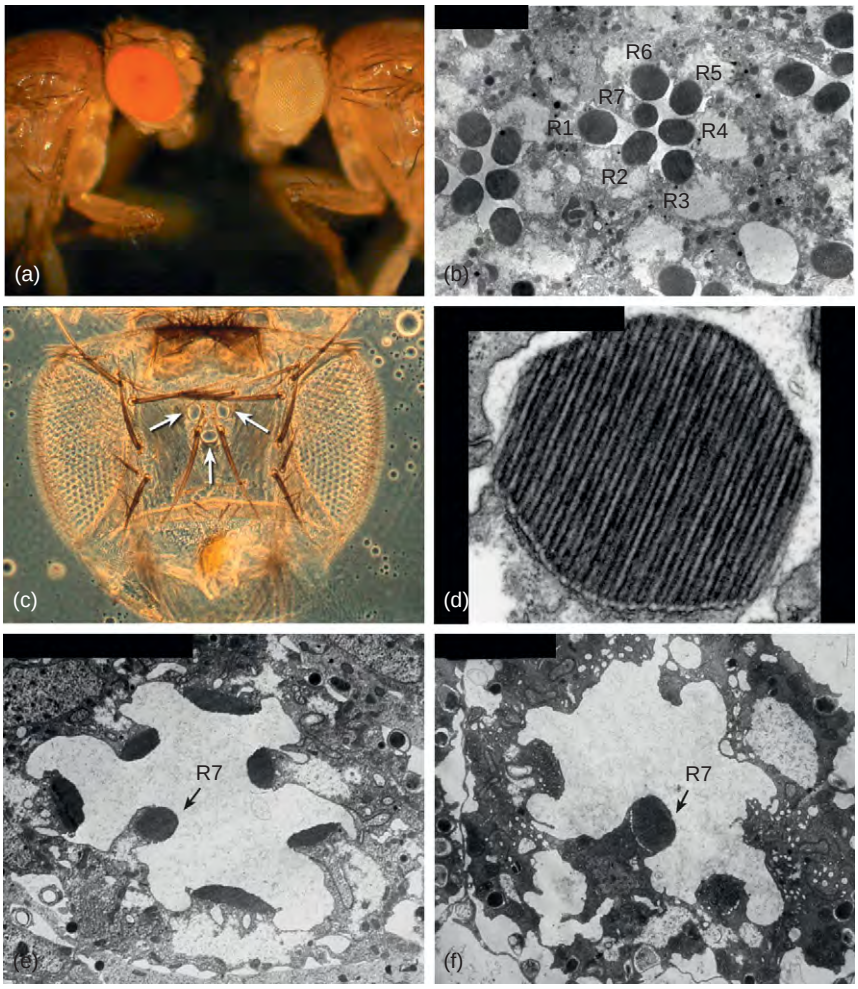

Figure 1 (a) Wild-type red-eyed fly, Canton S compared to a white-eyed mutant fly, w^{1118}. (b) Cross section through the compound eye showing the R1-7 photoreceptor cells and their photosensitive rhabdomeres (R). The R8 photoreceptor cell is located below the plane of the section. (c) The adult *Drosophila* visual system showing the two compound eyes and the three simple eyes (ocelli) located on the top of the head (arrows). (d) A higher magnification of a rhabdomere showing the microvilli. The rhabdomeres are made up of about 60 000 microvilli and are 50 nm in diameter and 1–2 μm in length. (e) A newly eclosed $ninaE^{I17}$ mutant fly, showing the reduced size of the rhabdomeres. $ninaE^{I17}$ is a null allele, so the flies completely lack Rh1 rhodopsin expressed in the R1-6 photoreceptor cells. (f) Six-day-old $ninaE^{I17}$ fly, showing that the rhabdomeres of the R1-6 photoreceptor cells are almost completely gone, but the R7 cell rhabdomere remains.

general principles that are fundamental to a wide spectrum of biological processes. Studies in *Drosophila* have led to conceptual and technical breakthroughs in the areas of development, gene expression, learning and memory, sleep, alcoholism, cocaine and nicotine addiction, ecology and evolution, olfaction, taste, mechanotransduction, vision, hearing, aging, pigmentation, biological clocks and circadian rhythms, courtship and mating behaviors, and human disease and the development of new pharmaceuticals.

In addition to sharing genes and signaling pathways with humans, flies are a powerful model for providing insights into human health and disease for other reasons. In spite of their small size, flies display complex rituals such as courtship behavior, so questions related to the genetic basis of complex behavior are tractable in the fly. The fruit fly uses the same or similar genes to develop from a fertilized egg to an adult, but they do it in the short time of about 11 days. A female will lay hundreds of eggs, allowing large numbers of genetically identical offspring to be obtained. Flies have a short life span of about 2 months, so the onset and progression of age-related retinal degeneration disorders or any other age-related degenerative process can be studied quite rapidly.

The eye is not essential for viability or fertility of the flies, therefore genes encoding proteins that are uniquely required for visual function may be easily manipulated and studied. Large-scale mutagenesis screens have been carried out, producing hundreds of thousands of mutant flies whose phenotypes can be analyzed to identify genes required for vision. In addition, second-site modifier screens have been used to identify novel genes in

signaling pathways. Fly models can be used to dissect the cell biological basis and physiological basis of retinal degeneration, and therefore can be used to obtain insights into mechanisms of degenerative disorders. Just like in humans, electroretinogram (ERG) recordings can be carried out, and they have proved to be an indispensable means for uncovering visual system defective phenotypes that would otherwise have remained unnoticed.

Transgenic flies can be easily produced and, as a result, mutant genes may be introduced and mutant phenotypes may be complemented with wild-type transgenes. Using specialized promoters, genes may be targeted to specific tissues and may also be overexpressed. The fly has a relatively small genome, made up of about 13 600 genes in four pairs of chromosomes. However, despite the dramatic differences in size and apparent complexity between humans and flies – we have less than twice as many genes as a fly – our genome is estimated to be made up of only 20 000–25 000 genes contained in 23 pairs of chromosomes. Therefore, despite the fly's perceived simplicity, or our perceived complexity, our genetic makeup may not be all that different. Its versatility for genetic manipulation and convenience for unraveling fundamental biological processes continue to guarantee the fly a place in the spotlight for unraveling the basis of and therapeutic treatments for human disease.

The Compound Eye and Phototransduction

The *Drosophila* compound eye is composed of approximately 800 individual eye units called ommatidia, each containing the outer, R1-6 photoreceptor cells that extend the full length of the retina and express the major rhodopsin in the eye, the blue-sensitive rhodopsin, Rh1 (**Figure 2**). Rh1 is encoded by the *ninaE* gene, and it displays 22% amino acid identity with human rhodopsin. The inner photoreceptor cells, R7 and R8, are arranged such that a subset of the R7 cells expresses the ultraviolet (UV)-opsin, Rh3. They pair with the R8 cells expressing the blue-sensitive opsin Rh5 (p-ommatidia), while the R7 cells expressing the UV-opsin Rh4 pair with the R8 cells expressing the green-sensitive opsin Rh6 (y-ommatidia). The R7 cells are located above their partner R8 cells (**Figures 1(b)** and **2**). Above the photoreceptor cells are four cone cells and two lens components; the pseudocone (also called the crystalline cone) and the corneal lens. Two primary pigment cells surround the cones and each ommatidium is optically isolated by a sheath of secondary and tertiary pigment cells (**Figure 2**). The adult visual system also contains three simple eyes, ocelli, located on the top of the head (**Figure 1(c)**). The ocelli express the violet-sensitive, Rh2 opsin. *Drosophila* photoreceptor cells contain specialized portions of the plasma membrane,

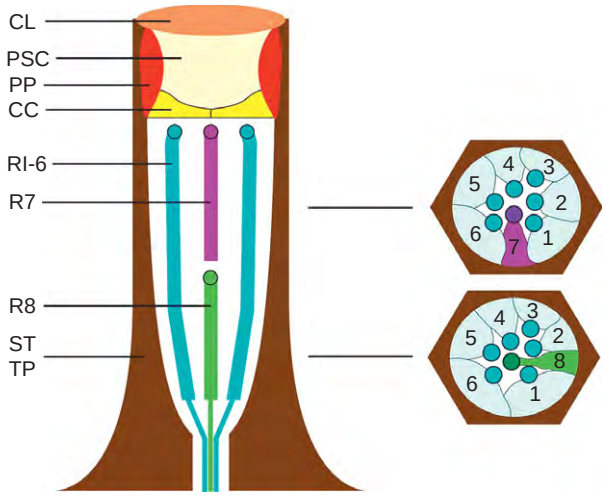

Figure 2 Schematic of an ommatidium. CL, corneal lens; PSC, pseudocone; PP, primary pigment cells; CC, cone cells; R1-6, R7, and R8 photoreceptor cells; SP and TP, secondary and tertiary pigment cells. Adapted from Tomlinson, A. and Ready, D. F. (1987). Cell fate in the *Drosophila ommatidium*. *Developmental Biology* 123: 264–275.

called rhabdomeres, which comprises approximately 60 000 tightly packed microvilli containing rhodopsin photopigments and other components of the phototransduction cascade (**Figure 1(b)** and **1(d)**). The microvillar processes of the rhabdomeres are functionally similar to the phototransducing disk membranes present in the vertebrate photoreceptor outer segments (**Figure 3**).

Phototransduction in *Drosophila* utilizes a signaling cascade in which light stimulation of rhodopsin leads to the activation of the heterotrimeric guanine-nucleotide-binding G protein (Gq) and the stimulation of phospholipase C beta (PLC-β), leading to the opening of the cation-selective transient receptor potential (TRP) and TRP-like (TRPL) channels. The photoreceptors depolarize as intracellular calcium dramatically rises from about 100 nm to about 10 μM. In the rhabdomeres, calcium rises even higher, to about 1 mM, and it is required for amplification, rapid response kinetics, and light adaptation in *Drosophila*. Calcium is subsequently removed from the rhabdomeres by a combination of sodium/calcium exchange and diffusion into the cell body where calcium increases to about 10 μM. Calcium in the cell body is buffered by calcium-binding proteins and is removed by uptake into intracellular stores by the sarco/endoplasmic reticulum (ER) calcium ATPase. The *Drosophila* phototransduction cascade shares some similarities with the phototransduction cascade in mammalian rod and cone photoreceptor cells. Both cascades are initiated by light-activation of rhodopsin that in turn leads to the stimulation of heterotrimeric G proteins. Phototransduction in *Drosophila* as well as in humans is terminated when the protein arrestin binds to light-stimulated rhodopsin and blocks the binding of rhodopsin

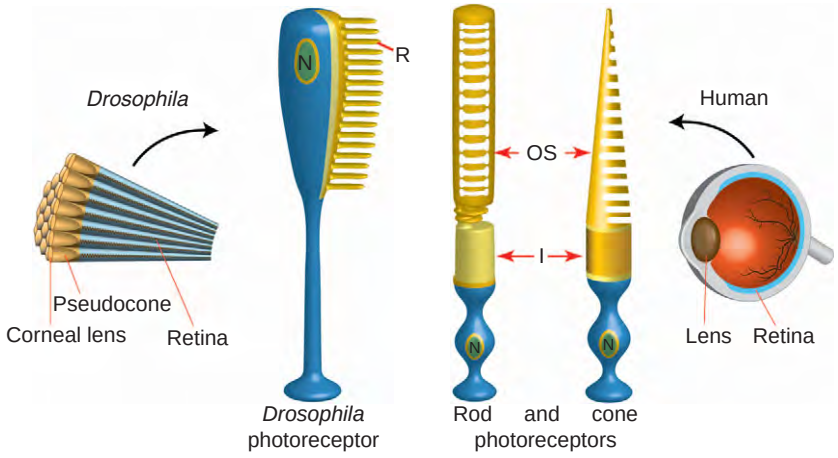

Figure 3 The *Drosophila* photoreceptor cell compared with human rod and cone photoreceptor cells. In *Drosophila*, the pseudocone cone (also called the crystalline cone) and the corneal lens are the lens elements, and they are secreted by the underlying cone cells. The *Drosophila* lens is comprised of droscrystallin, which is similar to insect cuticular proteins. R, rhabdomere; OS, outer segments; I, inner segments; N, nucleus. Photoreceptor cell drawings adapted from Chang, H. Y. and Ready, D.F. (2000). *Science* 290: 1978–1980.

to Gq. However, notable differences are that rod and cone channels are gated by cyclic nucleotides and they close in response to light, leading to a hyperpolarizing response.

Although certain features of phototransduction in *Drosophila* differ from rod and cone phototransduction, *Drosophila* phototransduction shares many common features with the cascade in intrinsically photosensitive retinal ganglion cells (ipRGCs). These cells function in circadian rhythm entrainment and pupil constriction. The light response in ipRGCs is initiated with absorption of light by melanopsin, which is more similar to *Drosophila* rhodopsins than to the photopigments in rods and cones. Light-stimulated melanopsin is thought to activate a phophoinositide cascade leading to the opening of channels that display similar properties to TRP channels. Therefore, *Drosophila* photoreceptor cells and ipRGCs share similar phototransduction cascades, and studies in flies will continue to provide insights into ipRGC function.

Genetic Screens Identify Retinal Degeneration Loci

Several forward genetic screens in *Drosophila* led to an explosion in the identification of many genes involved in retinal degeneration, and their counterparts in human disease. The approach has been to chemically mutagenize flies to disrupt photoreceptor cell function. The mutagenized flies are tested for function by ERG analysis, morphology by a deep pseudopupil (DPP), or Western blotting for the loss of candidate gene expression (such as arrestin). The ERG approach was pioneered by Bill Pak and co-workers in the 1960s and led to the isolation of over 200 ERG-defective mutants. In the 1980s, the development of gene-cloning techniques for *Drosophila* made it possible to isolate the corresponding genes. For example, *neither inactivation nor after potential E* (*ninaE*), a mutant isolated in the original ERG screen was later found to harbor a mutation in the structural gene for the major rhodopsin in *Drosophila*, Rh1. In 1985, almost a decade prior to the cloning of eyeless, *Drosophila* rhodopsin, Rh1, was cloned and sequenced by two groups and found to display 22% amino acid identity with bovine rhodopsin. In addition, the first evidence that mutations in a rhodopsin gene led to retinal degeneration came from elegant studies in the 1980s in *Drosophila*. The use of the ERG in *Drosophila* was an effective strategy to identify mutants in phototransduction and also in retinal degeneration.

The DPP is a sensitive phenotype in the eye that can be easily assessed in live flies. It is based on the precise packing of the photoreceptor cells. Any mutation leading to, even subtle, structural alterations in photoreceptor cells will cause attenuation in the DPP. For example, a reduction in rhodopsin levels in the R1-6 photoreceptor cells in *ninaE* mutants, leads to structural alterations in the photoreceptor cells (**Figures 1(e)** and **1(f)**) and attenuation in the DPP. A variety of mutants were isolated by this method, including dominant alleles of *ninaE* (rhodopsin), and alleles of two chaperone proteins, *ninaA* (cyclophilin) and *calnexin*. Both the ERG and the DPP screens accelerated the pace of identifying mutations that cause retinal degeneration in *Drosophila*.

Retinal Degenerations in Flies and Humans

Mutations in rhodopsin are the leading cause of blinding disease in RP. RP is a heterogeneous group of inherited disorders that is characterized by progressive retinal

degeneration and eventual blindness. RP may be inherited as an X-linked (about 5–15% of cases), autosomal recessive (50–60%), and autosomal dominant trait (30–40%). It affects one person in 4000 worldwide and is often restricted to the eye, but not always. In about 20–30% of the cases of RP, the genetic defects are not eye specific. There are approximately 30 syndromes that involve RP. One of the most common syndromes is Usher's syndrome. This syndrome is characterized by vision and hearing impairment, and mutations in myosin VIIA are responsible for one form, Usher 1B syndrome. Interestingly, loss of myosin VIIA function leads to deafness in *Drosophila*. In flies, like in humans, there are many examples of mutations in which the phenotype caused by the mutation is restricted to the eye, whereas there are others that are not. For example, mutations in the gene encoding rhodopsin (*ninaE*) and the *arrestin* gene cause defects that are restricted to the eye. Mutations in genes such as *retinal degeneration B* (*rdgB*, encoding a phosphatidylinositol transport protein), involve olfactory as well as visual defects.

Since the initial findings, in 1983, that mutations in *Drosophila* rhodopsin lead to retinal degeneration, over 100 mutations in human rhodopsin have been found to cause autosomal dominant RP (adRP). The first mutation identified in adRP patients, published by Dryja and coworkers in 1990, was a mutation that caused a proline residue located near the N-terminus of rhodopsin to be replaced by a histidine residue (Pro23His). A great majority of these mutants, including Pro23His, produce misfolded rhodopsin that is improperly transported through the secretory pathway. However, the mechanism by which the mutant rhodopsins cause dominant retinal degeneration was not known. In 1995, studies in *Drosophila* on rhodopsin mutations that act dominantly to cause retinal degeneration revealed that the retinal degeneration results from the interference in the maturation of normal rhodopsin by the mutant protein. These studies in *Drosophila* provided a mechanistic explanation for the cause of certain forms of adRP.

Mechanisms of Retinal Degenerations

Light-Dependent Retinal Degenerations

It is now widely appreciated that retinal defects and retinal degeneration can be triggered by mutations in almost every component of the photoreceptor cells. These mutations can be divided into two distinct classes. One class pertains to the unregulated activities of phototransduction and/or calcium toxicity. Mutations in this class lead to retinal degenerations that are dependent on or influenced by light stimulation of the cascade and the opening of the TRP and TRPL channels, and these are termed light dependent.

For example, some mutations in rhodopsin itself or mutations in the *arrestin* gene lead to light-dependent retinal degeneration. Arrestin is required for deactivating rhodopsin, and loss of arrestin causes unregulated rhodopsin and hence excessive activation of phototransduction. It is also thought that the loss of arrestin causes decreased endocytosis of Rh1 and all of these defects lead to retinal degeneration.

The precise spatial and temporal regulation of calcium is also essential for photoreceptor survival in flies and people. Prolonged elevation of cytosolic calcium or low levels of calcium can be toxic, leading to cell death and retinal degeneration. In *Drosophila*, mutations in *arrestin*, the $Na^{+}/Ca2^{+}$ exchanger (*calx*), the diacylglycerol kinase (*retinal degeneration A*, *rdgA*), and constitutively active TRP channels are all thought to trigger cell death by causing abnormally high levels of calcium. In humans, a lack of cyclic guanosine monophosphate (cGMP) phosphodiesterase (PDE), caused by mutations in *PDE6A* and *PDE6B*, leads to an elevation in the cGMP concentration in the outer segments, which in turn causes cGMP channels to be open, resulting in excessive levels of calcium. Defects in PDE6A and PDE6B cause recessive RP.

Light-Independent Retinal Degenerations

A second class of retinal degenerations involves defects in rhodopsin maturation and does not require activation of phototransduction by light. These are termed light independent. In *Drosophila*, as in humans, Rh1 is synthesized and glycosylated in the ER, binds its vitamin-A-derived chromophore (11-*cis* 3-hydroxyretinal), at a lysine residue in the seventh transmembrane domain, is transported through the various compartments of the Golgi, and is delivered to its final destination for phototransduction. The mechanisms that regulate rhodopsin maturation, such as its folding, glycosylation, chaperone interaction, chromophore attachment, and transport, are key to photoreceptor survival in flies and humans.

In flies, the transport of Rh1 from the ER to the rhabdomere requires the cyclophilin, NinaA. Cyclophilins are known to display peptidyl-prolyl *cis–trans* isomerase and are thought to play a role in protein folding during biosynthesis. Consistent with a role in protein folding, NinaA resides in the ER. In addition, NinaA is detected in secretory transport vesicles together with Rh1, and forms a specific and stable complex with Rh1, consistent with a broader role as a chaperone in the secretory pathway. Similarly, in mammals a cyclophilin-like protein (RanBP2/Nup358) modulates protein biogenesis. The *Drosophila* cyclophilin, NinaA, is a chaperone that is specifically required for Rh1 biosynthesis and maturation. Another chaperone required for Rh1 biosynthesis in *Drosophila* is calnexin and mutations in *ninaA* (cyclophilin), *ninaE* (Rh1), and *calnexin*

all lead to severe retinal pathology in flies. In mammalian photoreceptors, calnexin is also expressed in the ER. Although calnexin is not required for the expression of rod rhodopsin, cone M-opsin, or melanopsin (in the ipRGCs) in the mouse, it is required for proper retinal morphology.

Rhodopsin in both mammals and flies undergoes N-linked glycosylation during biosynthesis, and in flies, elimination of the glycosylation site, asparagine 20 (N20I), results in the retention of rhodopsin in the secretory pathway. Moreover, in both mammals and flies, genes involved in rhodopsin chromophore biosynthesis and transport are critical to rhodopsin maturation and expression as well as photoreceptor function. Defects in chromophore production in the *Drosophila* mutants *ninaB*, *ninaD*, *ninaG*, and *santa maria*, cause a failure in Rh1 transport from the ER to the rhabdomere, resulting in a severe reduction in Rh1 and retinal pathology. The *ninaB* gene encodes an enzyme that catalyzes the conversion of carotenoids to retinal (β, β′ – carotene-15, 15′-monoxygenase) and *ninaG* encodes an enzyme that acts to convert retinal to 3-hydroxyretinal (oxidoreductase). Two additional *Drosophila* loci, *ninaD* and *santa maria*, are both similar to the mammalian class B scavenger receptors and play a role in transporting β-carotene to cells. In flies, β-carotene is required in the diet for the production of all-*trans* retinol, which is in turn converted to 11-*cis* 3-hydroxyretinal. Upon light stimulation 11-*cis* 3-hydroxyretinal is photoconverted to all-*trans* 3-hydroxyretinal. Mutations in chromophore biosythesis result in defective Rh1 maturation, low levels of Rh1, and retinal pathology, establishing the importance of vitamin A in the fly.

Once rhodopsin exits the ER, it requires several Rab-guanosine triphosphate (GTP)ases for vesicular transport through the secretory pathway in flies and in mammals. Rab-GTPases are conserved from yeast to humans and are members of the Ras superfamily of small GTPases. They function in distinct steps in membrane trafficking pathways including vesicle formation, actin- and tubulin-dependent vesicle movement, and membrane fusion events. In *Drosophila*, Rab1, Rab6, and Rab11 mediate vesicular fusion between the ER and the Golgi (Rab1), intra-Golgi (Rab6), and post-Golgi (Rab11) transport of rhodopsin in *Drosophila.* Defects in Rab function cause inadequate Rh1 transport and retinal pathology. Therefore, the mechanisms that regulate Rh1 maturation, such as its folding, chaperone interaction, and chromophore binding and transport are essential for photoreceptor health in flies and humans.

Retinal Degenerations Caused by Mutations in Dual-Role Proteins

Although most retinal degenerations are classified as either light dependent or light independent, there is a growing list of retinal degenerations that fall into both classes. In these cases, the corresponding mutant proteins play dual roles. For example, as was described above, calnexin is a chaperone required for rhodopsin maturation. In addition, it is a calcium-binding protein for regulating calcium in photoreceptor cells. Mutations in *calnexin* lead to defects in Rh1 maturation and retinal degeneration. The degeneration due to defects in rhodopsin maturation is light independent, but *calnexin* mutants also display prolonged and elevated levels of calcium, following light stimulation. In the *calnexin* mutants, the retinal degeneration is enhanced by the stimulation of phototransduction by light. Therefore, calnexin plays a dual role: one in rhodopsin maturation and another in calcium modulation.

Summary

In the 1980s, *Drosophila* took on a surprising new role, as an animal model for retinal disease, when the genetic similarities and fundamental processes between flies and humans became apparent. It became clear that information obtained in flies was transferable to human blinding diseases. As a result, and since then, there has been an explosion in the use of *Drosophila* as an animal model for unraveling the molecular genetic basis of retinal degeneration disorders. Despite its perceived simplicity, the fruit fly is, indeed, a remarkably complex creature with a genetic makeup that is surprisingly similar to our own. Investigators continue to capitalize on a whole host of versatile genetic techniques together with the accessibility of the fly to dissect fundamental photoreceptor cell mechanisms *in vivo.* The short life span of the fly, only 2 months, allows for monitoring the onset and progression of retinal degeneration in a short time. These advantageous features place *Drosophila* at the forefront of current research efforts, aimed at unraveling the basis of and therapeutic treatments for retinal degenerative disorders.

Acknowledgments

Our research, on retinal degeneration in *Drosophila*, is supported by funding from the National Eye Institute, the Retina Research Foundation, and the Retina Research Foundation/Walter H. Helmerich Research Chair. I gratefully acknowledge C. Vang, E. Rosenbaum and B. Larson for assistance with preparing the figures. For the poem, I thank M. Annucci, author of Luck (Parallel Press) and member of the Department of Languages and Literatures at the University of Wisconsin-Whitewater.

See also: Circadian Photoreception; Circadian Rhythms in the Fly's Visual System; Coordinating Division and Differentiation in Retinal Development; Embryology and Early Patterning; The Evolution of Opsins; Ganglion Cell Development: Early Steps/Fate; Genetic Dissection of

Invertebrate Phototransduction; Histogenesis, Cell Fate, and Signaling Factors; Photoreceptor Development: Early Steps/Fate; The Photoreceptor Outer Segment as a Sensory Cilium; Phototransduction: Phototransduction in Rods; Phototransduction: Rhodopsin; Primary Photoreceptor Degenerations: Retinitis Pigmentosa; Primary Photoreceptor Degenerations: Terminology; Retinal Degeneration through the Eye of the Fly; Retinal Histogenesis; Secondary Photoreceptor Degenerations: Age-Related Macular Degeneration; Secondary Photoreceptor Degenerations; *Xenopus laevis* as a Model for Understanding Retinal Diseases; Zebrafish as a Model for Understanding Retinal Diseases: Pde6, Apoptosis, and the Bystander Effects; Zebrafish: Retinal Development and Regeneration.

Further Reading

Bok, D. (2007). Contributions of genetics to our understanding of inherited monogenic retinal diseases and age-related macular degeneration. *Archives of Ophthalmology* 125: 160–164.

Colley, N. J., Baker, E. K., Stamnes, M. A., et al. (1991). The cyclophilin homolog *ninaA* is required in the secretory pathway. *Cell* 67: 255–263.

Colley, N. J., Cassill, J. A., Baker, E. K., et al. (1995). Defective intracellular transport is the molecular basis of rhodopsin-dependent dominant retinal degeneration. *Proceedings of the National Academy of Sciences of the United States of America* 92: 3070–3074.

Graham, D. M., Wong, K. Y., Shapiro, P., et al. (2008). Melanopsin ganglion cells use a membrane-associated rhabdomeric phototransduction cascade. *Journal of Neurophysiology* 99: 2522–2532.

Greenspan, R. J. and Dierick, H. A. (2004). 'Am not I a fly like thee?' From genes in fruit flies to behavior in humans. *Human Molecular Genetics* 13(2): R267–R273.

Halder, G., Callaerts, P., and Gehring, W. J. (1995). Induction of ectopic eyes by targeted expression of the eyeless gene in Drosophila. *Science* 267: 1788–1792.

Hardie, R. C. and Postma, M. (2008). Phototransduction in microvillar photoreceptors of *Drosophila* and other invertebrates. In: Allan, A. K., Basbaum, I., Shepherd, G. M., and Westheimer, G. (eds.) *The Senses: A Comprehensive Reference* vol. 1, pp. 77–130. San Diego, CA: Academic Press.

Hartong, D. T., Berson, E. L., and Dryja, T. P. (2006). Retinitis pigmentosa. *Lancet* 368: 1795–1809.

Pak, W. L. (1995). *Drosophila* in vision research. The Friedenwald lecture. *Investigative Ophthalmology and Visual Science* 36: 2340–2357.

Reiter, L. T., Potocki, L., Chien, S., et al. (2001). A systematic analysis of human disease-associated gene sequences in *Drosophila melanogaster*. *Genome Research* 11: 1114–1125.

Rosenbaum, E. E., Hardie, R. C., and Colley, N. J. (2006). Calnexin is essential for rhodopsin maturation, Ca^{2+} regulation, and photoreceptor cell survival. *Neuron* 49: 229–241.

Rubin, G. M. and Lewis, E. B. (2000). A brief history of Drosophila's contributions to genome research. *Science* 287: 2216–2218.

Tomlinson, A. and Ready, D. F. (1987). Cell fate in the *Drosophila ommatidium*. *Developmental Biology* 123: 264–275.

Wang, T. and Montell, C. (2007). Phototransduction and retinal degeneration in Drosophila. *Pflugers Archiv* 454: 821–847.

Wernet, M. F., Celik, A., Mikeladze-Dvali, T., et al. (2007). Generation of uniform fly retinas. *Current Biology* 17: R1002–R1003.

Relevant Website

http://www.sph.uth.tmc.edu – Genes and mapped loci causing retinal diseases: Homepage.

Retinal Ganglion Cell Apoptosis and Neuroprotection

K M Coxon, J Duggan, L Guo, and M F Cordeiro, UCL Institute of Ophthalmology, London, UK

Glossary

Apoptosis – The process of programmed cell death, whereby the cell proceeds through a highly regulated series of morphological changes resulting in the controlled disassembly of the affected cell.
Bax, Bak, Bad, and Bid – Proapoptotic proteins.
Bcl-2 – B-cell CLL/lymphoma 2, an antiapoptotic protein.
Excitotoxicity – The process by which raised levels of neurotransmitters trigger cell death.
Glaucoma – A major cause of blindness worldwide, resulting from the loss of retinal ganglion cells, with raised intraocular pressure as a major modifiable factor.
Neuroprotection – The use of therapeutic agents to prevent or reverse neuronal damage thereby retaining physiological function.
Neurotrophic factors – The growth factors that promote the growth, differentiation, and survival of neurons.
Retinal ganglion cells – The neurons that relay visual information from their cell soma located in the retina, through their axons which project along the optic nerve to the brain.

Introduction

Retinal ganglion cells (RGCs) relay visual information from their cell soma located in the retina, through their axons which project along the optic nerve to the brain. Their loss is associated with various optic neuropathies such as Leber hereditary optic neuropathy, optic neuritis, anterior ischemic optic neuropathy, and glaucoma. The most prominent of these is glaucoma, which is a major cause of irreversible blindness worldwide. In this article, glaucoma is used to highlight the challenges involved in unraveling the complexities of RGC apoptosis and neuronal cell death in order to facilitate more effective treatment strategies.

Apoptosis

Unlike necrosis, apoptosis is a regulated process of cell death leading to chromatin condensation, DNA fragmentation, oxidative damage, and autophagic degeneration, commonly proceeding through either extrinsic or intrinsic caspase-dependent pathways outlined in Figure 1. Identifying which aspect of apoptosis regulation is susceptible in glaucoma has important implications for the elucidation of pharmacological targets.

Apoptosis in Glaucoma

The exact mechanism triggering RGC apoptosis in glaucoma is still unidentified, although the major modifiable risk factor identified is that of raised intraocular pressure (IOP) and is commonly used to investigate apoptotic mechanisms. Mitochondria play a fundamental role in RGC apoptosis, with raised hydrostatic pressure inducing apoptosis that is at least partially dependent on mitochondria. More specifically, Bax, a regulator of membrane permeability, has been suggested to be essential in triggering apoptosis, with RGCs-expressing mutant Bax showing complete resistance to raised hydrostatic pressure, even after axonal loss.

While the primary site of damage in RGCs appears to be the axon, leading to axonal degeneration, and a positive correlation between raised IOP and axon loss has been established, it does not inevitably lead to cell soma death. The contribution of axonal degeneration and secondary challenges to the cell soma are evaluated below.

Diagnosis and Measuring Glaucoma Progression

Traditionally, glaucoma is screened by monitoring changes in IOP using tonometry, a technique lacking sensitivity in glaucoma detection, as damage to the RGCs can occur in the absence of raised IOP. This lack of sensitivity sparked the development and introduction of alternative screening methods. Examples of these are standard automated perimetry to measure visual-field loss, optical coherence tomography, allowing the quantification of the retinal nerve fiber layer (RNFL) thickness, and disk tomography to assess any structural damage to the optic nerve head (ONH). The major drawback common to these methods is the inability to detect the disease before considerable damage to the retina has occurred. It is estimated that death of 50% of the RGCs occurs before there is a significant-enough visual loss to diagnose glaucoma. The development of detection of apoptosing retinal cell (DARC), a method of detecting RGC apoptosis in glaucoma before the onset of visual loss, may be instrumental in early diagnosis and successful treatment

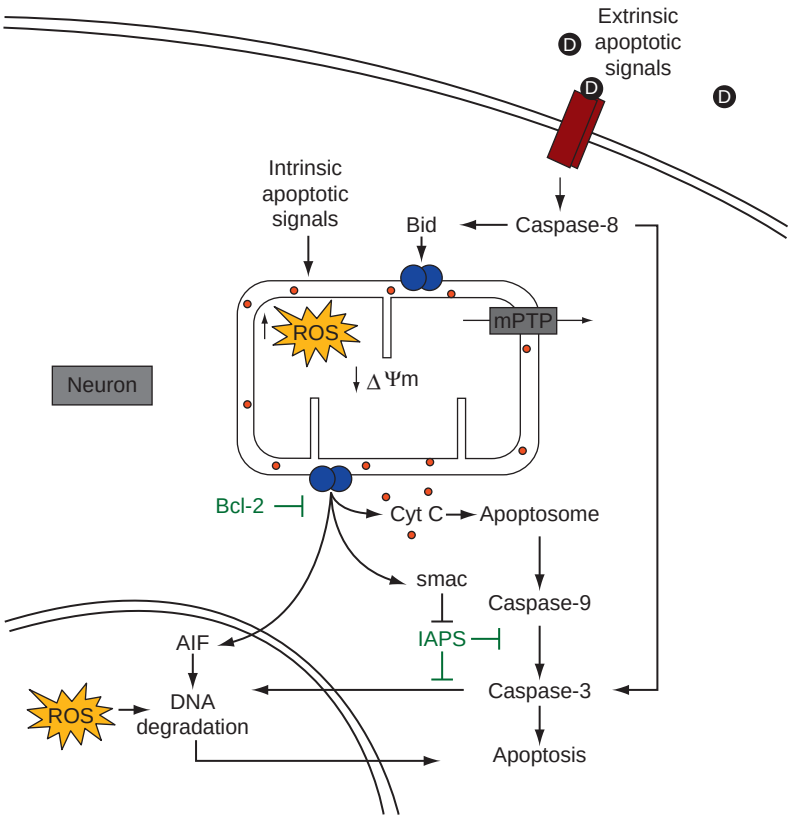

Figure 1 The intrinsic and extrinsic pathways of apoptotic cell death. Apoptosis can be triggered extrinsically through the binding of a death ligand to death receptors at the cell surface. The recruitment of procaspase-8 to the death receptors by adaptor proteins such as FADD follows allowing the conversion of procaspase-8 to its active form, caspase-8. Caspase-8 can cleave procaspase-3 triggering caspase cascade and the activation of the various effecter caspases which degrade DNA and various proteins. It can also act through a mitochondria-dependent manner, cleaving Bid, facilitating its translocation to the mitochondrial membrane and thereby initiating release of death mediators. Various intrinsic signals are also able to mediate apoptosis, through disruption of mitochondrial activity causing a subsequent decrease in the mitochondrial membrane potential ($\Delta\psi m$) and the activation of the mitochondrial permeability transition pore (mPTP), or through the actions of proapoptotic proteins such as Bax, Bak, Bad, and Bid. Following loss of mitochondrial stability various death mediators are released including cytochrome C (Cyt C), which in conjunction with APAF-1 and procaspase-9 forms the apoptosome which activates caspase-9 and triggers a caspase cascade. The release of Smac facilitates this process by inhibiting the actions of IAPS, an inhibitor of the caspase cascade. Various compounds, such as apoptosis-inducing factor (AIF), are also released from the mitochondria and are able to translocate to the nucleus where they trigger chromatin condensation and apoptosis. Mitochondrial dysfunction also leads to the increased generation of reactive oxygen species (ROS), which can trigger cell death through the modification of various molecules, including lipids, proteins, and DNA.

of the disease as well as a high-throughput screening method for new neuroprotectants.

Current Treatments for Glaucoma

Once diagnosed, the current treatments for glaucoma concentrate on lowering the raised IOP. First-line pharmacological therapies include prostaglandin analogs which increase aqueous humor outflow and beta-blockers to reduce aqueous humor formation. Alpha-agonists to increase the uveoscleral outflow of aqueous humor and carbonic anhydrase inhibitors suppressing enzymes involved in aqueous humor production are used as second-line treatments, while third- or fourth-line treatments rely on increasing trabecular outflow using cholinergenic agonists and miotic agents. The disadvantages all the drugs share are the potential side effects and the requirement for topical administration up to four times daily. Furthermore, the incidence of poor compliance and persistence with the topical application is high and so the success of glaucoma management is limited. In addition, glaucoma appears to progress in many sufferers despite the continued use of pharmacological treatments. In these cases, surgery such as trabeculoplasty to reduce resistance to the outflow of aqueous humor by modifying the trabecular meshwork or trabeculotomy to remove part of the trabecular meshwork, allowing enhanced drainage of the aqueous humor, may prove successful in reducing IOP. As the degeneration of visual field in glaucoma is known to progress through RGC apoptosis, research is currently underway to develop neuroprotective treatments for glaucoma.

Neuroprotection

Neuroprotection is defined as the use of therapeutic agents to prevent or reverse neuronal damage, thereby retaining physiological function. For example, neuroprotective treatments are being researched for diseases which progress through the death of neurons of the central nervous system such as Alzheimer's, Parkinson's, and Huntington's. The efficacy of these therapeutic agents in clinical trials has been somewhat controversial. A number of clinical trials performed on stroke patients testing different neuroprotective agents showed either little success or adverse side effects, while treating patients of spinal cord trauma with the neuroprotective agent methylprednisolone resulted in improved motor function. The variation in success of these agents is thought to be due to the mechanism of neuronal death in the different diseases. In strokes, neuronal injury occurs at the cell body, so irreversible cell death occurs instantly; therefore, treatment with a neuroprotective agent would be given too late. However, in spinal cord trauma, neuroprotective treatment may have the desired effect as injury occurs at the axon and death of the cell body results hours later. For this reason, the use of neuroprotection as a treatment for glaucoma, thought to be brought about by death of RGC axons, seems a promising option.

Research Models

Research into the eye disease uses models which are important tools allowing researchers to monitor the progression of the disease and test new therapies. In order for these models to provide informative and transferable data, similarity to the human disease and reproducibility is required. A number of different models are used in the study of the disease, all of which have their strengths and limitations.

In Vitro Glaucoma Models

Initial experiments for neuroprotection in glaucoma are likely to be carried out *in vitro*. A number of ocular cells have successfully been cultured and present a cost-effective alternative to animal models for studying the effects of apoptosis and neuroprotection. Cell cultures have the advantage of allowing rapid screening of potential therapies and observation of direct effects on the cultured cells, under strict environmental control. Cell culture also provides a greater understanding of how compounds function at a cellular level; however, the response of the isolated cells, maintained in an artificial environment, may differ from that *in situ*. For this reason and the contentious use of immortalized cells to study apoptosis, a number of *in vivo* glaucoma models have been developed.

In Vivo Glaucoma Models

Pioneered in rat and more recently developed in monkey, the optic nerve crush is a well-calibrated and reproducible model of glaucoma. Damage to the optic nerve results in cell-body death and subsequent secondary injury to adjacent neurons, as seen in glaucoma. Alternatively, RGC apoptosis can be induced by raising the IOP and causing retinal ischemia, typically achieved through blockage of the aqueous humor outflow, including injection of hypertonic saline into the episcleral veins, cauterization of the episcleral veins, and laser photocoagulation of translimbus. As an alternative, excessive exposure to excitotoxins, such as glutamate or *N*-methyl-D-aspartic acid (NMDA) by intravitreal injections can be used to induce RGC apoptosis. A further model can be generated by laser coagulation at the retina where RGC apoptosis is induced adjacent to the site of laser contact. The DBA/J2 mouse is a genetically determined glaucoma model showing increased IOP, RGC apoptosis, optic nerve atrophy, and ONH cupping.

Mechanisms of Apoptosis and Development of Neuroprotective Agents

Neurotrophic Factor Withdrawal

Deprivation of neurotrophic factors (NFs) induces apoptosis, and has been suggested to play a role in glaucoma as outlined in **Figure 2**. Raised IOP is proposed to lead to a blockade of anterograde and retrograde transports, preventing transport of NFs. The neuroprotective effects of neurotrophins (NTs), a family of NTFs, are thought to be mediated through the activation of phosphoinositide (PI)-(3)-kinase, the inhibition of which is sufficient to block the survival effects of NT. PI(3)K phosphorylates and activates Akt which is known to target several key apoptosis regulators, including Bcl-2 antagonist of cell death (Bad) and cyclic adenosine monophosphate (cAMP) response element binding protein (CREB). The phosphorylation of Bad promotes its sequestration by the chaperone protein 14-3-3, while CREB is activated by Akt (also known as protein kinase B), leading to the upregulation of B-cell CLL/lymphoma 2 (Bcl-2). The actions of Akt have downstream consequences for mitochondrial function and both caspase activation and increased ROS production have been attributed to loss of NT-stimulated pathways.

NFs as Neuroprotective Agents

Brain-derived neurotrophic factor (BDNF) has been showed in a number of studies to have neuroprotective effects. Intravitreal injections of the NT administered to rats, following optic nerve transection and IOP-induced ischemia, increased the survival of RGCs. In addition to BDNF, ciliary neurotrophic factor (CNTF), glial-cell-line-derived neurotrophic factor (GDNF), and pigment-epithelium-derived

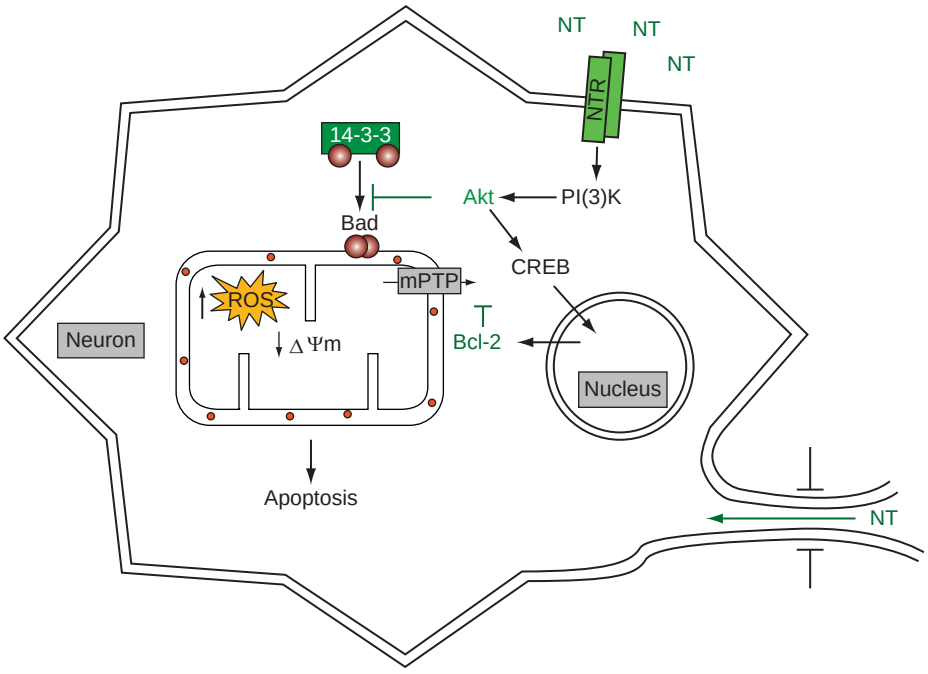

Figure 2 Apoptosis induced by neurotrophic factor withdrawal. Axotomy prevents the retrograde transport of both neurotrophins (NTs) and neurotrophic receptors (NTRs). NTs are able to suppress apoptotic signaling through the binding of NTR, the activation of phosphotidylinositol-3-kinase (PI(3)K), and subsequent activation of Akt. Akt promotes cell survival through multiple pathways, including the phosphorylation of Bad, which promotes its sequestration by the scaffold protein 14-3-3 and the activation of CREB, which promotes increased expression of Bcl-2. Bcl-2 is an essential antiapoptotic protein, which inhibits the release of death mediators, thereby preventing initiation of the caspase cascade.

growth factor (PEDF) have also demonstrated protection of RGCs in rat glaucoma models. The neuroprotective effects of the NFs are short-lived, with reduced survival of RGCs only weeks after a single injection. The longevity of the treatment has been addressed using a number of techniques. Injection of PEDF-peptide-loaded nanospheres into an ischemic rat model reduced RGC apoptosis over a longer period. The same technique was used to administer GDNF to the DBA/2J mouse glaucoma model and an ischemic rat model; again, increased survival of RGCs was observed over a longer period. An alternative method, meant to prolong the effects of the treatment, used an osmotic pump to administer NFs to an axotomized rat model. The technique was successful in reducing RGC apoptosis but most cells were dead within 1 month.

As an alternative to prolonged administration of NTs, researchers in this field have also looked toward gene transfer as a way of maintaining the required level of the NFs for long-term RGC survival. Transformation of a rat glaucoma model with the BDNF gene extended the life of the axotomized RGCs for a similar period. This work was furthered in the same model by injecting BDNF while simultaneously expressing the gene encoding the BDNF receptor, TrkB, known to show reduced expression in glaucoma models. The results showed increased survival of 76% of RGCs over a prolonged period.

Excitotoxicity

Glutamate is a neurotransmitter reported in raised concentrations in the vitreous of glaucoma patients and in animal models. RGCs are known to be highly susceptible to cell death through not only glutamate excitotoxicity and but also treatment with the glutamate analog, NMDA. This has lead to glutamate excitotoxicity being proposed as both a mechanism of primary insult upon RGCs and as a secondary insult following the death of RGCs and the release of further excitory amino acids and glutamate. At elevated levels, glutamate triggers the excessive activation of ionotrophic receptors, such as NMDA receptors, resulting in a subsequent influx of Ca^{2+} ions and an increase in oxidative stress leading to cell death as depicted in **Figure 3**.

Ca^{2+} is shown to increase mitochondrial permeability to ions and solutes and thought to regulate the mitochondrial permeability transition pore (mPTP), which is associated with the release of proapoptotic factors such as cytochrome C (Cyt C). Ca^{2+} has also been proposed to activate nitrous oxide synthase (NOS), leading to the generation of pathological quantities of nitric oxide (NO) and the subsequent production of reactive NO free radicals capable of triggering cell death, the full implications of which are discussed later.

Calpains are a family of cytoplasmic-calcium-activated cysteine proteases. Axotomy, ocular hypertension, and

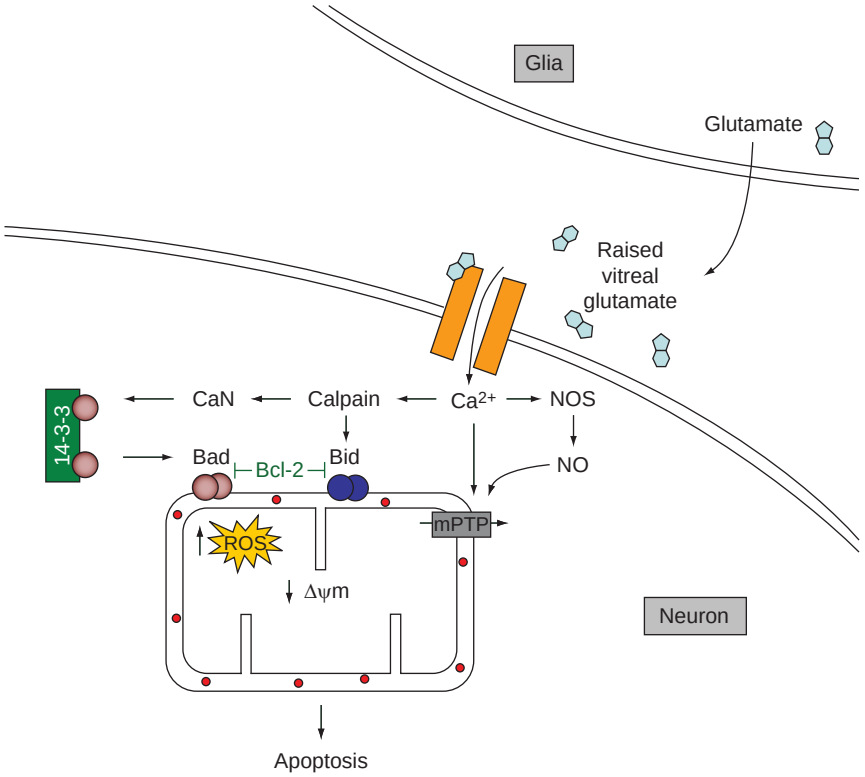

Figure 3 Excitotoxicity-induced apoptosis. Raised vitreal glutamate triggers the activation of ionotrophic calcium channels such as NMDA receptors. The resultant increase in intracellular calcium activates calpain and, in turn, calcineurin (CaN), which promote the translocation of Bad and Bid to the mitochondrial membrane, and the subsequent release of death mediators. Ca^{2+} also activates nitric acid synthase (NOS) which promotes mitochondrial dysfunction, ROS production, and activation of the mitochondrial permeability transition pore (mPTP). Increased cellular ROS and the release of death mediators, such as Cyt C and AIF, leads to apoptosis.

NMDA excitotoxicity all demonstrated calpain activity with inhibition showing reduced RGC loss. Increased Ca^{2+} in the retina correlates with increased calpain activity, which can activate the caspase cascade as well as lead to the phosphorylation of spectrin, Tau, and p35, and cleavage of known calpain substrates, including the autoinhibition domain of calcineurin (CaN).

In addition to activation by calpains, CaN has also been shown to undergo activating cleavage by caspases and interestingly raised IOP, although the mechanism of the latter is unknown. Sustained Ca^{2+} has also been shown to lead to increased levels of CaN, which induces apoptosis through the dephosphorylation of Bad, releasing the pro-apoptotic protein from sequestration by the chaperon protein 14-3-3. Bad is then able to translocate from the cytosol to the mitochondria, allowing it to heterodimerize with Bcl-2 and B-cell leukemia X_L (Bcl-X_L), leading to the release of Cyt C and the triggering of apoptosis. A role for CaN is further supported by the observation that dosing of cells with glutamate led to the translocation of a green fluorescent protein (GFP) fusion protein of Bad from the cytosol to the mitochondria, and the prevention of this in cells containing an inactive mutant form of CaN.

As mentioned previously, Bad phosphorylation is regulated by NT and treatment with NT is sufficient to confer resistance to excitotoxic insult. This suggests that excitotoxicity rather than working alone could act in conjunction with withdrawal of NFs to facilitate RGC apoptosis. Recent findings, however, have thrown doubt upon the hypothesis of glutamate excitotoxicity. Crucially, the raised glutamate levels observed in humans and animals have failed to be reproduced in follow-up studies. In addition, NMDA was able to induce apoptosis in the absence of Bax, a proapoptotic factor, suggested to be essential in apoptosis of RGCs in glaucoma. An alternative explanation for increased intracellular calcium and the subsequent triggering of apoptotic pathways is the activation of stress-activated channels by raised hydrostatic pressure.

NMDA-Antagonists and Neuroprotective Agents

This breakthrough of excess glutamate resulting in RGC apoptosis has led to considerable interest in the use of NMDA-receptor antagonists as neuroprotective therapies, many of which have been identified and characterized. MK801, a noncompetitive NMDA-receptor blocker, has been shown to protect RGCs from apoptosis in a number of experimental models including increased IOP and following intravitreal injections of NMDA in

rats. Despite showing promise as a successful neuroprotectant in the animal models, MK801 was never used in clinical trials due to its adverse side effects of inducing vacuole formation in neurons and neuronal necrosis.

Other NMDA-receptor antagonists were also studied for use as potential neuroprotectants. For example, detromethorphan was shown to aid the recovery of retinal activity in rabbits suffering from IOP-induced ischemia and flupirtine had a similar effect on the same model. Riluzole, an agent used for treatment of amyotrophic lateral sclerosis, reduced neuronal death following retinal ischemia brought about by raised IOP in rats. The most promising neuroprotective agent to date, memantine, is similar to MK801 but lacks the neurotoxic effects. Successfully used in the treatment of Alzheimer's disease (AD) and Parkinson's disease, memantine has also been shown to protect neurons from apoptosis in many different glaucoma models. Disappointingly, a recent second phase III clinical trial of memantine has revealed the compound to have no positive effect on visual-field deterioration in glaucoma patients.

Reactive Oxygen Species

Oxidative stress leading to neuronal apoptosis is an early event, occurring within hours of raised IOP, both *in vitro* and *in vivo*. Following atoxomy of RGCs, there is both an increase in reactive oxygen species (ROS) and cell death. Inhibition of ROS demonstrated a 50% reduction in RGC loss as did increasing expression of superoxide dismutase (SOD), known to be reduced in rat models with raised IOP.

The principal mechanism for ROS production is disruption of mitochondrial function, shown in **Figure 4**, leading to loss of mitochondrial membrane potential and subsequent release of death factors. In addition to raised IOP, light exposure has been suggested as a risk factor in glaucoma, through the increased generation of ROS. In addition, ROS can mediate apoptosis by reacting directly with various molecules including DNA, proteins, and lipids.

Mitochondrial Dysfunction and ROS Generation

ROS generation, particularly through the inhibition of complexes I and IV of the electron transport chain, has been implicated in various mechanisms of apoptosis, with treatment of antioxidants preventing apoptosis by inhibiting ROS generation and Cyt C release. A wide variety of antioxidants have been suggested as neuroprotectants in glaucoma, including vitamin E, 3-methyl-1,2-cyclopentanedione (MCP), and melatonin. Derivatives of catechin have been suggested to be potent antioxidants, and intravitreal co-addition of epigallocatechin was shown to attenuate the

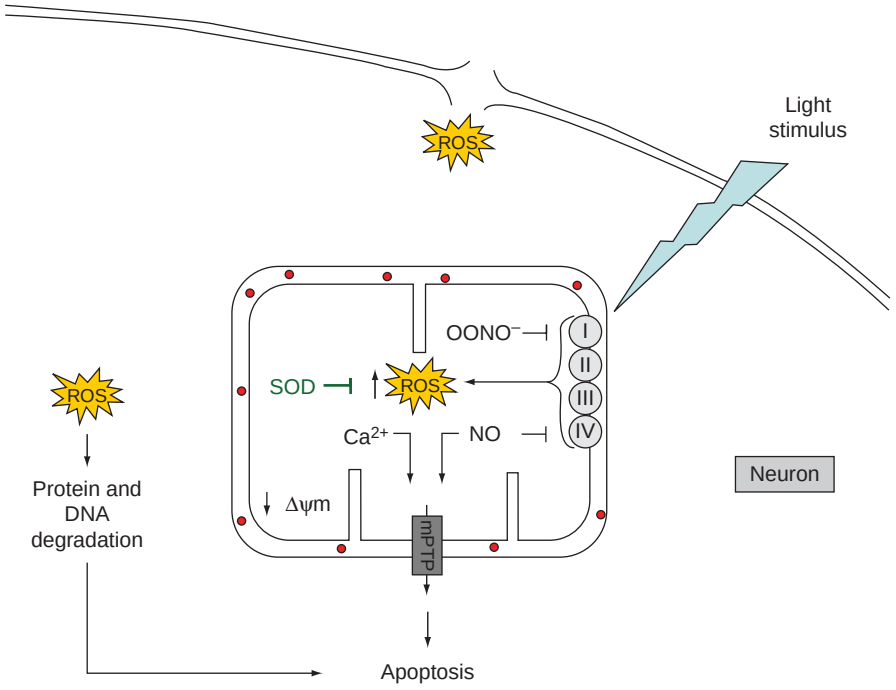

Figure 4 Reactive oxygen species (ROS) and mitochondrial dysfunction in apoptosis. Increased concentrations of ROS can lead to apoptosis through the modification of lipids, proteins, and DNA. Superoxide dismutase (SOD), a key enzyme involved in the removal of ROS, is reduced in glaucoma, potentiating the cells to increased damage by ROS. Inhibition of the electron transport chain by compounds, such as nitric oxide (NO) and peroxynitrite ($OONO^-$), leads to reduced mitochondrial membrane potential ($\Delta\psi m$) and increased generation of ROS, as has exposure to light. NO and Ca^{2+} can also promote mitochondrial dysfunction through activation of the mitochondrial membrane permeability transition pore (mPTP), and the release of death mediators.

retinal damage caused by treatment with the NO donor, sodium nitroprusside.

Ubiquinone (CoQ_{10}), a member of the electron transport chain, has been demonstrated to prevent lipid peroxidation and DNA damage. Furthermore, in recent tests in rats, the intraocular administration of CoQ_{10} afforded neuroprotective effects.

Antioxidants as Neuroprotective Agents

The most promising antioxidant treatment to date is that of orally administered *Gingko biloba* extract, which contains a number of substances shown to be effective in preventing mitochondrial damage through oxidative stress. Visual improvement has also been demonstrated in a double-masked long-term placebo-controlled study, with efficacy and safety reports suggesting a daily dose of 120 mg to be sufficient.

Protein Misfolding

The observation that AD patients demonstrated RGC loss typically associated with glaucomatous changes, including optic neuropathy and visual impairment, suggested possible mechanistic similarities. Supportive of mechanistic similarities between Alzheimer's and glaucoma is the observations of abnormal and phosphorylated Tau, a major plaque component, in the retina of glaucoma patients. β-Amyloid (Aβ), generated by the abnormal processing of amyloid precursor protein (APP), is another major component in Alzheimer's plaques. APP and Aβ are present in RGCs following elevation of IOP in rat models and in the DBA/2J mouse model. It has been shown *in vivo* that Aβ is neurodegenerative and that disruption of these APP processing pathways is sufficient to reduce RGC apoptosis in glaucoma models in rats.

In AD, mutations altering the function of APP processing proteins lead to increased Aβ production and, subsequently, increased apoptosis. A complementary mechanism, shown in **Figure 5**, has been implicated for glaucoma whereby normally rapid anterograde transport is blocked resulting in increased somal concentrations of APP. This has been proposed to trigger the abnormal processing of APP by caspase-3 in RGCs in glaucoma models generating increased Aβ in the retina and is supported by observations of decreased vitreal Aβ (suggesting increased deposition) in glaucoma patients.

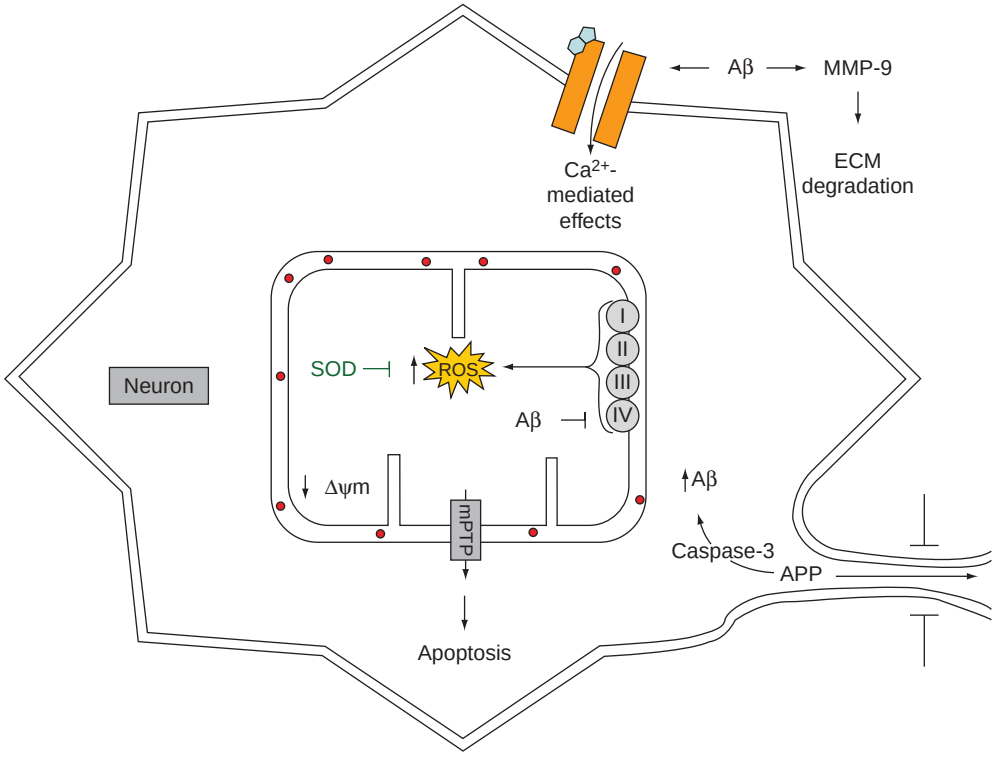

Figure 5 Aβ-induced apoptosis. The anterograde transport of amyloid precursor protein (APP) is blocked by axotomy, leading to increased somal concentrations of APP. At elevated concentrations, APP triggers the abnormal activation of caspase-3 which cleaves APP to yield Aβ, which has both intracellular and extracellular actions in promoting apoptosis. Aβ is shown to target the electron transport chain promoting increased reactive oxygen species (ROS) production and mitochondrial dysfunction. Additionally, Aβ upregulates the activity of ionotrophic calcium channels, increasing intracellular calcium and therefore promoting calcium-mediated apoptosis. Metalloproteinase-9 (MMP-9) also shows increased activity in the presence of Aβ, promoting increased extracellular matrix (ECM) degradation and apoptosis through anoikis.

Aβ is believed to induce apoptosis through elevated intracellular calcium and increased oxidative stress, as seen in AD, where oxidative damage is observed before significant plaque formation. Increased oxidative damage is indicative of mitochondrial dysfunction and both APP and Aβ have been shown to target mitochondria. At raised levels associated with glaucoma, APP has been shown to interact with mitochondria clogging them and preventing normal function. Aβ has been implicated in the inhibition of ketoglutarate dehydrogenase and complex IV of the electron transport chain, inhibition of both of which leads to increased ROS generation. This process could constitute a positive-feedback loop accelerating cell death, as the presence of ROS has been shown to facilitate Aβ production. Following mitochondrial dysfunction, apoptosis has ultimately been suggested to be mediated through the initiation of a caspase cascade.

Reduction of Misfolded Proteins in Neuroprotection

Recent *in vivo* studies have shown that a reduction in RGC apoptosis can be achieved by targeting the Aβ pathway. Inhibition of β-secretase, responsible for Aβ production, reduced plaque formation and RGC apoptosis. Increased plaque removal and inhibition of plaque formation had a similar effect. All of these mechanisms were shown to be effective in reducing RGC apoptosis, with the greatest benefit seen through the use of combination therapy, which resulted in a maximal reduction in RGC apoptosis of greater than 80%.

Glial–Neuronal Interactions

Glial cells, comprised of astrocytes, microglia, and Müller cells, act as support cells for neurons, maintaining their regular function by providing both neurotrophins and sustenance while removing toxic neurotransmitters and ions. Glaucoma induces dramatic changes in the glia gene expression patterns, potentially converting them from supportive to neurotoxic, as summarized in Figure 6. In the scope of this article, the impact of distinct types of glial cells are not differentiated, but evaluated as a whole.

Glial cell activation has been demonstrated in the glaucomatous optic nerve, in the retina of glaucoma

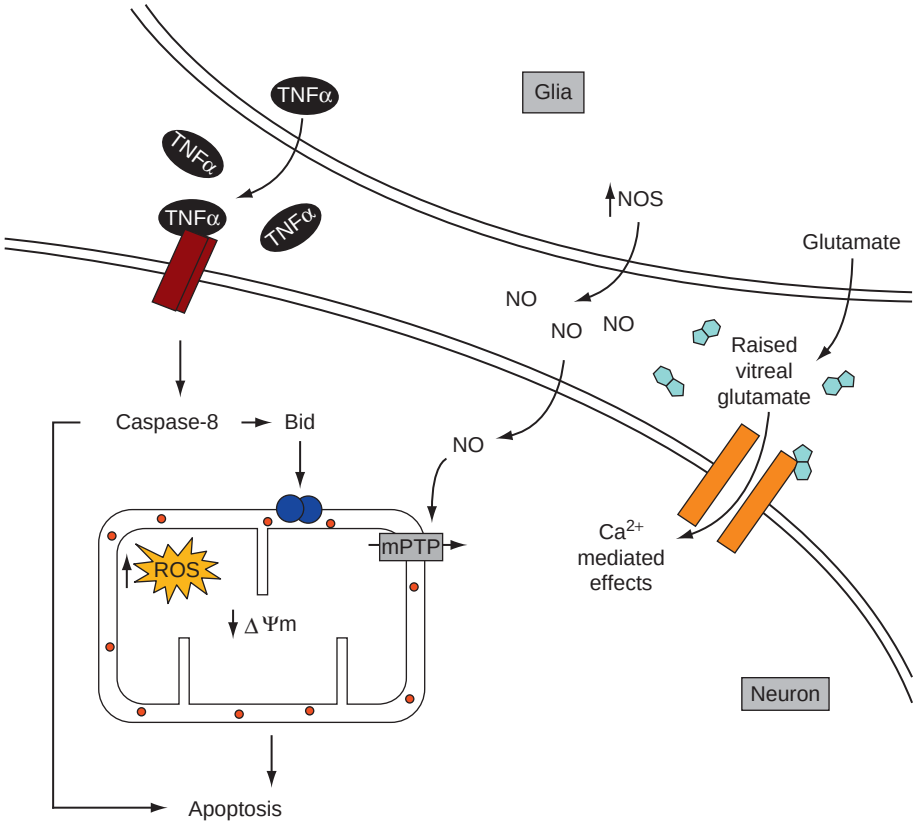

Figure 6 Apoptosis induced by glial–neuronal interaction. Glial cells release neurotoxic molecules such as TNF-α, glutamate, and nitric oxide (NO), which are known to induce apoptosis in RGCs. TNF-α is a death ligand and triggers caspase-8-mediated extrinsic apoptosis. Elevated intravitreal glutamate, due to increased secretion and decreased uptake by glia, leads to apoptosis through calcium-mediated mechanisms, while increased NO causes mitochondrial dysfunction and the subsequent release of death mediators as well as increased reactive oxygen species (ROS) and cytotoxic modifications to key cellular components.

patients and in glaucoma models showing altered levels of secretion. Increased secretion of NT appears to represent an attempted neuroprotective function, supporting damaged neuronal cells, while other changes, such as decreased secretion of interleukin (IL)-6 and increased secretion of NO and tumor necrosis factor (TNF)-α, which have been implicated in RGC apoptosis.

TNF-α, a trigger for extrinsic apoptosis, activates caspase-8 leading to activation of the caspase cascade, Bid activation, the loss of mitochondrial membrane potential, and the subsequent release of cell-death mediators such as apoptosis-inducing factor (AIF) and Cyt C. Increased secretion of TNF-α by glia has been shown to correlate with increased disease severity in glaucoma patients and is further accompanied by the upregulation of TNF receptor 1 (TNF-R1) in glial cells and in RGCs and their axons in glaucoma patients. TNF-α also represents a possible genetic component for glaucoma with the TNF-α-308 gene polymorphism identified in glaucoma patients suggesting a role for TNF-α signaling.

Glial cell secretion of NO, potentially stimulated by TNF-α, is raised in glaucoma with elevated NO concentrations shown to trigger axonal degradation and cell death in RGCs. There are three isoforms of NOS: neuronal (nNOS), inducible (iNOS), and endothelial (eNOS). Initially, iNOS received the most attention as it is induced under various stress conditions. It was suggested to be raised in the ONH of glaucoma patients and also shown to be raised in glaucoma rat model utilizing cauterization, where treatment with inhibitors was sufficient to abate apoptosis.

However, validation of this work in alternative models failed to produce correlating results, with both a murine model and a rat glaucoma model of IOP raised through intravitreal injections, failing to show the involvement of NOS or a reduction in RGC apoptosis by NOS inhibitors. It appears that iNOS upregulation could be due to secondary factors caused by the cauterization process and not raised IOP. While the role of iNOS in glaucoma has been called into doubt, it does not undermine the potential importance of NO signaling. nNOS and eNOS have been showed to be expressed at low levels in normal eyes in glial cells in the ONH, but shows dramatically raised levels in the ONH of glaucoma sufferers.

The main mechanism, through which NO triggers cell death, appears to be disruption of mitochondrial function. An interaction between NO and the mPTP directly facilitates the release of Cyt C and AIF, with mPTP inhibitors abating NO-induced neuronal apoptosis. Caspase-3 activation, however, has been shown without initial loss of mitochondrial membrane potential, suggesting activation may result from blockade of the electron transport chain and subsequent increased levels of ROS. Loss of mitochondrial membrane potential can be triggered as a downstream event, following prolonged inactivation of the electron transport chain.

NO binds complex IV of the electron transport chain, also known as cytochrome oxidase, reducing the enzyme's affinity for oxygen. Prolonged exposure to NO or peroxynitrite ($OONO^-$), a highly destructive molecule formed from ROS and NO, can lead to blockade of complex I of the electron transport chain. This facilitates further ROS production and $OONO^-$ synthesis, which are capable of extensively modifying cellular components leading to apoptosis, while antioxidant treatment in NO-induced apoptosis was shown to abate caspase activation.

Disruption of mitochondrial respiration has also been suggested to facilitate the disruption of Ca^{2+}, associating NO with excitotoxicity-induced apoptosis. This link was strengthened by observations that nNOS-deficient mice were resistant to NMDA-induced RGC death. NO induced modest increases in the amplitude of Ca^{2+} channels and the induction of the Ca^{2+}-mediated death effectors, the calpains.

Extracellular Matrix Degradation

Glaucomatous changes include extensive remodeling of the extracellular matrix (ECM), altering the levels of the various ECM components, including collagen I and IV, matrix metalloproteinases (MMPs), tissue inhibitors of metalloproteinases (TIMPs), transforming growth factor beta 2 (TGF-β2), and laminin.

MMP expression in particular has received attention, with expression in glaucoma patients being raised in comparison to normal patients. The condition of the ECM both regulates and is regulated by the expression and release of MMPs, with the subsequent reduced levels of laminin contributing to cell death, and significant RGC loss in the retina. Supportive evidence from the ability of TIMP-1 to abate neuronal apoptosis, as well as observations that MMP-9-deficient mice demonstrate reduced laminin degradation and increased resistance to neural trauma, further highlights the potential importance of MMPs in glaucoma.

It was recently demonstrated *in vivo* that raised IOP induced remodeling of the ECM within the retina. Raised IOP was shown to correlate to decreases in laminin and TGF-β2 and increased MMP-9, TIMP-1, and RGC apoptosis. Loss of survival signals from the ECM is thought to induce a specific form of apoptosis called anoikis.

Whether glaucomatous changes are initiated at the retina or ONH is still a matter of contention. Astrocytes in the ONH have been shown to be activated by raised IOP and produce MMPs that are able to remodel the ECM, possibly resulting in axonal compression and thereby facilitating apoptotic mechanisms associated with the blockade of anterograde and retrograde transport.

In addition to raised IOP, potential apoptotic mechanisms such as Aβ, NO, ROS, excitotoxicity, and TNF-α have all been implicated in triggering an increase in

MMP-9, suggesting that MMP-9 may represent an important downstream executor of apoptosis rather than a primary affecter.

Neuroprotective Vaccine

Studies using rat and mouse models of glaucoma have suggested a potential role for autoimmunity in the protection of neurons from secondary damage. Following the initial insult, nonspecific T-lymphocytes have been shown to accumulate at the primary lesion site. While nonspecific T-lymphocytes did not exhibit neuroprotection, effects were observed upon injection with myelin basic protein (MBP)-specific T-lymphocytes or immunization with MBP. Unfortunately, injections of anti-MBP-specific T-lymphocytes and MBP immunization induced the paralytic condition – experimental autoimmune encephalomyelitis (EAE).

Copolymer 1 (Cop 1), a synthetic peptide based on MBP, was discovered to suppress EAE and shown in clinical trials to be beneficial to patients with multiple sclerosis. Further studies have revealed that immunization with Cop 1 increases RGC survival following optic nerve crush, glutamate injections, and increased IOP in rats. This research shows that there is potential for the development of a glaucoma vaccine.

Summary

The primary mechanism of RGC loss in glaucoma is through apoptosis, which can be triggered through a variety of mechanisms both intrinsic and extrinsic. Apoptotic signaling shows a large level of redundancy with extensive cross talk. This redundancy poses a major problem in terms of neuroprotection with inhibition of one apoptotic pathway merely delaying apoptosis before mediation through an alternative pathway or the triggering of necrosis. It is still unclear as to the primary mechanism of apoptosis induction in glaucoma, although an increased understanding would aid a more effective development of neuroprotective strategies. Fundamental to the successful development of neuroprotective strategies is targeting the apoptotic pathway upstream and at multiple points to maximize effectiveness.

The studies of neuroprotective agents on glaucoma models carried out to date have shown great promise with many different agents demonstrating efficacy in a large number of models, summarized in Table 1. Unfortunately, translation of this research from animals through to clinical trials has exposed complications with side effects and inefficacy, hindering progression. However, due to the complicated nature and a number of different overlapping pathways inducing apoptosis, the identification of a multitude of potential neuroprotectants has been possible. One major problem still faced in the analysis of these compounds is the difficulties monitoring efficacy *in vivo*.

Table 1 Comparison of the models used to test the different neuroprotective agents

Neuroprotectant	*Animal*	*Model*
MK801	Rat	Increased IOP
		NMDA injection
Detromethorphan	Rabbit	Increased IOP
Flupirtine	Rabbit	Increased IOP
	Rat	Increased IOP
		NMDA injection
Riluzole	Rat	Increased IOP
Memantine	Monkey	Increased IOP
	Mouse	DBA/2J
	Rat	Glutamate injection
		Increased IOP
		Optic nerve crush
Brain-derived neurotrophic factor (BDNF)	Rat	Increased IOP
		Optic nerve transection
Ciliary neurotrophic factor (CNTF)	Rat	Increased IOP
		Optic nerve transection
Glial-cell-line-derived neurotrophic factor (GDNF)	Mouse	DBA/2J
	Rat	Increased IOP
Pigment-epithelium-derived growth factor (PEDF)	Rat	Increased IOP
		Optic nerve transection
Myelin basic protein (MBP) T-lymphocytes	Rat	Optic nerve transection
		Spinal cord contusion
Myelin basic protein (MBP)	Rat	Spinal cord contusion
Copolymer 1 (Cop 1)	Rat	Glutamate injection
		Increased IOP
		Optic nerve crush
Monoclonal anti-Aβ IgG	Rat	Increased IOP
Congo Red	Rat	Increased IOP
β-Secretase inhibitor	Rat	Increased IOP
Epigallocatechin (EGC)	Rat	NO donor
Ubiquinone (CoQ_{10})	Rat	Increased IOP
Vitamin E	–	Primary cultures
	Human	Glaucoma patients
Gingko biloba	Rat	Increased IOP
	Human	Glaucoma patients

It is hoped that the development of the novel DARC technique for early diagnosis of glaucoma may also be a valuable tool in the analysis of potential neuroprotectants.

See also: Biomechanics of the Optic Nerve Head; Glutamate Receptors in Retina; Information Processing: Ganglion Cells; Intraocular Pressure and Damage of Optic Nerve Axons; Primary Open-Angle Glaucoma.

Further Reading

Cheung, W., Guo, L., and Cordeiro, M. F. (2008). Neuroprotection in glaucoma: Drug-based approaches. *Optometry and Vision Science* 85(6): 406–416.

Cordeiro, M. F., Guo, L., Luong, V., et al. (2004). Real-time imaging of single nerve cell apoptosis in retinal neurodegeneration. *Proceedings of the National Academy of Sciences of the United States of America* 101(36): 13352–13356.

Grossmann, J. (2002). Molecular mechanisms of ''detachment-induced apoptosis – anoikis'' *Apoptosis* 7(3): 247–260.

Guo, L. and Cordeiro, M. F. (2008). Assessment of neuroprotection in the retina with DARC. *Progress in Brain Research* 173: 437–450.

Kuehn, M. H., Fingert, J. H., and Kwon, Y. H. (2005). Retinal ganglion cell death in glaucoma: Mechanisms and neuroprotective strategies. *Ophthalmology Clinics of North America* 18(3): 383–395, vi.

Lebrun-Julien, F. and Polo, A. D. (2008). Molecular and cell-based approaches for neuroprotection in glaucoma. *Optometry and Vision Science* 85(6): 417–424.

Lin, M. T. and Beal, M. F. (2006). Mitochondrial dysfunction and oxidative stress in neurodegenerative diseases. *Nature* 443(7113): 787–795.

Lipton, S. A. (2003). Possible role for memantine in protecting retinal ganglion cells from glaucomatous damage. *Survey of Ophthalmology* 48(supplement 1): S38–S46.

Wein, F. B. and Levin, L. A. (2002). Current understanding of neuroprotection in glaucoma. *Current Opinion in Ophthalmology* 13(2): 61–67.

Weinreb, R. N. and Lindsey, J. D. (2005). The importance of models in glaucoma research. *Journal of Glaucoma* 14(4): 302–304.

Yuan, J. and Yankner, B. A. (2000). Apoptosis in the nervous system. *Nature* 407(6805): 802–809.

Zhong, Y. S., Leung, C. K., and Pang, C. P. (2007). Glial cells and glaucomatous neuropathy. *Chinese Medical Journal (Engl)* 120(4): 326–335.

Retinal Histogenesis

J A Brzezinski, IV and T A Reh, University of Washington, Seattle, WA, USA

Glossary

Birthdate or born – The time when a progenitor permanently exits the cell cycle. Marking cells in their final division is referred to as birthdating.
Cell fate determination – The process by which a progenitor is programmed to become a specific cell type and its functional maturation. In the retina, a progenitor needs to acquire competence, exit the cell cycle, become specified, and differentiate.
Competence – The potential to adopt a certain cell fate(s).
Differentiation – The functional maturation of a specified cell.
Histogenesis – The development of a mature tissue from a naive progenitor population.
Lineage – A cohort of cells derived from division(s) of a common progenitor. This is also referred to as a clone.
Lineage tracing – The use of an indelible marker to label cells and all their descendants. Analysis at a later time point allows the inference of lineal relationships. This is also referred to as fate mapping.
Multipotent progenitor/progenitor – A cell that has competence to adopt several different fates. These cells may or may not be proliferative.
Progressive restriction model – A model of cell fate determination where multipotent progenitors lose the competence to adopt multiple cell fates over time. By this model, early progenitors have the competence to form all fates in a tissue.
Serial competence model – A variation on the progressive restriction model whereby multipotent progenitors transiently gain and subsequently lose competence for a subset of fates in a tissue over time. By this model, progenitors do not have the competence to form late fates at the earliest time points.
Specification or commitment – The point when a progenitor cell has irreversibly decided on a cell fate.

Birthdating

An interesting property of retinal cells is that they do not continue to divide after they differentiate. This means that at some point in development, a progenitor permanently exits the cell cycle, referred to as its birthdate. Investigators took advantage of this property and designed a clever pulse-chase experiment to investigate whether different cell types exited the cell cycle at characteristic times. Animals at various stages of development were given a pulse of ^{3}[H]-thymidine (3HdT). The 3HdT is incorporated into replicating DNA during synthesis (S)-phase and any excess is cleared from the body quickly. The incorporated 3HdT is maintained in the newly synthesized DNA permanently. If the cell continues to divide, it will dilute the 3HdT signal by one-half each division. Next, autoradiography was conducted after the retina was fully formed (the chase). Cells that retained maximum labeling are those that exited the cell cycle (born) on the day of 3HdT administration. More recently, birthdating studies have been conducted with synthetic nucleotides, such as 5-bromo-2-deoxyuridine (BrdU), which can be detected by antibodies instead of autoradiography.

About 50 years ago, Sidman used birthdating studies to test what order, if any, retinal cells were formed in the rodent retina. The observations of Sidman and future investigators revealed a stereotypical birth order that was broadly broken down into early and late groups (**Figure 1**). Retinal ganglion cells (RGCs) were born first, followed closely by horizontal cells, cones, and amacrines. The late cohort comprised rods, bipolar cells, and Müller glia. Birthdating has been conducted in several vertebrate species. While there are some small differences in the order, the first cells born in all species examined are RGCs. Although there is clearly an overall birth order, which is evident from the production onset of each cell type, there is also considerable overlap in the genesis of the cell types, such that multiple cell types are born on the same day of development (**Figure 1**). This overlap is also observed in species where retinal histogenesis is long, such as in monkey. These data implied that cell fate determination is not strictly regulated by measuring time (or cell cycles) during development. Nonetheless, the observance of a birth order indicated that there is a temporal input into cell fate determination.

These studies raised several questions about retinal progenitors. Are all retinal cell types derived from the progenitors in the optic cup? Are there different progenitors for each retinal cell type? Is fate choice predetermined or stochastic? These questions were addressed by tracing the fate of individual progenitors.

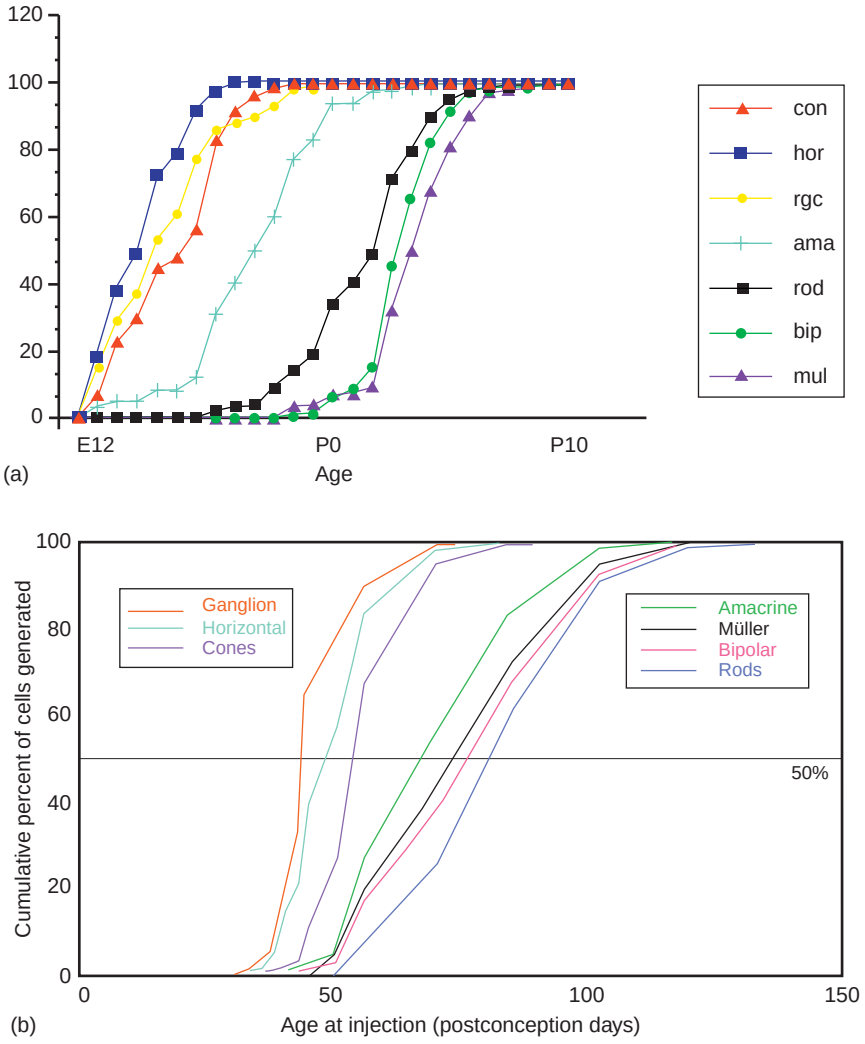

Figure 1 Birthdating. (a) Data from the rat retina showing the birthdates for each cell type as a percentage of its total. The progression from early to late cell-type generation that was first observed by Sidman can be clearly identified. CON, cone; HOR, horizontal cell; RGC, retinal ganglion cell; AMA, amacrine cell; BIP, bipolar cell; and MUL, Müller glia. (b) Similar thymidine labeling study in monkey shows a similar, though not identical, pattern of birthdates for the various types of retinal cells. Despite the fact that the patterns of generation are not identical, the early and late fates are largely segregated. (a) Data from Rapaport, D. H., Wong, L. L., Wood, E. D., Yasumura, D., and LaVail, M. M. (2004). Timing and topography of cell genesis in the rat retina. *Journal of Comparative Neurology* 474(2): 304–324. (b) Modified from La Vail, M. M., Rapaport, D. H., and Rakic, P. (1991). Cytogenesis in the monkey retina. *Journal of Comparative Neurology* 309(1): 86–114.

Lineage Tracing

To understand the behavior of progenitor cells, a way to trace the fate of individual progenitors was needed. Starting in the late 1980s, investigators designed elegant lineage-tracing (fate-mapping) experiments to study the retina. In rodents, Turner, Snyder, and Cepko used replication-incompetent retroviruses encoding a marker gene (e.g., *LacZ*) to infect retinal progenitors at various time points. These retroviruses can only infect dividing progenitors. Since the virus integrates into the genome, the progenitor and its descendents become permanently labeled. By adjusting the titer of the virus, individual progenitor lineages (clones) can be mapped from mature retinas (**Figure 2**).

The first set of retroviral lineage-tracing studies examined postnatal infections of rat retinas. In postnatal day 0 (P0) infections, majority of clones contained rods and were predominantly small (one to four cells). A large number of clones contained only rods, whereas others contained rods, amacrines, bipolars, and/or Müller glia (**Figure 2** and **Table 1**). There were few clones that did not contain any rods. Cell types born before P0 (e.g., cones, horizontals, and RGCs) were not observed in these clones, consistent with previous birthdating analyses. Clones generated from P2, P4, and P7 infections become progressively smaller. This reflects the progressive decrease in progenitor division that occurs in the first postnatal week. Clones were heterogeneous; some

contained multiple cell types and others one cell type or just a single cell. From all these time points, there was no obvious lineage hierarchy that could be constructed from the clone composition data. This showed that mammalian retinal cell fate determination is stochastic, or nondeterministic. Importantly, they observed two-cell clones that had different fates. This implied that fate choice is decided during or after the last cell division.

To see if the progenitors in the optic cup can give rise to all the retinal cell types, the investigators generated clones from embryonic (E) time points when few cells have exited the cell cycle. For this reason, they injected their retroviruses into the subretinal space of E13 and E14 mice *in utero*, a difficult procedure. The mice were allowed to mature and clone composition was examined. The clone size and composition were highly heterogeneous (Table 1). All seven cell fates were represented in these clones. Moreover, these clones never contained any other cell types (i.e., astrocytes, vascular endothelial cells, pigment epithelium, etc.). These early lineage traces showed that all seven retinal cell types derive solely from a retina-restricted progenitor pool. The heterogeneity in clone composition (there were few multicell clones alike) reinforced that fate choice is apparently stochastic. Consistent with retinal cell frequency (~78% are rods in mice), nearly all clones contained one or more rods. Clone size varied from 1 to

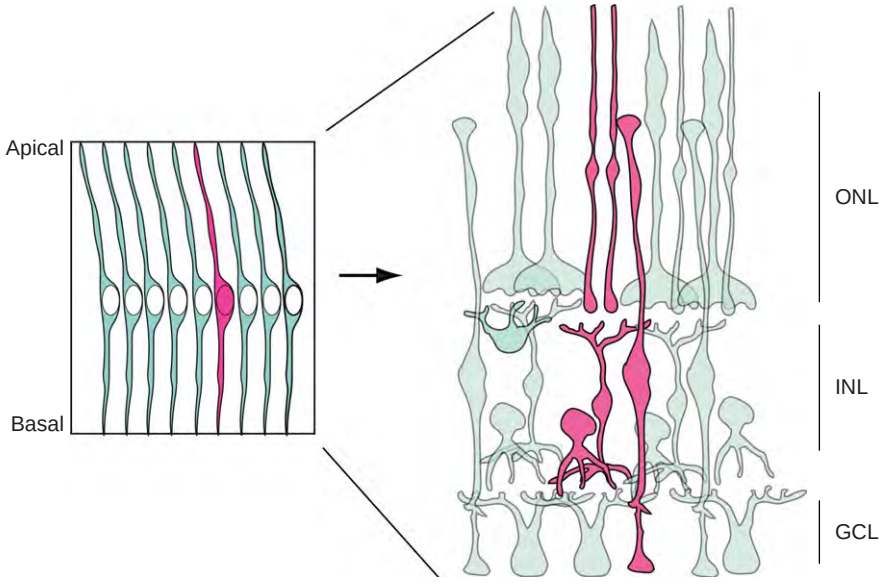

Figure 2 Lineage analysis. Diagram showing the basic strategy to track the lineages of the retinal progenitor cells. A progenitor cell is labeled (red) at an early stage of development, by using either a retroviral vector with a reporter gene, or a direct injection of a tracer. The cell undergoes multiple rounds of division in this case, and when the retina is examined in the adult animal, the different types of retinal cells can be identified by their laminar position and their morphology. In this case, two rods, a bipolar cell, an amacrine cell, and a Muller glial cell were derived from the progenitor. See Table 1 for more examples of the types of clones found in these experiments.

Table 1 Retroviral lineage tracing in rodents

Age of infection	*E13*	*E14*	*P0*	*P2*	*P4*	*P7*
Ave. clone size	46.4	26.3	2.5	1.6	1.4	1.1
Max. clone size	217	234	22	7	7	2
Cell fates[a]	r, b, a, c, m, g, h	r, b, a, c, m, g, h	r, b, a, m	r, b, m, a	r, b, m, a	r, m
Clone examples	1g	2c	4r	2r	1r, 1b	1r
	1c	1c, 1g	1a	1b	1r, 1m	1m
	1c, 1h	8r, 1c	3r, 1b	1r, 1b	2r	1r, 1m
	17r, 1c, 3b, 1m, 1a	51r, 6b, 1m	2r, 1b, 1a	1r, 1m	3r, 1b	2r
	43r, 1c, 7b, 2a	164r, 2c, 1h, 12b	2r, 1b, 1m	1r, 1a	1r, 1a	
	111r, 16b, 1m, 5a, 1g	28r, 9b, 3a, 1g	10r	3r, 1m	1r, 1b, 1a	

[a]Cell fates represented in clones (r, rod; b, bipolar; a, amacrine; c, cone; m, Müller; g, ganglion; h, horizontal) listed in decreasing frequency observed. In mice, the cell frequency in decreasing order is r, a, b, m, c, g, and h.
Data from Turner, D. L. and Cepko, C. L. (1987). A common progenitor for neurons and glia persists in rat retina late in development. *Nature* 328: 131–136; and Turner, D. L., Snyder, E. Y., and Cepko, C. L. (1990). Lineage-independent determination of cell type in the embryonic mouse retina. *Neuron* 4: 833–845.

234 cells and had a bimodal distribution. There were abundant small clones (<5 cells) and abundant large clones (>20 cells). The largest clones are simply too big to have been generated by simple asymmetric (one progenitor, one neuron) divisions in the time allotted for development. Based on the distribution of clone sizes, it is possible that progenitors preferentially utilize symmetric divisions during retinal histogenesis. Lineage-tracing studies have been conducted in other vertebrates, yielding similar results.

These lineage-tracing studies answered several questions. First, retinal progenitors in the optic cup are multipotent and give rise to all seven cell types. Second, there are no separate progenitors for each cell type. Nonetheless, rod-only clones were observed, raising the possibility of a rod-only progenitor. Since rods make up 78% of the mouse retina, small- to medium-sized rod-only clones are expected from multipotent progenitors. Fourth, cell fate choice is stochastic. Fifth, cell fate specification occurs during the last cell cycle or later. These data raised several more questions about the mechanisms of retinal histogenesis. Is fate determination a cell autonomous process, a cell nonautonomous process, or a combination of both? Do retinal progenitors have broad competence that is gradually lost, or are progenitors more limited in their cell fate choices during development? These questions have been addressed by manipulating the local cellular environment.

Environmental Challenge

Several approaches have been undertaken to discriminate between cell autonomous and cell nonautonomous control of retinal cell fate determination. Most of these experiments involve challenging retinal progenitors with different environments. Unlike the previous birthdating and lineage-tracing studies, these environmental challenge experiments are harder to interpret and, at times, yield conflicting results.

One type of experiment was designed to answer the question: What is the default state of retinal progenitors? For these experiments, retinal progenitors were labeled with 3HdT and dissociated to single cell density to examine their potential for differentiation in isolation. Reh and Kljavin saw that when rat progenitors were isolated from early stages of development, the majority of the progenitors differentiated into RGCs, while progenitors isolated from late stages of development differentiated into cell types normally generated late in development, like rods. A somewhat different result was obtained from similar studies in the chick embryo by Adler and colleagues, suggesting that cones were the default cell fate. However, subsequent studies in chick revealed a ganglion cell bias for the progenitors isolated from the earliest stages of retinal development. Together, these results led to the concept of a rolling default, or shifting competence in the progenitors; in other words, there is an intrinsic bias to the types of neurons generated by the progenitors that shifts progressively over developmental time. This idea has been recently supported by Notch-signaling studies. The Notch receptor is active in progenitor cells throughout development, and inhibition of signaling leads to premature progenitor differentiation. Inhibition of Notch in early progenitors leads to the overproduction of RGCs and cones, whereas inhibition of Notch function later in development results in overproduction of rods, but not of RGCs or cones. These results show that retinal progenitors change their competence intrinsically over time.

In the next type of experiment, investigators asked whether inductive interactions among the retinal cells played a role in their cell fate determination. Studies from *Drosophila* eye imaginal disk had shown an important role for cell–cell interactions in directing the ommatidial progenitors to their individual identities. In that tissue, the data were best fit by a sequential cell induction model in which the first cells, the R8 photoreceptors, induce the recruitment of the next type of photoreceptor, and so on. To test whether similar sequential inductions occurred in vertebrate retinas, investigators used heterochronic co-cultures, surrounding early embryonic progenitors with late-generated retinal cells. The groups of Raff and Reh co-cultured early embryonic rodent retinal cells with an excess of postnatal retinal cells. In both sets of experiments, the early progenitors were more likely to develop into rhodopsin expressing (rod photoreceptors) cells when compared to early progenitors cultured alone (which developed primarily early retinal fates). This increase was not seen when the challenging (older) cells were derived from the brain instead of the retina. Watanabe and Raff also found that the increase in rods was observed when the two cell populations were separated by a cell-impermeable membrane. Together, these data showed that a soluble factor(s) from late retina can promote rod fate in younger cells. In addition, very early mouse retinal progenitors (E11–E12) could form rods when cultured with an excess of older rat retinal cells; birthdating analyses indicate that rods are not normally generated by progenitors from this very early retina, which suggests that rod competence precedes rod genesis by at least 1 day. These experiments led to the idea that although progenitors may have an intrinsic bias in the types of cells they generate at any time in development, their fate can be influenced by factors in the microenvironment. Many subsequent studies have identified signaling factors in the developing retina that can influence the fate of the progenitors and, particularly, factors that can increase the percentage of these cells that differentiate into rods; however, since low-density cultures do not support robust rod differentiation (i.e., expression of

rhodopsin and other markers), it is possible that most of the factors identified to date have more of an effect on the expression of these identifiers, rather than the choice of the rod fate *per se*.

Another concept that emerged from the early studies of retinal development was the idea that specific cell types use feedback regulation to control their density. Elimination of dopaminergic amacrine cells in the developing frog leads to an overproduction of these cells by progenitors at the ciliary marginal zone. This suggested that there is a nonautonomous feedback regulation to negatively control amacrine cell number. *In vitro* experiments found a similar effect in developing rat retina. When E16 retinal cells were co-cultured with an excess of P0 cells, fewer amacrines were generated. However, when the P0 cells were depleted of amacrine cells, there was an increase in the number of amacrine cells generated by the E16 cells. When the converse experiment was done, P0 cells co-cultured with an excess of E16 cells, an increase in amacrines and bipolars was seen along with a decrease in rods. This confirmed the presence of negative feedback on amacrine cells and implied feedback regulation of bipolar cell genesis. The concept of feedback regulation of retinal cell production was extended to ganglion cells by Waid and McLoon. They examined the influence of a late retinal environment on RGC fate determination using heterochronic co-cultures in chick. Early cells were inhibited from RGC fate when co-cultured with late retinal cells. This inhibition was not observed when RGCs were depleted from the challenging (late) cell population, which showed that RGCs can nonautonomously feed back to inhibit further RGC production. In a subsequent study from the McLoon lab, they blocked Notch signaling (an RGC inhibitor) at different times. Interestingly, when later time points were examined, they saw newborn RGCs in areas where RGC genesis had ceased in controls. This suggested that RGC competence extends beyond RGC genesis.

Although the studies described above have supported a role for cell–cell interactions in the regulation of cell fate in the vertebrate retina, some types of studies have failed to find nonautonomous effects. Rapaport and colleagues conducted heterochronic transplants in frogs. When younger retinal tissue was transplanted into older hosts, the donor tissue did not adopt later fates or differentiate early. This result was also seen in co-cultured cells *in vitro*. Importantly, the donor cells directly adjacent to the older host cells were not fate shifted. This suggested that cell fate determination is not regulated by changing environmental stimuli, rather, that cell competence is limiting in frogs. Cayouette and colleagues combined lineage tracing and single cell culturing of rodent progenitor cells. In this experiment, E16–E17 rat progenitors were plated at single cell density and the resulting clones were examined 7–10 days later. In parallel, they conducted a retroviral lineage trace (similar to above) in E16–E17 retinal explants (intact tissue) cultured the same amount of time. The clones in both cases were screened for rod, bipolar, amacrine, and Müller glial cell fates. The clone composition and size in both experimental systems were similar in isolation and in explants. This suggested that fate choice is largely cell autonomous and that any given cell type is not required to induce (specify) another. In sum, while many studies have shown a role for cell–cell interactions in the control of retinal cell fate, the relative importance of intrinsic and extrinsic regulation is still not resolved.

These data have been used to assemble cell fate determination models (**Figure 3**). One model, progressive restriction, argues that early progenitors have competence to adopt all retinal cell fates and that this competence is gradually lost (restricted) over time. By this model, nonautonomous contributions are expected to specify cell fate in these multipotent progenitors over time. Early progenitors should be able to adopt late fates (if stimulated properly) and competence should extend beyond the normal genesis window to allow for feedback inhibition. Another model, serial competence, contends that progenitors have competence for only a few cell fates at any given time and that progenitors serially cycle through numerous restricted competence states. By this model, cell nonautonomous inputs are not required for fate specification. Presumably, the mechanism that controls competence dynamics would be reflected by the complement of transcription factors expressed in progenitors. In the next section, we discuss evidence that transcription factors regulate competence.

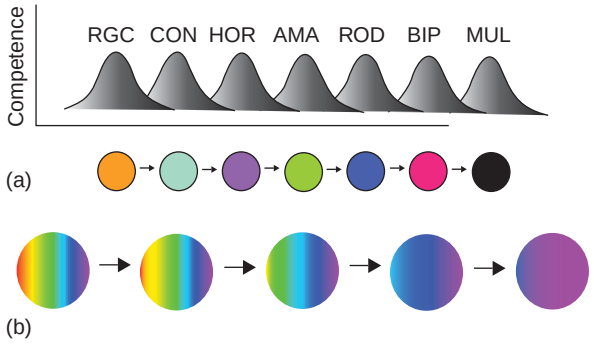

Figure 3 Cell fate determination models. (a) Serial competence model. The progenitor changes over time in their potential to generate different types of retinal cells. These changes in competence would be mediated by changes in the complement of transcription factors present in the cells. (b) Progressive restriction model. The progenitor can initially generate all types of retinal neurons, but over time loses one or another of the transcription factors needed for a specific fate. This is shown in the figure as what is initially a rainbow-colored cell, progressing into a cell that is only red. In principle, the progressive restriction could be due to a loss in key transcription factors, or alternatively by the addition of new repressors.

Transcription Factors and Competence

How transcription factors regulate retinal progenitor competence is beginning to be characterized (**Figure 4**). Although most of these transcription factors are expressed in the postmitotic cells, and therefore are unlikely to regulate the competence of the progenitor cells *per se,* there are members of several different transcription factor families that are expressed in the mitotically active cells. One transcription factor expressed by progenitors that appears to convey competence is *Pax6*. This eye-field transcription factor is expressed in all progenitors and directly promotes the expression of other transcription factors (*Ascl1*, *Ngn2*, *Atoh7*, etc.). Specific deletion of *Pax6* from progenitors leads to the apparent loss of competence to generate all retinal cell types except amacrine cells. A complementary result is obtained when *FoxN4*, a transcription factor expressed in a subpopulation of progenitors, is deleted in mice. In *FoxN4* null mice, amacrine cells fail to develop. This suggests that the combination of FoxN4 and Pax6 can convey progenitors with competence for all retinal cell fates. Ikaros is a transcription factor that is expressed primarily by early-staged progenitors, and mice deficient in this gene have fewer early-born neurons.

While these examples show that changes in transcription factors can affect the types of neurons produced by progenitors, and hence their competence to generate specific neuronal types in the retina, it has also become clear that a more general level of competence, to generate neurons versus glia, is also conveyed by these factors. Another transcription factor expressed in a subset of progenitors is *Ascl1* (*Mash1*), a member of the bHLH class. Prior to E15 in the rat retina, there is little *Ascl1* expression in the retina, though progenitors by this age are producing RGCs, cones, rods, and horizontal and amacrine cells. Even after E15, *Ascl1* is expressed in most, but not all, progenitors. Deletion of this gene in mice leads to an overproduction of Müller glia, apparently at the expense of rods and bipolar cells. It appears that *Ascl1* imparts retinal progenitors with the competence for late-generated retinal neurons, while also inhibiting Müller glial fate specification (**Figure 5**) in part by maintaining the expression of *Hes6*, but also by driving expression of key components of the Notch pathway, including *Hes5* and *Hes1*, to maintain the progenitors in an undifferentiated state while they generate additional neurons. When Notch signaling is reduced, even for times as short as 6 hours, the retinal progenitors are irreversibly committed to exit the cell cycle and differentiate. Since the Notch effector genes, *Hes1* and *Hes5* are normally regulated during the cell cycle, such they are lowest during the G2 and M-phases, one model for the mechanism by which progenitors initiate differentiation is through a progressive slowing of the cell cycle as development proceeds (**Figure 5**). Immunolabeling for the active Notch intracellular domain in mouse retina has confirmed that Notch signaling is lowest in cells whose nuclei are at the apical surface. However, this is apparently not the case in the fish retina. Live imaging studies in cortex by Kageyama's group confirm that Notch signaling oscillates through the cell cycle, with the lowest levels in the progenitors with nuclei located at the apical surface, those cells that are in G2- or M-phases of the cell cycle. Given the highly transient nature of Notch signaling and the very fast cell cycles in fish, further studies using highly destabilized reporters will be needed in the fish to determine whether this difference is real.

Another member of the bHLH class of transcription factors, *Atoh7* (*Math5*), is transiently expressed by a small subset of postmitotic progenitors. Lineage-tracing and genetic-deletion studies have shown that it is necessary for RGC competence. In addition to these transcription factors expressed in progenitors, there are many that are expressed in subpopulations of nascent neurons. For example, *Ptf1a*, *NeuroD1*, and *Math3* are expressed in amacrine cells, and loss of one or more of these genes leads to defects in amacrine cell fate determination or survival. Moreover, overexpression of transcription factors such as *NeuroD1* can drive progenitor differentiation into specific cell types, though the types appear to vary depending on the species and the method of

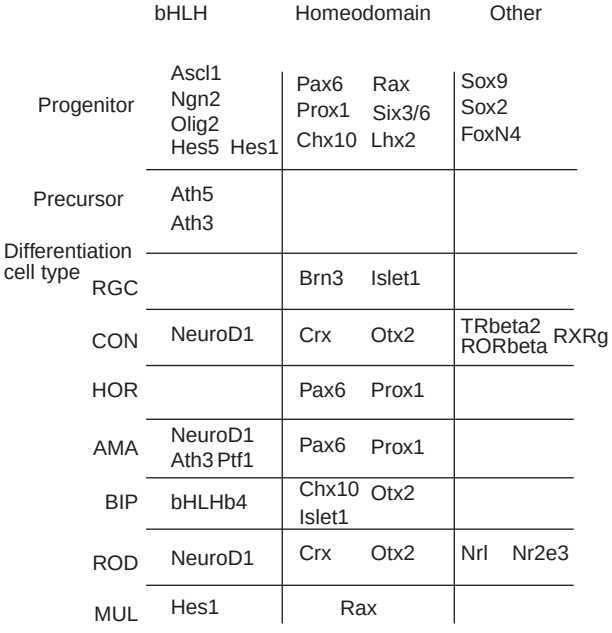

Figure 4 Transcription factor code. Kageyama and others have proposed that a combination of bHLH and homeodomain transcription factors specify each retinal cell type. Although most of these factors are expressed primarily in postmitotic cells, and therefore might not be candidates for the changing competence models described above, several lines of evidence indicate that these factors are necessary for the full differentiation of these cell types.

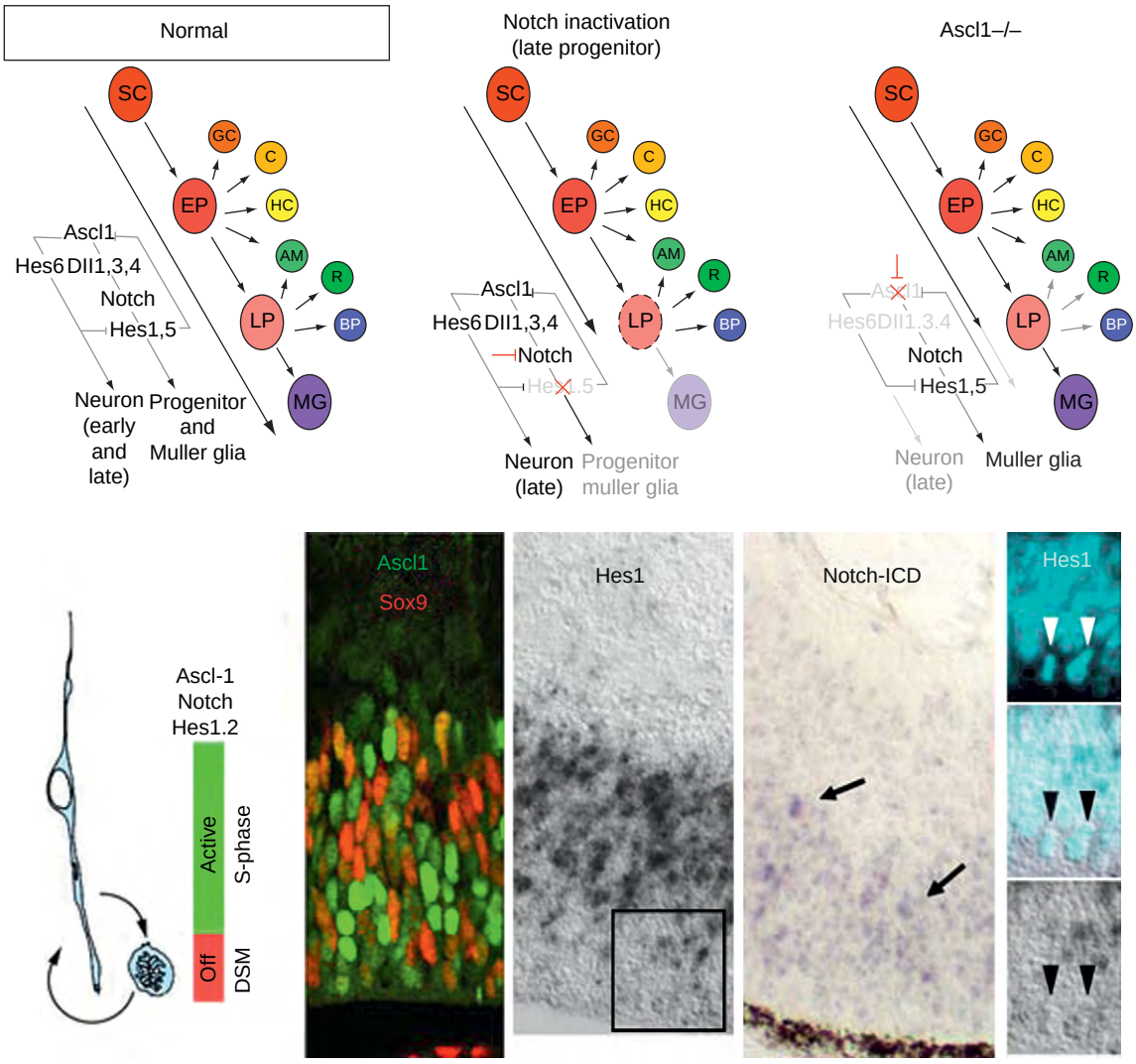

Figure 5 (Top row) *Ascl1/Mash1* functions to maintain neuronal competence in the progenitors. Deletion of this gene in mice leads to an overproduction of Müller glia, apparently at the expense of rods and bipolar cells. It appears that *Ascl1* imparts retinal progenitors with the competence for late-generated retinal neurons, while also inhibiting Müller glial fate specification by maintaining the expression of Hes6, and by driving expression of key components of the Notch pathway to maintain the progenitors in an undifferentiated state while they generate additional neurons. SC, stem cell; EP, early progenitor; LP, late progenitor; GC, ganglion cell; C, cone; HC, horizontal cell; AM, amacrine cell; R, rod; BP, bipolar cell; and MG, Müller glia. (Bottom row, left) Model of how Notch signaling changes with the cell cycle in mouse and chick retina. Notch signaling is high during the S-phase of the cell cycle and low to absent at the apical (ventricular) surface when cells are in G2 and M-phases of the cell cycle. This can be seen in the lower middle and right panels by the Notch ICD immunoreactivity (arrows) and the expression of Hes1, a downstream effector of Notch. By contrast, progenitor markers like Sox9 (red) and Ascl1-GFP (green), are expressed throughout the cell cycle in progenitor cells. Modified from Nelson, B. R., Hartman, B. H., Ray, C. A., et al. (2009). Acheate-scute like 1 (Ascl1) is required for normal delta-like (Dll) gene expression and notch signaling during retinal development. *Development Dynamics* 238: 2163–2178; and from Nelson, et al. (2007) Transient inactivation of notch signaling synchronizes differentiation of neural progenitor cells. *Developmental Biology* 304: 479–498.

overexpression. These studies show that few transcription factors fit cleanly in the simple models of progressive restriction or serial competence. Moreover, since few targets of these transcription factors have been identified, the nature of competence regulation remains unclear. Nevertheless, the transcription factor networks for two cell types, RGCs and rod photoreceptors, are beginning to be worked out.

Conclusions

A great deal has been done over the past 50 years to understand the developmental mechanisms of vertebrate retinal histogenesis. Birthdating studies have revealed a characteristic genesis order of the retinal cell types. Lineage-tracing experiments have shown that retinal progenitors are multipotent and that fate choice is stochastic.

Experiments that challenge the environment of retinal progenitors have revealed that both cell autonomous and cell nonautonomous factors contribute to fate determination. More recent techniques, such as expression fate mapping (lineage by gene expression) and live imaging of cell lineages, will further our understanding of retinal fate determination. In addition, the recent increase in early cell-type-specific markers will allow us to more precisely examine the effects of environmental challenges. While several factors have been identified, many more experiments are needed to elucidate the molecular mechanisms of retinal fate determination.

See also: Coordinating Division and Differentiation in Retinal Development; Ganglion Cell Development: Early Steps/Fate.

Further Reading

Cayouette, M., Barres, B. A., and Raff, M. (2003). Importance of intrinsic mechanisms in cell fate decisions in the developing rat retina. *Neuron* 40(5): 897–904.

Elliott, J., Jolicoeur, C., Ramamurthy, V., and Cayouette, M. (2008). Ikaros confers early temporal competence to mouse retinal progenitor cells. *Neuron* 60(1): 26–39.

Li, S., Mo, Z., Yang, X., et al. (2004). Foxn4 controls the genesis of amacrine and horizontal cells by retinal progenitors. *Neuron* 43(6): 795–807.

Marquardt, T., Ashery-Padan, R., Andrejewski, N., et al. (2001). Pax6 is required for the multipotent state of retinal progenitor cells. *Cell* 105(1): 43–55.

Nelson, B. R., Hartman, B. H., Ray, C. A., Hayashi, T., Bermingham-McDonogh, O., and Reh, T. A. (2009). Acheate-scute like 1 (Ascl1) is required for normal delta-like (Dll) gene expression and notch signaling during retinal development. *Development Dynamics* 238: 2163–2178.

Ohsawa, R. and Kageyama, R. (2008). Regulation of retinal cell fate specification by multiple transcription factors. *Brain Research* 1192: 90–98.

Rapaport, D. H., Wong, L. L., Wood, E. D., Yasumura, D., and LaVail, M. M. (2004). Timing and topography of cell genesis in the rat retina. *Journal of Comparative Neurology* 474: 304–324.

Reh, T. A. (1992). Cellular interactions determine neuronal phenotypes in rodent retinal cultures. *Journal of Neurobiology* 23: 1067–1083.

Reh, T. A. and Kljavin, I. J. (1989). Age of differentiation determines rat retinal germinal cell phenotype: Induction of differentiation by dissociation. *Journal of Neuroscience* 9(12): 4179–4189.

Shimojo, H., Ohtsuka, T., and Kageyama, R. (2008). Oscillations in notch signaling regulate maintenance of neural progenitors. *Neuron* 58: 52–64.

Turner, D. L. and Cepko, C. L. (1987). A common progenitor for neurons and glia persists in rat retina late in development. *Nature* 328: 131–136.

Turner, D. L., Snyder, E. Y., and Cepko, C. L. (1990). Lineage-independent determination of cell type in the embryonic mouse retina. *Neuron* 4: 833–845.

Waid, D. K. and McLoon, S. C. (1998). Ganglion cells influence the fate of dividing retinal cells in culture. *Development* 125: 1059–1066.

Watanabe, T. and Raff, M. C. (1992). Diffusible rod-promoting signals in the developing rat retina. *Development* 114: 899–906.

Retinal Pigment Epithelial–Choroid Interactions

K Ford and P A D'Amore, Schepens Eye Research Institute, Boston, MA, USA

Glossary

Angiogenesis – The formation of new blood vessels from preexisting ones.
Atrophy – To wither or deteriorate.
Blood–retinal barrier – Specialized, nonfenestrated, tightly joined endothelial cells that form a transport barrier for certain substances between the retinal capillaries and the retinal tissue.
Choroidal neovascularization – A condition whereby new blood vessels that originate from the choroid grow and break through Bruch's membrane into the subretinal pigment epithelium (sub-RPE) or subretinal space.
Dominant negative – A genetic mutation where the gene product adversely affects the normal, wild-type gene product within the same cell.
Fenestration – A small pore (60–80 nm in diameter) within the endothelium wall that allows the passage of small molecules and a limited amount of proteins.
Microphthalmia – An abnormal smallness of the eyes, occurring as the result of disease or of imperfect development.
Phagocytosis – The process in which phagocytes engulf and digest microorganisms and cellular debris.
Quiescence – The absence of proliferation.
Trophic factor – A molecule that promotes cellular growth and/or survival.

Introduction

Located at the back of the eye, the retinal pigment epithelium (RPE)–choroid complex is comprised of the RPE, a polarized, epithelial monolayer and the choroid, a highly fenestrated vascular bed. Separated by Bruch's membrane (BrM), an elastic lamina, the RPE and choroid each play a vital role in normal eye physiology. Considerable evidence indicates that there is not only a great deal of interaction between the RPE and choroid, but that the integrity of this interaction is critical to normal eye function. Examination of the morphology of the choroidal microvasculature reveals that the vessels are "polarized," with fenestrations preferentially localized to the capillary surface proximal to the RPE and BrM. Whereas the cytoplasm of the endothelial cell is thinnest in this region, endothelial cell bodies and nuclei are more prominent distal to the RPE. These observations led to the speculation that the RPE exerts an inductive effect on the choriocapillaris by releasing a factor that diffuses across BrM to provide a trophic effect and to mediate the anatomic specializations in the capillary endothelial cells. Preservation of a normal interaction between the RPE and choroid is required for proper eye physiology. This review explores the intricacies of the RPE and choroid, and their interactions during development, in the adult and with aging.

RPE–Choroid Complex Development

RPE Development

The development of the RPE is dependent upon the coordination of transcription factor expression and inductive signals received from the tissues surrounding the developing eye. Eye development proceeds from two principal tissue components: the neural ectoderm, which buds from the wall of the forebrain to form the optic vesicle, and the surface ectoderm, which forms the lens (**Figure 1**). When the optic vesicle comes in contact with the surface ectoderm, it invaginates, forming the optic cup. The optic cup consists of an inner layer, which gives rise to the neural retina, and an outer layer, which forms the RPE. At the optic cup stage, the presumptive RPE and retina are separated by a thin remnant of lumen, which becomes filled by a material known as the interphotoreceptor matrix (IPM). Coincident with this is the onset of the expression of RPE65, which encodes a protein involved in the conversion of all-*trans*-retinal to 11-*cis*-retinal. Prior to this stage, the RPE is a ciliated and pseudo-stratified epithelium; however, following IPM formation, RPE maturation commences. The onset of RPE maturation is marked by melanogenesis, which requires the activation of the tyrosinase promoter.

As the RPE continues to differentiate, it displays a complete apical to basolateral polarity, with short apical microvilli and small basolateral membrane infoldings, and the formation of tight junctions between the RPE cells, which can be divided into three stages. The early stage of tight junction formation is characterized by the expression of key tight junction proteins, such as zona occludens 1 (ZO-1), occludin, and claudins. However, these tight junctional complexes are rudimentary so the RPE lacks complete barrier properties and is therefore leaky. As the

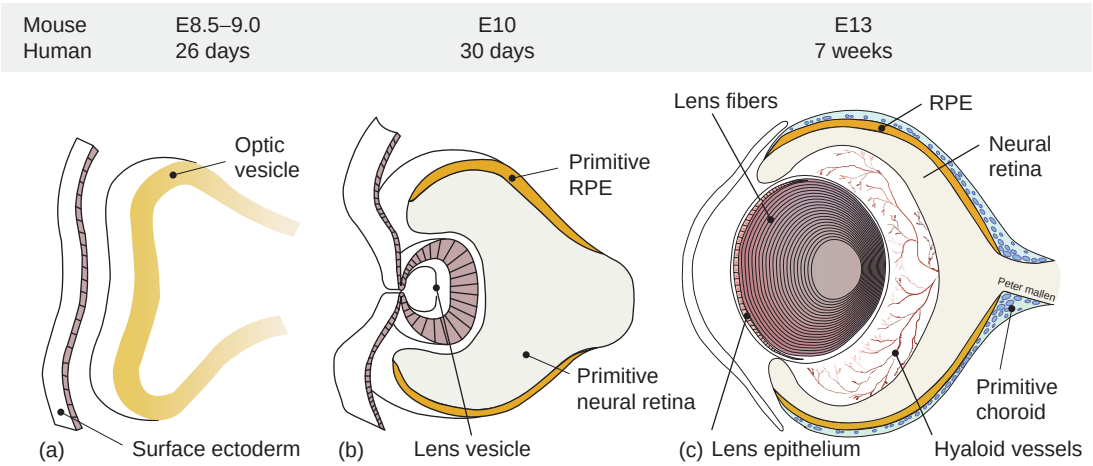

Figure 1 Development of the RPE and choroid. (a) Eye development begins with the budding of the neural ectoderm from the wall of the forebrain to form the optic vesicle. (b) When the optic vesicle comes in contact with the overlying surface ectoderm, it invaginates, forming the optic cup, which consists of an inner layer and an outer layer. The inner layer gives rise to the neural retina, and the outer layer eventually forms the RPE. Choroidal development proceeds from two embryonic tissues: the mesoderm and cranial neural crest cells. The endothelial cells of the choroidal blood vessels are derived from the mesoderm, whereas neural crest cells give rise to the stromal cells, melanocytes, and pericytes. (c) Choroid development begins early in eye development, as the oxygenation of the retina is supplied solely by the choroid and the transient hyaloid vascular system. Initially, tubes and spaces form in the surrounding periocular region of the optic vesicle, and eventually expand to form a plexus. Primitive capillaries develop from this plexus adjacent to the RPE as the optic vesicle invaginates. In humans, the choroidal plexus fuses to form a singular vessel known as the annular vessel at the anterior region of the optic cup during the second and third months of gestation. This primitive plexus is then organized into a complex network, and a well-defined choriocapillaris layer also appears at this stage.

early phase ends, Na^+ K^+ ATPase (ATPase, adenosine triphosphatase) becomes concentrated at the apical surface, and the apical microvilli begin to elongate. In the second stage, the tight junctions become increasingly less permeable, presumably due to the alterations in the distribution of various tight-junction proteins. At this stage, the RPE now prevents the free diffusion of membrane proteins, and the basolateral membrane is remodeled. In the last stage of tight-junction formation, the composition of tight-junction protein isoforms stabilizes and the RPE begins to display barrier properties characteristic of a tight epithelium. Following completion of tight-junction formation, the RPE begins to express specialized proteins, such as the glucose transporter, that aid in the transport of essential nutrients from the RPE to the photoreceptors. As RPE maturation concludes, the RPE becomes fully functional and is able to interact with the photoreceptors.

Choroid Development

Blood vessels develop by vasculogenesis and angiogenesis. In vasculogenesis, primitive vascular cells assemble into a primitive capillary plexus, which is remodeled to define the pattern of the vascular architecture, whereas in angiogenesis, new vessels develop as sprouts from preexisting vessels. It is thought that the superficial vessels of the retina form by vasculogenesis at the optic nerve and expand along a gradient from the posterior to the anterior retina. However, new vessels then sprout via angiogenesis and invade the retina to form intermediate and deep capillary beds. Nonetheless, the primitive vessels derived via vasculogenesis or angiogenesis must still be remodeled before they are considered mature. Remodeling involves the growth of new vessels and regression of others. In addition, alterations in lumen diameter and vessel wall thickness, which are dictated by the local needs of the tissue, must also occur.

The choroid develops from two principle embryonic tissues: the mesoderm and cranial neural crest cells. The mesoderm gives rise to the endothelial cells of the choroidal blood vessels, whereas the stromal cells, melanocytes, and pericytes are all derived from the neural crest cells. Choroid development begins early in eye development, which is not surprising considering that the differentiation of the ocular tissues relies upon the oxygen and nutrients supplied by the primitive vascular system. In early eye development, the oxygenation of the retina is supplied solely by the choroid and the transient hyaloid vascular system. The vascularization of the retina itself is actually a late event. Initially, tubes and spaces form in the surrounding periocular region of the optic vesicle. These tubes, which are lined by the mesodermal endothelium, expand to form a plexus as eye development proceeds. Concomitant with optic vesicle invagination, the primitive capillaries develop from this plexus adjacent to the RPE. In humans, choroidal capillaries completely encircle the optic cup by the 13-mm stage of development and remain separated from the retina by the basement

membrane of the RPE. At the anterior region of the optic cup, the choroidal plexus fuses to form a singular vessel known as the annular vessel, and during the second and third months of gestation, this primitive plexus is organized into a complex network. A well-defined choriocapillaris layer also appears at this stage. Pigmentation does not appear in choroidal melanocytes until late gestation – between 6 and 7 months; however, it is complete at birth.

BrM Development

In mice, the formation of the choroidal vessels precedes the deposition of BrM, and maturation of the BrM layers is not complete until 6 weeks following birth. However, in humans and monkeys, BrM layers are completely formed *in utero*. BrM formation commences near the RPE, and is initially comprised of a single basement membrane derived from the RPE. The RPE is able to synthesize many of the extracellular matrix (ECM) components that comprise BrM; therefore, it is not surprising that BrM development begins near the RPE. On the 17th to 18th day of gestation in rats, collagenous fibrils gradually accumulate in the space between the RPE and choriocapillaris endothelium and begin to form a three-dimensional meshwork within BrM. The meshwork consists of three sublayers: the basement membranes of the RPE and choriocapillaris endothelium, and a collagenous layer. The final component of BrM, the central elastic layer, appears on the fifth postnatal day. Initially, dense elastic deposits appear within the collagenous layer, and subsequently accumulate to form a single continuous layer, which separates the collagenous layer into an inner and outer layer. Finally, an immature, but five-layered BrM is formed by the ninth day after birth.

RPE–Choroid Complex: Structure and Function

RPE Structure and Function

It is apparent that the RPE performs a variety of complex functions that are essential for proper visual function. If any aspect of one of the many roles that the RPE serves is disrupted or fails, retinal degeneration, loss of visual function, and ultimately blindness may result. Therefore, the RPE is an indispensable component of the RPE–choroid complex. Anatomically, the RPE is juxtaposed to the outer segments of the photoreceptors at its apical surface, extending long apical microvilli that surround the outer segments. These microvilli provide a means for a complex structural interaction between the RPE and photoreceptors. BrM, which is at the basolateral side of the RPE, separates the RPE from the fenestrated endothelium of the choriocapillaris.

The RPE serves many functions that are vital to normal eye function and physiology. These functions have been categorized based on the characteristics of three classes of cells: epithelium, macrophage, and glia. The major function of an epithelium is to control the passage of substances from one extracellular space to another; therefore, the epithelial aspect of the RPE is its role in actively transporting ions, water, and metabolic end products from the subretinal space to the blood. The RPE is also involved in the uptake of nutrients, such as glucose, retinol, and fatty acids from the blood to nourish the photoreceptors. One of its most critical functions is the exchange of retinal with the photoreceptors. The photoreceptors are unable to reisomerize all-*trans*-retinal; therefore, it is transported to the RPE where it is reisomerized to 11-*cis*-retinal, and then transported back to the photoreceptors, a process known as the visual cycle of retinal.

The RPE also functions as a macrophage in that it phagocytoses the photoreceptor outer segments, which are constantly being renewed. As new membrane is added to the base of the outer segment, the older membrane is advanced toward the tip, and subsequently shed. The phagocytosis of the shed outer segments by the RPE is critical to normal photoreceptor function because it maintains the excitability of the photoreceptors. The vital nutrients, such as retinal, which are recycled and returned to the photoreceptors following outer segment digestion help rebuild the light-sensitive outer segments from the base of the photoreceptors.

The final role that the RPE plays is that of a glial cell. RPE resembles glial cells in the manner in which they respond electrically to changes in the concentration of extracellular K^+, which is determined by the photoreceptors. The RPE possesses tight junctions at both its basolateral and apical membranes, which generate transepithelial resistance (TER); furthermore, the tight junctions at the basolateral surface form the RPE portion of the blood–retinal barrier.

Choroid Structure and Function

The choroid is a vascular bed that supplies nutrients and oxygen to the RPE and outer nuclear layer of the retina. It consists of larger vessels and a highly fenestrated choriocapillaris (**Figure 2**), whose endothelial basement membrane comprises one layer of BrM. Fenestrated endothelium is a characteristic of tissues that are involved in secretion and/or filtration. The photoreceptors are metabolically very active and the fenestrated choriocapillaris facilitates the transport of oxygen and nutrients to fulfill their metabolic needs. RPE tight junctions, in combination with sophisticated transport systems, determine which components of the choriocapillary secretions are transported to the photoreceptors.

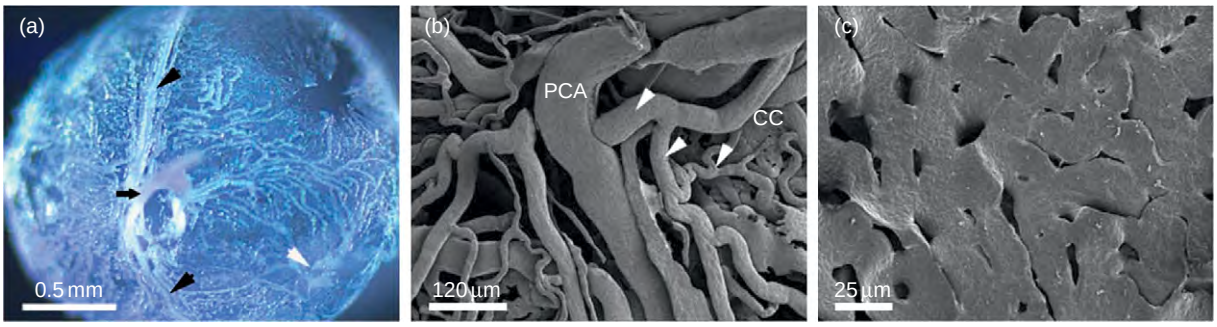

Figure 2 Corrosion cast of adult mouse choroidal vasculature. The choroid is a vascular bed that supplies nutrients and oxygen to the RPE and outer nuclear layer of the retina. It consists of larger vessels and a highly fenestrated capillary bed known as the choriocapillaris. (a) Scleral view of the entire adult choroid. Major vessels can be easily identified: posterior ciliary artery (black arrow), long posterior arteries (black arrowhead), and vortex vein (white arrowhead). (b, c) Scanning electron micrographs of vascular cast of the choroidal vasculature. (b) Posterior view showing one posterior ciliary artery (PCA) around the optic nerve. On each side, the artery divides regularly into smaller branches (arrows) and choriocapillaris (CC). (c) Anterior view showing the extremely dense choriocapillaris plexus.

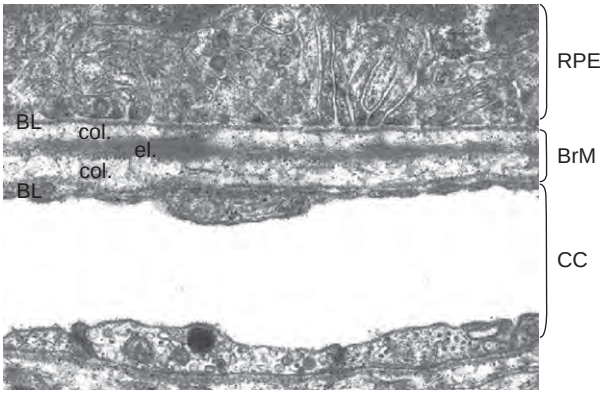

Figure 3 Ultrastructure of the RPE–BrM–choriocapillaris. The RPE and choriocapillaris are separated by a thick (1–4 μm) elastic lamina, BrM, which consists of five layers: the RPE basement membrane (BL), an inner collagenous layer (col), a central elastic layer (el), an outer collagenous layer (col), and the choriocapillaris (cc) endothelium basement membrane (BL), respectively, from top to bottom. BrM acts as a barrier for macromolecules and regulates the diffusion of small molecules between the RPE and the choriocapillaris.

BrM Structure and Function

Located between the RPE and the choriocapillaris, BrM is a thick (1–4 μm) pentalaminar ECM, which consists of the RPE basement membrane, an inner collagenous layer, a central elastic layer, an outer collagenous layer, and the choriocapillaris endothelium basement membrane (Figure 3). BrM is comprised of several types of extracellular components, including many types of collagen, laminin, fibronectin, and proteoglycans. The collagenous layers of BrM are primarily composed of type I collagen and collagenous-associated proteins. It is believed that these components fortify the framework of BrM and aid in the resistance to the force that intraocular pressure exerts on the back of the eye. The basement membranes of the RPE and choriocapillaris endothelium are composed of type IV collagen, which can indirectly interact with cells via laminin, and also binds to heparin and heparan sulfate proteoglycans. The central elastic layer consists of cross-linked elastin fibers that are associated with fibulin 5, an ECM protein that is thought to aid in elastin fiber assembly and serve as a link between the elastin fibers and cell surface receptors. BrM acts as a support and a barrier between the retina and the choroid, and is thought to support the many functions of the RPE. BrM is semi-permeable, and therefore controls the transfer of molecules and cellular components between the RPE and the choroidal vasculature.

RPE–Choroid Interactions

Interactions During Development

The presence of the RPE is required for proper choroid development. Studies have shown that an intact, fully differentiated RPE is required for normal choroidal development; when the RPE is transdifferentiated into a neural retina by expressing fibroblast growth factor (FGF)-9 under the control of the tyrosine-related protein 2 (TRP-2) promoter, the choroid fails to develop. This is further illustrated in humans with colombas where RPE differentiation has failed and there are abnormalities in development of both the choroid and sclera. Basic fibroblast growth factor (bFGF) has also been implicated in choroidal development. Transgenic mice in which a dominant-negative bFGF receptor (FGFR1) was overexpressed in the RPE displayed choroidal abnormalities, such as incomplete and immature choroidal vessels.

The RPE also secretes a variety of growth factors and an increasing body of evidence indicates that RPE-derived vascular endothelial growth factor (VEGF) is essential to choroidal development. Studies in humans and rodents have illustrated that both VEGF and its

receptor, VEGFR2, are highly expressed by the RPE and the underlying mesenchyme, respectively, at the time of choriocapillaris formation. Furthermore, mice with an RPE-specific deletion of VEGF presented a variety of defects, including microphthalmia, loss of visual function, and the complete absence of the choriocapillaris. In addition, the RPE itself was discontinuous, suggesting that RPE-derived VEGF is not only important for choroidal development, but also for RPE survival. Whether the RPE abnormality is secondary to the defects in choroidal development or due to a direct effect of VEGF on RPE has not been elucidated.

Interactions in the Adult

Normal RPE–choroid interactions are not only important during development, but also in the adult. Several studies have revealed the impact of RPE loss on choroidal structure and function. The presence of an intact RPE is critical to proper choroidal function, as surgical RPE removal causes several changes throughout the choroid. Both large choroidal vessels and the choriocapillaris display a reduction in circulation, and depending upon the extent of RPE removal, choroidal nonperfusion can be permanent due to fibroblast infiltration. A landmark study in which the RPE was selectively destroyed by sodium iodate treatment illustrated that within 1 week following iodate injection, the choriocapillaris had reduced fenestrations and displayed signs of atrophy, such as degenerating endothelial cells, and pericapillary basal laminae that had begun to separate from the apparently shrunken endothelium. Together, these data illustrate the critical role the RPE plays in both survival and in the maintenance of the choriocapillaris.

Growth factor secretion

RPE secretes a variety of growth factors, including VEGF, FGFs, transforming growth factor-β (TGF-β), and ciliary neutrophic factor (CNTF). The RPE also secretes pigment-epithelium-derived factor (PEDF), which functions not only to maintain the retina by acting as a neuroprotective factor, but also to provide antiangiogenic activity to inhibit endothelial cell proliferation, thereby stabilizing the choriocapillaris endothelium. VEGF, a well-characterized angiogenic factor, also plays a role modulating blood vessel permeability. Differential splicing of VEGF premessenger RNA (mRNA) gives rise to multiple isoforms, with the most notable being VEGF120, VEGF164, and VEGF188 in mice, and VEGF121, VEGF165, and VEGF189 in humans. VEGF120 does not bind heparin sulfate proteoglycans (HSPGs) and is readily diffusible, whereas VEGF164 is partially sequestered on the cell surface and in the ECM. VEGF188, with high affinity for heparan sulfate, is therefore primarily cell-surface- and matrix-associated. The RPE primarily expresses the diffusible isoforms, VEGF164 and VEGF120, while VEGF188 is virtually undetectable. RPE-derived VEGF is essential for both survival and maintenance of the underlying choriocapillaris endothelium. Interestingly, PEDF and VEGF are secreted by the RPE in a polarized fashion in opposing directions. PEDF is secreted to the apical surface of the RPE to support the neurons and photoreceptors of the retina, whereas VEGF is primarily secreted to the basolateral surface where it acts on the choroidal endothelium (**Figure 4**). Despite the fact that a small fraction of total VEGF, a potent angiogenic factor, is secreted to the apical surface by the RPE, the outer nuclear layer of retina remains completely avascular, presumably due to the balance between antiangiogenic (PEDF) and angiogenic (VEGF) factors.

Receptor expression

In parallel with the many factors secreted by the RPE, the choroid expresses a number of corresponding receptors, including FGF receptors, type I and II TGF-β receptors, and VEGFR2. Of particular interest is the fact that VEGFR2 is observed primarily in the choriocapillaris adjacent to the RPE, with substantially less VEGFR2 expression observed in the major vessels of the choroid. Furthermore, VEGFR2 is localized to the apical surface of the choriocapillaris endothelium and to the photoreceptors where it is constitutively activated, which is surprising given that adult choroidal vasculature is mature and quiescent.

Isoform-specific VEGF mouse model

In support of a critical role for RPE-derived VEGF in the maintenance of the adult choriocapillaris, we have shown that the absence of soluble VEGF isoforms in the RPE leads to changes that recapitulate the classical features of dry age-related macular degeneration (AMD). Mice expressing only VEGF188 (i.e., lacking the diffusible isoforms that they normally express) display signs of RPE dysfunction, such as increased autofluorescence, loss of barrier proprieties, and accumulation of basal deposits that are similar to drusen, extracellular deposits that build up beneath the basement membrane of the RPE within BrM. These changes occur prior to the formation of both focal choroidal atrophy and RPE attenuation, which progress to large areas of RPE loss. The abnormalities are age dependent and increase in severity over time.

Choroidal change impact on RPE

The RPE–choroid interactions do not merely function to serve the choroid; changes in the choroid have also been shown to impact the RPE. Choroidal ischemia has been reported to lead to opaque RPE lesions and subsequent serous retinal detachment. Furthermore, very early studies on the effects of choroidal congestion on RPE–retina function revealed that increased choroidal pressure may

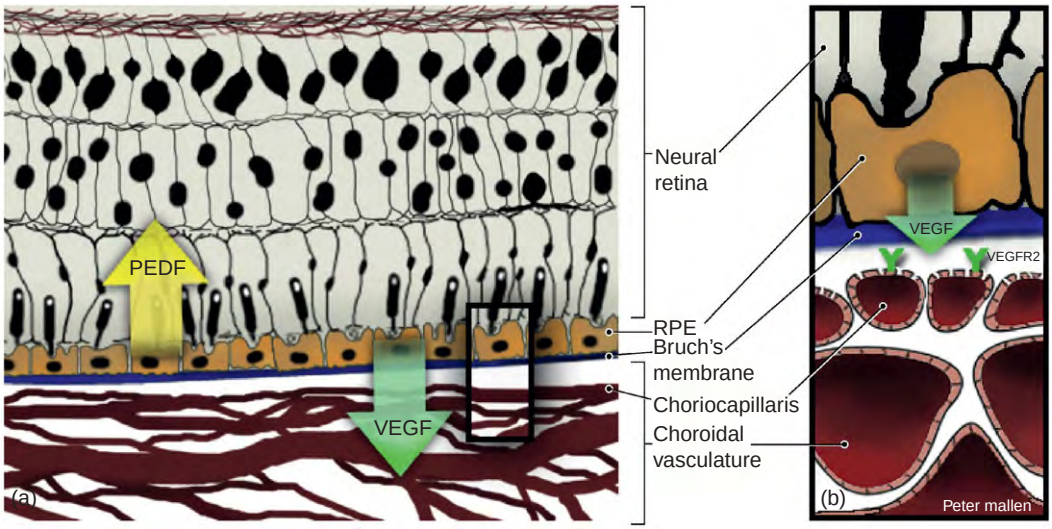

Figure 4 Polarized secretion by the RPE and localization of VEGFR2. (a) The RPE secretes both VEGF and PEDF in polarized fashion in opposing directions. PEDF is secreted to the apical surface of the RPE to support the neurons and photoreceptors of the retina, whereas VEGF is primarily secreted to the basolateral surface where it acts on the choroidal endothelium. RPE-derived VEGF is essential for both survival and maintenance of the underlying choriocapillaris endothelium, and PEDF functions not only as a neuroprotective factor, but also as an antiangiogenic factor to maintain the avascularity of the outer nuclear layer of the retina. (b) Higher magnification of selected area in (a) showing fenestrations in choriocapillaris and localization of the VEGFR2 receptor. In parallel with the VEGF secreted by the RPE, the choroid expresses the corresponding VEGF receptor, VEGFR2. VEGFR2 is observed primarily in the choriocapillaris adjacent to the RPE, with substantially less VEGFR2 expression observed in the major vessels of the choroid.

cause RPE–retina dysfunction by altering normal fluid movement across the RPE, modifying the integrity of the subretinal space.

RPE–Choroid Changes with Age

Various changes occur in the RPE–choroid complex with aging. In light of the close association among the RPE, BrM, and choroid, it is not surprising that an alteration in a single component of this complex compromises the normal RPE–choroid interaction and ultimately leads to disease. Studies have shown that the density and diameter of the choriocapillaris and medium-sized choroidal vessels substantially decline with age, resulting in decreased choroidal blood volume and blood flow. The aging RPE exhibit changes such as a reduction in cell density and a loss of RPE melanin. Melanin pigmentation is believed to play a protective role, acting to protect cells against oxidative stress. Oxidative changes in RPE melanin may be attributed to complexing of melanin with lipofuscin, pigment granules composed of lipid-containing residues of lysosomal digestion, which generate reactive oxygen species upon excitation with blue light, thereby making the aged RPE more susceptible to oxidative damage.

BrM Changes

Changes in BrM include increased thickness, accumulation of lipids, and subsequent alterations of the BrM permeability. Collectively, these changes can limit the diffusion of water-soluble proteins, leading to a range of problems. Furthermore, drusen are known to accumulate in the aging eye (**Figure 5**). There is a strong correlation between the presence of drusen and ocular pathology, such as AMD. It has been speculated that drusen lead to a gradual reduction in the diffusion of RPE-derived factors, such as VEGF, which may be causal in the atrophy of segments of the RPE and underlying choriocapillaris, known as geographic AMD. Drusen accumulation and coalescence may also lead to breaks in BrM that are believed to be the initiating event in the formation of choroidal neovascularization (CNV), in which new blood vessels sprout from preexisting choroidal vessels and invade the overlying RPE and retina. The development of CNV associated with wet AMD leads to visual loss due to the fact that the neovessels are leaky and cause damage to the surrounding tissues.

Gene Expression

Gene expression of the RPE–choroid also changes with age. There is considerable upregulation of the expression of genes and proteins involved in leukocyte extravasation, and the accumulation of leukocytes at the RPE–BrM interface suggests that leukocytes are possibly recruited to aid in the removal of cellular waste. Furthermore, there have been reports of increased macrophages in the aged RPE–choroid; mice harboring mutations that render them deficient in macrophage recruitment display hallmarks of

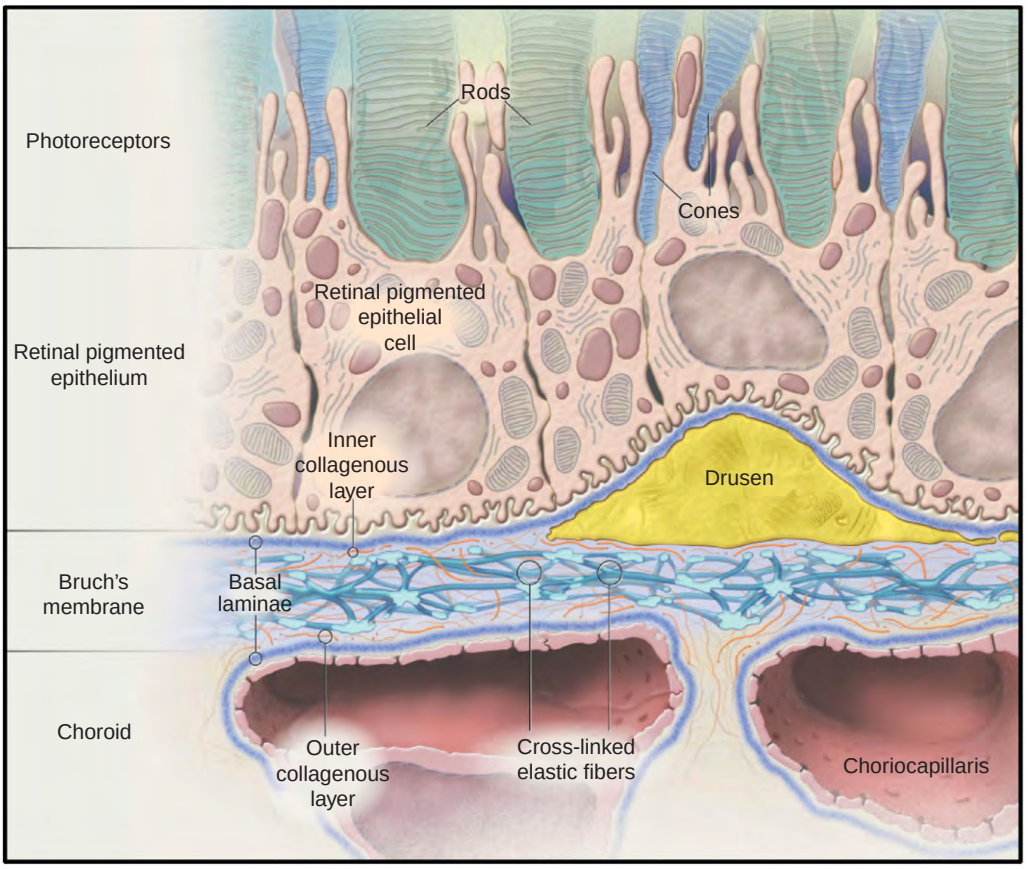

Figure 5 The accumulation of drusen beneath the RPE within BrM. In the aging eye, it is common for drusen to accumulate at the interface between the inner collagenous layer of BrM and the basal lamina of the RPE. Drusen are extracellular deposits that are strongly correlated with ocular pathology, such as age-related macular degeneration (AMD). It is proposed that drusen deposits between the RPE and the BrM as well as within BrM, and causes a gradual reduction in the diffusion of RPE-derived factors, such as VEGF, which may lead to the atrophy of segments of the RPE and underlying choriocapillaris, also known as geographic AMD. Drusen accumulation and coalescence may also cause breaks in BrM that are believed to be the initiating event in the formation of choroidal neovascularization (CNV), in which new blood vessels sprout from preexisting choroidal vessels and invade the overlying RPE and retina. Adapted from Johnson, L. V. and Anderson, D. H. Age-related macular degeneration and the extracellular matrix. *New England Journal of Medicine* 351(4): 320–322.

AMD. It is also thought that the aged RPE–choroid synthesizes proteins that not only attract leukocytes, but that also activate the complement pathway, which is a part of the immune response and can lead to inflammation. Recent associations between polymorphisms in a member of the complement pathway reinforce the role of inflammation in the development of AMD.

Conclusions

Despite the fact that the RPE and choroid are separated by BrM, there is a great deal of interaction between the tissues. The presence of an intact, fully differentiated RPE is not only required for proper choroidal development, but is also essential for survival and maintenance of adult choriocapillaris endothelium specializations (fenestrations) and integrity. The RPE secretes a variety of factors, one of the most notable being VEGF. The secretion of VEGF by the RPE is somewhat of a double-edged sword. Although VEGF is vital to choroidal homeostasis during both development and in adult, breakdown of the RPE barrier upon direct contact with choroidal endothelial cells is thought to involve a VEGF-mediated mechanism, for VEGF has been shown to mediate the vessel growth and permeability associated with wet AMD. Thus, maintenance of proper RPE–choroid interaction is vital to normal function, and any perturbation to this system can ultimately lead to disease.

See also: Angiogenesis in Response to Hypoxia; Angiogenesis in the Eye; Breakdown of the Retinal Pigmented Epithelium Blood–Retinal Barrier; Choroidal Neovascularization; Developmental Anatomy of the Retinal and Choroidal Vasculature; Immunobiology of Age-Related Macular Degeneration; Physiological Anatomy of the

Choroidal Vasculature; Retinal Pigmented Epithelium Barrier; Stability and Functional Integrity of New Blood Vessels; Vessel Regression.

Further Reading

Gogat, K., Le Gat, L., Van Den Berghe, L., et al. (2004). VEGF and KDR gene expression during human embryonic and fetal eye development. *Investigative Ophthalmology and Visual Science* 45(1): 7–14.

Hartnett, M. E., Lappas, A., Darland, D., et al. (2003). Retinal pigment epithelium and endothelial cell interaction causes retinal pigment epithelial barrier dysfunction via a soluble VEGF-dependent mechanism. *Experimental Eye Research* 77(5): 593–599.

Ivert, L., Kong, J., and Gouras, P. (2003). Changes in the choroidal circulation of rabbit following RPE removal. *Graefe's Archive for Clinical and Experimental Ophthalmology* 241(8): 656–666.

Korte, G. E., Reppucci, V., and Henkind, P. (1984). RPE destruction causes choriocapillary atrophy. *Investigative Ophthalmology and Visual Science* 25(10): 1135–1145.

Mancini, M. A., Frank, R. N., Keirn, R. J., Kennedy, A., and Khoury, J. K. (1986). Does the retinal pigment epithelium polarize the choriocapillaris? *Investigative Ophthalmology and Visual Science* 27(3): 336–345.

Marneros, A. G., Fan, J., Yokoyama, Y., et al. (2005). Vascular endothelial growth factor expression in the retinal pigment epithelium is essential for choriocapillaris development and visual function. *American Journal of Pathology* 167(5): 1451–1459.

Ramrattan, R. S., van der Schaft, T. L., Mooy, C. M., et al. (1994). Morphometric analysis of Bruch's membrane, the choriocapillaris, and the choroid in aging. *Investigative Ophthalmology and Visual Science* 35(6): 2857–2864.

Rousseau, B., Larrieu-Lahargue, F., Bikfalvi, A., and Javerzat, S. (2003). Involvement of fibroblast growth factors in choroidal angiogenesis and retinal vascularization. *Experimental Eye Research* 77(2): 147–156.

Saint-Geniez, M. and D'Amore, P. A. (2004). Development and pathology of the hyaloid, choroidal and retinal vasculature. *International Journal of Developmental Biology* 48: 1045–1058.

Saint-Geniez, M., Maldonado, A. E., and D'Amore, P. A. (2006). VEGF expression and receptor activation in the choroid during development and in the adult. *Investigative Ophthalmology and Visual Science* 47(7): 3135–3142.

Saint-Geniez, M., Maharaj, A. S., Walshe, T. E., et al. (2008). Endogenous VEGF is required for visual function: Evidence for a survival role on Müller cells and photoreceptors. *PLoS ONE* 3(11): e3554.

Steinberg, R. H. (1985). Interactions between the retinal pigment epithelium and the neural retina. *Documenta Ophthalmologica* 60: 327–346.

Strauss, O. (2005). The retinal pigment epithelium in visual function. *Physiological Reviews* 85(3): 845–881.

Zhao, S. and Overbeek, P. A. (2001). Regulation of choroid development by the retinal pigment epithelium. *Molecular Vision* 2(7): 277–282.

Retinal Pigment Epithelium: Cytokine Modulation of Epithelial Physiology

S S Miller, A Maminishkis, R Li, and J Adijanto, National Eye Institute, Bethesda, MD, USA

Published by Elsevier Ltd.

Glossary

Cytokines – A large and diverse family of polypeptide regulators that are used in cell regulation.
ELISA – The enzyme-linked immunosorbent assay is a biochemical technique that uses an enzyme-linked antibody to detect its corresponding ligand within a sample. It can be used to assay for chemokines and cytokines.
Subretinal space (SRS) – The extracellular space between the retinal photoreceptors and the apical surface of the retinal pigment epithelium.
Tight junctions – A structure of specialized proteins that form a seal between neighboring cells and regulate ion and small molecule selectivity and resistance in the paracellular pathway between epithelial cells. Tight junction proteins include occluding, claudins, and junction adhesion molecules (JAMs).

Introduction

In the back of the vertebrate eye, the apical membrane of the retinal pigment epithelium (RPE) and the photoreceptor outer segments form a very tight anatomical relationship (Figure 1). This structural feature supports a whole host of mechanical, electrical, and metabolic interactions that maintain the health and integrity of the neural retina throughout the life of the organism. Like all epithelia, the RPE plasma membrane contains a wide variety of proteins, enzymes, and small molecules that are specifically segregated to the apical or basolateral sides of the epithelium, which face the neural retina and choroidal blood supply, respectively (Figure 2).

The asymmetrical distribution of these functionally distinct molecules is maintained by junctional complexes that surround each cell and by the continuous synthesis and regulated traffic of these molecules to each membrane. Epithelial polarity is defined by the steady-state maintenance of this asymmetric distribution and is critical for the ongoing vectorial transport of ions, metabolites, fluid, and waste products across the RPE. Epithelial polarity is also fundamentally important for controlling changes in the volume and chemical compositions of the extracellular spaces on either side of the RPE, following transitions between light and dark. In the distal retina, the extracellular or subretinal space (SRS) separates the photoreceptor outer segments and the RPE apical processes. The chemical composition of this space is tightly buffered by the cells which surround it (Müller cells, photoreceptors, and RPE). On the opposite side of the RPE, an extracellular space is formed between its basolateral membrane and Bruch's membrane, which is adjacent to the choriocapillaris. The physiological and pathophysiological states of the RPE/distal retina complex are significantly affected by changes in the chemical composition of these extracellular spaces as evidenced in disease processes such as age-related macular degeneration (AMD) or uveitis. AMD develops within the RPE/distal retina complex and eventually leads to RPE impairment and loss of photoreceptor function. The RPE's ability to control and respond to varying levels of oxidative insult from light quanta, outer segment phagocytosis, vitamin A uptake and delivery, and oxygen consumption diminishes with age. These changes significantly affect the chemical composition of the surrounding extracellular spaces, SRS and choroid, and are a major factor in disease pathogenesis. In recent years, significant advances have been made in identifying the role of the immune system in neurodegenerative disease in general and in AMD, in particular (summarized by Hageman and colleagues and by Nussenblatt and Ferris). This article summarizes recent experiments from our lab and others, which show that inflammation induced changes in the environment surrounding human RPE can significantly alter intracellular signaling and physiology. This study provides a basis for understanding disease progression and regression.

This article is divided into three main parts. We begin with a description of our development of a robust and well-defined primary cell culture model of human fetal retinal pigment epithelium (hfRPE). We use this model to analyze how metabolic waste products, produced in the retina following light/dark transitions, can be disposed of by CO_2/HCO_3 and lactate transporters located in the apical and basolateral cell membranes. In the second part, we use this cell culture model to analyze RPE antioxidant mechanisms that are protective against disease processes, such as AMD or uveitis. In the third part, we describe a series of experiments that use this model to define the impact of cytokines on human RPE function. Finally, we briefly focus on the role of interferon gamma (INFγ) in controlling RPE physiology.

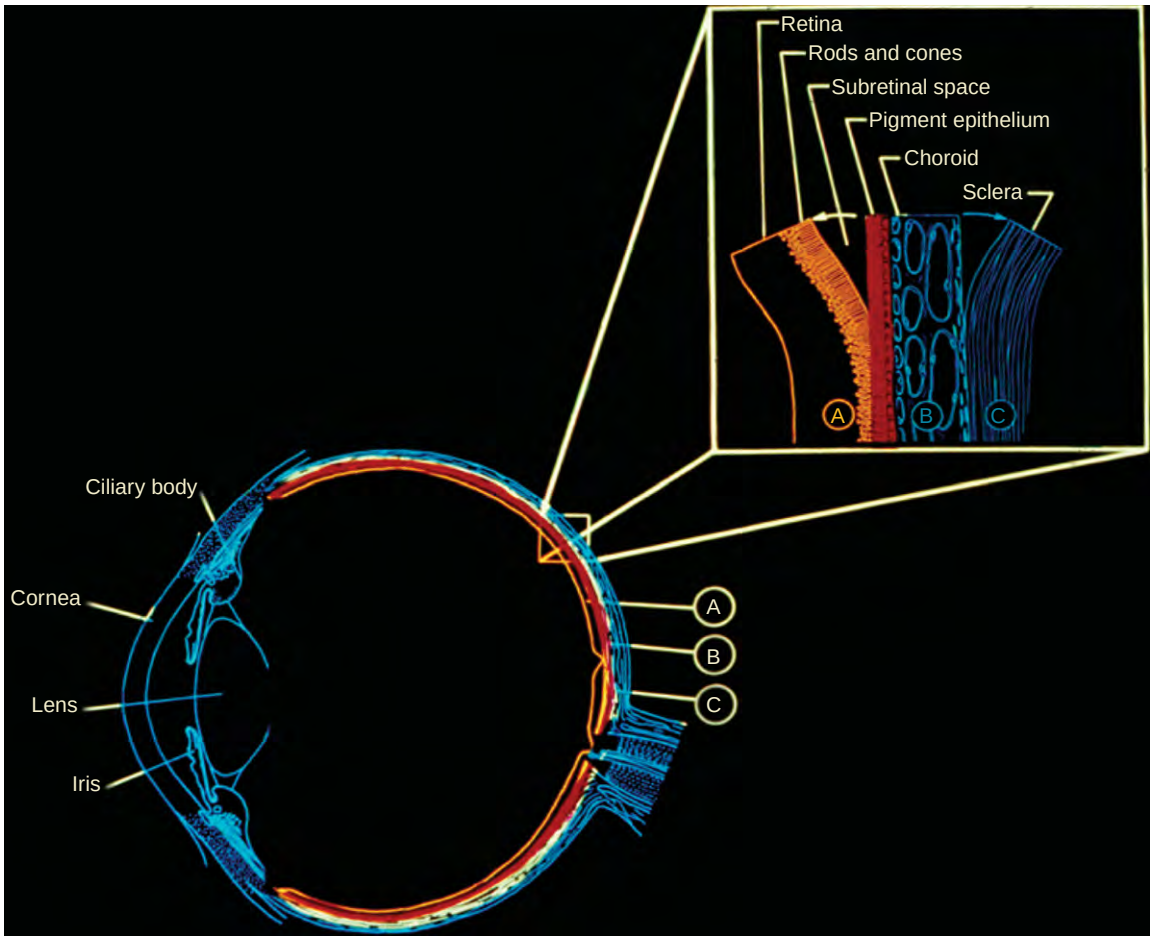

Figure 1 Schematic diagram of the eye. The retinal pigment epithelium is located in the back of the eye between neural retina and choroid.

Human RPE: Morphology, Polarity, and Function

The availability of native human tissue, fetal or adult, is limited and extant models of cultured human RPE have been, in varying degrees, less than adequately characterized or understood, not reproducible or available in large quantities, and lacking expression of melanin pigment and key functional proteins such as bestrophin (Best1), and RPE-specific protein 65 (RPE65). Therefore, we developed a set of standard procedures for producing confluent monolayers of hfRPE cells and demonstrated that they have the morphology, polarity, and function of the native tissue from which they were derived (Figure 3). Light and electron microscopy (EM) studies confirmed the presence of apical processes (microvilli) and basal infoldings that increased the elaboration of the apical and basolateral membranes, respective, in cultured hfRPE cells. We carried out immunoblot and immunofluorescence experiments for a variety of proteins to help define the polarity of this model. In the course of these experiments, we discovered that human RPE tight junctions contain a variety of membrane proteins (claudins) that are important for regulating the selectivity and conductance of the paracellular pathway, and we also confirmed the presence of several visual cycle and cytoskeleton proteins. Intracellular recordings confirmed many membrane physiological properties and demonstrated the polarity of purinergic and adrenergic receptors at the apical membrane, which serve to regulate cell calcium and transepithelial fluid absorption (Figure 2). By enzyme-linked immunosorbent assay (ELISA), we showed that these monolayers constitutively secrete pigment epithelium-derived factor (PEDF) to the apical bath and vascular endothelial growth factor (VEGF) to the basal bath; the former provides neuroprotection for the retina and the latter would allow active regulation of endothelial cell fenestration, a structural feature critical for choroidal circulation.

pH_i – Induced Changes in Fluid Absorption

In previous experiments we showed that acetazolamide, a carbonic anhydrase (CA) inhibitor, reduced net ^{36}Cl flux across frog RPE. Subsequent animal models and clinical

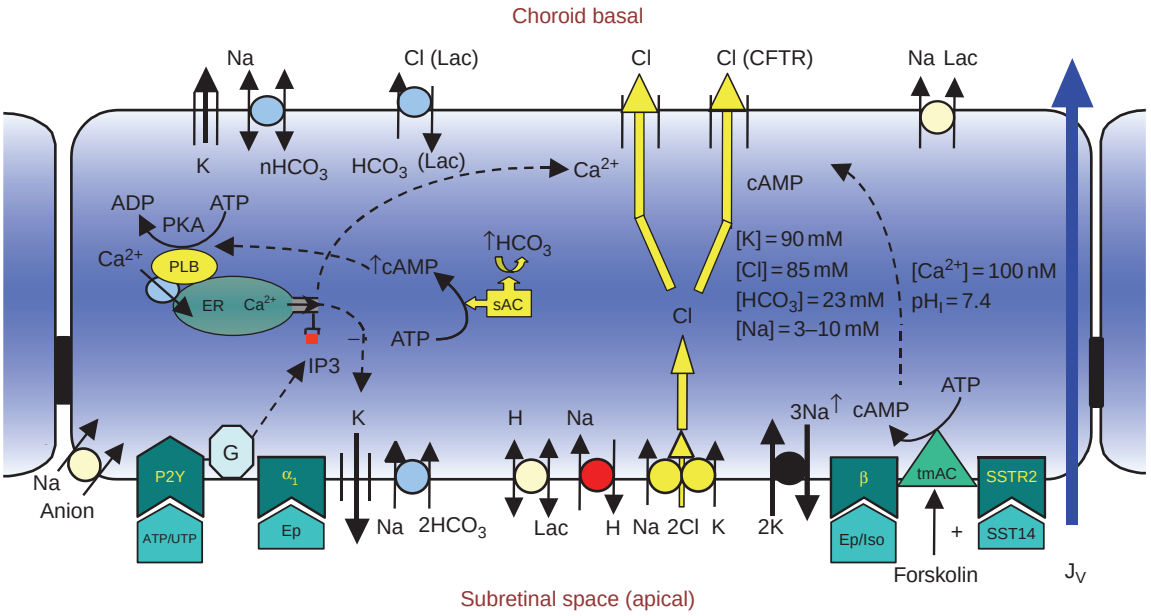

Figure 2 Schematic diagram of retinal pigment epithelium (RPE) summarizing some membrane proteins, channels, and receptors that are responsible for a variety of RPE functions such as fluid transport, pH maintenance, or cell-volume regulation. The arrows highlighted in yellow indicate a main pathway for solute-driven fluid transport across the RPE, consisting of a sodium, potassium, 2 chloride co-transporter (Na/K/2Cl co-transporter) at the apical membrane, and a cyclic AMP-activated chloride channel, CFTR (cystic fibrosis transmembrane conductance regulator), and Ca^{2+}-activated Cl-channels at the basolateral membrane. The apical membrane contains a variety of receptors, for example, purinergic (P2Y), adrenergic (α-1 and β), and somatostatin (SSTR2), which when bound to their specific ligands, activate Ca^{2+} and cAMP second-messenger signaling systems. The plasma membrane localization of previously described ion transporters such as the Na/2HCO_3 co-transporter, Na/H exchanger, 3Na/2K ATPase, H/Lac co-transporter, Cl/HCO_3 exchanger, and potassium channels are also shown. From Maminishkis, A., et al. (2002). *Investigative Ophthalmology and Visual Science* 43(11): 3555–3566. © Association for Research in Vision and Ophthalmology.

trials have utilized CA inhibitors to reduce disease-induced abnormal accumulation of retinal fluid. CAs catalyze the reversible hydration of CO_2 to HCO_3 and protons, which are transported across the plasma membrane (e.g., Na/HCO_3 or H/lactate co-transporters) to regulate cell pH. As a first step, we have identified and localized several highly expressed CAs in human RPE and begun study of their physiology. A total of 16 CAs have been identified in human tissues. In human fetal RPE cell cultures, 14 of the 16 known isozymes have been confirmed by quantitative real-time polymerase chain reaction (qRT-PCR). Immunocytochemical studies indicate that CA II is localized intracellularly, as in many other cell types. CA IV, XII, and XIV are localized to the apical surface, while CA IX, the most abundantly expressed isozyme in hfRPE cultures, is expressed apically and laterally (**Figure 4**). However, it should be noted that CA IX messenger RNA (mRNA) and proteins are not expressed in native adult or fetal human RPE. CA inhibitors have had limited success in alleviating the effects of retinal disease, partly because of systemic side effects, but mainly because of their lack of specificity. The positive clinical outcomes for some patients with retinal edema suggest that nonspecific CA inhibitors, such as acetazolamide, may be affecting multiple CAs or other transport-related mechanisms that can either increase or decrease net fluid absorption across the RPE in varying degrees in different patients. This is supported by *in vivo* animal studies, in which intravenous administration of acetazolamide to rabbits increased fluid clearance from the SRS. The regulatory role of CAs is potentially important in human RPE, which critically depends on HCO_3 transport to maintain fluid absorption (J_V) out of the SRS (**Figure 5**).

Modulation of SRS Metabolic Load and Chemical Composition

In the intact eye (cat/monkey), the transition from light to dark causes significant alterations in SRS pH, Ca^{2+}, and K. In addition, the transition from light to dark increases photoreceptor O_2 consumption by ≈2-fold as measured *in situ* in cat and nonhuman primate retina. The rates of retinal O_2 consumption in light and in dark were used by Linsenmeier and Winkler and their colleagues to estimate the associated changes in glucose metabolism that leads to the concomitant release of carbon dioxide, lactic acid, and water from the photoreceptor inner segments into the SRS. This metabolic acid load is potentially damaging to all of the cells that surround the SRS (i.e., photoreceptors, Müller cells, and RPE). It raises the

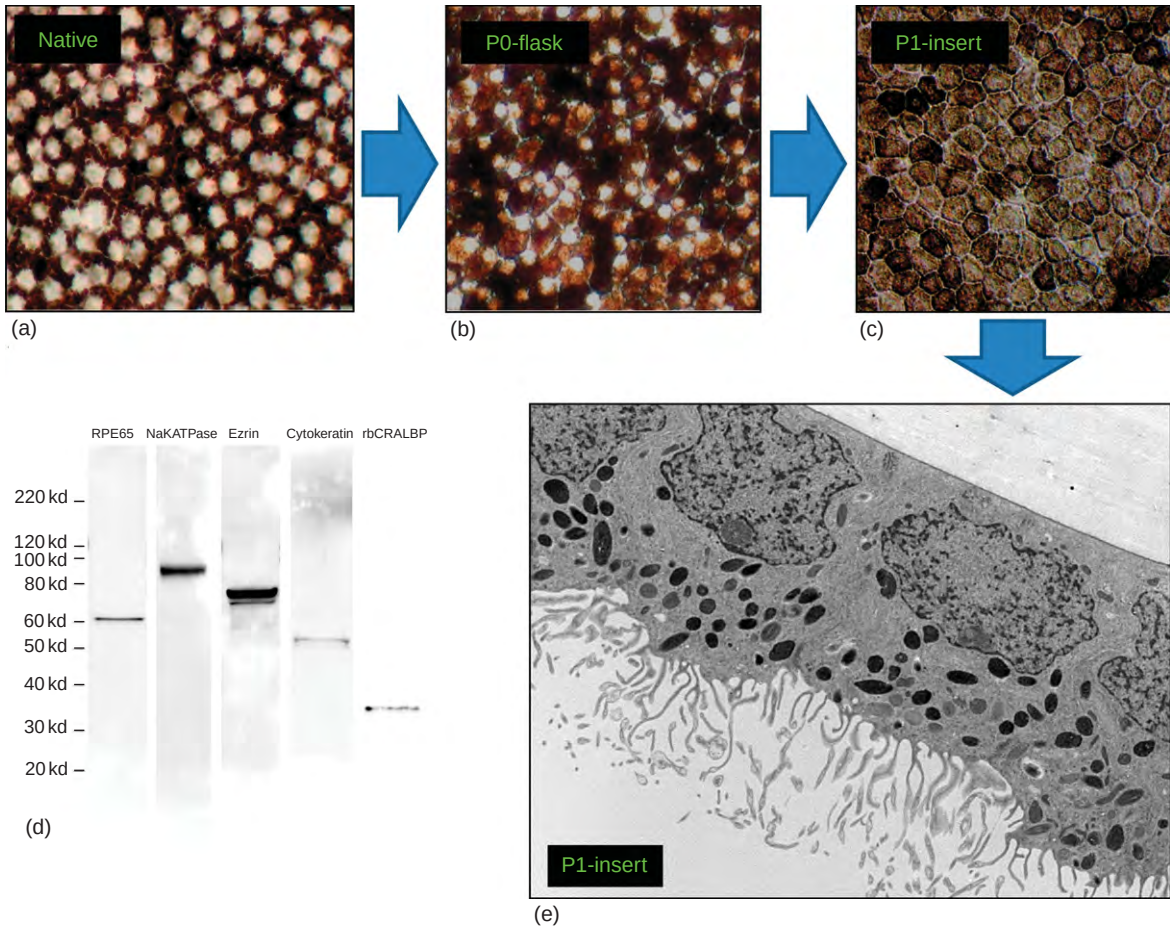

Figure 3 Photomicrographs showing native (a) and cultured human fetal retinal pigment epithelium (hfRPE) ((b) P_O cultured on flask; (c) P_1 cultured on insert). (d) Westerns blots for five hfRPE specific proteins. (e) Transmission-electron micrograph of hfRPE cells grown on inserts. From Maminishkis, A., et al. (2006). *Investigative Ophthalmology and Visual Science* 47 (8): 3612–3624. © Association for Research in Vision and Ophthalmology.

question of how the RPE could help prevent this accumulation of metabolic acid and water in the SRS.

In *in vivo* studies of rabbit eye, it was estimated that ≈70% of fluid absorption across the RPE is linked to metabolite transport to the choroidal blood supply. In addition, *in vitro* studies of frog RPE showed that steady-state fluid absorption decreased by ≈70%, following the removal of HCO_3 from both bathing solutions, implicating HCO_3 transport in a regulatory role on fluid transport. The RPE functionally expresses several different HCO_3 transport proteins at the apical and basolateral membranes as illustrated in **Figure 5**. In an earlier study, a 4,4′-diisothiocyano-2,2′-stillbene-disulfonic acid (DIDS)-sensitive electrogenic $Na/2HCO_3$ co-transporter was localized to the apical membrane of frog and bovine RPE; DIDS is a bicarbonate transport inhibitor. At the basolateral membrane, HCO_3 is transported out of the RPE through a pH-sensitive Cl/HCO_3 exchanger with a possible contribution from a Na/HCO_3 co-transporter. These HCO_3 transporters in the RPE are linked to Na and Cl transport, which are major driving forces for fluid transport. Recently, the identities of some of these HCO_3 transporters have been characterized in our laboratory and by other groups. NBC1 ($Na/2HCO_3$ co-transporter) and NBC3 (NBCn1; electroneutral Na/HCO_3 co-transporter) were localized to the apical membrane. AE2 (Cl/HCO_3 exchanger) mRNA transcripts were detected, but protein expression in the RPE remains to be determined. The identity of the basolateral membrane $Na/nHCO_3$ co-transporter (NBC) is still unknown.

In vitro, we mimic the increased retinal CO_2 production, following the transition from light to dark by increasing apical bath CO_2 level from 5% to 13%. This maneuver increased NaCl uptake at the apical membrane and can enhance CA-mediated Na/HCO_3 co-transport across the RPE, thus increasing net $NaHCO_3$ absorption. This increase in solute transport would drive additional fluid across the RPE as observed in *in vitro* experiments. The transport of metabolic waste products from the SRS to the choroidal blood supply by the RPE helps maintain ionic and pH homeostasis of the SRS. The RPE handles the increased metabolic load by transporting

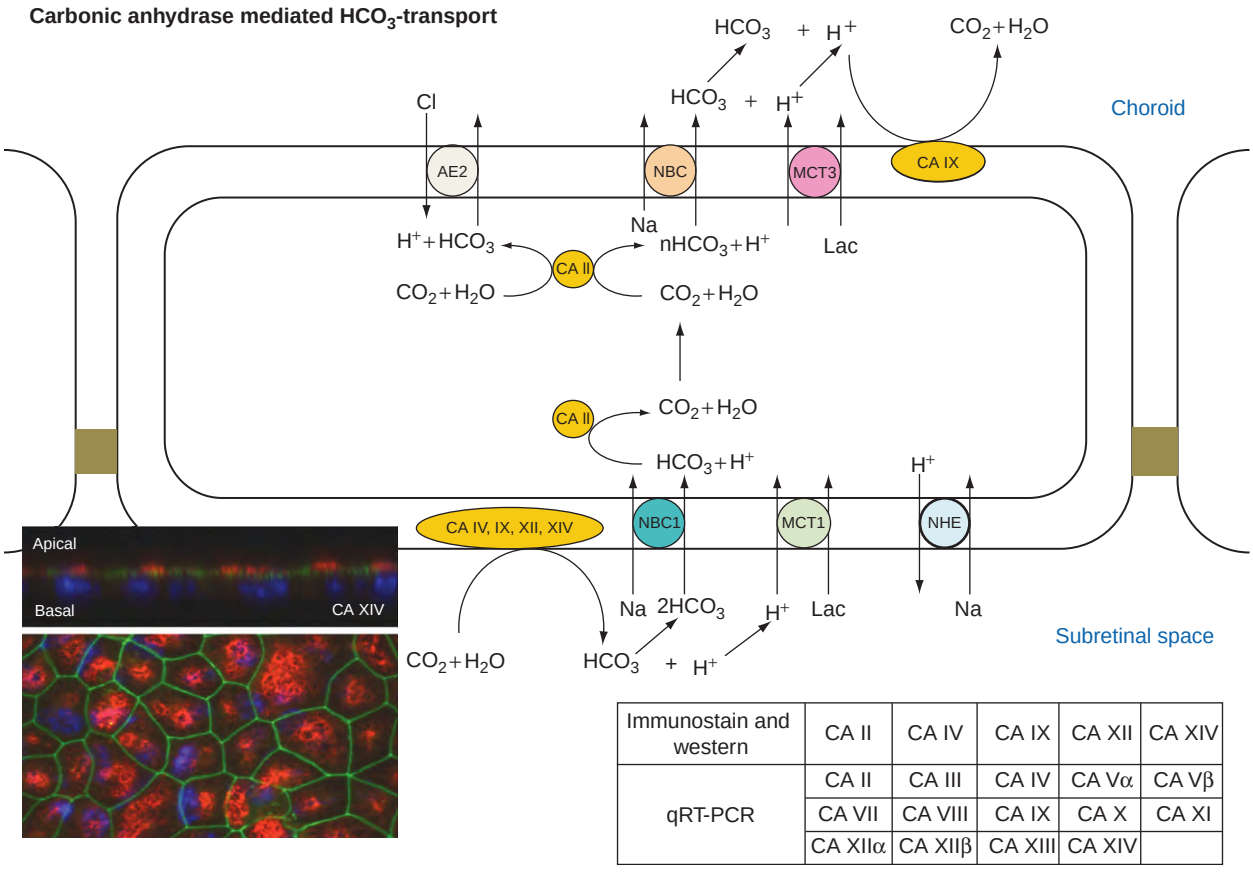

Immunostain and western	CA II	CA IV	CA IX	CA XII	CA XIV
qRT-PCR	CA II	CA III	CA IV	CA Vα	CA Vβ
	CA VII	CA VIII	CA IX	CA X	CA XI
	CA XIIα	CA XIIβ	CA XIII	CA XIV	

Figure 4 Carbonic anhydrase (CA)-mediated CO_2/HCO_3 transport in retinal pigment epithelium (RPE). Membrane-bound CA IV, XII, and XIV are expressed exclusively at the apical membrane (immunostaining of CA XIV shown in insert on lower left). CA IX is expressed at both the apical and basolateral membranes of cultured human fetal RPE. CA II is expressed in the cytosol and can be recruited to the inner leaflet of the membrane. Experimental data (immunostaining, Western blots, and RT-PCR) that support the localization of the various CAs are listed in the table (lower right). Membrane-bound CAs hydrate CO_2 into HCO_3 and H^+, which are substrates for NBC1 (sodium bicarbonate co-transporter) and MCT1 (proton lactate co-transporter) at the apical membrane. Cytosolic CA II regulates CO_2 and HCO_3 equilibrium in the RPE. The anion exchanger isoform 2 (AE2) mediates Cl/HCO_3 exchange at the basolateral membrane, while a sodium proton exchanger (NHE) at the apical membrane helps regulate intracellular pH.

CO_2 across the RPE in the form of HCO_3 through HCO_3-transporters, and this process is mediated by the catalytic activity of CAs. This increase in Na and HCO_3 absorption provides the driving force for increased net fluid absorption across the RPE, which dehydrates the SRS and creates retinal adhesion, thus allowing the RPE to maintain proper anatomical relationship with the photoreceptors.

In the retina, ≈95% of glucose consumption is metabolized through glycolysis into lactic acid, which is subsequently deposited into the SRS. In addition to the high glycolytic activity of the retina, several other mechanisms cause additional lactic acid to be released by the retina following light–dark transition: (1) increased glucose metabolism at the outer retina; (2) reduced retinal oxygen level in the dark-adapted eye, leading to an increased anaerobic lactate production; and (3) glutamate-induced lactate release from Müller cells. The RPE disposes of this metabolic load by transporting lactic acid to the choroid through monocarboxylate transporters (MCTs) of the MCT family. We previously demonstrated that the RPE is extremely resistant to pH change compared to other epithelia and that part of this regulation comes from H/Lac co-transporters at the apical and basolateral membranes.

In human RPE, Philp and colleagues showed that monocarboxylate transporter 1 (MCT1), a H/Lac co-transporter, is immunolabeled at the apical membrane (**Figure 5**). They also showed that MCT3, a H/Lac co-transporter expressed exclusively in the RPE and choroid plexus basolateral membranes, meditates lactate efflux from the RPE into the choroidal blood supply (**Figure 5**). In addition, a Cl/Lac exchanger, possibly anion exchanger 2 (AE2), has been shown to transport lactate at the basolateral membrane. The importance of lactate transport in the mammalian eye has also been demonstrated in mice lacking MCT1, MCT3, and MCT4 expression – the mutant mice gradually lose photoreceptor function and

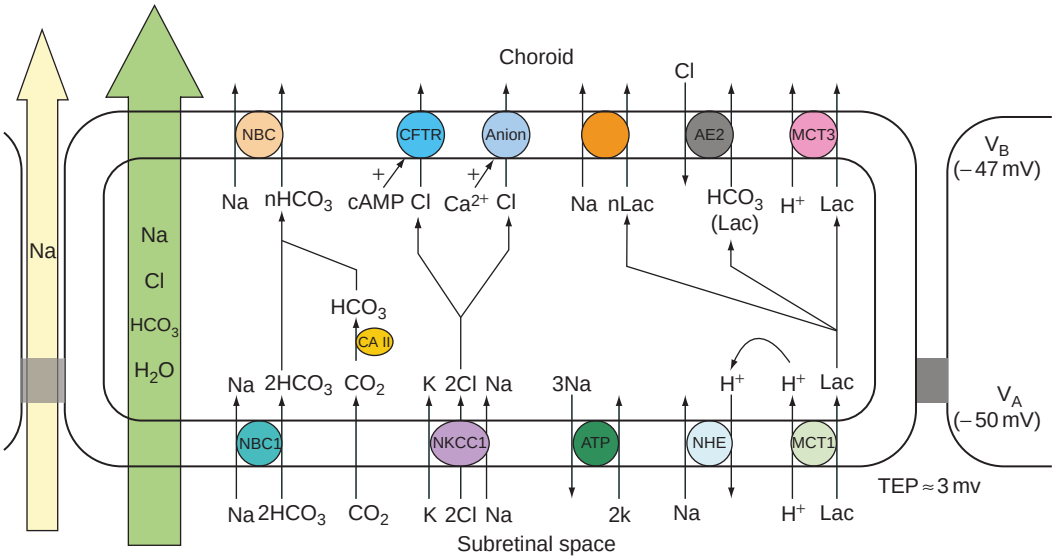

Figure 5 Na, Cl, HCO_3, and lactate transport mechanisms in retinal pigment epithelium (RPE). CO_2 enters the apical membrane via diffusion and HCO_3 is transported into the cell by NBC1 (sodium bicarbonate co-transporter). As CO_2 enters the cell, it can be hydrated into HCO_3 in a reversible reaction catalyzed by carbonic anhydrase II. Cl enters the apical membrane via NKCC1 (sodium potassium chloride co-transporter – Na/K/2Cl) and exits the basolateral membrane via CFTR or Ca^{2+}-activated Cl channels. Lactic acid is transported across the apical membrane by MCT1, and out of the basolateral membrane through MCT3 (H/Lac co-transporter) and AE2 (Cl/Lac exchanger). These ion-transport mechanisms at the apical and basolateral membranes mediate net solute transport across the RPE, which drives fluid absorption. The apical and basolateral membrane potentials are given by V_A and V_B, respectively, and their difference is the transepithelial potential (TEP).

were completely blind after 41 weeks. Further, altered visual function in MCT3-null mice demonstrates the importance of lactate transport specifically in the RPE.

Oxidative Stress

The RPE encounters significant levels of oxidative stress on a daily basis and this onslaught promotes mitochondrial (mt) damage and decreases in mt potential and respiration, which may contribute to inflammation and the onset of age-related diseases such as AMD (summarized by Jarrett and colleagues). In opposition to these oxidative stresses, there exist mt protective mechanisms that provide direct antioxidant protection and those that enhance glutathione (GSH) production; furthermore, there is evidence that all of these protective mechanisms weaken with age. Different cell types can exert different levels of protection; for example, it has been shown that hfRPE monolayers are significantly more resistant to oxidative stress than ARPE-19 cells. Volobouева and colleagues used the hfRPE primary cultures to examine mt and other pathways that are putative targets for therapeutic intervention against oxidative stress. In one set of experiments they studied the protective effects of α-lipoic acid (R-form), a potent intracellular antioxidant that has been shown in other systems, to induce all three cellular protective mechanisms. The R form of lipoic acid is a coenzyme in mt that has been shown to reverse the age-related decrease in mt function. Measurements of cell viability, mt potential, cell death, oxidative stress, apoptosis, and GSH/GSSH show that lipoic acid can protect hfRPE cells in three ways: (1) directly scavenge reactive oxidative species; (2) repair and protect mt enzymes; and (3) activate antioxidant defenses through phase 2 enzymes. Our results suggest that (R)-α-lipoic acid can be used as an all-purpose therapeutic intervention against the slow accumulation of oxidative damage that can occur in AMD.

Cigarette smoke is an important risk factor for AMD and causes significant oxidative damage in RPE that also can be mitigated by (R)-α-lipoic acid. RPE mitochondria are themselves a main generation site of oxidants and a critical and sensitive target of specific cigarette-smoke components. Acrolein is present in the gas phase of cigarettes (25–140 μg per cigarette), and it is estimated that the gas phase of one cigarette reaches a concentration of 80 μM in the airway surface fluid. Acrolein has a high hazard risk in cigarette smoke and causes oxidative stress in cells by reacting with sulfhydryl groups. In the physiological range (0.1–100 μM), it causes significant mt damage in hfRPE that can be ameliorated by (R)-α-lipoic acid, for example, by inducing GSH and other phase-2 antioxidant protective enzymes. Pretreatment by (R)-alpha-lipoid acid has a protective effect against peroxide induced mt oxidative stress in several ways: (1) by lowering cell calcium; (2) by increasing mt electron chain complexes I, II, and III

activity levels; (3) by increasing mt membrane potential; and (4) by increasing total antioxidant power as well as GSH peroxidase/GSH/superoxide dismutase levels. Collectively, these data indicate that lipoic acid may be an effective therapeutic strategy against age-related, oxidant-induced RPE degeneration.

As summarized recently by Dunaief, AMD patients have elevated levels of iron within the RPE that also can lead to oxidative damage to mitochondria. Based on that observation, Volobouéva and colleagues showed that ferric ammonium citrate increased intracellular iron and oxidant production and decreased GSH and mt complex IV activity in human fetal cultured RPE. They also showed that N-*tert*-butyl hydroxylamine (Nt-BHA), a known mt antioxidant, reduced oxidative stress, mt damage, and age-related iron accumulation. These data show that the application of Nt-BHA may be an effective therapeutic strategy against AMD.

RPE–Immune System Interactions in and around the SRS

The integrated effect of proinflammatory molecules on RPE function depends on the polarized location of the cognate receptors and the access of their ligands (cytokines and chemokines) to the apical and basolateral membranes, and the interactions of downstream signaling pathways. For the experiments summarized in **Table 1**, we used a mixture of three proinflammatory cytokines, interleukin 1 beta (IL-1β), interferon gamma (IFNγ), and tumor necrosis factor-alpha (TNF-α) to stimulate confluent monolayers of hfRPE. These proinflammatory cytokines are elevated in patients with uveitis and are detected in the vitreous and blood of patients with proliferative diabetic retinopathy (PDR) and AMD with choroidal neovascularization (CNV).

As a first step in understanding how the RPE *in vivo* can actively control the inflammatory environment in the SRS and choroid, Shi and colleagues used confluent monolayers of human fetal RPE primary cultures to (1) measure the constitutive and polarized secretion of angiogenic/angiostatic cytokines by the RPE; (2) determine how this pattern of polarized secretion changes in the inflammatory state; and (3) demonstrate that the inflammatory state alters RPE physiology. Constitutively, the human RPE secretes massive amounts of monocyte chemoattractant protein 1 (MCP-1) to the SRS and lesser amounts of IL-6 and IL-8 (**Table 1**), all of which contribute to the ongoing downregulation of the immune environment of the retina. RPE activation was achieved using a cocktail of IL-1β, TNF-α, and INFγ with similar concentrations as that detected in the diseased eye. We showed that IL-1β receptors are mainly localized to the apical membrane and TNF-α and INFγ (subunit 1) receptors are mainly localized at the basolateral membrane. This cocktail significantly increased the secretion of various cytokines/chemokines to both baths, but significantly more to the apical bath. The increase in angiogenic cytokine secretion exceeds the increase in angiostatic cytokine secretion. However, two chemokines generally thought to be angiostatic, interferon-inducible T-cell α-chemoattractant (I-Tac) and monokine induced by γ interferon (MIG), were secreted to the apical bath in significant quantities. The mechanisms by which these chemokines exert their effects and their role in eye physiology are not yet known. Similarly intriguing and not understood are the secretions into the apical bath of interferon-inducible protein 10 (IP-10), monocyte chemoattractant protein 3 (MCP-3), and the Rantes chemokine. In animal model experiments from Charlotte Reme's group, blue-light-induced oxidative damage induces the invasion of blood-borne monocytes and activation of retinal microglia, thus stimulating the secretion of cytokines to induce an inflammatory response. Our experiments strongly suggest that the RPE is a significant source of cytokines and chemokines. Thus both retinal microglia and RPE can contribute to the inflammatory response in a diseased eye. Our further demonstration that basolateral addition of the cocktail acutely increases fluid absorption across the RPE (**Figure 6**), from the apical to basal baths (retina to choroidal side of tissue), and significantly decreases transepithelial resistance after a 24-h treatment is important because of the possibility that with age or accumulated oxidative stress these changes can alter chemokine/cytokine gradients across the RPE. These gradients regulate the attraction of monocytes to the RPE basement membrane and, thus, play a role in the accumulation of drusen with age. We believe that this concept is important for understanding early events that underlie chronic disease processes, such as AMD, a notion revisited below.

Modulation of RPE Proliferation and Migration by Cytokines and Growth Factors

Breakdown of the inner or outer blood–retinal barrier can lead to significant alterations in the chemical composition of the SRS, including cytokines and growth factors, which trigger the activation of normally quiescent RPE cells. In proliferative vitreoretinopathy (PVR), RPE cells proliferate and migrate to the vitreous cavity along with other types of cells (e.g., glial cells, fibroblasts, and macrophages) and form fibrocellular membranes on the retinal surface or in the vitreous. These newly formed membranes, if left untreated, eventually contract, resulting in retinal detachment and eventual vision loss.

Several isoforms of platelet-derived growth factor (PDGF) are present in retinal membrane from patients

Table 1 Inflammatory cytokine mixture alters polarized secretion of chemokines and cytokines by cultured human fetal retinal pigment epithelium (hfRPE)

		Angiogenic								Angiostatic						
		MCP-1	IL-8	GRO-α	IL-6	MCP-2	MDC	MIP-1α	MIP-1β	12p40	12p70	MIG	ITAC	MCP-3	RANTES	IP-10
Stimuli	Secretion	pg/ml	pg/ml	pg/ml	pg/ml	pg/ml	pg/ml	pg/ml	pg/ml	pg/ml	pg/ml	pg/ml	pg/ml	pg/ml	pg/ml	pg/ml
None	Apical	9,495	647	70.2	55.1	9.6	3.0	7.9	18.6	9.7	1.1	8.8	8.2	14.4	0.6	11.1
	SD	5,285	979	45.9	28.2	6.9	1.4	3.1	17.0	12.9	0.5	6.0	8.6	5.8	0.8	4.0
	Basal	992	95.2	24.4	3.5	3.6	1.4	6.2	9.2	3.7	0.6	3.4	3.7	4.0	0.4	5.0
	SD	1,343	238	29.7	3.1	2.0	1.5	3.6	9.3	7.8	0.3	5.4	2.2	3.3	0.0	4.1
ICM (Ap)	Apical	212,408	110,865	72,097	125,167	34,185	21.9	143	39.5	63.3	40.1	8,518	89,126	22,431	21,067	239,839
	SD	52,434	33,309	1,518	6,565	2,575	2.8	115	13.6	7.2	13.5	3,550	3,409	2,381	2,237	37,493
	Basal	75,019	4,415	2,328	3,221	2,900	10.8	36.8	26.2	51.3	19.9	132	1,335	1,452	4,915	11,700
	SD	8,694	213	191	330	501	0.5	8.7	5.6	4.7	3.8	28.8	250	428	707	1,291
ICM (Ba)	Apical	179,247	22,567	8,375	7,108	6,613	12.9	44.2	24.2	66.2	36.3	202	3,623	1,741	1,088	17,626
	SD	36,462	11,316	2,710	1,457	1,844	1.7	7.5	3.6	6.5	5.8	61.6	1,390	431	244	5,605
	Basal	48,470	2,053	1,227	1,550	1,527	9.0	31.9	21.1	42.4	26.0	94.6	838	622	2,497	5,549
	SD	16,646	309	297	281	492	1.2	1.8	3.8	6.9	5.6	13.1	34.4	263	635	1,661
ICM (Ap & Ba)	Apical	314,290	112,416	39,406	52,479	21,120	11.7	249	81.8	29.2	58.6	6,668	66,863	8,415	9,277	132,548
	SD	99,378	20,528	19,909	26,200	8,537	7.6	104.9	30.3	27.2	55.9	3,754	22,992	4,342	6,159	62,068
	Basal	73,521	4,599	3,363	17,929	2,900	5.0	69.9	51.3	15.1	16.9	138	1,395	623	1,984	7,546
	SD	15,277	2,402	2,039	24,194	1,469	1.9	16.1	15.1	21.5	6.0	37.9	714	252	2,004	4,079

(a)

		Angiogenic								Angiostatic						
		MCP-1	IL-8	GRO-α	IL-6	MCP-2	MDC	MIP-1α	MIP-1β	12p40	12p70	MIG	ITAC	MCP-3	RANTES	IP-10
		pg/ml	pg/ml	pg/ml	pg/ml	pg/ml	pg/ml	pg/ml	pg/ml	pg/ml	pg/ml	pg/ml	pg/ml	pg/ml	pg/ml	pg/ml
IL-1β(Ap)	Apical	107,865	51,298	31,578	7,572	373	14.5	22.4	30.2	50.7	9.5	74.6	27.4	706	580	236
	SD	18,455	14,956	12,362	3,219	309	3.1	7.4	7.2	8.7	1.5	25.3	8.2	470	419	111
	Basal	19,902	1,420	805	318	13.4	4.4	5.8	7.0	23.8	2.6	50.9	30.1	17.5	25.4	184
	SD	9,520	971	634	15.7	3.2	0.5	2.5	2.1	10.3	0.4	53.6	32.4	2.0	16.8	270
[TNF-α, IFNγ](Ba)	Apical	73,113	2,358	514	729	14.0	6.5	3.1	10.2	29.7	4.3	153	184	30.3	40.8	3,155
	SD	1,294	1,422	504	30.1	5.0	1.5	0.0	2.1	8.7	1.3	57.0	49.9	7.7	20.2	472
	Basal	28,098	437	98.8	283	11.1	4.1	3.1	5.3	16.1	2.5	161	64.5	15.3	72.8	678
	SD	6,962	98.1	3.9	33.3	1.5	0.2	0.0	0.5	2.8	0.2	72.9	2.6	1.5	31.2	167
IL-1β(Ap) & [TNF-α, IFN]	Apical	169,963	66,722	42,890	9,935	586	16.5	18.4	28.6	42.1	8.9	282	453	584	1,005	5,524
	SD	35,717	2,751	27,066	4,532	170	4.4	6.4	11.6	5.5	2.4	33.1	544	479	638	1,954
	Basal	59,938	7,959	4,134	2,636	310	6.8	6.3	13.9	42.9	10.3	174	88.6	72.9	207	1,283
	SD	8,945	2,286	904	498	25.2	1.5	2.8	4.7	10.4	6.2	1.4	38.4	7.1	67.9	273

(b) P< 0.05 0.01 0.001 P>0.05

Source: From Shi, G., et al. (2008). Investigative Opthalmology and Visual Science 49: 4620–4623. Copyright Association for Research in Vision and Opthalmology.

The table summarizes the polarized secretions of simultaneously measured chemokines (12) and cytokines (3) using multiplex sandwich ELISAs. The left-hand column of this table defines the stimuli and the site of addition of pro-inflammatory mediators. These data are reported as actual concentrations and therefore corrected for transwell volume differences. Each Table entry is the mean ± SD for three experiments and the levels of significance are color coded for ease of comparison.

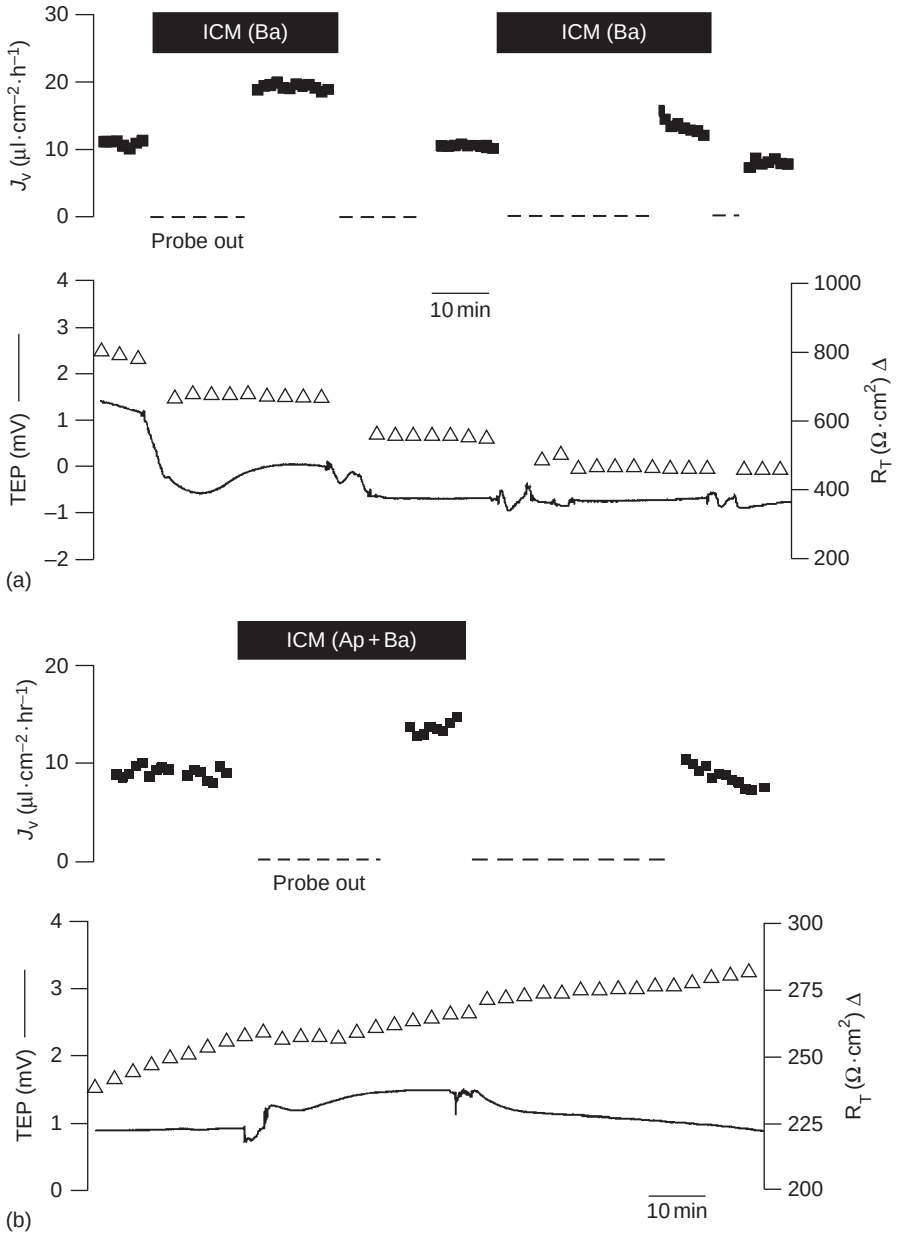

Figure 6 Inflammatory cytokine mixture (ICM) induced changes in hfRPE fluid transport (J_V). In all panels, the top trace is J_V, which is plotted as a function of time; net fluid absorption is indicated by positive values and TEP and total tissue resistance (R_T) are plotted in the lower traces. (a) Addition of ICM to the basal bath increased J_V by ≈13 μl ·cm^{-2}· hr^{-1} with no significant changes in TEP and R_T. (b) Concomitant addition of ICM to apical and basal baths increased J_V by ≈10 μl ·cm^{-2}· hr^{-1} with no change in TEP and a slight increase in resistance that is not statistically significant. From Shi, G., et al. (2008). *Investigative Ophthalmology and Visual Science* 49(10): 4620–4630. © Association for Research in Vision and Ophthalmology.

with PVR and PDR and are elevated in the vitreous of PVR eyes. Recently we showed that PDGF-C, -D are highly expressed in human fetal and adult RPE and that the mRNA levels of these two isoforms are up to 100-fold higher than PDGF-A and -B. PDGF-C and -D have been implicated in PVR and lens epithelial cell proliferation, but relatively little is yet known about their function in RPE. In other systems, they play an important role in angiogenesis and wound healing.

PDGFR-α and PDGFR-β, the receptors for PDGF-C and -D, respectively, are mainly localized to the apical membrane of human fetal RPE as shown in **Figure 7**. PDGF-CC, -DD, and -BB significantly stimulated hfRPE cell proliferation, while PDGF-DD, -BB, and -AB significantly stimulated cell migration. Furthermore, the stimulatory effects of PDGF were abrogated by a proinflammatory cytokine cocktail composed of TNF-α, IL-1β, and IFNγ. Comparison of the component effects

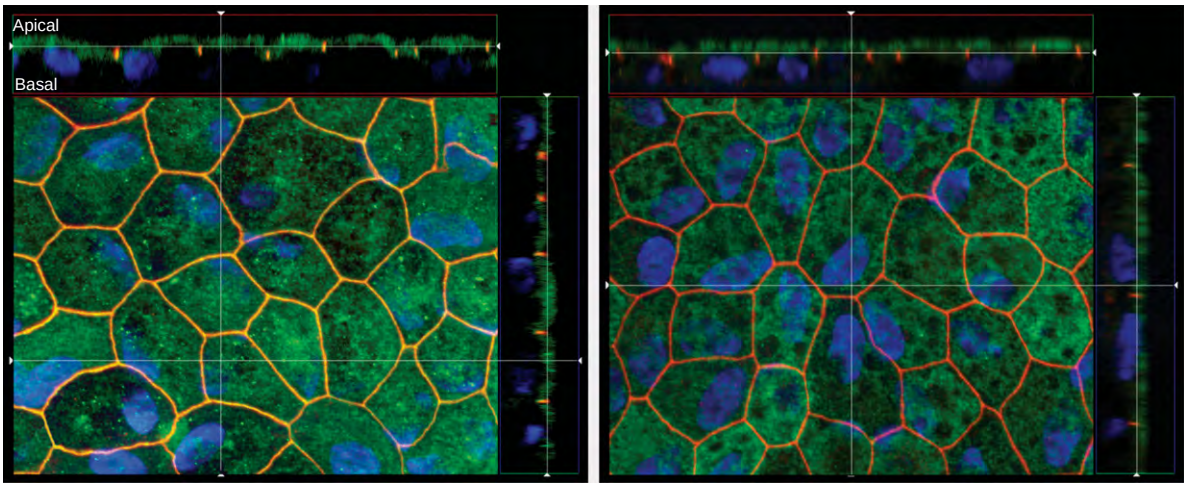

Figure 7 Immunofluorescence localization of PDGF receptors on hfRPE. The main part of each panel is an *en face* view of a cell culture monolayer shown as a maximum intensity projection through the *z*-axis. The top and right side of each panel is a cross section through the Z-plane of multiple optical slices obtained using the Apotome. In all experiments shown, the nucleus was stained with DAPI (blue), and the tight junction protein (ZO-1) was immunolabeled in red. The platelet-derived growth factor receptor PDGFR-α (green) is shown in (a), and while the beta subunit, PDGFR-β (green) is shown in (b). Both were detected on the apical membrane of hfRPE. From Li, R., et al. (2007). *Investigative Ophthalmology and Visual Science* 48(12): 5722–5732. © Association for Research in Vision and Ophthalmology.

showed that IFNγ was more effective in suppression than the entire cocktail or any subset of the cocktail, indicating that the downstream cytokine signaling pathways are interactive. Identifying the elements of this putative network and the specific nature of these interactions could provide targets for therapeutic intervention. For example, the proinflammatory cocktail may activate PDGF secretion by the RPE. In preliminary experiments, we showed that IFNγ increased the polarized secretion of PDGF-AA to the apical bath, providing a possible autocrine signal mediating RPE proliferation/migration. We have shown that the cytokine cocktail induces cell apoptosis, alters cytoskeleton distribution, and significantly decreases transepithelial resistance, which can help mediate leukocyte traffic to the SRS. The cytokine cocktail-induced in hibition of RPE proliferation/migration indicates a potential therapeutic role against proliferative responses at the retina/RPE/choroid interfaces.

Since IFNγ has a strong inhibitory effect on RPE proliferation and migration, it is natural to ask how this signaling pathway might provide the basis for inhibition. Native human adult RPE and hfRPE cells constitutively express two transcription factors, interferon regulatory factors 1 and 2 (IRF-1 and IRF-2), which are well-characterized members of the IFN regulatory family and key factors in the regulation of cell growth through their effects on cell cycle. In hfRPE, we showed that stimulation by IFNγ significantly increased IRF-1 protein levels with no effect on IRF-2. If these two transcription factors are mutually antagonistic, as shown in other systems, this may explain the strong inhibitory effect of IFNγ on RPE proliferation and migration, which we hypothesize is caused by an increase in the ratio of IRF-1/IRF-2.

IFNγ Regulation of RPE Fluid Transport

Immunoblots, immunofluorescence, intracellular recordings, pharmacology, and fluid transport data indicate a basolateral location of cystic fibrosis transmembrane conductance regulator (CFTR), a chloride channel, in native adult and fetal human RPE. As a first step in unraveling the network of cytokine interactions, we focused on INFγ since it is a main determinant of several key effects produced by the inflammatory cocktail. IFNγ has been implicated in the pathogenesis of a number of inflammatory diseases of infectious or presumed autoimmune origin and it has been detected in vitreous aspirates of patients with uveitis, PVR, and other inflammatory ocular diseases. In human RPE, IFNγ activates several intracellular signaling pathways, including the canonical janus-activated kinase and signal transducers and activators of transcription protein (JAK/STAT) pathway and P38 mitogen-activated protein kinase (MAPK), leading to the elevation of cyclic adenosine monophosphate (cAMP) and the subsequent activation of protein kinase A-dependent chloride channels – CFTRs. This results in a significant increase in net fluid absorption across the epithelium (**Figure 8**). These data and the data summarized below provide a possible basis for the etiology of chronic inflammatory diseases, such as posterior uveitis and AMD. In the diseased eye, the IFNγ-induced dehydration of the SRS

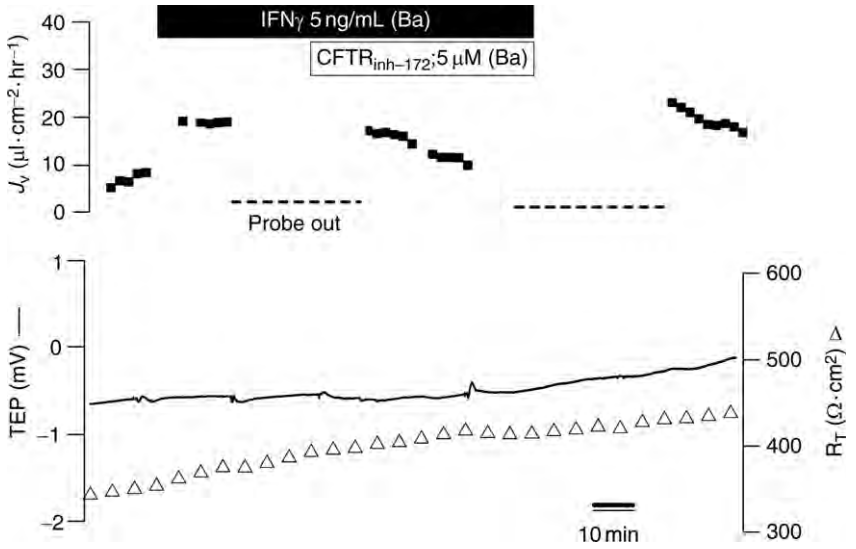

Figure 8 IFNγ-stimulated fluid transport (J_V) increase is inhibited by 5 μM $CFTR_{inh}$-172, an inhibitor of the cystic fibrosis transmembrane conductance regulator (CFTR), added to basal bath. J_V is plotted as a function of time in the top trace and net fluid absorption (apical to basal bath) is indicated by positive values; TEP (−) and R_T (△) are plotted as function of time in the two lower traces.

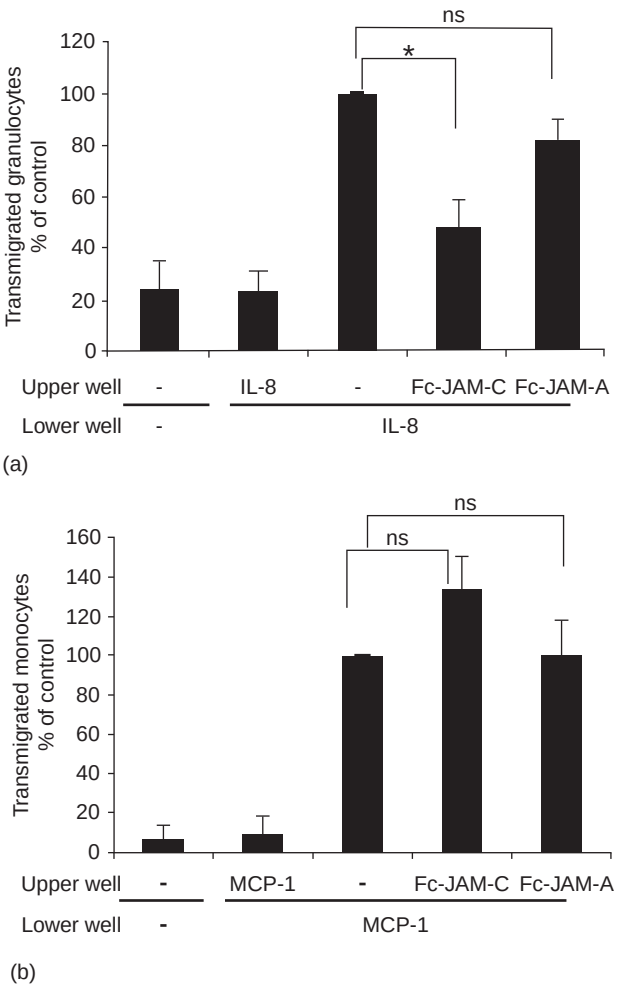

Figure 9 IL-8 and MCP-1 regulated transmigration of leukocytes. (a) Basolateral to apical transepithelial migration of granulocytes. The number of transmigrating granulocytes is shown as % of control. Exogenous addition of modified junctional adhesion molecule Fc-JAM-C competes with JAM-C/JAM-C interactions between adjacent cells, significantly reducing IL-8 induced transmigration of granulocytes. (b) In contrast, Fc-JAM-C had no significant effect on the basolateral to apical transepithelial migration of monocytes toward MCP-1. Addition of another RPE JAM isoform Fc-JAM-A, did not alter transmigration of granulocytes or monocytes. From Economopoulou, M., et al. (2009). *Investigative Ophthalmology and Visual Science* 50(3): 1454–1463. © Association for Research in Vision and Ophthalmology.

could increase the concentration of the already-accumulating chemokines and thereby help draw monocytes and neutrophils to the RPE basement membrane or across the RPE to the SRS. This helps control the continuing accumulation of debris from incompletely digested photoreceptors, oxidative stress, and accumulation of drusen that normally occur in and around the RPE over the first five decades of life. Based on a variety of risk factors that activate the immune system (e.g., monocytes), these protective gradients may dissipate with age, aided perhaps by the loss of RPE barrier function and the steady buildup of an immunologically hostile environment.

Leukocyte Migration across the RPE: A Model of Disease Progression

The integrity of the RPE monolayer depends on the inter-epithelial junctions that include tight and adherens junctions and desmosomes. The main constituents of tight junctions are three families of transmembrane proteins: occludins, claudins, and junctional adhesion molecules

(JAMs). The third member of the JAM family, JAM-C, has been identified in various cell types and implicated in inflammatory processes and shown to participate in the transmigration of leukocytes through endothelial and gut epithelial cells. Economopoulou and colleagues found that JAM-C is localized at the tight junctions of intact monolayers of adult and fetal human RPE, it is found at the initial cell–cell contacts of newly forming junctions, and that it helps initiate hfRPE junction formation and polarization. JAM-C also promotes the transepithelial migration of granulocytes through intact monolayers of cultured hfRPE driven by physiological gradients of interleukin 8 (IL-8). Thus, in the intact eye, JAM-C may be an important determinant of RPE initial junction formation, cell polarization, and immune-system-mediated pathophysiology at the retina–RPE interface (**Figure 9**). Recent animal model studies have implicated monocyte chemoattractant protein 1 (MCP-1) and fractalkine receptor in retinal microglia as critical regulators of drusen accumulation, local inflammation, and the development of AMD. As demonstrated by Shi and colleagues, the RPE secretes significant amounts of MCP-1 and IL-8 to the apical side in a polarized manner (**Table 1**). Both chemokines could form gradients across the RPE that coordinate monocyte and neutrophil movement to the RPE basement membrane. This could provide local surveillance/protection against the accumulation of immunologically active debris (drusen). The transformation over time of monocytes into macrophages would slowly degrade the RPE's ability to maintain protective chemokine gradients for the removal of immunologically active debris and eventually lead to degeneration/disease.

See also: Injury and Repair: Light Damage; Injury and Repair Responses: Retinal Detachment; Phototransduction: The Visual Cycle; Secondary Photoreceptor Degenerations: Age-Related Macular Degeneration.

Further Reading

Adijanto, J., Banzon, T., Jalickee, S., and Miller, S. S. (2009). CO_2-induced ion and fluid transport in human retinal pigment epithelium. *Journal of General Physiology* 133(6): 603–622.

Blaug, S., Quinn, R., Quong, J., Jalickee, S., and Miller, S. S. (2003). Retinal pigment epithelial function: A role for CFTR? *Documenta Ophthalmologica* 106: 43–50.

Bryant, D. M. and Mostov, K. E. (2008). From cells to organs: Building polarized tissue. *Nature Reviews. Molecular Cell Biology* 9(11): 887–901.

Daniele, L. L., Sauer, B., Gallagher, S. M., Pugh, E. N., Jr., and Philp, N. J. (2008). Altered visual function in monocarboxylate transporter 3 (Slc16a8) knockout mice. *American Journal of Physiology Cell Physiology* 295: C451–C457.

Donoso, L. A., Kim, D., Frost, A., Callahan, A., and Hageman, G. (2006). The role of inflammation in the pathogenesis of age-related macular degeneration. *Surveys of Ophthalmology* 51: 137–152.

Dunaief, J. L. (2006). Iron induced oxidative damage as a potential factor in age-related macular degeneration: The Cogan lecture. *Investigative Ophthalmology and Visual Science* 47: 4660–4664.

Economopoulou, M., Hammer, J., Wang, F., et al. (2009). Expression, localization, and function of junctional adhesion molecule-C (JAM-C) in human retinal pigment epithelium. *Investigative Ophthalmology and Visual Science*. 50: 1454–1463.

Fisher, S. K., Lewis, G. P., Linberg, K. A., and Verardo, M. R. (2005). Cellular remodeling in mammalian retina: Results from studies of experimental retinal detachment. *Progress in Retinal and Eye Research* 24: 395–431.

Gehrs, K. M., Anderson, D. H., Johnson, L. V., and Hageman, G. S. (2006). Age-related macular degeneration – emerging pathogenetic and therapeutic concepts. *Annals of Medicine* 38: 450–471.

Illek, B., Fu, Z., Schwarzer, C., et al. (2008). Flagellin activates inflammatory response and cystic fibrosis transmembrane conductance regulator-dependent Cl secretion: Role for p38. *American Journal of Physiology Lung Cell Molecular Physiology.* 295: L531–L542.

Jarrett, S. G., Lin, H., Godley, B. F., and Boulton, M. E. (2008). Mitochondrial DNA damage and its potential role in retinal degeneration. *Progress Retinal Eye Research* 6: 596–607.

Jia, L., Liu, Z., Sun, L., et al. (2007). Acrolein, a toxicant in cigarette smoke, causes oxidative damage and mitochondrial dysfunction in RPE cells: Protection by (R)-alpha-lipoic acid. *Investigative Ophthalmology and Visual Science* 48: 339–348.

Li, R., Maminishkis, A., Wang, F. E., and Miller, S. S. (2007). PDGF-C and-D induced proliferation/migration of human RPE is abolished by inflammatory cytokines. *Investigative Ophthalmology and Visual Science* 48: 5722–5732.

Maminishkis, A., Chen, S., Jalickee, S., et al. (2006). Confluent monolayers of cultured human fetal retinal pigment epithelium exhibit morphology and physiology of native tissue. *Investigative Ophthalmology and Visual Science* 47: 3612–3624.

Nussenblatt, R. B. and Ferris, F., 3rd (2007). Age-related macular degeneration and the immune response: Implications for therapy. *American Journal of Ophthalmology* 144: 618–626.

Philp, N. J., Ochrietor, J. D., Rudoy, C., et al. (2003). Loss of MCT1, MCT3, and MCT4 expression in the retinal pigment epithelium and neural retina of the 5A11/basigin-null mouse. *Investigative Ophthalmology and Visual Science* 44: 1305–1311.

Shi, G., Maminishkis, A., Banzon, T., et al. (2008). Control of chemokine gradients by the retinal pigment epithelium. *Investigative Ophthalmology and Visual Science* 49: 4620–4630.

Strauss, O. (2005). The retinal pigment epithelium in visual function. *Physiological Reviews* 85: 845–881.

Volobouеva, L. A., Killilea, D. W., Atamna, H., and Ames, B. N. (2007). *N*-tert-butyl hydroxylamine, a mitochondrial antioxidant, protects human retinal pigment epithelial cells from iron overload: Relevance to macular degeneration. *FASEB Journal* 21: 4077–4086.

Volobouеva, L. A., Liu, J., Suh, J. H., Ames, B. N., and Miller, S. S. (2005). (R)-alpha-lipoic acid protects retinal pigment epithelial cells from oxidative damage. *Investigative Ophthalmology and Visual Science* 46: 4302–4310.

Wangsa-Wirawan, N. D. and Linsenmeier, R. A. (2003). Retinal oxygen: Fundamental and clinical aspects. *Archives of Ophthalmology* 121: 547–557.

Winkler, B. S., Starnes, C. A., Twardy, B. S., Brault, D., and Taylor, R. C. (2008). Nuclear magnetic resonance and biochemical measurements of glucose utilization in the cone-dominant ground squirrel retina. *Investigative Ophthalmology and Visual Science* 49: 4613–4619.

Retinal Pigmented Epithelium Barrier

L J Rizzolo, Yale University School of Medicine, New Haven, CT, USA

Glossary

Adherens junctions – A component of the apical junctional complex that provides mechanical strength to cell–cell adhesions and, together with the tight junction, regulates cell size, shape, and proliferation.
Apical junctional complex – An assembly of tight, adherens, and gap junctions that join neighboring cells of an epithelial monolayer together. The junctions form a belt that completely encircles each cell at the apical end of the lateral membranes.
Apical membrane – The region of the plasma membrane that interdigitates with the photoreceptors of the neural retina. It is separated from the basolateral membranes by the apical junctional complex.
Basolateral membrane – The region of the plasma membrane that rests on Bruch's membrane and faces the choroid. It is separated from the apical membrane by the apical junctional complex.
Claudins – A family of proteins that forms tight junctional strands and determines the selectivity and permeability of the tight junctions.
Paracellular space – The space between the neighboring cells of an epithelial monolayer.
Subretinal space – The thin space that lies between the apical membrane of the retinal pigment epithelium and the photoreceptors. It becomes a wide space with retinal edema and detachment.
Tight junctions – A component of the apical junctional complex that regulates transepithelial diffusion through the paracellular space, retards diffusion of lipids and membrane proteins between the apical and basolateral membranes, and, together with the adherens junction, regulates cell size, shape, and proliferation.
Transepithelial electrical resistance (TER) – An amalgam of the electrical resistances of the apical membrane, basolateral membrane, and paracellular space. It is commonly used as a reflection of the electrical resistance of tight junctions. When the sum of the membrane resistances greatly exceeds the paracellular (shunt) resistance, the TER approximates the electrical resistance of the tight junctions.

Introduction

Blood–tissue barriers were first revealed by the inability of injected proteins, or protein-bound dyes, to move from the blood into certain tissues. Only the brain, testes, and placenta shared this property. The cells that formed the barrier exhibited reduced transcytosis and were bound together by seemingly impermeable tight junctions. Transcytosis is one mechanism to move serum solutes across the cells of the barrier, whereas tight junctions partially occlude the paracellular spaces to reduce transepithelial diffusion between the cells. This initial conception has since been expanded to include all mechanisms of transcellular transport and the metabolic and catabolic pathways that alter solutes during transport.

The blood–retinal barrier has two divisions. The inner layers of the retina are supplied by a vascular bed, whose endothelia form the inner blood–retinal barrier. This endothelial barrier typifies most of the blood–brain barrier. This article focuses on the outer blood–retinal barrier, which is more similar to the choroid plexus and testes blood–tissue barriers. These barriers are a collaboration of a fenestrated capillary bed with an epithelium. In the outer retina, the collaboration is between the choriocapillaris and the retina pigment epithelium (RPE). As fenestrae make the capillaries porous, the RPE forms the barrier to serum components (**Figure 1**). Certainly, the Bruch's membrane that separates the capillaries and RPE serves as a filter; however, this aspect of the outer blood–retinal barrier is discussed elsewhere in the encyclopedia. A good example of a metabolic pathway that participates in barrier function is the visual cycle. Vitamin A, transported by the serum, is endocytosed and transformed into *cis*-retinal as it is transported across the cell and exported to the photoreceptors. Ultimately, the paracellular and transcellular transport of ions and small organic solutes should be considered as a unit. Because explorations of how these pathways interact remain in their infancy, the two topics are discussed separately in this encyclopedia. This article focuses on the paracellular pathway, but includes the transcellular pathway whenever a connection between the two can be made. We discuss the assembly of RPE tight junctions, their retina-specific properties, and how the RPE and its tight junctions are regulated by the surrounding tissues.

Structure and Function

Tissue Level

The distinctive structure of the outer blood–retinal barrier leads to unique functions. Unlike other epithelia and endothelia, the RPE separates two solid tissues – the choroid and the neural retina. Early in embryogenesis, the apical surface of the RPE borders a fluid-filled lumen, the lumen of the optic vesicle. As development proceeds, this lumen is reduced to a potential space known as the subretinal space (Figure 2). In this space, the microvilli of the RPE's apical pole interdigitate with the outer segments of the photoreceptor cells. The intimate contact of the RPE and photoreceptors allows retinoids of the visual cycle to readily shuttle back and forth across the subretinal space, and allows disk membranes shed by the photoreceptors to be phagocytosed by the RPE. The ionic composition of the subretinal space is carefully regulated to support the functions of the photoreceptors and the RPE. To this end, the RPE absorbs water. Water continuously enters the retina from the inner vascular bed and vitreous and is transported by the RPE into the choroid for removal by the choroidal circulation. Failure of this process results in retinal edema and even retinal detachment. Contrast this with another region of the blood–brain barrier, the epithelium of the choroid plexus. The epithelium of the choroid plexus is also derived from the neuroepithelium, but in this case, the lumen of the neural tube expands to form the ventricular system. Rather than absorb fluid, the choroid plexus secretes copious volumes of cerebral spinal fluid. To understand the functional differences between the RPE and the epithelium of the choroid plexus, we need to look more closely at the structure of the barrier.

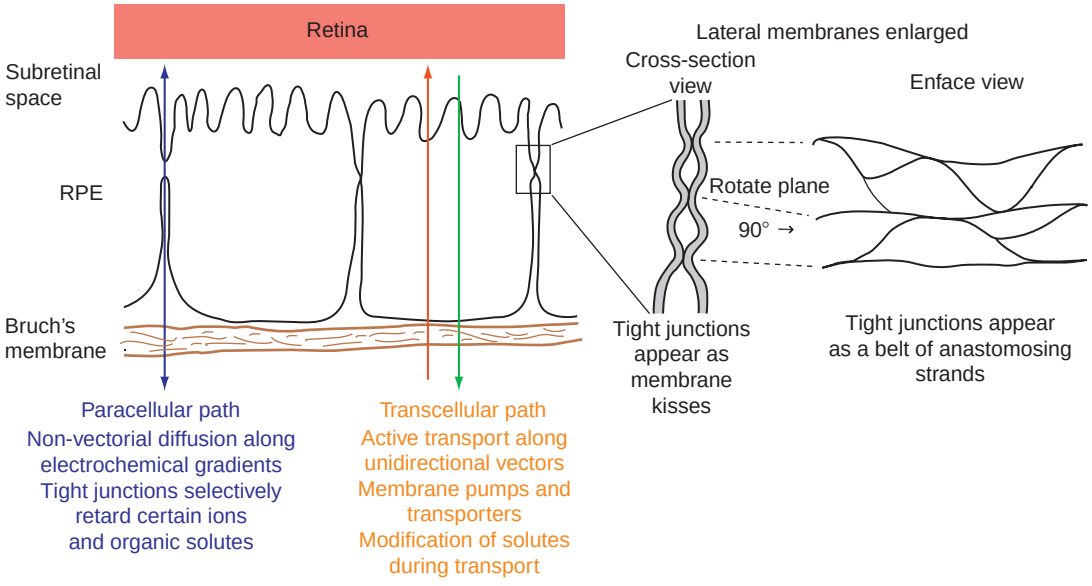

Figure 1 Mechanisms that regulate transport across the outer blood–retinal barrier.

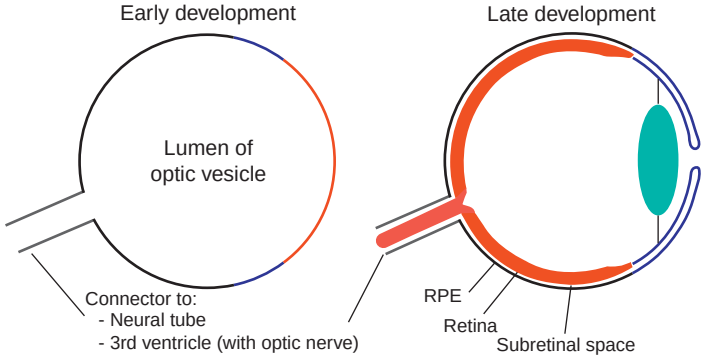

Figure 2 The lumen of the embryonic optic vesicle becomes the subretinal space.

Cellular Level

The RPE is a monolayer of cells that are joined by a complex of junctions known as the apical junctional complex. The apical junctional complex encircles each cell to bind the monolayer together much like the plastic rings that hold together a six-pack of canned beverages. The complex consists of three junctions (tight, adherens, and gap) whose functions are intertwined. Adherens junctions bind neighboring cells together. Tight junctions form a partially occluding seal that semiselectively retards diffusion through the paracellular spaces of the monolayer (**Figure 1**). Both junctions regulate proliferation, cell size, and the polarized distribution of plasma membrane proteins. The junctions of the complex work in concert, but we focus on how tight junctions contribute to barrier function.

Tight junctions form a barrier between the apical and basolateral poles of the cell. They work in conjunction with intracellular trafficking pathways to create and maintain an apicobasal polarity that is essential for the blood–retinal barrier to function. Unlike most epithelia, the Na,K-ATPase (ATP, adenosine triphosphate) is enriched in the apical membrane rather than localized to the basolateral membrane. Although this initial discovery suggested that the RPE is an upside-down epithelium, it is now known that only a few RPE proteins have an atypical distribution. What is crucial for RPE function is the distribution of membrane channels and transporters. The RPE and the epithelium of the choroid plexus both have an apical Na,K-ATPase that provides the energy for vectorial transport. It is the distribution of the various ion channels and transporters that determines whether the RPE absorbs water or the epithelium of the choroid plexus secretes it. Briefly, the polarized distribution of transporters in the RPE results in the active transport of chloride from the apical to basal side of the cell. As a result, the apical side of the monolayer has a positive charge relative to the basal side. Sodium and potassium are transported down this electrical gradient to balance the chloride transport. The osmotic gradient that results pulls water in the apical to basal direction. The polarized distribution of the various channels and transporters differs in the epithelium of the choroid plexus to support the opposite, basal to apical, transport of water. There are general housekeeping mechanisms that recognize the targeting signals encoded in a protein's structure to deliver it to the correct membrane. In some cases, different tissue-specific isoforms encode different targeting signals; in others, tissue-specific variations in the targeting machinery give each epithelium its unique character.

The vectorial transport mechanism outlined above would have little effect, if transepithelial ion gradients were dissipated by the paracellular pathway. Early microscopists believed that a zonular band of junctions occluded the paracellular space by completely encircling each cell. Their name for this junction, zonula occuldens or tight junction, is misleading because the junction is selectively leaky. The degree of leakiness, and selectivity for certain ions, not only varies among epithelia, but is essential for epithelial function as well. The permeability and semiselectivity of the junctions are matched to transcellular transport mechanism. For example, RPE tight junctions need to be leakier to sodium than to chloride, because RPE pumps chloride across the cell and needs a leak for cations to passively follow the chloride flux. The inadequate capacity for sodium and potassium to cross the cell is ameliorated by the sodium-selective leak through the tight junction.

A compelling example of how transcellular transport is matched to tight junction selectivity is provided by the kidney. The diuretic hormone, aldosterone, changes the flux of water by acting simultaneously on a membrane sodium channel and a tight junction protein that regulates sodium selectivity. In the retina, the volume and composition of the subretinal space vary with the day/night cycle. It remains to be investigated how the properties of tight junctions and membrane transporters are coordinated to manage the subretinal space during this cycle.

Molecular Level

Proteins of the apical junctional complex fall into transmembrane, adaptor, and signaling/regulatory categories. Adaptors link the transmembrane proteins to signaling proteins and a cortical band of actin filaments. Besides known members of the tight junction (**Figure 3**), proteomics suggest that over 912 proteins are associated with the tight junction. The adaptor proteins express multiple copies of PDZ domains. This protein-binding domain of approximately 100 amino acids takes its name from the three proteins that defined this class of protein-binding domain: postsynaptic density protein 95 (PSD-95), disks large, and zonula occludins 1 (ZO-1). PDZs are the largest family of protein-binding domains and form the basis of many protein complexes. Each adaptor protein expresses

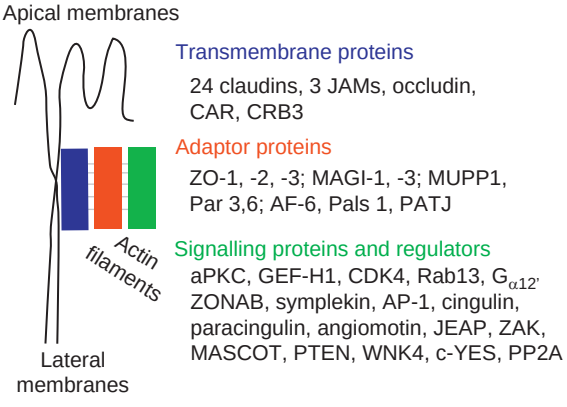

Figure 3 Composition of the tight junctions.

multiple homologs of PDZ domains that have distinct, but sometimes overlapping binding specificities. Together with other protein-binding motifs, for example, SRC homology 3 domain, guanylate kinase, bi-tryptophan domain that binds proline-rich peptides, Dilute domain, and Phox and Bem1P domain, the known adaptor proteins have the capacity to bind the large number of regulatory proteins that proteomics suggests. A junction of such complexity would be inconsistent with the original view of the tight junction as a static barrier.

The tight junction is a highly dynamic structure with the potential to rapidly respond to environmental stimuli. Photobleaching studies demonstrate that ZO-1 and occludin, a regulator of permeability, rapidly associate and dissociate from the junction. Occludin has a very short half-life and its degradation is regulated by endocytic and ubiquitin pathways. Therefore, the cell exerts a fine control over the properties of the tight junction that can rapidly respond to changes in the environment. This flexibility extends to the claudin family of transmembrane proteins. Membrane proteins typically have a half-life on the order of days, but the claudins that have been studied have a half-life of 4–12 h. Claudins form the anastomosing network of strands that are observed by freeze-fracture electron microscopy (**Figure 4**) and schematized in **Figure 1**. There are 24 or more claudins. Each epithelium expresses a subset of claudins. The subset of claudins, expressed and localized to the tight junction, determines the selectivity and permeability of the junction. In the kidney example given above, aldosterone decreases the expression of claudin 4 to increase the sodium leak through the tight junctions.

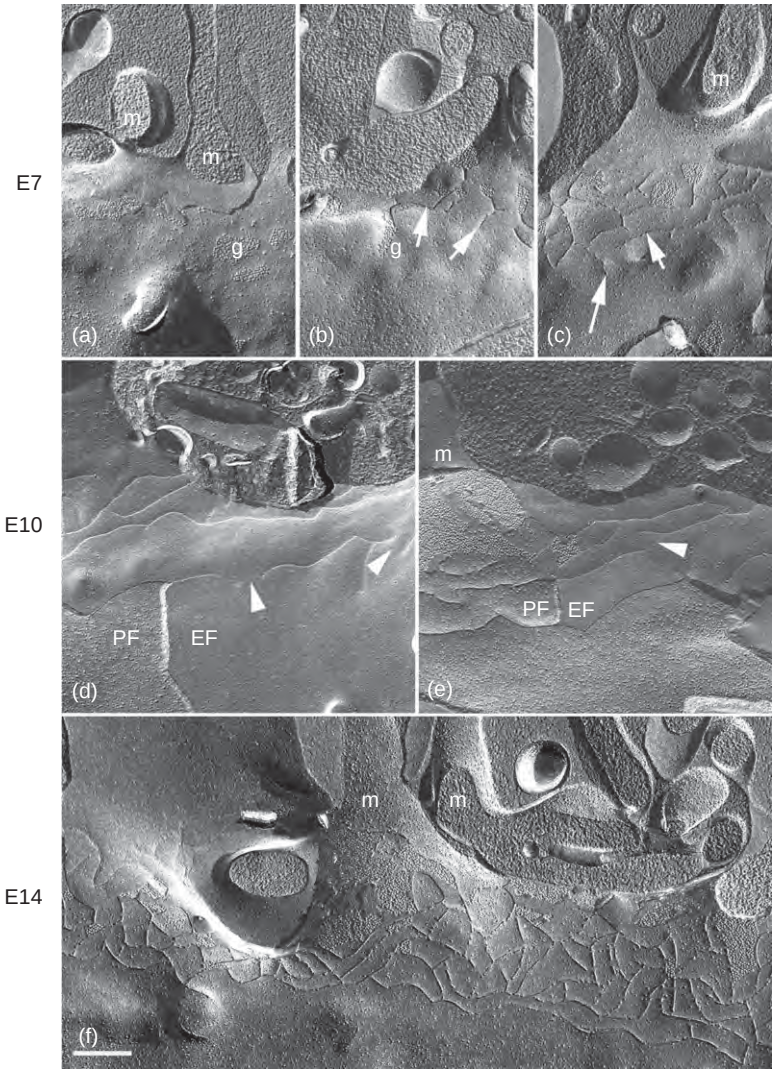

Figure 4 Strands of the tight junction gradually coalesce during development. Freeze-fracture replicas show how sparse, disconnected strands on E7 become a necklace of strands with discontinuities by E10 and a continuous, uninterrupted network by E14. Microvilli (m) at the top of each panel indicate the apical end of the lateral membrane. Arrows, tight junctional strands; Arrowheads, discontinuities. EF, E-face; PF, P-face; Bar = 0.25 μm.

Although the basic structure of the outer blood–retinal barrier is conserved among species, there are species-specific variations in the composition of the subretinal space, the properties of transmembrane transport, and the composition of the tight junctions. In human RPE, the principal claudins appear to be claudins 3, 10, and 19. Claudin 19 has been linked to kidney disease and visual impairment. By contrast, chick RPE expresses primarily claudins 1 and 20 with lesser amounts of claudins 2, 4L2, 5, and 12. Claudins 1 and 3 are fairly ubiquitous with most epithelia expressing one or the other. Claudin 2 increases sodium permeability in some contexts. However, the study of how claudins affect permeability is in its infancy particularly in regard to the effects of cellular context on function.

Regulation of RPE Tight Junctions

Clues from Embryonic Maturation

What is a mature, differentiated RPE monolayer? Which markers and how many should we use to render this judgment? Might enhancing the expression of some markers in a culture experiment lessen the expression of others? If cellular pathways form an integrated web, would over- or underexpression of a protein have deleterious effects? A default path for human embryonic stem cells appears to be an RPE-like cell, but those cells lack some RPE proteins and express non-RPE proteins. The RPE is the first retinal cell to form during development, but despite its undeniable RPE character, the early RPE cell is only partially differentiated. It will undergo many transformations, as the neural retina and choroid differentiate on either side of it. The RPE is very plastic. Depending upon pathology or culture conditions, one can observe many partially differentiated states, or even transform RPE to other phenotypes. This may be the reason why RPE transplants fail when retinal degeneration is advanced. Dedifferentiation would be a normal response of healthy RPE to this abnormal environment. In support of this hypothesis, RPE transplants were most successful when the RPE and neural retina were co-transplanted. In some ways, culture is like a disease state where a degenerate neural retina and choroid no longer send RPE the signals that maintain key functions. In the chick culture model described, we found that retinal secretions promote RPE differentiation over the course of days rather than the months required without the retina. More work will be needed to determine whether these findings apply to mammalian eyes.

A study of chick embryonic development illustrates the maturation process. We can describe early, intermediate, and late phases of development. The early phase extends from the time that the RPE forms on embryonic day 3 (E3) until the inner segments of photoreceptors protrude the outer limiting membrane on E9. The intermediate phase extends from E9 to E15, when photoreceptors begin to elaborate outer segments. The late phase extends from E15 until hatching on E21. During the intermediate phase, the layers of Bruch's membrane gradually form. Fenestrations in the walls of the choroidal capillaries begin to form in the intermediate phase, but are not fully elaborated until the middle of the late phase. In parallel with the formation of fenestrations in the capillaries, infoldings of the basolateral membrane begin to form in the intermediate phase, but are not completely elaborated until the middle of the late phase. As the basolateral membranes elaborate infoldings, apical membrane microvilli elongate in coordination with the elongation of photoreceptor inner and outer segments. Some plasma membrane proteins have a distribution that is polarized between the apical and basolateral membranes as early as E7. Nevertheless, some proteins become polarized later in development in parallel with the morphological changes of the apical and basolateral membranes. Examples include basigin, monocarboxylate transporters, and the Na,K-ATPase. This coordination of the development of photoreceptors, RPE plasma membranes, Bruch's membrane, and the choriocapillaris is conserved between chickens and mammals. It is in the context of this maturing environment that the RPE completes its differentiation.

The RPE is the first retinal layer to overtly differentiate. Despite an epithelial morphology and the expression of RPE markers, early embryonic RPE is still immature. Between E7 and E18 of chick development, 40% of the transcriptome changes with substantial effects on the extracellular matrix, junctional complexes, cell surface receptors, signal transduction pathways, cytoskeleton, regulators of gene expression, and transmembrane transport proteins. Some genes turned on and others off, but most changed their level of expression relative to one another. These data suggest why RPE cultures that express the same tissue-specific markers can function so differently. Without direction from the neural retina or choroid to establish balanced gene expression, cultured RPE can adopt the range of behaviors it displays during development *in vivo*.

Assembly of Tight Junctions during Differentiation

Most studies of the assembly of the apical junctional complex were performed in mouse blastocysts or in culture using kidney or intestinal cell lines. The rapid kinetics of assembly in these models makes it difficult to parse the role of the putative assembly proteins. The consensus is that a primordial adherens junction forms first, followed by the segregation of tight junction components into a nascent tight junction. Nectin, E-cadherin, and junctional

adhesion molecule-A (JAM-A) trigger the formation of the primordial adherens junction. These transmembrane proteins form homodimers with their counterparts on the neighboring cell. Their cytoplasmic domains crystallize a complex of proteins by binding an adaptor protein. For example, JAM-A binds the adaptors, AF-6 (Afadin), PAR3 (Partitioning defective-3 homologue), and ZO-1. Their multiple protein-binding domains enable these adaptors to assemble a complex. For example, PAR-3 binds PAR-6 (Partitioning defective-6 homologue) and the atypical protein kinase C, which contributes to cell polarity. JAM-A also localizes ZO-1 to the apical side of the complex to initiate the formation of a tight junction. The tight junction transmembrane proteins, occludin and claudin, bind this nascent complex. Anti-JAM-A antibodies block the formation of tight junctions, as evidenced by the mislocalization of occludin and a low transepithelial electrical resistance (TER). Nevertheless, the adherens junction did form, as evidenced by the localization of E-cadherin and ZO-1. Taken together, these data suggest that JAM-A may play a role in assembling adherens junctions, but plays a more critical role in assembling tight junctions.

As the apical junctional complex assembles slowly during normal RPE development, the process may be studied in greater detail. In chick, primordial adherens junctions are already present in the neuroepithelium that forms the RPE on E3, days before rudimentary tight junctions begin to form on E7. Many of the proteins described above in the assembly of the apical junctional complex are present at this time, but the adherens junction will remodel throughout development both morphologically and molecularly. In each phase of development, different cadherins will appear and disappear. The early phase includes many tight-junctional proteins: ZO-1, occludin, and the assembly proteins AF-6, JAM-A, PAR3, and PAR6. Nonetheless, tight junctions are absent until claudins expression begins on E7 and short, sparse tight-junctional strands begin to appear (**Figure 4**). During the intermediate phase, tight-junctional strands grow in number and length to gradually coalesce into a complete network that encircles each cell. The tight junction first becomes functional between E10 and E12 (defined by the ability to block the transepithelial diffusion of horseradish peroxidase). During the late phase, structural modifications of the tight junctions continue. Like the adherens junctions, these morphological changes are accompanied by molecular changes. Some claudin messenger RNAs (mRNAs) appeared early, but others appeared during the intermediate or late phases. The expression of some of the early-appearing claudins decreased during the late phase. During the intermediate phase, there was a switch in the expression of ZO-1 isoforms, an event also observed during tight-junction formation in pre-implantation embryos. ZO-3 did not appear until the late phase of development. Although changes in protein expression parallel gene expression to some extent, it appears that the claudins and ZO proteins are also regulated by effects on protein stability and subcellular localization.

The molecular and morphological changes in the apical junctional complex imply the function of the outer blood–retinal barrier changes during this long maturation process. The changes in claudin expression imply changes in the selectivity and permeability of the tight junctions. It would be reasonable to expect that this would be coupled with changes in transepithelial transport. Among the changes in the transcriptome, many involve membrane transporters. Several should be mentioned, because there is also physiological and cell biological data to corroborate the changes in gene expression. Changes in the expression and polarized distribution of the monocarboxylate transporters and Na,K-ATPase have already been mentioned. Early in development, several facilitated glucose transporters are expressed, but more are expressed later in development, including a sodium-coupled glucose transporter. The appearance of the latter transporters corresponds to the time that the tight junctions become relatively impermeable to glucose. These changes are essential because the retina has a high demand for glucose. It appears that housekeeping transporters that are sufficient for the RPE's individual needs are replaced by a transcellular, active transport mechanism at the time the blood–retinal barrier forms. These conclusions are based on studies of a primary cell culture model of RPE maturation.

Culture Models to Study Regulation of the Outer Blood–Retinal Barrier

RPE can be cultured on matrix-coated filters that are suspended in a culture dish (**Figure 5**). This architecture separates the media compartment into apical and basal chambers. The cultures spontaneously polarize with the basal membrane against the filter substrate and the apical microvilli projecting into the upper chamber. The culture architecture allows the cells to feed from the basolateral membranes, as *in vivo*. By contrast, plastic-grown cells need to feed from the apical membranes. Another advantage is that it is easy to measure barrier function by placing tracers in one medium chamber and measuring their flux

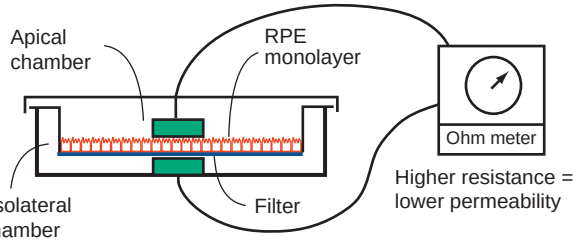

Figure 5 RPE cell culture.

across the monolayer into the opposite chamber. Further, electrodes may be placed to measure a TER. This flexibility is important because selectivity and permeability of tight junctions are regulated semi-independently. The TER is commonly used to assess tight junctions, but TER is an amalgam of transcellular and paracellular resistances to a current that is carried by all the ions of the extracellular space. The TER often approximates the resistance of the tight junctions, because the transjunctional current is often much greater than the transcellular current. Junctions of epithelia with a similar TER can differ in their ion selectivity. Therefore, it is valuable to measure ion fluxes directly. Further, the permeation of mannitol (a small organic tracer) can be modulated independently of TER, and vice versa. Accordingly, multiple assays of barrier function are required for a full assessment.

Although it is relatively easy to culture RPE from many species, including human adults, it is difficult to establish cultures that form an effective barrier. A good example of the problems encountered is the human-derived ARPE19 cell line. This spontaneously transformed cell line has many RPE-specific properties, but its tight junctions are immature. Many claudins were expressed that are undetected in native tissue, and some of the claudins expressed *in vivo* were undetected in ARPE19. By modifying culture conditions, barrier function, morphology, and melanin expression could be improved. Although claudin expression was affected somewhat, large differences between native RPE and ARPE19 remained. Like the chick studies described above, genomic analyses of native and cultured human RPE have become or are becoming available, which will allow a molecular definition that can compare native to cultured RPE.

Several culture systems have been devised that allow RPE to form a barrier that resembles native RPE. The most highly differentiated are primary or secondary cultures that were isolated from the intermediate phase of RPE development. This stage corresponds to E14 in the chick, postnatal day 5 in rat, and 18–22 weeks gestation in the human. Notably, human fetal RPE appears to have a broader window, as cultures isolated from 13-week fetuses also have excellent properties. Each culture relies on highly specialized medium that includes low amounts, or no, serum. In some cases, the medium appears to remove the need for choroidal or retinal stimulation, but these cultures require 1–2 months in culture to fully mature. Rat and chick cultures that were maintained in serum-free medium were very sensitive to the addition of serum to the apical medium chamber, as might be seen in pathology. For each species, apical serum decreased barrier function, as measured by the TER.

In contrast to the other models, the chick model was designed to study tissue interactions. It used primary cultures that formed incomplete tight junctions with a low TER in a serum-free medium. However, the cultures were very sensitive to retinal secretions. A medium conditioned by the organ culture of neural retinas induced the formation of complete tight junctions with a TER that was similar to native RPE. Reconstitution experiments showed that contact with the neural retina was required for the proper polarized distribution of the Na,K-ATPase and certain integrins. A central finding was that retinal interactions promoted differentiation on a timescale of days rather than months. Besides cellular junctions, the retinal conditioned medium affected the expression of genes related to the visual cycle, phagocytosis, cytoskeleton, and transmembrane transport. Besides gene expression, retinal conditioned medium affects the half-life and subcellular localization of claudins and ZO proteins. By regulating membrane transporters and tight junctions, the retina and RPE appear to collaborate in regulating the subretinal space. This is an area of research that needs to be explored in greater detail.

RPE in the Larger Context of Ocular Biology and Disease

Many diseases are coming to be viewed as a low-grade inflammatory process, including age-related macular degeneration. Investigations of inflammatory diseases of the intestine (Crohn's) and central nervous system (multiple sclerosis) demonstrate that disease can affect the tight junctions in part through the action of inflammatory cytokines. Certainly, disease also affects the membrane transporters of epithelia and endothelia. In the renal field, there has been progress in understanding the interrelationships of tight junctions and membrane transporters and how they are coordinately regulated. The retina field lags behind, but the availability of good culture models and the advances in genomics and systems biology hold great promise for the future.

See also: Breakdown of the Retinal Pigmented Epithelium Blood–Retinal Barrier; Phototransduction: The Visual Cycle; Retinal Pigment Epithelium: Cytokine Modulation of Epithelial Physiology.

Further Reading

Bradbury, M. W. B. (1979). *The Concept of a Blood–Brain Barrier*. New York: Wiley.

Burke, J. M. (2008). Epithelial phenotype and the RPE: Is the answer blowing in the Wnt? *Progress in Retinal and Eye Research* 27(6): 579–595.

Cereijido, M. and Anderson, J. M. (eds.) (2001). *Tight Junctions.* Boca Raton, FL: CRC Press.

Cereijido, M., Contreras, R. G., Shoshani, L., Flores-Benitez, D., and Larre, I. (2008). Tight junction and polarity interaction in the transporting epithelial phenotype. *Biochimica et Biophysica Acta* 1778: 770–793.

Grunwald, G. B. (1996). Cadherin cell adhesion molecules in retinal development and Pathology. *Progress in Retinal Eye Research* 15: 363–392.

Guillemot, L., Paschoud, S., Pulimeno, P., Foglia, A., and Citi, S. (2008). The cytoplasmic plaque of tight junctions: A scaffolding and signalling center. *Biochimica et Biophysica Acta* 1778: 601–613.

Klimanskaya, I., Hipp, J., Rezai, K. A., et al. (2004). Derivation and comparative assessment of retinal pigment epithelium from human embryonic stem cells using transcriptomics. *Cloning and Stem Cells* 6: 217–245.

Le Moellic, C., Boulkroun, S., Gonzalez-Nunez, D., et al. (2005). Aldosterone and tight junctions: Modulation of claudin-4 phosphorylation in renal collecting duct cells. *American Journal of Physiology – Cell Physiology* 289: C1513–C1521.

Radtke, N. D., Aramant, R. B., Petry, H. M., et al. (2008). Vision improvement in retinal degeneration patients by implantation of retina together with retinal pigment epithelium. *American Journal of Ophthalmology* 146: 172–182.

Rajasekaran, S. A., Beyenbach, K. W., and Rajasekaran, A. K. (2008). Interactions of tight junctions with membrane channels and transporters. *Biochimica et Biophysica Acta* 1778: 757–769.

Rizzolo, L. J. (2007). Development and role of tight junctions in the retinal pigment epithelium. *International Review of Cytology* 258: 195–234.

Strauss, O. (2005). The retinal pigment epithelium in visual function. *Physiological Reviews* 85: 845–881.

Van Itallie, C. M. and Anderson, J. M. (2006). Claudins and epithelial paracellular transport. *Annual Review of Physiology* 68: 403–429.

Wilt, S. D. and Rizzolo, L. J. (2001). Unique aspects of the blood–brain barrier. In: Anderson, J. M. and Cereijido, M. (eds.) *Tight Junctions*, pp. 415–443. Boca Raton, FL: CRC Press.

Retinal Vasculopathies: Diabetic Retinopathy

N C Steinle and J Ambati, University of Kentucky, Lexington, KY, USA

Glossary

Cotton-wool spots (CWSs) – Also known as soft exudates, these may be found in nonproliferative diabetic retinopathy (NPDR). They are composed of accumulations of neuronal debris within the retinal nerve fiber layer, and result from disruption and stasis of axoplasmic flow.
Diabetes control and complications trial (DCCT) – A study that contributed to our understanding that intensive glycemic control is associated with a reduced risk of newly diagnosed retinopathy and a reduced progression of existing retinopathy in people with diabetes.
Diabetes mellitus (DM) – A metabolic disorder characterized by sustained hyperglycemia secondary to lack or diminished efficacy of endogenous insulin.
Diabetic retinopathy (DR) – A retinal disease consequent to development of DM.
Insulin-dependent diabetes mellitus (IDDM) – A term sometimes used to refer to type I diabetes.
Intraretinal microvascular abnormalities (IRMAs) – The tortuous, hypercellular micro vessels that develop in NPDR.
New vessels elsewhere (NVE) – The neovascularization of the retina found greater than one disk diameter from the optic nerve head.
New vessels on disk (NVD) – The neovascularization on or within one disk diameter of the optic nerve head.
Non-insulin-dependent diabetes mellitus (NIDDM) – An older term for type II diabetes or adult-onset diabetes.
Nonproliferative diabetic retinopathy (NPDR) – DR characterized by intraretinal microvascular changes which precede the proliferative phase.
Optical coherence tomography (OCT) – A noninvasive imaging technique that permits analysis of retinal structure in the living eye.
Proliferative diabetic retinopathy (PDR) – DR characterized by the presence of retinal neovascularization.
The early treatment diabetic retinopathy study (ETDRS) – A large study of progression and treatment of DR.
United Kingdom Prospective Diabetes Study (UKPDS) – A study that contributed to our understanding that intensive glycemic control is associated with a reduced risk of newly diagnosed retinopathy and a reduced progression of existing retinopathy in people with diabetes.
Vascular endothelial growth factor (VEGF) – A growth factor that promotes development of endothelial cells.

Background

Diabetes mellitus (DM) is a metabolic disorder characterized by sustained hyperglycemia secondary to lack or diminished efficacy of endogenous insulin. The terminology used for classification of different types of diabetes is evolving and can be a source of confusion. Traditionally, there have been two types of DM: type I diabetes and type II diabetes (these terminologies are used throughout the remainder of this article). Immune-mediated diabetes is the latest, and perhaps most descriptive, terminology applied to type I diabetes. Autoimmune destruction of insulin-producing pancreatic islet cells is postulated as instrumental in the pathogenesis of type I diabetes. Previous terminology used for type I diabetes included insulin-dependent diabetes mellitus (IDDM), and juvenile-onset diabetes. Type II diabetes is characterized by relative deficiencies of insulin and/or peripheral insulin resistance. It was previously known as non-insulin-dependent diabetes mellitus (NIDDM) or adult-onset diabetes.

DM is a common medical problem and is a major global source of morbidity and mortality. The incidence of DM is thought to be increasing throughout the world in part due to an increasing incidence of obesity and sedentary lifestyles. In the United States, it is estimated that 7.8% of the total population has DM, and it causes a vast array of long-term systemic complications which have a significant impact on both quality and quantity of life. Patients with DM have heart disease, death rates, and stroke rates that are 2–4 times higher than adults without diabetes, and DM is the leading cause of end-stage renal disease in the United States. Further, people with diabetes are more susceptible to many other illnesses and, once acquired, often have worse prognoses (e.g., pneumonia).

From an ophthalmic standpoint, DM causes numerous complications. Chief among these complications are diabetic retinopathy (DR), unstable refractions, accelerated

cataracts, rubeosis iridis, which can lead to neovascular glaucoma, cranial nerve palsies, reduced corneal sensitivity, papillopathy, and poor wound healing. The incidence of blindness is 25 times higher in patients with diabetes than in the general population. Furthermore, DR is the most common cause of blindness in patients aged 20–74 years, accounting for 12 000–24 000 new cases of blindness in the United States each year.

Risk Factors for DR

The prevalence of DR in the diabetic population increases with the duration of diabetes and patient age. Studies have shown that after 20 years of diabetes, nearly 99% of patients with type I DM and approximately 60% of patients with type II DM have some degree of DR (**Figure 1**). DR rarely develops in children younger than 10 years of age, regardless of the duration of diabetes. The risk of DR increases after puberty. Approximately 5% of type II diabetics have DR at presentation; this observation is a reflection of the typically insidious onset of hyperglycemia in type II diabetes many years before the diagnosis is firmly established.

In addition to duration of DM, other risk factors for the development of DR include poor glycemic control, the type of diabetes (type 1 more than type 2), and the presence or absence of associated conditions such as hypertension, smoking, dyslipidemia, nephropathy, and pregnancy. The Diabetes Control and Complications Trial (DCCT) and the United Kingdom Prospective Diabetes Study (UKPDS) demonstrated that intensive glycemic control is associated with a reduced risk of newly diagnosed retinopathy and a reduced progression of existing retinopathy in people with DM (type I in DCCT (**Figure 2**) and type II in UKPDS). According to the DCCT, intensive insulin therapy reduced the incidence of new cases of DR by as much as 76% compared with conventional therapy. The UKPDS found similar results in type II diabetics; each 1% point reduction in glycosylated hemoglobin was associated with a 37% reduction in development of retinopathy. Further, the UKPDS showed that control of hypertension was also beneficial in reducing progression of DR. Pregnancy is occasionally associated with rapid progression of DR; thus, women with diabetes who become pregnant require more frequent evaluation of the retina. Pregnant women without any DR are at a 10% risk of developing nonproliferative diabetic retinopathy (NPDR) during their pregnancy. Of those with preexisting NPDR, 4% progress to proliferative retinopathy (**Figure 3**).

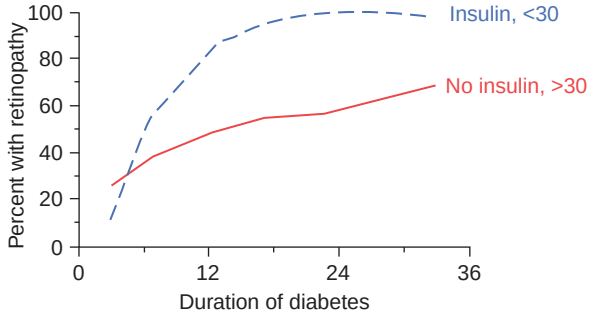

Figure 1 Incidence of diabetic retinopathy (DR) increases over time. Duration of DM is directly associated with an increased prevalence of DR in people with both type I and type II DM. The figure represents the percent of diabetic patients with retinopathy according to duration of disease in patients under the age of 30 years who were treated with insulin (primarily type I diabetics) and patients over the age of 30 years who were not treated with insulin (primarily type II diabetics). Retinopathy increased over time in both groups, affecting virtually all patients with type I diabetes by 20 years. The increased incidence in type II diabetes at 3 years is likely secondary to the difficulty in determining the exact time of onset of type II DM. Data from Klein, R., Klein, B. E., Moss, S. E., Davis, M. D. and DeMets, D. L. (1984). The Wisconsin Epidemiologic Study of Diabetic Retinopathy: III. Prevalence and risk of diabetic retinopathy when age at diagnosis is 30 or more years. *Archives of Ophthalmology* 102: 527.

Pathogenesis

The pathogenesis of DR is the current subject of intense research. It is theorized that exposure to chronic hyperglycemia results in a number of biochemical and physiologic alterations that ultimately produce retinal vascular changes and subsequent retinal injury and ischemia. The list of hematologic and biochemical abnormalities theorized to play a role in the development of DR

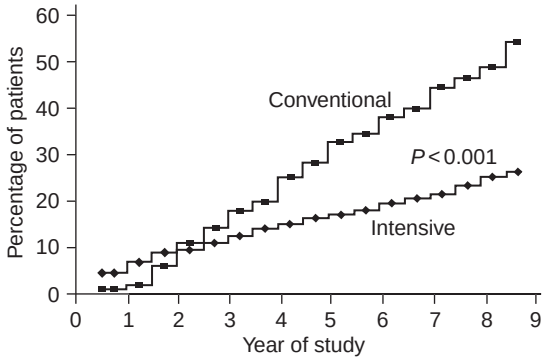

Figure 2 Intensive glycemic control slows progression of retinopathy. Cumulative incidence of progressive retinopathy in patients with type 1 diabetes and early nonproliferative retinopathy who were treated with either conventional or intensive insulin therapy for 9 years. Intensive glycemic control reduced the risk of DR progression over time by 54%, although intensive therapy was associated with transient worsening in the first year ($p < 0.001$). Data from Diabetes Control and Complications Trial Research Group (1993). The effect of intensive treatment of diabetes on the development and progression of long-term complications in insulin-dependent diabetes mellitus. *The New England Journal of Medicine* 329: 977.

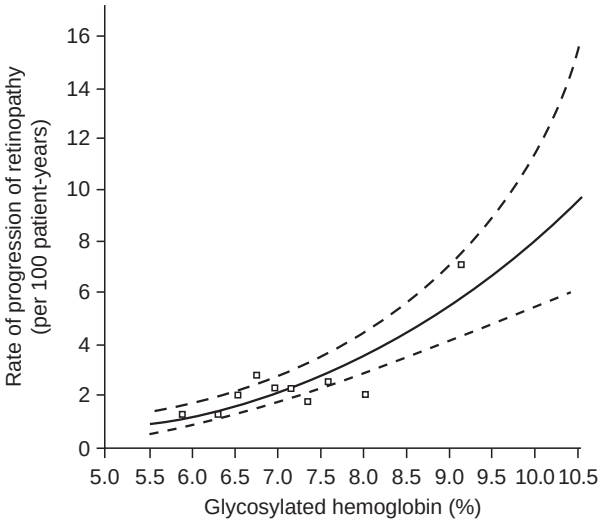

Figure 3 Progression of DR in relation to glycemic control. The figure shows the rate of progression of retinopathy in patients with type 1 diabetes according to mean glycosylated hemoglobin values (solid line). Better glycemic control was associated with slower rates of DR progression. The dashed lines represent the 95% confidence intervals. Data from Diabetes Control and Complications Trial Research Group (1993). The effect of intensive treatment of diabetes on the development and progression of long-term complications in insulin-dependent diabetes mellitus. *The New England Journal of Medicine* 329: 977.

includes the following: impairment of retinal blood vessel autoregulation, the occurrence of retinal microthrombosis and subsequent ischemia, accumulation of advanced glycosylation end products, and damage caused by reactive oxygen species. The role that growth factors (e.g., vascular endothelial growth factor (VEGF)) play in the formation of DR is discussed later. There have also been recent considerations of categorizing DR as an inflammatory disease. Trials investigating anti-inflammatory agents for prevention or treatment of DR in humans are ongoing.

Specific retinal vascular changes theorized to be instrumental in DR include the loss of pericytes, basement membrane thickening, and impaired endothelial cell function. The walls of retinal capillaries consist of endothelial cells and pericytes and are devoid of smooth muscle and elastic tissue. Endothelial cells form a single layer on a basement membrane and are linked by tight junctions that form the inner blood–retinal barrier. Pericytes are found external to the endothelial cells and have pseudopodial processes that envelop the capillary. It is believed that pericytes have contractile properties and are thought to participate in autoregulation of the microvascular capillary circulation (analogous in function to the smooth muscle found in larger arteries). The classic histologic finding of early DR in the human retina is the loss of microvascular pericytes; however, the exact mechanism by which pericytes are preferentially lost early in DR is unknown. Thickening of the retinal capillary basement membrane is another well-known lesion found in DR. In addition to basement membrane thickening, patients with DR are also found to have vacuolization and deposition of fibrillar collagen in their basement membranes. Similar to the loss of pericytes, the exact biochemical events that lead to basement membrane alterations in DR are not fully evident. Several studies implicate the sorbitol pathway in this process. The sorbitol pathway is the name given to the sequence of reactions that convert glucose to fructose involving the enzymes aldose reductase and sorbitol dehydrogenase. In this pathway, glucose is reduced first to sorbitol, which is then oxidized to fructose. However, since the latter reaction occurs slowly in many cells, sorbitol may build to high, and possibly, toxic concentrations. The toxicity of sorbitol is theorized to perhaps lead to basement membrane alterations. The final vascular change that appears to be instrumental in DR is the loss of endothelial cell function and the subsequent breakdown of the blood–retinal barrier. One possible cause of the blood–retinal barrier breakdown is opening of the tight junctions (zonulae occludentes) between adjacent microvascular endothelial cell processes. Several proteins are known to be involved with tight junction function, namely ZO-1, occluding and claudin. Studies have shown that high glucose levels appear to inhibit ZO-1 expression. Further experiments have shown reduced expression and anatomical distribution of occludin in experimental diabetes. Finally, studies have shown that intravitreal injections of the growth factor VEGF in rats increased production of nitric oxide (NO) and increased phosphorylation of ZO-1 and occludin, changes that result in increased breakdown of the blood–retinal barrier.

Advanced stages of DR are marked by the proliferation of new blood vessels. Retinal neovascularization is a devastating process that can lead to blindness in DR. Neovascularization develops through angiogenesis, in which capillaries develop from preexisting blood vessels. In DR, the regulatory mechanisms of angiogenesis can become compromised, which leads to uncontrolled endothelial cell division. On a molecular level, angiogenesis is a complicated pathway involving interplay between a number of angiogenic messengers, proteolytic enzymes, and the preexisting vessels themselves. The common final product in angiogenesis is activation of vascular endothelial cells. Several endothelial cell mitogens have been isolated and studied, including VEGF, platelet-derived growth factor (PDGF), insulin-like growth factor (IGF), basic fibroblast growth factor (bFGF), protein kinase C (PKC), antiopoietins, integrins, and ephrins. VEGF is commonly considered the most potent angiogenic factor, and some of the other molecules may act indirectly through VEGF. As the activated endothelial cells proliferate, they secrete proteolytic enzymes that degrade the parent vessel's basement

membrane as well as the extracellular matrix. Once the endothelial cells gain access to the extravascular space, they migrate and form new capillary sprouts. Mesenchymal cells are then recruited to form smooth muscle cells in arterioles and a new basement membrane is deposited to complete the process of angiogenesis. The resulting abnormal vessels lack structural integrity and are prone to leak fluid, leading to retinal edema. Further, the abnormal vessels often are associated with a fibrovascular membrane. This membrane can become adherent to both the retina and the posterior hyaloid face. As the vitreous contracts, the fibrovascular membrane can cause tractional forces on the retina, leading to retina edema, vitreous hemorrhages, retinal heterotropia, retinal tears, and tractional retinal detachments. Fortunately, the majority of DR follows a fairly predictable course; thus, screening examinations and prophylactic interventions can be implemented to reduce the devastating and potentially blinding consequences of advanced DR.

Classifications

The classification of DR is classically based on the severity of intraretinal microvascular changes and the presence or absence of retinal neovascularization. Thus, DR is divided into two main forms: nonproliferative and proliferative. NPDR is characterized by intraretinal microvascular changes which precede the proliferative phase. Proliferative diabetic retinopathy (PDR) is characterized by the presence of retinal neovascularization. These two classifications of DR (NPDR and PDR) have been useful for the analysis of treatment efficacy in the literature and serve as general indicators for treatment strategies. However, it should be noted that an individualized approach to the treatment of DR is prudent, as every patient with DR has a unique combination of findings, symptoms, and rate of progression.

Nonproliferative Diabetic Retinopathy

The retinal microvascular changes found in NPDR are, by definition, limited to the confines of the retina and do not extend beyond the innermost retinal layer – the internal limiting membrane. Characteristic findings in NPDR include microaneurysms, retinal hemorrhages, retinal edema, hard exudates, cotton-wool spots (CWSs), areas of capillary nonperfusion, intraretinal microvascular abnormalities (IRMAs), and venous beading. NPDR primarily causes visual decline through either capillary nonperfusion leading to macular ischemia, or through increased vascular permeability, resulting in macular edema.

The first visible sign of NPDR is the retinal capillary microaneurysm. Clinically, microaneurysms are identified as red dots from 15 to 60 μm in diameter (**Figure 4**).

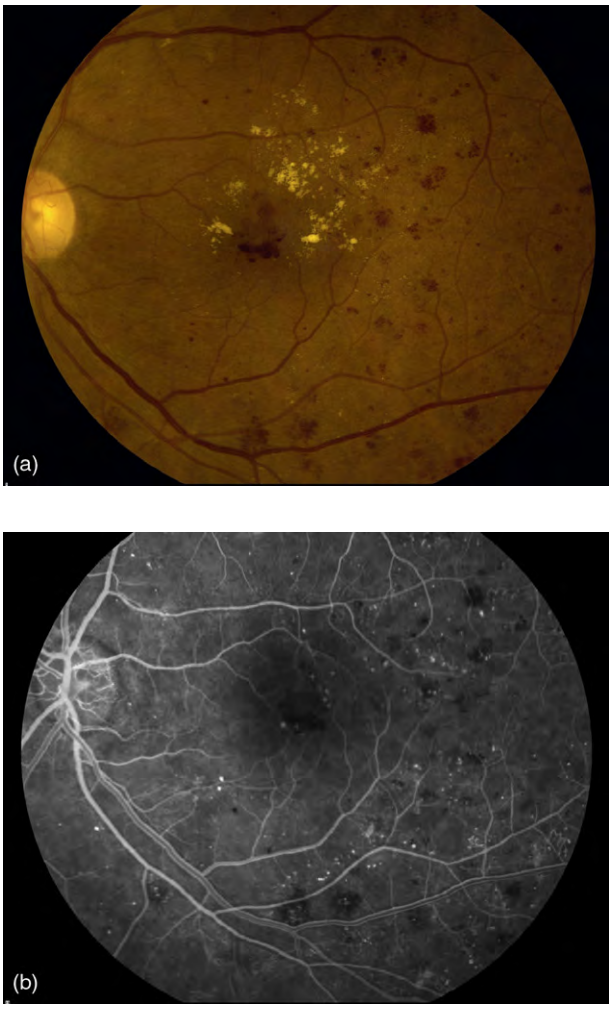

Figure 4 (a) Severe non-proliferative diabetic retinopathy. Color fundus photograph and a red-free fundus photograph of the left eye of a patient with severe NPDR. The photographs demonstrate numerous diffusely scattered microaneurysms, dot-blot hemorrhages, and hard exudates. (b) Microaneurysms and retinal hemorrhages. Arteriovenous phase fluorescein angiogram image of the same left eye (a). The microaneurysms demonstrate marked early hyperfluorescence, whereas the retinal hemorrhages block fluorescein and thus appear hypofluorescent.

On histologic examination, microaneurysms are hypercellular saccular outpouchings of the capillary wall. They are often found in relation to areas of capillary nonperfusion. Postulated mechanisms behind microaneurysm formation include the release of vasoproliferative factors (e.g., VEGF) with endothelial cell proliferation, weakness of the capillary wall secondary to the loss of pericytes, abnormalities of the adjacent retina, and increased intracapillary pressure. Microaneurysms can be differentiated from punctate retinal hemorrhages, which are also seen in DR, through fluorescein angiography. Microaneurysms will demonstrate marked early hyperfluorescence against the darker choroidal background; whereas, retinal hemorrhages

will block fluorescein and thus appear hypofluorescent (Figure 4(b)). Late fluorescein angiography frames often demonstrate leakage emanating from microaneurysms as a result of the breakdown in the blood–retinal barrier. Individual microaneurysms typically appear and disappear over time. Microaneurysms often foreshadow progression of DR as an increase in microaneurysms often is associated with progression of DR.

The retinal hemorrhages most commonly seen in NPDR include both dot-blot hemorrhages and retinal nerve fiber layer hemorrhages. Dot-blot hemorrhages are punctate, intraretinal hemorrhages that arise from the venous end of retinal capillaries and are located within the compact middle layers of the retina. These compact, vertically aligned, middle retinal layers confer upon the retinal hemorrhages their characteristic red, dot-blot appearance (Figure 4). Retinal nerve fiber layer hemorrhages arise from the more superficially located precapillary arterioles. The horizontal alignment of the retinal nerve fiber layer gives these hemorrhages their classic flame shape.

As discussed previously, another consequence of DR is excessive vascular permeability, which can result in retinal edema, usually in the macular region. Retinal edema is often accompanied by macular hard exudates, which are lipid deposits that accumulate in association with lipoprotein leakage from decompensated endothelial tight junctions. On clinical examination, hard exudates are yellowish intraretinal deposits often found at the border of edematous and nonedematous retinal tissue (Figure 4). Macular edema initially accumulates between the outer plexiform and inner nuclear layers. With chronic edema, the entire thickness of the retina becomes edematous and can assume a cystoid appearance. Retinal thickening secondary to macular edema is best detected by indirect slit-lamp biomicroscopy; in addition, optical coherence tomography (OCT), can be used to detect thickening and may be used to assess response to therapy (Figure 5).

CWSs, also known as soft exudates, may often be found in NPDR. CWSs are composed of accumulations of neuronal debris within the retinal nerve fiber layer. These result from disruption and stasis of axoplasmic flow. As CWSs heal, debris is removed from the nerve fiber layer by autolysis and phagocytosis. Clinically, CWSs are seen as yellowish, fluffy superficial lesions which obscure the underlying blood vessels. Interestingly, CWSs are only found in the postequatorial retina where the nerve fiber layer is of sufficient thickness to allow visualization of the CWSs.

As NPDR progresses, it can lead to the obliteration of retinal capillaries. These areas of capillary nonprofusion are seen on fluorescein angiography as patches of hypofluorescence. Adjacent to areas of nonperfusion, tortuous, hypercellular vessels often develop. It is difficult to determine whether these vessels are actually dilated preexisting capillaries or whether they represent new vessels forming within the retina. These vessels have been

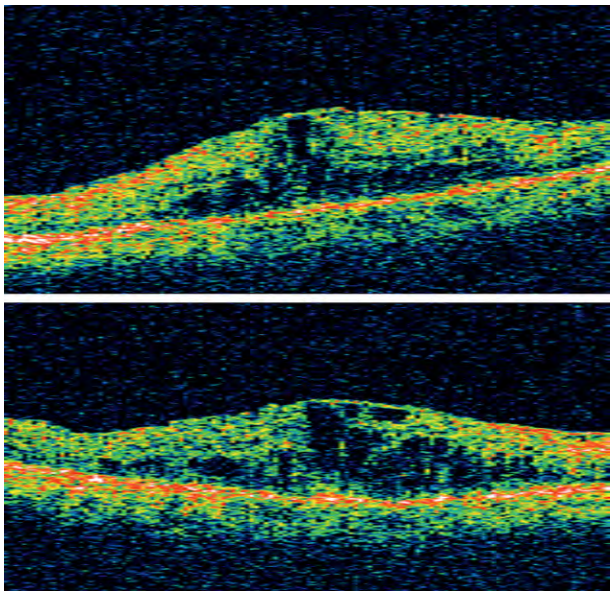

Figure 5 Macular edema secondary to diabetic retinopathy. OCT (two images) demonstrating retinal thickening and cystoid intraretinal spaces created by extensive capillary leakage and secondary macular edema in a patient with severe NPDR.

referred to as IRMAs, a term which encompasses both possibilities. The main distinguishing features of IRMAs are their intraretinal location, failure to cross major retinal blood vessels, and absence of leakage on flouroscein angiography. As areas of capillary nonperfusion become extensive, it is common to see an increase in intraretinal hemorrhages or dilated segments of retinal veins (referred to as venous beading). The degree of retinal capillary nonperfusion is directly associated with the severity of IRMAs, intraretinal hemorrhages, and venous beading.

NPDR is further categorized into four levels of severity: mild, moderate, severe, and very severe (Table 1). The clinical extent of microaneurysms, retinal hemorrhages, venous beading, and IRMA determine the level of severity of nonproliferative disease. Mild and moderate NPDR are characterized by relatively few microaneurysms and intraretinal hemorrhages and only minimal venous changes or IRMA. Severe NPDR is characterized by diffuse intraretinal hemorrhages, two quadrants of venous beading, or moderate IRMA in at least one quadrant. If any two of these features are present, the retinopathy is considered to be very severe NPDR. The Early Treatment Diabetic Retinopathy Study (ETDRS) found that severe NPDR had a 15% chance of progression to high-risk PDR within 1 year. Very severe NPDR had a 45% chance of progression to high-risk PDR within 1 year.

Macular Edema

Macular edema is the most common cause of visual impairment in patients with NPDR. Due to the

Table 1 Classification of diabetic retinopathy

Nonproliferative diabetic retinopathy (NPDR)
Mild NPDR: At least one microaneurysm Criteria not met for other levels of DR
Moderate NPDR: Hemorrhage/microaneurysm ≥standard photograph #2A or Soft exudates (cotton-wool spots), venous beading, and intraretinal microvascular abnormalities definitely present Criteria not met for severe NPDR, very severe NPDR, or PDR
Severe NPDR: Hemorrhage/microaneurysm ≥standard photograph #2A in all four quadrants or Venous beading in at least two quadrants or Intraretinal microvascular abnormalities ≥standard photograph #8A in at least one quadrant
Very servere NPDR: Any two or more of criteria for severe NPDR Criteria not met for PDR
Proliferative diabetic retinopathy (PDR)
Early PDR: New vessels Criteria not met for high-risk PDR
High-risk PDR: Neovascularization of the disk ≥1/4 to 1/3 disk area or Neovascularization of the disk and vitreous or preretinal hemorrhage or Neovascularization elsewhere ≥1/2 disk area and vitreous or preretinal hemorrhage
Advanced PDR: Posterior fundus obscured by preretinal or vitreous hemorrhage or Center of macula detached

breakdown of the blood–retinal barrier, leakage of fluid and plasma constituents leads to retinal edema (**Figure 6**). If the retinal edema threatens the center of the fovea, there is a higher risk of visual loss. In the ETDRS, the 3-year risk of moderate visual loss was 32% (moderate visual loss was defined as a doubling of the initial visual angle or a decrease of three lines or more on a logarithmic visual acuity chart). The ETDRS investigators classified macular edema by its severity. More specifically, macular edema was defined as clinically significant macular edema (CSME) if any of the following features were present: (1) thickening of the retina at or within 500 µm of the center of the macula; (2) hard exudates at or within 500 µm of the center of the macula, if associated with thickening of the adjacent retina; or (3) a zone of thickening larger than one disk area if located within one disk diameter of the center of the macula (**Table 2**). Many of the current treatment paradigms for the management of diabetic macular edema are derived from the ETDRS. The ETDRS demonstrated that eyes with CSME benefited from focal argon laser photocoagulation treatment when compared to untreated eyes in a control group. Furthermore, focal argon laser photocoagulation treatment for CSME reduced the risk of moderate visual loss, increased the chance of visual improvement, and was associated with only minor losses of visual field. Specifically, in patients with CSME involving the center of the macula, focal treatment reduced moderate visual loss by 60% after 3 years of follow-up. In patients with less than CSME, little difference was noted between the untreated and treated groups during the first 2 years of follow-up, after which there was a trend toward less frequent visual loss in the treated group.

Treatment patterns regarding CSME continue to evolve. In patients with refractory CSME, intravitreal administrations of corticosteroids have been shown to be beneficial. Intravitreal anti-VEGF agents have also been shown to improve CSME. Currently, several trials investigating corticosteroid use as well as anti-VEGF agents in the treatment of CSME are underway. Pars plana vitrectomy and detachment of the posterior hyaloid may also be useful for treating CSME. Surgical intervention may prove particularly beneficial when there is evidence of posterior hyaloidal traction and diffuse macular edema.

Proliferative Diabetic Retinopathy

As the degree of retinal ischemia increases, extensive hypofluorescent areas representing retinal nonperfusion are seen on fluorescein angiography. Eventually neovascularization may develop in an attempt to revascularize hypoxic retinal tissue. This neovascularization is the hallmark of PDR. It has been estimated that over one-quarter of the retina has to be nonperfused before PDR develops. PDR affects 5–10% of the diabetic population (**Figure 7**). Type I diabetics are at particular risk for PDR with an incidence of about 60% after 30 years. Although new vessels may arise from anywhere in the retina, neovascularization is particularly common on the optic disk itself (this location is termed new vessels on disk, or NVD). NVD is defined as neovascularization on or within one disk diameter of the optic nerve head. It can be differentiated from normal vessels by utilizing fluorescein angiography, which demonstrates profuse leakage in NVD but not in normal vasculature (**Figure 8**). Neovascularization of the retina found greater than one disk diameter from the optic nerve head is termed new vessels elsewhere, or NVE. NVE typically is found along the course of the major retinal vessels. The rate of growth of NVD or NVE is extremely variable. In some patients, neovascularization may show little change over many months, while in others definite changes in neovascularization may be seen in as little as 1–2 weeks. As neovascularization

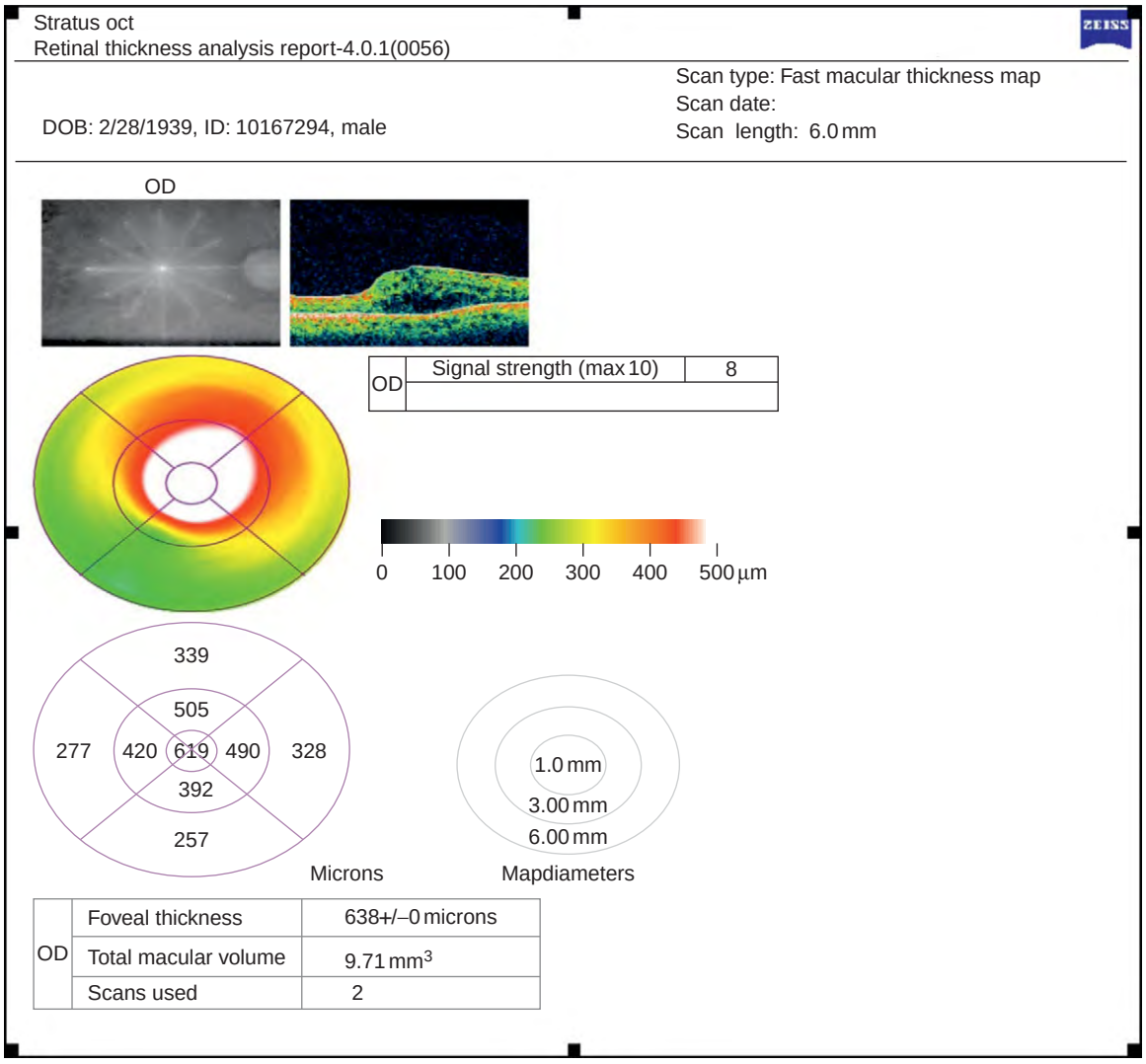

Figure 6 OCT demonstrating CSME. OCT of a diabetic patient with CSME. The patient has marked thickening of the central macula secondary to CSME. The OCT retinal cross section reveals cystic intraretinal and subretinal changes.

Table 2 Clinically significant macular edema as defined by ETDRS

Thickening of the retina ≤500µm from the center of the macula
or
Hard exudates and adjacent retinal thickening ≤500 µm from macular center
or
Zone of retinal thickening at least 1 disk area in size located <1 disk diameter from the center of the macula

progresses, a white fibrous membrane composed of fibrocytes and glial cells accompanies the growth of the new vessels. As mentioned previously, this membrane can become adherent to both the retina and the posterior hyaloid face. As the vitreous contracts, the fibrovascular membrane can cause tractional forces on the retina, leading to retina edema, vitreous hemorrhages, retinal heterotropia, retinal tears, and tractional retinal detachments. The main therapy used to prevent the devastating complications of PDR is the application of thermal laser photocoagulation in a panretinal pattern in order to induce neovascular regression. Numerous panretinal photocoagulation (PRP) application protocols exist.

The classification of PDR is determined by the location and size of the neovascularization, along with the presence or absence of vitreous hemorrhage (Table 1). The Diabetic Retinopathy Study (DRS) defined high-risk PDR as any one of the following: (1) mild NVD with vitreous or preretinal hemorrhage, (2) NVD $\geq$ 1/4 to 1/3 disk area with or without vitreous hemorrhage, (3) NVE $\geq$ 1/2 disk area with vitreous or preretinal hemorrhage. The DRS was designed to evaluate the effectiveness of photocoagulation for treating diabetic retinopathy. As complications from PDR can result in severe vision loss (SVL), the primary outcome measured in the DRS was SVL, defined as visual acuity of less than 5/200. The DRS found that PRP

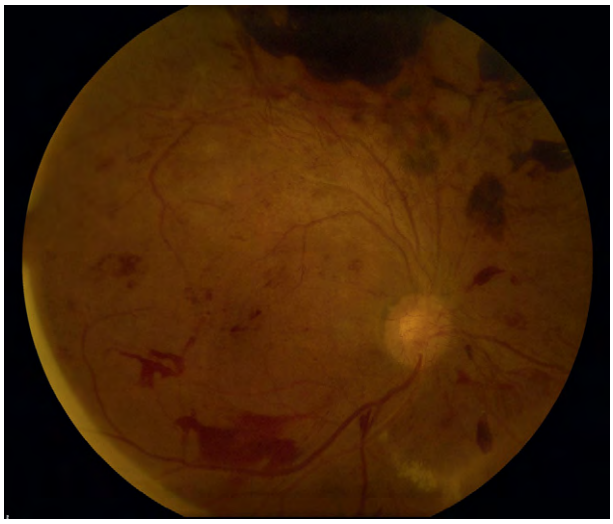

Figure 7 High-risk PDR. Color fundus photo of the right eye of a patient with high-risk PDR. Patient has significant NVD and NVE. This patient also has several areas of preretinal hemorrhages. CWSs can be seen inferior to the optic disk.

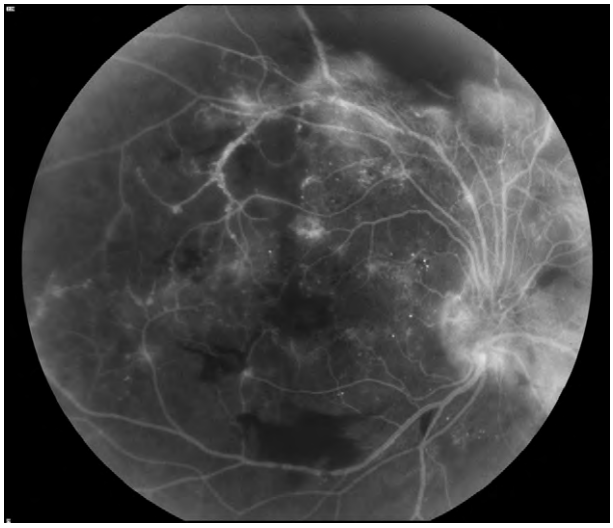

Figure 8 Leakage of NVD and NVE on fluorescein angiography. Fluorescein angiogram of the same patient seen in **Figure 7**. This patient has developed severe NVD and NVE causing significant hyperfluorescences secondary to profuse vascular leakage.

produced a 50% reduction in the rates of SVL in eyes treated with PRP compared to untreated control eyes during a follow-up of over 5 years. Treated eyes with high-risk PDR achieved the greatest benefit; thus, the DRS recommended prompt PRP treatment of eyes with high-risk PDR because this group had the highest risk of SVL.

Surgical management of PDR can be employed in patients with severe, persistent vitreous hemorrhages, progressive tractional retinal detachments, combined tractional and rhegmatogenous retinal detachments, and dense macular preretinal hemorrhages. Investigation into the use of anti-VEGF agents in the treatment of PDR is ongoing.

Screening for Diabetic Retinopathy

Proper screening for DR is critical as diabetic patients often do not experience visual disturbances until late in the disease course. Screening examinations allow for the prompt diagnosis and treatment of DR before the development of potentially blinding complications. In patients with type I diabetes, initiating screening examinations 3–5 years after diagnosis is recommended. In patients with type II diabetes, an initial examination upon diagnosis is recommended. Pregnant women with preexisting diabetes should undergo screening early in the first trimester. More frequent retinal evaluations are subsequently required during pregnancy and in the early postpartum period.

See also: Angiogenesis in the Eye; Pathological Retinal Angiogenesis; Stability and Functional Integrity of New Blood Vessels; Vessel Regression.

Further Reading

Aiello, L. M. (2003). Perspectives on diabetic retinopathy. *American Journal of Ophthalmology* 136: 122–135.

Centers for Disease Control and Prevention (2007). *National Diabetes Fact Sheet*. http://www.cdc.gov/diabetes/pubs/pdf/ndfs_2007.pdf (accessed June 2009).

Diabetes Control and Complications Trial Research Group (1993). The effect of intensive treatment of diabetes on the development and progression of long-term complications in insulin-dependent diabetes mellitus. *The New England Journal of Medicine* 329: 977–986.

Diabetes Control and Complications Trial Research Group (1995). Progression of retinopathy with intensive versus conventional treatment in the Diabetes Control and Complications Trial. *Ophthalmology* 102: 647–661.

Diabetic Retinopathy Study Research Group (1981). Photocoagulation treatment of proliferative diabetic retinopathy: clinical application of Diabetic Retinopathy Study (DRS) findings. DRS report 8. *Ophthalmology* 88: 583–600.

Early Treatment Diabetic Retinopathy Study Research Group (1987). Treatment techniques and clinical guidelines for photocoagulation of diabetic macular edema. ETDRS report 2. *Ophthalmology* 94: 761–774.

Early Treatment Diabetic Retinopathy Study Research Group (1991). Early photocoagulation for diabetic retinopathy. ETDRS report 9. *Ophthalmology* 98: 766–785.

Early Treatment Diabetic Retinopathy Study Research Group (1995). Focal photocoagulation treatment of diabetic macular edema. Relationship of treatment effect to fluorescein angiographic and other retinal characteristics at baseline. ETDRS Report 19. *Archives of Ophthalmology* 113: 1144–1155.

Kanski, J. J. (2007). *Clinical Ophthalmology*, 6th edn. Philadelphia, PA: Butterworth Heinemann-Elsevier.

Klein, R., Klein, B. E., Moss, S. E., Davis, M. D., and DeMets, D. L. (1984a). The Wisconsin Epidemiologic Study of Diabetic Retinopathy: II. Prevalence and risk of diabetic retinopathy when age at diagnosis is less than 30 years. *Archives of Ophthalmology* 102: 520–526.

Klein, R., Klein, B. E., Moss, S. E., Davis, M. D., and DeMets, D. L. (1984b). The Wisconsin Epidemiologic Study of Diabetic Retinopathy: III. Prevalence and risk of diabetic retinopathy when age at diagnosis is 30 or more years. *Archives of Ophthalmology* 102: 527–532.

Preferred Practice Patters Committee (2003). Retina Panel. *Diabetic Retinopathy.* San Francisco: American Academy of Ophthalmology; November 2003.

Ryan, S. J., Hinton, D. R., Schachat, A. P., and Wilkinson, C. P. (2006). Retina. 4th edn. Philadelphia, PA: Mosby-Elsevier.

United Kingdom Prospective Diabetes Study Group (1998a). Intensive blood-glucose control with sulphonylureas or insulin compared with conventional treatment and risk of complications in patients with type 2 diabetes. UKPDS 33. *Lancet* 352: 837–853.

United Kingdom Prospective Diabetes Study Group (1998b). Tight blood pressure control and risk of macrovascular and microvascular complications in type 2 diabetes. UKPDS 38. *British Medical Journal* 317: 703–713.

UpToDate (2008). *Prevention and treatment of diabetic retinopathy*. http://www.uptodate.com/online/content/topic.do?topicKey=diabetes/12336&selectedTitle=1~90&source=search_result (accessed June 2009).

Retinopathy of Prematurity

M E Hartnett, University of North Carolina, Chapel Hill, NC, USA

Glossary

Aggressive posterior retinopathy of prematurity (APROP) – Severe ROP manifesting at young ages in zone 1 with flat neovascularization. Outcomes may be poor with conventional management.
Avascular retina – Retina that lacks blood vessel growth in the inner capillary plexus.
Intravitreous neovascularization – Endothelial budding or blood vessels that grow above the inner limiting membrane of the neurosensory retina into the vitreous.
Oxygen-induced retinopathy – Includes a number of models of recently born animals of species that complete retinal vascular development after birth. Exposure to oxygen stresses varies depending on the model but shares the features of first avascular retina followed by intravitreous neovascularization.
Peripheral severe ROP (PSROP) – It refers to zone II, stage 2–3 ROP, plus disease, in this article.
Plus disease – A feature of severe ROP, it refers to the dilation and tortuosity of retinal arterioles and veins.
Postgestational age – The age measured in weeks that is the sum of the gestational age (age of preterm infant from conception or last menstrual period) and the chronologic age (age since the birth of the infant). For example, a 24-week gestational age infant who was born 16 weeks ago would have a postgestational age of 40 weeks. Similar terms used include postmenstrual age, postconceptual age, or corrected age.
Retinal detachment – A fluid develops between the photoreceptor outer segments and the retinal pigment epithelium. A traction retinal detachment occurs by vitreous tractional forces, a rhegmatogenous retinal detachment because of a break in the retina, and a serous retinal detachment from exudation often as a result of inflammation or leaky vessels, and is sometimes seen after treatment for severe ROP.

Clinical Background

Epidemiology

The Institute of Medicine reported that preterm births were up 30% from 1981 and now account for 12.5% of all births in the US. Furthermore, developing countries are witnessing an increase in retinopathy of prematurity (ROP); therefore, ROP has now become a leading cause of childhood blindness worldwide. A report from a national registry of children in the US (Babies Count) found that ROP was the earliest cause of visual impairment and one of the three most prevalent conditions to cause visual impairment along with cortical visual impairment and optic nerve hypoplasia. ROP of any stage affects approximately 16 000 infants yearly in the US. Most early stages of ROP resolve, but about 1100 infants require treatment. Even with treatment, blindness occurs in 550 infants per year. In the US, ROP is seen more commonly in Caucasians than African-Americans, but once severe ROP occurs, the outcomes appear similar. Asians also have an increased risk of ROP. ROP has been reported in preterm infants of larger birth weight and older gestational ages in developing nations compared to those in the US, possibly because of variations in ethnic groups, regulation and monitoring of oxygen delivery, and the availability of prenatal care.

Clinical Classification of ROP

Based on the International Classification of ROP (ICROP), it is characterized by several parameters: zone, stage, extent of stage, and the presence of plus disease.

The zone of ROP is the retinal area supplied by the retinal vasculature and is an indicator of the extent of retinal vascular development (**Figure 1(a)**). Zone I is the smallest, having the largest area of avascular retina. Zone II has a greater area of retinal vascularization than zone I, and less than zone III. When vascularization completely extends to the ora serrata, it is termed complete vascularization. The risk of a poor visual outcome is greatest when severe ROP occurs in zone I (**Figure 1(b)**) and is still substantial in zone II. The risks of severe ROP and poor vision are rare when retinal vascularization extends into zone III. There are five stages of ROP. Stages 1 through 3 are the acute forms of ROP and are named for the appearance of the retina at the junction of vascular and avascular retina. A line (stage 1) or ridge (stage 2, **Figure 2(a)**) can often regress and vascularization of the previously avascular retina can occur. Stage 3 ROP has intravitreous neovascularization, a feature of severe ROP (**Figure 2(b)**). Stages 4 (**Figure 2(c)**; also see **Figures 6(a)** and **5** (**Figures 2(d)** and **2(e)**) define partial or complete retinal detachment, respectively, and are associated with vitreous and fibrovascular changes. The extent of ROP indicates the number of clock hours of a stage. Plus disease

is the presence of dilated and tortuous retinal vessels in two or more quadrants around the optic nerve and is a feature of severe ROP (Figure 3).

There is a useful distinction to note between retinal drawings and images of dissected retinal flat mounts. The retina covers the inner sphere of the eyeball and, when dissected, must be cut with relaxing incisions in order to flatten it onto a microscope slide. The result is a clover-leaf appearance (Figure 4(a)). However, clinicians and surgeons represent the retina as a round clock face and use clock hours to describe the location of pathologic features on the retina determined in clinical examinations (Figure 4(b)).

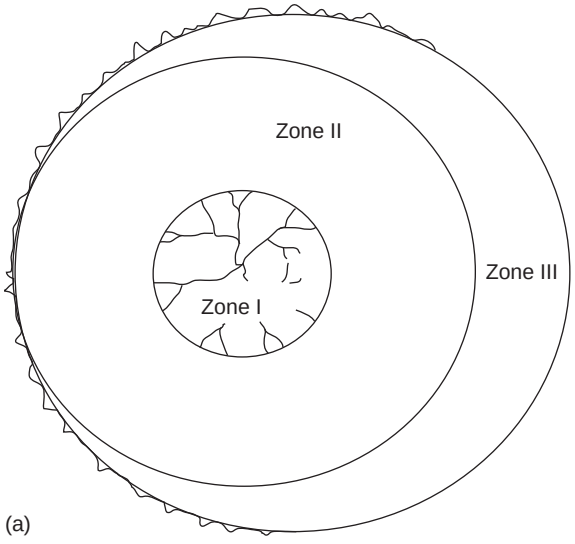

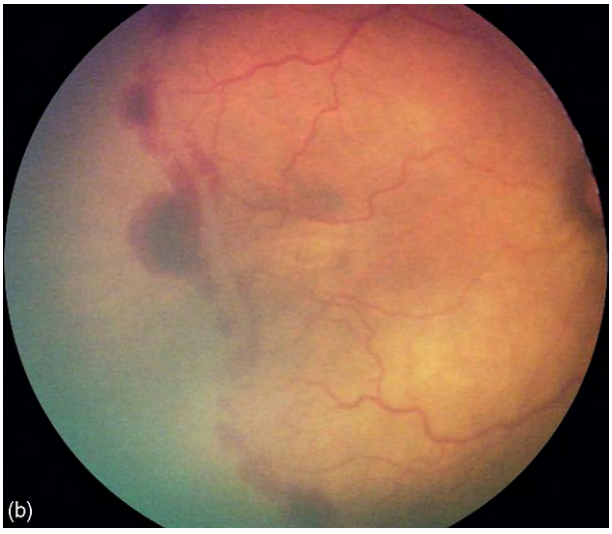

Figure 1 (a) Retinal drawing of left eye showing vascularization into zone I and the areas of the retina that would encompass zone II or zone III. (b) Image taken with wide-angle viewing system (Retcam, Clarity) of the right eye of an infant with zone I ROP (optic nerve barely visible at right of image); Courtesy Sarah Moyer, CRA, OCT-C.

Management of ROP

Based on the American Academy of Pediatrics and American Academy of Ophthalmology, infants born at or younger than 30 weeks gestational age or less than 1500 g birth weight are screened for retinal vascular development

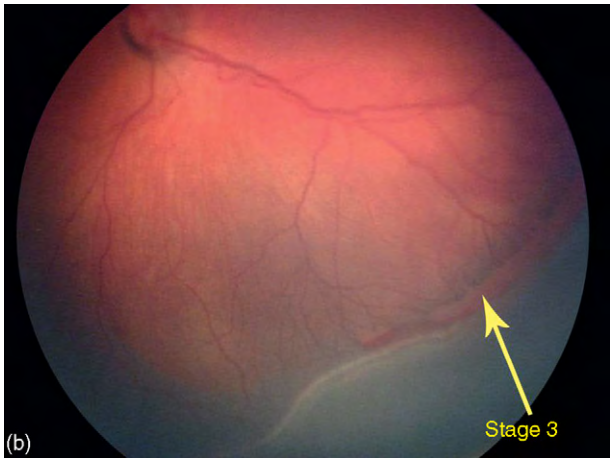

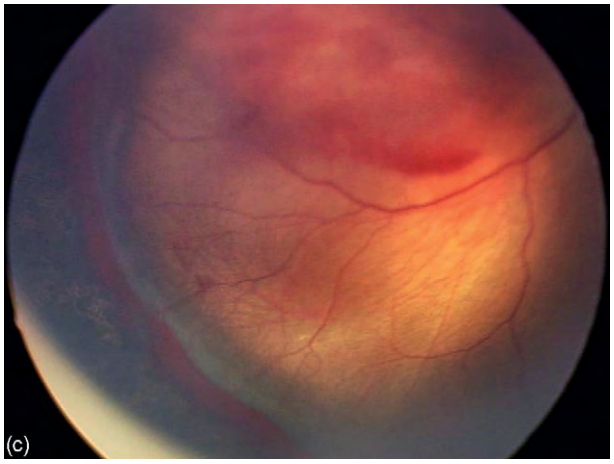

Figure 2 (Continued)

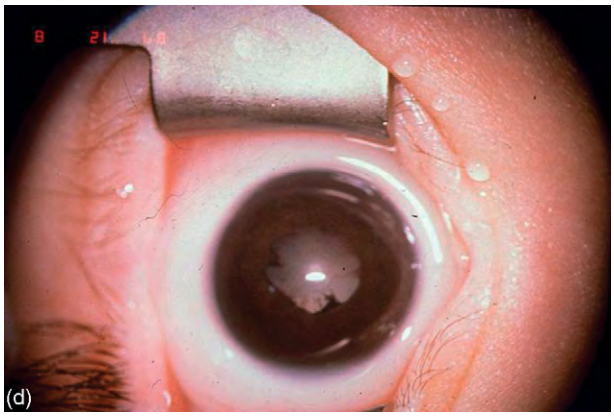

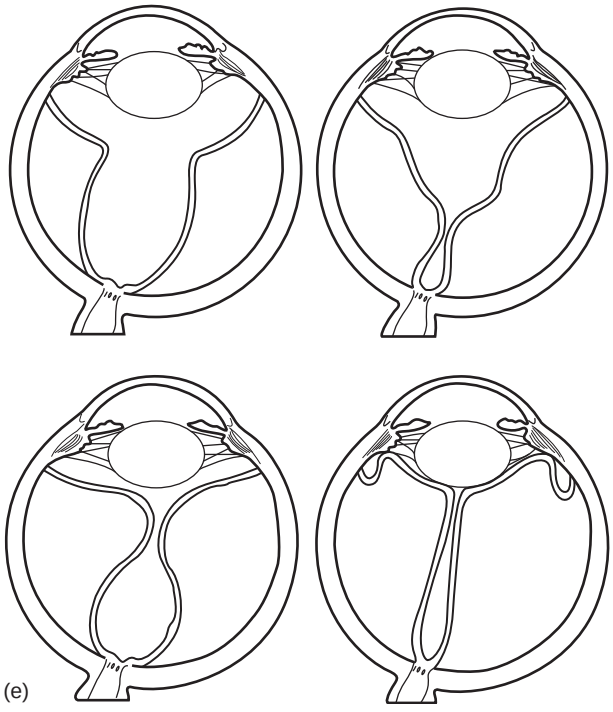

Figure 2 Images taken with wide-angle viewing system (Retcam, Clarity) of infant left eyes with (a) stage 2 ROP with early ridge and (b) stage 3 ROP with areas of intravitreous neovascularization (arrow) and hemorrhage adjacent to avascular retina (3–5 o'clock in image). Images of infant right eye with (c) early stage 4A ROP and (d) stage 5 ROP showing total retinal detachment with white pupil. (e) Diagram showing cross section of possible retinal appearances in stage 5 ROP; Figures 2(a), 2(b), and 2(c) courtesy Sarah Moyer, CRA, OCT-C. **Figure 2(e)** from Schepens' Retinal Detachment and Allied Diseases, 2nd edn (eds. Schepens, Hartnett, and Hirose) copyright 2000. Butterworth-Heinemann, Boston, MA: Figure 26-19, p. 534.

and the presence of ROP. The screening examination is performed 4–6 weeks after birth (chronologic age) or at 31 weeks postgestational age, whichever is older. (The postgestational age is the gestational age + chronologic age from birth in weeks and is similar in meaning to postmenstrual, postconceptual, or corrected ages). At any

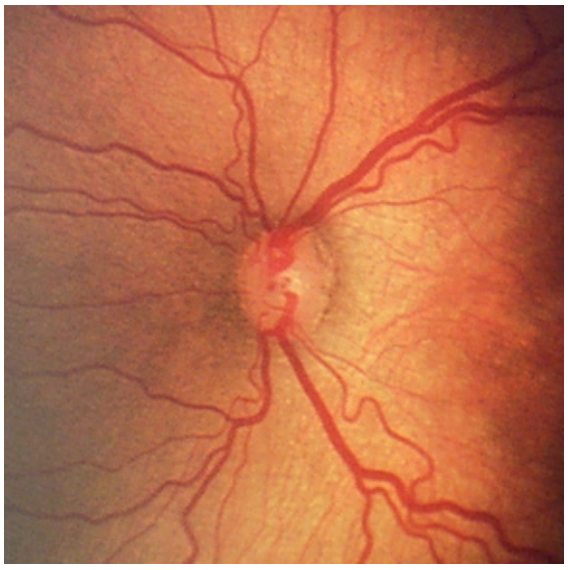

Figure 3 Plus disease (dilated and tortuous vessels in all four quadrants around optic nerve) of right eye in infant with severe ROP; Courtesy Sarah Moyer, CRA, OCT-C.

examination, the risk of a bad outcome depends on the presence of plus disease or stage 3 ROP (both features of severe ROP). Severe ROP develops at about 35–37 weeks postgestational age, regardless of the gestational age or birth weight of the infant.

At the screening examination, the extent of retinal vascular development is determined (i.e., the zone of ROP), along with the presence and stage of ROP and presence of pre-plus or plus disease. (Pre-plus is less severe than plus disease and alerts the clinician to follow the infant closely.) If ROP is not severe, follow-up examinations are performed until full vascularization of the retina occurs or until severe ROP develops, at which time the treatment for acute neovascular ROP is performed.

Treatment of ROP

Acute neovascular stages

Based on the Cryotherapy for Retinopathy of Prematurity (CRYO-ROP) and Early Treatment for Retinopathy of Prematurity (ETROP) studies, the treatment for ROP is strongly considered for infants with type 1 prethreshold ROP and almost always performed for infants with threshold ROP (**Table 1**). Laser is preferred to cryotherapy because it causes less inflammation, is less destructive, and is less often associated with myopia. The laser is applied to the peripheral avascular retina (**Figure 5**). Infants are then followed up weekly for regression of severe ROP or for the development of progressive stage 4 ROP.

Fibrovascular stages/retinal detachment

Stage 4 ROP refers to partial retinal detachment and develops as a result of fibrovascular changes and

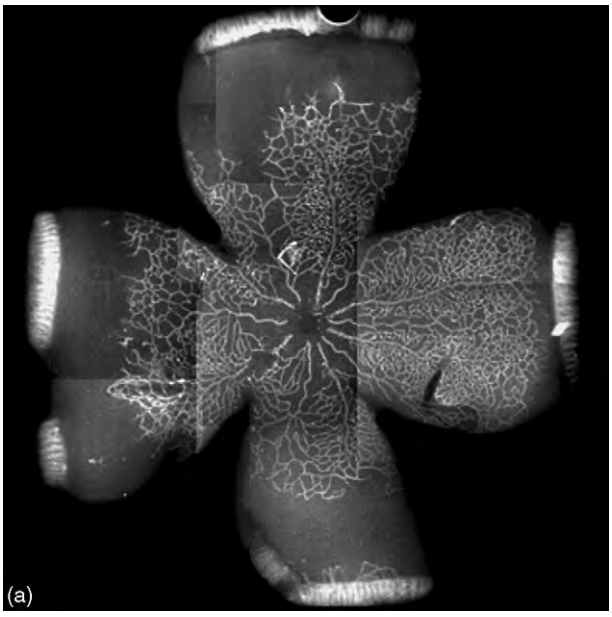

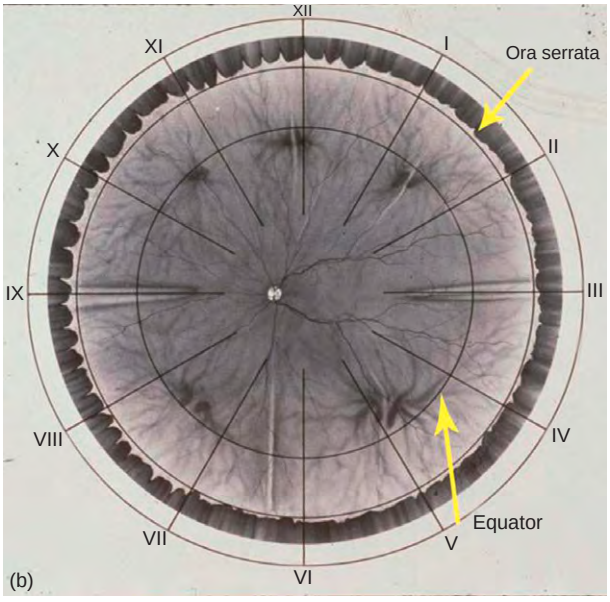

Figure 4 (a) Retinal flat mount stained with Alexa Fluor 568 conjugated isolectin B4 lectin (lectin-B4) to demonstrate vasculature from postnatal day 14 rat pup from the rat 50/10 oxygen-induced retinopathy model. (b) Artist's drawing of retina with clock hour delineations, often used clinically to localize regions of pathology on the retina. Innermost circle at vortex vein ampullae indicates equator of the globe; middle circle indicates ora serrata; and outermost circle indicates pars plana region in adult.

vitreoretinal traction that particularly occur at the junction of vascular and avascular retina and optic nerve to lead to retinal detachment (Figure 6(a)). The timing of the development of stage 4 ROP is often between 37 and 44 weeks postgestational age and represents a change

Table 1 Definitions of threshold and type 1 prethreshold retinopathy of prematurity

Threshold ROP (CRYO-ROP) (risk of unfavorable outcome approaches 50%)	Type 1 prethreshold (risk of unfavorable outcome is ≥15% – ETROP)
Zone I or II, stage 3 (5 contiguous or 8 total clock hours with plus disease*)	Zone I, any stage with plus disease*
	Zone I, stage 3 without plus disease*
	Zone II, stage 2 or 3 with plus disease*

CRYO-ROP – Cryotherapy for Retinopathy of Prematurity Study.
ETROP – Early Treatment for Retinopathy of Prematurity.
*The ETROP recognized plus disease as two quadrants of dilated and tortuous vessels whereas CRYO-ROP defined it as four quadrants.

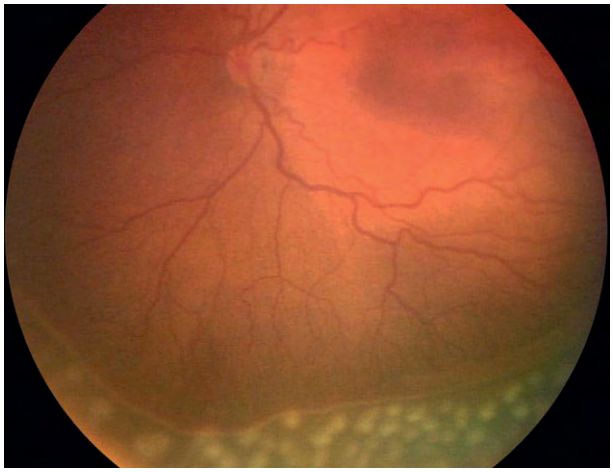

Figure 5 Type 1 prethreshold ROP (zone II, stage 2 severe ROP) after laser; it shows white spots from recently delivered laser to avascular retina and skipped areas between laser spots that will need to be filled in with laser in the left eye.

from neovascular to fibrovascular changes. Once progressive stage 4 ROP is diagnosed, surgery, preferably with a lens-sparing vitrectomy (Figure 6(b)), is performed to release vitreous tractional forces that detach the retina. The main forces addressed are those around the optic nerve, between the ridge and anterior aspect of the eye and lens, between the ridge and optic nerve, between the ridge and ora serrata, and from ridge to ridge (Figure 6(b)). The retina then reattaches in the postoperative period (Figure 6(c)), although the ridge and pulled-up retina often persist. Occasionally, a scleral buckle is performed, often when a break, that is, rhegmatogenous component, is present.

The decision to operate must be carefully considered in the preterm infant eye because there are surgical difficulties that make operating on an infant eye different from operating on an adult one. The infant eye is about two-thirds the diameter of the adult eye and the region of safe

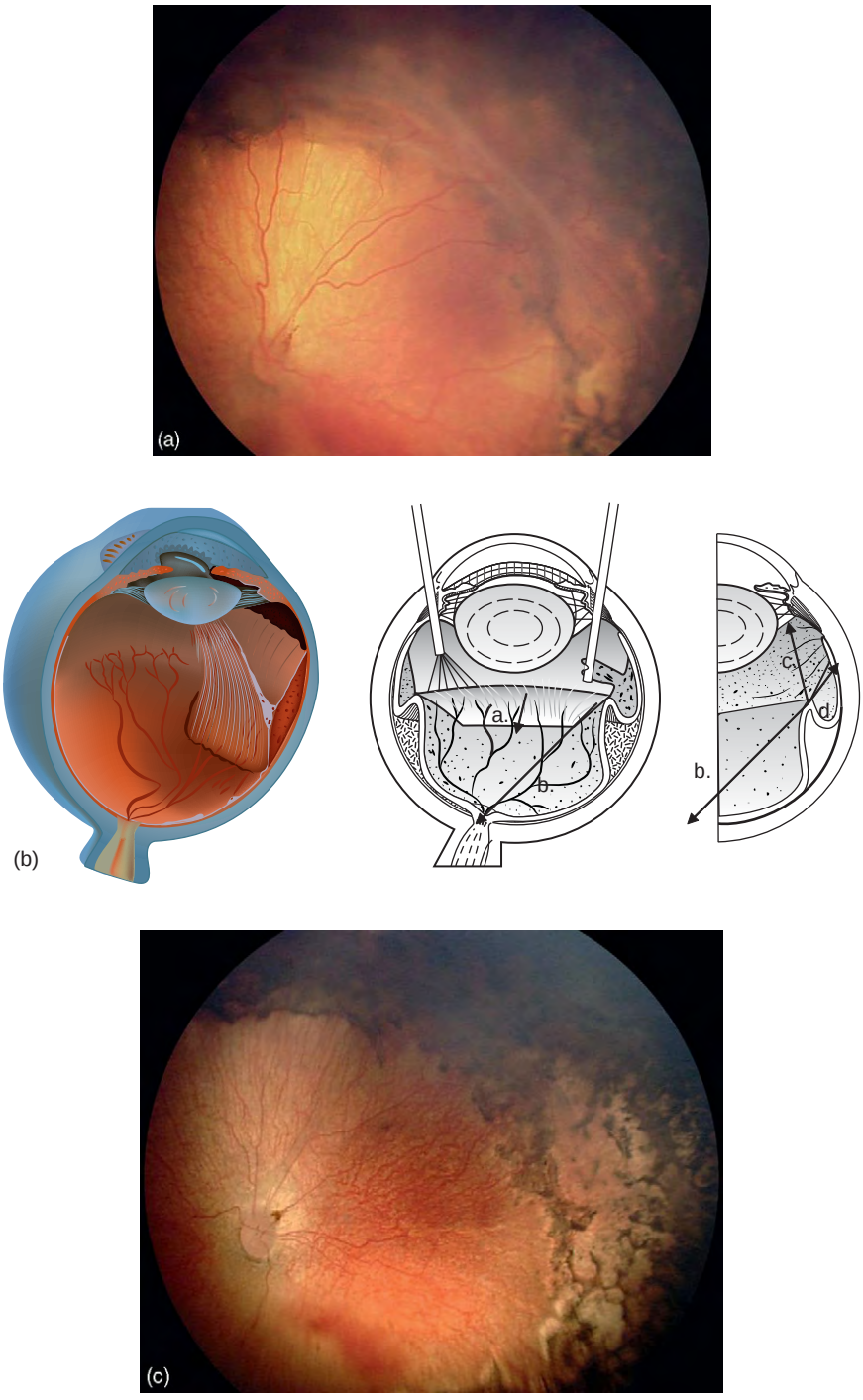

Figure 6 Image taken with wide-angle viewing system (Retcam, Clarity) of infant left eyes with (A) stage 4B ROP showing superior and temporal region of ridge with incorporated retinal detachment and retinal detachment extending posteriorly toward the optic nerve. Pigmented laser spots are in the peripheral region of avascular retina. Focus is on the retinal detachment posterior to the ridge; therefore ridge, which is more anterior in the eye, and optic nerve, which is posterior in the eye, are out of focus. Detachment extends from about 11 o'clock until 4 o'clock and involves the macular region; Courtesy of Sarah Moyer, CRA, OCT-C. (B) An artist's representation of traction retinal detachment and of lens-sparing vitrectomy on left. On the right, the vitrectomy is done to address the vitreous between the (a) ridge and the optic nerve, (b) around the optic nerve, (c) ridge to the anterior portion of the eye, and (d) ridge to the ora serrata. Care is taken not to cut the elevated ridge, which can have retina drawn into it, and risk causing a retinal break. At the end of the case, an air bubble is placed into the vitreous cavity to maintain the globe form while the sclerotomies are sewn closed. (C) 2-week postoperative image taken with wide-angle camera (Retcam, Clarity), showing the resolution of retinal detachment posterior to the ridge and elevated ridge/retinal detachment in the region of the pigmented avascular retina. In addition, note the reduction in plus disease. Residual vitreous hemorrhage is present along the inferior retinal arcade. Lens remains clear; Courtesy Sarah Moyer, CRA, OCT-C.

entry without damage to the retina is less than 1 mm in width compared to about 6 mm in the adult eye. Unlike in the adult, a retinal break can lead to an inoperable retinal detachment and blindness in an infant. The ridge/junction region often has retinal detachment incorporated into it. Therefore, in order to reduce the risk of causing an iatrogenic retinal break, the surgical strategy is to release vitreous traction rather than to remove the ridge or dissect preretinal tissue from it. In addition, injury to the lens can lead to cataract, amblyopia, and poor vision. Therefore, the timing of surgery is prior to that when the retina and ridge are pulled anteriorly to contact the posterior lens capsule.

Visual rehabilitation in preterm infants

Infants with ROP are more likely to be myopic and develop strabismus in childhood than full-term infants. The more severe the ROP, the greater the risk of developing high myopia. Infants who develop stage 5 ROP or total retinal detachment have very poor vision, and are usually legally blind (bilateral visual acuity $<20/200$) even after successful surgery to reattach the retina. Therefore, the goal in managing ROP is to prevent stage 5 ROP. Surgery at early stage 4 ROP often permit the retention of the lens which is important in visual development. Infants who have their lenses removed have compromised visual development and reduced visual acuity from aphakic amblyopia, even with optical means to correct aphakia.

Genetics Related to ROP

Based on retrospective analysis of monozygotic and dizygotic twins, a 70% variance in the susceptibility of ROP was found to be from genetic factors, suggesting that genetics plays a strong role in ROP. However, studies of candidate genes are not in agreement and suggest that a more complex situation exists, involving genetics and environmental factors such as nutrition, oxygen, and the health of the infant.

The Norrie disease gene produces the gene product, norrin, which is also a downstream ligand for receptors in the Wnt signaling pathway. Norrie disease is usually x-linked and causes visual and hearing loss. The Wnt pathway and norrin are important in retinal and vascular development. Genetic mutations in the Norrie disease gene [Xp11.2-11.3] were reported to account for 3% of the cases of advanced ROP, but were not found in a study in infants with severe ROP compared to control preterm infants with no or minimal ROP within a racially diverse population. Another study reported that mutations within the cysteine knot configuration of the Norrie disease gene were associated with severe retinal dysplasia, whereas other polymorphisms within the gene had less severe vitreoretinopathies.

Severe ROP has been reported in infants with certain polymorphisms in the gene of vascular endothelial growth factor (VEGF), but the same polymorphisms have not been confirmed in other studies. Despite the finding that low serum insulin-like growth factor-1 (IGF-1) was associated with more severe ROP, one study failed to show a relationship between a prevalent polymorphism in the IGF-1 receptor and the presence of ROP. The role of genetics requires greater study and will continue to be elucidated along with the effect of environmental factors on gene function.

Pathophysiology of ROP

To understand ROP, it is helpful to understand the known processes in human retinal vascular development. It is believed that vasculogenesis or *de novo* development of the central vasculature around the optic nerve occurs from angioblasts, or endothelial cell (EC) precursors. Angioblasts lack markers commonly thought to be present on ECs such as CD31, CD34, and von Willebrand's factor, but do express CD39 and CXCR4. Retinal vascular development is believed to be completed mainly through a process of angiogenesis, but the role of circulating endothelial precursors is being appreciated more. During angiogenesis, a front of migrating cells, astrocytes in cat or angioblasts in dog, sense physiologic hypoxia and express VEGF. The ensuing ECs are attracted to VEGF and migrate to create blood vessels. The VEGF signaling pathway has been found to regulate and integrate several cell processes important during sprouting angiogenesis. Whereas VEGF concentration is thought to regulate EC division rate, the presentation of VEGF, as in a gradient, may regulate filopodia formation of endothelial tip cells at the migrating front and direct the growth of ECs. The delta-like ligand 4/Notch1 (Dll4/Notch1) signaling pathway regulates VEGF-induced endothelial tip/stalk cells at the junction of vascular and avascular retina and permits ordered angiogenesis.

Role of Oxygen in Retinal Development

The oxygen level has been long recognized as important in the development of ROP. High unregulated oxygen at birth likely accounted for many of the early cases of ROP first described in the 1940s and 1950s. With improved oxygen monitoring and avoidance of hyperoxia, ROP virtually disappeared. However, as infants of younger gestational ages and lower birth weights survived, ROP re-emerged. Currently, it is recognized that fluctuations in oxygen, as well as high oxygen at birth, are important

risks for severe ROP. Although a multicenter clinical study (Supplemental Therapeutic Oxygen for Prethreshold Retinopathy of Prematurity) to test the effects of supplemental oxygen to prevent severe ROP found no adverse effect from supplemental oxygen and, perhaps, a benefit in a subgroup, some reports indicate that severe ROP is associated more commonly with infants who have had high oxygen saturations during their courses.

High oxygen early in development causes loss of perfused central capillaries and is the basis for the development of several animal models of oxygen-induced retinopathy (OIR) in cats, mice, beagles, and rats. One mechanism proposed is that hyperoxia inhibits basic fibroblast growth factor (bFGF)-induced angioblast differentiation into ECs *in vitro*. Although most models of OIR recapitulate this high constant hyperoxia, it is not relevant to what preterm infants experience in neonatal intensive care units (NICUs) in which oxygen is well regulated, in whom minute to minute fluctuations in oxygen have been measured rather than constant oxygen. Furthermore, almost all studies of the mechanisms of oxygen stress on retinal vessels have been performed using models that subject animals to high constant oxygen.

Table 2 Mouse and 50/10 rat models of OIR

Constant high hyperoxia: Mouse OIR model of human APROP	
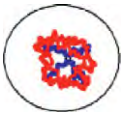	p12 Low retinal VEGF Central avascular retina p17 Intravitreous neovascular budding
Fluctuations in oxygen: Rat 50/10 OIR model of more common PSROP	
	p14 Rat 50/10 OIR; ~32 weeks premature infant High retinal VEGF
	p18 Rat 50/10 OIR; ~35-37weeks premature infant High VEGF164 and VEGFR2 signaling Intravitreous neovascularization
	~p30 Rat 50/10 OIR; 40 weeks preterm infant Intraretinal vascularization and regression of IVNV

Animal Models of Severe ROP

Models of severe ROP take advantage of the fact that several species undergo retinal vascular development after birth. Furthermore, the newly developed capillaries are susceptible to oxygen stresses such that high oxygen will cause loss of capillaries. No model uses premature animals. In addition, no model develops stage 4 or 5 ROP (retinal detachment). The beagle OIR model comes closest to stage 4 ROP with the development of tractional retinal folds, but does not develop stage 5 ROP.

Mouse OIR (model of aggressive posterior ROP)

The mouse OIR model also uses high constant oxygen and is probably the most useful to study mechanisms of extreme oxygen insult by using genetically modified animals (**Table 2** and **Figure 7**). This model may mimic aggressive posterior ROP (APROP, **Figure 8**), a less-common form of severe ROP, in which there are broad areas of central avascular retina. APROP may share the retinal oxygenation pattern as does the avascular hypoxic retina during relative hypoxia in the mouse OIR model. Fluorescein angiograms of infants with APROP demonstrated extensive capillary loss centrally that appeared similar to that seen in perfused retinas from the mouse OIR, and several studies have shown avascular retina in OIR models to be hypoxic.

Rat 50/10 OIR (model of peripheral severe ROP)

The rat 50/10 OIR model mimics the more common form of severe ROP, peripheral severe ROP (PSROP). Here, newborn rat pups are placed into an oxygen environment that cycles concentrations between 50% and 10% oxygen every 24 h for 14 days. The oxygen extremes in the rat 50/10 OIR model cause rat arterial oxygen levels to be similar to the transcutaneous oxygen levels measured in preterm infants who developed severe ROP. In addition, rather than constant oxygen used in other models, the 50/10 OIR model exposes pups to repeated fluctuations in oxygen, a risk factor for severe ROP. As in PSROP, in which there is reduced peripheral retinal vascularization and perfusion with minimal central nonperfusion, the rat 50/10 OIR model has mainly peripheral avascular retina and minimal central capillary loss (**Figure 4(a)**). The 50/10 OIR model reproducibly and consistently first develops avascular retina (analogous to human zone II ROP) and, subsequently, vessel tortuosity (analogous to human plus disease) and intravitreous neovascularization (analogous to human stage 3 ROP). All OIR models have regression of tortuosity and intravitreous neovascularization with later intraretinal vascularization; however, the beagle model takes the longest to regress.

Role of Avascular Retina

Although the size of the avascular retina does not always correlate with the presence of intravitreous neovascularization in animal models, multicenter clinical trials have shown that eyes with the largest peripheral retinal avascular zones have the worst outcomes from ROP. Furthermore, the avascular, hypoxic retina is believed to be a source of angiogenic

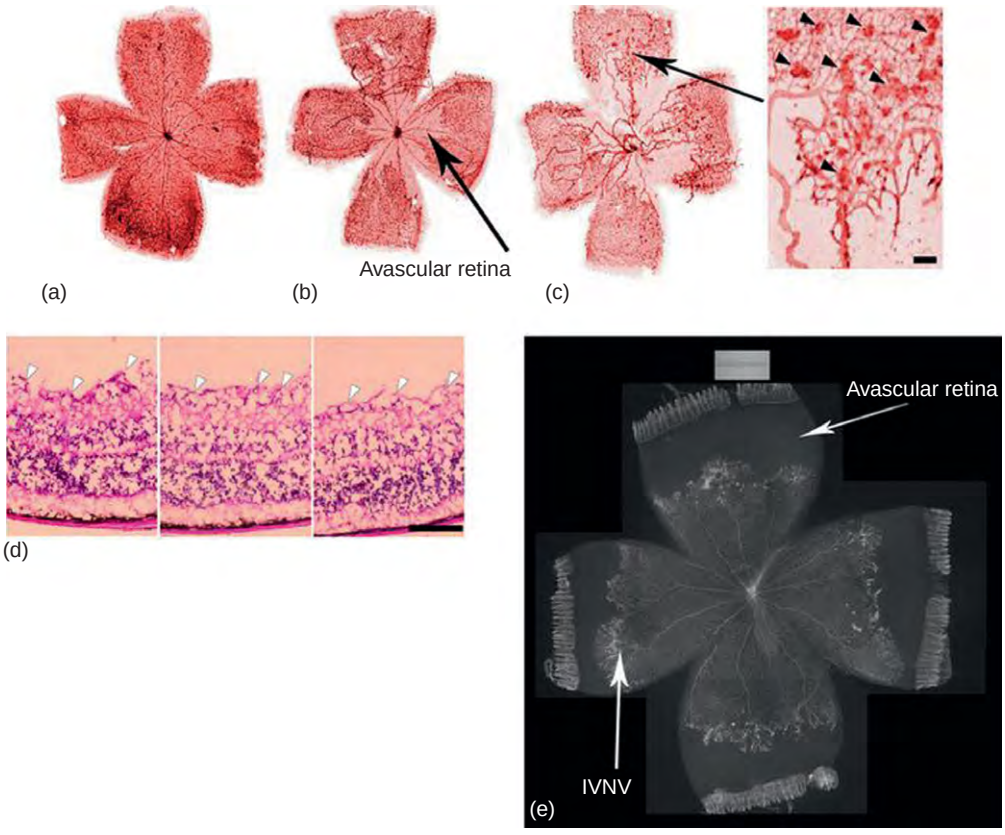

Figure 7 Retinal flat mounts from (a) room air raised mouse at postnatal day (p)12; (b) mouse raised in oxygen-induced retinopathy (75% constant oxygen for 5 days) with central capillary loss (arrow) at p12. ((c), left) After 5 days in room air (relative hypoxia) with capillary budding into the vitreous at p17, possibly mimicking aggressive posterior ROP (see **Table 2**). ((c), right) Enlargement of area centered at arrow; arrowheads indicate capillary budding; and (d) cross section of (c) showing endothelial budding into the vitreous (white arrowheads). (e) Lectin B4-stained retinal flat mount from rat 50/10 OIR model following oxygen fluctuations between 50% and 10% oxygen until p14, followed by 4 days of room air. At p18, intravitreous neovascularization (IVNV) appears at the junction of vascularized and peripheral avascular retina similar in appearance to peripheral severe ROP (see also **Table 2**).

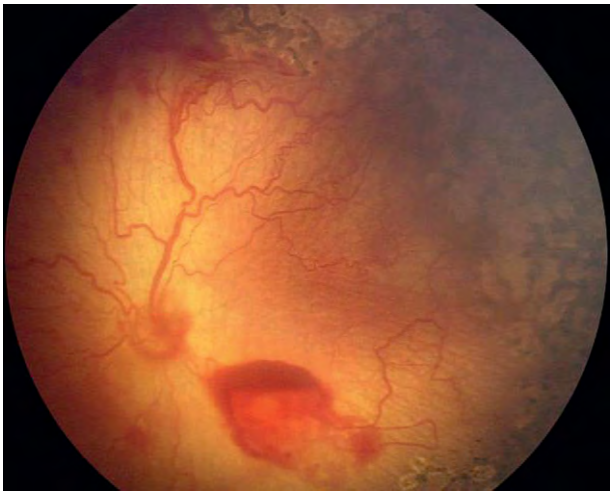

Figure 8 Preterm infant left eye with APROP after laser treatment showing pigmentation of laser to the right of image, plus disease, and vitreous hemorrhage inferior to optic nerve; Courtesy Sarah Moyer, CRA, OCT-C.

factors that cause pathologic intravitreous neovascularization in some models of ROP. What causes avascular retina remains largely unknown. Delayed retinal vascular development in B-cell lymphoma protein 2 ($bcl2^{-/-}$)-deficient mice that have a defect in protection against apoptosis supports the thinking that increased apoptosis of ECs or their precursors may contribute to avascular retina. Protection of newly formed capillaries from hyperoxia-induced endothelial death occurs by giving growth factors or nutritional supplements prior to the hyperoxic insult, and these protective agents largely prevent intravitreous neovascularization that would occur in the hypoxic phase of the mouse OIR model. The activation of nicotinamide adenine dinucleotide phosphate [NADPH] oxidase from repeated oxygen fluctuations in the rat 50/10 OIR model contributed to the avascular retina through apoptosis. Thus, the area of avascular retina appears to be one factor involved in the severity of human ROP, and apoptosis of ECs or their precursors may contribute to its size.

Role of Growth Factors

Molecular mechanisms of OIR have been identified mainly from the mouse OIR model, which mimics APROP, but does not mimic most cases of severe ROP.

Vascular Endothelial Growth Factor

VEGF is an important factor in retinal vascular development and is also neuroprotective. However, it is also one of the most important angiogenic factors involved in pathologic retinal and choroidal vascular diseases. Mice in OIR had reduced VEGF expression in association with capillary loss centrally when exposed to high constant hyperoxia. Subsequently, when placed into relative hypoxia that occurred in room air, VEGF messenger ribonucleic acid (mRNA) was overexpressed in association with the development of endothelial budding above the internal limiting membrane. If VEGF was given during hyperoxia, capillary loss could be reduced and, if agents to inhibit VEGF were given during relative hypoxia, endothelial budding into the vitreous was also reduced.

In the rat 50/10 OIR model, a relevant model of most cases of severe ROP in the US currently, neutralizing VEGF with an antibody made against $VEGF_{164}$ reduced tortuosity (analogous to plus disease) and intravitreous neovascularization (analogous to stage 3 ROP). Too low a dose appeared to lead to a rebound in intravitreous neovascularization and persistence of the avascular retina.

Clinical trials are underway, testing intravitreous injections of antibodies to VEGF in severe ROP. There are concerns regarding the effect of dose based on animal studies described above, and the possible adverse effect of inhibiting VEGF in the developing preterm infant. VEGF is neuroprotective and besides the possible local effect on the retina, there is the potential adverse effect systemically from the absorption of the antibody into the bloodstream. Compared to the adult, an intravitreous drug in the newborn can achieve a higher concentration in the bloodstream and affect measurable outcomes, such as body weight gain in animal models. However, in some forms of severe ROP, such as APROP, there are few other options to prevent retinal detachment and permit the development of vision in these infants. Therefore, clinical trials are necessary and the data obtained will be important in developing improved treatments for severe ROP.

IGF-1 – IGF 1BP3

IGF-1 is important in the physical growth of the infant. However, IGF-1 levels that occur *in utero* are not maintained upon birth in preterm infants. Low serum IGF-1 was found to correlate with greater avascular retinal area in human preterm infants. Furthermore, transgenic mice expressing a growth hormone antagonist gene, or wild-type mice treated with an inhibitor to growth hormone, had reduced intravitreous neovascularization in the mouse OIR model. IGF-1 was also found to be important for signaling through the mitogen-activated protein (MAP) kinase pathway, which is important in cell proliferation. In addition, VEGF and IGF-1 synergistically triggered the serine-threonine kinase, Akt, which is important in cell survival. Based on these findings, it is theorized that IGF-1, which is low in the preterm infant, is necessary for early retinal vascular survival and growth, but can result in later intravitreous neovascularization in ROP. However, the timing and dose of IGF-1 appear to be critical.

A hypoxia-regulated binding protein of IGF-1, IGF-1BP3, was shown to be important in reducing hyperoxia-induced capillary loss and in promoting vascular regrowth into the retina in the mouse OIR model. IGF-BP3 was shown to promote differentiation of endothelial precursor cells into ECs and in promoting angiogenic processes, such as cell migration and tube formation.

Erythropoietin

Erythropoietin is angiogenic, erythropoietic, and neuroprotective. It is upregulated after the stabilization of hypoxia-inducible factor (HIF)-1α in response to hypoxia. In the mouse OIR model, hyperoxia reduces the expression of erythropoietin. The administration of exogenous erythropoietin prior to hyperoxia reduced capillary loss, whereas giving erythropoietin during relative hypoxia in room air enhanced pathologic neovascularization. Clinical studies have reported an association between the number of administrations of erythropoietin for anemia of prematurity and the prevalence of severe ROP and have found that recombinant erythropoietin is an independent risk factor for severe ROP.

HIF 1α

The stabilization of HIF1α occurs under hypoxic conditions or secondary to reactive oxygen species (ROS) generated from NADPH oxidase, nitric oxide, mitochondria, and other enzymes. HIF1α binds to the hypoxia response elements to cause transcription of several genes including angiogenic factors, VEGF, and erythropoietin. A knock-out to HIF 1α is lethal, but a knock-out to the HIF-1α-like factor (HLF)/HIF-2α provided evidence that erythropoietin was a major gene involved in intravitreous neovascularization after relative hypoxia from hyperoxia-induced capillary loss in the mouse OIR model.

Role of Oxidative Stress

Oxidative stress has been proposed to be important in the development of ROP because the retina is susceptible to oxidative damage given its high metabolic rate and rapid rate of oxygen consumption. In addition, the premature infant has a reduced ability to scavenge ROS, increasing

its vulnerability to oxidative stress. End products of ROS, lipid hydroperoxides, were increased in the 50/10 OIR model at time points corresponding to intravitreous neovascularization. When injected into the vitreous, these compounds caused intravitreous neovascularization in the rabbit. In addition, ROS can trigger signaling pathways relevant to apoptosis or angiogenesis, both important in the pathogenesis of ROP.

The treatment of pups in the 50/10 OIR model or humans with ROP using a broad antioxidant, *N*-acetylcysteine, failed to show a reduction in clock hours of intravitreous neovascularization, or the avascular retinal area. In a clinical trial in preterm infants, there was no difference in the incidence in ROP between those receiving *N*-acetylcysteine or control. However, reduction in ROS with preparations of vitamin E or liposomes containing the antioxidant enzyme, manganese superoxide dismutase, reduced OIR severity. Also, a meta-analysis of human preterm infants treated with vitamin E showed a significant reduction in severity of ROP. Reducing the activation of NADPH oxidase, an enzyme that produces ROS, can also reduce the size of the avascular areas and subsequent intravitreous neovascularization in certain OIR models.

Light was proposed to be important in ROP development through photooxidation of polyunsaturated fatty acids within photoreceptor outer segments. On the other hand, during the dark, photoreceptors are more metabolically active. A clinical trial testing the effect of light or shade on the development of ROP showed no significant difference.

Future Treatment Considerations

There are difficulties in studying treatments for ROP in developing infants. Preterm infants with severe ROP often have other developmental and health problems, making it difficult to assess long-term complications of a drug in clinical trials. Inhibiting the bioactivity of VEGF has been reported to be beneficial in adult diseases, such as proliferative diabetic retinopathy, but this strategy has been reported to interfere with neuronal and endothelial survival in some animal models, and these are issues of concern in the developing preterm infant. Inhibition of ROS may be detrimental to the preterm infant, whose abilities to combat infection are limited. A reduction in inspired oxygen concentration may also be detrimental to the developing preterm infant brain and long-term effects of such reductions are unknown. The timing and dose of neuroprotective agents such as erythropoietin and growth factors are critical but vary among individual infants, so that an agent may worsen rather than lessen ROP severity. Currently, the optimal time or dose of an agent cannot be safely determined for an individual infant. However, the current standard of care laser treatment for severe ROP does not address vascular development that is ongoing in the developing human preterm infant. Better treatments for severe ROP are needed.

See also: Anatomy and Regulation of the Optical Nerve Blood Flow; Choroidal Neovascularization; The Evolution of Opsins; Genetic Dissection of Invertebrate Phototransduction; Microvillar and Ciliary Photoreceptors in Molluskan Eyes; Molecular Mechanisms of Angiostasis; Properties and Functions of the Vessels of the Ciliary Body.

Further Reading

Capone, A., Jr., Hartnett, M. E., and Trese, M. T. (2005). Treatment of retinopathy of prematurity: Peripheral retinal ablation and vitreoretinal surgery. In: Hartnett, M. E., Trese, M. T., Capone, A., Keats, B., and Steidl, S. (eds.) *Pediatric Retina*, pp. 417–424. Philadelphia, PA: Lippincott Williams and Wilkins.

Chen, J., Connor, K. M., Aderman, C. M., and Smith, L. E. (2008). Erythropoietin deficiency decreases vascular stability in mice. *Journal of Clinical Investigation* 118: 526–533.

Coats, D. K. (2005). Retinopathy of prematurity: Involution, factors predisposing to retinal detachment, and expected utility of preemptive surgical reintervention. *Transactions of the American Ophthalmological Society* 103: 281–312.

Geisen, P., Peterson, L. J., Martiniuk, D., et al. (2008). Neutralizing antibody to VEGF reduces intravitreous neovascularization and does not interfere with vascularization of avascular retina in an ROP model. *Molecular Vision* 14: 345–357.

Hartnett, M. E. (2003). Examination and diagnosis in the pediatric patient. In: Steidl, S. M. and Hartnett, M. E. (eds.) *Clinical Pathways in Vitreoretinal Disease*, pp. 341–373. New York: Thieme Medical Publishers.

Hartnett, M. E. and Toth C. A. (2010). Retinopathy of prematurity. In: Levin L. and Albert, D. (eds.) *Ocular Disease: Mechanisms and Management*. London: Elsevier.

Hartnett, M. E., Trese, M. T., Capone, A., Keats, B., and Steidl, S. (eds.) (2005) *Pediatric Retina.* Philadelphia, PA: Lippincott Williams and Wilkins.

Hartnett, M. E., Martiniuk, D., Byfield, G., Zeng, G., and Bautch, V. (2008). Neutralizing VEGF decreases tortuosity and alters endothelial cell division orientation in arterioles and veins in rat model of ROP: Relevance to plus disease. *Investigative Ophthalmology and Visual Science* 49: 3107–3117.

Hasegawa, T., McLeod, D. S., Prow, T., et al. (2008). Vascular precursors in developing human retina. *Investigative Ophthalmology and Visual Science* 49: 2178–2192.

McColm, J. R. and Hartnett, M. E. (2005). Retinopathy of prematurity: Current understanding based on clinical trials and animal models. In: Hartnett, M. E., Trese, M. T., Capone, A., Keats, B., and Steidl, S. (eds.) *Pediatric Retina*, pp. 387–410. Philadelphia, PA: Lippincott Williams and Wilkins.

McLeod, D. S., Hasegawa, T., Prow, T., Merges, C., and Lutty, G. (2006). The initial fetal human retinal vasculature develops by vasculogenesis. *Developmental Dynamics* 235: 3336–3347.

Penn, J. S., Henry, M. M., and Tolman, B. L. (1994). Exposure to alternating hypoxia and hyperoxia causes severe proliferative retinopathy in the newborn rat. *Pediatric Research* 36: 724–731.

Penn, J. S., Madan, A., Caldwell, R. B., et al. (2008). Vascular endothelial growth factor in eye disease. *Progress in Retina and Eye Research* 27: 331–371.

Saito, Y., Uppal, A., Byfield, G., Budd, S., and Hartnett, M. E. (2008). Activated NADPH oxidase from supplemental oxygen induces neovascularization independent of VEGF in retinopathy of prematurity model. *Investigative Ophthalmology and Visual Science* 49: 1591–1598.

Smith, L. E. H., Wesolowshi, E., McLellan, A., et al. (1994). Oxygen induced retinopathy in the mouse. *Investigative Ophthalmology and Visual Science* 35: 101–111.

Stone, J., Itin, A., Alon, T., et al. (1995). Development of retinal vasculature is mediated by hypoxia-induced vascular endothelial growth factor (VEGF) expression by neuroglia. *Journal of Neuroscience* 15: 4738–4747.

Relevant Websites

http://www.iom.edu – Institute of Medicine Statement on Prematurity.
http://www.nei.nih.gov – National Eye Institute statement on ROP.

Rhegmatogenous Retinal Detachment

S C Wong, Moorfields Eye Hospital, London, UK
Y D Ramkissoon, Royal Hallamshire Hospital, Sheffield, UK
D G Charteris, Moorfields Eye Hospital, London, UK

Glossary

Retinopexy – A Laser- or cryotherapy-induced chorioretinal adhesion surrounding a retinal break as prophylaxis for or during surgical treatment of rhegmatogenous retinal detachment.
***Rhegma* (Greek)** – A rupture, rent, or fracture.
Rhegmatogenous retinal detachment – A separation of the neurosensory retina from the retinal pigment epithelium associated with a full-thickness hole, break, or tear in the retina. The detachment occurs secondary to the passage of vitreous fluid through the break.
Tamponade – The plugging on a retinal break so that fluid can no longer pass through it (e.g., with a gas bubble).
Vitreous – Pertaining to the vitreous body of the eye located in the posterior chamber of the eye.

Rhegmatogenous retinal detachment (RRD) is defined as a separation of the neurosensory retina from the underlying retinal pigment epithelium (RPE) due to accumulation of subretinal fluid (SRF) via one or more full-thickness retinal breaks. With an incidence of 1 in 10 000 among the general population, RRD is relatively uncommon but remains an important cause of vision loss. In 1918, Jules Gonin recognized the importance of retinal breaks in the etiology of RRD and transformed the prognosis of this previously untreatable, blinding condition. Using thermocautery to seal retinal breaks, he demonstrated successful retinal reattachment in 30–40% of his cases. Modern vitreoretinal surgery can now achieve a final retinal reattachment rate of >95%.

Pathophysiology

Under physiological conditions, retinal attachment is principally maintained by the following mechanical and metabolic factors: (1) fluid or intraocular pressure (IOP) differentials (hydrostatic and osmotic forces); (2) glue-like interphotoreceptor matrix at the photoreceptor outer segment and RPE interface; and (3) RPE pump (NA^+–K^+ adenosine triphosphate (ATP)ase metabolic pump transporting ions and fluid across the subretinal space).

For RRD to occur, the following factors need to be present to overcome the attaching forces: (1) full-thickness retinal break in the neurosensory retina and (2) vitreous liquefaction and vitreoretinal traction. Vitreoretinal traction may coexist at the site of the retinal break, and varies depending on the type of break.

Full-thickness retinal breaks are classified as tractional tears, round holes, or dialyses.

Retinal tractional tears (also known as U, horseshoe, or flap tears) develop following posterior vitreous detachment (PVD) and are the most common causes of RRD. They occur at sites of enhanced vitreoretinal adhesion, such as in peripheral retinal lattice degeneration, chorioretinal scars, or at the posterior edge of the vitreous base. Persistent vitreous traction exerted on the flap of a tear promotes rapid, continuous recruitment of liquefied vitreous into the subretinal space and progression to retinal detachment, which usually occurs more rapidly than with a round hole or dialysis (where there is no posterior vitreous separation).

Retinal hole formation is not usually associated with overt vitreous traction. This is caused by localized retinal atrophy and occurs more commonly in myopic patients. The pathophysiology of progression from retinal hole to RRD is not entirely clear, as 5–10% of postmortem eyes have full-thickness retinal holes without RRD.

Retinal dialyses are circumferential retinal breaks occurring along the ora serrata with concurrent avulsion of the overlying vitreous base. There is often a history of ocular trauma, although spontaneous cases are not uncommon.

Clinical Features

Symptoms

Many patients present acutely with classic symptoms of flashing lights (photopsia) and visual floaters in the affected eye, usually resulting from PVD. Photopsia lasts for seconds, is more noticeable in dim light conditions, may be precipitated by ocular movements, and commonly occurs in the temporal field but is not localizing. Floaters in the visual field vary from a solitary floater (e.g., Weiss ring formation) to innumerable minute dark spots (pigment or hemorrhage in vitreous). As an RRD develops and progresses, patients may notice peripheral visual-field loss, which is often described as a black curtain,

shadow, or half-moon. Central vision is lost if SRF spreads to involve the macula and detaches the fovea.

In a minority of patients, RRD may be asymptomatic. Typically, this occurs in young myopic patients with atrophic round holes who often present late only when the detachment encroaches the macula.

Signs

Nonspecific signs of RRD may include reduced visual acuity, relative afferent pupillary defect, mild anterior uveitis, and low IOP compared to the fellow eye. Up to 2% of patients may present with raised IOP or Schwartz–Matsuo syndrome. This typically occurs in young patients with chronic RRD, and is due to rod photoreceptor outer segments passing into the anterior chamber and blocking trabecular outflow. A positive Shaffer's sign, defined as the presence of tobacco dust or pigment granules in the anterior vitreous, is highly predictive of a retinal break particularly when associated with any of the above symptoms.

Stereoscopic fundal examination reveals an elevated neurosensory retina in the area of the detachment, with reduced visibility of underlying choroidal markings. The detached retina has a convex configuration and may have a corrugated surface due to intraretinal edema. This is in contrast to tractional non-RRD, which has a concave configuration.

In addition, one or more full-thickness retinal breaks may be visible as evidenced by discontinuity of the retinal surface. These typically occur anterior to the equator. Visualization of the type, number, and distribution of all retinal breaks is important for surgical planning. This is best achieved with the aid of indirect ophthalmoscopy and scleral indentation. However, this may be difficult in the presence of media opacities. Identification of break type in RRD is crucial, as it determines the choice of appropriate surgical technique for repair.

Break type – identification

Retinal tears

1. Horseshoe or U-shaped tear (may be irregular; Figure 1).
2. Persistent point of vitreous traction present at anterior edge of flap.
3. Giant retinal tear (GRT) is a circumferential retinal tear of 3 or more clock hours.
4. Avulsion of the anterior flap of a retinal tear may result in a round break with overlying retinal operculum. A tear with an operculum that is fully separated from the retina is known as a fully operculated round hole (FORH).
5. Retina is visible anterior to break.

Retinal round holes

1. Round atrophic hole without overlying retinal operculum (Figure 2).
2. May be associated with retinal degeneration (e.g., peripheral lattice degeneration).
3. Retina is visible anterior to break.

Figure 1 Right eye. Retinal tear in the superotemporal retinal periphery causing an acute macular-sparing retinal detachment. HST, horseshoe tear; RRD, rhegmatogenous retinal detachment.

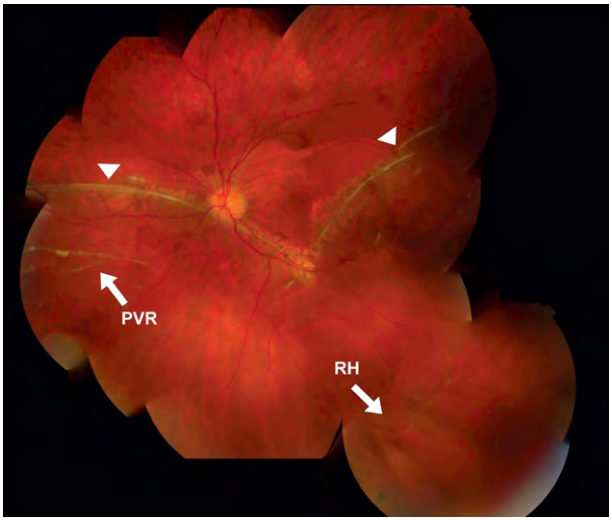

Figure 2 Left eye. Retinal round hole in the inferotemporal retinal periphery causing a chronic macular-sparing retinal detachment. A demarcation line (arrowhead) indicates several months of stasis and nonprogression of the retinal detachment. Proliferative vitreoretinopathy in the form of subretinal band formation is consistent with the chronicity of the detachment. RH, round hole; PVR, proliferative vitreoretinopathy.

Retinal dialyses

1. Circumferential retinal break at the ora serrata without a PVD (Figure 3).
2. No visible retina anterior to retinal break.

Lincoff first described the principles of predicting retinal break location, taking into account the effect of gravity on the spread of SRF from the primary break and the resultant topography of an RRD. This is influenced by anatomical limits such as the disc, the ora serrata, and any chorioretinal adhesions that might be present.

Break localization – principles based on topography of RRD

Superotemporal and superonasal

1. SRF descends on the same side of break toward the disc, then revolves around the inferior pole of the disc and rises on the opposite side.
2. SRF may rise as high on the opposite side of the disc as the level of the primary retinal break, but never as high as the fluid level on the primary side.
3. The primary break will be found within 1.5 clock hours of the highest border of the detachment in 98% cases.

Midline (12 o'clock meridian) and total detachments

1. Detachments that cross the 12 o'clock meridian originate from breaks at or near 12 o'clock.
2. These detachments can become total.
3. In subtotal detachments, if the break is slightly to one side of 12 o'clock, the fluid front will be more extensive on the side coincidental with the break.
4. The more posterior the break, the more it can deviate from 12 o'clock position and still cause a detachment that will cross the vertical meridian. Therefore, contour edges of the detachment are of less localizing value.

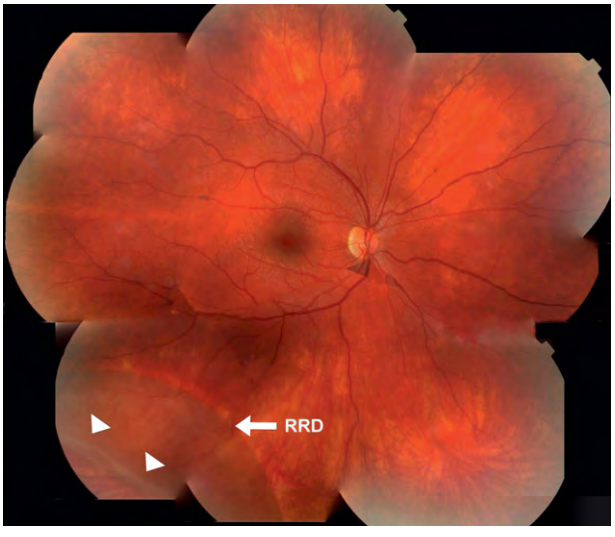

Figure 3 Right eye. Retinal dialysis (arrowhead) in the inferotemporal retinal periphery causing a macular-sparing retinal detachment.

Inferior

1. The SRF that arises from breaks below the level of the optic disc develops first around the break and then advances toward the disc and macula, rising higher on that side of the disc where the break lies.
2. The break need only be 1 or 2 mm from the 6 o'clock position for it to cause a difference in fluid levels.
3. When the levels are equal, the hole is at the 6 o'clock meridian.
4. Such detachments are never bullous.

Chronic RRD

The distinction between an acute and chronic RRD is important, as it may determine both the urgency of treatment and prognosis. Signs of chronicity are:

1. Retinal atrophy – retina may be thinned and atrophic.
2. Intraretinal cysts – these can develop in long-standing RRD, typically those over 12 months duration. At the time of surgery, they can be left undisturbed as they do not usually interfere with retinal reattachment and can subsequently collapse.
3. Subretinal demarcation lines – also known as high watermarks or tidemarks, these develop at the advancing front of the RRD as a result of proliferation of RPE cells. Their presence simply indicates a period of stasis of the RRD at the point of the demarcation line. However, it does not confer the strength of a chorioretinal scar that is generated by retinopexy; thus, RRD progression may still occur.
4. Proliferative vitreoretinopathy (PVR) (Figure 4) – This is a process of cellular proliferation and fibrocellular membrane contraction that complicates between 5% and 12% of all RRD, and is the most common reason for final failure of RRD surgery. PVR has a higher incidence in RRD secondary to GRTs (16–41%) and in eyes sustaining penetrating trauma (10–45%). Once PVR has developed, visual recovery is usually limited despite improving anatomical surgical success rates. The location and extent of epiretinal or subretinal proliferation have been classified by the Retina Society Terminology Committee in 1991 (Table 1).

Differential Diagnoses

RRD must be distinguished from other causes of retinal or choroidal elevation. Differential diagnoses include PVD, exudative RD, tractional RD, retinoschisis, choroidal lesions, and artifacts (Table 2).

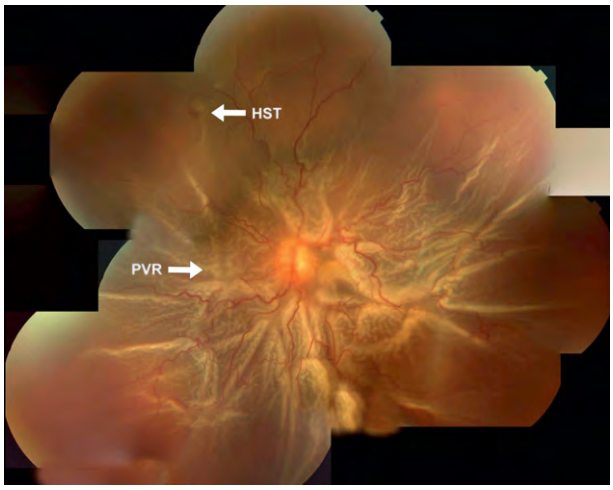

Figure 4 Right eye. Total rhegmatogenous retinal detachment secondary to a small superior retinal tear. Proliferative vitreoretinopathy is evidenced by posterior starfolds involving approximately 11 clock hours (PVR CP11). HST, horseshoe tear; PVR, proliferative vitreoretinopathy. Reproduced with kind permission from Paul M. Sullivan.

Table 1 Proliferative vitreoretinopathy classification by the Retina Society Terminology Committee

Grade (stage)	*Characteristics*
A	Vitreous haze; vitreous pigment clumps; and pigment clusters on inferior retina
B	Wrinkling of the inner retinal surface; rolled and irregular edge of retinal break; retinal stiffness; vessel tortuosity; and decreased vitreous mobility
C P 1 – 12 (clock hours)	Posterior to equator: focal, diffuse, or circumferential full-thickness retinal folds; and subretinal strands
C A 1 – 12 (clock hours)	Anterior to the equator: focal, diffuse, or circumferential full-thickness retinal folds; subretinal strands; anterior displacement; and condensed vitreous with strands

From Machemer, R., Aaberg, T. M., Freeman, M., et al. (1991). An updated classification of retinal detachment with proliferative vitreoretinopathy. *American Journal of Ophthalmology* 112: 159–165, with kind permission from Elsevier.

Management

The primary aim in the management of RRD is to prevent complete loss of central and peripheral vision, that is, progression to no perception of light. In patients with symptomatic RRD, the secondary aim of management is restoration/improvement of peripheral visual field and central vision. Depending on the type of retinal break, size, and rate of progression of the RRD and PVD status, treatment may be either conservative or active. Conservative management involves observation for progression of RRD without intervention. Active management includes either barrier laser demarcation to wall off the detachment and prevent further progression, or surgery to reattach the retina. The various treatment options are discussed in turn, categorized by type of causative retinal break.

Conservative

Conservative management consists of either self-monitoring by the patient for development or progression of RRD symptoms, and/or observation by regular clinical examinations charting any signs of an enlarging RRD. This option is usually reserved for patients with chronic RRD without clinical signs of recent progression who are often asymptomatic and discovered to have RRD as an incidental finding. Another group of patients, where conservative management may be appropriate, comprises those with such significant systemic comorbidity that active treatment cannot be safely administered. When considering conservative management regardless of the specific indication, the ophthalmologist should discuss in detail its risks and benefits versus active therapies with the patients, allowing them to make informed decisions regarding their care. In addition, it is important to ensure that the patient understands the symptoms of RRD progression, and are able to reliably monitor their vision monocularly to detect changes before macula detachment occurs.

RRD due to retinal tear

RRD due to retinal tears occurs following PVD and tends to be rapidly progressive in nature due to persistent vitreoretinal traction on the anterior edge of the tear. It is therefore unusual for this to be asymptomatic or present as chronic RRD, and so much less likely to be managed conservatively.

RRD due to retinal hole or dialysis

Both retinal holes and retinal dialyses are usually associated with an attached vitreous, that is, without a PVD. This is thought to account for the relatively slower progression of RRD compared to those caused by retinal tears. As such, these patients often present with signs of chronicity and nonprogression, and many are asymptomatic until the macula becomes involved. Conservative management may be considered with appropriate patient selection.

Laser Demarcation

Laser photocoagulation results in the formation of a chorioretinal scar, conferring enhanced adhesion between the neurosensory retina and RPE. Laser demarcation for RRD is applied to the area of attached retina immediately adjacent to the most posterior edge of the RRD, walling off the area of detachment and preventing further

Table 2 Differential diagnosis of rhegmatogenous retinal detachment

Differential diagnosis	*Features*
Posterior vitreous detachment	– Weiss ring, vitreous syneresis – Attached retina
Exudative RD	– RD configuration convex, but smooth without corrugated surface – Shifting SRF – configuration of RD responds to changes in posture and its gravitational effects – No full-thickness retinal breaks present – May be associated with uveitis, scleritis, tumor, vascular, and other disorders
Tractional RD	– Associated with proliferative diabetic retinopathy or penetrating ocular trauma – RD has concave configuration – No full-thickness retinal breaks present, unless combined tractional and rhegmatogenous – Limited retinal mobility; no shifting fluid – Retina less elevated, and associated with sites of vitreoretinal traction
Retinoschisis	– Age-related or congenital X-linked – Occurs secondary to intraretinal splitting (age-related: splitting at outer plexiform or less commonly inner nuclear layer. X-linked: splitting at nerve fiber layer) – Often bilateral, and more common in hypermetropes – Retinal elevation has concave configuration – No full-thickness retinal breaks present – Partial thickness retinal breaks may be visible involving the inner and/or outer leaf – Does not produce demarcation line – Produces absolute scotoma, unlike RD which produces relative scotoma – Laser reaction test – this can help differentiate retinoschisis from a retinal detachment. Low-energy argon green laser is applied to the area of retinoschisis. Intensity of gray burn reaction should be equal to a control shot in peripheral flat retina. No reaction is seen in RRD.
Choroidal lesions	– Choroidal detachments or choroidal masses (tumors or inflammatory lesions) – No full-thickness retinal breaks present – May be associated with exudative RD
Artifacts	
– Vitreous hemorrhage	– Hemorrhage in vitreous cavity – Absence of true retinal vessel configuration
– Lens opacity – cataract or pseudophakic capsule opacification	– No relative afferent pupillary defect – Visible lens opacity – No vitreous haze or pigment granules – No mobility of opacity – Attached retina on ultrasound B scan

progression. Two to three contiguous rows of laser are required, extending anteriorly up to the ora serrata on either side of the RRD. This is usually achieved using indirect laser ophthalmoscopy with scleral indentation. Increased adhesion at the site of laser photocoagulation is evident within 24 h in histological studies of animal and human eyes, and is twice normal by 2–3 weeks. Therefore, laser demarcation is only appropriate for RRD with signs of slow progression or recent stasis. Cryotherapy is not appropriate for RRD demarcation as a large area of retinopexy is required, causing more extensive tissue destruction and is less precise than laser.

RRD due to retinal tear

As discussed previously, acute RRD due to retinal tears tends to progress rapidly and is therefore not usually suitable for laser demarcation. Possible exceptions are localized RRD from a single small tear, particularly if within inferior retina.

RRD due to retinal hole or dialysis

Patients with limited or no symptoms from RRD secondary to retinal hole or dialysis, with associated signs of chronicity, may be suitable candidates for laser demarcation. Exceptions are patients with significant symptoms, especially visual field loss, signs of recent rapid progression, or when the SRF has progressed to the major vascular arcades. Laser demarcation limits rather than alleviates RRD symptoms. Laser-induced chorioretinal scars in the posterior pole can expand up to 13% per year, potentially causing a symptomatic central scotoma, if this is close to the macula.

Pneumatic Retinopexy

Pneumatic retinopexy for RRD was introduced by Hilton and Grizzard in 1986 as a two-step outpatient procedure without conjunctival incision. This involves an intravitreal

gas injection to temporarily close the retinal break preventing further recruitment of SRF from liquefied vitreous, followed by retinopexy (laser or cryotherapy) to permanently seal the break. Postoperative posturing for a minimum of 5 days is required in all patients. Careful case selection is required as not all patients are suitable for pneumatic retinopexy.

This procedure is not suitable in the following cases:

1. multiple breaks spanning over 3 clock hours;
2. giant retinal breaks;
3. inferior breaks involving inferior 4 clock hours;
4. presence of PVR grade C; and
5. inability to maintain postoperative posturing.

RRD due to retinal tear

Pneumatic retinopexy is most suitable for RRD with a single superior tear situated in the superior 8 clock hours. Patients must be able to posture, and attend clinic regularly in the early postoperative period to monitor the outcome of treatment. Additional gas injection or further surgery with scleral buckling or vitrectomy may be required in the event of treatment failure.

RRD due to retinal hole or dialysis

Pneumatic retinopexy is not suited to either of the following pathologies: RRD due to retinal hole or dialysis. The presence of an attached vitreous in both retinal holes and dialyses increases the risk of complications of the procedure, including new retinal break and formation of multiple small gas bubbles (see the section titled 'Complications').

Scleral Buckling

The concept of scleral buckling was introduced by Custodis in 1949. Prior to the advent of noncontact wide-angle viewing systems for vitrectomy, scleral buckling was the most commonly performed operation for RRD, and remains so in certain countries due to high primary success rates of over 90%. It is typically performed under general anesthesia, although local anesthesia may be used.

The basic principle of scleral bucking (**Figure 5**) is to close retinal breaks by indentation of the sclera, preventing further recruitment of fluid into the subretinal space. Scleral indentation is achieved by using a variety of explant materials sutured externally to the scleral surface. Encircling explants afford a permanent 360° indent, while segmental explants provide a localized indent, which supports the break for a period of several months until the indent fades. Segmental explants are preferred due to lower associated ocular comorbidity. Permanent break closure must be ensured by application of retinopexy, typically cryotherapy. Intraoperative drainage of SRF may be performed either to aid more rapid resolution of the RRD, or to create space within the vitreous cavity for the scleral indent by substituting SRF volume for the volume of indent, thus preventing excessive IOP elevation. Drainage of SRF involves surgical penetration of the sclera and choroid to the subretinal space. Indications for drainage remain controversial as this converts scleral buckling surgery from an external to an internal procedure, with associated increased risk of intraoperative complications (see the section titled 'Complications').

RRD due to retinal tear

RRDs due to a single tear, or a cluster of tears spanning 2–3 clock hours at the same anteroposterior position, are suitable for scleral buckling. Scleral buckling should be considered in patients with inferior tears, particularly as these are more difficult to effectively tamponade with a vitrectomy and gas procedure. Relatively young phakic patients are ideal candidates for scleral buckling as accommodation is preserved and the risk of developing cataract is small. Scleral buckling is not suitable for patients with significant media opacity, large tears, GRTs, or posterior breaks.

RRD due to retinal hole or dialysis

Patients with retinal holes or dialyses respond well to scleral buckling, typically with segmental explants. Primary reattachment rates of up to 100% have been reported.

Vitrectomy

Machemer performed the first pars plana vitrectomy in 1971. Since then, significant progress has been made in our understanding of vitreoretinal pathology alongside improvements in microsurgical instrumentation and techniques. In the United Kingdom, vitrectomy is now the most commonly performed procedure for both simple and complex RRD.

Vitrectomy (**Figure 6**) is performed via three pars plana sclerostomy ports. Standard 20-gauge (0.9 mm) instruments are most widely used. The technique involves removal of vitreous with relief of vitreous traction at the site of retinal breaks, followed by intraocular drainage of SRF, application of retinopexy (cryotherapy or laser), and intravitreal injection of gas or silicone oil tamponade. Noncontact wide-angle viewing systems allow for superior depth of field, visualization, and break localization compared to scleral buckling. This is particularly useful in pseudophakic patients and those with media opacities.

RRD due to retinal tear

In both the UK and USA, vitrectomy has become the treatment of choice for RRD due to retinal tears as there is usually a preexisting PVD. This simplifies

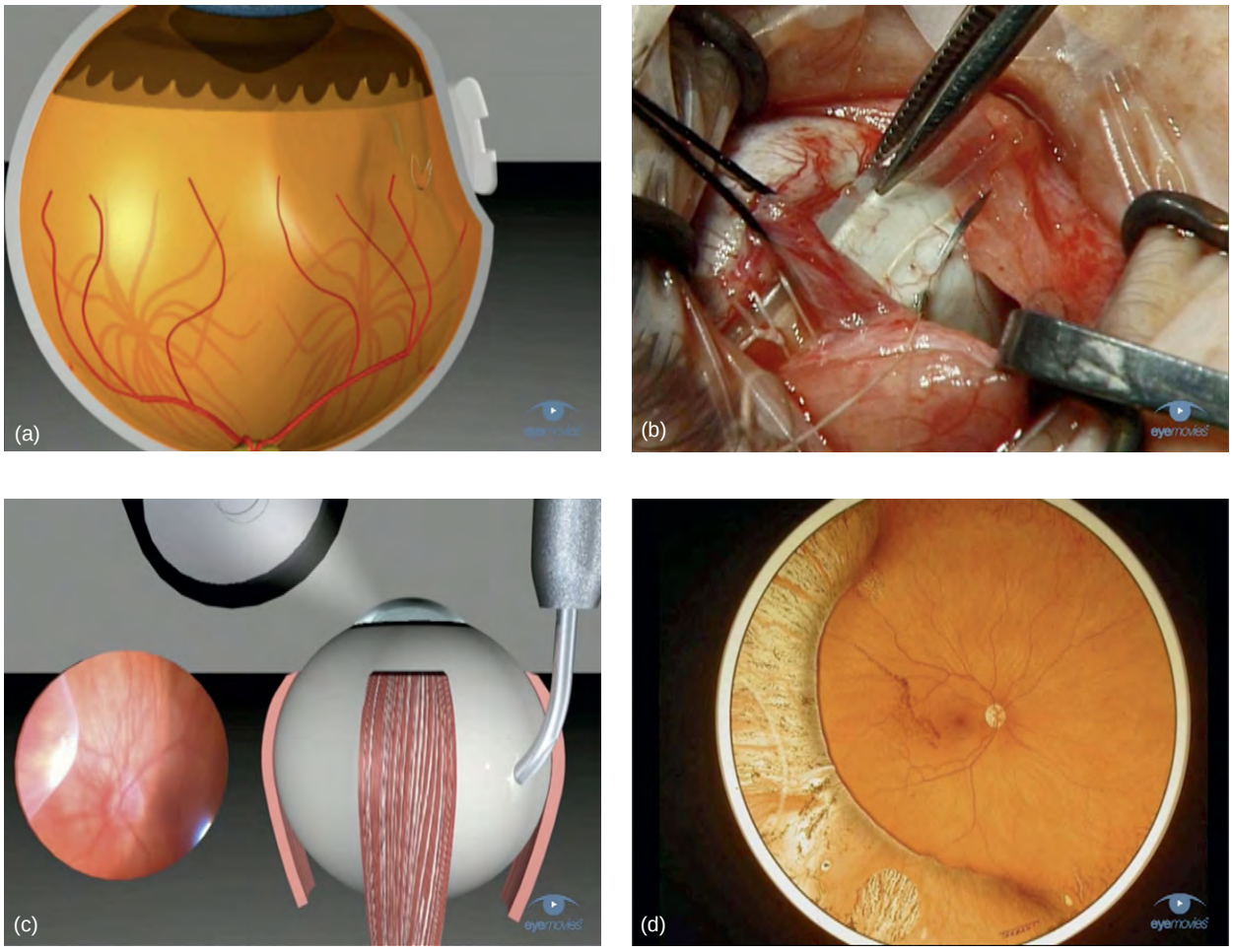

Figure 5 Scleral buckling surgery. (a) Schematic of explant placement on scleral surface. An underlying retinal tear is visible. (b) Silicone explant being secured to scleral surface using a 5/0 Ethibond suture. Part of the explant is positioned under a rectus muscle as shown. (c) Schematic of cryotherapy application to a retinal break viewing through an indirect ophthalmoscope. Inset photo demonstrates corresponding retinal whitening during cryotherapy application. (d) Schematic of postoperative scleral indent. Chorioretinal scars from previous cryotherapy are visible over the indent with successful retinal reattachment. Reproduced from Aylward, G. W., Sullivan, P. M., and Vote, B. (2007). *Vitreoretinal. Volume 1: Basic Techniques* (*DVD*). Surrey: Eye Movies, with kind permission from Eye Movies.

vitrectomy surgery as induction of a PVD is not required and direct relief of vitreoretinal traction at the tear can be achieved. A PVD is present in approximately 75% of people aged over 65. Therefore, the majority of patients with retinal tears is already presbyopic, minimizing the consequences of postoperative cataract formation.

RRD due to retinal hole or dialysis

Vitrectomy is rarely indicated in RRD secondary to retinal holes or dialyses, which usually have an attached vitreous. Surgically inducing a PVD in these typically young patients is often difficult, adding an unnecessary layer of complexity with increased risk of complications, for example, iatrogenic break formation. In addition, in the case of a dialysis, PVD induction would convert the break into a GRT.

Outcomes

Pneumatic Retinopexy

Pneumatic retinopexy is less invasive than scleral buckling or vitrectomy, with less local tissue damage and inflammation. Primary success rate in a selected patient group has been shown to be noninferior to scleral buckling in a multicenter, randomized, controlled trial by Tornambe and co-workers. A recent comprehensive review of 4128 eyes reported in the literature over a 21-year period (1986–2007) showed that pneumatic retinopexy has an overall primary retinal attachment rate of 74.4%, lower than scleral buckling or vitrectomy, with a final reattachment rate of up to 96.1%. Aphakic or pseudophakic patients appear to do less well, with primary retinal reattachment rates of 41–67%.

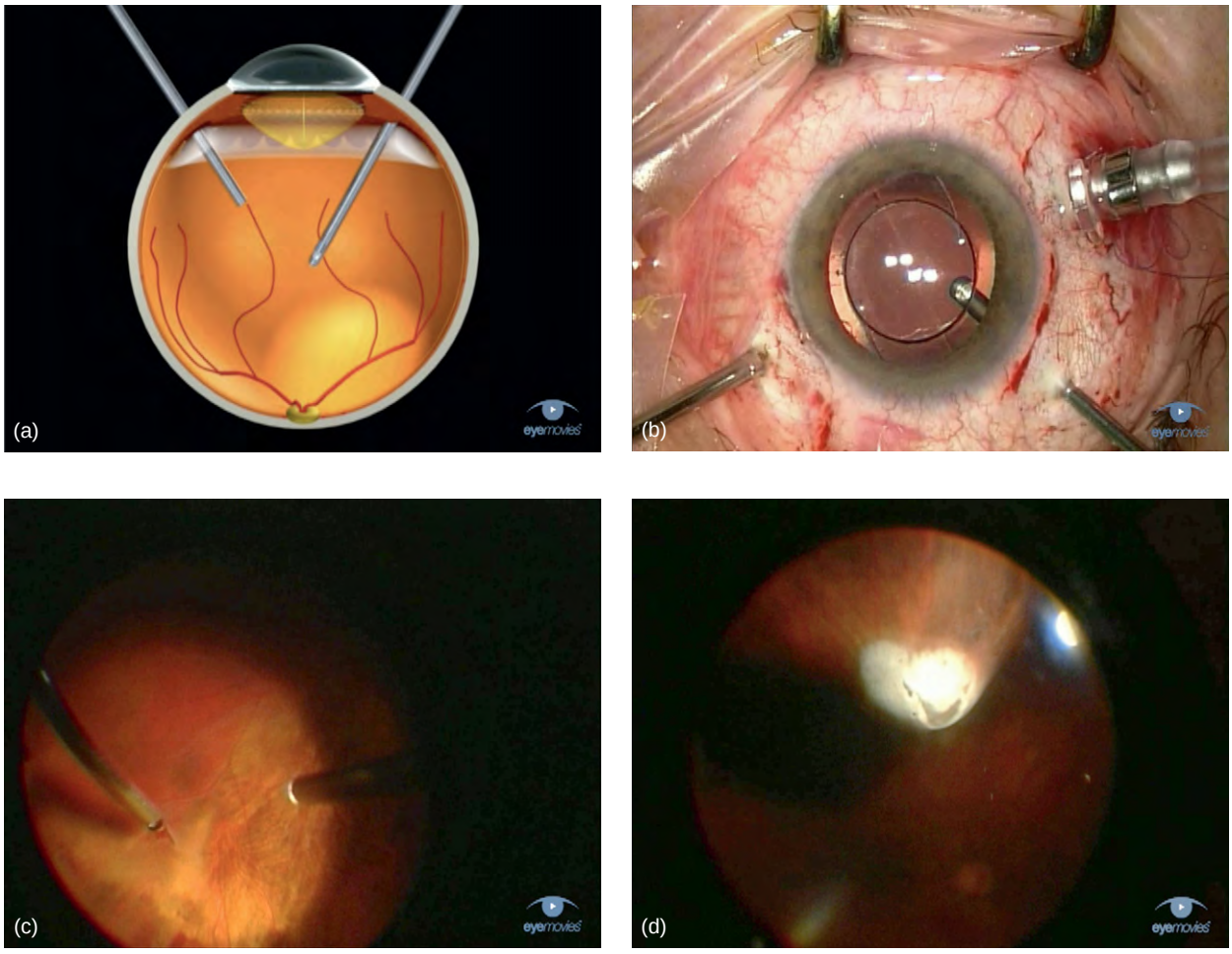

Figure 6 Pars plana vitrectomy. (a) Schematic of vitrectomy. Instruments are inserted 3.5–4mm posterior to the corneal limbus, entering the posterior segment through the pars plana. (b) Microscope view of standard instrumentation. Three scleral ports are usually required for vitrectomy. Instrumentation consists of a fluid infusion line, endoillumination, and vitrector (cutter). (c) Intraoperative view of vitrectomy for rhegmatogenous retinal detachment due to a retinal tear. Vitrectomy is being performed close to a retinal tear. (d) Intraoperative view of cryotherapy application to a retinal tear. Reproduced from Aylward, G. W., Sullivan, P. M., and Vote, B. (2007). *Vitreoretinal. Volume 1: Basic Techniques* (*DVD*). Surrey: Eye Movies, with kind permission from Eye Movies.

Scleral Buckling

Primary retinal reattachment occurs in over 90% of cases with scleral buckling alone, although up to 100% has been reported in small series. In patients with RRD and an attached macula, 90% achieve visual acuity of 20/30 or better at 6 months, although reduction in two Snellen lines of visual acuity occur in 10% despite anatomical success. Causes include macular epiretinal membrane and cystoid macular edema. Patients, who have their macular detached preoperatively, achieve a visual acuity of 20/50 or better in 38–71% of cases. A recent study involving foveal optical coherence tomography (OCT) imaging, by one of the authors (DGC), showed that postoperative resolution of foveal SRF can be delayed by over 6 weeks in 55% of patients, and complete resolution can take over 12 months. These patients have worse visual outcomes.

Pars Plana Vitrectomy

Primary retinal reattachment rates with vitrectomy are similar to scleral buckling, ranging from 65% to 100% with a mean of 85%. Final reattachment rate is 96–99%. Median visual acuity is 20/30 in macula-attached RRD, and 20/40 in macula-detached RRD. In an OCT imaging study by the same author (DGC), delayed resorption of foveal SRF was less common following vitrectomy, occurring in 15% of patients.

Complications

Intraoperative and postoperative complications for each procedure are discussed below.

Pneumatic Retinopexy

The main intraoperative complication of pneumatic retinopexy is formation of multiple small intravitreal gas bubbles or fish eggs during injection of gas, rather than a single large bubble as desired. This can result in subretinal gas migration, inadequate break tamponade, and treatment failure. This is principally managed by postoperative posturing to allow the gas bubbles to coalesce.

Postoperatively, new retinal break formation occurs in up to 20% of patients, and is a significant cause of surgical failure. PVR occurs in approximately 5% of patients.

Scleral Buckling

Intraoperative complications include inadvertent scleral perforation during suture placement, or SRF-drainage-related problems. Consequences include hypotony, choroidal or subretinal hemorrhage (with or without subfoveal tracking of blood), and retinal incarceration.

Postoperative complications include glaucoma, anterior segment ischemia (following encirclement), diplopia secondary to ocular dysmotility, change in refractive error and astigmatism, explant extrusion/intrusion or infection, and PVR. Contact lens users should be forewarned about possible lens-wear intolerance due to an irregular tear film and ocular surface following surgery, particularly as many patients who undergo scleral buckling are young myopes.

Pars Plana Vitrectomy

Intraoperative complications include iatrogenic retinal breaks, vitreous and retinal incarceration into the sclerostomy ports, lens trauma, and suprachoroidal hemorrhage.

Postoperatively, cataract formation is common and occurs in 81% of patients by 6 months. Raised IOP in the early postoperative period is common, and there appears to be an associated risk of late secondary glaucoma. PVR complicates between 5% and 12% of RRDs. Endophthalmitis following 20-gauge vitrectomy is rare.

Treatment Failure

In approximately 1 in 100 patients, it is not possible to reattach the retina despite multiple surgical attempts resulting in loss of vision. Consequences include chronic uveitis, rubeosis iridis, glaucoma, hypotony, band keratopathy, leukocoria, phthisis bulbi, and chronic ocular discomfort which may be severe enough to necessitate evisceration or enucleation of the eye.

New Developments

Smaller 25-gauge vitrectomy instruments were first introduced in 1990. Since then, techniques have evolved to enable sutureless transconjunctival surgery, with the benefits of reduced surgical time, less postoperative inflammation, more rapid wound healing, and improved patient comfort. As yet, small-gauge sutureless vitrectomy has not replaced 20-gauge systems, principally due to concerns regarding higher rates of endophthalmitis. A large retrospective series of 8601 patients from the Wills Eye Hospital demonstrated a 12-fold higher incidence of endophthalmitis with 25-gauge compared to 20-gauge vitrectomy. A smaller difference has been supported by other studies. Until this concern is adequately addressed, 20-gauge systems with conjunctival peritomy and suturing of ports will remain the gold standard.

The need for gas tamponade and postoperative posturing following vitrectomy for RRD has recently been challenged. A small prospective study of 60 patients by Martínez-Castillo and co-workers demonstrated a 98.3% primary reattachment rate without tamponade following complete drainage of SRF and laser retinopexy. This has not yet been supported by larger studies.

PVR remains to be the most important cause of failure of RRD treatment. Novel prophylactic treatment with adjunctive intraoperative 5-fluorouracil and low-molecular-weight heparin showed promise with decreased incidence of PVR in high-risk cases. However, this has not been reflected in unselected RRD undergoing primary vitrectomy, and may in fact be detrimental to visual acuity outcomes in patients with macula-attached RRD. Reducing the risk of PVR formation remains an important area of research.

See also: Proliferative Vitreoretinopathy.

Further Reading

Aylward, G. W., Sullivan, P. M., and Vote, B. (2007). *Vitreoretinal. Volume 1: Basic Techniques* (*DVD*). Surrey: Eye Movies.

Chan, C. K., Lin, S. G., Nuthi, A. S., and Salib, D. M. (2008). Pneumatic retinopexy for the repair of retinal detachments: A comprehensive review (1986–2007). *Survey of Ophthalmology* 53: 443–478.

Charteris, D. G. and Wong, D. (2007). The role of combined adjunctive 5-fluorouracil and low molecular weight heparin in proliferative vitreoretinopathy prevention. In: Kirchhof, B. and Wong, D. (eds.) *Vitreo-Retinal Surgery,* 1st edn., pp. 33–37. New York: Springer.

Kunimoto, D. Y. and Kaiser, R. S. (2007). Wills eye retina service. Incidence of endophthalmitis after 20- and 25-gauge vitrectomy. *Ophthalmology* 114: 2133–2137.

Lincoff, H. and Gieser, R. (1971). Finding the retinal hole. *Archives of Ophthalmology* 85: 565–569.

Machemer, R., Aaberg, T. M., Freeman, M., et al. (1991). An updated classification of retinal detachment with proliferative

vitreoretinopathy. *American Journal of Ophthalmology* 112: 159–165.

Martínez-Castillo, V., Zapata, M. A., Boixadera, A., Fonollosa, A., and García-Arumí, J. (2007). Pars plana vitrectomy, laser retinopexy, and aqueous tamponade for pseudophakic rhegmatogenous retinal detachment. *Ophthalmology* 114: 297–302.

Peyman, G. A., Meffert, S. A., and Conway, M. (eds.) (2007). *Vitreretinal Surgical Techniques,* 2nd edn. London: Informa UK.

Ryan, S. (ed.) (2006). *Retina, Vol. III: Surgical Retina,* 4th edn., 3 vols. Philadelphia, PA: Elsevier.

Wilkinson, C. P. and Rice, T. A. (eds.) (1997). *Michels Retinal Detachment,* 2nd edn. St. Louis, MO: Mosby.

Rod and Cone Photoreceptor Cells: Inner and Outer Segments

D H Anderson, University of California, Santa Barbara, CA, USA
D S Williams, UCLA School of Medicine, Los Angeles, CA, USA

Glossary

Cilium – An organelle that projects from a cell and contains a defined array of microtubules.
Electron microscope – A microscope that uses a particle beam of electrons to illuminate a specimen and create a highly magnified image. An electron microscope has much greater resolving power than a light microscope because the wavelength of an electron is much smaller than that of visible light.
Glycoconjugate – A class of carbohydrates covalently linked to proteins, lipids, and other types of molecules.
Mitochondrion – A cellular organelle that provides most of the chemical energy, in the form of adenosine triphosphate, for metabolism in eukaryotic cells.
Plasma membrane – A bilayer of lipid molecules that physically separates the interior of cells (i.e., cytoplasm) from the extracellular environment.

In this article, we focus on the organization of the photoreceptor inner and outer segments, with an emphasis on the structural similarities and differences between rods and cones. The process by which the photoreceptor outer segments replace their disk membranes; soma and synapse; and cilim, phototransduction, soluble protein dynamics, and the visual cycle are described elsewhere in this encyclopedia.

In the late nineteenth century, Schultze proposed an organizational framework for vertebrate photoreceptors that, today, has become a cornerstone of visual science. According to this duplicity theory, photoreceptors may be anatomically and functionally divided into two main groups: rods and cones. These terms emerged from early anatomical observations showing that the distal portions of photoreceptors, the so-called outer segments, are either cylindrical or conical in shape. However, it soon became clear that there were exceptions to the outer segment shape criterion, most notably in the foveas of some species where cone outer segments possess a distinct rod-like configuration. Therefore, with the passage of time, the definitions of rods and cones were relaxed somewhat to include the combined shapes of the outer and inner segments (**Figure 1**). More recently, light-sensitive ganglion cells without obvious outer segments have been identified.

Duplicity theory also stipulated that rods and cones may be distinguished functionally by the light levels to which they are tuned. Rods were regarded primarily as a sensitivity mechanism; whereas cones were considered to be an acuity mechanism, and a prerequisite for color vision. The predominance of rods in nocturnal species and of cones in diurnal species provided compelling evidence in support of this generalization.

With the advent of electron microscopy in the latter half of the twentieth century, it became apparent that there were also ultrastructural differences between rods and cones. In longitudinal sections, rod outer segments are visualized as a stack of hundreds of free-floating disks that resemble a stack of coins. The disk stack in rods is enclosed by, and separated from, the cell's plasma membrane, except at the base where new disks are formed (**Figure 2**, left). In cones, however, many and perhaps all of the disk membranes appear to be in continuity with the plasma membrane (**Figure 2**, right; **Figure 4**). This ultrastructural difference between rod and cone outer segments has been confirmed in a wide variety of vertebrates, and still remains a distinction with no known exceptions. In cross section, single-rod disks have a scalloped margin all of which are in alignment; in contrast, cone disks possess a single incisure that extends from the margin to the center of the disk.

The photoreceptor cell is the epitome of a specialized neuronal cell. It is dedicated to the absorption of light energy (photons) and transduction of that energy into an electrochemical signal that is transmitted throughout the retina and, ultimately, to the brain. The packing density of the inner and outer segments defines the spatial resolution of the retina. Where visual acuity is at a premium, the segments form a fine array, the density of which is limited only by the wave nature of light. Hence, in many retinas, the inner and outer segments are long, narrow structures that may be as small as 1 μm in diameter.

The photoreceptors form the outermost layer of the neural retina (**Figure 3**). Rod and cone outer segments are enveloped by microvilli (mv) that emanate from the apical surface of the retinal pigment epithelium (RPE). In rods, the outer segments abut the apical surface; but in many species, including humans, cone outer segments are slightly recessed from the apical surface (see **Figure 1**). A highly organized array of mv known as the cone sheath extends down from the apical RPE surface and ensheaths the cone outer segments. Cone outer and inner segments are also ensheathed by an extracellular matrix rich in glycoconjugates known as the cone matrix sheath (**Figure 4**). The inner segments lie between the outer segments and the photoreceptor cell nuclei. Broadly speaking, the inner segment provides the metabolic support for the outer segment.

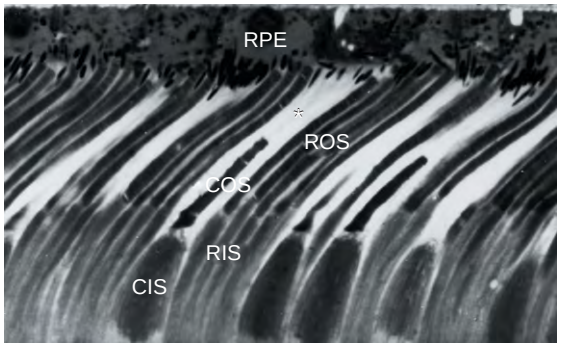

Figure 1 Light micrograph showing the photoreceptor cell layer in a monkey retina. RPE, retinal pigment epithelium; ROS, rod outer segment; RIS, rod inner segment; COS, cone outer segment; CIS, cone inner segment; *, cone sheath.

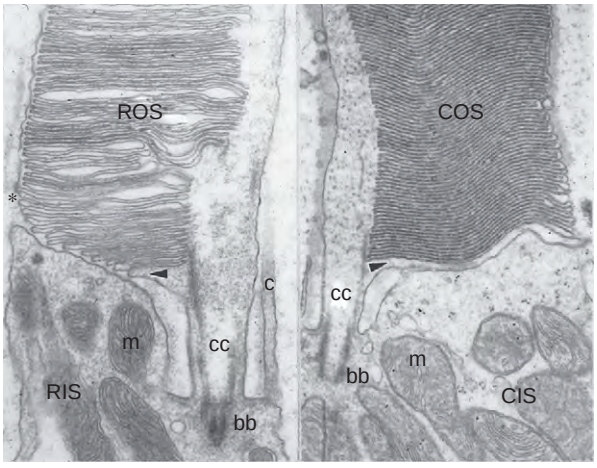

Figure 2 Electron micrographs illustrating the organization of disk membranes at the base of mammalian rod and cone outer segments. The only cytoplasmic link between inner and outer segments is through a connecting cilium. Arrowheads indicate growth points for the evagination of new disk membranes from the plasma membrane adjacent to the centric face of the connecting cilium. In cones, most disks retain a connection to the enclosing plasma membrane; whereas, in rods, only the most basal disks (below the asterisk) retain a plasma membrane connection. bb, basal body; c, ciliary process; cc, connecting cilium; CIS, cone inner segment; m, mitochondrion; RIS, rod inner segment.

The distal region of the inner segment, known as the ellipsoid, contains a high concentration of mitochondria that are excluded from the outer segment. The only cytoplasmic link between inner and outer segments is a connecting cilium (**Figure 2**). The proximal region of the inner segment, the myoid, is the primary site for the synthesis of proteins destined for the outer segment (**Figure 3**). Projecting from the lateral margin of the ellipsoid is an array of calycal processes containing longitudinally oriented, filamentous actin and myosin. In monkey cones, each ellipsoid contains an array of actin-containing cables that originate in the myoid region, converge as they course through the

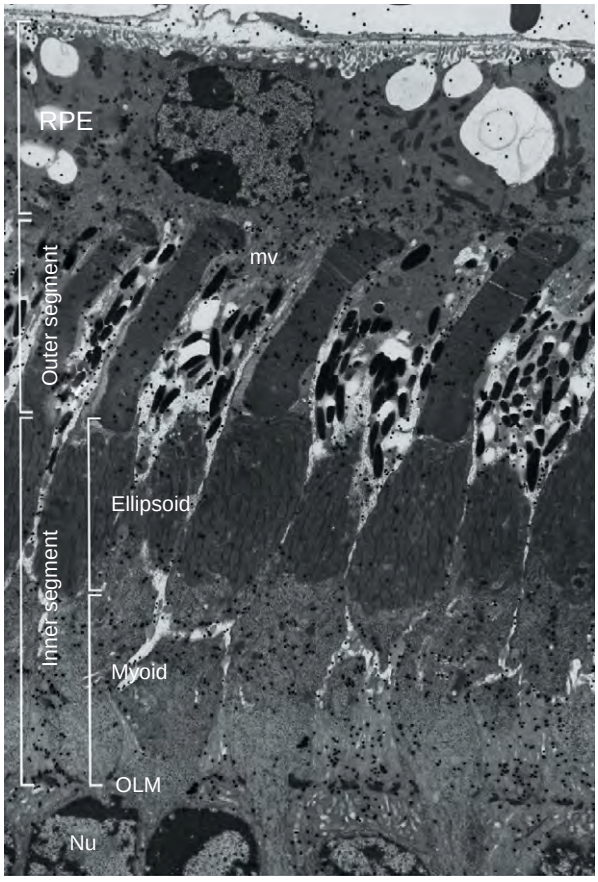

Figure 3 Low power electron microscopic autoradiogram of squirrel photoreceptors, illustrating the ellipsoid and myoid regions, the outer segments, and their relationship to the RPE. The black dots over the tissue are developed silver grains that signify sites of incorporation of a sugar residue (fucose) that had been labeled with a radioactive isotope (tritium). mv, microvilli; Nu, nucleus; OLM, outer limiting membrane; RPE, retinal pigment epithelium.

ellipsoid, and terminate within the calycal processes that form a circumferential ring at the base of the outer segments (**Figure 5**).

Just proximal to the myoid is the outer limiting membrane (OLM) (**Figure 3**). In longitudinal sections, the OLM appears as a demarcation line between the inner and outer retina. In reality, it is not a membrane but a series of aligned adherens junctions between photoreceptor cells, and between photoreceptor cells and adjacent radial glial cells (i.e., Mueller cells), that are linked to the cells' actin cytoskeleton. In lower vertebrates, the myoid region of the inner segment is quite labile, and is capable of expansion and contraction in response to changes in ambient lighting. These so-called retinomotor movements are considered to be a light-adaptive mechanism in many species of lower vertebrates.

Approximately 90% of the membrane protein in the rod disk and plasma membranes consists of the visual pigment opsin, a light-sensitive guanine nucleotide-binding protein

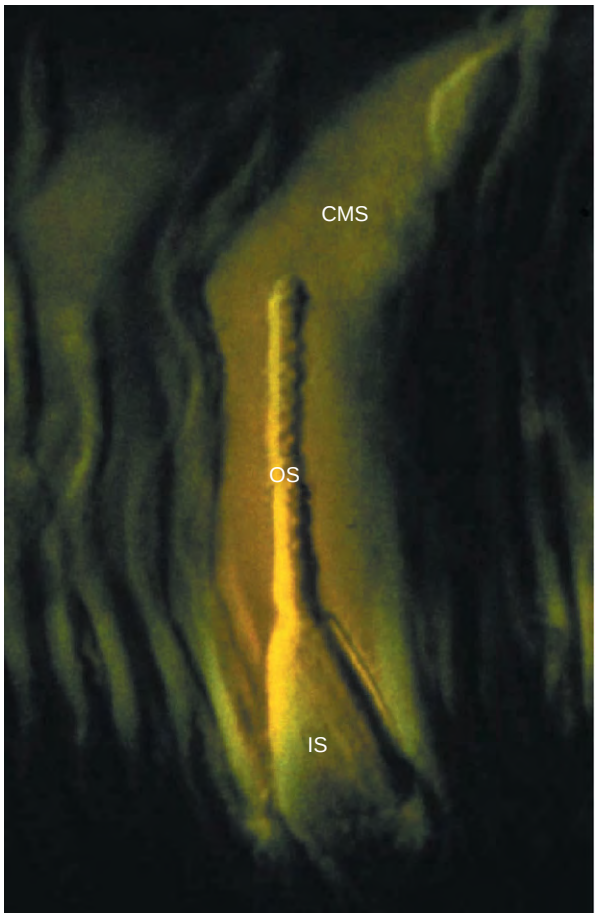

Figure 4 Longitudinal section of a human cone photoreceptor inner segment (IS) and outer segment (OS) labeled with a plant lectin (peanut agglutinin) conjugated to a fluorescent probe. The cone matrix sheath (CMS) (shown in yellow) is a distinct domain of the retinal interphotoreceptor matrix that is rich in glycoconjugates and envelops cone outer and inner segments. Modified from Hageman, G. S. and Johnson, L. V. (1991). Progress in Retina Research. In: Osborne, N. and Chader, J. (eds.) *Structure, Composition, and Function of the Retinal Interphotoreceptor Matrix*, Vol 10, Ch.9, p. 226.

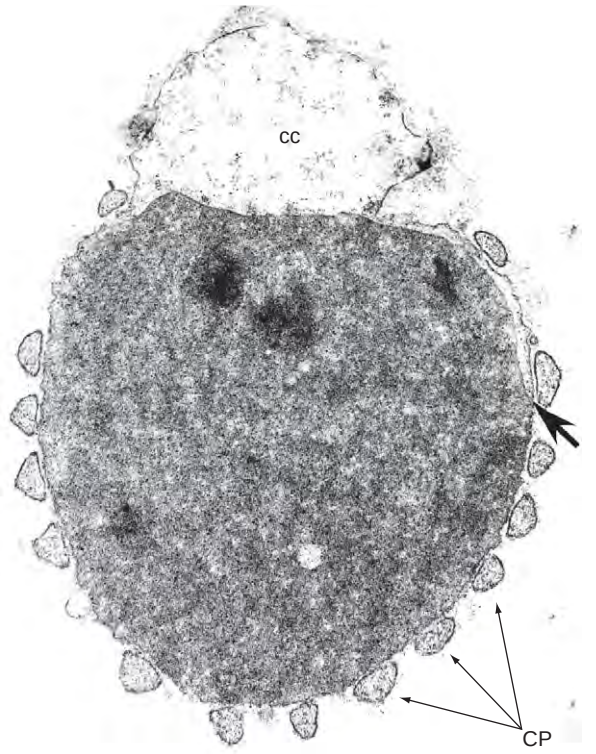

Figure 5 Electron micrograph of a tangential section through a monkey cone outer segment. The calycal processes (small arrows) that project from the ellipsoid form a basket at the base of the cone outer segment. At one point, the rim of the cone disk and the outer plasma membrane appear to be in continuity (large arrow), signaling a potential growth point. cc, connecting cilium; CP, calycal processes.

(G-protein)-coupled receptor. Cone outer segments contain homologous visual pigment proteins, also known as photopsins or iodopsins. Numerous other proteins that participate in the phototransduction cascade are also present in the outer segments. Rod outer segments, especially from bovine and rodent retinas, have been used widely in biochemical studies of structure and function. The ciliary connection between the inner and outer segments is quite fragile, such that outer segments are readily broken off in solution by shaking retinas that have been detached from the adjacent RPE. Following purification over a density gradient, relatively pure biochemical preparations of outer segments can be obtained. With additional steps, the disk and plasma membranes of rod outer segments can be separated from each other, and have thus been shown to contain some notable differences in protein composition. For example, the light-dependent cyclic nucleotide-gated channel and Na^+, K^+, Ca^{2+} exchanger proteins are restricted to the plasma membrane, while the retinal degeneration slow (peripherin/rds), rod outer segment membrane protein 1 (rom-1), and the ATP-binding cassette family A 4 (ABCA4) transporter proteins are present only in disk membranes. Opsin is present in both membrane domains. The disk membranes also contain two distinctive domains. Opsin is a ubiquitous component of rod disk membranes, except at their rims where a complex of peripherin/rds and rom-1 enables the formation of a loop that gives the disk its characteristic bilamellar structure.

In development, the outer segments form by repeated outgrowths or evaginations of the distal plasma membrane of the connecting cilium. In a mature photoreceptor cell, new rod and cone disks are also formed from evaginations originating from the centric face of the connecting cilium (**Figures 2** and **6**). The mature outer segment remains connected to the inner segment by what corresponds to the transition zone of the cilium, and what has been referred to historically as the ciliary stalk or connecting cilium. In recent years, it has been recognized that, while the photoreceptor cilium is highly unusual with its attached

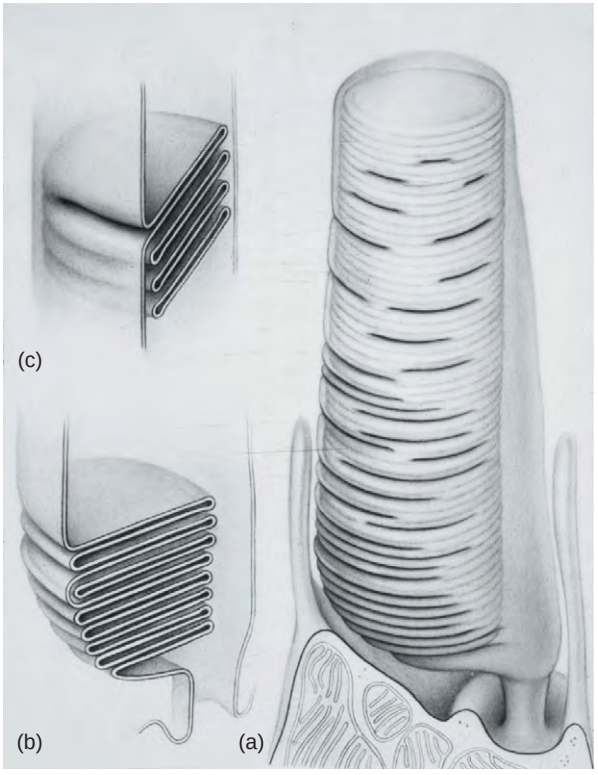

Figure 6 Schematic of the cone photoreceptor outer segment, inner segment, and connecting cilium (a). (b) Base of the cone outer segment and its relationship to the plasma membrane of the connecting cilium. (c) Illustration of the continuity between cone disks and the outer segment plasma membrane. From Anderson, D. H., Fisher, S. K., and Steinberg, R. H. (1978). Mammalian cones: Disc shedding, phagocytosis, and renewal. *Investigative Ophthalmology and Visual Science* 17(2): 130.

network of outer segment disks, it is homologous to other primary cilia located elsewhere in the body. For example, like other primary cilia, it possesses microtubule motor proteins that may function in the transport of outer segment components. There are numerous other proteins shared by primary cilia and photoreceptor cilia. Thus, despite the extraordinary specializations of the inner and outer segments, the connecting link between them is an organelle that is highly conserved. This point has been made most poignantly by demonstrations in a variety of syndromic disorders, such as Senior Loken and Bardet Biedel syndromes. These disorders are characterized, in part, by retinal degeneration, as well as kidney and other disorders, caused by mutations in genes which encode ciliary proteins that subserve shared functions.

See also: Circadian Photoreception; Cone Photoreceptor Cells: Soma and Synapse; Fish Retinomotor Movements; Light-Driven Translocation of Signaling Proteins in Vertebrate Photoreceptors; The Photoreceptor Outer Segment as a Sensory Cilium; Phototransduction: Adaptation in Rods; Phototransduction: Inactivation in Cones; Phototransduction: Inactivation in Rods; Phototransduction: Phototransduction in Cones; Phototransduction: Phototransduction in Rods; Phototransduction: The Visual Cycle; Rod and Cone Photoreceptor Cells: Outer-Segment Membrane Renewal; Rod Photoreceptor Cells: Soma and Synapse.

Further Reading

Anderson, D. H., Fisher, S. K., and Steinberg, R. H. (1978). Mammalian cones: Disc shedding, phagocytosis, and renewal. *Investigative Ophthalmology and Visual Science* 17(2): 117–133.

Besharse, J. C. and Horst, C. J. (1990). The photoreceptor connecting cilium: A model for the transition zone. In: Bloodgood, R. A. (ed.) *Ciliary and Flagellar Membranes*, pp. 409–431. New York: Plenum Press.

Cohen, A. I. (1970). Rods and cones. In: Fjuortes (ed.) *Handbook of Sensory Physiology,* vol. 7, part 1B, pp. 63–110. Berlin: Springer.

Molday, R. S. (2004). Molecular organization of rod outer segments. In: Williams, D. S. (ed.) *Photoreceptor Cell Biology and Inherited Retinal Degenerations.* Singapore: World Scientific Publishing.

Schultze, M. (1866). Anatomie und Physiologie der Nezhaut. *Archiv für mikroskopische Anatomie* 2: 175–286.

Spitznas, M. and Hogan, M. J. (1970). Outer segments of photoreceptors and the retinal pigment epithelium. *Archives of Ophthalmology* 84: 810–819.

Young, R. W. (1970). Visual cells. *Scientific American* 223: 80–91.

Rod and Cone Photoreceptor Cells: Outer-Segment Membrane Renewal

D S Williams, UCLA School of Medicine, Los Angeles, CA, USA
D H Anderson, University of California, Santa Barbara, CA, USA

Glossary

Autoradiography – A technique used to localize radioactivity emitted by cells, tissues, or organisms that have been treated or injected with a radioactive isotope.
Electron microscope – A microscope that uses a particle beam of electrons to illuminate a specimen and create a highly magnified image. An electron microscope has much greater resolving power than a light microscope because the wavelength of an electron is much smaller than that of visible light.
Lysosome – An organelle in a cell that contains digestive enzymes.
Phagocytosis – The engulfing and internalization of particles by a cell.
Retinal pigment epithelium – A single layer of pigmented epithelial cells that borders the back of the sensory retina. The outer segments of the photoreceptor cells interdigitate with the apical processes of the retinal pigment epithelium cells.

Based upon their observations of photoreceptor disk membrane-like inclusions in the cytoplasm of rodent retinal pigmented epithelial (RPE) cells, A. Bairati and N. Orzalesi proposed in 1963 that the disk membranes of photoreceptor outer segments were in a dynamic state of turnover. A few years later, in a classic series of autoradiographic studies, Richard Young and his colleagues provided the first direct evidence that vertebrate rod photoreceptors continually replace their disk membranes. Following injection of radiolabeled amino acids into a series of frogs, a transverse band of radioactive protein became apparent at the base of rod outer segments within 24 h following injection (**Figure 1**). We now know that the main proteinaceous component of the phototransductive disk membranes is the visual receptor, opsin. Over the ensuing days, the band became progressively displaced toward the tip of the outer segment, and eventually became evident in inclusions within the cytoplasm of the RPE cells. Electron microscopic observations later revealed that packets of disks derived from the tips of rod outer segments were engulfed by microvillous processes on the apical surface of the RPE cells and internalized into the RPE cytoplasm. These membrane-bound inclusions, called phagosomes, were then degraded by the RPE. Young proposed the term outer-segment renewal to refer to the overall turnover process. It encompasses a number of stages, including protein synthesis, transport to the outer segment, disk formation, disk displacement, shedding, phagocytosis and degradation, all of which result in the vectorial flow of membrane from the photoreceptor inner segment to the RPE (**Figure 2**).

Many cell types have short lives and are replaced on a regular basis. However in a terminally differentiated cell, such as a photoreceptor cell, the components must be turned over to prevent the formation and build up of macromolecular byproducts that can interfere with cellular function. Accordingly, it is widely believed that the turnover of phototransductive membrane is part of a normal preemptive process to replace macromolecules before they become dysfunctional. Because phototransductive membrane is typically an extremely amplified membrane system, its turnover involves an extraordinarily high rate of synthesis and degradation of membrane proteins. Some nocturnal arthropods provide the most extreme examples, with the turnover of nearly all of their phototransductive membrane each day. Even at the more pedestrian rate of 10% per day, as found in rodent and primate rods, the turnover of disk membranes represents a major metabolic challenge for the photoreceptor and RPE cells. In each human retina, which contains approximately 100 million photoreceptor cells, an average of 9 billion opsin molecules turn over every second. Not surprisingly, therefore, the processes involved in disk membrane turnover are critical for photoreceptor cell viability, as shown with some of the first-studied rodent models of retinal degeneration. For example, in the RCS rat, phagocytosis by the RPE is defective, and in the retinal degeneration slow (rds) mouse disk membrane morphogenesis is blocked; photoreceptor cell death and blindness ensues in both these models.

Whereas the experiments using radiolabeled amino acids convincingly demonstrated the renewal of the rod outer-segment membranes, and the involvement of the RPE in the degradation phase, the case for cone outer-segment renewal was less compelling. In contrast to rods, no discrete band of radioactivity was detected at the base of frog cone outer segments; instead, it appeared to be distributed diffusely throughout the cone outer segment. However, in the cones of diurnal rodents, quantitative electron microscopic autoradiographic studies showed that a

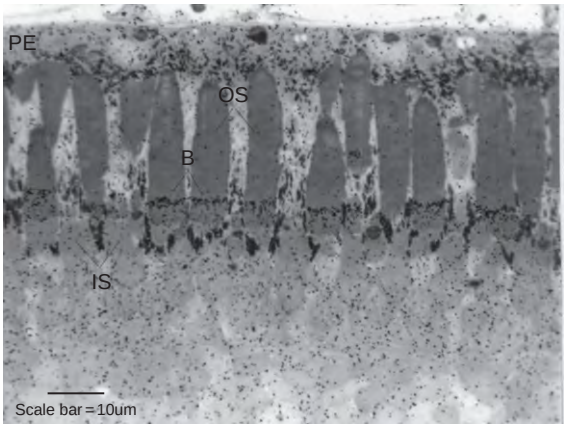

Figure 1 Light micrograph autoradiograph of a retina from a frog injected with radiolabeled amino acids, illustrating the band of radiolabeled protein (B) near the base of the outer segments (OS). IS, inner segments. Scale bar = 10 μm. From Hall MO, Bok D, and Bacharach ADE (1968) Visual pigment renewal in the mature frog retina. *Science* 161: 787–789.

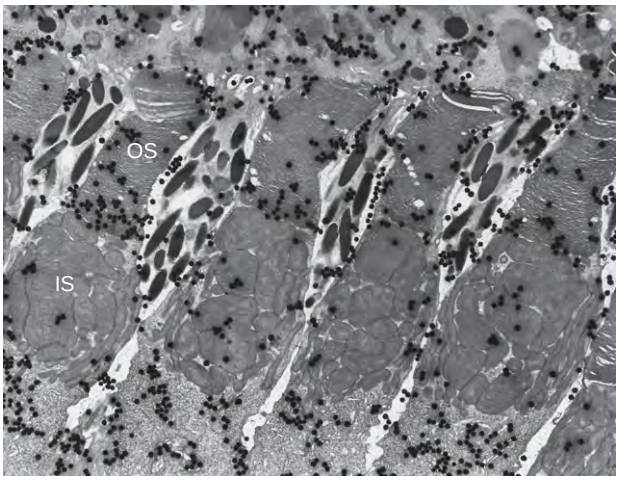

Figure 3 Electron micrograph autoradiograph of a retina from a ground squirrel, shortly after injection with radiolabeled fucose, illustrating the concentration of radiolabel near the base of the cone outer segments. OS, outer segment; IS, inner segment.

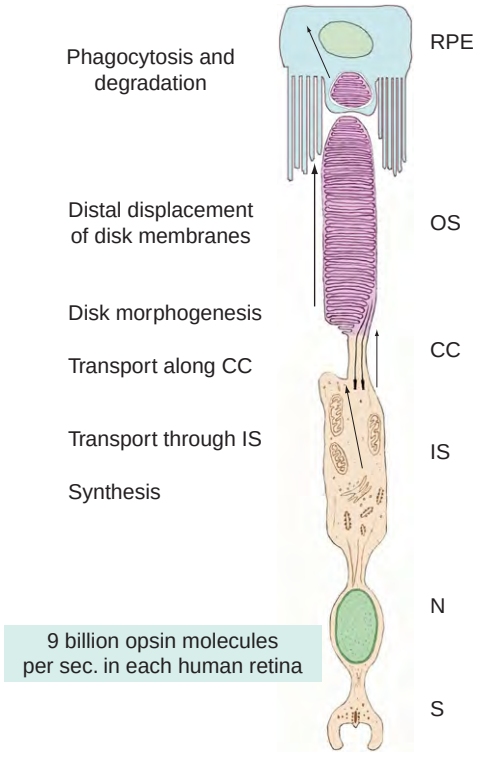

Figure 2 Illustration of the stages involved in the turnover of phototransductive membrane in vertebrate photoreceptor cells. Modified from Williams DS (2002) Transport to the photoreceptor outer segment by myosin VIIa and kinesin II. *Vision Research* 42: 455–462.

concentration of radioactive glycoconjugates could be detected in the proximal portion of cone outer segments within a few hours after injection of radiolabled fucose (Figure 3). In retrospect, it is now appreciated that the banding pattern in rods is due to the confinement of newly synthesized membrane proteins to rod disks, which mature into discrete units. In contrast, cone outer-segment disks remain interconnected, so that radiolabeled protein is free to diffuse longitudinally throughout the disk stack. Studies demonstrating the presence of disk shedding in cones, and the presence of phagosomes in RPE cells overlying regions of high cone density, such as in the human fovea and in all-cone retinas, also helped to demonstrate that the unidirectional flow of disk membrane proteins, from inner segment to outer segment, and then to the RPE, occurred in cones as well as rods.

The *de novo* synthesis of opsin-containing membranes occurs mainly in the proximal region of the inner segment (i.e., the myoid). Membranes containing newly synthesized protein are then transported from the *trans*-Golgi network, through the ellipsoid, to the base of the connecting cilium (Figure 2). Opsin contains motifs that appear to be important for its targeting to the outer segment. The best characterized are its C-terminal amino acids. Missense mutations that affect this region result in mistargeting of opsin and underlie forms of inherited retinal degeneration in humans. It seems likely that a molecular motor, like a dynein, which travels toward the minus ends of microtubules, is involved in this vectorial transport. In support of this notion is the finding that opsin binds to tctex-1, a light chain of dynein, *in vitro*. Further studies have reported roles for a number of other proteins that appear to be important for the targeting and fusion of membrane near the base of the cilium. These proteins include small GTPases, such as ADP ribosylation factor 4 (ARF4) and the RAS oncogene-related protein RAB8. It is likely that RAB8 promotes membrane fusion near the base of the cilium, and may be recruited to the post-Golgi membranes by a complex of Bardet–Biedl syndrome (BBS) proteins; mutations in BBS proteins are responsible for BBS, which includes photoreceptor degeneration

along with defects in cilia throughout the body. In photoreceptors that have a high rate of delivery of disk precursor membrane to the outer segment, the site of membrane fusion appears as a periciliary ridge complex, where the surface area of the plasma membrane has been greatly amplified by forming a series of ridges and grooves around the base of the cilium.

Transport along the cilium to the site of disk membrane morphogenesis involves molecular motors and associated proteins. Myosin VIIa, an actin-based motor, participates in this transport, although there is a clearer requirement for the kinesin-2 family of microtubule motors. In the absence of functional heterotrimeric kinesin-2, opsin delivery to the outer segment fails, and the ectopic build up of opsin causes rapid photoreceptor cell death. A homodimeric kinesin-2, KIF17, may also function in ciliary transport of outer-segment proteins. A group of intraflagellar transport proteins appear to function in concert with kinesin-2 motors. These proteins, which function in anterograde transport in primary cilia in other cells, are present in the photoreceptor axoneme, and IFT88 is required for the assembly and turnover of the outer-segment disk membranes. The specific cargoes of the different motor systems along the photoreceptor cilium are not known, but it is likely that there are a variety of different routes along the cilium. For example, evidence indicates that opsin and the rim-specific protein, peripherin-rds, are transported by different mechanisms.

Historically, the process of disk formation in rods was thought to result from an invagination of the outer plasma membrane toward the centric face of the connecting cilium. However, in 1980, an alternative evagination model of disk membrane morphogenesis was proposed that could account for disk morphogenesis in both rods and cones. Over the years, experimental evidence has been generated in support of this model. According to this model, as successive evaginations of new disk membrane occur, a second membrane growth phase forms the nascent rims around the newly formed evaginations. In rod cells, rim formation occurs relatively quickly, so that only a small number of disks at the base of the stack remain continuous with the outer plasma membrane. The vast majority of rod disks are discrete units that form a stack, completely surrounded by the plasma membrane. In cone cells, however, the process of rim formation remains incomplete and a connection(s) between the disk and the outer plasma membrane is retained in many, if not all cone disks.

Although there have been some challenges to the evagination model of disk membrane morphogenesis, some key observations provide strong support. First, in contrast to mature rod disks, the evaginating membranes can be labeled with tracer molecules, showing that they are open to the extracellular milieu. Second, the nascent disks contain specific membrane proteins that are not found in mature disks, and they lack the proteins added at the stage of rim formation. This latter observation indicates that there must be a mechanism(s) to sort different groups of outer-segment proteins prior to disk membrane morphogenesis.

Most cells are responsible for the complete turnover of their lipids and proteins. However, vertebrate photoreceptor cells are unusual in that they have recruited another cell type, the RPE cell, for the catabolic phase of disk membrane turnover. The disposal of the distal outer-segment disks requires an interaction between the photoreceptor and RPE cells. When the photoreceptors are detached from the RPE, the distal disks are not shed, indicating that disk membrane shedding and phagocytosis by the RPE are not independent events (**Figure 4**). In 1976, Matthew LaVail reported that rod disk shedding in rodents followed a daily rhythm, and that a peak of shedding was apparent near the

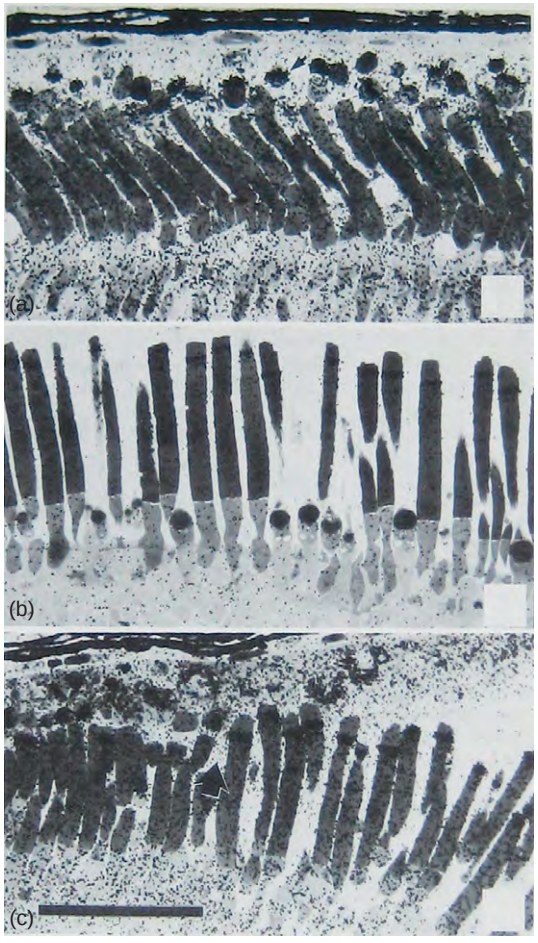

Figure 4 Light micrograph autoradiographs of retinas from frogs injected with radiolabeled amino acids. The band of radiolabel had migrated to the distal disks, and the eyecups were removed and placed in culture for the next shedding phase. Where the retina has remained attached to the RPE (a, and to the left of arrow in (c)), radiolabeled phagosomes are evident in the RPE. Where the retina was detached from the RPE (b, and to the right of arrow in (c)), the band of radiolabel is still evident at the distal end of each outer segment, indicating that the distal disks have not been shed. Scale bar = 50 μm. From Williams DS and Fisher SK (1987) Prevention of rod disk shedding by detachment from the retinal pigment epithelium. *Investigative Ophthalmology and Visual Science* 28: 184–187.

time of light onset. Subsequent studies have shown that the shedding of phototransductive membrane occurs at dawn in other vertebrates, as well as invertebrates. However, cone photoreceptors of most vertebrate species provide an exception to this rule; the peak of cone disk shedding typically occurs shortly after dusk (or light-offset). In crepuscular and nocturnal arthropods, the morphogenesis and shedding phases occur at dusk and dawn, respectively, resulting in different-sized light-absorbing structures (known as rhabdoms) between day and night. In this manner, the turnover of phototransductive membrane is coordinated to increase the efficiency of photon absorbance by individual photoreceptors at night.

The signaling mechanisms involved in the phagocytosis of disk membranes are not well understood; however, the requirement for a number of molecules has been determined. The c-mer proto-oncogene (*Mertk)* gene encodes a receptor tyrosine kinase, which is localized to the apical membrane of the RPE. In the absence of a functional form of this receptor, the ingestion of disk membranes does not occur, as is found in the retina of the RCS rat which carries a mutation in the *Mertk* gene. A role for the $\alpha v\beta 5$ integrin receptor and its ligand, milk fat globule EGF factor 8 (MFG-E8), has also been detected. This receptor appears to be required for the diurnal rhythm of shedding and phagocytosis since, in $\beta 5$ integrin knockout mice, disk membranes are still phagocytosed, but there is no peak of disk shedding at light onset.

Following internalization, the phagosomes are transported out of the apical region of the RPE where they subsequently fuse with lysosomes, and are degraded enzymatically. In mice lacking myosin VIIa, phagosome transport in the cytoplasm is impaired, thus indicating a role for this actin-based motor in the transport process. Microtubule motors also appear to be required in facilitating phagosome–lysosome fusion. A major enzyme in the degradation of opsin is cathepsin D, which is highly concentrated in the RPE lysosomes. Lysosomal enzymes have also been detected in RPE melanosomes, which may have a minor degradative role. The degradation of disk membrane proteins and lipids represents the end of the catabolic phase of the turnover process.

See also: Injury and Repair: Light Damage; Injury and Repair Responses: Retinal Detachment; Photoreceptor Development: Early Steps/Fate; The Photoreceptor Outer Segment as a Sensory Cilium; Phototransduction: Phototransduction in Cones; Phototransduction: Phototransduction in Rods; Phototransduction: Rhodopsin; Primary Photoreceptor Degenerations: Retinitis Pigmentosa; Rod and Cone Photoreceptor Cells: Inner and Outer Segments; Secondary Photoreceptor Degenerations: Age-Related Macular Degeneration.

Further Reading

Besharse, J. C. (1986). Photosensitive membrane turnover: Differentiated membrane domains and cell–cell interaction. In: Adler, R. and Farber, D. B. (eds.) *The Retina*, Part I, pp. 297–352. New York: Academic Press.

Deretic, D. (2006). A role for rhodopsin in a signal transduction cascade that regulates membrane trafficking and photoreceptor polarity. *Vision Research* 46: 4427–4433.

Insinna, C. and Besharse, J. C. (2008). Intraflagellar transport and the sensory outer segment of vertebrate photoreceptors. *Developmental Dynamics* 237: 1982–1992.

LaVail, M. M. (1976). Rod outer segment disk shedding in rat retina: Relationship to cyclic lighting. *Science* 194: 1071–1074.

Papermaster, D. S., Schneider, B. G., and Besharse, J. C. (1985). Vesicular transport of newly synthesized opsin from the Golgi apparatus toward the rod outer segment. Ultrastructural immunocytochemical and autoradiographic evidence in Xenopus retinas. *Investigative Ophthalmology and Visual Science* 26: 1386–1404.

Steinberg, R. H., Fisher, S. K., and Anderson, D. H. (1980). Disc morphogenesis in vertebrate photoreceptors. *Journal of Comparative Neurology* 190: 501–508.

Williams, D. S. (ed.) (2004). *Photoreceptor Cell Biology and Inherited Retinal Degenerations*, chs. 1, 3–6, and 13–15. Singapore: World Scientific Publishing.

Young, R. W. (1967). The renewal of photoreceptor cell outer segments. *Journal of Cell Biology* 33: 61–72.

Young, R. W. and Bok, D. (1969). Participation of the retinal pigment epithelium in the rod outer segment renewal process. *Journal of Cell Biology* 42: 392–403.

Rod Photoreceptor Cells: Soma and Synapse

R G Smith, University of Pennsylvania, Philadelphia, PA, USA

Glossary

Endocytosis – Active incorporation of external membrane into the cell, used to recover vesicular membrane that has fused with the external membrane at a chemical synapse.
Invagination – A permanent infolding of a cell's external membrane, associated in photoreceptors with their synaptic ribbons, and containing fine dendritic processes of bipolar and horizontal cells.
Mesopic – The 3-log unit range of background illuminance in which rod and cone signals temporally sum in cones and the cone bipolar pathway.
Poikilotherm – A species such as fish, turtles, and frogs whose body temperature varies with the environment.
Refractory period – A period immediately after an event, for example, the release of a vesicle of neurotransmitter, during which the next event cannot occur.
Rhodopsin – The rod pigment molecule that absorbs photons and starts the visual transduction cascade.
Ribbon – A presynaptic structure that collects vesicles of neurotransmitter for release.
Scotopic – The range of background illuminance from starlight to moonlight in which rods absorb one photon or less per integration time (~200 ms).
Spherule – The rod terminal, normally in the shape of a sphere, that contains synaptic ribbons.
Telodendria – Fine axonal processes extending laterally from the base of the cone terminal, which contact neighboring rod and cone terminals.

Introduction

Photoreceptors are the vertebrate retina's primary site for transduction of light into a neural signal. The rod photoreceptor is responsible for vision at night. Rods are essential for vision over the scotopic range (starlight through moonlight) into the mesopic range (twilight) where their signals mix with cone signals. In starlight they must transduce single-photon signals, but in twilight they function more like sensitive cones to temporally integrate photon signals and to adapt before finally saturating in bright daylight. The rod's exquisite combination of signal-processing mechanisms makes it a marvel of signal processing for a dedicated purpose.

Structure

Morphology and Topology

The rod is a specialized neuron consisting of an outer segment, inner segment, soma, axon, and axon terminal (Figure 1(a)). The biochemical pathways responsible for transducing light into an electrical signal are contained in the outer segment. The electrical signal passes to the inner segment where it is transformed by voltage-gated channels. The inner segment of the vertebrate rod lies just above the external limiting membrane. The rod soma lies in a variable location in the outer nuclear layer, connected to the inner segment above and the terminal below by the axon. For rods of most species, the soma is larger in diameter (~3–5 μm) than the outer segment. It contains the nucleus which holds the cell's DNA, necessary for development and to maintain the cell's biochemical machinery. Many mammalian species have ~20-fold more rods than cones, so the outer nuclear layer consists mainly of several layers of rod somas. Rods of most species fill the space between the cones, and are closely spaced (~100 000–200 000 mm^{-2}) to capture as many photons as possible.

Axon and Terminal

The rod axon, which carries the electrical signal from the soma to the axon terminal, varies in length depending on the species and the eccentricity (distance from central retina) of the rod. In para-foveal rods near the center of the primate eye, rod axons extend along with cone axons up to 200–400 μm laterally to allow the cone outer segments to be packed tightly together in the fovea and the axon terminals to be given adequate space outside the fovea to make their synaptic connections. In other mammals, the rod axon is shorter; in a cat it is vertical and typically extends ~50 μm through 6–10 layers of rod somas in the outer nuclear layer, and in guinea pig the axon is shorter, typically 10–25 μm, depending on the number of layers of rod somas. Typically, rod axons are ~0.5 μm in diameter, interspersed between rod somas and cone axons of 1–2 μm diameter (Figure 1(a)). The mammalian rod axon terminal is typically 2–3 μm in diameter, and is spherical; hence, it is

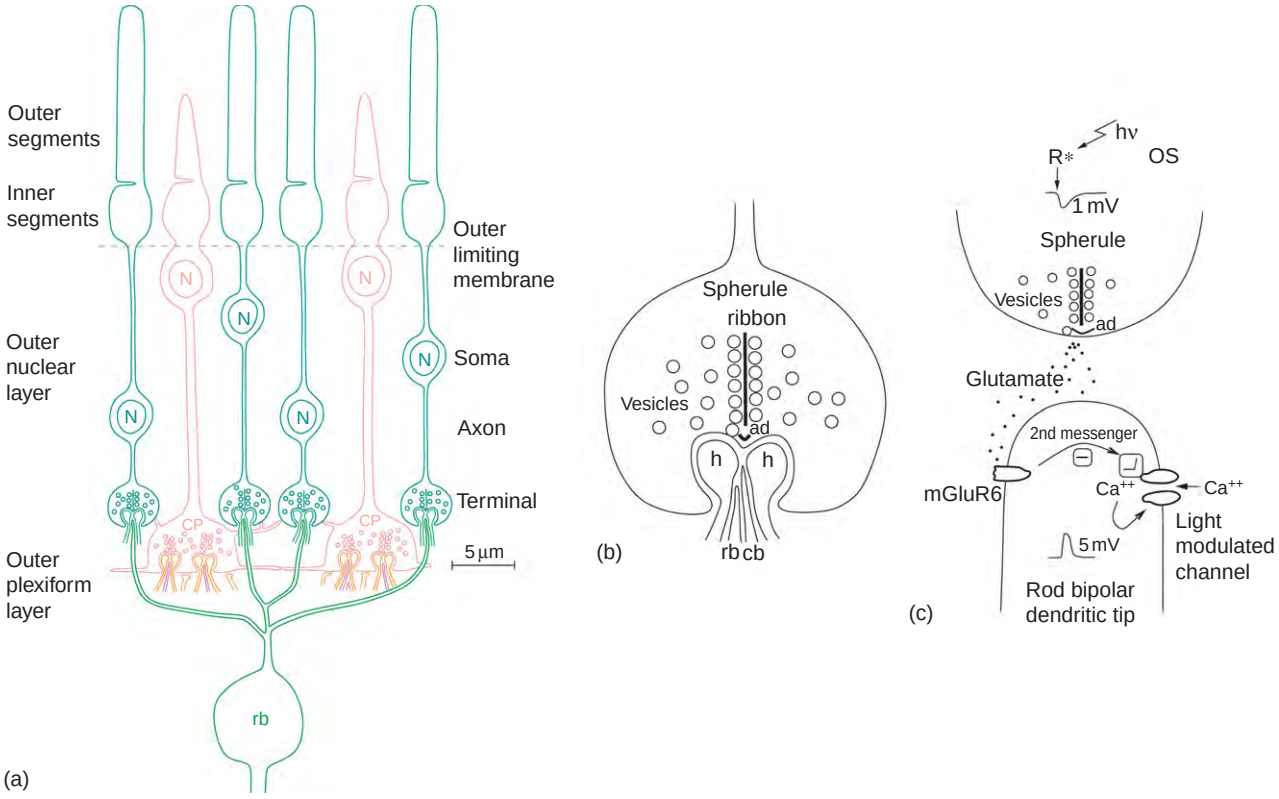

Figure 1 The rod is specialized to capture single photons in starlight but also functions in twilight. (a) Rods (blue-green) in most mammals and in distal primate retina extend vertically interspersed between cones (light red). The rod spherules are electrically coupled to cones at gap junctions on basal processes that emanate from cone terminals. At the bottom, a rod bipolar (green) collects signals from 20 to 100 rods, depending on the species. (b) The rod ribbon synapse sits at the apex of an invagination into the basal surface of the rod spherule. Attached to the ribbon are two rows of vesicles that contain glutamate. The vesicles are released at the active zone near the arciform density (ad). For each ribbon, two horizontal cell processes (h) and one invaginating rod bipolar cell dendrite (rb) extend into the spherule to receive glutamate from vesicles released at the ribbon. One type of OFF-cone bipolar (cb) also invaginates the spherule. (c) A photon absorption ($h\nu \rightarrow$ R*) in the rod outer segment (OS) generates a 1 mV hyperpolarizing signal, which travels down the axon to the rod spherule, where it slows glutamate release by the ribbon synapse. The glutamate level falls via transporters in the rod spherule's membrane and by diffusion out of the invagination. Glutamate unbinds from the mGluR6 receptors on the rod bipolar dendrite, which through an inverting second-messenger cascade opens the ion channel. The single-photon R* signal passes through two nonlinearities: the high-gain release of glutamate and the threshold nonlinearity in the second-messenger cascade. Calcium entering the rod bipolar's ion channel closes the channel after a delay, generating a ~5 mV response more transient than the rod's signal.

commonly called a spherule. The spherules of adjacent rods are located at different heights, allowing them to fit just above the cone terminals where they can be reached by cone telodendria and fine dendritic processes of bipolar cells.

Synapse

The rod makes chemical synaptic contacts onto one type of rod bipolar cell, one or more types of OFF-cone bipolar cell, and one type of horizontal cell at its axon terminal (**Figure 1(b)**). The synapse releases glutamate via small packets of membrane called synaptic vesicles, which are small (~30 nm) organelles, created by endocytosis from the cell's external membrane and filled with glutamate by transporter proteins. The vesicles diffuse freely around the cytoplasm while they are being filled. The presynaptic machinery in the terminal contains one or two dense structures called ribbons, because in cross section they are thin and extend vertically away from the cell's membrane, easily seen in electron micrographs or by confocal visualization of specific presynaptic proteins (ribeye, kinesin). The ribbon is thought to be a specialization to allow high release rates, for it collects several rows of vesicles and tethers them for release. The mechanism for vesicle release is complex and contains several dozen proteins, and its details are not yet understood, but it is known to be initiated by calcium ions binding to a receptor protein which causes the vesicle to fuse with the external membrane and thus release its contents into the extracellular space. The ribbon is thought to gather vesicles ready to be docked to provide a larger readily

releasable pool. As the rod is depolarized for long periods at night, its ribbon mechanism is specialized to release vesicles at a high rate continuously.

Invagination

The rod's ribbon synapse is located in a way similar to the cone's ribbon, in an extension of extracellular space into the bottom surface of the spherule called an invagination, where very fine processes of horizontal and bipolar cells extend to form postsynaptic specializations. Each invagination contains two ribbons, each of which is presynaptic to two horizontal cell dendrites from different horizontal cells. In addition, each ribbon is presynaptic to one rod bipolar cell, for a divergence from a rod to two rod bipolars. In addition, the rod terminal in some species contacts one or more types of OFF bipolar cells. The function of the invagination is unknown, but it has been suggested to limit diffusion of the neurotransmitter released by the cone or by horizontal cells for negative feedback.

Biophysical Properties

The inner segment and axon terminal of rods are similar to those of cones in that they contain several membrane-bound ion channels, including K_v, K_{Cn}, BK, and L-type Ca^{2+}. The K^+ channels (K_v, K_{Cn}, and BK) of the inner segment and soma are activated by depolarization, providing an outward current to balance the inward dark current through the light-modulated cyclic guanosine monophosphate (cGMP)-gated channels of the outer segment. These channels provide an adaptational influence, opposing the dark signal, and indirectly opposing the light signal by deactivating with hyperpolarization. The K_{Cn} channels in the soma, axon, and terminal underlying the hyperpolarization-activated current (I_h) provide a delayed depolarization when activated by hyperpolarization. The rod terminal's L-type Ca^{2+} channels ($Ca_v1.4$) uniquely include α 1F subunits and may have special gating properties in conjunction with CaBP4, a calmodulin-like binding protein that shifts the $Ca_v1.4$ gating activation curve to provide higher gain. In addition, the terminal contains a calcium-sensitive chloride current ($I_{Cl(Ca)}$) which provides signal enhancement because the chloride gradient is depolarizing in rods. However, the resulting chloride efflux is thought to downmodulate the calcium current. Further, the rod terminal contains a calcium-sensitive potassium current (BK) which limits depolarization and calcium entry, and calcium-induced calcium release (CICR) from internal stores which amplifies the internal calcium signal. The rod terminal contains a high-affinity calcium system which includes buffers, plasma membrane calcium ATPase pumps (PMCAs), ryanodine receptors, and inositol triphosphate (IP_3) receptors to modulate calcium release from internal stores. One possible reason for these specializations is that the calcium channels that trigger vesicle release must be modulated by a tiny single-photon signal and thus the system must have high gain. The rod terminal contains several transporters with special functions. Some of them transport glutamate, including at least two isoforms in the membrane of vesicles to load them with glutamate. A glutamate transporter sitting in the external membrane of the rod terminal is important for uptake of glutamate from the extracellular space.

Gap Junctions

The rod spherules in most vertebrates are electrically coupled by gap junctions to the neighboring cones. The gap junctions are made between the rod spherule and cone telodendria which are basal processes emanating from the cone terminals. This coupling allows rod signals to enter cones at twilight and to be carried through cone pathways to ganglion cells. In addition, rods in some, possibly all, mammals are directly coupled by small gap junctions which may reduce voltage noise in the rod terminal that originates in transduction and membrane ion channels.

Function

The Single-Photon Signal and Noise

The rod is faced with a difficult task. Vertebrate species active in night, such as most mammals, can see in starlight backgrounds when photons are rare and a rod receives a photon only every 20 min. Over the ~3-log unit range of scotopic backgrounds, a rod receives one photon or less per integration time (200 ms) so that its signal is binary. To generate a continuous visual image at such low backgrounds requires that signals from many rods be summed. A typical mammalian ganglion cell sums signals from several thousand rods, and can detect the signal from just one photon in that huge field. This extraordinary feat is a challenge because the single-photon signal is tiny, about 1 mV in amplitude. To detect such a tiny signal in a huge field of rods would be straightforward if all the rods were silent in the dark; but the mechanisms of transduction and synaptic transmission are noisy. The noise from the rods converging to a ganglion cell, if linearly summed with the single-photon signal, would completely mask it, preventing its transmission through the visual pathway. Therefore, the rod pathway has evolved mechanisms to remove the dark continuous noise before it is summed with photon signals.

Sources of Noise

The mammalian rod generates dark continuous noise of thermal origin in its transduction cascade with an amplitude of 10–30% of the peak single-photon signal.

In addition, the rod generates thermal isomerizations of its pigment molecule rhodopsin, called dark thermal events, at a rate equivalent to starlight on a cloudy night. The signals generated by dark thermal events are identical to the single-photon signal, so they appear as real photons from the visual environment and are sometimes referred to as dark light. Another source of noise is variability in the single-photon signal's amplitude. Further, the rod synapse generates robust noise from fluctuation in vesicle release, which masks single-photon events in a way similar to the dark continuous noise. These sources of noise would not be a problem for detecting a single-photon signal from one rod, but if the signals of more than 10 rods were linearly summed, the noise would mask the single-photon signal. To mitigate the problem, synaptic convergence in the rod pathway is accomplished in several stages. The first stage of convergence, from rods to the rod bipolar, is limited to between 20:1 and 100:1 depending on the species, but even this limited amount of convergence would mask the rod signal without special synaptic mechanisms.

Synaptic Transfer Function: High Gain and Temporal Filtering

The rod ribbon synapse is specialized to transmit the rod signal at scotopic backgrounds. It is thought to transmit a binary single-photon signal because, over the range of starlight to moonlight, single-photon events predominate, and when measured with brighter flashes, the variance of the rod bipolar response saturates at the single-photon level. The rod's presynaptic release function (vesicle release as a function of voltage) has very high gain, possibly as high as $\sim$1 mV e^{-1}-fold change, allowing the tiny single-photon signal to modulate a large fraction of the dark release rate. Indeed, the rod's calcium channels, high-affinity buffering, internal calcium stores, and PMCA are thought to participate in the high-gain release, to maximize modulation of vesicle release by the 1 mV hyperpolarization of the single-photon signal. In addition, the postsynaptic half of the rod synapse in the rod bipolar dendrite includes several mechanisms specialized for its unique single-photon function (**Figure 1(c)**). It contains a second-messenger cascade that inverts the signal. A photon signal causes a drop in the rod's glutamate release, which reduces glutamate binding to the postsynaptic mGluR6 receptor to deactivate the second-messenger cascade, opening the postsynaptic ion channels and depolarizing the rod bipolar. The second-messenger cascade includes several steps of temporal filtering, which remove the high-frequency components of the dark continuous noise. In some species (e.g., salamander), the synaptic filter in the rod synapse is $\sim$10-fold slower than the corresponding cone synapse. This matches the slower rod transduction response and allows more complete removal of the noise. In mammals, the light-modulated ion channel in the rod bipolar dendrite is blocked after a short delay by calcium entering the channel. The effect is to generate a transient that limits the duration of the light response in the rod bipolar.

Rate of Vesicle Release

The random release of vesicles by the rod ribbon is a major source of noise for the rod pathway. Although the details of the ribbon's release mechanism are not known, it is stochastic (noisy), similar to a modulated Poisson distribution, for which the standard deviation is equal to the square root of the mean. The rod's ribbon synapse is similar to other ribbon synapses in the cone and bipolar cell, but its challenge is simpler and yet more extreme. The rod's binary signal simplifies the requirements for the synapse; it must only transmit two discriminable levels, signifying the presence or absence of a photon. However, to transmit a discriminable level, the rod must drop its calcium level, in response to a 1 mV hyperpolarization, by a fraction adequate to modulate its random release by more than one standard deviation over the single-photon signal's rise time (100 ms). The rod's rate of vesicle release is thought to be $\sim$100 s^{-1}, equivalent to 10 vesicles in 100 ms, with a standard deviation of $\sim$3 vesicles, which would be adequate if the release were modulated by more than 30%, but the 1 mV single-photon signal is thought to modulate the rod's calcium channels by only 20%. This implies either (1) a higher release rate, for example, 250 ves/s, (2) a higher voltage gain for calcium-channel gating, (3) an unknown mechanism to remove vesicle fluctuation noise, or (4) an unknown mechanism for amplifying the single-photon signal so that it can modulate a greater fraction of release. There is some evidence of a refractory period that could generate more regular release. Protons released along with a cone photoreceptor's vesicles bind to the local calcium channels which may generate a short refractory period, allowing release to be more regular. If release in this case could be more regular than a Poisson distribution, it raises the question of why synaptic release is typically found to be Poisson-like.

Synaptic Transfer Function: Nonlinear Threshold

The second-messenger cascade in the rod bipolar dendritic tip contains a nonlinear threshold to process the single-photon signal embodied in the binding of glutamate to the mGluR6 receptor. The rod bipolar's dendritic ion channels do not open unless the rod signal rises above the nonlinear threshold. This mechanism removes much of the dark continuous noise remaining after the cascade's temporal filter. When the peak amplitude of the single-photon signal falls below the nonlinear threshold,

the photon signal is lost, resulting in a false-negative, reducing the quantum efficiency of vision. When the peak amplitude of the continuous dark noise rises above the nonlinear threshold, a false-positive event is generated, which may mask individual real photon events, confounding their detection. A high nonlinear threshold will reduce the false-positive rate, but cannot reduce the rate of dark thermal events because they are identical to real photon events. Therefore, the dark thermal rate will mask a low false-positive rate, obviating the need to reduce the false-positive rate to zero. The optimal level for the nonlinear threshold thus is a compromise between false-negative and false-positive rates, and depends on the level of continuous noise, the variability of the single-photon signal, and the thermal event rate. The optimal level for the threshold is suggested by some studies to be in the range of 0.4–0.8 times the peak amplitude of the single-photon signal, which will cause a false-negative rate of ~30–50%. In some studies, the optimal level was suggested to be 1.3 times the peak amplitude of the single-photon signal, thus losing most of the photon signals. The discrepancy between these studies emphasizes that not all the details of the rod synapse are understood. However, it is clear that when signals from 20 rods are summed in a rod bipolar cell, the nonlinear threshold reduces the noise level enough to allow a single-photon signal to be detected downstream in the visual pathway.

Electrical Coupling in Starlight

The electrical coupling between rods not only reduces their voltage noise by averaging their signals, but also reduces the amplitude of the single-photon signal. The amplitude of the single-photon signal is reduced proportionate to the equivalent number of rods, but the noise amplitude is reduced only by the square root of the equivalent number of rods coupled, which produces a net reduction in signal-to-noise ratio at each rod synapse. This type of lateral electrical coupling would not affect performance if the rod bipolar were to sum rod signals linearly, for example, without the nonlinear threshold, but in that case the noise would swamp single-photon signals as described above. The nonlinear synaptic threshold of the rod synapse depends, for its noise-reduction effect, on the amplitude of the single-photon signal, implying that electrical coupling between rods reduces the signal-to-noise ratio of the single-photon signal transmitted to the rod bipolar cell. This paradoxical result suggests that the gap junctions may be modulated by light or by the circadian clock. Alternately, the distribution of each single-photon signal to several nearby rod terminals by electrical coupling may allow vesicle fluctuation noise from rod ribbons to be averaged downstream. The amount of improvement in this case would depend on the gain and degree of nonlinearity and the amount of noise in rod vesicle release.

Electrical Coupling in Twilight

At mesopic backgrounds, rods receive ~1–1000 photons per integration time, so they temporally integrate photon signals and function more like cones except that their response gain is 30-to100-fold higher than the cone signal. As the rod synapse is specialized for single-photon signals and the rod bipolar pathway is specialized for high-gain spatial summation, the robust signals in rods at twilight need an alternate pathway. The electrical coupling between rods and cones allows twilight signals to pass from rods into neighboring cones and thence into cone pathways, where, as the background level increases, the rod component drops as rods saturate or adapt and the rod-cone coupling is downmodulated. In most mammals, the rod–cone coupling is not selective for cone type, so different cone spectral types have a similar rod contribution. This is convenient because opponent color signals computed by subtraction in retinal circuits can then remove the rod contribution. The mixing of the cone's signal with the higher-gain rod signal represents a form of adaptation because it extends by 2–3 log units the background range over which the cone ribbon synapse can transmit a signal. Rods of some species (frog, turtle, and fish) are much larger in diameter than mammalian rods and therefore, when warm, generate more dark thermal events and are more likely to receive multiple photon events at scotopic backgrounds; so in this case rod–rod coupling imitates mesopic cone–cone coupling and is advantageous. However, at low temperatures these poikilotherms (cold-blooded species) have a low dark thermal event rate and can respond to stimuli that evoke single-photon signals.

Negative Feedback

The rod ribbon synapse is similar to the cone ribbon synapse in that two horizontal cell dendritic processes are postsynaptic to each ribbon. The horizontal cell is the type B axon terminal (HBat; H1 in primate) which contacts only rods and is known to carry exclusively rod signals. The HBat is therefore considered to be electrically isolated from its cone-driven soma and dendritic tree. The function of this horizontal cell appendage is thought to be feedback to rods, but little evidence exists for negative feedback at the rod terminal. In salamander, the buffer 4-(2-hydroxyethyl)-1-piperazineethanesulfonic acid (HEPES) when applied in the perfusion bath *in vitro* blocks the shift in the calcium current originating in horizontal cells, suggesting that rod horizontal cell feedback functions in a way similar to cone horizontal cell feedback. The HBat collects from several hundred to several thousand rods, making it a good candidate to collect an average rod signal in starlight to control, through negative feedback, the rods' release of neurotransmitter. One likely possibility is that feedback to

rods helps to closely regulate the synaptic threshold for neurotransmitter release, to provide maximal gain for transmitting the tiny single-photon signal. Corroborating evidence for this role exists in recordings from ganglion cells at scotopic backgrounds where the antagonistic receptive field surround has been reported as hidden (summing nonlinearly with the receptive field center) and is only evident when a light stimulus is also applied to the center. This would be expected in the case where negative feedback from the HBat to the rod must pass through the rod synapse's nonlinear threshold to be sensed by the rod bipolar pathway.

Conclusion

The rod functions both at night and in twilight, but is specialized to transduce signals over the scotopic range of illuminance from starlight to moonlight where photons are rare. The single-photon signal is tiny and would be swamped by the dark continuous noise present in a large array of rods, but the rod ribbon synapse contains several mechanisms to reduce the noise and amplify the single-photon signal. Horizontal cells are thought to provide negative feedback at the rod synapse, and may provide a means to regulate the presynaptic release of neurotransmitter to optimize the single-photon signal. The balance between signal and noise in the rod's signal processing mechanisms is delicate. However, the rod's striking ability to capture and transmit single-photon signals suggests that each of its components has a specific function, and that biology has found for each a nearly optimal solution.

Acknowledgment

This work was supported by NEI grant EY016607.

See also: Physiology of Photoreceptor Synapses and Other Ribbon Synapses; Rod and Cone Photoreceptor Cells: Inner and Outer Segments.

Further Reading

Berntson, A., Smith, R. G., and Taylor, W. R. (2004). Postsynaptic calcium feedback between rods and rod bipolar cells in the mouse retina. *Visual Neuroscience* 21: 913–924.

Berntson, A., Smith, R. G., and Taylor, W. R. (2004). Transmission of single photon signals through a binary synapse in the mammalian retina. *Visual Neuroscience* 21: 693–702.

Field, G. D., Sampath, A. P., and Rieke, F. (2005). Retinal processing near absolute threshold: From behavior to mechanism. *Annual Review of Physiology* 67: 491–514.

Hagins, W. A., Penn, R. D., and Yoshikami, S. (1970). Dark current and photocurrent in retinal rods. *Biophysical Journal* 10: 380–412.

Heidelberger, R., Thoreson, W. B., and Witkovsky, P. (2005). Synaptic transmission at retinal ribbon synapses. *Progress in Retinal and Eye Research* 24: 682–720.

Hsu, A., Tsukamoto, Y., Smith, R. G., and Sterling, P. (1998). Functional architecture of primate cone and rod axons. *Vision Research* 38: 2539–2549.

MacLeish, P. R. and Nurse, C. A. (2007). Ion channel compartments in photoreceptors: Evidence from salamander rods with intact and ablated terminals. *Journal of Neurophysiology* 98: 86–95.

Migdale, K., Herr, S., Klug, K., et al. (2003). Two ribbon synaptic units in rod photoreceptors of macaque, human, and cat. *Journal of Comparative Neurology* 455: 100–112.

Okawa, H. and Sampath, A. P. (2007). Optimization of single-photon response transmission at the rod-to-rod bipolar synapse. *Physiology (Bethesda)* 22: 279–286.

Rodieck, R. W. (1998). *The First Steps in Seeing.* Sunderland, MA: Sinauer Associates.

Smith, R. G., Freed, M. A., and Sterling, P. (1986). Microcircuitry of the dark-adapted cat retina: Functional architecture of the rod–cone network. *Journal of Neuroscience* 6: 3505–3517.

Sterling, P. and Matthews, G. (2005). Structure and function of ribbon synapses. *Trends in Neuroscience* 28: 20–29.

Taylor, W. R. and Smith, R. G. (2004). Transmission of scotopic signals from the rod to rod bipolar cell in the mammalian retina. *Vision Research* 44: 3269–3276.

Thoreson, W. B. (2007). Kinetics of synaptic transmission at ribbon synapses of rods and cones. *Molecular Neurobiology* 36: 205–223.

van Rossum, M. C. W. and Smith, R. G. (1998). Noise removal at the rod synapse. *Visual Neuroscience* 15: 809–821.

Role of Complement in Ocular Immune Response

P Jha, P S Bora, and N S Bora, University of Arkansas for Medical Sciences, Little Rock, AR, USA

Glossary

Complement factor H (CFH) – It regulates the alternative pathway of complement activation.
Complement regulatory proteins (CRegs) – These regulate complement system.
Experimental autoimmune anterior uveitis (EAAU) – An animal model of human idiopathic autoimmune anterior uveitis.
Membrane attack complex (MAC) – The end product of complement activation that forms pore and cause lysis of cells.

Introduction

The complement system consists of a large group of plasma and membrane-bound proteins and is an important part of the innate immune system. It is critical for the defense against infection and in the modulation of immune and inflammatory responses. The components of the complement system can be divided into two categories: the first category is comprised of the proteins that initiate and participate in the activation of complement pathways, and the second category comprises the proteins that regulate complement activation (Figure 1). The proteins in the first category are present in an inactive form and are activated either by cleavage by other components or by conformational change in their structure leading to the activation of the complement cascade. The activation of the complement system leads to the release of biologically active peptides like anaphylotoxins (e.g., C3a, C4a, and C5a) and formation of membrane attack complex (MAC).

Activation of Complement System

The complement system can be activated via three distinct pathways, namely the classical, the alternative, and the lectin pathways. The classical pathway can be activated when complement component C1 (which is a complex of C1q, C1r, and C1s) binds to antigen-bound IgM or IgG or when it binds to substances such as C reactive protein. This binding induces changes in conformation of C1q, which results in sequential activation of C1r and C1s (both are serine proteases). The activated C1 complex then cleaves C4 and C2 to form the C4bC2a complex, which is called C3 convertase, because it cleaves C3. The alternative pathway provides a rapid, antibody-independent route of complement activation and amplification. In the alternative pathway, C3 is activated (cleaved) either directly by enzymes or spontaneously when it interacts with certain activating surfaces (e.g., zymosan and lipopolysaccharides). The membrane-bound C3b (cleaved fragment of C3) binds to complement factor B that is cleaved by complement factor D into Ba and Bb. The C3bBb complex then can cleave more C3 and thus activating and amplifying the whole complement cascade. The lectin pathway is activated by interaction of certain serum lectins, such as mannose-binding lectin (MBL), with mannose and *N*-acetyl glucosamine residues present surfaces of pathogens. The binding of lectins to mannose activates the MBL-associated serine proteases (MASP-1 and MASP-2) that are functionally similar to C1r and C1s of classical pathway. MASP-1 and MASP-2 then cleave C4 and C2 to generate C4bC2a complex (C3 convertase).

Although the complement system can be activated by three pathways, all the pathways converge to a common step that results in the formation of C3 convertase. After the C3 convertase is formed, the downstream process (also known as terminal pathway) is activated. Cleavage of C3 results in the release of the fragments C3a and C3b. C3b binds to the C3 convertase to form C5 convertase (C4b2a3b for classical as well as lectin pathway and C3bBb3b for alternative pathway). C5 convertase cleaves C5 into C5a and C5b. C5b binds to C6 to form C5b6 complex that subsequently binds to C7 and then C8. Once C8 is bound to the complex, then the C5b678 complex inserts into lipid membrane where several C9 molecules bind to the complex to form a pore-forming polymer on the membrane. The deposition of MAC on a cell surface such as those of bacteria causes the formation of pores in the membrane that leads to lysis of the cells.

Regulation of the Complement System

The second category of proteins of complement system comprises the family of proteins called complement regulatory proteins (CRegs). The activated complement system is not equipped to distinguish between self and non-self cells. Therefore, the complement system has a potential to also destroy self components if left unregulated. The body protects itself from complement-mediated damage by expressing various CRegs that regulate the complement system at different stages of the complement activation cascade. CRegs can be classified into two

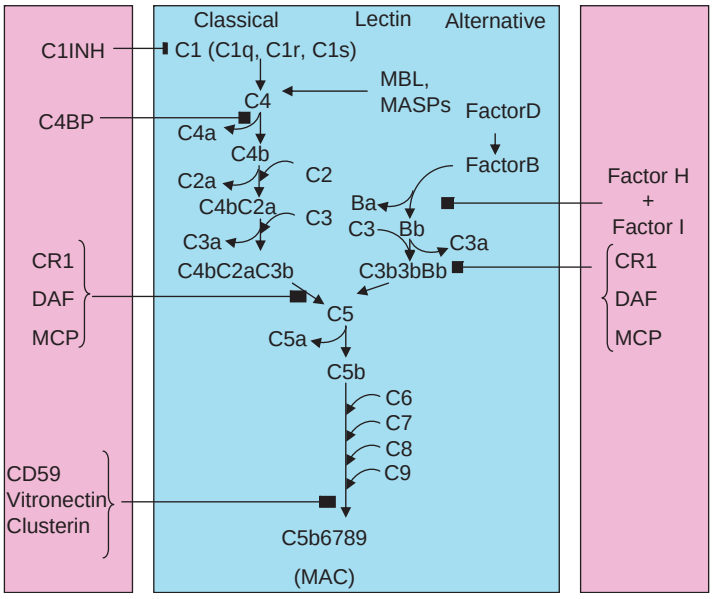

Figure 1 The complement system. Complement components and complement activation pathways are shown in the middle box. Complement regulatory proteins (CRegs) shown in the side boxes regulate the complement system at various check points.

categories: membrane bound and soluble proteins. Decay accelerating factor (DAF, CD55), membrane cofactor protein (MCP, CD46), complement receptor 1 (CR1, CD35), and membrane inhibitor of reactive lysis (MIRL, CD59) are important membrane bound CRegs. As mentioned before, these CRegs regulate the complement system by blocking/degrading the different components at various stages of the cascade. DAF regulates the activation of C3 and C5 and MCP acts as cofactor for factor I, which cleaves and inactivates C3b. CR1 has both DAF and MCP functions. CD59 regulates the assembly and function of MAC. Crry (512 antigen) is a membrane-bound CReg that is present only in rodents and has both decay accelerating and cofactor activities. C1 inhibitor (C1INH), C4-binding protein (C4bp), complement factor H (CFH), and complement factor I (CFI) are some of the important soluble CRegs. C1INH inhibits C1, whereas C4bp increases the cleavage of C4b by CFI. CFH is a cofactor for factor I-mediated cleavage of C3b and also has decay accelerating activity against the alternative pathway C3 convertase, C3bBb.

Complement System and Protection of Eye

The complement system is critical in protecting ocular tissues and is also involved in constant immune surveillance of the eye. A functionally active complement system that is activated at low levels is present in the normal eye even in the absence of any inflammation. Along with the functionally active complement system, several CRegs, such as DAF, MCP, CD59, factor I and factor H are also differentially expressed in eye. These CRegs are also functionally active and provide a perfect balance between the activation and regulation of the complement system. Any disturbance in this balance causes inflammation in the eye. For instance, if the CRegs present in the eye are inhibited, the activation of complement system is left unregulated and hence is amplified. This results in the inflammation of the eye. Similarly, if the complement system is activated by external factors such as zymosan, inflammation is initiated in the eye. This inflammation can be controlled by inhibiting the complement system. Therefore, the continuous presence of a functionally active complement system (i.e., finely regulated) ensures that a rapid immune response can be generated in case of a biological or chemical insult to the eye.

Complement System and Ocular Immune Responses

Ocular Tolerance

The eye is an immune-privileged site. If an antigen is introduced into the AC, there is a deviation of immune response to that antigen and systemic tolerance is developed against that particular antigen. This phenomenon is known as AC-associated immune deviation. Within the eye, iC3b, the activation product of C3, plays an important role in the generation and maintenance of tolerogenic/suppressive antigen-presenting cells (APCs). iC3b binds to complement receptor 3 (CR3) on the APCs (e.g., dendritic cells) and this interaction results in increased

expression of anti-inflammatory cytokines, such as TGF-β2 and IL-10, instead of inflammatory cytokines, such as IL-12. Thus, within the eye binding of iC3b to CR3 leads to the development of tolerance and ocular immune privilege.

Autoimmune Uveitis

Activation of complement system has been implicated in the pathogenesis of autoimmune anterior uveitis (AU) in humans and experimental autoimmune anterior uveitis (EAAU) in rats. EAAU is an animal model of human idiopathic AU and is induced in Lewis rats using antigens purified from the iris and ciliary body. There is a direct correlation between intraocular complement activation and disease activity in EAAU. In the EAAU model, the complement system is required to mount the antigen-specific CD4+ T-cell-mediated immune responses that cause inflammation in the anterior segment of the eye. The complement system contributes to the immune response in EAAU by regulating the production/expression of immune mediators, such as IFN-γ, IP-10, ICAM-1, and LECAM-1. The potential role of the complement in EAAU is summarized in **Figure 2**. In EAAU, the expression of various CRegs on ocular tissues is upregulated. If the function and/or expression of these CRegs is inhibited, then the inflammation is more severe and the duration of the disease is prolonged. This exacerbation of the disease is the result of excessive complement activation due to loss of regulation by CRegs. In the absence of CReg-mediated control of complement activation, more C3 convertases are formed, leading to more MAC formation and deposition. Apart from EAAU, the complement system also plays an important role in other animal models of uveitis such as experimental autoimmune uveoretinitis, which is an animal model for posterior uveitis. Although the complement system appears to be a potential target for therapeutic purposes, more research is required for designing anticomplement therapy to treat uveitis. Future studies identifying the contribution of each complement activation pathway will help in the development of more efficient and effective therapies for uveitis.

Complement and Age-Related Macular Degeneration

Age-related macular degeneration (AMD) is one of the leading causes of vision loss among the elderly population. As the name suggests, AMD is caused by the damage of macula that leads to the loss of central vision. There are

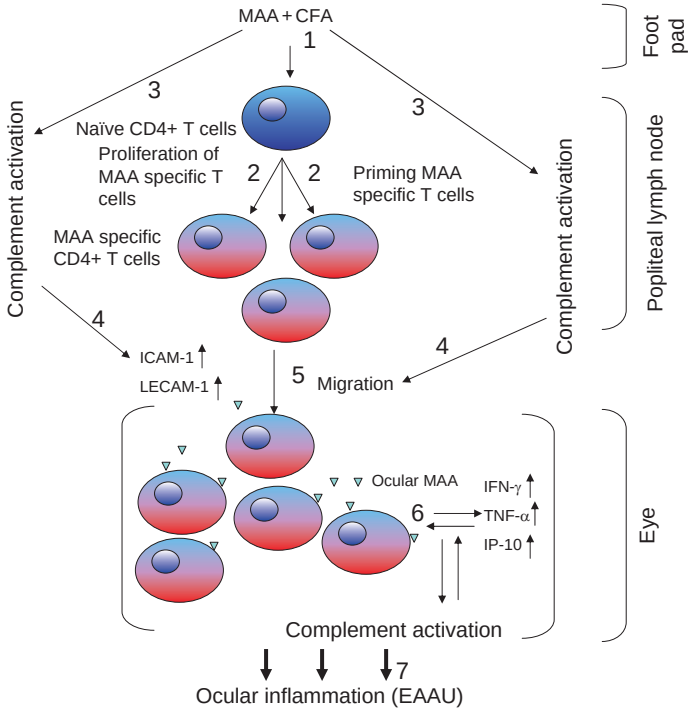

Figure 2 Role of the complement in EAAU. In EAAU animal model, ocular inflammation is induced by subcutaneous injection of melanin-associated antigen (MAA) emulsified in CFA (1) in the foot pad of male Lewis rats. This is followed by complement activation accompanied by priming and proliferation of MAA-specific $CD4^+$ T cells in popliteal lymph nodes (2). This step requires activation of the complement system because, in the absence of complement system, this step is inhibited. Complement activation (3) upregulates the expression of docking molecules like ICAM-1 and LECAM-1 (4), which results in migration of MAA-specific T cells to the eye (5). T cells recognize the MAA present within the eye and are further activated to express pro-inflammatory cytokines as well as chemokine (6). The complement system is also activated in the eye and results in ocular inflammation (7).

two types of AMD: dry (nonneovascular) and wet (neovascular). Studies conducted during the past 5 years have established that AMD is also an immunologic disease, as the complement system plays an important role in its development and its pathogenesis. In humans, unregulated complement activation is central to the pathogenesis of both types of AMD. In dry AMD, complement activation products are elevated in patient's serum. Drusen are the abnormal extracellular deposits underneath the basal surface of retinal-pigmented epithelium. The complement system has been implicated in the formation of drusen and various complement activation products (C3a, C5a, and MAC), and complement regulatory proteins (factor H, CR1, CD46, and Vitronectin) are present in drusen of patients with AMD.

One of the most convincing pieces of evidence that the complement system plays a central role in the immunopathogenesis of AMD is the association between polymorphisms of the complement factor H gene (HF1) and significantly increased risk of AMD in humans. This polymorphism occurs at position 402 of the codon-encoding factor H. If at this position a tyrosine residue is present, then the risk of AMD is reduced. However, if at this position a histidine residue is present, then there is a significantly higher risk to develop AMD. The variant of factor H with a tyrosine residue at position 402 (CFH_{YY402}) is called a protective variant and the variant with a histidine at position 402 (CFH_{HH402} or CFH_{YH402}) is called the risk variant for AMD. Due to the variation, the risk variant is less efficient in regulating the complement system compared to the protective variant. The replacement of a tyrosine residue results in a decreased ability of factor H to degrade C3. A similar polymorphism in complement component C2 and factor B is also associated with AMD. As mentioned before, both of these components belong to the first category of the complement system that participates in its activation. However, the effect of risk variation in these two complement components on their activity is different from that of factor H. In the case of factor H, the mutation that leads to the risk variant reduces the activity of factor H. In contrast, the mutation in the risk variant of factor B and C2 results in increased activity of these components. A reduction in complement activity of factor H and an increase in activity of factor B and C2 result in an overall increase in complement activation that initiates the inflammatory cascade and drusen formation in AMD.

The second form of AMD is wet AMD. Choroidal neovascularization (CNV) is the hallmark of wet AMD. The immunopathology and therapeutic strategies to treat wet AMD have been explored using various animal models of this disease. CNV can be induced in animals by rupturing Bruch's membrane with laser photocoagulation. In this animal model, the complement system plays an important role in CNV. The final product of complement activation, the formation of the MAC, is critical for the immune process leading to the development of CNV. Mice that are deficient in complement components C3 (C3−/−) do not develop CNV after laser photocoagulation. C3 is a key component of the complement system and is indispensable for the formation of MAC. In C3−/− mice the MAC formation is inefficient because of the unavailability of C3. If C3 is depleted in wild-type mice by administering cobra venom factor or if the MAC formation is inhibited directly by blocking complement component C6, the development of laser-induced CNV is inhibited. MAC formation is critical for the upregulation of various mediators of angiogenesis, such as VEGF, TGF-β2, and β-FGF. As mentioned earlier, MAC can be formed by classical, alternative, or the lectin pathways of complement activation. However, only alternative pathway activation is responsible for MAC formation and development of laser-induced CNV in mice (**Figure 3**). Similar to dry AMD in humans, factor B and factor H play an important role in the pathogenesis of laser-induced CNV in mice. Factor H levels decrease and factor B levels increase during CNV, which again demonstrates the importance of the critical balance between the complement activation and regulation in ocular immune responses. The importance of regulation of the complement system in the development of CNV is further evident by the decrease in the levels of CD59 (regulator of MAC) in eyes with CNV. Furthermore, laser-treated animals fail to develop CNV if CD59 is replenished by administration of exogenous recombinant CD59.

Keratitis

The cornea is the first barrier that protects the ocular tissue from the various insults including biological and

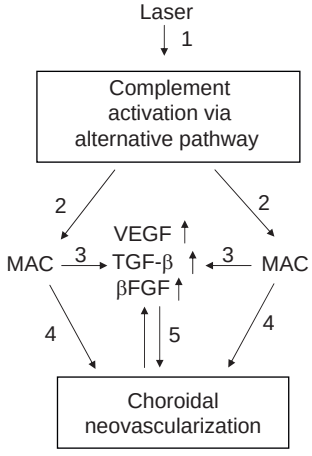

Figure 3 Role of the complement in CNV. The injury caused by laser treatment activates the complement system via the alternative pathway in the posterior segment of the eye (1). The activation of complement system leads to formation of MAC (2). MAC deposition on the cell surface leads to increased expression of growth factor (3). Increased production of growth factors and MAC deposition leads to the development of CNV (4).

environmental. Chronic activation of the complement system in the cornea ensures that this tissue is protected from various insults. It is due to the robust nature of the complement system, rapid activation and amplification of this defense system is possible in the case of any pathological condition, such as bacterial infection. The complement system is required to mount an immune response and protect the cornea from *Pseudomonas aeruginosa* infection. *P. aeruginosa* is the most common causative agent of microbial keratitis. However, unlike autoimmune uveitis and AMD, MAC does not play a critical role in protection against *P. aeruginosa* in microbial keratitis. The complement component C3 and functions associated with it, such as opsonization and regulation of phagocytosis, are important in protecting the cornea during microbial keratitis.

Glaucoma

Glaucoma is a leading cause of vision loss world-wide. Glaucoma is characterized by the slow, progressive loss of retinal ganglion cells and their axons, and by progressive excavation of the optic nerve head resulting in the loss of vision. Elevated intraocular pressure (IOP) is an important risk factor for glaucoma. Recent studies implicate autoimmune mechanisms in the development of glaucoma with the complement system as a key player. These studies provide an autoimmune basis for the development and progression of glaucoma. In animal models of glaucoma, inhibition of complement activation protects the optic nerve from damage induced by increased IOP. Furthermore, the complement component C1qs appear to play a major role in the immunopathogenesis of glaucoma, both in humans and rodents.

Retinal Disorders

The complement system has been implicated in the pathogenesis of several other retinal disorders, such as diabetic retinopathy, light-induced photoreceptor damage, and proliferative vitreoretinopathy (PVR). Unregulated complement activation, due to the loss of complement regulator, results in increased MAC formation. This leads to increased permeability and apoptosis of choriocapillaries in diabetic retinopathy.

Unregulated activation of the alternative pathway plays a critical role in the light-induced damage of photoreceptor cells in the retina. The regulation as well as the activation of alternative pathway is very important in the protection as well as maintenance of normal function of the retina.

PVR is another ocular disorder that affects the retina and complement activation has been associated with its pathogenesis in humans. Future studies investigating the exact role of the complement in the pathogenesis of PVR using animal models would help us understand and design better strategies to manage and treat PVR.

Acknowledgments

This work was supported by NIH grants EY016205 and EY 014623 and Pat and Willard Walker Eye Research Center, Jones Eye Institute, Little Rock, AR.

See also: Immunobiology of Age-Related Macular Degeneration; Immunopathogenesis of Experimental Uveitic Diseases; Innate Immune System and the Eye.

Further Reading

Atkinson, J. P. and Farries, T. (1987). Separation of self from non-self in the complement system. *Immunology Today* 8: 212–215.

Bora, N. S., Gobleman, C. L., Atkinson, J. P., Pepose, J. S., and Kaplan, H. J. (1993). Differential expression of the complement regulatory proteins in the human eye. *Investigative Ophthalmology and Visual Science* 34(13): 3579–3584.

Bora, N. S., Jha, P., and Bora, P. S. (2008). The role of complement in ocular pathology. *Seminars in Immunopathology* 30(2): 85–95.

Bora, N. S. and Kaplan, H. J. (2007). Intraocular diseases – anterior uveitis. *Chemical Immunology and Allergy* 92: 213–220.

Frank, M. M. and Fries, L. F. (1991). The role of complement in inflammation and phagocytosis. *Immunology Today* 12: 322–326.

Grisanti, S., Wiedemann, P., Weller, M., Heimann, K., and Zilles, K. (1991). The significance of complement in proliferative vitreoretinopathy. *Investigative Ophthalmology and Visual Science* 32(10): 2711–2717.

Jha, P., Bora, P. S., and Bora, N. S. (2007). The role of complement system in ocular diseases including uveitis and macular degeneration. *Molecular Immunology* 44(16): 3901–3908.

Jha, P., Sohn, J. H., Xu, Q., et al. (2006). Suppression of complement regulatory proteins (CRPs) exacerbates experimental autoimmune anterior uveitis (EAAU). *Journal of Immunology* 176(12): 7221–7231.

Morgan, B. P. and Harris, C. L. (1999). The complement system. In: Morgan, B. P. and Harris, C. L. (eds.) *Complement Regulatory Proteins*, pp. 1–13. San Diego, CA: Academic Press.

Ross, G. D. (1986). *Immunobiology of the Complement System*. Gainesville, FL: Academic Press.

Skerka, C., Lauer, N., Weinberger, A. A., et al. (2007). Defective complement control of factor H (Y402H) and FHL-1 in age-related macular degeneration. *Molecular Immunology* 44(13): 3398–3406.

Sivaprasad, S. and Chong, N. V. (2006). The complement system and age-related macular degeneration. *Eye* 20(8): 867–872.

Sohn, J. H., Bora, P. S., Suk, H. J., et al. (2003). Tolerance is dependent on complement C3 Fragment iC3b binding to antigen-presenting cells. *Nature Medicine* 9(2): 206–212.

Sohn, J. H., Kaplan, H. J., Suk, H. J., Bora, P. S., and Bora, N. S. (2000). Complement regulatory activity of normal human intraocular fluid is mediated by MCP, DAF, and CD59. *Investigative Ophthalmology and Visual Science* 41: 4195–4202.

Stein-Streilein, J. and Streilein, J. W. (2002). Anterior chamber associated immune deviation (ACAID): Regulation, biological relevance, and implications for therapy. *International Reviews of Immunology* 21(2–3): 123–152.

Role of Proteoglycans in the Trabecular Meshwork

T S Acott, K E Keller, and M J Kelley, Oregon Health and Science University, Portland, OR, USA

Glossary

Aqueous humor outflow resistance – A poorly understood physical resistance to aqueous humor outflow as it exits through the trabecular meshwork. This resistance is responsible for regulating intraocular pressure.
Extracellular matrix – The structural environment supporting and surrounding most cells that is comprised of a complex and highly organized group of many specialized proteins, glycoproteins, proteoglycans, and glycosaminoglycans.
Glycosaminoglycan – A highly charged carbohydrate chain composed of distinctive disaccharide repeats.
Juxtacanalicular or cribriform region – The deepest 10–20-μm-thick portion of the trabecular meshwork, which is adjacent to Schlemm's canal, is comprised of several layers of trabecular meshwork cells embedded in extracellular matrix, and is thought to be the site of the aqueous humor outflow resistance.
Proteoglycan – A protein with one or more glycosaminoglycan side chains. A glycoprotein is similar, except that the carbohydrate side chains are various monosaccharide patterns rather than disaccharide repeats.
Trabecular meshwork – A small fenestrated tissue surrounding the cornea on the inside of the eye that is responsible for providing and regulating resistance to aqueous humor outflow and maintaining intraocular pressure homeostasis.

Aqueous Humor Outflow Resistance

Trabecular Meshwork

The trabecular meshwork (TM) is thought to provide most of the flow resistance to aqueous humor outflow. Modulation of the trabecular outflow resistance is responsible for the regulation of intraocular pressure (IOP). In open-angle glaucoma, sustained increases in trabecular outflow resistance commonly result in elevated IOP, which is the primary risk factor for glaucomatous optic neuropathy and subsequent vision loss.

Site of Outflow Resistance

The outer uveal and corneoscleral portions of the TM are highly fenestrated and composed of several irregular layers of extracellular matrix (ECM) covered by TM beam cells. These beams become more flattened and sheet-like in the deeper portions of the TM. They are normally covered and maintained by continuous monolayers of TM cells, which reside on a basal lamina with a lamina rara and lamina densa. The center or stroma of the beams exhibits typical collagen fibrils, elastic fibers, and microfibril sheath-derived (SD) material. Between the beams and sheets, irregular intertrabecular spaces form tortuous flow channels leading to the cribriform or juxtacanalicular tissue (JCT) region, which lies adjacent to Schlemm's canal (SC). The size of the intertrabecular spaces is sufficiently large that it is unlikely that they contribute directly to the outflow resistance. The cells on the outer layers of the TM are actively phagocytic and are thought to act primarily as prefilters, removing debris from the aqueous humor prior to its passage through the less-porous inner JCT and SC regions.

Sequential serial dissection and microcapillary studies with perfused eyes suggest that the outflow resistance resides somewhere within the deepest one-quarter to one-third of the TM, approximately 7–14 μm from the inner wall of SC. This is approximately the thickness of the JCT region. This region is composed of an amorphous ECM with a discontinuous scattering of several layers of cribriform or JCT cells on the trabecular surface and embedded within the ECM. These JCT cells form occasional contacts with each other and with SC inner wall endothelial cells, often through extended processes using gap and adherens junctions. No continuous occludens junctions are apparent between JCT cells or between JCT and SC cells. Conversely, SC inner wall cells form a continuous monolayer and exhibit occasional gap junctions and extensive continuous tight occludens junctions. SC inner wall cells reside on a discontinuous basal lamina that may be affected by the movement of aqueous humor through these cells. Whether JCT cells have basal lamina is controversial. These cells have been considered to be fibroblast-like and thus without a basal lamina. However, basement membrane proteins, such as type IV collagen, laminin, and basement membrane proteoglycans (PGs), have been identified closely associated with the JCT cells. One study found basement membrane components adjacent to all JCT cells. This varied in amount and location with individual cells and was associated with at least half of the surface of most JCT cells.

It was generally not observed on the face of JCT cells, where they abut the apparent open spaces found scattered throughout the JCT region.

Extracellular Matrix

ECM, particularly the highly charged glycosaminoglycans (GAGs), has long been believed to contribute significantly to the outflow resistance, although some controversy about the exact nature of this contribution remains. Perfusion of the outflow pathway with several enzymes that degrade specific GAGs has been shown to increase outflow facility in several species, but the effects in primates and humans are ambiguous. Perfusion of both porcine and human anterior segments with enzyme inhibitors, which interfere with GAG biosynthesis or GAG sulfation, increased outflow facility. In addition, perfusion of human or porcine anterior segments with matrix metalloproteinases (MMPs) or with agents that stimulate MMP synthesis increased outflow facility, while perfusion with agents that specifically inhibit endogenous MMPs reversibly reduced outflow facility. Thus, ongoing ECM turnover, mediated by the MMPs, appears to be absolutely essential for maintaining the outflow resistance.

There is evidence for a direct involvement of JCT or SC cells or both in the resistance. Manipulations of the cellular cytoskeleton have strong and fairly immediate effects on outflow facility. Cells and ECM are highly interactive, thus separating their individual contributions is difficult.

Glycosaminoglycans

Structure and Properties

With the exception of hyaluronan, GAGs are synthesized directly as covalent side chains on serine/threonine or asparagine groups of specific PG core proteins (Figure 1). These are long carbohydrate chains composed of several distinctive disaccharide repeat units. They include hyaluronan or hyaluronic acid (HA), chondroitin sulfate (CS), dermatan sulfate (DS), keratan sulfate (KS), and heparan sulfate (HS). The defining disaccharide units are various alternating glucuronic acid (GlcA) and *N*-acetyl glucosamine (GlcNAc) or galactosamine (GalNAc), where some GlcAs are epimerized to iduronic acid (IdoA). They all have an abundance of carboxyl groups and many are O- or N-sulfated in complex patterns. Both carboxyl and sulfate groups are negatively charged at physiologic pH levels, giving a very high charge density along these chains.

GAG Biosynthesis

Hyaluronan is synthesized at the cell surface by an integral plasma membrane synthase and the growing GAG chain is extruded directly out of the cell and into the extracellular milieu. By contrast, HS, CS, DS, and KS are synthesized in the Golgi prior to secretion of the PG. HS, CS, and DS are *O*-linked to a consensus Ser-Gly/Ala-X-Gly motif of a core protein, while KS can be *N*-linked or *O*-linked. The resultant polysaccharide–protein conjugate is called a proteoglycan (Figure 2). Since KS is less abundant in the TM and utilizes a complex biosynthetic scheme, the nuances will not be presented herein. CS, DS, and HS GAG biosynthesis is initiated by transfer of a xylose (Xyl) onto the hydroxyl group of a Ser or Thr residue of a core protein (Figure 1). To the Xyl, two consecutive galactose (Gal) residues are added, followed by a GlcA. Synthesis of this initial chain is achieved by xylosyltransferase (XylT), galactosyltransferase I (GalT-I), galactosyltransferase II (GalT-II), and glucuronyltransferase I (GlcAT-I). XylT is highly regulated and this step is rate limiting. Distinctive GAG disaccharide repeats are

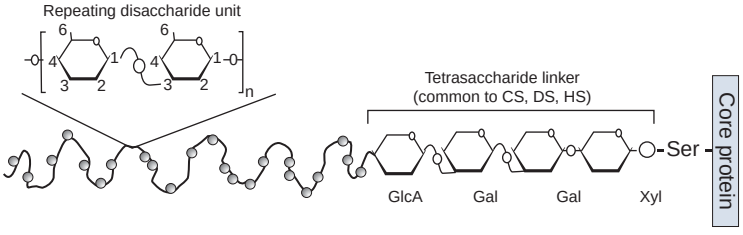

GAG class	Disaccharide	Modifications
Heparin/heparan sulfate (HS)	$GlcA/IdoA_{2x(\alpha/\beta1,4)}$-$GlcNAc_{NY,\ 3x,\ 6x\ (\alpha1,4)}$	X = sulfated; Y = acetylated/sulfated
Chondroitin sulfate (CS)/ dermatan sulfate (DS)	$GlcA/IdoA_{2x(\alpha/\beta1,3)}$-$GalNAc_{NAc,\ 4x,\ 6x\ (\beta1,4)}$	X = sulfated
Keratan sulfate (KS)	$Gal_{6x(\beta1,4)}$-$GlcNAc_{NAc,\ 6x(\beta1,3)}$	X = sulfated
Hyaluronic acid (HA)	$GlcA_{(\beta1,3)}$-$GlcNAc_{NAc(\beta1,4)}$	None

Figure 1 Glycosaminoglycan structures and sulfation. The identities of the disaccharide units are shown with the position and type of bonding between monosaccharides indicated by α or β. The position of acetylation or sulfation is indicated by the number associated with X or Y, for example, 2X represents 2-*O*-sulfation.

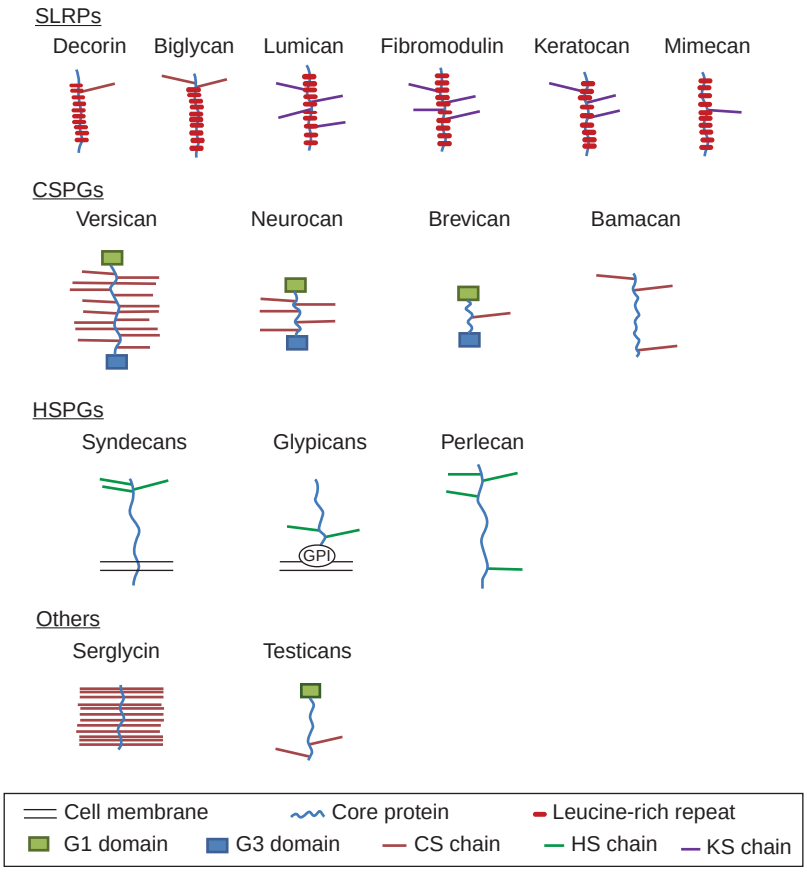

Figure 2 Typical proteoglycan structures are as shown with GAG side chains and approximate domain structures of the core proteins as indicated.

then added to this core tetrasaccharide linker by addition of either a GlcNAc or a GalNAc residue by the respective GlcNAc transferase-1 or GalNAc transferase-1. This step determines the identity of the final mature GAG chain as HS or CS/DS, respectively. Enzymes involved in the GAG-defining step must recognize other features of the core protein and more than just the common tetrasaccharide linker in order to extend the correct type of GAG chain. GAG chain extension steps are achieved by several exostosin (EXT) enzymes for HS or chondroitin synthases for CS or DS. Epimerization of GlcA in some CS chains to IdoA produces a DS chain. Some GlcA in HS chains are also epimerized.

All GAG chains, except HA, are sulfated in various positions and to varying degrees. For HS chains, GlcNAc residues can be N-acetylated or N-sulfated and sulfation then occurs at the 2-*O*, 3-*O*, and 6-*O* positions. Heparin (Hep) is more highly sulfated than HS. For CS/DS chains, the three main sulfation events are 4-*O* and 6-*O* sulfation of GalNAc and 2-*O* sulfation of GlcA/IdoA. The density of sulfation within regions of a GAG chain and length of chains is variable and carefully controlled. Thus, there is a potential for considerable diversity in GAG chain structure and properties.

GAGs of the TM

The GAG composition in TM extracts has been determined by sequential enzymatic degradation with various GAG-degrading enzymes. Sources included extracts of TMs from human eyes a few hours post mortem, stationary or perfused human anterior segment organ cultures, and densely confluent early-passage human TM cell cultures. Relatively good agreement was found in the amount of each type of GAG in the TM using these models and all of the normal GAGs were identified. Of the total human trabecular GAGs, approximately 20–25% is HA, 40–60% is CS and DS, 5–10% is KS, and 15–20% is HS. These percentages are based on GAG staining or ^{3}H- or ^{35}S-radiolabel incorporation and are not strictly calibrated molar amounts. When normalized to a relative ng amount based on GAG standards, HA was 15%, CS/DS was 38%, KS was 6.5%, and HS was 40% of the total. GAG distributions of other species are similar.

Localization of GAGs within the TM was determined by similar enzymatic degradation methods using various GAG stains and light or transmission electron microscopy (TEM). Hyaluronan-binding protein and GAG-specific antibodies have also been used to localize GAGs within

the TM. Most studies found HA primarily in the JCT region with less in the remainder of the TM. Since the other GAGs are sulfated, alternative staining methods are possible. When GAGs were stratified within the JCT of normal human eyes, fg μm^{-2} values obtained were 7.78 for HA, 8.18 for CS, 0.29 for DS, and 2.48 for HS (where HS included a small contribution from undegraded material). Using four-layer stratification, HA and HS were found to be higher near SC and declined somewhat toward the trabecular side of the JCT, while CS and DS were found to increase modestly toward the trabecular side of the JCT. Eyes from persons with glaucoma showed decreased HA and increased CS in all layers of the JCT.

Using antibodies specific to the various sulfated GAG chains, it was found that for all cell layers in the TM and JCT, CS, DS, and HS were present at higher levels just beneath the cells. CS/DS GAGs were also found as small clumps in the center of TM beams, apparently associated with collagen fibrils and elastin microfibrils. The JCT showed relatively dense staining throughout for CS, DS, and HS sulfated GAGs. Using Cuprolinic or Cupromeronic blue to stain sulfated GAG chains in conjunction with GAGase treatments, sulfated PGs have been localized at the ultrastructural level within the TM. With Cuprolinic blue staining, small, thin structures were found to be closely associated with collagen fibrils. A large, thick structure was located more peripherally, both with and between collagen fibril bundles, and was found associated with fine filaments. Both of these structures contained predominantly DS/CS GAGs. Basement-membrane-associated structures contained HS GAGs. Using Cupromeronic blue and a slightly different analysis, fairly similar distributions were obtained. In one study, sulfated GAGs were also found associated with JCT cell basement-membrane-like material.

GAG Turnover

GAG synthesis and degradation are tightly regulated in order to maintain a constant concentration within tissue. Several mammalian genes have been identified that degrade specific GAGs or remove sulfates. Targeted degradation of GAGs to smaller fragments, or removal of specific sulfates, modifies the function and/or biological activity of the GAG chain. Hence, some of these events may serve as functional processing steps rather than actual degradation. Superimposed on these specific GAG-chain-directed degradation events are targeted mechanisms for PG and other ECM component degradation, which involve MMPs and other proteinases. In these cases, the GAGs are likely captive bystanders and their subsequent degradation in lysosomes may not be as specific and may use more generic enzymes.

Hep/HS chains in mammals are degraded by heparanase-1 (HPSE-1), which is an endo-β-D-glucuronidase. This enzyme cleaves HS chains at only a few sites, resulting in HS fragments of appreciable size (5–10 kDa, 10–20 disaccharides). HPSE-1 is a pro-enzyme that is activated by removal of an N-terminal 6-kDa fragment. It is localized in endosomes/lysosomes in the cell and shows maximal endoglycosidase activity in acidic (pH 5.5–6.0) environments. However, active HPSE-1 can be secreted from intracellular compartments in response to certain stimuli, for example, tumor necrosis factor (TNF)-α and interleukin (IL)-1α, and it degrades syndecan-1 and perlecan at the cell surface. In addition, HPSE-1 enhances synthesis and shedding of the ectodomain of syndecan-1. Although heparinase-2 has been recently identified, no HS-degrading activity has been reported for this enzyme.

Hyaluronan synthesis and degradation are also tightly regulated to maintain a constant HA concentration within tissues. HA is catabolized rapidly in blood (half-life = 2–5 min), modestly in skin (~1 day), and relatively slowly in cartilage (1–3 weeks). HA catabolism is regulated by six hyaluronidase-like genes, HYALs 1–4, PH-20/SPAM1, and HYALP1. HYAL1 is a lysosomal enzyme, while HYAL2 is a glycosylphosphatidylinositol (GPI) lipid-anchored cell-surface protein. HYAL2 cleaves HA into ~20-kDa (~50 disaccharide units) fragments at the cell surface, which are then endocytosed by CD44, a cell surface receptor for HA. The rate-limiting step of HA catabolism is internalization. If HA is large or is bound by other PGs, then internalization is sterically inhibited. After uptake, HA fragments are delivered to lysosomes where HYAL1 degrades them into smaller tetrasaccharide units. HA fragments are inflammatory, immunostimulatory, and angiogenic. They can compete with larger HA polymers for cell-surface receptors such as CD44.

Sulfatases are also involved in GAG degradation. Human lysosomal sulfatases act on the GAG in an exoenzymatic fashion, only as specific residues are exposed at the nonreducing terminus by a glycosidase. A class of extracellular sulfatases, known as the Sulfs, is involved in cell signaling. Wnt, bound to HSPG, was released following 6-*O*-sulfate cleavage by Qsulf1, while desulfation of HS PGs by HSulf1 influences fibroblast growth factor (FGF) and epidermal growth factor (EGF) signaling pathways. Other known sulfatases are membrane-bound ER and Golgi network enzymes with a neutral pH optimum.

Proteoglycans

Structure and Properties

PG families

Proteoglycans (PGs) are a heterogeneous group of proteins with between 1 and over 100 GAG side chains of different lengths and a wide range of core protein sizes (**Figure 2**). The small leucine-rich PG (SLRP) family is comprised of 17 gene products, some of which are not true

PGs. Among these are biglycan, decorin, lumican, fibromodulin, keratocan, proline/arginine-rich end leucine-rich repeat protein (PRELP), and mimecan or osteoglycin. Different members have CS, DS, or KS GAG chains. A number of ocular disorders have been linked to these genes. Members of the SLRP family also affect cytokine and growth factor signaling pathways involving TNFα and insulin-like growth factor (IGF) and bind to and modulate bone morphogenic protein (BMP) and transforming growth factor (TGF)β receptors. They also serve in an array of ECM organizational functions, such as modulating collagen fibril formation.

Another family of PGs, the chondroitin sulfate proteoglycans (CSPGs) is the large aggregating and hyaluronan-binding family, including aggregan (CSPG 1), versican (CSPG 2), neurocan (CSPG 3), melanoma-associated proteoglycan (CSPG 4), and brevican. Versican (**Figure 3**) is comprised of four domains with numerous CS GAGs attached to two central GAG domains and a number of binding sites for other ECM proteins, cell surface receptors, cellular components, and HA. The other members of this family are similar, although each shows distinct characteristics and domains.

The cell surface HS PGs break down into three groups based on their mode of interaction with cells. Syndecans 1–4 are transmembrane proteins with small cytoplasmic tails and larger extracellular regions containing several HS chains and in some cases, a CS chain. The cytoplasmic tail has two conserved regions, C1 and C2, which are, respectively, proximal and distal to the inner surface of the plasma membrane and which sandwich a variable (V) domain. C1 and C2 bind, respectively, to actin-binding ezrin, radixin, and moesin (ERM) proteins and to post-synaptic density, disk large, and zo-1 protein domains (PDZ)-containing proteins such as syntenin. Binding to the V domain has not been defined, but appears to involve cell spreading, actin and fascin bundling, and ECM assembly. The ectodomains of syndecans bind a variety of ECM proteins, several cell surface receptors such as integrins, and numerous growth factors, for which they act as both sequestration and activation sites. They bind to the Hep II domain of fibronectin, which has been shown to modulate aqueous outflow facility. Under some conditions, the ectodomain is shed following a proteolytic event near the extracellular membrane surface. The soluble fragments then compete for binding sites. Signal transduction, both outside-in and inside-out, has been shown for the syndecans. There are phosphorylation sites on their cytoplasmic tails that are involved in their regulation.

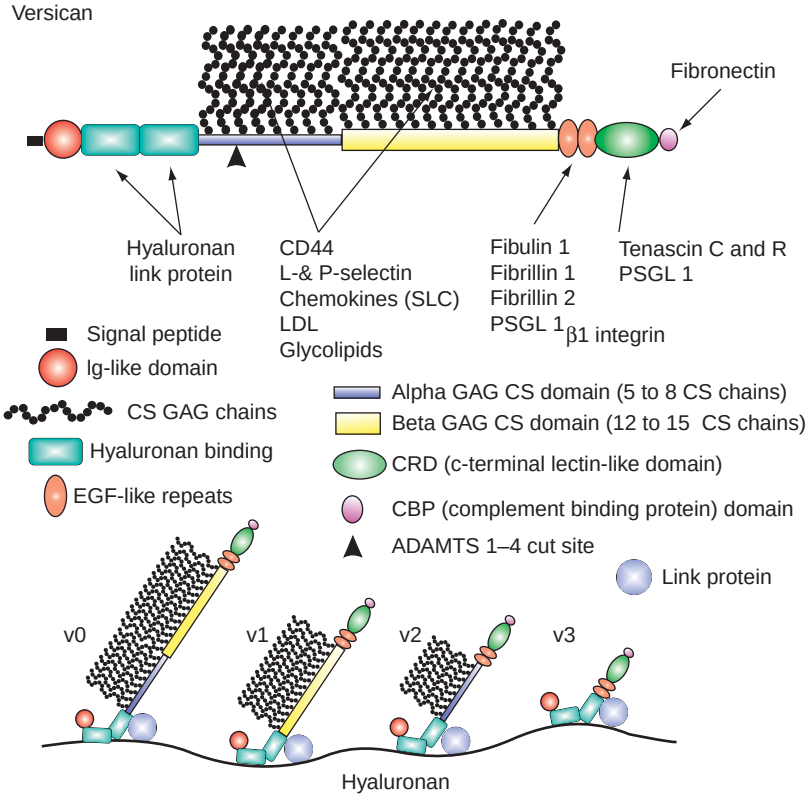

Figure 3 Versican domain structure, GAG attachment sites, binding sites of various binding partners, alternative splicing isoforms, a disintegrin and metalloproteinase with thrombospondin motifs (ADAMTS) cleavage sites, and hyaluronan binding with stabilization by link protein. Modified from Acott, T. S. and Kelley, M. J. (2008). Extracellular matrix in the trabecular meshwork (Review). *Experimental Eye Research* 86: 543–561.

A second group of HSPGs, glypicans 1–6, are cell surface PGs that attach to the cell through GPI lipid anchors. They typically have two HS chains attached near the plasma membrane and a conserved extracellular domain with 14 Cys residues. Glypicans are implicated in FGF, IGF, Wnt, BMP-2, and TGFβ signaling, development, axonal guidance, and have been associated with several genetic diseases and cancers. Evidence for glypican recycling between the cell surface and Golgi has been presented, although the functional significance of this process is not clear. They bind various ECM and cell surface proteins, including the Hep II domain of fibronectin, much as observed for the syndecans.

The third type of HSPGs cell surface attachment is through receptor binding or similar types of interactions and this includes the large basement-membrane HS PG, perlecan. Perlecan has a very large core protein with several HS chains and is an integral component of cellular basement membranes. Bamacan (CSPG 6), a similar large basement-membrane CS PG, is also important in basement membrane structure. Perlecan is thought to serve as a scaffold in basement membrane organization with various complex interactions between collagen type IV, laminins, nidogen, and a variety of other ECM and cell surface proteins. Perlecan normally has one HS chain near the C-terminus and three near the N-terminus. It has numerous laminin domains, laminin EGF-like domains, immunoglobin-like domains, EGF-like domains, and a nidogen-like domain that interacts with nidogen-1. The other perlecan domains interact with fibulin-2, fibrillin, fibronectin, integrin β1, α-dystroglycan, acetylcholinesterase, Hep, and others. The HS side chains bind heparin-binding growth factors such as FGF, vascular endothelial growth factor (VEGF), platelet-derived growth factor (PDGF), and connective tissue growth factor (CTGF). Fragments of perlecan, such as endorepellin, have other independent functions such as inhibiting angiogenesis. Perlecan can also modulate focal adhesion or focal contact function and impacts the C-terminal domain of focal adhesion kinase (FAK) (FRNK) and FAK cytoplasmic distributions and signaling.

Several ECM PGs only have GAG chains attached to some isoforms, often due to insertion of different domains by alternative mRNA splicing, as discussed later. Several collagens, such as types XII, XIV, and XV, are PGs in some instances. Another such molecule is CD44, a transmembrane glycoprotein with a large extracellular domain that functions in cell signaling, migration, adhesion, and cell–cell interactions. CD44 is a primary cellular hyaluronan receptor (**Figure 4**). Its large N-terminus also binds numerous other ECM components including, collagen, fibronectin, and osteopontin. Its cytoplasmic tail interacts with the cytoskeleton through actin-binding ERM proteins. Thus, CD44 is an important mediator of

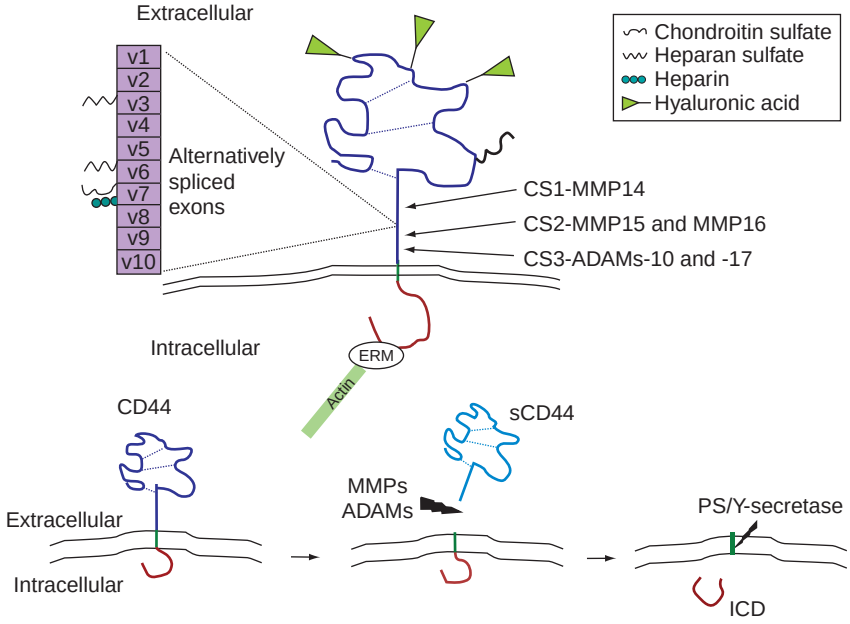

Figure 4 Schematic of CD44. CD44 is a transmembrane glycoprotein that binds hyaluronan and other proteins in the extracellular matrix and interacts with the intracellular cytoskeleton through ERM proteins. Up to 10 additional exons (v) can be included by alternative mRNA splicing and these may introduce additional GAG-binding sites. Proteolytic cleavage sheds the extracellular domain and the positions of three cleavage sites (CS) are shown. The lower diagram shows the sequential proteolytic cleavage events. Following proteolytic release of sCD44, presenilin (PS) or γ-secretase cleavage releases the intracellular domain (ICD), which is translocated to the nucleus where it affects transcription of itself and various other genes. MMP, matrix metalloproteinases; ADAM, a disintegrin and metalloproteinase; ERM, Ezrin/Radixin/Moesin.

extracellular signals. The N-terminal soluble ectodomain of CD44 (sCD44) can be shed from the parent molecule by proteinase cleavage. Shedding, or cleavage of membrane-anchored proteins, is one mechanism by which cell surfaces are modified and biologically active molecules are released. Regulated proteolysis also allows rapid down-regulation of adhesion molecules and ectodomain shedding may contribute to regulation of cell adhesion and migration. There are three cleavage sites implicated in shedding of CD44, involving MMPs and ADAMs (a disintegrin and metalloproteinases). These release sCD44 of different sizes and since the cleavage sites span the variant region, alternative splicing may affect cleavage activity or site selection. This also infers that sCD44 may also contain variant domains. Shedding can happen constitutively or in response to cytokine stimulation, and correlates with enhanced proteolytic degradation and matrix remodeling.

PGs of the TM

A number of PGs have been identified in the TM of anterior segments or in TM cells in culture. This includes a number of SLRPs, CSPGs, HSPGs, and other types of PGs, including CD44 and collagen types XII, XIV, and XV (**Table 1**).

Some specific core proteins have been localized to regions of the TM by immunohistochemistry using light or TEM. Perlecan was localized to the basement membranes of TM beams and SC inner wall cells. By immunofluorescence, syndecan 1 immunostaining in the TM/SC was light or absent. Syndecan 2, 3, and 4 immunostaining was observed through the TM/SC region with syndecan 3 immunostaining being somewhat stronger in the JCT/SC region. As would be expected for a transmembrane protein, syndecan immunostaining was strongest at the cell edges. At the ultrastructural level, decorin and versican immunostaining were found within electron-dense elastic fiber cores and the surrounding microfibril sheath material, both within TM beams and the JCT region. Both PGs were also localized to long-spaced collagen (100–120-nm periodicity) and normal collagen fibrils. With confocal immunofluorescence, we see similar versican and fibromodulin distributions with a significant amount also associated with the TM beam, JCT, and SC cells.

Many of these PGs have complex structures with multiple binding domains and exhibit alternative splicing. For example, versican (**Figure 3**) is a large lectican, which can bind to hyaluronan chains and interact with various other ECM proteins or cellular receptors. It has four alternative mRNA splicing variants, which appear to be important in TM function, as discussed later. Versican is also cleaved by specific proteinases at various sites, which results in fragments with very different activities such as stimulation of cell division, disruption of chemokine function,

Table 1 Trabecular meshwork proteoglycans

Proteoglycan	*GAG(s)*	*Type or family*	*Known alternative splicing*
CSPG 2, versican	CS	Large aggregating, HA binding	Yes, TM
CSPG 3, neurocan	CS	Large aggregating, HA binding	
CSPG 4, melanoma-associated	CS	Large aggregating, HA binding	
CSPG 6, bamacan	CS	Basement membrane CSPG	
HSPG 1, perlecan	HS	Basement membrane HSPG	Yes
HSPG 2, LDL receptor	HS	Cell surface HSPG	Yes
Biglycan	CS/DS	SLRP	Yes
Decorin	CS/DS	SLRP	Yes
Lumican	KS	SLRP	
Fibromodulin	KS	SLRP	
Mimecan, osteoglycin	KS	SLRP	Yes
Syndecan 1	HS	Cell surface transmembrane	
Syndecan 2	HS	Cell surface transmembrane	
Syndecan 3	HS	Cell surface transmembrane	
Syndecan 4	HS	Cell surface transmembrane	Yes
Glypican 3	HS	Cell surface GPI anchored	
Glypican 4	HS	Cell surface GPI anchored	
Glypican 5	HS	Cell surface GPI anchored	
CD44	HS/CS	Cell surface hyaluronan receptor	Yes, TM
Testican 1	CS	SPARC, osteonectin	Yes
Testican 3	CS	SPARC, osteonectin	Yes
Secretory granule PG 1	CS/HS	Serglycin	
Collagen XII	CS	Nonfibrillar collagen	Yes, TM
Collagen XIV	CS	Nonfibrillar collagen	Yes
Collagen XV	CS	Nonfibrillar collagen	Yes

These proteoglycans have been identified in the TM by Western immunoblots, immunohistochemistry, RT-PCR, cDNA libraries, microarray, or general proteomics approaches. For alternative splicing, yes indicates that it has been reported in other tissues and TM indicates that it has also been studied in the TM.

and apoptosis. In the TM, the versican fragment produced by ADAMTS (a disintegrin and metalloproteinase with thrombospondin motifs) 1- or 4-cleavage between Glu441 and Ala442 in the αGAG domain, is found in moderate abundance and may be higher in areas of high segmental outflow. Versican has also been shown to distribute with TM cell podosome- or invadopodia-like structures (PILS), functional units recently identified in the outflow pathway that appear to serve in targeted ECM turnover. Versican formed a novel ring around the center of the PILS in TM cells. The ADAMTS-4 cleaved form of versican also co-localized with these distinctive rings beneath TM cell PILS.

Recent studies have found that sCD44 is significantly increased in primary open-angle glaucoma (POAG) aqueous humor. Although shedding likely occurs elsewhere in the anterior chamber, aqueous sCD44 may affect TM cell function. When it flows through the TM, it may disrupt interactions of membrane-bound CD44 with its typical binding partners. This in turn may interfere with the normal function of CD44 in the TM. A previous study showed that sCD44 was cytotoxic to TM cells.

Alternative splicing

Many ECM genes, including numerous PGs, undergo alternative splicing, a process by which various exon sequences of the primary transcript are differentially included in the mature mRNA. This allows cells to produce multiple proteins with different domains included or excluded using variations of a single gene-coding sequence. The most common form of alternative splicing is exon skipping, which results in exclusion of certain regions from the protein. Since many PGs are comprised of protein domains encoded by single exons, exon skipping is a relatively common phenomenon. Other alternative splicing mechanisms include alternative 5′ and/or 3′ splice sites, intron retention, and mutually exclusive splicing, where one exon is selected from an array of two or more possible exon variants. Alternative splicing generates protein diversity, although in most cases the specific function of the alternatively spliced exon is not yet known.

The gene for versican contains two large central exons (7 and 8) that are alternatively spliced. These encode the αGAG and βGAG domains that are substituted with CS GAG chains (**Figure 3**). Four alternate transcripts are therefore expressed: V0, V1, V2, and V3, which contain both, either the βGAG or αGAG domain, or neither domain, respectively. Consequently, the number of GAG chains varies between alternate splice forms. The V1 isoform is the most abundant splice variant expressed by TM cells, and the proportion of V1 transcripts increased when TM cells were subjected to mechanical stretch. Concomitantly, total versican mRNA levels decreased. This results in a net reduction of CS GAG attachment sites in the TM and may affect structural organization and/or disrupt signaling systems in the TM. TGFβ treatment of TM cells produced the opposite effect, that is, it shifted toward more V0 splice variants with more potential GAG attachment sites per PG molecule. Both TNFα and IL-1α also modulate versican splicing.

CD44 is also well known for its complex alternative splicing (**Figure 4**). CD44 is composed of 20 exons, 10 of which can be regulated by alternative splicing. In human TM cells, three isoforms of CD44 were observed. These include CD44 that does not contain any variant exons, CD44v-I, which contains exons v3 and v7-v10, and CD44v-III, which contains exons v8 and v9. Mechanical stretching and TNFα or IL-1α treatment of porcine TM cells increased the amount of v7 exon included in CD44 transcripts. However, the function of these variant domains in TM cells is unknown.

A novel splice variant of syndecan-4 has been reported. It incorporates exon V-b as a terminal exon instead of the transmembrane-encoding exon V-a. This generates a soluble ectodomain of syndecan-4, which mimics that generated by proteolytic cleavage. Thus, the alternative splice form of exon V-b would have functional consequences that were similar to proteolytic shedding. Syndecan splicing has not yet been analyzed in TM cells.

Several other PGs also undergo alternative splicing. For instance, biglycan has several isoforms that have a truncated core protein with shorter CS/DS GAG chains. Decorin has two alternatively spliced leader exons in the 5′ untranslated region, while mimecan has three different-sized mRNA transcripts that suggest it also is alternatively spliced. A truncated form of testican-3, N-tes, is generated by alternative splicing. It lacks C-terminal GAG chain sites and inhibits MMP-14 and-17 activities, which in turn compromises pro-MMP2 activation. None of these splicing alternatives has been assessed in the TM at this time. The NC3 domain of collagen XII has two splice forms, a short and a long form. The long NC3 isoform is increased in TM cells subjected to mechanical stretch, which provides additional CS and heparin-binding sites not found in the short NC3 form.

See also: Biological Properties of the Trabecular Meshwork Cells; The Biology of Schlemm's Canal; Biomechanics of Aqueous Humor Outflow Resistance; Control of Aqueous Humor Flow; The Corneal Stroma; The Cytoskeletal Network of the Trabecular Meshwork; The Development of the Aqueous Humor Outflow Pathway; The Fibrillar Extracellular Matrix of the Trabecular Meshwork; Functional Morphology of the Trabecular Meshwork; Myocilin; Pharmacology of Aqueous Humor Formation; Pharmacology of the Aqueous Humor Outflow; Regulation of Extracellular Matrix Turnover in the Aqueous Humor Outflow Pathways; The Role of Oxidative Stress in the Trabecular Meshwork; Steroid-Induced Ocular Hypertension and Effects of Glucocorticoids on the Trabecular Meshwork; Uveoscleral Outflow.

Further Reading

Acott, T. S. (1992). Trabecular extracellular matrix regulation. In: Drance, S. M., Van Buskirk, E. M., and Neufeld, A. H. (eds.) *Pharmacology of Glaucoma*, pp. 125–157. Baltimore, MD: Williams & Wilkins.

Acott, T. S. (1994). Biochemistry of aqueous humor outflow. In: Kaufman, P. L. and Mittag, T. W. (eds.) *Textbook of Ophthalmology,* vol. 7, pp. 1.47–41.78. London: Mosby.

Acott, T. S. and Kelley, M. J. (2008). Extracellular matrix in the trabecular meshwork (Review). *Experimental Eye Research* 86: 543–561.

Acott, T. S. and Wirtz, M. K. (1996). Biochemistry of aqueous outflow. In: Ritch, R., Shields, M. B., and Krupin, T. (eds.) *The Glaucomas*, vol. I, pp. 281–305. St. Louis, MO: Mosby.

Borras, T. (2003). Gene expression in the trabecular meshwork and the influence of intraocular pressure. *Progress in Retinal and Eye Research* 22: 435–463.

Ethier, C. R. (2002). The inner-wall of Schlemm's canal. *Experimental Eye Research* 74: 161–172.

Farach-Carson, M. C. and Carson, D. D. (2007). Perlecan–a multifunctional extracellular proteoglycan scaffold. *Glycobiology* 17: 897–905.

Fears, C. Y. and Woods, A. (2006). The role of syndecans in disease and wound healing. *Matrix Biology* 25: 443–456.

Hernandez, M. R. and Gong, H. (1996). *Extracellular Matrix of the Trabecular Meshwork and Optic Nerve Head*. St. Louis, MO: Mosby.

Johnson, M. (2006). What controls aqueous humour outflow resistance? *Experimental Eye Research* 82: 545–557.

Kreis, T. and Vale, R. (eds.) (1999). *Guidebook to the Extracellular Matrix, Anchor, and Adhesion Proteins.* Oxford: Oxford University Press.

Lutjen-Drecoll, E. (1999). Functional morphology of the trabecular meshwork in primate eyes. *Progress in Retinal and Eye Research* 18: 91–119.

Prabhakar, V. and Sasisekharan, R. (2006). The biosynthesis and catabolism of galactosaminoglycans. *Advances in Pharmacology* 53: 69–115.

Sasisekharan, R., Raman, R., and Prabhakar, V. (2006). Glycomics approach to structure-function relationships of glycosaminoglycans. *Annual Review of Biomedical Engineering* 8: 181–231.

Yue, B. Y. J. T. (1996). The extracellular matrix and its modulation in the trabecular meshwork. *Survey of Ophthalmology* 40: 379–390.

Secondary Photoreceptor Degenerations*

M B Gorin, Jules Stein Eye Institute, Los Angeles, CA, USA

Glossary

Epigenetic – The heritable modifications of gene expression that are not the result of changes in the DNA sequence. This can include methylation of DNA that results in inactivation of gene transcription or factors that modify how RNA transcripts are spliced to form the final transcripts that are translated into peptide sequences.

Extrinsic factor – An agent external to the organism that contributes to or is causative of a disease state. This can include drugs, foods, normal nutrients (excess or deficiency), toxins, inhaled chemicals, infectious agents, and exposures to radiation such as light, sound, and high-energy particles.

Intrinsic factor – An agent that is inherent to the organism that contributes to or is causative of a disease state. While commonly these factors are genetic variants in the organism's DNA that may predispose (or be protective) of specific conditions, other intrinsic factors include epigenetic changes, aging changes, and the effects of the biology of symbiotic bacteria in the skin or gut. Another intrinsic agent is an organism's immunologic response behavior and memory (though obviously the immunologic memory is heavily affected by the exposure to extrinsic agents, such as viral infections).

Microbiomics – The genetic information expressed by the microbes that are indigenous to a host organism (e.g., bacteria colonized to the skin or intestinal tract).

Introduction

Secondary retinal degeneration occurs when cells in the retina die by a process triggered by factors not inherent to retina. Secondary retinal degeneration can be caused by trauma, infection, inflammation, toxins, anti-retinal antibodies, or as an adverse effect of medications.

In the past, clinicians have tended to view genetic and nongenetic etiologies of retinal degeneration as easily separated categories. The molecular studies of hereditary retinal degenerations have shown that, while some retinal conditions are caused by mutations in genes with photoreceptor-specific expression, many retinal conditions are the results of mutations in genes that are widely expressed in the body as well as from the secondary effects of metabolic changes caused by the expression of mutated genes in ocular cell types other than photoreceptors as well as from other organs and tissues distant from the eye. Based on our understanding of complex genetic disorders, we now realize that there can be interplay of genetic and nongenetic factors that run the entire spectrum of possibilities. For example, rhegmatogenous retinal detachments, which can lead to secondary photoreceptor degeneration, may be influenced or caused by genetic variants (e.g., COL11A1, VCAN, COL9A1, and COL2A1) that are expressed in nonretinal cells, and whose expression may be limited to a particular period in ocular development. Thus, we have to consider this continuum of causality as we attempt to make useful classifications that can guide diagnostics and therapy. In light of these complexities, we offer the following operational distinctions among primary and secondary photoreceptor and retinal degenerations that may be relevant to therapeutic approaches.

- If the genetic defect is such that it would require actual alteration of the gene expression in the photoreceptors to correct the abnormality and arrest the degeneration, then this can be considered a primary photoreceptor degeneration. The genetic alteration is necessary and sufficient to cause photoreceptor degeneration. The gene that is mutated may (e.g., opsin, peripherin/rds, cone transducin, AIPL1, and GUCY2D) or may not (e.g., splicing factors PRPF8, PRPF3, and PRPF31, IMPDH1, and CA4) be photoreceptor specific. For a primary photoreceptor degeneration, one would expect that the correction of the genetic alteration outside of the photoreceptors would not be sufficient to prevent photoreceptor degeneration. However, a secondary photoreceptor degeneration that results from loss of expression or expression of a mutated protein in either other retinal cells or the retinal pigment epithelium (RPE) (e.g., RPE-65, RGR, and LRAT) might be corrected by gene therapy to the key nonphotoreceptor cells in the retina or RPE.
- If one reviews the genes attributed to primary photoreceptor degenerations, it is clear that many of these causative genes are not limited to photoreceptor-specific

* All of the genes that are mentioned in this article are described in Table 2 of Chapter 210 (for the retinal degenerations), RetNet (www.sph.uth.tmc.edu/retnet/), and/or Online Mendelian Inheritance of Man (OMIM) (www.ncbi.nlm.nih.gov/Omim/).

expression. Mutations in these genes have been attributed to nonsyndromic primary photoreceptor degenerations (such as retinitis pigmentosa (RP), Leber congenital amaurosis (LCA), cone dystrophy, and cone–rod dystrophy) as well as syndromic forms (e.g., Usher syndrome, Bardet–Biedl syndrome, Alstrom disease, and Cohen syndrome). Most of these conditions are further described and discussed elsewhere in the encyclopedia. In some instances, the mechanisms of action of these genes may not be solely mediated through their direct effects on the photoreceptors, thus raising the possibility that, in some cases, the photoreceptor degeneration is mediated through a mixed primary and secondary photoreceptor degeneration model (see below). Two unique examples of this potential ambiguity are the ABCA4 (Stargardt disease, cone–rod dystrophy) and RS1 (X-linked retinoschisis) genes. Both genes are specifically expressed in the photoreceptors, but their mechanism of action appears to be mediated through other retinal/RPE cells that lead to a secondary photoreceptor degeneration (see below).

- If the photoreceptors degenerate as the result of an alteration in a gene whose expression is primarily in other retinal or RPE cells, then this would be a primary retinal degeneration with secondary photoreceptor degeneration. Correction of the genetic defect would require modification of the effects of those retinal/RPE cells. A primary retinal degeneration without photoreceptor degeneration can occur such as with optic neuropathies that lead to retinal ganglion cell loss without significant loss of photoreceptors (Table 1).
- A mixed model of primary and secondary photoreceptor degeneration can be considered in two different modes. One is when a genetic alteration within the photoreceptors themselves would not be sufficient to cause photoreceptor degeneration by itself but would predispose to degeneration in the presence of an extrinsic or intrinsic agent. The genetic alteration within the photoreceptors could be necessary, conditional, or probabilistic but not sufficient. An intrinsic agent could be a genetic alteration in nonphotoreceptor retinal cells or due to expression elsewhere in the body. As noted above, a number of genes that are expressed in photoreceptors and for whom there are mutations that are known to be responsible for photoreceptor degeneration also have expression in other retinal cells as well as in other tissues. In some of these cases, it is not always clear if the expression in the photoreceptors alone is sufficient to cause cell death or whether or not there is a component of photoreceptor degeneration that is secondary to the effects on other cells and tissues. The only way to distinguish a secondary effect from a primary one would be to create animal models in which the genetic alteration is limited to specific cell populations and to determine if the photoreceptors are spared when their gene expression is normal. This is especially true for the forms of RP that are associated with mutations in genes that affect metabolic processes throughout the body. Examples of these conditions include gyrate atrophy, Bietti crystalline retinopathy, abetalipoproteinemia, and Refsum disease. At this time, we simply cannot establish if the effects of these genetic mutations are mediated by a primary effect on the photoreceptors or by secondary mechanisms. In the case of gyrate atrophy and Refsum disease, there is evidence that nutritional therapy can ameliorate the progression of the condition, which suggests an interplay of a person's intrinsic genetic makeup and diet (an extrinsic agent), but we still do not know if the effect is due to the systemic reduction of toxic metabolites or a photoreceptor-specific mechanism is also involved. Similarly, with Bietti crystalline retinopathy, the defect in CYP4V2 has multitissue consequences but it is not known if a systemic correction of the metabolic defect would be sufficient to overcome the enzyme deficiency in photoreceptor cells. Only future studies will be sufficient to distinguish if these conditions are representative of a mixed model of photoreceptor degeneration or secondary photoreceptor degenerations of an intrinsic type (see below).

Table 1 Secondary photoreceptor degenerations associated with primary retinal/RPE degeneration/dystrophy

Gene involved, site of cell/tissue expression related to retinal degeneration (RPE-retinal pigment epithelium, RVE-retinal vascular endothelium, RVP-retinal vascular pericytes, MGC-Muller glial cells), and phenotype (LCA-Leber congenital amaurosis, RP-retinitis pigmentosa) (from RetNet)		
RPE65	RPE	LCA and RP
MERTK	RPE	RP
CRALBP	RPE, MGC	Bothnian dystrophy
LRAT	RPE, liver	RP
RGR	RPE	RP and dominant choroidal sclerosis
TIMP3	RPE, RVP	Macular dystrophy
C1QTNF5	RPE	Macular dystrophy
ABCC6	REV	Macular dystrophy
AMD-related genes	RPE, liver	Macular dystrophy
BEST1	RPE	Macular dystrophy

An extrinsic agent can be a drug or environmental exposure (including something in the diet). There are relatively few established human examples of this model for retinal degenerations, though retinal degeneration-B (rdgB) mutants in *Drosophila* show light-dependent photoreceptor degeneration. This mixed model could possibly account for some of the cases of photoreceptor degenerations with incomplete penetrance (individuals who have the disease-causing mutation but show no clinical evidence of retinal degeneration).

- If one could prevent the photoreceptor degeneration by preventing an individual's exposure to an extrinsic agent or condition (e.g., toxin, drug, infectious agent, light, and trauma), then this is secondary photoreceptor degeneration of the extrinsic type (even if the body converts that agent to a toxic form as part of a normal metabolic pathway – such as methanol to formaldehyde). Clearly, the primary method of management is to avoid exposure to the extrinsic conditions that would induce the degeneration. This form of degeneration can be due to exposure to an external agent as well as deprivation of a mandatory nutrient (such as vitamin A). The deficiency can be the result of a lack of intake or synthesis of the key nutrient (vitamin-A- or zinc-deficient diet) or due to the inability to process or use such a metabolite/nutrient. Examples would be malabsorption of vitamin A and zinc due to intestinal disorders or drugs which block utilization, such as fenretinide or accutane (Table 2).
- A second mode of a combined primary and secondary photoreceptor degeneration is when one group of photoreceptors, such as the rod photoreceptors, undergoes a primary degenerative process due to a mutation in a gene that is expressed in those photoreceptors that precipitates apoptosis. At the same time, there is a second group of photoreceptors, the cone photoreceptors, which undergoes a secondary degenerative process due to alterations in the cellular environment induced by the death of neighboring cells. This situation is actually very common among patients with retinal dystrophies such as rod–cone (e.g., RP) or cone–rod forms. Recent studies of several mouse models of RP due to rod-photoreceptor specific genes have showed that the nonautonomous death of the cone photoreceptors is influenced by activation of the rapamycin pathway that can be modified by exogenous insulin, suggesting a possible intrinsic mechanism that could be influenced by a systemic therapeutic approach. The importance of this mechanism cannot be overemphasized since preservation of cone photoreceptor cells and function in a patient with RP would have a dramatic impact on maintaining useful visual function and it does not necessarily require the correction of the primary photoreceptor degeneration mechanism in the rod photoreceptors.
- If one can prevent photoreceptor degeneration by correcting or reversing a systemic or ocular metabolic or immune process, then it is a secondary photoreceptor degeneration of the intrinsic type. A number of these conditions are driven or influenced by genetic etiologies (necessary and sufficient in the case of metabolic syndromes, but often conditional or probabilistic in immune-related conditions), but the retinal degeneration is still secondary. Intrinsic causes are not exclusively genetic, one may have to consider epigenetic factors as well as immunologic memory and the microbiomics of the natural flora. Clearly, one would primarily direct therapy to correcting the primary metabolic or immune disturbance rather than focusing on modifying the behavior of the photoreceptors. Therapy might be directed specifically to the affected eye(s), (such as periocular or intraocular steroid therapy) rather than systemically, but it would be intended to primarily modify effector cells in the tissue, rather than the photoreceptors themselves (Table 3).

Table 2 Retinotoxic drugs and agents, nutrient deficiencies, infectious agents, light injury, and trauma

Drugs
Ethambutol, aminoglycosides, epinephrine, desferroximine, antimalarials (hydroxychloroquine, chloroquine, quinine), vigabatrin, phenothiazines (e.g., fluphenazine, mellaril, and stellazine).
Nutrient deficiencies
Zinc, vitamin A, omega-3 fatty acids.
Infectious
Toxoplasmosis, cytomegalovirus, herpes simplex, varicella zoster, HIV, DUSN (nematode), rubella, syphilis, prion, corona virus, others.
Toxins
Cadmium, iron (siderosis), lead, mercury (suspected), copper (intraocular chalcosis), cobalt, iodoacetic acid (IAA), methanol.
Light
Solar, laser chronic exposure.
Trauma
Commotio, retinal detachment.
Vascular
Occlusive disease, embolic, inflammatory, retinopathy of prematurity (ROP), Coats disease.

Table 3 Intrinsic factors: genes, phenotypes (e.g., RP nonsyndromic, RP syndromic, and macular degeneration), mechanism (e.g. metabolic, immune, inflammatory (inflamm))

OAT	Gyrate atrophy	Metabolic
CYP4V2	Bietti crystalline retinopathy	Metabolic
PEX1, PEX2	Zellweger Syndrome	Metabolic
PEX7, PHYH	Refsum disease (adult)	Metabolic
MTP	Abetalipoproteinemia	Metabolic
PANK2	Hypoprebetalipoproteinemia	Metabolic
	Niemann–Pick	Metabolic
	neuronal ceroid lipofuscinosis	Metabolic
CTNS	Cystinosis	Metabolic
CA4 (carbonic anyhydrase 4)	RP	Metabolic
LRP5	FEVR	Metabolic
HLA-B27, A29, B7	Ankylosing spondylitis	Immune
	Birdshot choroidopathy	Immune
	Bechet's disease	Immune
Unknown, retinal antigens, cancer	Cancer-assoc. retinopathy	Immune
	Autoimmune retinopathy	Immune
CFH	Hemolytic uremia – mac deg	Inflamm

- A mixed intrinsic and extrinsic etiology for a secondary photoreceptor degeneration would be when a person has a genetic variant that creates a toxic metabolite in the presence of an extrinsic molecule that would normally not be encountered. A normal person would not experience a retinal degeneration under the same exposure conditions. This set of conditions has overlap with the purely extrinsic and intrinsic etiologies if the genetic variation simply shifts the dose–response characteristics of the host. For example, a person is genetically predisposed to react to an extrinsic molecule at levels in the normal environment, while another person would experience similar photoreceptor degeneration only when the exposure is at levels that would exceed normal exposures. Reduction of the extrinsic exposure below the normal levels could be beneficial for these individuals (such as Refsum disease or gyrate atrophy). Alternatively, correction of the genetic variant would allow the person to cope with normal exposure levels. An animal model of the mixed intrinsic and extrinsic secondary photoreceptor degeneration would be the RPE65-MET450 mutants (intrinsic) that have varying reduced sensitivity to light-induced (extrinsic) photoreceptor degeneration as compared to animals that have the LEU450 variant in the RP65 gene.
- We are only beginning to understand these types of situations, although it is likely that many of the idiosyncratic reactions that some patients experience to certain situations or medications are the result of genetic variations that affect drug bioavailability, mechanism of action, and elimination. One such example would be the patient who develops cystoid macular edema (CME) after uncomplicated surgery. The surgical intervention would be considered an extrinsic agent. While CME is common in cases of complicated surgery and postsurgical inflammation, it is relatively uncommon (but not rare) in individuals whose surgery and postoperative care are uneventful and have no predisposing clinical conditions. Yet, this is most likely due to intrinsic (nonphotoreceptor-specific) genetic factors that govern inflammation. Persistent CME can lead to secondary photoreceptor degeneration.

If the extrinsic exposure cannot be manipulated, then essentially, one is forced to treat the mixed etiology as a purely intrinsic issue. For example, if a person had a genetic condition from an intrinsic metabolic defect that is light sensitizing such that normal ambient light would trigger photoreceptor degeneration, the distinction between an intrinsic etiology and a mixed intrinsic/extrinsic etiology becomes almost meaningless, since having a person avoid all light exposure to prevent photoreceptor degeneration is neither feasible nor desirable. However, reduction of the light exposure might alter the rate of disease progression, but therapy directed toward the intrinsic factor(s) would be essential to preserve vision under normal exposure circumstances. This situation is comparable to the mixed primary and secondary photoreceptor degeneration category (such as a mutation in an photoreceptor-specific gene that is responsible for light-dependent degeneration) except that, instead of the intrinsic etiology being disconnected from the photoreceptors themselves, the photoreceptors are directly affected by a genetic variant that renders the photoreceptors vulnerable to the extrinsic factor (e.g., light). While the reduction of the extrinsic exposure would be desirable, it may not be realistic and thus therapy would also have to be directed to the photoreceptors themselves.

The combination of extrinsic and intrinsic factors that affect photoreceptor degeneration is comparable to the genetic and environmental interactions that are often discussed in the context of complex genetic diseases such as age-related macular degeneration. At this time, our understanding of these interactions is very limited, but there are some examples for simpler retinal conditions. Mice that are heterozygous for a deletion in the PDE6B subunit (the rd mouse), a dose of sildenafil citrate (Viagra) that would normally have no effect in the normal mouse, will show a major change in the electroretinogram. It is likely that some of the individuals who experience visual side effects from this medication may have a genetic variant that reduces the overall level of phosphodiesterase activity in their retinas, thus conferring sensitivity. Another mixed etiology of secondary photoreceptor dysfunction (which can ultimately lead to degeneration) can be seen in an individual with a normally adequate intake of vitamin A, who becomes vitamin A deficient due to an acquired or hereditary malabsorption syndrome (including postsurgical bowel resection or remodeling). The etiology may be intrinsic or iatrogenic, but the treatment is directed toward the extrinsic agent by increasing the dose or mode of absorption of the vitamin A.

Mechanisms of Secondary Photoreceptor Death

Photoreceptors can die from several mechanisms, including physical lysis, destruction by thermal denaturation (such as by laser), or by triggering the apoptotic pathways. Apoptosis can be triggered by a number of disruptions, including loss of key trophic factors such as vascular endothelial growth factor (VEGF), energy depletion through mitochondrial failure, oxidative damage of proteins and lipids, release of calcium by shifts in membrane permeability, which can be caused by deregulation of ionic channels, or from the fixation of complement to the membrane

surface. Light levels below those that cause thermal denaturation can lead to direct activation of caspases, calpain 2, and cathepsin D. In addition, mitochondrial-dependent apoptotic pathways also appear to be activated.

In a number of cases, signaling of the apoptotic pathway appears to be governed by at least two pathways: the Wnt pathway and the Jak–STAT pathway. A number of research groups are attempting to identify nonspecific therapies that can block or inhibit the pathways that result in photoreceptor death. The use of ciliary neurotrophic factor (CNTF) as a trophic factor to inhibit activation of the apoptosis pathway is currently in clinical trials to treat primary and secondary photoreceptor degenerations.

As one considers these multiple mechanisms of photoreceptor death, it becomes clear that a major value of experimental animal models for these conditions is to specifically determine the extent to which photoreceptor death is a primary event and if genetic defects within the photoreceptors themselves are necessary and sufficient to initiate apoptosis. At the same time, this does not negate the importance of understanding the intrinsic (both genetic and nongenetic) factors and extrinsic factors that either trigger or modify cell death that may be amenable to therapeutic intervention at a systemic level. Finally, even in the presence of a combination of factors that lead to photoreceptor death, there is the possibility of interrupting or inhibiting the common apoptosis signaling pathways within the photoreceptor cells and other retinal neurons in order to preserve function and vision.

See also: Primary Photoreceptor Degenerations: Retinitis Pigmentosa; Primary Photoreceptor Degenerations: Terminology; Retinal Ganglion Cell Apoptosis and Neuroprotection.

Further Reading

Glazer, L. C. and Dryja, T. P. (2002). Understanding the etiology of Stargardt's disease. *Ophthalmology Clinics of North America* 15(1): 93–100, viii.

Hackam, A. S. (2005). The Wnt signaling pathway in retinal degenerations. *IUBMB Life* 57(6): 381–388.

Ling, C. P. and Pavesio, C. (2003). Paraneoplastic syndromes associated with visual loss. *Current Opinion in Ophthalmology* 14(6): 426–432.

Poll-The, B. T., Maillette de Buy Wenniger-Prick, L. J., Barth, P. G., and Duran, M. (2003). The eye as a window to inborn errors of metabolism. *Journal of Inherited Metabolic Disease* 26(2–3): 229–244.

Punzo, C., Kornacker, K., and Cepko, C. L. (2009). Stimulation of the insulin/mTOR pathway delays cone death in a mouse model of retinitis pigmentosa. *Nature Neuroscience* 12(1): 44–52.

Rattner, A. and Nathans, J. (2006). An evolutionary perspective on the photoreceptor damage response. *American Journal of Ophthalmology* 141(3): 558–562.

Samardzija, M., Wenzel, A., Aufenberg, S., et al. (2006). Differential role of Jak–STAT signaling in retinal degenerations. *FASEB Journal* 20(13): 2411–2413.

Siu, T. L., Morley, J. W., and Coroneo, M. T. (2008). Toxicology of the retina: Advances in understanding the defence mechanisms and pathogenesis of drug- and light-induced retinopathy. *Clinical and Experimental Ophthalmology* 36(2): 176–185.

Stone, J., Maslim, K., Valter-Kosci, K., et al. (1999). Mechanisms of photoreceptor death and survival in mammalian retina. *Progress in Retinal and Eye Research* 18(6): 689–735.

Wenzel, A., Grimm, C., Samardzija, M., and Remé, C. E. (2005). Molecular mechanisms of light-induced photoreceptor apoptosis and neuroprotection for retinal degeneration. *Progress in Retinal and Eye Research* 24(2): 275–306.

Wu, J., Seregard, S., and Algvere, P. V. (2006). Photochemical damage of the retina. *Survey of Ophthalmology* 51(5): 461–481.

Yang, L. P., Zhu, X. A., and Tso, M. O. (2007). A possible mechanism of microglia–photoreceptor crosstalk. *Molecular Vision* 13: 2048–2057.

Relevant Website

http://www.sph.uth.tmc.edu – Retinal information network.

S

Secondary Photoreceptor Degenerations: Age-Related Macular Degeneration

L V Johnson, University of California, Santa Barbara, CA, USA

Glossary

Drusen – The abnormal deposits containing cellular debris and inflammatory molecules that form beneath the retinal pigmented epithelium (RPE) and are associated with the development of age-related macular degeneration.

Macula – The portion of the retina that is responsible for fine acuity vision in the central visual field. It is a small (~6 mm diameter) area located at the posterior pole of the eye near the optic nerve that is structurally unique and contains the highest concentration of cone photoreceptor cells in the retina.

Photoreceptor – The cells of the retina responsible for the absorption of light and its conversion to electrical signals that are transmitted to the brain. In humans, there are two types of photoreceptor cells: rods and cones. Rod photoreceptor cells are very sensitive in dim light situations but do not provide high resolution or color vision. Cone photoreceptor cells are less sensitive than rods but in bright light distinguish colors and provide for high-acuity vision owing to their concentration in the macula.

Retina – The light-sensitive part of the eye that lines its inner surface. It is a multilayered tissue that collects light, processes electronic signals produced by the light, and transmits those signals to the brain.

Retinal pigmented epithelium(RPE) – A pigmented monolayer of cells lying directly adjacent to the retina that provides support for the photoreceptor cells. Its functions include absorption of excess light; processing of molecules required for transduction of light into electrical signals; removal of cellular debris shed by photoreceptor cells; and transport of nutrients, waste products, and ions.

Introduction

Age-related macular degeneration (AMD) is a disease of the eye that causes loss of vision in the center of the visual field. Central vision is mediated by a region of the retina, known as the macula that is specialized for fine acuity vision such as that used for reading and other tasks that require fine focus and high resolution. While the macula comprises only 4% of the retina (it is only 6 mm in diameter), it is responsible for essentially all scotopic (bright light) vision and almost 10% of our visual field. In AMD, the light-sensitive photoreceptor cells in this critical region of the retina become dysfunctional and die resulting in symptoms ranging from slight visual distortions to complete loss of central vision.

Incidence

As the name implies, AMD is most common in the elderly, its incidence being highest in those over 50 years of age. It is the most common cause of irreversible blindness in elderly individuals worldwide and its clinical symptoms are recognized in more than one-third of persons over the age of 75 in industrialized societies. In 2004, it was estimated that over 9 million persons were affected by some form of AMD in the United States alone. It is expected that this number will reach almost 15 million by the year 2020. There are other diseases that affect the macula in younger individuals, but the frequencies of these are significantly less than for AMD and many of these are known to be monogenic diseases, that is, caused by single gene mutations (e.g., vitelliform macular dystrophy, Sorsby's fundus dystrophy, and malattia leventinese).

The Macula

It is not yet clear why the macula is preferentially affected in AMD. The term macula is derived from the Latin *macula lutea* (yellow spot) that describes the appearance of the macula in life due to the accumulation of two carotenoid pigments, lutein and zeaxanthin, in the macular retina. Lutein and zeaxanthin are thought to function as antioxidants and filters of high-energy blue light, and thus protect the macula from light-induced oxidative damage. The fovea is the centermost 2 mm of the macula and is the region of the retina where cone photoreceptor density is highest (up to 200 000 cells mm^2) and visual acuity is maximal. One factor that may contribute to macular sensitivity is its relative lack of vasculature compared to the rest of the retina. Despite the fact that photoreceptor cell density is highest in this region of the retina and photoreceptor cells consume oxygen at a higher rate than any other cells in the body, the inner retina here is thinned and avascular. As a consequence, macular photoreceptors appear to rely on the choroidal capillary bed, the choriocapillaris, as their primary source for oxygen and nutrients. Age-related decreases in choroidal vascular volume and flow could thus compromise macular photoreceptor cells. Age-related changes in Bruch's membrane that are more pronounced in the macular region than elsewhere in the eye may also contribute to the macula's particular susceptibility to pathogenic changes leading to AMD.

Clinical Symptoms

AMD is typically classified into early and late forms. Early AMD (dry or atrophic AMD) is characterized by the appearance of abnormal extracellular deposits known as drusen that form below the retinal pigmented epithelium (RPE) and by focal areas of increased or decreased pigmentation in the RPE and choroid. Drusen are classified as hard (small, distinct, and hemispherical) or soft (large, diffuse, and amorphous) based on their fundoscopic and histologic appearance. Late AMD has two forms: neovascular AMD (wet or exudative AMD) and geographic atrophy, the end stage of dry AMD when neovascularization does not occur (**Figure 1**).

Neovascular AMD is typified by the growth of blood vessels from the choroid into the RPE and the subretinal space (choroidal neovascularization or CNV) and subretinal hemorrhage that cause severe damage to the retina, leading to precipitous vision loss. Physicians

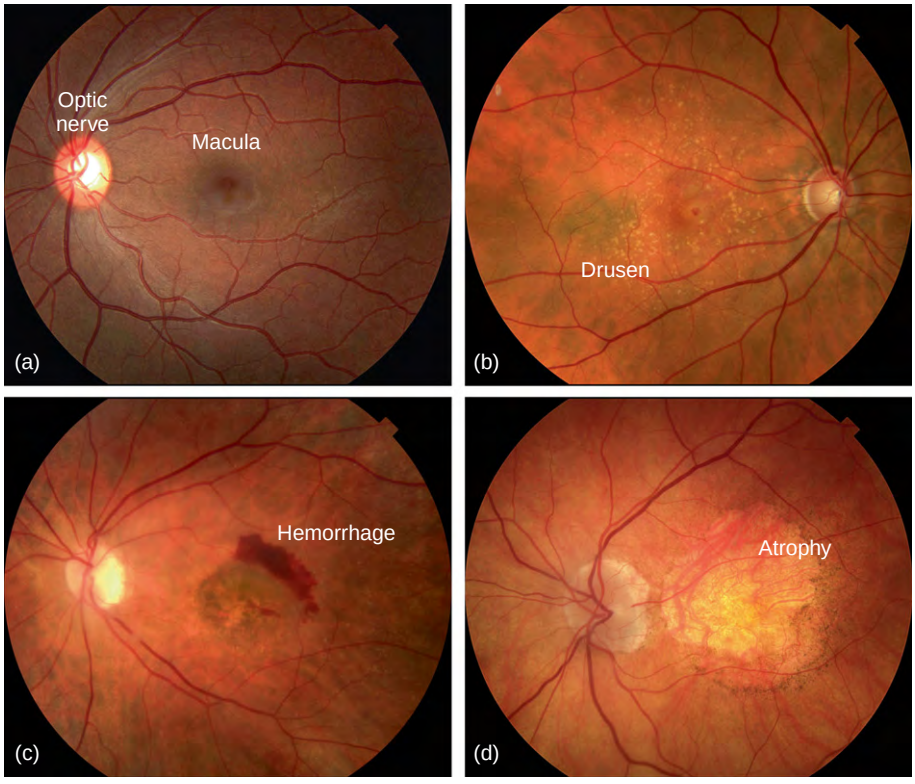

Figure 1 Fundus photographs. Characteristic examples of fundus photographs from a normal, nondiseased eye (a) and eyes with dry AMD (b), wet AMD (c), and geographic atrophy (d). In (b) the hard drusen (numerous small spots) that are characteristic of dry AMD can be seen surrounding the macula. In (c) an area of bleeding (hemorrhage) is present near the macula of an eye with wet AMD. In (d) a large area of atrophy encompassing the entire macular region can be seen in an eye with geographic atrophy. Photographs: courtesy of Dr. Robert Avery.

often use a procedure known as fluorescein angiography to assess the extent of CNV in patients suspected of having neovascular AMD. If untreated, neovascular AMD can lead to the development of a disk-shaped fibrovascular scar underlying the macula and severe loss of central vision (central scotoma). Individuals who develop neovascular AMD in one eye are likely to have it develop in the other (contralateral) eye and thus the risk of bilateral vision loss is high in neovascular AMD. Geographic atrophy is characterized by widespread areas of depigmentation that represent areas of degeneration of the RPE and adjacent photoreceptor cells of the retina. Atrophy of the capillary bed (choriocapillaris) of the choroid is also commonly associated with geographic atrophy. Ultimately, these areas coalesce to form a large distinct area of degeneration that encompasses the macula and causes loss of central vision.

In early, dry AMD, vision loss is gradual and progresses over many years. As such, individuals with early AMD are often unaware of their visual dysfunction. More rapid and severe vision loss is seen in individuals where early AMD progresses to geographic atrophy or neovascular AMD; this occurs in 10–15% of individuals in each case.

Histopathology

Numerous studies show that the earliest pathologic changes associated with AMD occur in the RPE and the adjacent extracellular matrix complex known as Bruch's membrane, which undergoes a substantial number of changes in association with aging and AMD. These include thickening, accumulation of lipids and cholesterol, decreased permeability, and development of deposits of extracellular debris between Bruch's membrane and the RPE. The most prominent of these deposits are known as drusen (German for geodes, because of their glittering appearance when first described) (Figure 2).

Large numbers and extensive areas of drusen deposits in the macula (especially soft drusen) are potent risk factors for the development of AMD. It is thought that drusen diminish access to vital nutrients and oxygen diffusing from the choroidal vessels, leading to the compromise of overlying RPE cells and secondarily to the dysfunction and death of the photoreceptor cells in the adjacent neural retina.

The process of drusen formation is poorly characterized. Drusen are comprised of protein and lipid molecules, many of which are known to be involved in inflammatory processes. These include activators of the complement system, activated complement components, and complement regulatory molecules. As such, it has been proposed that drusen formation is the byproduct of chronic local inflammatory processes. Many drusen components are normal constituents of circulating plasma and it has been suggested that reduced choroidal blood flow associated with AMD leads to increased hydrostatic pressure in the choroidal capillaries forcing plasma proteins extravascularly into the sub-RPE space. However, some drusen-associated molecules are known to be biosynthetic products of RPE cells and cellular debris, likely of RPE origin, is frequently observed in drusen. It is thus likely that RPE-derived molecules also contribute to drusen biogenesis; however, causative conditions and precise mechanisms remain to be identified. It has also been noted that some molecular constituents of drusen have been oxidatively modified, consistent with the idea that oxidative damage may be an important component of drusen formation and AMD pathogenesis.

Risk Factors

The two most significant risk factors for AMD are age and heredity. As noted above, the disease is most commonly diagnosed in individuals over 50 years of age. There is a

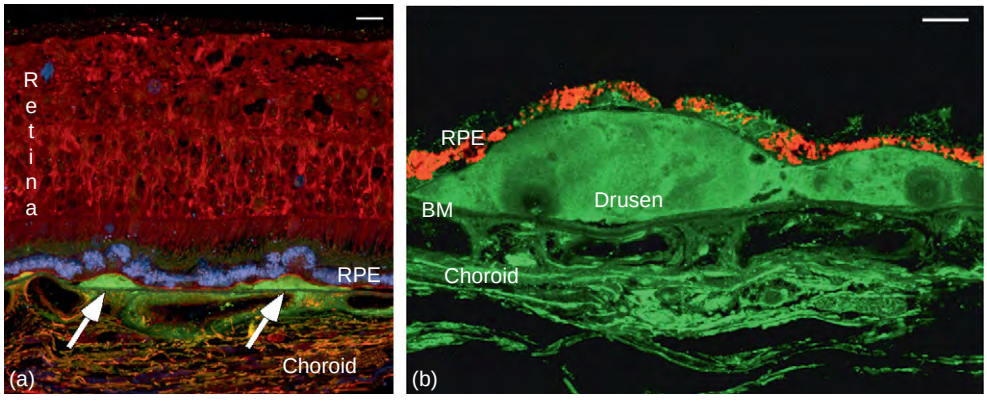

Figure 2 Drusen histology. (a) Two large drusen (green, arrows) are seen lying between the retinal pigmented epithelium (RPE, blue) and the choroid. The adjacent retina is stained red. Scale = 10 μm. (b) At higher magnification, two adjacent drusen (green) are seen displacing the RPE (red) from Bruch's membrane (BM). Scale = 5 μm.

significant increase in AMD risk if close family members are afflicted with the disease. Individuals who have a first-degree relative (parent or sibling) with the disease are more than twice as likely to be afflicted as those without afflicted relatives. They also tend to be affected at an earlier age. These results indicate that specific genetic attributes are likely to be involved in influencing an individual's susceptibility to AMD (see the section titled 'Genetics').

Of environmental risk factors, smoking is the most significant modifiable risk factor for AMD. One study indicates that approximately 25% of AMD cases in individuals over 70 may be attributable to risk conferred by smoking. The preponderance of epidemiological data shows that smokers have a two- to threefold increased risk of having late AMD, neovascular AMD, or geographic atrophy, compared to individuals who have never smoked. There is a dose–response effect in that the risk of developing AMD increases in relation to the duration and intensity of smoking history. It also appears that the average age of onset of AMD symptoms is earlier in smokers compared to nonsmokers, as is the likelihood of disease in both eyes. Stopping smoking, however, can have beneficial effects. While ex-smokers still have an increased AMD risk compared to never-smokers, it is significantly lower than for current smokers. It has been suggested that the increased AMD risk conferred by smoking is related to oxidative damage in the retina, induction of proinflammatory mediators, reduced choroidal blood flow, and decreased levels of protective carotenoid pigments (lutein, zeaxanthin) in the macular retina.

Obesity (or elevated body mass index) has also been linked to an increased risk of progression to late-stage AMD. It has been proposed that this relationship is due to increased oxidative stress, reduced antioxidant defense mechanisms, and/or increased incidence of chronic low-grade inflammation in obese individuals. Low-grade systemic inflammation may contribute to AMD pathogenesis directly through inflammatory damage at the level of the RPE and Bruch's membrane, or secondarily by reducing systemic availability of the macular pigments, lutein and zeaxanthin (increased body fat is associated with decreased serum and macular levels of carotenoids).

Reduced progression of early AMD and reduced risk for neovascular AMD is associated with dietary supplementation with antioxidant vitamins and minerals (the Age-Related Eye Disease Study (AREDS) supplement: 500 mg vitamin C, 50 mg vitamin E, 15 mg beta carotene, 80 mg zinc, and 2 mg copper daily). Diets high in foods that are good sources of the macular carotenoid pigments (e.g., certain green leafy vegetables) and omega-3 fatty acids (e.g., fatty fish and flaxseed) are also associated with decreased incidence of AMD. Interestingly, some epidemiological studies have noted a decreased risk of AMD in individuals who regularly use antacids or anti-inflammatory medications.

Genetics

Genes in two chromosomal regions, one on chromosome 1 (1q32) and one on chromosome 10 (10q26), have now been linked to a significant proportion of AMD cases. In both cases, certain single-base differences in DNA sequence (single-nucleotide polymorphisms or SNPs) in specific genes have been shown to be present at higher frequency in individuals with AMD than in those not afflicted with the disease. Together, genetic variants in these two chromosomal loci confer significant risk for AMD and can account for over half of AMD cases. The implicated gene on chromosome 1 is that for complement factor H (*CFH*), which lies within an area of the chromosome known as the regulator of complement activation (RCA) locus that is known to be involved in modulating activity of the complement system. The involvement of the complement system in AMD that is implied by these observations is consistent with pathological evidence suggesting that chronic inflammation has a primary role in the AMD disease process (see the section titled 'Histopathology'). The AMD-associated genes on chromosome 10 are tightly linked and include *PLEKHA1, ARMS2 (LOC387715)*, and *HTRA1*. The functions of the proteins encoded by these genes and their potential relationship to AMD pathogenesis are less well defined than for *CFH*. *HTRA1* encodes a serine protease and *PLEKHA1* a plekstrin-homology-domain-containing protein; the product of the *ARMS2* gene has not been completely characterized but may be a mitochondrial protein. Polymorphisms in the genes in these two chromosomal loci, especially *CFH* and *ARMS2/HTRA1* (see below), can account for a substantial number of AMD cases. Several additional genes, including those encoding complement component C3, complement factor B, the adenosine triphosphate (ATP)-binding cassette transporter (ABCA4), fibulin-5, apolipoprotein E, human leukocyte antigens, and others have been associated with smaller percentages of AMD cases.

CFH

A SNP (rs1061170) in the gene for *CFH* has been shown in numerous studies to be associated with increased risk for both forms of late AMD. The *CFH* gene is located on human chromosome 1 (1q32) in an area often linked to AMD in familial and population-based studies. The risk-conferring polymorphism in *CFH* results in a thymidine (T) to cytosine (C) substitution at nucleotide position 1277 in exon 9 of the gene. Individuals carrying one copy of the C allele (heterozygotes) are 2–5 times more likely to be afflicted with AMD and carriers of two copies (homozygotes) are 3–7 times more likely to be afflicted. The T → C nucleotide change leads to a tyrosine to histidine shift at amino acid position 402 (Y402H) of the

CFH protein. At the time of writing, the functional implications of this amino acid change have not been fully characterized but the affected site in the protein is one that is known to contribute to a number of CFH functions, including the binding of heparin and C-reactive protein. *CFH* is an important negative regulator of the alternative pathway of complement activation and it is hypothesized that the 402H variant of the molecule may have reduced inhibitory activity. Compromised regulation of the complement system could lead to inflammation and complement-mediated damage to the RPE, and secondary damage to the retina. Combined analyses of polymorphisms in *CFH* and genes encoding some other members of the complement system (complement factor B, complement component 2) indicate that their AMD risk-conferring variants can together account for nearly 75% of AMD cases. There is additional evidence that environmental risk factors, such as smoking and obesity, can combine with genetic risk to increase AMD susceptibility even further. For example, the risk of AMD is 8–10 times higher in individuals who are both homozygous for the risk-conferring C allele in the *CFH* gene and smoke. Additional variants in the *CFH* and related genes have also been linked to AMD risk. For example, deletion of two *CFH*-related genes (*CFHR1* and *CFHR3*) has been shown to have protective effects and decrease the likelihood of AMD.

ARMS2/HTRA1

Both the *ARMS2* and *HTRA1* genes contain polymorphisms that have been associated with increased risk for AMD and they exhibit a high degree of linkage disequilibrium (i.e., they are essentially always transmitted together). Because of this latter property it has been difficult to determine which of the polymorphisms is responsible for the associated AMD risk. In addition, biological evidence supporting a role for both has been presented. One *ARMS2* polymorphism (rs10490924) leads to a change in a region of the gene that is predicted to result in an amino acid change from alanine to serine at position 69 (A69S) of the ARMS2 protein. Some data suggest that the ARMS2 protein is located in mitochondria and that it is involved in modulating oxidative stress and associated apoptosis, but there is no direct evidence yet linking ARMS2 protein dysfunction and the AMD disease process. An additional *ARMS2* polymorphism that involves both deletion and insertion of genetic material has been shown to lead to messenger RNA (mRNA) instability and marked reduction in the levels of *ARMS2* transcripts, and is significantly associated with AMD risk. ARMS2 protein is highly expressed in the retina and it has been proposed that dysfunctional ARMS2 and/or reduced levels of ARMS2 in mitochondria-rich retinal photoreceptor cells may enhance susceptibility to age-associated mitochondrial dysfunction that leads to photoreceptor compromise and visual loss.

The AMD-linked polymorphism in the *HTRA1* gene (rs11200638) lies in the gene's promoter region and some data have suggested that the risk-conferring allele leads to altered binding of transcription factors, increased transcription of the gene, and elevated HTRA1 protein levels, but other studies have not confirmed this observation.

Treatments

Most therapeutic approaches for AMD have historically focused on the neovascular form of the disease, as it is the one which is responsible for the most severe and precipitous vision loss. Therapies for neovascular AMD have included thermal laser photocoagulation of leaky neovessels and photodynamic therapy that utilizes laser activation of an intravenously administered compound that damages the endothelial cells of neovessels, leading to thrombosis. These approaches were applicable to less than half the patients with neovascular AMD and thus, to less than 5% of all AMD patients. More recently, molecular inhibitors of vascular growth factors (primarily vascular endothelial growth factor, VEGF) have been exploited to limit neovascularization in a variety of ocular neovascular processes. Such VEGF inhibitors are generally administered in multiple intravitreal injections and act by inhibiting the interaction of VEGF with its receptor on the surfaces of vascular endothelial cells. The binding of VEGF to its receptor promotes endothelial cell proliferation, vessel growth, and increased vascular permeability, leading to the development of CNV in affected eyes. The most striking results to date have been provided by antibody-based compounds (Lucentis and Avastin) that are directed against VEGF and inhibit its function. These compounds have provided unprecedented benefits in terms of visual stabilization in most patients with CNV and visual improvement in many. It is anticipated that advances in the specificity, efficacy, durability, and deliverability of anti-VEGF compounds, as well as compounds directed against additional vascular growth factors, will continue to advance the physician's ability to combat neovascular AMD. However, similar therapeutic advances have not been made for the dry or atrophic forms of AMD that represent 85–90% of disease cases.

See also: Developmental Anatomy of the Retinal and Choroidal Vasculature; Physiological Anatomy of the Choroidal Vasculature; Physiological Anatomy of the Retinal Vasculature; Primary Photoreceptor Degenerations: Retinitis Pigmentosa; Primary Photoreceptor Degenerations: Terminology; Retinal Pigment Epithelium: Cytokine Modulation of Epithelial Physiology; Secondary Photoreceptor Degenerations.

Further Reading

Baird, P. N., Robman, L. D., Richardson, A. J., et al. (2008). Gene–environment interactions in progression of AMD – the CFH gene, smoking and exposure to chronic infection. *Human Molecular Genetics* 17: 1299–1305.

Berger, J. W., Fine, S. L., and Maguire, M. G. (1999). *Age-Related Macular Degeneration*. St. Louis, MS: Mosby.

Chong, E. W., Kreis, A. J., Wong, T. Y., Simpson, J. A., and Guymer, R. H. (2008). Dietary omega-3 fatty acid and fish intake in the primary prevention of age-related macular degeneration: A systematic review and meta-analysis. *Archives of Ophthalmology* 126: 826–833.

Cong, R., Zhou, B., Sun, Q., Gu, H., Tang, N., and Wang, B. (2008). Smoking and the risk of age-related macular degeneration: A meta-analysis. *Annals of Epidemiology* 18: 647–656.

Gehrs, K. M., Anderson, D. H., Johnson, L. V., and Hageman, G. S. (2006). Age-related macular degeneration – emerging pathogenic and therapeutic concepts. *Annals of Medicine* 38: 450–471.

Grisanti, S. and Tatar, O. (2008). The role of vascular endothelial growth factor and other endogenous interplayers in age-related macular degeneration. *Progress in Retinal and Eye Research* 27: 372–390.

Jager, R. D., Mieler, W. F., and Miller, J. W. (2008). Age-related macular degeneration. *The New England Journal of Medicine* 358: 2606–2617.

Johnson, E. J. (2005). Obesity, lutein metabolism and age-related macular degeneration: A web of connections. *Nutrition Reviews* 63: 9–15.

Klein, R. (2007). Overview of progress in the epidemiology of age-related macular degeneration. *Ophthalmic Epidemiology* 14: 184–187.

Lotery, A. and Trump, D. (2007). Progress in defining the molecular biology of age related macular degeneration. *Human Genetics* 122: 219–236.

Montezuma, S. R., Sobrin, L., and Seddon, J. M. (2007). Review of genetics in age related macular degeneration. *Seminars in Ophthalmology* 22: 229–240.

Pieramici, D. J. and Rabena, M. D. (2008). Anti-VEGF therapy: Comparison of current and future agents. *Eye* 20: 1330–1336.

Provis, J. M., Penfold, P. L., Cornish, E. E., Sandercoe, T. M., and Madigan, M. C. (2005). Anatomy and development of the macula: Specialization and the vulnerability to macular degeneration. *Clinical and Experimental Optometry* 88: 269–281.

Rattner, A. and Nathans, J. (2006). Macular degeneration: Recent advances and therapeutic opportunities. *Nature Reviews Neuroscience* 7: 860–872.

Scholl, H. P. N., Fleckenstein, M., Issa, P. C., et al. (2007). An update on the genetics of age-related macular degeneration. *Molecular Vision* 13: 196–205.

Sunness, J. S. (1999). The natural history of geographic atrophy, the advanced atrophic form of age-related macular degeneration. *Molecular Vision* 5: 25.

Relevant Websites

http://www.ahaf.org – American Health Assistance Foundation.
http://www.macular.org – American Macular Degeneration Foundation (AMDF).
http://www.eyesight.org – Macular Degeneration Foundation (MDF).
http://www.mayoclinic.com – Mayo Clinic.
http://www.nei.nih.gov – National Eye Institute (NEI).
http://www.nlm.nih.gov – National Library of Medicine, National Institutes of Health.

Stability and Functional Integrity of New Blood Vessels

A Uemura, Kobe University Graduate School of Medicine, Kobe, Japan

Glossary

Adherens junction – The protein complex at cell–cell junction in epithelial tissue, which appears as a band encircling the cell.
Extracellular matrix – The matrix surrounding cells that includes the interstitial matrix and the basement membrane. It provides structural support to the cells, serves as a reservoir of cytokines and growth factors, and mediates various biological functions.
Inflammation – The complex biological response of blood vessels to extrinsic stimuli, such as pathogens, involving the increased movement of plasma and leukocytes from the blood into the injured tissues.
Tight junction – The close association between two cells whose membranes join together to form a firm, impermeable barrier to fluid.
Weibel–Palade body – The endothelial organelle storing presynthesized molecules that are rapidly released in response to thrombin, histamine, serotonin, and other secretagogs. The stored molecules include von-Willebrand factor, P-selectin, angiopoietin-2, and others involved in the control of hemostasis, inflammation, or permeability.

Formation of New Blood Vessels During Development and Under Pathological Conditions

During development, an imbalance between oxygen supply and demand within growing organs or tissues results in physiological hypoxia, which triggers a series of cellular and molecular events leading to the formation of new blood vessels. This process is called angiogenesis. Among the increasing list of pro-angiogenic growth factors, the best characterized is vascular endothelial growth factor (VEGF, also referred to as VEGF-A), which binds to the receptor tyrosine kinases, VEGF receptor-1 (VEGFR-1; Flt-1) and VEGFR-2 (Flk-1; KDR). VEGF binding to VEGFR-2 on endothelial cells evokes multiple cascades of intracellular signaling events, which stimulate the proliferation and migration of endothelial cells, and increase vascular permeability. New blood vessels are initially leaky and unstable, but homotypic endothelial–endothelial contacts limit paracellular leakage and provide structural continuity, connecting the cytoskeletal structure of adjacent cells. In addition to these homotypic contacts, nascent endothelial cells also recruit pericytes, which become embedded in the vascular basement membrane and extend long cytoplasmic processes that make focal contacts with several different endothelial cells. Pericytes have long been assumed to simply support the mechanical integrity of the vascular structure, but recent studies have revealed that they also contribute to the stability of the vascular structure through the release, presentation, and activation of signals that act on endothelial cells and strengthen cell–cell and cell–matrix associations. The combination of homotypic and heterotypic cell–cell contacts produces an infrastructure that not only renders blood vessels quiescent, with endothelial cell turnover rates of months to years, but also renders them highly resistant to leakage and inflammation. However, this functional integrity of blood vessels is disrupted in some pathological conditions, such as certain ocular diseases, by pro-angiogenic insults. In diabetic retinopathy and age-related macular degeneration, angiogenesis occurs in response to ischemia or inflammation, but the newly formed blood vessels are unstable, resulting in prolonged retinal edema and hemorrhage. It is therefore clinically important to understand the complex mechanisms underlying the stability and functional integrity of new blood vessels. Recent studies have revealed the cellular and molecular bases responsible for the control of both the homotypic and heterotypic cellular interactions that take place in blood vessels. Surprisingly, the extracellular and intracellular signals involved in these events are closely associated, and provide potentially valuable information for the development of novel therapeutic modalities for restoring vascular integrity in retinal vascular disorders.

Cell–Cell Adhesive Junctions in Blood Vessel Walls

Cell–cell contacts in blood vessel walls are remarkably complex, comprising membrane-associated adhesion proteins, including vascular endothelial (VE)-cadherin and neural (N)-cadherin at adherens junctions, and occludin, claudins, and junctional adhesion molecules at tight junctions. Among these junctional proteins, VE-cadherin and claudin-5 are endothelial-specific molecules, present in most blood vessels. These adhesive junctions contribute to the lack of paracellular permeability, especially in the blood–retina barrier, where endothelial–endothelial interfaces are enriched in tight junctions. In addition, cell–cell contacts modulate various endothelial functions

through a network of intracellular signals. At adherens junctions, VE-cadherin is directly or indirectly bound inside the cells to multiple intracellular partners, including β-catenin, p120-catenin, plakoglobin, vascular endothelial protein tyrosine phosphatase (VE-PTP), density-enhanced phosphatase (DEP)-1, and others. The intracellular components at tight junctions are members of the zonula occludens protein (ZO) family (ZO-1, -2, and -3), AF6/Afadin, PAR-3/ASIP, MUPP-1, and others. Upon contact with neighboring endothelial cells, the formation of adherens junctions precedes that of tight junctions. Interestingly, in the course of junction formation, ZO-1, which is initially localized at adherens junctions, moves to the tight junctions. The nature of these junctions changes depending on the angiogenic status, allowing vessels to grow, or return to a quiescent state.

While tight-junction components interact with several signal transduction molecules, such as G proteins and protein kinases, intensive studies on adherens junctions have demonstrated the importance of VE-cadherin in mediating intracellular signals to control endothelial behavior (**Figure 1**). During the quiescent state, VE-cadherin clustering transmits intracellular signals that promote survival and inhibit the motility of endothelial cells, by regulating the activities of phosphoinositide 3-kinase (PI3-K) and the serine–threonine kinase Akt, as well as the small guanosine triphosphatases (GTPases), Ras-related C3 botulinum toxin substrate (Rac1) and Ras homolog gene family, member A (RhoA). PI3-K/Akt activation by VE-cadherin inactivates the forkhead transcription repressor FKHR (FOXO1), leading to upregulation of the claudin-5 gene, suggesting that molecular communication between adherens and tight junctions strengthens inter-endothelial cell contacts. Furthermore, VE-cadherin associates with VEGFR-2 and negatively regulates its intracellular signaling properties. For example, density-enhanced phosphatase-1 (DEP-1) and other phosphatases associated with the VE-cadherin/catenin complex dephosphorylate VEGFR-2 and inhibit its internalization, leading to reduced activation of mitogen-activated protein kinase (MAPK). These functions of VE-cadherin may partly explain the poor proliferative responses of quiescent vessels to stimulation by VEGF. However, during the angiogenic state, VEGF binding to VEGFR-2 activates nonreceptor Src family kinases that mediate VE-cadherin phosphorylation, leading to dissociation from p120- and β-catenin, internalization into clathrin-coated vesicles, and β-arrestin-dependent endocytosis of VE-cadherin. Thus, the increased vascular permeability mediated by VEGF signaling can be explained, at least in part, by the disassembly of adherens junctions, and subsequent disruption of the endothelial barrier function. Moreover, redistribution of VE-cadherin further enhances VEGF signaling through reduction of the activities of the c-Src tyrosine kinase (Csk), which can bind to phosphorylated VE-cadherin and inactivate Src family kinases. In addition to VEGF, fibroblast growth factor signaling also mediates decoupling of p120-catenin from VE-cadherin, leading to a loss of vessel integrity.

Recruitment of Pericytes in New Blood Vessels

While pericytes are assumed to belong to the same cell lineage as vascular smooth muscle cells (vSMCs), they are distinguished by their location: pericytes occur in intermediate- to small-sized vessels, while vSMCs occur in large arteries or veins. However, depending on the vascular beds, pericytes display remarkable heterogeneity in their morphology, as well as in their frequency relative to endothelial cells, which may reflect their diverse functions. Likewise, depending on the organs or tissues, pericytes have multiple origins, including mesoderm or neural crests. While pericyte differentiation from mesenchymal precursor cells can be induced by transforming growth factor (TGF)-β signaling in *in vitro* culture systems, variable effects of this signaling, both on endothelial cells and pericytes, have hindered a clear understanding of their *in vivo* functions in blood vessel formation. It should be noted that endothelial dysfunction accounts for many of the vascular abnormalities seen in mice with genetic mutations of the ligand TGF-β1, its receptors (activin-receptor-like kinase (Alk)-1 and -5, TGF-β receptor II, and endoglin), or its downstream effector (Smad5), as well as in human hereditary hemorrhagic telangiectasia (HHT) where the endothelial receptors endoglin (type 1 HHT) or Alk1 (type 2 HHT) are mutated. TGF-β modulates the differentiation, proliferation, or migration of endothelial cells, depending on distinct subsets of receptors and downstream effectors, whereas its antiproliferative and antimigratory effects are enhanced in the presence of clustered VE-cadherin.

During the maturation of blood vessels, the pericyte population is expanded by signals mediated by platelet-derived growth factor (PDGF)-B and its receptor β (PDGFRβ). In newly formed blood vessels, PDGF-B derived from endothelial cells, especially those residing at the sprouting vascular tips, promotes the proliferation and migration of PDGFRβ-expressing pericytes. In addition to its localized gene expression in the actively angiogenic endothelium, the spatial distribution of PDGF-B protein is strictly controlled by the binding of its retention motif to heparan sulfate proteoglycans. Disruption of either the PDGF-B or PDGFRβ gene in mice perturbs pericyte recruitment, leading to defective endothelial integrity. Interestingly, vascular dysfunction due to a lack of pericytes is most remarkable in the central nervous system, where pericyte recruitment depends exclusively on their migration from preexisting vessels to new vessel walls, rather than on their *de novo* induction from the

surrounding mesenchyme. This indicates less potential for PDGF-B/PDGFRβ involvement in the initial steps of pericyte differentiation.

Upon recruitment to new blood vessels, endothelial–pericyte contacts are promoted by N-cadherin, which is expressed in both endothelial cells and pericytes. The trafficking of N-cadherin to polarized plasma membrane

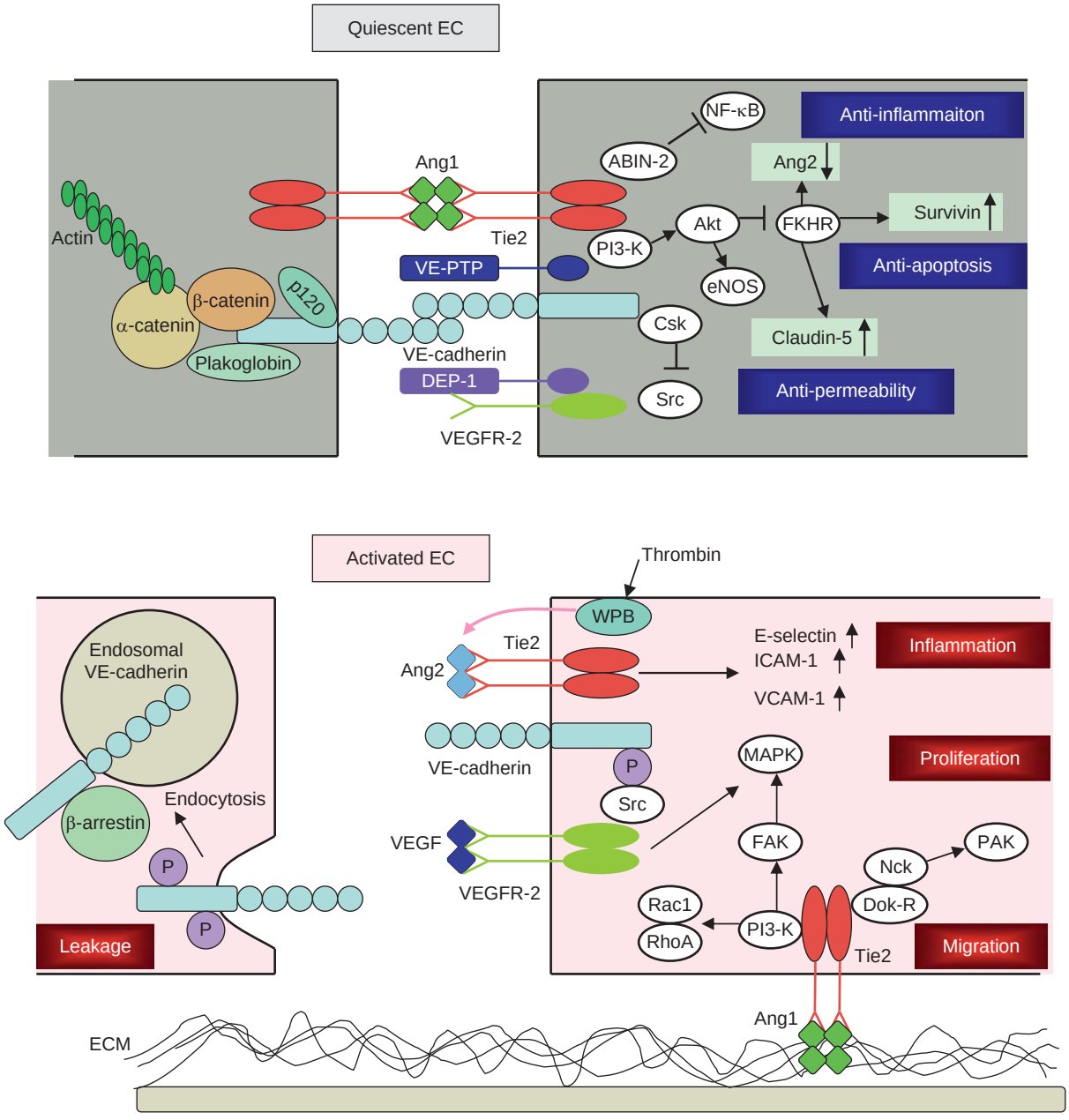

Figure 1 Extracellular and intracellular signals in quiescent and activated endothelial cells. In quiescent endothelial cells (EC), clustering of VE-cadherin at adherens junctions promotes the formation of multimolecular complexes in which plakoglobin and β-catenin directly associate with actin-binding proteins such as α-catenin. DEP-1 dephosphorylates VEGFR-2, whereas Csk negatively regulates Src-mediated VE-cadherin phosphorylation, leading to the maintenance of endothelial barrier function and vascular quiescence. At cell–cell contacts, *trans*-associated Tie2 complexes bridged by multimerized Ang1 comprise Tie1 and VE-PTP, and activate the PI3-K/Akt pathway, leading to enhancement of endothelial survival. Activated Tie2 also recruits ABIN-2 and suppresses inflammatory responses by inactivating NF-κB. On the other hand, Ang2 protein stored in Weibel–Palade bodies (WPB) is rapidly released upon stimulation by thrombin or other secretagogs, rendering EC highly responsive to pro-angiogenic and proinflammatory cytokines, such as VEGF and TNF-α, respectively. VEGF binding to VEGFR-2 activates Src, and subsequent phosphorylation and endocytosis of VE-cadherin impair junctional integrity, leading to increased vascular permeability. In the absence of cell–cell contacts, Ang1–Tie2 complexes anchor basal plasma membranes to the extracellular matrix (ECM) and preferentially activate signaling pathways involved in the control of cell migration, including Dok-R and FAK.

domains is facilitated by sphingosine-1-phosphate (S1P)-mediated activation of the G protein-coupled endothelial differentiation gene (EDG)-1 receptor, which is crucial for pericyte adhesion to endothelial surfaces.

Angiopoietin/Tie Signals as Regulators of Stability and Integrity of Blood Vessels

Angiopoietin-1 (Ang1) secreted from pericytes activates the Tie2 receptor tyrosine kinase expressed on endothelial cells. Whereas the Ang1/Tie2 signal regulates the dynamic, morphogenetic processes of growing vascular networks, constitutive Tie2 activation is further required for promoting endothelial survival and preventing vascular leakage and inflammation in quiescent blood vessels. By contrast, Ang2 counteracts the Ang1/Tie2 signaling axis, thereby rendering endothelial cells responsive to pro-angiogenic and proinflammatory stimuli. Thus, the Tie2 activation status determined by the balance between Ang1 and Ang2 is critical in the organization and stabilization of vascular structure.

Molecular Properties of Angiopoietins and Tie Receptors

Ang1, Ang2, Ang3, and Ang4 have been identified as endogenous ligands for Tie2, among which Ang1 and Ang2 have been characterized as the predominant regulators of Tie2 activities. The angiopoietins share a similar overall structure, with a short amino-terminal motif followed by a coiled-coil domain and carboxy-terminal fibrinogen-like domain. The fibrinogen-like domain is responsible for receptor binding, the coiled-coil domain is required for dimerization of angiopoietin monomers, and the short amino-terminal motif forms ring-like structures that cluster dimers into variable sized multimers, which is a necessary step in Tie2 activation. Ang1 and Ang2 have indistinguishable binding sites on Tie2 and similar binding affinities. Although Ang2 counteracts Ang1/Tie2 signaling in endothelial cells, direct evidence for an inhibitory effect of Ang2 on Tie2 phosphorylation is lacking. In *in vitro* culture systems, Ang2 can activate Tie2 transfected into nonendothelial cells, or even native Tie2 expressed on endothelial cells under certain experimental conditions. Indeed, Ang2 has been demonstrated to act as an autocrine factor that activates Tie2 *in vivo*, inhibiting apoptosis and vascular leakage in stressed endothelial cells. Ang2 might therefore be better considered as a partial agonist, rather than a full antagonist. In addition to Tie2, its close relative, Tie1, is also phosphorylated in endothelial cells by Ang1, but not by Ang2. It is likely that Ang1 activates Tie1 either directly, or indirectly through binding to Tie2, which forms a complex with Tie1. Moreover, Ang1 can bind to integrin $\alpha 5\beta 1$, an endothelial receptor for fibronectin, through the receptor-binding fibrinogen-like domain. Ang1-mediated bridging of Tie2, integrin, and fibronectin anchor endothelial membranes to the underlying extracellular matrix and enhance Ang1-activated endothelial adhesion and motility. By contrast, at endothelial–endothelial contacts, Ang1 induces the formation of homotypic Tie2–Tie2 *trans*-associated complexes that include VE-PTP and Tie1, leading to inhibition of paracellular permeability and promotion of endothelial quiescence. Intriguingly, distinct downstream signals are activated depending on the Tie2 localization, either at cell–matrix or cell–cell contacts, which may explain the differential effects of Ang1 in the formation and stabilization of blood vessels (**Figure 1**).

Regulation of Angiogenesis and Vascular Homeostasis by Ang/Tie Signals

Significant insights into the functional roles of Ang/Tie signals have been obtained from studies of genetically mutated mice. Defects in the remodeling of primary capillary networks, which show reduced morphological complexity with dilated vessels, diminished branching and sprouting, and vessel rupture, are common features of mouse models lacking the Tie2 or Ang1 gene. In these mutant mice, dysfunctional endothelial cells fail to properly associate with the underlying matrix and the pericytes. These findings suggest a critical role for the Ang1/Tie2 signal in the stabilization and maturation of vascular structure. This notion is further supported by the presence of leakage-resistant vessels in the skin of transgenic mice overexpressing Ang1 under the control of a keratinocyte-specific promoter. On the other hand, mice lacking Tie1 demonstrate a phenotype characterized by defective vascular integrity and quiescence, which is partially similar to, but distinct from, that seen in mice lacking Tie2 or Ang1.

In contrast to the relatively stable expression of Ang1 in pericytes, Ang2 expression occurs predominantly in areas where either vascular sprouting or regression is taking place. Transgenic mice overexpressing Ang2 under the control of an endothelium-specific promoter display a vascular phenotype similar to that observed in Ang1- or Tie2-deficient mice. These findings suggest that binding of Ang2 to Tie2 interferes with Ang1-induced vascular stabilization, making vessels more sensitive to the actions of other cytokines, such as VEGF. In this model, Ang2 acts as a pro-angiogenic cytokine in the presence of VEGF, whereas it induces vascular regression in the absence of VEGF. The latter scenario is consistent with the delayed regression of the hyaloid vessels seen in the eyes of Ang2-deficient mice. Interestingly, defective vascular phenotypes selectively seen in postnatal retinas, but not in other organs, of Ang2-deficient mice suggest that Ang2 is required for specific angiogenic processes, presumably those involved in sprouting angiogenesis.

In the adult vasculature, Ang1 derived from pericytes constitutively phosphorylates Tie2 at a low level to

maintain the mature phenotype of the endothelium. The importance of the degree of Tie2 activation is demonstrated by the observation that an activating mutation of the Tie2 gene causes venous malformations in humans. This Ang1/Tie2 signal can counteract leakage-inducing stimuli such as VEGF. Ang2 expression is almost absent in the quiescent vasculature, but Ang2 gene expression is dramatically upregulated, mainly in endothelial cells, in response to hypoxia or VEGF. Ang2 destabilizes the endothelial–pericyte association, thereby priming endothelial cells to respond to pro-angiogenic stimuli. In addition, upon stimulation by thrombin or other secretagogs, presynthesized Ang2 protein stored in Weibel–Palade bodies is rapidly released, rendering quiescent endothelium highly responsive to proinflammatory cytokines such as tumor necrosis factor (TNF)-α, leading to the upregulation of a number of endothelial–leukocyte adhesion molecules, including E-selectin, intercellular adhesion molecule-1 (ICAM-1), and vascular cell adhesion molecule-1 (VCAM-1). Thus, vascular homeostasis, maintained by the Ang1/Tie2 default pathway, can be disrupted by Ang2 activation.

Intracellular Signaling Cascades Mediated by Tie2 Activation

Ang1 binding to the Tie2 extracellular domain rapidly mediates receptor dimerization, activation of its kinase domain, and autophosphorylation of specific tyrosine residues in its intracellular domain. Among the intracellular events triggered by Tie2 activation, signaling through PI3-K appears to be essential for Tie2-mediated survival and motility of endothelial cells. Binding of PI3-K to the phosphorylated tyrosine residue in the Tie2 intracellular domain activates Akt, which in turn inactivates FKHR, leading to upregulation of the survivin gene and downregulation of the Ang2 gene. The PI3-K/Akt pathway further activates endothelial nitric oxide synthase (eNOS) that modulates various endothelial functions, including cell survival. These signals together exert anti-apoptotic effects and promote vascular quiescence. PI3-K also regulates the activities of intracellular signals involved in the control of cell adhesion and migration, including the focal adhesion kinase (FAK), RhoA, and Rac1, which may lead to Ang1-induced vascular sprouting and remodeling. Besides PI3-K, Tie2-mediated stimulation of endothelial migration involves recruitment of the adaptor protein, Dok-R, to activated Tie2, leading to the creation of binding sites for Nck and the serine kinase p21-activating kinase (PAK). Interestingly, distinct subsets of Tie2-mediated intracellular signals are preferentially enhanced depending on the endothelial cell microenvironment; Dok-R and FAK are activated at cell–matrix contacts in migrating endothelial cells, whereas Akt and eNOS are activated at homotypic endothelial cell–cell contacts to maintain vascular quiescence. Tie1, like Tie2, can activate PI3K/Akt, but it does not activate Dok-R/Nck/PAK, which may explain the differential effects of Tie1 and Tie2, especially in endothelial migration.

Although the mechanism whereby Tie2 mediates anti-leakage and antiinflammatory effects is poorly understood, several signaling events involved in these vasoprotective functions have recently been identified. Ang1 binding to Tie2 inhibits VEGF-mediated Src activation, thereby preventing the phosphorylation-dependent redistribution of VE-cadherin. On the other hand, Tie2 activation recruits the A20-binding inhibitor of nuclear factor κB-2 (ABIN-2), leading to the suppression of nuclear factor κB (NF-κB), a transcription factor critical for the regulation of inflammatory gene expression (**Figure 1**).

Stability and Functional Integrity of Retinal Blood Vessels

The retinas in both human and mouse embryos initially have no vascular systems, and the resulting hypoxia in the retinal neurons stimulates an influx of astrocytes from the optic nerves. Retinal astrocytes subsequently form fine networks within the superficial retinal areas and secrete VEGF and fibronectin, which cooperatively promote sprouting angiogenesis in the retinas of human embryos or mouse neonates. The extracellular fibronectin matrices serve as depositories of matrix-bound VEGF isoforms and contribute to the establishment of concentration gradients of VEGF proteins, which regulate the direction of endothelial sprouting. These extracellular fibronectin matrices also provide physical scaffolds to which α5β1 integrin-expressing endothelial cells adhere. Thus, retinal vascular networks migrate over the preexisting astrocyte networks, using them as templates. Upon contact with blood vessels, the astrocytes rapidly lose their pro-angiogenic properties by downregulating their expression of VEGF and fibronectin genes. They cover the blood vessel walls to contribute to establishment of the blood–retina barrier, in cooperation with tight junctions formed at endothelial–endothelial contacts.

Throughout the processes of retinal vascular development, pericytes are found over the entire vascular network, except at the sprouting vascular tips, although not all endothelial cells surfaces are covered by pericytes. Recruitment of pericytes in retinal blood vessels is largely dependent on PDGF-B/PDGFRβ signaling, as revealed by the complete inhibition of pericyte recruitment by pharmacological blockade of PDGFRβ. In the absence of pericytes, retinal vessels are enlarged, with multiple clefts formed in endothelial–endothelial junctions, leading to progressive edema and hemorrhage. Intriguingly, intraocular administration of Ang1 protein can suppress the vascular leakage and ameliorate the morphogenetic remodeling of vascular architecture, without restoration of pericyte recruitment. These direct actions of Ang1 on endothelial integrity

indicate that Ang1 plays central roles in pericyte-mediated vascular stabilization (Figure 2).

In the capillaries of adult retinas, pericytes are flattened and elongated with long cytoplasmic processes along the capillary axis, with a pericyte:endothelial cell ratio of 1:1, the highest in the body, implying their significant contribution to the maintenance of vascular integrity. Indeed, the loss of pericytes is regarded as a critical event triggering a series of vascular abnormalities seen in diabetic retinopathy, including microaneurysm formation, retinal hemorrhage and edema, and vascular obstruction. In contrast to the developmental period, pharmacological blockade of PDGFRβ in adult mice has no obvious effects on the retinal vascular structure. Together with the absence of endothelial PDGF-B expression in quiescent retinal vessels, it is less likely that the maintenance

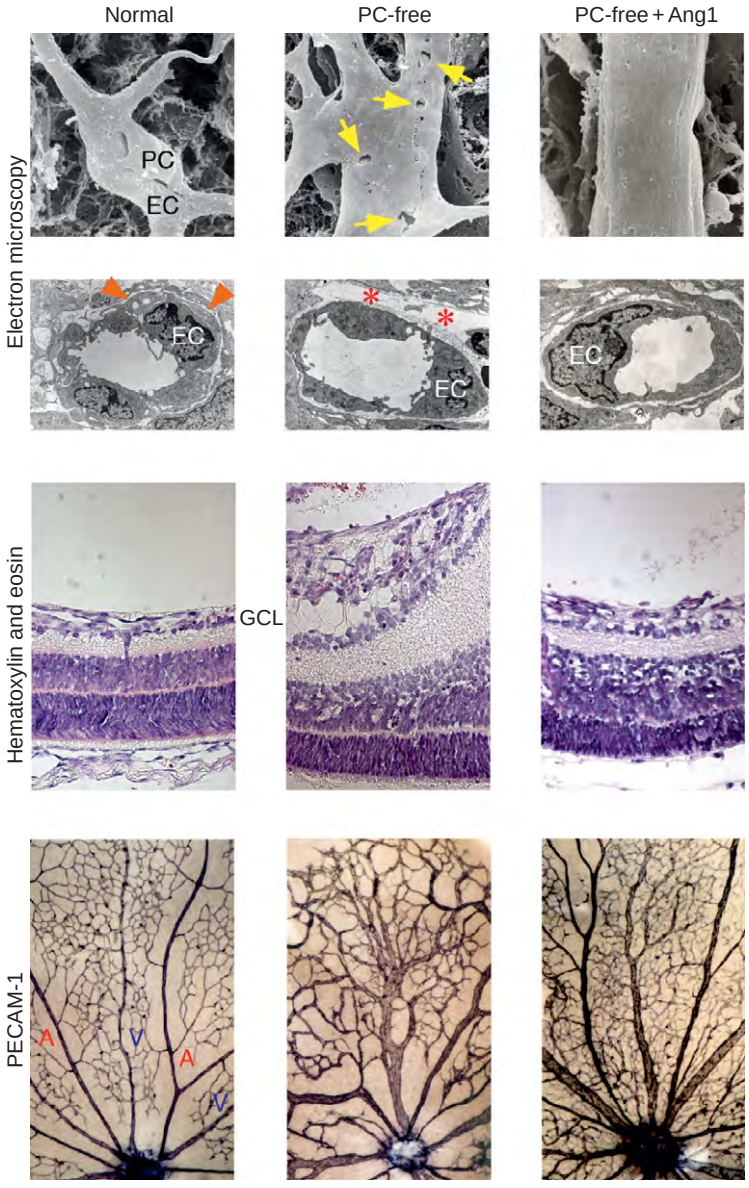

Figure 2 Ang1-mediated restoration of retinal vascular integrity in the absence of pericytes. In developing blood vessels of normal mouse retinas (left columns), pericytes (PC, arrowheads) extending long cytoplasmic processes associate with nascent endothelial cells (EC). The superficial vascular networks formed above the ganglion cell layer (GCL) undergo morphogenetic remodeling into arteries (A), veins (V), and capillaries, as demonstrated by whole-mount immunostaining with PECAM-1. Systemic injections of anti-PDGFRβ blocking antibody completely inhibit PC recruitment to retinal vessels (middle columns), resulting in multiple cleft formation at denuded endothelial cell–cell junctions (arrows), extraluminal fluid accumulation (asterisks), progressive exacerbation of edema and hemorrhage in the superficial retinal areas, and disorganized architecture of vascular networks. These defects in functional integrity, as well as morphogenetic remodeling of retinal blood vessels, can be substantially ameliorated by intraocular injection of Ang1 protein, even without restoration of pericyte recruitment (right columns). Adapted from Uemura, A. et al. (2002). *Journal of Clinical Investigation*.

of an endothelial–pericyte association constitutively requires PDGF-B/PDGFRβ signaling. By contrast, Ang2 is upregulated in the retinas of diabetic animal models, and direct administration of Ang2 protein into the eye induces pericyte loss from retinal microvessels. Furthermore, high glucose levels increase Ang2 transcription in cultured endothelial cells. These findings collectively suggest that upregulation of Ang2 in response to hyperglycemia could be partly responsible for the destabilization of vessel integrity in diabetic retinopathy.

Clinical Therapies to Restore Vascular Integrity in Retinal Vascular Disorders

Improvement of vision in diabetic retinopathy and age-related macular degeneration might be expected to be achieved either by inhibiting new vessel formation, or by stabilizing leaky blood vessels. Currently available anti-VEGF drugs are administered based on the theory that new blood vessels fail to recruit pericytes, thereby rendering naked endothelial cells, but not healthy blood vessels, selectively sensitive to VEGF deprivation. Indeed, inhibition of pericyte recruitment by pharmacological blockade of the PDGFRβ signal enhances the anti-angiogenic effects of VEGF neutralization in experimental models of choroidal neovascularization. However, the assumed lack of pericyte coverage of new blood vessels needs to be confirmed. This uncertainty could be due to difficulties in identifying all of the heterogeneous pericyte populations using a single marker, such as smooth muscle α-actin. Indeed, by combining multiple markers (desmin, PDGFRβ, NG2, or RGS5) and ultrastructural observations, new blood vessels in developing retinas, which were often previously reported to lack pericytes, have recently been shown to have abundant pericytes. It is notable that developing retinal vessels undergo regression, under hyperoxia or by VEGF neutralization, or even in the normal developmental course, despite their association with pericytes. This suggests that the presence of pericytes *per se* does not stabilize new blood vessels. The degree to which pericyte–endothelial contacts ensure vascular stability requires further elucidation.

In addition to the neutralization of VEGF signals, alternative therapeutic approaches aimed at achieving selective regression of abnormal vessels, while leaving normal vessels intact, should be evaluated. Interestingly, during tumor angiogenesis, a monoclonal antibody against a VE-cadherin epitope that is only accessible on endothelial cells forming new adherens junctions, has been demonstrated to specifically inhibit the formation of new blood vessels without affecting the permeability of resting blood vessels.

In addition to their anti-angiogenic ability, anti-VEGF drugs have also been proven to be effective in reducing vascular permeability. However, constitutive expression of cell-autonomous VEGF is reportedly required for endothelial homeostasis in healthy, quiescent, blood vessels. Furthermore, in adult retinas, both VEGF and VEGFR-2 are expressed by various types of neurons and Müller glia, indicating a constitutive requirement for this signal in retinal homeostasis. Indeed, sustained inhibition of VEGF signaling results in neuronal or glial cell death, leading to a decline in retinal function. These findings indicate the potential for adverse effects of anti-VEGF drugs used for retinal diseases. Alternatively, restricted manipulation of signaling molecules specifically responsible for vascular permeability may be a more desirable method of effectively restoring vascular integrity without affecting retinal function. VEGF-induced vascular permeability in retinas is inhibited by blockade of Src kinase, suggesting that this signaling molecule is a potential therapeutic target. Furthermore, the therapeutic potential of Ang1 is indicated by its ability to inhibit retinal vascular leakage induced by VEGF, inflammation, or the loss of pericytes. Ang2-neutralizing reagents may also be effective in restoring the quiescence of retinal blood vessels.

Conclusion

In blood vessel walls, multiple ligand–receptor systems and junctional protein complexes at homotypic and heterotypic cell–cell contacts act in concert to modulate intracellular signaling events to switch endothelial cells between quiescent and activated states, depending on their microenvironmental conditions. Accumulating evidence has determined that angiogenesis-regulating signals are also crucially involved in governing the stability of blood vessels. While a list of the extracellular and intracellular signals responsible for vascular stabilization is emerging, further investigations are needed to identify specific molecules relevant to the development of pinpoint therapies targeting the functional integrity of blood vessels in retinal vascular disorders.

See also: Angiogenesis in Inflammation; Angiogenesis in Response to Hypoxia; Blood–Retinal Barrier; Breakdown of the Blood–Retinal Barrier; Development of the Retinal Vasculature; Formation and Regression of the Primary Vitreous and Hyaloid Vascular System; Injury and Repair: Neovascularization; Macular Edema; Molecular Mechanisms of Angiostasis; Pathological Retinal Angiogenesis; Pericytes and Microvascular Remodeling: Regulation of Retinal Angiogenesis; Physiological Anatomy of the Choroidal Vasculature; Physiological Anatomy of the Retinal

Vasculature; Retinal Degeneration through the Eye of the Fly; Retinal Vasculopathies: Diabetic Retinopathy; Vessel Regression.

Further Reading

Aiello, L. P. (2008). Targeting intraocular neovascularization and edema – one drop at a time. *New England Journal of Medicine* 359: 967–969.

Andrae, J., Gallini, R., and Betsholtz, C. (2008). Role of platelet-derived growth factors in physiology and medicine. *Genes and Development* 22: 1276–1312.

Andreoli, C. M. and Miller, J. W. (2007). Anti-vascular endothelial growth factor therapy for ocular neovascular disease. *Current Opinion in Ophthalmology* 18: 502–508.

Betsholtz, C., Lindblom, P., and Gerhardt, H. (2005). Role of pericytes in vascular morphogenesis. In: Clauss, M. and Breier, G. (eds.) *Mechanisms of Angiogenesis*, pp. 115–126. Basel: Birkhäuser.

Brindle, N. P., Saharinen, P., and Alitalo, K. (2006). Signaling and functions of angiopoietin-1 in vascular protection. *Circulation Research* 98: 1014–1023.

Carmeliet, P. (2005). Angiogenesis in life, disease and medicine. *Nature* 438: 932–936.

Dejana, E., Orsenigo, F., and Lampugnani, M. Z. (2008). The role of adherens junctions and VE-cadherin in the control of vascular permeability. *Journal of Cell Science* 121: 2115–2122.

Erickson, K. K., Sundstrom, J. M., and Antonetti, D. A. (2007). Vascular permeability in ocular disease and the role of tight junctions. *Angiogenesis* 10: 103–117.

Folkman, J. (2006). Angiogenesis. *Annual Review of Medicine* 57: 1–18.

Fruttiger, M. (2007). Development of the retinal vasculature. *Angiogenesis* 10: 77–88.

Gerhardt, H. and Betsholtz, C. (2005). How do endothelial cells orient? In: Clauss, M. and Breier, G. (eds.) *Mechanisms of Angiogenesis*, pp. 3–16. Basel: Birkhäuser.

Motiejunaite, R. and Kazlauskas, A. (2008). Pericytes and ocular diseases. *Experimental Eye Research* 86: 171–177.

Risau, W. (1997). Mechanisms of angiogenesis. *Nature* 386: 671–674.

Uemura, A., Kusuhara, S., Katsuta, H., and Nishikawa, S. (2006). Angiogenesis in the mouse retina: A model system for experimental manipulation. *Experimental Cell Research* 312: 676–683.

Yancopoulos, G. D., Davis, S., Gale, N. W., et al. (2000). Vascular-specific growth factors and blood vessel formation. *Nature* 407: 242–248.

Stem Cells of the Ocular Surface

Y Du and J L Funderburgh, University of Pittsburgh, Pittsburgh, PA, USA

Glossary

Basement membrane – Every epithelial sheet elaborates a noncellular dual-layered membrane of collagen and proteoglycans to which the cells are anchored. In addition to anchoring the cells, basement membranes (also called basal laminae) serve to maintain epithelial differentiation and to provide a biological barrier preventing contact between the epithelial cells and the underlying mesenchymal tissue.
Cell therapy – Stem cells are injected directly into pathological tissues to restore tissue function.
Conjunctiva – The squamous epithelium overlaying the sclera and inner eyelid.
Corneal stroma – This tough connective tissue provides 90% of the corneal thickness and consists mostly of collagen, proteoglycans, and water. Cells make up 4% of the stromal tissue.
Crypts – These structures, originally named in the intestine, represent small dead-end tubes that protrude from the surface of an epithelial layer into the surrounding mesenchymal tissue.
Cytokeratin – Hair and the epidermis consist primarily of the fibrous proteins, keratins. Moist epithelia such as intestine and cornea were originally thought not to be 'keratinized' but the outer layers cells in these tissues express intracellular keratin proteins as they differentiate. Due to the large number of keratin genes, keratin expression is highly tissue specific.
Endothelium – Corneal endothelium is a single epithelial layer of cells on the posterior (inner) side of the cornea which provides a hydrodynamic pumping function to maintain corneal hydration. It is unrelated to vascular endothelium.
Keratocyte – These are dendritic, quiescent cells of the corneal stroma. They produce the complex extracellular matrix of the corneal stroma but, during wound healing, also produce an opaque scar tissue.
Limbus – In the eye, the border between the transparent cornea and the opaque sclera is known as the limbus. The limbal region of the overlying epithelia is continuous with no obvious boundary, but the conjunctival and corneal cells can be distinguished by the types of cytokeratins that are expressed.
Neural crest – In early embryonic development a small population of cells between the ectoderm and the neural tube migrates out into the embryo, differentiating into a wide variety of tissues including autonomic nerves, cartilage, smooth muscles, and melanocytes. A number of ocular tissues (corneal stroma and iris) are derived from neural crest.
Niche – A stem cell niche is a phrase loosely used to describe the microenvironment in which stem cells are found, which interacts with stem cells to regulate stem cell fate.
Squamous epithelium – Multilayered epithelia show differences between the basal cells attached to the basal lamina and the more superficial cells of the layer. The apical cells flatten and express tissue-specific keratins. These outer cells die by apoptosis and leave the layer (known as desquamation) to be replaced by underlying cells. Single-layer epithelia such as the corneal endothelium do not undergo the process of desquamation and renewal.

The Ocular Surface

Anatomy

Beneath the protective tear film, the human ocular surface is covered with a contiguous layer of moist squamous epithelium, consisting of the bulbar conjunctival epithelium over the sclera and the transparent corneal epithelium of the cornea (**Figure 1**). The bulbar conjunctival epithelium rests on a loose, vascularized connective tissue which allows the movement of the eyelid over the sclera and maintains the limbal vascular supply. This epithelium is contiguous with the corneal epithelium and with the conjunctiva of the fornix located in the folded region between the sclera and the eyelid. The conjunctival epithelium contains goblet cells – the source of soluble mucins in the tear film. These cells are an essential element in maintenance of the integrity of the ocular surface. The cornea is covered with a phenotypically unique epithelial sheet 5–11-cell layers deep which is transparent to light and devoid of goblet cells. The flattened cells of the corneal surface overlie wing-shaped cells – which, in turn, rest on a cuboidal basal epithelium. Unlike the conjunctival epithelium, the corneal epithelium is firmly connected to rigid tissue of the stroma via an anchoring complex involving keratin and collagen fibrils extending into the acellular anterior collagenous layer of the stroma. The interface between the corneal and conjunctival epithelium is known as the

corneoscleral limbus (Figure 1(a)). This region features a network of physical folds in the surface of stromal tissue known as the palisades of Vogt (Figure 1). As described below, the palisades harbor a small population of cells identified as limbal stem cells (LSC). The limbal region also contains pigmented cells and a population of immune cells related to the Langerhans' cells of the dermis.

Underlying the corneal epithelium is the corneal stroma, a tough, transparent connective tissue making up 90% of the thickness of the cornea (Figure 1(c)). The stroma contains layers (lamellae) of aligned collagen fibrils sandwiching quiescent keratocytes, flattened mesenchymal cells. The specialized arrangement of the collagenous ultrastructure in the stroma is responsible for the remarkable tensile strength of this tissue as well as its unique light transparency. On the posterior side of the stroma a single cell layer – the corneal endothelium – is separated from the stromal tissue by Descemet's membrane. The three tissue layers of the cornea each make an important physiological contribution to maintenance of corneal transparency. In addition, the cornea provides 75% of the refractive power required to focus the light on the retina and acts as an effective biological barrier.

Development

Formation of the human cornea begins at approximately 5–6 weeks of gestation. After the lens vesicle pinches off from the surface ectoderm of the head, the overlying ectoderm transforms into a layer of cuboidal epithelial cells, which continue to develop into the corneal epithelium. At 6–7 weeks, neural crest cells migrate between this epithelium and the lens, forming the corneal endothelium. Shortly afterward, a second wave of cell migration from neural crest forms the stroma – which then begins to generate collagenous matrix in the 8th week.

Homeostasis and Repair

The cellular layers of the cornea and conjunctiva differ markedly in several important characteristics of homeostasis and repair. In the corneal epithelium, the superficial cells are lost by exfoliation and replaced by the underlying wing cells. These, in turn, are continually replaced by mitotically active basal cells. In addition to the basal to superficial migration of corneal epithelial cells, there is a well-documented migration of epithelial cells from the periphery to the center of the cornea, measured at 2–3 μm per day. The dynamics of the corneal epithelium have been characterized as the X,Y,Z equation, in which the exfoliation rate (X) equals the rate of production of new cells from the basal cells (Z) plus cells added by the centripetal migration of cells (Y). When injured, the corneal epithelium closes wounds first by migration of the intact sheet over the denuded area, followed by a delay before increased cell division is observed. Bulbar conjunctival epithelium is contiguous with the corneal epithelium without any obvious physical barrier; however,

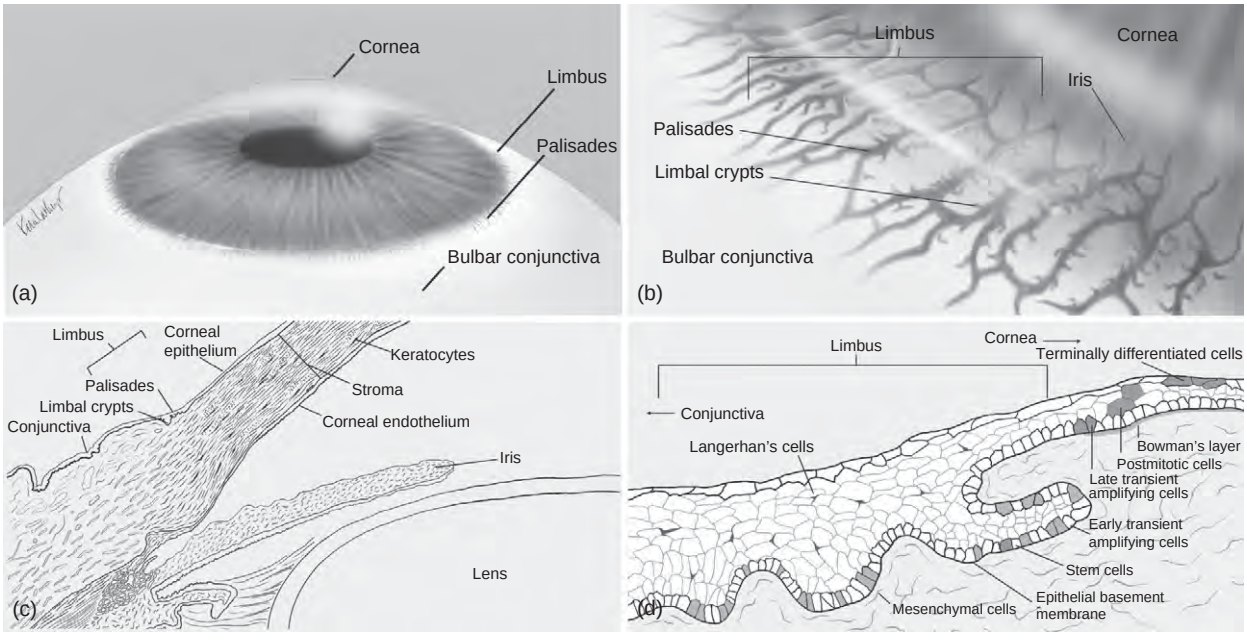

Figure 1 The ocular surface. (a) The location of the corneal, conjunctival, and limbal surfaces are displayed along with the location of the palisades of Vogt. (b) Artists rendering illustrating a close-up view of the anatomy of the palisades of Vogt and the dead-end crypts that branch off from these folds in the tissue. (c) Cross-sectional illustration of the corneoscleral junction. (d) Close-up illustration of the limbal epithelium region and limbal stem cell niche. Original drawings by Kira Lathrop.

these cells express different cytokeratin markers and are found not to migrate in the unwounded eye. Cell division by basal cells and exfoliation is observed throughout the conjunctiva.

The cells of the corneal stroma – the stromal keratocytes – show little cell division in normal adults. The keratocytes undergo rapid cell division after localization in the cornea in late embryogenesis, but, following birth, the keratocyte cell number stabilizes and little or no mitosis can be detected throughout life. In the case of inflammation or wounding, however, the stromal keratocytes become activated and mitotic. The activated keratocytes adopt a fibroblastic phenotype and, later, display characteristics of myofibroblasts. Connective tissue secreted by these cells during wound healing is not transparent but becomes opaque scar tissue. Following healing, the cells become quiescent, but human corneal scars are very slow to resolve; it is not clear if the resident cells ever return to a fully keratocytic phenotype. These properties suggest a limited process of tissue renewal in the corneal stroma.

Renewal of corneal endothelial cells is even more limited than that of the keratocytes. Following childhood, human corneal endothelial cells do not divide. Compensation for endothelial damage is accomplished by flattening of the remaining cells to cover the posterior surface of the cornea. *In vitro* as well, human corneal endothelial cells show only limited ability to divide following infancy.

These characteristics have led to a conventional view that, while the corneal epithelium is maintained by a stem cell population, the stroma and the endothelium – with limited ability for self-renewal – are not maintained by mitotically active, tissue-resident stem cells.

Properties of Stem Cells

Stem cells, by definition, undergo asymmetric cell division; that is, they undergo self-renewal while giving rise to differentiated daughter cells. Embryonic stem cells derived from the inner cell mass of the blastocyst are pluripotent, giving rise to most cells of the body. In culture, embryonic stem cells can be propagated indefinitely in an undifferentiated state. Although they can be isolated from umbilical cord blood, fully pluripotent stem cells are thought to be scarce or absent in adult tissues. Stem cells in adult organisms have long been associated with self-renewing tissues, such as the hematopoietic system, dermis, and intestine. The resident stem cells in these tissues are generally capable of generating only one type of cell, making them unipotent. In recent years, understanding of a new class of stem cells has emerged: known as mesenchymal stem cells (MSC), these cells appear to be present in small numbers in many somatic tissues and can also be isolated from bone marrow. Studies show these MSC to participate in injury repair, and – when expanded in culture – the MSC exhibit potential to differentiate into a number of lineages, and thus can be considered as being multipotent. Considerable effort has gone into identifying common characteristics of adult stem cells, but in spite of such efforts there appears to a dearth of global phenotypic markers for such cells. *In vitro*, clonal growth, extended life span, and the ability to express phenotypic markers of multiple differentiated cell types have been useful in stem cell identification, but cell surface markers for stem cells – as well as properties enabling isolation of these populations – often need to be defined for individual tissues.

In self-renewing tissues, stem cells appear to be localized in an anatomical niche, a restricted microenvironment which interacts with stem cells to regulate stem cell fate. The niche provides physical and chemical factors that both control the replication and maintain the differentiation potential of the stem cells. Typically, the niche is near a vascular bed, usually containing a population of unrelated cells that serve as feeder cells.

Stem Cells in the Corneal Epithelium

Characteristics of Limbal Stem Cells

Abundant research supports the idea that a stem cell population is localized in the corneoscleral limbal region. These cells – termed limbal stem cells (LSC) – share a number of features with the stem cells of other self-renewing tissues. They have small cell size and high nuclear-to-cytoplasmic ratio. They lack expression of differentiation markers expressed by corneal epithelial cells, specifically cytokeratins (CK) 3 and 12. Like stem cells in other self-renewing tissues, the LSC divide very infrequently (slow cycling), and, therefore, DNA-labeling agents – such as bromodeoxyuridine – are retained in these cells for months. Label retention has often been used in identifying stem cell candidates in intact tissues. Cells from the limbal region also grow clonally in large colonies known as holoclones, whereas clones from the central cornea are less abundant and grow through fewer population doublings. Furthermore, unlike central corneal cells, LSC proliferation is resistant to inhibition by phorbol esters. LSC express several genes linked to stem cell self-renewal, including CEBPD, Bmi1, and Notch1. Cornea-specific ablation of Notch1 resulted in differentiation of LSC into hyperplastic, keratinized, epidermal-like cells, indicating the probability that Notch1 expression is essential in maintenance of the LSC stem potential. LSC also express a transporter protein, ABCG2, responsible for efflux of fluorescent dye Hoechst 33342. Expression of ABCG2 enables isolation of cells using fluorescence-activated cell sorting (FACS). Cells isolated using this dye-efflux assay are known as a side population,

based on the distribution pattern of the fluorescent cells following FACS. Side-population cells from the corneal epithelium are present exclusively in the limbus; following sorting, they exhibit slow cycling and clonal growth properties consistent with their identification as stem cells. Ability to isolate LSC has allowed a detailed comparison of the differences between this population and the other cells of the corneal epithelium. A summary of these differences is given in **Table 1**.

Limbal Stem Cell Niche

Centripetal migration of pigmented cells in healing epithelial wounds was first observed in the 1940s, and, in 1971, Davanger and Evenson proposed that the source of the migrating cells was the palisades of Vogt. These are a series of radially oriented fibrovascular ridges concentrated along the upper and lower corneoscleral limbus (**Figure 1(a)** and **(b)**) described originally in the early twentieth century. The morphology of these features has been elucidated by Daniels and by Dua, showing that they are present throughout the limbus but more concentrated in the superior and inferior regions. The ridges and valleys of the palisades are maintained by a specialized vascular system and form an interwoven network, often terminating in tunnels or 'crypts' under the surface of the stroma (**Figure 1(b)**). The bases of these crypts contain cells strongly expressing the several marker genes used in identifying LSC (**Table 1**), providing further evidence that these crypts represent the LSC niche. Recently, it was observed that pigmented melanocytes in the limbal crypts express N-cadherin, as do the LSC. During expansion in culture the LSC lose N-cadherin expression as they differentiate. N-cadherin-dependent cell–cell interactions with melanocytes may consequently represent a feature of the niche environment involved in maintaining the slow cycling and stem cell potential of the LSC.

Table 1 Expression markers for determining epithelial stem cell differentiation

Gene	*Limbal stem*	*Cornea: Basal*	*Cornea: Apical*
Positive (stem cell) markers			
ΔN-p63α	++	−	−
ABCG2	+++	−	−
Vimentin	+++	−	−
Integrin α9	+++	+	−
Keratin 19	++	−	−
N-Cadherin	++	−	−
GDNF	+++	−	−
Integrin ß1			
a-enolase	+++	++	+
TrkA	+++	++	+
Notch1	+++	++	−
C/EBPdelta	+	−	−
Bmi1	+	−	−
Negative (differentiation) markers			
CK3/CK12	−	+++	+++
Involucrin	−	+++	+++
Integrin a6	−	+++	+++
Cx 43	−	+++	+++
E-Cadherin	+/−	+++	+++

Modified from Secker and Daniels (2008).

The presence of label-retaining cells in the limbus and the centripetal migration of the more rapidly dividing cells in the corneal epithelium prompted Schermer and colleagues to suggest that the slow-cycling LSC are precursors to the mitotic basal cells throughout the epithelium. These mitotic daughter cells are termed transient amplifying (TA) cells. The TA cells are hypothesized to migrate from the limbus throughout the central cornea before ceasing cell division and differentiating to the superficial cells of the corneal surface. Labeling with both tritiated thymidine and bromodeoxyuridine followed by various chase periods provided kinetics showing that migrating basal cells are indeed mitotic, but are not label retaining – that is, cycle faster than the LSC. The LSC appear small and round compared to the TA cells, thus may be more primitive than the TA cells. Cloning studies also show the mitotic cells in the central stroma to be less able than LSC to generate the large holoclones indicative of high replicative potential.

TA cells are not fully committed to corneal epithelial differentiation. TA cells in adult central corneal epithelium – when transplanted to embryonic dermis – have demonstrated potential to differentiate into hair follicles and other dermal tissue types. Thus, these basal cells of the central epithelium maintain a clear stem cell potential. Are these central corneal stem cells progeny of the LSC? DNA-labeling kinetics are consistent with an interpretation that slow-cycling cells in the limbus are the origin of mitotic cells of the central cornea. Lamellar keratoplasty in male rabbits with corneal tissue from females led to the gradual replacement of the sex chromatin in the central corneal graft, suggesting that LSC from the host were the source of the cells that mature and exfoliate from the superficial central cornea. In spite of these and a number of related studies, however, there is still only indirect evidence that LSC are the progenitors of the mitotic basal TA cells in undisturbed corneal epithelium. In fact (as discussed below), recent studies suggest the possibility that the LSC may contribute to the central corneal epithelial cell populations only in healing wounds.

Limbal Stem Cell Deficiency

It is well documented that, following wounding, the LSC become more mitotically active and participate in centripetal migration. Cells from the limbus can, in fact, rapidly repair wounds involving the entire central corneal epithelium. However, injuries or conditions resulting in loss or inactivation of the LSC present a markedly

different outcome. After loss of the limbal cells, cells from the conjunctiva – including goblet cells – migrate across the corneal surface. This conjunctivalization results in inflammation, neovascularization, and growth of a fibrovascular pannus which severely reduces visual acuity. This phenomenon, known as limbal stem cell deficiency, can result from either hereditary or acquired causes. Transplantation of central corneal tissue without the accompanying LSC provides only temporary amelioration of this condition. Successful treatment, however, can be affected by autologous transplantation of limbal tissue from a contralateral, unaffected eye to the conjunctivalized eye. Reestablishing the LSC population can restore a stable and transparent corneal epithelium both in experimental animal studies and in human patients. Allografts can serve the same purpose but require immune suppression to prevent rejections. Expansion of LSC in culture has also been used to prepare epithelial sheets that restore long-term human epithelial function as well. It is worth noting that autologous, cultured epithelial sheets from buccal epithelial cells – as well as from conjunctival cells cultured under conditions in which goblet cells do not form – can also restore epithelial function. The biological implications of this use of nonlimbal cells to restore corneal epithelial function have not been fully explored. It is not clear, for example, if stem cells in these cultured layers colonize the limbal crypts and become a kind of ectopic, but functional, LSC population. The conclusions of the studies on limbal stem cell deficiency and its therapy are that the LSC are effective in replacing the corneal epithelial layer in a wound healing situation, and that the LSC create a biological barrier preventing conjunctival migration onto the corneal surface.

Understanding the Role for LSC in Corneal Homeostasis

Several studies have suggested the possibility that during normal corneal homeostasis the LSC may not contribute cells to the corneal epithelium. Studies of the destrin-knockout mouse showed that these mice lack the centripetal migration of corneal epithelium. Destrin is an actin-binding protein involved in cytoskeletal dynamics and thus may be involved directly in such motility. The corneal epithelium forms correctly in these mice, but, later in life, the tissue becomes vascularized and hyperplastic. The presence of mitotic basal cells in the absence of migration suggests that the basal cells are not TA progeny of the LSC but arise from a distributed stem cell population in these mice. Thus, the LSC may not be necessary for establishing a fully differentiated corneal epithelium. In a later study using mice, limbal tissue expressing a β-galactosidase marker gene was transplanted to the limbus of non-β-Gal-expressing nude mice. Over a period of months, β-Gal was not found in the central cornea of unwounded mice, but β-Gal cells rapidly migrated into the central cornea after wounding. β-Gal-expressing cells from central cornea were able to reconstitute a full epithelial sheet following transplantation, and furthermore, the reconstitution after transplantation could be carried out serially. These results indicate the existence of a nonlimbal population of corneal epithelial stem cells in mice that can give rise to a functional corneal epithelium. Such studies indicate LSC may not be necessary for formation or normal homeostasis of mouse cornea but support the principle that the LSC does participate in restoration of the tissue after wounding. There are no experimental data extending these results to humans, but until such data are presented, the role of the LSC in normal tissue homeostasis of the central corneal epithelium should be considered as unresolved.

Conjunctival Stem Cells

The bulbar conjunctiva contains basal mitotic cells that migrate to the surface and become quiescent as they differentiate; however, the cell layer does not undergo a lateral migration similar to that of the cornea. Differentiated conjunctival epithelium also differs from corneal epithelium in the expression of cytokeratins. Whereas cornea is positive for CK3 and CK12, conjunctiva lacks these keratins while expressing CK19, an antigen absent in cornea. Label-retaining cells can be observed in the fornix region, and clonal culture of these gives rise to both epithelial cells and goblet cells. Thus, the fornix appears to contain bipotent stem cells. Similarly, cells in the fornix are more strongly stimulated to proliferate by phorbol ester than those in the bulbar epithelium. These studies support the idea of a stem cell population in a fornicial niche. Clonogenicity studies, however, support the idea that cells with extended replicative potential (e.g., stem cells) are present both in the fornix and the bulbar surface. The lack of lateral migration of the cells of the bulbar conjunctiva, however, strongly supports the idea that during normal tissue homeostasis the tissue is maintained by a distributed population of resident stem cells.

Careful examination of stem-like cells in the bulbar conjunctiva has identified rare clusters of cells expressing the CK3/12 keratins characteristic of the cornea. Furthermore, transplantation of limbal β-galactosidase-expressing tissue into the limbal region of nude mice showed that, following wounding, some of these cells migrate into the conjunctiva and differentiate to both conjunctival epithelial and goblet cell phenotypes. These studies suggest that some of the stem cells distributed in the bulbar conjunctiva may derive from the LSC. Conversely, cells cultured from the bulbar region can be used to reconstitute the corneal epithelium in transplantation studies. Following transplantation to the cornea, these conjunctival-derived cells express the cornea-specific keratins CK3/12. The idea of

conjunctival/corneal transdifferentiation, once popular, is currently out of favor; however, these experiments support the possibility that stem cells in both the conjunctiva and cornea can – and do, in fact – produce differentiated cells in the neighboring tissue. The extent and the conditions under which this phenomenon occurs require further elucidation.

Corneal Stromal Stem Cells

The corneal stroma is a mesenchymal connective tissue making up 90% of the corneal thickness, with physical properties that provide the cornea its essential character. The stroma is formed during late embryogenesis by a population of neural crest cells migrating from the periocular mesenchyme. Chicken keratocytes from late embryogenesis retain neural crest progenitor properties even after transplantation into a new environment along cranial neural crest migratory passageways. In adult mammals, however, numerous *in vitro* experiments show that keratocytes rapidly lose their characteristic phenotype following several population doublings. Such a loss of phenotype occurs in healing wounds *in vivo* as well as *in vitro*. Recently, the authors found that the stroma of bovine corneas contain a small population of cells exhibiting self-renewal ability for an extended number of population doublings in culture. These corneal stromal stem-like cells were clonogenic and proliferated *in vitro* for over 100 doublings. A similar population of stem cells was isolated from human corneas as a side population using FACS. These stromal stem cells demonstrated potential for differentiation into several noncorneal cell types – a characteristic similar to that found in adult stem cells from other mesenchymal tissues. These cells also expressed several genes clearly designating them as tissue-specific mesenchymal stem cells, including ABCG2, Notch1, BMI1, SIX2, and KIT. ABCG2-expressing cells were localized in the limbal stroma subjacent to the epithelial basement membrane in the regions near the LSC niche.

Human corneal stromal cells remained viable for months after injection into mouse corneal stroma and were able to increase the transparency of lumican-knockout mouse corneas. In serum-free monolayer culture, keratocytes express stroma-specific gene products, but do not accumulate or organize extracellular matrix resembling that of the corneal stroma. However, when human stromal stem cells were cultured in attachment-free conditions they produced a stromal-like tissue including the stroma-specific keratan sulfate proteoglycan keratocan and generated parallel layers of collagen fibers resembling those in the stroma. These results suggest the potential use of stromal stem cells in bioengineering of corneal stroma or in direct stem cell-based therapy for corneal scars or corneal dystrophies.

Corneal Endothelial Stem Cells

The corneal endothelium is a single layer of flat hexagonal cells forming a boundary between the corneal stroma and the anterior chamber. This layer of cells functions as a pump to regulate stromal hydration. Although – like the keratocytes – the corneal endothelium is derived from neural crest, the endothelial cell characteristics are different from those of keratocytes. The human corneal endothelial cells are arrested in G1 phase *in vivo* and do not normally replicate to replace dead or injured cells. This lack of cell division results in a physiological reduction of cell density of about 0.3–0.5% per year. Scattered evidence, however, suggests the potential for some mitotic events in human corneal endothelium. Mitotic figures were observed *in vivo* by specular microscopy study following a rejection reaction on a corneal graft. Clusters of cells smaller than surrounding cells suggested that, at least under some circumstances, mitosis occurs in the endothelium of the adult human cornea. Recently, Yokoo and coworkers identified cells in the human corneal endothelium able to form cell-spheres in attachment-independent culture. Cells in these spheres, formed under conditions similar to those used for isolation of neural stem cells, can be expanded and generate daughter cells expressing neuronal and mesenchymal molecular markers. These properties suggest a stem cell origin for the cells forming the spheres. The sphere-forming cells also adapted the polygonal morphology characteristic of endothelial cells, suggesting the presence of endothelial progenitors. These precursors were effective *in vivo* in restoring endothelial function in an animal model of corneal endothelial deficiency. Both peripheral and central rabbit corneal endothelia contain a significant number of precursors, but the peripheral endothelium contains more precursors and has a stronger self-renewal capacity than the central region by sphere-forming assay. As the long-term culture of human endothelial cells has not been carried out and because of a lack of both stem cell and endothelial markers, positive identification of the proposed endothelial stem cells *in situ* has yet to be accomplished.

Conclusions

The ocular surface contains multiple populations of cells with stem cell-like properties. Some of these are localized to a distinctive niche in the corneoscleral limbus but other populations are more dispersed. Stem cells also are present in corneal stroma and endothelium. Stem cells support self-renewal of the corneal and conjunctival epithelia and the limbal stem cells prevent conjunctivalization of the corneal surface; however, relationships among the different stem cell populations in normal tissue homeostasis – and in

response to wounding – are not yet fully characterized. Ocular-surface stem cells have a high potential for use in cell-based therapy for a variety of ocular pathologies, and in tissue engineering. Continuation of the characterization of ocular stem cells is, therefore, a high priority both for understanding the biology of the ocular surface and for development of sight-saving therapies.

Acknowledgments

The authors wish to thank Kira Lathrop for the excellent illustration and Martha Funderburgh for proofreading the manuscript. This work was supported by NIH Grant EY016415 and Research to Prevent Blindness Inc.

See also: Corneal Epithelium: Wound Healing Junctions, Attachment to Stroma Receptors, Matrix Metalloproteinases, Intracellular Communications; The Surgical Treatment for Corneal Epithelial Stem Cell Deficiency, Corneal Epithelial Defect, and Peripheral Corneal Ulcer.

Further Reading

Daniels, J. T., Dart, J. K., Tuft, S. J., and Khaw, P. T. (2001). Corneal stem cells in review. *Wound Repair Regen* 9(6): 483–494.

Daniels, J. T., Notara, M., Shortt, A. J., et al. (2007). Limbal epithelial stem cell therapy. *Expert Opinion on Biological Therapy* 7(1): 1–3.

Davanger, M. and Evensen, A. (1971). Role of the pericorneal papillary structure in renewal of corneal epithelium. *Nature* 229(5286): 560–561.

Du, Y., Funderburgh, M. L., Mann, M. M., SundarRaj, N., and Funderburgh, J. L. (2005). Multipotent stem cells in human corneal stroma. *Stem Cells (Dayton, Ohio)* 23(9): 1266–1275.

Lavker, R. M. and Sun, T. T. (2003). Epithelial stem cells: The eye provides a vision. *Eye (London, England)* 17(8): 937–942.

Lavker, R. M., Tseng, S. C., and Sun, T. T. (2004). Corneal epithelial stem cells at the limbus: Looking at some old problems from a new angle. *Experimental Eye Research* 78(3): 433–446.

Limb, G. A., Daniels, J. T., Cambrey, A. D., et al. (2006). Current prospects for adult stem cell-based therapies in ocular repair and regeneration. *Current Eye Research* 31(5): 381–390.

Majo, F., Rochat, A., Nicolas, M., Jaoude, G. A., and Barrandon, Y. (2008). Oligopotent stem cells are distributed throughout the mammalian ocular surface. *Nature* 456(7219): 250–254.

Mimura, T., Yokoo, S., Araie, M., Amano, S., and Yamagami, S. (2005). Treatment of rabbit bullous keratopathy with precursors derived from cultured human corneal endothelium. *Investigative Ophthalmology and Visual Science* 46(10): 3637–3644.

Secker, G. A. and Daniels, J. T. (2008). Corneal epithelial stem cells: Deficiency and regulation. *Stem Cell Reviews and Reports* 4(3): 159–168.

Shortt, A. J., Secker, G. A., Notara, M. D., et al. (2007). Transplantation of *ex vivo* cultured limbal epithelial stem cells: A review of techniques and clinical results. *Survey of Ophthalmology* 52(5): 483–502.

Thoft, R. A. and Friend, J. (1983). The X, Y, Z hypothesis of corneal epithelial maintenance. *Investigative Ophthalmology and Visual Science* 24(10): 1442–1443.

Steroid-Induced Ocular Hypertension and Effects of Glucocorticoids on the Trabecular Meshwork

A F Clark, North Texas Eye Research Institute, University of North Texas Health Science Center, Ft. Worth, TX, USA

Glossary

Arachidonic acid metabolism – The degradation of a membrane lipid that leads to the generation of inflammatory signaling molecules.
Cortisol – The endogenous glucocorticoid (GC) in man.
Cytoskeleton – The internal scaffolding inside cells that regulates a variety of cell functions as well as cell shape.
Extracellular matrix (ECM) – An organization of specific proteins outside cells and tissues.
Glucocorticoid (GC) – A steroid molecule that regulates carbohydrate, lipid, and protein metabolism, which is often used therapeutically as an anti-inflammatory agent.
Intraocular pressure (IOP) – The pressure inside the globe of the eye.
Ocular hypertension – The pressure inside the globe of the eye that is higher than normal.
Osteoporosis – A condition of thinning and weakening bone structure.
Posterior subcapsular cataract – The clouding that occurs at the back of the ocular lens.
Primary open-angle glaucoma (POAG) – The most common form of glaucoma in most populations.
Steroid glaucoma – The glaucoma that occurs in some individuals due to the therapeutic use of GCs.
Steroid responsiveness – The ability of an individual to develop ocular hypertension upon steroid therapy.
Trabecular meshwork (TM) – A tiny tissue located at the junction of the iris and cornea, which is responsible for drainage of aqueous humor from the eye.
Transcription factor – A special protein that binds to DNA and regulates gene expression.

Introduction

Glucocorticoids (GCs) physiologically regulate carbohydrate, lipid, and protein metabolism and are absolutely essential for life. GC receptors (GRs) are ubiquitously expressed and, therefore, almost all tissues are targets for GC action.

GCs have been used therapeutically for over 60 years and are unsurpassed in their broad-based anti-inflammatory and immunosuppressive activity. However, prolonged GC therapy can also cause undesired side effects, including osteoporosis, muscle wasting, thinning of the skin, altered distribution of body fat, immunosuppression, and psychological disturbances. In addition, GC therapy has been linked, as a causative factor, to ocular side effects such as posterior subcapsular cataracts as well as to the development of ocular hypertension and iatrogenic open-angle glaucoma.

The intraocular pressure (IOP) elevation induced by GCs is associated with GC-mediated changes in the trabecular meshwork (TM), a small, reticulated tissue at the junction of the iris and cornea. The TM regulates aqueous humor outflow resistance in the eye. This article briefly summarizes steroid-induced ocular hypertension and highlights the effects of GCs on the TM. Full citations for many of the topics discussed can be found in the recently published *Experimental Eye Research* review (see the section titled 'Further reading').

Steroid-Induced Ocular Hypertension

Therapeutic administration of GCs can cause ocular hypertension and steroid glaucoma in certain individuals. The propensity to develop GC-induced ocular hypertension depends on the route of administration, the duration of therapy, the potency of the therapeutic GC, and individual susceptibility. GC-induced ocular hypertension has been reported with topical ocular, intraocular, periocular, oral, inhalation, intranasal, and topical dermal administration. Although GC-induced ocular hypertension can occur within a week of administration in some individuals, it often takes one or more months for this condition to develop. The more potent and longer-acting GCs, such as dexamethasone (DEX), betamethasone, triamcinolone acetonide, and fluocinolone acetonide, are more likely to raise IOP compared to less potent and shorter-acting GCs. However, ocular hypertension has been reported even with weaker and shorter-acting GCs, such as fluoromethalone or medrysone, in some individuals.

GC-induced ocular hypertension is generally reversible upon discontinuation of GC therapy. There are some reported cases where IOP remains elevated after cessation of GCs. These cases may be due to extensive and irreversible GC-mediated damage to the outflow facility or could be due to the actual development of primary open-angle glaucoma (POAG), since most POAG patients are steroid responders (see below).

Not all individuals treated with GCs develop ocular hypertension, and there is considerable heterogeneity in individual responsiveness to this GC-mediated side effect. Early studies categorized three classes of steroid responsiveness in the normal population after frequent (q.i.d.) topical ocular dosing with potent GCs for 4–6 weeks. Approximately 5% of the individuals developed substantially increased IOPs and were termed high responders, while 33% had moderately elevated IOPs and were termed moderate responders. The remaining population were considered nonresponders with no or only slightly elevated IOPs. Therefore, approximately 40% of the population developed ocular hypertension after topical ocular GC treatment, and individual steroid responsiveness was reproducible. Identified steroid responders remained steroid responsive and nonresponders remained nonresponsive when rechallanged with GCs. It is interesting to note that this 40% responder rate also occurs in individuals who receive intravitreally injected triamcinolone acetonide as well as in individuals receiving oral GC therapy.

In contrast to the normal population, almost all POAG patients are steroid responders. Interestingly, descendents of POAG patients have a higher rate of steroid responsiveness, suggesting that steroid responsiveness may be heritable.

The clinical presentation and features of GC-induced ocular hypertension and GC-iatrogenic glaucoma are very similar to POAG in many aspects. In fact, GC treatment is one of the exclusionary factors for the diagnosis of POAG. IOP elevation in both conditions is due to compromised aqueous outflow and is associated with similar morphological and biochemical changes in the TM. Moreover, in both diseases, there are not only similar optic disk cupping and visual-field changes, but also increased deposition of extracellular material, including fibronectin, in the TM; however, in steroid glaucoma, there is also the deposition of fingerprint-like deposits in the TM.

GC-induced ocular hypertension is not unique to humans. Topical ocular administration of DEX also elevated IOP in monkeys, rabbits, cats, cows, sheep, rats, and mice and can cause similar ECM deposition and biochemical changes in the TM. In addition, DEX-induced ocular hypertension can occur in isolated perfusion-cultured human donor eyes, indicating that GCs act directly on the anterior segment outflow pathway.

A summary of the key features of GC-induced ocular hypertension and steroid glaucoma is given in **Table 1**.

Possible Role of GCs in POAG

There are several lines of evidence suggesting that GCs may play a role in the development of POAG. The endogenous GC in humans is cortisol, which is less potent than most therapeutic GCs. Several investigators have reported that POAG patients have elevated levels of plasma cortisol, although other studies have not found this association. One research group also reported abnormal cortisol metabolism in the TM and peripheral blood leukocytes of POAG patients. Others have suggested that changes in the activities of the 11β-hydroxysteroid dehydrogenases, which interconvert cortisol and cortisone, may regulate IOP in glaucoma patients, although there is no evidence yet that these steroid metabolic enzymes play any role in GC-induced ocular hypertension. Furthermore, there have been reports that POAG patients have increased sensitivity to GC-induced vasoconstriction in the skin, to plasma cortisol suppression after oral DEX, and to GC-induced suppression of a mitogen response in peripheral blood leukocytes, although others have not been able to reproduce the latter study.

Another line of evidence further suggests a link between GCs and POAG. Individuals who were classified as high responders to topical ocular GC administration were at significantly higher risk of developing POAG compared to nonresponders.

GC Effects on the TM

GCs have multiple effects on the TM. The TM contains GC receptors and is a GC-responsive tissue and cell type. GCs directly regulate a number of TM cell functions, including inhibition of phagocytosis, cell proliferation,

Table 1 Key features of glucocorticoid-induced ocular hypertension and glaucoma

- Therapeutic administration of GCs can cause elevated IOP (steroid responsiveness) and iatrogenic glaucoma in susceptible individuals
- Steroid responsiveness is higher in primary open-angle glaucoma patients and their descendents
- Steroid responsiveness is a risk factor for the development of primary open-angle glaucoma
- Clinical features mimic primary open-angle glaucoma
- Elevated IOP is due to increased aqueous humor outflow resistance in the conventional outflow pathway
- Associated with biochemical and morphological changes in the trabecular meshwork

and migration, as well as decreased cellular acidification (related to decreased metabolic activation). They also alter TM cell morphology with an overall increase in cell and nucleus size. GCs cause an activated intracellular morphology that includes increased levels of rough endoplasmic reticulum, Golgi apparatus, and secretory vesicles.

GCs and their receptors act as a ligand-dependent transcription factor; hence, it is not surprising that GCs alter TM cell gene expression. Myocilin (MYOC) was one of the first GC-induced genes discovered in the TM, and it also turned out to be the first glaucoma gene identified. MYOC is a secreted glycoprotein, currently of unknown function. Although several studies have shown that glaucomatous mutations in MYOC cause a gain-of-function phenotype that may account for the elevated IOP associated with MYOC glaucoma, currently there is no evidence that MYOC plays a role in GC-induced ocular hypertension. Overexpression of wild-type MYOC in mouse eyes does not elevate IOP or alter anterior segment morphology.

Five independent studies have evaluated the effect of DEX on global gene expression in cultured human TM cells. As expected, there is some overlap in the sets of GC-responsive genes between the studies, and many of the differences reported could be due to variability between the TM cell lines and the duration of DEX exposure. All the studies reported altered expression of MYOC, IGFBP2, SERPNA3, and GAS1. GCs induced the expression of alkaline phosphatase, which is suggested to be a marker for TM cell calcification. DEX treatment of perfusion-cultured anterior segments increased the expression of pigment-epithelium-derived factor (PEDF) in the TM. GCs also decreased the sensitivity of TM cells to four different growth factors, most likely mediated by decreased expression of their respective growth factor receptors.

GC treatment alters TM cell junctions. Exposure of cultured TM cells to DEX changes the morphology and distribution of gap junctions and increases the expression and distribution of several proteins associated with tight junctions. In addition, GCs change the expression of integrin $\alpha 2$, $\alpha 5$, and αV subunits, which may alter TM cell adhesion.

One of the most striking features of GC treatment is the increased deposition of ECM in TM cells and tissues. Expression of fibronectin, laminin, collagen, and elastin was increased in DEX-treated TM cells. Glycosaminoglycan (GAG) metabolism was also altered by GCs, with decreased hyaluronan and increased levels of chondroitin sulfate and GAGase-resistant material. GCs decrease TM ECM turnover by decreasing matrix metalloproteinases, urokinase plasminogen activator, and increasing levels of plasminogen activator inhibitor-1. They also increased the expression of the fibrogenic growth factor connective tissue growth factor (CTGF) and thrombospondin-1 (TSP-1), which helps bioactivate transforming growth factor (TGF)-β, further reinforcing ECM deposition.

A novel effect of GCs on TM cells is the reorganization of the actin cytoskeleton. Microfilaments bundled into stress fibers and actin networks in the cell periphery are the major actin structures in cultured TM cells as well as in TM cells *in situ*. Treatment of confluent human and bovine TM cells with GCs causes a major reorganization of the microfilaments to form geodesic-dome-like structures called cross-linked actin networks (CLANs) (**Figure 1**). GC-induced CLAN formation takes several days to develop and progresses over time, reaching a maximum after several weeks of GC exposure. These CLAN structures are reversible after withdrawal of the GC from the culture medium. GC-induced CLAN formation appears to be unique to the TM because it does not occur in many other ocular and nonocular cell types tested. In addition to cultured primary TM cells, GC treatment also induces CLANs in the TM of perfusion-cultured anterior segments. Intriguingly, alterations in the actin cytoskeleton, including very similar CLAN structures, are found in glaucomatous TM (GTM) cells and in the TM of glaucomatous donor eyes, even in the absence of exogenous GCs. GTM cells are more sensitive to GC-mediated CLAN formation. The actin cytoskeleton regulates a number of cellular functions, and a GC or glaucomatous reorganization of actin structures may compromise TM cell homeostasis. In addition to effects on the actin cytoskeleton, GCs also cause microtubule tangles in cultured TM cells. However, this effect on microtubules could be associated with TM cell size and shape changes and could be secondary to GC-mediated CLAN formation. Moreover, these findings may help explain the finding that DEX-treated cells are more resistant to microtubule-disrupting agents.

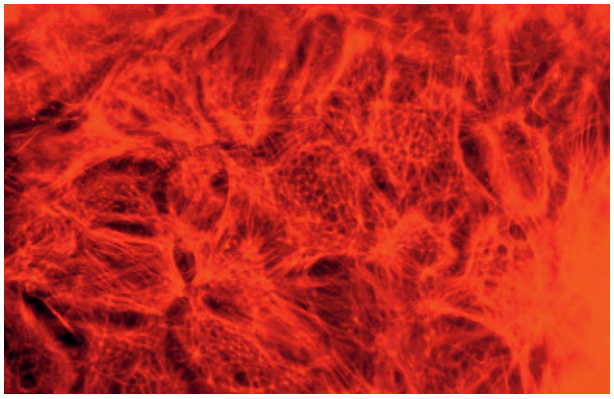

Figure 1 Steroid (DEX)-induced cytoskeletal reorganization to form cross-linked actin networks (CLANs) in trabecular meshwork cells.

Similar to their effects in other tissues, GCs also inhibit arachidonic acid metabolism in TM cells. Currently, there is evidence that IOP-lowering prostaglandin analogs (PGF2α agonists) increase conventional outflow through the TM, in addition to their effects on the uveoscleral outflow pathway. PGF2α is endogenously made by the TM and may play a role in maintaining normal outflow. Inhibition of PGF2α production by GCs may therefore compromise normal outflow.

As mentioned previously, there is considerable individual heterogeneity in the propensity to develop GC-induced ocular hypertension. What is the molecular mechanism(s) responsible for determining steroid responsiveness in normals and why are POAG patients steroid responders? The biological activities of GCs are mediated by the GR. However, there are two alternative forms of the human GR that are both encoded by exons 1–8, but are formed by alternative splicing of exons 9α and 9β. GRα (containing amino acids from exon 9α) is the biological, physiological, and pharmacological receptor for GCs that regulates gene expression in *cis* (through GC response elements (GREs) in the promoter of responsive genes) or in *trans* (through binding to and inhibiting other transcription factors, such as activator protein 1 (AP-1)). GRβ (containing amino acids encoded by exon 9β) lacks the carboxy terminal GC-binding domain and acts as a dominant negative regulator of GC action. Increased expression of GRβ has been implicated in GC resistance in a number of diseases such as rheumatoid arthritis, inflammatory bowel disease, and asthma, among others.

It is possible that altered expression of GRβ in the TM could be responsible for differences in GC sensitivity. In fact, differences in GRβ levels have been demonstrated between normal and GTM cells. GRβ expression is higher in normal TM cells compared to GTM cells, and therefore the GTM cells are more sensitive to GC induction of a GRE-luciferase reporter gene compared to normal TM cells. Transduction of TM cells with a GRβ expression vector makes TM cells more resistant to DEX induction of a GRE-luciferase reporter gene, DEX induction of fibronectin and MYOC, and DEX inhibition of TM cell phagocytosis.

In addition to differences in GRβ levels, there is another potential mechanism for GRβ regulation of GC responsiveness. Both GRα and GRβ are made in the cytoplasm and have to be translocated to the nucleus for their biological effects. GRα nuclear translocation is initiated by GC binding and is mediated by heat-shock protein 90 (hsp90), the immunophilin FK506-binding protein 52 (FKBP52), and the dynein microtubule motor protein complex. GRβ also utilizes hsp90 and dynein for nuclear translocation. However, in contrast to GRα, GRβ translocation to the nucleus is ligand independent and is mediated by the immunophilin FKBP51. In fact, overexpression of FKBP51 in the TM cells enhanced endogenous GRβ nuclear translocation, making these TM cells more GC resistant.

There are still many unanswered questions about the potential involvement of GRβ in GC responsiveness. What is the cause of altered GRβ expression between normal TM and GTM cells? A splicesome protein (SRp30c) responsible for this alternative splicing has been identified; can altered activity of this protein be responsible for different levels of expression in the TM? Could polymorphisms in GR, SRp30c, or FKBP51 lead to altered GRβ expression or activity? Is altered GRβ expression specific for the TM or is this a more generalized systemic phenomenon? Finally, does GRβ directly regulate GC-induced and/or glaucomatous ocular hypertension?

Summary

GC-induced ocular hypertension and iatrogenic glaucoma have been recognized for more than a half a century as serious side effects of GC therapy. This still is an important clinical condition, especially with the increased use of intraocular GCs for the treatment of several retinal conditions. In addition, GC-induced ocular hypertension is an important tool that provides a better understanding of POAG because there are many clinical, morphological, and biochemical similarities. GCs have a plethora of effects on the TM (**Table 2**; **Figure 2**). However, we still are unaware of not only which effect or combination of effects are responsible for the GC-mediated increased outflow resistance and elevated IOP, but also whether the endogenous GC cortisol plays any role in the pathogenesis of glaucoma. In the future, it may be possible to determine whether a person is a steroid responder prior to GC therapy, so that patients can be more closely

Table 2 Summary of effects of glucocorticoids on the trabecular meshwork

- TM cells and tissues express glucocorticoid receptors (GRs) and are targets for GC action
- Glucocorticoids alter TM cell gene and protein expression
  - Induction of the glaucoma gene myocilin
  - Suppression of growth factor receptor expression
- Glucocorticoids inhibit TM cell proliferation, migration, and phagocytosis
- Glucocorticoids promote extracellular matrix deposition in the TM through increased synthesis and decreased degradation
- Glucocorticoids reorganize the TM actin cytoskeleton (forming cross-linked actin networks)
- Levels of GRβ, an alternatively spliced form of the glucocorticoid receptor, regulate glucocorticoid sensitivity in TM cells

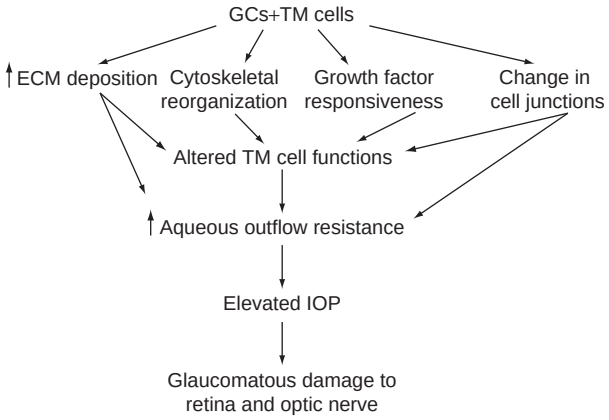

Figure 2 Effects of glucocorticoids on the trabecular meshwork and development of steroid glaucoma.

monitored, and to determine the potential enhanced risk for developing POAG.

See also: The Biology of Schlemm's Canal; Biomechanics of Aqueous Humor Outflow Resistance; The Fibrillar Extracellular Matrix of the Trabecular Meshwork; Functional Morphology of the Trabecular Meshwork; The Genetics of Primary Open-Angle Glaucoma: A Review; Myocilin; Pharmacology of the Aqueous Humor Outflow; Primary Open-Angle Glaucoma; Structural Changes in the Trabecular Meshwork with Primary Open Angle Glaucoma.

Further Reading

Clark, A. F. (1995). Steroids, ocular hypertension, and glaucoma. *Journal of Glaucoma* 4: 354–369.

Clark, A. F. and Morrison, J. C. (2003). Steroid-induced glaucoma. In: Morrison, J. C. and Pollack, I. P. (eds.) *Glaucoma: Science and Practice*, pp. 197–206. New York: Thieme.

Clark, A. F. and Wordinger, R. J. (2009). The role of steroids in outflow resistance. *Experimental Eye Research* 88: 752–759.

Johnson, D. H., Bradley, J. M., and Acott, T. S. (1990). The effect of dexamethasone on glycosaminoglycans of human trabecular meshwork in perfusion organ culture. *Investigative Ophthalmology and Visual Science* 31(12): 2568–2571.

Jones, R., 3rd and Rhee, D. J. (2006). Corticosteroid-induced ocular hypertension and glaucoma: A brief review and update of the literature. *Current Opinion in Ophthalmology* 17(2): 163–167.

Kersey, J. P. and Broadway, D. C. (2006). Corticosteroid-induced glaucoma: A review of the literature. *Eye* 20(4): 407–416.

Wordinger, R. and Clark, A. (1999). Effects of glucocorticoids on the trabecular meshwork: towards a better understanding of glaucoma. *Progress in Retina and Eye Research* 18(5): 629–667.

Structural Changes in the Trabecular Meshwork with Primary Open Angle Glaucoma*

E Lütjen-Drecoll and O-Y Tektas, University of Erlangen-Nürnberg, Erlangen, Germany

Glossary

Cribriform elastic network – A network of elastic-like fibers which is continuous with that part which forms the core of the trabecular lamellae, and which is connected to the inner wall of Schlemm's canal.
Elastic-like fibers – The elastic fibers in the trabecular meshwork which are different from ordinary elastic fibers as they contain little elastin, and are surrounded by a sheath of cross-linked fibrils (previously termed curly collagen).
Glaucomatous (POAG) SD plaques – The SD plaques to which fine fibrils (which are immunoreactive to type VI collagen) adhere, thereby forming irregular thickenings that are responsible for the increase in SD plaques' area in glaucoma eyes as compared to age-matched controls.
Sheath-derived (SD) plaques – Those parts of the elastic-like fibers and their cross-linked fibrillar sheath that are seen in ultrathin sections viewed by transmission electron microscopy.

Introduction

It is generally accepted that increased resistance to aqueous humor outflow is a predominant risk factor for the increase in intraocular pressure (IOP) in glaucomatous eyes. Neither the pathophysiology nor the structures responsible for the increase in outflow resistance are presently known. The main problem in this respect is the lack of an animal model that shows structural changes in the outflow pathways comparable to those seen in glaucomatous eyes.

It is known, however, that under physiological conditions ciliary muscle (CM) contraction can influence outflow resistance. With increasing age and development of presbyopia, the effect of CM contraction on outflow resistance is diminished and outflow resistance increases. Aging is a main risk factor for the development of primary open-angle glaucoma (POAG). We, therefore, assume that understanding the connection of the CM system with the trabecular meshwork (TM) and its age-related changes is a prerequisite for understanding why POAG develops mainly in elderly human eyes.

Effect of Accommodation on Outflow Resistance

Using serial tangential sections in parallel to the inner wall of Schlemm's canal (SC), Rohen and colleagues in 1967 found that the anterior tendons of the CM insert into the trabecular lamellae. Later on, these findings were confirmed by electron microscopical studies of tangential sections. The studies showed that the curled cribriform fibers in the juxtacanalicular region of the TM consist of bent fibrillar bundles connecting the cribriform elastic fiber network and the elastic fiber network of the TM to the inner wall endothelium of SC (the so-called connecting fibrils (CFs)). The elastic tendons of the outermost longitudinal CM fibers obliquely bend into the TM and insert either into the scleral spur or into the cribriform elastic fiber system (**Figures 1**, and **2(a)** and **(b)**).

The elastic tendons and the elastic fibers in the TM show a specific morphology and were therefore previously termed elastic-like fibers. The elastic fiber core contains only little elastin and is surrounded by elastic microfibrils and a sheath of cross-banded fibrils. The nature of these cross-banded fibrils is not yet known. Histologically, the sheath stains for type VI collagen. At the ultrastructural level, antibodies against various proteins seem not to penetrate into the banded fiber sheath. Here, only the fibrils entering the banded sheath stain for type VI collagen. In the ciliary body, type VI collagen connects basement membranes of smooth muscle cells and vascular endothelial cells with the surrounding connective tissue. In the TM, the elastic fiber network is connected to patches of basement membrane material of the cribriform cells and to the basement membrane or cell membrane of the endothelial lining of SC. The CFs are derived from the sheath of the elastic fibers and also contain type VI collagen.

The posterior elastic tendons of the CM insert into the choroidal elastic fiber system and Bruch's membrane. The ultrastructural details of the fibers differ from those seen at the anterior muscle tips and the TM. They contain large amounts of elastin and appear morphologically

* This article is an adaption and extension of the review entitled "Structural changes of the trabecular meshwork in different kinds of glaucoma" published in Experimental Eye Research (2009, 88, 769–755). Copyright Elsevier (2009).

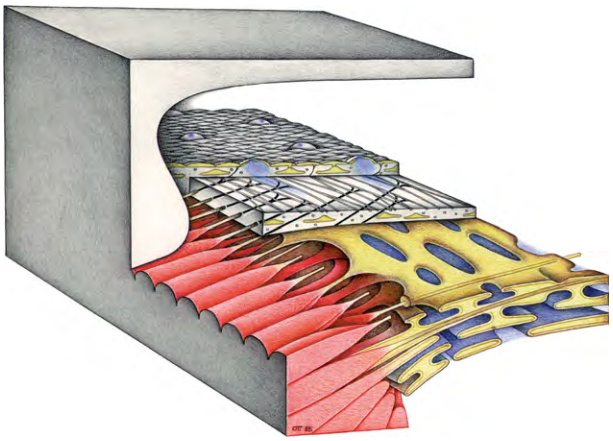

Figure 1 Three-dimensional structure of the trabecular meshwork and insertion of the anterior tendons of the ciliary muscle. The elastic tendons (black) of the outer most muscle fibers are fixed to the cribriform elastic fiber network connected to the inner wall of Schlemm's canal by bend connecting fibrils.

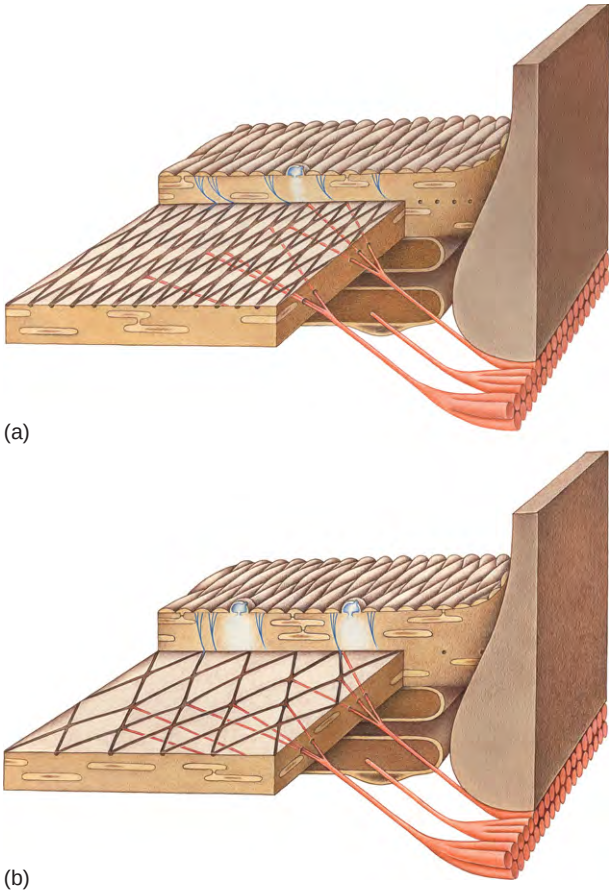

(a)

(b)

Figure 2 (a) Cribriform elastic network (black), outer elastic tendons of the ciliary muscle (red), and bend connecting fibrils (blue) in a relaxed ciliary muscle; (b) following ciliary muscle contraction. The spaces of the cribriform network are enlarged, the connecting fibrils straightened, and the subendothelial region widened through an inward movement of the ciliary muscle and its tendons.

nearly homogeneous. During accommodation and CM contraction, the posterior muscle tendons become elongated or stretched, and the muscle shortens posteriorly. The anterior muscle tips stay in place. The CM moves anterior inwardly, thereby expanding the TM. Expansion of the cribriform elastic network allows the bent CFs to straighten. This straightening of the fibers leads to an enlargement of the spaces in the cribriform elastic network, and to a widening of the subendothelial region of SC and its lumen (**Figures 2 (a) and 2(b)**). Physiologically, the morphological changes are accompanied by an increase in outflow facility. When Barany measured resting facility following CM contraction induced by pilocarpine treatment in Thailand stump-tailed macaques, there was a significant correlation between optically empty spaces in the subendothelial region of SC and resting outflow facility. It is possible that wash-out of extracellular matrix (ECM) from the subendothelial region contributes to the increase in outflow facility following CM contraction, at least in monkey eyes, and presumably also in younger human eyes.

Age-Related Changes of the CM–TM-System

With increasing age and the development of presbyopia not only the CM but especially the elastic tendons undergo age-related changes. The changes profoundly differ between anterior and posterior tendons. With age, the CM remains shortened, even in a relaxed position, following atropine treatment, indicating that the muscle cannot be pulled backwards in the same way as in young eyes. It is tempting to speculate that loss of elasticity of the posterior tendons might be involved in this diminished backward movement of the muscle.

The anterior elastic tendons of the muscle do not seem to lose elasticity as the tips of the muscle do not move backward, but stay in place at the scleral spur even in very old human eyes. This finding indicates that the special structural elements of the TM elastic fibers undergo different age-related changes than the posterior elastic tendons. The sheath of the anterior tendons and the TM elastic fibers significantly thicken with increasing age, whereas the diameter of the elastin-containing central core of the fibers remains constant throughout life. This thickening and presumably even stiffening of the fiber sheath prevents collapse of the TM and SC with age. On the other hand, thickening of the elastic fiber sheath leads to a decrease in size of the pores of the cribriform network. In addition, concomitant with the sheath, the CFs thicken. The resulting increase in the amounts of ECM in the outer TM might contribute to the increase in outflow resistance seen in normal elderly eyes. This hypothesis is supported by findings in elderly rhesus monkeys. Here, increase in cross-sectional area of the

elastic fibers with their sheaths in the outer TM is significantly correlated with increase in outflow resistance. This correlation exists, even if the absolute changes in the TM of old rhesus monkeys were found to be much less prominent than in human eyes of comparable relative ages. The morphology of the TM and CM in a (very old) 30-year-old rhesus monkey resembled that of a 30-year-old human eye. Age-related changes similar to that observed in the eyes of more than 60-year-old humans have not been observed in any animal model investigated so far.

In old human eyes, there is a steady decline in cells throughout life. Alvarado and colleagues found a decrease of 0.56% of cells per year. Grierson and colleagues recorded a decrease from 763 000 cells in 20-year-old humans to 403 000 in 80-year-olds, with a loss rate of 6000 cells/year. The loss of cells was least in the cribriform region of the TM. Only if increased cell loss occurs, fusion of denuded beams might contribute to collapse of the TM, and to an increase in outflow resistance.

Morphological Changes in the Outer TM of Eyes with POAG

In collaboration with Doug Johnson, we studied the morphological changes in the TM not only in trabeculectomy specimens from advanced-glaucoma patients undergoing surgery, but also from donor eyes with different stages of the disease. The morphology of the outer TM in eyes with POAG does not differ very much from that of age-matched controls; however, there are quantitative differences. The amount of SD plaques is significantly higher in glaucomatous than in normal eyes (**Figures 3(a)** and **3(b)**, and **4(a)** and **4(b)**). In a few eyes with advanced stages of POAG, it was possible to perform enzyme digestion studies on serial tangential sections and to study these sections electron microscopically. In these sections, fine fibrils adhered to the cribriform elastic network and to the CF. Most of the fibrils stained for type VI collagen (**Figure 5**). In nondigested specimens, they are surrounded and masked by glycoprotein and proteoglycan-rich ground substances also masking the banded sheath of the elastic fibers. In 2002, Ueda and colleagues found fibronectin, vitronectin, laminin, and tenascin as glycoproteins, decorin and versican as proteoglycans, as well as hyaluronan, collagen I, III–VI, MAGP-1, and fibrillin in the sheath material. In contrast to our previous findings, myocillin was also found, probably because of differences in the antibodies that were used for immunocytochemical staining.

Adherence of additional fibrillar material to the network of the TM, which is masked by the various ECM components, can explain why in eyes with POAG the thickness of the sheath is irregular and that plaque material can even be found separated from the elastic fibers (**Figure 4(b)**). In eyes with POAG, the CF are also surrounded by increased amounts of type VI collagen and various other components of the ECM. In more advanced cases of POAG, they form fibrous plates which could participate in blocking of outflow pathways.

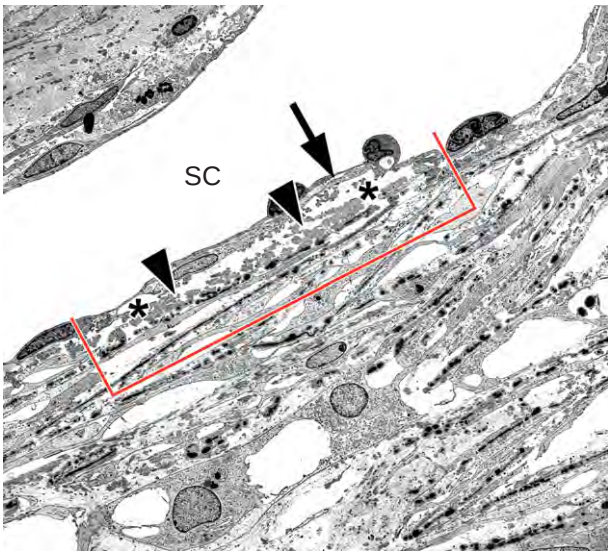

(a)

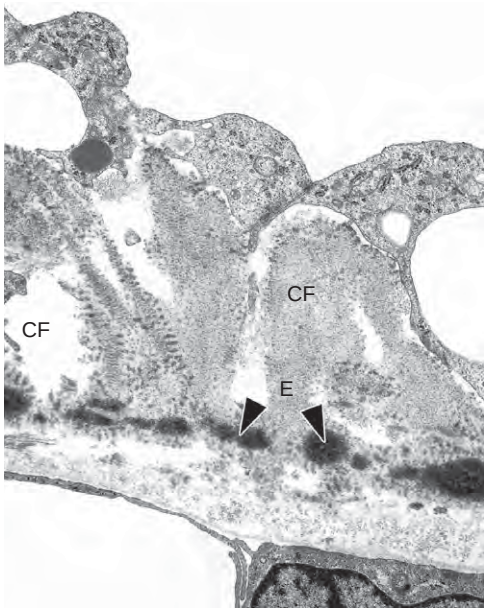

(b)

Figure 3 Inner wall regions of eyes with POAG. (a) The red lines indicate the area quantitatively evaluated by Gottanka and colleagues in 1997. The area of SD plaques (arrow heads), basement membrane-like material (arrow), optically empty spaces (asterisks), etc. were measured. There was a significant increase in SD plaques in glaucomatous eyes compared to age-matched controls. (b) Higher magnification of SD plaques. The cribriform elastic fiber network (E) and its CF are surrounded by a homogeneous sheath. Sections through the elastic fibers and sheaths, as well as through the CF and their surrounding extracellular material, were measured as SD plaques.

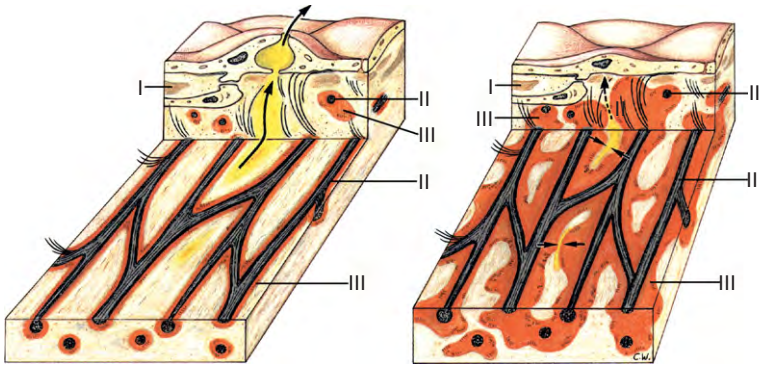

Figure 4 (a) The subendothelial elastic fiber network and its CF (II) in normal; (b) in glaucomatous eyes. The sheaths of the elastic fibers (red, III) thicken and become irregularly arranged in glaucomatous eyes thus narrowing the intertrabecular outflow channels (yellow, arrows). In cross sections, the elastic fibers and their sheaths form SD plaques. The basement membrane-like deposits adjacent to the inner wall endothelium (I) are not changed in glaucomatous eyes.

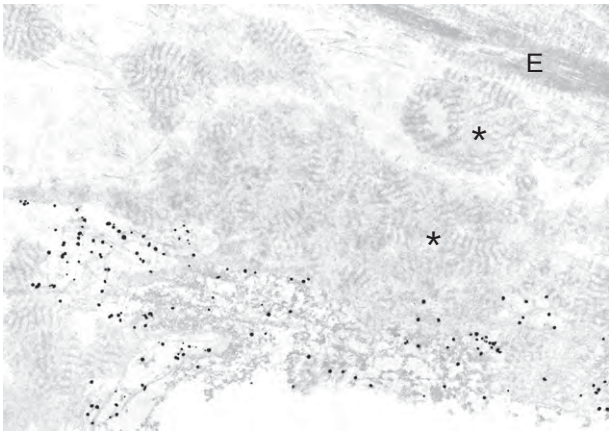

Figure 5 Immunogold labeling of type VI collagen fibrils. Oblique ultrathin section through the cribriform region. Note that the fine fibrils adhering to the sheaths (asterisks) of the elastic fibers (E) are type VI collagen immunoreactive.

Studies by Rohen and colleagues in 1993 enabled a comparison between POAG TM specimens that had been treated with antiglaucomatous drugs with specimens from patients who had not received any treatment. There was no difference in the amount of plaques between the two groups. Therefore, increased and irregular thickening of elastic fiber sheaths seems to be a sign for POAG disease, and is not caused by long-term treatment with antiglaucomatous drugs. This is supported by the fact that such thickening of elastic fiber sheaths is not seen in age-matched eyes suffering from pseudoexfoliation or steroid-induced glaucoma, but also having undergone long-term treatment.

Regional Differences

Sections from different parts in the circumference of the eye showed that there are marked regional differences in the individual eye with POAG. Pigmentation of trabecular cells appeared to be a marker for aqueous flow regions. In areas with thin trabecular lamellae covered by trabecular cells and with wide open spaces in the subendothelial region of SC, many cells contained pigment granules (**Figure 6(a)**). In other parts of the circumference nearly no pigment granules were present in the TM. In these regions the trabecular lamellae appeared thickened and fused (**Figure 6(b)**). Often, the SC filtration region appeared to be smaller and the cribriform region densified, presumably indicating a diminished perfusion.

Correlation between TM Changes and Axon Loss in the Optic Nerve

Interestingly, the area of SD plaques in POAG TM significantly correlates with axon loss in the optic nerve. As plaques in the TM cannot cause axon loss in the optic nerve, it is possible that common factors are responsible for both changes. The search for such factors has been undertaken mainly *in vitro*.

Many factors known to increase expression in other tissues or factors induced by oxidative damage are increased in the aqueous humor of a number of eyes with POAG.

One of the factors increased in the aqueous humor of nearly 50% of eyes with POAG is TGFβ_2. In fact, *in vitro* TGFβ_2 can stimulate trabecular cells to synthesize increased amounts of various ECM components, of the enzyme transglutaminase which cross-links proteins to complexes nondegradable by metalloproteinases and of plasminogen activator inhibitor that inhibits activation of metalloproteinases. Further studies will clarify which other factors could be responsible for induction of the TM changes seen in eyes with POAG.

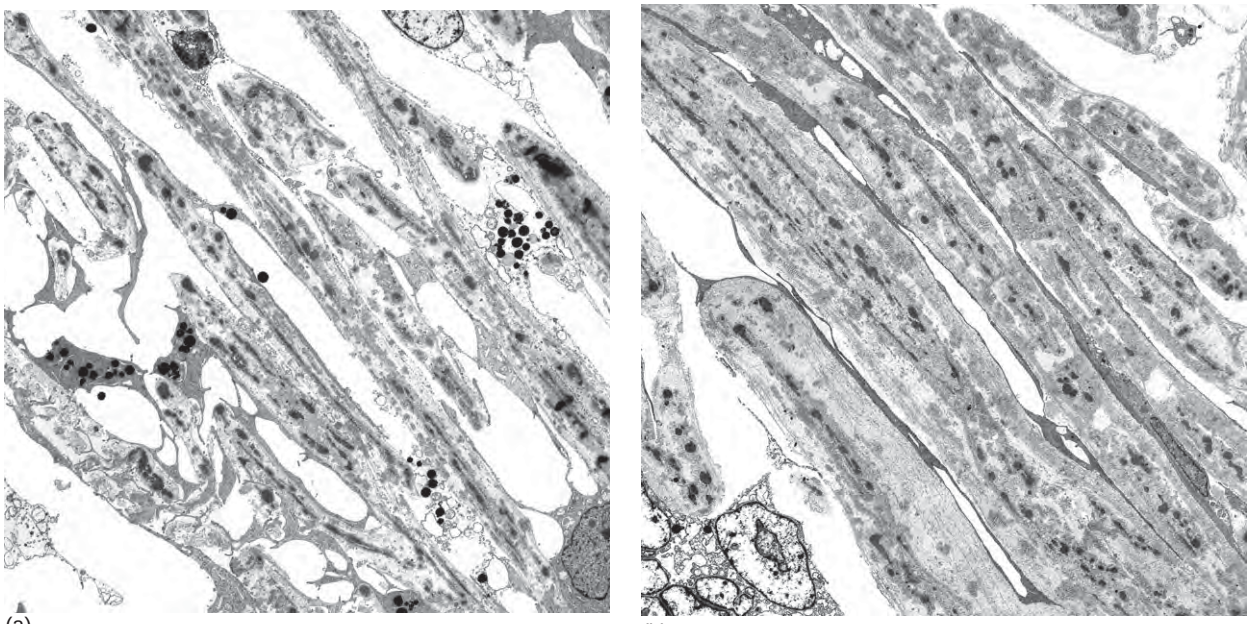

Figure 6 Electron micrographs of sagittal sections of the TM. (a) In areas with open intertrabecular spaces and thin lamellae, most of the trabecular cells contain pigment granules. (b) In areas with small or occluded intertrabecular spaces and thick lamellae, few cells contain pigment granules.

Acknowledgments

We are grateful to Doug Johnson for his collaboration in the study of morphological changes in the TM.

See also: Animal Models of Glaucoma; The Biology of Schlemm's Canal; Biomechanics of Aqueous Humor Outflow Resistance; The Fibrillar Extracellular Matrix of the Trabecular Meshwork; Functional Morphology of the Trabecular Meshwork; Primary Open-Angle Glaucoma; Regulation of Extracellular Matrix Turnover in the Aqueous Humor Outflow Pathways; Steroid-Induced Ocular Hypertension and Effects of Glucocorticoids on the Trabecular Meshwork.

Further Reading

Gottanka, J., Johnson, D. H., Martus, P., and Lütjen-Drecoll, E. (1997). Severity of optic nerve damage in eyes with POAG is correlated with changes in the trabecular meshwork. *Journal of Glaucoma* 6: 123–132.

Gottanka, J., Johnson, D. H., Martus, P., and Lütjen-Drecoll, E. (2001). Beta-adrenergic blocker therapy and the trabecular meshwork. *Graefe's Archive for Clinical and Experimental Ophthalmology* 239: 138–144.

Grierson, I., Howes, R. C., and Wang, Q. (1984). Age-related changes in the canal of Schlemm. *Experimental Eye Research* 39: 505–512.

Johnson, D. H. (2000). Myocilin and glaucoma: A TIGR by the tail? *Archives of Ophthalmology* 118: 974–978.

Johnson, D. H. (2005). Trabecular meshwork and uveoscleral outflow models. *Journal of Glaucoma* 14: 308–310.

Lütjen-Drecoll, E. (1999). Functional morphology of the trabecular meshwork in primate eyes. *Progress in Retinal and Eye Research* 8(1): 91–119.

Lütjen-Drecoll, E. and Rohen, J. W. (1996). Morphology of aqueous outflow pathways in normal and glaucomatous eyes. In: Ritch, R., Shields, M. B., and Krupin, T. (eds.) *The Glaucomas, Basic Sciences,* 2nd edn., vol. 1, pp. 89–123. St. Louis, MO: Mosby.

Lütjen-Drecoll, E. and Rohen, J. W. (2001). Functional morphology of the trabecular meshwork. In: Tasman, W. and Jaeger, E. A. (eds.) *Duane's Foundations of Clinical Ophthalmology,* 1st edn., vol. 1, ch. 10, pp. 1–30. Philedelphia, PA: Lippincott Williams and Wilkins.

Lütjen-Drecoll, E., Futa, R., and Rohen, J. W. (1981). Ultrahistochemical studies on tangential sections of the trabecular meshwork in normal and glaucomatous eyes. *Investigative Ophthalmology and Visual Science* 21: 563–573.

Streeten, B. W. (1993). Elastic fibers and microfibrils in the eyes. In: Lütjen-Drecoll, E. (ed.) *Basic Aspects of Glaucoma Research III,* 1st edn., pp. 67–94. New York: Schattauer.

Tamm, E. (2002). Myocilin and glaucoma: Facts and ideas. *Progress in Retinal and Eye Research* 21: 395–428.

Tektas, O.-Y. and Lütjen-Drecoll, E. (2009). Structural changes of the trabecular meshwork in different kinds of glaucoma. *Experimental Eye Research* 88: 769–755.

Structure and Evolution of Crystallins

G Wistow, National Eye Institute, Bethesda, MD, USA
C Slingsby, Birkbeck, University of London, London, UK

Published by Elsevier Ltd.

Glossary

Crystallins – The proteins that accumulate to very high levels in the cytoplasm of lens fiber cells, usually comprising more than 10% of the total protein. They may either belong to the group of classical crystallins, present in all vertebrate lenses, or be taxon specific. Taxon-specific crystallins, as the name suggests, are expressed in the lenses of species in a limited number of taxonomic groups.

Heat-shock proteins – The proteins that accumulate in cells in response to stress or that protect cells from stress. These proteins were originally named by their selective expression in cells exposed to elevated temperatures and for their ability to increase the temperature resistance of the cells in which they are expressed. Many proteins that, based on structural criteria, are heat-shock proteins are expressed constitutively and may protect cells from a variety of harmful insults.

Refractive index – In practical terms, this is the property that alters the speed of light passing through a substance. Lenses must have a refractive index that is different from the medium that surrounds them. The high protein concentration in biological lenses gives them a refractive index that is higher than the fluids around them.

What Are Crystallins?

To fulfill its function in light refraction and image formation in the vertebrate camera eye, the lens needs to have a high refractive index. This is largely conferred by high concentrations of soluble cytoplasmic proteins which as a group are known as the crystallins. The lenses of vertebrates contain three classes of crystallins, the α-, β-, and γ-crystallins, which must have been present in an early common ancestor. α-Crystallins belong to the small heat-shock protein (sHSP) superfamily, while the β- and γ-crystallins are related to each other and belong to another widespread superfamily. Other crystallins are taxon specific, restricted to specific evolutionary lineages. These crystallins are mostly enzymes and became crystallins through modification to their genes conferring greatly increased expression specifically in the lens, a process called gene recruitment.

Indeed, this is probably the mechanism by which all crystallins arose. This is illustrated most tellingly by the discovery of a protein related to β- and γ-crystallins that is expressed in cells of the primitive light-sensitive organ of the urochordate *Ciona intestinalis*, an organism which diverged from the vertebrate lineage before the development of the lens. When the promoter of the gene for the *Ciona* protein is transferred to amphibians, it directs expression in the lens and other parts of the visual system. This suggests that the most ancient crystallins arose from proteins with a functional role in the ancestral eye whose expression could be enhanced in the newly evolving lens and that the lens made use of elements of the transcriptional repertoire of light-sensitive cells (such as Pax6) that are still used in vertebrate eyes.

While different proteins serve as crystallins, not just any protein will do. Crystallins must be able to accumulate to high concentrations without aggregating, precipitating, or undergoing phase separations into protein-rich and protein-poor regions, any of which would give rise to light scattering that would render the lens opaque. Since the lens grows as layers of terminally differentiated fiber cells that lose their nuclei (probably to enhance transparency), crystallins have low (or no) turnover in the lens. They must be stable for the lifetime of the organism while subject to light exposure and the threats of oxidation and other insults. These requirements put constraints on the shape, thermodynamic stability, and surface properties of crystallins.

The selection of an existing protein as a crystallin would be more likely if the protein was already expressed at moderately high levels in the lens (or precursor cells) and if it had other useful features that might confer a selectable benefit on the lens, such as stabilization of unfolded proteins or protection from oxidative damage.

α-Crystallins

The lenses of all vertebrates contain α-crystallins, 18–20-kDa polypeptides which form large, polydisperse assemblies in the 600-kDa size range. In terrestrial species, two genes (Cryaa and Cryab), the result of an ancient duplication, provide all this protein. The two gene products (αA and αB-crystallin) belong to the widespread sHSP superfamily, part of a network of molecular chaperones. sHSPs have roles in binding, stabilizing, and solubilizing

unfolded or partially folded polypeptide chains. Unlike the HSP70 and HSP90 families, the sHSPs do not have adenosine triphosphate (ATP)-dependent active protein folding processes. Their role seems to be rescue or protection of unfolded proteins from aggregation before they can be refolded (or degraded) by other systems. They also associate with cytoskeleton and have activity in protecting or shepherding multimolecular assemblies in the cytoplasm and the cell nucleus. Since one of the most significant features of the cellular lens in vertebrates is the enormous elongation of fiber cells and the elaboration of very extensive cytoskeletal structures, high levels of proteins with sHSP activity is probably beneficial. Selection of a sHSP as a crystallin could have contributed both increased refractive index and improved stability of cytoarchitecture in the evolving lens.

Of the two α-crystallins, αB is most similar to the ancestral state since, although it is highly expressed in lens, it is also widely expressed in other tissues and is stress inducible. In contrast, αA-crystallin has become much more specialized for lens (although it does exhibit some nonlens expression, particularly in retina). This history of duplication and specialization has gone one step further in some fish. In zebrafish (*Danio rerio*), there has been a duplication of the gene for αB-crystallin. Recapitulating the original duplication in this family, one copy (αB1) is highly specialized for lens and has compromised some of its chaperone-like properties, while the other (αB2) is widely expressed and has normal chaperone properties. (Since specialization for lens is accompanied by a reduction in chaperone activity, this may not be of central importance to the role of α-crystallins in lens.)

Structure and Implications for Function

sHSPs contain a core domain of about 90 residues (known as the α-crystallin domain; ACD) in addition to highly variable N-terminal domain extensions (**Figure 1(a)**). X-ray structures have been solved for some nonlens sHSPs, although none from vertebrates and all contain a conserved β-sandwich in the ACD. The solved structures are for proteins that form well-defined multimers built up from dimers, unlike the polydisperse α-crystallins, but reveal significant variations in the way N- and C-terminal regions influence subunit interactions (**Figure 1**). In particular, the structure of the metazoan sHSP Tsp36 from the flatworm *Taenia saginata* shows differences in dimerization mechanism from the other solved sHSP structures. However, in all cases, the β-sandwiches have hydrophobic grooves that are filled by residues from N- or C-terminal extensions in self assembly. Acting as chaperones, these grooves could be used to stabilize various secondary structural elements of client proteins. Other metazoan sHSPs, including α-crystallins, are likely to show further variability in multimerization, but following this general mechanism.

The β- and γ-Crystallins

The β- and γ-crystallins belong to the same protein superfamily, the βγ-crystallins. They consist of polypeptides of 20–30 kDa and share many structural features. They also have major differences, the most obvious of which is that β-crystallins are multimeric, while γ-crystallins are monomers. β-Crystallins also have long N-terminal, and sometimes C-terminal, extensions that are subject to post-translational cleavage in the lens.

The βγ-Crystallin Fold and Tertiary Structure

The β- and γ-crystallins are the result of duplications of a distinctive structural motif of about 40 amino acid residues that conforms to a modified Greek key pattern of four β-strands (**Figure 2**). One motif cannot exist as a stable structure alone, but a pair of motifs can associate around a pseudo-twofold axis to create a highly stable, wedge-shaped domain, with two β-sheets sandwiching a tightly packed hydrophobic core capped with connecting loops that link the sheets.

If the strands of each motif are designated *a, b, c,* and *d,* the fold begins with an *ab* hairpin, which bends back on itself, and is defined by highly conserved residues giving a YxxxxF/YxG signature (**Figure 2(a)**). The glycine, lacking a side chain, is essential for the geometry of the fold. Strand *c* extends away so that strands *b* and *c* define the wedge shape of the domain. A long loop, often containing a helical stretch, connects across the top of the wedge to strand *d*, which contains a conserved serine that contributes to the structure of the folded *ab* hairpin. Thus, each β-sheet in a βγ-crystallin domain has four strands in the order *b, a, d,* and *c′* (with *c′* coming from the paired motif).

Two other secondary structural features are common (but not universal) in the βγ domain. One is a tyrosine corner in one motif (the second in β- and γ-crystallin domains) in which a tyrosine from the *c* strand hydrogen bonds to a main-chain carbonyl group of the *b* strand. The same motif also often possesses a tryptophan (Trp) corner, in which a Trp near the start of the *a* strand similarly hydrogen bonds to main chain at the end of the *d* strand of the other motif. Both these features stabilize the base of the domain wedge and contribute to correct folding (**Figure 2(b)**).

The β- and γ-crystallins have two domains that are linked by a connecting peptide (**Figure 3**). In γ-crystallins, the connecting peptide is bent and the two domains interact around another pseudo-twofold axis. In βB2-crystallin, a different arrangement occurs. The connecting peptide does not bend, so the two domains of one subunit cannot interact; instead, two subunits pair up head to tail and form interdomain contacts similar to those seen in γ-crystallins but with domains from the other subunit. This is an example of domain swapping in which

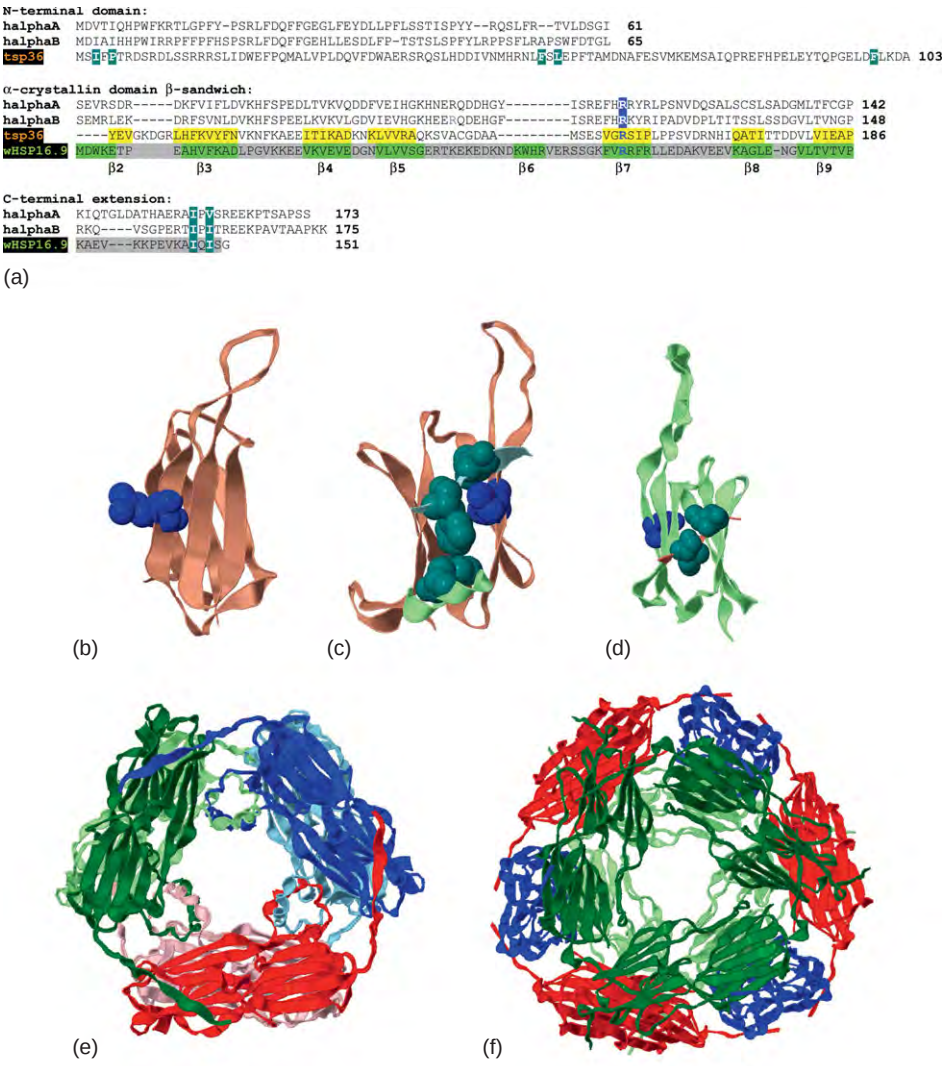

Figure 1 The conserved α-crystallin domain (ACD). (a) sHSPs have a variable N-terminal domain and a conserved ACD that includes a β-sandwich and an ordered extension (highlighted here in gray in the wheat HSP16.9 sequence). The sandwich β-strands, highlighted in bright green and yellow, are labeled. (b) The ACD β-sandwich, represented here by the one from the first ACD (it has two) from the flatworm protein tsp36, shown in salmon pink, taken from Protein Data Bank (PDB) 2bol. These sHSP beta-sandwiches have open, hydrophobic N-terminal (left) and C-terminal (right) sides that attract other hydrophobic sequences. The residue shown in blue space-fill in the model and in the alignment is a conserved arginine that when mutated in human αA- and αB-crystallins causes, respectively, cataract or myopathy. (c) This view of the tsp36 domain rotated 90° relative to (b) shows how hydrophobic residues from the variable N-terminal region, shown in dark green in the 3D structure and in the alignment, patch the open face of the sandwich, close to the conserved arginine. (d) The same region of wheat HSP16.9 (PDB 1gme) is shown in ribbon representation in pale green, with the ordered C-terminal extension of another subunit in salmon pink, to indicate that the interaction is between different chains in the 12-chain assembly structure. In this view, with the C-terminal side in the foreground, the open face is patched with hydrophobics from the ordered extension, shown in dark green in the 3D structure and the alignment, with the conserved arginine in the background. Different arrangements of subunits in two sHSP multimers from (e) wheat HSP16.9 and (f) archaebacterium (*M. jannaschii*), PDB 1shs. Dimers, colored in uniform color, show extensions interacting with beta-sandwiches from other dimers.

dimerization can occur in proteins by substituting interfor intramolecular contacts. However, there are alternative ways in which β-crystallins can dimerize. In a truncated version of βB1-crystallin (missing most of its N-terminal extension), the domains of one subunit associate in the γ-crystallin manner with a bent connecting peptide. Dimerization now occurs by side-to-side interactions of γ-like subunits similar to the way βB2 dimers associate with symmetry-related dimers in the crystal lattice. Mixed multimers of β-crystallin subunits may explore many modes of assembly.

Surface and sulfur

A striking feature of γ-crystallins is the high percentage of intramolecular surface ion pairs. This may reduce the amount of bound water, suitable for the dehydrated core

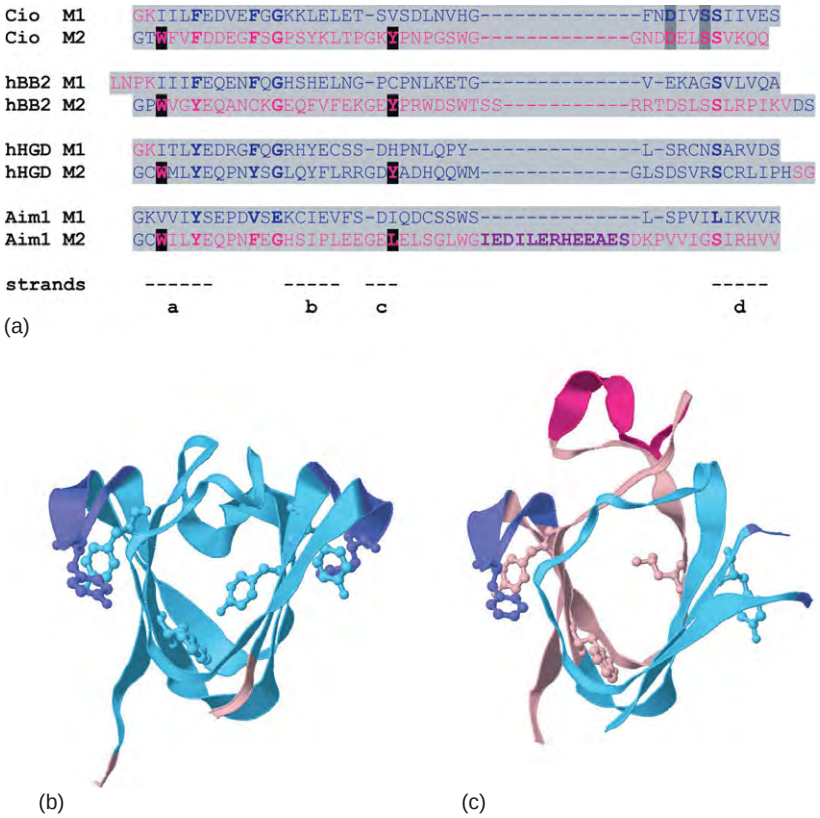

Figure 2 The βγ-crystallin motif and domain structure. (a) Sequence alignment of representative domains from the ancestral *Ciona* βγ-crystallin (cio); human βB2-crystallin (N-terminal domain) (hbb2); human gD-crystallin (N-terminal)(hGD) and Aim1 (domain 1); arranged so that the two Greek key motifs of each domain (M1, M2) are shown in pairs, aligned vertically, and color-coded to show the exons. For Cio, side chains that bind calcium are highlighted in dark gray. Residues corresponding to the βγ-crystallin fingerprint are in bold. The positions of *a, b, c,* and *d* strands are indicated. (b) The N-terminal domain of human γD-crystallin (PDB 1hk0), showing that most of the domain is encoded in a single exon, colored blue. The *ab* hairpins are colored purple and the fingerprint and corner aromatic residues have been appended as ball-and-stick models. The tyrosine corner residue is prominent in the center of the view. (c) The first βγ-domain of human AIM1 (PDB 3cw3). Sequences corresponding to separate exons are colored pink and blue and in general correspond to motifs. The same pattern is seen in β-crystallins. The absence of critical conserved residues in the second motif has resulted in a disordered conformation of the *ab* hairpin. The extra acidic insertion in the *cd* loop region is shown in crimson.

region of some hard lenses. Various cataract-causing mutations also show that small changes in surface residues can have major effects on solubility in γ-crystallins. It seems that polar groups on each γ-crystallin create characteristic molecular dipoles that may define the relative orientation of the molecules in solution. Disruption of the dipole by even a single side-chain alteration may disrupt the ordering of the proteins so that in dense solutions they undergo phase change or precipitation.

The γ-crystallins, particularly in fish, also have high contents of cysteines and methionines. These sulfur-containing side chains may contribute to stability or packing of crystallins at high density. Even in mammals the sulfur content of γ-crystallins is significant and may be a risk factor for oxidation in cataract.

Mapping of Protein and Gene Structure

The regular, repeated structure of β- and γ-crystallins is reflected in their gene structure, but with a characteristic difference (**Figures 2** and **3**). In the former, each motif is encoded in a separate exon, consistent with a history of duplication from an ancestral motif gene. One or more additional exons encode the N-terminal extension. γ-Crystallins (with the interesting exception of γN) lack the intron dividing the exons for each pair of motifs in one domain. Instead of one exon per motif they have one exon per domain.

Nonlens Relatives

The characteristic sequence signature of β- and γ-crystallins has allowed the identification of a βγ-crystallin superfamily that includes one, two, and six domain proteins in species ranging from prokaryotes to vertebrates (**Table 1**) Unlike the sHSP superfamily to which α-crystallins belong, the nonlens relatives of the βγ-crystallins do not reveal a clear common function. Two well-characterized members, the two-domain Protein S of the prokaryote *Myxococcus xanthus* and the one-domain spherulin 3a of the eukaryotic slime

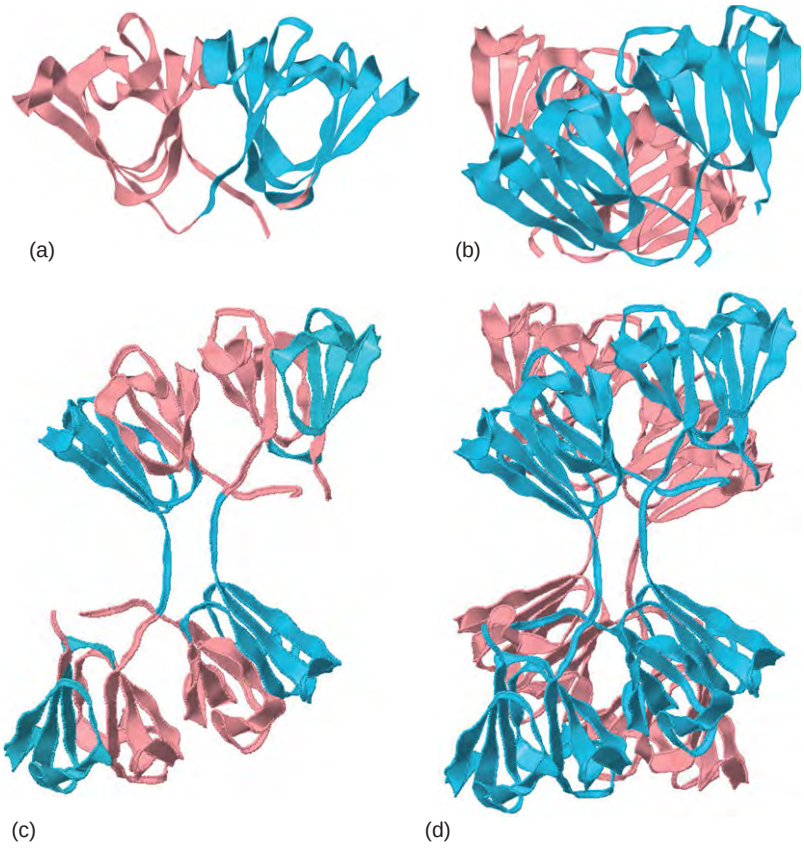

Figure 3 Modular domain interactions in βγ-crystallins. (a) Intramolecular domain pairing in a γ-crystallin (PDB 1hk0) with the N-terminal domain shown as a blue ribbon and the C-terminal domain in pink. The junction between exons 2 and 3 is in the middle of the connecting peptide. (b) A dimer of N-terminally truncated βB1-crystallin (PDB 1oki) with each chain in uniform color showing that each monomer has a similar domain organization as a γ-crystallin. (c) A dimer of βB2-crystallin (PDB 1ytq) with each polypeptide chain colored by exon showing that intrachain domains do not interact with each other, but that the interchain domain–domain interface is very similar in overall geometry to the intramolecular interface in monomeric γ-crystallin. (d) A tetramer of βB2-crystallin as observed in the crystal lattice showing a domain-swapped dimer in the foreground that is colored in blue, and a domain-swapped dimer in the background that is colored in pink. Note that the set of four upper domains (or four lower domains), all from different chains, has a similar organization to the βB1-crystallin dimer.

mold *Physarum polycephalum*, have well-defined calcium-binding sites and are induced in spore or cyst formation, suggesting possible roles in long-lived, dehydrated structures. The calcium-binding sites in these two proteins, distantly related in evolution, are very similar to those found in the one-domain *Ciona*-crystallin, but they are absent from the lens βγ-crystallins (**Figure 2**). (While low levels of calcium binding have been observed in β- and γ-crystallins, it is not clear whether this has physiological significance.)

The structure of Protein S also has remarkable similarities and differences with its lens relatives. Protein S too has tyrosine corners, but in the first motif of each domain rather than the second. Thus, while the motifs in the crystallins follow an ABAB pattern, in Protein S the pattern is BABA. Ancestral prototypes of A and B motifs may have existed as products of separate genes that folded together as a dimer of motifs. The genes may have fused in the order AB in the line leading to vertebrates and BA in the ancestors of *M. xanthus*.

Two other members of the superfamily may give clues to the functional role of βγ-crystallins in vertebrates. Epidermis differentiation specific protein 1 (EDSP or Ep37) of the newt *Cynops pyrrhogaster*, which has calcium-binding sites, is associated with plasma membrane in the developing epidermis. Absent in melanoma 1 (AIM1), which lacks calcium-binding sites, is encoded by a gene in a region of human chromosome 6 known to contain a suppressor of malignancy in melanoma. AIM1 expression is associated with changes in cell morphology that may reflect the formation of a more organized cytoskeleton. Thus, EDSP and AIM1 may have roles in control of cellular architecture.

AIM1 is also striking because it contains 12 βγ-crystallin motifs arranged as six domains with the

Table 1 Nonlens members of the βγ-crystallin superfamily

	Protein	*Distribution*	*Domains*
Eukaryote			
	AIM1 (and AIM1-like)	Vertebrates	6
	EDSP/ Ep37/ GEP	*Cynops pyrrhogaster* (newt)	2
	βγ-CAT	*Bombina maxima* (frog)	2
	Ciona crystallin	*Ciona intestinalis* (tunicate)	1
	Spherulin 3a	*Physarum polycephalum* (slime mold)	1
Prokaryote			
	Protein S	*Myxococcus xanthus*	2
	Yersina crystallin	*Yersinia pestis*	2 or 3
	Hahellin	*Hahella chejuensis*	1
	Caulollin	*Caulobacter crescentus*	1
	M-crystallin	*Methanosarcina acetivorans*	1

Other proteins have similar β-sheet topology to the βγ-crystallins but lack the characteristic folded hairpin and sequence signatures and are unlikely to be evolutionarily related.

crystallin-like ABAB pattern, perhaps forming a structure similar to a β-crystallin trimer. Indeed, AIM1 gene structure is like a β-crystallin with each motif encoded by a separate exon. Among the six AIM1 domains, numbers 1 and 6 show the greatest divergence from the canonical signatures of any superfamily member so far identified. In domain 1, residues of the characteristic folded hairpin of the first motif are not conserved, while the second motif lacks the tyrosine corner and contains a large insertion in the *c–d* loop (**Figure 2(a)**). X-ray analysis (**Figure 2(c)**) shows that the variant hairpin has no defined rigid structured but, while stability may be impaired, the domain folds compactly and follows βγ-crystallin domain topology.

In addition to the βγ-crystallin domains, AIM1 contains an alternatively spliced N-terminal extension that may be rod-like and a C-terminal ricin-like trefoil domain (a protein interaction domain found in many classes of proteins). Multidomain proteins may have arisen by fusion of genes encoding interacting partners. This raises the possibility that some other βγ-crystallins may have interactions with trefoil domains. Indeed, a multifunctional toxin secreted by the skin of a frog (*Bombina maxima*) is a heterodimer of an EDSP-like protein and a trefoil protein.

Gene Families

The β-crystallins are subdivided into two classes (A, acidic; B, basic) with three genes for each class giving rise to βA1/3, βA2, βA4, βB1, βB2, and βB3-crystallins (βA1 and βA3 are the products of the same gene through alternative translation start sites). This repertoire is present in vertebrates from fish (in which some members are duplicated) to mammals and birds (**Figure 4**). The diversification of these six genes must have occurred in a very early vertebrate ancestor and has been conserved through 300 million years of evolution. This may mean each β-crystallin has a very specific role in the organization or development of the lens. Conversely, since β-crystallins form a wide range of homo- and hetero-multimers, this may restrict the options for divergence in individual proteins.

Genes for β- and γ-crystallins are not randomly distributed in the genome. Those for βB1 and βA4 are arranged head to head on human chromosome 22, while 1.4 Mbp away on the same chromosome, the genes for βB2 and βB3 are also close together. The gene for βA2-crystallin is on human chromosome 2 about 1 Mbp away from a cluster of six γ-crystallin genes. Whether this degree of linkage for such ancient genes is related to coordination in regulation is not known.

While β-crystallins have orthologs in all vertebrate species examined, γ-crystallins are much more variable. Typical placental mammals, such as mice, have six closely related γ-crystallins, γA–F (85–98% identical in amino acid sequence), encoded by genes closely linked in a single chromosomal locus. They are highly expressed in the embryonic lens and contribute to the dense lens core region (the lens nucleus). They have no orthologs in nonmammals; in fish there are many γM-crystallins but these are highly divergent from the mammalian proteins (**Figure 4**).

The γ-crystallins are often associated with regions in the lens of higher refractive index. They are very abundant in fish and in the hard, spherical, myopic lenses of rodents. However, they are (essentially) absent from the softer, highly accommodating lenses of birds. In humans, the genes for γE and γF are nonfunctional, while expression of human γA and γB is low. γ-Crystallins may have evolved to provide the high refractive index needed to diffract and focus light under water in the aquatic ancestors of all vertebrates. In water, the cornea makes little contribution to focusing and therefore all the work must be done by the lens. The multiple, sulfur-rich γ-crystallins of fish provide the hard lens with a protein content that can reach 60% or more wet weight. In contrast, many terrestrial species need a softer lens for fine focusing and accommodation, adapting vision for near and far objects and in terrestrial vertebrates the lens has undergone major changes in γ-crystallin content (**Figure 5**).

The loss of γ-crystallins is most pronounced in birds and reptiles (although data on reptiles are still rather limited) where they have been replaced by taxon-specific crystallins. It seems likely that the reptile-like ancestors of mammals would similarly have lost or downregulated

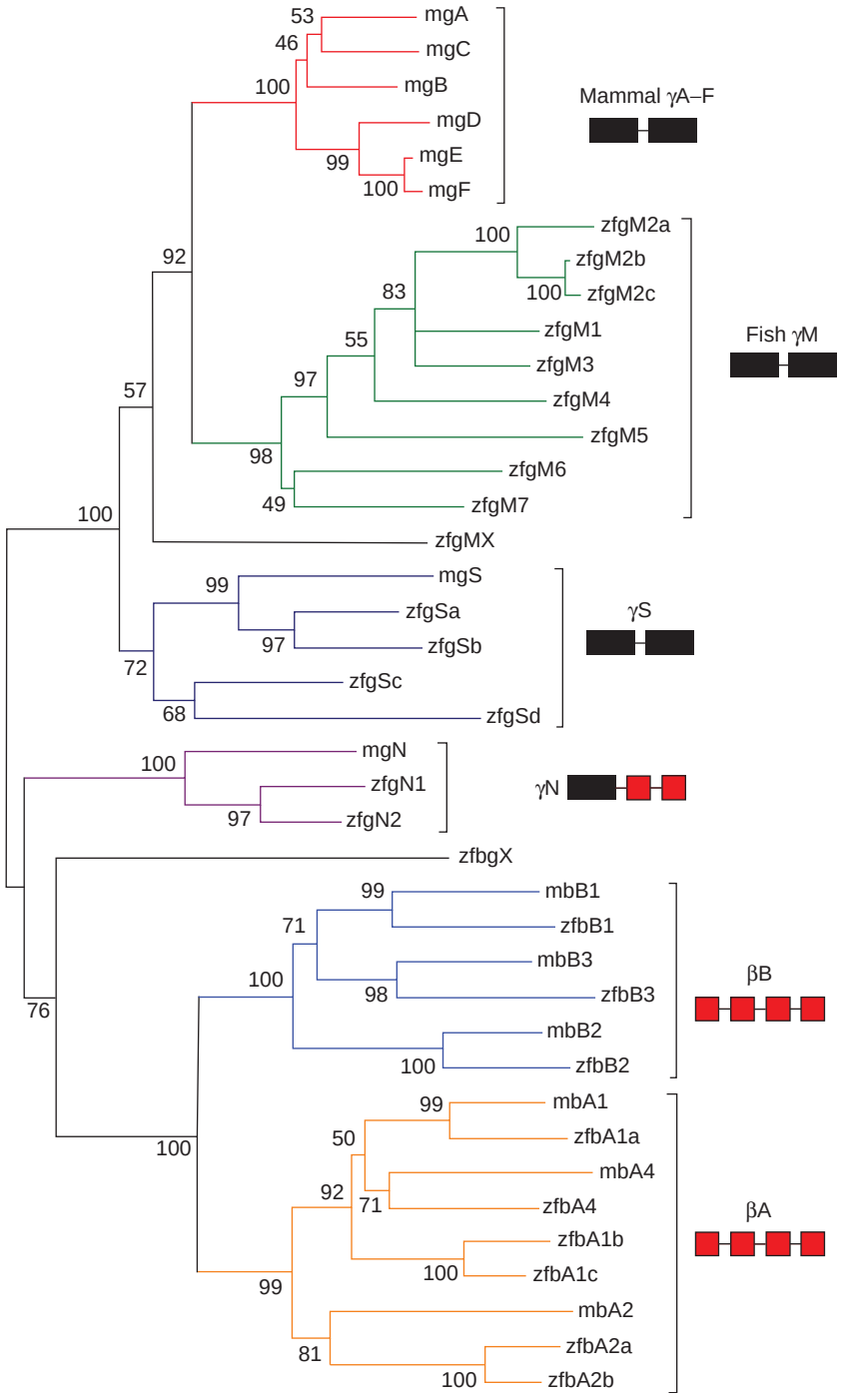

Figure 4 Family tree of β- and γ-crystallins. The complete repertoire of mouse (m) and zebrafish (zf) β- and γ-crystallins were aligned and a family tree constructed using the neighbor-joining procedure using the program MEGA. Mouse βA, βB, γS, and γN crystallins lie on the same branch as orthologs (sometimes duplicated) in zebrafish, showing strong conservation from ancestral sequences. However, γM and γA–F form separate branches, suggesting separate histories of divergence and duplication. For each branch, the exon structure encoding the βγ motifs and domains in each gene class is shown with small red boxes representing individual exons encoding individual motifs (typical of β-crystallins) and lager black boxes representing fused exons encoding both motifs of a single domain (typical of γ-crystallins). γN has hybrid gene structure suggesting it represents an evolutionary intermediate.

ancestral γ-crystallin genes and, yet in many modern mammals (such as mice), high contents of γ-crystallins are found in the lens. It is possible that the mammalian γA–F-crystallin gene cluster was reinvented through a series of duplications from a remaining γ-crystallin gene during a time when the ancestors of placental mammals were nocturnal, burrowing animals for whom a close-vision lens may have been advantageous. However, as

mammals diversified into other ecological niches in more recent evolutionary periods and the need arose once more for lenses capable of accommodation and distance vision, γ-crystallins again began to disappear in some lineages, often replaced with taxon-specific crystallins.

There are two other types of γ-crystallin that are not so tightly associated with the dense core of the lens and which are better conserved through evolution (**Figure 4**). One is γS-crystallin (~50% identical to γA–F), while the other is the recently discovered γN-crystallin. Both have orthologous genes in birds, although their level of expression is not yet known. They also have orthologs in reptiles (*Iguana*) and in fish. γS-crystallin is expressed at its highest levels in the adult lens, making major contributions to the softer lens cortical regions than to the harder nucleus, and is the most abundant γ-crystallin in the human lens. In mouse, γN is detectable at low levels in lens, while complementary DNA (cDNA) analysis suggests γN is moderately abundant in lenses of other species; however, in humans its gene may be nonfunctional, producing only rare aberrant transcripts. Similar to γE and F, it seems to have been deleted from the repertoire of the primate lens. In zebrafish, both γS and γN have undergone gene duplications to form families of two and four genes respectively (**Figure 4**).

γN has a particular significance in the evolution of β- and γ-crystallins. Cladistically, it is close to the division between the two classes. Furthermore, its gene structure is clearly intermediate between β and γ with the first domain encoded in one exon, like a γ gene, and the other encoded as separate motifs, like a β gene (**Figure 4**). The γ gene structure may have arisen by intron loss in a β-like gene (giving rise to γN), followed by loss of a second intron, perhaps by gene conversion.

Taxon-Specific Crystallins

The ancestral vertebrate lens evolved to suit the needs of aquatic species. During evolution, the composition of the

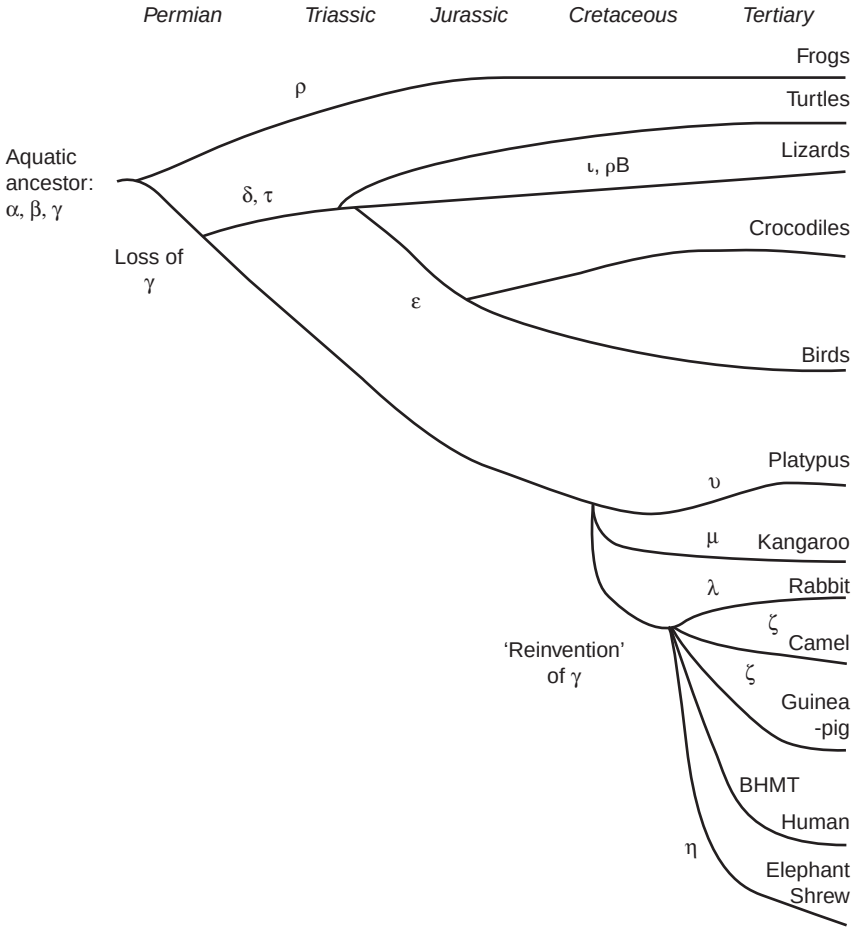

Figure 5 The evolutionary history of vertebrate crystallins. Some major lines of terrestrial vertebrates are shown along with the approximate appearance or disappearance dates for different crystallins by geological epoch. Ancestors of mammals may have lost, then reacquired abundant γ-crystallins during evolution. Different taxon-specific crystallins were recruited at different times, often replacing γ-crystallins in soft, accommodating lenses.

Table 2 Taxon-specific enzyme crystallins

Crystallin	*Distribution*	*Identity (or ~similar)*
δ	Most birds, reptiles	Argininosuccinate lyase
ε	Some birds, crocodiles	Lactate dehydrogenase B
ζ	Guinea pig, camel, llama	NADPH quinone oxidoreductase
η	Elephant shrew	Aldehyde dehydrogenase A1A
λ	Rabbit, hare	~Hydroxyacyl CoA dehydrogenase
?	Primates	Betaine-homocysteine methyltransferase
μ	Australian marsupial (kangaroo, etc.)	~Ornithine cyclodeaminase
ν	Monotreme (platypus)	Lactate dehydrogenase A
τ	Turtles, other reptiles	Enolase 1
ι	Gecko (*Lygodactylus*)	Retinol-binding protein 1
π	Gecko (*Pheksuma*)	Glyceraldehyde 3-phosphate dehydrogenase
ρ	Gecko (*Lepidodactylus*); frogs	~Aldose reductase

Several of these proteins, notably enolase and glyceraldehyde 3-phosphate dehydrogenase, are moderately abundant in lenses of many species where they do not count as crystallins. However, in the species listed, these enzyme crystallins may account for 5–50% of total lens protein and are unambiguously crystallins.

lens has been modified many times, to reengineer its optical properties for different needs (**Figure 5**). Often, this has involved loss and divergence of γ-crystallins. Another evolutionary strategy has been to acquire new crystallins, to replace or perhaps dilute the γ-crystallins. Remarkably, this usually involves the gene recruitment of different metabolic enzymes (**Table 2**). Examination of expressed genes in lenses of different species shows many moderately abundant housekeeping enzymes that occur at much higher levels as crystallins in other species. Thus, taxon-specific enzyme/crystallins have been selected from a pool of enzymes that were already moderately abundant in the lens. (In parallel, enzymes such as glutathione S-transferase have also been recruited as crystallins in the cellular lenses of some invertebrates, a remarkable instance of convergent evolution.)

In birds, the γ-crystallins of the lens core region have gone, replaced by high levels of δ-crystallin. δ-Crystallin is derived from the enzyme argininosuccinate lyase (ASL). Early in the bird and reptile lineage, this enzyme must have acquired high expression in lens as a crystallin. It underwent gene duplication and, as in the case of α-crystallins, one copy (δ2-crystallin) maintained the ancestral functional role, while the other (δ1-crystallin) specialized for lens and, in so doing, lost the enzyme activity that was not needed for the new role. In some birds, both proteins are expressed at high levels in lens, while in others the level of δ2-crystallin is decreased.

Birds and crocodiles also have another major taxon-specific crystallin: ε-crystallin, which is identical to the enzyme lactate dehydrogenase B (LDHB). Unlike δ-crystallin, this has not (yet) undergone duplication and separation of functions. As such, it carries the burdens of two functions: enzyme and crystallin. Indeed, these and other crystallins illustrate an important mechanism in protein evolution in which a single protein may acquire two roles, creating an adaptive conflict. This can be resolved by duplication allowing the duplicate genes to diverge and specialize. While α- and δ-crystallins may have relieved adaptive conflict by this mechanism, ε-crystallin has not, but perhaps this will occur in some lineage of birds in the future.

If enzyme/crystallins are at least partially involved in replacing the lens-hardening γ-crystallins, the same might be expected to have occurred in primate lenses in which γ-crystallins also seem to be on the way out. Indeed the embryonic lens in humans and other primates contains very high levels of the enzyme betaine–homocysteine methyltransferase (BHMT). Although this has not received the accolade of a Greek letter, BHMT certainly seems to fit the criteria for a taxon-specific crystallin, partially replacing γ-crystallins in the human lens core.

Several different enzymes serve as crystallins in different species. In all cases, the enzymes are so abundant in the lens that they exceed any conceivable metabolic requirement. Some (but not all) of them bind nicotinamide adenine dinucleotide phosphate (NAD(P)H) cofactors that could act as ultraviolet (UV) filters or as reservoirs of reducing potential, potentially useful additional effects of their recruitment in the lens. Since many enzymes associate with cytoskeleton, it is also possible that, like other crystallins, enzyme/crystallins help to maintain the architecture of the lens fiber cells. Indeed, there is one recruited enzyme that, although it does not reach the levels of abundance usually associated with crystallins, has a specialized role in lens associated with cytoskeleton. Lengsin is a member of the glutamine synthetase superfamily but has lost enzyme activity. It is conserved in all vertebrate lenses where it plays a role in interacting with the lens-specific beaded filaments in terminally differentiating fiber cells.

In terms of three-dimensional (3D) structural adaptations to the lens role, the enzymatically inactive duck δ1-crystallin shows specific changes in substrate-binding regions that presumably enhance its role as a crystallin. η-Crystallin, a type 1 aldehyde dehydrogenase that is a major component of the lens in the elephant shrew (*Elephantulus* sp.), shows reduced flexibility in regions related to the active site tunnel; the protein may have acquired increased stabilization of its tertiary structure in response to the requirements of the lens perhaps at the expense of the enzyme role.

Conclusions

Vertebrate crystallins are a diverse group of proteins that, fitting certain criteria of stability and solubility, form the bulk refractive structure of a cellular lens. The proteins need to be stable and to interact with each other and other lens components in an orderly way (including short-range order) that maintains the supramolecular structure of the lens cytoplasm, forming no centers for light scattering and thereby maintaining transparency. In addition to their roles in lens, crystallins and their relatives have functional roles in other tissues.

See also: Accommodation; Normal Age-Related Changes: Crystallin Modifications, Lens Hardening.

Further Reading

Aravind, P., Wistow, G., Sharma, Y., and Sankaranarayanan, R. (2008). Exploring the limits of sequence and structure in a variant βγ-crystallin domain of the protein absent in Melanoma-1 (AIM1). *Journal of Molecular Biology* 381: 509–518.

Bateman, O. A., Purkiss, A. G., van Montfort, R., et al. (2003). Crystal structure of η-crystallin: Adaptation of a class 1 aldehyde dehydrogenase for a new role in the eye lens. *Biochemistry* 42(15): 4349–4356.

Bloemendal, H., De Jong, W., Jaenicke, R., et al. (2004). Ageing and vision: Structure, stability and function of lens crystallins. *Progress in Biophysics and Molecular Biology* 86(3): 407–485.

Liu, S. B., He, Y. Y., Zhang, Y., et al. (2008). A novel non-lens betagamma-crystallin and trefoil factor complex from amphibian skin and its functional implications. *PLoS ONE* 3(3): e1770.

Purkiss, A. G., Bateman, O. A., Wyatt, K., et al. (2007). Biophysical properties of gammaC-crystallin in human and mouse eye lens: The role of molecular dipoles. *Journal of Molecular Biology* 372(1): 205–222.

Shimeld, S. M., Purkiss, A. G., Dirks, R. P., et al. (2005). Urochordate betagamma-crystallin and the evolutionary origin of the vertebrate eye lens. *Current Biology* 15(18): 1684–1689.

Stamler, R., Kappe, G., Boelens, W., and Slingsby, C. (2005). Wrapping the alpha-crystallin domain fold in a chaperone assembly. *Journal of Molecular Biology* 353(1): 68–79.

Wistow, G. (1995). *Molecular Biology and Evolution of Crystallins: Gene Recruitment and Multifunctional Proteins in the Eye Lens*. Austin, TX: R.G. Landes.

Wistow, G., Wyatt, K., David, L., et al. (2005). GammaN-crystallin and the evolution of the betagamma-crystallin superfamily in vertebrates. *FEBS Journal* 272(9): 2276–22791.

Wyatt, K., Gao, C., Tsai, J.-Y., et al. (2008). A role for lengsin, a recruited enzyme, in terminal differentiation in the vertebrate lens. *Journal of Biological Chemistry* 283(10): 6607–6615.

T

Tear Drainage

F P Paulsen and L Bräuer, Martin Luther University Halle-Wittenberg, Halle, Germany

Glossary

Dacryocystitis – An infection of the efferent tear ducts.
Dacryolithiasis – The formation and presence of dacryoliths.
Dacryostenosis – The obstruction or narrowing of one or both canaliculi or the nasolacrimal duct. It may be present at birth.
Epiphora – An abnormal overflow of tears down the face.
Horner's muscle – A branch of the orbicularis oculi muscle passing behind the lacrimal sac; it contributes to the lacrimal pump.
Natural killer (NK) cells – A type of cytotoxic lymphocytes that constitute a major component of the innate immune system.
Pseudostratified epithelium – A type of epithelium that, though comprising only a single layer of cells, has its cell nuclei positioned in a manner suggestive of stratified epithelia.
Rheology – The study of the flow of matter: mainly liquids but also soft solids or solids under conditions in which they flow rather than deform elastically. It applies to substances which have a complex structure, including muds, sludges, suspensions, polymers, many foods, bodily fluids, and other biological materials. The flows of these substances cannot be characterized by a single value of viscosity (at a fixed temperature) – instead the viscosity changes due to other factors.

The upper and lower canaliculi, lacrimal sac, and nasolacrimal duct are subsumed under the terms nasolacrimal ducts, efferent tear ducts, or lacrimal passages. After birth, the function of the nasolacrimal ducts is to drain tear fluid into the inferior meatus of the nose.

The physiology of lacrimal drainage has been under study for over a century. Various mechanisms have been proposed to explain tear drainage, reflecting the unique anatomic configuration of the efferent tear ducts (Table 1). These include an active lacrimal pump mechanism that functions by contraction of the orbicularis eye muscle; a wringing-out mechanism governed by a system of helically arranged fibrillar structures; the bulging and subsiding of a cavernous body that surrounds the lacrimal sac and nasolacrimal duct; the action of epithelial secretion products; and physical factors such as capillarity, gravity, respiration, evaporation, and absorption of tear fluid through the lining epithelium of the efferent tear ducts. Nevertheless, the complex mechanism by which the tear fluid is brought from the ocular surface to the inferior meatus of the nose is yet not completely understood.

The median transit time of a single applied teardrop containing fluorescein dye has been shown to be 4.5 min or 8 min, depending on whether the fluorescein is applied without or with anaesthetizing the ocular surface, respectively. Without anaesthetizing, some reflex tearing of the lacrimal gland is initiated that increases lacrimal fluid volume, which in turn shortens the dye transit time. However, the passage time is subject to distinctive intraindividual variability with a standard deviation of 3.23 min and minimum and maximum values between 15 s and more than 18 min, respectively. There may be several factors that determine the high level of intraindividual variability in dye transit time: fluctuations within a single individual over time, family predisposition, emotional status, the fluid balance, basal tear film production, atmospheric conditions of testing, tear pump efficiency, hormonal status, and blink rate.

History

The first exact description of the efferent tear duct system dates back to Giovanni Battista Carcano Leone (1574). Together with the work of Niels Stensen (1662) on tear secretions, Leone's explanations led to a plausible concept for the entire lacrimal system.

Table 1 Mechanisms of tear drainage

Active lacrimal pump mechanism aided by contraction of the lacrimal portion of the orbicularis muscle
Distension of the lacrimal sac by the action of the lacrimal portion of the orbicularis muscle
Epithelial secretion products (mucins, TFF peptides, and surfactant proteins) of the epithelia of the lacrimal sac and nasolacrimal duct
Wringing-out mechanism governed by a system of helically arranged fibrillar structures
Opening and closing of the lumen of the lacrimal passage effected by the bulging and subsiding of the cavernous body
Capillarity
Respiration
Evaporation
Absorption of tear fluid through the lining epithelia of the lacrimal sac and nasolacrimal duct

Development

During the third month of embryological development, the eyelid folds contact each other and fuse. The specialized structures of the eyelids develop during the period of fusion. Some epithelial cores from both margins of the lid folds get buried in them, at the inner sixth of the eyelids, to form the precursors of the puncta and canaliculi. The epithelial buds, which have grown inside the tarsus, become canalized, as do the epithelial cores that will form the puncta and canaliculi. In the sixth month, the nasolacrimal system becomes patent as a result of lysis in the central cells of both epithelial rods (one starting from the inner canthus and extending toward the nose and the other starting from the nasal mucosa and extending toward the inner canthus) at their site of junction. At birth, the nasolacrimal canal is patent from the puncta to the nasal mucosa, under the lower concha (also known as turbinate). The lower end of the lacrimal duct is separated from the inferior meatus of the nasal cavity by a membrane (Hasner's membrane) consisting of the apposed mucosa lining the nasal fossa and the lower end of the duct. Many newborns suffer from congenital obstruction of the lacrimal pathways. The rate of congenital membranous stenosis of the lacrimal excretory systems in newborns has been reported to be as high as 50%. Fortunately, there is a high rate of spontaneous relief of the epiphora within the first 9 months of life. The repair of a lacrimal duct obstruction should therefore only rarely be performed prior to this age.

Anatomy and Dimensions

The lacrimal passages consist of a bony passage and a membranous lacrimal passage. The bony passage is formed anteriorly by the frontal process of the maxilla and posteriorly by the lacrimal bone. The membranous part includes the lacrimal canaliculi, the lacrimal sac, and the nasolacrimal duct (**Figure 1**).

Each canaliculus starts with a 0.25 mm (upper) to 0.3 mm (lower) large, round, oval, or slit-like lacrimal punctum with a nearly 2-mm-long vertical part. Consequently, the lacrimal canaliculus nearly runs at a right angle into the horizontal part, which measures approximately 8 mm. In most cases (*c.* 65–70%), the two canaliculi join to form a common canal that penetrates the wall of the lacrimal sac regularly 2–3 mm below the apex of the sac, termed fornix or fundus sacci lacrimalis. The vertical diameter of the sac is close to 12 mm, the saggital 5–6 mm, and the transversal 4–5 mm. The nasolacrimal duct normally measures 12.4 mm in adults. The bony coat is nearly 10 mm long and has a diameter of 4.6 mm.

The upper and lower canaliculi are lined by pseudostratified/stratified columnar epithelium and surrounded by a dense ring of connective tissue as well as muscle fibers of the lacrimal portion of Horner's muscle (orbicularis oculi muscle and tensor tarsi muscle). The lacrimal sac and the nasolacrimal duct are lined with a double-layered epithelium, revealing a superficial columnar layer with microvilli and a deep flattened layer of basal cells. Both layers sometimes appear pseudostratified. Some cells of the nasolacrimal duct are lined by kinocilia (sincular kinocilium; a motile cilium on the apex of distinct cells, for example, cells covering the nasal cavity and nasal sinus). Besides epithelial cells, goblet cells are also integrated in the epithelium, sometimes forming intraepithelial mucous glands. Moreover, small seromucous glands are present in the lamina propria, especially in the fundus of the lacrimal sac.

Comparative Anatomy

Unlike the human and ape nasolacrimal systems composed of upper and lower canaliculi, the lacrimal sac, and the nasolacrimal duct, the lacrimal systems in dogs, rabbits, cats, deer, pigs, and rats consist solely of the upper and lower canaliculi, leading directly into the nasolacrimal duct. Human, ape, dog, rabbit, cat, deer, and pig tissues reveal a pseudostratified, columnar epithelium with double layering in most areas, a basal cell layer and a superficial columnar layer. The rat shows a multilayered epithelium. The upper cell layers consist of larger squamous elements over several layers of essentially cuboidal cells. Goblet cells are integrated in the epithelia of humans, rats, and cats as solitary cells and in human and rat epithelia as intraepithelial mucous glands. By contrast, the epithelia of apes, dogs, rabbits, deer, and pigs contain no goblet cells. However, ape, dog, rabbit, and pig epithelia do contain many epithelial cells that show mildly positive staining with alcian blue (pH 1.0) in the upper cytoplasm; from investigations in dogs, it is known that

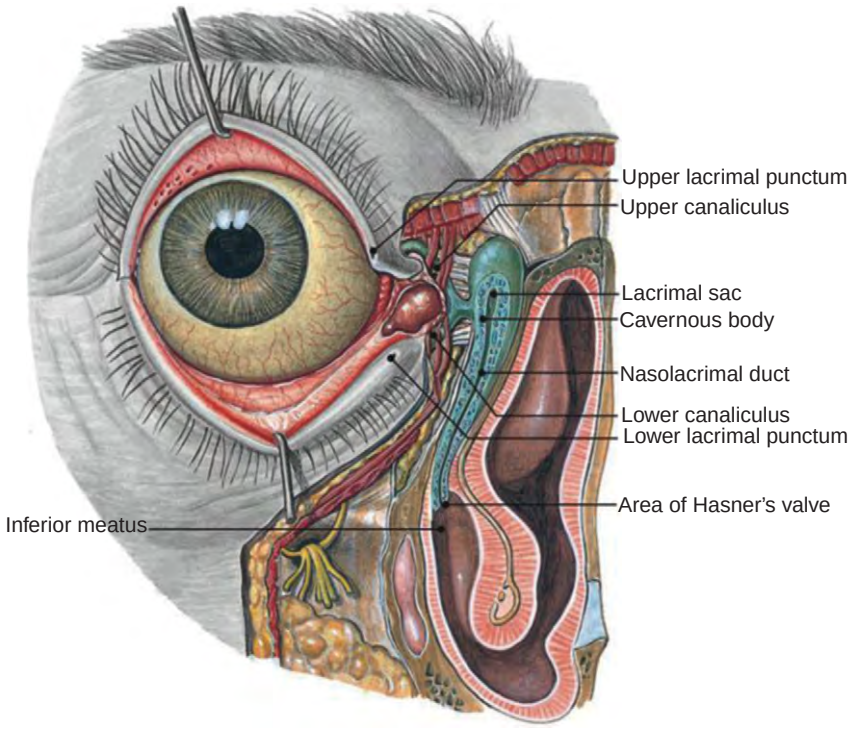

Figure 1 Nasolacrimal ducts. At the medial rim of the upper and lower lids, the lacrimal puncta open, leading into the lacrimal sac through the upper and lower canaliculi. The lacrimal sac is situated in the orbital lacrimal fossa and proceeds into the nasolacrimal duct. The nasolacrimal duct is surrounded by a bony canal created by the maxillary and lacrimal bones and opens into the inferior meatus of the nose. Both the lacrimal sac and nasolacrimal duct are surrounded by a vascular plexus comparable to a cavernous body that is connected to the cavernous system of the nose. From Putz / Pabst: Sobotta, Atlas der Anatomie des Menschen, 22. Auflage © 2006 Elsevier GmbH, Urban & Fischer Verlag München.

this positive staining corresponds to mucins (authors' observations). The cells with the mild staining are mostly arranged in cell groups. There are also epithelial areas without such cells or cell groups. Subepithelially, the lamina propria of the human lacrimal passage is composed of loose connective tissue containing elastic fibers and lymphatic cells and a rich venous plexus comparable to a cavernous body. A surrounding cavernous system of blood vessels is also found in apes, dogs, rabbits, deer, and pigs, but is absent in rats and cats. Small seromucous glands with excretory ducts opening into the lacrimal passage are integrated in the lamina propria of humans and pigs. None of the other animals possesses seromucous glands. Compared to humans, the efferent tear duct system of dogs and pigs is long. Therefore, the similarities between rabbit and human nasolacrimal ducts support the use of the rabbit for experimental studies of the efferent tear duct system.

Tear Transport through Canaliculi

The drainage of tears involves a number of different mechanisms that are not completely understood. It has been suggested that physical factors such as gravity, respiration, and evaporation might play a role in the drainage of tears through the lacrimal passage. Brienen and Snell postulated that the main, and presumably the sole, force that impels lacrimal flow from the conjunctival sac is the pressure brought about by closing of the eyes; in all probability, their expansions and contractions are secondary consequences of pressure fluctuations in the conjunctival sac. Jones introduced the concept of the lacrimal pump system which functions with blinking and might be responsible for lacrimal drainage by analyzing the structure of the medial palpebral ligament and the palpebral part of the orbicularis oculi muscle. It has also been shown that, during blinking movements, the canaliculi and medial canthal tendon are compressed and a uniform volume of lacrimal fluid is squirted into the lacrimal sac. The expansion of the lacrimal sac then causes suction during the opening phase of the blink, and, after the opening phase of the punctual areas, the canaliculi and lacrimal sac vacuum breaks to reload with tear fluid. The small canaliculi may also act as capillary tubes. Lacrimal fluid is attracted by capillarity into the lacrimal puncta, and, upon closing of the eyelids, the contraction of the preseptal muscle creates a negative pressure and sucks the tear fluid into the sac. The existence of negative pressure and the active transport of tears into the sac are, however,

questioned by many. Nevertheless, the importance of Horner's muscle becomes clear in cases of facial palsy. Tears are not pumped through the lacrimal system. Even with a Jones tube (a small tube allowing tears to drain into the nose) in place, there will be a decrease in tear flow if the orbicularis muscle function is insufficient. Support for the existence of a canalicular pump system on lid closure also came from experimental work carried out by others. Amrith et al. demonstrated that the puncta elevate and meet forcefully when the lids are half shut, and, on complete lid closure, the canaliculi and sac are compressed, forcing tears into the sac and nasolacrimal duct. The elastic expansion of the channels during lid opening and the drawing apart of the puncta break the vacuum, and the tear from the marginal strip is drawn into the puncta. Doane concluded that the force generated in the canaliculi during lid closure alone is sufficient to transport the non-reflex secretion, as it is less than 1 $\mu l\,min^{-1}$. If excess fluid is available, as in reflex tearing, it is possible that the sac may contribute to drawing the fluid. However, high-speed photographic and cinematographic techniques have not been useful in demonstrating what happens in the lacrimal sac during a blink. Even the role of gravity is not clear since Hurwitz concluded that gravity does play a significant role in the transport of tears.

Tear Transport through Lacrimal Sac and Nasolacrimal Duct

It is a popular misinterpretation that the tear fluid is drained into the inferior meatus of the nose by the contraction of musculature surrounding the lacrimal sac and/or nasolacrimal duct. Underneath the epithelium, the lamina propriae of the lacrimal sac and nasolacrimal duct consist of loose connective tissue containing a thin layer of elastic fibers and a rich venous plexus situated under this tissue that is connected caudally to the cavernous body of the nasal inferior turbinate. Collagen bundles as well as elastic and reticular fibers between the blood vessels of a rich venous plexus are arranged in a helical pattern and run spirally from the fornix of the lacrimal sac to the outlet of the nasolacrimal duct, where they contribute biomechanically to tear outflow during blinking. Specialized types of blood vessels are distinguishable inside the vascular tissue and are comparable to a cavernous body.

The blood vessels are specialized arteries (barrier arteries), venous lacunae (capacitance veins), veins (throttle veins), and arteriovenous anastomoses. They facilitate the opening and closure of the lumen of the lacrimal passage by swelling and shrinkage of the cavernous body. Swelling occurs when the barrier arteries (arteries with an additional muscular layer) are opened and the throttle veins (veins whose tunica media contains a muscle layer of helically arranged smooth muscle cells) are closed. Filling of the capacitance veins (widely convoluted venous lacunae) occurs at the same time as closure of the lumen of the lacrimal passage. By contrast, closure of the barrier arteries and opening of the throttle veins reduce the blood flow to the capacitance veins, simultaneously allowing blood outflow from these veins with resultant shrinkage of the cavernous body and dilatation of the lumen of the lacrimal passage. Arteriovenous anastomoses enable direct blood flow between arteries and venous lacunae; thus, the subepithelially located capillary network can be avoided and rapid filling of capacitance veins is possible when the shunts of the arteriovenous anastomoses are open. While regulating the blood flow, the specialized blood vessels permit opening and closing of the lumen of the lacrimal passage, effected by the bulging and subsiding of the cavernous body, and simultaneously regulate tear outflow.

The presence of the cavernous body is lacking in nearly all textbooks of anatomy and is therefore unknown to most nasolacrimal surgeons and radiologists. It is, however, densely innervated. Epiphora related to emotions such as sorrow or happiness occurs not only by increased tear secretion from the lacrimal gland and accessory lacrimal glands, but also by closure of the lacrimal passage. This mechanism acts, for example, to provide protection against foreign bodies that have entered the conjunctival sac: Not only is tear fluid production increased, but tear outflow is also interrupted by the swelling of the cavernous body to flush out the foreign body and protect the efferent tear ducts themselves. Moreover, it can be assumed that the valves in the lacrimal sac and nasolacrimal duct described in the past by Rosenmüller, Hanske, Aubaret, Béraud, Krause, and Taillefer could be caused by different swelling states of the cavernous body and must therefore be considered speculative.

In fact, the cavernous body of the efferent tear ducts plays an important role in the physiology of tear outflow regulation and can be influenced pharmacologically. Interestingly, administration of a decongestant drug or insertion of a foreign body at the ocular surface prolong the tear transit time significantly, but by different mechanisms (**Figure 2**). The application of a decongestant drug simultaneously with insertion of a foreign body shortens the tear transit time significantly compared to the effect of the decongestant drug alone, but there is no significant difference compared with application of a foreign body alone. The tear transit time is independent of side (right or left), gender, whether eyeglasses are worn, and whether the person is suffering from a common cold.

Tear outflow is further supported by the regional distribution of epithelial secretion products in the lacrimal sac and nasolacrimal duct (see the section titled 'Innate immune mechanisms'). These include membrane-bound and secretory mucins and trefoil factor family

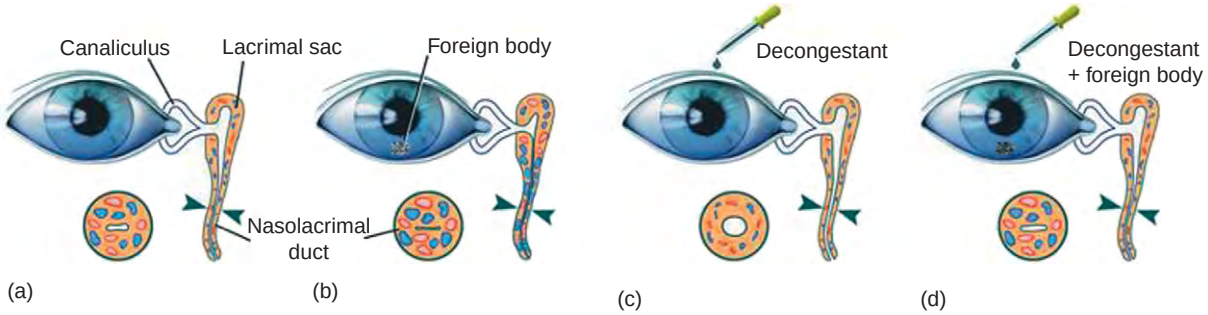

Figure 2 A Schematic/anatomical model of the state of the cavernous body and lacrimal passage in the (a) resting state and (b–d) under different experimental conditions, indicating the specific swelling and compression of the cavernous body and how it permits or restricts tear drainage. Reproduced from Paulsen, F. P., Schaudig, U., and Thale, A. B. (2003). Drainage of tears: Impact on the ocular surface and lacrimal system. *Ocular Surface* 1: 180–191.

(TFF) peptides and, as recently shown, surfactant proteins. The epithelial secretion products might influence the rheology and flow of tears through the efferent tear passages. There is speculation that at the ocular surface, mucin composition, distribution, and function are influenced by shear forces generated during blinking. Such forces are absent in the nasolacrimal ducts, and other mechanisms are necessary to ease the flow of tears. From the data available so far, it can only be said that mucins, TFF peptides, and surfactant proteins are likely to interact and may thus affect tear outflow. However, concrete data addressing this feature are lacking.

Table 2 Functions of the epithelia of the lacrimal sac and nasolacrimal duct

Secretion of antimicrobial substances (lysozyme, lactoferrin, secretory phospholipase A_2, bactericidal-permeability-increasing protein, heparin-binding protein, human β-defensins, and surfactant proteins A and D)
Secretion of mucins (MUC2, MUC5AC, MUC5B, MUC7, MUC8) and production of membrane-bound mucins (MUC1, MUC4, and MUC16)
Secretion of trefoil factor (TF) peptides (TFF1 and TFF3)
Secretion of surface active components (surfactant proteins B and C)
Production of lipids
Absorption of tear fluid components

Innate Immune Mechanisms

As is the case with all mucosae, the surfaces of the lacrimal sac and the nasolacrimal duct are in constant interaction with environmental microorganisms and are therefore vulnerable to infection. Similar to conjunctiva and cornea, the mucosa of the nasolacrimal ducts has developed a number of different nonspecific defense systems that can protect against dacryocystitis (**Table 2**); the epithelial cells thus produce a spectrum of different antimicrobial substances, such as lysozyme, lactoferrin, and secretory phospholipase A_2, as well as defensins, which protect against the physiological germ flora inside the lacrimal passage. When infectious and/or inflammatory dacryocystitis pose a threat, changes in the expression pattern occur, inducing the production of some of the antimicrobial substances, for example, antimicrobial peptides such as human inducible beta defensins 2 and 3, which are not produced under healthy conditions in the efferent tear ducts.

Besides supporting tear outflow, the product of the mucus component formed by goblet cells and epithelial cells has been attributed largely to immunological response. It contains mucins MUC1, MUC2, MUC4, MUC5AC, MUC5B, MUC7, MUC8, and MUC16 and probably additional mucins. Moreover, the epithelium of the nasolacrimal ducts expresses and produces – as already mentioned – the TFF peptides TFF1 and TFF3. Disturbances in the balance of single mucins or TFF peptides are important in the development of dacryostenosis, daryolithiasis, and daryocystitis. Mucins have several functions. In addition to lubricating the mucosa and waterproofing to regulate epithelial cell hydration, mucins protect mucosal surfaces against potentially harmful substances; however, a variety of oral and intestinal bacteria have been shown to produce sialidase, an enzyme that can degrade mucins by removing sialic acid. Additionally, oral and intestinal bacteria synthesize an array of other glycosidases that can attack the oligosaccharide residues of mucins. Early results of current investigations reveal that such glycosidases are also present at the ocular surface.

Finally, secretory immunoglobulin A (sIgA; the class of antibodies produced predominantly against ingested antigens, found in body secretions such as saliva, sweat, and tears, and functioning to prevent the attachment of viruses and bacteria to epithelial surfaces) is incorporated into the mucus layer of mucosal surfaces, supplementing the protective activity. It can interact with functionally diverse cells, including epithelial cells, B- and T-lymphocytes, natural killer (NK) cells, cells

of the monocyte/macrophage lineage, and neutrophils. All of these latter cell types, as well as sIgA, are present on and in the nasolacrimal ducts and belong to the lacrimal mucosal immune system (see below). This defense is supported by the collectins (surfactant-associated proteins) SP-A and SP-D in the service of nonspecific natural immune defense and in the activation of the adaptive immune system. As a substance intrinsic to drained tear fluid, they protect the ocular surface in conjunction with IgA, defensins, and mucins against infection by *Pseudomona aeruginosa*, *Staphylococcus aureus*, and other pathogenic microbes in preventing the formation of dacryocystitis.

Adaptive Immune Mechanisms

Subepithelially, lymphocytes and other defense cells are amply present inside the efferent tear ducts, sometimes aggregated into follicles. Aggregated follicles are present in nearly a third of nasolacrimal ducts from unselected cadavers with no known history of disease involving the eye, efferent tear ducts, or the nose. These aggregations and the surrounding tissue fulfill the criteria for designation as mucosa-associated lymphoid tissue (MALT). They consist of organized mucosal lymphoid tissue characterized by the presence of reactive germinal centers and mantle zones. Around the mantle zone, there is an additional zone of somewhat larger cells corresponding to marginal zone cells. These larger cells extend into the overlying epithelium, forming a lymphoepithelium.

In accordance with the terminology of MALT in other body regions, MALT of the human nasolacrimal ducts was termed TALT and, in conjunction with CALT of the conjunctiva, EALT for eye-associated lymphoid tissue. Current analysis of EALT, as well as different epithelial cells of the lacrimal passage, is interesting with regard to the induction of tolerance in the nasolacrimal system and at the ocular surface.

Specific secretory immunity depends on a sophisticated cooperation between the mucosal B-cell system and an epithelial glycoprotein called the secretory component. The initial stimulation of Ig-producing B-cells is believed to occur mainly in organized MALT. It has become evident that considerable regionalization or compartmentalization exists in MALT, perhaps determined by different cellular expression profiles of adhesion molecules and/or the local antigenic repertoire. The antigenic stimulation of B-cells results in the generation of predominantly IgA-synthesizing blasts (an immature stage in cellular development before the appearance of the definitive characteristics of plasma cells) that leave the mucosae through efferent lymphatics, pass through the associated lymph nodes into the thoracic duct, and enter the circulation. The cells then return selectively to the lamina propria (nasolacrimal ducts) as plasma cells or memory B-cells by means of homing mechanisms and contribute to mucosal sIgA.

Absorption of Tear Fluid Components

Recent animal experiments in rabbits have indicated that the components of tear fluid are absorbed in the nasolacrimal passage and transported into the surrounding cavernous body that is subject to autonomic control and regulates tear outflow. Under normal conditions, tear fluid components are constantly absorbed into the blood vessels of the surrounding cavernous body. These vessels are connected to the blood vessels of the outer eye and could act as a feedback signal for tear fluid production (**Figure 3**), which ceases if these tear components are not absorbed.

Conclusions

The human efferent tear ducts are part of the lacrimal system. They consist of the upper and the lower lacrimal canaliculi, the lacrimal sac, and the nasolacrimal duct. As a draining and secretory system, the nasolacrimal ducts play a decisive role in tear transport and nonspecific immune defense. In this context, an active lacrimal pump mechanism that functions by contraction of the orbicularis eye muscle has the major impact on tear transport from the ocular surface into the lacrimal sac. From here, tears are transported by a wringing-out mechanism governed by the helical arrangement of fibrillar structures within the vascular system surrounding the lacrimal sac and nasolacrimal duct, the action of epithelial secretion products such as mucins, TFF peptides, surfactant proteins as well as probably others, and physical factors such as capillarity, gravity, respiration, and evaporation.

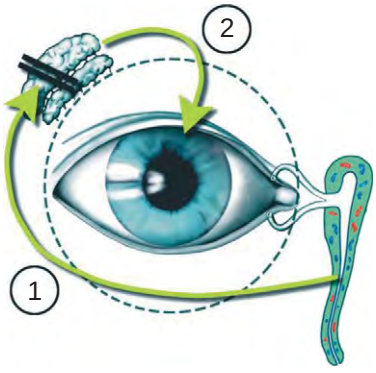

Figure 3 The normally constant absorption of tear fluid components into the blood vessels of the surrounding cavernous body of the nasolacrimal ducts and their transport to the lacrimal gland by blood vessel connections (1) could be a feedback signal for tear fluid production (2). Reproduced from Paulsen, F. P., Schaudig, U., and Thale, A. B. (2003). Drainage of tears: Impact on the ocular surface and lacrimal system. *Ocular Surface* 1: 180–191.

Moreover, components of the tear fluid are absorbed by the epithelium of the nasolacrimal passage and transported into the surrounding vascular system of the lacrimal sac and nasolacrimal duct. This system is comparable to a cavernous body that is subject to autonomic control and also regulates tear outflow from the sac into the inferior meatus of the nose. TALT is present in the efferent tear ducts, displaying the cytomorphological and immunophenotypic features of mucosa-associated tissue MALT.

See also: Adaptive Immune System and the Eye: Mucosal Immunity; Adaptive Immune System and the Eye: T Cell-Mediated Immunity; Conjunctiva Immune Surveillance; Conjunctival Goblet Cells; Defense Mechanisms of Tears and Ocular Surface; Inflammation of the Conjunctiva; Lacrimal Gland Overview; Ocular Mucins; Overview of Electrolyte and Fluid Transport Across the Conjunctiva; Tear Film Overview.

Further Reading

Amrith, S., Goh, P. S., and Wang, S-C. (2007). Lacrimal sac volume measurement during eyelid closure and opening. *Clinical and Experimental Ophthalmology* 35: 135–139.

Ayub, M., Thale, A., Hedderich, J., Tillmann, B., and Paulsen, F. (2003). The cavernous body of the human efferent tear ducts functions in regulation of tear outflow. *Investigative Ophthalmology and Visual Science* 44: 4900–4907.

Barishak, Y. R. (2001). *Embryology of the Eye and Its Adnexa*. Basel: Karger.

Bernal-Sprekelsen, M., Alobid, I., Ballesteros, F., et al. (2007). Dacryocystorhinostomy in children. In: Weber, R. K., Keerl, R., Schaefer, S. D., and Della Rocca, R. C. (eds.) *Atlas of Lacrimal Surgery*, pp. 69–71. Berlin: Springer.

Bräuer, L. and Paulsen, F. P. (2008). Tear film and ocular surface surfactants. *Journal of Epithelial Biology and Pharmacology* 1: 62–67.

Paulsen, F. (2003). The human nasolacrimal ducts. *Advances in Anatomy, Embryology, and Cell Biology* 170: 1–106.

Paulsen, F. (2006). Cell and molecular biology of human lacrimal gland and nasolacrimal duct mucins. *International Review of Cytology* 249: 229–279.

Paulsen, F. (2007). Pathophysiological aspects of PANDO, dacryolithiasis, dry eye, and punctum plugs. In: Weber, R. K., Keerl, R., Schaefer, S. D., and Della Rocca, R. C. (eds.) *Atlas of Lacrimal Surgery*, pp. 15–27. Berlin: Springer.

Paulsen, F. and Berry, M. (2006). Mucins and TFF peptides of the tear film and lacrimal apparatus. *Progress in Histochemistry and Cytochemistry* 41: 1–53.

Paulsen, F., Föge, M., Thale, A., Tillmann, B., and Mentlein, R. (2002). Absorption of lipophilic substances from tear fluid by the epithelium of the nasolacrimal ducts. *Investigative Ophthalmology and Visual Science* 43: 3137–3143.

Paulsen, F. P., Schaudig, U., and Thale, A. B. (2003). Drainage of tears: Impact on the ocular surface and lacrimal system. *Ocular Surface* 1: 180–191.

Paulsen, F., Thale, A., Hallmann, U., Schaudig, U., and Tillmann, B. (2000). The cavernous body of the human efferent tear ducts – function in tear outflow mechanism. *Investigative Ophthalmology and Visual Science* 41: 965–970.

Tear Film

J P Craig, University of Auckland, Auckland, New Zealand
A Tomlinson and L McCann, Glasgow Caledonian University, Glasgow, UK

Glossary

Fluorescein sodium – A topical agent used extensively as a diagnostic tool in ophthalmology to enhance tear film visibility or to highlight epithelial cell loss. The molecule is highly fluorescent, with excitation and emission occurring at 494 and 521 nm, respectively. Interference bandpass filters are commonly combined with the observation systems used in ophthalmology to optimize visualization of the fluorescence alone.
Lacrimal gland – The lacrimal gland is a compound tubuloalveolar gland, similar to the salivary gland, situated superotemporally in the orbit, which secretes aqueous tear fluid.
Lacrimal sac – The lacrimal sac forms part of the tear drainage system, collecting tear fluid from the ocular surface via the puncta and canaliculi. Blinking controls the pumping action of the lacrimal sac into the nasolacrimal duct for drainage into the nasal cavity.
Meibomian gland – Vertically oriented tubulo-acinar glands, embedded in the upper and lower tarsal plates, which release meibum (lipid).
Videokeratoscopy – A computerized, dynamic technique, based on the principle of keratoscopy, used traditionally to assess the shape of the anterior surface of the cornea (corneal topography) from the reflection of a series of projected concentric rings.

The tear film is a thin film of fluid, which covers the exposed ocular surface. Essential for the health and normal function of the eye and visual system, any abnormality in quantity or quality of the tear film can lead to signs and symptoms of dry eye disease and ultimately to a loss of vision.

The Role of the Tear Film

The tear film has a number of important functions, the first of which, as the most anterior element of the visual system, is maintenance of high-quality vision. Alterations in the stability of the tear film due to abnormal tear evaporation, production, and/or drainage can cause optical aberrations and adversely affect retinal image quality.

Secondly, the tear film plays an important role in ocular surface defence. Environmental challenges such as extremes of temperature or humidity, and exposure to irritants such as pollutants and allergens, can have a detrimental effect on the tear film. The tear film must be sufficiently robust to be able to withstand these challenges and be capable of responding rapidly with reflex tearing to help flush out irritants when required. External and adnexal infectious agents pose an additional risk to the exposed ocular surface. Antimicrobial components of the tear film, which include lysozyme, lactoferrin, and immunoglobulin A, help to protect the ocular surface from microbial infection.

Lubrication is another important tear film function. The non-Newtonian rheological properties of the tear film mucins enable the tear film to lubricate the corneal and mucosal surfaces. The normal blinking mechanism draws the tear film across the ocular surface, enhancing comfort and cushioning the ocular surfaces from the shearing forces present during the blink, while the mucins that trap and coat foreign particles in the tear film for removal at the caruncle, confer further epithelial surface protection.

Finally, the tear film plays a vital nutritive role in the transport of substances necessary for corneal metabolism and regeneration. Uniquely avascular for transparency, the cornea requires a nonvascular route for the supply of oxygen, electrolytes, growth factors, and nutrients to, and for the removal of metabolic by-products such as carbon dioxide from the ocular surface. While glucose diffuses primarily from, the aqueous humor, oxygen must be transported to the tissue through the tear film, either from the air in the open eye state or via the palpebral conjunctival vessels in the closed eye state.

Structure and Thickness of the Tear Film

Initial reports described the tear film as trilaminar in structure, consisting of a thin superficial lipid layer, an intermediate aqueous layer, and an underlying mucous layer. Each of these layers has the potential to be affected by different conditions resulting in qualitative and quantitative changes. Almost half a century later, it was proposed that interfaces existed between the layers, giving rise to a six-layer model, with an oily layer, a polar lipid monolayer, an absorbed mucoid layer, an aqueous layer, and a mucoid layer on a glycocalyx base. The carbohydrate-rich

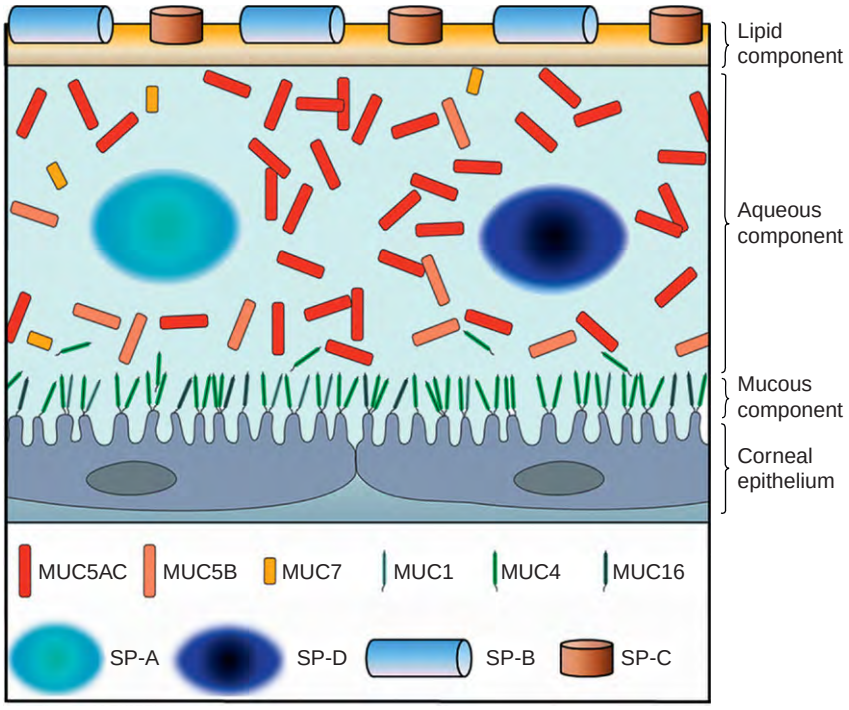

Figure 1 Diagrammatic representation of our current understanding of tear film structure. The tear film comprises a thin superficial lipid layer, and an aqueous-mucin continuum increasing in mucin concentration toward the glycocalyx, adjacent to the ocular surface epithelium. Adapted from Bräuer, L. and Paulsen, F. P. (2008). Tear film and ocular surface surfactants. *Journal of Epithelial Biology and Pharmacology* 1: 62–67, with permission.

glycocalyx, produced by the surface cells of the corneal epithelium and subsurface vesicles of the conjunctival epithelium, is believed to attach the tear film to the surface of the epithelial cells. The most recent studies do not differentiate this number of distinct layers, but instead suggest the existence of an aqueous-mucin continuum that contains a decreasing concentration of dissolved mucus toward the superficial lipid layer, and is anchored to the epithelium by glycocalyx (Figure 1).

The thickness of the precorneal tear film has proven to be a subject of great debate. Early estimates placed the thickness of the tear film in the region of between 4 and 8 μm. Later, on the basis of noninvasive techniques such as interferometry, it was proposed that due to a previously underestimated contribution from the mucous layer, the tear film thickness was closer to 40 μm in thickness. However, the most recent findings using techniques such as tomography and reflectance spectra propose values closer to the original measurements, suggesting that the tear film thickness is approximately 3 μm.

The Lipid Layer

The superficial lipid layer of the tear film forms the initial barrier between the ocular surface and the environment. This thin, oily layer approximates 100 nm in thickness, although values ranging between 10 and 600 nm have been reported. It is derived primarily from the meibomian glands, with additional lipid secreted by the eyelid glands of Moll and Zeiss. The lipids are excreted as meibum onto the ocular surface through the gland orifices located at the mucocutaneous junction of the lid margins.

Between blinks, the lipid layer forms in two distinct phases. An inner, thin, polar layer spreads as a monolayer across the aqueous in the initial phase after the blink, then a thicker, outer, nonpolar layer follows, creating a final lipid structure with multiple layers. The lipid layer must be spread evenly by the blink to form a continuous layer without excessively thin or thick patches in order to inhibit evaporation and to prevent accelerated tear breakup from mucin contamination, respectively.

Table 1 describes the proportions of the major lipid components of meibum. The polar layer consists of phospholipids, free fatty acids, and cerebrosides, while the less surface-active, nonpolar layer comprises mainly wax esters and sterol esters. The lipid layer confers a number of important protective functions including the formation of a hydrophobic barrier to prevent tear overflow onto the lids and to provide a water-tight seal during overnight lid closure, and the prevention of tear film contamination by skin lipids. However, arguably one of the most critical roles of the superficial lipid layer is to retard evaporation from the ocular surface. The polar lipids of the ocular tear film in the normal eye are capable of reducing its rate of evaporation by about 80–90%.

Tear Evaporation

Numerous investigators have measured evaporation of fluid from the tear film, since it was established that the lipid layer retarded evaporation in a rabbit model, in 1961. Later work, also in a rabbit model, passed dry air over a cornea enclosed within a chamber. From the weight of water collected, the evaporative rate was measured as 10.1×10^{-7} g cm^{-2} s^{-1}, and a fourfold increase in evaporation was found to occur with the removal of the rabbit tear film lipid layer. A similar increase in human tear film evaporation has since been confirmed in patients with incomplete or absent lipid layers (**Figure 2**).

The use of different techniques for measurement of tear film evaporation makes comparison of evaporation rates in different studies difficult because the absolute values recorded are technique-dependent. However, a pattern to the observations reported in the literature does exist, making evaporation rate a useful measurement in the differential diagnosis of dry eye. In most cases, significant increases from normal tear film evaporation are seen in patients with aqueous deficient dry eye (ADDE), evaporative dry eye (EDE), and meibomian gland dysfunction (MGD). The evaporation in normal eyes averages $13.57 \pm 6.52 \times 10^{-7}$ g cm^{-2} s^{-1}, while in ADDE the values average $17.91 \pm 10.49 \times 10^{-7}$ g cm^{-2} s^{-1}, and in EDE, $25.34 \pm 13.8 \times 10^{-7}$ g cm^{-2} s^{-1}.

Table 1 Major lipid components of meibum

Component	*Percentage (%)*
Synthesised lipids	
Wax esters	44
Sterol esters	33
Triglycerides	5
Diglycerides	2
Monoglycerides	Trace
Fatty alchohol	Trace
Hydrocarbons	2
Membrane-derived lipids	
Cerebrosides	4
Ceramides	Trace
Phospholipids	8
Degeneration products	
Free fatty acids	2

Adapted from McCulley, J. P. and Shine, W. E. (2003). Meibomian gland function and the tear lipid layer. *Ocular Surface* 1(3): 97–106, with permission.

The Aqueous Layer

The aqueous component of the tear film is a watery phase, bordering the lipid layer and comprising most of the tear film thickness. It is produced principally by the main lacrimal gland and accessory lacrimal glands of Krause and Wolfring although additional water and electrolytes are secreted by the epithelial cells of the ocular surface. The typical or basal level of tear flow present is believed to originate mainly from the accessory glands while the reflex tears, produced in response to mechanical, noxious, or emotional stimuli, arise from the main lacrimal gland.

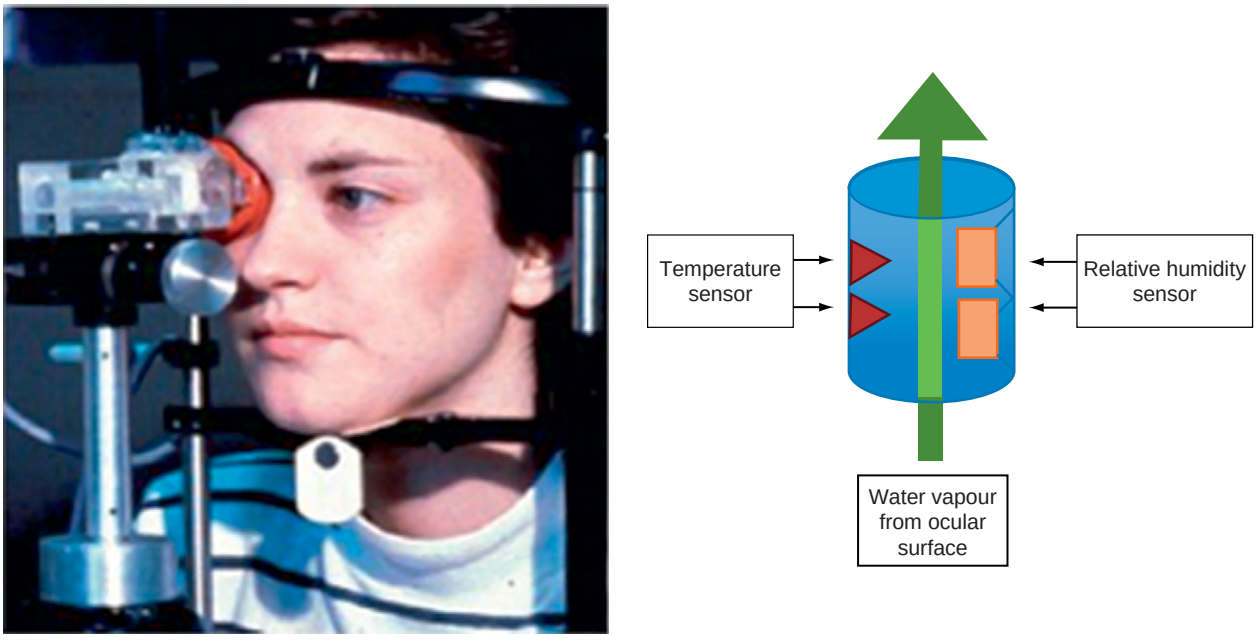

Figure 2 Tear film evaporation rate measured by a modified ServoMed EP-3 Evaporimeter (Kinna, Sweden). This technique involves the measurement of the vapor pressure gradient from recordings of relative humidity and temperature at two points a known distance above the ocular surface. Reprinted from *The Ocular Surface* (www.theocularsurface.com), with permission.

During sleep, tear production is minimal but in the normal eye, in the open eye state, sensory stimulation of the exposed ocular surface induces tear production at a rate that varies according to the demands of the external environment. The secretion of electrolytes, protein, and water onto the ocular surface serves to nourish and protect the epithelia and convey messages between the structures bathed in aqueous.

Corneal innervation is denser than that of any other part of the body, resulting in extreme pain if the corneal epithelium is damaged. Sensory nerve supply to the ocular surface arises from the trigeminal nerve. Stimulation of these nerve endings causes the release of neuropeptides such as substance P and calcitronin gene-related peptide (CGRP), which, through initiation of the inflammatory cascade, is believed to be an important step in the pathogenesis of many cases of dry eye.

The lacrimal and meibomian glands are innervated by parasympathetic efferent nerve fibers (muscarinic and vaso-intestinal peptide (VIP)-ergic fibers) and to some extent they, and the blood vessels supplying them, are sympathetically innervated through tyrosine hydroxylase (TH) and neuropeptide Y fibers. Parasympathetic efferent nerve terminals surrounding the goblet cells suggest that conjunctival secretions are also under neurogenic control.

The aqueous phase has a number of important responsibilities. These include creating a nurturing environment for the epithelial cells of the ocular surface, carrying essential nutrients and oxygen to the cornea, allowing cell movement over the ocular surface, and washing away epithelial debris, toxic elements, and foreign bodies. The major electrolytes present in the tear film are sodium, potassium, bicarbonate, and chloride, with magnesium, calcium, nitrate phosphate, and sulfate present in smaller quantities. The electrolytes dictate the osmolarity of tears, besides acting as a buffer to maintain pH and playing a role in maintaining epithelial integrity. An increase in the electrolyte concentration, described as hyperosmolarity, can cause damage to the ocular surface.

The tear film protein concentration is approximately 10% that of plasma. The proportion of lacrimal gland versus serum-derived proteins and enzymes varies with tear flow rate, epithelial surface stimulation, blinking, and ocular surface disease. The tear proteins are involved in defense of the ocular surface and the maintenance of tear film stability. Electrophoresis has confirmed the presence of approximately 80 different components of human tear proteins. Around 30 proteins have been identified, half of which are enzymes. The principal tear proteins are lysozyme, lactoferrin, albumin, tear-specific pre-albumin, and globulins. **Table 2** shows typical concentrations of the most significant tear proteins. The tear film also contains antioxidants such as vitamin C and tyrosine, which scavenge free radicals from within the tear film, while the abundance of growth factors facilitates constant epithelial regeneration and promotes wound healing.

Table 2 Average concentration of the principal tear proteins

Protein component	*Average concentration* ($mg\,ml^{-1}$)
Total protein	7.51
Lysozyme	2.36
Albumin	1.30
Tear specific prealbumin	1.23
Lactoferrin	1.84
Immunoglobulins (IgA, IgG, IgM, and IgE)	0.43

Adapted from Sariri R. and Ghafoori, H. (2008). Tear proteins in health, disease, and contact lens wear. *Biochemistry (Moscow)* 73(4): 381–392, with permission.

Alterations in tear composition or inflammatory changes within the conjunctival vascular endothelia can act as the stimulus to ocular surface inflammation in which both cellular and soluble mediators play a significant role. The numbers of T lymphocytes and the relative proportions of activated T cells are increased in dry eye. The ocular surface epithelial cells are directly involved in such ocular surface inflammation with the release of a number of pro-inflammatory cytokines such as interleukin (IL)-1α, IL-1β, IL6, IL8, transforming growth factor beta 1 (TGF-β1) and tumor necrosis factor alpha (TNFα), and increased expression of immune activation molecules such as CD54 and HLA-DR. Increased proteolytic enzyme levels and activity have been observed in dry eye with, in particular, high levels of matrix metalloproteinase 9 (MMP9), which are not present on the normal ocular surface. The inflammatory markers described as precipitating dry eye are also recognized to perpetuate ocular surface inflammation, triggering an escalating cycle of ocular irritation, inflammation, apoptosis, and tear film dysfunction and instability, epithelial cell disease, and disruption of corneal epithelial barrier function.

Tear Production

Traditional methods of measuring tear production rates are based on absorption of tears by Schirmer strips or cotton threads; however, both tests have been found to be poor quantifiers of tear production; the Schirmer test is marred by low specificity and sensitivity and the exact parameter measured with the cotton thread test has been questioned. As a result, a number of tests have been devised to measure the rate of disappearance of a dye marker placed in the tear film, as new tears are produced and the waste eliminated. In most studies in recent years, the rate of disappearance of instilled sodium fluorescein dye has been used to determine tear turnover (TTR) by the technique of fluorophotometry (**Figure 3**).

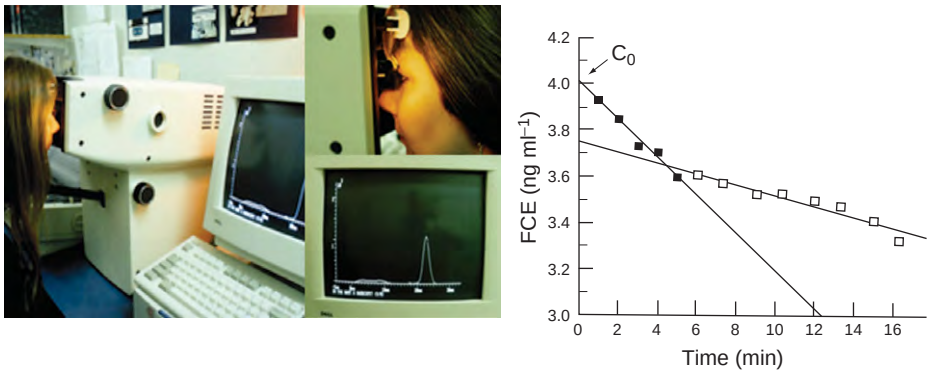

Figure 3 Commercial fluorophotometer (Fluorotron Master, Coherent Radiation Inc, CA, USA) shown with a typical trace of ocular surface fluorescence decay following instillation of fluorescein sodium into the eye. A biphasic curve of fluorescence is observed with initial rapid decay (due to reflex tearing) followed by a more gradual decay (due to basal tear turnover). Adapted from *The Ocular Surface* (www.theocularsurface.com), with permission.

The values reported for tear turnover (%min^{-1}) and tear flow (μl min^{-1}) in the major studies in the literature for normal and dry eye subjects of studies using the commercial fluorophotometer have recently been collated. The data reported for normals in the majority of studies ranges from 10% to 20% min^{-1}, which equates to an average basal tear flow rate of 1.03 ± 0.39 μl min^{-1} (16.19 ± 5.10% min^{-1}). For dry eye, in all its forms, it averages 0.58 ± 0.28 μl min^{-1} (9.36 ± 5.68% min^{-1}) and, within the dry eye subtypes, averages 0.40 ± 0.10 μl min^{-1} (7.71 ± 1.02% min^{-1}) and 0.71 ± 0.25 μl min^{-1} (11.95 ± 4.25% min^{-1}) for ADDE and for EDE, respectively. These are the rates of tear production under nonstimulated conditions in normal and dry eyes. However, the eye is capable of producing copious reflex tears under provocative conditions, providing the lacrimal gland has the ability to function at the required capacity. Reflex rates have been quoted as approximately 100-fold those under basal conditions.

The Mucin Layer

The innermost, mucin layer of the tear film lies adjacent to the hydrophobic epithelial cells of the ocular surface. The layer consists of soluble, gel-forming mucins, which are capable of retaining large quantities of water, and corneal and conjunctival epithelial mucins (principally MUC1, 2, 4, and 16), which form the glycocalyx. The glycocalyx functions, through the membrane-spanning domain of MUC1, to anchor the soluble mucin layer to the plasma membrane of the corneal and conjunctival epithelial cells, while the soluble mucins interact with these transmembrane mucins and with the overlying aqueous layer, to form a water-retaining gel. The most significant soluble mucin for the ocular surface is MUC5AC, secreted by the goblet cells of the conjunctiva.

The high-molecular-weight glycoproteins, with additional proteins, electrolytes, and cellular material that contribute to the mucous layer, enable fulfilment of several important functions in the maintenance of a healthy ocular surface. In addition to providing a hydrophilic surface upon which to support a stable aqueous layer, the mucous layer offers protection against the shear force of blinking and environmental insult, and facilitates maintenance of a smooth ocular surface for optical clarity. The constituents are also believed to protect the ocular surface by inhibiting inflammatory cell adhesion.

Tear Distribution and Stability

The distribution of tear fluid on the ocular surface is highly dependent on the blink. Lid closure during a blink progresses from the temporal to the nasal side of the eye spreading tears across the ocular surface and facilitating tear drainage through the lacrimal puncta. The inter-blink period in normal individuals averages 4.0 ± 2.0 s and is significantly decreased in patients with dry eye (to 1.5 ± 0.9 s); a high blink rate in dry eye patients maximizes the tear supply to the ocular surface. In detailed reading tasks, requiring concentration, the blink rate drops to about a half (from 22.4 ± 8.9 to 10.5 ± 6.5 min^{-1}).

In the clinical setting, tear film stability has traditionally been measured following the instillation of fluorescein sodium solution into the tear film, to improve visualization of the film. Tear breakup time has been defined as the time taken for the tear film to form a dark spot or streak, following a blink. However, subsequent awareness of the disruptive effect of fluorescein instillation on the tear film has encouraged use of noninvasive techniques where tear film stability is determined by observing mires reflected from the tear film surface, for signs of disruption or distortion following a blink. A tear breakup time of greater than 10 s is considered normal while values less than 5 s are suggestive of dry eye. Values between 5 and 10 s are

generally considered to correspond to borderline dry eye, although it should be noted that this reported range was originally established for Caucasian eyes, and Asian eyes may exhibit significantly shorter tear film stabilities. In noninvasive techniques, without instillation of fluorescein, the reported cut-off values are longer with mean values around double those of the traditional fluorescein breakup test.

The distribution of the tear film can further be observed *in vivo* using thin film interferometry. Interference fringes are produced by light reflected at the air-lipid and at the lipid-aqueous boundaries of the tear film due to the changes in refractive index. Specular reflection from the lipid layer precludes a clear view of the aqueous layer of the precorneal tear film although where the lipid layer is very thin or absent, aqueous fringes may be observed.

Based on this optical principle, a number of clinical instruments, together with qualitative grading systems have been developed. These are useful for observing the structure of the tear film and offer some insight into its stability. Significant differences in appearance (and grade) have been observed in dry eye conditions, with the partial or complete absence of the lipid layer being a feature. Recent work in this field has concentrated on developing quantitative analyses of interferometric images from the tear film of normal and dry eye patients (**Figures 4** and **5**, respectively). With the use of kinetic analysis of sequential interference images, it has been possible to quantify the lipid-spread time of tears in normal and dry eye patients. This spread time, defined as the time taken for the lipid film to reach a stable interference image, is significantly slower in ADDE, at 2.17 $\pm$ 1.09 s, than it is in normal eyes (0.36 $\pm$ 0.22 s). Because of this slower spread time, the resultant lipid film has been found to be thicker on the inferior cornea than the superior cornea, with the thickness being measured from a color reference chart created from the reflectance images of thin film interference generated by a white light source. Almost 90% of the patients with aqueous tear deficiency exhibit an interferometric pattern with vertical streaking, rather than the horizontal propagation typically observed in the superior corneal region.

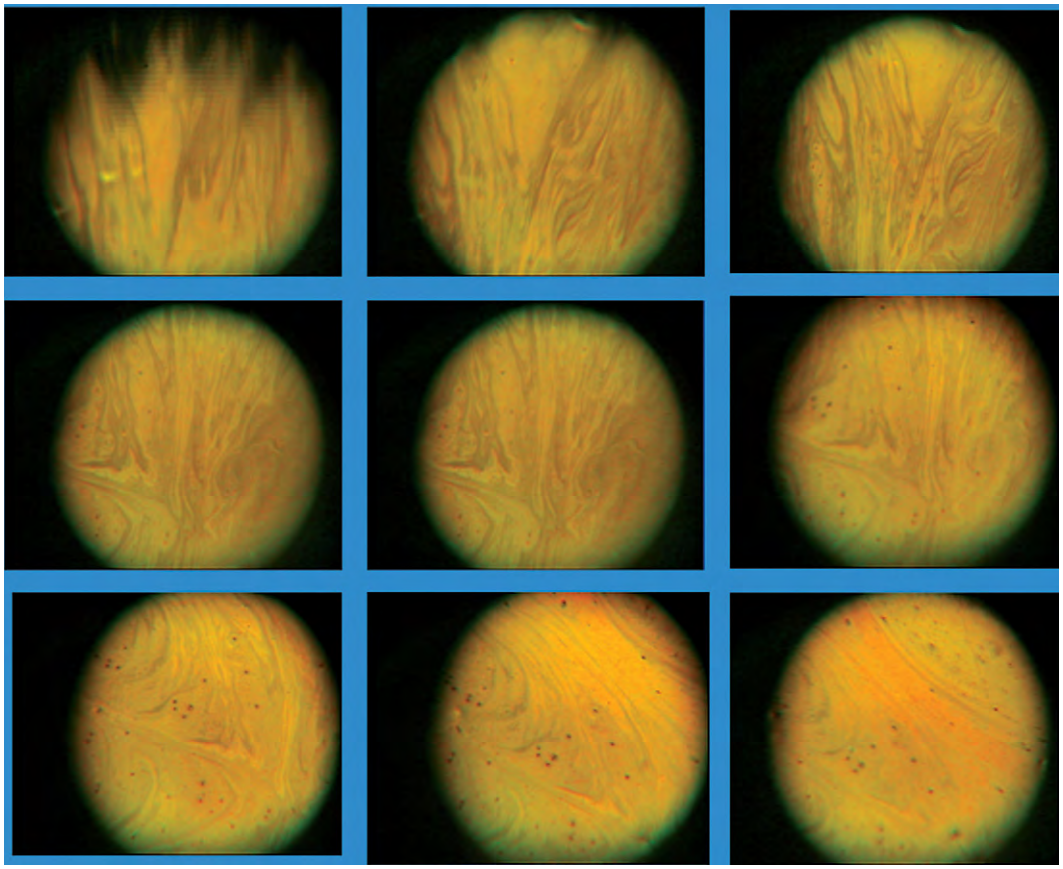

Figure 4 Series of images obtained by dynamic thin film interferometry in a normal, asymptomatic subject. The images are obtained at 1 s intervals, following a blink. The lipid layer of the normal tear film reaches a relatively stable pattern within the first second after the blink. This pattern is then stable for about 6 s. Reprinted from *The Ocular Surface* (www.theocularsurface.com), with permission.

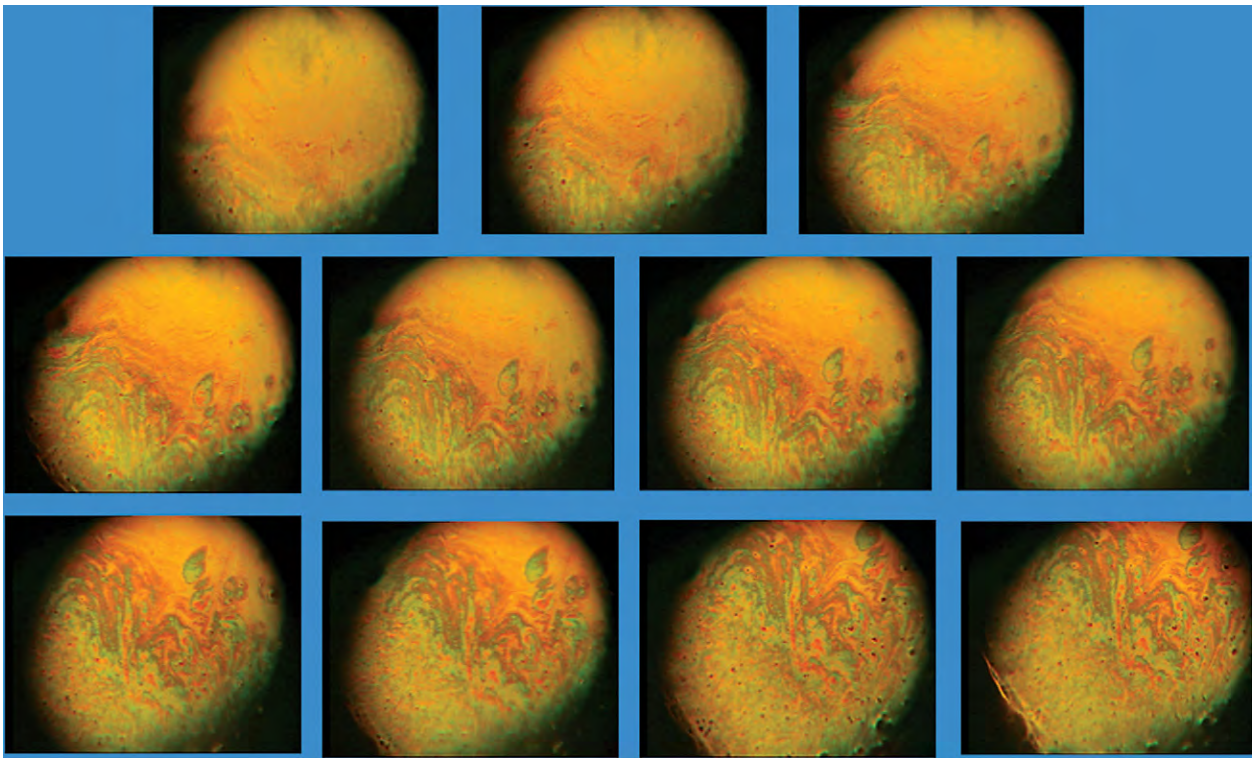

Figure 5 Series of thin film interferometry images obtained from a patient with severe dry eye. The patient had primary Sjögren's syndrome with a tear turnover rate of 4% min^{-1}, evaporation of 25.5 g cm^{-2} s^{-1}, volume of 3.9 μl and osmolarity of 337.6 mOsm ml^{-1}. The images are obtained at 1 s intervals following a blink. The lipid layer of the tear film is incomplete and variable in thickness, exhibiting color fringe patterns. A stable pattern is reached in 2–3 s after the blink, but this pattern begins to be disrupted within the next 3 s. Reprinted from *The Ocular Surface* (www.theocularsurface.com), with permission.

Evaluation of tear film particle movement can also provide an indication of the time necessary to obtain stability of the tear film after the blink. The observed particles are thought to be accumulations of newly secreted lipid from the meibomian glands. Measuring the displacement of these tear film particles immediately after a blink has shown that the time necessary to reach zero velocity (tear stabilization time) is 1.05 ± 0.3 s.

A commercial thin film interferometer has been developed, which enables the specular reflection from the tear surface to be monitored digitally and the tear film interference patterns classified. Research with this apparatus has shown that thicker lipid layers are associated with greater tear film stability. A number of grading systems have been developed mostly assessing the uniformity of the interference fringe pattern. A change in color and loss of uniformity in distribution indicates tear film instability. Such patterns are found more commonly in dry eyes in association with thin lipid layers and reduced stability.

Assessment of the reflected images from the cornea and tear film has been used to evaluate tear film quality and stabilization following the blink. High-speed videokeratoscopy assesses the regularity indices, such as surface regularity index (SRI) and surface asymmetry index (SAI), in the time interval following a blink. These indices have been found to correlate significantly with the results of standard diagnostic tests for dry eye, such as symptoms, tear breakup time, Schirmer test, fluorescein staining score, and best corrected visual acuity.

Tear Film Osmolarity

Adequate production, retention, distribution, and balanced elimination of tears are necessary for ocular surface health and normal function. Any imbalance of these components can lead to the condition of dry eye. A single biophysical measurement that captures the balance of inputs and outputs from the tear film dynamics is tear osmolarity, the end-product of variations in tear dynamics. Normal homeostasis requires regulated tear flow, the primary driver of which is osmolarity. Hyperosmolarity is thus an important biomarker for dry eye disease.

Tear hyperosmolarity has been found to be the primary cause of discomfort, ocular surface damage, and inflammation in dry eye. In studies of rabbit eyes, tear osmolarity has been found to be a function of tear flow rate and evaporation. In rabbit conjunctival cell cultures, hyperosmolarity has been demonstrated to decrease the density of goblet cells and, in humans, a 17% decrease in

goblet cells density for subjects with dry eye has been reported. Granulocyte survival is significantly decreased with increases in solute concentration. Rabbit cells cultured in hyperosmolar states, above 330 mOs ml^{-1}, show significant morphological changes, similar to those seen in subjects with dry eye. Hyperosmolarity-induced changes in surface cells in dry eye can be correlated with the degree and distribution of rose bengal staining.

Measuring tear osmolarity is of benefit in the diagnosis of conditions such as dry eye. In a meta-analysis of human tear osmolarity values recorded in studies between 1978 and 2004 with freezing point depression (FPD) and vapor pressure (VP) osmolarity tests, normal values averaged 302.0 $\pm$ 9.7 compared with 326.9 $\pm$ 22.1 mOs ml^{-1} for patients with dry eye disease.

Drainage of Tears

A principal means of elimination of tears from the eye is by drainage through the puncta of the eye. Tears then pass through the canaliculi, the lacrimal sac, and finally the nasolacrimal duct before reaching the nose. A technique for measuring tear turnover, which allows direct observation of tear drainage, involves instilling a radioactive dye into the tear film. In the technique of lacrimal scintigraphy a small quantity (0.013 mls) radioactive tracer such as technetium 99 (99M Tc), is introduced into the lower marginal tear strip. The distribution of the tracer is imaged serially by a gamma camera as it passes down the lacrimal drainage system (**Figure 6 a–c**). Images are typically taken at 10-s intervals for 1 min and then at less frequent intervals until all of the tracer has drained into the nasal cavity. The technique has been used to quantify tear turnover from the eye and drainage through the lacrimal system. The drainage through this system is not linear, as a significant number of naso-lacrimal folds and ducts offer physiological obstruction to normal tear flow, and variable tear flow has been shown to be a typical feature of the drainage facility in asymptomatic individuals (**Figure 6(d)** and **(e)**). Therefore, most models of lacrimal drainage favor compartmental analysis to evaluate tear flow through the system, with separate components for the conjunctival sac, lacrimal sac, the nasolacrimal duct, and the nasal cavity. Although most quantitative lacrimal scintigraphy measurements describe the transit time of the radioactive tracer through the system, the compartmental model has be used to estimate tear flow rates. Depending on the number of compartments considered, basal flow rates have been estimated to fall between 0.45 and 8 µl min^{-1}. Using a single compartment model for decay of the radioactive tracer on the conjunctival surface, mean values of reflex and basal turnover of 3.33 $\pm$ 1.95 µl min^{-1} and 0.56 $\pm$ 0.32 µl min^{-1}, respectively, have been recorded by gamma scintigraphy.

The mechanism of lacrimal drainage and the influence of blinking on the mechanics of the system have been observed by high-speed photography and by intracanalicular pressure measurements. Taking an anatomical approach and observing the lacrimal systems of human cadavers has shown that the surrounding vascular plexus of the lacrimal sac and the nasolacrimal duct is comparable to a cavernous body. While regulating the blood flow, the specialized blood vessels of this body permit opening and closing of the lumen of the lacrimal passage, which is effected by the bulging and subsiding of the cavernous body, thereby regulating tear outflow from the eye. Attempts have been made to quantify the regulation of tear outflow by measurement of the transit time of a fluorescein drop from the conjunctival sac into the inferior meatus

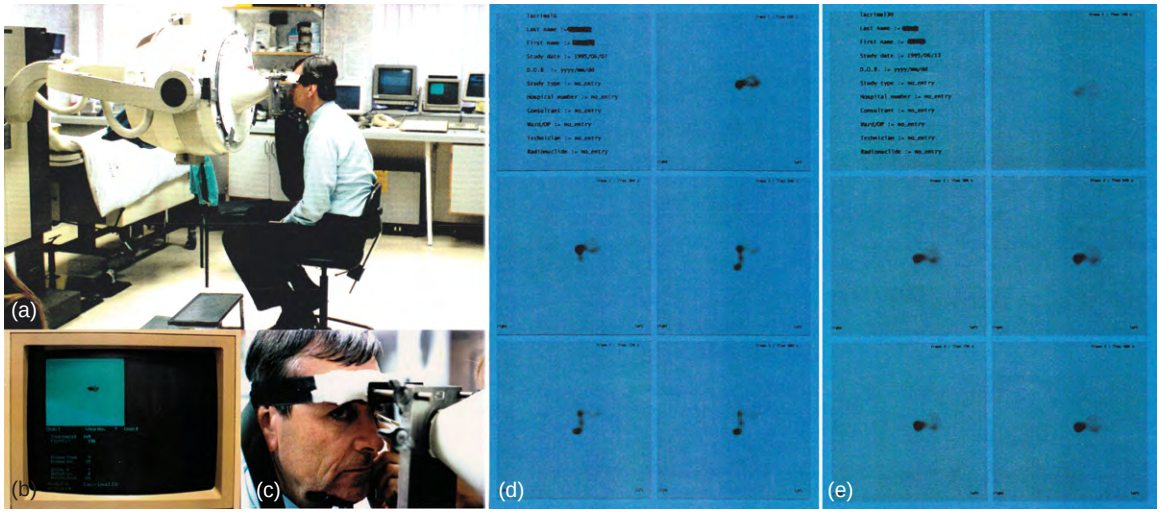

Figure 6 Gamma camera (a–c) used in the recording of intensity of a radioactive dye at various stages as it passes through the lacrimal system (d). In many cases of normal systems, the tracer does not proceed beyond the lacrimal sac (e). Reprinted from *The Ocular Surface* (www.theocularsurface.com), with permission.

of the nose. Application of a decongestant drug or placement of a foreign body on the ocular surface have both been found to significantly prolong the dye transit time, indicated restricted drainage through the lacrimal system in these conditions. It has therefore been concluded that the cavernous body of the lacrimal sac and naso-lacrimal duct plays an important role in the physiology of tear outflow regulation; it is subject to autonomic control and is integrated into a complex neural reflex feedback mechanism between the blood vessels, the cavernous body, and the ocular surface.

Absorption of Tears by the Ocular Surface

Another method by which tears can be eliminated from the eye is by absorption into the tissues of the ocular surface and the drainage system. The possibility has been suggested that the epithelial lining of the drainage system absorbs tear fluid before it reaches the nose. It has been shown in an animal model that lipophilic substances are absorbed from the tear fluid by the epithelium of the naso-lacrimal duct and that the cavernous body surrounding this duct may play a role in drainage of absorbed fluid. No quantification of fluid volume eliminated by this route has been reported. However, tears absorbed in the blood vessels of the cavernous body may, because these vessels connect to the blood vessels of the outer eye, have a role in a biofeedback mechanism for tear production.

Observations of the absorption of tear film onto the anterior ocular surface have been made in studies of corneal permeability. The proportion absorbed, in the absence of compromised corneal function, appears to be small at $0.24 \pm 0.13\%$ of the dye instilled in the eye.

The lacrimal system of the human eye is, in the vast majority of individuals, a robust system, which allows the ocular surface to maintain its health and normal function throughout life, and under modest provocation. It is only in a relatively small proportion ($\sim$15%) that the imbalance between evaporative loss and tear production results in dry eye. Recent research has confirmed that an increase in this ratio of approximately 2–3 times, as most often occurs in older individuals, appears to lead the condition of dry eye.

The tears covering the anterior ocular surface, form a dynamic structure with a complex nature and a number of important functions. The tear film components are interdependent and have a close relationship with those of the adjacent ocular tissues such that failure of any one of aspect of the tear film or lacrimal system can cause imbalance and result in dry eye.

See also: Blinking Mechanisms; Conjunctival Goblet Cells; Contact Lenses; Defense Mechanisms of Tears and Ocular Surface; Dry Eye: An Immune-Based Inflammation; Eyelid Anatomy and the Pathophysiology of Blinking; Inflammation of the Conjunctiva; Lacrimal Gland Overview; Lids: Anatomy, Pathophysiology, Mucocutaneous Junction; Meibomian Glands and Lipid Layer; Tear Drainage; Tear Film Overview.

Further Reading

Bron, A. J., Yokoi, N., Gaffney, E., and Tiffany, J. M. (2009). Predicted phenotypes of dry eye: Proposed consequences of its natural history. *Ocular Surface* 7(2): 78–92.

Craig, J. P. (2002). Structure and function of the preocular tear film. In: Korb, D. R. (ed.) *The Tear Film: Structure, Function and Clinical Examination*, pp. 18–50. London: Elsevier Health Sciences.

Dartt, D. A. (2004). Dysfunctional neural regulation of lacrimal gland secretion and its role in the pathogenesis of dry eye syndromes. *Ocular Surface* 2(2): 76–91.

Doane, M. G. (1994). Abnormalities of the structure of the superficial lipid layer on the *in vivo* dry-eye tear film. *Advances in Experimental Medicine and Biology* 350: 489–493.

Gilbard, J. P. (1985). Tear film osmolarity and keratoconjunctivitis sicca. *Contact Lens Association of Ophthalmologists Journal* 11(3): 243–250.

Gipson, I. K., Hori, Y., and Argüeso, P. (2004). Character of ocular surface mucins and their alteration in dry eye disease. *Ocular Surface* 2(2): 131–148.

King-Smith, P. E., Fink, B. A., Fogt, N., et al. (2000). The thickness of the human precorneal tear film: Evidence from reflection spectra. *Investigative Ophthalmology and Visual Science* 41(11): 3348–3359.

Mathers, W. D. and Choi, D. (2004). Cluster analysis of patients with ocular surface disease, blepharitis, and dry eye. *Archives of Ophthalmology* 122(11): 1700–1704.

McCulley, J. P. and Shine, W. E. (2003). Meibomian gland function and the tear lipid layer. *Ocular Surface* 1(3): 97–106.

Sariri, R. and Ghafoori, H. (2008). Tear proteins in health, disease, and contact lens wear. *Biochemistry (Moscow)* 73(4): 381–392.

Stern, M. E., Beuerman, R. W., and Pflugfelder, S. (2004). *Dry Eye and Ocular Surface Disorders; the Normal Tear Film and Ocular Surface*. New York: Marcel Dekker.

Tiffany, J. M. (2008). The normal tear film. *Developments in Ophthalmology* 41: 1–20.

Tomlinson, A. and Khanal, S. (2005). Assessment of tear film dynamics: Quantification approach. *Ocular Surface* 3(2): 81–95.

van Best, J. A., Benitez del Castillo, J. M., and Coulangeon, L. M. (1995). Measurement of basal tear turnover using a standardized protocol. European concerted action on ocular fluorometry. *Graefes Archive for Clinical and Experimental Ophthalmology* 233(1): 1–7.

Tear Film Overview

M Uchino and K Tsubota, Keio University School of Medicine, Tokyo, Japan

Glossary

Aqueous layer of the tear film – The middle watery phase of the tear film, approximately 6.5–7.5-μm thick.
Functional visual acuity – Sharpness of vision.
Higher order aberration (HOAs) – A distortion acquired by a wave front of light when it passes through an eye with irregularities of its refractive components.
Tear film – Fluid covering the ocular surface. The tear film is composed of mucin/aqueous gel next to the ocular surface that decreases in density toward the lipid layer, the outermost layer.
Tear-film break-up time (TFBUT) – A test to determine tear-film stability. In this test, the time taken for the first black spot to appear in the fluorescently labeled tear film is measured.
Tear lipids – Lipids secreted by the meibomian glands which comprise the outermost layer of the tear film.
Tear mucins – Proteins of a high molecular weight due to the presence of a large number of carbohydrate moieties covalently attached to the protein core. Mucins in the tear film provide lubrication to the ocular surface, allowing the eyelid margins and palpebral conjunctiva to slide smoothly.
Tear proteins – Proteins present in the tear film, mainly in the aqueous layer. Over 60 different proteins have been identified in human tears.
Tear-stability analysis – A test that measures the tear stability of the tear film as a function of serial surface regularity and asymmetry.
Visual maintenance ratio (VMR) – The percentage of time that a patient is able to maintain the best visual acuity over the entire time of the test.

The Structure and Function of the Tear Film

The tear film has been traditionally suggested to have a unique three-layer structure that enables it to perform many functions. These layers include an outer lipid layer, a middle aqueous layer, and an inner mucous layer. There is also a mucin-containing glycocalyx interface that extends from the apical membranes of the corneal and conjunctival epithelia which acts as an integral part of the tear film. However, several types of measurements question the existence of a free-fluid layer beneath the lipid layer. The currently proposed tear-film structure is that of a mucin/aqueous gel decreasing in density toward the lipid layer (**Figure 1**).

The major functions of the tear film are:

1. to maintain a smooth surface for light refraction as the tears form the first refractive surface encountered by light on its path to the retina. For clear vision, it is critical to maintain the transparency of the second refractive surface that rays of light encounter, that is, the cornea.
2. to lubricate of the eyelids, conjunctiva, and the cornea by providing a smooth surface, thus avoiding ocular surface mechanical damage from the surprisingly high pressures generated by each blink.
3. to supply the cornea with nutrients by transporting oxygen and a limited number of other nutrients to the avascular cornea, and regulation of the electrolyte composition and pH.
4. to provide white blood cells with access to the cornea and conjunctiva.
5. to remove foreign materials from the cornea and conjunctiva. The tear film protects the ocular surface from the external environment by responding dynamically to a wide range of external conditions and potentially damaging situations. These external stresses include desiccation, bright light, cold, mechanical stimulation, physical injury, noxious chemicals, and bacterial, viral, and parasitic infections.
6. to defend the ocular surface from the pathogens via specific and nonspecific antibacterial substances.
7. to protect the ocular surface from free-radical insults with antioxidants such as ascorbic acid, lactoferrin, uric acid, and cysteine. An increase in oxidative stress markers and changes in antioxidant-related gene expression can chronically distort the regenerative capacity of the corneal epithelial cells in dry eye conditions. This suggests a strong relationship between the accumulations of oxidative stress and the etiology of corneal epithelia alterations in the blink-suppressed dry eye.

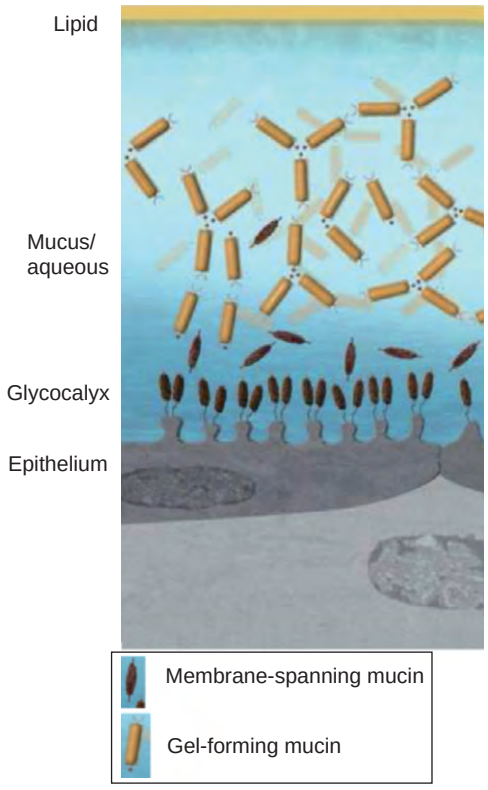

Figure 1 The structure of tear film.

The Function and Structure of the Lipid Layer of Tear Film

Lipids secreted from the meibomian glands are an essential component of the tear film, providing a smooth optical surface for the cornea and retarding evaporation from the eye. The meibomian lipids stabilize the tear film by lowering its free energy, carrying water into the tear film during its formation and interacting with lipid-binding proteins.

Meibomian glands secrete a complex fluid containing hydrocarbons, wax esters, triglycerides, diesters, free sterols, sterol esters, free fatty acids, and polar lipids. The polar lipids interact with the aqueous phase of the tear film and spread in advance of the nonpolar lipids.

The complexity of meibomian gland fluid reflects the products from the disintegrating cells as well as from the synthesized lipids. Meibomian gland lipids differ from cellular lipids in the acyl-chain and sterol types. The major classes of lipids are the wax monoesters and sterol esters that make up about 77% of the meibomian gland fluid. Other synthesized lipids are di- and triglycerides. A third type of lipid is the diesters that form ester linkages with fatty acids, fatty alcohols, or sterols. These diester compounds make up about 8% of the fluid. A new model of the structure of the lipid layer is described elsewhere in this encyclopedia.

The Relationship Between Tear-Film Lipids and Refraction

A stable tear film over the corneal surface is essential for achieving an optically smooth surface. The unstable and irregular tear film is disrupted over the irregular ocular surface in dry eye and is associated with poor quality of vision. Even a small change in tear-film stability and volume will significantly change the quality of vision (primarily contrast sensitivity). Functional visual acuity (FVA) measurements have shown impaired FVA in patients with dry eye during gazing. Moreover, investigators in several studies who measured continuous corneal topographic data or corneal and ocular wave front aberrations in the normal and dry eyes have reported that the dynamic changes in tear film affect the optical quality after blinking, with decreased optical quality in eyes of patients with dry eye. Recent studies have shown that corneal higher order aberrations (HOAs; a distortion acquired by a wave front of light when it passes through an eye with irregularities of its refractive components) after blinking tend to increase with dry eye, and both ocular and corneal HOAs are significantly greater than those in normal eyes.

The Structure and Function of Aqueous Layer of the Tear Film

The major, intermediate watery phase of the tear film is approximately 6.5–7.5-μm thick and contains dissolved ions and proteins. The aqueous phase originates from the main lacrimal gland and the accessory glands of Wolfring and Krause.

The electrolytes present in the tear film are responsible for the osmolality of the tears. These essential ions play an important role in maintaining epithelial integrity. Proteins present in the tears also serve many functions. These include a generalized wetting action by lowering the surface tension, and allowing the tear film to spread over and wet the corneal and conjunctival surfaces more effectively. Other important functions include metal transport, control of infectious agents, osmotic regulation, and buffering against pH changes that would affect ionic equilibrium and enzymatic activity.

More than 60 different protein components of the human tear have been identified. The major tear proteins from the lacrimal gland are lysozyme, lactoferrin, tear lipocalin, lacritin, secretory immunoglobulin A (IgA), and serum proteins such as albumin, transferrin, IgG, and IgM.

The relative proportions of the proteins present in an individual tear sample depend on the method of tear collection. Invasive methods, including filter paper

and cellulose sponges, stimulate the conjunctiva, induce serum leakage, and result in a higher proportion of plasma proteins. Samples collected by less invasive means, such as fine capillary tubes dipped into the tear meniscus, demonstrate a higher proportion of lacrimal gland proteins. Around 20–40% of total tear protein is made up of lysozyme, the most alkaline protein in tears. It has the ability to dissolve bacterial walls by enzymatic digestion of tissue mucopolysaccharides. Patients with Sjögren's syndrome have been reported to have decreased lysozyme production. Tear lipocalin is an acidic protein abundant in tears. The lipocalins, complexed with other tear components, may also contribute to the high, non-Newtonian viscosity of the tear film and its low surface tension – features which are essential for tear-film stability. IgA is the most abundant immunoglobulin of the tears and is normally attached to an antigenic fragment, secretory component. This has been proposed as the first line of the host defense mechanism by furnishing the conjunctiva with an immunologic coating.

The Structure and Function of Mucous Layer of the Tear Film

Ocular mucins provide lubrication to the ocular surface, allowing the eyelid margins and the palpebral conjunctiva to slide smoothly over one another with minimal friction during blinking and ocular rotational movements. Another important function is protection of the epithelial surfaces by covering foreign bodies with a slippery coating, thus protecting the cornea and conjunctiva.

The last 10 years have seen remarkable progress in understanding the structure and character of mucins which are heavily glycosylated glycoproteins with 50–80% of their mass comprised of carbohydrates. Molecular cloning and sequencing of genes encoding mucin apoproteins have extended the definition of glycoproteins from, "mucins are large molecules that have as their major mass carbohydrate" to include the fact that they have tandem repeats of amino acids rich in serine and threonine in their protein backbone that serve as sites for *O*-glycosylation.

Mucins have been given number designation in order of their molecular characterization. To date, although 20 numbers have been assigned, cloning has shown that several mucins are in fact the result of different gene products. For example, MUC3 and MUC5 have now been redesignated to include MUC3A, MUC3B and MUC5AC, and MUC5B.

Mucins can be either secreted or associated with the cell surface. The membrane-associated mucins form the scaffold for the mucous layer. The secreted mucins can either be small soluble mucins or large gel-forming mucins. They are stored in secretory granules in the condensed form and secreted with the appropriate stimulus. Soluble mucins are smaller in molecular weight than the gel-forming mucins, but are stored and secreted similarly to them.

Multiple mucins have been identified in tears and localized to corneal or conjunctival epithelial cells. The gel-forming mucin MUC5AC is secreted solely by the goblet cells. The membrane-bound mucins MUC1, MUC4, and MUC16 are produced in the stratified squamous cells of both the cornea and conjunctiva. In addition, the cornea and conjunctival epithelia also produce MUC2 and MUC7, and other membrane-bound mucins.

Methods to Evaluate the Ocular Surface Health and Tear Functions

Several methods have been developed to assess the health of the ocular surface epithelial cells. These include the use of vital stains and impression cytology.

Fluorescein Staining

Fluorescein staining indicates increased epithelial permeability of the cornea or conjunctiva by staining devitalized areas of the ocular surface. A minimal amount of dry fluorescein (1 μl of 1% fluorescein) is applied with a sterile disposable applicator using a micropipette, or by using a fluorescein-impregnated strip. The strip is wet with a drop of sterile preservative-free solution, the excess is shaken off, and the strip is touched to the lower fornix. The ocular surface is visualized using a yellow barrier-filter with the cobalt blue light of the slit lamp.

Rose Bengal/Lissamine Green Staining

Rose Bengal stains dead or degenerating conjunctival cells, corneal epithelial filaments, or areas not covered by mucins with a dark pink color. It is toxic to the epithelium and causes irritation on instillation even in small amounts. One microliter of 1% Rose Bengal is applied with a sterile disposable applicator. Lissamine green is similar to Rose Bengal in that it is seen best over the sclera and least over the dark iris, but it is less toxic and is better tolerated.

Impression Cytology

Impression cytology is a simple diagnostic method where a cellulose filter paper is placed onto the ocular surface epithelium following anesthesia and then removed. The superficial layer can be easily removed from the deeper epithelium layers by impression cytology, which allows

visualization of epithelial cells and quantization of goblet cells by staining the cells with stains such as alcian blue/Periodic Acid Schiff's reagent or by immunofluorescent techniques. This technique can also identify pathological alterations that develop in ocular surface disease and define the state of keratinization of the superficial epithelial layers. A nonkeratinized state of the ocular surface is crucial to its health.

Assessment of Tear Film Stability and Quantity

Assessment of the stability and quantity of the tear film are important parameters to diagnose dry eye. Tear-film stability is measured by determining the tear-film break-up time, while Schirmer's test measures the quantity of tears.

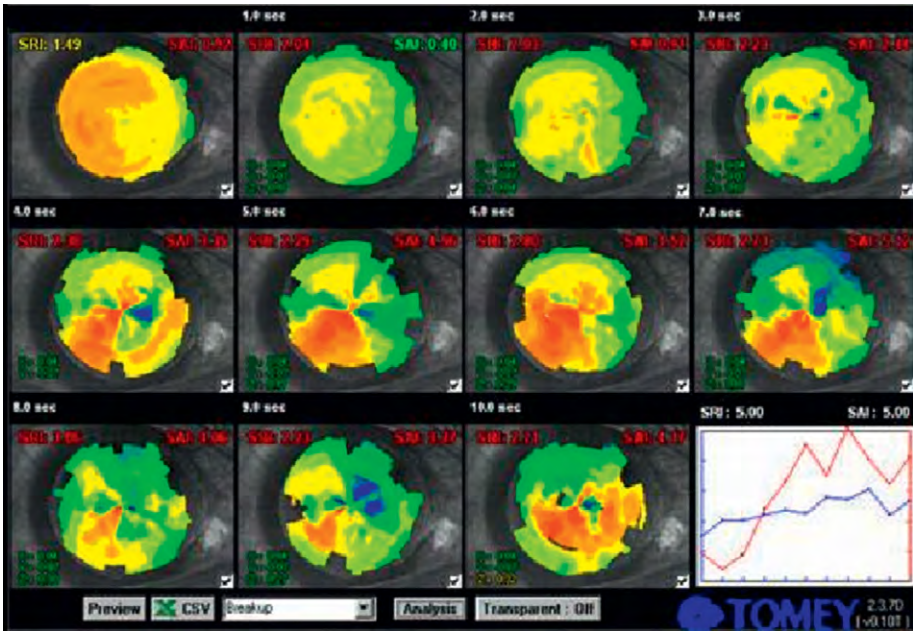

(a)

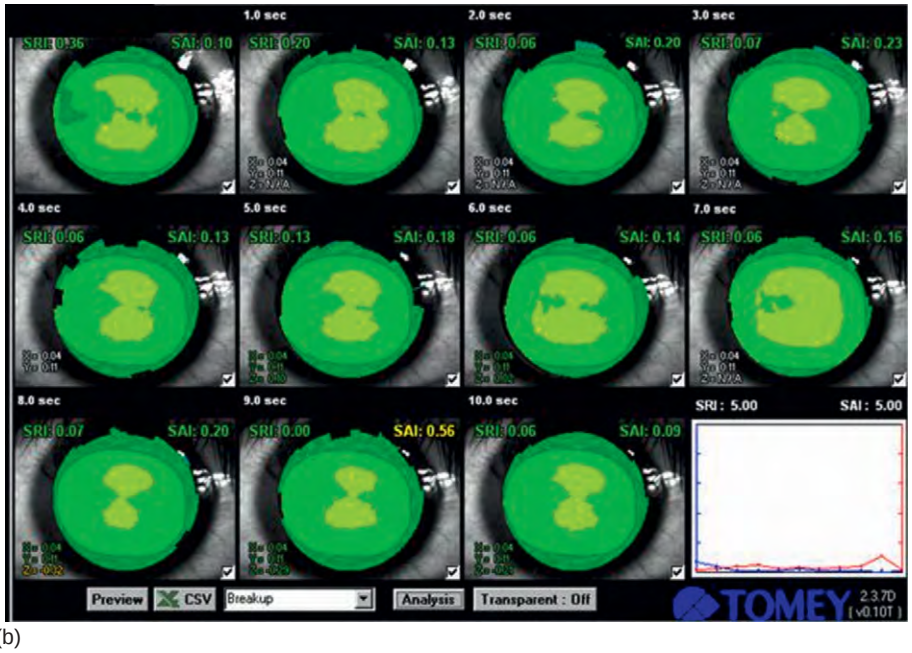

(b)

Figure 2 (a) Tear-stability analysis system (TSAS) in dry-eye patient. Tear-film break-up time is 3 s. Note the dramatic change in the TSAS pattern with time. The tears evaporate from the lower part of the cornea. (b) Tear-stability analysis system in normal subject. Tear-film break-up time is 12 s.

Tear-Film Break-Up Time (TFBUT)

This is carried out using a small amount of fluorescein, which is applied to the lower fornix using an applicator and the use of a yellow barrier-filter to enhance the visibility of the break-up of the fluorescent tear film. The patient is asked to blink and then keep the eyes open. The time taken for the first black spot in the stained tear film is recorded as the TFBUT. The test is ideally repeated 3 times and the mean is recorded as the TFBUT of that eye. Currently, a TFBUT value greater than 10 s is regarded as normal.

Schirmer's Test

Aqueous tear quantity is measured by Schirmer's test, which may be performed with or without the use of a topical anesthetic. For the Schirmer's test, a strip of filter is placed with its tip in the lower lateral conjunctival fornix, and the length of strip that becomes wet after 5 min is measured. The patient's eyes should be closed during the test. Aqueous deficiency is suspected if there is less than 5 mm of strip wetting after 5 min without anesthesia.

Assessment of Other Tear Functions

Tear Osmolarity

Although techniques to measure tear osmolarity are currently inaccessible to most practitioners, the development of commercial instruments may make such measurements feasible in the near future. As an objective measure of dry eye, hyperosmolarity is attractive as a signature feature, characterizing dryness. The diagnostic cut-off is in excess of 316 MOsm l^{-1}.

Lipid-Layer Interferometry

Interference cameras measure the tear-film lipid-layer interferometry. This can assist in analyzing the changes in thickness and the structure of the tear lipid layer. Reflective meniscometry measures the tear-meniscus curvature which has been shown to be decreased in patients with dry eye. This decrease correlates well with increased ocular surface staining. Lipid-layer interferometry, along with measurement of tear osmolarity is a potentially useful tool in the diagnosis of dry eye.

Tear-Stability Analyses

Tear-stability analysis measures tear stability as a function of serial surface regularity index and surface asymmetry index. These topographical indices assess the tear-film-related corneal surface changes. This analysis has shown a decrease in tear stability with increase in surface regularity index and surface asymmetry index in patients with dry eye. Tear-stability analysis has been found to be useful in evaluating the effects of punctum-plug treatment in patients with dry eye (Figure 2). Punctum-plug insertion is a treatment for patients with dry eye where the nasolacrimal punctum is plugged, thereby decreasing tear drainage.

Functional Visual Acuity

The FVA system continuously measures changes in visual acuity over time (Figure 3). The test begins with the best corrected Landolt visual acuity, which is the baseline of FVA. Landolt optotypes (consists of a ring that has a gap, thus looking similar to the letter C) are presented on the frame every second within a defined time (1–5 s), which increases in size when the answer is incorrect or when there is no response within the set display times, and decreases in size when the answer is correct. Each response is recorded on a table and as graphs, which are composed of points joining the correct answers only. FVA-test parameters include the mean FVA and visual maintenance ratio (VMR). VMR measures the percentage of the time a subject is able to maintain his or her best visual acuity over the present-time testing. The mean logMAR FVA and VMR scores have been reported to decrease in dry-eye patients compared to healthy control subjects. Both parameters improve with punctum-plug occlusion (Figure 4) but may deteriorate with epiphora (watery eyes).

Higher Order Aberration (HOA) Measurement

Wave front sensors can measure serial ocular HOAs continuously. During the measurement, each subject is instructed to blink every 10 s. The HOA data can analyze, in the central 4-mm cornea, up to the sixth-order aberrations by expanding the set of Zernike polymials (a sequence of

Figure 3 Functional visual acuity (FVA) system. This is a compact device developed to measure changes in continuous visual acuity over time.

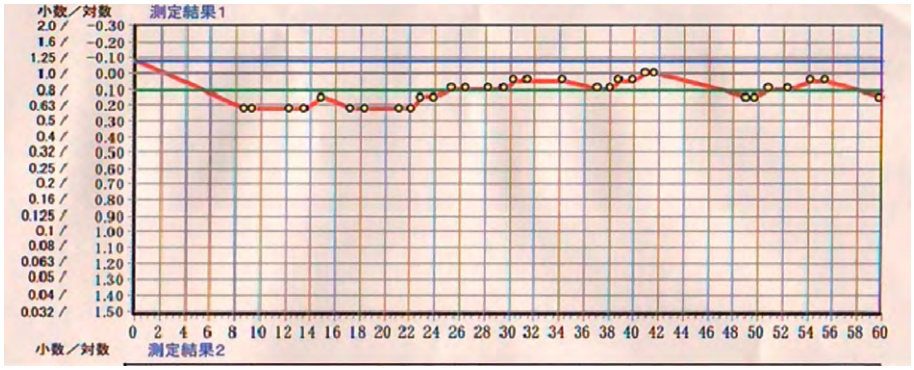

(a)

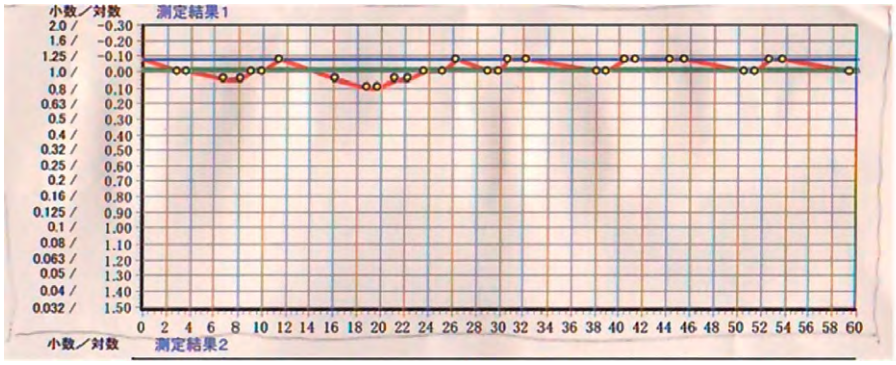

(b)

Figure 4 (a) The result of FVA in dry-eye patient. Baseline vision is 20/20, FVA is 0.775, VMR is 0.93. (b) The result of FVA in normal patient. Baseline vision is 20/20, FVA is 1.046, VMR is 0.98. FVA, Functional visual acuity; VMR, visual maintenance ratio.

polynomials that are orthogonal on the unit disk). Two quantitative indices are used to indicate the sequential changes in HOAs over time – the fluctuation index and the stability index of the total HOAs. The fluctuation index is defined as the fluctuations in the total HOAs obtained that showed the fluctuations in the total HOAs measured between blinks. Stability index is defined as the slope of the linear regression line of the total ocular HOAs between blinks. The total ocular HOAs are reported to be significantly greater in dry eye with central corneal staining than in dry eye without staining. The low tear volume in dry eye may not cause sequential increases in HOAs after blinking. Sequential assessment of HOAs may be useful for evaluating the sequential changes in corneal optical quality in patients with dry eye.

See also: Conjunctival Goblet Cells; Lacrimal Gland Overview; Lacrimal Gland Signaling: Neural; Meibomian Glands and Lipid Layer; Ocular Mucins.

Further Reading

Goto, E., Yagi, Y., Kaido, M., et al. (2003). Improved functional visual acuity after punctal occlusion in dry eye patients. *American Journal of Ophthalmology* 135: 704–705.

Ishida, R., Kojima, T., Dogru, M., et al. (2005). The application of a new continuous functional visual acuity measurement system in dry eye syndromes. *American Journal of Ophthalmology* 139: 253–258.

Koh, S., Maeda, N., Hirohara, Y., et al. (2008). Serial measurements of higher-order aberrations after blinking in patients with dry eye. *Investigative Ophthalmology and Visual Science* 49: 133–138.

Kojima, T., Ishida, R., Dogru, M., et al. (2004). A new noninvasive tear stability analysis system for the assessment of dry eyes. *Investigative Ophthalmology and Visual Science* 45: 1369–1374.

Lamberts, D. W. (1994). Physiology of the tear film. In: Smolin, G. and Thoft, R. A. (eds.) *The Cornea*, pp. 439–455. New York: Little Brown.

Lemp, M. A. and Blackman, H. J. (1981). Ocular surface defense mechanisms. *Annals of Ophthalmology* 92: 61–63.

Milder, B. (1987). The lacrimal apparatus. In: Moses, R. A. and Hart, W. M. (eds.) *Adler's Physiology of the Eye*, 8th edn., pp. 15–35. St. Louis, MO: Mosby.

The Active Pulley Hypothesis

J L Demer, University of California, Los Angeles, CA, USA

Glossary

Active pulley hypothesis (APH) – A kinematic hypothesis that explains how actively generated translational shifts in the positions of connective tissue pulleys in the orbit can control the pulling directions of the extraocular muscles so as to regulate how muscle pulling direction changes with eye orientation. The APH states that the orbital layers of the extraocular muscles translate the pulleys to control the muscle pulling direction, while the global layers rotate the eye directly in directions determined by pulley locations. The APH explains Listing's law as a mechanical phenomenon not explicitly commanded by innervation to torsionally acting extraocular muscles.

A-pattern strabismus – Horizontal binocular misalignment in which the eyes are more convergent (or less divergent) in upward gaze, and more divergent (or less convergent) in downward gaze.

Commutativity – A property of sequential mathematical operations whose outcome is identical regardless of the sequence of operations. For example, addition is a commutative operation. Sequential rotations of a solid object, however, are not commutative.

Craniosynostosis – A pathological condition in which the suture junctions between the bony plates of the skull fuse prematurely during maturation, resulting in deformity of the skull and often of the ocular orbit.

Esotropia – Convergent horizontal strabismus, in which the eyes are crossed.

Exotropia – Divergent horizontal strabismus, opposite to the misalignment of esotropia.

Excycloduction – Rotation about the line of sight so that the superior part of the eye or orbit is rotated away from the midline.

Extorted (position) – Oriented in a position achieved by excycloduction. This term may be applied to the eye or to the orbit.

Hypertropia – Strabismus in which the eyes are misaligned vertically, so that the visual direction of one eye is higher than that of the other.

Incomitant strabismus – A binocular misalignment that varies in degree or direction with the direction of gaze.

Incycloduction – Rotation about the line of sight so that the superior part of the eye or orbit is rotated toward the midline.

Intorted (position) – Oriented in a position achieved by incycloduction. This term may be applied to the eye or to the orbit.

Kinematic – Relating to the rotational motion of the eye.

Lateral enthesis – The lateral anchor of the pulley connective tissue system onto the lateral orbit at the orbital tubercle of the zygomatic bone (Whitnall's tubercle).

Levator aponeurosis – The expansion of the tendon of the levator palpebrae superioris that ultimately inserts into the skin of the upper eyelid.

Listing's law – A constraint on ocular torsion about the line of sight first described by von Helmholtz: with the head upright and stationary, torsional eye position is always that value attained by a rotation from a primary starting position about a single axis. All such physiologic axes lie in a single plane termed Listing's plane. An equivalent formulation of Listing's law in the velocity domain is termed the half-angle rule, wherein the velocity axis of the eye changes by half of eye position.

Medial enthesis – The medial anchor of the pulley connective tissue system onto the medial orbit at the posterior lacrimal crest.

Orbit – The tissues surrounding the ocular globe, including the bony eye socket.

Orbital pulley – A connective tissue structure that constrains the path of an extraocular muscle. Except for the rigid, cartilaginous trochlea of the superior oblique muscle, orbital pulleys consist of soft, ring-shaped specializations in posterior Tenon's fascia into which are attached the fibers of the orbital layers of their corresponding extraocular muscles.

Saccade – Rapid refixational eye movement executed in ballistic fashion without ongoing sensory feedback.

Secondary gaze position – An eye position achieved by a purely horizontal or vertical rotation from primary position.

Tertiary gaze position – An eye position achieved by a combination of horizontal and vertical rotations.

Trochlea – A cartilaginous structure in the superiomedial part of the orbit through which the

superior oblique runs and results in a complete change in superior oblique muscle path.
V-pattern strabismus – Horizontal binocular misalignment in which the eyes are more divergent (or less convergent) in upward gaze, and more convergent (or less divergent) in downward gaze.

Gross Anatomy of Orbital Tissues

The six striated ocular rotary extraocular muscles (EOMs) are configured as antagonist pairs. The medial rectus (MR) and the lateral rectus (LR) muscles rotate the eye horizontally, with the MR adducting (rotating toward the midline) the eye and the LR abducting it (rotating away from the midline). The superior rectus (SR) and the inferior rectus (IR) muscles form a vertical antagonist pair, but some vertical action is contributed by the oblique EOMs. The superior oblique (SO) muscle, seemingly paradoxical in view of its name, has an infraducting (downward rotating) action, while the inferior oblique (IO) muscle has a supraducting (upward rotating) action. More importantly, the oblique EOMs act torsionally to rotate the eye around the line of sight. The SO incycloducts the eye by rotating its superior pole toward the nose, while the IO muscle excycloducts the eye by an oppositely directed rotation around the line of sight.

Pulleys and Muscle Paths

Rectus EOMs originate deep in the orbit, traveling anteriorly toward insertions on the ocular globe. The EOMs were traditionally described as following the shortest paths from origin to scleral insertion, which implies that the EOMs sideslip over the sclera. The shortest-path concept also implies that the rotational axis imposed upon the eye by a rectus EOM is fixed in the orbit. The X-ray tomographic observations of Simonsz and magnetic resonance imaging (MRI) observations of Miller first showed that EOMs do not follow shortest paths from origins to insertions. In eccentric gaze, rectus EOM paths are inflected sharply at discrete points in the anterior orbit by pulleys that constrain sideslip and cause EOM pulling direction to change with eye position.

The modern concept of orbital pulleys describes a change in the anterior paths of rectus EOMs, and thus their pulling directions, in an orderly way during duction. This is shown in the axial MR images in **Figure 1**, illustrating that the IR's anterior path changes by half the change in the duction angle. MRI shows similar behavior for all rectus EOMs: the anterior direction changes by half the duction angle.

Connective tissue pulleys surround the rectus and IO EOMs at their points of perforation of posterior Tenon's

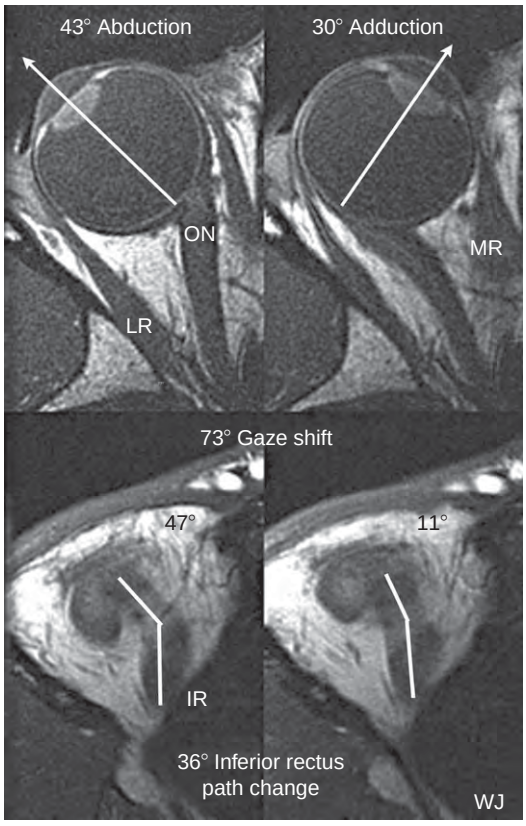

Figure 1 Axial magnetic resonance imaging views of human right orbit at the level of lens, fovea, and optic nerve (top row) and simultaneously in an inferior plane along the inferior rectus (IR) muscle path (bottom row), in abduction (left) and adduction (right). Note the two-part IR path, with an inflection corresponding to the IR pulley. For this 73° horizontal gaze shift, there was a corresponding 36° shift in IR muscle path anterior to its pulley. Reproduced from Demer, J. L. (2004). Pivotal role of orbital connective tissues in binocular alignment and strabismus. The Friedenwald lecture. *Investigative Ophthalmology and Vision Sciences* 45, 729–738, with permission from Association for Research in Vision Ophthalmology.

fascia. In secondary and tertiary gazes, EOM paths are inflected at these pulleys away from the shortest paths to EOMs' scleral insertions that have been shifted by ocular rotation. Since an EOM rotates the globe in a direction determined by the EOM's direction of pull as it departs the globe surface, path inflections influence an EOM's oculorotary direction. Systematic changes in EOM path direction produce a complex but systematic dependence of EOM pulling direction on instantaneous eye position, thus varying the amount of horizontal, vertical, and torsional rotation an EOM produces.

Structure of Pulleys

The overall structure of the orbital connective tissues is schematized in **Figure 2**. Points of rectus EOM inflection

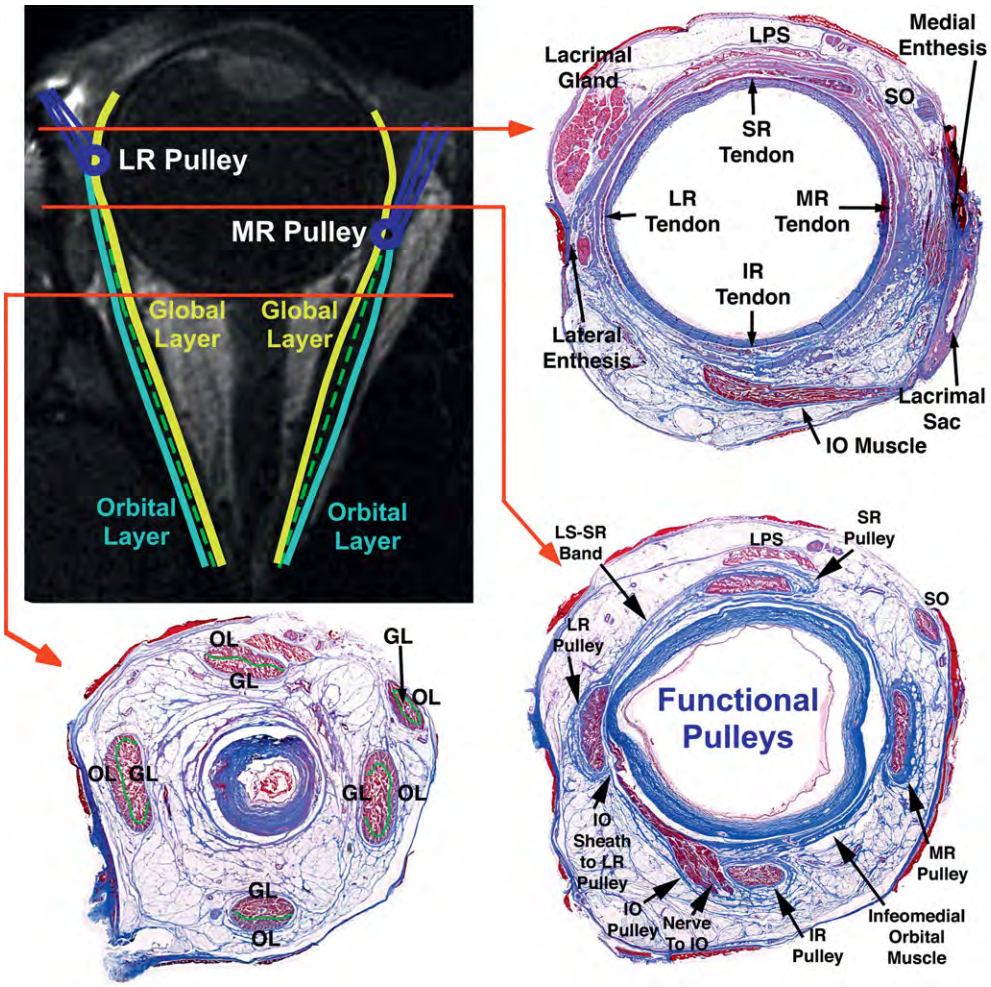

Figure 2 Anatomy of the human orbit. Axial magnetic resonance imaging (MRI) scan at upper left includes the medial (MR) and lateral rectus (LR) muscles whose orbital layers (OLs) and global layers (GLs) are demarcated by broken green lines. For each horizontal rectus EOM, the GL is illustrated as a yellow line that inserts upon the sclera, while the OL is illustrated as a light-blue line that terminates on the corresponding pulley (dark-blue ring). Pulleys are suspended from anteriorly located enthuses, attachments to the orbital wall. Superimposed on the MRI are three red lines denoting planes of coronal histological sections stained with Masson trichrome, which stains collagen blue and muscle in red. The upper right section is anterior to the globe equator, where the anterior pulley slings surrounding the thin rectus tendons are convex toward the orbital walls. The lower right section is posterior to the globe equator near the level of the functional pulleys, which appear as dense blue collagenous encirclements of the rectus and inferior oblique (IO) muscles. Note that the levator palpebrae superioris (LPS) muscle lacks a pulley. The lower left section is through the posterior pole of the globe, where the connective tissues have become attenuated to thin slings convex toward the globe. Each EOM exhibits an OL and GL, whose borders are demarcated by the broken green line. IR, inferior rectus muscle; LR, lateral rectus muscle; MR, medial rectus muscle; SO, superior oblique muscle; SR, superior rectus muscle.

constitute the functional orbital pulleys, and from the standpoint of ocular rotation, constitute functional EOM origins. Pulleys consist of discrete rings of dense collagen encircling the EOM, transitioning gradually into less substantial but broader collagenous sleeves (Figure 2). Anteriorly, these sleeves thin down to form slings convex to the orbital wall, and posteriorly the sleeves thin down to form slings convex toward the orbital center. The anterior pulley slings have also been called the intermuscular septum. Fibrils of collagen in the pulleys have an interlaced configuration suited to high internal rigidity. There are bands of smooth muscle in some pulley suspensions, and particularly in a distribution called the inframedial peribulbar smooth muscle between the MR and IR pulleys. The MR and LR pulleys are suspended by fibroelastic connective tissues from anteriorly located entheses, or anchors, on the orbital bones. The medial enthesis is at the posterior lacrimal crest, while the lateral enthesis is at the orbital tubercle.

IO and IR Pulleys

The IR pulley is coupled to the IO pulley in the central part of the inferior tarsal ligament (Lockwood's), the

connective tissue hammock spanning the inferior orbit. The IR and IO pulleys share a common collagenous sheath stiffened by dense elastin. The IR's orbital layer inserts on its pulley and does not continue anteriorly. The IO's orbital layer inserts partly on the conjoined IO–IR pulleys, partly on the IO sheath temporally and partly on the LR pulley's inferior aspect. As the orbital layer of the IR contracts during infraduction, the IR pulley shifts posteriorly to maintain a constant distance from the scleral insertion. Being only partially coupled to the IR pulley, the IO pulley shifts by half of this distance.

Elastin and smooth muscle are present in the region of the inferior tarsal ligament which supports the IR–IO pulleys. The inframedial peribulbar smooth muscle is positioned upon contraction to displace the IR pulley nasally. The smooth muscle retractors of the lower eyelid, the inferior tarsal muscle (Müller's muscle), and the connective tissues extending to the inferior tarsal plate are also coupled to the conjoint IR–IO pulley, coordinating lower eyelid position with the eye during vertical duction. Pulley smooth muscle has autonomic innervation, including: sympathetic with a norepinephrine projection from the superior cervical ganglion; cholinergic parasympathetic, probably from the ciliary ganglion; and nitroxidergic, probably from the pterygopalatine ganglion.

Trochlea

With its rigid pulley – the trochlea – the SO is unique that its orbital layer inserts via the SO sheath on the SR pulley's medial aspect. SO pulling direction changes half the duction angle because the thin, broad SO tendon wraps over the globe.

Functional Anatomy of Pulleys

According to the APH, the insertion of each rectus EOM's orbital layer on its pulley is the principal driving force translating (linearly moving) that pulley posteriorly during EOM contraction. In humans and monkeys, orbital layer fibers form small tendons that insert into the dense encircling tissue of the pulley system in a distributed manner over an anteroposterior region several millimeters (mm) in anteroposterior extent. MRI suggests that the pulley-system tissues move in coordination with the insertion and underlying sclera, although histological examinations show no direct connections between these tissues. The connective-tissue sleeves themselves have a substantial anteroposterior extent along which connective-tissue thickness varies.

Active Pulley Shifts

Since the EOMs pass through their encircling pulleys, physiological pulley locations are inferred from EOM paths. Pulley locations and shifts during ocular duction have been determined quantitatively from coronal MRIs in secondary and tertiary gazes. Imaging in tertiary (combined horizontal and vertical) gaze positions shows changes in anteroposterior positions of EOM path inflections. These data have confirmed that all four rectus pulleys move anteroposteriorly in coordination with their scleral insertions by the same anteroposterior amounts. MRI studies in living subjects have been consistent with histological examinations of the same regions in cadavers.

Pulley Positions

Although MRI indicates that rectus and IO pulleys are mobile along the axes of their respective EOMs, pulleys are located stably and stereotypically in planes transverse to the EOM axes. The 95% confidence intervals for horizontal and vertical coordinates of normal rectus pulleys range over less than $\pm$ 0.6 mm. Pulley stability in the coronal plane implies that pulleys are suspended by stiff tissues. The APH proposes that anteroposterior mobility of pulleys is accomplished by application of substantial force by each EOM's orbital layer. Aging causes inferior sagging of the horizontal rectus pulley positions, which shift downward by 1–2 mm from young adulthood to the seventh decade in people with normal binocular alignment, and more in people with strabismus or high axial myopia. Vertical rectus pulley positions change little with aging.

Globe Translation

The globe itself makes small translations – linear shifts – during normal ocular duction. The globe translates 0.8 mm inferiorly from 22° downward gaze to 22° upward gaze, and it also translates slightly nasally in both abduction and adduction. Even these small translations affect EOM force directions since the globe center is only 8 mm anterior to the plane of the rectus pulleys.

Pulley Translation

While pulleys limit EOM sideslip during globe rotations, small physiologic transverse shifts of rectus pulleys do occur. Coronal MRI shows that the MR pulley translates 0.6 mm superiorly from 22° infraduction to 22° supraduction. The LR pulley translates 1.5 mm inferiorly from infraduction to supraduction, opposite to the direction predicted by the shortest-path concept. The IR pulley shifts 1.1 mm medially in supraduction, but moves 1.3 mm temporally in infraduction. The SR pulley is relatively stable in the mediolateral direction, but moves inferiorly in supraduction and superiorly in infraduction.

Gaze-related shifts in rectus pulley positions are uniform among normal people.

Pulley Kinematics

Orbitally fixed pulleys make the eye's rotational axis dependent on eye position in a way important to ocular kinematics. Sequential rotations are mathematically non-commutative, so that final eye orientation depends on the order of rotations. Each combination of horizontal and vertical orientations could also be associated with many torsional orientations representing rotations around the line of sight, but the eye is constrained when the head is upright and immobile by Listing's law (LL): torsion in any gaze direction is that which the eye would have reached by a single rotation from primary eye position about an axis lying in Listing's plane (LP). LL is formulated in the kinematic position domain. Equivalent in the three-dimensional velocity domain, the half-angle rule states that LL is satisfied if the ocular rotational velocity axis shifts by half of the ocular duction. For example, if the eye supraducts 30°, then the vertical velocity axis about which it rotates for subsequent horizontal movement should tip back by 15°. Conformity to the half-angle rule makes the sequence of ocular rotations appear commutative to the brain, a property crucial to the control of ocular motility. It means that the brain does not need to keep track of the history of prior eye rotations in order to program subsequent eye rotations.

Active Pulley Hypothesis

Muscle Path Geometry

The APH explains how rectus pulley position can implement the half-angle kinematics required by the half-angle rule. EOMs rotate the globe about axes perpendicular to the tendon paths near the insertion. In **Figures 3(a)** and **(b)** it is seen from simple small-angle trigonometry that a horizontal rectus EOM's pulling direction tilts posteriorly by half the angle of supraduction when the pulley is located as far posterior to globe center as the insertion is anterior to globe center. Since all rectus EOMs and their pulleys are arranged similarly, all rotational forces acting on the eye-change direction by half of eye orientation. This configuration thus mechanically implements the half-angle rule, and thus LL.

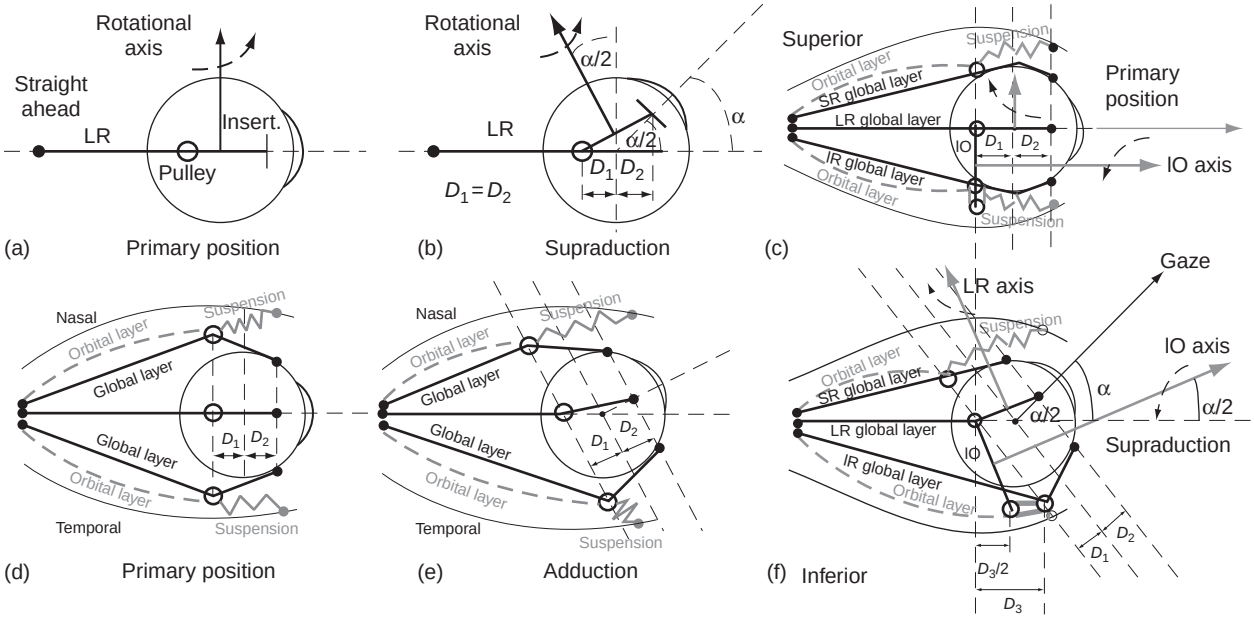

Figure 3 Diagram of extraocular muscle (EOM) and pulley behavior for half-angle kinematics conforming to Listing's Law. (a) Lateral view. EOM's rotational velocity axis is perpendicular to the segment from pulley to scleral insertion. The lateral rectus (LR) velocity axis is vertical in primary position. (b) Lateral view. In supraduction to angle alpha, the LR velocity axis tilts posteriorly by angle alpha/2 if distance D_1 from pulley to globe center is equal to distance D_2 from globe center to insertion. (c) Lateral view. In primary position, terminal segment of the inferior oblique (IO) muscle lies in the plane containing the LR and inferior rectus (IR) pulleys into which the IO's orbital layer inserts. The IO velocity axis parallels primary gaze. (d) Superior view of rectus EOMs and pulleys in primary position, corresponding to A. (e) Superior view. In order in adduction to maintain $D_1 = D_2$ in an oculocentric reference, the medial rectus (MR) pulley must shift posteriorly in the orbit, and the LR pulley anteriorly. This is proposed to be implemented by the orbital layers of these EOMs, working against elastic pulley suspensions. (f) Lateral view similar to (c). In supraduction to angle alpha, the IR pulley shifts anteriorly by distance D_3, as required by the relationship shown in E. The IO pulley shifts anteriorly by $D_3/2$, shifting the IO velocity axis superiorly by alpha/2. Reproduced from Demer, J. L. and Clark, R. A. (2005). Magnetic resonance imaging of human extraocular muscles during static ocular counter-rolling. *Journal of Neurophysiology* 94: 3292–3302, with permission from American Physiological Society.

Were primary and secondary gaze positions the only ones required, rectus pulleys could be rigidly fixed in the orbit. However, agonist–antagonist EOM alignment and conformity with LL are possible only if pulleys move in the orbit. Tertiary gazes, such as adducted supraduction, require the rectus pulleys to actively shift anteroposteriorly in the orbit, maintaining a fixed oculocentric relationship (**Figures 3(d)** and **(e)**). The APH explains that pulley shifts are generated by the contraction of the orbital layers acting against elasticity of the pulley suspensions, which are anchored from the bone of the anterior orbit at the entheses.

Muscle Commands

Despite coordinated movements, however, ocular rotation by the orbital layer and pulley translation by the global layer would require different EOM actions and neural commands. The global layer's mechanical load can be hypothesized to be predominantly the viscosity of the relaxing antagonist EOM. Viscosity is a resisting force proportional to rotational speed, and is a prominent mechanical feature of an EOM. The orbital layer's load, however, is postulated to be primarily due to the elasticity of the pulley suspension. Elasticity is a mechanical load independent of speed, but proportional to the duction angle. Electromyography (EMG) shows high, phasic global-layer activity during saccades, with a smaller-maintained tonic change in activity in eccentric gaze. The phasic activity of the global layer is thus appropriate to overcome viscosity of the relaxing antagonist EOM when the eye rotates quickly during a saccade, while the global layer's lesser tonic activity is appropriate to overcome the elastic forces of the opponent EOM and the connective tissues that oppose maintenance of an eccentric eye position. In the orbital layer, there is sustained, high EMG activity in eccentric gaze, but no phasic activity during saccades. The tonic activity of the orbital layer is appropriate to overcome mainly the elastic load of the connective tissues suspending an EOM's pulley. In cat, the most powerful and fatigue-resistant LR motor units, comprising 27% of all units, innervate both the orbital and global layers. Such bilayer motor units could command similar tonic contraction in the two layers, which may, in turn, maintain the pulley position relative to the EOM insertion. Other motor units project selectively to either the orbital or global layer, appropriate to differentiated muscle control.

Non-Listing's Kinematics in Convergence

Not all eye movements conform to LL. Violations of LL occur during the vestibulo-ocular reflex (VOR) and during convergence due to action of the oblique EOMs. Excycloduction refers to a rotation of the eye around the line of sight so that the superior pole of the eye shifts laterally. It occurs in convergence which violates LL. During asymmetrical convergence to a target aligned to one eye, this excycloduction is binocular, and interpretable as temporal tilting of LP for each eye. MRI during convergence to a target aligned to one eye has distinguished the effect of convergence from that of adduction. In the aligned orbit, there is extorsional shift of most rectus pulleys similar to globe extorsion. During convergence, the rectus pulley array rotates about the orbital axis in coordination with ocular torsion, changing the torsional pulling directions of all rectus EOMs but maintaining half-angle dependence on horizontal and vertical ductions. This would cause a parallel, torsional offset in LP.

An active mechanism probably implements torsional pulley shifts during convergence. The IO muscle's orbital layer inserts on the IR pulley and, at least in younger specimens, also on the LR pulley. Contraction of the IO orbital layer would excycloduct the LR and IR pulleys. Contractile IO thickening has been directly demonstrated by MRI during convergence. Inferior LR pulley shift would be coupled to produce lateral SR pulley shift because these pulleys are coupled by a ligament connecting the superior and lateral rectus pulleys, the LR–SR band. The SO muscle's orbital layer inserts on the SO sheath posterior to the trochlea, with both tendon and sheath passing anteriorly through the rigid pulley so that the SO sheath inserts on the SR pulley's nasal border. Relaxation of the SO orbital layer during convergence is consistent with single-unit recordings in the monkey trochlear nucleus and could contribute to pulley array excycloduction. The inframedial peribulbar smooth muscle may also contribute to rectus pulley excycloduction in convergence.

Non-Listing's Kinematics in Ocular Counterrolling

Ocular counterrolling (OCR) is a static torsional vestibulo-ocular reflex mediated by the otoliths of the inner ear. MRI during OCR shows coronal plane positions of the rectus EOMs being shifted torsionally in the same direction as the eye rotates about the line of sight. Pulley array torsion has been estimated to be roughly half the amount of OCR. Torsional shift of the rectus pulley array half of OCR would change rectus EOM pulling directions by one-quarter of OCR (**Figure 4**). During OCR, oblique EOMs exhibited changes in MRI cross section consistent with active roles in rotating the rectus pulley array. This finding suggests that the array of rectus pulleys constitutes a kind of inner gimbal conforming to Listing's half-angle kinematics for visually guided movements such as fixations and saccades, but that is rotated torsionally by

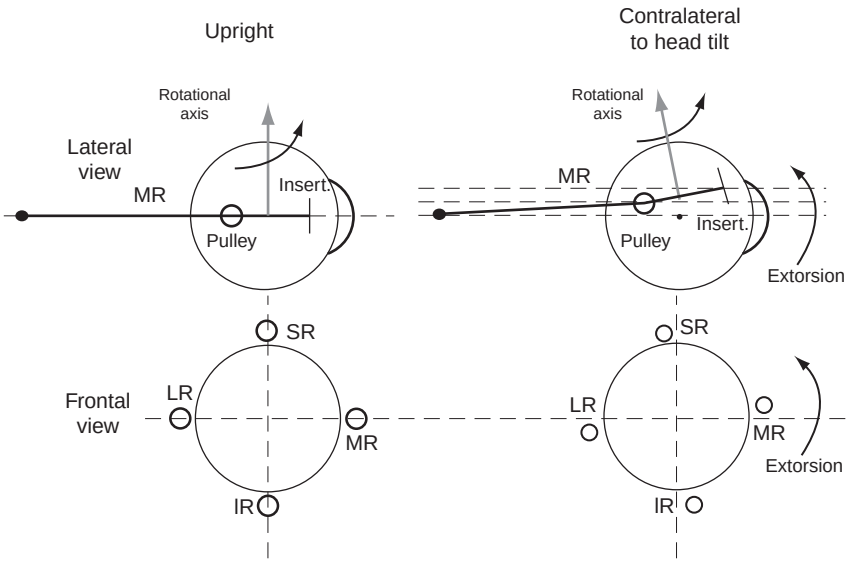

Figure 4 Diagram of effects of head tilt on rectus pulleys in lateral (top row) and frontal (bottom row) views. With head upright, the inferior (IR), lateral (LR), medial (MR), and superior rectus (SR) pulleys are arrayed in a cruciate pattern when viewed frontally. The MR passes through its pulley, represented as a ring, to its scleral insertion. The rotational velocity axis imparted by the MR is perpendicular to the segment from pulley to insertion. The pulley array extorts during contralateral head tilt. Since during head tilt the MR pulley shifts superiorly by the half the distance the insertion shifts, the MR's velocity axis changes by one-fourths of the ocular torsion. Reproduced from Demer, J. L. and Clark, R. A. (2005). Magnetic resonance imaging of human extraocular muscles during static ocular counter-rolling. *Journal of Neurophysiology* 94: 3292–3302, with permission from American Physiological Society.

the oblique EOMs to implement non-LL eye movements such as the slow and quick phases of the VOR.

Electrophysiologic Evidence for the APH

Electrophysiologic evidence supports the APH. Motor neurons innervating the vertical rectus and oblique EOMs in monkeys signal no neural commands for LL torsion during pursuit tracking, although pursuit conforms to LL. Direct electrical stimulation of the monkey abducens nerve evokes saccade-like movements that conform to the half-angle rule and thus to LL. These findings support the APH contention that the ocular torsion required by LL arises from mechanical properties of rectus EOMs and orbital connective tissues, rather than by explicit neural commands to the cyclovertical EOMs to generate ocular torsion.

Implications for Strabismus

As the EOM pulley array is anchored to the bony orbit, bony abnormalities may malposition pulleys to alter EOM pulling directions. Typically, the heterotopic array of rectus pulleys is extorted or intorted, not necessarily symmetrically. Computer simulations suggest rectus pulley malpositioning, as in craniosynostosis, can produce incomitant strabismus. Extorsion of the pulley array is associated with V patterns and intorsion associated with A patterns (**Figure 5**). Surgery for pulley disorders recently has emerged for treatment of three types of pathologies.

Pulley Heterotopy

Pulley heterotopy may involve stable malpositioning of one or several rectus pulleys. Initial efforts to treat heterotopy involved transpositions of the scleral insertions of EOMs whose pulleys were heterotopic, later augmented by fixations of EOM bellies to the underlying sclera ~8 mm posteriorly. MRI has demonstrated that this surgery shifts the involved rectus pulley somewhat toward the desired direction. However, because the pulley does not shift as far as the insertion, the operation introduces undesirable ocular torsion opposite to the direction of transposition. Since normal pulleys are not attached to sclera, posterior fixation compromises normal pulley kinematics and introduces abnormal globe translation during duction. Newer approaches to pulley heterotopy involve surgery on connective tissues suspending the pulleys without scleral suturing. A technically convenient approach to treatment of inferior displacement of the LR pulley is to shorten and stiffen the ligament coupling the LR and SR pulleys, the LR–SR band.

Extreme pulley heterotopy is associated with esotropia and hypotropia in axial high myopia. In this condition, historically called the heavy-eye syndrome, the LR pulley shifts inferiorly to approach the IR, and the globe

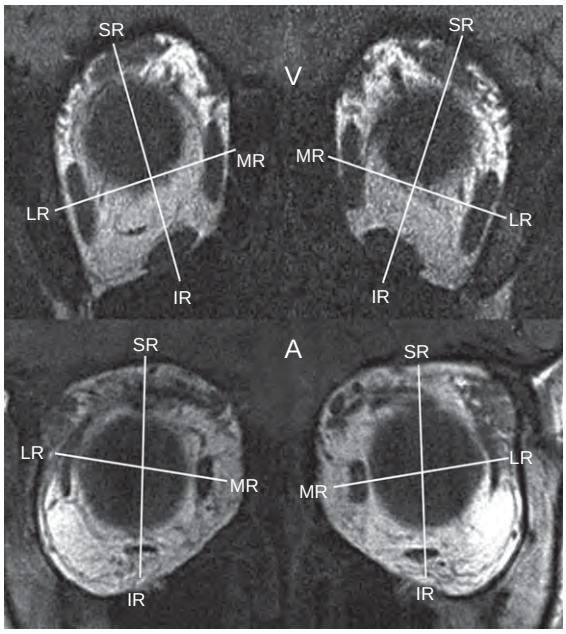

Figure 5 Magnetic resonance imaging scan showing typical pulley configurations for A and V patterns. A-pattern strabismus is a horizontal binocular misalignment in which the eyes are more convergent (or less divergent) in upward gaze, and more divergent (or less convergent) in downward gaze. V-pattern strabismus is a horizontal binocular misalignment in which the eyes are more divergent (or less convergent) in upward gaze, and more convergent (or less divergent) in downward gaze.

correspondingly shifts superotemporally in the orbit. A similar degenerative condition occurs in elderly, nonmyopic people, in whom it is termed the sagging-eye syndrome. Surgical anastamosis of the lateral margin of the SR belly with the superior margin of the LR belly may be effective in correcting esotropia associated with inferior displacement of the LR pulley, since the procedure normalizes EOM paths relative to the globe in a manner impossible for more conventional strabismus surgery.

Pulley Instability

Large gaze-related shifts or one or more pulleys are associated with incomitant strabismus. Pulley instability also has been termed gaze-related pulley shift. Inferior LR pulley shift in adduction produces restrictive hypotropia closely resembling Brown syndrome, caused by hindrance of SO travel in the trochlea, or X-pattern exotropia characterized by greater deviation in both up and down gaze compared to central gaze. Early efforts to treat pulley instability consisted of posterior fixation of the involved EOM to the underlying sclera. More recently, physiologically driven approaches involve tightening lax connective tissue bands in pulley suspensions.

Pulley Hindrance

In pulley hindrance, normal posterior shift with EOM contraction is mechanically impeded. This creates a mechanical restriction to ocular rotation in the field of action of the EOM. Intentionally created hindrance can be therapeutic, as done by the technique of posterior fixation (also known as retroequatorial myopexy and fadenoperation) of an EOM to the underlying sclera. Posterior fixation was postulated to work by reducing the EOM's arc of contact, diminishing its rotational lever arm. MRI demonstrates that posterior fixation works by hindering posterior shift of the contracting EOM's pulley, mechanically restricting EOM action. A technically simpler and safer modification of posterior fixation involves temporarily placing the MR-pulley suspension under tension, with the MR pulley sutured to the EOM belly. This operation is at least as effective as posterior fixation with scleral suturing in treatment of accommodative esotropia with excessive accommodative convergence.

Only relatively small shifts of pulleys are observed by MRI after simple transposition of the scleral insertions of rectus EOMs to treat paralytic strabismus. Posterior suture fixation of transposed EOMs shifts the pulley farther into the direction of the transposed insertion. This changes the pulling direction to mimic more closely that of the paralyzed EOM, increasing the effectiveness of transposition.

Conclusion

The ocular motor system consists of an intricate mechanical arrangement comprising a trampoline-like suspension supported by the rectus EOMs and their associated connective tissues, in turn circumferentially controlled by the oblique EOMs. Rectus EOMs and their connective tissue pulleys constitute the inner gimbal that is postulated to mechanically implement LL without explicit neural specification of ocular torsion. The inner gimbal has commutative properties that simplify neural commands for binocular coordination. The outer gimbal moves the inner by oblique EOM forces to generate ocular torsion not conforming to LL. Outer gimbal shift noncommutatively influences the inner gimbal in appropriate physiologic situations. While pathology of the orbital connective tissues may cause some forms of strabismus, the connective tissues are surgically accessible, so surgery on them may be therapeutic for specific types of disorders of ocular motility.

Acknowledgments

This study was supported by US Public Health Service, National Eye Institute: grants EY08313 and EY00331.

See also: Abnormal Eye Movements due to Disease of the Extraocular Muscles and Their Innervation; Congenital Cranial Dysinnervation Disorders; Cranial Nerves and Autonomic Innervation in the Orbit; Extraocular Muscles: Extraocular Muscle Anatomy; Extraocular Muscles: Functional Assessment in the Clinic; Imaging of the Orbit; Orbital Bony Anatomy and Orbital Fractures.

Further Reading

Clark, R. A., Miller, J. M., and Demer, J. L. (1997). Location and stability of rectus muscle pulleys: Muscle paths as a function of gaze. *Investigative Ophthalmology and Vision Sciences* 38: 227–240.

Clark, R. A., Miller, J. M., and Demer, J. L. (2000). Three-dimensional location of human rectus pulleys by path inflections in secondary gaze positions. *Investigative Ophthalmology and Vision Sciences* 41: 3787–3797.

Demer, J. L. (2004). Pivotal role of orbital connective tissues in binocular alignment and strabismus. The Friedenwald lecture. *Investigative Ophthalmology and Vision Sciences* 45: 729–738.

Demer, J. L. (2006). Current concepts of mechanical and neural factors in ocular motility. *Current Opinions in Neurology* 19: 4–13.

Demer, J. L. (2007). Mechanics of the orbita. *Developments In Ophthalmology* 40: 132–157.

Demer, J. L. and Clark, R. A. (2005). Magnetic resonance imaging of human extraocular muscles during static ocular counter-rolling. *Journal of Neurophysiology* 94: 3292–3302.

Demer, J. L., Miller, J. M., Poukens, V., Vinters, H. V., and Glasgow, B. (1995). Evidence for fibromuscular pulleys of the recti extraocular muscles. *Investigative Ophthalmology and Vision Sciences* 36: 1125–1136.

Demer, J. L., Poukens, V., Miller, J. M., and Micevych, P. (1997). Innervation of extraocular pulley smooth muscle in monkey and humans. *Investigative Ophthalmology and Vision Sciences* 38: 1774–1785.

Demer, J. L., Oh, S. Y., and Poukens, V. (2000). Evidence for active control of rectus extraocular muscle pulleys. *Investigative Ophthalmology and Vision Sciences* 41: 1280–1290.

Demer, J. L., Kono, R., and Wright, W. (2003). Magnetic resonance imaging of human extraocular muscles in convergence. *Journal of Neurophysiology* 9: 2072–2085.

Demer, J. L., Oh, S. Y., Clark, R. A., and Poukens, V. (2003). Evidence for a pulley of the inferior oblique muscle. *Investigative Ophthalmology and Vision Sciences* 44: 3856–3865.

Kono, R., Clark, R. A., and Demer, J. L. (2002). Active pulleys: Magnetic resonance imaging of rectus muscle paths in tertiary gazes. *Investigative Ophthalmology and Vision Sciences* 43: 2179–2188.

Kono, R., Poukens, V., and Demer, J. L. (2002). Quantitative analysis of the structure of the human extraocular muscle pulley system. *Investigative Ophthalmology and Vision Sciences* 43: 2923–2932.

Kono, R., Poukens, V., and Demer, J. L. (2005). Superior oblique muscle layers in monkeys and humans. *Investigative Ophthalmology and Vision Sciences* 46: 2790–2799.

Miller, J. M., Demer, J. L., Poukens, V., et al. (2003). Extraocular connective tissue architecture. *Journal of Vision* 2: 12–23.

Relevant Website

http://www.eidactics.com – Eidactics: Journal of Vision.

The Biology of Schlemm's Canal

W D Stamer, The University of Arizona, Tucson, AZ, USA

Glossary

Adherens junction – A type of cell–cell junction in which the cytoplasmic face of proteins in the junction complex is attached to actin filaments of the cytoskeleton.
Aqueous humor – A clear fluid that fills the anterior and posterior chambers of the eyeball and supplies the metabolic needs of the avascular lens, cornea, and trabecular meshwork.
Blood–aqueous barrier – Formed by the tight junctions (zonula occludens) of the nonpigmented ciliary epithelium, the endothelial cells of iris vessels, and the Schlemm's canal endothelium, to separate blood and aqueous humor compartments.
Collector channel – Openings in Schlemm's canal lumen that facilitates transport of aqueous humor to systemic venous system.
Endothelial cell – The flattened cell type that forms a sheet, the endothelium, lining blood vessels.
Gap junction – A communicating cell–cell junction that allows ions and small molecules to pass from the cytoplasm of one cell to the cytoplasm of a cell neighbor.
Giant vacuole – Cellular distention into Schlemm's canal lumen by endothelia that are formed by pressure gradient across the inner wall.
Integrins – The members of a large family of transmembrane proteins involved in the adhesion of cells to the extracellular matrix and to each other.
Juxtacanalicular tissue – The region of the conventional outflow pathway, including the cribiform (outermost) trabecular meshwork and inner wall of Schlemm's canal, where resistance to aqueous humor outflow is generated.
Syndecans – A family of glycoproteins at the plasma membrane of cells that act as receptors for extracellular matrix and are involved in intracellular communication.
Trabecular meshwork – The major component tissue of the conventional outflow pathway is located at the iridocorneal angle and consists of cells and extracellular matrix that functions to filter intraocular debris and regulate intraocular pressure.
Tight junction – A type of cell–cell junction that seals epithelial or endothelial cells together, forming a barrier such that even small molecules cannot pass between cells. An alternative term is zonula occludens.

Introduction

Intraocular pressure (IOP) is a function of the balance of aqueous humor secretion into and drainage out of the eye. Resistance generation that regulates the drainage of aqueous humor out of the eye is a dynamic process, maintaining IOP within a narrow range throughout a lifetime. Over a century ago, it was postulated that elevated IOP (ocular hypertension) in glaucoma is caused by increased resistance of aqueous humor drainage in the conventional outflow pathway. As it leaves the eye, the bulk of aqueous humor (70–90%) passes through the conventional outflow pathway, a complex pressure-sensitive tissue that is comprised of various cell types under constant mechanical strain (Figure 1). Multiple studies directed to identify the location of normal resistance generation in the conventional drainage tract implicate the juxtacanalicular tissue (JCT), a region populated by JCT–trabecular meshwork (TM) cells and the endothelium of Schlemm's canal (SC). The JCT region also appears to be the diseased tissue in glaucoma; implicated for generating the elevated outflow resistance associated with most forms of glaucoma. Still unknown today, however, are the mechanisms for aqueous humor outflow resistance generation, regulation, and why resistance becomes elevated in glaucoma, a group of diseases that affects ~70 million people worldwide. Significantly, even though the site of damage that leads to blindness in glaucoma is at the optic nerve head in the back of the eye, all current strategies to treat glaucoma (including normal-tension glaucoma) involve reducing IOP. In fact, results from multiple, large, clinical trials show that if IOP is lowered sufficiently and maintained over time, disease progression as indicated by visual performance is completely halted. Therefore, understanding the biology of SC endothelia in its contribution to the generation and regulation of outflow resistance is paramount to developing rational therapeutic strategies to intervene in those who suffer from glaucoma. This article reviews the biology of SC endothelia and the unique environment in which it functions.

Development

SC is vascular in origin, forming from the intrascleral venous plexus present in the developing human eye. Starting around week 17 of gestation, deep scleral vessels are observed in the SC region. By week E28, a complete SC can be seen in some regions of the eye. Soon afterward, around week 29 of gestation, some characteristic features (large, pressure-dependent distensions into the canal

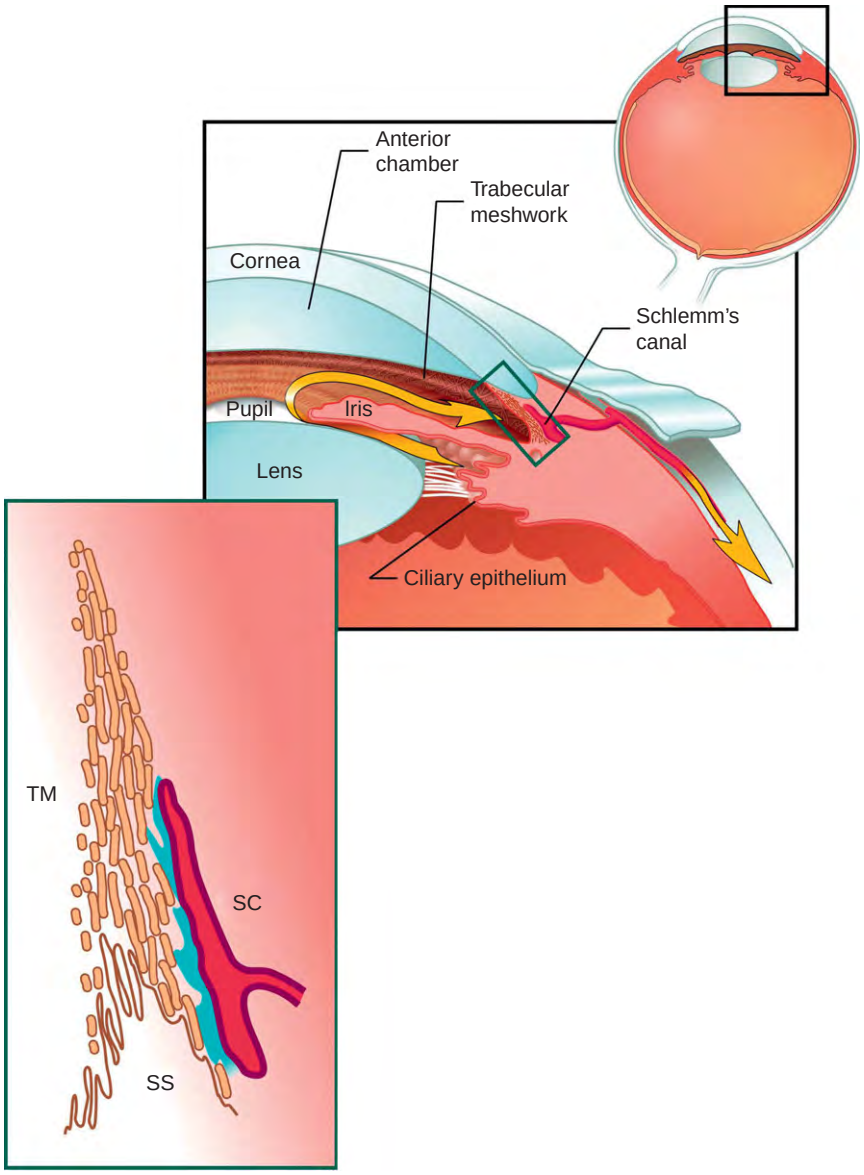

Figure 1 Flow pattern for aqueous humor and conventional outflow structures in the human eye. The black box indicates the region of the eye that is enlarged and structures labeled. Yellow ribbon arrows depict the origin of aqueous humor secretion by the ciliary epithelium and direction of flow into the posterior chamber, through the pupil, into the anterior chamber, and out through the conventional outflow pathway. The conventional outflow pathway is highlighted by a green rectangle and enlarged as an inset on the bottom left, showing the trabecular meshwork (TM), the scleral spur (SS), and Schlemm's canal (SC). The area shaded in blue is the juxtacanalicular region.

lumen called giant vacuoles; see below) are found in inner wall cells, indicating the presence of a pressure gradient and associated fluid flow. Preceding the formation of the SC, the TM tissues can be seen developing from the neural crest. TM cells start populating the regions contiguous with SC by week E16 and, by week E23, TM cells start interacting with the branching scleral vessels that will develop into the SC around week E28. Thus, it appears that the interactions between TM and SC cells begin early during development to guide the formation of a functional conventional outflow pathway, the primary route for aqueous humor to exit the eye.

The Conventional Outflow Pathway

Aqueous humor is drained from the human eye by two routes: the conventional pathway (also known as the trabecular pathway) and the unconventional pathway (also known as uveoscleral or uveovortex pathway). The unconventional pathway accounts for a small fraction (10–30%) of total aqueous humor drainage from the human eye and does not contribute significantly to normal outflow dynamics in older eyes, nor does it contribute to the generation of elevated outflow resistance in glaucoma, although the enhancement of uveoscleral outflow

underlies effectiveness of prostaglandin-$F_{2\alpha}$ analogs (current first-line therapy) in lowering IOP. The majority of aqueous humor leaves the eye through the conventional pathway, which is comprised of the TM, SC, and the collector channels/intrascleral venous plexus/aqueous veins (Figure 2). The TM is usually divided into three regions: the innermost uveal meshwork, the deeper corneoscleral meshwork, and the outermost JCT, which lies adjacent to SC, a ring-shaped venous vessel that encircles the eye at the corneoscleral junction. Collector channels and intrascleral aqueous plexus/aqueous veins connect SC lumen to the episcleral veins on the surface of the eye.

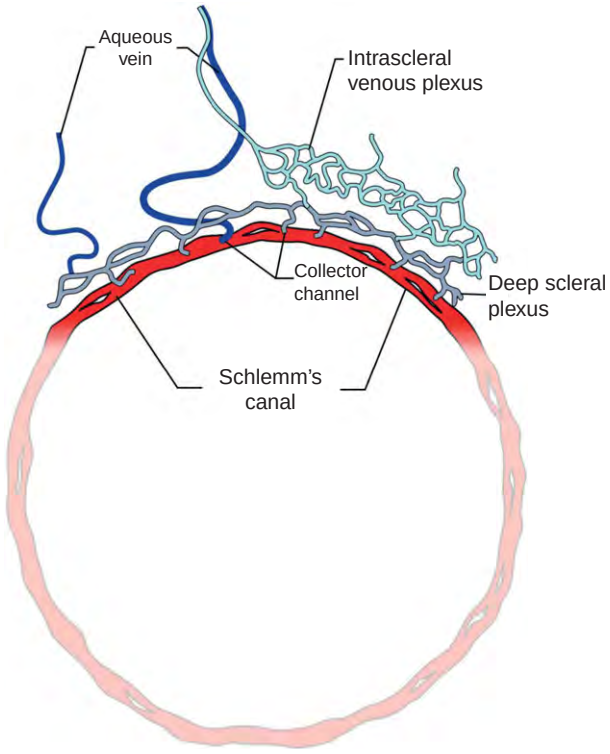

Figure 2 The morphology of Schlemm's canal and its relationship with distal venous system. The drawing shows complete vascular ring, which is Schlemm's canal. In the upper quadrant, detail is provided to reveal specific connections that collector channels make directly with aqueous veins or with deep scleral plexus and/or intrascleral venous plexus prior to joining aqueous veins.

Trabecular Meshwork

The majority of the TM, including the uveal and corneoscleral regions, is designed like a filter to intercept cell debris, including pigment, as it leaves the eye. Aqueous humor first encounters the uveal meshwork, which is made up of an irregular netlike structure of lamellae. Next, aqueous humor enters the corneoscleral meshwork, consisting of a number of porous sheets that are attached to the scleral spur posteriorly and the peripheral cornea at Schwalbe's line anteriorly. Both of these networks of extracellular matrix (ECM) are covered and maintained by resident TM cells. The openings in the uveal meshwork and in the sheets of the corneoscleral meshwork decrease progressively as they approach SC, creating turbulence, but neither generates any significant resistance to flow.

The final portion of the TM that aqueous humor encounters before reaching SC is known as the JCT, also called the endothelial meshwork or cribriform region. The JCT is bordered on one side by the innermost corneoscleral TM sheet and on the other by the basement membrane of the inner wall of Schlemm's canal – a separation distance of 10 μm on average. Cells that populate the JCT are not confluent monolayers similar to cells in the innermost TM regions, but suspended in ECM materials (mostly glycosaminoglycans), and make cell–cell attachments on corneoscleral TM, SC, and/or JCT–TM cells. At physiological IOPs (13–18 mm Hg) and episcleral venous pressures (7–8 mmHg in SC), a pressure gradient exists across the conventional outflow pathway, distending TM and inner wall tissues toward the outer wall of SC (Figure 3). Under the influence of a physiological pressure gradient, spaces between cells

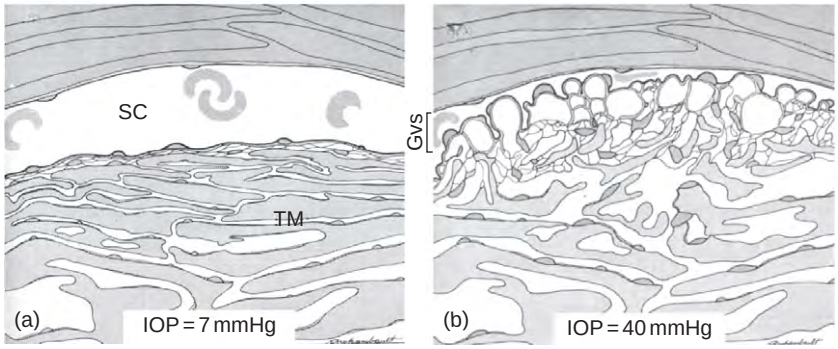

Figure 3 Changing configuration of trabecular meshwork (TM) tissue and Schlemm's canal (SC) inner wall endothelium at low (a) and high (b) perfusion pressure. Bracket indicates inner wall region where giant vacuoles (GVs) form in response to change in pressure gradient. Reproduced from Johnstone, M. A. and Grant, W. G. (1973). Pressure-dependent changes in structures of the aqueous outflow system of human and monkey eyes. *American Journal of Ophthalmology* 75: 365–383, with permission from Elsevier.

in the JCT emerge (1–3 μm in diameter). Together with associated ECM and the inner wall of SC, the JCT–TM likely generates a major portion of the resistance to outflow.

Schlemm's Canal

After passing by JCT–TM cells, aqueous humor encounters the inner wall of SC, the only continuous cell monolayer that aqueous humor must cross in the conventional outflow pathway. The inner wall of SC is characterized by predominantly elongated and flattened (thickness $\leq$ 1 μm) endothelial cells aligned parallel to the longitudinal axis of the canal (**Figure 4(a)**). While highly variable in appearance, these cells can be generally characterized as spindle shaped (100–150 μm in length and 8–10 μm in width). This confluent layer of cells is attached to one another by tight junctions and adhered to a discontinuous basement membrane. In contrast, the cells that populate the outer wall of SC are situated on a continuous basement membrane. Perhaps fluid flow across the inner, but not the outer wall of SC in the basal-to-apical direction, is responsible for such a difference.

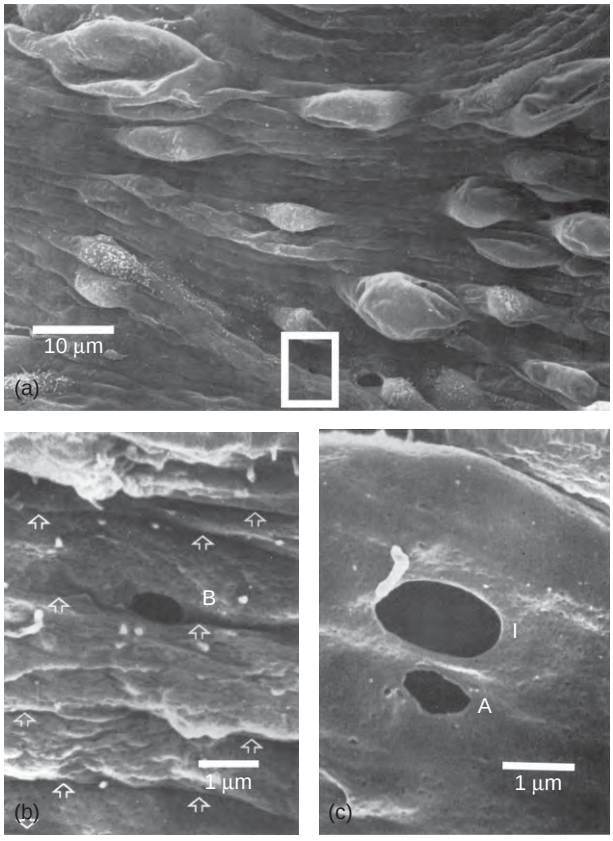

Figure 4 As viewed from the canal lumen, scanning electron micrographs showing morphology of inner wall of Schlemm's canal and two types of pore structures. (a) Overview of inner wall morphology. (b) A high-powered view of intercellular or border pore (*B*) from boxed area in (a). (c) A high-powered view of intracellular pore (*I*) and artifactual pore (*A*). Arrows in (b) point out cellular margins to demonstrate that ''B'' pore is intersected on each edge. From Ethier, C. R., Coloma, F. M., Sit, A. J., and Johnson, M. (1998). Two pore types in the inner wall endothelium of Schlemm's canal. *Investigative Ophthalmology and Visual Science* 39: 2041–2048. The Association for Research in Vision and Ophthalmology.

Driven by a pressure gradient, fluid flow across the inner wall of SC often creates structures that have been named giant vacuoles (**Figure 3**). Dimensions of giant vacuoles are 1–10 μm in width, 1–7 μm in height, and sometimes extending to 20 μm in length. Such significant morphological structures are not an intracellular compartment, but instead outpouchings of cells into its lumen caused by the pressure drop across the inner wall. In fact, the size and density of giant vacuoles positively correlate with IOP. Interestingly, vacuoles appear to be concentrated near collector channel ostia, suggesting that the pressure drop at these locations is greater; consistent with studies showing preferential flow patterns near collector channel ostia.

At the site of these outpouchings, the inner wall is very attenuated and thin; where the endothelial cells are most distended, unique pores appear to form. Inner wall pores usually range in size from 0.1 to 3 μm with an average diameter of about 1 μm. The majority (about 75%) of pores is transcellular and the minority is paracellular, located at the border of neighboring cells (**Figures 4(b)** and **4(c)**). For transcellular pores, the inner and outer plasma membranes of SC endothelial cells appear to have come together and fused, making membrane-limited openings (similar to fenestrae). While primarily found associated with giant vacuoles, pores are occasionally found on flat, thin portions of the inner wall; perhaps artifacts of fixation. Indeed, the original estimates of inner wall pores (2000 pores mm^{-2}) have been revised to less than 1000 pores mm^{-2} due to new methods that mark active pores and reveal that only a portion carries fluid into the canal lumen. These recent data are consistent with two previous studies showing that aqueous humor must pass through pores to access the SC lumen because: (1) tracer particles up to 1 μm in size pass freely through the conventional outflow pathway to enter SC and (2) the inner wall has an unusually high measured hydraulic conductivity compared to other endothelia. Potentially relevant to the pathology of glaucoma, fewer pores are observed in the inner wall in those with glaucoma compared to age-matched control eyes.

After passing through the inner wall endothelium, aqueous humor enters the SC lumen. In cross section, the canal's shape is that of a highly elongated ellipse with a diameter along its long axis that ranges between 190 and 350 μm. Often (about 40% of the time), SC divides into more than one lumen (**Figure 2**). Throughout the canal, but especially near collector channels, are septa that bridge between the inner and outer walls of the canal.

The proximity of these structures to collector channel ostia suggests that they prevent collapse of the canal lumen and subsequent occlusion of collector channel ostia that may occur at elevated IOP.

Once inside of the canal, aqueous humor travels circumferentially around the eye until reaching one of 20–30 collector channel ostia (tens of microns in diameter) that open from the outer wall of SC (**Figure 2**). Collector channels transport aqueous humor to the eye surface and the episcleral venous system through two parallel pathways: one pathway leads through an anastomotic system of intrascleral plexus and the other is a more direct pathway through a set of aqueous veins.

Mechanical Environment

The mechanical environment of SC is unique. In addition to the basal-to-apical pressure gradient, the inner wall endothelial cells are exposed to shear forces as aqueous humor travels circumferentially on its way to exit the canal lumen and enter a collector channel. The magnitude of shear force applied to SC endothelia is influenced by the separation of the inner wall from the outer wall. This separation, or canal height, is dependent upon IOP, which at higher levels progressively collapses the SC as conventional outflow tissues pressed exteriorly, toward the outer wall (**Figure 3**).

IOP varies with time and activity. Two recurring physiological factors that affect IOP, and thus the microenvironment of the inner wall endothelial cells, are ocular pulsations and circadian IOP cycles. Aqueous humor secretion is not constant throughout the day. Instead, it has a sinusoidal behavior where the maximum rate is found at night ($\sim$3.4 µl min^{-1}) and the minimum is in the morning ($\sim$1.5 µl min^{-1}). These circadian oscillations in secretion contribute to consequential changes in IOP that vary during the day (2–8 mmHg). Importantly, several studies observe that circadian fluctuations are often more severe in those with glaucoma or ocular hypertension. The second factor, pulsatile IOP associated with each heart beat (ocular pulse), has a magnitude of 1–4 mmHg (average is 2.7 mmHg) and a frequency of approximately 1 Hz. Such pulsations in pressure have been shown to modulate outflow resistance, presumably in the JCT–TM and/or SC.

In addition, other unavoidable everyday activities (i.e., ocular massage and squinting and/or postural variations) cause dramatic changes in IOP, often creating transient spikes in IOP that approach 100 mmHg. Interestingly, after such transient IOP elevations, IOP quickly returns to baseline levels, indicating that the conventional tissues including SC have the capacity to hold the displaced fluid without allowing it to enter the SC lumen and consequently decreasing IOP. The expansion of the JCT and inner wall into the SC lumen appears to act as a temporary reservoir.

Cell Attachments

Due to its unusual anatomy and physiology, the inner wall of SC must participate in the generation of outflow resistance (and thus IOP), provide a barrier for reflux of blood into the eye (part of the blood–aqueous barrier), accommodate the transendothelial passage of micron-sized cell debris, and stay in place in the face of a pressure gradient in the basal-to-apical direction (opposite of other vascular endothelia). To function in such a dynamic environment, SC relies on a variety of cell–cell and cell–matrix attachments.

Cell–Cell Interactions

Ultrastructural examination of the JCT under a pressure gradient shows that JCT cells have cytoplasmic processes that extend from the corneoscleral meshwork on one side to the subendothelial space/inner wall endothelium on the other, making contact on either its cell surface or basal lamina. These processes were proposed to provide an anchoring or tethering support to the inner wall to compensate for the discontinuous basement membrane underlying the inner wall endothelium and the unique direction of the pressure gradient across the endothelium. Thus, with increasing IOP, inner wall cell nuclei make a dramatical transition from a rounded into a fusiform shape tapering toward the processes, indicating the magnitude of force on the cells. The JCT cells connect the inner wall to the rest of the conventional outflow tissues, creating a mechanically continuous network for sensing, distributing, and transmitting forces. While the nature of the adhesions between JCT and SC cells is currently not known, SC–SC adhesions include gap, adherens, and occluding (tight) junctions.

Working together, tight, adherens, and gap junctions form a complex that contributes to stabilize cell–cell interactions. Electron microscopy studies demonstrate that tight junctions are continuous around the circumference of SC cells. However, inner wall tight junctions rarely branch or anastomose, forming a loose arrangement of parallel strands (<4 sealing strands). These structures appear to respond to elevated IOP by decreasing the number and/or complexity of strands. In the inner wall, tight-junction strands are transversed by maze-like pathways, which go from the basal to the apical side of the cells, and have been previously referred to as slit-pores or intrajunctional openings. Such openings are more frequent and apparent at elevated IOPs. The importance of intrajunctional openings in generating resistance to aqueous humor drainage is highlighted by effects of calcium chelators, which pull calcium from junctional complexes, resulting in junctional disassembly and associated decrease in outflow resistance. In contrast, the perfusion of human eyes with tracers such as cationic ferritin, which preferentially obstructs intrajunctional openings, increases outflow resistance.

The outer wall of SC rests on a more continuous basement membrane that is supported by sclera, is not involved in drainage of aqueous humor, and does not appear to have heterotypic cell–cell interactions (with subendothelial fibroblasts). Moreover, adhesions along the lateral borders between outer-wall cells reveal fewer junctional modifications compared to their inner wall counterparts. Hence, the mechanical and hydrodynamic environment of the inner wall compared to the outer wall is significantly different.

Cell–ECM Interactions

A complementary mechanism to secure inner wall cells to their substratum in the face of pressure differentials appears to involve tethering to the elastic fibers that originate in the ciliary muscle and extend out from the cribriform plexus through the JCT. Connecting elastic fibrils reach from the cribriform plexus into the JCT where they make contact with plaque material, basement membrane components, or inner wall cells. In fact, cell membranes of inner wall cells are densified where the elastic fibrils make contact, resembling adhesion plaques. Consistent with the idea that these fibrils support mechanical stress, the intracellular filaments of inner wall cells are often observed in the same orientation (mechanically continuous) as the connecting fibrils. The manner by which SC cells attach to elastic fibers is unknown, but is likely through integrin binding to components of elastic sheath material.

Also providing mechanical support for inner wall cells are adhesive interactions with their basement membrane; a discontinuous scaffold composed mostly of collagen I, IV, fibronectin, laminin 111, 211, and 511, and heparin sulfate proteoglycans (and to a lesser extent collagens III, V, and VI). Cell–ECM adhesions involving integrins and/or syndecans are likely involved in attaching the inner wall endothelium to the basement membrane.

The two major integrin pairs expressed by SC cells appear to be $\alpha_5\beta_1$ and $\alpha_6\beta_1$, binding fibronectin and laminin, respectively. SC also expresses $\alpha_v\beta_3$ integrin pairs, particularly in young eyes. Syndecans, particularly syndecan-3 and -4, bind collagen and fibronectin and likely participate in SC–ECM adhesion. As a potential mechanism to increase adhesion, SC cells extend finger-like processes that interdigitate into the basement membrane, anchoring the cell into the basement membrane and increasing the surface area for integrin or syndecan adhesion. Perfusion with a recombinant HepII domain of fibronectin, that includes both integrin- and syndecan-binding sites, decreases outflow resistance in human organ culture eyes. Emphasizing the importance of cell–ECM adhesion by SC, heparin-binding (HepII) domain treatment apparently separated inner wall cell linkages to elastic fibrils and their basement membrane.

Cell–Cell and Cell–ECM Adhesion Strength

To maintain the morphology and function of the outflow pathway, cell–cell and/or cell–ECM adhesions must be physically capable of supporting the loads arising from the pressure drop across these tissues. A clue as to the magnitude of the pressure gradient that the inner wall supports may be obtained by calculating the apparent strength of these various attachments.

For instance, the forces necessary to detach adherent cells from fibronectin-coated substrates typically range from 1 to 10 nN cell^{-1}, but can be as high as ~200 nN, depending upon the assay. Using the highest reported cellular adhesion strength of 200 nN and a cellular surface area for SC cells of approximately 450 μm^{-2}, the maximum pressure load that can be supported by SC is estimated to be approximately 3 mmHg. This calculation is consistent with recent data using modulus measurements of SC cells that estimates the inner wall would fail at pressure drops greater than 2.8 mmHg.

Mechanical force transmission between cells is typically mediated through cell–cell adhesions involving cadherins (as part of adherens junctions). While the strength of these adhesions is not as well characterized, it has been suggested that the strength of cadherin adhesions is similar to that of focal adhesions. If true for adhesions between inner wall cells and JCT cells, then cadherin adhesions would likely be mechanically challenged in their ability to support a significant pressure drop across the inner wall endothelium. It is unknown, however, how cell adhesion strength is affected by cell overlap and dynamic junctional remodeling, both of which are characteristic features of SC.

Since inner wall cell continuity is preserved despite IOPs of 30 mmHg or higher, it is possible that the combination of attachments that SC makes with cell neighbors and its substratum is synergistic and much stronger than those measured for other cell types *in vitro* or that only a small fraction of the total pressure drop in the aqueous outflow pathway occurs directly across the inner wall endothelium. This latter explanation is consistent with the funneling theory; predicting that, despite the inner wall pores acting to modulate resistance, the bulk of outflow resistance is generated within the JCT.

Funneling Theory

The best evidence indicates that aqueous humor crosses the endothelium of SC through micron-sized pores in an otherwise continuous and relatively impermeable endothelial monolayer. The wide pore separation distance of 20–30 μm (or greater) implies that flow must be nonuniform since the flow patterns must funnel or converge as flow approaches a pore. Since the JCT is immediately upstream of these pores, the flow patterns through the JCT must also be nonuniform (**Figure 5(a)**). The funneling theory predicts that such

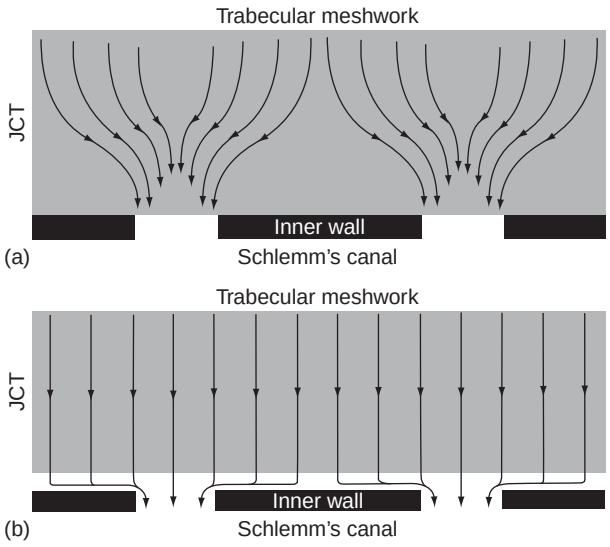

Figure 5 The streamlines of aqueous flow through the JCT across Schlemm's canal as predicted by the funneling hypothesis. (a) Shows that to enter Schlemm's canal, aqueous humor must converge onto discrete openings along the inner wall, which decreases the available area for flow and increases outflow resistance. (b) Demonstrates that treatments (such as H-7 or washout) that result in separation of the inner wall from the JCT eliminates the funneling pattern, increases the available area for flow, and increases outflow facility. Reproduced from Overby, D., Gong, H., Freddo, T., and Johnson, M. (2002). The mechanism of increasing outflow facility during washout in the bovine eye. *Investigative Ophthalmology and Visual Science* 43: 3455–3464. The Association for Research in Vision and Ophthalmology.

nonuniform flow patterns decrease the effective area available for flow through the JCT, which in turn increases the effective hydraulic resistance of this region. Modeling found that funneling increases the JCT flow resistance by a predicted 30-fold increase.

Physical evidence for funneling is found in tracer studies that observed nonuniform distribution of tracer along the inner wall. For example, a colloidal gold tracer occupied only 10–20% of the inner wall length and was found in sparse foci, consistent with funneling. Interestingly, when eyes were treated with 300 μM 1-(5-isoquinolinylsulfonyl)-2-methylpiperazine (H-7), a nonselective protein kinase inhibitor, gold particles redistributed to occupy >80% of the inner wall length in a more uniform pattern, suggesting that H-7 eliminates funneling (**Figure 5(b)**). New evidence suggests that H-7 works by separating the inner wall from underlying JCT, while connections between SC cells appear unaffected. Similar to previous studies, the change from a punctate to a uniform tracer decoration pattern and JCT expansion coincided with nearly a twofold decrease in outflow resistance, without a perceptible change in endothelial continuity. Importantly, the effects of H-7 upon outflow resistance were reversible 2.5 h after drug removal, coinciding with a return of inner wall/JCT morphology toward normal.

The importance of connectivity between JCT and inner wall cells in funneling is found with the phenomenon known as the washout effect. Washout is the progressive decrease in outflow resistance that occurs during prolonged perfusion of conventional outflow tissues of many species (e.g., bovine, porcine, canine, and monkey, but not human) with nutrient media. The name washout originated from the thought that perfusion of nutrient media was washing out ECM from the conventional outflow tissues. However, two studies that specifically examined ECM content following perfusion reveal no significant change over time. Recently, new evidence shows that washout is the result of a loss of mechanical tethering between the inner wall endothelium and the JCT. Similar to H-7 effects, perfusion of conventional outflow tissues physically separates the inner wall and JCT, apparently eliminating funneling (**Figure 5(b)**). By stopping perfusion and allowing SC and JCT to reestablish connections, washout can be reversed during a time frame too short to resynthesize and replace ECM materials. Taken with H-7 data, it appears that the relationship between the JCT–TM and SC is essential to facilitate funneling and create resistance.

Concluding Remarks

SC, and in particular its inner wall, has evolved unique features that enable it to function (1) to assist in the pressure-dependent regulation of IOP; (2) as a capacitor to accommodate transient spikes in IOP due to everyday activities; (3) in maintaining the blood–aqueous barrier; (4) to transport micron-sized cell debris/cells into canal lumen; and (5) as part of the venous system to return aqueous humor to the general circulation. Thus, to accommodate these diverse physiological responsibilities the inner wall endothelia have adapted features not found in other vascular endothelia. Therefore, while SC is continuous tight endothelia similar to other endothelia, its inner aspects sit on a discontinuous basal lamina and endure a pressure gradient and associated fluid flow in the basal-to-apical direction unlike its brethren. To fasten the inner wall in place, cells are anchored in spots by attachments to its discontinuous basement membrane and tethered by both elastic fibrils (that originate in the ciliary muscle) and cell processes from underlying JCT cells (anchored to cribiform plates). As cells lift off from their basement membrane and form giant vacuoles in response to transient or constant pressure gradient/waves, pressure relieving and regulating pores dynamically form and disappear to facilitate a relatively stable, pressurized ocular environment. Taken together, SC is defined by its unique name, morphology, physiology, and biological responsibilities.

See also: Biological Properties of the Trabecular Meshwork Cells; Biomechanics of Aqueous Humor Outflow

Resistance; The Development of the Aqueous Humor Outflow Pathway; The Fibrillar Extracellular Matrix of the Trabecular Meshwork; Functional Morphology of the Trabecular Meshwork; Pharmacology of the Aqueous Humor Outflow; Primary Open-Angle Glaucoma; Pseudoexfoliation Syndrome and Glaucoma; Role of Proteoglycans in the Trabecular Meshwork; Uveoscleral Outflow.

Further Reading

Epstein, D. L. and Rohen, J. W. (1991). Morphology of the trabecular meshwork and inner wall endothelium after cationized ferritin perfusion in the monkey eye. *Investigative Ophthalmology and Visual Science* 32: 160–171.

Ethier, C. R. (2002). The inner wall of Schlemm's canal. *Experimental Eye Research* 74: 161–172.

Grant, W. M. (1963). Experimental aqueous perfusion in enucleated human eyes. *Archives of Ophthalmology* 69: 783–801.

Grierson, I. and Lee, W. R. (1975). Pressure-induced changes in the ultrastructure of the endothelium lining Schlemm's canal. *American Journal of Ophthalmology* 80: 863–884.

Hamanaka, T., Bill, A., Ichinohasama, R., et al. (1992). Aspects of the development of Schlemm's canal. *Experimental Eye Research* 55: 479–488.

Johnson, M., Shapiro, A., Ethier, C. R., and Kamm, R. D. (1992). Modulation of outflow resistance by the pores of the inner wall endothelium. *Investigative Ophthalmology and Visual Science* 33: 1670–1675.

Johnstone, M. A. and Grant, W. G. (1973). Pressure-dependent changes in structures of the aqueous outflow system of human and monkey eyes. *American Journal of Ophthalmology* 75: 365–383.

Mäepea, O. and Bill, A. (1992). Pressures in the juxtacanalicular tissue and Schlemm's canal in monkeys. *Experimental Eye Research* 54: 879–883.

Overby, D., Gong, H., Freddo, T., and Johnson, M. (2002). The mechanism of increasing outflow facility during washout in the bovine eye. *Investigative Ophthalmology and Visual Science* 43: 3455–3464.

Overby, D. R., Stamer, W. D., and Johnson, M. (2009). The changing paradigm of outflow resistance generation: Towards synergistic models of the JCT and inner wall endothelium. *Experimental Eye Research* 88: 656–670.

Ramos, R. F., Hoying, J. B., Witte, M. H., and Stamer, W. D. (2007). Schlemm's canal endothelia, lymphatic or blood vasculature? *Journal of Glaucoma* 16: 391–405.

Rohen, J. W., Futa, R., and Lütjen-Drecoll, E. (1981). The fine structure of the cribriform meshwork in normal and glaucomatous eyes as seen in tangential sections. *Investigative Ophthalmology and Visual Science* 21: 574–585.

Sabanay, I., Gabelt, B. T., Tian, B., Kaufman, P. L., and Geiger, B. (2000). H-7 effects on the structure and fluid conductance of monkey trabecular meshwork. *Archives of Ophthalmology* 118: 955–962.

Stamer, W. D., Roberts, B. C., Howell, D. N., and Epstein, D. L. (1998). Isolation, culture, and characterization of endothelial cells from Schlemm's canal. *Investigative Ophthalmology and Visual Science* 39: 1804–1812.

Ye, W., Gong, H., Sit, A., Johnson, M., and Freddo, T. F. (1997). Interendothelial junctions in normal human Schlemm's canal respond to changes in pressure. *Investigative Ophthalmology and Visual Science* 38: 2460–2468.

The Circadian Clock in the Retina Regulates Rod and Cone Pathways

S C Mangel and C P Ribelayga, The Ohio State University College of Medicine, Columbus, OH, USA

Glossary

Circadian clock – A type of self-sustained molecular oscillator with a period of approximately 24 h.
Dopamine – The main retinal catecholamine produced by a type of amacrine or interplexiform cell. Dopamine activates D_1 and D_2 receptors and plays key roles in light-adaptive processes and in the effects of the retinal clock. Most of the effects of retinal dopamine are through volume transmission; thus, dopamine acts as a neurohormone in the retina.
Electrical conductance – A measure of how easily electrical current flows along a certain path that has a difference in voltage or potential.
Entrainment of a circadian clock – Altering the phase of a circadian oscillator due to the presence of environmental input (e.g., light/dark, temperature) generally in the early or late night.
Ganglion cell – The output neuron of the retina that sends its axon to other parts of the brain.
Gap junction – A type of electrical synapse that is comprised of intercellular channels that directly connect the cytoplasm of two cells and facilitate the cell-to-cell passage of ions and small molecules.
Horizontal cell – The second-order interneuron in the outer retina that regulates photoreceptor–bipolar cell synaptic activity.
Melatonin – The neurohormone produced by the retina in the photoreceptor cells and in the pineal gland and whose production is increased at night under the control of circadian clocks.
Mesopic – An adjective that describes the dim ambient light levels between the scotopic and photopic ranges, such as those observed at dawn and dusk, to which both rods and cones can respond.
Photopic – An adjective that describes the bright ambient light levels, such as those observed during a sunny day, to which cones, but not rods, can respond.
Rod (cone) pathway – The ensemble of retinal cells (circuit) that sequentially relay the electrical signals through the retina from the rods (cones) to the ganglion cells.
Scotopic – An adjective that describes the very dim ambient light levels, such as those observed during a moonless night, to which rods, but not cones, which have been separated from the retina, can respond.
Synapse – A zone of contact between two cells that allows the transmission of an electrical signal from one cell to the other. Although a synapse may be chemical or electrical (gap junction), when used alone, the term usually refers to a chemical synapse.

Introduction

Most vertebrate retinas contain both rods and cones, photoreceptor cells that detect and transduce visual images into neural signals. These neural signals are then transmitted to bipolar cells, second-order neurons that then signal ganglion cells, the output neurons of the retina (Figure 1). As we live on a planet that rotates, the ambient or background illumination during a bright sunlit day, compared to a moonless night, changes by approximately 20-billion-fold on a daily basis. The retina must be able to function effectively during this dramatic daily environmental change. At least three adaptive mechanisms are thought to have evolved in the vertebrate retina to facilitate its day/night operation. First, because isolated rods and cones, which have been dissociated from the retina, display high and low light sensitivity, respectively, it has been accepted that rods and cones function under different illumination conditions, that is, that rods mediate dim light (scotopic) vision at night and cones mediate bright light (photopic) vision during the day. Second, external environmental factors, such as the level of ambient illumination itself, can modulate the light responses of retinal neurons and alter the operating characteristics of neural networks within the retina. For example, although ganglion cells exhibit a center-surround receptive field under light-adapted conditions, such as occurs in a bright sunlit day, their receptive fields exhibit only center responses if the retina is subsequently maintained in the dark for 30–40 min, such as occurs if an animal moves from a brightly illuminated area to the shade for a prolonged period. Third, intrinsic retinal processes, such as the circadian (24-h) clock or oscillator in the retina, can also modulate the light responses of retinal neurons and alter the operating characteristics of neural networks within the retina. Although it was originally thought that the transition between day vision and night vision is a passive process driven by the intensity of ambient illumination, it is

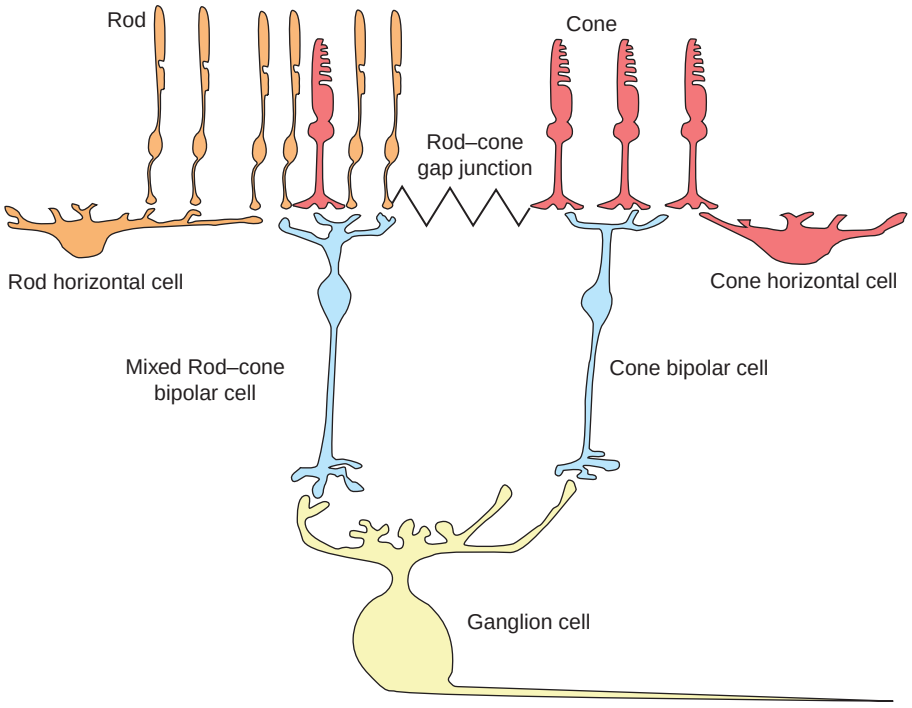

Figure 1 Rod and cone pathways in the goldfish retina. This schematic drawing shows retinal cell types and rod and cone pathways in the goldfish retina. In goldfish retina, as in all vertebrate retinas, rods and cones are anatomically connected or coupled by gap junctions, a type of electrical synapse. Both rods and cones synapse onto second-order neurons, the bipolar cells and horizontal cells, but with some degree of segregation. Mixed rod–cone bipolar cells in goldfish receive direct synaptic input from rods and cones. In the mammalian retina, a single class of rod bipolar cell makes synaptic contact exclusively with rods (not shown). In the goldfish, rod horizontal cells make synaptic contact only with rods and cone horizontal cells and cone bipolar cells make synaptic contact exclusively with cones. In goldfish, bipolar cells directly relay the photoreceptor light responses to ganglion cells, the output neurons of the retina. Individual ganglion cells in both fish and mammals can be driven by signals from both the rod and cone pathways. In mammals, however, rod bipolar cells do not directly synapse onto ganglion cells, but instead communicate rod signals to cone bipolar cells and then to ganglion cells through an interneuron, the AII amacrine cell (not shown).

now known that the retinal clock plays a key role in this mechanism.

A circadian clock is a biological oscillator that has persistent rhythmicity (i.e., a molecular process that rewinds itself) with a period of approximately 24 h under constant environmental conditions (e.g., constant darkness and temperature). Thus, day/night differences in biochemical, morphological, and physiological processes, which are observed under constant environmental conditions, can be attributed to the action of a circadian clock. In the vertebrate retina, many such day/night differences have been observed, including differences in neuronal light responses, dopamine and melatonin content and release, visual sensitivity, retinomotor movements, extracellular pH, photoreceptor disk shedding, and gene expression. A number of these day/night differences have been demonstrated to be under the control of the circadian clock in the retina, and not the circadian clocks located elsewhere in the brain (i.e., suprachiasmatic nucleus of the hypothalamus, pineal gland) or in peripheral organs (i.e., liver).

This article focuses on how the circadian clock in the retina regulates rod and cone pathways, especially concerning circadian regulation of rod–cone coupling. Our review focuses primarily on findings that have been obtained from the fish retina, because this aspect of circadian function has been most thoroughly studied in the fish. However, the available evidence suggests that the circadian mechanisms, discussed in this article, occur in the vast majority of vertebrate species, including both mammals and nonmammals. These similarities will be noted when evidence from mammalian and other nonfish species is available. Information on how the retinal clock regulates other retinal processes is dealt with elsewhere in this encyclopedia and in other recent reviews and papers, which are listed under the section, titled 'Further reading'.

Rod and Cone Pathways in the Fish Retina

As shown in Figure 1, rod signals can reach ganglion cells through at least two separate pathways in all vertebrate species that have both rods and cones. First, rod input can reach ganglion cells through cones. In both mammalian and nonmammalian retinas, rods and cones are anatomically connected or coupled by gap junctions, a type of electrical synapse at which rod input can enter the cone

circuit and thereby reach ganglion cells. Although it was thought that rod–cone electrical coupling is relatively weak, recent evidence has demonstrated that rod–cone coupling in both fish and mice is strong at night, but weak during the day due to the action of the retinal clock.

Second, rod input can reach ganglion cells through bipolar cell pathways that do not involve cones. Rods signal bipolar cells at chemical synapses in all vertebrates. In fish, these bipolar cells also receive synaptic contact from cones and, thus, are called mixed rod–cone bipolar cells (Figure 1). In contrast, in mammals, bipolar cells that receive rod input do not receive cone input. Individual ganglion cells in both fish and mammals can be driven by signals from both the rod and cone systems. In fish, mixed rod–cone bipolar cells synapse directly onto ganglion cells, whereas in mammals, rod bipolar cells do not directly synapse onto ganglion cells but instead provide indirect rod input to ganglion cells through AII amacrine cells, which then signal cone bipolar cells.

Day/Night Differences in the Light Responses of Neurons in the Fish Outer Retina

The first evidence that supported the idea that the retinal clock regulates rod and cone pathways by modulating the electrical synapses between rods and cones was obtained from electrical recordings of goldfish cone horizontal cells, second-order cells that receive synaptic contact from cones, but not from rods (Figure 1). Under dark-adapted conditions during the day, the hyperpolarizing light responses of these cells are cone driven (Figure 2). However, under dark-adapted conditions at night, the light responses of the cells are dominated by rod input. Specifically, the cells respond to light that is 100× dimmer at night, than in the day. In other words, the threshold stimulus that evokes a response is in the low scotopic range (i.e., intensities to which isolated rods, but not isolated cones, respond) at night, but in the low mesopic range (i.e., the threshold intensity of isolated cones) in the day. In addition, the light responses of dark-adapted cone horizontal cells at night, but not in the day, have a time course that is similar to that of rod horizontal cells; they are slower and of longer duration, especially to brighter light stimuli. Additional support that the cells receive rod input at night, but not in the day, was the demonstration that the L-type (or H1) cone horizontal cells, which make synaptic contact with red (long-wavelength)-sensitive cones, are most sensitive to long-wavelength stimuli during the day, but are most sensitive to middle-wavelength stimuli at night, which is typical of rods. Interestingly, the light responses of rod horizontal cells, which make synaptic contact with rods, but not with cones (Figure 1), are similar in the day and night under dark-adapted conditions (Figure 2).

The day/night differences in the light responses of cone horizontal cells described above are due to the action

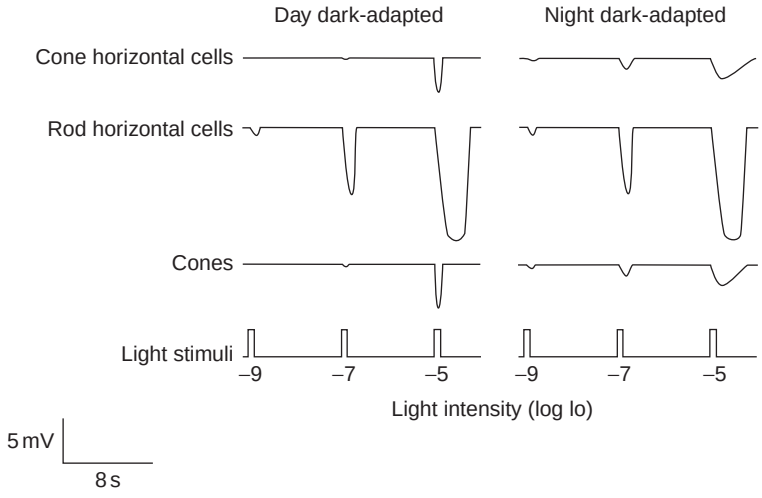

Figure 2 The light responses of goldfish cones and cone horizontal cells depend on the time of day. Schematic intensity-response series are shown for a cone horizontal cell (top trace), a rod horizontal cell (middle trace), and a cone (bottom trace) in the goldfish retina during the day under dark-adapted conditions (left column) and during the night under dark-adapted conditions (right column). At night, the rising and falling portions of the light responses of cones and cone horizontal cells are slower, response duration is longer than stimulus duration, and response threshold is approximately 2 log units lower, compared to daytime. These light-response characteristics are similar to those of rod horizontal cells (although the light responses of rod horizontal cells are larger at night), indicating the presence of significant rod input to cones and cone horizontal cells at night. In contrast, the low-threshold, slow rod-driven light responses of rod horizontal cells do not change between day and night. The light response traces were generated from the averaged response latency, time-to-peak, response duration and amplitude of the cells. Stimuli were full-field white light. Light intensity is relative to a standard (*Io*), with $Io = 2.0\,\text{mW cm}^{-2}$.

of a circadian clock, and not the result of acute dark-adaptive or other environmental effects, because similar day/night differences are observed when the fish and/or their *in vitro* retinas are maintained in constant darkness and temperature for 24–72 h. In addition, prior reversal of the 12-h light/12-h dark cycle in which the fish are maintained, reverses the day/night differences in the light responses of the cone horizontal cells. As circadian clocks can be entrained or phase-shifted by the light/dark cycle, this finding demonstrates that the observed day/night differences in the light responses of L-type cone horizontal cells are circadian in nature, and not due to day/night differences in environmental factors.

More recently, electrical recordings of the light responses of goldfish cones in the day and night, following 24–72 h of constant darkness, revealed that they are also under circadian control. Specifically, the cone light response threshold is 100× lower at night (i.e., low scotopic) than in the day (**Figure 2**). In addition, the light responses of dark-adapted cones at night, but not in the day, have a time course that is similar to that of rod horizontal cells; they are slower and of longer duration, especially to brighter light stimuli. Moreover, although recorded cones can be distinguished as either blue (short-wavelength)-sensitive, green (middle-wavelength)-sensitive, or red (long-wavelength)-sensitive during the day, all recorded cones at night are most sensitive to middle-wavelength light, and their sensitivity closely matches that of rods.

The circadian clock regulates the light responses of cones and cone horizontal cells in part through activation of the D_2 family of dopamine receptors. Dopamine receptors have been divided into the D_1 and D_2 receptor families based on their opposite effects on the level of intracellular cyclic adenosine monophosphate (cAMP) and the difference in their affinity for dopamine. D_1 receptors are approximately 500× less sensitive to dopamine than D_2 receptors, and D_1 receptor activation increases cAMP, whereas D_2 receptor activation decreases it. Substantial evidence indicates that both the D_1 and D_2 families of receptors are found in the retina and that rods and cones express D_2 receptors, whereas rod and cone horizontal cells express D_1 receptors. Moreover, the retinal clock produces a circadian rhythm in dopamine release through melatonin. Specifically, the clock increases melatonin synthesis and release at night, compared to the day. As melatonin inhibits dopamine release, a circadian rhythm in dopamine release is generated, but one in which extracellular dopamine levels are higher in the day, than at night (i.e., the dopamine and melatonin rhythms are in antiphase).

The retinal clock produces a variety of circadian rhythms in the retina, including daily rhythms in retinomotor movements and cyclic guanosine monophosphate (cGMP)-gated cationic channels in cones, by increasing dopamine levels in the day so that D_2 receptors are activated. The clock does not appear to utilize D_1 receptors, apparently because it does not increase dopamine levels sufficiently to activate the low-affinity D_1 receptors in the retina. Similarly, the retinal clock modulates the strength of rod input to cones and cone horizontal cells by increasing the activation of the D_2 receptors on rods and cones during the day. When D_2 receptor activation is minimal at night, as evidenced by the lack of effect of D_2 receptor antagonists at night, rod input dominates the light responses of cones and cone horizontal cells. In contrast, when the retinal clock activates D_2 receptors in the day, rod signals do not reach cones and cone horizontal cells, as evidenced by the finding that application of D_2 receptor antagonists during the day increases rod input to cones and cone horizontal cells. Indirect evidence based on data obtained from cone horizontal cells further suggests that the decrease in intracellular cAMP in rods and cones that is evoked by D_2 receptor activation in the day eliminates rod input to cones and cone horizontal cells. Although this idea requires further direct testing on cones, a circadian rhythm of cAMP content in retinal photoreceptors, with high levels at night, has been described in several vertebrate species.

The Circadian Clock in the Retina, and Not the Retinal Response to the Ambient Illumination, Controls Rod–Cone Coupling

The day/night differences in the strength of the rod input to cones and cone horizontal cells originate in part from changes in the conductance of rod–cone gap junctions. Following the injection of a membrane-impermeant, gap-junction-permeant, biotinylated tracer (biocytin) during the day, the tracer accumulates in the injected goldfish cone. However, when the experiment is conducted at night, the tracer diffuses to many cones and rods in the vicinity of the injected cell, consistent with an increase in the conductance of the rod–cone gap junctions. The tracer experiments demonstrate that the modulation of the rod–cone gap-junctional conductance is the primary means through which the retinal clock controls the strength of the rod signal that flows into cones and cone horizontal cells (**Figure 3**).

Consistent with the effects of the clock on the light responses of cones and cone horizontal cells described above, the clock uses dopamine to control the extent of rod–cone tracer coupling. Specifically, the clock-controlled daytime increase in dopamine decreases rod–cone tracer coupling, whereas the nighttime drop in dopamine levels is required to increase the coupling. The day/night difference in rod–cone coupling can be pharmacologically manipulated and the results are consistent with the involvement of D_2, and not D_1, dopamine receptors. Thus, by increasing dopamine release and D_2 receptor activation during the day, the retinal clock decreases rod–cone coupling and

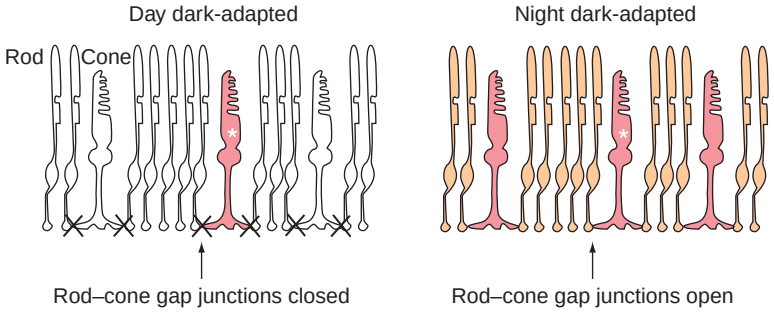

Figure 3 Day/night changes in rod–cone gap-junctional coupling. This drawing illustrates that following injection of the biotinylated tracer biocytin into a single goldfish cone (indicated by an asterisk) during the day (left panel), the tracer remains restricted to the injected cone (filled cone). In contrast, injection of biocytin into a single cone at night (right panel) leads to tracer staining of numerous rods and cones (filled cells) in the vicinity of the injected cell. Since biocytin is a membrane-impermeant molecule that can diffuse through gap junctions, these observations demonstrate that the rod–cone gap junctions are closed during the day and open at night. A similar day/night difference in rod–cone tracer coupling occurs in the mouse.

thereby decreases rod input to cones and cone horizontal cells. Conversely, the nighttime decrease in dopamine release enhances rod–cone coupling and increases rod input to cones and cone horizontal cells.

Interestingly, the effects of the clock on rod–cone tracer coupling and on cone light responses are not altered when dim background lights are present. More specifically, similar results are obtained in the day and night, with and without dopamine D_2 receptors blocked, when the intensity of the ambient illumination is very dim (i.e., low scotopic), as occurs on a moonless night, or is brighter, but still dim (i.e., mesopic), as occurs on a moonlit night. Most significantly, at night, the extent of rod–cone tracer coupling and the strength of rod input to cones and cone horizontal cells are not decreased even when the intensity of the ambient illumination is in the mesopic range. As the background light level at night normally varies between very dim starlight and dim moonlight conditions, these results indicate that the retinal clock, and not the retinal response to the normal visual environment at night, regulates rod–cone coupling. The clock decreases rod–cone coupling at dawn by increasing D_2 receptor activation and increases rod–cone coupling at dusk by reducing D_2 receptor activation.

The Circadian Clock in the Mammalian Retina Controls Rod–Cone Coupling

Although it may be thought that circadian regulation of retinal function occurs in nonmammals, and not in mammals, substantial evidence indicates that the circadian clock in the mammalian retina regulates a variety of cellular phenomena, including melatonin and dopamine production and release, neuronal activity, rod disk shedding, extracellular pH, and rod–cone coupling. Recent findings, using bath application of the gap-junction-permeant, tracer molecule neurobiotin onto mouse retinas that had been cut in pieces with a razor, indicated that neurobiotin diffused extensively through photoreceptor cell gap junctions under dark-adapted conditions at night and in the day when D_2 receptors were blocked, but diffused significantly less under dark-adapted conditions in the day. Thus, it seems likely that the retinal clock controls the strength of rod–cone coupling in most, if not all, mammalian and nonmammalian retinas that have both rods and cones. Moreover, in most vertebrate species, including mammals, the fact that (1) rods and cones are connected by gap junctions, (2) D_2 receptors are expressed by rods and cones, but not by horizontal cells, and (3) the retina contains a circadian clock supports this view. Although the clock increases the conductance of rod–cone gap junctions at night, evidence to date does not address whether at night the clock also increases the conductance of cone–cone and/or rod–rod gap junctions, which are also found in vertebrates.

A Circadian Clock Pathway in the Retina

The circadian clock in the fish retina regulates the light responses of cones and cone horizontal cells in part through a melatonin/dopamine pathway that controls rod–cone coupling (Figure 4). Specifically, the clock regulates melatonin synthesis, so that melatonin synthesis and release are kept low during the day and dramatically increased at night. Melatonin inhibits dopamine release from dopaminergic interplexiform cells, and consequently, the extracellular levels of dopamine are the lowest at night. The relief in the inhibition of dopamine release during the day generates an increase in the extracellular levels of dopamine in the day, so that the D_2 receptors on photoreceptor cells are activated, which then lowers intracellular cAMP and protein kinase A (PKA) levels in the photoreceptors, decreasing the conductance of rod–cone gap junctions. As a consequence, rod input to cones and cone horizontal cells is decreased. At night, because the clock decreases

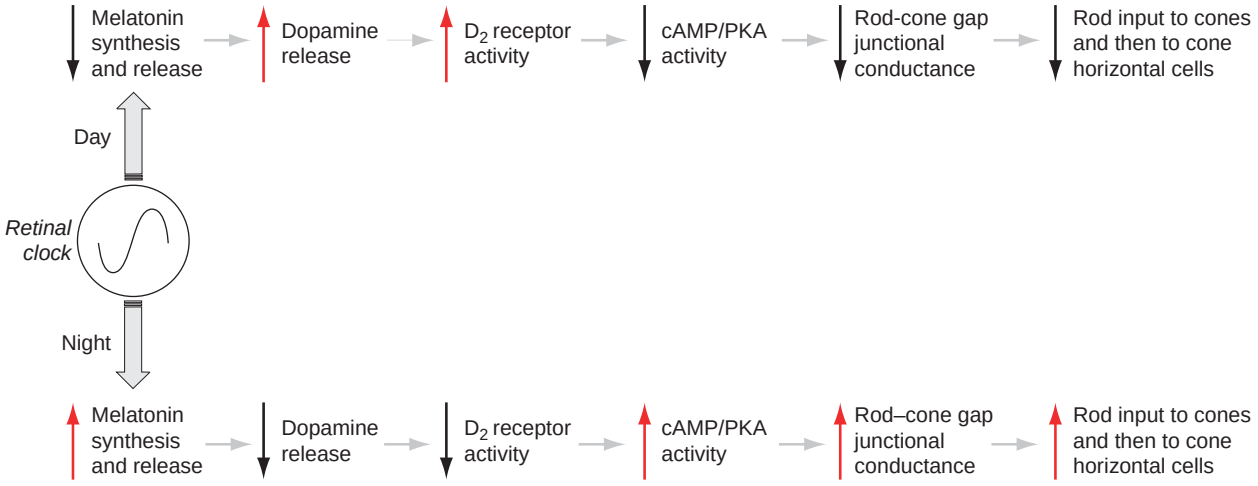

Figure 4 A retinal circadian clock pathway that controls rod–cone coupling. The circadian clock in the retina utilizes melatonin and dopamine to control rod–cone coupling. Specifically, the clock exerts transcriptional and post-translational control of melatonin synthesis, so that melatonin synthesis and release are kept low during the day and dramatically increased at night. Melatonin inhibits dopamine release and consequently extracellular levels of dopamine are the lowest at night. The relief in the inhibition of dopamine release during the day generates an increase in the extracellular levels of dopamine in the day so that the D_2 receptors on photoreceptor cells are activated, which then lowers intracellular cAMP and protein kinase A (PKA) levels in photoreceptors, decreasing the conductance of rod–cone gap junctions. As a consequence, rod input to cones and cone horizontal cells is decreased. At night, because the clock decreases dopamine levels below the threshold of D_2 receptor activation, the intracellular cAMP level in photoreceptor cells increases, raising the conductance of rod–cone gap junctions and increasing rod input to cones. As a result, rod signals are transmitted to cone horizontal cells, even though these cells do not make direct synaptic contact with rods. In the daytime and nighttime sequences of events that are illustrated, upward pointing red arrows and downward pointing black arrows indicate increases and decreases, respectively, in the events with which they are associated. Although the pathway illustrated here has been established from data collected in goldfish, accumulative evidence indicates that this pathway is likely conserved among vertebrates.

dopamine levels below the threshold of D_2 receptor activation, the intracellular cAMP level in photoreceptor cells increases, raising the conductance of rod–cone gap junctions and increasing rod input to cones. As a result, rod signals are transmitted to cone horizontal cells, even though these cells do not make direct synaptic contact with rods. Although the circadian pathway illustrated here has been established from data collected in goldfish, accumulative evidence indicates that this pathway is likely conserved among vertebrates, including mammals. However, it is still unresolved as to whether the clock in the mammalian retina increases dopamine release in the day by generating a melatonin rhythm, as occurs in nonmammals, or by direct control of dopamine metabolism in dopaminergic cells.

It is interesting to note that circadian clock pathways in the retina may be different from light-responsive and light/dark-adaptive pathways. As described above, the retinal clock, and not the retinal response to the level of ambient illumination, uses specific neurotransmitters (i.e., melatonin), neurotransmitter receptors (i.e., melatonin receptors, dopamine D_2 receptors), and synaptic processes (i.e., rod–cone gap junctions) to control the strength of rod–cone electrical coupling, These physiological processes, which participate primarily in circadian clock pathways within the retina, may be distinct from other processes that primarily respond to light stimuli, such as those that mediate bright light adaptation (i.e., D_1 receptors). In the case of dopamine receptors, this segregation of pathways may be explained by the difference in the affinity of D_1 and D_2 receptors for endogenous dopamine. Although the retinal clock increases extracellular dopamine levels sufficiently to activate the high-affinity D_2 receptors on rods and cones, the low-affinity D_1 receptors on horizontal cells are not activated, as evidenced by the absence of a day/night difference in horizontal-cell gap-junctional coupling under dark-adapted conditions. Instead, horizontal cell coupling, which is modulated by D_1 receptor activation, is decreased by bright light stimulation during the day, which increases extracellular dopamine levels sufficiently to activate the D_1 receptors on horizontal cells. Viewed from this perspective, the D_1 and D_2 receptor systems in the retina function in a complementary manner; the retinal clock activates D_2 receptors at dawn and reduces their activation at dusk, whereas bright lights activate D_1 receptors during the day. Retinal function (neurotransmitters, synapses, pathways, adaptation, etc.) may therefore arise from the interplay of both light-responsive and circadian clock pathways.

Functional Implications of Circadian Clock Control of Rod–Cone Coupling

As the retinal clock increases the strength of the electrical synapses between rods and cones at night, very dim light

signals from rods can reach cones and then cone horizontal cells at night. Thus, although individual cones that have been separated from the intact retina cannot respond to very dim light (i.e., low scotopic) stimuli, dark-adapted cones in the intact retina at night can do so because the clock opens the electrical synapse between rods and cones at night. Circadian control of rod–cone electrical coupling therefore serves as a synaptic switch for the direct introduction of rod signals to cones and cone pathways at night, but not in the day.

In addition to enabling rod signals to reach cones at night, the circadian increase in rod–cone electrical coupling may also enhance the detection of very dim, large light stimuli by the rod to bipolar cell to ganglion cell circuit. Many rods converge onto each bipolar cell, summing visual signals over a large spatial area at synapses that are highly nonlinear. Although noise in one photoreceptor cell is independent of the noise in nearby photoreceptor cells, dim, large visual objects will produce similar or correlated responses from nearby photoreceptor cells. As a result, an increase in electrical coupling between nearby photoreceptor cells will decrease photoreceptor noise more than it reduces their light responses to dim, large objects. Increased photoreceptor coupling at night will therefore augment the signal-to-noise ratio and the reliability of rod responses to dim, large stimuli before the nonlinear rod to bipolar cell synapse distorts the signal and the noise. Circadian control of rod–cone electrical coupling thus enhances the detection of very dim, large objects at night, and by decreasing rod–cone coupling at dawn, improves the detection of small objects in the day. The absence of rod signals in the cone pathways during the day facilitates the processing of high acuity and color information by the cone pathways during the day. In contrast, the increase in rod–cone coupling at night may maximize nighttime vision and tune the retina to detect large, dim objects. Moreover, circadian control of rod–cone coupling may also mediate in part the circadian rhythm in visual sensitivity that occurs in many vertebrates, including fish and human.

Finally, the nighttime increase in rod–cone coupling may influence photoreceptor survival. Specifically, the metabolic exchange of small signaling molecules and nutrients will likely occur between rods and cones each night because open gap-junctional channels are large enough to allow the diffusion of such small molecules between coupled cells. Healthy rods might improve cone survival by providing coupled cones with nutrients and protective factors at night and/or dying rods might facilitate the death of coupled cones through the diffusion of pro-apoptotic factors each night.

See also: Anatomically Separate Rod and Cone Signaling Pathways; Chick Metabolism in the Chick Retina; Circadian Regulation of Ion Channels in Photoreceptors; Fish Retinomotor Movements; *Limulus* Eyes and Their Circadian Regulation; Morphology of Interneurons: Amacrine Cells; Morphology of Interneurons: Bipolar Cells; Morphology of Interneurons: Horizontal Cells; Morphology of Interneurons: Interplexiform Cells; Neurotransmitters and Receptors: Dopamine; Neurotransmitters and Receptors: Melatonin Receptors; Physiology of Photoreceptor Synapses and Other Ribbon Synapses.

Further Reading

Barlow, R. B. (2001). Circadian and efferent modulation of visual sensitivity. *Progress in Brain Research* 131: 487–503.

Bloomfield, S. A. and Dacheux, R. F. (2001). Rod vision: Pathways and processing in the mammalian retina. *Progress in Retinal and Eye Research* 20: 351–384.

Copenhagen, D. R. (2004). Excitation in the retina: The flow, filtering, and molecules of visual signaling in the glutamatergic pathways from photoreceptors to ganglion cells. In: Chalupa, L. M. and Werner, J. S. (eds.) *The Visual Neurosciences*, pp. 320–333. Cambridge, MA: MIT Press.

Dowling, J. E. (1987). *The Retina, an Approachable Part of the Brain*. Cambridge, MA: Harvard University Press.

Green, C. B. and Besharse, J. C. (2004). Retinal circadian clocks and control of retinal physiology. *Journal of Biological Rhythms* 19: 91–102.

Iuvone, P. M., Tosini, G., Pozdeyev, N., et al. (2005). Circadian clocks, clock networks, arylalkylamine *N*-acetyltransferase, and melatonin in the retina. *Progress in Retinal and Eye Research* 24: 433–456.

Raviola, E. and Gilula, N. B. (1973). Gap junctions between photoreceptor cells in the vertebrate retina. *Proceedings of the National Academy of Sciences of the United States of America* 70: 1677–1681.

Ribelayga, C. and Mangel, S. C. (2003). Absence of circadian clock regulation of horizontal cell gap junctional coupling reveals two dopamine systems in the goldfish retina. *Journal of Comparative Neurology* 467: 243–253.

Ribelayga, C., Cao, Y., and Mangel, S. C. (2008). The circadian clock in the retina controls rod–cone coupling. *Neuron* 59: 790–801.

Ribelayga, C., Wang, Y., and Mangel, S. C. (2002). Dopamine mediates circadian clock regulation of rod and cone input to fish retinal horizontal cells. *Journal of Physiology (London)* 544: 801–816.

Ribelayga, C., Wang, Y., and Mangel, S. C. (2004). *A circadian clock in the fish retina regulates dopamine release via activation of melatonin receptors. Journal of Physiology (London*) 554: 467–482.

Tessier-Lavigne, M. and Attwell, D. (1988). The effect of photoreceptor coupling and synapse nonlinearity on signal:noise ratio in early visual processing. *Proceedings of the Royal Society of London, Series B* 234: 171–197.

Wang, Y. and Mangel, S. C. (1996). A circadian clock regulates rod and cone input to fish retinal cone horizontal cells. *Proceedings of the National Academy of Sciences of the United States of America* 93: 4655–4660.

Warrant, E. J. (1999). Seeing better at night: Life style, eye design and the optimum strategy of spatial and temporal summation. *Vision Research* 39: 1611–1630.

Witkovsky, P. (2004). Dopamine and retinal function. *Documenta Ophthalmologica* 108: 17–40.

The Colorful Visual World of Butterflies

F D Frentiu, University of Queensland, St. Lucia, QLD, Australia

Glossary

Gene duplication – Duplication of a region of DNA containing a gene, thought to be one of the most powerful evolutionary mechanisms for diversification.
Filtering pigment – Molecules present in photoreceptor cells that act as spectral filters by absorbing particular wavelengths of light.
λ_{max} – Wavelength of peak spectral absorbance of a visual pigment, measured in nm.
Neofunctionalization – The origin of a new gene function by mutation.
Phylogeny – A description of the evolutionary relationships among species inferred to have descended from a common ancestor.
Positive selection – Process through which advantageous mutations increase in frequency in a population.
Visual pigment – An opsin protein bound to a light-sensitive molecule, the chromophore, which is derived from retinal.

Introduction

Butterflies are some of the most colorful animals on the planet. The diversity of their wing colors and patterns has not only inspired human artistic expression but it has also made these animals prominent study systems in biology. For example, butterflies have become leading model animals for the study of evolution and development, particularly of how wings are patterned. Equally, our understanding of defensive signaling is based largely on butterflies, for example, mimicry in *Heliconius* species where two butterflies unpalatable to predators resemble one another in color and pattern. Butterflies also play an important ecologic and economic role by pollinating flowers and orchard crops, where they utilize vision among other senses to find sources of nectar. Understanding vision in butterflies therefore gives us a fascinating insight into how these animals might see their surroundings, their own wing colors, and may also inform us on their patterns of habitat use and pollination.

So what do butterflies see? Can they see in color and if so, how do they use color vision? Here, what we currently know about color vision in the butterflies within an evolutionary context has been reviewed. First, this article provides an overview of the butterfly group and its evolutionary history. Subsequently, a mechanistic account of how the structure of the butterfly eye makes color vision possible is provided, paying particular attention to the molecular basis of the visual pigments that enable this type of vision to occur. Next, is discussed the evolutionary processes that have led to a diversification of the visual systems present in this group that is unparalleled in other insects. Finally, the ecological significance of color vision in the butterflies is explored.

The Butterflies and Their Evolutionary History

The butterflies (Rhopalocera) are a charismatic group of insects that includes an estimated 15 000 species. This is a recently evolved group within the order Lepidoptera, which includes the moths. The Rhopalocera comprises the true day-flying butterflies (Papilionoidea), the skippers (Hesperioidea), and a newly identified group of nocturnal butterflies (Hedyloidea) (**Figure 1**). Within the true butterflies (Papilionoidea), which are the subject of most studies, five families are recognized. The families are: the Papilionidae (including the swallowtails and birdwings), the Pieridae (including the whites and sulfurs), the Lycaenidae (the blues and coppers), the Nymphalidae (the brush-footed butterflies, including the famous monarch, the morphos, and frittilaries), and the Riodinidae (the metalmarks) (**Figure 1**).

The butterflies are thought to have originated on the ancient continent of Gondwana during the Cretaceous period, sometime prior to the extinction of dinosaurs at the Cretaceous–Tertiary (K/T) boundary and possibly concurrent with the radiation of the flowering plants. However, the paucity of fossil butterflies has led to scientific disagreement as to the exact date of when butterflies first appeared, with estimates of their age ranging from 150 to 70 Ma. New molecular approaches are helping resolve some of these controversies. Molecular phylogenies (i.e., reconstructions of the lineages of species using DNA sequence data) have indicated that the Nymphalidae and the Pieridae families were probably present at the K/T boundary, around 65 Ma, and in the case of the Pieriae, may date to 100 Ma. Definitive resolution of the age of the butterflies and timing of divergence of the major families, however, awaits the development of additional molecular markers.

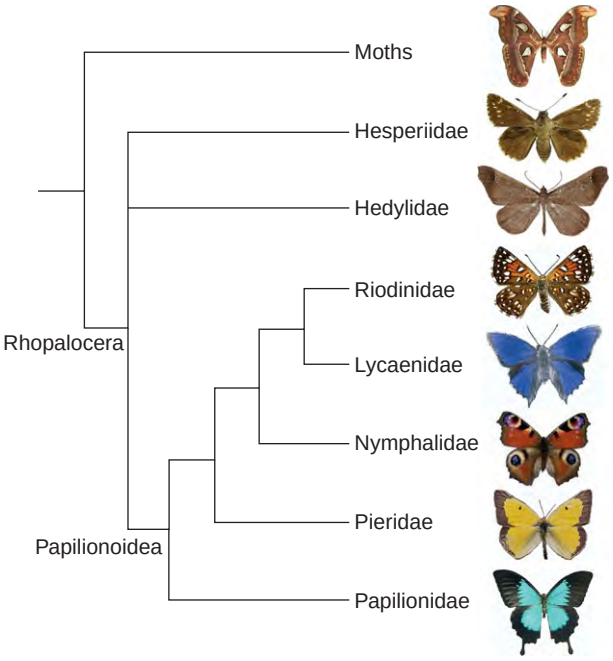

Figure 1 Evolutionary relationships of the major lineages in the Rhopalocera.

Color Vision and the Butterfly Eye

Most organisms detect light through the presence of photosensitive molecules located in specialized organs, such as eyes. However, only arthropods (the phylum that includes insects, spiders, and crustaceans) and vertebrates have developed eyes capable of true color vision. Color vision is the ability to discriminate between two visual stimuli based on their wavelength regardless of their relative intensities. Color vision also requires the presence of at least two photoreceptors with overlapping spectral ranges so that the same point in space can be compared.

Despite the observations that butterflies use colored flowers as food sources and that they employ color-based signaling via their wings, it was only relatively recently that color vision was demonstrated in butterflies using behavioral tests. *Papilio* butterflies were trained to associate rewards containing sucrose with particular colors. When butterflies were behaviorally tested, a majority of animals chose colors previously associated with food rewards among an array of colors regardless of their intensity.

Butterflies, like other insects, have compound eyes that contain thousands of units called ommatidia (**Figure 2(a)**). In butterflies, each ommatidium contains nine photoreceptor cells (cells R1 to R9) (**Figure 2(b)**), that is, cells that possess light-sensitive visual pigments that make color vision possible. The cell membranes of the photoreceptors are folded into microvilli (cell membrane projections) that form the rhabdomeres. The rhabdomeres

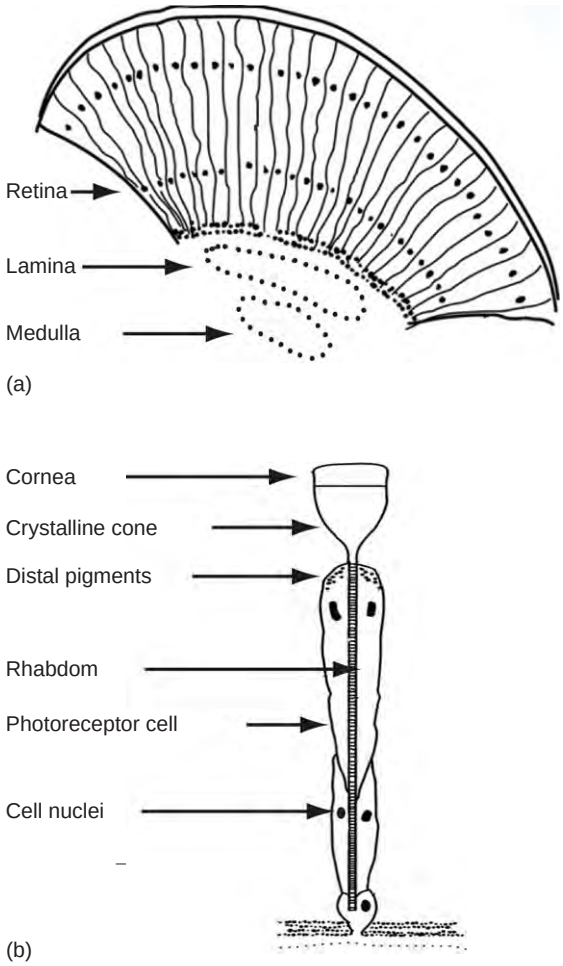

Figure 2 Schematic diagram of the butterfly compound eye. (a) Diagram of a longitudinal section through the eye showing the numerous repeated ommatidia comprising the butterfly retina as well as non photoreceptor regions (lamina and medulla). (b) Diagram of a longitudinal cross-section of an individual ommatidium. Reproduced from Frentiu, F. D., et al. (2007). © National Academy of Sciences USA.

of one ommatidium form a cylinder (the rhabdom) that acts as an optical waveguide for light passing through (**Figure 2(b)**). Light passes through the lens and is focused by the crystalline cone onto the rhabdom. When light propagates down the rhabdom, the majority of it is absorbed by the visual pigments in the photoreceptor cell membranes. Light that is not absorbed by the visual pigments is reflected back by the tapetum, a structure that sits at the base of the ommatidium and is found in most butterflies except papilionids and the pierid genus *Anthocharis*. In addition to visual pigments, butterflies also possess filtering pigments that surround the rhabdom and act as spectral filters by absorbing wavelengths of light and shifting the peak spectral sensitivity of their photoreceptors to longer wavelengths.

Key to color vision in both arthropods and vertebrates are the visual pigments and, most importantly, the presence of at least two spectrally distinct types of visual

pigments. Neural inputs from at least two types of photoreceptor cells that bear different visual pigments are required for color discrimination. A visual pigment comprises of an opsin protein bound to a light-sensitive molecule, the chromophore (**Figure 3**) that, in butterflies, is 11-*cis*-3-hydroxyretinal. Photons reaching the chromophore cause its photoisomerization and induce a conformational change in the opsin protein. In turn this activates a guanine nucleotide-binding protein (G-protein) that initiates the phototransduction cascade that converts light into signals to the brain through a series of biochemical reactions. The eyes of invertebrates employ fundamentally different phototransduction cascades than those of vertebrates.

The absorbance spectrum of a visual pigment depends on the interaction of the chromophore with critical amino acids in the opsin protein. By itself, the chromophore has a wavelength of maximum absorption (the λ_{max} value) in the ultraviolet (UV) part of the light spectrum at approximately 380 nm. However, through the chromophore interacting with key amino acids in the binding pocket of the opsin protein, a diversity of visual pigment λ_{max} values can be achieved, a phenomenon called spectral tuning. The sensitivities of different photoreceptors to light (**Figure 4**) are determined by the opsins that they express and any associated filtering pigments they may contain. The visual pigments of butterfly species sampled to date range in λ_{max} from 340 to 600 nm (**Table 1**), although the exact opsin amino acids involved in producing this diversity remain to be elucidated.

The opsins that form the basis of visual pigments are ancient molecules that belong to the large G-protein-coupled receptor family. They have a seven transmembrane domain structure, with a diagnostic lysine residue in the seventh helix that binds to the chromophore. The opsin family predates the emergence of the major groups of animals present today. Phylogenetic reconstructions suggest that the ancestral arthropod may have been able to see in color, including in the ultraviolet. Insect ultraviolet/blue (UV/B) and blue-green opsins originated early in arthropod evolution. Distinct insect UV and B opsins then evolved via duplication of the ancestral UV/B opsin and the long wavelength (LW) opsin evolved from a duplication of the ancestral blue-green opsin. The blue-green opsin was however lost in most insects, with the exception of some flies (e.g., *Drosophila*). Insects such as bees, butterflies, and moths now possess at least three classes of visual pigment in their photoreceptors that enable them to see in the UV (UV, 300–400 nm), blue (B, 400–500 nm), and long wavelength (LW, 500–600 nm) parts of the light spectrum. However, compared to moths and bees, butterflies display an unusual diversification of their visual systems. In the following, I explore the diversification of butterfly eyes and the evolutionary processes that have produced it.

Spectral Heterogeneity of Butterfly Eyes

Although ommatidia are anatomically identical in structure, they are spectrally very heterogeneous: that is, they hold different complements of photoreceptors that express different visual pigments; different photoreceptors within an ommatidium are designated as R1-R9 and may express different pigments. Using molecular genetic techniques such as *in situ* hybridization to visualize patterns of opsin mRNA has allowed us to map the types of ommatidia present in the butterfly eye. Three types of ommatidia exist in the main retinas of butterflies, with all types of ommatidia expressing LW visual pigments but differing in the expression of the UV and B visual pigments.

The extent of spectral heterogeneity of butterfly eyes differs among the major butterfly families. For example,

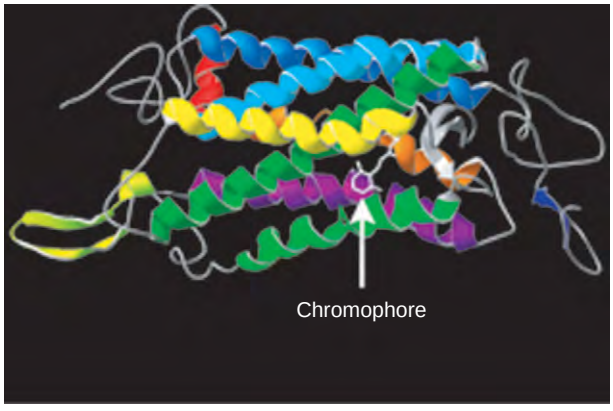

Figure 3 Three-dimensional model of a visual pigment comprising a seven-transmembrane opsin protein and a chromophore (indicated by the arrow). The seven transmembrane domains are shown in different colors. Reproduced from Frentiu, F. D., et al. (2007). © National Academy of Sciences USA.

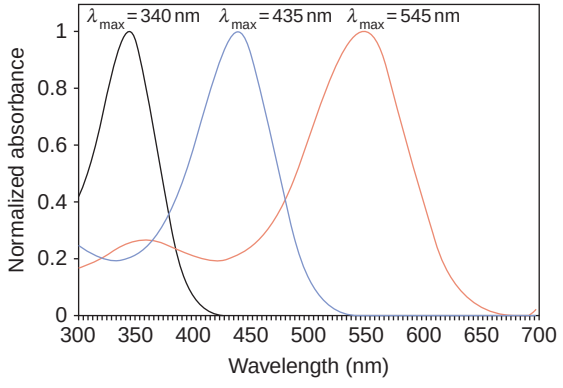

Figure 4 Normalized absorbance spectra of visual pigments in the eye of the monarch, *Danaus plexippus*. Wavelengths of peak absorbance (λ_{max}) for the three visual pigments are estimated to be 340, 435, and 545 nm. Peak absorbance values from Stalleicken et al. (2006) *Journal of Comparative Physiology A* 192: 321–331.

Table 1 Approximate λ_{max} of visual pigments in different butterfly species.

Family	*Subfamily*	*Species*	*UV*	*B*	*LW*
Lycaenidae	Lycaeninae	*Lycaena rubidus*	360	437, 500	568
		Lycaena heteronea	360	437, 500	568
		Lycaena dorcas	360	437, 500	568
		Lycaena nivalis	360	437, 500	568
Nymphalidae	Apaturinae	*Asterocampa leilia*	–	–	530
		Sasakia charonda	345	425, 440	540
	Charaxinae	*Archeoprepona demophon*	–	–	565
	Danainae	*Danaus plexippus*	340	435	545
	Heliconiinae	*Agraulis vanillae*	–	–	555
		Heliconius charitonia	–	–	550
		Heliconius erato	370	470	555
		Heliconius hecale	–	–	560
		Heliconius sara	–	–	550
	Limenitidinae	*Limenitis archippus archippus*	–	–	514
		Limenitis archippus floridensis	–	–	514
		Limenitis arthemis astyanax	–	–	545
		Limenitis lorquini	–	–	530
		Limenitis weidemeyerii	–	–	530
	Nymphalinae	*Aglais urticae*	380	460	530
		Anartia jatrophae	–	–	530, 565
		Euphydryas chalcedona	–	–	565
		Inachis io	–	–	530
		Junonia coenia	–	–	510
		Nymphalis antiopa	–	–	534
		Polygonia c-album	–	–	532
		Polygonia c-aureum	350	450	540, 565
		Siproeta stelenes	–	–	522
		Vanessa cardui	360	470	530
	Satyrinae	*Hermeuptychia hermes*	–	–	530
		Neominois ridingsii	–	–	515
		Oeneis chryxus	–	–	530
		Pararge aegeria	360	460	530
Papilionidae	Papilioninae	*Papilio xuthus*	360	460	530, 515, 575
Pieridae	Pierinae	*Pieris rapae*	360	425, 453	563
Riodinidae	Riodininae	*Apodemia mormo*	340	450	505, 600

the eyes of Nymphalidae species are quite simple in terms of ommatidial heterogeneity. Studies of Nymphalidae species to date show that they have only three types of ommatidia in the main retina and one type in the dorsal rim area (DRA) of the eye, which is an eye region specialized for the detection of polarized skylight. All ommatidial types in the main retina express long wavelength visual pigments in their R3-R8 photoreceptor cells, but the expression of the UV and B opsins in the R1 and R2 cells is variable (the R9 cell expresses the LW opsin in the main retina and may express the UV opsin in the DRA). One ommatidial type contains one UV and one blue receptor, the second has two blue receptors, and the third has two UV receptors. In the DRA ommatidia, the R1-R8 cells express the UV opsin. This type of eye employs a straightforward, one-to-one relationship between the type of visual pigment expressed and spectral phenotype of the photoreceptor cell. It may also best represent the ancestral butterfly eye and it resembles the eyes of bees and moths.

By contrast, the eyes of other families of butterflies are much more diverse in their spectral complements. For example, the butterfly *Pieris rapae* (family Pieridae) expresses four opsins but photoreceptors with seven different peak sensitivities have been identified, due to the presence of filtering pigments. Perhaps the most spectrally diverse butterfly eye studied so far belongs to the papilionid butterfly, the Japanese swallowtail, *Papilio xuthus*. *Papilio xuthus* expresses five different opsins in the eye, has eight different types of photoreceptors, and employs tetrachromatic color vision. In these animals, both opsin gene duplications and pigments acting as spectral filters have led to spectral diversification of visual systems. Below, I consider the evolutionary mechanisms that have led to butterfly visual system diversity.

Diversification of Visual Pigments via Gene Duplication and Positive Selection

The eyes of some butterflies express a larger number of visual pigments than the three UV, B, and LW known to

be present in bees and moths. The diversity of visual pigments is primarily due to opsin gene duplications that have occurred independently in different butterfly families (**Figure 5**). Duplications of the B opsin gene have occurred independently in two of the five butterfly families: the Pieridae and the Lycanenidae, giving rise to four different visual pigments. In the Pieridae, as exemplified by the well-studied *Pieris rapae* (the cabbage white), duplicate B opsins have diversified into violet- ($\lambda_{max} = 425$ nm) and blue-absorbing ($\lambda_{max} = 453$ nm) visual pigments. In the Lycaenidae, duplication of the B opsin has also facilitated the emergence of two visual pigments. However, the peak wavelength sensitivities in species such as *Polyommatus icarus* are different from those found in the Pieridae, with one visual pigment absorbing in the blue ($\lambda_{max} = 437$ nm) and the other in the blue-green ($\lambda_{max} = 500$ nm).

Duplications of the LW opsin gene have occurred independently in three butterfly families, also leading to diversification of visual pigments. In the Papilionidae, three LW opsins are now expressed in the eye, each the result of a round of gene duplication. In *Papilio xuthus*, these duplicated opsins now encode three different visual pigments with λ_{max} values ranging from 515 to 575 nm. The LW opsin gene duplications have also occurred in two species of butterflies in the Nymphalidae and one in the Riodinidae families. In total, of more than 50 butterfly species studied to date, 7 LW opsin duplicates have been identified. The most red-shifted visual pigment known to date in the riodinid butterfly *Apodemia mormo*, with a λ_{max} of 600 nm, has resulted from a gene duplication specific to the family Riodinidae. Molecular evidence has also suggested that duplication was followed by elevated rates of amino acid evolution in one of the LW duplicates. However, not all opsin duplications have resulted in visual pigments expressed in the eye, with some expressed in the optic lobes and brain.

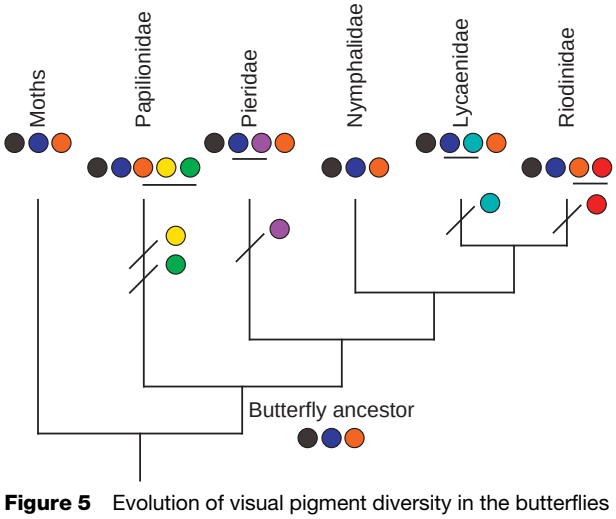

Figure 5 Evolution of visual pigment diversity in the butterflies and hypothesized complement of pigments in the ancestral butterfly eye. Circles indicate UV (gray), blue (blue), and long wavelength (orange) visual pigments. Diagonal lines along the branches of the phylogeny denote opsin duplications.

In addition to gene duplication, a mechanism that generates spectral diversity in butterflies is positive selection on single opsin genes, whereby novel mutations that enhance an organism's fitness spread through a population and may replace other genetic variants. The most striking example of this process to date comes from the North American butterfly genus *Limenitis*. Butterflies in this group have radiated across the North American continent from a European ancestor during the past 3–4 My. The genus is best known for species that display wing color pattern mimicry such as the viceroy *Limenitis archippus*, which mimics the monarch *Danaus plexippus*, and *L. arthemis astyanax*, which mimics the more toxic pipevine swallowtail *Battus philenor*. An unusual diversity in λ_{max} values of the LW visual pigment has been found in this group of butterflies, suggesting that their visual systems had diversified in tandem with wing color patterns (**Figure 6**). Reconstruction of phylogenetic relationships within the genus indicated that a shift in spectral sensitivity towards the blue part of the light spectrum had occurred (**Figure 6**). Wavelength sensitivities of LW visual pigments had diversified from an ancestral λ_{max} of 545 nm in *L. arthemis astyanax* to a λ_{max} of 515 nm in *L. archippus archippus*.

Using several molecular evolutionary analyses, the signature of positive selection was found at several amino acid sites in *Limenitis* LW opsins. The *Limenitis* opsin protein was modeled against the bovine rhodopsin crystal structure (homology modeling) in order to visualize where the amino acid sites were located. The results indicated that some of the amino acids found to be under positive selection were located in the chromophore-binding pocket, strongly suggesting that they interact with the chromophore to determine spectral sensitivities. The same amino acids were found to change in parallel in butterfly species that were distantly evolutionarily related to the *Limenitis* genus but that also showed a shift in λ_{max} in the same direction (**Figure 6**). Interestingly, one of the amino acid sites under positive selection in butterflies is evolutionarily homologous to an amino acid site in the cone opsin of humans that is responsible for a 5–7 nm shift to the blue part of the light spectrum and which is under balancing selection in New World monkeys. These findings suggest a common molecular basis for spectral shifts in insects and vertebrates, a feature that has been retained across more than 540 My of evolution. However, opsin amino acid sites suggested by molecular evolutionary analyses to be involved in the spectral tuning of butterfly visual pigments need to be tested and functionally characterized experimentally.

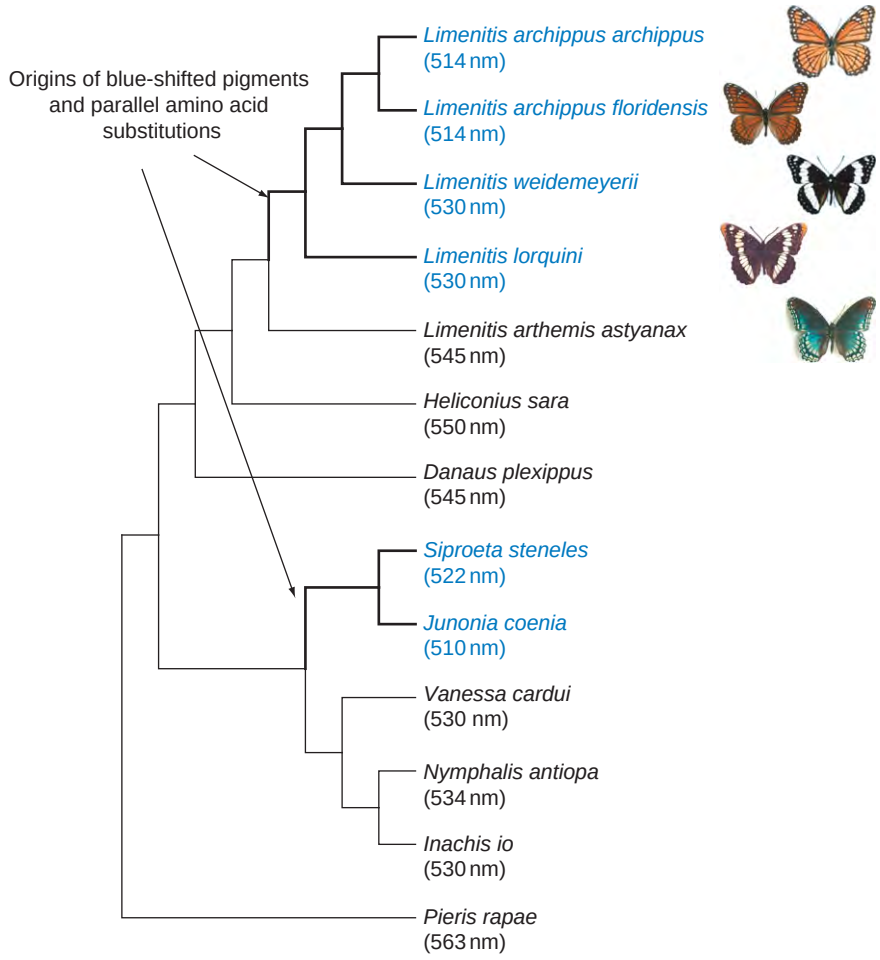

Figure 6 Diversification of wing colors and LW visual pigment spectral sensitivities in the genus *Limenitis* following colonization of North America. Blue-shifted visual pigments ($\lambda_{max} \leq 530$ nm) in evolutionarily independent lineages of butterflies in the family Nymphalidae display parallel substitutions in the opsin protein at key amino acid sites that interact with the chromophore. Reproduced from Frentiu, F. D., et al. (2007). © National Academy of Sciences USA.

Diversification of Photoreceptor Types via Filtering Pigments

Some butterflies possess photoreceptor cells containing filtering pigments that coat the rhabdom (**Figure 1**), which are red, orange, and yellow in color. Filtering pigments act as spectral filters by absorbing particular wavelengths of light traveling down the rhabdom. Whilst the breadth of wavelength sensitivity of a photoreceptor is determined by the opsin it expresses, by absorbing shorter wavelengths of light, filtering pigments shift the λ_{max} of some photoreceptors towards longer wavelengths. The color discrimination abilities of butterflies in a particular wavelength range are thus enhanced by comparing neural inputs from two types of photoreceptors that express the same opsin but have differing peak spectral sensitivities (λ_{max}) due to the presence or absence of filtering pigments.

Filtering pigments play a role in the diversification of the peak spectral sensitivity of photoreceptors in the ommatidia of some butterflies. The same visual pigment, in conjunction with filtering pigments, is used to expand photoreceptor sensitivities in *Heliconius* butterflies. For example, in *Heliconius erato*, two types of LW photoreceptors express the same LW visual pigment but differ in peak spectral sensitivity as a result of the presence of a red-filtering pigment. This expanded wavelength discrimination in the LW range is used in foraging behavior. In *Pieris rapae*, filtering pigments expressed in conjunction with the same LW opsin are used to produce two additional photoreceptor types that enhance wavelength discrimination in the red part of the light spectrum, although the behavioral and ecological reasons for this pattern are unclear.

Currently very little is known about the genetic basis, molecular identity, evolution, and ecological significance of butterfly filtering pigments. Both *Pieris* and *Papilio* butterflies have lateral filtering pigments suggesting that filtering pigments are an evolutionarily old feature of the butterfly eye. Some of the pigments used in butterfly wing

colors are molecularly similar to eye pigments found in *Drosophila*, although butterflies may employ a much larger repertoire of pigments than flies. Tantalizing clues from a handful of studies suggest that, aside from diversifying photoreceptor sensitivities, filtering pigments may play a role in the co-evolution of photoreceptors and color-based mating signals. The same genes that mediate both spectral sensitivities in photoreceptors via filtering pigments may also influence the expression of wing pigments expressed in butterfly wings. However, this hypothesis remains to be tested empirically by identifying and molecularly characterizing the genes involved. Filtering pigments and their expression in the butterfly eye offer a fruitful avenue for research into the co-evolution of animal color-based signals and the ability to perceive them.

Evolution of Sexually Dimorphic Eyes: Opsin Duplications and Sex-Specific Filtering Pigment Expression

One of the most interesting aspects of butterfly vision is that some species display sexually dimorphic eyes: males and females detect different colors in the same areas of the eye. This feature appears to have evolved independently in two butterfly families, the Lycaenidae and the Pieridae, via two different mechanisms. In the North American butterfly *Lycaena rubidus* (Lycaenidae), duplication of the B opsin has facilitated the evolution of a sexually dimorphic eye. The eyes of this butterfly express four opsin genes, one UV, two B (B1 and B2), and one LW. In the dorsal part of the eye, *L. rubidus* males exclusively express the B1 opsin in the R3-R8 photoreceptors, whereas in the female both B1 and LW are expressed. The R1 and R2 cells primarily express UV opsins in this dorsal part of the eye. Therefore, duplication and neofunctionalization of the B1 domain of expression have potentially allowed the evolution of dichromatic and trichromatic color vision in this part of the eye in males and females respectively. The male *L. rubidus* may use dichromatic color vision in the dorsal part of the eye in behaviors associated with defense of its mating territory. If opsin duplication has facilitated the evolution of sexually dimorphic eyes, we may yet discover these eyes to be more prevalent in the butterflies than previously thought given how frequently such duplications have occurred in this group of insects.

In *Pieris rapae* subspecies *crucivora* (Pieridae), sexually dimorphic eyes have also been documented, however in this case mediated by the sexually differentiated expression of filtering pigments in some photoreceptors. The sexual dimorphism occurs in the violet photoreceptors of this species present in some ommatidia. In females, violet photoreceptors match their expected peak spectral sensitivity ($\lambda_{max} = 425$ nm). However, in males, the expression of a violet-absorbing filtering pigment modifies violet photoreceptors into double-peaked blue photoreceptors that have a much narrower spectral sensitivity, with a λ_{max} of 416 nm. This sexual dimorphism may aid males in discriminating the different wing colors of males and females that differ in the short wavelength part of the spectrum, but this hypothesis requires empirical testing through behavioral tests. Not all subspecies of *Pieris rapae* show sexually dimorphic filtering pigment expression, suggesting that pigment-mediated changes in spectral sensitivities may rapidly facilitate fine-tuning of visual systems according to the ecology of a particular species or subspecies.

Ecological Significance of Butterfly Visual System Diversity

Why are butterfly eyes so diverse? What are the ecological reasons for such a diversity of color vision systems? To date, however, the ecological and life history factors driving the diversity observed have been far less thoroughly investigated than the molecular basis of this pattern. No clear adaptive matching of the visual pigments to ambient light, as demonstrated in fish, has ever been found in butterflies. For example, the coelacanth lives at a depth of 200 m and only receives light at around 480 nm in wavelength. Its two visual pigment sensitivities peak at around 475 and 485 nm, suggesting adaptive matching to the light environment in this species. In cichlids, visual system spectral sensitivities also seem to match the ambient light environments of these species. In butterflies, the limited evidence available to date suggests that visual pigment diversity may be driven by the social signaling and foraging needs of the animals rather than their particular light environment.

Like many other insects, butterflies utilize vision for a whole range of tasks. They use vision to locate food sources, select suitable oviposition sites, and in intraspecific communication. *Papilio* butterflies use two of their duplicated LW opsins to see in the green part of the light spectrum when ovipositing and foraging. The lycaenid butterfly *Polyommatus icarus* uses one of the duplicate B opsins together with the LW opsin-based visual pigment to see green up to 560 nm when foraging. Importantly, opsin gene duplications resulting in the diversification of photoreceptor types have clearly impacted on the foraging behavior of butterflies.

Mate choice in many butterfly species also occurs via color-based signaling. For example, *Heliconius* butterflies appear to use both colored and polarized light for finding mates. The size of UV-reflecting eye spots on the wings seems to correlate with mating success in *Bicyclus anynana*. These observations suggest that there might be selective pressure for visual systems to evolve to detect the specific

spectral signals of wings. Correlative evidence suggests that photoreceptor sensitivities have evolved in tandem with wing coloration but empirical evidence is needed.

Conclusions

It is clear that the visual systems enabling butterflies to see in color are functionally very diverse compared to other insects, particularly their moth ancestors. Visual system diversity has been achieved primarily through opsin gene duplication, positive selection at single opsin loci, and heterogeneous expression of filtering pigments in photoreceptors. The evolutionary basis of this pattern of diversification has recently received significant attention, however the exact molecular basis of spectral tuning of butterfly visual pigments remains unknown. Butterfly visual systems offer an excellent opportunity to study the evolutionary and functional genetic links from genotype to phenotype through to behavioral and ecological consequences. To this end, further work is required to explicitly link the pattern of photoreceptor diversification in different butterflies to their ecology, behavior, and life history traits. Only then will we gain a complete understanding of the evolutionary significance of visual system diversification in these insects.

See also: Circadian Rhythms in the Fly's Visual System; Color Blindness: Acquired; Color Blindness: Inherited; Microvillar and Ciliary Photoreceptors in Molluskan Eyes; Photoresponse in Squid; Phototransduction: Rhodopsin; Phototransduction: The Visual Cycle.

Further Reading

Arikawa, K., Wakakuwa, M., Qiu, X., Kurasawa, M., and Stavenga, D. G. (2005). Sexual dimorphism of short-wavelength photoreceptors in the small white butterfly, *Pieris rapae crucivora*. *Journal of Neuroscience* 25: 5935–5942.

Bernard, G. D. (1979). Red-absorbing visual pigment of butterflies. *Science* 203: 1125–1127.

Bernard, G. D. and Remington, C. L. (1991). Color vision in *Lycaena* butterflies: Spectral tuning of receptor arrays in relation to behavioral ecology. *Proceedings of the National Academy of Sciences of the United States of America* 88: 2783–2787.

Briscoe, A. D. (2008). Reconstructing the ancestral butterfly eye: Focus on the opsins. *Journal of Experimental Biology* 211: 1805–1813.

Frentiu, F. D., Bernard, G. D., Sison-Mangus, M. P., Brower, A. V. Z., and Briscoe, A. D. (2007). Gene duplication is an evolutionary mechanism for expanding spectral diversity in the long-wavelength photopigments of butterflies. *Molecular Biology and Evolution* 24: 2016–2028.

Frentiu, F. D., Bernard, G. D., Cuevas, C. I., et al. (2007). Adaptive evolution of color vision as seen through the eyes of butterflies. *Proceedings of the National Academy of Sciences of the United States of America* 104: 8634–8640.

Frentiu, F. D. and Briscoe, A. D. (2008). A butterfly eye's view of birds. *BioEssays* 30: 1151–1162.

Kelber, A. (1999). Ovipositing butterflies use a red receptor to see green. *Journal of Experimental Biology* 202: 2619–2630.

Kelber, A. and Pfaff, M. (1999). True color vision in the orchard butterfly, *Papilio aegeus*. *Naturwissenschaften* 86: 221–224.

Kinoshita, M., Shimada, N., and Arikawa, K. (1998). Colour vision of the foraging swallowtail butterfly *Papilio xuthus*. *Journal of Experimental Biology* 202: 95–102.

Sison-Mangus, M. P., Bernard, G. D., Lampel, J., and Briscoe, A. D. (2006). Beauty in the eye of the beholder: The two blue opsins of lycaenid butterflies and the opsin gene-driven evolution of sexually dimorphic eyes. *Journal of Experimental Biology* 209: 3079–3090.

Stalleicken, J., Labhart, T., and Mouritsen, H. (2006). Physiological characterization of the compound eye in monarch butterflies with focus on the dorsal rim area. *Journal of Comparative Physiology A - Neuroethology Sensory Neural and Behavioral Physiology* 192: 321–331.

Stavenga, D. G. and Arikawa, K. (2006). Evolution of color and vision of butterflies. *Arthropod Structure and Development* 35: 307–318.

Terakita, A. (2005). The opsins. *Genome Biology* 6: Article No 213.

Wahlberg, N., Braby, M. F., Brower, A. V. Z., et al. (2005). Synergistic effects of combining morphological and molecular data in resolving the phylogeny of butterflies and skippers. *Proceedings of the Royal Society B: Biological Sciences* 272: 1577–1586.

Wakakuwa, M., Stavenga, D. G., Kurasawa, M., and Arikawa, K. (2004). A unique visual pigment expressed in green, red and deep-red receptors in the eye of the small white butterfly, *Pieris rapae crucivora*. *Journal of Experimental Biology* 207: 2803–2810.

The Corneal Stroma

J L Funderburgh, University of Pittsburgh, Pittsburgh, PA, USA

Glossary

Adherens junctions – Protein complexes that occur at cell–cell junctions, involving calcium-dependent homophilic interactions of a family of transmembrane proteins called cadherins.
Connexin – Gap-junction proteins; family of structurally related transmembrane proteins that assemble to form vertebrate gap junctions. Each gap junction is composed of two hemichannels, or connexons, which are themselves each constructed out of six connexin molecules.
Corneal dystrophies – Group of disorders characterized by a noninflammatory, inherited, bilateral opacity of the cornea.
Crystallins – Water-soluble structural proteins found in the lens of the eye, accounting for the transparency of the structure.
Ectomesenchyme – It has similar properties to mesenchyme. The major difference is that ectomesenchyme arises from neural crest cells, which are a critical group of cells that form in the cranial region during early vertebrate development.
Glycan – It refers to a polysaccharide or oligosaccharide. Glycan may also be used to refer to the carbohydrate portion of a glycoconjugate, such as a glycoprotein, glycolipid, or a proteoglycan.
Glycosaminoglycans – Long, linear carbohydrate polymers that are negatively charged under physiological conditions, due to the occurrence of sulfate and uronic acid groups.
Hurler's syndrome – Known as mucopolysaccharidosis type I (MPS I), Hurler's disease, or gargoylism, this genetic disorder results in the buildup of mucopolysaccharides due to a deficiency of alpha-L iduronidase, an enzyme responsible for the degradation of mucopolysaccharides in lysosomes. Without this enzyme, a buildup of dermatan sulfate occurs in the body. Symptoms appear during childhood and early death can occur due to organ damage.
Keratan sulfate – Also called keratosulfate, it is any of several sulfated glycosaminoglycans (structural carbohydrates) found especially in the cornea, cartilage, and bone. Keratan sulfates are large, highly hydrated molecules which, in joints, can act as a cushion to absorb mechanical shock.
Keratocytes – The basic cell type found in the corneal stroma. The keratocytes are sparse in distribution, occupying less than 5–10% of the stromal volume.
Lamellae – A lamella is a thin plate-like structure, often one among many lamellae very close to one another, with open space between.
Lumican – Also known as LUM, it is a human gene. This gene encodes a member of the small, leucine-rich proteoglycan (SLRP) family that includes decorin, biglycan, fibromodulin, keratocan, epiphycan, and osteoglycin. In these molecules, the protein moiety binds collagen fibrils and the highly charged hydrophilic glycosaminoglycans regulate interfibrillar spacings. Not only is lumican the major keratan sulfate proteoglycan of the cornea, but it is also distributed in interstitial collagenous matrices throughout the body. Lumican may regulate collagen fibril organization and circumferential growth, corneal transparency, and epithelial cell migration and tissue repair.
Macular corneal dystrophy – An autosomal recessive condition, which is the least common but the most severe of the three major stromal corneal dystrophies. It is characterized by multiple, gray-white opacities that are present in the corneal stroma and that extend out into the peripheral cornea.
Mesenchyme – Loosely organized connective tissue present in the embryo regardless of origin. Viscous in consistency, mesenchyme contains collagen bundles and fibroblasts.
Myofibroblast – Cell with a phenotype between a fibroblast and a smooth muscle cell in differentiation. It can contract by using smooth muscle-type actin–myosin complex, rich in a form of actin called alpha-smooth muscle actin. These cells are then capable of speeding wound repair by contracting the edges of the wound.
Neural crest – Transient component of the ectoderm, located between the neural tube and the epidermis of an embryo during neural tube formation. Neural crest cells migrate during neurulation, an embryological event marked by neural tube closure.
Proteoglycan – Special class of glycoproteins that are heavily glycosylated. They consist of a core protein with one or more covalently attached glycosaminoglycan (GAG) chain(s).
Scheie's syndrome – Mildest form of mucopolysaccharidosis type I (MPS I) (see Hurler's syndrome).

Sutural fibers – The elasmobranch (sharks, skates, and rays) cornea resists swelling because of unique structural adaptations in the stroma called sutural fibers. These are collagen fibers running anterior-to-posterior, perpendicularly to the stromal lamellae, tying the anterior limiting lamella to Descemet's membrane.

Transforming growth factor-beta – Transforming growth factor-beta (TGF-β) is a small protein-growth factor with a broad array of functions. It controls proliferation, cellular differentiation, and other functions in most cells. It plays a role in immunity, cancer, and heart disease.

Stromal Anatomy

In humans, the cornea has a diameter of about 11.5 mm and a thickness of 0.5–0.6 mm in the center and 0.6–0.8 mm at the periphery. Almost 90% of the human cornea is composed of stroma (**Figure 1(a)**). By weight, water in the extracellular matrix makes up 65% of the stroma and cellular water 11%. This hydration is roughly similar to that of cartilage, but surprisingly, it is higher than that of bone, muscle, or adipose tissue. As discussed below, the proteoglycans of the stroma are hydrophilic and, given free access to water, the tissue will imbibe up to 10-fold its normal content of water. Thus the tissue composition, particularly its hydration, is a dynamic property.

The majority of the stroma consists of thin sheets (lamellae) of tightly packed collagen fibrils. In human corneas, there are up to 200–250 such lamellae, each about 2-μm thick. Within each lamella, the collagen fibrils run parallel to the corneal surface, parallel to one another, and regularly spaced. Ends of the fibrils are not abundant and thus fibrils extend essentially the entire width of the cornea. The lamellae are largely self-contained, but occasional bundles of fibrils extend from one lamella to another. Directional orientation of the fibril layers varies between neighboring lamellae. In the posterior stroma the fibril orientation is almost perpendicular from one layer to the next. Anteriorly, it is more oblique. This arrangement of layers of parallel rigid rods in a friable matrix is not unlike that of composite structural materials such as fiberglass or reinforced concrete. Such an arrangement gives the cornea its remarkable toughness and tensile strength.

Numerous electron micrographic studies have documented the striking regularity of the collagen in the stroma. The collagen fibrils in central stroma have a diameter of about 31 nm and the distribution of diameters is narrow, giving a remarkably homogeneous distribution of collagen within each fibril bundle. Within the fibril bundles electron-dense material, identified as proteoglycans, encase the individual fibrils and form bridges between neighboring fibrils (**Figure 1(b)**). In central stroma of normal human cornea, the proteoglycan bridges occur at highly regular intervals, and the bridging structures are of uniform lengths, about 1.8 nm. Such tight interaction between fibrils is considered to participate in generating the parallel alignment of the fibrils in each bundle and the highly regular spacing between neighboring fibrils. As discussed below, this lattice-like structure of the collagen fibrils in the central stroma is thought to be essential for corneal transparency.

The anterior portion of most corneal stromas is limited by an acellular layer of dense, irregularly organized collagen immediately subjacent to the epithelial basement membrane. This anterior limiting lamella (ALL) is also known as Bowman's layer or Bowman's membrane. In human corneas, the ALL is about 10-μm thick in the central cornea and absent in the periphery. ALL is also prominent in chickens and some other terrestrial mammals, but it is very thin or not detected in other species such as felines. Collagen fibrils in the ALL are randomly interwoven to form a dense, felt-like sheet composed primarily of collagen types I, III, and V. Collagen VII, associated with anchoring fibrils of the overlying epithelium, is also present within the ALL. The posterior of the ALL merges with the lamellar stroma via oblique fibril bundles, recently revealed using two-photon microscopy. These connecting fibers appear to serve as a stabilizing feature, anchoring the anterior lamellae to the more rigid ALL and indirectly to the epithelial basement membrane. These anterior anchoring fibers appear analogous to the well-known sutural fibers present in corneas of some species of sharks. The sutural fibers traverse the cornea perpendicular to the orientation of the lamellae and prevent the stroma from swelling when exposed to water. The oblique anterior anchoring fibrils recent identified in human corneas may provide a similar function in that studies show the swelling of human corneas in water occurs almost exclusively in central and posterior stroma. The extremely dense collagen in the ALL has prompted speculation that it may serve as a defense against bacterial or viral infection; however, little hard evidence supports such a role.

Stromal Development

The embryonic origins of the corneal stroma were detailed in a elegant study by Hay and Revel in 1969. In developing chicks, a wave of migrating neural crest cells, destined to become corneal endothelium, moves between the overlying ectoderm and the lens during early embryogenesis. Shortly thereafter, the epithelium secretes an acellular layer of matrix, termed the primary stroma, which becomes hydrated and swells before a second wave of neural crest cells move into the stroma and begins active

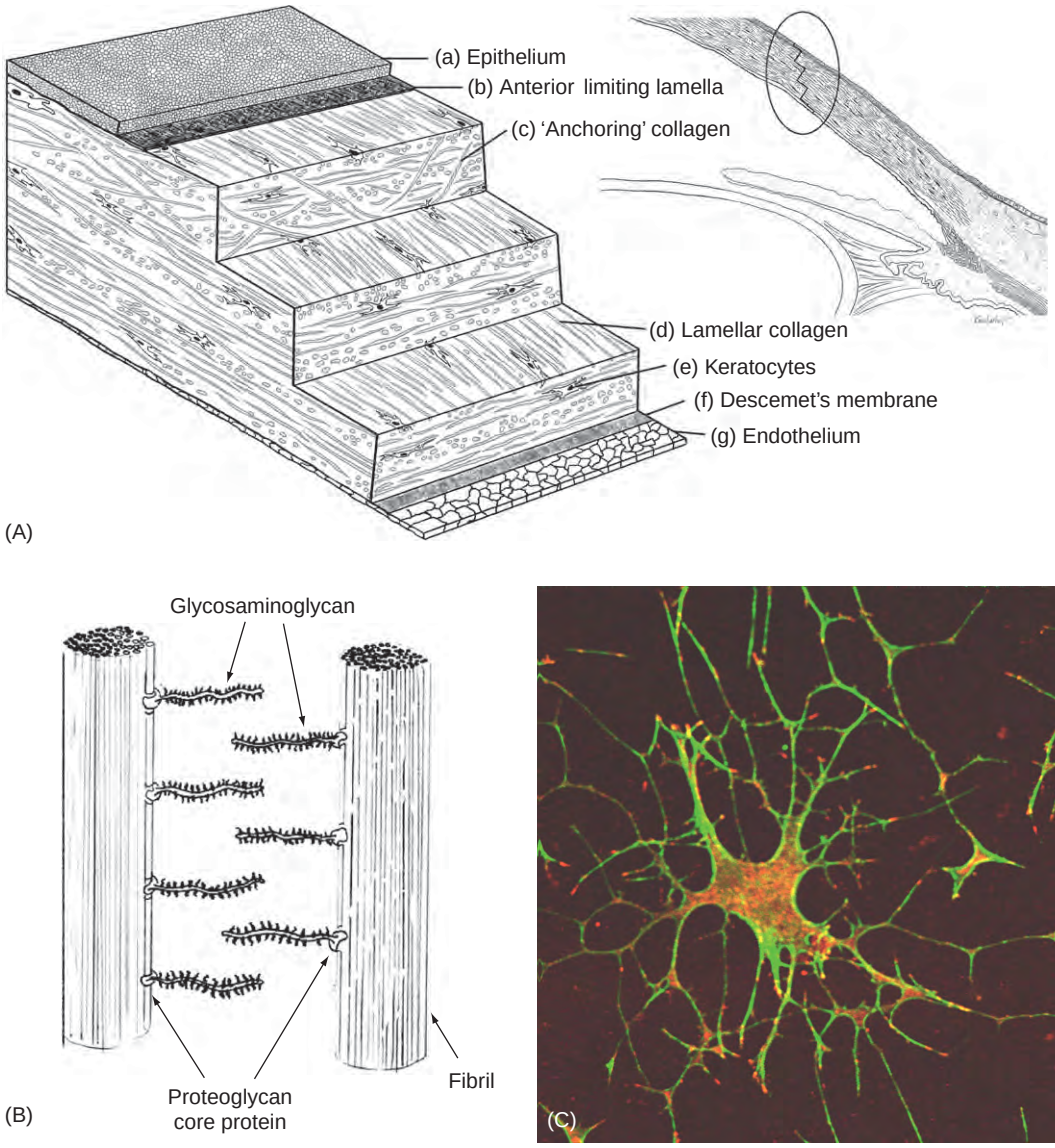

Figure 1 Components of the corneal stroma. (A) Cross section of the cornea with the expanded cutaway illustrating (a) epithelium, (b) anterior limiting lamella, (c) anterior 'anchoring' collagen fibrils, (d) aligned lamellar collagen in central and posterior stroma, (e) keratocytes sandwiched between lamellae, (f) Descemet's membrane (g) endothelium. (B) Interaction between collagen fibrils and stromal proteoglycans. The core proteins bind fibrillar collagen at regular intervals and glycosaminoglycan chains protrude into the interfibrillar space. (C) Cultured primary bovine keratocyte with its extensive cellular processes (Green, actin; Red, vinculin).

secretion of the abundant extracellular matrix of the stroma. The orientation of collagen in the primary stroma is thought to direct formation of lamellae elaborated by the invading stromal cells. At day 14 (before hatching at day 21), the stroma undergoes dehydration in response to thyroxine, leading to thinning of the stroma and initiation of stromal transparency. Mammalian corneas show a somewhat different developmental pattern. No obvious primary stroma is present, and the endothelium and stromal cells are formed after a single influx of neural crest cells. After the endothelium is formed, neural crest cells in the stroma begin to elaborate new extracellular matrix. In mice and rabbits, cells in the stroma are mitotically active until after birth. In mice, approximately at the time of eye opening (12–14 days postnatal) a decrease in the number of stromal cells occurs along with thinning and dehydration of the stroma. Simultaneously, the cornea-specific glycosaminoglycan – keratan sulfate – appears in the stroma, the stromal cells become quiescent, stromal proteins known as corneal crystallins accumulate in keratocytes, and transparency of the cornea increases significantly. Human stroma, by contrast, matures earlier in development. Keratan sulfate and corneal transparency are observed in embryos at 10–12 weeks of gestation, and infants are born with fully transparent corneas. Despite these species-related differences, the pattern of neural

crest population of the stromal space, secretion of corneal-specific matrix components following formation of the endothelial barrier, and corneal thinning due to dehydration present a common pattern of stromal development.

Stromal Cells

Cells populating the adult stroma are known as keratocytes. Although the same term has been used for fish epidermal cells, corneal keratocytes are neural crest-derived mesenchymal cells (ectomesenchyme). In adult tissue, the keratocytes are located between collagenous lamellae, exhibiting a flattened cell body with numerous extended cellular processes (**Figure 1(c)**). Keratocytes are the population of cells responsible for deposition and maintenance of the extracellular matrix which provides strength and transparency to the cornea. This population of cells is highly interconnected via their processes with numerous junctions between neighboring cells. At sites of contact, gap junctions containing connexin 43 and adherens junctions with cadherin 11 are present. A localized stimulus, such as an epithelial scratch, activates keratocytes throughout the stroma, as indicated by uptake of the dye neutral red. Such a global response to a localized stimulus demonstrates presence of a network of active cell–cell communications maintained by interconnected keratocytes. Following maturity, keratocytes remain quiescent, almost never exhibiting mitotic nuclei or uptake of DNA precursors. Studies of keratocyte turnover in mammals find half-lives too long to estimate accurately. DNA of keratocytes in adult humans shows a high incidence of acquired chromosomal abnormalities, but that of infants and children does not. This fact suggests that keratocytes do not regularly enter the cell cycle in which DNA repair is initiated, but accumulate damage from environmental exposure to light and oxidative stresses over long periods of time. Thus, in the nonwounded cornea, keratocytes may exist for years or decades without turnover.

In spite of their quiescence, keratocytes maintain an active synthesis of the extracellular matrix. Proteoglycan secretion is maintained at a high rate throughout life. Because collagen becomes cross-linked in adult corneas, however, collagen turnover is reduced in adult keratocytes compared to that in embryonic tissue. Adult keratocytes also retain the ability to enter the cell cycle and divide. Nearly 100% of keratocytes isolated by collagenase digestion of bovine corneas enter the cell cycle when exposed to serum or mitogens. Collagenase-isolated primary keratocytes cultured in serum-free conditions maintain the keratocyte phenotype, as defined by quiescence – a dendritic morphology (**Figure 1(c)**) – and expression of high levels of cornea-specific products (**Table 1**); however, when exposed to serum or other mitogens, these cells dedifferentiate into a fibroblastic phenotype similar to that of other mesenchymal cells cultured in serum. Following short-term culture in serum, some keratocyte properties return under quiescent conditions, but after multiple passages in culture transition to the fibroblast phenotype appears to be irreversible. When cultured corneal fibroblasts are exposed to transforming growth factor-beta (TGF-β), the cells express mRNA and protein for alpha-smooth muscle actin and assume a contractile phenotype known as the myofibroblast. TGF-β also induces a range of new gene products, many associated with corneal scarring or fibrosis *in vivo*. Genes and gene products which have been identified in corneal fibrotic (scar) tissue and also as products of myofibroblasts are shown in the top rows of **Table 1**. These include cell-associated markers such as Thy-1, matrix proteins (fibronectin, SPARC, tenascin c, etc.), collagens, proteoglycan proteins (biglycan), and glycosaminoglycans. The last four entries of **Table 1** show components expressed at high levels in keratocytes which are reduced or disappear in corneal scars and are not expressed by myofibroblasts. These include corneal crystallins (such as ALDH3), the keratan sulfate proteoglycan keratocan, and the cell-surface marker CD34. As described below, the characteristic changes in collagens, crystallins, and proteoglycans occurring during keratocyte–myofibroblast transition directly impact stromal transparency. Thus, loss of transparency in extracellular matrix deposited in response to wound healing can be directly attributed to responses of the keratocytes to wounding. Smooth muscle actin-containing cells appear in healing corneas 1–2 weeks following wounding, and this appearance can be blocked with antibodies to TGF-β. This inhibition suggests that *in vivo*, as *in vitro*, TGF-β is an important inducer of fibrotic scar tissue. Several weeks following healing of corneal wounds, smooth muscle actin-containing cells are no longer seen in the wound area. It not clear, however, that the loss of smooth

Table 1 Markers of stromal fibrosis

Gene or product	*Normal stroma*	*Fibrotic stroma and myofibroblast*
Dermatan sulfate	+	+++
Hyaluronan	0	++++
Biglycan	+/–	+++
Tenascin C	0	+++
SPARC	0	+++
Fibrillin-1	0	+++
Collagen 1	++	++++
Collagen 3	+/–	++
Thy-1	+/–	++
Aldehydehyde dehydrogenase 3A1	++++	+
Keratocan	+++	+
Keratan sulfate	++++	0
Collagen a3(IV)	++	0
CD34	+++	0

muscle actin expression corresponds to a return to normal stromal extracellular matrix production. In fact, experimental animal studies show expression of fibrotic markers for months following wounding, and human scar tissue can persist for many decades.

In addition to keratocytes, other cell types have been observed in the stroma. Most prominent are bone marrow-derived cells. Mice in which bone marrow cells express green fluorescent proteins have about 10% of stromal cells demonstrating fluorescence. Most stromal leucocytes express the CD11b marker, but not other dendrite, granulocyte, T-cell, or NK markers, placing them in the monocyte/macrophage lineage. Following minor damage to the epithelium, the number of green inflammatory cells in the stroma increases dramatically within a few hours. These transient inflammatory cells are primarily neutrophils.

A population of stem or progenitor cells has also been identified in the corneal stroma. Transplantation of avian corneal keratocytes into the neural crest migratory pathways of early embryos showed that some of the transplanted cells changed phenotype, migrating and differentiating into a variety of neural crest-derived tissues, thus demonstrating that progenitor cell potential is maintained following stromal differentiation. In mammals, similarly, stromal cells with stem cell properties can be isolated using a variety of techniques including spheroid culture, cloning, and fluorescence-activated cell sorting. These cells exhibit multipotent differentiation, clonal growth, and expression of a number of stem-cell-associated genes. These stromal stem cells do not express characteristic keratocyte markers, but can do so under selected culture conditions or when injected into corneal stroma *in vivo*. These stromal stem cells can restore transparency to lumican null mice with stromal haze, suggesting they may be appropriate for cell-based therapy of corneal diseases. The stromal stem cells appear to reside in the anterior region of the stroma near the limbus, but it is currently unknown what specific roles they play in corneal maintenance or repair.

Transparency

The cornea is one of the few complex biological tissues with high transparency to light, and the biophysical properties which allow such transparency have been the subject of debate for decades. In most transparent tissues such as the lens, all structures have a similar index of refraction so that light is not scattered as is passes through the tissue. Birefringence studies of the cornea, however, demonstrate that the corneal collagen has an index of refraction different from the extrafibrillar matrix surrounding it, and thus should scatter light, producing an opalescent or white appearance. David Maurice proposed, in 1957, that the highly regular structure of the collagen fibrils in the stroma functioned like a crystal, producing destructive interference of scattered light, allowing nonscattered light to pass. Mathematical models by McCally, Farrell, and others supported this concept, suggesting that, as long as the collagen fibrils were small, tightly packed, and aligned, transparency was possible. The crystal-like regularity of the stromal collagen allows for analysis using classical techniques such as X-ray diffraction. In a large number of such studies, Keith Meek and collaborators have confirmed the high regularity of spacing of nearest neighbor collagen fibrils and loss of that regularity in virtually every instance in which the cornea loses transparency. These studies have confirmed stromal hydration as one of the most critical parameters in maintenance of transparency. Excess water is adsorbed by the proteoglycans between collagen fibrils, disrupting the critical spacing and eliminating the order essential for transparency. Stromal transparency is consequently a highly dynamic property, dependent both on the removal of water from the tissue by the pumping action of the endothelial layer and by the water-binding properties of the stromal proteoglycans.

Recently, a new aspect of corneal transparency has come to notice with the discovery of abundant soluble proteins in keratocytes and other cellular tissues of the cornea. These proteins, termed corneal crystallins, are typically enzymes with housekeeping functions present in corneal cells at concentrations vastly exceeding that in other tissues. This group of proteins includes isoforms of aldehyde dehydrogenase (ALDH), transketolase, and up to a dozen or more unrelated enzymes. The variety of proteins involved and their unusual abundance has led to the suggestion that – like lens crystallins – these proteins serve to alter the refractive index of cells, thus reducing light scatter by corneal cells. Studies by Jester and coworkers have shown light scatter by keratocytes correlates with abundance of corneal crystallins in these cells, supporting a role for crystallins in stromal transparency.

Stromal Extracellular Matrix

Collagens are the most abundant proteins in the cornea, and most of the collagen in the stroma is involved in the collagen fibrils of the lamellae. Studies by Birk and coworkers have shown that fibrils in the stroma are heterotypic, containing both types I and V collagens in the same fibril. The triple-helical domain of the type V collagen molecules is buried within the fibril with its NH2-terminal domains exposed at the fibril surface. These exposed domains alter lateral association of collagen molecules during fibrillogenesis and, therefore, limit fibril diameter. The abundance of collagen type V is a likely factor in the small diameter of the stromal fibrils compared to fibrils in dermis and sclera, which contain mostly collagen types I and III. In corneal scarring and

haze, collagen type III is elevated in the stroma suggesting a direct correlation between the abundance of the small type I and V fibrils and corneal transparency.

Type XII collagen is found associated at regular intervals with stromal fibrillar collagen. The long form of this fibril-associated (FACIT) collagen can be modified with chondroitin sulfate, making it also a fibril-associated proteoglycan. Mice expressing a truncated form of type XII show altered collagen fibril spacing in the stroma. In addition to fibrillar collagen, stroma is very rich in type VI – a nonfibrillar collagen. This protein interacts with cells and numerous components of the stroma forming a beaded network throughout the stroma. Type VI microfibrils can be visualized running perpendicularly to the fibrils in lamellae and may help stabilize the lamellar structure. Numerous other collagen types have also been identified in the stroma in small amounts. Type IV collagens, often associated with basement membrane, are seen in the stroma to be associated with keratocytes. One of these, alpha3(IV) is downregulated as keratocytes become activated by wound healing or mitogens, and thus serves as a marker of keratocyte phenotype.

Proteoglycans are the second most abundant component of the corneal stroma. The corneal proteoglycans all belong to the small leucine-rich proteoglycan (SLRP) family, consisting of proteins of about 40 kDa, decorated with several N-linked oligosaccharides and one to two glycosaminoglycan chains. Normal adult stroma has one proteoglycan protein, decorin, which is modified with dermatan sulfate and three more SLRP proteins– lumican, keratocan, and osteoglycin (mimecan) – which have keratan sulfate chains. During healing, a fifth SLRP protein, biglycan, is detected in the stroma. Biglycan joins decorin as a second dermatan sulfate-containing proteoglycan in scar tissue. These SLRP proteoglycans contain multiple leucine repeat regions (LRR) – motifs involved in protein–protein binding. Each of the stromal proteoglycans binds collagen in a repeating pattern along the length of the fibrils with the keratan sulfate-containing SLRP's binding sites different from that of decorin. X-ray studies and molecular modeling reveal that SLRP proteins fold into compact horseshoe-shapes with the glycosylation on the convex portion of the curve and the collagen-binding region on the inner face. Thus, proteoglycan association with collagen produces glycosaminoglycan chains protruding from the fibril with a 'bottle brush' like appearance, as documented by deep freeze etch electron microscopy (**Figure 1(b)**). The interactions between proteoglycan and collagen has an effect on the rate and size of the fibrils formed during fibrillogenesis, effecting the diameter and length of the collagen fibrils, and thus the physical properties of the tissue. Decorin-knockout mice thus have weakened skin, whereas lumican-knockout mice exhibit large and heterogeneous collagen fibrils in the posterior corneal stroma leading to corneal haze. These *in vivo* models confirm the importance of the SLRP proteins in maintenance of the stromal ultrastructure required for vision. In addition to structural roles, the SLRP proteins interact directly with cells and growth factors. Decorin activates the EGF receptor on cell surfaces and also binds to and inactivates TGF-β, leading to reduced fibrosis in experimental models. Lumican stimulates attachment of macrophages and also has been shown to stimulate the healing of corneal epithelial wounds. Lumican-knockout mice show reduced responsivness to lipopolysaccharide-induced septic shock, and poor induction of proinflammatory cytokines. Lumican core protein also binds the CXC-Chemokine KC (CXCL1) and thus regulates neutrophilic infiltration. The SLRP proteins, therefore, clearly play important roles in mediating the response of the stroma to injury and inflammation.

The glycosaminoglycan chains (glycans) – decorating SLRP proteins – constitute about half of the molecular weight of the proteoglycans. Because of their high level of sulfation, these glycans are hydrophilic, providing the impetus for influx of water into the stroma against which the endothelium provides an active pump. Dermatan sulfate is a widespread and abundant glycan which, in the cornea, is less highly sulfated than in skin or sclera. Keratan sulfate, while detectable in many tissues, is present in abundance only in cartilage and cornea. In addition, only in the cornea are lumican, keratocan, and mimecan glycanated with keratan sulfate, making the stromal keratan sulfate proteoglycans an abundant, structurally unique, tissue-specific class of matrix molecules. Keratan sulfate binds water differently than dermatan sulfate, and it is clear that the ratio of these glycosaminoglycans in the stroma is important for stromal transparency. In genetic diseases such as Scheie's and Hurler's syndromes, dermatan sulfate cannot be degraded and accumulates in the cornea. In such cases, intense corneal opacity occurs early in life. In macular corneal dystrophy, keratan sulfate is not properly sulfated. In this disease, the cornea loses transparency in the second decade of life. It is notable that, in scar tissue, keratan sulfate is absent or greatly reduced, whereas dermatan sulfate is more abundant and highly sulfated. It is thought that such long-term differences in the glycosaminoglycan content of scar tissue contributes to light scattering as a result of differential water binding by the two types of glycosaminoglycan.

Biosynthesis of glycosaminoglycans is controlled differently from that of the proteins to which they are attached. For example, TGF-β treatment of keratocytes *in vitro* causes little change in lumican or decorin secretion; however, keratan sulfate modifying the lumican becomes dramatically shorter and virtually unsulfated during this treatment and dermatan sulfate modifying the decorin becomes longer and much more highly sulfated. These changes in glycanation can have dramatic effects on the properties of the proteoglycan. Lumican with short, unsulfated glycan chains serves as an

attachment substratum for macrophages and stimulates cell migration. Lumican modified with highly sulfated keratan sulfate, on the other hand, is antiadhesive and serves as a barrier for migrating cells. Thus the state of the glycan chains of the SLRP proteins serves not only to regulate water binding, but also other biological properties of the molecules. Modification of synthesis of the glycosaminoglycan is complex and not yet fully understood. Initiation, elongation, and sulfation of dermatan sulfate requires the participation of up to 16 different glycosyltransferase and sulfotransferase enzymes. For keratan sulfate, not all of participating enzymes are known as yet. One important gene has been clearly identified, however. CHST6 codes for a cornea-specific keratan sulfotransferase. This enzyme is mutated or nonfunctional in macular corneal dystrophy, leading to undersulfation of keratan sulfate.

In healing wounds and fibrotic corneas, not only are keratan sulfate and dermatan sulfate altered but another glycosaminoglycan, hyaluronan (HA), is present. This glycan, not present in normal corneal tissue, appears rapidly in the stroma in most pathological conditions and remains for many months following healing. The hyaluronan biosynthetic enzyme HAS2 is upregulated in keratocytes in response to mitogens and TGF-β. Mice lacking HAS2 in the stroma do not express HA in response to induced inflammation, demonstrating that upregulation of HAS2 mRNA in the keratocytes is the source of HA during stromal pathology. Hyaluronan is a simple, unsulfated, acidic polysaccharide but is known to exhibit a large number of biological activities. It is associated with cell motility, inflammation, and with metastatic potential of cancer cells. In culture, knockdown of HAS2 mRNA reduces keratocyte ability to respond to TGF-β with fibrotic matrix components. These results suggest that HA might represent an extracellular signal that mediates scarring in the stroma.

A final class of matrix components important to stromal function are the noncollagenous matrix proteins. Some of these are listed in **Table 1**. Another member of this group is protein BIGH3 (TGF-β-inducible gene H3). This secreted protein interacts with collagen and contains an RGD amino-acid sequence. It promotes cell attachment and in a number of systems the BIGH3 protein inhibits cell growth and motility. In the cornea, it has been shown that mutations in the gene coding for this protein (TGFBI) lead to a variety of corneal dystrophies presenting as opaque deposits in the stroma, usually in adults. Some of the specific syndromes caused by BIGH3 are granular dystrophy, Groenouw type I, Reis–Bucklers, lattice dystrophy type I, and Avellino dystrophy. The discovery that a minor component of the stromal extracellular matrix leads to marked disruption of vision attests to the complex biophysical equation involved in maintenance of stromal transparency. There are likely to be more important components of this system yet to be discovered.

Conclusion

The corneal stroma is a physically tough tissue with the remarkable property of transparency to light. Stromal transparency is essential for vision, and corneal scarring obscures vision for millions of individuals worldwide. Although we have gained an understanding of how stromal fibrosis disrupts vision, we do not yet understand how this process might be reversed biologically. An important challenge for the future is to employ our understanding of stromal biology to design pharmaceutical or cell-based treatments to reverse the scarring process and restore the complex balance of cells, molecules, and water in order to provide vision for those affected by corneal blindness.

Acknowledgments

The authors wish to thank Kira Lathrop and Martha Funderburgh for the excellent illustrations. This work was supported by NIH Grant EY016415 and Research to Prevent Blindness Inc.

See also: Artificial Cornea; Corneal Dystrophies; Corneal Imaging: Clinical; Corneal Scars.

Further Reading

Birk, D. E. (2001). Type V collagen: Heterotypic type I/V collagen interactions in the regulation of fibril assembly. *Micron* 32(3): 223–237.

Farrell, R. A., McCally, R. L., and Tatham, P. E. (1973). Wave-length dependencies of light scattering in normal and cold swollen rabbit corneas and their structural implications. *Journal of Physiology* 233(3): 589–612.

Fini, M. E. (1999). Keratocyte and fibroblast phenotypes in the repairing cornea. *Progress in Retinal and Eye Research* 18(4): 529–551.

Guerriero, E., Chen, J., Sado, Y., et al. (2007). Loss of alpha3(IV) collagen expression associated with corneal keratocyte activation. *Investigative Ophthalmology and Visual Science* 48(2): 627–635.

Hay, E. D. and Revel, J. P. (1969). Fine structure of the developing avian cornea. *Monographs in Developmental Biology* 1: 1–144.

Jester, J. V. (2008). Corneal crystallins and the development of cellular transparency. *Seminars in Cell and Developmental Biology* 19(2): 82–93.

Maurice, D. M. (1957). The structure and transparency of the cornea. *Journal of Physiology* 136(2): 263–286.

McCally, R. L. and Farrell, R. A. (1982). Structural implications of small-angle light scattering from cornea. *Experimental Eye Research* 34(1): 99–113.

Meek, K. M., Leonard, D. W., Connon, C. J., Dennis, S., and Khan, S. (2003). Transparency, swelling and scarring in the corneal stroma. *Eye (London, England)* 17(8): 927–936.

Meek, K. M. and Quantock, A. J. (2001). The use of X-ray scattering techniques to determine corneal ultrastructure. *Progress in Retinal and Eye Research* 20(1): 95–137.

Morishige, N., Petroll, W. M., Nishida, T., Kenney, M. C., and Jester, J. V. (2006). Noninvasive corneal stromal collagen imaging using two-photon-generated second-harmonic signals. *Journal of Cataract and Refractive Surgery* 32(11): 1784–1791.

The Cytoskeletal Network of the Trabecular Meshwork*

B Tian, B'Ann T Gabelt, and P L Kaufman, University of Wisconsin, Madison, WI, USA
B Geiger, Weizmann Institute of Science, Rehovot, Israel

Glossary

Actomyosin – The contractile cytoskeletal system, consisting of actin and myosin that, together with additional regulatory components, constitutes a force-generating system in muscle and nonmuscle cells.
Adherens junctions – The cell–cell adhesion sites (commonly referred to as: junctions) that are associated with the actin cytoskeleton, via cadherin receptors.
ATP – Adenosine 5′-triphosphate (ATP) is a multifunctional nucleotide that is most important as a molecular currency of intracellular energy transfer. In the context of this article, ATP plays a major role in cytoskeletal contraction.
Cytoskeleton – The internal network of fibers present within the cell's cytoplasm, composed largely of actin filaments, intermediate filaments, and microtubules.
Focal adhesions – Also known as focal contacts, these are specific types of large, membrane-bound macromolecular assemblies through which cells attach to the extracellular matrix (ECM). They are associated with the actin cytoskeleton, and their adhesion to the ECM is mediated by integrin receptors.
Glaucoma – A group of eye diseases characterized by a specific loss of the retinal nerve fiber layer, excavation of the optic disk, and visual-field deficits, typically caused by an intolerance to elevated or even normal intraocular pressure, and potentially leading to blindness.
Phosphorylation – The addition of a phosphate group to an organic molecule, thereby affecting the biological properties of the phosphorylated molecule. For example, phosphorylation of protein molecules (by enzymes, known as protein kinases) can affect their overall structure, interactions with other molecules, and biological activity.
Polymerization – A chemical process whereby individual components (defined as monomers) interact with each other, forming a stable molecular chain.
Schlemm's canal – A circular endothelium-lined channel that is located in the front of the eye internal to the limbus. It collects aqueous humor from the anterior chamber and drains it into the general circulation.
Trabecular meshwork – An area of tissue composed of arrays of collagen beams covered by endothelial-like cells with ECM occupying the spaces. It is located in the angle of the anterior chamber internal to Schlemm's canal and allows aqueous humor to drain into Schlemm's canal from the anterior chamber.

Actomyosin System in the Trabecular Outflow Route

Aqueous humor enters the posterior chamber of the eye from the ciliary processes, flows around the lens and through the pupil into the anterior chamber, and leaves the eye primarily through the trabecular route and the uveoscleral route at the anterior chamber angle. The trabecular route is the predominant outflow pathway in human eyes and consists of the trabecular meshwork (TM) and Schlemm's canal. The TM is composed of arrays of collagen beams covered by endothelial-like cells, with loose extracellular matrix (ECM) occupying the spaces between the cells of the adjacent beams. The outermost, juxtacanalicular (JCT) or cribriform region has no collagenous beams, but rather several cell layers immersed in a loose web of ECM fibrils. The adjacent Schlemm's canal is a continuous endothelium-lined channel that drains aqueous humor to the general venous circulation. TM structure and experimental flow studies suggest that flow resistance is maximal in the JCT region and/or the inner wall of Schlemm's canal, although the exact location of the major resistance barrier is not clear. Glaucoma is an ophthalmologic disorder responsible for visual impairment. Generally, glaucoma is characterized by progressive optic neuropathy usually associated with elevated or intolerable intraocular pressure (IOP), consequent to abnormally high flow resistance in the TM. Since glaucomatous eyes exhibit fewer TM cells and abnormally appearing JCT ECM compared to the eyes of age-matched normal individuals, cells and ECM in the JCT region may be critical in resistance regulation. In the last two decades, dynamics of the actin cytoskeleton in TM/Schlemm's canal cells have been confirmed to play important roles in the regulation of aqueous humor outflow.

*An adaptation and extension of Tian, B., Gabelt, B. T., Geiger, B., and Kaufman, P. L. (2009). The role of the actomyosin system in regulating trabecular fluid outflow. *Experimental Eye Research* 88: 713–717. Copyright Elsevier (2008).

The actomyosin system, composed of actin microfilaments and associated proteins, is one of the three major systems (the actomyosin system, the microtubule system, and the intermediate filament system) of the cytoskeleton. Microfilaments assemble within cells into complex bundles or three-dimensional meshworks located subjacent to the plasma membrane, and attach to the plasma membrane at a variety of sites, including adherens cell–cell junctions and focal adhesions, through specific receptors, namely cadherins and integrins, respectively. This link is mediated through a network of anchor proteins and additional structural and signaling molecules. The actomyosin system is present in essentially all cells, including TM and Schlemm's canal cells. Microfilament-based structures, such as adherens cell–cell junctions, focal contacts, and microfilament bundles, are highly organized in the cells along the trabecular outflow pathway (**Figure 1**). Intact microfilament bundles in TM/Schlemm's canal cells are essential to maintain physiological contractility of the JCT–Schlemm's canal region. Conversely, a physiologically contracted state of the JCT–Schlemm's canal region is required to maintain the microfilament-related structures in the outflow pathway. Microfilaments are involved in a variety of cellular processes from cell adhesion and motility to organelle trafficking to adhesion-mediated signal transduction. Therefore, microfilament dynamics play important roles in cellular morphogenesis, such as changes in cell shape, volume, contractility, and adhesion to neighboring cells and to the ECM. These changes in TM and/or Schlemm's canal cells, which could affect trabecular outflow resistance by altering the dimensions or direction of flow pathways, the amount and composition of the ECM, and the structures of adherens cell–cell junctions and focal adhesions, can be modulated directly by actin-disrupting agents or indirectly by inhibition of specific protein kinase(s) or cellular contractility through administration of protein kinase inhibitors or gene therapies. In addition, since the three cytoskeleton systems function in concert, changes in the microtubule system or intermediate filament system can also induce radical changes in the actomyosin system itself.

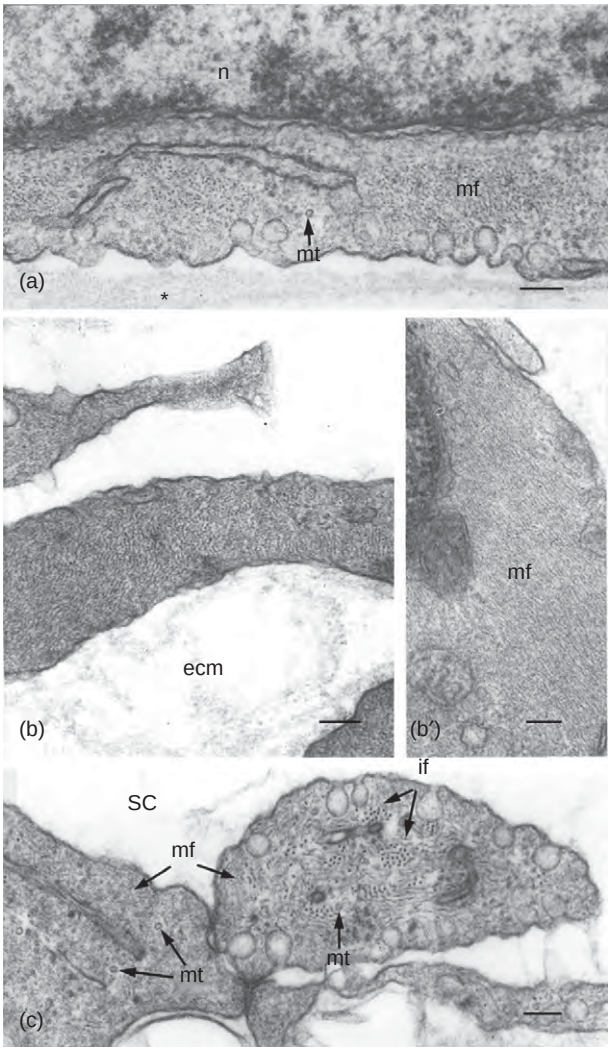

Figure 1 Transmission electron microscopy showing abundance of cytoskeletal filaments in different cellular compartments of the trabecular outflow pathway in a monkey eye. (a) Ventral aspect of a TM cell, which interacts with underlying collagen beam (*) through many focal-adhesion-like structures, is highly enriched with cytoskeletal filaments, including actin-rich microfilaments (mf) and microtubules (mt); n, nucleus. (b, b′) Juxtacanalicular cells displaying numerous microfilaments (mf), seen in cross section (b) or longitudinal (b′) section; ECM, extracellular matrix. (C) Inner-wall endothelial cells of Schlemm's canal (SC), displaying numerous intermediate filaments, organized in discrete bundles (if). Microtubules (mt) are also present. Microfilaments (mf) are usually seen in the cortical cytoplasm and near cell–cell junctions. Magnification = 0.1 μm. from Tian, B., Geiger, B., Epstein, D. L., and Kaufman, P. L. (2000). Cytoskeletal involvement in the regulation of aqueous humor outflow. *Investigative Ophthalmology and Visual Science* 41: 619–623. Reprinted with permission of ARVO.

Trabecular Outflow Enhancement Following Actomyosin Inhibition

Disruption of Microfilaments

The actin microfilament (filamentous actin; F-actin), which is the major component of the actomyosin system, is composed of many G-actin (globular actin) monomers. Pharmacological disruption of microfilaments in TM and Schlemm's canal cells alters the cell shape, inhibits cellular contractility, affects adhesions of cell–cell and cell-ECM, and in turn decreases outflow resistance in the trabecular outflow pathway.

Cytochalasins

Cytochalasins are fungal metabolites that interfere with the polymerization process by which G-actin aggregates into F-actin. Anterior chamber infusion of microgram to milligram doses of cytochalasins B or D, in live monkey

eyes and/or organ cultures of enucleated postmortem human eyes, cause distension of the cribriform meshwork, separation of its cells, and ruptures of the inner-wall endothelium of Schlemm's canal, leading to washout of ECM and significant increases in trabecular outflow facility. This is completely independent of ciliary muscle contraction, because the effect persists in the ciliary muscle-disinserted live monkey eye and in the cultured human anterior segment in which the ciliary muscle is not functionally interacting with the TM. Subthreshold doses of cytochalasin B and the trabecular outflow enhancer H-7 (see below) significantly increased outflow facility in living monkeys, indicating that the pathways by which the two drugs reduce aqueous humor outflow resistance converge at some point presumably involving deterioration of actin microfilaments in TM/Schlemm's canal cells. *In vitro* studies with cultured human and monkey trabecular cells confirm the alteration of cell shape and, with human cells grown on filters, the increased hydraulic conductivity.

Latrunculins

Latrunculins, which are macrolides produced by the marine sponge *Negombata magnifica*, are specific and potent actin-disrupting agents. They sequester monomeric G-actin, leading to massive disassembly of the polymeric form, namely F-actin. The addition of latrunculin A or B causes destruction of microfilament bundles and associated proteins in a wide variety of cultured cells, including human TM cells. This effect is manifested by cell rounding and retraction of the lamellipodium, and is accompanied by an apparent arborization of the cells. In living monkey eyes or organ cultures of enucleated porcine or postmortem human eyes, latrunculin A or B induces major increases in outflow facility and/or decreases IOP. Morphological studies indicate that the latrunculin-B-induced decrease in outflow resistance is associated with microfilament-disruption-related structural changes in the TM. Electron microscopy of the live monkey eye has revealed substantial ballooning of the JCT region following latrunculin B treatment, leading to a substantial expansion of the space between the inner wall of Schlemm's canal and the trabecular collagen beams without observable separations between inner-wall cells (**Figure 2**). In postmortem human eyes, the facility increase is accompanied by increased openings between inner-wall cells (more border or paracellular pores) with only very modest rarefaction of the JCT tissue and separation of the inner wall of Schlemm's canal from JCT tissue.

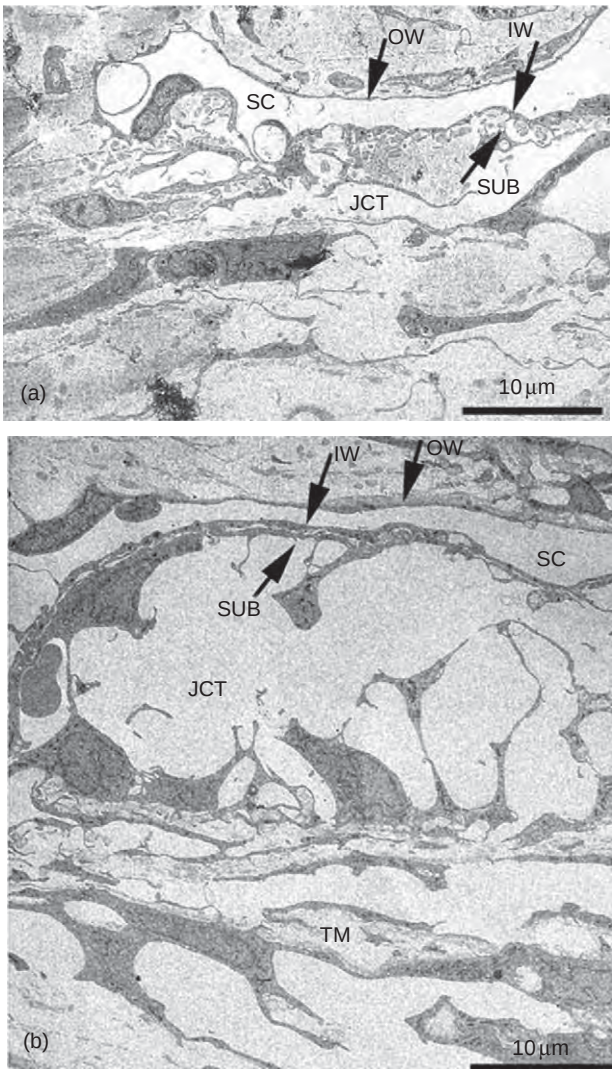

Figure 2 Transmission electron microscopy of the trabecular meshwork (TM) of a monkey eye following vehicle or LAT-B treatment: (a) shows normal JCT region and its circumjacent structures (vehicle-treated eye); (b) indicates the massive ballooning of the JCT region and the retention of close contact between IW and SUB (LAT-B-treated eye). IW, inner wall; JCT, juxtacanalicular region; OW, outer wall; SC, Schlemm's canal; SUB, subcanalicular cells. Modified from Sabanay, I., Tian, B., Gabelt, B. T., Geiger, B., and Kaufman, P. L. (2006). Latrunculin B effects on trabecular meshwork and corneal endothelial morphology in monkeys. *Experimental Eye Research* 82: 236–246. Copyright Elsevier.

Swinholide A

Unlike latrunculins, swinholide A, another marine macrolide, severs microfilaments but stabilizes the dimeric form. However, swinholide A significantly increases outflow facility in living monkeys similar to latrunculins. Since swinholide A decreases the level of F-actin without significantly increasing the concentration of G-actin, its positive effect on outflow facility further indicates that microfilament depolymerization or consequent disorganization of the actomyosin system in the TM/Schlemm's canal, and not the increase in G-actin concentration, is the major mechanism responsible for the latrunculin-induced increase in outflow facility.

TM Contractility Inhibition

Muscle and nonmuscle cellular contraction is associated with Ca^{2+}-dependent activation of myosin light-chain kinase (MLCK) and consequently phosphorylation of the regulatory myosin light chain. This phosphorylation, and consequent contraction, can be greatly enhanced by G-protein-mediated activation, in which the small G protein known as Rho activates a protein kinase, namely Rho kinase (ROCK). Rho, as well as other G proteins, including Rac and Cdc42 (signaling proteins that are activated by guanosine triphosphate (GTP), thereby regulating the activity of different partner proteins which, in turn, regulate the organization of the actin cytoskeleton) play key roles in the regulation of cellular contraction. Rho-activated Rho kinase triggers myosin II activity by inhibiting myosin light-chain phosphatase as well as by phosphorylating the myosin II regulatory light chain. Myosin II is the major cytoskeletal protein that drives the assembly of contractile bundles of actin and myosin, known as stress fibers in nonmuscle cells and is responsible for the generation of cellular tension. The TM possesses smooth-muscle-like properties and the actomyosin system in TM cells plays a key role in its contraction. Expression of nonmuscle myosin IIA and IIB has been confirmed in human TM cells, suggesting that myosin II activity is also involved in the actomyosin-driven TM contractility. Pharmacological inhibition of TM contractility enhances trabecular outflow facility in living animals and cultured anterior segments of enucleated animal or human eyes.

Broad specificity protein kinase inhibitors (H-7)

H-7, a broad spectrum serine–threonine kinase inhibitor, dramatically inhibits actomyosin-driven contractility. This leads to cellular relaxation, deterioration of the microfilaments and perturbation of their membrane anchorage, and loss of stress fibers and focal contacts in many types of cultured cells. H-7 increases outflow facility and decreases IOP in living monkeys and/or organ cultures of enucleated porcine, monkey, or postmortem human eyes, similar to actin disruptors. Morphological studies in the live monkey eye indicate that the H-7-induced increase in outflow facility is associated with cellular relaxation and drainage-surface expansion of the TM and Schlemm's canal, accompanied by loss of ECM. The inner-wall cells of Schlemm's canal become highly extended, yet cell–cell junctions are maintained (**Figure 3**). The morphological changes in the TM of live monkey eyes are consistent with functional changes in isolated bovine TM strips, where the TM precontracted by carbachol was relaxed by H-7. In postmortem cultured anterior segments of human eyes, H-7 causes a partial loss of the endothelial lining of Schlemm's canal.

The specific target kinases affected by H-7 are not well defined, because H-7 inhibits multiple protein kinases, including MLCK, Rho kinase, and protein kinase C (PKC). Studies have confirmed that the nonselective PKC inhibitor staurosporine, the specific PKC inhibitors chelerythrine and GF109203X, and the specific MLCK inhibitor ML-7 similarly increase outflow facility in living monkeys or cultured porcine anterior segments.

Rho-kinase inhibitors (Y-27632, Y39983, HA-1077, H-1152, and INS117548)

Inhibition of Rho kinase may play a key role in regulating trabecular outflow. A specific Rho kinase inhibitor, Y-27632, induces reversible changes in cell shape and decreases in actin stress fibers, focal adhesions, and protein phosphotyrosine staining in human TM cells and Schlemm's canal cells. In isolated bovine TM strips, Y-27632 completely blocks Ca^{2+}-independent phorbol myristate acetate or endothelin-1-induced contraction. As expected, Y-27632 and other Rho kinase inhibitors (such as Y-39983, HA-1077, H-1152, and INS117548) increase outflow facility and/or decrease IOP in living rabbits, rats, monkeys, and/or enucleated porcine eyes, similar to H-7. A recent morphological study in bovine eyes indicates that, with

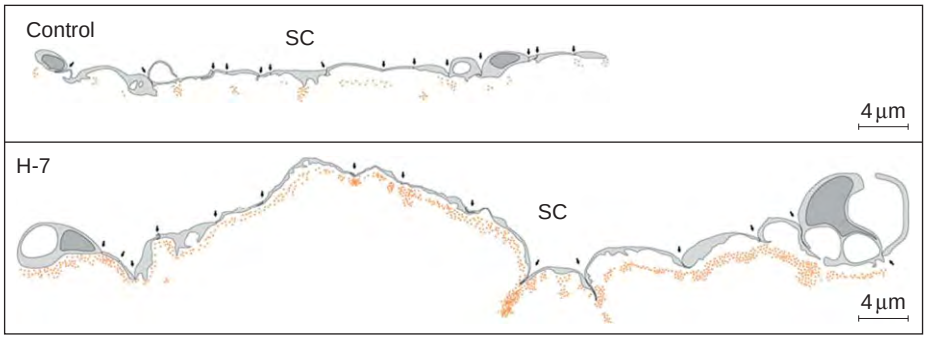

Figure 3 Schematic drawing depicting 15-cell stretches (cell–cell junctions marked by arrows) along Schlemm's canal (SC) and distributions of perfused gold particles that crossed the juxtacanalicular area of control and H-7-treated monkey eyes. Location of individual gold particles represented by red dots. Modified from Sabanay, I., Gabelt, B. T., Tian, B., Kaufman, P. L., and Geiger, B. (2000). H-7 effects on the structure and fluid conductance of monkey trabecular meshwork. *Archives of Ophthalmology* 118: 955–962, with permission from American Medical Association.

Y-27632, the inner wall of Schlemm's canal and the JCT connective tissue are significantly distended compared to control eyes, with discernible separation between the inner wall and JCT connective tissue (**Figure 4**). The average percent effective filtration length of the inner wall of Schlemm's canal (filtration length/total length × 100) is threefold larger in Y-27632-treated eyes than in controls. A significant positive correlation is found between the average percent effective filtration length of the inner wall and the average percent separation length (separation length/total length × 100, where separation length is the length exhibiting separations between the JCT connective tissue and inner wall), suggesting that the structural correlate to the increase in outflow facility after Y-27632 is physical separation between the JCT connective tissue and the inner wall of Schlemm's canal. The Y-27632-induced TM structural changes are consistent with those induced by latrunculin B or H-7, further indicating that cellular relaxation and drainage surface expansion in the TM are likely the key mechanisms by which cytoskeletal agents increase outflow facility. Recently, a ROKβ/ROCK-I and ROKα/ROCK-II inhibitor, INS117548, was confirmed to induce a dose-dependent decrease in the number of stress fibers, focal adhesion size, and numbers in HeLaJW cells. INS117548 also significantly lowered IOP in living monkeys. Since prolonged, acute exposure of formulated INS117548 produced no observable effects on the ocular surface at nearly threefold of a minimally effective IOP-lowering dose, INS117548 could be a potential efficacious and well-tolerated IOP-lowering agent for glaucoma therapy.

Myosin II inhibitors (blebbistatin)

Blebbistatin is a highly specific inhibitor of myosin II that inhibits both the adenosine triphosphatase (ATPase) and gliding motility activities of myosin II without inhibiting MLCK. It does not affect ATP binding or hydrolysis, but instead binds to the myosin–ADP–Pi complex, interfering with phosphate release, keeping myosin in an actin-detached state and preventing actomyosin interaction.

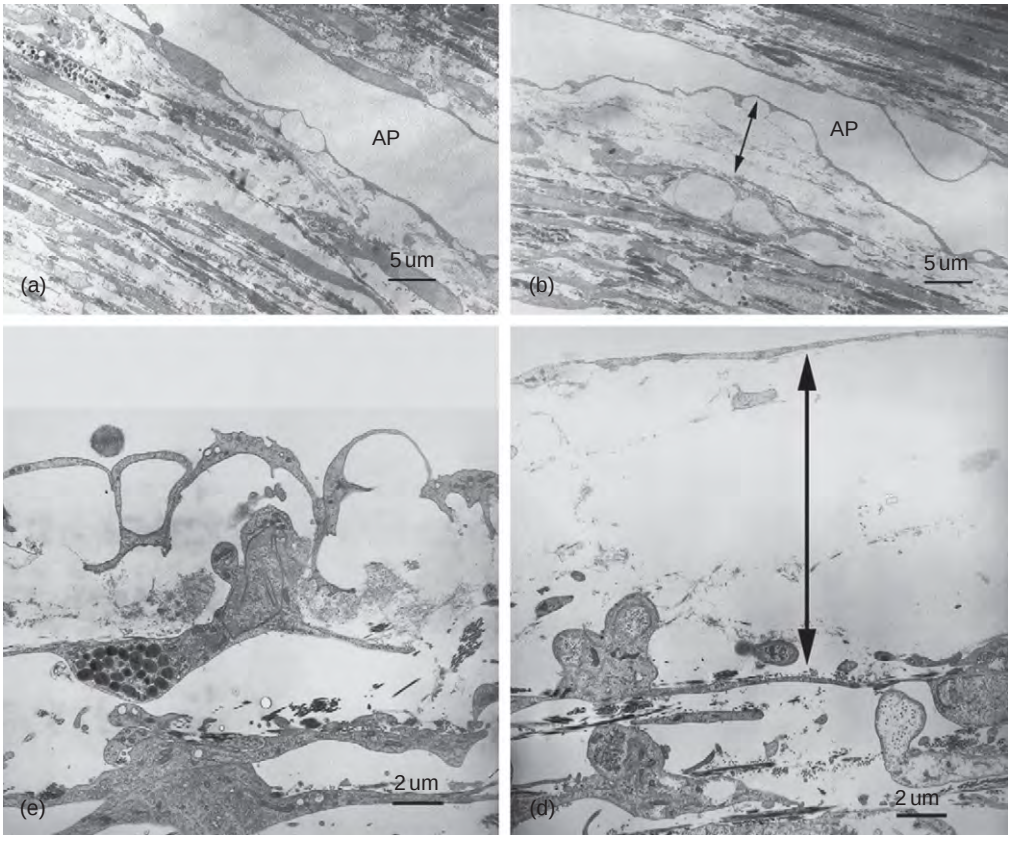

Figure 4 Electron microscopic analysis of the trabecular meshwork of bovine eyes. (a) In a control eye, the inner wall of Schlemm's canal and JCT tissue were more in contact with underlying structures, the JCT tissue appeared compact and without separation between the inner wall and JCT tissue. (b) In a Y-27632-treated-eye, the inner wall appeared distended, the JCT tissue was loose with significant separation between the inner wall and JCT tissue (double arrow). (c) In areas without separation, the connection between the inner wall and JCT cells and between the inner wall and JCT matrix were maintained. (d) In separated areas, the connection between the inner wall and JCT cells and between the inner wall and JCT matrix were lost (double arrow). Modified from Lu, Z., Overby, D. R., Scott, P. A., Freddo, T. F., and Gong, H. (2008). The mechanism of increasing outflow facility by rho-kinase inhibition with Y-27632 in bovine eyes. *Experimental Eye Research* 86: 271–281. Copyright Elsevier.

Confluent cultures of primary porcine TM cells treated with blebbistatin in the presence of serum have revealed dose-dependent changes in cell morphology, decreases in actin stress fibers, and in focal contacts and cell–cell adherens junctions. Perfusion of anterior segments of enucleated porcine eyes with blebbistatin significantly increases outflow facility. The effects of blebbistatin on TM cell morphology and actomyosin cytoskeletal organization are consistent with the effects of the inhibitors of Rho kinase, PKC, and MLCK on TM cells. However, unlike these inhibitors, which mediate their effects by inhibiting myosin II activity through decreased MLC phosphorylation, blebbistatin mediates its effects without affecting the phosphorylation status of MLC in TM cells, confirming its specificity to myosin II ATPase activity. Since the integrity of the inner wall of aqueous plexi in blebbistatin-perfused porcine eyes is intact, and the TM cell morphology after the drug appears to be similar to that noted in vehicle-treated eyes, observable structural deterioration in the TM may not be the main mechanism for the drug-induced increase in outflow facility, but rather the cellular relaxation of the trabecular outflow pathway following blebbistatin may be involved.

Actomyosin-Modulating Gene Therapy

Modulating proteins that negatively regulate actin–myosin interactions can also induce TM relaxation. Caldesmon is such a protein, whose function is the regulation of actomyosin contractility. When caldesmon is overexpressed, actin becomes uncoupled from myosin, which can affect both actomyosin-driven contractility and actin polymerization. In addition, exoenzyme C3 transferase may also affect actin–myosin interactions. Rho GTPases are the preferred intracellular targets of exoenzyme C3 transferase. The latter specifically inhibits Rho-GTP at the beginning of the Rho activation cascade, thereby blocking the whole Rho cascade. Adenovirus-delivered exoenzyme C3 transferase (C3-toxin) complementary DNA (cDNA) and nonmuscle caldesmon cDNA have been successfully expressed in cultured human TM cells. Perfusions in organ-cultured human or monkey eyes following overexpression of these genes have shown significant increases in outflow facility. Specific inhibition of Rho-kinase activity in the TM by dominant-negative Rho expression also increases outflow facility in organ-cultured anterior segments of postmortem human eyes. All these suggest that, similar to pharmacological approaches, gene therapies may also inhibit actomyosin system in the TM and in turn increase trabecular outflow facility through blocking the Rho activation pathway and overexpressing modulating proteins.

Microtubule Inhibition

The microtubule system consists of microtubules and associated proteins. Similar to microfilaments, microtubules are also highly organized in cells of the trabecular outflow route (**Figure 1**). They are not intrinsically contractile, but are important for directional cell motility and driven by specific microtubule motor proteins for cytoplasmic trafficking of vesicles and organelles. Associated proteins that bind to microtubules can affect the latter's stability and potentially attach the latter to other cytoskeletal filaments (e.g., microfilaments). Microtubule function could affect outflow pathway events through direct cellular mechanical effects (e.g., tensegrity), influences on ECM or cell membrane turnover (through vesicle movement), or through secondary signaling (e.g., leading to activation of the actin cytoskeleton).

Ethacrynic acid, known to be a potent microtubule inhibitor, reduces outflow resistance in enucleated calf and human eyes and in living monkey eyes, and concomitantly reduces IOP in live rabbit, monkey, and human eyes. Although ethacrynic acid primarily inhibits microtubule assembly, it also induces a rapid decrease in phosphotyrosine levels of focal adhesion kinase and a more subtle decrease in paxillin phosphorylation. Dephosphorylation of these proteins disrupts signaling pathways that normally maintain the stability of the actin microfilaments and cellular adhesions, and consequently induces the onset of retraction, stress fiber disruption, or complete disruption of focal adhesions. This indicates a close relationship between the microtubule system and the actomyosin system. Several new derivatives of ethacrynic acid significantly decrease IOP in cats and monkeys. These derivatives are more potent than ethacrynic acid in terms of inducing cell-shape alterations and decreasing actin stress fibers in human TM cells, suggesting that microtubule disruption may reduce outflow resistance at least partially through perturbation of the actomyosin system.

Significance of Actomyosin Inhibition in Glaucoma Therapy

Glaucoma is one of the most common causes of irreversible blindness in the world. At present, the only effective approach available to treat glaucoma is to reduce IOP. Pharmacologically reducing IOP is usually the first choice in glaucoma therapy. Medications used clinically to decrease IOP include aqueous humor secretory inhibitors (e.g., beta-adrenergic receptor antagonists, alpha2-adrenergic agonists, and carbonic anhydrase inhibitors), uveoscleral-outflow enhancers (e.g., prostaglandin analogs), cholinergic drugs that affect trabecular outflow indirectly by contracting the ciliary muscle and deforming the TM, and epinephrine drugs that work on both the TM (inducing changes in cell shape through a beta-adrenergic receptor-cyclic adenosine monophosphate (cAMP)/PKA-mediated cellular relaxation) and the uveoscleral (mediating endogenously synthesized prostaglandins) outflow routes. Secretory

suppression may affect supplies of oxygen and nutrients to the nonvascularized cornea, lens, and TM. Prostaglandin analogs do not substantially improve trabecular outflow. Cholinergic drug effects on the pupil and accommodation limit their clinical use. Epinephrine-like drugs are no longer used clinically because of their local and systemic side effects. Thus, there are no TM-selective outflow enhancers in current clinical use.

Since evidence has shown, as discussed in this article, that cytoskeletal agents or relevant gene therapies decrease outflow resistance by a mechanism directly related to the TM/Schlemm's canal, pharmacological or genetic perturbation of the actomyosin system in the TM may have potential to open a new avenue in glaucoma treatment. However, although cytoskeletal drugs effectively increase outflow facility and decrease IOP, they could, in principle, have detrimental effects on other anterior segment tissues, especially the cornea. Lower drug concentrations in larger volumes could minimize corneal toxicity without significantly sacrificing the drug's effect on the TM following topical administration. However, the potential cornea toxicity is still an obstacle to the use of higher concentrations of the drugs topically for a greater outflow facility increase. To overcome this problem, novel methods of drug delivery need to be developed. Receptors might be different in different cell types or ECM; therefore, a better understanding of the biomolecular differences between cornea and TM, the different molecular targets or mechanisms for different actin-disrupting agents, and a pro-drug, gene therapy or other site-activated approach, could facilitate the development of TM-selective drugs that reduce outflow resistance without affecting other ocular tissues.

Acknowledgments

This study was supported by grants from the US National Eye Institute (EY002698 and EY016665), Research to Prevent Blindness, the Wisconsin Alumni Research Foundation, and the Ocular Physiology Research and Education Foundation. BG is the incumbent of the E. Neter Chair in Cell and Tumor Biology.

The authors would also like to disclose here that the University of Wisconsin and the Weizmann Institute of Science hold a patent related to cytoskeletal compounds, (latrunculins and H-7), and that patent has been licensed by Inspire Pharmaceuticals; accordingly, Drs. Kaufman (UW) and Geiger (WIS) have a proprietary interest. Additionally, Inspire conducts research in Dr. Geiger's and Dr. Kaufman's laboratories, and both Dr. Kaufman and Dr. Geiger serve as advisors/consultants to Inspire. Inspire also provides unrestricted support for research in Dr. Kaufman's laboratory.

See also: Biological Properties of the Trabecular Meshwork Cells; The Biology of Schlemm's Canal; Biomechanics of Aqueous Humor Outflow Resistance; The Fibrillar Extracellular Matrix of the Trabecular Meshwork; Functional Morphology of the Trabecular Meshwork; Pharmacology of the Aqueous Humor Outflow; Regulation of Extracellular Matrix Turnover in the Aqueous Humor Outflow Pathways; Role of Proteoglycans in the Trabecular Meshwork; Structural Changes in the Trabecular Meshwork with Primary Open Angle Glaucoma.

Further Reading

Ethier, C. R., Read, A. T., and Chan, D. W. (2006). Effects of latrunculin-B on outflow facility and trabecular meshwork structure in human eyes. *Investigative Ophthalmology and Visual Science* 47: 1991–1998.

Gabelt, B. T., Hu, Y., Vittitow, J. L., et al. (2006). Caldesmon transgene expression disrupts focal adhesions in HTM cells and increases outflow facility in organ-cultured human and monkey anterior segments. *Experimental Eye Research* 82: 935–944.

Geiger, B., Yehuda-Levenberg, S., and Bershadsky, A. D. (1995). Molecular interactions in the submembrane plaque of cell–cell and cell–matrix adhesions. *Acta Anatomica (Basel)* 154: 46–62.

Honjo, M., Tanihara, H., Inatani, M., et al. (2001). Effects of rho-associated protein kinase inhibitor Y-27632 on intraocular pressure and outflow facility. *Investigative Ophthalmology and Visual Science* 42: 137–144.

Liu, X., Hu, Y., Filla, M. S., et al. (2005). The effect of C3 transgene expression on actin and cellular adhesions in cultured human trabecular meshwork cells and on outflow facility in organ cultured monkey eyes. *Molecular Vision* 11: 1112–1121.

Lu, Z., Overby, D. R., Scott, P. A., Freddo, T. F., and Gong, H. (2008). The mechanism of increasing outflow facility by rho-kinase inhibition with Y-27632 in bovine eyes. *Experimental Eye Research* 86: 271–281.

Olson, M. F. (2008). Applications for ROCK kinase inhibition. *Current Opinion in Cell Biology* 20: 242–248.

Peterson, J. A., Tian, B., Bershadsky, A. D., et al. (1999). Latrunculin-A increases outflow facility in the monkey. *Investigative Ophthalmology and Visual Science* 40: 931–941.

Rao, P. V. and Epstein, D. L. (2007). Rho GTPase/Rho kinase inhibition as a novel target for the treatment of glaucoma. *BioDrugs* 21: 167–177.

Rao, P. V., Shimazaki, A., Ichikawa, M., Alvarado, J. A., and Epstein, D. L. (2005). Effects of novel ethacrynic acid derivatives on human trabecular meshwork cell shape, actin cytoskeletal organization, and transcellular fluid flow. *Biological and Pharmaceutical Bulletin* 28: 2189–2196.

Sabanay, I., Gabelt, B. T., Tian, B., Kaufman, P. L., and Geiger, B. (2000). H-7 effects on the structure and fluid conductance of monkey trabecular meshwork. *Archives of Ophthalmology* 118: 955–962.

Tian, B., Kaufman, P. L., Volberg, T., Gabelt, B. T., and Geiger, B. (1998). H-7 disrupts the actin cytoskeleton and increases outflow facility. *Archives of Ophthalmology* 116: 633–643.

Vittitow, J. L., Garg, R., Rowlette, L. L., et al. (2002). Gene transfer of dominant-negative RhoA increases outflow facility in perfused human anterior segment cultures. *Molecular Vision* 8: 32–44.

Wiederholt, M., Thieme, H., and Stumpff, F. (2000). The regulation of trabecular meshwork and ciliary muscle contractility. *Progress in Retinal and Eye Research* 19: 271–295.

Zhang, M. and Rao, P. V. (2005). Blebbistatin, a novel inhibitor of myosin II ATPase activity, increases aqueous humor outflow facility in perfused enucleated porcine eyes. *Investigative Ophthalmology and Visual Science* 46: 4130–4138.

The Development of the Aqueous Humor Outflow Pathway

E R Tamm, University of Regensburg, Regensburg, Germany

Glossary

Corectopia – Distorted or displaced pupils.
Mesenchyme – An embryonic connective tissue that usually derives from the mesoderm. Only in the cranial region, mesenchyme derives from the neural crest.
Neural crest – Originates from the ectoderm and is located between the neural tube and the surface ectoderm. Neural crest cells migrate extensively during development and give rise to multiple cell types. Cranial neural crest cells largely contribute to the ocular mesenchyme.
Polycoria – Extra holes in the iris.
Transcription factor – A protein that binds to DNA, and controls the transcription of genetic information from DNA to RNA.

Anterior Eye Development

Eye development begins when the two optic vesicles appear as lateral outgrowths of the prosencephalon (forebrain). Both vesicles grow and get into contact with the cells of the adjacent surface ectoderm that respond by forming a local thickening which is called lens placode. Upon contact with the lens placode, the distal part of the optic vesicle is invaginated into its proximal part, and the optic vesicle converts into a double-layered optic cup. The neural retina derives from the inner layer of the optic cup, while the retinal pigmented epithelium differentiates from the outer layer. In a parallel process, the lens placode enlarges and deepens to form the lens pit. The lens pit subsequently forms the lens vesicle, which remains in contact with the surface epithelium with the help of the lens stalk. Finally, the lens stalk detaches from the surface epithelium, and the lens vesicle invaginates into the optic cup (**Figure 1(a)**).

Ocular Mesenchyme and Development of the Chamber Angle

In the human eye, ocular mesenchyme is first seen around the sixth week of development (**Figure 2(a)**). By then, the lens stalk has already separated from the surface epithelium, and the lens vesicle has invaginated into the optic cup. There is evidence from fate-mapping studies in the avian eye, from cell-grafting and labeling experiments in the mouse eye, and from transgenic mouse models that the ocular mesenchyme largely derives from the neural crest. In addition, there appears to be some contribution from cells that derive from the cranial paraxial mesoderm. The mesenchymal cells which migrate to the eye are first seen in the space between surface epithelium and lens epithelium, where they form several layers of loosely aggregated, star-shaped cells (**Figure 1(a)**). The cells condense into a dense layer that finally forms the corneal endothelium, while mesenchymal cells continue to migrate into the space between the surface epithelium and the developing corneal endothelium to form the future corneal stroma (**Figure 1(b)**).

The cells in this area differentiate into keratocytes or corneal stroma fibroblasts, the cell type that is critically required for synthesis of the extracellular matrix of the transparent cornea. The surface epithelium covering the anterior eye differentiates into the corneal epithelium. While the cells at the innermost layer of the corneal stroma differentiate into the corneal endothelium, the inner epithelial layer of the future cornea, the lens becomes separated from the cornea by a fluid-filled space (**Figure 3(a)**). Subsequently, the peripheral edge of the optic cup starts to elongate and grow toward the fluid-filled space to form the ciliary body and the iris, and finally divides the space into an anterior and a posterior chamber. At the same time, in a second migratory wave, mesenchymal cells arrive at the angle between the future cornea and the edge of the optic cup. They continue to grow along the optic-cup-derived epithelial layers of iris and ciliary body to form the stroma of both structures (**Figure 3(b)**).

Finally, trabecular meshwork and Schlemm's canal develop. Around the 15th to 17th week of human embryonic development, shortly after the optic cup has started to elongate to form iris and ciliary body, neural-crest-derived mesenchymal cells form a dense mass of cells in the chamber angle, which extends onto the anterior surface of the developing ciliary body/iris (**Figure 2(b)**). About a month later, the mesenchymal cells in the chamber angle are separated from each other by small fluid-filled spaces (**Figure 2(c)**). Consequently, extracellular matrix is deposited in the spaces, while vessels grow toward the chamber angle from the immediate adjacent sclera. During this period, the chamber angle cells that give rise to the trabecular meshwork are still localized at or behind the posterior border of the chamber angle, and are covered by uveal tissue that extends from the iris rot. In the next

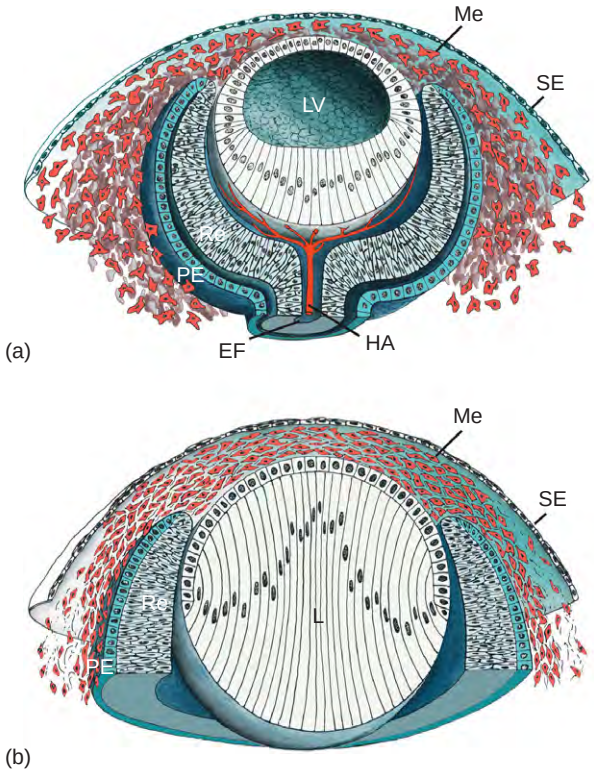

Figure 1 Schematic diagram of ocular mesenchyme development in the mouse eye between embryonic days (E) 12.5–14.5. (a) At E 12.5–13.5, the lens vesicle (LV) has detached from the surface epithelium (SE) and become invaginated into the optic cup. Mesenchymal cells (ME) start to migrate into the space between the anterior epithelium of the lens vesicle and the surface ectoderm. The inner layer of the optic cup forms the neural retina (Re), the outer layer, the retinal pigmented epithelium (PE). The optic cup is incompletely inferior at the so-called embryonic (choroidal) fissure (EF), which is used by the hyaloid artery (HA) to pass into the optic cup. (b) At E 13.5–14.5, the mesenchyme cells condense to form several flat layers that are separated from each other by a loose fibrillar extracellular matrix. In the lens (L), the primary lens fibers elongate to close the lumen of the lens vesicle. Adapted from Cvekl, A. and Tamm, E. R. (2004). Anterior eye development and ocular mesenchyme: New insights from mouse models and human diseases. *BioEssays* 26, 374–386, with permission from John Wiley & Sons, Inc.

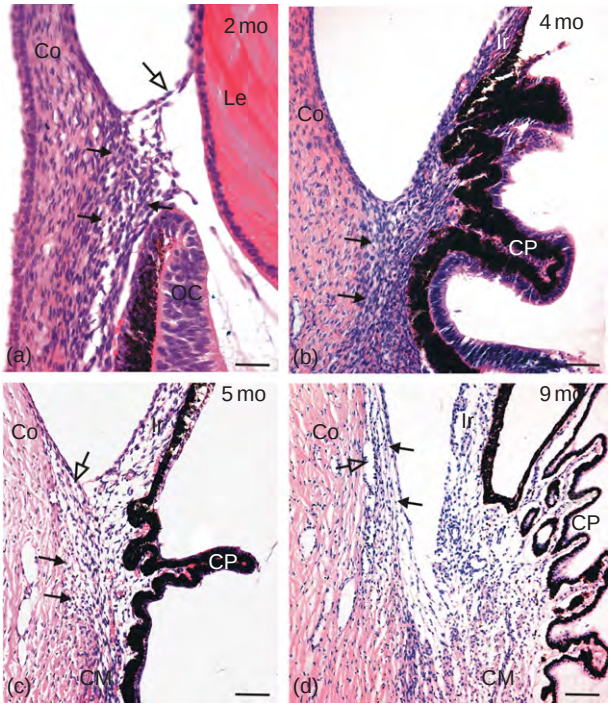

Figure 2 Development of the chamber angle and trabecular meshwork in human embryonic and fetal eyes at 2 (a), 4 (b), 5 (c), and 9 (9) months of development. (a) At 2 months, mesenchymal cells (arrows) are seen between the anterior edge of the optic cup (OC) and the future cornea (Co). Cells of the anterior pupillary membrane (white arrow) extend from the peripheral cornea to the anterior surface of the lens. (b) At 4 months, mesenchymal cells (arrows) form a dense mass at the chamber angle, which extends onto the anterior surface of the developing iris (Ir). (c) In 5-month-old fetal eyes, the cells of the future trabecular meshwork (solid arrows) are separated from each other by small open spaces. Uveal tissue (open arrow) covers the anterior surface of the trabecular meshwork. (d) At term, most of the trabecular meshwork (solid arrows) is exposed to the anterior chamber. Schlemm's canal (open arrow) is seen at the outer side of the trabecular meshwork. CP, ciliary process; CM, ciliary muscle. Sections kindly provided by Dr. Christian Vorwerck, Department of Ophthalmology, University of Magdeburg, Germany. Magnification bars: (a) = 20 μm; (b) = 30 μm; (c) = 40 μm; (d) = 60 μm. Adapted from Tamm, E. R. (2004). Genetic changes and their influence on structure and function of the eye in glaucoma. In: Grehn, F. J. and Stamper, R. (eds.) *Essentials in Ophthalmology. Glaucoma.* Berlin, Heidelberg, New York: Springer, with permission from Springer Science+Business Media.

months, the extracellular fibers in the chamber angle become organized into trabecular meshwork beams or lamellae, which are covered by flat trabecular meshwork cells. In parallel, the vessels in the adjacent scleral coalesce to form a circumferential Schlemm's canal. Maturation of the trabecular meshwork and optic cup occurs alongside a posterior move of the peripheral margin of the anterior chamber and the chamber angle. Thereby, the anterior surface of the trabecular meshwork becomes exposed to the anterior chamber and the aqueous humor within (Figure 2(d)).

The critical morphogenetic steps of trabecular meshwork development become complete around the time of birth. Still, some minor modeling of the trabecular meshwork continues throughout the first years of life. Between the trabecular meshwork lamellae and the endothelial lining of Schlemm's canal, there still remain some cells with a stellate phenotype that do not cover the trabecular lamellae. Instead, these cells develop cell-to-cell contacts with the endothelial cells of the Schlemm's canal on one side and the cells covering the trabecular beams on the other side, and form the juxtacanalicular or cribriform layer of the trabecular meshwork, where most of the resistance to aqueous humor outflow is located.

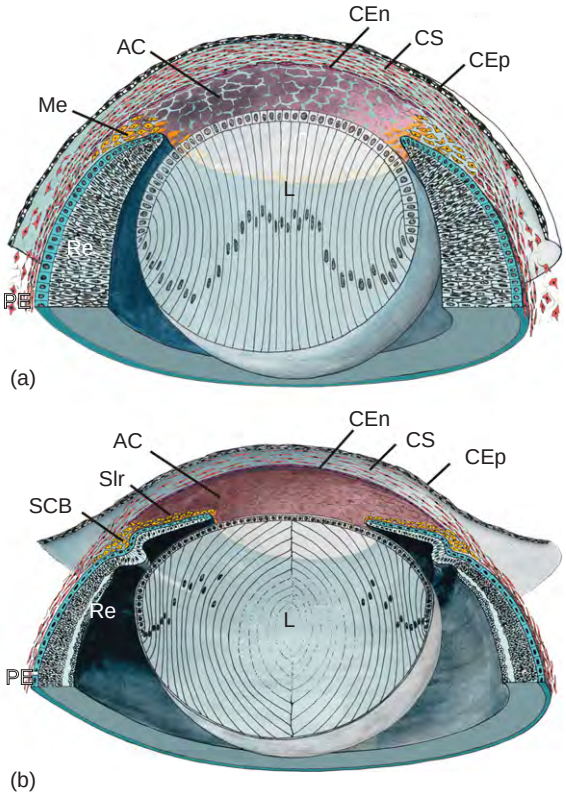

Figure 3 Schematic diagram of ocular mesenchyme development in the mouse eye between embryonic days (E) 14.5–19.5. (a) At E 14.5–15.5, the posterior mesenchyme cells closest to the lens flatten, become connected by apicolateral contacts, and form an endothelial monolayer. At the end of this process, all layers of the future cornea have been defined. The endothelial monolayer that has been formed from the posterior mesenchyme cells becomes the corneal endothelium (CEn), and the surface ectoderm that covers the anterior side of the mesenchyme becomes the corneal epithelium (CEp). Mesenchyme cells between the corneal epithelium and endothelium differentiate into keratocytes, the specific cell type of the corneal stroma. During differentiation of the corneal endothelium, the lens (L) detaches from the future cornea and a fluid-filled cavity, the anterior chamber (AC) is generated between both the structures. In parallel, a new group of mesenchyme cells (Me) arrives at the angle between the future cornea and the anterior edge of the optic cup. (b) Beginning at approximately E 15.5, the anterior edge of the optic cup enlarges to form the iris and ciliary body. Mesenchyme cells migrate along the epithelial layers of both structures and finally differentiate into the stroma of the iris (Slr) and ciliary body (SCB). Adapted from Cvekl, A. and Tamm, E. R. (2004). Anterior eye development and ocular mesenchyme: New insights from mouse models and human diseases. *BioEssays* 26, 374–386, with permission from John Wiley & Sons, Inc.

In the mouse eye, an animal model that is commonly used to study developmental aspects of chamber angle formation and its genetic control, the morphogenetic processes are very similar. A minor difference appears to be the formation of the corneal endothelium, which is not formed in the mouse before multiple layers of cells have filled the space between the lens and the surface epithelium (**Figure 1(a)**). The development of the trabecular meshwork and the Schlemm's canal starts at postnatal day 1, and is completed at around postnatal day 21. The principal morphogenetic processes of chamber angle development are essentially similar to that seen in humans (**Figure 4**).

Anterior Segment Dygenesis

Typical clinical disorders that occur from failure of correct mesenchyme differentiation during anterior eye development are part of the broad spectrum of Axenfeld–Rieger's syndrome which includes Rieger's anomaly or syndrome, Axenfeld's anomaly, and iridogoniodysgenesis. All of these conditions are commonly inherited in an autosomal-dominant fashion, and affected patients may develop juvenile glaucoma in about 50% of cases. Rieger's anomaly is characterized by midperipheral adhesions from the iris to the cornea (**Figure 5(b)**). In addition, there are structural defects, such as polycoria and corectopia, and a marked iris hypoplasia. When ocular changes are associated with systemic developmental defects, such as dental or facial abnormalities, the term Rieger's syndrome is used. In Axenfeld's anomaly, iris strands attach to a structure called posterior embryotoxon, which is a ring of collagenous fibers at the peripheral end of Descemet's membrane forming a prominent Schwalbe's line (**Figure 5(a)**). Posterior embryotoxon presents clinically as a ring-shaped opacity in the peripheral cornea. Patients with iridogoniodysgenesis have an iris with hypoplastic stroma, abnormal chamber angle tissue, and glaucoma.

The broad spectrum of different specific clinical phenotypes, which are all part of Axenfeld–Rieger's syndrome, results from mutations in two genes, the bicoid-like homeobox gene *PITX2*, or the forkhead/winged-helix transcription factor gene *FOXC1*. Both genes encode for transcription factors that obviously control the morphogenetic processes of anterior eye development and the role of the ocular mesenchyme therein.

Peters Anomaly

Another phenotype that is seen in anteriorsegment dysgenesis is Peters anomaly. Peters anomaly is characterized by central corneal opacities (leukoma) that are associated with abnormalities of the deepest corneal stromal layers and local absence of the corneal endothelium (**Figure 5(c)**). The lens may adhere to the back of the corneal opacity and show signs of an anterior polar cataract. Peters anomaly is often associated with iris hypoplasia and corectopia, and with iridocorneal adhesions that arise from the pupillary region. About 50–70% of the cases may develop abnormally high

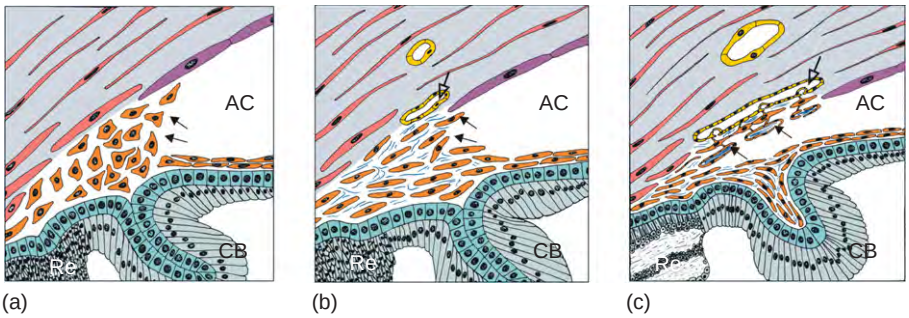

Figure 4 Schematic diagram of the development of chamber angle and trabecular meshwork in the mouse eye between postnatal days (P) 1–14. (a) From P1 to P4, the chamber angle is occupied by a dense mass of mesenchymal cells (arrows). (b) From P4 to P10, chamber angle cells (solid arrows) become separated from each other by small open spaces that are partially filled with extracellular fibers, while vessels appear in the immediate adjacent sclera (open arrows). During this period, the chamber angle is level with the anterior border of the future trabecular meshwork. (c) From P11 to P14, the extracellular fibers in the chamber angle organize themselves into trabecular beams that become covered by trabecular meshwork cells, while the scleral vessels next to the chamber angle coalesce to Schlemm's canal. In parallel, the peripheral margin of the anterior chamber moves posteriorly and the inner surface of the trabecular meshwork becomes exposed to the anterior chamber. Adapted from Cvekl, A. and Tamm, E. R. (2004). Anterior eye development and ocular mesenchyme: New insights from mouse models and human diseases. *BioEssays* 26, 374–386, with permission from John Wiley & Sons, Inc.

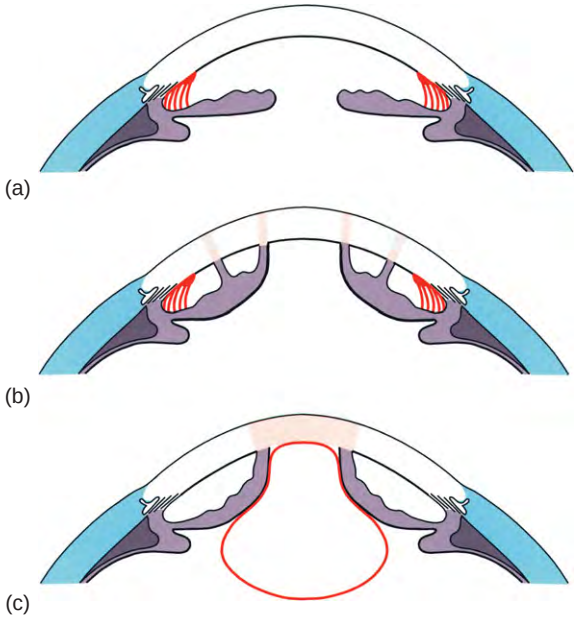

Figure 5 Schematic drawing of typical phenotypes seen in the spectrum of anterior segment dysgenesis. (a) In Axenfeld's anomaly, iris strands traverse the chamber angle and insert into a prominent Schwalbe's line (posterior embryotoxon). (b) In Rieger's anomaly, midperipheral adhesions from the iris to cornea are seen in addition to Axenfeld's anomaly. (c) The phenotype of Peters anomaly consists of a central corneal opacity (leukoma), with local absence of the corneal endothelium. The lens may adhere to the back of the corneal opacity. Peters anomaly is usually associated with iridocorneal adhesions that arise from the pupillary region. Adapted from Tamm, E. R. (2004). Genetic changes and their influence on structure and function of the eye in glaucoma. In: Grehn, F. J. and Stamper, R. (eds.) *Essentials in Ophthalmology. Glaucoma.* Berlin, Heidelberg, New York: Springer, with permission from Springer Science+Business Media.

intraocular pressure and glaucoma, very likely due to dysgenesis and/or malfunction of the aqueous humor outflow tissues in the iridocorneal angle. In humans and in mice, mutations in several transcription factors such as *PITX2, PITX3, FOXC1, FOXE3, MAF, SOX11*, and *PAX6* have been found in Peters anomaly associated with anterior segment dysgenesis.

Aniridia

Pax6, a transcription factor that is characterized by a paired domain and paired-like homeodomain, is also critically required for the morphogenesis of the anterior eye. It is a key regulator of eye development in both vertebrates and invertebrates. Patients with heterozygote mutations in *PAX6* develop the phenotype aniridia, which is commonly associated with iris hypoplasia, corneal opacification, cataract, and foveal dysplasia. In addition, mutations in *PAX6* may also cause Peters anomaly, and about 50–75% of patients with aniridia develop juvenile glaucoma.

Anterior Segment Dysgenesis and Glaucoma

Juvenile glaucoma develops in about 50% of patients with Axenfeld–Rieger's syndrome. The electron microscopy of affected patients reveals considerable amounts of amorphous extracellular material in the juxtacanalicular or cribriform region of the trabecular meshwork, for example, the part of the trabecular meshwork outflow pathways which is most critical for outflow resistance

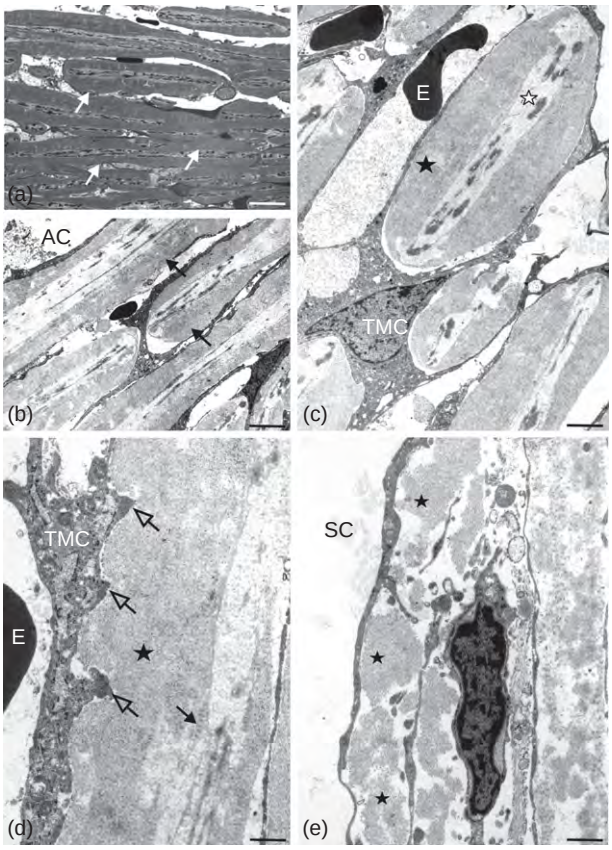

Figure 6 Light (a) and electron microscopy (d-e) of the trabecular meshwork (TM) in a 24-year-old patient with Axenfeld's syndrome and glaucoma. (a, b) The intertrabecular spaces are markedly narrowed because of an abnormally thickened basement membrane in the TM lamellae (arrows). (c) The basement membrane (black asterisk) surrounds the central core of TM lamellae (white asterisk), which is of normal thickness. (d). Processes of TM cells (open arrows) protrude into the thickened basement membrane (asterisk), which appears granular and contains aggregates of broad-banded material (solid arrow). (e) The extracellular spaces of the juxtacanalicular meshwork contain numerous aggregates of sheath-derived plaque material (asterisks). AC, anterior chamber; TMC, trabecular meshwork cell; SC, Schlemm's canal; E, erythrocyte. Magnification bars: (a) = 4 μm; (b) = 1.7 μm; (c) and (e) = 1 μm; (d) = 0.7 μm. Adapted from Tamm, E. R. (2004). Genetic changes and their influence on structure and function of the eye in glaucoma. In: Grehn, F. J. and Stamper, R. (eds.) *Essentials in Ophthalmology. Glaucoma.* Berlin, Heidelberg, New York: Springer, with permission from Springer Science+Business Media.

(Figure 6). In addition, the extracellular matrix of the trabecular lamellae was found to be markedly thickened due to an increase in electron-dense material in the basement membrane of trabecular meshwork cells (Figure 6).

Haploinsufficiency in *FOXC1* or *PITX2* may lead to an abnormal turnover of the extracellular matrix in the juxtacanalicular trabecular meshwork during development, which continues into childhood and adolescence. An abnormal quantity and/or quality of the extracellular matrix in the trabecular meshwork may finally lead to an increase in aqueous humor outflow resistance and cause glaucoma in Axenfeld–Rieger's syndrome.

Glaucoma in patients with aniridia appears to result from a different mechanism. Studies in mouse strains with mutations in *Pax6* indicate that the trabecular meshwork does not differentiate and Schlemm's canal is absent.

Primary Congenital Glaucoma

Primary congenital glaucoma is an inherited developmental defect in the trabecular meshwork and chamber angle that manifests in the neonatal or infantile period. Increased intraocular pressure, corneal enlargement, and optic nerve cupping are typical signs. Several histopathological studies describe that the iris insertion and anterior ciliary body overlap the posterior portion of the trabecular meshwork, but leave the angle open. Apparently, during chamber angle development, the iris and the ciliary body fail to recede posteriorly. In addition, an increase in extracellular matrix has been described in the trabecular meshwork. In familial cases of primary open angle, an autosomal recessive mode of inheritance is commonly observed, and mutations in the gene *CYP1B1* coding for the enzyme cytochrome P4501B1 were found to be causative for some forms.

The ocular substrate for cytochrome P4501B1 is not known, but it is reasonable to assume that it is a part of an important signaling pathway during development, and possible candidates are steroids, all-*trans*-retinol, fatty acids, or arachidonic acid.

Acknowledgments

This work was supported by DFG Research Unit 1075 (TP 5).

See also: Animal Models of Glaucoma; Functional Morphology of the Trabecular Meshwork; Molecular Genetics of Congenital and Juvenile Glaucoma; The Role of the Ciliary Body in Aqueous Humor Dynamics. Structural Aspects.

Further Reading

Alward, W. L. (2000). Axenfeld–Rieger syndrome in the age of molecular genetics. *American Journal of Ophthalmology* 130: 107–115.

Anderson, D. R. (1981). The development of the trabecular meshwork and its abnormality in primary infantile glaucoma. *Transactions of the American Ophthalmological Society* 79: 458–485.

Ashery-Padan, R. and Gruss, P. (2001). Pax6 lights up the way for eye development. *Current Opinion in Cell Biology* 13: 706–714.

Baulmann, D., Ohlmann, A., Flügel-Koch, C., et al. (2002). *Pax6* heterozygous eyes show defects in chamber angle differentiation

that are associated with a wide spectrum of other anterior eye segment abnormalities. *Mechanisms of Development* 118: 3–17.

Chow, R. L. and Lang, R. A. (2001). Early eye development in vertebrates. *Annual Review of Cell and Developmental Biology* 17: 255–296.

Cvekl, A. and Tamm, E. R. (2004). Anterior eye development and ocular mesenchyme: New insights from mouse models and human diseases. *BioEssays* 26: 374–386.

Gehring, W. J. and Ikeo, K. (1999). Pax 6: Mastering eye morphogenesis and eye evolution. *Trends in Genetics* 15: 371–377.

Gould, D. B. and John, S. W. (2002). Anterior segment dysgenesis and the developmental glaucomas are complex traits. *Human Molecular Genetics* 11: 1185–1193.

Lines, M. A., Kozlowski, K., and Walter, M. A. (2002). Molecular genetics of Axenfeld–Rieger malformations. *Human Molecular Genetics* 11: 1177–1184.

Schottenstein, E. M. (1996). Peters anomaly. In: Ritch, R., Shields, M. B., and Krupin, T. (eds.) *The Glaucomas*, pp. 887–897. St. Louis, MS: Mosby.

Stoilov, I., Akarsu, A. N., and Sarfarazi, M. (1997). Identification of three different truncating mutations in cytochrome P4501B1 (CYP1B1) as the principal cause of primary congenital glaucoma (Buphthalmos) in families linked to the GLC3A locus on chromosome 2p21. *Human Molecular Genetics* 6: 641–647.

Stoilov, I., Jansson, I., Sarfarazi, M., and Schenkman, J. B. (2001). Roles of cytochrome p450 in development. *Drug Metabolism and Drug Interactions* 18: 33–55.

Tamm, E. R. (2004). Genetic changes and their influence on structure and function of the eye in glaucoma. In: Grehn, F. J. and Stamper, R. (eds.) *Essentials in Ophthalmology. Glaucoma*, pp. 1–28. Berlin: Springer.

The Epidemiology of Cataract

S K West, Johns Hopkins University School of Medicine, Baltimore, MD, USA

Glossary

Etiology – A causal relationship underlying a condition or disease. In this sense, high sunlight exposure has been shown to be part of the etiology of cortical cataracts.
Incidence – The rate at which a condition appears in a population over time. Incidence studies measure the rate at which cataracts appear in a population from baseline values established using prevalence data.
Prevalence – The occurrence of a trait or disease, in this case cataract, in a population.

Introduction

As the leading cause of blindness worldwide, cataract is and should be a primary focus for public health in ophthalmology. The World Health Organization estimates 36.9 million persons are blind. Forty-eight percent of all blindness worldwide is due to cataract. A recent review suggests that there has been a decrease in global blindness, about 15 million fewer cases than had been projected, and not as many blind from cataract, despite the increase in the age group 50 years and older worldwide. The authors attribute this success to an increase in the quantity and quality of cataract surgery, helped by the advent of low-cost intraocular lenses. However, cataract is not yet preventable, and this success will continue only if there is vigilance in restoring sight lost from cataract through high-quality surgery and continued research efforts on prevention.

Considerable progress has been made in understanding the epidemiology of cataract. Leads from this research point to very promising directions for further work. The next sections review the progress made in the epidemiology of cataract and suggest future work.

Cataract Classification Systems: Characterization of Phenotype

Rigorous investigations into the etiology of cataract have been considerably enhanced by the development of valid and reliable classification systems to assess the presence and severity of different cataract types. Differentiation of nuclear, cortical, and posterior subcapsular (PSC) lens opacities is important, as it has permitted careful phenotypic description of the type of cataract and better characterization of the distribution of cataract types in populations, which provide clues into possible causal factors. Moreover, as the different cataract types have been associated with different etiologies, precision in characterization of cataract is critical in epidemiological studies.

The classification systems are based on images of the lens taken in standardized fashion, and largely rely on graders who compare features of the images to standard photographs and grade severity. At least four classification systems have been developed, which differ largely in the standards photographs used. Unfortunately, many of the major cataract epidemiological studies have used different grading schemes and, more importantly, different cutoff points to define opacification. This makes comparisons more difficult. Reliability between graders using any of these systems, based on photographs, is usually very good, but adapting these grading methods to assessment in the eye clinic has proved more difficult. To address this problem, the World Health Organization developed a clinical tool for simple assessment of cataract type at the slit lamp. This tool may prove to be useful for surveys of patients during treatment.

Attempts have been made to automate image analyses, with varying results. Most success has been achieved quantifying the density of nuclear opacification, but this still relies on specification of the nuclear region by a grader. A recent study, using anterior segment ocular coherence tomography (OCT) to determine the degree of nuclear opalescence, showed some promise, as it removes some of the variability in slit lamp and flash settings in subjective assessment of nuclear density. However, further work is needed to test the value of this approach in the assessment of cortical and posterior subcapsular opacities. This is especially true because, for these opacities, there need to be multiple scans in several meridians and OCT appears to be subject to the production of artifacts from the anterior surface. Analysis of the loss of retinal image clarity is associated with cataract severity. However, this approach cannot determine the type of cataract and does not detect the early stages of opacification.

Further investigations of automated grading systems and better, low-cost, digital-image capture systems for cortical cataracts and PSCs are warranted, as this would substantially reduce the cost of cataract assessment.

However, the systems that are already available permit careful characterization of cataract type. These have, and will continue to enable the precise identification of the risk factors for cataract.

Distribution of Different Lens Opacity Types in Different Racial Groups or Populations

Differences in the distribution of the cataract types within racial or ethnic populations point to potential differences in genetic, genetic/environment or environmental exposures that could be exploited to find the causes of cataract. For example, population studies in Barbados and Salisbury, Maryland, have shown that African Americans/Caribbeans have a higher prevalence of cortical cataract and lower occurrence of nuclear and posterior subcapsular opacities, when compared to Caucasians. Incidence rates of cortical opacities are high in African Americans/Caribbeans as well, confirming the difference seen in prevalence studies. In the Salisbury study, this difference was not explained by differences in sunlight exposure, diabetes, or gender, suggesting other exposures and/or a strong genetic component may be operative.

There is conflicting evidence about rates of occurrence of PSCs in Chinese as compared to Caucasians. Based on two Asian studies, which used clinical grading rather than image assessment, rates appear to be higher in Asian subjects. However, in the most recent lens opacity study in Beijing, there was no substantial difference in the rates of PSCs among Chinese, compared to similarly aged Caucasians in the Salisbury study. Comparisons between Latinos and Caucasians for rates of specific cataract types are somewhat hampered, as the two Latino studies relied on clinical grading and did not use image-based cataract assessment systems. With this caveat in mind, Latinos in Los Angeles appear to have higher rates of PSC, compared to the rates in Caucasians. However, this may also be due to differential access to cataract surgical services.

There are sex differences in the prevalence of lens opacities, with women having consistently higher rates of cortical opacities than men. This gender difference is not explained by any difference in diabetes, sunlight exposure, or age. The 10-year, age-adjusted incidence rates of nuclear and cortical opacities were higher in females than males in the Caucasian populations of Blue Mountain, Australia. Similarly, 10- and 15-year, age-adjusted incident nuclear opacities were higher in females in Beaver Dam, USA. There is less evidence for a gender difference in PSC. The reason(s) for a gender difference in cataract are not clear. However, a study of expression differences in the lens proteomes between male and females rats suggested potential differences in oxidative stress regulation that deserves further research. There is considerable evidence for higher rates of vision loss caused by cataract in females worldwide, which is discussed in more detail below.

These population differences provide clues about the etiology of cataracts. Future research is needed to discover why such differences exist.

Risk Factors for Cataract

An exhaustive review is beyond the scope of this article, so this section covers only highlights and recent literature. Readers are also directed to the reviews listed in the section titled 'Further reading'.

Diabetes

By the 1950s the development of cataract in a diabetic rat model was fairly well established. Despite differences in animal and human lens, researchers suspected that diabetes was a cause of cataract in human diabetic patients as well. There was good biological plausibility to expect diabetes was a risk factor for cataracts, based on the effects of elevated levels of glucose on the sorbitol pathway, and increased free radical production leading to oxidative damage. Recent work on calpains provides further insight into diabetes-induced cataracts.

Population-based studies have identified the excess risk of cortical and PSC lens opacities in persons with diabetes. The risk appears to increase with increasing duration of diabetes. The level of control of blood glucose, as measured by levels of glycated hemoglobin, is related to the prevalence, onset, and progression of opacity. Diabetes is not usually associated with increased risk of nuclear cataracts.

There are no data on the differential effect, if any, of diabetes on cataract formation in different racial or ethnic populations. The risk of cataracts attributable to diabetes in African/Caribbeans is estimated at 14%, but is likely to be different among other populations, depending upon the prevalence of diabetes and the level of control of blood sugar.

Chronic Ultraviolet Light Exposure

Early work in animal models identified exposure to optical radiation as a cataractogenic agent, with an action spectrum that implicated ultraviolet light B (UVB; 290–320 nm). Recent work in rabbit lenses suggest that cumulative effect of repeated UVB radiation is more harmful to the lens metabolic profile than the same dose as a single irradiation. Geographic differences in cataract risk were long associated with differences in ambient sunlight. Population-based

surveys over large geographical areas, using latitude as the marker of exposure, found elevated risk of cataract where ambient UVB exposure was highest.

However, such studies are subject to bias known as ecologic fallacy, wherein many other risk factors could vary along with ambient sunlight, producing a spurious association. A classic example was the fall in diarrheal disease with the rise in home televisions (TVs), where clearly TV was just another marker of improved socioeconomic status and not an etiological agent. The imprecision of the measure of ocular exposure to UV light was also a hindrance, with many studies using ambient UV or skin sunburns as indices. Methods to estimate ocular exposure in a more precise way were developed, using a Maryland Sun Year as a unit of measure. This metric was tied to the average amount of UVB that falls on a flat plane in Maryland in a year, as measured over several years. Ocular radiation was estimated by factoring in the use of a brimmed hat, sun or corrective eyeglasses, season, time of day, and geographic location, coupled with self-report of being outside during daylight hours. This detailed assessment of cumulative ocular exposure to UV light in a high-risk group, Maryland fishermen, showed a dose–response relationship between exposure and risk of cortical opacities. However, there were no African Americans or females in the study. A subsequent evaluation in a population-based study demonstrated that, for all groups including women and African-Americans, there was an increased risk of cortical opacity with increasing ocular exposure to UVB, even with the type of exposure found in a general population. For every 0.01-MSY increase in ocular exposure, there was a significant, 10% increase in the risk of cortical opacity.

The public health ramifications of this association between UV light exposure and lens opacity extend to global warming and increases in lens opacity have been predicted, based on various scenarios attributable to the ozone hole. However, exposure to UVB can be limited through very simple measures; wearing plastic glasses or sunglasses when outside or wearing a brimmed hat. These measures have become part of the sun awareness campaigns carried out in Australia, Canada, and, by the US Environmental Protection Agency's SunWise program, in the United States.

Other Radiation Exposure

Cataract formation has long been known to result from exposure to ionizing radiation. Fortunately, the atmosphere filters ionizing radiation and human populations are not exposed from solar sources. Human populations have been exposed as atomic bomb survivors, nuclear reactor survivors, or through exposure to therapeutic radiation. Earlier reports suggested that the minimum dose required to produce a detectable cataract was 1.5 Gy (single exposure). Such data supported the recommendations of the National Council on Radiation Protection, which state that single 2-Gy dose is the minimum required to produce a detectable cataract, with a 5-Gy limit for a fractioned dose.

Recent data from exposed populations challenge the threshold recommendations. A recent re-analyses of cataract prevalence among the atomic bomb survivors in Japan suggests no evidence for a threshold effect. Cataract among the 8607 cleanup workers at the nuclear site in Chernobyl was assessed at 12 and 14 years after exposure. PSC and cortical cataract rates were present in a dose-dependent fashion, suggesting a threshold under 1 Gy. Using cataract extraction as a surrogate for cataract, a study in 35 705 radiologic technologists followed up for 20 years found that those reporting three or more X-rays to the head and neck were 25% more likely to have a cataract extraction. In addition, the technologists who worked in the highest category of exposure (mean 60 mGy) were 18% more likely to have cataract extraction compared to those in the lowest category of exposure (5 mGy), although the latter difference was not statistically significant. These differences suggest that there may be no threshold, or at least that the threshold is considerably less than current recommendations of the National Council on Radiation Protection.

Other Oxidative Stress

Most ocular tissues are vascularized and supplied with ample levels of oxygen, except the lens whose cells are normally hypoxic. Animal models suggest that the lens may have difficulty controlling the consumption of oxygen. Increasing oxygen exposure to the posterior lens surface is associated with higher consumption of oxygen by the lens. Such a scenario may lead to increased production of reactive oxygen species, known to contribute to opacification.

One mechanism by which increasing levels of oxygen may reach the posterior lens is through breakdown in vitreous gel that lies between the lens and retina, or removal of vitreous altogether. Vitrectomies are associated with rapid development of nuclear opacities, and exposure of the posterior lens to higher-than-normal levels of oxygen is felt to be the mechanism. It may also explain age-related nuclear opacification; one study has already shown that there is an association between age-related vitreous liquefaction and nuclear opacification. The observational studies that have shown a relationship of early-onset myopia (not myopic shift due to nuclear cataract) to nuclear cataract may also be explained by the association of myopia with vitreous degeneration. However, not all studies have found an association of myopia with nuclear cataract; some report that another cataract type, PSC, is related to myopia.

If oxidative stress is cataractogenic, then prevention or amelioration of the stress should be protective. This has led to the postulate that antioxidant nutrients, vitamins, or supplements may be protective against cataractogenesis. However, numerous studies have attempted to demonstrate a protective effect of antioxidant nutrients, vitamins, and supplements against cataract with no clear, consistent findings. Notably, several clinical trials of antioxidant vitamins in diverse populations have failed to demonstrate any consistent, protective effect for cataract. The Age-Related Eye Disease Study (AREDS) clinical trial followed up 4629 patients randomized to four combinations of antioxidants with zinc and placebo. No protective effect was seen on incidence or progression of lens opacities. A more recent study of 1020 participants randomized to multivitamin versus placebo, using the same AREDS grading scheme, found a protective effect of supplementation for nuclear opacity, and a twofold increased risk for PSC. All these trials have been criticized for not including the correct supplement, or dosing for too short a period of time, or being conducted in study populations which are already taking supplements outside the trial. Considering the huge investment in research in this area, and the conflicting findings across many different populations and study designs, this field deserves a thorough and careful review with recommendations of promising approaches before any further research is warranted.

Medications

The promise of medication to prevent or retard cataract growth has proved elusive. Initial hope for aspirin or non-steroidal anti-inflammatory agents as anticataract agents was not supported by research. The seemingly protective effect of hormone replacement therapy in women was not borne out in the longitudinal follow-up in both Beaver Dam and Salisbury populations. It is likely that other endogenous hormonal effects are implicated in cataractogenesis in women. Two reports of protective effect of long-term statin use against nuclear cataract or any cataract are intriguing, due to the anti-inflammatory and antioxidant effects of these medications. However, the findings were in a small sample of the Beaver Dam and Blue Mountains populations (in the latter there was insufficient power to evaluate cataract subtypes). This observation deserves confirmation in other studies designed to specifically evaluate the possible protective effect of statins.

Other medications have been shown to be cataractogenic. Oral steroids, particularly in high doses or with prolonged use, have long been implicated in PSC. Early studies suggested an absence of increased risk for inhaled corticosteroids. However, these were criticized for being conducted in primarily young populations or for being confounded by oral steroid use as well. Several studies have now reported increased risk of cataract among users of inhaled steroids. A dose–response relationship was reported from the study by Mitchell and co-workers, lending more weight to the association. Steroids may appear to be a risk factor for PSC and, interestingly, for nuclear opacity as well.

Topical medications for lowering intraocular pressure were associated with incident nuclear opacity in a population-based study of African Caribbean persons in Barbados, an association that was confirmed in the Early Manifest Glaucoma (EMG) trial. The most frequently used medication in the Barbados study was topical beta-blockers. After careful adjustment to exclude high intraocular pressure itself as the risk factor, a consistent elevated risk was observed. Another large study of glaucoma treatment, the Ocular Hypertensive Treatment Study (OHTS) did not detect an increased risk of lens opacity after treatment with glaucoma medications. This might be attributed to the cross-sectional assessment of cataract after a large proportion of persons in the medication treatment arm had already had cataract surgery. The initial findings in a population-based study resulted in cataract components being added to the OHTS and EMG clinical trials to provide more information about this potentially damaging consequence of glaucoma medication. These findings could have considerable clinical relevance when treating older persons, who are at risk for both diseases.

Smoking

Since the first epidemiological reports of smoking associated with nuclear cataract, a large and consistent body of literature has supported this relationship. A dose–response relationship exists, and smoking increases the incidence and progression of nuclear opacification. Smoking cessation appears to reduce the risk of cataract, which may be due to either the lower cumulative doses smoked by those who stopped, or some reversible damage. The consistency of the association, the presence of a dose–response relationship, and findings of change after cessation provide strong evidence for causality, with smoking now a well-accepted risk for nuclear cataract. Cataract has now been added to the US Surgeon General's report on health effects of smoking, the first ocular condition to have this dubious distinction. An estimated 20% of cataract cases in the US may be attributable to smoking. In countries such as China, where smoking is common, cataract is and will continue to be epidemic.

Genetics and Cataract

The likelihood of a genetic predisposition to nuclear and cortical cataract has been evaluated in several population studies. In studies of monozygotic and dizygotic Caucasian twins in the UK, the heritability of nuclear cataract

was estimated at 48%, with unique environmental factors estimated to account for another 14% of the variability. The heritability in sibling pairs has been estimated at 36% in an older cohort in Salisbury after adjusting for smoking. In extensive analyses in the Beaver Dam cohort pedigrees that included smoking, the data suggest contributions to nuclear cataractogenesis from multiple genes, characteristic of a complex disorder. Promising work has been carried out investigating mutations in the crystalline genes, using congenital or autosomal dominant nuclear cataract cases, but further work linking these to age-related cataract is needed.

Similarly, there appears to be a strong genetic component to cortical cataract. In the UK Twin Study, additive and dominant genes accounted for 53–58% of the variability in cortical cataract, with unique environmental factors accounting for 26–37%. The heritability for cortical cataract in the Salisbury sibling pairs was 24%.

To date, much research has identified polymorphisms and mutations that are associated with autosomal dominant or recessive congenital cataracts, with some work in age-related cataract. This is a growing field that will continue to evolve. Fascinating work on the crystalline genes has provided not only leads into cataractogenesis, but also associations with other neurological, cardiac, and muscular disorders that will likely provide insights into the aging process.

Cataract as a Predictor of Mortality

A provocative link between lens opacity and increased risk of early mortality has now been reported from several, although not all, epidemiological studies. Nuclear opacity and mixed opacity in particular have been found to be independent risk factors for mortality, adjusted for health status, frailty, and other confounders. This association is clearly not causal, but suggests that the lens may well be a natural window into the aging process. This is being explored by cell biologists interested in aging tissues, especially in lens proteins. Further research may well involve development of lens biomarkers that serve as an index of early senescence

Cataract Surgery and Outcomes

In addition to playing a major role in understanding cataract etiology, epidemiological research has also helped to identify issues relating to access and barriers to cataract surgery, the outcomes of cataract surgery, methods to improve the cost effectiveness, and the impact of cataract and cataract surgery on quality of life. These important accomplishments could be the subject of another review, so only highlights are covered here.

The development of the simple tool, called Rapid Assessment of Cataract Surgical Services, has allowed countries to determine how well the cataract blind are accessing surgery. This reporting tool has been invaluable for the VISION 2020 community to chart the coverage of its mission to reduce cataract as an avoidable cause of blindness by the year 2020.

However, surgical coverage indices alone are not a complete indicator of success in reduction of cataract blindness. For example, when coverage improved in India under a World Bank program to increase cataract surgery, epidemiological assessments of outcomes showed that vision restoration was less than ideal, with the potential for higher rates of poor visual outcome occurring in the rush to increase coverage. These findings were instrumental to the institution of surgical audits of outcomes to be certain that quality was not sacrificed for quantity.

Surgical coverage may not be equitable. Women experience more barriers to cataract surgery, especially in countries were gender equality is less than ideal. The rates of blindness and visual loss due to cataract are significantly higher in women compared to men in many countries. Women have more difficulty accessing the resources necessary to obtain cataract surgery and cataract campaigns are not designed especially to encourage women. Further operational research designed to determine barriers specific for women, and especially cost-effective strategies to eliminate these barriers, should be undertaken.

Barriers are not confined to less-wealthy countries. In the US, African-Americans are less likely to have cataract surgery, compared to Caucasians, despite having similar or higher rates of disability due to an opacified lens. The reasons for this health disparity are unknown. Language and financial barriers have been identified as impediments among Latinos in the US who need cataract surgery. Recent efforts to document the inequities in eye care delivery should now be expanded to determine why such inequities exist and how these disparities in underserved minorities may be eliminated.

The use of large, simple trial methodology has demonstrated that medical testing before cataract surgery does not improve outcomes and could be eliminated with significant cost savings. The use of large existing databases is becoming a valuable resource to study small, increased risks with changes in methods for cataract surgery, or to investigate large population inequities in access to services where generalizability is important.

The development of self-reported quality-of-life tools for use in studying the impact of visual impairment began with research on cataract surgery patients, demonstrating how sensitive these tools were to improvement in vision following surgery. The original tool, Activities of Daily Vision, was followed by the development of shorter sets of

questions specifically for cataract surgery, such as the visual function 14 (VF-14) questionnaire. These have been used to document patient complaints due to cataract, complaints that are not necessarily captured by tests of acuity or contrast sensitivity. Recognition of the broad impact of cataract on patient function led to a change in surgery best practices. This guideline states that, in addition to deficits in visual acuity, cataract surgery may be indicated when patient function is compromised.

Summary

The epidemiologic study of cataract and lens opacity has made great strides in determining the magnitude of the problem and the burden that cataract places on human populations. Considerable progress has been made in characterizing different opacity phenotypes, ethnic and racial population differences, and identifying risk factors with public health importance. Future research must address the questions of why these population differences exist, using creative collaborations in diverse population laboratories.

While the risk of cataract can be reduced, it cannot be prevented. Therefore, continued emphasis on health services research is needed, using effective methodologies to identify disparities and inequities in access to surgical treatment for cataract. Links with systemic models of aging are at the forefront of research and deserve special attention for the broader implications that may be revealed by findings markers for early senescence.

See also: Genetics of Age-Related Cataract; Genetics of Congenital Cataract.

Further Reading

Abou-Gareeb, I., Lewallen, S., Bassett, K., and Courtright, P. (2001). Gender and blindness: A meta analyses of population-based surveys. *Ophthalmic Epidemiology* 8: 39–56.

Abraham, A. G., Congdon, N. C., and Gower, E. W. (2006). The new epidemiology of cataract. *Ophthalmology Clinics North America* 19: 415–425.

Age-Related Eye Disease Study Group (2001). A randomized placebo controlled clinical trial of high dose supplementation with vitamins C and E and beta carotene for age related cataract and vision loss: AREDS report no 9. *Archives of Ophthalmology* 119: 1439–1452.

Holekamp, N. M., Shui, Y. B., and Beebe, D. C. (2005). Vitrectomy surgery increases oxygen exposure to the lens: A possible mechanism for nuclear cataract formation. *American Journal of Ophthalmology* 139: 302–310.

International Commission on Radiological Protection (1990). *Recommendations of the International Commission on Radiological Protection*. Oxford: Pergamon Press.

Limburg, H., Foster, A., Vaidyanathan, K., and Murthy, G. V. (1999). Monitoring visual outcome of cataract surgery in India. *Bulletin of the World Health Organization* 77: 455–460.

O'Day, D. and The Cataract Management Guideline Panel of the Agency for Health Care Policy and Research (1993). Management of cataract in adults. Quick reference guide for clinicians. *Archives of Ophthalmology* 111: 453–459.

Resnikoff, S., Pascolini, D., D'etyale, D., et al. (2004). Global data on visual impairment in the year 2002. *Bulletin of the World Health Organization* 82: 844–851.

United States Department of Health and Human Services (2004). *2004 Surgeon General's Report: The Health Consequences of Smoking*, pp. 777. Atlanta, GA: Centers for Disease Control and Prevention, Office on smoking and health. US Government Printing Office, Washington, DC.

West, S. K., Duncan, D. D., Munoz, B., et al. (1998). Sunlight exposure and risk of lens opacities in a population-based study: The salisbury eye evaluation project. *Journal of the American Medical Association* 280: 714–718.

West, S. K., Munoz, B., Istre, J., et al. (2000). Mixed lens opacities and subsequent mortality. *Archives of Ophthalmology* 118: 393–397.

Wu, S. Y. and Leske, M. C. (2000). Antioxidants and cataract formation: A summary review. *International Ophthalmology Clinics* 40: 71–81.

Zhang, X., Saaddine, J. B., Lee, P. P., et al. (2007). Eye care in the United States: Do we deliver to high risk people who can benefit most from it? *Archives of Ophthalmology* 125: 411–418.

The Evolution of Opsins

T H Oakley and D C Plachetzki, University of California, Santa Barbara, Santa Barbara, CA, USA

Glossary

Bilaterian – A major family of animals characterized by bilateral symmetry, including insects, nematode worms, mollusks, vertebrates, echinoderms, and other animals.

Chromophore – A light-reactive chemical that binds to a protein, such as opsin, and which allows biological sensitivity to light.

Ciliary – Relating to cilia, which are subdivided into motile and sensory types. Ciliary photoreceptors are those in which phototransduction occurs in a sensory cilium.

CNG (cyclic nucleotide-gated ion channel) – A family of proteins that acts (along with other functions) as the ion channel in ciliary photoreceptor cells. CNG proteins open in the presence of cyclic nucleotides to allow positively charged ions such as calcium to flow into the cell.

Cnidaria – A group of animals that includes jellyfish, anemones, hydras, and corals.

Co-duplication – The simultaneous duplication during evolution of interacting components (e.g., genes or proteins).

Co-option – The pattern or process whereby existing components (e.g., genes or proteins) are used in the evolution of a new structure or function.

Eumetazoa – A major group of animals characterized by the presence of numerous cell types, tissues, and organs and that includes bilaterians and cnidarians.

GPCRs – Guanine-nucleotide-binding protein (G-protein)-coupled receptors form a class of proteins that functions by embedding in cell membranes. These proteins function to detect a signal outside the cell and then signal to proteins inside through a G protein to the cell to change the cell's state in some way.

G protein (Gt, Gq, Go, Gs) – A family of multi-unit proteins that are activated by GPCR receptor proteins to transmit signals into cells. Gt, Gq, Go, and Gs are subfamilies of G-alpha proteins activated by opsins.

Photopic vision – The vision in high light levels, which may include color vision.

Phototransduction – The conversion of a light signal received by an animal opsin to an electrical signal that is transmitted to the nervous system.

Rhabdomeric – A type of photoreceptor cell with numerous microvilli. It is also called microvillar photoreceptors.

Rhodopsin – A name originally given to isolated visual pigments that contained both opsin protein and nonprotein chromophore. Today the term still applies to visual pigments, and is also used commonly to describe the opsin protein expressed in vertebrate rod (dim-light) photoreceptors, and the opsins of certain organismal groups, such as bacteria.

Scotopic vision – A monochromatic vision in low light levels.

Spectral tuning – The changes in specific amino acids of opsin proteins that mediate the maximum sensitivity to different wavelengths of light of different visual pigments.

Tetrachromatic – A visual system based on four classes of visual pigments with four different λ-*max* values.

Trichromatic – A visual system based on three classes of visual pigments with three different λ-*max* values.

TRP (transient receptor potential ion channel) – A family of proteins that acts (along with other functions) as the ion channel in rhabdomeric photoreceptor cells. TRP proteins open in the presence of products derived from the lipid diacylglycerol to allow positively charged ions to flow into the cell.

Type I opsin – The retinylidene proteins present in bacteria and algae, which are referred to by various names, including bacteriorhodopsin, bacterial sensory rhodopsins, channelrhodopsin, halorhodopsin, and proteorhodopsin. These proteins have varied functions, including bacterial photosynthesis (bacteriorhodopsin), which is mediated by pumping protons into the cell, and phototaxis (channelrhodopsin), which is mediated by depolarizing the cell membrane.

Type II opsin – The retinylidene proteins present for approximately 600 million years in eumetazoans (animals not including sponges), and unknown from sponges or any nonanimals. The proteins of this family have varied functions, including phototransduction and vision, circadian rhythm entrainment, mediating papillary light reflex

(pupil constriction), and photoisomerization (recycling the chromophore).
λ-max – The wavelength of light to which a visual pigment (opsin plus chromophore) is maximally sensitive.

Introduction

Opsins are a group of proteins that underlie the molecular basis of various light-sensing systems, including phototaxis, circadian (daily) rhythms, eye sight, and a type of photosynthesis. They are sometimes called retinylidene proteins because they bind to a light-activated, nonprotein chromophore called retinal (retinaldehyde). Opsins are also, in some cases, called rhodopsins, a name originally given to isolated visual pigments that contained both opsin protein and nonprotein chromophore in a time before the two separate components were known. Today, the term rhodopsin is used commonly to describe the opsin expressed in vertebrate rod (dim-light) photoreceptors, and the opsins of certain organismal groups, such as bacteria.

General Opsin Structure and Function

Opsins are light-sensitive proteins that snake in and out of a cell membrane 7 times. Crystal structures of opsins have been generated, which allows a detailed understanding of this protein structure. Opsin light sensitivity is mediated by light-sensitive chemicals called chromophores. Opsin proteins covalently bind a chromophore through a Schiff base linkage to a lysine amino acid in the seventh membrane-spanning region of the protein. The absorption of a photon of light results in a photoisomerization, or shape change, of the chromophore. Photoisomerization then causes a shape change in the liked opsin protein.

Type I and Type II Opsins

Two major classes of opsins are defined and differentiated based on primary protein sequence, chromophore chemistry, and signal transduction mechanisms. Several lines of evidence indicate that the two opsin classes evolved separately, illustrating an amazing case of convergent evolution.

Type I opsins are present in bacteria and algae and are referred to by various names, including bacteriorhodopsin, bacterial sensory rhodopsins, channelrhodopsin, halorhodopsin, and proteorhodopsin. These opsins have varied function, including bacterial photosynthesis (bacteriorhodopsin), which is mediated by pumping protons into the cell, and phototaxis (channelrhodopsin), which is mediated by depolarizing the cell membrane. Type II opsins are present in eumetazoans (animals not including sponges), but are unknown from sponges or any nonanimals. As opsins are known from cnidarians and bilaterian animals (animals with bilateral symmetry, including humans, flies, and earthworms), type II opsins are inferred to have been present in their common ancestor, which lived about 600 million years ago. These opsins have varied function, including phototransduction and vision, circadian rhythm entrainment, mediating pupillary light reflex (pupil constriction), and photoisomerization (recycling the chromophore).

Despite their functional similarity and despite both being seven-transmembrane proteins, multiple lines of evidence indicate that type I and type II opsins evolved independently. First, the primary amino acid sequences of type I and type II opsins are no more similar than expected by chance. Second, the orientation of the transmembrane domains differs between the major groups. Third, the major opsin groups differ in chromophore chemistry. Prior to light activation, the chromophore of type I opsins is an all-*trans* isomer. Light activation then involves isomerization of the chromophore to 13-*cis* retinal. In contrast, prior to light activation, the chromophore of type II opsins is 11-*cis* retinal. Light activation of type II opsins involves isomerization to all-*trans* retinal (**Figure 1**). Fourth, type II opsins belong to the larger protein family called G-protein-coupled receptors (GPCRs), which transmit varied signals from outside to inside cells by activating guanosine triphosphate (GTP)ase proteins, which in turn signal to second messengers that affect the state of the cell in various ways. Type I opsins do not activate G proteins. Furthermore, type II opsins are more closely related to nonopsin, light-insenstive GPCRs than they are to type I opsins.

Major Type II Opsin Classes

Based on phylogenetic analyses, there are four major classes of type II opsins in animals: cnidops, retinal G-protein receptor (RGR)/Go, rhabdomeric (Gq), and ciliary (Gt) (**Figure 2**).

Cnidops

In 2007, a new major class of opsins was described based on analyses of whole genome sequences of the phylum Cnidaria, which includes sea anemones and jellyfish. This cnidarian-specific class of opsins is called cnidops. The molecular details of cnidops-mediated phototransduction are not yet fully elucidated, but box jellyfish cnidops appears to activate Gs-class G proteins, which in turn activate adenylyl cyclase. For what might cnidarians be using opsins? Some jellyfish are known to use light cues to

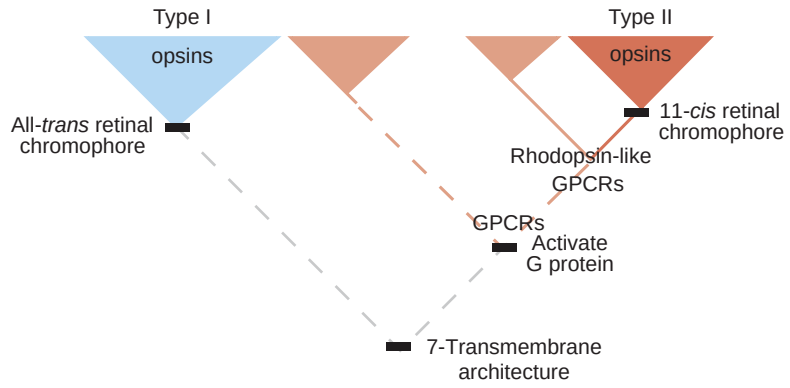

Figure 1 Evolutionary relationships of type I and type II opsins, and G-protein-coupled receptors (GPCRs). Triangles represent major groups with many genes from many species. Solid lines indicate good support for evolutionary relationship (common descent) based on sequence similarity and other evidence. Dashed lines indicate there is no evidence for common ancestry beyond random similarity of sequences and similar function. Type I opsins are well known from bacteria and function in a type of photosynthesis and, in some cases, to mediate movement toward or away from light. Type II opsins are found only in animals (see **Figure 2** and **Table 1**), and are likely related to nonopsin GPCRs, which include chemoreceptor and other proteins that detect a signal outside a cell, and mediate a response inside the cell. A chromophore is a light-sensitive chemical that is bound to opsin. Type I and type II opsins use different chromophores.

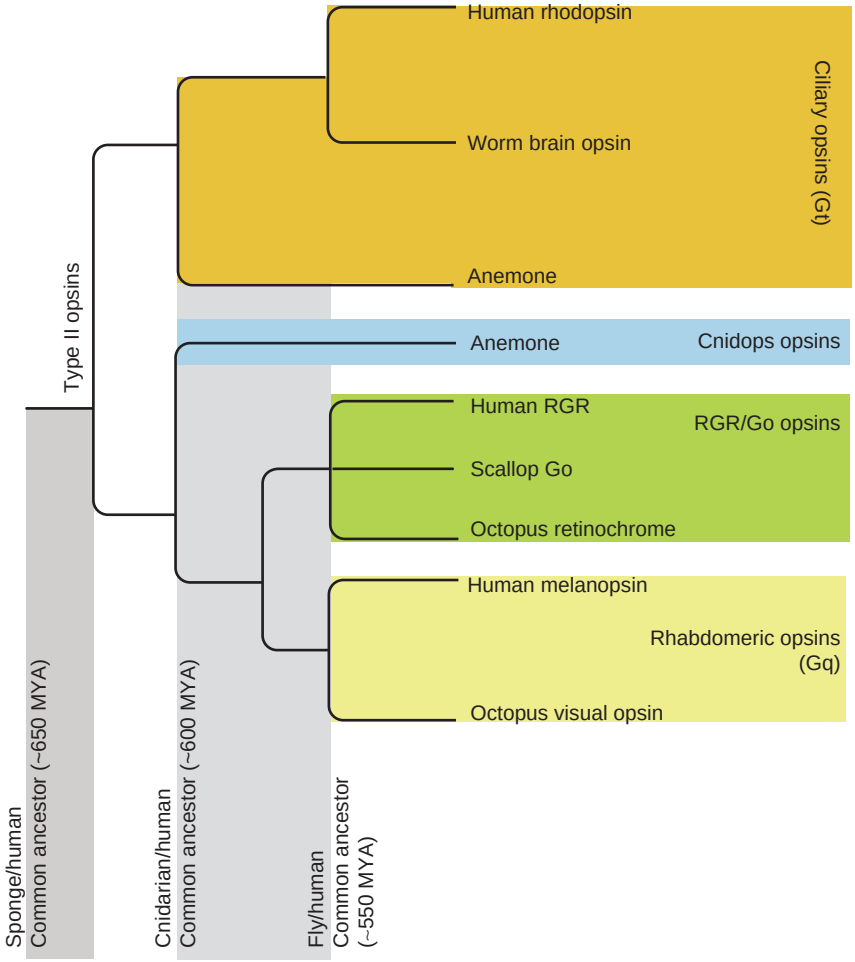

Figure 2 Illustrated are possible evolutionary relationships of the major groups of opsin genes (ciliary, cnidops, RGR/Go, and rhabdomeric). Here, each major group is represented by genes from one to three species, but each major opsin group is found in many other species as well. **Table 1** shows names of other opsins, some not on this figure, and the major opsin group to which they belong. Based on presence in anemone (a cnidarian) and bilaterian animals (humans and annelid worms), ciliary opsins and therefore all type II opsins originated before the common ancestor of cnidaria and bilateria, which lived some 600 million years ago.

regulate their depth in the water column and their swimming speed, while others (box jellyfish) possess sophisticated camera eyes analogous those of humans. These complex cnidarian eyes may be capable of image-forming vision, and are used for obstacle avoidance and perhaps for hunting prey. At present, there is no evidence for cnidops-mediated color vision.

Retinal G-Protein Receptor/Go

Retinal G-protein receptor (RGR) and Go opsins are functionally distinct from each other, but sometimes group together in phylogenetic analyses, indicating they may share more recent common ancestry with each other than with the other major opsin classes. Opsins grouping in this clade include those from vertebrates, cephalochordates (invertebrate chordates represented by the lancelet *Branchiostoma*), and mollusks.

In humans, three opsins often fall within the RGR/Go group: peropsin, neuropsin, and RGR. Cephalopod mollusks also possess a related opsin called retinochrome. Interestingly, members of this opsin class have not been noted from any arthropod or any other ecdysozoan (a group of molting invertebrates, including arthropods and nematode worms).

The RGR opsins are not well understood, but some important clues to their function exist. These opsins preferentially bind an all-*trans* isomer of retinal, contrasting with rod and cone opsin, which require 11-*cis* retinal for function. When tested in specific wavelengths of light that ranged from blue to ultraviolet (UV), RGR was able to convert all-*trans* retinal to the 11-*cis* isomer. Thus, it would seem that RGRs function to provide fresh retinal of the functional 11-*cis* conformation that is required for proper rod and cone opsin function. Retinochrome opsins from mollusks also have this photoisomerase function.

In addition, in mollusks and cephalochordates are opsins that may interact with a Go-class G protein, and as such are called Go opsins.

Rhabdomeric (Gq)

Opsins belonging to the rhabdomeric (Gq) class are present in bilaterian animals (animals with left and right sides), but unknown from Cnidaria. Where known, these opsins activate Gq-class G proteins, which drive phospholipase C second messengers. The opsins are sometimes called rhabdomeric opsins, because they tend to be expressed in specific cell types (rhabdomeric photoreceptor cells) that increase cell surface area using microvilli. Gq opsins are well known for mediating vision of many invertebrate animals, and are particularly well studied in the compound eyes of the fly *Drosophila melanogaster*. In chordates, including humans, Gq opsins are not expressed in the primary visual photoreceptors; instead, a Gq opsin, called melanopsin is known to be expressed in retinal ganglion cells, which are among the cells that relay signals from the primary photoreceptors to the optic nerve. Melanopsin is also involved in mediating the papillary reflex.

Ciliary (Gt)

Opsins belonging to the ciliary (Gt) class are present in eumetazoan animals, including vertebrates, annelid worms, and cnidarians (anemones and jellyfish). In vertebrates, these opsins activate Gt-class G proteins (transducins), which drive phosphodiesterase (PDE) enzymes. In invertebrates, the G protein that is activated by ciliary opsins is unknown. This class of opsins is often called ciliary opsins because they are known to be expressed in ciliary photoreceptor cells, which assemble a phototransduction organelle from a sensory cilium membrane. In annelids and bees, ciliary opsins are expressed in the brain. Although the organismal function of ciliary opsins is unknown in invertebrates, some have suggested a role in entraining circadian rhythms. In vertebrates, ciliary (Gt) opsins are expressed in the primary photoreceptors, the rods and cones, with different subclasses of opsin expressed in rods versus cones and further subclasses expressed in different cones to mediate color vision. Ciliary opsins with extraretinal expression are also known from vertebrates, and have been given various monikers, often named for their site of expression, such as pinopsin, parapinopsin, and tmt opsin. Details about the molecular and organismal functions of these extraretinal ciliary opsins are scarce (**Table 1**). One opsin in this class, parietopsin, is expressed in the parietal eye of a lizard and activates a Go-class G protein.

Opsin and Color Vision

Color vision, the ability to discriminate between light information of different wavelengths, is present in various groups of animals including insects and vertebrates, and involves opsin genes. Although color vision is a behavioral phenomenon that involves processes of both physical detection and neurobiological comparison, duplicated opsin proteins expressed in the retina directly mediate the physical detection of different wavelengths of light.

The specificity of a given opsin protein to a given wavelength of light is summarized by its λ-*max*, a measure of the peak absorbance across the light spectrum. The specific λ-*max* of a given opsin protein is largely a function of its amino acid sequence. Opsins representing the different spectral classes are specifically expressed in individual photoreceptor neurons called cone cells. When stimulated by light of the proper wavelength, opsins trigger a cellular response, leading to a change in the resting electric charge, or potential, of a photoreceptor cell. Color vision emerges from this system through the comparison

Table 1 Various names for type II opsins

Name	*Major clade*	*Taxon*	*Expression*	*Function*
Encephalopsin/ panopsin	Ciliary		Brain	Retinoid Receptor?
Exo-rhodopsin	Ciliary	Zebra fish	Pineal	Unknown
Parapinopsin	Ciliary	Vertebrates	Parapineal, pineal	
VA/VAL opsin	Ciliary	Vertebrates	Horizontal and amacrine cells, pineal, brain	Unknown
Cone L-opsin	Ciliary	Vertebrates	Cone cells	Photopic Vision
Cone M-opsin	Ciliary	Vertebrates	Cone cells	Photopic Vision
Cone S-opsin	Ciliary	Vertebrates	Cone cells	Photopic Vision
Cone V-opsin	Ciliary	Vertebrates	Cone cells	Photopic Vision
Pinopsin	Ciliary	Vertebrates	Brain, pineal organ	
Pteropsin	Ciliary	Bees, Mosquitoes	Brain	Unknown
Rhodopsin	Ciliary	Vertebrates	Rod cells	Scotopic Vision
TMT opsin	Ciliary	Teleost fishes	Many tissues	Unknown
Parietopsin	Ciliary	Zebra fish, fugu, Xenopus, lizard	Parietal eye	Photoreception
Cnidops	Cnidops	Cnidarians (hydra, anemone, and jellyfish)	Neurons	Light perception
Neuropsin	RGR/Go	Mammals	Testes, brain, spinal cord, eye	Photoisomerase?
Peropsin	RGR/Go	Mammals	RPE	Photoisomerase?
RGR	RGR/Go		RPE and Müller cells	Photoisomerase
Retinochrome	RGR/Go	Cephalopoda	Retina	Photoisomerase
Go	RGR/Go	Scallop, lancelet	Scallop eye	Photoreception
Arthopsin	Rhabdomeric	Daphnia	Unknown	Unknown
Melanopsin	Rhabdomeric	Vertebrates	Retinal ganglion cells	Circadian rhythms, papillary reflex
Rhabdomeric (Gq) opsin	Rhabdomeric	Invertebrates	Eye	Vision

of the resultant potentials of cone cells with those that express opsins of differing *λ-max* expressed in adjacent cone cells. For instance, humans possess three cone-opsins with *λ-max* values falling roughly into the categories of blue, blue–green, and yellow–green. Compared to other vertebrates, human opsins represent a single blue S opsin and two M opsins (blue–green and yellow–green) that resulted from a primate-specific gene duplication event. When red light falls upon a cone cell that is sensitive to yellow–green, it activates opsin signaling because light of this wavelength falls within the activity spectrum of this protein. However, red light does not fall within the sensitivity spectra of either the blue or blue–green opsins. Together, comparisons made between activated and non-activated cone cells lead to the human perception of red light. In most vertebrates, these comparisons are made by additional cells in the retina (i.e., the horizontal and ganglion cells) and also in a portion of the brain called the visual cortex.

In vertebrates, four distinct opsin classes, each with distinct sensitivities, accomplish the full spectral range. These include violet-(V) short-(S), middle-(M), and long-(L) wavelength varieties. Studies in the sea lamprey, a distant vertebrate relative of humans, have provided data that allow scientists to infer that the four major classes of vertebrate retinal opsins are the result of ancient gene duplication mutations that likely occurred before the origin of all living vertebrates. This implies that major opsin clades must have been lost in various vertebrate lineages. For instance, placental mammals likely originated from nocturnal ancestors that lost the V and M spectral classes of opsin. In addition, some marine mammals are known to have further lost the S class of opsin and are cone monochromats. Similar losses have been reported in a deep-dwelling, Lake Baikal fish. In general, each of these examples of opsin loss can be correlated to photoecology. When spectral sensitivity of a given wavelength is not required, selection against mutations at these loci is relaxed, allowing the loss of functional copies. However, on numerous occasions, photoecology has provided a generative context for the origination of new opsin genes and classes in vertebrate and invertebrate lineages alike. Often, these new visual repertoires converge both in spectral sensitivity (i.e., *λ-max*) and in the specific mutations that have lead to the functional shift.

Despite major differences between insect-faceted eyes and vertebrate camera-like eyes, both eye types utilize opsins in a similar way to achieve color vision. Similar to vertebrate color vision, insect color vision is based on a process of physical detection of light by opsins of differing *λ-max*, followed by neurobiological comparison of these light data. In insects and other arthropods, the neurobiological basis for color vision is less well understood but

likely involves a part of the insect brain called the medulla. While the neurobiological basis for insect color vision requires further clarification, it is clear that opsin gene duplication has been a driving force for the evolution of color vision in insects and other invertebrates. For example, the duplicated opsin genes of fruit flies are well studied. Two fly opsins are maximally sensitive to UV (345, 375 nm), one to blue (437 nm), two to blue–green (420, 480 nm), and one to green (508 nm) light.

Molecular Basis of Wavelength Sensitivity

Different *λ-max* values of different opsins are mediated by specific amino acid differences, which in some cases have been experimentally demonstrated. For example, in primates, three amino acid sites have a dominant role in differentiating red-sensitive and green-sensitive opsins. In birds, one opsin gene is blue sensitive in some species, and UV-sensitive in other species, a difference that is mediated by a single amino acid change. Changing the 84th amino acid of a zebra finch opsin allowed the protein's sensitivity to change from UV to blue when the protein was expressed in cultured cells. Conversely, pigeon and chicken blue-sensitive opsins became UV sensitive in cell culture after a change of the 84th amino acid. The combination of gene duplication and differential changes in amino acids of duplicated opsins has generated a diversity of proteins in different species.

Opsin and Modes of Phototransduction Evolution

As discussed above, opsin genes were very often duplicated and retained during animal evolution. Early opsin gene duplications led to the major opsin groups and more recent duplications mostly led to additional specializations, such as the ability for color vision. As members of highly coordinated protein networks, changes in opsin proteins are sometimes correlated with changes in partnering proteins. The interaction of two evolutionary processes has resulted in the diversity of opsin-based phototransduction pathways observed today that contains a combination of shared and distinct interactions. First, co-option refers to instances where an opsin recruited different intracellular signaling components than its ancestor during evolution. Second, co-duplication involved the simultaneous duplication of multiple genes of an ancestral network. Co-option and co-duplication are not discrete alternatives; instead, some genes of a network originated by co-duplication, whereas others joined the network by co-option. This becomes especially clear if we examine the evolution of particular networks at multiple timescales, or at increasing spatial scales by increasing the number of interactions considered.

An example of phototransduction pathways that evolved largely by co-duplication is the different pathways used in rod and cone cells of vertebrate retinas. Rods are specialized for dim light (scotopic) vision, and cones are specialized for bright light (photopic) vision. Rods and cones utilize different, duplicated opsins as well as different duplicated genes downstream of opsin. Multiple rod-specific and cone-specific genes originated through large-scale segmental duplication of an ancestral vertebrate genome before the origin of gnathostomes (jawed vertebrates) and after the split of vertebrates and their closest nonvertebrate relatives. As such, the duplication of multiple genes in these pathways maps to the same time interval and is consistent with co-duplication.

Examples of the origin of new opsin pathways involving co-option probably include the origin the major opsin groups, which signal to different G proteins. In particular, the rhabdomeric opsins are the only opsins to signal through Gq G proteins and transient receptor potential (TRP) ion channels. Since rhabdomeric opsins originated in the ancestor of living bilaterally symmetric animals, and are unknown from Cnidaria, they have a more recent evolutionary origin than ciliary opsins, which are present in Cnidaria. This pattern indicates co-option: at or near their origin, rhabdomeric opsins began signaling to Gq and TRP, proteins that predate bilaterian animals.

See also: Circadian Rhythms in the Fly's Visual System; Color Blindness: Inherited; The Colorful Visual World of Butterflies; Genetic Dissection of Invertebrate Phototransduction; *Limulus* Eyes and Their Circadian Regulation; Microvillar and Ciliary Photoreceptors in Molluskan Eyes; The Photoreceptor Outer Segment as a Sensory Cilium; Phototransduction in *Limulus* Photoreceptors; Phototransduction: Phototransduction in Cones; Phototransduction: Phototransduction in Rods; Phototransduction: Rhodopsin; Polarized-Light Vision in Land and Aquatic Animals; Rod and Cone Photoreceptor Cells: Inner and Outer Segments.

Further Reading

Arendt, D. (2003). Evolution of eyes and photoreceptor cell types. *International Journal of Developmental Biology* 47(7–8): 563–571.

Briscoe, A. D. and Chittka, L. (2001). The evolution of color vision in insects. *Annual Review of Entomology* 46: 471–510.

Fernald, R. D. (2006). Casting a genetic light on the evolution of eyes. *Science* 313(5795): 1914–1918.

Hardie, R. C. and Raghu, P. (2001). Visual transduction in *Drosophila*. *Nature* 413(6852): 186–193.

Lamb, T. D., Collin, S. P., and Pugh, E. N. (2007). Evolution of the vertebrate eye: Opsins, photoreceptors, retina and eye cup. *Nature Reviews. Neuroscience* 8(12): 960–975.

Land, M. F. and Nilsson, D-E. (2002). *Animal Eyes.* (Willmer, P. and Norman, D. (eds)). Oxford: Oxford University Press.

Nathans, J. (1999). The evolution and physiology of human color vision: Insights from molecular genetic studies of visual pigments. *Neuron* 24(2): 299–312.

Oakley, T. H. and Pankey, M. S. (2008). Opening the ''black box'': The genetic and biochemical basis of eye evolution. *Evolution Education and Outreach* 4: 390–402.

Plachetzki, D. C. and Oakley, T. H. (2007). Key transitions during animal eye evolution: Novelty, tree thinking, co-option and co-duplication. *Integrative and Comparative Biology* 47: 759–769.

Salvini-Plawen, L. V. and Mayr, E. (1977). *On the Evolution of Photoreceptors and Eyes.* New York: Plenum Press.

Spudich, J. L., Yang, C. S., Jung, K. H., and Spudich, E. N. (2000). Retinylidene proteins: Structures and functions from archaea to humans. *Annual Review of Cell and Developmental Biology* 16: 365–392.

Terakita, A. (2005). The opsins. *Genome Biology* 6(3): 213.

Yokoyama, S. and Yokoyama, R. (1996). Adaptive evolution of photoreceptors and visual pigments in vertebrates. *Annual Review of Ecology and Systematics* 27: 543–567.

F

The Fibrillar Extracellular Matrix of the Trabecular Meshwork

M K Schwinn, J A Faralli, M S Filla, and D M Peters, University of Wisconsin, Madison, WI, USA

Glossary

Actomyosin network – A complex of myosin and actin filaments that regulates cell contractility.
Alternative splicing – The mechanism by which introns (noncoding regions) are removed from eukaryotic pre-messenger RNAs (mRNAs) to produce several different mature mRNAs and protein products from one gene.
Basement membrane – A thin layer of extracellular matrix proteins under a cell layer that supports cell attachment.
Cooperative signaling – Occurs when activation of one cell surface receptor activates or enhances activity of another cell surface receptor.
Exons – The coding sequences of genes.
Matrix metalloproteinases – A family of endopeptidases that cleave extracellular matrix proteins.
Mechanochemical – The conversion of mechanical stimuli into intracellular chemical signals.
RGD – The three-letter code for the amino acid sequence of arginine–glycine–asparagine. This amino acid sequence is found in many extracellular matrix proteins that bind integrins.
Rho GTPase – A member of the Ras family of guanine-nucleotide-binding proteins that control the polymerization of actin filaments and serves as a molecular switch to regulate cell proliferation, morphogenesis, migration, and gene expression.

Introduction

Intraocular pressure (IOP) is maintained through a delicate balance between aqueous humor (AH) production and its drainage through the trabecular meshwork (TM) and ciliary muscle. A major regulatory site of AH drainage in humans resides within the extracellular matrix (ECM) of the juxtacanalicular tissue (JCT) and the underlying inner wall of Schlemm's canal. The role the ECM plays in regulating AH outflow is unknown. One theory suggests that the ECM acts as a passive filter that restricts outflow across the TM by providing physical resistance to the movement of AH. Increases in fibronectin and collagen deposition could conceivably clog the filter and restrict AH movement. More recent studies, however, suggest that changes in the composition of the ECM would affect AH outflow by altering either the compliance of the TM or the contractile properties of the trabecular cells in the TM. In this article, we discuss the properties of collagen and fibronectin fibrils and how they might affect AH outflow.

Collagen: Structure and Localization

Collagens are composed of three α-chains that intertwine to form stable triple helical protomers. The protomers are either homo- or heterotrimers that assemble into unique supramolecular complexes. In vertebrates, there are at least 28 different types of collagens which are divided into several families based upon their structure. A number of collagens have been identified in the TM (**Table 1**); however, comparatively little is known about their molecular composition, relative abundance, or function within the TM. This article focuses on two of the major collagens found in the TM types I and IV collagen.

The collagens are highly conserved in terms of both their structure and function. Type I collagen is a heterotrimer of two identical chains called α1(I)-chains and one chain called α2(I)-chain. Each α-chain is synthesized from a single gene as a precursor molecule called procollagen that contains additional peptide extensions on both the N- and C-termini of the α-chains. These extensions referred to as propeptides maintain the solubility of type

Table 1 Collagens found in the trabecular meshwork

Family	*Type*	*Molecular form*	*Localization*
Fibril forming 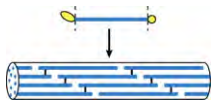	I III V XI	$[\alpha1(I)]_2\alpha2(I)$ $[\alpha1(III)]_3$ $[\alpha1(V)]_3$ $[\alpha1(V)]_2\alpha2(V)$ $\alpha1(V)\alpha2(V)\alpha3(V)$ $\alpha1(XI)\alpha2(XI)\alpha3(XI)$	Core of beams, JCT
Type IV 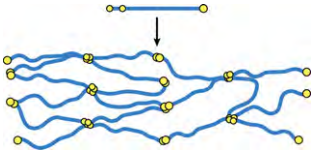	IV	$[\alpha1(IV)]_2\alpha2(IV)$ $\alpha4(IV)$-$\alpha6(IV)$*	Basement membranes of inner wall, along beams and underneath trabecular cells in JCT
Hexagonal networks 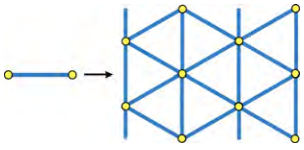	VIII	$[\alpha1(VIII)]_2\alpha2(VIII)$	Corneoscleral meshwork; within the JCT; both walls of Schlemms's canal
Beaded filaments 	VI	$\alpha(VI)\alpha2(VI)\alpha3(VI)$	Core and basement membrane of beams; JCT; outer wall of Schlemm's canal
FACITs 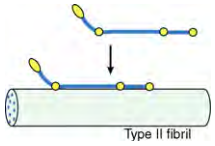	XII XIV XXII	$[\alpha1(XII)]_3$ $[\alpha1(XIV)]_3$ $\alpha1(XXII)$*	Gene level only
Multiplexins	XV	$[\alpha1(XV)]_3$	Gene level only

*Molecular form unknown.
Modified from Myllyharju, J. and Kivirikko, K. (2004). Collagens, modifying enzymes and their mutations in humans, flies and worms. *Trends in Genetics* 20: 33–43, with permission from Elsevier.

I collagen at physiological pH and play a regulatory role in modulating fibril formation. The propeptides are cleaved off by the specific proteases, procollagen N-proteinase and procollagen C-proteinase, which then triggers the spontaneous self-assembly of type I collagen molecules into fibrils. Within fibrils, type I collagen molecules are staggered relative to a neighboring molecule to create a striated collagen fibril exhibiting a 67-nm banding pattern. Type I collagen fibrils are found in the center of the trabecular beams, in the basement membrane along the beams and throughout the JCT. They are responsible for providing tensile strength to the TM, which is an essential physical requirement given the biomechanical demands on the TM. Type I collagen fibrils are often co-assembled into fibrils with types III and V collagen. Both these collagens are also found in the center of the beam and the JCT, but it is not known whether they are co-assembled with type I collagen into the same fibril and how this affects the function of the TM.

In addition to type I collagen, another major collagen in the TM is type IV collagen. In mammals, there are six homologous α-chains, α1(IV)–α6(IV), that are assembled into five distinct heterotrimeric protomers (**Table 1**). Each α-chain is characterized by three domains: a cysteine rich N-terminal 7S domain, a central triple helical domain, and a globular C-terminal noncollagenous domain (NC1). The central collagenous domain is interrupted by several noncollagenous sequences, which presumably contribute to the increased flexibility of type IV collagen relative to type I collagen. The assembly of the type IV chains is

different from that of type I chains in that the propeptides are not cleaved from the type IV molecule and the flexible type IV chains assemble into a network of filaments rather than linear fibrils.

Another interesting difference is that the NC1 domains of type IV collagen can exist as biologically active fragments in tissues or in the circulation. For instance, the isolated NC1 domains of the α1, α2, and α3 chains referred to as arrestin, canstatin, and tumstatin, respectively, are inhibitors of angiogenesis. *In vitro*, NC1 domains of type IV collagen regulate cell attachment, migration, proliferation, and gene expression. In particular, the NC1 domains control expression of matrix metalloproteinases (MMPs) that are important in the regulation of AH outflow. The activities of the NC1 domains are only expressed after type IV collagen has undergone proteolytic degradation. This implies that the activities of the NC1 domains are conformation dependent and would only be exposed in the TM as the ECM is remodeled. The release of these domains and additional upregulation of the MMP activity could be one way that matrix turnover and outflow are enhanced.

Type IV collagen is a major constituent in basement membranes and comprises approximately 50% of all basement membranes. In the TM, type IV collagen is found in the basement membranes covering the trabecular beams, along the inner and outer walls of Schlemm's canal and underneath the TM cells in the JCT. Together with laminin, type IV collagen is crucial for the stability and function of basement membranes. The functional specificity of the different basement membranes is derived in part from the different type IV collagens expressed in the tissue. For example, in kidney at least three distinct type IV collagens can be found. Bowman's capsule basement membrane contains the $[\alpha1(IV)]_2\alpha2$ (IV) protomer and perhaps the $[\alpha5(IV)]_2\alpha6$ (IV) protomer, while glomerular basement membrane contains the $\alpha3(IV)\alpha4(IV)\alpha5(IV)$ protomer. Whether there is any heterogeneity among the various basement membranes in the TM is not known, but clearly if there was, it could play a role in imparting different functional properties to the layers of the TM.

The synthesis of all collagens involves the coordination of several post-translational modifications that require specific enzymes and chaperones. These enzymes include the three collagen hydroxylases: prolyl 4-hydroxylase, lysyl hydroxylase, and prolyl 3-hydroxylase. The hydroxylation of proline and lysine residues is unique to collagens and is needed to stabilize the formation of the triple helix. These enzymes require ascorbate as a cofactor, which could explain one reason why ascorbate is found in high concentrations in the AH. It would also explain why ascorbate has been found to enhance collagen deposition into the ECM. Collagen synthesis also involves two collagen glycosyltransferases (galactose transferase and glucose transferase) that add galactose and glucose to hydroxylysyl and galactosylhydroxylysyl residues, respectively. This glycosylation is distinct from *O*- and N-glycosylation that occurs on most other proteins and is another unique post-translational modification of collagen precursors. Another post-translational modification includes the removal of the *N*- and C-propeptides by procollagen N-proteinase and procollagen C-proteinase. Procollagen C-proteinase belongs to the tolloid family and was originally called bone morphogenic protein-1 (BMP-1). Finally, collagen synthesis involves two isomerases (peptidyl-prolyl *cis–trans* isomerase and protein disulfide isomerase), an oxidase (lysyl oxidase), and a collagen-specific chaperone (HSP47). Together, these proteins mediate the assembly of collagen molecules into fibrils and create the covalent cross-links that are necessary for normal tensile strength and function of the fibril.

Fibronectin: Structure and Localization

Fibronectin is another major ECM fibrillar protein in the TM. Similarly to type I collagen, it is found in the core of the trabecular beams as well as along the basement membranes on the beams. In addition, fibronectin can be found in the sheath material surrounding the elastin tendons, in the amorphous fibrogranular material in the JCT and scattered along the basement membranes of the inner wall of Schlemm's canal. Fibronectin is also found as a soluble protein in AH.

An important feature of fibronectin's activity is its modular and flexible structure. As a soluble protein, fibronectin exists as a soluble, compact protein with many of its biological domains inaccessible. The active form of fibronectin is generally thought to be an extended protein assembled into an insoluble fibril. In contrast to the self-assembly of collagen fibrils, fibronectin fibrillogenesis is a highly controlled cell-mediated process involving integrins (especially α5β1) and cell contractility. Any changes in this process are likely to affect outflow facility because it would affect the incorporation of fibronectin into the ECM in much the same way as changes in the levels of fibronectin expression would.

Although single chain forms of fibronectin have been found in cartilage and zebra fish, human fibronectin primarily exists as a dimer composed of two nonidentical polypeptide chains that are disulfide bonded at their carboxyl termini (**Figure 1**). Each chain contains a series of homologous units called type I, II, and III repeats. The type III repeats comprise the majority of each chain and play a critical role in determining the activity of fibronectin in part because their conformation is sensitive to proteolysis or mechanical perturbations. Perturbations in the tertiary structure of the type III repeats expose novel cryptic sites with unique biological activities. For example, a 30–35% stretch applied to immobilized fibronectin revealed a cryptic site in the III1 repeat that promotes the assembly of fibronectin fibrils and stimulates cell growth and contractility.

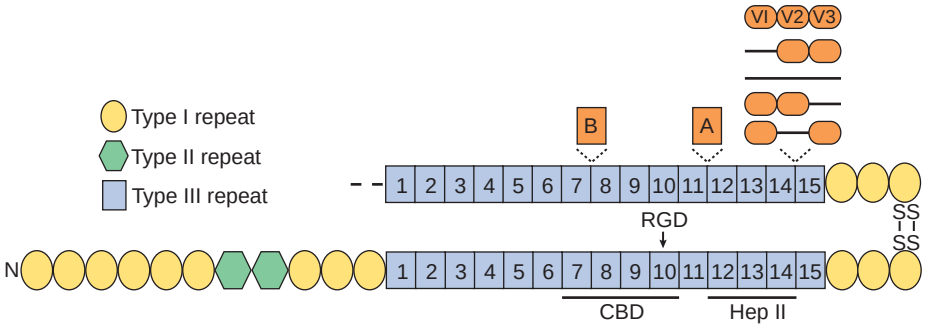

Figure 1 Fibronectin. Two nonidentical polypeptide chains consist of homologous type I (circles), II (hexagons), and III (squares) repeats that are disulfide bonded at the C-termini. Omitted portion of top strand (dashes) is identical to bottom strand. The RGD containing cell-binding domain (CBD) and the HepII domain are underlined. Alternatively spliced exons (EDA, EDB, and V) are offset from the fibronectin chain.

The flexibility of these repeats is retained even after fibronectin has been assembled into a fibril. Thus, a fibronectin fibril is elastic and can stretch about 4 times its original length. The force required to unfold these repeats and stretch a fibronectin fibril can be generated by the actomyosin network. This suggests that changes in contractility, or IOP, which stretch the TM, would alter the biological activity of fibronectin in the matrix. Interestingly, not all fibrils exhibit the same level of stretch, which implies that fibronectin fibrils could have different activities in different regions of the TM.

Fibronectin is a multidomain protein with each domain exhibiting a remarkable number of biological activities, including cell adhesion, migration, proliferation, differentiation, apoptosis, and gene expression. These domains also regulate growth factor signaling and the organization of the actin cytoskeleton. Since many of the domains are resistant to proteolysis and can be isolated without a loss in activity, it is possible that similar to the NC1 domain of type IV collagen, small bioactive domains of fibronectin could be available in the TM *in vivo* during ECM turnover.

The HeparinII (HepII) domain of fibronectin is an example of such a domain. This domain is especially relevant to the regulation of outflow resistance, because when it is perfused into either human- or monkey-cultured anterior segments, outflow facility is increased. This domain consists of the 12th–14th type III repeats (**Figure 1**) and can bind heparan sulfate proteoglycans (HSPGs) either on the cell surface or in the ECM. It also binds myocilin, a glucocorticoid response protein associated with glaucoma and vascular endothelial growth factor (VEGF), which is present in AH and upregulated in glaucomatous eyes.

The HepII domain regulates a number of biological activities, including cell survival and MMP expression. This domain, however, is probably best known for its ability to regulate the organization of the actin cytoskeleton and the contractile properties of the TM which play an important role in regulating outflow facility (see **Figure 2(a)**).

Fibronectin is a highly conserved protein. The sequence homology among mammals is greater than 90% and between chickens and mammals, the homology is greater than 80%. As many as 20 variants of fibronectin are derived from a single gene. These forms arise from alternative splicing of three exons called EDA (or EIIIA), EDB (or EIIIB), and IIICS (or V). The exons for EDA and EDB are spliced out entirely whereas the V exon undergoes exon subdivision to generate a V1, V2, or V3 region (**Figure 1**). In primary porcine TM cells, fibronectin messenger RNA (mRNA) contains all three regions of the V exon, but it lacks both the EDA and EDB exons. This is consistent with the observation that the EDA and EDB exons are mainly expressed in embryonic tissues or in some disease states.

In the TM, alternative splicing of these regions can be regulated by stretch or the growth factors, transforming growth factor beta 1 (TGF-β1) and TGF-β2. For example, in stretched porcine TM cells, the V1 and V3 regions are expressed, but the V2 region is spliced out. Stretch does not significantly affect expression of the EDA and EDB exons, since at least 90% of the transcripts from stretched porcine TM cells lack the EDB exon and none of the transcripts contains the EDA exon. In contrast, TGF-β1 and TGF-β 2 upregulate the expression of the EDA and EDB exons. Thus, patients with primary open-angle glaucoma, in which the levels of TGF-β2 are elevated, are more likely to express EDA- and EDB-containing fibronectin.

Expression of the splice variants is likely to alter the biological activity of fibronectin in the TM and consequently AH outflow. It still needs to be determined exactly how expression of the different variants of fibronectin affects outflow facility. Theoretically, inclusion of the EDA domain could increase outflow facility because it triggers the reorganization of actin stress fibers into cortical actin filaments and induces MMP-1, MMP-3, and MMP-9 expression. Inclusion of the EDA domain, on the other hand, could decrease outflow facility because it also promotes the assembly of fibronectin matrices. Alternative splicing of the V region is likely to affect the contractile properties of the TM because that would remove several binding sites that cells use to regulate adhesion and the contractile properties of cells. Alternative splicing of the V region could also modify the

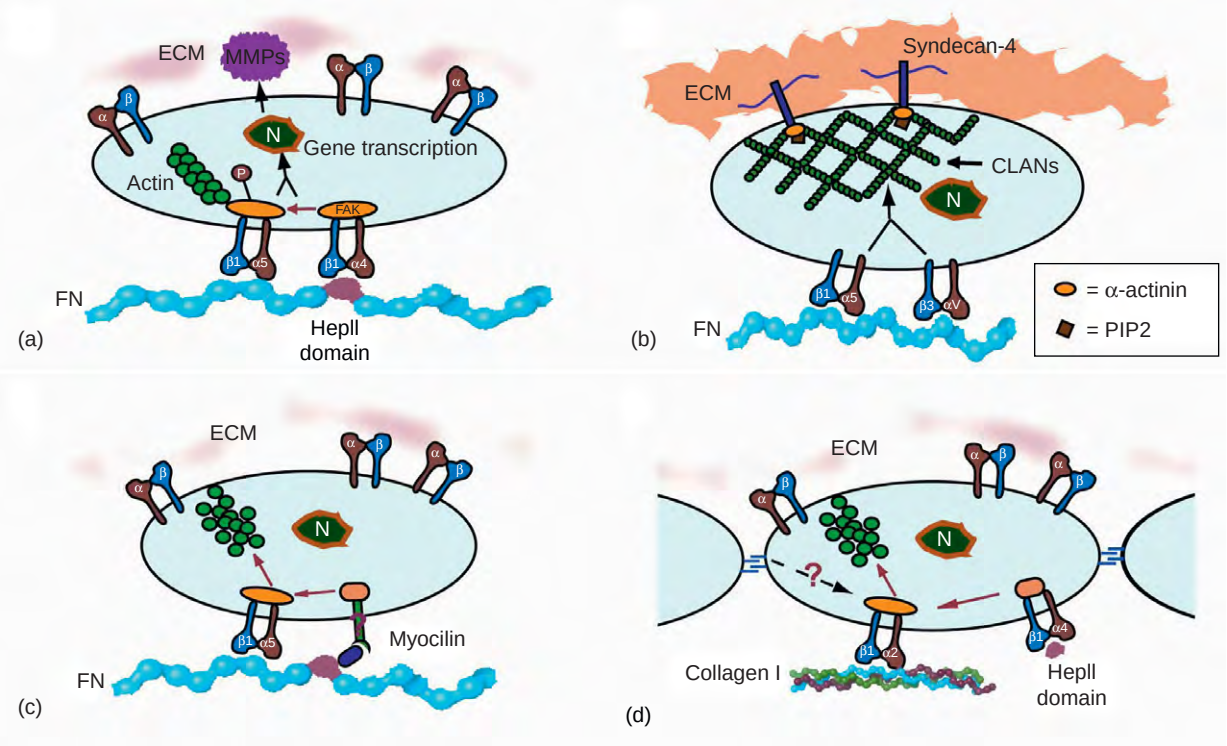

Figure 2 Model of fibronectin (FN) signaling in the TM. (a) In subconfluent cells, engagement of α4β1 integrin by the HepII domain initiates co-signaling with α5β1, which induces phosphorylation of FAK and enhances actin stress fiber and focal adhesion (FA) formation. This co-signaling could also trigger changes in gene transcription and levels of MMPs resulting in less ECM. (b) Cooperative signaling between β1 and β3 integrins enhances cross-linked actin network (CLAN) formation in TM cells. Molecules such as syndecan-4, α-actinin and PIP2 have been shown to localize to the vertices of CLANs. (c) Myocilin downregulates the assembly of actin stress fibers when TM cells or fibroblasts are plated on FN. It is not known how myocilin does this. It may be due to signaling through an unknown receptor or by binding to the HepII domain of FN and inhibiting signaling through α4β1 integrins. (d) In confluent TM cell monolayers, co-signaling from the HepII domain bound to α4β1 integrins and collagen engaged integrins (i.e., α2β1) results in the disassembly of cell–cell contacts and stress fiber disassembly.

adhesive properties of the heparin-binding activity of the HepII domain of fibronectin, switching it from a HSPG-dependent binding domain to a HSPG-independent-binding domain. This could affect the ability of the HepII domain to regulate AH outflow because it could alter how the HepII domain interacts with the ECM and cell surface receptors. Finally, alternative splicing of the V region has been shown to modulate the ability of the HepII domain to regulate MMP expression and cell survival that could also affect outflow facility. In summary, fibronectin has a modular and flexible structure which could provide a unique mechanochemical mechanism that the ECM can use to mediate AH outflow.

Factors that Affect Collagen and Fibronectin Expression and Assembly into the ECM

Although a number of studies have reported increases in ECM deposition in glaucoma and during aging, it is unknown whether this is due to an increase in the synthesis and deposition of collagen and fibronectin and/or a decrease in turnover of fibronectin and collagen fibrils. Factors that have been shown to increase the expression of types I and IV collagen and fibronectin in the TM as well as increase outflow resistance include: glucose, glucocorticoids, ascorbic acid, TGF-β1, and TGF-β2. Glucocorticoids, TGF-β1, and ascorbate could also alter the assembly of collagen fibrils. Glucocorticoids lead to a downregulation of type I C-propeptides and the α2(I) chain in the TM, while ascorbate and TGF-β1 lead to an increase in the hydroxylation of prolyl and lysyl residues used to stabilize the triple helix. TGF-β1 enhances the hydroxylation of prolyl residues because it increases the expression of the gene for protein disulfide isomerase which is essential for proline hydroxylation.

Elevated levels of TGF-β2, which have been reported in glaucoma patients, would also promote the accumulation of collagen and fibronectin into the ECM because it activates tissue transglutaminase. Tissue transglutaminase is a calcium-dependent enzyme that promotes the cross-linking of collagen and fibronectin via the formation of an isopeptide bond. This would modify the stability of the collagen and fibronectin fibrils in the ECM by rendering them more resistant to degradation. Tissue transglutaminase has also

been reported to form a cross-linked complex with fibronectin. Interestingly, this complex has been shown to amplify signaling to Rho guanosine triphosphate (GTP)ases which would increase the contractile properties of the TM and reduce outflow facility.

Age-related changes in collagen fibrils are also likely to occur, especially if there is a slower turnover of collagen. One critical change would be the formation of new cross-links derived from sugar through the Maillard reaction. In hyperglycemic conditions, excess sugar accelerates this reaction, leading to an accumulation of advanced glycation end products (AGEs) and a subsequent increase in collagen-collagen cross-links. Increased levels of AGEs have been correlated with diabetes mellitus, a condition that is considered a possible risk factor for glaucoma. The resulting cross-links are not readily broken down by the enzymes capable of degrading type I collagen. MMP-1 is only capable of digesting native type I collagen fibrils, while the other enzymes, called gelatinases, degrade collagen only after it has been cleaved by MMP-1 or if it is denatured. Thus, in the aging eye or in diabetic patients, turnover of the ECM could lead to the formation of a matrix that consists of highly cross-linked collagen fragments or partially cleaved fibrils. The presence of this fragmented and cross-linked matrix would impair the structural and mechanical properties of the ECM in the TM. This could lead to alterations in the compliancy of the ECM, a decrease in the contractile properties of the TM, changes in the expression of genes such as MMPs, and even cell death.

Finally, despite the fact that over 1100 mutations have been reported to occur in types I, II, III, IV, and VII collagens, nothing is known about how about these mutations may affect the function of the deposition and remodeling of collagen fibrils. Interestingly, mice that have a targeted mutation in type I collagen that impairs collagen remodeling exhibited ocular hypertension.

Collagen and Fibronectin Receptors

Extensive literature from other cell types suggests that fibronectin, collagen, and their receptors provide mechanical support for cell attachment and activate signaling pathways that regulate many of the biological processes involved in modulating outflow resistance, including matrix production, ECM turnover, gene expression, growth factor signaling, and cytoskeletal organization. Furthermore, fibronectin and collagen receptors modulate mechanochemical responses to physical forces such as stretch.

Many of the biological activities of collagen and fibronectin are mediated via interactions with integrins. Integrins are heterodimeric transmembrane receptors composed of α- and β-subunits. Those found in the TM include α2β1 and α1β1. α2β1 integrins preferentially bind type I collagen, while α1β1 integrins bind type IV collagen. The integrin α11β1 also binds type I collagen but, as of yet, this integrin has not been identified in the TM. The TM also contains the integrins α3β1, αvβ1, α5β1, αvβ6, α4β1, and α4β7 that bind fibronectin and the integrins αvβ3 and αvβ5 that bind both fibronectin and type IV collagen. These integrins are distributed throughout the TM with the heaviest localization observed along cells on the beams.

The major integrin-binding site in fibronectin for all integrins, except α4β1, is the arg–gly–asp (RGD) sequence in the III10 repeat. The α4β1 integrin binds RGD homologs found in five different regions of fibronectin. They are: the KLDAPT sequence in the III5 repeat, the EDGIHEL sequence in the EDA domain, the IDAPS sequence in the III14 repeat of the HepII domain, and the LDV and REDV sequences in the V1 and V3 regions of fibronectin, respectively (**Figure 1**).

The integrin-binding site in type IV collagen is in the NC1 domain and appears to be specific for the various α(IV)-chains. Hence, the α1(IV) NC1 domain binds α1β1 integrins, the α2(IV) NC1 domain binds α1β1, αvβ3, and αvβ5 integrins, and the α3(IV) NC1 domain binds αvβ3 and αvβ5 integrins. Additional binding sites for α1β1 and α2β1 can also be found in the collagenous regions α1(I)CB3 and α1α2(IV)CB3 in types I and IV collagen, respectively. Although the sequence GRGDTP was initially reported as the integrin-binding sequence for type I collagen, several reports now show that the GER motif, in particular, the hexapeptide GFOGER, may be the more crucial sequence for binding integrins particularly to type I collagen fibrils. GER-containing motifs are not the only sequence recognized by the collagen integrins, αvβ3 and αvβ5 integrins may use both RGD and non-RGD motifs in the NC1 domain of type IV collagen. The collagen integrins appear to have specific activities. α1β1 integrins downregulate collagen synthesis and upregulate cell proliferation, while α2β1 integrins upregulate collagenase and collagen synthesis. The α2β1 integrin may also preferentially interact with type I collagen fibrils, whereas the α1β1 integrin binds monomeric type I collagen.

Integrin signaling in the TM is likely to be complex and controlled in part by the presence of other receptors and matrix proteins that co-direct signaling events with integrins. This process, referred to as cross talk, can be either cooperative or antagonist. For example, cooperative signaling between β1 and β3 integrins enhances the formation of cross-linked actin networks in TM cells (**Figure 2(b)**), while the matrix protein myocilin downregulates the assembly of actin networks formed when TM cells or fibroblasts are plated on fibronectin (**Figure 2(c)**). In subconfluent proliferating TM cells plated on fibronectin, activation of α4β1 integrins by the HepII domain triggers cross talk with α5β1 integrins bound to a fibronectin substrate (**Figure 2(a)**). Activation of the α4β1/α5β1 integrin signaling pathway enhances cell attachment to fibronectin by increasing actin stress fiber formation and focal adhesion kinase (FAK) phosphorylation. In contrast, co-signaling between the collagen integrin, α2β1,

and α4β1 appears to trigger the disassembly of actin filaments in confluent TM cultures. Integrin signaling is also likely to be controlled by the specific molecules associated with the cytoplasmic tails of the integrins, such as paxillin and talin.

Another major family of receptors for fibronectin and collagen in the TM are the syndecans, which are transmembrane HSPGs that typically use their heparan sulfate chains to interact with a heparin-binding motif that is rich in highly basic amino acids. All four members of the syndecan family are found in the TM, but only syndecans-1, -2, and -4 bind to fibronectin and only syndecan-1 has been reported to interact with types I and IV collagen. The most prominent syndecan in the TM is syndecan-4. It is best known for its role in focal adhesion formation, and organization of the actin cytoskeleton.

Integrins and syndecans are ideal candidates to regulate outflow facility. They control cell adhesion, growth factor signaling, and assembly and turnover of extracellular matrices. They also activate members of the Rho GTPase family which control the contractility of the actomyosin network and play a critical role in regulating AH outflow. In addition, integrin and syndecan signaling is responsive to stretch, steroids, and TGF-β; all factors that affect IOP. In the TM, stretch upregulates the expression of αv, α5, and β1 integrins. Steroids, on the other hand, downregulate the expression of αv integrins in TM cells, but upregulate the expression of the α5 integrins. To date, it is not known if TGF-β affects integrin and syndecan expression in the TM. In other cell types, TGF-β increases the expression of α5, αv, β1, and β3 integrins and syndecan-1. In some instances, integrin expression may not be affected by these factors, but its activity is. For example, α4β1, α5β1, α2β1, and αvβ3 integrins can switch from an inactive (low-affinity) state to an active (high-affinity) state in response to stretch and external stimuli. ECM signaling through integrins and syndecans, therefore, could easily be adapted to meet changes in IOP and potentially play an important role in the maintenance of AH homeostasis.

Summary and Future Perspectives

In conclusion, very little is known about how the ECM contributes to the regulation of outflow facility. As discussed in this article, changes in both the relative amounts of collagen and fibronectin deposition as well as their level of cross-linking by tissue transglutaminase in the TM have been reported in glaucomatous tissues. However, it is not known how these changes could affect outflow facility. Will they only affect the compliance and permeability of the TM? Or will the changes also affect ECM-mediated signals responsible for cellular function and survival? Clearly, studies are needed in order to better understand how alterations in collagen and fibronectin deposition contribute to the pathophysiology of glaucoma.

See also: The Biology of Schlemm's Canal; Biomechanics of Aqueous Humor Outflow Resistance; The Cytoskeletal Network of the Trabecular Meshwork; Functional Morphology of the Trabecular Meshwork; Myocilin; Primary Open-Angle Glaucoma; Regulation of Extracellular Matrix Turnover in the Aqueous Humor Outflow Pathways; Role of Proteoglycans in the Trabecular Meshwork; Steroid-Induced Ocular Hypertension and Effects of Glucocorticoids on the Trabecular Meshwork; Structural Changes in the Trabecular Meshwork with Primary Open Angle Glaucoma.

Further Reading

Acott, T. S. and Kelley, M. J. (2008). Extracellular matrix in the trabecular meshwork. *Experimental Eye Research* 86: 543–561.

Calderwood, D. A. (2004). Integrin activation. *Journal of Cell Science* 117: 657–666.

Filla, M. S., David, G., Clark, A., Kaufman, P. L., and Peters, D. M. P. (2006). β1 and β3 integrins cooperate to induce syndecan-4 containing cross-linked actin networks (CLANs) in human trabecular meshwork (HTM) cells. *Investigative Ophthalmology and Visual Science* 47: 1956–1967.

Gabelt, B. T. and Kaufman, P. L. (2005). Changes in aqueous humor dynamics with age and glaucoma. *Progress in Retinal and Eye Research* 24: 612–637.

Gonzalez, J. M., Jr., Peterson, J. A., Peters, J. M., Newman, J., and Peters, D. M. P. (2006). Effect of Heparin II domain of fibronectin on actin cytoskeleton and adherens junctions in human trabecular meshwork cultures. *Investigative Ophthalmology and Visual Science* 47: 2924–2931.

Heino, J. (2000). The collagen receptor integrins have distinct ligand recognition and signaling functions. *Matrix Biology* 19: 319–323.

Hynes, R. O. (1990). *Fibronectins*. New York: Springer.

Kaufman, P. L. (2008). Enhancing trabecular outflow by disrupting the actin cytoskeleton, increasing uveoscleral outflow with prostaglandins, and understanding the pathophysiology of presbyopia: Interrogating mother nature: Asking why, how, recognizing the signs, following the trail. *Experimental Eye Research* 86: 3–17.

LeBleu, V. S., MacDonald, B., and Kalluri, R. (2007). Structure and function of basement membranes. *Experimental Biology and Medicine* 232: 1121–1129.

Lütjen-Drecoll, E. (1998). Functional morphology of the trabecular meshwork in primate eyes. *Progress in Retinal and Eye Research* 18: 91–119.

Mao, Y. and Schwarzbauer, J. (2005). Fibronectin fibrillogenesis, a cell-mediated matrix assembly process. *Matrix Biology* 24(3): 89–399.

Myllyharju, J. and Kivirikko, K. (2004). Collagens, modifying enzymes and their mutations in humans, flies and worms. *Trends in Genetics* 20: 33–43.

Ortega, N. and Werb, Z. (2002). New functional roles for non-collagenous domains of basement membrane collagens. *Journal of Cell Science* 115: 4201–4214.

Pankov, R. and Yamada, K. M. (2002). Fibronectin at a glance. *Journal of Cell Science* 115: 3861–3863.

Peterson, J. A., Shiebani, N., David, G., Garcia-Pardo, A., and Peters, D. M. P. (2005). Heparin II domain of fibronectin uses α4β1 integrins to control focal adhesion and stress fiber formation independent of Syndecan-4. *Journal of Biological Chemistry* 280: 6915–6922.

Rao, V. P. and Epstein, D. L. (2007). Rho GTPase/Rho kinase inhibition as a novel target for the treatment of glaucoma. *BioDrugs* 21: 167–171.

Rohen, J. W. and Lütjen-Drecoll, E. (1989). Morphology of aqueous outflow pathways in normal and glaucomatous eyes. In: Ritch, R., Shields, M. B., and Krupin, T. (eds.) *The Glaucomas*, pp. 41–74. St. Louis, MS: CV Mosby.

Schwartz, M. A. and Ginsberg, M. H. (2002). Networks and crosstalk: Integrin signaling spreads. *Nature Cell Biology* 4: E65–E68.

The Genetics of Primary Open-Angle Glaucoma: A Review*

R R Allingham and Y Liu, Duke University, Durham, NC, USA

Glossary

Association – A statistical statement used to describe the co-occurrence of alleles or phenotypes.
Chromosome – A linear structure found in all nucleated cells consisting of both DNA and proteins. Genes are organized on strands of DNA. The normal human complement consists of 23 pairs of chromosomes.
Complex disease – A disorder that is inherited in a manner not consistent with conventional Mendelian genetics that are controlled by a single locus or gene. The phenotype of a complex disorder results from the contribution of multiple genes in combination with environmental factors.
Gene – The DNA or RNA that codes for a functional RNA or protein product.
Linkage analysis – A statistical and biomolecular approach to determine the location of a gene or genes in an organism.
Locus (plural: loci) – The physical or relative location of a gene within a chromosome.
Mutation – A heritable change in genetic material that can potentially be passed from parent to offspring. This change may occur in a gene or in a chromosome and can result from the loss, gain, or rearrangement of genetic material.
Polymorphism – A piece of DNA that has more than one form (allele), each of which occurs with at least 1% frequency is said to be polymorphic. Polymorphisms are a normal part of genetic variability, and they may or may not result in functional changes of the gene.
Single nucleotide polymorphism (SNP) – It consists of a single base change in a DNA sequence.

Introduction

Glaucoma is a heterogeneous group of disorders which constitute the leading cause of irreversible blindness worldwide. It is a pathologic condition in which there is a progressive loss of retinal ganglion cells, specific visual-field deficit, and a characteristic excavative atrophy of the optic nerve. Primary open-angle glaucoma (POAG) is the most common type of glaucoma and is characterized by the presence of glaucomatous optic neuropathy in the absence of an identifiable secondary cause (**Figure 1**). Abnormally elevated intraocular pressure (IOP) is frequently associated with glaucoma and is a major risk factor for this disease.

POAG as a Complex Inherited Disorder

The familial nature of POAG has been recognized for decades. In studies of patients with POAG, up to 50% have a positive family history. In a large population-based study conducted in the Netherlands, Wolfs and coworkers examined family members of individuals with and without POAG. These investigators found that first-degree relatives of an affected individual had a 22% risk of developing POAG compared with only a 2.3% risk in family members of controls. The overall risk of developing POAG among first-degree relatives of an affected individual is increased from three- to ninefold. These evidences strongly suggest that specific genetic defects contribute to the pathogenesis of POAG.

Our modern understanding of the genetic architecture of POAG has been steadily evolving since the first gene for POAG, myocilin (MYOC), was mapped and identified. The MYOC gene and other reported genes for POAG were mostly identified from large families with glaucoma inherited in a Mendelian pattern, where the altered function of a single gene is sufficient to cause the disease. However, it has become increasingly clear that POAG, in most cases, is inherited as a complex trait, where the disease results from the interaction of multiple genes and environmental factors. This should not come as a surprise since the glaucoma phenotype itself is quite complex, resulting from diverse pathological processes that involve, but are not limited to, the aqueous humor outflow pathway, the retina, and optic nerve.

Genetic Approaches to Gene Identification

Identifying genes that either cause or contribute to the development of disease is challenging, especially in complex disorders such as POAG. The most commonly used method to identify genes that are transmitted in a Mendelian pattern, such as an autosomal dominant or

*Adapted from Allingham, R. R., Liu, Y., and Rhee, D. J. (2009). The genetics of primary open-angle glaucoma: A review. *Experimental Eye Research* 88(4): 837–844.

recessive trait, is genetic linkage analysis. This method employs the use of families where multiple members are affected. The power to detect linkage is proportional to the number of individuals affected within families and the total number of families. Once linkage to a specific chromosomal locus is identified, analysis of the genes and their variants that are within the region of interest is conducted. To date, disease genes for the vast majority of inherited disorders have been identified using traditional linkage analysis. However, despite this success, more than 90% of the genetic contribution for POAG still remains to be determined.

In an effort to address the challenges associated with gene identification for common, complex disorders that do not exhibit classical Mendelian inheritance patterns, newer and more robust methods have been developed. The most promising of these is genome-wide association with high-density single-nucleotide-polymorphism (SNP) arrays and massive enlargement of cohort sizes. This approach utilizes data sets containing large numbers of unrelated cases and controls to determine statistical associations between common genetic variations within the human genome and disease. SNPs are the mainstay of this type of analysis and, numbering in the millions, they are dispersed throughout the human genome – making them ideal for genetic analysis. Although the theory underlying this approach has been known for decades, only recent advances in massive throughput genotyping have made this approach practical. It is now possible to genotype 1 million SNPs per individual on large data sets containing thousands of samples in just a few days. This approach has led to the identification of common disease-associated genetic variants in chronic disorders, including diabetes mellitus, heart disease, cancer, and others. Ophthalmology has greatly benefitted from this approach. Major, common genetic variants that predispose to age-related macular degeneration (CFH) and pseudoexfoliation syndrome (LOXL1) have recently been identified by genome-wide association studies.

In addition to whole-genome association, there are additional methods being developed to determine the cause of inherited disease. Admixture mapping is a method used to localize disease-associated genetic variants that differ in frequency across populations. This powerful method has been successfully used to locate the chromosomal location for a gene that causes prostatic cancer and is currently being used to locate disease-associated variants for POAG in the African-American population. Another area of intense interest is the role that DNA copy number variants and genetic imprinting may have in a variety of human disorders including POAG. As these approaches are increasingly used, additional susceptibility loci and genes for POAG will likely be discovered.

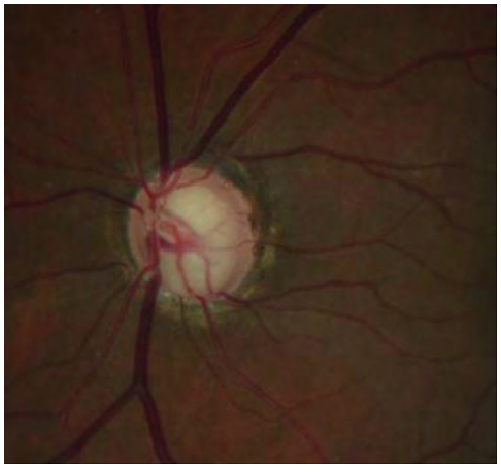

Figure 1 The optic disk photo demonstrates moderate to advanced optic disk cupping in a patient with POAG. There is complete loss of the inferior neuroretinal rim.

Chromosomal Loci for POAG

A genetic locus (singular; loci is plural) refers to a specific physical region of a chromosome that defines an area harboring a gene or genes that are associated with a specific phenotype or disease. Currently 14 chromosomal loci for POAG (GLC1A-N) are listed by the Human Genome Organization (HUGO; Geneva, Switzerland) and many more have been reported in the literature (Table 1). In most cases, these loci have been identified in family datasets using genetic linkage analysis. Three genes associated with glaucoma have been identified within these loci, including myocilin/TIGR (GLC1A), optineurin (GLC1E), and WDR36 (GLC1G).

Myocilin

MYOC was identified by Stone and coworkers in the GLC1A, which was the first locus for POAG located

Table 1 Currently reported POAG chromosomal loci

Chromosomal location	*POAG phenotype*	*Locus name*	*Candidate gene*
1q23-q24	JOAG, adult-onset	GLC1A	MYOC
2cen-q13	Adult-onset	GLC1B	
2p12	Elevated IOP		
2p16.3-p15	JOAG, Adult-onset	GLC1H	
3p22-p21	Adult-onset	GLC1L	
3q21-q24	Adult-onset	GLC1C	
5q22.1	Adult-onset	GLC1G	WDR36
5q22.1-q32	JOAG	GLC1M	
7q35-q36	Adult-onset	GLC1F	
8q23	Adult-onset	GLC1D	
9q22	JOAG	GLC1J	
10p13	Adult-onset, NTG	GLC1E	OPTN
15q11-q13	Adult-onset	GLC1I	
15q22-q24	JOAG	GLC1N	
19p13.2	Elevated IOP		
20p12	JOAG	GLC1K	

on chromosome 1. The MYOC protein was previously known as trabecular-meshwork-inducible glucocorticoid response protein or TIGR. Disease-associated mutations of MYOC are generally associated with a juvenile or early adult form of POAG. This genetic form of glaucoma is typically associated with high IOPs and frequently requires surgical intervention for disease control. In adult POAG populations, the prevalence of MYOC mutations in POAG cases varies between 3% and 5% making it the most common form of inherited glaucoma currently known.

The MYOC gene consists of three exons. MYOC protein has sequence similarities to the muscle protein myosin at the N-terminus, from which it gets its name, and olfactomedin at the C-terminus. Most glaucoma-associated mutations in the MYOC gene are located within the third exon which codes for the olfactomedin-like domain. MYOC is expressed by most tissues of the eye and multiple tissues throughout the body. Although MYOC is widely expressed, the only disorder that results from genetic variants of this gene is glaucoma.

MYOC-associated glaucoma is transmitted as an autosomal dominant Mendelian trait. Carriers of disease-associated mutations develop the glaucoma phenotype in an estimated 90% of cases. Interestingly, individuals who are homozygous, where both MYOC copies are abnormal, for certain MYOC mutations Gln368STOP and Lys423Glu do not appear to develop glaucoma. However, one patient with a congenital form of open-angle glaucoma was reportedly homozygous for the Gln48His MYOC mutation. Although MYOC mutations generally cause an earlier-onset form of glaucoma, some variants such as the Gln368Stop mutation often have a later adult onset.

When first discovered, MYOC was a novel gene and protein. Over the past decade, our knowledge about the physiological role of MYOC is improving. Although MYOC protein expression is greatly increased upon administration of glucocorticoids in trabecular meshwork (TM) cells, this property does not appear to be related to steroid-induced ocular hypertension. Fautsch and coworkers demonstrated that the introduction of MYOC protein increases outflow resistance in the perfused human anterior segment model system, while Caballero and coworkers showed that overexpression of the N-terminal domain of MYC results in an increase of outflow facility in perfused anterior segment model system.

A number of animal model studies of MYOC have been conducted in the genetic mouse model. Neither absence of MYOC nor increased expression of wild-type MYOC in the TM produces elevated IOP. In a transgenic mouse model, the effect of a mutated form of MYOC, Tyr423His, was studied. Similar to humans, the mutated form of MYOC was not secreted and accumulated in the TM but failed to elevate IOP. However, in other studies utilizing the same MYOC mutation, increased IOP did occur which was associated with loss of retinal ganglion cells, findings being consistent with glaucoma.

Interestingly, MYOC protein is normally found in the aqueous humor of many species including humans; however, this protein is absent in the aqueous humor of patients with glaucoma-associated MYOC mutations. Recent studies have shown that MYOC is associated with the shedding of small vesicles called exosomes into the aqueous humor. In other tissues, exosomes contain ligands that participate in autocrine and paracrine signaling, and thus serve as vehicles that may play a role in TM homeostasis. It is possible that interference in this pathway induced by mutations in MYOC may play a role in causing glaucoma.

These data suggest that mutant, disease-associated forms of MYOC interfere with protein trafficking and result in the intracellular accumulation of misfolded protein. How this process causes an increase in aqueous humor outflow resistance and why the onset of glaucoma in most cases takes decades to occur remains to be determined. However, it is clear that the discovery of MYOC is leading to a better understanding of the pathobiology of POAG.

Optineurin

The second gene discovered that is associated with POAG was optineurin (OPTN). OPTN is located in the GLC1E locus on chromosome 10. The phenotype for affected individuals with OPTN variants was remarkable for glaucoma associated with normal IOP, or normal-tension glaucoma (NTG), in a large percentage of affected family members.

The original report identified OPTN variants in over 16% of open-angle glaucoma families. Subsequently, disease-associated variants have been reported by other investigators. However, most investigators have found that OPTN variants are uncommon in POAG and NTG cases. Of those OPTN mutations studied to date, the E50K variant, although rare, appears to be most strongly associated with open-angle glaucoma, particularly of the normal-tension type. Furthermore, it is reported that NTG patients who have the E50K mutation have a more severe form of glaucoma compared to NTG patients that lack the mutation. These mutation carriers appear to have a younger age of onset, develop more advanced optic nerve cupping, and require surgical intervention more frequently than their NTG counterparts.

Other investigators have also reported association between OPTN variants and glaucoma. Forsman and coworkers found that three OPTN SNPs, Thr34Thr, Glu163Glu, and 553-5C, were associated with an increased risk of glaucoma. In addition, specific OPTN variants have been associated with a higher IOP in a glaucoma population in India. Although controversial, the more common Met98Lys polymorphism of OPTN has been reported to increase susceptibility to normal-tension forms of open-angle glaucoma, especially in Asian populations.

It has been reported by Funayama and coworkers that the synonymous variant Thr34Thr is associated with POAG in the Japanese population. It was also reported that certain tumor necrosis factor-alpha (TNFα) variants in combination with OPTN variants were higher in POAG patients compared with controls and that these patients had a worse prognosis. This interaction between TNFα and OPTN is consistent with the belief that frequently the glaucoma phenotype is polygenic in origin. Although interesting, most of these associations remain to be corroborated.

Similar to MYOC, the mechanistic role of OPTN in the pathogenesis of glaucoma is unclear. Studies of OPTN expression in the human anterior segment perfusion model have produced conflicting results. There is evidence that OPTN may play a neuroprotective role by reducing retinal ganglion cell susceptibility to apoptosis. It has been reported that in response to apoptotic stimuli, OPTN translocates from the Golgi to the nucleus in a manner dependent on the guanosine triphosphate (GTP) ase activity of Rab8. Overexpression of OPTN blocks cytochrome c release from mitochondria and protects cells from hydrogen-peroxide-induced cell death. The OPTN E50K mutation inhibits translocation to the nucleus. Overexpression of this variant compromises the mitochondrial membrane integrity by increasing the susceptibility to death from external stressors. The protection against apoptosis may not translate to other tissues as overexpression in the lens of transgenic mice failed to protect against transforming growth factor-beta 1 (TGFβ1)-induced apoptosis of lens epithelial cells.

In studies examining the cellular role of the OPTN, investigators have found that OPTN negatively regulates TNFα-induced nuclear factor kappa-light-chain-enhancer of activated B cells (NF-κB) activation. TNFα-stimulated NFκB-dependent gene transcription is greatly enhanced if the level of expression of OPTN is reduced, lowering the apoptotic threshold. Other investigators have observed that the OPTN E50K mutation increases binding to TANK-binding kinase 1 (TBK1), which forms a complex that regulates TNFα and its proapoptotic effects. It is suggested that the OPTN E50K mutant may cause aberrant activation of TBK1, which may underlie increased susceptibility to ganglion cell loss in subjects with familial NTG. These and other studies are bringing us closer to the role of OPTN variants and the pathogenesis of glaucoma.

WDR36 (WD40-Repeat 36)

In 2005, it was reported that sequence variants in WDR36 gene cause POAG. WDR36 encodes a protein with 951 amino acids. It is located in the GLC1G locus on chromosome 5q22. Similar to both MYOC and OPTN, the messenger RNA (mRNA) transcript is ubiquitous, and is found in various tissues of the body and throughout the structures of the eye. The prevalence of WDR36 sequence variations has been estimated to be present between 1.6% and 17% of POAG patients. Subsequent studies in a sample of West Africans as well as in other POAG families with autosomal dominant POAG have mapped to this region on chromosome 5, but have failed to identify genetic variants in WDR36 as the causative agent. Most investigators find little or no evidence for an association between WDR36 variants in POAG compared with controls. In one report, POAG patients with WDR36 sequence variations were associated with a more severe disease phenotype than those without, suggesting that sequence variants in WDR36 may play a role in disease susceptibility rather than causation. WDR36 functions in ribosomal RNA processing and interacts with p53 stress response pathway, suggesting the possible involvement of p53 in glaucoma.

Gene Variants Associated with POAG

In addition to the genes described above, over 20 gene variants have been associated with POAG as summarized in Table 2. These include apolipoprotein E (APOE), optic atrophy 1 (OPA1), tumor protein p53 (TP53), TNF, interleukin-1 (IL-1), and cytochrome P450 1B1 (CYP1B1). CYP1B1 has been reported to be associated with early onset POAG in Spanish, French, and Indian populations. Variants of OPA1 have been associated with normal-tension glaucoma in Japanese and Caucasian populations. OPA1 variants are not associated with glaucoma in Caucasian, African-American, and West-African POAG cases with elevated IOP. Most candidate gene associations with POAG have not been corroborated by other investigators or in other populations.

POAG Genetics and the Future

Clearly, an explosion in the understanding of the underlying genetic architecture of complex inherited disorders is underway. This is being driven by powerful new methods for genetic discovery, logarithmic growth in genotyping technology, and the assemblage of increasing large, robust clinical datasets. This knowledge will ultimately lead to a vastly improved understanding of the molecular mechanisms of complex diseases such as glaucoma. As the underlying genetics of POAG improve so will the contribution of environmental factors, which to date, is poorly understood.

Ultimately, genetic screening will greatly improve our ability to predict the risk of developing disease as well as disease severity. Importantly, expanding comprehension of the molecular pathways that produce disease will guide the development of more effective treatment options for individuals as well as their families. For diseases such as POAG, where end-organ damage is untreatable, the

Table 2 Gene variants associated with POAG

Gene symbol	*Gene name*	*Genomic location*	*OMIM*	*KEGG pathway*	*POAG phenotype*	*Population*
AGTR2	Angiotensin II receptor, type 2	Xq22-q23	300034	Renin–angiotensin system	NTG	Japanese
ANP	Atrial natriuretic polypeptide	1p36.2	108780		POAG	Caucasian
APOE	Apolipoprotein	19q13.2	107741	Neurodegenerative diseases, Alzheimer's disease	NTG, POAG	Japanese, Chinese, Tasmanian, French
CDH-1	Cadherin 1	16q22.1	192090	Cell adhesion molecule	POAG	Chinese
CYP1B1	Cytochrome P450, 1B1	2p22-p21	601771	Tryptophan metabolism	POAG	Indian, French, Spanish
EDNRA	Endothelin receptor type A	4q31.2	131243	Calcium signaling pathway	NTG	Korean, Japanese
GSTM1	Glutathione S-transferase M1	1p13.3	138350	Glutathione metabolism	POAG	Arabs, Turkish, Estonian
HSPA1A	Heat-shock 70-kDa protein 1A	6p21.3	140550	MAPK signaling pathway	POAG, NTG	Japanese
IGF2	Insulin-like growth factor 2	11p15.5	147470		POAG	Chinese
IL1α	Interleukin-1α	2q14	147760	MAPK pathway, apoptosis	POAG	Chinese
IL1β	Interleukin-1β	2q14	147720	Apoptosis, MAPK and toll-like receptor signaling pathway	POAG	Chinese
MTHFR	Methylene-tetrahydrofolate reductase	1p36.3	607093	Folate biosynthesis, methane metabolism,	NTG, POAG	Korean, German
NOS3	Nitric oxide synthase 3	7q36	163729	Arginine and proline metabolism, calcium and VEGF pathway	POAG with migraine history	Caucasian
OCLM	Oculomedin	1q31.1	604301		POAG	Japanese
OLFM2	Olfactomedin 2	19p13.2			POAG	Japanese
OPA1	Optic atrophy 1	3q28-q29	605290		NTG	Japanese, Caucasian
P21	P21	6p21.2	116899	p53 signaling pathway	POAG	Chinese
PON1	Paraoxonase 1	7q21.3	168820		NTG	Japanese
TAP1	ABC transporter, MHC,1	6p21.3	170260	ABC transporters	POAG	Chinese
TLR4	Toll-like receptor 4	9q32-q33	603030	Toll-like receptor signaling pathway	NTG	Japanese
TNFα	Tumor necrosis factor alpha	6p21.3	191160	MAPK and toll-like receptor pathway, apoptosis	POAG	Japanese, Chinese
TP53	Tumor protein 53	17p13.1	191170	MAPK and p53 pathway, apoptosis	POAG	Chinese, Caucasian

KEGG, Kyoto Encyclopedia of Genes and Genomes; OMIM, Online Mendelian Inheritance in Man.

ability to accurately predict disease prior to symptomatic vision loss is critical.

See also: Molecular Genetics of Congenital and Juvenile Glaucoma; Myocilin; Primary Open-Angle Glaucoma; Pseudoexfoliation Syndrome and Glaucoma.

Further Reading

Manolio, T. A., Collins, F. S., Cox, N. I., et al. (2009). Finding the missing heritability of complex diseases. *Nature* 461: 747–753.

McKusick, V. A. (2006). A 60-year tale of spots, maps, and genes. *Annual Review of Genomics and Human Genetics* 7: 1–27.

Pasquale, L. R. and Kang, J. H. (2009). Lifestyle, nutrition, and glaucoma. *Journal of Glaucoma* 18: 423–428.

Zhang, F., Gu, W., Hurles, M. E., and Lupski, I. R. (2009). Copy number variation in human health, disease, and evolution. *Annual Review of Genomics and Human Genetics* 10: 451–481.

Relevant Website

http://www.genenames.org/index.html – HUGO Gene Nomenclature Committee.

The Immunological Aspects of Aqueous Humor Turnover

F Bock and C Cursiefen, Friedrich-Alexander University Erlangen-Nürnberg, Erlangen, Germany

Glossary

Antigen presenting cells (APCs) – Cells that display foreign antigens together with a major histocompatibility complex (MHC) receptor on its surface. T cells are activated by these antigens via their T-cell receptors.
Aqueous humor – A clear body fluid in the posterior and anterior chamber of the eye supporting the vessel-free parts of the eye like the cornea and the lens with nutrients and contributing to the transparency of the cornea.
Delayed type hypersensitivity (DTH) – It belongs to the four groups of hypersensitivity which describes damaging or rejection reactions produced by the normal immune system. A hypersensitivity reaction is elicited by a presensitization of the host. The DTH is a cell-dependent immune reaction which is mainly triggered by T cells.
Glycoproteins – Proteins that contain covalently attached oligosaccharide chains (glycans) to the side chains of the polypeptide.
Lymphangiogenesis – Formation of lymphatic vessels from preexisting lymphatic vessels.
Lymphatic vessels – A vessel type comparable to blood vessels, but instead of blood, lymphatic vessels drain fluid (lymph) out of the tissue together with proteins and cells of the immune system through the draining lymph nodes back into the bloodstream.
Neuroendocrine – A hormone which is released into the circulating blood by neuroendocrine cells in response to a neural stimulus.
Plasminogen – A circulating proenzyme that is converted by cleavage into the active enzyme plasmin, which, for example, degrades fibrin.
T lymphocyte – One of the white blood cells known as lymphocytes, responsible for the cell-mediated immunity. In contrast to B cells, T cells mature in the thymus.

Aqueous Humor and the Immune Privilege of the Eye

For the immune response after organ or tissue transplantation, an analogy to the neural reflex arc was introduced named immune reflex arc. Herein the afferent limb is defined as an antigenic signal captured in the periphery and transmitted to secondary lymphoid tissues through lymphatic vessels. At the central processing mechanism, the antigenic signal is transduced into effector modalities such as antibodies and effector T cells. At last, the efferent limb represents the delivery of the effectors through the blood to the site of antigen, leading to its elimination.

The presentation of antigens in the anterior chamber (AC) provokes a series of immunological responses, which are characterized by the generation of noncomplement antibodies (IgG1), the formation of cytotoxic T lymphocyte (CTL) precursors and an obvious absence of a normal delayed-type hypersensitivity (DTH) response. For example, DBA/2-mice-derived P815 mastocytoma cells with a naturally fast immunogenic effect after subcutaneous transplantation into allogenic BALB/c mice can escape the immunologic rejection when injected in the AC. The fact that P815 tumor allografts were consequently rejected outside the eye shows that the growth of these highly immunogenic tumors in the eye is facilitated by the downregulation of a cell-mediated immunity (CMI). So, CD8+ CTL precursors invading in the intraocular tumor are not able to differentiate completely to gain their cytolytic function.

The CMI is also inhibited systemically. BALB/c mice which were primed with P815 DBA/2 mastocyte cells in the AC were unable to reject orthotopic DBA/2 allografts nor were able to reject skin allografts of third-party donors. Therefore, the systemic CMI of the host is inhibited actively. The AC priming with several antigens leads to the generation of regulatory T cells which impair the DTH. One population of the generated T cells is CD4+ and affects the afferent arm, and a CD8+ population affects the efferent arm of the immune response arc. These regulatory T cells secrete the transforming growth factor-β_2 (TGF-β_2), which is not only anti-inflammatory but also prevents the activation of CD4+ T cells which induce DTH. According to these findings, it became clear that this immune deviation induced by AC priming is a characteristic of the AC and therefore it was termed anterior chamber-associated immune deviation (ACAID).

The immune privilege of the AC is achieved by several unique features of this site.

1. One is the absence of blood and lymphatic vessels in the surrounding tissues (cornea, lens, and aqueous humor (AqH)).
2. Further important features are soluble immunomodulatory factors in the AqH, which are secreted from the

ciliary body. AqH from healthy eyes has been shown to have an inhibitory effect on many cells and factors involved in inflammation and immune response: (a) CD4+ T cells, which are inhibited in proliferation and secretion of effector cytokines, polymorphonuclear neutrophilic leukocytes inhibited in release and destructive potential of the cellular content; (b) macrophages activated by bacterial lipolysaccharides and IFN-γ, which reduced the production of reactive oxygen intermediates and nitric oxide; (c) natural killer (NK) cells, which reduced the capacity to lyse appropriate target cells and complement components C1q and C3 NK cells. On the other hand, AqH does not impair the capacity of functional cytotoxic T cells to lyse their specific targets and neutralizing, noncomplement-fixing antibodies retain their properties when AqH is present.

Furthermore, cell-surface immunomodulatory factors constitutively expressed on the pigment epithelium and corneal endothelium do also contribute to the immune privilege. It was shown that T cells are altered in their immunological function when passing the ocular pigment epithelium.

3. The immunosuppressive factors such as the TGF-β, thrombospondin 1 and 2 (TSP-1/ TSP-2) and prostaglandin E2 have been shown to be secreted from the cornea, the iris pigment epithelium (IPE) and the retinal pigment epithelium (RPE).
4. In addition, corneal endothelial cells secrete several molecules suppressing lymphocyte activation and inflammation and express molecules on their apical surface, which inhibit complement activation like CD46, CD55, CD59 and promote apoptosis by the CD95 ligand at CD95+ cells getting in contact with them.
5. The ability of the corneal endothelium which expresses CD95 ligand constitutively, but low levels of major histocompatibility complex (MHC) class I molecules to prevent intraocular activation of innate immune effectors prevents destruction by NK cells and neutrophils, and protects the visual axis from distortion by macrophage and complement-mediated inflammation. In addition, in the normal uninflamed cornea MHC class II-negative Langerhans cell (LaC)-type dendritic cells (DCs) in an immature state are present.

The AqH Combines Immune Modulation and Angiogenic Privilege

The AqH is supplied with antiangiogenic and immune modulatory factors from the AC circumscribing tissues such as the ciliary body, the trabecular meshwork, and the corneal endothelium.

In addition to maintaining corneal transparency through a pump-leak mechanism, the corneal endothelium plays an active role in the transport of certain proteins to supply nutrients for the stroma and to remove metabolites. So the agile exchange between the AqH and the cornea supports the theory that the AqH might contribute to the antiangiogenic privilege of the cornea.

Lymphangiogenesis and inflammation are intimately connected. Long-term clear allografts displayed an antigen-specific downregulation of DTH. Another connection between inflammation and lymphangiogenesis is that during DTH, macrophages are recruited through activated T-effector cells (Th1); Maruyama and Cursiefen described in 2005 that inflammatation-induced lymphangiogenesis in the cornea arises from CD11b-positive macrophages.

Thrombospondin

Like the macrophages the well-known antiangiogenic factor TSP also displays effects on both the immune and the angiogenic privilege in the anterior segment. TSPs are generated from a family of five genes encoding glycoproteins that regulate multiple extracellular matrix functions. Within this family, TSP-1 and -2 constitute a subfamily with strong antiangiogenic effects. TSP-1 can bind to latent TGF-β and promote its activation. It might inhibit angiogenesis through direct effects on endothelial cell migration and survival, for example, by inducing vascular endothelial cell apoptosis through its binding to CD36 as well as through indirect effects on growth factor mobilization, for example, by binding heparan sulfate proteoglycans. TSP-2 lacks a TGF-β binding site. It is also a multifunctional protein with antiangiogenic properties that binds to multiple receptors and is capable of inhibiting cell-cycle progression in endothelial cells in the absence of apoptosis. The exact mechanisms by which TSP-1 and -2 achieve their antiangiogenic effects are not yet fully understood. However, both TSP-1 and -2 have been shown to inhibit basic fibroblast growth factor (bFGF)-induced corneal neovascularization. TSP-1 and -2 are expressed in the normal cornea and in the AqH of healthy rat and bovine eyes, whereas they are significantly decreased in diabetic rat AqH. Thus, TSP1 may play a role in ocular vascular homeostasis and its absence may contribute to vascular dysfunctions associated with diabetes. On the other hand, TSP can also upregulate the expression of macrophage-inflammatory protein-2 (MIP-2), TGF-β_2, and tumor necrosis factor alpha which are all required to mediate tolerance induced by TGF-β-treated antigen presenting cells (APCs).

The AqH also contains many factors contributing to the immune privilege of the AC. Taylor and colleagues mentioned that only a few have been studied for their role in suppressing induction of DTH. They defined the criteria for such a immunosuppressive factor as that such a factor has to be physically present in the normal AqH,

second that the AqH concentration of such a factor has to have an *in vitro* immunosuppressive activity similar to whole AqH, and finally that neutralization of such a factor also leads to a neutralization of some aspects of AqH immunosuppressive activity. According to these criteria, only TGF-β_2, calcitonin gene-related peptide (CGRP), α-melanocyte-stimulating hormone (α-MSH), and vasoactive intestinal peptide (VIP) are identified so far as ocular immunosuppressors of DTH.

α-Melanocyte Stimulating Hormone

On the one hand, α-MSH suppresses antigen-stimulated effector T cells and IL1/TNF-induced thymocyte proliferation (IL, interleukin; TNF, tumor necrosis factor); on the other hand, it activates through the melanocortin 1 receptor (MC-1R) the activating protein 1 (AP-1), a transcription factor which binds the TPA (12-*O*-tetradecanoylphorbol 13-acetate) response element (TRE; nucleotide sequence: TGAG/CTCA). Most matrix metalloproteinases (MMPs) contain the TRE and so the following antiangiogenic MMPs might be expressed subsequently: MMP2, cutting plasminogen resulting in the antiangiogenic factor angiostatin and cutting off the ectodomain of the fibroblast growth factor receptor 1 (FGFR1), so the angiogenic activity of FGF is inhibited; MMP7, cutting plasminogen resulting in the antiangiogenic factor angiostatin: MMP9, cutting collagen XVIII, resulting in endostatin and cutting collagen VI , resulting in tumstatin, and cutting plasminogen resulting in the antiangiogenic factor angiostatin; and MMP3, 12, 13 and 20, cutting collagen XVIII, resulting in endostatin. The α-MSH receptor MC-1R has been shown to be expressed on human dermal microvascular endothelial cells.

α-MSH also has a proangiogenic effect which can be provoked by this hormone: α-MSH leads also to the release of interleukin 8 (IL8; CXCL8). This chemokine was shown to have a para- and autocrine angiogenic effect via nuclear factor kappa B (NFκB). Therefore, the antiangiogenic effect on blood endothelial cells (BECs) through different MMPs might be outbalanced by the autocrine proliferative effect of IL8 on endothelial cells, whereas this balance might be shifted in favor of the antiangiogenic effect in lymphangiogenesis.

Vasoactive Intestinal Polypeptide

VIP is a neuroendocrine factor and a 28-amino acid residue that was first isolated from hog upper intestinal tissue. This peptide is also found to be widely distributed in both the central and peripheral nervous system as a neurotransmitter. VIP has several biological functions such as intestinal water and electrolyte secretion, vasodilation, smooth muscle relaxation, thyroid hormone secretion, modulation of leukocyte migration, immunoglobulin production, and growth stimulation of B cells. The peptide also inhibited *in vitro* invasion and migration of murine colon 26-L5 carcinoma cells without affecting their growth and establishment of their liver metastases in mice probably by suppressing their arrest in the liver. The process of angiogenesis by endothelial cells is considered to be functionally similar to that of invasion by tumor cells, so VIP may affect angiogenic responses of endothelial cells by regulating their invasive and motile activities. It was demonstrated that VIP inhibited the morphogenesis of hepatic sinusoidal epithelial (HSE) cells into capillary-like structures on Matrigel-coated wells.

As far as the vascular endothelial cell growth factor (VEGF) activation of endothelial cells can lead to upregulation of the antiapoptotic molecule, Bcl-2, that in turn promotes the expression of endothelial cell-derived IL8, VIP could also inhibit the expression of IL8 in endothelial cells in a similar manner as in monocytes.

Transforming Growth Factor β

The TGF-β family consists of TGF-β1, TGF-β2, and TGF-β3. These are polypeptides of approximately 25 kDa produced by a variety of tissues. TGF-β forms an active complex with a dimeric latency-associated peptide (LAP). This complex binds with high affinity to the extracellular matrix, thereby creating pools of the latent growth factor. The growth factor is activated by proteolytic dissociation. By binding to the TGF-β glycoprotein receptors I, II, and III, a wide range of signaling pathways is activated: for example, regulation of cell growth and differentiation, extracellular matrix production, or changes in cell morphology. Besides the inhibition of epithelial, endothelial, and leukocyte cell growth, TGF-β is thought to stimulate proliferation of fibroblasts. The AqH contains up to 700 pg ml^{-1} latent TGF-β which is produced by the ciliary body and trabecular meshwork. If activated, it has an inhibitory effect on proliferation and motility. It was shown that TGF-β has antiangiogenic properties in the anterior segment at the concentrations present in the aqueous humor. Its proangiogenic effect in the cornea, however, remains controversial. Most important is the leading role of TGF-β in the induction of the AC-associated immune deviation (ACAID), by what the anterior segment becomes an immunologically privileged site avoiding visual damage due to cell-mediated inflammation. Through activation and binding of TGF-β2 to APCs by TSP-1, TGF-β2 impairs these cells to generate T-cell activating CD40 and IL-12, but juxtaposed T cells are promoted to further secrete TGF-β2 and other immunosuppressive factors. APCs migrate from the eye to the marginal zone of the spleen and interact with NK cells. The antigen-specific regulatory T cells are then guided by cytokines back to the eye preventing a delayed hypersensitivity response to the antigen. But at the same time, NK cells still have the ability to lyse their appropriate targets in the eye.

Calcitonin Gene-Related peptide

Another neuropeptide found in the AqH, the sensory neurons of the iris and the ciliary body, is CGRP. CGRP is a 37-amino acid neuropeptide. It is known to inhibit the mechanisms of antigen presentation by macrophages and dermal dendritic cells (Langerhans' cells) to induce DTH and contact hypersensitivity. In addition, CGRP inhibits in macrophages the production of reactive oxygen intermediates induced by IFN-γ. Thus, CGRP seems to suppress immunogenic inflammation induced by antigen-presenting cells and is an opponent of inflammatory cytokines produced by inflammatory T cells. So CGRP plays an important role by the mediation of immunosuppression in the AC.

In contrast to these immunosuppressive abilities, it was shown that CGRP also can promote localized inflammatory activity. In tissues with acute and chronic phases of inflammation, the CGRP concentration is raised. This increase of CGRP is also associated with the induction of neurogenic and endotoxin-induced ocular inflammation.

AqH suppression of DTH has mostly been described by its immunosuppressive effects on effector T-cell activity (Figure 1). CGRP mediates the suppression of DTH by inhibiting IFN-γ-induced inflammatory activity of macrophages, independent of neuropeptides and growth factors mediating T-cell-directed immunosuppression.

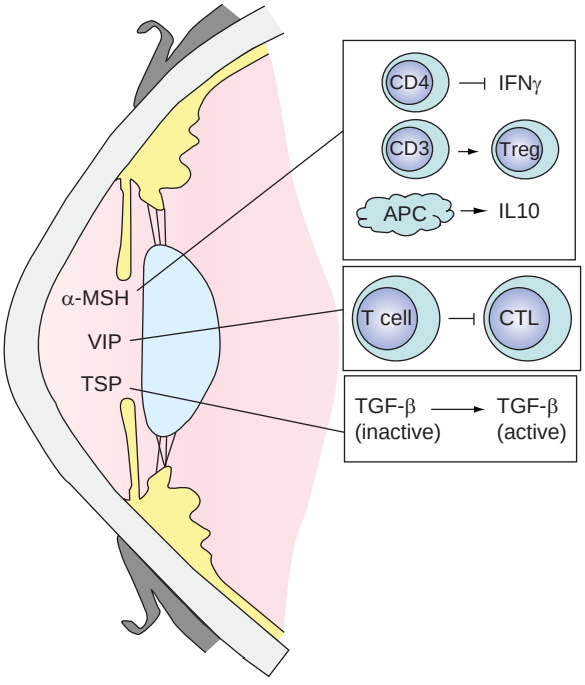

Figure 1 Aqueous humor factors that suppress delayed-type hypersensitivity (DTH). α-Melanocyte stimulating hormone (α-MSH), vasoactive intestinal peptide (VIP), and TSP are present in the aqueous humor and are known to suppress DTH. α-MSH inhibits the production of interferon (INF)-γ by CD4+ T cells, promotes the transformation of CD3+ T cells to T regulatory (Treg) cells, and promotes the release of interleukin (IL)10 from antigen presenting cells (APCs). VIP inhibits the transformation of T cells to cytotoxic T cell (CTL). TSP promotes activation of latent transforming growth factor (TGF)-β and promotes its activation.

By the help of CGRP AqH becomes anti-inflammatory, so the immune-privileged ocular microenvironment seems to suppress not only the T cells that trigger DTH, but also IFN-γ-dependent inflammation. CGRP regulates the inflammatory activities of T cells and macrophages in the ocular microenvironment, so the suppression of macrophage activity could prevent inflammation triggered by factors other than activated T cells.

Therefore, the AqH appears to carry multiple mechanisms to affect T-cell activation, IFN-γ production, macrophage activation, and lymphangiogenesis to suppress inflammation in the eye at multiple levels.

See also: Angiogenesis in the Eye; Concept of Angiogenic Privilege; Functional Morphology of the Trabecular Meshwork; Neuroendocrine Properties of the Ciliary Epithelium; Regulation of Extracellular Matrix Turnover in the Aqueous Humor Outflow Pathways; The Role of the Ciliary Body in Aqueous Humor Dynamics. Structural Aspects.

Further Reading

Cousins, S. W., McCabe, M. M., Danielpour, D., and Streilein, J. W. (1991). Identification of transforming growth factor-beta as an immunosuppressive factor in aqueous humor. *Investigative Ophthalmology and Visual Science* 32: 2201–2211.

Cursiefen, C., Masli, S., Ng, T. F., et al. (2004). Roles of thrombospondin-1 and-2 in regulating corneal and iris angiogenesis. *Investigative Ophthalmology and Visual Science* 45: 1117–1124.

Ferguson, T. A. and Griffith, T. S. (1997). A vision of cell death: Insights into immune privilege. *Immunological Reviews* 156: 167–184.

Lawler, J. (2002). Thrombospondin-1 as an endogenous inhibitor of angiogenesis and tumor growth. *Journal of Cellular and Molecular Medicine* 6: 1–12.

Maruyama, K., Ii, M., Cursiefen, C., et al. (2005). Inflammation-induced lymphangiogenesis in the cornea arises from CD11b-positive macrophages. *Journal of Clinical Investigation* 115: 2363–2372.

Masli, S., Turpie, B., and Streilein, J. W. (2006). Thrombospondin orchestrates the tolerance-promoting properties of TGFbeta-treated antigen-presenting cells. *International Immunology* 18: 689–699.

Niederkorn, J. Y. (1990). Immune privilege and immune regulation in the eye. *Advances in Immunology* 48: 191–226.

Rundhaug, J. E. (2005). Matrix metalloproteinases and angiogenesis. *Journal of Cellular and Molecular Medicine* 9: 267–285.

Sonoda, Y., Sano, Y., Ksander, B., and Streilein, J. W. (1995). Characterization of cell-mediated immune responses elicited by orthotopic corneal allografts in mice. *Investigative Ophthalmology and Visual Science* 36: 427–434.

Streilein, J. W. (1993). Immune privilege as the result of local tissue barriers and immunosuppressive microenvironments. *Current Opinion in Immunology* 5: 428–432.

Streilein, J. W. (1999). Regional immunity and ocular immune privilege. *Chemical Immunology* 73: 11–38.

Streilein, J. W. (2003). Ocular immune privilege: The eye takes a dim but practical view of immunity and inflammation. *Journal of Leukocyte Biology* 74: 179–185.

Streilein, J. W. and Stein-Streilein, J. (2000). Does innate immune privilege exist? *Journal of Leukocyte Biology* 67: 479–487.

Streilein, J. W., Takeuchi, M., and Taylor, A. W. (1997). Immune privilege, T-cell tolerance, and tissue-restricted autoimmunity. *Human Immunology* 52: 138–143.

Taylor, A. W. (1999). Ocular immunosuppressive microenvironment. *Chemical Immunology* 73: 72–89.

The Photoreceptor Outer Segment as a Sensory Cilium

J C Besharse and C Insinna, Medical College of Wisconsin, Milwaukee, WI, USA

Glossary

Axoneme – The cytoskeletal backbone of cilia and flagella composed of nine microtubule doublets aligned in a cylindrical array. Motile axonemes, generally referred to as 9 + 2 axonemes, contain a pair of central singlets and dynein arms.
Basal body – A centriole that becomes associated with the cell membrane for the nucleation of a cilium. Doublet microtubules of cilia in most animals are extensions of triplets of the basal body.
Centriole – A barrel-shaped or cylindrical organelle composed in most animals of nine triplet microtubules. A pair of centrioles, surrounded by an amorphous zone containing many proteins, constitutes the centrosome.
Cilia – The extensions of the cell surface that have a plasma membrane and contain a cytoskeletal core of microtubules, called an axoneme, which extends out from the basal body. They may be motile, as in the airway epithelium in humans, or nonmotile and sensory in function. Cilia and flagella have the same organization, but flagella are generally motile and are longer.
Intraflagellar transport – A microtubule-based trafficking pathway required for the formation and maintenance of cilia and flagella. Intraflagellar transport (IFT) involves the bidirectional transport of a protein adaptor complex composed of highly conserved IFT proteins. The pathway requires kinesin 2 family motors in the outward (anterograde) direction and a cytoplasmic dynein in the return (retrograde) direction. The pathway is equally important in cilia and flagella.
Kinesins – The plus-end-directed motor proteins powered by adenosine triphosphate hydrolysis to walk along microtubules. These are involved in multiple cellular functions, including transport of cargo, mitosis, and meiosis. Many different genes encode kinesins with different properties and functions.
Microtubules – The cytoskeleton tubules assembled from protofilaments composed of linear polymers of α- and β-tubulin heterodimers. These are asymmetric hollow cylinders with plus and minus ends that differ in polymerization rate and binding proteins. They form a dynamic network within the cell and organize themselves into complex structures, such centrioles, basal bodies, and cilia.
Microvilli – The membrane protrusion from the cell surface composed of cytoplasm and dense bundles of actin filaments serving to increase the surface area of the cell.
Sensory cilia – The cilia that contain membrane receptors and signaling components. These often have a nonmotile 9 + 0 axoneme, but actively motile cilia may also serve a sensory function.

Introduction

There are at least two fundamentally different designs for visual photoreceptors, generally referred to as the rhabdomeric type and the ciliary type. Rhabdomeric photoreceptors are widely represented among invertebrates and have been intensively studied in the horseshoe crab, fruit fly, and squid. Rhabdomeric photoreceptors concentrate the visual pigment for photon capture in a highly replicated array of microvilli, each containing an actin cytoskeletal core. The array of microvilli is called the rhabdomere. The visual pigment of ciliary photoreceptors is also concentrated in a photon capture organelle called the outer segment (OS). However, the OS is derived from the plasma membrane of a cilium and retains the microtubule-based cytoskeletal core, called an axoneme, which is common to all cilia. Often, rhabdomeric and ciliary photoreceptors are referred to as invertebrate and vertebrate types, respectively, but this distinction can be misleading. Both photoreceptor types appeared early in animal evolution and are present in multiple invertebrate phyla. Furthermore, some animals have both photoreceptor types, and the retina in the compound eye of the scallop contains a layered juxtaposition of both rhabdomeric and ciliary photoreceptors. Although vertebrate photoreceptors with true rhabdomeres have not been identified, the recent discovery of intrinsically light-sensitive ganglion cells (ipGCs) has led to the realization that their melanopsin photopigment and transduction pathway have features in common with rhabdomeric rather than ciliary photoreceptors. This suggests that ipGCs may have originated from an evolutionary ancient rhabdomeric precursor.

Turnover of the OS and Phototransduction Machinery

The light-sensitive OS of vertebrate photoreceptors is an elegantly complex organelle that serves as the starting

point for highly sensitive nighttime vision (rods) as well as high acuity, color vision (cones) in the daytime. The OS consists of a stack of membrane disks containing a photopigment (opsin) of the guanine-nucleotide-binding protein-coupled receptor (GPCR) family, and a large array of cytosplasmic, cytoskeletal, membrane, and membrane-associated proteins that are essential for phototransduction. The phototransduction cascade begins with photon absorption by the vitamin-A-derived chromophore of opsin and proceeds through activation of transducin, a guanine-nucleotide-binding protein (G-protein), which in turn activates a phosphodiesterase that reduces cytoplasmic cyclic guanosine monophosphate (cGMP) levels. The photoresponse is a hyperpolarization event that occurs when declining local cGMP levels result in closure of the cGMP-gated channel in the OS plasma membrane. The high sensitivity of the rod cells, which can respond to single-photon absorption events, and the rapid responses of cone cells in bright light, depend on the integrity of the disk stack and close juxtaposition of the protein components of the transduction cascade. Optimal function also depends on other OS proteins that support transduction such as membrane guanylyl cyclases (GC1 and GC2), which regenerate cGMP, a Na^+/Ca^{2+} exchanger which regulates Ca^{2+} levels, anaerobic glycolysis, which supplies a portion of the adenosine triphosphate (ATP), and the pentose phosphate shunt which supplies nicotinamide adenine dinucleotide phosphate (NADPH), essential for conversion of the all-*trans* retinaldehyde to retinol in the visual pigment cycle.

Two additional interdependent features of OS organization, essential for optimal visual function, are proper targeting of the phototransduction proteins to the OS and long-term maintenance through OS renewal. A striking feature of normal rods and cones is the high level to which phototransduction proteins are concentrated in the OS. Since those proteins are all synthesized at polyribosomes in the inner segment, a great deal of recent focus has been on those mechanisms that are essential for proper trafficking of OS proteins. This is a major problem throughout the life of the cell because OSs renew at a particularly high rate (see **Figure 1**). In the 1960s, Richard Young, then at the University of California at Los Angeles, thoroughly documented the fact that rod OSs are renewed through continuous new disk assembly adjacent to the inner segment. Furthermore, Young along with Dean Bok determined that OS length is maintained through a compensatory shedding of disks from the distal tip where they are phagocytized and degraded by the retinal pigment epithelium. In the 1970s, these same concepts were extended to include the cone OSs. The turnover of OSs is highly conserved, but occurs at very different rates in different species. In mice, rod OSs turnover once every 10 days.

The Photosensitive Organelle as a Sensory Cilium

With the advent of transmission electron microscopy in the 1950s, photoreceptors were an early subject of analysis, particularly by Eduardo de Robertis in Argentina and Kiyoteru Tokuyasu and Eichi Yamada in Japan. Those early studies showed that developing photoreceptors have the basic organization of cilia. During early differentiation, a centriole pair moves to the plasma membrane where one member serves as a template for assembly of a microtubule cytoskeletal structure called an axoneme (**Figure 2**); the other centriole is generally seen next to the basal body as an accessory centriole. Centrioles consist of an array of nine triplet microtubules and each triplet has an A-, B-, and C-tubule. The A-tubule is a complete microtubule comparable to cytoplasmic microtubules, but the B subtubule is a partial microtubule built on the wall of the A-tubule. Likewise, the C-tubule is built on the wall of B. The centriole that associates with the plasma membrane is called a basal body because it serves as a template for outgrowth of doublet microtubules that form the axoneme. As a consequence of basal body templating, the axoneme grows out as an array of nine doublet microtubules that are direct extensions of the A- and B-tubules of the basal body. The photoreceptor and other sensory cilia are generally said to have a 9 + 0 axoneme, in contrast to motile cilia, which have a 9 + 2 axoneme; the 2 in the latter designation refers to a central pair of single microtubules within the core of the axoneme. Although the 9 + 2 axoneme is found in a wide array of motile cilia, 9 + 0 cilia are sometimes motile. For example, the rotatory cilia of the embryonic Henson's node have a 9 + 0 axoneme.

As the axoneme elongates in rodents, the plasma membrane expands at the distal end of the cilium, and membrane vesicles and tubules accumulate (**Figure 2**). At this early stage, the photopigment apoprotein, opsin, is localized within the plasma membrane of the distal end of the cilium, and membrane vesicles and tubules accumulate. This region expands in the early stages of OS formation, quickly taking the form of an orderly stack of membrane disks (**Figure 2**). Frog OSs, as described by S. E. Nilsson in 1964, exhibit ordered disks from the very beginning of differentiation. At later stages, and, presumably during early development, new membrane disks are thought to form as evaginations of the ciliary membrane. The most proximal part of the cilium emanating from the basal body, called the connecting cilium by Eduardo de Robertis in 1956, connects the photosensitive OS with the cells synthetic machinery in the inner segment; components of the phototransduction machinery in the OS are synthesized in the inner segment and must be transported to the OS through the connecting cilium.

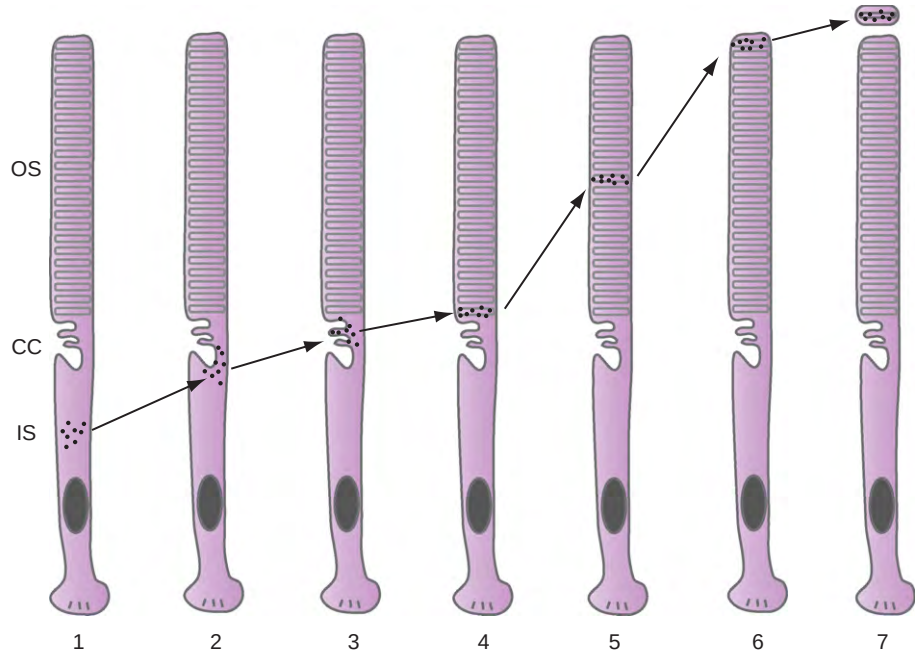

Figure 1 Conceptual diagram of a pulse chase autoradiography experiment revealing OS turnover in rod cells. Radioactive amino acids provided as a pulse at 1 (left) were incorporated into protein, mainly rhodopsin, in the inner segment (IS). Over the next few hours (2–3) radioactive protein was transported to the apical inner segment and disk-forming region at the connecting cilium (CC), and incorporated into newly formed disks creating a discrete radioactive band (4). Over the next ≈10 days (mammals), the band was gradually displaced toward the distal end of the OS (5–6) until discarded in a process called disk shedding (7). Discarded disks (7) are phagocytized by adjacent retinal pigment epithelium (not shown). From Young, R. W. (1967). The renewal of photoreceptor cell outer segments. *Journal of Cell Biology* 33: 61–72.

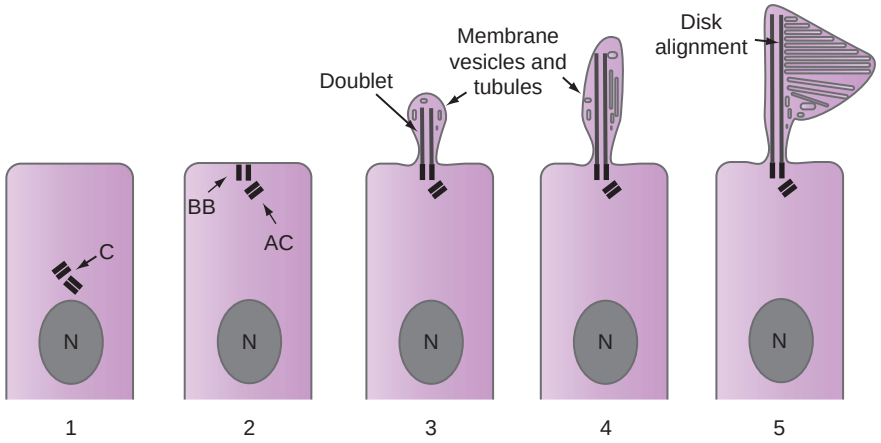

Figure 2 Early development of the outer segment. After the last mitotic division the centriole pair (1, left) moves to the cell surface (2). One member of the centriole pair associates with the plasma membrane where it is called a basal body (BB); the second centriole is often seen adjacent to the basal body in EM images where it is called the accessory centriole (AC). The basal body nucleates the extension of doublet microtubules at the cell surface to elongate the cilium (3). In the early stages of cilium elongation membrane vesicles and tubules are seen in the ciliary cytoplasm (3–4). Finally, disks align perpendicular to the axoneme composed of doublet microtubules (5). Based on early EM analysis by Tokuyasu, K. and Yamada, E. (1959). The fine structure of the retina studied with the electron microscope. IV. Morphogenesis of outer segments of retinal rods. *Journal of Biophysical and Biochemical Cytology* 6: 225–230; De Robertis, E. (1960). Some observations on the ultrastructure and morphogenesis of photoreceptors. *Journal of General Physiology* 43(6) supplement, 1–13; and Greiner, J. V., Weidman, T. A., Bodley, H. D., and Greiner, C. A. M. (1981). Ciliogenesis in photoreceptor cells of the retina. *Experimental Eye Research* 33: 433–446.

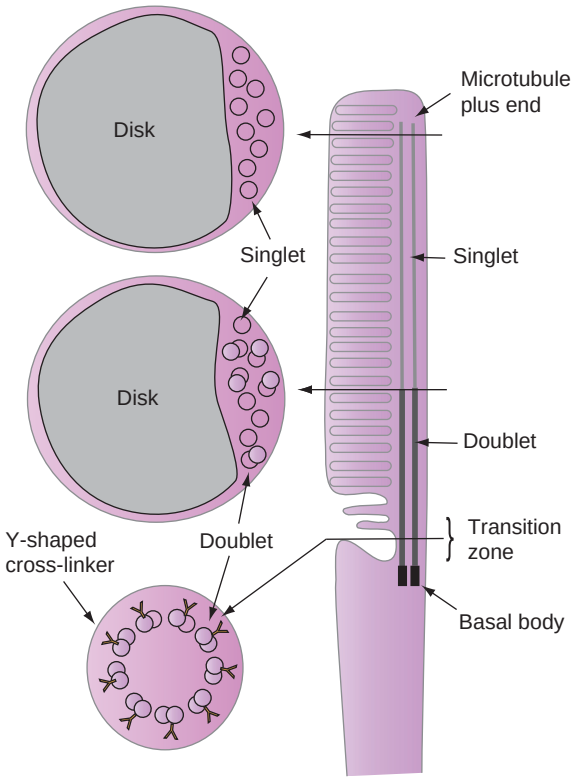

Figure 3 Structure of the ciliary axoneme of a mature photoreceptor. Longitudinal view is shown on the right and magnified cross sections at the position of the arrows on the left. The axoneme grows out of the basal body as an array of nine doublet microtubules. The microtubule plus ends extend distally and the minus ends are anchored in the basal body. The region adjacent to the basal body is a transition zone in which doublets are closely linked with the plasma membrane by Y-shaped cross-linkers (lower diagram on left); this region is often referred to as the connecting cilium. The region immediately distal to the transition zone is the site of new disc assembly. Within the OS the doublets loose their B-tubule to become singlets in the distal OS. This is shown as an abrupt transition on the right, but conversion to singlets appears to occur gradually leaving mixtures of singlets and doublets (middle diagram on left). The distal OS only has singlets.

The term connecting cilium refers to that portion of the cilium between the basal body and the disk-forming region of the OS. As originally demonstrated by Pal Röhlich in 1976, the connecting cilium is actually comparable to the transition zone, a structure common to all eukaryotic cilia and flagella (**Figure 3**). Here, the plasma membrane is closely linked to the doublet microtubules of the axoneme by cross-linkers that extend from the doublet microtubule to the plasma membrane. These cross-linkers are stable structures that remain bound to the axoneme after detergent extraction and link the axoneme to cell surface glycoconjugates through transmembrane connections. Although these microtubule-membrane cross-linkers exhibit a conserved Y-shaped structure across many cilium types, their molecular composition has not been determined. Recently, a number of cilium proteins relevant to human photoreceptor degenerative disease, such as retinitis pigmentosa guanosine triphosphate (GTP)ase regulator (RPGR) and RPGR-interacting protein 1 (RPGRIP), have been localized to the transition zone and some may be components of the cross-linking structures. Further high-resolution analysis of the composition of cross-linkers may lead to a better understanding of the function of connecting cilium proteins that are relevant to human disease.

Distally, beyond the transition zone, the axoneme extends deep into the OS (**Figure 3**). This point requires emphasis because the term connecting cilium refers to the link between inner and OS and the term is often used with the implication that this is the entire cilium. However, both early electron microscopic studies and numerous immunocytochemistry studies have shown that photoreceptor axonemes extend through much of the length of the OS (**Figure 4**); in some cases, they extend all the way to the distal tip. The recent finding of extremely long axonemes in mouse, frog, and zebrafish OSs, along with earlier studies showing much shorter axonemes, suggests that they may vary significantly in their length. The reason for variability in axoneme length observed in various studies is not known. A possible explanation, however, is that the distal axoneme is dynamic and unstable, resulting in some cases in poor preservation for morphological studies. The principles governing these length variations in either rods or cones remain unknown, but are likely to be relevant to the finding that OSs maintain a relatively constant length through many cycles of OS turnover.

Evidence for Intraflagellar Transport in Photoreceptors

Recently our work has demonstrated that the assembly of photoreceptor OSs depends on a highly conserved microtubule-based trafficking pathway called intraflagellar transport (IFT). IFT was originally discovered in the motile flagella of the green alga *Chlamydomonas rheinhartii* and quickly extended to the sensory cilia *Caenorhabditis elegans*. The essential components of IFT are the kinesin and dynein molecular motors that drive movement along axonemal microtubules and multiprotein IFT particles that are thought to link cargo such as cytoskeletal and phototransduction proteins to the IFT motors (see **Figure 5**). For example, at least 16 different proteins assemble to form two large protein complexes referred to as IFT particles (**Figure 5**), and all of these proteins are highly conserved between *C. rheinhartii* and man. IFT transport is bidirectional. In anterograde IFT plus-end-directed motors of the kinesin 2 family move IFT particles with attached cargo toward the plus end of the axoneme, while in retrograde IFT a minus-end-directed dynein motor returns the IFT machinery for exchange with a pool in the cell body. Again, the pathway is highly conserved in that the same molecular

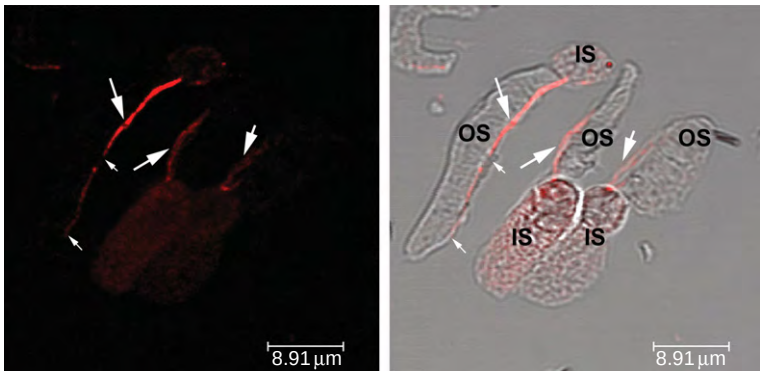

Figure 4 Immunocytochemical labeling of the axoneme of cone OSs from zebrafish. An antibody to α-tubulin was used to label (red) the microtubules of the axoneme (large arrows). An immunofluorescence image is on the left and for orientation this image is merged with a phase image of the same cells on the right. The image includes a long single cone (upper left) and a double cone (lower right). Note that the axoneme staining is attenuated distally (small arrows), particularly in the long single cone. Magnification bars in lower right equal 8.91 µm. IS, inner segment; OS, outer segment.

motors identified in *C. rheinhartii* and *C. elegans* perform similar functions in virtually all eukaryotic cilia including those in man. For example, heterotrimeric kinesin II, assembled from the kinesin family member 3A and 3B (KIF3A, KIF3B) along with kinesin-associated protein 3 (KAP3) proteins, is the canonical anterograde motor, while a dynein containing the cytoplasmic dynein 2 heavy chain (DNCH2) is the canonical retrograde motor.

A prominent role for IFT in photoreceptor OS formation is now well established. Four of the IFT proteins (IFT88, IFT57, IFT52, and IFT20) have been localized along photoreceptor axonemes and photoreceptor OS assembly defects have been fully characterized in rods of mice with a mutation in IFT88. This has been extended to cone cells with targeted, cone-specific deletion of IFT20, which results in disrupted OS assembly. A central feature of the IFT model is the multi-protein IFT particle (**Figure 5**). IFT particles containing IFT88, IFT57, IFT52, and IFT20 can be isolated from bovine photoreceptor outer segments. The photoreceptor IFT particle is large, fractionating in sucrose gradients at a peak size of ~500–750 kDa and has properties remarkably similar to those originally described in *C. rheinhartii*. This implies that the photoreceptor particle contains additional IFT proteins for which antibodies have not yet been generated. Evidence for photoreceptor IFT is also based on analysis of its canonical motors. All three subunits of kinesin II as well as DNCH2 have been localized to photoreceptor axonemes. Furthermore, conditional deletion of the KIF3A subunit of kinesin II disrupts OS assembly, causes rhodopsin mislocalization, and results in photoreceptor cell death.

A Special Role for KIF17 in Photoreceptors

The foregoing description of photoreceptor IFT describes conditions and expectation of a canonical IFT model that has applicability in virtually all ciliated cells. However, a novel feature of photoreceptor IFT is the critical involvement of an additional kinesin motor, the homodimeric kinesin family member 17 (KIF17). As illustrated in **Figure 5**, both kinesin II and KIF17 are associated with the IFT particle along doublet microtubules in the proximal OS, but KIF17 alone is associated with movement of the IFT particle along singlet microtubules in the distal OS. Our recent work has demonstrated that KIF17 is required to form outer segments, but does not simply replace kinesin II function; both kinesins are required. An interesting feature of this work is that while reduced kinesin II function disrupts both photoreceptor and kidney cilium elongation, knockdown of KIF17 results in failed OS assembly with no apparent effect in the kidney. The importance of KIF17 is likely related to the presence of singlet microtubule extensions in photoreceptors (see **Figure 3**). While singlet extensions are prominent in photoreceptor cilia, as originally illustrated in the older EM literature, singlet extensions in kidney sensory cilia are either very short or not present at all.

Work from the laboratory of Jonathan Scholey at the University of California at Davis has shown that the *C. elegans* KIF17 homolog, osmotic avoidance abnormal protein (OSM-3), is also required for sensory cilium elongation, specifically in cilia with singlet extensions. In *C. elegans* cilia OSM-3 serves as an accessory IFT motor along with kinesin II. Specifically, either kinesin motor can function and compensate for loss of the other motor in the proximal cilium, which contains doublet microtubules, but only OSM-3 can extend and move along the distal singlets. In fact, it was the existence of singlet extensions in photoreceptors that drew our attention to KIF17 and led to our finding of a prominent role of this accessory kinesin motor. However, the simple model for dual IFT kinesins in *C. elegans* does not fully explain findings in photoreceptors. The *C. elegans* model predicts that knockdown of KIF17 would result in short OSs that fail to elongate.

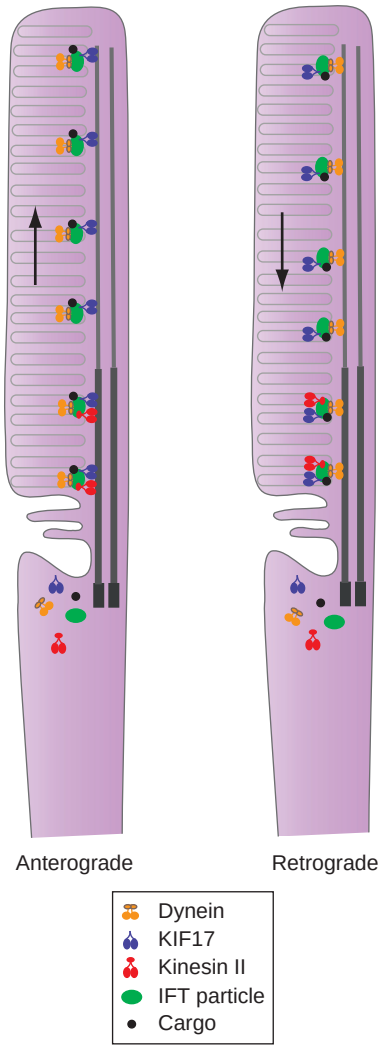

Figure 5 Conceptual diagram of intraflagellar transport (IFT) in photoreceptors. (Left) Anterograde IFT uses the plus end directed kinesin motors, kinesin II and KIF17, to move IFT particles with attached 'cargo' toward the distal, plus end of the axoneme (arrow). Note that the minus-end-directed motor, dynein, is illustrated as cargo for anterograde IFT. Based largely on work in *C. elegans*, it is hypothesized that kinesin II and KIF17, move cooperatively on doublets in the proximal outer segment and that KIF17 operates alone on singlets in the distal outer segment. (Right) Retrograde IFT uses a cytoplasmic dynein motor to return IFT particles and cargo to the inner segment. Note that kinesin II and KIF17 are illustrated as cargo for retrograde IFT. IFT complexes along with cargo and molecular motors are thought to assemble into large complexes in the inner segment in the region adjacent to the basal body.

Results from direct comparison of mutated forms of the KIF3B subunit of kinesin II and KIF17 suggest that the motors carry out nonredundant functions and suggest that, in addition to a role for KIF17 in distal cilium extension, the motor may also be involved in transport of proteins that are essential for disk assembly in the proximal outer segment. Although knockdown of KIF17 results in ablation of OS formation, a recent mutagenesis study of a consensus calcium, calmodulin kinase II (CaMKII) phosphorylation site in the KIF17 tail region, demonstrates that KIF17 plays a critical role in the distal OS in the control disk shedding (see **Figure 1**).

What Is the IFT Cargo?

The requirement for IFT in ciliogenesis has led to the general idea that the IFT particle serves as an adaptor to link IFT cargo to the requisite IFT motors. Some of the early evidence for cargo relates to the motors themselves. Since the axoneme plus end is at the distal end of the cilium, the minus-end-directed dynein motor required for retrograde IFT cannot move from the cell body to the distal tip on its own and available data suggest that it is cargo during anterograde IFT. Likewise, recycling of the plus-end-directed kinesins back to the inner segment appears to require retrograde IFT (see **Figure 5**). Another feature of axoneme organization is that its microtubules can assemble or disassemble only at the plus end, which is located distally. Since the axoneme can both elongate and shorten, its building blocks are likely cargo in both directions. It is important to point out that since the axoneme provides the principle cytoskeletal scaffold for the OS, IFT would be of great significance if its main purpose were to maintain axoneme structure. Recent evidence, however, suggests that IFT transports membrane components of the OS as well.

The photoreceptor OS provides a special challenge in that the components of phototransduction are present in high abundance and turn over rapidly. The question is: Which of these components is moved to the OS by IFT? One reasonably clear conclusion is that not all OS components require IFT. For example, some phototransduction proteins, such as arrestin and transducin, move between inner and OS in relationship to light and dark adaptation and a strong case can be made for free diffusion as the underlying mechanism for movement of abundant freely soluble proteins. Current evidence favors the idea that many membrane and membrane-associated proteins may require IFT. In *C. rheinhartii* and *C. elegans*, where real time imaging is feasible, movement of specific membrane proteins has been detected along the cilium. Rigorous proof that a particular protein is IFT cargo requires direct demonstration that it is linked to the IFT machinery and moves with IFT components, and there are no examples of this type of evidence outside of *C. rheinhartii* and *C. elegans*.

Nonetheless, mutation of the KIF3A subunit of the kinesin II motor, and mutation of the IFT88 subunit of the IFT particle both result in rhodopsin mislocalization, suggesting that rhodopsin is carried as IFT cargo. In support of the specificity of this effect, we recently demonstrated that expression of a dominant-negative

form of the KIF3B subunit of kinesin II in zebrafish cones results in cone opsin mislocalization, but dominant-negative KIF17 blocks OS elongation without causing opsin mislocalization. Since studies of protein mislocalization in cells carrying mutations is an inherently indirect measure, we have recently used a variety of pull-down assays to isolate IFT protein complexes containing the two kinesin motors as well as rhodopsin and another OS membrane protein, retinal guanylyl cyclase 1 (RetGC1 also called GUCY2E). The work with GC1 is particularly interesting because we have identified a small chaperone protein (DNAJB6) that binds specifically to IFT88 in the IFT particle and to the kinase homology domain in the cytoplasmic tail region of GC1. We have proposed that this is the key linkage required for association of membrane GC1 with the IFT machinery and that the binding can be regulated directly through the ATPase activity of heat-shock cognate protein 70 (HSC70). This represents the first specific model for the molecular linkage of a cargo protein with the IFT machinery.

Summary and Perspective

The fact that photoreceptor OSs are sensory cilia has been known for many years, but recent advances in understanding the mechanisms underlying ciliogenesis, including the IFT pathway, are likely to have a large impact on our understanding of the cell biology of photoreceptors. Although mutations in genes involved in ciliogenesis often cause embryonic lethal phenotypes and will not frequently appear among the causes of photoreceptor-specific degenerative disease, our understanding of disease mechanisms are likely to improve through understanding which photoreceptor proteins are IFT cargo. For example, human GC1 contains three human disease causing mutations in the domain that we have recently shown to bind a linker chaperone that couples GC1 to the IFT machinery. This has led us to propose that those human mutations lead to abnormal ciliary trafficking. The importance of photoreceptor cilia also provides a basis for understanding syndromic diseases such a Bardet–Biedl syndrome, which includes RP among a complement of other abnormalities. Such diseases are now referred to as ciliopathies because cilia provide a common basis for understanding pathology in the different tissues that are affected. Finally, placement of photoreceptor OSs in their appropriate niche as a special type of sensory cilium provides evolutionary perspective on pathways common to all cilia that emerged early in eukaryote evolution.

See also: Circadian Photoreception; Genetic Dissection of Invertebrate Phototransduction; *Limulus* Eyes and Their Circadian Regulation; Light-Driven Translocation of Signaling Proteins in Vertebrate Photoreceptors; Microvillar and Ciliary Photoreceptors in Molluskan Eyes; Photoresponse in Squid; Phototransduction: Adaptation in Rods; Phototransduction in *Limulus* Photoreceptors; Phototransduction: Inactivation in Cones; Phototransduction: Inactivation in Rods; Phototransduction: Phototransduction in Cones; Phototransduction: Phototransduction in Rods; Phototransduction: Rhodopsin; Phototransduction: The Visual Cycle; Retinal Degeneration through the Eye of the Fly; Rod and Cone Photoreceptor Cells: Outer-Segment Membrane Renewal.

Further Reading

Baker, S. A., Freeman, K., Luby-Phelps, K., Pazour, G. J., and Besharse, J. C. (2003). IFT20 links kinesin II with a mammalian intraflagellar transport complex that is conserved in motile flagella and sensory cilia. *Journal of Biological Chemistry* 278: 34211–34218.

Besharse, J. C. and Horst, C. J. (1990). The photoreceptor connecting cilium. A model for the transition zone. In Bloodgood, R. A. (ed.) *Ciliary and Flagellar Membranes*, pp. 389–417. New York: Plenum.

Bhowmick, R., Li, M., Sun, J., et al. (2009). Photoreceptor IFT complexes containing chaperones, guanylyl cyclase 1, and rhodopsin. *Traffic* 10(6): 648–663.

De Robertis, E. (1960). Some observations on the ultrastructure and morphogenesis of photoreceptors. *Journal of General Physiology* 43(6): supplement, 1–13.

Eckmiller, M. S. (1996). Renewal of the ciliary axoneme in cone outer segments of the retina of *Xenopus laevis*. *Cell Tissue Research* 285: 165–169.

Hong, D. H., Yue, G. H., Adamian, M., and Li, T. S. (2001). Retinitis pigmentosa GTPase regulator (RPGR)-interacting protein is stably associated with the photoreceptor ciliary axoneme and anchors RPGR to the connecting cilium. *Journal of Biological Chemistry* 276: 12091–12099.

Inglis, P. N., Ou, G., Leroux, M. R., and Scholey, J. M. (2007). The sensory cilia of *Caenorhabditis elegans*. *WormBook* March 8: 1–22.

Insinna, C. and Besharse, J. C. (2008). Intraflagellar transport and the sensory outer segment of vertebrate photoreceptors. *Developmental Dynamics* 237: 1982–1992.

Insinna, C., Pathak, N., Perkins, B., Drummond, I., and Besharse, J. C. (2008). The homodimeric kinesin, Kif17, is essential for vertebrate photoreceptor sensory outer segment development. *Developmental Biology* 316: 160–170.

Maerker, T., van Wijk, E., Overlack, N., et al. (2008). A novel Usher protein network at the periciliary reloading point between molecular transport machineries in vertebrate photoreceptor cells. *Human Molecular Genetics* 17: 71–86.

Marszalek, J. R., Liu, X., Roberts, E. A., et al. (2000). Genetic evidence for selective transport of opsin and arrestin by kinesin-II in mammalian photoreceptors. *Cell* 102: 175–187.

Pazour, G. J., Baker, S. A., Deane, J. A., et al. (2002). The intraflagellar transport protein, IFT88, is essential for vertebrate photoreceptor assembly and maintenance. *Journal of Cell Biology* 157: 103–113.

Rohlich, P. (1975). The sensory cilium of retinal rods is analogous to the transitional zone of motile cilia. *Cell Tissue Research* 161: 421–430.

Tokuyasu, K. and Yamada, E. (1959). The fine structure of the retina studied with the electron microscope. IV. Morphogenesis of outer segments of retinal rods. *Journal of Biophysical and Biochemical Cytology* 6: 225–230.

Young, R. W. (1967). The renewal of photoreceptor cell outer segments. *Journal of Cell Biology* 33: 61–72.

Young, R. W. and Bok, D. (1969). Participation of the retinal pigment epithelium in rod outer segment renewal process. *Journal of Cell Biology* 42: 392–403.

The Physiological Consequences of Vitreous Composition

T M Ranchod, D T Goldenberg, and M T Trese, Associated Retinal Consultants, Royal Oak, MI, USA

Glossary

Chromovitrectomy – The use of dyes during vitrectomy to identify and facilitate removal of the vitreous, epiretinal membranes, or internal limiting membrane.
Enzymatic posterior vitreous detachment – The posterior vitreous detachment induced by an enzyme injected into the vitreous cavity.
Posterior vitreous detachment (PVD) – The detachment of the vitreous cortex and posterior hyaloid face from the internal limiting membrane of the sensory retina.
Vitrectomy – The surgical removal of the vitreous body from the posterior segment of the eye.
Vitreoretinal interface – The site where vitreous collagen fibrils bind the internal limiting membrane of the sensory retina with the aid of glycoproteins.

Anatomy and Physiology of the Nonvitrectomized Eye

Vitreous is composed predominantly of water (99%) and the main extracellular matrix components are collagen and glycosaminoglycans. Vitreous collagen is predominantly type II; however, type IX, type V/XI, and small amounts of type VI are also present. Within the vitreous, collagen fibrils are interspersed with molecules of the glycosaminoglycan hyaluronan. Collagen fibrils are distributed unevenly throughout the vitreous body; they are most dense at the vitreous base, followed by the posterior vitreous cortex, then the anterior vitreous cortex, and they are least dense in the central vitreous body. The distribution of hyalocytes is similarly uneven, roughly corresponding to the distribution of collagen.

The vitreous body is bounded anteriorly by the lens–zonule–ciliary body–iris diaphragm and elsewhere by the neurosensory retina, of which the internal limiting membrane (ILM) is the innermost layer. Attachments of the vitreous body to adjacent structures are strongest at the vitreous base, which spans across the ora serrata, from the pars plana to the anterior retina. The next strongest adhesion exists at the borders of the optic disk. When a spontaneous posterior vitreous detachment (PVD) occurs, glial cells from the disk margin can remain on the posterior hyaloid face, seen clinically as a Weiss ring. The vitreous also adheres to the major retinal vessels, accounting for occasional avulsion of retinal vasculature during the process of PVD. A firm attachment is also present in the macula. Weaker adhesions are present anteriorly where the vitreous meets the posterior lens capsule, known as Wieger's ligament.

The structure of the vitreous body changes with age, as the gel matures into fluid pockets alternating with patches of condensed collagen (syneresis). A large fluid pocket, or lacune, often forms in the central vitreous body where collagen is least dense, and this pocket is frequently visible on anterior slit lamp examination as well as during vitrectomy surgery. Detachment of the posterior hyaloid from the retina (PVD) occurs spontaneously with age as well, and a Weiss ring may or may not be visible. The incidence of PVD increases with age, but the overall prevalence of partial or complete PVD may be lower than previously thought. The vitreous in children warrants special consideration. Vitreous adhesions are much stronger in children than in adults, making complete surgical removal of the vitreous difficult without the aid of enzymes (discussed below). Furthermore, the vitreous architecture is distinctly abnormal in children with retinopathy of prematurity (ROP), familial exudative vitreoretinopathy (FEVR), and some retinal dystrophies. In these patients, the vitreous cortex is composed of alternating layers of liquid and solid gel. The precise orientation of these sheets has not been clearly delineated, but removal of vitreous cortex layers can be confused for removal of the posterior hyaloid during surgery, resulting in unwanted residual vitreous following vitrectomy. Splitting of the posterior hyaloid, vitreoschisis, has also been noted in adult patients with proliferative diabetic retinopathy.

Mechanical Vitrectomy

Standard vitrectomy involves the creation of two or three full-thickness scleral incisions (sclerotomies) through the pars plana. Instruments and infusions are delivered through these ports during surgery, and the sclerotomies are traditionally sutured at the end of surgery with 20-gauge instruments. More recently, sutureless vitrectomy has become possible with 23- or 25-gauge and even with 20-gauge instruments. During vitrectomy surgery, the bulk of the vitreous is generally removed initially (core vitrectomy). If a PVD is not already present, the posterior hyaloid face is usually detached deliberately in

order to facilitate removal of the posterior vitreous cortex. It is often assumed that this is done leaving a collagen-clean anterior retinal surface but vitreoschisis can result. Vitreous cortex in the periphery may be trimmed to varying degrees depending on the goals of surgery, and some degree of peripheral cortex at the vitreous base invariably remains at the end of surgery. In some cases, such as rhegmatogenous retinal detachment, residual peripheral vitreous may act as a scaffold for cellular proliferation (proliferative vitreoretinopathy, or PVR); hence, meticulous removal of peripheral vitreous is warranted.

Pharmacologic Vitreous Manipulation

Several enzymatic agents have been used to alter vitreous structure in preparation for or in lieu or surgery. Hyaluronidase injected into the vitreous cavity results in vitreous liquefaction but does not cause a PVD. More recently, autologous plasmin enzyme and recombinant microplasmin (ThromboGenics Ltd., Dublin, Ireland) were shown to successfully cause vitreous liquefaction as well as complete PVD, and animal models have confirmed increased vitreous diffusion coefficients after microplasmin, consistent with reduced vitreous viscosity.

The presence or absence of attached posterior hyaloid may influence the flux of molecules across the vitreoretinal junction, either as a physical barrier or through molecular binding. In hyaluronidase-injected cat eyes (vitreous liquefaction without PVD) and in control eyes (no liquefaction and no PVD), the cortical vitreous appeared more densely compressed at the retinal surface than in microplasmin-injected eyes which demonstrated a smooth retinal surface free of cortical vitreous. Glycoproteins at the vitreoretinal interface may also bind free proteins, thereby preventing retinal penetration (**Figures 1–3**). Laminin and fibronectin are the main glycoproteins that bind vitreous collagen fibers of the posterior vitreous cortex to the ILM. The failure of tissue plasminogen activator (tPA) to penetrate the retina has been attributed to its specific binding to fibronectin, in addition to other proteins at the vitreoretinal juncture. Plasmin enzyme and microplasmin are able to hydrolyze laminin and fibronectin at the vitreoretinal junction, and studies are currently underway to determine if a microplasmin-induced PVD increases retinal penetration of tPA. A rabbit model has demonstrated that bevacizumab injected into the vitreous cavity achieves higher retinal penetration in the presence of microplasmin-induced PVD, supporting the hypothesis that attached posterior hyaloid plays a barrier role to molecular flux across the vitreoretinal border. Rapid transport of oxygen in and out of the vitreous cavity after enzymatic PVD is also consistent with this vitreoretinal barrier theory.

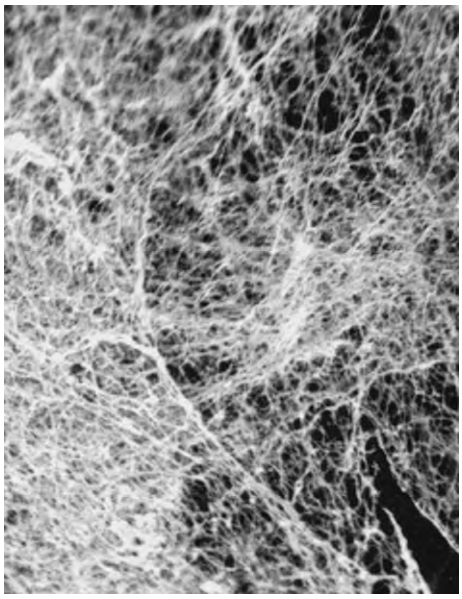

Figure 1 A scanning electron microscopy (SEM) image of the cat vitreoretinal interface demonstrates a network of cortical vitreous fibers adherent to the internal limiting membrane, consistent with the absence of a posterior vitreous detachment (PVD).

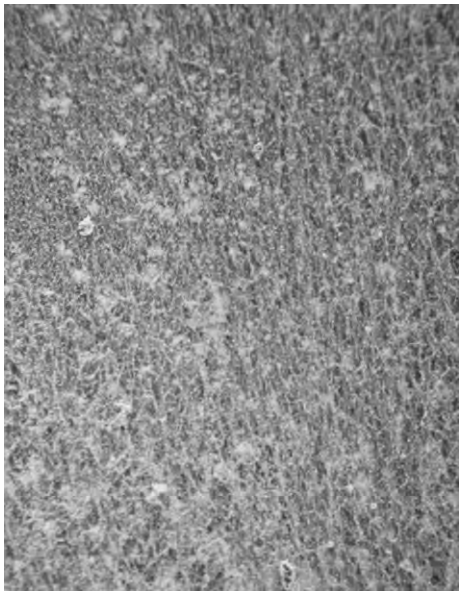

Figure 2 A scanning electron microscopy (SEM) image of the vitreoretinal interface after intravitreal injection of hyaluronidase demonstrates cortical fibers adherent to the internal limiting membrane. Hyaluronidase causes vitreous liquefaction without posterior vitreous detachment.

In adults, the utility of autologous plasmin has been demonstrated in several small series. Preoperative intravitreal injections of autologous plasmin were shown to induce PVD and increase resolution of macular edema in diabetic patients with advanced retinopathy. When used as an adjunct for macular hole repair surgery,

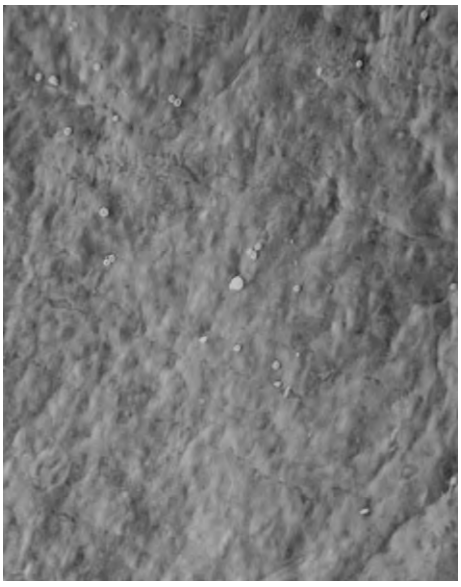

Figure 3 A scanning electron microscopy (SEM) image of the vitreoretinal interface after intravitreal injection of microplasmin demonstrates a smooth internal limiting membrane surface free of cortical vitreous, consistent with vitreous detachment. Microplasmin causes both vitreous liquefaction and posterior vitreous detachment.

autologous plasmin resulted in spontaneous PVD and reduced surgical time. In primary vitrectomy in the pediatric population, autologous plasmin allows for PVD creation and more complete vitreous removal. Microplasmin, a recombinant plasmin enzyme, is undergoing human clinical trials in both the United States and Europe.

Tractional Release During Vitrectomy

Vitrectomy may relieve traction on the neurosensory retina and consequently allow partial or complete restoration of normal retinal architecture in tractional disorders. Vitreous traction on the neurosensory retina is directly implicated in certain disease states such vitreomacular traction (VMT), a subset of diabetic macular edema, and macular hole formation.

During vitrectomy for conditions involving vitreoretinal traction, the ILM is often mechanically removed. The ILM is the innermost layer of the neurosensory retina, and adhesions between the ILM and vitreous cortex exist in normal eyes. Of importance during surgery, ILM adherence to underlying retinal structures is heterogeneous. Adhesions between the ILM and nerve fiber layer (NFL) are firm outside of the macula but much weaker within the macula due to attachment plaque distribution. Visually significant vitreoretinal traction occurs within the macula, where the ILM can be safely peeled due to weaker NFL adhesions. Peeling of the ILM becomes risky outside of the macula because strong NFL adhesions increase the risk of a retinal tear.

Cataract Formation after Vitrectomy

The incidence of visually significant cataract increases following vitrectomy, likely due to altered physiology of the rentrolenticular environment both during and after surgery. The human lens exists in a relatively hypoxic environment, and normal oxygen gradients within the vitreous cavity are lost when the vitreous is removed and replaced with fluid.

The infusate during vitrectomy surgery (most commonly a balanced salt solution, or BSS) contains oxygen at ten times the tension of oxygen in normal vitreous. Oxygen tension within the vitreous cavity remains elevated months after surgery compared to normal values, and the lens is therefore exposed to elevated oxygen tensions both during and after vitrectomy.

Other Molecular Changes after Vitrectomy

The flow of molecules within the vitreous cavity changes significantly after vitrectomy. The viscosity of aqueous humor or BSS is several 100-fold lower than that of vitreous gel. Consequently, the diffusion of oxygen, cytokines, and other molecules increases greatly when the vitreous gel is replaced by fluid. After vitrectomy, oxygen may circulate more freely from well-oxygenated retina to hypoxic retina, thereby decreasing the stimulus for vascular endothelial growth factor (VEGF) production. Furthermore, vitrectomy allows the diffusion of growth and permeability factors away from the retinal surface, likely reducing their stimulus on the sensory retina.

In certain pathologic states, such as retinal neovascularization in diabetes, vitreous oxygen tension is elevated in the immediate vicinity of the neovascularization. Immediately following vitrectomy, this local oxygen gradient dissipates, presumably due to high rates of diffusion in liquid compared to vitreous.

While increased diffusion within the vitreous cavity may alter oxygen circulation, the specific presence of a PVD appears to increase baseline oxygen tension within the vitreous cavity. When vitreous liquefaction was induced using hyaluronidase in an animal model, no PVD occurred and vitreous oxygen tension remained unchanged. When microplasmin was injected, causing both vitreolysis and spontaneous PVD, oxygen tension increased. This result might be explained by posterior vitreous cortex and the hyaloid face acting to reduce oxygen diffusion from the retinal circulation into the vitreous cavity, but the precise mechanism is not known.

Several vitreoretinal diseases are characterized by the presence of proinflammatory and angiogenic cytokines. Both VEGF and angiopoietin 2 are elevated in the vitreous in patients with proliferative diabetic retinopathy, and this elevation seems to be independent of PVD status. VEGF levels remain elevated immediately after vitrectomy, suggesting that changes in intravitreal VEGF following vitrectomy may occur due to flow and circulation of various factors rather than absence of vitreous alone.

Reactive oxygen species are elevated in the vitreous of patients with diabetic retinopathy. Oxidative stress, resulting from reactive oxygen species, may play a role in pathogenesis and correlate with severity of retinal microangiopathies such as diabetes, and it is not known if levels of reactive species change following vitrectomy.

When vitrectomy is combined with lensectomy, the eye effectively becomes unicameral, with oxygen tensions equalizing between the anterior and posterior segments. The anterior-chamber oxygen tension decreases from approximately 30 to 20 mmHg, while the posterior-segment oxygen tension remains near 20 mmHg. This equilibration may explain the increased rate of iris neovascularization seen following vitrectomy and lensectomy.

Chromovitrectomy

A variety of dyes may be used during vitrectomy in order to facilitate identification and removal of the vitreous, epiretinal membranes, or ILM. The most commonly used chromovitrectomy agents include indocyanine green (ICG), trypan blue, and triamcinolone acetonide.

ICG demonstrates a high affinity for the ILM and is therefore used during vitrectomy to identify and peel the ILM. ICG stains epiretinal membranes relatively poorly compared to other agents. At high doses, intraocular injections of ICG may cause retinal ganglion cell apoptosis, and subretinal injections in rats result in toxicity to the retinal pigment epithelium (RPE). During vitrectomy, however, small amounts of ICG are delivered in proximity to the macula for a brief period of time before removal, thereby limiting retinal exposure and potential toxicity. ICG may be delivered as a thin solution or as thicker solution when mixed with glucose. Experimental evidence for retinal toxicity at doses used during surgery is variable and inconclusive.

Trypan blue stains dead tissues and cells and is used during vitrectomy to selectively stain epiretinal membranes. As with ICG, experimental studies of retinal toxicity have yielded variable results.

Triamcinolone acetonide, a synthetic steroid used clinically for its anti-inflammatory effects, may be used during vitrectomy to help visualize vitreous. Triamcinolone is available in a preserved form as well as in a preservative-free form. The preserved form contains particles which may settle during surgery and help delineate epiretinal membranes, but the benzyl alcohol vehicle may have toxic effects. Toxicity concerns are relatively minor, as intraocular injections are tolerated well at high doses and subretinal injections have not shown significant toxicity to the retina or RPE.

Vitreous Replacements

During vitrectomy, the vitreous cavity may be filled with a variety of substances other than the default infusate, BSS. Some substances, such as perfluorinated liquids, are used temporarily, while others such as air, gas, and silicone oil may be left in the eye at the end of surgery.

Air is nonexpansile and absorbs within 1 week after surgery. Patients may be positioned postoperatively so that the air bubble tamponades a particular region such as the macula or an area of retinal detachment. Air is nontoxic to the retina but may prevent retinal reattachment if migration into the subretinal space occurs through a retinal break.

The most common gases used as vitreous replacements are sulfur hexafluoride (SF_6) and perfluoropropane (C_3F_8). SF_6 expands to double its original volume over a period of 24–78 h and absorbs over a period of roughly 2 weeks. C_3F_8 expands to 4 times its original volume over a period of 72–96 h and absorbs over a period of roughly 6 weeks when used at a nondiluted concentration. Nonexpansile concentrations may be used if volume expansion is not desired in the immediate postoperative period. As with air, patients may be positioned postoperatively in order to tamponade retinal breaks.

Silicone oil is generally used as a vitreous replacement in more complex surgeries such as repair of diabetic tractional retinal detachments or retinal detachments with PVR. Silicone oil does not change in volume and is not absorbed over time. The oil may be removed at the surgeon's discretion or left in place indefinitely in the absence of complications such as band keratopathy, elevated intraocular pressure (IOP), or cataract. Available *in vitro* evidence suggests that silicone oil has intrinsic antimicrobial effects with respect to causative agents of endophthalmitis. Silicone oil has a refractive index of 1.40, resulting in a hyperopic shift in the phakic patient, but this can be corrected with appropriate refraction. By comparison, useful refraction is not easily achievable in gas-filled eyes.

Silicone oil has a higher viscosity and lower specific gravity than saline. The lower specific gravity causes the oil to float within saline or aqueous. As oil is immiscible in water, surface tension is created at the interface, although less so than between gas and saline. The surface tension allows silicone oil to exert a tamponade effect on the

retina. Viscosity varies and the two main viscosities used are 1000 and 5000 centistoke. Lower viscosity is used more widely in the United States due to availability but is thought to have a higher rate of emulsification. Emulsification occurs when small droplets break off from the main oil bubble. The smaller droplets may travel into the anterior chamber, particularly in aphakic or pseudophakic patients. Silicone oil in the anterior chamber may be visible at the slit lamp as an inverted clear hypopion but is not necessarily clinically detectable. IOP may rise if oil enters the angle and prevents normal function of the trabecular meshwork. The degree of IOP elevation is proportional to the amount of emulsified oil in the anterior chamber. Elevated IOP in oil-filled eyes may also occur due to pupillary block or lens–iris diaphragm shift related to choroidal effusion.

There is some evidence that silicone oil in the vitreous cavity blocks diffusion of oxygen out of the anterior chamber into the posterior segment, thereby increasing anterior segment oxygen tension. This may help to explain why rates of iris neovascularization are reduced in eyes filled with silicone oil. Within the posterior segment, proteins and cytokine concentrations appear to be concentrated within the remaining fluid that bathes the oil bubble.

Perfluorocarbon (PFO) heavy liquids are sometimes used as a temporary vitreous substitute during vitreoretinal surgery. There is some evidence in animal models that because of greater oxygen solubility in PFO compared to BSS, eyes filled with PFO are less susceptible to ischemic retinal damage than eyes filled with BSS. PFO liquid has been safely used as a short-term postoperative tamponade after vitrectomy for retinal detachment, but animal data suggest retinal toxicity with long-term intravitreal use.

Sclerotomy Sites after Vitrectomy

During vitrectomy, instruments are inserted into the vitreous cavity through sclerotomy incisions. Incisions for traditional 20-gauge surgery are created using a sharp blade, after which instruments are inserted and removed through the wounds. Sclerotomies for small-gauge surgery are frequently created using trocars. The trocar is removed, leaving a cannula through which surgical instruments are inserted and removed for the duration of surgery, thereby minimizing trauma to the wound edges. At the end of surgery, sclerotomies are traditionally sutured after 20-gauge procedures and left sutureless after small-gauge surgery unless leakage is detected. Scleral wounds do not regain normal architecture postoperatively. In 20-gauge surgery, when sutures support wound closure integrity, wound gape may still occur. In sutureless surgery, a 5% rate of hypotony on the first postoperative day emphasizes the variable integrity of wound closure. Fibrovascular proliferation occurs at 10–15% of sclerotomy sites, and postoperative vitreous hemorrhage is more difficult to treat when associated with fibrovascular proliferation. In addition, trauma and traction on retinal tissue around sclerotomy sites may result in retinal breaks in both the early and late postoperative periods.

See also: Hyalocytes; Molecular Composition of the Vitreous and Aging Changes; Pharmacological Vitreolysis; Vitreous Anatomy, Aging, and Anomalous Posterior Vitreous Detachment.

Further Reading

Balazs, E. A. (1973). Fine structure and function of ocular tissues. The vitreous. *International Ophthalmology Clinics* 13: 169–187.

Gandorfer, A., Messmer, E. M., Ulbig, M. W., and Kampik, A. (2000). Resolution of diabetic macular edema after surgical removal of the posterior hyaloid and the inner limiting membrane. *Retina* 20: 126–133.

Goldenberg, D. T. and Trese, M. T. (1998). Pharmacologic vitreodynamics: What is it? Why is it important? *Expert Review of Ophthalmology* 3: 273–277.

Holekamp, N. M., Shui, Y. B., and Beebe, D. C. (2005). Vitrectomy surgery increases oxygen exposure to the lens: A possible mechanism for nuclear cataract formation. *American Journal of Ophthalmology* 139: 302–310.

Saxena, S. and Gopal, L. (1996). Fluid vitreous substitutes in vitreo retinal surgery. *Indian Journal of Ophthalmology* 44: 191–206.

Sebag, J. (1998). Macromolecular structure of vitreous. *Progress in Polymer Science* 23: 415–446.

Stefansson, E. (2006). Ocular oxygenation and the treatment of diabetic retinopathy. *Survey of Ophthalmology* 51: 364–380.

Trese, M. T. (2000). Enzymatic vitreous surgery. *Seminars in Ophthalmology* 15: 116–121.

Williams, J. G., Trese, M. T., Williams, G. A., and Hartzer, M. K. (2001). Autologous plasmin enzyme in the surgical management of diabetic retinopathy. *Ophthalmology* 108: 1902–1905.

The Role of Acetylcholine and its Receptors in Retinal Processing

K T Keyser, V E Wotring and C E Strang, The University of Alabama at Birmingham, Birmingham, AL, USA

Glossary

Acetylcholine – A neurotransmitter ($C_7H_{17}NO_3$) released at autonomic and central nervous system synapses and neuromuscular junctions; it is synthesized from choline.
Agonist – A ligand or a drug that binds to and activates a specific receptor.
Antagonist – A ligand or a drug that opposes the action of an agonist by interacting with the receptor.
Ligand-gated ion channel – A membrane-spanning ion channel that is opened by the binding of a specific ligand, typically a neurotransmitter at a chemical synapse.
Nicotinic acetylcholine receptor – A neurotransmitter receptor comprising five subunits that contain a cation channel. The channel can be opened by the binding of acetylcholine, nicotine, and other substances to the receptor. These receptors are found at neuromuscular junctions, and at autonomic and central nervous system synapses.

Introduction

Studies in the 1970s revealed that acetylcholine (ACh) in the retina is synthesized in and released from two populations of amacrine cells. A population in the ganglion cell layer (GCL) releases ACh in response to light onset, and another population in the inner nuclear layer (INL) releases ACh in response to light offset. These amacrine cells are frequently referred to as starburst amacrine cells because of their distinctive morphology. The enzyme responsible for ACh synthesis is choline acetyltransferase (ChAT) and ChAT immunoreactivity is apparent in the starburst cells and their dendrites that narrowly ramify in the ON and OFF sublamina of the inner plexiform layer (IPL) in mammalian and nonmammalian retinas (Figure 1).

Under voltage clamp, starburst cells respond to light with slow graded currents, and release both ACh and γ-aminobutyric acid (GABA) in response to K^+ depolarization. While the tonic and light-evoked release of ACh by the starburst cells is commonly accepted as the only source of ACh in the retina, ChAT immunoreactivity has been reported in the A6 amacrine cell of the ground squirrel, a cell type that stratifies in the OFF sublamina of the IPL, and an alternative ChAT splice variant (pChAT), detected in the rat peripheral nervous system, has been reported to be expressed by retinal ganglion cells (GCs). The pChAT enzyme appears to be involved in the synthesis of ACh for release at retinorecipient sites, as it can only be detected in GCs when retinofugal axonal transport is blocked.

Physiological studies have shown that the activation of nicotinic acetylcholine receptors (nAChRs) by nicotine, choline, or ACh can have profound effects on the response properties of many GCs (including those that display directional selectivity) and on subpopulations of transient and sustained GCs. This article provides an overview of our current understanding of the expression of nAChRs in the retina and the functional consequences of nAChR activation.

nAChRs Receptors

Neuronal nicotinic acetylcholine receptors are ligand-gated, mixed cation channels that belong to the ligand-gated ion channel (LGIC) superfamily, which includes $GABA_A$, glycine, and 5-hydroxytryptophan-3 (5-HT3) receptors. Complementary DNAs (cDNAs) encoding nine α subunits (α2–α10) and three β subunits (β2–β4) of neuronal nAChRs have been cloned. In the vertebrate nervous system, nAChRs composed of α7, α8, α9, or α10 subunits exist either as homomers, in combination with each other (for α7 and α8), or with other as yet-unidentified subunits. The α subunits for these receptors contain both principal and complementary binding components. They form receptors that bind, and are blocked by, alpha bungarotoxin (αBgt), a high-affinity competitive antagonist from the venom of the banded krait.

Heteromeric nAChRs are composed of combinations of subunits α2–α6 assembled with subunits β2–β4 and are αBgt-insensitive. The α subunits carry the principal component for agonist binding, while the non-α-subunits have the complementary component. Agonist binding occurs at the interfaces of the α and β subunits. The known subunits in different combinations can theoretically yield a vast number of different receptor complexes. Studies in expression systems show that nAChRs with different subunit compositions differ in their ligand-binding affinities and in their physiological characteristics. Subunit composition also confers channel properties such as open times and desensitization rate.

nAChR Subunits in the Vertebrate Retina

Neuronal nAChR subunits are expressed in the retinas of many vertebrate species, although there are species differences. For example, nAChR subunits α2–α7 and β2–β4, but not α8,are present in mammalian retina. There are indications that α9 and α10 subunits, first discovered in the auditory system, may be expressed in retina; however, this is yet to be definitively demonstrated.

While α7 subunits are almost certainly assembled into the homomeric α7 nAChR subtype in the mammalian retina, or the α7α8 subtype in avian retinas, the determination of the subunit composition of heteromeric nAChRs has proven to be more difficult. Biochemical studies and labeling experiments using rodent, rabbit, and chick retinas have demonstrated the expression of simple heteromeric subtypes, including α2β2, α3β2, α3β4, α4β2, and α6β2 nAChRs. There are also indications that more complex heteromeric nAChRs are expressed, including α2α4β2, α6α3β4, or α6β2β3 subtypes. In addition, the expression levels of some nAChR subtypes are developmentally regulated, suggesting that the functional requirements for nAChRs change throughout development.

In order to understand the functional consequences of nAChR expression in the retina, considerable effort has been directed toward understanding the distribution of nAChRs in specific retinal circuits. The following two sections describe nAChR localization as revealed by methods, including radiolabeling, ligand-binding, immunohistochemistry, and *in situ* hybridization. While these studies were able reveal the expression patterns of one or more nAChR subunits, they do not provide information about the subunit composition of the assembled receptors.

Distribution of αBgt-Sensitive nAChRs

Radiolabeled or fluorescently labeled αBgt has been used to determine the localization of homomeric nAChRs. In live cells, αBgt binds only to receptors inserted on the cell surface. Thus, while αBgt binding is indicative of functional receptor expression, it has less utility in the determination of expression by specific cell types since binding is predominantly limited to the synaptic layers of the retina.

αBgt-sensitive nAChRs have been detected in the outer plexiform layer (OPL) of amphibian and avian species, while αBgt binding is broadly distributed throughout the IPL in both mammalian and nonmammalian tissue. The distribution in the IPL is more extensive than the narrow bands of ChAT immunoreactivity, suggesting the expression of nAChRs at a distance from the sites of ACh release.

As αBgt binding does not discriminate among the homomeric nAChR subtypes, specific antibodies have been used by themselves or in concert with αBgt binding to determine the expression patterns of αBgt-sensitive subunit expression.

In chick retina, α7, α8, and α7α8 nAChRs are widely expressed in subpopulations of amacrine and GCs, while a subpopulation of bipolar cells expresses α8-containing nAChRs. Immunohistochemical studies in rabbit retina have identified amacrine, ganglion, and three separate populations of ON bipolar cells that express α7 nAChRs (**Figure 2**). These include calbindin- and glycine-positive bipolar cells. The third bipolar cell type is neither calbindin nor glycine immunoreactive. Subpopulations of GABAergic and glycinergic amacrine cells and subpopulations of GCs also exhibit immunoreactivity to antibodies against the α7 subunit. The α7 immunoreactivity within the IPL closely correlates with concurrent fluorescent αBgt binding, supporting the specificity of the immunoreactivity.

The identification of expression patterns of α7 nAChRs by immunohistochemistry has been more problematic in

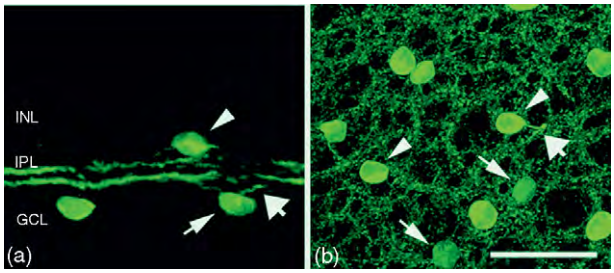

Figure 1 Choline acetyltransferase (ChAT) immunoreactivity in rabbit retina. (a) Vertical section through rabbit retina and (b) horizontal view of whole-mount rabbit retina demonstrate that two populations of amacrine cells are immunoreactive to antibodies against ChAT. The somas of the first population are located in the INL (arrowheads) with processes (arrowheads) descending to the OFF sublamina of the IPL. The second population consists of immunoreactive cells with somas in the GCL (arrows) and processes (broad arrows) ascending to the ON sublamina of the IPL.

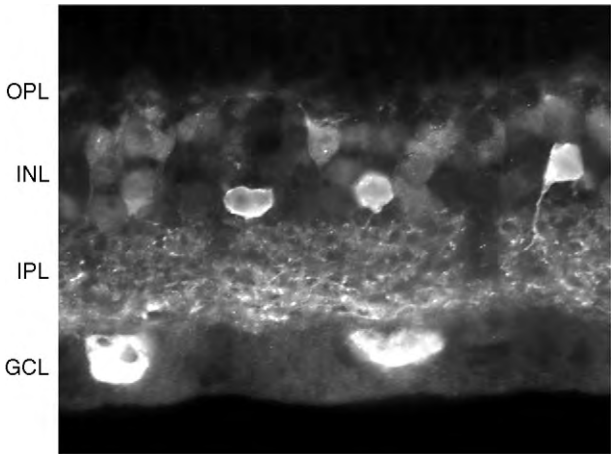

Figure 2 Expression of α7 nAChRs in rabbit retina. Immunoreactivity to an antibody generated against the α7 subunit demonstrates that α7 nAChRs are expressed by bipolar cells, amacrine cells, and ganglion cells. Labeling is distributed throughout the IPL, but is more intense in the ON sublamina (below, near ganglion cells). This may be accounted for by the populations of ON bipolar cells that express the α7 receptor.

the mouse retina. Studies using α7 knock-out mice have called into question the specificity of commonly used antibodies made against the α7 nAChR subunit. In some studies using homozygous α7 knock-out mouse tissue, there is residual anti-α7 antibody labeling in selected nonretinal parts of the brain. The residual immunoreactivity may be due to a lack of specificity, in that the antibodies also recognize an epitope on the α9 or α10 subunit or some other tissue constituent. Alternatively, in the case of a knock-out that has been generated by exon deletion, truncated nonfunctional proteins that contain the antibody-binding epitope may continue to be transcribed.

αBgt-Insensitive nAChR Expression in the Retina

Multiple αBgt-insensitive nAChR subtypes are widely expressed in the vertebrate retina. For example, in the chick, nAChRs that include β2, α3, or α5 subunits are expressed by amacrine and GCs, with the highest density of nAChR-expressing GCs in central retina. The α3β2 nAChR subtype is thought to be a major subtype, although binding and immunoprecipitation experiments have confirmed the presence of α4β4 and α6β4 nAChRs.

Heteromeric αBgt-insensitive nAChRs are also expressed in the mammalian retina and are distributed across much of the IPL, with bands of denser labeling overlapping the dendrites of the starburst cells (Figure 3). In rabbit retina, at least 60% of GCs in the visual streak display immunoreactivity to antibodies against the α3 subunit, as do many amacrine cells.

Most of the α3 subunit protein extracted from the rabbit retina can be co-precipitated with a specific β2 antibody, demonstrating co-assembly. However, a small but significant fraction of the α3 protein is not co-assembled with the β2 subunit, suggesting that there are nAChRs containing α3 and an alternative β subunit, perhaps the β4 subunit. The β4 subunit has been localized in the ground squirrel retina by immunohistochemistry and *in situ* hybridization in medium- to large-bodied GCs in the GCL, as well as in the INL and IPL. The β4 subunit gene is clustered with the α3 subunit gene, and both genes are expressed by amacrine and GCs in the developing rat retina. Co-localization with antibodies against glycine and GABA demonstrate that nAChRs are expressed by most glycinergic amacrine cells and by subsets of GABAergic amacrine cells in the rabbit retina. Interestingly, a small but variable fraction of starburst amacrine cells have been reported to express nAChRs.

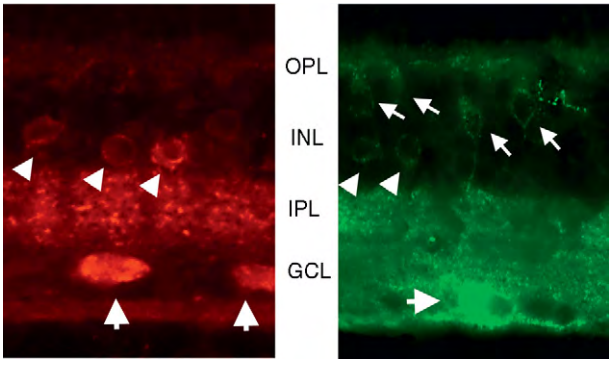

Figure 3 Distribution of heteromeric non-α7 nAChRs in rabbit (left) and mouse (right) retina. Amacrine (arrowheads) and ganglion cells (large arrows) of both species are immunoreactive to mAb210, and immunoreactivity is distributed throughout the IPL. However, bipolar cells (small arrows) are immunoreactive in mouse, but not rabbit retina. OPL, outer plexiform layer; INL, inner nuclear layer; IPL, inner plexiform layer; GCL, ganglion cell layer.

In the rat retina, *in situ* hybridization studies detected transcripts for the α2–α6 and β2–β3 nAChR subunits in the INL and GCL. The distribution of α4 and β3 subunit transcripts is relatively the same between the INL and GCL, transcripts for the α5 subunit are more abundant in the INL than in the GCL, and the α2 subunit appears restricted to the INL. Transcripts for α3, α6, and β3 are distributed more strongly in the GCL relative to the INL.

In summary, nAChRs are localized predominantly in the inner retina of mammalian and nonmammalian species, although nAChRs have also been identified in the outer retina of nonmammalian species. In all species studied to date, nAChRs are expressed by subsets of bipolar, amacrine, and GCs; the distribution in the IPL is not restricted to the sublaminae containing starburst cell processes. Thus, while the identity of the particular receptor subtypes may vary, the commonalities in overall expression indicate that ACh exerts its effects via the activation of nAChRs expressed by many cells in diverse inner retinal circuits. That ACh may be able to act at a distance in the retina is supported by electrophysiological data. For example, subsets of rabbit αGCs respond to the application of nicotine and/or choline but do not co-stratify with cholinergic dendrites. Additionally, subsets of cholinoceptive amacrine and GCs express more than one nAChR subtype. Expression by inhibitory amacrine cells suggests that ACh may influence the overall excitability of the retina as well as modulate GC responses. Thus, the nAChR distribution suggests that ACh has the potential to exert complex effects on retinal responses.

nAChR Pharmacology

Pharmacological agents are widely used for identification of the receptor subtypes involved in nicotinic responses. While the crystal structure and mechanistic details of the interactions of ligands with nAChRs are increasingly being well understood, many of the agents available fail to exhibit ideally discriminative properties. However,

important information can be gained from pharmacology experiments, providing that caution is exercised in experimental design and interpretation of results.

Agonists

The endogenous agonist of all known nAChRs is ACh, although there is evidence that choline may act as an agonist at α7 and α9 subtypes. While many exogenous compounds are effective agonists, none of them exhibits strong selectivity, so the rank order of agonist potency has long been used as a tool for the determination of receptor subtype. Several of the commonly used nicotinic agonists are structurally similar which may, at least partially, explain their lack of specificity. All of those discussed below appear to interact with elements of the acetylcholine-binding site.

Nicotine

Nicotine is the agonist for which the entire class of nicotinic acetylcholine receptors is named and was originally isolated from tobacco leaves. It is not broken down by the enzyme acetylcholinesterase, which makes it a useful drug in preparations with active enzymes. It is a potent agonist of the heteromeric (α3-, α4-, α6-containing) αBgt-insensitive nAChR subtypes and of α8-containing receptors, while it is somewhat less effective at α7 homomeric nAChRs.

Carbamylcholine

Carbamylcholine or carbachol is an esterified form of choline that activates both nicotinic and muscarinic acetylcholine receptors. It is not metabolized by acetylcholinesterase, which makes it a useful drug *in vivo* or *ex vivo*. In the retina, α4-containing nAChRs would be most affected, while there would be somewhat less activity at α7-containing receptors. It also activates muscarinic AChRs, which greatly limits its experimental utility.

Cytisine

Cytisine is a plant alkaloid that is most active at α8 nAChRs, followed by α3-, α6-, and some α4-containing receptors. It may be less effective at α7.

Epibatidine

Epibatidine was originally isolated from the poison dart frog *Epipedobates* sp. and was first investigated as a potential analgesic. It is now used as an exquisitely sensitive (effective in the pM range) nAChR ligand in binding assays. Epibatidine is the most potent agonist at α3-, α4-, and some α6-containing receptors, but is not very effective at αBgt-sensitive receptors. However, it has been recently reported to bind 5-HT3 receptors, which could confound results in preparations where serotonin receptors may be expressed.

Choline

Choline is transported into cells through a high-affinity transporter and subsequently made into acetylcholine. It is not an effective agonist of any heteromeric retinal nAChR subtypes, but it is nearly as effective as ACh at α7 nAChRs. Choline sensitivity is frequently used as one indication of α7 receptors; however, choline is also an effective agonist at muscarinic AChRs, and a subtype-specific antagonist must be used to confirm α7 expression.

Antagonists

d-Tubocurarine (Curare)

This was the first antagonist used in experiments at the neuromuscular junction, and has been used in neuronal preparations as well. It acts through a competitive mechanism and blocks all nAChR subtypes with little specificity. It has also been shown to block $GABA_A$, glycine, and 5-HT3 receptors and some potassium channels. With such a wide range of activities, d-tubocurarine is of limited utility.

Dihydro-β-erythroidine

Dihydro-β-erythroidine (DHβE) is another plant-derived competitive antagonist of heteromeric nicotinic receptors. It is somewhat more effective at α4- and β2-containing receptors than at those containing α3 and is much less effective at α7 nAChRs. Its reversibility and specificity make DHβE an experimentally useful drug.

Hexamethonium and mecamylamine

These are classical blockers of autonomic ganglia nAChRs. They are used to block central nAChRs and also act through noncompetitive mechanisms, probably by occluding the channel pore. Blockade may be voltage dependent, which is an important caveat in electrophysiology experiments. They are considered nonselective among nAChR subtypes, although hexamethonium is somewhat more effective at receptors containing α3 or α6. Both require ~10-fold higher concentrations to block α7 nAChRs and are reversible as well; there is no evidence that either interacts with other LGICs. These facts, coupled with relatively low cost, make these drugs experimentally attractive blockers of nAChRs.

α-Bungarotoxin (α-Bgt)

The bungarotoxins are components of venom from the banded krait (*Bungarus multicinctus* and other species). αBgt binds homomeric α7–α9 receptors with high affinity and slow kinetics and is the ideal ligand for these receptor subtypes. The binding is of such high affinity, however, that it is essentially irreversible. There is a report that αBgt also binds β3-containing heteromeric $GABA_A$ receptors. This GABA receptor subtype is relatively of low abundance in the rest of the brain, but care should be exercised in retinal preparations.

α-Conotoxins

Among the many components of cone snail (family: Conidae) venom are the α-conotoxins. α-Conotoxin IMI is a

competitive antagonist of α7 at ~100 nM, and of α9 at 10-fold higher concentrations. α-Conotoxin AuIB is fairly specific for α3-containing nAChRs, and also acts through a competitive mechanism. α-Conotoxin MII competitively blocks α6-containing nAchRs.

Methyllycaconitine (MLA)

Methyllycaconitine is an antagonist of α6-, α7-, α8-, and possibly α9-, and α10-containing nAChRs at nM concentrations, but is nonspecific at μM concentrations.

While the pharmacology of nAChRs is clearly complex, the situation is made even more difficult by the nonselective effects of agonists and antagonists used in the study of other LGICs. The classical $GABA_A$ antagonist, picrotoxin, has been shown to block α3β4 and α7 nAChR subtypes with IC_{50} values of 96.1 ± 5.5 and 194.9 ± 19.2 μM, respectively. It also blocks glycine receptors and 5-HT3 receptors at ~30 μM. The cross-reactivity among LGICs has yielded interesting information about picrotoxin's mechanism and highlights the similarity among members of the picrotoxin family, but renders picrotoxin of limited use. Another commonly used $GABA_A$ antagonist, bicuculline, also inhibits nAChRs while gabazine seems to be a more specific antagonist, and should probably be used in lieu of picrotoxin or bicuculline.

Another example of a nonspecific LGIC antagonist is strychnine, which has been employed by physiologists to study the contribution of glycine receptors to retinal information processing. Unfortunately, strychnine is also a competitive antagonist of α7–α10 at ~1 μM. It also blocks heteromeric nAChRs at about 10-fold higher concentrations.

Atropine is often used at a concentration of 0.5–1 μM to block activity mediated by muscarinic acetylcholine receptors. It has also been found to block α3- and α7-containing nAChRs while potentiating those containing α4 subunits.

nAChR Function in the Retina

Physiological studies in the retina demonstrate that effects of cholinergic agents applied to the retina are complex. In rhesus monkey, the pattern electroretinogram (ERG) is enhanced by the ACh precursor L-α-glycerylphosphorylcholine. In cat, the application of ACh first enhances and then inhibits the ERG b-wave, an indicator of bipolar cell activation. These effects are attenuated by both nicotinic and muscarinic antagonists. The effects of ACh are more pronounced on the cone-driven ERG than on the rod-driven ERG, which is consistent with a report of α7 nAChR expression by cone, but not by rod bipolar cells in the rabbit retina. The subsequent inhibition of the b-wave may be due to either the desensitization of α7 nAChRs, or the expression of multiple types of AChRs, including muscarinic AChRs. In contrast to the cat, the frog ERG b-wave is inhibited by ACh, possibly through a cholinergic–glycinergic feedback loop onto the bipolar cells, or through activation of nAChRs on horizontal cells.

While *in vivo* ERG measurements provide important information about global or population responses to cholinergic agents, *in vitro* techniques have been used to explore the effects of nAChR activation on the responses of specific retinal cell types. For example, the application of ACh to isolated cat retina increases the responses of certain transient GCs, decreases the spontaneous firing of sustained ON cells with high background rates, and increases the spontaneous rate of sustained OFF cells with low background rates. It has been reported that, in some preparations, every GC tested responded to cholinergic agents. In the rabbit retina, ACh increases the activity of brisk GCs and ON-sluggish GCs. Brisk ON and OFF wide-field GCs are also affected by nicotinic agonists but are less sensitive.

In carp and rabbit, the effects of exogenously applied cholinergic ligands on many GCs persist after blockade of synaptic transmission, demonstrating the activation of nAChRs on the cells' surfaces. ACh application decreases a tonic inward current in dissociated rat GCs, and gates inwardly, rectifying cation channels in GCs dissociated from cat retina and in retinal slice preparations. Nicotine application also increases intracellular free calcium in many different GC classes, an effect that may be due in part to the activation of α7 nAChRs. These receptors are not very specific cation channels and sufficient Ca^{2+} can enter through them to regulate calcium-dependent events such as the activation of signal transduction pathways, including those mediating neuroprotection from glutamate excitoxicity. nAChR-mediated depolarization can also activate voltage-gated calcium channels providing an additional avenue for the initiation of calcium-dependent events.

There is evidence that the effects of cholinergic agonists on GCs are mediated by multiple nAChR subtypes. Evidence for α7 nAChRs includes blockade by MLA of responses to semiselective α7 nAChR agonists, including choline or anatoxin-a. Functional α3β4 (choline-sensitive; MLA-insensitive), and α4β4 and/or α3β2 (DHβE, nicotine-sensitive, MLA-insensitive) subtypes have also been identified.

The effects of cholinergic agents on retinal light responses appear to be mediated through multiple cell types. While there are limited data concerning the function of nAChR subtypes expressed by cells in the INL, nAChR-mediated depolarization of bipolar or amacrine cells can enhance or reduce the effects of activation of nAChRs expressed by GCs. These interactions have the potential to modulate complex operations in the retina, including GC center-surround receptive field organization, as well as directional selectivity.

Directional Selectivity

Directionally selective GCs (DS GCs) are perhaps the best-known cholinoceptive cells in the retina. The receptive fields of DS GCs are organized such that the cells respond preferentially to stimuli moving in one direction, for instance, the preferred direction, while responses to movement in the opposite, for example, the null direction, are reduced or absent. The dendrites of ON–OFF DS GCs co-stratify with those of the two populations of starburst amacrine cells. Although the details of the circuitry that underlie the DS mechanism remain uncertain, there is strong evidence that there is asymmetric inhibition of the responses to stimulus motion in the null direction. Current data suggest that, at least for simple stimuli, the asymmetry is generated by the starburst amacrine cell. Movement in the null direction results in GABA release that is thought to suppress the glutamate-mediated excitatory input from cone bipolar cells.

The role of ACh in directional selectivity is less clear. ACh contributes to, but is not required for, the preferred direction response to a moving bar or spot of light in turtle, chick, and rabbit. The cholinergic agonist dimethylphenylpiperazinium (DMPP) eliminates DS by increasing spontaneous firing to a level that masks the preferred response. Cholinergic blockade by mecamylamine decreases spontaneous firing and attenuates, but does not eliminate, preferred direction responses. Simultaneous blockade of ACh and *N*-methyl-D-aspartic acid (NMDA) receptors further attenuates the preferred response without completely abolishing DS. Interestingly, the preferred response is also attenuated by α7 nAChR-specific concentrations of MLA or α-conotoxin MII, suggesting that both αBgt-sensitive and αBgt-insensitive nAChRs are involved. In contrast to the responses to moving bars or spots, ACh is required for the DS response to a moving low spatial frequency grating in the rabbit. Curare blocks DS responses to moving gratings by decreasing the preferred response and enhancing the null response, indicating that in this case, DS is dependent on the activation of nAChRs. Application of physostygmine, an acetylcholinesterase inhibitor, also eliminates DS, presumably through saturating nAChRs. The activation of α7 nAChRs is also involved in DS responses to other complex stimuli such as moving sheets of spots and transparent motion.

nAChRs in Retinal Development

αBgt-sensitive and αBgt-insensitive nAChR expression in the retina is developmentally regulated and driven by intrinsic genetic programs as well as by visual experience. In chick retina, transcripts for structural nAChR subunits are detectable at embryonic day 6 (E6), increasing through and stabilizing after E10. In rat retina, multiple nAChR subtypes including αBgt-sensitive, α6-containing, α4-containing, and non-α6/non-α4 nAChR subtypes increase through postnatal day 21. Visual deprivation decreases the amount of α2, α6, and β3 subunits, and increases the amount of α4 and β2 subunits. Interestingly, while visual experience has effects on the expression patterns of some nAChR subtypes, the development of directional selectivity is independent of visual experience and cholinergic waves.

Spontaneous waves of activity are detectable in the GCL early in retinal development. The waves that occur during ganglion and amacrine cell synaptogenesis depend upon the activation of nAChRs, and may be involved in axon pathfinding. Retinal waves are altered in α3 or β2 nAChR knock-out mice, and projections to the LGN in β2 knock-out mice are altered. However, appropriate retinal organization and retinal projections recover after blockade of cholinergic retinal waves in non-knock-out animals. In fact, spontaneous activity in the retina recovers after conditional knock-out of ChAT eliminates retinal cholinergic activity. This evidence suggests that there are compensatory mechanisms for maintaining the integrity of the structure of the retina and the adult visual system.

Conclusions/Summary

ACh and choline exert their effects in the retina through the activation of nicotinic and muscarinic AChRs. The expression of several nAChR subtypes by neurons in diverse retinal circuits suggests that ACh and choline can affect many aspects of retinal information processing. Molecular, protein, and physiological experiments have aided in the understanding of these effects and the nAChR subtypes involved. However, our understanding of the role of nAChRs in retinal processing is based on studies that often involve pharmacological agents. Data from such studies must be interpreted with care, due to the limited specificity of currently available pharmacological agents.

See also: Information Processing: Amacrine Cells; Information Processing: Contrast Sensitivity; Information Processing: Ganglion Cells; Information Processing: Horizontal Cells; Information Processing: Retinal Adaptation; Intraretinal Circuit Formation; *Limulus* Eyes and Their Circadian Regulation; Morphology of Interneurons: Amacrine Cells; Morphology of Interneurons: Interplexiform Cells; The Role of Acetylcholine and its Receptors in Retinal Processing; Vitreous Anatomy, Aging, and Anomalous Posterior Vitreous Detachment.

Further Reading

Clementi, F., Fornasari, D., and Gotti, C. (2000). Neuronal nicotinic receptors, important new players in brain function. *European Journal of Pharmacology* 393: 3–10.

Famiglietti, E. V. (1991). Synaptic organization of starburst amacrine cells in rabbit retina: Analysis of serial thin sections by electron microscopy and graphic reconstruction. *Journal of Comparative Neurology* 309: 40–70.
Horenstein, N. A., Leonik, F. M., and Papke, R. L. (2008). Multiple pharmacophores for the selective activation of nicotinic alpha7-type acetylcholine receptors. *Molecular Pharmacology* 74(6), 1496–1511.
Keyser, K. T., MacNeil, M. A., Dmitrieva, N., et al. (2000). Amacrine, ganglion and displaced amacrine cells in the rabbit retina express nicotinic acetylcholine receptors. *Visual Neuroscience* 17: 743–752.
Lindstrom, J. M. (2000). The structures of neuronal nicotinic receptors. In Clementi, F., Fornasari, D., and Gotti, C. (eds.) *Handbook of Experimental Pharmacology,* vol. 144, pp. 101–162. Berlin: Springer.
Masland, R. H. and Raviola, E. (2000). Confronting complexity: Strategies for understanding the microcircuitry of the retina. *Annual Review of Neuroscience* 23: 249–284.
Schoepfer, R., Conroy, W. G., Whiting, P., et al. (1990). Brain alpha-bungarotoxin binding protein cDNAs and MAbs reveal subtypes of this branch of the ligand-gated ion channel gene superfamily. *Neuron* 5: 35–48.
Zhou, Z. J. and Lee, S. (2008). Synaptic physiology of direction selectivity in the retina. *Journal of Physiology* 596: 4371–4376.
Zhou, Z. J. and Zhao, D. (2000). Coordinated transitions in neurotransmitter systems for the initiation and propagation of spontaneous retinal waves. *Journal of Neuroscience* 20: 6570–6577.

Relevant Websites

http://www.nature.com – British Journal of Pharmacology.
http://www.sigmaaldrich.com – Sigma-RBI handbook of receptor classification and signal transduction, acetylcholine receptors (Nicotinic).
http://www.tocris.com – Tocris Bioscience: Scientific Literature.

The Role of Oxidative Stress in the Trabecular Meshwork

P Gonzalez, Duke University, Durham, NC, USA

Glossary

8-oxo-2,7-dihydro-2′-deoxyguanosine (oxo8dG) – One of the more than 20 DNA adducts, or pieces of DNA covalently bonded to a chemical, generated by oxidation of DNA. oxo8dG can be removed from damaged DNA through cellular processes of DNA repair involving nuclease activity. As it is relatively easy to quantify, the content of oxo8dG is the more frequently used method to evaluate oxidative damage to nucleic acids.

Free radicals – The atoms, molecules, or ions with one or more unpaired electrons on an open-shell configuration. The presence of unpaired valence-shell electrons makes them highly reactive and usually short lived.

Lipid peroxidation – The oxidative modification of lipids by a process in which reactive oxygen species steal electrons from the lipids in cell membranes. This process affects preferentially polyunsaturated fatty acids, because they contain multiple double bonds containing methylene (CH_2) groups that are particularly susceptible to interactions with reactive oxygen species.

Protein carbonylation – A terminal oxidative modification of amino acid side chains of proline, arginine, lysine, and threonine that results in the formation of glutamic semialdehyde and aminoadipic semialdehyde. Unlike oxidative modifications of proteins, such as the formation of methionine sulfoxide and cystein disulfoxide bonds, protein carbonylation is irreversible.

Reactive oxygen species (ROS) – The molecules or ions formed by the incomplete reduction of oxygen that results in the presence of unpaired valence-shell electrons. These reactive oxygen intermediates include singlet oxygen; superoxides; peroxides; hydroxyl radical; and hypochlorous acid.

Introduction

Denham Harman proposed in 1956 the free-radical theory of aging based on the similarities between the effects of ionizing radiation and aging, and the discovery that radiolysis of water generates free radicals. Harman hypothesized that endogenous oxygen-radical generation occurs *in vivo* as a by-product of enzymatic redox chemistry, and that this process contributes to cellular damage and aging. Initially, Harman's ideas did not gain much attention because the traditional thought was that free radicals were too reactive to exist in biological systems. However, the discovery of the enzyme superoxide dismutase (SOD) by McCord and Fridovich in 1969 provided compelling evidence of the generation of free radicals *in vivo*, and gave credibility to Harman's hypothesis. There is currently extensive evidence supporting the generation of free radicals in aerobic organisms. The major source of free radicals in living cells is believed to be the mitochondria. Electron transport in the respiratory chain appears to be imperfect and generates several reactive oxygen species (ROS). One-electron reduction of oxygen that takes place in the mitochondria leads to the generation of superoxide (O_2^-). Since spontaneous and enzymatic dismutation of O_2^- yields hydrogen peroxide (H_2O_2), both O_2^- and H_2O_2 are constantly generated as by-products of mitochondrial metabolism. In the presence of free transition metals, such as iron and copper, O_2^- and H_2O_2 generate the extremely reactive hydroxyl radical (^-OH), which is believed to be the species responsible for initiating most of the oxidative tissue damage. In addition to O_2^-, H_2O_2, and ^-OH, two energetically excited species of oxygen termed singlet oxygens can result from the absorption of energy (e.g., from ultraviolet light). Additional sources of free radicals *in vivo* include the beta-oxidation of fatty acids in peroxisomes, which generates H_2O_2 as a by-product, the microsomal cytochrome P-450 enzymes that metabolize xenobiotic compounds by catalyzing their univalent oxidation or reduction, and the respiratory burst of phagocytic cells that respond to pathogens with the production of a mixture of free radicals and other oxidants. The massive generation of oxidants by immune cells has led to the speculation that chronic inflammation, frequently associated with aging, may constitute a major contributing factor for oxidative damage. A variety of other enzymes are capable of generating free radicals and other oxidants, frequently in a tissue-specific manner. For instance, monoamine oxidase generates H_2O_2 in some neurons and has been implicated in the etiology of Parkinson's disease. Finally, the catalytic generation of nitric oxide by the isozymes of nitric oxide synthase, involved in some biological processes, can lead to the formation of several reactive species including the powerful oxidant peroxynitrite ($ONOO^-$).

The realization that other oxidants such as peroxides and aldehydes (that are not strictly free radicals) are also generated *in vivo* and contribute to oxidative damage in cells has led to a generalization of the free radical theory, now frequently referred to as the oxidative stress theory of aging. The current view of this theory is that cells of aerobic organisms are subjected to a chronic state of oxidative stress even under normal physiological conditions because of an imbalance between oxidant production and antioxidant defense mechanisms. This imbalance leads to a steady-state accumulation of oxidative damage in a variety of macromolecules and cellular structures, resulting in the functional alterations characteristic of the aging process and some age-related pathologies.

The concept that oxidative stress is one of the most significant determinants of the life span is currently supported by a large body of evidence from comparative studies of antioxidant defenses, ROS generation, and accumulation of oxidative damage in species with different maximum life-span potentials. It is, therefore, well accepted that oxidants are generated *in vivo* and can contribute to aging and numerous pathologies. However, until recently, the role of oxidative stress in the outflow pathway has not received much attention. Therefore, there is still relatively little evidence about how the cells of the aqueous humor (AH) outflow pathways cope with oxidative stress, the extent of oxidative damage that may occur with aging and glaucoma, and the consequences of oxidative stress in the physiology of the outflow pathways.

Antioxidant Mechanisms in the Outflow Pathways

Similar to other tissues, the conventional outflow pathway, formed by the trabecular meshwork (TM) and the Schlemm's canal (SC), has a variety of mechanisms to prevent oxidative damage by scavenging ROS as well as mechanisms to repair or replace oxidized molecules and cellular structures. Studies on enucleated calf eyes have shown the ability of the outflow pathway tissues to completely remove H_2O_2 at physiological concentrations present in the AH (25 μM). Some of the mechanisms to remove ROS studied in the TM include high concentration of reduced glutathione (GSH), as well as SOD and catalase activities. In addition, the outflow pathway may be protected against oxidative damage by the activity of other tissues that contribute to eliminate ROS in the AH that is drained out of the eye through the TM. In particular, the ciliary epithelium appears to provide a significant contribution to the elimination of ROS in the AH by releasing detoxifying enzymes such as glutathione peroxidase.

The ability of the TM and other tissues to eliminate ROS in the AH may be important in the maintenance of normal levels of outflow resistance. While exposure to H_2O_2 is known to have no direct effect on outflow facility in the normal eyes, the same treatment in eyes with the GSH-depleted TM results in a significant decrease in outflow facility. This observation suggests that, although GSH may not contribute directly to AH outflow regulation, a decrease in the ability to prevent TM H_2O_2-induced oxidative damage may result in an increase in outflow resistance.

The effectiveness of antioxidant defenses in many tissues declines during the process of normal aging as well as in certain pathologic conditions. The resultant increase in oxidative stress is believed to contribute to the functional alterations of these tissues in aging and contribute to the progression of some age-related pathologies.

Although a similar age-related decline in antioxidant protection seems likely to take place in the TM, experimental evidence is still limited to observations including the decrease of SOD activity in the TM of normal cadaver eyes.

There is, however, more information supporting a decrease of antioxidant defenses in the TM associated with glaucoma. Several studies have been conducted analyzing AH samples from glaucoma patients and nonglaucoma cataract age-matched controls. The AH of glaucoma donors has been shown to contain significantly lower levels of ascorbic acid. Perhaps more importantly, the total antioxidant redox potential (TRAP) of the AH was found to be noticeably lower than that of the nonglaucoma controls. Additional studies have been conducted in trabeculectomy specimens from patients with various stages of POAG and showed a decrease in GSH content that correlates with the stage of the disease.

Evidence of Oxidative Stress in the Outflow Pathway

Several attempts to quantify the levels of H_2O_2 and other ROS in the AH that suggest the presence of relatively high levels of H_2O_2 in the anterior chamber of the eye have been reported in the literature. However, since the direct quantification of ROS in living tissues is technically challenging because of the high instability of these molecules, the results from these studies remain controversial. Nevertheless, there is currently substantial evidence supporting the presence of oxidative stress in the TM. Most of this evidence has been provided by studying the presence of oxidation products of lipids, proteins, and nucleic acids, which constitute the main targets of ROS in living tissues. The first line of evidence is the observation that extracts from AH, TM, and SC show a significant increase in the accumulation of the primary, secondary, and end products of lipid peroxidation (diene and triene conjugates, Schiff's bases) in patients with primary open-angle glaucoma (POAG) as compared to nonglaucoma age-matched controls. This observation is potentially relevant, not only

because it supports the pathological relevance of oxidative stress in the TM, but also because such end products of lipid peroxidation are known to react with proteins to form adducts that induce protein dysfunctions and alter cellular responses. Therefore, a significant elevation of lipid peroxidation products could contribute to the functional alterations of the TM in glaucoma.

Further support for the presence of oxidative stress in the TM comes from the observation of protein oxidation in the TM: the presence and accumulation of oxidized proteins in the TM have been demonstrated by several laboratories. Reactive oxygen and nitrogen species can generate several oxidative modifications of proteins, including methionine sulfoxide, formation of free carbonyl groups, polypeptide backbone fragmentation, and cross-linking through disulfoxide bonds. An increase in methionine sulfoxide content that results from oxidation of methionine residues has been observed in the aging TM. Similarly, a significant increase in carbonyl groups, which results from terminal oxidation of amino acid residues, has been reported in primary cultures of TM cells from old donors when compared to those from young donors. Such increase in protein carbonylation appears to be associated with a decline in the ability of the proteasome to degrade proteins. This observation suggests that oxidative stress may be accompanied by a progressive loss of proteasomal function, which may contribute to the observed increase in the accumulation of oxidized proteins.

Finally, in addition to protein oxidation, there is also evidence for nucleic acid oxidation in the TM: oxidative damage of DNA results in the formation of several adducts of base and sugar groups, single- and double-strand breaks, and cross-links to other molecules. More than 20 different products are known to result from DNA oxidation. One of them, 8-oxo-2,7-dihydro-2′-deoxyguanosine (oxo8dG), is relatively easy to quantify and has been used extensively as a method to assess oxidative damage to DNA. Measurements of 8-OH-dG levels in TM specimens demonstrated a higher level of oxidative damage to the DNA in glaucoma patients compared to age- and sex-matched controls. Furthermore, this increase in 8-OH-dG correlated significantly with the severity of the disease evaluated by the degree of visual-field loss and intraocular pressure (IOP) elevation.

Additional indirect evidence of the role of oxidative stress in glaucoma is suggested by the observation that TM cells from glaucoma donors appear to exhibit a constitutive activation of a stress response. This sustained stress response has been observed in both cultured cells and tissue specimens and includes the activation of the transcription factor nuclear factor kappa B (NF-κB), the upregulation of inflammatory markers such as endothelium leukocyte adhesion molecule 1 (ELAM-1), as well a marked increase in the production of ROS by the mitochondria that is associated with decreased mitochondrial membrane potential. Upregulation of ELAM-1 has also been detected in the TM of glaucoma donors by gene-array analysis as well as in the aqueous outflow pathway of porcine eyes with induced glaucoma. The presence of inflammatory markers in the TM of glaucoma patients might be relevant to the pathogenesis of glaucoma. There is increasing evidence supporting a role for chronic inflammation as an underlying mechanism for the molecular alterations that link aging and major age-related diseases such as atherosclerosis, arthritis, osteoporosis, and cardiovascular diseases. Such chronic inflammatory response in aging tissues appears to be mediated by oxidative stress and the concomitant generation of intracellular ROS. An increase in ROS generation has been shown to activate an intracellular signaling cascade that can stimulate a chronic state of inflammation. Some of the key players involved in this process are believed to include the transcription factor NF-κB, cytokines interleukin 1 beta (IL-1b), and IL-6, and adhesion molecules such as ELAM-1. The reported upregulation of some of these markers in glaucoma supports the concept that oxidative stress may lead to chronic inflammation in the TM, which could contribute to both the aging process of the tissue and the pathologic manifestations associated with glaucoma. Experimental data in other systems suggest that the suppression of this age-related chronic inflammation helps to delay the progression of several age-related pathologies. Therefore, the observed activation of a chronic stress response in the TM deserves special attention in regard to new approaches for glaucoma therapy based on the suppression of proinflammatory mediators.

One general note of caution that has to be taken into consideration in these studies is that most glaucoma donors are treated with IOP-lowering agents that could potentially have effects on the redox status of TM. Topical AH suppressants inhibit active transport and might lead to a decrease in ascorbic acid and other protective agents in the anterior chamber of the eye. Carbonic anhydrase inhibitors could lead to acidosis and subsequent oxidative stress. Finally, although prostaglandins are likely to exert protective effects against oxidative damage, some preservatives such as benzalkonium chloride may increase oxidative stress.

Effects of Oxidative Stress on the Outflow Pathway

Despite the potential role of oxidative stress on the pathological changes of the TM during aging and glaucoma, very little experimental work has been conducted to investigate the effects of ROS on TM cells. Cultured bovine TM cells subjected to oxidative stress *in vitro* show a marked increase in the aggregation of damaged and cross-linked proteins. Short-term sublethal oxidative stress has also been demonstrated to have important effects

on the cytoskeleton and adhesive properties of TM cells. Treatment with 1 mM of H_2O_2 for 10 or 30 min significantly reduces the adhesion of TM cells to fibronectin, laminin, and collagen types I and IV. This short-term loss of cell–matrix adhesiveness is associated with increased levels of transcription factor NF-κB and NF-κB-binding activity, as well as with rearrangement of cytoskeletal structures. Although such changes are reversible, it is likely that repeated oxidative stress *in vivo* may result in a prolonged decrease in TM cell adhesion, leading to cell loss, and compromising TM integrity. Indeed, studies conducted using models of chronic oxidative stress provide evidence of a variety of permanent changes in TM cells. Incubation of TM cells at hyperoxic conditions (40% oxygen) leads to the accumulation of nondegradable material within the lysosomal compartment, which results in diminished lysosomal activity. Since the lysosomal system is responsible for the continuous turnover of cellular organelles, these results suggest that impaired lysosomal activity subsequent to chronic oxidative stress may lead to progressive failure of cellular TM function. In addition, chronic oxidative stress induced by repeated treatment with sublethal doses of H_2O_2 has been shown to increase the endogenous production of ROS by the mitochondria in TM cells, which in turn induces a sustained stress response characterized by activation of NF-κB and expression of inflammatory markers. Such endogenous production of ROS by TM cells resulting from chronic oxidative stress could potentially contribute to the pathogenesis of the TM by inducing the expression of inflammatory mediators previously observed in the TM of glaucoma donors and by increasing the levels of oxidative damage in the tissue. Interestingly, such increase in the endogenous generation of ROS and the subsequent upregulation of inflammatory mediators induced by chronic oxidative stress can be prevented *in vitro* by the naturally occurring polyphenol resveratrol, suggesting that it may be possible to develop effective therapeutic strategies aimed at delaying some of the alterations induced by oxidative stress in the cells of the outflow pathway (**Figure 1**).

Conclusions and Future Perspectives

A growing body of experimental evidence supports the concept that oxidative damage accumulates in the cells of the TM with aging and in glaucoma. However, the extent of the contribution of oxidative damage to the pathogenesis of the TM in glaucoma and the specific mechanisms by which it may contribute to an increase in AH outflow

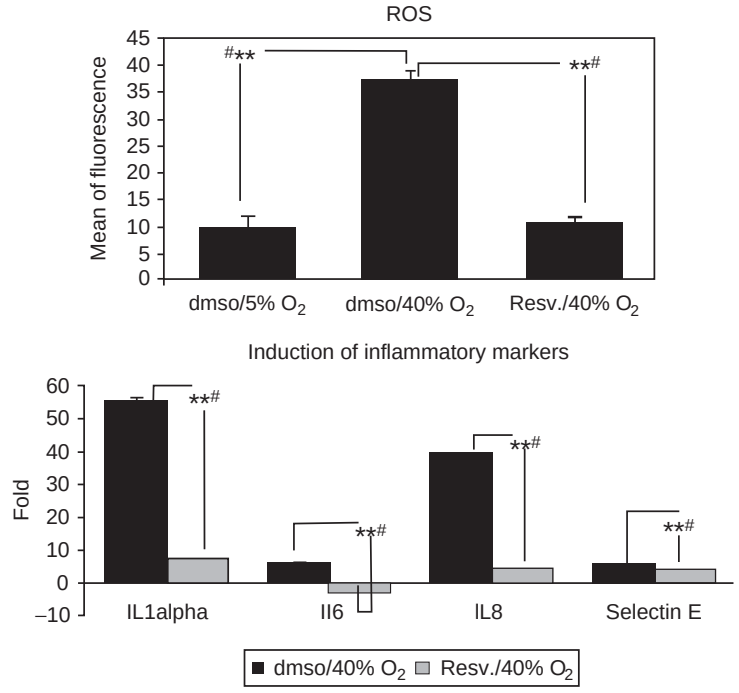

Figure 1 Effect of resveratrol treatment on the induction of endogenous generation of ROS (left) and the expression of inflammatory markers (right) mediated by chronic oxidative stress in porcine TM cells. Levels of ROS were measured by H2DCFDA and the expression of inflammatory markers was monitored by rt-Q-PCR in cells incubated at 40% oxygen and treated with resveratrol or vehicle and compared to cells incubated at physiological oxygen conditions (5%) ($N = 3$, t-test ,$^{**}P \leq 0.001$, # Kruskal–Wallis test $P \leq 0.049$). Adapted from figures 2 and 3 in Luna, C., Li, G.,Liton, P. B., et al. (2008) Resveratrol prevents the expression of glaucoma markers induced by chronic oxidative stress in trabecular meshwork cells. *Food and Chemical Toxicology* 47(1), 198–204, with permission from Elsevier Ltd.

resistance remain to be elucidated. Future research should help to clarify the extent of the role that oxidative damage may play in the aging of the TM and the pathological alterations of this tissue in glaucoma. An ongoing trend in the field of oxidative stress is the increasing recognition that ROS can play important roles as signaling molecules and may mediate some of the cellular responses relevant to understanding the process of cell aging. Similarly, there is increasing attention to the close relationship between oxidative stress and the activation of a chronic inflammatory response that may contribute to the pathologic alterations associated with aging in many tissues. Finally, a topic that deserves special attention is the study of the signaling networks that coordinately regulate the levels of ROS within the cell and the mechanisms protecting against oxidative damage. The identification of the pathways that regulate the longevity in yeast, *Caenorhabditis elegans*, and *Drosophila* suggest the existence of key regulators of the level of resources used by the cells to prevent and repair oxidative damage such as the sirtuin and FOXO families. Other examples may include p66SHC, Nrf2-ARE, and p53. Increasing our understanding on how these regulatory networks modulate the intracellular levels of ROS and the cellular defenses is currently a critical step to evaluate the importance of oxidative stress in glaucoma and could eventually lead to the development of new therapeutic strategies for this disease.

See also: Animal Models of Glaucoma; Biological Properties of the Trabecular Meshwork Cells; The Biology of Schlemm's Canal; Biomechanics of Aqueous Humor Outflow Resistance; Control of Aqueous Humor Flow; The Development of the Aqueous Humor Outflow Pathway; Functional Morphology of the Trabecular Meshwork; The Genetics of Primary Open-Angle Glaucoma: A Review; The Immunological Aspects of Aqueous Humor Turnover; Molecular Genetics of Congenital and Juvenile Glaucoma; Primary Open-Angle Glaucoma; Pseudoexfoliation Syndrome and Glaucoma; Retinal Ganglion Cell Apoptosis and Neuroprotection; Structural Changes in the Trabecular Meshwork with Primary Open Angle Glaucoma; Uveoscleral Outflow.

Further Reading

Aslan, M., Cort, A., and Yucel, I. (2008). Oxidative and nitrative stress markers in glaucoma. *Free Radical Biology and Medicine* 45(4): 367–376.

Davies, K. J. (1995). Oxidative stress: The paradox of aerobic life. *Biochemical Society Symposium* 61: 1–31.

Freedman, S. F., Anderson, P. J., and Epstein, D. L. (1985). Superoxide dismutase and catalase of calf trabecular meshwork. *Investigative Ophthalmology and Visual Science* 26: 1330–1335.

Harman, D. (1956). Aging: A theory based on free radical and radiation chemistry. *Journal of Gerontology* 11: 298–300.

He, Y., Leung, K. W., Zhang, Y. H., et al. (2008). Mitochondrial complex I defect induces ROS release and degeneration in trabecular meshwork cells of POAG patients: Protection by antioxidants. *Investigative Ophthalmology and Visual Science* 49(4): 1447–1458.

Izzotti, A., Bagnis, A., and Sacca, S. C. (2006). The role of oxidative stress in glaucoma. *Mutation Research* 612: 105–114.

Izzotti, A., Sacca, S. C., Cartiglia, C., and De Flora, S. (2003). Oxidative deoxyribonucleic acid damage in the eyes of glaucoma patients. *American Journal of Medicine* 114: 638–646.

Kahn, M. G., Giblin, F. J., and Epstein, D. L. (1983). Glutathione in calf trabecular meshwork and its relation to aqueous humor outflow facility. *Investigative Ophthalmology and Visual Science* 24: 1283–1287.

Li, G., Luna, C., Liton, P. B., et al. (2007). Sustained stress response after oxidative stress in trabecular meshwork cells. *Molecular Vision* 13: 2282–2288.

Liton, P. B., Lin, Y., Luna, C., et al. (2008). Cultured porcine trabecular meshwork cells display altered lysosomal function when subjected to chronic oxidative stress. *Investigative Ophthalmology and Visual Science* 49(9): 3961–3969.

McCord, J. M. and Fridovich, I. (1969). Superoxide dismutase. An enzymic function for erythrocuprein (hemocuprein). *Journal of Biological Chemistry* 244: 6049–6055.

Spector, A., Ma, W., and Wang, R. R. (1998). The aqueous humor is capable of generating and degrading H2O2. *Investigative Ophthalmology and Visual Science* 39: 1188–1197.

Wang, N., Chintala, S. K., Fini, M. E., and Schuman, J. S. (2001). Activation of a tissue-specific stress response in the aqueous outflow pathway of the eye defines the glaucoma disease phenotype. *Nature Medicine* 7: 304–309.

Zanon-Moreno, V. and Pinazo-Duran, M. D. (2008). Oxidative stress theory of glaucoma. *Journal of Glaucoma* 17(6): 508–509.

Zhou, L., Li, Y., and Yue, B. Y. (1999). Oxidative stress affects cytoskeletal structure and cellmatrix interactions in cells from an ocular tissue: The trabecular meshwork. *Journal of Cell Physiology* 180: 182–189.

The Role of the Ciliary Body in Aqueous Humor Dynamics Structural Aspects

E R Tamm, University of Regensburg, Regensburg, Germany

Glossary

Ciliary body – It consists of ciliary processes and ciliary muscle and is the anterior continuation of retina and choroid.
Ciliary epithelium – It consists of two epithelial layers, the nonpigmented epithelium (NPE) that covers the surface of the ciliary body, and the pigmented epithelium that lies underneath the NPE. Both epithelial layers are required for active secretion of aqueous humor.
Ciliary muscle – A smooth muscle in the ciliary body that is required for accommodation. The anterior tendons of the ciliary muscle attach to the scleral spur and the trabecular meshwork. Contraction of the ciliary muscle causes an increase in trabecular outflow facility.
Desmosome – A spot-like junctional complex arranged on the lateral sides of cell membranes. This helps to resist shearing forces. An alternative term is macula adherens.
Gap junctions – These connect the cytoplasm of two neighboring cells by forming hemichannels (connexons) that connect across the intercellular space. These junctions allow molecules smaller than 1000 Da to pass through. An alternative term is nexus.
Tight junctions – A type of a junctional complex in which the membranes of two cells join together, thereby forming a barrier that is largely impermeable to fluid. An alternative term is zonula occludens.
Zonular fibers – The structural elements of the ciliary zonula that connects the ciliary body with the lens equator to form the suspensory ligaments of the lens. Zonular fibers are 10–12-nm microfibrils, and their major structural component is fibrillin-1, a secreted 350-kDa glycoprotein.

Introduction

The ciliary body in the anterior eye is the anterior continuation of retina and choroid. It consists of two parts: the posterior pars plana and the anterior pars plicata (Figure 1). The pars plana forms a smooth surface that is in contact with the anterior vitreous. The pars plicata gives rise to 70–80 radiating ridges, the ciliary processes. The stroma of the ciliary body contains the ciliary muscle, a smooth muscle that is required for accommodation. In a meridional section through a human eye, the ciliary muscle has the form of a right-angled triangle in which the angle is localized anterior-inward underneath the ciliary processes (Figure 1). The anterior muscle bundles of the ciliary muscle attach to scleral spur and trabecular meshwork, forming the main attachment site of the uvea to the outer coats of the eye. In the valleys between the ciliary processes, the zonular fibers originate that connect the lens with the ciliary body. The ciliary body is involved in two critical functional processes in the eye, namely accommodation and aqueous humor turnover. This article focuses on the roles of the ciliary body in aqueous humor dynamics.

Ciliary Processes

Each of the ciliary processes is filled with numerous capillaries (Figure 2). The capillaries are supplied by arterioles that originate from the major arterial circle of the iris.

The arterioles emerge from the major arterial circle and enter the anterior part of the ciliary processes to form a network of capillaries that frequently anastomose with each other. A larger capillary bends to the margin of each process to become the marginal venule that drains the blood into the veins of the posterior pars plana. Endothelial cells of ciliary process capillaries and marginal venule are of the fenestrated type and form numerous small openings that are covered by a diaphragm (Figure 3).

The diaphragmed fenestrae of the ciliary process capillaries are the reason for the high permeability of the capillaries that facilitates ultrafiltration of water and ions into the adjacent stroma. In addition, the fenestrated capillaries allow larger plasma-derived proteins, such as myoglobulin or gammaglubulin, to enter the stroma, an effect that leads to a high oncotic pressure in the ciliary process stroma. In younger eyes, the extracellular space between the basal laminae of capillaries and pigmented ciliary epithelium (PE) is relatively small, but increases with age. In the eyes of older humans, the stroma of the ciliary processes may contain large amounts of extracellular matrix that appear hyalinized in light microscopical sections (Figure 4).

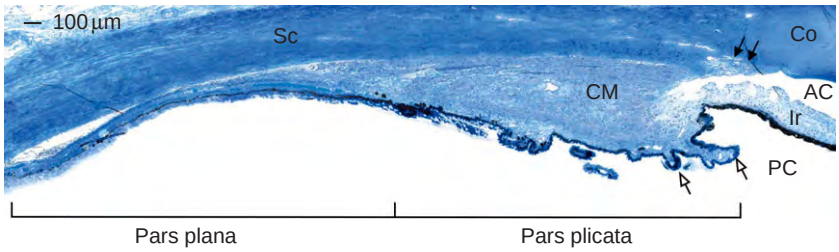

Figure 1 Meridional section through the ciliary body of a 49-year-old human. Solid arrows indicate the position of trabecular meshwork and Schlemm's canal. Open arrows point to ciliary processes. Semithin section stained with Richardson's stain. Sc, Sclera; CM, ciliary muscle; Co, cornea; Ir, iris; AC, anterior chamber; PC, posterior chamber.

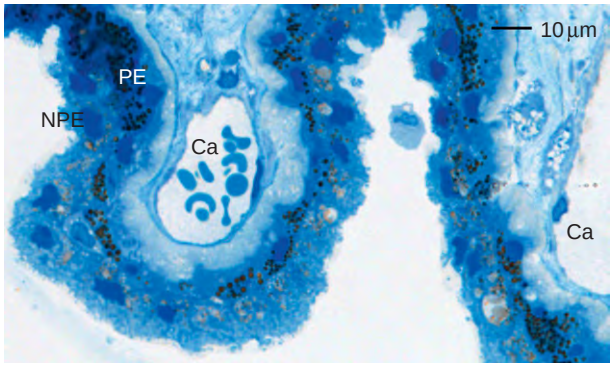

Figure 2 Meridional section through the tips of ciliary processes. Each ciliary process is covered by a pigmented (PE) and nonpigmented (NPE) epithelial layer, and contains numerous capillaries (Ca). Semithin section stained with Richardson's stain.

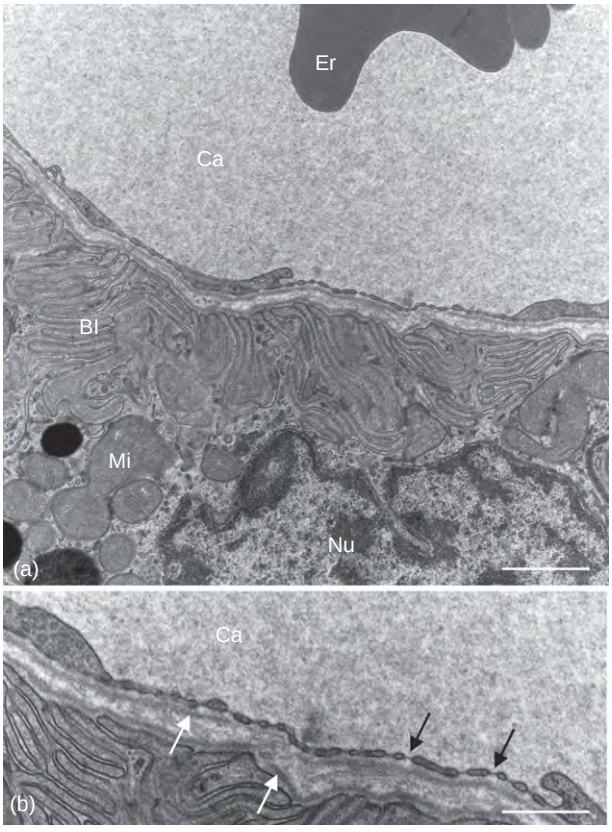

Figure 3 Electron microscopy of ciliary process capillaries ((b) is a higher magnification of (a)). (a) Electron micrograph of a ciliary process capillary (Ca) next to a cell of the pigmented ciliary epithelium (PE) with nucleus (Nu), numerous mitochondria (Mi), and basal infoldings (BI). An erythrocyte (Er) is present in the lumen of the capillary. (b) The endothelial cells of the capillary wall next to the basal laminae of capillary endothelium and PE (white arrows) form numerous fenestrae that are covered with a diaphragm (black arrows). Magnification: (a) 1 µm; (b) 500 nm.

In addition, there is a substantial thickening of the pigmented epithelium (PE) basal lamina (**Figure 5(a)**), which becomes increasingly multilamellated (**Figure 5(b)**). The age-related increase in extracellular matrix in the ciliary process stroma likely causes or contributes to the age-related decline in aqueous humor production.

The ciliary processes are covered by two epithelial layers of secretory cells (**Figure 6**). The pigmented outer epithelial layer (PE, pigmented epithelium) lies adjacent to the ciliary body stroma, contains pigment granules, and is a direct continuation of the retinal pigmented epithelium. The nonpigmented inner epithelial layer (NPE, nonpigmented epithelium) is a direct continuation of the retina. The two-layered ciliary epithelium originates in embryonic eye development when the optic vesicle invaginates to form the optic cup. As a result, the basal side of the NPE, which faces the posterior chamber and the vitreous, is covered by a basal lamina that is a direct continuation of the internal limiting membrane of the retina (**Figure 6**).

The cells of the ciliary epithelium form all the ultrastructural characteristics that are typically found in cells that are actively involved in energy-dependent transport processes. Accordingly, the basolateral surfaces of both NPE and PE form an elaborate system of cytoplasmic infoldings (**Figures 3, 6, and 7(a)**). The cell membrane of the infoldings shows intense histochemical and immunohistochemical staining for the enzymes Na-K-adenosine triphosphate (ATP)ase and carbonic anhydrase. To direct fluid transport across an epithelium, polarity between its luminal and basolateral membranes must be maintained. The tight junctions or zonulae occludentes that are required for this purpose are localized between the apical–lateral cell membranes of NPE cells, close to their contact with the cells of the PE. The tight junctions between the cells of the NPE form the

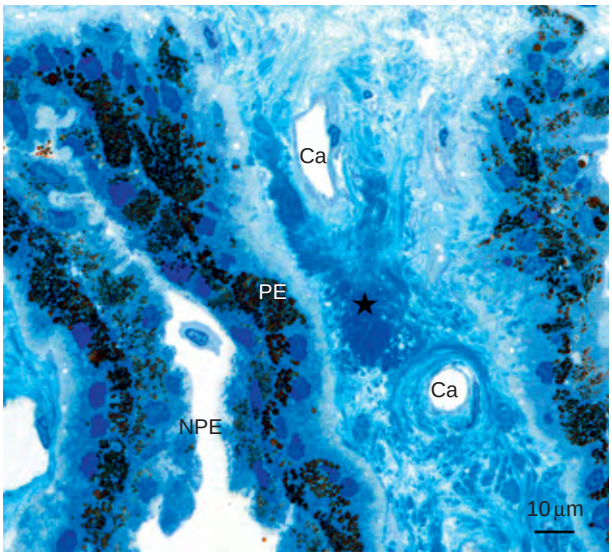

Figure 4 Light micrograph of ciliary processes in the eyes of a 78-year-old human. The stroma of the ciliary processes shows advanced signs of hyalinization and is filled with dense extracellular material (asterisk). Semithin section stained with Richardson's stain. NPE, nonpigmented ciliary epithelium; PE, pigmented ciliary epithelium; Ca, capillaries.

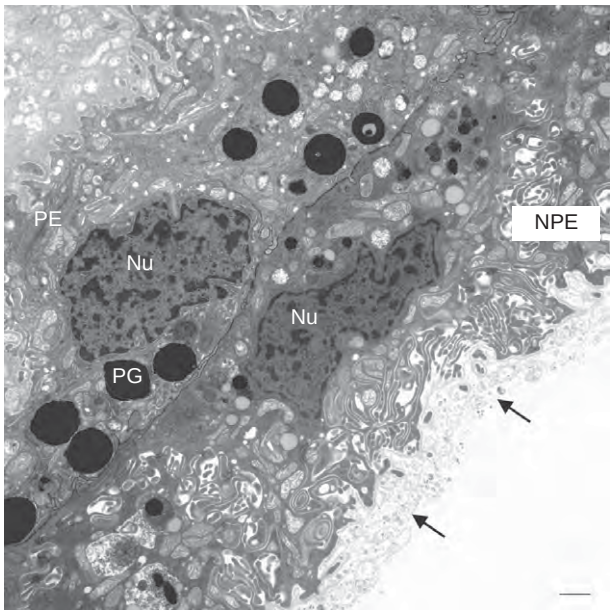

Figure 6 Electron micrograph of pigmented (PE) and nonpigmented (NPE) ciliary epithelium. Arrows point to the internal limiting membrane, which forms the basal lamina of the NPE. Magnification: 1000 nm. Nu, nucleus; PG, pigment granules.

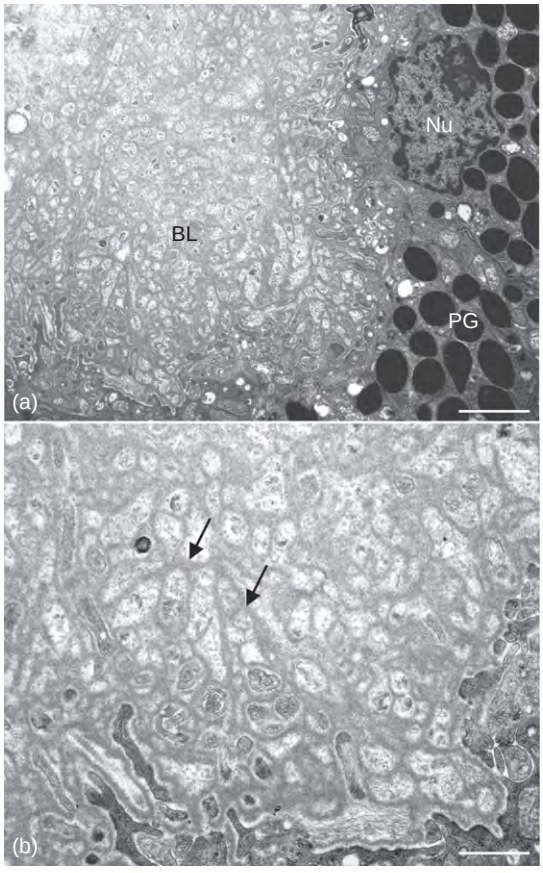

Figure 5 Electron micrographs of the basal lamina (BL) of the pigmented ciliary epithelium in a 78-year-old human; (b) is magnification of (a). The basal lamina consists of multiple layers (arrows) that surround osmiophilic granular material. Magnification: (a) 2000 nm; (b) 1000 nm. PG, Pigment granules; Nu, nucleus.

blood–aqueous barrier that is impermeable to plasma proteins or tracers such as horseradish peroxidase. While plasma proteins that leak from the capillaries of the ciliary body cannot pass the blood–aqueous barrier, they may move to the iris stroma and diffuse into the anterior chamber through the anterior surface of the iris, which is not covered by an epithelial layer. On the basal side of the tight junctions, adherens-type junctions are frequently observed.

Another type of junction that appears to be critically required for secretion of aqueous humor across the epithelial layers of the ciliary processes is gap junctions. Gap junctions, which allow ions and other molecules smaller than 1000 Da to pass through, are abundant in both layers of the ciliary epithelium. They are particularly numerous between NPE and PE (**Figure 7(d)**). The intense electrical coupling between both epithelial layers generates a functional syncytium that allows ions taken up from the stroma by cells of the PE to pass from PE to NPE. Ion transport between the epithelial layers appears to be critically required for secretion of aqueous humor as mice with a conditional inactivation of connexin 43 do not form gap junctions between both epithelial layers and show a substantial reduction in aqueous humor production.

To maintain the mechanical integrity of the NPE, the lateral sides of adjacent NPE cells are connected by well-differentiated desmosomes (**Figures 7(a),** and **7(b)**). At the adjacent cytoplasmic sides of the desmosomes, which are separated by a cleft 17 nm wide, electron-dense plaques are present, which are associated with 9–10-nm tonofilaments. Desmosomes of the NPE frequently form desmosomal–mitochondrial complexes in which the tonofilaments

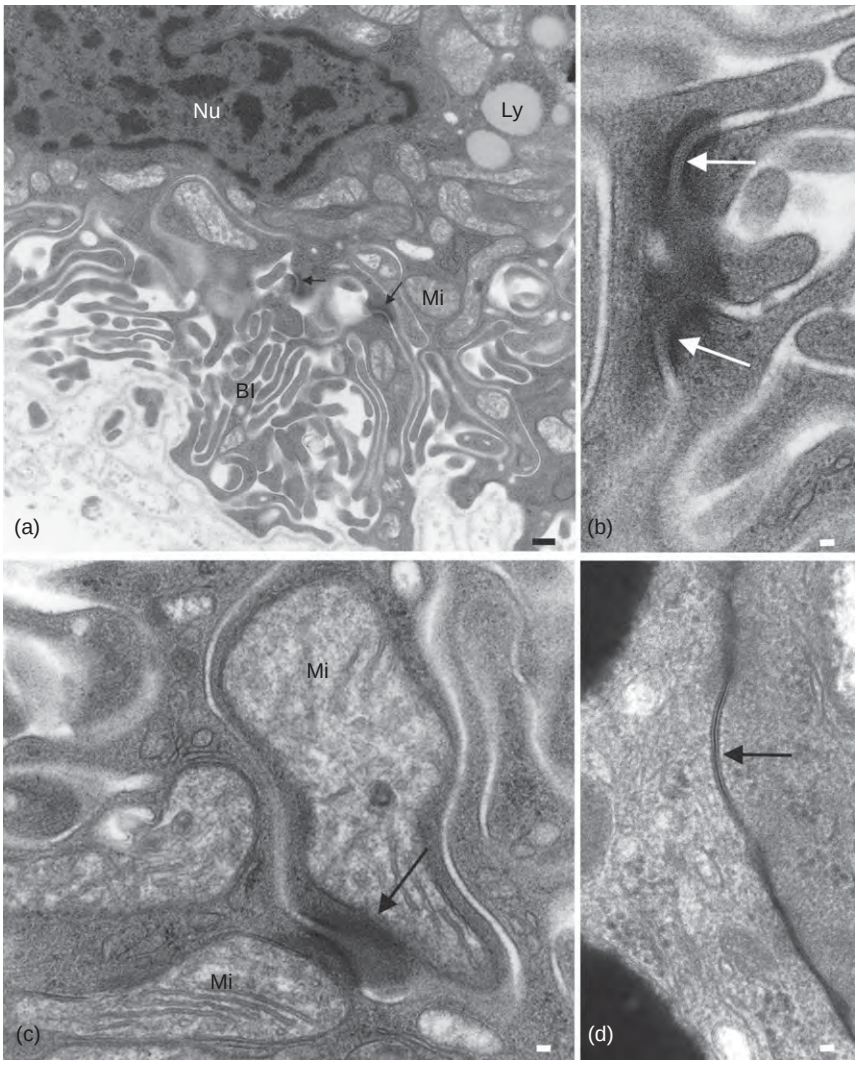

Figure 7 Electron microscopy of the nonpigmented ciliary epithelium. (a) The basal and lateral sides of nonpigmented ciliary epithelial cells form numerous infoldings (BI). Immediately adjacent to the infoldings are numerous mitochondria (Mi). Asterisks point to desmosomes that connect two adjacent epithelial cells. Ly, lysosome. (b) Higher magnification of two desmosomes (arrows) connecting two nonpigmented ciliary epithelial cells. (c) Desmosomal–mitochondrial complexes in the nonpigmented ciliary epithelium. The tonofilaments of the desmosomes contact the outer mitochondrial membrane. (d) Gap junction (arrow) between cells of the pigmented and nonpigmented ciliary epithelium. Magnification: (a) 250 nm; (b–d) 50 nm.

contact the outer mitochondrial membranes. The functional significance of the desmosomal–mitochondrial complexes has not been finally clarified. Since calcium has been demonstrated in the associated mitochondria, the hypothesis has been put forward that the mitochondria may serve as buffers for intracellular calcium by controlling the local calcium concentration. This scenario might be advantageous for stability and functional integrity of desmosomal junctions in secretory or actively transporting epithelia with high endogenous calcium levels.

Mechanical stability is required for the epithelial layers of the ciliary body, as the zonular fibers which suspend the lens attach to the basal lamina of the NPE (Figure 8). While most of the zonular fibers originate in the posterior region of the pars plana, secondary tension fibers attach in the valleys between the ciliary processes to act as a fulcrum (pivot point). Accordingly, adherens-type junctions between NPE and PE have reported to be more numerous in the valleys between the ciliary processes than at their tips. In addition, the cytoplasm of the NPE contains less mitochondria in the valleys between the processes than at their tips, while the NPE cell membranes in the valley do not stain for Na-K-ATPase or carbonic anhydrase. Taken together, aqueous humor secretion appears to occur mainly at the tips of the ciliary processes, while the valleys between the processes primarily serve a mechanical function.

Cells of the ciliary epithelium typically show Golgi complexes and single cisternae of rough endoplasmic

reticulum (rER) that are both localized close to the nucleus. In the posterior part of the ciliary processes, cisternae of rER are more numerous and may form large aggregates with a fingerprint-like arrangement (**Figure 9(b)**). Proteins or peptides that are secreted into the aqueous humor may be produced in the fingerprint-like structures. Candidates are growth factors such as transforming growth factor-β2 or signaling molecules such as endothelin-1, which are both found in the aqueous humor and are synthesized by cells of the ciliary epithelium *in vitro*. In the eyes of older humans, lysosomes and lipofuscin particles may accumulate in the apical parts of NPE cells (**Figure 9(a)**).

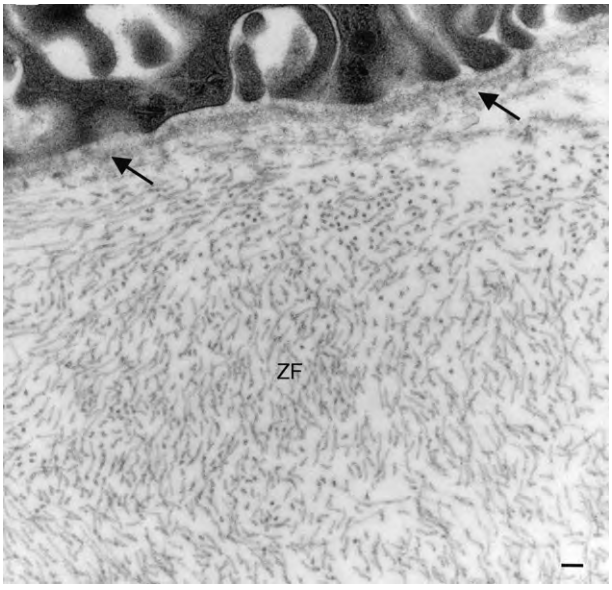

Figure 8 Attachment of zonular fibers (ZF) to the basal lamina (arrows) of the NPE. Electron micrograph. Magnification: 100 nm.

Ciliary Muscle

The stroma of the ciliary body is largely occupied by the ciliary muscle. While the main function of the ciliary muscle is related to accommodation, it is also critically involved in both conventional trabecular and unconventional uveoscleral aqueous humor outflow. Ciliary muscle contraction influences trabecular outflow due to the site of the anterior attachment of the muscle. The muscle bundles of the radial portion of the ciliary muscle and the inner bundles of its longitudinal portion form tendons in region of their anterior insertion that are continuous with the extracellular matrix of the trabecular meshwork beams (**Figure 10(a)**).

The tendons of the inner muscle bundles of the longitudinal portion pass the scleral spur at its inner aspect to continue to the trabecular meshwork (**Figure 10(b)**). The same banded material that forms the sheaths of the elastic fibers in the core region of the trabecular beams is the main structural element of the tendons. The banded material comes in direct contact with the cell membrane of the muscle cell, which forms dense bands at the cytoplasmic site (**Figure 10(c)**). In region of contact with the tendons, the muscle bundles taper and form deep furrows, which are filled with banded material. The outer muscle

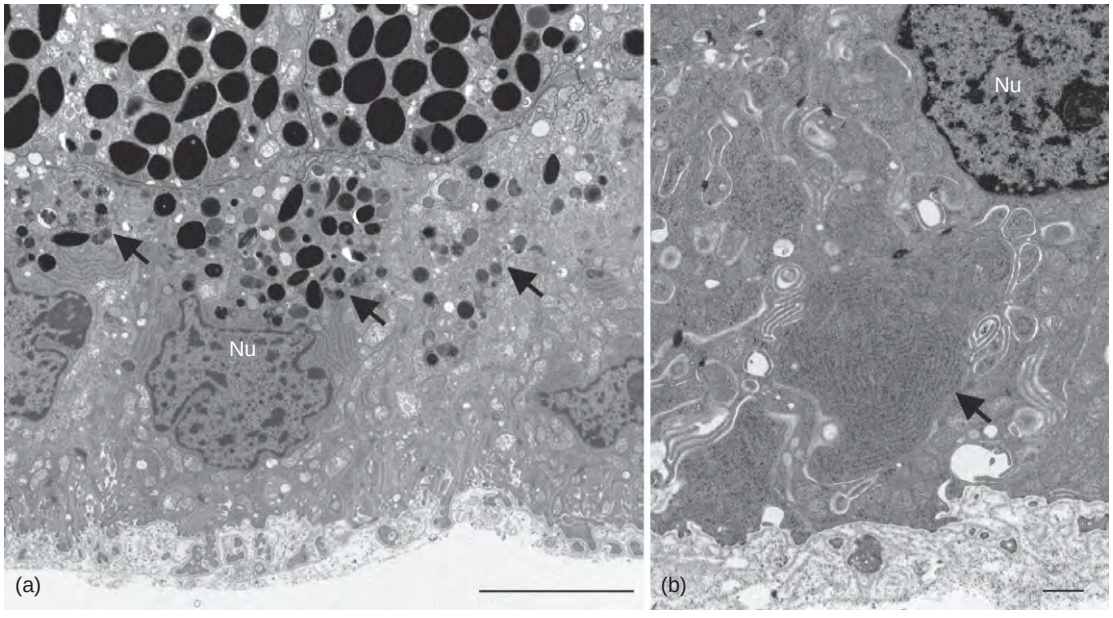

Figure 9 Electron micrographs of NPE cells. (a) NPE cells containing large amounts of lysosomes and lipofuscin particles in their apical cytoplasm (arrows). (b) Numerous cisterns of rough endoplasmatic reticulum arranged in a fingerprint-like pattern (arrow) in the cytoplasm of an NPE cell. Magnification: (a) 5000 nm; (b) 1000 nm.

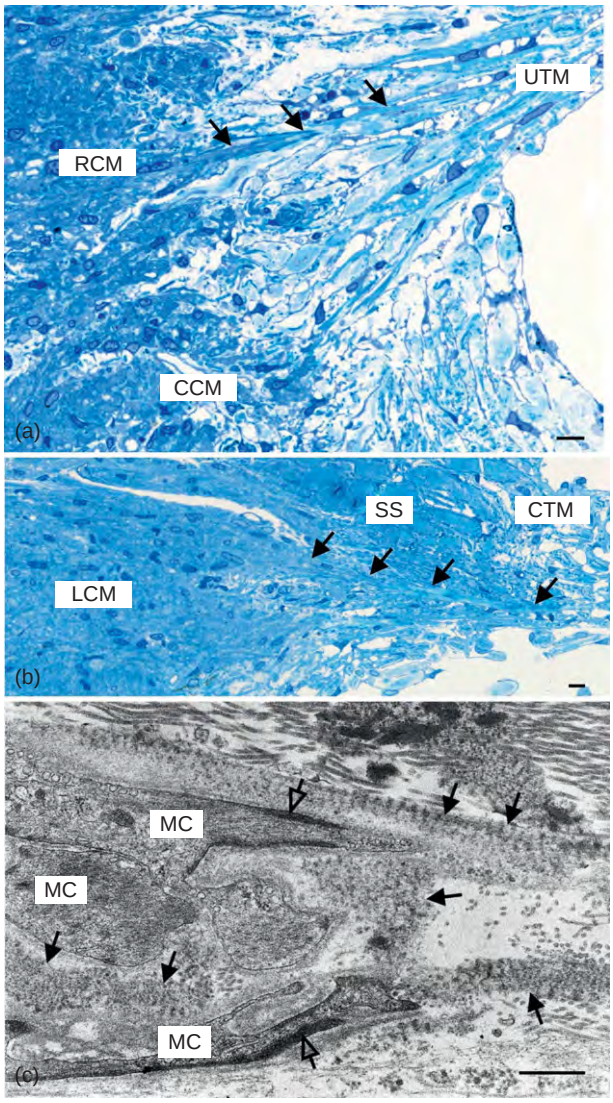

Figure 10 Light (a, b) and electron microscopy (c) of anterior ciliary muscle tendons. (a, b) The muscle bundles of the radial portion of the ciliary muscle (RCM, (a)) and the inner bundles of its longitudinal portion (LCM, (b)) form tendons (arrows) in region of their anterior insertion that are continuous with the extracellular matrix of the trabecular meshwork beams. (a) The tendons of the radial portion continue to the uveal trabecular meshwork (UTM). (b) The tendons of the inner muscle bundles of the longitudinal portion pass the scleral spur (SS) at its inner aspect to continue to the corneoscleral trabecular meshwork (CTM). (c) The banded material of the ciliary muscle tendons (solid arrows) comes in direct contact with the cell membrane of the muscle cell (MC), which forms dense bands at the cytoplasmic site (open arrows). In region of contact with the tendon, the muscle cell forms deep furrows which are filled with banded material. CCM, circular portion of the ciliary muscle. Magnification: (a, b) 10 μm; (c) 500 nm. From Tamm, E. R. (2009). The trabecular meshwork outflow pathways. Functional morphology and surgical aspects. In: Shaarawy, T. M., Sherwood, M. B., Hitchings, R. A., and Crowston, J. G. (eds.) *Glaucoma*, vol. II, pp. 31–44. Saunders, UK: Elsevier.

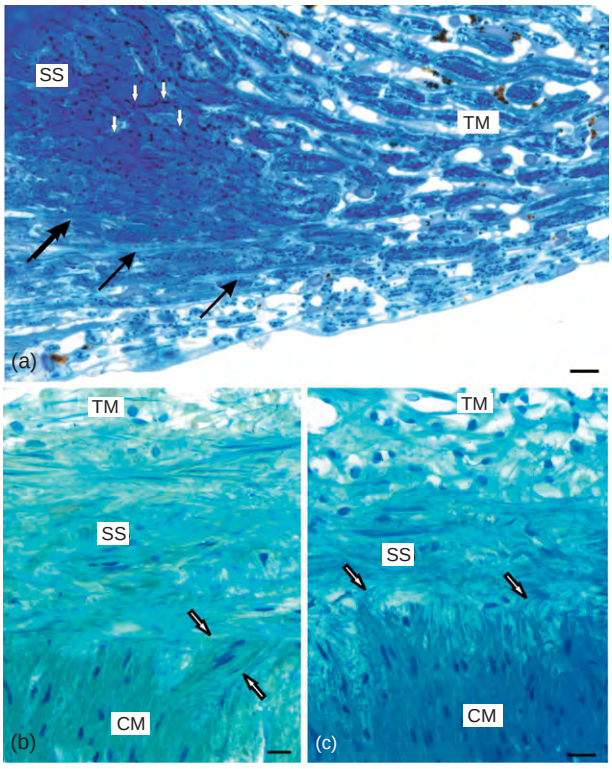

Figure 11 Meridional (a) and tangential sections (b, c) of the scleral spur (SS) and the anterior insertion of the ciliary muscle (CM). (a) The scleral spur contains numerous elastic fibers (white arrows), which are continuous with those of the trabecular meshwork (TM). Solid arrows denote anterior tendons of the longitudinal portion of the ciliary muscle. (b) Near its insertion to the scleral spur, a muscle bundle bends in the circular direction (arrows). (c) Ciliary muscle bundles insert to the scleral spur by means of elastic tendons which form arcades finally bending in a circular direction (arrows). Magnification: (a) 10 μm; (b, c) 20 μm. (a, b) From Tamm, E. R. (2009). The trabecular meshwork outflow pathways. Functional morphology and surgical aspects. In: Shaarawy, T. M., Sherwood, M. B., Hitchings, R. A., and Crowston, J. G. (eds.) *Glaucoma*, vol. II, pp. 31–44. Saunders, UK: Elsevier. (c) From Tamm, E., Flügel, C., Stefani, F. H., and Rohen, J. W. (1992). Contractile cells in the human scleral spur. *Experimental Eye Research* 54: 531–543.

bundles of the longitudinal portion of the ciliary muscle also form tendons, but connect with the extracellular matrix fibers of the scleral spur. The scleral spur contains collagen and elastic fibers that are circumferentially arranged (**Figure 11(a)**).

The elastic fibers are continuous with those of the core of the corneoscleral meshwork beams, or the cribriform plexus in the juxtacanalicular tissue. The outermost muscle bundles of the longitudinal portion of the ciliary muscle bend clockwise or counterclockwise before they attach to the scleral spur (**Figure 11(b)**). More inwardly, they do not bend, but insert to elastic fibers that are continuous with the circumferentially arranged elastic fibers of the scleral spur (**Figure 11(c)**). Because of the

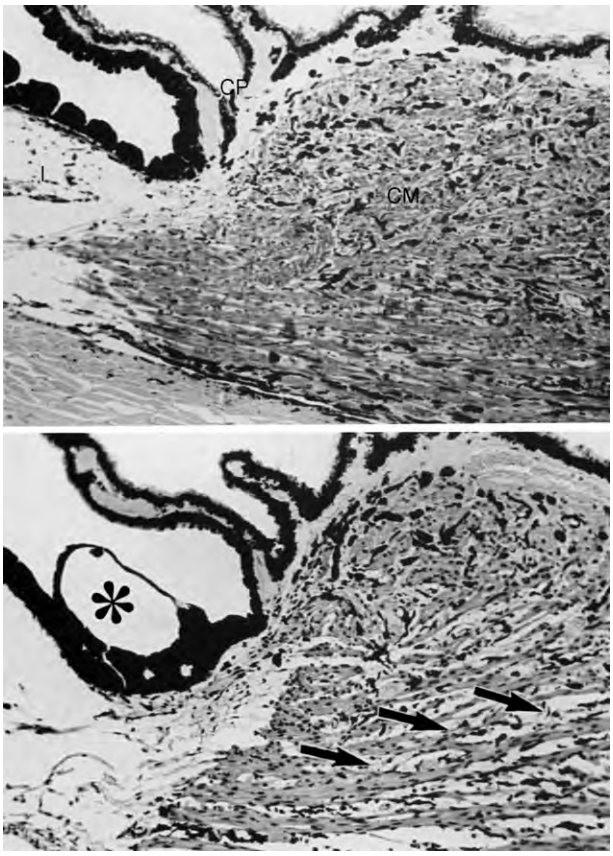

Figure 12 Sagittal section through the anterior portion of the ciliary body (Crossmon's stain, ×135). (a) Vehicle-treated control eye. CM, ciliary muscle; I, iris; CP, ciliary processes. (b) Following treatment with $PGF_{2\alpha}$for 4 days, enucleation 4.5 h after last treatment. Note the enlarged spaces between the thin muscle fiber bundles in the prostaglandin-treated eye (arrows). No edema of the ciliary processes is seen in this section. Asterisk: Greeff's vesicle. From Lütjen-Drecoll, E. and Tamm, E. (1988). Morphological study of the anterior segment of cynomolgus monkey eyes following treatment with prostaglandin $F_{2\alpha}$. *Experimental Eye Research* 47: 761–769.

structural connections between ciliary muscle and scleral spur, contraction of the ciliary muscle pulls the spur posteriorly and widens the trabecular spaces, thereby inducing changes in the geometry of the trabecular meshwork that lead to a reduction in outflow resistance. The intraocular pressure (IOP)-lowering effects of cholinergic parasympathomimetic agents, such as pilocarpine, are mediated through ciliary muscle contraction through its anterior insertion to scleral spur and trabecular meshwork. In monkeys, surgical disinsertion of the muscle from its anterior attachment abolishes the IOP-lowering effect of pilocarpine.

The ciliary muscle is not only involved in conventional trabecular outflow, but does also play a critical role in unconventional or uveoscleral outflow. The uveoscleral outflow route is open to the aqueous humor at the chamber angle in region of the anterior insertion of the ciliary muscle, as there is no complete endothelial or epithelial layer that covers the anterior surface of the ciliary body. When passing through the uveoscleral outflow pathways, aqueous humor exits the anterior chamber through the extracellular spaces between the ciliary muscle bundles, into the supraciliary and suprachoroidal space and out through the sclera into the extraocular tissues. Fluid in the uveoscleral pathways ultimately drains into the lymphatic system. Depending on the method that is used to measure it, unconventional or uveoscleral outflow is found to account for 10% or 25–57% of the total outflow in the human eye. In contrast to the conventional trabecular outflow, which is increased upon ciliary muscle contraction, uveoscleral outflow decreases, most likely because the available extracellular space is largely diminished in the contracted ciliary muscle. This pathway is important to understanding the mechanism of action of prostaglandin analogs in the treatment of glaucoma. In monkey eyes, treatment with prostaglandin analogs causes a widening of the extracellular spaces between the ciliary muscle bundles, resulting in an increase of available uveoscleral outflow pathways (**Figure 12**). This effect appears to be mediated through degradation of extracellular matrix compounds in the intramuscular connective tissue of the ciliary muscle.

Acknowledgments

This work was supported by: DFG Research Unit 1075 (TP 5). The author would like to thank Margit Schimmel for the expert technical help in processing of the micrographs.

See also: Ciliary Blood Flow and its Role for Aqueous Humor Formation; Control of Aqueous Humor Flow; Functional Morphology of the Trabecular Meshwork; Ion transport in the Ciliary Epithelium; Neuroendocrine Properties of the Ciliary Epithelium; Pharmacology of the Aqueous Humor Outflow; Uveoscleral Outflow.

Further Reading

Alm, A. and Nilsson, S. F. (2009). Uveoscleral outflow – a review. *Experimental. Eye Research* 88: 760–768.

Barsotti, M. F., Bartels, S. P., Freddo, T. F., and Kamm, R. D. (1992). The source of protein in the aqueous humor of the normal monkey eye. *Investigative Ophthalmology and Visual Science* 33: 581–595.

Bill, A. (1975). Blood circulation and fluid dynamics in the eye. *Physiological Reviews* 55: 383–417.

Calera, M. R., Topley, H. L., Liao, Y., et al. (2006). Connexin43 is required for production of the aqueous humor in the murine eye. *Journal of Cell Science* 119: 4510–4519.

Flügel, C. and Lütjen-Drecoll, E. (1988). Presence and distribution of NA^+/K^+-ATPase in the ciliary epithelium of the rabbit. *Histochemistry* 88: 613–621.

Freddo, T. F. (1988). Mitochondria attached to desmosomes in the ciliary epithelia of human, monkey and rabbit eyes. *Cell and Tissue Research* 251: 671.

Funk, R. and Rohen, J. W. (1990). Scanning electron microscopic study on the vasculature of the human anterior eye segment, especially with respect to the ciliary processes. *Experimental Eye Research* 51: 651–661.

Hara, K., Lütjen-Drecoll, E., Prestele, H., and Rohen, J. W. (1977). Structural differences between regions of the ciliary body in primates. *Investigative Ophthalmology and Visual Science* 16: 912–924.

Kaufman, P. L. and Bárány, E. H. (1976). Loss of acute pilocarpine effect on outflow facility following surgical disinsertion and retrodisplacement of the ciliary muscle from the scleral spur in the cynomolgus monkey. *Investigative Ophthalmology and Visual Science* 15: 793–807.

Lütjen-Drecoll, E. and Tamm, E. (1988). Morphological study of the anterior segment of cynomolgus monkey eyes following treatment with prostaglandin F_2 alpha. *Experimental Eye Research* 47: 761–769.

Lütjen-Drecoll, E., Lönnerholm, G., and Eichhorn, M. (1983). Carbonic anhydrase distribution in the human and monkey eye by light and electron microscopy. *Graefe's Archive for Clinical and Experimental Ophthalmology* 220: 285–291.

Ober, M. and Rohen, J. W. (1979). Regional differences in the fine structure of the ciliary epithelium related to accommodation. *Investigative Ophthalmology and Visual Science* 18: 655–664.

Raviola, G. (1971). The fine structure of the ciliary zonule and ciliary epithelium. *Investigative Ophthalmology and Visual Science* 10: 851–869.

Raviola, G. (1977). The structural basis of the blood–ocular barriers. *Experimental Eye Research* 25(supplement): 27–63.

Rohen, J. W. (1979). Scanning electron microscopic studies of the zonular apparatus in human and monkey eyes. *Investigative Ophthalmology and Visual Science* 18: 133–144.

Schlötzer-Schrehardt, U., Müller, H.-G., Wirtz, M., and Naumann, G. O. H. (1990). Desmosomal–mitochondrial complexes in human nonpigmented ciliary and retinal pigment epithelia. *Investigative Ophthalmology and Visual Science* 31: 664–669.

Tamm, E., Flügel, C., Stefani, F. H., and Rohen, J. W. (1992). Contractile cells in the human scleral spur. *Experimental Eye Research* 54: 531–543.

Tamm, E., Rittig, M., and Lütjen-Drecoll, E. (1990). Elektronenmikroskopische und immunhistochemische Untersuchungen zur augendrucksenkenden Wirkung von Prostaglandin F2 alpha. *Fortschritte der Ophthalmologie* 87: 623–629.

Tamm, E. R. (2009). The trabecular meshwork outflow pathways. Functional morphology and surgical aspects. In: Shaarawy, T. M., Sherwood, M. B., Hitchings, R. A., and Crowston, J. G. (eds.) *Glaucoma* vol. II, pp. 31–44. Saunders, UK: Elsevier.

Tamm, E. R. and Lütjen-Drecoll, E. (1996). Ciliary body. *Microscopy Research and Technique* 33: 390–439.

The Role of the Vitreous in Macular Hole Formation

W E Smiddy, Bascom Palmer Eye Institute, Miami, FL, USA

Glossary

Henle's nerve fiber layer – The inner layer of cones at the fovea lacking overlying nerve fiber or inner nuclear layer cells that have the most attenuated internal limiting membrane covering; could be the most susceptible location for a breach in that layer that might initiate macular hole formation.
Internal limiting membrane – The confluence of inner footplates of Müller cells of retina that forms a membrane-like structure delimiting inner retinal surface where it contacts the posterior hyaloidal elements.
Macula – The retina that subserves central vision, populated by the most dense distribution of cone photoreceptors to offer the best visual resolution; this term is somewhat imprecisely used among clinicians (broader, perhaps 2 disk diameter zone) and histologists (more narrowly used to central point).
Posterior hyaloid – The most posterior elements of the vitreous body; this structure is more complex than previously thought, frequently exists as a multilaminated structure, and composed primarily of type IV collagen, but may be impregnated with cellular components.
Vitreoschisis – A phenomenon that is usually not visible, but could be important pathogenically whereby the vitreous body develops a splitting of some of its layers, most notably just anterior to the posterior hyaloidal attachment to the macula.

The pathogenesis of macular holes has undergone at least one full cycle of thought. Since macular holes were first identified following trauma, it was natural for early clinicians to deduce that a coup–countrecoup force transmitted through the vitreous caused macular hole formation. However, as it became apparent that trauma was only infrequently associated with the finding of a macular hole, other mechanisms were proposed as first summarized by Aaberg. Three principal, possibly coexisting, enhanced mechanisms have been proposed including unroofing or dissolution of the attenuated inner retinal layer of cystoid edema due to a range of etiologies, atrophy or degeneration of the retina, and vitreomacular traction. Advances in imaging have allowed unprecedented resolution which has ratified vitreomacular traction as the most prominent component, if not the basic underlying mechanism, of macular hole formation.

Undeniably, the vitreoretinal interface is the battlefront of macular hole formation and therapeutics. Some observations do not fully conform to the model of vitreomacular traction as the sole and universal cause of macular hole formation, but these may be consequences of vitreomacular traction or factors contributing to or potentiating vitreous traction. Thus, it is possible that the vitreous may play a prime-mover role, an innocent bystander role, or a collaborative role in the formation of macular holes. This article reviews the evidence and perspective of the role of the vitreous in macular hole formation.

Vitreous Anatomy and Biochemistry

The vitreous body has a much more complex structure and physiology than might initially be apparent from its transparent, paucicellar, predominantly aqueous appearance. It is a nonhomogeneous biochemical complex of collagen and hyaluronan. The physical structure of the vitreous is an extensive cisternal system of cavitated, more liquefied portions lined by extenuated and thickened walls. This seems to be accentuated with age (syneresis) or in certain disease states. Most specifically, the concept of a posterior precortical vitreous pocket and, consequently, a cortical vitreous layer has been defined and to a large degree imaged which, by its proximity to the fovea, mostly likely plays some role in the genesis of vitreous forces at the fovea. Improved optical visualization of the fine structure of the vitreous has allowed clinical detection of this pocket, and its size has been hypothesized to be proportional to the amount of tangential traction generated at the fovea.

The vitreous dual senescent processes of synchesis and syneresis render a posterior vitreous detachment (PVD) to be a much more complex process than the casual observer might suspect.

Vitreous Traction

Peripheral retinal breaks form at the time of a PVD. Thus, it was a natural step to conceive of the PVD as playing a formative role in causing macular holes. Gass' seminal grading scheme standardized observations of the stages involved in macular hole formation and it remains generally accepted. Its clinical relevance was immediately

seized upon and preventative surgery aimed at inducing the posterior vitreous separation before a macular break could occur led to several surgical investigations that seemed to offer promising results initially, but a randomized trial failed to establish the efficacy of this preemptive strategy. The surgical strategy employed at the time was to remove the cortical vitreous, which itself may reflect an incomplete or overly simplified understanding of the pre-hole dynamics.

Various clinical studies identified a lack of PVD to be associated with a higher risk of macular hole formation in the fellow eyes of patients with macular holes compared to fellow eyes with incident posterior vitreous separations. Histopathologic series not only established that posterior vitreous separation was more common among patients with full-thickness macular holes, but also made the observation that persistent attachments of the vitreous and associated cystic changes may imply a more complex mechanism than simple posterior vitreous separation.

The earliest imaging studies included ultrasound tests which also seem to establish the strong association of vitreous separation with macular hole formation. Subsequently, imaging with optical coherence tomography (OCT) depicted a compelling role for vitreous traction.

However, other observations have suggested that while traction at the time of posterior vitreous separation may well be important, it may be part of a more complex scenario. The fellow eyes of patients develop macular holes much more frequently than in the general populations, suggesting a constitutional susceptibility to macular hole formation, presumably at the time of posterior vitreous separation.

Vitreoretinal Interface

The second iteration of the vitreous separation at the fovea has focused on the nature and actions that occur at the vitreofoveal interface. Formerly, a vitreous separation was simplistically thought of as a clean, total separation of the hyaloid from the internal limiting membrane (ILM). However, the concept of an anomalous posterior vitreous separation at the fovea is what is probably most consistent with both the clinical behavior and the imaging appearances. Vitreous cortex remnants have been identified at the fovea and perifoveal area after apparent spontaneous posterior vitreous separation. In this way, the vitreous may be a necessary substrate for action at the fovea. Histopathologic studies have also suggested or have identified numerous other possible substrates that might mediate traction, but more of a delayed or tangential nature than the expected anterior-to-posterior traction of the simplified posterior vitreous separation. Anatomic features at the fovea are unique and may also account for what are incidental vitreoretinal forces elsewhere. For example, the fovea is thin centrally and the ILM as well as the basal lamina of the vitreous are extremely thin at the fovea. At the fovea, the outer plexiform layer and the photoreceptor layer (Henle's nerve fiber layer) are more exposed and the ILM is even more attenuated in this area. The tangential orientation of the fibers, their delicate nature, and the thin overlying ILM may make this layer more susceptible to incidental trauma at the time of vitreous separation at the fovea.

These anatomic and theoretic features seem to be consistent with other clinical observations, including the apparent predecessor lesion as a cyst. Thus, the question of the pathogenic role of the vitreous becomes open to its possible chronic role in inducing an inner cystic change, or its subsequent action on the weakened inner cystic layers to precipitate the full-thickness hole. Careful biomicroscopic study of the vitreous at the fovea can demonstrate vitreous separation or, more importantly, a partial vitreous separation at the fovea. Other imaging modalities besides OCT, including laser biomicroscopy kinetic ultrasound and retinal thickness analysis, also demonstrate these findings. The most convincing evidence for this role comes from the more newly advanced and available optical coherence tomography images which have corroborated the apparent impact of the vitreous at the fovea (**Figure 1**). This concept is demonstrated by cases with spontaneous closure of a macular hole after release of the persistent vitreofoveal attachment, whether in traumatically induced or in idiopathic cases. Applying this observation therapeutically, others have performed vitrectomy relieving the traction with peeling of the posterior hyaloid, vitrectomy with removal of the ILM, or even vitreolysis of its persistent attachment without a larger vitrectomy with resolution of a macular hole as well. However, the indication for intervention is not well established, and occasionally, the apparent vitreofoveal traction will spontaneously release (**Figure 2**).

Numerous case reports of macular hole formation associated with seemingly unrelated diseases share themes of vitreous traction in the setting of intravitreal injection, fungal endophthalmitis, and laser-assisted *in situ* keratomileusis (LASIK) associated with formation of full-thickness macular holes. A corollary of the role of the vitreous attachment at the fovea is that other case reports have suggested a sort of accomplice role that the vitreous may play in transmitting tractional effects from seemingly unassociated conditions as they burst as hemorrhage from a retinal microaneurysm, LASIK, transpupillary thermal therapy, yttrium aluminum garnet (YAG) laser injury, and subhyaloid hemorrhage. The possible contractile-potent quality of tissue in the vitreous is demonstrated by the ultrastructural analyses of removed tissue specimen from patients with impending macular holes which

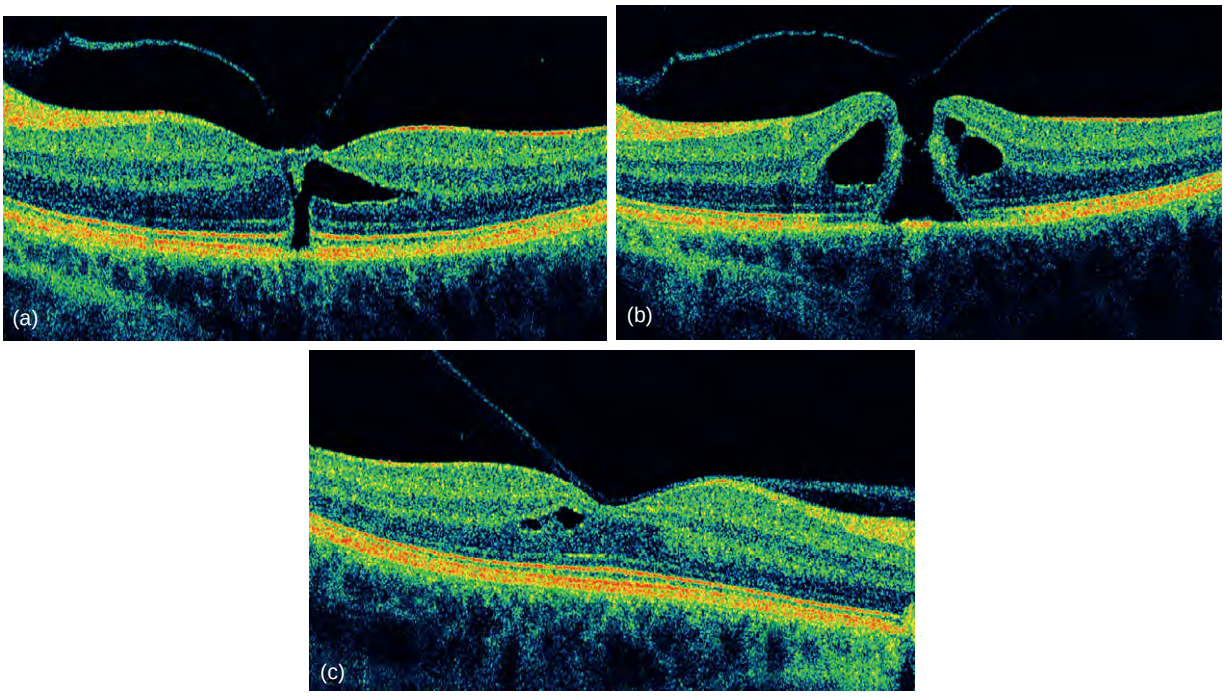

Figure 1 (a) Spectral domain OCT of right eye of a 60-year-old female with a visual acuity of 20/40 and a 2-week history of central visual disturbance. There is vitreous adherence at the fovea with associated cystic changes. (b) Spectral domain OCT 2 weeks later; the visual acuity has decreased to 20/70 with completion of a macular hole. (c) Fellow eye showing normal foveal contour with mild cystic change and with vitreous adherence at the fovea.

demonstrate glial-type tissue that might cause such a secondary tractional effect.

Confounding Observations

However, some macular holes have been observed under circumstances that do not seem to follow the mold of a direct or secondary, tractionally induced macular hole formation via active vitreous traction. These include macular hole cases that seemed to have been observed distantly after a documented short-term or long-term PVD, following the repair of retinal detachment repair or even after a vitrectomy for seemingly unrelated disorders. In addition, macular holes have been found to reopen clearly in the absence of any vitreous which would have been systematically removed at the time of previous surgery.

These observations have caused some to consider other possible mechanisms that may cause macular hole formation or may influence the vitreous role in macular hole formation. A leading mechanism besides vitreous traction as a primary element is the possible role of cystoid foveal changes. The finding of cystoid changes may represent a confounding of previously, undetected vitreous traction that might have been released, but may play a prominent role in the circumstances apparently leading to the macular hole by compromising the integrity of the already-delicate foveal elements. Unroofing of cystoid changes has been implicated in a variety of again, seemingly unrelated associations of macular hole formation with conditions including idiopathic juxtafoveal telangiectasis following uncomplicated phacoemulsification surgery and the presumed pseudophakic cystoid edema, macular edema for a branch vein occlusion, eyes with retinitis pigmentosa, and eyes as part of the Alport syndrome. The reopening of macular holes has been demonstrated to be preempted by some cystoid changes that seem to have no relationship to the vitreous since the vitreous was previously removed. Another case report of a formation of a macular hole after an OCT documented release of the posterior cortical remnant had been demonstrated a year and a half previously further brings into question the tractional induced role. The cystic changes observed might possibly be secondary to small breaks in the ILM or Henle's nerve fiber layer, which subsequently lead to hydration with secondary stiffening of the retina and extension of a separation into the deeper layers of the retina.

There are numerous elements that have been delineated above that may persist in the foveal area that could have contractile potential and lead to the separation of the foveal layers.

Figure 2 (a) Fundus appearance of left eye of a 70-year-old female with a visual acuity of 20/50 and a few months' history of an apparently nonprogressive central visual disturbance. (b) Time domain OCT shows vitreofoveal traction and mild cystic changes. (c) The clinical appearance and symptoms are unchanged 6 months later, but the OCT shows a more elongated vitreous attachment at the fovea. (d) There was a mild clinical improvement 3 months later, with visual acuity at 20/40, and the OCT appearance depicts spontaneous release of the vitreofoveal attachment.

Summary

The pathogenesis of macular holes has been widely reviewed. Undoubtedly, the vitreous plays a pivotal role in the formation of most, if not all, macular holes. Its actual role could vary from being the prime initiator and executor of traction at the fovea to being a sort of accomplice by transmitting traction generated elsewhere to being an innocent bystander to some other anatomic circumstances.

Cystoid changes seem to occur at least after a macular hole has occurred and very possibly before a macular hole is actually apparent. This could be because of hydration from a discontinuity in the Henle's nerve fiber layer or ILM break, or it could be a reflection of some other biochemical process that is occurring, possibly as a response to persistent vitreous traction. The formation of a macular hole in at least many cases is probably not simply from the vitreous separating, but rather from some abnormal features that are consummated by otherwise inconsequential persistent vitreous traction.

See also: Acuity; Adaptive Optics; Histogenesis, Cell Fate, and Signaling Factors; Hyalocytes; Pharmacological Vitreolysis.

Further Reading

Aaberg, T. M. (1970). Macular holes. A review. *Survey of Ophthalmology* 15: 139–162.

de Bustros, S. (1994). Vitrectomy for prevention of macular holes. Results of a randomized multicenter clinical trial. Vitrectomy for Prevention of Macular Hole Study Group. *Ophthalmology* 101: 1055–1059 discussion 1060.

Ezra, E., Wells, J. A., Gray, R. H., et al. (1998). Incidence of idiopathic full-thickness macular holes in fellow eyes: A 5-year prospective natural history study. *Ophthalmology* 105: 353–359.

Gass, J. D. M. (1988). Idiopathic senile macular hole: Its early stages and pathogenesis. *Archives of Ophthalmology* 106: 629–639.

Gass, J. D. M. (1995). Reappraisal of biomicroscopic classification of stages of development of a macular hole. *American Journal of Ophthalmology* 119: 752–759.

Green, W. R. (2006). The macular hole. Histopathologic studies. *Archives of Ophthalmology* 124: 317–321.

Hee, M. R., Puliafito, C. A., Wong, C., et al. (1995). Optical coherence tomography of macular holes. *Ophthalmology* 102: 748–756.

Kiry, J., Ogura, Y., Shahidi, M., et al. (1993). Enhanced visualization of vitreoretinal interface by laser biomicroscopy. *Ophthalmology* 100: 1040–1043.

Kishi, S., Demaria, C., and Shimizu, K. (1986). Vitreous cortex remnants at the fovea after spontaneous vitreous detachment. *International Ophthalmology* 9: 253–260.

Lipham, W. J. and Smiddy, W. E. (1997). Idiopathic macular hole following vitrectomy: Implications for pathogenesis. *Ophthalmic Surgery and Lasers* 28: 633–639.

McDonnell, P. J., Fine, S. L., and Hillis, A. I. (1982). Clinical features of idiopathic macular cysts and holes. *American Journal of Ophthalmology* 93: 777–786.

Sebag, J. (1998). Macromolecular structure of vitreous. *Progress in Polymer Science* 23: 415–446.

Sebag, J. (2004). Anomalous posterior vitreous detachment: A unifying concept in vitreo-retinal disease. *Graefe's Archive for Clinical and Experimental Ophthalmology* 242: 690–698.

Smiddy, W. E. and Flynn, H. W., Jr. (2004). Pathogenesis of macular holes and therapeutic implications. *American Journal of Ophthalmology* 137: 525–537.

Smiddy, W. E., Michels, R. G., Glaser, B. M., and deBustros, S. (1988). Vitrectomy for impending idiopathic macular holes. *American Journal of Ophthalmology* 105: 371–376.

Worst, J. G. F. (1977). Cisternal systems of the fully developed vitreous body in the young adult. *Transactions of the Ophthalmological Societies of the United Kingdom* 97: 550–554.

The Surgical Treatment for Corneal Epithelial Stem Cell Deficiency, Corneal Epithelial Defect, and Peripheral Corneal Ulcer

N Koizumi and S Kinoshita, Kyoto Prefectural University of Medicine, Kyoto, Japan

Glossary

Allogeneic – Taken from different individuals of the same species.
Aniridic keratopathy – The corneal opacification in congenital absence of the iris.
Atopic or vernal keratoconjunctivitis – The ocular conditions resulting from allergies. Type I and IV hypersensitivities have been demonstrated to play a role in the allergic response. Both disease processes manifest with classical symptoms of ocular allergy.
Cicatrization – The formation of scar tissue.
Corneal lenticules – Corneal disks, usually obtained from a donor.
Keratoepithelioplasty (KEP) – The transplantation of peripheral corneal lenticules harvested from donor tissue for the treatment of severe ocular surface diseases.
Keratolimbal allograft (KLAL) – A surgical procedure in which limbal tissue with peripheral cornea is obtained from donor eyes and transplanted to the recipient eyes. KLAL is performed to treat severe bilateral ocular surface disorders combined with limbal stem cell deficiencies.
Lamellar keratoplasty – An operation in which diseased corneal tissue is removed and replaced by lamellar corneal tissue from a donor. The procedure is performed either to improve vision (optical keratoplasty) or to provide structural support for the cornea (tectonic keratoplasty).
Limbal transplantation – The transplantation of limbal tissue including stem cells. Autografts and allografts of limbal transplantations were developed to improve the outcome of ocular surface reconstruction.
Mooren's ulcer – A rapidly progressive, painful, ulcerative keratitis, which initially affects the peripheral cornea and may spread circumferentially and then centrally.
Ocular cicatricial pemphigoid (OPC) – A chronic disease that produces adhesions and progressive cicatrization and shrinkage of the conjunctival, oral, and vaginal mucous membranes.
Penetrating keratoplasty – The corneal transplant involving the replacement of all layers of the cornea, yet retaining the peripheral cornea.
Stevens–Johnson syndrome – A condition affecting the skin in which cell death causes the epidermis to separate from the dermis. The syndrome is thought to be a hypersensitivity complex affecting the skin and the mucous membranes.
Superficial keratectomy – The removal of corneal epithelium and anterior stroma.
Symblepharon – Adhesion of the eyeball to one or both eyelids.
The *ex vivo* expansion of corneal epithelial cells/oral mucosal epithelial cells – A form of ocular surface reconstruction using cultivated corneal epithelial/oral mucosal epithelial cell sheets that are developed using tissue engineering techniques. Several types of cultivated epithelial sheets, with or without carrier materials, are used for the treatment of severe ocular surface diseases, such as Stevens–Johnson syndrome, ocular cicatricial pemphigoid, and severe chemical burns.

Introduction

The concept of an ocular surface has been widely accepted in the field of ophthalmology and investigations in this area have greatly improved our understanding of the important role that the ocular surface plays in the maintenance of vision and ocular health. The healthy ocular surface is composed of corneal and conjunctival epithelia, each of which has a distinct cellular phenotype. These two types of epithelia, with the presence of an intact tear film, maintain the ocular surface integrity. The corneal epithelium, especially, plays a critical role in maintaining corneal transparency and avascularity. On the basis of numerous investigations, it is now believed that corneal epithelial stem cells exist in the basal layer of the limbal regions where palisades of Vogt are seen in normal human subjects. Severe damage to the limbal

region, for example, damage caused by limbal stem cell deficiencies, results in serious corneal surface problems such as persistent epithelial defects, conjunctivalization with superficial vascularization, keratinization, scarring, etc., with an associated severe loss of vision.

In order to rescue such damaged ocular surfaces, surgical modalities have been developed over the past 20 years that are aimed at reconstructing the diseased ocular surface epithelium. In this article, we explain the surgical treatment for total stem cell deficiency.

Corneal Epithelial Transplantation for Total Stem Cell Deficiency

In Vivo Expansion of Corneal Epithelial Cells (Keratolimbal Allografts)

History and concept of ocular surface reconstruction

The concept of ocular surface reconstruction was first introduced via an autologous conjunctival transplantation for unilateral chemical injury reported in 1977 by Thoft. Thereafter, Thoft described a new technique known as keratoepithelioplasty (KEP), which involves the transplantation of peripheral corneal lenticules harvested from donor tissue for the treatment of severe ocular surface diseases. Following this development, autografts or allografts of limbal transplantations were developed to improve the outcome of ocular surface reconstruction. These surgical procedures, which involve the utilization of donor limbal stem cells in conjunction with the peripheral corneal lenticules, are now classified as keratolimbal allografts (KLALs), a kind of *in vivo* expansion of limbal stem cells.

Indications

KLAL is a procedure in which limbal tissue with peripheral cornea is obtained from donor eyes and transplanted to the recipient eyes. KLAL is performed to treat severe bilateral ocular surface disorders combined with limbal stem cell deficiencies. This procedure is also applicable to patients with unilateral disease who do not wish to use limbal tissue obtained from their healthy eye. KLAL is a surgery most suitable for diseases with total stem cell deficiency with less inflammation and less conjunctival cicatrization, such as ocular surface tumors (conjunctival intraepithelial neoplasia or squamous cell carcinoma) or aniridic keratopathy. For cases involving stem cell deficiency with severe inflammation, such as those resulting from chemical injury, Stevens–Johnson syndrome (SJS), or ocular cicatricial pemphigoid (OCP), a KLAL is applicable if the inflammation can be well controlled prior to surgery by steroid and immunosuppressive treatment and if conjunctival involvement is not severe. When the conjunctival scarring is severe, amniotic membrane (AM) transplantation combined with a KLAL is performed to reconstruct the conjunctival fornix (**Figure 1**).

Surgical procedure

For KLAL, fresh donor corneoscleral tissue preserved at 4 °C is used. Ideally, the donor tissue should be as fresh as possible when used, with surgery being performed within 6 days after preparation. After the central cornea of the donor tissue is excised with a 7.0–7.5-mm trephine, the peripheral cornea with scleral rim is sectioned into four to five pieces of lamellar grafts (lenticules). The residual corneoscleral rim after conventional penetrating keratoplasty is also useful. Under a surgical microscope, the excess peripheral scleral tissue of each lenticule is removed by scissors. Then, the posterior two-thirds of the corneal stroma that is attached by Descemet's membrane and the corneal endothelium are removed by lamellar dissection using spring scissors. After trimming the edge of each lenticule by spring scissors, the lenticules are placed onto the limbal area of the patient's eye and secured with two to three interrupted sutures per lenticule using 10-0 nylon. Immediately after surgery, a therapeutic soft contact lens is placed on the ocular surface to prevent donor epithelial damage and promote smooth corneal epithelial healing.

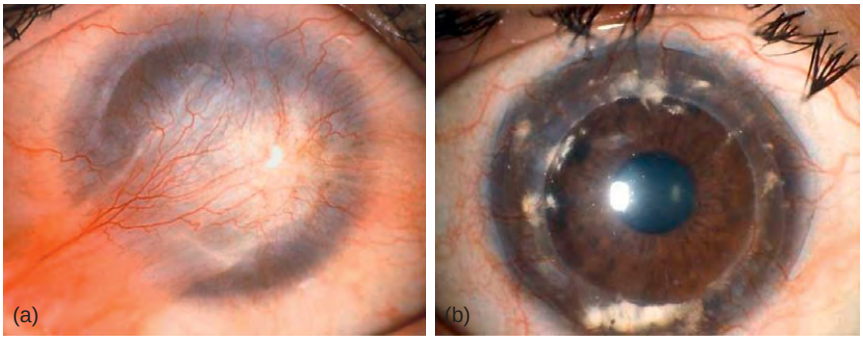

Figure 1 Keratoepithelioplasty combined with lamellar keratoplasty and amniotic membrane transplantation for chemical injury. (a) Before surgery, the patient's cornea was covered with conjunctival tissue. (b) One year after surgery, the corneal surface is covered with clear corneal epithelium and the patient recovered good vision.

Postoperative management

Compared to conventional penetrating keratoplasty, limbal allografts are at significantly higher risk for immunological rejection. Postoperatively, 0.1% dexamethasone and 0.05% cyclosporine A should be instilled topically, and dry-eye patients should receive preservative-free artificial tears. Systemic corticosteroids (betamethasone, 1 mg per day), cyclosporine A (3 mg per kg of body weight per day), and cyclophosphamide (1 mg per day), as well as mycophenolate mofetil (1 g per day), in some cases, should be used to prevent postoperative inflammation and immunological rejection. Systemic immunosuppression as described above should be used for at least 6 months postoperatively, after which it can be gradually reduced depending on clinical characteristics (Table 1). In many cases, it is necessary to administer a low dose of cyclosporine A (1 mg per kg of body weight per day) for up to 2–3 years.

A therapeutic soft contact lens should be used for several years after surgery, changing the lens once every 2–4 weeks, as it has been shown that continuous coverage of the corneal surface including the limbal area by use of a soft contact lens is effective for preventing immunological rejection as well as mechanical damage of the corneal epithelium. Although the working mechanism is unknown, it is speculated that the continuous soft contact lens wear may prevent the exposure of the donor limbal tissue to host immunocompetent lymphocytes in tears.

Other surgical procedures

Conjunctival limbal autograft (CLAU) is a procedure used for a unilateral stem cell deficiency, in which limbal tissue attached to a conjunctival carrier is transplanted from the healthy eye of the patient. The biggest advantage of this procedure is that no immunosuppression is required for an autograft. Living-related conjunctival limbal allograft (LR-CLAL) is a similar surgery to CLAU, yet in this procedure, a living relative of the patient is the source of the limbal tissue used for transplantation. LR-CLAL is applicable for bilateral stem cell deficiency. A major concern associated with both CLAU and LR-CLAL is the risk of stem cell deficiency of the donor eye. Prior to the surgery, it is vital to exclude any possibility of limbal stem cell damage in the donor eye, and it is important to continue observing the condition of the donor eye through postsurgical follow-up. Compared to the KLAL, the amount of limbal tissue that can be taken from the donor eye is limited in CLAU and LR-CLAL. Thus, partial stem cell deficiency is the appropriate condition for the use of those two procedures.

Table 1 Immunosuppressive treatment after all-corneal epithelial transplantation

Agent	*Dose and duration*
Topical	
corticosteroids	4 times per day, several years
Cyclosporine A	4 times per day, several years
Systemic	
corticosteroids	2–4 mg per day, 2–4 weeks
Cyclosporine A	100–200 mg per day, 6 months
Mycophenolate	1 g per day, 6 months
Cyclophosphamide (for Stevens–Johnson syndrome)	50–100 mg per day, 3 months

Ex Vivo Expansion of Corneal Epithelial Cells

History and concepts

There is no doubt that corneal epithelial transplantations, including limbal autografts and KLALs, have helped to improve the outcome of ocular surface reconstruction in a number of situations. However, in severe ocular surface diseases, such as SJS or OCP, severe inflammation interferes with *in vivo* epithelial healing and results in a persistent epithelial defect. An alternative concept to the *in vivo* expansion of corneal epithelial cells is the *ex vivo* expansion of corneal epithelium using a tissue engineering technique.

For this purpose, many investigators endeavored to reconstruct corneal epithelial sheets on carrier materials, such as collagen sheets, and corneal stromal carriers to create stratified corneal epithelial cell layers. Some groups tried to reconstruct not only the epithelial sheet, but also three layers of corneal tissue – a corneal equivalent – using cell-line cells supported by natural and synthetic polymers. This kind of corneal equivalent is now ready to be used for testing toxicity and drug efficacy, but it is not ready for clinical application.

Despite the potential drawbacks of cultivated corneal epithelial transplantation, its first clinical application was demonstrated in 1997. A method was developed to reconstruct stratified corneal epithelial cell sheets on petrolatum gauze or a soft contact lens as a carrier. Two patients, who had unilateral chemical burns, were treated by transplanting cultivated corneal epithelial cells taken from the limbus of the healthy contralateral eye. The well-established keratinocyte-culturing method, which involves the use of 3T3 feeder layers to help maintain epithelial stem cells, was used.

AM as a suitable carrier for corneal epithelial cell culture

Researchers soon realized the potential of AM as a carrier for corneal epithelial stem cell culture. AM is the innermost layer of the fetal membrane, and it is composed of a monolayer of amniotic epithelial cells, a thick basement membrane, and an avascular stroma. AM has been used for several years in a range of ocular surgeries, with or

without limbal transplantation, and has proven to be useful for the treatment of thermal and chemical injuries, severe pterygium, persistent or deep corneal ulcers, OCP, SJS, and other limbal stem cell deficiencies.

AM is known to have many unique characteristics that are beneficial to ocular surface reconstruction. Notably, AM inhibits conjunctival fibroblasts by suppressing the transforming-growth-factor-beta signaling system, and it also prevents myofibroblastic differentiation of normal fibroblasts. Furthermore, the normal differentiation of conjunctival epithelial cells is encouraged after AM transplantation. The basement membrane of AM is reported to resemble that of the conjunctival epithelium as well as that of corneal epithelium. In addition, growth factors, such as epidermal growth factor (EGF), keratinocyte growth factor (KGF), and hepatocyte growth factor (HGF), detected in AM may also play a role in accelerated epithelialization after AM transplantation. A high and therapeutic level of nerve growth factor (NGF) is also reported to be present in AM. It has been reported that AM has anti-inflammatory effects by inducing the suppression of interleukin 1α and interleukin 1β in limbal epithelial cells, as well as by trapping and preventing polymorphonuclear cells from infiltrating into corneal stroma.

Based on these interesting clinical and laboratory findings, preserved AM is considered to be one of the most appropriate carrier materials for transplantation of cultivated corneal epithelial cells. Although there is still debate surrounding its use, including the merits and demerits of the denuding process for amniotic epithelial cells and controversy regarding methods, the clinical results of cultivated corneal epithelial transplantation using an AM carrier are encouraging.

Cell culture procedure

Denuded AM is useful to promote the prompt migration of corneal epithelial cells *in vitro*, and AM has the potential to make well-stratified and differentiated corneal epithelial cell layers that express corneal-epithelium-specific keratins K3 and K12. In our clinical experiences, we have found that the ocular surface condition of candidates for cultivated corneal epithelial transplantation is very severe, often accompanied by complications such as severe aqueous-deficient dry eye and eyelid abnormality. For these patients, we consider it essential to transplant well-stratified epithelial cell layers that have developed barrier functions with well-controlled proliferative activity in basal cells and differentiated superficial cells. For this purpose, a culture system using an air-lifting method to promote epithelial cells via tight-junction formation was developed. By air-lifting, we have obtained cultivated epithelial cell sheets with smaller intercellular spaces in the superficial cells and with an epithelial barrier function. We have also attempted to transplant cultivated corneal epithelial cells, including limbal stem cells, and have developed a cell-suspension culture system capable of supplying cultivated corneal epithelial sheets that are well developed, potentially allowing the transplantation of more corneal epithelial stem cells.

Indications

In 1999, the Institutional Review Board of Kyoto Prefectural University of Medicine, Kyoto, Japan, approved the transplantation of cultivated corneal epithelial cell sheets. The use of cultivated corneal epithelial sheet transplantation was restricted to those patients who had poor visual prognosis with conventional corneal epithelial transplantation, such as a KLAL. Thus, cultivated corneal epithelial transplantation was performed on 39 eyes of 36 patients with total stem cell deficiencies such as severe chemical injury, SJS, and OCP (**Figure 2**). While the acute-phase eyes with persistent epithelial defects received cultivated corneal epithelial transplantation for the purpose of covering the corneal surface, alleviating intensive inflammation, and avoiding complications that accompany persistent epithelial defects, the chronic-phase eyes

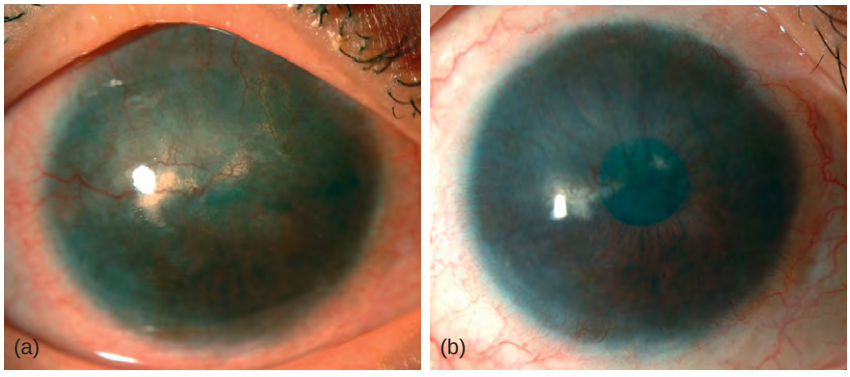

Figure 2 Ocular surface reconstruction using *ex vivo* expanded corneal epithelial cells for the chronic phase of Stevens–Johnson syndrome. (a) Before surgery, the patient suffered from total stem cell deficiency. (b) One year after surgery, the corneal surface is covered with clear corneal epithelium.

received cultivated corneal epithelial transplantation to obtain better visual function.

Surgical procedure

In our surgical procedure, scarred conjunctival tissue overlying the ocular surface from the cornea is removed up to approximately 3 mm outside of the limbus. After removing the subconjunctival tissue, the small tips of several microsponges containing 0.04% mitomycin C are placed in the subconjunctival space adjacent to the cornea for 5 min and vigorous saline washing is then performed to prevent the development of subconjunctival fibrosis after surgery. A cultivated corneal epithelial sheet on AM is then transplanted onto the corneal surface and sutured using 10-0 nylon. A therapeutic soft contact lens is then applied. For the chronic-phase eyes with corneal stromal scarring, lamellar keratoplasty is first performed with the use of preserved donor grafts to replace the scarred corneal stroma, followed by cultivated corneal epithelial transplantation.

Postoperative management

Postoperatively, 0.1% dexamethasone and 0.05% cyclosporine A are instilled topically, and dry-eye patients receive preservative-free artificial tears. Systemic corticosteroids (betamethasone, 1 mg per day), cyclosporine A (3 mg per kg of body weight per day), and cyclophosphamide (1 mg per day), as well as mycophenolate mofetil (1 g per day), in some cases, should be used to prevent postoperative inflammation and immunological rejections. Systemic immunosuppression as described above should be used for at least 6 months postoperatively, after which it can be gradually reduced depending on clinical characteristics (Table 1). In many cases, it is necessary to administer a low dose of cyclosporine A (1 mg per kg of body weight per day) for up to 2–3 years.

Clinical outcome of allogeneic cultivated corneal epithelial transplantation

The epithelial integrity was satisfactory in all cases, as evidenced by the fact that the transplanted corneal epithelium did not stain with sodium fluorescein just after being transferred onto the ocular surface during surgery. In addition, in every case there was no epithelial damage to the transplanted corneal epithelium 48 h after transplantation. The transplanted AM did not disturb the visual acuity, and clarity increased day by day. Surprisingly, the preoperative ocular surface inflammation, which had not been controlled by conventional treatment, decreased rapidly after surgery in all of the acute-phase patients.

In the chronic-phase eyes, the long-term visual prognosis and epithelial stability were varied in the three kinds of diseases discussed below. In the case of severe chemical injury, the transplanted corneal epithelium was clear and stable up to 8 years after transplantation, and very little conjunctival inflammation was present during the entire postoperative period. On the other hand, in patients with Stevens–Johnson syndrome, mild to moderate ocular surface inflammation occurred several months after surgery, and then decreased during the following 18 months. Whereas subconjunctival fibrosis had not progressed in the eyes with SJS, conjunctival scarring such as symblepharon and shortening of the fornix had progressed in the eyes with OCP. In most of the chronic-phase patients with SJS and OCP, the phenotypes of ocular surface cells on AM gradually changed from donor to host epithelial cells over a couple of years; however, subepithelial scarring and neovascularization did not progress. In other words, host conjunctival epithelium replacement on AM occurred without scarring. This phenomenon is considered to be partly due to a mild rejection of the transplanted corneal epithelial cells. Although graft survival was not very long in some eyes in these chronic cases, the ocular surface maintained its transparency and the patients obtained a better visual function than before surgery. It is possible to perform regrafting of cultivated corneal epithelium in which the severity of epithelial opacity progressed after an episode of rejection or persistent conjunctival inflammation.

In unilateral cases, autologous cultivated corneal epithelial transplantation is applicable. There is less damage to the contralateral eye than has been the case with limbal autografts, and the cultivated corneal epithelial sheets formed well-stratified epithelial layers from the very small amount of limbal tissue. After a substantial follow-up period, the transplanted epithelium remained transparent and stable, and the patient achieved good visual acuity with no complications in the healthy contralateral eye.

Ex Vivo Expansion of Oral Mucosal Epithelial Cells

Concept

Due to the fact that severe ocular surface diseases are usually bilateral, allogeneic corneal epithelial transplantation (either KLAL or cultivated corneal epithelial transplantation) is normally performed. However, these procedures not only require sufficient donor tissue, but they also are accompanied by the risk of rejection; therefore, prolonged immunosuppression is required that severely affects the clinical results. With these drawbacks in mind, we have established cultivated oral mucosal epithelial transplantation using autologous tissue.

Cell culture procedure

Small oral biopsies (approximately 2–3 mm in size) are obtained from the oral cavity under local anesthesia. The biopsy specimens are then incubated with enzymatic reagents, such as dispase and trypsin – ethylenediaminetetraacetic acid (EDTA), to separate the cells from the underlying connective tissue. The resultant single-cell suspension

of oral mucosal epithelial cells is then co-cultured for 2–3 weeks on a denuded AM carrier with inactivated 3T3 fibroblasts. Toward the end of the culture period, an air-lifting technique is used to facilitate epithelial differentiation and stratification. The oral mucosal epithelial cells cultivated on AM will show five to six layers of stratification and appear very similar to *in vivo* normal corneal epithelium. The cultivated oral mucosal epithelial sheet will show non-keratinized, mucosal-specific keratins 4 and 13, and cornea-specific keratin 3; however, keratinization-related keratin 1 or keratin 10 will not be detectable. Under appropriate culture conditions, oral mucosal epithelial cells cultivated on AM have the potential ability to differentiate into cornea-like epithelial cells.

Indications

In our clinical trials, we applied cultivated oral mucosal epithelial transplantation in two different forms of surgery with a total of 50 eyes. One form of surgery was reconstruction of the corneal surface of a severe bilateral corneal stem cell deficiency, using a cultivated oral mucosal epithelial sheet instead of allogeneic corneal epithelium. The other was reconstruction of the conjunctival fornix in patients with OCP, SJS, and chemical and thermal burns (**Figure 3**).

Surgical procedure and postoperative medications

The surgical procedure is almost the same as that of cultivated corneal epithelial sheet transplantation. After complete removal of damaged tissue on the corneal surface and subconjunctival fibroblastic tissue, residual subconjunctival tissue is treated for 5 min with 0.04% mitomycin C, followed by vigorous repeated washing with saline in order to suppress the excessive preoperative inflammation and subconjunctival fibrosis. Then, the cultivated oral mucosal epithelial sheet on AM is transplanted onto the corneal surface and secured with 10-0 nylon sutures at the limbus. The integrity of the cultivated oral mucosal epithelium is then confirmed via intraoperative fluorescein staining, and a therapeutic soft contact lens is applied. Postoperatively, topical antibiotics and corticosteroids are usually applied. Due to the fact that it is an autograft, immunosuppressives are not necessary, except for corticosteroids and cyclosporine to control the inflammation of the original disease.

Clinical outcome of cultivated autologous oral mucosal epithelial transplantation

Using slit-lamp examination with fluorescein staining, the survival of the transplanted epithelium can be confirmed 48 h after surgery. An epithelial phenotype of transplanted cultivated oral mucosal epithelium will be somewhat distinguishable from the conjunctival epithelium by fluorescein staining. Our preliminary data show the successful survival of autologous cultivated oral mucosal epithelium on the ocular surface without returning to an *in vivo* oral tissue phenotype, as was previously the case with oral mucosal transplantation. This major difference can be explained by the elimination of the subconjunctival fibrous tissue and vascular component in oral mucosa during the tissue culture system. It is possible that AM has some effect on this phenomenon as well. One adverse effect of this procedure is that the transplanted cultivated oral mucosal epithelium can sometimes show some neovascularization in the peripheral cornea with epithelial thickening. For cases with poor visual recovery due to the optical corneal opacity, the two-step surgical combination of cultivated autologous oral mucosal epithelial transplantation followed by penetrating keratoplasty is advised.

Cultivated oral mucosal epithelial transplantation is also useful for reconstruction of the conjunctival fornix; this form of surgery is successful in cases of cicatricial pemphigoid, chemical injury, etc. However, it is important to be aware of abnormal postoperative fibrovascular proliferation caused by primary diseases, which is still critical to the long-term prognosis.

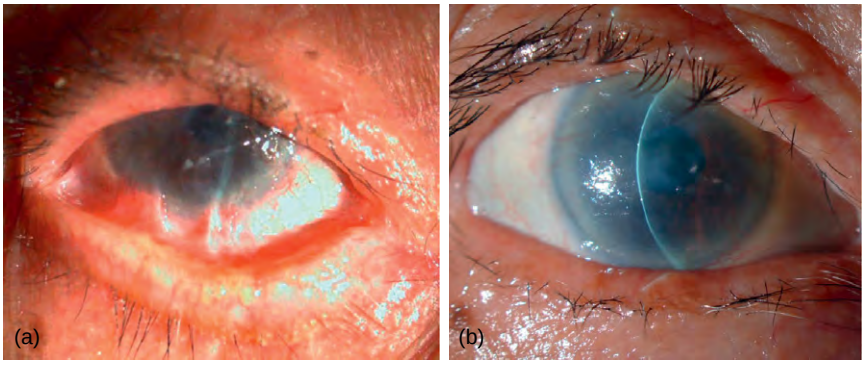

Figure 3 Ocular surface reconstruction using cultivated autologous oral mucosal epithelium for severe total stem cell deficiency in ocular cicatricial pemphigoid. (a) Before surgery. (b) Two months after surgery, the corneal surface is covered with cultivated oral mucosal epithelium and the fornix is well reconstructed by the surgery.

Phototherapeutic Keratectomy for Corneal Epithelial Disorders

Phototherapeutic keratectomy (PTK) using an excimer laser is a good therapeutic tool for a variety of corneal surface disorders, including corneal degenerations and dystrophies, epithelial adherence problems, persistent epithelial defects, corneal irregularities, and superficial stromal scars. PTK, with or without manual superficial keratectomy, can make the patient's corneal surface smooth and can effectively improve visual acuity or relieve symptoms such as pain, glare, and tearing.

PTK for Corneal Epithelial Defect

Indications

Recurrent epithelial erosions associated with posttraumatic or epithelial basement dystrophy resistant to the conventional therapy, including lubricative medications, bandage soft contact lens, or epithelial debridement, are good indications for PTK. PTK is also very effective for Schield ulcer seen in patients with either vernal or atopic keratoconjunctivitis.

Surgical procedure

Prior to an excimer laser abrasion to the surface, any disadherent epithelium adjacent to the epithelial defect, but not degenerated epithelium, should be removed by gentle manual debridement. Then, a 10–20-0m abrasion should be performed either focally or diffusely depending on the area for treatment. The area to be abraded should encompass the area of epithelial defect and include 1 mm of adjacent cornea. Application of artificial-tear eye drops just prior to laser abrasion will enhance the smoothness of the cornea surface.

Postoperative management

After the laser abrasion, a disposable bandage contact lens is applied to enhance reepithelialization and reduce the pain. For the best results, the patient should wear the contact leans for up to 3 months to establish permanent epithelial-basement-membrane adhesions. Topical antibiotics and corticosteroids are essential to prevent infection and decrease postoperative inflammation. We suggest the instillation of 0.1% betamethasone and 0.3% levofloxacin 4 times per day for 2 weeks, followed by a tapering-off of the dosage.

Tectonic Lamellar Keratoplasty for Peripheral Corneal Ulcers

Concept

Lamellar keratoplasty is an operation in which diseased corneal tissue is removed and replaced by lamellar corneal tissue from a donor. The procedure is performed either to improve vision (optical keratoplasty) or to provide structural support for the cornea (tectonic keratoplasty). Lamellar keratoplasty can be performed to replace just a portion of the corneal thickness when the endothelium is healthy. Depending on the location of the corneal abnormality, it may be sufficient to replace just the anterior layers with lamellar keratoplasty, or the full thickness of the corneal stroma without endothelium, with deep lamellar keratoplasty. Postoperative care involving the use of appropriate immunosuppressive therapy often influences the results of optic keratoplasty as well as tectonic keratoplasty.

Rheumatoid Arthritis

Peripheral corneal ulceration is associated with scleral or episcleral inflammation in rheumatoid arthritis (RA) patients. When corneal thinning progresses or perforation occurs in reaction to conventional steroid therapy, KEP combined with peripheral lamellar keratoplasty is effective. In RA patients, paracentral corneal perforation is also often observed. Small-size lamellar keratoplasty is a good surgical treatment for paracentral corneal perforation. However, it is important to bear in mind that the prognosis for penetrating keratoplasty is not good for RA patients.

Pre- and postoperative antirheumatic therapies improve surgical results. We recommend the application of therapeutic soft contact lenses at the conclusion of surgery; these should then be continuously used for several years to avoid the infiltration of immunoreactive cells from tears and prevent the recurrence of ulceration. Topical corticosteroids and antibiotic drops should be applied 4 times per day. The frequency should then be decreased as inflammatory signs subside to a level of two to three drops per day for several months. Careful removal of the sutures is performed during the first and second postoperative months to avoid epithelial damage. To avoid the recurrence of the original disease, corticosteroid drops should be continued once or twice per day for a number of years.

Mooren's Ulcer

For the treatment of severe Mooren's ulcer, which does not respond to steroids or immunosuppressive therapy using cyclosporine A, one surgical option which is available is KEP, with or without lamellar keratoplasty. By transplanting the Bowman's layer with a thin corneal stroma onto the sclera adjacent to the ulcerated area, inflamed conjunctival tissue is unable to invade the corneal surface and cellular infiltration of the ulcerated peripheral cornea is prevented (**Figure 4**). Pre- and postoperative anti-inflammatory therapy, including systemic cyclosporine A, is important for the achievement of good surgical results. In our cornea service, we administer oral

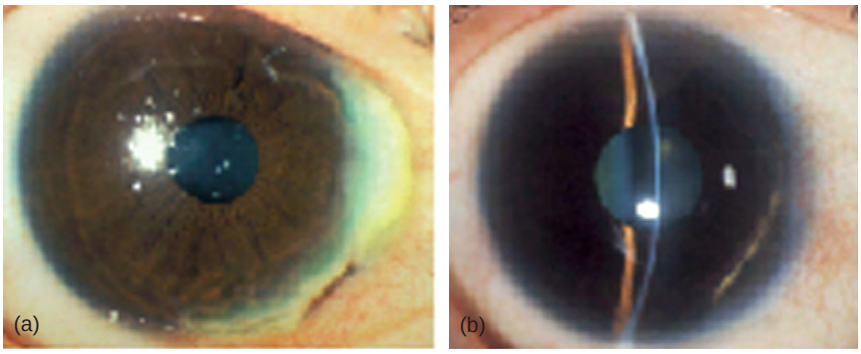

Figure 4 Keratoepithelioplasty for Mooren's ulcer. (a) Before surgery (visible from the 1 o'clock to 6 o'clock position). (b) Ten years after keratoepithelioplasty. There was no recurrence of Mooren's ulcer.

cyclosporine A (100–200 mg per day) and oral betamethasone (2–4 mg), as well as topical 0.1% dexamethasone (4 times per day) and antibiotics (0.3% ofloxacin).

As mentioned earlier, careful removal of the sutures is performed during the first and second postoperative months to avoid epithelial damage. To avoid the recurrence of the original disease, the extended use of therapeutic soft contact lenses and corticosteroid eye drops (1–2 times per day) should be continued for as many years as possible.

See also: Contact Lenses; Corneal Epithelium: Cell Biology and Basic Science; Corneal Epithelium: Wound Healing Junctions, Attachment to Stroma Receptors, Matrix Metalloproteinases, Intracellular Communications; Defense Mechanisms of Tears and Ocular Surface; Lids: Anatomy, Pathophysiology, Mucocutaneous Junction; Stem Cells of the Ocular Surface.

Further Reading

Das, S. and Seitz, B. (2008). Recurrent corneal erosion syndrome. *Survey of Ophthalmolgy* 53: 3–15.

Dua, H. S. and Azuara-Blanco, A. (1999). Amniotic membrane transplantation. *British Journal Ophtalmology* 83: 748–752.

Holland, E. J., Schwartz, G. S., and Nordlund, M. L. (2005). Surgical technique for ocular surface reconstruction. In: Krachmer, J. H., Mannis, M. J., and Holland, E. J. (eds.) *Cornea,* 2nd edn., pp. 1799–1812. Philadelphia, PA: Elsevier Mosby.

Kenyon, K. R. (1989). Limbal autograft transplantation for chemical and thermal burns. *Developments in Ophthalmology* 18: 53–58.

Kinoshita, S., Koizumi, N., and Nakamura, T. (2004). Transplantable cultivated mucosal epithelial sheet for ocular surface reconstruction. *Experimental Eye Research* 78: 483–491.

Kinoshita, S., Koizumi, N., Sotozono, C., et al. (2004). Concept and clinical application of cultivated epithelial transplantation for ocular surface disorders. *Ocularsurface* 2: 21–33.

Kinoshita, S., Ohashi, Y., Ohji, M., and Manabe, R. (1991). Long-term results of keratoepithelioplasty in Mooren's ulcer. *Ophthalmology* 98: 438–445.

V

The Vascular Stem Cell

A V Ljubimov, Cedars-Sinai Medical Center, Los Angeles, CA, USA
L C Shaw, S Li Calzi, J V Kielczewski, S Caballero, M E Boulton, and M B Grant, University of Florida, Gainesville, FL, USA

Glossary

Angioblast – One of two products derived from a hemangioblast; an undifferentiated endothelial progenitor cell that has yet to integrate into a blood vessel.
Angiogenesis – The formation of new blood vessels from preexisting ones; it involves sprouting of endothelial cells that contribute to the growing blood vessel.
CD34$^+$ cells – It is derived from HSCs, referred to as an endothelial progenitor cell, which can give rise to mature endothelial cells, that make up blood vessels. It expresses the CD34 early developmental cell marker.
Chimeric mice – The hybrid mice that are reconstituted with murine donor green fluorescent protein (GFP$^+$) hematopoietic stem cells (HSCs) via a bone marrow transplant, as well as a small subset of their own resident HSCs, which were not depleted after lethal body irradiation.
Choroid – A thin, vessel enriched membrane lying between the retina and the sclera that provides oxygen and nourishment to the outer layers of the retina.
CFU – Colony-forming unit, a measure of viable cells in which a colony represents an aggregate of cells derived from a single progenitor cell.
Differentiation – The process by which an unspecialized primitive cell acquires the features of a specialized cell, such as a heart, liver, or muscle cell. As cells differentiate they become more committed toward a final fate, losing the expression of early developmental markers.
Endothelial progenitor cell (EPC) – A bone-marrow-derived cell that circulates in the blood and has the ability to differentiate into an endothelial cell, the cells that make up the lining of blood vessels.
Hematopoietic stem cell (HSC) – The stem cell that originates from the bone marrow, which gives rise to all the blood cell types.
Homing – The process by which EPCs or HSCs, once in the bloodstream, extravasate and head to the area of injury where they are needed for tissue repair.
Ischemia – The deficient supply of blood to a body part that is due to obstruction of the inflow of arterial blood, resulting in tissue damage.
Neovascularization – The process involving abnormal formation of new blood vessels, usually in or under the retina. The new blood vessels are usually fragile, which tend to hemorrhage causing blood to leak into the eye and impairing vision. It can lead to vision loss or even blindness in diabetic retinopathy, macular degeneration, and other vascular occlusive diseases.
Stromal cell-derived factor-1 (SDF-1) – A chemokine with unique functions, including a role in the trafficking of EPCs. It is a potent migratory stimulus and upon injury recruits EPCs to sites of damage. SDF-1 exerts its action through binding to and activation of its cell surface receptor, CXCR4, expressed on EPCs and HSCs.
Vascular endothelial growth factor (VEGF) – One of the most important endothelial growth factors; it is often secreted by oxygen-deprived cells. VEGF stimulates new blood vessel formation by binding to specific receptors on nearby blood vessels, stimulating new blood vessels to form.
Vasculogenesis – The formation of new blood vessels from vascular stem cells; it involves incorporation of stem cells into the growing blood vessel and their differentiation into endothelial cells.

The Discovery of the Endothelial Precursor Cell and Circulating Endothelial Cells

By the early 1960s, patients with cardiovascular disease were undergoing artificial vascular grafts which, upon later excision, were covered by a layer of endothelial cells (ECs). While it was believed that the endothelium found on these vascular grafts grew from the original vessel ends at the site of anastomosis, Stump and co-workers determined that circulating cells could colonize this artificial substrate. This was cleverly tested by suspending a piece of Dacron material within a pig aortic graft and isolating the surface of the Dacron material from any microvasculature. Two weeks later they observed patches of endothelium on the graft, and by 20 days, the graft segment was completely lined by endothelium, concluding that circulating endothelial cells (CECs) must have attached and proliferated to coat the suspended material. Ten years later, Gaynor and co-workers measured the number of CECs in the blood of rabbits and demonstrated an increase in CEC concentration after endotoxin administration. He was the first to suggest that CECs might be a biomarker to measure vascular injury. Now it is well established that CEC levels reflect vascular injury and disease following coronary angioplasty, acute coronary syndromes, unstable angina, and in patients with diabetic retinopathy. Increased CECs are associated with peripheral vascular disease, inflammatory vasculitis, and during organ transplant rejection. The concentration of CECs in the blood of healthy individuals is quite low (about 3 cells ml^{-1}), but, as described above, this number is dramatically increased in disease.

In 1997, Asahara and co-workers purified a population of circulating cells that displayed properties of both ECs and progenitor cells, which he termed endothelial progenitor cells (EPCs); they were purported to give rise to differentiated ECs in a process termed postnatal vasculogenesis. Before this exciting finding, vasculogenesis was thought to occur only in the developing fetus when progenitors of endothelium (angioblasts) differentiate to form growing vessels in developing tissues. Vascular remodeling in the adult, however, involves the recruitment of not only endothelial progenitors, but also numerous different cells in an intricate collaboration. As elegantly described by Schatteman and co-workers, sprouted endothelium may line the vessel lumen, while other cells support vessel formation through secretion of cytokines.

Whereas the existence of EPC is no longer in question and the significance of CECs as biomarkers of vascular health is well accepted, the field now suffers from the lack of clarity in the identification of EPC populations and their precise function. Different cell types are involved in postnatal vasculogenesis, but they are all lumped together as EPCs. The origin of EPC is also in question and debate continues about lineages and their derivation.

Bone Marrow Microenvironment for the Hematopoietic Stem Cells

Hematopoietic stem cells (HSCs) are believed to be the source of EPCs by many investigators, whereas others believe that the vessel wall can also be a source of these precursors. The bone marrow (BM) stem cell niche consists of a specialized microenvironment that nurtures and regulates the stem cell pool (**Figure 1**). Parmar and co-workers showed that a relatively low level of oxygenation is a hallmark of the BM stem cell niche and that primitive hematopoietic cells in the BM are sequestered in a hypoxic microenvironment. This implies that low oxygen levels play a fundamental role in the maintenance of normal function of BM stem cells that are typically non-cycling with less metabolic need for oxidative respiration. Furthermore, quantitative proteomic analysis of isolated BM populations indicates that these cells express high levels of glycolytic and oxidative repair proteins, supporting that these cells are adapted to anaerobic metabolism. Moreover, hematopoiesis is improved *ex vivo* by maintaining cell cultures at levels of between 1% and 3% O_2. When mice were infused with Hoechst dye, which stains cells based on their proximity to blood vessels, the lowest Hoechst perfused BM fraction contained 90- to 200-fold more HSCs compared to the highest perfused fraction, supporting that HSCs are located in regions of the lowest oxygen concentration. These low Hoechst cells were also found to be hypoxic by co-staining with antibody to pimonidazole (PIM), a chemical marker for hypoxia. PIM binding and low Hoechst staining identified the long-term retaining (LTR)-HSC population. The oxygen gradient within the BM seems to provide a positional effect that not only defines the spatial organization of the hematopoietic system and confers a primary physiological role in maintaining stem cell homeostasis, but also provides a microenvironment protected from the toxic and mutagenic effects of oxygen-generated free radicals.

Clonal Relationship of EPCs to HSCs

In the original description of colony-forming unit (CFU)-ECs by Asahara and co-workers, 27.2% of the cultured cells retained cluster of differentiation 45 (CD45) expression and 6% expressed the hematopoietic antigen CD68. Hematopoietic antigen expression in the primary culture was taken as an indication for a relationship between CFU-ECs and HSCs. We proposed that any common precursor for both hematopoietic and endothelial lineages might be evaluated in long-term repopulating HSC transplant studies. Transplanting single HSCs into animals that subsequently underwent retinal injury, we observed that some of the vessels newly formed after injury to the retinal vasculature were derived from the donor stem cells. These results led us to

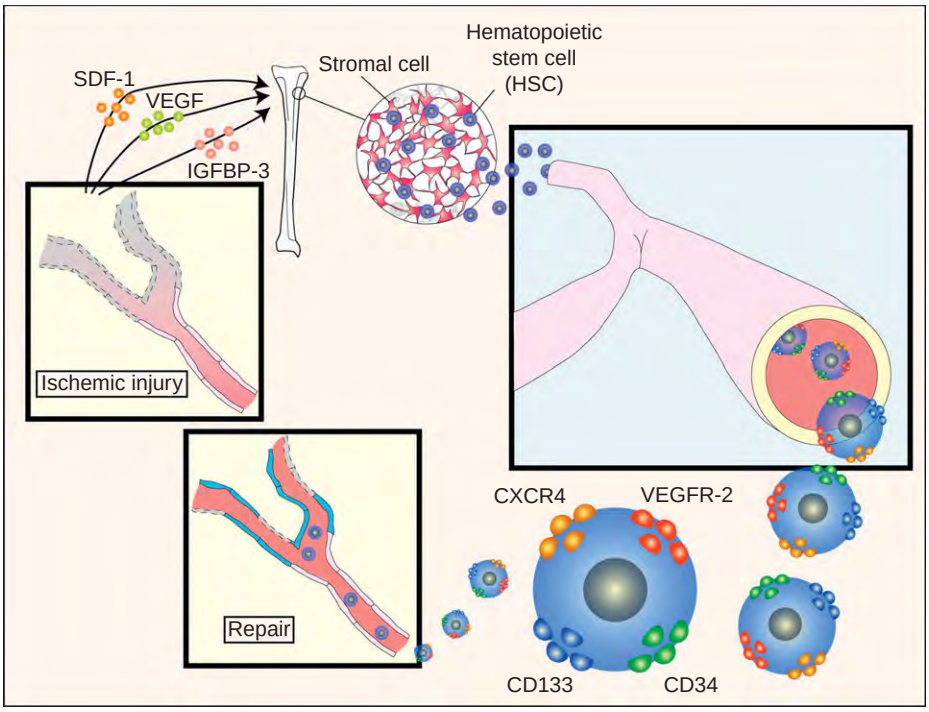

Figure 1 Schematic representation showing pro-angiogenic growth factors such as IGFBP-3, SDF-1, and VEGF, being released from ischemic blood vessel injury sites. The three ischemia-induced growth factors have a profound effect on $CD34^+$ EPCs, which reside in the bone marrow niche. IGFBP-3, SDF-1, and VEGF stimulate $CD34^+$ cells to migrate out of the bone marrow niche into the circulation where they home to sites of injury and actively participate in vascular repair and re-endothelialization.

conclude that HSC can generate all the blood elements and blood vessels and that a hemangioblast-like cell can persist into adulthood, and that these cells are derived from the same HSCs that have a long-term hematopoietic repopulating ability. Cogle and co-workers utilized the same murine retina injury model, but the injury was preceded with transplants of human umbilical cord blood (CB)-derived $CD34^+$ cells, which again repopulated the murine hematopoietic system; they also noted that human donor cells contributed to the murine host neovasculature, and speculated that only hematopoietic cell progenitors participated in blood reconstitution and blood vessel repair.

Nomenclature of the EPC

A complex relationship exists among EPC types and mononuclear cell (MNC) subtypes. The use of different isolation procedures from peripheral blood (PB) further complicates the comparisons. Recently, Yoder and colleagues have attempted to simplify the nomenclature in the field of EPC-related research and have integrated information on the phenotype of the cultured cells and their properties *in vivo*, thus taking on the task of classifying the different *in vitro* features and extrapolating to their *in vivo* origins (hematopoietic or nonhematopoietic) in these cells involved in repair of the vasculature. They conclude, as does Dimmler's group, that the vast majority (>99.99%) of $CD45^+$ MNCs are hematopoietic elements.

There are several common methods of EPC culture from the MNCs of the blood. To isolate CFU-EC includes a 5-day process wherein nonadherent MNCs give rise to an EPC colony. This is the approach used by Asahara to identify EPC for the first time. These represent a small fraction of blood MNCs, roughly in the range of 50–500 cells ml^{-1} of adult PB. Circulating angiogenic cells (CACs) are the adherent MNCs of a 4- to 7-day culture procedure. CAC cultures typically do not display colony formation. A major portion of circulating mononuclear phagocytes (roughly 5% of PB MNCs) has been termed CAC, a critically important cell to the healing process. The Yoder group hypothesized that CACs constitute a heterogeneous population of mostly differentiated myeloid cells. The detailed profile of cells within CAC cultures has not yet been established, but CACs have been reported to constitute 2% of all blood MNCs.

Endothelial colony-forming cells (ECFCs) are derived from adherent MNCs cultured for 7–21 days in conditions favoring endothelial differentiation, and colonies display cobblestone morphology. CFU-ECs are hematopoietic by clonal lineage tracking, a feature likely to be shared by CACs.

Based on *in vivo* studies using the retinal vasculature as the model system, single cell transplantation, and serial

transplantation, we concluded that HSCs give rise to all EPC populations. Yoder and colleagues disagree and expand on this by stating that the hematopoietic progenitor cells (HPC or HSC) overlap with CFU-ECs to a degree that has yet to be determined, and that the CAC population does not overlap with the HPC population. They propose that CD45 expression distinguishes hematopoietic from non-hematopoietic EPC populations and further propose that the nonhematopoietic CEC population constitutes a much smaller fraction of MNCs than do hematopoietic CAC and CFU-EC populations. They propose that ECFCs reside within the CEC population and that ECFCs display all the properties of a circulating endothelial progenitor. They also reported that ECFCs reside throughout the vascular endothelium and hypothesized that these ECFCs may get mobilized to become a propose that ECFCs reside within the CEC population. ECFCs are found at a concentration of about 0.05–0.2 cells ml^{-1} in adult PB, whereas CECs occur at a frequency of 3 cells ml^{-1} in adult PB. Thus, in human subjects, ECFCs appear to arise independently of hematopoietic precursors.

The complexity is increased by the common belief that the majority of work conducted in the field of EPC replacement therapy has been focused on cells that do not give rise to vessels, but which recruit or facilitate the cells that do. Recruitment has emerged as a critically relevant step in the healing process, which can be illustrated by the vast number of inflammatory cells at sites of ischemic injury, including the involvement of myeloid cells at those sites. Further research is required to link the processes involved in the recruitment of hematopoietic elements necessary for vascular repair to the endothelial progenitor recruitment from either the vessel wall or the circulation.

Making New Blood Vessels with BM Cells

Angiogenesis occurs in both the adult and embryo and is a process wherein differentiated ECs proliferate and migrate as the extracellular matrix is degraded at sites along existing blood vessels, allowing sprouts to form new tubes. Initially, capillaries are formed, some of which go on to recruit smooth muscle cells and mature into arterioles. Adult EPCs appear to contribute to this process (**Figures 2** and **3**). Schatteman and co-workers found that capillary-like structures are formed in $CD14^+$ BM-derived cell cultures through vacuolization and coalescence of multiple cells, a process normally associated with angiogenesis. Numerous papers have reported the sporadic integration of BM-derived cells into EC tubes *in vitro* and blood vessels *in vivo*, again consistent with a role for BM-derived cells in angiogenesis (**Figure 4**).

Studies of BM-derived cells indicate that this process can occur in the adult as well. Asahara showed the formation of blood-island-like structures by $CD34^+$-enriched BM-derived cells *in vitro*; however, more importantly, the formation of blood vessels *in situ* from BM-derived cells was subsequently reported *in vivo*, both of which are suggestive of adult vasculogenesis.

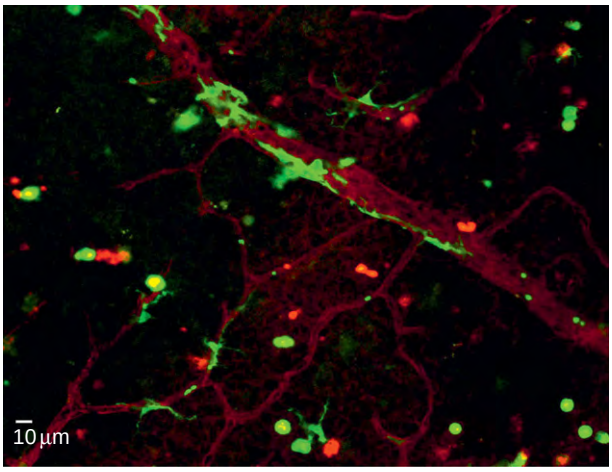

Figure 2 Laser injury promotes recruitment of bone-marrow-derived GFP^+ HSCs to the retinal vasculature. Confocal microscopy image of a retinal flat mount, from a chimeric mouse that underwent laser retinal vessel occlusion injury, double stained with rhodamine-agglutinin (red), to reveal blood vessels, and anti-GFP (green), to reveal GFP^+ $c\text{-}kit^+$, $Sca\text{-}1^+$ HSC. Scale bar = 10 μm.

Blood vessels can be formed by intussusception, which occurs in both the embryo and adult. This is the formation of a vascular network by division of larger vessels into smaller through focal insertion of a tissue pillar or by longitudinal fold-like splitting of a vessel. This process is difficult to study and, to our knowledge, no one has looked at intussusception in vessels of BM origin. A new process, the drilling of tunnels by monocytes, was described only recently. In this process, $F4/80^+$ monocyte/macrophages pattern the tissue space by degrading the extracellular matrix, thereby facilitating the penetration of EC precursors and other cells. In addition, the $F4/80^+$ cells can themselves form lumens and line the resulting tubes, apparently rapidly establishing a local microcirculation. The $F4/80^+$ cells may also stimulate differentiation of progenitors in the tube. The origin of the ECs that ultimately come to line these drilled tunnels is not yet known.

With the onset of neovascularization due to hypoxia, injury, or other stimuli, one might anticipate that the contribution of BM-derived cells to the endothelium would increase, and this has been observed repeatedly. For example, 8.3–11.2% of total ECs in the neovessels of an implanted angiogenic sponge and ischemic limb were found to be of BM origin. Similarly, the contribution of BM-derived cells to skin graft neovascularization was ~15–20% of new ECs. In addition, when a gradient of hypoxia was created in skin wounds in mice, recruitment

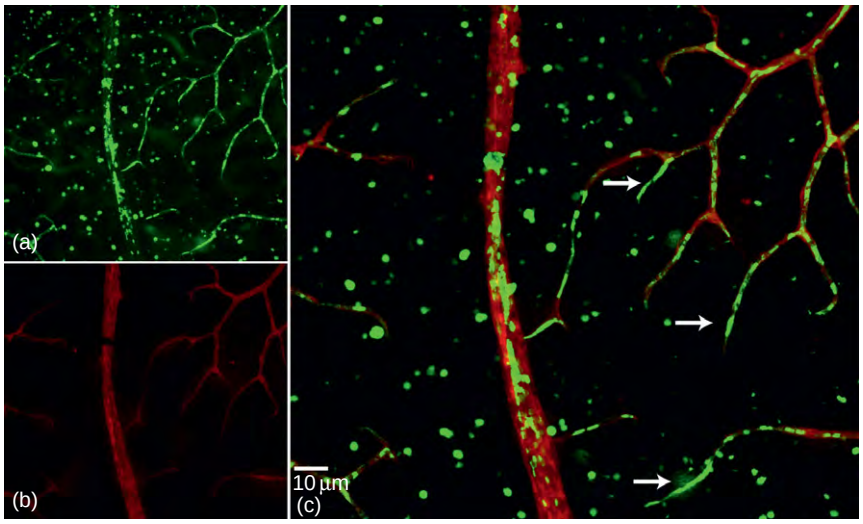

Figure 3 Insulin-like growth factor binding protein-3 (IGFBP-3) promotes recruitment of bone-marrow-derived GFP$^+$ HSCs to the retinal vasculature in the absence of injury. Confocal microscopy images of a retinal flat mount, from a chimeric mouse that underwent intravitreal injection of an IGFBP-3-expressing plasmid, double stained with rhodamine-agglutinin (red), to reveal blood vessels, and anti-GFP (green), to reveal GFP$^+$ c-kit$^+$, Sca-1$^+$ HSC. Green channel (a), red channel (b), and merged image (c) are shown. Arrows in (c) show areas where the GFP$^+$ HSCs appear to form new vessels and sprouts from existing vessels. Scale bar = 10 μm.

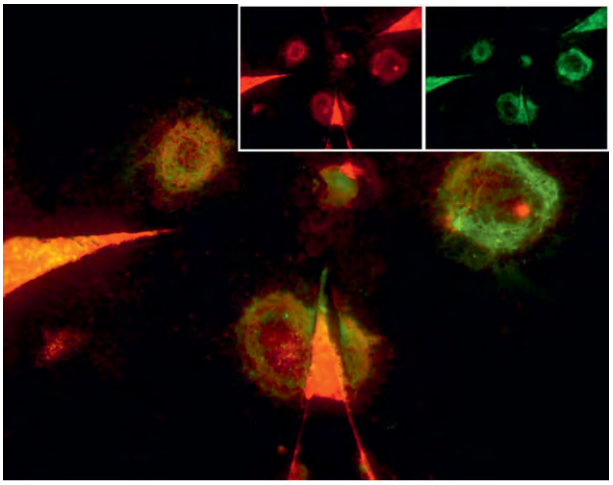

Figure 4 Normal mice whose bone marrow was ablated by lethal irradiation and reconstituted with bone-marrow-derived Lin$^-$/c-kit$^+$/Sca-1$^+$ HSC from homozygous GFP transgenic donors were subjected to Bruch's membrane rupture by laser injury. Two weeks after injury, the eyes were enucleated, preserved, reacted with rhodamine-conjugated *Ricinus communis* agglutinin I to visualize vasculature, and finally mounted flat for fluorescence microscopy. Representative image captures show the vascular lesions (red inset) and GFP-expressing cells (green inset) localizing to the CNV. These GFP$^+$ cells could only have come from the reconstituted bone marrow, thus indicating the participation of HSC in adult angiogenesis in the eye.

of BM-derived cells followed the gradient, and the greatest number of cells homed to and integrated into vessels of the most ischemic tissue. In addition, the proportion of EPC in the pancreas of mice after streptozotocin treatment (which is toxic to the pancreas) was 17.8%.

In contrast, engraftment of BM-derived ECs was only 1.6% in the peritubular endothelium of the kidney. When supraphysiological levels of growth factors are introduced, even greater BM-derived cell recruitment can be seen. In mice implanted subcutaneously with fibroblast growth factor-2-impregnated Matrigel plugs, 26.5% of ECs in the neovasculature were BM-derived.

EPCs as a Source of Paracrine Growth Factors for Vessel Growth

Whereas not everyone agrees on the source of EPCs, the general contention is that the cells contribute to the repair of endothelium, yet just how they do this is under debate. The recruitment of endogenous EPCs and treatment with exogenous EPCs (such as autologous cells injected systemically or locally) stimulate vascular growth in animal models and in patients subjected to clinical trials. One of the most striking features of EPC-mediated vascular growth is the rapidity with which it occurs. In some murine models, improvements are apparent within 2 days after treatment.

The functional integrity of the endothelium correlates with the number and activities of EPC, whereas EPC senescence is also associated with endothelial dysfunction. The argument continues whether EPCs can express hematopoietic markers or not; however, EPCs do express both endothelial and progenitor cell markers, some of which are species specific. A key EPC marker in humans is CD34. In contrast, EPCs in mice are lin$^-$ BM cells and

spinocerebellar ataxia type 1 (Sca-1$^+$) lin$^-$ circulating cells. Some EPC markers are expressed by both rodent and human EPCs such as vascular endothelial growth factor receptor 2 (VEGFR2) and CD133 (AC133).

However, with the exception of the retina, in most cases, the increase in neovascularization is not directly related to the differentiation of EPCs into ECs. Despite profound improvements in vascular growth, often few EPC are found in the neovascular endothelium. This has led to a revised hypothesis that the primary function of EPC is to secrete factors that stimulate vascular growth. Thus, the actual long-term physical participation of these cells in the growth of neovessels is probably highly dependent on the vascular bed, the nature of growth stimulus, and the characteristics of the individual (diabetic or nondiabetic).

What Are EPCs Doing in the Eye? When Are They Good? When Are They Bad?

EPC in the Cornea

Implantation of VEGF- or other growth-factor-impregnated pellets in the cornea results in corneal neovascularization. It has been found, using lethally irradiated mice transplanted with β-galactosidase-expressing BM cells, that in case of VEGF, corneal neovasculature had about 17.7% of BM-derived ECs. In another study using the same model, only 7.3% was reported in the absence of simvastatin, whereas drug treatment increased the percentage to 25.7%. In mice injected intraperitoneally with granulocyte-macrophage colony-stimulating factor (GM-CSF), corneal neovascularization in the micropocket assay was enhanced. EPCs that contributed to this enhanced neovascularization were also mobilized from BM as identified by the expression of β-galactosidase regulated by EC-specific Tie-2 promoter. Contrary to the data obtained with VEGF, implantation of fibroblast growth factor 2 (FGF-2) pellets did not lead to any contribution of the BM-derived cells to EC present in the corneal neovasculature as observed with green fluorescent protein (GFP) as BM cell marker. Instead, a large number of pericytes (53% total) originated from BM-derived cells. Another example of BM-derived cells differentiating into other cell types than EC came from the study of Nakamura and co-workers, who used intravenous transplantation of (lin$^-$, Sca-1$^+$) HSCs from GFP$^+$ transgenic mice. The progeny of these cells expressing GFP was found in the corneal stroma, where they apparently migrated from the limbal vessels at the corneal periphery. As calculated on corneal sections, GFP$^+$ cells comprised 27.3% (BM) and 24.0% (HSC) of total cells in the peripheral corneal stroma. In the central stroma, GFP$^+$ cells were 7.58% (BM) and 8.06% (HSC) of total cells. These data raise the possibility that the actual fate of EPC coming from the BM as a response to a stimulus may strongly depend on the nature of pertinent growth factor. In diseased conditions of the cornea, CD34$^+$ BM-derived cells were found in the stromal neovascularization associated with Mooren's ulcer.

EPC in Age-Related Macular Degeneration

Age-related macular degeneration (AMD) is the primary cause of blindness in people aged 50 years or more. The wet form leads to severe loss of central vision and is due to choroidal neovascularization (CNV). Moreover, the most common cause of blindness in the elderly in advanced countries is AMD with CNV. CNV is characterized by the subretinal invasion of a pathologic new vessel complex from the choriocapillaris. Although CNV is traditionally considered to consist of ECs, its cellular population is likely more complex in nature, comprising several different cell types. Knowledge of the cellular composition and origin might help understand the pathogenic mechanisms controlling CNV severity, as well as indicate potential targets for therapeutic intervention. We have examined whether the CNV cell population has a dual origin, circulating versus resident populations, and whether BM-derived cells participate in CNV. These studies were performed using GFP chimeric mice that were generated from highly enriched Sca-1$^+$, c-Kit$^+$, lin$^-$ cells, and following stable reconstitution underwent laser rupture of Bruch's membrane. Eyes were enucleated at 1, 2, 3, and 4 weeks after laser injury and CNV was examined by confocal microscopy of retinal flatmounts. We found that laser injury alone was sufficient to induce stem cell recruitment and subsequent CNV. GFP$^+$ cells formed part of the functional vasculature in the choroid as early as 1 week after injury and were present for the duration of the study (**Figure 4**). Interestingly, we found that the relative EPC contribution to CNV remained fairly constant throughout the study and constituted almost 50% of the total vasculature. We concluded that adult stem cells are recruited from the BM to the choroid in a model of CNV, where they contribute to forming aberrant new vessels, and targeting stem cell recruitment to the eye may offer a novel therapeutic strategy for AMD.

These studies were corroborated and extended by two other groups. Tomita and co-workers used a similar approach, however, with unfractionated (whole) BM from GFP$^+$ mice. Upon immunohistochemical analysis of the lesions, they observed that the vascular wall cells of the CNV expressed both GFP and CD31, indicating that the newly developed blood vessels in the CNV were derived from the BM cells. Espinosa-Heidmann and co-workers used the whole BM transplantation from GFP$^+$ mice and showed that GFP-labeled cells represented 17% of the total cell population in the lesion. Many of the GFP-labeled cells were immunoreactive for α-smooth muscle actin (39%), desmin, NG2, CD31 (41%), BS-1

lectin, or F4/80. GFP-labeled cells in CNV were morphologically indistinguishable from cells normally present in CNV lesions. They concluded that BM-derived progenitor cells not only are a source of endothelial, but also of smooth muscle-like cells.

Caicedo and co-workers used similar strategy to determine the relative role of recruited blood-derived macrophages versus resident microglia in the retina associated with CNV. They found that the cell adhesion molecules such as vascular cell adhesion molecule 1 (VCAM-1), intercellular adhesion molecule 1 (ICAM-1), and platelet endothelial cell adhesion molecule 1 (PECAM-1, CD31) were strongly upregulated in retinal blood vessels of the CNV lesion, that the GFP-labeled cells were immunoreactive for the macrophage marker F4/80, and that the density of resident microglia did not increase. Most GFP-labeled cells were found in close proximity to activated Müller cells. They then depleted circulating macrophages with clodronic acid and showed that the density of F4/80 immunoreactive cells, as well as the density of pERK-immunoreactive Müller cells in the retina, under CNV, decreased. They concluded that recruitment of blood-derived macrophages, more than resident microglia, seems to be associated with CNV. In addition, using GFP chimeric mice generated from whole BM transplantation, Espinosa-Heidmann quantitated the participating cell types in more detail. He found that macrophages represented 20%, ECs 25%, vascular smooth muscle cells 11%, retinal pigment epithelial (RPE) cells 12%, and nonlabeled cells 32% of the cells in the lesion. The macrophage population was mostly derived from circulating monocytes at all time points studied (70% were GFP-labeled), whereas endothelial and vascular smooth muscle cells were partly BM-derived (50–60% were GFP-labeled), and RPE cells appeared to be entirely derived from preexisting tissue-resident cells. They concluded that BM-derived progenitor cells contribute significantly to the vascular and inflammatory components of CNV.

Csaky and co-workers, utilizing GFP chimeras in which the BM was derived from mice expressing LacZ driven by the endothelial-specific Tie-2 promoter and injecting adenoviral vector expressing $VEGF_{165}$ subretinally to induce CNV, found that EPCs contribute to the formation of neovascularization in this VEGF-driven system. It is apparent from these studies that BM-derived ECs contribute to the pathological CNV in both laser-induced or VEGF-induced CNV.

EPC in the Retinal Disease

We have developed a novel model of retinal neovascularization in adult GFP chimeric mice to examine the role of EPC in revascularizing ischemic retinas. We showed that the recruitment of endothelial precursors to sites of ischemic injury had a significant role in neovascularization in the retina (Figure 2). Otani and co-workers showed that intravitreally injected lin^- BM cells selectively target retinal astrocytes, cells that serve as a template for both developmental and injury-associated retinal angiogenesis. When lin^- BM cells were injected into neonatal mouse eyes, they extensively and stably incorporated into forming retinal vasculature. When EPC-enriched HSCs were injected into the eyes of neonatal rd/rd mice, whose vasculature ordinarily degenerates with age along with photoreceptors, they rescued and maintained a normal vasculature. In contrast, normal retinal angiogenesis was inhibited when EPCs expressing a potent angiostatic protein were injected. They also showed that BM cells and astrocytes specifically interact with one another during normal angiogenesis and pathological vascular degeneration in the retina. The authors concluded that selective targeting with HSC may be a useful therapeutic approach for the treatment of many ocular diseases.

Hypoxia-Regulated Factors Recruit EPC to the Ischemic Retina

It remains unknown whether stem cells with tissue-specific antigenic repertoires reside in and move out of the BM when signaled to or whether generic stem cells modulate their phenotype before or after leaving the BM in response to a particular type of stimulus. In any case, the retrieved total peripheral blood mononuclear cells (PBMCs) produce more ECs in culture after these stimuli. This has been attributed to mobilization; however, this also may simply indicate that circulating cells have modulated their phenotype in response to the stimulus.

One of the most potent stimuli recruiting BM-derived cells to any tissue is ischemia. Ischemia leads to an influx of inflammatory cells that release cytokines, pro-angiogenic factors, matrix-degrading proteinases, and other effector molecules. Along with the influx of inflammatory cells, BM-derived cells expressing surface markers of EC precursors, including Sca-1, Tie-2, Fms-related tyrosine kinase 1 (Flt-1), vWF, VEGFR2, and CD133, are recruited in response to ischemia. Hypoxia-induced factors released at sites of tissue ischemia promote the recruitment of cells from the circulation into ischemic tissues. VEGF, stromal-derived factor-1 (SDF-1), erythropoietin (EPO), and, more recently, insulin-like growth factor binding protein-3 (IGFBP-3) have been shown to increase EPC recruitment to the retina (Figure 3). IGFBP-3 mediates EPC migration, differentiation, and capillary formation *in vitro*. Targeted expression of IGFBP-3 by genetically modified HSC resulted in the protection of the vasculature from hyperoxia-induced damage in the mouse oxygen-induced retinopathy (OIR) model.

Considering the pleiotropic effects of VEGF on ECs, it is not surprising that it can stimulate differentiation and proliferation of EC precursors. VEGF can mobilize and

recruit EC precursors from the BM into tissues. VEGF mobilization appears to be isoform-specific, because $VEGF_{165}$, but not $VEGF_{189}$, induced a rapid mobilization of $VEGFR2^+$ cells into the circulation. Like VEGF, the VEGF family member placental growth factor (PlGF) may also modulate recruitment or function of BM-derived EC precursors. Embryonic vessel growth is unaffected, but arteriogenesis is delayed in mice lacking PlGF. However, if the BM of $PlGF^{-/-}$ mice is replaced by wild-type BM, normal arteriogenesis is restored, suggesting that BM-derived cells stimulate vascular growth or stabilization through PlGF and its receptor VEGFR1. By increasing signaling through VEGFR1, PlGF amplifies the responsiveness of ECs to VEGF. Together, these data suggest that PlGF probably does not play a role in the differentiation of BM-derived cells to ECs, but may induce proliferation in the partially differentiated cells. It could also stabilize larger vessels.

Serum SDF-1 mobilizes hematopoietic stem and progenitor cells from the BM, as does the CXCR4 (the SDF-1 receptor) antagonist AMD3100, which disrupts the interactions of EC precursors with BM stromal cells. SDF-1 is chemotactic for EC precursors, and *in vitro* data suggest that it is required for recruitment of EC precursors to sites of injury. Studies with human into mouse BM transplants support this conclusion, because blockade of CXCR4 abrogated human $CD34^+$ BM-derived cell homing to the liver, whereas local injection of SDF-1 increased their homing.

In humans, vitreal SDF-1 concentration increases as diabetic retinopathy progresses to the proliferative stage. Treatment of patients with triamcinolone decreases SDF-1 levels in the vitreous, with marked disease improvement. SDF-1 induces human retinal EC to increase the expression of VCAM-1, a ligand of very late antigen-4 (VLA-4) found on many hematopoietic progenitors, and to reduce cellular tight junctions by suppressing occludin expression. Both changes would serve to recruit HSC and EPC along an SDF-1 gradient. We showed, using a murine model of branch retinal vein occlusion, that the majority of new vessels formed in response to oxygen starvation originates from HSC-derived EPCs. We also showed that the levels of SDF-1 found in patients with proliferative diabetic retinopathy induce neovascularization in our murine model. Intravitreal injection of blocking antibodies to SDF-1 prevented retinal neovascularization in this model, even in the presence of exogenous VEGF. Together, these data demonstrate that SDF-1 plays a major role in proliferative diabetic retinopathy and may be an ideal target for the prevention of its development.

However, studies in vascular beds outside the eye showed that overexpression of SDF-1 in the absence of VEGF failed to recruit BM-derived cells to the liver, whereas blocking CXCR4 decreased BM-derived cells in the liver even in the presence of high levels of VEGF. Together, these data suggest that SDF-1 is not sufficient to recruit the BM-derived cells to the tissue in the absence of another signal, such as VEGF or one of its targets. Instead, SDF-1 may play a crucial role in sequestering BM-derived cells at the site of injury once they have arrived. Furthermore, three studies have shown that the molecule is required for adhesion of BM-derived cells at sites of injury. Hypoxia is a potent mobilizer of BM-derived cells, and hypoxia-inducible factor-1α (HIF-1α) activity is induced by hypoxia. VEGF, in turn, is induced by HIF-1α, which then upregulates SDF-1 and CXCR4. A positive-feedback loop occurs because HIF-1α also induces SDF-1, which is a weak inducer of VEGF. This evidence supports the idea that VEGF and SDF-1 work in concert, such that VEGF and SDF-1 induce each other, SDF-1 mobilizes BM-derived cells, VEGF (or a VEGF-induced factor) recruits the cells, SDF-1 sequesters the arriving BM-derived cells, and VEGF promotes the differentiation and proliferation of the sequestered cells.

SDF-1 and its cognate receptor CXCR4 clearly play important roles in BM-derived cell differentiation and ability to induce vascular growth. Recently, a new receptor for SDF-1 has been found: the orphan receptor RDC1 (CXCR7). This finding will undoubtedly make sorting out their precise functions even more difficult. Another factor that may be critical in the HIF-1α/SDF-1 pathway is monocyte chemoattractant protein-1 (MCP-1). Monocytes are attracted to sites of injury, and once there, they secrete MCP-1, which, in turn, stimulates HIF-1α activity. Responsiveness of monocytes to VEGF is reduced in people with diabetes, resulting in fewer monocytes being recruited to sites of injury, the failure of which may lead to lower HIF-1α activity and reduced engagement of the VEGF/SDF-1 system. Attracted monocytes may also have an important role in laying out the scaffold on which neovessels will form.

EPO is a potent stimulator of vascular growth, and, like SDF-1, it is strongly induced by hypoxia. EPO increases the number of circulating $CD34^+VEGFR2^+$ BM-derived cells, whereas in another study of 28 patients with congestive heart failure, long-term EPO treatment failed to increase the number of $CD34^+$, $CD34^+CD45^+$, $CD34^+CD133^+$, $CD34^+VEGFR2^+$, or $CD34^+CD133^+$ $VEGFR2^+$ cells in the circulation. EPO has direct effects on EC precursors, stimulating proliferation of $CD14^+$ BM-derived cells and their differentiation into ECs as well as their adhesion to vascular ECs. Recently, Chen and co-workers showed that EPO increases the number of pro-angiogenic stem cells in the retina. They found that EPO treatment (5000 U kg^{-1}, i.p. P6 and P7) increases the number of $CD34^+$ EPCs per vessel length by approximately 80% in the retinas of postnatal day 8 mice exposed to oxygen. These results suggest that in addition to acting locally through EPO receptors in the retina, EPO can also

promote retinal vascular repair by recruiting BM-derived pro-angiogenic cells to the retina.

The angiopoietins have a role in mobilization and function of EC precursors. Angiopoietin-1 appears to regulate initial commitment to the EC lineage, whereas angiopoietin-2 induces BM-derived EC expansion *in vitro* and stimulates formation of neovessels by BM-derived cells *in vivo*. It was found that complete blockade of Tie-2 (angiopoietin-1 receptor) leads to rapid EC precursor death in culture (G. C. Schatteman and C. Jiao, unpublished observations). *In vivo*, $CD34^+$ BM-derived cells tend to localize near the sites of angiopoietin-1 and -2 immunoreactivity. Like VEGF, angiopoietin-1 can mobilize $VEGFR2^+$ cells, but the mobilization is delayed relative to response to VEGF. Tie-2^+ but not Tie-2^- BM-derived cells can differentiate into ECs in culture.

Do Cell Therapies Have a Role in the Eye? If so, Who Will Benefit?

Many ocular diseases, such as AMD, are diseases of the elderly, a population that should best benefit from cellular therapy. Interestingly, the number of HSCs in the circulation does not decrease with age, nor is the ability of HSCs to reconstitute the BM lost with age. Old cells cycle more frequently and home less efficiently than do young cells, indicating more subtle functional problems. Treatment of skin wounds with old lin^- BM-derived cells profoundly inhibited vascular growth, whereas young cells stimulated it. These experiments were performed in young mice, so the dysfunction was intrinsic to the BM-derived cells. A reduction in the repair capacity of mesenchymal stem cells with age has also been observed.

Type 1 Diabetes Induces BM-Derived Cell Dysfunction

Individuals with type 1 diabetes and vascular complications would potentially benefit from cellular therapy, but their EPCs are dysfunctional. HSCs and EPCs from adult type 1 diabetic patients produce fewer ECs, and their EC show reduced proliferative potential and migratory function. Diabetes disrupts normal signaling through pathways such as nuclear factor-kappa B (NF-κB), mitogen-activated protein kinases (MAPK), protein kinase C (PKC), and insulin receptor substrate (IRS); chronic activation of these pathways blunts acute responses. The increased nicotinamide adenine dinucleotide phosphate (NADPH) oxidase and NF-κB expression in diabetes contribute to enhanced EPC oxidative stress. Recently, we showed that activation of SR1B (the high-density lipoprotein (HDL) receptor) is protective to diabetic EPC, whereas activation of oxidized low-density lipoprotein (ox-LDL) receptor downregulates endothelial nitric oxide synthase (eNOS) leading to reduced vascular reactivity and vasoconstriction. Accumulation of reactive oxygen species (ROS) increases cellular/replicative senescence, which is defined as the loss of division potential and the simultaneous change in morphology. Diabetes accelerates the onset of EPC senescence, which is accompanied by impairment of migration and proliferation capacities. Several atherosclerotic factors, such as angiotensin II, ox-LDL, and homocysteine, directly accelerate the onset of EPCs senescence and lead to cellular dysfunction.

Revascularization is impaired when dysfunctional EPCs from type 1 diabetic mice are injected into diabetic mice. Hemoglobin A1c levels inversely correlate with the number of EPCs that can be derived from PB of type 1 diabetic patients. Moreover, these cells show a reduced ability to integrate into EC tubes *in vitro*. We showed that when $CD34^+$ cells from healthy donors were tested for their potential to re-endothelialize ischemia-injured retinas, they induced repair of capillary endothelium, whereas diabetic $CD34^+$ cells did not.

Can Diabetes Alter Cytokine Secretion by EPCs?

It is now recognized that EPCs promote vascular growth by secreting pro-angiogenic factors. Thus, changes in the secretory profile of these cells as a function of diabetes is a relevant parameter to investigate. It is interesting to explore the possibility that diabetic EPCs secrete distinct and detrimental cytokines compared to nondiabetic cells. The release of such cytokines after injury would not potentiate healing and repair, but rather hinder this process and adversely affect vessel function.

Cytokines that may be dysregulated in diabetic EPCs include tumor necrosis factor-alpha (TNFα), interleukin-1 beta (IL-1β), and MCP-1. TNFα is an inflammatory cytokine that is rapidly upregulated after injury, and that directly and indirectly regulates many additional pro-angiogenic factors. It induces expression of molecules on ECs that mediate adhesion of inflammatory cells, intensifying the response. IL-1β, another important early mediator of inflammation, is both induced by and induces TNFα, so that these factors act synergistically to support inflammation. MCP-1 is essential for arteriogenesis, and recent work has shown it to be a key factor in FGF-2 mediated arteriolar growth as well, although its direct effects on capillary growth are modest. MCP-1 can be induced by TNFα. Monocytes secrete TNFα and MCP-1 when activated by IL-1β and other factors, so their arrival and activation in injured tissue initiate a positive-feedback loop that recruits more monocytes. Preliminary data from

our laboratory indicate that the cytokines released by EPC populations are specific to a particular subpopulation.

Type 1 Diabetes Induces Nitric Oxide Dysfunction in EPCs

Nitric oxide (NO) has an essential role in the mobilization and migration of $CD34^+$ cells into the sites of engraftment. NO also regulates survival by activating telomerase and delaying cell senescence. We and others have shown that diabetic EPCs have reduced bioavailable NO and decreased eNOS activity. More importantly, exogenous NO can correct the migratory defect in these cells. Diabetes is associated with increased oxidative stress due to upregulation of NADPH oxidase and eNOS uncoupling. As we have observed, pharmacological and molecular inhibition of NADPH oxidase restores bioavailable NO and improves the engraftment potential of EPCs. The impaired *in vivo* re-endothelialization capacity of human diabetic EPCs was restored by small interfering RNA silencing of NADPH oxidase subunit p47(phox). Propofol, a peroxynitrite scavenger, inhibits NF-κB activation, increases NO production, and protects cells from apoptosis. The Ox-LDL increase in diabetes directly inhibits EPCs survival, induces senescence, and inhibits eNOS. High glucose also enhances EPC senescence, and impairs migration and tube formation. Moreover, the deleterious effects of high glucose can be ameliorated by co-incubation with the NO donor sodium nitroprusside and worsened by eNOS inhibitors. Diabetic EPC dysfunction improves with peroxisome proliferator-activated receptor-gamma (PPAR-γ) activation. PPAR-γ agonists improve NO bioavailability and reduce arterial inflammation and oxidative stress. Rosiglitazone, a PPAR-γ agonist, was documented to promote the differentiation of angiogenic progenitor cells toward the endothelial lineage. Similarly, mice treated with pioglitazone exhibited increased EPC number and migratory activity, and reduced rate of EPC apoptosis.

Of note, the negative effects of C-reactive protein on EPC survival, differentiation, and angiogenic function were abrogated by pretreatment of EPCs with rosiglitazone, providing direct evidence of the salutary impact of anti-inflammatory eNOS-enhancing agents on EPC biology. The precise mechanisms involved in EPC stimulation by PPAR-γ agonists have yet to be investigated, while no data are still available on humans. PPAR-γ agonists should decrease EPC oxidative stress, induce mobilization, and improve functionality of EPCs, at least in theory.

As described above, reduced levels of bioavailable NO can be due to increased oxidative degradation of NO, and also reduced NO synthesis. Elevated blood levels of asymmetric dimethylarginine (ADMA), an analog of the amino acid L-arginine that inhibits the formation of NO, seem to augment vascular oxidative stress, partly through eNOS uncoupling, which results in the generation of higher superoxide radicals that are increased in diabetes. The latter finding was also confirmed by recent *in vitro* observations, showing that ADMA represses EPC proliferation, differentiation, and function in a concentration-dependent manner. The dimethylarginine dimethylaminohydrolase (DDAH) enzymes inactivate ADMA, co-segregate with NOS, and regulate NO production. Over-expression of DDAH *in vitro* results in increased endothelial NO production and overexpression of human DDAH in mice leads to increases in NO production and improvements in vascular resistance.

Drug Modulation of EPC Function

As discussed above, EPC functional activity may be impaired in disease conditions, such as diabetes. At the same time, proliferative diabetic retinopathy needs treatments inhibiting new retinal blood vessel formation, including EPC recruitment and engraftment therein. Conversely, other sites and disease conditions may actually need an increase of EPC activity toward tissue repair, for example, in myocardial infarction or stroke. The previous sections have emphasized the role of NO in maintaining normal function of BM-derived EPC. Certain agents increasing NO and NOS activity could be potentially used to boost EPC activity in patients who suffer from decreased EPC function, such as the elderly and diabetics. Not much is known about the ways of inhibiting EPC function and engraftment to sites of unwanted neovascularization as observed in tumors and retinopathies. The few emerging data, however, show that tumor cell-mediated recruitment and engraftment of BM-derived EPC can be specifically inhibited. This concerns inhibiting CXCR4, the receptor for SDF-1 that is important for tumor vasculogenesis, or infusion of endostatin into tumor-bearing animals. In our recent work, BM-derived GFP^+ EPC incorporation into hypoxia-induced retinal neovasculature in the mouse oxygen-induced retinopathy (OIR) model was examined. It was shown that EPC engraftment was substantially inhibited by systemically administered inhibitors of protein kinase CK2, a key enzyme in cell cycle, proliferation, and migration. One can hypothesize that blocking of EPC incorporation into neovasculature may be one of the mechanisms of action of a variety of anti-angiogenic drugs that have shown promise in animal studies. The use of antagonists of specific growth factors and their receptors (antibodies, soluble receptors, chemicals, and RNA interference) may emerge as another powerful approach to inhibiting EPC engraftment during pathological vasculogenesis.

See also: Angiogenesis in Inflammation; Angiogenesis in Response to Hypoxia; Angiogenesis in the Eye; Angiogenesis in Wound Healing; Physiological Anatomy of the Retinal Vasculature; Stability and Functional Integrity of New Blood Vessels.

Further Reading

Asahara, T., Murohara, T., Sullivan, A., et al. (1997). Isolation of putative progenitor endothelial cells for angiogenesis. *Science* 275: 964–967.

Anghelina, M., Moldovan, L., Zabuawala, T., Ostrowski, M. C., and Moldovan, N. I. (2006). A subpopulation of peritoneal macrophages form capillary like lumens and branching patterns in vitro. *Journal of Cellular and Molecular Medicine* 10: 708–715.

Caicedo, A., Espinosa-Heidmann, D. G., Pina, Y., Hernandez, E. P., and Cousins, S. W. (2005). Blood-derived macrophages infiltrate the retina and activate Muller glial cells under experimental choroidal neovascularization. *Experimental Eye Research* 81: 38–47.

Castellon, R., Hamdi, H. K., Sacerio, I., et al. (2002). Effects of angiogenic growth factor combinations on retinal endothelial cells. *Experimental Eye Research* 74: 523–535.

Cogle, C. R., Wainman, D. A., Jorgensen, M. L., et al. (2004). Adult human hematopoietic cells provide functional hemangioblast activity. *Blood* 103: 133–135.

Csaky, K. G., Baffi, J. Z., Byrnes, G. A., et al. (2004). Recruitment of marrow-derived endothelial cells to experimental choroidal neovascularization by local expression of vascular endothelial growth factor. *Experimental Eye Research* 78: 1107–1116.

Dimmeler, S., Burchfield, J., and Zeiher, A. M. (2008). Cell-based therapy of myocardial infarction. *Arteriosclerosis, Thrombosis, and Vascular Biology* 28: 208–216.

Espinosa-Heidmann, D. G., Reinoso, M. A., Pina, Y., et al. (2005). Quantitative enumeration of vascular smooth muscle cells and endothelial cells derived from bone marrow precursors in experimental choroidal neovascularization. *Experimental Eye Research* 80: 369–378.

Gaynor, E. (1973). The role of granulocytes in endotoxin-induced vascular injury. *Blood* 41: 797–808.

Grant, M. B., May, W. S., Caballero, S., et al. (2002). Adult hematopoietic stem cells provide functional hemangioblast activity during retinal neovascularization. *Nature Medicine* 8: 607–612.

Karmerov, A. A., Saghizadeh, M., Caballero, S., et al. (2008). Inhibition of protein kinase CK2 suppresses angiogenesis and hematopoietic stem cell recruitment to retinal neovascularization sites. *Molecular and Cellular Biochemistry* 316: 177–186.

Li Calzi, S., Purich, D. L., Chang, K. H., et al. (2008). Carbon monoxide and nitric oxide mediate cytoskeletal reorganization in microvascular cells via vasodilator-stimulated phosphoprotein phosphorylation: Evidence for blunted responsiveness in diabetes. *Diabetes* 57: 2488–2494.

Parmar, K., Mauch, P., Vergilio, J. A., Sackstein, R., and Down, J. D. (2007). Distribution of hematopoietic stem cells in the bone marrow according to regional hypoxia. *Proceedings of the National Academy of Sciences of the United States of America* 104: 5431–5436.

Segal, M. S., Shah, R., Afzal, A., et al. (2006). Nitric oxide cytoskeletal-induced alternations reverse the endothelial progenitor cell migratory defect associated with diabetes. *Diabetes* 55: 102–109.

Schatteman, G. C., Dunnwald, M., and Jiao, C. (2007). Biology of bone marrow-derived endothelial cell precursors. *American Journal of Physiology. Heart and Circulatory Physiology* 292: H1–H18.

Stump, M. M., Jordan, G. L., Jr., Debakey, M. E., and Halpert, B. (1963). Endothelium grown from circulating blood on isolated intravascular Dacron hub. *American Journal of Pathology* 43: 361–367.

Tomita, M., Yamada, H., Adachi, Y., et al. (2004). Choroidal neovascularization is provided by bone marrow cells. *Stem Cells* 22: 21–26.

Yoder, M. C., Mead, L. E., Prater, D., et al. (2007). Redefining endothelial progenitor cells via clonal analysis and hematopoietic stem/progenitor cell principals. *Blood* 109: 1801–1809.

Thyroid Eye Disease

M N Stan and R S Bahn, Mayo Clinic, Rochester, MN, USA

Glossary

Chemosis – Swelling of the conjunctiva.
Erythema – Redness of the skin resulting from inflammation, often due to capillary congestion.
Graves' disease – An autoimmune disease causing overproduction of thyroid hormones and associated with eye and skin manifestations.
IGF-1 receptor – A transmembrane tyrosine kinase receptor that mediates the action of insulin-like growth factor.
Proptosis – The forward protrusion of the globes from the orbit; often found in patients with GO.
RANTES (Regulated on Activation, Normal T cell Expressed and Secreted) – A member of the IL-8 superfamily of cytokines, selective for monocytes and memory T cells.
TRAb – Autoantibodies directed against the thyrotropin receptor.
TSH receptor – A G-protein-coupled receptor found on the surface of thyroid and other cells that binds TSH and autoantibodies.

Introduction

Thyroid eye disease (TED) is an inflammatory disorder that develops in the orbit in association with autoimmune thyroid disease (AITD). In the majority of cases, TED is associated with autoimmune hyperthyroidism, or Graves' disease (GD), and has therefore also has been termed Graves' ophthalmopathy or Graves' orbitopathy (GO). It is additionally referred to in the clinical literature as thyroid associated orbitopathy (TAO). For consistency, we will employ the abbreviation GO since it is the abbreviation used by EUGOGO (the EUropean Group On Graves' Orbitopathy), the only organization that has so far put forth a set of clinical guidelines for this entity.

The clinical presentation of GO is quite variable (Figure 1). Most patients have minimal symptoms of corneal irritation associated with some periocular swelling, eyelid retraction, and conjunctival injection. Only in a minority of cases (5%) is the disease severe and potentially sight-threatening, with severe inflammation, corneal ulceration, or optic neuropathy. The natural history of the disease is one of rapid deterioration that generally occurs over several months' time, followed by a plateau phase of variable length, and then gradual improvement toward the baseline. While the inflammatory signs and symptoms generally abate, resolution of proptosis and extraocular dysfunction may be incomplete.

Epidemiology

The incidence of GO varies depending on the criteria used to define its presence. On conservative clinical grounds, with lid signs not included, the incidence is 10–25%, whereas with orbit imaging, computerized tomography (CT), magnetic resonance imaging (MRI), or ultrasound, up to 90% of cases have evidence of ocular involvement. Fortunately, the vast majority of cases are mild, and only 5% of patients have severe disease. The incidence based on data from Olmsted County, Minnesota is, respectively, 16 cases for women and 2.9 cases for men per 100 000 per year. The clinical association between the onset of Graves' hyperthyroidism and the onset of GO is strong; 80% of patients afflicted with one of these conditions develop the other within 18 months.

Etiology

No single factor has been identified that universally induces GO. Rather, a number of factors of varying degree of importance appear to work together to cause or worsen the disease. We discuss here the most commonly accepted contributors to disease etiology.

Genetic Contributions

Familial aggregation of autoimmune thyroid disease (AITD; GD and Hashimoto's disease, also known as lymphocytic thyroiditis) has been known for some time. The prevalence of AITD in siblings of patients with GD is 33%, and is similar to the 36% incidence of AITD in the families of patients with GD or GO. Polymorphic forms of several genes involved in the regulation of the immune system, including HLA-DR3, CTLA-4, CD40, PTPN22, as well as several thyroid-associated genes, including thyroid-stimulating hormone (TSH) receptor and thyroglobulin, are associated with GD. However, studies have not identified any stronger links between these polymorphisms and susceptibility to GO in GD patients.

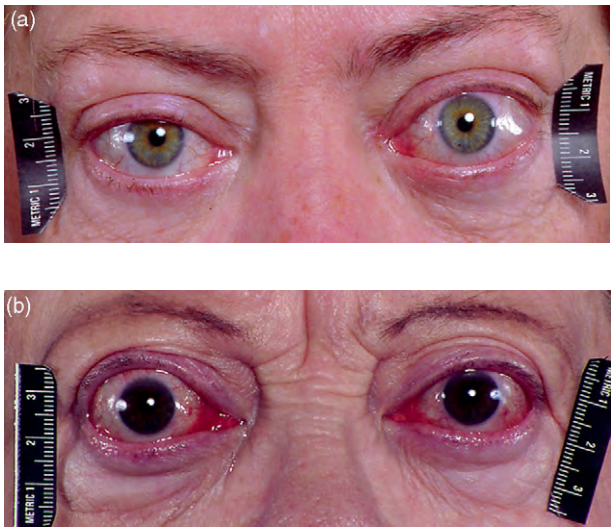

Figure 1 Photographs of two patients with GO: (a) asymmetric eyelid retraction with periocular edema and mild conjunctival congestion; (b) significant eyelid erythema and swelling with caruncular inflammation and conjunctival injection.

Similarly, other genes that have been found to confer susceptibility to GD with low relative risk, including T-cell receptor (TCR)-β-chain, tumor necrosis factor-β (TNF-β), and some immunoglobulin heavy chain-associated genes, confer no additional susceptibility to GO than to GD itself. This suggests that environmental factors may play a more significant role than genetic factors in the development of the ocular manifestations of GD.

Mechanical Factors

The bony confines of the orbit restrict the posterior expansion of the inflamed tissues within the GO orbit. Therefore, the increased volume of the orbital fat and extraocular muscle may lead to anterior displacement of the globe, or proptosis. This serves as a natural orbital decompression to relieve the intraorbital pressure. In addition to proptosis, other signs and symptoms of GO are attributable to mechanical pressures within the noncompliant bony orbit which may impair venous and lymphatic outflow and result in chemosis, periorbital edema, and increased inflammation. The latter is likely secondary to impaired drainage of inflammatory mediators. Individual anatomic variations in the orbital contour or the venous or lymphatic vessels may make some patients with GD more prone to the development of clinically significant GO or might explain the asymmetric eye disease seen in some patients. The trauma delivered by orbital tissue expansion within a noncompliant bony orbit may aggravate the underlying inflammatory process. This could further stimulate release of proinflammatory cytokines and chemokines and lead to augmentation of the orbital autoimmune process.

Uncontrolled Thyroid Dysfunction

Both hyper- and hypothyroidism have been shown in several case series and retrospective cohorts to be associated with increased risk for development of GO. DeGroot in a cohort of 264 patients found an odds ratio (OR) of 2.8 for development or worsening of preexistent GO in patients requiring more than a single treatment with radioactive iodine to control hyperthyroidism, compared with patients receiving only a single treatment. Prummel found, in a case series of 90 GO patients, that either hypothyroidism or hyperthyroidism increases the risk for severe GO almost twofold. In a smaller case series, Karlsson reported occurrence of GO after a period of hypothyroidism in 50% of patients, and Tallstedt in a retrospective cohort analysis found that patients who experienced hypothyroidism following radioactive iodine therapy for GD have an increased risk and an OR of 1.63 for development/worsening of GO compared to patients in whom hypothyroidism was prevented with early thyroid hormone replacement.

Tobacco Smoking

Smoking is the primary risk factor known for the development of GO in patients with GD; the relative risk, compared with nonsmokers with GD, is between 1.3 and 3.1. The risk is proportional to the number of cigarettes smoked per day, and former smokers have significantly lower risk than current smokers, even after adjusting for lifetime cigarette consumption. This suggests a direct and immediate effect of smoking on the development of GO. Smoking is additionally highly associated with more severe GO, with failure of immunosuppressive therapy and with worsening of GO after radioiodine treatment.

Mechanisms underlying the association between smoking and GO are unclear. Smoking has been associated with other autoimmune diseases, such as rheumatoid arthritis and Crohn's disease, suggesting that it increases the risk for immune self-attack with subsequent development of autoimmune conditions. Circulating levels of systemic cytokines do not appear to differ between smokers and nonsmokers, except for the presence of higher levels of interleukin (IL)-6 receptor in the former. However, these systemic levels might not be an appropriate surrogate for levels of these compounds within the GO orbit. Although patients with GO have higher levels of circulating IL-6 receptor than do GD patients without clinical GO, smoking and nonsmoking GO patients do not differ in this regard. Orbital fibroblasts cultured under hypoxic conditions produce increased levels of hyaluronic acid, and exposure of these cells to cigarette smoke extract appears to stimulate both adipogenesis and hyaluronic acid secretion.

Radioiodine Therapy for Graves' Disease

Studies have suggested that treatment with radioiodine may exacerbate eye disease in patients with GD who have preexisting, active GO. In one large study, patients were prospectively treated with radioiodine, methimazole, or a combination of radioiodine and prednisone. Within 6 months of treatment, mild progression of ocular disease was seen in 15% of patients treated with radioiodine alone, in approximately 3% of patients treated with methimazole, and in none of the patients treated with the combination of radioiodine and prednisone. By 1 year, the differences between the groups had almost disappeared, with only 5% of the radioiodine group having persistent symptoms that required additional treatment. Patients who experienced progression after receiving radioiodine were most commonly smokers and individuals with preexisting active GO. In addition, the higher incidence of hypothyroidism in the radioiodine group might have played a role in the outcome. Thus, it appears that progression of preexisting GO due to radioiodine therapy does occur in some patients. However, it is generally mild, temporary, and can be prevented by concurrent administration of corticosteroids. Patients with preexisting eye disease, smokers, those with high titers of autoantibodies directed against the thyroidal TSH receptor (TRAb), or those with severe thyrotoxicosis, high triiodothyronine (T3) levels, appear to be more likely to experience this complication. Ocular disease progression was not seen in another study in which postradioiodine hypothyroidism was carefully prevented by early thyroid hormone replacement, suggesting that hypothyroidism itself might play a role and should be avoided. Mechanisms responsible for ocular disease progression following radioiodine are unclear, but might include increased TRAb production, release of autoantigen from the thyroid, or destruction of radiosensitive suppressor T cells within the thyroid.

Pathophysiology

A number of factors appear to contribute to the pathogenesis of GO. Although we will describe each separately, their interplay determines the clinical outcome in a given patient (Figure 2).

Histology

The volume of the orbital adipose/connective tissue compartment and extraocular muscles is increased in GO. The muscle fibers are largely intact, but widely separated by edematous material composed largely of glycosaminoglycans (GAGs). Enlargement of these tissues can be ascribed in part to enhanced proliferation and secretion of hydrophilic GAG by orbital fibroblasts. In addition, new fat cell development, or adipogenesis, is active within the orbit and results in the observed expansion of the orbital adipose tissues. Within these tissues is found an infiltration of macrophages, T lymphocytes and to a lesser extent B lymphocytes, and natural killer cells. Further characterization of the activated T lymphocytes reveals increases in both CD4- and CD8-expressing populations and restriction in the T cell receptor repertoire. T-cell

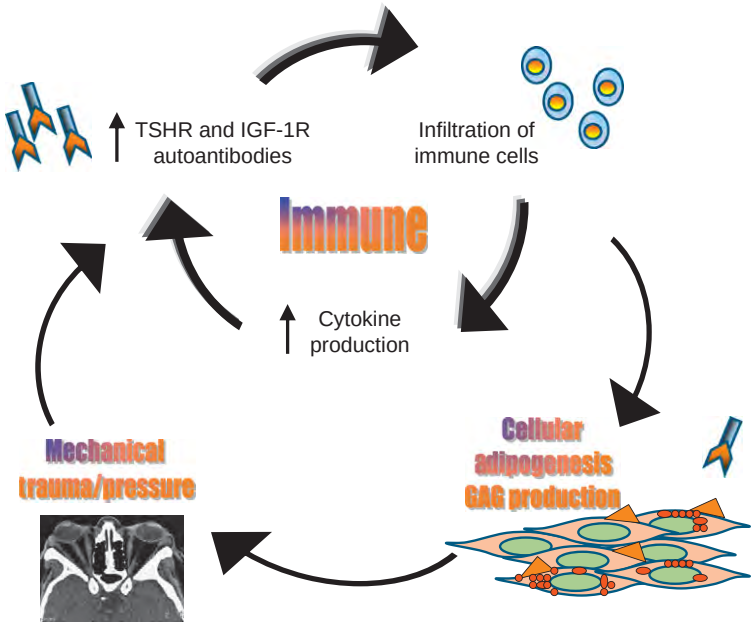

Figure 2 Immunological, cellular, and mechanical factors interact in a positive feedback loop to contribute to the development and progression of GO. TSHR – thyroid-stimulating hormone receptor. IGF-1R – insulin-like growth factor-1 receptor.

phenotyping has shown the presence of both Th1 and Th2 cytokine profiles of helper T cells (Th). Evidence suggests that the predominant profile found might depend on the stage of disease, with Th1 cells, which participate in cell-based immunity, appearing in early disease and the Th2 cells, which participate in antibody-mediated immunity, appearing in later stages.

Orbital fibroblasts are phenotypically heterogeneous multipotent cells. Subpopulations of these cells, distinguishable on the basis of the cell surface marker thymocyte differentiation antigen-1 (Thy-1), can be identified even within a single tissue. Approximately 20% of fibroblasts found within the normal orbital adipose/connective tissue compartment do not express this antigen and are preadipocyte fibroblasts capable of differentiating into adipocytes. The remainder are Thy-1 positive and do not possess adipogenic potential. In contrast, essentially all perimysial fibroblasts, those that form the individual fascicles within the muscles, are Thy-1 positive and therefore cannot differentiate into mature fat cells. A recent study showed an increase in Thy-1 positive cells within the adipose/connective tissues of the GO orbit, perhaps representing an adaptive response that limits disease progression. Individual differences in the distribution of cells expressing this antigen within the GO orbit may help to explain why some patients have predominant eye muscle disease while others have increased orbital adipose tissue volume as the predominant feature.

Cytokines

Orbital fibroblasts are capable of initiating lymphocyte recruitment via their secretion of proinflammatory cytokines which, in turn, stimulate the production of chemoattractant molecules by T cells. Two such molecules, IL-16 and RANTES, appear to account for the majority of T-lymphocyte migration initiated by orbital fibroblasts. Other cytokine-induced responses with potential relevance to GO include the inhibition of adipogenesis in orbital fibroblasts by transforming growth factor-β (TGF-β), interferon-γ (IFN-γ), and TNF-α, and its promotion by IL-6. Orbital fibroblasts also produce IL-1, IL-6 and IL-8, as well as prostaglandins, in response to ligation of their CD40 receptors by CD154 on T cells.

Orbital Autoantibodies

It is well accepted that autoantibodies against the TRAb are responsible for the hyperthyroidism of GD. The close clinical and temporal associations between Graves' hyperthyroidism and GO have led to the hypothesis that TRAb may also underlie the pathogenesis of GO. Indeed, the occurrence of GO is greatest in GD patients with the highest levels of circulating TRAbs, and the clinical activity of the disease correlates with serum levels of these autoantibodies.

A qualifying requirement to link TRAbs to the pathogenesis of GO is that the TSH receptor be expressed in orbital tissues. Recent studies have shown this to be the case as both TSH receptor mRNA and protein have been demonstrated in GO orbital adipose tissue specimens. Further, expression levels are higher in GO tissues than in orbital tissues obtained from normal individuals and a positive correlation has been shown between clinical activity scores and TSH receptor mRNA levels in patients' orbital tissues.

Studies *in vitro* show that orbital preadipocyte fibroblasts can be induced to differentiate into mature adipocytes and in doing so increase their expression of TSH receptor. When cultured in the presence in adipogenic agonists, levels of TSH receptor mRNA, as well as mRNA encoding various adipocyte-associated genes, increase roughly 10-fold in these cells. Studies of uncultured orbital fat specimens obtained from GO patients also show high levels of these genes compared with normal orbital fat specimens, suggesting that adipogenesis is increased within the orbit in GO. Whether this is directly caused by TRAb targeting TSH receptor on these cells is an area of active investigation.

Recent studies have implicated insulin-like growth factor-1 (IGF-1) receptor as another important autoantigen in GO. Human orbital fibroblasts have high-affinity IGF-1 binding sites, and immunoglobulin G (IgG) from the sera of GD patients interacts with these sites, while normal IgG does not. This IgG stimulates orbital fibroblasts to produce IL-16 and RANTES and to enhance their synthesis of hyaluronic acid. Evidence points toward these effects being mediated through the IGF-1 receptor, suggesting a possible role for IGF-1 receptor autoantibodies in the pathogenesis of GO.

Future Management

Current medical management of GO is inadequate, generally benefitting patients only modestly while they await spontaneous improvement in the disease. While orbital decompression surgery has proven beneficial to patients with severe disease, the prevention of this surgery is a primary goal of medical management. Recent progress in the understanding of GO pathogenesis has led to the identification of several potential targets for novel therapeutic agents. Both the production of autoantibodies by B cells and the release of proinflammatory cytokines by activated T cells can be impacted by targeting the initial stages of lymphocyte activation. As such, costimulation inhibitors (CTLA4-Ig or alefacept) could be of therapeutic benefit in early GO, and similar agents might ultimately hold promise in prevention.

Growing evidence for the involvement of autoantibodies directed against the TSH and IGF-1 receptors in GO has excited interest in the potential clinical utility of rituximab. This anti-B-cell monoclonal antibody targets the CD20 antigen and impacts antigen presentation and early steps in B-cell maturation. Trials of rituximab in the treatment of rheumatoid arthritis have shown significant improvement in active disease with decreases in serum activity markers. Results of uncontrolled trials of this agent in GO are promising and have paved the way for randomized controlled trials now underway.

The participation of proinflammatory cytokines and chemokines in the development of GO suggests that monoclonal antibodies targeting these molecules might be useful in treatment. In particular, biological agents that block TNF-α (infliximab, adalimumab, etanercept) or IL-1 receptor (anakinra) are attractive candidates for therapeutic trials in patients with active GO.

See also: Extraocular Muscles: Extraocular Muscle Anatomy; Extraocular Muscles: Extraocular Muscle Metabolism; Imaging of the Orbit; Orbital Bony Anatomy and Orbital Fractures; Orbital Masses and Tumors.

Further Reading

Bahn, R. (2008). The EUGOGO consensus statement on the management of Graves' orbitopathy: Equally applicable to North American clinicians and patients. *Thyroid* 18(3): 281–282.

Bartalena, L., Baldeschi, L., Dickinson, A. J., et al. (2008). Consensus statement of the European group on Graves' orbitopathy (EUGOGO) on management of Graves' orbitopathy. *Thyroid* 18(3): 333–346.

Bartalena, L., Mercocci, C., Bogazzi, F., et al. (1998). Relation between therapy for hyperthyroidism and the course of Graves' ophthalmopathy. *The New England Journal of Medicine* 338(2): 73–78.

Brent, G. A. (2008). Clinical practice. Graves' disease. *The New England Journal of Medicine* 358(24): 2594–2605.

Dickinson, A. J. and Perros, P. (2001). Controversies in the clinical evaluation of active thyroid-associated orbitopathy: Use of a detailed protocol with comparative photographs for objective assessment. *Clinical Endocrinology* 55(3): 283–303.

Garrity, J. A. and Bahn, R. S. (2006). Pathogenesis of Graves' ophthalmopathy: Implications for prediction, prevention, and treatment. *American Journal of Ophthalmology* 142(1): 147–153.

Hales, I. B. and Rundle, F. F. (1960). Ocular changes in Graves' disease. A long-term follow-up study. *Quarterly Journal of Medicine* 29: 113–126.

Khoo, T. K. and Bahn, R. S. (2007). Pathogenesis of Graves' ophthalmopathy: The role of autoantibodies. *Thyroid* 17(10): 1013–1018.

Lehmann, G. M., Feldon, S. E., Smith, T. J., and Phipps, R. P. (2008). Immune mechanisms in thyroid eye disease. *Thyroid* 18(9): 959–965.

Mourits, M. P., Prummel, M. F., Wiersinga, W. M., and Koornneef, L. (1997). Clinical activity score as a guide in the management of patients with Graves' ophthalmopathy. *Clinical Endocrinology* 47(1): 9–14.

Naik, V., Khadavi, N., Naik, M. N., et al. (2008). Biologic therapeutics in thyroid-associated ophthalmopathy: Translating disease mechanism into therapy. *Thyroid* 18(9): 967–971.

Perros, P., Crombie, A. L., and Kendall-Taylor, P. (1995). Natural history of thyroid associated ophthalmopathy. *Clinical Endocrinology* 42(1): 45–50.

Terwee, C. B., Gerding, M. N., Dekker, F. W., Prummel, M. F., and Wiersinga, W. M. (1998). Development of a disease specific quality of life questionnaire for patients with Graves' ophthalmopathy: The GO-QOL. *British Journal of Ophthalmology* 82(7): 773–779.

Wiersinga, W. M. (2007). Management of Graves' ophthalmopathy. *Nature Clinical Practice Endocrinology and Metabolism* 3(5): 396–404.

Wiersinga, W. M., Prummel, M. F., and Terwee, C. B. (2004). Effects of Graves' ophthalmopathy on quality of life. *Journal of Endocrinological Investigation* 27(3): 259–264.

U

Unique Specializations – Functional: Dynamic Range of Vision Systems

A C Arman and A P Sampath, University of Southern California, Los Angeles, CA, USA

Glossary

Dynamic range – The full range of light levels over which retinal cells or pathways can dynamically modify their function to encode.
Mesopic vision – Intermediate light level vision mediated by both rod and cone photoreceptors under conditions where both are responsive, allowing a seamless transition from rod to cone vision.
Photopic vision – High light level vision mediated by cone photoreceptors.
Ribbon synapse – Synapses where a ribbon-like structure is present that optimizes the continuous release of neurotransmitter.
Rod spherule – The specialized synaptic terminal of the rod photoreceptor.
Scotopic vision – Low light vision mediated by rod photoreceptors.

Introduction

Nearly all sensory systems must find a way to represent a wide range of input signals and translate them into meaningful neural responses. The human visual system is able to operate effectively from starlight to bright sunlight, a range that spans about 12 orders of magnitude of light intensity. The pupil serves as the first stage of sensitivity control by changing the amount of the light reaching the photoreceptors. The diameter of the pupil can change by a factor of 4, allowing light intensity to change by a factor of 16. However, this alone cannot account for the complete range of light to which the mammalian retina is sensitive. To reliably transmit changes in light stimuli over this range, the mammalian retina has evolved several specializations to report changes in the light environment that include: (1) the evolution of two photoreceptor types, the rods and cones, that operate at different light levels; (2) several neural pathways with which to encode the output of these photoreceptors; and (3) adaptive mechanisms at all levels of retinal processing to modulate light sensitivity based on light history.

Rods versus Cones

The evolution of the duplex retina in vertebrates with two classes of photoreceptors, the rods and cones, marks a departure from the single type of photoreceptor present in many invertebrates. The use of two photoreceptor subtypes with different sensitivities to light allows the vertebrate retina to respond over a greater range of light intensities. By switching between rods and cones, the vertebrate retina is thus able to maximize visual sensitivity depending on the ambient light level. It is now believed that such an arrangement allows the vertebrate retina to reduce energy consumption in daylight, when the rods are not responsive.

Rods mediate vision when photons are scarce; their design and cytoarchitecture are optimized for maximal sensitivity to incoming photons and are capable of generating a reproducible response to a single absorbed photon, which is critical for setting the sensitivity of scotopic vision when the retinal circuitry pools thousands of rods (see the section titled 'The pathways concept' below). As the mean background light level increases, rods themselves are able to adapt, which allows them to signal light intensities up to ~1000 R^* or more per second.

Cone photoreceptors are ~100-fold less sensitive than rods, and are critical for our daytime vision under conditions when the exquisitely sensitive rod photoreceptors are saturated. The reduced sensitivity of cones arises from reduced amplification within cone phototransduction, and mechanisms designed to shut off phototransduction more quickly than rods. Furthermore, even in

the brightest light the cone photocurrent does not remain saturated, which leaves open the ability to adapt and signal changes in light intensity even under conditions where a majority of the photopigment is bleached. The optimizations of cones to function in bright light with virtually little overlap with rod light levels allows for a smooth transition from rod to cone vision, in what is referred to as the mesopic range.

The Pathways Concept

The adaptive features of the rod and cone light response allow these photoreceptors to remain responsive over a larger range of light intensities by preventing response saturation. However, the dynamic range of the rods and cones themselves cannot account for the ~12 orders of magnitude in light intensity we experience. Another strategy used by the mammalian retina to extend further the dynamic range of vision is to utilize multiple neural pathways to carry light-evoked signals. The functional properties of these pathways (e.g., convergence, gain, and adaptation) can then be adjusted to maximize the visual system's ability to remain responsive over the largest range of light intensities. To date, the most-studied retinal pathways in mammals are those that carry signals from rod photoreceptors to ganglion cells. These include the circuits that carry light information near scotopic threshold (rod bipolar pathway or classical rod pathway), and those that operate at higher rod light levels that may provide a seamless mesopic transition (rod–cone and rod–OFF pathways) to photopic vision. Rather less is known about the functional properties of the cone pathways that maximize dynamic range.

Rod Bipolar Pathway

Psychophysical studies have demonstrated at the limits of scotopic vision that the human visual system is capable of detecting the absorption of a few photons of light. This remarkable sensitivity arises from the fact that individual rods can reliably signal the absorption of a single photon, and that a specialized retinal circuitry referred to as the rod bipolar pathway can combine these signals such that a ganglion cell projecting centrally can pool thousands of rod signals. The discovery of a dedicated depolarizing bipolar cell and an amacrine cell that carries rod signals in the rabbit retina leads to the finding that this circuit appears conserved across all mammalian species. A hallmark of this pathway is the convergence of rod signals at many stages of processing that is critical for our scotopic sensitivity. For instance, as many as 20–100 rods converge on a rod (ON) bipolar cell, and 20–30 rod bipolar cells converge on an AII amacrine cell. Thus, a ganglion cell that sums the output of many AII amacine cells can pool upward of 10 000 rods. Ultimately, by pooling rod signals and eliminating rod noise to preserve best the single-photon response from individual rods, the rod bipolar pathway can extend the dynamic range of vision down to light levels where a small fraction of the rods absorb a photon.

Signal transfer from rods to rod bipolar cells

At scotopic threshold, vision relies on a sparse number of photons at the retina that produce few photon absorptions per thousands of rods within the 0.2-s integration time of the rod photoresponse. Under these conditions, the transmission of a small, graded hyperpolarization upon photon absorption requires that rod synapse is appropriately optimized. The transmission of small, graded single-photon responses at the rod synaptic terminal is aided by two specializations. First, the resting dark membrane potential, or voltage, sits at approximately –40 mV, near the steepest point in the relationship between voltage and L-type Ca^{2+} channel opening (**Figure 2**). Thus, small changes in membrane potential produce substantial changes in the number of open channels, thereby altering glutamate release. Second, if the rod bipolar cell is sensing reductions in glutamate release due to photon absorption, then statistical lapses of glutamate release in darkness would mimic light absorption. Thus, the high rate of glutamate release generated in darkness by the specialized synaptic ribbon in the rod spherule reduces the probability of these lapses. Together, these synaptic properties allow the small, light-evoked signals from rods to be reproducibly transferred to downstream neurons.

Despite the rod synaptic specializations for the transmission of single-photon absorptions, the depolarization in darkness due to open cyclic guanosine monophosphate (cGMP)-gated channels is also a complicating factor in the detection of these sparse signals. Open cGMP-gated channels in turn will report internal fluctuations in cGMP, produced by the phototransduction mechanism, which are commonly referred to as dark noise. Since rods generate a small, graded hyperpolarization upon photon absorption, the downstream convergence of thousands of rod signals would cause the light-evoked response from a single rod to be overwhelmed by the dark noise of the majority. Given the magnitude of dark noise in individual rods, it has been proposed that some type of nonlinear combination of rod signals would be required to increase the detection of the single-photon responses in downstream cells. Since rod photoreceptors are relatively depolarized in darkness, the steady release of glutamate from the synapse provides some insights into potential mechanisms. Postsynaptic saturation at the rod-to-rod bipolar synapse would allow noise generated by open cGMP-gated channels in the rod outer segment to be eliminated. It was proposed that the saturation of postsynaptic glutamate receptors would provide a nonlinear way to eliminate the rod noise, since the synapse would not be

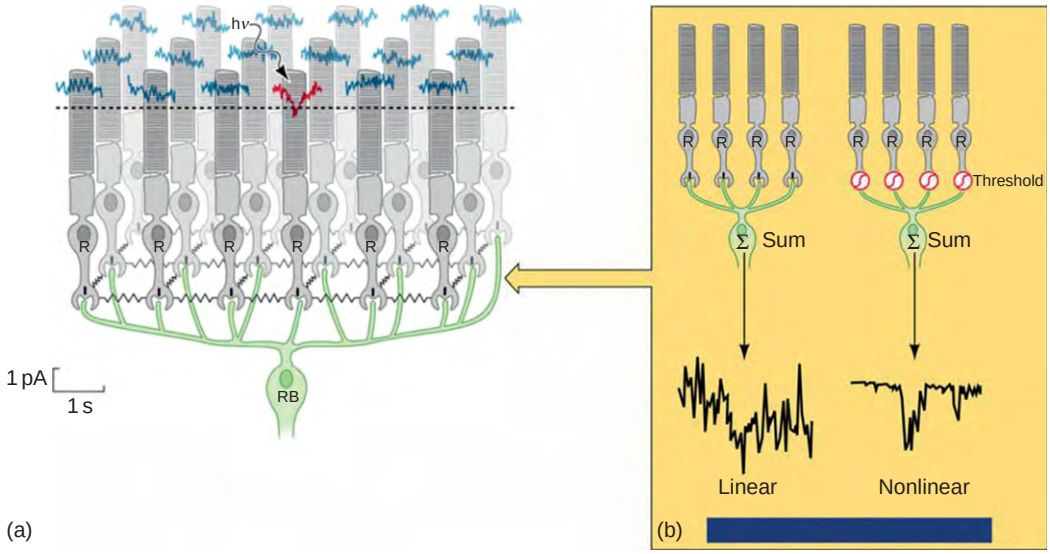

Figure 1 Convergence at the rod-to-rod bipolar synapse. (a) A rod bipolar cell pools inputs from many rods, but near absolute visual threshold only one rod may absorb a photon (red), while the remaining rods are generating electrical noise (blue). A nonlinear threshold (dashed) may improve photon detection at this synapse by retaining responses in rods absorbing a photon and discarding responses of the remaining rods. (b) Nonlinear signal processing can improve the fidelity of rod signals. If rod outputs from (a) are simply summed, the resulting trace is noisy, but when summed after applying a threshold for each rod in (a), the response is more detectable. From Okawa, H. and Sampath, A. P. (2007). Optimization of single-photon response transmission at the rod-to-rod bipolar synapse. *Physiology* 22: 279–286. With kind permission from The American Physiological Society.

able to relay small changes in membrane potential that reflect rod noise. Later work suggested that such thresholding is critical for maximizing the detection of the single-photon response in retinal neurons downstream of the rods (**Figure 1**). In particular, the extent of nonlinear signaling appears to be set to separate optimally the rod single-photon response from rod noise, allowing scotopic vision to reach the highest possible sensitivity.

The mechanism that underlies the nonlinear threshold at the rod synapse has been studied to some extent, but is hindered by a lack of identification of the components of the signaling pathway. Light-evoked signaling between rod photoreceptors and rod (ON) bipolar cells results in a membrane depolarization, effectively inverting the sign of the rod's hyperpolarizing light response. The postsynaptic mechanism underlying this sign inversion is a G-protein signaling pathway initiated by the metabotropic glutamate receptor, mGluR6. mGluR6, in turn, activates a guanine nucleotide-binding protein, $G_o\alpha$, which leads to a series of unidentified events that close a cationic transduction channel of unknown identity. Thus, upon light-absorption, glutamate release from rods is reduced, thereby reducing the activity of the mGluR6 signaling pathway and allowing transduction channels to open and depolarize the cell (**Figure 2**).

In the context of the mGluR6 signaling cascade, it now appears that the nonlinear threshold that eliminates rod noise is due to saturation within the signaling cascade, and not at the level of the glutamate receptors. Furthermore, evidence from axotomized rod bipolar cells indicates that nonlinear signal transfer does not arise due to feedback in the inner plexiform layer. Saturation of the mGluR6 signaling cascade allows the elimination of noise by making the rod bipolar cell insensitive to small fluctuations in glutamate, driven by noise in the rod photoreceptor. Only when the rod's membrane potential is hyperpolarized sufficiently does the glutamate concentration in the synaptic cleft reduce enough to relieve the synapse from saturation. Such an operation thus allows larger hyperpolarizations due to light absorption to cross the rod synapse, while masking smaller fluctuations that are more likely due to noise in the rod photocurrent or synaptic transmission. Near absolute visual threshold, such synaptic processing is necessary to maximize the detectability of rod signals.

Signal transfer from rod bipolar cells to AII amacrine cells

The convergence of the rod bipolar pathway moving from rods to rod bipolar cells and, finally, AII amacrine cells, requires the further accentuation of the single-photon response. Two main specializations between these cells appear well tuned to further improve the detection of the single-photon response, and thus push the dynamic range of vision to lower light intensities. First, a specialized ribbon synapse between the rod bipolar cell and the AII amacrine cells allows the coordinated release of multiple vesicles upon stimulation. Such multivesicular release increases the amplitude of the AII amacrine cell response, allowing it to be distinguished from vesicular release due to noise in the rod bipolar cell. Second, the electrical coupling

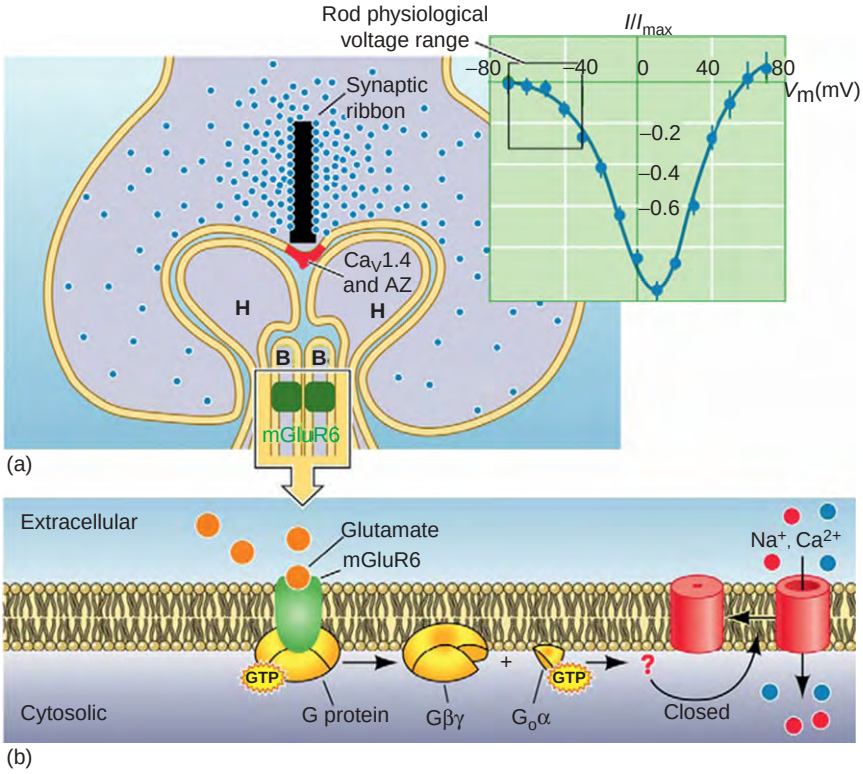

Figure 2 Structure and signal transfer at the rod-to-rod bipolar synapse. (a) The rod spherule is a specialized invaginating structure where the dendrites of horizontal (H) and rod bipolar cells (RB) are apposed to a glutamate release site controlled by a ribbon. Ca^{2+} channels ($Ca_V1.4$) are located near the active zone (AZ) and allow the continuous release of glutamatergic vesicles in darkness. In ON rod bipolar cells, glutamate is sensed by mGluR6 receptors located near the mouth of the invagination. (Inset) Release of glutamate is dependent on Ca^{2+} influx through Ca^{2+} channels, which is graded by voltage over the physiological range. (b) The signaling cascade in rod bipolar cell dendrites is poorly understood. mGluR6 activation leads to the activation of $G_o\alpha$, which through unknown mechanisms leads to the closure of a nonselective cation channel whose identity is also unknown. The light-evoked reduction in glutamate release relieves activity in this cascade and opens cation channels leading to depolarization. From Okawa, H. and Sampath, A. P. (2007). Optimization of single-photon response transmission at the rod-to-rod bipolar synapse. *Physiology* 22: 279–286. With kind permission from The American Physiological Society.

of AII amacrine cells by connexin 36 appears to reduce noise in the network, allowing an improved signal-to-noise ratio.

Ganglion cell sensitivity

Retinal ganglion cells can also relay single-photon responses to higher visual centers, a requirement for the high sensitivity of rod vision. Through the process of neural convergence, as well as the mechanisms described above, ganglion cells and AII amacrine cells have about the same flash sensitivity. Recordings of many groups from dark-adapted cat retinal ganglion cells indicate bursts of ~2–3 action potentials occurred with a frequency consistent with an upstream origin that may be the rods. The frequency of these bursts increased with background light, suggesting that the bursts were related to photon absorption. Similar conclusions have been drawn using a cross-correlation analysis from paired ganglion cell recordings in the presence and absence of background lights.

Rod–Cone Pathway

A consequence of the high sensitivity of the rod bipolar pathway is that it saturates at modest light levels where the rods themselves are not saturated. To capture light-evoked signals from rods until they themselves saturate additional pathways are required. Studies of the ultrastructure of the outer plexifom layer reveal that gap junctions exist between rods and rods, and rods and cones. The nature of the rod-to-rod gap junction is unclear, but has been proposed to dissipate small rod signals into the network allowing signal averaging at the cost of a twofold elevation in visual threshold. The rod-to-cone gap junctions have been studied in more detail and are found in a majority of rods. Evidence points to the expression of the gap junction subunit connexin 36 in cones, but not in rods. Thus, the electrical gap junctions between rods and cones must be heterologous. Given the lower input impedance of cones, signal transfer will preferably travel from rods to cones, which would allow these signals to be relayed to ganglion cells through the cone circuitry.

Physiological recordings have indicated robust rod signals in the cone photoreceptors of several species. In particular, measurements from dark-adapted retina indicate that rod-to-cone coupling must exist, going against the idea that, to maximize visual sensitivity, the rods and cones should be uncoupled in darkness. Recordings from mouse retinal whole mounts suggest that the signals through this pathway are 10-fold less sensitive than for the rod bipolar pathway. These physiological data correspond well with psychophysical experiments indicating a secondary rod pathway with a 10-fold lower sensitivity than the primary pathway.

Rod–OFF Pathway

A third rod pathway has been identified in some species of mammals. Under conditions where the rod–bipolar and rod–cone pathways are blocked or eliminated, OFF signals with rod sensitivity have been shown to persist in the mouse retina. Direct synaptic contacts have been identified anatomically in mice, rats, and rabbits. However, direct contacts between rods and OFF bipolar cells have not yet been reported in higher mammals. It is possible that an OFF rod pathway evolved as a specialization in nocturnal rodents to sense dark objects against a light sky.

The rod–OFF pathway is believed to be active at 5–10-fold higher light intensities than the rod bipolar pathway. Its prominence as a signaling circuit in rodents appears to vary based on the percentage of the OFF cone bipolar cell population that sees direct signals from rods. It is now believed that between 5% and >25% of cone OFF bipolar cells may see direct contacts from rods, the upper end suggesting that this pathway may play an integral role in visual processing.

Despite attempts by various groups to characterize the physiological response properties of the rod pathways, the exact sensitivities and operating ranges of each pathway remain unclear. The lack of physiological evidence elucidating the role of these pathways in rod vision arises from common signaling mechanisms used by each. Thus, genetic or pharmacological manipulation of each rod-signaling pathway will also influence other pathways, making it impossible to unambiguously identify the properties of each. Nevertheless, the evidence now points to the rod bipolar pathway as the primary carrier of single-photon responses near absolute visual threshold, with an ~5–10-fold reduction in the sensitivity of the rod–cone and rod–OFF pathways that may carry signals at higher light levels where cone function is merged.

Cone Pathways

Our understanding of the cone pathways is far less complete than our understanding of rod pathways in the mammalian retina. The physiological properties of the cones and cone pathways remain as one of the frontiers in retinal neurobiology, especially as cone function dominates our visual experience. To date, as many as nine types of cone bipolar cells have been identified in mammalian retinas, which may connect to as many as 10–15 types of retinal ganglion cells. Other than the specific pathway for S-cones, there is presently little understanding of specific circuits that carry cone responses to ganglion cells.

Adaptation to Mean Background Light

A common feature of all sensory systems is the ability to adapt to increases in the mean level of a stimulus by reducing the gain of the system. Such sensitivity adjustments allow the sensory system to remain maximally responsive as the stimulus intensity changes. Both rods and cones in the retina, as well as their circuitry, exhibit adaptive mechanisms that are designed to increase the dynamic range of the receptor. However, in the context of the dynamic range of the visual system, the influences of adaptation on the lower limit of scotopic and upper limit of photopic vision are opposite. To retain maximal sensitivity near absolute visual threshold, the retina must maximize its gain for the single-photon response and any adaptive mechanism would allow the rod circuitry to aid in the transition from scotopic to mesopic vision. Conversely, the upper light limits of our visual experience are ultimately defined by adaptation in the cone photoreceptors, which continue to operate even when a majority of the photopigment is bleached.

Adaptation: Rod Pathways

Adaptation within a neural circuit with considerable convergence will begin centrally and move peripherally. Under these circumstances, downstream cells will be the first to detect sufficient signal to adapt for the weakest stimuli, and the rod pathways are no exception. In the rod bipolar pathway, weak background light begins to reduce the gain of ganglion cells and AII amacrine cells before adaptation is detectable in rod bipolar cells or rod photoreceptors. Some mechanisms that provide this gain reduction have been identified, particularly at the rod-to-rod bipolar, and the rod bipolar-to-AII amacrine synapses. For instance, at the rod-to-rod bipolar synapse, the influx of Ca^{2+} through mGluR6 transduction channels reduces the bipolar cell gain for subsequent stimulation. In addition, at the rod bipolar-to-AII amacrine synapse depression mediated by depletion of the available pool of vesicles can be evoked at individual synapses by single-photon responses. These adaptive mechanisms allow the rod bipolar pathway to extend its range to higher light levels

where they merge with the other rod pathways. However, the extension of the dynamic range of vision to lower light levels requires that the retina remains maximally responsive to single photons, and thus these adaptive mechanisms would impair absolute threshold.

Adaptation: Cone Pathways

It has been well documented that adaptation of ganglion cell responses in the cone pathways occurs at lower light levels than where adaptive features of cone pathways have been documented. Cone and horizontal cell recordings have demonstrated that cone adaptation is observed at light levels that exceed those required for the adaptation of cone-driven signals in ganglion cells. This adaptation of the postsynaptic cone circuitry, in turn, prevents these pathways from saturating, thereby allowing the extension of the cone operating range through mesopic to photopic vision. Adaptation, both in the cones and in the postreceptoral circuitry, have been found to be mutually exclusive. Ultimately, the upper limits of cone vision are directly imposed by receptoral adaptation of the cones themselves and not by the postsynaptic circuitry.

Conclusions

The vertebrate retina has developed many strategies to maximize the dynamic range of vision. At the initial stages of light detection the evolution of two photoreceptor types, the rods and cones, allows the visual system to signal a wide range of light intensities. By dividing the output of these receptors across many retinal pathways, each of which is subject to its own optimization and adaptation, the human eye is capable of providing the brain with information that extends the range of vision to encompass approximately 12 orders of magnitude of light intensity.

See also: Anatomically Separate Rod and Cone Signaling Pathways; Information Processing: Bipolar Cells; Information Processing: Ganglion Cells; Morphology of Interneurons: Bipolar Cells; Phototransduction: Adaptation in Cones; Phototransduction: Adaptation in Rods; Phototransduction: Phototransduction in Cones; Phototransduction: Phototransduction in Rods; Rod Photoreceptor Cells: Soma and Synapse.

Further Reading

Barlow, H. B. (1956). Retinal noise and absolute threshold. *Journal of the Optical Society of America* 46: 634–639.

Barlow, H. B., Levick, W. R., and Yoon, M. (1971). Responses to single quanta of light in the retinal ganglion cells of the cat. *Vision Research Supplement* 3: 87–101.

Baylor, D. A., Lamb, T. D., and Yau, K. W. (1979). Responses of retinal rods to single photons. *Journal of Physiology* 288: 613–634.

Dacheux, R. F. and Raviola, E. (1986). The rod pathway in the rabbit retina: A depolarizing bipolar and amacrine cell. *Journal of Neuroscience* 6: 331–345.

Dunn, F. A. and Rieke, F. (2008). Single photon absorptions evoke synaptic depression in the retina to extend the operational range of rod vision. *Neuron* 57: 894–904.

Dunn, F. A., Lankheet, M. J., and Rieke, F. (2007). Light adaptation in cone vision involves switching between receptor and post-receptor sites. *Nature* 449: 603–606.

Field, G. D. and Rieke, F. (2002). Nonlinear signal transfer from mouse rods to bipolar cells and implications for visual sensitivity. *Neuron* 34: 773–785.

Hecht, S., Schlaer, S., and Pirenne, M. H. (1942). Energy, quanta, and vision. *Journal of General Physiology* 25: 819–840.

Hornstein, E. P., Verweij, J., Li, P. H., and Schnapf, J. L. (2005). Gap-junctional coupling and absolute sensitivity of photoreceptors in macaque retina. *Journal of Neuroscience* 25: 11201–11209.

Okawa, H. and Sampath, A. P. (2007). Optimization of single-photon response transmission at the rod-to-rod bipolar synapse. *Physiology* 22: 279–286.

Sampath, A. P. and Rieke, F. (2004). Selective transmission of single photon responses by saturation at the rod-to-rod bipolar synapse. *Neuron* 41: 431–443.

Singer, J. H., Lassova, L., Vardi, N., and Diamond, J. S. (2004). Coordinated multivesicular release at a mammalian rod synapse. *Nature Neuroscience* 7: 826–833.

Smith, R. G., Freed, M. A., and Sterling, P. (1986). Microcircuitry of the dark-adapted cat retina: Functional architecture of the rod–cone network. *Journal of Neuroscience* 6: 3505–3517.

Sterling, P., Freed, M. A., and Smith, R. G. (1988). Architecture of rod and cone circuits to the on-beta ganglion cell. *Journal of Neuroscience* 8: 623–642.

van Rossum, M. C. and Smith, R. G. (1998). Noise removal at the rod synapse of mammalian retina. *Visual Neuroscience* 15: 809–821.

Uveoscleral Outflow*

A Alm, University of Uppsala, Uppsala, Sweden

Glossary

Aqueous humor – The clear fluid found between the cornea and the iris.
Bulk flow – The proteins following fluid transport in proportion to its concentration in the fluid.
Ciliary muscle – The muscle that controls the eye's accommodation for viewing objects allowing the lens to focus on near, distant, and intermediate objects.
Glaucoma – An eye disease associated with increased intraocular pressure which can damage the optic nerve and may lead to vision loss.
Goldmann equation – The equation that describes the relationship between intraocular pressure, aqueous flow, outflow through the trabecular meshwork, and episcleral venous pressure.
LYVE-1 – A marker for lymphatic vessels, which is also expressed on some blood vessels and macrophages.
Prostaglandins – A group of lipid compounds, which act as a hormone-like substance that mediate many bodily functions.
Pseudoexfoliation – The abnormal deposits of white substance seen on the lens and usually associated with glaucoma.
Uveitis – The inflammation of the middle layer of the eye.

The circulation of aqueous humor through the anterior segment of the eye serves several purposes. It nourishes the avascular lens and cornea, rids the anterior chamber from inevitable debris accumulated during the years, and it maintains sufficient pressure within the eye to keep the eye globe rigid during eye movements. It has long been known that the fluid filling the anterior and posterior chamber, aqueous, is not a stagnant pool, but that there is a continuous secretion of aqueous from the ciliary processes, and that aqueous leaves the eyes through the tissues of the anterior chamber. The structures of the trabecular or conventional outflow route are well known. As this anatomical arrangement seems to fulfill the purpose of circulating aqueous it was long accepted that this was a complete description of the aqueous humor circulation, with the possible exception of some leakage to the vitreous and diffusion into nearby tissues. A second outflow route was, however, discovered when Anders Bill noted that in young monkeys about half of the aqueous leaves the eye by bulk flow through what became termed the unconventional or uveoscleral outflow.

Morphology

Thus the trabecular outflow route seems to provide all that is necessary in order for aqueous to circulate and pass out of the eye through bulk flow. It even permits very large particles, such as red blood cells (**Figure 1**), to leave the anterior chamber, a necessity for saving sight after trauma. Still, in retrospect, it may seem obvious that some aqueous can leave the eye through other tissues in the chamber angle than the trabecular meshwork. As seen in **Figure 2** there is no epithelial barrier between the anterior chamber and the iris/ciliary muscle and at least water and small molecules should be able to pass this way. The intermuscular connective tissue between the ciliary muscle bundles is sparse in young human eyes (**Figure 3(a)**). In monkeys even 1-μm large latex spheres can pass between the muscle bundles. From the supraciliary or suprachoroidal space, 0.1-μm spheres can enter the perivascular spaces in the sclera and 10-nM Thorotrast particles enter the sclera. In human donor eyes, stained gelatine or methyl methacrylate injected into the suprachoroidal space can be found in the perivascular spaces between the adventitia of the vessels and scleral fibrils (**Figure 4**), and even in direct channels from the suprachoroidal space communicating with the scleral venous plexus (**Figure 5**). Thus, proteins accumulating in the extravascular space of the highly permeable choroidal vessels can leave the eye through these routes, a task normally handled by lymphatic vessels. It has long been accepted that there are no lymph vessels in the eye. However, recent development of new markers for lymphatic endothelium has renewed interest on this subject. A network of channels stained with a specific marker for lymphatic endothelium has been seen in the ciliary muscle and processes of human eyes (**Figure 6**) and LYVE-1 positive macrophages, but no classical lymphatic vessels, are found in the choroid. However, the role of these new findings in the removal of proteins from the suprachoroidal and supraciliary spaces remains to be determined.

* Adapted from Alm, A. and Nilsson, S. F. E. (2009). Uveoscledral outflow – a review. *Experimental Eye Research* 88: 760–768.

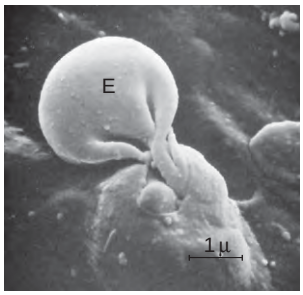

Figure 1 Detail of the inner wall of Schlemm's canal in a rhesus monkey. The anterior chamber had been perfused with red cells. An erythrocyte (E) was on its way out of a bulging structure into the canals of Schlemm at the moment of fixation. Procedure: formalin fixation; ethanol dehydration; air-drying; opening of the canal. Adapted from Bill, A. (1970). Scanning electron microscopic studies of the canal of Schlemm. *Experimental Eye Research* 10: 214–218.

Figure 2 The anterior segment of a cynomolgus monkey. Courtesy of P. Naeser.

Techniques to Determine the Rate of Uveoscleral Flow

Experimental Animals

Aqueous flow can be determined in experimental animals where the anterior chamber is perfused with a large-molecular-weight tracer. Small tracers, such as sodium fluorescein that pass through the cornea, are used for clinical studies but about 10% is lost by diffusion into the surrounding tissues. Very little albumin is lost by diffusion and it leaves the anterior chamber mainly by bulk flow. In his search for a suitable tracer to determine aqueous flow in monkeys, Anders Bill noted that about

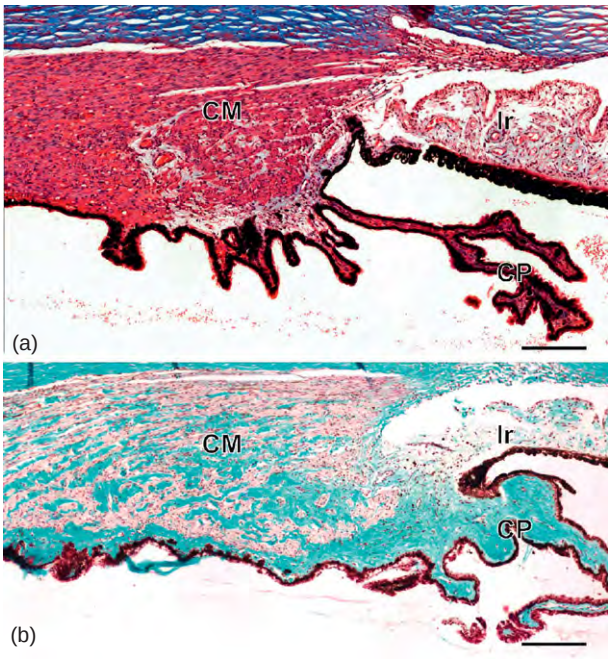

Figure 3 Ciliary body (pars plicata) of a 34-year-old (a) and an 80-year-old human donor stained after Masson (a) or Masson–Goldner (b), respectively. Smooth muscle cells of the ciliary muscle (CM) are labeled in red while extracellular fibrillar material is labeled in blue (a) or green (b). In the older eye, there is considerably more fibrillar extracellular material between the ciliary muscle cells and in the stroma of the ciliary processes (CP) as compared to the younger eye. Magnification = 200 μm; I, iris. Adapted from Tamm, S., Tamm, E., and Rohen, J. W. (1992). Age-related changes in the human ciliary muscle. A quantitative morphologic study. *Mechanisms of Ageing and Development* 62: 209–221.

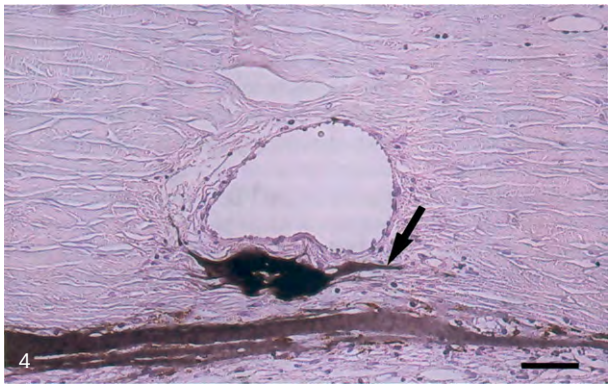

Figure 4 Histological cross section of an anterior ciliary vein in the anterior part of the sclera. Black gelatine from the suprachoroidal space fills the perivascular space (arrow) between the adventitia of the vessel and the scleral fibrils. H.E. stain; original magnification: ×200. Bar = 50 μm. Adapted from Krohn, J., and Bertelsen, T. (1998). Light microscopy of uveoscleral drainage routes after gelatine injections into the suprachoroidal space. *Acta Ophthalmologica Scandinavica* 76: 521–527.

half of the tracer injected into the anterior chamber did not appear in blood until much later. The lost albumin could be found in the ciliary muscle and the suprachoroidal space. Large-molecular-weight tracers have since been used for determination of aqueous flow in experimental animals. In order to determine uveoscleral flow, the concentration of labeled albumin in the anterior chamber is followed continuously and the animals are sacrificed after a fixed time. Albumin drained by the conventional outflow route is determined by following the appearance of radioactivity in blood samples. Albumin drained by the uveoscleral outflow route can then be calculated as the concentration in the ocular tissues, after removal of all aqueous, divided by the mean concentration in aqueous during the experiment. A second technique is based on near-continuous calculation of aqueous humor flow, and conventional outflow is determined by following the appearance of the labeled albumin in plasma. The rate of uveoscleral is then the difference between aqueous flow and conventional outflow during the experiment.

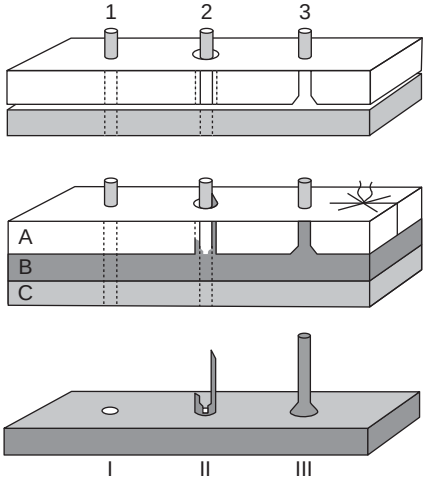

Figure 5 Schematic vessels in the corrosion cast of human cadaver eyes where methylmetacrylate had been injected into the suprachoroidal space on the average 48 h postmortem. (a) Sclera; (b) methyl methacrylate in the suprachoroid space; (c) choroid. 1. Perforating blood vessel passing through the suprachoroidal space. 2. Perforating blood vessel, surrounded by perivascular connective tissue. 3. Scleral channel, arising directly from the suprachorodial space. I: Small hole right through the cast. II: Irregular branch, deriving close to a hole. III: Smooth circular branch, deriving from a plain surface. Adapted from Krohn, J. and Bertelsen, T. (1997). Corrosion casts of the suprachoroidal space and uveoscleral drainage routes in the human eye. *Acta Ophthalmologica Scandinavica* 75: 32–35.

Human Eyes

There is no technique for direct, noninvasive measurements of uveoscleral flow in human eyes. The Goldmann equation, adjusted for uveoscleral flow, establishes the relationship between the IOP, aqueous flow (F_{IN}), uveoscleral flow (F_{US}), outflow facility through the trabecular meshwork (C), and episcleral venous pressure (P_{EV}).

$$\text{IOP} = P_{EV} + \frac{(F_{IN} - F_{US})}{C}$$

Thus

$$F_{US} = F_{IN} - C^{*}(\text{IOP} - P_{EV})$$

Unfortunately, determining the other components of aqueous humor dynamics will not provide sufficiently precise measurements to make calculations of F_{US} from the Goldmann equation meaningful. IOP and F_{IN} can both be determined with reasonable precision, but they are measured under markedly different conditions. IOP is an instant measurement and F_{IN} is averaged over several hours. Techniques to determine P_{EV} are difficult and it is usually assumed to be 8 or 9 mmHg. Clinical tonography is the weak link for clinical determination of F_{US}. It requires a marked increase in IOP and the measurement error is large. As aqueous flow, determined with a fluorophotometric technique, and IOP can be measured with reasonable precision, a clinical technique that is

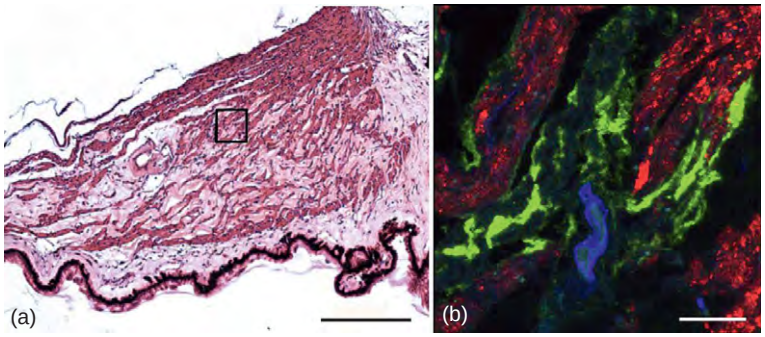

Figure 6 D2-40-immunoreactive lymphatic channels seen in human ciliary body. (a) H- and E-stained human ciliary body (calibration bar indicates 250 μm). (b) Confocal projection image (1 5 μm thick, 0.5 μm step, 60× oil immersion) taken from an area in the ciliary muscle (the square in (a)). D2-40-positive lymphatic channels (green) are seen along SMA-positive smooth muscle fiber bundles (red) and are distinct from CD34-blood vessel endothelium (blue) in the ciliary body (calibration bar indicates 40 μm). Courtesy of N. Gupta.

independent of C is now the technique that is usually applied for clinical determination of uveoscleral flow. IOP and F_{IN} are determined at two different levels, before and after administration of a combination of oral acetazolamide and a topical adrenergic β-receptor antagonist, timolol. Neither drug is expected to change F_{US}, C, or P_{EV}. A reasonable value for P_{EV} is usually assumed, and C can then be calculated as $\Delta F_{IN}/\Delta$IOP. The technique has obvious advantages over calculations based on standard tonography but it is sensitive to the difference between IOP and P_{EV} and even a small change in estimated P_{EV} would have a marked effect on the calculated uveoscleral flow, particularly in eyes with normal levels of IOP.

Normal Values

Values Obtained with Tracers in Different Species

Direct measurements of uveoscleral flow with tracers have been done in several species, including a few human eyes scheduled for enucleation (Table 1). In nonhuman primates 38–55% of aqueous flow left the eye through the uveoscleral route, while much lower values were found in rabbits (3–8%), cats (3%), and dogs (15%). The values for human eyes were much lower than in nonhuman primates, 4–14% respectively in two eyes. This may, however, reflect the fact that these values were determined in elderly eyes and there are good reasons to believe that uveoscleral flow is reduced with age (see below). When values obtained in nonhuman eyes are compared, there is a marked species difference that seems to reflect the degree of development of the ciliary muscle.

Table 1 Uveoscleral flow in different species determined with labeled tracers

Species	*F_{US} (μL min^{-1})*	*% of F_{IN}*	*Reference*
Human	nd/0.28	4/14	Bill and Phillips (1971)
Monkey			
Cynomolgus	0.96	55	Bill (1971)
Vervet	0.65	38	Bill (1971)
Cat	0.36	3	Bill (1966c)
Rabbit (albino)	0.11–0.26	3–8	Bill (1966d), Poyer et al. (1992)
Dog (beagle)	n.d.	15	Barrie et al. (1985)

n.d., not determined; F_{US}, uveoscleral flow; F_{IN}, aqueous flow.
Adapted from Alm, A. and Nilsson, S. F. E. (2009). Uveoscledral outflow – a review. *Experimental Eye Research* 88: 760–768.

Calculated Values from Human Eyes

Values calculated from measurements of aqueous humor dynamics in human eyes have, as a rule, provided considerably higher values for uveoscleral flow than that determined with labeled albumin in human eyes. Although, as pointed out above, clinical techniques are likely to be less precise than experiments with labeled tracers, the results are reasonably consistent suggesting that between 30% and 50% of aqueous leaves the anterior chamber of the human eye by the uveoscleral outflow route in young individuals (Table 2).

Effect of Age

Comparing uveoscleral flow in different species determined with tracers (Table 1), it is striking that the values reported for two human eyes are much lower than in nonhuman primates. Obviously, a true species difference may be involved; however, it is also possible that the main reason is that uveoscleral flow is reduced with age. The two human eyes were from patients aged 54 and 63 years, respectively. Both aqueous flow and outflow facility is reduced with age with little overall effect on IOP in Western populations. A similar, modest reduction seems to take place with uveoscleral flow. Clinical studies (Table 2) found a significant reduction in uveoscleral flow with age from 1.52 µl min^{-1} in eyes aged 20–30 years to 1.10 µl min^{-1} in eyes older than 60 years. The morphology of the ciliary muscles supports the concept that uveoscleral flow is age dependent. The spaces between the ciliary muscle bundles are markedly reduced with age. Connective tissue is increased from about 20% of the total area in human eyes between the age of 30 and 40 to more than 50% in eyes at an age of 60 or more in the reticular portion of the ciliary muscle, facing the anterior chamber (Figure 3(b)). This is likely to reduce the amount of aqueous passing through the uveoscleral route.

Table 2 Values for F_{US} determined in human eyes from indirect calculations

Age	*Diagnosis*	*F_{US} (μL min^{-1})*	*% of F_{IN}*	*Reference*
21–27	Normal	0.80	36	Townsend and Brubaker (1980)
20–30	Normal	1.52	54	Toris et al. (1999a)
≥60	Normal	1.10	46	Toris et al. (1999a)
	Normal	0.14–1.09	12–42	Toris et al. (1993, 2002), Johnson et al. (2008)
33–84	OH	0.12–1.24	5–40	Toris et al. (1995a,b, 1999b, 2002, 2004) Johnson et al. (2008)
72 (8)	PEX with or without OH	0.11	5	Johnson et al. (2008)

F_{US}, uveoscleral flow; F_{IN}, aqueous flow.
Adapted from Alm, A. and Nilsson, S. F. E. (2009). Uveoscledral outflow – a review. *Experimental Eye Research* 88: 760–768.

Physiology

Effect of IOP

Flow through the uveoscleral outflow occurs by bulk flow, which is always pressure dependent, but the unconventional outflow route is often referred to as pressure independent. This is because uveoscleral flow does not depend on the IOP to the same extent as trabecular outflow does. Within the normal range of IOP flow through the trabecular meshwork increases almost linearly, while uveoscleral flow is relatively stable (**Figure 7**). The main resistance to trabecular outflow is located in the trabecular meshwork. Measurements of pressure in the anterior chamber and in Schlemm's canal in monkeys have shown that the pressure in Schlemm's canal is only slightly higher in eyes with a marked artificial increase in IOP. Thus, as IOP is raised there is a concomitant and almost equal increase in pressure across the main resistance of the trabecular outflow route.

The pressure gradients for the uveoscleral flow are quite different. The fact that the sclera offers little resistance to flow, and that the choroidal vessels probably easily can absorb the small amount of aqueous delivered, makes it likely that the main resistance is within the ciliary muscle. Removing this resistance by cyclodialysis (surgery to create a hole between anterior chamber and suprachoroidal space) causes a very marked increase in uveoscleral flow in rabbits and monkeys. In addition, the previously mentioned parallel between age-related changes within the ciliary muscle and reduction in uveoscleral flow rate with age supports this assumption. Then the pressure gradient that determines uveoscleral flow is the one between the anterior chamber and the supraciliary and suprachoroidal spaces. This pressure gradient is only a few mmHg and as pressure in the supraciliary and suprachoroidal spaces increases if IOP is increased, there will be no or only a small effect on the pressure gradient for flow through the ciliary muscle when IOP is increased. This will cause an impression of a pressure-independent flow if only IOP is considered. Moreover, compression of the spaces between the ciliary muscle bundles at high IOP will increase resistance to flow and tend to compensate for the small increase in the pressure gradient. At a very low IOP, below 4 mmHg, the pressure gradient over the ciliary muscle becomes very low and uveoscleral flow is much reduced.

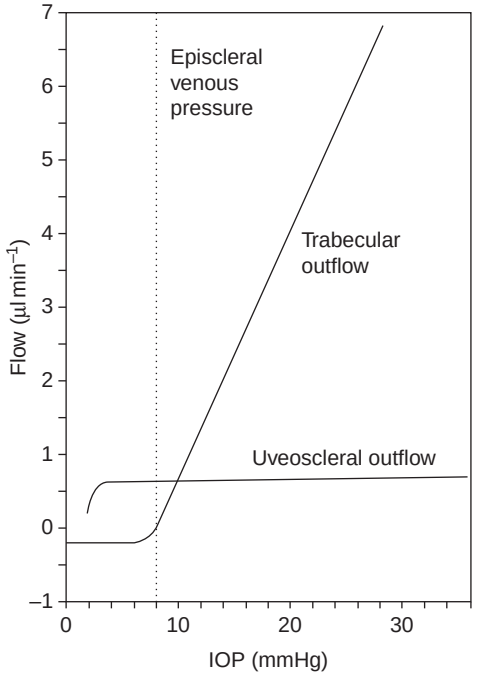

Figure 7 Influence of the intraocular pressure (IOP) on outflow through Schlemm's canal (trabecular outflow) and the uveoscleral pathway. Adapted from Nilsson, S. F. E. and Bill, A. (1994). Physiology and neurophysiology of aqueous humor inflow and outflow. In: Kaufman, P. L, Mittag, T. W., Podos, S. M., and Yanoff, M. (eds.) *Textbook of Ophthalmology, Vol. 7: Glaucoma.* London: Mosby.

Effect of Ciliary Muscle Tone

The tone of the ciliary muscle has an effect on uveoscleral flow, contraction reduces it and relaxation increases it, most likely by its influence on the volume of the extracellular space between the muscle bundles. Thus, atropine increases and pilocarpine reduces uveoscleral flow (see below). The effect has mainly been studied in short-term experiments, but studies on monkeys with or without pretreatment with pilocarpine provided the first support that prostaglandins decreased IOP by increasing flow through the ciliary muscle (see below). In addition, the age-related changes in ciliary muscle morphology and uveoscleral flow mentioned above support the general assumption that the permeability of the ciliary muscle is an important determinant for the rate of uveoscleral flow.

Pharmacology

Cholinergic Agents

The first drugs tested for a possible effect on uveoscleral flow were drugs active on the cholinergic receptors. Pilocarpine markedly reduced uveoscleral flow in human and nonhuman primate eyes, and this was prevented by atropine, which when given alone, has a moderately increasing effect on uveoscleral flow in anesthetized monkeys. Pilocarpine also has a marked effect on the conventional outflow route mediated by the ciliary muscle which, when contracted, separates the lamellae of the trabecular meshwork and reduces outflow resistance. As pilocarpine is a potent ocular hypotensive drug, it is clear that the

IOP-lowering effect on the trabecular meshwork outweighs the reduction in uveoscleral flow and pilocarpine, thus both redirect and increase aqueous outflow.

Adrenergic Agents

Sympathetic tone has no effect on the uveoscleral flow but topical application of epinephrine increases uveoscleral outflow. In monkey eyes, it is almost doubled. Epinephrine is a nonselective adrenergic receptor agonist and the mechanism of action is not clear; part of it may be due to relaxation of the ciliary muscle induced by stimulating the β-adrenergic receptor. Considering the marked effect on uveoscleral flow in anesthetized monkeys, much larger than the effect seen with atropine, one must assume that other adrenergic mechanisms are involved. It seems likely that at least part of the effect is mediated by β-adrenergic receptors since studies both on nonselective (isoproterenol) as well as β_2-adrenergic receptor agonists (terbutaline and salbutamol) have shown that these tend to increase uveoscleral flow in monkey and human eyes. Still, the effect of β-adrenergic receptors on the normal uveoscleral flow rate is probably small and there is no known effect of topically applied β-adrenergic receptor blockers, such as timolol, on uveoscleral flow. It has also been suggested that stimulating the α_2-adrenergic receptor increases uveoscleral flow but results obtained with apraclonidine and brimonidine have been inconclusive.

Prostaglandins

Prostaglandins are a family of local hormones that are involved in many physiological processes and in inflammation. Inhibitors of prostaglandin synthesis have long been used clinically as nonsteroidal anti-inflammatory agents. The development of prostaglandin analogs to reduce IOP has had a marked impact on the treatment of open-angle glaucoma. Prostaglandin, mainly prostaglandin $F_{2\alpha}$ ($PGF_{2\alpha}$), is a powerful ocular hypotensive agent in many species, including rabbits, cats, dogs, and monkeys. In monkey eyes, it is clear that its mechanism of action is mediated through an increase in uveoscleral flow. Among the first observations supporting that prostaglandins affect flow through the ciliary muscle were studies that demonstrated that contraction of the ciliary muscle by pretreatment with pilocarpine reduced or eliminated the effect of prostaglandin $PGF_{2\alpha}$ on IOP. Morphological studies on monkey eyes treated for several days with $PGF_{2\alpha}$ showed enlarged spaces between the ciliary muscle bundles. Thus, it seems clear that prostaglandins remodel the extracellular matrix of the ciliary muscle and reduce flow resistance between the muscle bundles. Since prostaglandins relax the ciliary muscle, part of the early effect may be due to this; however, the long-term effect is due to remodeling of the extracellular matrix. As a consequence, $PGF_{2\alpha}$ and $PGF_{2\alpha}$ analogs do not reach their maximal effect on IOP until after 8–12 h, and after withdrawal of latanoprost, a $PGF_{2\alpha}$ analog, IOP is only slowly returning to pretreatment values over several weeks (**Figure 8**). Studies in human eyes have shown that prostaglandins and prostaglandin analogs have little or no effect on aqueous flow, and it is clear that the effect on IOP observed for the various $PGF_{2\alpha}$ analogs now in clinical use is on outflow. As pointed out above, clinical tonography cannot adequately separate between outflow through the trabecular meshwork and the uveoscleral outflow route, but the effects seen on outflow facility, determined with clinical tonography, have usually been too small to explain the effect on IOP. It seems reasonable that $PGF_{2\alpha}$ analog exerts its main effect also in the human eye by increasing uveoscleral flow.

The mechanism of action behind the remodeling of the ciliary muscle has been studied *in vitro* on cells and muscles from human and nonhuman primate eyes. Thus, topical application of $PGF_{2\alpha}$ as well as latanoprost reduce several collagens in the ciliary muscle of monkeys (**Figure 9**). Increased metalloproteinases (MMPs) have also been recorded in human ciliary muscle cells exposed to $PGF_{2\alpha}$ or latanoprost. The increased expression of MMPs seems to be a consequence of an increased expression of c-Fos in ciliary muscle cells. Factors other than reduction of collagen may well be involved. The shape of ciliary muscle cells exposed to latanoprost changes with alterations in the localization of the cytoskeleton proteins, actin and vinculin.

These changes in the ciliary muscle are likely to be mediated by prostaglandin FP receptors that have been identified in the ciliary muscle. The importance of the FP receptor for the effect on IOP is supported by observations that neither latanoprost nor bimatoprost has any effect on IOP in homozygous knock-out mice. Still, receptors other than the FP-receptor may well have been involved in the effect of $PGF_{2\alpha}$ and the prostanoid

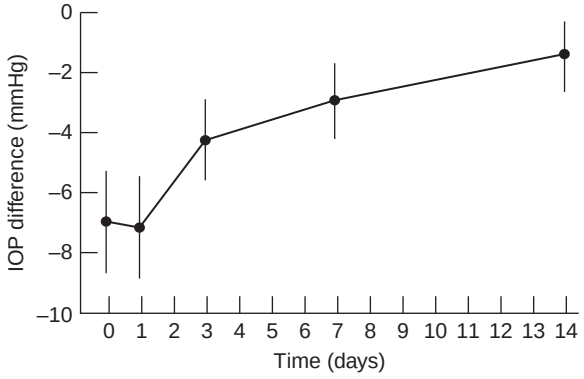

Figure 8 Mean difference (pretreatment IOP – IOP during follow up) versus time after cessation of latanoprost treatment. Error bars denote 95% confidence interval ($n = 26$). Adapted from Lindén, C., Nuija, E., and Alm, A. (1997). Effects on IOP restoration and blood-aqueous barrier after long term treatment with latanoprost in open angle glaucoma and ocular hypertension. *British Journal of Ophthalmology* 81: 370–372.

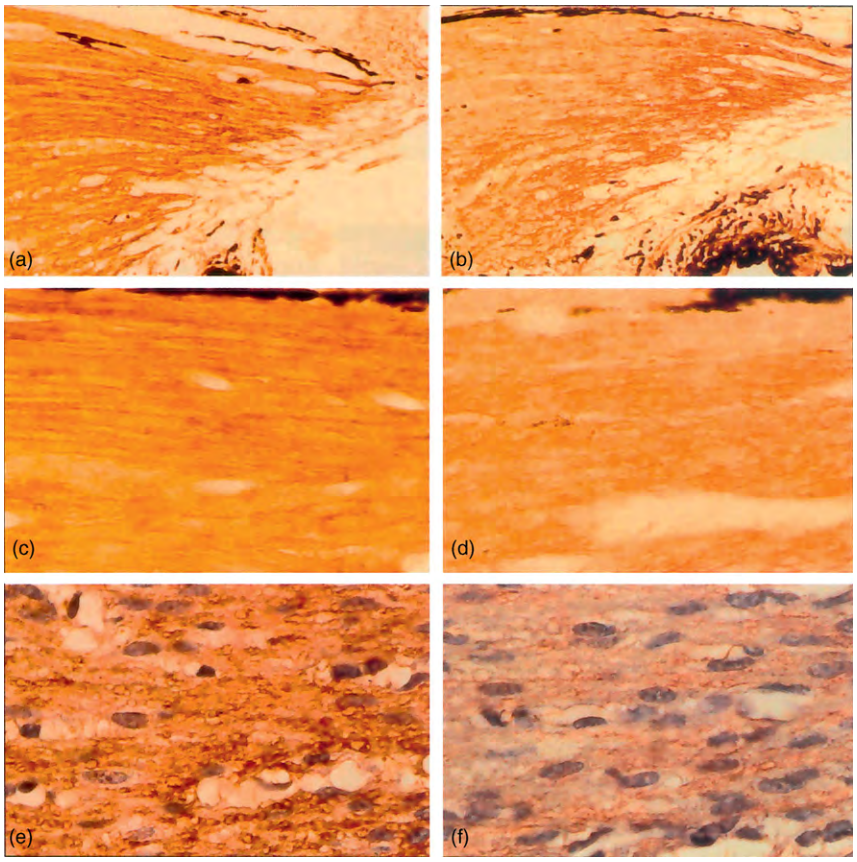

Figure 9 Immunoperoxidase stainings of the ciliary muscle from two cynomolgus monkeys 10 days after unilateral topical treatment with placebo (left panels) or 3 μg day^{-1} latanoprost (right panels). (a)–(d) collagen IV and (e, f) collagen VI. (a, b) ×100; (c)–(f) ×400. Apparent decreases in collagen types IV and VI immunoreactivity are seen in these latanoprost-treated eyes. Adapted from Ocklind, A. (1998). Effect of latanoprost on the extracellular matrix of the ciliary muscle. A study on cultured cells and tissue sections. *Experimental Eye Research* 67: 179–191.

EP_2 receptor agonist butaprost has also been shown to increase uveoscleral outflow in monkeys. Thus, receptors other than the FP receptor may contribute to a reduction of IOP, which may well be the case with $PGF_{2\alpha}$, which is not highly selective for the FP receptor.

Role of Uveoscleral Flow in Normal and Diseased Eyes

The physiological role of the uveoscleral outflow route is not clear. It removes a sizable fraction of aqueous in younger individuals, but seems to be markedly reduced with age, as a consequence of age-related changes in the ciliary muscle. This has no obvious effect on IOP, perhaps due to concomitant, modest, age-related reductions in both aqueous flow and outflow facility. There are also large species differences in the development of uveoscleral flow without any evidence of malfunction. One can then conclude that the lack of an epithelial barrier to prevent flow through the iris and ciliary muscle has no obvious negative consequences.

Thus, the uveoscleral route permits the passage of large molecules between the anterior chamber and the extravascular spaces of the uvea. The small amount of proteins present in aqueous is likely to be a result of some leakage of proteins from the supraciliary space and obviously large molecules in the anterior chamber can go in the other direction as demonstrated by the tracer methods for studies of uveoscleral flow. Albumin injected into the anterior chamber can be found in the suprachoroidal space as far back as the optic nerve (**Figure 10**). This is a consequence of the slow removal of proteins from the suprachoroidal space, mostly by passage through the sclera. For smaller molecules, however, such as drugs that can pass through the cornea the turnover in the suprachoroidal space is much faster and most of them will remain there for less than a minute. Other factors, such as polarity and lipofilicity, will affect the fate of a small molecule in the suprachoroidal space, but as a rule only a very modest improvement in drug concentration in the posterior suprachoroidal space can be expected for molecules small enough to penetrate the cornea.

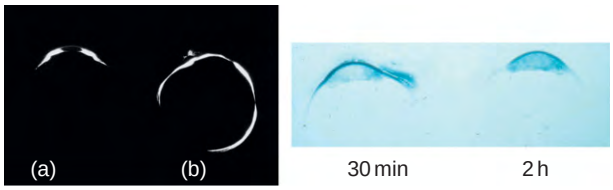

Figure 10 Autoradiograms from monkey eyes. (Right) Labeled albumin had been injected into the anterior chamber in the two eyes, one untreated (a) and one that had received $PGF_{2\alpha}$-1-isopropylester topically (b). (Left) Latanoprost had been applied to the eye 30 min of 2 h earlier. Note that unlike albumin latanoprost cannot be seen in the suprachoroidal space. Courtesy of J. Stjernschantz.

Glaucoma

As uveoscleral flow seems to decrease markedly with age in the human eye, a further reduction would probably have only a modest effect on IOP. It is not known if uveoscleral flow in human eyes with primary open-angle glaucoma (POAG) is reduced and studies in eyes with ocular hypertension (OH) have been inconclusive. In eyes with pseudoexfoliations, however, there is a markedly reduced uveoscleral flow, but the effect on IOP is small, only 2–3 mmHg compared to eyes without pseudoexfoliations. The main role for uveoscleral outflow in glaucoma may then well be the possibility to increase it and thereby reduce IOP.

For clinicians it is obvious that the effect of cholinergic agonists on the ciliary muscle, and its marked effect on uveoscleral flow, makes a combination of prostaglandins and miotics questionable. Still, clinical studies have demonstrated that combined 2% pilocarpine added to latanoprost is additive, and in normal eyes the effect of combining a strong miotic (physostigmin) and latanoprost on IOP was mainly additive. A likely explanation is that an intense contraction of the ciliary muscle is only seen for about 30 min after application of physostigmin permitting the much longer-acting drug, latanoprost, to exert its action on the ciliary muscle.

Uveitis

It is clear that, whether by design or not, the uveoscleral outflow route becomes important in eyes with uveitis. Cells and debris can be expected to congest the conventional outflow route, while prostaglandins released by the inflammation will increase outflow through the uveoscleral outflow route. In experimental uveitis in monkeys, there is a fourfold increase in uveoscleral flow, which in combination with a reduction of aqueous flow to less than half the normal values resulted in ocular hypotony, a condition not unusual in clinical practice.

See also: Biomechanics of Aqueous Humor Outflow Resistance; Functional Morphology of the Trabecular Meshwork; Pharmacology of the Aqueous Humor Outflow.

Further Reading

Alm, A. and Nilsson, S. F. E. (2009). Uveoscledral outflow – a review. *Experimental Eye Research* 88: 760–768.

Alm, A. and Weinreb, R. N. (eds.) (1998). *Uveoscleral Outflow.* London: Mosby–Wolfe.

Bill, A. (1975). Blood circulation and fluid dynamics in the eye. *Physiological Review* 55: 383–417.

Gabelt, B. T. and Kaufman, P. L. (2003). Aqueous humor dynamics. In: Kaufman, P. L. and Alm, A. (eds.) *Adler's Physiology of the Eye,* 10th edn., pp. 237–289. London: Mosby.

Gabelt, B. T. and Kaufman, P. L. (2005). Changes in aqueous humor dynamics with age and glaucoma. *Progress in Retinal and Eye Research* 24: 612–637.

Gupta, N., Patel, M., Ly, T., et al. (2008). Evidence of a new uveolymphatic outflow pathway in human and sheep: Implications for aqueous humor drainage and glaucoma. *Investigative Ophthalmology and Visual Science* 49: E-Abstract 2879.

Nilsson, S. F. E. and Bill, A. (1994). Physiology and neurophysiology of aqueous humor inflow and outflow. In: Kaufman, P. L., Mittag, T. W., Podos, S. M., and Yanoff, M. (eds.) *Textbook of Ophthalmology, Vol. 7: Glaucoma*, pp. 1.17–1.34. London: Mosby.

Schroedl, F., Brehmer, A., Neuhuber, W. L., et al. (2008). The normal human choroid is endowed with a significant number of lymphatic vessel endothelial hyaluronate receptor 1 (LYVE-1)-positive macrophages. *Investigative Ophthalmology and Visual Science* 49: 5222–5229.

Vessel Regression

H-P Hammes, University of Heidelberg, Mannheim, Germany

Glossary

Advanced glycation end products (AGE) – Highly reactive metabolic intermediates with the potential to modify structural and functional proteins such as matrix proteins, growth factors, and transcription factors.
Intercellular adhesion molecule 1 (ICAM-1) – It mediates adhesion of leukocytes to endothelial cells and is activated by inflammatory cytokines.
Platelet-derived growth factor B (PDGF-B) – Factor involved in promoting endothelial surival and pericyte recruitment.
Protein kinase C (PKC) – Enzyme transfering phosphates to serin and threonine residues; central role in regulation of important cellular functions such cell growth, survival, permeability, and motility.
Reactive oxygen species (ROS) – Short-lived highly reactive molecules involved in cell signaling under physiological conditions, but also in promotion of tissue damage under disease conditions.
Vascular endothelial growth factor (VEGF) – It describes a group of factors involved in angiogenesis; works also as survival factor and strong permeation factor.

Introduction

Vasoregression or the development of capillary obliteration in the retina of a diabetic patient represents the first and crucial step in the evolution of diabetic retinopathy. Its causal link to chronic hyperglycemia has been firmly established by both, experimental and clinical studies. All subsequent steps of progressive affection, detectable by the retinal expert through direct ophthaloscopy, are responses to this incipient injury. The underlying mechanisms of incipient vasoregression are highly complex, and to date not fully elucidated in their temporal and spatial relevance. However, novel concepts and innovative techniques have given some deeper insight into fundamental processes involved in capillary vasoregression.

Vasoregression in Diabetic Retinopathy

The term vasoregression in the diabetic retina relates to the vasoobliteration of previously unaffected capillaries. The first demonstration of vascular nonperfusion in diabetic retinopathy came from India ink-injection of autoptic (after autopsy) eyes from diabetic patients. The retinal vascular system was visualized by injecting India ink postmortem into the central retinal artery. Areas of exclusive capillary nonperfusion were identified in whole mounts of retinal tissue. Of note, retinal capillary microaneurysms were concentrated in these areas.

Using retinal digest preparations, capillary areas were identified in human diabetic retinae and in diabetic animal models which were devoid of the regular cellular composition of endothelial cells and intramural pericytes. These acellular capillaries were subsequently identified as regions of capillary nonperfusions by several techniques. An example of the widely used diabetic rat model of experimental retinopathy is shown in **Figure 1**.

The mere presence of acellular capillaries is not sufficient to claim the existence of diabetic retinopathy. The occurence of obliterations in isolated capillaries during incipient periods of diabetes is clinically irrelevant due to the density of the capillary network compensating for these minor lesions and the occasional presence of acellular capillaries in retinas of nondiabetic individuals. Importantly, the transition into stages where more capillaries become occluded marks the moment when diabetic retinopathy ensues, and represents the most important event that can elicit hypoxic tissue responses.

The Role of Pericytes in Vasoregression

The first structural capillary lesion observed in animals that is representative for the incipient stages of diabetic retinopathy is pericyte dropout. Pericytes are enigmatic cells. Their diverse ancestry reflected by a lack of a pancellular marker, and their complex functions in the various vascular beds are foiled by the fact that they are uniformely lost prior to the development of acellular capillaries in all experimental diabetic models studied in a diabetic time course. Pericyte loss precedes the formation of acellular capillaries by several months in rodent models and in dogs. In diabetic rodent models, pericyte loss commences 8 weeks after diabetes induction, while increasing numbers of acellular capillaries are not observed before 4–6 months of hyperglycemia.

Under normal conditions – and during developmental angiogenesis – pericyte coverage is thought to stabilize vessels. The concept was developed that pericytes inhibit endothelial cell proliferation requiring direct cell–cell

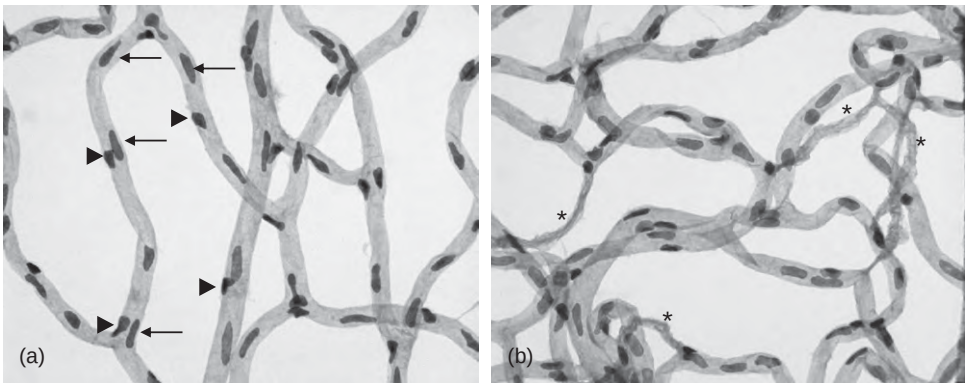

Figure 1 Retinal digest preparation of a nondiabetic (a) and a diabetic (b) rat retina. In the nondiabetic retina, an equal distribution of endothelial cells (arrow) and pericytes (arrowhead) in a uniform basement membrane tube system is depicted. In the diabetic retina (diabetes duration: 26 weeks), acellular occluded capillary segments (asterisks) are visible. Retinal digests were stained with period-acid Schiff base and hematoxyllin. Original magnification 400×.

contacts with activation of latent transforming growth factor (TGF). This general concept was supported by data from mice with a homozygous deletion of platelet-derived growth factor (PDGF)-B. As these mice die around birth when retinal vessels have not yet formed, vessels from the brain were studied. The absence of pericytes correlated with endothelial hyperplasia, increased capillary diameter, abnormal shape and ultrastructure of endothelial cells, and changes in the cellular distribution of junctional proteins such as VE-cadherin, occludin, and ZO-1. As the prenatal lethality of these mice precluded effects of pericyte deficiencies on the retinal vasculature, which in mice develops only postnatally, mice with an endothelium-restricted ablation of PDGF-B were analyzed. In these mice, an inverse correlation of pericyte density with microvascular abnormalities was observed. In particular, when pericyte deficiency was less than 50%, numerous capillary regression profiles were noted. When pericyte deficiency exceeded 50%, retinal neovascularizations occurred. Moreover, retinas of mice heterozygous for PDGF-B yielded a 30% reduction of pericyte coverage coinciding with an approximately 50% increased in the number of acellular capillaries. Thus, the concept prevails that pericytes control endothelial survival and proliferation in a coverage-dependent manner.

However, it must be noted that pericytes are absent from extended areas of diabetic capillaries without vasoproliferative activities. On the other hand, microaneurysms – which are considered as abortive attempts of neovascularizations can harbor pericytes – suggest that the link between pericyte loss and endothelial cell response may be more complex in the human diabetic retina.

The Mechanisms Leading to Pericyte Dropout

Pericyte apoptosis

For many years, the toxicity of metabolic intermediates accumulated in pericytes was considered primary in the sequence of events leading to pericyte dropout. For example, advanced glycation end products (AGEs) were found to accumulate in pericytes either upon injection in normal animals, or as the result of endogenous excess formation in diabetic animals. However, inconsistency between the time course of AGE accumulation (delayed) and pericyte loss (early) in animal models precluded a causal link. Differential susceptibility toward modified or irregular plasma proteins and the selective activation of proapoptotic pathways were documented as further mechanisms inducing diabetic pericyte loss. Thus, the loss of pericytes by apoptosis is considered one important mechanism.

Pericyte migration

Alternatively, migration of pericytes away from their allocated position in the capillary has been proposed as a mechanism of early pericyte loss preparing for diabetic vasoregression. In this context, the angiopoietin/Tie receptor system which is involved in pericyte recruitment during retinal vessel development and stabilization is important. The interaction of angiopoietin 1 (Ang-1) with Tie-2 is crucial for the timely and coordinated recruitment of pericytes to the developing vascular system. The notion that angiopoietin-2 acts as natural antagonist of Ang-1 led to the hypothesis that diabetic pericyte loss could be the result of a change of the Ang-1/Ang-2 ratio. Thus, the expression of Ang-1 and-2 was studied in a diabetic rat model, in which the onset of pericyte dropout was known. It was found that Ang-2 which is almost absent in the mature retinal vasculature, was excessively upregulated in a diabetic rat retina prior to the onset of pericyte dropout. Injection of recombinant Ang-2 into the vitreous of nondiabetic rats reproduced pericyte dropout within days. Studies in mice which lacked 50% of Ang-2 gene dose demonstrated the prevention of diabetic pericyte loss, suggesting that hyperglycemic Ang-2 overexpression was crucially involved in pericyte loss. Furthermore, constitutive overexpression of

Ang-2 in photoreceptor cells reduced pericyte coverage in the deep capillary layers of the retina during retinal development.

The next question is how hyperglycemia-induced upregulation of Ang-2 contributes to retinal pericyte loss. Quantitation of pericyte subpopulations in diabetic retinae demonstrated that only one subset of pericytes was lost upon hyperglycemic exposure over time, that is, pericytes positioned on straight parts of capillaries. Notably, pericytes which loosened the contact to intact capillaries were found more frequently, both – in diabetic mice and in mice with retinal overexpression of Ang-2 – while Ang-2-deficient mice completely lacked the hyperglycemia-induced increase in pericyte migration. These data support the hypothesis that pericyte loss pertains to one specific pericyte subpopulation, and may involve active migration.

Rather than opposing other concepts such as pericyte apoptosis, it complements them. Ang-2 expression is induced by hypoxia, cytokines, and, as noted recently, by hyperglycemia. A brief appraisal of the biochemistry of diabetic vasculopathy should be prepended.

The Biochemistry of Microvascular Damage and Vasoregression

The four biochemical pathways that have been discussed over years to be involved in the damage of blood vessels by chronic hyperglycemia are an increased activity of the polyol-pathway, the activation of PKC-isoforms by *de novo* synthesis of diacylglycerol, an increased flux through the hexosamine-pathway, and the excess flow of glycolytic intermediates to form AGEs. By increasing sorbitol and fructose levels, and reducing the cofactor nicotinamide adenine dinucleotide phosphate (NADPH) necessary to replenish an important intracellular antioxidant, glutathion, the activation of the polyol pathway was thought to reduce vascular resistance to increased oxidative stress. The effects of PKC activation were summarized as follows: blood-flow alterations through changes in the balance of vasoconstrictors and vasodilators; increased vessel permeability through activation of vascular endothelial growth factor (VEGF); vascular occlusion through increased matrix production and decreased fibrinolytic activity; and perpetuation of oxidative stress through activation of prooxidative pathways. The intracellular overproduction of AGE precursors appears to damage vascular cells by three mechanisms: (1) modification of intracellular proteins including those implicated in gene transcription; (2) modification of extracellular matrix molecules after diffusion out of the cells; and (3) activation of AGE receptors, causing production of inflammatory cytokines and growth factors affecting vessels. Finally, the increased hexosamine pathway activity was found to result in pathological changes in gene transcription by modifications of transcription factors through the hexosamine pathway product *N*-acetyl-glucosamine.

A novel concept was recently proposed, linking metabolic changes associated with increased intracellular AGE (most prominently methylglyoxal) with altered transcription of genes relevant in vascular remodeling such as Ang-2. Increased glycolytic flux – as observed in cells exposed to high glucose and unable to downregulate glucose transport – caused methylglyoxal modifications of the transcriptional corepressor mSin3A. These modifications caused the recruitment of the O-GlcNAc (O-glycosidic linkage) transferase to mSin3A, complexed with the transcriptional suppressor Sp3, which then modified Sp3 by O-linked *N*-acetylglucosamine. Modified Sp3 was less bound to a glucose-responsive GC box in the Ang-2 promoter resulting in the upregulation of Ang-2. The mechanism was found in renal microvascular endothelial cells as well as in retinal Müller cells.

Endothelial Damage and Loss Leading to Vasoregression

As mentioned, chronic hyperglycemia has been identified as the major underlying cause of diabetic microvessel damage. The explanation that endothelial cells are the primary target of hyperglycemia-induced injury was based on *in vitro* studies showing that endothelial cells in contrast to smooth muscle cells were unable to downregulate inward glucose transport in the presence of high ambient glucose. The resulting increased flux through glycolysis and the impact on mitochondrial reactive oxygen species (ROS) production has been identified as the unifying mechanism linking the four seemingly independent pathways with chronic hyperglycemia as the primary event. In cells exposed to normal ambient glucose, glucose is metabolized through glycolysis and the tricarbon cycle to generate electron donors for the mitochondrial respiratory chain that finally generated adenosine triphosphate (ATP). In hyperglycemic cells, increased flux through glycolysis and the tricarboxylic acid (TCA) cycle generates a voltage gradient of electrons surpassing a threshold which is blocked at the transition to complex III of the mitochondrial electron-transport chain. From complex III, the surplus of electrons is purported to coenzyme Q together with molecular oxygen-producing superoxide. The mitochondrial isoform of superoxide dismutase detoxifies this radical via hydrogen peroxide to water in the presence of oxygen. The link between the four biochemical pathways and the mitochondrial overproduction of ROS was made when it became evident that an important change in hyperglycemic cells and in experimental animals was the reduced activity of the glycolytic enzyme glyceraldehyde-3-phosphate dehydrogenase (GAPDH).

When examining for biochemical modifications of the enzyme, it was observed that hyperglycemia-induced superoxides caused polymers of adenosine diphosphate (ADP)-ribose to attach to the enzyme and reduce its activity. These changes were prevented with the inhibition of superoxide generation, and with the inhibition of the nuclear enzyme poly-ADP-ribose polymerase (PARP) using a specific PARP inhibitor. The latter is activated upon DNA strand brakes known to form in hyperglycemic cells. Reduced GAPDH activity induced by PARP activates the biochemical pathways by increasing intermediates such as diacyl-glycerol (protein kinase C (PKC) pathway), glyceraldehyde-3-phosphate (AGE pathway), fructose-6-phosphate (hexosamine pathway), and intracellular glucose (sorbitol pathway). Experimental proof-of-concept was provided by studies demonstrating that endothelial cells which lack a functional mitochondrial electron transport chain did not produce ROS when exposed to high ambient glucose, and that ROS overproduction was prevented upon overexpression of uncoupling protein (UCP)-1 or Mn-superoxide dismutase (SOD). Together, these data indicate that hyperglycemia leads to increased oxidative stress from mitochondrial sources which activate biochemical abnormalities known to induce endothelial damage and, ultimately, vasoregression.

The Mediators of Vasoregression

The ultimate process leading to capillary obliteration has yet to be determined. Since the primary histological step is pericyte dropout, the definitive damage converting a perfused into a nonperfused capillary must affect the endothelial cell. As outlined above, oxidative stress and the progressive exhaustion of antioxidative defense systems which are upregulated during the early course of diabetic retinopathy may account for the stepwise, exponential increase in capillary obliteration. Mechanisms thought to contribute to capillary dropout include increasing lumen narrowing by basement membrane thickening, cumulative deposition of cellular debris from platelets and leukocytes, endothelial detachment from the increasingly modified matrix, and endothelial death by apoptosis.

Basement membrane (BM) thickening as a cause of vaso-obliteration is no longer discussed since the overproduction of matrix material by endothelial cells and pericytes is now considered an epiphenomenon rather than a cause. It has been demonstrated that the relative degree of luminal narrowing, and the time course of BM-thickening versus the formation of acellular capillaries precluded a significant causal contribution.

Direct evidence for a causal role of platelet aggregation or deposits of coagulation proteins has been scarce. Platelet aggregation and fibrin deposits have been observed in postmortem eyes of diabetic individuals and were twice as frequent as in nondiabetic individuals. In experimental diabetes, microthromboses were only reported in conjunction with severe hypertension. In diabetic animals and in humans, administration of platelet inhibitors or aspirin at low doses were unable to prevent capillary obstruction, suggesting that platelet aggregation/microthrombosis was not a primary mechanism of progressive capillary dropout.

Schmidt–Schönbein's group first reported that activated leukocytes adhere and possibly obliterate diabetic retinal capillaries. Further studies showed that leukocytes both adhere to and transmigrate through the capillary wall – a process that was associated with increased vascular leakage and that could be blocked by an antibody against intracellular adhesion molecule-1 (ICAM-1). Thus, leukostasis seemed to coincide and correlate with the onset of diabetic vascular damage. Studies in diabetic monkeys which develop retinopathy similar to humans revealed a higher number of neutrophils in the retina. Of note, neutrophils were preferentially located in areas of capillary dropout and microaneurysms, supporting the role of leukostasis in capillary nonperfusion. Subsequently, several studies indicated the preponderance of the 2-integrin-ICAM-1 system in the interaction between neutrophils and endothelial cells. In particular, the formation of acellular capillaries was reduced in diabetic ICAM 1/and CD 18/mice which led to the conclusion that chronic leukostasis in the retina, and the resulting leukocyte-mediated endothelial injury was causal for vasoregression. However, it has to be considered that despite the strong correlation between the apparent leukocyte–endothelial interaction and the occurrence of vasoregression, it is still unclear whether there is a causal relationship – or an epiphenomenon – since several questions remain to be clarified. Usually, leukocyte–endothelial interactions do not cause damage to the endothelial monolayer even under inflammatory conditions. Leukocytes transmigrate through endothelial cells without affecting junctional integrity. As the leukocyte–endothelial interactions in the retina reportedly result in endothelial injury and death, in direct injury of supportive cells like pericytes, and in the opening of tight junctions, this interaction must be unique to the retina, as opposed to other tissues where the same interactions do not cause any vascular damage. The glucose dependence of the interaction is questioned by the fact that nonhyperglycemic, insulin-resistant models exhibit increased leukostasis, and that increased interactions can occur at glucose levels as low as 5.5 mmol. Thus, leukostasis and the consequences of the interactions with endothelial cells is possibly less evident as suggested by recent studies.

A less well-studied, but possible mechanism leading to acellularity of capillaries in the retina, is endothelial cell detachment. Proper cell adhesion is dependent on a variety of mechanisms for each of which profound

diabetes-induced changes were reported. These include changes in the composition of extracellular matrix molecules, posttranslational modification by AGE, and modifications of binding sites for adhesion molecules. The levels, compositions, and binding capacities of heparan sulfate proteoglycans are affected by hyperglycemia leading to changes in the availability of survival promoting angiogenic factors. Intracellularly stored growth factors such as basic fibroblast growth factor (bFGF) are modified by intracellular glycation, and AGE formation, while the activation of the hexosamine pathway cooperates in the upregulation of Ang-2 which reduces the growth promoting action of Ang-1. In endothelial cells, junctional proteins and integrins may become altered due to hyperglycemia resulting in impaired attachment to the underlying matrix. Together, the mutual interaction of endothelial cells and the underlying matrix in the diabetic capillaries can result in a traceless loss of endothelial cells compensated by neighboring endothelial cells or by anchoring of bone marrow-derived precursor cells. A very low proliferation index of capillary endothelial cells, and the fact that only endothelial precursor cells of nondiabetic, but not from diabetic, origin can replace detached endothelial cells may explain the progressive failure to compensate for endothelial damage and loss. An increased number of circulating endothelial cells (also termed endothelemia) has been reported in diabetic patients and animal models. However, the retina as origin has not been specified.

Finally, endothelial cell apoptosis as the result of increasing damage and reduced survival promotion has been found in retinas of both, diabetic humans, and in diabetic rodent models. In experimental models, apoptosis of vascular cells becomes only apparent at the time when acellular capillaries increase in numbers, that is, they do not precede their formation. Despite the low numbers of apoptotic endothelial cells in a given retina, and the technical limitation to detect the cumulative damage exerted by apoptosis to retinal capillaries over time, the process, in general, may be sufficient to account for capillary degeneration.

Prevention of Vasoregression

The numerous mechanisms outlined above that participate in capillary obliteration in the diabetic retina were addressed in studies with equally numerous readouts. Therefore, the final part of this article focuses on those experimental therapies that affected vasoregression in animal (preferably rat and mouse) models.

Biochemial Pathway Inhibitors

Aldose reductase inhibitors have been extensively studied, using many different chemically unrelated compounds. Recently, a significant effect of sorbinil on capillary obstruction was recently reported in diabetic rats, while a study in dogs using the same drug did not inhibit vasoregression. The crucial question to explain the existing controversies about the relative importance of this pathway is to what extent the respective compound inhibited flux through the pathway (as compared with absolute, but static levels of aldoses).

PKC inhibitors have been used in rat models to demonstrate corrections on functional readouts such as vascular permeability and leukostasis. However, no data have been provided as to whether PKC inhibition is capable to prevent capillary regression.

Inhibitors of AGE formation had a substantial effect on vascular regression in several model systems. Aminoguanidine – which traps highly reactive dicarbonyls such as methylglyoxal – was the first to be tested in various animal models. Aminoguanidine reduced tissue levels of AGEs, inhibited extracellular crosslinks, and intracellular sequelae of AGE formation. It consistently prevented the formation of acellular capillaries by approximately 80% and the loss of pericytes to a lesser degree. It was also found that aminoguanidine inhibits oxidative stress, the activation of PKC and the upregulation of VEGF. Thus, the protection from diabetic vascular regression by aminoguanidine may be the result of the disruption of several pathogenetically important abnormalities.

Pyridoxamine was originally described as a post-Amadori inhibitor of the formation of AGEs, but also inhibits the formation of advanced lipoxidation end products (ALEs) on protein during lipid-peroxidation reactions. Treatment over 28 weeks of 1 g l^{-1} in the drinking water reduced diabetic capillary regression in diabetic rats by 71%. Whether this treatment also inhibits pericyte loss is unclear to date.

LR-90 (methylene bis [4,4prime-(2 chlorophenylureido) phenoxyisobutyric] acid) was developed as a member of a new class of multistage glycation inhibitors. *In vitro*, LR-90 exhibited general antioxidant properties by inhibiting metal-catalyzed reactions and ROS and reactive carbonyl species (methlyglyoxal and glyoxal) generations. The compound also prevents AGE-protein cross-linking reactions. It was recently shown to reduce both – acellular capillaries and the diabetic loss of pericytes.

No hexosamine pathway inhibitor has been developed to be tested in diabetic retinopathy models to date.

Metabolic Signal Blockers

Novel therapeutic approaches for the prevention and treatment of diabetic retinopathy were based on the unifying hypothesis, in particular metabolic signal blockers, and catalytic antioxidants.

The first class of new compounds emerged from an obvious feature of the unifying hypothesis, that is, the substrate accumulation upstream of the inhibited enzyme

GAPDH and shunted into the four biochemical pathways mentioned before. As two of the accumulating glycolytic metabolites – fructose-6-phosphate and glyceraldehyde-3-phosphate – are also products of the transketolase reaction, it was reasoned that the activation of transketolase should reduce the pathway overload f.e. on AGE formation, if the substrate flux could be directed toward the pentose phosphate pathway. Benfotiamine was selected because of its high activating efficiency *in vivo*, and was given to diabetic rats for 9 months. The treatment completely inhibited the formation of acellular capillaries. The effect of benfotiamine was also tested in a secondary interventional approach. The failure of many therapeutic concepts to translate into human diabetic retinopathy is often attributed to the secondary intervention character of human compared with animal studies. Benfotiamine (80 mg kg^{-1}) was given for 26 weeks to diabetic animals following a 26-week period of no treatment. Compared with untreated diabetic animals, secondary intervention with benfotiamine halted further progression of capillary obliteration almost completely, suggesting that the mode of action interfered with mechanisms that cause hyperglycemic memory.

A second concept in the group of metabolic signal blockers is PARP inhibition. PARP activation, as described above, is the result of mitochondrial overproduction of ROS and the cause for the inhibition of the glycolytic enzyme GAPDH. PARP inhibitors have been tested for microvascular damage, including diabetic retinopathy. PJ-34 – a potent PARP inhibitor – was given for 9 months to diabetic rats, and inhibited the development of acellular capillaries and pericyte ghosts. *In vitro* data suggested that PARP inhibition blocked the endothelial activation of nuclear factor kappa B (NFκB) and downstream increases of proinflammatory cytokine production while unpublished *in vivo* data suggest that PARP inhibition affects AGE formation and downstream activation of Ang-2.

Tenilsetam [(+)-3-(2-thienyl)-2-piperazinone] is a dicarbonyl scavenger (i.e., an AGE inhibitor) in the millimolar range and a transition metal ion chelator in the micromolar range. It was administered to diabetic rats at a dose of 50 mg kg^{-1} body weight, and reduced the formation of acellular capillaries by 70%. However, it did not affect pericyte loss. This study is the first of its kind to suggest that the primary target of treatment is the endothelial cell. In further *in vitro* studies, it was found that tenilsetam, given in a dose too low to exert an anti-AGE action, stimulated VEGF production in endothelial cells. Although VEGF is upregulated in the diabetic rat retina suggesting an increased need for survival factors rather than a stimulus for neovascularization, beneficial effects on vasoregression were observed when compounds were given that either reduced (aminoguanidine) or increased

Table 1 Summarizes the effects of pharmacological intervention with a focus on acellular capillaries and pericyte dropout

Agent	*Mechanism*	*Model*	*Effect on AC**	*Effect on PC**	*References*	
LR-90	Age-inhibition, multiple others	STZ-diabetic rat	+	+	Bhatwadekar et al.	
Valsartan	AT-1R blockade	STZ-diabetic ren2 rat	+	nd	Wilkinson-Berka et al.	
Tenilsetam	AGE-inhibition, VEGF stimulation	STZ-diabetic rat	+	−	Hoffmann et al.	
ALA	Catalytic antioxidant	STZ-diabetic	+	+	Lin et al.	
PJ-34	PARP-inhibition	STZ-diabetic rat	+	+	Zheng et al.	
Sorbinil	AR-inhibition	STZ-diabetic rat	+	**	Dagher et al.	** Reduced apoptosis
Benfotiamine	Metabolic signal blocker	STZ-diabetic rat	+	(–)*	Hammes et al.	* Unpublished observation
Multiple	Antioxidant	STZ-diabetic rat	+	+	Kowluru et al.	
Aminoguanidine	AGE-inhibition, multiple others	+	+	+*	Kern et al.	* Partial improvement
Captopril	ACE-inhibition	STZ-diabetic rat	+	nd	Zhang et al.	
Nepafenac	Antiinflammatory	STZ-diabetic rat	+	+	Kern et al.	
Aspirin	Multiple	STZ-diabetic rat	+	+*	Sun et al.	* Reduced apoptosis
Green Tea	Multiple	STZ-diabetic rat	+	+	Mustafa et al.	
Pyridoxamin	AGE-inhibition	STZ-diabetic rat	+	nd	Stitt et al.	
Nicanartine	Antioxidant	STZ-diabetic rat	−	+	Hammes et al.	
NGF	Multiple	STZ-diabetic rat	+	+	Hammes et al.	

AT-1R – angiotensin 1 receptor; AGE – advanced glycation endproducts; VEGF – vascular endothelial growth factor; PARP – poly-ADP-ribose polymerase; AR – aldose reducatase; ACE – angiotensin-converting enzyme; STZ – streptozotocin; AC – acellular capillaries; PC – pericyte cells.

(tenilsetam) retinal VEGF. Thus, more studies are needed to dissect the role of VEGF in the preservation of diabetic vascular obstruction.

Catalytic Antioxidants

Increased mitochondrial ROS due to chronic hyperglycemia favors a second class of compounds to be tested for its efficacy against diabetic capillary dropout, that is, antioxidants. Classical antioxidants are less favorable as they work stochiometrically and do not penetrate into the compartments of primary ROS overproduction. Only when given in combination, did antioxidants such as a-tocopherol, Trolox, or *N*-acetylcysteine prevent acellular capillary formation. Interestingly, two antioxidant compounds – nicanartine and probucol – failed to prevent the formation of acellular capillaries over 6 months, but significantly reduced pericyte loss, indicating that some of the ROS-dependent mechanisms leading to pericyte loss are amenable to antioxidant therapy, while many others linked to endothelial damage are resistant to classical antioxidant treatment.

One antioxidant, R-alpha-lipoic acid (ALA) is an exception because of three important aspects: it distributes to the mitochondria, it is regenerated by hyperglycemia-dependent mechanisms, and it has a very low redox potential. In fact, apart from a beneficial effect on parameters of oxidative stress, NFκB activation, and Ang-2 overexpression, long-term ALA treatment substantially reduced acellular capillaries, and pericyte loss in diabetic rats.

An obvious additional candidate to be used for the prevention of vasoregression is the mitochondrial form of superoxide dismutase. SOD mimetics have not yet entered the feasibility phase of long-term experiments in models. Therefore, animals with genetic gain- and loss-of-function modifications were studied for retinal pathology in diabetes. Unfortunately, meaningful results in particular with regard to the prevention of vasoregression were not to be achieved since both, SOD-overexpressing as well as SOD-deficient mice were prone to retinal degeneration.

A variety of chemically defined compounds have been tested in animal models. Furthermore, growth factors, antibodies against growth factors and inflammatory cytokines, and antisense oligos have been tested with varying results – in particular, on vasoregression.

Table 1 summarizes the effects of pharmacological intervention with a focus on acellular capillaries and pericyte dropout.

Acknowledgments

This was funded by grants from the Deutsche Forschungsgemeinschaft, the German Diabetes Association, the EFSD, and the Juvenile Diabetes Foundation International.

See also: Angiogenesis in the Eye; Angiogenesis in Wound Healing; Development of the Retinal Vasculature; Formation and Regression of the Primary Vitreous and Hyaloid Vascular System; Molecular Mechanisms of Angiostasis; Pathological Retinal Angiogenesis; Retinopathy of Prematurity; Stability and Functional Integrity of New Blood Vessels.

Further Reading

Adamis, A. P. and Berman, A. J. (2008). Immunological mechanisms in the pathogenesis of diabetic retinopathy. *Seminars in Immunopathology* 30(2): 65–84.

Ashton, N. (1959). Diabetic retinopathy: A new approach. *Lancet* 2(7104): 625–630.

Brownlee, M. (2005). The pathobiology of diabetic complications: A unifying mechanism. *Diabetes* 54(6): 1615–1625.

Caballero, S., Sengupta, N., Afzal, A., et al. (2007). Ischemic vascular damage can be repaired by healthy, but not diabetic, endothelial progenitor cells. *Diabetes* 56(4): 960–967.

Frank, R. N. (2004). Diabetic retinopathy. *New England Journal of Medicine* 350(1): 48–58.

Hammes, H. P., Du, X., Edelstein, D., et al. (2003). Benfotiamine blocks three major pathways of hyperglycemic damage and prevents experimental diabetic retinopathy. *Nature Medicine* 9(3): 294–299.

Kowluru, R. A., Tang, J., and Kern, T. S. (2001). Abnormalities of retinal metabolism in diabetes and experimental galactosemia: VII. Effect of long-term administration of antioxidants on the development of retinopathy. *Diabetes* 50(8): 1938–1942.

Saint-Geniez, M., Maharaj, A. S., Walshe, T. E., et al. (2008). Endogenous VEGF is required for visual function: Evidence for a survival role on Müller cells and photoreceptors. *PloS ONE* 3(11): e3554.

Yao, D., Taguchi, T., Matsumura, T., et al. (2007). High glucose increases angiopoietin-2 transcription in microvascular endothelial cells through methylglyoxal modification of mSin3A. *Journal of Biological Chemistry* 282(42): 31038–31045.

Zheng, L., Szabo, C., and Kern, T. S. (2004). Poly(ADP-Ribose) polymerase is involved in the development of diabetic retinopathy via regulation of nuclear factor-{kappa}B. *Diabetes* 53(11): 2960–2967.

Vitreous Anatomy, Aging, and Anomalous Posterior Vitreous Detachment

J Sebag, University of Southern California, Los Angeles, CA, USA

Glossary

Anomalous posterior vitreous detachment – The result of vitreous gel liquefaction without concurrent dehiscence at the vitreo-retinal interface.
Hyalocytes – Mononuclear phagocytes embedded within the posterior vitreous cortex.
Pharmacologic vitreolysis – The use of drugs (enzymes and nonenzymatic agents) to induce gel liquefaction (liquefactants) and dehiscence at the vitreo-retinal interface (interfactants) resulting in prophylactic posterior vitreous detachment (PVD).
Posterior vitreous cortex – The outer shell of the vitreous with a higher density of collagen fibrils and hyaluronan than elsewhere in the vitreous body.
Synchisis – Liquefaction of the gel vitreous.
Syneresis – Collapse of the gel vitreous that results from profound synchisis.
Vitreoschisis – Splitting of the posterior vitreous cortex that results from anomalous PVD that leaves the outermost layer of vitreous attached to the retina, usually in the macula.

Invisible by design (**Figure 1**), vitreous was long unseen as an important part of the eye. In recent years, however, the roles of vitreous in ocular physiology and the pathobiology of various retinal diseases have been increasingly appreciated. As a result, the contribution of vitreous to blindness is being treated with ever-evolving therapeutic modalities, for the most part surgical. The future, however, will see the use of pharmacologic agents for therapy and prevention. To do so successfully requires an understanding of vitreous anatomy and biochemistry as well as an appreciation of how these change with aging and disease. In particular, many retinal diseases can now be conceived as anomalies in the process of posterior vitreous detachment (PVD). This unifying concept of vitreo-retinal diseases is known as anomalous PVD.

Vitreous Anatomy

Vitreous Body

In an emmetropic adult human eye (**Figure 2**), vitreous is approximately 16.5 mm in axial length, with a depression just posterior to the lens (patellar fossa). The hyaloideocapsular ligament (of Weiger) is the annular region 1–2 mm in width and 8–9 mm in diameter where vitreous is attached to the posterior lens. Erggelet's or Berger's space is at the center of the hyaloideocapsular ligament. Arising from this space and coursing posteriorly through the central vitreous is Cloquet's canal – the former site of the hyaloid artery in the primary vitreous. The former lumen of the artery is an area devoid of vitreous collagen fibrils, surrounded by multi-fenestrated sheaths that were previously the basal laminae of the hyaloid artery wall. Posteriorly, Cloquet's canal opens into a funnel-shaped region anterior to the optic disk known as the area Martegiani.

Dissection of the outer layers of the eye (sclera, choroid, and retina) can be performed and the naked vitreous body can be maintained intact and attached to the anterior segment of the eye (**Figure 1**). Studies have identified that within the adult human vitreous there are fine, parallel fibers coursing in an anteroposterior direction (**Figure 3**). These fibers, which probably represent bundles of vitreous collagen fibrils, attach into the vitreous base where they splay out anterior and posterior to the ora serrata. As the peripheral fibers course posteriorly, they are circumferential with the vitreous cortex, while central fibers undulate in a configuration parallel with Cloquet's canal. The fibers are continuous and do not branch. Posteriorly, these fibers attach into the posterior vitreous cortex, but not the retina.

Ultrastructural studies have demonstrated that vitreous collagen tends to be organized into bundles of parallel fibrils (**Figure 4**). It has been hypothesized that, initially, the collagen fibrils within these bundles are spaced apart by the chondroitin sulfate chain of type IX collagen, but with aging the chondroitin sulfate is lost and there is progressive aggregation of the fibrils leading to the formation of thick fibers. Eventually, the fibers attain sufficiently large proportions that they can be visualized *in vitro* (**Figures 3** and **4**) and clinically. The areas adjacent to these large fibers have a low density of collagen fibrils in association with hyaluronan (HA) molecules and, therefore, do not scatter light as intensely as the larger bundles of aggregated collagen fibrils. Furthermore, these adjacent areas offer relatively little resistance to bulk flow through vitreous, since they are largely occupied by hydrated HA.

Vitreous Base

The vitreous base is a three-dimensional zone that extends 1.5–2 mm anterior to the ora serrata, 1–3 mm posterior to the ora serrata, and several millimeters into the vitreous

body itself. The vitreous base posterior to the ora serrata varies in width depending on age. More than half of the population over 70 years of age have a posterior vitreous base wider than 1.0 mm. The width increases with increasing age to nearly 3.0 mm, bringing the posterior border of the vitreous base closer to the equator. This widening of the vitreous base is most prominent temporally. It has been proposed that the intra-retinal synthesis of collagen fibrils that penetrate the internal limiting lamina of the retina and splice with vitreous collagen fibrils, which may explain the increased vitreo-retinal adhesion at the vitreous base, traction, and retinal tears/detachment.

Vitreous Cortex

The vitreous cortex is defined as the peripheral shell of the vitreous body that courses forward and inward from the anterior vitreous base to form the anterior vitreous cortex, and posterior from the posterior border of the vitreous base to form the posterior vitreous cortex (**Figure 5**).

The anterior vitreous cortex, also called the anterior hyaloid face, begins about 1.5 mm anterior to the ora serrata. Here, the vitreous collagen fibrils are parallel to the surface of the cortex and are densely packed with looser collagen-fibril packing in the subjacent vitreous, giving the appearance of lamellae. The anterior vitreous cortex varies in thickness from 800 to 2000 nm with connections to the loose fibrils in the anterior vitreous and multiple interconnections with a branching fibrillar network in the posterior chamber.

The posterior vitreous cortex is 100–110 μm thick and consists of densely packed collagen fibrils. The organization of these collagen fibrils is lamellar, presenting a sheet-like appearance on immunohistochemistry (**Figure 6**). These potential tissue planes are important as sites of tissue separation during PVD (see Section Vitreoschisis) as well as during surgery while peeling membranes off the macula.

Hyalocytes (**Figure 7**) are bone marrow-derived cells widely spread apart in a single layer situated 20–50 μm from the retina in the posterior vitreous cortex and basal vitreous. The highest density of hyalocytes is in the region of the vitreous base, followed next by the posterior pole, with the lowest density at the equator.

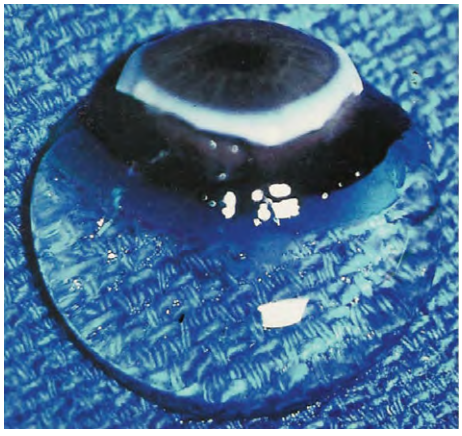

Figure 1 Human vitreous structure in a 9-month-old child.

Vitreoretinal Interface

There is a basal lamina on the inner surface of the retina to which the cortical and basal vitreous are attached. The basal lamina posterior to the ora serrata, known as the internal limiting lamina (ILL) of the retina, is actually the basement membrane of retinal Müller cells. Immediately

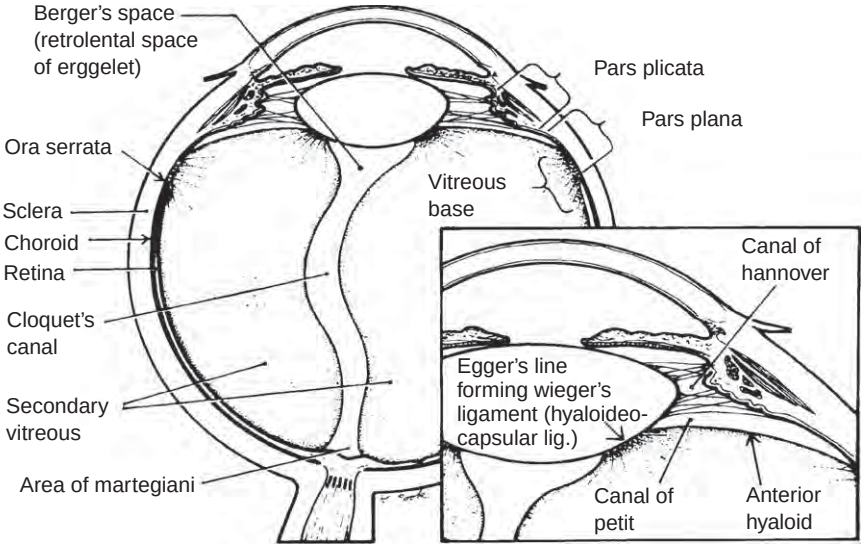

Figure 2 Schematic diagram of vitreous anatomy.

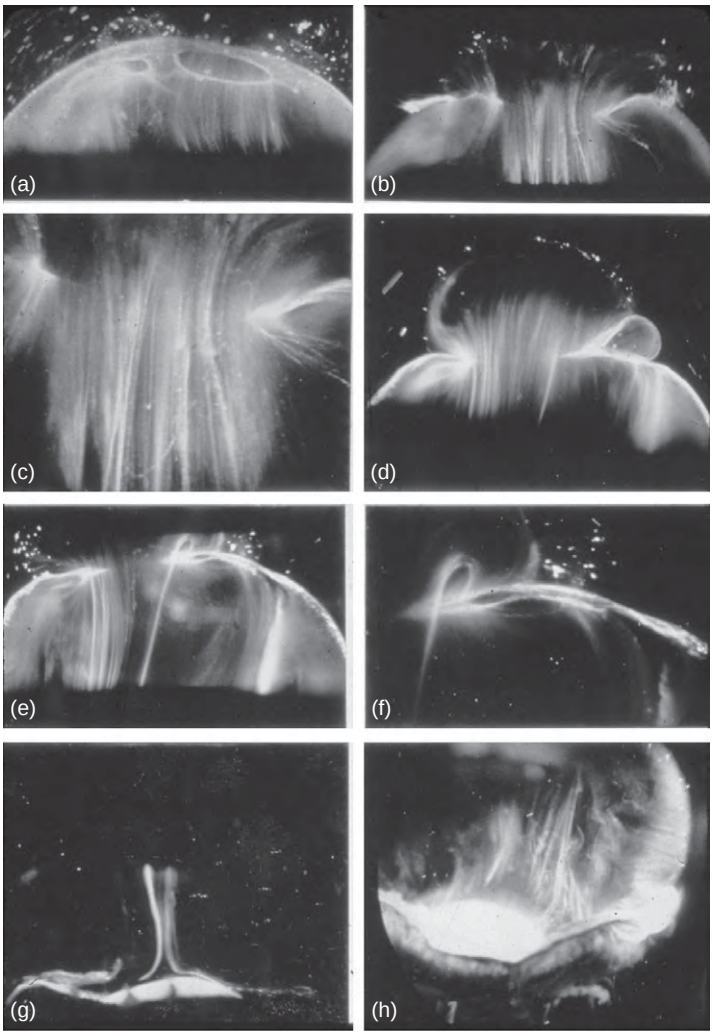

Figure 3 Dark-field slit-lamp microscopy of human vitreous. (a) Left eye of a 52-year-old man. The prepapillary hole in the vitreous cortex is to the left. (b) A 57-year-old man in whom a large bundle of prominent fibers is seen coursing anteroposteriorly and entering the preretinal space through the premacular vitreous cortex. (c) Same view as upper right at higher magnification. (d) A 53-year-old woman in whom there is posterior extrusion of vitreous out the prepapillary hole (to the right) and premacular (large extrusion to the left) vitreous cortex. Fibers course anteroposteriorly in the central vitreous and out into the preretinal, space. (e) Same specimen as second row right. A large fiber courses posteriorly from the central vitreous and inserts into the premacular vitreous cortex. (f) Same view as (e) at higher magnification. The curvilinear appearance is due to traction by vitreous extruding into the retro-cortical space. Because of its attachment to the posterior vitreous cortex, the fiber arcs back to its point of insertion. (g) Cloquet's canal is seen in this 33-year-old woman, forming the retro-lental space of Berger. (h) A 57-year-old man in whom the lens are surrounded by fibers coursing anteroposteriorly that insert into the vitreous base. These fibers splay out to insert anterior and posterior to the ora serrata.

adjacent to the Müller cell is a lamina rara (0.03–0.06 μm thick) that demonstrates no species variations, nor changes with topography or age. The lamina densa (i.e., the basement membrane itself) is thinnest at the fovea (0.01–0.02 μm) and disk (0.07–0.1 μm). It is thicker elsewhere in the posterior pole (0.5–3.2 μm) than at the equator or vitreous base. The existence of lamellae within the ILL has relevance to the pathophysiology and surgical repair of macular holes.

The vitreous is known to be most firmly attached at the vitreous base, at the disk and macula, and over retinal blood vessels. The posterior aspect (retinal side) of the ILL demonstrates irregular thickening the farther posteriorly one goes from the ora serrata. So-called attachment plaques between the Müller cells and the ILL have been described in the basal and equatorial regions of the fundus but not in the posterior pole, except for the fovea. It has been hypothesized that these plaques develop in response to vitreous traction on the retina. The thick ILL in the posterior pole dampens the effects of this traction except at the fovea where the ILL is thin. The thinness of the ILL and the purported presence of attachment plaques at the central macula could explain the predisposition of this region to changes induced by traction.

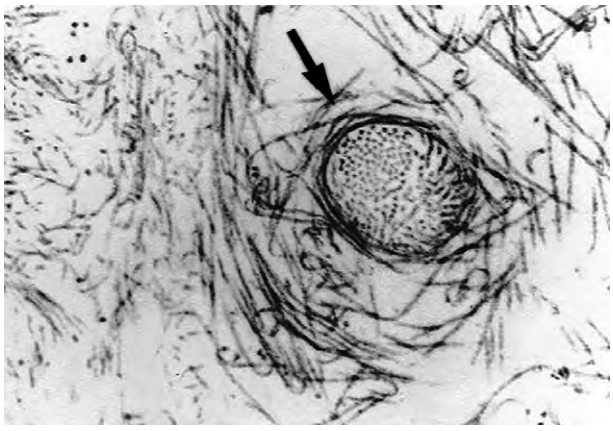

Figure 4 Transmission electron microscopy of human vitreous. Transmission electron microscopy of human vitreous demonstrates collagen fibrils organized in a bundle of parallel fibrils as seen here in cross-section.

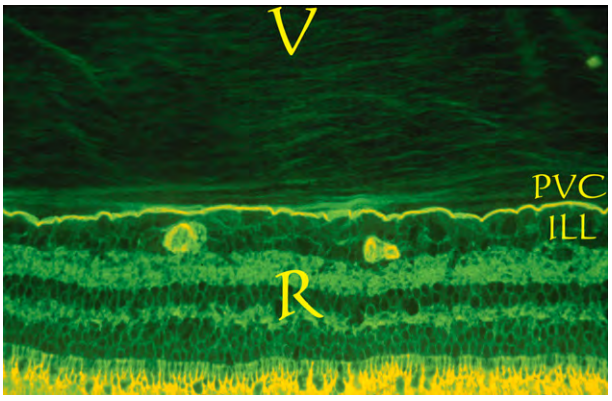

Figure 6 Immunohistochemistry of the human vitreoretinal interface demonstrates intense staining of the internal limiting lamina (ILL) with anti-ABA antibodies. This lectin binding is also evident, although less intense, in the lamellae of the posterior vitreous cortex (PVC, above the bright line in the middle – which is the ILL). Courtesy of Greg Hageman, PhD, University of Iowa.

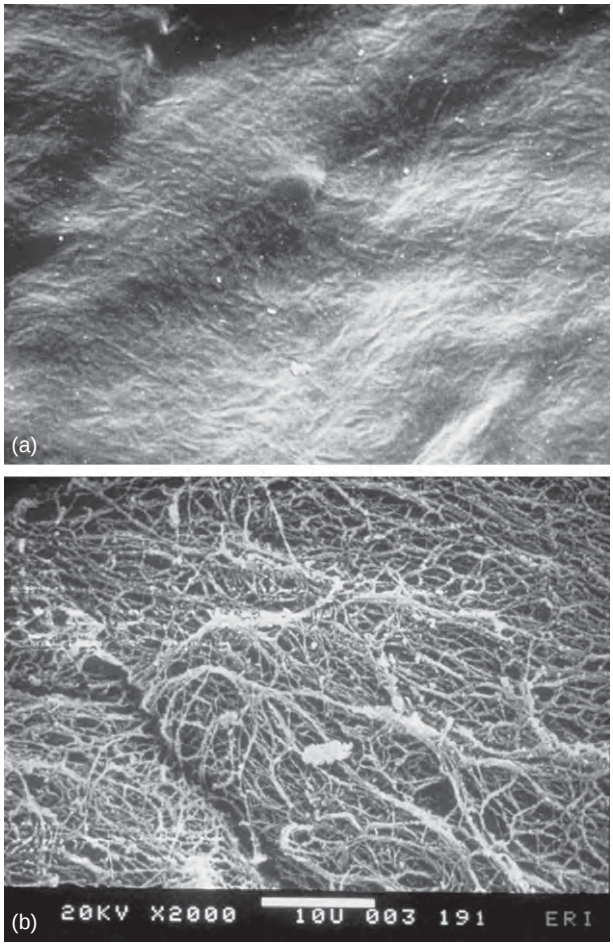

Figure 5 Scanning electron microspcopy of human vitreoretinal interface. (a) Scanning electron microscopy of posterior aspect of posterior vitreous cortex and (b) anterior surface of internal limiting lamina of retina.

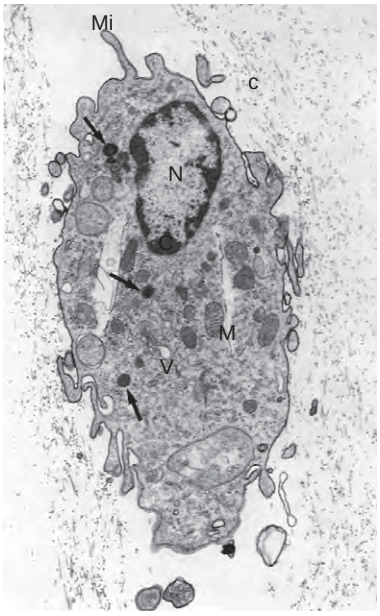

Figure 7 Ultrastructure of the human hyalocyte. A mononuclear cell is seen embedded within the dense collagen fibril (black C) network of the vitreous cortex. There is a lobulated nucleus (N) with dense marginal chromatin (white C). In the cytoplasm there are mitochondria (M), dense granules (arrows), vacuoles (V), and microvilli (Mi) (×1670). Courtesy of JL Craft and DM Albert, Harvard Medical School, Boston.

Aging Changes

Throughout life, there are changes in vitreous structure (Figure 8). During late prenatal and early postnatal stages, there are no structures within the vitreous body other than the remnants of the hyaloid artery oriented

toward the prepapillary region (**Figure 8**, top row). The vitreous body is relatively small and has an overall dense appearance with marked density at the outermost shell corresponding to the vitreous cortex. The generalized density of the vitreous likely relates to the fact that, at this stage of development, collagen and proteoglycan(s) other than HA are the principal structural components. HA synthesis begins following birth, increasing transparency by the aforementioned mechanisms. During childhood, only the vitreous cortex scatters incident light and thus appears dense upon dark-field slit microscopy. There are no visible fibers within the vitreous until middle age (**Figures 3** and **8** – middle row). During old age, these fibers become thickened and tortuous, associated with many pockets of liquid vitreous and a collapsed (syneretic) appearance (**Figure 8**, bottom row). These changes are the result of age-related biochemical alterations in the composition and organization of the molecular components that simultaneously result in vitreous liquefaction and fiber formation. Pockets of liquid vitreous have classically been called lacunae. In addition to having a low density of collagen during youth, the central vitreous is the first region to undergo liquefaction during middle age. A large autopsy study of human eyes found that more than one-half of the vitreous was liquefied in 25% of persons in the age range of 40–49 and that this increased to 62% of individuals in the age range of 80–89. In another study, ultrasonography was used *in vivo* to detect echoes from gel–liquid interfaces in 444 normal human eyes and observed echoes in 5% of young persons, in more than half of those in the age range of 51–60, and in more than 80% of persons over 60 years. However, there is evidence of liquid vitreous following the age of 4 years and, by the time the human eye reaches its adult size (age range: 14–18 years), approximately 20% of the total vitreous volume consists of liquid vitreous.

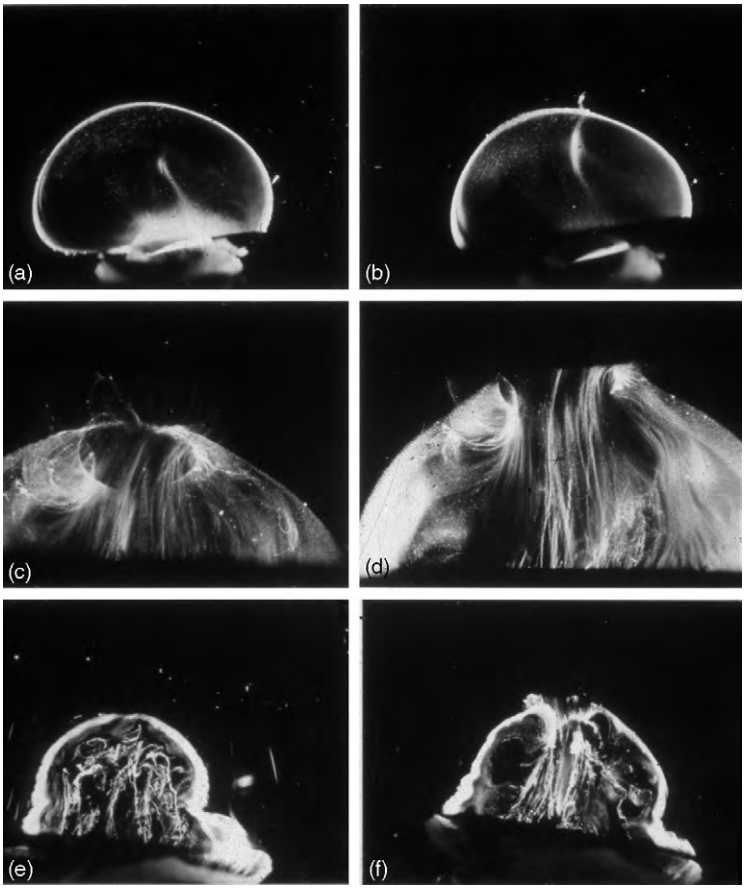

Figure 8 Changes caused by aging in human vitreous structure. (a, b) Dark-field slit microscopy of the posterior and central vitreous in a 33-week-old human embryo shows considerable light scattering arising from the vitreous cortex, due to densely packed collagen fibrils. In the central vitreous is the remnant of the hyaloid artery oriented toward the prepapillary posterior vitreous cortex. This structure is destined to become Cloquet's canal. (c, d) Vitreous structure in adults is characterized by macroscopic fibers with an antero-posterior orientation, inserting into the vitreous base. (e, f) In old age, there is aggregation of the fibers into tortuous structures with adjacent pockets of liquid vitreous that ultimately form lacunae (left side of photograph on right, bottom panel).

Posterior Vitreous Detachment (PVD)

True PVD (Figure 9) is a separation between the posterior vitreous cortex and the ILL of the retina. PVD can be localized, partial, or total (throughout the entire posterior pole up to the posterior border of the vitreous base). Although there are various methods for examining the vitreous, it is difficult to accurately determine the presence or absence of true PVD both in research and clinical settings. The future, however, may see improvements in this diagnostic acumen through the use of new diagnostic technologies, such as dynamic light scattering.

Epidemiology of PVD

In clinical studies, the incidence of PVD has been purported to be 53% in persons older than 50 and 65% in those older than 65. Autopsy studies revealed an incidence of 27–51% in the seventh decade and 63% in the eighth decade. It is not certain, however, that these are not overestimates owing to the suspension-in-air methods employed in these postmortem studies. PVD is more common in myopic patients, occurring 10 years earlier than in emmetropia and hyperopia. This is likely the result of myopic vitreopathy Cataract extraction in myopic patients introduces additional effects. In one study, PVD was present in 102 of 103 myopic eyes with myopia greater than −6 D that had undergone cataract extraction (presumably intracapsular).

There is a higher incidence of PVD in women than men, a finding that may be due to hormonal changes following menopause. This hypothesis is supported by findings that glycosaminoglycan synthesis can be influenced by a variety of hormones. There is also evidence that sex hormones can affect glycosaminoglycans metabolism, for example, there are variations in the concentration of HA following hormonal treatment. The vitreous HA concentrations in men ($120.89 \pm 75.44\,\mu g\ ml^{-1}$) is significantly greater than in women ($79.53 \pm 48.17\,\mu g\ ml^{-1}$; $p < 0.01$). This may be related to low estrogen levels in postmenopausal women and may explain why PVD is more common in women than men. Furthermore, all these lines of evidence support the concept that insufficient or abnormal HA destabilizes the gel state of vitreous contributing to liquefaction and PVD.

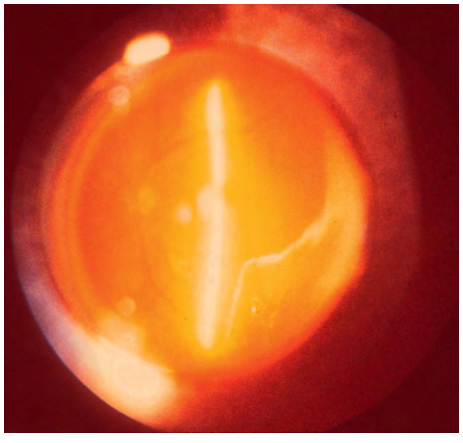

Figure 9 Posterior vitreous detachment. Preset lens biomicroscopy of the left eye in a patient with a complete PVD. The optic disk and retinal vessels can be seen to the left and the detached posterior vitreous cortex, which is brightly illuminated by the slit beam, is located to the right. Courtesy of C. L. Trempe, MD, Boston.

Pathogenesis of PVD

Several studies have shown that PVD begins at the posterior pole. PVD results from concurrent changes within the vitreous body and at the vitreoretinal interface. Whether due to age-related changes in collagen structure, HA conformation and/or concentration, light-induced or metabolically derived free radicals, hormonal effects, or combinations of all these factors, there is a disruption of the normal collagen–HA association transforming the gel vitreous to liquid. Dissolution of the ILL–vitreous cortex adhesion at the posterior pole allows this liquid vitreous to dissect a retro-cortical plane, resulting in collapse of the vitreous body. Further studies on the nature of HA–collagen interactions and the forces underlying posterior vitreous cortex–ILL adhesion should help to further identify the changes that result in PVD. Elucidating these mechanisms may enable the development of techniques by which liquefaction and PVD could be induced or prevented, depending on the clinical circumstances.

Sequela of PVD

In youth, the vitreous body is normally clear and has little or no effect on glare sensitivity. In old age, the aggregation of vitreous collagen fibrils into thick, irregular, visible fibers (Figures 3 and 8) can induce glare sensitivity, which may be subjectively bothersome. Furthermore, the high incidence of PVD in old age may also induce glare owing to scattering of light by the dense collagen fibril network in the posterior vitreous cortex (Figure 5). A group of individuals in whom glare diskomfort is a common complaint comprises patients who have undergone scleral buckling surgery for rhegmatogenous retinal detachment. The complaint of glare appears to be due to postoperative vitreous turbidity and not due to a change in the threshold sensitivity of retinal receptors. Scleral buckle surgery adds to the preexisting vitreous inhomogeneity by inducing temporary dysfunction of the blood ocular barriers – causing an influx of serum proteins and other macromolecules, as well as creating an inflammatory response and influx of cellular elements.

Floaters are the most common complaint of patients with PVD. These usually result from entopic phenomena caused by condensed vitreous fibers, glial tissue of epi-papillary origin, and/or intravitreal blood. Floaters move with vitreous displacement during eye movement and scatter incident light, casting a shadow on the retina that is perceived as a gray, hair-like or fly-like structure. In an autopsy series of cases with complete PVD, 57% had glial tissue on the posterior vitreous cortex and, in a study of cases of floaters, glial tissue was detected on the posterior vitreous cortex in 83% of patients.

Anomalous PVD

PVD is innocuous when gel liquefaction, which causes vitreous body destabilization – develops in tandem with dehiscence at the vitreo-retinal interface. If the degree of vitreo-retinal dehiscence is sufficient to allow syneresis (collapse), the vitreous body pulls away from the retina without untoward sequela (**Figure 9**). When there is insufficient vitreo-retinal dehiscence, the destabilized, liquefied vitreous cannot pull away cleanly, resulting in the development of anomalous PVD. There are various sequela to anomalous PVD (**Figure 10**).

When the entire (full-thickness) posterior vitreous cortex separates from the macula, but induces peripheral vitreo-retinal traction, retinal tears and detachments are induced. Posterior full-thickness traction can pull on the macula and induce vitreo-macular traction syndrome or place traction upon the optic disk, exacerbating neovascularization in proliferative diabetic retinopathy or other ischemic retinopathies, inducing vitreous hemorrhage, or resulting in vitreo-papillary traction syndromes. Partial PVD with splitting of the posterior vitreous cortex (vitreoschisis) may be the first event in macular pucker and macular hole pathogenesis.

Retinal Tears

Autopsy studies found that PVD is associated with retinal breaks in 14.3% of all cases. A degree of vitreous hemorrhage occurs in 13–19% of cases with PVD and, when patients suffer a severe vitreous hemorrhage that obscures the view of the fundus on ophthalmoscopy, there is a high-incidence of retinal tears (67%) and retinal detachments (39%).

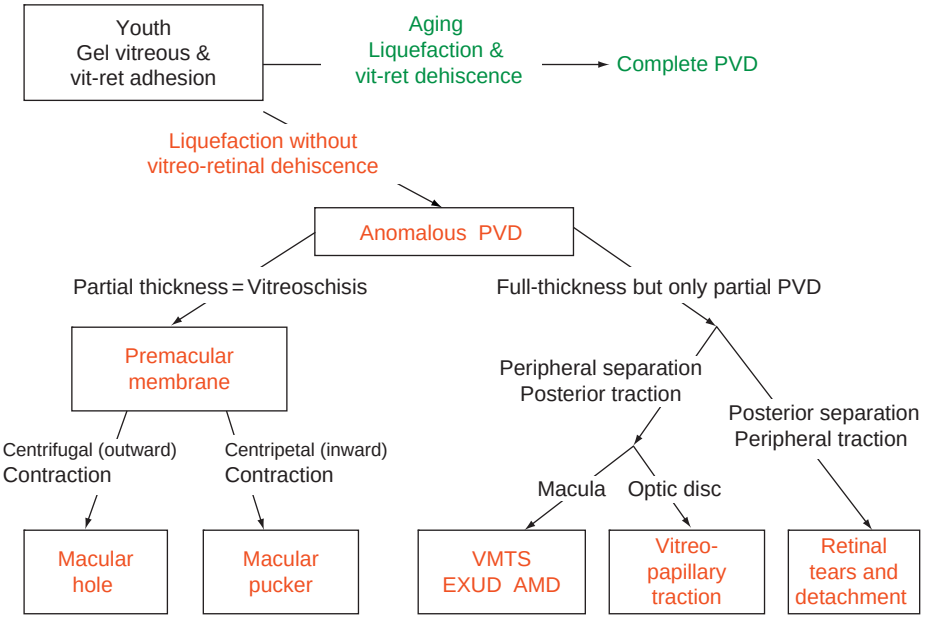

Figure 10 Schematic diagram of anomalous PVD. This schematic diagram demonstrates the various possible manifestations of anomalous PVD. When gel liquefaction and weakening of vitreoretinal adhesion occur concurrently, the vitreous separates away from the retina without sequela (top of diagram). If the separation of vitreous from retina is full-thickness but incomplete, there can be different forms of partial PVD (right side of diagram). Posterior separation with persistent peripheral vitreoretinal attachment can induce retinal breaks and detachments. Peripheral vitreoretinal separation with persistent full-thickness attachment of vitreous to the retina posteriorly can induce traction upon the macula, known as the vitreo-macular traction syndrome (VMTS). This phenomenon appears to be highly associated with exudative age-related macular degeneration (AMD). Persistent attachment to the optic disk can induce vitreo-papillopathies and also contribute to neovascularization and vitreous hemorrhage in ischemic retinopathies. If, during PVD, the posterior vitreous cortex splits (vitreoschisis), there can be differences depending upon the level of the split. Vitreoschsis anterior to the level of the hyalocytes leaves a relatively thick, cellular membrane attached to the macula. Inward (centripetal) contraction of this membrane induces macular pucker. If the split occurs at a level posterior to the hyalocytes, the remaining premacular membrane is relatively thin and hypocellular. Outward (centrifugal) tangential traction can induce a macular hole.

Vitreo-Macular Traction Syndrome

Vitreo-macular traction syndrome (VMTS) results when there is peripheral PVD but persistent attachment of full-thickness (i.e., not split) posterior vitreous cortex to the macula. This induces axial traction upon the macula with thickening due to both the effects of traction as well as edema. Full-thickness vitreo-macular adhesion may also be important in patients with age-related macular degeneration (AMD). Recent studies have identified that true PVD is protective against wet AMD, while anomalous PVD with persistent vitreo-macular adhesion may promote choroidal neovascularization.

Vitreoschisis

PVD is associated with vitreous cortex remnants at the fovea in 44% of human eyes studied at autopsy with scanning electron microscopy. When these remnants are a layer or sheet of posterior vitreous cortex, the term vitreoschisis is appropriate. On clinical examination, the inner wall of the vitreoschisis cavity may be clinically confused with a PVD when the posterior layer of the split vitreous cortex remains attached to the ILL of the retina.

Ulltrasonography (Figure 11) can, at times, detect the split layers in vitreoschisis – depending upon the thickness of the layers. Vitreoschisis has been detected by ultrasound in 20% of eyes with proliferative diabetic retinopathy and optical coherence tomography detected vitreoschisis in about one-half of patients with macular pucker and macular holes.

Figure 11 Ultrasonography of vitreoschisis. B-scan ultrasound of vitreoschisis in a human demonstrates the inner (I) and outer (P) walls of a split posterior vitreous cortex. The arrow indicates the schisis cavity created by the split.

Macular Pucker

Following vitreoschisis, premacular membranes can contract and cause significant visual impairment and metamorphopsia, sometimes necessitating surgical intervention. Studies of excised tissue have demonstrated the presence of astrocytes and retinal pigmentary epithelium (RPE) cells, but there can likely be other cells that can have similar appearances – such as hyalocytes. It has been hypothesized that macular pucker results when vitreoschisis splits the cortex anterior to hyalocytes leaving this cellular membrane attached to the macula.

Recent studies have identified that nearly one-half of all eyes with macular pucker have more than one site of retinal contraction (Figure 12). There is a higher incidence of intra-retinal cysts and significantly more macular thickening with increasing foci of retinal contraction.

Macular Holes

The precise pathogenesis of macular holes is unknown, although several hypotheses have been presented over the years. Initial theories cited anteroposterior traction by vitreous fibers, while more recent hypotheses incriminate tangential traction upon the macula. Advanced imaging using combined optical coherence tomography and scanning laser ophthalmoscopy has determined that nearly all subjects with macular holes have vitreo-papillary adhesion – suggesting that this might alter the vectors of force upon the macula inducing outward (centrifugal) tangential traction inducing a central hole.

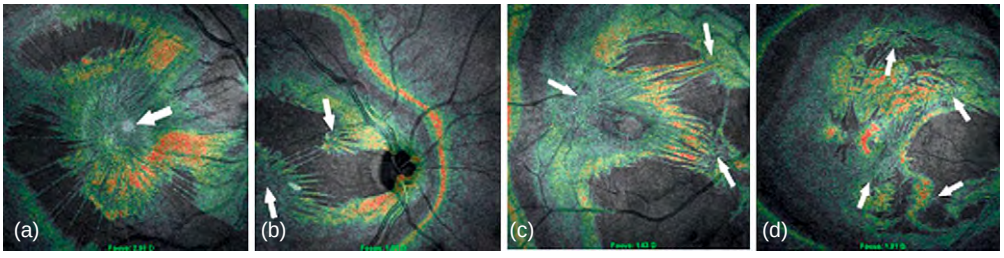

Figure 12 Multi-focal retinal contraction in macular pucker. Superimposed coronal plane OCT images upon the SLO fundus images reveal multi-focality (arrows) in the pattern of macular pucker. (a) 1 pucker center, (b) 2 pucker centers, (c) 3 pucker centers, and (d) 4 puckers centers.

See also: Hyalocytes; Molecular Composition of the Vitreous and Aging Changes; Pharmacological Vitreolysis; The Role of the Vitreous in Macular Hole Formation.

Further Reading

Green, W. R. and Sebag, J. (2001). Vitreous and the vitreo-retinal interface. In: Ryan, S. J. (ed.) *Retina* vol III, pp. 1882–1960. St. Louis, MO: Mosby.

Gupta, P., Sadun, A. A., and Sebag, J. (2008). Multifocal retinal contraction in macular pucker analyzed by combined optical coherence tomography/scanning laser ophthalmoscopy. *Retina* 28: 447–452.

Krebs, I., Brannath, W., Glittenberg, K., et al. (2007). Posterior vitreo-macular adhesion: A potential risk factor for exudative age-related macular degeneration. *American Journal of Ophthalmology* 144: 741–746.

Robison, C., Krebs, I., Binder, S., et al. (2009). Vitreo-macular adhesion in active and end-stage age-related macular degeneration. *American Journal of Ophthalmology* 148(1): 79–82.

Sebag, J. (1989). *The Vitreous – Structure, Function, and Pathobiology*. New York: Springer.

Sebag, J. (1991). Age-related differences in the human vitreo-retinal interface. *Archives of Ophthalmology* 109: 966–971.

Sebag, J. (1992). The vitreous. In: Hart, W. M., Jr. (ed.) *Adler's Physiology of the Eye*, pp. 268–347. St. Louis, MO: Mosby.

Sebag, J. (1998). Pharmacologic vitreolysis. *Retina* 18: 1–3.

Sebag, J. (2004). Anomalous PVD – a unifying concept in vitreo-retinal diseases. *Graefe's Archive for Clinical and Experimental Ophthalmology* 242: 690–698.

Sebag, J. (2005). Molecular biology of pharmacologic vitreolysis. *Transactions of the American Ophthalmological Society* 103: 473–494.

Sebag, J. (2007). Surgical anatomy of vitreous and the vitreo-retinal interface. In: Tasman, W. and Jaeger, E. A. (eds.) *Clinical Ophthalmology* vol. 6, ch. 51, pp. 1882–1960. Philadelphia, PA: JB Lippincott.

Sebag, J. (2008). Vitreoschisis. *Graefe's Archive for Clinical and Experimental Ophthalmology* 246: 329–332.

Sebag, J. and Balazs, E. A. (1989). Morphology and ultrastructure of human vitreous fibers. *Investigative Ophthalmology and Visual Science* 30: 1867–1871.

Sebag, J., Gupta, P., Rosen, R., Garcia, P., and Sadun, A. A. (2007). Macular holes and macular pucker: The role of vitreoschisis as imaged by optical coherence tomography/scanning laser ophthalmoscopy. *Transactions of the American Ophthalmological Society* 105: 121–131.

Sebag, J. and Yee, K. M. P. (2007). Vitreous – from biochemistry to clinical relevance. In: Tasman, W. and Jaeger, E. A. (eds.) *Duane's Foundations of Clinical Ophthalmology* vol. 1, ch. 16, pp. 1–67. Philadelphia, PA: Lippincott Williams and Wilkins.

Wang, M. Y., Nguyen, D., Hindoyan, N., Sadun, A. A., and Sebag, J. (2009). Vitreo-papillary adhesion in macular hole and macular pucker. *Retina* 29(5): 644–650.

X

Xenopus laevis as a Model for Understanding Retinal Diseases

O L Moritz and D C Lee, University of British Columbia, Vancouver, BC, Canada

Glossary

AP20187 – A small molecule modeled on a dimer of the immunosuppressive drug FK506. One molecule of AP20187 can bind with high affinity to two FK506-binding protein (Fv) domains. Thus, Fv domains can be used to produce fusion proteins that will dimerize in the presence of AP20187. This in turn can be used to control the activity of proteins or enzymes whose activities are influenced by dimerization, such as caspases.

Bardet–Biedl syndrome – An autosomal recessive disorder characterized by obesity, retinal degeneration, polydactyly, hypogonadism, developmental delay, and mental retardation. Genes implicated in this syndrome are involved in ciliary transport processes.

Caspase-9 – An initiator caspase in the apoptotic cascade. Caspases are a family of cysteine proteases, which play essential roles in programmed cell death. Once activated, caspase-9 triggers activation of other caspases, precipitating the apoptotic process.

Optical coherence tomography (OCT) – A technique that permits three-dimensional imaging within tissues that scatter light. The technique is frequently used in ophthalmology to noninvasively image the cell layers of the retina.

Peripherin/RDS – A transmembrane glycoprotein found in the outer segment of both rod and cone photoreceptor cells. It is thought to be a structural protein important for disk morphogenesis. Mutations in the gene encoding peripherin/RDS are associated with a variety of autosomal dominant retinal dystrophies; also referred to in publications as rds, peripherin, or peripherin-2.

Rab proteins and Arf4 – The members of the Ras superfamily of monomeric guanine-nucleotide-binding proteins (G proteins), which are involved in the regulation of membrane trafficking.

Retinal degeneration – A phenotype associated with many different retinal disorders, involving progressive death of retinal cells, usually of a specific cell type.

Retinitis pigmentosa – A hereditary retinal dystrophy characterized by defective dark adaptation, progressive loss of peripheral vision that may eventually extend to loss of central vision, and the appearance of black pigment in the fundus.

RNA helicase Ddx39 – A member of the DEAD box protein family of putative RNA helicases. Family members are characterized by the conserved motif Asp-Glu-Ala-Asp (D-E-A-D), and are involved in RNA metabolism.

Stargardt's disease – An autosomal recessive juvenile-onset form of macular dystrophy arising from mutations in the *ABCA4* gene. The *ABCA4* gene product is expressed in photoreceptor cells and is thought to be an ATP-dependent transporter for N-retinylidene-PE.

Introduction

The amphibian retina has many unique properties that have intrigued visual scientists for decades. Many studies have been conducted on the retina of *Xenopus laevis*, a frog species commonly used as a laboratory animal. These frogs were introduced to the research community in the 1930s and soon became widely available, after the discovery that they can be induced to lay eggs by injection of human chorionic gonadotropin (known as the Hogben test for pregnancy). As a research subject, *X. laevis* have advantages over other amphibians in that they have low maintenance

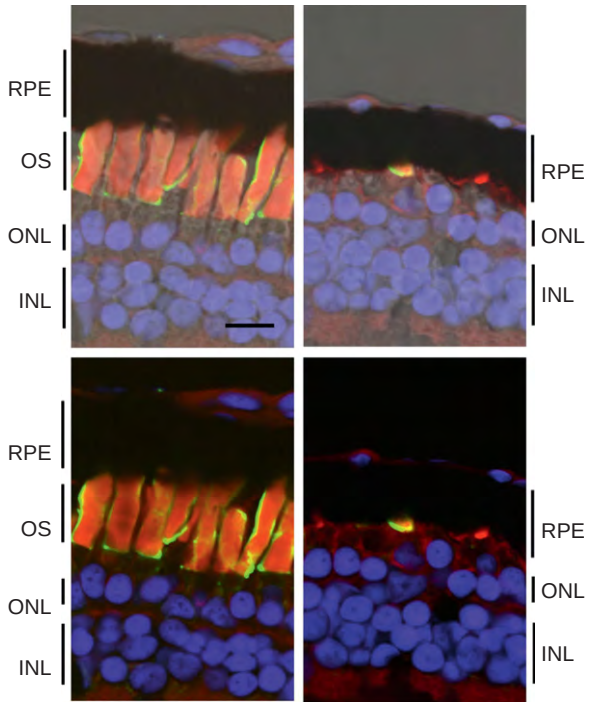

Figure 1 Expression of a bovine rhodopsin P23H mutant transgene causes retinal degeneration in *Xenopus laevis*. Combined confocal/DIC (upper panels) or confocal micrographs (lower panels) of developmental stage 47/48 wild-type retinas (left panels) or transgenic retinas expressing bovine-rhoP23H (right panels). Animals were raised in bright cyclic light for 2 weeks, beginning at fertilization. The 12-μm retinal cyrosections were stained with wheat germ agglutinin (red), B630N anti-rhodopsin (green), and Hoechst 33342 nuclear stain (blue). The central retinas of animals expressing bovine P23H rhodopsin (right panels) have almost no remaining rods, with those that remain having short and irregular outer segments. Note the relatively large diameter (7 μm) of the rod photoreceptors relative to those of the mammalian retina. Due to the relatively large diameter of the photoreceptors, only a single row of nuclei is required in the ONL. RPE, retinal pigment epithelium; OS, outer segment; INL, inner nuclear layer; ONL, outer nuclear layer. Scale = 10 μm.

requirements (they are entirely aquatic and do not require live food), and they can easily be induced to lay eggs. This made them a desirable model organism for developmental biologists studying fertilization and embryonic development; however, they have also been adopted by vision researchers as a model amphibian retina. The large size of the principle rod photoreceptors makes them highly amenable to biochemical, morphological, and electrophysiological studies (**Figure 1**). Early studies on the properties of the *X. laevis* visual system laid the groundwork for the use of this animal as a model organism for the study of visual disorders, while more recently developed techniques for genetic manipulation have resulted in *X. laevis* models of inherited retinal disease that are particularly amenable to certain forms of analysis.

Early Work on *X. laevis* – Biochemistry, Electrophysiology, and Microscopy

Modern research on the amphibian retina dates back to the extraordinary anatomical studies of Cajal and others in the 1800s that defined many of the principal cell types of the retina. Most early studies dealt with *Rana* and *Bufo* species. However, *X. laevis* have been used as a subject of retinal research dating back more than 50 years. In the 1950s, Wald and co-workers used *X. laevis* for investigations of visual pigment biochemistry. From the most abundant rod photoreceptors, it was found that the principal pigment exhibited maximal absorbance at 523 nm.

The amphibian retina is also of interest to electrophysiologists. Although the first electroretinogram (ERG) was recorded by Holmgren in the 1860s from a frog eye, *X. laevis* frogs were not used extensively for electrophysiological studies until the 1970s, with initial studies of *X. laevis* retinal physiology performed by Ripps and co-workers, correlating visual pigment content and photoreceptor threshold.

In the 1950s and 1960s, detailed analysis of the ultrastructure of photoreceptors was obtained by electron microscopy, leading to the current understanding of photoreceptor disk membrane structure, and the mechanisms of disk membrane synthesis and renewal. Many of these studies utilized amphibian retina, again typically *Rana* species, although Lanzavecchia examined the ultrastructure of *X. laevis* rods and cones in 1960. Further studies by Kinney and Fisher further characterized the morphogenesis and ultrastucture of the principal rod photoreceptor in *X. laevis*.

In the 1940s and 1950s, work by Sperry and co-workers demonstrated regeneration of the optic nerve after transection in various amphibians. Beginning in the late 1960s, Jacobson and co-workers conducted investigations of retinal development in *X. laevis*, with particular emphasis on the development of retinotectal projections. These studies employed embryonic surgery (e.g., inversion of the eye) to identify the origin of signals for optic nerve axon guidance, and demonstrated that the location of synapses of ganglion cell axons in the optic tectum are specified by the location (dorsal, ventral, nasal, or temporal) of the cell bodies in the retina.

These early investigations established the *X. laevis* retina as a viable subject for retinal research that is still in use, including ongoing studies of *X. laevis* disk shedding and renewal, electrophysiology, biochemistry, and retinal development, that are further improving our understanding of retinal function. Additionally, several studies discussed below have directly modeled human retinal disorders in *X. laevis*, in order to better understand retinal dysfunction.

X. laevis as a Model for Vitamin A Deprivation

One of the first instances of modeling retinal disease in *X. laevis* was a study by Witkovsky and co-workers on vitamin A deprivation in tadpoles. This model reproduced features of night blindness (i.e., decreased rod sensitivity) seen in vitamin-A-deprived patients. Among other novel findings, the authors demonstrated that bleaching of photopigment causes a greater reduction in photoreceptor sensitivity than can be accounted for by reduction in pigment quantity alone. This was accounted for in later studies, which demonstrated that opsin has a greater tendency to activate the visual transduction cascade than rhodopsin. More recently, studies on vitamin A deprivation in *X. laevis* have been continued by Solessio and co-workers, who have also pioneered the use of psychophysical measurements of *X. laevis* visual sensitivity.

X. laevis as a Model for Glaucoma

Early studies by Jacobson and Keating involving optic nerve transection in *X. laevis* are similar to paradigms currently used in research of optic nerve injury or glaucoma, although more typically the research subject is a mammal. However, unlike a mammalian optic nerve, a severed *X. laevis* optic nerve regenerates (a property that would be highly desirable in glaucoma patients). Research focused on *X. laevis* models of retinal regeneration of this type is currently being continued by Belecky-Adams and co-workers, who recently identified a possible role of the RNA helicase Ddx39 in the regulation of stem cells in the retina.

X. laevis and Studies of the Transport of Rhodopsin

The first investigations of the mechanism of outer segment renewal utilized amphibians injected with radioactive amino acids in a pulse–chase paradigm that allowed newly synthesized membranes to be visualized by autoradiography. The original experiments by Young and coworkers demonstrated that new disks were formed at the base of the rod outer segment, and subsequently became discontinuous with the outer segment plasma membrane. These studies were further extended by Besharse and Hollyfield, who examined the influence of light on disk synthesis in *X. laevis* photoreceptors, demonstrating diurnal regulation of disk membrane synthesis. Collectively, these studies demonstrated the extremely high rate of rod photoreceptor disk membrane synthesis in *X. laevis* retina, estimated at roughly 50-fold higher than in mammalian photoreceptors.

These findings suggested that, due to the enormous rate of outer segment membrane synthesis, the amphibian retina would be an excellent choice for studying the biosynthesis of rhodopsin. This work was pioneered by Papermaster and Dreyer, and subsequently continued by Papermaster and co-workers. These studies largely used *Rana* and *Xenopus* species, and resulted in identification of molecular and ultrastructural details of the rhodopsin transport pathway. Components of the biosynthetic machinery and transport mechanisms first identified in amphibia included associated features of the connecting cilium (the pericilliary ridge complex), and vesicles transporting rhodopsin (RTCs or rhodopsin transport carriers). Deretic was able to reconstitute rhodopsin transport in amphibian retinal extracts, and using this assay demonstrated that the rhodopsin transport signal was located in the cytoplasmic C-terminal domain. This *in vitro* assay and associated methodologies subsequently led to identification of a number of molecules associated with rhodopsin transport, including the small G proteins, rab6, rab8, rab11, and arf4.

However, due to the lack of an effective system for culturing photoreceptors, it was not possible to incorporate molecular biology approaches into the study of amphibian rhodopsin transport pathways until the 1990s, when techniques for the production of transgenic *X. laevis* developed by Kroll and Amaya, and cloning of promoters suitable for driving expression in *X. laevis* rods, allowed the study of rhodopsin transport in a genetically manipulated amphibian retina. Tam and colleagues found that rhodopsin-green fluorescent protein (GFP) fusion proteins expressed in *X. laevis* retina were transported correctly to rod outer segments. This allowed further identification and *in-vivo* demonstration of the function of the outer segment localization signal QVAPA, located at the extreme C-terminus of rhodopsin. Several mutations affecting this region cause retinitis pigmentosa (RP). These studies also demonstrated the extraordinary utility of transgenic *X. laevis* for conducting comparisons between transgenic animals, as numerous primary transgenic animals carrying different transgenes can be generated in a relatively short amount of time. For example, the rhodopsin outer segment localization signal was identified and refined using 15 distinct transgene constructs.

Using the same transgenic *X. laevis* system, the function of rab8 in rhodopsin transport was explored using dominant-negative and constitutively active mutants. Expression of these mutant rab8-GFP fusion proteins in *X. laevis* rods generated the first *X. laevis* models with an inherited retinal degeneration (RD) phenotype, as these fusion proteins proved to be quite toxic to retinal rods,

and the phenotype was passed to F1 offspring. The expression of dominant-negative GFP-rab8T22N caused a particularly rapid death of photoreceptors associated with accumulation of rhodopsin-containing intracellular vesicles in the vicinity of the base of the connecting cilium. Although it was not clear at the time, subsequent studies indicate that the resulting phenotype may be closely related to the RD associated with Bardet–Biedel syndrome (BBS). Similar investigations of the small G-protein Arf4, which binds the rhodopsin outer segment localization signal, are ongoing.

The RD observed in this study demonstrated a unique central-to-peripheral distribution subsequently seen in all other *X. laevis* models of RD. This is associated with the rapid growth of the eye in young *X. laevis*, which results in continuous addition of new photoreceptors to the peripheral retina. Thus, a single cryosection can demonstrate all stages of photoreceptor degeneration moving from central retina to periphery.

Modeling RP in Transgenic *X. laevis*

Subsequently, genetically modified transgenic *X. laevis* was used in a number of studies that directly examined mutations associated with the human disorder RP, an inherited form of RD. The pioneering study involved transgenic expression of mutant forms of peripherin/rds, a protein found at the periphery of rod outer segment disks. Peripherin/rds and its mutants were expressed as GFP fusion proteins using the rod opsin promoter to drive expression in retinal rods, at levels sufficiently high to cause RD in some cases. Confocal microscopy of the intrinsic GFP fluorescence showed that several fusion proteins had unique localization patterns distinct from wild type that respectively suggested either specific disruptions in normal function, or misfolding and endoplasmic reticulum (ER) retention. Furthermore, electron microscopy revealed unique abnormalities in disk organization, possibly associated with disruption of the normal functions of the peripherin/rds C-terminus.

Previous attempts to use rhodopsin-GFP fusion proteins to develop similar models of RP were unsuccessful, most likely due to low expression levels. In order to adapt the system for the study of RD induced by rhodopsin mutants, a system was devised for detection of nonfluorescent transgene products based on nonconserved rhodopsin antibody epitopes, such that epitope tags involving minimal (or no) sequence changes could be introduced. Initially, this system was applied to the study of an RP-causing mutation (Q348ter) that disrupts the previously identified rhodopsin outer segment localization signal. In these studies, the power of the *X. laevis* system for drawing comparisons between transgenes was further expanded. Rhodopsin mutants defective in signal transduction properties were combined with rhodopsin mutants responsible for RP to dissect the role of rhodopsin signal transduction in rod cell death pathways. The results demonstrated rhodopsin mislocalization was associated with axonal sprouting and cell death, regardless of whether rhodopsin signal transduction properties were inhibited.

The same system was subsequently applied to the study of the rhodopsin mutation P23H, the most common cause of autosomal dominant RP in North America. Despite numerous studies of this rhodopsin mutant in cultured cells and transgenic rodents, there was no clear consensus as to the effects of this mutation on rhodopsin function; in cultured cells, it was classified as a mutant defective in folding and ER exit, while transgenic animal studies suggested it was transported correctly to rod outer segments, where it caused RD that was exacerbated by light.

Studies in transgenic *X. laevis* compared several different forms of P23H rhodopsin, including P23H rhodopsins based on different species, and P23H rhodopsins defective in signal transduction and chromophore binding. Interestingly, all forms of P23H rhodopsin caused RD, but varied in terms of ER retention, expression level, and light sensitivity. P23H rhodopsins that exhibited dramatic ER retention (*X. laevis* P23H rhodopsin) caused RD under all circumstances, while P23H rhodopsins that were transported in small quantities to the OS (bovine P23H rhodopsin) caused RD only on light exposure (**Figure 1**). Furthermore, for bovine P23H rhodopsin, disruption of the chromophore-binding site was associated with reduced expression levels and RD, regardless of light exposure. This result reconciles the differences seen between previous studies, suggesting that in some forms of P23H-induced RD, chromophore binding promotes ER exit of newly synthesized rhodopsin. The dramatic sensitivity of these phenotypes to the underlying rhodopsin sequence was confirmed by Zhang and colleagues, who demonstrated light-sensitive RD in an *X. laevis* rhodopsin that differed from that used previously only in the sequences of the epitope tags. In addition to providing insight into the mechanisms underlying RD, these studies dramatically emphasize the difficulties in extrapolating results reported from a single disease model to human disease states.

A unique finding in this system was the presence of considerable quantities of truncated P23H rhodopsin, in which a significant portion of the N-terminal domain (including the mutated H23 residue) was removed; in fact, this was the dominant species observed in retinas expressing bovine P23H rhodopsin. This truncated species was also previously observed in cultured cells, although in smaller quantities. Identification of this species in other transgenic models would be difficult due to lack of a suitable reagent for detection, but was readily

achieved in *X. laevis* due to the availability of both N- and C-terminal specific antibodies that did not cross-react with endogenous rhodopsin.

Subsequent studies of the same *X. laevis* models of P23H-rhodopsin-induced RD probed the association of chromophore binding and ER exit. In order to address the question of whether the causative factor in light-induced RD was a reduction in the supply of free 11-*cis* retinal, or isomerization of 11-*cis* retinal bound to P23H rhodopsin as chromophore, the sensitivity of RD to different wavelengths of light was examined. It was determined that the profile of light sensitivity was consistent with photoisomerization of rhodopsin (which maximally absorbs green light) rather than free chromophore (with maximal absorbance in the UV). This also brings to mind similar studies of the constitutively active rhodopsin mutant K296E, classified as misfolding by some studies in cultured cells, suggesting that the active conformation of rhodopsin and/or loss of chromophore can be associated with altered kinetics of ER exit.

Studies of additional RP-causing rhodopsin mutations in transgenic *X. laevis* are ongoing, and have been reported at international meetings, including K296E rhodopsin and the glycosylation-defective mutants T4K and T17M. Glycosylation-defective rhodopsin mutants are also reported to be associated with light-exacerbated RD in *X. laevis*.

Inducible RD

In an alternate approach to modeling RP in the transgenic *X. laevis* retina, Hamm and co-workers designed a drug-inducible model of RD driven by a modified form of caspase-9. Dimerization and subsequent activation of this caspase-9 transgene is driven by AP20187, a small molecule based on a dimer of FK506. Administration of AP20187 to these transgenic *X. laevis* induces rapid RD that is not dependent on any particular environmental condition (such as special lighting). The system is designed to examine the effects of rod degeneration on other cell types, including cone photoreceptors and cells of the inner nuclear layer, and to examine the capacity for regeneration of rods in the *X. laevis* retina. This study was also the first to provide functional (i.e., electrophysiological) data for an *X. laevis* model of RD.

Interestingly, this model demonstrated a dramatic reduction in electrophysiological responses to stimuli designed to isolate cone function (e.g., a rapid flicker stimulus), despite the fact that no associated cone death was detected. This reduction in cone sensitivity may be associated with the cones themselves, or with other cells associated with the cone pathway and the ERG B-wave (e.g., cone bipolar cells and/or Müller glia). The restoration of responses to flicker stimuli was associated with a thickening of the inner nuclear layer, and a similar thickening can be observed by optical coherence tomography (OCT) in human RP patients.

Other Transgenic *X. laevis* Models of Retinal Disease

In addition to rhodopsin and peripherin/rds mutations responsible for RP, gene products related to Stargardt's disease have been expressed in *X. laevis* retina as GFP fusion proteins in order to examine their localization properties, although this has not yet resulted in a replication of a RD phenotype.

In studies by Kefalov and colleagues, cone opsins were expressed in *X. laevis* rods. As cone photoreceptors are considerably noisier than rod photoreceptors, this allowed a determination of the proportion of cone dark noise (activation of transduction in the absence of photons) that is purely due to the cone pigment sequence, and not other aspects of the transduction cascade or photoreceptor environment. Although generating a model of disease was not a goal of this study, the resulting animals could be considered a model for congenital stationary night blindness, which is due to abnormally high activity of the visual transduction cascade in the absence of photons.

X. laevis as a Model for Eye Development/ Developmental Disorders

The rapid development of the *X. laevis* embryos makes these animals of particular interest to developmental biologists, including those concerned with eye development. The first studies of the development of the *X. laevis* eye were conducted by Hollyfield through radioactive monitoring of the growth of the developing retina. Chung and colleagues histologically monitored the structural changes in the developing larval *X. laevis* retina and correlated these changes with electrophysiological changes, notably that while the receptive field of a ganglion cell remains constant in the developing larvae through metamorphosis, the inhibitory peripheral region expands to the entire retina of the adult *X. laevis*.

The development of the *X. laevis* eye has been manipulated by both the overexpression and by the knockdown of transcription factors. El-Hodiri and colleagues have extensively studied the transcriptional regulation of photoreceptor development. More recently, they identified a retinal homeobox gene family member, Rx-L, which regulates photoreceptor-specific gene expression. Expressed in developing embryos, the knockdown of Rx-L expression

adversely affected photoreceptor development, causing subtle phenotypes of altered photoreceptor morphology.

Using a similar embryonic transfection paradigm, Knox and colleagues found that overexpression of the transcription factors, *Nrl* and *Nr2e3*, in *X. laevis* retina resulted in an increase in numbers of rods, with concomitant reduction in cone photoreceptors, indicative of the roles of these factors in determining the developing photoreceptor cell fate. This system may prove extremely useful in modeling developmental disorders of the retina with similar underlying mechanisms.

X. laevis Models of Retinal Regeneration

Some recent studies have investigated the fascinating capacity of the *X. laevis* retina to repair itself after severe traumatic injury. In these studies, the entire retina is excised from an *X. laevis* tadpole eye. The retina subsequently demonstrates a dramatic capacity to completely regenerate by transdifferentiation of the remaining cells of the retinal pigment epithelium (RPE). Certain aspects of this transdifferentiation can be reproduced in culture, and it appears to be dependent on diffusible factors (possibly fibroblast growth factor 2 (FGF2)) released from the choroid. These results could have implications for traumatic eye injuries such as retinal detachment, retinal degenerative disorders, and glaucoma.

Summary

As an unconventional system for modeling retinal disease, *X. laevis* presents a number of advantages. As it is quite easy to generate transgenic *X. laevis*, they are an excellent system for comparing the effects of multiple transgenes. Other advantages include the relative ease of microscopic and electrophysiological studies due to the large size of the photoreceptor cells, regenerative capacity of the retina, and non-cross-reactivity of mammalian antibodies. However, there are also significant disadvantages, such as the current lack of knock-out or gene-replacement capabilities, long generation time (1 year), pseudotetraploid genome, and relatively small eyes, such that it is clearly not an ideal system appropriate for all experiments. Rather, *X. laevis* models of retinal disease are a very useful addition to the library of systems and models available to vision researchers.

See also: The Photoreceptor Outer Segment as a Sensory Cilium; Primary Photoreceptor Degenerations: Retinitis Pigmentosa; Primary Photoreceptor Degenerations: Terminology; Retinal Degeneration through the Eye of the Fly; Secondary Photoreceptor Degenerations: Age-Related Macular Degeneration; Secondary Photoreceptor Degenerations; Zebrafish as a Model for Understanding Retinal Diseases: Pde6, Apoptosis, and the Bystander Effects; Zebrafish: Retinal Development and Regeneration.

Further Reading

Araki, M. (2007). Regeneration of the amphibian retina: Role of tissue interaction and related signaling molecules on RPE transdifferentiation. *Development, Growth and Differentiation* 49: 109–120.

Besharse, J. C., Hollyfield, J. G., and Rayborn, M. E. (1977). Turnover of rod photoreceptor outer segments. II. Membrane addition and loss in relationship to light. *Journal of Cell Biology* 75: 507–527.

Deretic, D., Williams, A. H., Ransom, N., et al. (2005). Rhodopsin C terminus, the site of mutations causing retinal disease, regulates trafficking by binding to ADP-ribosylation factor 4 (ARF4). *Proceedings of the National Academy of Sciences of the United States of America* 102: 3301–3306.

Hamm, L. M., Tam, B. M., and Moritz, O. L. (2009). Controlled rod cell ablation in transgenic *Xenopus laevis*. *Investigative Ophthalmology and Visual Science* 50(2): 885–892.

Hollyfield, J. G. (1971). Differential growth of the neural retina in *Xenopus laevis* larvae. *Developmental Biology* 24: 264–286.

Pan, Y., Nekkalapudi, S., Kelly, L. E., and El-Hodiri, H. M. (2006). The Rx-like homeobox gene (Rx-L) is necessary for normal photoreceptor development. *Investigative Ophthalmology and Visual Science* 47: 4245–4253.

Papermaster, D. S., Schneider, B. G., Zorn, M. A., and Kraehenbuhl, J. P. (1978). Immunocytochemical localization of opsin in outer segments and Golgi zones of frog photoreceptor cells. An electron microscope analysis of cross-linked albumin-embedded retinas. *Journal of Cell Biology* 77: 196–210.

Sperry, R. W. (1944). Optic nerve regeneration with return of vision in Anurans. *Journal of Neurophysiology* 7: 57–69.

Tam, B. M. and Moritz, O. L. (2007). Dark rearing rescues P23H rhodopsin-induced retinal degeneration in a transgenic *Xenopus laevis* model of retinitis pigmentosa: A chromophore-dependent mechanism characterized by production of N-terminally truncated mutant rhodopsin. *Journal of Neuroscience* 27: 9043–9053.

Tam, B. M., Moritz, O. L., Hurd, L. B., and Papermaster, D. S. (2000). Identification of an outer segment targeting signal in the COOH terminus of rhodopsin using transgenic *Xenopus laevis*. *Journal of Cell Biology* 151: 1369–1380.

Tam, B. M., Xie, G., Oprian, D. D., and Moritz, O. L. (2006). Mislocalized rhodopsin does not require activation to cause retinal degeneration and neurite outgrowth in *Xenopus laevis*. *Journal of Neuroscience* 26: 203–209.

Witkovsky, P., Gallin, E., Hollyfield, J. G., Ripps, H., and Bridges, C. D. (1976). Photoreceptor thresholds and visual pigment levels in normal and vitamin A-deprived *Xenopus* tadpoles. *Journal of Neurophysiology* 39: 1272–1287.

Young, R. W. and Droz, B. (1968). The renewal of protein in retinal rods and cones. *Journal of Cell Biology* 39: 169–184.

Zhang, R., Oglesby, E., and Marsh-Armstrong, N. (2008). *Xenopus laevis* P23H rhodopsin transgene causes rod photoreceptor degeneration that is more severe in the ventral retina and is modulated by light. *Experimental Eye Research* 86: 612–621.

Z

Zebrafish as a Model for Understanding Retinal Diseases: Pde6, Apoptosis, and the Bystander Effects

A A Lewis, C C Heikaus, and S E Brockerhoff, University of Washington, Seattle, WA, USA

Glossary

Achromatopsia – A disease characterized by defects in the cone photoreceptors resulting in extreme light sensitivity and color blindness or rod monochromacy.
Apoptosis or programmed cell death – A form of cell death characterized by a series of biochemical and morphological changes resulting in the formation of apoptotic bodies and removal by the immune system.
Bystander effect – This describes the transmission of death from mutant or injured cells to healthy neighboring cells.
Cyclic guanosine monophosphate (cGMP) – A cyclic nucleotide derived from guanosine triphosphate (GTP). cGMP acts as a regulator of the cyclic-nucleotide-gated ion channels in photoreceptors.
Cyclic nucleotide phosphodiesterases (Pde) – A family of enzymes that hydrolyze the phosphodiester bond in the second-messenger molecules cAMP and cGMP. They regulate the localization, duration, and amplitude of cyclic nucleotide signaling.
Electroretinography (ERG) – A method for evaluating visual response. Electrodes are placed against the cornea and used to measure the electrical responses of various cell types in the retina to a light flash of varying intensity.
GAF domains – A large group of protein domains that bind small molecules; in the Pde proteins these domains bind cyclic nucleotides. The GAF acronym comes from the names of the first three different classes of proteins identified to contain them: cGMP-specific and-regulated cyclic nucleotide phosphodiesterase, adenylyl cyclase, and *E. coli* transcription factor FhlA.
Gap junctions – The intercellular connections that occur between some types of cells. These junctions allow the movement of various molecules and ions between cells.
Optokinetic response (OKR) – A method for evaluating zebrafish vision. Fish are placed in a small dish in the center of a rotating drum decorated with vertical stripes. If the fish can see, its eyes will follow the rotating stripes with regular reflexive saccades.
Retinitus pigmentosa (RP) – A group of diseases characterized by defects in the rod photoreceptors resulting in night blindness. Progressive RP often results in cone loss and tunnel vision in some cases progressing to total blindness.
Scotopic vision – The low light vision that is produced exclusively by rod function.
Zebrafish or *Danio rerio* – A tropical freshwater fish of the minnow family that has gained prominence as a scientific animal model. For further information see the Zebrafish Information Network (ZFIN), an online database of zebrafish genetic, genomic, and developmental information.

Introduction

Inherited photoreceptor degenerations are a major cause of incurable blindness. Degenerations can affect rods, causing night blindness, cones, causing color and daylight blindness, or both cell types, leading to complete blindness. Although there are many models of retinal degeneration caused by variety of mutations in different genes, it is still not possible to completely describe the molecular cascade causing cell death in any of these disorders and therefore it is equally difficult to prevent the degenerative

process. Fundamental new information about the biochemistry of photoreceptor cell death is required to enhance our understanding of retinal degeneration and to develop new successful therapies. Zebrafish have gained prominence as a model organism for studies of retinal development, disease, and vision because they offer some distinct advantages over other genetically tractable systems. Zebrafish develop rapidly *ex utero* and can be maintained transparent allowing cells in the retina to be visualized in live larvae in real time using confocal and multiphoton imaging techniques. This provides the opportunity to visualize morphological and biochemical changes occurring in diseased photoreceptors with cellular and subcellular resolution. Here, we describe two mutations in the zebrafish cone phosphodiesterase (*pde6c*) gene that result in retinal degeneration. These mutants provide a unique opportunity to learn more about the biochemical triggers and inhibitors of cell death within the retina.

Retinal Disease

Photoreceptors are the primary sensory cells within the visual system. There are two main types of photoreceptors within the vertebrate eye: rods, which are monochromatic and respond in low light levels, and cones, which respond to higher light levels and specific wavelengths within the visual spectrum. The system of light absorption, ion fluctuation, and neuronal transmission are processes that require significant energy and, thus, the retina is one of the highest-energy-consuming tissues in the body. The high level of oxygen consumption by photoreceptors makes them particularly susceptible to injury and perturbation often resulting in cell death. Retinal degeneration is a leading cause of blindness in the developed world. The most common form of degeneration is age-related macular degeneration, which first affects the cones within the central retina (macula) and then progresses to the periphery.

Retinal degeneration can also occur as a result of genetic mutations. Achromatopsia and Retinitis pigmentosa (RP) together define a large class of heritable diseases that affect vision in humans. Both of these diseases are caused by a wide variety of mutations that disrupt visual transduction and photoreceptor maintenance. Achromatopsia is characterized by defects in the cone photoreceptors while rods remain functional, resulting in extreme light sensitivity and color blindness or rod monochromacy. Achromatopsia symptoms are generally seen at birth and the vision loss is only rarely progressive. RP, in contrast, develops during childhood and in later stages of life starting with degeneration of the rod photoreceptors, and progressing in some cases to total blindness. RP is estimated to affect 1 in 10 000 people. Due to the diversity of genes associated with these disease states, most therapeutics have focused on the general prevention of cell death as a method for limiting progressive vision loss.

Animal Models of Vision

Many animal models are used to study the visual system, and each possesses various strengths and weaknesses. By using a variety of systems scientists are able to capitalize on the strengths of all of them. The two most common systems for retinal modeling have been the fruit fly, *Drosophila melanogaster*, and mice, with a variety of work occurring in related species such as rabbit or ferret.

Drosophilae have mainly been used to study ocular development and patterning. Surprisingly, despite the obvious structural differences between the insect compound eye and our own, many of the same signaling cascades are used to establish the structure and patterning of the *Drosophila* eye. *Drosophilae* have an extremely short gestation period and well-established methods for rapid genetic manipulation, and these features have been used to understand the roles of multiple genes in eye development. However, there are still many limitations in the use of this organism, particularly in the modeling of retinal disease. Several differences exist between the insect and mammalian phototransduction cascade, and the structural differences of the compound eye also limit the applicability of this organism for disease studies.

The most commonly used mammalian animal model of the retina is the mouse. Mice have a number of advantages as a model system. There is an extensive literature on a variety of mutants that have been studied for many years. There are also multiple techniques for genetic manipulation, including the ability to modify genes and genomic loci and several techniques for retinal explantation for *in vivo* imaging. However, mice are nocturnal creatures and depend primarily on their olfactory system for foraging and predator identification. As a result, unlike the human retina, the mouse retina is dominated by rod photoreceptors and contains only 3% cone photoreceptors. While this makes mice ideal for studying rod photoreceptor disease and function, the study of cone physiology and function is less straightforward in this system. Additionally, mouse eye development occurs *in utero*, making it difficult to image and understand the early stages of eye development and retinal perturbation.

The Advantages and Techniques of the Zebrafish Model System

The zebrafish system has a number of benefits for studying visual development and disease. First, zebrafish vision, similar to humans, is cone dominated. They rely upon their vision for food acquisition and have four different

cone types: red, green, blue, and ultraviolet. In the zebrafish, ocular development occurs externally over the first 5 days postfertilization (dpf). During zebrafish development, the cone photoreceptors mature first between 3–5 dpf followed by the rods, which mature between 15–20 dpf. Thus, early zebrafish vision is dependent solely on cone-mediated vision. The rapid development of the visual system and early cone dominance have facilitated several genetic screens using young embryos to select specifically for cone related defects (see below).

Zebrafish were originally developed as a model system because they are inexpensive to keep, and take only 3 months to reach sexual maturity after which a mating pair will produce 200–300 eggs per week for at least a year. Further, development of many different genetic tools has added greatly to the versatility of this model for scientific study. In particular, mutagenesis protocols were optimized in the mid-1990s to introduce high frequencies of mutations. This made it possible to conduct large-scale forward genetic screens. Hundreds of different mutants affecting many aspects of vertebrate development and function have been identified. The constantly improving annotation of the nearly completed genome makes identifying mutated genes straightforward, and an impressive collection of vision mutants is available.

Another advantage is that cellular behavior can be observed in the intact, living organism. During the first 2 weeks of development, zebrafish larvae can be maintained in a translucent state and visualized live using either exogenous or genetically encoded fluorescent markers (see examples in **Figure 1**). Zebrafish can be maintained alive and healthy in agar on the microscope stage for days. Thus, cells can be imaged over the course of development or degeneration without perturbing the extracellular environment. At this point, transgenic lines containing fluorescent markers in various cell types are simple to generate and maintain. Transient injection of plasmid DNA at the one-cell stage will also produce a mosaic expression of genes throughout the fish allowing for the study of isolated cells within the intact animal. Multiple promoters have been developed to drive expression in various types of cells within the eye.

While no procedures exist to manipulate specific genes within the genome, several methods have been developed which allow scientists to circumvent this limitation. Morpholinos are synthetic RNA-like oligonucleotides that can be injected at the one-cell stage or electroporated into the fish at later stages. These morpholinos bind to corresponding RNA sequences within the cell, resulting in the degradation of the RNA and loss of protein expression. The loss-of-protein function is not as complete as is seen in knockouts and is only transient, but it has allowed researchers to study the effects of specific knockdowns during development. Additionally, several labs have developed a method known as targeting-induced local lesions in genomes (TILLING) in which high-throughput polymerase chain reaction (PCR) methods are used to identify specific gene mutations from libraries of randomly mutagenized fish.

Very recently, another method has been established in which nucleases are used to produce double-strand breaks at specific loci within the genome. These double-strand breaks are repaired by nonhomologous end joining, often resulting in deletions or insertions at the break site that can lead to frame-shift mutations in the target gene. The targeting specificity of these double-strand breaks is established by fusion to an array of zinc finger domains that bind to specific DNA sequences. Each zinc finger recognizes a 3-bp sequence and three zinc fingers are fused together to create a 9-bp recognition domain. Further, these zinc finger nuclease arrays must dimerize to activate the nuclease such that a total 18-bp recognition sequence is required.

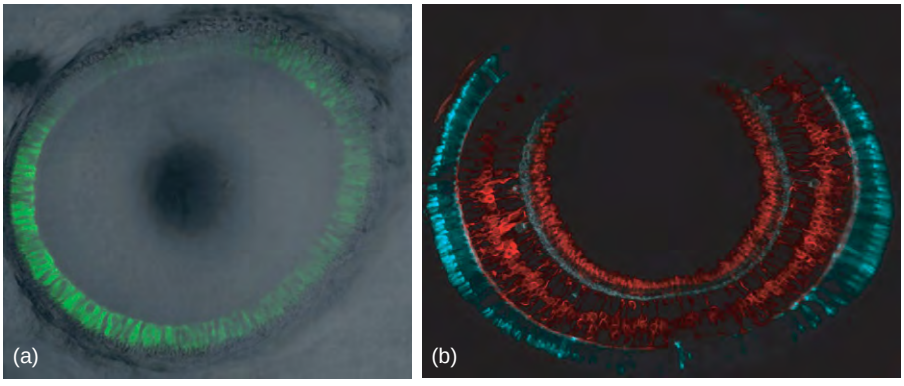

Figure 1 The zebrafish eye. These images illustrate the translucence of the eye and the ability to image the eye *in vivo*. For these experiments, zebrafish are anesthetized and embedded in a 0.5% agar solution during imaging. The zebrafish can survive under these conditions for up to 2 days. (a) A fluorescent image of the eye with the cone photoreceptors expressing the transgene for green fluorescent protein (*GFP*) under the control of a cone-specific promoter (*TαCP*), shown over the differential interference contrast (DIC) image of the eye. (b) An eye showing the photoreceptors in blue, expressing the transgene for cyan fluorescent protein under a cone-specific promoter (*Tg(TαCP:MmCFP)*) and the secondary layer of neurons or bipolar cells in red, expressing yellow fluorescent protein under a bipolar-specific promoter, (*Tg(nyc:mYFP)*).

Currently, the technology for generating the zinc finger arrays is cumbersome, but soon this will be a rapid and convenient way to generate targeted zebrafish mutants.

Methods have also been developed to create chimeric fish allowing for the rapid evaluation of the cell autonomous nature of genetic phenotypes. To produce these fish, eggs are grown to the blastula stage and then cells from one egg are removed and inserted into another egg. This procedure does not affect fish development and wild-type chimeras grow normally. The production of chimeric fish can be used to determine the critical cell population for the phenotypic changes associated with a mutation. It can also be useful for the evaluation of neighboring and surrounding effects.

Zebrafish have one other major advantage for the study of disease, which is the aqueous environment in which they reside. Methods are being developed for rapid high-throughput drug screens using zebrafish by adding compounds to their water and evaluating the effects. Most of the current studies with this method use fluorescent cell markers to indicate the presence or absence of various cells. This technique has been used with fluorescent hair cells to identify compounds that prevent hair cell death in the presence of the ototoxic agent neomycin. As zebrafish are small and easy to maintain, they are the best vertebrate model for this type of shotgun approach to drug development.

Evaluating zebrafish vision

There are several ways of evaluating zebrafish vision. The simplest involves a manipulation of the fish instinct to maintain its position within a moving stream. In this test, groups of fish can be placed in a long dish with a series of moving bars along its side. As the bars move, the fish respond to the apparent current by swimming to maintain their position with the bars. Thus, shoals of fish can be tested simultaneously for their ability to see and respond to the moving lines. This is known as the optomotor response. A related test called the optokinetic response (OKR) is done with a single fish placed in a small dish in the center of a rotating drum decorated with vertical stripes. In this test, the fish's eye will follow the stripes with periodic involuntary saccades. This is a very sensitive measure of an individual fish's ability to perceive its visual environment. Several labs have identified blind fish in mutagenesis screens using the optomotor response and/or the OKR. These screens have yielded a variety of mutants that can be used as models for retinal disease.

Another method that has been used to measure fish vision is the electroretinogram (ERG), which is a stimulated measure of the electrical response of the eye to a flash of light. In these measurements, the fish are dark adapted and a small electrode is placed on the cornea. The eye is then stimulated with a light flash and the electrical response is recorded. This technique records both the primary photoreceptor response, which appears as a negative spike at the beginning of the recording known as the a-wave, and the response of the secondary neurons, which is a large secondary positive response following the a-wave, known as the b-wave.

The Visual System: Phosphodiesterase and Phototransduction

Cyclic GMP (cGMP) phosphodiesterase (Pde) is an important enzyme in the process of phototransduction. During phototransduction the 11-*cis* retinal absorbs a single photon of light and alters the conformation of the opsin protein to activate the associated heterotrimeric guanosine triphosphate (GTP)-binding protein, transducin. The activated transducin removes the inhibitory gamma subunit from phosphodiesterase, which then degrades cGMP in the outer segments (for a schematic see Figure2).

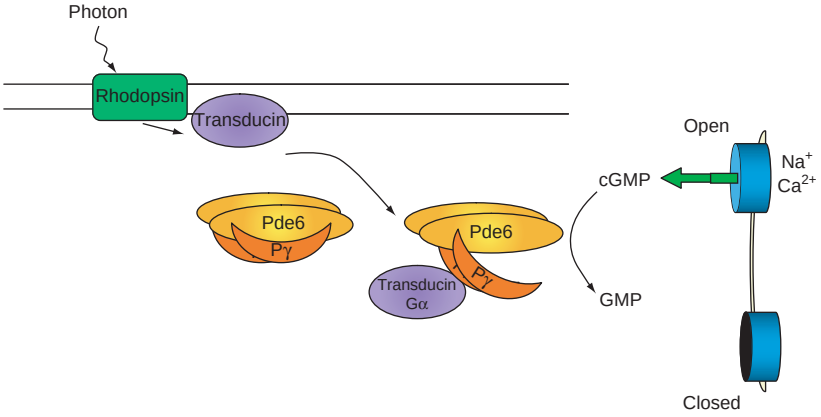

Figure 2 A schematic of the initial steps of phototransduction. The absorbance of a photon activates the 11-*cis* retinal of rhodopsin, which in turn activates the heterotrimeric GTP-binding protein, transducin. The Gα subunit of transducin binds to the inhibitory Pγ subunit of the Pde6 holoenzyme and relieves the inhibition of the catalytic domain. Pde6 then cleaves cGMP, resulting in a drop in cGMP levels that causes the closure of cGMP-gated ion channels in the plasma membrane.

The lowering of cGMP levels stimulates the closure of cyclic-nucleotide-gated ion channels in the plasma membrane, causing hyperpolarization and a decrease in neurotransmitter release at the synapse, initiating light signaling to downstream neurons. Channel closure also interrupts Ca^{2+} influx leading to a decrease in intracellular $[Ca^{2+}]_i$. The drop in intracellular $[Ca^{2+}]_i$ activates a Ca^{2+}-sensitive guanylyl cyclase, restoring cGMP to presignaling levels. Both types of photoreceptors have a similar phototransduction cascade, but use different genetically encoded enzymes to accomplish each task. Therefore, a mutation in the cone phosphodiesterase will not affect rod phototransduction.

The photoreceptor Pde (Pde6) is a multisubunit enzyme that differs slightly in rods and cones. In both cells the catalytic domain is a dimer that is bound and inhibited by the regulatory gamma subunit called Pγ. During phototransduction, activated transducin binds to Pγ and exposes the catalytic cGMP-binding site allowing the catalytic domain to cleave cGMP. In rod photoreceptors, two related but different proteins, Pα and Pβ, form the Pde6 catalytic domain. In cones, the catalytic domain consists of a dimer of one protein Pα', also known as Pde6c.

Retinal Degeneration in *pde6* Mutants: Primary Degeneration

Mutations in the Pde gene (*pde6)* are found in several families with RP and similar mutations have been used for many years as a model for RP in mice. The oldest and most commonly used mouse model of RP is the retinal degeneration 1 (*rd1*) mouse that contains a mutation in the Pβ rod-specific subunit of Pde6, the *pde6b* gene. In this model, rod degeneration is apparent by postnatal day 8 and nearly all of the rods are lost by 3 weeks of age. Despite many years of study, the process of primary photoreceptor degeneration in the *rd1* mouse is not well understood. Initial work has implicated programmed cell death pathways. The death of rods is associated with the extreme DNA cleavage that accompanies apoptosis, and this DNA cleavage can be detected with the terminal deoxynucleotidyl transferase biotin-dUTP nick end labeling (TUNEL) assay. However, several studies suggest that the standard apoptotic cascades, including a group of cysteine proteases known as the caspases, and other typical apoptotic effectors, are not involved. Instead, recent work implicates intracellular calcium concentration ($[Ca^{2+}]_i$) and the calpains, a calcium-activated set of proteases found in the mitochondria, as the relevant initiators of photoreceptor programmed cell death.

In *rd1* mice, the absence of Pde6 results in elevated levels of cGMP even under dark conditions, and it has been hypothesized that this results in the greater open probability of the cyclic-nucleotide-gated ion channels leading to increased $[Ca^{2+}]_i$ levels and apoptosis. However, little is known about the distribution of $[Ca^{2+}]_i$ during the death of cones. An initial report using the Ca^{2+} channel blocker, D-*cis*-diltiazem, to inhibit $[Ca^{2+}]_i$ accumulation showed a decrease in apoptosis. However, other labs using the same and other Ca^{2+} channel blockers have been unable to repeat these results. Due to the difficulty of imaging a mouse retina *in vivo* over long time periods, none of these studies has examined the levels of $[Ca^{2+}]_i$ within the cells *in vivo*. The translucence of the zebrafish retina enables *in vivo* imaging of both the morphological changes of degeneration as well as changes in levels of signaling molecules, such as Ca^{2+} or cGMP.

Retinal Degeneration in *pde6* Mutants: Secondary Retinal Degeneration, the Bystander Effect – Models and Mechanisms

In humans, RP is characterized by a lack of night vision, but often progresses over time to tunnel vision and, in some cases, complete blindness. This progression of the disease is due a gradual death of cones by apoptosis. Cell death begins in the peripheral retina where the number of rods is highest and moves toward the central retina. The cone photoreceptors are fully functional and do not use the mutated genes for phototransduction. However, the death of the mutant rods causes healthy cones to die apoptotically. This transmission of death to healthy neighboring cells is a process known as the bystander effect. The death of these cones represents the most debilitating part of this disease, and has significant potential for therapeutic intervention.

In addition to retinal degeneration, the bystander effect has been seen in a variety of diseases, including cancerous tumors, and can be either beneficial or detrimental to therapeutic efforts. One of the first descriptions of the bystander effect occurred during studies of gene therapy for cancer in which malignant tumors were injected with viruses containing suicide genes, which convert a prodrug into a lethal compound inside cells. Researchers found that, although only a small population within the tumor expressed the detrimental genes, significant portions of the tumor mass still died, suggesting that virally transfected cells were able to induce death in untransfected neighboring cells. Recently, researchers have found a similar occurrence in cells exposed to radiation therapy. In this case, cells that have not been irradiated show the genetic instability associated with radiation exposure.

In general, apoptosis does not affect the health of neighboring cells and it is unclear why in some instances there is a spread of death across a population. There are currently several hypotheses for how healthy cells are

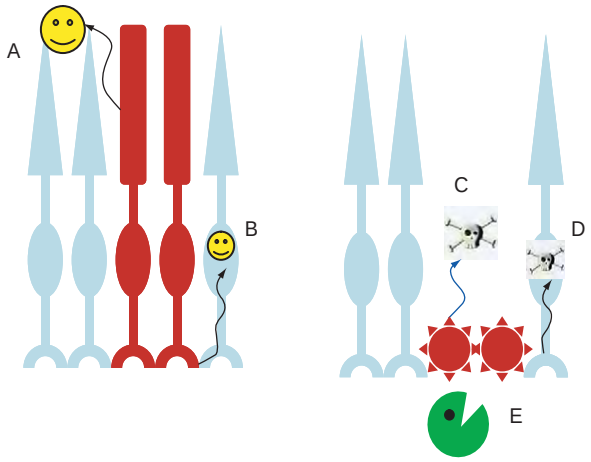

Figure 3 Schematic of some of the possible sources of the bystander effect. (a, b) Live cells release trophic factors (happy faces) that help neighboring cells and are lost when the mutant cells (in red) die. These factors could be released exogenously (a) or through gap junctions between cells (b). (c, d) Dying cells release toxic factors (skulls) that kill neighboring cells, again either exogenously (c) or through gap junctions (d). (e) The immune response to the presence of dying cells could have a deleterious effect on the remaining healthy cells.

induced to die. One possibility is that live cells release a trophic factor that stimulates the growth and differentiation of their neighbors and is required for their proper maintenance. For instance, it has been suggested that rods release a factor that stimulates the growth of cones. Another possibility is that dying cells release toxic factors that kill neighboring cells. A potential corollary to both of these hypotheses is that either toxic or trophic factors are released to neighboring cells through gap junctions. It is also possible that the immune response triggered by the removal of apoptotic cells has a deleterious effect on the neighboring cells. See Figure 3 for a schematic of these possibilities. Understanding the source of the bystander effect will suggest other methods by which it might be prevented.

Levels of the Bystander Effect in Photoreceptor Degeneration

The extent of bystander cell death is not the same for all cases of retinal degeneration. The death of cones in rod–cone dystrophies has been extensively studied in human patients and in a variety of animal models, including the *rd1* mouse. Mutations in rod phototransduction, resulting in rod death, almost always lead to some cone degeneration. However, the number of cells that die within the central fovea varies significantly from patient to patient. Mutations in genes required for cone phototransduction and their effects on rods are less well studied. Cone–rod dystrophies are conditions in which degeneration of the cones causes a decrease in scotopic vision, low light vision that is produced exclusively by rod function. Little is known about the state of rods in these patients, but it is thought that there is some degeneration associated with the visual loss. In contrast, some patients with cone dystrophies have cone death without affecting the rods or scotopic vision.

Differences in the connections between cells in a population might account for the variable levels of bystander death. In particular, it is thought that gap junctions between rods and cones in mammals may be predisposed to allow the flow of materials from the rods to the cones, but not from the cones to the rods. Thus, it may be possible that the flow of information would be asymmetrical between cell types and this could lead to differences in the effects on neighboring cells.

In order to better understand the bystander effect, an important first step is to determine how death progresses throughout the population and which populations of cells are capable of propagating apoptotic signals to healthy neighbors. For this type of analysis, zebrafish provide an ideal system. Not only are mosaic animals easy to generate, but the transparency of the embryo make it possible to analyze the transmission of death *in vivo*. This feature combined with the other tools described above provides a novel and powerful approach to examining the bystander effect within the photoreceptor population.

Zebrafish Models of Retinal Degeneration: Mutations in *pde6c*

Mutations in the zebrafish cone phosphodiesterase have been identified in two separate genetic screens for fish lacking OKR at 5 dpf. One of the mutations is a null mutant (*w59*), while the other is a missense mutation in a conserved amino acid (*els*). Recently, recessive mutations in *pde6c* were also identified in mice and in three human families with achromatopsia. Preliminary results indicate that in humans this form of achromatopsia may be progressive, suggesting the possibility of a bystander-associated death of rods.

pde6c^{w59}

pde6c^{w59} is a mutation in the splice site between exons 11 and 12 in the *pde6c* gene. The abnormal splicing caused by this mutation introduces a premature stop codon generating a null mutant. Zebrafish, homozygous for the *pde6c*^{w59} mutation, are viable and form normal swim bladders, a marker of general fish health, but must be raised with higher-than-normal food concentrations, as their visual defects impair acquisition of food (Figure 4(a)). In these fish, cone photoreceptors initially develop normally. However, at 4 dpf, when fish first respond to light, the cone photoreceptors in the central retina begin to

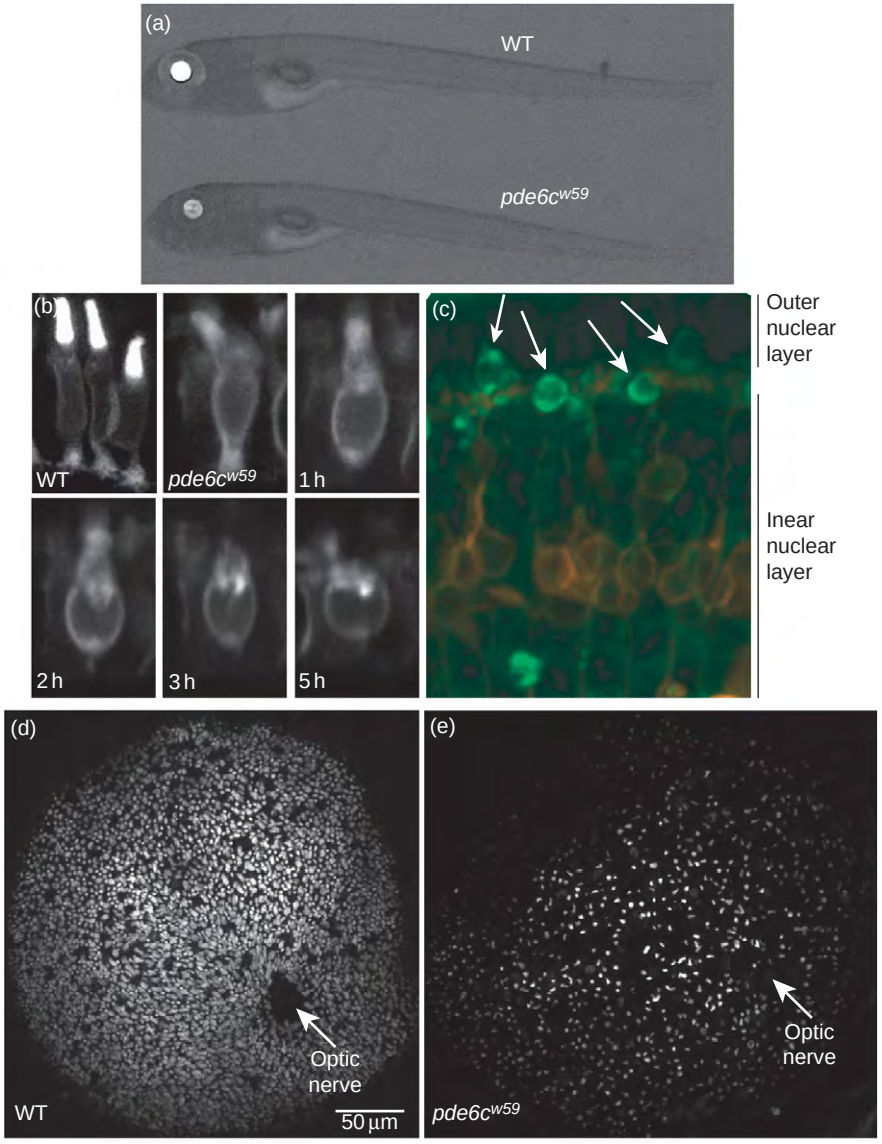

Figure 4 Images of the *pde6c*^{w59} mutant fish. (a) Homozygous *pde6c*^{w59} mutant fish have swim bladders, and are generally healthy. These fish contain the transgene *Tg(TαCP:MmCFP)*, which causes expression of membrane-tagged cyan fluorescent protein (MmCFP) specifically in cone photoreceptors. The level of fluorescence in the mutant eye is decreased due to the degeneration of cone photoreceptors. (b) A time-lapse sequence of a single mutant cone photoreceptor undergoing apoptosis. The initial picture is an image of wild-type cones. The subsequent pictures are a single *pde6c*^{w59} mutant cell over a 5-h time course. As the cells die, they retract their synaptic connections and round up to form apoptotic bodies which are eventually removed by the immune system. (c) Apoptotic photoreceptors (green) viewed using the membrane label boron-dipyrromethene (BODIPY), which labels all cellular membranes in the fish. Apoptotic bodies are clearly visible in the outer nuclear layer (arrows). Bipolar cells express yellow fluorescent protein (*Tg(nyc:mYFP)*) and are shown here in red. (d, e) The dramatic loss of fluorescently labeled photoreceptors in the whole eye of *Tg(TαCP:MmCFP) pde6c*^{w59} mutant. Eyes were removed from euthanized and fixed 6-day-old *Tg(TαCP:MmCFP)* WT (d) and *pde6c*^{w59} (e) mutant animals. Fluorescently labeled cone photoreceptors were viewed with confocal microscopy. From Lewis, Wong and Brockerhoff, in preparation.

degenerate. The *pde6c*^{w59} mutants exhibit a flat ERG at 5 dpf, indicating a total lack of photoreceptor response to light and no signaling to downstream neurons. At this stage in development, zebrafish vision relies on cones, so a flat ERG is consistent with the rapid cone degeneration observed in these fish. As the cone photoreceptors die, they retract their synaptic connections and outer segments and become spherical. Time-lapse images of this process are shown in **Figure 4(b)**. In the final stages of cell death, only the rounded apoptotic bodies remain (**Figure 4(c)**, arrows). This cell debris travels out of the outer nuclear layer and is disposed of by the macrophages of the immune system.

Within the central retina of the *pde6c*^{w59} mutant, a majority of cones die by 5 dpf. **Figures 4(d)** and **4(e)**

show the central retina of a wild-type (d) and mutant (e) eye, expressing membrane-tagged cyan fluorescent protein (MmCFP) specifically in the cone photoreceptors. The MmCFP accumulates in the outer segments of the cones. In **Figures 4(d)** and **4(e)**, the eye is visualized by removing it from a day-6 zebrafish larva and inverting it onto a microscope slide. In the wild-type eye, the central retina is densely populated with cones that show a regular mosaic pattern (**Figure 4(d)**). In the *pde6c*^{w59} eye, most of the cone photoreceptors have died and been removed from the retina, and many of the remaining outer segments appear dystrophic (**Figure 4(e)**).

Unlike humans or mice, fish continue to produce photoreceptor cells throughout their life. At the periphery of the eye is a region of cells known as the circumferential marginal zone, in which new photoreceptors are generated by multipotent stem cells. In this zone, young cones are constantly differentiating throughout the life of the animal. Even in adult *pde6c*^{w59} mutants, there are always cones in this region of the eye, indicating that there is no defect in cone morphogenesis or differentiation, but that cones die as they mature. The circumferential marginal zone is not visible in **Figures 4(d)** and **4(e)** but can be seen in **Figure 4(a)** as a faint ring of fluorescence around the periphery of the *pde6c*^{w59} eye.

The rods in the central retina also deteriorate during early development in *pde6c*^{w59} mutants but later recover. At 7 dpf, the rods appear normal and are slightly more clustered than in wild type, but not reduced in number. At 8–9 dpf, the number of rods begins to decrease in the central retina. The outer segments of the remaining rods in the central retina appear dystrophic. The deterioration of the rods continues through at least 6 weeks postfertilization. These data were the first evidence that zebrafish can undergo a bystander effect in the retina (i.e., mutant cones kill neighboring healthy rods).

The multipotent stem cells in the circumferential marginal zones of the eye can differentiate into rods throughout the life of the animal. Additionally, in cases of damage or injury, the Müller glia can also enter a mitotic state and produce stem cells capable of forming all types of retinal neurons. In the *pde6c*^{w59} mutants, this continuous regeneration eventually replenishes the small number of rods that have died. Thus, by 3 months postfertilization, the retina is completely populated with rods. Interestingly the *pde6c*^{w59} mutants never develop a scotopic ERG or OKR, indicating that even the remaining rods are unable to form proper connections with the downstream neurons in the eye. Unlike human and mouse eyes, zebrafish do not have separate rod and cone bipolar cells. The bipolar cells that connect to rods also connect to cone photoreceptors. The lack of scotopic vision in the *pde6c*^{w59} mutant suggests that the cones are necessary for the proper connections of the rods with their bipolar targets. In support of this theory, the bipolar cells of the *pde6c*^{w59} embryos often show an altered morphology with axons that extend into the ganglion cell layer and dendritic branches that send filopodia into the photoreceptor layer.

The *pde6c*^{w59} mutant allows for exceptional visibility of photoreceptor degeneration. Due to the rapid degeneration of the cones and rods in the central retina, it is possible to monitor many aspects of cell death as they are occurring. However, in the human diseases of RP and Achromatopsia, retinal degeneration can be a slow process occurring over several years. Thus, although it is easier to visualize cell death and develop drugs that will combat the rapid loss of photoreceptors in the *pde6c*^{w59} mutation, it would also be useful to have a mutant where degeneration occurred over a more protracted period of time. Recently the *els* mutant was identified as a mutation in *pde6c* that results in slow cone degeneration.

els

The *els* mutation produces a single amino acid change; methionine (M) 175 is mutated to an arginine (R) (M175R) in the first GAF domain of Pde6c. At 5 dpf, when zebrafish vision is cone dependent, fish that are homozygous for the *els* mutation have a flat ERG and no OKR, although initially the cones appear morphologically normal. This indicates that phototransduction is disrupted but surprisingly cell death has not been triggered. This finding suggests that the *els* allele is not null for the Pde6c protein, but that secondary defects within the *els* cones may be disrupting phototransduction, resulting in a flat ERG. One finding in support of this idea is that, although all four types of cones are initially present in the *els* mutant, the localization of various opsins within the photoreceptors is abnormal. Generally, opsins are found only in the outer segments, but in the *els* mutant, opsin proteins are found throughout the cell. At this stage, there is also a small but significant increase in the number of apoptotic cells in the *els* retinas. By 3 weeks postfertilization, the cones and rods in the central retina have begun to show an altered morphology, and the number of cone cells has decreased. However, despite their slightly altered morphology, rod maturation occurs in these fish and by 3 weeks postfertilization the fish respond to OKR under scotopic conditions.

As the *els* fish matures, the cones continue to deteriorate and by 6 months postfertilization the retina no longer contains cones, but consists entirely of rods. The rods are morphologically normal and, unlike those found in *pde6c*^{w59}, functional. This suggests that the significantly slower death of cones in *els* compared to *pde6c*^{w59} fish allows rods to form proper synaptic connections with bipolar cells. Interestingly, the total number of cells in the inner retina is decreased in this mutant; however, the ratio of inner retinal cells to rods has increased over wild type, suggesting that the rods are forming more

connections in the mutant than they do in the wild-type retina. The number of mitotically dividing cells in the retina is also increased in the mutant, suggesting that there is an increase in cellular proliferation probably resulting from the death of the cone photoreceptors.

Pde6 Structure

Recent work on the structure and function of Pde6c has shed some light on the potential effects of the *els* mutant for the Pde6c holoenzyme. The catalytic subunit of the Pde6 protein consists of two domains: a regulatory domain with two GAF domains, one of which (GAF A) binds cGMP, and a catalytic domain that has phosphodiesterase activity. The inhibitory subunit Pγ binds to the GAF A domain though its C terminus and the catalytic domain through interactions with its N terminus. Recent work with the rod Pde6 has suggested that the binding of cGMP to the GAF A domain may increase the binding affinity of the N terminus of Pγ for the catalytic domain. Thus, the binding of cGMP to the GAF A domain may help to regulate the activity of Pde6c *in vivo*. Met175 is located within the allosteric cGMP-binding site of the GAF A domain of Pde6c (**Figure 5(a)**). A recently determined crystal structure of the GAF A domain from chicken Pde6c reveals that the side chain of Met175 (equivalent to Met179 in chicken Pde6c) is in close proximity to the cyclic phosphate group of cGMP, although it does not directly interact with the cyclic nucleotide. As in other cyclic-nucleotide-binding Pde GAF domains, the phosphate group of the ligand is stabilized through the positive dipole of helix α3 (**Figure 5(b)**). The mutation M175R (equivalent to M179R in chicken Pde6c) introduces a larger and positively charged side chain into the binding pocket and thereby changes the cGMP-binding environment and, potentially, the binding affinity for the allosteric regulator cGMP (**Figure 5(c)**). A model in which a methionine side chain is substituted for an arginine side chain suggests three potential consequences of the M175R mutation. First, the R175 side chain clashes with helix α3, which may disrupt the dipole interaction between the helix and the phosphate group. Second, the R175 side chain clashes directly with the phosphate group of cGMP. Third, R175 might form a salt bridge with the phosphate group. In the former two scenarios, R175 would disrupt cGMP binding and lower the binding affinity of the GAF domain for cGMP, whereas in the latter scenario, R175 may cause a higher affinity for cGMP.

In either model, it is likely that the M175R mutation interferes significantly with cGMP binding and the sensitive regulatory mechanism of Pde6 through its GAF A domain. This, in turn, may lead to impaired Pde6 function and cause over- or underexpression of Pde6 protein, thereby disrupting the cone photoreceptor function. No data are available on the stability or functionality

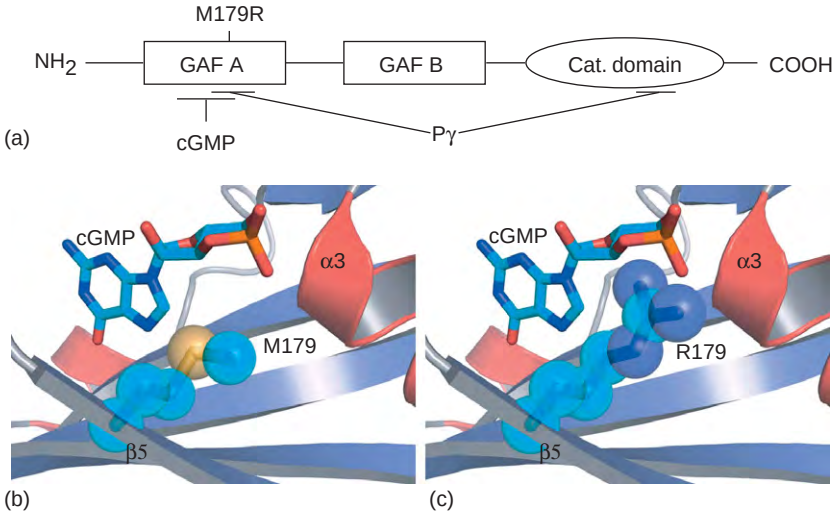

Figure 5 Structural consequences of M179R mutant in Pde6c GAF A. (a) Domain organization of Pde6c. The C-terminal catalytic domain is regulated by allosteric noncatalytic binding of cGMP to the N-terminal GAF A domain and binding of the inhibitory Pγ-subunit. The methionine (M)179 to arginine (R) mutation in chicken Pde6c, for which there is a crystal structure, is equivalent to the *els* Met175R mutation in zebrafish. (b) Experimentally determined structure of wild-type cGMP-binding pocket of chicken Pde6c GAF A (pdb-code: 3dba). α-Helices are shown in red, β-strands are shown in blue. cGMP and Met179 are shown in sticks with carbon atoms in cyan. Met179 is also highlighted through spheres. The figure was prepared with PyMOL, a molecular modeling program. (c) Model of M179R mutant cGMP-binding pocket of Pde6c GAF A. M179 was mutated to R179 through the mutation-function of PyMOL. In the absence of some structural rearrangements in the binding pocket, the longer side chain of R179 clashes with the phosphate group of cGMP and helix α3. α-Helices are shown in red; β-strands are shown in blue. cGMP and R179 are shown in sticks with carbon atoms in *cyan*. R179 is also highlighted through spheres.

of the *els* mutant protein. However, the phenotypic comparison with the *w59* mutant suggest that the *els* mutant is not a null mutation, but creates a more subtle effect on the levels or activity of the Pde6c protein. The proximity of the mutation to the cGMP-binding site in the GAF A domain implicates a possible disruption of the intramolecular allosteric regulation of catalytic activity ascribed to this portion of Pde6c.

The *els* mutant represents a unique opportunity to understand more about the enzymatic functions of Pde6 and its role in retinal degeneration. The slower degeneration of this mutation compared to the *w59* allele more accurately reflects slower human forms of degeneration. These two zebrafish *pde6c* mutants will provide complementary tools for studying Achromatopsia and apoptosis due to phosphodiesterase deficiency.

Conclusion

Zebrafish have gained prominence as a model for retinal disease. Cone-based vision, visual translucence, inexpensive maintenance, and rapid external embryologic development help make this model particularly exciting for retinal studies. Several genetic screens for blind fish have identified a variety of mutants that mimic human retinal disease. Among these, the *pde6c* mutants are a particularly good example of a retinal model that has been studied for many years in mice, and will benefit from the types of study available in the zebrafish system. In particular, the potential for live imaging of cells *in vivo* in an intact animal presents a novel opportunity to visualize and understand the source of photoreceptor degeneration.

One of the largest differences between the eyes of zebrafish and humans is the continuous growth of the zebrafish eye, and its regenerative ability in response to damage. Although this regenerative potential can complicate the evaluation of zebrafish as a model organism, it also presents a novel possibility to understand and imitate a natural system of retinal stem cell regeneration. By studying the differences between the zebrafish and mammalian systems it may be possible to stimulate our own potential for retinal regeneration.

The zebrafish model also offers an unprecedented potential for high-throughput drug screening. Using fluorescent cell markers and fluorescent plate readers, it will soon be possible to do large-scale screening of drugs that affect the levels of retinal degeneration. This method can also be used to test permeability and the toxicity of drugs. This is the first vertebrate animal model that provides a method for this type of rapid drug development.

See also: Color Blindness: Inherited; Phototransduction: Phototransduction in Cones; Phototransduction: Phototransduction in Rods; Phototransduction: Rhodopsin; Primary Photoreceptor Degenerations: Terminology; Secondary Photoreceptor Degenerations; Zebrafish: Retinal Development and Regeneration.

Further Reading

Brockerhoff, S. E., Hurley, J. B., Janssen-Bienhold, U., et al. (1995). A behavioral screen for isolating zebrafish mutants with visual system defects. *Proceedings of the National Academy of Sciences of the United States of America* 92(23): 10545–10549.

Cote, R. H. (2007). Photoreceptor phosphodiesterase (PDE6): A G-protein-activated PDE regulating visual excitation in rod and cone photoreceptor cells. In: Beavo, J. A., Francis, S. H., and Houslay, M. D. (eds.) *Cyclic Nucleotide Phosphodiesterases in Health and Disease*, pp. 165–193. Boca Raton, FL: CRC Press/ Taylor and Francis.

Doyon, Y., McCammon, J. M., Miller, J. C., et al. (2008). Heritable targeted gene disruption in zebrafish using designed zinc-finger nucleases. *Nature Biotechnology* 26(6): 702–708.

Goldsmith, P. and Harris, W. A. (2003). The zebrafish as a tool for understanding the biology of visual disorders. *Seminars in Cell and Developmental Biology* 14(1): 11–18.

Hamada, N., Matsumoto, H., Hara, T., and Kobayashi, Y. (2007). Intercellular and intracellular signaling pathways mediating ionizing radiation-induced bystander effects. *Journal of Radiation Research (Tokyo)* 48(2): 87–95.

Martinez, S. E., Heikaus, C. C., Klevit, R. E., and Beavo, J. A. (2008). The structure of the GAF A domain from phosphodiesterase 6C reveals determinants of cGMP binding, a conserved binding surface, and a large cGMP-dependent conformational change. *Journal of Biological Chemistry* 283(38): 25913–25919.

Morris, A. C., Scholz, T. L., Brockerhoff, S. E., and Fadool, J. M. (2008). Genetic dissection reveals two separate pathways for rod and cone regeneration in the teleost retina. *Developmental Neurobiology* 68(5): 605–619.

Muto, A., Orger, M. B., Wehman, A. M., et al. (2005). Forward genetic analysis of visual behavior in zebrafish. *PLoS Genetics* 1(5): e66.

Nishiwaki, Y., Komori, A., Sagara, H., et al. (2008). Mutation of cGMP phosphodiesterase 6alpha'-subunit gene causes progressive degeneration of cone photoreceptors in zebrafish. *Mechanisms of Development* 125(11–12): 932–946.

Paquet-Durand, F., Johnson, L., and Ekstrom, P. (2007). Calpain activity in retinal degeneration. *Journal of Neuroscience Research* 85(4): 693–702.

Ripps, H. (2002). Cell death in retinitis pigmentosa: Gap junctions and the 'bystander' effect. *Experimental Eye Research* 74(3): 327–336.

Sancho-Pelluz, J., Arango-Gonzalez, B., Kustermann, S., et al. (2008). Photoreceptor cell death mechanisms in inherited retinal degeneration. *Molecular Neurobiology* 38(3): 253–269.

Stearns, G., Evangelista, M., Fadool, J., and Brockerhoff, S. E. (2007). A mutation in the cone specific pde6 gene causes rapid cone photoreceptor degeneration in zebrafish. *Journal of Neuroscience* 27(50): 13866–13874.

Wissinger, B., Chang, B., Dangel, S., et al. (2007). Cone phosphodiesterase defects in the murine cpfl1 mutant and human achromatopsia patients. *Investigative Ophthalmology and Visual Science* 48(5): 4521.

Zhang, X. J., Cahill, K. B., Elfenbein, A., Arshavsky, V. Y., and Cote, R. H. (2008). Direct allosteric regulation between the GAF domain and catalytic domain of photoreceptor phosphodiesterase PDE6. *Journal of Biological Chemistry* 283(44): 29699–29705.

Zebrafish: Retinal Development and Regeneration

T J Bailey and D R Hyde, University of Notre Dame, Notre Dame, IN, USA

Glossary

BrdU (bromodeoxyuridine) labeling – The synthetic nucleoside which is incorporated into nascent DNA during replication and is detectable by antibodies to indicate what cells have divided since exposure to BrdU.

CMZ (circumferential marginal zone) – The region of the retina distal to the optic stalk and proximal to the ciliary margin and lens. Here, retinal cells are continually born throughout the life of the zebrafish. CMZ cells express genes found in the neuroretina of the developing zebrafish embryo.

Homeobox transcription factors – The proteins that pattern tissue in that they regulate gene transcription by binding to a specific DNA sequence, the homeobox, in the target gene promoter.

Morpholino – Similar to RNA, this polymerized oligomer with a morpholino (rather than ribose) backbone, can base pair with ribonucleic acid (RNA) molecules, and persists in the cell as it is not easily degraded by RNases. Morpholinos interfere either with ribosomal processing of the messenger RNA into protein or spliceosome processing of premessenger RNA into mRNA, thus depleting the amount of protein produced.

Notch signaling – The plasma membrane-bound receptor that regulates the cell fate choice of individual neurons. Intracellular cleavage product can act as a transcription factor and regulate the expression of pro-neural genes such as basic helix–loop–helix (bHLH) transcription factors.

Pcna (proliferating cell nuclear antigen) – A marker for DNA replication in that it is a protein that functions as a trimer to promote DNA polymerase δ processivity.

Shh (sonic hedgehog) signaling – The Shh family members act as morphogens to pattern tissue. Signaling pathway proteins and pathways are reutilized in more specific cell fate specification as tissues are patterned.

TUNEL (terminal deoxynucleotidyl transferase dUTP nick end labeling) – A hallmark of apoptotic cells is genomic DNA fragmentation by specific nucleases that cleave DNA between histones. This process results in semi-uniform lengths of DNA with overhanging hydroxyl groups. Terminal transferase efficiently polymerizes labeled nucleotides to DNA hydroxyl groups without the need of a template. TUNEL is used to detect the genomic fragmentation of an apoptotic cell.

Introduction

Zebrafish has rapidly become a leading model system to study a variety of developmental processes, due to its large clutch size, external development of transparent embryos, and the rapid development of the embryo. Large and small genetic screens identified hundreds of mutants that affect the development of various tissues, including the retina. The ease in generating transgenic zebrafish lines has permitted a detailed cellular analysis of organ development without harm to the embryo. For example, transgenes that label specific cells are used to follow cell fates in the transparent embryo during tissue development. Alternatively, transgenes that express molecules that lead to cell death have been used to ablate cells to study either the disruption of development or organization of a tissue. Furthermore, the nearly complete sequence of the zebrafish genome has allowed comparative analyses with other vertebrate genomes to predict the presence of orthologous genes and developmental processes. Combined with the ability to direct the transient reduction in expression of desired proteins, it is possible to functionally analyze the potential role of different signaling pathways in the development of various tissues. Our understanding of zebrafish retinal development, from a sheet of neuroepithelial cells to a laminated and functional neural tissue, has benefited significantly from all of these approaches.

In addition to being an excellent model system to study early development, zebrafish has quickly become the premier model system to study tissue regeneration. In addition to exhibiting rapid and functional regeneration of the fin, liver, and heart, zebrafish also regenerate neuronal tissues, including the spinal cord, brain, and retina. Using mutants and transgenic lines that are readily available in zebrafish, a detailed comparison of the genes, molecules, and process that are required for retinal development and retinal regeneration is starting to be generated. While it may initially seem reasonable that regeneration would recapitulate the mechanisms that are involved in retinal development, recent studies revealed that regeneration may utilize the same genes and proteins as

development, but in a different context. This becomes most obvious when one compares the development of a laminated retina from an unpatterned neuroepithelium to the regeneration of single neuronal cell type from an existing laminated retina. To fully appreciate the differences between these two processes and the mechanisms involved in regeneration, it is important to contrast our understanding of the general events involved in retinal development with our recently acquired knowledge of the processes underlying retinal regeneration.

Embryonic Eye Patterning

Zebrafish Eyes Form from a Single Field in the Anterior Neural Plate

There is a large body of knowledge regarding the genes and genetic pathways that are required for the proper formation of the vertebrate eye. Around 10 h postfertilization (hpf), several secreted proteins induce the most anterior region of the anterior ectoderm to become the neural plate. Several signaling pathways (wingless (Wnt), fibroblast growth factor, and insulin-like growth factor) then further subdivide the anterior neural plate to produce the presumptive eye field. Some anterior-most cells then begin expressing several homeobox transcription factors, such as the retinal progenitor genes visual system homeobox 2 (*vsx2*), paired box gene 6 (*pax6*), and retinal homeobox (*rx*), which further restrict their fates to be retinal progenitor cells. The midline of the underlying head mesoderm then expresses several secreted, signaling molecules (such as the sonic hedgehog-related protein, sonic-you), which induces the eye field in the anterior neural plate to split into two distinct regions. This yields the first morphological sign of the developing visual system, the bilateral evagination of a single-cell thick epithelium from the anterior end of the neural keel, which will develop into the optic lobe. The optic lobes are morphologically visible by 12 hpf (**Figure 1(a)**). Each optic lobe expresses diffusible signals that induce the overlying naïve epithelium to commit to form the lens. As the lens placode starts to thicken (18 hpf, **Figure 1(b)**), it produces soluble signaling molecules that promote the underlying optic lobe to proliferate and invaginate, which results in the formation of a concave neuroepithelium – the optic cup. Expression of the transcription factor genes microphthalmia-associated transcription factor (*mitf*) in the ventral optic cup and *vsx2* in the dorsal optic cup commits those cells to develop into the retinal pigmented epithelium and neural retina, respectively. The region that lies at the junction of the *mitf* and *vsx2* expressing cells later becomes one region of persistent retinal neurogenesis in the adult retina, the circumferential marginal zone (CMZ, discussed below).

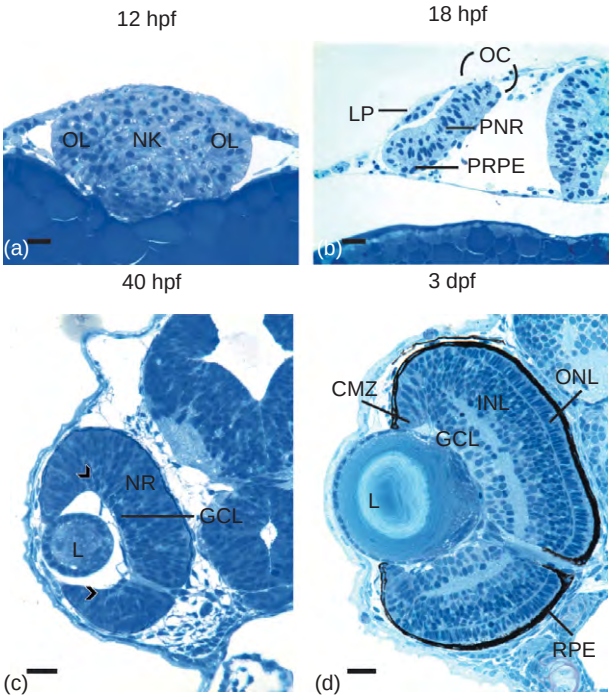

Figure 1 Zebrafish retinal development. (a) Cells evaginate bilaterally from the anterior neural keel (NK) to form the optic lobes (OL), which are morphologically distinguishable by 10–12 h postfertilization (hpf). (b) By 18 hpf, the proliferating cells of the presumptive neuroretina (PNR) have induced the overlying ectoderm to thicken into the lens placode (LP). The retina then invaginates to form the OC, with the thicker dorsal cells, or presumptive neuroretina, expressing *vsx2* and the thinner ventral cells, or presumptive retinal pigmented epithelium (PRPE), expressing *mitf*. (c) The cells in the neural retina continue to proliferate until a wave of sonic hedgehog (Shh) signaling induces the first retinal ganglion cells (RGCs) in the most basal nuclear layer, the ganglion cell layer (GCL: between the arrowheads), to differentiate around 40 hpf in the center of the retina, whereas cells in the retinal margin remain in an uncommitted state. (d) Additional waves of Shh signaling produce three nuclear layers, the ganglion cell layer (GCL), inner nuclear layer (INL), and outer nuclear layer (ONL). The ONL is immediately below the retinal pigmented epithelium (RPE), which is now darkened with pigment granules by 3 days postfertilization (dpf). Scale bars represent 20 μm. OC, optic cup; NK, neural keel; NR, neural retina; RPE, retinal pigmented epithelium; CMZ, circumferential marginal zone; GCL, ganglion cell layer; INL, inner nuclear layer; L, lens; LP, lens placode; OL, optic lobe; ONL, outer nuclear layer; PNR, presumptive neuroretina; PRPE, presumptive retinal pigmented epithelium.

The Laminar Structure of the Retina Forms as Cells Exit the Cell Cycle and Differentiate

The number of cells in the NR increases through cell proliferation until the diffusible signaling protein sonic hedgehog (Shh) is produced in a ventronasal patch of the NR. The Shh protein initiates a wave of expression of the basic helix–loop–helix (bHLH) transcription factor atonal homolog 7 (Atoh7) that sweeps radially toward the dorsal retina that induces the differentiation of the retinal

ganglion cells (RGCs) (**Figure 1(c)**). Shh is then secreted from the newly specified RGCs to sequentially induce the apically located naïve mitotic cells to exit the cell cycle and commit to the other retinal neuronal identities. Later, Shh signaling from the RPE is required for proper photoreceptor differentiation. This process results in the formation of the terminally laminated retina, which is composed of three nuclear layers (ganglion cell layer, inner nuclear layer (INL), and outer nuclear layer) and two synaptic layers (inner plexiform layer and outer plexiform layer) by 72 hpf (**Figure 1(d)**).

Intrinsic commitment and specification of the different retinal cell types also requires the expression of homeobox transcription factors and pro-neural genes of the Notch signaling pathway. Experiments aimed at determining when the different retinal cell types are committed (neuronal birthdating) established a bias of early committing cells to the RGC, amacrine cell, cone, and horizontal cell classes, followed by the bipolar and rod photoreceptor cells, and lastly the Müller glial cells. The reproducible timing observed with these different cell types suggests that a molecular clock modulates their commitment and differentiation. This model proposes that the commitment of a retinal progenitor cell to a particular neuronal cell type corresponds to when the progenitor cell exits the cell cycle, with early committed cells localizing more basally in the retina. Thus, retinal progenitor cells divide and some daughter cells become ganglion cells, while the remaining daughter cells continue to divide. Some of these retinal progenitors exit the cell cycle and differentiate as amacrine cells and others continue as retinal progenitors. These progenitors continue their asymmetrical cell division to produce some retinal neurons with each round of cell division, until the final retinal progenitors are committed to become Müller glial cells. This suggests that the Müller glia is the retinal cell type that is most recently differentiated from the retinal progenitor cell. This model also allows for the presence of external signals to influence the commitment of the cell, which also changes over time. These mechanisms appear to be conserved across species.

Addition of Retinal Cells Throughout the Life of a Zebrafish

Unlike mammals, the zebrafish eye continuously grows throughout the lifetime of the fish. This growth requires the continual generation of new retinal neurons in a process called persistent neurogenesis. These additional retinal cells are produced from two adult stem cell niches, the CMZ (**Figure 1(d)** and **Figure 2(a)**) and an INL stem cell niche (**Figure 2(a)**). The stem cells within the CMZ continue to express the cell cycle genes and the embryonic retinal progenitor genes, such as orthodenticle homolog 2 *otx2*, *pax6*, and *rx,* throughout the life of the fish. These stem cells proliferate to yield daughter cells that ultimately differentiate into ganglion cells, amacrine cells, horizontal cells, cone photoreceptors, bipolar neurons, and Müller glial cells, but not rod photoreceptors. Rods arise from the INL stem cell niche as described below. The addition of these newly differentiated cells to the region adjacent to the CMZ (**Figure 2(c)** and **2(d)**) results in the radial growth of the adult retina.

The INL stem cells have recently been demonstrated to correspond to the Müller glial cells. Unlike the CMZ stem cells, however, the asymmetric division of the Müller glia ultimately produce only rod photoreceptors during persistent neurogenesis (**Figure 2**). Relatively few Müller glia are actively dividing at any given moment. The asymmetric division of the Müller glial cell produces neuronal progenitor cells (**Figure 2(a)**), which continue to proliferate as they migrate to the outer nuclear layer, where they are called rod precursor cells and continue to undergo cell division (**Figure 2(b)**). Unlike the pluripotent CMZ stem cells, these Müller glial-derived rod precursor cells are committed to differentiate into only rod photoreceptors during persistent neurogenesis (**Figure 2(c)**). As the adult eye enlarges, the distance between the originally differentiated rod photoreceptors increases. The Müller glial-derived rods fill in this space. Thus, persistent neurogenesis in the zebrafish retina encompasses both the radial growth of the retina by addition of all retinal cell types by the CMZ and the slow production of additional rod photoreceptors by the Müller glia (**Figure 2(d)**).

Regeneration in the Zebrafish Retina

Zebrafish regenerate all retinal neurons

Persistent neurogenesis involves the continual generation of new neurons in the adult retina, without any prior loss of retinal neurons that must be replaced. It should be noted that the scientific literature often uses retinal regeneration to define the reprojection of axons from viable neuronal soma to replace damaged axons, such as the reprojection of axons from RGCs subsequent to an optic nerve crush or severing. For this discussion, retinal regeneration refers to the replacement of entire neuronal cells that were lost through retinal insult or genetic causes. Zebrafish respond to the loss of retinal neurons by significantly increasing both the number of Müller glia that reenter the cell cycle and the rate of proliferation in the neuronal progenitor cells, relative to that observed during persistent neurogenesis. This amplified proliferation response appears to be proportional to the amount of damage suffered. In contrast to persistent neurogenesis, these Müller-glial-derived neuronal progenitors are not committed to become only rod photoreceptors. These neuronal progenitors proliferate, migrate to the retinal layer that contains the missing neurons, and differentiate specifically into the lost neurons. Thus, the damage response alters the persistent neurogenesis program to

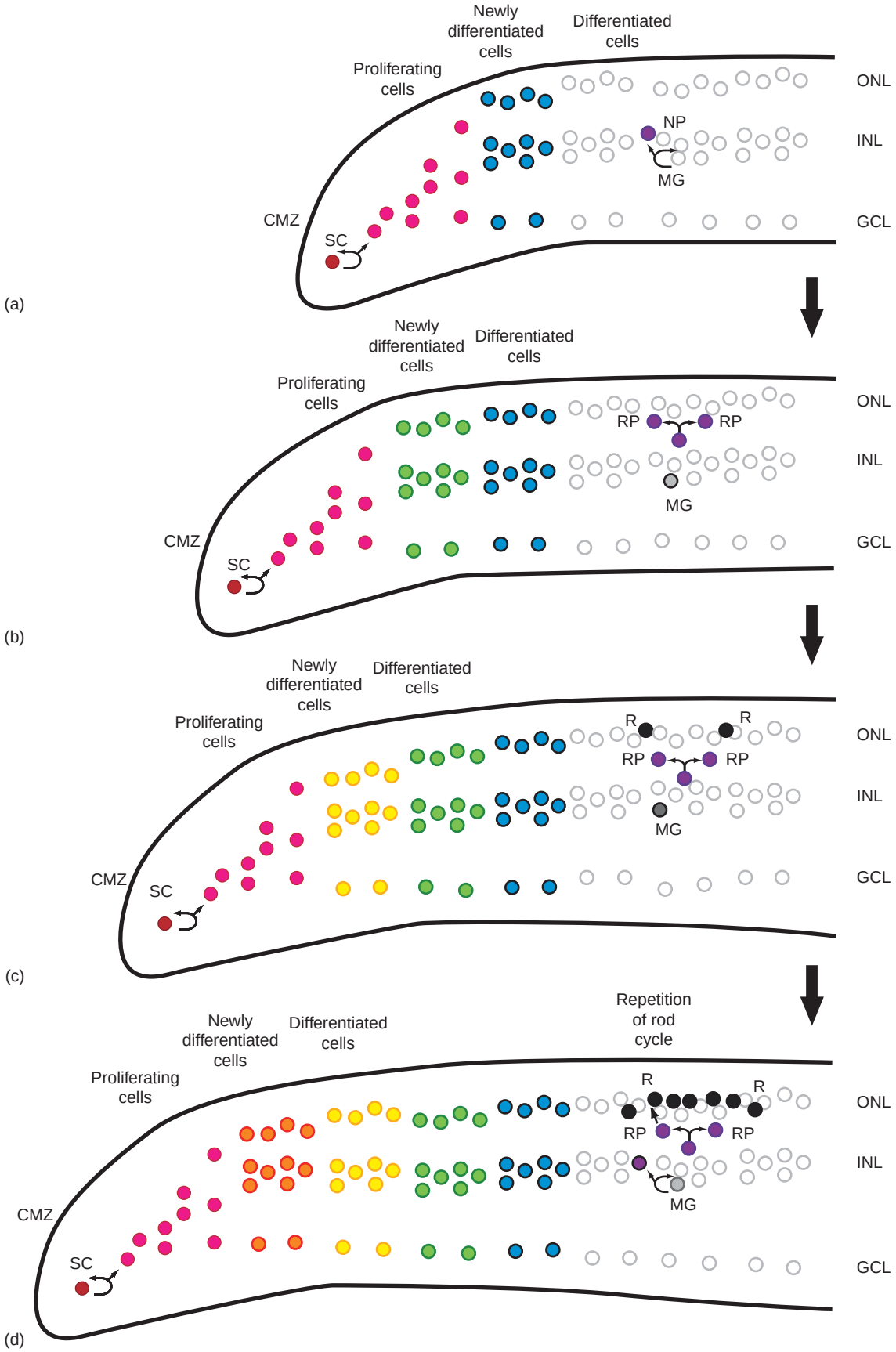

Figure 2 Continued

significantly increase the number of neuronal progenitors and allow them a greater breadth of cell differentiation potential.

A variety of damage paradigms have been studied in the zebrafish retina. For example, simple surgical lesion induces cells proximal to the cut site to die, which usually results in the death of all the retinal cell types in a small area of the retina. Similarly, heat caused by either a high temperature probe or laser ablation, or high concentrations of ouabain (Na, K-ATPase inhibitor), often causes loss of cells from all three retinal layers. In contrast, other damage models exhibit more restricted cell-type loss. For example, intravitreal injection of low concentrations of ouabain causes the loss of ganglion cells and INL neurons, without the loss of significant numbers of rod and cone photoreceptors. Constant intense light, in contrast, causes apoptosis of only the rod and cone photoreceptors, primarily in the dorsal and central retina, with no detectable cell death in the INL or GCL layers. An advantage of the light damage model is that only two neuronal classes are lost, rod and cone photoreceptors, which limits the complexity of the regeneration response. Furthermore, the light damage extends across a large region of the retina, which induces the participation of a very large number of Müller glia and neuronal progenitor cells. This results in an amplification of the signals and processes that are required for regeneration, which should increase the likelihood of their identification.

Constant Intense Light Kills Photoreceptors, Which Are then Regenerated by Müller Glia

Zebrafish rods and cones die by apoptosis upon exposure to prolonged high-intensity light. Apoptosis is a genetically programmed cell death mechanism, in which the dying cell fragments its DNA and the cell body (blebs) to produce easily phagocytosed cell corpses. Terminal deoxynucleotidyl transferase-mediated dUTP nick-end labeling (TUNEL), is a standard method to detect this fragmented genomic DNA. Fragmentation of the DNA produces large numbers of free 3′-hydroxyl ends that can be used by terminal deoxynucleotidyl transferase to add dUTP nucleotides that are covalently modified to a detectable molecule, such as biotin or fluorescein (**Figure 3**).

The light-induced photoreceptor cell death is rapid, with TUNEL-positive cells first detected in the ONL as early as 3 h after initiating the light treatment. By 16 h of constant light, the photoreceptor cell death is evident based on the reduction in the number of ONL nuclei relative to undamaged retina and is striking by 3 days of constant light (**Figure 4(a)** and **4(b)**). In addition to the strong TUNEL-positive signal that is detected in the ONL, a weaker TUNEL signal is observed throughout the Müller glial cells in the INL. Strikingly, this INL TUNEL signal is neither restricted to, nor predominantly localized in, the Müller glia nuclei, which demonstrates that the Müller glial cells are not apoptotic. Rather, the colocalization of some proteins derived from apoptotic rods with the TUNEL signal in the Müller glia suggests that the Müller glia selectively engulf dying rod photoreceptors. These data are consistent with results in the degeneration model of the *Tg*(*Xops:mCFP*) transgenic line, which expresses membrane-bound cyan fluorescent protein (mCFP) from the *Xenopus rod opsin* promoter (*Xops*) in only zebrafish rods. The *Tg*(*Xops:mCFP*) retina exhibits a persistent loss of only rod photoreceptors, even in the absence of any retinal insult, such as constant bright light. Furthermore, the *Tg*(*Xops:mCFP*) retina revealed TUNEL labeling in the INL in a morphology similar to Müller glia. Thus, the engulfment of apoptotic rod photoreceptors by Müller glia is a common early feature of the damaged zebrafish retina and may be required for regenerative Müller glial cell stimulation. TUNEL labeling in the Müller glia can be detected early, within the first 12 h of light treatment, and represents one of the earliest signs of Müller glial response to apoptotic photoreceptor damage. Robust regeneration of the light-damaged zebrafish retina follows and a normal complement of rod and cone photoreceptors reform within 28 days after terminating the constant light treatment (**Figure 4(c)**).

Figure 2 Schematic of persistent neurogenesis in the adult zebrafish retina. (a) In the adult retina, stem cells (SC) in the circumferential marginal zone (CMZ) continue to proliferate through asymmetric cell division to produce neuronal progenitor cells (pink circles), which then exit the cell cycle to become newly differentiated cells (blue circles). These CMZ-derived cells differentiate into cone, horizontal, bipolar, amacrine, and ganglion neurons, as well as Müller glia (not labeled), but not rod cells. Throughout the remainder of the retina, a limited number of Müller glial cells (MG) divide asymmetrically to produce a Müller glial cell and a neuronal progenitor cell (NP). (b) As the CMZ stem cells continue to produce neuronal progenitors (pink circles), there is a radial growth of the adult retina, with the most recently differentiated neurons (green circles) located closer to the CMZ than the older neurons (blue circles). In the central region of differentiated retina, the new NP cell continues to divide and migrates to the ONL. Once these NP cells reach the ONL, they are termed rod precursor cells (RP). (c) The CMZ continues producing new retinal cells (yellow circles), which are located closest to the CMZ. The RP cells in the ONL continue to proliferate, with some of the daughter cells differentiating into rod photoreceptors (purple circles). The newly differentiated rod cell intercalates between differentiated cone cells to maintain the density of rod photoreceptors during the radial expansion of the retina. (d) Persistent neurogenesis continues as the CMZ-based retinal stem cells and the Müller-glial-derived neuronal progenitors continue to produce new neurons at the margin and central retina, respectively. CMZ, circumferential marginal zone; GCL, ganglion cell layer; INL, inner nuclear layer; MG, Müller glial cell; ONL, outer nuclear layer; NP, neuronal progenitor; RP, rod precursor cell; SC, stem cell.

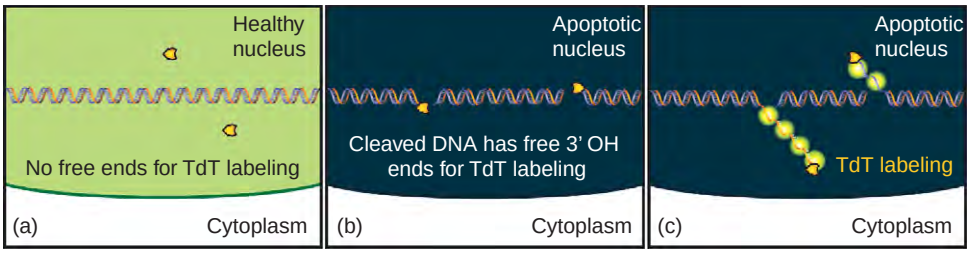

Figure 3 TUNEL assay detects the fragmented DNA in apoptotic nuclei. (a) A healthy nucleus contains intact DNA, which contains only a single 3′ hydroxyl group at the end of each chromosome. The terminal deoxynucleotidyl transferase enzyme (TdT), which can add polymerized stretches of deoxyuridine triphosphate (dUTP), without the need for a complementary strand of DNA with which to pair nucleotides (template-independent). TdT binds to both ends of the linear chromosomal DNA and adds only a few dUTPs per healthy nucleus. (b) Apoptosis results in the fragmentation of the DNA, which generates a very large number of free 3′ hydroxyl ends. (c) TdT adds dUTPs to each of the now many generated 3′ hydroxyl ends. The large number of dUTP molecules can either directly fluoresce because they are tagged with a fluorochrome or, in the case of biotinylated-dUTP, are detected by tagged Streptavidin molecule to generate a strong fluorescent signal in the apoptotic nucleus. Because of the absence of the genomic DNA in the cytoplasm, little, if any, fluorescent signal is present in the cytoplasm of an apoptotic cell.

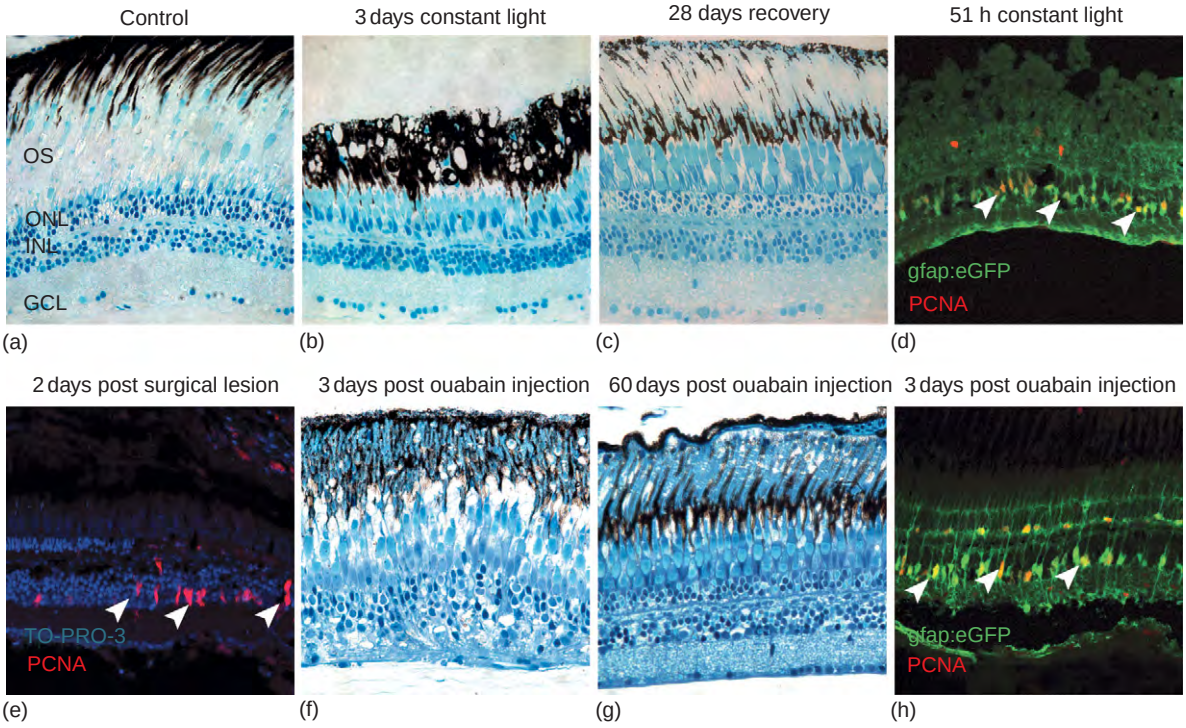

Figure 4 Cell-type restricted retinal damage in zebrafish. (a) Histological section of an undamaged zebrafish retina (control) with the following labeled: outer segments (OS), outer nuclear layer (ONL), inner nuclear layer (INL), and ganglion cell layer (GCL). (b) After 3 days of constant light, the loss of photoreceptor nuclei in the ONL and reduced outer segment integrity relative to the control are evident. (c) Photoreceptors are regenerated only 28 days post light treatment based on the nuclear density and thickness of photoreceptor nuclei in the ONL and the restoration of the photoreceptor outer segments. (d) A transgenic zebrafish line, *Tg*(*gfap:eGFP*), expresses EGFP in the Müller glia from the *gfap* promoter. Light-induced damage of this transgenic line induces proliferating cell nuclear antigen (Pcna-red) in a subset (arrowheads) of the Müller glial cells (green) after only 51 h of constant intense light. (e) Proliferating cell nuclear antigen (Pcna-red) immunolabeling Müller glial cells (arrowheads) at 2 days after a surgical lesion (TO-PRO-3 labeling of nuclei-blue) is very similar to the response observed in the light-damaged retina (d). (f) Three days after intraocular injection of ouabain, the damaged retina revealed lost retinal ganglion cells and INL neurons, without significant loss of ONL photoreceptors. (g) Sixty days after ouabain injection, the regenerated retina revealed a GCL and INL that is nearly indistinguishable from wild type (a). (h) The *Tg(gfap:eGFP)* line revealed that Pcna was detected in a subset of Müller glial cells (arrowheads) at 3 days after intraocular injection of ouabain.

In light-damaged zebrafish retinas, the Müller glia exhibit increased expression of proliferating cell nuclear antigen (Pcna), which is a component of the DNA replication machinery. The expression of this protein in the Müller glia indicates their reentry into the cell cycle (**Figure 4(d)**). To confirm that the Müller glia were proliferating, light-damaged *Tg*(*gfap:EGFP*) retinas, which express enhanced green fluorescent protein (EGFP) specifically in the Müller glial cells from the zebrafish glial fibrillary acidic protein (*gfap*) promoter, were coimmunolabeled for the expression of the proliferation marker Pcna. The number of actively dividing Müller glia, coexpressing EGFP and the red fluorescing anti-Pcna antibody, increases through 51 h of constant intense light treatment (**Figure 4 (d)**), at which point the Müller glial-derived INL neuronal progenitor cells continue to proliferate to produce clusters of 8–12 progenitor cells associated with a single Müller glial cell. While this suggests that all the neuronal progenitor cells in a cluster are derived from a single Müller glial cell and remain associated with that glial cell, this has not been formally demonstrated. This Müller glial cell-based regeneration response is conserved throughout a number of different damage models. For example, either surgical lesion or ouabain injection results in the death of many different neuronal cell types in the retina, and they both exhibit increased proliferation of the Müller glial cells (**Figure 4(e)–4(h)**).

Curiously, not all of the Müller glial cells proliferate in response to constant intense light treatment. Earlier reports suggested that a threshold of rod cell death was required to induce the Müller glial proliferation response. However, intravitreal injection of a low concentration of ouabain into the zebrafish retina resulted in massive death of the neurons in both the ganglion cell and INLs, with minimal cell death of photoreceptors (**Figure 4(f)**). Regeneration of the ouabain-damaged retina takes longer than the light-damaged retina, but still produces a relatively normal retina by 60 days post ouabain injection (**Figure 4(g)**). This demonstrates that significant rod or cone cell death is not required to induce retinal regeneration from the Müller glia (**Figure 4(h)**). Furthermore, this suggested that the number of apoptotic neurons, rather than the type of neuron, was critical for inducing this regeneration response.

To address if only rod photoreceptor cell death was sufficient to induce a Müller glial-derived regeneration response, the *Tg*(*Xops:mCFP*) transgenic line and the phosphodiesterase 6c (*pde6c*) mutant line were analyzed. The *pdge6* mutant line fails to maintain cone cells, in contrast to the rod photoreceptor cell death in the *Tg*(*Xops:mCFP*) fish. While no detectable Müller glial proliferation response was observed in the *Tg*(*Xops:mCFP*) line, a small, but significant, Müller glial proliferation response was detected in the *pdge6* mutant line. This suggested that loss of rods requires only increased proliferation of the ONL rod precursor cells that were derived from the neuronal progenitor cells during persistent neurogenesis, while loss of cones requires the increased proliferation of the pluripotent Müller glia.

To further test this hypothesis, a *Tg*(*zop:ntr*) transgenic line was generated that expresses the bacterial *nitroreductase b* (*ntr*) gene from the zebrafish *rhodopsin promoter* (*zop*). The NTR enzyme converts the prodrug, metronidazole, into a cell-autonomous toxin within NTR producing cells. Exposing a *Tg*(*zop:ntr*) transgenic line, expressing NTR in all rod photoreceptors, to metronidazole results in the death of only rod photoreceptors and the induction of a Müller glial proliferation response. Addition of metronidazole to a similar transgenic line that expresses NTR in only a subset of rods, however, failed to induce the Müller glial response. These data suggest that it is the magnitude of the cell death that determines if the Müller glia exhibit a robust proliferation response. The failure of the *Tg*(*Xops:mCFP*) transgenic line to induce the Müller glial proliferation response may be due to the rod cell death being small and chronic relative to the massive and acute cell death observed in the metronidazole-treated *Tg*(*zop:ntr*) transgenic retinas that express NTR protein in all the rod photoreceptors.

Discovery and Analysis of Candidate Genes Involved in Retinal Regeneration

Several groups have performed microarray analyses of mRNA expression patterns in different retinal damage models to determine what genes might change their expression during specific points of regeneration. In both the surgical-lesioned and light-damaged models, signal transducer and activator of transcription 3 (*stat3*) and its negative regulator suppressor of cytokine signaling 3 (*socs3*) exhibited increased expression shortly after the retinal insult (e.g., within 16 h of starting the constant intense light treatment). The increased *stat3* expression suggests that Gp130 receptor signaling is involved in the early damage response. Gp130 is a promiscuous receptor that binds a number of different extracellular signaling molecules, such as cytokines, to activate the Stat3 transcription factor in neuronal niches to promote cell proliferation in the adult vertebrate brain. The *socs3* gene, which is transcriptionally activated by the Stat3 protein, encodes a protein that binds the activated receptor to prevent further Stat3 activation. Increased *stat3 expression* is also known to occur in RGCs following optic nerve crush, further supporting Stat3's role in the damage response. Microarrays also revealed that both the achaete-scute complex-like 1a (*ascl1a*) pro-neural gene and the notch pathway genes were upregulated in the surgical-lesioned and light-damaged retinal models. By contrast, retinal progenitor genes, such as *rx* and *vsx2*, whose expression are maintained in the CMZ throughout life, are not significantly increased in expression in the damaged retina.

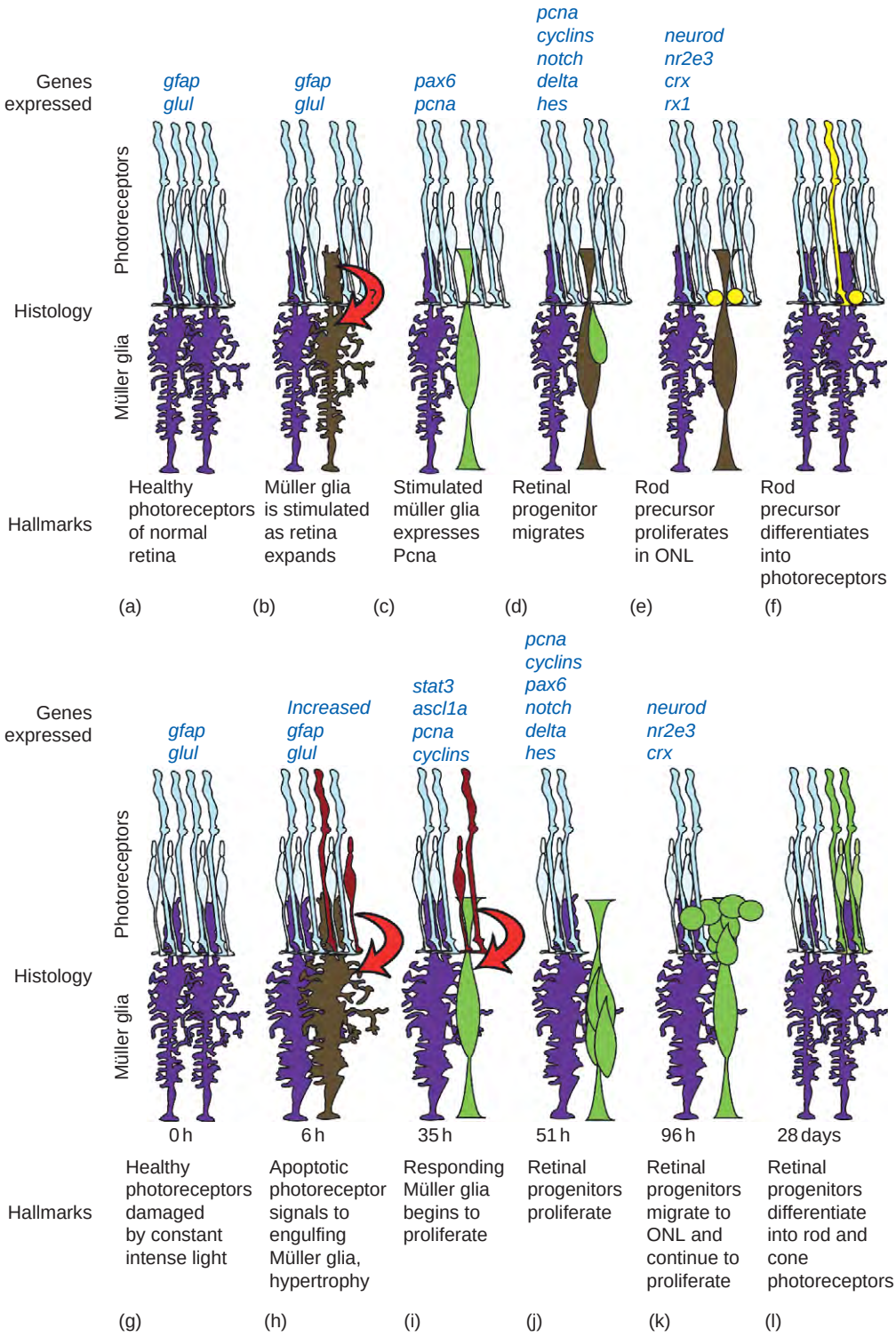

Figure 5 Schematic comparison of zebrafish retinal development and regeneration. (a) The healthy retina is made up of rod (tall dark blue) and cone (short light blue) photoreceptors interdigitating with the processes of Müller glial cells (purple). Other retinal neurons are neglected for simplicity. Müller glial cells express genes indicative of their differentiated state, glial fibrillary acidic protein (gfap) and glutamine synthetase (glul). (b) As the retina expands, a Müller glial cell becomes stimulated to proliferate (brown), possibly due only to slow or sporadic progression through the cell cycle. (c) The stimulated Müller glial cell (green) expresses *pcna* and *pax6* as it begins to divide. (d) The cell division in panel C produces a daughter Müller glial cell (brown) and a neuronal progenitor cell (green), which expresses *pcna, cyclins, notch, delta*, and *hes* genes as it migrates to the photoreceptor layer. (e) This neuronal progenitor cell reaches the ONL and is now called a rod precursor cell (yellow), as it expresses *neurod* and the rod specification genes *nr2e3, crx,* and *rx1*. (f) The rod precursor cell divides with one daughter cell differentiating into a rod photoreceptor (green). (g) The undamaged retina,

This suggests that Müller glia exhibit a state of competency that is downstream of the CMZ stem cells, but upstream of retinal neuron differentiation.

The ability to test the function of these various candidate genes in the regenerating retina has been recently advanced by the development of a method to electroporate morpholinos into the adult retina. Morpholinos are modified oligonucleotides that contain a morpholine ring, rather than deoxyribose. The morpholinos, which are complementary to a specific mRNA sequence, can base pair with and transiently block the efficient translation of the target mRNA. Because some protein could still be correctly translated in the presence of a morpholino, these loss-of-function experiments and organisms are termed knockdowns and morphants, respectively. Morpholinos have traditionally been introduced into zebrafish embryos by direct injection into either the relatively large cells of the early embryo (1–32 cell stage) or the yolk. The morpholinos then diffuse into the daughter cells as they divide during embryonic development. This approach has tested the function of numerous proteins in zebrafish development. Recently, morpholinos that are covalently attached to a positively charged fluorochrome, lissamine, have been injected into the vitreous and then electroporated into the adult retina. These morpholinos can disrupt retinal regeneration if they are electroporated into the retina to knockdown the expression of a target protein prior to its role in regeneration.

Proof-of-principle experiments to test the effectiveness of this method were shown for the requirement of Pcna in retinal regeneration. Morpholino-induced knockdown of Pcna expression resulted in the Müller glia failing to proliferate in the light-damaged retina, which led to the premature death of the stimulated Müller glial cells due to their inability to proceed through the S phase of the cell cycle. Retinas that were injected and electroporated with anti-Pcna morpholinos also failed to upregulate expression of the retinal progenitor cell marker *pax6* in the Müller glial-derived neuronal progenitor cells. Similar morpholino knockdown studies revealed that Stat3 and Pax6 are also required at different steps in the regeneration process. Microarray analyses of mRNA expression at different time points during regeneration of the surgical-lesioned and light-damaged retinas have revealed numerous candidate genes for functional study. The electroporation of morpholinos will permit a relatively rapid loss-of-function analysis to elucidate the genes that are required for regeneration and the key steps and processes underlying retinal regeneration.

Events Underlying Regeneration of the Light-Damaged Retina

Adult Müller glial cells are characterized by the expression of cell-specific markers (**Figure 5(a)**), such as glutamine synthetase (Glul) and glial fibrillary acidic protein (Gfap) among others. During persistent retinogenesis, rods are added to the established repeating mosaic of cone and rod photoreceptors from the Müller glial cell population. It is not clear if there is a signal (arrow) to stimulate Müller glia proliferation or if a small subset of Müller glia remain in a slow cell cycle (**Figure 5(b)**). This limited number of proliferating Müller glia can be detected by Pcna and Pax6 expression (**Figure 5(c)**). The small number of dividing Müller glial cells produce a daughter Müller glial cell (**Figure 5(d)**, brown) and a neuronal progenitor cell (green), which continues to express genes important in the cell cycle (Pcna and cyclins) and genes required for cell specification signaling (*notch, delta,* and *hes*). The neuronal progenitor continues to proliferate and migrates to the ONL. As the neuronal progenitor reaches the ONL (where it is now called a rod precursor), it continues dividing or begins to differentiate, expressing rod specification genes (neurogenic differentiation (*neurod*), nuclear receptor subfamily 2e3 *nr2e3, crx,* and *rx1*) and giving rise only to rod photoreceptors (**Figure 5(f)**, green).

Upon light-induced retinal damage (or other forms of retinal insult), Müller glia hypertrophy and transiently increase their expression of Glul and Gfap (**Figure 5(h)**). If the number of dying rods and cones (**Figure 5(h)**, red) is sufficiently large, the Müller glial cells increase their expression of the *ascl1a* and *signal transducer* (*stat3* genes (**Figure 5(i)**) through unclear mechanisms. Electroporation of morpholinos into the retina prior to inducing retinal damage revealed that both *stat3* and *ascl1a* are independently required for the Müller glial proliferation response. The reentry of these Müller glia into the cell cycle is accompanied by the increased expression of the

identical as in 4A is repeated here for comparison. (h) Photoreceptors (light blue) begin to undergo apoptosis (red) within 6 h of entering constant intense light treatment (rod precursors have been ignored for simplicity). The damaged photoreceptors signal (arrow) a subset of the Müller glial cells (brown) to hypertrophy, increase expression of *gfap,* and *glul,* and phagocytose the apoptotic rod cell bodies. (i) At 35 h, responding Müller glial cells (green) increase expression of the early response genes, such as *stat3* and *ascl1a,* and the cell cycle regulatory genes, the *cyclins.* Loss of Pcna expression by morpholino-induced knockdown, results in the failure of responding Müller glial cells to proliferate and regenerate the lost rods and cones. Similarly, morpholino-induced knockdown of Stat3 expression significantly reduces the number of proliferating Müller glial cells. (j) Pcna-positive neuronal progenitor cells are clustered around a Müller glial cell and exhibit increased expression of retinal progenitor genes, such as *pax6*, and genes involved in intracellular signaling pathways, such as Notch. (k) Pcna-positive neuronal progenitors display several neuronal and photoreceptor differentiation markers, including *neurod, nr2e3*, and *crx*, as they migrate to the damaged ONL. (l) One month after exiting the constant intense light treatment, regenerated photoreceptors (green) have differentiated and are indistinguishable from the undamaged photoreceptors.

cell cycle regulatory proteins, the cyclins. The Müller glial cell divisions produce neuronal progenitor cells, which continue to proliferate (expressing Pcna and the cyclins) and begin to express the retinal progenitor gene *pax6* and genes in the Notch and Delta neuronal signaling pathways (**Figure 5(j)**). As the neuronal progenitor cells migrate toward the ONL, they begin to express genes that are required for the commitment and differentiation of rod and cone photoreceptors (*neuroD, nr2e3*, and *crx*; **Figure 5(k)**). Within 28 days of ending the constant intense light treatment, the rod and cone photoreceptors have regenerated (**Figure 5(l)**).

Vestigial Retinal Regeneration Activity in Mammals

The finding that the Müller glial cell acts as an adult neuronal stem cell in the regeneration of the damaged zebrafish retina suggests that it potentially could produce a similar regeneration response in the damaged mammalian retina. Recent studies support the hypothesis that mammalian Müller glia possess some of the features of adult neuronal stem cells. Transplanted rodent Müller glia into a damaged retina will produce rhodopsin-positive cells. As expected, intraocular injection of neurotoxic doses of *N*-methyl-D-aspartic acid (NMDA), which is a synthetic amino acid that binds a glutamate receptor, results in the death of many retinal cell types. However, NMDA damage in the rat retina is followed by a small number of Müller glia proceeding through one cell division to yield a limited number of cells that differentiate into photoreceptors and bipolar cells. This Müller glial cell proliferation and regeneration response can be slightly enhanced with the addition of various growth factors. Injection of the toxin *N*-methyl-N-nitrosourea (NMU) into the adult rat eye, which specifically kills photoreceptors, induces Müller glial hypertrophy and increased expression of GFAP and the neural stem cell marker, nestin, followed by the proliferation of some Müller glia. While BrdU labeling confirmed that the Müller glia actively divided in response to the NMU damage, only 42% of the BrdU-labeled cells remained 2 weeks after the NMU injection. Of these surviving BrdU-labeled cells, which were all located in the INL, 58% expressed glutamine synthetase (suggesting they corresponded to Müller glial cells that initially divided) and only 8% expressed rhodopsin. Thus, there were very few rhodopsin-positive cells produced by this Müller cell division and the ones that were generated, failed to properly migrate to the ONL. Expression or addition of various growth factors increased the number of proliferating Müller glia only to a small extent. Activation of various signaling pathways, such as Notch, similarly resulted in only a slight increase in the number of Müller glial-derived neuronal progenitors in the damaged rodent retina. While retinal damage induced some mammalian Müller glia to proliferate and various growth factors or signaling pathways slightly increased that number, there remained an insufficient number of proliferating Müller glial cells and neuronal progenitor cells to properly regenerate all the neurons lost from the retinal damage. Analyzing the mechanisms underlying the robust Müller glial proliferation response in the light-damaged zebrafish retina will provide important clues as to why the regenerative capacity of the mammalian retina is so limited.

Similarities and Differences of Development with Retinal Ontogeny/Genesis

As discussed above, Müller glia and the neuronal progenitor cells respond to retinal damage by increasing the expression of many of the retinal progenitor genes, such as *pax6*, that are expressed during embryogenesis and near the CMZ throughout the life of the fish. The inability of the mammalian Müller glial cells to mount a sufficiently robust proliferative and regenerative response may be due to differences in the signals that stimulate the Müller glia to respond. All attempts to stimulate sufficient levels of Müller glial proliferation in the mammalian retina have met with very limited success. Conversely, the failure to robustly proliferate may be due to intrinsic differences between the mammalian and zebrafish Müller glial cells. For example, transplanted mammalian Müller glial cells into a damaged retina will differentiate into rhodopsin-positive cells that are predominantly restricted to the INL, rather than repopulating the ONL. Thus, a further understanding of the signals that stimulate the zebrafish Müller glial and neuronal progenitor cells to proliferate and migrate may reveal insights into how to better manipulate the mammalian retina, and by extension, potentiate human retinal regeneration.

See also: Color Blindness: Inherited; Injury and Repair: Light Damage; Retinal Histogenesis.

Further Reading

Bailey, T. J., El-Hodiri, H., Zhang, L., et al. (2004). Regulation of vertebrate eye development by Rx genes. *International Journal of Developmental Biology* 48: 761–770.

Bernardos, R. L., Barthel, L. K., Meyers, J. R., and Raymond, P. A. (2007). Late-stage neuronal progenitors in the retina are radial Muller glia that function as retinal stem cells. *Journal of Neuroscience* 27: 7028–7040.

Fausett, B. V. and Goldman, D. (2006). A role for alpha1 tubulin-expressing Muller glia in regeneration of the injured zebrafish retina. *Journal of Neuroscience* 26: 6303–6313.

Fimbel, S. M., Montgomery, J. E., Burket, C. T., and Hyde, D. R. (2007). Regeneration of inner retinal neurons after intravitreal injection of ouabain in zebrafish. *Journal of Neurosciences* 27: 1712–1724.

Kassen, S. C., Ramanan, V., Montgomery, J. E., et al. (2007). Time course analysis of gene expression during light-induced

photoreceptor cell death and regeneration in albino zebrafish. *Developmental Neurobiology* 67: 1009–1031.

Malicki, J. (2000). Harnessing the power of forward genetics – analysis of neuronal diversity and patterning in the zebrafish retina. *Trends in Neurosciences* 23: 531–541.

Morris, A. C., Scholz, T. L., Brockerhoff, S. E., and Fadool, J. M. (2008). Genetic dissection reveals two separate pathways for rod and cone regeneration in the teleost retina. *Developmental Neurobiology* 68: 605–619.

Morris, A. C., Schroeter, E. H., Bilotta, J., Wong, R. O., and Fadool, J. M. (2005). Cone survival despite rod degeneration in XOPS-mCFP transgenic zebrafish. *Investigative Ophthalmology and Visual Science* 46: 4762–4771.

Otteson, D. C. and Hitchcock, P. F. (2003). Stem cells in the teleost retina: Persistent neurogenesis and injury-induced regeneration. *Vision Research* 43: 927–936.

Raymond, P. A., Barthel, L. K., Bernardos, R. L., and Perkowski, J. J. (2006). Molecular characterization of retinal stem cells and their niches in adult zebrafish. *BMC Developmental Biology* 6: 36.

Raymond, P. A. and Hitchcock, P. F. (2000). How the neural retina regenerates. *Results and Problems in Cell Differentiation* 31: 197–218.

Thummel, R., Kassen, S. C., Enright, J. M., et al. (2008). Characterization of neuronal progenitors in zebrafish adult retinal regeneration. *Experimental Eye Research* 87: 433–444.

Thummel, R., Kassen, S. C., Montgomery, J. E., Enright, J. M., and Hyde, D. R. (2007). Inhibition of Muller glial cell division blocks regeneration of the light-damaged zebrafish retina. *Developmental Neurobiology* 68: 392–408.

Vihtelic, T. S. and Hyde, D. R. (2000). Light-induced rod and cone cell death and regeneration in the adult albino zebrafish (*Danio rerio*) retina. *Journal of Neurobiology* 44: 289–307.

Vihtelic, T. S., Soverly, J. E., Kassen, S. C., and Hyde, D. R. (2006). Retinal regional differences in photoreceptor cell death and regeneration in light-lesioned albino zebrafish. *Experimental Eye Research* 82: 558–575.

Yurco, P. and Cameron, D. A. (2005). Responses of Muller glia to retinal injury in adult zebrafish. *Vision Research* 45: 991–1002.